

Annual Cumulated Index

ACCESSION NOS. A71-10001 to A71-45384

INTERNATIONAL AEROSPACE ABSTRACTS

PART 2, SUBJECT INDEX, M - Z

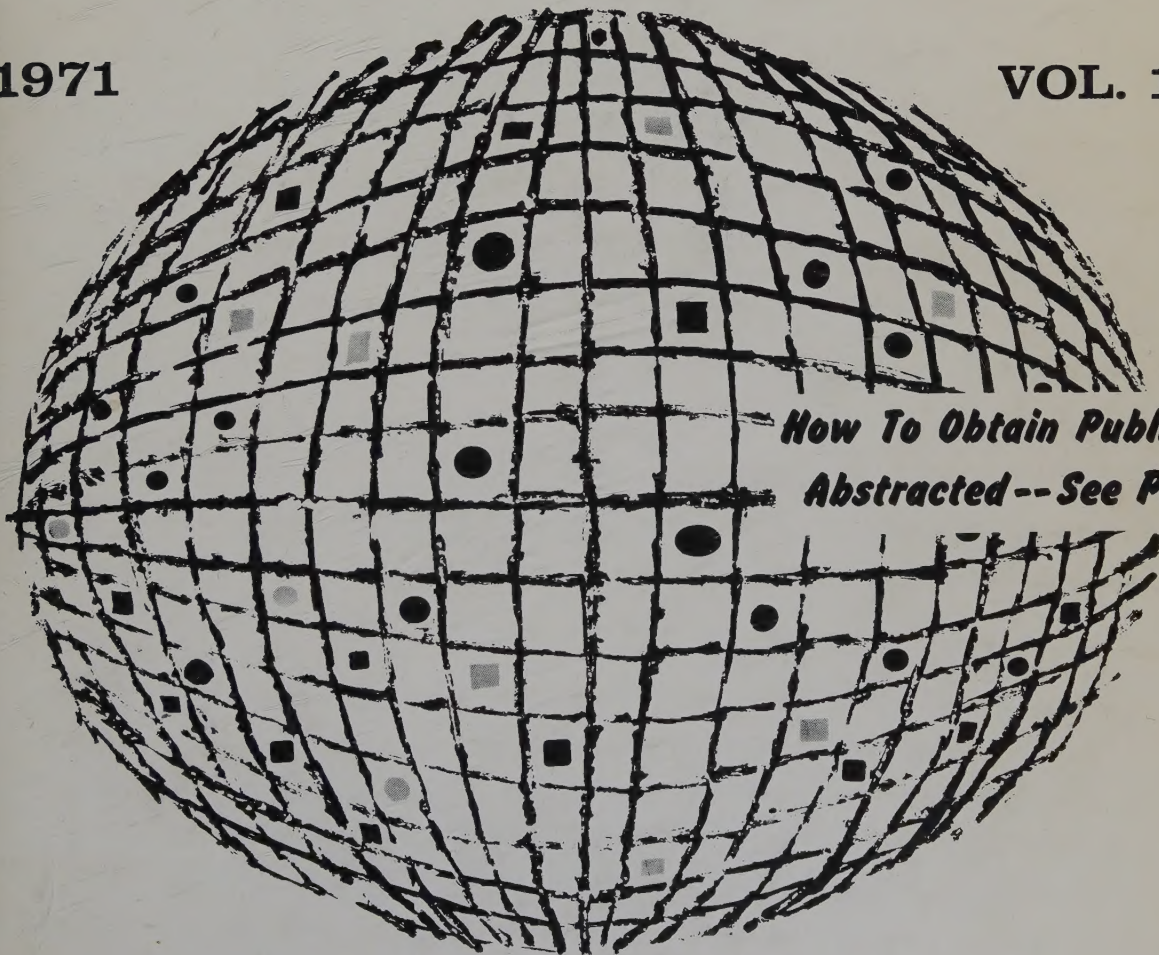
U. of ILL. LIBRARY

JAN 17 1972

CHICAGO CIRCLE

1971

VOL. 11



*How To Obtain Publications
Abstracted--See Page V*

PUBLISHED BY THE TECHNICAL INFORMATION SERVICE
AMERICAN INSTITUTE OF AERONAUTICS AND ASTRONAUTICS

TL
500
I 57
Vol. 11
1971
subj. index
M-Z
n/c

Science

INTERNATIONAL AEROSPACE ABSTRACTS

**ANNUAL
CUMULATED
INDEX**

**PART 2
SUBJECT INDEX, M – Z**

**VOLUME 11
JANUARY – DECEMBER
1971**

ACCESSION NUMBERS A71-10001 to A71-45384

INTERNATIONAL AEROSPACE ABSTRACTS is prepared and published semimonthly (except June and December, which have three issues) by the Technical Information Service, American Institute of Aeronautics and Astronautics, Inc., for the Institute and the National Aeronautics and Space Administration under Contract No. NASW-1949. Editorial and Subscription Offices: 750 Third Avenue, New York, N. Y. 10017. Copyright © 1971 by the American Institute of Aeronautics and Astronautics, Inc. (The indexes, however, may be reproduced for any bibliographic purpose.)

Telephone: 212 TN-7-8300

TWX: 212 867-7265

SUBSCRIPTION INFORMATION. Semimonthly issues: United States and Possessions, 1 year, \$110 postpaid; Foreign Countries, 1 year, \$125 postpaid. Cumulated Index Volumes: United States and Possessions, 1 year, \$75 postpaid; Foreign Countries, 1 year, \$90 postpaid. Second-class postage paid at Phillipsburg, N. J.

INTRODUCTION

INTERNATIONAL AEROSPACE ABSTRACTS (IAA) is an abstracting and indexing service covering the world's published literature in the field of aeronautics and space science and technology. IAA is issued semimonthly, on the 1st and 15th of each month.

Coverage of Published Literature

The following types of publications are covered in IAA:

- Periodicals (including government-sponsored journals) and books.
- Meeting papers and conference proceedings issued by professional societies and academic organizations.
- Translations of journals and journal articles.

Coverage of Reports ("Unpublished" Literature)

Abstracts and indexes of report literature are issued in SCIENTIFIC AND TECHNICAL AEROSPACE REPORTS (STAR), which is published by the Scientific and Technical Information Office, National Aeronautics and Space Administration.

By special arrangement between NASA and the American Institute of Aeronautics and Astronautics, IAA is issued in coordination with the twice-monthly schedule of STAR, which appears on the 8th and 23rd of each month.

IAA and STAR both utilize identical subject categories and indexes, which are described below.

Thus the two services provide comprehensive access to the national and international unclassified report and published literature of current significance to aerospace science and technology.

Arrangement of the Semimonthly Issues

IAA is arranged in two major sections:

- (1) Abstracts Section. This section contains complete bibliographic citations with informative abstracts, arranged by appropriate subject categories to facilitate scanning. The subject categories are numbered from 01 to 34, and the scope of each category is outlined in the Table of Contents and again at the beginning of each category in the Abstracts Section. Each abstract is prefixed by the IAA accession number.
- (2) Index Section. Five indexes are contained in this section: Subject, Personal Author, Contract Number, Meeting Paper and Report Number, and Accession Number. Each index is prefaced by explanatory notes to guide the user to the desired abstract.

Cumulated Indexes

The semi-annual cumulated index is issued promptly at the end of the first six months and the annual cumulated index is issued promptly at the end of the twelve-month period.

Each cumulated index contains the following sections: A—Subject Index, B—Personal Author Index, C—Contract Number Index, D—Meeting Paper and Report Number Index, and E—Accession Number Index.

Indexing Vocabulary

The Preliminary Edition of the NASA THESAURUS (December 1967) (NASA SP-7030) is the authority for the indexing vocabulary that appears in the subject indexes to STAR and IAA. The NASA Thesaurus should be consulted for a total picture of the current indexing vocabulary and associated cross-reference structure. Copies of the NASA Thesaurus may be obtained from the National Technical Information Service or the U.S. Government Printing Office at a price of \$8.50 for the three-volume set.

Information regarding SCIENTIFIC AND TECHNICAL AEROSPACE REPORTS and the availability of INTERNATIONAL AEROSPACE ABSTRACTS to organizations having contractual arrangements with NASA may be obtained from the following address:

National Aeronautics and Space Administration
Scientific and Technical Information Office
Attention: Code KSI
Washington, D. C. 20546

how to obtain publications abstracted

All documents abstracted are available from the AIAA Technical Information Service as follows:

- Paper copies of accessions announced in IAA and of other published articles in the TIS library are available at \$5.00 per document up to a maximum of 20 pages. The charge for each additional page is \$0.25.
- Paper copies of accessions announced in Scientific and Technical Aerospace Reports (STAR) and of similar unpublished reports in the TIS library are available at the rate of \$0.25 per page, minimum order \$5.00.
- Microfiche of documents announced in IAA are available at the rate of \$1.00 per microfiche on demand. Documents available in this manner are identified by the symbol # following the accession number in the Abstracts Section and in the Meeting Paper and Report Number and the Accession Number Indexes.
- Minimum air-mail postage to foreign countries is \$1.00.
- A number of publications, because of their special characteristics, are available only for reference in the library.

PLEASE REFER TO THE ACCESSION NUMBER WHEN REQUESTING PUBLICATIONS

Address all inquiries and requests to:

Technical Information Service
American Institute of Aeronautics
and Astronautics, Inc.
750 Third Avenue, New York, N. Y. 10017

Telephone: 212 TN-7-8300
TWX: 212 867-7265

CROSS REFERENCES

The subject index includes two types of cross references to aid the user of the index in locating the material being sought:

1. "USE" references (U) direct the user to alternate headings under which material on the subject will be found, for example

COLUMBIUM
U NIOBIUM

2. "NARROWER TERM" references (NT) refer the user to more specific headings in the same subject area, for example

LUMINESCENCE
NT ELECTROLUMINESCENCE

A Notation of Content, rather than the title of the publication, appears under each subject heading; it is listed under several subject headings which provide multiple access to the subject of each accession. The IAA accession number is located under and to the right of the Notation of Content. It is preceded by numbers identifying the issue and page of *International Aerospace Abstracts* where the abstract is located.

To illustrate:

Issue Number	Page Number	Accession Number
05	p795	A71-16573

M

M WINGS

U VARIABLE SWEEP WINGS

MACH CONES

Lunar Mach cone in flow of magnetized warm collisionless solar plasma from Explorer 35 observations
01 p0162 A71-11489

Detonation waves Mach configuration, noting frontal structure similarity, lead shock velocity and non-reactive blast wave model
05 p0833 A71-16507

Mach cones reflection at thin wing subsonic leading edges in supersonic flow, considering axial disturbance velocity and pressure distributions
09 p1384 A71-23616

Shock standoff distance and Mach disk diameter measurements in underexpanded sonic jets, using nitrogen dioxide-tetroxide working fluid
17 p2670 A71-34895

MACH INERTIA PRINCIPLE

Critique on Mach principle, discussing incompatibility between system inertia in universe and general relativity theory
09 p1522 A71-22980

MACH NUMBER

Blunt body problem with detached shock, considering methods of lines and integral relations agreement for wide range of Mach numbers
03 p0344 A71-14449

Incident shock test time and reflected pressure for turbulent boundary layer at high Mach numbers in air and nitrogen
04 p0563 A71-14663

Laminar and turbulent boundary layer effects on flow velocity and Mach number behind shock front
04 p0567 A71-14664

Finite difference simulation of high energy Mach 120 to 40 air shock experiment
04 p0565 A71-14678

Steady two dimensional ideal gas flow past blunt body at incident infinite Mach number, obtaining gas dynamic variable asymptotic expansions as kappa approaches infinity
04 p0528 A71-15553

Shock initiated detonation wave propagation in combustible hydrogen oxygen flow in constant area duct, considering wave initiation Mach number and ignition temperature
05 p0834 A71-16519

Shock waves in nitrogen, carbon dioxide and mixtures, measuring Mach number for deviation evaluation from vibrational and dissociation equilibria
05 p0835 A71-16522

Turbulent boundary layer separation at low supersonic Mach numbers based on blowdown wind tunnel tests
05 p0735 A71-16582

Gaseous film cooling effectiveness under varying conditions of free stream turbulence intensity, hot gas acceleration, Mach number and film coolant flow rate
07 p1219 A71-18760

Axial Mach number distribution of supersonic flow in rocket nozzle with Rao optimum contour
07 p1093 A71-20366

Mach disk in underexpanded exhaust plume predicted by dividing flow field into subregions [AIAA PAPER 70-231]
09 p1382 A71-22097
Cut-off Mach number of sonic bang propagation on ground for flight track in relation to atmospheric parameters
09 p1383 A71-23577

Unsteady low Mach number flow calculation by singular perturbation method with matched asymptotic expansions, considering application to aerodynamic noise
10 p1549 A71-23936

Sound generation by frontal collision of double pair vortices, showing pressure proportional to Mach number
10 p1641 A71-24346

Triple point trajectory of shock-shock Mach reflection off plane wall, comparing to Whitham theory
11 p1752 A71-26192

Shock wave incidence on wedge moving at supersonic speed, considering uniform flow region on upper wedge surface for specific values of Mach number and vertex angle
12 p1897 A71-27445

Alpha radiation machmeter with semiconductor pulse detectors, discussing supersonic regime effects on rate variations
12 p1908 A71-27607

Isomagnetic potential discontinuity of electrostatic character in collisionless plasma shock waves, studying Mach number effect
13 p2105 A71-28169

Altitude-airspeed and Mach number pressure transducer with diaphragm free of temperature and vibration effects
14 p2243 A71-30322

Hypersonic wakes behind wedges for various angles of attack, determining near and far wakes [AIAA PAPER 71-563]
15 p2344 A71-31558

Collisionless small amplitude shocks in plasmas, considering wave dispersion and critical Mach number effects
15 p2459 A71-32561

Mach number effects on axial flow transonic compressor characteristics, using empirical corrections based on measured three dimensional grid characteristics
15 p2471 A71-32715

Shock wave diffraction patterns on plane walled convex corners in air, nitrogen and carbon dioxide at various Mach numbers
16 p2556 A71-32918

High temperature high Mach number expansion tube flows, determining impurities by time integrated spectroscopic measurements
16 p2551 A71-33155

Mach number effects on flow field in gas bearings at high subsonic and supersonic tangential speeds based on perturbation theory [ASME PAPER 71-APM-U]
18 p2926 A71-36263

Implicit continuous fluid Eulerian time dependent multidimensional fluid flows calculation at arbitrary Mach number based on finite difference approximation
18 p2908 A71-36345

Pressure distribution over deflected flap as function of boundary layer separation, flap geometry, Reynolds number and Mach number
18 p2972 A71-36435

Gas flow through hypersonic conical nozzle in shock-gun tunnel, measuring pressure ratio and Mach number distributions at test section
18 p2849 A71-37024

Gas resonant oscillations in closed end tube, describing time-periodic motion by perturbation method with Mach number as flow parameter
20 p3211 A71-39078

Two dimensional supersonic base flow with small Mach number recirculation zone, determining jet line by variational principle of Poisson equation
20 p3176 A71-39414

High Alfvén Mach number collisionless plasma flow in weak magnetic field, investigating momentum transfer mechanisms and coupling lengths
22 p3581 A71-41890

High Mach number turbulent magnetosonic shocks generation by driving reflecting piston into plasma, simulating by electromagnetic particle code
23 p3708 A71-42893

Two dimensional supersonic variable area nozzle geometry calculation as function of Mach number

23 p3626 A71-44071

Establishment time measurement for laminar separated flow, using shock tunnel driver section to give long test time at low incident Mach number

24 p3818 A71-44628

Mach number distribution along critical streamline in compressed layer in front of cylinder in supersonic flow

24 p3790 A71-45101

MACH-ZEHNDER INTERFEROMETERS

Relativistic self confined electron beam produced plasmas, measuring electron density profile by multiple pass Mach-Zehnder laser illuminated interferometer

02 p0289 A71-11946

Thermal radiation-conduction interaction in horizontal fluid layer, obtaining temperature profiles with Mach-Zehnder interferometer

04 p0685 A71-15515

Mach-Zehnder interferometer measurements of average temperature and heat transfer rate in free convection on heated vertical flat plate

04 p0599 A71-15522

Iterative technique using continuous gas laser for alignment of Mach-Zehnder interferometer for monochromatic and white light fringes

09 p1453 A71-23692

Flame structure and propagation studied by modified Mach-Zehnder interferometers with He-Ne laser source, describing optical arrangements

10 p1623 A71-25125

Superheterodyne radiometers for millimeter and submillimeter waves, using Mach-Zehnder interferometer frequency mixer for parasitic signal suppression

12 p1886 A71-26847

Interferometric gas diagnostics by hook method, using Mach-Zehnder interferometer and stigmatic spectrograph

16 p2578 A71-33157

Laser illuminated Mach-Zehnder interferometer system including high speed cameras for studying flame propagation among polythene particles suspended in air

19 p3064 A71-38063

Mach-Zehnder interferometric measurement of modulation transfer function of optical instrument disturbed by turbulent atmosphere

23 p3679 A71-43893

MACHINE LEARNING

U LEARNING MACHINES

MACHINE LIFE

U SERVICE LIFE

MACHINE ORIENTED LANGUAGES

NT ALGOL

NT FORTRAN

NT PL/I

Programming language translator system, describing syntactic specifications for input-output relationships

01 p0045 A71-10190

SYMPLE/Syntax Macro Preprocessor for Language Evaluations/ for processing higher level language texts

01 p0045 A71-10191

LEAF/LISP Extended Algebraic Facility/ as FORTRAN dialect in list structure, extending LISP arithmetic functions to algebraic language level

01 p0045 A71-10192

On-line machine language dynamic debugger for Operating System 360, using graphic display terminal or operator typewriter

01 p0045 A71-10193

PL/I compiler for system programming in high speed binary machine object code

01 p0045 A71-10194

MOBSSL-UAF block structured simulation language for digital and hybrid computers

01 p0046 A71-10200

Hybrid computer simulation program for analyzing large circuits intractable by conventional methods using PACTOLUS language

01 p0048 A71-10225

High speed real time interpretive language for biological calculations with PDP-8 computer

01 p0049 A71-10244

PERL programming language for on-line control of industrial processes and scientific experiments

01 p0051 A71-11186

Multiple dialect automatic test language for avionics industry, considering software design

03 p0381 A71-13077

Artificial intelligence computer programming system for continuum mechanics, discussing capabilities of CONFORM as mathematical language

03 p0382 A71-13548

Programming language for computerized circuit design and analysis, considering techniques for input statements translation

03 p0382 A71-14306

MITOL problem-oriented compiler language for real time and postflight telemetry data processing

04 p0556 A71-15295

Complex digital computer systems effectiveness measurement, using simulation program with programming language SIMSCRIPT [AIAA PAPER 71-229]

07 p1068 A71-19707

Problem Oriented Languages for consulting and construction engineering problem solving by translator-generator for time shared system

09 p1412 A71-23278

User-oriented conversational language computer program for Jet Propulsion Laboratory digital control random excitation environmental test system for spacecraft

11 p1736 A71-26498

Principal program languages application and classical mathematical notation

14 p2206 A71-29562

Real time systems programming techniques based on modular programs, integrated data stores, multiprocessing and special computer languages

14 p2208 A71-30381

Higher order computer language architecture for aerospace software production problems, discussing real time constraints, hardware tradeoffs, memory, computer design and logic circuitry

17 p2712 A71-35777

ALOFT computer language for checkout and operation of complex space oriented equipment such as space shuttle

18 p2885 A71-36446

TOTAL checkout computer language for future space vehicles, considering objectives, characteristics and merits

18 p2885 A71-36447

Syntactical characterization of tautologies for deductive systems and theories based on formalized algorithmic languages

18 p2942 A71-36822

Algorithms and operator matrix language for infinite linear automata analysis, synthesis and identification

19 p3024 A71-37223

F-bounded erasing operator in abstract family of language for mapping, applying to families defined by tape-bounded Turing acceptors

20 p3201 A71-38846

Time-bounded grammars and languages capable of simulation by Turing acceptors in automata theory

20 p3202 A71-39050

Abbreviated test language for avionics systems, discussing program organization, statement formats, vocabulary and syntax diagrams

21 p3351 A71-40812

Pattern recognition problems, using on-line picture language program with flying spot scanner

22 p3519 A71-42767

MACHINE RECOGNITION

U ARTIFICIAL INTELLIGENCE

MACHINE STORAGE

U COMPUTER STORAGE DEVICES

U CORE STORAGE

MACHINE TOOLS

NT BORING MACHINES

NT GRINDING MACHINES

NT LATHES

Automated machinery for reinforced plastic structural products manufacture by filament winding [SME PAPER EM-70-135]

01 p0089 A71-11261

Electrochemical machining package consisting of machine tool, electrolyte system and power supply [SME PAPER MR-70-512]

01 p0090 A71-11268

Computer controlled laser machining system for cutting integrated circuit masks in thin films deposited as fused silica substrates

03 p0433 A71-14342

Apparatus for rolling and stretching metals at cryogenic temperatures, describing structural features

08 p1300 A71-21810

Carbon dioxide lasers for industrial material processing, discussing machine tool reliability, maintenance, various automation approaches and economic efficiency

09 p1457 A71-23403

Machine tool friction slides dynamics simulation for phase diagrams analysis, using Szoke model

10 p1614 A71-23994

Three dimensional isostatic pressing process, discussing equipment, tooling and forging preforms and finished parts production

10 p1618 A71-24764

Tools production and shaping for extrusion of light metal profiles

10 p1619 A71-25032

Carbon-graphite bound electrochemical grinding wheel, describing composition formulation, fabrication techniques, mechanical and electrical properties and performance criteria

14 p2263 A71-29654

Cutting angle effect on service life of broaching tools for Ti alloys annealed forgings, using high-speed P18 tool steel

14 p2259 A71-30271

Extrusion tools development since 1930, emphasizing economic aspects

14 p2253 A71-30470

Centerless grinding control high precision automatic invariant systems synthesis, outlining machine tool working elements inductive setters

15 p2415 A71-32185

Laser interferometer application in machine tool calibration, digital readout and feedback system, discussing advantages and limitations [SME PAPER IQ-71-745]

15 p2421 A71-32433

Tridea ALTAPE /automatic line tracing and programming/ system for drawing data conversion to tape for machining surfaces in direct numerical control applications

19 p3068 A71-37244

Book on lubrication systems selection, application, handling and maintenance covering journal and thrust bearings, nuclear reactors and machine tools

19 p3069 A71-37523

Molins 24 integrated automatic complete-processing system for small light-metal parts, using numerically controlled machine tools integrated with palletized feeder system

23 p3681 A71-43473

Complex variable solutions to electrochemical machining with two dimensional straight sided tool

23 p3682 A71-44142

MACHINE TRANSLATION

Programming languages expansion by users, considering language elements important in flow control or formulation of translation processes

19 p3025 A71-37423

MACHINERY

Long term planning of technological and scientific development of machine design and construction on national industrial and enterprise levels

02 p0336 A71-11860

Reliability prediction for machine parts subjected to cyclic stresses, using statistical analysis of fatigue data for failure rate calculation

02 p0327 A71-12367

Machine assemblies forced vibrations equations of motion determination, considering elastic dissipative qualities, structural hysteresis and damping

03 p0503 A71-13410

Machine components resistance to low temperature failure, considering threaded joints, gears and shafts for strength and plasticity characteristics

05 p0827 A71-16764

Forced dynamic regimes of machines and mechanisms, evaluating role of second order acceleration

13 p2099 A71-27806

Electrical DC collector machines and MHD magnetic systems design using superconductors, describing models

15 p2355 A71-32274

Machine structural elements endurance margin prediction from limited tests, proposing statistical method of integral estimates and tolerance factors

16 p2651 A71-33064

Machine design strength criteria in development of formulas for lower bound estimates of mechanical components structural reliability

16 p2582 A71-33293

Machine components resistance to low temperature brittle failure, considering threaded joints, gears and shafts for strength and plasticity characteristics

17 p2832 A71-35463

Machinery failure prediction under high vibration amplitudes using stochastic excursions principles [ASME PAPER 71-VIBR-60]

21 p3460 A71-40305

Computer method to simulate dynamic behavior of two dimensional machine systems with linkage elements [ASME PAPER 71-VIBR-111]

21 p3386 A71-40334

Design and technological calculations in machine building, analyzing flow, creep and elastoplastic deformation theories

21 p3472 A71-41144

Vibration tests of instruments, machines and apparatus, allowing for functional reliability

22 p3536 A71-41441

Stress relaxation equation for arbitrary initial tensile stresses and pliabilitys applied to machine element design

23 p3778 A71-44044

Material properties, metallurgy, production technology and operational factors effects on machinery structural strength

23 p3779 A71-44207

Unified electrical machine theory with allowance for space harmonics effects, transforming time-dependent linear differential equations into linear time-invariant equations

24 p3793 A71-44657

MACHINING

NT CHEMICAL MACHINING

NT ELECTROCHEMICAL MACHINING

NT HOT MACHINING

NT MILLING [MACHINING]

NT SPARK MACHINING

NT ULTRASONIC MACHINING

Ti and Ti-Al alloys machinability, discussing physical properties, dynamic deformation behavior and optimal cutting, milling and drilling [SME PAPER EM-70-101]

01 p0089 A71-11254

Large Al forgings machining cost reduction via stress relief involving mechanical working following quench

01 p0091 A71-11547

Epitrochoidal profile machining methods and tools for chamber surface in Wankel engine

02 p0257 A71-12560

Soviet book on machinability of titanium alloys covering microstructure, physical properties, surface finish and fatigue properties, tooling for industrial machining operations, etc

06 p0903 A71-17444

Concorde airframe structures, discussing numerically controlled machining of aluminum alloy integral units

06 p0904 A71-17954

Lasers applications to materials working including welding, cutting, machining, etc

06 p0908 A71-18069

Holographic lens used with pulsed ruby laser for machining single and multiple spots on Ti thin film on glass

07 p1122 A71-19205

Metal cutting on lathes, discussing machining conditions optimization based on productivity and cost criteria and linear programming solution

07 p1117 A71-19367

Fiber reinforced materials machining, considering deformation and stress fields, forces required for continuous machining

07 p1120 A71-20133

High temperature austenitic steels, Ni and Co alloys machining, considering deformation resistance and strain hardening

09 p1456 A71-23297

Aircraft engines and stationary gas turbines high precision components, discussing die forging and machining combined with joining processes

09 p1456 A71-23299

Laser welding, machining and safety - Conference, Pennsylvania State University, July 1969

09 p1457 A71-23401

Continuously pumped Q switched neodymium doped YAG laser micromachining tool for resistor trimming, resonator/filter frequency tuning and diode/transistor vaporizing

09 p1457 A71-23402

Laser thermal energy-materials interaction, discussing excess heat buildup, power generation, reflectivity and repetition rates

09 p1458 A71-23406

Laser microwelding, discussing focusing properties, high power radiation interactions, metal working, machining and microelectronic applications

09 p1458 A71-23407

Cutting angle effect on service life of broaching tools for Ti alloys annealed forgings, using high-speed P18 tool steel

14 p2259 A71-30271

High strength steels and Ti alloys machining, discussing hardness levels, cutting speeds, tool chip contact area, and reasonable production rates [SME PAPER MR-71-819]

15 p2416 A71-32426

Ni-base alloys machining, discussing special tools and manufacturing methods with special reference to machinability of Inconel 718, Rene 41 and 95 [SME PAPER MR-71-825]

15 p2416 A71-32427

Boron and graphite fiber reinforced plastics machining, discussing tools, operating parameters and process limitations [SME PAPER MR-71-820]

15 p2416 A71-32429

Carbon dioxide laser beam machining, describing accessories for cutting, drilling, scribing and welding [SME PAPER MR-71-807]

15 p2416 A71-32431

Aluminum-boron composite forming and cutting processes covering milling, grinding, abrasive cutoff, drilling, piercing, electrodischarge machining, blanking, punching and shearing

18 p2928 A71-36666

High quality continuous tone micromachining and image recording on metal thin films by low power pulsed gas laser heating

19 p3071 A71-37213

Machining integrated circuit metal film masks with continuously operating carbon dioxide laser and high pressure pulsed He-Ne laser

19 p3069 A71-38234

Hot extrusion properties of free machining Al alloys with low melting point Pb as chip breakers

21 p3384 A71-40026

Ion machining techniques for cutting accurate and repeatable pumping grooves in gas bearing component materials typified by boron carbide

22 p3551 A71-41665

Machining effects on martensitic stainless steels corrosion resistance, showing formation of defects and internal stresses in surface layers

23 p3692 A71-44028

MACROPHAGES

Peritoneal macrophagocytic ingestive capacity decrease in mice under hypobaric hypoxia, indicating infection susceptibility in altitude environments

22 p3486 A71-41832

MACROSCOPIC EQUATIONS

Entropy-disorder concepts relation in teaching thermodynamics, urging treatment as macroscopic theory

01 p0126 A71-10134

Crystal time reversal symmetry for macroscopic laws determination, discussing spontaneous electric and magnetic moments and magnetically ordered systems

01 p0138 A71-10348

Gravitational field equations in classical Newtonian mechanics within framework of macroscopic gravitation theory

09 p1523 A71-23074

Nonlinear optics classical macroscopic treatment with Maxwell equations

13 p2078 A71-28517

Closed system of macroequations for mass and energy conservation along symmetry axis of steady rarefied supersonic gas flow in front of blunt body

13 p1991 A71-29151

Arbitrary periodic composite structure system with local interactions, obtaining macroscopic properties from unit cell boundary value problems

14 p2323 A71-29812

Hyperelastic continuous bodies with periodic structure, developing macroscopic model based on boundary value problem for unit cell

14 p2323 A71-29813

Linearized gravitation theory in macroscopic media, deriving refraction of gravitational waves based on classical electromagnetism

17 p2777 A71-34585

Macroscopic derivation of Onsager relations for nonoscillatory processes with linear flow in isotropic media

18 p2852 A71-36964

Gas dynamic model for coupled vibrational and radiative nonequilibrium in carbon dioxide, obtaining macroscopic collisional and radiative transfer equations

21 p3418 A71-40233

MACULAR VISION

U VISION

MAGIC TEES

Compact Q band magic tee with matched loads to check noise performance of two-input switched radiometer

16 p2579 A71-33385

Dielectric articles thickness and flaw control by microwave magic tee junction waveguide, describing instrument design and operating characteristics

22 p3521 A71-41772

MAGMA

Geothermometer based on plagioclase-magmatic liquid equilibrium

05 p0751 A71-16411

Chemical elements abundance in ordinary chondrites, terrestrial magma and lunar rocks, considering Alven theory of solar system origin

10 p1665 A71-23741

Lunar 12 spinel compositional variation and textures as petrogenetic indicators, showing magma differentiation by crystal settling after lunar surface extrusion

10 p1672 A71-24394

Cooling history of magma containing spinelulite growth forms on basis of morphological variations in glassy and crystalline rocks

19 p3051 A71-37673

Rare earth, alkali and alkaline earth elements content of phenocrysts and acidic igneous magma

23 p3734 A71-43246

Apollo 12 crystalline rocks composition from microprobe analyses, indicating undercooled magmatic fractional crystallization

23 p3742 A71-43639

MAGNESIUM

NT MAGNESIUM ISOTOPES

Mg, Al and Si ions spectral analysis, discussing energy levels and transition lines

01 p0129 A71-10136

Mg I and II vacuum UV emission series, presenting quantum defect plot

01 p0129 A71-10137

Magnesium particle combustion in rarefied air at various pressures

01 p0182 A71-11444

Dense plasma cluster charge exchange in supersonic Mg jet, examining par collision model, particle scattering, target thickness and Q switching

02 p0292 A71-12614

Copper oxide-magnesium thermal cells open circuit voltage drop in latter discharge stages, discussing cuprous ion activity at cathode

02 p0197 A71-12959

High purity Mg deformation by remelting and rolling, investigating grain growth based on size measurement

03 p0445 A71-14341

Magnesium and manganese ferrite ion states under heat treatment using X ray and Mossbauer methods

05 p0793 A71-16832

Mg slurry fuel mixing, ignition and combustion characteristics for injection into high speed air flow [AIAA PAPER 71-6]

06 p1007 A71-18480

Li and temperature effects on mechanical properties of Mg base single crystals in basal and prismatic slip

08 p1309 A71-21525

Polyfraction Mg particles suspension in active gaseous medium, studying ignition and burnout

08 p1376 A71-21909

Burning mechanism of condensed ballistite compositions with metallic particles of aluminum, magnesium and ammonium perchlorate

08 p1376 A71-21912

Solar color index calibration from Mg b triplet photoelectrical measurement for dwarfs and Jupiter satellites

09 p1516 A71-22064

Solar atmosphere center limb observations, describing line intensity fluctuations in Na D and Na 5688 doublets and Mg 4571 line

13 p2140 A71-29044

Mg and Al particles burning in air, water vapor, Cl and nitrous oxide

14 p2337 A71-30614

Ignition initiation, burning time and particle size distribution determination for dispersed Mg and Al particles in condensed system

14 p2337 A71-30615

Magnesium vapor-oxygen low pressure diffusion flames temperature profile measurement, using subminiature thermocouple [WSS/ICI PAPER 71-22]

15 p2464 A71-31631

Identifying magnesium dayglow measurement in sporadic E layer by rocket-borne UV spectrometer, determining ion to atom ratio

15 p2398 A71-31765

Primary high purity Mg refining technique, composition, oxidation and structure

15 p2435 A71-32338

Singly ionized magnesium CW laser oscillation in He-Mg discharge at micron wavelengths with possible extension to visible and UV spectrum

15 p2420 A71-32386

Ca, Mg, B and Al prominent resonance transitions radiative lifetimes and absolute oscillator strengths

15 p2452 A71-32596

Relative excitation functions for electron impact with Mg in crossed beam experiment, considering simultaneous ionization of neutral Mg

16 p2614 A71-33331

Quasi-stellar objects, investigating velocity dispersion, column densities and abundance of Mg and Fe in absorbing region by Stromgren method of line pairs

17 p2797 A71-34371

Ca and Mg light emission and ionization cross section measurements at simulated meteor conditions, using photomultiplier and optical filters

17 p2798 A71-34374

High rate quasi-static dynamic pressure deformation hardening of magnesium single crystals

18 p2934 A71-35990

Solar Mg II H and K line profiles from rocket-borne echelle interferometer spectrograph and densitometer data

19 p3135 A71-37612

Stellar chromosphere characteristics from OAO observation of magnesium II emission in late type stars

19 p3137 A71-37628

Al and Mg powder dispersed in solid ammonium perchlorate oxidizer, investigating various combustion mechanics

19 p3120 A71-38120

Magnesium diatomic metal static and dynamic properties, using multiple electron and ion analysis system

24 p3839 A71-45118

MAGNESIUM ALLOYS

Self ignition temperature of aerogels of Al-Mg alloys during heating of powders

01 p0182 A71-11448

Grain boundary sliding on Mg-Al alloy polycrystalline specimens measured at successive strains during creep under 2800 psi stress

03 p0443 A71-14184

AlZnMgCu alloys fracture behavior, examining aging conditions, rolling, forging, cracking, tensile strength and chemical composition

04 p0613 A71-15745

Tensile-compressive yield strengths of wrought Mg alloy, noting plastic deformation by slip on basal plane

04 p0614 A71-15786

Al and Mg alloys mechanical and microstructural changes under low temperature conditions, optimizing casting component ratios

05 p0767 A71-16765

Al-Mg alloy oxide film morphology and composition under various oxidation conditions, using electron microscopy and diffraction

05 p0770 A71-17100

Tubular Mg and Ti alloy samples under tension and compression load, observing creep properties

07 p1211 A71-19195

MACROCLIMATE

U CLIMATE

MACROMOLECULES

U MOLECULES

Mg alloys mechanical properties and microstructure changes under static tension in temperature range 20-293 K

07 p1131 A71-19363

Mg-Cd single crystals deformation by prismatic slip as function of testing temperature and state of order

07 p1132 A71-19437

Mechanical properties, crack formation sensitivity, corrosion resistance and stress cracking behavior of Al-Zr-Mg alloys welded joints

07 p1136 A71-19633

Alloying elements, mechanical working and heat treatment effects on vibration damping of Mg-Zr alloys, using Fastov device

07 p1136 A71-19634

Magnesium indium alloys single crystal plastic deformation, investigating basal and prismatic slip at various temperatures

08 p1309 A71-21528

Mg-Y alloy age hardening due to coherent metastable phase precipitation

08 p1312 A71-21548

Al and Mg alloys mechanical properties anisotropy as function of loading conditions, taking into account stress condition effect

09 p1467 A71-22315

Al-Mg alloy oxidation, observing Be, B, Mo and Zr addition effects

09 p1468 A71-22656

Annealed Al-Mg alloys mechanical measurement, noting low temperature tensile strength and yield point variations with specimen composition and temperature

09 p1473 A71-23230

Mg-Al eutectic alloy and commercial-purity Zr stress relaxation tests and mechanical behavior

11 p1780 A71-26022

Polycrystalline pure Al and Al-Mg alloy strength, investigating temperature and strain rate effects

13 p2084 A71-28112

Al-Mg-Si alloy development with low quenching sensitivity and high tensile strength

14 p2259 A71-30471

Metal particle agglomeration during burning of Al-Mg alloy in ballistic powder, using high speed burning track microphotography

14 p2260 A71-30619

Particle size effect on self ignition temperature of powdered Al-Mg alloys

14 p2285 A71-30621

Magnesium corner of Mg-Li-Sn system phase diagram, detecting two invariant transformations in Mg-rich alloys

15 p2425 A71-31403

Medium strength corrosion resistant weldable Al-Mg alloy for aircraft jettisonable tanks, napalm containers and jet shroud pipes fabrication

15 p2426 A71-31437

Soviet papers on physical metallurgy of light metal alloys covering high strength, grain size effect, heat treatment, structural dependent properties and melt refining

15 p2434 A71-32326

Ultralight magnesium based alloys classification by Li content, noting lattices, structural composition, specific weight, plastic properties and impact strength

15 p2435 A71-32336

Deformable magnesium alloys, discussing applications and semifinished products manufacturing equipment

15 p2435 A71-32337

Chemical composition effect on corrosion resistance of Mg-Li system with alloying additions

15 p2435 A71-32339

Mechanical properties, crack formation sensitivity, corrosion resistance and stress cracking behavior of Al-Zr-Mg alloys welded joints after prolonged heating

16 p2593 A71-33629

Alloying elements, mechanical working and heat treatment effects on vibration damping of Mg-Zr alloys

16 p2593 A71-33630

Zinc and misch metal in Mg alloys, detailing rare earth metals distributions in various phases

16 p2594 A71-33714

Al-Cu-Li-Mn and magnesium/rare-earth-element alloys heat resistance and microhardness, determining strengthening by intermetallics

16 p2597 A71-33926

Storing and plastic deformation effects on artificial aging of Al-Zn-Mg alloy, using thin foil electron microscopy and hardness measurements

17 p2755 A71-34417

Al-Mg-Si alloy vibration creep endurance under single step loading, emphasizing strain and defect accumulation

17 p2757 A71-34593

Al and Mg alloys mechanical and crystal microstructural changes under low temperature conditions, optimizing casting component ratios

17 p2760 A71-35464

Mg-Ge alloys liquid and two phase mixtures thermodynamic properties at 660-1130 C, using galvanic cell with magnesium chloride electrolyte

19 p3080 A71-37715

Al-Zn-Mg alloy welded joints under repeated static loads, determining shape, filler wire composition and aging effects on fatigue strength

19 p3083 A71-38425

Salt solution treated and quenched Mg-Al alloy rods tests in distilled water, investigating transgranular stress corrosion cracking and deformation twinning

19 p3083 A71-38722

Weldable Al-Zn-Mg alloys with cathodic polarization protection, noting decrease in stress corrosion crack propagation rate

22 p3560 A71-41625

Age hardenable Mg-Y alloys, investigating impurity phase in solution heat treatment

23 p3696 A71-44292

Liquid Mg-Al alloys thermodynamic properties determination by electrochemical and barometric methods

24 p3840 A71-45372

MAGNESIUM CELLS

Development and performance characteristic of batteries including Zn and Mg dry cells, metal air, organic electrolytic, organic cathode and secondary systems

24 p3793 A71-45133

MAGNESIUM CHLORIDES

Scanning electron microscopic observation of fracture surface of austenitic stainless steels for stress corrosion cracking in magnesium chloride and calcium chloride solution

23 p3693 A71-44073

MAGNESIUM COMPOUNDS

NT CHLOROPHYLLS

NT ENSTATITE

NT MAGNESIUM CHLORIDES

NT MAGNESIUM FLUORIDES

NT MAGNESIUM OXIDES

NT TALC

Phase relationships in magnesium ferrate-magnesium chromate systems subjected to annealing in air and hydrogen atmospheres

01 p0107 A71-10403

Thermal conductivity of Li and Na carbonates alone and combined in mixture with magnesia at various temperatures

08 p1377 A71-21933

Mg compounds family of antifluorite structured small-gap semiconductors, investigating surface light scattering properties by Raman scattering techniques

19 p3119 A71-37870

Lithium magnesium zinc silicates crystallization phase equilibria, noting temperature effects, structure, melting and solubility

20 p3253 A71-38818

MAGNESIUM FLUORIDES

High intensity vacuum UV solar simulator, using high pressure jet pinched xenon arc lamp with magnesium fluoride envelope

11 p1747 A71-26515

Fluorine chemical shift tensor measurements in magnesium fluoride, using multiple pulse NMR technique

13 p2025 A71-28031

MAGNESIUM ISOTOPES

Mg 26 isotopic abundance in meteoritic, lunar and terrestrial feldspar by mass spectrometry, suggesting limits on Al 26 in early solar system

06 p0966 A71-17896

Mg 24 photodisintegration rate in stellar silicon burning process, presenting reactions at low alpha particle energies

23 p3723 A71-42952

Li, B, Mg and Ti isotopic abundances and search for trapped solar wind Li in Apollo 11 and 12 rocks

23 p3752 A71-43708

Mg isotopes in solar atmosphere, analyzing absorption bands in sunspot spectrum

23 p3767 A71-43837

MAGNESIUM OXIDES

Sunspot observation of 22 June 1959, discussing two MgO bands spectrographic analysis

02 p0313 A71-12536

Ceramic particle compaction as function of size, shape, loading rate and hardness for fused alumina, magnesia and mullite

03 p0448 A71-12973

Integrating sphere coatings bidirectional reflectance characteristics, describing reflectometer data for smoked magnesium oxide and Au coated sandpaper samples

06 p0902 A71-18534

Nickel ion diffusion coefficients in high purity magnesium oxide single crystals in high temperature argon atmosphere

08 p1343 A71-20664

MgO single crystals dominant coloration in solar spectral region by electron hole pair diffusion, trapping and recombination

11 p1808 A71-26234

Magnesia rich magnesium aluminum oxide spinel ceramics, discussing sintering, grain growth inhibition and strength increase

13 p2092 A71-28662

Thermodynamic equilibrium constants of Fe-MgO-SiO₂-O₂ system reactions at one atmosphere and 900-1300 C

14 p2190 A71-29875

Search for upper atmosphere MgO content, using modified Ebert spectrometer with photomultiplier detection to measure twilight excited scattered and resonance radiation

23 p3670 A71-43191

LiF and MgO high purity single crystals plastic deformation geometric characteristics, discussing nucleation probability on different slip planes

24 p3859 A71-44450

MAGNESYN (TRADEMARK)

U SERVOMOTORS

MAGNETIC ABSORPTION

U ELECTROMAGNETIC ABSORPTION

MAGNETIC AMPLIFIERS

Rotating accelerometer with magnetic amplifier for angular acceleration detection, investigating static, dynamic and frequency response characteristics

02 p0252 A71-12421

Defectoscopes with current regulation by magnetic amplifiers, describing circuitry and remanent magnetization of components with AC and rectified half wave currents

08 p1273 A71-21894

Modulated power control for fusion welding, considering modification to conventional magnetic amplifier controlled power sources

13 p2076 A71-29093

MAGNETIC ANNULAR ARC

Magnetic annular arc accelerator for high pressure high enthalpy flow test facility

07 p1083 A71-19880

Magnetic annular arc continuous operation at atmospheric pressure, determining arc velocity and rotational frequency as functions of magnetic flux density and arc current

17 p2788 A71-34901

MAGNETIC ANOMALIES

NT GEOMAGNETIC HOLLOW

Ionospheric vertical wind role in anomaly of quiet sun diurnal geomagnetic variation at magnetic equator

02 p0243 A71-11764

Electromagnetic induction by plates with nonuniform conductivity distribution, applying results to North German anomaly

05 p0745 A71-17190

Geomagnetic secular variations from various surveys, noting negative value for Gulf of Aden anomaly chart

05 p0745 A71-17192

Geomagnetic field anomalous variations due to solar eclipse of 22 September 1968

05 p0746 A71-17211

Ionospheric absorption winter anomaly observation based on Loran-A pulse signals during IQSY, noting diurnal variation

06 p0889 A71-17685

Atmospheric Coulomb interaction influence on longitude dependence of electron intensity in anomaly region

06 p0963 A71-18255

Spherical harmonic analysis of geomagnetic field strength for global magnetic anomaly charts

06 p0894 A71-18267

Autocorrelation functions of anomalous gravitational and magnetic fields for ocean lines, relating Mohorovičić boundary and Curie isotherm

06 p0894 A71-18268

Geomagnetic cavity heuristic model with solar wind driven unipolar induction current in ionosphere

08 p1280 A71-21218

Geomagnetic disturbance field asymmetry Fourier analysis for amplitude G and local time phase of first diurnal harmonic for IGY

10 p1600 A71-24295

Ionization crests of equatorial anomaly at magnetic L values from Ariel 2 satellite electron probe measurements

11 p1754 A71-25603

F 2 layer critical frequency abnormal latitudinal distributions, using Alouette 1 satellite data

12 p1900 A71-26935

Geomagnetic secular variations from various surveys, noting negative value for Gulf of Aden anomaly chart

13 p2059 A71-28248

Geomagnetic field anomalous variations due to solar eclipse of 22 September 1968

13 p2060 A71-28266

Ionospheric absorption winter anomaly including temporal and local variations and frequency dependence, examining possible correlations with stratospheric and mesospheric phenomena

14 p2237 A71-30943

Localized abnormal geomagnetic disturbance near polar cap and simultaneous ionospheric variation during auroral zone weak magnetic activity periods

22 p3536 A71-42625

Aircraft permanent magnetic fields strength variation, observing magnetic anomaly detection equipment performance degradation

23 p3674 A71-42923

MAGNETIC CIRCUITS

Counterrotating antenna without mechanical contact, using magnetic bearings for spin stabilized geostationary telecommunications satellites

18 p2892 A71-36574

Differential magnetic circuit sensor with movable screen, analyzing neutral point lag for calculation of emf distributed output winding and neutral point displacement

24 p3810 A71-45153

MAGNETIC COILS

Electromagnetic transducer DC rotor magnetic state diagram, describing simulation procedure for moment pickup

06 p0899 A71-17933

Gyrocompass strapdown three coil synchro sensor magnetometer in conjunction with vertical gyro, eliminating azimuth detector inertial platforms

07 p1156 A71-20340

Analog computer power relay analysis simulating flux, coil current, moving mass motion and magnetic and spring forces as function of time

13 p2001 A71-28839

Auxiliary propulsion system using low power MPD thrusters, discussing feasibility of thrust vectoring with skewed magnetic coil arrangement [AIAA PAPER 71-695]

14 p2293 A71-30754

Inductive voltage divider bridge network for ferrite coils inductance and Q measurements

17 p2723 A71-35713

German monograph on calibrating induction coil and proton precession magnetometers for polar electrojet rocket experiments

18 p2915 A71-35922

Inertialess glow discharge ignition in triotron controllable crossed field cold cathode tube, comparing with magnetic coil initiation

19 p3028 A71-37785

MAGNETIC COMPASSES

Strapdown solid state compass based on magnetometer principle, describing gyro feedback correction system and circuitry

08 p1287 A71-21171

MAGNETIC CONTROL

Critical velocity and elastic panel flutter stabilization in magnetohydrodynamic flow by distributed magnetic field control

02 p0293 A71-12628

Nonlinear resonant roll motion of passive magnetic attitude control satellites, using Hill and Mitropolskii methods

11 p1837 A71-25458

Optimal control of oscillations of electrically conducting fluid by magnetic field in plane channel with free boundaries, using dynamic programming

13 p2107 A71-28728

Auxiliary propulsion system using low power MPD thrusters, discussing feasibility of thrust vectoring with skewed magnetic coil arrangement [AIAA PAPER 71-695]

14 p2293 A71-30754

Aeros satellite active magnetic attitude control system design, operation and testing

15 p2499 A71-31210

In-flight operation of Azur satellite magnetic attitude control system during period between booster separation and steady orbital motion [DGLR-71-012]

15 p2501 A71-32782

Seasonal and annual longitudinal variations in ionospheric ion distribution, stressing solar geomagnetic control importance

16 p2567 A71-33762

Interelectrode gap position control of discharge in coaxial gas heater with arc rotated by magnetic field

17 p2676 A71-34509

Magnetic torquer for satellite attitude control consisting of solenoid with hard magnetic material core

18 p2973 A71-36463

German monograph on locking process in earth satellites with passive magnetic attitude control covering satellite rotational motion mathematical model, stability analysis, etc

21 p3455 A71-40773

MAGNETIC CORES

Stapleblock fabrication method for low mass, high strength ferrite core memory storage blocks in space travel applications

02 p0232 A71-12071

Earth satellites ferrite core buffer storage replacement by magnetic tape unit noting design, performance, volume and operation [DGLR-70-082]

05 p0726 A71-15952

HF microcircuits packaging inside magnetic cores, discussing inherent advantages of RF interference and radiation shielding and heat transfer properties

12 p1888 A71-27433

Ferrite core memories for information storage of digital computer onboard Eole satellite, discussing design and reliability measures

18 p2891 A71-36560

Phase sensitive magnetic semiconductor pulse width modulator with diode bridge consisting of single saturable-core choke input and transistor circuit output arms

24 p3810 A71-45155

MAGNETIC DIFFUSION

Cosmic rays compound diffusion, considering combined effects of one dimensional diffusion along interstellar magnetic field lines and field lines three dimensional random walk

14 p2301 A71-30434

MAGNETIC DIPOLES

Charged particle motion in magnetic dipole field, investigating singularity and topological flow nature

01 p0127 A71-10382

Relativistic kinetic theory of particles with magnetic dipole moment in external EM field, deriving transport equations for distribution function

03 p0463 A71-13425

Solar wind torque on earth magnetic dipole based on magnetosphere model analytic solution in rotating reference frame

06 p0891 A71-17885

Cosmic plasma stream capture by magnetic dipole of neutron star in binary system

07 p1192 A71-19287

Geomagnetic field modeling facility based on nine-dipole model parameters

07 p1100 A71-19406

Satellite altitude dipole source effectiveness in lower ionosphere, comparing to ground based source with same dipole moment

07 p1064 A71-20319

Compressible isotropic plasma slab effect on magnetic dipole radiation pattern, using reciprocity theorem

08 p1253 A71-21274

High latitude magnetosphere structure, using two dipole model

09 p1437 A71-22665

Near earth motion equations for electrically charged dust particles in gravitating dipole magnetic fields, using zero-relative-velocity surfaces and energy integral

09 p1437 A71-22832

Plasma-free point magnetic dipole in field-free stationary plasma, determining magnetopause or free boundary by moment technique

09 p1503 A71-22865

Earth-ionosphere waveguide model of VLF signals propagation with perturbed ionosphere, considering magnetic dipole transmitting antenna array

09 p1410 A71-23575

Lunar surface electromagnetic sounding, presenting analysis of radiation fields and polarization characteristics for magnetic dipole situated on layered half space

10 p1576 A71-24054

Atmospheric electric ring current in higher atmosphere with equatorial flow across magnetic lines, using dipole tensor conductivity model

10 p1603 A71-24701

Sunspots forbidden Fe I lines, calculating magnetic dipole and electric quadrupole transition probabilities

11 p1830 A71-26112

Zero relative velocity surfaces in bounded circular three body problem in presence of magnetic dipole, deriving Jacobi integral

12 p1947 A71-26634

One magnon Raman scattering induced by light magnetic dipole coupling with YIG coherent spin waves

12 p1913 A71-26860

Cosmic rays origin from pulsar model with particles accelerated by magnetic dipole radiation, producing equal energy spectrum

12 p1948 A71-27365

Magnetic dipole field second invariant and drift frequency in terms of pitch angle and energy from analytical approximation to trapped charged particle bounce period

13 p2055 A71-27925

Geomagnetic field modeling facility based on nine-dipole model parameters

19 p3053 A71-37830

Two dimensional magnetospheric model, investigating magnetic line dipole field confinement in empty cavity by tail-like infinitely conducting plasma at constant pressure

20 p3286 A71-38732

Magnetosphere neutral layer plasma conductivity determination from model of linear magnetic dipole in conducting fluid flow

20 p3216 A71-39138

Pulsar radiation from oscillating interface with steady current sheet between rotating radiating magnetic dipole and external plasma

20 p3285 A71-39952

Magnetospheric midday boundary width dependence on geomagnetic dipole axis orientation, discussing different positions for magnetosphere boundary

24 p3824 A71-45319

MAGNETIC DISKS

Magnetic disk storage media for recording and reproducing wideband instrumentation data

01 p0082 A71-10893

EDITOR program for writing, reading, copying or altering data on file disk via display station

13 p2035 A71-29015

Computer-disk interface system photooptical instrumentation for weather data acquisition, analysis and display

18 p2884 A71-36078

MAGNETIC DISPERSION

Magnetospheric cold plasma dispersive and amplifying combined effects on pearl elements spectral shape, considering wave packet propagation applications

11 p1730 A71-25543

Steady LF geomagnetic pulsations, deriving dispersion equation relating plasma electron frequency, hot ion velocity and particle radii and drift frequencies

17 p2735 A71-35243

MAGNETIC DISTURBANCES

NT MAGNETIC STORMS

Sunward magnetosheath magnetic field fluctuations, noting power levels spatial variations, transverse shock aligned fields and longitudinal waves

01 p0075 A71-11493

Kelvin-Helmholtz instability at magnetopause, initiating semiannual variation of geomagnetic disturbances

01 p0075 A71-11495

Large fluxes of energetic neutral atomic hydrogen at 800 km preceding geomagnetic disturbance, using sounding rocket electrostatic analyzer

01 p0148 A71-11526

Diurnal variations of polar aurora-magnetic activities correlation at high latitudes

02 p0242 A71-11758

Nighttime polar aurora zone during IGY and IQSY related to magnetic activity

02 p0242 A71-11759

F region electron density profile changes during negative magnetic bays, deriving ionization drift from continuity equation

02 p0243 A71-11771

Simultaneous sudden magnetospheric compressions and geomagnetic bay onsets correlation, using IGY data

02 p0245 A71-11967

Nondissipative focusing and ionospheric reflecting effects on MF radio wave absorption measurements for magnetically quiet and disturbed periods

03 p0409 A71-13391

Auroral oval transverse magnetic disturbance, examined as field aligned current models

03 p0419 A71-14523

Magnetic disturbances effect on drift behavior and anisotropy parameters of E and F region irregularities

05 p0740 A71-16433

Magnetic disturbances effect on F2 critical frequencies in Australasian zone during IGY-IGC, correlating to equatorial electrojet

05 p0741 A71-16438

Coronal magnetic structure mechanical diagnosis, using flare associated hydromagnetic disturbances

05 p0799 A71-16471

Dawn chorus western drift and relationship to magnetic disturbances on night side

05 p0745 A71-17189

Inner radiation zone electrons loss and replenishment observation by Pegasus satellite during magnetically quiet and active periods

06 p0949 A71-17264

Penetrating electron flux relation to magnetic perturbations and auroral substorms development

07 p1185 A71-19392

Solar wind fast shock wave and simultaneous ground geomagnetic disturbance related to magnetospheric deformation

07 p1185 A71-19396

Polar magnetic disturbances in electrojet, studying Hall conductivity, electric field behavior and auroral ionosphere ionization

07 p1101 A71-19415

Upper atmosphere balloon altitudes electron flux dependence on magnetosphere magnetic perturbation

08 p1351 A71-20957

H Lyman alpha auroras during May 18-27, 1967 magnetic disturbance from satellite observation

08 p1283 A71-21637

Dynamo role in magnetospheric disturbances and ionospheric inhomogeneities, allowing for charged particle concentration height dependence

09 p1435 A71-22430

Magnetic disturbances caused by magnetospheric-solar wind filamentary inhomogeneity interaction observed by Pioneer 6

09 p1513 A71-22560

Magnetospheric electric field diagnosis, using geomagnetic disturbances in equatorial plane and pulsations in middle and high latitudes

09 p1441 A71-23639

Low latitude air density correlation to magnetic disturbance deduced from Ariel 2 satellite spin rate changes

10 p1602 A71-24552

Generation mechanism of 27-day recurrent geomagnetic disturbances sudden commencements, analyzing interrelationship between recurrent disturbances, solar data and solar plasma physical parameter

10 p1607 A71-25119

Generation mechanism of magnetohydrodynamic shock waves associated with sudden commencements of 27e day recurrent geomagnetic disturbances 10 p1608 A71-25120

Solar activity and geomagnetic disturbance effects on upper atmosphere density from ATS 2 satellite orbit observations 12 p1899 A71-26886

Dawn chorus westward drift and relationship to polar substorm and magnetic disturbances on night side 13 p2059 A71-28246

Geomagnetic disturbance vector distribution, computing three dimensional ring and ionospheric currents system models 14 p2229 A71-29672

Diurnal correlation between cosmic ray meson intensity and atmospheric ozone content on magnetically undisturbed days 14 p2231 A71-29723

Polar magnetic disturbances, discussing correlation with interplanetary magnetic field and interaction effects between solar wind and magnetosphere 14 p2231 A71-29907

Magnetometer network operation during IQSY, establishing Sq variations in polar regions on quiet days and nature of geomagnetic disturbances 15 p2396 A71-31607

Thermospheric density response to auroral heating during geomagnetic disturbances simulation assuming impulse heat input into small latitude band within auroral ovals 15 p2398 A71-31770

Joule heating and winds in upper atmosphere due to geomagnetic disturbances at 140 km altitude, deriving set of nonlinear partial differential equations 16 p2564 A71-33726

Air density observation near 150 km heights from Cosmos 316 orbit, noting geomagnetic disturbance effects and semiannual variation 16 p2569 A71-33806

Earth bow shock internal structure based on correlated observations of magnetic field, ELF magnetic fluctuations and suprathermal electrons by OGO 5 satellite 16 p2628 A71-33943

High latitude sudden impulses, calculating transverse hydromagnetic waves propagation from magnetosphere equatorial plane 17 p2733 A71-34777

Pc 3 and 4 micropulsations period structure data, observing multiple frequencies during magnetically active times 19 p3048 A71-37397

Penetrating electron flux relation to magnetic perturbations and auroral substorms development 19 p3127 A71-37816

Solar wind fast shock wave and simultaneous ground geomagnetic disturbance related to magnetospheric deformation 19 p3127 A71-37820

Polar magnetic disturbances in electrojet, studying Hall conductivity, electric field behavior and auroral ionosphere ionization 19 p3054 A71-37839

Upper atmosphere supplementary electron flux data following geomagnetic disturbance from high altitude balloon experiments 19 p3129 A71-38357

F1 region ion structure during ionospheric magnetic disturbances by numerical simulation of quiet and disturbed conditions based on electron concentration profiles 19 p3057 A71-38368

Magnetic perturbations in near polar region and morning-night sectors of auroral oval as function of current sources and modulation by universal time 19 p3059 A71-38397

German monograph on electron flux properties in polar atmosphere, discussing pitch angle distribution, energy spectrum and relation to geomagnetic field disturbances 19 p3130 A71-38646

Upper atmosphere density variations and time lag with respect to geomagnetic disturbances, using satellite drag measurements 20 p3223 A71-39709

Neutral atmospheric composition and density variations during geomagnetic disturbances from OGO-6 satellite quadrupole mass analyzer measurements 20 p3223 A71-39711

Steady state magnetospheric convection pattern from synoptic maps of magnetic disturbance and auroral motions 20 p3230 A71-39879

Polar cap electric field and relationship to magnetic disturbances from measurements on Ba ion clouds released by rockets 20 p3230 A71-39883

Magnetosphere-ionosphere electric coupling for polar magnetic disturbances and auroral break-up origin, discussing thermal particles precipitation due to transient electric field 21 p3375 A71-41354

Localized abnormal geomagnetic disturbance near polar cap and simultaneous ionospheric variation during auroral zone weak magnetic activity periods 22 p3536 A71-42625

Geomagnetic bay-like disturbances formation and decay during multiple midlatitude 6300 A auroral arc after magnetic storm, observing time variation of current system pattern 23 p3672 A71-43981

Solar unipolar magnetic regions relation to geomagnetic disturbances variability, discussing 11 year cycle 24 p3823 A71-45036

Geophysical data analysis for high latitude negative geomagnetic disturbances revealing geomagnetic pulsations during auroral arcs passage 24 p3823 A71-45037

MAGNETIC DOMAINS

Orthoferrite cylindrical magnetic domains in memory and logic devices, considering conductor, angelfish and in-plane rotating field circuits 01 p0047 A71-10211

Supercritical Permalloy thin films thickness effect on magnetic domain structure 06 p0941 A71-17401

Epitaxial garnet films magnetic anisotropic models, describing mobile cylindrical domains 12 p1943 A71-26854

Magnetic thin film domain wall velocity dependence on magnetic field intensity as function of film thickness, discussing nonlinearity causes 18 p2955 A71-36938

Transcritical Permalloy thin film domain structure, investigating external field effect on powder depositions and proposing model 18 p2955 A71-36942

Gunn diodes stable high field domains parameters and behavior, considering hole effects in various carriers 19 p3028 A71-37861

MAGNETIC EFFECTS

NT MAGNETIC RIGIDITY

Te-doped In Sb single crystal growth in transverse magnetic fields, using Czochralski crystal puller 01 p0100 A71-10281

Drift causes in floated-rotor integrating gyros used as accelerometers, discussing gyromotor magnetic field effects 01 p0080 A71-10535

Nonlinear magnetoelasticity theory applied to deformation of elastic bodies by magnetic field, considering ferromagnetic membrane deflection and flexible conductor equilibrium 01 p0171 A71-10661

Distribution function for two circularly polarized modes in laser with axial magnetic field derived by master equation transformation to Fokker-Planck equation 01 p0094 A71-10745

Optically thin medium convective instability, examining radiant pressure and magnetic field effects 01 p0158 A71-10804

Arc oscillation spectra in MPD thruster operation at low magnetic field 01 p0142 A71-10959

Axisymmetric bulge region formed in long uniform plasma column by reduction of external magnetic field 01 p0134 A71-11004

Magnetic field effects on electron heating by strong electric field in n-Ge single crystals 01 p0140 A71-11459

Magnetoconcentrating effect in diodes with hemispherical p-n junction and semiorganic base in longitudinal magnetic field 01 p0057 A71-11461

Magnetic field confinement of ionized plasmas generated by laser-irradiated lithium hydride solid particle 01 p0137 A71-11483

Satellite oscillations about center of mass, allowing for energy dissipation due to magnetic hysteresis 02 p0319 A71-11907

Damping in gravity graded satellite passive stabilization systems under eddy currents and dry friction induced by magnet motion 02 p0319 A71-11908

Uniaxial satellite rotational motion, examining magnetic and gravitational torque effects on gyro dynamic properties 02 p0320 A71-11975

Magnetic field effect on boundary temperature in axisymmetric MHD flow in vortex chamber, using dissipationless approximation 02 p0293 A71-12633

Uniform magnetic field effects on electroconducting fluids turbulent flow and heat transfer characteristics 02 p0293 A71-12649

Multicomponent ionized gases mixture transport coefficients for field-free and strong magnetic field cases 03 p0463 A71-13471

Circular Al rings under radial impulsive loading by curved magnetically driven Al flyer plates, recording strain-time histories on oscilloscopes [SESA PAPER 1644] 03 p0509 A71-13778

Swept electron beam scanning in microwave beam-wave interaction devices via periodic magnetic fields 03 p0385 A71-13794

Nonuniform magnetic field cyclotron heating, presenting stochastic criteria in terms of Larmor rotation phase randomization 03 p0462 A71-13928

Magnetic field effect on mean electron impact ionization probability in valent semiconductors with ellipsoidal equienergetic surfaces 03 p0467 A71-13978

Sudden impulses in geomagnetic field, discussing synchronous equatorial orbit-satellite magnetometer observations 03 p0421 A71-14537

Surface impedance of thin metal plate excited by RF electromagnetic field as function of external DC magnetic field 04 p0636 A71-14972

Thermal conductive liquid hydrodynamic stabilized Hartmann flow in rectangular canal with transverse field, examining magnetic effect on heat transfer 04 p0635 A71-15509

Magnetohydrostatic stellar interior instability, noting magnetic buoyancy 05 p0802 A71-15938

Magnetic and thermal pressures in solar wind from Explorer 34 data 05 p0797 A71-16016

Angular distribution and polarization of solar X-ray bremsstrahlung, taking into account magnetic field effects 05 p0000 A71-16032

Geomagnetic field effects on cosmic radiation, determining muon component momentum distribution and charge ratio 05 p0798 A71-16219

Electron heating in weakly ionized plasma by magnetic perturbation 05 p0787 A71-16291

Magnetic disturbances effect on drift behavior and anisotropy parameters of E and F region irregularities 05 p0740 A71-16433

Dynamic I-V characteristics of megawatt pulsed MPD-arc plasma thruster under various axial magnetic fields given for Ar and hydrogen propellants [AIAA PAPER 70-164] 05 p0796 A71-16574

Shock structure at Venus and Mars dependence on interplanetary magnetic field orientation from Mariners 4 and 5 data, indicating magnetosheaths existence 05 p0810 A71-16636

Magnetic field effects on biological systems, discussing ergometer measurements of human subjects muscular contractions 05 p0714 A71-16896

Fe powder filled tubular shell compression by magnetic fields and pulse sequences 05 p0759 A71-17168

Geocentric distances to subsolar point on magnetospheric boundary as function of magnetic activity state, discussing auroral oval position 05 p0744 A71-17180

Magnetically confined plasma dynamic stabilization, using HF potential 06 p0933 A71-17473

Dynamic stabilization of MHD instability of low current z-pinch by HF quadrupole and oscillating magnetic fields 06 p0935 A71-17486

Ray tracing near reflection level in ionosphere, considering magnetic field effect 06 p0927 A71-17687

Anomalous viscous fluid in channel with nonconducting walls, considering magnetic field effect on heat transfer 06 p0937 A71-17738

Cosmic ray intensity variations from magnetic fields of micrometeor streams in interplanetary plasma 06 p0954 A71-18126

Energetic solar wind particles, discussing interplanetary magnetic field curvature and gradient effects 06 p0956 A71-18142

Quartz astatic galvanometer resistant to geomagnetic field variations, vibrations or microseismic noise 06 p0901 A71-18286

Magnetic pulse technique connecting Al pipe with steel pipe, determining mechanical and physical parameters 06 p0906 A71-18713

Uniform magnetic field parallel alignment effects on incompressible electrically conducting free two dimensional jet flow stability at large Reynolds number 07 p1084 A71-18745

Maserlike pulsar radiation mechanism using Coulomb bremsstrahlung near strong quantizing magnetic field 07 p1190 A71-18858

Magnetoreflexion of helicon wave from n-InSb semiconductor in microwave range 07 p1176 A71-19270

Oscillatory magnetic field superimposition effects on flux flow properties of superconducting metal foils 07 p1177 A71-19596

Permanent magnets for footwear restraint and mobility in zero gravity spacecraft, testing neutral buoyancy and six degree of freedom simulation effects
[IEEE PAPER 2.2] 07 p1048 A71-19607

Magnetic field effects on collisionless plasma sheath near planar electrode, solving electric and magnetic potentials nonlinear differential equations by numerical scheme 07 p1171 A71-20290

Subinoculations of bacterial strains under constant, varying and pulsed magnetic fields, producing sensitivity increase or decrease to antibiotics 08 p1247 A71-20856

Irregularity levels changes in interplanetary magnetic field during solar activity cycle from cosmic ray neutron component measurement data obtained on azimuthal muon telescopes 08 p1353 A71-20976

Polar substorms electric current systems and magnetic effect below and above ionosphere 08 p1279 A71-21211

Plasma HF heating boundaries by magnetic traps, noting diamagnetic effects due to ion and electron heating 08 p1339 A71-21480

Two fluid continuum theory of Thomson scattering extended to uniform DC magnetic field and electron drift, finding backscattered power dependent on magnetism 08 p1283 A71-21640

High pressure electrodeless HF gas discharge plasmas, investigating effects of external magnetic field, gas and pressure on discharge rotation frequency 08 p1342 A71-21915

Confined plasma drift instability universal eigenmode stabilization by magnetic field shear 09 p1500 A71-22246

Electron loss by resonant interaction with whistlers in nonuniform magnetic field, taking Fokker-Planck equation as distribution function 09 p1513 A71-22423

Magnetic disturbances caused by magnetosphere-solar wind filamentary inhomogeneity interaction observed by Pioneer 6 09 p1513 A71-22560

Magnetic damper motions in rapidly spinning satellite 09 p1533 A71-23140

Artificial earth satellite orbit perigee motion, calculating perturbation effect due to gravitational and magnetic fields on orientation and rotation 09 p1523 A71-23150

Magnetoionic theory for drifting plasma whistler mode propagation, deriving magnetic field effects on imaginary and real parts of complex refractivity 09 p1505 A71-23385

Reflected radiative shock wave propagation velocity under transverse magnetic field, taking into account radiation pressure and energy 09 p1506 A71-23588

High power magnetically tunable microwave interference filters based on spin waves magnetic field dependent dispersion in ferrimagnetic materials 09 p1421 A71-23721

Electrical resistive incompressible fluid motion past thin airfoils in oblique field, showing inverse dependence of lift on magnetic Reynolds number 10 p1648 A71-23956

Soviet book on homogeneous plasma instabilities covering oscillations, magnetic effects, particle velocities, Landau damping, dielectric permittivity, electron fluxes and ion-cyclotron instabilities 10 p1648 A71-24016

Astrophysics - Conference, University of Nice, France, April 1969 10 p1670 A71-24186

Neutrino luminosity in strongly magnetized degenerate relativistic electron gas plasma from URCA energy loss rate calculations 10 p1671 A71-24303

Single-mode He-Ne laser, investigating longitudinal magnetic field effect on output amplitude, frequency and polarization characteristics 10 p1620 A71-24343

High purity GaAs transverse magnetophonon amplitudes, investigating magnetic field dependence and Landau level collision broadening 10 p1621 A71-24537

Hall effect mechanical vibration transducer with indium arsenide semiconductors and elastically suspended magnets 10 p1612 A71-24639

Spatially uniform external periodic magnetic field effect on wave propagation perpendicular to hot electron plasma, obtaining dispersion relation from hydrodynamic equations 10 p1578 A71-24655

High beta turbulent plasmas radiation scattering due to magnetic field strength and direction fluctuations from optical Faraday rotation observation 10 p1652 A71-24660

Pulsar oblique magnetic rotator model, noting large amplitude EM traveling wave effects on electron motion 10 p1679 A71-24956

Magnetic field effects on plane wave propagation in plasma, reducing motion data problem to vectorial differential equation with mean electronic velocity as only unknown 11 p1804 A71-25174

Attenuation and phase velocity of ELF and VLF radio waves propagating under anisotropic ionosphere, discussing geomagnetic field effect 11 p1731 A71-25602

Data reading function synchronized digital mass spectrometer with incremental scan by magnetic field sweeping, describing method for polynomial fitting of data 11 p1762 A71-25663

Laser-blowoff metal plasma interaction with strong transverse magnetic field, observing velocity reduction due to inhibited ambipolar electron-ion energy transfer 11 p1805 A71-25794

Longitudinal magnetic field effect on output power, polarization and lasing frequency of He-Ne laser operating at 0.63 micron wavelength 11 p1774 A71-26003

Nematic liquid crystal ultrasonic measurements at room temperature, showing anisotropic attenuation dependence on magnetic field orientation 11 p1808 A71-26149

Hamiltonian optics based model of ionospheric radio propagation, discussing earth magnetic field effects on radio wave angle-of-arrival changes 12 p1879 A71-27058

Magnetic field effect on emission spectrum and intensity at electron cyclotron frequency harmonics from PIG Reflex discharge, discussing electron oscillations excitation in plasma 12 p1938 A71-27214

Satellite rotation about center of mass, allowing for energy dissipation due to magnetic hysteresis 13 p2144 A71-28194

Damping in gravity gradient satellite passive stabilization systems under eddy currents and dry friction induced by magnet motion 13 p2144 A71-28195

Geocentric distances to subsolar point of magnetospheric boundary as function of magnetic activity state, discussing auroral oval position 13 p2059 A71-28237

Interplanetary magnetic field angular gradient and sectorial effects on solar wind, discussing wind velocity 13 p2128 A71-28527

Solar wind deflection due to permanent lunar surface magnetism 13 p2129 A71-28780

Relativistic thermo-magnetoelastic wave propagation, considering elastic solid under magnetic and thermal fields 13 p2101 A71-29105

Apollo 11 lunar rock and microbreccia examination for natural remanent magnetization, emphasizing viscous magnetization effect in terrestrial magnetic field 14 p2303 A71-29534

Circular lead specimens in water flow, determining external magnetic field effects on cavitation and erosion 14 p2278 A71-29613

Auroral electrons interaction with atmosphere from Fokker-Planck equation, considering angular diffusion, energy loss and geomagnetic field convergence effects 14 p2235 A71-30345

Geomagnetic pulsation effect on charged particles motion, based on Mead magnetosphere analytic model, using Parker perturbation method 14 p2235 A71-30346

Gravitational instability of heat conducting compressible fluid relative to class of axisymmetric perturbations, considering viscosity, magnetic field and uniform rotation 14 p2226 A71-30397

Monograph on instabilities in ion beam-plasma system covering surface wave propagation, magnetic effect and ion cyclotron radiation characteristics 14 p2281 A71-30507

Low temperature plasma MHD waves propagation in inhomogeneous magnetic fields, comparing numerical solutions with experimental results 14 p2282 A71-30559

Stellar and interstellar magnetic fields effects on plasma instabilities in Colgate cosmic ray model, using computer simulation 14 p2282 A71-30644

Cosmic ray modulation by solar wind, developing model with time variations based on magnetic bending power 14 p2302 A71-30647

Hydrogen plasma HF heating boundaries by magnetic traps, noting diamagnetic effects due to ion and electron heating 14 p2282 A71-30667

MHD three dimensional flow between rotating and stationary disks in transverse magnetic field with uniform suction at stationary disk 14 p2283 A71-30839

Vertical magnetic field and Coriolis forces effect on equilibrium of heavy viscous incompressible infinitely conducting rotating fluid 15 p2453 A71-31183

DC magnetic field effect on organism sympathoadrenal system, noting hypokinesia reduction of noradrenalin in hypothalamus and myocardium 15 p2357 A71-31311

Cosmic ray muon-neutrinos sea level energy spectra at low energies for horizontal and vertical directions, estimating geomagnetic cut-off effects for various geomagnetic latitudes 15 p2477 A71-31799

Magnetic stabilization of transverse plasma instabilities, considering waves propagating transversely to plasma direction in presence of uniform external magnetic field 15 p2460 A71-32658

HF magnetic field effects on LF plasma instability and oscillation spectrum 16 p2615 A71-32794

Mathematical theory of planetary atmosphere oscillations, considering coriolis, magnetic and viscous forces effects 16 p2561 A71-32804

Magnetic field perturbation and electric current injection techniques for characterizing high strength alloys fatigue microcracks 16 p2581 A71-32865

Elektron 2 and 4 satellites rotary motion with orbital variance of precession parameters and kinetic angular momentum vector, considering gravitational and magnetic effects 16 p2645 A71-33438

Zenomagnetic core-mantle coupling and fluctuations in period of rotation of Jupiter Great Red Spot 16 p2637 A71-33515

Electron temperature profiles in ionosphere from rocket probes, noting correlation with geomagnetic activity indexes 16 p2569 A71-33798

Magnetic drift wave instabilities in plasmas with nonuniform density and temperature gradient 16 p2572 A71-33949

Velocity and magnetic field equations of electroconductive fluid vortex motion due to annular receptacle insulating walls rotation 16 p2620 A71-34057

Boundary shock waves in electrically conducting gas under magnetic field, deriving Rankine-Hugoniot jump relations analogs and Prandtl relation 16 p2660 A71-34128

Ohmically heated collision plasma confinement in Uranian racetrack stellarator with large shear, describing magnetic field topography effects and plasma lifetime 17 p2785 A71-34196

Equilibrium state linear theta pinch plasma confinement dependence on magnetic force lines curvature radius 17 p2786 A71-34278

Moving plasma beam capture by transverse magnetic field due to polarization space charges electrostatic separation 17 p2786 A71-34280

Thin elastic shallow cylindrical panel in steady conducting supersonic gas flow, detailing magnetic field effects on static and dynamic stability and flutter 17 p2816 A71-34326

Pulsed emission and modulation of output power of He-Ne laser at 0.63 and 1.15 micron wavelengths as function of external longitudinal magnetic field 17 p2751 A71-34385

He-Ne laser emission and discharge plasma parameters, detailing variable magnetic field effects on modulation 17 p2752 A71-34389

Sq day to day variability relation to interplanetary plasma parameters including magnetic field and solar wind velocity and kinetic energy 17 p2801 A71-34625

Transverse magnetic field influence on heat transfer of conductive fluid/mercury/ in electrically insulated pipe subjected to uniform heat flux 17 p2788 A71-34660

Sunspot convective heat transfer in terms of magnetic field convection theory, considering motion in photosphere 17 p2802 A71-34826

Transverse magnetic field effects on Ar cross flow arc in constant velocity mainstream 17 p2788 A71-34868

Magnetic field effects on ruby laser radiation kinetics and spectral composition, studying crystal heating and light emission 17 p2753 A71-35242

High pressure electrodeless HF gas discharge plasmas, investigating effects of external magnetic field, gas and pressure on discharge rotation frequency 17 p2789 A71-35260

- Plane plasma layer stabilization by force-free magnetic field 17 p2789 A71-35342
- Time and space variable magnetic field effects on plane unsteady MHD boundary layer flow separation 17 p2789 A71-35343
- Electron bombardment mercury ion rocket engine, considering mass flow rate and magnetic field strength effect on performance 17 p2794 A71-35540
- Reynolds magnetic number effect on MHD channel conducting gas flow current distribution, taking into account Hall effect 17 p2790 A71-35642
- Anomalous microwave heating of electrons in magnetized plasma, showing resonances dependence on magnetic fields and charged particles concentration 17 p2790 A71-35735
- Variable and magnetic stellar model hypothesis concerning long period modulation due to radial and non-radial oscillation mode coupling beat in dipole magnetic field 18 p2962 A71-36152
- Solar corona model for structure and dynamic properties, investigating gas-magnetic field interactions 18 p2966 A71-36737
- Transcritical Permalloy thin film domain structure, investigating external field effect on powder depositions and proposing model 18 p2955 A71-36942
- MHD channels end effects at finite magnetic Reynolds numbers, discussing wall conductivity and external magnetic field geometry effects 19 p3108 A71-37078
- Reflection and transmission coefficients for electromagnetic propagation across magnetic field in parabolic plasma layer, determining EM-plasma wave conversion efficiency 19 p3014 A71-37079
- Rotating magnetic field plasma pinch, discussing streak and framing photography, electron line density profiles, magnetic probes and ion and electron temperature measurements 19 p3111 A71-37632
- Electromagnetic radiation from beam-plasma system in strong magnetic field, noting maximum microwave emission near electron cyclotron frequency 19 p3116 A71-38252
- Magnetic storm effect on integral electron content in F2 layer and in outer ionosphere 19 p3058 A71-38383
- Magnetic activity effect on pitch angle distribution of low energy auroral electrons from ESSO 1A measurements 19 p3060 A71-38575
- Magnetic field effect on emission spectrum and intensity at electron cyclotron frequency harmonics from PIG Reflex discharge, discussing electron oscillations excitation in plasma 19 p3117 A71-38626
- Double scattering of plasma stream in bi-thermal ionosphere, noting ion density perturbation under external magnetic field 20 p3272 A71-38748
- Pulsar periods change rate and radio luminosity decay, discussing magnetic field braking 20 p3286 A71-38762
- Uniform magnetic field effects on beam-plasma waves, using scalar pressure hypothesis 20 p3274 A71-39049
- Astronomical models of solar wind interaction with interstellar medium, determining magnetic field effects on shock wave 20 p3278 A71-39139
- Charged particle motion in constant magnetic field under random electric field, deriving maximum energy and diffusion coefficient 20 p3269 A71-39163
- Viscous electrically conducting laminar fluid steady flow through insulated MHD duct under uniform external magnetic field by extended Kantorovich method 20 p3275 A71-39561
- Nonflare solar X-ray emission from Cosmos 230 observation, noting presence of sunspot groups with complicated magnetic fields during enhanced short wave emission 20 p3283 A71-39749
- Pulsar radiation beaming due to strong magnetic field, computing Compton scattering and opacity 20 p3285 A71-39953
- Magnetic fluid sloshing in solenoidal magnetic field, describing fluid free surface waves similarity to ordinary liquid waves in reduced gravity field [ASME PAPER 71-VIBR-24] 21 p3366 A71-40281
- Magnetic field stabilizing effect on free shear layer of electrically conducting fluid at small Reynolds number 21 p3421 A71-40637
- Vertical magnetic field effects on stability of variable density compressible inviscid fluid, solving by variational principle 21 p3415 A71-40666
- MHD flow stability under arbitrary three dimensional disturbances, considering energy estimate for interaction between magnetic field and velocity field at critical Reynolds number 21 p3422 A71-40676
- Electrically conducting fluid flow resistance in plane insulated channel in presence of transverse magnetic field, determining pressure, velocity and electric potential distributions 21 p3422 A71-40677
- Confined plasma drift instability universal eigenmode stabilization by magnetic field shear 21 p3424 A71-41135
- Self magnetic field effect on I-V characteristics of Cs-Ba thermionic converter, noting effects of pressure differential due to ponderomotive forces action 21 p3326 A71-41294
- Bismuth telluride single crystals thermal conductivity and thermoelectric power temperature dependence 2.3-100 K, discussing magnetic field effects 21 p3433 A71-41314
- Cubic nonlinearity in p-type germanium semiconductor in constant magnetic field 21 p3435 A71-41337
- Te-doped n-type GaSb semiconductor negative magnetoresistance and magnetothermoelectric power dependence on longitudinal magnetic field 21 p3436 A71-41349
- Fluorescence of iodine molecule excited at 5017 and 5145 Å by ionized Ar laser, observing magnetic depolarization/Hanle effect/ 22 p3555 A71-41623
- Homogeneous positive plasma column perturbation analysis in axial magnetic field, deriving model for ionization waves dispersion characteristics 22 p3582 A71-41898
- Alouette and Isis satellites flight data comparison with attitude and spin dynamics theory, considering solar radiation pressure and gravitation and magnetic field effects 22 p3609 A71-41997
- Antiferromagnetic semiconductors and metals in magnetic field, obtaining Fourier components of electromagnetic fluctuation correlators for dielectric permittivity and magnetic permeability tensors 22 p3586 A71-42062
- Pulsar radio emission from expanding charge sheets moving relativistically along dipolar magnetic field near neutron star polar caps, calculating energy distribution 22 p3604 A71-42336
- Schwarzschild constants evaluation from coupled gyroscopes spin axes observation, noting axes high angular velocities due to gravomagnetic effect in gravitational interaction 22 p3605 A71-42338
- Resonant coupling of two electron plasma waves with ion sound wave at large electron Larmor radii under weak magnetic field 22 p3583 A71-42418
- Coronal flare onset, examining dynamic processes of plasma compression with longitudinal magnetic field 22 p3606 A71-42610
- Microwave emission from plasmas in InSb with and without magnetic fields, deriving pseudolongitudinal wave interaction theory for explanation 23 p3714 A71-42914
- Solar wind velocity increase by magnetic field energy conversion to kinetic energy, constructing steady state MHD one fluid model 23 p3719 A71-42949
- Radio reflection and transmission coefficients for thin highly ionized layers under earth magnetic field, based on numerical integration of differential equations 23 p3665 A71-42962
- Ionospheric geomagnetic field effect on ELF/VLF radio propagation 23 p3643 A71-42967
- IGY interplanetary field independent storm sudden commencement triggered magnetospheric polar substorms, indicating sympathetic flare analogy 23 p3668 A71-43164
- Magnetic drift waves near proton cyclotron frequency, noting magnetic field gradient role in plasma instability 23 p3709 A71-43181
- Midlatitude sporadic E layer changes during increased geomagnetic activity, considering skin effect and current shear 23 p3670 A71-43189
- Magnetic field effects on complex Young and shear moduli for nonferromagnetic metals, describing experimental technique and frequency resolution criterion 23 p3689 A71-43206
- Thin nickel films elastoresistance properties, examining magnetic state effects 23 p3691 A71-43361
- Particle collisions and relativistic effects on electromagnetic wave propagation within plasma in direction normal to external magnetic field near gyrofrequencies 23 p3645 A71-43559
- Electromagnetic wave reflection from ferrite plate in external alternating magnetic field, showing frequency change due to moving domain wall 23 p3645 A71-43568
- Plane supersonic ionizing shock wave in magnetic field under small wave plane perturbation from equilibrium position, calculating stability from linearized equations 23 p3663 A71-43575
- Heliographic longitude effect on delay time between solar proton observation and flare occurrence from HEOS A1 data, noting magnetic field influence 23 p3768 A71-43852
- Plasma acceleration of low pressure toroidal gas discharge, measuring plasma velocity as function of radial magnetic field for different pressures 23 p3711 A71-43874
- Planetary atmospheric motions, discussing solar radiation, internal heat sources, planetary rotation and magnetic field effects 23 p3672 A71-43891
- Strong magnetic field effects on acoustic oscillations and instability in stationary inhomogeneous low temperature plasma flow in crossed fields 23 p3712 A71-43917
- MnAlGe crystal domain structure observed for behavior with smaller crystal dimensions and changes in applied magnetic field orientation and strength 23 p3717 A71-43949
- Spread F configuration irregularities at Nairobi, investigating nocturnal and seasonal variations and magnetic and solar activity effects 23 p3672 A71-43979
- Large geomagnetic diurnal variations effects period determination by statistical method, considering partial ring currents in night magnetosphere 23 p3673 A71-43985
- Self magnetic impulses in gas discharge configuration as function of current and anode-cathode radii ratio 24 p3851 A71-44431
- Molecular gas dissociation equilibrium and carbon monoxide overtone line widths dependences on magnetic field strength in sunspots 24 p3868 A71-44459
- Magnetic energy pumping into plasma by slowly modulating plasmon frequency-dependent external magnetic field 24 p3851 A71-44485
- Steady state problem of energy spectrum of variable magnetic field accelerated electrons, considering synchrotron X ray emission of Crab Nebula and pulsar 24 p3869 A71-44802
- Poloidal magnetic field effects on polytropic oscillation modes, using second order tensor virial equations 24 p3871 A71-44909
- Stress and magnetic field induced spin density wave polarization vectors rotation in Cr single crystals, accounting for Young modulus temperature and magnetic field dependence 24 p3861 A71-45131
- Refraction of electromagnetic wave with electric field perpendicular to applied magnetic field in anisotropic plasma cylinder cross section 24 p3858 A71-45236
- He-Ne laser discharge gap oscillation modes observation, noting applied magnetic field, gas parameters and cathode type effects on stimulated emission 24 p3835 A71-45239
- Magnetospheric midday boundary width dependence on geomagnetic dipole axis orientation, discussing different positions for magnetosphere boundary 24 p3824 A71-45319
- Predawn effect on hot and cold electrons at magnetopause point in F2 layer, discussing electron shock wave speed and thermal collisionless wave energy dissipation 24 p3824 A71-45321

MAGNETIC EQUATOR

- Whistler ducts as enhanced ionization fromOGO 3 satellite observations near magnetic equator, noting magnetospheric ionization hydrostatic model and predicted cut-off 01 p0076 A71-11499
- Magnetospheric VLF electric field emissions above electron cyclotron frequency fromOGO 5 observation at magnetic equator 01 p0076 A71-11500
- Ionospheric vertical drift velocities and east-west electric fields at magnetic equator from incoherent scatter observations 01 p0076 A71-11505
- Directional differential energy spectra for proton intensities in outer radiation zone near magnetic equator from satellite observations 06 p0949 A71-17261
- Magnetic storm of 31 October 1968, observing charged particle increase at geomagnetic equator 06 p0961 A71-18172
- Quiet day geomagnetic field measurements at synchronous orbit ATS 1, calculating equatorial component of interaction force between solar wind and earth 07 p1102 A71-19664

Electron continuity equation for lower F 2 layer near dip equator, estimating photoionization and recombination rates

08 p1278 A71-21203

Steady state streaming of cold magnetospheric plasma in magnetic equatorial plane near plasmopause

10 p1650 A71-24557

Plasma sheet proton ring current, trapping boundary and plasmopause interrelations near magnetic equator and local midnight by satellite-borne analyzer array

10 p1605 A71-24781

Spectral lines of O/IS/ generated by oxygen molecule dissociative recombination in upper atmosphere observed in nightglow at geomagnetic equator with Fabry-Perot spectrometer

14 p2229 A71-29663

Traveling ionospheric disturbances at magnetic equator, determining electron concentration profiles by incoherent scatter radar

15 p2398 A71-31771

Geomagnetic equatorial ionospheric ion temperature, comparing incoherent scatter radar and OGO-D retarding potential analyzer values

16 p2573 A71-33956

Nighttime sporadic E layer behavior near magnetic equator, discussing occurrence frequency, seasonal variation and solar activity effects

19 p3055 A71-38037

Equatorial modulation in pulsating aurora, discussing electron measurements with channel multipliers and electrostatic analyzers aboard ESRO Skylark S29/2

20 p3228 A71-39841

Ionospheric properties at geomagnetic equator from ionograms by automatic sounder at Thumba, noting F 2 layer ionization frequencies solar cycle variations altitude dependence

21 p3373 A71-40376

MAGNETIC FIELD INTENSITY

U MAGNETIC FLUX

MAGNETIC FIELDS

NT FORCE-FREE MAGNETIC FIELDS

NT GEOMAGNETISM

NT INTERPLANETARY MAGNETIC FIELDS

NT INTERSTELLAR MAGNETIC FIELDS

NT LUNAR MAGNETIC FIELDS

NT MAGNETOSTATIC FIELDS

NT NONUNIFORM MAGNETIC FIELDS

NT PALAEOMAGNETISM

NT PLANETARY MAGNETIC FIELDS

NT SOLAR MAGNETIC FIELD

NT STELLAR MAGNETIC FIELDS

NT TRAPPED MAGNETIC FIELDS

Magnetic field generation during radiation era, discussing generating mechanism by angular momentum transfer between ion and electron-photon gases in expanding plasma

01 p0148 A71-10024

Radio galaxies emission source, examining Patchy model for prestellar matter magnetic field strength

01 p0150 A71-10063

Electric current carrying plasma with finite and anisotropic conductivity in longitudinal magnetic field, determining equilibrium and stability

01 p0132 A71-10173

Parabolic particle distribution stability in plasmoids in guiding magnetic field under diffusion due to electron-ion collisions

01 p0133 A71-10680

Torsional and compressional hydromagnetic wave propagation in inhomogeneous magnetic fields

01 p0134 A71-11001

Electrons motion across gas plasma magnetic field under stochastic electric field, noting accelerating effect

01 p0135 A71-11032

Two dimensional inhomogeneities effects on electrical resistance of plasma with nonuniform density in strong magnetic field

01 p0135 A71-11065

Self similar unsteady waves in cold plasma containing magnetic field, determining plasma oscillations

01 p0135 A71-11095

Self gravitating fluid spheroid oscillations in hydrostatic equilibrium with magnetic fields using variational principle

01 p0129 A71-11336

Quasi-nucleon nuclear interactions of high energy protons in photoemulsion irradiated in pulsed magnetic field

01 p0131 A71-11368

Longitudinal electrical and thermal conductivities of fully ionized plasma in strong external magnetic field

01 p0136 A71-11473

Electron gas column rotating about axis parallel to uniform external magnetic field, considering equilibria within Vlasov-Maxwell model

01 p0136 A71-11478

Power transfer in plasma heating with combined RF and steady magnetic fields

01 p0137 A71-11481

Weak magnetic field measurement using magnetometer with digital technique time coding

02 p0247 A71-11722

Thermomagnetic gas torque within kinetic theory framework for collinear static and alternating magnetic fields

02 p0291 A71-12316

Transformation properties of radiation field and electromagnetic energy fluxes of relativistic charged particles in magnetic field

02 p0312 A71-12362

Astrophysical bodies dynamo equations describing large scale magnetic fields generation by small scale cyclonic turbulence in rotating fluid body

02 p0314 A71-12588

Earth gravitational and magnetic field correlation, determining undulations on core-mantle interface

02 p0247 A71-12953

Ionizing shock wave interaction with transverse magnetic field, examining magnetic field distribution behind shock front, interface discontinuity and wave reflection

03 p0462 A71-13234

Conducting fluids Rayleigh-Taylor instability in vertical magnetic field, taking into account Hall currents

03 p0463 A71-13473

High beta plasma, calculating turbulence for fast shock propagating perpendicular to magnetic field

03 p0496 A71-14514

Nonpotential ion cyclotron waves propagation at very large angles to unperturbed magnetic field, obtaining dispersion relation numerical solutions

03 p0420 A71-14530

Charged particle trajectory under dipole magnetic field, deriving Stoermer orbit existence and uniqueness proof

04 p0625 A71-15081

Ionizing shock wave interaction incident on transverse magnetic field

05 p0786 A71-15975

Primeval intergalactic magnetic field existence, observing radio sources rotation distribution and red shift

05 p0805 A71-16108

Incompressible inviscid perfectly conducting cylindrical plasma stability against azimuthal disturbance in monotonic decreasing magnetic field with constant pitch, using energy principle

05 p0787 A71-16478

Electron-hole plasma in current carrying wire azimuthal magnetic field, noting electric field intensity by hydrodynamic approximation

05 p0790 A71-16880

Lower ionosphere magnetic fields generated by three dimensional Alfvén waves, analyzing spatial phase and amplitude distribution

05 p0745 A71-17199

Polyatomic gases thermal conductivity coefficient, examining magnetic field effect

06 p1005 A71-17316

High-beta sharp-boundaried stellarator plasma column feedback stabilization with helical fields

06 p0932 A71-17463

Dynamic stabilization of drift dissipative instability by inhomogeneous RF electric field parallel to magnetic field

06 p0934 A71-17475

Dynamic stabilization of magnetoplasma drift dissipative instability by HF oscillating magnetic field, discussing helium and hydrogen afterglow plasmas

06 p0934 A71-17481

Dynamic control of steady state plasma loss in cusped magnetic field, considering density and electron and ion temperatures

06 p0935 A71-17490

Hot electron plasma confinement in cusped magnetic field, considering production in electron cyclotron resonance region by pulsed microwaves

06 p0935 A71-17491

Anomalous viscous fluid in channel with nonconducting walls, considering magnetic field effect on heat transfer

06 p0937 A71-17738

Whistler wave packet propagating in ambient magnetic field direction, computing nonlinear particle trajectories

06 p0869 A71-17987

Geomagnetic field daily variation, discussing ambient field weakening on night side

06 p0893 A71-17992

Purely azimuthal magnetic toroidal-meridional component poloidal field conversion by slow precessional motion superimposition on rotating fluid under uniform current distribution

06 p0894 A71-18016

Inhomogeneous plasma flute instability in presence of gravitational field and supported by magnetic fields

06 p0938 A71-18425

Transverse velocity shear effects on low-beta resistive plasma LF stability in uniform magnetic field

07 p1166 A71-18882

Collisional drift plasma wave instability nonlinear analysis, calculating wave amplitude as function of magnetic field based on two fluid theory

07 p1166 A71-18883

Plasma instabilities under radial magnetic field effect across homogeneous field, considering oscillation modes

07 p1167 A71-19231

Helicon wave resonance excitation and indication in intermediate magnetic fields in semiconductors

07 p1176 A71-19274

Ionospheric inhomogeneities effect on dipole current system produced magnetic field, deriving analytical expressions as function of distance from current carrying layer and inhomogeneity center

07 p1099 A71-19381

Diffusion coefficient estimation for energetic charged particles across magnetic fields from mathematical model

07 p1186 A71-19631

Hydrodynamic stability of viscous conducting fluid plane Couette-Poiseuille flow in transverse magnetic field by linear theory, considering complete spectrum of small disturbances

07 p1169 A71-19722

Unsteady viscous incompressible electrically conducting fluid flow past accelerated conductor or insulator flat plate in uniform transverse magnetic field

07 p1169 A71-20022

Nondissipative heterogeneous shear flow stability in presence of uniform magnetic field in streaming direction

07 p1169 A71-20023

Pressure shocks propagation through electrically and thermally conducting viscous gas in presence of uniform magnetic field

07 p1169 A71-20025

Parabolic particle distribution stability in plasmoids in guiding magnetic field under diffusion due to electron-ion collisions

07 p1170 A71-20141

N-type InSb microwave noise radiation and attendant RF current oscillations under magnetic field

07 p1180 A71-20177

Single mode gas ring laser in longitudinal magnetic field, deriving lasing equations from semiclassical theory

07 p1129 A71-20532

Plane steady state MHD shock wave structure in infinitely conducting fluid under magnetic field perpendicular to shock velocity, introducing quadratic artificial viscosity factor

07 p1174 A71-20616

Voltage induction in superconductors by superimposed AC and DC magnetic fields

08 p1343 A71-20881

Electromagnetic wave scattering by perfectly conducting cylinder in anisotropic plasma with external magnetic field, deriving radiation pattern from asymptotic expression

08 p1253 A71-21295

Plasma configurations kinetic description by differential equations based on Vlasov and Maxwell equations, obtaining boundary layer distribution between plasma and magnetic field

08 p1340 A71-21492

Low density plasma in magnetic field, investigating existence possibilities of stationary isothermal jump and plane wave periodic solution

08 p1340 A71-21493

Electron fluxes hydrodynamic stability in vacuum confined by external electric and magnetic fields and inertia forces, noting electron oscillations possibility

08 p1340 A71-21494

Pulsed coaxial plasma accelerator, measuring longitudinal gas pressure distribution, particle emission and magnetic fields characteristics under various operating conditions

08 p1341 A71-21496

Moving magnetic field lines identification, applying to moving nonrigid conductor

08 p1283 A71-21648

Magnetic field generation in acoustically turbulent medium, deriving spectral function equation

08 p1341 A71-21795

High pressure electrodeless HF gas discharge plasmas, investigating effects of external magnetic field, gas and pressure on discharge rotation frequency

08 p1342 A71-21915

Self similar unsteady waves in cold plasma containing magnetic field, determining plasma oscillations

08 p1342 A71-21953

Interaction between perfect gas ionizing shock wave and transverse magnetic field in coaxial channel, indicating incident wave attenuation and reflected shock wave formation

09 p1498 A71-22128

Electrodynamical forces distribution in conducting bodies in two traveling magnetic fields with different frequencies and pole spacings

09 p1499 A71-22137

Electromagnetic effects in infinite conducting layer situated in field of inductors with mutually opposed traveling magnetic fields

09 p1499 A71-22138

Weak magnetic field disturbance by strong spherical shock wave propagation in finite conductivity gas

09 p1430 A71-22140

- Radiative instability of nonequilibrium plasmas in magnetic traps, considering circularly polarized oscillations propagating along magnetic field
09 p1500 A71-22241
- Fluctuations effect on MHD shock wave propagating in plasma perpendicular to external magnetic field, obtaining field amplitude distribution function
09 p1500 A71-22242
- Unitary potential method for numerical separation of subterranean three dimensional gravitational and magnetic fields
09 p1436 A71-22608
- Boundary condition effects on thermomagnetic torque from moment method solution for Boltzmann equation for diatomic molecular gas in magnetic field and cylindrical geometry
09 p1502 A71-22853
- Plasma flow interaction with nozzle-shaped magnetic field generated by current loop with strong Hall effect
09 p1504 A71-23309
- Plasma confinement in Heliotron magnetic field discussing equilibrium and stability problems
09 p1505 A71-23442
- Longitudinal plasmon decay in strong magnetic field into neutrino-antineutrino pair
09 p1527 A71-23533
- Quasi-radial hypervelocity approximation of rotating azimuthally dependent solar wind under magnetic field
09 p1515 A71-23709
- Angular dependence of specularly parameter /probability of specular scattering of electron incident upon surface/ via magnetic field dependence of magnetomorph harmonic oscillations
10 p1655 A71-23771
- Observation range determination numerically for cyclotron resonances of effective scattering cross section of light wave by collisionless plasma in magnetic field
10 p1646 A71-23848
- Stationary shock wave propagation perpendicular to magnetic field in Vlasov collisionless plasmas
10 p1647 A71-23892
- Soviet book on large pulsed currents and magnetic fields technology covering condenser bank discharge systems and components design, electrical characteristics and structural details
10 p1557 A71-24014
- Conducting fluid in transverse magnetic field at low Reynolds numbers, deriving laminar boundary layer universal equations in Crocco or Mises variables
10 p1648 A71-24028
- Polar cap as distinct geophysical entity, considering open magnetic field lines for connectedness to interplanetary plasma and particle input to lower latitudes
10 p1600 A71-24308
- Polar caps magnetic field variations, considering relationship to auroral phenomenon and ionospheric conductivity variations
10 p1600 A71-24314
- Uniform magnetic field effect on rarefied gas slip flow over porous flat plate for skin friction response, using velocity and temperature fields equations
10 p1649 A71-24407
- Wall conductivity effects in MHD rectangular duct flow at high Hartmann numbers with uniform magnetic field applied parallel to one pair of duct sides
10 p1649 A71-24419
- Astrophysical objects magnetic field generation, examining behavior at large dynamo numbers
10 p1676 A71-24494
- High purity GaAs transverse magnetophonon amplitudes, investigating magnetic field dependence and Landau level collision broadening
10 p1621 A71-24537
- Electromagnetic extraordinary wave propagation in toroidal plasma with sheared magnetic field, discussing ordinary component generation at upper hybrid frequency
10 p1650 A71-24629
- Poloidal magnetic field measurements in toroidal pinch by Thomson scattered carbon dioxide laser beam
10 p1651 A71-24631
- Nonhomogeneous plane parallel cold plasma flows in external magnetic field, deriving energy transfer between two sliding plasmas
10 p1651 A71-24634
- Very weak magnetic field measurements by highly rarefied gases as sensors
10 p1642 A71-24697
- Turbulent plasma heating in current sheet between opposed magnetic fields
10 p1653 A71-24891
- Stochastic particle acceleration in random electromagnetic field determination by turbulent plasma motion in external homogeneous magnetic field
10 p1655 A71-25075
- Ionospheric drift mechanism in midlatitude F region, discussing ground level magnetic field, E region side effects, horizontal winds and polarization fields
11 p1753 A71-25550
- HF electromagnetic waves absorption as function of discharge current intensity in ionized H₂ using gas pressure or uniform magnetic field as parameters
11 p1805 A71-25598
- Rotating plane layer viscous incompressible conducting fluid flow between two parallel walls with temperature gradient subject to perpendicular gravitational and magnetic fields
11 p1757 A71-25767
- Magnetic field components of local ionospheric current for LF oscillation range including micropulsation frequencies, discussing spatial and frequency distribution
11 p1758 A71-25790
- Tangential velocity profile in steady incompressible electrically conducting viscous axial flow between concentric rotating cylinders with radial magnetic field, solving Navier-Stokes equations
11 p1752 A71-26048
- Linear and nonlinear laser induced ion emission from solid targets with and without magnetic field, considering electron space charge accelerator
11 p1775 A71-26085
- Spiral galaxies orientation anisotropy explanation by hypothetical model of cosmological magnetic field
11 p1831 A71-26166
- MHD oscillations of homogeneous compressible self gravitating fluid spheroid in static equilibrium with poloidal magnetic field inside and dipole field outside
11 p1831 A71-26167
- Spontaneous magnetic fields in laser produced plasmas explained as thermoelectric currents
11 p1807 A71-26406
- Modified Landau-Lipschitz equation of thin ferromagnetic film for slowly reversing magnetic fields solved by interpolation, discussing magnetization curve subrelaxation segment
11 p1809 A71-26547
- Monograph on marginal stability analysis of MHD instabilities by force free magnetic fields in plasma-vacuum systems covering gravitational, pinch and shearless models
12 p1934 A71-26569
- Collisionless motion of solar wind ions in helical magnetic field, giving transfer function of charged particles
12 p1947 A71-26636
- Plasma instabilities under radial magnetic field effects across homogeneous field, considering oscillation modes
12 p1934 A71-26749
- Current distribution effect on stability of exploding and collapsing accelerated cylindrical plasma shell in axial and azimuthal magnetic field
12 p1935 A71-26765
- Ne absorption tube in alternating magnetic field for He-Ne laser frequency stabilization reference, discussing laser output SNR effects
12 p1913 A71-26926
- Nondestructive magnetic method for measuring longitudinal residual stress in outer portions of ferromagnetic cylindrical bars
12 p1974 A71-26948
- Milky Way galaxy radio halo, investigating background brightness distribution and local spiral arm magnetic field structure
12 p1963 A71-27078
- Electric and magnetic fields of fundamental modes in cylindrical and rectangular dielectric microwave resonators, classifying transmission lines connections
12 p1888 A71-27613
- Traveling wave tube magnetic field focusing and accelerating voltage effects on power output
12 p1889 A71-27627
- Collisionless plasma with thermal ions in magnetic field absence, investigating stationary ion shock wave propagation
12 p1941 A71-27767
- Polarization behavior of radio waves propagating through magnetoionic medium near and across transversal point of magnetic field
13 p2028 A71-27997
- Lower ionosphere magnetic fields generated by three dimensional Alfvén waves, examining amplitude and phase spatial distribution and frequency dependence
13 p2059 A71-28254
- Collisionless plasma thermal shock wave, showing heat in electron component transportable along magnetic field at lower rates than thermal velocity
13 p2106 A71-28425
- Diffusion measurement of highly ionized thermal Cs plasma in magnetic field by Langmuir probe, determining density profile
13 p2106 A71-28450
- Nonhomogeneous turbulent flow with magnetic field, deriving MHD turbulence model neglecting velocity correlation time
13 p2107 A71-28565
- Collisionless heat propagation along plasma magnetic field, showing relation to ion sound velocity
13 p2107 A71-28568
- Permanent magnet system design, deriving optimal field configurations and maximum magnetic energy
13 p1999 A71-28637
- Group properties of laminar boundary layer equations for incompressible binary fluid under various magnetic field distributions and reaction rates
13 p2048 A71-28735
- Helicon and magnetoacoustic waves instability during passage through hot collisionless plasma with current transverse to weak external magnetic field
13 p2107 A71-28851
- Hydrogen plasma internal magnetic field determination, using spectral characteristic measurements due to level interconversion
13 p2108 A71-29030
- Scott effect observation of superrotation of upper atmosphere, relating temperature gradient, magnetic field and gas rotation
13 p2063 A71-29095
- Distant geomagnetic tail longitudinal magnetic field gradient model based on pressure balance between internal field and solar wind, discussing tail flux content
13 p2064 A71-29162
- Solar wind-magnetosphere interaction based on electric fields and currents, discussing energy transfer and magnetic field reversal at magnetopause
13 p2064 A71-29165
- Adiabatic flow model of noiseless magnetic neutral sheet of finite width, discussing particle trajectory and charge density distribution
13 p2109 A71-29166
- Kinetic theory of two dimensional boundary layer between plasma and magnetic field, using computer for vector potential differential equations solution
13 p2109 A71-29214
- Magnetic corrections to Boltzmann distribution function by power expansion, determining current density in system of free electrons accelerated by crossed electric and magnetic fields
13 p2109 A71-29288
- Intense magnetic fields in astrophysics, emphasizing flux conservation law and quantum effects
13 p2144 A71-29436
- Conducting incompressible liquid in transverse magnetic field, considering plane steady motion of isothermal MHD boundary layer
14 p2278 A71-29604
- Ideally conducting compressible liquid flow near arbitrary geometrical thin profile form in transverse magnetic field
14 p2278 A71-29608
- Bounded flow incident on cylindrical body in transverse magnetic field, determining constraints effects on dynamic and structural characteristics
14 p2278 A71-29609
- Nonuniform conductivity effect on cosmic magnetic fields structure with zero Lorentz force, using Maxwell equations and Ohm law
14 p2274 A71-29982
- Integral coefficient of correlation between gravitational and magnetic fields with geological element
14 p2235 A71-30189
- German monograph on application of theory of optical pumping with crossed light beams to magnetic fields vector measurement
14 p2242 A71-30230
- Massive rotating plasma cloud contraction with magnetic field perpendicular to rotation axis, causing magneto-rotational explosions
14 p2312 A71-30386
- Afterglow plasma drift-dissipative instability stabilization by RF magnetic and electric fields
14 p2280 A71-30504
- Millimeter wave semiconductor isolator using circular waveguide with coaxial n-type InSb in longitudinal magnetic field
14 p2212 A71-30510
- Magnetic field generation from coaxial plasma gun, discussing mechanism in terms of azimuthal plasma mass motion imparted during initial gas discharge
14 p2281 A71-30543
- Large scale kinematic dynamo theory for magnetic field generation in turbulent fluids based on Lorentz force helicity
14 p2314 A71-30646
- Atmospheric spectral and structural characteristics, reviewing studies of source phenomena and related electric, magnetic and electromagnetic fields
14 p2237 A71-30965
- Monograph on planetary nebulae covering structure, luminosity, spectra, origin, chemical composition, temperature, magnetic fields, etc
15 p2481 A71-31148
- Coaxial plasma beam polarization interaction in toroidal magnetic field with diverter, showing axial stream trapping in hollow plasma cylinder
15 p2453 A71-31244
- Electron hole plasma in plate shaped semiconductor under rapidly increasing external magnetic field, examining density
15 p2453 A71-31247
- Magnetic cut-off system reducing length of high density jet flows from plasma guns, using axially asymmetric field configurations
15 p2455 A71-31644
- Electron cluster formation in klystron buncher, calculating focusing longitudinal magnetic field variation for maximum electron radial stability
15 p2376 A71-31742

Magnetic field and electron plasma observations near dawn magnetopause by triaxial spectrometer and fluxgate magnetometer on satellite OGO 5

15 p2485 A71-31754

Hydromagnetic waves, micropulsations and temporal variations in vector geomagnetic field at 6.25 earth radii

15 p2397 A71-31759

Complex refractive index equation of ionosphere for large values of vertical component of magnetic field, showing imaginary part independent of temperature effects

15 p2449 A71-31849

Similarity solutions describing flow characteristics behind plane hydromagnetic shock propagating into uniform ideal gas at rest in presence of transverse magnetic field

15 p2391 A71-32074

Soviet papers on gas discharge plasmas and strong magnetic fields covering plasmatrons, MHD generators, electric arc combustion, etc

15 p2457 A71-32266

Electrical breakdown in transverse magnetic field and Ar plasma flow in pressure range 0.2-1400 mm Hg and velocity range 0-50,000 cm/sec

15 p2457 A71-32272

Ferromagnetic shields effectiveness against magnetic fields, permitting solutions to nonlinear shielding problems

15 p2377 A71-32369

Guiding center equations for charged particle motion and statistical fluctuations of plasma in magnetic field, using Krylov-Bogoliubov transformation

15 p2458 A71-32393

Ion motion effect on first order oscillations in infinite homogeneous two-component cold plasma in constant magnetic field and circularly polarized external field

15 p2459 A71-32651

Magnetogravitational instability model with allowance for finite Larmor radius effect, considering plasma rotation parallel to magnetic field

15 p2459 A71-32654

Radiative energy transfer equations solution in magnetic field, facilitating magnetograph calibration

15 p2496 A71-32740

Critique of papers on line formation in absorption fields, discussing dispersion in absorption matrix

15 p2496 A71-32741

Square cross section rectangular rotating grains dynamic behavior in magnetic fields, obtaining orientation data with Monte Carlo method

15 p2498 A71-32772

Conductivity measurement of shock generated nitrogen plasma in transverse magnetic field, considering vibrationally excited molecules role in electron collision frequency

16 p2616 A71-32899

Shock wave reflection process model in magnetic fields, describing time development of interaction process

16 p2616 A71-32901

Closed path recycling shock tubes, presenting numerical simulation of circular path continuous shock wave driven by successive electrical discharges in presence of perpendicular magnetic field

16 p2551 A71-32917

Magnetoelastic oscillations of thin conducting plate in magnetic field, solving electrodynamic equations

16 p2647 A71-32928

Electric field in flow of medium with tensor conductivity due to Hall effect, studying eddy currents structure in magnetic field variation region

16 p2616 A71-32929

Plasma configurations kinetic description by differential equations based on Vlasov and Maxwell equations, obtaining boundary layer distribution between plasma and magnetic field

16 p2618 A71-33043

Low density plasma in magnetic field, investigating existence possibilities of stationary isothermal jump and plane wave periodic solution

16 p2618 A71-33044

Pulsed coaxial plasma accelerator, measuring longitudinal gas pressure distribution, particle emission and magnetic fields characteristics under various operating conditions

16 p2618 A71-33046

Galaxy formation in expanding universe, discussing primordial plasma and photon gas turbulent medium for magnetic field amplification by dynamo mechanism

16 p2625 A71-33052

Lower limit on size of matter and antimatter regions in vanishing baryon number cosmology based on homogeneous intergalactic magnetic field existence

16 p2632 A71-33237

Specific heat measurement in magnetic field for graphite under neutron irradiation at low temperatures, noting Schottky anomaly

16 p2600 A71-33379

Schuster hypothesis on celestial object relation between angular momentum and magnetic fields

16 p2637 A71-33513

Magnetic field generation in acoustically turbulent MHD medium, deriving spectral function equation and eigenvectors

16 p2619 A71-33545

Plasma beams injection into toroidal magnetic field along gradient or radius, using polarizational interaction

17 p2786 A71-34281

Plasma interchange instability in multipole magnetic field, including disturbance wavelength comparable to ion cyclotron radius

17 p2786 A71-34282

Partial differential equations governing second order correlation functions for velocity and magnetic field in isotropic conducting turbulent flow

17 p2789 A71-35443

S shock wave and magnetic field interaction at supersonic speed, using shock tube and MHD channel with sectioned electrodes

17 p2790 A71-35643

Combustion systems ionic wind velocities, investigating gauze parameters, magnetic fields and mixture inhomogeneity effects

17 p2785 A71-35703

Superconducting phase transition temperature measurements as function of magnetic field in thin film hollow Al and In cylinders

17 p2791 A71-35742

Particle gyration in homogeneous magnetic field and perpendicularly propagating electrostatic wave, calculating wave-particle energy transfer and wave-amplitude limiting effects

18 p2950 A71-35862

Lunar stratified composition based on electrical conductivity profile from magnetic field fluctuations measurement in terms of two layer model

18 p2961 A71-35993

Electric and magnetic fields effect on turbulent boundary layer of conducting gas near electrode in MHD channel with insulated walls

18 p2951 A71-36113

Double electron-nuclear resonance spectrometer using HF modulation of magnetic field for observation of electron paramagnetic resonance signal

18 p2924 A71-36626

Magnetic thin film domain wall velocity dependence on magnetic field intensity as function of film thickness, discussing nonlinearity causes

18 p2955 A71-36938

Weakly ionized gas plasma confined by cylindrical electrodes and dielectric fronts, calculating rotational movement behavior in transverse electric and longitudinal magnetic fields

18 p2952 A71-36943

Kinematic dynamo theory application to infinite stationary media with large scale magnetic field components and isotropic turbulence

18 p2967 A71-37025

Parametric plasma instability in HF electric field and constant magnetic field, noting longitudinal plasma oscillations growth

19 p3108 A71-37130

Ion charge composition in plasma-electron beam system in strong longitudinal magnetic field, noting multiply charged ions production under high temperature conditions

19 p3109 A71-37132

Stationary plasma flow interaction with axisymmetric spatially periodic magnetic field in presence of Hall effect, determining electric currents structure

19 p3109 A71-37139

Magnetopause current layer equilibrium based on numerical solution of uniform magnetic field confinement by warm plasma with net parallel velocity

19 p3132 A71-37355

Magnetic field aligned electric field production by hot magnetospheric plasma interaction with cold ionosphere

19 p3048 A71-37401

Milky Way galaxy radio halo, investigating background brightness distribution and local spiral arm magnetic field structure

19 p3133 A71-37428

Stellar atmosphere line formation in magnetic fields, considering Milne-Eddington model

19 p3133 A71-37507

Hydrodynamic equations for anisotropic plasma in magnetic fields, considering collisionless and collisional transport effects

19 p3111 A71-37634

Surface wave patterns created by constant velocity pressure point on inviscid plasma bounded by magnetic field

19 p3111 A71-37637

Ion-exosphere in open magnetic field, calculating number density, particle, moment and energy flux distribution from simple mathematical model

19 p3138 A71-37737

Helium plasma interaction with inhomogeneous transverse magnetic field, noting plasma electron temperature and density increase

19 p3112 A71-37743

Magnetospheric electric field dynamics, examining resonant protons role in magnetic storms

19 p3127 A71-37760

Ionospheric inhomogeneities effect on dipole current system produced magnetic field, deriving analytical expressions as function of distance from current carrying layer and inhomogeneity center

19 p3052 A71-37810

Transverse waves and electromagnetic instabilities propagating along magnetic field in homogeneous plasma, discussing ions and electrons energy losses and plasma dispersion

19 p3114 A71-38206

Finite Larmor radius equations for collisionless plasmas in magnetic fields, noting application to axisymmetric systems stability

19 p3115 A71-38209

Electromagnetic wave scattering on single ellipsoidal inhomogeneity in cylindrical waveguide, obtaining relationship for electric and magnetic waves reflection coefficient

19 p3019 A71-38330

H wave propagation in waveguide consisting of two parallel plates with longitudinal rectangular grooves, determining electric and magnetic fields by reduction method

19 p3019 A71-38331

Asymmetrical single ring resonator with electric and magnetic waves, determining intrinsic fields

19 p3019 A71-38340

Axial and radial components of magnetic induction of steady plane meridional field from rectangular region with azimuthal current density

19 p3000 A71-38638

One dimensional ambipolar diffusion parallel to magnetic field lines, considering plasma cloud imbedded in weakly ionized gas with homogeneous field

20 p2315 A71-38737

RF magnetic field radial distribution measurement in thermal argon induction plasma flame

20 p2373 A71-38841

Nonlinear Faraday effect in nonparabolic semiconductors subjected to strong electromagnetic field and steady magnetic field, deriving distribution function of charge carriers

20 p3276 A71-39010

Coherent small amplitude hydromagnetic wave propagation in magnetic field with time independent random component

20 p3274 A71-39057

Stability of plane rotating galaxies in magnetic field parallel to axis of rotation, showing linearized MHD equations self conjugate for radial disturbance case

20 p2389 A71-39298

Satellite data on solar wind velocity, ion composition, temperature and magnetic field characteristics near earth orbit

20 p3279 A71-39445

Marginal stabilization of MHD instabilities of linear pinch by force free magnetic fields, comparing with energy method

20 p3275 A71-39462

Shearless magnetic fields discontinuities in marginal stabilization of MHD instabilities for constant pinch force free fields, including toroidal effects

20 p3275 A71-39463

Homogeneous large scale intergalactic magnetic field evidence in terms of Faraday rotation measurements of extragalactic radio sources

20 p3294 A71-39541

H, He and O ion fluxes along exospheric magnetic field lines, determining flux energy and direction from RF mass spectrometer measurements onboard Elektron 4 satellite

20 p3226 A71-39742

Ionospheric model for magnetic perturbation field global distribution during polar magnetic substorm, considering ground level geomagnetic effects from Birkeland and Pedersen currents

20 p3229 A71-39857

Artificial auroral experiment by Aerobee rocket-borne electron accelerator generated monoenergetic electron beam injection onto magnetospheric field

20 p3231 A71-39885

MHD power generator for converting heat into electricity by interacting magnetic field with flowing electrically conducting fluid

21 p3436 A71-40020

Collisionless plasma thermal shock wave, showing heat in electron component transportable along magnetic field at lower rates than thermal velocity

21 p3421 A71-40083

Plane waves propagation in viscoelastic body representing parallel union of Kelvin and Maxwell bodies in magneto-thermal field

21 p3463 A71-40577

Projective numerical solution of integral equations arising in boundary value problems of electric and magnetic field theory

21 p3416 A71-40846

Longitudinal and transverse magnetostriction of polycrystalline iron garnets containing Gd, Tb, Dy and Ho in high magnetic fields

21 p3428 A71-41116

Charged particles acceleration in homogeneous magnetic field varying periodically with time /Alfvén magnetic pumping/

21 p3424 A71-41117

Atomic level interference and hyperfine splitting effects on angular and polarization distributions of resonantly scattered light in magnetic field

21 p3420 A71-41120

Radiative instability of nonequilibrium plasmas in magnetic traps, considering circularly polarized oscillations propagating along magnetic field

21 p3424 A71-41130

Fluctuations effect on MHD shock wave propagating in plasma perpendicular to external magnetic field, obtaining field amplitude distribution function

21 p3424 A71-41131

Magnetospheric plasma instabilities from velocity distribution anisotropies and nonuniform plasma and magnetic field distributions

21 p3374 A71-41180

Kinematic dynamo equations for turbulent generation of large scale magnetic and small scale turbulent fields, presenting exact treatment of fluctuation and ordered field equations

21 p3416 A71-41194

Temperature, magnetic field and pressure dependence of electrical conductivity, thermal emf, Hall effect and transverse Nernst-Ettingshausen effect in indium-doped lead telluride

21 p3429 A71-41210

Magneto-optical oscillatory absorption spectrum of tin oxide crystal at 1.3 K observed beyond band-absorption edge with peaks as function of magnetic field

21 p3431 A71-41235

Electron gas in constant crossed E and H fields, deriving nonlinear conductivity theory

21 p3424 A71-41260

Sound wave dispersion in metals in inclined magnetic field, noting sound velocity deviation

21 p3417 A71-41265

Turbulent plasma heating in current sheet between opposed magnetic fields

21 p3424 A71-41270

Plasma shock wave propagation along weak magnetic field, considering energy dissipation

21 p3425 A71-41279

Nonelectrostatic helicon and magnetoacoustic waves instability during passage through hot collisionless plasma with current transverse to weak external magnetic field

21 p3425 A71-41280

Microwave plasma generation in magnetic field, detecting expansion related to electron cyclotron frequency harmonics

21 p3426 A71-41287

Relativistic neutralized cylindrical electron beam paraxial motion through uniform longitudinal magnetic field

21 p3426 A71-41289

GaAs luminescent p-n junction diode spontaneous emission measurement in magnetic field, noting redistribution in Lorentz force direction

21 p3432 A71-41303

Micropolar, homogeneous, isotropic and centrosymmetric medium under external mechanical factors and embedded in magnetic field, investigating magnetoelasticity problems

21 p3417 A71-41361

Gravitational wave impingement upon static magnetic field, noting EM waves excitation

21 p3417 A71-41397

Rotating plane layer viscous incompressible conducting fluid flow between two parallel walls with temperature gradient subject to perpendicular gravitational and magnetic fields

22 p3532 A71-41535

Magnetic field components of local ionospheric current for LF oscillation range including micropulsation frequencies, discussing spatial and frequency distribution

22 p3532 A71-41558

Short wavelength instabilities in collision dominated plasma confinement by rotating magnetic field, interpreting in terms of equivalent negative resistance

22 p3579 A71-41579

Laminar collisionless shock propagation perpendicular to magnetic field into hot plasma, calculating temperature effects on leading edge growth rate

22 p3579 A71-41580

Plasma/magnetic field pressure ratio and inductance per unit length in Tokamak plasma pinch with arbitrary cross section

22 p3579 A71-41583

Plasma flow around disk in single ended Q machine with magnetic field parallel to flow velocity, measuring density profile for wake structure

22 p3580 A71-41587

Varying magnetic field disturbance by eddy currents in conductive elliptical cylinder, obtaining field vector potential and magnetic induction vector

22 p3528 A71-41769

High beta laser produced spherical plasma expansion in background magnetic field and ambient plasma, treating electrons as inertialess fluid

22 p3581 A71-41891

LF waves and instabilities on positive column in magnetic field, comparing three theories for helical modes for He at low pressures

22 p3582 A71-41897

Electron plasma waves and free streaming bursts response to fast rising voltage step in low density cylindrical plasma in strong magnetic field

22 p3582 A71-41899

LF wave propagation in weakly ionized plasma under magnetic field, observing forward and backward waves dispersions near cathode

22 p3582 A71-41905

Rotational energy electron beam-plasma interactions in static magnetic field, showing exponential saturated intensity variation

22 p3582 A71-41906

Cosmic ray transport in random magnetic fields, deriving coupled integrodifferential equations for radiant intensity and flux

22 p3592 A71-41915

Tunable spin-flip magneto-Raman IR laser, describing indium antimonide scattering, tuning range and applications

22 p3557 A71-42133

Insulating circular cylinder steady axial motion in conducting fluid permeated by uniform transverse magnetic field, determining flow along cylinder at field tangency points

22 p3583 A71-42198

N-type In-Sb continuous coherent microwave oscillation under transverse magnetic field, discussing helical frequency instability on threshold and growing wave conditions

22 p3586 A71-42347

Ion cloud expansion perpendicular to initially homogeneous magnetic field, estimating maximum radius with energy balance and expansion process

23 p3667 A71-43132

Explorer 12 magnetic field observations of magnetopause current layer during magnetic storm, interpreting data by magnetosphere model

23 p3668 A71-43160

Weakly ionized decaying plasma potential fluctuations and instability in magnetic field, using electrostatic probes

23 p3709 A71-43262

Longitudinal ambipolar sound instability effect on duration of plasma particle motion to wall across magnetic field, using phase method

23 p3709 A71-43263

Electric parameters of cold hollow cathode discharge and effect, controlling electron free paths by electric or magnetic field

23 p3710 A71-43276

Scale effect in semiconductor magnetoresistance due to carrier separation across plate thickness under perpendicular magnetic field

23 p3715 A71-43476

Plane vortex sheet in inviscid incompressible finitely conducting fluid under uniform magnetic field, considering hydromagnetic stability

23 p3663 A71-43490

Liquid flow rate measurement by determining fall time of emf generated in sensor coil by fluid nuclei precessing freely in magnetic field

23 p3678 A71-43536

Stationary toroidal plasma under external magnetic field, investigating classical resistive diffusion velocity with one fluid MHD equations

23 p3713 A71-44147

Characteristic modes theory for radiation and scattering by conducting bodies, considering electric and magnetic fields

23 p3660 A71-44161

Plasma current driven sheet at neutral point of cusp and quadrupole magnetic field for space physical simulation of solar flare and geomagnetic tail

23 p3714 A71-44277

Equilibrium plasma in perfectly conducting rigid wall with closed magnetic field lines, deriving necessary conditions for MHD stability

24 p3852 A71-44496

Metagalactic X ray and cosmic electrons power spectra explanation by electron acceleration and scattering in turbulent plasma with frozen-in magnetic field

24 p3865 A71-44568

Plasma perturbations in curved magnetic field due to electron thermal conductivity finiteness

24 p3856 A71-45053

Laser radiation intensity modulation by time varying magnetic field

24 p3834 A71-45055

Oxygen viscosity variation under strong magnetic field, comparing angular dependence of Senfleben effect

24 p3802 A71-45116

Hot electrons in semiconductors within crossed and parallel electric and quantizing magnetic fields, examining collision frequencies and energy relaxation

24 p3861 A71-45165

Spark source generated electron beam interaction with plasma in uniform magnetic field, estimating HF longitudinal oscillation power

24 p3857 A71-45233

MAGNETIC FILMS

Mated magnetic film memory design employing continuous vacuum deposition fabrication

01 p0047 A71-10213

MOS transistors as high speed switches in magnetic film memory selection matrix, discussing requirements for drive current pulse yield, signal power and dissipation

02 p0229 A71-11815

Supercritical Permalloy thin films thickness effect on magnetic domain structure

06 p0941 A71-17401

Pulse rise time effect on nanosecond magnetic thin film switching with flux reversal and stray field interaction

09 p1508 A71-22704

Mathematical models and flux measurements of external magnetic fields of plane film elements, evaluating dipole, spheroidal and equivalent coil

09 p1387 A71-23170

Conductivity in microwave Permalloy thin films without external magnetic field comparing Fuchs-Sondheimer theory

10 p1656 A71-24213

Polycrystalline copper and magnetic films thin intermediate layers, showing prevention of epitaxial growth

12 p1943 A71-26855

Magnetic field detection by magnetometer with coherent magnetization rotation in thin magnetic film

12 p1906 A71-26856

Bloch-wall Permalloy films coercive force effects on low frequency creep, using high resolution Bitter pattern observation technique

15 p2461 A71-32003

Magnetic thin films - Conference, Prague, September 1970

18 p2954 A71-36936

EuO, YIG, GdIG and ferrite magnetic oxide thin films growth techniques and magnetic properties comparison with bulk materials

18 p2954 A71-36937

Magnetic thin film domain wall velocity dependence on magnetic field intensity as function of film thickness, discussing nonlinearity causes

18 p2955 A71-36938

Mossbauer effect applications to magnetic thin films, discussing electric and magnetic hyperfine interactions and experimental difficulties

18 p2955 A71-36939

LF ferromagnetic resonance in anisotropic polycrystalline thin magnetic films, noting dependence on magnetization inhomogeneity

18 p2955 A71-36940

Transcritical Permalloy thin film domain structure, investigating external field effect on powder depositions and proposing model

18 p2955 A71-36942

High density redundant information storage in magnetic holography with Curie point writing on thin films and magneto-optic readout

19 p3065 A71-38237

Ni-Fe film exposure to continuous IR laser light for laser radiation structure

23 p3686 A71-44056

MAGNETIC FLUX

Magnetic flux transfer measurement at hyperbolic neutral point resulting in plasma compression

01 p0136 A71-11474

Phased array radar systems accuracy increase, using ferrite core magnetic flux feedback for phase shifter control

02 p0215 A71-12174

Admittance first derivative interpretation in flux sounding by electromagnet field stabilization

04 p0581 A71-15068

Circular polarization measurement in various lines, finding magnetic field strength influenced by line absorption coefficient variations from photosphere to spot and faculae

05 p0803 A71-16025

Electromagnetic transducer DC rotor magnetic state diagram, describing simulation procedure for moment pickup

06 p0899 A71-17933

Geomagnetic field daily variation, discussing ambient field weakening on night side

06 p0893 A71-17992

Time linear increase of magnetic flux flow through superconducting Nb-Zr wall, inferring empirical critical current density model agreement with measured flow rate

07 p1179 A71-20156

Stable ellipsoidal plasma configurations in alternating electrode annular system, considering longitudinal magnetic field strength, electrode voltage and gas discharge chamber pressure

07 p1171 A71-20185

He-Ne laser spontaneous emission intensity in N synchronized longitudinal modes as function of intermediate beat frequency and longitudinal magnetic field strength

07 p1127 A71-20376

Galactic cosmic rays interaction with interplanetary magnetic field from Venera 4 measurements June-October 1967

08 p1354 A71-21015

Geomagnetic activity indices-overall diurnal interplanetary magnetic field strength correlation by satellite magnetometer data

08 p1360 A71-21016

LF electrostatic waves axisymmetric and nonaxisymmetric propagation modes in weakly ionized plasma column under weak magnetic field

09 p1504 A71-23051

Mathematical models and flux measurements of external magnetic fields of plane film elements, evaluating dipole, spheroidal and equivalent coil

09 p1387 A71-23170

Strongly magnetized relativistic degenerate electron gas proton-proton reaction rates and electron capture over various temperatures, densities and magnetic field strengths

10 p1661 A71-24305

High beta turbulent plasmas radiation scattering due to magnetic field strength and direction fluctuations from optical Faraday rotation observation

10 p1652 A71-24660

Optimal location of nonreciprocal disk shaped YIG element of traveling wave quantum ruby paramagnetic amplifier for weak magnetic field levels

10 p1585 A71-24883

Pulsar mechanism relation to solar cycle mechanism, discussing magnetic flux correlation to period

10 p1681 A71-25073

First order EM discontinuities propagation in nonlinear centrosymmetric isotropic material with displacement field dependent on electric field and induction field dependent on magnetic intensity

11 p1798 A71-25568

Star formation angular momentum and magnetic flux problem, investigating collapsing dust cloud theory

11 p1830 A71-26108

Radial velocity fields-magnetic fields relationship in solar atmosphere active and quiet regions

12 p1955 A71-26587

Color frequency-time spectrograms of VLF electric and magnetic field Poynting flux data from Injun 5 satellite

13 p2054 A71-27914

Oscillating artificial earth satellite orientation determination from geomagnetic field strength vector, using least squares method

13 p2145 A71-28205

Permeance and magnetic pull curves for miniature reed switch with wire pressed blades in sealed glass, using computer program

13 p2001 A71-28843

Driving modes and operation characteristics of reed switches with permanent magnets

13 p2001 A71-28844

Magnetic field strength measurements from Zeeman splittings of sunspots molecular lines, considering saturation effects

13 p2140 A71-29047

Spherical harmonic expansion for volumes of tubes of unit flux in geomagnetic field for use in magnetospheric dynamics

14 p2229 A71-29668

Sunspot umbra, calculating vertical magnetic field strength distribution from Fraunhofer lines

14 p2308 A71-29979

Solar atmospheric active regions, comparing longitudinal and transverse magnetic field strengths at various levels

14 p2308 A71-29981

Pinch devices under laser heating, determining plasma density and temperature and confining magnetic field strength with thermodynamic model

15 p2458 A71-32396

Pc 2-4 pulsations relationship to interplanetary magnetic field strength and orientation, using IMP 3 and 4 satellite data

15 p2401 A71-32732

Extragalactic radio sources millimeter wavelength spectra measurements, investigating electron energy loss mechanism, magnetic field strengths and dynamics

16 p2631 A71-33234

Critical current density in niobium alloy with disperse superconducting phase as function of transverse magnetic field strength

16 p2593 A71-33653

Plasma jet formation within high pressure discharges in air at atmospheric pressure, discussing electrode configuration, current density and accelerating magnetic field strength

17 p2787 A71-34285

Galactic high energy electron differential spectrum, estimating spatial distribution and random magnetic field intensity

19 p3129 A71-38358

Solar prominences magnetic fields, determining strength and orientation with Zeeman effect

19 p3146 A71-38572

Wide angle paraboloid reflector electromagnetic field intensity distribution measurements in focal region

19 p3035 A71-38601

Thermal motion effects on space charge waves propagation along plasma columns in weak magnetic field, comparing measured wavelength/frequency relationship with theoretical prediction

20 p3273 A71-38879

Milky Way galaxy internal small scale magnetic field generation, relating strength to cyclonic turbulence properties and large scale shear

20 p3287 A71-39055

Galactic cosmic rays interaction with interplanetary magnetic field from Venera 4 measurements of June-October 1967

20 p3280 A71-39595

Geomagnetic activity indices-overall diurnal interplanetary magnetic field strength correlation by satellite magnetometer data

20 p3294 A71-39596

Galactic cosmic rays and interplanetary magnetic field flux measurements onboard Venera 4 space probe, noting lack of correspondence with Forbush decrease

20 p3282 A71-39737

Pulsar radio emission via maser amplification, presenting model based on electrons behavior in intense magnetic field

20 p3285 A71-39949

Current and potential distributions in lossless nonequilibrium MHD plasmas at high magnetic field strengths, using method of characteristics

21 p3423 A71-40946

Large scale spiral variations of interplanetary magnetic field related to structures in solar wind, including polar field and out of ecliptic models

21 p3453 A71-41181

Magnetosphere aerodynamic parameters, discussing lift and drag coefficient, shape, magnetic field gradients and tail

21 p3374 A71-41353

Small scale structure of extragalactic compact radio sources at 6 and 18 cm, obtaining magnetic field strengths and maximum brightness temperatures

22 p3598 A71-41912

Dense plasma heating by electron beam in magnetic trap as function of cyclotron frequency and field strength, noting strong microwave emission

22 p3583 A71-42064

Extragalactic radio sources polarized radiation intensity statistical analysis, calculating magnetic field scale

22 p3602 A71-42175

Aircraft permanent magnetic fields strength variation, observing magnetic anomaly detection equipment performance degradation

23 p3674 A71-42923

Plasma jet injection stoppage and reflection in strong transverse magnetic field, considering instability due to flow interactions

23 p3709 A71-43265

Mott exciton differential absorption spectrum in parallel and crossed electric and strong magnetic fields

23 p3716 A71-43479

Lunar atmosphere as source of lunar surface gaseous elements, calculating ions trajectory and impact energy as function of interplanetary magnetic field strength

23 p3754 A71-43728

MAGNETIC FORMING

Alumina trichite reinforcement of nickel base matrix using magnetic alignment and sintering under low pressure below melting point

[ONERA-TP-911]

11 p1777 A71-25238

Inductor winding dependent magnetic pulse deformation of cylindrical blanks allowing for mutual electromagnetic and mechanical coupling

15 p2417 A71-32525

MAGNETIC INDUCTION

Solar wind lunar impingement induction of magnetic fields used for global sounding of moon structure

03 p0486 A71-13323

Magnetic thermometry below 3 K using stable AC mutual inductance bridge

03 p0427 A71-13915

High temperature permeameters for measuring magnetizing force and magnetic induction, presenting normal induction curves as function of temperature

03 p0430 A71-14413

Shape and dimensions of magnetoresistance sensors as transducers in magnetic induction comparators field measurement error analysis

04 p0599 A71-15571

Electromagnetic induction by plates with nonuniform conductivity distribution, applying results to North German anomaly

05 p0745 A71-17190

Electromagnetic induction in plate with two dimensional conductivity distribution for case of E polarization, representing field by Green functions

06 p0928 A71-18264

Three dimensional electromagnetic induction problem of magnetovariational and magnetotelluric sounding at flat earth

07 p1099 A71-19394

Voltage induction in superconductors by superimposed AC and DC magnetic fields

08 p1343 A71-20881

Magnetic field of currents in earth induced by external field with known distribution, representing earth conductivity by thin conducting spherical shell

08 p1278 A71-21200

Geomagnetic cavity heuristic model with solar wind driven unipolar induction current in ionosphere

08 p1280 A71-21218

EM induction in flat plates with two dimensional conductivity distribution, describing approximation method

09 p1492 A71-22425

Magnetically coupled tunnel diode oscillator with square loop core, calculating leakage and source inductances effect on switching pattern

[IEEE PAPER 11.4]

09 p1416 A71-22593

First order EM discontinuities propagation in nonlinear centrosymmetric isotropic material with displacement field dependent on electric field and induction field dependent on magnetic intensity

11 p1798 A71-25568

High temperature permeameter for measuring magnetizing force or magnetic induction in vacuum or inert atmosphere

15 p2401 A71-31194

Thin metallic body of revolution under electromagnetic pulse, predicting transient induced currents with radiation condition in finite difference solution

15 p2372 A71-32368

Steady one dimensional MHD flow under transverse magnetic induction, determining maximum power of incompressible fluid generator

16 p2620 A71-34144

Thermal electrodeless plasma generation below RF range through magnetic induction heating, applying to argon glow and arc discharges

17 p2788 A71-34869

Coupling effects between two Permalloy films for different interface treatments, using standing spin wave resonances

18 p2955 A71-36941

Three dimensional electromagnetic induction problem of magnetovariational and magnetotelluric sounding at flat earth

19 p3053 A71-37818

Axial and radial components of magnetic induction of steady plane meridional field from rectangular region with azimuthal current density

19 p3000 A71-38638

Lunar electrical induction presence of subsurface spherical conducting bodies, determining tangential magnetic field component amplification at surface

21 p3453 A71-41358

Varying magnetic field disturbance by eddy currents in conductive elliptical cylinder, obtaining field vector potential and magnetic induction vector

22 p3528 A71-41769

RF power absorption by magnetized uniform hot electron-ion plasma column submitted to TE and TM waves

24 p3852 A71-44498

Magnetic induction by HF current passing over conducting torus enclosed by larger torus, obtaining vector potential, current density and inductance expressions

24 p3857 A71-45232

MAGNETIC INDUCTION PROBES

U MAGNETIC PROBES

MAGNETIC LENSES

Two lens high current plasma accelerator with closed electron drift, using crossed electric and magnetic fields

14 p2282 A71-30664

Electron cluster formation in klystron buncher, calculating focusing longitudinal magnetic field variation for maximum electron radial stability

15 p2376 A71-31742

MAGNETIC MATERIALS

NT FERRIMAGNETIC MATERIALS

NT FERROMAGNETIC FILMS

NT FERROMAGNETIC MATERIALS

NT MAGNETITE

NT PERMALLOYS [TRADEMARK]

Room temperature curing rubber for detection of cracks and other surface flaws in magnetic materials, revealing cracks in specimen by distinct dark lines

10 p1615 A71-24100

Magnetism and magnetic materials - IEEE-AIP Conference, Miami Beach, November 1970

12 p1943 A71-26853

Miniature dry reed switch for latching and speech path, using semihard magnetic material, sealing glass and electroplated rhodium contact

13 p2001 A71-28842

Book on materials for magnetic functions covering magnetic materials and devices, magnetic phenomena, parameters and interrelations, ferrites chemistry, microstructure and processing, etc

13 p2112 A71-29443

Meteoritic material magnetic fraction determination by chemical analysis for spherules in soil surrounding meteorite craters at Henbury, Australia
15 p2488 A71-32351

Magnetic fluid sloshing in solenoidal magnetic field, describing fluid free surface waves similarity to ordinary liquid waves in reduced gravity field
[ASME PAPER 71-VIBR-24] 21 p3366 A71-40281

Electron scattering magnetic impurities effect in insulator layer of tunnel junction on superconductor current
22 p3585 A71-41818

Compact optical Faraday rotation isolator using terbium-aluminum garnet and high field permanent magnets of rare earth alloys
22 p3559 A71-42566

Quasi-optical waveguide system for measuring electrical properties of dielectric and magnetic materials in submillimeter band
23 p3677 A71-43530

Color photography of magnetic particle and penetrant indications, discussing light sources, camera types, filter and film selection, exposure and spectral characteristics of indications
24 p3829 A71-45283

MAGNETIC MEASUREMENT

Magnetic fields measurement in plasmas by laser scattering, discussing theory and applications
01 p0133 A71-10747

Position finding for auroral electrojet using magnetometer measurements onboard Black Brant 3 rockets
01 p0075 A71-11331

Magnetic flux transfer measurement at hyperbolic neutral point resulting in plasma compression
01 p0136 A71-11474

Weak magnetic field measurement using magnetometer with digital technique time coding
02 p0247 A71-11722

Solar general magnetic field determination by measuring visually small displacements on photographic plate
02 p0316 A71-12752

Electric field strength measurement at rocket surface in ionosphere by electrostatic fluxmeter, obtaining E and F region ion drift velocities
03 p0417 A71-14035

Longitudinal magnetic field component measurement quiescent prominences, relating to angle between prominence and north-south direction on sun
05 p0804 A71-16026

Geomagnetic components measurement from moving platforms, discussing coordinate system stabilization methods for errorless time averaging of measurements
05 p0756 A71-17194

Pi2 geomagnetic pulsation polarization characteristics observations, using photoelectric fluxmeters
05 p0747 A71-17213

Solar polar magnetic field simultaneous measurements at Crimea and Mount Wilson from magnetographs
06 p0967 A71-17901

Indirectly stabilized magnetometers on moving carrier, examining techniques for geomagnetic field vector component measurements
06 p0899 A71-17932

Quiet day geomagnetic field measurements at synchronous orbit ATS 1, calculating equatorial component of interaction force between solar wind and earth
07 p1102 A71-19664

Geomagnetic PP type oscillations recordings, using fluxmetric rings and galvanometer
07 p1104 A71-20049

Electromagnetic device with superconducting elements for magnetic monopole detection in Apollo lunar samples, describing operation principle, amplifier, sample container and transport system
09 p1446 A71-22733

Geomagnetic field measurements by ATS 1 in synchronous equatorial orbit, determining pulsations types during magnetically quiet and geomagnetic storm periods
09 p1440 A71-23636

Very weak magnetic field measurements by highly rarefied gases as sensors
10 p1642 A71-24697

Magnetic field detection by magnetometer with coherent magnetization rotation in thin magnetic film
12 p1906 A71-26856

Interplanetary magnetic field north-south component from Mariner 2, 4 and 5 measurements
13 p2131 A71-27907

Nonmagnetic high pressure cell for pulsed and wide line nuclear magnetic resonance measurements
13 p2066 A71-28157

Nondestructive testing, discussing visual, liquid penetrant, thermal, X and gamma rays, ultrasonics, magnetic, electrical and eddy currents methods
13 p2073 A71-28218

Geomagnetic components measurement from moving platforms, discussing coordinate system stabilization methods for errorless time averaging of measurements
13 p2067 A71-28249

Pi2 geomagnetic micropulsation polarization characteristics, using photoelectric fluxmeters
13 p2060 A71-28268

Quartz magnetometer design and operation for simultaneous geomagnetic field declination and horizontal component measurements
13 p2067 A71-28270

Geomagnetic T and Z components variation measurements, discussing design and operation of magnetic survey device
13 p2067 A71-28271

Planetary magnetic activity measure based on K indices of antipodal observations
14 p2235 A71-30353

Magnetic properties measurement of Co-rare earth permanent magnets, using Nb-Sn superconducting solenoid
14 p2284 A71-30704

High temperature permeameter for measuring magnetizing force or magnetic induction in vacuum or inert atmosphere
15 p2401 A71-31194

Solar protons penetration over polar cap during 25 February 1969 event from particle and magnetic field measurements inside and outside magnetosphere by satellites
16 p2628 A71-33934

Geomagnetic micropulsation data, emphasizing behavior during 11 year solar cycle
17 p2732 A71-34671

Lunar magnetic fields measured by magnetometers placed by Apollo 12 and 14 astronauts, considering permanent fields due to fossil magnetic material and transient fields
17 p2811 A71-35734

German monograph on geomagnetic reference field for rocket measurements covering mathematical model for northern Scandinavia
18 p2913 A71-36682

Telescopic phase retardation effect on polarization in Zeeman split Fraunhofer line, discussing consequence for solar magnetic field determination
18 p2965 A71-36732

Polar substorms relation to interplanetary magnetic field from IMP 3 satellite magnetic measurements
19 p3132 A71-37396

Optical space observations need in solar physics, stressing 0.2 sec angular resolution for extreme UV and magnetic field measurement
19 p3136 A71-37619

Magnetic field measurements on Outer Planets Grand Tour to yield solar system origin and evolution and interstellar medium data
19 p3139 A71-37918

Plasma wave instrument for measuring AC electrical and magnetic field levels in outer planets missions
19 p3064 A71-37939

Lunar interior electrical conductivity and temperature three-layer model from magnetic transient response measurement in solar wind
20 p3301 A71-39877

Earth bow shock multiple crossings identification by magnetic field experiment onboard Pioneer 8 at geocentric distances
20 p3230 A71-39878

Theta /north-south/ component in spherical polar coordinates of interplanetary magnetic field from Explorer 33 and 35 measurements
23 p3734 A71-43155

Magnetic shell parameter L approximation simplifying McIlwain expression
23 p3669 A71-43179

LF eddy current bridge to measure small magnetic permeability changes in weakly ferromagnetic materials, applying to nondestructive tests of austenitic stainless steels
23 p3681 A71-43193

Apollo 12 magnetic measurements of lunar interior electroconductivity simultaneously on lunar surface and in circumlunar orbit
23 p3762 A71-43789

Lunar electrical conductivity profile from joint power spectral density analysis of Apollo 12 and Explorer 35 magnetometer data
23 p3762 A71-43790

Magnetic modulation observation in plasma light scattering spectra experiments, noting dependence on angle between scattering and magnetic field vectors
23 p3713 A71-44150

Transverse magnetic field measurement over sunspot in chromosphere, noting fan-shaped field line divergence
24 p3870 A71-44817

Magnetic leakage flux method for nondestructive detection of structural defects
24 p3870 A71-44817

Aerospace industry magnetic particle inspection problem identification in complex ferromagnetic structures
24 p3831 A71-45277

MAGNETIC MEMORIES
U **MAGNETIC STORAGE**
MAGNETIC METALS
U **MAGNETIC MATERIALS**
U **METALS**

MAGNETIC MIRRORS

Electron diffusion in trap with magnetic mirrors under pulsed field perturbations, determining coefficients by numerical integration of drift equation
09 p1513 A71-22551

Flute oscillations stability in low density plasma within strong magnetic field of mirror geometry, calculating unstable oscillation spectrum by Galerkin method
10 p1650 A71-24526

Magnetic mirror confined microwave heated plasmas stability based on uniform collisionless plasma model
10 p1651 A71-24632

Magnetic mirror confined plasma diagnostics, considering hot electron density, X ray pulse height and synchrotron radiation measurement techniques
10 p1651 A71-24651

Bounce effects in negative mass instability of plasma in short mirror magnetic bottle with ion cyclotron frequency dispersion
10 p1652 A71-24652

Limiting frequency for Ar plasma absorption of HF waves, observing plasma production in open magnetic mirror configuration
14 p2282 A71-30668

Magnetic mirror system measured axial energy distribution of electron beams conversion to equivalent electrostatic analyzer
14 p2249 A71-30886

Free-free bremsstrahlung emission in anisotropic hot electron plasma in magnetic mirror, measuring polarization by Compton scattering
17 p2788 A71-34853

Finite beta microinstabilities inherent in magnetic mirror confined plasmas, considering wave propagation across magnetic field at multiples of ion cyclotron frequency
18 p2950 A71-35861

Stochastic model for electron-cyclotron plasma heating by high power microwaves in magnetic mirror
21 p3422 A71-40762

Electrostatic mode wave equations for low beta plasma microinstabilities in axisymmetric magnetic mirror machines, including effects of particle cyclotron, bouncing and drift motions
22 p3582 A71-41902

Electron distributions in afterglow of hot electron mirror contained plasma as function of time, using bremsstrahlung spectra measurement
22 p3582 A71-41903

Supersonic plasma flow interaction with mirror field studied by changing ion-ion collision mean free path in BSG-1A device
24 p3852 A71-44489

Injected ion beam interaction with hot plasma in cylindrical magnetic mirror, noting acoustic frequency oscillation heating effect
24 p3854 A71-44514

Temporal electron and ion temperature behavior for pulsed beam-plasma discharge interaction in prokotron mirror-like device
24 p3854 A71-44515

Thermal and nonequilibrium microwave emission from colliding plasma beams in transverse magnetic mirror field
24 p3854 A71-44517

Hydrogen plasma generation by microwave field in magnetic-mirror device due to electron cyclotron resonance, measuring transverse diffusion coefficient dependence on magnetic field
24 p3858 A71-45235

MAGNETIC MOMENTS

Crystal time reversal symmetry for macroscopic laws determination, discussing spontaneous electric and magnetic moments and magnetically ordered systems
01 p0138 A71-10348

Diamagnetic moment of strong shock waves from high temperature light spark explosion in gases
06 p0930 A71-17399

Electromagnetic transducer DC rotor magnetic state diagram, describing simulation procedure for moment pickup
06 p0899 A71-17933

Polarization of LF oscillation branch of uniaxial ferrites in noncollinear phases analyzed by four column matrix, considering magnetic moments terminal points
09 p1507 A71-22291

Plasma-free point magnetic dipole in field-free stationary plasma, determining magnetopause or free boundary by moment technique
09 p1503 A71-22865

Neutrino magnetic moment spin precession effects on solar magnetic fields, discussing electromagnetic field-charged particles interaction
09 p1528 A71-23593

Materials with prescribed magnetic properties and expansion coefficients developed using relationships between solid solutions structure and physical properties
10 p1623 A71-23901

- Asteroid magnetospheres effects on magnetic moments and whistler mode noise propagation in solar wind 18 p2964 A71-36292
- Lunar rocks 12002 and 12022 remanent magnetic moment as evidence for ancient lunar magnetic field 23 p3763 A71-43795

MAGNETIC PERMEABILITY

- Electromagnetic wave reflection from ferrite moving domain wall, considering wave separation and permittivity and magnetic susceptibility tensors 01 p0138 A71-10435
- Thin uniaxial ferromagnetic metal films blocking curve verification using rotational hysteresis and transverse susceptibility measurements 07 p1180 A71-20171
- Ferrite microstrip microwave phase shifters with transverse and longitudinal magnetization, calculating diamagnetic and permeability tensor effects 08 p1263 A71-20768
- EMC susceptibility test equipment consisting of portable buzzing relay noise generator 13 p2045 A71-28874

- High temperature permeameter for measuring magnetizing force or magnetic induction in vacuum or inert atmosphere 15 p2401 A71-31194

- Stony, stony-iron and iron meteorites magnetic properties relating susceptibility to nickel iron content 17 p2810 A71-35720

- MHD detonation waves in relativistic perfect fluid of magnetic permeability μ immersed in electromagnetic field 18 p2951 A71-36189

- Single crystal vanadium carbide magnetic susceptibility decrease with increasing carbon content attributed to orbital paramagnetism 21 p3395 A71-40025

- Heisenberg ferromagnet magnetic and thermodynamic properties in random phase approximation, determining magnetization and susceptibility with Green function theory 21 p3476 A71-40897

- Rh and Ag-Pd alloys magnetic susceptibility, investigating hydrostatic pressure effects 21 p3432 A71-41269

- Microhardness and magnetic permeability and viscosity changes during fatigue loading of steel parts, describing electromagnetic fatigue testing method 22 p3554 A71-41771

- Antiferromagnetic semiconductors and metals in magnetic field, obtaining Fourier components of electromagnetic fluctuation correlators for dielectric permittivity and magnetic permeability tensors 22 p3586 A71-42062

- LF eddy current bridge to measure small magnetic permeability changes in weakly ferromagnetic materials, applying to nondestructive tests of austenitic stainless steels 23 p3681 A71-43193

- Zirconium monocarbide electrical conductivity, Hall coefficient, thermal emf and magnetic susceptibility measurements for temperature dependence at 500-1000 C in homogeneity region 23 p3692 A71-44021

- Electromagnetic scattering of plane wave obliquely incident on infinitely long circular cylinder with radially varying permittivity and permeability 24 p3805 A71-45179

MAGNETIC PISTONS

- Pulsed magnetic piston produced shock waves propagation along field in collisionless hydrogen plasma 10 p1654 A71-24894

- Pulsed magnetic piston produced shock waves propagation along field in collisionless plasma 21 p3425 A71-41274

MAGNETIC POLES

- Auroral oval continuity during winter /1969-1970/ from jet aircraft ionospheric instrumentation, showing band distribution along geomagnetic pole 03 p0419 A71-14526

- Low energy precipitating auroral particle fluxes over magnetic poles delineating polar cap, noting electron precipitated flux 14 p2299 A71-30030

- Heavily ionized particles search at sea level for magnetic monopoles existence evidence in highest energy cosmic rays 19 p3124 A71-37285

- Metric frequency solar radio noise active regions relationship to interplanetary magnetic field polarity distribution 22 p3597 A71-41471

MAGNETIC PROBES

- Magnetic probes effectiveness study of electron heating behind shock wave front in plasma, measuring electron temperature 02 p0288 A71-11636

- Collisionless shock waves generation in theta pinches, plasma formation, experimental devices, diagnostic methods and magnetic probes 07 p1172 A71-20507

MAGNETIC PROPERTIES

NT ANTIFERROMAGNETISM

NT CURIE TEMPERATURE

NT DIAMAGNETISM

NT FERROMAGNETISM

NT GEOMAGNETISM

NT GYROFREQUENCY

NT MAGNETIC EFFECTS

NT MAGNETIC INDUCTION

NT MAGNETIC MOMENTS

NT MAGNETIC PERMEABILITY

NT MAGNETIC RIGIDITY

NT MAGNETIC SUSPENSION

NT MAGNETOACOUSTICS

NT MAGNETOACTIVITY

NT MAGNETORESISTIVITY

NT MAGNETOSTRICTION

NT PALEOMAGNETISM

NT PARAMAGNETISM

NT POLARIZATION CHARACTERISTICS

NT RELUCTANCE

NT REMANENCE

NT SPIN-LATTICE RELAXATION

NT THERMOMAGNETIC EFFECTS

- Apollo 11 magnetic rocks and Apollo 12 rocks dating 06 p0966 A71-17742

- Sintered Al-Ni-Co alloys, investigating magnetic properties and density after heat treatment 06 p0913 A71-18099

- Subdomain magnetic particles ferrofluid colloidal dispersions, for energy conversion devices, viscous dampers, accelerometers, gyroscope supports and specific gravity meters 07 p1178 A71-19611

- Soviet papers on solid state electronics problems covering semiconductors photoelectric, magnetic, surface properties, autoemission, photoemission, etc 07 p1178 A71-19917

- High temperature blank heating and cutting during magnetic alloy machining for optimal cutter stability 08 p1296 A71-20844

- Molybdenum Permalloy powder cores heat treatment effects on permeability, magnetic loss and brittleness control, using metallographic techniques 09 p1466 A71-22171

- Materials with prescribed magnetic properties and expansion coefficients developed using relationships between solid solutions structure and physical properties 10 p1623 A71-23901

- Excess Knight shift due to spin polarization in electron gas by magnetic impurity Fermi contact coupling as function of distance from nucleus 11 p1801 A71-25373

- Magnetostriction in hydrated cesium manganese chloride, examining dimensional changes as function of magnetic field and temperature through antiferromagnetic, spin flopped and paramagnetic phases 11 p1807 A71-25559

- Eighteen layer hexagonal ferrite magnetic properties in various fields and temperatures, noting magnetization and crystal structure 12 p1943 A71-26862

- Solar wind-Mercury interaction, discussing planet physical properties, magnetized wind parameters and bow shock wave existence 13 p2120 A71-27924

- Short wave radio reception and signal paths at magnetically conjugate point in Southern Hemisphere, using 40-110 msec delay times 13 p2030 A71-28536

- Rarefied collisionless plasma, obtaining hydrodynamic equations for magnetic viscosity and thermal conductivity 13 p2106 A71-28564

- Magnetic properties of sintered cobalt-rare earth alloy magnets using Sm, Pr, La or Ce misch metal for microwave device applications 14 p2284 A71-30703

- Magnetic properties measurement of Co-rare earth permanent magnets, using Nb-Sn superconducting solenoid 14 p2284 A71-30704

- Galvanomagnetic properties of solid refractory zirconium and titanium compounds in two-band representation, measuring Hall effect and reluctance vs external magnetic field 15 p2426 A71-31512

- Magnetic properties of contained plasma, discussing equilibrium equations and pressure profiles 17 p2788 A71-35025

- Thermally stabilized volcanic rock magnetic properties and coupling hysteresis effect changes due to reheating in weak magnetic field 18 p2912 A71-36197

- EuO, YIG, GdIG and ferrite magnetic oxide thin films growth techniques and magnetic properties comparison with bulk materials 18 p2954 A71-36937

- Mossbauer effect applications to magnetic thin films, discussing electric and magnetic hyperfine interactions and experimental difficulties 18 p2955 A71-36939

- Lunar mechanical and magnetic properties, discussing impact craters, rocks, soil iron abundance, mascons and convection processes 19 p3142 A71-38020

- Heisenberg ferromagnet magnetic and thermodynamic properties in random phase approximation, determining magnetization and susceptibility with Green function theory 21 p3476 A71-40897

- Size distribution and concentration of magnetic spherules in troposphere from electron and optical microscopy 23 p3665 A71-42965

- Neutron diffraction studies of Apollo 12 lunar samples 12070,119, 12071,6 and 12008,7, observing magnetic ordering 23 p3759 A71-43761

- Magnetic properties of glass spherules from Apollo 11 and 12 fines, determining oxidation effect 23 p3762 A71-43791

- * Apollo 12 lunar soil and igneous rocks magnetic properties 23 p3763 A71-43792

- Apollo 12 fines and Apollo 11 microbreccias and rocks magnetic properties, discussing remanent magnetization 23 p3763 A71-43793

- Apollo 12 lunar soil samples magnetic resonance properties, determining temperature, frequency and thermal annealing dependence 23 p3763 A71-43796

- Ni-Co maraging steels with improved combination of mechanical and magnetic properties at elevated temperatures 24 p3836 A71-44441

MAGNETIC PUMPING

- Electromagnetic radiation pumping by stimulated Compton scattering near pulsars, determining secondary emission frequencies from energy and momentum conservation laws 07 p1192 A71-19292

- Gain and noise characteristics of reactive phase/amplitude modulation ferrite amplifier as function of pumping power and resonator coupling 12 p1886 A71-26845

- Cross field magnetic discharge stabilization of plasma column in flowing CW electrically initiated chemical laser 12 p1940 A71-27278

- Magnetic pumping of collisionless turbulent plasma with LF Alfvén and magnetosonic waves, assuming high initial plasmon energy 13 p2105 A71-28175

- Charged particles acceleration in homogeneous magnetic field varying periodically with time /Alfvén magnetic pumping/ 21 p3424 A71-41117

- Magnetic energy pumping into plasma by slowly modulating plasmon frequency-dependent external magnetic field 24 p3851 A71-44485

MAGNETIC RECORDING

- Magnetic disk storage media for recording and reproducing wideband instrumentation data 01 p0082 A71-10893

- Machine-to-machine compatibility in wideband magnetic tape recording, discussing record-head gap width variations effects on record transfer characteristics 01 p0033 A71-10895

- Astronomical objects light polarization recording on magnetic video tape, providing digitized data for computer input 03 p0424 A71-13631

- High speed magnetic printing apparatus for digital computers, discussing ferrographic process 03 p0382 A71-13819

- Magnetographic defectoscopy, discussing defect field magnetic recording techniques quality 07 p1106 A71-19143

- Magnetic hologram reconstruction process, discussing diffracted field, polarization properties and efficiency [IEEE PAPER 8.2] 07 p1112 A71-19610

- Magnetic recording device for defect field recording by ferromagnetic tape polarization 08 p1273 A71-21900

- Magnetic tape recording systems nonlinear amplitude distortion in terms of transfer function characteristics applied to analog instrumentation 09 p1449 A71-22786

- Thermomagnetic modulated Kerr effect readout and magneto-optical laser recording at high output on cobalt base metallic films 10 p1613 A71-25108

- Magnetic recording of heart electrical activity by cryogenic magnetometer with two Josephson junction quantum interference reduction device 22 p3504 A71-42341

MAGNETIC RELAXATION

NT SPIN-LATTICE RELAXATION

MAGNETIC RESONANCE

NT ELECTRON

PARAMAGNETIC

RESONANCE

NT FERROMAGNETIC RESONANCE

NT NUCLEAR MAGNETIC RESONANCE

NT PROTON MAGNETIC RESONANCE

NT PROTON RESONANCE

Magnetoplasma electric and magnetic resonances by Voigt configuration, noting similarity to single particle scattering and particle size dependence 05 p0787 A71-16497

Magnetic field and trapped electron/proton correlated pulsations due to magnetospheric field line resonance, using model based on Maxwell equation two dimensional solution 10 p1664 A71-24786

Magnetically tunable microwave bandpass and bandstop filters with yttrium-iron garnet /YIG/ single crystal 11 p1737 A71-25625

ULF geomagnetic pulsations interpretation based on Kelvin-Helmholtz magnetospheric instability mechanism and bounce resonance wave excitation, considering energy exchange with energetic protons 14 p2202 A71-30954

CH free radicals detection in oxyacetylene flame magnetic resonance absorption spectrum by IR water vapor laser 15 p2420 A71-32380

Magnetospheric hydromagnetic resonances, considering resonant poloidal-toroidal coupling 20 p3215 A71-38745

Dual beam pulsed gas laser magnetic resonance spectrometer for magneto-optic studies of solids in far IR frequencies 20 p3244 A71-39177

Apollo 12 lunar soil samples magnetic resonance properties, determining temperature, frequency and thermal annealing dependence 23 p3763 A71-43796

Abrikosov vortex lattice in superconductors, calculating resonance linewidth and vacancy formation energy 24 p3860 A71-45119

MAGNETIC RIGIDITY

Solar protons and electrons latitude profiles, discussing dependence on magnetic rigidity 06 p0964 A71-17276

Primary cosmic ray solar modulation calculations using Trilling formula for response functions and upper limiting rigidity to diurnal variation 06 p0953 A71-18119

Forbush decrease rigidity dependence relation to cosmic ray solar modulation, using neutron monitors counting rate variations at different vertical cut-off rigidities 06 p0956 A71-18136

Primary cosmic ray electrons energy spectrum measurement at Fort Churchill, examining geomagnetic cut-off rigidity daily variations 06 p0959 A71-18159

Cosmic ray intensity variations, discussing trajectory-derived cut-off rigidities for neutron monitor data analysis 06 p0959 A71-18160

Cosmic ray mean intensity drop observation after Forbush decrease, noting rigidity dependence and daily variation from exponential recovery curve 15 p2474 A71-31777

Balloon-borne magnetic spectrograph for primary cosmic ray particle trajectory and rigidities measurement 15 p2407 A71-31812

Radiation belt particles nonadiabatic changes, calculating rigidity as function of magnetic field lines 21 p3439 A71-41357

MAGNETIC SHIELDING

Cosmic rays sidereal diurnal variations, considering interplanetary magnetic field shielding effect 07 p1185 A71-19378

Magnetic shielding of various shaped enclosures such as rectangular or cylindrical cross sections in terms of normalized parameters 13 p2039 A71-28870

Magnetic shield design for protecting cylindrical space vehicle from space electron radiation, using simulator for engineering data 15 p2500 A71-32042

Ferromagnetic shields effectiveness against magnetic fields, permitting solutions to nonlinear shielding problems 15 p2377 A71-32369

Cosmic rays sidereal diurnal variations, considering interplanetary magnetic field shielding effect 19 p3127 A71-37803

MAGNETIC SIGNATURES

DP 2 fluctuations and polar substorm activity morphological distinctions, using worldwide magnetograms 11 p1753 A71-25545

Magnetic storms sudden commencements /SSC/ occurrence over 1949-1968 period based on original magnetogram observation 12 p1900 A71-26891

Lunar diamagnetic cavity signatures from Ames magnetometer experiment on Explorer 35 orbiter, indicating solar wind interaction 13 p2132 A71-27909

Substorm signature in interplanetary medium relating southward component with solar wind energy transformation 19 p3132 A71-37356

MAGNETIC SPECTROSCOPY

Magnetic mass spectrometer for ionosphere composition measurements permitting single spectrum analysis of plasma of negative and positive ions 10 p1608 A71-23817

Balloon-borne magnetic spectrograph for primary cosmic ray particle trajectory and rigidities measurement 15 p2407 A71-31812

Hypersonic magnetic spectrometer-relaxometer, comparing direct and indirect recording methods for hypersonic in metals at helium temperatures 16 p2580 A71-33928

Cosmic ray muons energy loss rate measurement in Fe using Durham magnetic spectrograph 18 p2957 A71-35930

Absolute measurement of vertical cosmic ray muon intensity at 3-50 GeV/c, using solid iron magnetic spectroscopy 21 p3438 A71-40587

MAGNETIC STARS

Ap-type magnetic stars wavelength dependent polarization, discussing polarimetric observations in different spectrum regions 01 p0153 A71-10355

Electrical polarization of vacuum around rotating magnetic Newtonian star, evaluating electrostatic potential 04 p0643 A71-14912

Magnetic stars, discussing stellar magnetic fields, Ap stars, crossover effect, period line width correlation, overabundances and models 04 p0648 A71-15245

Magnetic stars with brightness variations in visual and blue light, noting method for period determination 04 p0650 A71-15397

Magnetic stars models on possibility of rotational deceleration by hydromagnetic waves radiation without mass loss 07 p1190 A71-18857

Alfven waves and magnetosonic radiation by rotating magnetic stars and planets 07 p1193 A71-19293

Magnetic white dwarf G195-19 circularly polarized light, confirming handedness and approximate magnitude 07 p1199 A71-19833

Sr-Cr-Eu class Ap magnetic stars mean surface field estimates, using broadened absorption line measurements 08 p1359 A71-20939

Pulsars as rotating magnetic neutron stars, examining radio emission via maser amplification 08 p1363 A71-21174

Pulsar model consisting of rotating neutron star with strong magnetic field 09 p1517 A71-22337

Book on stellar spectroscopy for peculiar stars covering hot star spectra emission lines, novae, magnetic, metallic line and related stars 10 p1675 A71-24477

Periodic rotational LF synchrotron model of magnetic neutron star for pulsar radiation 12 p1947 A71-26649

Magnetic stars as cosmic ray generators, considering interstellar gas particle acceleration by EM forces produced by rotating stellar magnetic field 16 p2625 A71-33324

Cosmic ray injection by clusters of dense magnetic neutron stars, giving particle number for Galaxy 18 p2957 A71-35962

Variable and magnetic stellar model hypothesis concerning long period modulation due to radial and non-radial oscillation mode coupling beat in dipole magnetic field 18 p2962 A71-36152

Rotating magnetic white dwarf stars possibility as X ray sources with thermal spectrum, considering evidence based on Sco X-1 emission relationship to bremsstrahlung 19 p3127 A71-38010

Magnetic A stars accretion model, investigating spectra, abundances, ion capture and braking 21 p3439 A71-40051

Photoelectric observations of magnetic variable stars with five color photometer, giving light and color curves parallel to main sequence 21 p3440 A71-40057

Static magnetic fields configurations of magnetic and rotating neutron stars, considering general relativistic effects 21 p3450 A71-40714

MAGNETIC STORAGE

NT CORE STORAGE

NT MAGNETIC DISKS

Mass fabrication of three hole integrated Permalloy sheet magnetic memories 01 p0047 A71-10212

Magnetic disk storage media for recording and reproducing wideband instrumentation data 01 p0082 A71-10893

Solar spectrograph data transmission to digital computer, discussing intermediate magnetic tape storage 04 p0590 A71-14841

Integrated telescope computer system, including magnetic disk storage, digital encoding, drive control and automatic guiding 17 p2711 A71-34984

Laser Curie point writing characteristics and diffraction efficiencies of MnBi thin films for holographic recording 19 p3062 A71-37143

High density redundant information storage in magnetic holography with Curie point writing on thin films and magneto-optic readout 19 p3065 A71-38237

Storage arrays of high operational speed with field effect transistors, evaluating contributions to access and cycle times 21 p3354 A71-40734

Thermoremanent recording by Curie point writing in thin manganese-bismuth films for magneto-optic mass memories 22 p3587 A71-42473

MAGNETIC STORMS

Polar magnetic substorms perturbation pattern westward motion related to ionospheric current lengthening 01 p0077 A71-11512

F region electron concentration distribution during global magnetic storm, latitude and diurnal variation effects and radio wave reflections diffusion 02 p0243 A71-11770

Electron concentration and temperature data from Langmuir probe on Explorer 22, discussing magnetic storms effects 02 p0244 A71-11910

Midlatitude atmospheric gravity waves generation by auroral heating during magnetic substorms 02 p0245 A71-11965

Space shuttle reentry in quiet and geomagnetic storm perturbed atmosphere with reference to density variations, using San Marco 2 satellite [ICAS PAPER 70-04] 03 p0497 A71-13149

Solar flare particles effects on magnetospheric energetic particle population, discussing magnetic activity effects on trapped particles [AIAA PAPER 70-1357] 03 p0473 A71-13578

Diurnal minimum and geomagnetic storms effect on equatorial air density from San Marco 2 satellite drag experiment 03 p0415 A71-14024

Inner belt electron flux variations following geomagnetic storms from satellite instrument data 03 p0418 A71-14212

Solar radio centers and interplanetary sector structures in connection with recurrent geomagnetic storms 03 p0496 A71-14512

Magnetopause inward motion before substorm, showing association with interplanetary field vertical component reversal 03 p0496 A71-14515

Geomagnetic tail configuration during substorms from Imp 4 magnetic field and auroral index measurements 03 p0419 A71-14516

Auroral oval electrojet poleward expansion correlation to energetic electron enhancement in magnetotail during substorm from satellite observation 03 p0419 A71-14518

Energetic electron magnetospheric motion and acceleration during substorms, examining fault line existence at near local midnight 03 p0419 A71-14519

Conjugate observations of ionospheric absorption associated with electron precipitation during sudden commencement of magnetic storm 03 p0419 A71-14520

Interplanetary medium during magnetic storm periods, noting pressure and density increases of various energy flows of media and static pressure/magnetic pressure ratio 05 p0744 A71-17179

Spherical harmonic analysis of worldwide cosmic ray variations during geomagnetic storms, using ground station and satellite data 06 p0949 A71-17253

Magnetopause crossing observation of ATS 5 satellite during magnetic storm 06 p0887 A71-17258

Geomagnetic storm disturbance fields measurement by ATS 1 satellite compared with simultaneous low altitude observation, noting cavity sudden commencement compression effect 06 p0887 A71-17259

Midlatitude F 2 layer electromagnetic drift during magnetic storm 06 p0888 A71-17287

Geomagnetic storm on 24 March 1969, obtaining upper atmosphere emission data in middle latitude zone 06 p0894 A71-17996

Magnetic storm of 31 October 1968, observing charged particle increase at geomagnetic equator 06 p0961 A71-18172

Electron concentration disturbances in outer ionosphere and F 2 maximum on daylight side during magnetic storm 06 p0894 A71-18257

- Cosmic ray intensity Forbush decrease on 23 September 1966 coincidence with magnetic storm sudden commencement from satellite and ground based monitors data
07 p1184 A71-18750
- Longitudinal drift of auroral ionization in substorm recorded at different stations
07 p1099 A71-19388
- Electromagnetic and thermal energy fluxes during magnetic storms, using interplanetary spacecraft and D variation data
07 p1099 A71-19397
- Altitudinal storm effect in electron concentration in outer atmosphere during nighttime hours
07 p1100 A71-19398
- Ring currents and polar magnetic substorms during intensive charged particle flux period in nighttime magnetosphere
07 p1101 A71-19414
- Recurrent solar cosmic ray events and M region magnetic storms
07 p1186 A71-19654
- High energy electron injection into magnetosphere inner region during magnetic storms
08 p1350 A71-20956
- Low latitude geomagnetic substorm development model due to increased resistance in magnetosphere tail current sheath
08 p1278 A71-20107
- Polar substorms electric current systems and magnetic effect below and above ionosphere
08 p1279 A71-21211
- Equatorial ring current asymmetry and change during magnetic storms studied by DR indices
08 p1279 A71-21212
- Substorm related magnetic field variations in near geomagnetic tail from OGO 5 inbound pass
08 p1283 A71-21643
- Nighttime E layer behavior during geomagnetic storms in quiet sun years, investigating corpuscular flux effects
08 p1356 A71-21854
- Occurrence frequencies of recurrent geomagnetic storms with gradual and sudden commencements
09 p1434 A71-22260
- Solar wind electric field relation to ground magnetic disturbances during magnetic storm from Explorer 28 and ground data
09 p1435 A71-22433
- Neutral and ionized atmosphere parameter variations and circulation during magnetic storms observed at various heights
09 p1436 A71-22550
- Adiabatic drawing of quasi-captured charged particles by geomagnetic trap field during phase recovery period of magnetic storm
09 p1513 A71-22572
- Auroral protons and substorm resonance concept, eliminating discrepancy between hydrogen emission spectroscopic and direct measurements
09 p1513 A71-22674
- Lower ionospheric region parameters during 24 and 30 March 1968 substorms, determining auroral electron precipitation effects
09 p1440 A71-23630
- Interplanetary shock waves sounding and geomagnetic storm forecasting based on cosmic ray intensity increases from ground observations
09 p1515 A71-23633
- Geomagnetic field measurements by ATS 1 in synchronous equatorial orbit, determining pulsations types during magnetically quiet and geomagnetic storm periods
09 p1440 A71-23636
- Auroral zone magnetic substorm correlation to magnetospheric plasma drift
09 p1441 A71-23640
- Ring current indices by IGY data, attributing differences during great magnetic storms main phase to asymmetry of magnetospheric ring current
10 p1603 A71-24598
- Hydrogen ion concentration measurements by OGO 5 in plasmasphere during intense magnetic storms accompanied by stable auroral red arcs
09 p1605 A71-24787
- Low latitude DS ionospheric current component and auroral electrojet intensity for intense geomagnetic storms, considering particle observations by ATS 5 synchronous satellite
10 p1605 A71-24790
- Polar substorm energy from auroral region size and brightness photographic observations, discussing total flux dependence on magnetic field disturbance intensity
10 p1606 A71-24917
- DP 2 fluctuations and polar substorm activity morphological distinctions, using worldwide magnetograms
11 p1753 A71-25545
- Sudden geomagnetic storm effects on low ionosphere state, discussing solar X-ray and particle radiation
11 p1815 A71-25581
- Storm time variations of F 2 layer electron concentration and critical frequency at Australasian stations
11 p1754 A71-25606
- Midlatitude F layer electron concentration increase during magnetic storm, assuming auroral zone heating of horizontal winds
11 p1754 A71-25607
- Latitudinal profiles of geomagnetic H and Z components due to return current of auroral zone electrojet during polar substorms
11 p1756 A71-25757
- Sudden commencements occurrence frequency diurnal and seasonal variations from worldwide magnetic storms data
11 p1758 A71-25793
- Lower ionosphere ionization response to auroral particle fallout during 1968 substorms, using geomagnetic, VLF and balloon measurements
12 p1899 A71-26642
- German low altitude polar orbiting research satellite AZUR orbital characteristics and bearing on auroral zone substorm phenomena
12 p1899 A71-26833
- Magnetic storms sudden commencements (SSC) occurrence over 1949-1968 period based on original magnetogram observation
12 p1900 A71-26891
- Multiple midlatitude auroral arcs during geomagnetic storm recovery phase /8-9 March 1970/, noting correlation with recorded geomagnetic field intensity variations
12 p1902 A71-27670
- Auroral zone X ray events due to electron precipitation, considering relationship to polar magnetic substorms
13 p2119 A71-27797
- Temporal history of 25-26 August 1967 magnetospheric substorm, discussing magnetotail plasma sheet thinning, partial ring current buildup and magnetic bays development
13 p2132 A71-27912
- Band limited micropulsations observed in space during magnetospheric substorm by fluxgate magnetometer on OGO 5
13 p2119 A71-27913
- Ionospheric electron concentration and temperature data from Langmuir probe on Explorer 22, discussing magnetic storms effects
13 p2058 A71-28197
- Interplanetary medium characteristics during geomagnetic storms, discussing changes in pressures, energy flux densities, acoustic velocities and static/magnetic pressure ratio
13 p2058 A71-28236
- Decreasing period micropulsations during elementary magnetospheric substorms, discussing relation to ring current asymmetry development
13 p2061 A71-28546
- Earth magnetosphere boundary position, head shock wave, transition region width and current magnetic field changes during magnetopause in geomagnetic storm periods
13 p2061 A71-28549
- Auroral absorption and DR currents development during magnetic storms, discussing corpuscular fluxes arrival from magnetospheric tail into lower ionosphere
13 p2062 A71-28563
- Daily Ap activity response of magnetosphere to sunspots, using 38 year geomagnetic storminess levels
13 p2062 A71-28785
- Turbopause oxygen/nitrogen decrease effect on ion and neutral composition changes in thermospheric region during magnetic storm, using simultaneous ionospheric and atmospheric equations
14 p2229 A71-29665
- Midlatitude ionosphere dusk sector total electron content during geomagnetic storm time increase
14 p2229 A71-29666
- Initial phase duration of geomagnetic storms inverse dependence on sudden commencement amplitude in accord with solar wind-magnetosphere interaction
14 p2231 A71-29724
- Magnetic cutoff variations during geomagnetic storm from counting rates of neutron monitors, noting cosmic ray intensity augmentation
14 p2298 A71-29748
- Upper atmosphere exploration by San Marco 2 satellite, studying diurnal density variations and effects of large geomagnetic storms
14 p2236 A71-30817
- Magnetospheric plasma clouds equatorial observation by ATS 5 satellite, revealing plasma injection during substorms and dispersion by earth magnetic and electric fields
15 p2397 A71-31755
- Auroral 1.2-4 second periodicity X ray pulsations during magnetic storms, using omnidirectional detector at balloon altitude
15 p2474 A71-31775
- Total electron content and F region plasma frequencies height during magnetic storm of 8 March 1970
16 p2563 A71-33393
- Neutral upper atmosphere properties, discussing temperature, density and wind variations during disturbed conditions associated with geomagnetic storms
16 p2565 A71-33727
- Electron and proton precipitation, studying effects at high latitudes on 2 February 1969 magnetic storm
16 p2627 A71-33795
- Thermospheric convective instability as interpretation of north polar cap high speed winds observed by satellite at 200 km altitude during magnetic storm of May 1967
16 p2572 A71-33847
- Magnetotail changes relationship to solar wind magnetic field and magnetospheric substorms from ground and satellite data
16 p2629 A71-33944
- OGO-2 rubidium vapor magnetometer measurements comparison with surface magnetic observatory data during geomagnetic storms, considering asymmetric ring current
16 p2572 A71-33946
- Relativistic electron precipitation during magnetic storms, showing cyclotron resonances with electromagnetic ion cyclotron waves
16 p2629 A71-33948
- Low energy auroral thermal electrons flux after geomagnetic substorm, entering magnetosphere from solar wind
16 p2629 A71-33953
- Large scale traveling ionospheric disturbances at midlatitudes related to polar substorms on statistical basis
16 p2573 A71-33955
- Plasmapause position during stormtime increase in trapped energetic electrons, measuring near prime geomagnetic meridian by whistler techniques
16 p2629 A71-33969
- Magnetospheric observations by Imp 3 satellite of energetic electron and magnetotail field variations near neutral sheet as function of substorm time
16 p2574 A71-33971
- Energetic electrons pitch angle scattering during magnetic storms due to resonant interaction with proton generated Doppler shifted ion cyclotron waves
16 p2574 A71-33972
- Bibliography on magnetosphere covering structure, magnetopause, geomagnetic tail, plasma sheet, convection plasmapause, storm and substorms, ring current and energetic particles
17 p2732 A71-34468
- Model interpretation of Pc pulsations during geomagnetic storms, analyzing plane HM-wave resonance in horizontally stratified middle-low geomagnetic latitude lower magnetosphere
17 p2734 A71-35190
- Solar corona formation relation to geomagnetic storm generation
17 p2734 A71-35191
- Longitudinal dynamic stability of space shuttle during geomagnetic entry, noting magnetic storms effects
19 p3151 A71-37322
- Substorm signature in interplanetary medium relating southward component with solar wind energy transformation
19 p3132 A71-37356
- Electron and proton fluxes intercorrelation in recovery phase of auroral substorm
19 p3125 A71-37362
- Thermospheric winds measurement during geomagnetic storms with Fabry-Perot interferometer from Doppler shift of two 6300 Å fringe profiles
19 p3047 A71-37366
- Magnetospheric electric field dynamics, examining resonant protons role in magnetic storms
19 p3127 A71-37760
- Polar auroras production by electric fields and electron precipitation from magnetospheric magnetic storms
19 p3052 A71-37761
- Longitudinal drift of auroral ionization in substorm recorded at different stations
19 p3052 A71-37813
- Electromagnetic and thermal energy fluxes during magnetic storms, using interplanetary spacecraft and D variation data
19 p3053 A71-37821
- Altitudinal storm effect in electron concentration in outer atmosphere during nighttime hours
19 p3053 A71-37822
- Ring currents and polar magnetic substorms during intensive charged particle flux period in nighttime magnetosphere
19 p3054 A71-37838
- Interplanetary plasma and magnetic field interaction with earth magnetosphere using spacecraft measurements during storms
19 p3145 A71-38272
- Magnetic storm effect on integral electron content in F 2 layer and in outer ionosphere
19 p3058 A71-38383
- Auroral substorms development phases, noting auroral arcs latitudinal shifting during genesis phase
19 p3059 A71-38394
- Geomagnetic storms association with atmospheric pressure trough development during sporadic solar activity
20 p3214 A71-38729

Low latitude geomagnetic substorm development model due to increased resistance in magnetosphere tail current sheath

20 p3219 A71-39597

Magnetospheric electrons and protons acceleration and slot injection between radiation belts during magnetic storms, using flux measurements onboard Molniya 1 satellite

20 p3282 A71-39738

Plasmaspheric ambient hydrogen and helium atomic cations density measurement by OGO 5 ion mass spectrometer during magnetic storm, noting relationship to auroral red arcs

20 p3227 A71-39833

F 2 and D regions disturbances associated with magnetic storms, emphasizing airglow effects

20 p3227 A71-39836

Auroral morphology, covering static and dynamic ovals, polar cap and dayside auroras, auroral zones, substorms and electron precipitation

20 p3227 A71-39838

Auroral zone X ray events in midnight sector associated with substorm and electron precipitation following electrojet, using balloon-borne detector measurements

20 p3284 A71-39851

Auroral substorm model refinements for proton aurora by classifying substorms according to intensity or magnitude

20 p3284 A71-39858

Infrasound waves correlation to superionic auroral motions and polar electrojet during substorm periods

20 p3229 A71-39859

Magnetotail plasma sheet variations association with auroral display features during substorms from all sky photography

20 p3230 A71-39880

Geomagnetic horizontal field decrease from magnetospheric tail field annihilation during magnetic storm, considering polar ionospheric current generation mechanism

22 p3533 A71-41560

Sudden commencements occurrence frequency diurnal and seasonal variations from worldwide magnetic storms data

22 p3533 A71-41561

Geomagnetic Pi 2 pulsations association with magnetic storm onset in quiet conditions, discussing plasma sheet and pause theories

22 p3535 A71-42051

Worldwide geomagnetic disturbance during magnetic storm using DR-indices to express magnetospheric ring current induced perturbation

22 p3536 A71-42624

Quiet and stormy day diurnal variations of geomagnetic field, investigating ionospheric contribution

23 p3665 A71-42968

Midlatitude ionosphere and magnetosphere thermal protons dynamic behavior, investigating magnetic storm effects

23 p3720 A71-43129

Explorer 12 magnetic field observations of magnetopause current layer during magnetic storm, interpreting data by magnetosphere model

23 p3668 A71-43160

OGO 5 polar cusp observations showing dayside magnetosheath plasma penetration during magnetic storm

23 p3668 A71-43162

Magnetospheric substorms observations by satellite and balloon-borne X ray detectors, considering auroral arc brightening and energetic electron flux enhancement in magnetotail

23 p3668 A71-43163

Earth corotating plasma tail evidence in plasmapause variations from high resolution proton distribution data obtained by Ogo 4 satellite during magnetic storm

23 p3668 A71-43166

Magnetotail magnetic fluctuation observation during polar magnetic substorms, noting localized character

23 p3669 A71-43178

Magnetospheric substorms relationship to interplanetary magnetic field and solar wind plasma parameters, noting dominant effect of interplanetary southward component

23 p3734 A71-43183

Low latitude whistler propagation characteristics associated with magnetic storms in March 1970 at Sugadaira/Japan/

23 p3644 A71-43364

Geomagnetic bay-like disturbances formation and decay during multiple midlatitude 6300 A auroral arc after magnetic storm, observing time variation of current system pattern

23 p3672 A71-43981

Solar radio burst generation model based on effects of strong shock waves during chromospheric flares for geomagnetic storm prediction

24 p3867 A71-45081

MAGNETIC SURVEYS

Geomagnetic field intensity during past 2000 years from global data, noting cyclic variations

05 p0745 A71-17193

Geomagnetic field secular variations in Drake passage (Antarctic Ocean), applying absolute magnetic surveys

05 p0747 A71-17215

Three dimensional electromagnetic induction problem of magnetovariational and magnetotelluric sounding at flat earth

07 p1099 A71-19394

German monograph on geomagnetic reference field for rocket measurements covering mathematical model for northern Scandinavia

18 p2913 A71-36682

Three dimensional electromagnetic induction problem of magnetovariational and magnetotelluric sounding at flat earth

19 p3053 A71-37818

MAGNETIC SUSCEPTIBILITY

U MAGNETIC PERMEABILITY

MAGNETIC SUSPENSION

Magnetic suspension apparatus for temperature measurement near interface of sliding bodies in vacuum

03 p0397 A71-13914

Thirring effect experimental measurements in gravitation theory, magnetic suspension system or torsion balance with two rotating disks generating angular momentum

10 p1642 A71-24467

Magnetically suspended laminar supersonic cone wake stability from hot wire fluctuation and spectral components amplitude/phase measurements

11 p1702 A71-25475

Stability control of magnetic suspension with stabilizer allowing for energy dissipation in electromagnet, using Lagrange-Maxwell electromechanical equations

15 p2353 A71-32080

Asymptotic high velocity lift drag ratios for sheet and loop magnetic suspension train tracks

22 p3574 A71-41728

Optimal control of self excited vibration of high speed rotor with thrust magnetic bearing, using analog simulation

23 p3681 A71-43311

MAGNETIC TAPE RECORDERS

U MAGNETIC RECORDING

U TAPE RECORDERS

MAGNETIC TAPES

Magnetic tape recording system FM distortion derivation from head-to-tape spacing transfer function

01 p0033 A71-10892

Instrumentation magnetic tape recorder reproduce systems equalization using active circuits and signal processing to develop required transfer function

01 p0082 A71-10894

Notch power ratio noise tests on magnetic tape recorder/reproducer using direct recording in baseband

01 p0034 A71-10910

Solar spectrograph data transmission to digital computer, discussing intermediate magnetic tape storage

04 p0590 A71-14841

Aerospace systems instrumentation magnetic tape standardization and testing

04 p0597 A71-15298

Signals measurement distortions in FM recording-reproducing channel due to recorder magnetic tape speed fluctuations, discussing compensation methods

05 p0752 A71-16724

Switch series data checking and sequence identification in program controlled computer systems, exemplifying tape reading procedure

11 p1734 A71-25637

MAGNETIC TRANSDUCERS

Shape and dimensions of magnetoresistance sensors as transducers in magnetic induction comparators field measurement error analysis

04 p0599 A71-15571

Electromagnetic transducer DC rotor magnetic state diagram, describing simulation procedure for moment pickup

06 p0899 A71-17933

MAGNETIC TRAPS

U PLASMA CONTROL

MAGNETIC VARIATIONS

NT GEOMAGNETIC MICROPULSATIONS

NT GEOMAGNETIC PULSATIONS

NT NOCTURNAL VARIATIONS

Magnetic field fluctuations in magnetosheath from Pioneer observations, noting bow shock correlation

01 p0075 A71-11492

Rapid geomagnetic field variations relationship with auroral luminosity fluctuations at 4278 A

01 p0076 A71-11501

Quiet day magnetic field variations at geosynchronous satellite ATS 1, comparing magnetospheric models

03 p0419 A71-14522

Lunar and solar periodic magnetic variations, using time series analysis based on discrete Fourier transforms for frequency spectrum lines

04 p0582 A71-15097

Geomagnetic field secular variation subdivision based on time effect, noting harmonic processes with 20 year period

05 p0745 A71-17191

Geomagnetic secular variations from various surveys, noting negative value for Gulf of Aden anomaly chart

05 p0745 A71-17192

Sporadic E layers magnetic field variations, examining charged particle redistribution with air turbulence model

05 p0746 A71-17203

Geomagnetic T and Z components variation measurements, discussing design and operation principles of magnetic survey device

05 p0756 A71-17217

Geomagnetic activity relation to large scale variations in interplanetary magnetic field and solar wind deformation velocity, using satellite and space probe observations

06 p0963 A71-18254

Geomagnetic field variations recording by two variometers, correcting for variation components effects by instruments orientation

06 p0901 A71-18284

Quartz magnetic variometer allowing simultaneous recording of magnetic field variations and suspension axis inclination changes

06 p0901 A71-18285

Cyclic variations in geomagnetic field from 1550 through 1960 using spherical harmonic analysis of magnetic declination

07 p1099 A71-19395

Quiet time galactic component of geomagnetic field variations excluding solar-terrestrial disturbances

08 p1363 A71-21199

Substorm related magnetic field variations in near geomagnetic tail from OGO 5 inbound pass

08 p1283 A71-21643

Midlatitude spread F, sunspot activity and geomagnetic activity variations related, discussing fast solar particles

09 p1437 A71-22938

Perturbed magnetic surfaces topology in quadrupole, estimating local imperfections size for plasma control

10 p1652 A71-24661

Magnetic field and trapped electron/proton correlated pulsations due to magnetospheric field line resonance, using model based on Maxwell equation two dimensional solution

10 p1664 A71-24786

Pulsar mechanism relation to solar cycle mechanism, discussing magnetic flux correlation to period

10 p1681 A71-25073

Sudden commencements occurrence frequency diurnal and seasonal variations from worldwide magnetic storms data

11 p1758 A71-25793

Geomagnetic field secular variation subdivision based on time effect, noting harmonic processes with 20 year period

13 p2059 A71-28247

Geomagnetic secular variations from various surveys, noting negative value for Gulf of Aden anomaly chart

13 p2059 A71-28248

Sporadic E layers magnetic field variations, examining charged particle redistribution with air turbulence model

13 p2059 A71-28258

Geomagnetic T and Z components variation measurements, discussing design and operation of magnetic survey device

13 p2067 A71-28271

Magnetic cutoff variations during geomagnetic storm from counting rates of neutron monitors, noting cosmic ray intensity augmentation

14 p2298 A71-29748

Geomagnetic field daily variation amplitude increase under equatorial electrojet during 7 July 1966 solar proton flare

16 p2567 A71-33768

Earth upper mantle electrical conductivity as function of depth based on geomagnetic variation field spatial distribution data

16 p2572 A71-33907

Magnetospheric observations by Imp 3 satellite of energetic electron and magnetotail field variations near neutral sheet as function of substorm time

16 p2574 A71-33971

Geomagnetic diurnal variations near Sq current vortex focus, indicating existence of ionospheric diverging or converging currents

18 p2912 A71-36298

Cyclic variations in geomagnetic field from 1550 through 1960, using spherical harmonic analysis of magnetic declinations

19 p3053 A71-37819

Five component electromagnetic field station to record geomagnetic field magnetic and electric components variations

19 p3042 A71-38374

Charged particles eruptions effects on relation of magnetic perturbations to integral auroral luminance intensity from whole sky photometry measurements

19 p3059 A71-38398

- Solar regular daily geomagnetic variations - Conference, Potsdam, East Germany, April 1970
20 p3216 A71-39508
- Magnetospheric interactions with ionosphere for solar regular daily geomagnetic variations, discussing dynamo region electric fields effects
20 p3217 A71-39509
- Daily geomagnetic variations ionospheric current systems calculation from total magnetic field data obtained at ground stations during IGY
20 p3217 A71-39511
- Geomagnetic activity daily variability index statistical dependence on geomagnetic latitude, noting maximum below equatorial electrojet
20 p3217 A71-39513
- Lunar and solar daily geomagnetic variation morphology correlation based on atmospheric dynamo model
20 p3217 A71-39515
- Emf dynamo nonuniformities effect on magnetospheric field aligned electric currents associated with solar quiet geomagnetic variations, calculating ionospheric electrostatic fields
20 p3217 A71-39516
- Atmospheric dynamo equations derivation based on Maxwell equations and Ohm law with anisotropic and asymmetric electric conductivity tensor for quiet geomagnetic variations explanation
20 p3217 A71-39518
- Automated diurnal variation analysis program applied to IGY observed solar quiet day geomagnetic variations
20 p3218 A71-39520
- Dynamo theory for ionospheric thin shell model, considering wind fields determination from diurnal geomagnetic variations
20 p3218 A71-39522
- Equatorial electrojet region ionospheric currents during magnetically quiet day and nighttime from rocket measurements
20 p3218 A71-39524
- Polar cap magnetic variation mechanism based on electric field aligned continuity of Hall current auroral electrojets, noting ionospheric electron density gradients effects
20 p3230 A71-39862
- Geomagnetic field horizontal component H daily variation astute, using graphs to show increases above or decreases below given level
21 p3373 A71-40050
- Worldwide geomagnetic disturbance during magnetic storm using DR-indices to express magnetospheric ring current induced perturbation
22 p3536 A71-42624
- Quiet and stormy day diurnal variations of geomagnetic field, investigating ionospheric contribution
23 p3665 A71-42968
- Lunar daily geomagnetic variations separation into oceanic and ionospheric origin in Indian region
23 p3667 A71-43149
- Dynamo theory of solar and lunar magnetic fields diurnal variations, determining ionospheric wind velocities and pressure changes
23 p3669 A71-43174
- Model prediction for magnetospheric electric field dependence on solar wind velocity, comparing results with plasmaspheric measurements for different Kps
23 p3721 A71-43177
- Magnetotail magnetic fluctuation observation during polar magnetic substorms, noting localized character
23 p3669 A71-43178
- Least geomagnetic diurnal variation effects period determination by statistical method
23 p3673 A71-43984
- Large geomagnetic diurnal variations effects period determination by statistical method, considering partial ring currents in night magnetosphere
23 p3673 A71-43985
- MAGNETICALLY TRAPPED PARTICLES**
- NT INNER RADIATION BELT
- NT OUTER RADIATION BELT
- NT PROTON BELTS
- NT RADIATION BELTS
- Plasma containment in adiabatic magnetic traps, discussing particles, Coulomb collisions, instabilities, cyclotron resonance masers, Van Allen belts, etc
07 p1166 A71-19097
- Adiabatic drawing of quasi-captured charged particles by geomagnetic trap field during phase recovery period of magnetic storm
09 p1513 A71-22572
- Two-stream instability for magnetically confined pure electron gas column resulting from surface wave interaction
18 p2950 A71-35864
- Finite-beta stabilization of collisionless trapped particle mode in toroidal plasma confinement devices, using magnetic well dug by plasma diamagnetism
19 p3112 A71-37742
- Collisions or weak turbulence caused noise effects on broadening of echo pulses in magnetically trapped particles, using propagator formalism
19 p3113 A71-37746
- Aerospace industry magnetic particle inspection problem identification in complex ferromagnetic structures
24 p3831 A71-45277
- Nonadiabatic and atmosphere induced energy losses as causes of proton capture in geomagnetic field
24 p3867 A71-45320
- MAGNETITE**
- Magnetic particles in Orgueil meteorite, discussing high symmetry morphology and generation
03 p0487 A71-13333
- MAGNETIZATION**
- High temperature permeameters for measuring magnetizing force and magnetic induction, presenting normal induction curves as function of temperature
03 p0430 A71-14413
- Ferrite microstrip microwave phase shifters with transverse and longitudinal magnetization, calculating diamagnetic and permeability tensor effects
08 p1263 A71-20768
- Quantum mechanical relation for magnetized electron gas in constant magnetic field and thermal equilibrium
08 p1337 A71-21192
- Defectoscopes with current regulation by magnetic amplifiers, describing circuitry and remanent magnetization of components with AC and rectified half wave currents
08 p1273 A71-21894
- Generalized Watson sums calculation with application to magnetization of anisotropic ferromagnet for Callen type decoupling schemes
09 p1506 A71-22149
- Carbonaceous chondrites natural remanent magnetization, revealing grey spinel oxide, Ni-Fe and iron sulfide as principal opaque minerals
10 p1674 A71-24429
- Magnetic field detection by magnetometer with coherent magnetization rotation in thin magnetic film
12 p1906 A71-26856
- Magnetization discontinuities in cobalt-rare earth particles at discrete imperfection levels as function of chemical, mechanical and heat treatment, noting Co-Y rectangular loop
12 p1943 A71-26861
- Eighteen layer hexagonal ferrite magnetic properties in various fields and temperatures, noting magnetization and crystal structure
12 p1943 A71-26862
- Anisotropic Heisenberg antiferromagnet sublattice magnetization, obtaining temperature dependence
13 p2100 A71-28675
- Apollo 11 lunar rock and microbreccia examination for natural remanent magnetization, emphasizing viscous magnetization effect in terrestrial magnetic field
14 p2303 A71-29534
- Microwave scattering by DC magnetized ferrimagnetic circular cylinder in rectangular waveguide
14 p2212 A71-30512
- LF ferromagnetic resonance in anisotropic polycrystalline thin magnetic films, noting dependence on magnetization inhomogeneity
18 p2955 A71-36940
- Heisenberg ferromagnet magnetic and thermodynamic properties in random phase approximation, determining magnetization and susceptibility with Green function theory
21 p3476 A71-40897
- Mn-Ge solid solutions coercive force and magnetization, investigating temperature dependence and heat treatment effects
21 p3432 A71-41264
- MAGNETO-OPTICS**
- High speed small aperture electro-optic, acousto-optic and magneto-optic modulators for optical communications, considering capabilities and limitations
02 p0231 A71-12003
- High density redundant information storage in magnetic holography with Curie point writing on thin films and magneto-optic readout
19 p3065 A71-38237
- Dual beam pulsed gas laser magnetic resonance spectrometer for magneto-optic studies of solids in far IR frequencies
20 p3244 A71-39177
- Magneto-optical oscillatory absorption spectrum of tin oxide crystal at 1.3 K observed beyond band-band absorption edge with peaks as function of magnetic field
21 p3431 A71-41235
- Orientational magneto-optic effect in nickel and ferrosilicon monocrystals, discussing anisotropy influence on frequency dependence
21 p3431 A71-41263
- Thermoremanent recording by Curie point writing in thin manganese-bismuth films for magneto-optic mass memories
22 p3587 A71-42473
- MAGNETOACOUSTIC WAVES**
- VHF radiation from plasma during electron beam interaction with fast magnetoacoustic wave stimulated by external spatially periodic currents
01 p0132 A71-10155
- Magnetosonic wave instability in differentially rotating gas
01 p0160 A71-11119
- Quasi-Alfvén and acoustic wave coupling in inhomogeneous stratified plasma within intense magnetic field as function of directional pressure
02 p0292 A71-12627
- Low energy magnetoacoustic wave with finite conductivity, determining gas parameters near singular points
06 p0936 A71-17652
- Alfvén waves and magnetosonic radiation by rotating magnetic stars and planets
07 p1193 A71-19293
- Alfvén wave transformation into magnetosonic wave during passage across boundary between two media in strong magnetic field, considering reflection and refraction laws
07 p1195 A71-19381
- Ion acoustic and helicon waves nonlinear interactions in plasma, evaluating whistler buildup rate
09 p1501 A71-22536
- Magnetosonic waves generation by interaction of bow shock with frozen tangential discontinuities in solar wind
09 p1521 A71-22866
- MHD wave propagation in magnetoplasma perturbed by LF magnetoacoustic waves, considering wave scattering and polarization
09 p1505 A71-23566
- Magnetoacoustic wave propagation in magnetic plasma traps by geometrical optics methods, considering annular traps existence
10 p1651 A71-24638
- Steady state scattering of cylindrical magnetoacoustic waves traveling along axis of rigid ideally conducting static cylinder
13 p2105 A71-28281
- Magnetosphere transmittance for fast magnetosonic waves, considering refraction, reflection and earth surface intersection
13 p2060 A71-28531
- Helicon and magnetoacoustic waves instability during passage through hot collisionless plasma with current transverse to weak external magnetic field
13 p2107 A71-28851
- Finite ion temperature effect on large amplitude magnetosonic disturbances and collisionless shock waves formation in plasmas, using one dimensional macroparticle code
15 p2458 A71-32394
- Arbitrary amplitude magnetoacoustic waves under gravitational field effects, obtaining exact Riemann wave solutions to MHD equations for compressible medium
19 p3112 A71-37741
- Alfvén wave transformation into magnetoacoustic wave during passage across boundary between two media in strong magnetic field, considering reflection and refraction laws
19 p3138 A71-37806
- Short periodical pulsations in solar atmosphere related to magnetosound propagation in area of temperature minimum with directed perpendicular magnetic field
20 p3290 A71-39305
- HF plasma heating in Tokamak torus device by magnetosonic wave energy absorption in high density region via Buchsbaum hybrid resonance
21 p3422 A71-40764
- Nonelectrostatic helicon and magnetoacoustic waves instability during passage through hot collisionless plasma with current transverse to weak external magnetic field
21 p3425 A71-41280
- High Mach number turbulent magnetosonic shocks generation by driving reflecting piston into plasma, simulating by electromagnetic particle code
23 p3708 A71-42893
- Cyclotron magnetoacoustic wave generation by planets and binary stars in circular orbits, deriving interstellar gas density variations
24 p3869 A71-44804
- Weakly damped Alfvén ion-cyclotron waves and fast magnetoacoustic waves in infinite plasma cylinder inserted into current bearing finite coil
24 p3858 A71-45245
- MAGNETOACOUSTICS**
- Magnetoacoustic instabilities in weakly ionized gas flow, using adiabatic approximation
05 p0788 A71-16602
- Electron-nuclear interactions in ruby by magnetoacoustic double resonance, comparing experimental and theoretical data
07 p1181 A71-20526
- Magnetic field generation in acoustically turbulent medium, deriving spectral function equation
08 p1341 A71-21795
- Magnetic field generation in acoustically turbulent MHD medium, deriving spectral function equation and eigenvectors
16 p2619 A71-33545
- Electromagnetoacoustic ultrasonic vibrations radiation and reception angular orientation as function of

transducer design parameter, frequency and propagation velocity
22 p3528 A71-41756

MAGNETOACTIVITY
NT **MAGNETORESISTIVITY**
Magnetoactive cold plasma wave interaction theory, investigating energy transfer
07 p1167 A71-19230
Magnetoactive spatially homogeneous plasma parallel and perpendicular waves derivation from hydrodynamic equations in quasi-linear approximation, noting resonances and nonlinear effects
12 p1937 A71-27181
Magnetoactive plasma layer in strong constant magnetic field, computing dispersion equation for large amplitude thermomagnetic wave propagation
15 p2456 A71-31745
Magnetoactive spatially homogeneous plasma parallel and perpendicular waves derivation from hydrodynamic equations in quasi-linear approximation, noting resonances and nonlinear effects
22 p3583 A71-42458

MAGNETOCARDIOGRAPHY
Magnetic recording of heart electrical activity by cryogenic magnetometer with two Josephson junction quantum interference reduction device
22 p3504 A71-42341

MAGNETOELASTIC VIBRATIONS
U **MAGNETOELASTIC WAVES**
U **MAGNETOELASTIC WAVES**
NT **MAGNETOACOUSTIC WAVES**
Soviet papers on wave propagation in viscoelastic and elastoplastic media covering shock wave interaction, magnetoelastic waves, etc
12 p1980 A71-27444
Magnetic pumping of collisionless turbulent plasma with LF Alfvén and magnetosonic waves, assuming high initial plasmon energy
13 p2105 A71-28175
Relativistic thermo-magnetoelastic wave propagation, considering elastic solid under magnetic and thermal fields
13 p2101 A71-29105
Magnetoelastic oscillations of thin conducting plate in magnetic field, solving electrodynamic equations
16 p2647 A71-32928
Magnetostriction and magnetoelastic quantum oscillations in p-PbTe, using thermodynamic derivatives of Lifshitz-Kosevich expression for oscillatory part of electronic free energy
17 p2791 A71-34860

MAGNETOELASTICITY
U **MAGNETOSTRICTION**
U **MAGNETOELECTRIC MEDIA**
Plane electromagnetic waves reflection and transmission at boundary of semiinfinite magnetolectric medium
23 p3642 A71-42918

MAGNETOGASDYNAMICS
U **MAGNETOHYDRODYNAMICS**
MAGNETOGRAMS
U **MAGNETIC SIGNATURES**
MAGNETOGRAPHS
U **MAGNETOMETERS**
U **RECORDING INSTRUMENTS**
MAGNETOHYDRODYNAMIC ACCELERATION
U **PLASMA ACCELERATION**
MAGNETOHYDRODYNAMIC FLOW
Slowly varying plane flows of highly conducting inviscid quasi-neutral gas plasma in channel with solid metallic walls as electrodes
01 p0133 A71-10790
Steady supersonic conducting gas flow in channel with nonconducting walls, calculating electric and gas dynamic parameters for different imposed magnetic field geometries
01 p0133 A71-10791
One dimensional motion of unsteady incompressible conducting free jet in transverse magnetic field, noting computer solution by characteristics method
01 p0133 A71-10792
Shock tube generated Ar plasma electric conductivity augmentation by electrical discharge through supersonic plasma flow in Faraday tube
01 p0134 A71-10998
Polytrope solar wind equations, expressing distance and flow velocity as functions of mass density
01 p0147 A71-11510
Two parameter asymptotic solutions for viscous model of solar wind flow
01 p0147 A71-11511
Supersonic electrically conducting gas flow in flat channel with dielectric walls in inhomogeneous magnetic field
02 p0289 A71-11926
Nonlinear electrostatic vibrations in colliding antiparallel flows of rarefied plasma
02 p0289 A71-11928
Small size calorimetric probe for measuring enthalpy, temperature and pressure in high velocity dense plasma flow
02 p0290 A71-12194

Mean and pulsation characteristics of velocity and temperature in turbulent conducting jets under longitudinal and transverse magnetic fields
02 p0292 A71-12626
Critical velocity and elastic panel flutter stabilization in magnetohydrodynamic flow by distributed magnetic field control
02 p0293 A71-12628
Inviscid ideally conducting fluid flow past thin foil in transverse magnetic field, using small parameter method
02 p0186 A71-12629
Mass transfer and Biot diffusion in MHD flows with mixed boundary reaction kinetics, considering Hartmann and plate problems
02 p0293 A71-12632
Magnetic field effect on boundary temperature in axisymmetric MHD flow in vortex chamber, using dissipationless approximation
02 p0293 A71-12633
Nitrogen plasma flow over flat plate, comparing probe and probeless methods for boundary layer concentration profile measurement
02 p0254 A71-12648
Uniform magnetic field effects on electroconducting fluids turbulent flow and heat transfer characteristics
02 p0293 A71-12649
Nonstationary rotating MHD viscoplastic medium between coaxial cylinders in crossed electric and magnetic fields, determining zone interface position and stress distribution
03 p0464 A71-13601
Unsteady MHD forced flow of viscous incompressible electrically conducting fluid against rotating disk
03 p0459 A71-13902
Moving plasma hydrodynamic equations of motion, continuity and energy in axially symmetric coordinate system
03 p0464 A71-13904
Multielectrode MHD channels, investigating relaxation effects on two dimensional current distribution and plasma properties
03 p0466 A71-14319
Ionizable gas flow through two dimensional nozzle under transverse magnetic field, using quasi-one dimensional approximation
03 p0466 A71-14553
Viscous incompressible conducting fluid steady flow in rectangular channel under normal external magnetic field
03 p0466 A71-14554
Conducting fluid flow in rectangular channel with electrodes under longitudinal magnetic field
03 p0466 A71-14555
Viscous incompressible conducting fluid steady laminar flow in rectangular channel with two insulating and two arbitrarily conducting walls under external magnetic field
03 p0466 A71-14556
One dimensional ionized gas flow behind shock wave propagating in MGD duct
03 p0466 A71-14569
Incident shock tube flow interaction with one dimensional MHD channel flow
04 p0632 A71-14687
Ionizing shock wave propagation through MHD channel flow, determining induction emf current and electron density and concentration
04 p0632 A71-14691
Steady high power plasma flows using three phase AC generator
04 p0632 A71-14794
MHD conducting lubricant composite slider bearing in transverse magnetic field, calculating conductivity effect on load capacity
04 p0602 A71-14801
Ionized gas flow temperature distribution effects on half width of H beta line
04 p0633 A71-15064
Air/Ar with ionizable lithium oxide plasma stream electric properties determination by shock tube wall electrode pair, using ambipolar diffusion theory
04 p0634 A71-15113
Variable properties effects on MHD flow in ducts with finite aspect ratio and electrically insulating walls, noting current distribution
04 p0634 A71-15179
MHD generalized Couette flow by splitting linear time dependent flow into simultaneous solution of boundary and initial value problems
04 p0571 A71-15201
Heat transfer in laminar MHD boundary layers on moving flat plate in magnetic field
04 p0635 A71-15468
MHD channel flow with axial conduction and third kind boundary condition, investigating thermal entry region heat transfer
04 p0684 A71-15506
Viscous incompressible MHD fluid steady laminar flow past semiinfinite flat plate, noting heat transfer characteristics
04 p0635 A71-15508

Thermal conductive liquid hydrodynamic stabilized Hartmann flow in rectangular canal with transverse field, examining magnetic effect on heat transfer
04 p0635 A71-15509
Soviet book on fundamentals of heat transfer theory covering thermodynamic equations, steady, unsteady, turbulent, incompressible and MHD flows, etc
05 p0831 A71-16196
Hydrodynamic model describing intermediate stages of propagation of plasma shock wave created by laser light focusing
05 p0787 A71-16333
Partially ionized rotating plasma centrifuge for isotope and element separation, controlling velocity distribution of conducting magnetic fluid by isorotation law
05 p0788 A71-16607
Plasmas and liquids inhomogeneous flow oscillations, determining resonance points effect on stability and oscillatory properties
05 p0790 A71-16825
Plane steady incompressible MHD flow past slender nonconducting profile, determining magnetic field components boundary conditions
05 p0695 A71-16892
Low pressure toroidal plasma confinement with flow in axially symmetric configurations, using numerical model
06 p0935 A71-17554
Plane incompressible MHD boundary layer on porous plate, considering heat and mass transfer in blowing or suction velocity distribution
06 p0936 A71-17736
MHD oscillating flow along infinite unmagnetized conducting plane porous wall, deriving temperature field in boundary layer
06 p0937 A71-18231
Supersonic flow of rarefied plasma around plane bodies, allowing for electric field effect on ion motion
06 p0842 A71-18252
Rotating fluid cylinder in magnetic field parallel to rotation axis, discussing hydromagnetic precession rate, resonance phenomena and magnetic Reynolds number flows
06 p0882 A71-18319
Ionizational and electron thermal nonequilibrium effects in insulator boundary layer of potassium-seeded nitrogen MHD accelerator
06 p0939 A71-18581
MHD boundary layers with nonequilibrium ionization and recombination at finite rates
06 p0939 A71-18582
Fully ionized quasi-one dimensional magnetic nozzle flow analysis, including effects of unequal electron and ion temperatures and electron thermal conductivity
06 p0939 A71-18584
Negatively charged conical electrostatic probe characteristics determination in supersonic plasma stream, using shock tube
06 p0939 A71-18586
Hydromagnetic boundary layer free convection past vertical flat plate, discussing flow rates, temperature profiles and skin friction for high and low Prandtl numbers
07 p1165 A71-18744
Uniform magnetic field parallel alignment effects on incompressible electrically conducting free two dimensional jet flow stability at large Reynolds number
07 p1084 A71-18745
Far wake asymptotic structure in rarefied plasma flow past charged bodies
07 p1165 A71-18878
Weakly ionized gas discharge three dimensional unsteady motion of viscous incompressible gas discharge plasma in homopolar device curvilinear channel, emphasizing secondary overflow during acceleration
07 p1167 A71-19235
Two dimensional flow MHD in plasmas with anisotropic pressure, considering weak shock waves parameter changes in linear approximation
07 p1168 A71-19726
One dimensional steady supersonic motion of partially ionized two temperature argon-caesium plasma in disk type Hall MHD generator channel
07 p1023 A71-19728
Unsteady viscous incompressible electrically conducting fluid flow past accelerated conductor or insulator flat plate in uniform transverse magnetic field
07 p1169 A71-20022
Pressure shocks propagation through electrically and thermally conducting viscous gas in presence of uniform magnetic field
07 p1169 A71-20025
Viscous conducting fluid MHD fluctuating flow over porous flat plate with time dependent suction, determining skin friction and transient velocity profiles
07 p1169 A71-20028
Unsteady MHD channel flow between two semiinfinite harmonically oscillating and perfectly conducting solids, determining liquid velocity profile curves
07 p1169 A71-20032

MHD Couette flow at stationary plate under transverse magnetic field, discussing effect on heat transfer between electrically conducting walls

07 p1170 A71-20099

Low density plasma flow past bodies, measuring disturbed zone velocity, density and temperature distributions by Langmuir probes

07 p1173 A71-20528

Plasma ring vortices in crossed electrical discharges attributed to shock wave induced plasma flow across lines of force of azimuthal magnetic field

08 p1338 A71-20785

Time estimation for plasma front propagation in quartz glass circular pipes without imposition of axial magnetic field

08 p1338 A71-20829

Electron density profiles in supersonic plasma jet, using immersed microwave probe [AIAA PAPER 71-272]

08 p1342 A71-21998

One dimensional nonstationary motion of compressible electrically conducting gas with allowance for heat conductivity and viscosity, solving MHD equations

09 p1499 A71-22129

Boundary value problem of end effect in MHD channel with semiinfinite electrodes for arbitrary Reynolds numbers

09 p1499 A71-22130

Three dimensional end effects on MHD flow in rectangular channel with nonconducting walls

09 p1499 A71-22133

Laminar flow of viscous electrically conducting fluid in traveling magnetic field, examining channel flow in traveling wave field of one directional and two directional inductor

09 p1499 A71-22134

Inviscid incompressible electrically conducting fluid flow past slender profile investigated by asymptotic power expansion of reciprocal magnetic Reynolds number

09 p1382 A71-22135

Nonlinear MHD equations solution for laminar flow of electrically conducting fluid in cylindrical channel in traveling magnetic field

09 p1499 A71-22191

Supersonic collisionless plasma flow around flat plate and expansion into vacuum, using Poisson equation

09 p1500 A71-22233

MHD accelerator in pulsed mode with crossed fields, studying one dimensional steady inviscid flow

09 p1501 A71-22407

Plasma blowing and suction through channel wall electrodes in two dimensional stationary flow, taking into account Hall effect

09 p1502 A71-22537

Electrohydrodynamic flow in plane channel with conducting walls and axial emitter electrode, determining velocity and pressure profiles distortion

09 p1502 A71-22538

Collisionless plasma steady flow past thin symmetrical semiinfinite wedge, considering dispersion due to finite Larmor radius

09 p1504 A71-23052

Thin airfoils theory in nonequilibrium magnetogasdynamics with nonuniform nonequilibrium free stream, using Green function technique

09 p1383 A71-23200

Plasma flow interaction with nozzle-shaped magnetic field generated by current loop with strong Hall effect

09 p1504 A71-23309

Ion currents to cylindrical electrodes in mobility dominated plasma flow from thin sheath theory involving convection currents

09 p1505 A71-23374

Spherical magnetogasdynamic shock production in conducting gas by explosion into homogeneous self gravitating system, assuming density dependence on inverse power of distance

09 p1505 A71-23585

Two group model of stationary plasma flow in magnetosphere with space charges due to inertia drift and forbidden regions

09 p1529 A71-23710

MHD Hg flow between concentric cylinders with nonconductive walls, comparing pressure loss and voltage measurements with theoretical predictions for large Hartmann numbers

10 p1647 A71-23862

Conducting fluid in transverse magnetic field at low Reynolds numbers, deriving laminar boundary layer universal equations in Crocco or Mises variables

10 p1648 A71-24028

Pseudo-stationary shock wave in plane MHD flow of conducting gases, deriving existence theorem for linear relations between vorticity and current density

10 p1648 A71-24281

Charged particles velocity distribution effect on plasma flow in transverse nonuniform magnetic field, observing configuration/trajectory distortion and particle dispersion

10 p1649 A71-24319

Mixing layer of turbulent flows in homogeneous nonconducting and conducting incompressible fluids, extending approximate solution to flow in longitudinal magnetic field

10 p1593 A71-24366

Friction drag and energy losses of steady plane incompressible boundary layer flow of viscous liquid on nonconducting wall in MHD channel

10 p1649 A71-24377

MHD effects on transpiration cooled Couette flow through porous wall, considering magnetic drag produced pressure differential and shear recovery rates

10 p1649 A71-24404

Steady two dimensional MHD laminar flow between two parallel circular porous disks in transverse magnetic field, determining velocity, pressure and shear stress distribution

10 p1649 A71-24408

Wall conductivity effects in MHD rectangular duct flow at high Hartmann numbers with uniform magnetic field applied parallel to one pair of duct sides

10 p1649 A71-24419

Steady state streaming of cold magnetospheric plasma in magnetic equatorial plane near plasmopause

10 p1650 A71-24557

Soviet book on MHD flow of incompressible electrically conducting fluid past bodies covering inviscid flows and viscous flows of Stokes and Oseen type

10 p1596 A71-24669

Helical motions with vorticity-velocity and conduction current-free force magnetic vectors parallelisms

11 p1804 A71-25177

Hydromagnetic flow of conducting viscous incompressible fluid in rotating straight annular pipe under constant pressure gradient

11 p1804 A71-25433

Plane unsteady polytropic MHD flow equations reduced to time independent system, using complex variable techniques

11 p1804 A71-25439

Preionization and velocity effects in MHD channels containing potassium seeded argon plasma at atmospheric pressure

11 p1804 A71-25488

Rotating plane layer viscous incompressible conducting fluid flow between two parallel walls with temperature gradient subject to perpendicular gravitational and magnetic fields

11 p1757 A71-25767

Restricted set of correlated measurements with inductive theta pinch in MHD plasma accelerators, determining electromagnetism field structure and electron density distribution

11 p1766 A71-26288

Nonstationary three dimensional weakly ionized incompressible viscous gas plasma flow in homopolar device, noting effects on ionization- diffusion balance

12 p1935 A71-26753

Automatic control application to liquid metal and semiconductor materials, plasma flows, charged particle beams and similar media interacting with magnetic fields

12 p1936 A71-26972

Solar plasma emission capacity, using atmospheric ionization theory

12 p1964 A71-27084

Magnetoactive spatially homogeneous plasma parallel and perpendicular waves derivation from hydrodynamic equations in quasi-linear approximation, noting resonances and nonlinear effects

12 p1937 A71-27181

Three dimensional MHD flows with strong transverse magnetic fields variable area rectangular ducts with conducting sides

12 p1938 A71-27216

Unsteady mass exchange during laminar MHD free convection on vertical plate, deriving time dependence expression for external magnetic field

12 p1938 A71-27242

Forced convection effects on characteristics of steady state cross flow arc in presence of applied transverse magnetic field

12 p1938 A71-27265

Soviet book on MHD flows in channels covering one dimensional theory, viscous fluids, boundary layers, electric fields, laminar flow, etc

12 p1940 A71-27294

Pulsed MPD arc experiment, determining voltage characteristics and rotating current spokes occurrence and behavior

12 p1941 A71-27567

Resistance and heat transfer coefficients in hydrodynamically and thermally developed MHD pipe flow

12 p1941 A71-27740

Neutral stability of laminar free boundary layer in mixing incompressible MHD half jets at low Reynolds number

13 p2103 A71-27842

Interplanetary magnetic field angular gradient and sectorial effects on solar wind, discussing wind velocity

13 p2128 A71-28527

Discrete ionospheric model of supersonic two dimensional low density plasma flow past large bodies, using quasi-neutrality condition

13 p1990 A71-28532

Compressible electrically conducting liquid two dimensional steady state laminar flow calculations in MHD duct

13 p2109 A71-29294

Steady flow of electrically conducting incompressible viscous fluid in rotating parallel- plane channel under constant transverse magnetic field

13 p2110 A71-29296

Electric circuits calculation in MHD problems such as MHD channel flow, electrodynamic plasma, etc

14 p2277 A71-29558

Conducting incompressible liquid in transverse magnetic field, considering plane steady motion of isothermal MHD boundary layer

14 p2278 A71-29604

Spatial MHD flow in diffuser bounded by two diverging and two parallel walls, showing solutions with axial symmetry in cylindrical and spherical coordinate systems

14 p2278 A71-29605

MHD flow abrupt widening and narrowing, considering M shaped velocity profiles

14 p2278 A71-29606

MHD flow in rectangular channel with two conducting walls, investigating velocity structure

14 p2278 A71-29607

Argon plasma jet velocity distribution at MHD channel exit with magnetic quadrupole, using calorimetric plasma velocity measurements and Doppler shift observations

14 p2278 A71-29611

Rectangular cross section MHD channel spatial electrical field distribution, obtaining electrostatic potential, boundary conditions and efficiency

14 p2278 A71-29612

Flow transition to laminar drag law for thin cylinder freely suspended in Hg in rotating vertical cylindrical MHD channel

14 p2279 A71-29615

Electrode voltage of rectangular cross section MHD channel in conductive flowmeter, investigating magnetic field inhomogeneity and velocity profile effects

14 p2279 A71-29617

Group-invariant properties of boundary layer flow differential equation for electrically conducting liquid in magnetic field

14 p2279 A71-29629

Heterogeneous fluid flow-chemical processes interaction in low density plasma flow two phase boundary layer seeding, using physiochemical model

14 p2279 A71-29878

Supersonic plasma flow effects on neutral hydrogen, helium and charged particle density and velocity profiles in polar ionosphere

14 p2234 A71-30040

High latitude upper ionospheric structures and plasma flow in magnetosphere from Alouette/ISIS topside sounders, noting solar UV and particle ionization sources

14 p2234 A71-30042

Spectral lines self reversal effects on plasma temperature and density measurement in MHD duct boundary layer

14 p2279 A71-30046

Collisionless plasmas stationary flow hydrodynamic equations applied to plasma waves analysis

14 p2280 A71-30211

Hydrogen plasma transport in linear magnetic quadrupole field, studying polarization potential and density distribution

14 p2282 A71-30669

MHD three dimensional flow between rotating and stationary disks in transverse magnetic field with uniform suction at stationary disk

14 p2283 A71-30839

German monograph on similarity transformations application to MGD channel flows covering mechanical, electromagnetic and thermodynamic equations

14 p2283 A71-30863

Small size calorimetric probe for measuring enthalpy, temperature and pressure in high velocity dense plasma flow

15 p2454 A71-31500

Porous refractory materials for thermochemical protection against high temperature plasma flow, discussing effectiveness in erosive wear reduction

15 p2432 A71-32164

Electrical breakdown in transverse magnetic field and Ar plasma flow in pressure range 0.2- 1400 mm Hg and velocity range 0-50,000 cm/sec

15 p2457 A71-32272

Plasmas and liquids inhomogeneous flow oscillations, determining resonance points processes effect on stability and velocity

15 p2459 A71-32504

MHD rectilinear two dimensional flows at high Hartmann number, including extension to three dimensional problems

15 p2459 A71-32560

Two dimensional MHD flow past flat plate with magnetic field aligned with flow field, using method of matched asymptotic expansions

16 p2615 A71-32860

Fast argon plasma flow interaction with strong magnetic fields, describing ionization relaxation phenomena behind magnetically reflected shock fronts

16 p2615 A71-32898

Electric field in flow of medium with tensor conductivity due to Hall effect, studying eddy currents structure in magnetic field variation region

16 p2616 A71-32929

Flame, laser and shock wave plasma generation, considering afterglows, ionized gas flows and high temperature effects

16 p2617 A71-32958

Rarefied plasma flow generation by Q-switched laser pulse focusing on solid target, measuring plasma properties with Langmuir probes and microwave interferometers

16 p2586 A71-33162

Plasma flow wave propagation, investigating compressibility, radiation and finite electrical conductivity effects with plane asymptotic solution combinations

16 p2618 A71-33173

Neutral current sheets in slow moving plasma with frozen-in magnetic field with null force line

16 p2638 A71-33651

Velocity and magnetic field equations of electroconductive fluid vortex motion due to annular receptacle insulating walls rotation

16 p2620 A71-34057

Axisymmetric blunted body heating by high temperature plasma flow as function of geometry, pressure and stagnation enthalpy

17 p2669 A71-34207

Moving plasma beam capture by transverse magnetic field due to polarization space charges electrostatic separation

17 p2786 A71-34280

Cold plasma flow rate determination from emission inhomogeneities, using time of flight method and high speed streak photography for instantaneous velocity measurements

17 p2787 A71-34286

Steady plasma flow velocity measurements, describing two channel high resolution spectrometer

17 p2787 A71-34390

Perturbed two dimensional laminar boundary layers of incompressible conducting fluid flow along insulated concave wall in transverse magnetic field, investigating three dimensional instability

17 p2788 A71-34642

Magnetic annular arc continuous operation at atmospheric pressure, determining arc velocity and rotational frequency as functions of magnetic flux density and arc current

17 p2788 A71-34901

Time and space variable magnetic field effects on plane unsteady MHD boundary layer flow separation

17 p2789 A71-35343

Reynolds magnetic number effect on MHD channel conducting gas flow current distribution, taking into account Hall effect

17 p2790 A71-35642

S shock wave and magnetic field interaction at supersonic speed, using shock tube and MHD channel with sectioned electrodes

17 p2790 A71-35643

Compressible electrically conducting gas boundary layer on MHD channel electrode, deriving equations for ambipolar region with finite ionization and recombination rates

17 p2790 A71-35644

Positive biased ionospheric probes in steady state plasma flow, presenting self consistent parameter computation

18 p2915 A71-36013

Vlasov-Poisson equations of collisionless plasma flow around conducting cylinder without magnetic effects, using nonrestrictive hybrid simulation techniques

18 p2951 A71-36025

Streamlines geometry in hydromagnetic inviscid nonheat conducting compressible flow in magnetic field, taking into account force vectors and energy/mass distributions

18 p2951 A71-36183

Weakly interacted laminar MHD flow growth in entrance region of plane channel with wall conductances investigated by momentum integral method

18 p2951 A71-36251

Numerical analysis of plasma expansion confined by magnetic field, emphasizing boundary oscillation and temperature rise, based on hyperbolic and parabolic system equations

18 p2952 A71-36308

Steady inviscid fluid flows in plane channel and in axially symmetric nozzle, considering external magnetic field effects with electroconductive fluid

18 p2907 A71-36327

MHD equations of motion solved for conducting fluid interaction with electromagnetic field in porous media in range of Darcy law

18 p2953 A71-36948

Plane MHD Couette flow stability with asymmetric velocity profile shaped by transverse magnetic field, considering Hartmann flow

19 p3108 A71-37077

MHD channels end effects at finite magnetic Reynolds numbers, discussing wall conductivity and external magnetic field geometry effects

19 p3108 A71-37078

Viscous incompressible conducting fluid at constant flow rate under magnetic field variation, investigating laminar unsteady MHD Couette flow problem with approximate solution

19 p3108 A71-37092

Poloidal Hall current calculation in hydrodynamic approximation for stationary weakly interacting and conducting cylindrical plasma flow with uniform transverse flow parameter distribution

19 p3109 A71-37138

Stationary plasma flow interaction with axisymmetric spatially periodic magnetic field in presence of Hall effect, determining electric currents structure

19 p3109 A71-37139

Solar plasma emission capacity, using atmospheric ionization theory

19 p3133 A71-37434

Ideally conducting magnetostatic equilibria and associated time dependent resistive flows from two dimensional solution for MHD equations

19 p3115 A71-38211

Double scattering of plasma stream in bithermal ionosphere, noting ion density perturbation under external magnetic field

20 p3272 A71-38748

Magnetosphere neutral layer plasma conductivity determination from model of linear magnetic dipole in conducting fluid flow

20 p3216 A71-39138

Viscous electrically conducting laminar fluid steady flow through insulated MHD duct under uniform external magnetic field by extended Kantorovich method

20 p3275 A71-39561

Time dependent plasmopause motion after increase and decrease in magnetic activity based on analytical model of plasma flow

20 p3232 A71-39897

MHD power generator for converting heat into electricity by interacting magnetic field with flowing electrically conducting fluid

21 p3436 A71-40020

Shock free transonic deceleration of solar wind due to ionizing interactions, discussing plasma flow

21 p3438 A71-40604

MHD flow stability under arbitrary three dimensional disturbances, considering energy estimate for interaction between magnetic field and velocity field at critical Reynolds number

21 p3422 A71-40676

Electrically conducting fluid flow resistance in plane insulated channel in presence of transverse magnetic field, determining pressure, velocity and electric potential distributions

21 p3422 A71-40677

Hydrodynamic stability of incompressible conducting fluid flow between two moving linearly and rotating coaxial cylinders in longitudinal magnetic field

21 p3367 A71-40688

Probe size and orientation effects in turbulent plasma flow diagnostics, considering electrostatic probes frequency filtering and wake effects

21 p3423 A71-40979

Supersonic collisionless plasma flow around flat plate and expansion into vacuum, using Poisson equation

21 p3424 A71-41113

Stationary collisional shock observation in continuous supersonic plasma wind tunnel involving Q device modified into magnetic de Laval nozzle

21 p3426 A71-41403

Rotating plane layer viscous incompressible conducting fluid flow between two parallel walls with temperature gradient subject to perpendicular gravitational and magnetic fields

22 p3532 A71-41535

High Alfvén Mach number collisionless plasma flow in weak magnetic field, investigating momentum transfer mechanisms and coupling lengths

22 p3581 A71-41890

Insulating circular cylinder steady axial motion in conducting fluid permeated by uniform transverse magnetic field, determining flow along cylinder at field tangency points

22 p3583 A71-42198

Plane MHD boundary layer growth and separation in viscous incompressible flow past cylinder under abrupt motion and transverse magnetic field

22 p3584 A71-42685

Steady laminar viscous hydromagnetic flow in annulus with porous walls of different permeability, giving wall friction coefficients and velocity distribution

23 p3708 A71-43099

Plasma jet injection stoppage and reflection in strong transverse magnetic field, considering instability due to flow interactions

23 p3709 A71-43265

Transient pressure measurement in plasma exhaust flow of 500 microsec duration, discussing discharge temporal behavior and cold gas pressure front existence

23 p3711 A71-43598

Carbon dioxide additions effect on electron temperature relaxation and electron concentration distribution in expanding supersonic flow of low temperature Ar plasma

23 p3713 A71-44065

Plasma current driven sheet at neutral point of cusp and quadrupole magnetic field for space physical simulation of solar flare and geomagnetic tail

23 p3714 A71-44277

Supersonic plasma flow interaction with mirror field studied by changing ion-ion collision mean free path in BSG-IA device

24 p3852 A71-44489

Stability of dissipative shear flow of inviscid incompressible electrically conductive fluid in presence of magnetic field, deriving instability modes phase velocity limiting conditions from MHD equations

24 p3855 A71-44645

Ion current sheath-convection effects with flush mounted electrostatic probes in high pressure flowing plasmas

24 p3826 A71-44792

Natural trihedrons associated with stationary or nonstationary flows in hydrodynamics and MHD, using moving reference theory

24 p3856 A71-44795

Hartmann number for velocity pulsation free transition from turbulent MHD flow to laminar, noting difference relative to linear stability theory

24 p3856 A71-45059

Unsteady state MGD equations and Alfvén velocity behavior, examining triple orthogonal curves system formed by magnetic, principal normal and binormal lines

24 p3857 A71-45186

MAGNETOHYDRODYNAMIC GENERATORS

End loss elimination in MHD induction generators via nonconducting baffles and end coils

01 p0143 A71-10965

Book on direct energy conversion principles and methods covering fusion, fuel cells, MHD, thermoelectric, thermionic, photovoltaic, electrohydrodynamic, piezoelectric and ferroelectric power generation

01 p0006 A71-11193

Transverse current leakage effect on energy conversion and Hall characteristics of MHD generator

02 p0290 A71-12195

Energy converters for satellite nuclear power plants, discussing rotating, MHD, thermionic and thermoelectric systems

02 p0282 A71-12306

Oscillation application to steady current in MHD generator to stabilize electrothermal instability

05 p0791 A71-16938

Carbon dioxide laser excitation using nonequilibrium MHD generator

[AIAA PAPER 71-67] 06 p0938 A71-18526

Gas laser using nonequilibrium MHD generator with He, carbon dioxide and Cs mixture

[AIAA PAPER 71-68] 06 p0940 A71-18656

Nonequilibrium plasma molecular impurities effect on electron energy balance, considering importance in closed cycle MHD generators

08 p1342 A71-21916

Pulsed MHD generator model with nonequilibrium plasma, obtaining I-V characteristics

08 p1237 A71-21929

MHD generator with Ar-K plasma, examining electrical insulation behavior

08 p1237 A71-21930

Load currents and preionization of large nonequilibrium segmented Faraday MHD generator

09 p1386 A71-22072

Optimal inlet parameters of MHD generator channel employing kerosene-gaseous oxygen combustion products

09 p1386 A71-22136

Hall MHD generator duct optimization, using digital calculation for Carter integral minimum for size under required power output

09 p1512 A71-23441

Mathematical model for fields and currents calculation for asynchronous linear motors and MHD converters by Fourier transformation

09 p1387 A71-23650

Gas agent temperature measurement by sodium spectral line reversal method using MHD generators experimental research

09 p1512 A71-23671

Excitation schemes, fluid velocity and power of jet MHD induction generator

11 p1709 A71-25456

Soviet book on thermionic and MHD energy conversion covering gas ionization, converter operation and low temperature plasma physics

11 p1715 A71-26099

Time dependent current flow measurements and energy losses in capacitor discharge of electrodeless MHD motor

11 p1716 A71-26290

Rotating spole in unstable pulsed MPD arc, noting rotation frequency and resemblance to plasma rotation [AIAA PAPER 69-234]

12 p1941 A71-27568

Hydrodynamic instabilities of MHD plasma with current, using two fluid model in crossed magnetic-electric fields

13 p2105 A71-27879

Soviet book on liquid metals nonstationary flow in ducts of MHD devices covering laminar flow at constant and variable flow rates

14 p2277 A71-29526

Linear nonequilibrium shock tunnel driven super-sonic MHD generator operation under large scale power extraction and strong electromagnetic-rare gas interactions

14 p2287 A71-29879

Electrode size effects on voltage loss and boundary layer conductivity of combustion driven MHD generator

14 p2287 A71-29880

Turbo-MHD cycle technology of nuclear electric power systems with high temperature reactor for space and terrestrial applications [AIAA PAPER 71-638]

14 p2273 A71-30716

Soviet papers on gas discharge plasmas and strong magnetic fields covering plasmatrons, MHD generators, electric arc combustion, etc

15 p2457 A71-32266

Coaxial type MHD generator with steady magnetic field and plasma consisting of inert gases and ionizable alkali metal additives, obtaining electrical conductivity

15 p2355 A71-32268

Steady one dimensional MHD flow under transverse magnetic induction, determining maximum power of incompressible fluid generator

16 p2620 A71-34144

Low temperature high conductivity nonequilibrium plasma creation in MHD generators by microwave ionization

17 p2676 A71-34193

Nonequilibrium plasma molecular impurities effect on electron energy balance, noting importance in closed cycle MHD generators

17 p2789 A71-35261

Pulsed MHD generator model with nonequilibrium plasma, obtaining I-V characteristics

17 p2677 A71-35273

Electrical insulation behavior of MHD generator channel having Ar-K plasma, noting temperature dependence of surface conductivity

17 p2789 A71-35274

MHD generator duct external loop electric current maximization by working material resistivity tensor optimal distribution

19 p3108 A71-37102

Combustion oscillator for MHD energy conversion, using products flow modulation by traveling pressure wave

19 p2998 A71-38099

Performance potential of MHD generators utilizing nonequilibrium ionization in nuclear space power systems

20 p3264 A71-38930

MHD power generator for converting heat into electricity by interacting magnetic field with flowing electrically conducting fluid

21 p3436 A71-40020

Liquid metal MHD cycles for spacecraft power supply systems, proposing counterflow condensation at nozzle outlet

22 p3574 A71-42431

Transverse current conduction through MHD generator seeded hot plasma flow, showing Joule heating dominance in cathode boundary layer due to thermal instability

22 p3584 A71-42596

MAGNETOHYDRODYNAMIC STABILITY

Electron cyclotron drift instability shown by numerical simulation as cause for anomalous plasma diffusion and heating

01 p0132 A71-10147

Ellipsoidal plasmoid equilibrium in external HF field, calculating rotation rate and potential energy

01 p0132 A71-10151

Dissipating instability in plasma by variational method, using relation between energy balance of wave and medium

01 p0132 A71-10152

Electric current carrying plasma with finite and anisotropic conductivity in longitudinal magnetic field, determining equilibrium and stability

01 p0132 A71-10173

Feedback instability of LF oscillations in high pressure plasma diode

01 p0133 A71-10685

Magnetosonic wave instability in differentially rotating gas

01 p0160 A71-11119

Electron beam nonlinear interaction with plasma, considering electrostatic wave propagation, instability and dispersion equation

01 p0135 A71-11209

Quasi-transverse extraordinary wave interaction with density fluctuations in inhomogeneous magnetized plasma, using modulation measurement for instability diagnosis

01 p0136 A71-11440

Transverse wave instability of unmagnetized collisionless plasma subjected to shear flow

01 p0136 A71-11477

Electron gas column rotating about axis parallel to uniform external magnetic field, considering equilibria within Vlasov-Maxwell model

01 p0136 A71-11478

Regular and stochastic oscillations in plasma beam discharge produced by beam instability from observing time dependent variations in spectral line luminescence intensities

02 p0288 A71-11634

Inhomogeneous plasma oscillations excitation by high intensity electron beam, causing instability greater than hydrodynamic beam mode

02 p0288 A71-11890

Electron density fluctuations in nonstationary plasma under crossed electric and magnetic fields, relating times of instability development and background relaxation

02 p0289 A71-12179

Beam current instability and plasma heating by electron beam generated in linear discharge, discussing electron beam-cold plasma interactions

02 p0291 A71-12501

Plane and cylindrical MHD wave propagation in conducting compressible fluid under Hall effect, examining flow perturbation

02 p0291 A71-12533

Quasi-neutral electron beam instabilities in plasmas within longitudinal magnetic field with ion compensated space charge

02 p0291 A71-12546

Nonlinear stabilization of beam instability during electron beam interaction with decay plasma, determining distribution function in damping dynamics of HF vibrations

02 p0292 A71-12610

Stability of finite pressure plasma trapped by magnetic field, discussing trapped particle effects

03 p0463 A71-13296

Decaying helium gas plasma particles diffusion across magnetic fields by combined microwave and Langmuir electron density probes, considering instabilities

03 p0463 A71-13470

Neutral atoms collision effects on partially ionized plasmadynamic stability, considering fluid medium model with one dimensional density gradient

03 p0464 A71-13927

Electron plasma waves one dimensional quasi-linear instability with allowance for spontaneous emission

03 p0464 A71-13929

Corrugated theta pinch stabilization, considering variable axial HF current and quadrupole magnetic field

03 p0464 A71-13930

Anisotropic plasma stability, taking into account self gravitation, finite ion Larmor radius, Hall current and rotation

03 p0465 A71-14263

Strong turbulence theory of ionospheric cross field instability of weakly ionized plasma

03 p0420 A71-14533

Electromagnetic instability of counterstreaming electron plasmas with anisotropic temperatures, using Vlasov equation

04 p0633 A71-15032

Inhomogeneous magnetoplasma electrostatic LF oscillations, discussing wave modes and instability conditions

04 p0634 A71-15257

Magnetohydrostatic stellar interior instability, noting magnetic buoyancy

05 p0802 A71-15938

Hydrogen plasma turbulent heating, simulating ion-acoustic instability

05 p0786 A71-16226

Coronal magnetic structure mechanical diagnosis, using flare associated hydromagnetic disturbances

05 p0799 A71-16471

Incompressible inviscid perfectly conducting cylindrical plasma stability against azimuthal disturbance in monotonic decreasing magnetic field with constant pitch, using energy principle

05 p0787 A71-16478

Electromagnetic instability growth in counterstreaming nonrelativistic plasmas, comparing electrostatic rate

05 p0788 A71-16601

Magnetoacoustic instabilities in weakly ionized gas flow, using adiabatic approximation

05 p0788 A71-16602

Nonuniformly rotating Hg fluid, noting hydromagnetic stability and velocity control by imposed radial current distribution between coaxial ring shaped electrodes

05 p0788 A71-16608

Two component hydromagnetic system Kelvin instability due to tangential velocities discontinuity, using normal mode analysis

05 p0788 A71-16626

Collisional effects on Taylor and Kelvin instabilities in composite medium, considering longitudinal wave propagation mode

05 p0788 A71-16627

Rotating streaming plasma stability, including ion Larmor finite radius effects in presence of coriolis forces

05 p0788 A71-16628

Global stability of closed plasma configurations relation to dynamical principle of least constraint and space-time and gage symmetries of flow fields

05 p0789 A71-16651

Weakly ionized magnetoplasma waves and instabilities due to effects of electrons parallel, Hall and diamagnetic drifts relative to ions

05 p0789 A71-16653

Velocity space diffusion and collision effects on fully ionized inhomogeneous plasma instability, using Fokker-Planck kinetic equation

05 p0789 A71-16654

Collisionless plasma shock longitudinal wave propagation perpendicular to magnetic field, demonstrating ion acoustic/electron Bernstein modes instability

05 p0789 A71-16655

Plasmas and liquids inhomogeneous flow oscillations, determining resonance points effect on stability and oscillatory properties

05 p0790 A71-16825

Density thresholds for anisotropy and loss-cone instabilities onset in hot electron plasmas as function of frequency, wavelength and propagation direction of oscillations

05 p0790 A71-16937

Oscillation application to steady current in MHD generator to stabilize electrothermal instability

05 p0791 A71-16938

Convective cyclotron instability in whistler mode, discussing magnetosphere as generation mechanism and taking into account magnetospheric plasma inhomogeneity

05 p0743 A71-17003

Plasma instabilities role in ionospheric heating and radio wave attenuation

06 p0888 A71-17288

Current-interchange instability in plasma turbulent heating by current

06 p0930 A71-17395

Plasma stabilization, considering feedback loop system with Maxwell-Vlasov equations

06 p0931 A71-17452

Plasma stability criterion for feedback systems limitations, noting geometrical and electronic effects on phase and amplitude

06 p0931 A71-17454

Plasma stabilization, discussing external feedback system model

06 p0931 A71-17456

Fusion reactor plasma feedback stabilization by nonlinear interaction of two carbon dioxide IR laser beams to produce difference frequency near hybrid resonance

06 p0931 A71-17457

MHD continua z-theta pinch stabilization, discussing analytical models for determining feedback spatial and temporal resolution

06 p0931 A71-17458

Plasma stabilization by nonlinear bang-bang feedback

06 p0932 A71-17459

Cylindrical plasma Kruskal-Shafranov modes, examining active feedback stabilization

06 p0932 A71-17461

Tokamak copper shell as feedback control device for toroidal plasma, considering stabilization of thermal instability

06 p0932 A71-17462

High-beta sharp-boundaried stellarator plasma column feedback stabilization with helical fields

06 p0932 A71-17463

Collisional drift instability remote feedback suppression in Q machine Cs plasma by microwave modulation at upper hybrid frequency

06 p0932 A71-17464

Drift type plasma instabilities, discussing feedback stabilization and remote sensing

06 p0932 A71-17465

Plasma LF instabilities, observing temporal growth and effect on confinement by switching feedback control off

06 p0932 A71-17466

Q-machine with boundary segments to provide passive feedback for reducing Kelvin-Helmholtz instability and plasma losses

06 p0933 A71-17467

- Plasma transverse Kelvin-Helmholtz instability, describing stabilization by feedback controlled electron sink
06 p0933 A71-17468
- Electron-hole plasmas feedback stabilization, considering instability coefficients measurement
06 p0933 A71-17470
- Hot electron plasma, observing flute instabilities with feedback
06 p0933 A71-17471
- Dynamic plasma stabilization, discussing closed and open loop approaches
06 p0933 A71-17472
- Inhomogeneous collisionless low beta plasma drift wave instability dynamic stabilization, considering AC electric field parallel to confining field
06 p0933 A71-17474
- Dynamic stabilization of drift dissipative instability by inhomogeneous RF electric field parallel to magnetic field
06 p0934 A71-17475
- HF stabilization of plasma instabilities, noting electrostatic instability suppression by ordinary and helicon type waves
06 p0934 A71-17476
- Electron-ion collision effects on parametric instability growth rate in plasma dynamic stabilization
06 p0934 A71-17477
- Dynamic stabilization of high-beta plasmas with sharp boundary, illustrating model effect on stability by numerical calculation
06 p0934 A71-17478
- MHD dynamic stabilization, deriving stability conditions from periodic solutions of time dependent equations in Eulerian form
06 p0934 A71-17479
- Dynamic stabilization of instability in bumpy theta pinch by generalization of energy principle
06 p0934 A71-17480
- Dynamic stabilization of magnetoplasma drift dissipative instability by HF oscillating magnetic field, discussing helium and hydrogen afterglow plasmas
06 p0934 A71-17481
- Drift wave instability suppression by homogeneous RF electric field in DC discharge diffused plasma
06 p0934 A71-17482
- Dynamic stabilization of two stream ion instability in collisionless plasma
06 p0934 A71-17483
- Dynamic stabilization of MHD instability of low current z-pinch by HF quadrupole and oscillating magnetic fields
06 p0935 A71-17486
- Plasma stabilization in screw pinch, using combined inertial forces and dynamic shear in diffuse column
06 p0935 A71-17487
- Dynamic stabilization of MHD instabilities in high beta plasma column, using superposed fluids parametric resonance model
06 p0935 A71-17488
- Dynamic stabilization of helical and sausage instabilities of p-indium antimonide electron-hole plasmas, using Ioffe type RF energized magnetic quadrupoles
06 p0935 A71-17489
- MHD system hydrodynamic stability using propellant and fuel filled reactor cavity to form three region two fluid vortex
06 p0882 A71-18318
- Cosmic plasma dynamics collective phenomena, investigating models, instabilities, nonlinear interactions, wave transformations, turbulence, cosmic rays and radiative acceleration
06 p0972 A71-18330
- Energetic lifetime, equilibrium and thermal insulation of ohmically heated plasma in stellarator
06 p0937 A71-18350
- Inhomogeneous plasma flute instability in presence of gravitational field and supported by magnetic fields
06 p0938 A71-18425
- Steady state current-free magnetized plasma generation by microwave discharge, using feedback control to reduce power fluctuations
06 p0938 A71-18458
- Transverse velocity shear effects on low-beta resistive plasma LF stability in uniform magnetic field
07 p1166 A71-18882
- Collisional drift plasma wave instability nonlinear analysis, calculating wave amplitude as function of magnetic field based on two fluid theory
07 p1166 A71-18883
- Coulomb collisions effect on instability of cold and warm monoenergetic electron beams in plasma
07 p1166 A71-18885
- Finite amplitude helical instability effect on microwave beam phase propagated through plasma column
07 p1166 A71-18888
- Plasma containment in adiabatic magnetic traps, discussing particles, Coulomb collisions, instabilities, cyclotron resonance masers, Van Allen belts, etc
07 p1166 A71-19097
- MHD Rayleigh-Taylor instability in galvanic approximation, demonstrating Hartmann number stabilizing effect
07 p1167 A71-19188
- Inhomogeneous collisionless plasma stability, showing small pressure gradient effects
07 p1167 A71-19228
- Plasma nonlinear drift oscillation instabilities, discussing plasma interaction with HF electromagnetic fields
07 p1167 A71-19229
- Plasma instabilities under radial magnetic field effect across homogeneous field, considering oscillation modes
07 p1167 A71-19231
- Hydrodynamic stability of viscous conducting fluid plane Couette-Poiseuille flow in transverse magnetic field by linear theory, considering complete spectrum of small disturbances
07 p1169 A71-19727
- Nondissipative heterogeneous shear flow stability in presence of uniform magnetic field in streaming direction
07 p1169 A71-20023
- Feedback instability of LF oscillations in high pressure plasma diode
07 p1170 A71-20147
- Plasma-electron beam interaction instability transition from absolute to convective in hydrogen tube system at various pressures, considering electron collision effects
07 p1170 A71-20181
- Plasma heated by cyclotron resonance using waveguide method, considering properties, confinement conditions and instabilities
07 p1170 A71-20182
- Stable ellipsoidal plasma configurations in alternating electrode annular system, considering longitudinal magnetic field strength, electrode voltage and gas discharge chamber pressure
07 p1171 A71-20185
- HF plasma instabilities driving mechanisms and distribution types, considering beam plasma computer simulation example
07 p1173 A71-20508
- Noncollisional plasma LF instabilities, discussing flutelike, drift wave and trapped particle modes from spatially confined plasma Vlasov equation
07 p1173 A71-20509
- Plasma instabilities and mode stabilization, discussing density-gradient-driven drift waves in collision-dominated regime
07 p1173 A71-20510
- High beta plasmas instabilities, discussing collisionless bode model of theta pinch and diagnostic measurements
07 p1173 A71-20511
- Finite and large pressure inhomogeneous plasma with finite electron heat conduction, calculating instability
07 p1173 A71-20534
- Cross field instability effect on weakly ionized plasmas with ionization density gradients under crossed electric and magnetic fields, using linear analysis
08 p1339 A71-21207
- Current carrying plasma in toroidal trap, studying instability and equilibrium due to captured and escaping particles
08 p1339 A71-21476
- Electron fluxes hydrodynamic stability in vacuum confined by external electric and magnetic fields and inertia forces, noting electron oscillations possibility
08 p1340 A71-21494
- Incompressible equilibrium plasma ellipsoid stability in electromagnetic traveling wave field
08 p1341 A71-21500
- Ionization instabilities feedback suppression in magnetized nonisothermal plasma
08 p1342 A71-21932
- Radiative instability of nonequilibrium plasmas in magnetic traps, considering circularly polarized oscillations propagating along magnetic field
09 p1500 A71-22241
- Confined plasma drift instability universal eigenmode stabilization by magnetic field shear
09 p1500 A71-22246
- Interplanetary plasma electron density inhomogeneities formation explained by instability due to electron stream curvilinearity obtained from spacecraft data
09 p1518 A71-22435
- One dimensional plasma wave nonlinear dispersion relation, stability and harmonic generation from statistical properties of trapped particle orbits in random potential
09 p1503 A71-22862
- Stability of finite pressure plasma trapped by magnetic field, discussing trapped particle effects
09 p1504 A71-23269
- Plasma confinement in Heliotron magnetic field discussing equilibrium and stability problems
09 p1505 A71-23442
- Steady nonlinear amplitude of electrothermal instability in nonequilibrium plasma derived by expanding electrothermal equations in terms of perturbation about equilibrium state
09 p1387 A71-23649
- Weak turbulence analysis of Maxwellian plasma waves nonlinear interactions effects on two stream instability with Gaussian momentum distribution
10 p1647 A71-23886
- Hall current effects on plasma screw pinch stability, obtaining dispersion relation from perturbations characteristic equations
10 p1647 A71-23889
- Soviet book on homogeneous plasma instabilities covering oscillations, magnetic effects, particle velocities, Landau damping, dielectric permittivity, electron fluxes and ion-cyclotron instabilities
10 p1648 A71-24016
- Short wave HF instabilities in strongly inhomogeneous plasma with hot electrons, considering ion acoustic oscillations and electron cyclotron harmonics
10 p1650 A71-24525
- Flute oscillations stability in low density plasma within strong magnetic field of mirror geometry, calculating unstable oscillation spectrum by Galerkin method
10 p1650 A71-24526
- Inhomogeneous collisionless plasma instabilities under dense blanket of neutral gas, investigating Alfvén type oscillation
10 p1650 A71-24628
- Magnetic mirror confined microwave heated plasmas stability based on uniform collisionless plasma model
10 p1651 A71-24632
- Plasma feedback stabilization, investigating flute instabilities
10 p1651 A71-24633
- Collisional plasma background influence on classification of two stream instability, considering lines of equal asymptotic growth rates in parameter space
10 p1651 A71-24635
- Strong interaction between plasma forward wave and electron beam slow wave at equal densities, causing double stream instability nonlinear limitations
10 p1651 A71-24636
- Bounce effects in negative mass instability of plasma in short mirror magnetic bottle with ion cyclotron frequency dispersion
10 p1652 A71-24652
- Atmospheric electrical effects due to aurora, discussing negative space charge, bremsstrahlung flux and electrojet plasma instability
10 p1604 A71-24703
- Ion beam deceleration and effective energy transfer to plasma at nonisothermal acoustic velocities in presence of ion acoustic instability
10 p1653 A71-24892
- Anomalous dispersion and instability in solar wind plasma with thermal anisotropy and high beta ratio, applying magnetosonic wave-particle interactions
11 p1816 A71-25754
- Monograph on marginal stability analysis of MHD instabilities by force free magnetic fields in plasma-vacuum systems covering gravitational, pinch and shearless models
12 p1934 A71-26569
- Anisotropic instability in velocity distribution of ions in plasmas under external RF electric field
12 p1934 A71-26572
- Inhomogeneous collisionless plasma stability, showing small pressure gradient effects
12 p1934 A71-26746
- Plasma nonlinear drift oscillation instabilities, discussing plasma interaction with HF electromagnetic fields
12 p1934 A71-26747
- Plasma instabilities under radial magnetic field effects across homogeneous field, considering oscillation modes
12 p1934 A71-26749
- Current distribution effect on stability of exploding and collapsing accelerated cylindrical plasma shell in axial and azimuthal magnetic field
12 p1935 A71-26765
- Drift waves dynamic stabilization in collisionless plasma, considering AC electric field effects on low frequency instabilities
12 p1935 A71-26914
- Linear longitudinal ion wave instabilities in electrostatic shock in plasma by double humped /bump in tail/ velocity distribution
12 p1935 A71-26916
- Stability and oscillation of zero-beta magnetically confined plasmas, applying to multipole configuration
12 p1935 A71-26917
- Anomalous resistance and turbulent heating of strongly nonisothermal plasma in strong magnetic field due to electron scattering by ion-acoustic turbulent pulsations beats
12 p1936 A71-27032
- Short wave ion-cyclotron plasma oscillations excitation by electrons drifting in magnetic field for wavelength much less than ion Larmor radius
12 p1936 A71-27033
- Hot plasma oscillations analysis for instabilities as function of magnetic viscosity and heat fluxes, using inertial waves dispersion equations
12 p1937 A71-27202

Weakly ionized plasma instabilities in high frequency field exceeding electron collision frequency, considering waves parametric excitations

12 p1937 A71-27204

Wall-stabilized arc column optimization from energy balance solutions, considering temperature and pressure effects on Ar arcs

12 p1939 A71-27275

Cross field magnetic discharge stabilization of plasma column in flowing CW electrically initiated chemical laser

12 p1940 A71-27278

Plasma jet drift stabilization in toroidal magnetic field with diverter producing 180 degree field line rotation

12 p1941 A71-27548

Parametric dissipative plasma instability in HF electric field, showing plateau formation in velocity distribution function causes Cerenkov dissipation decrease

12 p1941 A71-27765

Cold plasma convection production by ion driven LF drift instability, noting tokamaks and stellarators stabilization

13 p2104 A71-27850

Ion beams heating by ion-ion two stream instability perpendicular to magnetic field with cold electron background

13 p2104 A71-27851

Acoustic instability of plasma with current under ionizational equilibrium and moderate neutral gas pressures

13 p2105 A71-27878

Equatorial electrojet model instability to gradient instability and electron density irregularities

13 p2055 A71-27922

Cyclotron instability of outer radiation belt under growing waves self modulation conditions, describing discrete signals production by continuous excitation

13 p2128 A71-28171

MHD wave coupling in homogeneous plasma in field dependent on single coordinate, obtaining modified Alfvén and acoustic waves stability conditions

13 p2106 A71-28498

MHD waves nonlinear interaction in magnetosphere, calculating transverse Alfvén and magnetosonic and longitudinal acoustic wave decay instabilities

13 p2106 A71-28562

Helicon and magnetoacoustic waves instability during passage through hot collisionless plasma with current transverse to weak external magnetic field

13 p2107 A71-28851

States stabilization in low density plasma layer in ion-accelerating constant external electric field

13 p2108 A71-28857

Gravitohydrodynamic instability of static and counterstreaming composite systems composed of infinitely conducting fluids, using normal mode analysis

13 p2108 A71-29164

Wave propagation near upper hybrid frequency in mirror-confined hot electron unstable plasma

13 p2109 A71-29242

Plasma ion-sound instability feedback stabilization with remote modulated source at electron cyclotron resonance frequency

13 p2109 A71-29245

Ion wave frequency shift and instability suppression by RF electric field, examining wave-field coupling

13 p2110 A71-29334

Soviet book on inhomogeneous plasma instabilities covering spatial gradients, charged particles collisions, temperature effects, steady electric fields and magnetic shear

14 p2279 A71-29942

Afterglow plasma drift-dissipative instability stabilization by RF magnetic and electric fields

14 p2280 A71-30504

Monograph on instabilities in ion beam-plasma system covering surface wave propagation, magnetic effect and ion cyclotron radiation characteristics

14 p2281 A71-30507

High beta diffuse plasma pinch configurations, deriving stability requirement hydromagnetic energy principle

14 p2281 A71-30540

Unstable collisional drift waves in high density ionized Li arc plasma, possibly causing anomalous losses and fluctuations

14 p2281 A71-30544

Theorem proving impossibility of stabilizing unstable MHD configuration with nondissipative plasma in vacuum surrounded by superconducting wall by means of finite electrical conductivity wall

14 p2282 A71-30557

Dynamic stabilization of plasma column drift dissipative instability by inhomogeneous RF electric field, using two fluid macroscopic equations

14 p2196 A71-30560

Stellar and interstellar magnetic fields effects on plasma instabilities in Colgate cosmic ray model, using computer simulation

14 p2282 A71-30644

Equilibrium of current carrying plasma in toroidal system, studying instabilities due to trapped and slowly drifting particles

14 p2282 A71-30662

Stable plasma resonance behavior, calculating small signal and nonlinear responses for theory verification and diagnostic techniques

14 p2283 A71-30948

Incompressible frictionless helical flows hydromagnetic stability in cylindrical circular space

15 p2387 A71-31166

Relativistic electron beams in plasma, considering electrostatic instability conditions and critical currents

15 p2453 A71-31235

Electron density fluctuations in nonequilibrium plasma under crossed electric and magnetic fields, relating ionization instability development and background relaxation times

15 p2454 A71-31488

Structural stability for two beam plasma model with proportional controller using distributed feedback

15 p2456 A71-31846

Steady state of nonequilibrium Ar-Ca plasma in electric field, attributing instability to plasma radiation effect

15 p2457 A71-32273

Quasi-neutral electron beam instabilities in plasmas within longitudinal magnetic field with ion compensated space charge

15 p2459 A71-32502

Plasmas and liquids inhomogeneous flow oscillations, determining resonance points processes effect on stability and velocity

15 p2459 A71-32504

Magnetogravitational instability model with allowance for finite Larmor radius effect, considering plasma rotation parallel to magnetic field

15 p2459 A71-32654

Magnetic stabilization of transverse plasma instabilities, considering waves propagating transversely to plasma direction in presence of uniform external magnetic field

15 p2460 A71-32658

HF magnetic field effects on LF plasma instability and oscillation spectrum

16 p2615 A71-32794

Feedback stabilization of linear distributive systems in form of second-order evolutionary equation in Hilbert space, applying to plasma stabilization

16 p2618 A71-33006

Incompressible equilibrium plasma ellipsoid stability in electromagnetic traveling wave field

16 p2618 A71-33048

Plasma instabilities effectiveness for high energy cosmic rays confinement in galactic disk

16 p2625 A71-33238

Plasma energy cumulation by concentric spherical and cylindrical waves, calculating stability limit by integral solution

16 p2619 A71-33355

Magnetic drift wave instabilities in plasmas with nonuniform density and temperature gradient

16 p2572 A71-33949

Nonisothermal collisionless low beta plasma with electron temperature greater than ion, investigating low frequency potential modes for Kelvin-Helmholtz instability

16 p2620 A71-34167

Electron beam nonlinear interaction with plasma, considering electrostatic wave propagation, instability and dispersion equation

17 p2786 A71-34261

Plasma interchange instability in multipole magnetic field, including disturbance wavelength comparable to ion cyclotron radius

17 p2786 A71-34282

Plasma fluctuations and diffusion correlation analysis in linear octupole magnetic confinement, determining dispersion relation for interchange instability

17 p2786 A71-34283

Anisotropy instabilities of hydromagnetic wave propagation at small angle perpendicular to magnetic field above ion cyclotron frequency, calculating dispersion relation

17 p2788 A71-34664

Ionization instabilities suppression in magnetized nonisothermal plasma by feedback control

17 p2789 A71-35276

Plane plasma layer stabilization by force-free magnetic field

17 p2789 A71-35342

Explosive instability effect on plasma distribution function, field energy level and time response

18 p2950 A71-35863

Two-stream instability for magnetically confined pure electron gas column resulting from surface wave interaction

18 p2950 A71-35864

Bernstein mode wave instability growth rate in collisionless shocks propagating perpendicular to magnetic field, including pressure gradient effects

18 p2950 A71-35928

Decay instability at ion-sound frequency induced by large amplitude Bernstein mode wave in plasma

18 p2951 A71-35929

MHD systems equilibrium and stability involved in quiescent prominences, considering temperature dependence of heat conductivity, magnetic field and initial gas compression

18 p2967 A71-36927

Parametric plasma instability in HF electric field and constant magnetic field, noting longitudinal plasma oscillations growth

19 p3108 A71-37130

Dissipative plasma instability in lower E region investigation by alkali plasma clouds injection, observing irregular echo behavior by coherent pulse Doppler radar

19 p3110 A71-37365

Electric field fluctuations in magnetosheath plasma at multiples of local electron gyrofrequency due to plasma instability

19 p3048 A71-37368

Plasma drift cyclotron instability feedback stabilization, using immersed modulated electron sources

19 p3111 A71-37636

Finite-beta stabilization of collisionless trapped particle mode in toroidal plasma confinement devices, using magnetic well dug by plasma diamagnetism

19 p3112 A71-37742

Linear and nonlinear two-stream instability under relative motion between cold plasma components from Hamiltonian derivation for plasmons

19 p3112 A71-37744

Transverse waves and electromagnetic instabilities propagating along magnetic field in homogeneous plasma, discussing ions and electrons energy losses and plasma dispersion

19 p3114 A71-38206

Resistive instability in uniformly rotating magnetoplasmas with finite Larmor radius, using guiding center equations

19 p3115 A71-38208

Short wave HF instabilities in strongly inhomogeneous plasma with hot electrons, considering ion acoustic oscillations and electron cyclotron harmonics

19 p3116 A71-38251

Ion acoustic instability in ionosphere in presence of fast particles inhomogeneity, estimating ions and electrons drift velocities

19 p3129 A71-38366

Hot plasma oscillations analysis for instabilities as function of magnetic viscosity and heat fluxes, using inertial waves dispersion equations

19 p3116 A71-38614

Weakly ionized plasma instabilities in high frequency field exceeding electron collision frequency, considering waves parametric excitations

19 p3117 A71-38616

Marginal stabilization of MHD instabilities of linear pinch by force free magnetic fields, comparing with energy method

20 p3275 A71-39462

Shearless magnetic fields discontinuities in marginal stabilization of MHD instabilities for constant pinch force free fields, including toroidal effects

20 p3275 A71-39463

Auroral radio reflections mechanism in terms of auroral plasma instability processes, identifying ion acoustic wave characteristics among other echo components

20 p3199 A71-39852

Large and small scale auroral formation dynamics, covering precipitating electron and proton acceleration and plasma instabilities role

20 p3229 A71-39860

VLF ion wave instabilities in polar wind based on plasma kinetic theory, comparing with electrostatic wave observation by OV3-3 satellite

20 p3231 A71-39890

E x B plasma instability in auroral arcs, deriving dispersion relation

21 p3373 A71-40045

Radiative transfer effects on hydromagnetic stellar atmospheres thermal-convective instability in presence of uniform rotation and uniform magnetic field

21 p3421 A71-40579

Plasma ordinary wave mode electromagnetic cyclotron instability, discussing Dory-Guest-Harris type loss cone distributions

21 p3421 A71-40627

Magnetic field stabilizing effect on free shear layer of electrically conducting fluid at small Reynolds number

21 p3421 A71-40637

Long wavelength ion acoustic instability of two temperature collisional fully ionized plasma with heat transfer, noting additional destabilizing currents

21 p3422 A71-40708

Ion-cyclotron perturbation build-up in inhomogeneous plasma, investigating ion magnetic drift instability dependence on pressure

21 p3422 A71-40760

Unified linear theory for MHD waves in weakly ionized radiating plasma, deriving two-fluid model set of equations corresponding to magnetoacoustic, thermal, electrothermal and ionization rate waves

21 p3423 A71-40945

Natural potential and nonpotential electron oscillations excitation in plasma by transverse wave field, determining wave amplitude threshold and excitation instability 21 p3424 A71-41125

Confined plasma drift instability universal eigenmode stabilization by magnetic field shear 21 p3424 A71-41135

Magnetospheric plasma instabilities from velocity distribution anisotropies and nonuniform plasma and magnetic field distributions 21 p3374 A71-41180

Ion beam deceleration and effective energy transfer to plasma at nonisothermal acoustic velocities in presence of ion acoustic instability 21 p3425 A71-41272

Nonelectrostatic helicon and magnetoacoustic waves instability during passage through hot collisionless plasma with current transverse to weak external magnetic field 21 p3425 A71-41280

Electron beam heating of cold plasma in magnetic trap as function of plasma density, showing two stream instability due to Cerenkov effect 21 p3425 A71-41285

Low density collisionless plasma stabilization in ion-accelerating external DC electric field 21 p3426 A71-41293

Semiconducting plasma carrier density gradient instability, investigating threshold curve for n-type germanium 21 p3434 A71-41330

Short wavelength instabilities in collision dominated plasma confinement by rotating magnetic field, interpreting in terms of equivalent negative resistance 22 p3579 A71-41579

High pressure collisional plasma instabilities caused by spatial gradients from quasi-stationary state transport equations derivation 22 p3580 A71-41585

Weakly ionized magnetoplasma with no axial drift, investigating collisional drift-type instability by linearized two fluid hydrodynamic numerical analysis 22 p3580 A71-41586

Slow toroidal theta-Z pinch experiment, describing measurements temperature distribution with emphasis on transitions between stable and unstable states 22 p3580 A71-41588

LF waves and instabilities on positive column in magnetic field, comparing three theories for helical modes for He at low pressures 22 p3582 A71-41897

Threshold AC electric field calculation for inhomogeneous plasma parametric instability excitation, noting role of electron plasma wave energy propagation from unstable region 22 p3582 A71-41901

Electrostatic mode wave equations for low beta plasma microinstabilities in axisymmetric magnetic mirror machines, including effects of particle cyclotron, bouncing and drift motions 22 p3582 A71-41902

Inhomogeneous high-beta collisionless plasma temperature gradient effects on ion-acoustic and Alfvénic drift instabilities 22 p3583 A71-41907

Ionospheric small scale electron content irregularities and electrostatic plasma instabilities correlated with electrojet current intensity 22 p3535 A71-42223

Electrostatic plasma instabilities under HF alternating electric field oscillating at plasma frequency 22 p3584 A71-42465

Mathematical model for solar flares formation based on magnetic/kinetic energy conversion, investigating plasma instability 23 p3719 A71-42950

Weakly ionized cesium plasmas produced in sealed diodes, examining LF instabilities with fluid equations 23 p3708 A71-43083

Suprathermal electron beam induced HF wave instability in solar wind upstream from earth bow shock, interpretingOGO 5 observations 23 p3720 A71-43158

Barium ion cloud release at 194 km, observing striation formation for instability characteristics evaluation 23 p3669 A71-43170

Magnetic drift waves near proton cyclotron frequency, noting magnetic field gradient role in plasma instability 23 p3709 A71-43181

Acoustic instability of Joule heated nonisothermal electron plasma 23 p3709 A71-43261

Weakly ionized decaying plasma potential fluctuations and instability in magnetic field, using electrostatic probes 23 p3709 A71-43262

Longitudinal ambipolar sound instability effect on duration of plasma particle motion to wall across magnetic field, using phase method 23 p3709 A71-43263

Nonlinear stabilization of beam instability in plasma with comparable phase velocity, electron capture and decay effects 23 p3709 A71-43264

Plasma jet injection stoppage and reflection in strong transverse magnetic field, considering instability due to flow interactions 23 p3709 A71-43265

Plane vortex sheet in inviscid incompressible finitely conducting fluid under uniform magnetic field, considering hydromagnetic stability 23 p3663 A71-43490

Spatially separated plasma beams of different temperatures, determining amplified wave instability boundaries and growth increments by quasi-hydrodynamic approximation 23 p3711 A71-43557

Fully ionized plasma particle collision effects on surface oscillation stability 23 p3711 A71-43558

Plane supersonic ionizing shock wave in magnetic field under small wave plane perturbation from equilibrium position, calculating stability from linearized equations 23 p3663 A71-43575

Strong magnetic field effects on acoustic oscillations and instability in stationary inhomogeneous low temperature plasma flow in crossed fields 23 p3712 A71-43917

Bounded plasma ionization instability inhomogeneity scale evaluation, assuming negligible electron energy losses due to heat conduction as compared to elastic losses 23 p3712 A71-43923

Longitudinal magnetic field inhomogeneity influence on inhomogeneous plasma Alfvén instability, considering magnetic field pressure and trapped particles 23 p3713 A71-44151

Stratified nonequilibrium plasma ionization instability in crossed fields investigated by physical model without diffusion processes and boundary effects, considering space-time behavior of perturbation 23 p3713 A71-44152

Wide wavelength parametric plasma instability in constant magnetic and weak HF electric fields above ion gyroscopic frequency 23 p3714 A71-44327

Equilibrium plasma in perfectly conducting rigid wall with closed magnetic field lines, deriving necessary conditions for MHD stability 24 p3852 A71-44496

Rarefied theta pinch plasma collective interactions, examining kinetic instability, electron energy distribution, anisotropy, suprathermal microwave emission, cyclotron harmonics and oscillations 24 p3854 A71-44513

High current pulsed arc in hydrogen plasma at 400 atm, showing instability with rising pressure and arc length 24 p3854 A71-44519

Transverse instability of charged particle beam in segmented linear accelerators due to beam encounter with wall 24 p3855 A71-44522

Relativistic electron beam propagation in decelerating medium in crossed electric and magnetic fields, noting nonrelativistic instability condition 24 p3856 A71-44669

Stepwise ionization effects on ionic wave propagation and oscillation stability in inert gas DC discharges 24 p3857 A71-45230

Inhomogeneous high-collision finite-pressure plasma stability, finding thermal instability development under uniform temperature and arbitrary pressure 24 p3858 A71-45243

MAGNETOHYDRODYNAMIC TURBULENCE

NT PLASMA TURBULENCE

Type IV solar radio emission broadband intensity fluctuations explained by MHD pulsations in flux tubes in corona 01 p0162 A71-11387

Burger model equations for MHD turbulence with analog in gas dynamics for nondissipative case 09 p1432 A71-22703

Second order correlation functions of velocity and magnetic field for homogeneous unsteady isotropic hydromagnetic turbulence in incompressible conducting fluid 11 p1805 A71-25599

Isotropic MHD turbulence in incompressible fluid by diagrammatic representation, obtaining approximation with transfer functions and scalar equations for correlation 11 p1805 A71-25600

Nonhomogeneous turbulent flow with magnetic field, deriving MHD turbulence model neglecting velocity correlation time 13 p2107 A71-28565

Large scale kinematic dynamo theory for magnetic field generation in turbulent fluids based on Lorentz force helicity 14 p2314 A71-30646

Magnetic field generation in acoustically turbulent MHD medium, deriving spectral function equation and eigenvectors 16 p2619 A71-33545

Electric and magnetic fields effect on turbulent boundary layer of conducting gas near electrode in MHD channel with insulated walls 18 p2951 A71-36113

Kinematic dynamo theory application to infinite stationary media with large scale magnetic field components and isotropic turbulence 18 p2967 A71-37025

MAGNETOHYDRODYNAMIC WAVES

NT ELECTROSTATIC WAVES

NT PLASMA WAVES

Torsional and compressional hydromagnetic wave propagation in inhomogeneous magnetic fields 01 p0134 A71-11001

Hydromagnetic waves interaction with time dependent inhomogeneous background fluid, using Hamilton principle 01 p0136 A71-11475

Quasi-Alfvén and acoustic wave coupling in inhomogeneous stratified plasma within intense magnetic field as function of directional pressure 02 p0292 A71-12627

Radiation effects on cylindrical magnetohydrodynamic shock propagation in plasma, deriving jump conditions in terms of Mach number and pressure ratios 02 p0294 A71-12847

MHD parameters in photospheric plasmas of giant and dwarf stars, noting electric conductivity, Joule dissipation, Reynold and Lundquist numbers 03 p0490 A71-13938

MHD shock waves structure capable of ionizing gases, using law of conductivity variation with temperature 03 p0465 A71-14063

Monograph on helicon and Alfvén wave propagation in nonmagnetic semiconductors and semimetals covering active and passive waves 04 p0635 A71-14808

Ionospheric and exospheric ELF magnetic waves generation by high altitude nuclear explosions, discussing hydromagnetic waves propagation 04 p0581 A71-14981

Lower ionosphere magnetic fields generated by three dimensional Alfvén waves, analyzing spatial phase and amplitude distribution 05 p0745 A71-17199

Polarization splitting of EW and NS Alfvén oscillations in axisymmetric magnetosphere 06 p0894 A71-18269

Interstellar gas acceleration and heating by cosmic rays streaming along uniform magnetic field faster than Alfvén speed 07 p1190 A71-18854

Alfvén waves and magnetosonic radiation by rotating magnetic stars and planets 07 p1193 A71-19293

Charged particles interactions with shock fronts or MHD discontinuities, indicating contributory effects to cosmic rays acceleration 07 p1184 A71-19376

Alfvén wave transformation into magnetoacoustic wave during passage across boundary between two media in strong magnetic field, considering reflection and refraction laws 07 p1195 A71-19381

Hydromagnetic wave propagation with coupled isotropic and guided modes, obtaining steady state solution with toroidal, plasma resonance induced period dependent reflecting barrier 07 p1197 A71-19767

Alfvén irregularities near plasmapause, discussing significance in relation to geomagnetic micropulsations based onOGO-3 and ground station observations correlation 07 p1104 A71-20008

Plane steady state MHD shock wave structure in infinitely conducting fluid under magnetic field perpendicular to shock velocity, introducing quadratic artificial viscosity factor 07 p1174 A71-20616

Fluctuations effect on MHD shock wave propagating in plasma perpendicular to external magnetic field, obtaining field amplitude distribution function 09 p1500 A71-22242

Lower ionosphere geomagnetic induction effect on geomagnetic field guided MHD wave propagation, considering Hall effect 09 p1435 A71-22436

Cyclotron instability of high energy protons in magnetosphere with refraction of growing Alfvén waves 09 p1435 A71-22437

Deceleration of low energy cosmic rays in solar wind involving Fermi acceleration by MHD waves and adiabatic energy change 09 p1514 A71-22802

MHD wave propagation in magnetoplasma perturbed by LF magnetoacoustic waves, considering wave scattering and polarization 09 p1505 A71-23566

Radiative flux effect on magnetogasdynamic shock in selfgravitating gaseous stars 09 p1506 A71-23589

Alfven waves effect on MHD fast shock from numerical solution of extended Rankine-Hugoniot equations 10 p1667 A71-23798

Wave propagation with frequency inferior to gyrofrequency of ions in collisionless hydrogen plasma, showing Alfven wave reflection on discontinuity surface parallel to magnetic field 10 p1599 A71-23846

Relativistic MHD waves based on ideal fluid compressibility and statistical mechanics for given spacetime 10 p1650 A71-24586

Highly underexpanded plasma jet structure with coaxially superimposed arc discharge, investigating stationary MHD normal shock in jet core [DFVLR-SONDDR-108] 10 p1650 A71-24600

Inhomogeneous collisionless plasma instabilities under dense blanket of neutral gas, investigating Alfven type oscillation 10 p1650 A71-24628

Hydromagnetic shock wave structure, treating plasma in two fluid approximation with collisional transport coefficients in changing density and temperature 10 p1596 A71-24657

Homogeneous wave turbulence-MHD tangential discontinuity structures interaction, resulting in shear stress across discontinuity surface 10 p1652 A71-24663

Magnetohydrodynamic Kelvin-Helmholtz problem in Hall plasma, discussing case of hot unmagnetized fluid juxtaposed to cold magnetized plasma 10 p1653 A71-24664

Geomagnetic Pc1 pulsations propagation in F region, deriving hydromagnetic waves equations by ray tracing method and waves refractivity index in extraordinary mode 10 p1607 A71-25118

Generation mechanism of magnetohydrodynamic shock waves associated with sudden commencements of 27-day recurrent geomagnetic disturbances 10 p1608 A71-25120

MHD oscillations of homogeneous compressible self gravitating fluid spheroid in static equilibrium with poloidal magnetic field inside and dipole field outside 11 p1831 A71-26167

MHD waves incident at density step, calculating reflection, refraction and transmission coefficients and coupling modes 11 p1807 A71-26429

Quasi-steady spectrum of hydromagnetic noise in proton belt, using random excited broad wave fields in nonisothermal magnetosphere 12 p1947 A71-26643

Potential and nonpotential equation for Alfven waves and ion cyclotron oscillations in low density nonisothermal plasma 12 p1936 A71-27035

Cosmic rays resonant interaction with hydromagnetic waves, determining turbulent source for confining high energy radiation to Galactic disk 12 p1948 A71-27366

Induction and wave drag due to Alfven waves on long cylindrical satellite in ionosphere, investigating radiated power integral 12 p1973 A71-27576

Hydromagnetic wave coupled solar wind-plasma sheet effects on resonant oscillations of geomagnetic tail, using two dimensional model 13 p2119 A71-27910

Magnetic pumping of collisionless turbulent plasma with LF Alfven and magnetosonic waves, assuming high initial plasmon energy 13 p2105 A71-28175

Lower ionosphere magnetic fields generated by three dimensional Alfven waves, examining amplitude and phase spatial distribution and frequency dependence 13 p2059 A71-28254

MHD wave coupling in homogeneous plasma in field dependent on single coordinate, obtaining modified Alfven and acoustic waves stability conditions 13 p2106 A71-28498

MHD waves nonlinear interaction in magnetosphere, calculating transverse Alfven and magnetosonic and longitudinal acoustic wave decay instabilities 13 p2106 A71-28562

Stellar wind flow models associating energy transport with propagation and dissipation of hydrodynamic waves and heat conduction 14 p2297 A71-29586

Collisionless magnetic slow shocks laminar wave train structure, using two-fluid hydromagnetics with ion cyclotron radius dispersion 14 p2782 A71-30558

Low temperature plasma MHD waves propagation in inhomogeneous magnetic fields, comparing numerical solutions with experimental results 14 p2282 A71-30559

Dynamic nonshock properties of large amplitude microscale Alfven waves in interplanetary medium, using plasma and magnetic field data from Mariner 5 15 p2456 A71-31752

Hydromagnetic waves, micropulsations and temporal variations in vector geomagnetic field at 6.25 earth radii 15 p2397 A71-31759

Similarity solutions describing flow characteristics behind plane hydromagnetic shock propagating into uniform ideal gas at rest in presence of transverse magnetic field 15 p2391 A71-32074

Unsteady one dimensional MHD shock wave evolution and separation in shock tube, using single fluid continuum equations with numerical dissipation 15 p2457 A71-32389

Relativistic kinetic theory of large amplitude transverse Alfven wave, discussing propagation in collisionless plasma 15 p2459 A71-32653

MHD planetary waves existence on sun, estimating mean toroidal solar magnetic field and rotation rate 15 p2497 A71-32756

Slow MHD shock wave profile discontinuity corresponding to conventional gas dynamics isothermal jump 16 p2615 A71-32793

Plane and cylindrical waves three dimensional propagation, investigating finite electrical fluid conductivity and radiation effects in MGD 16 p2618 A71-33172

Plasma flow wave propagation, investigating compressibility, radiation and finite electrical conductivity effects with plane asymptotic solution combinations 16 p2618 A71-33173

Anisotropy instabilities of hydromagnetic wave propagation at small angle perpendicular to magnetic field above ion cyclotron frequency, calculating dispersion relation 17 p2788 A71-34664

High latitude sudden impulses, calculating transverse hydromagnetic waves propagation from magnetosphere equatorial plane 17 p2733 A71-34777

MHD detonation waves in relativistic perfect fluid of magnetic permeability μ immersed in electromagnetic field 18 p2951 A71-36189

Hall fields effect on interaction of MHD waves in inhomogeneous plasma, considering MHD wave dispersion 19 p3109 A71-37134

Second order MHD equations for density fluctuations driven by Alfven waves with relation to solar wind 19 p3110 A71-37352

Plasmapause Alfven, ion-acoustic, electron and ion drift wave modes coupling, calculating instability condition and growth rate 19 p3110 A71-37371

Charged particles interactions with shock fronts or MHD discontinuities, indicating contributory effects to cosmic rays acceleration 19 p3127 A71-37801

Alfven wave transformation into magnetoacoustic wave during passage across boundary between two media in strong magnetic field, considering reflection and refraction laws 19 p3138 A71-37806

Solar wind acceleration due to Alfven wave pressure gradient, taking into account coronal parameters of temperature, magnetic field and energy density 19 p3128 A71-38162

Magnetospheric hydromagnetic resonances, considering resonant poloidal-toroidal coupling 20 p3215 A71-38745

Coherent small amplitude hydromagnetic wave propagation in magnetic field with time independent random component 20 p3274 A71-39057

Magnetospheric high energy protons relaxation due to interaction with Alfven waves, presenting Einstein-Kolmogoroff equation numerical solution for particle momentum distribution function 20 p3278 A71-39074

Transverse hydromagnetic shock structure in partially ionized gas, calculating ions, electrons and atoms temperatures, velocities and momentum 21 p3444 A71-40239

Outwardly propagating coronal Alfven waves pressure exertion on solar wind, using one fluid polytropic model 21 p3438 A71-40423

Fluctuations effect on MHD shock wave propagating in plasma perpendicular to external magnetic field, obtaining field amplitude distribution function 21 p3424 A71-41131

Solar wind theory, discussing thermal conduction and MHD wave energy supply mechanisms of large scale solar corona expansion 21 p3439 A71-41183

Electromagnetic HF wave field pressure effects on slow transverse magnetic wave propagation along

plasma layer, noting dispersion equations difference from linear theory 21 p3426 A71-41400

Mgd shock propagation in viscous heat conducting gas, investigating radiation escape effect 23 p3708 A71-43100

MHD wave spectrum relaxation during wave-plasma interactions in weakly turbulent plasma, treating associated triplasma processes as elementary events 24 p3855 A71-44661

Weakly damped Alfven ion-cyclotron waves and fast magnetoacoustic waves in infinite plasma cylinder inserted into current bearing finite coil 24 p3858 A71-45245

MAGNETOHYDRODYNAMICS

Shock wave propagation in channel with MHD interaction between compressed gas and nonuniform magnetic field 01 p0132 A71-10662

Linear MHD theory of inhomogeneities in axisymmetric models of universe with cosmological magnetic field 01 p0160 A71-11093

Voltage distribution measurements between electrodes of MHD Faraday nozzle across ionized Ar plasma supersonic flow 01 p0136 A71-11373

Infinite MHD journal bearing with electrically conducting fluid lubricant in radial magnetic field, obtaining pressure distribution, load capacity and driving torque 02 p0258 A71-12601

Compressible magnetofluid dynamics studies in cesium shock tube 04 p0632 A71-14690

Energy deposition by MHD into supersonic argon plasma flow in shock tube 05 p0787 A71-16537

MHD discontinuities effects on earth magnetosphere from satellite observation, discussing head shock wave and magnetopause positions 05 p0745 A71-17197

Auroral phenomena, using dimensional analysis to examine MHD equations for fields and plasmas in magnetosphere 06 p0888 A71-17286

Variational principle for MHD of ideal fluid, determining canonical variables and Hamiltonian 06 p0929 A71-17378

Plane grid condenser movement through magnetized plasma, calculating resistance by quasi-hydrodynamic approximation for plasma dielectric tensor 06 p0936 A71-17731

Finite wall conductance effect on performance /pressure and load capacity/ of MHD hydrostatic thrust bearings [ASME PAPER 70-LUB-1] 07 p1117 A71-19503

Weak discontinuities propagation and growth in MGD with finite electrical and thermal conductivity, calculating shock wave generation critical time 07 p1170 A71-20094

Solar cosmic ray interaction with oblique shock wave MHD discontinuity, noting energy particle buildup and acceleration 08 p1351 A71-20964

Magnetohydrodynamical effects of spirally twisted interplanetary field on solar wind velocity and density 08 p1355 A71-21420

Linear MHD theory of inhomogeneities in axisymmetric models of universe with cosmological magnetic field 08 p1366 A71-21951

Stationary motion stability of shaft in cylindrical MHD finite length bearing, assuming incompressible lubrication and small lubrication clearance 09 p1453 A71-22139

MHD equations for charged conducting fluid behavior in first postNewtonian approximation to general relativity, obtaining conservation laws 09 p1518 A71-22339

One dimensional plane adiabatic MHD free expansion of relativistic plasma 10 p1676 A71-24495

Variational principle for ideal fluid MHD, determining canonical variables and Hamiltonian 12 p1940 A71-27456

Low pressure paramagnetic regime axially symmetric hydromagnetic equilibria with spherical plasma-vacuum interfaces, extending solution to high pressure diamagnetic regime 13 p2104 A71-27843

MHD discontinuities effect on earth magnetosphere, computing bow shock wave and magnetopause positions from satellite observation data 13 p2059 A71-28252

Oscillatory hydromagnetic dynamo model of large scale solar magnetic field of variable sign, using Bernad convective cell with Coriolis velocity disturbance 13 p2137 A71-28529

MHD processes of upper atmosphere in mesospheric cloud formation, discussing solar wind-magnetic field interactions and equilibrium for Pikelner bomb 14 p2232 A71-29960

Shock wave propagation in channel with MHD interaction between compressed gas and nonuniform magnetic field 14 p2283 A71-30995

Small monochromatic disturbances propagation in stable ideal MHD fluid by geometric optics method, solving point source radiation at short wavelengths 15 p2459 A71-32652

Magnetohydrodynamic model system numerical integration as initial value problem, using finite difference scheme or differential equation conversion method 16 p2620 A71-34081

Multiply connected domain with Hilbert reduced problem, applying to MHD problems 18 p2953 A71-36950

Solar wind MHD interaction with magnetosphere, taking into account photospheric origin, velocity in interplanetary space and Parker theory 19 p3126 A71-37460

Solar and lunar hydromagnetic tides in earth magnetosphere obtained from electrostatic fields in dynamo region 19 p3142 A71-38030

Large scale alternating solar magnetic field generation by outer shell convective flow, constructing oscillator hydromagnetic dynamo model 19 p3145 A71-38353

Milky Way galaxy poloidal magnetic field generation with hydromagnetic dynamos, showing galactic cosmic rays as major driving force 20 p3287 A71-39056

Stability of plane rotating galaxies in magnetic field parallel to axis of rotation, showing linearized MHD equations self conjugate for radial disturbance case 20 p3289 A71-39298

MHD models of photospheric layers of sunspots emphasizing magnetic forces distribution 20 p3292 A71-39444

Submerged vehicle drag reduction and turbulence transition damping by MHD boundary layer control, using Lorentz force and optimum magnetic field 20 p3214 A71-39963

Symbolic ALGOL programming of partial differential equations applied to three dimensional MHD fields 21 p3351 A71-40847

Quasi-steady MPD thrusters performance correlation with structural and operational parameters 22 p3589 A71-42040

Dense hydromagnetic plasmoid interaction with nonuniform axisymmetric magnetic field using two dimensional fully ionized two temperature model 24 p3852 A71-44487

Digital computer numerical procedure to solve dynamo theory MHD equations for earth nucleus, using combination of Fourier and finite difference methods for integration 24 p3823 A71-45038

MAGNETOHYDROSTATICS

Magnetohydrostatic stellar interior instability, noting magnetic buoyancy 05 p0802 A71-15938

Rotating inertia effects on step-type MHD hydrostatic thrust bearing characteristics, discussing disk shape and operating conditions for improvement 17 p2748 A71-34641

MAGNETOIONIC PLASMA

U PLASMAS (PHYSICS)

MAGNETOIONICS

Magnetoionic theory for drifting plasma whistler mode propagation, deriving magnetic field effects on imaginary and real parts of complex refractivity 09 p1505 A71-23385

Reciprocity theorem for magnetoionic modes, considering arbitrary plane slab within magnetoplasma with parameter variation in direction normal to horizontal plane of stratification 10 p1577 A71-24293

Polarization behavior of radio waves propagating through magnetoionic medium near and across transversal point of magnetic field 13 p2028 A71-27997

Magnetoionic component with fluctuating elliptical polarization during wave reflection from F 2 layer, discussing suppression mechanism 13 p2030 A71-28537

Coupled longitudinal-transverse wave modifications of electrostatic dispersion relation with ion gyrofrequency instabilities in magnetized plasma 18 p2950 A71-35866

Magnetoionic mode coupling of HF radio waves, considering Faraday rotation of satellite signals 23 p3642 A71-42963

MAGNETOMETERS

NT VARIOMETERS

Weak magnetic field measurement using magnetometer with digital technique time coding 02 p0247 A71-17122

Solar magnetograph with potentiometers, recording magnetic fields, emission and absorption lines, radial velocity and brightness 04 p0589 A71-14836

Magnetometers for space research, discussing instrumentation, spacecraft response, data, earth orbit, lunar, planetary and interplanetary measurements 05 p0748 A71-16228

ALSEP magnetometer design and performance 05 p0755 A71-17127

Quartz magnetometer design and operation for simultaneous geomagnetic field declination and horizontal component measurements 05 p0756 A71-17216

Indirectly stabilized magnetometers on moving carrier, examining techniques for geomagnetic field vector component measurements 06 p0899 A71-17932

Magnetographic defectoscopy, discussing defect field magnetic recording techniques quality 07 p1106 A71-19143

Pulkovo observatory six channel two slit single photomultiplier rotating photographic plate magnetograph, for solar spectra polarization and radial velocities observation 07 p1109 A71-19337

Sunspot observations on 3 July and 14 September 1967, examining transverse magnetic field distribution and radial gas velocities and motion with magnetograph 07 p1195 A71-19338

Gyrocompass strapdown three coil synchro sensor magnetometer in conjunction with vertical gyro, eliminating azimuth detector inertial platforms 07 p1156 A71-20340

Solar disk active region gas development radial velocities on two levels /4 July 1966/, using double magnetograph 07 p1205 A71-20636

Strapdown solid state compass based on magnetometer principle, describing gyro feedback correction system and circuitry 08 p1287 A71-21171

Fossil lunar magnetism observations, using magnetometer data from orbiter Explorer 35 08 p1365 A71-21747

Very weak magnetic field measurements by highly rarefied gases as sensors 10 p1642 A71-24697

Magnetometer for indicating position of constant level meteorological balloons provided with solar sensors 10 p1612 A71-24759

Magnetic field detection by magnetometer with coherent magnetization rotation in thin magnetic film 12 p1906 A71-26856

Quartz magnetometer design and operation for simultaneous geomagnetic field declination and horizontal component measurements 13 p2067 A71-28270

Time dependence of signal emf induced in toroidal proton precession magnetometer sensor with elliptical cross section 14 p2246 A71-30481

Optically pumped magnetometers for earth and interplanetary magnetic fields measurement, using Zeeman effect 15 p2405 A71-31409

Magnetometer network operation during IQSY, establishing Sq variations in polar regions on quiet days and nature of geomagnetic disturbances 15 p2396 A71-31607

Simultaneous two magnetometer measurements of weak magnetic fields in interplanetary space, near moon and planets by satellites in presence of spacecraft field 15 p2406 A71-31753

Radiative energy transfer equations solution in magnetic field, facilitating magnetograph calibration 15 p2496 A71-32740

OGO-2 rubidium vapor magnetometer measurements comparison with surface magnetic observatory data during geomagnetic storms, considering asymmetric ring current 16 p2572 A71-33946

Forty channel magnetography system including CRT display, digital controlled heliostat, real time computer and optical transducer 17 p2740 A71-34988

German monograph on rocket measurements in auroral zone with proton magnetometer covering magnetosphere, spin-lattice and spin-spin relaxation time and data processing 18 p2910 A71-35885

German monograph on three component magnetometer for position determination of polar electrojet by sounding rocket 18 p2915 A71-35921

German monograph on calibrating induction coil and proton precession magnetometers for polar electrojet rocket experiments 18 p2915 A71-35922

MAGNETOMETRY

U MAGNETIC MEASUREMENT

MAGNETOPAUSE

Sunward magnetosheath magnetic field fluctuations, noting power levels spatial variations, transverse shock aligned fields and longitudinal waves 01 p0075 A71-11493

Kelvin-Helmholtz instability at magnetopause, initiating semiannual variation of geomagnetic disturbances 01 p0075 A71-11495

Solar wind and magnetopause shock front location at 1969 maximum, examining proton parameters from Heos 1 observations 03 p0482 A71-14513

Magnetopause inward motion before substorm, showing association with interplanetary field vertical component reversal 03 p0496 A71-14515

Quiet day variations in earth surface magnetic field, examining magnetopause, neutral sheet and ring nonionospheric current models 03 p0421 A71-14535

MHD discontinuities effects on earth magnetosphere from satellite observation, discussing head shock wave and magnetopause positions 05 p0745 A71-17197

Magnetopause crossing observation of ATS 5 satellite during magnetic storm 06 p0887 A71-17258

Low energy electron and proton fluxes observation by Isis 1 satellite, concluding solar wind penetration to low altitudes through magnetopause cusp 07 p1186 A71-19659

Magnetopause electric field accounting for ATS 5 energetic proton and electron flux measurements, comparing to various models 07 p1186 A71-19660

Multiple magnetopause crossings in equatorial plane by OGO 5, showing magnetopause motion composed of two oscillations 08 p1282 A71-21631

Pressure conditions across distant magnetopause from interplanetary magnetic field measurements, comparing Pioneer 7 plasma data with Explorer 33 distant geomagnetic tail field magnitudes 08 p1285 A71-21692

Plasma-free point magnetic dipole in field-free stationary plasma, determining magnetopause or free boundary by moment technique 09 p1503 A71-22865

MHD discontinuities effect on earth magnetosphere, computing bow shock wave and magnetopause positions from satellite observation data 13 p2059 A71-28252

Earth magnetosphere boundary position, head shock wave, transition region width and current magnetic field changes during magnetopause in geomagnetic storm periods 13 p2061 A71-28549

Solar wind-magnetosphere interaction based on electric fields and currents, discussing energy transfer and magnetic field reversal at magnetopause 13 p2064 A71-29165

Magnetic field and electron plasma observations near dawn magnetopause by triaxial spectrometer and fluxgate magnetometer on satellite OGO 5 15 p2485 A71-31754

Exact charge neutral magnetopause equilibrium, discussing microinstabilities as trapped particle flow cause 16 p2563 A71-33233

Space radio astronomy, discussing frequency range in terrestrial atmosphere, RAE-1 satellite, cosmic and solar emissions and magnetopause generation, propagation and absorption processes 17 p2797 A71-34243

Magnetopause current layer observations based on numerical solution of uniform magnetic field confinement by warm plasma with net parallel velocity 19 p3132 A71-37355

Magnetopause and bow shock location from IMP measurements, discussing solar wind momentum flux induced orbit-to-orbit changes in boundary positions 23 p3667 A71-43159

Explorer 12 magnetic field observations of magnetopause current layer during magnetic storm, interpreting data by magnetosphere model 23 p3668 A71-43160

Magnetopause current layer deflection during OGO 5 crossings, noting independence on sun-earth-satellite angle 23 p3668 A71-43161

MAGNETOPLASMAS

U PLASMAS (PHYSICS)

MAGNETORESISTANCE

U MAGNETORESISTIVITY

MAGNETORESISTIVITY

Magnetoresistance of coil surrounded electromagnetic mechanisms air gaps, noting potential distribution at pole aperture axis 05 p0705 A71-17175

Te-doped n-type GaSb semiconductor negative magnetoresistance and magnetothermoelectric power dependence on longitudinal magnetic field 21 p3436 A71-41349

Scale effect in semiconductor magnetoresistance due to carrier separation across plate thickness under perpendicular magnetic field 23 p3715 A71-43476

MAGNETOSONIC RESONANCE

MAGNETOSONIC RESONANCE

Wave kinetics in anisotropic plasma of weakly damped magnetosonic vibrations, using Lagrangians of three and four wave interactions

04 p0633 A71-15108

Electron-nuclear interactions in ruby by magnetoacoustic double resonance, comparing experimental and theoretical data

07 p1181 A71-20526

Anomalous dispersion and instability in solar wind plasma with thermal anisotropy and high beta ratio, applying magnetosonic wave-particle interactions

11 p1816 A71-25754

HF plasma heating in Tokamak torus device by magnetosonic wave energy absorption in high density region via Buchsbaum hybrid resonance

21 p3422 A71-40764

Magnetosonic wave excitation and electron heating in magnetically confined hydrogen plasma hybrid resonance region

24 p3853 A71-44502

MAGNETOSPHERE

NT GEOMAGNETIC TAIL

NT MAGNETOPAUSE

Auroral ionization relationship to incident magnetospheric electrons based on atmospheric model

01 p0073 A71-10253

Solar wind injection into magnetosphere, noting effects of magnetopause outward velocity and electric field strength

01 p0146 A71-11452

Directed proton fluxes measurements in bow shock, magnetosheath and solar wind by OGO 5 satellite ion spectrometer

01 p0147 A71-11491

Magnetic field fluctuations in magnetosheath from Pioneer observations, noting bow shock correlation

01 p0075 A71-11492

Magnetosphere thermal ion density and temperature in dawn and morning quadrants from OGO 5 satellite measurements

01 p0147 A71-11498

Magnetospheric VLF electric field emissions above electron cyclotron frequency from OGO 5 observation at magnetic equator

01 p0076 A71-11500

Compressible corotation of model magnetosphere, considering electric field induced by earth rotation

01 p0077 A71-11514

Plasma motion in magnetosphere under undisturbed geomagnetic conditions, taking solar wind into account

02 p0244 A71-11919

Boundary position and thickness between geomagnetic field and solar wind plasma, simulating interaction with magnetosphere

03 p0473 A71-13107

Effective electron collision frequency and RF conductivity along geomagnetic lines in magnetosphere

03 p0377 A71-13272

Solar flare particles effects on magnetospheric energetic particle population, discussing magnetic activity effects on trapped particles

03 p0473 A71-13578

Magnetospheric processes and structure, discussing solar wind interaction, magnetopause and shock wave formation, geomagnetic tail geometry, etc

03 p0410 A71-13822

Energetic electron magnetospheric motion and acceleration during substorms, examining fault line existence at near local midnight

03 p0419 A71-14519

Thermal magnetospheric plasma densities from hydromagnetic whistlers dispersion characteristics by normalized dispersion curve method

03 p0419 A71-14521

Quiet day magnetic field variations at geosynchronous satellite ATS 1, comparing magnetospheric models

03 p0419 A71-14522

Geomagnetic microfluctuations noting magnetospheric dimensions, solar wind velocity, magnetic activity indicators and latitude effects on rapid variations

04 p0584 A71-15369

Jupiter magnetosphere size, shape, structure, energetic particles and expected and potential energy sources

04 p0659 A71-15852

Zone of unstable radiation in magnetosphere localizing auroral and quasi-captured particles

05 p0798 A71-16046

Magnetospheric whistlers, deriving group refractive index and velocity, propagation time and various L values

05 p0721 A71-16443

Jupiter rotating inner magnetosphere plasma density distribution, using Lorentz term in force balance equation

05 p0810 A71-16631

High energy particle interaction with magnetospheric tail neutral layer, determining limiting shape of pitch angle particle distribution

05 p0800 A71-17176

Charged particle acceleration by electrical mechanism in magnetosphere, evaluating particle flux penetration into ionosphere

05 p0800 A71-17177

Resonant proton drift in axisymmetric rotating magnetosphere, discussing flow from boundary or tail to auroral region

05 p0800 A71-17178

Geocentric distances to subsolar point on magnetospheric boundary as function of magnetic activity state, discussing auroral oval position

05 p0744 A71-17180

Solar electrons access to closed field lines in geomagnetosphere quasi-trapping region from satellite observation

06 p0949 A71-17257

Pitch angle distribution of protons and helium ions in magnetosphere from numerical solution of Fokker-Planck equation

06 p0964 A71-17285

Auroral phenomena, using dimensional analysis to examine MHD equations for fields and plasmas in magnetosphere

06 p0888 A71-17286

Magnetospheric sudden impulses amplitude and rise time distributions observation by OGO 3 and 5 satellites

06 p0889 A71-17686

Solar wind torque on earth magnetic dipole based on magnetosphere model analytic solution in rotating reference frame

06 p0891 A71-17885

Magnetospherically reflecting nonducted whistler mode waves propagation noting dispersion, hybrid frequencies, ray curvature and field lines

06 p0868 A71-17983

High latitude neutron monitors during 15 November 1960 solar cosmic ray event, calculating asymptotic directions for protons with magnetospheric model

06 p0959 A71-18161

Jupiter magnetospheric rotation period based on RF observations

06 p0971 A71-18240

Magnetospheric plasma concentration from geomagnetic pulsations periods

06 p0894 A71-18270

Nondipole geomagnetic field effect on magnetosphere boundary, presenting graphs for distance dependence on polar angle

06 p0895 A71-18271

Jupiter and Saturn magnetosphere calculations, considering solar wind characteristics and planetary magnetic fields

[AIAA PAPER 71-30]

06 p0977 A71-18494

Space station plasma physics experiments, investigating electron and ion wakes, resonance, VLF electromagnetic energy propagation and magnetospheric phenomena

[AIAA PAPER 71-71]

06 p0938 A71-18529

Earth immersion in glowing He ions, studying magnetosphere structural dynamics by observations from cavity

07 p1095 A71-18742

Magnetospheric Debye radius, critical electric field voltage and normal and anomalous conductivities from low energy plasma concentration and temperature measurements

07 p1098 A71-19377

Whistler indicator generation, relating VLF emissions to iono-acoustic oscillations in magnetosphere

07 p1099 A71-19387

Magnetospheric boundary Pc2-4 pulsations period relationship based on Explorer 12 daytime magnetosphere data

07 p1101 A71-19416

Magnetospheric convection and polar wind influence on outer radiation belt energetic electron loss, subjecting previously large fluxes of lower energy electrons to trapping limit

07 p1186 A71-19661

Dawn to dusk magnetospheric electric field effect on energetic stably trapped particle drift shell pitch angle degeneracy

07 p1103 A71-19675

Polar auroras, lower magnetosphere and geomagnetic perturbations, as effect of corpuscular fluxes penetration into lower ionosphere

07 p1104 A71-20046

Whistler wave propagation along bell shaped ducts of enhanced ionization in magnetosphere

07 p1064 A71-20321

High energy electron injection into magnetosphere inner region during magnetic storms

08 p1350 A71-20956

Upper atmosphere balloon altitudes electron flux dependence on magnetosphere magnetic perturbation

08 p1351 A71-20957

Solar flare electron spectra in interplanetary space and within earth magnetosphere, investigating simultaneous observations by satellite-borne magnetic electron spectrometers

08 p1354 A71-21037

Book on ionosphere and magnetosphere covering temperature, composition ionizing radiations, radio communication electron production and loss, etc

08 p1363 A71-21164

Dynamo theory for electric current variations in magnetosphere-ionosphere interactions, discussing electrostatic fields mapping and plasma particle drift motion production

08 p1279 A71-21213

Electric currents in undisturbed magnetospheric tail, discussing interplanetary magnetic field polarity effect and neutral sheet characteristics

08 p1280 A71-21214

Dungey model generated by interplanetary magnetic field addition to closed magnetospheric model, discussing adiabatic theory breakdown for model current sheet

08 p1280 A71-21217

Magnetospheric electric fields properties via simultaneous balloon flights between plasmopause and polar cap, indicating fields and bulk plasma flow turbulence

08 p1282 A71-21632

Naturally generated electromagnetic waves interaction with electron flux in magnetoplasma, noting gyroresonance

09 p1501 A71-22304

Magnetic disturbances caused by magnetosphere-solar wind filamentary inhomogeneity interaction observed by Pioneer 6

09 p1513 A71-22560

Soft electron fluxes spatial distribution and temporal variations in magnetosphere based on Elektron 2 charged particle trap data

09 p1513 A71-22573

Plasmasphere ion concentration measurements on-board Elektron 2 and 4 satellites, observing dependence on geomagnetic activity

09 p1513 A71-22574

High latitude magnetosphere structure, using two dipole model

09 p1437 A71-22665

Solar wind static and dynamic pressures on earth magnetosphere, using geomagnetic parameters

09 p1514 A71-23152

Geomagnetic micropulsations distribution in magnetosphere, using OGO 3 and 5 data

09 p1440 A71-23635

Pc and Pi micropulsations, correlating magnetospheric cavity eigenmodes with sunspot activity

09 p1440 A71-23637

Magnetospheric electric field diagnosis, using geomagnetic disturbances in equatorial plane and pulsations in middle and high latitudes

09 p1441 A71-23639

Plasma intrusion into simulated magnetosphere compared with satellite observations, discussing spatial distribution and interplanetary magnetic field effects

09 p1529 A71-23707

Two group model of stationary plasma flow in magnetosphere with space charges due to inertia drift and forbidden regions

09 p1529 A71-23710

SIRIO project mission analysis, discussing space communication and magnetospheric investigations by scientific satellite in geostationary orbit

10 p1670 A71-24268

Steady state streaming of cold magnetospheric plasma in magnetic equatorial plane near plasmopause

10 p1650 A71-24557

Ring current indices by IGY data, attributing differences during great magnetic storms main phase to asymmetry of magnetospheric ring current

10 p1603 A71-24598

Solar wind-magnetosphere interaction modes from Explorer 33 and 35 interplanetary plasma and magnetic field data

10 p1663 A71-24780

Magnetospheric numerical model with two-monoenergy-component proton distribution function, examining ring current belt formation causing inflation

10 p1663 A71-24782

Magnetic field and trapped electron/proton correlated pulsations due to magnetospheric field line resonance, using model based on Maxwell equation two dimensional solution

10 p1664 A71-24786

Magnetospheric VLF banded emissions spectral analysis, investigating OGO-5 data by high time resolution spectral techniques

10 p1579 A71-24788

Magnetospheric model characteristics, discussing auroral phenomena energy sources, magnetotail length, polar cusp, auroral oval and electrojet relationships, polar and magnetospheric substorms

10 p1606 A71-24802

Solar wind distribution with respect to interplanetary magnetic field structure, interaction with planets and effect on earth magnetosphere

11 p1814 A71-25262

Energetic charged particle motion in magnetosphere, considering radiation belt dynamics

12 p1949 A71-27372

- Cosmic ray particles propagation anisotropies in model magnetosphere, suggesting detection interplanetary medium with geostationary satellites
12 p1950 A71-27377
- Pulsar electrodynamics, considering oblique rotator with dense magnetosphere to supply particles for Gunn-Ostriker mechanism
12 p1968 A71-27539
- Earth plasmasphere annual and sunspot cycle variations, considering observations with respect to whistler paths and Pc4 pulsations mean period variations
12 p1902 A71-27669
- Magnetospheric electron echo probe experiment, using sounding rocket and injecting gun for controlled particle trapping investigation
12 p1953 A71-27674
- Temporal history of 25-26 August 1967 magnetospheric substorm, discussing magnetotail plasma sheet thinning, partial ring current buildup and magnetic bays development
13 p2132 A71-27912
- Frequency vs time spectral shapes of magnetospheric VLF discrete emissions for field line and electron stream parameters
13 p2027 A71-27916
- Magnetospheric location of SAR-arc field lines, discussing proximity to plasmapause, electron trough and ring current
13 p2055 A71-27918
- Vacuum merging speed and magnetospheric cross tail electric field inverse proportionality to plasma sheet particle concentration
13 p2056 A71-27934
- Plasma motion in magnetosphere under undisturbed geomagnetic conditions, taking into account solar wind
13 p2058 A71-28206
- High energy particle interaction with magnetospheric tail neutral layer, determining particle pitch angle distribution limiting shape
13 p2128 A71-28233
- Charged particles acceleration by electric field in magnetosphere, evaluating injected particles flux into ionosphere under quiet conditions
13 p2128 A71-28234
- Resonant proton drift in asymmetric rotating magnetosphere, discussing flow from boundary or tail to auroral zone
13 p2128 A71-28235
- Geocentric distances to subsolar point of magnetospheric boundary as function of magnetic activity state, discussing auroral oval position
13 p2059 A71-28237
- Magnetospheric two component plasma model, considering thermal and suprathermal spectra
13 p2060 A71-28432
- Magnetosphere transmittance for fast magnetosonic waves, considering refraction, reflection and earth surface intersection
13 p2060 A71-28531
- Hall effect and magnetic field characteristics in lower ionosphere by vertical magnetospheric currents, using gyrotopic model
13 p2061 A71-28534
- Decreasing period micropulsations during elementary magnetospheric substorms, discussing relation to ring current asymmetry development
13 p2061 A71-28546
- MHD waves nonlinear interaction in magnetosphere, calculating transverse Alfvén and magnetosonic and longitudinal acoustic wave decay instabilities
13 p2106 A71-28562
- Daily Ap activity response of magnetosphere to sunspots, using 38 year geomagnetic storminess levels
13 p2062 A71-28785
- Solar wind-magnetosphere interaction based on electric fields and currents, discussing energy transfer and magnetic field reversal at magnetopause
13 p2064 A71-29165
- Magnetospheric model calculation for self oscillation period and amplitude dependence on longitude and plasma density estimation from observed geomagnetic pulsation period
14 p2228 A71-29531
- Magnetospheric tail models for Uranus type planet with viscous and magnetic coupling compared to geomagnetic configuration
14 p2305 A71-29664
- Spherical harmonic expansion for volumes of tubes of unit flux in geomagnetic field for use in magnetospheric dynamics
14 p2229 A71-29668
- Magnetosphere structure, considering geomagnetic field lines configuration in magnetotail
14 p2229 A71-29669
- Ionospheric currents due to electric polarization field transfer from magnetosphere under quiet and disturbed conditions, using Ba ion cloud and geomagnetic measurements
14 p2230 A71-29715
- Energetic electron power spectrum effect on synchrotron radiation from magnetosphere
14 p2298 A71-29722
- Initial phase duration of geomagnetic storms inverse dependence on sudden commencement amplitude in accord with solar wind-magnetosphere interaction
14 p2231 A71-29724
- Polar magnetic disturbances, discussing correlation with interplanetary magnetic field and interaction effects between solar wind and magnetosphere
14 p2231 A71-29907
- Polar ionosphere and magnetospheric processes - Conference, Kjeller, Norway, April 1969
14 p2299 A71-30027
- Solar wind compressed magnetic field in sunward magnetosphere and extended geomagnetic tail observation by Pioneer 7 spacecraft
14 p2234 A71-30028
- Low energy electron and proton fluxes in geomagnetic tail of equatorial magnetosphere forming plasma sheet related to auroral oval
14 p2299 A71-30029
- Upper F region transpolar plasma distribution from Alouette 1 data, relating results to satellite measurements of magnetospheric low energy charged particles
14 p2234 A71-30041
- High latitude upper ionospheric structures and plasma flow in magnetosphere from Alouette/ISIS topside sounders, noting solar UV and particle ionization sources
14 p2234 A71-30042
- Geomagnetic pulsation effect on charged particles motion, based on Mead magnetosphere analytic model, using Parker perturbation method
14 p2235 A71-30346
- Nonequatorial charged particle radial diffusion in asymmetric magnetosphere by third adiabatic invariant violation, using Kosik model
14 p2235 A71-30347
- Magnetospheric tail regions, investigating McIntosh effect in AE and Dst indices daily variations
14 p2236 A71-30354
- Radio science - Conference, Ottawa, August 1969, Volume 1, Ionosphere, magnetosphere, radio noise
14 p2201 A71-30939
- Satellite measurements of cold plasma density and plasmapause in magnetosphere, comparing Whistler, Langmuir probe and ion trap data
14 p2237 A71-30951
- Hydromagnetic approximation of ELF propagation modes and emission in magnetosphere, using satellite and ground based observations
14 p2202 A71-30953
- DC electric fields measurements in magnetosphere at equator, midlatitudes and close to or inside auroral arcs
14 p2237 A71-30955
- Electromagnetic waves in interplanetary space and effects on magnetosphere, considering solar wind characteristics due to wave interactions
14 p2202 A71-30956
- Asymmetries in magnetospheric shock layer due to upstream interplanetary magnetic field, considering forward stagnation region of solar wind-magnetosphere interaction
15 p2395 A71-31546
- Magnetospheric plasma clouds equatorial observation by ATS 5 satellite, revealing plasma injection during substorms and dispersion by earth magnetic and electric fields
15 p2397 A71-31755
- Local time variations of power spectra of magnetospheric electric field from balloon flight data
15 p2397 A71-31758
- Ground based HF radio sounding of earth magnetosphere echoes due to propagation along electron density enhancement
15 p2398 A71-31769
- Magnetospheric resonator properties bounded by ionosphere/earth system lines of force, examining nonuniform plane wave generation and standing wave pulsation period
15 p2401 A71-32731
- Density distribution of plasmaspheric particles in equatorial plane via model of plasmasphere streaming, noting current system production in lower ionosphere
16 p2562 A71-32806
- Charged particles distribution in magnetosphere beyond radiation belts, proposing unstable radiation zone model containing auroral and semitrapped particles
16 p2626 A71-33450
- Normal angle determination by rocket observations for whistler mode waves propagation through magnetosphere and ionosphere from conjugate VLF ground station signals
16 p2569 A71-33805
- Swedish space research activity covering upper atmospheric physics, ionosphere, magnetosphere and solar phenomena
16 p2665 A71-33853
- Solar protons penetration over polar cap during 25 February 1969 event from particle and magnetic field measurements inside and outside magnetosphere by satellites
16 p2628 A71-33934
- Magnetotail changes relationship to solar wind magnetic field and magnetospheric substorms from ground and satellite data
16 p2629 A71-33944
- Low energy auroral thermal electrons flux after geomagnetic substorm, entering magnetosphere from solar wind
16 p2629 A71-33953
- Magnetospheric observations by Imp 3 satellite of energetic electron and magnetotail field variations near neutral sheet as function of substorm time
16 p2574 A71-33971
- Bibliography on magnetosphere covering structure, magnetopause, geomagnetic tail, plasma sheet, convection plasmapause, storm and substorms, ring current and energetic particles
17 p2732 A71-34468
- High latitude sudden impulses, calculating transverse hydromagnetic waves propagation from magnetosphere equatorial plane
17 p2733 A71-34777
- Model interpretation of Pc pulsations during geomagnetic storms, analyzing plane HM-wave resonance in horizontally stratified middle-low geomagnetic latitude lower magnetosphere
17 p2734 A71-35190
- French monograph on ULF geomagnetic field variations covering plasmapause, geomagnetic pulsations, WKB limit and magnetospheric density
17 p2735 A71-35248
- German monograph on rocket measurements in auroral zone with proton magnetometer covering magnetosphere, spin-lattice and spin-spin relaxation time and data processing
18 p2910 A71-35885
- Earth upper atmosphere superrotation due to zonally averaged magnetospheric electric fields
18 p2911 A71-35992
- Quadrupole probe for measuring magnetospheric electric currents, noting transfer impedance dependence on probe motion relative to ambient plasma
18 p2912 A71-36198
- Jovian magnetospheric plasma densities, discussing roles of centrifugal ejection, solar wind plasma injection and photoelectron diffusion
18 p2964 A71-36291
- Asteroid magnetospheres effects on magnetic moments and whistler mode noise propagation in solar wind
18 p2964 A71-36292
- Plasma in dayside polar magnetosphere, analyzing Imp 5 and other earth satellites measurements data
19 p3047 A71-37357
- Diurnal variations in equatorial and precipitating low energy solar proton-produced gamma rays in magnetosphere
19 p3125 A71-37359
- Equatorial and precipitating solar proton fluxes interrelationship in magnetosphere from riometer absorption in auroral and polar cap regions
19 p3125 A71-37360
- Balloon-measured magnetospheric electric fields comparison with all sky camera pictures of large scale visible auroral form motions, noting relationship
19 p3047 A71-37363
- Electric field fluctuations in magnetospheric plasma at multiples of local electron gyrofrequency due to plasma instability
19 p3048 A71-37368
- Magnetospheric conjugate ducts characteristics for HF radio propagation from Alouette 2 topside sounder ionograms analysis
19 p3016 A71-37369
- Magnetospheric whistler mode signal propagation paths and amplification, investigating echoes of ground to satellite transmission
19 p3016 A71-37400
- Magnetic field aligned electric field production by hot magnetospheric plasma interaction with cold ionosphere
19 p3048 A71-37401
- Solar wind MHD interaction with magnetosphere, taking into account photospheric origin, velocity in interplanetary space and Parker theory
19 p3126 A71-37460
- Magnetospheric electric field dynamics, examining resonant protons role in magnetic storms
19 p3127 A71-37760
- Polar auroras production by electric fields and electron precipitation from magnetospheric magnetic storms
19 p3052 A71-37761
- Magnetospheric Debye radius, critical electric field voltage and normal and anomalous conductivities from low energy plasma concentration and temperature measurements
19 p3052 A71-37802
- Whistler indicator generation, relating VLF emissions to iono-acoustic oscillations in magnetosphere
19 p3052 A71-37812
- Magnetospheric boundary Pc2-4 pulsations period relationship based on Explorer 12 daytime magnetosphere data
19 p3054 A71-37840

Crab Nebula pulsar timing measurement leading to model involving inflation of closed magnetosphere with explosively released plasma 19 p3142 A71-38007

Solar and lunar hydromagnetic tides in earth magnetosphere obtained from electrostatic fields in dynamo region 19 p3142 A71-38030

Whistlers as diagnostic tools in space plasma, measuring electron densities at large distances in earth outer atmosphere within magnetosphere 19 p3116 A71-38246

Interplanetary plasma and magnetic field interaction with earth magnetosphere using spacecraft measurements during storms 19 p3145 A71-38272

Transverse electric field in ionosphere and magnetosphere during inhomogeneities consisting of fast electrons 19 p3057 A71-38367

Solar wind proton penetration through earth magnetosphere, taking into account drift, force lines curvature and nonstationary plasma boundary 19 p3129 A71-38377

Charged particle acceleration by nonstationary sinusoidal electric fields in earth magnetosphere based on mathematical model 19 p3129 A71-38377

Noncircular ionospheric current conversion into longitudinal currents in magnetosphere along lines of force of geomagnetic field 19 p3057 A71-38380

Magnetospheric field model, assuming magnetostatic problem solution facilitated by equation linearity 19 p3059 A71-38395

Magnetospheric current effects on geomagnetic field structure, noting electron and proton precipitation into auroral zone 19 p3059 A71-38396

Cyclotron resonance energization of trapped electrons in magnetosphere from plasma pseudopotential shape calculation, noting geophysical effect 19 p3117 A71-38724

Narrow band magnetospheric radio noise between electron plasma and upper hybrid resonance frequencies from satellite observations 20 p3285 A71-38728

Two dimensional magnetospheric model, investigating magnetic line dipole field confinement in empty cavity by tail-like infinitely conducting plasma at constant pressure 20 p3286 A71-38732

Magnetospheric hydromagnetic resonances, considering resonant poloidal-toroidal coupling 20 p3215 A71-38745

Magnetospheric high energy protons relaxation due to interaction with Alfvén waves, presenting Einstein-Kolmogoroff equation numerical solution for particle momentum distribution function 20 p3278 A71-39074

Interplanetary and magnetospheric magnetic force lines reconnection and effects on geomagnetic activity 20 p3289 A71-39126

Scintillation spectrometers sensitivity evaluation for low energy electrons in various regions of magnetosphere 20 p3234 A71-39127

Magnetosphere neutral layer plasma conductivity determination from model of linear magnetic dipole in conducting fluid flow 20 p3216 A71-39138

Magnetospheric interactions with ionosphere for solar regular daily geomagnetic variations, discussing dynamo region electric fields effects 20 p3217 A71-39509

Three dimensional atmospheric dynamo models in quasi-stationary and stationary approximation for ionospheric and magnetospheric electric fields and currents production during quiet conditions 20 p3217 A71-39512

Emf dynamo nonuniformities effect on magnetospheric field aligned electric currents associated with solar quiet geomagnetic variations, calculating ionospheric electrostatic fields 20 p3217 A71-39516

Plasmasphere evening ionization anomalies observations from spherical electrostatic analyzers onboard OV3-1 polar orbiting satellite, noting thermal plasma depletion during orbit night sector 20 p3225 A71-39741

Steady state magnetospheric convection pattern from synoptic maps of magnetic disturbance and auroral motions 20 p3230 A71-39879

Magnetospheric plasma convection electric field double-probe measurement at high latitude by Injun-5 satellite, noting east-west velocity reversals or discontinuities at auroral zone 20 p3230 A71-39882

Artificial auroral experiment by Aerobee rocket-borne electron accelerator generated monoenergetic electron beam injection onto magnetospheric field 20 p3231 A71-39885

Broadband electrostatic VLF wave observation in polar magnetosphere by OV3-3 satellite, noting emission power spectra density relationship to frequency 20 p3199 A71-39889

Crab Nebula pulsar magnetosphere, considering model of rotating magnetized neutron star rate of energy generation and rotation law exponent 20 p3305 A71-39948

Crab Nebula pulsar and extra emission from collapsed star magnetosphere, accounting for physical characteristics with nonthermal plasma mechanism 20 p3285 A71-39954

Magnetospheric plasma observation by Sirio 1 satellite, measuring protons, electrons and magnetic field with sensors 20 p3307 A71-39959

Magnetospheric VLF waves growth rate variations, calculating frequency spectrum and intensity with self consistent solution 21 p3346 A71-40046

Magnetospheric plasma instabilities from velocity distribution anisotropies and nonuniform plasma and magnetic field distributions 21 p3374 A71-41180

Magnetosphere aerodynamic parameters, discussing lift and drag coefficient, shape, magnetic field gradients and tail 21 p3374 A71-41353

Magnetosphere-ionosphere electric coupling for polar magnetic disturbances and auroral break-up origin, discussing thermal particles precipitation due to transient electric field 21 p3375 A71-41354

Ring current location in magnetosphere, noting electromagnetic ion cyclotron instability region as stable proton trapping boundaries 22 p3532 A71-41446

HEOS-A2 eccentric orbit satellite for interplanetary space and high latitude magnetosphere data, discussing onboard experiments, major subsystems and design philosophy 22 p3607 A71-41505

Magnetospheric VLF transverse wave propagation along geomagnetic field, examining dispersion relation 22 p3533 A71-41797

Worldwide geomagnetic disturbance during magnetic storm using DR-indices to express magnetospheric ring current induced perturbation 22 p3536 A71-42624

Midlatitude ionosphere and magnetosphere thermal protons dynamic behavior, investigating magnetic storm effects 23 p3720 A71-43129

Atmospheric triggered VLF emissions theory, examining magnetospheric whistler Morse pulses 23 p3643 A71-43135

OGO 5 polar cusp observations showing dayside magnetosheath plasma penetration during magnetic storm 23 p3668 A71-43162

Magnetospheric substorms observations by satellite and balloon-borne X ray detectors, considering auroral arc brightening and energetic electron flux enhancement in magnetotail 23 p3668 A71-43163

Triggered whistler emissions in magnetosphere, considering nonlinear interaction between whistler wave and resonating particles 23 p3643 A71-43175

Model prediction for magnetospheric electric field dependence on solar wind velocity, comparing results with plasmaspheric measurements for different Kps 23 p3721 A71-43177

Electron periodic energization by magnetospheric RF wave propagation, examining cyclotron resonant interaction 23 p3644 A71-43321

Artificial magnetosphere interaction with 8 keV electrons in hydrogen plasma beam simulating solar wind, noting penetration caused by boundary instability 24 p3823 A71-45043

Magnetospheric midday boundary width dependence on geomagnetic dipole axis orientation, discussing different positions for magnetosphere boundary 24 p3824 A71-45319

MAGNETOSPHERIC ELECTRON DENSITY

Magnetospheric electron density trough measurements by Explorer 22 Langmuir probe during rising solar cycle 03 p0420 A71-14529

Ionosphere and magnetosphere daily electron content change measurement, describing satellite beacon experiment 07 p1096 A71-19017

Radio signal receiving system design for group delay experiments with geostationary ATS-F for ionospheric and magnetospheric electron content 07 p1206 A71-19033

Altitudinal storm effect in electron concentration in outer atmosphere during nighttime hours 07 p1100 A71-19398

Electric field formation of field aligned electron density irregularities in magnetosphere 08 p1280 A71-21215

Midlatitude whistlers propagation paths during minimum solar activity for estimating magnetospheric electron density profile 10 p1580 A71-25135

Shot noise effect on ambient plasma magnetosphere electric field measurements with Langmuir and double probes for electron density and temperature 11 p1756 A71-25644

Magnetic field and electron plasma observations near dawn magnetopause by triaxial spectrometer and fluxgate magnetometer on satellite OGO 5 15 p2485 A71-31754

Ground based HF radio sounding of earth magnetosphere echoes due to propagation along electron density enhancement 15 p2398 A71-31769

Altitudinal storm effect in electron concentration in outer atmosphere during nighttime hours 19 p3053 A71-37822

Magnetospheric electrons and protons acceleration and slot injection between radiation belts during magnetic storms, using flux measurements onboard Molniya 1 satellite 20 p3282 A71-39738

MAGNETOSPHERIC INSTABILITY

Auroral magnetoionospheric perturbations processes, discussing space charge electric field structure and plotted altitude dependences 01 p0073 A71-10070

Stability analysis of magnetosphere whistler amplification, discussing energetic electron interaction with background plasma 01 p0038 A71-11308

Kelvin-Helmholtz instability at magnetopause, initiating semiannual variation of geomagnetic disturbances 01 p0075 A71-11495

Simultaneous sudden magnetospheric compressions and geomagnetic bay onsets correlation, using IGY data 02 p0245 A71-11967

Sudden impulses in geomagnetic field, discussing synchronous equatorial orbit-satellite magnetometer observations 03 p0421 A71-14537

Geomagnetic tail tearing instability nonlinear evolution, discussing quasi-linear theory 05 p0742 A71-16630

Convective cyclotron instability in whistler mode, discussing magnetosphere as generation mechanism and taking into account magnetospheric plasma inhomogeneity 05 p0743 A71-17003

MHD discontinuities effects on earth magnetosphere from satellite observation, discussing head shock wave and magnetopause positions 05 p0745 A71-17197

Electric field strength in earth ionosphere and magnetosphere during irregular motion of fast ions and electrons 06 p0894 A71-18253

Polarization splitting of EW and NS Alfvén oscillations in axisymmetric magnetosphere 06 p0894 A71-18269

Solar wind fast shock wave and simultaneous ground geomagnetic disturbance related to magnetospheric deformation 07 p1185 A71-19396

Low latitude geomagnetic substorm development model due to increased resistance in magnetosphere tail current sheath 08 p1278 A71-21017

Solar wind flux correlation with earth EM field pulsations, noting flare-generated shock front effects on magnetosphere 09 p1513 A71-22422

Dynamo role in magnetospheric disturbances and ionospheric inhomogeneities, allowing for charged particle concentration height dependence 09 p1435 A71-22430

Cyclotron instability of high energy protons in magnetosphere with refraction of growing Alfvén waves 09 p1435 A71-22437

Auroral zone magnetic substorm correlation to magnetospheric plasma drift 09 p1441 A71-23640

Long period, pearls and irregular geomagnetic pulsations for plasma diagnostics in magnetosphere 11 p1756 A71-25647

Comparative proton flux and Pc-1 pulsations from Explorer 26 satellite and ground observations 11 p1756 A71-25648

Quasi-steady spectrum of hydromagnetic noise in proton belt, using random excited broad wave fields in nonisothermal magnetosphere 12 p1947 A71-26643

MHD discontinuities effect on earth magnetosphere, computing bow shock wave and magnetopause positions from satellite observation data 13 p2059 A71-28252

Plasma electron and proton motion in equatorial plane of magnetosphere under geomagnetic disturbance generated electric field
13 p2060 A71-28530

Conjugate duct irregularities in magnetosphere involving interchange of plasma tubes by spatially varying electric fields, applying to spread F formation
14 p2230 A71-29714

ULF geomagnetic pulsations interpretation based on Kelvin-Helmholtz magnetospheric instability mechanism and bounce resonance wave excitation, considering energy exchange with energetic protons
14 p2202 A71-30954

Synchronous and oscillatory energy gain with electron-wave resonance time in collision magnetospheric plasma
15 p2371 A71-32024

Linear and nonlinear whistler mode cyclotron instability, discussing VLF emissions generation mechanism in magnetosphere
16 p2615 A71-32803

Exact charge neutral magnetopause equilibrium, discussing microinstabilities as trapped particle flow cause
16 p2563 A71-33233

Solar wind fast shock wave and simultaneous ground geomagnetic disturbance related to magnetospheric deformation
19 p3127 A71-37820

Low latitude geomagnetic subsystem development model due to increased resistance in magnetosphere tail current sheath
20 p3219 A71-39597

Ring current location in magnetosphere, noting electromagnetic ion cyclotron instability region as stable proton trapping boundaries
22 p3532 A71-41446

IGY interplanetary field independent storm sudden commencement triggered magnetospheric polar substorms, indicating sympathetic flare analogy
23 p3668 A71-43164

Magnetospheric substorms relationship to interplanetary magnetic field and solar wind plasma parameters, noting dominant effect of interplanetary southward component
23 p3734 A71-43183

Auroral plasma particle discharge during motion in strong magnetic field, discussing magnetospheric instability due to temperature anisotropy
24 p3867 A71-45309

MAGNETOSPHERIC ION DENSITY

NT MAGNETOSPHERIC PROTON DENSITY
Whistler ducts as enhanced ionization from OGO 3 satellite observations near magnetic equator, noting magnetospheric ionization hydrostatic model and predicted cut-off
01 p0076 A71-11499

Enhanced ionization density duct propagation of VLF radio waves in magnetosphere
07 p1062 A71-19578

Hydrogen ion concentration measurements by OGO 5 in plasmasphere during intense magnetic storms accompanied by stable auroral red arcs
10 p1605 A71-24787

Magnetospheric cold plasma dispersive and amplifying combined effects on pearl elements spectral shape, considering wave packet propagation applications
11 p1730 A71-25543

Midday ion composition altitude variations in midlatitude trough region and plasmasphere, observing light ion concentrations
15 p2398 A71-31767

Plasmaspheric ambient hydrogen and helium atomic cations density measurement by OGO 5 ion mass spectrometer during magnetic storm, noting relationship to auroral red arcs
20 p3227 A71-39833

Whistling atmospherics generation mechanism, showing ionic sound excitation by hydromagnetic wave propagation through magnetospheric rapid plasma concentration change regions
24 p3823 A71-45035

MAGNETOSPHERIC PROTON DENSITY

Periodic drift echoes in magnetospheric energetic proton fluxes from satellite observation
06 p0950 A71-17283

Anomalously low magnetospheric He alpha/proton flux ratio in terms of electrostatic radial diffusion taking into account charge exchange and pitch angle loss processes
06 p0964 A71-17284

Solar flares of 25-27 February 1969 effects on polar cap and interplanetary space flux rates, confirming magnetospheric modulation of proton density peaks
06 p0958 A71-18151

Magnetospheric electrons and protons acceleration and slot injection between radiation belts during magnetic storms, using flux measurements onboard Molniya 1 satellite
20 p3282 A71-39738

MAGNETOSTATIC FIELDS

Energy conversion efficiency from microwave into magnetostatic waves propagation inside cylindrical ferromagnetic substance
08 p1265 A71-21276

Magnetostatic sunspot model with twisted field showing radial dependence of azimuthal component
10 p1666 A71-23789

Cold Hg plasma in composite HF and magnetostatic field near electron cyclotron resonance, obtaining electron and ion energy spectra
10 p1650 A71-24527

MAGNETOSTATICS

Deizner magnetostatic sunspot model enhancement by surface boundary condition derivation for horizontal pressure difference effect of photosphere
05 p0801 A71-15934

Absorption peaks mode numbers and separation using magnetostatic spin waves in axially magnetic YIG rods
07 p1180 A71-20172

Magneto-electrostatic containment ion thruster, considering adaptation for Hg operation based on discharge chamber loss comparison with Cs [AIAA PAPER 71-692]
15 p2470 A71-32288

Ideally conducting magnetostatic equilibria and associated time dependent resistive flows from two dimensional solution for MHD equations
19 p3115 A71-38211

Magnetospheric field model, assuming magnetostatic problem solution facilitated by equation linearity
19 p3059 A71-38395

MAGNETOSTRICTION

Nonlinear magnetoelasticity theory applied to deformation of elastic bodies by magnetic field, considering ferromagnetic membrane deflection and flexible conductor equilibrium
01 p0171 A71-10661

Magnetoelastic anisotropy and low temperature annealing effects on coercive force of ferromagnetic Fe-Ni foils
01 p0138 A71-10669

Magnetostriction in hydrated cesium manganese chloride, examining dimensional changes as function of magnetic field and temperature through antiferromagnetic, spin flopped and paramagnetic phases
11 p1807 A71-25559

Magnetostriction in cobalt and nickel-cobalt ferrites from room temperature to 300 C
15 p2426 A71-31514

Magnetostriction and magnetoelastic quantum oscillations in p-PbTe, using thermodynamic derivatives of Lifshitz-Kosevich expression for oscillatory part of electronic free energy
17 p2791 A71-34860

Papers on ultrasonic transducer materials covering magnetostrictive metals and alloys and piezoelectric crystals and ceramics
20 p3236 A71-39253

Magnetostrictive metals and piezomagnetic ceramics as transducer materials for ultrasonic wave generation, detection and filtration
20 p3236 A71-39254

Longitudinal and transverse magnetostriction of polycrystalline iron garnets containing Gd, Tb, Dy and Ho in high magnetic fields
21 p3428 A71-41116

Micropolar, homogeneous, isotropic and centrosymmetric medium under external mechanical factors and embedded in magnetic field, investigating magnetoelasticity problems
21 p3417 A71-41361

Magnetostriction in antiferromagnetic, spin flopped and paramagnetic phases of hydrated cesium manganese trichloride, studying volume changes and thermal expansion near phase transition
22 p3585 A71-41885

MAGNETOTELLURIC PROFILING

U GEOMAGNETISM

U MAGNETIC SURVEYS

MAGNETOVARIOGRAPHS

U VARIOMETERS

MAGNETRONS

Optimal input stage interaction height in large scale operation of two-stage magnetron amplifier
03 p0385 A71-13791

Computer design of magnetron gun forming electron beam of specific pervance and oscillatory energy in converging magnetic field
03 p0385 A71-13796

Magnetron oscillators frequency and oscillation stability, examining phase mismatch angle, filament current and cathode thermal balance
03 p0386 A71-13805

Computerized statistical simulation of steady state, ergodic, self oscillatory processes in plane magnetron
03 p0386 A71-13811

Modified waveguide magnetrons for continuous 1.3 mm waves, discussing construction and operation
07 p1081 A71-20454

Electron beam shaping by inverted coaxial magnetron gun with steady oscillatory energy exceeding analogous value
09 p1415 A71-22462

Magnetron devices with anode voltage as independent variable, calculating output characteristics based on electron cluster model
09 p1415 A71-22463

High efficiency and power long life cross field amplifier generator for solar energy conversion in space into microwave, discussing magnetron and amplifron
13 p2000 A71-28668

Space charge delay angle, RF induced current and mode instability interrelated for actual high power heavy duty magnetrons, using electron bunch model
14 p2211 A71-29831

Magnetron crossed field amplifier multistage frequency multiplier HF field properties, obtaining numerical solutions for nonlinear governing equations
22 p3522 A71-42315

Magnetron manometer calibration to .001 picotorr for hydrogen, using condensate pump
23 p3674 A71-43273

Spectroscopic analysis of pulsed gas discharge in crossed electric and magnetic fields of gas magnetron diode in 3100-4660 A wavelength range
23 p3712 A71-43933

MAGNETS

NT CRYOGENIC MAGNETS

NT ELECTROMAGNETS

NT HIGH FIELD MAGNETS

NT SUPERCONDUCTING MAGNETS

Permanent magnet optimal size selection from initial operating point on demagnetization curve
05 p0705 A71-17173

Permanent magnet system as nonlinear computer problem, using Newton method and equivalent circuits with lumped parameters
05 p0705 A71-17174

Permanent magnet system design, deriving optimal field configurations and maximum magnetic energy
13 p1999 A71-28637

Driving modes and operation characteristics of reed switches with permanent magnets
13 p2001 A71-28844

Magnetic properties of sintered cobalt-rare earth alloy magnets using Sm, Pr, La or Ce misch metal for microwave device applications
14 p2284 A71-30703

Magnetic properties measurement of Co-rare earth permanent magnets, using Nb-Sn superconducting solenoid
14 p2284 A71-30704

Mo additions to Co rich ductile permanent magnet alloys, obtaining higher coercive forces and energy products
23 p3694 A71-44283

MAGNIFICATION

Beam-combining prism/magnifier eyepiece configuration with miniature CRT for superimposing magnified virtual image upon user visual field
04 p0597 A71-15362

Holographic lens magnification aberrations in various Fourier transform optical data storage geometries
15 p2412 A71-32592

Magnification level for optimum performance at microminiature inspection with binocular microscope, minimizing time
17 p2689 A71-34704

MAGNIFIERS

U MAGNIFICATION

Phonon-magnon absorption bands temperature dependences in Ni, Co and Li ferrimagnetic spinels, giving graphical data for Curie points
04 p0637 A71-15106

Yttrium-iron garnet single crystals angle between variable and constant fields influence on spin wave thresholds
05 p0794 A71-16883

Absorption peaks mode numbers and separation using magnetostatic spin waves in axially magnetic YIG rods
07 p1180 A71-20172

High power magnetically tunable microwave interference filters based on spin waves magnetic field dependent dispersion in ferrimagnetic materials
09 p1421 A71-23721

Ferromagnetic and antiferromagnetic characteristics relation to electromagnet and spin waves coupling in nonresonant and resonant regions
10 p1656 A71-24317

One magnon Raman scattering induced by light magnetic dipole coupling with YIG coherent spin waves
12 p1913 A71-26860

One dimensional acoustic tunnel effect for incident wave normal to barrier analogous to macroscopic spin waves and quantum mechanics
15 p2449 A71-31703

Grain scattering in unstable spin wave region of parametrically excited magnons in polycrystalline YIG
21 p3428 A71-41047

Stress and magnetic field induced spin density wave polarization vectors rotation in Cr single crystals, accounting for Young modulus temperature and magnetic field dependence
24 p3861 A71-45131

MAGNUS EFFECT

MAGNUS EFFECT

- Roll resonance in reentry body motion under non-linear pitch, damping and Magnus moments, using multiple scales method
[AIAA PAPER 71-47] 06 p0979 A71-18508
- Magnus effects on Apache sounding rocket at supersonic speeds, discussing spinning model and static tests
[AIAA PAPER 70-207] 07 p1205 A71-18893
- Magnus or Robins effect on rotating spheres, obtaining lift coefficients from conical pendulum periodic time measurements 15 p2346 A71-31927

MAIN SEQUENCE STARS

- Pre-main sequence stellar evolution - Conference, Liege, Belgium, June-July 1969 01 p0157 A71-10757
- Open cluster NGC 7789 blue stragglers data acquisition from image tube spectrograms and four color and H beta photometry, obtaining location along main sequence 02 p0314 A71-12583
- Internal constitution and kinematics of main sequence stars regarding age, evolution and formation place during hydrogen burning phase 04 p0646 A71-15233
- Hertzsprung-Russell diagram calibration in terms of age and mass for main sequence B and A stars 04 p0646 A71-15234
- Main sequence stars upper mass limit, using linear nonadiabatic analysis for composition dependence and nonlinear hydrodynamic calculations for mass excess 05 p0801 A71-15933
- Normal main sequence B stars, distinguishing features from rapid rotators and supergiants by photometric scheme 05 p0805 A71-16118
- Unstable massive main sequence stars nonlinear pulsation, using small amplitude tests of approximation technique 05 p0806 A71-16202
- G5-K5 stars 3600-4000 A region, determining forbidden Fe/H lines for G8-K3 giants 07 p1201 A71-20436
- Predicted UV fluxes for main sequence stars, comparing stellar observations with models described by Kucz, Carbon and Gingerich 09 p1522 A71-22962
- He I lines in OB spectra, examining main sequence stars 11 p1830 A71-26111
- Open star cluster NGC 6819 photoelectric and photographic data, indicating age, color magnitude diagram and main sequence turnoff 11 p1831 A71-26134
- Mass exchange during main sequence evolution of close binaries with shell hydrogen burning 11 p1832 A71-26185
- Young cluster NGC 2264 main sequence A and F stars four color and H beta observation, suggesting evidence of circumstellar gas shells 12 p1956 A71-26615
- Main sequence stars hydrogen burning stage, examining neutrino emission and nuclear process effects in stellar evolution 16 p2625 A71-33230
- Equivalent width of metallic lines for pole-on main sequence stars, examining effect of rotational axis inclination with respect to line of sight on washout of lines 16 p2633 A71-33334
- Main sequence A and early F stars with shallow convective envelopes, investigating particle diffusion effects on element abundance data 18 p2960 A71-35939
- Three color photometry of star field in Sagittarius cloud, determining interstellar absorption, density and luminosity for main sequence stars 19 p3144 A71-38169
- Massive main sequence stars in rapid differential rotation, investigating structure, energy transport, luminosity and circulation time scale 21 p3444 A71-40241
- Photographic photometry of M67 to 200-inch telescope limit for main sequence star evolution track 21 p3446 A71-40414
- Massive main sequence stars pulsation kinetics, examining amplitude growth, time scale ratios and evolutionary stabilization 22 p3596 A71-41447
- MAINTAINABILITY**
- Meteorological instrument design, emphasizing reliability and maintainability 08 p1293 A71-21734
- Large aperture telescope on-orbit maintainability packaging, examining optical systems replacement tolerances and astronauts EVA mode accessibility 09 p1446 A71-22742
- Failure rate data in reliability analysis, considering material failure phenomena, and maintainability 12 p1909 A71-26665
- FAA aircraft design appraisal for maintainability, considering maintenance concepts and adverse airworthiness situations [SAE PAPER 710431] 13 p2073 A71-28316

- Airline operator evaluation of maintainability, considering costs and investment return 13 p2073 A71-28317
- Civil aircraft antenna design mechanical and environmental aspects and electrical performance, considering serviceability and duplication 14 p2218 A71-31061
- Reliability and maintainability - ASME/SAE/AIAA Conference, Anaheim, California, June 1971 16 p2582 A71-33284
- Reliability and maintainability as concepts in life cycle costs applied to airline operations 16 p2552 A71-33287
- Statistical procedure for maintainability allocation during early system design to meet specified overall goal 16 p2583 A71-33299
- Synthesis method for combining individual part repair time distributions for maintainability prediction using computer 16 p2552 A71-33301
- Producer risk determination and tables for Method 4 maintainability demonstration plan of MIL-STD-471 16 p2583 A71-33303
- Cost distribution theory for various costs of failure, using probability distribution functions for modeling maintainability and reliability 16 p2583 A71-33305
- System effectiveness tasks of producibility analysis, maintainability evaluation and tradeoff studies 16 p2664 A71-33316
- Nuclear power station design for optimal reliability levels, noting maintainability requirements 18 p2928 A71-36807
- F 101 30,000 lb thrust augmented turbofan engine for B-1 bomber, considering maintainability and bird ingestion tolerance 19 p3122 A71-37491
- Optimal design for system reliability and maintainability, using dynamic programming model 21 p3407 A71-40363
- Priority standby redundant system consisting of two repairable units, considering preemptive and non-preemptive repair for system failure 21 p3386 A71-40364

MAINTENANCE

- NT AIRCRAFT MAINTENANCE**
- NT SPACE MAINTENANCE**
- Optimal periodicity of computer systems remedial and preventive maintenance operations based on reliable operation maximum duration 01 p0049 A71-10530
- Single repairable unit system with spares deterioration in storage, calculating long-run availability and time to system failure 02 p0258 A71-12590
- Satellite communications system earth station operation and reliability, discussing staffing, main and supporting communication equipment maintenance, utilities and redundancy 02 p0224 A71-12825
- Military earth communication station maintenance, noting mobility, environment, logistics and reliability 02 p0224 A71-12827
- Large earth station operation and maintenance for international communications, noting control consoles, static tracking, aerial flexibility, transmitter reliability, etc 02 p0224 A71-12828
- Computer simulation for evaluating equipment effect on weapon mission success, considering failure time, repair cycle, operational and maintenance parameters 03 p0431 A71-13090
- Fluid logic automatic control systems troubleshooting, discussing circuit and components design for quick malfunction analysis and repair 07 p1023 A71-19995
- Quality control role in meteorological instruments maintenance 08 p1329 A71-21730
- Soviet book on aircraft ground support and onboard radio equipment operation and reliability increase by redundancy and rational methods, discussing preventive maintenance 10 p1583 A71-24670
- Reliability of redundant repairable systems with preventive maintenance, determining mean time between failures 11 p1769 A71-25660
- Allocation, assessment and demonstration of system mean-time-to-repair in complex multiple failure situations 16 p2583 A71-33300
- Maintenance replacement sequence selection for minimizing equipment repair time, noting dependence on failure rate 16 p2552 A71-33310
- Maintenance aids evaluation for government contracting and decision making, including cost model based on life cycle economics 16 p2552 A71-33311
- Premature scheduled maintenance, providing model for duplication between repair and overhaul/replacement cost 16 p2552 A71-33313

- Computer program for prediction of repair time elements for versatile avionics test 16 p2545 A71-33314

- Electronic equipment maintenance simplification by proceduralized troubleshooting method for malfunction isolation and tests and checks selection and sequencing, noting technician training cost reduction 17 p2689 A71-34702
- Hydraulic system and fluid cleanliness maintenance, discussing contamination sources and prevention techniques including filtration, dehydration and degasification 19 p2999 A71-38319
- Hydraulic fluid filtering and maintenance techniques, discussing component life optimization and adverse environment handling problems 19 p3000 A71-38325
- Reliability controlled maintenance plan for avionics equipment based on mean time between failures 20 p3203 A71-39087
- Independent sideband transmitter checkout and maintenance for maximum communication circuit performance 21 p3353 A71-40519
- Soviet book on automatic control and computer components reliability, explaining redundancy principles and test and repair procedures 22 p3526 A71-41820
- Computerized simulation of maintenance man hour loading for communication system based on repair, failure and availability distributions 22 p3554 A71-42113
- Cost based algorithm for allocating availability parameters/repair times and failure rates/to system components 22 p3566 A71-42115
- Optimal redundancy and availability allocation for MTBF and time to repair in multistage system, using dynamic programming 22 p3518 A71-42116
- Electric circuit component failure prediction and probability distribution in troubleshooting search 23 p3638 A71-42900
- MAJORITY CARRIERS**
- Neutron induced lifetime damage short term annealing dependence on minority carrier density in p-type silicon, considering majority carrier repulsion by positively charged centers 07 p1175 A71-19061
- Highly ordered pressure-annealed pyrolytic graphite majority carrier electrons and holes locations in Brillouin zone from measurements in magnetic fields 08 p1344 A71-21363
- Nonlinear planar transistor model, analyzing majority carrier current flow fields in base due to injection of emitter and collector p-n junctions 12 p1888 A71-27612
- Capacitance and conductivity in metal dielectric semiconductor during majority current carrier population depletion by pulsed voltage, discussing concentration and mobility determination 24 p3859 A71-44376
- MALAYA**
- Oklahoma and Malaysia thunderstorms comparison based on weather reconnaissance aircraft measurements, considering turbulence patches 14 p2266 A71-29752
- MALFUNCTIONS**
- Malfunction probabilities in presence of wideband noise for tunnel diode binary logic element /flip-flop/ pulse triggered into either of two output states 11 p1740 A71-26543
- MAC malfunction detection, analysis and recording system applications in commercial airlines, emphasizing real time response for maintenance function [SAE PAPER 710425] 13 p1995 A71-28311
- Electrical and physical nature of microbial membranes implicated in aircraft fuel quantity probe malfunction [SAE PAPER 710439] 13 p2113 A71-28321
- Economically optimal operation of circuits protecting object subject to stationary random process, determining object malfunction intensity 19 p3025 A71-37572
- MAMMALS**
- NT BATS**
- NT CATS**
- NT CATTLE**
- NT CHIMPANZEES**
- NT DOGS**
- NT GUINEA PIGS**
- NT HAMSTERS**
- NT HUMAN BEINGS**
- NT MICE**
- NT MONKEYS**
- NT PRIMATES**
- NT RABBITS**
- NT RATS**
- NT RODENTS**
- NT SNAKES**
- NT TURTLES**
- Mammal species body temperature during 24 hr periodic light cycle, using statistical data analysis 01 p0020 A71-11570

Bacteria and mammalian cells radiosensitization, using phenylglyoxal and various carbonyl compounds 07 p1034 A71-18944

Age dependent changes in mammalian cells radiosensitivity, emphasizing endogenous nonprotein sulphhydryl effects 07 p1034 A71-18945

Mammalian tolerance to low body temperatures, discussing limits to spontaneous unassisted recovery and recovery assisted with reanimation and resuscitation procedures 07 p1041 A71-19523

Hyperresponsiveness in hibernating mammals, discussing responsiveness increase with body temperature decrease as compensating mechanism for sensitivity loss 07 p1041 A71-19524

Physiological characteristics in llamas pulmonary circulation at sea level and changes after 5 and 10 weeks at 3,420 m above sea level, noting arterial hypertension 08 p1237 A71-20678

Area analysis of pressure-volume hysteresis in mammalian lungs by slowly filling with air and saline 12 p1870 A71-27132

Biosynthesis control of melatonin and other methoxyindoles in mammalian pineal organ 14 p2182 A71-29631

Papers on anatomy and mechanisms of mammalian sensory systems including vision, audition and touch 14 p2183 A71-30251

Mammalian cells cultivation at suboptimal temperatures, considering reproduction and cytophysiological changes 20 p3188 A71-39220

Mammal extraocular muscle fiber structural and functional properties, discussing histological arrangement, fiber type classification and motor nerve endings 22 p3488 A71-42434

MAN

U HUMAN BEINGS

MAN MACHINE SYSTEMS

Flight training by simulator, discussing justification and effectiveness criteria, transfer of learning to real flight situations, information flow models, full mission simulation, etc 01 p0066 A71-10019

Centralized inquiry-response systems for information retrieval, analyzing voice-data communications interaction 01 p0048 A71-10220

Man role in future navigation from SAC viewpoint, considering relationships to mission and machine 01 p0123 A71-10502

Commercial and military aircraft navigator future role, considering increasing task requirement stringency and growing navigational aids availability 01 p0124 A71-10505

Avionics system maximizing pilot chances of surviving mission and destroying selected target by removing mental limitations 01 p0124 A71-10506

Space navigator operations, procedures and computer interface and manually aided onboard Apollo cislunar navigation system possible improvement 01 p0124 A71-10510

Space vehicle onboard navigation and guidance systems capability, considering Apollo transition from direct task interaction and supervision to functional man machine communication 01 p0124 A71-10511

Man machine considerations in all-weather low level navigation system design, noting off-course error reduction by command information display to pilot 01 p0125 A71-10515

Complex navigation systems training philosophy emphasizing functional approach to system and components 01 p0023 A71-10523

Biomedical experiments and man machine relationship on Soyuz 9 record endurance flight 01 p0164 A71-11457

Bioelectric control, man and automatic systems - Conference, Yerevan, U.S.S.R., September 1968 03 p0365 A71-12976

Operator behavior in man/machine system, using multidimensional manual control system model with random sampling time and information theory method 03 p0368 A71-12996

Human behavior during machine control learning, modeling habit development as automatic control system 03 p0368 A71-12997

Human operator thinking and decision making model for man-machine interaction 03 p0368 A71-12999

Aircraft information display simulation and flight tests of experimental display systems, discussing man machine communication systems development [DFVLR-SONDDR-81] 03 p0396 A71-13344

Man-machine graphics, discussing research in mass data reduction, production scheduling, speech synthesis, etc 03 p0372 A71-13500

Spacecraft and aircraft automatic control man machine interface, bionics and traffic control systems 03 p0455 A71-14393

Military helicopter design and weaknesses correction, considering man/machine combat survivability and operational accidents reduction 04 p0534 A71-15447

Computer operators activity analysis, suggesting computer center layout 04 p0547 A71-15847

Human sleep deprivation research, discussing task performance, man machine interaction and work-rest cycles 04 p0540 A71-15848

Aircraft longitudinal control during landing approach, investigating back side operation characteristics by closed loop system analysis regarding pilot and aircraft as elements 05 p0696 A71-16388

Human factors engineering in man machine systems, evaluating biotechnology and aeronautical medicine relationship 05 p0715 A71-16935

Operator reliability control models, discussing rational work-rest schedule for man machine systems 05 p0731 A71-17017

OAO for observations of stars, galaxies, planets and nebulae, discussing ground system and men and data systems integration 05 p0734 A71-17130

Memoscope for communications between operator and machine during biological image studies 06 p0864 A71-18696

Human role in manned observatory/laboratory spacecraft, taking into account sensor payload, on-board analysis equipment and astronaut training 07 p0146 A71-18803

National Airspace System air traffic control automation man machine considerations, noting controller productivity increase, input difficulties and symbology clutter [AIAA PAPER 71-246] 07 p0149 A71-19720

Lunar Module physical characteristics and control system function, emphasizing automated vs manual flight degree and astronaut overriding capability 07 p1208 A71-19915

Human operator psychophysiological characteristics as cybernetic man machine system components, emphasizing human memory activity 07 p1050 A71-20117

Manned aircraft crew long range navigation, discussing sensor, information processing and display systems for future commercial and military missions 07 p1157 A71-20343

Man-machine considerations in all-weather low-altitude navigation system design, discussing computer generation of roll command guidance, visual display and pilot modeling 07 p1157 A71-20344

Human role in Aerospace Defense Command navigation, discussing Airborne Warning And Control System and navigational aspects of ADC mission 07 p1157 A71-20346

Two dimensional adaptive pattern-recognizing model of human operator in visual-manual compensatory tracking task 07 p1053 A71-20406

Earth resources survey remote sensor system with human for spatial and machine for spectral data processing 08 p1257 A71-20691

Interactive computer graphics in cartography, considering on-line updating of digital topographic map file by human decision making 08 p1281 A71-21248

Clustering and decision making with interactive a priori problem knowledge insertion in subcategory mean vectors and covariance matrices form for pattern recognition and learning 08 p1260 A71-21664

Man oriented program system for industrial facilities engineering design with modular structure, operating in time sharing mode 09 p1412 A71-23275

Man machine interactive computer graphics for design molding during evolution by computer with nonlinear programming algorithm 09 p1412 A71-23276

Civil Engineering Systems Laboratory remote terminal interactive time sharing computer facility, discussing consulting engineer design office experiences and computing center management 09 p1412 A71-23277

Aircraft display designs, emphasizing man machine problems 09 p1402 A71-23621

Man-machine interactive scanned-display computer graphics system implemented on Honeywell DDP-224 computer 10 p1581 A71-23967

Man machine systems classification, suggesting machine-only system for decision making 10 p1567 A71-23998

Aerospace research bionics and bioengineering, considering adaptation of man to environment and matching of man and machine 10 p1568 A71-24221

Book on digital computers in engineering covering systems, man machine communication, numerical analysis, network analysis program, circuits, devices, control, etc 10 p1581 A71-24476

Influence sources affecting self organization of man machine systems, discussing human pilot model 10 p1571 A71-24760

Displaced and delayed retinal feedback adaptation theory for human factors problems in man machine systems 10 p1571 A71-24825

Apollo hybrid simulator for man-machine interface in low orbit lunar landmark tracking 11 p1796 A71-25850

User-oriented conversational language computer program for Jet Propulsion Laboratory digital control random excitation environmental test system for spacecraft 11 p1736 A71-26498

Miss/stick oscilloscope techniques in signal and switching relay testing with automated human-interactive time-and-level-measurement machine 13 p2001 A71-28840

Quantitative performance evaluation of man machine systems in stochastic environments, deriving simulation algorithm 13 p2021 A71-29286

SIMCON simulation of physical systems using IBM 360/91 computer illustrated by satellite attitude control application 14 p2207 A71-30022

Man and equipment instrumentation in simulated space environment, considering training and interface of man and life support systems 14 p2188 A71-30312

Nationwide man machine remote employment/personal services system including synchronous communication satellite, information and control network and remote terminals 14 p2199 A71-30914

Controlled aircraft motion under strict kinematic constraints in terms of simple subsystems, noting pilots role in Newmark theory 14 p2177 A71-31024

Man machine system dynamic properties and biomechanical model concepts, determining random vibration effects on sitting and working human body 15 p2366 A71-32728

Human performance reliability data system using taxonomic structure for classifying behavioral studies and predicting man-machine performance 16 p2536 A71-33318

Optimization and operational problems of man powered aircraft, noting Kremer Competition design [AIAA PAPER 71-798] 16 p2525 A71-34023

Soviet book on aircraft automatic control systems covering linear theory, design, autopilot, man machine performance, operation modes, etc 17 p2771 A71-34473

Interactive digital computing systems survey, describing one language AMTRAN system as example 17 p2710 A71-34621

Mathematically oriented digital computer system implemented on IBM 360 with graphic remote consoles for engineering problems 17 p2710 A71-34622

Man-teleoperator-robot teams for space exploration facilities construction and operation, discussing lunar programs [AIAA PAPER 71-823] 17 p2723 A71-34722

Two dimensional adaptive model of human operator control in visual-manual compensatory tracking task using pattern recognition 17 p2691 A71-35046

Information transfer in all-weather aircraft operation, discussing pilot role in overall reliability based on man machine system information process 17 p2693 A71-35209

Automatic electronics design, analyzing visual and graphic devices for initial data preparation, introduction, operator computer interaction and results extraction 18 p2887 A71-35878

Operator-computer communication devices with graphic data display, discussing construction and operation 18 p2884 A71-35879

Weightlessness simulation for orbital man machine experimentation, discussing teterboard and cargo transfer examples [AIAA PAPER 71-850] 18 p2871 A71-36643

Human performance in optical high inertia tracking system interface, considering proprioceptive feedback, display magnification, control dynamics view field and anticipatory processes effects 18 p2873 A71-36912

Ergonomic evaluation of flight crew working conditions from viewpoint of static and dynamic adaptation

of aircraft system design to human psychophysical capabilities

19 p3007 A71-38016

Data display units as man machine interface elements in data processing operations, discussing combined alphanumeric/graphic CRT units

20 p3202 A71-38885

Display devices components in highly interactive man machine systems, noting drawbacks of CRT

20 p3233 A71-39059

Fast time digital computer simulation model for evaluation of man-machine interface /display/ problem of ATC system including personnel and equipment

21 p3412 A71-40112

Display devices in aircraft cockpit providing pilots with information from various sources, considering head-up display and CRT

21 p3376 A71-40113

ATC display device man-computer interaction faults and delays effects on operator performance

21 p3413 A71-40119

Computerized interactive stereographics by treating line identification as primitive, enabling rapid access to stereo pair for speed advantage

21 p3376 A71-40124

Interactive graphical computer system with remote on-line consoles for engineering problem modeling and analysis, giving illustrative examples

22 p3516 A71-41868

Synthesis models and methods for large scale automated control systems with human elements, discussing mathematical models and computerized design

22 p3528 A71-42858

Man machine system dynamic properties and biomechanical model concepts, determining random vibration effects on sitting and working human body

23 p3639 A71-43299

Automatic flight control systems, discussing pilot as systems manager or retained in control loop

24 p3845 A71-44454

MANAGEMENT

NT CONFIGURATION MANAGEMENT

NT CONTRACT MANAGEMENT

NT DATA MANAGEMENT

NT ENGINEERING MANAGEMENT

NT FINANCIAL MANAGEMENT

NT INDUSTRIAL MANAGEMENT

NT INFORMATION MANAGEMENT

NT LOGISTICS MANAGEMENT

NT PERSONNEL MANAGEMENT

NT PROCUREMENT MANAGEMENT

NT PRODUCTION MANAGEMENT

NT RESEARCH MANAGEMENT

NT SAFETY MANAGEMENT

NT WATER MANAGEMENT

Characteristics study of technical entrepreneurs, considering family background, education and motivation

19 p3173 A71-37631

MANAGEMENT ANALYSIS

MACE /management aid to compatibility engineering/, consisting of analysis routines for IBM 7030 and Univac 1108 computers

13 p2032 A71-28871

British civil aircraft airworthiness requirements, discussing aircraft industry management philosophy ensuring quality standards in design, development, production, inspection and product support

18 p2989 A71-36673

Large project management model, presenting schematic diagrams for nature and interrelation of functions

23 p3784 A71-43452

MANAGEMENT INFORMATION SYSTEMS

International HEOS project organization, discussing communication, task delegation, decision making and structure

23 p3785 A71-43455

Management information techniques, discussing project reports, meetings, decision process, work breakdown, planning schedules and computerization

23 p3785 A71-43457

MANAGEMENT METHODS

Power spectrum in project management of matrix organizations involving support personnel cooperation

07 p1225 A71-20014

Defense management efficiency improvement concepts for weapon systems programs, discussing elimination of bureaucracy, communication between organizational levels, mission instead of function orientation, etc

12 p1988 A71-27246

International space exploration management and organization, emphasizing NASA cooperative programs

16 p2665 A71-33587

Payload cost and response time reductions for shuttleborne space experiments, examining NASA Ames airborne research program management technique [AIAA PAPER 71-808]

17 p2813 A71-34731

Program management techniques, discussing organization, planning, systems engineering and personnel selection

23 p3785 A71-43453

Project management methods oversophistication, discussing French space activity and managerial apprenticeship

23 p3785 A71-43454

Space project management techniques under European conditions, covering requirements, style, motivations, concepts and rules

23 p3785 A71-43458

MANAGEMENT PLANNING

NT PRODUCTION PLANNING

NT PROJECT PLANNING

Technical work evaluation in cost-plus contracts for management control

01 p0184 A71-11190

Rational structure selection for scientific research organizations, using systems analysis

02 p0335 A71-11855

Long term planning of technological and scientific development of machine design and construction on national industrial and enterprise levels

02 p0336 A71-11860

Computer aided network analysis for multiple project planning facilitating readjustments and budgeting

02 p0336 A71-12122

Airport planning by management systems approach, considering airspace, taxiways, runways, terminals, parking lots and roadways

03 p0522 A71-12962

Design management, discussing organization, planning and control

03 p0524 A71-13743

Defense and space programs management systems, discussing structured activities planning for efficient resources use

[ASME PAPER 70-WA/MGT-5] 03 p0524 A71-14097

Space shuttle program plans, economics, operational characteristics, contracting and management planning

04 p0689 A71-14929

NASA multiple interagency interfaces, surveying work and resource integration, space programs and agency structure

04 p0690 A71-14937

Cost efficiency, management and economics of airport operation, considering facilities relationship to airline operations

04 p0690 A71-14993

Aerospace contractor management program projected through 1975 in terms of system engineering, configuration and financial management, with Minuteman Missile as example

04 p0691 A71-15291

Aerospace systems project management using graphic networking critical path method for planning and control

04 p0691 A71-15293

Europa 3 experimental preparatory program, discussing hardware development and project management planning and control

05 p0839 A71-15949

Optimal space experiments selection for satellites and space probes, discussing criteria and techniques for guidance in program management decision making

05 p0816 A71-16138

Production startups deviation from increased productivity anticipation patterns, noting management actions minimizing losses

05 p0840 A71-16742

R and D money optimal reallocation due to total research budget decrement, based on computer program

05 p0840 A71-16743

R and D management decision making process structural model, discussing technological forecasting based on organized technical information, quantitized judgments, optimum resource allocation and hybrid technique

05 p0840 A71-16744

Earth resources satellite systems R and D planning, using case study approach in economic benefit analysis for parametric requirements determination

[AIAA PAPER 68-1077] 05 p0840 A71-17050

Complex supply system large quantity data handling and cost savings through optimum planning of storage points and transport using linear separable programming

06 p1010 A71-17746

Quality management planning for 1970s, discussing reliability, maintainability and production quality programs

07 p1225 A71-19558

Uncertainty factors in management decisions and operations optimization in international air transportation industry

10 p1698 A71-24265

Experiment planning in electronic component design and microelectronics, using mathematical theory for optimal strategies

12 p1885 A71-26712

Soviet airlines operations planning, discussing principal objectives, methodology and organizational principles

12 p1988 A71-27144

NASA past and future space programs, examining operations analysis problems associated with space missions planning

13 p2133 A71-28030

Technical, sales/marketing and management - Conference, Coronado, California, May 1971

13 p2091 A71-28164

Processes involved in obtaining materials required for socialist organization operation, discussing operations, cost reduction by work mechanization and optimum data processing

13 p2167 A71-28492

German monograph on game theory and planning techniques for aircraft evaluation

13 p1996 A71-28880

Logistics planning as integral part of phased program planning process, considering preliminary analysis, definition, design, development, fabrication, test and operations phases

13 p2167 A71-28895

Experimental computer-aided system evolution to integrate technology plans and evaluate potential resource allocations for mission-oriented technology programs

14 p2339 A71-29853

Aviation within total transport system, discussing decision making and management planning

14 p2341 A71-30165

Criteria for converting aeronautical project operational targets into actual requirements and technical specifications, emphasizing cost effectiveness

14 p2177 A71-30824

Logistics support planning technique for determining number of spares with prechosen probability level, using asymptotic approximation method

16 p2552 A71-33302

Airline fleet equipment planning, discussing management decision making based on aircraft and ground equipment life cycle costs

16 p2522 A71-33307

Organizing space activities for world needs - Conference, New York, October 1968

16 p2664 A71-33580

Large software systems development management, discussing steps including program design before analysis, documentation, testing, monitoring and cost effectiveness

17 p2709 A71-34618

Large software systems development management, discussing pending disaster early identification, relationship to hardware, integrating contractor and programming tools

17 p2710 A71-34619

Apollo real time control center large software systems development management covering implementation, integration, testing, operation and maintenance

17 p2710 A71-34620

Parallel strategies effectiveness in R and D projects, discussing learning rate as critical parameter in project management decision making process

19 p3173 A71-37629

French monograph on medium term planning process for large basic research laboratory based on information system of functional activities presentations

19 p3174 A71-38548

Computerized reliability optimization system program for electronic equipment design and management methods to achieve high reliability and low cost

22 p3517 A71-42105

Program management techniques, discussing organization, planning, systems engineering and personnel selection

23 p3785 A71-43453

Incentive contract with contractor profit based on achievement in cost, schedule and technical performance

23 p3786 A71-43467

Soviet aircraft industry R and D organizations and management

23 p3786 A71-44189

Strategies and tactics for industrial R and D problems selection and solution for products innovation, noting element of chance

24 p3891 A71-44364

Technology transfer management, distinguishing between active and passive pursuit of technology, catalyst and vertical and horizontal transfer [AIAA PAPER 71-1008]

24 p3891 A71-44593

Pure and pragmatic science in future NASA programs, discussing interagency cooperation, communications, ATC, education, earth resources, space science, meteorology, budgets and program management

[AIAA PAPER 71-1021] 24 p3892 A71-44599

Commercial air transportation industry trends and optimal planning requirements, discussing airline economic viability, industry regulation, public service and environmental compatibility

[AIAA PAPER 71-1022] 24 p3892 A71-44600

MANAGEMENT SYSTEMS

NT MANAGEMENT INFORMATION SYSTEMS

Flight crew training, describing systematic tools, learning elements, managing systems and course organization
[SAE PAPER 710474] 13 p2016 A71-28303

Logistics planning as integral part of phased program planning process, considering preliminary analysis, definition, design, development, fabrication, test and operations phases 13 p2167 A71-28895

Integrated vehicular information management systems consisting of computers, multiprocessors, multiplexers, dedicated subsystem processors, sensors and effectors 17 p2743 A71-35057

MANDELSTAM REPRESENTATION
Stimulated Mandelstam-Brillouin, Rayleigh line wing and thermal light scattering, discussing fine structure, glass fracture and components shift 10 p1621 A71-24837

MANDRELS
Contoured silicone internal pressure bag mandrels for helicopter rotor blades fabrication 10 p1615 A71-24096

Design, fabrication and testing of electrically heated externally configured thermionic diodes with emitter using mandrel side of CVD fluoride tungsten for electrode surface 11 p1715 A71-25911

MANEUVERABILITY
Optimum VTOL aircraft landing maneuverability, using short range three dimensional surveillance system and ground computer 03 p0454 A71-13574

Flight simulator efficiency for optimal vehicle characteristics, considering in-flight, digital and manned techniques involving horizon indication and maneuver applications [DGLR-70-072] 05 p0732 A71-15960

A-7 low altitude tactical fighter spin evaluation program, discussing maneuvering capability, external stores and departure mode 07 p1018 A71-19094

Large variable sweep wing maneuver load relief system with allerons reducing resulting bending moment at pivot 15 p2348 A71-31600

Space flight aerodynamic problems and wind tunnel simulation, considering satellites, maneuverability for landing and synergetic orbit rotation, hypersonic problems of reentry, etc 18 p2846 A71-36408

Double gimbal control moment gyro systems for spacecraft attitude control, providing three axis attitude stabilization, precision pointing control and maneuverability [AIAA PAPER 71-937] 19 p3097 A71-37182

MANEUVERABLE SATELLITES
U MANEUVERABLE SPACECRAFT
U SATELLITES

MANEUVERABLE SPACECRAFT
NT APOLLO SPACECRAFT
NT LIFTING REENTRY VEHICLES

Rotating dumbbell shaped satellites orientation optimization by system of jets, calculating energy losses 16 p2646 A71-33672

Space shuttle attitude control propulsion and orbit maneuver, considering high and low chamber pressure gaseous systems 18 p2973 A71-36456

On-line radar tracking of six orbital elements of thrust maneuvering spacecraft, obtaining discrete non-linear measurement and dynamical equations [AIAA PAPER 71-902] 19 p3095 A71-37153

MANEUVERS
NT EARTH ORBITAL RENDEZVOUS
NT LUNAR ORBITAL RENDEZVOUS
NT ORBITAL RENDEZVOUS
NT SIDESLIP
NT SPACECRAFT DOCKING
NT SPACECRAFT MANEUVERS

Maneuvering vehicles behavior model selection for real time Kalman filter tracking algorithm, based on accuracy predictions and empirical performance 08 p1270 A71-21349

Flight time, path and fuel consumption in climb at constant radius turn, variable or constant velocity and constant engine power, deriving approximate simple formulas 08 p1232 A71-22050

Control parameter optimization of dynamic system for single and series maneuvers 10 p1637 A71-24846

MANGANESE
NT MANGANESE ISOTOPES
High carbon Cr and Mn steels martensitic transformation points, ascertaining short range order occurrence by electron microscopic study 07 p1130 A71-19278

Internal friction from hydrogen dissolved in Ti-Mn alloys, considering solute interstitial atoms caused asymmetrical distortion decrease with increased Mn concentration 10 p1625 A71-24008

Activator Mn impurity effect of carrier redistribution and partial photoionization of photoconductivity spectra of ZnS single crystals 21 p3430 A71-41218

Thermoremanent recording by Curie point writing in thin manganese-bismuth films for magneto-optic mass memories 22 p3587 A71-42473

MANGANESE ALLOYS
Cu-Ni-Mn alloys hardening by heat treatment, describing various critical temperature measurement methods and micrographic analysis 01 p0105 A71-11622

Austenitic steel containing Cr, Cr and Mn, investigating W, Mo, V and Nb effect on structure and mechanical properties 04 p0616 A71-15804

V-Mn-B, Mo-Mn-B and W-Mn-B systems phase equilibria, describing diagrams isothermal sections at specific temperature 09 p1470 A71-23065

Addition effects on ordering kinetics in Ni-Mn based ternary alloys, using Rawar neutronography 12 p1918 A71-27543

Austenite and carbide chromium manganese steel boron distribution obtained by tracing elements 15 p2425 A71-31397

Chemical composition effect of low carbon alloys metallic matrix on abrasive wear resistance, showing austenitic manganese alloys superiority to martensitic or ferritic alloys 16 p2593 A71-33626

Nitrogen alloying effects on relaxation resistance of Cr-Mn austenitic steel 21 p3402 A71-41092

Mo, W and Al alloying additives effects on mechanical properties and wear resistance of austenitic high Mn electrosag melted steel 21 p3403 A71-41106

Mn-Ge solid solutions coercive force and magnetization, investigating temperature dependence and heat treatment effects 21 p3432 A71-41264

Co-Mn binary alloy phase diagram redetermination, noting sigma phase formation after heavy deformation 23 p3689 A71-42933

Mn-Zn ferrite for pulse transformers, discussing permeability and temperature range 23 p3650 A71-43348

Electron microscopic study of antiphase domains size and shape in Ni-Mn alloy after annealing 23 p3692 A71-44009

Strain hardening effect of Ni, Mn and Mo in Cr steel after high temperature annealing 23 p3693 A71-44216

MANGANESE COMPOUNDS
NT MANGANESE OXIDES
NT PERMANGANATES

Magnesium and manganese ferrite ion states under heat treatment using X ray and Mossbauer methods 05 p0793 A71-16832

Laser Curie point writing characteristics and diffraction efficiencies of MnBi thin films for holographic recording 19 p3062 A71-37143

Rhodochrosite /manganese carbonate/ complex refractivity determination for correlation between optical reflection, attenuation and scattering coefficients 20 p3269 A71-39185

MnSe-CdSe mixed crystals growth investigation by elements, binary compounds and solid solutions vapor transport properties 21 p3427 A71-40214

MnAlGe crystal domain structure observed for behavior with smaller crystal dimensions and changes in applied magnetic field orientation and strength 23 p3717 A71-43949

MANGANESE IONS
Manganese, iron and vanadium ion ordering in orthorhombic zoisite structure by electron paramagnetic resonance technique 07 p1053 A71-18741

MANGANESE ISOTOPES
Mn 53 age measurement of galactic cosmic rays 05 p0797 A71-15930

Solar protons contribution to spallogenic Mn 53 production in Apollo 12 lunar rock and soil from neutron activation analysis 23 p3755 A71-43734

MANGANESE OXIDES
Manganese dioxide depolarizer for biomedical electrodes, discussing electrochemical and toxicological characteristics 01 p0021 A71-10239

MnO oxidation reduction kinetics measurement in carbon monoxide/dioxide atmospheres by gravimetry and electrical conductivity 08 p1318 A71-20698

MANGANESE 53
U MANGANESE ISOTOPES
MANGANESE 54
U MANGANESE ISOTOPES
MANGANESE 56
U MANGANESE ISOTOPES

MANIFOLDS
Trojan periodic orbits interpretation to establish manifolds evolution for mass ratio variations 04 p0652 A71-15702

MANIFOLDS [MATHEMATICS]
Commutative nilpotent semigroups, discussing necessary and sufficient conditions for freedom within manifolds 02 p0276 A71-11725

Flows on 3-manifolds near isolated invariant sets 04 p0620 A71-15727

Neron-Tate height fine structure of points on Abelian manifolds, considering canonical bounded and diophantine problems 06 p0917 A71-17571

Closed invariant sets of smooth flow on compact manifold involving homoclinic or heteroclinic point theory of Poincare 06 p0918 A71-17640

Dynamic systems toroidal manifolds disturbance, discussing invariant torus preservation 08 p1336 A71-22017

Variational and boundary value problems in regular regions containing manifolds with dimensionalities lower than n minus one 09 p1485 A71-22289

Boiling of relativistic heat conducting fluid in normal space-time manifold for nonstrict hyperbolic system, using Eckart scheme 10 p1694 A71-23831

Natural symplectic structure for twistors on cotangent bundle over space-time manifold, considering Lagrange identity for Jacobi fields 16 p2609 A71-33264

Einstein equations solution as hypersurface of four dimensions in Euclidean space, investigating imbedded manifold deformations 16 p2610 A71-33272

Differential equations optimization method based on auxiliary functional and minimization at simple structure manifold 17 p2765 A71-34849

Perturbation theory of invariant manifolds of dynamic systems based on Green function, deriving new existence theorems 17 p2781 A71-34930

Bounded integral manifolds existence for perturbed system of nonlinear differential equations near critical point, periodic orbit or periodic surface 17 p2769 A71-35795

Excising neighborhood of singularity from manifold with vector field definition, making possible regularization of two and three body problems 20 p3254 A71-38900

MANIPULATION
U MANIPULATORS
MANIPULATORS

On-orbit payload handling for space shuttles, including manipulator arms for drawing docking vehicles together, closed circuit TV and airlocking [AIAA PAPER 71-811] 17 p2814 A71-35427

MANNED ORBITAL LABORATORIES
NT MANNED ORBITAL RESEARCH LABORATORIES

Human role in manned observatory/laboratory spacecraft, taking into account sensor payload, on-board analysis equipment and astronaut training 07 p1046 A71-18803

SkyLab as orbital factory, worksite and observatory for experiments in science, technology, materials science and manufacturing 15 p2500 A71-31460

SkyLab manned earth orbital artificial gravity experiment, describing mission objectives and requirements [AIAA PAPER 71-861] 18 p2975 A71-36649

Space station biological/medical laboratories, discussing physiology, pathology, hematological, static and dynamic equilibrium, neuropsychic, dietetic, radiobiological, hygiene and prophylaxis departments 19 p3006 A71-37308

Manned orbital operations economy for space station utilization, discussing laboratory equipment, on-orbit supervision, maintenance and remote communications limitations [MDAC-WD-1746] 22 p3611 A71-42030

MANNED ORBITAL RESEARCH LABORATORIES
Manned space station research capabilities in earth orbital environment for agravic force field, hard vacuum, cosmic radiation and spatial disposition [SAE PAPER 700758] 02 p0237 A71-11685

SkyLab workshop as orbital manned platform for scientific investigation, discussing system design details and technical evaluation 10 p1682 A71-24276

General purpose manned space laboratory concept for multidisciplinary long term shuttle supported research investigations [AIAA PAPER 71-814] 17 p2812 A71-34727

Manned orbital research modules design for atmospheric physics, weather and earth resources observations and stellar astronomy [AIAA PAPER 71-815] 17 p2814 A71-35426

Skylab manned scientific space laboratory for medical, solar astronomy, earth resources, technology and engineering experiments 22 p3608 A71-41950

MANNED ORBITAL SPACE STATIONS

U ORBITAL SPACE STATIONS

MANNED ORBITAL TELESCOPES

NT APOLLO TELESCOPE MOUNT

ATM for manned solar observation, discussing thermal design, thermal vacuum test philosophy, mathematical models and analytical and test data correlation [AIAA PAPER 71-433] 11 p1838 A71-26222

MANNED SPACE FLIGHT

NT APOLLO FLIGHTS

NT APOLLO 7 FLIGHT

NT APOLLO 8 FLIGHT

NT APOLLO 9 FLIGHT

NT APOLLO 11 FLIGHT

NT APOLLO 12 FLIGHT

NT APOLLO 13 FLIGHT

NT APOLLO 14 FLIGHT

NT APOLLO 15 FLIGHT

NT GEMINI 4 FLIGHT

NT GEMINI 10 FLIGHT

Star charts as orientation and navigation aids in manned space flight 01 p0125 A71-10517

Medical support of extended manned space missions, considering functional disturbances, diseases, drug reactivity and timing of in-flight aid 01 p0024 A71-11133

Ground based biomedical supervision of crew members during extended space missions, discussing data acquisition and transmission, astronaut medical competence, etc 01 p0027 A71-11451

Biomedical experiments and man machine relationship on Soyuz 9 record endurance flight 01 p0164 A71-11457

Frequency spectra and cosinor for circadian rhythms in rodents and in man during Gemini and Vostok flights, considering future biosatellites 01 p0020 A71-11569

Space station crew operations, discussing vehicle and research duties, habitability, etc 02 p0203 A71-11976

Manned space flight escape systems evolution, examining requirements and devices from X-15 to Apollo program 02 p0320 A71-11977

Skylab design and mission objectives, describing attitude control, MDA, quarters, Apollo telescope mount and proposed experiments 02 p0321 A71-12738

Soyuz 9 scientific and technical experiments during prolonged orbital flight, discussing day and night horizon 03 p0495 A71-14391

Soyuz 9 prolonged space flight biomedical effects on human organism, emphasizing weightlessness 03 p0365 A71-14392

Vestibular problems in long manned space flight, discussing weightlessness and rotating environment for artificial gravity 04 p0541 A71-14753

Manned artificial satellites, discussing problems of orbiting and interplanetary space stations with reference to U.S./U.S.S.R. future projects 05 p0816 A71-16195

Manned space flight missions in next decade, discussing potential payloads and compatibility to proposed mission structure [AIAA PAPER 71-69] 06 p0977 A71-18527

Common module series for NASA candidate experiment program for manned space stations in 1975-1985 era, discussing configuration and subsystem design [AIAA PAPER 71-70] 06 p0980 A71-18528

Soviet book on manned space flight covering spacecraft design, life support systems, mission characteristics, medical considerations, etc 06 p0864 A71-18700

Scientist-astronauts work in manned space flight program support/backpack crews and Skylab missions scientific/medical experiments 07 p1046 A71-19089

Manned space flight data processing system data storage, describing data base structure, direct access display and batch processing [AIAA PAPER 71-237] 07 p1068 A71-19713

Star maps for recognition and attitude orientation aids as function of stereographic display realism in manned space flight 07 p1157 A71-20348

Medical flight information on astronauts response to space flight environment in confined and unconfined state and during intra- and extravehicular activities 08 p1246 A71-20731

Soyuz 9 flight manned biomedical mission, evaluating 18 day exposure effect on human physiology and work capacity 08 p1246 A71-20820

Recreational preferences among potential space crews from questionnaire analysis 08 p1248 A71-21231

Acceptable gamma radiation dosages for extended manned space flights based on prolonged irradiation of dogs 09 p1388 A71-22193

German book on space medicine covering stresses on human organism during ascent into space, weightlessness and radiation effects, spacecraft environment, nutritional problems, etc 10 p1558 A71-23753

Computer methods for automatic diagnosis program applied to future manned space vehicles, discussing cost relationship to fault isolation techniques and component reliability 13 p2044 A71-27940

Manned mars exploration, discussing excursion module, surface rover and base construction 13 p2143 A71-29251

Manned planetary precursor missions size, cost and operational characteristics, discussing effects of transportation system for projection 14 p2319 A71-30247

Manned space projects U.S./European cooperation, discussing economic and population factors involved in international space cooperation programs 14 p2341 A71-30261

Microbiological respirometer for oxidative metabolism for plants and small animals, considering manned space flight applications 14 p2189 A71-30344

Human energy requirements in weightless environments, correlating metabolic data from Gemini and Apollo missions with food consumption and energy balance measurements 16 p2532 A71-33778

Tektite II program of underwater research as future manned space flight operations model, discussing mission structure, crew selection and communications [AIAA PAPER 71-828] 17 p2690 A71-34718

Reverse osmosis application to wash water recovery in manned space mission life support systems, emphasizing membranes development 18 p2864 A71-36368

Automated self sterilizing breadboard unit for potable water reclamation from urine by electrolysis-electrodialysis for long term space missions [ASME PAPER 71-AV-11] 18 p2866 A71-36378

Water vapor electrolysis for oxygen generation and humidity control in long term manned space flight [ASME PAPER 71-AV-24] 18 p2868 A71-36391

Long term spaceflight crew personal hygiene, discussing human waste processing and/or utilization, microbiological control and medical infirmary-dispensary-laboratory requirements [AIAA PAPER 71-878] 18 p2870 A71-36631

Manned earth-orbital missions performance assessment experiments, studying effects of artificial and zero gravity spacecraft environments on humans [AIAA PAPER 71-891] 18 p2857 A71-36641

Unmanned spacecraft pursuit of evading manned vehicle by game theory, assuming full information availability to both players 19 p3038 A71-38014

Electrical or electromagnetic acceleration of ionized gas to obtain high velocity rocket exhaust for deep space manned flight 19 p3123 A71-38249

Nuclear safety considerations for ground checkout, launch and in-orbit operations of reactors for earth orbital manned space stations 20 p3262 A71-38920

Safe disposal for nuclear zirconium hydride reactors for manned space base mission 20 p3263 A71-38921

Continuous solar UV and X rays monitoring by SOLRAD 10 satellite, investigating solar activity and flares effect on shortwave communications and manned space travel 20 p3294 A71-39580

Experiences of living on moon, discussing effects on task performance and physical movements and observations of lunar surface, lighting and color 20 p3295 A71-39614

Active biological immunity development in long term space flights, discussing natural and nonspecific resistance to viruses and recurrent infections 21 p3332 A71-40552

Human microbial flora and immunologic response in long term space missions, describing environmental parameters and factors and work-rest schedules effects 21 p3332 A71-40553

Human body immune status normalization in prolonged space flight, investigating ribonucleic acid stimulated antibody formation 21 p3332 A71-40554

Prolonged manned space flight infectious disease hazards, discussing confinement, zero gravity, high oxygen content, personal hygiene, waste disposal and preflight immune status 21 p3333 A71-40561

Decontaminating methods for water regenerated from urine under space flight conditions by filtering water condensate through sorbents 22 p3506 A71-42815

Balanced space programs for 1970s and beyond, discussing unmanned planetary missions, manned Apollo, Skylab and space shuttle projects, private, foreign and international programs [AIAA PAPER 71-1020] 24 p3892 A71-44598

MANNED SPACE FLIGHT NETWORK

Unified S band communication system for manned space flight network ground stations 01 p0035 A71-10916

Manned space flight network telemetry system modification for Skylab, ERTS and Apollo 1 missions, giving data flow diagrams and equipment electrical characteristics 01 p0035 A71-10917

Computerized interactive scheduling system for modeling, optimization and priority requirements for NASA manned space flight network 10 p1581 A71-24297

MANNED SPACECRAFT

NT APOLLO SPACECRAFT

NT LUNAR MODULE

NT MANNED ORBITAL LABORATORIES

NT MANNED ORBITAL RESEARCH LABORATORIES

NT ORBITAL SPACE STATIONS

NT ORBITAL WORKSHOPS

NT SOYUZ SPACECRAFT

NT SPACE SHUTTLES

NT SPACE STATIONS

NT VOSTOK 2 SPACECRAFT

Soyuz 9 scientific and technical experiments during prolonged orbital flight, discussing day and night horizon 03 p0495 A71-14391

Lifting body flight test program applications in manned space shuttle 04 p0661 A71-14819

Manned space vehicle unsteady aerodynamics, considering flow separation, vortex interference, shock and stall flutter problems in space shuttle design 04 p0526 A71-15337

Thermonuclear microbombs for manned spacecraft propulsion to solar system boundary, describing system design and performance 04 p0625 A71-15647

Human role in manned observatory/laboratory spacecraft, taking into account sensor payload, on-board analysis equipment and astronaut training 07 p1046 A71-18803

Spacecraft cabin atmospheres, discussing controlled atmosphere composition, barometric pressure, physiological effects, trace constituents, fire hazards, etc 08 p1245 A71-20729

Space based reusable manned/unmanned tug, discussing potential missions, system requirements and auxiliary hydrogen oxygen propulsion system [AIAA PAPER 70-719] 09 p1511 A71-22902

Manned spacecraft maintenance simulation model, applying complex systems operational availability assessments 12 p1894 A71-26689

Photometric analysis of manned spacecraft twilight brightness photographs for spherical atmosphere in single scattering approximation 12 p1901 A71-27103

Materials selection for manned spacecraft, discussing environmental interactions between man, materials and atmosphere 16 p2601 A71-33874

Long mission duration manned spacecraft contaminant control system design, discussing catalytic, oxidation, chemisorption and charcoal adsorption removal techniques and computerized performance prediction [ASME PAPER 71-AV-19] 18 p2867 A71-36386

Critical solar cell battery power system design parameters and performance characteristics affecting post 1977 satellites and manned vehicles design 20 p3179 A71-38902

NiCd battery and third electrode characteristics for different charge and discharge rates, considering end-of-charge control system optimized for satellites and manned spacecraft applications 20 p3179 A71-38904

Manned spacecraft life support system dehydrated food ration effects on human organisms health, metabolism and immunoreactivity during long space flight 22 p3507 A71-42823

Manned spacecraft hazard from charged particles radiation during solar flares and trapped particles by geomagnetic field, recommending protection methods 24 p3865 A71-44887

Cosmic ray dosimetric monitoring in manned spacecraft, discussing ionization, thermoluminescent and nuclear photoemulsion methods of radiation measurement 24 p3826 A71-44888

Manned spacecraft radiation protection against cosmic rays, considering proton attenuation in shielding materials and dose formation in body tissues 24 p3801 A71-44889

MANOMETERS

- Manometric apparatus determining solubility of inert gases in water, blood and other liquids, establishing partition coefficients of ethyl ether 06 p0862 A71-18390
- Manometric equipment arrangement in nose cone of oriented satellite with aerodynamic system stabilization 08 p1287 A71-21022
- Manometric equipment arrangement in nose cone of oriented satellite with aerodynamic system stabilization 20 p3240 A71-39602
- Lower thermosphere vertical temperature distribution measurements, using ionization and heat manometers 20 p3222 A71-39702
- Magnetron manometer calibration to .001 picotorr for hydrogen, using condensate pump 23 p3674 A71-43273

MANPOWER

- NT SCIENTISTS
- Engineers time and intellectual utilization in industry dependence on local company attitudes, suggesting better management appreciation of motivation factor [ASME PAPER 70-WA/MGT-12] 07 p1225 A71-19501

MANTLE [EARTH STRUCTURE]

U EARTH MANTLE

MANUAL CONTROL

- Spacecraft navigation, guidance and control for manual rendezvous with orbiting target, examining error sources perturbing effects 01 p0022 A71-10513
- Human foot-balancing reflex as basis for hands-free EVA control system [RE-352J] 01 p0068 A71-11306
- Manual tracking systems identification and real time display, developing software system 01 p0027 A71-11437
- Aircraft manual flight control analysis using continuous mathematical pilot model for closed loop digital simulation 02 p0188 A71-11787
- Human operator adaptive response characteristics to step changes in compensatory tracking system dynamics 02 p0207 A71-12349
- Operator behavior in man/machine system, using multidimensional manual control system model with random sampling time and information theory method 03 p0368 A71-12996
- Human motor skills acquisition during manual control problem solving, modeling operator as single channel data processing system 03 p0368 A71-12998
- Stepped wideband radio signal power generator with manually controlled signal attenuator 06 p0876 A71-18078
- Helicopter automatic and manual low visibility landing systems evaluation by hybrid computer simulation 06 p0880 A71-18423
- F-104D aircraft side stick control system design and function, curriculum maneuvers and component reliability 07 p1018 A71-19092
- Lunar Module physical characteristics and control system function, emphasizing automated vs manual flight degree and astronaut overriding capability 07 p1208 A71-19915
- Two dimensional adaptive pattern-recognizing model of human operator in visual-manual compensatory tracking task 07 p1053 A71-20406
- Manual vs automatic contouring, comparing accuracy and economy 08 p1281 A71-21256
- Manual onboard orbit determination assuming electronic equipment failure, discussing geometric in-plane orbital parameters and safe orbit check [AIAA PAPER 70-159] 09 p1521 A71-22910
- Two dimensional adaptive model of human operator control in visual-manual compensatory tracking task using pattern recognition 17 p2691 A71-35046
- Foot operation of pedals, investigating speed and accuracy of lower leg motion in different directions 18 p2873 A71-36972
- Spacecraft manual control investigation, using human operator models described by linear transfer function with variable coefficients 20 p3193 A71-39226
- Integrated system for aircraft control and operation with visualization and manual regulation techniques, emphasizing interconnections with onboard electronic equipment 24 p3791 A71-44353

MANUFACTURING

- Stapleblock fabrication method for low mass, high strength ferrite core memory storage blocks in space travel applications 02 p0232 A71-12071

Service life and manufacturing yield of Apollo 25-IRIG/inertial reference integrating gyroscope/ ball bearing 02 p0252 A71-12458

Cryogenic tanks manufacture from Al alloys 07 p1118 A71-19801

High strength and modulus continuous carbon fibers, discussing preparation and quality control [PLASTICS INST. PAPER 5] 08 p1297 A71-20925

Zinc electrodes manufacturing processes, describing materials used in electrodeposition and pressed powder methods, quality control procedures and Zn-Ag batteries electrical characteristics 08 p1297 A71-21088

Refractory metals forming, coating, machining and joining operations, discussing parts manufacture 08 p1299 A71-21683

Reliability assurance in product manufacturing, discussing specific tasks during design, preproduction and production phases 12 p1910 A71-26672

Buckling load scatter reduction in axially compressed thin walled circular shells as function of manufacturing accuracy [DFVLR-SONDDR-92] 12 p1974 A71-26869

Acoustic emission application to nondestructive testing of materials, manufacturing processes and structural components failures 13 p2073 A71-27939

Ultrasonic vibration energy surface and volume effects, obtaining static forces reduction, processing rate increases, technique shortening and surface finish improvement in manufacturing processes 13 p2075 A71-28949

Carbon/carbon composites, describing manufacturing techniques for fiber reinforced matrix structures 14 p2261 A71-29640

Failure mechanisms and manufacturing improvement of sealed nickel cadmium batteries 14 p2181 A71-29701

Complex structural aircraft components manufacture, using group technology principle based on subdivision of parts classes 14 p2252 A71-30267

Preliminary circuit-stage alignment procedures in multistable triggers manufacture with counter input based on tunnel diodes and transistors 14 p2213 A71-30632

Gas laser construction and processing techniques, considering operating temperature, cathode processing, bore design and Brewster window material 14 p2255 A71-30706

Radome design and production, considering construction, materials, shape, manufacturing techniques and technological problems 14 p2218 A71-31067

Ni-base alloys machining, discussing special tools and manufacturing methods with special reference to machinability of Inconel 718, Rene 41 and 95 [SME PAPER MR-71-825] 15 p2416 A71-32427

Aircraft manufacturing techniques, discussing structural components fabrication, economics, lightweight, high strength and heat resistance [SME PAPER MR-71-725] 15 p2417 A71-32436

Manufacturing processes in orbital workshop, considering metal and optical lenses casting crystal growth and gravity lack effects 16 p2606 A71-32856

Safety engineers integration into overall system through basic development programs, involving management, manufacturing, testing and integrated logistic support 16 p2664 A71-33309

Semifinished product production technology influence on heat resistant alloys mechanical properties, considering forging, rolling, casting, melting, diffusion welding and powder metallurgy 18 p2937 A71-36725

Spherical indium crystal manufacture in space, suspending and positioning weightless containerless melt in air and vacuum by adhesion and cohesion for crystal growth 20 p3247 A71-38767

Economical alternative construction materials selection for partmaking cost reduction while maintaining quality 20 p3251 A71-39338

Automated electrical wire harness manufacturing for Boeing 747 aircraft, discussing development of numerical control program 21 p3386 A71-40441

Laser development and applications in telephone communications, manufacturing and holographic memory 21 p3393 A71-40877

Single channel electron multiplier manufacture and performances, discussing test equipment and procedures 24 p3811 A71-45331

MANY BODY PROBLEM

- Quasi-stationary spherical various mass star system, applying ergodic theory in stellar dynamics 01 p0150 A71-10058

Gravitating particle system phase density, finding differential and integral equations for Fourier transform 01 p0150 A71-10064

N-body problem real singularities in celestial mechanics, considering present status and holomorphic motion 01 p0154 A71-10384

Celestial mechanics, Volume 1, Dynamical principles and transformation theory covering quasi-periodic motions, many body problems, Lie groups, etc 02 p0316 A71-12774

Newtonian gravitational system of n mass particles, noting solutions by deterministic approach analysis and Poincare theory 04 p0652 A71-15707

Collision periodic orbit sets in restricted n body problem for various mass ratios 04 p0654 A71-15715

Photo-Neptune system implications for solar system evolution theories, discussing deterministic and statistical models and n body problem approaches 04 p0655 A71-15726

Hill lunar solution of n planet problem in rectangular heliocentric coordinates 04 p0656 A71-15733

Space-time and time correlation functions for classical many body system, proving Chapman-Enskog equivalence to correlation function methods 05 p0786 A71-16864

Gravitational n-body calculation in discrete phase space using game model and finite difference scheme 06 p0927 A71-17555

Celestial mechanics n body equations simultaneous integration, using Taylor-Steffensen numerical method 09 p1525 A71-23335

N body system variables evolution, discussing complete scattering based on mean quadratic and harmonic distances 10 p1642 A71-24432

Newtonian gravitational system n body problem in finite time approach, obtaining spatial distribution of star clusters 11 p1819 A71-25208

Stellar cluster evolution equations in terms of free particle physics based on Boltzmann equation, describing computerized integrations 12 p1960 A71-26785

Gravity decrease effects on planetary orbits, considering two bodies in circular and elliptical orbits and many bodies solar system with interaction between planets 16 p2631 A71-33167

Celestial body mass determination in many body problem, using Kalman-Bucy filtering for Taylor series approximation linearized problem 18 p2960 A71-35935

Electron-electron correlation effects in photoabsorption induced double electron ejection process, using many body perturbation theory 22 p3577 A71-41628

Periodic solutions to Hamiltonian systems with convex potential, considering application to n-body problem 22 p3568 A71-42694

N-body integrated reference trajectories and navigation requirements for extended Venus/Mercury 1973 mission midcourse correction [AAS PAPER 71-362] 23 p3729 A71-43032

Fast spacecraft trajectory computation in n-body inverse square force field, developing closed form recurrence formula for onboard computers [AAS PAPER 71-382] 23 p3731 A71-43052

MANY PARTICLE THEORY

U MANY BODY PROBLEM

MAP MATCHING GUIDANCE

High aperture wide angle lens design for compact electro-optical systems of airborne moving map projection navigational instruments 18 p2947 A71-36605

Avionics combined display system for area navigation, discussing design, color map projection, overlays, CRT unit and viewability 21 p3413 A71-40137

MAPPING

NT ICE MAPPING

NT ORTHOPHOTOGRAPHY

NT SOIL MAPPING

Conjugate mirror point locations for world geomagnetic contour maps, noting use for particle tracing 01 p0077 A71-11516

Pseudoazimuthal, polycylindrical pseudocylindrical secant and tangential, isoparametric nonorthogonal cartographic projections 03 p0418 A71-14351

Admittance first derivative interpretation in flux sounding by electromagnetic field stabilization 04 p0581 A71-15068

Thunderstorms anvil cloud high level outflow mapping by Doppler radar at various heights and elevation angles 05 p0721 A71-16669

Mars Mercator projection photomap, using Mariner 6 and 7 spacecraft TV images

06 p0965 A71-17629

Stereo-orthophoto mapping system design and operation

06 p0901 A71-18289

Automatic cartography, describing data conversion, EDP and instrumentation

06 p0895 A71-18291

Automatic cartography, using plotting machine digital output via attached shaft encoders

06 p0895 A71-18292

Mapping by position data extraction from airborne high resolution side-looking radar

06 p0869 A71-18295

Normalized hodographic mapping for constrained trajectory families, discussing mapping concepts, information content and applications [AIAA PAPER 69-924]

07 p1199 A71-19884

Weather radar plan position indicator automatic film reading for digital mapping of rainfall intensity, discussing raindrop sizing

08 p1286 A71-20690

Computer plotting of living units, business and industrial plant location for public utilities planning

08 p1280 A71-21246

Map preparation techniques and cartographic design for cost reduction and production speeding

08 p1280 A71-21247

Interactive computer graphics in cartography, considering on-line updating of digital topographic map file by human decision making

08 p1281 A71-21248

Integrated data processing of stereotriangulation system providing automatic map plotting

08 p1281 A71-21249

Department of Defense data processing equipment for all weather airborne terrain imaging radar mapping sensor

08 p1288 A71-21250

Manual vs automatic contouring, comparing accuracy and economy

08 p1281 A71-21256

Standard printing color identification system for DOD mapping, charting and geodesy services standardization

08 p1281 A71-21259

Automatic adaptive pattern recognition in photomapping

08 p1259 A71-21438

Expansive mappings as generalizations of expansive homeomorphisms, proving nonexistence of expansive functions on open unit interval

09 p1485 A71-22587

Ground wave propagation over nonuniform overburden with arbitrarily varying complex dielectric coefficient and depth, discussing application to water table mapping

09 p1436 A71-22644

Side-looking radar, thermal IR scanner and passive microwave radiometers for remote sensors for geologic mapping

09 p1452 A71-23215

Cartographic characteristics and applications of airborne radar sensors, stressing synthetic aperture radar and electronic techniques and equipment

09 p1452 A71-23219

Chromosome mapping of *Pasteurella pseudotuberculosis* by interrupted mating, indicating chromosome transfer in more than one linkage group

09 p1396 A71-23474

Polar cap lower ionosphere mapping by solar and magnetospheric charged particles, considering disturbances in polar regions

10 p1661 A71-24312

Mars surface maps from visual and photographic observations for TV picture interpretation of Mariner orbital flights

11 p1834 A71-26432

Recursion formulas for mapping entire earth ellipsoid on plane in single zone of Gauss-Kruger projection

12 p1900 A71-26970

Flight tests of inertial navigation system in aerial geodetic mapping, achieving automatic side-lap, verticality and line position control

12 p1927 A71-27256

Satellite scale imagery potential for land-use mapping, using photomosaic simulation at 1/400000 scale

13 p2064 A71-29395

Land use classification schemes selection with orbital imagery for U.S. thematic mapping

13 p2064 A71-29397

ATC radar display systems mapping techniques using vectors and optical projections

14 p2271 A71-30014

Geophysical map preparation by automatic procedure using polynomial representation of fields in iteration process

16 p2563 A71-33460

Meteorological uses of stereographic horizon map projection, permitting placement of map center at any point on earth

16 p2564 A71-33538

Sikhote-Alin 1967 meteoritic expedition, discussing collected fragments and soil samples, crater and hole structures and mapped sites

17 p2809 A71-35715

Jet streams simulation method by electrohydrodynamic analog, using principle of mapping free lines of flow

19 p3043 A71-37542

Function classes of n-dimensional nonlinear mappings generalizing matrices, including convergence for Jacobi and Gauss-Seidel process

19 p3088 A71-38311

F-bounded erasing operator in abstract family of language for mapping, applying to families defined by tape-bounded Turing acceptors

20 p3201 A71-38846

Noise equivalent irradiance evaluation of passive IR scanners for target thermal mapping systems operating in earth atmosphere, determining figure of merit

22 p3545 A71-42150

IR linescan technique for airborne terrain mapping, discussing choice of waveband, system parameters and display techniques with emphasis on film recording

22 p3546 A71-42425

Mars surface cartography and orbit determination using TV data from Mars orbiting spacecraft

23 p3730 A71-43043

Isodensity mapping with digital computer symbol selection and cathode ray X-Y plotter, showing photographic image display and enhancement of density or height information

24 p3826 A71-44787

MAPS

NT ASTRONOMICAL MAPS

NT LUNAR MAPS

NT METEOROLOGICAL CHARTS

NT RADAR MAPS

NT RELIEF MAPS

Geomagnetic field intensity maps of vertical, horizontal, northern and eastern components of geomagnetic field and of magnetic inclination for 1965

11 p1757 A71-25779

Classification changes in IQSY Auroral Atlas, considering symbolism, synoptic map plotting and data reduction

15 p2396 A71-31608

Global geomagnetic field intensity maps of vertical, horizontal, northern and eastern components of geomagnetic field and of magnetic inclination for 1965

22 p3532 A71-41547

MARAGING

Fe-Ni-Mo alloys maraging process kinetics at various temperatures, measuring hardness, electrical resistance and lattice constants

02 p0266 A71-12653

Potentiokinetic study of anodic polarization in maraging Fe alloys, considering relationship to structural transformations during tempering

05 p0765 A71-16200

MARAGING STEELS

High strength and plasticity maraging steels of Fe-Ni-Co-Mo system, noting surface crack sensitivity in tension

01 p0103 A71-11071

Maraging steel welded plates edge displacements under linear multiflame burner heating, determining temporal deformations by heat distribution from additional source

01 p0088 A71-11098

Ni maraging steel weldments stress corrosion cracking characteristics in air and pentaborane by electron microscopy

02 p0262 A71-11707

Ni maraging steel cantilever beams intergranular stress corrosion cracking in aqueous solutions, noting heat treatment effects

02 p0267 A71-12881

Ni maraging steels weld heat-affected zone, showing liquid grain boundary film formation due to titanium sulfide inclusions constitutional liquation

04 p0603 A71-14921

Ti-Al and Al alloys and Ni maraging steel creep behavior during high stress, elevated temperatures and rapid heating

04 p0617 A71-15909

Maraging steel weldability, examining crack origin and fracture toughness

05 p0770 A71-17246

Maraging steels precipitation hardening due to alloying with Si, obtaining improved strength with satisfactory plasticity

08 p1305 A71-21026

Maraging steels thermal embrittlement, discussing austenite grain boundaries inclusions, carbide networks precipitation and carbon concentration

08 p1305 A71-21027

High strength high Ni maraging steels crystal structures, alloying elements effects on mechanical properties, applications, etc

08 p1305 A71-21028

High strength and plasticity maraging steels of Fe-Ni-Co-Mo system, noting surface crack sensitivity in tension

08 p1305 A71-21036

Ni maraging steel fatigue properties in relation to Ti and Al content

08 p1312 A71-21553

Maraging steel structural analysis under heat treatment, noting age hardening time and temperature

11 p1778 A71-25855

High temperature tensile strength, creep rupture behavior and high temperature exposure effects on subsequent room temperature properties of maraging steel plates and welds

12 p1918 A71-27314

Welding of maraging steels, discussing metallurgical aspects of weldments and advantages/disadvantages of various techniques

12 p1918 A71-27465

Tensile strength and plasticity of hot rolled maraging steel at low temperatures

13 p2082 A71-27869

Mechanical properties, hardness and dislocation structure of Ti bearing maraging steels, considering Mo role in strength and plastic properties improvement

13 p2086 A71-28581

Precipitation kinetics and austenite formation during aging of Fe-Ni-Mo and Fe-Ni-Co-Mo maraging alloys from dilatometry, electrical resistivity measurement and electron microscopy

14 p2257 A71-29838

Structural evolution of Ni-Co-Mo maraging steel during martensite reversion at rapid heating, studying heating rate effect on alpha-gamma transformation

14 p2257 A71-29839

Heat treatment effect on electrochemical behavior of Ni-Co-Mo maraging steel in sulfuric acid aqueous solution, studying anodic polarization

14 p2257 A71-29840

Strengthening mechanism of Cr-Ni and Ni maraging steels related to dislocation stress field

15 p2427 A71-31524

High tensile strength maraging steels aging, discussing dispersed precipitates formation by homogeneous nucleation

15 p2427 A71-31525

Co-Mo and Co-Mo-Ti stainless maraging steels tensile strength after quenching, establishing Mo and Co alloying limits

15 p2427 A71-31526

Heat treatment effects on high strength maraging steel tensile, fracture toughness and stress corrosion properties, discussing reversion to austenite

15 p2433 A71-32175

Creep rupture behavior and high temperature exposure effects on room temperature properties of Ni-Cr-Mo maraging steel plates and welds

15 p2434 A71-32256

Stress corrosion fatigue crack growth in Ni-Cr-Mo maraging steel, using controlled-potential techniques, pH measurements and fractographic analysis

16 p2590 A71-32942

Refining and hardening reactive additions effect on slow cooling grain boundary embrittlement response of maraging steel

17 p2756 A71-34490

Stress corrosion cracking in Ni maraging steel in NaCl solution, using electrochemical polarization and potential analysis

18 p2934 A71-35989

Nickel maraging steel in NaCl solution, investigating susceptibility to stress corrosion cracking

18 p2935 A71-36595

Neutron diffraction analysis of atomic arrangements in maraging steel, discussing interatomic attractions

19 p3081 A71-37722

Co, Mo, Ti and Cr effect on mechanical properties and microstructure of maraging weld metals

19 p3083 A71-38491

Corrosion fatigue crack propagation in Ni-Cr-Mo maraging steel in room temperature NaCl solution at various stress intensity ranges

20 p3248 A71-38778

Charpy impact test measurement of maraging steel thermal embrittlement, observing fracture mode and toughness changes with heat treatment

21 p3398 A71-40467

Strength, ductility and notch toughness research on base materials and welds of nickel maraging steel rocket motor cases

21 p3389 A71-40913

Low temperature aging behavior of maraging stainless steels from electrical resistivity measurements

22 p3562 A71-41948

Crystal microstructure of strengthening precipitates in Ni maraging steel, giving electron diffraction patterns

22 p3562 A71-41949

Explosive peening effects on weld fatigue in Ni maraging steel, Fortiwell and Al-Zn-Mg alloy

23 p3682 A71-43877

Loading modes effect on stress corrosion cracking of Ni maraging steel in NaCl solution

23 p3693 A71-44074

Ni-Co maraging steels with improved combination of mechanical and magnetic properties at elevated temperatures 24 p3836 A71-44441

MARIA
NT LUNAR MARIA

MARINE BIOLOGY
Aerial and orbital remote sensing of water quality, considering waste materials effect on coastal marine environment 11 p1760 A71-26504

MARINE NAVIGATION
U SURFACE NAVIGATION

MARINE PROPULSION
Aircraft gas turbine condition analysis instrumentation used for status diagnosis of naval turbine engines, discussing sensor and electronic data interpretation progress [ASME PAPER 71-GT-86] 11 p1813 A71-25994
SK-5 air cushion vehicles evaluation including search/rescue, aids to navigation, law enforcement, safety logistics and oil pollution [AHS PREPRINT 572] 14 p2180 A71-31113

MARINE TECHNOLOGY
Marine traffic control via satellite telemetry, describing merchant and powered fishing fleet distribution and navigation requirements 01 p0125 A71-10978
Maritime and aeronautical technology - Conference, Paris, May 1970 04 p0571 A71-15204

MARINER PROGRAM
NT MARINER VENUS-MERCURY 1973
NT MARINER-MERCURY 1973
Mariner 1969 flyby Mars UV spectrum observations, interpreting data in terms of atmospheric, topographic and polar cap adsorptive characteristics 17 p2799 A71-34501
Planetary quarantine constraints for Mariner Mars 1971 orbiter missions, considering heliocentric and areocentric phases [AAS PAPER 71-318] 23 p3725 A71-42992
IR radiometer experiment for Mariner 1971 Mars orbiter mission, describing objectives and instrumentation 23 p3676 A71-43510

MARINER SPACE PROBES
NT MARINER VENUS-MERCURY 1973
NT MARINER 5 SPACE PROBE
NT MARINER 6 SPACE PROBE
NT MARINER 7 SPACE PROBE
NT MARINER-MERCURY 1973
Mars atmospheric data from Mariner flights, discussing north polar haze, bright surface features morphology, multiring structures and water vapor exchange 06 p0965 A71-17627
Mariner photometric data, examining variations in Martian surface limb darkening with reciprocity principle 06 p0898 A71-17633
Mariner near encounter pictures with maximum discriminability, applying algorithms for contrast and resolution enhancement and noise removal 06 p0898 A71-17634
Mars surface maps from visual and photographic observations for TV picture interpretation of Mariner orbital flights 11 p1834 A71-26432
In-flight UV spectrometric measurements of simulated Jupiter atmosphere, using sunlit gas mixture released from Mariner spacecraft in interplanetary space 14 p2308 A71-29914
Solar wind turbulence spectrum from Mariner 6 and 7 space probe radar measurements, using differenced range vs integrated Doppler technique 16 p2627 A71-33728
Mars surface features observed during opposition in August 1971, discussing canal controversy, life, dark areas shift and Mariner probes results 18 p2959 A71-35908
Mariner 6 and 7 Mars color TV recording of craters, chaotic terrain and canals, using wide and narrow angle cameras 20 p3297 A71-39628
Planetary quarantine constraints for Mariner Mars 1971 orbiter missions, considering heliocentric and areocentric phases [AAS PAPER 71-318] 23 p3725 A71-42992
Covariance analysis of Mars gravity harmonics, ephemeris and radiation pressure from Mariner 1971 range and Doppler radio tracking data [AAS PAPER 71-343] 23 p3727 A71-43016
Least squares and sequential estimation techniques application to Mariner 6 and 7 tracking data analysis, verifying Einstein relativity theory on electromagnetic radiation propagation [AAS PAPER 71-384] 23 p3731 A71-43054
Mariner 9 Mars 71 mission orbit determination, trajectory and maneuver strategy for near earth, cruise, planetary approach and satellite phases, using in-flight tracking data [AAS PAPER 71-391] 23 p3732 A71-43059

Atomic hydrogen dayglow Lyman alpha structure of Mars exosphere from Mariner 6 and 7 UV spectrometric observations 23 p3734 A71-43156
Photochemical mechanism of atomic carbon production in Mars and Venus atmospheres, comparing dayglow emissions with Mariner results 23 p3734 A71-43157
Atomic oxygen and hydrogen identification in Mars upper atmospheric emission spectra by Mariner UV spectrometer, inferring carbon monoxide presence by self absorption 23 p3735 A71-43330
Mariner S-band occultation experimental data compared with theory for accuracy of physical characteristics of Mars and Venus atmosphere, reviewing data reduction and error analysis 23 p3735 A71-43331
Mars surface mapping, discussing computer reconstruction process for Mariner 6 and 7 TV picture quality improvement 24 p3875 A71-45266

MARINER SPACECRAFT
Design, testing and flight performance of sealed AgO-Zn cells of Mariner Mars 1969 spacecraft 03 p0350 A71-13029
Mariner Mars 1969 navigation, guidance and control systems design, mechanization and flight testing 03 p0455 A71-14073
Mariner Mars 1969 TV cameras instrument design and calibration techniques 06 p0898 A71-17632
Planetary atmosphere Mariner spacecraft occultation experiments, showing neglect of latitudinal and longitudinal variations introduce serious errors 06 p0970 A71-17984
Low energy protons radial gradient in interplanetary space measured with intercalibrated solid state detectors on Venus bound Mariner 5 and earth orbiting Explorer 33 06 p0952 A71-18113
Thermal/vacuum space simulation assembly level testing for prelaunch confidence of Mariner spacecraft 12 p1893 A71-26680
Mariner 9 spacecraft mission, discussing configuration, data handling and TV surface mapping of Mars 24 p3876 A71-45267

MARINER VENUS-MERCURY 1973
N-body integrated reference trajectories and navigation requirements for extended Venus/Mercury 1973 mission midcourse correction [AAS PAPER 71-362] 23 p3729 A71-43032

MARINER 5 SPACE PROBE
Venera satellites and Mariner 5 radio wave fluctuations and discontinuities of refractive index in Venusian atmosphere, considering atmospheric turbulence 05 p0719 A71-16042
Radio signal refractive index fluctuations in Venus atmosphere from Mariner 5 data 07 p1197 A71-19762
Venus atmosphere determinations by Mariner 5 radio occultation measurements, deriving altitude profiles of refractivity, molecular number density, pressure, temperature and radio frequency absorption 10 p1669 A71-24176
Ionic and thermal structure model of daytime Venus ionosphere with solar wind heating based on Mariner 5 flyby mission 14 p2305 A71-29661
Venera satellites and Mariner 5 radio wave fluctuations and discontinuities of refractive index in Venusian atmosphere, considering atmospheric turbulence 16 p2542 A71-33446
Solar wind angular momentum flux transport from nonradial velocity components measurements by Mariner 5, noting agreement with comet tail observations 21 p3438 A71-40428

MARINER 6 SPACE PROBE
Mars Mariner 6 and 7 flyby missions, discussing surface and atmospheric information and data processing techniques 06 p0965 A71-17626
Mars Mercator projection photomap, using Mariner 6 and 7 spacecraft TV images 06 p0965 A71-17629
Mars surface areodetic control net from Mariner 6 and 7 TV pictures, determining initial coordinate points and far and near encounter frames 06 p0965 A71-17630

MARINER 7 SPACE PROBE
Mars Mariner 6 and 7 flyby missions, discussing surface and atmospheric information and data processing techniques 06 p0965 A71-17626
Mars Mercator projection photomap, using Mariner 6 and 7 spacecraft TV images 06 p0965 A71-17629
Mars surface areodetic control net from Mariner 6 and 7 TV pictures, determining initial coordinate points and far and near encounter frames 06 p0965 A71-17630

MARINER-MERCURY 1973
Mariner mission to Venus and Mercury in 1973, discussing special opportunity characteristics, mission options, real time TV picture transmission, trajectory analysis, etc 05 p0814 A71-17230

MARKERS
Geodetic marker preservation program establishing horizontal and vertical control networks in U.S. 08 p1281 A71-21251
Optimal shapes and sizes of marker signs used in calibrating aerial photographs 12 p1906 A71-26971

MARKET RESEARCH
Book on aviation technology and market structure covering technological and scientific effects on industry innovative behavior, R and D programs, operating costs, etc 10 p1698 A71-23982
Boron and graphite fiber market competition, considering aerospace application 11 p1860 A71-25400
Passenger travel demand model for STOL transportation in underdeveloped areas 18 p2987 A71-36348
Civil aircraft market analysis, examining replacement cycle and used aircraft market based on aircraft histories 18 p2989 A71-36676

MARKETING
Concorde role in air traffic market, discussing operating costs and profit potential 02 p0190 A71-12746
Aerospace industry engineering company management and marketing, discussing corporate strategy, production control, market analysis and professionally trained managers 05 p0840 A71-17148
Optimal reliability proposals for industry competitive posture improvement in difficult market environment, recommending military electronics reliability standards specification 12 p1909 A71-26669
Technical, sales/marketing and management - Conference, Coronado, California, May 1971 13 p2091 A71-28164

MARKING
NT ISOTOPIC LABELING
Concorde aircraft components electrochemical marking, considering stamping and engraving unacceptability for highly stressed thin material parts 09 p1459 A71-23582

MARKOV CHAINS
Limit theorems for spacewise inhomogeneous random walks on straight line with Markov chain transition probabilities 01 p0110 A71-10099
PCM telemetry data transmission bit error probability confidence intervals upper bounds based on Markov chain model analysis 01 p0032 A71-10877
Book on stochastic processes covering random events, Markov chains, fixed terminal time, discounted cost problem, optimal control and stability theory 08 p1268 A71-21310
Optimal reception of Markov radio signals with intrapulse FM, using nonlinear filtration theory 10 p1578 A71-24711
Target trajectory detector optimization, using surveillance radar data and Markovian chain apparatus 13 p2033 A71-28993
Accelerated procedures for Markov chain model optimal control problems solution with computation time advantage over usual dynamic programming 17 p2719 A71-34737
Waiting time distribution in computer controlled queueing system with Poisson input, deriving formulas on basis of total probability and Markov chain theory 24 p3806 A71-44654

MARKOV PROCESSES
NT MARKOV CHAINS
Time distribution of first passage through fixed level for regeneration vector Markov process with step trajectories 01 p0110 A71-10095
Dwell time of semiMarkov system in given state with mixed Erlang and exponential distribution functions 01 p0110 A71-10096
Dynamic programming and Bayes algorithm for self organizing and self adjusting Markovian systems 03 p0389 A71-13515
Optimal and nonoptimal signal reception under conditions of incomplete a priori information based on approximation by Markov processes in white noise 05 p0730 A71-16000
Algorithms for optimal detection of weak determinate signal on background of Markov process approximated non-Gaussian noises 05 p0719 A71-16009
Markov process optimal stoppage, using strongly supermedian functions 05 p0773 A71-16157

- One dimensional Markovian process residence probability in region with variable boundaries
05 p0732 A71-17021
- NonMarkoffian kinetic theory for hierarchical structure of clusters in expanding universe
06 p0964 A71-17314
- Soviet book on limit theorems for random walks covering random walk functionals, zero mean value, finite dispersion, sequences, normalized sums, Markov functionals, etc
07 p1148 A71-20300
- Book on probability theory and applications covering stable distributions, renewal theory, large numbers laws, central limit theorem, Markov processes, random walks, etc
08 p1325 A71-21655
- Nonlinear fluctuation-dissipation thermodynamics with time-even and time-odd parameters concerning four index relations for nonquantum Markovian case
09 p1544 A71-22366
- General Markov processes, considering topological space E and semigroup t equal to or greater than zero
12 p1922 A71-26819
- Asymptotic methods and Markov processes theory extension to unsteady vibration of nonlinear systems with slowly varying parameters and random perturbation
12 p1930 A71-27173
- Book on nonlinear modulation based on optimum estimation theory covering phase synchronization, analog data transmission, digital and analog systems performance, Markov processes, etc
13 p2029 A71-28041
- Time sharing digital computers busy period task completions modeling as semi-Markov process
13 p2035 A71-28974
- Book on dynamic probabilistic systems, Volume 1, covering Markov models, linear processes, systems analysis, statistics, recurrent events, population models, time variations, etc
15 p2440 A71-31196
- Book on dynamic probabilistic systems, Volume 2, covering semi-Markov and decision processes
15 p2440 A71-31197
- Signal detection in stationary, Markov and other noise background, discussing functional method of statistical and probabilistic representation
15 p2370 A71-31589
- Markov process models of failure times of repairable systems, using lumping and decomposing techniques
15 p2415 A71-32340
- Stationary narrow band Gaussian vibration excursion probability based on Markov point process
[ASME PAPER 71-APM-19] 16 p2655 A71-33210
- Transition probabilities of random processes with rapid variability, using continuous Markov smoothing under Fokker-Planck equation
16 p2612 A71-33520
- Kolmogoroff differential equations for probabilities of system states, showing validity for Markovian random processes and processes with aftereffects
16 p2603 A71-33891
- Signal to quantizing noise ratios for differential PCM systems used to encode analog signals from Markov processes into digital form
22 p3514 A71-42391
- Probabilistic system observation at random times, calculating Markov renewal processes optimal long run control
22 p3527 A71-42628
- Optimal and nonoptimal signal reception under conditions of incomplete a priori information based on approximation by Markov processes in white noise
22 p3527 A71-42749
- Algorithms for optimal detection of weak determinate signal on background of Markov process approximated non-Gaussian noise
22 p3515 A71-42760
- Signal filtration algorithms and parameter estimation in additive non-Gaussian noise background by conditional Markov process theory
23 p3644 A71-43290
- Electron motion in plasma under stochastic electric field, emphasizing distribution function dependence on velocity and time
24 p3853 A71-44510
- MARROW**
Rat bone marrow chromosomes radiation protection, using 5-hydroxytryptamine
07 p1038 A71-18973
- MARS [PLANET]**
Carbon dioxide clathrate in Martian ice cap suggested from hydrate stability relative to solid phase and water ice as function of temperature
01 p0148 A71-10002
- Soil microorganisms multiplication under simulated Martian conditions in limonite and garden soil mixture
01 p0019 A71-11558
- Planet Mars polar and equatorial radii optical measurements comparison with radar and Mariner probes occultations results, determining optical ellipticity
03 p0493 A71-14200

- Ozone in Mars solid carbon dioxide polar cap, using UV reflection-absorption spectra
04 p0661 A71-15897
- Shock structure at Venus and Mars dependence on interplanetary magnetic field orientation from Mariners 4 and 5 data, indicating magnetosheaths existence
05 p0810 A71-16636
- Meteorites as information sources on interplanetary space beyond Martian orbit and asteroid belt, discussing possible magnetic barrier and galactic field modulation
05 p0813 A71-16857
- Statistical analysis for parabolic approximation of phase dependence observations of integral Mars brightness
06 p0975 A71-18446
- Earth based orbit determination for Mars orbiting spacecraft, comparing batch and sequential tracking filter data processing methods
[AIAA PAPER 71-119] 06 p0978 A71-18657
- Mars photographic positions on double short focus astrophotograph with random error for ascent and declination
07 p1194 A71-19332
- Deimos and Phobos position measurements by photographic observations, including refractor and astrophotograph errors
07 p1194 A71-19333
- Deimos photographic observations on Pulkovo normal astrophotograph during 1967 Mars opposition
07 p1194 A71-19334
- Deimos and Phobos photographic observations with light reducing slit attenuator diaphragm on refractometer
07 p1195 A71-19335
- Near equilibrium shock layers nonequilibrium radiant emission calculation, noting application to Mars entry conditions
[AIAA PAPER 70-773] 07 p1091 A71-19914
- Martian satellites nature and evolution, facts, theories, hypotheses and speculations
07 p1202 A71-20516
- Planetary surface smoothness factor determination by disk brightness, Mars red light and phase curves methods, indicating superiority of visual observation
09 p1520 A71-22828
- Hydrogen isotopes around terrestrial planets, discussing H and deuterium dynamic behavior in Venus and Mars coronas
10 p1668 A71-24001
- Mars observations at August 1971 opposition, discussing dark spots, polar cap and darkening, atmosphere, etc
10 p1670 A71-24277
- Venus, Mars, Jupiter and lunar thermal emission data in 7-25 micron region
11 p1824 A71-25698
- Parabolic approximation of total Mars brightness phase dependence observations, using statistical analysis
12 p1955 A71-26596
- Chemical evolution and extraterrestrial life detection, noting cell proliferation methods, automatic biological stations and Mars microorganisms
13 p2009 A71-28680
- Visible and UV photometric recording of microorganism reproduction in liquid medium for application to Mars extraterrestrial life detection
13 p2019 A71-28682
- Space vehicle observation effect on Mars and Venus conceptions, considering origins of life, runaway greenhouse effect on earth and atmospheric circulation
14 p2308 A71-29909
- Mars and Jupiter radio emission at 2.3 mm and 8.15 mm, determining brightness temperature and electrical and thermal waves soil penetration depth ratio
15 p2490 A71-32413
- Mars microwave brightness temperature measurements, defining planetary spectra
15 p2490 A71-32415
- Mars radio spectrum discrepancy with elementary theory, assessing microwave observations
15 p2490 A71-32416
- Mariner 1969 flyby Mars UV spectrum observations, interpreting data in terms of atmospheric, topographic and polar cap adsorptive characteristics
17 p2799 A71-34501
- Mars, Uranus and Jupiter observations with Sao Paulo Observatory Danjon astrolabe, presenting east and west transits right ascension and declination tables
18 p2961 A71-35943
- Martian satellites motion along arbitrary elliptical orbits, expressing planet gravitational potential
18 p2962 A71-36108
- Mars motion 1751-1969, comparing Clemence theory and Newcomb Tables of sun with meridian and radar ranging Mars observations
19 p3144 A71-38166
- Statistical processing of phase dependence of Martian integral brightness at 0.3-1.1 microns, noting abrupt reflectivity decrease
20 p3290 A71-39308

- General relativistic time delay and moon-earth masses and Mars mass-eccentricity ratios from S-band range and Doppler tracking
20 p3296 A71-39623
- Size classification of limonite Mars simulation samples, noting surface roughness of 0.02-10 microns
21 p3449 A71-40642
- Soviet papers on terrestrial planets, discussing Mercury, Venus and Mars atmosphere, surface, internal structure and physical conditions
21 p3452 A71-40882
- Mars mass, dimensions, configuration, internal structure, magnetic field, color evolution, surface properties, atmospheric parameters, etc
21 p3452 A71-40885
- Martian polar caps heat balance, noting albedo differences due to irregularities in solid carbon dioxide cover
22 p3603 A71-42190
- Mars coordinate shift from ecliptic to equator system, considering precession and orientation data
22 p3607 A71-42871
- Mars orbiting spacecraft trajectory from spacecraft based TV pictures of Phobos and Deimos
[AAS PAPER 71-372] 23 p3730 A71-43042
- Batch and sequential consider filters data processing methods for Mars orbiting spacecraft state estimation, investigating error sources
[AAS PAPER 71-385] 23 p3731 A71-43055
- Unified procedure for detection of life on Mars by Viking program missions, using mass spectrometer for remote biologically oriented experiments
23 p3736 A71-43541
- High resolution Mars photographs obtained with 61-in reflector telescope
24 p3872 A71-44998
- Mars telescopic observations, emphasizing south polar cap prominences around edge
24 p3872 A71-44999
- Deimos and Mars photography observation by 400 mm astrophotographic camera, introducing corrections for irregularities in satellite motion and planet phase
24 p3874 A71-45177
- MARS ATMOSPHERE**
Photochemistry, diffusion and escape of atomic and molecular hydrogen on Mars, noting water vapor spectroscopy consistent with temperature profiles
01 p0162 A71-11488
- UV effect on airborne bacteria survival in simulated Martian dust clouds
01 p0019 A71-11557
- Martian exospheric temperatures diurnal variations during Mariner 4, 6 and 7 observations by solving time dependent heat balance equations
02 p0305 A71-11972
- Martian surface environment from biological viewpoint, considering atmosphere, radiation field, temperature, polar caps, composition, granularity and topography
02 p0310 A71-12161
- Martian atmospheric water vapor latitude distribution, evaluating high dispersion spectroscopic observations
03 p0488 A71-13555
- Atmospheric aerosols role in Martian opposition effect, applying Mie theory to integrated scattering intensities calculation for submicron particles
03 p0489 A71-13558
- Mars atmosphere carbon dioxide condensate cloud layer implications, considering temperature lapse rate and water condensation at lower levels
03 p0489 A71-13608
- Space capsule reentry into Martian atmosphere for soft landing, using onboard nonlinear filter and stochastic control for random wind gusts
03 p0500 A71-14479
- Martian dayglow spectrum, examining excitation processes for carbon monoxide Cameron bands
03 p0497 A71-14544
- Mars atmosphere carbon dioxide photodissociation via pressure independent one step process
03 p0497 A71-14548
- Goethite stability on Mars, considering dehydration-rehydration cycle and time average atmospheric water vapor content
04 p0645 A71-15132
- Mars atmospheric water vapor detection during Southern Hemisphere spring and summer season
04 p0645 A71-15139
- Mars and Mercury polarization measurements, investigating Rayleigh scattering in atmospheres
05 p0806 A71-16204
- Mars atmospheric data from Mariner flights, discussing north polar haze, bright surface features morphology, multiring structures and water vapor exchange
06 p0965 A71-17627
- Downward atmospheric radiation fluxes incident on Martian surface horizontal plane, tabulating atmospheric composition, surface pressures and temperatures and effective sky temperatures
07 p1199 A71-19874

Organic compounds biosynthesis in simulated Mars atmosphere, using UV irradiation for photocatalytic production from CO and water mixtures

09 p1403 A71-22647

Mars yellow clouds extent during near perihelion apparitions since 1877, considering dust storm origin in Southern Hemisphere

09 p1520 A71-22698

Martian studies during opposition, discussing atmosphere, optical thickness, pressure, brightness phase dependences over land and sea, crust material and dust clouds

10 p1677 A71-24584

Upper Martian atmosphere UV emission spectrum observation noting carbon dioxide photoionization, ion fluorescent scattering and photon/electron dissociative excitation

10 p1604 A71-24776

Mars atmospheric CO abundances and rotational temperature from Voigt line profiles

10 p1646 A71-24993

Martian ionosphere below 80 km, developing positive and negative ion chemistry model

11 p1821 A71-25548

Mars monochromatic albedos, investigating longitudinal variations and opposition effects

11 p1824 A71-25707

Martian atmosphere Mie scattering analysis, using limonite and bulk solid carbon dioxide complex refractivity to interpret polarization effects

11 p1825 A71-25708

Mars UV polarization and atmospheric opacity measurements, using ground based polarimetric data at near maximum elongation

11 p1825 A71-25709

Similarity comparisons of isotropic and anisotropic scattering patterns in cloudy atmospheres for haze effects on Mars image contrast, using asymptotic method

11 p1825 A71-25710

Martian atmospheric pressure carbon dioxide abundance variations correlated with waxing and waning of polar caps or Mars season

11 p1825 A71-25712

Water vapor latitude variation on Mars from Coude spectrograph of 107 inch telescope

11 p1826 A71-25716

Martian atmospheric water vapor abundance during 10 February-25 April 1969 Mars opposition by spectroscopic observations

11 p1826 A71-25717

Martian cloud motions from Lowell Observatory plates following local positions of well-defined clouds

11 p1826 A71-25722

Oxygen atom deficiency and very low exospheric temperature in Mars and Venus upper atmospheres, considering photochemical processes and molecular diffusion

11 p1826 A71-25723

Carbon dioxide cations emission bands in Mars and Venus dayglows, suggesting fluorescent scattering and photoionization as main excitation sources

11 p1827 A71-25724

Mariner 6 and 7 UV spectrometers, describing technical details, operating characteristics and calibration of planetary coronagraph and Ebert-Fastie monochromator used for Martian atmosphere analysis

11 p1766 A71-26301

Mars atmosphere optical thickness by polarimetric /ground and spacecraft/ observations, considering light areas roughness /smoothness/ factor variation with wavelength

12 p1964 A71-27086

Atmospheric viscous dissipation energy relationships, calculating Martian atmosphere thermal structure

12 p1965 A71-27192

Jupiter Red Spot, zonal wind and banded appearance, Venus vertical temperature structure and atmospheric motions, and Mars circulation, dust phenomena and atmosphere stratification

14 p2313 A71-30499

URSI-IAU-COSPAR Woods Hole Conference on lunar emission and Mercury surface temperature from radiometry, discussing Mars and Venus atmosphere measurements

14 p2316 A71-30967

Radiative heat transfer equilibrium in earth, Venus and Mars atmospheres, taking into account interaction with ground

15 p2395 A71-31448

Carbon dioxide electron impact energy loss spectrum and molecular orbit calculations, discussing fourth positive bands production in Mars upper atmosphere UV dayglow

15 p2398 A71-31766

Carbon suboxide polymers formation in Martian atmosphere, examining carbon monoxide photolysis and radiolysis processes enhanced by solar ionizing radiation

15 p2491 A71-32420

Diurnal variation of Venus and Mars exospheric temperatures, using neutral heating efficiency calculation based on molecular theory

16 p2641 A71-33769

Large meteoroids ablation and breakup mathematical model, estimating Mars atmosphere effectiveness as shield against surface impact craters production

16 p2643 A71-33968

Mars atmosphere high resolution line spectra, calculating carbon dioxide abundance, rotational temperature and surface pressure

17 p2800 A71-34588

Astigmatic image distortion in low temperature multiple reflection White cell with aluminum dewar assembly for Martian IR interpretation

18 p2914 A71-35844

Martian surface topography effects on mean wind from time independent and frictionless thermal wind equation solution for radiative-convective atmospheres at scaling analysis level

18 p2964 A71-36287

Martian blue haze clearings and flash phenomena meteorological mechanism, considering atmospheric clearing due to water precipitation

18 p2966 A71-36767

Mars, Venus and earth atmospheres, considering abundance of volatiles such as carbon dioxide, water, oxygen, nitrogen, argon, carbon monoxide, chlorine and fluorine

18 p2968 A71-37032

Lifting entry and terminal phase system optimization for 1975 Mars Viking lander, considering graphical tradeoff approach including design parameter and atmosphere model variations

19 p3148 A71-37171

Mars atmosphere optical thickness by polarimetric /ground and spacecraft/ observations, considering light areas roughness /smoothness/ factor variation with wavelength

19 p3133 A71-37436

Martian lower ionospheric models during solar proton event, determining electron density profiles

20 p3286 A71-38741

Mars short-wave line spectra from measurement with reflector, estimating nitrogen dioxide content in atmosphere

20 p3290 A71-39307

Annual heat balance in Martian northern polar cap, considering atmospheric, ground and solar heat flux absorbed by snow

20 p3290 A71-39309

Mars and Venus atmospheres, considering energetics, mean winds, temperature differences, circulations and climates

20 p3296 A71-39624

Mars ionosphere radio wave absorption integral coefficients, studying electron concentration and electron/gas molecular collisions frequency vertical profiles

20 p3297 A71-39629

Gamma radiation due to cosmic rays interaction with Mars surface/atmosphere and natural radioactive rocks elements decay, calculating intensity and spectral composition

20 p3280 A71-39630

Mars mass, dimensions, configuration, internal structure, magnetic field, color evolution, surface properties, atmospheric parameters, etc

21 p3452 A71-40885

Ion anemometer for measuring wind velocity magnitude and direction in rarefied Martian atmosphere

22 p3600 A71-41960

Mars IR spectra with Connes-type interferometer, noting atmospheric absorption and albedo drop due to surface water

22 p3602 A71-42176

Atomic hydrogen dayglow Lyman alpha structure of Mars exosphere from Mariner 6 and 7 UV spectrometric observations

23 p3734 A71-43156

Photochemical mechanism of atomic carbon production in Mars and Venus atmospheres, comparing dayglow emissions with Mariner results

23 p3734 A71-43157

Carbon dioxide photolysis at 1740-2100 A applied to photochemistry of Mars lower atmosphere

23 p3641 A71-43327

Atomic oxygen and hydrogen identification in Mars upper atmospheric emission spectra by Mariner UV spectrometer, inferring carbon monoxide presence by self absorption

23 p3735 A71-43330

Mariner S-band occultation experimental data compared with theory for accuracy of physical characteristics of Mars and Venus atmosphere, reviewing data reduction and error analysis

23 p3735 A71-43331

Mars atmospheric carbon dioxide dissociation, solving and comparing diffusion equations to Mariner oxygen and carbon dioxide observations

23 p3735 A71-43332

Mars and Venus carbon dioxide atmospheres, covering solar EUV heating efficiency, upper atmosphere temperature and chemical recombinations

23 p3735 A71-43334

Mars and Venus upper atmospheric electron distribution compared with theoretical ionospheric models, considering solar wind as ionization source

23 p3736 A71-43342

Mars physicochemistry, discussing Wright effect /blue veil/, atmosphere, polar cap migration, Phobos acceleration and relief inversion darkening

23 p3736 A71-43360

Onboard computation of Mars atmospheric density and temperature, evaluating error covariance

23 p3774 A71-44095

Martian dust storm observation by telescope in New Mexico, noting brilliant yellow cloud cover

24 p3872 A71-45000

MARS ENVIRONMENT

NT MARS ATMOSPHERE

Martian environment simulator chamber for pressure, visible light, biological objectives UV irradiation and daily temperature cycle

01 p0068 A71-11559

Martian surface environment from biological viewpoint, considering atmosphere, radiation field, temperature, polar caps, composition, granularity and topography

02 p0310 A71-12161

Thermogravimetric analysis of goethite-rich sample of Mars type limonite, considering sorption process relation to Mars environment and polar caps

04 p0644 A71-15131

Extraterrestrial life hypotheses, citing astronomical considerations, inorganic chemical evolution and prebiotic synthesis with emphasis on Mars exploration for microorganisms

07 p1044 A71-20374

Spectroscopic search for water on Mars during 1963-1970, summarizing conclusions concerning quantity and variations with location, season and from year to year

11 p1826 A71-25715

Simple organisms resistance and adaptation to low pressure, anoxia, intense cooling, UV irradiation and Mars conditions

13 p2009 A71-28687

Mars physical conditions compared to earth, simulating Martian conditions and low temperature and UV effects on proteins

13 p2009 A71-28688

Xerophyte soil microorganisms reproductive stability in artificial Mars environment chamber at maximum hygroscopic moisture

13 p2019 A71-28690

Living organisms life-sustaining possibility under simulated Martian temperature, humidity and atmospheric composition conditions, emphasizing unicellular organisms radiation resistance

21 p3334 A71-40572

Simulated Martian environment effects on terrestrial microorganisms survival

22 p3487 A71-42227

Microorganisms survival in simulated Martian environment noting culture cells concentration increase

22 p3507 A71-42826

Simulation chamber for experimental investigation of organisms reactions to Mars environment

22 p3507 A71-42827

MARS EXCURSION MODULE

Manned Mars exploration, discussing excursion module, surface rover and base construction

13 p2143 A71-29251

MARS LANDING

Space capsule reentry into Martian atmosphere for soft landing, using onboard nonlinear filter and stochastic control for random wind gusts

03 p0500 A71-14479

Mars lander deorbit trajectory sensitivity analysis for fixed flight path and communications angles at atmospheric entry, comparing with Monte Carlo simulation

06 p0978 A71-18628

Viking Mars 1975 surface meteorological transducers, discussing measurements, environment and mission constraints

09 p1448 A71-22773

Manned Mars exploration, discussing excursion module, surface rover and base construction

13 p2143 A71-29251

MARS PROBES

NT MARINER 6 SPACE PROBE

NT MARINER 7 SPACE PROBE

NT VIKING LANDER SPACECRAFT

NT VIKING MARS PROGRAM

NT VIKING ORBITER SPACECRAFT

Mariner Mars 1969 navigation, guidance and control systems design, mechanization and flight testing

03 p0455 A71-14073

Mariner photometric data, examining variations in Martian surface limb darkening with reciprocity principle

06 p0898 A71-17633

Ion source for double focusing magnetic mass spectrometer for use with gas chromatograph on Mars mission, requiring electron beam stabilization in space

07 p1113 A71-19851

Planetary quarantine analysis for unmanned Mars orbiter, considering accidental spacecraft impact, loose particles and gases used for attitude control and pressurization

16 p2537 A71-33799

Phobos and Deimos missions, examining lander and lander/orbiter configurations and Titan-Centaur and space shuttle-Centaur launch systems
[AIAA PAPER 71-830] 17 p2802 A71-34716

Viking Mars 1975 mission analysis software system for trajectory optimization, describing condensed format print and contour plot program
[AAS PAPER 71-311] 23 p3725 A71-42987

Mars surface cartography and orbit determination using TV data from Mars orbiting spacecraft
[AAS PAPER 71-373] 23 p3730 A71-43043

Mars Viking Lander camera system with solid state focus switching, radiometry and solar imaging survivability 23 p3677 A71-43517

Mars orbiters and Kepler laws, discussing planetary motion, satellite orbits and orbital characteristics 24 p3875 A71-45268

MARS SPACECRAFT U MARINER SPACECRAFT MARS SURFACE

Mars surface environment from biological viewpoint, considering atmosphere, radiation field, temperature, polar caps, composition, granularity and topography 02 p0310 A71-12161

Annular structures on earth, moon and Mars, explaining cosmic origin on basis of lens-shaped subsurface breccia 02 p0310 A71-12298

Spectral reflectance measurement, comparing oxidized meteoritic material and Martian surface 03 p0489 A71-13559

Martian north polar cap observations, discussing physical aspects and seasonal regression curves 03 p0489 A71-13560

Goethite stability on Mars, considering dehydration-rehydration cycle and time average atmospheric water vapor content 04 p0645 A71-15132

Single module unmanned Mars roving vehicle with flexible metal toroidal hoop-spoked wheels, discussing remote controlled scale model design for simulation on earth 04 p0566 A71-15333

Mars atmospheric data from Mariner flights, discussing north polar haze, bright surface features morphology, multiring structures and water vapor exchange 06 p0965 A71-17627

Mars surface TV pictures from Mariner 6 and 7, including cratered and uncratered terrains, light and dark markings and south polar cap 06 p0965 A71-17628

Mars Mercator projection photomap, using Mariner 6 and 7 spacecraft TV images 06 p0965 A71-17629

Mars surface areocentric control net from Mariner 6 and 7 TV pictures, determining initial coordinate points and far and near encounter frames 06 p0965 A71-17630

Digital computer techniques for Mars surface imagery systematic video data distortions quantification and correction onboard Mariner 6 and 7 06 p0871 A71-17631

Mariner photometric data, examining variations in Martian surface limb darkening with reciprocity principle 06 p0898 A71-17633

Moon and Mars brightness distribution, considering surface roughness, albedo, fragmentation and walls between pores 06 p0975 A71-18447

Martian radio emission measurements at millimeter wavelength and surface thermal and electric parameters estimation 07 p1193 A71-19314

Downward atmospheric radiation fluxes incident on Martian surface horizontal plane, tabulating atmospheric composition, surface pressures and temperatures and effective sky temperatures 07 p1199 A71-19874

Surface navigation system and error analysis for Martian roving vehicle, using continuous tracking of pole star and local vertical 08 p1332 A71-21350

Bands and gray levels number selection for Mars surface multispectral imaging 09 p1447 A71-22750

Mars border-disk brightness comparison noting atmospheric transparency effects 09 p1520 A71-22837

Mercator chart of Mars surface between 70 deg north and 70 deg south latitude from Mariner 6 and 7 photography 09 p1452 A71-23220

Martian studies during opposition, discussing atmosphere, optical thickness, pressure, brightness phase dependencies over land and sea, crust material and dust clouds 10 p1677 A71-24584

Colorimetry of Mars surface from dual beam area scanner, considering light and dark areas contrast during 1969 opposition 11 p1824 A71-25706

Martian surface pressure from 1967-1969 apparition observations, discussing micron bands carbon dioxide abundances 11 p1825 A71-25711

Relative elevation differences on Mars surface revealed by near IR carbon dioxide bands spectroscopic observations 11 p1825 A71-25713

Mars surface pressure and elevation differences determined by spectroscopic observation of carbon dioxide band 11 p1825 A71-25714

Liquid water natural occurrence on Martian surface, considering possibility of ice melting by sunlight or other heat sources 11 p1826 A71-25718

Cloud activity on Mars near autumn equinox of Northern Hemisphere, comparing 1937 and 1969 oppositions 11 p1826 A71-25721

Mars surface maps from visual and photographic observations for TV picture interpretation of Mariner orbital flights 11 p1834 A71-26432

Mars 1969 opposition effects, describing Syrtis Major, Arabia and disk brightness, color and spectrum 11 p1835 A71-26456

Moon and Mars brightness distribution, considering surface roughness, albedo, fragmentation and walls between pores 12 p1955 A71-26597

Mars regolith carbon dioxide, water and Kr adsorption, explaining diurnal brightness phenomena 12 p1961 A71-26875

Mars atmosphere optical thickness by polarimetric /ground and spacecraft/ observations, considering light areas roughness /smoothness/ factor variation with wavelength 12 p1964 A71-27086

Martian continents, seas and polar caps spectrum analysis, noting spectral reflectivity and brightness distributions 12 p1965 A71-27225

Optimal mineral-organic nutrient medium and soil selection for microorganism detection on Mars 13 p2009 A71-28681

Mars map based on computer cataloged planetary patrol photographs 13 p2143 A71-29342

Martian radio emission measurements at millimeter wavelength and surface thermal and electric parameters estimation 15 p2486 A71-31894

Heat balance and 8.22 mm radio emission of Mars, evaluating surface thermal and electrical parameters including brightness temperature 15 p2490 A71-32411

Mars microwave spectrum, discussing brightness temperature increase towards short wavelengths in terms of surface material thermal, electrical or chemical properties 15 p2490 A71-32417

Mars surface features contrast reduction, discussing forward scattering haze as possible cause 15 p2491 A71-32418

Mars IR spectral geometric albedo of bright and dark regions for surface composition model 15 p2491 A71-32419

Mars Meridiani Sinus region map preparation from computer reconstruction of near and far encounter pictures taken by Mariner 6 and Mariner 7 15 p2492 A71-32464

Lunar and Martian subsurface liquid water under porous rock layers and permafrost, using terrestrial hydrogeology analogs 15 p2494 A71-32491

Existence conditions for liquid water on Mars, considering freezing depression, condensation, capillary evaporation and permafrost melting 15 p2494 A71-32492

Lunar-Martian craters relationship, discussing volcanic model of lava infilling, caldera floors and magmatic pressure 15 p2494 A71-32494

Lunar and Martian cratering possibility by cometary icy blocks based on sonic impact fluidation experiments 16 p2636 A71-33508

Mars surface harmonics and continental drift from radar and spectroscopic topographic height determination 16 p2638 A71-33519

Martian surface relief details observation from earth distance, showing telescope resolution requirements above dense atmospheric layers 16 p2639 A71-33698

Polar asymmetry between distribution of surface features on earth, moon, Mars and Mercury 17 p2801 A71-34670

Mars surface features observed during opposition in August 1971, discussing canal controversy, life, dark areas shift and Mariner probes results 18 p2959 A71-35908

Martian surface topography effects on mean wind from time independent and frictionless thermal wind

equation solution for radiative-convective atmospheres at scaling analysis level 18 p2964 A71-36287

Roving vehicle design for 1979 Mars mission 18 p2898 A71-36445

Mars surface narrow-band spectrophotometric observation, obtaining spectral reflectivities for geometric albedos calculation 18 p2970 A71-37048

Martian continents, seas and polar caps spectrum analysis, noting spectral reflectivity and brightness distributions 19 p3132 A71-37377

Mars atmosphere optical thickness by polarimetric /ground and spacecraft/ observations, considering light areas roughness /smoothness/ factor variation with wavelength 19 p3133 A71-37436

Astronomical telescopic observations of Mars for map updating, discussing surface colors 19 p3145 A71-38570

Annual heat balance in Martian northern polar cap, considering atmospheric, ground and solar heat flux absorbed by snow 20 p3290 A71-39309

Mariner 6 and 7 Mars color TV recording of craters, chaotic terrain and canals, using wide and narrow angle cameras 20 p3297 A71-39628

Gamma radiation due to cosmic rays interaction with Mars surface/atmosphere and natural radioactive rocks elements decay, calculating intensity and spectral composition 20 p3280 A71-39630

Martian features nomenclature based on Schiaparelli application of ancient geographical and mythological names 21 p3448 A71-40520

Martian surface clouds distribution in graph, noting statistical correlation with surface radar altitude 21 p3450 A71-40712

Mars mass, dimensions, configuration, internal structure, magnetic field, color evolution, surface properties, atmospheric parameters, etc 21 p3452 A71-40885

Mars IR spectra with Connex-type interferometer, noting atmospheric absorption and albedo drop due to surface water 22 p3602 A71-42176

Injection laser range finder with avalanche photodiode for Mars rover obstacle sensing, discussing range data processing methods 22 p3529 A71-42772

Infusoria adaptation ability to extreme environmental conditions with emphasis on Mars surface 22 p3496 A71-42825

Mars surface cartography and orbit determination using TV data from Mars orbiting spacecraft [AAS PAPER 71-373] 23 p3730 A71-43043

Martian surface materials determination by comparing albedo and brightness with spectral and photometric characteristics of crushed reddish volcanic rock and silicate sand mixed with limonite 23 p3770 A71-44052

Mars surface soil thermophysical properties, temperature and thermal emission from Mariner spacecraft IR radiometer data, correlating with visual images 24 p3867 A71-44439

Martian height gradients from 1.6 micron carbon dioxide band intensity, using telescopes with prismatic quartz spectrometer 24 p3869 A71-44807

Semitransparent particle model of Martian surface for reflective power at various incidence and reflection angles, discussing packing density and optical parameters 24 p3869 A71-44808

Mars surface mapping, discussing computer reconstruction process for Mariner 6 and 7 TV picture quality improvement 24 p3875 A71-45266

Mariner 9 spacecraft mission, discussing configuration, data handling and TV surface mapping of Mars 24 p3876 A71-45267

MARS 69 PROJECT

Mariner Mars 1969 TV cameras instrument design and calibration techniques 06 p0898 A71-17632

Bacterial spore distribution and dry heat resistance on Mariner-Mars 1969 spacecraft, using randomly selected aerobic mesophilic isolates 19 p3002 A71-37646

MARS 71 PROJECT

Mars 1971 orbiter mission, investigating orbit determination accuracy during approach phase [AIAA PAPER 71-189] 06 p0978 A71-18627

LF vibration qualification tests for Mariner Mars 1971 propellant tanks 11 p1746 A71-26494

Covariance analysis of Mars gravity harmonics, ephemeris and radiation pressure from Mariner 1971 range and Doppler radio tracking data [AAS PAPER 71-343] 23 p3727 A71-43016

Mariner 9 Mars 71 mission orbit determination, trajectory and maneuver strategy for near earth, cruise, planetary approach and satellite phases, using in-flight tracking data
[AAS PAPER 71-391] 23 p3732 A71-43059
IR radiometer experiment for Mariner 1971 Mars orbiter mission, describing objectives and instrumentation 23 p3676 A71-43510

MARTENSITE

Fe-Ni martensite crystals microstructure, using Kossel method and electron microscopes 01 p0106 A71-10278
Steels prior austenite and martensite grain size control by thermal cycling 03 p0446 A71-14492
Martensite formation and fracture toughness in TRIP steels, examining effects of plastic zone ahead of crack tip and triaxiality ahead of notch 04 p0615 A71-15792
Austenite-martensite transformation effects on Fe-Ni-Co alloys low temperature thermal conductivity 05 p0768 A71-16771
High carbon Cr and Mn steels martensitic transformation points, ascertaining short range order occurrence by electron microscopic study 07 p1130 A71-19278
Chemical composition effect of low carbon alloys metallic matrix on wear resistance in abrasive medium, showing austenitic manganese alloys superiority to martensitic or ferritic alloys 07 p1136 A71-19630
Co-Ni-Cr-Mo alloys hardening mechanisms, noting martensitic transformation role 08 p1312 A71-21551
High strength martensite beta Ti alloy microstructure, discussing ductility and age hardening 08 p1312 A71-21552
Martensitic transformation-induced plasticity in austenitic Fe alloys, examining strain rate and chemical composition effects 08 p1312 A71-21554
Deformation-induced martensitic transformation effects on Fe-Ni-Cr-C alloy plastic behavior 08 p1313 A71-21555
Fe-Ni-Co alloy strengthening by martensite to austenite transformation taking into account microstructure 08 p1313 A71-21556
Martensitic transformation in NiAl oxidation-resistant coatings on Ni superalloys heated for 300 hr at 1093 C 09 p1472 A71-23132
Ti-Nb alloys constitution, discussing alpha-bis martensite dissolution and undercooled beta phase decomposition 10 p1623 A71-23902
Fast heated titanium-vanadium martensite beta-phase transformations comparison with slow heated structures 11 p1782 A71-26472
Aging behavior of Nb-containing Fe-Ni alloys, considering austenite and martensite in twinned and massive form 13 p2089 A71-29412
Shape-memory effect in equiatomic Ti-Nb alloys with reversible martensitic transformation 14 p2259 A71-30392
Chemical composition effect of low carbon alloys metallic matrix on abrasive wear resistance, showing austenitic manganese alloys superiority to martensitic or ferritic alloys 16 p2593 A71-33626
Equiatomic TiNi martensite crystal structure and internal defects investigation by electron microscopy and electron and X ray diffractions 16 p2598 A71-34045
Fe-Ni-V-C alloy strengthening by cyclic martensitic phase transformation 17 p2756 A71-34487
Martensite-type omega phase formation in Ti alloys during grinding by abrasive wheels and tapes, noting dependence on plastic deformation 19 p3078 A71-37474
Intermetallic compound Ti-Ni phase transformations, relating martensite crystal structure with pre-martensitic instability 21 p3397 A71-40433
Ti-Ni alloy martensitic thermoelastic transformation and memory effect, using optical microscopy to examine change in lattice discontinuity 21 p3398 A71-40459
Alloying elements effects on martensite decomposition and carbide phase formation during tempering of chromium steels 21 p3401 A71-41085
Transformation zones of Ti alloy in isothermal conditions after tempering, showing martensite decomposition and omega phase detection by hardness measurements 22 p3560 A71-41624
Tempering anomalies of austenitic stainless steels partially transformed into martensite, using

dilatometry, resistivity and internal friction measurements 22 p3562 A71-42244

Carbon effects on fracture phenomena in martensitic transformation of steels under heat and thermomechanical treatments 22 p3563 A71-42322

Isothermal martensite transformations in Fe-Ni-Cr alloys, explaining kinetics difference in terms of elastic parameters small variations 23 p3688 A71-42925

Near equiatomic TiNi thermal martensite transformation premonitory events, discussing crystal structure, mechanical instability and lattice vibrations 23 p3694 A71-44280

Interstitial solute carbon distribution in martensite, using generalized perfect lattice gas statistical mechanics 23 p3694 A71-44281

Alloying elements effects on high-carbon steels phase transformation under shock loading to form martensite-austenitic structure 24 p3840 A71-45376

MARTENSITIC STAINLESS STEELS

Martensitic stainless steels structure related to energy dissipation capability, obtaining damping mechanism as magnetomechanical hysteresis 07 p1142 A71-20477

Martensitic transformation of Fe-Ni-Si alloys under tensile plastic strains at 233-373 K 09 p1469 A71-22849

Cr and V diffusion plating influence on principal characteristics of highly alloyed martensitic and carbon steels 12 p1912 A71-27690

Tempered martensite and lower bainite in high purity carbon steels, discussing impact toughness due to internal twinning, grain boundary precipitation and carbide morphology 15 p2432 A71-32173

Metallographic examination of inorganic, metal plated and intermetallic coatings on martensitic stainless steels for pitting and surface corrosion prevention 19 p3081 A71-37902

Electron beam welding of martensitic turbine grade steel thick sections, showing accelerating voltage and focus coil current effect on weld profile 19 p3070 A71-38314

Fe-C alloys martensitic transformation, investigating high quench rate effects 21 p3397 A71-40451

Crystallographic habit plane and martensite plate orientation in Fe-Ni and Fe-Ni-C dilute alloys 21 p3397 A71-40452

Hardness, internal friction, microstress, martensite lattice and density changes during aging of precipitation hardening Fe-Cr-Ni steel, using dilatometric and X ray analysis 21 p3402 A71-41086

Phase transformations and mechanical properties of heat resistant martensitic stainless steel during precipitation aging at prolonged high temperature exposures 23 p3690 A71-43280

Machining effects on martensitic stainless steels corrosion resistance, showing formation of defects and internal stresses in surface layers 23 p3692 A71-44028

MASCONS

Lunar surface mascon structure and origin from mass estimates, noting contributions to lunar gravity field variations 02 p0306 A71-11990

Lunar mascon origin, considering primordial atmosphere and hydrosphere formation from internal heating with resultant mass imbalance and isostatic compensation 03 p0492 A71-14053

Lunar mascons interpretation as meteorites impact, discussing use as gravitational waves detectors 04 p0661 A71-15904

Gravitational anomaly of mascons formation on lunar surface from geological data analysis 09 p1519 A71-22532

Vertical motions on moon resulting from stress differences leading to isostatic equilibrium, discussing maria, craters and mascons 16 p2636 A71-33504

Lunar anorthositic crust flotation, fractional crystallization process in seas and mascons genesis based on experimental data and petrogenetic scheme 16 p2636 A71-33505

Lunar gravitational field interpretation based on Apollo data, considering mascons creation, isostasy, thermal history and maria orientation hypotheses 16 p2636 A71-33506

MASER OUTPUTS

Multiple region hydrogen maser using Teflon coated cylindrical vessel to reduce atom-wall collision frequency shift 01 p0096 A71-11223

Pulsars as rotating magnetic neutron stars, examining radio emission via maser amplification 08 p1363 A71-21174

Prototype two stage maser extended passband broadening and stability increase at high cooling temperature 13 p2078 A71-28374

Pulsar radio emission via maser amplification, presenting model based on electrons behavior in intense magnetic field 20 p3285 A71-39949

Two stage decimeter wavelength quantum paramagnetic amplifier, noting noise temperature and gain 23 p3652 A71-43529

MASER RESONATORS

U MASERS

MASERS

NT GAS MASERS

NT TRAVELING WAVE MASERS

Optically pumped rubidium maser short term frequency instability caused by thermal noise and resonator temperature and pumping power fluctuation 01 p0095 A71-11211

Radiation frequency control in cyclotron resonance maser via TEM wavelength oscillations in Fabry-Perot resonator produced by screw electron beam 01 p0095 A71-11212

Steady state quantum analysis of linear distributed systems applied to attenuator, maser amplifier and multiterminal-pair networks 02 p0213 A71-12017

Solar coronal plasma electromagnetic wave amplification, discussing maser action effect on radar echoes 02 p0306 A71-12078

Hydroxyl and water vapor emission properties in interstellar medium attributed to maser action 02 p0313 A71-12498

Coherent radiation mechanisms characterizing cosmic masers in molecular lines, sporadic radio emission and pulsar radiation 03 p0486 A71-13321

Papers on solid state maser development covering theory, materials and applications 03 p0435 A71-13531

German monograph on polycrystalline ferrites studies with quasi-optical resonators in mm wave range 05 p0791 A71-16125

X band gas tube attenuator for ruby maser saturation protection in pulsed high power radar 07 p1070 A71-18866

Solar coronal plasma electromagnetic wave amplification, discussing maser action effect on radar echoes 08 p1361 A71-21128

Book on lasers and masers covering electric and magnetic dipole transitions, electron oscillator, collision broadening, optical resonators, waveguides, etc 09 p1466 A71-23725

Double resonator ruby maser for observing transitions of interstellar hydroxyl, noting incorporation in modulation radiometer of astronomical telescope 13 p2077 A71-28373

Field components, frequency, quality and filling factors effects of storage quartz bulbs in maser microwave cavities 14 p2254 A71-30563

Superconducting magnetic systems for traveling wave quantum paramagnetic amplifiers, considering minimum weight maser systems 15 p2376 A71-32275

Long baseline radio interferometers, considering quasars, interstellar masers, geodesy and geology applications 15 p2412 A71-32705

Optically pumped rubidium maser short term frequency instability caused by thermal noise and resonator temperature and pumping power fluctuations 17 p2750 A71-34262

Centimeter TEM waves excitation in Fabry-Perot cavity of cyclotron resonance maser by helical electron beam 17 p2750 A71-34263

Soviet book on microwave quantum amplifiers covering traveling wave and multicavity masers calculation, design, tests, applications and basic components 17 p2753 A71-34474

Transfer function for transmission through maser medium, cancelling signal distortions due to propagation 20 p3242 A71-38877

Emissive molecular beam masers, discussing cavity resonators, spectroscopy, amplifiers characteristics, oscillators behavior and electrostatics 20 p3247 A71-39873

Laser pumped solid state masers operational characteristics, describing spontaneous emission noise 23 p3683 A71-43084

MASKING

Masking techniques for printed and thin film circuits and semiconductor devices fabrication 05 p0759 A71-16775

Muscle reflex action role in contralateral retinal masking at high auditory signal sound pressure levels 08 p1246 A71-20803

Interaural phase angle control, using equal masker/signal narrow noise bands and phase shifting network between channels

12 p1871 A71-27534

Speech envelope masking noise generation with constant S/N ratio for intelligibility studies

15 p2372 A71-32297

Neural network hypothesis for mechanism of backward masking and disinhibition in visual perception

17 p2684 A71-35253

Visual perceptual masking under binocular and dichoptic conditions separating peripheral and central interference effects

21 p3342 A71-40225

Memory cell fault tolerant sequential machine synthesis, considering masking feasibility and lower bounds on minimum redundancy

21 p3351 A71-41036

Masking techniques in monolithic IC production in microelectronics, emphasizing contactless, lens, holographic and electron beam projection methods

22 p3325 A71-41713

Comparative residual and reversed microinterval masking signals and human auditory perception capacity measurements using sound level estimates

22 p3490 A71-42579

Visual masking effects in cat striate cortex single cell activity, using moving slit and diffuse flashing light stimuli

24 p3799 A71-45140

MASKS

Computer controlled laser machining system for cutting integrated circuit masks in thin films deposited as fused silica substrates

03 p0433 A71-14342

German monograph on photographic masks as position frequency filters covering pattern recognition, transfer functions, etc

15 p2410 A71-32309

Machining integrated circuit metal film masks with continuously operating carbon dioxide laser and high pressure pulsed He-Ne laser

19 p3069 A71-38234

Holographic methods for etching masks of IC and other semiconductor components

21 p3354 A71-40731

MASS

NT CRITICAL MASS

NT ELECTRON MASS

NT PARTICLE MASS

NT PLANETARY MASS

NT STELLAR MASS

Spheroidal solutions near center for free oscillations of self gravitating rheological spherical mass

01 p0127 A71-10462

Spiral galaxies mass-luminosity relationship from optical and radio astronomy data

02 p0308 A71-12102

Quasar mass lower limit estimation from emission and absorption red shift data

15 p2483 A71-31368

Celestial body mass determination in many body problem, using Kalman-Bucy filtering for Taylor series approximation linearized problem

18 p2960 A71-35935

Upper limits to quasars masses with optical emission lines inside radio sources, using method independent of red shift composition

18 p2961 A71-35965

Mass and discrepant red shifts theory, discussing time dependent gravitational constant, Friedmann cosmological model and Dirac equation

20 p3305 A71-39956

MASS BALANCE

Mass balance stability in closed life support systems, using mathematical model

01 p0024 A71-11127

Cosmic gas dynamics, discussing galactic mass balance, dark matter and interstellar gas kinetic energy, temperature and density

06 p0971 A71-18327

Astronomical mirror mass balancing system, discussing counterweights and levers arrangement and error and temperature compensation

15 p2411 A71-32526

Aircraft loading system consisting of onboard weight and balance equipment and fully mechanized cargo pallet transfer, using computerized simulation model for parametric evaluation [SAWE PAPER 900]

17 p2676 A71-35811

STAN/MASS system aircraft weight and balance determination, discussing basic concepts, design requirements and applications [SAWE PAPER 896]

17 p2834 A71-35816

Automatic balance control device for regulating vibration caused by rotating ill-balanced mass system

21 p3388 A71-40755

MASS DISTRIBUTION

Faint sporadic meteors mass distribution from forward and backscatter of radio echoes

01 p0151 A71-10254

Fibrous body optimum material distribution, considering arbitrary density continuous three dimensional bar network

01 p0177 A71-11285

Spinning space stations with mass geometry changes, discussing attitude and angular velocity optimal control

01 p0164 A71-11435

Micrometeorites composition and mass distribution in earth orbit vicinity, describing spaceborne and ground based data acquisition

02 p0313 A71-12470

Elastic column optimization, examining material distribution for minimum volume without buckling

03 p0501 A71-13023

Galaxy clusters stabilization by cosmological constant, considering clusters mass discrepancy

03 p0489 A71-13561

Shock-reflection interferometry of electron and mass density profiles of ionized argon end wall thermal layer

04 p0674 A71-14701

Plasmoid mass and velocity distribution in pulsed plasma accelerators, using mass spectrometers and platinum thermal probe

04 p0634 A71-15111

Expanding universe adiabatic density fluctuation evolution, describing photon distribution function collision equation for plasma recombination

05 p0801 A71-15929

Tapered cantilever beam with variable bending rigidity and concentrated mass, investigating nonlinear flexural vibration

05 p0820 A71-15986

Panel with segment-wise constant mass distribution structural optimization design, considering flutter

05 p0824 A71-16577

Double galaxies mass distribution from pair components motion dependence on radial velocity

06 p0966 A71-17750

Satellite orbital motion, discussing idealized perturbations limiting problem from point mass

08 p1360 A71-21004

Mean luminous cosmic matter density calculations, using galaxy counts and mass data eliminating luminosity functions

09 p1516 A71-22060

Angular motion of deformable earth satellite as solid-elastic system with distributed masses, applying automatic control transfer function

09 p1491 A71-22548

Stokes earth shape formula derivation without removing continental masses for regularization requirement

09 p1438 A71-23181

Rotating self gravitating axisymmetric fluid mass structure steady state equations, examining Clairaut theory asymptotic nature

09 p1527 A71-23532

Lunar surface mass distribution, using dynamic point mass solution

09 p1530 A71-23717

Orthotropic shells of revolution with concentrated masses and oscillator inclusions and reinforced by stringers and ribs, calculating free vibration by Ritz method

10 p1690 A71-24570

Hinged sandwich beams loaded by concentrated masses, calculating natural vibration frequencies with and without allowance for rotatory mass inertia

10 p1690 A71-24571

Cometary nucleus radius, mass, composition and icy-conglomerate model

10 p1677 A71-24687

Sweptback thin cantilever wing transonic flutter density and velocity coefficients, investigating engine pod shaped concentrated mass location effects

11 p1706 A71-25189

Cometary atmosphere photometric data, determining particle distribution and ejection rate, temperature, molecular lifetime, acceleration and emission velocity

11 p1821 A71-25542

Interstellar matter, emphasizing H I and H II regions temperatures, dust, magnetic fields, intermediate and high velocity clouds

12 p1959 A71-26779

Statistical analysis of gravitational instability for isotropic cosmological models, examining density perturbations as random functions of coordinates and comparing with galactic mass statistics

12 p1965 A71-27178

Mass distribution of compact galaxies, obtaining average mass/luminosity ratio

13 p2138 A71-28762

Coma galaxy clusters missing mass observations by gravitational lens effect

14 p2305 A71-29676

Transverse free vibrations of beam with one end fixed and other supported on bilinear spring and carrying concentrated mass

14 p2323 A71-29847

Planetary mass distribution, considering accretional theory of gas condensation into particles and particle accretion by growing embryo

14 p2312 A71-30389

Variable mass body rotational motion stability in central Newtonian field with gyroscopic on symmetry axis

14 p2275 A71-30880

Low degree gravity harmonics source, discussing upper mantle hypothesis of mass anomalies location

16 p2563 A71-33150

Classical gravitational field equations modification for virtual quantized matter, taking into account additional mass due to attractive forces

16 p2610 A71-33271

F-4E stall/spin development and flight tests, relating mass distribution and angle of attack aerodynamic design [AIAA PAPER 71-772]

16 p2524 A71-34008

Oceanic masses vertical gravity gradient, noting slight decrease with depth

16 p2575 A71-34065

Multiple mass rheonomic vibrational systems dynamic stability, presenting approximate solution and critical dissipation level for damping parametric resonances

17 p2777 A71-34346

Spherical harmonic expansion of nonhomogeneous oblate spheroid mass distribution potential, giving convergence criterion

17 p2733 A71-35029

Earth masses substitution by nearly minimum number of point sources of gravity anomalies

17 p2734 A71-35188

Meteor bodies mass distribution function for Geminid stream, determining parameter S from radio echoes

19 p3145 A71-38528

Globular clusters with inhomogeneous composition, deriving partial densities of masses

20 p3291 A71-39318

Satellite orbital motion, discussing idealized perturbations limiting problem from point mass

20 p3294 A71-39584

Sporadic and shower meteoroids mass distribution temporal variations as function of magnitude and solar longitude from visual and radio echo measurements

20 p3298 A71-39643

Total mass density in neighborhood of sun and Galactic force law from stellar motions perpendicular to Galactic plane, using King pseudomoments method

21 p3440 A71-40061

Linear second order multidegree of freedom vibrational system with singular mass matrix, determining response to excitation

[ASME PAPER 71-VIBR-10] 21 p3457 A71-40272

Distributed mass and elastic damping finite element model for turborotor system on fluid film bearings

[ASME PAPER 71-VIBR-56] 21 p3385 A71-40301

Stability of rotating unsymmetrically mass distributed cantilever shaft with unsymmetrical rotor, determining unstable region boundaries by theoretical analysis and experiment

[ASME PAPER 71-VIBR-58] 21 p3385 A71-40303

Linear multidegree of freedom shock isolation system optimum design, masses, spring and damping coefficients, using mathematical programming

[ASME PAPER 71-VIBR-81] 21 p3461 A71-40317

Galaxies clusters mass determination with aid of virial theorem based on velocity dispersion, emphasizing black holes existence

21 p3450 A71-40713

Mercury perihelion advance due to solar mass distribution departure from spherical symmetry because of negative eddy viscosity

21 p3439 A71-41422

Relative abundances and mass measurements of Li and B isotopes in primary low energy cosmic rays

22 p3593 A71-42339

Statistical analysis of gravitational instability for isotropic cosmological models, examining density perturbations as random functions of coordinates and comparing with galactic mass statistics

22 p3605 A71-42452

Spiral galaxy M33 observations at 21 cm, deriving hydrogen atoms distribution and kinematic properties

23 p3722 A71-42938

Liquid drop deformation and mass loss in high speed gas flow at high Weber numbers due to capillary surface waves

23 p3662 A71-43371

Rotor elements eccentricity effect on rotor dynamic deflection, discussing rotor unbalance determination

24 p3884 A71-45010

MASS FILTERS

U FLUID FILTERS

MASS FLOW

Swirling flow through multiple nozzles of simulated solid propellant rocket motors, determining thrust and mass flow effects on passage

01 p0072 A71-11592

Solar chromosphere mass motion, studying macroturbulence influences on visible spectrum lines high resolution profiles from rocket spectrograms

06 p0967 A71-17904

- Incompressible fluid steady laminar flow free convection and various gas species mass diffusion from hot horizontal plate surface
06 p1007 A71-18074
- Incompressible laminar boundary layer flow with mass and heat sources, calculating thermal and friction stress distribution
08 p1277 A71-22037
- Hydrodynamic study of systematic errors of mass flowmeters, considering effects of working fluid, sensitive elements and secondary motions
10 p1610 A71-24168
- Dust devil vortex model, considering boundary layer velocity profiles and thickness and integrated radial and vertical mass flows
11 p1794 A71-25470
- Electric arc motion division into relative velocity of arc phenomenon with respect to mass flow and mass motion
12 p1938 A71-27264
- Hypersonic reentry heat shielding problem, considering axisymmetric laminar boundary layer flow with local coolant mass injections at multiple stations
13 p1990 A71-29127
- Circumferential traversing probe technique for intrastage analysis of axial flow compressors, considering mass flow averaging data reduction technique [ASME PAPER 71-FE-33]
13 p2118 A71-29468
- Magnetic field generation from coaxial plasma gun, discussing mechanism in terms of azimuthal plasma mass motion imparted during initial gas discharge
14 p2281 A71-30543
- Incompressible laminar flow between rotating and stationary disks with small gap width and radial mass flow, using Navier-Stokes and continuity equations
15 p2387 A71-31168
- Closed circuit electrical, mass and heat flow stability analysis, showing capacities or inductances trace effects
16 p2607 A71-32991
- Transverse acoustic wave amplification due to mass injection around submerged nozzle in solid propellant rocket engines, noting annular flow role
22 p3589 A71-42034
- Jet mixing in cross flow at different velocity ratios and incidence angles, calculating momentum and mass flow
23 p3664 A71-43831
- Compressible gas flow in two dimensional porous wall, calculating heat transfer and mass flow by conformal mapping for Laplace equation solution
24 p3889 A71-44972
- MASS FLOW FACTORS**
Eddy diffusivity of mass in air measurement discrepancies in circular duct, considering axial concentration and radial distributions
14 p2339 A71-30934
- Mass flow function diagram for axisymmetric isentropic compressible swirling flow in annular duct
24 p3820 A71-44960
- MASS FLOW RATE**
Rapid mass transport to Pt electrodes in foamed electrolytes, examining current density-anode overpotential relationship
02 p0210 A71-12957
- High secondary/primary mass ratio multinozzle jet pump/ejector/operation feasibility [AIAA PAPER 70-579]
03 p0344 A71-14452
- Bulk solids melting on inclined plane heated surface, investigating heat transfer and mass flow rates, fluid driving force and pressure gradient
04 p0678 A71-15456
- Novae, symbiotic, T Tauri, U Geminorum and UV Ceti type stars, determining mass loss rate
06 p0973 A71-18338
- Solid propellant combustion instability, considering burning propellant mass flux response to periodic thermal radiation [AIAA PAPER 71-209]
06 p0948 A71-18645
- Small curvature radius/throat radius ratio supersonic nozzles mass flow rate coefficients at high Reynolds numbers, appraising isentropic flow prediction methods
07 p1015 A71-19877
- Supersonic molecular beams with cycling-pressure sources, investigating mass flow rate effects on skimmer interference
07 p1164 A71-19900
- Air mass flow rate in can type gas turbine combustion chambers
13 p2117 A71-28747
- Supersonic mass flux probe description, discussing inlet geometry, angle of attack and Reynolds and Mach numbers effects on performance
14 p2239 A71-29925
- Real gas mass flow rate computation through sonic nozzle
14 p2239 A71-29927
- Methane and natural gas flow through critical flow nozzles, calculating real gas effects on mass flow rate
14 p2224 A71-29937
- Gas generator with high thrust-weight ratio, discussing thermodynamic cycles, mass flow rates and combustion chamber
15 p2471 A71-32571
- Oxygen sorption rate by Ti at low pressure from measurement in stainless steel ultrahigh vacuum chamber
17 p2695 A71-35139
- Electron bombardment mercury ion rocket engine, considering mass flow rate and magnetic field strength effect on performance
17 p2794 A71-35540
- Discharge coefficient correction factor for curvature effect on mass flow rate measurement by sonic throat for axisymmetric nozzles [ONERA-TP-956]
18 p2915 A71-36024
- Mass flow rate measurements and calibration in heterogeneous medium with hot wires tested on Freon mixtures
19 p3163 A71-37894
- Capacitance measurement technique for density and mass flow measurements for hydrogen slush storage and transfer
20 p3237 A71-39276
- Volume fraction analysis of coaxial flow gas core nuclear rocket for mass flow ratios, fuel radius and density, using free jet computer code and eddy viscosity equations
22 p3573 A71-41638
- MASS RATIOS**
NT PAYLOAD MASS RATIO
Earth-moon mass ratio correction, observing artificial satellite motion near triangular libration point
02 p0308 A71-12100
- High secondary/primary mass ratio multinozzle jet pump/ejector/operation feasibility [AIAA PAPER 70-579]
03 p0344 A71-14452
- Trojan periodic orbits interpretation to establish manifolds evolution for mass ratio variations
04 p0652 A71-15702
- Collision periodic orbit sets in restricted n body problem for various mass ratios
04 p0654 A71-15715
- Critical periodic orbits for main families and all mass ratios, considering stability in restricted problem
04 p0655 A71-15729
- Earth-moon mass ratio correction, observing artificial satellite motion near triangular libration point
08 p1362 A71-21150
- Massive body gravitational to inertial mass ratio from equilibrium assembly model of particle interactions
13 p2139 A71-28997
- Double stars astrometry, discussing proper motions, parallaxes and mass ratios of visual binaries
14 p2310 A71-30359
- Multistep rocket mass ratios optimization, including exhaust gas velocities, structure and efficiency
16 p2644 A71-32843
- Fuel cell system steam/hydrogen mixture mass ratio detector using fluidic delay line oscillator
17 p2745 A71-35294
- General relativistic time delay and moon-earth masses and Mars mass-ephemeris ratios from S-band range and Doppler tracking
20 p3296 A71-39623
- Three body problem involving large mass ratio by backward numerical integration in constant density resisting medium
22 p3601 A71-42164
- MASS SPECTRA**
Valeraldehyde o-nitrophenylhydrazine mass spectrum with low intensity peak due to combined hydroxyl and water loss from molecular ion
02 p0209 A71-12573
- Synthesized amino esters and ketones with varying distance between functionalities, examining mass spectral fragmentation
02 p0209 A71-12574
- Mass spectral properties of alkoxy-cyclohexanol trimethylsilyl ethers and alkoxy-cyclohexyl trimethylsilanes, using deuterium labeling
02 p0209 A71-12575
- Computer program for interpretation of residual gas analyzer mass spectra, considering vacuum environmental testing of spacecraft
11 p1730 A71-26505
- Mass spectrum of stopping heavy cosmic ray particles at sea level observed, interpreting flux as deuteron production by high energy protons and neutrons
13 p2122 A71-28067
- Shock tube production of vibrationally excited molecules for mass spectra studies in hot gases
16 p2613 A71-32894
- Massive pulsationally unstable stars dynamic analysis, formation and upper mass limits
18 p2960 A71-35934
- MASS SPECTROMETERS**
Solar wind elemental and isotopic He and Ne compositions from mass spectrometry of ions collected in metal foils deployed during Apollo 11 and 12 landings
01 p0146 A71-11486
- Computer controlled mass spectrometer system, processing spectral information data for on-line graphic system output
02 p0253 A71-12550
- Small mass spectrometers as substance specific detectors for gas chromatography, differential thermal analysis and thermogravimetry
04 p0601 A71-15916
- Mass spectrometer with electron impact ion source, evaluating instrument linearity and reproducibility
05 p0754 A71-16948
- Paper chromatography combination with dinitrophenyl amino acids mass spectrometry for analyzing purine and pyrimidine bases
06 p0865 A71-17574
- Mass spectrometer application to study of secondary ion emission during metal surface bombardment by argon ion beam
07 p1112 A71-19621
- Ion source for double focusing magnetic mass spectrometer for use with gas chromatograph on Mars mission, requiring electron beam stabilization in space
07 p1113 A71-19851
- Electronic compensation of water vapor effects in respiratory mass spectrometry
07 p1052 A71-20335
- He ion vertical concentration profiles from space probe mass spectrometer measurements
08 p1278 A71-21020
- Mass spectrometer ion source modifications for temperature range extension in high temperature research
09 p1450 A71-23068
- Magnetic mass spectrometer for ionosphere composition measurements permitting single spectrum analysis of plasma of negative and positive ions
10 p1608 A71-23817
- Data reading function synchronized digital mass spectrometer with incremental scan by magnetic field sweeping, describing method for polynomial fitting of data
11 p1762 A71-25663
- Mass spectrometric technique for investigation of hydrazine catalytic decomposition on heated platinum at low pressure, considering advantages of quadrupole spectrometer
11 p1765 A71-26280
- Positive H, He and O ions in exosphere from mass spectrometers mounted on Elektron 4 satellite
12 p1899 A71-26644
- Ion source of mass spectrometer for high temperature composition studies of gas phase
14 p2247 A71-30588
- Ammonium perchlorate propellants sterilizability, using medium resolution mass spectrometer and regression analysis of results in thermal stability studies [AIAA PAPER 71-718]
14 p2286 A71-30769
- Spatially periodic static field mass spectrometers for upper atmosphere composition measurements on board satellite and sounding rocket
15 p2400 A71-32350
- Computer controlled data handling system for quadrupole mass spectrometer performing on-line chemical analysis of rocket chamber combustion gases [JPL-TR-32-1518]
16 p2578 A71-33182
- Quadrupole mass spectrometer ultimate characteristics concerning resolution, range, recording speed, working pressure and sensitivity
17 p2737 A71-34288
- Mass and charge dependent ion discrimination in linear pulsed time of flight mass spectrometer, using electric field for source storage and count enhancement
18 p2922 A71-36590
- He ion vertical concentration profiles from space probe mass spectrometer measurements
20 p3219 A71-39600
- Crystall growth of III-V compound semiconductors from vapor phase, studying deposition processes chemistry by mass spectrometry
21 p3427 A71-40216
- Mass spectrometer application to gas analysis of samples from turbulent wake of hypervelocity projectiles
21 p3362 A71-40384
- High vacuum mass spectrometric hazardous gas detection system used during cryogenic loading of Saturn vehicles, discussing application to environmental pollution detection
22 p3542 A71-41988
- Unified procedure for detection of life on Mars by Viking program missions, using mass spectrometer for remote biologically oriented experiments
23 p3736 A71-43541
- Mass spectrometer measurements of hydrogen, helium, nitrogen, oxygen and nitrogen oxide ion concentrations vertical profiles in ionosphere at midlatitudes
24 p3824 A71-45311
- Mullard channel electron multipliers applications to space research, scientific instruments, vacuum devices and mass spectrometers
24 p3811 A71-45332

MASS SPECTROSCOPY

Human blood gases continuous measurement in vivo by mass spectrography, considering arterial nitrogen washout and cerebral blood flow determination

01 p0021 A71-10237

Mass and phase spectrometry in modulated laser beam experiment for neutral particles velocity measurement prior to ionization

01 p0028 A71-11303

Mass spectroscopic determination of geometric isomers of alpha, beta-unsaturated carboxylic acids, noting various modes of fragmentation

01 p0028 A71-11304

Rocket-borne mass spectrometer observation of NO in auroral arc

01 p0077 A71-11522

Remote group interactions after electron impact in 4-substituted cyclohexanones, investigating mass spectrometry in structural and stereochemical problems

02 p0209 A71-12548

TiS vaporization thermodynamics at high temperature mass spectrometry, considering ionic fragmentation and ionization cross section errors

07 p1054 A71-19368

Gas pressure conversion for spacecraft outgassing products investigation by mass spectrometer analysis, noting plastic decomposition products calibration

07 p1023 A71-20067

Mass spectrometric determination of vapor phase dissociation energies of scandium dicarbide and scandium tetracarbide

08 p1250 A71-20673

Computerized method of interpreting low resolution mass spectra in organic chemical analysis, describing inference maker program applications and results

09 p1403 A71-22471

Service life of solid molybdenum sulfide based plastic coatings with different binders under high vacuum friction investigated by mass spectroscopy

09 p1454 A71-22819

Quadrupole mass spectroscopy of spacecraft critical surfaces vapor contamination, using lubricating oil covered titanium dioxide colorimetric sample

10 p1609 A71-23930

Autoionic mass spectroscopy, discussing emitters, ion sources and mass spectra of deuterized benzene, chlorobenzene and chloroform molecules during electron ionization and autoionization

10 p1611 A71-24383

Atomic oxygen and carbon dioxide measurement in lower thermosphere by mass spectroscopy

10 p1606 A71-24803

Mass spectroscopy - Conference, Kyoto, September 1969

11 p1819 A71-25217

Mass spectroscopy applications to neutral and ionized terrestrial upper atmosphere, lunar atmosphere and space research

11 p1726 A71-25218

Real time high resolution mass spectroscopy using digital computer techniques for data acquisition, processing and presentation

11 p1761 A71-25220

Positive diatomic nitrogen ions dissociation during collisions with inert gas atoms, measuring mass and energy distributions from focusing parabolic spectrograph

11 p1801 A71-25227

Modulated molecular beam mass and phase spectroscopy applications in hot oxygen radiative attachment, crossed beam chemical kinetics and neutrals clustering in free jets

11 p1727 A71-25228

Hydrocarbons pyrolysis in Knudsen cells at low pressures, using mass spectrometry to study reactions and products

11 p1727 A71-25229

Alpha-beta unsaturated carboxylic acids geometric isomers determination by mass spectroscopy

11 p1727 A71-25230

Mass spectrometric studies of laser beams interaction with solids, discussing surface temperature reached by solid during irradiation

11 p1775 A71-26081

Ultrahigh vacuum gas analysis by mass spectrometry, discussing quadrupole and omegatron mass spectrometers performance with special reference to reversible adsorption characteristics

11 p1763 A71-26187

Reacting gases analysis by mass spectroscopy, discussing stable products microprobe and molecular beams effective samplings for free radicals and active atoms

11 p1765 A71-26278

Quadrupole mass spectrometry in studies of heterogeneous and flash photolytic reactions and unstable intermediates detection

11 p1765 A71-26279

Mass spectrometric investigation of high power laser beam plasma on solid target, determining multicharged ion yield, energy, angular distribution and recombination effect

15 p2418 A71-31191

Sterols isolation and identification from Pleistocene sediment by gas-liquid chromatography and combined gas chromatography-mass spectrometry

15 p2366 A71-31367

Arc-heated nonequilibrium air expansion flow mass spectroscopic analysis, noting reservoir entropy effect [AIAA PAPER 71-621]

15 p2366 A71-31550

Open microcracks and internal microdefects detection during long term strength testing in vacuum by mass spectrography

15 p2383 A71-31653

ClF diluted solutions in Ne, investigating thermal decomposition mechanism behind shock waves by mass spectroscopy

15 p2367 A71-31874

ZrC vaporization at high temperatures, investigating dissociation into components by mass spectroscopy

15 p2431 A71-32158

Vaporization thermodynamics of lanthanum carbides from Knudsen effusion mass spectrometry

16 p2538 A71-32812

Ion mass spectrometry in plasma analysis, reviewing complex ionized gaseous media investigations and specific reactions

16 p2576 A71-32962

Mass spectroscopy of upper atmosphere neutral composition at equatorial, middle and polar latitudes from meteorological rockets

16 p2566 A71-33758

Polynuclear aromatic hydrocarbons in Murchison meteorite, determining distribution by gas chromatography and mass spectrometry

17 p2799 A71-34503

Mass spectrometric studies of origin of light elements Li, Be and B in universe, considering spallation of stellar and galactic gases by high energy particles

18 p2959 A71-35914

Mass spectrometric investigation of plasma created in atomization of Ni and Y ferrites by laser radiation

19 p3110 A71-37142

Mass spectrometric measurements of negative ion concentration in D and lower E regions

19 p3127 A71-38031

Mass spectrometric measurement of negative ion concentration in nighttime D region

19 p3128 A71-38033

Bound sugar content in marine sediments by capillary gas chromatographic-mass spectrometric analysis of trimethylsilyl derivatives

19 p3055 A71-38146

Pulsed Nd laser source mass spectroscopy application to geological material analysis, tabulating assessed limits of detection for various elements

20 p3245 A71-39422

Photoionization mass spectrometry, considering application to appearance potentials determination, ion-neutral reactions and gas analysis

22 p3537 A71-41649

Corrosive oxide layer formation kinetics during interaction of oxygen with polycrystalline W at 500-1000 K, using desorption mass spectrometry

23 p3641 A71-42907

Gas-liquid chromatography and mass spectrometry of lunar fines and glass constitution by preparing trimethylsilyl derivatives of discrete silicate ions

23 p3746 A71-43668

Spark mass spectrometric analysis of major and trace elements abundance in Apollo 11 and 12 lunar rocks and soil samples, comparing with standard basalt

23 p3749 A71-43686

Thermal analysis-quadrupole mass spectrometric analyses on inorganic released gases of Apollo 11 and 12 samples and synthetic lunar analogs

23 p3750 A71-43699

Knudsen cell-mass spectrometric study of Apollo 12 samples vaporization process

23 p3750 A71-43700

Ar, Kr and Xe emanation during stepwise heating of lunar rocks under slow neutron irradiation in pile, using mass spectroscopy

23 p3754 A71-43726

Apollo 12 lunar surface samples analysis for organic compounds by mass spectroscopy and pyrolysis-gas chromatography

23 p3756 A71-43741

Tektite organic constituents evidence from high temperature mass spectrometry, investigating relation to formation process and terrestrial contamination

23 p3769 A71-43926

MASS TRANSFER

Ni diffusion and electric transfer in Ni-Mo alloy, using isotope tracer technique

01 p0097 A71-10043

Porous metal fiber laminar vacuum insulation, calculating steady state heat and mass transfer

01 p0179 A71-10615

Spherical alcohol droplet vaporization in acoustically disturbed medium, considering convective heat and mass transfer

01 p0179 A71-10798

Steady isothermal plane gas flow between infinite parallel plates at arbitrary Knudsen numbers, obtaining linear differential equations of mass transfer

01 p0071 A71-11114

Digital simulation mathematical model describing simultaneous energy and mass transfer process in clothing-airspace-skin system

02 p0203 A71-11806

Two free homogeneous turbulent coaxial air jet mixing, showing mass transfer between boundary layers and interface presence

02 p0185 A71-12409

Semidetached eclipsing binary stars mass exchange, examining stellar evolution, luminosity, mass loss and exchange and Roche limit

02 p0313 A71-12497

Mass transfer and Biot diffusion in MHD flows with mixed boundary reaction kinetics, considering Hartmann and plate problems

02 p0293 A71-12632

Rapid mass transport to Pt electrodes in foamed electrolytes, examining current density-anode overpotential relationship

02 p0210 A71-12957

Variational problem for turbulent liquid flow mass transport on inclined flat plate, using plane Poiseuille flow solution

03 p0398 A71-13101

Base pressure variation by mass injection in turbulent supersonic axisymmetric near wake at high Mach numbers

03 p0399 A71-13457

Close binary star evolution, discussing mass exchange in system with 7 solar mass primary

03 p0490 A71-13939

Severe storm mass and energy convective transport characteristics, using ATS-3 cloud photographs and three layer model

03 p0454 A71-14204

Convective heat and mass transfer - ASME Conference, New York, November-December 1970

04 p0674 A71-14777

Gas to gas film cooling, describing physical processes and performance prediction method based on heat and mass transfer analogy

04 p0676 A71-14978

German monograph on mass transfer between close binaries from hydrodynamic standpoint

04 p0644 A71-15099

Soviet monograph on mass exchange in solid-liquid system covering soluble material extraction and absorption, interphase mass transfer and dissolving process

04 p0677 A71-15446

Turbulent boundary layer equations for heat and mass transfer in incompressible and compressible flows, using eddy viscosity formulation

04 p0680 A71-15479

Free stream turbulence enhanced stagnation line heat and mass transfer on two dimensional blunt body

04 p0681 A71-15481

Turbulent heat and mass exchange intensity at gas screen, investigating nonisothermality and wall penetrability effects

04 p0683 A71-15497

Translatory vapor bubbles motion in binary liquid mixtures under heat and mass transfers

04 p0687 A71-15534

Liquid-vapor system in closed container, investigating transient pressure rise under heat and mass transfer interactions including incipient and nucleate boiling

04 p0687 A71-15535

Nonlinear integrodifferential equations of heat and mass transfer problems, discussing asymptotic solution method

04 p0688 A71-15542

Friction, mass and heat transfer in turbulent boundary layers of fluid flows past obstacles

04 p0577 A71-15619

Convective mass transfer, velocity and concentration fields during nonNewtonian fluid motion in circular pipe with diffusion flow at wall

04 p0579 A71-15798

Soviet book on supersonic turbulent boundary layer covering gas flow molecular theory, heat and mass transfer at porous surfaces, etc

06 p0841 A71-17439

Oceanic rise crest heat flow model, examining vertical velocity distribution of mass transport

06 p0889 A71-17635

Plane incompressible MHD boundary layer on porous plate, considering heat and mass transfer in blowing or suction velocity distribution

06 p0936 A71-17736

Laminar flow convective heat and mass transfer on end walls of vortex chambers

06 p1005 A71-17737

Moving condensate film effect on velocity profile and mass transfer rate from gas-vapor mixture by Crank-Nicholson method

06 p1006 A71-18070

Submerged arc welding process, observing arc motion and metal transfer with X ray high speed photography

06 p0905 A71-18090

Interstellar gas and star mass interchange, discussing balance and galactic and stellar evolution models

06 p0972 A71-18334

Heat and mass transfer in turbulent boundary layers - Conference, Herceg Novi, Yugoslavia, September 1968, Volume 1

07 p1219 A71-18751

High velocity liquid flow past rough plate surface, investigating boundary layer cavitation effects on convective heat and mass transfer

07 p1086 A71-18774

Heat and mass transfer investigation in nucleate boiling boundary layer by salt depositions

07 p1221 A71-18787

Binary fluids boiling heat and mass transfer in boundary layer, discussing bubble growth rate, surface roughness effects and burnout heat flux

07 p1221 A71-18791

Heat and mass exchange coefficients and critical separation for turbulent boundary layer during nonuniform blowing under nonisothermal conditions

07 p1087 A71-18918

Mass transfer net rate /evaporation plus entrainment/ from thin liquid film, using methanol, water, butanol and RP-1 as coolants

07 p1222 A71-18997

Turbulent transfer model in wall region, estimating mean surface renewal frequency for mass momentum and heat transfer rates and velocity, temperature and concentration profiles

07 p1092 A71-20224

Membrane separate systems ion and water mass transport, noting effect on anolyte concentration and alkaline battery performance

08 p1234 A71-21092

Boundary layer model of laminar viscous flow around high speed slender bodies with surface mass transfer

[AIAA PAPER 68-719] 09 p1381 A71-22084

Uniform two dimensional incompressible turbulent boundary layer with uniformly distributed surface mass injection, correlating results on basis of turbulent kinetic energy equation

09 p1430 A71-22105

Thermodynamic system with concentrated loads due to heat and mass transfer or chemical reactions, analyzing wave processes and system stability

09 p1544 A71-22269

Book on dynamic characteristics of aerosol particles in terms of classical mechanics covering continuum approximation, single particles heat and mass transfer, diffusion, dispersion, etc

09 p1431 A71-22284

Meteoritic masses evaporation during flare, showing discrepancies for luminosity factors

09 p1520 A71-22830

Book on homogeneous flows aerothermochemistry covering chemical reactions, heat and mass transfer, entropy production, species continuity, momentum and energy equation

09 p1547 A71-23674

Mass entrainment products effect on radiative and convective heat transfer during decomposition of graphite blunt body in steady hypersonic flow of radiating air

10 p1696 A71-24364

Soviet papers on heat and mass transfer covering conduction, transport in capillary and dispersed systems, irreversible thermodynamics, material drying, etc

10 p1696 A71-24481

Heat and mass transfer in supersonic laminar boundary layers with light gas injection, deriving approximate solution for binary mixture flow with variable fluid properties

10 p1598 A71-25097

Compressible similar laminar boundary layer equations for zero wall shear and mass addition, describing heat transfer reduction and boundary layer growth by asymptotic analysis

11 p1750 A71-25479

Planetary nebulae mass ejection by radiation pressure, describing mathematical models for time independent outflowing envelopes

11 p1821 A71-25537

High temperature heat pipes material corrosion problems, considering mass transfer from cooling zone into heating zone

12 p1917 A71-26975

Unsteady mass exchange during laminar MHD free convection on vertical plate, deriving time dependence expression for external magnetic field

12 p1938 A71-27242

Transverse acoustic wave amplification in solid propellant rocket motor, using discrete mass injection as excitation source

12 p1946 A71-27565

Heat and mass transfer in monatomic molecular gases and gas mixtures, discussing energy exchange during collision and thermal diffusion effect on thermal conductivity

13 p2159 A71-28186

Optimal control synthesis of one dimensional stochastic heat and mass transfer processes with distributed parameters

13 p2161 A71-28727

Two phase critical flow of one component mixtures in nozzles, orifices and short tubes, considering interphase heat, mass and momentum transfer rates [ASME PAPER 70-WA/HT-5]

13 p2049 A71-28980

Heat and mass transfer in triple interline region of stationary evaporating meniscus on flat plate immersed in liquid pool

13 p2164 A71-29006

Boundary conditions formulation for energy and mass transfer in weakly rarefied gas flows past bodies

13 p1991 A71-29149

Axisymmetric flow effects on surface mass injection at supersonic and hypersonic speeds, streamline inclinations and surface pressures generation by turbulent viscous dissipation

14 p2223 A71-29874

Mass injection effect on heat transfer reduction to three dimensional stagnation points as function of shape, enthalpy and gas properties

14 p2335 A71-29891

Heat and mass transfer optimization in hydrogen-oxygen fuel cells with ion exchange membrane

14 p2181 A71-30050

Heat transfer processes in heat pipes, examining heat and mass transport mechanisms between heat source and sink

14 p2336 A71-30243

Equations for radiative contribution to energy and mass transfer in monatomic and ionized gas flow in local thermodynamic nonequilibrium

14 p2338 A71-30819

Temperature fields and mass and heat transfer at surface of solid spherical particle in laminar viscous fluid flow

16 p2557 A71-32931

Integral analysis of incompressible turbulent boundary layer with mass transfer and pressure gradient, including Stevenson velocity profiles and skin friction law

16 p2559 A71-33221

Heat and mass transfer during deposition on heated surfaces in nonisothermal gas flow with suspended solid particles, using motion of continuous Newtonian medium

17 p2836 A71-34305

Convective mass or heat transfer to or from uniform or size distributed drops, bubbles or solid particles at high Peclet and low particle Reynolds numbers

17 p2837 A71-34690

Mass transfer in turbulent flow region downstream of circular pipe sudden enlargement for high Schmidt numbers, using diffusion controlled electrolysis technique

17 p2837 A71-34692

Mass transfer in close binaries, determining gaseous ring formation conditions and properties from ejected particle trajectories computation

17 p2809 A71-35594

Light wave Rayleigh interferometer for concentration gradient measurements in liquid systems with mass transport

18 p2917 A71-36052

Close binary systems evolutionary processes, considering mass transfer and gas dynamics

18 p2968 A71-37033

Turbulent rotating tube flows kinematic similarities, deriving heat and mass transfer, swirl damping and axial and rotational velocity profile

19 p3043 A71-37127

Bulk vapor formation processes during laser beam heating of metals, considering effect on mass transfer

19 p3072 A71-37586

Dissolution rate of vertical nickel cylinder in liquid aluminum under free convection, showing fluid boundary layer mass transfer role

19 p3079 A71-37709

Rotating disk flow system for Fe vaporizing into cold Ar atmosphere, investigating effect of condensation in boundary layer on mass transfer

19 p3162 A71-37727

Matter effluence forming comet Bennett 1969 i tail, calculating particle ejection acceleration as function of intrinsic anomaly of nucleus

19 p3138 A71-37783

Curvature effect on heat and mass transfer from isothermal sphere in potential flow [ASME PAPER 71-HT-7]

19 p3164 A71-37984

Heat and mass transfer through porous plate into turbulent two dimensional incompressible boundary layer, using van Driest damped mixing length

[ASME PAPER 71-HT-10] 19 p3045 A71-37986

Mass transport at high current densities in Al and Mo thin film conducting stripes, noting effect on IC life

19 p3119 A71-38511

French monograph on free and forced convection and external radiation from hot gas oscillating in resonance tube, considering heat balance and mass exchange

19 p3172 A71-38649

Planetary capture in restricted three body problem and bridge formation between galaxies

20 p3286 A71-38761

Heat and mass exchange coefficients and critical separation for turbulent boundary layer with secondary fluid injection under nonisothermal conditions

20 p3210 A71-38897

Heat and mass transfer calculation in turbulent boundary layer on rough surface

20 p3315 A71-39793

Observation probability of orbital motion and mass transfer of pulsars in close binary systems, excluding supernova explosion origin for runaway velocities

20 p3304 A71-39943

Unsteady state boundary layer equations solution in laminar flow systems with free surface and transfer of heat or mass

21 p3370 A71-40990

Surface roughness and mass transfer influence on boundary layer and friction coefficient for turbulent flow over flat plate

21 p3371 A71-40997

Radioisotope testing methods for dissolution and mass transfer of alloying additives in Pb-Sb alloys during preparation in electromagnetic pumps

22 p3553 A71-41765

Boundary layer asymptotic solutions for free convection in laminar three dimensional systems, determining rapid mass transfer and centrifugal forces effects

22 p3619 A71-41870

Laminar free convective heat transfer on vertical cylinder with concentration gradients, considering mass transfer effects prediction

22 p3620 A71-41882

Thin liquid films under simultaneous shear and gravity forces, noting data incorporation into transport equations for heat and mass transfer

22 p3620 A71-41884

Approximate solutions to Stefan nonlinear heat and mass transfer problem under various boundary conditions and phase transformation temperature

22 p3622 A71-42687

Spin stabilized spacecraft inversion by mass translation with momentum vector fixed in inertial space, calculating control mass dynamics

22 p3612 A71-42777

Lead isotopes volatile transfer in Apollo 11 and 12 lunar soil samples, discussing lunar age estimates

23 p3752 A71-43714

Heat and mass transfer in binary laminar boundary layer with free convection on vertical porous surface, integrating momentum and energy equations for upper limits

24 p3887 A71-44744

Laminar boundary layer calculation for simultaneous heat and mass transfer in evaporating liquid layer on flat plate in parallel gas flow, considering variable material parameters

24 p3888 A71-44965

Monatomic gas flow in radiation field, noting effects on mass transfer

24 p3821 A71-45182

MASTOIDS

Mechanical impedance measurement of artificial and human mastoids for bone vibrator calibration as function of frequency

11 p1725 A71-26189

MATCHING

Single thin lens for Gaussian laser mode matching, discussing position and focal length determination

12 p1905 A71-26809

Transient matrix heat transfer test data reduction, discussing direct curve matching methods implementation by distance function minimization

17 p2835 A71-34178

Mean value theorem for broadband matching of source with known resistance and parasitic capacitance matched to load resistance

22 p3510 A71-42247

MATERIAL ABSORPTION

Amino silica gels absorption properties with respect to carbon dioxide, hydrogen sulfide and water vapor, comparing affinity

20 p3193 A71-39233

MATERIAL BALANCE

NT WATER BALANCE

MATERIAL REMOVAL [MACHINING]

U MACHINING

MATERIALS EROSION

U EROSION

MATERIALS HANDLING

NT GROUND HANDLING

NT PROPELLANT TRANSFER

NT REMOTE HANDLING

Complex supply system large quantity data handling and cost savings through optimum planning of storage points and transport using linear separable programming

06 p1010 A71-17746

Material point motion in conveyor horizontal pipe drums with screw surface on inner walls, using law of addition

13 p1998 A71-28297

- Melbourne/Tullamarine airport, describing facilities, capacity, road system, cargo and passenger handling areas and runway layout 13 p2045 A71-29310
- Intravascular manual cargo transfer, using water immersion technique for zero gravity simulation [ALAA PAPER 71-851] 18 p2871 A71-36642
- Exchange regulation of standardized container loading units in air freight transportation 19 p3173 A71-38220

MATERIALS RECOVERY

NT WATER RECLAMATION

- Aluminum compression microstructure under various strain rates and temperatures, discussing dynamic recovery role 02 p0267 A71-12877
- Deformed metals stage I recovery, considering plastic deformation microscopic description, defect creation, interstitials and experimental methods 03 p0441 A71-13348
- Thermal recovery in stainless steel after explosive shock loading and forming 04 p0614 A71-15781
- Co-ti alloy hardness recovery, noting dependence on solid solution structure after low temperature aging 05 p0768 A71-16855
- Self pulsing in homogeneously broadened oscillator, using materials with short recovery time for appreciable inverted population density modulation 18 p2929 A71-35901
- Tantalum and niobium ternary oxides recovery from liquid potassium solution, determining composition and crystallographic modifications by chemical and X ray diffraction analyses 20 p3194 A71-39372

MATERIALS SCIENCE

- Steels and weld metal alloying for stable austenitic structure under long term cryogenic conditions, investigating optimal Cr, Ni, Mn and nitrogen combinations 01 p0085 A71-10087
- Materials R and D economic considerations, emphasizing processing and assembly costs reduction and user benefits 01 p0183 A71-10279
- Fiber reinforced materials technology, reviewing basic principles, existing technologies and future trends, various composite materials characteristics, etc 01 p0107 A71-10315
- Papers on bearings covering types, materials, lubricants, applications, etc 01 p0088 A71-10813
- Ducting materials and joints technology fallout from aerospace projects, discussing reliability in terms of corrosion resistance, fatigue strength and thrust compensating duct design 01 p0007 A71-11431
- Soviet book on oxide and silicate materials chemistry and technology covering corrosion, thermophysical properties shear stress, drying, etc 02 p0272 A71-11825
- Materials science and manufacturing in space, discussing potential technologies and laboratory techniques using vacuum, weightlessness, temperature and radiation environment 02 p0255 A71-11973
- Superconductivity in physical metallurgy, discussing flux line structure and lattices, grain boundaries, stacking faults, etc 02 p0266 A71-12876
- Nb high purity binary alloys preparation and processing 02 p0270 A71-12933
- Continuum internal thermodynamic constraints effect on materials response, assuming workless stress tensor 03 p0506 A71-13694
- Space research benefits from applications technology satellites and materials utilization, reviewing satellite communication networks, meteorology geodesy, navigation, geology and agriculture 03 p0524 A71-14245
- Homogeneous and inhomogeneous photoelectric semiconductors, examining photomagnetolectric, photomechanic, photovoltaic and Dember effects 03 p0468 A71-14303
- Fine coherent precipitate morphologies by spinodal mechanism, reviewing clustering in binary solid solutions 03 p0446 A71-14491
- Materials corrosion, discussing measurement, prevention, secondary interactions, R and D, etc 04 p0613 A71-15776
- Gas turbine engines materials and components equivalent service life estimation 05 p0796 A71-16753
- Solid deformable body combined brittle and plastic elements model for strain analysis 05 p0827 A71-16758
- Solid state physicists and metallurgy, discussing high strength materials, composites, radiation tolerance, fatigue, oxidation, superconductors, etc 05 p0794 A71-16957

- Materials properties measurement by laser, describing methods for stress investigation in glass and electron density measurement in plasmas 05 p0764 A71-16969
- Corrosion damage relationship to military aircraft accidents, discussing quality control, material selection and manufacturing processes 06 p0911 A71-17415
- Soviet book on materials strength covering physical properties, stress-strain state, elastic bodies, loading conditions, shear, torsion, bending, buckling creep, etc 06 p0984 A71-17448
- Short term creep effect on high speed air flows, investigating material behavior under vibration loads, corrosion and erosion 07 p1130 A71-19163
- Failure theory for anisotropic homogeneous materials, discussing interaction factor, resistance, orthotropism and planar stress 07 p1214 A71-20011
- Low temperature material properties analyzer with superconducting microwave resonant cavity 07 p1179 A71-20160
- Space shuttle structures and materials, considering booster arrangements thermal protection, high temperature metals and composite materials 07 p1216 A71-20228
- Materials durability in presence of stress concentration under biharmonic loading 09 p1538 A71-22626
- Substrate materials for microwave integrated circuits, comparing dielectric constants, surface finishes and thermal conductivity for alumina, sapphire, magnesium titanite, YIG and beryllium oxides 09 p1418 A71-23156
- Carbon dioxide lasers for industrial material processing, discussing machine tool reliability, maintenance, various automation approaches and economic efficiency 09 p1457 A71-23403
- Material thermal removal by electrical discharge, electron beam and laser machining, discussing effects on surface integrity 09 p1458 A71-23411
- Structural materials dynamic analysis, considering viscous, hysteresis and viscoelastic damping [ALAA PAPER 71-349] 11 p1843 A71-25328
- Viking rocket heat shield material mechanical properties, examining time-temperature superposition with continuous stress relaxation data measured in vacuum 11 p1791 A71-26518
- Materials evaluation system for aerospace structural application 12 p1919 A71-27678
- Book on materials for magnetic functions covering magnetic materials and devices, magnetic phenomena, parameters and interrelations, ferrites chemistry, microstructure and processing, etc 13 p2112 A71-29443
- Soviet book on aircraft materials science and treatment covering steel/cast iron processing, metallurgy, heat/thermochemical conditioning, surface protection and corrosion prevention 14 p2256 A71-29529
- Aerospace materials - Conference, Anaheim, California, April 1971 14 p2261 A71-29633
- Advanced composite vs conventional material components in cost comparison for aircraft parts 14 p2263 A71-29656
- Low ductility materials, considering applications to stress analysis, failure criteria, fatigue, physical metallurgy and polymer mechanics 14 p2251 A71-29893
- Brittle structures and materials fracture strength, using linear fracture mechanics as analytical basis for testing 14 p2258 A71-29895
- Steels and weld metal alloying for stable austenitic structure under long term cryogenic conditions, investigating optimal Cr, Ni, Mn and nitrogen combinations 16 p2584 A71-33643
- Thermoelastic materials thermodynamic properties, developing coldness as universal function of viscous heat conducting fluids 17 p2837 A71-34694
- Gas turbine engines materials and components equivalent service life estimation 17 p2793 A71-35452
- Vibration and corrosion-erosion damage effects on material behavior during short term creep in high speed air flows 17 p2760 A71-35659
- Premium mechanical properties for materials in space shuttle orbiter project, emphasizing cost and weight reductions 18 p2979 A71-36465
- Materials behavior at low temperatures, investigating lattice vibrational spectra relation to specific heat, conducting electron energies, thermal expansion, etc 20 p3270 A71-39242

- Laser holography and interferometry in materials science, evaluating displacement and deformation within nondestructive testing 20 p3245 A71-39342
- Holographic interferometry for structure and material deformation measurement, presenting static loading and resonant vibration surveys 20 p2338 A71-39346
- Materials research - Conference, Kyoto, September 1970 21 p3400 A71-40830
- Metal and polymer matrix materials research based on stringent requirements for thermal reactors, jet engines and space vehicles, discussing tests and analysis methods 21 p3401 A71-40901
- MATERIALS TESTS**
- Electroinductive defectoscopy using eddy currents as nondestructive materials testing method 01 p0079 A71-10335
- Fiberglass reinforced plastics heavy duty structural parts quality control, discussing strength parameters, safety coefficients, testing methods, etc 01 p0088 A71-10689
- Airplane materials mechanical properties degradation due to fatigue, discussing breaking strain of Al alloy 01 p0104 A71-11395
- Al-Zn-Mg-Cu type high strength Al alloys mechanical properties evaluation by fracture mechanics methods 01 p0104 A71-11540
- Soviet book on material analysis by nuclear radiation covering heavy elements concentration in ores, radioisotope devices and gamma ray capture spectroscopy 02 p0283 A71-12721
- Composite materials testing, standards and design, considering flat laminates, honeycombs and construction weight savings 03 p0448 A71-13535
- Continuous filament composite materials fabrication and tests for dynamic deformation, fracture and wave propagation properties, considering axially reinforced cylindrical body compression 03 p0508 A71-13768
- Rigid-perfectly plastic model for real materials behavior, considering modification for strain hardening and elastic effects under various load conditions 03 p0509 A71-13780
- Launching intermediate velocity thin plastic sheets for short duration pressure pulse studies of dynamic materials properties 03 p0427 A71-13916
- Material testing - Conference, Budapest, October 1970, Section 3, Spectrochemical analysis 03 p0375 A71-13968
- Plastic, elastomeric, ceramic glass, metallic and composite materials rain erosion resistance at supersonic speeds, examining rate-velocity dependence 03 p0444 A71-14288
- Rain and sand erosion materials tests, considering temperature and atmosphere pressure effects and relation between fatigue behavior and erosion/cavitation strength 03 p0444 A71-14289
- Polymeric materials plastic deformation properties during service and storage, discussing prediction and testing methods 03 p0448 A71-14300
- Material testing - Conference, Budapest, October 1970, Metal physics and test methods, Volume 1, Part 1 04 p0665 A71-14876
- Material testing - Conference, Budapest, October 1970, Metal physics and test methods, Volume 2, Part 2 04 p0666 A71-14885
- Ultrasonic viscosimeter for gamma irradiation effects on materials structure, determining fluid viscosity changes from rate of damping of plate vibrations 04 p0594 A71-14918
- Whisker technology developmental history and current state, discussing composite material production and whisker testing methods 04 p0611 A71-14941
- Testing methods for mechanical properties of individual whiskers, describing tensile machines, shear stress measurement torsion device and Young modulus measurement method 04 p0603 A71-14945
- Thermal conductivity determination for materials by pulsed laser or flash lamp energy absorption 04 p0595 A71-14961
- Stainless steel physicochemical properties stability, discussing equipment for industrial materials testing under various environmental and loading conditions 05 p0769 A71-16897
- Material stiffness/weight ratio effects on helicopter blades uncoupled flapwise, chordwise and torsional natural frequencies by rapid estimation 06 p0985 A71-17691

Test facility for acoustic fatigue of materials and structural elements

07 p1083 A71-19167

Shock tube testing of acoustic materials at high sound amplitudes

07 p1083 A71-19586

Rail shear test theoretical and experimental analysis, comparing high modulus reinforced composites test data with predicted values from lamination theory

07 p1215 A71-20128

Universal materials testing system control using digital computer and changeable programs

07 p1069 A71-20201

Automatic materials testing device for thermal fatigue and strength under programmed loading

08 p1271 A71-20838

Gas dynamic test stand for cyclic thermal load testing of gas turbine engine materials and components at variable heating and cooling rates and mechanical loads

08 p1271 A71-20839

Friction and wear tests on materials of various speeds, loads and temperatures at high relative humidity

09 p1426 A71-22325

Materials mechanical properties measurement methods and equipment at cryogenic temperatures including microscopes, X ray cameras, microhardness tester, fatigue and impact strength testing machines

09 p1468 A71-22329

Thermal fatigue testing of materials under static load with allowance for creep

09 p1426 A71-22497

Grain size influence on deformation characteristics of commercial Ti with oxygen and Fe impurities, discussing test results on various mechanical properties

09 p1479 A71-23688

Ablative thermal insulation materials testing for naval missile propulsion system application

11 p1789 A71-26032

Polymeric ablation materials testing in arc image furnace over various temperatures, pressures and thermal flux

11 p1790 A71-26045

Fracture toughness and critical strain rate measurements in unidirectional glass reinforced plastics as function of resin, hardener, fiber and degree of cure

11 p1790 A71-26387

High temperature heat pipes material corrosion problems, considering mass transfer from cooling zone into heating zone

12 p1917 A71-26975

Explosive shock loading effect on materials properties, describing test equipment

12 p1895 A71-27689

Acoustic emission application to nondestructive testing of materials, manufacturing processes and structural components failures

13 p2073 A71-27939

Destructive and nondestructive material testing techniques, discussing equipment design and procedures standardization

13 p2074 A71-28493

Machine for corrosion testing materials under various static and dynamic axial tension, torsion and bending loads

13 p2045 A71-29374

Materials and structural design development by high velocity impact testing due to transport and subsonic military aircraft susceptibility to bird collision damage

14 p2221 A71-29642

Nondestructive testing techniques for discrete local materials properties evaluation, allowing nonstatistical analysis of thermomechanical stress behavior

14 p2251 A71-29900

Light transmission homogeneity measurements of optical materials, using Murty interferometer

14 p2242 A71-30154

Absorbent materials test methods and acoustic data reduction with simulation principle

14 p2275 A71-30525

Impact reaction intensity test, determining fire or explosion hazards of materials exposed to liquid oxygen

14 p2222 A71-30549

Flash points, fire points and impact sensitivity of materials under gaseous oxygen pneumatic and mechanical impact

14 p2222 A71-30550

Holography in nondestructive materials testing, describing laser interferometry and reproduction techniques for deformation and torsional, bending, thermal and vibrational behavior

15 p2402 A71-31217

Open microcracks and internal microdefects detection during long term strength testing in vacuum by mass spectrography

15 p2383 A71-31653

Fiberglass shift moduli based on twist tests, using ratio of deformations on adjacent faces

15 p2438 A71-31654

Structural materials low temperature testing using cryogenic chambers, high power tensile test machines,

semiconductor thermometers and resistance wire strain gauges

15 p2408 A71-31854

Materials dynamic characteristics determination by acoustic input signal impedance measurement, presenting expressions as functions of reflection factor and signal propagation phase shift

15 p2409 A71-32186

Materials evaluation of SNAP 8 power conversion system breadboard assembly after 8700 hour test, extrapolating service life for space flight application

15 p2448 A71-32222

Dynamic hysteresis loop measurement of energy dissipation in materials, showing deformation effects on accuracy

15 p2508 A71-32233

Energy dissipation in material under complex vibrations, noting role of summary shear stress

15 p2508 A71-32234

Finite element analysis with material nonlinearities, obtaining linear incremental elastoplastic stress-strain relation

16 p2652 A71-33084

Automatic testing machine for materials corrosive strength under varying and combined complex static or dynamic stresses

16 p2580 A71-33687

Advanced testing techniques - ASTM Conference, Philadelphia, June 1969

17 p2820 A71-34552

Toughness testing for low ductility fracture due to crack development in elastic stress field

17 p2757 A71-34557

German monograph on correlation of Vickers and Rockwell C hardness testing methods covering indentation form measurements, deformation work, etc

17 p2739 A71-34797

Inductive extensometers with spherical tips for materials testing, noting Young modulus and Poisson ratio determination

17 p2744 A71-35239

Test equipment for acoustic fatigue of materials and structural elements

17 p2724 A71-35663

Low temperature test facility for cryogenic and rocket materials under combined tension and torsion

18 p2900 A71-36726

Contact materials effects on X band FM noise and current fluctuations of Gunn elements

19 p3029 A71-38073

Pulsed ruby laser holographic instrumentation for materials tests, detailing reflected wave front complex amplitude characterization

20 p3245 A71-39347

Fracture mechanics application to proof testing for components life determination, exemplifying concept by flawed pressure vessel

20 p3308 A71-39459

Cryogenic fracture toughness testing - ASTM-ASME Conference, Toronto, June 1970

21 p3401 A71-40914

Testing machine stiffness determination during strain rate variation and stress relaxation tests for metallic and nonmetallic engineering materials plastic properties assessment

22 p3559 A71-41589

Radiation flaw detection by fast neutrons, monitoring thick lead plates and three-layer articles

22 p3528 A71-41761

Automatic measurement of materials nonlinear deformation, considering Morrow mechanical strain rate for plastic deformation

23 p3774 A71-42895

Holographic nondestructive testing of materials, using laser for object illumination and interferometry

23 p3682 A71-43951

Postoperative states of turbine disk alloys at 280-500 and 550-630 C, noting lower durability values

23 p3779 A71-44211

MATHEMATICAL ANALYSIS

U APPLICATIONS OF MATHEMATICS

MATHEMATICAL LOGIC

NT ALGORITHMS
NT AXIOMS
NT BOOLEAN ALGEBRA
NT BOOLEAN FUNCTIONS
NT BOREL SETS
NT EQUIVALENCE
NT FORMULAS [MATHEMATICS]
NT LATTICES [MATHEMATICS]
NT SET THEORY
NT THRESHOLD LOGIC

MATHEMATICAL MODELS

NT DIGITAL SIMULATION
NT THOMAS-FERMI MODEL

Mathematical model for interaction between solar wind and interstellar gas

01 p0144 A71-10066

Commercial transport aircraft maintenance simulation Monte Carlo Modeling techniques, considering application to airline operations

[SAE PAPER 700345]

Batch/Time-Sharing Monitor for achieving balance of digital computer systems efficiency and responsive-

01 p0067 A71-10128

ness, discussing performance modeling and empirical measurements

01 p0043 A71-10178

Mathematical model for laser-induced supersonic crack propagation in crystals with weak cleavage planes

01 p0092 A71-10293

Ion exchange kinetics during pulsating fluid flow, developing approximate mathematical model

01 p0070 A71-10619

PCM telemetry data transmission bit error probability confidence intervals upper bounds based on Markov chain model analysis

01 p0032 A71-10877

Radiative transfer in plane layer of nongray absorbing and emitting medium bounded by black parallel plates, using rectangular model

01 p0180 A71-10945

Tangential momentum transfer accommodation coefficient for gas flow based on monocrystalline molecular model of gas-solid interface

01 p0071 A71-10949

ATC communication environment simulation via mathematical model based on ATC statistics

01 p0126 A71-10979

Mass balance stability in closed life support systems, using mathematical model

01 p0024 A71-11127

Atmospheric boundary layer motion and transports applied to mathematical atmospheric circulation models

01 p0121 A71-11355

Stochastic model for analysis of track-while-scan technique for aircraft search radar, based on Kalman filter theory

01 p0065 A71-11393

Iterative forces and gas theories from Newton to Lennard-Jones, discussing hypothetical deductive atomic models relation to gas properties

01 p0129 A71-11401

Thermal design of space experiment by analytical model for temperature regime acceptable to all experimental elements

01 p0017 A71-11454

Stationary waves produced by earth bow shock, calculating cyclotron radiation amplitude and polarization characteristics by thin current sheet model

01 p0075 A71-11490

Homogeneous and composite polycrystalline materials macroscopic thermoelastic characteristics determination based on structural model

02 p0324 A71-11750

Mathematical model and digital simulation for nonlinear characteristics of prototype integrated actuator package for fighter aircraft control

02 p0190 A71-11783

Aircraft manual flight control analysis using continuous mathematical pilot model for closed loop digital simulation

02 p0188 A71-11787

Digital simulation mathematical model describing simultaneous energy and mass transfer process in clothing-airspace-skin system

02 p0203 A71-11806

Cardiovascular system blood flow mathematical model parameter optimization by simulation on hybrid computer, using OPTTRAN program

02 p0203 A71-11807

Mathematical model for optimizing observational data sampling and working time losses by scientific research personnel

02 p0336 A71-11859

Pseudoshock mechanism model, explaining supersonic diffuser main flow static pressure increase and decrease alternately and wall increase monotonously

02 p0239 A71-11870

Optical scatter channel transmission characteristics, using mathematical model consistent with radiative transfer theory and probability-computing receiver

02 p0249 A71-12012

Pole Chandler motion, discussing residual deviations distributions in Jeffreys and Arato-Kolmogorov models

02 p0309 A71-12105

Identification problems in mathematical model of respiratory function

02 p0206 A71-12108

Thermionic emitter metal surface adsorption, investigating impurities and additives effects by analytical model

02 p0295 A71-12231

Hydride thermionic reactor system transient behavior dynamic mathematical model and digital simulation

02 p0281 A71-12262

Thermionic reactor analytical model for systems analysis, considering complex interactions between reactor physics, thermionics and thermal/hydraulics

02 p0281 A71-12265

Elastic theory problems, deriving continuum spectral models in Cartesian coordinate system

02 p0327 A71-12404

A-B-A block copolymers statistical thermodynamics, describing postulated microstructure theoretical model for phase transition prediction 02 p0273 A71-12450

Perturbation theory of Hooke's law model for He atom, obtaining ground state energy through third order 02 p0287 A71-12494

Discrete linear plant identification, using generalized Kalman models 02 p0236 A71-12624

Dynamic systems synthesis by exponential power input packet 02 p0285 A71-12670

Blade bound vortex system mathematical model for optimum heavily loaded ducted fans, including thrust, power and efficiency design parameters 02 p0299 A71-12677

Model performance index /Pi providing criterion for approximating one dynamic flight control system by another based on geometrical representation of linear autonomous systems 02 p0189 A71-12682 [AIAA PAPER 69-885]

Creep failure model, using wedge crack nucleation in polycrystalline materials due to grain boundary sliding 02 p0329 A71-12716

Monograph on corrections to Holtsmark continuum model for plasma fluctuations covering probability distributions, quantum mechanical corrections for hot plasmas, etc 02 p0293 A71-12843

Tubular gas turbine engine combustor design by combining turbulent flame speed, microvolume burning and stirred reactor models 02 p0299 A71-12852

Cool flames theoretical model, formulating flame propagation equations based on mass, momentum and energy conservation and Fick mass diffusion law 02 p0210 A71-12859

Monte Carlo simulation model program, evaluating automatic test equipment design influence 03 p0381 A71-13089

Approximate minimum energy control for time variable linear system, using mathematical model 03 p0389 A71-13447

Mathematical model for determining thrust interplanetary spacecraft orbit, considering time history of position, velocity and thrust acceleration [AIAA PAPER 69-901] 03 p0487 A71-13451

Mathematical models for heat transfer by laminar free convection to rotating central plate passing through synchronously rotating surroundings, considering Coriolis effect 03 p0518 A71-13617

Edge jet Hovercraft dynamic stability in heaving motion, deriving two dimensional mathematical model [ASME PAPER 70-APM-QQQ] 03 p0348 A71-13712

Anisotropic materials ductile fracture involving crack initiation and propagation, using Dugdale mathematical model [SESA PAPER 1729] 03 p0507 A71-13760

Mathematical stress wave model for sandwich plates under high velocity impact, considering structural multiple reflections and various material combinations [SESA PAPER 1653] 03 p0508 A71-13774

Human left ventricle mathematical models, determining physiological response oriented mechanical parameters with diagnostic significance [ASME PAPER 70-WA/BHF-14] 03 p0373 A71-14112

Dynamic response of linear systems with parameters subjected to step perturbations, obtaining quasi-linear mathematical model describing parameter-perturbation transmission path 03 p0394 A71-14483

Computation scheme for hinged plate systems subject to arbitrarily oriented loads based on two layer flexible base model 04 p0664 A71-14601

Soviet book on self adjusting control systems with reference models covering harmonic linearization method, phase plane technique, deterministic signals, etc 04 p0560 A71-14641

Stratospheric ozone, comparing observations to numerical models of formation, distribution and destruction 04 p0582 A71-15071

Fick diffusion model for Haxo-Blinks electrochemical determination of photosynthetic oxygen evolution 04 p0546 A71-15169

Feedback control system parameters optimization by target model method, with automatic pilot example 04 p0560 A71-15205

Kalman filtering sequential estimates convergence theorems for identifying modeling errors 04 p0561 A71-15328

Wing representation by lifting line lattice as computation method for complex configurations unsteady aerodynamic forces, presenting numerical program for wings in two parallel planes [ONERA-TP-891] 04 p0526 A71-15356

Living human tissue thermal behavior analytical modeling including internal heat generation and blood flow effects 04 p0539 A71-15460

Ettingshausen refrigerator dynamic behavior mathematical models, using current density and potential gradient as controlling variables 04 p0678 A71-15465

Turbulent film boiling on vertical surfaces, proposing theoretical model with interfacial wave disturbances taken into account for heat transfer calculation 04 p0686 A71-15527

Nonlinear model equation for hydrodynamic perturbations, discussing solution at large Reynolds numbers for one dimensional flow 04 p0575 A71-15609

Consistent finite element model for two dimensional continuum problems on basis of virtual work principle 04 p0672 A71-15770

Semicircular canal ducts dynamic behavior, using mathematical model for wave transmission of elastic fluid-filled toroidal shell in rigid channel 04 p0547 A71-15772

Data reduction for badly conditioned systems, describing general classical and modified linear statistical models for parameter determination from erroneous measurements data [DGLR-70-084] 05 p0726 A71-15950

Inertial gyro testing, measuring coefficients for performance model equation [AGARDOGRAPH-128] 05 p0750 A71-16306

Inertial quality accelerometer tests, including mathematical models and error analysis [AGARDOGRAPH-128] 05 p0750 A71-16307

Hydrodynamic model describing intermediate stages of propagation of plasma shock wave created by laser light focusing 05 p0787 A71-16333

Hydrogen-oxygen catalytic ignition system steady state model for predicting temperature and concentration profiles 05 p0795 A71-16350

Mathematical model linear in mass and stiffness but nonlinear in damping, considering causal anomalies in hypothetical models and absent in real 05 p0825 A71-16606

Artificially produced holes closing in clouds, investigating role of water vapor and droplets turbulent diffusion by mathematical model 05 p0777 A71-16668

Dynamic objects optimal linear model existence and uniqueness conditions, considering gradient technique and stochastic approximation algorithms convergence 05 p0731 A71-16794

Quasi-means definition and auxiliary system introduction for models including negative four-fermion interaction, solving limiting expressions problem for free energy 05 p0775 A71-16865

Operator reliability control models, discussing rational work-rest schedule for man machine systems 05 p0731 A71-17017

Wideband FSK system involving direct and reflected path transmission, predicting diversity performance from mathematical model 05 p0724 A71-17057

Electro-hydraulic servomechanisms dynamic performance variation probabilistic model, presenting sixth order system variable parameters for Monte Carlo simulation 06 p0848 A71-17318

Control system synthesis and analysis, using time and frequency domain methods 06 p0878 A71-17427

Plasma stabilization, discussing external feedback system model 06 p0931 A71-17456

MHD continua z-theta pinch stabilization, discussing analytical models for determining feedback spatial and temporal resolution 06 p0931 A71-17458

Dynamic stabilization of high-beta plasmas with sharp boundary, illustrating model effect on stability by numerical calculation 06 p0934 A71-17478

Analog to digital conversion mathematical model, considering comparators dynamic properties effects on optimal algorithms selection 06 p0871 A71-17523

Low pressure toroidal plasma confinement with flow in axially symmetric configurations, using numerical model 06 p0935 A71-17554

Gravitational n-body calculation in discrete phase space using game model and finite difference scheme 06 p0927 A71-17555

Nucleus energy spectra projection from Hartree-Fock intrinsic wave functions model space, using coupled orbital matrix elements 06 p0929 A71-17578

Linear dynamic object output reaction prediction by Kalman method constructed model 06 p0879 A71-17673

Electric discharge carbon dioxide mixing laser, presenting model with chemical, vibrational and thermal nonequilibrium effects 06 p0909 A71-18525 [AIAA PAPER 71-66]

Airflows in two dimensional nonuniformly sheared slipstreams, predicting pressure distribution from mathematical model for comparison with measurement [AIAA PAPER 71-94] 06 p0843 A71-18549

Orientation vector differential equation formulation for strapdown inertial navigation, applying to rigid body rotation problem 07 p1154 A71-18832

Guided weapons modeling techniques, discussing use of mathematical models for analog, digital and hybrid computerized design of missile systems 07 p1207 A71-19419

Austenitic stainless steel intergranular corrosion model for thermodynamic analysis leading to grain boundary diffusion and Cr concentration profiles determination 07 p1134 A71-19566

Three element model for choice behavior binary prediction consisting of logical, experimental and error components 07 p1048 A71-19595

Probability theory for viable microorganism exposure in fractured contaminated solid, using quantal response model 07 p1048 A71-19600

Fluid inertia effect on porous thrust plate, using mathematical model for prediction [ASME PAPER 70-LUB-18] 07 p1088 A71-19625

Computational model for post acceleration propagation of solar flare charged particles 07 p1185 A71-19652

Diffusion coefficient estimation for energetic charged particles across magnetic fields from mathematical model 07 p1186 A71-19662

Diatom molecular autoionization model, calculating limit of high vibrational and electronic principal quantum numbers 07 p1164 A71-19687

Liquid rocket propellant engine exhaust plume flow field, discussing mathematical models for combustion chamber, throat region and nozzle [AIAA PAPER 70-844] 07 p1183 A71-19861

Phase change solidification phenomena in n-hexadecane for spacecraft thermal control systems, considering two or three dimensional models 07 p1223 A71-19876

Jet plume in subsonic cross flow, calculating counterrotating vortices as function of distance along trajectory from semiempirical model 07 p1090 A71-19901

Pressure wave distortion effects on combustor acoustic mode instability based on model with burning rate related to Reynolds number 07 p1224 A71-19906

Alternate reduced order particle dynamics model in aircraft mission analysis featuring instantaneously variable speed by time scale separation 07 p1019 A71-19913

Heat treatment and deformation effects on blended metal powder compacts homogenization, using mathematical model 07 p1137 A71-19976

Linear mathematical model for human visual edge contrast by delineating and emphasizing image contours 07 p1043 A71-20101

Mathematical model for perpendicular coordinate transformation from pattern to sensation in central visual field 07 p1050 A71-20106

Mathematical simulation of human recognition by black box approach as information conversion process 07 p1050 A71-20109

Vision mathematical model based on homogeneous medium thermal conductivity equation 07 p1043 A71-20112

Nervous and muscular tissues excitability during subthreshold rhythmic stimulation, discussing mathematical model for compounding polarization induced electrotonic fluctuations 07 p1050 A71-20115

Human eye information processing algorithms mathematical model technological materialization 07 p1051 A71-20119

Optical perception constancy of object size, developing mathematical models of accommodation, convergence and retinal image size 07 p1051 A71-20120

Mathematical simulation of visual distance perception capacity of man from ground reference landmarks observation during vertical flight 07 p1051 A71-20121

Mathematical model of visual information of edge contrast effects in human eye as functions of image brightness and viewing angle 07 p1051 A71-20123

Crystal dislocation core analytical model, examining short range interactions 07 p1180 A71-20163

Cyclic stress-strain behavior prediction by mathematical model and computer simulation, applying to Al alloy fatigue

07 p1216 A71-20204

Turbulent transfer model in wall region, estimating mean surface renewal frequency for mass momentum and heat transfer rates and velocity, temperature and concentration profiles

07 p1092 A71-20224

Turbulent pipe, channel and plane Couette flow by Prandtl model equations, comparing with experimental data

07 p1092 A71-20278

Giant pulse amplification in Nd ion doped glass analysis using model, taking into account sublevels and multiplicity

07 p1127 A71-20387

High beta plasmas instabilities, discussing collisionless bounce model of theta pinch and diagnostic measurements

07 p1173 A71-20511

Satellite-borne long wave transmitting antenna excitation, calculating electromagnetic field near earth surface by earth-ionosphere waveguide model

08 p1252 A71-20744

Mathematical model of nonstationary intake and exhaust gas motion in two cycle internal combustion engine cylinders

08 p1347 A71-20780

Buckling loads prediction for conservative elastic systems from vibration data by stochastic and deterministic models, providing nondestructive testing procedure

08 p1368 A71-20804

Stagnation point flow flame sheet model, showing density-viscosity product variation for injection rate effect on velocity profile

08 p1375 A71-20865

Polytropic models second order pulsations, evaluating stellar pulsational stability and thermal imbalance

08 p1359 A71-20941

Zn-Ag oxide cell discharge, determining heat generation rate and voltage production model

08 p1235 A71-21099

Maneuvering vehicles behavior model selection for real time Kalman filter tracking algorithm, based on accuracy predictions and empirical performance

08 p1270 A71-21349

Curved space-time mathematical structure /quasi-groups/, investigating 10-parametric classes of coordinate systems and Poincare groups

08 p1334 A71-21358

Nonpairwise van der Waal interactions effects on vacancy formation energies in monatomic solids, using Lorentz oscillator and two body models for comparison

08 p1344 A71-21367

Diagnostic numerical model of frontal vertical circulation in atmospheric boundary layer using local parameters

08 p1326 A71-21448

Isotropic material structures under static external loads, considering stress rupture strength models

08 p1371 A71-21608

Short term creep and rupture model, considering strain hardening effect

08 p1371 A71-21610

Soviet book on research and design work optimization and automation based on mathematical methods and computer techniques

08 p1299 A71-21650

Solar photosphere facula, applying Schuster-Schwarzschild model for molecular lines and bedding level of carbon hydride

08 p1365 A71-21772

Theoretical model of elastic medium with diverse tensile and compression resistances under finite deformation

08 p1373 A71-21944

Boundary layer model of laminar viscous flow around high speed slender bodies with surface mass transfer

09 p1381 A71-22084

Heart, lungs and erythropoiesis optimum functional parameters mathematical model based on oxygen transport minimum losses

09 p1388 A71-22126

Mathematical model for brain arteries hemodynamic resistance, using blood pressure data

09 p1390 A71-22261

Blast wave propagation following explosions at center of generalized Roche model, discussing core radius and envelope thickness

09 p1431 A71-22371

Mathematical model for calculating plates of variable thickness referred to curvilinear triorthogonal coordinate system

09 p1536 A71-22411

General nonlinear elasticity theory including applications, deformation laws, complex nonlinear equations solutions, equilibrium and stability problems, experimental methods and mathematical models

09 p1536 A71-22512

Positive curvature type shallow shells computation for optimum efficiency and minimum material expenditure by dimensionless modeling method

09 p1537 A71-22517

Mathematical model for optimal control of spacecraft reentry into atmosphere

09 p1519 A71-22558

Pattern recognition feature subset selection based on sequential decision model for on-line processes

09 p1411 A71-22624

Discrete fluidic element dynamic tests, using magnified models with similarity criteria

09 p1386 A71-22653

Model of curved channel multipliers saturation gain at high applied voltages

09 p1446 A71-22736

Weakly ionized plasma density fluctuations and diffusion from kinetic equations for electron-space density cross correlation, assuming BGK model

09 p1503 A71-22863

Book on matrix structural analysis covering transformation, structure idealization, displacement method, finite element theory, nonlinear aspects, etc

09 p1539 A71-22873

Mathematical model system analysis methods for reliability assurance, discussing worst case and Monte Carlo techniques

09 p1423 A71-23040

Models for nonferromagnetic solid body mechanics allowing for relationships among mechanical, thermal and electromagnetic processes

09 p1509 A71-23076

Mathematical models and flux measurements of external magnetic fields of plane film elements, evaluating dipole, spheroidal and equivalent coil

09 p1387 A71-23170

Mathematical model for interaction between solar wind and interstellar gas

09 p1514 A71-23259

Inhomogeneous semiconductor model leading to anomalously high apparent mobility

09 p1510 A71-23486

VLF electromagnetic propagation, calculating mode conversion efficiency at solar terminator on angle based on flat model with finite wall conductivities

09 p1411 A71-23576

Wave propagation in elastoviscoplastic medium in temperature field under complex dynamic and thermal conditions, considering mathematical models and mechanical properties changes

09 p1543 A71-23611

Mathematical model for fields and currents calculation for asynchronous linear motors and MHD converters by Fourier transformation

09 p1387 A71-23650

Fracture models of stress field produced by accelerating crack under shear loading, using pulse diffraction method

10 p1684 A71-23932

Baroclinic instability problem analytical solutions for models with linear wind profiles, presenting growth rate variations and unstable waves phase velocity

10 p1638 A71-23962

Mathematical model for secondary flow in turbulent boundary layer in corners and salients, confirming existence of transversal pressure gradient variation

10 p1592 A71-23979

Electro-optical devices evaluation search model, considering imagery and image transmission

10 p1610 A71-24062

Visual recognition process for simple achromatic image confined within simultaneous-perception viewing angles, deriving hypothetical model based on psychological factors

10 p1567 A71-24162

Excitable myocardium cell simplified model based on artificial membrane excitation phenomena, using hybrid computer complex analog section

10 p1567 A71-24166

Vestibular system functions physical analog model, predicting responses to motion inputs and possible problems for flight situations

10 p1569 A71-24237

Elementary component constant failure rate for systems with prolonged operation without maintenance, determining mathematical model for confidence levels and dependability figures

10 p1617 A71-24266

Ionospheric computer model, describing electron and ion densities in middle latitudes as function of latitude, longitude, altitude, season, time and solar activity

10 p1577 A71-24290

Two phase mixture nonequilibrium flow mathematical model with allowance for colliding droplets coagulation and atomization based on high speed photographic studies

10 p1551 A71-24380

Brittle fracture mechanism models and connection with rheological properties of material, deriving relations for Griffith energy criterion

10 p1688 A71-24388

Research and development project funds allocation, developing mathematical dynamic modeling method for cost management

10 p1699 A71-24539

Van der Waal bound lamellar solids interlayer binding energy computational model, discussing talc and pyrophyllite equilibrium stacking arrangements and force constants

10 p1573 A71-24541

Absolute and relative visual movement perception quantitative models relevant to length perception theory

10 p1570 A71-24603

Optimal models for time shared computer systems with real time multiprogramming

10 p1581 A71-24727

System identification, considering input signals classification, model structure, linear/nonlinear systems identifying and on-line/real time techniques

10 p1586 A71-24736

Model theory identification application to aeronautical systems, discussing transfer function representation, state variable and direct methods

10 p1587 A71-24748

Computer generated visual simulation of three dimensional objects, using geometric modeling technique for mathematical representation of photographic process

10 p1581 A71-24775

Short carbon and glass fiber reinforced composites, calculating modulus of elasticity from mathematical model

10 p1635 A71-24806

Flexible tires theoretical models application to wheel shimmy analysis, examining stretched string and point contact theories validity

10 p1557 A71-24864

Atmospheric boundary layer numerical modeling, discussing subgrid scale mixing processes and parameterization

10 p1639 A71-25067

Predictive stochastic optimal control model for saccadic eye movements in visual target tracking based on target motion estimate

11 p1723 A71-25142

Mathematical model for heat transfer coefficients between two identical metal surfaces in contact

11 p1853 A71-25157

Sturm oscillation theorems for second order elliptic equation nonlinear partial derivatives, using linear Picone identity

11 p1791 A71-25176

Bayesian modeling of nonstationary Poisson process with probabilistic lambda in time

11 p1791 A71-25252

Model concepts and mathematical methods for planned economy conditions and goals representation, considering prediction reliability

11 p1860 A71-25257

Prandtl equations derivation, initial value problem and similarity theory models for steady plane incompressible laminar flow

11 p1749 A71-25302

Aircraft tires mechanical data from small models, discussing mechanical properties, tire stresses and tire temperatures

11 p1707 A71-25325

High speed tracked air cushion vehicles dynamic interactions with guideways, considering model of lumped double-sprung vehicle masses traveling in tandem along simply supported beams

11 p1846 A71-25350

Gas dynamic effects of reaction center in explosive gas mixture, using model and numerical computation

11 p1854 A71-25452

Ammonium perchlorate deflagrations, determining intrinsic stability of one dimensional burning configuration based on flame structure modeling

11 p1809 A71-25455

Fatigue failure probabilistic model under variable amplitude loading, considering relation between safety factor and fatigue failure probability

11 p1848 A71-25492

Deterministic steady state error model for floated inertial gyroscope, considering lateral or rotational float displacement and temperature distribution variations

11 p1761 A71-25517

Thermodynamic properties of interstitial solid solutions with fcc metals from atomically discrete model by computer simulation

11 p1778 A71-25531

Planetary nebulae mass ejection by radiation pressure, describing mathematical models for time independent outflowing envelopes

11 p1821 A71-25537

Creep rupture data analysis model based on minimum commitment station function approach, generalizing hypothesized time temperature stress relation

11 p1848 A71-25561

Fiber reinforced composites, predicting mechanical properties, stress-strain behavior, interface failure, creep and fatigue by mathematical model

11 p1849 A71-25655

Variable sweep wing aircraft angular motion mathematical model, analyzing inertial moments influence on control dynamics

11 p1708 A71-25661

Compton electrons produced ring current effects on geomagnetic fields for gamma quantum source and air molecular interactions, considering exact analytical model

11 p1817 A71-25777

Relativistic effects and optimization in Doppler geodetic measurements, using model computations for satellite azimuth-elevation relation

11 p1732 A71-25832

Macroscopic working model for CVD tungsten assuming change of substrate work function and preferential crystal orientation by impurity adsorbed molecules

11 p1808 A71-25861

Lagerstrom mathematical model for two dimensional viscous flow at low Reynolds number, discussing asymptotic solutions for limit process expansions analysis

11 p1752 A71-26010

Gas dynamics models for plasma production by irradiating solids with laser beams, taking into account spatial inhomogeneity of absorption process

11 p1775 A71-26090

Spherical plasma ball thermokinetic expansion model, considering solid state laser irradiation

11 p1806 A71-26091

Expanding laser generated plasma self similarity model from hydrodynamic equations, describing thermokinetic properties

11 p1806 A71-26092

Optimal reliability of system with nonlinear constraints, using mathematical model and sequential unconstrained minimization technique

11 p1771 A71-26161

Limited reliability mathematical model for radioisotopic thermoelectric generators semiconductor couples based on catastrophic failures

11 p1715 A71-26165

Mechanical waves propagation in elastic viscoplastic medium in presence of temperature field, using mechanical and mathematical models

11 p1850 A71-26177

ATM for manned solar observation, discussing thermal design, thermal vacuum test philosophy, mathematical models and analytical and test data correlation [AIAA PAPER 71-433]

11 p1838 A71-26222

Numerical and scale modeling interaction for spacecraft thermal design verification [AIAA PAPER 71-439]

11 p1838 A71-26227

Reflectance measurements of dielectric coating on metallic substrate, comparing with analytical model [AIAA PAPER 71-448]

11 p1799 A71-26233

Paint absorbance values effect on passive thermal control system primary component, using calibrated computer satellite model [AIAA PAPER 71-455]

11 p1859 A71-26238

Bidirectional reflectance model for randomly rough surface, using distribution function for macroscopic probability of microscopic surface roughness elements with specific slopes [AIAA PAPER 71-465]

11 p1800 A71-26246

Spherically symmetric radiative transfer problems, constructing model with neutron transport theory [AIAA PAPER 71-466]

11 p1859 A71-26247

Free flight ranges application to high temperature gas dynamics, using mathematical model to relate sub and full scale observations

11 p1705 A71-26269

Radio interference suppression rules optimization, using mathematical model to characterize interference voltage, antenna sensitivity and radio transmitter field strength

11 p1733 A71-26339

Meteor streams dynamic properties, computing mean orbit elements with statistical mathematical model

11 p1835 A71-26458

Signals as information carriers, comparing bounded spectrum carrier model, Gabor model, analytical signal model, steady random process model with bounded spectrum and Rice-Bunimovich model

11 p1734 A71-26463

Service life testing and reliability estimation, using ordinary and empirical Bayes approach in failure model with gamma probability distribution

12 p1910 A71-26685

Manned spacecraft maintenance simulation model, applying complex systems operational availability assessments

12 p1894 A71-26689

Experimental plan group characteristics, describing main goals, construction methods, mathematical models and data analysis procedures

12 p1988 A71-26706

Equations of motion for variable mass system of bodies, developing mathematical model of flight vehicle as six degrees of freedom control plant

12 p1926 A71-26728

Hot water vapor curve of growth, using statistical band model with exponential line intensity distribution yielding spectral absorption coefficients

12 p1904 A71-26793

Epitaxial garnet films magnetic anisotropic models, describing mobile cylindrical domains

12 p1943 A71-26854

Atom rigid rotor problem, applying generalized phase shift rotational excitation treatment in lowest approximation

12 p1932 A71-26949

Response strategies in two-choice reaction task with continuous cost for time, confirming fast-guess model prediction

12 p1873 A71-27008

Small signal characteristics mathematical models of carotid sinus baroreceptors of rabbits

12 p1870 A71-27133

Cloud formation two dimensional model simulation by numerical integration of hydrodynamic and thermodynamic equations, considering condensation, evaporation, coagulation and water drops terminal fall velocity

12 p1925 A71-27196

Quasi-classical ionization model under assumption of straight-line electron trajectories, presenting Hamilton-Jacobi equations solution

12 p1932 A71-27241

Three dimensional Monte Carlo simulation of extensive air shower development, comparing fireball and mathematical models for mean total hadronic energy spectra

12 p1951 A71-27388

Muon spectra and charge ratios at sea level, analyzing by collision model and one dimensional diffusion equations

12 p1933 A71-27406

Flow field model for steady asymmetric vortex system shed from slender body of revolution in coning motion [AIAA PAPER 70-52]

12 p1865 A71-27552

Human body thermal behavior modeling, obtaining steady state analytical solution for various boundary conditions and parameters

12 p1875 A71-27563

Nonlinear planar transistor model, analyzing majority carrier current flow fields in base due to injection of emitter and collector p-n junctions

12 p1888 A71-27612

Turbulent diffusion Langevin model with pressure-viscous stress interaction, calculating particle dispersion, Reynolds number, Richardson law time span and Eulerian-Lagrangian relations

12 p1898 A71-27730

Crack extension criterion for time dependent spallation, correlating simple mechanistic model with Al alloys data

12 p1919 A71-27774

Consistent discrete models of continuous bodies electrothermoelastic behavior, using finite element formulations for general energy balance equations derivation

13 p2099 A71-27785

Forced dynamic regimes of machines and mechanisms, evaluating role of second order acceleration

13 p2099 A71-27806

Lake Erie steady state wind driven currents numerical solutions, using shallow lake model for velocity as function of depth and horizontal position

13 p2054 A71-27857

Self- and mutual admittances for axial rectangular slots in inhomogeneous cylindrical plasma layer, giving coupled radial transmission line model for propagation

13 p2105 A71-28002

Fireball model at various energies, describing multiple meson production at very high energy

13 p2058 A71-28049

Air showers nuclear active and muon components simulation in space and time, using different shower models based on isobar-fireball concept

13 p2125 A71-28090

Cerenkov light distribution calculation from gamma ray initiated air shower model obtained from Monte Carlo computer program

13 p2125 A71-28093

Fiberglass reinforced plastics under constant strain rate, deriving failure models as random process for microscopic crack propagation

13 p2148 A71-28115

Diffused fracture model as basis for plotting delayed fracture curves in space of principal stresses

13 p2149 A71-28119

Modeling of differences between actual and estimated flight times over radio beacon, obtaining cumulative frequency distributions

13 p2167 A71-28490

Dense liquid thermodynamic model, using approximate equation of state

13 p2160 A71-28571

Radiant heat transfer measurements on sintered gauzes, considering mathematical model of porous wall with sweat cooling

13 p2161 A71-28750

Identification by minimization of Gaussian-Markovian representation of stochastic process, considering positive linear systems and algorithm for matrix calculation

13 p2043 A71-28818

Mathematical model for harmonic emission spectrum in FM and PM communication transmitters modulated by random signal

13 p2032 A71-28875

Monograph on potential flow interaction between blade rows in axial flow compressors covering mathematical model, numerical analysis and experiment

13 p1990 A71-28883

Probabilistic cyclic queue model of overhead time and channel utilization in multiprogrammed computer systems under demand memory paging

13 p2035 A71-28973

Time sharing digital computers busy period task completions modeling as semi-Markov process

13 p2075 A71-28978

Electron beam welding, calculating penetration depth from mathematical model [ASME PAPER 70-WA/HT-2]

13 p2075 A71-28978

Gas particle radial reflection model application to hypersonic nearly-free molecular flow about convex bodies, solving steady state problem

13 p1991 A71-29153

Correlation model of stability and onset of turbulent motions for incompressible fluid, noting inconsistency of Keller-Friedman equations

13 p2050 A71-29206

Quasi-one dimensional nonlinear model of electrohydrodynamic stability and control of current carrying semiinsulating jets at supercritical and subcritical regimes

13 p2118 A71-29249

Solar arrays for satellite electrical power supply, discussing mathematical model for reliability calculation

13 p2002 A71-29273

Mathematical and mechanical models of human thermal system thermodynamic/transport processes and external regulation devices for single elements and entire body

13 p2023 A71-29400

Visual perception theoretical models for liminal contrast prediction

13 p2023 A71-29442

Boundary layer equations based on eddy viscosity model for turbulent free shear flow, solving numerically in Crocco coordinate plane [ASME PAPER 71-FE-17]

13 p2052 A71-29456

High entrainment constant area multiple nozzle ejectors with two mixing tube lengths for boundary layer control, estimating performance with analytical model [ASME PAPER 71-FE-34]

13 p2053 A71-29469

Respiratory air flow optimal regulation hypothesis, testing analytic prediction model results with experiment under stress and rest conditions

13 p2023 A71-29491

Ionospheric VLF signal propagation paths based on earth atmospheric simulation and mathematical models

14 p2228 A71-29513

Galactic dynamo generated magnetic field periodic modes based on mathematical model involving cyclonic turbulence and nonuniform rotation of gaseous disk

14 p2303 A71-29591

Geomagnetic disturbance vector distribution, computing three dimensional ring and ionospheric currents system models

14 p2229 A71-29672

V/STOL aircraft gust effects prediction with mathematical models based on nonlinear hybrid simulation at takeoff and landing altitudes

14 p2173 A71-29775

Spalling fatigue life prediction in rolling contact, studying ductility, compressive stresses, inclusions, surface imperfections and bearing ring deflections effects with mathematical model

14 p2251 A71-29830

Mathematical programming models for resource allocation and project selection decision in R and D

14 p2340 A71-29855

Steady state wind driven currents velocity in Lake Erie, using shallow lake level model in numerical calculation

14 p2231 A71-29935

Linear filter to represent diffusion in numerical models of large scale atmospheric circulation

14 p2269 A71-29948

Internal gravity waves numerical model allowing momentum transport interaction with mean flow

14 p2269 A71-29950

Harmonic vibration analysis methods, discussing mathematical model, ground tests, structure suspension exciter and pickup location eigenvalue measurement and mode research

14 p2175 A71-30058

Biomathematical model and least square estimation from time series data of discrete particle population in stochastic compartmental system

14 p2265 A71-30181

Mathematical model for short term adaptation to vestibular stimuli, deriving transfer function relating angular velocities of nystagmus and head rotation

14 p2182 A71-30250

General atmospheric circulation mean time distribution, kinetic energy, regional interactions and mathematical simulation

14 p2236 A71-30492

Cosmic ray shower evolution model based on passive baryon existence and direct energy transfer to gamma quanta hypotheses

14 p2302 A71-30593

Ion thruster ion beam current density profiles mathematical representation by two parameter equation

[AIAA PAPER 71-693] 14 p2293 A71-30752

Modular concept mathematical model for combustion and pollution formation processes in jet engine combustors, including turbulent mixing and reaction kinetics

[AIAA PAPER 71-714] 14 p2294 A71-30766

Gated phase locked loop system characteristics based on sampled data model, comparing with continuous loop operation

14 p2214 A71-30795

Complex media and plasticity theory deformation models based on central friction mechanism, discussing elastic spring analog

14 p2332 A71-30879

Crack tip strain problem in elastic body, relating fracture energy criterion with mathematical models

14 p2334 A71-31002

Nonlinear mathematical model for dynamical behavior of extensible towing cable subjected to aerodynamic forces generated by uniform flow field, discussing system stability

14 p2171 A71-31026

Wake model and computer program to compute geometries, flows and velocity influence coefficients for helicopter blade load calculations

[AHS PREPRINT 523] 14 p2172 A71-31089

Mathematical model for predicting microwave signal fading characteristics due to reflections from ocean surface

15 p2368 A71-31140

Optimum configuration/cost design of computer graphics systems, using mathematical model involving response time prediction by queueing analysis

15 p2374 A71-31181

Book on dynamic probabilistic systems, Volume 1, covering Markov models, linear processes, systems analysis, statistics, recurrent events, population models, time variations, etc

15 p2440 A71-31196

Analytical model of oscillatory combustion in aircraft engine augmentors

[AIAA PAPER 71-700] 15 p2466 A71-31324

Jet noise reduction by foam injection, developing mathematical model for foam behavior in sound field

[AIAA PAPER 71-734] 15 p2388 A71-31327

Energy output of left ventricle and congestive heart failure mechanism, approximating blood velocity in aortic system by mathematical model

15 p2363 A71-31443

Atmospheric primitive equation prediction model, discussing four processor version

15 p2374 A71-31516

Mathematical modeling and convergence analysis of nonscanning self adaptive control systems for linear objects, using Liapunov second method

15 p2379 A71-31519

Unenclosed laminar jet diffusion flame phenomenological analysis predicting flame height relationship to fuel flow rate and atmospheric density and oxygen concentration

[WSS/CI PAPER 71-12] 15 p2513 A71-31622

Monatomic gas interaction with solid phase surface, deriving three dimensional theoretical model including hard spheres collision and surface energy

15 p2451 A71-31675

Atmospheric cosmic ray propagation based on phenomenological model of hadron-nucleus collisions, predicting sea level nucleon, pion and muon energy spectra and ionization profile

15 p2474 A71-31732

Mathematical model of multidimensional system stability for random vibration spectra control, including white noise generators, spectrum shaper/analyzer and summator

15 p2380 A71-31847

Mathematical models for boundary lubrication, computing specific liquid lubricant/surface wear rates in machine element design

15 p2414 A71-31950

Crack propagation model in linearly viscoelastic solid strip based on thermodynamics first law

15 p2506 A71-32011

Nonconservative elastic system involving standard double pendulum model under retarded follower load, calculating damping, time delay and parameter variations effects on stability

15 p2449 A71-32012

Room with windows and open doors under sonic boom, determining cavity resonance model for impulsive loading conditions

15 p2450 A71-32514

Color conversion model of equivalences under various illuminants, reducing problem to chromatic adaptation with nonlinear von Kries formulation

15 p2412 A71-32599

Mathematical models to optimize successive fault finding programs in complex control systems with/without recovery

15 p2382 A71-32618

Steady nonlinear regime of Benard convection in uniformly rotating fluid, using two-dimensional primitive equation numerical model with rigid boundaries

15 p2393 A71-32638

Solar photosphere and faculae temperature, gas/electron pressures, density and turbulence velocity from Schuster-Schwarzschild model

15 p2495 A71-32677

Time domain model of device-circuit characteristics of TRAPATT diode microwave oscillator

15 p2378 A71-32699

Linear two shaft turbojet model development and conditions for stability, observability, controllability and feedback loop parameters

15 p2383 A71-32711

Polycrystalline graphite total creep time dependent effects based on mathematical model of nonlinear hereditary theory

16 p2600 A71-32799

Mathematical theory of planetary atmosphere oscillations, considering coriolis, magnetic and viscous forces effects

16 p2561 A71-32804

Shock wave reflection process model in magnetic fields, describing time development of interaction process

16 p2616 A71-32901

Frequency spectrum of lightning discharges, developing mathematical model to account for atmospheric difference between cloud-ground and cloud-cloud discharges

16 p2604 A71-33070

Variational principles in solid continua mechanics, describing finite element models

16 p2651 A71-33078

Inertial properties of segmented cadaver trunk for mathematical model of spinal response to impact in seat ejection acceleration injuries in high speed aircraft

16 p2528 A71-33117

Thin elastic shells Koiter-Sanders mathematical model finite element analysis using Ritz method

[ASME PAPER 71-APM-32] 16 p2655 A71-33197

Kinetic theory of gases in general relativity, including model of matter particle structure

16 p2610 A71-33267

Relativistic cosmological models with nonzero pressure, considering matter as perfect gas-radiation mixture and isotropic/homogeneous three space

16 p2611 A71-33274

Gravitation phenomena based on uniformly expanding universe cosmological model for acceleration field

16 p2612 A71-33281

Information model for simulating systems reliability estimates uncertainty, noting state transition matrix, methodology and sensitivity analysis of effectiveness

16 p2583 A71-33304

System safety evaluation model with state-space network for representation of mission phase and hazard degradation

16 p2602 A71-33308

Mathematical model for combustion processes, obtaining computerized approximate solutions for momentum, heat and mass transfer partial differential equations

16 p2663 A71-33362

N-order continuous linear automatic control system compensation method, using model of sampled systems with duration modulation

16 p2549 A71-33377

Clutter signals simulation with predetermined auto- and cross correlation, describing mathematical method for filter weighting function

16 p2541 A71-33424

German book on problems, mathematical foundations and investigation methods of technical reliability covering Boole model, random variables, distribution functions, failure rates, etc

16 p2583 A71-33524

Chemical bonds types in intermetallic, metal-like and nonmetallic compounds, stressing model based on valence electrons configuration localization

16 p2622 A71-33919

Large meteoroids ablation and breakup mathematical model, estimating Mars atmosphere effectiveness as shield against surface impact craters production

16 p2643 A71-33968

Combat aircraft vulnerability to projectile impact predicted by model giving target penetration, damage size and structural response

[AIAA PAPER 71-777] 16 p2660 A71-34013

Diffusion flame theoretical model characterization as singular perturbation problem

16 p2664 A71-34073

Magnetohydrodynamic model system numerical integration as initial value problem, using finite dif-

ference scheme or differential equation conversion method

16 p2620 A71-34081

Temperature dependent electron structure model of free energy decomposition of beta phase in Ti alloys

16 p2599 A71-34085

Na and K transition oscillator strengths, noting core polarization effects on mathematical model

16 p2615 A71-34088

Balance equations expansion for giant-pulse Q switched laser model, considering output intensity

16 p2589 A71-34138

Extension of Heisenberg model for spectral transfer to second order fluids in turbulent shear flow, noting accompanying weakening of anisotropic influences

17 p2725 A71-34181

Two vortex model for downwash variations in supersonic flow past thin delta wing with separation at leading edges

17 p2669 A71-34190

Mathematical fatigue models based on permeability variations in synaptic membranes and feedback regulation due to working organ metabolic changes

17 p2687 A71-34354

Quantum mechanics model of optical parametric amplifier, considering performance of optical information systems

17 p2698 A71-34409

ATC system models, covering surface movement, runway utilization, terminal areas and enroute traffic

17 p2771 A71-34523

Dugdale mathematical model for cylindrical bending of thin plates, finding resulting plastic zone dependence on applied moment and normal coordinate

[SESA PAPER 1854A] 17 p2819 A71-34538

Real turbulent fluctuations superimposed on metric and satisfying free space Einstein equations, basing model on oscillating gravitation and elementary particles as excitons

17 p2777 A71-34586

Elementary particle geometrical-group model assuming negative curvature de Sitter space inside and flat space outside

17 p2778 A71-34627

Rhodopsin kinetics mathematical analysis by cyclic five-component model, applying to flash and extended photolysis in rat retina

17 p2680 A71-34653

Tornado and waterspouts, using concentrated vortices produced in laboratory rotating tanks and mathematical models

17 p2726 A71-34657

Continuously stratified fluid flow into contraction, assuming constant upstream dynamic pressure and density gradient/Long model/

17 p2726 A71-34661

Monograph on statistical theory for weak homogeneous turbulence covering mathematical model, wave correlation functions, Bogoliubov expansion method, kinetic equation, nonlinear interactions, etc

17 p2727 A71-34771

Stress hybrid finite element model for boundary conditions in solid continua with nodal values as final set of matrix equations

17 p2825 A71-34893

Slightly nonlinear structures vibration, examining experimental means for mathematical models development and coefficients determination

17 p2779 A71-34906

Rotational ocular nystagmus phases induced by head rotation, developing vestibulo-ocular system mathematical model

17 p2691 A71-35045

Two dimensional nonlinear discrete /pulse frequency modulation/ control system stability, using Liapunov direct method and mathematical model

17 p2721 A71-35134

Analytical model for molecular flow of reactive gaseous species through cylindrical reactors with apertures at either end, evaluating surviving flux magnitude

17 p2695 A71-35137

Mathematical models of distance perception under flight conditions according to visible brightness of luminous surface

17 p2691 A71-35166

Robots structural description and computer modeling based on various algorithms

17 p2691 A71-35167

Adaptive mathematical model of human operator during pursuit tracking, synthesizing brain in accordance with arbitrary reasonability criterion

17 p2692 A71-35169

Mathematical models of color data coding and decoding, studying light emissions transformations in visual organs and engineering systems

17 p2692 A71-35173

Visual adaptation mathematical model, studying relation of brightness static transformation into luminance

17 p2692 A71-35174

Dynamic system impulse response model for goodness of fit and linearity hypothesis tests by computer simulation

17 p2722 A71-35181

French monograph on system reliability of particle detection device covering methodology, functional models, Monte Carlo simulation, spectrometers and DC/DC converters

17 p2767 A71-35231

Picosecond duration coherent light pulse propagation in resonant medium, discussing basic equation, self induced transparency, Bloch equations, soluble model and higher conservation laws

17 p2754 A71-35375

Tasks with subject guiding vehicle at arbitrary speed along tolerance band defined course, considering prediction model for velocity-bandwidth relationship

17 p2693 A71-35437

Probability density function for parameter of exponential measurement model based on structural inference theory, developing prediction densities as life test inferences

17 p2768 A71-35537

Stellar atmospheres mathematical model, considering transfer equation reduction to linear equations set

17 p2808 A71-35556

Long time failure modeling of real structure behavior in short times by scale and mathematical models, noting nonaccountability of crack propagation time

17 p2834 A71-35669

Composite failure model tested for short term creep and rupture in Mo alloy at constant loads and 785-1400 C, considering strain hardening

17 p2834 A71-35670

Ammonium chloride specific heat measurement near order-disorder transition, comparing results to Ising model behavior

17 p2791 A71-35743

Jumbo jet trailing vortex mathematical model for studying effect on penetrating aircraft

17 p2673 A71-35754

Rotating liquid flow impulsive spin-up and spin-down in finite cylindrical containers, deriving simplified mathematical model at Reynolds number 1002

18 p2901 A71-35853

Externally excited moving striations measurement in low pressure Ar discharge, comparing with ion acoustic wave propagation derivation from model

18 p2948 A71-35859

Large amplitude whistler as collisionless laminar shock model, showing instability for oblique perturbation propagation

18 p2950 A71-35865

Consecutive toroidally circulating buoyant elements interactions by numerical simulation, including vortex formation process effects

18 p2901 A71-35954

Dynamic rate equation model of single wavelength flash lamp pumped rhodamine dye laser accounting for short molecular triplet state lifetimes

18 p2929 A71-35958

Fireball model of meson production in high energy nucleons collisions

18 p2949 A71-36210

Laminated composite beam microstructure continuum model, calculating equations of motion and boundary conditions with Hamilton principle

[ASME PAPER 71-APM-S] 18 p2978 A71-36261

Rigid sphere and concentric shells models approximation to turbulent motion in liquid-filled precessing spherical cavity

[ASME PAPER 71-APM-Y] 18 p2904 A71-36265

Shock wave structure prediction by nonlinear kinetic models with Monte Carlo solutions of full Boltzmann equation

18 p2907 A71-36334

Compressible three dimensional nonsimilar laminar boundary layers numerical analysis using two layer heuristic model

18 p2845 A71-36336

Plane Poiseuille flow at constant rate, developing numerical simulation of transition and turbulence

18 p2845 A71-36337

Computer simulation model for experimental data in post-Skylab space station design

18 p2973 A71-36458

Mathematical model of arc Pioneer 6/7 plasma probe electrostatic analyzer responding to monoenergetic unidirectional charged particle beam

18 p2952 A71-36583

Hot water vapor total emissivity charts at various temperatures, using band model parameters with spectroscopic data

18 p2985 A71-36592

Mathematical model for underwater simulation of astronaut extravehicular activities in weightless conditions, using computer program

[AIAA PAPER 71-852] 18 p2872 A71-36644

Weightless environment effects on fluid behavior and heat transfer in life support systems, obtaining analytical models

[AIAA PAPER 71-864] 18 p2909 A71-36652

Mathematical model of hemispherical inclusion in elastic half space for estimating plastic deformation

18 p2937 A71-36772

Mathematical model for continuous elastoplastic transition stress-strain response of steels and nonferrous metals

18 p2937 A71-36835

Mathematical model for human thermal system, checking accuracy

18 p2873 A71-36899

One-dimensional numerical model of nonisothermal plasma, showing soliton separation from leading front by ion-acoustic shock waves after reversal stage

19 p3042 A71-37076

Aircraft position errors computation for ATC mathematical surveillance models, estimating collision risk

[AIAA PAPER 71-927] 19 p3097 A71-37173

Twin wheel momentum bias/reaction jet spacecraft attitude control system, presenting mathematical model, stability analysis and design

[AIAA PAPER 71-951] 19 p3099 A71-37192

Optimal Kalman filter gyro drift rate mathematical models for limiting inertial navigation errors

[AIAA PAPER 71-971] 19 p3100 A71-37212

Viscous relativistic fluid plane laminar flow, discussing incompressible thermally nonconducting case and stationary models

19 p3044 A71-37640

Work hardening materials yield criterion derivation from mathematical model for inclusions embedded in elastoplastic matrix

19 p3078 A71-37644

Human operator models parameter estimation by stochastic approximation, considering continuous and sampled data models

19 p3007 A71-37648

Optimal models for time shared computer systems with real time multiprogramming

19 p3025 A71-37692

Isolated buoyant thermal motion asymptotic behavior derivation from simplified model, comparing results with experiment

19 p3162 A71-37732

Cardiovascular system mathematical model for evaluating system parameters effects on circulatory indices including minute volume and arterial tension

19 p3007 A71-37777

Polymer materials strength and lifetime prediction under natural conditions from mathematical model based on laboratory accelerated test data

19 p3084 A71-37781

S-N curve and structural failure probability due to combined random and primary loads based on mathematical model

19 p3157 A71-37847

Heat transfer to transpired turbulent boundary layer, reviewing theoretical models and experimental results for friction coefficient and Stanton number

[ASME PAPER 71-HT-44] 19 p3166 A71-38003

Solid propellant combustion pressure oscillations amplification, developing mathematical model as function of reaction rate constant, chamber pressure, frequency and solid properties

19 p3123 A71-38096

Theoretical model of excess surface current in p-n junctions, based on surface-controlled tetrode transistor experiment for bipolar transistors I-V characteristics explanation

19 p3029 A71-38142

Neutron star models based on Nemeth-Sprung equation of state, discussing dynamic stability and Crab pulsar central density

19 p3143 A71-38161

One layer midlatitude beta plane channel model of incompressible fluid for study of systematic error propagation on nearly stationary synoptic scale wave

19 p3090 A71-38268

Signal propagation in model neuron network in terms of differential equations system, representing retina major cell types in planar model

19 p3003 A71-38276

Simulation model for optimal cost time-independent component replacement of complex system subject to probabilistic deterioration

19 p3069 A71-38288

Two dimensional seismic mathematical and scale techniques appropriate to inertial navigation devices test pads noise isolation examination

[AIAA PAPER 71-912] 19 p3056 A71-38326

Charged particle acceleration by nonstationary sinusoidal electric fields in earth magnetosphere based on mathematical model

19 p3129 A71-38377

Environment, coupling and electronic equipment modeling for electromagnetic compatibility analysis

19 p3031 A71-38440

Co-site analysis model automated for evaluation EM compatibility of single site employing large number of transmitting and receiving equipments

19 p3032 A71-38457

Radar antenna interference determination based on model using electrical and physical characteristics of

reflector type antenna for statistical gain distribution prediction

19 p3021 A71-38458

Stochastic passband model of tropospheric communications channel, denoting random frequency duration above threshold level

19 p3022 A71-38501

Criterion selection and minimum margin search for optimization of complex electronic circuit parameters described by mathematical models

19 p3039 A71-38503

Theoretical model for initial stage of cloud condensation developing at constant air cooling rate

19 p3092 A71-38684

Linear-elastic fracture mechanics limits concerning toughness based on elastic-plastic rupture model for yielding materials

19 p3161 A71-38726

Ternary solid solutions with substitutional and interstitial solute atoms, developing statistical mechanical interaction model

20 p3194 A71-38805

Electric discharge carbon dioxide laser gas temperature, electron and current densities radial distribution from mathematical model

20 p3242 A71-38844

Long life radioisotope thermoelectric generator, discussing mathematical model to simulate expected performance profiles

20 p3266 A71-38958

Decomposition matrix Cauer model for multivariable control systems analysis and design

20 p3207 A71-38995

Parameter estimation algorithms for state variable models of multivariable linear control systems from noisy input-output records

20 p3208 A71-38999

Incompressible turbulent boundary layer with pressure gradients, calculating Clauser equilibrium model and flow with constant wall shear stress

20 p3210 A71-39030

Higher order noisy optical pulse intensity correlations interpretation by statistical model, estimating spike amplitude

20 p3196 A71-39103

Cylindrical shell stability under radial pressure or axial compression from load-distributing filler model solution

20 p3308 A71-39166

Schottky barrier diodes as photodetectors in hot electron mode, deriving ballistic transport model for scattering mechanisms effects

20 p3236 A71-39191

Meteorological prediction from joint frequency of initial and final weather elements conditions, developing conditional probability models from bivariate normal distribution tables and Markov process

20 p3256 A71-39204

Meteorological rocketsonde film mounted thermistor bead temperature sensor, developing mathematical model for thermometric correction formulas in automatic data processing

20 p3236 A71-39208

Variable thickness ice film water-to-cryogen heat exchanger design, presenting mathematical model for performance calculation by modified integration digital analog simulator computer program

20 p3314 A71-39291

Atmospheric transmissivity measurement from backscattered light intensity, deriving model based on light beam geometry and path

20 p3238 A71-39333

Dynamo equations solution for electrostatic potential, discussing three dimensional model for ionospheric equatorial conditions and Northern-Southern Hemispheres coupling

20 p3218 A71-39519

Sealing coefficient and leakage performance model for multiple thread rarefied gas viscoelastic

20 p3241 A71-39801

Time dependent plasmopause motion after increase and decrease in magnetic activity based on analytical model of plasma flow

20 p3232 A71-39897

Mathematical model for studying solar radiation pressure effects on artificial satellite motion

21 p3438 A71-40104

Non-LTE picket fence model in radiative equilibrium solutions for thermal coupling and line strength parameter

21 p3438 A71-40243

Automatic computational algorithm for parameter identification of nonlinear systems, using deterministic time invariant model with memory and gain functions

21 p3407 A71-40261

Lumped parameter models for description of continuous one dimensional and Bernoulli-Euler beam vibration, compared on basis of maximum system strain energy

[ASME PAPER 71-VIBR-5] 21 p3456 A71-40268

Lumped parameter modeling of fluid elastic vibration response of nonlinear piston driven pneumatic-

mechanical system, using finite element control volumes [ASME PAPER 71-VIBR-41] 21 p3459 A71-40291

Discrete renewal processes applied to mathematical modeling of physical processes, using statistics of complicated events in reliability analysis 21 p3407 A71-40361

Computer model for dynamical evolution of isolated disks of stars with initial velocity dispersions corresponding to Toomre criterion, noting instability relative to large scale modes 21 p3445 A71-40410

Recovery-strain hardening rate model for steady state creep 21 p3462 A71-40430

Time optimal self alignment methods for inertial platforms, using mathematical model based on torque iteration and bang bang misalignment angles control 21 p3413 A71-40544

Mathematical model of electrocardiographic QT-RR relationship, showing agreement with membrane theories 21 p3343 A71-40586

Retinal directional effect measurements confirming mathematical model based on Gaussian distribution of retinal cones orientation, explaining brightness stimuli effectiveness and hue shift 21 p3335 A71-40670

Vacancy absorption model for fatigue crack propagation in Al based on X ray inspection and transmission electron microscopy 21 p3399 A71-40698

Transition layer structure formation of epitaxial semiconducting films, discussing model for dislocations origin 21 p3427 A71-40727

Stochastic model for electron-cyclotron plasma heating by high power microwaves in magnetic mirror 21 p3422 A71-40762

High data rate optical communication system bit error rate determination from models for noncoherent digital baseband and subcarrier modulation formats 21 p3348 A71-40804

Particle model measurements of collision and heating times in two dimensional thermal computer plasma 21 p3423 A71-40843

Molecular beam extraction from equilibrium gas flows, describing shock beam formation model with associated escape probability 21 p3419 A71-40956

Mechanical properties of muscular organs, presenting mathematical model for biological fluid flow analysis 21 p3336 A71-40984

Electrical heart activity and ECG mathematical model with nonlinear oscillator system construction for normal and abnormal rhythms 21 p3336 A71-40986

Numerically simulated turbulent velocity field, covering Navier-Stokes and energy conservation equations 21 p3371 A71-40996

Two dimensional supersonic turbulent free shear layer recompression process from flow model numerical calculation 21 p3371 A71-40998

Zero-charge and scale-invariance problems in solvable field theory model, considering Green function and vertex parts behavior under perturbation theory invalidity 21 p3420 A71-41128

Mathematical description by Gaussian error function for metals diffusive saturation and diffusion constants determination 21 p3403 A71-41160

Signal process models choice in Kalman-Bucy filtering, proving smallest error covariance matrix existence 21 p3349 A71-41190

Mathematical model of emission spectrum for PKZ radiosonde and radiosondes using superregenerative transceivers 21 p3383 A71-41243

Dead ended compartments concentration and current distributions calculation in space hydrogen-oxygen fuel cells, using mathematical model with convective diffusion equation 21 p3326 A71-41249

Numerical modeling and analysis of homocentric light beams propagation in cubic and nonlinearity saturation medium, using parabolic equation approximation 21 p3417 A71-41259

Soviet book on mathematical plasticity theory covering stress/strain flow and deformation, stress/strain tensors statistical averaging methods and hardening conditions 21 p3473 A71-41370

Numerical model of three dimensional convection in atmosphere with vertical wind shear, solving system of differential equations 21 p3411 A71-41385

Numerical model of turbulence effect on cumulus cloud mesoscale convective motion 21 p3411 A71-41386

Mathematical model for atmospheric carbon monoxide production from methane 21 p3375 A71-41423

One dimensional structure failure calculation, using mathematical programming static method for load limit approximation 22 p3613 A71-41430

Apparent motion effects associated with stationary flashing lights configurations, noting frequency response characteristics analogous to real motion effects in human visual system model 22 p3498 A71-41487

Compton electrons produced ring current effects on geomagnetic fields for gamma quantum source and air molecular interactions, considering exact analytical model 22 p3532 A71-41545

Incompressible inviscid fluid free droplet surface layer tension determination as function of curvature from mechanical moment model 22 p3613 A71-41565

Linear system model for multiple scattering light transmission through optically thick clouds, calculating optical effects by four dimensional linear superposition integral 22 p3575 A71-41789

Dynamical formation and structure of plasma focus, using two dimensional numerical fluid model 22 p3581 A71-41892

Earth-orbiting space vehicle attitude motion under constantly acting disturbances based on mathematical total stability of equilibrium 22 p3608 A71-41968

Space shuttle trajectory design optimization by nonlinear programming, proposing mathematical model to handle equality and inequalities constants 22 p3600 A71-42013

Charged pions differential photoproduction cross section description by theoretical model 22 p3578 A71-42060

Analytical model for air navigation and ATC system design, demonstrating system parameters effects on lateral separation standards for parallel flight lanes 22 p3571 A71-42083

Validity study of mathematical models representing failure rate variations of electronic components, considering thermal and electrical stresses 22 p3517 A71-42109

Statistical fatigue life models, surveying failure probability distributions in reliability studies 22 p3566 A71-42117

Computerized electrostatic field model of biological cell membrane 22 p3487 A71-42119

Semiempirical model for molecular band mean transmission, applying to ammonia 10 and 16 micron lines 22 p3602 A71-42179

Mathematical models for microorganism exponential die-off rate and variance estimation from decontamination data 22 p3504 A71-42231

Mathematical model for pulse waveform identical with single integrator delta modulator, using analog techniques of angle modulation and sampling 22 p3522 A71-42276

Lumped model for two dimensional current flow in grown junction transistor base, predicting small signal common emitter short circuit input impedance 22 p3523 A71-42359

Mathematical models for computerized ATC automatic aircraft flight tracking logics without tracks smoothing 22 p3573 A71-42396

Sea level high energy cosmic ray muon spectra calculation based on phenomenological model of nucleon-nucleus collisions 22 p3594 A71-42408

Model aspects of sea echoes and clutter unsteadiness on radar 22 p3514 A71-42470

Early effect incorporation in Ebers-Moll simulation model for junction transistor large signal behavior to obtain current gain and conductance dependence on voltage 22 p3523 A71-42484

Diffraction phenomena numerical modeling by Monte Carlo statistical analysis, using Heisenberg uncertainty principle 22 p3576 A71-42556

Nonlinear finite element analysis of sandwich arches elastic buckling, using straight beam-column type model 22 p3618 A71-42586

Steady state transition layer between cold solar plasma flow and geomagnetic field in one dimensional model 22 p3536 A71-42622

Flip-flop circuits nonlinear distributed network mathematical model, investigating oscillations nonexistence 22 p3527 A71-42626

Linear and nonlinear models for computer aided circuit design involving Zener diodes, providing for thermal effects 22 p3524 A71-42762

Static joint wear role in overall machine reliability and service life under working loads from mathematical prediction 22 p3619 A71-42852

Synthesis models and methods for large scale automated control systems with human elements, discussing mathematical models and computerized design 22 p3528 A71-42858

Mathematical modeling and convergence analysis of nonscanning self adaptive control systems for linear objects, using Liapunov second method 22 p3528 A71-42884

Mathematical model for solar flares formation based on magnetic/kinetic energy conversion, investigating plasma instability 23 p3719 A71-42950

Viking vehicle structural flexibility and propellant sloshing effects on thrust vector control dynamics, obtaining computer simulated responses for hybrid and discrete coordinate models [AAS PAPER 71-348] 23 p3773 A71-43021

Mathematical model of solar radiation pressure force and torque acting on spacecraft surface intercepting solar photon stream [AAS PAPER 71-352] 23 p3728 A71-43024

Field effect devices mathematical modeling for computer aided circuit design, using unified approach 23 p3649 A71-43069

Vortice generation in laminar boundary layer of water flow under hydraulic pressure reduction, proposing mathematical model 23 p3662 A71-43315

Spectral model of warm bubble motion in neutral surroundings from anelastic equations for shallow convection, comparing results with similarity theory and numerical models 23 p3781 A71-43336

Large project management model, presenting schematic diagrams for nature and interrelation of functions 23 p3784 A71-43452

Heat treatment specifications selection for Ni alloy by mathematical method based on cylindrical specimens elongation under tensile loads 23 p3691 A71-43523

Laser resonator natural field amplitude fluctuation calculation based on two- and four-level models for photon number dispersion 23 p3685 A71-43560

Traveling wave laser emission phase and amplitude fluctuations and spectral line width determination from single-mode distributed parameter model 23 p3685 A71-43563

Global atmospheric research program, discussing circulation, weather forecasts, numerical modelling and observational system 23 p3701 A71-43822

Kraichnan turbulence theory based on exact solution of model equations presenting strong structural similarities with turbulent Navier-Stokes equations 23 p3701 A71-43976

Statistical modeling technique for approximate numerical solution of unsteady heat conductivity inverse problem, obtaining foam chamotte and magnesite temperature field data 23 p3782 A71-44059

Stochastic optimal control theory application to airplane rescheduling model, obtaining dynamic programming algorithm for optimal landing and takeoff rules 23 p3702 A71-44104

Linear dynamic systems suboptimal control determination from lower dimension models, characterizing system and model outputs as Hilbert space elements 23 p3660 A71-44121

Soviet book on rational, irrational and transcendental transfer functions electronic modeling covering mathematical theory and applications to control plants 23 p3648 A71-44185

High Prandtl/Schmidt/number fluids turbulent flow temperature profile derivation by turbulent transport mathematical model 23 p3664 A71-44199

Grainy composite material structural analysis, presenting statistical mathematical model 23 p3698 A71-44224

Stable austenitic stainless steels and fcc metals plastic deformation flow curve model, presenting stress-strain relation 23 p3695 A71-44284

Flow models for turbomachinery, averaging equations for flow through blade cascades across pitch 23 p3627 A71-44348

Continuous chemical laser model for constant gain method exposure, emphasizing strong radiation-chemistry coupling, molecular J-shift, output power limiting behavior and lasing efficiency 24 p3832 A71-44373

Rod buckling under creep conditions, evaluating stability with Shenley model 24 p3877 A71-44405

Acoustical harmonic point source in motion relative to surrounding fluid, using Fourier integrals for mathematical representation 24 p3847 A71-44418

Analytical model of eclipsing binary star systems, testing validity through numerical integration error analysis 24 p3867 A71-44437

One dimensional diffusion model for on state propagation along p-n-p-n structure, determining propagation velocity as function of structural parameters and current density 24 p3859 A71-44462

Generalized eddy viscosity model application to quiescent and coflowing axisymmetric turbulent jets mixing 24 p3818 A71-44626

Couple-stress theory application to body model with constrained rotations, discussing elasticity theory modifications in relation to real physical phenomena 24 p3848 A71-44643

Polymer systems molecular rheology based on statistical mechanics and simplified structural models 24 p3841 A71-44644

Geometrical least squares model extension to maximum likelihood method for linear processes with additive Gaussian error 24 p3843 A71-44704

Computer systems design for complex process control, constructing models with differential equations and Boolean functions 24 p3806 A71-44714

Numerical modeling of Venus atmosphere taking into account short wave radiation absorption, boundary layer, mesoscale convection and horizontal friction 24 p3870 A71-44819

Thunderclouds and torrential clouds classification from radar data, developing algorithm model with Bayes method 24 p3845 A71-44884

Two phase nonequilibrium flow mathematical model with allowance for colliding droplets coagulation and atomization based on high speed photographic studies 24 p3790 A71-44927

Slit tube flat-to-circular transition during extension, considering mathematical model for curvature change, modulus of elasticity and Poisson ratio effects 24 p3884 A71-44959

Respiratory sinus arrhythmia by spectral analysis and digital filtering, using linear model to approximate lung volume relationship to heart rate during normal breathing 24 p3802 A71-45067

Ocean surface wave height /sea state/ measurement by high resolution random-signal radar based on model characterized by Poisson distributed scatterer density function 24 p3823 A71-45082

Analog modeling of enzyme and biochemical systems with fixed and variable functional properties, using operational amplifier integrator 24 p3802 A71-45109

Newtonian analog construction, examining relativistic homogeneous anisotropic models 24 p3873 A71-45110

Nonlinear controlled plant dynamic behavior sensitivity in parameter perturbation derived from mathematical model, applying to satellite attitude control [ASME PAPER 70-WA/AUT-5] 24 p3816 A71-45136

Computer model of microchannel electron multiplier plates in imaging devices using Monte Carlo method 24 p3811 A71-45328

Surface potential barrier models for thermionic and photoelectric emissions from semiconductors in Schottky deviation region 24 p3862 A71-45350

MATHEMATICAL STATISTICS

U STATISTICAL ANALYSIS

MATHEMATICS

Mathematics role in human activities relating to technology and pure thinking, discussing computer technology, cybernetics and mathematical models 01 p0112 A71-11159

MATHEU EQUATION

U MATHEU FUNCTION

MATHEU FUNCTION

Parametric resonance and first order instability region of Mathieu equation in nonlinear systems 04 p0620 A71-15737

Nonlinear Mathieu equation response in first unstable region, comparing results to computer simulation 07 p1161 A71-19958

Numerical method for Mathieu equation solution applicable to ordinary and asymptotic problems 13 p2094 A71-28229

Out-of-plane motion about libration points within framework of elliptic restricted three body problem, using Mathieu and Hill equation [AAS PAPER 71-336] 23 p3727 A71-43009

MATRICES

Stresses and deformation in circular matrix subject to internal pressure gradients, assuming cylindrical anisotropy on macroscopic scale 03 p0504 A71-13463

Multidirectional reinforced resin matrix composites inspection and nondestructive analysis by film/neutron radiography and X ray Vidicon 14 p2263 A71-29659

Prisoner dilemma game matrix, noting response patterns to various formats 18 p2863 A71-37017

MATRICES [CIRCUITS]

Structured or array logic configurations based on transistorized matrices with programmable interconnections for large scale integration in computer design 01 p0044 A71-10182

Silicon-on-sapphire complementary MOS circuits for high speed associative memory arrays, discussing system, circuit and device processing concepts 01 p0047 A71-10209

N-port networks interconnection by NASAP-70 transfer function capability for large scale circuit problems, considering Laemmel and Cascade Parameter methods 03 p0390 A71-14309

Network synthesis of beam-forming matrices feeding linear and rectangular antenna arrays 05 p0719 A71-16145

Butler matrix antenna array feed network extension to increased number of ports, considering relationship between beams and radiation pattern 06 p0875 A71-17726

Inhomogeneous heat transfer lines analysis by matrix method in form of power converging series by Laplace operator 07 p1221 A71-18925

Plasma display panel with rectangular gas discharge cells array separated by thin dielectric sheets, discussing operation principles 14 p2249 A71-31030

Discrete closed loop system stability with Kalman filter by determining z plane poles of special augmented transition matrix 19 p3036 A71-37235

Frequency dependent conductor coating matrices for lossy cylindrical conductors with circular section, using diffusion equation 20 p3197 A71-39450

Monolithic alphanumeric array of planar light-emitting GaAsP diode matrix on common chip for programmed function keyboard use in display devices 21 p3349 A71-40108

Red and green light emitting GaP junction diodes and monolithic arrays for display devices, discussing fabrication and properties 21 p3352 A71-40110

Low voltage IR image converter display system using scanned line array of GaAsP light-emitting junction diodes 21 p3352 A71-40117

Minimum elements number on discrete two dimensional hologram with constant distance between elements, considering reduction of matrix elements 22 p3546 A71-42311

MATRICES [MATHEMATICS]

NT ADJOINTS

NT CANONICAL FORMS

NT EIGENVALUES

NT EIGENVECTORS

NT JORDAN FORM

Error bounds for inverted nonsingular matrices using interval arithmetic in ALGOL-60 01 p0049 A71-10325

Matrix perturbation methods for nonlinear perturbed systems, involving variational equations solution of regularized Keplerian motion 01 p0154 A71-10380

Sparse matrices inverses and eigenvectors computation methods, giving bibliography 02 p0276 A71-11802

Linear matrix equations explicit solution representation techniques 02 p0276 A71-11803

Bounded plasma wave interaction matrix elements calculation from orthogonal system formation by normal waveguide modes 02 p0289 A71-11891

Successive approximations of order K iterative methods for calculating inverse matrix, yielding lower and upper bounds 03 p0449 A71-13111

Partial differential equation approximate solution by matrix transformation, reducing boundary or mixed problem to n independent linear ordinary differential equations 03 p0449 A71-13117

Book on applied matrix and tensor analysis covering coordinate systems, vectors, transformations, etc 03 p0450 A71-13569

Symmetric sparse matrices transformation to triple diagonal form, giving algorithms for nonzero elements growth minimization 03 p0450 A71-13623

Plane contours problems analytic solution by least squares method approximation, giving matrices of linear equations systems 04 p0602 A71-14605

Gaussian probability density functions covariance matrices dimension-reducing mapping using confidence spaces 04 p0619 A71-15331

Navier-Stokes equation solution in cylindrical coordinates, using finite difference scheme with brute force matrix methods 04 p0572 A71-15551

Hadamard transform spectroscopy, discussing spectral intensity calculation for cyclic measurement matrices 04 p0549 A71-15690

Book on optimization methods covering matrix algebra, n dimensional geometry, search techniques, linear and nonlinear programming, etc 05 p0774 A71-16475

Identical V antennas coplanar array admittance matrix, showing mutual conductance and susceptance as function of spacing 06 p0875 A71-17727

Linear sequential circuits feedforward inverse transfer function matrix existence condition and construction procedure 07 p1081 A71-18735

Minimization with superlinear convergence based on second derivative matrix successive approximation scheme 07 p1146 A71-19176

Two nonlinear coupled second order differential equations finite difference solution, using nonsquare and nonuniform grids for minimum error 07 p1149 A71-20612

Perturbation theory for reduced density matrices representable as functions of independent parameters 08 p1332 A71-20660

Spacecraft motion parameters maximum probability estimates, using approximate weight-matrix inversion techniques 08 p1360 A71-21003

Lower triangular matrices and associated foldant algorithm application to network analysis 08 p1268 A71-21271

Logical functions for constructing graph with fundamental cutset matrix equal to given fundamental cutset matrix 08 p1268 A71-21282

Kalman filter application as observer of observable signals derivatives, using gain matrix to minimize variance estimate for instrument landing systems 08 p1269 A71-21343

Transform coding techniques using orthogonal matrices to implement bandwidth or dimensionality reduction for image processing in digital communication systems 08 p1259 A71-21591

Matrix multiplication algorithm based on degrees of freedom analysis for various transformations and spectral analysis 08 p1260 A71-21662

Liapunov matrix equation for linear and nonlinear automatic control systems stability 08 p1325 A71-21976

Boundary value problems in noncylindrical domains investigated by Green matrix 09 p1484 A71-22176

Multicomponent microwave equipment, discussing design automation by matrix notation with computer calculations 09 p1416 A71-22468

Book on matrix methods in stability theory covering matrix algebra, Liapunov theory and functions, stability matrices properties and optimal control theory applications 09 p1539 A71-22872

Modules and matrices over semilattice ordered semigroup, developing algebraic foundation for Boolean matrix theory 09 p1485 A71-22960

Emission line profile and source function in finite optical thickness plane layer, using matrix equation 09 p1525 A71-23195

Automatic generator for finite rectangular/isoparametric element stiffness and mass matrices, discussing memory requirements and computation time optimization 09 p1542 A71-23280

Element stiffness matrix generator in terms of material and geometric properties by computer algorithm, using displacement functions, transformation matrices and strain energy expression 09 p1542 A71-23281

Return-difference matrix for optimal stationary Kalman-Bucy filter behavior examination in associated feedback system, noting spectral factorization and signal/noise separation 09 p1425 A71-23683

Growth minimization of nonzero elements in sparse matrix during reduction to Hessenberg triangular form by Gaussian similarity transformations 10 p1635 A71-23775

Covariance matrix of coordinate fluctuations of instantaneous radar center of reflection from set of scatterers 10 p1578 A71-24709

Misconceptions and distortions in n dimensional covariance matrices interpretation regarding probability confidence levels to error ellipsoid and hyperellipsoid 11 p1791 A71-25485

- Density matrix components for multiconfiguration wave functions, constructing N electron /spin free/ Hamiltonian configuration interaction matrix
11 p1802 A71-26056
- Spacecraft flight trajectory parameters estimation from unknown second moment matrix of navigation measurement errors
12 p1957 A71-26628
- Second order experimental plans, obtaining regression analysis for matrix elements and regression coefficients variance
12 p1988 A71-26707
- Probability theory application to entropy and conductivity matrices
12 p1986 A71-26960
- Minimization algorithms unified derivation, using Hessian matrix inverse
12 p1923 A71-27727
- Planar elliptic restricted three body problem, calculating variational equations separation with matrix approach
13 p2136 A71-28359
- Eigenvalue problem for transfer matrix of two dimensional Ising lattice with free boundaries perpendicular to transfer direction, calculating correlation function between spins
13 p2094 A71-28777
- Structural properties of equilibrium solutions of quadratic matrix equation, using variational interpretation of associated Riccati equation, transform techniques and Parseval formula
13 p2095 A71-28815
- Identification by minimization of Gaussian- Markovian representation of stochastic process, considering positive linear systems and algorithm for matrix calculation
13 p2043 A71-28818
- Numerical technique for two dimensional non-similar unsteady laminar boundary layer in oscillatory flow by integral matrix method
13 p2052 A71-29451
- Soviet book on multiloop automatic control systems covering matrix notation, stability and accuracy, invariance principle, compensating cross couplings, etc
14 p2218 A71-29527
- Rectangular section microstrip lumped capacitance calculation by matrix methods
14 p2210 A71-29571
- Inelastic scattering transition densities in single particle operator reduced matrix elements between initial and final nuclear states for nucleon angular momentum calculations
14 p2276 A71-30013
- Digital communication system frame synchronizer performance analysis, using mean time formula and state transition matrices
14 p2201 A71-30925
- Finite element midincrement stiffness matrices in postbuckling analysis of imperfect strut and rectangular plate
15 p2503 A71-31420
- Gyroscopic system nonstationary operation mode analysis, utilizing asymptotic method with linear matrix equation
15 p2410 A71-32454
- Mixed finite element formulation for shallow shells, discussing element matrix generation phase and governing variational principle
16 p2652 A71-33080
- Transient matrix heat transfer test data reduction, discussing direct curve matching methods implementation by distance function minimization
17 p2835 A71-34178
- Linear differential equations system with periodic coefficients, determining solutions by stationary components matrix location on complex plane
17 p2766 A71-34933
- Discrete Kalman filter computational efficiency improvement by iterative processing technique for covariance matrix updating
17 p2722 A71-35182
- Soviet book on algorithms for electronic circuit analysis covering linear and nonlinear transistor or tube circuits matrix-topological description and frequency-time domain solutions
17 p2717 A71-35219
- Natural vibration parameters of cantilevered isotropic plates, using finite difference method with matrix form solution
17 p2829 A71-35308
- Classes of n dimensional functions nonlinear matrix mapping, emphasizing block-Jacobi and block-Gauss-Seidel process convergence for continuous surjective M functions
17 p2767 A71-35524
- Eigenvalues of band matrices with nonzero elements below main diagonal or differing from Toeplitz matrix in first row
17 p2768 A71-35687
- Orthogonal matrix estimate by iterative algorithm with given order of convergence
17 p2769 A71-35692
- Correlation coupling matrix elements for one electron transfer and ion-ion recombinations in Landau-Zener calculations
18 p2948 A71-35839
- Degree reduction of scattering matrix by factorization, deriving necessary and sufficient conditions by methods based on Hankel matrices and on Smith-MacMillan form
18 p2941 A71-36237
- Projection iterative method for solving singular linear equations, noting use for matrix conversion
18 p2942 A71-36699
- Strassen algorithm as matrix products representation in seven dimensional space
18 p2942 A71-36700
- Complementary variational principles, noting application to differential, integral and matrix equations
18 p2943 A71-36957
- Algorithms and operator matrix language for infinite linear automata analysis, synthesis and identification
19 p3024 A71-37223
- Direct modification procedure for matrix displacement method
19 p3086 A71-37887
- Solution of higher order linear partial differential equations with variable coefficients, using functions of multidimensional matrices
19 p3086 A71-38012
- First and second order density matrices calculation of pure state N fermion systems, using higher random phase approximation
19 p3107 A71-38054
- Atomic structure constants numerical calculation, obtaining H matrix of complex including spin-orbit interaction and configuration mixing
19 p3142 A71-38155
- Function classes of n-dimensional nonlinear mappings generalizing matrices, including convergence for Jacobi and Gauss-Seidel process
19 p3088 A71-38311
- Computer aided digital transform natural image processing, using Fourier, Hadamard and Haar matrix algebra
19 p3026 A71-38404
- Dipole antenna with parallel parasitic element, investigating resonant length variation as function of spacing with matrix inversion method
19 p3035 A71-38599
- Sequence convergence of similarity transformations in matrix balancing for accurate eigenvalues computation
20 p3254 A71-38756
- Stationary covariance generation of matrix of rational functions of complex variable, solving factorization equation via algebraic Riccati equation
20 p3207 A71-38990
- State feedback decoupling sensitivity of time invariant linear multivariable system, using Liapunov matrix equations
20 p3207 A71-38992
- Decomposition matrix Caer model for multivariable control systems analysis and design
20 p3207 A71-38995
- Three-pole theory of amplifiers, deriving operational resistances as function of wave resistance and control parameters by current-voltage matrices
20 p3205 A71-39467
- Spacecraft motion parameters maximum probability estimates, using approximate weight-matrix inversion techniques
20 p3294 A71-39583
- Water radiolysis measurement in nuclear reactor tests, discussing experiment design as doubly telescoping sequences of blocks
21 p3345 A71-40202
- Linear second order multidegree of freedom vibrational system with singular mass matrix, determining response to excitation
21 p3457 A71-40272
- Initial conditions influence on transfer matrices of real zero leakage hydraulic tubing
21 p3326 A71-40595
- Canonical approximation of state correlation matrix and threshold crossings of variable systems with random turbulence type input vectors representing flight environment
21 p3408 A71-40614
- Real symmetric matrix eigenvectors calculation with differential equation, using Liapunov function
21 p3409 A71-41080
- Extreme eigenvalues of Toeplitz matrices associated with Laguerre and Jacobi polynomials, using finite difference operators
21 p3410 A71-41084
- Holomorphic matrix valued function on connected open subset of complex plane, obtaining conditions for satisfying homogeneous linear differential equation
21 p3410 A71-41185
- Signal processing models choice in Kalman-Bucy filtering, proving smallest error covariance matrix existence
21 p3349 A71-41190
- Singularities of Green matrix in steady state wave propagation in homogeneous anisotropic media
21 p3416 A71-41245
- Kinetic wave equation matrix elements for three resonantly coupled electrostatic plasma waves noting application to electron plasma coupling with ion sound waves
22 p3582 A71-41900
- Computer program for on-line determination of minimal realizations of transfer function matrices, using Rosenbrock system matrix formulation
22 p3526 A71-42285
- Multicomponent diffusion process calculation using eigenvalues of Onsager diffusion matrix
22 p3575 A71-42371
- Ax equals lambda Bx eigenvalue problem, presenting Perron and Frobenius results and dual characteristics
22 p3567 A71-42627
- Finite Fourier transforms from finite dimensional algebraic viewpoint, deriving fast Fourier transform algorithm via tensor products induced matrix factorization
23 p3698 A71-42920
- Herrick-Gibbs preliminary orbit determination method in matrix form for spacecraft extended to process greater than three inertial position vectors [AAS PAPER 71-317]
23 p3725 A71-42991
- Simultaneous iterative solution for obtaining dominant subset of unsymmetric matrix eigenvalues and eigenvectors
23 p3698 A71-43098
- Iterative solution of eigenvalue problems for positive real symmetric matrices without first approximation of eigenvalues and eigenvectors, constructing by powers of spectral decomposition
23 p3699 A71-43488
- Generalized matrix inverses application to estimation of state vector in dynamic control system, determining covariance matrix of estimator
23 p3700 A71-44117
- Pole placement design of dynamic compensators for linear time invariant multivariable systems, using transfer function matrices
23 p3660 A71-44119
- Sequential zero-pole placement technique for multivariable control systems, developing algorithm for computing closed loop transfer function matrix
23 p3660 A71-44120
- Necessary and sufficient conditions for separating regular multiplier from matrix polynomial, presenting method for determining regular multiplier real factors
24 p3842 A71-44477
- Jones reflection and transmission matrices representation for beam splitters, investigating reversibility and action on incident light amplitude and/or phase
24 p3849 A71-45210
- MATRIX ALGEBRA**
U MATRICES [MATHEMATICS]
MATRIX ANALYSIS
U MATRICES [MATHEMATICS]
MATRIX METHODS
Cryptographic techniques applications to data processing systems, considering digital substitution and digital route transposition matrix
01 p0044 A71-10187
- Comparative shallow shell finite element analyses using different stiffness matrices
01 p0175 A71-11012
- Hybrid computer structural response simulation for helicopter fuselage, using matrix displacement method
02 p0227 A71-11790
- Matrix algorithm using difference-differential method for thin wall moments of varied thickness anisotropic cylindrical shell
02 p0328 A71-12561
- Matrix method for multiple scattering extended to polarized light
03 p0458 A71-13611
- Thin shells of revolution formed of closed box sections, using numerical integration and stiffness matrix for solution [ASME PAPER 70-PVP-12]
04 p0665 A71-14770
- Redundant structure dynamic analysis for forced and free vibrations, using finite element rank force method
05 p0829 A71-17120
- Matrix displacement /finite element/ method for elastic structures analysis
06 p1001 A71-18050
- Book on computer methods of structural analysis concentrating on frame systems, stiffness matrix techniques and Fortran IV
07 p1210 A71-19099
- Cylindrical, conical and spherical shells natural frequencies and vibration modes determination using matrix series
07 p1212 A71-19365
- Bending stiffness matrix for sandwich folded plate, reproducing core shearing deformations
08 p1367 A71-20748
- Nonlinear analysis of cable and truss structures, using computerized stiffness matrix method
08 p1367 A71-20749
- Optimal thin walled structures design, using discrete matrix methods for computer programming
08 p1368 A71-20791

Periodically supported and damped closed circular beam structure, determining frequency response matrix

08 p1374 A71-22026

Book on matrix structural analysis covering transformation, structure idealization, displacement method, finite element theory, nonlinear aspects, etc

09 p1539 A71-22873

Matrix force method for structural cut-out problems, using undetermined multipliers to incorporate modifications

09 p1540 A71-22993

Statistically indeterminate modified structures automated design reanalysis by displacement method, using matrix formulations, numerical computation and computer operations

09 p1542 A71-23282

Structural system analysis by partial decomposition of flexibility and stiffness matrices, obtaining coordinate deformations for computer and hand applications

10 p1691 A71-24693

Lumped parameter torsional and flexural system synthesis for vibratory characteristics, using transfer matrices

10 p1692 A71-24925

Structural dynamics motion matrix Newmark generalized acceleration operator, Wilson averaging variant and Gurtin variational principle investigations for stability and approximation viscosity

10 p1693 A71-25050

Positive rotational transformations of stress vectors for anisotropic lamina in matrix notation

11 p1852 A71-26393

Finite element for torsion of thin walled open tubes, applying to matrix force analysis

12 p1974 A71-26871

Photoelastic materials polarization characteristics analysis using Muller matrix method

12 p1976 A71-27115

Spring loaded intermittent contact devices vibrating system parameters for computer programmed transfer matrix solution, noting gravity loaded variant

12 p1931 A71-27480

Stress analysis of thin walled framed structures of variable cross section by second order differential buckling equations, using matrix method

14 p2321 A71-29539

Rectangular cylindrical shell finite element, deriving stiffness matrix with stress distribution

15 p2510 A71-32516

Matrix methods of structural analysis and design - Conference, Tokyo, August 1969

16 p2651 A71-33076

Matrix force analysis, discussing methods for expressing elastic behavior of semiconocque polygon membrane and isotropic polygon bending elements

16 p2652 A71-33082

Stiffness matrices determination for flat plate elements under tangential and normal loadings by collocation, using exact polynomial solutions

16 p2652 A71-33083

Elastoplastic analysis by matrix displacement method, discussing perforated plate under tension and bar thermal stress due to rapid heating

16 p2652 A71-33085

Dynamic vibration analysis of mechanical structures, considering transfer and stiffness matrix methods

16 p2653 A71-33091

Elastic-plastic stiffness matrix methods, applying linear and nonlinear programming techniques to framed structures analysis

16 p2653 A71-33094

Finite element procedure for plate large deflection by considering effects of element membrane forces due to initial deflection and bending on stiffness matrices

17 p2825 A71-34872

Torsion free, rigid and elastic stiffness matrices of thin walled bars, noting transformation to eccentric nodal points

17 p2832 A71-35399

Influence coefficient matrix method for discretized Poisson equation solution

18 p2905 A71-36306

Large stiffness matrices building and manipulation, including structural analysis computer programs input determination, coupling techniques and eigenvalue problems solution

19 p3161 A71-38654

Modified Newton-Raphson stiffness matrices and initial value formulations to geometrically nonlinear structural analysis for beam and plane stress triangular elements

20 p3311 A71-39870

Algorithm for linearly elastic structures vibration natural undamped frequency computation, assuming known dynamic stiffness matrix

20 p3311 A71-39964

Cyclic discrete holonomic mechanical systems Liapunov stability analysis, developing matrix formalism for kinetic energy, Routhian, Hamiltonian and dynamic potential energy quadratic approximation

21 p3454 A71-40097

Exact calculations of prestressed networks of arbitrary form and magnitude based on matrix displacement method

21 p3456 A71-40156

Direct solution for divergence speed of lifting surface using matrices of structural and static aerodynamic influence coefficients

21 p3456 A71-40171

Transfer matrix and finite element combination technique for plates and shells vibration analysis [ASME PAPER 71-VIBR-85]

21 p3461 A71-40321

Axially coupled turborotors, calculating coupling characteristics, disk inertia and gyroscopic effects on dynamic response, by transfer matrix techniques [ASME PAPER 71-VIBR-108]

21 p3462 A71-40332

Koiter theory for structural snap-through buckling behavior, using discretized matrix procedure based on finite element idealization

22 p3613 A71-41436

Quasi-static thermoelasticity and dynamic thermal stress equations solution in matrix form by Fourier transform and Hilbert-Levy method

22 p3614 A71-41567

Vehicle attitude determination and guidance sensor orientation by vector space matrix method, minimizing errors by weighted least squares affine transformation technique

23 p3773 A71-43064

Stiffness and consistent mass matrices for beam bending finite element containing integration parameters

23 p3776 A71-43374

Stiffness matrix algorithm for triangular plate bending elements using hierarchy of interpolation polynomials

24 p3879 A71-44637

Hermite polynomials application to stiffness matrix determination in plate finite element method for disk under plane stress, presenting digital computer program flow diagram

24 p3880 A71-44641

Geodetic grid points coordinates accuracy estimate based on normal equations system cracovian matrix, determining arbitrary elements by numerical process without error equations linearization

24 p3822 A71-44768

Approximate periodic Green matrix solution to equilibrium equations in displacements for shell of revolution under linear loads

24 p3881 A71-44826

Numerical evaluation of structures buckling loads, considering matrix equation application to elastic stability problems

24 p3883 A71-44870

Systems synthesis by Liapunov direct method, developing vector-matrix equations for systems classes satisfying specified Liapunov scalar functions [ASME PAPER 70-WA/AUT-3]

24 p3816 A71-45135

MATRIX STRESS CALCULATION

U MATRIX METHODS

MATRIX THEORY

Error bounds for inverted nonsingular matrices using interval arithmetic in ALGOL-60

01 p0049 A71-10325

Conjugate direction minimization procedure based on sequences and inferred second partial derivative matrix inverse

01 p0112 A71-10962

Sparse matrices inverses and eigenvectors computation methods, giving bibliography

02 p0276 A71-11802

Linear matrix equations explicit solution representation techniques

02 p0276 A71-11803

Existence and construction of modified L lag inverses solution method for linear dynamical systems

03 p0393 A71-14482

Matrix algorithms for linear and nonlinear inequalities, discussing rank generation and matrix inversion

05 p0774 A71-16398

Axisymmetric isotropic shells of revolution, using matrix-operator notation for differential equations systems solution

06 p0995 A71-17835

Matrix eigenvalue problem solution by reducing to nonlinear algebraic equations for iterative solution or integration by Runge-Kutta method

06 p0921 A71-18342

Algorithm for simultaneous estimate of spacecraft state and covariance matrix with observation error vector

07 p1148 A71-19882

Logical functions for constructing graph with fundamental cutset matrix equal to given fundamental cutset matrix

08 p1268 A71-21282

Book on matrix methods in stability theory covering matrix algebra, Liapunov theory and functions, stability matrices properties and optimal control theory applications

09 p1539 A71-22872

Modules and matrices over semilattice ordered semigroup, developing algebraic foundation for Boolean matrix theory

09 p1485 A71-22960

Complex zeros of complex polynomials, matrix inequalities and nonlinear programming, constructing areas intersection in complex plane defined by inequality bounds on eigenvalues of companion matrix

09 p1485 A71-22970

Growth minimization of nonzero elements in sparse matrix during reduction to Hessenberg triangular form by Gaussian similarity transformations

10 p1635 A71-23775

General nonorthogonal coordinate systems operation techniques, modifying matrix theory for vector equations handling in classical mechanics

15 p2442 A71-32111

Monograph on algebraic theory for ordinary linear time invariant difference systems covering constant shift operators, matrix formalism, operational calculus, etc

16 p2602 A71-33397

Matrix trace method for identities relating eigenvalues of singular ordinary differential operators and zero Bessel functions

16 p2603 A71-33593

Array design by matrix inversion for specified pattern in far zone field exceeding number of independent excitation voltages

17 p2715 A71-34766

Eigenvalues of band matrices with nonzero elements below main diagonal or differing from Toeplitz matrix in first row

17 p2768 A71-35687

Degree reduction of scattering matrix by factorization, deriving necessary and sufficient conditions by methods based on Hankel matrices and on Smith-MacMillan form

18 p2941 A71-36237

Direct modification procedure for matrix displacement method

19 p3086 A71-37887

Analysis and synthesis of linear optical systems involving polarization effects by Pauli algebra of complex second order matrices

20 p3267 A71-38775

Iterative solution of eigenvalue problems for positive real symmetric matrices without first approximation of eigenvalues and eigenvectors, constructing by powers of spectral decomposition

23 p3699 A71-43488

MATTER (PHYSICS)

Uniform matter fragmentation under gravitational influence, examining approximate solution for density perturbations

01 p0150 A71-10062

Cosmological plasma physics, considering matter, antimatter, electrodynamics, ambiplasma, annihilation and heavy nuclei

07 p1196 A71-19649

Hot universe model, discussing small scale entropy, matter distribution, adiabatic density perturbations, energy balance, formation of galactic clusters, galaxies, globular clusters and quasars

09 p1527 A71-23531

Matter and antimatter separation mechanism in universe based on thermal radiation thermodynamic properties

10 p1665 A71-23739

Hydrodynamics of matter-antimatter in contact, discussing coalescence, particles annihilation pressure and energy balance

11 p1821 A71-25539

Matter density in universe, comparing delayed galactic growth with observed radio sources and quasars

14 p2305 A71-29675

Cl chondrites approximating primordial solar system matter condensable fractions based on isotopic/elemental abundance continuity, fractionation patterns and chondrules absence

14 p2306 A71-29708

Plasma as fourth state of matter, including high temperature behavior, radiation emission, applied electric/magnetic fields effects and laboratory generation

16 p2617 A71-32953

Lower limit on size of matter and antimatter regions in vanishing baryon number cosmology based on homogeneous intergalactic magnetic field existence

16 p2632 A71-33237

Kinetic theory of gases in general relativity, including model of matter particle structure

16 p2610 A71-33267

Classical gravitational field equations modification for virtual quantized matter, taking into account additional mass due to attractive forces

16 p2610 A71-33271

Cosmological implications of microscopic charge-parity violation, considering redefinition of matter and antimatter in time-inverted expansion

16 p2611 A71-33278

Critique of cosmological theories based on spontaneous matter creation in strong gravitational fields, deriving particles discrete number constancy in general relativity

20 p3268 A71-38834

MATURING U GROWTH

MAXIMUM LIKELIHOOD ESTIMATES

Spacecraft motion parameters maximum probability estimates, using approximate weight-matrix inversion techniques
08 p1360 A71-21003

Maximum likelihood estimates for deterministic signal parameter during optimal reception on stationary normal noise background
09 p1405 A71-22465

Maximum likelihood method for accuracy of spacecraft trajectory determination by complex expressions in multidimensional geometric representation
12 p1957 A71-26629

Optimal measurement programs for instrument controlled spacecraft trajectory sections, using maximum likelihood method
12 p1957 A71-26630

PAM data transmission systems timing recovery, discussing maximum likelihood estimation method for timing parameter from random data
15 p2377 A71-32314

Human inferences based on partially reliable reports, studying likelihood ratio estimates and probabilistic relations in nature
16 p2534 A71-33103

Maximum likelihood estimates potential accuracy in presence of interfering parameters, presenting analysis method based on Fisher information matrix
16 p2542 A71-33489

Navigational accuracy improvement by combining VOR/DME information with airspeed and heading data via maximum likelihood filter, using small airborne computer [AIAA PAPER 71-928]
19 p3097 A71-37174

Noise variance maximum likelihood estimate based on order statistics for first order Reed-Muller code transmission over zero-mean white Gaussian noise channel
20 p3202 A71-38875

Spacecraft motion parameters maximum probability estimates, using approximate weight-matrix inversion techniques
20 p3294 A71-39583

Accuracy in maximum likelihood estimate for correlation function parameter of random process in signal reception on normal noise background
20 p3199 A71-39816

Open clusters membership probabilities and frequency distribution function parameters calculation by fitting relative proper motions to model with maximum likelihood procedure
22 p3601 A71-42165

Maximum likelihood estimation algorithm for arrival direction of narrowband signal under correlated noise
22 p3510 A71-42258

Geometrical least squares model extension to maximum likelihood method for linear processes with additive Gaussian error
24 p3843 A71-44704

MAXIMUM PRINCIPLE

Cylindrical shells and circular plates optimal limiting and adaptable loads calculation by Pontryagin maximum principle
01 p0170 A71-10639

Optimal control with equality type phase operator constraints, obtaining multiplier rules for necessary conditions in maximum principle form
04 p0561 A71-15870

Optimal process control with various delay times, discussing maximum principle variant and calculus of variations
06 p0879 A71-17671

Trajectory optimization, using Pontryagin maximum principle for differential inclusions
07 p1146 A71-19178

Distributed parameter control systems optimality conditions, using Pontryagin maximum principle
09 p1425 A71-23469

Search scanning system synthesis based on forces optimal distribution over investigated field, using Pontryagin maximum principle
10 p1586 A71-24167

Spring coupled inertially damped instrument servomechanisms design, applying phase margin maximization criterion
11 p1716 A71-26417

Computational approach to maximum principle in control theory, considering canonical problem
13 p2035 A71-28996

Extremum principle for structures in creep under cyclic loading for time dependent stable dissipative material
15 p2505 A71-31944

Optimal control synthesis for saturating time-varying and stationary sampled data systems, using integral performance index and extended maximum principle
16 p2551 A71-34169

Optimal design of axisymmetrical annular plate and cylindrical and spherical shells by maximum principle
17 p2833 A71-35621

Convergence estimation of locally one dimensional scheme for multidimensional heat conduction boundary value problem solution on nonuniform grids using maximum principle
19 p3171 A71-38415

Turbulent flow stability with respect to small disturbances, applying maximum stability principle to stable averaged flow
20 p3210 A71-38895

MAXIMUM USABLE FREQUENCY

Short radio wave propagation over single jump lines in F2 critical frequency gradient presence, examining maximum usable frequency increase
09 p1405 A71-22439

Ionospheric propagation forecasting as function of solar and magnetic activity conditions for maximum usable communications frequencies, using F2 layer peak electron density
10 p1575 A71-23865

Satellite data for ionospheric radio communication forecasting involving maximum usable radio frequencies, discussing F2 region large scale disturbances
10 p1575 A71-23868

Ionospheric propagation prediction accuracy problems, considering numerical mapping, horizontal gradients, absorption, scatter, maximum usable frequency and transequatorial propagation
14 p2202 A71-30949

MAXWELL BODIES

Optimal relaxation time existence for Maxwell solid cylinder bonded to thin casing during forced vibration of rocket assembly, discussing Voight solid
03 p0497 A71-13469

Plane waves propagation in viscoelastic body representing parallel union of Kelvin and Maxwell bodies in magneto-thermal field
21 p3463 A71-40577

MAXWELL EQUATION

Plasma stabilization, considering feedback loop system with Maxwell-Vlasov equations
06 p0931 A71-17452

Log periodic dipole antennas Maxwell equations solution in cylindrical coordinates for all boundary conditions
06 p0874 A71-17706

Maxwell theory analogy with Cosserat continuum moving dislocations, studying kinematic and dynamic equations common features
07 p1161 A71-20016

Static cylindrically symmetric universes consisting of Einstein-Maxwell gravitational and electromagnetic fields, discussing central axial mass and charge or current density
08 p1334 A71-21361

Plasma configurations kinetic description by differential equations based on Vlasov and Maxwell equations, obtaining boundary layer distribution between plasma and magnetic field
08 p1340 A71-21492

Steady electromagnetic oscillation amplitude calculation from solution kernel to Maxwell equations boundary value problems through orthogonal coordinate transformation to Fredholm integral equations
09 p1495 A71-23431

Maxwell equations analog for gravitational fields, considering Maldybaeva equation as condition for gravitational waves existence in Riemann manifold
12 p1931 A71-27243

Nonlinear optics classical macroscopic treatment with Maxwell equations
13 p2078 A71-28517

Third harmonic component generation in reflected and transmitted waves from magnetoplasma slab, using Boltzmann transport equation and Maxwell equation
13 p2109 A71-29243

Nonuniform conductivity effect on cosmic magnetic fields structure with zero Lorentz force, using Maxwell equations and Ohm law
14 p2274 A71-29982

Plasma configurations kinetic description by differential equations based on Vlasov and Maxwell equations, obtaining boundary layer distribution between plasma and magnetic field
16 p2618 A71-33043

Wave fronts in Einstein-Maxwell theory, showing perturbation propagation along background spacetime metric field
16 p2609 A71-33261

Plane electromagnetic wave diffraction on ideally conducting convex body of large electrical dimensions, obtaining Maxwell equations asymptotic solution
16 p2542 A71-33485

Gravitational equations in Maxwellianized form, investigating Bianchi qualities
17 p2778 A71-34631

Tensors in relativistic asymmetrical field theory, generalizing Einstein gravitation and Maxwell electromagnetic equations for electrogravitational fields
19 p3105 A71-38580

Light ponderability in gravitation theory, discussing hypothetical Freundlich effect of light velocity dependence on radiation field intensity, based on Maxwell electrodynamics nonlinear generalization
20 p3270 A71-39457

Atmospheric dynamo equations derivation based on Maxwell equations and Ohm law with anisotropic and asymmetric electric conductivity tensor for quiet geomagnetic variations explanation
20 p3217 A71-39518

Electromagnetic field theory formulation, using Maxwell equations for spinors
23 p3705 A71-43827

MAXWELL-BOLTZMANN DISTRIBUTION FUNCTION

Maxwellian distribution function calculation for molecules during initial phase of chemical reaction by successive approximations and Chapman-Enskog method
03 p0376 A71-14065

Combustion, reaction and flame propagation during gas mixtures burning, allowing for disruption of Maxwell-Boltzmann molecular velocity distribution
13 p2162 A71-28957

MAXWELL-MOHR METHOD

Topological methods of linear electric circuits analysis, considering Kirchhoff, Maxwell and Mason methods
11 p1743 A71-26464

MAXWELLIAN DISTRIBUTION (DENSITY)

U MAXWELL-BOLTZMANN DISTRIBUTION FUNCTION
MCDONNELL AIRCRAFT
NT DC 10 AIRCRAFT
NT F-4 AIRCRAFT
MCDONNELL MILITARY AIRCRAFT
U MILITARY AIRCRAFT
MEAN

Shear-invariant mean value of positive-definite operator on bicompart group in form function of integral sequence, considering ergodic theorem
01 p0110 A71-10097

Quasi-means definition and auxiliary system introduction for models including negative four-fermion interaction, solving limiting expressions problem for free energy
05 p0775 A71-16865

MEAN FREE PATH

Ultrahigh energy electrons and gamma quanta in ground produced by cosmic rays, plotting mean free path vs energy
03 p0478 A71-13868

Electron scattering out of electron beam in beam plasma, presenting evidence for nonlinear effective inverse mean free path
06 p0935 A71-17485

Sn additives effect on In thin film superconducting transmission lines, comparing with Pippard nonlocal theory for mean free path reduction
07 p1179 A71-20155

Relativistic electron beam instability and mean free path in dense plasma target, using Vlasov equation
09 p1500 A71-22238

Interplanetary magnetic field irregularities and solar proton diffusion mean free path during 25 February 1969 event
10 p1677 A71-24556

Large angle Rayleigh light scattering for density fluctuations determination in dilute gases with wavelength comparable to mean free path
10 p1642 A71-24835

Relativistic quarks in cosmic rays at sea level and at mountain altitude, estimating production cross section vs absorption mean free path and mass
11 p1815 A71-25589

Atmospheric scintillation light detection from air shower, determining interaction mean free path of 10-10 million TeV primary particles
13 p2122 A71-28070

Compressible rarefied gas Couette flow over plane wall, calculating mean free path with Boltzmann equation relaxation model
13 p2051 A71-29357

Relativistic electron beam instability and mean free path in dense plasma target, using Vlasov equation
21 p3424 A71-41124

Ultrahigh energy electrons and gamma quanta in ground produced by primary cosmic rays, plotting mean free path vs energy
22 p3595 A71-42669

Electric parameters of cold hollow cathode discharge and effect, controlling electron free paths by electric or magnetic field
23 p3710 A71-43276

Supersonic plasma flow interaction with mirror field studied by changing ion-ion collision mean free path in BSG-1A device
24 p3852 A71-44489

MEAN TIME BETWEEN FAILURES

U MTBF
MEASURANDS
U MEASUREMENT

MEASURE AND INTEGRATION

NT BINARY INTEGRATION
NT BOREL SETS
NT FUNCTIONAL INTEGRATION
NT INTEGRAL CALCULUS
NT LEBESGUE THEOREM

NT NUMERICAL INTEGRATION
 NT RUNGE-KUTTA METHOD
 NT STIELTJES INTEGRAL
 NT WEIGHTING FUNCTIONS
 Triple integrals approximation using cubature formulas symmetrical with respect to parallelepiped center

06 p0921 A71-18344

Semiimplicit time integration scheme application to grid point atmospheric models of primitive meteorological equations

06 p0924 A71-18411

Compressible turbulent boundary layers integral solution based on entrainment theory

07 p1090 A71-19903

Complex hydrodynamic systems nonlinear differential motion equations integration, taking friction forces into account

08 p1299 A71-21620

Stellar mass relativistic integral theorems and upper and lower bounds for gravitational potential theory

11 p1830 A71-26106

Inertial instruments with outputs indicative of time integral and time double integral of vehicle acceleration for velocity and distance determination

14 p2245 A71-30343

Integral containing Heaviside and Dirac delta function in integrand with minus and plus infinity limits, computing value using thin spherical shells in general relativity

16 p2656 A71-33263

Integration method for second order nonlinear differential equation describing vibrational processes in mechanics, physics and engineering

17 p2766 A71-34913

Friction forces in complex hydrodynamic systems nonlinear differential motion equations integration

17 p2749 A71-35680

Channel type closed shallow shells stress states calculation, applying asymptotic integration technique to load decomposition

18 p2976 A71-36178

Nonlinear operators differentiation and integration, considering Gateaux and Frechet derivatives and Riemann integral

18 p2943 A71-36953

Asstatic gyroscope mounted on aircraft moving arbitrarily near earth surface, obtaining integrals of kinematic equations

24 p3828 A71-45160

MEASURE THEORY

U MEASURE AND INTEGRATION

MEASUREMENT

Weather radar echoes quantization following detection, discussing subsequent digital processing

01 p0049 A71-10591

MEASURES

Quantitative and qualitative philosophical aspects of measure and forecasting applied to patent handling

02 p0336 A71-11861

MEASURING

U MEASUREMENT

MEASURING APPARATUS

U MEASURING INSTRUMENTS

MEASURING INSTRUMENTS

NT ACCELEROMETERS
 NT ACTINOMETERS
 NT ALTIMETERS
 NT AMMETERS
 NT ANALYZERS
 NT ANEMOMETERS
 NT APPROACH INDICATORS
 NT ATOMIC CLOCKS
 NT ATTITUDE INDICATORS
 NT BAROMETERS
 NT BOLOMETERS
 NT CALORIMETERS
 NT CERENKOV COUNTERS
 NT CHRONOMETERS
 NT CLOCKS
 NT CLOUD HEIGHT INDICATORS
 NT COMPARATORS
 NT COMPASSES
 NT COULOMETERS
 NT COUNTERS
 NT DEFORMETERS
 NT DENSITOMETERS
 NT DICKE RADIOMETERS
 NT DIFFRACTOMETERS
 NT DISTANCE MEASURING EQUIPMENT
 NT DOSIMETERS
 NT DYNAMOMETERS
 NT ELECTROMETERS
 NT ELECTRON COUNTERS
 NT ELECTRON PROBES
 NT ELECTROPHOTOMETERS
 NT ELECTROSTATIC PROBES
 NT ELLIPSOMETERS
 NT ENGINE ANALYZERS
 NT ENGINE MONITORING INSTRUMENTS
 NT ERGOMETERS
 NT EXTENSOMETERS
 NT FABRY-PEROT INTERFEROMETERS
 NT FABRY-PEROT SPECTROMETERS
 NT FLAME PROBES
 NT FLIGHT LOAD RECORDERS

NT FLIGHT RECORDERS
 NT FLOW DIRECTION INDICATORS
 NT FLOWMETERS
 NT FUEL GAGES
 NT GALVANOMETERS
 NT GAS METERS
 NT GEIGER COUNTERS
 NT GEODIMETERS
 NT GOLAY DETECTOR CELLS
 NT GONIOMETERS
 NT GRAVIMETERS
 NT GRAVITY GRADIOMETERS
 NT GYRO HORIZONS
 NT GYROCOMPASSES
 NT HELIOMETERS
 NT HODOSCOPES
 NT HOT-FILM ANEMOMETERS
 NT HOT-WIRE ANEMOMETERS
 NT HOT-WIRE FLOWMETERS
 NT HYGROMETERS
 NT HYPSONOMETERS
 NT IMPEDANCE PROBES
 NT INDICATING INSTRUMENTS
 NT INFRARED DETECTORS
 NT INFRARED INSTRUMENTS
 NT INFRARED SCANNERS
 NT INFRARED SPECTROMETERS
 NT INFRARED SPECTROPHOTOMETERS
 NT INTERFEROMETERS
 NT ION PROBES
 NT ION TRAPS [INSTRUMENTATION]
 NT IONIZATION GAGES
 NT IONOSONDES
 NT KNUDSEN GAGES
 NT LASER ALTIMETERS
 NT LASER RANGE FINDERS
 NT LIGHT SCATTERING METERS
 NT LUNAR SEISMOGRAPHS
 NT MACH-ZEHNDER INTERFEROMETERS
 NT MAGNETIC PROBES
 NT MAGNETOMETERS
 NT MANOMETERS
 NT MASS SPECTROMETERS
 NT METEOROLOGICAL INSTRUMENTS
 NT MICHELSON INTERFEROMETERS
 NT MICRODENSITOMETERS
 NT MICROMETERS
 NT MICROWAVE INTERFEROMETERS
 NT MICROWAVE PLASMA PROBES
 NT MICROWAVE PROBES
 NT MICROWAVE RADIOMETERS
 NT MICROWAVE SENSORS
 NT MILLIVOLTMETERS
 NT MOISTURE METERS
 NT MONOCHROMATORS
 NT NEUTRON COUNTERS
 NT NOISE METERS
 NT OCULOMETERS
 NT OMEGA NAVIGATION SYSTEM
 NT OPTICAL MEASURING INSTRUMENTS
 NT OPTICAL PYROMETERS
 NT OPTICAL RANGE FINDERS
 NT OPTICAL SCANNERS
 NT OSCILLOGRAPHS
 NT OXYGEN ANALYZERS
 NT PARTICLE TELESCOPES
 NT PENETROMETERS
 NT PENNING GAGES
 NT PHASE SWITCHING INTERFEROMETERS
 NT PHOTOGONIOMETERS
 NT PHOTOMETERS
 NT PIEZOELECTRIC GAGES
 NT PLAN POSITION INDICATORS
 NT PLASMA PROBES
 NT PNEUMATIC PROBES
 NT POLARIMETERS
 NT POLARISCOPES
 NT POSITION INDICATORS
 NT POTENTIOMETERS [INSTRUMENTS]
 NT PRESSURE GAGES
 NT PROPORTIONAL COUNTERS
 NT PSYCHROMETERS
 NT PYROHELIOMETERS
 NT QUANTUM COUNTERS
 NT RADIATION COUNTERS
 NT RADIATION DETECTORS
 NT RADIATION MEASURING INSTRUMENTS
 NT RADIATION PYROMETERS
 NT RADIO ALTIMETERS
 NT RADIO DIRECTION FINDERS
 NT RADIO FREQUENCY IMPEDANCE PROBES
 NT RADIO INTERFEROMETERS
 NT RADIOMETERS
 NT RADIOSONDES
 NT RAIN GAGES
 NT RANGE FINDERS
 NT RATIOMETERS
 NT RAWINSONDES
 NT REFLECTOMETERS
 NT REFRACTOMETERS
 NT RESISTANCE THERMOMETERS
 NT RESONANCE PROBES
 NT RESPIROMETERS
 NT RHEOMETERS
 NT RIOMETERS

NT SCINTILLATION COUNTERS
 NT SEISMOGRAPHS
 NT SHOCK MEASURING INSTRUMENTS
 NT SIGNAL ANALYZERS
 NT SILICON RADIATION DETECTORS
 NT SOLAR SPECTROMETERS
 NT SONDES
 NT SONIC ANEMOMETERS
 NT SPACECRAFT POSITION INDICATORS
 NT SPARK CHAMBERS
 NT SPECTROMETERS
 NT SPECTROPHOTOMETERS
 NT SPECTRODIAMETERS
 NT SPEED INDICATORS
 NT STRAIN GAGE BALANCES
 NT STRAIN GAGES
 NT TEMPERATURE MEASURING INSTRUMENTS
 NT TEMPERATURE PROBES
 NT TENSOMETERS
 NT THEODOLITES
 NT THERMAL CONDUCTIVITY GAGES
 NT THERMOBALANCES
 NT THERMOCOUPLE PYROMETERS
 NT THERMOMETERS
 NT THRESHOLD DETECTORS [DOSIMETERS]
 NT TIME MEASURING INSTRUMENTS
 NT TIMING DEVICES
 NT TORQUEMETERS
 NT TURBULENCE METERS
 NT ULTRAVIOLET SPECTROMETERS
 NT VACUUM GAGES
 NT VARIOMETERS
 NT VIBRATION METERS
 NT VISCOMETERS
 NT VOLTMETERS
 NT WATTMETERS
 NT WEIGHT INDICATORS

Instrument for measuring cross and autocorrelation functions with capability of extracting signal masked by noise by averaging operations

01 p0079 A71-10313

Czech circumzenithal instrument used with astronomical telescope for equal altitude stellar observation, discussing optical system, electronics and measurement results

01 p0082 A71-10872

Universal UHF telemetry system for use on artillery projectiles and gun launched probes, describing components

01 p0034 A71-10911

Discrete servo position gage accuracy in presence of high uncorrelated noise level, using Markov chain

01 p0038 A71-11233

MOS capacitors as low mass micrometeoroid detectors in near-earth space, discussing fabrication and environmental tests

01 p0083 A71-11310

Time-pulse converter for semiconductor triodes DC amplification factor measurement

02 p0230 A71-11832

Q switched ruby laser-Raman radar for real time air pollution probe

02 p0213 A71-12014

Molecular mass gage with chambers interconnected by porous membranes for injected small gas samples

02 p0250 A71-12137

Book on mechanical vibration and shock measurements covering periodic and random vibrations characteristics, instrumentation, control, etc

02 p0251 A71-12175

Fluidic sensors for automatic control systems parameter measurement

02 p0196 A71-12625

Electrical measuring device error caused by longitudinal instability of frame held in tensile suspension during casing transverse vibration

02 p0253 A71-12635

Ballistic projectile velocity measurement using condenser charged thin wire circuit

03 p0422 A71-13273

Prismatic absorption type wavemeter consisting of frequency divider and Fabry-Perot interferometer, considering tests in millimeter and submillimeter range

03 p0386 A71-13801

High impedance source with shunt capacitance, discussing periodic output measurement using operational amplifier

03 p0427 A71-13923

Electric field strength measurement at rocket surface in ionosphere by electrostatic fluxmeter, obtaining E and F region ion drift velocities

03 p0417 A71-14035

Vortex angular rate sensor flow characteristics, solving Navier-Stokes equations by numerical technique

[ASME PAPER 70-WA/FE-5]

03 p0402 A71-14127

High temperature permeameters for measuring magnetizing force and magnetic induction, presenting normal induction curves as function of temperature

03 p0430 A71-14413

Astronomical instrument manufacture - Conference, Pulkovo, U.S.S.R., November 1967

04 p0587 A71-14826

Automatic solar and lunar reference guidance system with balanced photoelectric measuring equipment

04 p0591 A71-14846

Apparatus for thermal diffusivity measurements under gas atmosphere at high temperature, using flash method

04 p0595 A71-14962

Multiproperty apparatus for high temperature determination of tungsten thermal properties, using direct electrical heating methods

04 p0595 A71-14967

Automatic transistor noise factor measurement equipment consisting of noise source, signal amplifier, synchronizing oscillator, controllable attenuator and automatic control circuits

04 p0557 A71-15078

Air pollution monitoring instrument for measuring mass concentration of aerosols and particulates in atmosphere

04 p0597 A71-15288

Soviet papers on astronomical devices covering stellar transit and observation, photoelectronic instruments and recordings

04 p0598 A71-15376

Photoelectric stellar transit instrument lens with increased spherical aberration based on light beam passage analysis

04 p0598 A71-15379

Stellar transit time photoelectric instruments time lag measurements by variable flux light source

04 p0599 A71-15382

Measuring instrument for lunar surface layer heat flow, temperature and thermal conductivity

04 p0599 A71-15543

Digital measurement equipment production and circuit design principles, considering decimal memory elements in adder and divider circuits, miniaturization, reliability and integration

04 p0599 A71-15566

High temperature plasma electron density and ion signal intensity measuring apparatus for reaction rate evaluation

04 p0600 A71-15591

Modified buried collector gauge performance over He pressure range, determining sensitivity dependence on filament geometry

05 p0748 A71-16231

Measuring instruments for hyperabrupt varactor tuning diodes in RF, VHF and UHF ranges

05 p0728 A71-16396

Analog periodometer with short response time for helicopter blade vibration studies

05 p0752 A71-16736

Pi2 geomagnetic pulsation polarization characteristic observations, using photoelectric fluxmeters

05 p0747 A71-17213

Geomagnetic T and Z components variation measurements, discussing design and operation principles of magnetic survey device

05 p0756 A71-17217

Wall thickness measurement by ultrasonic tests in presence of corrosion, discussing instruments development

06 p0897 A71-17416

Hydrazine concentration measurement in potassium hydroxide, describing instrument design and operation

06 p0900 A71-18014

Device for jet fuels antiwear properties measurement under rolling friction

07 p1111 A71-19493

Geomagnetic PP type oscillations recordings, using fluxmetric rings and galvanometer

07 p1104 A71-20049

Soviet book on fog, cloud and humidity measuring instruments, discussing artificial fog formation and natural fog dispersion problems

07 p1114 A71-20298

Four-ring stable capacitor for reference standard and application to precision angle measurement

07 p1080 A71-20315

Free-space focused microwave system for determining materials complex permittivity to temperatures over 2000 C

07 p1115 A71-20357

Rocket-borne HF capacitance probe for measuring ionospheric electron density profile

07 p1116 A71-20498

FM type system for measurement of wear narrow band noise power based on phase components processing

08 p1253 A71-21289

Microwave methods for nitrogen or hydrogen densities and flow rate measurement in single phase liquid and slush state

[NAS PAPER M-1]

08 p1292 A71-21696

Accuracy, calibration, maintenance and optimum design of scientific instruments for meteorological measurements

08 p1293 A71-21735

Defectoscopes with current regulation by magnetic amplifiers, describing circuitry and remanent magnetization of components with AC and rectified half wave currents

08 p1273 A71-21894

High temperature apparatus for enthalpy and specific heat measurements of refractory metals

08 p1273 A71-21936

Measuring instrument for determining shear strength of adhesive bond

09 p1443 A71-22503

Weak ion concentration in stratosphere and mesosphere measured by accumulated capacity amplifier

09 p1443 A71-22676

Instrumentation - Conference, Pittsburgh, October 1970, Part 2, Advances in Instrumentation

09 p1443 A71-22705

Fatigue life gages performance test using calibration program for cryogenic temperature applications

09 p1444 A71-22716

High accuracy temperature measurements using type K thermocouples

09 p1445 A71-22724

Balloon flight instrumentation for solar cell I-V measurements, using semiconductor selection circuits and RF telemetry

09 p1446 A71-22734

Measuring instrument for amorphous and polycrystalline materials resistivity and Seebeck coefficient as function of temperature and pressure

09 p1446 A71-22737

Torsion pendulum for measuring internal friction and shear modulus of refractory metals and alloys

09 p1452 A71-23333

Astrometric instruments optimal spatial sampler with parallel slits grill in focal plane, studying error minimization

10 p1608 A71-23825

Ultrasonic energy density measurement over various frequencies in liquids, using instrument unperturbed by standing acoustic waves

10 p1612 A71-24682

Source-subject coupling, reactive near field, multipath components and arbitrary polarization in hazardous EM fields quantification, discussing measuring techniques and instruments

11 p1717 A71-25286

Standard equipment and procedures for aircraft gas turbine engine exhaust smoke measurement

[ASME PAPER 71-GT-88]

11 p1813 A71-25995

Measuring system for 180 degree Raman scattering in single crystals, powders, liquids and strongly absorbent solutions

12 p1915 A71-27673

Nonmagnetic high pressure cell for pulsed and wide line nuclear magnetic resonance measurements

13 p2066 A71-28157

Pi2 geomagnetic micropulsation polarization characteristics, using photoelectric fluxmeters

13 p2060 A71-28268

Geomagnetic T and Z components variation measurements, discussing design and operation of magnetic survey device

13 p2067 A71-28271

RF noise measurement instrumentation using statistical analysis for better interference characterization

13 p2035 A71-28865

Quartz-tube LF measuring generator with low linear instability, using frequency divider and narrow band RC filter

13 p2040 A71-28936

Instrument for skin friction measurements in adiabatic turbulent compressible boundary layers

[ASME PAPER 71-FE-27]

13 p2072 A71-29463

True time averaged oscillating pressure measurements and testing in turbomachinery, including hydraulic, mechanical and evaluation methods

[ASME PAPER 71-FE-28]

13 p1995 A71-29464

Circumferential traversing probe technique for intrastage analysis of axial flow compressors, considering mass flow averaging data reduction technique

[ASME PAPER 71-FE-33]

13 p2118 A71-29468

Soviet book on experimental aerodynamics covering wind tunnels, shock tubes, liquid and gas physical properties, flow parameter measurement equipment, etc

14 p2221 A71-29524

Measuring instrument for solar radio emission at 8 mm, using GaAs Schottky barrier diode mixer for system noise temperature reduction

14 p2239 A71-29916

Supersonic mass flux probe description, discussing inlet geometry, angle of attack and Reynolds and Mach numbers effects on performance

14 p2239 A71-29925

Apparatus for measuring polar liquids dielectric permittivity and losses at microwave frequencies over wide temperature and pressure ranges

14 p2222 A71-30583

Minuteman 2 third stage rocket engine instrumentation performance evaluation for oscillatory combustion characteristics analysis

[AIAA PAPER 71-755]

14 p2248 A71-30789

High temperature permeameter for measuring magnetizing force or magnetic induction in vacuum or inert atmosphere

15 p2401 A71-31194

Ultrasonic rotameter for turbulent wind velocity circulation measurement, using cylindrical elec-

troacoustic capacitor converter with solid dielectric for radiators and receivers

15 p2444 A71-31447

Titanium and silicon tetrachlorides oxygen-containing impurities determination without hydrolysis, describing measuring device design

15 p2383 A71-31659

Dispersionless delay line design producing signal frequency shifts for calibration tests of wideband Doppler shift measuring equipment

15 p2373 A71-32632

Shock wave propagation in ducts and cavities of different shapes and cross sections, compensating errors in recorded signals for shock tube pressure measuring equipment development

16 p2555 A71-32885

Arterial or venous blood oxygen tension continuous measurement, describing electrode cuvette design with response time of less than 3 sec

16 p2535 A71-33248

Enthalpy probe heat response dependence on surface thermal load amplitude

16 p2581 A71-34033

Frequency stabilized He-Ne laser wave secondary length standard for automatic measurements, discussing electronic control, accuracy, line width, pressure, current and magnetism effects

16 p2588 A71-34119

Filtering methods for reducing systematic errors of measuring system with structural redundancy

17 p2740 A71-34964

High temperature apparatus for enthalpy and specific heat measurements of refractory metals

17 p2724 A71-35278

Gages using X radiation for measuring thickness range, linearity and response time, noting application of absorption and fluorescence techniques

17 p2744 A71-35287

Photogrammetric three dimensional digitizer for automatically measuring and recording automotive models dimensions

17 p2744 A71-35288

Electrosensing liquid level gage using electrochemical charge transfer through fluid

17 p2744 A71-35290

Ion cyclotron resonance spectroscopy, discussing fundamentals, instrumentation and ion-molecule chemistry applications

17 p2695 A71-35522

Inductive voltage divider bridge network for ferrite coils inductance and Q measurements

17 p2723 A71-35713

Accommodometer for automatic measurement of eye response to accommodation stimulus

18 p2863 A71-35849

Multichannel sound level meter capable of direct and continuous measurement and recording

18 p2897 A71-36221

Range and range rate measuring equipment for PCM-TDMA satellite communications system data feed and orbit observation

18 p2879 A71-36533

Measuring apparatus for envelope distortion of transmitted high-energy transversely polarized pulses through ionizable or partially ionized gas

18 p2952 A71-36589

Instrumentation and techniques of torsional pendulum and braid analyses, studying trace moisture and cure cycle effects on thermomechanical spectra of polymeric materials

18 p2939 A71-36596

Rogowski belts application to pulsed discharges current measurements, describing measuring circuits and calibration

18 p2924 A71-36758

High speed system for thermophysical properties measurement of electrical conductors above 2000 K in subsecond experiments

19 p3062 A71-37246

Radio astronomy, covering invisible stars discovery and instrumentation techniques comparison with UV and X ray astronomy

19 p3131 A71-37342

Beam splitting photocell for pulsed laser power and energy measurement

19 p3072 A71-37551

Plasma wave instrument for measuring AC electrical and magnetic field levels in outer planets missions

[AAS PAPER 71-125]

19 p3064 A71-37939

Panels and cassettes mechanical design for Camac modular construction of electronic analog and digital measuring instruments based on integrated circuits

19 p3029 A71-38065

Autoclave chronic catheter system and restraining box for blood sampling and pressure measurement for hibernating marmots

19 p3010 A71-38568

Ballistic measurement system for photographing satellites, illustrating minimum brightness relation to satellite distance

20 p3240 A71-39536

Broadcast sound loudness level monitor as measuring and indicating instrument, discussing technological and psychoacoustical evolution

20 p3271 A71-39763

Radiotelemetrical equipment for continuous subcutaneous measurements of circadian body temperature rhythm in rats

21 p3335 A71-40634

Logarithmic rate meter computer aided design, taking into account components tolerances for desired accuracy over selected frequency range

21 p3379 A71-40650

Soviet papers on meteorological observation and instrument testing covering precipitation gages, hygrometers, humidity gages, anemometer testing, mobile monitoring, pyrliometers, etc

21 p3383 A71-41376

Vibration tests of instruments, machines and apparatus, allowing for functional reliability

22 p536 A71-41441

Ultrasonic immersion echo pulse thickness meter for single side access measurement in Al and Zr alloys

22 p528 A71-41759

Coercive force and specimen thickness effects on outputs of meters with attached electromagnets

22 p553 A71-41766

Ferrite coercimeter with attached electromagnet and compensation winding, deriving analytical expressions for demagnetization and compensation currents

22 p521 A71-41767

Velocity and frequency drifting measurement apparatus developed for rotating machinery study

22 p523 A71-42474

Graphite high modulus fiber material tensile strength, modulus of elasticity and elongation measurement method and equipment

23 p3696 A71-42898

Waveguide system for measuring semiconductor electrical and photoelectric properties at SHF, observing temperature effects

23 p3652 A71-43531

Transistorized amplifier circuit for measuring power of CW emission from He-Ne laser

23 p3685 A71-43532

Device for dry friction determination at low temperatures

23 p3678 A71-43537

Static and dynamic measurement errors in contact and contactless sensors of automatic dimensional control of finished product sorting

23 p3679 A71-43866

Fokker-Planck-Kolmogoroff equation for radar tracking meter with nonlinear discriminator and second-order smoothing loops, obtaining steady solution by separated variables method

24 p3815 A71-44702

Automatic collimator for measuring tube lateral deflection in universal astronomical instruments

24 p3829 A71-45300

MECHANICAL DEVICES

Mechanical transducers for generating and detecting second sound in He isotopes at millidegree temperatures, discussing construction and performance

02 p0250 A71-12135

Soviet optomechanical instruments for metallurgy and high temperature metallography

02 p0254 A71-12711

Optimum synthesis of mechanical systems using effort functions

04 p0625 A71-15061

Intelsat 3 satellite mechanical and electronic components fabrication, emphasizing quality and reliability assurance procedures and assembly techniques

06 p0905 A71-18403

Control function synthesis by linearization for maintenance of uniform motion of driven component in mechanical system including motor, variator and operating machine

07 p1116 A71-19358

Mechanical systems partial differential equations solution through reduction to infinite systems of ordinary differential equations, considering Cauchy problem power series solution

09 p1492 A71-22523

High performance precision shaft and face seal design and applications

10 p1617 A71-24417

Soviet book on mechanical systems oscillations with allowance for imperfect elasticity covering energy dissipation, linear asymptotic methods, etc

10 p1691 A71-24729

Force springs flexural pivots and miniature incandescent lamp tests failure distribution analysis for comparing mechanical vs electrical components

12 p1911 A71-27326

Stationary motions of holonomous five degree of freedom mechanical system of rod suspended homogeneous symmetrical body in central gravitational field

13 p2100 A71-28730

Azur satellite structure and mechanism requirements, design and tests, noting damping characteristics and Yo-Yo system

15 p2501 A71-32783

Mechanical elements and systems optimal design, discussing variational and programming techniques application to machine elements design optimization

21 p3385 A71-40306

Timer devices and applications, discussing timing and power functions, switching cycles, mechanisms, ratings and life/cost evaluation

21 p3379 A71-40672

Composites and mechanical systems dynamic behavior prediction, calculating Hugoniot with effective modulus

21 p3465 A71-40792

Stiffness and load capacity control by self compensating flow restrictor for externally pressurized gas lubricated thrust bearing design

22 p3552 A71-41673

MECHANICAL DRAWINGS

U ENGINEERING DRAWINGS

MECHANICAL DRIVES

NT HELICOPTER PROPELLER DRIVE

Gear drives operating in vacuum conditions, calculating friction coefficient with dimensional analysis

02 p0258 A71-12598

Communication satellite earth station steerable antennas drive train resonance and traction drive wheel slippage control by differential velocity feedback, discussing analog simulation

02 p0222 A71-12790

Power train systems gear induced noise analysis, using in-flight vibration and noise measurements for comparison with calculated noise spectra

[ASME PAPER 70-WA/DGP-1] 03 p0471 A71-14137

Transmission impending failure detection via lubricating oil monitoring for metal particle content

04 p0532 A71-15415

Numerical and graphic drive shaft motion trajectories in dynamic gyroscopic system with four degrees of freedom

06 p0928 A71-18232

Equatorially mounted parabolic reflector radio telescope, discussing structural design, mechanical drives and electronic control system

08 p1271 A71-21152

Maximum efficiency of turbine for driving auxiliary equipment, noting design constraints

08 p1349 A71-22046

Mossbauer spectrometer with constant speed mechanical drive, describing special design features to avoid vibration induced lowering of spectral resolution

09 p1442 A71-22319

Fan propulsion power plants with mechanical and gas dynamical energy distribution systems for commercial VTOL aircraft

09 p1511 A71-22964

Boron-glass-epoxy lightweight composite gear case for aircraft engine reduction gearbox, describing design, molding, machining and testing

[ASME PAPER 71-GT-85] 11 p1771 A71-25993

Reliable brushless direct-drive system design for controlling position and rate of solar power arrays on orbiting spacecraft

12 p1869 A71-27432

Reduction gearbox reliability problems from development and service experience with PT6A turboprop engine

[SAE PAPER 710433] 13 p2073 A71-28318

Optimal quick response control synthesis for hydraulic drive with throttle, using two step phase space method

13 p2002 A71-28937

Solid propellant rocket engine design, discussing combustion instability technology applications in damping and driving mechanisms influence determination

[AIAA PAPER 71-754] 14 p2296 A71-30788

Digital computer process controller for telescope with driving system consisting of single worm wheels for tracking and slewing

17 p2740 A71-34985

Tapered roller bearing lubrication, considering application to CH-47 Boeing helicopter transmission

17 p2749 A71-35300

Inclined radial jet drive systems for noiseless gas bearings, comparing with turbine driven device

22 p3553 A71-41681

Large telescope design - Conference, Geneva, March 1971, covering telescope projects, optical properties, mountings and control and drive systems

22 p3542 A71-42120

Adjustable speed drive with brushless DC synchronous motor using rotor position sensor and three phase bridge inverter

23 p3630 A71-43499

MECHANICAL ENGINEERING

Petroleum mechanical engineering and pressure vessels and piping - ASME Conference, Denver, September 1970

04 p0665 A71-14767

Multicomponent plane flap mechanism with transmission angles diverging minimally from ninety degrees, discussing synthesis by least squares method

07 p1117 A71-19361

Rumanian book on nonlinear and random vibrations covering dissipative and conservative nonlinear mechanical systems, deterministic excitation and applications of mathematics

09 p1543 A71-23619

Nonlinear static structural mechanical problems solution, using self correcting initial value formulations

21 p3467 A71-40959

MECHANICAL IMPEDANCE

Cantilever beam bending vibration, measuring driving point impedance and natural frequencies at low strain amplitudes for Mg alloy, Mn-Cu and coated Al beams

03 p0502 A71-13299

Optimal lining impedance for jet engine inlet duct, yielding discrete frequency, flow velocity and geometry on basis of minimum radiated power

08 p1349 A71-21661

Mechanical impedance measurement of artificial and human mastoids for bone vibrator calibration as function of frequency

11 p1725 A71-26189

Interchangeable head vibration exciter for 200g large object testing and measurement of structural modes, impedances, transfer functions and calibration

11 p1746 A71-26495

Impedance testing techniques based on ratio of mechanical input force to velocity response for structures and systems behavior evaluation under dynamic loads

14 p2252 A71-30054

Time dependence of radial mechanical driving point impedance of Al cylindrical shell immersed in two anechoic tanks related to chemical reaction

23 p3662 A71-43215

MECHANICAL MEASUREMENT

NT DISPLACEMENT MEASUREMENT

NT DRAG MEASUREMENT

NT FLOW MEASUREMENT

NT FRICTION MEASUREMENT

NT PRESSURE MEASUREMENTS

NT STRESS MEASUREMENT

NT THRUST MEASUREMENT

NT VELOCITY MEASUREMENT

NT VIBRATION MEASUREMENT

NT WIND MEASUREMENT

NT WIND VELOCITY MEASUREMENT

Single edge notch tension Al alloy specimens mechanical compliance measurement, solving stress functions for various gage length-sample width combinations

07 p1110 A71-19469

Pneumatic resistance transducer for fluidic measurement of mechanical quantities

07 p1030 A71-20598

Materials mechanical properties measurement methods and equipment at cryogenic temperatures including microscopes, X ray cameras, microhardness tester, fatigue and impact strength testing machines

09 p1468 A71-22329

Mobility definition and measurement methods, discussing portable instrument and vibration testing application

14 p2252 A71-30056

Dynamic hysteresis loop measurement of energy dissipation in materials, showing deformation effects on accuracy

15 p2508 A71-32233

Gyroscope rotor axial moment of inertia of measurement by connection to small vibrator device

19 p3062 A71-37148

Epoxy resin plate mechanical stress measurement under impact load, using laser light source three beam interferometric assembly with photographic recorder

22 p3555 A71-41613

MECHANICAL OSCILLATORS

NT GYROSCOPIC PENDULUMS

NT PENDULUMS

Book on mechanical vibration and shock measurements covering periodic and random vibrations characteristics, instrumentation, control, etc

02 p0251 A71-12175

Nonlinear closed loop-shape characteristics of vibrational mechanical systems, using forced vibration analysis

02 p0284 A71-12284

Soviet book on mechanical oscillator threshold sensitivity to small moment of forces, covering light friction and radiometric oscillatory instability effects and estimates

02 p0285 A71-12839

Mechanical oscillator mean square response to non-stationary random excitation

04 p0669 A71-15200

Air lubricated mechanical oscillator dynamics and modes of operation as function of system parameters, using analog computer

05 p0758 A71-16352

Oscillatory systems with nonlinear elastic arresting devices, calculating dynamic characteristics and motion stability

08 p1332 A71-20687

Oscillations generating mechanism in resonance tube fed by subsonic gas jet, determining oscillations amplitude and frequency at resonance

09 p1382 A71-22406

Hall effect mechanical vibration transducer with indium arsenide semiconductors and elastically suspended magnets

10 p1612 A71-24639

Lumped parameter torsional and flexural system synthesis for vibratory characteristics, using transfer matrices

10 p1692 A71-24925

Holographic method for investigating piston type oscillations with phase modulated reference light beam

24 p3829 A71-45270

MECHANICAL PROPERTIES

NT ABRASION RESISTANCE
NT AEROELASTICITY
NT ANELASTICITY
NT BRITTLENESS
NT BULK MODULUS
NT COLD STRENGTH
NT COMPRESSIBILITY
NT COMPRESSIVE STRENGTH
NT CREEP PROPERTIES
NT CREEP RUPTURE STRENGTH
NT CREEP STRENGTH
NT DIMENSIONAL STABILITY
NT DUCTILITY
NT ELASTIC PROPERTIES
NT ELASTOPLASTICITY
NT ELECTROSTRICTION
NT FATIGUE LIFE
NT FIBER STRENGTH
NT FLEXIBILITY
NT FRACTURE STRENGTH
NT HARDNESS
NT HIGH STRENGTH
NT HYDROELASTICITY
NT HYPOELASTICITY
NT IMPACT STRENGTH
NT MAGNETOSTRICTION
NT MICROHARDNESS
NT MODULUS OF ELASTICITY
NT NOTCH SENSITIVITY
NT NOTCH STRENGTH
NT PHOTOELASTICITY
NT PHOTOVISCOELASTICITY
NT PIEZOELECTRICITY
NT PLASTIC PROPERTIES
NT POISSON RATIO
NT PROPORTIONAL LIMIT
NT SHEAR CREEP
NT SHEAR PROPERTIES
NT SHEAR STRENGTH
NT SHELL STABILITY
NT STEADY STATE CREEP
NT STIFFNESS
NT STRESS CYCLES
NT STRESS RATIO
NT STRESS RELAXATION
NT STRUCTURAL STABILITY
NT TENSILE CREEP
NT TENSILE PROPERTIES
NT TENSILE STRENGTH
NT THERMAL RESISTANCE
NT THERMOELASTICITY
NT THERMOPLASTICITY
NT THERMOVISCOELASTICITY
NT TOUGHNESS
NT VISCOELASTICITY
NT VISCOPLASTICITY
NT WELD STRENGTH
NT YIELD POINT
NT YIELD STRENGTH

Two-phase composites stability at various temperatures, noting failure regularities dependence on components mechanical properties relationship

01 p0106 A71-10083

Mechanical properties effect on steels fatigue crack growth rate as function of stress intensity factor

01 p0099 A71-10167

Synthetic plastic materials mechanical and electrical properties for electronics industry use, emphasizing injection molded polymers, pressed molding compounds and casting resins

01 p0051 A71-10285

Fiber reinforced materials industrial applications based on various matrix-fiber combinations, considering manufacturing processes, chemical and mechanical properties, etc

01 p0107 A71-10316

Fiberglass reinforced plastics heavy duty structural parts quality control, discussing strength parameters, safety coefficients, testing methods, etc

01 p0088 A71-10689

Thin wires mechanical properties compared for epoxy resin reinforcement applications, considering ductility, temperature and aging effects, cost, etc

01 p0108 A71-10694

Glass fiber reinforced durometer and hard foam sandwich structures deformation characteristics under static loads, presenting theoretical and experimental results

01 p0172 A71-10700

Microstructure and mechanical properties of weldable heat resistant Ni alloy containing carbon and boron

01 p0103 A71-11068

Mechanical properties, long term strength and corrosion resistance of low alloy chromium steel with nitrogen

01 p0103 A71-11069

German monograph on stress strain state calculation in strengthening material disks

01 p0176 A71-11221

Modular ratios effect on structural composites, predicting property values from structural measurements

01 p0103 A71-11276

Diffusion bonding cycles for Al-B composite materials fabrication, relating strength enhancement to residual stress relief

01 p0104 A71-11284

Airplane materials mechanical properties degradation due to fatigue, discussing breaking strain of Al alloy

01 p0104 A71-11395

Glass properties and applications, discussing strengthening, surface etching and structure modification

01 p0109 A71-11432

Be mechanical and physical properties, corrosion behavior, toxicity, fabrication and application as aircraft and spacecraft structural material

01 p0104 A71-11539

Al-Zn-Mg-Cu type high strength Al alloys mechanical properties evaluation by fracture mechanics methods

01 p0104 A71-11540

High strength steel weld metal, determining gaseous impurities effects on mechanical properties degradation

02 p0262 A71-11710

Inconel 718 arc welding procedures and weldments mechanical properties, discussing impact strength and ductility improvement by heat treatment

02 p0255 A71-11711

Gaseous atmospheres environmental effects on metal mechanical properties at high temperatures, discussing failure mode with crack growth rate dependence on pressure

02 p0263 A71-11864

Ni-Al-Ti alloys strength, investigating matrix precipitate lattice parameter mismatch effects

02 p0263 A71-11865

Mechanical characteristics of generalized Rayleigh waves in piezosemiconductors of cubic symmetry, deriving amplification and damping factors for zero diffusion coefficient

02 p0294 A71-11894

Runways, aprons and taxiways strengthening to accommodate higher tire pressures and landing speeds, heavier aircraft and surface riding requirements

02 p0238 A71-12169

Carbon fiber reinforced plastics, discussing mechanical and nondestructive testing for performance factors

02 p0274 A71-12482

Reinforced plastic laminates structural integrity, describing procedure for mechanical property evaluation

02 p0274 A71-12484

Carbon fiber composites, examining epoxy resin matrix effects on mechanical performance and heat tolerance

02 p0274 A71-12486

Longitudinal and cross rolling effects on anisotropy of mechanical properties and deep drawability of sintered thin sheet Mo

02 p0257 A71-12518

Alloying effects on room temperature mechanical properties of vacuum melted Mo-C-Ti, Mo-C-Zr and Mo-Ti-Zr under plastic deformation and recrystallization

02 p0265 A71-12520

Mechanical properties of Ti alloys subjected to rolling and heat treatment

02 p0265 A71-12522

Temperature and plastic deformation rate effects on plasticity and strength of cast iron, Ti and steels

02 p0257 A71-12525

Niobium with various interstitial and substitutional type impurities, examining plastic deformation and mechanical properties at various temperatures

02 p0269 A71-12927

Nb binary solid solutions with various Ti, Mo and Zr percentages, examining structure and mechanical properties

02 p0270 A71-12931

Nb alloys in hypersonic glider fabrication, discussing mechanical properties, oxidation resistance and sandwich panel design

02 p0270 A71-12935

Niobium mechanical properties temperature dependence from plastic deformation tests, taking into account interstitial and substitutional impurity concentrations

02 p0271 A71-12936

Apollo 11 and 12 lunar rocks physical and mechanical properties and chemical composition compared with terrestrial rocks

03 p0487 A71-13421

Polymer materials linear photocreep characteristics description in terms of differential and integral equations

MECHANICAL PROPERTIES

tions, discussing relationship between optical and mechanical properties

03 p0514 A71-14357

Ultrafine grain metals strength properties at cryogenic temperatures and near melting point, discussing grain boundaries

03 p0446 A71-14487

Powder metallurgy for fine grain metals and alloys, discussing grain size-mechanical properties relationship

03 p0446 A71-14490

Ni-Fe-Cr alloys microduplex structure, describing mechanical properties and workability

03 p0447 A71-14499

Energy accumulation effects on pressure vessels strength and failure mode, examining crack propagation and arrest

03 p0517 A71-14586

Al-Zn-Mg ternary alloys stress corrosion cracking resistance relation to mechanical strength decrease, quenching rate increase and solution treatment temperature

04 p0609 A71-14772

Fiber reinforced plastics testing and mechanical parameters measurement, considering materials strength and fracture probability

04 p0618 A71-14887

Rigid cellular plastics mechanical properties based on model assuming pentagonal dodecahedron cell form

04 p0667 A71-14894

Papers on whisker technology covering mechanical properties, crystal growth, composite materials, etc

04 p0611 A71-14940

Sapphire whiskers production by melt growth technique, describing process and whiskers mechanical properties

04 p0636 A71-14944

Testing methods for mechanical properties of individual whiskers, describing tensile machines, shear stress measurement torsion device and Young modulus measurement method

04 p0603 A71-14945

Ceramic and metallic whiskers mechanical properties, discussing failure and deformation mechanisms

04 p0611 A71-14946

Whisker composites mechanical properties analysis, discussing stiffness and strength under static loads, elastic moduli, stress analysis, statistical tensile failure model, etc

04 p0667 A71-14947

Whisker composites tensile and fatigue properties, fracture toughness and mechanical properties at high temperatures

04 p0611 A71-14951

Aluminum bicrystals mechanical properties under high strain rates, considering changes in surface structure, active slip planes and dislocation

04 p0612 A71-15077

Soviet book on perforated plates and shells covering strength, rigidity, lattice tension and bending, stress and strain states, boundary value problems, etc

04 p0671 A71-15398

Polarization-optical method of stress analysis problems, explaining high polymers physicochemical properties with Boltzmann-Volterra integral equations

04 p0671 A71-15557

Ferromagnetic dielectric composites physicochemical properties, considering thermal conductivity, density, linear expansion, resistivity, thermal stability and magnetic permeability

04 p0618 A71-15570

Thin gas turbine disk strength under axisymmetric flexural vibrations, noting agreement of calculated and experimental rotor rpm danger zone

04 p0671 A71-15639

Al alloys extrusion and chemical composition relationship to mechanical properties, examining various metallurgical processes

04 p0604 A71-15743

Elastic solids mechanical characterization using finite element formulation of minimum potential energy theorem

04 p0671 A71-15751

Microstructure effect on metastable beta Ti alloy strength, toughness, stress corrosion cracking susceptibility

04 p0614 A71-15780

Mo wire annealing with degassing, investigating temperature effect on mechanical properties

04 p0616 A71-15802

Austenitic steel containing C, Cr and Mn, investigating W, Mo, V and Nb effect on structure and mechanical properties

04 p0616 A71-15804

Ti-Ag contact N-P and P-N single crystal Si solar cells electrical and mechanical performance characteristics

05 p0700 A71-16069

Titanium alloys for drop and press formed airframe, engine, rocket and spacecraft components, presenting physical and mechanical properties for various alloys and applications

05 p0757 A71-16136

Monograph on cobalt base superalloys covering mechanical properties relation to microstructure, carbides, heat treatment, aging, intermetallic precipitation and dislocation

05 p0765 A71-16198

Interlayer rigidity effects on strength of fiber reinforced composite materials under plane loads

05 p0771 A71-16366

Elasticity and strength anisotropy changes of unidirectional fiberglass reinforced plastics during winding

05 p0759 A71-16372

Annealed Al bars mechanical properties and stress-strain curves dependence on strain rates under loading

05 p0766 A71-16390

Structural elements carrying capacity increase by strain hardening and nonuniform quenching

05 p0826 A71-16752

Al and Mg alloys mechanical and microstructural changes under low temperature conditions, optimizing casting component ratios

05 p0767 A71-16765

Beta stabilizers effects on Ti strength, plasticity and stress concentration sensitivity at low temperatures

05 p0767 A71-16766

Austenitic steels and Ti and Al alloys with stress raisers, studying low temperature mechanical properties

05 p0767 A71-16768

Al-Zn-Mg alloys low temperature mechanical properties dependence on aging treatment

05 p0767 A71-16769

Molybdenizing effects on Cr-Ni-Ti steel strength and stability in liquid Li

05 p0768 A71-16772

Human skin biomechanical properties, observing extensibility, resiliency and elasticity

05 p0710 A71-16807

Tensile test equipment for fiberglass reinforced plastics strength measurement under shear

05 p0772 A71-16888

Stainless steel physicochemical properties stability, discussing equipment for industrial materials testing under various environmental and loading conditions

05 p0769 A71-16897

Tensometer for measuring strain rate effects on composites mechanical properties

05 p0734 A71-16930

Weight-optimal cylindrical shells of revolution with uniform strength edge reinforcement, discussing pressure vessel design

06 p0982 A71-17356

Soviet book on materials strength covering physical properties, stress-strain state, elastic bodies, loading conditions, shear, torsion, bending, buckling creep, etc

06 p0984 A71-17448

Matrix and round inclusion two component composite equilibrium, considering crack effect on strength

06 p1000 A71-17938

Cured thermosetting polymers, investigating water effect on microstructure and mechanical properties

06 p0916 A71-17945

Mechanical property data for silicon nitride-silicon carbide fiber ceramic composites having high fracture values

06 p0916 A71-18035

Unidirectional discontinuous fiber composite longitudinal strength calculation based on perturbation effect and distortional energy criterion, using finite element method

06 p1001 A71-18100

Cancellous bones mechanical properties from compression testing of human femora, vertebrae and cranial bones

[AIAA PAPER 71-111]

06 p0863 A71-18561

Nb-W single crystal deformation, discussing athermal solid solution strengthening

06 p0914 A71-18683

Recrystallized annealed Ta, examining strain rate effect on mechanical properties

06 p0914 A71-18684

Strength characteristics of thin walled anisotropic shells, using difference-differential method to reduce partial differential equations

06 p1005 A71-18709

Mg alloys mechanical properties and microstructure changes under static tension in temperature range 20-293 K

07 p1131 A71-19363

Al cast alloys mechanical properties and sensitivity to stress concentration at low temperatures

07 p1131 A71-19366

Intermetallic compounds structural component applications, considering crystal growth, alloy constitution and development, mechanical properties and processing technology

07 p1131 A71-19427

NiMo alloy fcc disordered structure and mechanical properties correlation to domain size and orientations from thin film transmission electron microscopy

07 p1132 A71-19435

Mechanical properties of supersaturated Ni-Al alloys aged at 700 F, discussing composition effects on single crystals deformation and polycrystal strength variation

07 p1133 A71-19442

Ordered phases precipitation in ternary and quaternary ferritic alloys, investigating morphology, structure, distribution, coarsening kinetics and mechanical properties

07 p1133 A71-19443

Binary Ti-Al and ternary Ti-Al-X alloys precipitation strengthening, investigating structure, mechanical properties and deformation behavior

07 p1133 A71-19444

Refractory metals and alloys fabrication and mechanical and physical properties at high temperatures

07 p1134 A71-19581

Optimal heat resistance, mechanical properties and microstructure of steam pipe Cr-Mo-V steel

07 p1135 A71-19618

Oxygen effect on mechanical properties of Ti alloys with V and V-Al content, showing strengthening up to 400 C

07 p1136 A71-19631

Mechanical properties, crack formation sensitivity, corrosion resistance and stress cracking behavior of Al-Zr-Mg alloys welded joints

07 p1136 A71-19633

Mechanical and plastic properties of Ni-Mo alloys subjected to hot working, determining tensile strength as function of test temperature

07 p1136 A71-19635

Glass fiber reinforced thermoplastics with increased room temperature mechanical properties, noting effect of heat, aging and chemical environment exposure

07 p1145 A71-19692

Stainless steel coatings vacuum deposition on Ti alloy plates, considering product cryogenic and mechanical properties

07 p1118 A71-19853

Mechanical properties at different temperatures and allowable design stress for aluminum alloy

07 p1137 A71-19966

Wrought high strength Al alloy nonequilibrium second phase particles formation effect on mechanical behavior during solidification

07 p1137 A71-19978

Stacking sequence effect on laminate strength, considering specific layer orientations for optimal protection against delamination under uniaxial static and fatigue loadings

07 p1216 A71-20130

Mo-Re-Hf ternary alloys physical and mechanical properties, considering workability, electrical resistivity and expansion coefficient

07 p1140 A71-20237

Structure and mechanical properties of Mo alloy weld metal as function of Re concentration, using metallography, electron microscopy, X ray analysis and autoradiography

07 p1120 A71-20245

Dynamic strength of elastic elements from wire and tapes of Mo-Re alloy

07 p1120 A71-20249

Mechanical, heat resistant and thermoelectric properties of W-Re alloys for thermocouples

07 p1114 A71-20250

Discrete structure continuous medium model with internal degrees of freedom, studying physicochemical properties in elastic materials

07 p1217 A71-20455

Composition and annealing effects on mechanical and thermoelectric properties of sintered wire W-Re alloys

07 p1143 A71-20493

Automatic materials testing device for thermal fatigue and strength under programmed loading

08 p1271 A71-20838

Carbon fiber reinforced plastics mechanical properties, discussing batch processing and specimen geometry variables effects on laminates

[PLASTICS INST. PAPER 24]

08 p1318 A71-20893

Carbon fiber and carbon fiber-polytetrafluoroethylene composites high temperature

[PLASTICS INST. PAPER 35]

08 p1319 A71-20899

Graphite fiber reinforced plastics adhesion and orientation effects on mechanical properties

[PLASTICS INST. PAPER 27]

08 p1320 A71-20906

Composite materials with metallic matrix and carbon fibers, discussing production techniques and mechanical properties

[PLASTICS INST. PAPER 15]

08 p1320 A71-20907

Carbon fibers production by polyacrylonitrile fibers spinning, discussing stretching temperature effects on mechanical properties

[PLASTICS INST. PAPER 12]

08 p1320 A71-20909

High performance graphitized carbon/carbon composites, discussing mechanical properties improvement by fiber content optimization and heat treatment

[PLASTICS INST. PAPER 37]

08 p1321 A71-20910

Carbon fiber/carbon composites produced by moulded carbon technique, discussing mechanical properties and applications in rocket motors

[PLASTICS INST. PAPER 38]

08 p1348 A71-20914

Fiber content effect on mechanical properties of carbon felt/carbon matrix composites

[PLASTICS INST. PAPER 40]

08 p1321 A71-20915

Mechanical properties of plastic composites with boron, beryllium, silicon carbide and graphite fiber reinforcement

[PLASTICS INST. PAPER 29]

08 p1321 A71-20917

Tensile, flexural and compressive shear, impact and fatigue characteristics of carbon fiber-epoxy resin composites

[PLASTICS INST. PAPER 26]

08 p1322 A71-20923

Carbon fiber reinforced plastics potential aerospace structural applications, considering weight saving, mechanical properties, thermal expansion, stress concentration, impact resistance, corrosion and lightning problems

[PLASTICS INST. PAPER 43]

08 p1369 A71-20927

Carbon fiber composites utilization problems for product and tool designers, considering mechanical properties anisotropy, fiber alignment and bundle strength

[PLASTICS INST. PAPER 42]

08 p1322 A71-20931

Cemented carbides based on TiC-molybdenum carbide-Ni, studying properties as function of molybdenum carbide and C contents in primary solid solution

08 p1304 A71-20994

Forged superhigh density sintered steels strength and fracture mechanism

08 p1304 A71-20995

High strength high Ni maraging steels crystal structure, alloying elements effects on mechanical properties, applications, etc

08 p1305 A71-21028

Vacuum-melted and deformed Mo alloys tests, showing long term strength decrease under cyclic heating

08 p1305 A71-21030

Recrystallized and overrecrystallized Al alloys, investigating factors controlling anisotropy of mechanical properties

08 p1305 A71-21033

Al-Be-Mg alloys under solution treatment, noting aging and prolonged heating effects on mechanical properties from solid solution decomposition diagram

08 p1305 A71-21034

Microstructure and mechanical properties of weldable heat resistant Ni alloy containing carbon and boron

08 p1305 A71-21035

Cohesive strength of flame sprayed metallic coatings of various thicknesses

08 p1297 A71-21064

Manufacture and mechanical properties of sintered silver electrodes involving oxide, powder and resin bonding methods

08 p1297 A71-21089

Tubular compression members, examining residual stress profile effects on strength reduction

08 p1370 A71-21411

Strength of metals and alloys - Conference, Pacific Grove, California, August-September 1970

08 p1306 A71-21501

Bcc metals low temperature strength, examining solution softening in Fe-Mo alloys

08 p1307 A71-21506

Nb single crystals dislocation substructure correlation with strength properties

08 p1307 A71-21508

Solid solution hardening theories, discussing point obstacles random distribution effect on strength and superposition of multiple hardening mechanisms

08 p1309 A71-21522

Li and temperature effects on mechanical properties of Mg base single crystals in basal and prismatic slip

08 p1309 A71-21525

Ordered states effects on mechanical properties of Va-Co-Ni ternary alloys, considering creep behavior difference between ordered and disordered structures

08 p1309 A71-21526

V-Ti alloys high temperature behavior dependence on Ti content, examining interstitial impurities effects on mechanical properties

08 p1310 A71-21532

Electrochemical polarization effects on Ni single crystals mechanical behavior under tensile deformation

08 p1310 A71-21539

Discrete particles dispersion effects on polycrystals mechanical properties, examining various models

08 p1311 A71-21540

Guinier-Preston zone formation by mixed substitutional-interstitial solute-atom clustering in bcc metals, considering steel strengthening

08 p1311 A71-21541

Ti effects on Ni-Mo-Cr alloy strengthening, correlating microstructures and mechanical properties

08 p1311 A71-21542

Ni-Cr thoria dispersion strengthened alloys, determining texture effects on high temperature mechanical properties

08 p1311 A71-21545

Mo-Hf alloy dispersion hardening by internal nitriding, examining structure and high temperature mechanical behavior

08 p1311 A71-21546

Nb-Hf alloys alpha precipitation strengthening via aging at various temperatures, examining mechanical properties

08 p1312 A71-21549

Fe-Ni-Co alloy strengthening by martensite to austenite transformation taking into account microstructure

08 p1313 A71-21556

Ternary Mo-Hf-C alloys thermomechanical and mechanical property relationship, obtaining yield strength at various temperatures

08 p1313 A71-21557

Aged Al alloys dislocation substructure effect on mechanical properties at elevated temperatures

08 p1313 A71-21559

High strength corrosion resistant superalloy structure and mechanical properties

08 p1314 A71-21566

Ni superalloys plane front cast structure through controlled unidirectional solidification, discussing improved mechanical properties

08 p1314 A71-21567

High temperature alloys oxidation resistance and strength characteristics, considering influence of various alloying compositions via use of oxide mapping method

08 p1314 A71-21573

Titanium-steel continuously reinforced composites strength to weight ratings, describing ausforming process and fatigue tests

08 p1316 A71-21587

Single crystal TiC-VC alloys mechanical properties, considering room temperature hardness, high temperature deformation and brittle to ductile transition temperature

08 p1316 A71-21589

Polycrystalline Nb under plastic deformation and annealing, examining dislocation structure and mechanical properties

08 p1316 A71-21611

Low alloy Mo mechanical characteristics relation to structural states obtained during tensile and bending tests

08 p1316 A71-21613

Stress distribution and mechanical properties of adhesive bonded metal and plastic lap joints, using statistical analysis

08 p1372 A71-21711

Adhesive bonding of materials with different coefficients of expansion, discussing strength vs stress relief

08 p1372 A71-21712

Multilayer insulation systems for cryogenics protection aboard spacecraft, considering mechanical properties, radiation shielding, component evacuation rate and outgassing

08 p1375 A71-21748

Microstructure and mechanical properties of heat resistant alloy under homogenization and subsequent isothermal heat treatment

08 p1317 A71-21764

Steels mechanical properties factor analysis, considering Brinell hardness, tensile strength, yield point, relative contraction, elongation and impact strength

09 p1467 A71-22312

Al and Mg alloys mechanical properties anisotropy as function of loading conditions, taking into account stress condition effect

09 p1467 A71-22315

Cryostat design and operation for investigating solids mechanical properties and structure at liquid He temperature

09 p1426 A71-22321

Mechanical characteristics of extruded thermally hardened aluminum alloys determined by eddy current method

09 p1468 A71-22326

Materials mechanical properties measurement methods and equipment at cryogenic temperatures including microscopes, X ray cameras, microhardness tester, fatigue and impact strength testing machines

09 p1468 A71-22329

Filler and reinforcing agent effects on polypropylene rigidity, tensile strength and creep resistance at elevated temperatures

[PLASTICS INST. PAPER 11]

09 p1481 A71-22342

Deformation and strength characteristics of fiber composite thermoplastic resins in terms of stiffness and reinforcement factors

[PLASTICS INST. PAPER 3]

09 p1481 A71-22343

Mechanical property modifications of polytetrafluoroethylene by filler additions, noting improved wear resistance

[PLASTICS INST. PAPER 13]

09 p1482 A71-22346

Multicomponent Ti alloys mechanical properties for cryogenics applications, describing alloying advantages with tantalum

09 p1468 A71-22601

Kovpak method for estimating and extrapolating heat resistance characteristics, considering alloy long term strength

09 p1538 A71-22627

Ultrahigh tensile steels for landing gear and other aircraft design applications, discussing composition, mechanical properties, quality requirements, manufacture and testing

09 p1454 A71-22996

Granulometric composition effects on stainless steel powders bulk weight, friability and compactability, taking into account particle shape

09 p1470 A71-23062

Models for nonferromagnetic solid body mechanics allowing for relationships among mechanical, thermal and electromagnetism processes

09 p1509 A71-23076

Cr steel cyclic strength and elastic properties after combined high temperature thermomechanical treatment and cold working

09 p1471 A71-23079

Beta Ti alloy sheet and foil mechanical property tests, honeycomb core fabrication, forming and welding evaluations

[ASM PAPER W71-23.1]

09 p1455 A71-23095

Soviet papers on alloys crystal structure and properties covering electron microscopy, X ray analysis, heat treatment and pressure effects on phase transformations

09 p1473 A71-23223

High temperature Ni and Co alloys for stationary gas turbines and jet engine parts, considering microstructure and mechanical behavior under stress and temperature

09 p1475 A71-23302

Forging conditions effects on Ti alloys mechanical properties, considering ingot conversion to semifinished product

09 p1475 A71-23304

Discrete phase vs binder strength of inorganic brittle polycrystalline powder metallurgy materials, including alumina and magnesia

09 p1483 A71-23398

Arc weld metal carbon content effects on welded joints mechanical properties in Ni at low and high temperatures, noting crack reduction

09 p1479 A71-23422

Grain size influence on deformation characteristics of commercial Ti with oxygen and Fe impurities, discussing test results on various mechanical properties

09 p1479 A71-23688

Opaque ceramic armor materials for lightweight personnel and equipment ballistic protection applications, discussing mechanical properties and fabrication techniques

09 p1484 A71-23689

Adhesive bonded joints mechanical behavior relation to materials, processes and experimental techniques, developing statistical analysis and formulas for orthotropic-elastic joints

10 p1614 A71-24087

Strength characteristics of machine parts with cracks calculated by graphoanalytic procedure

10 p1686 A71-24192

Thermoviscoelasticity approximate method for materials with nonstationary nonuniform temperature distribution dependent mechanical properties, using time-temperature analogy principle

10 p1688 A71-24360

Al alloys microstructure and mechanical properties after rapid solidification, considering rapid quenching techniques and resulting metastable variations

10 p1627 A71-24596

Powder metallurgy superalloy parts, discussing production methods and mechanical properties comparison with conventional process products

10 p1618 A71-24763

Composite morphology and mechanical properties relationship, considering reinforcing effect, filamentous systems, whisker growth ladder molecules synthesis and material production

10 p1635 A71-24768

Three dimensional composite reinforcement principles, discussing thermal strain reduction and mechanical properties

10 p1691 A71-24772

Thornel graphite fibers modulus of elasticity, mechanical properties, applications and price

10 p1635 A71-24773

Time and temperature effects on epoxy composites mechanical behavior, changing from brittle to ductile to rubbery failure mode

10 p1635 A71-24805

Epoxy bond strength, cracking and failure of lapped joints as function of composition and mechanical properties

10 p1618 A71-24826

Hardened and glass reinforced epoxy resin mechanical properties after 180 day hold in water, acid and alkaline solutions

10 p1635 A71-24827

Aircraft continuous elastomechanical system parameters determination by ground vibration tests, using integral equation, phase resonance and separation technique

[DFVLR-SONDDER-103]

10 p1692 A71-24946

Luna 16 lunar rock samples mechanical properties and chemical and mineralogical compositions for regolith origin determination

10 p1681 A71-25116

High strength stainless steel dislocation structure and mechanical properties, discussing tempering, tensile strength, precipitation hardening and temperature effects

11 p1776 A71-25167

Aircraft tires mechanical data from small models, discussing mechanical properties, tire stresses and tire temperatures

[AIAA PAPER 71-346]

11 p1707 A71-25325

Mechanical properties and performance characteristics comparison of syntactic foams fabricated by conventional mixing or vacuum impregnation, including filler packing factors

11 p1784 A71-25394

Graphite fibers mechanical properties based on rayon and polyacrylonitrile, considering tensile, flexural, compressive and shear strength

11 p1784 A71-25398

Fiber reinforced composites, predicting mechanical properties, stress-strain behavior, interface failure, creep and fatigue by mathematical model

11 p1849 A71-25655

Glass fiber reinforced plastics mechanical properties, strain-stress characteristics and anisotropy, deriving orthotropic laminates tensile stiffness under deformation

11 p1849 A71-25656

Pyrolytic graphite, discussing fabrication by chemical vapor deposition process, mechanical and physical properties, residual stresses, applications in reentry vehicle heat shields, rocket nozzle throats, etc

11 p1789 A71-25743

Surface structure and environment effects on mechanical behavior of crystalline inorganic solids, giving stress-strain diagrams

11 p1808 A71-25999

Cr and Zr additives influence on Al-Zn-Mg-Cu alloys quench sensitivity, discussing mechanical properties and electron microscopic investigation of microstructural characteristics

11 p1780 A71-26021

Mg-Al eutectic alloy and commercial-purity Zr stress relaxation tests and mechanical behavior

11 p1780 A71-26022

Stress-strain states of physically nonlinear anisotropic media, showing boundary value problem equivalent to variational problem

11 p1850 A71-26179

Fracture mechanics and time dependent strength of elastic or viscoelastic solids adhesively jointed by soft polymeric bonding layer

11 p1851 A71-26383

Ti-Zr alloying in for microstructural hardness and mechanical strength increases, discussing Zr concentrations at Nb granular boundaries

11 p1782 A71-26470

W-Mo-Ta system alloys investigated along four radial sections from tungsten corner, establishing Ta additions effect on maximal strength

11 p1782 A71-26473

High energy hydrogen-oxygen launch vehicle thermal insulation system, discussing closed cell rigid polyvinyl chloride foam mechanical characteristics, use and tests

12 p1985 A71-26835

Al-Ni alloys rapidly quenched from melt, determining solid solutions mechanical and microstructural properties

12 p1916 A71-26893

Material properties, impregnation, shaping, hardening and structural design in mass production of reinforced laminates for aircraft construction

12 p1920 A71-26954

Filament winding techniques for glass fiber reinforced plastics, discussing processes, configurations and materials for achieving optimum strength

12 p1920 A71-27011

Stiffness factor in reinforced thermoplastics mechanical properties as function of glass fiber content, working temperature and duration of loading

12 p1920 A71-27012

Aged beta Ti alloy microstructure and mechanical properties, examining initial dislocation structure and interstitial concentration effects

12 p1917 A71-27297

Small deformation theory of thermoplasticity with medium mechanical characteristics dependent on tem-

perature, noting use in nonmechanical structural transformations and radioactive irradiation
12 p1978 A71-27348

Cr and V diffusion plating influence on principal characteristics of highly alloyed martensitic and carbon steels
12 p1912 A71-27690

Gas turbine blades cast heat treated superalloys high temperature mechanical properties during aging
12 p1919 A71-27778

Stress raisers effect on mechanical properties of fcc materials at cryogenic temperatures
13 p2083 A71-27871

Mechanical properties and heat treatment of Ti-V and Ti-V-Al alloys in quenched and quenched-aged states
13 p2083 A71-27872

Mechanical properties of Ti-Al-Cr and Ti-Al-Cr-Mo alloys annealed below solidus temperatures
13 p2083 A71-27873

Beta stabilizers effect on mechanical properties of alpha structure Ti-Al-V alloys subjected to different heat treatments
13 p2083 A71-27874

Mechanical properties of welded joints in Ti alloys with high oxygen content
13 p2072 A71-27875

Polyimide plastics, considering mechanical properties high temperature applications and cost effectiveness
13 p2091 A71-28165

Filament reinforced composite materials, considering spacecraft and missile applications mechanical and physical properties
13 p2144 A71-28166

High strength alloys fatigue in terms of irreversible microplastic deformations accumulations, discussing fatigue crack mechanisms and cyclic straining effects on bulk properties
13 p2152 A71-28219

Refractory materials production using chemical deposits from gaseous phase, discussing mechanical, physical and thermal properties of obtained coatings
13 p2074 A71-28526

Nb single crystals structure and properties after cold rolling and annealing, determining crystallographic parameters of plastic deformation
13 p2086 A71-28579

Mechanical properties, hardness and dislocation structure of Ti bearing maraging steels, considering Mo role in strength and plastic properties improvement
13 p2086 A71-28581

Mechanical properties of carbon fibers thinly coated with TiC by chemical vapor deposition from hydrogen, methane and titanium tetrachloride vapor mixture
13 p2092 A71-28627

Probability characteristics of glass/epoxy plastics mechanical properties, considering tangential and axial tensile and bending strength, modulus of elasticity, buckling and compression strength
13 p2092 A71-28653

Magnesia rich magnesium aluminum oxide spinel ceramics, discussing sintering, grain growth inhibition and strength increase
13 p2092 A71-28662

Optimization of mechanical characteristics of asynchronous capacitor microengine designs with asymmetric stator circuit for prolonged continuous operation with negligible steel wear
13 p2002 A71-28929

Aircraft engine production components and alloys mechanical properties evaluation for improved reliability of mass produced products
13 p2075 A71-28944

Mechanical properties and strain rates determination at high temperature, using automatic loading system with strain gage dynamometer and oscillograph
13 p2045 A71-29375

Mo and W single crystals mechanical properties, considering C and iron group additions influence
14 p2255 A71-29516

Temperature dependence and mechanical properties of Mo materials with various diffusive protective base coatings based on continuity and density
14 p2256 A71-29623

Shelf stable two component urethane adhesives with prepolymer reactive silane coupling agents for high peel strength retention in humid environment
14 p2261 A71-29637

Mechanical and thermal properties of chemical vapor deposited carbon composite felt material for reentry heat shielding
14 p2262 A71-29648

Pyrrone foams molding, considering chemically blown and syntactic foams mechanical properties
14 p2262 A71-29650

High modulus organic fiber for aerospace use, considering fiber-epoxy composite mechanical and physical properties
14 p2263 A71-29658

Mechanical properties of fiberglass-epoxy cross-ply laminates, considering tensile strength, crack propagation and ultimate stress and strain
14 p2264 A71-29837

Advanced filamentary composite materials behavior, discussing limited ductility, sensitivity to stress concentrations, fatigue and viscoelastic properties
14 p2264 A71-29897

Nondestructive testing techniques for discrete local materials properties evaluation, allowing nonstatistical analysis of thermomechanical stress behavior
14 p2251 A71-29900

Beta stabilizing Mo and Cr effects on mechanical properties of welded and heat treated Ti alloys
14 p2260 A71-30490

Optical, mechanical, thermal and electrical properties of IR sensor materials at low operating temperatures
14 p2284 A71-30545

Animal urinary bladder mechanical properties from controlled stretch tests, identifying viscoelastic, elastostatic and creep elements
14 p2186 A71-30566

Composite materials application to V/STOL prop/rotors, determining material properties parametric effect on frequencies and weight by Southwell coefficients
14 p2180 A71-31106

Al-base alloys granules dimension and shape effects on extruded semifinished product mechanical properties and structural stability
15 p2424 A71-31242

Microstructure and mechanical properties of Ti-rich alloys of Ti-W system, constructing phase diagram
15 p2425 A71-31402

Strengthening mechanism of Cr-Ni and Ni maraging steels related to dislocation stress field
15 p2427 A71-31524

Elastic interaction between specimen and testing machine in mechanical property tests, considering drawbacks to machine stiffness calculation methods
15 p2414 A71-31947

Single crystal and polycrystalline alumina specimens strengthening by annealing with various metal oxide powders
15 p2438 A71-31975

Unidirectionally solidified Ti-base eutectic composites and alloys strength and microstructural stability under heat treatment
15 p2432 A71-32170

Dispersion hardened Co strength and plasticity temperature dependence, determining Ti and Nb carbides additives effects
15 p2434 A71-32327

Al alloys high temperature thermomechanical treatment, discussing mechanical properties, enhanced plasticity and roughness
15 p2434 A71-32327

Grain size effect on corrosion resistance and mechanical properties of Al alloy sheets between final annealing and quenching
15 p2434 A71-32329

Fine structure variations of Al alloy after aging, using harmonic analysis for calculating matrix microdeformation for correlation with mechanical properties
15 p2435 A71-32332

Book on viscoelasticity covering isothermal stress-strain relations, wave propagation, mechanical properties, thermodynamics and nonisothermal effects
15 p2509 A71-32438

Loading history effect on optical and mechanical properties of polymethyl methacrylate under uniaxial tension
16 p2600 A71-32815

Human alveolar wall tissue length-tension characteristics, noting age, sex and expiratory flow relationships
16 p2530 A71-33246

Machine design strength criteria in development of formulas for lower bound estimates of mechanical components structural reliability
16 p2582 A71-33293

Ordered structure recovery in Fe-Co-V alloy from elasticity limit behavior, studying duration effect on mechanical properties of strain hardened samples
16 p2591 A71-33370

Specific strength of unidirectional fiber reinforced metal matrix composites, showing dependence on volume ratio and transmission coefficient
16 p2592 A71-33412

Oxygen effect on mechanical properties of Ti alloys with V and V-Al content, showing strengthening up to 400 C
16 p2593 A71-33627

Mechanical properties, crack formation sensitivity, corrosion resistance and stress cracking behavior of Al-Zr-Mg alloys welded joints after prolonged heating
16 p2593 A71-33629

Mechanical and plastic properties of Ni-Mo alloys subjected to hot working, determining tensile strength as function of test temperature
16 p2593 A71-33631

Two-phase composites stability at various temperatures, studying mechanical properties dependence on second phase proportion
16 p2593 A71-33639

Polymer binder setting degree effect on maximum strength of fiberglass cross reinforced plastic, analyzing compressive, bending, hardness, impact, thermal and porosity properties
16 p2601 A71-33682

Mo single crystals physicomechanical and microstructural anisotropy under tension at different temperatures, noting strength and plasticity dependence on crystallographic orientation
16 p2596 A71-33888

Polymers mechanical losses temperature-frequency dependence, using nonlinear viscoelastic theory
16 p2602 A71-33982

Mechanical properties, fracture and limited high temperature oxidation resistance of carbon fiber reinforced Ni composites
16 p2599 A71-34086

Deformation temperature effects on microstructure and mechanical properties of low alloy Mo, considering cold brittleness temperature and associated plasticity
17 p2755 A71-34418

Fe-Ni-V-C alloy strengthening by cyclic martensitic phase transformation
17 p2756 A71-34487

Strength and toughness optimization in high strength stainless steels by austenitizing and removing delta ferrite by isothermal transformation
17 p2756 A71-34491

Ti alloys metastable omega phase precipitation effect on mechanical properties, using thin film microscopy
17 p2756 A71-34492

Niobium alloy use for space shuttle thermal protection, examining oxidation and mechanical properties
17 p2757 A71-34495

Mechanical properties of explosively clad plates, considering stainless steel/mild steel and brass/mild steel composites
17 p2757 A71-34663

Electroslag welding of large pressed Al-Mg alloys sections, using electrodes to reduce weld grain size and obtain high mechanical properties
17 p2748 A71-34807

Steady wave propagation in laminated media, developing mechanical theory for composite response with hydrodynamic, thermodynamic and strength effects
17 p2823 A71-34808

German book on welding conditions and material composition effects on structural changes and heat-affected zone mechanical properties of high strength structural steels
17 p2748 A71-34851

Wrought precipitation hardened Co-base alloy, investigating Ti and Al additives effects on tensile and stress rupture strengths, microstructure and fabricability
17 p2758 A71-35147

Iron based Cr-Co-Mo alloys equilibrium diagrams and phase transformations at various temperatures, emphasizing intermetallic compounds effects on mechanical properties
17 p2758 A71-35148

Lunar surface and soil mechanical properties statistical analysis covering Alphonus event, cratering and erosion
17 p2805 A71-35179

Soviet monograph on plasticity and strength of solid bodies at low temperatures covering solidifying gases, static tests, dynamic properties and creep
17 p2724 A71-35186

Solid state diffusion bonded boron-aluminum composites, discussing mechanical properties, weight and cost reduction and applications
17 p2758 A71-35204

Filament wound glass-reinforced plastic struts for cryogenic tank supports in long term planetary missions, testing thermal and mechanical properties
17 p2762 A71-35205

Fiber reinforced resins mechanical properties determination based on component materials characteristics
17 p2763 A71-35441

Al and Mg alloys mechanical and crystal microstructural changes under low temperature conditions, optimizing casting component ratios
17 p2760 A71-35464

Beta stabilizers effects on Ti base binary alloys strength, plasticity and stress concentration sensitivity at low temperatures
17 p2760 A71-35465

Niobium dislocation and electronic structure and mechanical properties after plastic deformation and annealing from electron beam studies
17 p2760 A71-35671

Molybdenum mechanical characteristics relation to structural states obtained during tensile and bending tests
17 p2760 A71-35673

Mechanical properties in glass fiber optics, measuring tensile strength and modulus, Poisson ratio and fatigue

18 p2939 A71-36074

Hybrid circuits thick film technology, discussing printed circuits fabrication processes and electrical and mechanical properties

18 p2888 A71-36224

Axial flow turbines, calculating effects of axial clearance between stator and rotor blades on rotor impulse blades bending vibration strength

18 p2979 A71-36299

Premium mechanical properties for materials in space shuttle orbiter project, emphasizing cost and weight reductions

18 p2979 A71-36465

Diffusion bonding as economical fabrication process for aerospace applications involving Ti alloys, emphasizing mechanical properties and structural reliability improvement

[SME PAPER AD-71-245] 18 p2927 A71-36661

Large deformation stress and mechanical resistance of thin glass circular plates by bending test involving concentric rings

18 p2940 A71-36697

Carbon effects on strength, ductility, brittle transition and plastic strains of tungsten at high temperatures

18 p2936 A71-36713

Semifinished product production technology influence on heat resistant alloys mechanical properties, considering forging, rolling, casting, melting, diffusion welding and powder metallurgy

18 p2937 A71-36725

Carbon fiber reinforced plastics, reviewing properties, performance, development, applications and potential cost reduction

18 p2940 A71-36765

Blue edge anodize technique for revealing segregation in Ti alloys without affecting mechanical properties

18 p2938 A71-37058

Ni-Cr-Mo cermet alloys sinterability, physicochemical properties and microstructure

19 p3075 A71-37109

Physicochemical properties of cermet sintered thermoelectric materials, considering n- and p-type samples of Si-Ge alloys

19 p3075 A71-37111

Mechanical properties of carburized cermet steel with hypereutectic structure after water quenching and tempering at 300 C

19 p3076 A71-37113

High temperature strengthening of vacuum melted W-Ti alloys with Mo and Zr additions

19 p3076 A71-37267

Deformation rate and temperature effects on optimum strength and ductility of die forged and extruded Mo-Ti alloys

19 p3077 A71-37269

Mo effect on high temperature strength, heat resistance, plasticity and toughness of austenitic Cr-Mn-Ni-Al steel

19 p3077 A71-37465

Phase equilibria of Al-Mg-Li-Mn system in Al-rich region, noting composition effects on mechanical properties

19 p3078 A71-37470

Concentration effects of Nb and Ta on strengthening in tetrahedral section of W-Mo-Nb-Ta system at temperatures from 20 to 1100 C

19 p3078 A71-37473

Polymer materials strength and lifetime prediction under natural conditions from mathematical model based on laboratory accelerated test data

19 p3084 A71-37781

Lunar mechanical and magnetic properties, discussing impact craters, rocks, soil iron abundance, mascons and convection processes

19 p3142 A71-38020

Metallurgical and mechanical properties of Ti-Al-V joints produced by thin film diffusion brazing with copper

19 p3070 A71-38316

Tungsten carbide-cobalt alloys, investigating binder metal mechanical properties relationship to composition by chemical analysis and X ray inspection

19 p3083 A71-38475

Polyamides reinforced with finely chopped glass fiber, noting mechanical strength, Martens yield temperature and heat stability

19 p3085 A71-38476

Co, Mo, Ti and Cr effect on mechanical properties and microstructure of maraging weld metals

19 p3083 A71-38491

Multilayer insulation systems development and selection for cryogenics thermal protection on space vehicles, considering mechanical properties, radiation shielding, components, evacuation rate and outgassing

19 p3171 A71-38547

Arc melting consolidated W-Re-Hf-C alloy mechanical properties from tensile, creep and bend tests

20 p3247 A71-38766

Thermal protection and electrical and mechanical evaluation of SNAP 19 radioisotope thermoelectric generator for integration with Viking Mars lander

20 p3267 A71-38964

Heat resistant material properties under power and chemical plant conditions - Conference, Mala Fatra, Czechoslovakia, September 1971

20 p3249 A71-39013

High temperature properties of weld metals formed by electrodes for welding of low alloy heat resistant Cr-Mo and Cr-Mo-V steels

20 p3249 A71-39014

Creep test results scatter, considering non-homogeneity of specimen properties and deviation from test conditions

20 p3250 A71-39021

Creep tests effect on Cr-Mo-V steels mechanical properties during alternating stress fatigue testing, considering preliminary static prestressing

20 p3250 A71-39023

Luna 16 automatic probe drilling experiment, obtaining lunar rocks physicochemical properties for comparison with terrestrial rocks

20 p3209 A71-39131

Book on engineering properties of Ni and Ni alloys covering Ni-Cr alloys, Ni-base superalloys, Cu-base Ni alloys, conversion factors, etc

20 p3251 A71-39199

Corrosion resistant materials evaluation for suitability in high strength fasteners, considering mechanical properties, stress corrosion cracking and hydrogen embrittlement problems

20 p3251 A71-39340

Commercial Ti alloys homogeneity as function of ingot diameter, noting mechanical properties of semifinished products

20 p3252 A71-39544

Chemical vapor deposited tungsten or other refractory metal alloys mechanical properties evaluation at high temperature, describing hoop stress measurement apparatus for induction heated specimens

[ECS PAPER 384-RPN] 20 p3252 A71-39553

Viscoelastic polar materials thermomechanical behavior, deriving stress tensor, couple stress tensor, entropy density and linear constitutive equations

20 p3309 A71-39562

Frozen bipropellants as self supporting structural member for booster weight reduction, considering mechanical and thermal properties and melting rate requirement

20 p3276 A71-39609

Lunar soils structural-mechanical properties and composition, discussing volcanic origin and terrestrial analogs

20 p3295 A71-39618

Exact solutions for cord reinforced materials with thermomechanical constraints of incompressibility and inextensibility and thermal constraint on temperature gradient

20 p3310 A71-39869

Refractory diborides in oxidizing environments, considering mechanical strength, thermal stability, oxidation resistance, heat conductivity, thermal expansion, specific heat and electrical resistance

21 p3405 A71-40138

Ni-Cu-Nb age hardenable steel mechanical properties, examining hot rolling and heat treatment effects

21 p3387 A71-40455

Explosively shock strengthened austenitic stainless steel, investigating mechanical properties at elevated temperatures

21 p3398 A71-40462

Glass-fiber/glass-bead/resin beam stiffness and strength improvement with sandwicheing between layers of unidirectional carbon fiber composite

21 p3405 A71-40597

Hysteresis to strength relationship and particulate filler effect on reinforcement of rubbers and plastics

21 p3405 A71-40601

Mechanical and frictional properties of sintered copper matrix glass compacts, considering lubricating or seizure preventing effects of glass presence

21 p3406 A71-40759

Mechanical properties, applications and peculiarities of polymer composite materials reinforcement fibers

21 p3406 A71-40777

Shock waves and mechanical properties of solids - Conference, Raquette Lake, New York, September 1970

21 p3464 A71-40784

Strain rate and temperature effects on polycrystalline Al-Mg alloy strength, considering deformation mechanism

21 p3400 A71-40834

Mechanical properties of muscular organs, presenting mathematical model for biological fluid flow analysis

21 p3336 A71-40984

High strength stainless steel dislocation structure and mechanical properties, discussing tempering, tensile strength, precipitation hardening and temperature effects

21 p3402 A71-41088

Low carbon austenitic Cr-Mn steels, noting Ni and Al combined alloying effects on structure and mechanical properties

21 p3403 A71-41101

Gas turbine blades cast heat treated superalloys high temperature mechanical properties during aging

21 p3403 A71-41103

Mo, W and Al alloying additives effects on mechanical properties and wear resistance of austenitic high Mn electroslog melted steel

21 p3403 A71-41106

Mechanical properties of various polymeric solids under compressive loading cycles of 100 microsecond duration and under steady state compressive loads

21 p3406 A71-41427

Flexible polyurethane foam plastics under high rate loading, investigating strain rate and structural parameters effects on mechanical properties

22 p3565 A71-41592

Ni-Cr-Mo-Co steel microstructures after austenitizing, quenching and tempering, correlating with mechanical properties

22 p3560 A71-41594

Glass fiber reinforced flame retardant thermoplastic resins, tabulating flammability resistance and mechanical properties

22 p3565 A71-42076

Oxygen concentration and heat treatment effects on structure and mechanical properties of Nb-Zr alloys

22 p3563 A71-42366

Physical and mechanical properties of controlled flow vacuum cured glass reinforced polyimide prepreg laminates

22 p3565 A71-42595

Stress concentration factors of bonded single lap joints by finite element method as functions of dimensionless, geometric and material parameters

22 p3619 A71-42835

Synthetic fibers and plastics development, chemical composition, physical and mechanical properties, production growth rates and applications

23 p3696 A71-43107

Reduced oxygen effect on structure and mechanical, technological and corrosive properties of stainless steel melted in open and vacuum furnaces

23 p3690 A71-43279

Phase transformations and mechanical properties of heat resistant martensitic stainless steel during precipitation aging at prolonged high temperature exposures

23 p3690 A71-43280

Structure, hardness, density and electrical resistance of binary alloys V-Ti, V-Cr, V-Al and V-Sn

23 p3691 A71-43283

Ni-based alloy strength characteristics dependence on heat treatment during melting and casting in vacuum and in air

23 p3691 A71-43425

Lithium additions effect on hydrogen content and mechanical properties of molten aluminum specimens

23 p3691 A71-43522

Bimetallic plated high strength steel, noting transition zone effects on mechanical properties

23 p3692 A71-44026

Polyethylene coating physicochemical properties under UV radiation, discussing density and modulus of elasticity, internal stresses, microcrack formation and preventive heat treatment

23 p3697 A71-44032

Soviet book on diffusion coatings effects on steel structural elements strength covering cementation, nitriding, sulfidizing, boronizing, siliconizing, chromizing and calorizing processes, etc

23 p3693 A71-44183

Diffusive metal coatings stress-strain state effect on composite Mo material strength, deformation and creep characteristics

23 p3697 A71-44206

Material properties, metallurgy, production technology and operational factors effects on machinery structural strength

23 p3779 A71-44207

Heat resistant steels long time strength determination by graph-analytical time-temperature extrapolation

23 p3693 A71-44213

Brittle ceramic materials strength, showing porosity effect dependence on Weibull homogeneity parameter value

23 p3698 A71-44225

Heat resistant ZrSiO₄ alloy precision and ground cast specimens, determining short and long term strength and fatigue

23 p3780 A71-44236

Mechanical properties of Al-aluminum intermetallic eutectic alloys after rapid solidification in semicontinuous casting technique, noting flow stress and tensile strength increase

23 p3695 A71-44286

Carbon fiber reinforced plastics featuring high strength and Young modulus and low density for engineering applications

24 p3840 A71-44363

Ni-Co maraging steels with improved combination of mechanical and magnetic properties at elevated temperatures

24 p3836 A71-44441

Fiber-reinforced composites mechanical properties based on analytical treatment as homogeneous orthotropic bodies

24 p3841 A71-44573

Ti, Zr and Nb carbides alloying effects on deformed and annealed Mo alloys cellular structure and mechanical properties

24 p3836 A71-44672

Mechanical properties of fiber reinforced heat-resistant alloys

24 p3837 A71-44726

Heat resistant Nichrome composite alloy with tungsten filament reinforcement, discussing manufacture and mechanical properties at 1100 C

24 p3837 A71-44730

Plasma metal coating facility, noting antifriction and mechanical properties

24 p3816 A71-44864

Glass rods loading tests after exposure to hydrogen, nitrogen and argon under high pressure, noting strength improvement by Ar impregnation

24 p3841 A71-44868

Hardened cast Al alloys with Cu additions, investigating correlation between mechanical properties and structure at room temperature

24 p3840 A71-45377

MECHANICAL RESONANCE U RESONANT VIBRATION MECHANICAL SHOCK

Automatic equalizer-analyzer system for random or shock vibration testing, including narrow-band equalization, simplified display techniques and self-calibrating procedures

11 p1747 A71-26514

Frequency analysis and Fourier transform evaluation of mechanical shocks and single impulses, outlining theory for filter response to pulses

11 p1853 A71-26521

High pressure gaseous oxygen impact testing method incorporating drop plummet system for specimens flammability screening

14 p2222 A71-30547

Flash points, fire points and impact sensitivity of materials under gaseous oxygen pneumatic and mechanical impact

14 p2222 A71-30550

MECHANICAL TWINNING

Stacking fault formation and mechanical twinning in Ni base superalloy during tensile deformation at high temperature

08 p1315 A71-21581

Fast brittle crack slowing by mechanical twins in transformer steel and by slip bands in LiF and NaCl crystals

09 p1468 A71-22625

Prior deformation and subsequent annealing influence on fatigue response of coarse grained alpha Ti, evaluating relative effects of dislocation locking and mechanical twinning

10 p1626 A71-24445

Aging behavior of Nb-containing Fe-Ni alloys, considering austenite and martensite in twinned and massive form

13 p2089 A71-29412

Swaged high purity fine grained Ti stress-strain behavior below 424 K, emphasizing mechanical twinning in plastic deformation

23 p3695 A71-44289

MECHANICS (PHYSICS)

Applied mechanics - Conference, Bucharest, June 1969

02 p0284 A71-12401

Applied mechanics - Harvard University, June 1970

06 p0927 A71-18219

Solid mechanics boundary value problems solution by cylindrical functions addition theorem in polar and curvilinear orthogonal coordinates

07 p1162 A71-20648

Applied mechanics - Conference, Bucharest, June 1969

09 p1496 A71-23610

Damped mechanical systems sinusoidal vibration analysis, using four pole parameters

12 p1928 A71-26701

Theoretical and applied mechanics - Conference, Tokyo, November 1968

13 p2158 A71-29426

Applied mathematics and mechanics - Conference, Delft, Netherlands, April 1970

15 p2502 A71-31152

Nonlinear mechanical system stationary random forcing input and output response data, determining statistical linearization coefficients in Kazakov-Bootton method

19 p3037 A71-37347

Holographic applications in mechanics - ASME Conference, University of Southern California at Los Angeles, August 1971

21 p3377 A71-40226

Fluid and solid mechanics - Conference, University of Notre Dame, South Bend, Indiana, August 1971

21 p3468 A71-40982

Theoretical and applied mechanics - Conference, Haifa, September 1971

23 p3775 A71-43368

MECHANIZATION

Motion simulation in flight training devices, discussing basic phenomena, minimum requirements and methods of mechanization with regard to equipment design features and maintainability

01 p0066 A71-10017

MECHANORECEPTORS

Cardiovascular and respiratory systems afferent innervation in cats investigating pericardial, expiratory and pneumo-vascular mechanoreceptors

05 p0707 A71-16343

Gastric and rectal mechanoreceptor stimulation influences on vestibular rotation nystagmus in rabbits

06 p0856 A71-18466

Instantaneous postural reaction of cattle to brain concussion indicating mechanoreceptor HF discharge impulse pathophysiological mechanism

11 p1720 A71-26122

Gravity orientation in insects, discussing different mechanoreceptors role

21 p3327 A71-39990

MEDIA

NT ANISOTROPIC MEDIA

NT ELASTIC MEDIA

NT INTERGALACTIC MEDIA

NT INTERPLANETARY DUST

NT INTERPLANETARY GAS

NT INTERPLANETARY MEDIUM

NT METEOROID DUST CLOUDS

NT ZODIACAL DUST

Resonance line formation in multidimensional media, applying to non-LTE line transfer for two dimensional temperature variations

08 p1359 A71-20942

Wave propagation through random inhomogeneous media, discussing mean wave profile modification due to scattering from density inhomogeneities

09 p1434 A71-23168

Self referencing holographic system for image compensation in fluctuating random medium, describing homodyning procedure

21 p3382 A71-40935

MEDIASTINUM

Mediastinum effect on human esophageal pressure and lung compliance measurements

10 p1565 A71-24678

MEDIATION

Physicochemical aspects of conditioned reflexes, including membrane mechanisms, effectiveness of synapses, mediation processes, ribonucleotides function and subcellular structures dynamics

17 p2685 A71-35364

MEDICAL ELECTRONICS

Linear beat by beat cardiachometer, describing amplifier design and operation

01 p0021 A71-10242

Adapted multichannel analyzer for cardiology visualizing vectorcardiographic loops

02 p0206 A71-12107

Ultrasonic Doppler techniques in medical diagnosis, measuring ultrasonic probes directivities by echo amplitudes from various target configurations

03 p0373 A71-14422

Cathode ray tubes as real time display device in various types of professional equipment, describing functional performance and related tube design aspects

06 p0872 A71-17319

Polarographic blood oxygen measurement by principle of oxygen liberation into physical solution by potassium ferricyanide

07 p1053 A71-20337

Holography with fiber optics, allowing three dimensional photography of inaccessible objects in biomedical research and other applications

08 p1291 A71-21400

Astronaut electrode-amplifier helmet harness for cable and radiotelemetry acquisition of EEG, EGO, EMG and blood pressure data on noninterference basis

10 p1570 A71-24475

Percutaneous access to implanted electrodes, discussing metal plaque-needle system and connection to instruments

11 p1724 A71-25436

Wired monitoring system for continuous interference-free twelve-lead ECG recording before, during and after exercise

12 p1876 A71-27630

Small scale solid state digital computer for experimental medical data statistical processing

15 p2365 A71-32534

Medical screening techniques, discussing sensitive, specific, reliable, fail-safe and self calibrating instrumentation systems

17 p2689 A71-34609

MEDICAL EQUIPMENT

NT ARTIFICIAL EARS

NT ARTIFICIAL HEART VALVES

NT CARDIOTACHOMETERS

NT PROSTHETIC DEVICES

Ultrasonics applications in surgery, therapy and diagnosis, discussing physical principles, piezoelectric transducers, tissue acoustic properties and measurement methods

03 p0372 A71-13351

Laser applications in biology and medicine covering surgery, ophthalmology, microorganisms, viruses, tissue culture, tumor eradication, radiation hazards, etc

04 p0541 A71-14722

Electrically rotating chair transmitting medicobiological information of functional state of vestibular analyzer and statokinetic stability

05 p0715 A71-17027

Laser systems for biomedical applications, considering ophthalmology, dermatology, surgery, biological and cellular research, analytical and diagnostic medicine

07 p1049 A71-19782

Waist seal design providing discrete anatomical placement, subject comfort, ingress/egress ease and size accommodation for lower body negative pressure devices

11 p1725 A71-26130

Electrical medical apparatus with electrodes and intracardiac catheters, considering electric current danger threshold, electrocution hazards and safety precautions

17 p2693 A71-35486

Radioisotope thermoelectric generators in micro/milliwatt power range for biomedical applications

20 p3192 A71-38912

Cryogenics applications to cryosurgery and long term low temperature storage of living cells and tissues

20 p3189 A71-39252

Carbon fiber reinforced plastics, considering aerospace and medical applications

21 p3406 A71-40702

MEDICAL PERSONNEL

NT FLIGHT SURGEONS

MEDICAL PHENOMENA

NT PHENOMENOLOGY

MEDICAL SCIENCE

NT ANESTHESIOLOGY

NT EPIDEMIOLOGY

NT HISTOLOGY

NT IMMUNOLOGY

NT NEUROLOGY

NT ORTHOPEDICS

NT OTOLARYNGOLOGY

NT PATHOLOGY

NT PHENOMENOLOGY

NT PSYCHIATRY

NT RADIATION MEDICINE

NT RADIOBIOLOGY

NT RADIOLOGY

NT RADIOPATHOLOGY

NT SYMPTOMOLOGY

NT UROLOGY

NASA program for aerospace technology application to medicine

04 p0546 A71-15281

Survival and rescue medical aspects, discussing water and food intake, dehydration, hygiene, sanitation, rest, injuries, heat and cold exposure, illnesses, rescue operations, etc

08 p1245 A71-20718

Space research utilization in medicine, discussing remote blood pressure measurements, seismocardiography visual analysis, sterilization procedures and equipment for physically handicapped

10 p1571 A71-24754

Soviet army medical appraisal of chronic microwave field induced affections, noting evaluation procedures inadequacy

16 p2534 A71-32827

Soviet papers on biological and medical cybernetics covering control principles in living organisms, heuristic programming, higher nervous activity models, learning problems, etc

17 p2691 A71-35164

Frequency power and resolution effects on ultrasonic holography for medical diagnosis involving information processing on computer

19 p3066 A71-38240

SkyLab manned scientific space laboratory for medical, solar astronomy, earth resources, technology and engineering experiments

22 p3608 A71-41950

MEDICAL SERVICES

Medical support of extended manned space missions, considering functional disturbances, diseases, drug reactivity and timing of in-flight aid

01 p0024 A71-11133

Ground based biomedical supervision of crew members during extended space missions, discussing data acquisition and transmission, astronaut medical competence, etc

01 p0027 A71-11451

Space base biomedical center based on Integrated Medical and Behavioral Laboratory Measurement System /IMBLS/ concept

04 p0546 A71-15280

Flight surgeons guidance criteria for flying personnel, detailing individual areas examination, documentation and clinical findings 08 p1245 A71-20719

Statistical survey of aeromedical and human aspects of airports, discussing population, facilities, accident treatment, design guide and requirements 11 p1725 A71-26127

Medical planning and first aid in disasters at airports 11 p1725 A71-26128

Epidemiological aspects of airport medicine in relation to global public health and international cooperation 11 p1725 A71-26129

Functions of medical services charged with ensuring flying personnel fitness, stressing aging process 13 p2018 A71-28487

Biomedical requirements and emergency planning for aerodromes, surveying U.S. airports 18 p2864 A71-35999

Medical and technical aspects of air rescue and survival of astronauts in mountainous remote areas, noting dogs use for disaster victims location 22 p3482 A71-41982

Experimental ATS-1 satellite medical network for geographically and climatically isolated areas, noting impact on emergency treatment and anxiety level reduction [AIAA PAPER 71-1003] 24 p3801 A71-44592

MEDICINE

Medications stability regarding high temperature, humidity, ambient gas composition, increased oxygen content, radiation, vacuum, vibrations and accelerations 01 p0025 A71-11144

MEDITERRANEAN SEA

Meteorological satellite system for weather forecasting in Mediterranean area, including visible and IR ranges survey and automatic stations and buoys interrogation 16 p2604 A71-32846

Italian weather satellite system for Mediterranean meteorology, noting social and economic aspects 19 p3150 A71-37313

MEDIUM SCALE INTEGRATION

Aerospace digital computer partitioning based on MOS MSI technology using functional building blocks /FHB/ 03 p0384 A71-13281

MEETINGS

U CONFERENCES

MEISSNER EFFECT

U DIAMAGNETISM

U SUPERCONDUCTIVITY

MELTING

NT ARC MELTING

NT FUSION (MELTING)

NT VACUUM MELTING

Snowflakes melting region radar observation, discussing fall speed, reflectivity profile, particle size distribution, Doppler characteristics, etc 01 p0117 A71-10575

High purity Mg deformation by remelting and rolling, investigating grain growth based on size measurement 03 p0445 A71-14341

Thermophysical properties of methane, considering virial coefficients, vapor and melting pressures 04 p0674 A71-14728

Wave formation behavior on melting surface of flat plate in heated air stream 04 p0678 A71-15455

Bulk solids melting on inclined plane heated surface, investigating heat transfer and mass flow rates, fluid driving force and pressure gradient 04 p0678 A71-15456

Alloy melting technique and heat treatment effects on elastic limit and modulus of elasticity 06 p0912 A71-17947

Halophilic bacteria growth in freeze-thaw environment, investigating cooling and warming rates and solute concentrations 09 p1388 A71-22131

One dimensional heat conduction with freezing or melting in bodies with variable cross sectional areas, using phase boundary rate of propagation equations 10 p1698 A71-25099

Surface melting, spallation and stress response prediction for metals under pulsed electron beam heating, using one dimensional finite difference computer program 15 p2390 A71-32005

Pulsed electron beam heating of metals, determining surface melting, spallation and induced stresses with one dimensional computer programs 15 p2429 A71-32006

Silicon-boron melts, investigating B and C concentration effects on carbide layer thickness on graphite/melt interface 15 p2439 A71-32144

One dimensional two phase Stefan problem solution for melting of heated thin plate, comparing iterative methods 16 p2662 A71-33065

Gravity induced free convection effects in melting phenomena for thermal control, predicting temperature distributions and solid-liquid interface profiles by two dimensional model 20 p3314 A71-39354

Heat resistant and refractory materials contact eutectic melting for surface coating production 21 p3390 A71-41175

Inconel superalloy microscopic observation of local melting and hot ductility behavior during weld thermal cycles to clarify cracking cause in heat affected zone 22 p3564 A71-42494

Combined and individual effects of UV light, X ray irradiation and freezing-thawing cycles on ribonuclease 22 p3496 A71-42830

MELTING POINTS

Molybdenum borocarbide synthesis and properties, discussing melting temperature, electrical and heat conductivity, thermal emf, microhardness, etc 01 p0100 A71-10402

Solidified Ni-Mo-Al gas turbine guide vane alloy with improved melting point, creep rupture strength and structural stability 03 p0431 A71-13256

Electron beam welding penetration depth, using constant melt temperature boundary interface [ASME PAPER 70-WA/HT-2] 03 p0432 A71-14094

Thermal diffusivity and total emissivity measurements of solids between 1500 K and melting point, using arc image furnace 04 p0595 A71-14966

Solid/vapor surface energies of metals at melting point related to heat of sublimation 07 p1134 A71-19518

Adiabatic and melting point gradients in earth core, discussing temperature distribution inhibition to convection radial components 09 p1436 A71-22642

Mo high temperature melting point and electrical resistivity measurement by pulse heating method 10 p1624 A71-23912

Dissimilar metals welding, emphasizing melting point, linear expansion coefficient, thermal conductivity, electrical resistivity and polymorphic transformation 13 p2072 A71-27887

Refractory and rare metals absolute melting temperature dependence on atomic number, lattice constant, charge negativity and crystallographic, thermodynamic and mechanical parameters 16 p2594 A71-33878

Zirconium oxide-lanthanum oxide systems near melting point, plotting solidification and phase diagrams 20 p3254 A71-39962

Gaseous medium composition and multiple freezing temperature effects on catalase activity 22 p3497 A71-42831

Vacuum fusion sintered rhodium borides melting point, microhardness and conductivity and thermal emf temperature dependences determination by thermal metallographic and X ray analyses 23 p3717 A71-44024

MEM (EXCURSION MODULE)

U MARS EXCURSION MODULE

MEMBRANE ANALOGY

U MEMBRANE STRUCTURES

U STRUCTURAL ANALYSIS

MEMBRANE STRUCTURES

NT SKIN (STRUCTURAL MEMBER)

Inner ear basilar membrane motions estimation for lower hearing threshold, using nonlinear model 02 p0201 A71-12474

Corrugated membrane of nonuniform profile calculated as variable thickness orthotropic plate, considering corrugations deformation due to bending 02 p0329 A71-12640

General nonlinear finite deformation shell and strain membrane theories in terms of reference state quantities by direct physical derivation 03 p0502 A71-13353

Stereophotogrammetric measurement of plastic deformations of circular Al membrane loaded by pressure pulse, using high speed cameras 03 p0428 A71-13948

Fluid-loaded rectangular plates and membranes random vibration excitation by turbulent boundary layer flow [ASME PAPER 70-WA/DE-15] 03 p0511 A71-14147

Pressurized toroid modified linear membrane theory, presenting approximate solutions for derived boundary value problem by variational calculus methods [ASME PAPER 70-WA/APM-49] 03 p0512 A71-14168

Cord reinforced elastic homogeneous isotropic cylindrical membrane axisymmetric deformation, using strain energy function 03 p0514 A71-14348

Nonlinear elastic membranes large axisymmetric deformation, deriving initial value problem with differential equations 04 p0667 A71-15183

Axisymmetric free transverse vibration frequencies of centrally clamped spinning membrane disks 04 p0668 A71-15186

Thin elastic toroidal shells under nonsymmetric harmonic loadings, reducing problem to membrane and edge effect linear solutions 06 p1002 A71-18415

Flat triangular elements for shell analysis, describing membrane and bending displacements by identical quadratic polynomials [AIAA PAPER 71-114] 06 p1003 A71-18564

Circular membranes and plates with arbitrary hole distribution, deriving natural vibrations frequency characteristic equations by infinite determinants 07 p1218 A71-20464

Membrane separate systems ion and water mass transport, noting effect on anolyte concentration and alkaline battery performance 08 p1234 A71-21092

Unsteady interaction of compressible fluid and flat circular deforming elastic membrane analyzed coupled computer program method [AIAA PAPER 70-75] 09 p1430 A71-22085

Dynamic behavior of circular and rectangular membrane panels with time and space dependent boundary conditions for aerospace structures 09 p1544 A71-23736

Excitable myocardium cell simplified model based on artificial membrane excitation phenomena, using hybrid computer complex analog section 10 p1567 A71-24166

Circular plates with radially symmetric membrane stresses and thickness, investigating stability under peripheral-moving load excitations 10 p1692 A71-24995

Pneumatic membrane logic elements on basis of figure of merit characterizing usability in system engineering 11 p1709 A71-25570

Temperature and membrane thermal stress distribution in finite rectangular plate with insulated circular hole, considering steady state heat conduction equation 11 p1852 A71-26404

Axial wave propagation in linearly elastic membrane shells of revolution, using dynamic finite element technique 13 p2147 A71-27786

Porous glass hyperfiltration membranes stabilization by aluminum chloride solution, noting retreatment need 13 p2026 A71-29377

Closed membrane shell of revolution finite creep due to uniform pressure, applying large deformation incremental theory 14 p2328 A71-30396

Multilobed inflated membranes stability under finite deformation, deriving system instability critical conditions 15 p2503 A71-31421

Cylindrical membrane aeroelastic stability and flutter analysis at high supersonic or low hypersonic Mach numbers 15 p2506 A71-32019

Nonhomogeneous Helmholtz vibration equation for sectorial-annular membranes and plates under arbitrary load, using Fourier method 15 p2508 A71-32231

Matrix force analysis, discussing methods for expressing elastic behavior of semiconvex polygon membrane and isotropic polygon bending elements 16 p2652 A71-33082

Contact problems of inflated cylindrical membranes with quadrature reduction under normal stress applied to loaded floating and submerged life raft [ASME PAPER 71-APM-11] 16 p2656 A71-33215

Nonlinear creep analysis of clamped pressurized circular cylindrical sandwich shells representing stress, membrane force and bending moment as displacement based on Mises criterion 17 p2816 A71-34297

Finite element procedure for plate large deflection by considering effects of element membrane forces due to initial deflection and bending on stiffness matrices 17 p2825 A71-34872

Reverse osmosis application to wash water recovery in manned space mission life support systems, emphasizing membranes development [ASME PAPER 71-AV-1] 18 p2864 A71-36368

Wrinkled flat membranes analogy to very thin plates in flexure 18 p2982 A71-36836

Membrane theory of anisotropic shells, using three dimensional elasticity theory 20 p3308 A71-39366

Membrane and bending stresses analysis around elliptic hole in long thin circular cylindrical shell, using perturbation technique 20 p3309 A71-39776

Mathematical model of electrocardiographic QT-RR relationship, showing agreement with membrane theories 21 p3343 A71-40586

I-V characteristics and temperature responses of negative S and N-type resistances in niobium-niobium oxide-indium structures, considering use as active elements in membrane circuits 24 p3859 A71-44380

Stereophotogrammetric measurements of displacements and strains in Al membrane during explosive forming 24 p3825 A71-44755

MEMBRANE THEORY

U MEMBRANE STRUCTURES
U STRUCTURAL ANALYSIS

MEMBRANES

NT CHOROID MEMBRANES

NT ION EXCHANGE MEMBRANE ELECTROLYTES

NT MEMBRANE STRUCTURES

NT PLEURAE

NT SKIN [STRUCTURAL MEMBER]

Anatomy and function of normal pericardium including removal effect in mammals, fish and amphibians 03 p0362 A71-13328

Small-tipped microelectrode minimizing capacitative artifacts during current passage through bath in membrane potential measurement 03 p0372 A71-13912

Carbonic acid effect on isolated skeletal muscle, discussing membrane potential and ion content measurements 05 p0710 A71-16941

Ultrastructure changes of membrane and sarcoplasmic reticulum of myocardial cells in squirrels during hibernation 06 p0850 A71-17412

Electron microscopic studies of nerve membrane fine structure, discussing cell membrane multienzyme and macromolecular energy and information transduction, protein synthesis and nucleic acids interrelations 06 p0850 A71-17500

Ehrlich ascites tumor cell membrane potassium and electrophoretic mobility loss, investigating radiation effects under radiosensitizing and radioprotecting drugs 07 p1036 A71-18956

Polymeric materials for silver zinc battery separators, discussing porous and solvent-type pore free membranes 08 p1234 A71-21091

Semipermeable polyethylene grafted membranes/separators/ for extended cycle life in silver zinc cells 08 p1235 A71-21094

Mitosis control assuming existence of functional relationship between potential level and mitotic activity, using classical membrane potential theory 18 p2853 A71-35893

Rapid scanning dual wavelength spectrophotometer for recording oxidation-reduction and membrane bound reactions in turbid suspensions of biological materials 18 p2922 A71-36580

Fundamental frequency of star shaped membrane with boundaries described by polar coordinates in Fourier series form 20 p3308 A71-39039

Physical determinants of gravity receptor mechanisms, discussing hydrostatic stress effects on membranes and gravity influence on enzymatic transport 21 p3339 A71-39972

Low temperature effects on succinate oxidase activity of mitochondrial membranes in hibernating squirrels 21 p3336 A71-40854

Heart excitation and membrane permeability effects on two component action potentials in human atrial muscle strips, using microelectrodes 21 p3336 A71-40865

Computerized electrostatic field model of biological cell membrane 22 p3487 A71-42119

MEMORY

Equations of state for materials with memory, discussing derivation methods based on nonlinear functional analysis and applications 01 p0175 A71-11037

Cerebellum substrate for memory list processing in brain assuming Perceptron mechanism 01 p0015 A71-11313

Complex human memory processes large scale simulation/cybernetic modeling/ based on information handling probability and retrieval 07 p1050 A71-20105

Human operator psychophysiological analysis by memory-activity interdependence simulation, noting buffer memory, reflex system and habit acquisition 07 p1050 A71-20107

Redundancy effects on human memorization working capacity, noting application to memory systems design 07 p1043 A71-20113

Human operator psychophysiological characteristics as cybernetic man machine system components, emphasizing human memory activity 07 p1050 A71-20117

Biophysical nature of human memory, investigating electrosensitivity phase modulators and variations by supraincident light stimulus to eye and adjustment reflex 09 p1391 A71-22484

Biological learning, considering EEG wave activity association with structural change underlying information storage in cerebral tissue 10 p1562 A71-24226

Globus pallidus damage in cats, investigating effects on conditioned motor reflexes, learning and memory 10 p1564 A71-24466

Memory behavior in floating gate avalanche injection MOS structure, considering long term charge storage in insulated gate field effect device 13 p2036 A71-28045

Eye movements and visual perception, describing scan path for memory traces 14 p2188 A71-29801

Recognition response time experiments for word number effects in target set, discussing familiarity judgment and response decision 17 p2683 A71-35250

Extraretinal correction and memory for target position, suggesting corrective tendency of eye movements in dark 19 p3004 A71-38286

Eye pupil response during short term memory task, noting postsignal cycle of dilation-constriction 23 p3638 A71-43112

Presentation modality as encoding variable in short term memory, obtaining mean recall score as function of trials 23 p3639 A71-43113

Proactive reaction time inhibition as indicator of immediate memory retention intensity in subjects receiving interpolated acoustic stimuli 23 p3634 A71-43865

MEMORY STORAGE UNITS

U COMPUTER STORAGE DEVICES

U CORE STORAGE

MENISCI

Heat and mass transfer in triple interline region of stationary evaporating meniscus on flat plate immersed in liquid pool 13 p2164 A71-29006

Meniscus induced thinning of tear films due to fluid film fracture and straining 17 p2687 A71-35803

MENTAL PERFORMANCE

Visual task vigilance deterioration under hypoxia, considering work-rest schedule effect and IQ scores 01 p0017 A71-11418

Time judgment error as function of angular velocity during body rotation 07 p1043 A71-20216

Rheoencephalography of cerebral hemodynamics during mental work, showing left hemisphere hyperemia 08 p1242 A71-21960

Human operators performance under control problem programs, determining training and fatigue effects 09 p1398 A71-22483

ATC automation system design, considering controllers decision time savings 10 p1640 A71-24271

Human brain subcortical formations slow electrical processes during memory tests 13 p2005 A71-28377

EEG and derivative spectral characteristics evaluation in determining pilot mental activity during flight 15 p2362 A71-31250

German monograph on human mental performance under simultaneous mental and above normal muscular stress involving signal response in double choice reaction problems 15 p2360 A71-32306

Operator mental performance reliability prediction from heart beat rate and electromyogram 16 p2534 A71-32826

Pilot psychic states in flight, including preliminary demobilization, drowsiness, stunning, euphoria and phobias 16 p2536 A71-33576

Factor analysis of phase discrimination in mental fatigue during diurnal variation of cortical functions in railroad traffic control center operators 17 p2688 A71-34362

Telemetric accelerograph for assessing mental performance under industrial working conditions for work characterized by periodically repeated stereotyped movements 17 p2688 A71-34363

Mental load physiological parameters determination by binary choice task, noting changes in heart and respiratory rates and systolic and diastolic pressure 17 p2688 A71-34364

Human violent exercise burst effect on cognitive task, noting mild hypoxia irrelevance to skills decrements 17 p2686 A71-35436

Target value and exposure duration effects on recall in visual search tasks, discussing results in relation to previously reported inconsistencies 18 p2854 A71-36103

Mental reactive exertion increase phenomenon, investigating achievement under various degrees of carefulness and fatigue 18 p2862 A71-36945

Visual signal detection from noise, investigating mental images effects in six sense modalities 18 p2862 A71-37016

Human visual mental imagery for oscillation rate estimation of subfusional light, using critical flicker frequency test 18 p2863 A71-37020

Human EEG changes and motor analyzer activity during mental visualization of motions 19 p3002 A71-37445

Mental work capacity investigation methodology, including Kekcheev, Kosilov, Zinchenko, Pratushevich and Kraepelin tests 19 p3006 A71-37446

Test equipment for evaluating human higher nervous activity, noting use for radiotelegraphist selection 19 p3007 A71-37775

Intraocular pressure distribution of healthy mental workers in 25-40 years age range, noting symmetry 20 p3189 A71-39234

Computer generated buffered displays for psychological experiments involving interception, tracking, steering, memory and calculation tasks 21 p3341 A71-40136

Human response time for urgent signal after operational rest, showing effect of additional activation during waiting period 21 p3337 A71-41060

Pilot EEG, behavioral and subjective correlates of natural and drug induced sleep at atypical hours, using calculation and vigilance tests 22 p3502 A71-41835

MENTAL STRESS

U STRESS [PSYCHOLOGY]

MERCAPTAN

U THIOLS

MERCAPTO COMPOUNDS

U THIOLS

MERCATOR PROJECTION

Mars Mercator projection photomap, using Mariner 6 and 7 spacecraft TV images 06 p0965 A71-17629

Mercator chart of Mars surface between 70 deg north and 70 deg south latitude from Mariner 6 and 7 photography 09 p1452 A71-23220

MERCURY [METAL]

NT MERCURY VAPOR

Submillipound mercury electron bombardment ion thruster efficiency, noting cathode pole piece, baffle position and geometry influence on ion chamber performance [AIAA PAPER 70-616] 01 p0143 A71-11577

Solar Hg abundance low value by photosphere spectrum absence of Hg I lines, comparing higher content in carbonaceous chondrites 02 p0306 A71-12048

Cs atom ionization cross section during type II collision with resonantly excited Hg atom 02 p0287 A71-12197

Mercury droplet dynamics in conducting liquid within electromagnetic field under reduced gravitation 02 p0293 A71-12631

Horizontal cylindrical heaters heat transfer to pool boiling Hg at heat fluxes up to burnout [ASME PAPER 70-HT-R] 03 p0519 A71-13698

Heat transfer to concentric annular turbulent mercury flow, determining wetting effect, velocity profiles, eddy diffusivity of momentum transfer and friction factors 04 p0570 A71-15172

Nonuniformly rotating Hg fluid, noting hydromagnetic stability and velocity control by imposed radial current distribution between coaxial ring shaped electrodes 05 p0788 A71-16608

Hg content determinations in meteorite specimens, comparing to magnetic rock of earth crust 05 p0814 A71-17165

SERT II electron bombardment thruster operation with Ar and Hg propellants [AIAA PAPER 71-157] 06 p0947 A71-18599

Parameters influence on mercury hollow cathode neutralizers for Kaufman ion thruster [AIAA PAPER 70-1090] 07 p1184 A71-19863

Mercury intrusion porosimetry application to pore size and shape measurements for porous solids, discussing solid and air compressibilities, surface tension, contact angle, etc 09 p1453 A71-22168

MHD Hg flow between concentric cylinders with nonconductive walls, comparing pressure loss and voltage measurements with theoretical predictions for large Hartmann numbers 10 p1647 A71-23862

Induced electrostatic field in forced Hg vortex of ideal viscous electrically conducting fluid under axial magnetic field 10 p1649 A71-24456

- Low specific impulse hollow cathode mercury thruster for deep space electric propulsion, using SERT 2 configuration
[AIAA PAPER 70-1099] 11 p1811 A71-25526
- Lunar surface rocks Hg content under daytime temperatures volatilization conditions, considering cold trap and lunar atmosphere 12 p1958 A71-26692
- Hg content determinations in meteorite specimens, comparing to magnetic rock of earth crust 12 p1968 A71-27454
- Cs atom ionization cross section during type 2 collision with resonantly excited Hg atom 15 p2451 A71-31503
- SNAP-8 mercury Rankine system performance data, investigating design change for reduced reactor operating temperatures 15 p2447 A71-32201
- Local forced convection heat transfer data and empirical correlations for boiling Hg in single wetted Ta tube with composite helical inserts [GESP-450] 15 p2447 A71-32216
- Unalloyed tantalum as containment material in mercury Rankine cycle SNAP 8 system boiler for 5 year service life 15 p2448 A71-32221
- Photoelastic determination of stress distribution in thin square plates subjected to gravitational forces multiplied by immersion in Hg 16 p2647 A71-32824
- Luminescence quenching in Hg tube activated ZnS-Cu phosphors under action of ruby laser red light 17 p2752 A71-34404
- Transverse magnetic field influence on heat transfer of conductive fluid /mercury/ in electrically insulated pipe subjected to uniform heat flux 17 p2788 A71-34660
- Ionization and excitation kinetics of Hg in relaxation flow zone behind shock wave front, considering electron impact role in ground state atoms ionization 18 p2951 A71-35980
- Pulsed plasma rail mercury propellant thruster for satellite attitude control, measuring thrust and exhaust velocity with balance and Langmuir probe respectively 18 p2956 A71-36243
- Mercury properties, chemistry, safety, handling and corrosion in nuclear coolant applications 19 p3102 A71-37071
- He-Ne laser discharge tube using water cooled mercury cathode with supplementary molybdenum anode 19 p3073 A71-37789
- Mercury determination in terrestrial and nonterrestrial rock samples by atomic absorption spectroscopy, noting high temperature release patterns 21 p3346 A71-40863
- Ion engine development at Farnborough /England/, considering 10 mN mercury electron bombardment thruster system with hollow cathode 22 p3588 A71-41508
- Radiation quenching and depopulation of excited Hg atoms by collisions with ground state hydrogen molecules, using steady state flowing afterglow method 23 p3712 A71-43996
- MERCURY (PLANET)**
- Mercury planet average dark side temperature indicating top surface layer similarity with moon 01 p0148 A71-10004
- Mercury microwave and IR observations interpreted for thermophysical models for planetary subsurface, discussing rotation and heating 03 p0492 A71-14069
- Mercurian atmosphere models, discussing replenishing processes involving chemical reactions in thin and thick models 04 p0650 A71-15583
- Gravitational and tidal torque effects on Mercury spin rate as model of passage through resonance 04 p0657 A71-15738
- Mars and Mercury polarization measurements, investigating Rayleigh scattering in atmospheres 05 p0806 A71-16204
- Mercury spin orbit resonance probability computation, making a priori assumptions for long term orbital variations, tidal torque and equatorial asymmetry 07 p1203 A71-20521
- Cassini second and third laws generalization to energy extremes, discussing Mercury shape 07 p1203 A71-20523
- Mercury drawings from refractor observations /1964-1967/ 09 p1520 A71-22834
- Mercury transit across solar disk on 9 May 1970, using photographic micromasurements 10 p1677 A71-24587
- Mercury and Venus transit periodicity before solar disk, examining celestial mechanics and solar system distances determination 10 p1680 A71-25003
- Venus-Mercury flyby vehicle solar cells, cover glasses, adhesives and Kapton film, investigating space radiation effects on kapton absorptance and transmittance [AIAA PAPER 71-452] 11 p1859 A71-26236
- Solar wind-Mercury interaction, discussing planet physical properties, magnetized wind parameters and bow shock wave existence 13 p2120 A71-27924
- Planet Mercury density, discussing optical and radar measurements and theory comparison with observation 14 p2306 A71-29728
- URSI-IAU-COSPAR Woods Hole Conference on lunar emission and Mercury surface temperature from radiometry, discussing Mars and Venus atmosphere measurements 14 p2316 A71-30967
- Intra-Mercurial planets and comets discovered during solar eclipses, discussing size, orbital eccentricity, albedo and equilibrium temperature 16 p2642 A71-33830
- Action-at-a-distance theory of gravitation generalized to tensor interactions of all orders, considering special relativity demands and perihelion advance of Mercury 17 p2797 A71-34368
- Polar asymmetry between distribution of surface features on earth, moon, Mars and Mercury 17 p2801 A71-34670
- Mercury transit across solar disk, discussing visual and photographic observations with Repsold and sun refractors and coronagraphs 17 p2809 A71-35579
- Ephemerical times of ingress and egress times of Mercury transit across solar disk 17 p2809 A71-35580
- Stray-light and sunspot intensity measurements of sunspot umbra and aureole during Mercury transit 19 p3147 A71-38668
- Sunspot intensity during 9 May 1970 Mercury transit with corrections for scattered light from solar limb observations 19 p3147 A71-38669
- Soviet papers on terrestrial planets, discussing Mercury, Venus and Mars atmosphere, surface, internal structure and physical conditions 21 p3452 A71-40882
- Mercury visual, radar and radio data, describing rotation, temperature, surface properties, subsurface layers and atmospheric model 21 p3452 A71-40883
- Mercury perihelion advance due to solar mass distribution departure from spherical symmetry because of negative eddy viscosity 21 p3439 A71-41422
- Probe for circular polar Mercury orbit, obtaining missions values 22 p3600 A71-42010
- Radiative heat transfer from lunar and Mercurian surfaces during eclipse 22 p3603 A71-42188
- MERCURY ALLOYS**
- NT MERCURY AMALGAMS**
- MERCURY AMALGAMS**
- Semiconductor thermoelectric battery p-n cell elements joining with mercury amalgam for commutating 14 p2181 A71-29953
- MERCURY ARCS**
- Cs doped Mg vapor arc discharge, determining electron mobility and diffusion cross section 02 p0286 A71-12180
- Microwave scattering from nonuniform plasma of low pressure mercury arc in glass tube, describing density profile 03 p0463 A71-13474
- Plasma temperature determination in Hg high pressure discharge with TII addition 05 p0786 A71-16224
- Partially ionized Hg plasma electrical conductivity at various pressures and temperatures 05 p0790 A71-16787
- Partially ionized Hg plasma electrical conductivity at various pressures and temperatures 16 p2618 A71-33039
- Langmuir paradox problem concerning electron energy distribution function and anisotropy in low pressure DC Hg vapor discharge positive column plasma 23 p3710 A71-43402
- Dense low temperature Ar and Hg plasmas, observing correlation between electrical conductivity and optical emission 23 p3712 A71-43914
- MERCURY COMPOUNDS**
- NT MERCURY OXIDES**
- NT MERCURY TELLURIDES**
- MERCURY OXIDES**
- Mercuric oxide-cadmium batteries optimum cell design for low temperature operating conditions and elevated temperature storage life 03 p0351 A71-13038
- MERCURY TELLURIDES**
- P-n junction formation in zinc mercury telluride samples, using heat treatment to control carrier concentration 01 p0140 A71-11464
- Cadmium mercury telluride solid solutions electron energy spectrum at low temperatures, calculating electron mobility in crystals with zero forbidden band 13 p2110 A71-27955
- Solid solution electron energy spectrum at low temperatures, considering electron mobility in cadmium-mercury telluride crystals with zero forbidden band 21 p3435 A71-41342
- HgTe-CdTe thin films structural and optical properties, measuring absorption spectra in UV, IR and visible regions to determine Te contents effect 24 p3862 A71-45251
- MERCURY VAPOR**
- Kaufman electrostatic ion thruster using electron bombardment ionized mercury vapor in cylindrical vessel and acceleration by electrostatic field 02 p0283 A71-12310
- Equilibrium, highly imperfect, partially ionized Hg and Li vapor plasmas, examining charged and neutral particle interaction forming charged clusters 02 p0292 A71-12617
- Two phase Hg tunnel for shock wave visualization by RF discharge between test model body and external ring, comparing measurements with supersonic flow theory 08 p1272 A71-21751
- Hg vapor thermal conductivity measurement at 300-900 C and atmospheric pressure, using hot wire method 08 p1376 A71-21919
- Cold Hg plasma in composite HF and magnetostatic field near electron cyclotron resonance, obtaining electron and ion energy spectra 10 p1650 A71-24527
- Liquid and gaseous Hg thermoelectric power measurements at sub and supercritical temperatures and various pressures 13 p2000 A71-28676
- NASA Lewis Research Center Hg electron bombardment ion thrusters research programs 14 p2288 A71-29931
- Tantalum/stainless steel mercury boilers for SNAP 8, evaluating performance 15 p2448 A71-32219
- Magneto-electrostatic containment ion thruster, considering adaptation for Hg operation based on discharge chamber loss comparison with Cs [AIAA PAPER 71-692] 15 p2470 A71-32288
- Monatomic mercury gas excitation and ionization mechanisms ahead of and behind shock front, establishing electron gas heating kinetics in relaxation zone 16 p2616 A71-32902
- Electronic to vibrational energy transfer in mercury vapor reaction with hydrogen fluoride, studying IR emission and scattering cross section 18 p2874 A71-35834
- Cs and Hg vapors compressibility factor in supercritical range as function of density, considering charged particles and atoms polarization interactions in ionized metal vapors 19 p3111 A71-37590
- Saturated Hg vapor pressure at 650-900 K by boiling point method 19 p3162 A71-37591
- LF oscillations excitation and resonance amplification in mercury vapor plasma discharge 21 p3425 A71-41283
- Hg condensation characteristics on Cs substrate in high velocity nitrogen carrier gas, formulating one dimensional flow model based on two phase three component gas dynamics 22 p3620 A71-41876
- Langmuir paradox problem concerning electron energy distribution function and anisotropy in low pressure DC Hg vapor discharge positive column plasma 23 p3710 A71-43402
- MERIDIANALS**
- U LATITUDE**
- U LONGITUDE**
- MERIDIONAL FLOW**
- Carbon dioxide band radiances measured by Nimbus 3 satellite IR spectrometer, noting seasonal temperature changes in stratosphere due to meridional circulation 01 p0119 A71-10743
- Meridional ionization cross section in ionosphere between Leningrad and Murmansk with local anomaly and diurnal reversing of F 2 probability 02 p0243 A71-11766
- Semiannual atmospheric wind and pressure oscillations relation to seasonal meridional baric systems displacements, considering cosinusoidal wave motion variations between Northern and Southern Hemispheres 04 p0621 A71-14639
- Equatorial electric field generation by ionosphere dynamo region neutral wind meridional component 07 p1101 A71-19409
- Latitudinal variations in adiabatic production and destruction of kinetic energy by meridional and zonal motions of atmosphere 09 p1488 A71-23025
- Diurnal variations of meridional winds by dynamo electric field in troposphere, comparing with Thomson scattering 09 p1490 A71-23646

Yearly cosmic rays intensity variations in meridional plane from 1955-1969 ionization temperature coefficient recordings as function of solar activity levels

11 p1817 A71-25783

Atmospheric energy storage and meridional transport, calculating annual cycle in Northern Hemisphere

12 p1925 A71-27193

Propagation of 26-month oscillations in meridional component of wind velocity in stratosphere at extra-tropical latitudes from hydrothermodynamic equations solution

13 p2057 A71-28021

Sensitive heat meridional transport frequency spectra wavenumber in Southern Hemisphere midtroposphere

13 p2063 A71-29108

Angular momentum meridional transport flux wave number-frequency spectral characteristics in mid-troposphere of Southern Hemisphere

13 p2063 A71-29109

Mesospheric extraterrestrial dust and trapped water model of noctilucent cloud formation in high latitude summer conditions, using meridional trajectories

14 p2231 A71-29721

Summertime meridional wind component profile construction and hydrodynamic model for semidiurnal fluctuations in upper atmosphere

15 p2399 A71-31962

Solar eclipse effects on atmospheric structure, circulation and meridional flow, using rocket measured temperature and wind data for pressure and density variations near stratopause

16 p2567 A71-33764

Equatorial electric field generation by ionosphere dynamo region neutral wind meridional component

19 p3053 A71-37833

Sweep and dihedral geometry effects on blade to blade and meridional flows in turbomachinery blade rows, using actuator disk theory

19 p2994 A71-38274

Seasonal variations of kinetic energy balance of mean meridional circulation in Northern Hemisphere

20 p3257 A71-39436

Seasonal variations in vertical distribution of ozone at high latitudes, using Murgatroyd model of looped meridional atmospheric circulation

21 p3375 A71-41395

Yearly cosmic rays intensity variations in meridional plane from 1955-1969 ionization temperature coefficient recordings as function of solar activity levels

22 p3591 A71-41551

Blade cascade design for meridional flow, using finite difference method for universal computer program

23 p3626 A71-43550

MEROMORPHIC FUNCTIONS

NT ELLIPTIC FUNCTIONS

NT RATIONAL FUNCTIONS

Soviet monograph on meromorphic functions covering behavior variables, asymptotic properties and defects and Riemann surfaces application for values distribution analysis

05 p0773 A71-16249

MESH

Simply supported double layered rectangular mesh grids, solving finite difference equations under arbitrary loading

08 p1370 A71-21409

Elastic collapse analysis of shell structures with variable rectangular grid spacing based on modified finite difference computer program

11 p1844 A71-25338

Convergence and strain accuracy of finite element solutions for nodal displacements in plane elastic mesh

24 p3842 A71-44633

MESON-NUCLEON INTERACTIONS

Charged scalar static model, using dispersion theory to include two-meson effects in two nucleons binding energy at zero separation

05 p0785 A71-16449

Nucleon-nucleon and meson-nucleon collisions, determining secondary cosmic ray multiplicity dependence on primary particles energy spectra

13 p2121 A71-28057

MESONS

Strong cosmic ray interactions, considering meson production in accelerators

03 p0475 A71-13835

Fireball model at various energies, describing multiple meson production at very high energy

13 p2058 A71-28049

Atmospheric very high energy cosmic ray propagation by three dimensional Monte Carlo simulation, employing H quantum and fireball models for multiple meson production

13 p2122 A71-28065

Diurnal correlation between cosmic ray meson intensity and atmospheric ozone content on magnetically undisturbed days

14 p2231 A71-29723

Cosmic ray nucleon-meson and barometric pressure data continuous recording equipment, comparing system to conventional instruments

14 p2248 A71-30602

Nuclear soft core potential reproduction by isoscalar vector meson in nonlocal field theory of fireball in high energy cosmic ray collisions

15 p2472 A71-31151

Proportional counters design for ionizing radiation detection, examining cosmic ray meson component

15 p2408 A71-31814

Fireball model of meson production in high energy nucleons collisions

18 p2949 A71-36210

Strong cosmic ray interactions and meson production in accelerators

22 p3594 A71-42636

Underground meson telescope coupling functions calculations, using effective primary threshold energy

23 p3720 A71-43152

MESOPAUSE

Internal gravity waves in atmospheres with realistic dissipation and temperature, considering thermal tides excited below mesopause

05 p0739 A71-16425

Mesopause thermal transitions during spring and autumn based on noctilucent cloud observations, discussing stratospheric-mesospheric coupling effects

15 p2400 A71-31988

Atmospheric temperature and density scale height seasonal variations near mesopause, using meteor theory mass and luminosity equations

17 p2737 A71-35740

MESOPHILES

Thermophilic, mesophilic and psychrophilic anaerobes fatty acid composition, discussing results obtained by mass spectral analysis

15 p2360 A71-32050

MESOSPHERE

Stratospheric and mesospheric water vapor content by satellite-borne spectral measurements

01 p0120 A71-11103

Upper stratosphere and mesosphere concentrations of Ne, Ar, and Kr from rocket-borne cryogenic air sampler

02 p0246 A71-12701

Noctilucent clouds, discussing mesosphere thermodynamics and water vapor content, solar rain, etc

03 p0414 A71-14019

Mesosphere and lower thermosphere probing, noting electron and ion densities distributions, collision frequencies and ionospheric loss rates

05 p0740 A71-16427

Mesosphere and lower thermosphere heat input rates and circulation, calculating worldwide average eddy diffusion coefficient

06 p0892 A71-17978

Carbon dioxide and carbon monoxide atmospheric distribution dependence on combined effects of photochemical production, loss and transport in mesosphere and upper stratosphere

06 p0893 A71-17980

Charged particle balance equations for stratosphere and mesosphere, noting particle composition investigation and formation and annihilation processes

06 p0963 A71-18261

Stratospheric and mesospheric water vapor content by satellite-borne spectral measurements

08 p1277 A71-20847

Mesosphere and stratosphere data from high level observations for supersonic transport and reentering space vehicle operations

08 p1328 A71-21724

Weak ion concentration in stratosphere and mesosphere measured by accumulated capacity amplifier

09 p1443 A71-22676

Ozone distribution measurements in mesosphere and stratosphere by rocket during seasonal ionospheric disturbance and solar eclipse

09 p1490 A71-23562

Electrical processes in stratosphere and mesosphere - Conference, Madrid, September 1969

10 p1603 A71-24698

Mesosphere charged particles concentration and mobility measurements, using rocket-borne aspiration probes

10 p1604 A71-24705

Energy flux of tropospheric mesoscale waves and heat influx into upper mesosphere caused by energy absorption, discussing wavelength and latitude effects

12 p1924 A71-26735

Stratospheric and mesospheric wind measurements over Leba sounding rocket station

12 p1900 A71-27066

Neutral fluctuations of zonal winds in stratosphere and mesosphere from flow equations, noting flow instability role in generation mechanism

13 p2057 A71-28020

Seasonal-climatic vertical distributions of radiative heat sources and sinks calculation for Northern Hemisphere stratosphere and lower mesosphere

13 p2057 A71-28023

Stratosphere and lower mesosphere seasonal climatic temperature profiles calculation from radiation

transport and balance equations, noting turbulent heat influxes role in stratification formation

13 p2057 A71-28024

Concentration and transport from auroral zone of minor constituents in mesosphere and lower thermosphere during anomalous midlatitude radio absorption periods

14 p2230 A71-29711

Mesospheric extraterrestrial dust and trapped water model of noctilucent cloud formation in high latitude summer conditions, using meridional trajectories

14 p2231 A71-29721

Mesospheric /noctilucent/ cloud physics - Conference, Riga, November 1968

14 p2231 A71-29955

Noctilucent cloud formation from water vapor concentrations in mesosphere and lower thermosphere of arctic and midlatitude regions measured by rocket-borne RF mass spectrometers

14 p2232 A71-29957

Mesospheric height-temperature measurements in noctilucent cloud zone of Southern Hemisphere

14 p2232 A71-29958

Twilight OH emission intensity and rotational temperature in mesosphere as function of solar position below horizon

14 p2232 A71-29959

MHD processes of upper atmosphere in mesospheric cloud formation, discussing solar wind-magnetic field interactions and equilibrium for Pikelner bomb

14 p2232 A71-29960

Mesospheric cloud statistics compared with 200 MHz solar radio emission during summers of 1958-1966

14 p2232 A71-29961

Soviet research program relative to climatology, physical nature, morphology and dynamics of mesospheric clouds, discussing observational and experimental methods

14 p2233 A71-29968

Noctilucent clouds observations and data acquisition, considering cloud amount and thickness calculations

14 p2233 A71-29969

Noctilucent cloud observations at Tomsk, Novosibirsk and other Siberian locations from 1965 to 1968

14 p2233 A71-29970

Noctilucent clouds occurrence frequency relationship to mesospheric circulation

14 p2235 A71-30351

Ionospheric absorption winter anomaly including temporal and local variations and frequency dependence, examining possible correlations with stratospheric and mesospheric phenomena

14 p2237 A71-30943

Cluster ions concentration and nitric oxide in mesosphere D region, considering electron density profiles

15 p2394 A71-31430

Soviet papers on processes in upper layers of atmosphere covering troposphere, stratosphere and mesosphere over Northern and Southern Hemispheres

15 p2399 A71-31961

Northern Hemisphere upper stratosphere and lower mesosphere synoptic meteorological chart construction, using aerological network and rocket radio sounding data

15 p2400 A71-31967

Southern Hemisphere stratosphere and mesosphere meteorological parameters seasonal variation, comparing rocket sounding data with standard models

15 p2400 A71-31968

Mesospheric noctilucent cloud formations observations from space by cosmonaut on 9 June 1970 over Arabian peninsula

15 p2496 A71-32727

Seasonal temperature and density models for stratosphere and mesosphere from observations by resistance thermometers at Heiss Island Soviet rocket station

16 p2566 A71-33743

Spring and autumn cyclonic circulation in stratosphere and mesosphere up to 95 km, using ionospheric radiosonde and rocket data

17 p2730 A71-34301

Polar mesosphere internal gravity waves generation and propagation, using temperature and wind profiles from rocket granade method

20 p3221 A71-39693

Mesosphere and stratosphere ozone vertical density distribution from sounding rocket data, considering photochemical theory and hydrogenic reductions

20 p3221 A71-39694

Lower thermosphere and mesosphere water vapor and neutral composition spectrometric measurements, estimating hydrogen and oxygen atom recombination coefficient limits with mass analyzers

20 p3221 A71-39696

Mesospheric soft corpuscular radiation flux and temperature rocket observations, during solar flare activity

20 p3222 A71-39704

Stratosphere and mesosphere physics and dynamics, studying composition, radiation fields, tempera-

ture, winds, wave phenomena and relations to meteorological theory 20 p3230 A71-39872

MESSAGES

Two-directional digital data transmission system, determining probability of not obtaining message for arbitrary interrogation signals number 01 p0039 A71-11319

Message distortions analysis in PCM communications systems due to phase fluctuations of synchronization signal 19 p3022 A71-38494

METABOLIC WASTES

NT HUMAN WASTES

Regenerated nutrients as foods for long duration space missions, discussing physicochemical methods for metabolic waste products conversion into safe synthetic nutrient compounds 01 p0026 A71-11250

Potential foods synthesis for long duration space missions by physicochemical methods, discussing regeneration of carbohydrates from metabolic waste carbon dioxide and electrolytic byproduct hydrogen 07 p1056 A71-20375

Biowaste restructojet engine design and performance for various propellants and propellant mixtures [AIAA PAPER 71-687] 15 p2470 A71-32293

Urinary metabolites relationship to fatigue, considering excretion of proteins, electrolytes, simple organic compounds and hormones 17 p2679 A71-34357

Sodium and cations elimination by kidneys during water-salt metabolism changes due to high temperature and hypodynamia 20 p3189 A71-39232

Antiradiation drugs effects on healthy and irradiated rats gastrointestinal tract evacuatory motor function 22 p3492 A71-42707

Humans under constant diet feeding in closed ecological system, demonstrating instability in elimination process of various elements 22 p3506 A71-42817

METABOLISM

NT ADRENAL METABOLISM

NT CALCIUM METABOLISM

NT CARBOHYDRATE METABOLISM

NT ELECTROLYTE METABOLISM

NT ENZYME ACTIVITY

NT HORMONE METABOLISMS

NT HYPERGLYCEMIA

NT LIPID METABOLISM

NT OXYGEN METABOLISM

NT PHOSPHORUS METABOLISM

NT PROTEIN METABOLISM

Air carbon dioxide role in rabbits metabolism, using C 14 radioactive tracer technique 01 p0012 A71-11061

Human gas metabolism under rarefied atmosphere via gas chromatography, discussing pulmonary ventilation determination and exhaled samples collection equipment 01 p0025 A71-11142

Metabolic rate and ergometric data recording by analog and digital systems 01 p0026 A71-11409

Skin temperature and metabolism changes magnitude, duration and variability in unacclimatized male subjects during cold stress 02 p0208 A71-12836

Pulmonary gas exchange relation to cyclical pattern of ventilatory flow, considering alveolar dead space and metabolic and respiratory rate effects 03 p0361 A71-13183

Diurnal variations due to actual heat output, oxygen consumption and carbon dioxide production in rats undergoing eating habit changes 04 p0539 A71-15157

Metabolic processes in bone tissues as basis for fighting bone disease, emphasizing enzymes role 05 p0710 A71-16858

Clinical, physiological and metabolic changes in human body during 120 day bed rest 06 p0855 A71-18371

Toxic substances absorption, metabolism and excretion by man, discussing role of solubility, transfer through membrane tissue, liver and kidney as metabolizing and excreting organs 07 p1042 A71-19700

Chlorophenoxyisobutyric acid action on human cholesterol metabolism, suggesting cholesterol synthesis inhibition 07 p1044 A71-20353

Ventricular controllers automatism suppression by HF electric stimulation, examining energy metabolism inhibitors effects 08 p1240 A71-21793

Cerebral lipid fractions, examining relation between physiological functions and metabolism 09 p1391 A71-22481

L-dopa multiinjection timed effects on rat brain norepinephrine metabolites concentrations, observing zero time control rated modifications 09 p1393 A71-22649

Corneal transparency in metabolic activity absence, using acid mucopolysaccharide depletion and prolonged gamma irradiation 09 p1393 A71-22985

Metabolic energy cost prediction equation for level or grade walking with/without loads 09 p1401 A71-23372

Central nervous system role in body metabolism effects on cardiac output, measuring 2,4-dinitrophenol /DNP/ dosage effect on arterial pressure and oxygen consumption in dogs 09 p1396 A71-23541

Secretory function intensity of salivary glands, liver and stomach of animals and humans with different water-salt metabolism conditions 11 p1719 A71-25669

Isocarbic metabolic acidosis effects on blood plasma, electrochemical potential differences and cerebrospinal fluid pH 11 p1722 A71-26361

Long term immersion effects on human water-salt metabolism, noting increased erythrocyte water contents and hematocrit index 13 p2006 A71-28403

Postflight metabolism and renal function of Soyuz 6, 7 and 8 crewmembers, associating weight loss during flight with water and salt discharges 13 p2006 A71-28409

Food choice, consumption control and metabolism, discussing homeostatic alimentary theories, nerve signals and appetite regulation 13 p2010 A71-28719

Metabolic, ventilator and cardiovascular response during free swimming and treadmill walking, relating oxygen consumption to work intensity 13 p2024 A71-29500

Gas exchange metabolic fluctuations of nitrogen fixation, hydrogen evolution and photoreduction in Rhodospirillum rubrum as function of culture conditions and age 16 p2528 A71-33059

Pyridoxine and serotonin metabolism changes and vestibular disorders observation in space flight 16 p2532 A71-33677

Human erythrocyte 2, 3-diphosphoglycerate concentration elevation effects on glycolytic metabolism and intracellular pH 16 p2533 A71-34090

Energy metabolism disturbance effect on dissolved and undissolved collagen fractions content of aorta connective tissue 17 p2679 A71-34223

Skin temperature and perspiration role in metabolic heat elimination, considering evaporation coefficient relationship to convection coefficient 18 p2859 A71-36873

Noisy environment effects on circulatory, respiratory and metabolic parameters during physical exercise, measuring heart rate, systolic blood pressure, oxygen intake and respiratory quotient 20 p3185 A71-38889

World champion marathon runner metabolic responses during submaximal and maximal treadmill running, recording oxygen consumption, heart rate and lactic acid 20 p3185 A71-38890

Prolonged hypokinesia effect on rats serotonin /5-HT/ metabolism, noting pronounced blood content deviation from normal during first to third and thirteenth to fifteenth day 20 p3187 A71-39218

Aminazine and chloral hydrate effects on metabolism intensity of rats brain gangliosides components including N-acetylneuramine acid and N-acetylglucosamine 21 p3337 A71-41055

Glycerides metabolism in rats brain under normal conditions and during hypoxia, showing diglycerides role in triglycerides and phospholipids biosynthesis 21 p3337 A71-41056

Water immersion or bed rest effects on basic metabolism and external respiration under simulated weightlessness 22 p3495 A71-42794

Human nitrogen and water-salt metabolisms and respiratory activity during prolonged confinement in small volume chamber with cyclic varying hypoxic air 22 p3495 A71-42799

Serotonin metabolism of helicopter pilots, showing effects of emotional factors due to flight inexperience 23 p3632 A71-43220

Elevated basal metabolism in man under simultaneous altitude hypoxia and cold acclimatization 23 p3636 A71-44239

Brain monoamines localization and metabolism and endocrine function, discussing pituitary secretion and neurotransmitter input 23 p3637 A71-44274

Preoptic and environmental temperature effects on hibernator thermoregulatory responses, noting changes in metabolic rates 23 p3637 A71-44301

Water-salt metabolism in human blood and urine under high temperature conditions after residence in different climatic zone 24 p3794 A71-44414

Moderate heat exposure effects on human circadian variations in body temperature, heart and metabolic rates and water loss 24 p3797 A71-44779

METAGALAXY

U UNIVERSE

METAL AIR BATTERIES

NT ZINC-OXYGEN BATTERIES

Zinc air battery, evaluating materials capable of peroxide decomposition as low cost oxygen electrodes 03 p0351 A71-13040

Development and performance characteristic of batteries including Zn and Mg dry cells, metal air, organic electrolytic, organic cathode and secondary systems 24 p3793 A71-45133

METAL ALLOYS

U ALLOYS

METAL BONDING

NT METAL-METAL BONDING

Solid metal-licrubic films bonding by ion plating using diode method, noting interface type and structure examination by electron microscopy 01 p0087 A71-10483

Secondary fabrication of boron reinforced aluminum matrix composite sheets for aerospace sub-components, detailing joining and autoclave bonding [SME PAPER EM-70-126] 01 p0089 A71-11260

Combined vacuum furnace brazing with diffusion welding for joining high strength Ni base superalloys 02 p0255 A71-11708

Nb-sheathed insulators of three coaxial cylinders with ceramic bonding for thermionic converter, discussing pressure bonding techniques and stress relieving properties 02 p0232 A71-12248

Shearing strength of and lubrication effect on metal-plastic adhesion bond, using solid rotating indenter technique 05 p0759 A71-16363

Adhesive resin metal bond stability, examining surface finish and atmospheric moisture effects at various temperatures on exfoliation 06 p0904 A71-17944

Metal gluing with synthetic polymer based adhesives, discussing history, technology and high temperature resistance 06 p0905 A71-18093

Heat and corrosion resistant vacuum tight ceramic to metal brazed seals 07 p1119 A71-19972

Diffusion bonding for vacuum tight heat resistant and oscillation proof large area joints 09 p1459 A71-23584

Surface treatment effects on high shear strength adhesive bonding of fiber reinforced plastics to metal substructures 10 p1630 A71-24069

Alloy and heat treatment effect on Ti bondability for adhesive bonded aircraft structure, using annealed and aged Ti-6Al-4V and Ti-6Al-6V-2Sn alloys for testing 10 p1615 A71-24093

Al alloys and ferrous metals adhesive bonding, discussing surface preparation and surface exposure time influence on bonded joint strength for various epoxy adhesive types 10 p1615 A71-24095

Coupling agents in urethane and epoxy adhesives, discussing lap shear and T-peel tests on mild and stainless steels, Al and glass cloth substrates 10 p1616 A71-24108

Structural adhesive bonding of plastics and metals, emphasizing fast curing, high bond strength, environmental resistance and bonding ability 11 p1768 A71-25393

Spreading, wettability, diffusion and aggressive properties of nickel base brazing filler metals on stainless steels 11 p1769 A71-25750

Titanium carbide based cermet materials with alloy steel binder, investigating production conditions, hardness, machining and quenching properties 15 p2429 A71-32139

Radiation effects on bonding characteristics of epoxy-metal and epoxy-glass adhesive joints 15 p2439 A71-32511

Metal joint explosive bonding, investigating wavy interface formation mechanism by aerohydrodynamic analogy 17 p2748 A71-34494

Elastic adhesive interlayer effect on bond fracture strength, considering propellant-liner- steel combination in solid rocket motors 18 p2977 A71-36245

Bulk and surface diffusion roles in clean and contaminated Cu-Ni surfaces adhesion 19 p3080 A71-37713

Bonding conditions effect on wave mode formation at explosive bonded interface in bullet experiments on thin metal targets 22 p3617 A71-42495

Soviet book on microwelding by pressure covering semiconductor-metal bonding, ultrasonic soldering and thermal processes

23 p3682 A71-44125

METAL CARBIDES

U CARBIDES

METAL COATINGS

NT ALUMINUM COATINGS

NT GOLD COATINGS

NT NICKEL COATINGS

Boride coatings for Fe-Si alloy, testing corrosion and wear resistances in aqueous salt, acid and alkali solutions

01 p0097 A71-10039

Composite Ni coatings, adding mullite crystals to enhance oxidation resistance

01 p0102 A71-10784

Tungsten plasma coatings on steel, examining shear strength dependence on vaporization distance, microstructure and residual stresses

01 p0088 A71-10788

Soviet book on boride coatings on iron and steels covering physicochemical interactions and properties

02 p0263 A71-11848

Lunar Module Ag coated stranded Cu wire, analyzing fluorine contamination with proton microprobe

02 p0209 A71-12592

Cr and Mo thin film coatings on Si-Fe, examining effect on plastic deformation and mechanical properties

02 p0266 A71-12655

Niobium aluminide pest, investigating oxidation effects on Nb-Al protective coatings from 600 to 1400 C

02 p0271 A71-12942

Fuel cell electrodes preparation by sputtering thin Ta and Pt layers on porous Vycor

03 p0353 A71-13056

Ti alloys crack initiation by solid Cd coating under tensile stress with intimate contact, noting time and temperature effects

03 p0441 A71-13318

Chromium steel surface diffusion saturation by sublimated Mo, examining process kinetics

03 p0442 A71-13400

Ni coated carbon fibers tensile properties, examining thickness, stress-strain curve, plasticity and grain size

03 p0448 A71-14185

Cu and Ni electroless deposition on carbon fibers for composites

05 p0759 A71-16927

Metal coatings and thin films wetting by soldering materials, emphasizing oxide removal

06 p0903 A71-17426

Cohesive strength of metal coatings obtained by simultaneous vacuum condensation of strengthening phase and matrix material vapors

07 p1130 A71-19157

Electrodeposition of coherent coatings of zirconium diboride from solution of zirconium tetrafluoride and boron oxide in molten eutectic mixture of NaF-KF-LiF

07 p1118 A71-19567

Steel coatings produced by boriding, investigating structure and wear resistance properties

07 p1118 A71-19583

Plated wire storage element for military and aerospace scratch pad, main and mass memories of various speeds

[IEEE PAPER 7.6]

High temperature oxidation of Cr-Ti-Si coatings on Nb alloy

07 p1077 A71-19608

Stainless steel coatings vacuum deposition on Ti alloy plates, considering product cryogenic and mechanical properties

07 p1118 A71-19853

CW GaAs semiconductor laser fabrication by liquid epitaxy, noting Ag plating role in output power

07 p1126 A71-20196

Cohesive strength of flame sprayed metallic coatings of various thicknesses

08 p1297 A71-21064

Fluoride overcoated Al resistance measurements and polarization effects at various angles of incidence, noting utilization in vacuum UV instrumentation

08 p1335 A71-21381

Metallic coating effects on aircraft high strength steel fatigue, considering chromium plating, shot peening and plasma spraying

[NACE PAPER 23]

Martensitic transformation in NiAl oxidation-resistant coatings on Ni superalloys heated for 300 hr at 1093 C

09 p1469 A71-22889

Elastomeric seals for aircraft fastener countersinks, providing corrosion protection to static metal surface treatments and organic coatings

10 p1633 A71-24118

Ti-V alloys electrolytic deposition, discussing electrolyte composition, current density, temperature and coating thickness

10 p1627 A71-24646

Refractory metals coating of various substrates by gaseous phase chemical deposition, discussing diffusion

process theoretical analysis, experimental apparatus and coatings mechanical and physical properties

11 p1768 A71-25391

Superalloy dispersion strengthened and fused slurry silicide coatings for aircraft gas turbine engines and space shuttle heat shields

11 p1778 A71-25555

Boride coated steels and cast iron surfacing with nonconsumable tungsten electrode for higher abrasive wear resistance

12 p1917 A71-27125

Mechanical properties of carbon fibers thinly coated with TiC by chemical vapor deposition from hydrogen, methane and titanium tetrachloride vapor mixture

13 p2092 A71-28627

Metal coated superalloys evaluation for gas turbine engine components, including corrosion, impact and fatigue tests

14 p2256 A71-29635

Microdefects of lattice structure of molybdenum plasma coatings dependent on spray gun nozzle-surface distance

15 p2437 A71-32671

Refractory tungsten boride with iron or nickel for powdery surfacing mixtures, showing hardness and wear resistance dependence on low melting component

15 p2438 A71-32675

Lateral surface heat transfer effect on thermophysical characteristics in thin layer coatings, discussing temperature gradients in corundum and zirconium oxide on copper

17 p2836 A71-34308

Adhesive strength of metal coatings obtained by simultaneous vacuum condensation of strengthening phase and matrix material vapors

17 p2760 A71-35655

High temperature tensile strength of Ta-W-Hf alloy sheet with protective Si-Ti coating in vacuum and air

18 p2933 A71-35951

Thin thermally insulating film on metallic sample, showing vapor layer elimination during liquid nitrogen quenching

18 p2934 A71-36172

Optical properties of metallized fluorinated ethylene propylene Teflon films with various thicknesses, discussing suitability as spacecraft thermal control surface

[ASME PAPER 71-AV-35]

18 p2869 A71-36402

Metallographic examination of inorganic, metal plated and intermetallic coatings on martensitic stainless steels for pitting and surface corrosion prevention

19 p3081 A71-37902

Electric contact resistance of various conductive metal coatings on aluminum corrosion free joints

19 p3031 A71-38449

Ni and Ni-base alloys gaseous carburization by circulation method, investigating gas flow velocity effect on metal diffusive saturation

21 p3389 A71-41165

Boridosilicide and boridoaluminide diffusion coatings on iron and steel, investigating formation kinetics structure and properties

21 p3390 A71-41171

Vacuum contactless metallization of carbon steels, stainless steels and nickel alloys, considering Si, Cr and Al coatings

21 p3390 A71-41172

Heat resistant and refractory materials contact eutectic melting for surface coating production

21 p3390 A71-41175

Chromium and Ni-Cr electrodeposition from amide solvent system, describing water and sulfur ligands effects on plating efficiency

22 p3554 A71-42528

Reflection coefficients measurement for scanning two-mirror interferometer with absorbing Ni film matched to external medium, discussing multilayered coatings

23 p3676 A71-43399

Bimetallic plated high strength steel, noting transition zone effects on mechanical properties

23 p3692 A71-44026

Soviet book on diffusion coatings effects on steel structural elements strength covering cementation, nitriding, sulfidizing, boronizing, siliconizing, chromizing and carburizing processes, etc

23 p3693 A71-44183

Diffusive metal coatings stress-strain state effect on composite Mo material strength, deformation and creep characteristics

23 p3697 A71-44206

Plasma spraying steel coating process, establishing regularity of particle flight velocity variation with distance from burner nozzle

24 p3829 A71-44737

Boron silicide coatings wear resistance in vacuum and air, determining slipping rate and working medium influence on friction process in active surface layers

24 p3830 A71-44859

Plasma metal coating facility, noting antifriction and mechanical properties

24 p3816 A71-44864

METAL COMBUSTION

Magnesium particle combustion in rarefied air at various pressures

01 p0182 A71-11444

Flame temperature and combustion characteristics of model fuel-oxidizer-metal powder systems, using spectral and photometric techniques

03 p0376 A71-13988

Limiting temperature and size conditions for aluminum particle ignition in mixtures of oxygen with argon and nitrogen

03 p0468 A71-13990

Hafnium droplets burning in ultrapure oxygen at various pressures, considering combustion induced natural mode periodic oscillations

[WSS/CI PAPER 70-14]

Zirconium droplet combustion in oxygen-rare gas mixtures, observing transient burning phenomena, oxidation conditions and luminosity-time records

07 p1223 A71-19623

Metal powders hypergolic ignition in gaseous chlorine trifluoride, examining use in air augmented rockets primary combustors

07 p1183 A71-19875

Burning mechanism of condensed ballistite compositions with metallic particles of aluminum, magnesium and ammonium perchlorate

08 p1376 A71-21912

Rocket propellant performance improvement with boron, giving boiling temperature vs pressure and calculation methods for combustion products composition

11 p1809 A71-25573

Metals bulk ignition temperature in oxygen atmospheres, emphasizing preignition surface oxidation effects

14 p2337 A71-30456

Mg and Al particles burning in air, water vapor, Cl and nitrous oxide

14 p2337 A71-30614

Ignition initiation, burning time and particle size distribution determination for dispersed Mg and Al particles in condensed system

14 p2337 A71-30615

Alkali metal, alkaline earth metal nitrates and sodium perchlorate mixed with powdered magnesium burned in rarefied air

14 p2338 A71-30616

Physicochemical properties of powdered Al and Al-Mg-Zn alloy combustion products from chemical, electron microscopic and X ray analysis

14 p2191 A71-30617

Metal particle agglomeration during burning of Al-Mg alloy in ballistite powder, using high speed burning track microphotography

14 p2260 A71-30619

Burning rate of Al particles suspended in polymer propellant gas flow with inorganic oxidizers

14 p2285 A71-30620

Particle size effect on self ignition temperature of powdered Al-Mg alloys

14 p2285 A71-30621

Oxide films effect on metal particles ignition

15 p2511 A71-31378

Amorphous boron powder total burning time in premixed laminar boron-propane-oxygen-nitrogen flames at atmospheric pressure, noting variation as function of oxygen initial partial pressure

15 p2511 A71-31472

Boron combustion characteristics as function of temperature, pressure and gaseous fuel mixture ratio, using color photography

[WSS/CI PAPER 71-19]

Boron particles ignition theory and shock tube experiments, measuring ignition delay as function of temperature, pressure, gas composition and particle size

[WSS/CI PAPER 71-20]

Be droplet burning rate in oxygen-argon mixtures, using laser ignition technique

[WSS/CI PAPER 71-23]

Al particles combustion kinetics in propellant flames, showing gas composition and pressure effects on burning rate

[WSS/CI PAPER 71-24]

Metal particle nonequilibrium effects in mixing and combustion of ducted particle laden flow in air breathing engines

[AIAA PAPER 71-722]

Liquid Zr drops combustion in oxygen-nitrogen atmospheres, examining critical conditions for sac formation with homogeneous bubble nucleation theory

17 p2837 A71-34511

Aluminum particles ignition by focused laser flux in controlled oxygen-Argon environment, observing by cinephotomicrography throughout entire burning time

19 p3169 A71-38114

Al and Mg powder dispersed in solid ammonium perchlorate oxidizer, investigating various combustion mechanics

19 p3120 A71-38120

Photographic study of acceleration and pressure effects on Al agglomerates and combustion processes on solid propellant surface, describing pit growth by combustion model

19 p3120 A71-38121

METAL COMPOUNDS

Soviet book on Mg, Ca, Fe and Sn high temperature borates formation covering optimum synthesis conditions, properties, stability analysis, etc
02 p0208 A71-1800

Soviet book on chemistry of titanium covering intermetallic compounds, hydroxides, dioxide, titanates, halides, sulfates, titanium ores, deposit sites, etc
02 p0209 A71-1847

Refractory metals and carbides and borides, investigating laws governing electrodes erosion during electric spark breakdown
07 p1139 A71-20205

Alkali and rare earth metal hexaborides energetic structure, discussing semiconducting, semimetallic and metallic compounds on basis of energy bands and effective valence
12 p1944 A71-27094

D-transition metal carbides properties based on electron configuration localization model
15 p2429 A71-32138

Rare earth metals di- and sesqui-carbides physical characteristics, establishing changing properties patterns during phase transitions
15 p2461 A71-32153

Hot pressed transition metal carbide samples microhardness measurement, interpreting results in terms of atomic electron configurations
15 p2431 A71-32162

Chemical bonds types in intermetallic, metal-like and nonmetallic compounds, stressing model based on valence electrons configuration localization
16 p2622 A71-33919

Metals and intermetallic chemical compounds, examining heat and oxidation resistance, magnetic and semiconductor properties, superconductivity and electron emissivity
16 p2597 A71-33924

Binary and ternary metal compounds superconductivity parameters comparison, considering crystal structure, valence electron concentration, component position and processing techniques
16 p2622 A71-33925

METAL CORROSION

U CORROSION

METAL CRYSTALS

Fe-Ni martensite crystals microstructure, using Kossel method and electron microscopes
01 p0106 A71-10278

Cr-alloyed Fe powders fine crystalline structure from X ray analysis
01 p0102 A71-10789

Iron single crystal wavy slip pattern of plastic deformation under tension at room temperature, noting relation between yield point and crystal orientation
01 p0105 A71-11621

Soviet book on crystallite boundaries in cast metals and alloys covering solute distribution, lattice imperfections, fracture mechanisms, etc
02 p0263 A71-11845

Electrolytic saw for slicing strain-free metal crystals without damage, noting improved surface flatness
02 p0255 A71-12141

Zinc single crystals plastic deformation and dislocations movement enhancement under pulsating direct current, noting stress peaks-voltage relationship
02 p0296 A71-12297

Transition metal carbides and nitrides, observing metallic and nonmetallic sublattice dynamic characteristics by X ray diffraction
02 p0266 A71-12672

Kinetic, morphological and crystallographic effects of Nb crystals oxidation during growth at various temperatures and pressures
02 p0272 A71-12948

Zn deposition on Zn single crystals in KOH solution, examining time and potential effects on deposit morphology
02 p0210 A71-12956

Strain rate effect on critical shear and cross slip stresses of Al and Al-Mg single crystals, obtaining stacking fault energy
03 p0442 A71-13364

Ultrafine grain metallic structures by solidification, describing various techniques
03 p0446 A71-14488

Powder metallurgy for fine grain metals and alloys, discussing grain size-mechanical properties relationship
03 p0446 A71-14490

Work hardening model for grain size effects on metals flow stress, discussing dislocation density as stress-strain function
03 p0447 A71-14494

Aluminum bicrystals mechanical properties under high strain rates, considering changes in surface structure, active slip planes and dislocation
04 p0612 A71-15077

Ti microcrystals on single crystal tungsten substrate, discussing phase transformations
05 p0768 A71-16854

Structure changes of Al single and polycrystals with initial cube orientation under cold rolling
06 p0913 A71-18420

Uniaxial stress effect on morphology changes of coherent gamma prime precipitates in nickel base superalloy crystals
06 p0914 A71-18682

Lattice defect and grain boundary influence on metal dissolution in electrolyte and stress corrosion cracking
07 p1134 A71-19604

Hydrogen and nitrogen chemisorbed species interactions on 1100/ tungsten crystals, using flash desorption methods
07 p1056 A71-19846

Thermal and electrical transport in tungsten crystal for strong magnetic fields and liquid helium temperatures
08 p1344 A71-21365

Tungsten crystal Fermi surface galvanomagnetic coefficients in scattering process by semiempirical scheme
08 p1344 A71-21366

Bcc metals plastic deformation, discussing active slip systems, stress asymmetry, dislocation dynamics, interstitial and substitutional alloys, defect configurations, etc
08 p1307 A71-21502

Plastic anisotropy in bcc metal crystals, measuring flow strength for various plane strain compression states
08 p1308 A71-21513

Bcc metals slip band formation, investigating deformation and fraction behavior
08 p1308 A71-21515

Segmented slip theory of hardening application to bcc metals, discussing dislocation locking and virtual athermal dislocation model
08 p1308 A71-21516

Superconducting transition effects on metal and alloy single and polycrystals plasticity
08 p1344 A71-21520

Electrochemical polarization effects on Ni single crystals mechanical behavior under tensile deformation
08 p1310 A71-21539

Guinier-Preston zone formation by mixed substitutional-interstitial solute-atom clustering in bcc metals, considering steel strengthening
08 p1311 A71-21541

Radiation-anneal hardening and radiation effects on yield stress temperature dependence in bcc metals
08 p1312 A71-21550

Grain boundary sliding and shear deformation in bcc metal Al and Al-Co solid solutions
08 p1345 A71-21576

High purity Ge crystals growth, studying Hall effect and resistivity for semiconductor detector fabrication
08 p1345 A71-21841

Nonelastic unloading microstrains in Cu crystals after stage II macroscopic prestraining, discussing stresses action on dislocations
09 p1468 A71-22700

Contact potential measurements of work function dependence on adsorption of alkali metals on Ta(110) and W(100) crystals under ultrahigh vacuum
09 p1497 A71-22701

Sudden thermionic emission in surface ionization at near threshold temperatures of cesium activated tungsten single crystals
09 p1494 A71-22879

Electron microscope investigation of packing defect energy effect on structure of crystal dislocations in hardened metals during annealing and deformation
09 p1473 A71-23226

Deformed Mo single crystals, noting polygonization processes relation to recrystallization during annealing
09 p1476 A71-23318

Cut metal crystal orientation planes and dislocation structure determination, using Bragg reflection of monochromatic X ray beam
09 p1452 A71-23319

Crystal lattice type influence on volume and boundary diffusion mobility of iron group metals atoms
09 p1510 A71-23325

Elastic ultrasonic vibrations effects on metals and alloys microstructure and elastic and nonelastic properties
09 p1477 A71-23326

Strain effect on ultrasound damping in single W crystals, considering microhardness
09 p1477 A71-23328

Metals crystallization in ultrasonic field, investigating structural change as function of energy and impedance factors and cavitation effects in fine grain formation
10 p1626 A71-24136

Eighteen layer hexagonal ferrite magnetic properties in various fields and temperatures, noting magnetization and crystal structure
12 p1943 A71-26862

Coarse grain Al sheet deformation, determining dislocations distribution with etching defects method
12 p1919 A71-27691

Polycrystalline pure Al and Al-Mg alloy strength, investigating temperature and strain rate effects
13 p2084 A71-28112

Temperature dependent diffusion coefficient of yttrium in refractory metal single crystals of Mo, W, Nb and Ta, using radiometric analysis
14 p2258 A71-30005

Structural disorientation dependent recrystallization of cold rolled and annealed Mo single crystals
14 p2258 A71-30006

Absorbed energy spectra and absorption frequencies from elastic constants of vibrating metals with cubic lattice structure, using cold neutron scattering
14 p2190 A71-30149

Stable eta phase precipitation at dislocations in Al-Zn alloy, using X ray diffraction and electron microscopy
14 p2260 A71-30477

Boron solubility in molybdenum, showing grain size decrease, plastic deformation change and elongation
15 p2425 A71-31399

Binding states, adsorbate densities and desorption kinetics of hydrogen on crystal planes of tungsten
15 p2367 A71-31676

Stress-microstrain relationship for metal crystals prestrained in easy glide, obtaining mobile inelastic dislocation density and internal stress
16 p2654 A71-33102

Anodic dissolution of aluminum bicrystals in electrolytes containing perchloric acid during electropolishing, showing anisotropic layer existence
16 p2592 A71-33371

Polyhedral Nb single crystals production from niobium pentachloride and hydrogen reaction, determining growth rate
16 p2594 A71-33877

Oriented Mo single crystals substructure during growth, showing crystallographic orientation
16 p2595 A71-33879

Tungsten single crystals under deuteron bombardment, noting structural defects formation as function of irradiation energy
16 p2595 A71-33883

Addition effects on polygonization of deformed single crystals of Mo and W with Re, using X ray analysis
16 p2596 A71-33887

Yield point thermal component in bcc metals at low temperatures as function of hydrostatic compression, noting interionic reaction potential nonspphericity
16 p2596 A71-33889

Thermal polymorphous metals and alloys crystal structure, discussing plastic deformation due to formation of cubic lattice and metallic bonds
16 p2597 A71-33915

Fractographic investigation of fatigue crack propagation in pure monocrystalline and polycrystalline Al
16 p2599 A71-34095

Statistical microstructural analysis for nucleation and growth kinetics of recrystallization nuclei of metal single crystals
17 p2755 A71-34414

Al and Mg alloys mechanical and crystal microstructural changes under low temperature conditions, optimizing casting component ratios
17 p2760 A71-35464

High rate quasi-static dynamic pressure deformation hardening of magnesium single crystals
18 p2934 A71-35990

Critical growth work hardening germination and recrystallization of oriented compression deformed Nb, Mo and W refractory cubic centered crystals
18 p2935 A71-36200

Ni-Mo single crystals under isothermal aging, observing long range order parameter, domain size and microstrains
19 p3077 A71-37411

Interstitial solute thermomigration of C in Ti, V, Fe, Co, Ni and Pd, using radioactive tracer technique
19 p3079 A71-37710

Electrical resistivity of structural metal crystal defects in terms of Ziman-Harrison pseudopotential theory
21 p3395 A71-40023

Metallic polycrystal deformation equations, obtaining creep, Norton law dependences and thermally dissipated energy
22 p3560 A71-41606

LEED studies of oxygen adsorption on 111/ and 110/ surfaces of Al single crystals
22 p3561 A71-41730

Tungsten and molybdenum oxide crystals shape and size during annealing in various gas atmospheres and vacuum conditions
23 p3690 A71-43255

Zone refined Fe crystals under room temperature compression, examining lattice defects with X ray synergy method
23 p3695 A71-44287

Microalloying effects on phase composition, surface phenomena, fine crystalline structure and microstructure of E1417L steel
24 p3836 A71-44374

Crystal Al powder electrolytic production in inert atmosphere, discussing fractional composition, current efficiency, gravimetric density and particle morphology
24 p3837 A71-44734

Semiconductor applications of alpha SiC single crystals, showing mechanical separation of polytypes from druses

24 p3841 A71-44742

Elastoplastic deformation of Zn single crystals under uniaxial tensile loads, noting critical stresses relationship to current pulses

24 p3838 A71-45100

Pressure effects on Fermi surface of metals, examining crystal lattice parameters influence on electrons energy spectrum

24 p3839 A71-45168

Surface segregation, adhesion and friction of monocrystalline Cu-Al, Cu-Sn and Fe-Al alloys from Auger emission spectroscopy and low energy electron diffraction experiments [ASLE PREPRINT 71LC-5]

24 p3839 A71-45287

Diffusion acceleration in bcc Ti due to imperfections of fine structure created during polymorphous transformation

24 p3840 A71-45379

METAL CUTTING

Ni and Ti cutting, examining wear for various microcutter refractory materials

05 p0759 A71-16862

Metal cutting on lathes, discussing machining conditions optimization based on productivity and cost criteria and linear programming solution

07 p1117 A71-19367

Rectangular, square and circular cross section blanks dynamic metal cutting process by method of characteristics

08 p1295 A71-20794

High temperature blank heating and cutting during magnetic alloy machining for optimal cutter stability

08 p1296 A71-20844

High melting compound tools wear resistance during Ti and Ni continuous microcutting

08 p1297 A71-21065

Plasma flame temperature and flow characteristics in plasma jet transfer-type metal cutters from spectroscopic measurement and high speed streak camera photography

09 p1454 A71-23032

Cut metal crystal orientation planes and dislocation structure determination, using Bragg reflection of monochromatic X ray beam

09 p1452 A71-23319

German monograph on hot machining of high temperature steels by flame heating with propane-oxygen and plasma arc burners

14 p2252 A71-30232

Cutting angle effect on service life of broaching tools for Ti alloys annealed forgings, using high-speed P18 tool steel

14 p2259 A71-30271

Aluminum-boron composite forming and cutting processes covering milling, grinding, abrasive cutoff, drilling, piercing, electrodischarge machining, blanking, punching and shearing

18 p2928 A71-36666

METAL DRAWING

Inductor winding dependent magnetic pulse deformation of cylindrical blanks allowing for mutual electromagnetic and mechanical coupling

15 p2417 A71-32525

METAL FATIGUE

High fatigue resistance in metals and alloys - Conference, Atlantic City, July 1969

01 p0098 A71-10161

Metal fatigue relationship to cyclic plastic deformation resistance, considering fracture behavior, stress-strain curve, hardening and ductility

01 p0098 A71-10162

High metal fatigue resistance obtained via metallurgical means, discussing plastic deformation, crack initiation and propagation mechanisms, etc

01 p0099 A71-10165

Mechanical properties effect on steels fatigue crack growth rate as function of stress intensity factor

01 p0099 A71-10167

Discrete coatings, surface diffusion and thermomechanical surface treatments for metal fatigue strengthening

01 p0099 A71-10169

High compressive residual stress and high hardness for long life fatigue strength in nonrotating bending of notched machine parts

01 p0167 A71-10171

Fatigue effects on metallic materials elastoviscoplasticity properties

01 p0175 A71-11025

Al fatigue testing by cyclic uniaxial tensile load, examining deformation, internal friction ductility and plastic strain

02 p0262 A71-11683

Metal fatigue research, examining crack initiation and propagation mechanism, stress-strain relationship and statistical nature

02 p0325 A71-12074

Si-Fe fatigue crack growth in vacuum at various temperatures, discussing stress intensity, cleavage and ductility effects

02 p0267 A71-12882

Ni base superalloy single crystal fatigue crack propagation

02 p0268 A71-12886

Ti-Al-V hydrogen induced fatigue crack growth at room temperature under sustained load

02 p0268 A71-12891

High stress cycles and impact fatigue behavior of common case hardened carburized gear steels under loading

03 p0441 A71-13253

Accelerated creep rupture tests on metals and solder alloys, comparing constant stretch rate and load methods [SESA PAPER 1672]

03 p0508 A71-13762

Pinned steel lug joints fretting fatigue, examining cumulative damage under constant amplitude and narrow band random loading

03 p0513 A71-14244

Grain size effects on metal fatigue, considering work hardening and crack initiation and propagation

03 p0447 A71-14495

Intergranular failure modes in polycrystalline metals and alloys, discussing boundary sliding, cracking and structure

03 p0447 A71-14496

Brittle fracture resistance of mild steel after low cycle fatigue damage

03 p0516 A71-14579

Metal fatigue crack initiation and propagation by continuum mechanics approach, considering dislocation, stress and deformation conditions and load cycle effects

04 p0666 A71-14888

Central hole effect on flat metal sheet fatigue under tension-compression load cycles, noting application to aircraft materials

04 p0670 A71-15389

Energy dissipation patterns of metal fatigue failure during static and cyclic loading applied to untreated and heat treated steel samples

04 p0671 A71-15637

Energy dissipation during torsional and flexural vibrations of steel and duralumin specimens subjected to plastic deformation, accounting for discrepancies due to methodical errors

04 p0671 A71-15640

Shock pulse measurements for detecting damage to ball and roller bearings due to fatigue

04 p0604 A71-15673

Residual and mean stresses effects on fatigue strength of specimens with longitudinal nonload-carrying fillet welds

04 p0613 A71-15763

Damage and fracture mechanisms in high temperature low cycle fatigue of cast nickel-based superalloys, noting grain boundaries oxidation role in crack nucleation and propagation

04 p0615 A71-15789

Fatigue crack propagation in aluminum alloy sheet, determining relationship between propagation rate and stress intensity factor and crack initiation conditions

05 p0766 A71-16296

Subgrain volume and orientation effects at tip of fatigue crack on propagation rate

05 p0821 A71-16348

Aircraft light alloys fatigue characteristics for component endurance evaluation

05 p0767 A71-16757

Soviet book on machinability of titanium alloys covering microstructure, physical properties, surface finish and fatigue properties, tooling for industrial machining operations, etc

06 p0903 A71-17444

Metal endurance dependence on simultaneous oxygen corrosion and cyclic loading frequency at various temperatures and pressures

06 p1000 A71-17934

Duraluminum with anodic film, examining fatigue and corrosion-fatigue rupture

06 p0911 A71-17935

Differential equations derivation for metal fatigue point defect colonies concentration changes, discussing diffusion and dislocation interactions

06 p1002 A71-18418

Crystal dislocations and vacancy colonies complexes generation, discussing metal fatigue microcracks mechanism

06 p1002 A71-18419

Refractory alloys fatigue cracks kinetics based on endurance characteristics reflecting resistance to variable loads

07 p1129 A71-19153

Physical analogy treating low cycle metal fatigue relation to stress growth in plastic region, discussing cracking mechanisms

07 p1211 A71-19166

Vibration tumbling duration effects on surface quality, fatigue strength and damping properties of titanium alloy structural parts

07 p1130 A71-19169

Steel under cyclic loads, observing relationship between changes in microstructure and temperature curve shape in fatigue failure process

07 p1211 A71-19194

Ni base superalloys fatigue behavior, emphasizing role of ordered gamma prime precipitate in two phase materials

07 p1133 A71-19447

Austenitic stainless steel dislocation structures during fatigue deformation under cyclic loading, observing slip lines and lattice strain morphology

07 p1136 A71-19699

Electronic recording of cyclic strain diagrams of metals in wide loading frequency range using dynamic hysteresis method

07 p1218 A71-20485

Axial compressor blades surface finish and fatigue strength restoration by vibrational tumbling

08 p1295 A71-20843

Energy dissipation-fatigue strength relationships during vibrations for prestrained metals and alloys

08 p1369 A71-21118

Ni maraging steel fatigue properties in relation to Ti and Al content

08 p1312 A71-21553

Precipitation hardened Ni base superalloys fatigue deformation, investigating correlation between metal-lurgical structure characteristics and high-cycle fatigue behavior

08 p1314 A71-21570

Ductile metals fatigue crack propagation model applications to brittle metals, discussing crack initiation effects on high strength steels failure modes

09 p1467 A71-22285

Six position machine for fatigue testing in corrosive medium of circular rotating metal specimen with cantilever bending

09 p1426 A71-22327

Thermal fatigue tests of high temperature Ni and Co base alloys by fluidized bed technique

09 p1469 A71-22812

Metallic coating effects on aircraft high strength steel fatigue, considering chromium plating, shot peening and plasma spraying [NACE PAPER 23]

09 p1469 A71-22889

Al alloys HF accelerated fatigue testing, using magnetostrictive transducer excited mechanical resonance and electronic circuitry

09 p1428 A71-22939

Fatigue life and crack propagation of sheet, plate, extrusions and forgings in annealed and solution treated aged Ti-Al-V-Sn alloy [ASM PAPER W71-22.5]

09 p1471 A71-23096

Aerodynamic heating effects on fatigue and creep properties of supersonic aircraft alloys at high temperatures, considering deformation mechanisms interaction

09 p1472 A71-23204

Ti alloys in aircraft industry, considering jet engines applications and structural stability improvements related to fracture toughness, fatigue and stress corrosion

09 p1474 A71-23292

Strain hardening and grain size effects on early fatigue damage of polycrystalline metal under fluctuating stress, using micromechanics theory

10 p1685 A71-23933

Thermal fatigue and service life of thin walled tubular pearlite steel notched specimens in various oxidizing media

10 p1626 A71-24191

Kinetic crack propagation theory of fatigue fracture toughness for notched and unnotched asformed high strength and heat treated ball bearing steels

10 p1687 A71-24307

Multiplication, diffusion and vanishing of dislocations, slip band formation mechanism and lattice defects interactions during metal fatigue

10 p1626 A71-24386

Prior deformation and subsequent annealing influence on fatigue response of coarse grained alpha Ti, evaluating relative effects of dislocation locking and mechanical twinning

10 p1626 A71-24445

Al alloys one step fatigue tests under combined high temperature and structural vibration conditions

10 p1628 A71-24821

Fatigue crack propagation rates in Al under constant low stress, discussing data processing methods

10 p1629 A71-25053

Al alloy and carbon steel low cycle fatigue and fracture surface topography transition from static dimple to striation type by electron fractography

11 p1777 A71-25266

Metals mechanical properties under vacuum conditions, discussing alternate bending tests of Cu and Al specimens under range of oxygen pressures

11 p1777 A71-25389

Ti hot salt stress corrosion, considering effects of oxygen, air velocity, moisture, thermal cycling, fatigue and type of salt

11 p1781 A71-26261

Fractographic analysis of failure kinetics and crack formation in Al alloys, showing microfatigue intrusions and extrusions for various initial stress levels

12 p1919 A71-27682

Fatigue corrosion resistance of duraluminum anodized at various temperatures

13 p2082 A71-27823

Fatigue crack growth rate in plates of anisotropic materials, considering Al and Ti alloys under cyclic loads

13 p2082 A71-27826

Refractory and structural steels and Al alloys, obtaining low cyclic plastic deformation and breaking stress curves

13 p2148 A71-28116

Temperature variations of effective fracture surface energy of metals and alloys and relation to crack growth in high temperature creep

13 p2085 A71-28505

High strength steel delayed fracture, applying Yokobori stochastic-kinetic theory of fatigue crack propagation for time to fracture calculation

13 p2155 A71-28790

Notch effect on ductile fracture, considering plastic stress and strain concentration in stainless steel, brass, copper and mild steel

13 p2088 A71-29343

Stage 1 fatigue fracture mechanism in Ni-based superalloy single crystals, observing air and vacuum effects

13 p2088 A71-29405

Thermally activated plastic deformation of metals at low temperatures, determining stress flow, creep properties and upper yield limit

14 p2258 A71-30007

Notched age hardening Al alloys sheets, obtaining fatigue damage test data and S-N curves

14 p2326 A71-30067

Accelerated semiempirical method determining metallurgical processing techniques effects on steel and titanium alloy compressor blades fatigue life, comparing results with experimental data

14 p2252 A71-30269

Vibration fatigue of metallic materials in vacuum and different gas atmospheres, considering fcc metals, Al alloys and steels

[DFVLR-SONDRER-62] 14 p2259 A71-30466

Fretting fatigue test apparatus with load monitoring as function of cycles for relating quantitatively damage to life

14 p2248 A71-30883

Ti-Al-V alloy forgings fatigue strength improvements, discussing surface finish, heat treatments and alpha and beta grain size

[AHS PREPRINT 553] 14 p2261 A71-31105

Deformation work for strained copper during tensile testing until fracture as function of slenderness in neck

15 p2427 A71-31700

Fatigue crack propagation anisotropy in hot rolled steel plate, demonstrating crack growth rate sensitivity to microconstituents orientation

15 p2508 A71-32255

Thermomechanical damage by pulsed lasers in metals, discussing energy deposition and stress wave generation for optimal fracture conditions

15 p2422 A71-32555

Grain size effect on fatigue life during tension and compression tests of alpha brass, copper and aluminum, considering slip character

15 p2437 A71-32578

Magnetic field perturbation and electric current injection techniques for characterizing high strength alloys fatigue microcracks

16 p2581 A71-32865

Stress corrosion fatigue crack growth in Ni-Cr-Mo maraging steel, using controlled-potential techniques, pH measurements and fractographic analysis

16 p2590 A71-32942

Stress intensity history effect on metal fatigue crack growth rate, using closed loop hydraulic testing machine with stepwise increments in sinusoidal tension-tension load cycles

16 p2591 A71-32948

Flight mission severity in cumulative damage/low cycle fatigue and creep stress rupture/ not detected by usual nondestructive testing in aircraft gas turbine industry

16 p2624 A71-33298

Aircraft structures fatigue properties, discussing stresses, life estimates, safety factors and descriptive curves

16 p2656 A71-33343

Fatigue S-N curves discontinuities associated with plastic yield and crack path tested on mild steel notched specimens

16 p2591 A71-33346

Fatigue limits of Ti alloy by Wohler and Locati loading methods

16 p2592 A71-33406

Crack propagation resistance-cyclic fracture strength relation for austenitic and Mn-Cr-V steels, considering thermomechanical working effects

16 p2592 A71-33408

Surface effects of transverse slip screw dislocations in metal fatigue crack nucleation, relating stacking fault energy and number of cycles to failure

16 p2593 A71-33681

Flexural-torsional fatigue fracture of duraluminum, noting dependence on cyclic stress, frequency and medium

16 p2593 A71-33689

Thermostable and heat resistant steels and alloys vibration loading frequency effects on fatigue at high temperatures

16 p2598 A71-33992

Neuber elastoplastic analysis of residual notch stresses for improved cumulative damage predictions applied to aluminum alloy under overload

[AIAA PAPER 71-776] 16 p2659 A71-34012

Fractographic investigation of fatigue crack propagation in pure monocrystalline and polycrystalline Al

16 p2599 A71-34095

Fatigue crack propagation model for explosion bonded titanium-steel system under constant load amplitude conditions

16 p2600 A71-34096

Room temperature ultrasonic frequency fatigue behavior of Ni-base superalloy single crystals

17 p2756 A71-34493

Environmental effects on SST structural materials fatigue, discussing Ti alloys studies involving temperature effects, crack propagation and residual strength

17 p2821 A71-34556

Fatigue crack propagation dependence on strain energy release rate and crack opening displacement, analyzing data on high yield strength steels, Ti and Al alloys

17 p2826 A71-35152

Fatigue crack propagation in Al alloy panels stiffened with bolted and integral stringers, determining stress intensity factor/crack growth rate relationship

17 p2827 A71-35156

Metal fatigue crack failure prediction for arbitrary uniaxial cyclic loading, discussing method based on treatment of crack growth as continuous stochastic process

17 p2758 A71-35158

Al alloy sheet fatigue crack closure under cyclic tensile loading, deriving expression for crack propagation rate in terms of effective stress amplitude

17 p2828 A71-35162

Light alloys fatigue characteristics for aircraft components endurance evaluation

17 p2759 A71-35456

Refractory alloys fatigue cracks formation kinetics based on endurance characteristics during symmetrical and asymmetrical load cycles

17 p2760 A71-35652

Physical analogy treating low cycle metal fatigue relation to stress growth in plastic region, discussing cracking mechanisms

17 p2834 A71-35662

Vibrotumbling duration effects on surface quality, fatigue resistance and damping properties of titanium alloy structural parts

17 p2760 A71-35665

Environment and frequency effects on fatigue properties of age hardening Al-Cu-Mg alloy

18 p2933 A71-35876

Notch effect on metallographic characteristics of fatigue crack initiation and propagation in Al-Mg alloy

18 p2933 A71-35877

Structural steels fatigue resistance, investigating processing technique, chemical composition, plastic and hot working and heat treatment effects

18 p2934 A71-36149

Metal structure, crack nucleation and propagation during fatigue under cyclic stress

18 p2936 A71-36693

Stochastic character of metal fatigue fracture and fatigue life dependence on stress cycle amplitude, using equiprobability curves

18 p2936 A71-36694

Deformation kinetics and failure of high melting Nb and Mo base alloys in plastic state under low cyclic fatigue

18 p2936 A71-36710

Fatigue crack propagation in thin aluminum plates under fluctuating tensile loads, concerning Forman model

18 p2938 A71-36851

Cavitation damage in water to unalloyed metals and Ni superalloy, using ultrasonic vibratory testing with magnetostrictive transducer

19 p3081 A71-37904

Copper single crystals fatigue as statistical work hardening phenomenon

19 p3081 A71-38072

Ni-Mo-V, Ni-Cr-Mo-V and Cr-Mo-V high strength rotor forging steels fatigue crack growth characteristics tests at room temperature

20 p3247 A71-38768

Fatigue crack propagation in high yield strength steels at room temperature in air environments, considering primary influence of applied stress intensity range

20 p3248 A71-38769

Corrosion fatigue crack propagation in Ni-Cr-Mo maraging steel in room temperature NaCl solution at various stress intensity ranges

20 p3248 A71-38778

Tensile, impact and fatigue properties of welded Ti alloys, determining joint quality and friction welding sensitivity in highly stressed gas turbine components

21 p3387 A71-40619

Vacancy absorption model for fatigue crack propagation in Al based on X ray inspection and transmission electron microscopy

21 p3399 A71-40698

Statistical analysis of endurance limits for castings and forgings of die forged and cast steel, using rotating beam fatigue tests

21 p3388 A71-40754

Temperature effect on fatigue strength of Ni steel by tension-compression fatigue test at low temperatures

21 p3400 A71-40832

Dislocation structures in austenitic steel fatigued at various stress cycles and tensioned at various strains, using transmission electron microscopy

21 p3400 A71-40833

Carbon and stainless steels chemical composition effects on diffusion layer structure and fatigue strength after diffusive boriding

21 p3403 A71-41162

Steels fatigue behavior and cumulative damage effect prediction under strain controlled conditions, comparing with experimental data

22 p3559 A71-41593

Fracture mechanics analysis of metal fatigue crack growth as function of stress intensity factor

22 p3560 A71-41641

Thick Al alloy sheet with central slot under cyclic loads, examining striation spacings and fatigue crack propagation rates with electron fractography

22 p3561 A71-41708

Fracture mode transition under varied mean stress levels in metal fatigue at constant crack growth rate

22 p3561 A71-41711

Microhardness and magnetic permeability and viscosity changes during fatigue loading of steel parts, describing electromagnetic fatigue testing method

22 p3554 A71-41771

Hold time effects on plastic deformation and fracture in high temperature low cycle metal fatigue

22 p3561 A71-41942

Fatigue, necked-out and intermediate fracture types observation in load-controlled low-cycle fatigue tests of rolled steel

22 p3617 A71-42496

Pure Al annealed polycrystal electron microscopic observation for fatigue deformation at room and elevated temperatures, noting dislocation loop role in crack initiation and propagation

22 p3564 A71-42497

Asymmetrical metal fatigue cracks development under infrequent compression cycles alternating with fundamental cycles of tension

23 p3774 A71-42896

Temperature effects on fatigue response and tensile properties of coarse grained alpha Ti containing 0.085 wt pct oxygen

23 p3688 A71-42924

Explosive peening effects on weld fatigue in Ni maraging steel, Fortiwell and Al-Zn-Mg alloy

23 p3682 A71-43877

Duralumin fatigue process in air and corrosive medium, showing loading frequency and time dependence effects

23 p3692 A71-44027

Gas turbine blades of cast Zr56K heat resistant alloy, investigating structural strength from fatigue test data

23 p3779 A71-44208

Gas turbine blade models of heat resistant Zr56K alloy under operational temperature variations, observing fatigue strength

23 p3779 A71-44209

Failure and crack formation in gas turbine engine compressor disks under variable stresses from fatigue tests, considering safety factors

23 p3779 A71-44210

Solid powder metallurgy tungsten alloys, determining scale factor effect on bending strength and fatigue limit

23 p3693 A71-44226

Fatigue strength of two phase Ti alloys, considering work hardening, electrochemical finishing, electropolishing and protective media

23 p3694 A71-44232

Heat resistant Zr56K alloy precision and ground cast specimens, determining short and long term strength and fatigue

23 p3780 A71-44236

High cycle fatigue resistance improvement of age hardened Al-Zn-Mg-Cu alloys through thermomechanical treatments

23 p3695 A71-44290

Fatigue lifetime of overlapping joint spot welds of Al alloys, investigating shrinkage crack initiation and propagation

24 p3830 A71-44786

Prestraining effect on D16 duraluminum corrosion fatigue and tensile strengths

24 p3838 A71-44856

Metal fatigue strength evaluation for nonstationary loading and complex stress-amplitude variation

24 p3886 A71-45364

METAL FILMS

- Solid metal lubricant films bonding by ion plating using diode method, noting interface type and structure examination by electron microscopy
01 p0087 A71-10483
- Electrical resistivity and structure of thin films of W, Mo and Cr evaporated in vacuum by neodymium laser
01 p0101 A71-10674
- Metallized capacitors types and properties, considering extra thin dielectric films and high field strength
02 p0230 A71-11817
- Vacuum deposited Bi thin films on glass substrates at liquid He temperature, investigating characteristics of critical thickness
03 p0466 A71-13291
- Chemisorption layer kinetics of oxygen on thin Ta films at room temperature and low pressures
03 p0441 A71-13359
- Chemisorption and sticking probability of nitrogen on Ta films, considering relationship to temperature and pressure
03 p0441 A71-13360
- Chemisorption rate and physical adsorption of nitrogen on Ta films as function of temperature
03 p0441 A71-13361
- Calorimetric measurements determining total hemispheric emittance of thin gold films as function of temperature, demonstrating film thickness effect
[AIAA PAPER 70-63] 03 p0522 A71-14456
- Ultrahigh vacuum deposited Ni, Fe, W and Mo films, determining molecular oxygen adsorption efficiencies
04 p0636 A71-15015
- Thin metallic films thermal radiation properties at cryogenic temperatures, calculating spectral normal emissivity as temperature wavelength and thickness function
04 p0684 A71-15510
- Vacuum deposited Mo and Ru films optical properties, emphasizing reflectance measurements
04 p0627 A71-15693
- Ni-Fe alloy films composition gradients produced by W boats evaporation, noting vapor pressures effect
05 p0791 A71-16230
- Superconducting niobium aluminide and niobium aluminide-Ge films formation on Nb substrate
05 p0792 A71-16238
- Acoustic and surface plasma waves in superconducting semiconductor metal films and laminates
05 p0793 A71-16826
- Al-Mg alloy oxide film morphology and composition under various oxidation conditions, using electron microscopy and diffraction
05 p0770 A71-17100
- Holographic lens used with pulsed ruby laser for machining single and multiple spots on Ti thin film on glass
07 p1122 A71-19205
- Al alloy rapidly crystallized film structure, studying atomic diffusion mobility effects on formation of supersaturated solid solutions
07 p1130 A71-19299
- Metal film resistors rapid evaluation method including thermal, load and shock tests devised by British electronic component manufacturers
07 p1076 A71-19553
- Fcc metals film growth on air- and vacuum-cleaved PbS, using electron diffraction and conventional electron microscopy
07 p1178 A71-19848
- Be films evaporated in vacuum on W single crystals, investigating adsorption and electron emission by field emission microscopy
07 p1178 A71-19918
- Thin uniaxial ferromagnetic metal films blocking curve verification using rotational hysteresis and transverse susceptibility measurements
07 p1180 A71-20171
- Vacuum deposited Cr film formation as function of condensation rate
09 p1469 A71-22847
- Radar backscattering from thin metallic conductive films, giving results for Al and Ni from anechoic chamber measurements
09 p1410 A71-23517
- Thermomagnetic modulated Kerr effect readout and magneto-optical laser recording at high output on cobalt base metallic films
10 p1613 A71-25108
- Reflecting Au films deposition on glass substrates by evaporation in vacuo, discussing optical devices, reproduction and bonding improvements
11 p1809 A71-26431
- Polycrystalline copper and magnetic films thin intermediate layers, showing prevention of epitaxial growth
12 p1943 A71-26855
- Nickel alloys crystallization at superhigh cooling rates by dropping liquid metals on rotating copper cylinders to obtain films
12 p1917 A71-27301

- Thin film compound Au-Al intermetallic structure of CsCl type with lattice period of 3.140 plus or minus 0.003 Å from electronographic measurement
12 p1917 A71-27308
- Copper wire laser welding to film on Cr substrate exhibiting nonhomogeneous columnar structure and recrystallization
12 p1912 A71-27779
- Metal and alloys condensates corrosion tests based on recording changes in electrical resistance
15 p2427 A71-31651
- Gas-solid interaction by shock tube method, determining thickness and thermal accommodation effects on thin metal film resistance thermometer response
16 p2576 A71-32922
- Sputtered tantalum films oxygen content determination by anodization current efficiency measurements
16 p2621 A71-33187
- Strain analysis based on thin metallic film optical measurements, determining principal strain directions from wrinkle and microfracture patterns
[SESA PAPER 1828A] 17 p2820 A71-34551
- Thickness monitoring technique for thin films, using silicon solar cell mounted adjacent to substrate with iron deposition
18 p2922 A71-36591
- Vacuum deposited thin Cr films on glass substrate, describing hydrogen adsorption effects
19 p3076 A71-37116
- Vacuum deposited thin Cr films on glass, investigating substrate temperature and inert gas pressure effects on texture
19 p3076 A71-37117
- High quality continuous tone micromachining and image recording on metal thin films by low power pulsed gas laser heating
19 p3071 A71-37213
- Specific contact resistance at zero bias as measure of ohmic or rectifying behavior of metal-semiconductor barrier under operating conditions
19 p3117 A71-37485
- Machining integrated circuit metal film masks with continuously operating carbon dioxide laser and high pressure pulsed He-Ne laser
19 p3069 A71-38234
- Failure prediction for metal film semiconductor contacts on silicon substrate by electromigration, considering current density and temperature gradients
19 p3119 A71-38510
- Mass transport at high current densities in Al and Mo thin film conducting stripes, noting effect on IC life
19 p3119 A71-38511
- Failure analysis of vacuum deposited Al film interconnections at contact windows, considering grain size effect and reliability improvement techniques
19 p3119 A71-38512
- Thin gold films strain distribution determination from X ray diffraction peaks, noting elasticity theory
20 p3276 A71-39012
- Ga spreading over Ag and Au thin films surfaces from electronographic and optical experiments, noting volume heterodiffusion
20 p3276 A71-39153
- Evaporated Permalloy films deposition temperature measurement by vacuum evaporated Chromel-constantan thin film thermocouple, noting temperature difference between film and glass substrate
21 p3384 A71-40220
- Epitaxial metal film formation on Al-Ni fibers in Al matrix during electropolishing
21 p3387 A71-40456
- Copper wire laser welding to film on Cr substrate, exhibiting nonhomogeneous columnar structure and recrystallization
21 p3389 A71-41104
- Optical investigation of metal-semiconductor interface blocking layer and photo-Hall effect in high resistivity crystals
21 p3433 A71-41316
- Thin bismuth films thermal and electrical conductivities and thermoelectric power measurements, examining preparation methods
21 p3435 A71-41338
- Metal film ohmic contacts to n-type GaP devices operating at high ambient temperatures
22 p3520 A71-41687
- Low temperature proton irradiation damage and recovery in discontinuous Ta films sputtered in oxygen and nitrogen
22 p3585 A71-41804
- Experimental observation of 10.6 micron guided waves in Ge thin films, noting application to carbon dioxide laser communication
22 p3587 A71-42568
- Thin nickel films elastoresistance properties, examining magnetic state effects
23 p3691 A71-43361
- Reflection coefficients measurement for scanning two-mirror interferometer with absorbing Ni film matched to external medium, discussing multilayered coatings
23 p3676 A71-43399

- Critical current of ideally homogeneous second class superconducting film, noting lattice resistance to small displacements
23 p3715 A71-43414
- Ni-Fe film exposure to continuous IR laser light for laser radiation structure
23 p3686 A71-44056
- Niobium carbide film formation in pseudoliquidified layer on graphite at 3000 C in argon metal vapor mixtures with/without hydrogen
23 p3696 A71-44317
- W and Mo thin films phase diagrams, determining surface energies and heats for transformations
24 p3860 A71-44718
- Surface oxide, organic and lead film effects on friction and plastic deformation of Zn single crystal during sliding
24 p3839 A71-45288
- Quartz crystal mass monitor study of monolayer oxygen adsorption on Al films, noting surface roughness variation with deposition temperature
24 p3803 A71-45348
- ### METAL FINISHING
- #### NT ELECTROPOLISHING
- #### NT PEENING
- Metal microfinishing technique, evaluating surface integrity degrading effects and total time requirements
05 p0759 A71-16464
- Metal finishing tests on bronze in presence and absence of surface active agents, considering abrasive working
13 p2072 A71-27816
- Metal removal rate optimization in electrodischarge machining process, considering governing parameters of relaxation circuit
13 p2075 A71-28947
- Photochemical machining applied to thin complex flat metal parts manufacture, discussing tooling, prototype, production costs and dimensional requirements
[SME PAPER MR-71-813] 15 p2416 A71-32430
- Fatigue strength of two phase Ti alloys, considering work hardening, electrochemical finishing, electropolishing and protective media
23 p3694 A71-44232
- ### METAL FOILS
- Magnetoelectric anisotropy and low temperature annealing effects on coercive force of ferromagnetic Fe-Ni foils
01 p0138 A71-10669
- Solar wind elemental and isotopic He and Ne compositions from mass spectrometry of ions collected in metal foils deployed during Apollo 11 and 12 landings
01 p0146 A71-11886
- Multilayer composites preparation by cold rolling packets of alternating Al and Sn foils, determining tensile strength relation to layer thickness
02 p0264 A71-12278
- Thin web shear test device demonstrated on aluminum foil and glass fiber composites
03 p0508 A71-13765
- Subnanosecond laser pulses interaction with thin Ni foil targets leading to energetic pulsed plasma beam production
04 p0608 A71-15134
- Ti-Al-V foils by electron beam vapor deposition, discussing metallurgical characteristics
05 p0765 A71-16237
- Oscillatory magnetic field superimposition effects on flux flow properties of superconducting metal foils
07 p1177 A71-19596
- Composite plastic aircraft structures lightning protection, considering hazard to composite materials and use of metal filled or plasma sprayed coatings and metal foil coverings
07 p1021 A71-19943
- Methanol stress corrosion cracking of Ti-Al-V foil inhibited by pretreatment in aqueous solutions of electrolytes, discussing colloidal character of microcrystallites
07 p1142 A71-20362
- Be, V, Cu and Al foils low temperature integral radiant emission, describing calorimetric assembly
09 p1466 A71-22264
- Beta Ti alloy sheet and foil mechanical property tests, honeycomb core fabrication, forming and welding evaluations
[ASM PAPER W71-23.1] 09 p1455 A71-23095
- Thermal conductivity anomalies in thin superconducting metal foils in contact with two superfluid He basins at low temperatures, examining surface electron phonon interactions
10 p1640 A71-23832
- Thin metal foils total energy flux, electron/phonon temperatures and thermal conductivity anomalies at liquid He temperatures
10 p1657 A71-24457
- Laser pulse produced energetic ion and plasma measurements fore and aft side of targets including Al and Au foils
11 p1775 A71-26084
- X ray interference lines widening in Al-Mo alloy foil obtained from melt by rapid cooling attributed to stress relieving
14 p2258 A71-30008

Nitrogen beam foil spectrum analysis, calculating transitions and decay times 15 p2452 A71-32598

Coaxial cable antenna lead with shield or external conductor in form of slotted corrugated metal foil, testing performance 20 p3197 A71-39469

Copper wire laser welding to film on Cr substrate, exhibiting nonhomogeneous columnar structure and recrystallization 21 p3389 A71-41104

Irradiation dose effect on alpha particle irradiated Al foil electrical resistivity recovery, using Wheatstone bridge measurement 23 p3689 A71-42934

METAL FORGING

U FORGING

METAL FORMING

U FORMING TECHNIQUES

U METAL WORKING

METAL FUELS

Cobalt 60 oxides as thermionic fuels, discussing high temperature properties, fabrication and irradiation techniques 02 p0280 A71-12256

Flame propagation along interface between fuel slab /polymers, aluminum and tungsten powders/ and oxidizer slab /inorganic salts and oxides/ 03 p0521 A71-14278

Particulate B fuels combustion and ignition working models in air at ambient pressures, using levitation cell and pulsed Nd doped laser [WSS/CIPAPER 70-13] 06 p0943 A71-17659

Amorphous boron powder total burning time in premixed laminar boron-propane-oxygen-nitrogen flames at atmospheric pressure, noting variation as function of oxygen initial partial pressure 15 p2511 A71-31472

METAL GRINDING

Martensite-type omega phase formation in Ti alloys during grinding by abrasive wheels and tapes, noting dependence on plastic deformation 19 p3078 A71-37474

Adhesion effects on interactions between abrasive and metal surfaces in grinding operations as function of grinding speed and contact surfaces properties 24 p3830 A71-44860

METAL HALIDES

NT ALKALI HALIDES

NT ALUMINUM CHLORIDES

NT BARIUM FLUORIDES

NT CALCIUM CHLORIDES

NT CALCIUM FLUORIDES

NT CESIUM FLUORIDES

NT CESIUM IODIDES

NT CHROMIUM BROMIDES

NT COPPER CHLORIDES

NT IRON CHLORIDES

NT LEAD CHLORIDES

NT LITHIUM FLUORIDES

NT MAGNESIUM FLUORIDES

NT POTASSIUM BROMIDES

NT POTASSIUM CHLORIDES

NT SILVER HALIDES

NT SILVER IODIDES

NT SODIUM CHLORIDES

NT SODIUM FLUORIDES

NT SODIUM IODIDES

NT TUNGSTEN FLUORIDES

NT ZIRCONIUM IODIDES

METAL HARDENING

U HARDENING [MATERIALS]

METAL HYDRIDES

NT ALUMINUM HYDRIDES

NT BERYLLIUM HYDRIDES

NT LITHIUM HYDRIDES

NT SODIUM HYDRIDES

TiH metallographic and lattice parameters variation with hydrogen content 07 p1139 A71-19993

Transition metals hydrides electrical resistance calculation based on theory of hydrogen electrodiffusion /occlusion/ into incomplete d-states 09 p1473 A71-23232

METAL INSULATOR SEMICONDUCTORS

U MIS [SEMICONDUCTORS]

METAL IONS

NT FERRIC ION

NT MANGANESE IONS

Mg, Al and Si ions spectral analysis, discussing energy levels and transition lines 01 p0129 A71-10136

Mg I and II vacuum UV emission series, presenting quantum defect plot 01 p0129 A71-10137

Solid metal lubricant films bonding by ion plating using diode method, noting interface type and structure examination by electron microscopy 01 p0087 A71-10483

Copper oxide-magnesium thermal cells open circuit voltage drop in latter discharge stages, discussing cuprous ion activity at cathode 02 p0197 A71-12959

Electron excitation coefficient rate of green coronal line by quantum defect method, discussing energy levels of Fe ions 04 p0643 A71-14906

Metal ions effect on oxygen toxicity in rats, noting convulsions and lung edema alleviation through mixed Mg-Mn ion treatment 04 p0537 A71-15053

EPR spectrum of tetravalent vanadium ions in gamma irradiated corundum at liquid He temperatures, showing equidistant lines width temperature dependence 04 p0637 A71-15105

Eu II and La II line profiles in sunspots and undisturbed photosphere 05 p0803 A71-16022

Cr and Ti ionization rates, CO and NO reaction kinetics and decomposition products in shock tubes 05 p0716 A71-16521

Anomalous Cu concentration profile due to migrating Cu ions-GaAs crystal defects interaction 05 p0794 A71-16877

Highly ionized line spectra of Fe, Co, Ni and Cu belonging to Na I and Mg I isoelectronic sequences 05 p0717 A71-16909

Interlocking via photoexcitations and deexcitations due to lanthanide rare earths weak line solar spectra and ion atomic structure 06 p0969 A71-17970

Noise spectra of CW hollow cathode zinc ion laser comparison with conventional discharges, noting gain per unit length on transitions 06 p0910 A71-18662

Cysteamine and penicillamine effects on copper ion charge transfer, using electron spin resonance and optical absorption measurements 07 p1033 A71-18935

Electron paramagnetic resonance and optical absorption spectra of transition metal ions in zoisite crystal 08 p1343 A71-20658

Nickel ion diffusion coefficients in high purity magnesium oxide single crystals in high temperature argon atmosphere 08 p1343 A71-20664

Temperature induced spectral line widening of trivalent positive Pr ions in lanthanum niobate crystals 09 p1507 A71-22391

Spectrograms of potassium and iron ions radiated by laser plasma 09 p1462 A71-22403

X ray emission from optical and inner shell transitions of multiply ionized Cu, Fe, and Ti in low pressure discharge dense plasma 09 p1501 A71-22414

Secondary ion component on tungsten target surface during sputtering by alkali metal ions 09 p1494 A71-22878

Diffusion-ion capture and heat transfer by phonons in solid and liquid metals 09 p1494 A71-22882

Solar flare spectral line features at 1.9 A, considering iron ion origin 10 p1660 A71-23797

Emission spectra, wavelengths and photoelectric intensities of triply-ionized gadolinium, using hollow cathode source with Czerny-Turner vacuum spectrograph 11 p1801 A71-25137

Extreme UV spectra of Sc XIV, Ti XV and V XVI, identifying and classifying lines in 18-25 A range 11 p1729 A71-26140

Fe ion photodetachment cross section polarization dependence on a sites in YIG-Si to explain photoinduced uniaxial anisotropy, using crystal field theory 12 p1943 A71-26858

Fe XIV intensities in solar EUV spectrum, calculating equilibrium population of energy levels in coronal conditions 12 p1970 A71-27704

Sporadic E wind shear theory, discussing time variation in metallic ion content 13 p2055 A71-27923

Integral equations for source functions of Ca II H, K and IR triplet lines for transfer through homogeneous stellar atmosphere 14 p2276 A71-30298

Solar corona visible lines, identifying V VI to Fe IX electron transitions with variable inductance three electrode spark source 14 p2314 A71-30650

Chromatographic separation of molybdenum, niobium and tungsten based on metal ions absorption by aluminum oxide 15 p2367 A71-31647

Ionized magnesium dayglow measurement in sporadic E layer by rocket-borne UV spectrometer, determining ion to atom ratio 15 p2398 A71-31765

Calcium ions effects on electrophysiological properties of portal vein muscle cells in rats 16 p2533 A71-34109

Cd ion laser with He-Ne, suggesting Cd ion excitation by Penning process 18 p2929 A71-35981

METAL MATRIX COMPOSITES

Quantum counter action in various media including trivalent and divalent rare earth ions, Fe group transition metal ions, semiconductors and gases 18 p2930 A71-36145

Stellar chromosphere characteristics from OAO observation of magnesium II emission in late type stars 19 p3137 A71-37628

Emission lines of star S22 in Large Magellanic Cloud, identifying H, Fe II and forbidden Fe II and Ni II lines 19 p3144 A71-38167

Ion pairing study in unresolved metal hyperfine splitting spectral region, using electron spin resonance line shape analysis 21 p3345 A71-40372

Serotonin and gamma-aminobutyric acid loss and interaction in rat midbrain slices incubated in media containing Na, K and Ca ions 21 p3338 A71-41073

Solar far UV Fe and Ni ion lines 23 p3723 A71-42951

Barium ion cloud release at 194 km, observing strati-formation for instability characteristics evaluation 23 p3669 A71-43170

METAL JOINTS

NT SPOT WELDS

NT WELDED JOINTS

Furnace fluxless brazing of Al with metallic getters, discussing techniques and joint design 02 p0255 A71-11706

Machine screws and metal joints stress distribution, using electric simulation with adaptability to digital computation 03 p0432 A71-13957

Pinned steel lug joints fretting fatigue, examining cumulative damage under constant amplitude and narrow band random loading 03 p0513 A71-14244

Service life of pin jointed connections with elastoplastic strains in bore walls 04 p0602 A71-14606

Assembling accuracy of three dimensional joints using assembly holes in aircraft construction 04 p0602 A71-14609

Continuous seam diffusion bonding of Ti alloy thin gage and sandwich structures in air, considering joint types [ASM PAPER W71-23.4] 09 p1455 A71-23094

Aluminum-epoxy joints stress corrosion cracking inhibition and crack tip plastic deformation by scanning electron microscopy 10 p1615 A71-24091

Bimetallic refractory metal joints electron beam welding and aging for applications to in-pile thermionic converters 11 p1769 A71-25857

Copper wire laser welding to film on Cr substrate exhibiting nonhomogeneous columnar structure and recrystallization 12 p1912 A71-27779

Preliminary corrosion effect on fatigue strength of Al joints, noting insufficient anticorrosive anodic film and additional protection by paint and varnish 16 p2584 A71-33688

Metallurgical and mechanical properties of Ti-Al-V joints produced by thin film diffusion brazing with copper 19 p3070 A71-38316

Electric contact resistance of various conductive metal coatings on aluminum corrosion free joints 19 p3031 A71-38449

Resistance NOR Ti BOND joining of Ti shapes, forming Ti-Cu eutectic at Cu plated Ti joint interface 21 p3387 A71-40620

Copper wire laser welding to film on Cr substrate, exhibiting nonhomogeneous columnar structure and recrystallization 21 p3389 A71-41104

Statistical analysis of spot welded and adhesive joints of high strength Al alloy sheet in aircraft structures 24 p3831 A71-45012

METAL MATRIX COMPOSITES

Secondary fabrication of boron reinforced aluminum matrix composite sheets for aerospace sub-components, detailing joining and autoclave bonding [SME PAPER EM-70-126] 01 p0089 A71-11260

Metal matrix composites fabrication techniques, discussing isostatic hot pressing, explosive processing and in situ fibering [SME PAPER EM-70-125] 01 p0090 A71-11264

Metal matrix composites formation methods, emphasizing diffusion bonding and plasma spray deposition [SME PAPER EM-70-124] 01 p0090 A71-11265

Thermal cycling effect on Al-B composites, considering surface roughening and crack initiation 01 p0103 A71-11279

Metal matrix and polymer matrix composite materials in aerospace industry, discussing selection factors for specific applications 01 p0104 A71-11283

Diffusion bonding cycles for Al-B composite materials fabrication, relating strength enhancement to residual stress relief 01 p0104 A71-11284

Ceramic fibers formation by particles mechanical deformation by extrusion in W matrix, describing grain structure of various extruded metal oxides
02 p0273 A71-12149

Carbon base multifiber yarns for metal matrix composites reinforcement, considering fiber strength degradation minimization methods
03 p0449 A71-14419

Thermal expansion of dilute binary composites concerning ceramic-glass, glass-metal, metal-metal and organic-metal systems
03 p0449 A71-14458

Metal whisker composite technology based on unidirectionally solidified eutectics, discussing mechanical behavior of whisker phase isolated from matrix
04 p0611 A71-14950

Carbide particles mean interparticle spacing and low alloyed steels dislocation density determination by planar and volume methods for metal matrix
04 p0612 A71-15076

Boron fiber-Al alloy composites linear thermal expansion as function of fiber volume fraction and orientation
04 p0615 A71-15788

Tungsten fiber reinforced brass composites, studying multiple necking phenomena during tensile tests
04 p0615 A71-15794

Fiber reinforced Al and Al alloys, discussing physical properties and manufacturing methods
05 p0764 A71-15921

Steel wire reinforced Al manufacture and properties, discussing wire-matrix bonding
05 p0764 A71-15922

Reinforced Ni-based composites, discussing barrier coating for tungsten fibers
05 p0769 A71-16860

Filamentary metal matrix composite superconductors for magnet construction
05 p0769 A71-16926

Fiber composites reinforcement obtained in oriented solidification by structural precipitation hardening of matrix
[ONERA-TP-920] 06 p0913 A71-18094

Continuous filament metal matrix composites fabrication from hot pressed composites by diffusion reaction process
06 p0915 A71-18688

Mechanical and interface reaction properties of alumina reinforced Ti-Al-V alloy composites fabricated by vacuum diffusion bonding
07 p1137 A71-19965

Fracture toughness of aluminum oxide composite containing ductile Mo fibers
08 p1304 A71-20700

Carbon fiber-metal composites fabrication and properties, discussing coating, compaction, electroforming, mixed metal powder hot working and liquid metal infiltration techniques
[PLASTICS INST. PAPER 14] 08 p1319 A71-20898

Composite materials with metallic matrix and carbon fibers, discussing production techniques and mechanical properties
[PLASTICS INST. PAPER 15] 08 p1320 A71-20907

Carbon fiber reinforced Al composites fabrication and evaluation by metallographic examination, considering tensile strength
[PLASTICS INST. PAPER 17] 08 p1322 A71-20930

Metals and alloys strengthening by in situ grown transition metal carbide fibers, noting whisker-like characteristics
08 p1315 A71-21586

Titanium-steel continuously reinforced composites strength to weight ratings, describing ausforming process and fatigue tests
08 p1316 A71-21587

Iron and fcc metal composite wires, determining fiber thickness and strength relationship
08 p1323 A71-21588

W fibers reinforced Cu matrix work hardening rates as function of fiber diameter and volume fraction, using isolated tension pile-up model
09 p1535 A71-22279

Heat resistant dispersion strengthened and fiber reinforced metal matrix superalloys for high temperature applications, considering superstrength alloys development
09 p1478 A71-23397

Co-Cr and Ni-Cr eutectic alloys with single crystal TaC fiber reinforcement, discussing unidirectional solidification
09 p1479 A71-23623

Alumina trichite reinforcement of nickel base matrix using magnetic alignment and sintering under low pressure below melting point
[ONERA-TP-911] 11 p1777 A71-25238

Metal matrix composite fabrication procedures for gas turbine engine fan blades, stressing diffusion bonding process susceptibility to blades volume producibility
[ASME PAPER 71-GT-46] 11 p1770 A71-25979

Design and fabrication of Borsic aluminum composite fan blades for supersonic turbofan engines, considering 430 F application without severe vibratory stress
[ASME PAPER 71-GT-90] 11 p1771 A71-25997

Orientation dependent impact toughness and crack resistance of brittle fiber-ductile matrix composite of solidified carbide reinforced Co-Cr eutectic
11 p1782 A71-26386

Fracture mechanics of metal matrix composite with ductile stainless steel reinforcing fibers
12 p1985 A71-27775

Composite heat resistant Ni alloy production using refractory oxide phase dispersion hardening
13 p2083 A71-27893

Al alloy matrix-graphite fiber reinforcement composites, discussing strength, temperature properties and processing techniques
13 p2092 A71-28660

Ni-Ni Nb eutectic composite, investigating monotonic mechanical response, deformation and fracture mechanisms
13 p2088 A71-29401

Fiber strengthening of Cu-Fe-Cr wire by cold drawing and annealing, discussing age hardening process of chromium ferrite needles in ductile Cu matrix
13 p2088 A71-29402

Particle-matrix interface strength of dispersion strengthened Ni alloys, developing direct tensile stress measurement method
13 p2089 A71-29408

Al matrix-stainless steel composites under tensile loading parallel to reinforcement direction, noting creep behavior at ambient temperature
13 p2089 A71-29413

Uniaxially reinforced W-Cu matrix composite material dynamic compressive load properties, considering strain rates and yield stress
14 p2257 A71-29643

Low cost metal matrix composite fabrication, discussing plasma spraying and continuous casting
14 p2263 A71-29655

Impact strength of Cu, Cu-Ni alloy and superalloy matrices reinforced with W fibers, studying temperature, heat treatment and fiber content and toughness effects
14 p2258 A71-29919

Critical aspect ratio of W fibers in metal matrix composites for stress rupture applications
14 p2258 A71-29921

Mechanical properties of composites consisting of Al matrix reinforced by boron fibers, considering high temperature creep, corrosion and thermal shock resistivity
14 p2259 A71-30473

Unidirectionally solidified Ti-base eutectic composites and alloys strength and microstructural stability under heat treatment
15 p2432 A71-32170

Thermally induced residual stresses effect on yield behavior of unidirectionally solidified eutectic composites
15 p2432 A71-32171

Specific strength of unidirectional fiber reinforced metal matrix composites, showing dependence on volume ratio and transmission coefficient
16 p2592 A71-33412

Metal matrix composites fractured and cut surfaces analysis using scanning electron microscopy
[ASM PAPER W71-3.4] 16 p2579 A71-33541

Microhardness dependent saturation of glass powders by iron, nickel and titanium during sintering of cermet metal matrix materials in vacuum
16 p2601 A71-33573

Mechanical properties, fracture and limited high temperature oxidation resistance of carbon fiber reinforced Ni composites
16 p2599 A71-34086

Solid state diffusion bonded boron-aluminum composites, discussing mechanical properties, weight and cost reduction and applications
17 p2758 A71-35204

Metal-reinforced glass plastic composite conical shell with positive Gaussian curvature, estimating reliability and stability based on static tests
17 p2830 A71-35316

Optimal design of locally orthotropic elastic flat bodies of fiber reinforced plastics or metals
17 p2763 A71-35620

Fiber volume content, fiber-matrix bonding, heat treatment and age hardening effects on transverse modulus and tensile strength of unidirectional Al matrix fibrous composites
18 p2935 A71-36597

Aluminum-boron composite forming and cutting processes covering milling, grinding, abrasive cutoff, drilling, piercing, electrodischarge machining, blanking, punching and shearing
18 p2928 A71-36666

Microradiographic and acoustic evaluation of fracture in boron filament aluminum matrix composite under tensile stress
19 p3081 A71-37903

Composite heat resistant Ni alloy production using refractory oxide phase dispersion hardening
21 p3396 A71-40084

Epitaxial metal film formation on Al-Ni fibers in Al matrix during electropolishing
21 p3387 A71-40456

Carbon fiber/metal matrix composites fabrication by electrodeposition, discussing aluminum warp sheet lamination and filament wound techniques
21 p3387 A71-40599

Carbon and boron fibers and whisker reinforced plastics fabrication, properties and costs, noting materials and optimum matrix combination
21 p3405 A71-40600

Mechanical and frictional properties of sintered copper matrix glass compacts, considering lubricating or seizure preventing effects of glass presence
21 p3406 A71-40759

Metal and polymer matrix materials research based on stringent requirements for thermal reactors, jet engines and space vehicles, discussing tests and analysis methods
21 p3401 A71-40901

Glass particles crystallization in sintered metal matrix glass materials, examining microcracks and temperature and cyclic heating effects
23 p3696 A71-43251

Fiber reinforced metallic matrix composite under creep, discussing rigidity, stress distribution, rupture strength and failure time
23 p3697 A71-44201

Fibers-matrix force interaction effects in metal composites, analyzing stress-strain state of reinforced plate
23 p3697 A71-44202

Diffusive metal coatings stress-strain state effect on composite Mo material strength, deformation and creep characteristics
23 p3697 A71-44206

Heat resistant Ni-base composite stiffened with W wires, investigating interaction between alloy and fibers from metallographic and X ray diffraction microscopy data
23 p3693 A71-44214

Precipitation hardenable Cr-Cu liquid phase sintered powder composite, showing matrix properties variations
23 p3695 A71-44291

Nichrome matrix composites with W and Mo reinforcements
24 p3837 A71-44727

Tungsten filaments as reinforcing agent of heat resistant composite chromium alloy, investigating long term high temperature effects
24 p3837 A71-44728

Heat resistant Nichrome composite alloy with tungsten filament reinforcement, discussing manufacture and mechanical properties at 1100 C
24 p3837 A71-44730

METAL OXIDE SEMICONDUCTORS

Silicon-on-sapphire complementary MOS circuits for high speed associative memory arrays, discussing system, circuit and device processing concepts
01 p0047 A71-10209

High performance LSI main frame MOS flip-flops memory module for digital computers
01 p0047 A71-10210

MOS capacitors as low mass micrometeoroid detectors in near-earth space, discussing fabrication and environmental tests
01 p0083 A71-11310

MOS multiphase LSI circuits design using computer program
02 p0228 A71-11651

Schottky diode bipolar IC and silicon gate MOS LSI techniques in manufacturing
02 p0228 A71-11652

MOS LSI bipolar random access memory feasible at costs competitive with magnetics
02 p0228 A71-11653

MOS transistor inverters static and dynamic characteristics in IC assemblies
02 p0228 A71-11656

P-channel MOSFET tetrodes static and dynamic characteristics compared to conventional MOS triode, considering transfer and gate threshold voltage
02 p0229 A71-11811

MOS transistors as high speed switches in magnetic film memory selection matrix, discussing requirements for drive current pulse yield, signal power and dissipation
02 p0229 A71-11815

Carrier mobility dependence on channel transverse electric field in MOS transistor
02 p0231 A71-11841

Basic digital circuits with integrated TTL and MOS structural elements, giving diagrams for dual counters, frequency dividers, adders and shift registers
02 p0231 A71-11862

Acoustic surface wave amplification using accumulation layer on Si in MOS structures
02 p0249 A71-12039

MOS junction transistor operation governing equations and electron distribution, using numerical analysis

02 p0233 A71-12423

Aerospace digital computer partitioning based on MOS MSI technology using functional building blocks (FBB)

03 p0384 A71-13281

Semiconductor developments, discussing field effect transistors, MOS, microwave components, piezoelectric effects, optoelectronics and galvanomagnetism

03 p0384 A71-13534

Minority carrier bulk lifetime from large signal response time of MOS capacitor in deep inversion

03 p0388 A71-14474

MOS transistor and circuits in digital applications, presenting current-voltage characteristics, conduction resistance, transconductance, etc

04 p0557 A71-15083

MOSFET transistors instabilities due to charge exchange near oxide-silicon interface states, determining energy levels distribution and time constants

05 p0791 A71-16165

MOSFET inverter pulse response analysis using hyperbolic functional description

05 p0726 A71-17086

MOS large scale IC phosphosilicate glass substrate vapor deposits effects, including hardness, pinhole density and electromigration

07 p1070 A71-18868

Permanent IR electron radiation effects on hardened MOS integrated inverter circuits, using units with plasma grown and vapor deposited aluminum oxide

07 p1174 A71-19053

Long term IR X ray irradiation effects on complementary MOS logic networks with several p and n channels on single silicon, determining radiation induced failure modes

07 p1174 A71-19054

Silicon dioxide space charge distribution dependence on photoinjected currents in MOS structures, showing charge effects on I-V characteristics

07 p1174 A71-19055

Ionizing radiation effects on monolithic metal oxide semiconductor inverters, including testing and hardening techniques

07 p1070 A71-19060

Inhomogeneous crystals frequency properties calculation by admittance averaging method, deriving expressions for metal semiconductor contact impedance

07 p1175 A71-19222

MOS transistors for high digital logic speed and microwave performance, discussing fabrication by double diffusion through mask opening

07 p1078 A71-19998

MOS transistors and bipolar microcircuits mobile charge density, observing p-n junction effects

07 p1079 A71-20175

Charging carriers of MOS structure interface states, considering effect on static transistor characteristics

08 p1265 A71-21291

MOSFET data systems evolution for IMP, discussing effects on system design and reliability approach

08 p1267 A71-21844

MOS transistor cascade amplifiers, discussing monolithic integrated circuits

09 p1416 A71-22492

Metal-oxide-metal tunnel diode properties, discussing parametric effects on small and large signals detector operation

09 p1416 A71-22684

Epitaxial deposition of discrete separated p- and n-type silicon on single sapphire substrate, considering technique for MOS devices fabrication

09 p1509 A71-23116

Capacitance voltage measurements on interface of pyrolytically deposited n-type silicon dioxide-InAs MOS diodes as function of admittance at room and 77 K temperatures

10 p1582 A71-23774

Linear sawtooth generator, using MOS unijunction transistors to switch and maintain constant discharge current from timing capacitor

11 p1740 A71-26549

MOS transistors on P substrates, investigating ionizing radiation effects on I-V characteristics

12 p1885 A71-26830

Transient characteristics of MOS channel transistors, solving nonlinear differential equations describing current and potential distribution

12 p1886 A71-26850

Complementary symmetry MOS technology for logic circuit design of inverters, gates, flip-flops, switches and storage units

12 p1883 A71-27044

Thermal oxidation and metal evaporation effects on electrical properties of silicon-silicon dioxide wafer interface in MOS structures

12 p1944 A71-27096

MOS transistor saturation range transconductance, internal resistance and gain factor calculation, allowing for field effect on space charge near drain

12 p1889 A71-27626

Customized MOS arrays computer aided preliminary layout design methodology, using four phase clocking schemes

12 p1890 A71-27772

Memory behavior in floating gate avalanche injection MOS structure, considering long term charge storage in insulated gate field effect device

13 p2036 A71-28045

P channel enhanced MOS transistors, logic elements and digital integrated circuits in silicon films on sapphire substrates

13 p2038 A71-28716

Metal oxide semiconductor digital circuit supply voltage, load capacitance and standby power drain

14 p2206 A71-29547

Capacitance/voltage characteristics of MOS capacitors before/after 25 MeV proton irradiation

14 p2210 A71-29797

Channel P MOS memory elements, discussing factors governing electrical energy dissipation and consumption

17 p2715 A71-34684

Semiconductor behavior of zirconium oxide formed on Zr substrate with n-type below 685 C and p-type above

17 p2759 A71-35222

MOS sandwich grid diode for gas ionization and field electrons generation at solid-gas phase boundaries

17 p2717 A71-35448

High density MOS memory circuits, using multilayer ceramic substrate board for demonstration

17 p2712 A71-35787

Large scale MOS IC digital VOR navigation converter, comparing accuracy, size, weight and cost with standard design

17 p2776 A71-35789

High reliability integrated complementary MOS circuit fabrication chain in Concerto satellite program, discussing technological process with account of physicochemical data

18 p2890 A71-36536

Channel P doped MOS memory elements, discussing factors governing electrical energy dissipation and consumption

18 p2891 A71-36561

Integrated complementary MOS circuit technology, discussing low power consumption, high speed, n and p regions realization on Si plates and design parameters relations

18 p2891 A71-36562

MOS field effect transistors operation and DC characteristics including threshold voltage and substrate doping effects

19 p3027 A71-37562

Gain and stability of MOS transistor small signal amplifier as function of frequency, using lumped element equivalent circuit

19 p3028 A71-37563

Free carrier surface density and mobility in large MOS transistors from conductivity and Hall measurements

19 p3028 A71-37564

MOS transistors thin monocrystalline silicon layers formation by epitaxial growth and substrate selective electrochemical etching

19 p3028 A71-37565

Digital integrated circuits technology with MOS transistors packed on crystal wafer without isolation diffusions

19 p3028 A71-37566

Vacuum deposition of silica and alumina thin films on silicon substrate MOS diodes, using CW carbon dioxide laser

19 p3074 A71-38233

Insulator surface ion migration effects on MOS and bipolar integrated circuits, describing inversion voltage and surface conductivity and recombination velocities

19 p3033 A71-38505

Room temperature ionic instability on p channel silicon gate MOS devices due to processing method, noting threshold voltage change

19 p3033 A71-38506

Equivalent circuits for planar devices behavior under ionizing radiation, considering bipolar and MOS transistors

19 p3034 A71-38521

Silicon gate process effect on MOS circuits application, noting bipolar compatibility, circuit layout compactness and reliability

21 p3354 A71-40729

Impurity diffusion self aligned MOS and lateral transistors used in IC

21 p3354 A71-40730

Fast read only memory design implemented in MOS and bipolar technology, noting low access times

21 p3355 A71-40735

C-MOS integrated circuit technology emphasizing reliability, design, failure mechanisms and performance parameters
[DFVLR-SONDDR-100] 21 p3355 A71-40737

Leadless electronic packaging system for MOS LSI for low cost, high reliability and heat transfer advantages 21 p3356 A71-40745

LSI logic arrays testing problems minimization by test procedures based on circuit design characteristics and MOS structure properties 21 p3356 A71-40803

Beam-lead technology application to complementary MOS IC processing 21 p3357 A71-40814

Ion implanted depletion mode MOS/LSI devices in conjunction with conventional P channel processing 21 p3358 A71-40821

Distributed gate multielectrode MOS transistor, presenting negative resistance operation mode 22 p3520 A71-41685

Illumination effects on drain current for p channel enhancement type MOS transistor, attributing photoresponse to electron excitation in conduction band 22 p3523 A71-42481

Charge injection in metal-aluminum oxide-silicon dioxide-silicon systems using capacitance voltage technique 22 p3587 A71-42531

Flatband voltage stabilization of metal-glass-oxide-silicon systems for phosphosilicate glass 22 p3587 A71-42532

Silicon Schottky tunnel MOS diodes, discussing effect of thin interfacial film between metal and semiconductor on I-V characteristics 23 p3652 A71-43936

Tunnel MOS diode oxide thickness and thermal equilibrium considerations, emphasizing reverse bias case AC conductance, capacitance and DC I-V characteristics 23 p3652 A71-43937

MOS transistors operating in unsaturated region, discussing source and drain series resistance measurement techniques 24 p3808 A71-44656

Ion implantation technique utilization for reducing MOSFET devices threshold voltage and gate drain capacitance 24 p3808 A71-44725

Impurity redistribution errors in C-V characteristics of MOS capacitors due to Si thermal oxidation 24 p3809 A71-44993

Microstrip line on silicon-silicon oxide system, investigating propagation modes and fringing effect by parallel-plate waveguide model 24 p3809 A71-45091

Two component 1/f noise measurements in p-channel MOS transistors 24 p3812 A71-45352

Substrate effect on MOSFET noise and y-parameters using wave equation 24 p3862 A71-45354

Input admittance, drain noise and induced gate noise measurements in search for excess gate noise in large geometry MOSFET 24 p3863 A71-45355

Nonequilibrium negative bias effects on n-type metal oxide semiconductor tunnel currents 24 p3812 A71-45356

Low temperature noise in p and n channel MOST amplifiers 24 p3812 A71-45361

METAL OXIDES

NT ALUMINUM OXIDES
NT BARIUM OXIDES
NT BERYLLIUM OXIDES
NT BISMUTH OXIDES
NT CALCIUM OXIDES
NT CHROMITES
NT CHROMIUM OXIDES
NT COBALT OXIDES
NT COPPER OXIDES
NT HAFNIUM OXIDES
NT ILMENITE
NT IRON OXIDES
NT LANTHANUM OXIDES
NT LEAD OXIDES
NT LITHIUM OXIDES
NT MAGNESIUM OXIDES
NT MAGNETITE
NT MANGANESE OXIDES
NT MERCURY OXIDES
NT MOLYBDENUM OXIDES
NT NICKEL OXIDES
NT NIOBIUM OXIDES
NT POTASSIUM OXIDES
NT RUTILE
NT SAPPHIRE
NT SCANDIUM OXIDES
NT SILVER OXIDES
NT SODIUM PEROXIDES
NT TANTALUM OXIDES
NT THORIUM OXIDES
NT TIN OXIDES
NT TITANIUM OXIDES

- NT TUNGSTEN OXIDES
 NT URANIUM OXIDES
 NT VANADIUM OXIDES
 NT YTTRIUM OXIDES
 NT ZINC OXIDES
 NT ZIRCONIUM OXIDES
- Ceramic fibers formation by particles mechanical deformation by extrusion in W matrix, describing grain structure of various extruded metal oxides
 02 p0273 A71-12149
- Metal oxide particle temperature determination in flames
 03 p0376 A71-14283
- Metal coatings and thin films wetting by soldering materials, emphasizing oxide removal
 06 p0903 A71-17426
- Soviet book on multicomponent systems of oxides covering solid state structure, mathematical techniques, metal-metal and metal-oxide binary systems, etc
 06 p0865 A71-17436
- Gallium oxide particles effects on Ag-Ga matrix single crystals critical resolved shear stress
 08 p1311 A71-21543
- Metal friction surface oxide thin films and secondary structures thickness determination using electron microscope method
 09 p1454 A71-22311
- Discrete phase vs binder strength of inorganic brittle polycrystalline powder metallurgy materials, including alumina and magnesia
 09 p1483 A71-23398
- Physical properties, structure and sintering of refractory oxides of rare earth elements and actinides, including chromia
 09 p1478 A71-23399
- Cement systems based on metal oxides and organic compounds, stressing acidity factor for organic component selection
 13 p0290 A71-28007
- Dielectric properties of barium titanate with Nb, noting metal oxide additives effects on conductivity
 13 p0292 A71-28661
- Oxide films effect on metal particles ignition
 15 p2511 A71-31378
- Fifth group transition elements V, Nb and Ta, showing most stable metal dioxide gaseous compounds
 15 p2424 A71-31391
- Single crystal and polycrystalline alumina specimens strengthening by annealing with various metal oxide powders
 15 p2438 A71-31975
- Ternary Co-Cr-Al alloy oxidation data, detailing kinetics, products, mechanisms, resistance behavior and rate
 16 p2589 A71-32870
- Ternary Co-Cr-Al alloy oxidation resistant composition selection, using oxide maps superimposed on phase diagram
 16 p2590 A71-32872
- Group 3A suboxides IR absorption spectra at liquid helium temperatures, measuring bending frequencies and modes
 16 p2538 A71-32875
- Surface/volume damage induced by Nd-YAG laser irradiation to LiNbO₃ and KDP crystals in frequency doublers and Pockels cells, using scanning electron micrographs
 17 p2790 A71-34376
- Sodium superoxide isothermal decomposition, detailing metallic oxide effects with differential thermal analysis, thermogravimetry and differential thermogravimetry
 17 p2694 A71-34672
- EuO, YIG, GdIG and ferrite magnetic oxide thin films growth techniques and magnetic properties comparison with bulk materials
 18 p2954 A71-36937
- Photocatalytic stimulation of UV radiation photolysis of amino acids and pentoses in aqueous solutions by metal oxide sols
 21 p3345 A71-40574
- UV radiation effect on amino acids and peptides in different gas atmospheres in presence of salts and metal oxides
 22 p3496 A71-42829
- Armalcolite and ilmenite basalt in Apollo 11 lunar samples, discussing formation process of titanium, potassium and silicon oxides
 23 p3734 A71-43247
- Thin film oxide, ferroelectric and bismuth titanate dielectrics for high capacitance microwave IC technology
 23 p3651 A71-43429
- Tunnel MOS diode oxide thickness and thermal equilibrium considerations, emphasizing reverse bias case AC conductance, capacitance and DC I-V characteristics
 23 p3652 A71-43937
- Free radical induced high temperature oxidation degradation curtailment of polyphenyl ethers by oxides, hydroxides and carbonates of alkali metals and Be
 [ASLE PREPRINT 71LC-11] 24 p3842 A71-45290
- METAL PARTICLES
 NT METAL POWDER
- NT POWDERED ALUMINUM
- Thermal conductivity and diffusivity determination of powders by introducing dispersed metal particles
 01 p0182 A71-11447
- Metal shaping process during angle steel ream-type rolling, determining metal particles velocity fields, strain energy and total metal pressure on rollers
 02 p0257 A71-12566
- Condensed metal particle size distribution measurement at ambient conditions by photography using electron microscope
 02 p0333 A71-12854
- Transmission impending failure detection via lubricating oil monitoring for metal particle content
 04 p0532 A71-15415
- Polyfraction Mg particles suspension in active gaseous medium, studying ignition and burnout
 08 p1376 A71-21909
- Magnetization discontinuities in cobalt-rare earth particles at discrete imperfection levels as function of chemical, mechanical and heat treatment, noting Co-Y rectangular loop
 12 p1943 A71-26861
- Metal particle agglomeration during burning of Al-Mg alloy in ballistic powder, using high speed burning track microphotography
 14 p2260 A71-30619
- Focused laser beam interaction with liquid metal particles, discussing fluid phase light screening effect, droplet evaporation and mass expulsion characteristics
 17 p2750 A71-34291
- Apollo 12 lunar soil particles observation for reduced metal meteoritic inclusions, suggesting shock impact effects during meteoritic bombardment of moon
 23 p3739 A71-43619
- Trace elements concentration and metallic particles analysis from Apollo 12 lunar igneous rocks, soils and breccias, noting relation to sample location and exposure age
 23 p3748 A71-43681
- Electron spin resonance studies of Apollo 11 and 12 lunar soil samples, determining ferromagnetism due to Fe particles
 23 p3763 A71-43797
- METAL PLATES
- Metal sheet plate and bar fabrication, calculating minimum bend radii from ductility ratings
 01 p0087 A71-10457
- Maraging steel welded plates edge displacements under linear multilayer burner heating, determining temporal deformations by heat distribution from additional source
 01 p0088 A71-11098
- Hot forming/die quenching of aluminum and titanium alloy integrally stiffened panels
 [SME PAPER EM-70-178] 01 p0089 A71-11259
- Clamped rectangular metal plates dynamic plastic behavior under uniformly distributed impulsive velocities
 02 p0321 A71-11678
- Bending of plate of nonuniform elasticity over thickness due to gas surface layer saturation during heating prior to rolling
 02 p0328 A71-12513
- Elastic metal thin plates transverse resonant free vibrations, analyzing viscoelastic coatings damping effects
 [ASME PAPER 70-DE-E] 03 p0506 A71-13709
- Surface impedance of thin metal plate excited by RF electromagnetic field as function of external DC magnetic field
 04 p0636 A71-14972
- Ti alloy plate multipass welding process, describing temperature measurement techniques for multiple thermal cycles
 04 p0604 A71-15910
- Abnormal microstructure in hot rolled plates and sheets of alpha plus beta Ti alloys
 05 p0766 A71-16349
- Solid metal plates breakdown mechanism at high temperatures and supersonic plasma jet action
 05 p0768 A71-16778
- Supercritical behavior of metallic plates, using nonlinear equilibrium and strain compatibility equations
 06 p0987 A71-17765
- Full penetration argon arc welding of titanium alloy plates without edge preparation
 09 p1457 A71-23357
- Thin metallic disk radar cross sections for near resonance frequencies backscatter, comparing experimental and computer results
 09 p1410 A71-23518
- Input resistance of electric dipole above metallic disk lying on homogeneous conducting half space at HF, using compensation theorem
 09 p1495 A71-23573
- Heat conductivity anomalies of thin metallic plates at very low temperatures, discussing secondary phonons angular distribution and electron energy flux
 10 p1640 A71-23816
- Metal plates and sheets stress corrosion cracking velocities, using torsion crack propagation specimen at constant load or deflection
 10 p1627 A71-24474
- High temperature tensile strength, creep rupture behavior and high temperature exposure effects on subsequent room temperature properties of maraging steel plates and welds
 [ASME PAPER 71-MET-E] 12 p1918 A71-27314
- Particle flux toward charged metal plate / flat probe/moving relative to plasma
 13 p2134 A71-28238
- Al-Zn-Mg alloy plates welded with Al-Mg filler metals, observing ghost defects in radiographs
 13 p2074 A71-28524
- Instability limit curves for twisted square metal plates under vertical loads with transition from antinastic to synclastic deformation
 13 p2158 A71-29431
- Fatigue crack propagation anisotropy in hot rolled steel plate, demonstrating crack growth rate sensitivity to microconstituents orientation
 15 p2508 A71-32255
- Residual stress determination from stress intensity factor measurements, describing application to electron beam welded aluminum plate
 15 p2508 A71-32259
- Solid metal plates erosion mechanism at high temperatures under supersonic plasma jet action, noting dependence on specific heat and latent heat of fusion
 16 p2591 A71-33030
- Mechanical properties of explosively clad plates, considering stainless steel/mild steel and brass/mild steel composites
 17 p2757 A71-34663
- Double exposure pulsed laser holographic interferometry application to transverse wave propagation in Al plate
 18 p2977 A71-36233
- Two dimensional dynamic thermal stresses in Al plate, allowing for Newtonian surface heat exchange
 18 p2981 A71-36720
- Thin circular annular Al plate buckling under uniform radial compression
 19 p3157 A71-37872
- Semiempirical modification of Irwin fracture analysis for semielliptical surface crack in metal plate
 20 p3248 A71-38781
- Electron microprobe analysis of cavity surface and lip of cosmic dust impact craters in stainless steel plates exposed at 400 km altitude in Gemini S-010 experiment
 20 p3299 A71-39652
- Surface strain cyclic flaw growth rates for Al and Ti plates, using end point, flaw opening and striation measurements
 22 p3560 A71-41643
- Pressure and mass velocity profiles behind two dimensional shock wave generation on Al flat plates explosive surface
 24 p3839 A71-45228
- METAL POLISHING
 NT ELECTROPOLISHING
- Heat resistant alloys face polishing with ultrasonically cleaned grinding wheel abrasive rim surface
 13 p2075 A71-28942
- METAL POWDER
 NT POWDERED ALUMINUM
- Isostatic pressing for large complex metal powder parts, comparing with die-compacting
 01 p0088 A71-10814
- Self ignition temperature of aerogels of Al-Mg alloys during heating of powders
 01 p0182 A71-14448
- Self ignition temperature of aerosols of Al-Si powders as function of dispersion and alloy composition
 01 p0182 A71-14449
- Transition metals powders and carbides sintering by high temperature hot pressing in homogeneity region, determining optimum conditions and activation energy
 02 p0256 A71-12276
- Hydraulic hot pressing equipment for producing large parts from high melting point metal powders and compounds by induction heating of dies
 02 p0238 A71-12282
- Quench atomization of iron alloys to powders, using liquid metal two fluid nozzle method
 05 p0758 A71-16245
- Powdered W, Mo, Nb and Ta sulfides and compacts thermal vacuum behavior, examining phase compositions and transformations
 05 p0769 A71-16861
- Fe powder filled tubular shell compression by magnetic fields and pulse sequences
 05 p0759 A71-17168
- Metal powders sintering computer simulated dynamic volume diffusion model based on Laplace equation, comparing calculated growth rates with electron microscope data
 06 p0903 A71-17344
- Metal powders hypergolic ignition in gaseous chlorine trifluoride, examining use in air augmented rockets primary combustors
 07 p1183 A71-19875
- Heat treatment and deformation effects on blended metal powder compacts homogenization, using mathematical model
 07 p1137 A71-19976

Stress reduction in metal powders compaction at different temperatures and deformation rates

08 p1305 A71-21059

Fe powder concentration in Ni powder by spectral analysis, examining particle size and HF generator spark condensation effects

08 p1306 A71-21066

Sponge iron sintered powder compacts deformation behavior from uniaxial compression tests, proposing plasticity prediction criteria

09 p1466 A71-22169

Molybdenum Permalloy powder cores heat treatment effects on permeability, magnetic loss and brittleness control, using metallographic techniques

09 p1466 A71-22171

Granulometric composition effects on stainless steel powders bulk weight, friability and compactability, taking into account particle shape

09 p1470 A71-23062

Thoria containing Ni and Co base powders reduction in hydrogen atmosphere for precipitation hardened materials production, determining optimal thermodynamic and reaction kinetic factors

09 p1475 A71-23306

Soviet papers on powder metallurgy covering metal powder fabrication, forming and sintering techniques and materials for friction, antifriction, and heat resistant applications

09 p1478 A71-23388

Thermal reduction methods for refractory metal powders of W, Mo, Zr, V, Hf, Nb, Ta and Ti

09 p1457 A71-23389

Solid state sintering of metal ceramics, discussing diffusion-viscous, pure diffusion and activation mechanisms

09 p1457 A71-23390

Cermet antifriction and friction powder metallurgy sintered materials for working at high temperatures without lubricants, in vacuum and inert gases

09 p1483 A71-23392

Iron base, white cast iron and high alloy powder metallurgy products for antifriction bearing elements

09 p1478 A71-23393

Refractory oxygenless powder metallurgy products in high temperature technology, considering covalent bond formation

09 p1478 A71-23395

Sintering and pressing techniques for compact semifinished products of refractory metal powders including W, Mo, Ta, Nb, Zr and Ti

09 p1457 A71-23396

Powders and torch techniques for brazing, including Mn-Ni-Co, Cu-Mn-Ni, Zr-Ti-Be, Ti-Cu-Ni and Zr-Be alloys

11 p1769 A71-25746

Metal powders role in brazing, considering melt atomization and mechanical comminution

13 p2075 A71-29089

Amorphous boron powder total burning time in premixed laminar boron-propane-oxygen-nitrogen flames at atmospheric pressure, noting variation as function of oxygen initial partial pressure

15 p2511 A71-31472

Plastically deformed Ni powder specimens residual microstresses as function of applied hydrostatic pressure, using X ray diffraction measurements

15 p2429 A71-31996

Superconducting Nb-Sn intermetallic compound synthesis from elemental powders by converging shock waves

15 p2461 A71-32378

Pressed or sintered steel powder joining to wrought mild steel parts, evaluating welded joints with torsion test

15 p2417 A71-32615

Refractory tungsten boride with iron or nickel for powdery surfacing mixtures, showing hardness and wear resistance dependence on low melting component

15 p2438 A71-32675

Hot compaction of tungsten and pseudoalloys powders in terms of volumetric-viscous flow dependence on isothermal exposure time, using Kovalchenko-Samsonov equation

16 p2592 A71-33572

Stress annealing effects on Al 27 NMR lineshapes in pure Al powders filed and stored at room temperature, considering residual stress

17 p2759 A71-35225

Prealloyed Al powder liquid phase sintering without precompact, discussing oxidation and density control

18 p2928 A71-36667

Sealing porous metal castings and powdered parts, discussing impregnation by vacuum-pressure and internal circulatory methods and sealant types

18 p2928 A71-36838

Electrolytic production of metal powder in continuously operating facility, using vibrating cathodes with chambers filled with granulated anode metal

19 p3068 A71-37105

Pressure distribution during cold rolling of metallic powders of stainless steels, iron, titanium and copper, using dynamometer mounted in roll

19 p3075 A71-37107

Nichrome powder microstructure characteristics effect on hot compaction kinetics, considering temperature, pressure and preliminary heat treatment effects

19 p3075 A71-37108

Boron powder combustion at elevated pressures, observing preignition metastable surface reactions, self sustained diffusion burning and decay

19 p3170 A71-38116

Transparent scandium oxide powder development by hot pressing, plotting IR transmission vs wavelength

20 p2353 A71-38819

Creep rupture behavior of electron beam melted polycrystalline sheet and powdered rhenium

21 p3397 A71-40454

Porous Cu and W shock loading properties, discussing principal Hugoniot data for P alpha dynamic response model

21 p3466 A71-40796

Austenitic stainless steels diffusion layer formation and structure by gaseous calorization with Fe-Al-ammonium chloride powder mixture, describing elements redistribution

21 p3390 A71-41166

Ferromagnetic Co phase nondestructive determination in hard powdered-metal alloys by permanent magnet ponderomotive force measurement based on relationship to ferromagnetic alpha phase

22 p3561 A71-41775

Porous materials prepared from electrolytic Cr powder, noting high permeability and strength and filter applications

23 p3689 A71-43252

Nickel-chromium system powders physicochemical properties, noting use as high temperature cermet packing materials

23 p3690 A71-43256

Precipitation hardenable Cr-Cu liquid phase sintered powder composite, showing matrix properties variations

23 p3695 A71-44291

Titanium carbide powder corrosion resistance to sulphuric acid-hydrogen peroxide system at various temperatures

24 p3838 A71-44739

METAL PROPELLANTS

Al particle burning in oxygen and water vapor, examining surface oxide film role in ignition mechanism

08 p1376 A71-21908

Polyfraction Mg particles suspension in active gaseous medium, studying ignition and burnout

08 p1376 A71-21909

Continuous burning rate measurement for metalized composite solid propellants, using optical sensor for servo tracking propellant surface

14 p2244 A71-30328

Pulsed T-burner testing of oscillatory combustion and droplet damping of aluminized solid propellants as function of frequency and sample properties

14 p2289 A71-30713

Comparative variable area, pulsed and modified T burners for testing oscillatory combustion and stability of propellants containing aluminum

14 p2289 A71-30714

Ignition and combustion tests of storable boron/magnesium/hexane slurry injected directly in high speed air stream

14 p2286 A71-30773

Acceleration dependent burning rate increases of aluminized composite solid propellants induced by combined erosive and acceleration

21 p3436 A71-40943

METAL SHEETS

Metal sheet plate and bar fabrication, calculating minimum bend radii from ductility ratings

01 p0087 A71-10457

Flaw detection system for wide Al sheets, using eddy current equipment with modulation analysis principle

01 p0087 A71-10458

Plastic deformation rate effect on deep drawing of sintered and vacuum melted thin sheet Mo

02 p0256 A71-12516

Temperature effect on ductility of thin sheet sintered or vacuum melted Mo during deep drawing

02 p0257 A71-12517

Longitudinal and cross rolling effects on anisotropy of mechanical properties and deep drawability of sintered thin sheet Mo

02 p0257 A71-12518

Flat products skin milling work determination from microgrid deformation graphs, using continuum mechanics equations

04 p0602 A71-14607

Strain ratio measurement of pure sintered molybdenum and boron alloyed molybdenum sheets, discussing deformation anisotropy and texture

04 p0609 A71-14748

Central hole effect on flat metal sheet fatigue under tension-compression load cycles, noting application to aircraft materials

04 p0670 A71-15389

Thermal recovery in stainless steel after explosive shock loading and forming

04 p0614 A71-15781

Sulfide precipitates shape preservation in high strength low alloy hot rolled steel sheets, discussing effects of various additive elements

04 p0614 A71-15782

State definition international standardization for cold rolled Al sheets, examining yield curves and strain energy

05 p0764 A71-15923

Temperature gradients and cooling rates of Ti alloy sheet moving arc weld pools, discussing instantaneous solidification

05 p0757 A71-16212

Fatigue crack propagation in aluminum alloy sheet, determining relationship between propagation rate and stress intensity factor and crack initiation conditions

05 p0766 A71-16296

Thin metal sheet reinforcements effect on slow stable tear and catastrophic failure

[AIAA PAPER 71-113]

06 p1003 A71-18563

Thin nickel aluminate sheets and small particles long range ordering, discussing antiphase boundary energy effects

07 p1133 A71-19441

Swept lightning stroke effects on aircraft design involving Ti and Al sheets

07 p1020 A71-19936

Hot working cast nickel based alloy for thin gage sheet, noting electroslag remelting increased temperature range

07 p1136 A71-19964

Low alloy Mo sheet recovery and aging characteristics studied by X ray scattering

08 p1305 A71-21031

Metal sheet failure kinetics, investigating tensile stress and cycle frequency during fatigue crack growth and extension rate effects

09 p1468 A71-22508

Beta Ti alloy sheet and foil mechanical property tests, honeycomb core fabrication, forming and welding evaluations

09 p1455 A71-23095

Ferrous and nonferrous sheet metals neck formation prevention for increasing elongation in tensile tests, using continuous plastic bending method

09 p1479 A71-23697

Metal plates and sheets stress corrosion cracking velocities, using torsion crack propagation specimen at constant load or deflection

10 p1627 A71-24474

Room temperature rated coercive force measurements of Ni sheet specimens in torsional bending cycles for saturation value, using ballistic method

11 p1778 A71-25563

Temperature distribution in metal sheets due to point and circular surface heat sources for laser welding applications, using power supply approximation model

12 p1985 A71-26571

High chromium hot corrosion resistant superalloys in sheet form, noting precipitation hardening and creep resistance equivalent to Nimonic alloys

12 p1916 A71-26922

Coarse grain Al sheet deformation, determining dislocations distribution with etching defects method

12 p1919 A71-27691

Be sheet plastic bend ductility and yield strength, considering purity and processing effects

13 p2088 A71-29403

Compression rolled and hot upset Be sheet stress-strain behavior and deformation dynamics, emphasizing temperature and strain rate effects on polycrystalline flow stress

13 p2088 A71-29404

German monograph on Mo sheets textures and plastic anisotropy covering recrystallization processes, crystallography, etc

14 p2256 A71-29580

Notched age hardening Al alloys sheets, obtaining fatigue damage test data and S-N curves

14 p2326 A71-30067

Thin sheet Nb-Zr alloy welds, detailing residual stresses in butt joints

15 p2413 A71-31204

Sheet metal fatigue test method for transverse 100-1000 Hz bending at normal and high temperatures, applying to 1.5 mm Ti alloy sheet

15 p2505 A71-31864

Failure and forming limit diagrams in biaxial tension for sheet metal with preexisting inhomogeneities based on Marciniak concept

15 p2505 A71-31945

Grain size effect on corrosion resistance and mechanical properties of Al alloy sheets between final annealing and quenching

15 p2434 A71-32329

Mo sheet electron beam penetration during welding, calculating heat-affected zone temperature distribution

15 p2435 A71-32466

Fabrication, texture, alloying, substructure and fracture effects on bend ductility and toughness of beryllium sheet

15 p2436 A71-32509

- Minimum output power required for CW carbon dioxide laser drilling of thin stainless steel sheets in vacuum and air, using cylindrical source model
17 p2750 A71-34369
- Heat treatment effect on fracture behavior of aged Al alloy sheet, investigating toughness dependence on microstructure
17 p2756 A71-34486
- Residual stress measurement in thin contoured Ti alloy sheets by X ray diffraction, using stress camera in normal incident beam mode
17 p2757 A71-34537
- Thickness effect on fracture toughness and crack propagation of Al alloy sheets used for aircraft skins
17 p2758 A71-35153
- Fatigue crack propagation in Al alloy panels stiffened with bolted and integral stringers, determining stress intensity factor/crack growth rate relationship
17 p2827 A71-35156
- Al alloy sheet fatigue crack closure under cyclic tensile loading, deriving expression for crack propagation rate in terms of effective stress amplitude
17 p2828 A71-35162
- Temperature dependent directional differences of modulus of elasticity of Mo sheet, using resonance technique
18 p2936 A71-36711
- Edge cracked metal sheet elastoplastic strain distribution determination, using optical interference, moire technique and plane stress model finite element method
18 p2983 A71-36848
- Small holes effect on Ni base superalloy wrought thin sheets fatigue strength under pulsating tension load, analyzing crack initiation, propagation and critical length
18 p2938 A71-36850
- Plastic zones and stable crack growth at notches in thin high strength sheet alloys, using replication technique
18 p2938 A71-36853
- High temperature four point bending vacuum furnace machine testing thin refractory sheets, noting strain rate, velocity jump and relaxation on tantalum carbide
19 p3063 A71-37554
- Creep rupture behavior of electron beam melted polycrystalline sheet and powdered rhenium
21 p3397 A71-40454
- Width/thickness ratio effect on steel, brass and molybdenum sheet specimens plasticity and deformation under tension at room temperature
23 p3694 A71-44233
- Wall thickness change to prescribed value by controlling stress-strain state in sheet stamping operations
24 p3831 A71-45013
- Mo sheet anisotropic dynamic strain aging at high temperatures, noting plastic strain contribution to texture formation and dislocation consolidation
24 p3840 A71-45378
- METAL SHELLS**
- Thin walled two layer bimetallic shells of revolution under large deformation, analyzing equilibrium by zero moment theory
06 p0998 A71-17856
- Liquid filling effect on oscillation modes of ellipsoidal stainless steel shell in vibrator
07 p1218 A71-20471
- Metallic spherical shell shielding of electromagnetic waves, deriving approximation for first n terms for EM fields inside due to impinging plane monochromatic wave
09 p1405 A71-22683
- Cylindrical Duralloy shells critical strain measurement in axial compression under creep conditions
10 p1690 A71-24575
- Inelastic scattering cross sections, using measured neutron leakage spectra from thick spherical shells of Ta, W, Mo and Be
11 p1802 A71-25556
- Thin walled stiffened Duralumin box spars bending stress-strain states under unsteady creep
12 p1981 A71-27496
- Strain gage method for residual stress determination in thin walled brass cylindrical shells produced by deep drawing
13 p2066 A71-28034
- Deformation substructures, strain rates and terminal properties of explosively-formed thin walled stainless steel cylinders, using transmission electron microscopy
13 p2153 A71-28501
- Thin metallic body of revolution under electromagnetic pulse, predicting transient induced currents with radiation condition in finite difference solution
15 p2372 A71-32368
- Circular cylindrical shell stability under combined axial tensile/compressive loads and torque, verifying theory by experiments on stainless steel shell
17 p2817 A71-34336
- Superconducting phase transition temperature measurements as function of magnetic field in thin film hollow Al and In cylinders
17 p2791 A71-35742

Test apparatus for studying stress-strain behavior of thin walled metal tubes in torsion, examining strain rate and history effects
18 p2935 A71-36234

Long small bore metal tube internal diameters calculation from capacitance comparison with cylindrical coaxial probes
18 p2922 A71-36581

Time dependence of radial mechanical driving point impedance of Al cylindrical shell immersed in two anechoic tanks related to chemical reaction
23 p3662 A71-43215

Metal cylindrical shells plastic collapse under axial compression, deriving theoretical load/deflection relationship
24 p3883 A71-44875

METAL SPINNING

Carbon fibers production by polyacrylonitrile fibers spinning, discussing stretching temperature effects on mechanical properties
[PLASTICS INST. PAPER 12]
08 p1320 A71-20909

METAL STRIPS

Plane electromagnetic wave diffraction on infinite system of parallel metallic strips, determining natural frequencies
04 p0549 A71-14611

Plane TM wave scattering by systems of two parallel conducting elliptical cylinders, metal tapes and combinations
09 p1407 A71-23106

Scattering structures of two parallel elliptical cylinders, tapes or combinations, deriving surface current density distribution under plane TM wave excitation
09 p1407 A71-23107

Metal strip with circular hole under tension, calculating plastic strain and stress concentration coefficients
10 p1687 A71-24199

Metal strips with holes under tensile loads, determining plastic region boundaries with photostress method
17 p2821 A71-34592

Residual stress magnitude and distribution in metal strips rolled with ultrasonic vibrations
21 p3389 A71-41093

Plane electromagnetic wave diffraction by infinite system of parallel metallic strips, determining natural frequencies and eigenfunctions
22 p3510 A71-42251

Strain hardening narrow strip lateral instability under bending in plane of maximum rigidity, deriving critical moment formula
24 p3883 A71-44854

METAL SURFACES

Diffusion boride protective coatings on Nb, Ta, Mo and W against carbon diffusion from carburizing agents
01 p0100 A71-10401

Combustion residues particle size and distribution during rocket plume impingement on Al surface
01 p0183 A71-11594

Hot electron gas on metal surface under strong heat flux as function of crystal lattice temperature at Fermi level
02 p0332 A71-12196

Electron emission formulation for cesiated metal surfaces in thermionic converter in terms of work function, using Swanson-Strayer correlation
02 p0295 A71-12210

Thermionic emitter metal surface adsorption, investigating impurities and additives effects by analytical model
02 p0295 A71-12231

Desorption and migration of Cs adsorbed on W surface under electric field, using field emission microscope
02 p0296 A71-12340

Statistical study of microhardness across thickness of gas saturated layer distribution on surface of Ti alloys
02 p0265 A71-12524

Polyatomic organic adsorbates effect on field emission total energy distribution from W and Mo surfaces, discussing electronic and phononic spectra
02 p0297 A71-12733

Imaging gas-metal surface interaction in evaporation field by ion microscopy, discussing molecular ion identification and dipole attraction due to electronic rearrangement
02 p0209 A71-12735

Nb surface contamination by oxidation during electrolytic polishing and vacuum annealing
02 p0269 A71-12928

Surface oxidation kinetics of iron by solid electrolyte techniques, comparing weight gain method
03 p0374 A71-13122

Sliding friction and wear of metal pairs under vacuum, using gravimetric and electron optical methods
03 p0432 A71-13366

Machine part surface layers properties effect on vibration decrement
03 p0503 A71-13414

Steam turbine blade metal removal rates by repetitive water drop impact, using hydrodynamic model
03 p0405 A71-14290

Gold plated Ge surfaces, investigating LEED patterns and electronic properties
04 p0636 A71-15016

Input resistance and effective height of gap excited metallic and dielectric antennas in conductive environment
04 p0558 A71-15220

Static metallic adhesion model for sliding friction, using contact resistance measurements
05 p0758 A71-16239

Refractory metal surfaces behavior in ultrahigh vacuum, using LEED and Auger electron spectroscopy
05 p0766 A71-16240

Gravitationally induced electric field shielding using whisker model with conducting metal surface for reducing strain dependence on altitude
05 p0792 A71-16315

Surface temperature of metal target heated by single laser pulse or pulse sequences, relating various parameters
05 p0764 A71-17042

Virgin surfaces adhesion under normal loads, testing Pb, Zn and Cd polycrystal specimens
05 p0759 A71-17167

Handedness formula for elliptical polarization after specular metallic reflection of linearly polarized light
07 p1111 A71-19485

Solid/vapor surface energies of metals at melting point related to heat of sublimation
07 p1134 A71-19518

Mass spectrometer application to study of secondary ion emission during metal surface bombardment by argon ion beam
07 p1112 A71-19621

Hydrogen adsorption behavior on polycrystalline nickel surfaces, using electron impact desorption flash filament with gas phase and ion spectrometer and vapor deposition
07 p1055 A71-19843

Chemisorption energies of organics on Pb surface by extended Hueckel molecular orbital technique
07 p1055 A71-19845

Point matching techniques, discussing effects of metal boundary on divergence of series and error from numerical examples of rectangular waveguide and scattering
08 p1252 A71-20755

Electrochemical metal machining tool profile two dimensional steady state problem, solving for cathode surface changes as function of interelectrode potential
08 p1296 A71-20854

Two phase oxygen adsorption at molybdenum surface, using secondary ion-ion emission measurements
08 p1306 A71-21489

Rolled metals crystallographic texture and pole figure determination using X ray diffractometer
09 p1467 A71-22307

Metal friction surface oxide thin films and secondary structures thickness determination using electron microscope method
09 p1454 A71-22311

Metallic and nonmetallic objects phase separation and honeycomb structures adhesion lack, analyzing defects by surface temperatures distribution determination
09 p1450 A71-22893

Metals and welded joints corrosion resistance at high temperatures and pressures, describing tests in autoclave with pneumatic loading
09 p1429 A71-23050

Metal surface layers structural changes during fretting corrosion, analyzing strain effects
09 p1455 A71-23081

Solid metals and alloys electron emission, considering applications in surface phenomena observation
09 p1473 A71-23224

Metallic target in radiation damage from focused ruby laser beams as function of energy and luminous pulse duration
09 p1465 A71-23563

Metallic surfaces adhesive properties and adsorptive capacity from nondestructive testing by peeling
10 p1616 A71-24105

Temperature field influence on hysteresis in Cs surface ionization on metal surfaces, observing adsorption phase fine structure and ion current density increase
10 p1657 A71-24542

Mathematical model for heat transfer coefficients between two identical metal surfaces in contact
11 p1853 A71-25157

Al alloy and carbon steel low cycle fatigue and fracture surface topography transition from static dimple to striation type by electron fractography
11 p1777 A71-25266

Virgin metal surfaces adhesion under normal loads, testing Pb, Zn and Cd polycrystal specimens
12 p1912 A71-27461

Metallographic equipment for metal surface microstructure observations of samples under tensile loads at temperatures from 4.2 to 300 K 12 p1908 A71-27757
 Adsorption states of Mo and Re surfaces during oxidation at low oxygen pressures and temperatures up to 2300 K, using noble gas molecular beams 14 p2190 A71-30402
 Two phase oxygen adsorption on molybdenum surface from secondary ion-ion emission 14 p2260 A71-30678
 Sealing materials adhesion to fiberglass and metals based on rupturing force in loading tests 15 p2414 A71-31655
 Surface melting, spallation and stress response prediction for metals under pulsed electron beam heating, using one dimensional finite difference computer program 15 p2390 A71-32005
 Pulsed electron beam heating of metals, determining surface melting, spallation and induced stresses with one dimensional computer programs 15 p2429 A71-32006
 Cathode damage of nanosecond atmospheric arcs on silver, gold, tungsten and palladium contacts, using scanning electron microscope 15 p2376 A71-32022
 Chromium carbides or borides high melting wear resistant surfacing material for machine components subjected to abrasive wear 15 p2418 A71-32669
 Redistribution of carbon, copper, nickel and chromium on friction surfaces of powder metallurgy antifriction cermet slide bearings by spectral analysis 15 p2418 A71-32673
 Metals and alloys surface deformation stages by exoelectron emission method, discussing mechanical energy absorption and dissipation 16 p2580 A71-33930
 Laser spectral-isotopic determination of oxygen content in metals, noting analysis variant dependence on metal purity 17 p2751 A71-34384
 Machine part surface layers properties effect on internal friction from transverse vibration decrement measurement 17 p2826 A71-35021
 Plastic deformation resistance of rough metal surfaces under heavy loads, discussing mechanical contact changes due to asperities reactions as coherent block 18 p2926 A71-36186
 Silicon reactions with aluminum surfaces, using low energy electron diffraction technique 20 p3194 A71-38882
 Vacuum UV reflecting surfaces deterioration by intermetallic formation, recommending separation by dielectric barrier layer 20 p3236 A71-39196
 Inert gases energy accommodation coefficients dependence on clean metal surface temperature based on lattice theory 21 p3415 A71-40538
 Field adsorption of inert gas atoms at metal surface from variational calculation 21 p3419 A71-40887
 Ultrasonic immersion echo pulse thickness meter for single side access measurement in Al and Zr alloys 22 p3528 A71-41759
 Eddy current field formation of defect on extended surface crack in ferromagnetic and nonferromagnetic metals, investigating superposed transformer detector inductor coil effects 22 p3529 A71-41770
 Nitrogen ions surface interactions with Al surfaces at and above earth satellite speeds, measuring normal and tangential momentum accommodation coefficients 22 p3577 A71-41980
 Gas molecular interactions, energy and momentum transfer and scattering from clean metal surfaces 22 p3577 A71-41996
 Rough metal surface smoothing through annealing in vacuum, deriving governing equations from Mullins theory of thermal grooving and solid surface capillary morphology 22 p3554 A71-42424
 Quasi-stationary electric field in toroidal metallic ionization chamber with meridional and equatorial slots, deriving formulas for components as function of coordinates 24 p3857 A71-45231
 Energy deposition, vacuum expansion and vaporization of barium in two phase jets, using combustion and solid state shock waves 05 p0836 A71-16538
 He-Zn vapor lasers excitation mechanism, presenting Penning and charge transfer cross sections 06 p0910 A71-18670
 Al particle burning in oxygen and water vapor, examining surface oxide film role in ignition mechanism 08 p1376 A71-21908
 Infrared laser output from giant pulse laser beam photoexcited alkali metal vapors, assuming buffer gas collisional mechanism 09 p1464 A71-23380
 Refractory metals coating of various substrates by gaseous phase chemical deposition, discussing diffusion process theoretical analysis, experimental apparatus and coatings mechanical and physical properties 11 p1768 A71-25391
 Neutral gas cloud expansion into vacuum explained by high altitude rocket released metal vapor molecules collisions and release mechanism characteristics 14 p2223 A71-29662
 Molten Co-Sn alloys, detailing vaporization rate, vapor pressure and partial and integral isothermal and isobaric formation potentials 15 p2425 A71-31394
 Zirconium iodide vapor deposition kinetics, determining activation temperature 15 p2425 A71-31395
 Magnesium vapor-oxygen low pressure diffusion flames temperature profile measurement, using subminiature thermocouple 15 p2464 A71-31631
 Bulk vapor formation processes during laser beam heating of metals, considering effect on mass transfer 19 p3072 A71-37586
 Low pressure trimethylaluminum vapor and oxygen flat diffusion flame structure, observing separation, formation and growth 19 p3121 A71-38299
 Expanding metal vapor density-radius measurements in wire explosions, using twin tube flash X ray unit 20 p3311 A71-38827
 Condensate removal devices for potassium vapor Rankine space power turbines to prevent blade erosion and efficiency degradation 20 p3262 A71-38918
 Spatially periodic inhibition of gold vapor condensation by intense optical standing wave using Q switched laser radiation 20 p3245 A71-39403
 GaAs contacts fabrication by successive metals or alloy evaporation, examining surface distribution by X ray microprobe 22 p3585 A71-41703
 METAL WHISKER REINFORCEMENT
 U WHISKER COMPOSITES
 METAL WORKING
 NT AUSFORMING
 NT BULGING
 NT CLADDING
 NT COINING
 NT EXPLOSIVE FORMING
 NT FORGING
 NT MAGNETIC FORMING
 NT METAL DRAWING
 NT METAL SPINNING
 NT SIZING (SHAPING)
 Al alloys improved fatigue resistance via thermomechanical processing, considering microstructure and deformation characteristics 01 p0099 A71-10168
 Electrochemical machining for aircraft engine metal components, discussing cost, time comparisons, tooling techniques and applications 01 p0089 A71-11252
 [SME PAPER MR-70-206] Ti and Ti-Al alloys machinability, discussing physical properties, dynamic deformation behavior and optimal cutting, milling and drilling 01 p0089 A71-11254
 [SME PAPER EM-70-101] Metal matrix composites fabrication techniques, discussing isostatic hot pressing, explosive processing and in situ fibering 01 p0090 A71-11264
 [SME PAPER EM-70-125] Peen forming of large complex parts from sheet and plate, illustrating dihedral break in airplane wing skin 01 p0091 A71-11550
 Laser systems for metal working, discussing operation modes, workpiece properties and optical systems 02 p0259 A71-11697
 Sintered W rolling in vacuum over reduction and temperature ranges 02 p0256 A71-12514
 Mechanical properties of Ti alloys subjected to rolling and heat treatment 02 p0265 A71-12522
 Plastic flow of metal during rolling in T groove, determining particle velocity and strain energy distributions 02 p0257 A71-12565
 Metal shaping process during angle steel ream-type rolling, determining metal particles velocity fields, strain energy and total metal pressure on rollers 02 p0257 A71-12566
 Groove depth/residual deformation/in vibrational rolling of Ti cylindrical samples, considering impression force, cylinder and steel spheres diameters 02 p0258 A71-12641
 Refractory Nb alloys with high creep strength, good ductility and moderate density, heat treatment and workability 02 p0271 A71-12937
 Alloying elements, mechanical working and heat treatment effects on vibration damping of Mg-Zr alloys, using Fastov device 07 p1136 A71-19634
 Comparative review of friction welding mechanisms, including inertia and metallurgical aspects 07 p1121 A71-20548
 [SME PAPER AD-70-574] Refractory metals forming, coating, machining and joining operations, discussing parts manufacture 08 p1299 A71-21683
 Vertical hydraulic press for metal extrusion at temperatures from 4 to 77 K, discussing design 08 p1299 A71-21809
 Apparatus for rolling and stretching metals at cryogenic temperatures, describing structural features 08 p1300 A71-21810
 High temperature austenitic steels, Ni and Co alloys machining, considering deformation resistance and strain hardening 09 p1456 A71-23297
 Metals ultrasonic welding, discussing welded elements interactions in terms of thermal and diffusive phenomena, sample preparation, transducers, electric generators and process control systems 10 p1617 A71-24134
 Metals crystallization in ultrasonic field, investigating structural change as function of energy and impedance factors and cavitation effects in fine grain formation 10 p1626 A71-24136
 Pure W single crystals grown by electron beam zone melting technique, noting rolling workability 12 p1919 A71-27761
 High strength Ni base superalloy workability, investigating microstructure relation to mechanical properties 13 p2090 A71-29419
 Hydrostatic extrusion, emphasizing prismatic products fabrication from industrial metals and alloys 14 p2252 A71-30469
 Hot rolled powder metallurgy Mo, noting texture during annealing and cold rolling 15 p2425 A71-31396
 Metal specific work breakdown during crack propagation, investigating thermal effect of plastic deformation with thermocouples 15 p2413 A71-31479
 Superplastic metal alloys microstructure, development history and shaping technology, noting Zn-Al alloy for auto bodies fabrication 15 p2429 A71-32004
 Manufacturing processes in orbital workshop, considering metal and optical lenses casting crystal growth and gravity lack effects 16 p2606 A71-32856
 Alloying elements, mechanical working and heat treatment effects on vibration damping of Mg-Zr alloys 16 p2593 A71-33630
 Titanium and composite fabrication for F-14 aircraft, discussing hot forming, chemical milling and electron beam welding 16 p2585 A71-34156
 Superalloy investment casting, discussing production processes, shell molding technique, applications, cost control, solidification, ductility improvement and cooling rate 18 p2927 A71-36659
 [SME PAPER CM-71-160] Aluminum bronze alloy forming dies fabrication and repair, discussing surfacing, hot working grinding, machining and welding methods 18 p2928 A71-36855
 AMg6M alloy hot rolling butt joints, showing ductility and strength of welds 19 p3070 A71-38424
 Metal deformation processing in solid mechanics, discussing plastic idealization for viscous behavior theorems, Ekstein paradox, free surface problems and incremental forging 21 p3389 A71-40983
 Displacement fields for two dimensional minimum weight frames for load dispositions analogous to perfectly plastic plane flow in metal working 21 p3391 A71-41428
 Superplasticity and materials forming methods for metal alloys, considering reformation speed increase by finer grained and stable alloys development 22 p3563 A71-42323
 Machining effects on martensitic stainless steels corrosion resistance, showing formation of defects and internal stresses in surface layers 23 p3692 A71-44028

Laser beam interactions with metal in hole gouging operations, determining optimal laser modes at energy densities short of metal evaporation

24 p3833 A71-44861

Metal hardening by dispersion of spherical ordered and coherent precipitates from statistical theory

24 p3861 A71-45196

METAL-GAS SYSTEMS

Cryogenic austenitic steels embrittlement dependence on nitrogen content, noting second phase precipitation role

01 p0098 A71-10086

Quasi-spherical divergent shock waves produced by Pt wire explosion in air

02 p0332 A71-12336

Statistical study of microhardness across thickness of gas saturated layer distribution on surface of Ti alloys

02 p0265 A71-12524

Nb binary alloys room temperature brittleness in hydrogen atmosphere

02 p0270 A71-12932

Nitrogen diffusion and solubility in W, deriving expression for permeation constant

04 p0614 A71-15784

Oxygen solubility and activity in Fe-Al and Fe-Ti melts, using neutron activation analysis

04 p0614 A71-15785

Nb-N and Nb-Zr-N alloys phase composition, examining microconstituents at various temperatures after quenching

04 p0616 A71-15905

Nitrogen-alloyed austenitic steels precipitation hardening, discussing aging and strengthening rates

05 p0767 A71-16767

Nitrogen chemisorption and absorption on polycrystal Ta ribbons, using static method in ultrahigh vacuum

06 p0940 A71-17298

Nitrogen chemisorption on Ta by field emission microscopy, taking into account work function changes

06 p0940 A71-17299

Interstitial nitrogen effects on thermally activated flow in Nb single crystals, determining yield and flow stresses and strain-rate sensitivity dependences on temperature

08 p1307 A71-21504

Interstitial role in bcc metals slip anisotropy at low temperatures, examining stress differential effect in Nb-oxygen solid solutions

08 p1307 A71-21505

Al particle burning in oxygen and water vapor, examining surface oxide film role in ignition mechanism

08 p1376 A71-21908

Metals electronic structure effects on hydrogen diffusion mobility

09 p1471 A71-23082

Cryogenic austenitic steels embrittlement dependence on nitrogen content, noting second phase precipitation role

16 p2593 A71-33642

Thin thermally insulating film on metallic sample, showing vapor layer elimination during liquid nitrogen quenching

18 p2934 A71-36172

Shatter crack incubated nucleation in relation to heat treatment effects on hydrogen elimination in steels, comparing with thermal explosion mechanism

21 p3402 A71-41090

METAL-METAL BONDING

Fcc metals cohesion strengths, using fracture technique with subsequent cold welding

02 p0267 A71-12879

Stationary edge dislocation interaction with partially bonded bimetallic interface, noting isotropic elastic continuum approximation

04 p0670 A71-15383

Volatile adhesive curing effect on metal-metal bond fatigue strength

05 p0772 A71-16955

Adhesive/metal interface corrosion resistance tests, discussing salt fog chamber for shear, compression buckling and cleavage stresses

05 p0770 A71-17248

Explosive metal welding bond interface, investigating heat treatment effect on microstructure

06 p0914 A71-18680

Corrosion resistance of adhesive bonded airframe structure components under outdoor weather and salt spray conditions, discussing test results with Al alloy specimens

09 p1459 A71-23690

Metal-metal bonded structures corrosion resistance improvement by use of primers or Al alloy honeycomb core

10 p1626 A71-24110

Metal-metal adhesive bonds temperature effects, long term static loads, dynamic strength and aging behavior

10 p1618 A71-24684

Heat affected zone crack filling and weld metal-base metal interactions of high strength alloys in dissimilar gas arc welding

11 p1769 A71-25749

Electron beam welding of metal-metal and metal-ceramic joints and sapphire sealing under vacuum

11 p1745 A71-26399

Fatigue life, fail-safe capability and corrosion resistance of commercial aircraft structures improved through adhesive metal-metal bonding

[ASME PAPER 71-DE-27] 12 p1978 A71-27325

Traversing Infrared Inspection System for C-5 aircraft fail-safe strap panels of bonded Ti-Al laminates, discussing design and application

[ASME PAPER 71-DE-37] 12 p1911 A71-27327

Book on electron beam welding covering generation and control, thermal effects, techniques and equipment, metallurgical and mechanical properties, etc

13 p2074 A71-28736

Optimal electron beam welding of Nb alloy to bronze, showing high mechanical properties due to deep Cu diffusion

14 p2253 A71-30491

Resistance NOR Ti BOND joining of Ti shapes, forming Ti-Cu eutectic at Cu plated Ti joint interface

21 p3387 A71-40620

Corrosive delamination occurrence, reduction and prevention in metal-metal adhesive bonded aircraft structures

22 p3555 A71-42594

METAL-WATER REACTIONS

Corrosion rate of Nb in aqueous solutions as function of temperature, using electrochemical potential measurements

03 p0442 A71-13363

Iron corrosion product deposition on pipe wall from aqueous stream dependent on shear rate, using radioactive tracer technique

03 p0442 A71-13368

METALLIC PLASMAS

Dense Li plasma pulsed power discharge temperature, structure, propagation velocity and emission characteristics

02 p0290 A71-12183

Cesium consumption rates and content in thermionic converter components affecting system performance indicated via integral adsorption reservoir

02 p0195 A71-12245

Dispersion equations for complex transmission coefficients of submillimeter EM waves in solid state InSb plasma, applying plasma effects to control elements

03 p0467 A71-13797

Partially ionized Hg plasma electrical conductivity at various pressures and temperatures

05 p0790 A71-16787

Plasma formation from transition metal target under monopause laser radiation, noting absorbed surface density energy role in onset

07 p1171 A71-20191

Computer simulation of strongly ionized potassium and hydrogen plasmas relaxation during rapid electrode cooling by He atoms, noting population inversions

08 p1342 A71-21913

Soviet papers on low temperature plasma physics covering production and diagnostic techniques, electrokinetic and optical characteristics, electromagnetic and shock effects, metal plasmas, etc

10 p1648 A71-24188

Hypervelocity impact produced metallic plasmas equilibrium composition and radiation, calculating radiative energy as function of wavelength and internal partition functions

11 p1804 A71-25510

Laser-blowoff metal plasma interaction with strong transverse magnetic field, observing velocity reduction due to inhibited ambipolar electron-ion energy transfer

11 p1805 A71-25794

K giants, subgiants, M67 and NGC 188 abundances, noting high metallicities

13 p2136 A71-28431

Dense Li plasma pulsed power discharge temperature, structure, propagation velocity and emission characteristics

15 p2454 A71-31491

Partially ionized Hg plasma electrical conductivity at various pressures and temperatures

16 p2618 A71-33039

Computer simulation of strongly ionized potassium and hydrogen plasmas relaxation during rapid electrode cooling by He atoms, noting population inversions

17 p2788 A71-35257

Electrical insulation behavior of MHD generator channel having Ar-K plasma, noting temperature dependence of surface conductivity

17 p2789 A71-35274

Charged particles elastic interaction and recombination in low temperature weakly ionized potassium plasma

19 p3109 A71-37135

Langmuir paradox problem concerning electron energy distribution function and anisotropy in low pressure DC Hg vapor discharge positive column plasma

23 p3710 A71-43402

METALLIZING

Vapor phase aluminization in Ar atmosphere furnace, discussing physicochemical aspects, thermal cycles and deposition kinetics

01 p0099 A71-10267

Soviet book on boride coatings on iron and steels covering physicochemical interactions and properties

02 p0263 A71-11848

Ni aluminoborizing process by circulation method, discussing thermodynamic analysis for saturation possibility and parameters experimental determination

03 p0432 A71-13961

Molybdenizing effects on Cr-Ni-Ti steel strength and stability in liquid Li

05 p0768 A71-16777

Gas permeability of polymeric foils reduction by vapor metallization in vacuum, noting dependence on surface state, diffusion layer and macroporosity

16 p2601 A71-33684

Metals and systems for semiconductor devices metallization, evaluating conductivity, adhesion, contact resistance, deposition ease, electrochemical corrosion, reliability and stability

21 p3356 A71-40802

Vacuum contactless metallization of carbon steels, stainless steels and nickel alloys, considering Si, Cr and Al coatings

21 p3390 A71-41172

Gas turbine engine turbine blades service life increase by Cr and Al vacuum diffusion metallization, presenting full scale endurance test results

21 p3390 A71-41173

Emitter-base W metallized contacts RF power transistors for improved hot spotting and breakdown reliability, comparing with Al

23 p3651 A71-43441

METALLOGRAPHY

Metal flaw size measurement, discussing ultrasonic echo amplitude and defect scanning methods

01 p0086 A71-10304

Soviet optomechanical instruments for metallurgy and high temperature metallography

02 p0254 A71-12711

W and thoriated W grain boundaries topography by trace analysis and field evaporation, observing curved surface with ledges, protrusions and serrations

02 p0266 A71-12737

Metallographic specimens etching by cavitation damage, testing performance by ultrasonic vibration technique

03 p0445 A71-14420

Li concentration effect on CdS single crystals brittle fracture anisotropy by metallographic techniques

06 p0941 A71-18083

Computer calculation of phase diagrams from thermochemical data for Cr-Mo and Mg-Cd systems

07 p1054 A71-19519

TiH metallographic and lattice parameters variation with hydrogen content

07 p1139 A71-19993

Soviet papers on physics of metals and metallography covering residual stresses, energy dissipation after plastic deformation, heat treatment, etc

08 p1317 A71-21759

Shock reheated chondrites metal phases, discussing postshock cooling thermal histories by metallographic and electron microprobe studies

09 p1519 A71-22643

Primary, secondary and combinatory recrystallization kinetics and textures in tungsten wire of different compositions over 900-2300 C using X ray analysis and metallography

09 p1476 A71-23323

Subgrain growth kinetics for tungsten deformed by rolling and polygonizing annealing, using metallography, X ray microradiography and crystal spectrometry

09 p1476 A71-23324

Metal carbide grain boundary precipitates effect on austenitic stainless steels high temperature fatigue fracture behavior

11 p1782 A71-26439

Metallographic equipment for metal surface microstructure observations of samples under tensile loads at temperatures from 4.2 to 300 K

12 p1908 A71-27757

Notch effect on metallographic characteristics of fatigue crack initiation and propagation in Al-Mg alloy

18 p2933 A71-35877

Metallographic techniques - Conference, Cleveland, November 1970

19 p3081 A71-37901

Metallography of 700 C precipitation hardening in Fe-Ni alloy containing Be, using transmission electron microscopy

21 p3404 A71-41417

Cr-Ni alloy heat treated cast specimens microstructure, metallographic, X ray and spectral investigation, noting chemical inhomogeneity

24 p3836 A71-44484

Ni-base superalloys metallography, investigating catastrophic cracking in weld heat affected zones by electron microscopy

24 p3839 A71-45139

METALLOIDS
 NT ANTIMONY
 NT ARSENIC
 NT BORON
 NT BORON ISOTOPES
 NT GERMANIUM
 NT SILICON ISOTOPES
 Alkali and rare earth metal hexaborides energetic structure, discussing semiconducting, semimetallic and metallic compounds on basis of energy bands and effective valence
 12 p1944 A71-27094

METALLOGRANIC COMPOUNDS
 U ORGANOMETALLIC COMPOUNDS

METALLURGY
 High metal fatigue resistance obtained via metallurgical means, discussing plastic deformation, crack initiation and propagation mechanisms, etc
 01 p0099 A71-10165
 Polycrystalline material nonisothermal plastic deformation, using model based on metals and alloys properties and microstructure
 02 p0324 A71-11749
 Superconductivity in physical metallurgy, discussing flux line structure and lattices, grain boundaries, stacking faults, etc
 02 p0266 A71-12876
 Surface flaws in metallurgical products for aircraft building, welds and castings, noting material faults-failure relation and acceptance criteria
 03 p0431 A71-13251
 Ultrafine-grain metals - Conference, Raquette Lake, New York, August 1969
 03 p0445 A71-14486
 Grain size refinement by alloy solute additions inhibition effect on growth and recrystallization, reducing boundary migration
 03 p0446 A71-14489
 Al alloys extrusion and chemical composition relationship to mechanical properties, examining various metallurgical processes
 04 p0604 A71-15743
 Pure metal structure effect on friction and lubrication under steady slip in ultrahigh vacuum at low temperatures
 05 p0757 A71-16185
 Ti-Al-V foils by electron beam vapor deposition, discussing metallurgical characteristics
 05 p0765 A71-16237
 Solid state physicists and metallurgy, discussing high strength materials, composites, radiation tolerance, fatigue, oxidation, superconductors, etc
 05 p0794 A71-16957
 Metallic construction materials creep rupture behavior, discussing primary, secondary and tertiary creep metallurgical and physical processes
 06 p0911 A71-17346
 Ordered alloys structural applications and physical metallurgy - Conference, Lake George, New York, September 1969
 07 p1131 A71-19426
 Soviet papers on phase transformations covering Mo-Nb-Hf, Nb-Al, Fe-Cr-Zr systems, rhenium steels, Bi-Sn alloys, etc
 07 p1135 A71-19612
 X ray Debye chambers and diffractometer cameras for high temperature investigations of metal systems phase equilibrium
 07 p1112 A71-19620
 Soviet papers on structure and properties of metals covering crystal properties, yield strength theories and heterogeneous phase systems
 09 p1476 A71-23320
 Soviet monograph on physical metallurgy of refractory metals and alloys covering applicability, structure, phase diagrams, properties, chemistry, working, welding, etc
 11 p1777 A71-25270
 Plastic deformation and alloying effect of small additions of interstitial elements on decomposition of metastable beta phase
 13 p2086 A71-28580
 Low ductility materials, considering applications to stress analysis, failure criteria, fatigue, physical metallurgy and polymer mechanics
 14 p2251 A71-29893
 Dislocation theory and crystallography in metallurgy, discussing edge and screw dislocation motion and interactions, Burgers vectors and gliding planes
 15 p2427 A71-31530
 Soviet papers on physical metallurgy of light metal alloys covering high strength, grain size effect, heat treatment, structural dependent properties and melt refining
 15 p2434 A71-32326
 Pattern recognition techniques application to metallurgical data analysis, discussing spatial filtering and classification process
 17 p2749 A71-35791
 Metallurgical and mechanical properties of Ti-Al-V joints produced by thin film diffusion brazing with copper
 19 p3070 A71-38136

German book on metallurgy, production and application of rare metals, discussing high vacuum technology
 21 p3399 A71-40783
 Material properties, metallurgy, production technology and operational factors effects on machinery structural strength
 23 p3779 A71-44207

METALS
 NT ACTINIDE SERIES
 NT ALKALI METALS
 NT ALKALINE EARTH METALS
 NT ALUMINUM
 NT ALUMINUM COATINGS
 NT ALUMINUM ISOTOPES
 NT ALUMINUM 26
 NT ALUMINUM 27
 NT ANTIMONY
 NT BARIUM
 NT BERYLLIUM
 NT BERYLLIUM 7
 NT BERYLLIUM 9
 NT BERYLLIUM 10
 NT BISMUTH
 NT CADMIUM
 NT CADMIUM ISOTOPES
 NT CALCIUM
 NT CALIFORNIUM ISOTOPES
 NT CERIUM
 NT CERIUM ISOTOPES
 NT CERIUM 144
 NT CESIUM
 NT CESIUM ISOTOPES
 NT CESIUM VAPOR
 NT CESIUM 133
 NT CHROMIUM
 NT COBALT
 NT COBALT ISOTOPES
 NT COBALT 60
 NT DYSPROSIUM
 NT ERBIUM
 NT EUROPIUM
 NT FERROUS METALS
 NT GADOLINIUM
 NT GALLIUM
 NT GOLD
 NT GOLD COATINGS
 NT HAFNIUM
 NT HOLMIUM
 NT IRIIDIUM
 NT IRON
 NT LANTHANUM
 NT LEAD [METAL]
 NT LIQUID METALS
 NT LITHIUM
 NT LUTETIUM
 NT MAGNESIUM
 NT MANGANESE
 NT MANGANESE ISOTOPES
 NT MERCURY [METAL]
 NT MOLYBDENUM
 NT NEODYMIUM
 NT NICKEL
 NT NIOBIUM
 NT NOBLE METALS
 NT NONFERROUS METALS
 NT OSMIUM
 NT PALLADIUM
 NT PLATINUM
 NT PLUTONIUM
 NT POTASSIUM
 NT PRASEODYMIUM
 NT PROMETHIUM
 NT RARE EARTH ELEMENTS
 NT REFRACTORY METALS
 NT RHENIUM
 NT RHODIUM
 NT RUBIDIUM
 NT RUTHENIUM
 NT SAMARIUM
 NT SILVER
 NT SODIUM
 NT STRONTIUM
 NT TANTALUM
 NT TECHNETIUM
 NT TERBIUM
 NT THALLIUM
 NT THORIUM
 NT TIN
 NT TITANIUM
 NT TRANSITION METALS
 NT TRANSURANIUM ELEMENTS
 NT TUNGSTEN
 NT ULTRAPURE METALS
 NT URANIUM
 NT VANADIUM
 NT YTTRIUM
 NT ZIRCONIUM
 Cracked metals brittle fracture statistical analysis, discussing plastic deformation under load
 01 p0166 A71-10080
 Rapid identification of steels and other metals by chemical, instrumental and organoleptic methods
 01 p0183 A71-10256

Rapid internal standard identification method for metals by atomic absorption spectrophotometry, using diluted acid solution of specimen
 01 p0028 A71-10257
 Nondestructive high reliability rapid comparison and identification of metals by electrical interpretation method for product variation control and laboratory unknowns determination
 01 p0085 A71-10258
 Metal products structural failure analysis, discussing laboratory equipment and analyst experience and ingenuity
 01 p0087 A71-10455
 Metallic materials semimicroscopic damage in fatigue of S/N gage under constant strain
 01 p0104 A71-11396
 Metal hardening under cyclic thermal loads, determining deformation, breakdown, creep and stress-strain relation
 02 p0324 A71-11752
 Gaseous atmospheres environmental effects on metal mechanical properties at high temperatures, discussing failure mode with crack growth rate dependence on pressure
 02 p0263 A71-11864
 M type supergiants atmospheric metals abundances from high dispersion spectrograms analysis
 02 p0308 A71-12095
 Strain rate effects on plastic properties of various metals and alloys
 02 p0265 A71-12568
 Inelastic scattering by impurities and phonons in metals, determining energy level structure from nonlinear corrections to Ohm law
 02 p0297 A71-12615
 Deformed metals stage I recovery, considering plastic deformation microscopic description, defect creation, interstitials and experimental methods
 03 p0441 A71-13348
 Spectrographic method for simultaneous determination of constituents in hard metals by rotating disk solution technique
 03 p0375 A71-13972
 Anisotropic plasticity theories for metals predicting load-deformation relations
 {ASME PAPER 70-WA/APM-17}
 03 p0443 A71-14154
 Metal and glass composites with similar residual stress states under axial loading, examining yielding and fracture behavior
 03 p0443 A71-14186
 Ultrafine grain metals strength properties at cryogenic temperatures and near melting point, discussing grain boundaries
 03 p0446 A71-14487
 Monograph on helicon and Alfvén wave propagation in nonmagnetic semiconductors and semimetals covering active and passive waves
 04 p0635 A71-14808
 Material testing - Conference, Budapest, October 1970, Metal physics and test methods, Volume 1, Part 1
 04 p0665 A71-14876
 Notched tensile tests for measuring metal ductile-brittle transition temperature, deriving proportionality law
 04 p0666 A71-14877
 Metallic components strain localization and concentration factors under high pressures or temperatures involving plastic strain, noting static and cyclic load effects
 04 p0666 A71-14882
 Material testing - Conference, Budapest, October 1970, Metal physics and test methods, Volume 2, Part 2
 04 p0666 A71-14885
 Stress-strain function for metal fatigue including mean stress effect
 04 p0610 A71-14890
 Yield point in metals, using Cottrell theory of atmospheres of foreign atoms near dislocations
 04 p0612 A71-15062
 Laser radiation metal fracture, using pulsed X ray metallography and high speed photography for cavity depth and material ejection time dependences
 04 p0608 A71-15116
 Metal-rich star evolution from main sequence to red giant, examining mass, nuclear reactions and theoretical models
 04 p0648 A71-15247
 Thermophysical properties of solids at high temperatures concerning zirconium carbide, corundum, metals and Ba-Cs system
 04 p0612 A71-15578
 Electron gas problem in metal physics by self-consistent Green function formalism, presenting momentum-space Feynman rules and integral equations derivation
 04 p0631 A71-15795
 Old subgiant delta Pavonis composition, suggesting metal rich state
 04 p0658 A71-15839
 Metal galvanomagnetic properties for specific Fermi surface and conduction electron scattering model, solving linearized Boltzmann equation
 05 p0792 A71-16317

Metals and alloys with bcc structure, investigating ductile-to-brittle transition by ultrasonic MHz technique 05 p0770 A71-17251

Hard metals and WC-Co alloy stress and heat treatment effect on coercive force, crack formation energy and abrasive resistance 06 p0911 A71-17342

Metal fretting corrosion energy analysis in terms of thermodynamics of irreversible process 06 p0904 A71-17942

High strength metal and ceramic reinforcement fibers, discussing properties and fabrication for plastic composites 06 p0916 A71-18088

Volume spectra during heat treatment in metallic systems, using automatic dilatometry 07 p1112 A71-19613

Plastics and metals as construction materials in aircraft, missile and rocket design 07 p1215 A71-20044

Book on yield point phenomena in metals and alloys covering Fe, V, Cr, Ni, Mo, Ta, W, Al and alloys, hydrogen in metals and fcc lattices 08 p1304 A71-20999

Amplitude dependence of Young modulus defect in metals during large stress HF oscillations 08 p1369 A71-21121

M type supergiants atmospheric metals abundances from high dispersion spectrograms analysis 08 p1362 A71-21145

Cold creep effect on stress corrosion testing of metals under uniaxial bending and constant strain 08 p1306 A71-21439

Strength of metals and alloys - Conference, Pacific Grove, California, August-September 1970 08 p1306 A71-21501

Soviet papers on physics of metals and metallography covering residual stresses, energy dissipation after plastic deformation, heat treatment, etc 08 p1317 A71-21759

Metals and nonmetals orbital atomic radii and lattice parameters 08 p1345 A71-21762

Harmonic analysis of metals and alloys fine structure X ray photographs via digital computers 08 p1293 A71-21765

High temperature tensile strength testers for metallic and carbon filaments 09 p1446 A71-22735

Solid metals and alloys electron emission, considering applications in surface phenomena observation 09 p1473 A71-23224

Temperature and pressure effects on phase transformations, structural changes and related processes in metals, comparing thermographic and calorimetric methods 09 p1547 A71-23227

Resilient metal seals for extreme temperatures or minimum leakage and weight 12 p1911 A71-27060

Metallic materials static to dynamic transition in creep noting temperature and purity effects 13 p2084 A71-28110

Metallic body motion in strongly rarefied plasma, determining compensating surface current distribution 13 p1991 A71-29158

Super metal rich K giant stars atmospheric model, obtaining abundances and turbulent velocity parameter 14 p2305 A71-29674

Stellar initial metal content effect on nuclear abundance distributions synthesized under explosive carbon, oxygen and silicon burning conditions 16 p2631 A71-33231

Cracked metals brittle fracture statistical analysis, discussing plastic deformation under loading 16 p2658 A71-33636

Nonlinear dependence of resistance in metals on impurity concentration and temperature due to umklapp electron phonon interaction and anisotropy of phonon spectrum 16 p2593 A71-33654

Anisotropic carbon-graphite materials and metals temperature dependence of thermal expansion coefficients, noting approximation by Debye heat capacity function 16 p2601 A71-33710

Small elastoplastic cyclic strain effects on internal friction and energy dissipation in metals during vibrations 16 p2598 A71-33983

Idealized model for anisotropy of metals inelastic characteristics due to plastic prestraining, demonstrating applicability to polycrystalline materials 16 p2659 A71-33989

Coolant thermophysical properties effect on heat transfer intensity in porous metals, analyzing differential equations 17 p2835 A71-34204

Laminar semiconductor and metallic structures electromagnetism impedance dependence on layers thickness, resistances and permittivities 18 p2953 A71-35873

Metals and alloys thermal conductivity prediction using Lorentz ratio and electrical resistivity measurements 18 p2938 A71-36991

Test facility for studying temperature dependence of thermal diffusivity and true heat capacity of metals between minus 150 and plus 400 C 19 p3063 A71-37588

Interlaboratory program to evaluate thermocouple pyrometric practices in metals high temperature testing 19 p3065 A71-38136

Calculation method for standard potentials and enthalpies of metals during oxidation and chlorination, representing molar functions dependence on temperature 19 p3082 A71-38153

Magnetostrictive metals and piezomagnetic ceramics as transducer materials for ultrasonic wave generation, detection and filtration 20 p3236 A71-39254

Diffusion processes electron mechanism in metal-metal and metal-nonmetal systems, using configurational model for valence electrons localization 21 p3403 A71-41159

Mathematical description by Gaussian error function for metals diffusive saturation and diffusion constants determination 21 p3403 A71-41160

Antiferromagnetic semiconductors and metals in magnetic field, obtaining Fourier components of electromagnetic fluctuation correlators for dielectric permittivity and magnetic permeability tensors 22 p3586 A71-42062

Beta cephei stars atmospheric He and metal abundances, comparing line spectra data with other early B stars sample 23 p3723 A71-42947

Magnetic field effects on complex Young and shear moduli for nonferromagnetic metals, describing experimental technique and frequency resolution criterion 23 p3689 A71-43206

Orthogonal experiment plans application to metal elastic stiffness description as function of temperature and strain rate 24 p3840 A71-45375

METAMORPHISM [GEOLOGY]

Na and Mn homogeneity in chondritic meteorites, discussing accretion processes, metamorphisms, weathering effects and specimens size 04 p0659 A71-15855

Chondrites bibliography and review, considering classification, metamorphism, ages and thermal history, achondrites and organic compounds 17 p2798 A71-34454

Potassium-argon age determination for shock-metamorphosed anorthositic of Manicouagan-Mushalagan Lakes structure 19 p3049 A71-37657

K-Ar dating of shock metamorphosed rocks from Brent impact crater (Ontario, Canada) 19 p3050 A71-37658

Shock metamorphism of Coconino sandstone at Meteor Crater (Arizona), examining porosity role in rock compression and in high pressure phases formation 19 p3050 A71-37659

Coesite-stishovite content in Ries crater nonporous crystalline rocks of variable composition and degree of shock metamorphism 19 p3050 A71-37660

Refractive index changes by shock compression metamorphism of tektite, soda lime and silica glasses 19 p3084 A71-37661

Progressive metamorphism and classification of shocked and brecciated crystalline rocks at impact craters 19 p3050 A71-37665

Detritus and breccias occurrence, composition, shock metamorphism, ejection mode and deposition at terrestrial single impact crater formations based on petrographic observation 19 p3051 A71-37667

Igneous rocks origin associated with shock metamorphism, considering geochemical investigations of Canadian craters 19 p3051 A71-37668

Impact metamorphism effects in Apollo 12 microbreccias from Oceanus Procellarum 23 p3745 A71-43659

METASTABILITY

U METASTABLE STATE

METASTABLE ATOMS

Nitrogen molecule collision with metastable inert gas atoms and ions, investigating energy exchange mechanism 08 p1337 A71-20670

Bright quiescent solar prominences metastable He excitation, studying electron temperatures and densities in interfilament areas 09 p1525 A71-23197

Metastable atom destruction, collision-radiative recombination and electron heating in low temperature

decaying helium plasmas, using spectroscopic resonance line measurements 10 p1654 A71-24896

Cross sections of metastable H formation by charge transfer of hydrogen ion beam on helium, argon, nitrogen and oxygen targets 11 p1803 A71-26371

Oxygen (super 1S) effective lifetime measurements in pulsating aurora, discussing mechanisms, quenching coefficients and heights 15 p2397 A71-31762

Time of flight energy spectra of high lying and Rydberg metastable atoms by electron impact dissociation of molecular oxygen, noting atmospheric applications 16 p2614 A71-34043

He-Ne lasers noise modulation at DC excitation, confirming existence of critical frequency related to metastable atom lifetime 21 p3392 A71-40373

Metastable atom destruction, collision-radiative recombination and electron heating in low temperature decaying helium plasmas, using spectroscopic resonance line measurements 21 p3425 A71-41276

Visible coherent radiation generation mechanism in ionized oxygen and nitrogen, considering free radical stabilized on discharge tube wall and metastable atom creation 23 p3706 A71-42889

Low temperature kinetics of metastable He atom pair collisions, investigating temperature dependence of plasma ionization 24 p3856 A71-45054

METASTABLE STATE

Alpha and beta Ti alloys metastable phases decomposition behavior, using electrical resistance measurements and X ray analysis 02 p0266 A71-12651

Metastable atomic oxygen ion production in F region plasma due to photoionization by solar XUV radiation 03 p0462 A71-13271

Microstructure effect on metastable beta Ti alloy strength, toughness, stress corrosion cracking susceptibility 04 p0614 A71-15780

Oxygen and nitrogen metastable constituents in daytime atmosphere airglow, obtaining altitude density distributions 07 p1103 A71-19764

Metastable Al-rich Al-Fe solid solutions decomposition during isothermal and isochronal annealing, from X ray diffraction patterns 07 p1137 A71-19979

Metastable beta phase Ti-Mo and Ti-V alloys ternary additions effect on decomposition 07 p1138 A71-19982

Metastable radiative lifetimes of molecular states of nitrogen and CO, using time of flight and high resolution electron gun techniques 09 p1497 A71-22417

Electron beam current density measurement using neutral Ar atoms electron impact excitation to metastable states 09 p1497 A71-22731

Metastable oxygen ion distribution and related optical emission rates in aurora, discussing line intensities, charge transfer efficiency and ionization peaks 09 p1441 A71-23642

Isothermal transformation of metastable beta Ti-Mo alloys, considering contraction start point coincidence with point of quenched omega transformation to aged omega in TTT diagram 10 p1625 A71-24006

Zr effect on Ti-Mo beta alloy stability, considering Zr suppression and retardation of omega precipitation on basis of TTT diagram and tensile tests 10 p1625 A71-24007

Al alloys microstructure and mechanical properties after rapid solidification, considering rapid quenching techniques and resulting metastable variations 10 p1627 A71-24596

Rapid melt quenching in Al alloys metastably extended supersaturated solid solutions, discussing strengthening mechanisms, high temperature decomposition and powder metallurgy utilization 10 p1628 A71-25027

Metastable state gas flow experiment, investigating laminar boundary layer change in presence of flat plate surface catalytic reaction 11 p1705 A71-26276

Thin gallium films metastable gamma and delta phase ring diagrams using electron diffraction techniques 12 p1942 A71-26821

Predeformation effects on metastable Ni base Ti alloys precipitation aging at extrinsic stacking faults, using thin foil microscopy 12 p1916 A71-26894

Plastic deformation and alloying effect of small additions of interstitial elements on decomposition of metastable beta phase 13 p2086 A71-28580

Monoclinic, stabilized and metastable tetragonal and cubic zirconias, noting IR and Raman spectra 13 p2093 A71-28991

Carbon monoxide in metastable state, considering quenching and radiative lifetime 16 p2615 A71-34089

Ti alloys metastable omega phase precipitation effect on mechanical properties, using thin film microscopy 17 p2756 A71-34492

White dwarf and neutron stars magnetic field generation, noting system in metastable Lofar state 18 p2963 A71-36242

High strength metastable austenitic steels fractography, showing alloy composition, strain rate and temperature effects 19 p3080 A71-37717

Ti-Mo base metastable beta Ti alloy tensile properties anomalies at elevated temperatures, examining strain rate and annealing conditions effect 21 p3399 A71-40699

Metastable beta type Ti binary alloys isothermal transformation microstructure observation by microscopic and X ray diffraction methods 22 p3562 A71-41947

Sgr B2 region interstellar gas microwave emission spectrum, observing inversion transitions in metastable rotational levels of ammonia 24 p3872 A71-44916

METAZOA

U ANIMALS

METEOR BURSTS

U METEOROID SHOWERS

METEOR HAZARDS

U METEOROID HAZARDS

METEOR TRAILS

Telescopic and photographic meteors brightness distribution curves 01 p0149 A71-10051

Neutral atmospheric wind measurements at 75-110 km by radar observation of meteor trail drift, discussing diurnal variations 03 p0407 A71-13308

Double photographic techniques for meteors and trails, discussing assembly, control and operation 04 p0589 A71-14831

Ionic meteor emission spectra calculation using two-step ionization and excitation model, accounting for atmospheric molecules and vapor atoms collisions 05 p0812 A71-16693

Delay time between beams reflected from different parts of meteor trail, using phase invariant and frequency scanning methods 06 p0869 A71-18263

Photographic observations of meteors with flares, noting particle, solar and earth atmosphere role 07 p1193 A71-19315

Meteor atmospheric paths, relating appearance height, maximal brightness and disappearance to velocity, mass, path inclination and ablation coefficient 07 p1194 A71-19317

Telescopic and photographic meteors brightness distribution curves 08 p1361 A71-21045

Upper atmosphere wind measurement by meteor trails radar sounding, discussing seasonal variations, amplitudes and phases of harmonic components 09 p1487 A71-22302

Meteor trails isotropic diffusion in presence of moving point source of ionization with variable intensity, calculating plasma density on and near trajectory 09 p1518 A71-22447

Small meteor streams trajectories and radiants from epsilon-Lyrids, alpha-Coronids and phi-Draconids observations by amateur astronomers 09 p1520 A71-22841

Meteor trails ionization probability determination based on data since 1948, comparing results of theoretical, semiempirical, experimental and simulation method 10 p1669 A71-24031

Ionization mechanisms for deviation of experimental altitude vs velocity curves of meteor trails, considering various electron and ion emissions and dissociation effects 10 p1669 A71-24032

Meteor trails distance determination by radar pulses reflection observation, estimating reflected signal delay dispersion and plotting mean square errors 10 p1576 A71-24037

Meteor trails azimuth angle measurement by radar interferometry, describing system advantages with respect to receiver noise, angular resolution and calibration 10 p1576 A71-24053

Laboratory and meteoric cluster ions formation, using mass spectrometric techniques 11 p1802 A71-25630

Calcium H and K line anomaly in faint meteor spectra, discussing brightness correlation with aerodynamic flow and resonant charge exchange with ionized nitrogen 12 p1957 A71-26626

Atmospheric currents and turbulence determination from meteor trail photographic observations 12 p1901 A71-27075

Upper atmosphere aeronomy historical review, considering meteor trails, radio waves, auroral photography, terrestrial magnetic field and spectroscopy 14 p2229 A71-29704

Optical anomalies associated with Tungusk meteorite fall in 1908, noting volcanic activity and noctilucent cloud formations 14 p2233 A71-29964

Micrometeor mass data from radiometer measurements, detailing Cu and lanthanum hexaboride ionization probability 14 p2315 A71-30652

Wind profile determinations at 90-100 km from meteor trail drift and ionosphere inhomogeneity radar data, noting semidiurnal harmonics in wind components 15 p2395 A71-31450

VLF atmospherics integrated intensities changes probably due to ionization by meteors 15 p2371 A71-31839

Photographic observations of meteors with flares, noting particle, solar and earth atmosphere role 15 p2486 A71-31895

Meteor atmospheric paths, relating appearance, height, maximal brightness and disappearance to velocity, mass, path inclination and ablation coefficient 15 p2486 A71-31897

Lost City /Oklahoma/ meteorite photometric and trajectory data, comparing flight characteristics with other fireballs 15 p2489 A71-32360

Upper atmosphere He, Ne, Na and K atoms collisions with molecular oxygen, determining ejected electron energy during fast Na, K, Rb and Cs ionization for meteor phenomena modeling 16 p2639 A71-33695

Meteors light curves, showing maximum brightness distribution in visible trajectory 16 p2639 A71-33700

Antenna azimuthal radiation patterns and meteor radiant distribution effects on wind velocity measurement by radar observation of meteor trains 19 p3145 A71-38372

Wind velocity vertical component determination through meteor trail drift observation, presenting mean diurnal measurements data 19 p3059 A71-38393

Radar equipment for meteor velocity and radiants measurement at VHF by pulse diffraction method 19 p3067 A71-38635

Computer techniques for meteor stream trails recognition, considering stream concept extension to groupings of asteroid orbits 20 p3298 A71-39641

Incident meteor flux density seasonal variations from radio reflections from trains and light scattering from micrometeoroids 20 p3298 A71-39642

Soviet monograph on astronomical foundation of meteor communications, covering radio wave scattering by meteor trails and computer simulation of signal time-amplitude characteristics 21 p3349 A71-41373

Multicomponent meteoritic composition effects on meteor trails radio wave reflections, obtaining ionospheric electron concentration distribution 24 p3804 A71-45033

METEORITE COLLISIONS

Large meteor masses collisions with earth and moon, implying lunar craters endogeneous origin based on meteor dimension data extrapolation 01 p0149 A71-10050

Saturn satellite Iapetus periodic light variation curve explanation in terms of meteoroids impact erosion 04 p0660 A71-15861

Lunar mascons interpretation as meteorites impact, discussing use as gravitational waves detectors 04 p0661 A71-15904

Large meteor masses collisions with earth and moon, implying lunar craters endogeneous origin based on meteor dimension data extrapolation 08 p1361 A71-21044

Aubrite radiation age dating for stony meteorites lifetimes as function of collisional destruction, using Ne 21/Al 26 methods 10 p1680 A71-24989

Diamonds in ureilites and carbonaceous chondrites, discussing formation due to recrystallization during asteroid collisions 17 p2810 A71-35723

Small bodies collisions in solar system, using Newtonian mechanics to indicate formation of meteor and asteroid streams 18 p2967 A71-36923

Meteorite impact and volcanism - Conference, Houston, October 1970 19 p3049 A71-37651

Morphology and geology of Lappajarvi structure /Finland/, suggesting meteorite impact evidence 19 p3049 A71-37652

Small lunar and terrestrial craters, determining impact or volcanic origin by depth-diameter ratio 19 p3137 A71-37677

Gegenschein as zodiacal light illuminated lunar dust ejected from meteorite impacts 20 p3286 A71-38730

Apollo 12 lunar soil particles observation for reduced metal meteoritic inclusions, suggesting shock impact effects during meteoritic bombardment of moon 23 p3739 A71-43619

Lunar breccia sample matrix composition characteristics examination by transmission electron microscope, suggesting condensation from rock volatilized by meteorite impact heat 23 p3745 A71-43663

Apollo 12 returned Surveyor 3 samples examination for meteoroid and lunar ejecta impacts evidence by optical and electron microscopy 23 p3766 A71-43819

METEORITE COMPRESSION TESTS

U COMPRESSION TESTS

U MECHANICAL PROPERTIES

U METEORITES

METEORITE CRATERS

Lunar crater origin determination by terrestrial volcanic and meteoritic craters and maars geological criteria application to Lunar Orbiter 5 photographs 02 p0313 A71-12549

St. Magnus Bay meteorite crater, discussing topographical, petrological and mineralogical evidence and criteria for impact origin 05 p0809 A71-16458

Hypothetic meteorite crater in southeastern Mongolia from on-spot observation and aerial photography 07 p1098 A71-19318

Meteorite craters in U.S.S.R., discussing impact, explosive and complex craters 09 p1520 A71-22842

Lunar impact cratering in geologic time, deriving meteoritic flux mass approximation and planetesimals origin 13 p2134 A71-28288

Hypothetic meteorite crater in southeastern Mongolia from on-spot observation and aerial photography 15 p2399 A71-31898

Meteoritic material magnetic fraction determination by chemical analysis for spherules in soil surrounding meteorite craters at Henbury, Australia 15 p2488 A71-32351

Campo del Cielo, Argentina meteorite crater structural analysis, discussing dimensions, energy of formation, mass, impact velocity, etc 15 p2488 A71-32352

Russian /Popigay river basin/ hollow as meteoritic explosion crater 15 p2496 A71-32734

Lunar vs terrestrial origin of tektites, discussing meteoritic impact craters, age factor and properties 16 p2637 A71-33517

Large meteoroids ablation and breakup mathematical model, estimating Mars atmosphere effectiveness as shield against surface impact craters production 16 p2643 A71-33968

Impact craters and depressions on earth, examining meteoritic origin, characteristic features, energy release and cryovolcanism 17 p2805 A71-35376

Sikhote-Alin 1967 meteoritic expedition, discussing collected fragments and soil samples, crater and hole structures and mapped sites 17 p2809 A71-35715

Sikhote-Alin meteorite shower expedition, describing craters and pits identification 17 p2809 A71-35716

Sikhote-Alin expedition geological survey, examining crater and pit structural characteristics 17 p2810 A71-35717

Australian Liverpool and Strang way craters as probable meteoritic impact origin from topographic and petrographic data 19 p3049 A71-37653

Ries structure in southern Germany, considering complicated crater geometry revealed by surface topography and geophysical investigations 19 p3049 A71-37654

Rochechouart meteorite impact structure located in granites and gneisses of Hercynian age in south-central France 19 p3049 A71-37655

K-Ar dating of shock metamorphosed rocks from Brent impact crater /Ontario, Canada/ 19 p3050 A71-37658

Shock metamorphism of Coconino sandstone at Meteor Crater /Arizona/, examining porosity role in rock compression and in high pressure phases formation 19 p3050 A71-37659

Coesite-stishovite content in Ries crater nonporous crystalline rocks of variable composition and degree of shock metamorphism 19 p3050 A71-37660

Progressive metamorphism and classification of shocked and brecciated crystalline rocks at impact craters

19 p3050 A71-37665

Hypervelocity impact melts, considering meteorite crater igneous rocks or glasses associated with shock deformation

19 p3051 A71-37666

Detritus and breccias occurrence, composition, shock metamorphism, ejection mode and deposition at terrestrial single impact crater formations based on petrographic observation

19 p3051 A71-37667

Pueblito de Allende meteorite craters, discussing crater formation and impact direction in comparison with experimental airdrop craters

19 p3052 A71-37684

Micrometeorite craters on lunar rock surfaces, suggesting cosmic particles impact

19 p3138 A71-37686

Planetary and lunar meteorite craters classification according to radius logarithm to base ten, covering diameter size from 2 microns to 2000 km

21 p3444 A71-40206

Lunar near surface seismic velocity distribution for cold accretion and meteorite impact models, comparing travel times

21 p3450 A71-40645

Physical chemistry of Aouelloul impact crater glass, suggesting meteoritic origin of tektites

21 p3450 A71-40647

METEORITES

NT ACHONDRITES

NT AUSTRALITES

NT CARBONACEOUS METEORITES

NT CHONDRITES

NT IRON METEORITES

NT KAPOETA ACHONDRITE

NT MURRAY METEORITE

NT ORGUEIL METEORITE

NT STONY METEORITES

NT TEKTITES

NT TUNGSKU METEORITE

Meteorites as information sources on interplanetary space beyond Mariner orbit and asteroid belt, discussing possible magnetic barrier and galactic field modulation

05 p0813 A71-16857

Morphology, mineralogy and chemistry of Ashmore meteorite

11 p1835 A71-26482

Spherules and finely dispersed meteorite materials on earth, discussing detection, collection, morphology phase and chemical composition, incidence and formation mechanisms

12 p1965 A71-27224

Extraterrestrial microorganisms penetration into rocks and meteorites under various climate conditions, noting effects of humidity

13 p2010 A71-28693

Lattice defect mechanism for high coercive force remanence production in meteorites and lunar samples by cosmic ray exposure

14 p2308 A71-29913

Long range thermoluminescent dating of meteorites and tektites, discussing dependence on thermal release of trapped carriers, radiation saturation and instrumental errors

16 p2638 A71-33518

Small meteor bodies fragmentation, using radar diffractional pictures

16 p2639 A71-33697

Meteorites, covering impact on earth, craters, astrometries, tektites, carbonaceous chondrites properties, collisions, fragmentation, etc

17 p2809 A71-35714

Ural fireball observations, noting accompanying meteorite falls

17 p2810 A71-35727

Spherules and finely dispersed meteorite materials on earth, discussing detection, collection, morphology phase and chemical composition, incidence and formation mechanisms

19 p3132 A71-37376

Uncataloged meteorites presumed to have fallen in Poland, using historical records reporting meteoritic metal for metallurgical applications

19 p3137 A71-37645

Meteorite falls in Germany, discussing composition, surface properties, microstructure, weights and circumstances of observation and discovery

21 p3448 A71-40521

METEORITIC COMPOSITION

Apollo 12 lunar core and soil samples indicating meteoritic trace elements abundance

01 p0148 A71-10003

Laser microspectral investigations of meteorites microregions and nonhomogeneities relevant to astrophysics and nucleosynthesis

01 p0158 A71-10764

Spectra of faint optical meteors for chemical abundance, discussing radiative processes during atmospheric entry, Leonid meteors and data acquisition

01 p0161 A71-11275

Flanged australite and australasian microtektites chemical compositions, using electron microprobe analysis

01 p0162 A71-11427

Chondrites Li content, using atomic absorption spectroscopy

01 p0162 A71-11429

Meteoritic iron oxides abundances from recoilless resonance absorption spectra

02 p0306 A71-11993

Meteorites and earth core composition and models for terrestrial planets internal constitution

02 p0310 A71-12159

Elemental abundances of microtektites and tektites, noting differences from Apollo samples

02 p0312 A71-12363

Micrometeorites composition and mass distribution in earth orbit vicinity, describing spaceborne and ground based data acquisition

02 p0313 A71-12470

Primordial trapped planetary noble gases and solar isotopic ratios in separated meteoritic minerals from Orgueil carbonaceous chondrite

02 p0318 A71-12901

Isotopic Rb/Sr age and initial chondritic ratio for silicate inclusions in Colomera iron meteorite

02 p0318 A71-12902

Al and Si abundances of Italian chondrites by instrumental pile neutron activation analysis

02 p0318 A71-12903

Nonseparated grain low iron olivine and pyroxene in carbonaceous meteorite Orgueil, using optical and electron probe microanalysis

02 p0318 A71-12904

Magnetite particles in Orgueil meteorite, discussing high symmetry morphology and generation

03 p0487 A71-13333

Pitts iron meteorite exposure history, noting consistency of rare gases isotopes contents in separated metal phase with prehistoric radiation flux increase

03 p0487 A71-13334

Mg-Cr and Ba-rare earth relationships in stony meteorites and Apollo 11-12 soil and rocks

03 p0487 A71-13335

Eucrites Nuevo Laredo and Stannern significance in lunar-meteorite composition studies

03 p0487 A71-13336

Fe, Si, Mg, Ca, Al, Ti, Mn, K and P concentration differences in L and H group common chondrites

03 p0487 A71-13337

Spectral reflectance measurement, comparing oxidized meteoritic material and Martian surface

03 p0489 A71-13559

Extraterrestrial abiotic amino acids and hydrocarbons in type II carbonaceous chondrite at Murchison, Australia

03 p0493 A71-14209

Australian tektites population polygons of bulk specific gravity and refractive index, indicating variations in chemical composition

04 p0582 A71-15133

Na and Mn homogeneity in chondritic meteorites, discussing accretion processes, metamorphisms, weathering effects and specimens size

04 p0659 A71-15855

Hg content determinations in meteorite specimens, comparing to magnetic rock of earth crust

05 p0814 A71-17165

Stony meteorite fragments, using X ray powder method for diamond detection

06 p0967 A71-17900

Cubic iron carbide identification from iron meteorites by X ray powder photography and electron microscopy

07 p1200 A71-20057

Terrestrial and stony meteorite carbon, investigating similarity in isotopic composition

07 p1201 A71-20399

Murchison meteorite composition analysis, investigating nonprotein amino acids of extraterrestrial origin

07 p1201 A71-20400

Galactic primary cosmic rays nuclei tracks in meteorite olivine, studying intensity of VH and VVH groups

08 p1351 A71-20961

Gadolinium isotopic composition and neutron capture effects in meteorites

08 p1365 A71-21693

Rock material density, mineral fragments and metallic iron content, indicating part of chondrite stony meteorite

09 p1521 A71-22928

Mafic silicates condensation in primordial solar nebula, explaining meteoritic abundance patterns by two component elemental volatility model and trace element distribution

09 p1521 A71-22932

Radiation measurements near thunderstorms and tornadoes, testing hypothesis of meteoritic matter-antimatter annihilation mechanism for ball lightning

10 p1599 A71-23752

Gas rich Kapoeta howardite composition, evolution, high particle fossil track densities and normal track rich crystals spatial relations

10 p1672 A71-24392

Superheavy transuranic elements in meteorites and lunar dust by fossil track microscopy

10 p1673 A71-24424

Carbonaceous chondrites natural remanent magnetization, revealing grey spinel oxide, Ni-Fe and iron sulfide as principal opaque minerals

10 p1674 A71-24429

Meteoritic graphite, silicon carbide and silicates to explain observed interstellar grains properties

10 p1675 A71-24471

Mesosiderites silicate textures and compositions and metal-silicate relationships from mineralogical, petrographical and chemical data

10 p1602 A71-24504

Sulfide formation process from solar composition cooling gas, examining constrained equilibrium theory

10 p1676 A71-24505

Cosmic rays produced He, Ne and Ar isotope concentrations in iron meteorite separated phases, using Rudstam spallation model

10 p1676 A71-24506

Orgueil carbonaceous chondrite organic matter, detecting homologous compounds, optically active species, isotopes, bacteria and organized elements

10 p1565 A71-24612

Montmorillonite and serpentine as major crystalline constituents of Orgueil meteorite

10 p1679 A71-24983

Clear taenite formation in bronzite and hypersthene chondrites studied by metallographic and electron microprobe

10 p1680 A71-24985

Gas rich meteorites and carbonaceous chondrites with trapped argon, noting isotopic correlation with neon

10 p1680 A71-24988

Meteoritic Xe isotopes production mechanism covering spallation, neutron absorption, extinct I 129 and Pu 244 radiative decay and Xe component trapping

11 p1819 A71-25223

Fe meteorite Grant, measuring radial distribution of cosmogenic nuclides of K, Ca, Ti, V, Cr and Mn produced by cosmic rays

11 p1819 A71-25224

Rare earth and heavy elements determination in olivine hypersthene and enstatite chondrites by spark source mass spectroscopy, noting Fe meteorite silicate inclusions composition

11 p1819 A71-25225

Earth and meteorites evolution, discussing material transport between lower and upper mantles and crust based on model of trace elements

11 p1820 A71-25226

Soviet book on diamonds in meteorites covering abundance and origin in stony and iron meteors, distribution and structure

11 p1833 A71-26326

Mineralogy, petrology, chemistry and microstructure of Valdivia meteorite

11 p1835 A71-26480

Petrography, chemistry and mineralogy of El Paso meteorite

11 p1835 A71-26481

Morphology, mineralogy and chemistry of Ashmore meteorite

11 p1835 A71-26482

Chemical analysis and petrography of Murchison meteorite compared to Murray meteorite

11 p1836 A71-26483

Spherules and finely dispersed meteorite materials on earth, discussing detection, collection, morphology phase and chemical composition, incidence and formation mechanisms

12 p1965 A71-27224

Hg content determinations in meteorite specimens, comparing to magnetic rock of earth crust

12 p1968 A71-27454

Iron and stony iron meteorites chemical classification, noting Ni, Ga, Ge and Ir concentrations and metal phases

13 p2134 A71-28290

Hydrocarbons, amino acids and large molecule organic compounds formation in chondrite meteorites by abiogenic reactions

13 p2010 A71-28692

Chemical fractionations in meteorites, considering trace elements abundance in L chondrites and implications for cosmochemistry

13 p2141 A71-29097

Equilibrium temperatures, pressures and oxygen fugacities of equilibrated chondrites in meteorites

13 p2141 A71-29098

Stony-iron meteorites composition, considering Ca/Al ratio in mesosiderites

13 p2142 A71-29141

Horse Creek, Mount Egerton and Norton County enstatite meteorites metal phases and perryite inclusions from electron microprobe data

13 p2144 A71-29474

Chromite and ilmenite analysis in pallasites, mesosiderites, achondrites and meteorites with electron microprobe
14 p2310 A71-30173

Photometric meteor mass calculations from observational data, discussing Fe and Cu photographic luminous efficiency measurements accuracy and interpretation
14 p2314 A71-30651

Carbonaceous chondrites total nitrogen and carbon abundances, using gas chromatography
15 p2486 A71-31990

Meteoritic material magnetic fraction determination by chemical analysis for spherules in soil surrounding meteorite craters at Henbury, Australia
15 p2488 A71-32351

Campo del Cielo, Argentina meteorite crater structural analysis, discussing dimensions, energy of formation, mass, impact velocity, etc
15 p2488 A71-32352

Lost City /Oklahoma/ and Suchy Dul /Czechoslovakia/ bronzite chondrites stable rare gas concentration determination
15 p2488 A71-32354

Lost City /Oklahoma/ chondrites, determining alkali, alkaline earth and rare earth element concentrations and Rb-Sr model age
15 p2489 A71-32355

Lost City /Oklahoma/ meteorite classification as type H5 chondrite based on bulk chemical composition, mineralogy and petrography
15 p2489 A71-32356

Lost City /Oklahoma/ and Ucera /Venezuela/ meteorites cosmogenic radionuclides data, using non-destructive analysis by gamma-gamma-coincidence counting system
15 p2489 A71-32357

Radionuclides and noble gas isotopic abundances in recently fallen meteorites for cosmic ray exposure ages estimates
15 p2489 A71-32358

Lost City meteorite secular and encounter perturbation effects on orbital evolution, interpreting short lived cosmic radiogenic isotopes formation
15 p2489 A71-32359

Cosmic ray intensity gradient measurement from Lost City meteorite Ar 37/Ar 39 ratio
15 p2479 A71-32361

Lost City /Oklahoma/ meteorite chemical and mineral composition analysis by X ray diffraction and optical emission spectroscopy
15 p2489 A71-32362

Cosmic ray produced radionuclides in Lost City meteorite, determining concentrations by nondestructive two-parameter gamma ray analysis
15 p2479 A71-32363

Lost City meteorite Ar isotopes radioactivity measurements, considering cosmic ray flux radial gradient variations during meteoroid orbit
15 p2479 A71-32364

Lost City /Oklahoma/ meteorite mineralogical and chemical investigations, comparing with Pribram and Ucera meteorites
15 p2489 A71-32365

Murchison, Murray and Allende carbonaceous chondrites water extractable amino acids composition
16 p2630 A71-32950

Terrestrial basalts and lunar rocks volatile element concentrations comparison, noting relationship to abundance in chondrites
16 p2633 A71-33348

Meteorite structure and chemical composition, describing investigation methods, origin and evolution
16 p2639 A71-33691

Cuban tektite classification based on age, discussing physical properties and chemical composition
17 p2797 A71-34275

Bibliography and review of noble gases isotopic abundance in meteorites and lunar material, considering cosmic ray interactions, radiation ages and extinct radionuclides
17 p2798 A71-34451

Bibliography and review of age determination of meteorites and lunar samples, considering chondrites, achondrites and iron meteorites
17 p2798 A71-34452

Bibliography and review of meteorites not classified as chondrites, considering achondrites, stony irons and iron meteorites
17 p2798 A71-34453

Polynuclear aromatic hydrocarbons in Murchison meteorite, determining distribution by gas chromatography and mass spectrometry
17 p2799 A71-34503

Carbonaceous chondrites chemical and mineralogical composition densities and structure due to condensation at various temperatures within early solar nebula
17 p2799 A71-34512

Kyle /Texas/ chondrite classification based on chemical composition, mineralogy and structure
17 p2800 A71-34513

Cosmic radiation and gas retention ages of Chassigny achondrite by measuring Al, K and noble gases contents and production rates in meteorites
17 p2800 A71-34514

Carbon and nitrogen abundances in howardites, enstatite and hypersthene achondrites
17 p2800 A71-34515

Nazareth /Texas/ meteorite chemical composition and structure, showing Neumann bands in kamacite fields
17 p2800 A71-34516

Stony meteorites relicts in mesozoic formation of central Urals, discussing chemical and mineralogical composition and structure
17 p2800 A71-34517

De Kalb /Missouri/ chondrite structure and mineral composition, noting olivine and bronzite presence
17 p2800 A71-34518

Sikhote-Aline shower region soil samples and meteorite and micrometeorite fragment morphology, emphasizing silicate spherules
17 p2810 A71-35718

Stony, stony-iron and iron meteorites magnetic properties relating susceptibility to nickel iron content
17 p2810 A71-35720

Stony meteorite Bushkhof mineral composition data, detailing measured quantities, distribution and appearance
17 p2810 A71-35721

Canyon Diablo iron meteorite optical microscopic and X ray structural analysis finding moissanite /or carborundum/
17 p2810 A71-35722

Zemaitemis /Lithuania/ meteorite mineralogical composition, noting rhagmaglypts formations, micro- and macrochondrules and Ni-Fe inclusions in cleavage area
17 p2810 A71-35726

Cosmic dust separation from terrestrial material, using vibrating tray to roll spherical particles from bulk of demagnetized and dried material
17 p2811 A71-35729

Mineral and chemical composition of Krasnyi Kluch meteorite, characterizing as recrystallized chondrite containing chondrules
17 p2811 A71-35731

Microscopic analysis of secondary minerals in molten meteorite crusts and dust
17 p2811 A71-35732

Spherules and finely dispersed meteorite materials on earth, discussing detection, collection, morphology phase and chemical composition, incidence and formation mechanisms
19 p3132 A71-37376

Extraterrestrial amino acids identification in carbonaceous chondrite Murray meteorite by gas chromatographic method
19 p3132 A71-37414

Uncataloged meteorites presumed to have fallen in Poland, using historical records reporting meteoritic metal for metallurgical applications
19 p3137 A71-37645

Detritus and breccias occurrence, composition, shock metamorphism, ejection mode and deposition at terrestrial single impact crater formations based on petrographic observation
19 p3051 A71-37667

Crustal and meteoritic abundances of elements and water, considering chondritic and achondritic composition
19 p3055 A71-38145

Vertical 1 single stage geophysical rocket design and instrumentation for X rays, solar UV and meteoritic composition measurements
19 p3154 A71-38530

Variable Nb composition of meteoritic rutile grains from quantitative electron microprobe analysis
20 p3292 A71-39384

Heavy rare gases adsorption on terrigenous sediments, comparing earth atmospheric composition with meteoritic planetary primordial component
20 p3194 A71-39385

Uranium content correction for Ivory Coast microtektites, discussing effects on age values and correlation between tektite falls, geomagnetic reversals and faunal changes
20 p3292 A71-39405

Meteorite falls in Germany, discussing composition, surface properties, microstructure, weights and circumstances of observation and discovery
21 p3448 A71-40521

Soviet monograph on Canyon Diablo/Arizona/ meteorite covering chemical composition, minerals, isotope composition, history, geology and impact recrystallization
21 p3452 A71-40874

Iron meteorites total N abundances determination by inert carrier gas fusion extraction gas chromatography
23 p3734 A71-43243

Tridymite structure in lunar pigeonite porphyry 12021 by single crystal X ray diffraction, comparing with meteorite and silica brick
23 p3738 A71-43613

Apollo 12 lunar soil particles observation for reduced metal meteoritic inclusions, suggesting shock impact effects during meteoritic bombardment of moon
23 p3739 A71-43619

Meteoritic material characterization from trace elements in Apollo lunar soil, core samples, breccia and anorthositic fragments by neutron activation analysis
23 p3747 A71-43678

CrN discovery in iron meteorites, determining carlsbergite mineral composition by electron microprobe
23 p3770 A71-44015

Multicomponent meteoritic composition effects on meteor trails radio wave reflections, obtaining ionospheric electron concentration distribution
24 p3804 A71-45033

METEORITIC DAMAGE

Low micrometeoroid flux on lunar surface from comparative Surveyor 3 and Apollo 12 pictures
03 p0490 A71-13783

Glazed lunar rocks, explaining origin as result of nearby meteoritic impact
13 p2137 A71-28515

Russian /Popigay river basin/ hollow as meteoritic explosion crater
15 p2496 A71-32734

Tunguska explosion of 30 June 1908, determining air waves propagation velocity
16 p2639 A71-33696

Charlevoix structure impactite description, discussing meteoritic impact origin from petrographic and chemical data
19 p3049 A71-37656

METEORITIC DIAMONDS

Stony meteorite fragments, using X ray powder method for diamond detection
06 p0967 A71-17900

Soviet book on diamonds in meteorites covering abundance and origin in stony and iron meteoroids, distribution and structure
11 p1833 A71-26326

Diamonds in ureilites and carbonaceous chondrites, discussing formation due to recrystallization during asteroid collisions
17 p2810 A71-35723

METEORITIC DUST

U MICROMETEORITIDS

METEORITIC IONIZATION

U ATMOSPHERIC IONIZATION

U METEOR TRAILS

METEORITIC MICROSTRUCTURES

Iron meteorites microstructure investigation by light and transmission electron microscopy, determining plastic deformation and cooling rate from thermomechanical history
06 p0964 A71-17343

Mineralogy, petrology, chemistry and microstructure of Valdinizza meteorite
11 p1835 A71-26480

Petrographic study of Allende carbonaceous chondrite by high voltage transmission electron microscopy, comparing substructure with terrestrial rocks
14 p2308 A71-29912

Meteorite structure and chemical composition, describing investigation methods, origin and evolution
16 p2639 A71-33691

Kyle /Texas/ chondrite classification based on chemical composition, mineralogy and structure
17 p2800 A71-34513

Nazareth /Texas/ meteorite chemical composition and structure, showing Neumann bands in kamacite fields
17 p2800 A71-34516

Stony meteorites relicts in mesozoic formation of central Urals, discussing chemical and mineralogical composition and structure
17 p2800 A71-34517

De Kalb /Missouri/ chondrite structure and mineral composition, noting olivine and bronzite presence
17 p2800 A71-34518

Zemaitemis /Lithuania/ meteorite mineralogical composition, noting rhagmaglypts formations, micro- and macrochondrules and Ni-Fe inclusions in cleavage area
17 p2810 A71-35726

Uranium content correction for Ivory Coast microtektites, discussing effects on age values and correlation between tektite falls, geomagnetic reversals and faunal changes
20 p3292 A71-39405

Meteorite falls in Germany, discussing composition, surface properties, microstructure, weights and circumstances of observation and discovery
21 p3448 A71-40521

METEOROID CONCENTRATION

Meteor population radar observation data at Antarctica station, noting monthly variations
01 p0149 A71-10054

Optical evidence of meteoric aerosols in upper atmosphere at maximum Orionids, showing double red luminosity of sky above Adi Ugrí
03 p0489 A71-13750

Atmospheric meteor zone turbulent motions under Archimedes forces based on radio observations
07 p1101 A71-19412

METEOROID CRATERS

- Meteor population radar observation data at Antarctica station, noting monthly variations
08 p1361 A71-21048
- Sporadic meteoroid particles in ionospheric spatial density determined from kinetic energy measurements
09 p1519 A71-22562
- Meteorite masses evaporation during flare, showing discrepancies for luminosity factors
09 p1520 A71-22830
- High order conditional algebraic equations in determination from azimuthal radar observation sporadic meteor density distribution over celestial sphere, discussing solution procedure and convergence
10 p1571 A71-24030
- Meteor streams dynamic properties, computing mean orbit elements with statistical mathematical model
11 p1835 A71-26458
- Terrestrial influx of small meteoric particles, discussing data uncertainties
14 p2307 A71-29902
- Lunar surface meteoroid activity from Surveyor 3 sample examination, comparing with predictions by cumulative-flux and near-earth models
16 p2643 A71-33849
- Atmospheric meteor zone turbulent motions under Archimedes forces based on radio observations
19 p3054 A71-37836
- Combined micrometeoroid collection and detection rocket experiment using foil penetration and plasma emission at impact for flux, masses and particle velocity determination
20 p3299 A71-39645
- Space vehicle measurements of sporadic meteor particle flux near earth, using detectors insensitive to acoustic and vibrational noise
20 p3299 A71-39648
- Sporadic and cometary meteor particles concentration along earth orbit, using optical and radiant measurements
20 p3299 A71-39650
- Cosmic dust particles impact craters searched for in lunar samples by binocular and electron scanning microscopes, relating to early solar system meteoroid flux
23 p3765 A71-43807

METEOROID CRATERS

- U METEORITE CRATERS
- METEOROID DUST CLOUDS
- NT ZODIACAL DUST
- Circumterrestrial meteoroid dust cloud properties based on night sky brightness photometric observation
12 p1964 A71-27090
- Hydrodynamic model of coalescing meteors substantiating cosmogonic Laplace-Schmidt hypotheses of solar system planetary formation from cosmic dust
13 p2131 A71-27892
- Geminid meteoroid dust particles detection, determining velocity and orbital elements from OGO 3 flux measurements
16 p2640 A71-33741
- Laser radar investigation of upper atmosphere dust layer, obtaining evidence for Silverberg cometary micrometeoroid shower hypothesis
16 p2641 A71-33760
- Circumterrestrial meteoroid properties based on night sky brightness photometric observation
19 p3133 A71-37440

METEOROID HAZARDS

- Grand Tour meteoroid environment analysis, considering different asteroid and cometary particle models
19 p3139 A71-37910
- [AAS PAPER 71-110]
- METEOROID PROTECTION
- Fracture of bumper protected fuel tanks subjected to hypervelocity meteoroid impact, applying method of characteristics to stress wave propagation in tank walls
03 p0500 A71-14431
- [AIAA PAPER 69-369]
- Construction and hypervelocity impact tests of penetration resistive dual bumper wall for spacecraft meteoroid protection
11 p1843 A71-25318
- [AIAA PAPER 71-339]
- NASA space station design, describing operational procedures, structure, meteoroid, thermal and radiation insulation and living quarters
15 p2498 A71-31137
- Large meteoroids ablation and breakup mathematical model, estimating Mars atmosphere effectiveness as shield against surface impact craters production
16 p2643 A71-33968

METEOROID SHOWERS

- NT GEMINID METEORIODS
- NT LEONID METEORIODS
- NT ORIONID METEORIODS
- NT PERSEID METEORIODS
- Small meteor streams trajectories and radiants from epsilon-Lyrids, alpha-Coronids and phi-Draconids observations by amateur astronomers
09 p1520 A71-22841
- Meteor showers of March 1969, noting delta Lyrids, gamma Cygnids and beta Urs Minoris observations
16 p2639 A71-33699
- Sikhote-Alin meteorite shower expedition, describing craters and pits identification
17 p2809 A71-35716

- Sikhote-Aline shower region soil samples and meteorite and micrometeorite fragment morphology, emphasizing silicate spherules
17 p2810 A71-35718
- Ural fireball observations, noting accompanying meteorite falls
17 p2810 A71-35727
- Computer techniques for meteor stream trails recognition, considering stream concept extension to groupings of asteroid orbits
20 p3298 A71-39641
- Sporadic and shower meteoroids mass distribution temporal variations as function of magnitude and solar longitude from visual and radio echo measurements
20 p3298 A71-39643
- Micrometeoroid flux acoustic measurements by Cosmos 135 and 163, discussing detection of shower activity
20 p3299 A71-39649
- Sounding rockets sampling of cosmic dust in upper atmosphere during and after Zeta Perseid and Arietid meteor showers
20 p3299 A71-39651

METEORIODS

- NT BOLIDES
- NT GEMINID METEORIODS
- NT LEONID METEORIODS
- NT METEOROID DUST CLOUDS
- NT MICROMETEORIODS
- NT ORIONID METEORIODS
- NT PERSEID METEORIODS
- NT RADIO METEORIODS
- NT SPORADIC METEORIODS
- NT ZODIACAL DUST
- Asteroids, comets and meteor dynamics in solar system, examining motion and orbital evolution by computer techniques
01 p0155 A71-10437
- Radar astronomy principles, applications and types of measurements, discussing solar, lunar, planetary and meteor observations
02 p0313 A71-12490
- Amino acid synthesis in simulated primitive environments, discussing possible effects of meteoric kinetic energy and lightning-associated shock waves
03 p0358 A71-13015
- Prairie Network bright meteors, discussing constraints on meteoroid structure, photometric and dynamic masses and classical single body theory variations
03 p0490 A71-13934
- Electron line density determination by relative aerial power pattern effect on observed meteor echo amplitude
03 p0490 A71-13935
- Ionic meteor emission spectra calculation using two-step ionization and excitation model, accounting for atmospheric molecules and vapor atoms collisions
05 p0812 A71-16693
- Faint meteor orbit characteristics, observing distribution, eccentricities, dimensions and inclinations to ecliptic plane
07 p1194 A71-19316
- Artificial meteors ablation and luminosity measurements, using ballistic range shadowgraph and radiometric equipment for velocity history, shock wave formation and mass loss process
07 p1223 A71-19674
- Meteor observations by radar, determining number, range, velocity, deceleration, duration, radiants, orbits and densities
09 p1517 A71-22212
- Nomograms for meteor geocentric velocity and trajectory with correction for zenith attraction and radiant
09 p1520 A71-22831
- Orbital elements of small high velocity meteors determined by oblique radio sounding
09 p1520 A71-22840
- Meteor-reflected radio wave propagation directivity and diurnal and annual variations, comparing experimental and theoretical calculation results
10 p1576 A71-24033
- Meteor-reflected radio wave propagation diurnal and annual variations prognosis, discussing indispensability of incident meteor particle velocity and density distributions
10 p1669 A71-24034
- Wind velocity data processing technique for azimuthal radar observations in meteor zone, using least squares method
10 p1600 A71-24035
- Atmospheric turbulence parameters determination from radar meteor observation, calculating antenna radiation patterns effect on error
10 p1583 A71-24036
- Meteoroids orbital elements statistically compared to asteroids
11 p1820 A71-25246
- Earth outward winding by cosmic particle gravitational accretion, examining individual meteor counts crossing celestial meridian in WE and EW directions
12 p1966 A71-27232
- Meteor particle speed and size estimation using accelerated glass microsphere bombardment in plasmod
13 p2133 A71-28201

- Bibliography on lunar and planetary subjects covering astrobology, comets, cratering, meteors temperature, structure, asteroids, tektites surface features, etc
13 p2135 A71-28293
- Electron attachment rate determination by combined photographic and radar observation of meteors
13 p2137 A71-28545
- Faint meteor spectra recording, using high sensitivity image orthicon
13 p2070 A71-29017
- Photometric meteor mass calculations from observational data, discussing Fe and Cu photographic luminous efficiency measurements accuracy and interpretation
14 p2314 A71-30651
- Faint meteor orbit characteristics, observing distribution, eccentricities, dimensions and inclinations to ecliptic plane
15 p2486 A71-31896
- Meteor spectrum analysis presenting tables for Soviet observations
16 p2639 A71-33694
- Meteoroid velocity measurement by satellite-borne meteoroid detectors, giving Geminid meteor shower measurements results
16 p2639 A71-33724
- Lunar, meteoroid and asteroid surface erosion, investigating hypervelocity impact, solar wind flux and ion sputtering effect
16 p2642 A71-33818
- Ca and Mg light emission and ionization cross section measurements at simulated meteor conditions, using photomultiplier and optical filters
17 p2798 A71-34374
- Book on space science covering celestial coordinates, time and mechanics, planetary atmospheres and interiors, comets, meteors, stellar structure, etc
18 p2963 A71-36246
- Earth outward winding by cosmic particle gravitational accretion, examining individual meteor counts crossing celestial meridian in WE and EW directions
19 p3132 A71-37384
- Meteor streams effect on atmospheric motions turbulence intensity based on radar observations
19 p3054 A71-37972
- Hydrodynamic model of adhering meteors substantiating cosmogonic Laplace-Schmidt hypotheses of solar system planetary formation from cosmic dust
21 p3441 A71-40076
- METEOROLOGICAL BALLOONS
- Magnetometer for indicating position of constant level meteorological balloons provided with solar sensors
10 p1612 A71-24759
- Eole project for atmospheric phenomena studies, describing meteorological satellite/balloons arrangements, equipment and operational methods
15 p2500 A71-31824
- Worldwide data acquisition and tracking of meteorological balloon stations by flyby gravity stabilized satellite
18 p2878 A71-36528
- Hybrid thin film radiosonde transmitter design for atmospheric temperature and humidity data transmission from meteorological sounding balloon to ground station
19 p3035 A71-38539
- METEOROLOGICAL CHARTS
- Synoptic and moisture content charts from Kosmos-243 satellite measurements of escaping thermal RF flux
01 p0073 A71-10540
- Traffic radar generated weather contours for air traffic controller in helping aircraft avoid thunderstorms
01 p0118 A71-10587
- Northern Hemisphere upper stratosphere and lower mesosphere synoptic meteorological chart construction, using aerological network and rocket radio sounding data
15 p2400 A71-31967
- Meteorological uses of stereographic horizon map projection, permitting placement of map center at any point on earth
16 p2564 A71-33538
- Middle stratosphere monthly mean temperature maps based on radiosonde measurements, confirming anomalies with satellite IR spectrometer radiances
16 p2641 A71-33755
- Cloud cover charts for North Atlantic-European-North African region, comparing satellite and ground station visual observations
20 p3258 A71-39552
- METEOROLOGICAL FLIGHT
- Spatial correlations between inside cumulus cloud conditions and precipitation onset and intensity for modification experiments from aircraft penetration measurements
08 p1326 A71-21450
- Southern Hemisphere general atmospheric circulation data, using constant volume balloons dispersion
11 p1755 A71-25641
- Atmosphere meteorological sounding, measuring geodetic quadrangle sides and diagonals by aircraft radio direction finder
19 p3065 A71-38175

Meteorological rocketsonde film mounted
thermist bead temperature sensor, developing
mathematical model for thermometric correction for-
mulas in automatic data processing 20 p3236 A71-39208

METEOROLOGICAL INSTRUMENTS

NT BAROMETERS

NT CLOUD HEIGHT INDICATORS

NT RADIOSONDES

NT RAIN GAGES

NT RAWINSONDES

Meteorological satellite atmospheric parameter ob-
servations, discussing instruments and techniques for
temperature and pressure profiles, wind patterns and
cloud image data 01 p0164 A71-11360

Upper atmosphere meteorological sounding facility
for recording position and telemetry data from bal-
loons, rocket payloads and meteor trails
[AIAA PAPER 70-1392] 03 p0397 A71-13673

Nimbus meteorological sensor and photographic
data application to geology and hydrology for repeat
global and synoptic observations, terrestrial mapping
and event classification 04 p0583 A71-15290

NASA satellites meteorological IR instruments,
considering purpose, design, operation and per-
formance 04 p0598 A71-15365

Dew point hygrometer with constant resistance hu-
midity transducer, using salt solution phase transition
principle 08 p1292 A71-21456

Meteorological observations and instrumentation -
Conference, Washington, D.C., February 1969
08 p1327 A71-21714

Observational data statistical evaluation, consider-
ing meteorological instrument bias, corresponding in-
strument fluctuations and noise/signal separation by
linear algebraic filter 08 p1329 A71-21726

Quality control role in meteorological instruments
maintenance 08 p1329 A71-21730

Meteorological instrument design, discussing
response, errors, accuracy, range and standardization
08 p1293 A71-21733

Meteorological instrument design, emphasizing re-
liability and maintainability 08 p1293 A71-21734

Accuracy, calibration, maintenance and optimum
design of scientific instruments for meteorological
measurements 08 p1293 A71-21735

Meteorological equipment development and test
program, discussing technical objectives, feasibility
and user requirements 08 p1330 A71-21736

Solar radiation flux standard instruments develop-
ment for meteorological measurements, discussing
calorimetric techniques and high precision radiome-
ters 08 p1293 A71-21737

Viking Mars 1975 surface meteorological transdu-
cers, discussing measurements, environment and mis-
sion constraints 09 p1448 A71-22773

Instrument tilt effect on atmospheric turbulence
measurements, presenting transformation equations
for turbulence characteristics 09 p1488 A71-23028

Rocketsonde instrumentation noise separation from
stratospheric variability, discussing paired soundings
based large scale discrepancies in temperature and
wind observations 11 p1794 A71-25386

Meteorological IR radiometer with thermosensitive
element, chopper circuit and AC microvoltmeter, out-
lining calibration procedure 11 p1763 A71-26174

Self contained lightweight airborne data acquisition
system for atmospheric and meteorological research,
using analog recorder and telemetry system 14 p2243 A71-30311

Nimbus weather satellite with IR spectrometer,
Michelson interferometer and selective chopping
radiometer for atmospheric temperature remote
sounding 15 p2445 A71-32295

Laser radar system for measuring atmospheric den-
sity above troposphere, discussing equipment design
and construction 16 p2542 A71-33534

Fog drop size distribution measurement with laser
hologram camera 16 p2604 A71-33535

Radio controlled small aircraft as measurement plat-
form for meteorological sensors, discussing develop-
ment and performance from field tests 17 p2675 A71-35334

Automatic analyzer for rapid counting and sizing of
raindrops, using collimated flashlamp source for illu-
mination 18 p2918 A71-36076

Computer-disk interface system photooptical instru-
mentation for weather data acquisition, analysis and
display 18 p2884 A71-36078

Portable run-of-wind recorder featuring variable
gear changes to facilitate range adjustments 18 p2925 A71-36960

Mean dry bulb temperature estimation during
daylight hours by subtracting proportion of average
daily range from daily maxima average 18 p2944 A71-36961

Meteorological and instrumental options for at-
mospheric vertical temperature soundings from
geosynchronous satellites, noting Nimbus 3 and ATS
measurements of cloud cover and radiance levels 20 p3240 A71-39674

Soviet papers on meteorological observation and in-
strument testing covering precipitation gages,
hygrometers, humidity gages, anemometer testing,
mobile monitoring, pyrhieliometers, etc 21 p3383 A71-41376

Dew point /frost point/ reference hygrometer for
humidity gage testing in thermohygrostat
hygrochamber 21 p3384 A71-41379

Mobile monitoring and testing meteorological
laboratory design and equipment for automated sta-
tion network, considering pressure sensors, ther-
mohygrostat and wind measurement 21 p3365 A71-41381

Atmospheric self-aligning dual-scatter laser Doppler
velocimeter, calculating backscattered power, range,
wavelength and scatter centers number relationships
22 p3359 A71-42564

METEOROLOGICAL PARAMETERS

Meteorological, optical and coronographical obser-
vations of total solar eclipse of 7 March 1970
01 p0151 A71-10116

Meteorological observations during solar eclipse of
7 March 1970 concerning temperature, wind, humidi-
ty, pressure, air circulation and optical phenomena
01 p0151 A71-10118

Aircraft measurement of vertical and horizontal
structures of temperature, moisture, refractivity and
turbulence for atmospheric convection patterns, com-
paring radar structure to meteorological soundings
01 p0116 A71-10561

Mesoscale meteorological structure during radar
CAT detection at Wallops Island during January-
March 1968 and 1969 01 p0116 A71-10568

Atmospheric turbulence characteristic parameters
determination by two narrow laser beams 01 p0119 A71-10833

Soviet book on meteorological conditions and su-
personic aircraft flight covering atmospheric composi-
tion and structure, temperature distribution, wind ef-
fects, etc 02 p0278 A71-12840

Weather effects on pilot performance 03 p0369 A71-13021

Three dimensional numerical model of unstable
planetary boundary layer integrated for convecting
and turbulent region height, mean lateral shear and
Reynolds flux direction 03 p0453 A71-13612

Tropical storms and cyclones development numeri-
cal simulation with ten-level model, considering radia-
tional cooling and physical parameters effects 03 p0453 A71-14202

Computer algorithm for distribution functions of
meteorological element on isobaric surface 06 p0922 A71-17506

Space metric as similarity criterion for meteorologi-
cal element field synoptic setup, discussing probability
for forecasting by analogy 07 p1150 A71-18872

Convective and nonconvective heat release in
mesoscale parameterization improving numerical
weather prediction 08 p1326 A71-21447

Numerical weather prediction models, discussing
automatic data processing meteorological parameter
requirements 08 p1328 A71-21723

Meteorological data quality control, discussing in-
consistencies, data interrelationships and frequency
distribution 08 p1329 A71-21729

Meteorological observations for terminal weather
modification in aviation, noting airport fog dispersal
08 p1329 A71-21732

Lower atmosphere meteorological parameters
remote determination by acoustic sounding,
discussing range and resolution characteristics 08 p1330 A71-21743

Tropospheric height integral of refractivity for pre-
dicting atmospheric electromagnetic range at arbitrary
elevation angle from surface weather data 08 p1257 A71-21881

Atmospheric turbulence parameters determination
from radar meteor observation, calculating antenna
radiation patterns effect on error 10 p1583 A71-24036

Linear vector differential Fridman equations for
cosmic and telluric effects on earth atmosphere
facilitating dynamic climate forecasts 10 p1639 A71-25115

Four dimensional space-time meteorological obser-
vation data assimilation schemes and problems 13 p2096 A71-28014

Nonzonal atmospheric motion effects on
meteorological elements 26-month oscillations stabi-
lity in equatorial zone from linear hydrothermodynamic
equations 13 p2057 A71-28022

Radio propagation attenuation calculation by
tropodiffusion, using meteorological parameters from
Brazilian weather stations 14 p2192 A71-29573

Southern Hemisphere stratosphere and mesosphere
meteorological parameters seasonal variation, com-
paring rocket sounding data with standard models 15 p2400 A71-31968

Complex monitoring of aerological information on
geopotential and temperature of principal isobaric sur-
faces by static method and optimal interpolation on
semiautomatic basis 17 p2769 A71-34299

German monograph on lower atmospheric turbu-
lence and gustiness coefficients in connection with
large scale parameters, deriving climatological flow
characteristics from wind measurements 17 p2770 A71-35233

Cross power spectral analysis of atmospheric elec-
tric potential gradient relation to meteorological
parameters, noting diurnal variations 18 p2944 A71-36010

Meteorological problems of operation of com-
mercial supersonic aircraft, including sonic boom intensity
and extent [CASI PAPER 72/7] 19 p2996 A71-37597

Meteorological prediction from joint frequency of
initial and final weather elements conditions, develop-
ing conditional probability models from bivariate nor-
mal distribution tables and Markov process 20 p3256 A71-39204

Earth surface characteristics relationship to
meteorological elements based on interpretation of
color space photographs from automated Zond 7 sta-
tion 20 p3260 A71-39687

Vortex wakes transport and decay for various air-
craft types, flight modes and meteorological condi-
tions 21 p3320 A71-40499

Atmospheric wind, temperature, turbulence,
hydrometeors, ozone, cosmic radiation and radio ac-
tivity effects on commercial SST Concorde flight 21 p3325 A71-40829

Weather interruption effects on air transportation
operations and economics, considering fog, snow,
freezing rain, thunderstorms, winds, CAT and runway
conditions 24 p3845 A71-44983

METEOROLOGICAL PROBES

U SONDES

METEOROLOGICAL RADAR

Radar meteorology - Conference, Tucson,
November 1970 01 p0113 A71-10551

Hail detection by dual wavelength radar overcoming
prior limitations, discussing equipment design and
technique limitations 01 p0115 A71-10552

CAT radar observation from instrumented and unin-
strumented jet fighter flights, analyzing data statisti-
cally for spatial correspondence of ground and air-
borne observations 01 p0116 A71-10566

Thin CAT layer detection in lower stratosphere by L
band radar complemented by radiosonde and U-2 air-
craft probes 01 p0116 A71-10567

CAT layer simultaneous radar and instrumented air-
craft observations, noting eddy dissipation rate com-
putation from radar reflectivity measurement 01 p0116 A71-10570

Convective thunderstorm propagation from Doppler
radar velocities at leading edges 01 p0117 A71-10571

Severe thunderstorm warning by single pulse Dop-
pler radar plan shear indicator 01 p0117 A71-10572

Dual Doppler radar method of convective storms
observation, noting optimization via COPLAN
scanning 01 p0117 A71-10574

Snowflakes melting region radar observation,
discussing fall speed, reflectivity profile, particle size
distribution, Doppler characteristics, etc 01 p0117 A71-10575

Radar attenuation along slant paths due to precipita-
tion, comparing ATS-5 direct measurements with cal-
culations based on backscatter and sky temperature
measurements 01 p0030 A71-10579

Radar precipitation measurement accuracy improvement, using various Z-R relationships for correlation of radar data and rainfall rates

01 p0117 A71-10581

Meteorological radar rainfall estimates comparison with dispersed tipping bucket gage measurements during storms

01 p0118 A71-10582

Storm reflectivity models using weather radar and surface rainfall data correlations

01 p0118 A71-10585

Traffic radar generated weather contours for air traffic controller in helping aircraft avoid thunderstorms

01 p0118 A71-10587

In- and outflow fields in hurricane Debbie, using airborne radar echoes and ATS 3 satellite pictures

01 p0118 A71-10589

Contour-mapped and digital data field processing and analysis for National Severe Storms Laboratory (NSSL) radar signal processing and recoding system

01 p0118 A71-10590

Weather radar echoes quantization following detection, discussing subsequent digital processing

01 p0049 A71-10591

Solid state digital integrator for weather radar signals, using recursive integration scheme

01 p0050 A71-10593

Weather radar automatic data processing system for digitizing echo reflectivity by Video Integrator and Processor

01 p0050 A71-10594

Radar weather echo data processing by digital computer, providing economical means for analyzing large quantities of data

01 p0050 A71-10596

Weather radar resolution enhancement by pulse compression system for signal bandwidth increase by phase coding

01 p0030 A71-10597

Weather radar signals decorrelation times due to vertical wind shear and azimuth scanning

01 p0030 A71-10598

Autocorrelation of weather radar precipitation patterns by incoherent optical method

01 p0030 A71-10599

Clear air convective processes radar observations, discussing development stages of convective field and individual cells

03 p0453 A71-13609

Airborne severe storm surveillance, including radar detection hurricane model

07 p1058 A71-18826

Weather radar plan position indicator automatic film reading for digital mapping of rainfall intensity, discussing raindrop sizing

08 p1286 A71-20690

High sensitivity S band meteorological radar detecting clear air echoes from low horizontal layers and high altitude turbulence

12 p1880 A71-27156

Variable target reflectivity effect on weather radar measurements, using extended echo fluctuation theory for average and maximum signals

13 p2031 A71-28723

Meteorological tower high resolution CW-FM radar measurements for studies of temperature inversions, waves, thermal plumes and convection in atmospheric boundary layer

14 p2192 A71-29707

High power 10 cm radar as CAT detector, comparing with radar and aircraft data coincident in space and time

14 p2267 A71-29761

Meteorologic bistatic radar equation for randomly distributed targets, applying to raindrops, refractivity perturbations, etc

14 p2197 A71-30830

Onboard meteorological pulse radars for cloud formations detection, navigational aids, ground reference points determination and relief surveillance

15 p2371 A71-31920

Storm models for space-path attenuation calculations using digitized weather radar data for fine structure and surface rainfall data for extrapolation

17 p2704 A71-35090

High power radar identification of preferred areas of shower development, analyzing thermal convective areas distribution

19 p3089 A71-37503

Automated meteorological radar information operation methods for cloud fields, discussing data analysis and processing

19 p3094 A71-38702

Radar Meteor 50 PPI taken pictures concerning Adriatic regions meteorologic situations

21 p3411 A71-40828

Signal reception noise stability by superregenerative transceiver in meteorological system

21 p3383 A71-41242

Parasitic radar echoes of meteorological, ground and sea origin

22 p3514 A71-42468

Laser radar for lower cloud boundary measurements, using information theory for potentials evaluation

22 p3550 A71-42850

Solid state airborne weather radar for civil aviation, discussing design, weight and power requirement reduction

23 p3647 A71-44273

Soviet papers on radar meteorology covering formations classification, signal intensity measurement, detection probability, efficiency and errors

24 p3844 A71-44876

Meteorological formation classification problems from radar data, discussing optimal solution with discrete selection space

24 p3844 A71-44877

Thunderclouds and torrential clouds classification from radar data, developing algorithm model with Bayes method

24 p3845 A71-44884

Radar vs visual observation of cloudiness and hazardous weather phenomena, emphasizing storm warnings

24 p3845 A71-44885

METEOROLOGICAL ROCKETS **U SOUNDING ROCKETS**

METEOROLOGICAL SATELLITES **NT AEROS SATELLITE**

NT ELEKTRON SATELLITES

NT ELEKTRON 2 SATELLITE

NT ELEKTRON 4 SATELLITE

NT NIMBUS SATELLITES

NT NIMBUS 2 SATELLITE

NT NIMBUS 3 SATELLITE

NT NIMBUS 4 SATELLITE

NT SAN MARCO SATELLITE

NT SAN MARCO 2 SATELLITE

NT SYNCHRONOUS METEOROLOGICAL SATELLITE

NT TIROS SATELLITES

Meteorological satellite atmospheric parameter observations, discussing instruments and techniques for temperature and pressure profiles, wind patterns and cloud image data

01 p0164 A71-11360

Soviet book on nephanalysis for synoptic forecasting covering meteorological satellite observations and network characteristics, photointerpretation, data processing, cloud identification, weather charts, etc

02 p0278 A71-12842

Atmospheric humidity and cloud moisture determination, considering meteorological satellites radio measurements errors relation to turbulent sea surface spectral radiant emittance ambiguity

04 p0621 A71-14638

Satellite meteorology, discussing system, observational data, weather prediction, communications sensors, TV imaging and global atmospheric research program

04 p0621 A71-15308

ITOS-1 meteorological satellite launch and operational sequences in orbit, discussing thermal and attitude control, power and communications and sensor equipment

04 p0663 A71-15314

Soviet monograph on thermal sounding of atmosphere by satellite covering moisture content, cloud surfaces and stratosphere temperatures and thermal radiation distribution

05 p0738 A71-16197

Meteorological satellite systems, discussing earth image transmission by TV cameras IR photography, data processing and cloud pictures

05 p0817 A71-16641

Simultaneous meteorological satellite IR radiation measurements and cloud photographs for superposition and mutual interpretation

05 p0752 A71-16676

Vertical temperature distribution measurements by meteorological satellites distribution measurements applied to numerical weather forecasting

05 p0778 A71-17044

Soviet papers on satellite meteorology covering atmospheric radiation fields, wind determination, temperature distribution transformations and cloud forms identification

06 p0922 A71-17507

Meteorological satellite data interpretation, including atmospheric layers thermal balance and global absorbed and outgoing radiation distribution mapping

06 p0923 A71-17508

Radiation temperature fields and cloud distributions seasonal and latitude characteristics by meteorological earth satellite data

06 p0924 A71-17517

Meteorological satellites scan zones latitudinal overlap for circular or elliptical orbits

06 p0898 A71-17649

Meteorological satellites remote sensing advanced instruments and techniques, discussing retrograde polar and synchronous satellite orbits

08 p1366 A71-21744

Weather satellite data for numerical analysis and forecasts, reconstructing geopotential field

09 p1486 A71-22300

Launch time selection for meteorological earth satellites, discussing launching sites, orbital altitude variations and orbit inclination

11 p1793 A71-25172

Cloud shape data, comparing meteorological satellite measurements and ground based visual observations

11 p1795 A71-26559

Instrumentation and orbital parameters of meteorological satellites observing winds, tropical circulations, heat budget, hydrology and ocean surfaces

14 p2270 A71-30498

Eole project for atmospheric phenomena studies, describing meteorological satellite/balloons arrangements, equipment and operational methods

15 p2500 A71-31824

European meteorological satellite system, discussing measurement program, data management, orbital parameters and stability, satellite positioning and instrumentation

16 p2644 A71-32844

Meteorological satellite system for weather forecasting in Mediterranean area, including visible and IR ranges survey and automatic stations and buoys interrogation

16 p2604 A71-32846

Meteorological satellites characteristics, reviewing Tiros, Itois, Nimbus, ATS, SMS and IGAR programs and vehicles

17 p2812 A71-34244

Satellite communication technology in next decade covering Intelsat 4 characteristics, meteorological satellites, navigation aids, multichannel telephone and TV circuits and frequency assignment

17 p2699 A71-34677

Itois 1 and Noaa 1 meteorological satellite systems design and operation, outlining attitude and thermal control, sensors, power supply and orbital performance

[ALAA PAPER 71-836]

17 p2814 A71-35432

Meteorological objectives, radiometry and ground stations for Meteosat weather prediction system using geostationary satellite

18 p2878 A71-36527

Worldwide data acquisition and tracking of meteorological balloon stations by flyby gravity stabilized satellite

18 p2878 A71-36528

French space programs, discussing European and international activities, telecommunication, meteorology, data collecting, natural resources and air and sea traffic control

18 p2975 A71-36753

Italian weather satellite system for Mediterranean meteorology, noting social and economic aspects

19 p3150 A71-37313

Meteosat satellite for taking earth photographs and relaying between weather stations

19 p3154 A71-38474

Earth surface effective temperature map from meteorological satellites IR imagery interpretation

20 p3260 A71-39686

Meteorological satellite IR imagery for calculating spectral values of cloudiness radiation contrasts against underlying surface background

20 p3261 A71-39689

Tracking meteorological satellite receiving antenna orientation data computer calculation, obtaining methods for geographic picture gridding

21 p3410 A71-40824

APT weather satellite cloud pictures over sea southwest of Kyushu showing striated cloud pattern transformation into closed cellular pattern, discussing lower atmospheric layer moisture budget

22 p3568 A71-41859

ITOS meteorological satellite scanning radiometer using point detector optical system for earth imaging

23 p3676 A71-43511

Cumulus clouds photographs above Northern Hemisphere by meteorological satellite during active periods of earth atmospheric circulation

23 p3701 A71-44047

Radio brightness temperature relationship to sea surface state, noting ocean storm regions determination from radiometric satellite data

23 p3673 A71-44050

METEOROLOGICAL SERVICES

Kennedy Space Center Meteorological Tower Facility, describing equipment and data acquisition mission

02 p0277 A71-12528

Global computer processing scheme for aerological radiosonde observation, using coded telegrams as primary information data

06 p0922 A71-17502

Coded recording technique for microfilming daily aerological data, decoding by computer in rapid and compact search and recognition procedure

06 p0922 A71-17503

Global meteorological systems, discussing variables information content, measurements frequency and accuracy, horizontal/vertical resolution, sensor bearing platform and cost

08 p1327 A71-21715

World Meteorological Organization global weather observing, discussing coordinate function, developing countries technical assistance, observing systems planning and UN relations

Advanced technology influence on world meteorological service requirements

Observational data characteristics analysis as contributor to knowledge and utilization of all atmospheric physical occurrences

Meteorological observing program execution legal and legislative aspects, noting social adjustment to weather effects

World Weather Watch global telemetry system including observing stations, and rockets, balloons and satellite-borne sensors, determining atmospheric states on ground and sea

Soviet papers on analysis and forecasting of meteorological conditions for aircraft flying in troposphere and stratosphere

Apollo 14 communications support by USAF, discussing voice and data relay between spacecraft and control center, global weather support, cartographic and geodetic services, etc

Soyuz 9 cosmonaut meteorological experiments, observations and atmospheric formations photographs

French-American Eole project for meteorological prediction systems development, discussing balloon sounding and satellite data transmission

24 p3876 A71-45274

METEOROLOGICAL STATIONS

U WEATHER STATIONS

METEOROLOGY

NT AEROLOGY

NT HYDROMETEOROLOGY

NT LONG RANGE WEATHER FORECASTING

NT MICROMETEOROLOGY

NT NUMERICAL WEATHER FORECASTING

NT POLAR METEOROLOGY

NT RADIO METEOROLOGY

NT STATISTICAL WEATHER FORECASTING

NT SYNOPTICAL METEOROLOGY

NT TROPICAL METEOROLOGY

NT WEATHER FORECASTING

Space technology utilization in weather problems, considering tornado and other meteorological phenomena similarity to swirling vortex formation during missile flight

Soviet papers on mechanical processing methods for aerological observations covering weather forecasting, dew point deficit computer control, etc

Poor visual flight meteorological conditions, discussing instrumental and visual aids, airport landing and approach, holding patterns and overshoots

Semiimplicit time integration scheme application to grid point atmospheric models of primitive meteorological equations

Supersonic transport air traffic meteorology, considering high altitude and flight velocities, applications technology satellites for lower stratosphere thunderstorms, clear air turbulence, etc

Solar and lunar modulation of geophysical parameters, atmospheric electricity and thunderstorms in complex space-meteorology scope

Flow theorem as circulation extension for closed curves in autobarotropic fluids in meteorology and hydrography

Single anemometer wind measurement required for aircraft landing, comparing data from different sampling periods

Meteorological research on upper atmosphere energy sinks/sources, composition, density, turbulence, winds and thermal structure

Millimeter and visible waves propagation through clear atmosphere and precipitation

Meteorological planning study for 1973 African solar eclipse observation site selection

Rumanian space research, reviewing participation in socialist nations programs in physics, meteorology, communications and biology

Japanese space research report to COSPAR, discussing meteorology, atmospheric electricity, ionosphere, magnetosphere, galactic radiation, life sciences and planetology

16 p2666 A71-33860

Report to COSPAR on French space program covering ionosphere and magnetosphere physics, meteorology, cosmic rays and earth resources

German Democratic Republic space research, reviewing meteorological, ionospheric, geomagnetic and solar physics studies

West German space research activities during 1970 on meteorology, ionospheric physics, solar radiation, cosmic rays and life sciences

Global atmospheric research with balloons, buoys and orbiting satellites for meteorological and oceanographic data recovery

Stratosphere and mesosphere physics and dynamics, studying composition, radiation fields, temperature, winds, wave phenomena and relations to meteorological theory

SST sonic boom generation, discussing aircraft design and atmospheric conditions effects and property damage

Atmospheric conditions for hailstone evolution process, using convection theory and kinetic particle model

Meteorological formation classification problems from radar data, discussing optimal solution with discrete selection space

Radar echoes maximal intensity measurements from meteorological formations, describing pulse by pulse recording system

24 p3826 A71-44883

METEORS

U METEOROIDS

METERS

U MEASURING INSTRUMENTS

METHACRYLATE RESINS

U ACRYLIC RESINS

METHANE

Turbojet engine design for methane element of liquefied natural gas as aircraft fuel, discussing supersonic transport applications

Natural gas organic Rankine cycle system for commercial on site electrical power generation and heating-cooling purposes

Spectrophotometry of methane and ammonia absorption bands indicating decrease toward Jupiter disk edge

Thermophysical properties of methane, considering virial coefficients, vapor and melting pressures

German monograph on open turbulent methane-oxygen flame temperature and concentration distribution determination from jet density measurements, using radiometric method

Commercial sodium bicarbonate powder for methane air diffusion flames extinction, noting particle surface areas

Methane and ethane binary mixtures with chlorine, determining main combustion products under flame propagation

Apollo 12 sample 12023 fines carbon, carbides and methane determination by hydrolysis and vacuum pyrolysis

Flame propagation dynamics of layered methane-air mixtures in vertical tubes, using interferometric techniques

Water vapor condensation effects on methane-air combustion gases for aerodynamic test medium

Methane spectral band analysis, examining J manifolds self broadening coefficients of R branch

Methane and deuteromethane released from Apollo 11 and 12 lunar fines by deuterated acid etch, using gas chromatography for carbon compounds separation

Thermodynamic properties prediction for liquefied natural gas and other cryogenic fluids, using two fluid method

Precision Stark spectroscopy of methane by nonlinear laser absorption, observing Lamb-dip spectra by tuning stable single mode laser

Methane and natural gas flow through critical flow nozzles, calculating real gas effects on mass flow rate

Methane high temperature oxidation in steady flow system, predicting change rate of species concentrations and gas properties during reaction

14 p2285 A71-30457

METHOD OF CHARACTERISTICS

Pressure-induced absorption in planetary atmospheres from hydrogen-methane collisions, stressing resulting thermal opacity

Liquefied gas solutions of methane in carbon tetrafluoride and propylene, calculating pressure and temperature dependence of density

Saturn polarimetric observation, noting rings polarization Stokes parameters, methane absorption bands and continuous spectrum

Saturn atmospheric structure and optical properties, investigating methane absorption bands

Reflecting layer model for methane band absorption spectrum in Jovian atmosphere

Perchloric acid reactivity with respect to hydrogen, methane, ethane and ethylene by flow method, using twin concentric jet reactor of Pyrex glass

Air-methane supersonic diffusion flame in duct, comparing pressure measurement and gas sampling data with two dimensional combustion analysis

Absorption intensities of R branch J manifolds of methane band, using half widths and pressure shifts

Injection conditions effect on ignition temperature of methane and hydrogen in hot Mach 2 air stream

High temperature oxidation of ammonia, carbon monoxide and methane by nitrous oxide in shock tubes, using optical interferometry and UV/IR emission

Gaseous hydrogen and methane injection into supersonic air stream heated by plasma burner, studying combustion effects on flow field

Counterflow methane diffusion flames structure in forward stagnation region of porous cylinder, measuring velocity, temperature, concentration, reaction rate and heat release rate profiles

Jovian planets methane and ammonium absorption bands spectrophotometric investigation, noting Saturn spectral variations

Mathematical model for atmospheric carbon monoxide production from methane

Methane atmosphere polymerization by solar UV to form primordial oil slick, discussing importance to life development

Saturn polarimetric observation, noting rings polarization, Stokes parameters, methane absorption bands and continuous spectrum

Saturn atmospheric structure and optical properties, investigating methane absorption bands

N-heptane, carbon dioxide and Freon 13 droplet vaporization measurements at supercritical pressure, comparing with film theory calculation

24 p3890 A71-45072

METHIONINE

Chemohautotroph Thiobacillus neapolitanus growth inhibition by histidine, methionine, phenylalanine and threonine under imbalance conditions

Methionine S 35 uptake rate changes in auditory analyzer receptors and neurons due to sonic stimulation in guinea pigs

06 p0850 A71-17393

METHOD OF CHARACTERISTICS

Transform for hydrogen ion exchange perturbation problem, involving first order partial differential equations and method of characteristics

Supersonic overexpanded jet flow past cone, determining impingement point by method of characteristics

Surface construction of body of revolution in supersonic gas flow from distribution of velocity vector modulus along generatrix of body, using Frankl method of characteristics

Longitudinal waves propagation in viscoelastic semifinite rod under constant velocity impact, solving by characteristics and finite difference methods

Method of characteristics application to steady rarefied gas flow from spherical source or sink

Stress tensor components partial differential equations solution by method of characteristics, using isochromatic fringes

Nonlinear hyperbolic equations integration, considering characteristic, mesh finite difference and particle in cell techniques

15 p2441 A71-31355

German monograph on characteristics and upper and lower bound methods in plastic layer theory, deriving static and kinematic equations
17 p2748 A71-34798

Method of characteristics application to supersonic jet and nozzle gas flow with allowance for equilibrium and nonequilibrium condensation
17 p2673 A71-35636

Hyperbolic and parabolic system three dimensional boundary layer equations, discussing characteristics and subcharacteristics roles in influence and dependence zones determination
18 p2902 A71-36039

Numerical integration of Euler equations for three dimensional time dependent unsteady flow by extension of method of characteristics
18 p2904 A71-36302

Second order accuracy and stability analysis of method of characteristics application to three dimensional steady supersonic flow
18 p2907 A71-36329

Frictionless hypersonic flow around body by time dependent numerical processes and method of characteristics
18 p2846 A71-36423

Oswatitsch expansion method of characteristics for weak perturbations in nonlinear propagation processes
19 p2992 A71-37452

Transonic flow theory and experiment, considering hodograph method, integral equation method, parabolic method and method of characteristics
19 p2992 A71-37454

Numerical methods for unsteady compressible flows, considering method of characteristics, Lax-Wendroff and particle-in-cell method
19 p2992 A71-37456

Nonlinear vibrating system characteristics relationship to transient process, deriving Abel integral equations for damping coefficient and restoring force
19 p3104 A71-38483

Current and potential distributions in lossless nonequilibrium MHD plasmas at high magnetic field strengths, using method of characteristics
21 p3423 A71-40946

Hypersonic flow over rearward facing step by rotational characteristics method, describing inviscid and viscous dominated regions
21 p3324 A71-40969

Perturbations generated by two dimensional supersonic channel flows with walls oscillating with harmonic time dependence and small pressure amplitude computed, using linearized method of characteristics
24 p3819 A71-44951

Conical and cylindrical shell deformation with nonlinear one dimensional wave processes, describing algorithm for method of characteristics application
24 p3885 A71-45341

METHODOLOGY

Scientific research methods and tendencies, discussing theoretical and applied aspects, deductive and empirical procedures, technology interaction, practice criteria, etc
02 p0335 A71-11853

Blunt body problem with detached shock, considering methods of lines and integral relations agreement for wide range of Mach numbers
03 p0344 A71-14449

French book on method of equal heights in astronomy covering history, general formulas, universal time and latitude measurements, star catalog, planetary observations, etc
05 p0808 A71-16450

Static computations of thin walled shells and honeycombs, examining variational, matrix, finite element, initial function, small parameter and plate bending methods
06 p0999 A71-17867

Human time estimation tests, describing methods of reproduction, verbal estimation and production in randomized blocks of trials
10 p1562 A71-24207

Large system performance test resources allocation priorities determination methodology using decision theory, discussing extensive and diminutive forms
12 p1895 A71-27438

Visual double stars observation techniques coordination - Conference, Nice, September 1969
14 p2310 A71-30356

Aircraft engine noise test methods for acoustic certification, investigating jet and compressor silencing, absorbent materials, rotor and propeller noise and psychoacoustic tests
15 p2385 A71-31890

Methodology of fatigue assessment - Conference, Kyoto, September 1969
17 p2687 A71-34352

Methodological features of programmed control of human upper extremities movements, using six-channel bioelectric system
17 p2692 A71-35170

Distributed parameter system measurement optimization devices location for error estimation cost minimization by disturbances statistical characteristics and boundary conditions
17 p2722 A71-35211

METHODS

U METHODOLOGY

U PROCEDURES

METHOXY SYSTEMS

Aminoethylisothiuronium and methoxy-tryptamine synergism quantitative analysis by pharmacological methods of radioprotective effect in X irradiated mice
07 p1038 A71-18971

Biosynthesis control of melatonin and other methoxyindoles in mammalian pineal organ
14 p2182 A71-29631

METHYL ALCOHOLS

Methyl alcohol detection in Sagittarius, examining radio line emission at 834 MHz
05 p0802 A71-15945

Methanol stress corrosion cracking of Ti-Al-V foil inhibited by pretreatment in aqueous solutions of electrolytes, discussing colloidal character of microcrystallites
07 p1142 A71-20362

Ethyl and methyl alcohol droplets vaporization rate variation with respective distance from photographic observations
14 p2285 A71-30612

Methyl alcohol transitions in Orion at 1 cm noting emission source coincidence with IR nebula
21 p3447 A71-40445

METHYL CHLORIDE

Spectroscopy and collisional transfer in methyl chloride by microwave laser double resonance, measuring population changes in various rotation vibration levels
12 p1877 A71-27004

METHYL COMPOUNDS

Ethylene oxide and methyl bromide sporadic activity compared for spacecraft sterilization of *B. subtilis* var niger spores
01 p0027 A71-11565

Methyl radicals reactions produced by azomethane or ethane pyrolysis in reflected shock waves, describing chain reaction mechanism
08 p1250 A71-20668

Atomic and molecular hydrogen yields of propyne photolysis at 1470 Å Xe resonance line
09 p1403 A71-23378

Styrene-methyl methacrylate and -acrylonitrile copolymers linear and mass regression rates in hybrid rocket fuels combustion
15 p2464 A71-31640

Carbon and methyl radical formation, studying emission intensities and chemi-ionization rates in hydrogen-oxygen flames with hydrocarbons
19 p3013 A71-38090

Millimeter emission lines from interstellar methyl cyanide transitions, noting kinetic temperature and hydrogen density
21 p3447 A71-40446

Toluene and aniline-methylcyclohexane and toluene-aniline nonideal liquid systems, measuring molecular diffusion coefficients as function of concentration by Savart plate birefringent interferometer
24 p3820 A71-45074

METHYLENE

Flash photolysis produced methyl and methylene radical transitions maximum extinction coefficients and oscillator strength in vacuum UV
12 p1876 A71-26788

METHYLHYDRAZINE

Methylhydrazine radiosensitization of Ehrlich ascites tumor cells, investigating X radiation enhanced cell killing effect via deoxyribonucleic acid strand breakage
07 p1035 A71-18955

Acute inhalation toxicity of monomethylhydrazine vapor on rats, mice, beagles, squirrels and rhesus monkeys, considering hematology and blood chemistry tests
07 p1046 A71-19000

Tannic acid and water washing effects on prevention of monomethylhydrazine absorption through skin in dogs
16 p2535 A71-33119

METRIC PHOTOGRAPHY

Lunar mapping metric camera subsystems stellar calibration for photography maximum usability in photogrammetric data reduction
13 p2071 A71-29348

METRIC SPACE

NT HILBERT SPACE

Real turbulent fluctuations superimposed on metric and satisfying free space Einstein equations, basing model on oscillating gravitation and elementary particles as excitons
17 p2777 A71-34586

Exact solutions to radiation-filled Brans-Dicke cosmologies, using Robertson-Walker metric
20 p3294 A71-39558

Spherically symmetric Gaussian coordinate systems completeness in spaces analogous to Lemaitre and Kruskal spaces in general relativity
24 p3848 A71-44658

METROLOGY

Laser metrology, discussing precise distance measurement techniques based on modulated CW and

pulse sources, laser systems for constructional angular alignment and materials spectrography
04 p0606 A71-14719

Nondestructive monitoring calibration and alignment with standard specimens conforming with metrological regulations
08 p1300 A71-21895

Metrological holographic interferometry, discussing speckle pattern application for wavefront phase samples
10 p1613 A71-25092

Equivalent circuit concepts in diagnostic metrology as converging logical-physical process, stressing electronic failure analysis
12 p1890 A71-26666

Phase modulation in far IR interferometers applied to Fourier spectrometry and metrology, obtaining modulus, phase, absorption and refraction spectra
14 p2238 A71-29742

Nucleon-nucleon and nucleon-nucleus interaction energy measuring system at mountain elevation, discussing components and design
14 p2247 A71-30600

Gravitational constant measurement by resonance method, describing experimental device
16 p2575 A71-34060

Holographic interferometry for speckle pattern interpretation in metrology, using video techniques
18 p2917 A71-36056

MICA

NT MUSCOVITE

Epitaxial deposition of Au on ultrahigh vacuum cleaved mica during early nucleation and growth
14 p2284 A71-30072

Mica selection quality criteria for capacitors, outlining electrical, physical and optical properties standards
22 p3520 A71-41712

MICE

Arterioles, arteriovenous anastomoses and efferent veins functional behavior in anesthetized white mice ears
01 p0007 A71-10035

Audioconditioned convulsive response /ACCR/ characterization, investigating age, auditory conditioning and environmental noise effects on sound-induced seizures in mice
03 p0360 A71-13162

Circadian patterns of deer mice oxygen consumption in constant dark and thermally neutral zone
06 p0856 A71-18381

Mouse Ehrlich ascites tumor cells, examining Co-60 gamma ray influence in presence of radiosensitizing 5,8-dihydroxypsoralen
07 p1035 A71-18953

O-barenylacetic and methyl-o-barencarboxylic acids effects on mice radiosensitivity to fast neutrons and gamma rays
07 p1038 A71-18976

Seasonal effect on daily periodicity of mice radiosensitivity related to changes in bright/dark day time proportion and feeding
10 p1565 A71-24654

Fighting between male mice isolated at early age or reared in small groups, considering ontogenetic and experiential determinants
13 p2011 A71-28805

MICHELSON INTERFEROMETERS

Atmospheric turbulence effects on stellar Michelson interferometry
02 p0308 A71-12099

Single mode polarization in simple gas laser for long path difference Michelson interferometry
03 p0436 A71-13653

IR Q switched gas laser with Michelson interferometer for plasma diagnostics, describing equipment operation
03 p0439 A71-14056

Atmospheric turbulence effects on stellar Michelson interferometry
08 p1362 A71-21149

High resolution laser homodyne interferometer for determining small time resolved optical path length variations, using Michelson interferometer with He-Ne laser
10 p1611 A71-24507

Variable output coupling far IR gas lasers, using Michelson interferometer with polyethylene or polypropylene beam splitter
11 p1773 A71-25805

High resolution far IR interferometer in Michelson configuration for measuring gas optical properties in symmetric or asymmetric operation mode, testing performance
12 p1904 A71-26799

Submillimeter wave region solar radiation atmospheric absorption by Fourier spectrometry and double output Michelson interferometer with Golay cell detectors
14 p2307 A71-29740

Phase modulation theory for two-beam far IR Michelson interferometers, discussing application to Fourier transform spectrometry
14 p2238 A71-29741

Selective modulation spectroscopy by taking interference between reflected and diffracted beams of modified Michelson interferometer

14 p2241 A71-30137
Michelson interferometer onboard Nimbus 4 satellite for recording earth IR emission spectrum
14 p2241 A71-30140
Nimbus weather satellite with IR spectrometer, Michelson interferometer and selective chopping radiometer for atmospheric temperature remote sounding

15 p2445 A71-32295
Infrared Michelson interferometer system digital data processing by computer, developing spectral density plots

18 p2920 A71-36092
Relaxation processes in Michelson interferometer as integral part of carbon dioxide laser cavity in phase Q switching regime

19 p3071 A71-37389
Solar brightness temperature measurements using balloon-borne Michelson interferometer

19 p3135 A71-37613
Spectral density modulation visibility at Michelson interferometer exit illuminated with white light parallel beam

21 p3375 A71-40072
Stratospheric submillimeter wave emission and water vapor mixing ratios measurements, using Michelson interferometer with phase modulation and Fourier spectroscopy methods

22 p3545 A71-42145
Book on interference of electromagnetic waves covering Michelson-Fizeau and Fabry-Perot interferometers, Fourier transform spectroscopy, etc

22 p3576 A71-42429
Atmospheric background radiation measurements with balloon-borne Michelson interferometer, noting data reduction and calibration methods

22 p3549 A71-42563
Far IR spectrum analysis using Michelson interferometer with beam splitter

23 p3676 A71-43400
Laser mode suppression arrangements consisting of Michelson interferometers with polarization prism as beam splitting element

24 p3835 A71-45264
MICROANALYSIS
Spectrochemical analysis of alloy steels using microspark method

03 p0375 A71-13974
Quantitative spectrographic microanalysis using laser pulse vaporization and spark discharge
03 p0438 A71-13975

Scanning electron microscope for surface morphological investigations of materials after laser irradiation

07 p1113 A71-19793
Intracrystal liquefaction in Ni alloys containing Nb studied with microanalyser

09 p1480 A71-23702
X ray absorption and atomic number corrections in quantitative microprobe analysis of metals

14 p2277 A71-30476
Sn-Pb alloy solidification point analysis around liquid-solid front with interface visualization by electron microprobe

20 p3238 A71-39416
Vacuum pumped Apollo 12 lunar soil sample 12001,118 gas exposure effects, interface microanalysis and adhesion measurements in ultrahigh vacuum system

23 p3759 A71-43767
Microelement extraction from mineralized biological samples in food rations and human excretions

24 p3800 A71-44540

MICROBE

U MICROORGANISMS

MICROBEAMS
Laser microbeam welding, drilling and trimming of electronic devices

07 p1118 A71-19787

MICROBIOLOGY

NT BACTERIOLOGY

Blue green algae activity in Kratz-Myers medium, noting C 14 uptake changes for monocultures and mixed cultures of *Acanthocyclops* and *Synechocystis aquatilis*

06 p0858 A71-17392
Automatic cytophotometric techniques including microphotometer, ultramicrospectrophotograph, microanalyser, microinterferometers, cytofluorometer and differential microfluorometer

06 p0864 A71-18693
Follow-up scanning system input of microobject data with maximum contraction for biological computer analysis, noting karyotype or blood formula applications

06 p0864 A71-18698
Organic free radical photographic films for biomedical microimaging

07 p1110 A71-19475

Skin tissues automicroflora composition and natural immunity indices changes after 18 day orbital flight from microbiological and immunological examinations

09 p1389 A71-22204
Pretertiary invertebrate fossil remnants and microcoprolites found in Lower Himalayan Basin

11 p1721 A71-26318
Microbiological contamination of jet aircraft fuel tanks in tropical regions, considering maintenance [SAE PAPER 710438]

13 p1996 A71-28320
Microbiological respirometer for oxidative metabolism for plants and small animals, considering manned space flight applications

14 p2189 A71-30344
Substrate and light dependent fixation of molecular nitrogen in *Rhodospirillum rubrum* tested for nitrogenase activity by manometric measurement

16 p2527 A71-33057
Photoreduction regulation in *Rhodospirillum rubrum* by ammonium chloride, discussing nitrogen fixation and protein metabolism

16 p2527 A71-33058
Ion-membrane hydrogen oxygen fuel cell, using microbially or biochemically produced hydrogen by enzymatic reactions

16 p2527 A71-33550
Microbial contamination of human skin and upper respiratory tract during long term isolation in sealed environment

21 p3333 A71-40559
Microbiological analysis for surviving terrestrial microorganisms from Apollo 12 retrieved Surveyor 3 spacecraft electrical cabling

23 p3633 A71-43814
Pharyngeal streptococcal flora of men confined in sealed chamber, observing microbial transfer

24 p3800 A71-44530

MICROCALORIMETERS

U CALORIMETERS

MICROCHANNELS

Surface electronic conductivity in oxide glasses for microchannel electron multipliers, noting heat treatment and chemical composition effects

24 p3862 A71-45327
Computer model of microchannel electron multiplier plates in imaging devices using Monte Carlo method

24 p3811 A71-45328
Photoelectric tubes microchannel plates degassing during bake-out or during operation by electron bombardment, discussing desorption elimination by multiplier treatment before tube sealing

24 p3811 A71-45337

MICROCIRCUITS

U MICROELECTRONICS

MICROCLIMATOLOGY

Hypodynamia effects on human hemodynamics under various microclimatic conditions, noting hormonal activity changes in sympathoadrenal system

10 p1563 A71-24339

MICROCRACKS

Crystal dislocations and vacancy colonies complexes generation, discussing metal fatigue microcracks mechanism

06 p1002 A71-18419
Fracture kinetics, emphasizing plastic deformation, dislocation and diffusion micromechanics, point defects effects and microcrack formation

08 p1371 A71-21606
Microcrack formation in carbon fiber-resin matrix composites under thermal stress

12 p1920 A71-27013
Optical holographic interferometry for radial microcracks detection from bolt holes in high strength aircraft steel

[ASME PAPER 71-MET-C] 12 p1911 A71-27312
Thermally activated crystal microcrack initiation by fusion of leading and following dislocations

13 p2149 A71-28118
Open microcracks and internal microdefects detection during long term strength testing in vacuum by mass spectrography

15 p2383 A71-31653
Acoustic indicator for remote detection of microcracks in systems with high gas or vapor pressures

15 p2409 A71-32189
Microcracks detection in high strength steel by optical holographic interferometry, comparing results with magnafux, eddy current and X ray inspection methods

15 p2409 A71-32258
Magnetic field perturbation and electric current injection techniques for characterizing high strength alloys fatigue microcracks

16 p2581 A71-32865
Strain analysis based on thin metallic film optical measurements, determining principal strain directions from wrinkle and microfracture patterns

[SESA PAPER 1828A] 17 p2820 A71-34551
Microcracks analysis by micropolar continua theory, presenting solution for circular hole in infinite plate

17 p2832 A71-35421

Fracture kinetics, emphasizing plastic deformation, dislocation and diffusion micromechanics, point defects effects, microcrack formation and interstitial mechanisms

17 p2834 A71-35667
Pure Al annealed polycrystal electron microscopic observation for fatigue deformation at room and elevated temperatures, noting dislocation loop role in crack initiation and propagation

22 p3564 A71-42497
Glass particles crystallization in sintered metal matrix glass materials, examining microcracks and temperature and cyclic heating effects

23 p3696 A71-43251

MICROCRYSTALS
Ti microcrystals on single crystal tungsten substrate, discussing phase transformations

05 p0768 A71-16854
Microcrystal orientation in recrystallized tungsten structure by charged particles channelography

18 p2954 A71-36804

MICROCYSTIS

Blue-green algae *Microcystis aeruginosa* central zone cellular structure electron microscopic investigation, noting absence of distinct boundary between central and peripheral regions

23 p3640 A71-44054

MICRODENSITOMETERS

Elastomer O ring vacuum device for positive holding of Schumann film for precise microdensitometry during rocket flight in 7 March 1970 solar eclipse

14 p2249 A71-30887
X-Y programmed microdensitometer for stellar spectra analysis, imaging adjustable slit on spectrogram by interchangeable microscope objectives, using Kohler illumination

17 p2742 A71-35000
High resolution microdensitometry image interpretation and manipulation by digital computer, discussing radiation coherence problems

17 p2742 A71-35002

MICROELECTRONICS

NT LARGE SCALE INTEGRATION

NT MEDIUM SCALE INTEGRATION

Command system and associated algorithm for synthesis of integrated microcircuits composed of components with memories

01 p0051 A71-10090
Feedback circuit for constant current stimulation through intracellular microelectrode

01 p0021 A71-10245
Sequential environmental testing effects on large hybrid microcircuit packages, reviewing solder sealing processes and repair methods

01 p0053 A71-10732
Hybrid microcircuits reliability, discussing test data regarding receiving and sample inspection, environmental and performance testing, etc

01 p0053 A71-10733
Microelectronic remanent type /latching/ circulating, switching and phase-shifting microwave devices design and performance

02 p0228 A71-11654
Microelectronics technology effects on electronics engineer education, considering data processing applications and circuit types

03 p0388 A71-13005
Small-tipped microelectrode minimizing capacitive artifacts during current passage through bath in membrane potential measurement

03 p0372 A71-13912
Reciprocal thermal influence, temperature areas and conduction distance of electronic components in compact circuits

03 p0387 A71-14325
Microcircuits component vulnerability, deriving time independent nonlinear terminal I-V characteristics, electrical switching response and ionizing radiation induced transient response

07 p1070 A71-19059
Plastics for long life microcircuit encapsulation, investigating materials properties and failure mechanisms for device reliability assessment

07 p1077 A71-19561
Plastics for long life microcircuit encapsulation, investigating water absorption and resin-to-lead adhesion effects on reliability

07 p1077 A71-19562
MOS transistors and bipolar microcircuits mobile charge density, observing p-n junction effects

07 p1079 A71-20175
Low noise C band beam lead tunnel diode amplifiers characteristics and application in low cost microstrip reflection amplifiers

08 p1262 A71-20759
Low noise microstrip microwave mixer-preamplifier on thin polyolefin reinforced with Al, discussing design and manufacture

08 p1263 A71-20771
Wideband X band microstrip image rejection balanced mixer design

08 p1263 A71-20772

Microelectronic circuits reliability in aircraft engine control applications, discussing testing and selection for severe temperature and vibration environments [SAE PAPER 700822] 08 p1265 A71-21369

Hybrid integral microcircuits with thin film resistor heat sources, determining temperature fields on substrate and boundaries 09 p1416 A71-22495

IC quality control by temperature fields contactless measurement, using microthermographs 09 p1450 A71-22894

Laser microwelding, discussing focusing properties, high power radiation interactions, metal working, machining and microelectronic applications 09 p1458 A71-23407

Noise analysis of microelectronic active RC filters by cascade of passive and active networks, considering low pass filter 10 p1582 A71-23915

Experiment planning in electronic component design and microelectronics, using mathematical theory for optimal strategies 12 p1885 A71-26712

Direct analysis of IC by laser beams, considering homogeneity test scanning of Ge semiconductor crystals through photovoltaic injector microscopy 12 p1914 A71-27041

HF microcircuits packaging inside magnetic cores, discussing inherent advantages of RF interference and radiation shielding and heat transfer properties 12 p1888 A71-27433

Batch fabricated three dimensional planar coaxial microelectronic interconnection and packaging technique for semiconductor chips 12 p1890 A71-27771

Ion and electron beams technology application to microelectronics, discussing limitations imposed by electron/ion optical effects 14 p2277 A71-30701

Thick film microcircuit DC-TO-DC converter electronics design for TOPS spacecraft power subsystem 14 p2214 A71-30801

Book on solid state power supplies covering transistorized DC/DC converters and DC/AC inverters, oscillators, power amplifiers, transformers, inductors, magnetic amplifiers, voltage regulators, etc 14 p2182 A71-30857

Microstrip microwave amplifier design using common emitter configuration and quarter wave impedance matching transformer 16 p2545 A71-33395

Electron-optical system with electro- and magneto-static lenses, ensuring large image reduction for producing printed microcircuits 16 p2579 A71-33500

Optimal design of logic networks in homogeneous microelectronic structures, using shortest link search and graph continuity parameters 16 p2545 A71-33704

Space tractography radars for measurements on military firing ranges and civil space centers, using microelectronics for data processing 16 p2544 A71-34098

Redundant modules introduction in microelectronic systems for increased reliability 17 p2716 A71-34954

Redundancy method for correct performance of flexible structure with faulty elements prepared from microelectronic information media 17 p2720 A71-34955

Densely packaged microelectronics thermal control, using immersion cooling in dielectric fluids 17 p2718 A71-35786

Minerva digital computing system with learning cells and electronic microcircuit elements capable of self organizing similar to human intelligence 19 p3025 A71-37420

Digital integrated circuits technology with MOS transistors packed on crystal wafer without isolation diffusions 19 p3028 A71-37566

Plastic encapsulation for microcircuits including packaging, failure mechanisms, military qualifications and economic factors 19 p3033 A71-38508

Hybrid microelectronics IC S band double conversion phase locked receiver, discussing fabrication, process requirements and component selection criteria 19 p3035 A71-38538

Microelectronics high power hybrid circuit design, discussing application of packaging techniques to 10 Amp series regulator 21 p3353 A71-40440

Distributed RC network application as microelectronic delay line, discussing delay response improvement by compensating network 21 p3353 A71-40589

Microelectronics - Conference, Munich, November 1970 21 p3353 A71-40726

Precision relaxation oscillators design and error sources, discussing miniaturization by microelectronic approaches 21 p3355 A71-40736

Cholesterol liquid crystals technique for thermal analysis of microcircuits, multilayer circuit boards, semiconductor devices and other electronic components 21 p3355 A71-40738

Masking techniques in monolithic IC production in microelectronics, emphasizing contactless, lens, holographic and electron beam projection methods 22 p3525 A71-41713

Wireless assembly methods for thin and thick film hybrid and monolithic IC, emphasizing flip-chip elements microelectronic devices fabrication and interconnection 22 p3525 A71-41714

Cost effective general purpose minicomputer PDP-11/45 design and technology using Schottky TTL/MSI, semiconductor memories, multiple buses, microprogramming and floating point units 22 p3519 A71-42761

Thick film hybrid microcircuits for spacecraft electronic systems component reliability 23 p3650 A71-43123

Book on thick film microelectronics covering microcircuit design, fabrication, packaging and applications 23 p3650 A71-43224

Conventional components in hybrid circuits, using leadless inverted device, SOT-23 transistor and multilayer ceramic capacitors 23 p3655 A71-43349

Thick film technology and tests for hybrid microcircuits and semiconductor packaging 23 p3651 A71-43430

Thin film circuit microstructures and integrated microcircuits with distributed parameters, discussing analytical determination of microcell parameters 24 p3807 A71-44378

MICROFILMS

Computer output microfilm /COM/ technology, describing recorders and applications 01 p0047 A71-10218

Computer microfilm data recorder for output speed increase and information retrieval, discussing cost reduction 01 p0048 A71-10219

Coded recording technique for microfilming daily aerological data, decoding by computer in rapid and compact search and recognition procedure 06 p0922 A71-17503

MICROGRAPHY

U PHOTOMICROGRAPHY

MICROHARDNESS

Molybdenum borocarbide synthesis and properties, discussing melting temperature, electrical and heat conductivity, thermal emf, microhardness, etc 01 p0100 A71-10402

Statistical study of microhardness across thickness of gas saturated layer distribution on surface of Ti alloys 02 p0265 A71-12524

Vanadium and niobium carbides as function of C content, studying lattice constants, microhardness and electrical resistivity 06 p0912 A71-18086

Mo-Ti-C ternary alloy, examining solid state solubility, equilibrium conditions and microhardness 10 p1628 A71-24647

Mo-Fe-C ternary system, investigating various concentrations, microhardness measurements, solid state solubility and ductility 10 p1628 A71-24648

Ti-Zr alloying in for microstructural hardness and mechanical strength increases, discussing Zr concentrations at Nb granular boundaries 11 p1782 A71-26470

Boron or phosphorus doping of silicon, noting microhardness increase and friction coefficient reduction 12 p1911 A71-26820

Disintegration energy of hard compounds /carbides, nitrides and borides/ related to wear resistance and microhardness of alloys 13 p2072 A71-27818

W, Mo, Ta and W-Mo alloys hardness integrity, using high temperature microhardness tester 13 p2084 A71-28113

Transition metals addition effects on cast Zr grain size, microhardness and electrical resistivity, explaining results in terms of solid state electron theory 15 p2424 A71-31239

Hot pressed transition metal carbide samples microhardness measurement, interpreting results in terms of atomic electron configurations 15 p2431 A71-32162

Microhardness dependent saturation of glass powders by iron, nickel and titanium during sintering of cermet metal matrix materials in vacuum 16 p2601 A71-33573

Al-Cu-Li-Mn and magnesium/rare-earth-element alloys heat resistance and microhardness, determining strengthening by intermetallics 16 p2597 A71-33926

High temperature creep of niobium alloy, obtaining creep limit, microhardness and gas analysis data 18 p2936 A71-36715

Structure, superconductivity transition temperature, microhardness and electrical resistivity of V-Ta-Ti cast alloys 19 p3078 A71-37468

Orientation dependent microhardness and columnar and feather crystal structures of directionally cast Al alloys in tensile test bars 21 p3399 A71-40471

Elastoplastic work hardening material characteristics, using microhardness analysis 21 p3468 A71-41001

Microhardness, thermo-emf and phase composition of Al coatings on Armo iron and steel under furnace and rapid electric heating 21 p3389 A71-41096

Microhardness and magnetic permeability and viscosity changes during fatigue loading of steel parts, describing electromagnetic fatigue testing method 22 p3554 A71-41771

Sintering of Ni based heat resistant alloy, determining phase composition, lattice constant and microhardness of compressed specimens 23 p3691 A71-43521

Vacuum fusion sintered rhodium borides melting point, microhardness and conductivity and thermal emf temperature dependences determination by thermal metallographic and X ray analyses 23 p3717 A71-44024

Temperature effects on niobium carbide friction process in vacuum conditions, considering surface layer microhardness and X ray and metallographic analyses 23 p3692 A71-44030

Vacuum annealing and residual gas effects on Mo single crystal dislocation structure and microhardness 23 p3838 A71-44740

Homogenizing annealed TiC-WC carbides properties at room temperature, investigating microhardness, microbrittleness and resistivity 24 p3838 A71-44741

Titanium, niobium and tungsten carbides microhardness temperature dependence at 77-1973 K, discussing activation energy and deformation mechanism 24 p3838 A71-44741

MICROINDENTATION

U MICROHARDNESS

MICROINSTRUMENTATION

Microsensor measurement of spatial correlation between pressure fluctuations of turbulent boundary layer 04 p0600 A71-15636

Materials microstrain determination using automatic capacitance bridge gage and analog or hybrid computer for measurement signal processing 10 p1609 A71-23916

Mercury transit across solar disk on 9 May 1970, using photographic micromasurements 10 p1677 A71-24587

MICROMANOMETERS

U MANOMETERS

MICROMETEORITES

U MICROMETEORITIDS

MICROMETEORITIDS

NT METEOROID DUST CLOUDS

NT ZODIACAL DUST

MOS capacitors as low mass micrometeoroid detectors in near-earth space, discussing fabrication and environmental tests 01 p0083 A71-11310

Meteor particle speed and size estimation using accelerated glass microsphere bombardment in plasmoid 02 p0304 A71-11914

Micrometeorites composition and mass distribution in earth orbit vicinity, describing spaceborne and ground based data acquisition 02 p0313 A71-12470

Upper atmosphere micrometeorite research with sounding rockets, considering interplanetary particle flux 03 p0485 A71-13250

Calibration of condenser microphone micrometeoroid sensor, using bead drop and hypervelocity impact tests 03 p0422 A71-13284

Micrometeorite sputtering in ionosphere producing influx of meteorite atoms and ions in atmosphere, considering temperature dependence of stone meteorite sputtering coefficient 03 p0486 A71-13309

E layer meteor ionization, considering ablation processes effects of meteoroids evaporation and micrometeorites sputtering 03 p0486 A71-13310

Low micrometeoroid flux on lunar surface from comparative Surveyor 3 and Apollo 12 pictures 03 p0490 A71-13783

Cosmic dust fluxes determination by rocket-borne micrometeorite experiments, using piezoelectric acoustic type impact detectors 03 p0492 A71-14017

Micrometeorites orbital elements, evaluating cosmic dust experiment data from Pioneer 8 03 p0496 A71-14505

Cosmic ray intensity variations from magnetic fields of micrometeor streams in interplanetary plasma
06 p0954 A71-18126

High velocity microparticle simulation techniques for studying properties, dynamics and origin of micrometeoroids, considering accelerators and impact results
[AIAA PAPER 70-30] 09 p1425 A71-22099

Micrometeoroid detector design for hypervelocity particle impacts, discussing solar radiation pressure effects on satellite measurements
11 p1761 A71-25544

OGO 4 satellite micrometeoroid flux detection, emphasizing noise control procedures for data correlation
13 p2145 A71-28700

Terrestrial influx of small meteoric particles, discussing data uncertainties
14 p2307 A71-29902

Micrometeor mass data from radiometer measurements, detailing Cu and lanthanum hexaboride ionization probability
14 p2315 A71-30652

Micrometeoroids bibliography and review, considering ground based photometry and scattering theory, satellite flux measurements, particle collection and craters
17 p2798 A71-34456

Sikhote-Alin shower region soil samples and meteorite and micrometeorite fragment morphology, emphasizing silicate spherules
17 p2810 A71-35718

Heating, fusion and atomization of meteoric bodies in earth atmosphere
17 p2810 A71-35724

Microcrater morphology in lunar soil glass, oligoclase and olivine, determining projectile velocity, impact angle and shape effects
18 p2961 A71-35947

Microcrater morphology in soda-lime-silica glass by polystyrene spheres, detailing shape, density, velocity and incidence angle effects
18 p2961 A71-35948

Micrometeorite craters on lunar rock surfaces, suggesting cosmic particles impact
19 p3138 A71-37686

Outer planets missions combined zodiacal experiment, examining meteoric, asteroidal and satellite particles distribution and orbits
[AAS PAPER 71-127] 19 p3064 A71-37919

Pioneer 8 and 9 micrometeorite measurements of particles kinetic energy, momentum, velocity and direction, correlating measured particle flux rates with predictions based on zodiacal light
20 p3297 A71-39634

Galactic cosmic ray effects on interplanetary dust particles erosion and spurious counts in micrometeoroid sensors, microphones and capacitor detectors
20 p3280 A71-39635

Zodiacal light lines in interplanetary dust particle flux diagram, suggesting agreement with micrometeorite data
20 p3298 A71-39636

Incident meteor flux density seasonal variations from radio reflections from trains and light scattering from micrometeoroids
20 p3298 A71-39642

Italian soil particles of cosmic origin, noting space research activities relation to micrometeorites and dust studies
20 p3298 A71-39644

Combined micrometeoroid collection and detection rocket experiment using foil penetration and plasma emission at impact for flux, masses and particle velocity determination
20 p3299 A71-39645

Micrometeoroid flux acoustic measurements by Cosmos 135 and 163, discussing detection of shower activity
20 p3299 A71-39649

Qualitative micrometeoroid model for predicting results of in situ experiments, considering correlation to Pioneer 8 and 9 results
20 p3300 A71-39654

Micrometeoroid flux determination from impact sites on Surveyor 3 TV camera optical filter surfaces, noting agreement with Pioneer, Cosmos and Pegasus spacecraft measurements
23 p3766 A71-43820

MICROMETEOROLOGY
Turbulent mixing and radiative transfer relationship to micrometeorological temperature structure of atmospheric boundary layer
10 p1638 A71-23878

Agna rocket engine pollutants, considering pollution control by scrubbers, engine system modification and micrometeorological data gathering
[AIAA PAPER 71-716] 14 p2294 A71-30768

MICROMETEORS
U MICROMETEORIODS
MICROMETERS
Circumzenithal micrometric recording of aluminic passages of stars
03 p0422 A71-13011

Automatic micrometer for measurement of limb graduations and scales, basing method on Archimedes rotating spiral principle
04 p0591 A71-14851

Micrometer screw revolution value determined by method of scale pairs for Bamberg zenith telescope, noting dependence on temperature and declination differences of star pairs
08 p1292 A71-21675

Ocular micrometer screw revolution value of instruments of astronomical universal type from scale pair outside of meridian
08 p1292 A71-21676

Screw run and period error stability of eyepiece micrometer of universal astronomical instruments showing dependence on attitudes in space
09 p1451 A71-23179

Orbit computation and measurement errors of visual binaries by wire micrometer distance method
14 p2312 A71-30372

International zenith telescopes micrometer value, determining correction for ocular screw from latitude observations
23 p3680 A71-44261

MICROMINIATURIZATION
NT LARGE SCALE INTEGRATION
Data reduction for information retrieval, considering electron beams application for electronic circuit ultraminiaturization
06 p0871 A71-17525

Superconductivity based cryogenic electronics, considering thin film IC, miniaturization, microwave circuits, memory elements, etc
08 p1263 A71-21067

Microencapsulation of bonded reactive resins in packaging, logistics and adhesive applications at room and elevated temperatures
10 p1634 A71-24120

Magnification level for optimum performance at microminiature inspection with binocular microscope, minimizing time
17 p2689 A71-34704

MICROMINIATURIZED ELECTRONIC DEVICES
NT MICROMODULES
Optimized low loss microstrip microwave filters on silica substrates by photolithographic reduction of LF models
19 p3026 A71-37218

Permittivity increase in fluor-substituted barium titanate solid solutions for ceramic capacitor microminiaturization
24 p3859 A71-44387

MICROMODULES
Integrated S band microstrip parametric amplifier modules with self contained Gunn effect pump oscillator for space flight applications
14 p2210 A71-29570

MICROMOTORS
Dual phase asynchronous or hysteretic micromotors powering with two transistorized static DC to AC voltage converter circuits
13 p1999 A71-28629

Symmetrical hysteretic micromotors stator structure with windings around unilateral crowned teeth, calculating maximum EM power in starting mode
13 p1999 A71-28631

Optimization of mechanical characteristics of asynchronous capacitor microengine designs with asymmetric stator circuit for prolonged continuous operation with negligible steel wear
13 p2002 A71-28929

MICROORGANISMS
NT AEROBES
NT ANAEROBES
NT BACILLUS
NT BACTERIA
NT BACTERIOPHAGES
NT ESCHERICHIA
NT HYDROGENOMONAS
NT KLEBSIELLA
NT MESOPHILES
NT MICROCYSTIS
NT PARAMECIA
NT PROTOZOA
NT PSEUDOMONAS
NT PSYCHROPHILES
NT SPORES
NT STAPHYLOCOCCUS
NT STEAROTHERMOPHILUS
NT STREPTOCOCCUS
NT STREPTOMYCETES
NT VIRUSES
Soil microorganisms multiplication under simulated Martian conditions in limonite and garden soil mixture
01 p0019 A71-11558

Free radicals role in photodynamic inactivation of Rhodotorula glutinis subjected to high intensity light irradiation
01 p0019 A71-11560

Dry heat destruction rates for microorganisms encapsulated in and on spacecraft hardware, concluding temperature and water conditions in spore as major factors
01 p0027 A71-11564

Spacecraft sterilization by microbial inactivation, comparing thermoradiation and dry heat methods
06 p0853 A71-17959

Probability theory for viable microorganism exposure in fractured contaminated solid, using quantal response model
07 p1048 A71-19600

Extraterrestrial life hypotheses, citing astronomical considerations, inorganic chemical evolution and prebiotic synthesis with emphasis on Mars exploration for microorganisms
07 p1044 A71-20374

Apollo 11 lunar samples effect on terrestrial microorganisms, noting pigment production effects of Fe leaching from bulk fines and core samples
10 p1566 A71-23747

Terrestrial microorganisms adaptation to simulated methane-ammonia-hydrogen Jupiter atmosphere
10 p1566 A71-24688

Electrical and physical nature of microbial membranes implicated in aircraft fuel quantity probe malfunction
[SAE PAPER 710439] 13 p2113 A71-28321

Optimal mineral-organic nutrient medium and soil selection for microorganism detection on Mars
13 p2009 A71-28681

Visible and UV photometric recording of microorganism reproduction in liquid medium for application to Mars extraterrestrial life detection
13 p2019 A71-28682

Extraterrestrial life detection by measuring microorganism breeding dynamics with photometric, radiometric and bioluminescent methods from chemiluminescent reactions
13 p2068 A71-28686

Simple organisms resistance and adaptation to low pressure, anoxia, intense cooling, UV irradiation and Mars conditions
13 p2009 A71-28687

Xerophyte soil microorganisms reproductive stability in artificial Mars environment chamber at maximum hygroscopic moisture
13 p2019 A71-28690

Extraterrestrial microorganisms penetration into rocks and meteorites under various climate conditions, noting effects of humidity
13 p2010 A71-28693

Combined dry heat and ionizing radiation for spacecraft sterilization process, detailing synergistic effect on microbes
16 p2537 A71-33770

Spores released from solids interiors by aeolian erosion on planetary surface, noting application to microbes in planetary quarantine
16 p2537 A71-33796

Microorganisms under closed environmental ecological conditions with reference to astronauts infectious diseases, discussing bacteria growth in Biosatellite 2 and earth based closed chamber experiments
21 p3343 A71-40562

Gas exchange between air or gas mixture flows and terrestrial soil in extraterrestrial microorganisms detection, using continuous sampling and gas chromatography
21 p3346 A71-40575

Simulated Martian environment effects on terrestrial microorganisms survival
22 p3487 A71-42227

Mathematical models for microorganism exponential die-off rate and variance estimation from decontamination data
22 p3504 A71-42231

Microorganisms survival in simulated Martian environment noting culture cells concentration increase
22 p3507 A71-42826

Unicellular organisms increased tolerance to UV radiation, discussing cells repairing ability in dark and pigments and protective compounds screening role
22 p3496 A71-42828

Microbiological analysis for surviving terrestrial microorganisms from Apollo 12 retrieved Surveyor 3 spacecraft electrical cabling
23 p3633 A71-43814

MICROPARTICLES
Magnetite particles in Orgueil meteorite, discussing high symmetry morphology and generation
03 p0487 A71-13333

Emissivity and temperature measurement of assembled microscopic particles in black body cavity
04 p0676 A71-14954

High velocity microparticle simulation techniques for studying properties, dynamics and origin of micrometeoroids, considering accelerators and impact results
[AIAA PAPER 70-30] 09 p1425 A71-22099

Extinction parameters of submicron carbon, tungsten and Si particles in hydrogen measured at various temperatures, discussing scattering amplitude functions and Monte Carlo calculations
[AIAA PAPER 70-838] 11 p1854 A71-25507

Spherical microparticles in atmospheric boundary layer and fallout above Pacific Ocean correlated to extraterrestrial origin
17 p2810 A71-35719

MICROPHONES

- Glow discharge microphone for acoustic pressure detection and measurement at ultrasonic frequencies
02 p0232 A71-12140
- Calibration of condenser microphone micrometeoroid sensor, using bead drop and hypervelocity impact tests
03 p0422 A71-13284
- Condenser microphones aerodynamically induced noise, investigating acoustic pressure lower limit dependence on air flow velocity and turbulence
12 p1888 A71-27063

MICROPHOTOMETERS

U PHOTOMETERS

MICROPLASMAS

- Microplasma low temperature noise spectra in Si and Ge avalanche diodes
03 p0387 A71-13981
- Light emission of microplasmas and mesoplasmas in silicon p-n junctions, determining spectral distribution
09 p1507 A71-22190
- Si p-n junctions microplasmas I-V characteristics, discussing avalanche breakdown, temperature dependence and light emission
18 p2953 A71-35872

- Electrical, photoelectric and electroluminescent properties of reverse biased GaP p-n structures at room temperature, considering isolated microplasmas
21 p3430 A71-41217
- Low temperature investigation of microplasma breakdown in steep p-n junctions of Sb-doped n-type Ge
22 p3587 A71-42874

MICROPOROSITY

- Microporosity morphology relationship to grain size and boundaries in alloys solidification and pores removal kinetics from castings by sintering
07 p1119 A71-19977
- Carbon vapor deoxidized W on thermionic converter emitters, investigating deposition parameters effect on microporosity
11 p1807 A71-25860

MICROPROGRAMMING

- Microprogramming by Computer Design Language for describing digital computer functional configuration and sequential operation
07 p1069 A71-20404
- Microprogrammable hardware interpreter design in LSI multiprocessing system, emulating instruction set with software functions
17 p2712 A71-35776

MICROPULSATIONS

- NT GEOMAGNETIC MICROPULSATIONS
- Polar aurora pulsations of 4-12 sec intensity with associated cosmic radio noise absorption, using photometric measurements
02 p0242 A71-11761
- Solar wind parameters-terrestrial electromagnetic field micropulsations relation based on interplanetary probes and time correlated ground observations
05 p0800 A71-17170
- Micropulsations dynamic properties and resonant cavity modes, obtaining coupled toroidal and poloidal modes solution
06 p0969 A71-17976
- Solar radio emission micropulsations observations at 10 cm, discussing primary and secondary bursts from different disk regions and radio telescope
07 p1189 A71-20639
- Micropulsations power spectrum from magnetospheric model based on transient current sheets, approximating background frequency dependence and daytime/nighttime spectral line widths
09 p1441 A71-23638

MICROROCKET ENGINES

- Submillipound mercury electron bombardment ion thruster efficiency, noting cathode pole piece, baffle position and geometry influence on ion chamber performance
[AIAA PAPER 70-616] 01 p0143 A71-11577
- Cs ion microrocket engine development, discussing Cs fueling device, ionizer heating, fabrication and control methods
[ONERA-TP-847] 04 p0639 A71-15351
- Spacecraft attitude control microthrusters utilizing catalytically reactive gas mixtures during pulse mode and steady state operation
[AIAA PAPER 70-614] 07 p1183 A71-19859
- Colloid microthruster system life test, discussing design and steady state performance
[AIAA PAPER 70-1110] 07 p1184 A71-19864
- Low, medium and high specific impulse microthrusters development in France, using cold gases, subliming solids, hydrazine, ammonia and cesium ions
[AIAA PAPER 70-617] 07 p1184 A71-19865
- Ion microthruster for satellite orbit and position corrections, describing optimum performance characteristics and test facility
[DGLR-71-032] 17 p2795 A71-35548

MICROSCOPES

- NT ELECTRON MICROSCOPES
- NT ION MICROSCOPES
- NT OPTICAL MICROSCOPES

- Cytophotometric method using digital computer program and scanning microscope
06 p0864 A71-18694

MICROSCOPY

- Holography developments concerning interferometry, microscopy, display systems, data storage and ultrasonic tests
04 p0587 A71-14724
- Papers on optics, Volume 8, covering synthetic apertures, light beating spectroscopy, multilayer antireflection coatings, interference microscopy, photoelectron counting, human eye performance, laser light, etc
05 p0713 A71-16481
- Holographic microscopy technique fundamentals and electrically activated integrated circuit changes inspection
07 p1113 A71-19786
- Superheavy transuranic elements in meteorites and lunar dust by fossil track microscopy
10 p1673 A71-24424
- Field ion emission microscopic study of isothermal order-disorder transformation kinetics in water quenched Ni-Mo alloys
13 p2085 A71-28577
- Holography background, classification and application to microscopy, particle size analysis, interferometry, optical elements and data storage
13 p2071 A71-29349
- Magnification level for optimum performance at microminiature inspection with binocular microscope, minimizing time
17 p2689 A71-34704
- X-Y programmed microdensitometer for stellar spectra analysis, imaging adjustable slit on spectrogram by interchangeable microscope objectives, using Kohler illumination
17 p2742 A71-35000
- Microscopic analysis of secondary minerals in molten meteorite crusts and dust
17 p2811 A71-35732
- Holography, covering thin, thick, transmission, reflection, amplitude and phase type holograms principles and applications in interferometry, microscopy, imaging, optical data processing, etc
22 p3546 A71-42476

MICROSTRUCTURE

- NT METEORITIC MICROSTRUCTURES
- NT WIDMANSTATTEN STRUCTURE
- Annealed steels strengthening and structural changes under explosive shock wave
01 p0085 A71-10037
- Fe-Ni martensite crystals microstructure, using Kossel method and electron microscopes
01 p0106 A71-10278
- Laser microspectral investigations of meteorites microregions and nonhomogeneities relevant to astrophysics and nucleosynthesis
01 p0158 A71-10764
- Microstructure and mechanical properties of weldable heat resistant Ni alloy containing carbon and boron
01 p0103 A71-11068
- Boron addition distribution in iron microstructure, using nuclear track radiography
01 p0103 A71-11072
- Metallic materials semimicroscopic damage in fatigue of S/N gage under constant strain
01 p0104 A71-11396
- Homogenization and dehomogenization phenomena at high temperature of Cr-Ni austenitic steels, discussing electron microscope microstructural examinations after heat treatment
01 p0105 A71-11617
- A-B-A block copolymers statistical thermodynamics, describing postulated microstructure theoretical model for phase transition prediction
02 p0273 A71-12450
- Aluminum compression microstructure under various strain rates and temperatures, discussing dynamic recovery role
02 p0267 A71-12877
- Substructures and properties of Ni, Chromel A, Inconel 600 and TD-NiCr following explosive shock load deformation, using electron microscope
02 p0268 A71-12889
- Doped W wire core porosity and anomalous recrystallization behavior microstructural observation by electron microscopy
02 p0268 A71-12890
- Lunar continent surface microstructure from UV and IR spectra, discussing photometric function determination by geometric shadows and diffraction effects
03 p0492 A71-14055
- Solar wind microscopic structure, examining interplanetary wave-particle interactions
03 p0480 A71-14068
- Thermoelastic deformation of elastic media with stochastically inhomogeneous microstructure, characterizing physical properties as steady random variables
03 p0514 A71-14358
- Ultrafine grain metallic structures by solidification, describing various techniques
03 p0446 A71-14488

- Superplastic alloys fabrication and applications, discussing grain size and surface area roles
03 p0516 A71-14498
- Ni-Fe-Cr alloys microduplex structure, describing mechanical properties and workability
03 p0447 A71-14499
- Microstructure changes during austenite isothermal decomposition in Fe-Mo-C alloys
04 p0614 A71-15778
- Microstructure effect on metastable beta Ti alloy strength, toughness, stress corrosion cracking susceptibility
04 p0614 A71-15780
- Nb-N and Nb-Zr-N alloys phase composition, examining microconstituents at various temperatures after quenching
04 p0616 A71-15905
- Lunar dust samples 10084 and 12070 texture studies with electron microscope, noting difference from meteoritic or lunar rock matter
05 p0807 A71-16299
- Abnormal microstructure in hot rolled plates and sheets of alpha plus beta Ti alloys
05 p0766 A71-16349
- Doped tungsten high temperature behavior, discussing hypotheses regarding doping agents microstructural effects
05 p0767 A71-16599
- Al and Mg alloys mechanical and microstructural changes under low temperature conditions, optimizing casting component ratios
05 p0767 A71-16765
- Fused titanium carbide structure and property changes during annealing
05 p0769 A71-16863
- Ultrastructure changes of membrane and sarcolemmal reticulum of myocardial cells in squirrels during hibernation
06 p0850 A71-17412
- Soviet book on machinability of titanium alloys covering microstructure, physical properties, surface finish and fatigue properties, tooling for industrial machining operations, etc
06 p0903 A71-17444
- Cured thermosetting polymers, investigating water effect on microstructure and mechanical properties
06 p0916 A71-17945
- Stress rupture properties at elevated temperature of nickel base superalloys with varying Ti and Al additions, investigating microstructural and age hardening effects
06 p0913 A71-18676
- Explosive metal welding bond interface, investigating heat treatment effect on microstructure
06 p0914 A71-18680
- Scanning electron microscopy for microstructures of various eutectic Ni alloys, discussing rod-plate transition
06 p0914 A71-18681
- He embrittled stainless steel stress-rupture behavior under vacuum and elevated temperature conditions, discussing microstructural characteristics
06 p0914 A71-18685
- Follow-up scanning systems and reading volume reduction in biological image descriptions facilitating computer aided microstructure analysis
06 p0871 A71-18697
- Steel under cyclic loads, observing relationship between changes in microstructure and temperature curve shape in fatigue failure process
07 p1211 A71-19194
- Mg alloys mechanical properties and microstructure changes under static tension in temperature range 20-293 K
07 p1131 A71-19363
- Ni-Mn, Ni-Fe and Ni-Fe-Al alloys yield behavior and microstructure as result of ordering and disordering treatments, using center annealing technique
07 p1132 A71-19434
- Alloy matrix short range ordered particle microstructures and properties, correlating electron diffraction and field ion microscopy studies
07 p1132 A71-19439
- Ni base superalloys mechanical properties relationship to microstructure, considering precipitate dispersion and phase state effects on flow stress and creep strength
07 p1133 A71-19445
- Optimal heat resistance, mechanical properties and microstructure of steam pipe Cr-Mo-V steel
07 p1135 A71-19618
- Microstructural variables effects on fracture stress in alpha beta Ti alloy having Widmanstätten structure
07 p1139 A71-19992
- W-Re alloy ingot nonmetallic inclusions complex phase structure, using electron probe, metallographic and electrolytic techniques
07 p1141 A71-20239
- W-Re alloy microstructure creep, long term strength and plastic properties as function of temperature, using electron microscopy
07 p1141 A71-20241
- Structure and mechanical properties of Mo alloy weld metal as function of Re concentration, using

metallography, electron microscopy, X ray analysis and autoradiography 07 p1120 A71-20245

Ni-Ti alloy structural modulation during aging, examining effect on yield stress by X ray diffraction and tensile tests 07 p1143 A71-20494

Nonuniform feed effects on height of electrosark surface machining microasperities, investigating linear elliptical interpolator pulse sequence 08 p1296 A71-20851

Carbon fibers structural features, confirming model of slowly undulating ribbons of sp 2 carbons as basic structural elements by high resolution dark field micrographs [PLASTICS INST. PAPER 9] 08 p1319 A71-20895

Microstructure crystallites and voids of polyacrylonitrile based carbon fibers, using X ray diffraction and electron microscopy measurements [PLASTICS INST. PAPER 8] 08 p1320 A71-20901

Recrystallized and nitrated Mo alloy microstructure under plastic deformation by tension at high temperatures 08 p1305 A71-21029

Mo microstructure changes at high temperatures noting polygonization, grain migration and crack propagation during failure 08 p1305 A71-21032

W and Mo single crystals metallographic microanalysis for temperature cycles effects on microstructure 08 p1305 A71-21056

Structural and kinetics investigation of oxides formation in silver-argentine oxide-argentine oxide system, using electron microscopy and electron diffraction methods 08 p1234 A71-21087

Nb single crystals dislocation substructure correlation with strength properties 08 p1307 A71-21508

Ti effects on Ni-Mo-Cr alloy strengthening, correlating microstructures and mechanical properties 08 p1311 A71-21542

Mo-Hf alloy dispersion hardening by internal nitriding, examining structure and high temperature mechanical behavior 08 p1311 A71-21546

Al-Cu precipitation hardened alloys, determining microstructure effects on fatigue life and flow stress 08 p1312 A71-21547

High strength martensite beta Ti alloy microstructure, discussing ductility and age hardening 08 p1312 A71-21552

Fe-Ni-Co alloy strengthening by martensite to austenite transformation taking into account microstructure 08 p1313 A71-21556

Thermomechanical treatment effects on microstructure and fracture toughness of extruded Beta III titanium alloy 08 p1313 A71-21558

Al microstructure and strength, investigating prior deformation and temperature effects 08 p1313 A71-21561

High strength corrosion resistant superalloy structure and mechanical properties 08 p1314 A71-21566

Ni superalloys plane front cast structure through controlled unidirectional solidification, discussing improved mechanical properties 08 p1314 A71-21567

Co-Cr-W alloy systems equilibrium and precipitation effects, investigating microstructural properties at elevated temperatures 08 p1314 A71-21569

Co base superalloys fracture toughness microstructural aspects, considering effects of interdendritic carbides and carbide precipitation on aging at elevated temperatures 08 p1314 A71-21572

Low alloy Mo mechanical characteristics relation to structural states obtained during tensile and bending tests 08 p1316 A71-21613

Composition, microstructure, heat treatment and properties of Ni alloy with high rupture strength and hot corrosion resistance for turbine blade applications 08 p1299 A71-21687

Metals and nonmetals orbital atomic radii and lattice parameters 08 p1345 A71-21762

Microstructure and mechanical properties of heat resistant alloy under homogenization and subsequent isothermal heat treatment 08 p1317 A71-21764

High vacuum low temperature fatigue tests, describing design and operation of equipment for microstructural observation 09 p1427 A71-22511

Metal surface layers structural changes during fretting corrosion, analyzing strain effects 09 p1455 A71-23081

Al-Zn-Mg alloys stress corrosion, using electron transmission microscopy for microstructural investigation 09 p1472 A71-23125

Fracture toughness relationship to microstructure in alpha-beta Ti alloy heat treated to constant yield strength, considering crack propagation 09 p1472 A71-23126

Cr specimens containing Y, investigating microscopic breakdown at high temperatures as function of deformation during vacuum rolling 09 p1474 A71-23235

Aluminum high temperature resistant diffusion type coatings structure and chemical composition, outlining turbine blades testing for thermal shock, oxidation and sulfur and sea salt corrosion 09 p1474 A71-23287

High temperature Ni and Co alloys for stationary gas turbines and jet engine parts, considering microstructure and mechanical behavior under stress and temperature 09 p1475 A71-23302

Nickel under slow loading conditions at various temperatures, examining disorientation angles of substructure 09 p1476 A71-23317

Elastic ultrasonic vibrations effects on metals and alloys microstructure and elastic and nonelastic properties 09 p1477 A71-23326

Loading rate effect on Ni creep characteristics and substructure 09 p1477 A71-23330

Stress corrosion failure prevention in susceptible Al alloys, considering metallurgical structure, environment and stress distribution 09 p1478 A71-23417

Microstructural defects responsible for tensile strength reduction in carbon fibers subjected to high temperature graphitization, using transmission electron microscopy 09 p1483 A71-23653

Grain size influence on deformation characteristics of commercial Ti with oxygen and Fe impurities, discussing test results on various mechanical properties 09 p1479 A71-23688

Thermal, microstructural and X ray analyses of Al-Ti alloys phase diagrams, measuring hardness and conductivity 09 p1480 A71-23704

Phase diagram isothermal cross sections of Ti-Zr-Nb alloys for various temperatures and heating periods by X ray and microstructural analysis 09 p1480 A71-23705

Metals crystallization in ultrasonic field, investigating structural change as function of energy and impedance factors and cavitation effects in fine grain formation 10 p1626 A71-24136

Carbon fiber strength/microstructure relationship, examining failure mechanism initiated by graphite crystallites shearing 10 p1634 A71-24446

Variational principles for initial boundary value problem of fully coupled linear thermoelasticity for inhomogeneous anisotropic materials with microstructure 10 p1689 A71-24512

Ti-Al-Cr-Fe alloys microstructure, investigating alpha and beta phases with X ray diffraction 10 p1627 A71-24531

Al alloys microstructure and mechanical properties after rapid solidification, considering rapid quenching techniques and resulting metastable variations 10 p1627 A71-24596

Cr and Zr additives influence on Al-Zn-Mg-Cu alloys quench sensitivity, discussing mechanical properties and electron microscopic investigation of microstructural characteristics 11 p1780 A71-26021

Al coating of Nb and Nb alloys by pack cementation, discussing coating structural states, heating cycle temperatures and growth kinetics 11 p1781 A71-26295

Ti-Zr alloying in for microstructural hardness and mechanical strength increases, discussing Zr concentrations at Nb granular boundaries 11 p1782 A71-26470

Fast heated titanium-vanadium martensite beta-phase transformations comparison with slow heated structures 11 p1782 A71-26472

Al-Ni alloys rapidly quenched from melt, determining solid solutions mechanical and microstructural properties 12 p1916 A71-26893

Aged beta Ti alloy microstructure and mechanical properties, examining initial dislocation structure and interstitial concentration effects 12 p1917 A71-27297

Inhomogeneous microstructure elastoplastic medium, examining strain and work in plastic deformation 12 p1982 A71-27516

Boron solubility in Mo-W solid solution, discussing microstructure, electrical and mechanical properties for range of alloying ratios 12 p1918 A71-27660

Metallographic equipment for metal surface microstructure observations of samples under tensile loads at temperatures from 4.2 to 300 K 12 p1908 A71-27757

Chemical composition effects on microstructure and high temperature properties of cast Cr-Ni-Al steels containing Ti, B, Ce and Zr 13 p2084 A71-28035

Graphite epoxy composites fiber microstructure and surface condition, noting tensile fracture, crack propagation and brittleness 13 p2092 A71-28594

Strain and strain rate effect on flow stress and microstructure of Al-Cu eutectic alloy during superplastic deformation, deriving stress-strain diagrams 13 p2086 A71-28624

Steatites replicas electron microscopy for microstructure variations with composition and firing conditions differences, discussing protoenstatite crystallization and glass phase formation 13 p2093 A71-28664

Lead borosilicate glass with crystalline opacifiers, observing microstructure and reflectance 13 p2093 A71-28990

Cold rolled recrystallized Ni-Fe alloy, considering short range order structure effect on elastic limit 13 p2087 A71-29264

Hot ductility correlation with microstructure from nickel softening and fracture mechanisms interaction 13 p2089 A71-29410

High strength Ni base superalloy workability, investigating microstructure relation to mechanical properties 13 p2090 A71-29419

Microfossil structures from morphological alterations of proteinoid microspheres due to inclusion of organic or synthetic polyamino acids 14 p2190 A71-30178

Shape instabilities for eutectic alloys composite microstructure at elevated temperatures 14 p2259 A71-30413

Al-base alloys granules dimension and shape effects on extruded semifinished product mechanical properties and structural stability 15 p2424 A71-31242

Microstructure and mechanical properties of Ti-rich alloys of Ti-W system, constructing phase diagram 15 p2425 A71-31402

Cast Nb-W-Mo-Zr-C alloys heat treatment effect on microstructure and phase composition, noting ductility improvement 15 p2426 A71-31406

Substrate emitter monolithic inverted transistor structure for low-power high-current gain application 15 p2375 A71-31474

High chromium low carbon steel, detailing oxygen content effects on high temperature reduction intercrystalline corrosion and grain growth 15 p2427 A71-31528

Superplastic metal alloys microstructure, development history and shaping technology, noting Zn-Al alloy for auto bodies fabrication 15 p2429 A71-32004

Nb-Re-C system, investigating polythermal NbC-Re cross section structure by metallographic chemical and X ray analyses and microhardness and melting point measurements 15 p2430 A71-32148

Unidirectionally solidified Ti-base eutectic composites and alloys strength and microstructural stability under heat treatment 15 p2432 A71-32170

Aluminum single crystals tensile deformation and annealing to produce polygonized substructure 15 p2432 A71-32172

Grain refinement in dilute Al alloys, comparing peritectic reaction effect for Ti, Zr and Cr as alloying components 15 p2433 A71-32181

Monograph on ductile fracture covering electron microscopy of fracture surfaces and microstructures of Al alloys 15 p2434 A71-32301

Structural inhomogeneity effect on fatigue strength of Al alloys, considering microstructure qualitative estimation on basis of microplastic deformation 15 p2434 A71-32330

Fine structure variations of Al alloy after aging, using harmonic analysis for calculating matrix microdeformation for correlation with mechanical properties 15 p2435 A71-32332

Strength, plastic properties, electrical conductivity and fine structure associated with decomposition kinetics of Al alloy supersaturated solid solution 15 p2435 A71-32333

Fabrication, texture, alloying, substructure and fracture effects on bend ductility and toughness of beryllium sheet 15 p2436 A71-32509

Multipass low alloy steel weld metal strength dependence on microstructural changes due to thermal effects 15 p2437 A71-32614

Age hardenable Inconel X-750 superalloy mechanical response to tensile loads for identifying microstructural changes due to deformation 15 p2437 A71-32616

Microstructure and chemical composition of lunar soil sample collected by Luna 16 16 p2630 A71-32838

Stress-microstrain relationship for metal crystals prestrained in easy glide, obtaining mobile inelastic dislocation density and internal stress 16 p2654 A71-33102

Transition metals effect on Ti alloys grain size, suggesting La, Y, Ni, Pd and Pt effectiveness in crystal structure refinement 16 p2593 A71-33628

Oriented Mo single crystals substructure during growth, showing crystallographic orientation 16 p2595 A71-33879

Mo single crystals physicochemical and microstructural anisotropy under tension at different temperatures, noting strength and plasticity dependence on crystallographic orientation 16 p2596 A71-33888

Thermal strain hardening influence on structural changes in coarse grain Ni under creep tests during heat treatment 16 p2598 A71-33990

Recrystallization of heat treated Fe-Ni alloys microstructures after hammer hardening 16 p2598 A71-34051

Stratospheric extraterrestrial particles identification from balloon-collected electron microscope photographs, suggesting cometary origin 16 p2644 A71-34127

Randomly distributed domain structure of ordered Ni-Cr alloy, using electron microscopy and neutron diffraction 17 p2755 A71-34413

Statistical microstructural analysis for nucleation and growth kinetics of recrystallization nuclei of metal single crystals 17 p2755 A71-34414

Deformation temperature effects on microstructure and mechanical properties of low alloy Mo, considering cold brittleness temperature and associated plasticity 17 p2755 A71-34418

Heat treatment effect on fracture behavior of aged Al alloy sheet, investigating toughness dependence on microstructure 17 p2756 A71-34486

Gallium antimonide-germanium system solid solution lattice constant determination, using X ray and microstructural analysis and microhardness measurements 17 p2791 A71-34566

Electroslag welding of large pressed Al-Mg alloys sections, using electrodes to reduce weld grain size and obtain high mechanical properties 17 p2748 A71-34807

German book on welding conditions and material composition effects on structural changes and heat-affected zone mechanical properties of high strength structural steels 17 p2748 A71-34851

German monograph on heat transfer from vertical heating surfaces to liquids at rest in nucleate boiling, showing microstructure interaction with interfacial tension 17 p2838 A71-34852

Wrought precipitation hardened Co-base alloy, investigating Ti and Al additives effects on tensile and stress rupture strengths, microstructure and fabricability 17 p2758 A71-35147

Columnar grained Ni superalloy lifetimes and transverse creep ductilities enhancement and microstructural alterations due to Hf additions 17 p2759 A71-35394

Al and Mg alloys mechanical and crystal microstructural changes under low temperature conditions, optimizing casting component ratios 17 p2760 A71-35464

Microphase separation in homopolymer-block copolymer mixtures as function of composition, molecular weight and interaction parameters 17 p2695 A71-35525

Molybdenum mechanical characteristics relation to structural states obtained during tensile and bending tests 17 p2760 A71-35673

Creep rate enhancement by additional microplastic deformation in refractory alloys during thermal cycling 17 p2761 A71-35678

Two dimensional flow of non-Newtonian fluids with rigid spherical substructure, solving linear coupled ordinary differential equations for spin and velocity field [ASME PAPER 71-APM-N] 18 p2926 A71-36257

Laminated composite beam microstructure continuum model, calculating equations of motion and boundary conditions with Hamilton principle [ASME PAPER 71-APM-S] 18 p2978 A71-36261

Metal structure, crack nucleation and propagation during fatigue under cyclic stress 18 p2936 A71-36693

Nichrome powder microstructure characteristics effect on hot compaction kinetics, considering temperature, pressure and preliminary heat treatment effects 19 p3075 A71-37108

Ni-Cr-Mo cermet alloys sinterability, physicochemical properties and microstructure 19 p3075 A71-37109

Cermet iron chromosilicidization and sinter compactness effects on depth and structure, noting wear, corrosion and thermal resistance 19 p3075 A71-37110

Spherulitic linear polyethylene rod cold drawing, observing fibrous structure formation by light and electron microscopy and X ray scattering 19 p3084 A71-37650

Scanning electron microscope and petrographic observations of glass particles from Apollo 12 lunar soil sample, revealing surface features and origin 19 p3137 A71-37674

Precipitation strengthened Fe-Ni-base superalloy microstructure, investigating phase relationships 19 p3079 A71-37711

Unsteady flow of incompressible micropolar fluid due to sphere oscillations, calculating velocity, drag and stress components 19 p3045 A71-37799

Collisionless plasma shock front microstructure, examining isomagnetic discontinuity with high spatial resolution probes 19 p3045 A71-37853

Ti alloys heat resistant properties evaluation for long service under various heat treatment conditions, considering tensile properties, fracture toughness and microstructure 19 p3082 A71-38420

Co, Mo, Ti and Cr effect on mechanical properties and microstructure of maraging weld metals 19 p3083 A71-38491

Droplet clouds microstructure and phase state occurrence as function of temperature, size distribution and water content based on experimental data 19 p3091 A71-38680

Cumulus clouds macro- and microstructural parameters measurements including convective flow, temperature, water content, droplet concentration and size 19 p3091 A71-38681

Evaporated pure Ni coatings effects on carbon fiber fracture strength and microstructure at room temperature 20 p3248 A71-38815

Generalized continuum of interleaved microstructures coupled by forces, investigating equations of motion, tensor indices and asymmetrical effects 20 p3309 A71-39566

Lunar surface microstructure inhomogeneities bimodal distribution from IR and UV spectral analysis 20 p3295 A71-39617

Eutectic Al alloys parallel alignment formation by stable isothermal boundary surface, investigating microstructure 21 p3396 A71-40029

Fe-Al alloy fine lamellar microstructure from light microscopy and X ray examination 21 p3396 A71-40032

Precipitation hardened Ti-Nb alloy, correlating room temperature tensile properties with microstructure from step aging 21 p3387 A71-40461

Macroscopic residual stress and strain measurement and crack tip substructure, discussing crystal plastic deformation effect on fatigue crack propagation 21 p3466 A71-40831

Carbon fibers grown on graphite by thermal decomposition of hydrocarbons, investigating external morphology and structure 21 p3406 A71-40837

High strength stainless steel dislocation structure and mechanical properties, discussing tempering, tensile strength, precipitation hardening and temperature effects 21 p3402 A71-41088

High strength steel structural transformations under arc melting, cooling and electroslag remelting, noting delta ferrite precipitation with hot stage microscope 21 p3402 A71-41089

Microstructural characteristics of Fe-Ni alloy plastic deformation at 20-500 C during cold and hot rolling, noting intergranular shear processes 21 p3402 A71-41095

Low carbon austenitic Cr-Mn steels, noting Ni and Al combined alloying effects on structure and mechanical properties 21 p3403 A71-41101

Copper wire laser welding to film on Cr substrate, exhibiting nonhomogeneous columnar structure and recrystallization 21 p3389 A71-41104

Longitudinal, transverse and vertical wind distribution microstructure during convection from airborne experiments 21 p3412 A71-41388

Prior stressing and thermal treatments effect on shock induced substructures in polycrystalline Mo, using transmission electron microscopy 21 p3404 A71-41416

Ni-Cr-Mo-Co steel microstructures after austenitizing, quenching and tempering, correlating with mechanical properties 22 p3560 A71-41594

Ultrasonic defectoscopy of steel samples, considering grain size effects on SNR 22 p3528 A71-41757

Ti alloy microareas alloying element concentration quantitative analysis by EPMA program, obtaining working curves for Al, Fe, Cr, Mo and V 22 p3561 A71-41944

Ti-Fe and Ti-Cr binary alloys microsegregation genetic trend measurement by electron probe microanalysis, observing critical cooling rate from beta phase 22 p3562 A71-41945

Metastable beta type Ti binary alloys isothermal transformation microstructure observation by microscopical and X ray diffraction methods 22 p3562 A71-41947

Crystal microstructure of strengthening precipitates in Ni maraging steel, giving electron diffraction patterns 22 p3562 A71-41949

Microstructure, yield point and creep rupture strength of Nb-Ti alloy, investigating oxygen concentration and temperature effects 22 p3563 A71-42365

Oxygen concentration and heat treatment effects on structure and mechanical properties of Nb-Zr alloys 22 p3563 A71-42366

Accelerated intergranular corrosion tests under high humidity on Zn-Al alloy with lamellar eutectoid microstructure due to postforming heat treatment 22 p3564 A71-42534

AlCu alloy cellular dendritic substructure segregation observation by electron microprobes 23 p3689 A71-42931

Fibrous carbon structure determination by high resolution electron microscopy, establishing relationship between graphite planes and catalyst particles orientation 23 p3696 A71-43141

Optical, chemical and structural properties of lunar bytownite twin from U stage, microprobe and X ray measurements 23 p3738 A71-43612

Apollo 12 lunar soil and breccia core tube and surface samples optical and electron microscope and microprobe analysis, relating data to geologic processes 23 p3744 A71-43656

Lunar breccia sample matrix composition characteristics examination by transmission electron microscope, suggesting condensation from rock volatilized by meteorite impact heat 23 p3745 A71-43663

Lunar glassy objects and mineral grains surface microstructure by optical and scanning electron microscopy, comparing with tektites and terrestrial volcanic analogs 23 p3745 A71-43664

Surface morphology of free-growing ilmenites and chromites from lunar vuggy rocks by scanning electron microscopy and electron microprobe 23 p3745 A71-43665

Ultramicroscopic texture and radiation damage in Apollo 11 and 12 micron sized lunar dust grains compared with meteoritic rocks 23 p3758 A71-43756

Regular particle morphology and petrostatistics in Apollo 11 and 12 lunar fines and conglomerates, using phase contrast and scanning microscopes 23 p3758 A71-43757

Electron microscopic study of antiphase domains size and shape in Ni-Mn alloy after annealing 23 p3692 A71-44009

Microalloying effects on phase composition, surface phenomena, fine crystalline structure and microstructure of E1417L steel 24 p3836 A71-44374

Tensile and creep rupture strength and microstructure of Co-Fe-Ta alloys at elevated temperatures 24 p3836 A71-44442

Cr-Ni alloy heat treated cast specimens microstructure, metallographic, X ray and spectral investigation, noting chemical inhomogeneity 24 p3836 A71-44484

Ti, Zr and Nb carbides alloying effects on deformed and annealed Mo alloys cellular structure and mechanical properties 24 p3836 A71-44672

Phase and microstructure changes during nitriding process of Fe-Ti alloys, stressing Ti concentration effect 24 p3837 A71-44733

TiTe thin films phase composition and structural properties as functions of component contents, deposition conditions and annealing parameters, using X ray diffractometer and IR microscope 24 p3862 A71-45252

Microinhomogeneous elastic media with moduli as coordinate random function, investigating stress and strain tensors

24 p3849 A71-45345

MICROTHRUST

Microthrust powered spacecraft earth escape, using lunar attraction by orbiting spacecraft with vector opposite to moon

12 p1968 A71-27579

High thrust density colloid emitting source development as basic microthrustor for electrostatic propulsion systems [ALAA PAPER 71-694]

14 p2293 A71-30753

MICROWAVE AMPLIFIERS

YIG C band microwave amplifier using longitudinal pumping, comparing to other systems

02 p0228 A71-11692

Remotely controlled room temperature microwave parametric amplifier design for shipboard satellite telegraphy terminal

02 p0234 A71-12813

Uncooled low noise microwave parametric amplifier for small receiving earth stations, describing three stage design, gain and bandwidth

02 p0234 A71-12814

Wideband low noise parametric amplifier design, discussing noise temperature improvement by refrigeration at microwave frequencies

02 p0234 A71-12815

Nondegenerate parametric amplifiers above X band for satellite communication systems, discussing circuitry, varactors, diode packaging and solid state pump sources improvements

02 p0235 A71-12906

TWT microwave amplifier parameters effect on power threshold for electron beam signal control loss

03 p0385 A71-13790

Cyclotron electron beam transverse waves interaction in microwave amplifier resonant coupling element with double spiral

03 p0385 A71-13795

Broadband hybrid UHF integrated power amplifiers providing high output, noting integration techniques, design, fabrication and characterization

04 p0559 A71-15876

C band field effect transistor amplifiers with stable power gain, discussing circuit analysis, design parameters and test results

05 p0729 A71-16917

CW microwave reflection-type amplification from circuit stabilized epitaxial GaAs transferred electron devices, observing gain and hysteresis

05 p0729 A71-16918

Silicon junction avalanche diodes as S band oscillators and amplifiers, presenting peak power efficiency and gain data

05 p0729 A71-16921

Broadband IMPATT diode multistage transmission amplifiers computer aided design and X band performance

07 p1073 A71-19114

Low gain microwave amplifier cascade DC to RF conversion efficiency analysis

07 p1073 A71-19115

One watt CW high efficiency X band avalanche diode amplifier with in-band and second harmonic impedance control

07 p1073 A71-19117

Injection phase locked oscillator as input microwave limiting amplifier for noise measuring microwave discriminator

07 p1074 A71-19126

Multisignal characteristics of high power noise modulated microwave traveling wave tube amplifiers

07 p1080 A71-20452

Low noise C band beam lead tunnel diode amplifiers characteristics and application in low cost microstrip reflection amplifiers

08 p1262 A71-20759

K band double-tuned nondegenerative parametric amplifier using single-packaged GaAs varactor diode, discussing design and performance

08 p1262 A71-20763

Wide band low noise millimeter wave parametric amplification using wafer varactor diodes with Schottky barrier junctions

08 p1263 A71-20769

K band cryogenically cooled wideband /600 MHz/ low noise parametric amplifier for millimeter wave satellite communication earth terminals, discussing design

08 p1263 A71-20770

Low noise microstrip microwave mixer-preamplifier on thin polyolefin reinforced with Al, discussing design and manufacture

08 p1263 A71-20771

Microwave amplifier resonant gain frequencies as function of tunnel diode circuit, proposing low input design formulas

08 p1264 A71-21069

Microwave multistage transistor amplifier with IC configuration, discussing design and performance

08 p1265 A71-21287

Frequency characteristics calculation of regenerative two cavity microwave bandpass amplifiers, applying to parametric and quantum amplifiers and underexcited microwave relaxation oscillators

09 p1413 A71-22157

Symmetrical amplitude-frequency characteristics of microwave reflection amplifiers with active resonators connected in series by nonhalf wave transmission line

10 p1584 A71-24879

Microwave amplification using negative resistance device in prototype filter equalization networks, permitting realization of wideband amplifiers for C band and superhigh frequencies

11 p1736 A71-25140

Unilateral GaAs traveling wave microwave amplifier based on space charge growth in domain-stabilized transferred electron semiconductors, considering power, noise, gain and efficiency

11 p1736 A71-25234

Microwave front end designs for low noise operation, discussing FET applications and mixer conversion loss reductions

11 p1731 A71-25673

He-Ne laser cavity amplifier performance analysis, indicating usefulness as scanning interferometer for high resolution analysis of other laser outputs

11 p1776 A71-26430

Broadband multicavity multimegawatt klystron design for superpower amplifiers in radars and particle accelerators

11 p1734 A71-26433

Gunn diode operation at below threshold bias voltage, investigating microwave oscillations amplification

13 p2036 A71-27953

Small-signal gain radial variation in cylindrical electrically excited carbon dioxide laser amplifier, characterizing discharge properties by modified Schottky analysis

13 p2080 A71-29330

Integrated S band microstrip parametric amplifier modules with self contained Gunn effect pump oscillator for space flight applications

14 p2210 A71-29570

Power gain of Q-band GaAs FET with Schottky-barrier gate, giving amplifier and oscillator designs

14 p2210 A71-29800

Transistor minimum noise figure in low noise microwave amplifier circuit

15 p2378 A71-32635

Microstrip microwave amplifier design using common emitter configuration and quarter wave impedance matching transformer

16 p2545 A71-33395

Transistorized microwave amplifier/limiter for upper part of decimeter wave range, suggesting limitation in automatic gain control transistors

16 p2547 A71-33499

Microwave amplifiers gain fluctuations effect on Dicke radiometers minimum detectable temperature difference, considering traveling wave tubes and tunnel diode and mixer IF amplifiers

16 p2548 A71-34133

Parametric microwave amplifier feasibility with laser pumped electro-optical crystal as nonlinear element

16 p2589 A71-34135

Soviet book on microwave quantum amplifiers covering traveling wave and multicavity masers calculation, design, tests, applications and basic components

17 p2753 A71-34474

Low noise microwave transistor amplifiers technology, discussing performance levels in frequency coverage, SNR, gain flatness and power output

17 p2714 A71-34604

Low noise TWT amplifiers, performance, reliability and cost reduction

17 p2714 A71-34605

Communication satellite ground station transmitting equipment, discussing carrier waves, FM, frequency converters and microwave amplifiers characteristics

17 p2717 A71-35515

Transverse wave tubes with cyclotron and synchronous wave interactions as microwave amplifiers, analyzing energy exchange mechanism and axial beam velocity spread

18 p2888 A71-36128

IMPATT diode amplifiers and oscillators AM and FM noise spectra and SNR prediction for comparison with experiment

18 p2888 A71-36271

Transferred electron /Gunn/ amplifiers and oscillators for microwave applications, considering electronic and mechanical tuning over large frequency ranges

18 p2894 A71-36977

Microwave transistor amplifier dynamic range performance, comparing low noise and high power capabilities with traveling wave tubes

19 p3029 A71-38295

Linearization techniques for multiple signal interference reduction in broadband transistor power amplifiers in 225-400 MHz range

19 p3030 A71-38434

Cryogenic refrigeration requirements of low noise microwave amplifiers in satellite communications, discussing solid state masers and liquid helium parametric amplifiers

20 p3204 A71-39251

Maximum efficiency of 10-20 W output semiconductor amplifier at 2.3 GHz, discussing possible replacement of vacuum tubes

20 p3205 A71-39456

Transistorized microwave amplifiers with dissipative equalizing networks, describing transistor equivalent circuit

20 p3205 A71-39810

Hybrid integrated wideband linear microwave power amplifiers for S and C bands, discussing construction and performance

21 p3357 A71-40817

Gunn diode operation at below threshold bias voltage, investigating microwave oscillations amplification

21 p3358 A71-41339

Supercritical transfer electron amplifier using GaAs CW Gunn diode with cathode doping notch and profiles sloping upward for stabilization

22 p3521 A71-42204

Wideband microwave amplifier with two antiparallel high efficiency avalanche diode pairs, presenting fishbone shaped tuning plate for bandwidth widening

23 p3653 A71-43961

Silicon avalanche diodes for microwave TRAP-PATT amplifiers and self excited oscillators with IMPATT triggering

23 p3653 A71-43964

Series stabilization reflection type tunnel diode microwave amplifier synthesis with allowance for real circulator reactance

24 p3810 A71-45259

MICROWAVE ANTENNAS

L and S band paraboloidal dish antenna stellar calibration technique using absolute flux density from Cassiopeia A or Cygnus A

01 p0032 A71-10888

Microwave receiving and transmitting antennas proximity effects on permittivity measurements of dielectric layer

01 p0057 A71-11206

Cassegrain antenna electrical and structural design and control system for microwave propagation and communication research, using moon reflected signals as atmospheric probes

02 p0234 A71-12806

Maintenance free cryogenic noise temperature standard for continuous microwave antenna operation independent of elevation angle

04 p0550 A71-14658

Antenna synthesis by microwave holography, using interference pattern approximations for series of holograms construction

06 p0898 A71-17723

Planar microwave array antenna for scan requirement, discussing tilt angle and element arrangement optimization

06 p0876 A71-18097

Pulkovo radio telescope reflector adjustment by phase comparator, using centimeter wave transmitting-receiving antenna for sun, moon and Venus observations

07 p1083 A71-19344

Impedance antenna with slow wave structure of zig-zag shaped wires

07 p1079 A71-20260

Dual channel rotary joint combining Tm and Te modes in circular waveguide for X band antenna high average power operation

08 p1252 A71-20758

Planar microwave array antenna for scan requirement, discussing tilt angle and element arrangement optimization

08 p1229 A71-22030

Circularly polarized parabolic reflector UHF antenna with helical feed for direct TV reception from satellite, discussing design and performance

09 p1417 A71-23034

External and transistor noise temperature effects on SNR of transistorized microwave receiving antennas

09 p1417 A71-23038

Helios solar probe antenna system for S-band radio communication, discussing electrical and mechanical design

09 p1533 A71-23734

Wideband gas discharge duplexer as transmitter receiver microwave antenna switch in H/01/ mode circular waveguide

10 p1584 A71-24720

Field correlation diffraction theory of symmetrical microwave Cassegrain antenna, calculating main reflector focused field by spherical wave expansion

13 p2028 A71-27992

Monograph on tolerance effects and performance degradation in microwave aerials covering axial displacement, active array, radiation pattern prediction and mutual coupling

13 p2037 A71-28495

MICROWAVE ATTENUATION

Microwave receiving antenna with solid state power rectifier for converting energy from space solar cell array into DC power on earth 13 p2000 A71-28671

Electromagnetic compatibility, measuring microwave antennas characteristics, including frequency range, gain, beamwidth, voltage standing wave ratio, impedance and radiation patterns 13 p2039 A71-28877

High efficiency autotrack strip-line-fed dipole antenna array for L and S band airborne telemetry 14 p2198 A71-30905

Four arm conical spiral microwave antenna with circularly polarized hemispherical radiation pattern for satellite and rocket applications 14 p2216 A71-31042

Flush mounted aeronautical waveguide antennas with dielectric plug for 5GHz operation 14 p2216 A71-31043

Low carrier power aircraft antenna module for airborne UHF communications system, considering range/field strength measurements 14 p2216 A71-31046

VHF and UHF ground reflection measurements for antenna site layout, showing feasible operations at short ranges 14 p2217 A71-31050

Quasi-isotropic directional, omnidirectional and auxiliary antennas of Helios Solar Probe S band system, discussing design, radiation patterns, adaptability and X band measurements 14 p2217 A71-31052

Aircraft phased arrays for L-band ATC satellite system application, alleviating problems of power budget and vulnerability to multipath and interference 14 p2217 A71-31054

L band aircraft antenna array consisting of circularly polarized elements and static electronic steering circuits for synchronous satellites radio links 14 p2273 A71-31074

Microwave antenna far field radiation pattern determination from Brown transmission equation solution 15 p2368 A71-31143

High directional microwave antennas optical simulation, design and measurement based on coherent optics and holography 15 p2375 A71-31282

Circular aperture microwave antenna near field calculations based on ray diffraction theory in geometrical optics 15 p2372 A71-32366

Pseudorandom binary codes for improved microwave antenna range measurements by suppressing unwanted reflections 15 p2373 A71-32370

Microwave receiving and transmitting antennas proximity effects on permittivity measurements of dielectric layer 17 p2697 A71-34258

Wideband Cassegrain microwave antenna for space communication, discussing reflecting horn for maximum radiation gain 17 p2715 A71-34686

Fixed multiple beam toroidal reflector antenna operating above 12 GHz, analyzing 10 by 15 ft scaled model parabolic torus 17 p2704 A71-35091

Wide angle microwave antenna radiation beam steering with fixed parabolic reflectors, using adaptive primary feed for intercepted field spatial Fourier transformation 17 p2708 A71-35493

Antenna system design for communication satellite ground station operating in 10.7-35 GHz range 18 p2881 A71-36556

Multiple channel fringe counting interferometer for remote monitoring of large diameter microwave antenna under test in simulated solar thermal and vacuum environment 20 p3235 A71-39186

Microwave antenna near field apparent image and phase-amplitude distribution measurement with photocontrolled semiconductor panel 22 p3523 A71-42318

Circularly polarized parabolic SHF antenna with plane and parabolic reflectors, testing radiation pattern performance 22 p3515 A71-42521

Turnstile loop Yagi and hexafilar contrawound spiral antennas for microwave telemetry rocket data reception, describing design and radiation patterns 23 p3643 A71-43095

Receiving and transmitting antennas directional gain effect on microwave long range tropospheric propagation 23 p3644 A71-43289

High power multielement electronically scanned array of microwave log periodic monopole antennas for ionospheric backscattering measurements 23 p3653 A71-44155

Precision pointing correction /boresight calibration/ of microwave antennas, using sun as test source 23 p3654 A71-44158

Wideband transistorized active dipole antenna for reception at 100-1000 MHz, calculating impedance and effective height by linear theory 24 p3807 A71-44360

MICROWAVE ATTENUATION

Microwave attenuation cross section of wet ice spheres, tabulating as function of wavelength, sphere diameter and water thickness 01 p0030 A71-10555

Millimeter waves attenuation in fog, showing strong temperature dependence and correlation with visibility 01 p0117 A71-10580

Atmospheric water vapor dimers absorption of microwaves, computing total absorption coefficient 03 p0378 A71-13295

Rain and drizzle millimeter wave attenuation and radar scattering cross section calculation 05 p0718 A71-15988

Submillimeter wave attenuation measurement over 1 km path during summer rainstorms, comparing results with millimeter waves 05 p0718 A71-15989

Submillimeter and millimeter waves attenuation in rain, comparing calculation results with measurement 05 p0718 A71-15990

Submillimeter wave attenuation in snow, comparing results of calculation based on Mie theory with measurement 05 p0718 A71-15991

Decimeter radio wave propagation in Venusian atmosphere, determining refraction and absorption coefficients height dependence based on Venera spacecraft data 05 p0718 A71-15993

Wideband microwave absorbing wall using dielectric material of foamed polystyrol powder coated with graphite, discussing design procedure and thickness reduction 08 p1253 A71-21297

Atmospheric scintillation, refractive and diffusive attenuation of microwaves from outer space at low elevation angles 08 p1364 A71-21421

Atmospheric water vapor dimers microwave absorption, computing total absorption coefficient 09 p1408 A71-23268

Dielectric constant and loss tangent measurements at 60 and 90 GHz for Teflon, polystyrene and Lucite sheets, using Fabry-Perot interferometer 09 p1418 A71-23415

Microwave signal attenuation in LF oscillation beam plasma discharge, comparing to braking cyclotron absorption effect 10 p1653 A71-24880

Flame plasma temperature determination by microwave attenuation measurements, discussing measured values comparison with predictions by thermal ionization equation 11 p1804 A71-25193

Microwave power transmission from satellite solar energy station to earth, discussing atmospheric attenuation mechanisms and wavelength and power density optimization 13 p2000 A71-28670

Absorption, divergence and scattering attenuations and scintillation of microwaves from space sources, calculating frequency and distance dependence characteristics 13 p2034 A71-29390

Superhigh frequency microwave absorption region localization in collisionless plasmas by plasma parameters measurement in toroidal magnetic field 15 p2370 A71-31373

Frequency response of rainfall attenuation for various drops size distributions, plotting measured values at 890 and 110 GHz 15 p2374 A71-32696

Statistical analysis of radiometer measurement data of solar emission atmospheric attenuation at 19 GHz 15 p2496 A71-32710

Highly ionized plasma column anomalous microwave absorption near critical density as function of plasma frequency 16 p2619 A71-33176

Rain and drizzle submillimeter wave attenuation and radar scattering cross section calculation 22 p3515 A71-42737

Submillimeter wave attenuation measurement over 1 km path during summer rainstorms, comparing results with millimeter waves 22 p3515 A71-42738

Submillimeter waves attenuation in rain, comparing calculation with measurement 22 p3515 A71-42739

Submillimeter wave attenuation in snow, comparing results of calculation based on Mie theory with measurement 22 p3515 A71-42740

Decimeter radio wave propagation in Venusian atmosphere, determining refraction and absorption coefficients height dependence based on Venera spacecraft data 22 p3515 A71-42742

Vertically polarized millimeter and submillimeter wave attenuation measurement in rain 23 p3646 A71-43569

Precision compact rotary vane microwave attenuator, presenting modified law to extend dynamic attenuation range and reduce rotor section length 24 p3809 A71-45089

MICROWAVE CIRCUITS

Thin film lumped element microwave integrated circuits from concept to final functional devices 01 p0053 A71-10735

Thin film methods applied to microwave integrated circuits for compactness, reliability and low cost 01 p0053 A71-10736

Computer analysis of microwave circuit parameters effects on limited space charge accumulation oscillation in CW transferred electron devices 01 p0055 A71-11169

Microelectronic remanent type latching/ circulating, switching and phase-shifting microwave devices design and performance 02 p0228 A71-11654

Quasi-optical waveguide components for millimeter and submillimeter waves, considering couplers, attenuators, isolators, bandpass and bandstop filters 02 p0235 A71-12907

Microwave transistor circuit simplified noise figure expression including feedback and parasitics effects 05 p0719 A71-16164

Wideband interdigital microwave circuits using lithium niobate crystals for electro-optic modulation of light, discussing design and performance tests 05 p0762 A71-16336

Microwave integrated circuit technology, discussing substrates, conductors, dielectrics and resistors materials and design data and fabrication techniques 05 p0728 A71-16914

Microwave circuit with coupled TEM bars for L band Si avalanche diodes 05 p0729 A71-16920

Microwave semiconductor limiter diode for decimeter operation using spark gap analog 06 p0873 A71-17540

Thermal resistance of thermal p-n junction semiconductor microwave limiter diodes in continuous and pulsed mode operation 06 p0873 A71-17543

Loss resistance and dissipated power dependence on crystal configuration of microwave semiconductor junction diode 06 p0873 A71-17544

Microwave Gunn diodes made from GaAs single crystals, describing fabrication by diffusion process 06 p0876 A71-18082

Microwave transmitting and receiving duplexers for Intelsat 3 satellite, discussing design, operation and performance 06 p0877 A71-18402

Parasitic reactances in Gunn effect device packages from microwave equivalent circuit parameters 07 p1072 A71-19104

Compact microwave circuits for high efficiency operation of high power transferred electron oscillators 07 p1072 A71-19107

Large signal microwave equivalent circuits analysis of IMPATT diodes, allowing carrier multiplication by impact ionization at every point in diode 07 p1072 A71-19108

Avalanche diodes Evans circuit low pass filter located one half wavelength from diode/ analytic theory, developing expressions for efficiency and diode impedance 07 p1074 A71-19121

Compact microstrip high power high efficiency L band avalanche diode oscillator 07 p1074 A71-19123

MOS transistors for high digital logic speed and microwave performance, discussing fabrication by double diffusion through mask opening 07 p1078 A71-19998

Interdigital capacitors frequency response and application to lumped element microwave integrated circuits 08 p1261 A71-20753

Microwave circuits and components design using generalized rational function approximation in finite intervals with Zolotarev functions 08 p1252 A71-20757

Microwave dual mode reciprocal ferrite phasers, deriving insertion phase variations as function of ambient temperature and high average power heating 08 p1262 A71-20760

Slot transmission line bandpass and bandstop filters and hybrid couplers for microwave IC applications, presenting experimental performance data 08 p1262 A71-20761

Dual mode latching reciprocal ferrite microwave phase shifter, discussing operation principles, design and performance 08 p1262 A71-20764

Elliptic-function low pass microwave filters and other C sections applications including broadband impedance transformers 08 p1262 A71-20766

Automated network design optimization trends and role in computer aided design of lumped-distributed and microwave networks, emphasizing adjoint network method

08 p1268 A71-20767

Ferrite microstrip microwave phase shifters with transverse and longitudinal magnetization, calculating diamagnetic and permeability tensor effects

08 p1263 A71-20768

Wideband X band microstrip image rejection balanced mixer design

08 p1263 A71-20772

Bipolar silicon microwave transistors process technology improvements related to extensions of frequency, power handling or low noise performance

08 p1263 A71-20991

Superconductivity based cryogenic electronics, considering thin film IC, miniaturization, microwave circuits, memory elements, etc

08 p1263 A71-21067

Microwave diode technology, discussing Schottky barrier, p-i-n junction, varactor, tunnel, bulk effect and avalanche diodes performance and applications

08 p1266 A71-21622

Integrated microwave circuits substrate materials, discussing fabrication techniques with attention to mechanical, thermal and electrical characteristics

09 p1418 A71-23059

Substrate materials for microwave integrated circuits, comparing dielectric constants, surface finishes and thermal conductivity for alumina, sapphire, magnesium titanite, YIG and beryllium oxides

09 p1418 A71-23156

Varactor tuned X band Gunn oscillator with lumped thin film microwave circuits, discussing GaAs materials, output powers and bandwidths

09 p1421 A71-23722

C and higher-band pulse modulated signal generation with nanosecond duration, using TEM-mode pulse-forming network

10 p1577 A71-24211

Spurious spikes in microwave circulators due to hybrid resonant modes of ferrite post open-resonator structure

10 p1583 A71-24212

Microwave devices with transmission lines excited by curvilinear electron beams, deriving dispersion equations for TWT with allowance for space charge effect

10 p1584 A71-24717

P-n junction controlled discrete microwave commutation diodes performance calculation and design optimization

11 p1741 A71-26554

Decimeter range diode commutation devices, calculating speed, wideband capability, noise level and maximum power

11 p1741 A71-26555

Microwave integrated circuits lumped elements, including microstrip transmission lines configurations and electrical parameters

12 p1886 A71-26988

Single diode microwave circuit for simultaneous function as frequency doubler and parametric up-converter

12 p1887 A71-26999

Microstrip microwave circuit design by complex admittance measurement and computer modeling

12 p1892 A71-27149

Microwave meander line/coupled parallel commensurate conductors array/network analysis and synthesis, using equivalent circuit transformation for computerized design

14 p2219 A71-29565

Computerized design of optimally efficient dual-series fed microwave networks for waveguide phased arrays

14 p2209 A71-29566

Rectangular section microstrip lumped capacitance calculation by matrix methods

14 p2210 A71-29571

Equivalent circuit parameters of microwave planar power transistors at high injection levels, indicating parameters frequency dependence determination

14 p2213 A71-30627

Ferrimagnetic components in microwave IC, considering junction circulators, planar phase shifters, etc

16 p2547 A71-33551

Lumped elements in microwave IC, considering networks design, fabrication and performance in active and passive circuits

16 p2547 A71-33552

Integrated wideband low-noise X-band sweeping superheterodyne receiver, demonstrating advantages of microwave IC techniques application

16 p2547 A71-33553

S-band hybrid microwave IC module for phased arrays, presenting mechanical and electrical design details and performance test data

16 p2547 A71-33554

L band microwave IC front end for identification friend or foe (IFF) receiver, noting environmental and filtering requirements

16 p2547 A71-33556

SHF low noise IC mixer, considering effects of series resistance and barrier capacitance in diode and internal resistance of local oscillator

16 p2548 A71-33558

Microwave IC bandpass filters, utilizing dielectric resonators for high Q values

16 p2548 A71-33559

High power microwave phase shifter, using beryllium oxide filler ceramic dielectrics to obtain thermal coupling between ferrite element and waveguide wall

17 p2713 A71-34396

Low loss surface oriented waveguide for millimeter IC, using high permittivity rectangular dielectric image line

17 p2714 A71-34603

Book on microwave fields and circuits covering waveguides, transmission lines, impedance matching, sources, resonators, antennas, etc

17 p2716 A71-34772

Continuously variable microwave stripline phase shifter with linear shift by frequency by dielectric constant variation

18 p2889 A71-36272

Gridistor microwave FET for space communication equipment, combining advantages of FET and bipolar transistors

18 p2892 A71-36565

Microwave acoustic delay device incorporated in phase discriminator for AFC, FM noise meters and pseudo-superheterodyne receivers

18 p2893 A71-36599

Avalanche diode microwave oscillator design, comparing coaxial lumped, lumped element, microstrip and waveguide circuits

18 p2893 A71-36600

IC applications to microwave frequencies, relating circuit performance to substrate roughness and thickness of thin film metal adhesion layers

18 p2895 A71-36981

Noise temperature in microwave frequency mixers using nonlinear resistors, giving rectifier and diode loss formulas for rectangular and sinusoidal waves

19 p3027 A71-37494

Computer programming for on-line correction of microwave measurements of loss and reflection effects between network analyser and device/circuit under test

20 p3205 A71-39377

Microwave waveguide semiconductor modulator with p-n-n diode as control element, taking into account semiconductor control element conductivity change along waveguide wall

20 p3206 A71-39813

Microwave MESFET HF circuits, discussing noise factor advantage over bipolar transistors in low noise preamplifiers

21 p3355 A71-40743

Computerized optimal design of L band phase shift networks for broadband performance

21 p3361 A71-40816

Microwave bipolar transistors computer aided design, describing optimization and synthesis procedures and RF performance

23 p3649 A71-43067

Frequency and power limits of field effect triodes, noting application to gridistor for millimeter waves

23 p3653 A71-43950

Phase shift and attenuation measurements in high power microwave ferrite tetrodes circuits, using semiconductor transducers/digadectors/

24 p3809 A71-44871

MICROWAVE COUPLING

NT COUPLING CIRCUITS

Microwave bandpass filter design with couplings between nonadjacent resonant circuits for generating attenuation pole and increasing slope steepness

03 p0387 A71-13875

Dielectric loaded waveguide electromagnetic field and coupling matrix derived by finite element computer program, presenting dispersion curves and field plots

08 p1262 A71-20765

Gunn diode with capacitive probe on side surface for signaling strong field domain passage, calculating maximum permissible microwave coupling

10 p1584 A71-24721

Microwave resonator Q factor and coupling and matching characteristics measurement using line probe with AM and FM signals

10 p1584 A71-24724

Ferrite resonator coupled to microwave transmission line, deriving instability effects threshold power level for comparison with measurement

10 p1584 A71-24725

MICROWAVE EQUIPMENT

NT BACKWARD WAVE TUBES

NT CATHODE RAY TUBES

NT COLD CATHODE TUBES

NT GAS DISCHARGE TUBES

NT GYRATORS

NT MICROWAVE ANTENNAS

NT MICROWAVE FILTERS

NT MICROWAVE INTERFEROMETERS

NT MICROWAVE OSCILLATORS

NT MICROWAVE PLASMA PROBES

NT MICROWAVE PROBES

NT MICROWAVE RADIOMETERS

NT MICROWAVE TUBES

Multi octave microwave frequency synthesizer by subharmonic synthesis and frequency multiplication under digital programmed commands

01 p0054 A71-10972

Microwave negative resistance diode avalanche region, deriving four element incremental signal model

01 p0055 A71-11168

Microwave Gunn diodes I-V characteristics as function of carrier concentration

01 p0057 A71-11213

Variable microwave thermal noise temperature standard generator with output ranging from below 40 to above 370 K

02 p0250 A71-12139

Transmitter system for Skynet spacecraft performance tests using calibrated automatic level control and microwave calorimeters

62 p0218 A71-12442

L band DME and TACAN improvements, emphasizing use of static broadband amplifiers

02 p0235 A71-12905

STOL navigation equipment and microwave landing instruments test programs, noting data recording and flight operations

03 p0454 A71-13286

Waveguide microwave load element with separate adjustment for reflection coefficient phase and magnitude

03 p0378 A71-13397

Semiconductor developments, discussing field effect transistors, MOS, microwave components, piezoelectric effects, optoelectronics and galvanomagnetism

03 p0384 A71-13534

Swept electron beam scanning in microwave beam-wave interaction devices via periodic magnetic fields

03 p0385 A71-13794

Prismatic absorption type wavemeter consisting of frequency divider and Fabry-Perot interferometer, considering tests in millimeter and submillimeter range

03 p0386 A71-13801

Stable tunable microwave source for spectroscopy using Gunn diode, giving microwave cavity spectrometer block diagram

03 p0428 A71-13924

Ar-Ag arc, microwave discharge and plasma torch techniques in emission spectroscopy of trace elements in biological materials

03 p0377 A71-14421

Precision electromagnetic measurements - Conference, Boulder, June 1970

04 p0585 A71-14651

Microwave phase measuring system using programmable digital dividing circuits, considering application to plasma diagnostics

04 p0586 A71-14655

Microwave systems for cryogenic liquid and slush density and flow velocity measurements

04 p0586 A71-14659

Piezoelectric surface waves physical characteristics, examining excitation relationship to construction of microwave devices

04 p0550 A71-14742

German monograph on polycrystalline ferrites studies with quasi-optical resonators in mm wave range

05 p0791 A71-16125

Matched impedance microwave vacuum feedthrough

05 p0757 A71-16234

Millimeter wave lensless Fourier transformation/LFT/holographic imaging, discussing equipment and performance

05 p0754 A71-17081

High Q microwave diodes on n-type germanium using carrier counterdiffusion in reducing atmosphere

06 p0873 A71-17539

Integrated electro-optical microwave radar and laser/lidar systems for earth oriented, environmental and domestic applications

07 p1095 A71-18827

Wideband microwave monopulse radar direction finding techniques, discussing concept, operation theory, characteristic equations and error analysis

07 p1059 A71-18846

Packaged microwave avalanche diodes negative resistance properties three-parameter characterization at low current densities

07 p1074 A71-19125

Microwave plasma device development, noting beam plasma amplifiers and quiescent source

07 p1167 A71-19257

Free-space focused microwave system for determining materials complex permittivity to temperatures over 2000 C

07 p1115 A71-20357

V/STOL microwave scanning beam approach and landing system, describing ground and airborne station equipment and operation

08 p1332 A71-21680

Microwave methods for nitrogen or hydrogen densities and flow rate measurement in single phase liquid and slush state

08 p1292 A71-21696

Multicomponent microwave equipment, discussing design automation by matrix notation with computer calculations

09 p1416 A71-22468

Varactor-tuned avalanche microwave source, using interchangeable iris shims at output cavity for passive stabilization, power output and tuning variability

09 p1418 A71-23155

Symmetric self-calibrating attenuator consisting of rotatable grid between two fixed grids for application at submillimeter wavelengths

09 p1421 A71-23682

Microwave and modular solid state ILS designs, discussing accelerated progress, international standard and present system life expectancy

10 p1639 A71-23943

Microwave tunnel diode oscillator, representing nonlinear characteristics with Taylor series

11 p1737 A71-25666

Soviet papers on nonlinear and microwave radio engineering systems covering antenna arrays, tunnel diode multivibrators and binary logic elements, subharmonic oscillators, etc

11 p1739 A71-26535

Reinforced plastics components in supersonic transport nose radome and missile radar antennas, discussing molding, sandwich materials and computer controlled spraying techniques

12 p1887 A71-27016

Annular solid state microwave diodes temperature distribution at diode/heat sink interface, presenting closed form solution for calculation of absolute temperature rise

12 p1889 A71-27699

Microwave phase discriminators sensitivity and linearity performance improvement, noting diode detectors nonideal nature

13 p2038 A71-28779

Semiconductor materials technologies, discussing optoelectronic and microwave components, photodiode arrays, HF diodes and transistors and IC Doppler radar units

13 p2111 A71-28908

Thin film hybrid IC microwave component development, noting market and consumer applications

13 p2039 A71-28909

Microwave frequency mixer using two inverted tunnel diodes in series connection

14 p2211 A71-30116

Arbitrarily dimensioned microwave dielectric modules complex permittivity calculation

14 p2212 A71-30511

Magnetic properties of sintered cobalt-iron earth alloy magnets using Sm, Pr, La or Ce misch metal for microwave device applications

14 p2284 A71-30703

Small signal impedance of avalanche region in microwave IMPATT diode

14 p2215 A71-30833

Microwave responders in FM or AM modes with cavity resonator, considering use in medium distance telemetering or telemonitoring

14 p2215 A71-30911

Microstrip p-i-n diode controlled L band digital phase shifter for aircraft-satellite communication

14 p2217 A71-31055

Microwave spectrum analyzer, discussing capabilities and applications in ECM, surveillance, communications, circuit design and analysis and electromagnetic compatibility

15 p2368 A71-31208

Transient response and design formulas for microwave power stabilizer with nonlinear inertial feedback containing semiconductor attenuator

15 p2378 A71-31230

Book on hot electron microwave generators covering semiconductor physics, collision theory, Gunn effect, domain dynamics, avalanche breakdown, etc

15 p2375 A71-31509

Microwave transistor case design, considering RF parasitics, thermal dissipation, environmental mechanical factors, ceramic technology and sealing

15 p2377 A71-32500

Microwave Gunn diodes I-V characteristics as function of carrier concentration and power efficiency

17 p2713 A71-34264

Millimeter system, devices and guides - Conference, Los Angeles, August 1970, Volume 14

17 p2714 A71-34601

Millimeter wave systems applications to plasma probes, radar, radiometry and communications

17 p2699 A71-34602

Parametric up-converters for low noise broadband microwave receivers, discussing electronically tunable pump frequency accuracy and stability

17 p2714 A71-34606

Superheterodyne wideband microwave receiver requirements, design and performance

17 p2699 A71-34607

General purpose pulsed microwave radar receiver, describing balanced mixer and transistorized IF amplifier design and construction

18 p2887 A71-36015

Low noise microwave transistor, describing geometry and diffusions optimization, power gain, reliability and base resistance

18 p2892 A71-36564

High power microwave CW tubes and power amplifier requirements for communication satellites

18 p2892 A71-36571

Microwave avalanche diodes, considering drift velocity and power efficiency limitations of IMPATT mode

18 p2894 A71-36976

Silicon microwave transistors frequency response theory, considering application as small-signal and power amplifiers

18 p2894 A71-36978

Schottky barrier, point contact and Ge back diodes for microwave mixers and detectors, noting burnout characteristics

18 p2894 A71-36979

Bulk semiconductor microwave control components, considering dielectric and conductive properties of plasma state

18 p2894 A71-36980

Semiconductor instability effects on reflection and transmission coefficients of microwave control devices

19 p3026 A71-37252

Acoustic or microwave hologram reconstruction into visible three dimensional image in real time

19 p3066 A71-38412

Hybrid microelectronics IC S band double conversion phase locked receiver, discussing fabrication, process requirements and component selection criteria

19 p3035 A71-38538

Microwave instrumentation for measuring cryogenic fluids density and flow rate, noting slush

20 p2327 A71-39277

Multilayer microwave semiconducting film piezoelectric acoustic transducer loss and frequency response derivation from electromechanical power conversion theory

20 p3240 A71-39764

Terrain and atmospheric parameters affecting radar system design at microwave frequencies, discussing radar backscatter cross section and attenuation

20 p3200 A71-39904

Gunn effect devices properties and applications, discussing microwave energy sources tunable and local oscillators, parametric amplifier pumps and radar transmitters

21 p3357 A71-40819

Coherent microwave holographic radar systems, discussing mono and bistatic versions, far field performance, pulse compression techniques and signal processing

22 p3540 A71-41751

Modular step scan microwave aircraft landing system (TALAR)/ design and operation, noting short takeoff and landing

22 p3572 A71-42088

Doppler scanning landing microwave system for air-derived azimuth and elevation angle aircraft guidance by frequency coding and reference carrier transmission

22 p3572 A71-42089

Operational requirements of microwave guidance systems, comparing guidance and position measurement applied to aircraft approach and landing

22 p3572 A71-42092

Microwave biased germanium IR photoconductive detector for optical communication systems, describing operation principles, signal demodulation and performance

22 p3543 A71-42123

Microwave quasi-holographic techniques, discussing synthetic aperture, chirp radar, rotating target imaging system and beam forming method

22 p3546 A71-42477

Satellite-borne minimum bulk and weight K-band transmitter and receiver frequency converters design features and performance

22 p3524 A71-42522

IMPATT diode development for millimeter wave applications including oscillators, sweep generators and Doppler radar

22 p3524 A71-42763

German monograph on analysis and design of digital microwave phase shifters for phase controlled antennas covering admittance loaded lines, transmission and reflection behavior

23 p3649 A71-42999

Precision compact rotary vane microwave attenuator, presenting modified law to extend dynamic attenuation range and reduce rotor section length

24 p3809 A71-45089

Microwave structures symmetry analysis based on group theoretic concepts application to vector electromagnetic fields, investigating single wire helix

24 p3809 A71-45090

MICROWAVE FILTERS

Polynomial microwave frequency filter composed of random symmetric components of randomly selected circuit

01 p0057 A71-11217

Microwave bandpass filter design with couplings between nonadjacent resonant circuits for generating attenuation pole and increasing slope steepness

03 p0387 A71-13875

Book on electrical, microwave and digital filter systems and design covering approximations, phase shift, ladder networks, frequency transformation, time domain, etc

04 p0560 A71-15075

Slot transmission line bandpass and bandstop filters and hybrid couplers for microwave IC applications, presenting experimental performance data

08 p1262 A71-20761

Four-cavity elliptic waveguide microwave bandpass filter design and performance prediction from mathematical model

08 p1262 A71-20762

Elliptic-function low pass microwave filters and other C sections applications including broadband impedance transformers

08 p1262 A71-20766

X- to K-band harmonic generator using nonlinear capacitance of varactor diode, deriving maximum efficiency, optimum load and generator impedances

09 p1417 A71-23036

Waveguide and stripline bandstop filters for pass-band loss minimization, using Chebyshev response curves

09 p1418 A71-23158

High power magnetically tunable microwave interference filters based on spin waves magnetic field dependent dispersion in ferrimagnetic materials

09 p1421 A71-23721

Magnetically tunable microwave bandpass and bandstop filters with yttrium-iron garnet (YIG)/ single crystal

11 p1737 A71-25625

Low pass equiripple insertion loss functions roots for commensurate microwave filters with stubs and unit elements

13 p2038 A71-28610

Two cavity ring-type channel dropping filters for millimeter wave guided communication system, calculating pulse response and interchannel crosstalk characteristics

14 p2210 A71-29569

Millimeter wave waveguide time delay distortion characteristics equalization using directional filter cascades

14 p2210 A71-29572

TEM mode delay line microwave filters, deriving relationships between risetime, settling time, bandwidth and Q

14 p2219 A71-29601

UHF head for 225-400 MHz AM receiver, emphasizing choice of ring mixer and passband filter switching principle

16 p2548 A71-34124

Polynomial microwave frequency filters composed of random symmetric components of randomly selected circuit

17 p2718 A71-34268

Optimized low loss microstrip microwave filters on silica substrates by photolithographic reduction of LF models

19 p3026 A71-37218

Microwave narrow bandpass filters design using microstrip lines

21 p3354 A71-40733

MICROWAVE FREQUENCIES

NT C BAND

NT EXTREMELY HIGH FREQUENCIES

NT P BAND

NT SUPERHIGH FREQUENCIES

Automatic RF and microwave test equipment for communication, navigation, radar and tactical systems

03 p0395 A71-13083

Impedance measurement and standing wave ratios at microwave frequencies, using directional couplers

03 p0377 A71-13269

Nonautonomous operation of reflex klystron coupled to multifrequency waveguide, noting response to microwave signal

03 p0385 A71-13792

Calorimetric method for measuring high signal reflection coefficients at microwave frequencies

04 p0586 A71-14656

Instantaneous radar pulse frequency measurement for microwave bands, discussing multiplexed filters, wideband discriminators, dissipative frequency sensitive attenuators and band division receivers

04 p0555 A71-15360

Crab Nebula pulsar PSR 0531 plus 21 at 410-1664 MHz, noting mean pulse profiles and spectral indices

05 p0812 A71-16697

Microwave measurements of semiconductors and semiconductor films including resistivity, permittivity and carrier mobility

06 p0873 A71-17538

Microwave frequency measuring techniques extension into IR, developing Si point contact diode with nonlinear I-V characteristics

07 p1125 A71-19797

Microwave noise generation by triboelectric charging of dielectric surfaces

07 p1063 A71-19932

Fading microwave radio channel baseband gain and noise stability, assuming nonuniform frequency selective fading effects

07 p1066 A71-20426

Microwave irradiation effects on peripheral blood and bone marrow in dogs and rabbits

07 p1053 A71-20539

Noise behavior of Schottky barrier gate FET at microwave frequencies, discussing effects of carrier velocity saturation and parasitic resistances on noise parameters and measurement method

08 p1261 A71-20741

Limited space charge accumulation layer diodes operating characteristics, using GaAs devices with uniform doping for microwave peak power

08 p1266 A71-21624

High order harmonic mixing of klystron microwave and far IR laser radiation using Josephson junction

09 p1464 A71-22766

Epitaxial InP three level oscillators in K and Q bands /18-40 GHz/, suggesting optimum operating frequency determined by defined transit velocity

09 p1421 A71-23719

Conductivity in microwave Permalloy thin films without external magnetic field comparing Fuchs-Sondheimer theory

10 p1656 A71-24213

LF plasma beam density oscillation spectra from microwave emission amplitude modulation

10 p1648 A71-24316

Microwave frequency sound generation in solids with Q switched ruby laser

10 p1621 A71-24838

Microwave/high frequencies safe exposure limits, discussing radiating aerial near field, radar hazards and human body absorption

10 p1573 A71-25080

Thermal and nonthermal effects of microwave and RF radiation in biological systems, discussing dielectric constant and conductivity for high water content tissues

11 p1716 A71-25281

Italian book on microwave propagation covering electromagnetic wave attenuation, rainfall space-time structure and radioelectrical/meteorological data recording

11 p1731 A71-25650

Fast shock waves electromagnetic production in light gases, discussing interferometric measurements at optical and microwave frequencies in H

11 p1764 A71-26272

Microwave emission from North Sea and North Atlantic at surface wind speeds of 5-25 m/sec, measuring brightness temperature

12 p1902 A71-27199

Constant emf in bulk age and SiN-type semiconductors under multifrequency microwave electric field

13 p2111 A71-28368

Apparatus for measuring polar liquids dielectric permittivity and losses at microwave frequencies over wide temperature and pressure ranges

14 p2222 A71-30583

Absolute calibration of radio sources with variable flux density in microwave region

14 p2316 A71-30976

Binary optical detour phase holograms formation in measurements with centimeter electromagnetic waves, describing dielectric diffusers for microwaves

15 p2405 A71-31280

Low temperature high conductivity nonequilibrium plasma creation in MHD generators by microwave ionization

17 p2676 A71-34193

Solar X-ray flares recorded by SOLRAD-9 on Explorer 37 satellite occurring in optical flares-microwave bursts-X ray flares sequence

17 p2796 A71-35391

Impedance variations vs electrophysical properties of epitaxial and diffusive semiconductor structures for electronic equipment, applying microwave fields for parameter control

18 p2954 A71-35874

Semiconductor device with stable negative conductance over wide range of microwave frequencies and power levels, using transferred electron effect in epitaxial GaAs

18 p2895 A71-36985

Solar radio bursts circular polarization data, presenting single and multiple inversion analysis at microwave frequencies

19 p3128 A71-38170

Atmospheric water vapor effects on microwave frequencies refraction index structure

19 p3024 A71-38611

Liquid nitrogen cooled microwave low temperature noise standard in WR-51 waveguide

20 p3202 A71-38832

Scorpius X-1 radio emission detection at 1415 MHz, discussing brightness distribution

21 p3441 A71-40068

Microwave photoconductivity of boron single crystals under pulsed illumination, determining temperature effects on carrier mobility, recombination coefficients and relaxation times

21 p3428 A71-41202

Solar flux density measurements at 2980 MHz, noting integration with spectral curve

22 p3590 A71-41463

Solar proton flare prediction with microwave radio burst data, using satellite measurements

22 p3590 A71-41464

Solar proton events intensity forecasts using time parameters of microwave bursts

22 p3590 A71-41465

Scanning microwave landing guidance system coordinates choice, discussing signal format, antennas planar or conical beams and V/STOL application

22 p3572 A71-42090

Impedance and capacitance frequency dependence of p-i-n junction diodes at microwave frequencies with high injection levels

23 p3650 A71-43308

Upwind/downwind differential Doppler spectra of radar sea echo for P, L and C bands

23 p3646 A71-44173

Plasma microwave harmonic generation conversion efficiency, applying field gradient theory to case of positive column placed through rectangular waveguide

24 p3803 A71-44648

Hydrogen plasma generation by microwave field in magnetic-mirror device due to electron cyclotron resonance, measuring transverse diffusion coefficient dependence on magnetic field

24 p3858 A71-45235

He-Ne laser radiation modulator at 1.5 GHz using X and Z cut lithium niobate crystals in toroidal microwave cavity

24 p3835 A71-45265

MICROWAVE IMAGERY

Microwave holography with artificial reference wave and receiver multiplier, improving linear resolution in image

02 p0248 A71-11876

Millimeter wave holographic imaging for concealed weapon detection by phase-only hologram, discussing recording and reconstruction systems configurations

22 p3546 A71-42485

MICROWAVE INTERFEROMETERS

Microwave interferometer for low density electron laboratory plasmas

03 p0428 A71-13926

Broadband phase switch designs for high sensitivity RF and microwave interferometry at low signal power levels

12 p1889 A71-27698

X band focused beam interferometer for plasma phase shift measurement independent of propagation path attenuation over 30 dB dynamic range

14 p2214 A71-30804

Optical wave reconstruction from microwave holograms and application to interferometry, considering resolving power and visible images of microwave transparencies

15 p2405 A71-31281

Charge density fluctuation measurements in ionized turbulent hypersonic sphere wakes, using Langmuir and continuum electrostatic probes and microwave interferometric and scattering equipment

21 p3363 A71-40388

MICROWAVE OSCILLATORS

NT BACKWARD WAVE TUBES

NT GAS DISCHARGE TUBES

Microwave emission from InSb due to sound amplification by piezoelectric electron-phonon coupling at low magnetic fields

01 p0052 A71-10321

Computer analysis of microwave circuit parameters effects on limited space charge accumulation oscillation in CW transferred electron devices

01 p0055 A71-11169

Widely separated microwave oscillators phase synchronization via satellite transponder

02 p0216 A71-12330

Liapunov stability prediction of minimum length for distributed oscillators of superconductive tunnel junction strip line

03 p0388 A71-14475

Optimal design of low noise multistage microwave oscillator, discussing quartz master oscillator frequency effects

05 p0727 A71-16001

Silicon junction avalanche diodes as S band oscillators and amplifiers, presenting peak power efficiency and gain data

05 p0729 A71-16921

Coplanar n-type GaAs Gunn effect microwave oscillators failure mechanism, suggesting role of current filament formation in thermal breakdown

06 p0874 A71-17665

Microwave local oscillator and beacon generator for Intelsat 3, discussing design, operation and performance

06 p0877 A71-18400

Neutron radiation damage on high efficiency microwave avalanche diode sources /TRAPATT oscillators/

07 p1071 A71-19068

Frequency saturation effects in transferred electron /Gunn/ microwave oscillators mechanical tuning characteristics in conventional waveguide cavities

07 p1072 A71-19105

Postcoupled waveguide cavity Gunn effect microwave oscillator equivalent circuit analysis, using lumped constant elements

07 p1072 A71-19106

Waveguide cavity CW Gunn microwave oscillator bias voltage controlled amplitude and frequency modulation

07 p1073 A71-19110

X band IMPATT oscillator, discussing frequency stability, rms noise deviation, admittance characteristics, output power loss, temperature effects and power stability

07 p1073 A71-19111

Broadband pulling cavity stabilized X band Gunn oscillator, using measured circuit and diode admittance

07 p1073 A71-19112

Injection locked microwave oscillators nonlinear differential equation reduction to nonlinear algebraic equation, calculating AM limiting and output power increment as injected signal amplitude functions

07 p1073 A71-19113

Rucker multidevice symmetrical microwave oscillator analysis, overcoming nonlinearity difficulties in eigenvector approach

07 p1073 A71-19118

Microwave oscillator circuit with cap structures for testing millimeter wave IMPATT diodes

07 p1073 A71-19119

Frequency variation with temperature in coaxial cavity avalanche transit time microwave oscillators explained by diode junction capacitance and cavity length changes with temperature

07 p1074 A71-19120

Metal ceramic microstrip L band oscillator circuit with high efficiency silicon avalanche diodes in capacitively loaded TEM coupled lines

07 p1074 A71-19122

Compact microstrip high power high efficiency L band avalanche diode oscillator

07 p1074 A71-19123

Phase locked avalanche transit time oscillators FM noise spectra

07 p1074 A71-19124

Injection phase locked oscillator as input microwave limiting amplifier for noise measuring microwave discriminator

07 p1074 A71-19126

Frequency modulation technique based on injection phase locking theory applied to microwave oscillator Q measurement

07 p1074 A71-19127

Composite silicon IMPATT diode oscillator for 110 GHz operation with 140 mW output power

07 p1075 A71-19264

X band multiple IMPATT oscillator combining 12 packaged diodes in waveguide cavity for 10.5 watt CW output at 9.1 GHz, noting clean spectrum

07 p1075 A71-19266

Superconducting microstrip microwave resonators with high Q, using vacuum deposited lead on alumina substrate

07 p1079 A71-20162

Efficiency deterioration of M type backward wave oscillators /M-BWO/ from cyclotron wave interactions

07 p1080 A71-20453

IMPATT and Gunn microwave oscillators injection phase locking, discussing stationary state synchronization theory and phase vs frequency deviation measurements

08 p1263 A71-20990

Microwave oscillators with Gunn effect device resonant circuit and YIG tuning, discussing design and performance

08 p1263 A71-20992

Light-microwave signal relation in optical pumping and detection in Rb atomic oscillator

08 p1289 A71-21273

Submillimeter wave oscillations possibility by Bloch oscillation of conduction electrons in ideal crystal with periodic energy band structure

08 p1343 A71-21280

Bulk effect microwave oscillators energy source design, considering operation mode and circuit tuning control parameters

08 p1266 A71-21623

Tunnel diode microwave oscillator design, discussing fixed frequency or varactor tuned operation, power instabilities and load variations

09 p1415 A71-22457

Si Read diode computer simulated large-signal operation, determining temperature effect on microwave oscillating efficiency

09 p1417 A71-22966

Epitaxial InP three level oscillators in K and Q bands /18-40 GHz/, suggesting optimum operating frequency determined by defined transit velocity
09 p1421 A71-23719

CW X band frequency-locked Gunn oscillators as frequency demodulator with millivolt range detection sensitivity
09 p1421 A71-23720

Varactor tuned X band Gunn oscillators with lumped thin film microwave circuits, discussing GaAs materials, output powers and bandwidths
09 p1421 A71-23722

X band Schottky barrier diodes RF impedance mismatch and noise factor, calculating dependence on microwave oscillator voltage-standing wave ratio
09 p1421 A71-23723

Avalanche diode microwave oscillator stabilized by two external resonant circuits, investigating self oscillation characteristics
10 p1582 A71-23808

IMPATT diode oscillators noise and injection phase locking, discussing theoretical refinements of original simple model by Read
10 p1584 A71-24818

Microwave discriminators with IF error signal ensuring high stabilization of master oscillator frequency without complex tuning operations
11 p1737 A71-25939

X band reflex klystron oscillator with frequency stability comparable to high quality quartz clock by coupling to superconducting cavity
11 p1739 A71-26368

Tunnel diode microwave oscillator design, using circle diagrams of operational and load characteristics
12 p1888 A71-27513

Hybrid M-type microwave oscillators including backward and traveling wave tubes with crossed fields in large amplitude mode, considering power efficiency and frequency control
12 p1888 A71-27620

Temperature compensation for frequency changes stabilization of avalanche transit time diode microwave oscillator, using loop circuits and high dielectric constant ceramics
13 p2036 A71-27938

Unmodulated microwave oscillations power stabilizer with semiconductor attenuator
13 p2036 A71-28367

High efficiency and power long life cross field amplifier generator for solar energy conversion in space into microwave, discussing magnetron and ampliflon
13 p2000 A71-28668

Solid state local oscillator for radio relay systems microwave receivers
13 p2039 A71-28899

Microwave integrated stripline Gunn oscillators with fixed/variable frequency tuning in X band
13 p2039 A71-28911

Integrated S band microstrip parametric amplifier modules with self contained Gunn effect pump oscillator for space flight applications
14 p2210 A71-29570

Frequency-length relationship for bulk InP microwave oscillators in 10-100 micron thickness range, obtaining threshold field and average transit velocity
14 p2210 A71-29791

Power gain of Q-band GaAs FET with Schottky-barrier gate, giving amplifier and oscillator designs
14 p2210 A71-29800

Microwave oscillators Rieke diagram semiautomatic plotting by injection phase locking, using network analyzer for impedance measurement
14 p2211 A71-29823

Optical and microwave multifrequency autooscillatory drift and reflex klystrons, TWT and electronic oscillators, comparing to He-Ne lasers
14 p2211 A71-30091

Microwave oscillations small phase difference variation measurement, using polarization effects
14 p2196 A71-30636

Transferred electron microwave oscillators high efficiency operation mode with more severe limitation than limited space charge accumulation mode
14 p2215 A71-30826

Double cavity tuning of Gunn oscillators at mm wavelengths achieving output power improvements
14 p2215 A71-30831

Spectral theory of linear differential operators for microwave oscillatory systems synthesis from inhomogeneous line segments, determining line characteristic impedances and local reflection function
15 p2369 A71-31233

Metal-semiconductor-metal low noise microwave oscillator, using single crystal n-type Si wafers sandwiched between two PtSi Schottky barrier contacts
15 p2377 A71-32315

IMPATT diode oscillator for CW Doppler radar, microwave detection and communications systems, emphasizing cost reduction
15 p2377 A71-32522

Time domain model of device-circuit characteristics of TRAPATT diode microwave oscillator
15 p2378 A71-32699

Large signal saturation effects in cyclotron resonance oscillators, using helical electron beam-cavity interaction model
16 p2545 A71-33394

Varactor tuned FM pulsed Gunn oscillator for testing X band delay lines for pulse compression radar
16 p2546 A71-33415

Ku band monopulse receiver with electronically tunable Gunn oscillator, discussing negative resistance diodes dynamic impedance properties
16 p2547 A71-33557

High power efficiency solid state UHF sources, comparing Gunn and avalanche diodes performance
17 p2715 A71-34685

Sensitive mm wave receivers, using local oscillator and mixer functions in single Gunn diode for large dynamic signal input range and wide IF bandwidth capability
17 p2717 A71-35111

Silicon IMPATT microwave oscillators, calculating CW power as function of frequency by scaling approximation
18 p2888 A71-36129

High efficiency avalanche diode microwave oscillator design guidelines based on oscillation mode theory, covering CW and pulsed operations
18 p2888 A71-36131

Temperature and bias circuit frequency modulation in CW X band Gunn oscillators
18 p2888 A71-36132

X-band Gunn oscillator equivalent circuit parameters determination for baseband and RF noise contribution to AM and FM noise
18 p2888 A71-36270

IMPATT diode amplifiers and oscillators AM and FM noise spectra and SNR prediction for comparison with experiment
18 p2888 A71-36271

Avalanche diode microwave oscillator design, comparing coaxial lumped, lumped element, microstrip and waveguide circuits
18 p2893 A71-36600

Harmonic generation in trapped-plasma-mode IMPATT diode microwave oscillators with waveguide-coaxial cavity
18 p2894 A71-36828

Transferred electron /Gunn/ amplifiers and oscillators for microwave applications, considering electronic and mechanical tuning over large frequency ranges
18 p2894 A71-36977

IMPATT diode microwave oscillator temperature effect on operation, comparing with Read diode small signal admittance characteristics
18 p2895 A71-36986

Temperature variations effect on TRAPATT microwave oscillator parameters, considering upper temperature limit dependence on heat dissipated in diode and heat sink thermal resistance
18 p2895 A71-36988

Tunnel diode oscillator equivalent circuits with frequency variance by changing load susceptance
19 p3026 A71-37145

Equivalent circuit parameters determination for baseband and microwave noise from Gunn oscillator, using AM-FM correlation coefficient
19 p3028 A71-37699

X band output power and FM noise of parallel multicontact Gunn oscillators
19 p3029 A71-38074

FM noise in output spectrum of low level operating IMPATT diode microwave oscillators
19 p3029 A71-38217

High-power high-efficiency CW X band Gunn oscillators on diamond heat sinks, noting operation in waveguide cavities
19 p3029 A71-38219

High peak power microwave oscillators, discussing pulsed limited space charge accumulation and TRAPATT diodes pulsed radiation sources performance
19 p3029 A71-38294

Microwave discriminators with IF error signal ensuring high stabilization of master oscillator frequency without complex tuning operations
20 p3205 A71-39259

X band Gunn diode oscillator pulsed operation starting delay time relationship to CW operation frequency/temperature characteristics, suggesting contact resistance role
21 p3359 A71-41411

Si Pt-n-p transit time microwave diode source noise measurement, noting low noise characteristics and suitability for local oscillator applications
21 p3359 A71-41413

Microwave Si MESFET for 15 GHz oscillation with reduced gate metallization resistance and pad parasitics, improving gain and noise figure
22 p3520 A71-41683

Single cavity multiple device microwave oscillator with 12 IMPATT diodes combined output power, presenting proof for circuit configuration stable operation free from moding problems
22 p3524 A71-42631

Optimal design of low noise multistage microwave oscillator, discussing quartz master oscillator frequency effects
22 p3524 A71-42750

Multilayer epitaxial InP transferred electron microwave oscillator I-V characteristics and frequency dependence on layer thickness
23 p3649 A71-42912

Microwave planar Gunn oscillators performance in X band, giving pulsed and CW I-V characteristics
23 p3649 A71-42913

Microwave emission from plasmas in InSb with and without magnetic fields, deriving pseudolongitudinal wave interaction theory for explanation
23 p3714 A71-42914

GaAs LSA mode V band oscillator CW and pulsed operations power and efficiency limitations
23 p3649 A71-42915

German monograph on Gunn oscillators frequency stabilization by synchronization with external oscillator emitting HF signals
23 p3649 A71-43045

Reactive impedance matching of Gunn or IMPATT diodes for microwave oscillators by dielectric tuning
23 p3650 A71-43071

Gunn oscillator frequency stabilization at minus 10 to 60 C by high Q single tuned oscillator circuit, considering requirements for 20 GHz radio relay system
23 p3651 A71-43438

CW avalanche microwave oscillator frequency modulation /pulling/ by injected RF signal, discussing theory and experiment
23 p3646 A71-43903

Silicon avalanche diodes for microwave TRAPATT amplifiers and self excited oscillators with IMPATT triggering
23 p3653 A71-43964

Transmission and reaction cavity stabilized Gunn microwave oscillators AM and FM noise spectra, extending calculations based on Kurokawa theory to high modulation frequencies
23 p3653 A71-43967

Microwave power distributed self excited oscillator synchronization using elements insensitive to external disturbances
23 p3655 A71-44318

X band microwave oscillator design for matched cavity reactance and maximized power by coupling Gunn and IMPATT diodes to coaxial transmission line
24 p3807 A71-44362

MICROWAVE PLASMA PROBES

Radial density distribution in plasmoid and radial expansion of plasmoid investigated by microwave measurements
06 p0940 A71-18703

Cold bounded nonuniform magnetoplasma harmonic generations model for small collision frequencies
07 p1166 A71-18889

Electron density profiles in supersonic plasma jet, using immersed microwave probe [AIAA PAPER 71-272]
08 p1342 A71-21998

Microwave probing of electron number density and collision frequency in slightly ionized plasmas
15 p2458 A71-32395

Microwave and laser diagnostics of plasmas based on interaction with electromagnetic fields
16 p2617 A71-32960

Langmuir probe and microwave measurements of density, velocity and electron and ion temperatures in streaming plasmas generated by focused laser pulse
19 p3112 A71-37740

Electrical microwave probe for measuring HF potential oscillations in low temperature plasma
19 p3064 A71-37787

Monograph on electron drift rate measurement in low pressure arc discharge using microwave dragging technique
19 p3116 A71-38549

Plasma diffusion lifetime and electron concentration measurements in Tokamak-3 by pulsed neutral hydrogen injection and microwave multichord probing
24 p3852 A71-44488

Millimeter band plasma microwave radiation receivers for emission measurement, presenting schematic diagrams for superheterodyne
24 p3825 A71-44507

MICROWAVE PROBES

NT MICROWAVE PLASMA PROBES

Cassegrain antenna electrical and structural design and communication system for microwave propagation and communication research, using moon reflected signals as atmospheric probes
02 p0234 A71-12806

Near field electromagnetic radiation probe for microwave measurements in proximity of hazard source
09 p1453 A71-23626

Gunn diode with capacitive probe on side surface for signaling strong field domain passage, calculating maximum permissible microwave coupling
10 p1584 A71-24721

Thermoelectric microwave radiation sensors with small area n-n junctions, investigating carrier heating effects on I-V characteristics

10 p1584 A71-24723

Microwave resonator Q factor and coupling and matching characteristics measurement using line probe with AM and FM signals

10 p1584 A71-24724

Microwave dielectric meter measurement system sensitivity to electric field energy in dielectric non-magnetic specimen

12 p1889 A71-27621

Ionization measurement in detonation and shock waves in reactive gas mixtures by microwave cavity techniques

15 p2411 A71-32556

Dielectric articles thickness and flow control by microwave magic tee junction waveguide, describing instrument design and operating characteristics

22 p3521 A71-41772

Shock wave attenuation in two diaphragm tube, obtaining velocity profiles with microwave phase detector system

23 p3674 A71-43086

MICROWAVE RADIATION

U MICROWAVES

MICROWAVE RADIOMETERS

Noise temperature measurement of mismatched cryogenic generator, using compensation method

01 p0056 A71-11198

Microwave radiometry for earth terminal and communication satellite performance measurements, including gain, tracking, noise temperature, radome attenuation, power and transfer characteristics

02 p0218 A71-12446

Absolute measurements of solar flux density at 9500 MHz, comparing Nagoya and Heinrich-Hertz Institute radiometric observations

02 p0302 A71-12760

Brightness temperature of vertically structured medium in microwave radiometry

04 p0552 A71-15212

Microwave radiometric techniques for continuous all-weather remote sensing of sea conditions from satellites, discussing foam and surface ripple effects [AJAA PAPER 70-318]

05 p0743 A71-17101

Atmospheric moisture field radiometric microwave sounding statistical treatment, noting latitudinal dependence over oceans from Cosmos 243 satellite measurements

09 p1486 A71-22301

Side-looking radar, thermal IR scanner and passive microwave radiometers for remote sensors for geologic mapping

09 p1452 A71-23215

Cloud radiation measurements by ground based microwave radiometer

11 p1794 A71-25380

Microwave radiometers transfer calibrations by noise injection through avalanche diode directional coupler similar to plasma tube

11 p1739 A71-26438

Sky noise temperature measurements for ATS-5 millimeter wave radiometers, taking into account variations due to atmospheric temperature and humidity conditions

12 p1877 A71-26608

Superheterodyne radiometers for millimeter and submillimeter waves, using Mach-Zehnder interferometer frequency mixer for parasitic signal suppression

12 p1886 A71-26847

Statistical analysis of radiometer measurement data of solar emission atmospheric attenuation at 19 GHz

15 p2496 A71-32710

Remote sensors for hydrogeologic prospecting in arid terrains, recommending vertical and horizontal polarized microwave radiometers

18 p2913 A71-36362

Microwave sounding of ocean and earth surface thermal emission and atmospheric water vapor content by Cosmos 243 satellite-borne radiometers

20 p3259 A71-39672

Simultaneous CW microwave radiometer and laser probing of hypersonic wake ionization and turbulence, relating radiation temperature, radar echo and mechanical flow field structure

21 p3392 A71-40387

Global three dimensional atmospheric temperature mapping by selective chopper radiometer on Nimbus 4 satellite, measuring carbon dioxide IR emission

22 p3533 A71-41629

MICROWAVE RESONANCE

IR microwave double resonance of ammonia during IR vibration-rotation transitions induced by pumping of nitrous oxide laser

03 p0440 A71-14198

Microwave amplifier resonant gain frequencies as function of tunnel diode circuit, proposing low input design formulas

08 p1264 A71-21069

Spurious spikes in microwave circulators due to hybrid resonant modes of ferrite post open-resonator structure

10 p1583 A71-24212

Microwave resonator Q factor and coupling and matching characteristics measurement using line probe with AM and FM signals

10 p1584 A71-24724

Ferrite resonator coupled to microwave transmission line, deriving instability effects threshold power level for comparison with measurement

10 p1584 A71-24725

Josephson junction I-V characteristics self resonant current peaks calculation by finite difference scheme simulation, comparing results with perturbation technique and experiment

11 p1742 A71-25800

Thermal noise measurement of superconducting coaxial lambda/2 resonator at 2.46 GHz with ruby traveling wave maser and tunnel diode amplifier setup

12 p1887 A71-27010

Electric and magnetic fields of fundamental modes in cylindrical and rectangular dielectric microwave resonators, classifying transmission lines connections

12 p1888 A71-27613

Electron density distribution determination from microwave resonant frequencies of parallel plate cavity containing cold, collisionless, isotropic plasma

13 p2105 A71-27994

Cylindrical microwave cavity partially containing cold nonuniform plasma enclosed by quartz tube, calculating resonant frequency by exact, multistrata and series methods

13 p2029 A71-28500

Microwave resonator Q factor measurement by reflection coefficient method, using swept signal generator to eliminate incidental FM problem

15 p2376 A71-32310

Open microwave resonators self oscillations damping, using Sommerfeld radiation conditions

16 p2546 A71-33479

Contactless piston resonator ensuring one parallel resonance in tuning range, using quadrupole theory

19 p3030 A71-38341

Electron density measurement in microwave cavity resonator as function of plasma parameter or time, using digital control system

20 p3274 A71-39428

Microwave upper hybrid resonance absorption, emission and heating of nonuniform axially magnetized afterglow plasma column in waveguide geometry

24 p3851 A71-44430

SHF resonator small resonant frequency shift and Q factor changes measurement based on FM signal envelope shape analysis

24 p3858 A71-45237

MICROWAVE SCATTERING

Complex dielectric structure simulation for microwave scattering purposes using rotating target and zone technique

01 p0051 A71-10255

Radar reflectivities in South Dakota hailshafts from hailstone momentum data, applying microwave scattering theory

01 p0115 A71-10557

Microwave signal scattering by LF oscillations in electrodeless induction discharge plasma

01 p0135 A71-11031

Microwave scattering from plasma fluctuations produced by forcing gas in turbulent flow through discharge tube, investigating frequency spectrum broadening

01 p0136 A71-11480

Microwave scattering from nonuniform plasma of low pressure mercury arc in glass tube, describing density profile

03 p0463 A71-13474

Microwave scattering from gaseous plasmas, discussing EM waves, fluctuation and diagnostics problems

07 p1172 A71-20503

Longitudinal electron plasma waves generated by electron beam-plasma interactions, discussing simultaneous radiation and incoherent microwave scatter measurements in relation to theory

08 p1341 A71-21746

Absorption, divergence and scattering attenuations and scintillation of microwaves from space sources, calculating frequency and distance dependence characteristics

13 p2034 A71-29390

Microwave scattering by DC magnetized ferrimagnetic circular cylinder in rectangular waveguide

14 p2212 A71-30512

Microwave reflection from semiconductor wafers with dielectric film, presenting electromagnetic field parameters as function of electrophysical properties

19 p3117 A71-37264

Electromagnetic wave scattering from turbulent plasma at 31 GHz, determining cross section dependence on bistatic angle and electron density

19 p3017 A71-37868

Multiple scattering of VHF and UHF radio waves from bundle conductor high voltage power transmission lines

19 p3021 A71-38446

Microwave scattering noise spectrum from turbulent rocket-exhaust jet illuminated by plane wave

22 p3510 A71-42208

Scattering from turbulent rocket-exhaust jet illuminated by focused microwave beam, calculating noise spectrum by approximate theory

22 p3510 A71-42209

Raman microwave scattering on Langmuir oscillations, showing suprathermal emission origin in theta pinch plasma

24 p3853 A71-44505

Diffraction angular microwave beam scattering in fluctuating dense plasma, determining spatial scale of turbulence and permittivity

24 p3853 A71-44506

MICROWAVE SENSORS

Zero point fluctuations measurement standards for thermal and quantum noise, considering microwave network analytic application

11 p1733 A71-26366

MICROWAVE SPECTRA

Stable tunable microwave source for spectroscopy using Gunn diode, giving microwave cavity spectrometer block diagram

03 p0428 A71-13924

Galactic sources 18 cm OH emission and/or absorption observation

04 p0657 A71-15759

Statistical analysis of center-limb variations of intensity, spectrum and polarization of solar microwave impulsive bursts

08 p1364 A71-21419

High microwave power for studying interactions in high concentration linear Ar discharge plasma waveguide in magnetic field

08 p1339 A71-21479

Holographic spectrum analyzer for plasma diagnostics in microwave band, deriving formulas for emission spectrum based on interference patterns intensities in waveguide

09 p1499 A71-22150

Venus atmosphere composition and structure from microwave spectrum, noting surface pressure and temperature and water vapor

11 p1823 A71-25694

Geomagnetic crochet associated solar optical flares and microwave bursts during four year period, showing north-south asymmetry over disk

12 p1947 A71-26768

Intense solar microwave burst indication of high energy electron production, discussing synchrotron radiation, interplanetary medium particle propagation and cosmic ray modulation

12 p1950 A71-27381

High microwave power for studying interactions in high density linear Ar discharge plasma waveguide in magnetic field

14 p2282 A71-30666

Microwave spectrum analyzer, discussing capabilities and applications in ECM, surveillance, communications, circuit design and analysis and electromagnetic compatibility

15 p2368 A71-31208

Uranus and Neptune microwave emission spectra and atmospheric temperatures, comparing with Jupiter and Mars

15 p2490 A71-32410

Mars microwave brightness temperature measurements, defining planetary spectra

15 p2490 A71-32415

Mars microwave spectrum, discussing brightness temperature increase towards short wavelengths in terms of surface material thermal, electrical or chemical properties

15 p2490 A71-32417

Solar microwave bursts spectrum, calculating maximum radiation fluxes and frequencies from statistical data

15 p2480 A71-32749

Extragalactic radio sources millimeter wavelength spectra measurements, investigating electron energy loss mechanism, magnetic field strengths and dynamics

16 p2631 A71-33234

Papers on astronomy and astrophysics, Volume 8, covering lunar microwave thermal emission observation and origin

17 p2804 A71-35176

Lunar microwave thermal emission observation and theoretical predictions based on lunar surface models

17 p2804 A71-35177

Homologous solar microwave bursts from different active centers recorded with 7 GHz polarimeter

18 p2957 A71-35964

Frequencies, rotational constants, molecular structure and moments of inertia of five isotopic species of vinylene carbonate from microwave spectrum analysis

19 p3011 A71-37373

Spectral analysis of solar microwave bursts, examining flux and energy variation with frequency

19 p3146 A71-38577

Microwave spectral line receivers for radio astronomy observation of molecular clouds in interstellar space

20 p3238 A71-39401

Microwave molecular lines of CO, CN and CS emission from infrared object IRC plus 10216

22 p3599 A71-41929

- Interstellar formamide detection in Sgr direction by microwave emission, showing hyperfine components and rest frequencies 22 p3599 A71-41930
- Green Bank sky survey of radio sources at 1400 MHz, discussing 5C1 spectral analysis and overlaps 22 p3601 A71-42163
- Spectral representation and propagation mode of microwave transmission line on circular waveguides at great distance 24 p3803 A71-44361
- Microwave detection of anomalous interstellar electronic recombination line emission toward W49 A, using radio telescopes 24 p3871 A71-44904
- Sgr B2 region interstellar gas microwave emission spectrum, observing inversion transitions in metastable rotational levels of ammonia 24 p3872 A71-44916
- Microwave radiation intensity and spectral frequencies of Knudsen discharge in cesium plasma 24 p3858 A71-45244
- MICROWAVE SWITCHING**
- Circulation adjustment of m-port waveguide single junction circulator by scattering matrix eigenvalues 01 p0056 A71-11197
- German book on switching theory of linear microwave networks, covering waveguides for n-port network, network modeling, interconnections, etc 02 p0215 A71-12315
- Short-slot waveguide latching ferrite switch structure, operation principle, phase constants calculation and isolation characteristics 08 p1262 A71-20756
- Power losses and construction of microwave switch, using orthogonal striplines around thin ferromagnetic film on nonmagnetic substrate 11 p1741 A71-26551
- Compact Q band magic tee with matched loads to check noise performance of two-input switched radiometer 16 p2579 A71-33385
- MICROWAVE TRANSMISSION**
- Wall loss influence on energy flow center velocity of rectangular carrier pulses in circular waveguide for long distance transfer 01 p0056 A71-11195
- Gallium arsenide devices in microwave communications, discussing Gunn oscillators, PET, varactors and radar applications 02 p0231 A71-12049
- Test laboratory for Skynet spacecraft communications subsystems at microwave frequencies 02 p0238 A71-12443
- Precision measurement of satellite microwave flux and polarization at ground, involving Skynet tests 02 p0218 A71-12444
- ATS 5 satellite millimeter wave earth-space propagation and communications equipment 04 p0551 A71-15009
- Spatial statistical coherence of X band propagation over path near ground 04 p0552 A71-15211
- Rectangular waveguide with T junction, deriving characteristic impedance, maximum power and damping constant 05 p0719 A71-15997
- Low elevation polarimetric recordings of 136.44 MHz transmission from Early Bird geostationary satellite 07 p1206 A71-19022
- Cyclotron wave rectifier for S band and X band microwave conversion to DC or LF AC power 07 p1080 A71-20451
- Energy conversion efficiency from microwave into magnetostatic waves propagation inside cylindrical ferromagnetic substance 08 p1265 A71-21276
- Multiple reflections method for complex reflection and transmission coefficients of microwave transmission line permitting use of digital computers 09 p1413 A71-22151
- Pi-section waveguide with narrow slot in broad wall, calculating reflection and transmission coefficients as function of design parameters 10 p1584 A71-24719
- Y-shaped microwave power splitter, using dielectric wedge partially extending into rectangular metallic waveguide 11 p1733 A71-26349
- Wire grid simulation of electron density, transmission and reflection of lossless and lossy reentry plasma sheath under microwave radiation at X and K bands 12 p1935 A71-26767
- Self trapping of intense microwave signal penetrating dense transcrystal plasma 13 p2105 A71-28174
- Microwave propagation in cylindrical waveguide containing inhomogeneous gas discharge plasma 13 p2029 A71-28363
- Cylindrical waveguide with three differential phase shift sections, deriving microwave output magnitude

- and polarization for comparison with ferrite experiment 13 p2037 A71-28604
- Microwave power transmission from orbiting solar power station to earth, discussing design optimization problems 13 p1999 A71-28666
- Microwave power transmission for supplying electric power to space station complex for performing scientific experiments over long periods in earth orbits 13 p2000 A71-28667
- Reflection, diffraction and transmission of plane microwave incident on conducting screen perforated periodically with circular holes, using transmission line analysis and dipole moments method 14 p2192 A71-29568
- Two cavity ring-type channel dropping filters for millimeter wave guided communication system, calculating pulse response and interchannel crosstalk characteristics 14 p2210 A71-29569
- Integrated flight test data system combining digital airborne data acquisition/recording system with telemetry/microwave link to computerized ground station 14 p2243 A71-30318
- Microwave wideband and multiband radome design for strength, environmental and electrical requirements, achieving transmission efficiencies with dielectric and wall thickness selection 14 p2216 A71-31037
- Communication blackout during missile and spacecraft high altitude flight, considering convective effects on gas breakdown by microwaves 14 p2206 A71-31071
- Mathematical model for predicting microwave signal fading characteristics due to reflections from ocean surface 15 p2368 A71-31140
- Deep Space Communications System low noise microwave receiver, discussing operating noise temperature calibration, error analysis and programming 15 p2372 A71-32311
- Microwave reflection factor analytical and graphical dependences on resistivity of variable thickness semiconductor layers 16 p2544 A71-34032
- Book on microwave fields and circuits covering waveguides, transmission lines, impedance matching, sources, resonators, antennas, etc 17 p2716 A71-34772
- Intelsat satellite-earth station communications technology, considering microwave line of sight techniques 17 p2707 A71-35333
- Wall impedance method application to long distance transmission elliptical, parabolic and circular waveguides 17 p2707 A71-35480
- Thermal self focusing of pulsed millimeter waves transmitted through cylindrical plasma, observing power dependence and beam asymmetry 18 p2951 A71-35986
- European 12 GHz regional satellite telecommunications systems, discussing band assignment limitation and frequency reuse 18 p2877 A71-36517
- Phase and amplitude variations of multipath fading of microwave signals relating atmospheric irregularities 19 p3015 A71-37221
- Rain attenuation measurements, noting limitations on microwave transmission at SHF 19 p3024 A71-38612
- Italian Sirio synchronous satellite for SHF propagation and communication experiments on fading statistics, frequency dependence, path diversity and TV transmission 21 p3347 A71-40474
- Microwave communication transistors, considering power, low noise, digital and CATV types 21 p3358 A71-40820
- Line-of-sight microwave multipath fading, predicting attenuation distribution as function of pathlength by piecewise linear approximation of atmospheric refraction index 21 p3349 A71-41196
- Field configuration of TM mode in elliptical waveguide, showing inaccuracy of microwave theory 22 p3522 A71-42279
- Rectangular waveguide with T shaped pedestal, deriving characteristic impedance, maximum power and damping constant 22 p3515 A71-42746
- Receiving and transmitting antennas directional gain effect on microwave long range tropospheric propagation 23 p3644 A71-43289
- Low loss microwave iris-loaded circular TE mode waveguide delay line for pulse compression at X band 23 p3653 A71-43963
- Spectral representation and propagation mode of microwave transmission line on circular waveguides at great distance 24 p3803 A71-44361

- Microwave radio signals refraction angles and group delay times for biexponential model of ionospheric electron density profile 24 p3805 A71-45253
- MICROWAVE TUBES**
- NT BACKWARD WAVE TUBES
- NT CATHODE RAY TUBES
- NT COLD CATHODE TUBES
- NT GAS DISCHARGE TUBES
- NT MICROWAVE OSCILLATORS
- Transverse wave tubes with cyclotron and synchronous wave interactions as microwave amplifiers, analyzing energy exchange mechanism and axial beam velocity spread 18 p2888 A71-36128
- Waveguide mounted X band CW Gunn effect oscillators load impedance characteristics, proposing lumped equivalent circuit 18 p2894 A71-36830
- Spurious emissions from CW and pulsed GaAs solid state oscillators as function of material active layer thickness and contacting procedure 19 p3032 A71-38460
- Book on electronic components covering radio, cathode ray and microwave tubes, telecommunication, ceramic materials, light conversion to electricity, integrated circuits, etc 20 p3205 A71-39775
- Phase shift and attenuation measurements in high power microwave ferrite tetrodes circuits, using semiconductor transducers/digadectors/ 24 p3809 A71-44871
- MICROWAVES**
- NT DECIMETER WAVES
- NT MILLIMETER WAVES
- Microwave permittivity dispersion in segnetoelectrics as function of single crystal domains size, considering barium titanate dielectric spectrum resonance 01 p0138 A71-10433
- Very long baseline interferometry of galactic hydroxyl radical microwave emission sources 02 p0310 A71-12327
- Solar microwave bursts and associated optical flares homologous characteristics, discussing radio emission mechanism 02 p0302 A71-12763
- Microwave effects on living creatures, considering thermal and nonthermal effects on individual body organs and systems, permanent changes and protective measures 02 p0208 A71-12845
- Solar proton flares associated with 1968 and 1969 strong particle events, noting correlation with hard X ray and microwave bursts 03 p0478 A71-14037
- North-south asymmetry in solar disk microwave bursts sources distribution 03 p0496 A71-14536
- Perturbation method in microwave electromagnetic field pattern determination and resonator design 04 p0586 A71-14657
- Coronal condensations emission changes after microwave solar bursts, discussing circular polarization and flare mechanism based on collisionless dissipation of magnetic energy 05 p0804 A71-16029
- Solar microwave bursts correlation to solar proton emissions 05 p0798 A71-16115
- Lunar microwave emission effects and local surface temperature variations due to outward heat flow and low thermal conductivity 05 p0809 A71-16459
- Microwave holography application to monopole antenna radiation field mechanism, using liquid crystals for optical reconstruction 05 p0756 A71-17231
- Collisional drift instability remote feedback suppression in Q machine Cs plasma by microwave modulation at upper hybrid frequency 06 p0932 A71-17464
- Asynchronous tunnel diode microwave detector, considering frequency properties and sensitivity 06 p0874 A71-17547
- Nonsteady third harmonic generation due to plasma interaction with microwave 06 p0937 A71-18041
- Finite amplitude helical instability effect on microwave beam phase propagated through plasma column 07 p1166 A71-18888
- Magnetoreflexion of helicon wave from n-InSb semiconductor in microwave range 07 p1176 A71-19270
- N-type InSb microwave noise radiation and attendant RF current oscillations under magnetic field 07 p1180 A71-20177
- Microwave theory and techniques - IEEE Conference, Newport Beach, California, May 1970 08 p1261 A71-20751
- Microwave noise emission in He negative glow plasma frequency range, discussing high energy electron densities near cathode 09 p1502 A71-22694

Microwaves anomalous skin effect in high density gaseous magnetoplasma, comparing experimental electromagnetic field penetration increase due to thermal electron motion with theoretical prediction
09 p1502 A71-22800

Solar impulsive microwave bursts, showing association with types D, E and F sunspots
10 p1667 A71-23792

Stiles-Crawford effect interpretation by geometrical optics interferences, microwaves and diffraction scalar theory, calculating retinal cones mean diameters
10 p1560 A71-23991

Magnetic mirror confined microwave heated plasmas stability based on uniform collisionless plasma model
10 p1651 A71-24632

Coagulative and delayed cumulative cataract production by microwaves investigated by hypothermic technique
10 p1572 A71-25077

Microwave energy dissipation as heat in eye, using agar for eye model construction
10 p1572 A71-25078

Pathophysiological aspects of microwave irradiation, considering thermal response of human and animal organisms to electromagnetic radiation exposure
10 p1573 A71-25079

Microwave radiation nonthermal and cumulative biological effects, discussing dose/irradiation safety standards
11 p1717 A71-25283

Negative heart rate response during low level microwave irradiation of dorsal head in rabbits
11 p1717 A71-25284

Microwave radiation nonthermal biological damage, describing beetle pupae irradiation and radiant heating experiments
11 p1717 A71-25285

Microwave biological exposure systems implementation in limited space, describing focused prolate spheroid, absorber-lined horn and compact range illumination system
11 p1723 A71-25288

Radio frequency and microwave radiation hazards determination and elimination aboard naval ships
11 p1723 A71-25290

Life prolongation during high intensity microwave exposures with ambient air temperature control for radiation bioeffects studies
11 p1717 A71-25291

Cataract production from microwave radiation exposure by lens nutrition alteration and surface shape changes
11 p1718 A71-25292

Microwave irradiation of animals, noting analeptic effect and increased alertness
11 p1718 A71-25293

Cosmic microwave background measurements at 8 mm wavelength, examining isotropy
12 p1956 A71-26614

Energetic solar X-rays, microwaves and EUV ionizing radiation during periodic bursts of solar flare
12 p1953 A71-27655

Satellite solar power station for microwave generation, transmission and energy conversion to electrical power on earth
13 p1999 A71-28665

Microwave exposure effects on organisms and biological functions responses and thermal stresses as function of specific frequencies, power density and environmental temperature
13 p2021 A71-29325

Electron beam interaction with external harmonic microwave field in planar diode gap, calculating electric field current and voltage distribution functions
14 p2211 A71-30084

Anomalous microwave energy dissipation and electron heating in collisionless plasma without decay at high collision frequencies
14 p2281 A71-30539

Field components, frequency, quality and filling factors effects of storage quartz bulbs in maser microwave cavities
14 p2254 A71-30563

Resonant plasma heating at electron cyclotron frequency second harmonic, studying interactions with microwave electromagnetic radiation in adiabatic trap
15 p2455 A71-31736

Mars radio spectrum discrepancy with elementary theory, assessing microwave observations
15 p2490 A71-32416

Solar microwave burst frequency occurrence statistical analysis
15 p2495 A71-32687

Soviet army medical appraisal of chronic microwave field induced affections, noting evaluation procedures inadequacy
16 p2534 A71-32827

Anomalous microwave heating of electrons in magnetized plasma, showing resonances dependence on magnetic fields and charged particles concentration
17 p2790 A71-35735

Harmonic generation due to strong microwaves nonlinear mixing in He plasma, noting resonances at fundamental frequencies
18 p2951 A71-35932

Microwave radiation biological effects review and bibliography covering protein activity, genetic, central nervous system and cardiovascular effects
18 p2864 A71-35956

Reentry plasmas ionization and microwave and optical radiation properties, considering radar echo, electromagnetic scattering, thermal equilibrium and ablation products
18 p2952 A71-36422

Statistical determination of solar radio emission S-component average flux spectrum during solar cycle peak phase
18 p2966 A71-36739

Kinematic illusions in connection with retardation effects involving extragalactic sources with varying microwave output, noting occurrence in quasars 3C 279
18 p2925 A71-36924

Two dimensional structures of 76 extragalactic radio sources at 1425 MHz in tabular and graphical forms
18 p2970 A71-37064

Slow wideband excitation of ultrasonic waves with piezoelectric crystal delay line subject to microwave radiation
19 p3015 A71-37251

Gas concentration, field frequency and applied power level for control over electron temperature and emission spectra in microwave gas discharge plasma
19 p3113 A71-37764

Electromagnetic radiation from beam-plasma system in strong magnetic field, noting maximum microwave emission near electron cyclotron frequency
19 p3116 A71-38252

Double standard for national levels of exposure and biological hazards of microwave radiation, comparing Soviet work to U.S.
19 p3008 A71-38442

Aircraft sounding of atmospheric microwave radiation transfer compared with IR method, measuring optical Mie characteristics, water vapor content, cloudiness, ice cover, etc
20 p3259 A71-39673

Microwave emission measurement of earth surface from Cosmos 243 satellite, detecting radio brightness temperature dependence on latitude and local features
20 p3260 A71-39685

Microwave water emission in Comet Bennett, deriving column density for various temperatures of cometary gas
21 p3443 A71-40190

Radio telescopic search for extraterrestrial oxygen 18 containing water microwave emission, suggesting water vapor maser pumping mechanism dependence on isotopic species
21 p3444 A71-40223

Microwave plasma generation in magnetic field, detecting expansion related to electron cyclotron frequency harmonics
21 p3426 A71-41287

Dense plasma heating by electron beam in magnetic trap as function of cyclotron frequency and field strength, noting strong microwave emission
22 p3583 A71-42064

N-type In-Sb continuous coherent microwave oscillation under transverse magnetic field, discussing helical frequency instability on threshold and growing wave conditions
22 p3586 A71-42347

Planetary nebulae microwave radiation emission survey by Algonquin Radio Observatory, determining flux densities
23 p3769 A71-43988

Atmospheric vertical humidity profile determination by measuring microwave radiation from satellite
24 p3822 A71-44350

Off-resonance electron heating by microwaves in mirror contained high beta plasmas
24 p3852 A71-44486

Thermal and nonequilibrium microwave emission from colliding plasma beams in transverse magnetic mirror field
24 p3854 A71-44517

Light velocity measurements by optical and microwave techniques, noting electromagnetic constant error and role in distance measurement and physical theories development
24 p3827 A71-44996

MICROWEIGHING

U WEIGHT MEASUREMENT

MICTURITION

U URINATION

MIDAIR COLLISIONS

Aircraft midair collision avoidance, discussing Elimination Range Zero system operation procedures and cost
07 p1154 A71-19079

ATC system analysis, discussing airport and airspace utilization, area navigation, midair collisions and traffic mix
09 p1491 A71-22470

Midair collisions analysis for civil-military integrated ATC air space, discussing near miss volume, random heading aircraft density and pilots evasive action vs avoidance percentages
12 p1927 A71-27599

Inertial navigation impact on aircraft safety, discussing error sources and midair collision risks
22 p3571 A71-42079

MIDCOURSE GUIDANCE

Spacecraft midcourse guidance technique for lunar and interplanetary trajectories based on matched asymptotic expansions
06 p0978 A71-18567

N-body integrated reference trajectories and navigation requirements for extended Venus/Mercury 1973 mission midcourse correction
23 p3729 A71-43032

Midcourse and planetary approach guidance by on-board optical measurements, noting application to earth-Mars trajectories and Grand Tour missions
23 p3702 A71-43061

Optimal timing for interplanetary midcourse guidance maneuvers for realistic cost function, indicating first and last maneuver sensitivity
23 p3702 A71-43939

MIDCOURSE TRAJECTORIES

Planetary quarantine constraint effect on multiple outer planet missions, considering navigation error sources and midcourse maneuvers
19 p3002 A71-37917

MIDDLE EAR

Direct electrical stimulation of musculus tensor tympani on click elicited responses in cochlea and cochlear nucleus
13 p2003 A71-27832

Tympanic-cavity nerve plexus electric stimulation effects on cerebral blood circulation and overall arterial pressure in dogs and cats
16 p2533 A71-34108

Kinematic analysis and simulation of transmission modes of sound energy through middle ear
19 p3002 A71-38062

MIDDLE EAR PRESSURE

Vertigo due to increased middle ear pressure, discussing etiology from experience of aeromedical consultation service
22 p3502 A71-41833

MIDLATITUDE ATMOSPHERE

Midlatitude atmospheric gravity waves generation by auroral heating during magnetic substorms
02 p0245 A71-11965

Midlatitude topside ionosphere electron density diurnal variations, discussing F 2 layer seasonal anomaly altitudinal extension
03 p0409 A71-13390

Midlatitude nighttime D region ionization source, considering precipitating energetic electrons
03 p0420 A71-14527

F 1 layer development at summer midday midlatitude, noting role of molecular ions composition
05 p0745 A71-17200

Midlatitude F 2 layer electromagnetic drift during magnetic storm
06 p0888 A71-17287

Midlatitude wind vector longitudinal and transverse components correlation functions for different isobaric surfaces in summer and winter
06 p0924 A71-17647

Irregularities heights in ionospheric refractivity responsible for radio-satellite scintillation from spaced receiver experiments at midlatitude and subauroral locations
06 p0868 A71-17985

Geomagnetic storm on 24 March 1969, obtaining upper atmosphere emission data in middle latitude zone
06 p0894 A71-17996

Midlatitude scintillation diurnal and seasonal variations, using satellite communications data
07 p1095 A71-19003

Stable midlatitude red arc in night sky south of auroral zones, reviewing observed features, ionospheric behavior and formation theories
07 p1098 A71-19322

Morphology and dynamics of low intensity monochromatic midlatitude auroral arcs of 6300 A /O I/, comparing results with observation during IGY
07 p1103 A71-19766

Middle latitude night E region ionization, describing solar EM and corpuscular radiation absorption effects
08 p1286 A71-21853

F 2 layer nighttime ionization at midlatitudes, investigating conjugate point effects on observation point
09 p1434 A71-22426

Midlatitude upper atmospheric low energy proton intensity obtained from meteorological rocket data
09 p1513 A71-22579

Solar activity effects on midlatitude upper atmosphere corpuscular radiation intensity studied by rocket sounding
09 p1513 A71-22580

Midlatitude spread F, sunspot activity and geomagnetic activity variations related, discussing fast solar particles

09 p1437 A71-22938

Midlatitude stratosphere and lower ionosphere density model, discussing vertical, diurnal and seasonal variations effects on spacecraft trajectories

09 p1438 A71-23137

Ionspheric computer model, describing electron and ion densities in middle latitudes as function of latitude, longitude, altitude, season, time and solar activity

10 p1577 A71-24290

Midlatitude D region considering electron concentration height distribution, ionization process and solar activity effects

10 p1606 A71-24916

Midlatitude F2 region diurnal variations in peak electron density critical frequency and height, noting electric field and ion drag effects

10 p1606 A71-24921

Midlatitude whistlers occurrence rates, dispersion and structural features sampled recording over North Italy

10 p1579 A71-25002

Midlatitude whistlers propagation paths during minimum solar activity for estimating magnetospheric electron density profile

10 p1580 A71-25135

Neutral air winds and ionospheric continuity equation, calculating midlatitude electron concentration longitudinal variations

11 p1754 A71-25605

Midlatitude ionosphere electron production rates during quiet solar activity, deriving seasonally varying electron density profiles

11 p1755 A71-25609

Midlatitude topside ionospheric electron density mean diurnal and seasonal variations from Alouette 1 satellite observation

11 p1757 A71-25784

Midlatitude VLF hiss distinction from discrete emissions /chorus/ based on event tape recording and spectrum analysis

12 p1878 A71-26892

F layer vertical drifts due to winds at midlatitudes, computing longitudinal variations

13 p2054 A71-27793

F 1 layer development at summer midday midlatitude, analyzing molecular ions composition effect

13 p2059 A71-28255

Radio communication accuracy characteristics in calculation of maximum frequency, skip distance and emission angle by transmission curves for midlatitude ionosphere

13 p2030 A71-28544

Midlatitude ionospheric signatures from narrow beam HF radar backscatter sounder, discussing diurnal and seasonal occurrences

13 p2031 A71-28782

Midlatitude daytime ionospheric electron density profile during low solar activity based on rocket sounding data

14 p2228 A71-29535

Midlatitude ionosphere dusk sector total electron content during geomagnetic storm time increase

14 p2229 A71-29666

Noctilucent cloud formation from water vapor concentrations in mesosphere and lower thermosphere of arctic and midlatitude regions measured by rocket-borne RF mass spectrometers

14 p2232 A71-29957

Midlatitude D region electron density winter variability causes consideration based on enhancements, absorption and ionization changes data during stratospheric warming

14 p2237 A71-30944

IQSY data analysis of pulse reflection measurements from midlatitude station, determining polar cap and auroral absorption

15 p2396 A71-31611

Solar eclipse on 7 March 1970, determining midlatitude geomagnetic pulsations with dynamic power spectral analysis

15 p2397 A71-31761

Midday ion composition altitude variations in midlatitude trough region and plasmasphere, observing light ion concentrations

15 p2398 A71-31767

Empirical atmospheric model derivation from midlatitude density data

16 p2566 A71-33759

Upper atmospheric winds viscous damping energy deposition calculation for midlatitude profiles

16 p2568 A71-33789

Midlatitude E region electron density profile data for various solar activity levels, investigating formation theory and atmospheric models

16 p2570 A71-33822

Low and midlatitude ionospheric motion determination using barium ion cloud release technique

16 p2570 A71-33827

Midlatitude nighttime F region electron concentration enhancements as downward diffusion flux from protonosphere induced by ionospheric substorm associated electric fields

16 p2573 A71-33958

One layer midlatitude beta plane channel model of incompressible fluid for study of systematic error propagation on nearly stationary synoptic scale wave

19 p3090 A71-38268

Midlatitude sporadic E layer formation mechanism, considering wind shear theory

19 p3061 A71-38630

Midlatitude solar quiet geomagnetic field dynamics morphology, emphasizing regular diurnal and annual changes and irregular fluctuations

20 p3217 A71-39510

Midlatitude lower thermosphere atomic and molecular oxygen rocket measurements, presenting concentration and vertical distribution data

20 p3222 A71-39700

Mid- and high-latitude ionospheric radio wave transmission from spacecraft during solar cycle, considering latitudinal and longitudinal gradients and electron content change rate

20 p3197 A71-39715

Midlatitude ionospheric irregularities, electron density vertical distribution and electron and ion temperature variation measurements, during solar eclipse of 22 September 1968

20 p3224 A71-39716

Midlatitude ionospheric electron density and electron temperature measurements by rocket experiments, noting diurnal and seasonal variations

20 p3224 A71-39718

Plasma transport processes role in E region from midlatitude nocturnal and auroral ionospheric models in terms of transport equations

20 p3232 A71-39893

Peak electron density variations during midlatitude F region storm, investigating electrodynamic drift effects

21 p3372 A71-40037

Midlatitude topside ionospheric electron density mean diurnal and seasonal variations from Alouette 1 satellite observation

22 p3532 A71-41552

Midlatitude sporadic E layer changes during increased geomagnetic activity, considering skin effect and current shear

23 p3670 A71-43189

Rocket and radio wave wind profiles from 60 km to E region near 53N, presenting partial reflections and zonal winds time cross section

23 p3700 A71-43343

Geomagnetic bay-like disturbances formation and decay during multiple midlatitude 6300 A auroral arc after magnetic storm, observing time variation of current system pattern

23 p3672 A71-43981

Hysteresis effect at solar cycle maximum for midlatitude E layer electron density response to solar activity

24 p3824 A71-45125

Mass spectrometer measurements of hydrogen, helium, nitrogen, oxygen and nitrogen oxide ion concentrations vertical profiles in ionosphere at midlatitudes

24 p3824 A71-45311

MIDLATITUDES

U TEMPERATE REGIONS

MIE SCATTERING

NT RAYLEIGH SCATTERING

Mie extinction parameters tabulation for computed signal transmission through rain at microwave and visible frequencies

01 p0029 A71-10469

Atmospheric aerosols role in Martian opposition effect, applying Mie theory to integrated scattering intensities calculation for submicron particles

03 p0489 A71-13558

Zodiacal light theoretical models, considering interplanetary particles optics, Mie theory and multicolor polarization

03 p0491 A71-14011

Submillimeter wave attenuation in snow, comparing results of calculation based on Mie theory with measurement

05 p0718 A71-15991

UBV colors and polarization models for reflection nebulae based on Mie scattering functions for exponential size distribution of silicate particles

09 p1517 A71-22332

Martian atmosphere Mie scattering analysis, using limonite and bulk solid carbon dioxide complex refractivity to interpret polarization effects

11 p1825 A71-25708

Water and ice cloud discrimination by angular distribution measurement of various polarization parameters of scattered laser beam radiation, using Mie theory

11 p1776 A71-26298

Monodispersed particle semiinfinite atmosphere, calculating invariance principles of diffused radiation based on Mie theory

12 p1960 A71-26823

Angular function computation in Mie theory of light scattering, considering sequential computer programming economics

14 p2207 A71-30150

German monograph on ozone determination from sky radiance, considering Rayleigh and Mie scattering

17 p2733 A71-34794

Solar radiation field in polluted atmosphere, measuring intensity, polarization and flux due to aerosol scattering for comparison with Mie theory computation

17 p2736 A71-35563

Optical properties of graphite-iron-silicate grain mixtures from Mie theory for spherical particles, noting models consistency with interstellar extinction and backscattering observations

21 p3444 A71-40242

Submillimeter wave attenuation in snow, comparing results of calculation based on Mie theory with measurement

22 p3515 A71-42740

Intensity and polarization for meteorological spherical and nonspherical particle size parameters, comparing exact Mie scattering and ray optics

23 p3704 A71-43337

Resonance scattering laser radar for atmospheric pollution detection, discussing Rayleigh and Mie scattered light suppression

24 p3803 A71-44570

MIE THEORY

U MIE SCATTERING

MIGRATION

Austenitic stainless steels point defect migration sensitivity, measuring dislocation damping during recovery after quenching

02 p0267 A71-12883

Circannual biological clock operation without environmental signals based on squirrel hibernation and bird migration studies

10 p1563 A71-24298

MILITARY AIR FACILITIES

Bare base shelter/hangar expandable structures for rapid worldwide Tactical Fighter Organization deployment, noting foam and honeycomb fabrication [AIAA PAPER 71-398]

11 p1744 A71-25274

MILITARY AIRCRAFT

Combat aircraft cockpit temperature control system design and operation

01 p0004 A71-10270

Avionics system maximizing pilot chances of surviving mission and destroying selected target by removing mental limitations

01 p0124 A71-10506

Flight control systems influence on military aircraft design and performance, discussing static stability, ride quality, flutter margin and maneuver load controls [AIAA PAPER 69-767]

02 p0190 A71-12683

Electric power source requirements of USAF aircraft, missile and spacecraft electrical systems

03 p0351 A71-13036

STOL aircraft for tactical support, discussing USAF intertheater requirements

04 p0529 A71-15024

WG.13 Lynx battlefield helicopter design and performance

04 p0529 A71-15394

Reliability and maintenance problems of U.S. Army operational environment, noting inadequate design and test criteria during development

04 p0530 A71-15402

Army rotorcraft hot day standard design hover criterion, developing analytical models for hovering aircraft, cost, climatology and environmental features

04 p0533 A71-15431

Corrosion damage relationship to military aircraft accidents, discussing quality control, material selection and manufacturing processes

06 p0911 A71-17415

Development program for multiple access real time tactical information distribution system, designing and constructing tactical air control system test facility [AIAA PAPER 71-243]

07 p1156 A71-19718

Military aircraft zinc silver oxide battery service requirements and performance

08 p1236 A71-21103

FAA flying and handling qualities program, discussing development of optimum and minimum acceptable flight characteristics criteria for new civilian and military aircraft designs [SAE PAPER 710372]

10 p1554 A71-24241

Medium weight NAMC C-1A tactical transport aircraft technical specifications

11 p1706 A71-25231

Military aircraft flight test establishments, discussing airframe, engine, flight control and weapons delivery systems tests work flow integration requirements

11 p1708 A71-26315

Terrain following radar for airborne guidance of low flying military aircraft

12 p1927 A71-26881

Nervous/cardiovascular systems and blood composition changes in moderate duration military transport flights

12 p1874 A71-27163

Landing load estimation methods for preliminary design weight prediction for military aircraft

13 p1995 A71-28211
Optimization of military VTOL aircraft secondary power systems, considering alternate power source for aircraft hydraulics, pneumatic drives, etc [SAE PAPER 710445]

13 p1998 A71-28326
Military/commercial STOL transport design, discussing performance, payload and equipment requirements with emphasis on production cost benefits

[SAE PAPER 710468] 13 p1996 A71-28336
Commercial vs military design criteria for STOL transport aircraft, noting landing and takeoff distances and noise levels

[SAE PAPER 710465] 14 p2176 A71-30536
Army aircraft automatic inspection and maintenance monitoring system, considering feasibility, technology approach and effectiveness

[AIAA PAPER 71-649] 14 p2177 A71-30726
Multimission strategic aircraft installation effects testing in propulsion and aerodynamic wind tunnels, yielding flowfield definition, inlet internal performance, drag, forebody shape and orientation

[AIAA PAPER 71-759] 14 p2171 A71-30792
Flightworthy 25-foot diameter propotor wind tunnel test, considering civil and military need for VTOL transportation

[AHS PREPRINT 501] 14 p2177 A71-31077
Lower extremity Army aviator amputee retention on flight status regarding service need, amputation and prosthetic fit, age, career, hours flown and time in military

16 p2535 A71-33120
Lateral-directional handling qualities and roll control power requirements for executive jet and military class II airplanes in landing approach flight phase

[AIAA PAPER 71-771] 16 p2524 A71-34007
Sight line autopilot (SLAP) for side-firing aircraft pointing accuracy improvement, using optimal regulator theory to generate control gains

[AIAA PAPER 71-960] 19 p3099 A71-37201
Mortality in survivable or partially survivable U.S. Army aircraft accidents, observing death relationship to aircraft duty and seat location and type

23 p3640 A71-44248

MILITARY AVIATION

Flight simulators use in UK military flight training, discussing Full Mission Simulators concept and Royal Navy viewpoints

01 p0066 A71-10014
Man role in future navigation from SAC viewpoint, considering relationships to mission and machine

01 p0123 A71-10502
Navigator role in Military Airlift Command (MAC) as navigator, weather analyst, fuel manager and flight planner

01 p0123 A71-10504
USAF navigator training, discussing operational demands, philosophy, present and future training capabilities, etc

01 p0022 A71-10520
Standardized EEG data recordings in Air Force neurological evaluations

02 p0208 A71-12393
Legal aspects of military sonic booms, discussing administrative remedies, liability and various cases

08 p1379 A71-21830
Psychoreactive action caused by flying accident in group, discussing repercussions in civil and military aviation fields

10 p1572 A71-24982
Fog clearance from airport runways, discussing available techniques, economic aspects and importance for military operations

12 p1925 A71-27247
Military aviation greases for subsonic commercial airplane lubricants, discussing economic and technical benefits based on service experience and testing

[SAE PAPER 710411] 13 p2091 A71-28304
Army rotorcraft performance data, discussing hovering and forward flight performance out of ground and level flight power requirements and drag and compressibility effects

[AHS PREPRINT 500] 14 p2177 A71-31076
Civil and military aviation operational problems, including cloud masses and CAT detection, landing aids and radar navigation

15 p2446 A71-31917
Military and civil aircraft navigation systems development, emphasizing self contained airborne equipment

17 p2775 A71-35374
UK military and civil ATC coordination, discussing Mediator plan for modernization of communication and navigation equipment and techniques

22 p3570 A71-41519

MILITARY HELICOPTERS

NT CH-3 HELICOPTER

NT CH-46 HELICOPTER

NT CH-47 HELICOPTER

NT CH-54 HELICOPTER

NT H-53 HELICOPTER

NT H-56 HELICOPTER

NT OH-6 HELICOPTER

NT UH-1 HELICOPTER

Sand and dust effects on military helicopter flight controls and equipment service life, discussing relief program

04 p0533 A71-15430
Environmental development and testing of OH-58A light observation helicopter for close ground support, noting particle separator and injection seals

04 p0534 A71-15439
Military helicopter design and weaknesses correction, considering man/machine combat survivability and operational accidents reduction

04 p0534 A71-15447
Height velocity (H-V) flight testing, giving results from OH-58A Kiowa and AH-1G Huey Cobra helicopters

07 p0108 A71-19093
Soviet Mil V-12 heavy lift helicopter for civil and military missions, noting turbine engines, rotor configuration, cargo hold and navigation system

14 p2175 A71-30420
Weapons delivery computer for attack helicopters, using planar distributed function generator for general closed form instantaneous solution capability

[AHS PREPRINT 531] 14 p2209 A71-31092
Lynx military helicopter design high reliability and low maintenance demands

16 p2523 A71-33457

MILITARY PSYCHIATRY

U MILITARY PSYCHOLOGY

MILITARY PSYCHOLOGY

Superior jet pilots social, military and flying case histories, noting predominance of firstborn children with close father-son relationships

03 p0371 A71-13325
Aerospace psychiatry, discussing relationships between personality patterns and environmental factors, adaptability to occupational situations in combat flying and space activities

08 p1238 A71-20722
Psychopathological causes for French Air Force flying personnel inaptitude, considering motivational problems and age factor

22 p3500 A71-41575

MILITARY SATELLITES

NT VELA SATELLITES

MILITARY SPACECRAFT

NT VELA SATELLITES

Military earth communication station maintenance, noting mobility, environment, logistics and reliability

02 p0224 A71-12827
S band transponder for vehicle-space-ground link subsystem (VSGLS) of USAF integrated telemetry, tracking and command system

05 p0719 A71-16151
USAF space missions information processing requirements relative to space transportation system, emphasizing real time image processing

05 p0727 A71-17229
Receiving equipment for navigation satellites of Naval Weapons Laboratory, considering 150 MHz channel

07 p1205 A71-19015
Tacsat 1 telecommunications relay system, discussing UHF-SHF antenna radiation patterns, ground terminal equipment, nutation dampers and attitude and orbital correction procedures

12 p1882 A71-27611

MILITARY TECHNOLOGY

Airborne military multiprocessor compatible with commercial computers, discussing executive control, input-output interrupts, load balancing, self diagnosis, etc

01 p0046 A71-10206
Army avionics technology transfer to civil aviation, discussing communication systems, flight control and landing aids

04 p0557 A71-15017
USAF weapons and support systems, discussing military R and D funding and resulting constraints

05 p0839 A71-16285
USAF technology programs providing near term particular capability needs and long term fundamental incremental gains

05 p0839 A71-16286
U.S. tactical missile program evolution since WW II, discussing technology, air defense, assault/antitank weapons, interdiction and battlefield combat support

05 p0818 A71-17149
Properly fitting flight helmets for U.S. Army aviation personnel in Vietnam

06 p0859 A71-17616
Computer controlled time division multiple access control system for U.S. Army Satellite Communication Agency, discussing tests and operational details

07 p1057 A71-18820
Real time tracking filter candidates for implementation in systems tracking maneuvering vehicles compared in terms of accuracy and computer requirements for tactical applications

07 p1069 A71-18837
Soviet book on thermal radiation sensing covering system functional circuits, radar conversion, military application and personnel training

07 p1060 A71-19100

Plated wire storage element for military and aerospace scratch pad, main and mass memories of various speeds

[IEEE PAPER 7.6] 07 p1077 A71-19608
Human role in Aerospace Defense Command navigation, discussing Airborne Warning And Control System and navigational aspects of ADC mission

07 p1157 A71-20346
Computer generated profile maps to fill military need for rapidly produced, easily interpreted terrain map

08 p1280 A71-21242
USAF Camera Calibration Facility, describing precision multibank collimator for measuring focal length, distortion, prism effect, fiducial center and other camera parameters

08 p1272 A71-21258
Plastics as potting compounds in military aircraft electrical systems, investigating resistance to reversion and hydrolytic stability

10 p1633 A71-24115
Hybrid simulation to increase hit possibility of rocket fired from military tanks at moving targets

11 p1735 A71-25848
Statistical nature of time to complete MIL-STD-781 reliability sequential tests for military and space equipment, giving information about MTBF

12 p1908 A71-26656
Reliability experience acquired in collecting, processing and analyzing U.S. Army test and field data, stressing field data reduction work

12 p1909 A71-26662
MAC malfunction detection, analysis and recording system applications in commercial airlines, emphasizing real time response for maintenance function

[SAE PAPER 710425] 13 p1995 A71-28311
All-weather landing systems military constraints and requirements, considering ground equipment mobility and insensitivity topographic environments

15 p2445 A71-31908
ONR human engineering research program concerning information input, display and processing concepts, decision making and motor output and control

16 p2536 A71-33529
Naval Air Rework Facility, discussing primary mission, technical disciplines and operational performance feedback

[AIAA PAPER 71-765] 16 p2523 A71-34003
Flying qualities military specification, discussing longitudinal static stability, transonic flight relaxation, control forces in maneuvering flight, lateral-directional oscillations, etc

[AIAA PAPER 71-766] 16 p2523 A71-34004
Aerospace business future, discussing political, military and social factors effect

17 p2841 A71-34575
USAF total in-flight simulator model-following feedback control system, discussing conceptual design and flight test results

[AIAA PAPER 71-961] 19 p2995 A71-37202
Plastic encapsulation for microcircuits including packaging, failure mechanisms, military qualifications and economic factors

19 p3033 A71-38508
Cost effective integrated logistics support documentation system for military contractors

23 p3661 A71-43196

MILKY WAY GALAXY

Elliptic integrals for gravitational potential in symmetry plane of Milky Way galaxy

01 p0148 A71-10033
Turbulent diffusion role in magnetic fields origin in sun, planets and galactic gaseous disk

01 p0162 A71-11419
Planetary nebulae and scattered stellar cluster visible coincident distribution near galactic center

02 p0308 A71-12103
Cepheids in Milky Way spherical component, emphasizing brightness and color curves and spectral characteristics

03 p0485 A71-13261
Extragalactic LF background radiation spectra, using model for free-free absorption in galactic disk

03 p0473 A71-13563
Cosmic ray nuclei galactic disk confinement determination, considering particle mean age by radioactive Be10 tracer method

03 p0480 A71-14052
Population I Cepheids studies applied to galactic rotation and solar motion parameters estimation, discussing stellar distances inaccuracy effects

04 p0643 A71-14908
Blue and red supergiants ratio as function of radial distance from Galactic center, noting distribution in M33

05 p0805 A71-16119
Galactic magnetic field generation by dynamo process with nonuniform rotation and turbulence in gaseous disk

05 p0811 A71-16687
H I gas kinematics in Galactic anticenter region from Gaussian components of emission line profiles at 21 cm observations

06 p0964 A71-17349

Galactic structure derived from neutral hydrogen observations, using kinematic models based on density wave theory 06 p0969 A71-17972

Interstellar gas dynamic characteristics, discussing galactic large scale features 06 p0971 A71-18328

Visible brightness of Milky Way for various galactic structure models, discussing star and dust distribution effects 06 p0975 A71-18444

Ammonia inversion radiation at 1.25 cm in direction of three galactic center sources, setting upper limits on densities in other areas 07 p1188 A71-19834

Galactic center region far IR map in 75-125 microns spectral interval with 6 minute resolution 07 p1199 A71-19835

Neutral hydrogen subsystem rotation in inner Galaxy from equal angular velocity surfaces 09 p1518 A71-22375

Milky Way northern portion absorption values obtained from star cluster data 09 p1524 A71-23184

Stellar UVB photographic photometry of specific Milky Way oblong region 09 p1527 A71-23525

O and B type stars galactic Keplerian parameters statistical distributions based on galaxy point model 11 p1820 A71-25248

Southern galactic plane search for high dispersion pulsars, giving calibration data for Molonglo searches 11 p1820 A71-25295

Visible brightness of Milky Way for various galactic structure models, discussing star and dust distribution effects 12 p1955 A71-26594

Gravitational wave bursts emanating from direction of center of Milky Way Galaxy, considering pulsating neutron star as source 12 p1958 A71-26694

Galactic radio emission, considering continuum radiations, radio polarization, H I regions structure and physics, recombination and absorption lines 12 p1959 A71-26778

Milky Way Galaxy X ray sources, discussing bremsstrahlung, synchrotron radiation, Compton effect optical objects, supernova remnants and X ray astronomy 12 p1959 A71-26780

Terrestrial, solar and galactic magnetic fields, discussing generation by combined nonuniform rotation and cyclonic turbulence based on dynamo equation 12 p1961 A71-26859

Milky Way galaxy radio halo, investigating background brightness distribution and local spiral arm magnetic field structure 12 p1963 A71-27078

Soft X ray background source, discussing north polar galactic spur as supernova outburst remnant 14 p2298 A71-29732

Central Galactic region star distribution, considering RR Lyrae and metal-rich stars 15 p2495 A71-32704

Milky Way galaxy interstellar neutral hydrogen rolling motion phenomenon confirmed by 21 cm line survey data 16 p2630 A71-33053

Cosmic rays lifetime in Galaxy in presence of particle acceleration in interstellar space 16 p2626 A71-33463

Spiral structure of Galaxy, using perturbation method for analysis of steady state interstellar gas with differential rotation due to coupling with stellar gas 16 p2643 A71-34069

Stellar movement in Galactic field, discussing observational and mathematical techniques for stellar orbits and velocities determination 17 p2801 A71-34697

Dynamic formulation for number of communicative civilizations in Milky Way galaxy suitable for digital simulation 18 p2965 A71-36295

Local group stellar systems including Galaxy, Magellanic Clouds, Andromeda galaxy, triangulum and spherical dwarf galaxies 18 p2966 A71-36759

IR radiation sources, discussing intermediate and early stars, galactic nucleus and extragalactic sources 18 p2958 A71-37029

Milky Way galaxy radio halo, investigating background brightness distribution and local spiral arm magnetic field structure 19 p3133 A71-37428

Extragalactic Faraday rotation models, examining galactic plane and Galaxy supercluster 19 p3142 A71-38005

Galactic central region gas motions, discussing hypothetical explosive expulsion of matter from galactic nucleus 19 p3143 A71-38165

Milky Way galaxy internal small scale magnetic field generation, relating strength to cyclonic turbulence properties and large scale shear 20 p3287 A71-39055

Milky Way galaxy poloidal magnetic field generation with hydromagnetic dynamos, showing galactic cosmic rays as major driving force 20 p3287 A71-39056

UV radiation in space and Venus atmosphere, studying L-alpha lines luminescence hot stars intensity, Milky Way brightness and hydrogen envelope existence 20 p3282 A71-39748

Pulsars luminosity, z-distance and period distribution in Galaxy, comparing supernova remnants 20 p3303 A71-39933

Galactic nucleus map and flux at 10 microns scanned with 5.5 arcsec beam on Catalina observatory telescope 20 p3305 A71-39957

Total mass density in neighborhood of sun and Galactic force law from stellar motions perpendicular to Galactic plane, using King pseudomoments method 21 p3440 A71-40061

Compact radio sources in galactic nucleus, examining relation to IR emission 21 p3449 A71-40609

Spiral wave dispersion, wave number and amplitude relationship in Galaxy near inner Lindblad resonance, noting correlation with ionized hydrogen density 21 p3451 A71-40855

Balloon-borne far IR survey of sky portions in Galactic plane 23 p3736 A71-43539

Southern Milky Way isophote maps by near-UV surface photometry, showing brightest areas in Sgr/Scor, Car, Vel/Pup and Cyg 24 p3867 A71-44436

Galactic nucleus X ray source observations by Uhuru satellite, discussing emission and absorption spectra 24 p3866 A71-44915

Pulsar JP 1933 distance lower limit from 21 cm absorption and galactic rotation model, noting scintillation parameters consistency with observations in thin screen model 24 p3873 A71-45141

MILLIMETER WAVES

Radio astronomy in millimeter and submillimeter ranges, surveying programs and equipment at various observatories 01 p0156 A71-10450

Millimeter waves attenuation in fog, showing strong temperature dependence and correlation with visibility 01 p0117 A71-10580

Millimeter and submillimeter radio waves propagation, outlining molecular and aerosol attenuation in real atmosphere together with transmitters and receivers 02 p0212 A71-11872

Lunar radio emission measurements at 1.42 mm, using radio telescope and wideband superheterodyne radiometer 02 p0309 A71-12104

Earth station mixers design as wideband millimeter wave up- and down-converters for satellite communication systems 02 p0234 A71-12818

Quasi-optical waveguide components for millimeter and submillimeter waves, considering couplers, attenuators, isolators, bandpass and bandstop filters 02 p0235 A71-12907

Solar mm bursts impulsive component correlation with associated soft X ray burst 03 p0473 A71-13184

ATS 5 satellite millimeter wave earth-space propagation and communications equipment 04 p0551 A71-15009

Saturn millimeter wave spectrum and brightness temperature measurements, showing ammonia absorption characteristics in atmosphere 04 p0659 A71-15851

Mars, Jupiter, Saturn and Uranus millimeter wave radiation brightness temperatures, considering search for variations with time or phase angle 04 p0660 A71-15860

Rain and drizzle millimeter wave attenuation and radar scattering cross section calculation 05 p0718 A71-15988

Submillimeter and millimeter waves attenuation in rain, comparing calculation results with measurement 05 p0718 A71-15990

German monograph on polycrystalline ferrites studies with quasi-optical resonators in mm wave range 05 p0791 A71-16125

TWT noise level minimization in 8 mm band with circular spiral slow wave structure and five electrode gun 05 p0723 A71-16874

Millimeter wave lensless Fourier transformation /LFT/ holographic imaging, discussing equipment and performance 05 p0754 A71-17081

Diffusion varactor and Schottky barrier semiconductor diodes for frequency multiplication at millimeter wave frequency range 06 p0873 A71-17545

Solar radio bursts monitoring at 71 GHz /July 1967-December 1969/ 06 p0968 A71-17914

Solar 3.3 mm bursts observation, showing temporal correlation with soft X ray bursts 06 p0968 A71-17915

Microwave oscillator circuit with cap structures for testing millimeter wave IMPATT diodes 07 p1073 A71-19119

Atmospheric absorption by clouds, fog and rain on earth-space path at 90 GHz, using sun tracker 07 p1060 A71-19215

Martian radio emission measurements at millimeter wavelength and surface thermal and electric parameters estimation 07 p1193 A71-19314

Pulkovo radio telescope resolution improvement by range extension into millimeter wavelength region 07 p1109 A71-19341

Pulkovo radio telescope antenna surface precision and electrical characteristics at eight mm, using ground oscillators and solar, lunar and Venusian observations for radiation pattern 07 p1075 A71-19342

Pulkovo radio telescope effective frequency range extension beyond minimum 3 cm wavelength into millimeter range, installing high precision reflecting mirror surfaces 07 p1083 A71-19343

Modified waveguide magnetrons for continuous 1.3 mm waves, discussing construction and operation 07 p1081 A71-20454

Radio emission observations at 8 mm wavelength from 3C 273 and 3C 279 07 p1204 A71-20626

Wide band low noise millimeter wave parametric amplification using wafer varactor diodes with Schottky barrier junctions 08 p1263 A71-20769

Lunar radio emission measurements at 1.42 mm, using radio telescope and wideband superheterodyne radiometer 08 p1362 A71-21151

Long distance PCM-AM pulse regenerator for 4 GHz band and millimeter wave communication 08 p1265 A71-21285

Automatic control circuits for millimeter wave backward wave tube frequency tuning and supply voltage regulation 08 p1267 A71-21804

Phase regulated AFC system design for millimeter and submillimeter wave backward wave tubes 08 p1267 A71-21805

Fabry-Perot interferometer for dielectrics permittivity and loss measurements in millimeter and submillimeter ranges, discussing design, tests and accuracy 08 p1294 A71-21806

Atmospheric emission and absorption measurements at millimeter wavelengths, comparing with radiative transfer equation values 08 p1257 A71-21880

Solar radio bursts power spectra associated with proton events, noting extension to millimeter waves 09 p1514 A71-22933

Amplitude discriminating Goto circuit with four tunnel diodes operating on negative and positive half periods as amplitude distribution analyzer at 40 MHz 10 p1582 A71-23954

InP pulsed and CW millimeter wave oscillators at frequencies above 30 GHz 11 p1739 A71-26367

Millimeter backward wave oscillators, discussing cooling, operating characteristics, frequency pulling and pushing, life and reliability 11 p1739 A71-26436

Superheterodyne radiometers for millimeter and submillimeter waves, using Mach-Zehnder interferometer frequency mixer for parasitic signal suppression 12 p1886 A71-26847

Radio astronomy in millimeter and submillimeter ranges, surveying programs and equipment at various observatories 12 p1967 A71-27421

Chromospheric millimetric emission through 250 GHz atmospheric passband on isophoto maps, showing higher brightness temperatures compared with solar disk 12 p1969 A71-27649

Phase measurement at millimeter wavelengths in free space, using reference signal and interference pattern of slowly varying electric field 13 p2030 A71-28609

Two cavity ring-type channel dropping filters for millimeter wave guided communication system, calculating pulse response and interchannel crosstalk characteristics 14 p2210 A71-29569

Millimeter wave waveguide time delay distortion characteristics equalization using directional filter cascades

14 p2210 A71-29572

Measuring instrument for solar radio emission at 8 mm, using GaAs Schottky barrier diode mixer for system noise temperature reduction

14 p2239 A71-29916

Radio source 3C 273 observation at 8.2 mm wavelength, using traveling wave maser on radio telescope for tenfold sensitivity improvement

14 p2253 A71-29989

Millimeter wave semiconductor isolator using circular waveguide with coaxial n-type InSb in longitudinal magnetic field

14 p2212 A71-30510

Double cavity tuning of Gunn oscillators at mm wavelengths achieving output power improvements

14 p2215 A71-30831

Millimeter and visible waves propagation through clear atmosphere and precipitation

14 p2204 A71-30971

Radio power, insertion loss, frequency and dielectric measurements at mm wavelengths

14 p2205 A71-30982

Martian radio emission measurements at millimeter wavelength and surface thermal and electric parameters estimation

15 p2486 A71-31894

Heat balance and 8.22 mm radio emission of Mars, evaluating surface thermal and electrical parameters including brightness temperature

15 p2490 A71-32411

Uranus radio emission measurement at 8.22 mm, obtaining brightness temperature

15 p2490 A71-32412

Mars and Jupiter radio emission at 2.3 mm and 8.15 mm, determining brightness temperature and electrical and thermal waves soil penetration depth ratio

15 p2490 A71-32413

Mercury, Mars, Venus, Jupiter and Saturn temperatures at 9.55 mm wavelength, calibrating antenna gain with radio sources

15 p2490 A71-32414

Frequency response of rainfall attenuation for various dropsize distributions, plotting measured values at .890 and 110 GHz

15 p2374 A71-32696

IR stars and galaxies measurements, determining 3.5 mm continuum radiation intensity

15 p2498 A71-32775

Millimeter broadband high power traveling wave transmitter tubes with stub voltage tuning for ground stations of satellite communication systems

16 p2545 A71-32975

Extragalactic radio sources millimeter wavelength spectra measurements, investigating electron energy loss mechanism, magnetic field strengths and dynamics

16 p2631 A71-33234

Radio contour map of Crab nebula at 3.5 mm, giving brightness distribution and flux density

16 p2632 A71-33235

Fence guide waveguide on dielectric substrate for millimeter wave, applying to power dividers, directional couplers, hybrid rings and resonators

17 p2713 A71-34444

Millimeter wave systems applications to plasma probes, radar, radiometry and communications

17 p2699 A71-34602

Sensitive mm wave receivers, using local oscillator and mixer functions in single Gunn diode for large dynamic signal input range and wide IF bandwidth capability

17 p2717 A71-35111

Thermal self focusing of pulsed millimeter waves transmitted through cylindrical plasma, observing power dependence and beam asymmetry

18 p2951 A71-35986

Polarized solar millimeter emission associated with sunspot magnetic field compatible with multiple sources from chromosphere

18 p2966 A71-36762

Experimental comparison between double drift and single drift region mm wave IMPATT diodes on room temperature metal heat sinks

18 p2895 A71-36984

Filled aperture antennas for radio astronomy, considering mm wave observations, parabolic cylinder antennas and active/passive control of antenna surfaces

18 p2901 A71-37036

Discrete galactic and extragalactic radio sources observations at 3.3 mm, detailing flux and variability measurements

18 p2970 A71-37067

Atmospheric noise temperature variation with frequency in 2.53 mm molecular oxygen rotation line, considering Zeeman effect

19 p3048 A71-37402

Radio emission detection of para-formaldehyde and 2 mm formaldehyde distribution in Orion IR nebula

20 p3287 A71-39112

Millimeter and submillimeter laser action in symmetric tip molecules optically pumped via parallel absorption bands

20 p3246 A71-39759

Millimeter emission lines from interstellar methyl cyanide transitions, noting kinetic temperature and hydrogen density

21 p3447 A71-40446

Broadband helical antenna feeds for millimeter wave parabolic reflectors and lenses, determining beamwidths and polarizations as functions of helix parameters and frequency

21 p3359 A71-41408

Millimeter wave holographic imaging for concealed weapon detection by phase-only hologram, discussing recording and reconstruction systems configurations

22 p3546 A71-42485

IMPATT diode development for millimeter wave applications including oscillators, sweep generators and Doppler radar

22 p3524 A71-42763

Millimeter transverse electric wave diffraction by spherical plasma, interpreting interferometric measurements of electron density

23 p3708 A71-43085

Polarized solar radio emission at millimeter wavelength in active regions associated with sunspot magnetic fields

23 p3733 A71-43125

Millimeter and submillimeter wave radiation detection by paramagnetic materials, noting noise equivalent power dependence on various parameters

23 p3717 A71-44293

Millimeter band plasma microwave radiation receivers for emission measurement, presenting schematic diagrams for superheterodyne

24 p3825 A71-44507

Q band relative phase measurement using single sideband suppressed carrier ferrite modulator in serrodyne phase bridge

24 p3803 A71-44649

Multiple mismatch reflection and mode conversion echo effect on error rate in guided millimeter wave phase shift keying systems

24 p3804 A71-44989

Composite quasi-optical-broad waveguide transmission lines for millimeter and submillimeter waves with spectrum phase correction

24 p3810 A71-45258

MILLING [MACHINING]

Flat products skin milling work determination from microgrid deformation graphs, using continuum mechanics equations

04 p0602 A71-14607

Milling, band grinding, final manual polishing and tumbler polishing effect on fatigue life and surface finish of steel compressor blades

12 p1912 A71-27680

Wing models development by tangent milling on jig-borer, approximating cross section by hand finish smoothed polygon

15 p2413 A71-31439

Cutting speed, feed rate, tool geometry and other machining factors effects on surface finishes of face milled steels, titanium and nickel base alloys [SME PAPER MR-71-146]

18 p2927 A71-36663

Ion beam milling techniques for device fabrication involving atomic interactions on solid surfaces

21 p3384 A71-40219

MILLIVOLTMETERS

Single thermocouple temperature measurement, discussing millivoltmeters wiring method with resistance matching to ensure accuracy

03 p0430 A71-14329

MINER RULE

U PALMGREN-MINER RULE

MINERAL DEPOSITS

Kaersutite amphibole formation from pargasite amphibole interaction with basanite, discussing Fe, Ti, K, Mg, Si, Na and Cr contents

10 p1601 A71-24415

Lunar soil albedo, discussing radiation darkening, lunar rock particles size and mineral contents effects

11 p1835 A71-26460

Human waste product utilization possibility through mineralization by wet combustion method

22 p3507 A71-42820

Thermal combustion produced biocomplex vegetable waste mineralization effect on furnace working surface oxide film

22 p3507 A71-42821

MINERAL OILS

Vapor pressure measurements of mineral oils for hydraulic power systems, using transpiration method

09 p1484 A71-23666

Spherical cap bubbles in water and mineral oil at various dynamic viscosities, measuring laminar and turbulent wakes character, rise speed and shape

21 p3365 A71-40017

MINERALOGY

Opaque minerals in Apollo 12 rocks, emphasizing spinel compositions

01 p0162 A71-11426

Apollo 11 crystalline igneous rocks mineralogy and petrology, suggesting origin from pyroxenite mantle melting

02 p0305 A71-11982

Petrographic microscope and electron microprobe analysis of Apollo 12 rock 12013, noting biminerallitic composition with dominant potassic feldspar plus silica

03 p0493 A71-14214

Apollo 12 lunar rock 12013 mineralogy, identifying whitlockite, plagioclase, alkali feldspar, ilmenite, quartz and minerals encrusted with quartz

03 p0493 A71-14215

Apollo 12 lunar rock 12013 petrologic and mineralogic characteristics, discussing data on isotopic Xe and Gd composition

03 p0494 A71-14217

Mineralogy and chemistry of earth upper mantle, using partial fusion-partial crystallization model

04 p0583 A71-15266

Mesosiderites silicate textures and compositions and metal-silicate relationships from mineralogical, petrographical and chemical data

10 p1602 A71-24504

Luna 16 lunar rock samples mechanical properties and chemical and mineralogical compositions for regolith origin determination

10 p1681 A71-25116

Mineralogy, petrology, chemistry and microstructure of Valdinizza meteorite

11 p1835 A71-26480

Petrography, chemistry and mineralogy of El Paso meteorite

11 p1835 A71-26481

Morphology, mineralogy and chemistry of Ashmore meteorite

11 p1835 A71-26482

Lunar samples mineralogy, petrology and geochemistry, considering lunar surface processes, cosmic ray flux and solar wind

12 p1967 A71-27414

Lost City /Oklahoma/ meteorite classification as type H5 chondrite based on bulk chemical composition, mineralogy and petrography

15 p2489 A71-32356

Lost City /Oklahoma/ meteorite mineralogical and chemical investigations, comparing with Pribram and Uchra meteorites

15 p2489 A71-32365

Kyle /Texas/ chondrite classification based on chemical composition, mineralogy and structure

17 p2800 A71-34513

Stony meteorites relicts in mesozoic formation of central Urals, discussing chemical and mineralogical composition and structure

17 p2800 A71-34517

De Kalb /Missouri/ chondrite structure and mineral composition, noting olivine and bronzite presence

17 p2800 A71-34518

Lunik 16 soil samples physical properties, rock types, chemical analysis, mineral composition and petrology, comparing to Apollo project

17 p2805 A71-35332

Stony meteorite Bushkhof mineral composition data, detailing measured quantities, distribution and appearance

17 p2810 A71-35721

Zemaitkemis /Lithuania/ meteorite mineralogical composition, noting rhygmaglypts formations, micro- and macrochondrules and Ni-Fe inclusions in cleavage area

17 p2810 A71-35726

Mineral and chemical composition of Krasnyi Kliuch meteorite, characterizing as recrystallized chondrite containing chondrules

17 p2811 A71-35731

Physical, chemical, mineralogical and biological analysis of Apollo 14 lunar rocks and fines

19 p3144 A71-38179

Physical properties, mineralogy and chemical composition of lunar regolith sample returned by unmanned Lunik 16 probe

23 p3737 A71-43602

Opaque minerals in Apollo 12 lunar rocks from Oceanus Procellarum by reflected light microscopy and electron microprobe analysis, including ilmenite, chromite and troilite

23 p3739 A71-43622

Mineralogical, petrological and chemical features of four Apollo 12 lunar microgabbros

23 p3740 A71-43625

Apollo 12 crystalline rocks mineralogy, petrology and chemical composition, considering magmatic origin

23 p3740 A71-43626

Mineralogy and petrology of Apollo 12 igneous rocks 12004, 12008, 12009 and 12022, noting ilmenite, olivine and spinel content and metal grains composition

23 p3740 A71-43627

Mineralogy, petrology and chemical composition of Apollo 12 rocks and fines

23 p3740 A71-43628

Petrography and mineral composition of Apollo 12 crystalline rocks

23 p3740 A71-43629

Apollo 12 lunar rocks and fines mineralogy and petrology, using optical and electron microscopy, electron and X ray diffraction and electron probe microanalysis

23 p3741 A71-43630

Mineralogy, chemistry and origin of KREEP/potassium, rare earth element and phosphorus component in Apollo 12 soil and breccia samples from Ocean of Storms

23 p3741 A71-43632

Normative mineralogy of lunar basaltic rocks from Apollo 11 and 12 samples, comparing with terrestrial and meteoritic analogs

23 p3742 A71-43637

Apollo 11 and 12 crystalline rocks petrographical analysis and textural-mineralogical-chemical group classification, considering local stratigraphy reconstruction

23 p3742 A71-43638

Crystalline and glassy phases electron probe analysis for picrite basalts, ferrobasalts, feldspathic norites and rhyolites from Apollo 12 lunar soil samples

23 p3743 A71-43645

Petrography, mineral composition and grain size distribution of Apollo 12 lunar fines

23 p3743 A71-43649

Mineralogical composition, modal distribution and bulk chemical analysis on Apollo 12 lunar fines

23 p3744 A71-43652

Lunar fines samples 10084,148 and 12070,98, investigating grain size, mineral and chemical composition and optical properties

23 p3744 A71-43655

Lunar rocks 12063,9 and 12004,11 opaque mineralogy and textural feature, comparing to apollo 11 samples

23 p3745 A71-43661

Chemical element composition and mineralogy of powdered lunar surface material, comparing Surveyor, Apollo and Lunik missions data

23 p3748 A71-43682

MINERALS

NT ALUMINUM SILICATES

NT AMPHIBOLES

NT ANDESITE

NT ARAGONITE

NT ASBESTOS

NT CALCITE

NT CHROMITES

NT COESITE

NT CRYOLITE

NT ENSTATITE

NT FELDSPARS

NT FLUOROSILICATES

NT GARNETS

NT ILMENITE

NT KAOLINITE

NT LIMONITE

NT MAGNETITE

NT MICA

NT MONTMORILLONITE

NT MOSCOVITE

NT OLIVINE

NT PEROVSKITES

NT PYROPHYLLITE

NT PYROXENES

NT SERPENTINE

NT SILICATES

NT SPINEL

NT TALC

NT TROILITE

NT YTTRIUM-ALUMINUM GARNET

NT YTTRIUM-IRON GARNET

NT ZINCBLENDE

Soviet book on material analysis by nuclear radiation covering heavy elements concentration in ores, radioisotope devices and gamma ray capture spectroscopy

02 p0283 A71-12721

Rare earth element concentrations in zircons and apatites separated from dacites and granites, explaining partition coefficients between phenocrysts and groundmass by crystal structure

03 p0407 A71-13338

Undoped and Nd doped synthetic fluorapatite single crystals heat capacity, thermal expansion and thermal conductivity measurements, yielding Debye temperature

07 p1180 A71-20164

Heavy ion track registration in nonconductor minerals, discussing radiation damage and atomic species along trajectory

07 p1158 A71-20270

Electron paramagnetic resonance and optical absorption spectra of transition metal ions in zoisite crystal

08 p1343 A71-20658

Artificial mineralization of water regenerated from human waste products in space flight

15 p2362 A71-31309

Laboratory approach to circumstellar mineral condensation, demonstrating fractional condensation

15 p2486 A71-31989

Lost City /Oklahoma/ meteorite chemical and mineral composition analysis by X ray diffraction and optical emission spectroscopy

15 p2489 A71-32362

Optical fluorescence spectra of rock forming minerals for quantitative analysis of lunar surface

15 p2411 A71-32471

Microscopic analysis of secondary minerals in molten meteorite crusts and dust

17 p2811 A71-35732

Diaplectic glass formation by experimental shock loading of orthoclase in porous mixtures

19 p3084 A71-37662

Fission track and K-Ar ages of coexisting minerals in drill core from heat-flow boreholes in western central Sierra Nevada batholith

21 p3374 A71-40649

Apollo 12 lunar igneous rocks and breccia opaque minerals examined by optical and electron microprobe techniques

23 p3739 A71-43621

Lunar glassy objects and mineral grains surface microstructure by optical and scanning electron microscopy, comparing with tektites and terrestrial volcanic analogs

23 p3745 A71-43664

Microelement extraction from mineralized biological samples in food rations and human excretions

24 p3800 A71-44540

MINIATURE ELECTRONIC EQUIPMENT

Intracranial pressure measurement by miniature transducer with modifications for baseline reading and calibration checking throughout implantation period, giving circuit diagram

01 p0021 A71-10241

Broadband mini ferrite T circulator and isolator for X band

03 p0384 A71-13274

Oxygen partial pressure measurements in myocardium of beating heart by miniature glass needle and surface electrodes

05 p0714 A71-16598

ECG miniaturized single channel biotelemetry transmitter, discussing lightweight design and power supply

10 p1570 A71-24487

Base metal impurity effects on coercive force and contact properties of miniature multilayered diffused reed switches

13 p2038 A71-28837

Miniature dry reed switch for latching and speech path, using semihard magnetic material, sealing glass and electroplated rhodium contact

13 p2001 A71-28842

Permeance and magnetic pull curves for miniature reed switch with wire pressed blades in sealed glass, using computer program

13 p2001 A71-28843

Miniature transducers design and fabrication for fluctuating pressure measurements in jet engine testing, noting frequency response and power dissipation

14 p2244 A71-30324

Miniature integrated sensor pressure transducers for inlet air flow distortion and buffet studies of wind tunnel models

14 p2245 A71-30336

Eight channel micropowered miniature biomedical PAM/FM telemetry system for implantation in research subjects aboard orbiting space station

14 p2189 A71-30930

Visual displays preview, noting miniature eight-character alphanumeric, tabular, video, telephone and graphical displays

18 p2924 A71-36619

Precision relaxation oscillators design and error sources, discussing miniaturization by microelectronic approaches

21 p3355 A71-40736

Semiconductor package designs for high performance miniature IR sensors, including flat packs, TO, custom metal and glass dewar configurations

23 p3676 A71-43509

Miniature battery operated electromagnetic blood flowmeter for data acquisition from unrestrained animals

24 p3801 A71-44783

MINIATURIZATION

NT MICROMINIATURIZATION

NT SUBMINIATURIZATION

Operating experience with miniature thermionic radioisotope-fueled batteries, using thermal-thermionic models

02 p0196 A71-12273

Miniature pressure transducer with extended temperature capability, discussing design and operation

09 p1445 A71-22723

Fast miniature shielded pitot pressure transducer for spatial resolution of flow details

09 p1453 A71-23728

Miniature aerodynamic turbulence gage using axisymmetric lifting body sensor

13 p2066 A71-28158

Miniature 20-watt CW TWT with samarium cobalt focusing magnets for fitting X-band waveguide, comparing performance, size and weight with conventional design

15 p2375 A71-31206

Heat exchanger miniaturization for avionics applications, discussing design and fabrication [HEAT EXCH. CONF. PAPER 15]

15 p2376 A71-31636

Miniature high speed expansion turbines for helium liquefiers and refrigerators, discussing turbine flow passages and gas lubricated bearings

20 p3184 A71-39246

Miniature self regulating rapid cooling Joule-Thomson cryostat, noting purging of accumulated contaminants

20 p3184 A71-39274

MINIMAX TECHNIQUE

Optimal multiimpulse compensation for dynamic system external disturbances by minimax differential game approach, restricting impulse number and magnitude

01 p0059 A71-10429

Two body pursuit problem minimax and optimum absorption time control algorithm

07 p1082 A71-20642

Conflicting and relaxed minimax controls for Weierstrass E condition or Pontryagin maximum principle

11 p1792 A71-25752

Linear system programmed maxim transfer time problem solvability, investigating control process theory with time inversion

12 p1931 A71-27523

Minimization of convex maxim functions, obtaining formula for derivative with respect to direction

14 p2265 A71-29553

Algorithm for minimax and maxim problems in theory of differential games

14 p2265 A71-29555

Differentiation of maxim function with respect to direction, analyzing theorems on differentiability

14 p2265 A71-29563

Closed-loop control of discrete time systems with uncertainty, discussing minimax reachability of target sets and tubes

14 p2219 A71-29698

Two theorems on minimax transversal filter equalization at receiver for digital communication systems distortion reduction

14 p2193 A71-30012

Controlled objects convergence game, constructing optimal minimax pursuer strategy

18 p2948 A71-36779

Computer designed optimal or suboptimal feedback controllers, considering least-pth and minimax cost functions

18 p2886 A71-36832

Optimal control with minimax cost for systems of n first-order state equations with performance measured by Chebyshev type functional over state trajectory

19 p3039 A71-38716

Optimal design procedure as experimental design finite decision problem, using Bayes and minimax techniques

21 p3408 A71-40879

Optimal nonlinear discrete filters with finite memory for polynomial signals, discussing synthesis with aid of minimax method

22 p3527 A71-42856

Minimax groups relation to group classes with maximality and minimality conditions

24 p3843 A71-44825

MINIMIZATION

U OPTIMIZATION

MINIMUM DRAG

Civil aircraft aspect ratio relationship to commercial viability, considering need for minimum induced drag at wing loading to improve payloads, speeds and ranges

01 p0005 A71-11628

Pointed body of revolution in gravitationally stratified atmosphere, discussing supersonic boom and minimum drag

05 p0694 A71-16712

Hypersonic minimum drag slender wing leading edge shape for given airfoil section, using Newtonian theory

08 p1229 A71-22039

Numerical solution of axisymmetric minimum drag bodies in hypersonic viscous gas flow, obtaining coefficient of friction by local variations method

10 p1551 A71-24370

Minimum drag surface shape of thick lifting delta wing integrated with conical fuselage for supersonic cruising speed

12 p1866 A71-27716

Minimum drag wing-fuselage combination for supersonic speeds and prescribed lifting force, longitudinal moment and volume, using method of successive approximations

13 p1992 A71-29182

Variational principle for obtaining upper and lower bounds on minimum drag on body of given volume in slow viscous flow

20 p3177 A71-39500

Minimum drag and lifting line characteristics of large aspect ratio wing in uniform shear flow with velocity variations along span 23 p3625 A71-43312

MINING

CERCHAR low speed wind tunnel design details, operational characteristics and utilization of facility for coal mine safety 10 p1589 A71-24287

MINKOWSKI SPACE

Quantum electrodynamics on null planes in Minkowski space, discussing applications to lasers, wave packet construction, Heisenberg and Furry pictures and Compton scattering 13 p2080 A71-28998

Minkowski space-time concept, developing deviation function from geometric analysis 15 p2481 A71-31145

Deformation field of continuous medium in Minkowski space-time, defining tensor in Euclidean space of initial configuration 18 p2947 A71-36191

MINNESOTA

Lunar and terrestrial ilmenite basalt, considering hornfels from Keweenaw Duluth complex in Minnesota and Apollo 11 samples 09 p1529 A71-23657

MINORITY CARRIERS

Minority current carrier mobility in anisotropic semiconductors, using Dember and photomagnetic effects 01 p0139 A71-11035

High resistance semiconductors minority carriers mean diffusion length based on induced charge dependence on applied voltage during illumination by absorbable light 02 p0294 A71-11898

Minority carrier bulk lifetime from large signal response time of MOS capacitor in deep inversion 03 p0388 A71-14474

Neutron induced lifetime damage short term annealing dependence on minority carrier density in p-type silicon, considering majority carrier repulsion by positively charged centers 07 p1175 A71-19061

Forward biased asymmetric p-n junction diodes with arbitrary impurity distributions, measuring minority carrier lifetimes by refined step recovery technique 09 p1414 A71-22448

GaAs lasers p-n junction active region thickness from minority carrier mobility and spontaneous emission measurements in threshold current determination 09 p1460 A71-22305

Semiconductor radiation detectors, discussing minority charge carrier diffusion length measurements by nuclear method 13 p2065 A71-27957

Semiconductor radiation detectors, discussing minority charge carrier diffusion length measurements by nuclear method 21 p3383 A71-41346

Gold doping effect on minority carrier lifetime and other electrical properties of epitaxial Si transistors 22 p3520 A71-41702

Minority carriers charge distribution at boundary between neutral base and collector transition region of one dimensional n-p-n transistors 23 p3653 A71-43965

Excess minority carrier diffusion length measurement in thin silicon wafers, using light-spot and dark-spot methods 24 p3861 A71-45202

Irradiation defects and electrical quality of ion implanted silicon, using minority carrier lifetime measurements 24 p3863 A71-45357

MINUTEMAN ICBM

Computerized data management program for Minuteman radio telemetry instrumentation systems 01 p0050 A71-10884

Minuteman missile technology application as boosters for near earth spacecraft launching, emphasizing tradeoff between reliability and cost 04 p0663 A71-15313

Quality control for Minuteman zinc silver oxide battery production 08 p1298 A71-21109

Minuteman 2 third stage rocket engine instrumentation performance evaluation for oscillatory combustion characteristics analysis [AIAA PAPER 71-755] 14 p2248 A71-30789

Missile component vibration environments generation by Minuteman 2 and 3 third stage motors solid propellant oscillatory burning [AIAA PAPER 71-756] 14 p2296 A71-30790

MINUTEMAN MISSILES

U MINUTEMAN ICBM

MIRAGE 3 AIRCRAFT

Mach 2 Mirage Milan ground attack fighter, noting lift and moustache, low speed and steep approach handling from short airstrips 02 p0190 A71-12740

Extreme turbulence measurement during low level flights of Mirage A3-76 fighter aircraft, determining

true gust velocities and power spectral energy distributions 14 p2267 A71-29756

MIRRORS

NT MAGNETIC MIRRORS

NT PARABOLOID MIRRORS

NT ROTATING MIRRORS

Reflecting telescope with six meter mirror, describing optical and control systems and structure 02 p0254 A71-12712

Be mirrors thermal dimensional instabilities dependence on crystalline anisotropy, discussing X ray quality control technique 03 p0424 A71-13637

Carbon dioxide laser plasma lensing effect used as mirror curvature compensation for maximum output power 03 p0436 A71-13641

Vibrating mirror for continuously pumped ND/YAG laser repetitive Q switching 03 p0438 A71-13888

Solar telescope coelostat and auxiliary mirror hydropneumatic unloading mechanism 04 p0566 A71-14870

Three-mirror telescope third order dioptrics of astigmatism and coma suppression 06 p0901 A71-18313

Holographic interferometric recording of vibration patterns of plexiglass cored construction mirrors [AIAA PAPER 71-180] 06 p0903 A71-18619

Small sealed low power carbon dioxide lasers, noting signature variations as function of mirror distance variations 06 p0910 A71-18669

Pulkovo radio telescope effective frequency range extension beyond minimum 3 cm wavelength into millimeter range, installing high precision reflecting mirror surfaces 07 p1083 A71-19343

Plasma refractive index effects in pulsed HCN lasers, calculating stable cavity mirror curvatures construction as function of electron density by ray matrix approach 07 p1124 A71-19795

Paraboloidal, hyperboloidal and flattened spheroidal telescope mirrors testing with optical compensation lenses by Foucault shadow and Ronchi methods 07 p1116 A71-20641

Fabry-Perot resonator with anisotropic medium, deriving reflection mirror shape for optimizing diffraction loss and resonant conditions for extraordinary waves 08 p1289 A71-21284

Low energy proton irradiation induced thin polymer contaminant films effect on far UV reflecting mirrors reflectance and scattered light 08 p1290 A71-21382

Large spaceborne telescope primary mirrors materials under microstructural loads, considering low expansion ceramics and metallic applications 09 p1446 A71-22743

Thermal deflection tests of fused silica mirror blanks by holographic interferometry 09 p1447 A71-22745

Mirror reflection coefficients effect on fringe characteristics of multibeam series interferometer, showing improvement by Fabry-Perot etalon system 09 p1451 A71-23174

Heated mirrors and hot plasma column effects on diffraction losses and power output of gas lasers 10 p1623 A71-25093

Interferential spectrometer with selection by amplitude modulation with double passage mirrors arrangement for obtaining double resolution 12 p1905 A71-26811

Laser resonator properties with flat outlying mirrors, examining stimulated radiation generation and energy distribution 12 p1916 A71-27764

Substrates, films and laser mirrors production, discussing material combinations and evaporation processes 13 p2080 A71-29087

Tenzaloy Al mirrors for IR astronomy, discussing results of Hartmann tests for optical stability 14 p2241 A71-30144

Two beam holographic interferometer based on spherical mirrors with laser beam splitting by semitransparent plate and image reconstruction in monochromatic and nonmonochromatic light 15 p2402 A71-31257

Astronomical mirror mass balancing system, discussing counterweights and levers arrangement and error and temperature compensation 15 p2411 A71-32526

Plane mirror ruby laser pseudosteady regime, discussing fundamental TEM mode case 16 p2588 A71-34062

Laser beam reflection from arbitrary geometric surface, considering reverse problem of response of flat or curved mirror to incident collimated light 18 p2929 A71-36055

Diffraction loss equality in field distribution at con-focal laser resonator mirrors with circular coupling holes 20 p3242 A71-38850

Aspheric lenses and mirrors testing by single and double exposure two-wavelength visible light holography for obtaining interferogram 20 p3235 A71-39182

Mirror meridian circle of zero expansion glass for reduction of flexure and refraction instrument errors in astrometry 20 p3240 A71-39539

Paraboloid-hyperboloid Cassegrain telescope mirror centering, describing stigmatic point position permanent control in focal plane by geometrical method 21 p3375 A71-40066

Ten cm aperture penta and roof-penta mirror assemblies for telescope internal optical alignment 22 p3549 A71-42553

Gas ring laser lock-in zone, showing dependence on resonator mirror curvature radius and mode competition between oppositely directed waves 23 p3683 A71-43393

Laser vibration noise produced by piezoelectric transducer induced forced vibrations of resonator mirror, determining translational and rotational amplitude limits for laser output fluctuation 23 p3686 A71-43999

Ruby laser radiation modulation by ultrasonic mirror oscillations, discussing mechanism 24 p3836 A71-45269

MIS (SEMICONDUCTORS)

Electron tunneling through interfaces of MIS structures, calculating conductance and current characteristics 01 p0140 A71-11413

Tunneling in boron doped p-type silicon metal-semiconductor and MIS tunnel junctions 04 p0636 A71-14973

Electron trapping in MIS transistor, discussing thermal annealing process activation energy and trap production by radiation 07 p1076 A71-19499

Gate voltage drift in enhanced p-channel MIS transistors having either pure silicon dioxide insulation or silicon dioxide with silicon nitride 09 p1413 A71-22156

Metal-oxide-metal tunnel diode properties, discussing parametric effects on small and large signals detector operation 09 p1416 A71-22684

Dielectric layer surface electric charge movement determination by measuring metal-insulator-semiconductor (MIS) capacity response at very low frequency 12 p1942 A71-26829

MIS structure voltage-farad characteristics, determining surface state densities for silicon compound dielectric films 18 p2954 A71-35875

Electrons interaction with impurities and longitudinal optical phonon in metal-insulator-semiconductor tunnel junctions 19 p3119 A71-37869

Charge injection in metal-aluminum oxide-silicon dioxide-silicon systems using capacitance voltage technique 22 p3587 A71-42531

Cost effective general purpose minicomputer PDP-11/45 design and technology using Schottky TTL/MSI, semiconductor memories, multiple buses, microprogramming and floating point units 22 p3519 A71-42761

Capacitance and conductivity in metal dielectric semiconductor during majority current carrier population depletion by pulsed voltage, discussing concentration and mobility determination 24 p3859 A71-44376

Current carrier mobility and concentration measurements in inversion metal dielectric semiconductor channels by Hall method 24 p3808 A71-44384

MISALIGNMENT

Photographic measuring method for angular mis-alignment associated with broken ball bearing 01 p0086 A71-10296

Ball bearing cage life, examining angular misalignment effect 01 p0086 A71-10297

Launch vehicle under influence of random fin misalignments, predicting roll rate by statistical analysis [AIAA PAPER 70-1382] 03 p0498 A71-13665

Control of time varying mechanical torque normal to ball bearing pair common spin axis by cross torque control through misalignment coupling [ASLE PREPRINT 70LC-9] 08 p1298 A71-21156

Interaction between two rectilinear cracks, noting angle and disorientation effects 23 p3777 A71-44034

MISCIBILITY

U SOLUBILITY

MISFIRES

U FIRING (IGNITING)

MISMATCH

U IMPEDANCE MATCHING

MISORIENTATION

U MISALIGNMENT
MISS DISTANCE

Midair collisions analysis for civil-military integrated ATC air space, discussing near miss volume, random heading aircraft density and pilots evasive action vs avoidance percentages

12 p1927 A71-27599

Radar avoidance action logic for converging aircraft safe passage, discussing near miss and collision situations

12 p1927 A71-27600

MISSILE ANTENNAS

Nulls of radiation and input impedance of flush mounted rocket antennas for telemetry and transponder systems

02 p0228 A71-11674

Flush mounted annular slot missile antenna theory application to near zone field strength instrumentation calibration and plane wave electromagnetic field pulse response determination

10 p1580 A71-25071

Missile system passive radar echo enhancement, discussing dielectric enhancers comprising antennas and corner reflectors

14 p2206 A71-31070

Missile circumferential current density for plane wave electromagnetic field illumination, using Kao shadowing theory

15 p2372 A71-32367

Tuned loop antenna for missile telemetric data transmission, discussing design, implementation and impedance and radiation measurements

17 p2718 A71-35749

Theoretical signal strength reduction on USAF Eastern Test Range based on missile antenna radiation pattern characteristics

18 p2876 A71-36471

MISSILE BODIES

Finned missiles aerodynamics at high angle of attack, examining body vortex wake region interaction with fins

[AIAA PAPER 71-50] 06 p0980 A71-18511

MISSILE CASES

U MISSILE BODIES

MISSILE COMPONENTS

NT MISSILE ANTENNAS

NT MISSILE BODIES

Ten-year old missile battery reliability programs based on two aspects of remotely activated one-shot battery

08 p1236 A71-21110

Semiconductor element design flexibility, providing greater reliability and reduced size/weight for space vehicles and missiles

09 p1445 A71-22722

MISSILE CONFIGURATIONS

Asymmetric missile nonlinear angular motion, describing quasi-linear relations for frequencies, damping rates and swerving motion amplitude

[AIAA PAPER 70-534] 09 p1532 A71-22906

Control jets interaction with airstream surrounding typical tactical missile configuration, considering rear mounted bistable fluidic thrusters and circular sonic jets

11 p1837 A71-25506

Cone-cylinder-cone missile type body in transonic buffeting environment determining static and fluctuating wall pressure distribution

[ONERA-TP-942] 18 p2843 A71-36020

MISSILE CONSTRUCTION

U MISSILE STRUCTURES

MISSILE CONTROL

Inertially stabilized tactical missile control system performance analysis using hybrid computer simulation methods

02 p0226 A71-11785

Kalman-Bucy linear filtering algorithm application to nonlinear estimation of single channel missile attitude control system parameters

07 p1081 A71-18835

Nonlinear proportional navigation guided homing missile and minimum time to turn, developing quadratic equation with close larger positive root approximation

07 p1156 A71-19878

Subsonic tactical missile hydraulic and fluidic autopilot systems for directional control, considering costs, reliability, vulnerability, maintainability, weight and mobility

[SME PAPER MS-70-524] 07 p1024 A71-20547

Missile fluidic attitude control system, discussing integrator, transducer amplifiers and circuits

07 p1028 A71-20583

Missile roll axis attitude control system based on fluid amplifiers, describing fluidic integrator and chain

07 p1028 A71-20584

Dynamic instability of finned missiles occurring as angle of attack undamping and caused by differential lift from windward and leeward fins

[AIAA PAPER 70-206] 09 p1530 A71-22075

Control and instrumentation fluidics, describing equipment, circuits and applications to jet engine con-

trols, missile guidance, flight control, ordnance and machine tool control

09 p1386 A71-22775

Modified steepest descent algorithm for optimum trajectory computation applied to interceptor missile control

14 p2207 A71-30018

Control, navigation and guidance review, considering application of earth reference coordinates for aircraft, missiles and spacecraft

14 p2272 A71-30710

Linear closed loop optimal intercept guidance law compensating for short range tactical missile time lag, guidance command saturation and target acceleration

15 p2446 A71-32113

Soviet book on radio control of various flight vehicles covering closed loop synthesis, missile guidance, spacecraft trajectory correction and air traffic control

17 p2775 A71-35403

Avionic and missile computer control systems, describing universal function unit design and digital processing requirements

17 p2711 A71-35775

Fluidic inertial platform feasibility model for line of sight guidance of air to surface missile

18 p2945 A71-36483

Jet tab thrust vector control system for tactical missile applications, describing operational principles, design details and performance characteristics

[AIAA PAPER 71-752] 18 p2956 A71-36773

Kalman filter for computerized optimal SRAM air to surface missile alignment, discussing design, digital simulation and flight tests

[AIAA PAPER 71-948] 19 p3098 A71-37189

Space and missile guidance performance analysis based on error sources, using Monte Carlo simulation

19 p3101 A71-37754

Proportional navigation for trajectory control of missile homing on target in planar pursuit

20 p3261 A71-38856

MISSILE DEFENSE

Ballistic reentry warheads atmospheric interception, investigating defensive nuclear bursts effects

01 p0163 A71-10268

MISSILE DEFENSE SYSTEMS

U MISSILE SYSTEMS

MISSILE DESIGN

Error model and digital computer simulation programs for technical management of missile development and testing

01 p0068 A71-10883

Multistage rocket propelled strategic ballistic missiles and space boosters design and trajectory optimization, using SWORD computer program

04 p0556 A71-15292

Guided weapons modeling techniques, discussing use of mathematical models for analog, digital and hybrid computerized design of missile systems

07 p1207 A71-19419

Plastics and metals as construction materials in aircraft, missile and rocket design

07 p1215 A71-20044

Operational research in designing ground-to-air launch weapons, considering model, effectiveness measure, decision and experiment

09 p1532 A71-22992

MISSILE DETECTION

NT RADAR DETECTION

MISSILE ENGINE CASES

U ROCKET ENGINE CASES

MISSILE GUIDANCE

U MISSILE CONTROL

MISSILE LAUNCHERS

Vibrational damping, composition and structural design of cast polyurethane elastomers for Poseidon missile launch tube liner

08 p1367 A71-20694

Launch and data reduction in supersonic wind tunnel free flight testing of high fineness ratio bodies

[AIAA PAPER 71-278] 08 p1228 A71-22003

Operational research in designing ground-to-air launch weapons, considering model, effectiveness measure, decision and experiment

09 p1532 A71-22992

Solid propellant missiles underground silo self eject mode launching simulation, obtaining heat transfer, pressure and acoustic measurements

[AIAA PAPER 71-707] 15 p2385 A71-32576

MISSILE RANGES

Theoretical signal strength reduction on USAF Eastern Test Range based on missile antenna radiation pattern characteristics

18 p2876 A71-36471

MISSILE ROLL CONTROL

U LATERAL CONTROL

U MISSILE CONTROL

MISSILE SILOS

Solid propellant missiles underground silo self eject mode launching simulation, obtaining heat transfer, pressure and acoustic measurements

[AIAA PAPER 71-707] 15 p2385 A71-32576

MISSILE SIMULATION [MATH MODELS]

U MATHEMATICAL MODELS

U MISSILES

MISSILE SIMULATORS

Missile six degree of freedom simulation by hybrid computer, discussing roll and pitch dynamics

02 p0227 A71-11798

MISSILE SIMULATORS [TRAINING]

U MISSILES

U TRAINING SIMULATORS

MISSILE STABILIZATION

U MISSILE CONTROL

U STABILIZATION

MISSILE STAGING

U MISSILES

U STAGE SEPARATION

MISSILE STRUCTURES

Asymmetric missile angular response to spin varying through resonance

[AIAA PAPER 71-46] 06 p0979 A71-1850

Pulse response of unshathed coaxial umbilical cable connector mounted flush with missile skin

10 p1585 A71-25072

Filament reinforced composite materials, considering spacecraft and missile applications mechanical and physical properties

13 p2144 A71-28166

Composite structures development, discussing wing, fuselage, aeropropulsion and missile development, weight savings of hardware and fighter empenage applications

[AIAA PAPER 71-367] 18 p2979 A71-36275

MISSILE SYSTEMS

Real time missile radio telemetry data transmission to ground station, using instrumented aircraft

04 p0554 A71-15321

U.S. tactical missile program evolution since WW II, discussing technology, air defense, assault/antitank weapons, interdiction and battlefield combat support

05 p0818 A71-17149

Guided weapons modeling techniques, discussing use of mathematical models for analog, digital and hybrid computerized design of missile systems

07 p1207 A71-19419

Structural bonding with polyurethane adhesives in missile systems

10 p1615 A71-24094

Short range air to ground attack missile system, discussing nuclear warhead, propulsion system, performance characteristics and program cost analysis

10 p1682 A71-24286

French National Strategic Force sea-ground and ground-ground ballistic missiles characteristics and performances

16 p2646 A71-34095

MISSILE TEST LABORATORIES

U LABORATORIES

U MISSILE TESTS

MISSILE TEST RANGES

U MISSILE RANGES

MISSILE TESTS

Error model and digital computer simulation programs for technical management of missile development and testing

01 p0068 A71-10883

Tactical missile flight test planning using digital simulation data reduction techniques for fast cost effective trajectory synthesis

02 p0226 A71-11784

Missile prototype reliability prediction, using reliability theory concepts in establishing computation and test programs without damage probability determination

02 p0298 A71-12366

Air-to-air, air-to-ground and USN surface-to-air guided weapons operational assessment in military environment

09 p1532 A71-22991

Shillelagh missile reliability program development/deployment using part qualification levels and fly-before-buy procurement

12 p1885 A71-26684

Theoretical signal strength reduction on USAF Eastern Test Range based on missile antenna radiation pattern characteristics

18 p2876 A71-36471

MISSILE TRACKING

Directional antenna with parabolic reflector for missile tracking in telemetry band, considering radiation diagrams and design approach

07 p1078 A71-20012

Optimal tracking of goal seeking vehicles, evaluating Luenberger formulation for tracking error sensitivity

15 p2380 A71-31937

Optical tracking system for high angular acceleration missile flights, using movable mirrors with motion picture camera interfaced with computer

18 p2900 A71-36906

Optical target detection and position error signal system for boost phase missiles, using TV with digital computer controlled dual tracking electronics

18 p2883 A71-36911

Estimation error covariance matrices of linearized Kalman tracker for ballistic reentering missiles, observing strong coupling of range and range rate with ballistic coefficient

23 p3646 A71-44083

MISSILE TRAJECTORIES

Tactical missile flight test planning using digital simulation data reduction techniques for fast cost effective trajectory synthesis

02 p0226 A71-11784

Missiles and aircraft trajectories computation time reduced via time sharing and hybridization

02 p0227 A71-11794

Soviet book on rocket flight dynamics covering center of mass motion characteristics, guided missiles, external ballistics, multistage design and flight optimization

02 p0320 A71-12724

Hybrid computer simulation of three degree of freedom surface to air missile trajectory, obtaining cluster of points for position errors

04 p0642 A71-14798

Interceptor missiles minimum flight time control, describing modified steepest descent algorithm for optimal trajectories

[AIAA PAPER 71-19]

06 p0979 A71-18486

Craters produced by oblique trajectory missile impact, suggesting crater dimension dependence on target material and missile kinetic energy

19 p3156 A71-37683

Convergence improvement in parallel tangent/penalty function solutions for missile trajectory optimization with terminal constraints, comparing with steepest descent method

23 p3659 A71-44102

MISSILE VIBRATION

Missiles free flexural vibrations on moving or stationary launching pad calculated by matrix method

16 p2656 A71-33340

Missile vibrations during acceleration calculated in matrix form for Saturn 5/Apollo booster configuration

20 p3306 A71-39412

Natural frequencies and vibration mode shapes of missile with idealized air friction force tangent to instantaneous neutral axis

21 p3455 A71-41012

MISSILE WINGS

U LOW ASPECT RATIO WINGS

MISSILES

NT AIR TO AIR MISSILES

NT AIR TO SURFACE MISSILES

NT ANTIMISSILE MISSILES

NT ANTITANK MISSILES

NT BALLISTIC MISSILES

NT INTERCONTINENTAL BALLISTIC MISSILES

NT MINUTEMAN ICBM

NT SHILLELAGH MISSILES

NT SHORT RANGE BALLISTIC MISSILES

NT SURFACE TO AIR MISSILES

NT SURFACE TO SURFACE MISSILES

Soviet book on rocket flight dynamics covering center of mass motion characteristics, guided missiles, external ballistics, multistage design and flight optimization

02 p0320 A71-12724

MISSILERY

U MISSILES

MISSION PLANNING

Man role in future navigation from SAC viewpoint, considering relationships to mission and machine

01 p0123 A71-10502

Mission requirements in decision processes for guidance and control system design of aerospace vehicles

[AIAA PAPER 70-1231]

01 p0126 A71-11301

Skyet satellite mission profile, onboard equipment and control system, discussing communications, command/telemetry processing equipment, electrical power sources, and secondary propulsion

02 p0320 A71-12429

High bypass ratio jet engine noise reduction in relation to mission requirements

[ASME PAPER 70-WA/GT-13]

03 p0471 A71-14121

Cooperative international space ventures, discussing mission programs, global needs, successes and deficiencies

04 p0690 A71-14935

Unmanned scientific missions to outer planets in late 1970s, discussing instruments requirements, flight paths, spacecraft designs and payloads

04 p0649 A71-15347

Space station and interplanetary flight research programs, discussing design, grand tour and Jupiter flyby

05 p0817 A71-16642

OAO experiments instrument packages for UV observations from orbit, discussing telescopes pointing accuracy and stability, mission objectives, etc

05 p0755 A71-17129

Mariner mission to Venus and Mercury in 1973, discussing special opportunity characteristics, mission options, real time TV picture transmission, trajectory analysis, etc

05 p0814 A71-17230

Manned space flight missions in next decade, discussing potential payloads and compatibility to proposed mission structure

[AIAA PAPER 71-69]

06 p0977 A71-18527

Jupiter atmospheric probe approach trajectory uncertainties and navigation requirements during 1978 mission

[AIAA PAPER 71-120]

06 p0926 A71-18569

Electric propulsion spacecraft mission performance scaling laws for invariant trajectory, obtaining optimum gross payload over wide range of system input parameters

[AIAA PAPER 71-160]

06 p0981 A71-18602

Grand Tour mission design, discussing navigation, trajectory parameters, launch vehicles and satellite flybys

[AIAA PAPER 71-187]

06 p0978 A71-18626

Alternate reduced order particle dynamics model in aircraft mission analysis featuring instantaneously variable speed by time scale separation

07 p1019 A71-19913

Space based reusable manned/unmanned tug, discussing potential missions, system requirements and auxiliary hydrogen oxygen propulsion system

[AIAA PAPER 70-719]

09 p1511 A71-22902

Mission objectives and orbit parameters of Azur satellite, considering satellite control and data transmission as function of ground support system

10 p1589 A71-23927

SIRIO project mission analysis, discussing space communication and magnetospheric investigations by scientific satellite in geostationary orbit

10 p1670 A71-24268

Mission reliability calculations for systems with redundant units, considering design of airborne warning and control system and other radar control systems

12 p1885 A71-26675

Statistical analysis of equipment selection for multipurpose scientific laboratory onboard space stations under economic and time constraints

13 p2094 A71-28187

Sounding rockets, outlining experimental missions, design and payload varieties, auxiliary systems and electronic equipment

15 p2499 A71-31213

European scientific experiments satellite, describing design features and mission capabilities

15 p2501 A71-32693

Jupiter atmospheric entry probe missions to cloud layers base, discussing tradeoffs between various types of mission trajectories and technologies

[AIAA PAPER 71-834]

17 p2801 A71-34713

Venus planetology missions, discussing objectives, experimental packages, payloads, costs and entry/lander configurations

[AIAA PAPER 71-829]

17 p2802 A71-34717

Computer programs for functional analysis, planning and control of space stations and shuttles operation

18 p2885 A71-36459

Long duration orbital simulator for technical planning activities, discussing capabilities, options, accuracy and central processing unit usage

18 p2885 A71-36460

Consumable usage as function of mission time computed with computer program simulating NASA Skylab mission

18 p2885 A71-36461

Franco-German Symphonic communication satellite, discussing missions and subsystems design features

18 p2974 A71-36522

Jupiter grand tour mission, discussing objectives and technical aspects of unmanned Pioneer F and G vehicle

18 p2965 A71-36684

Jupiter orbiters and probes noting objectives, spacecraft design and mission description

[AAS PAPER 71-103]

19 p3152 A71-37905

Pioneer F and G spacecraft Jupiter flyby post-encounter mission options ranging from solar system escape to high-inclination low-perihelion trajectories

[AAS PAPER 71-136]

19 p3139 A71-37921

Mission analysis for multi-planet flyby and major satellites close encounter to determine solar system planetary evolution data, presenting Grand Tour trajectory parameters

[AAS PAPER 71-137]

19 p3139 A71-37922

Balanced terrestrial and outer planets NASA solar system exploration strategy for 1970s, outlining earth based observations and flight missions program

[AAS PAPER 71-100]

19 p3140 A71-37930

Pioneer F/G spacecraft Jupiter missions, trajectories and objectives with relation to outer system

[AAS PAPER 71-101]

19 p3140 A71-37931

Multipoint gravity assist grand tours in outer solar system, discussing launch opportunities and mission effects on spacecraft design

[AAS PAPER 71-102]

19 p3140 A71-37932

Navigation, orbit and trajectory analysis of 1979 Jupiter-Uranus-Neptune Grand Tour mission, assuming deep space network tracking

[AAS PAPER 71-117]

19 p3101 A71-37936

Launch opportunities for Grand Tour outer planets missions using Saturn-Jupiter instead of Jupiter-Saturn flyby sequence

[AAS PAPER 71-139]

19 p3140 A71-37943

Jovian probe and spacecraft mission feasibility, discussing launch opportunities, targeting, objectives and data transmission

[AAS PAPER 71-141]

19 p3141 A71-37944

Scientific unmanned exploration of near stellar systems, discussing target star selection, extraterrestrial life, propulsion systems and kinematic and energy requirements

[AAS PAPER 71-166]

19 p3141 A71-37963

ATS F and G satellites for half earth surface full time communication coverage, discussing mission objectives

20 p3306 A71-39607

Dust environment estimation in asteroid belt during trans-Martian spacecraft missions, considering cosmological, dynamical and observational evidence

20 p3297 A71-39633

Outer planet explorers design for Grand Tour mission, discussing launch parameters, flight paths, environmental hazards, communications, ground control, navigation and power generation

22 p3601 A71-42028

Radiation effects on components of science instruments used on outer planets Grand Tour mission

22 p3574 A71-42299

Trajectory aiming plane in optimum satellite orbit selection for planetary flyby and orbiter missions

[AAS PAPER 71-305]

23 p3724 A71-42981

Viking Mars 1975 mission analysis software system for trajectory optimization, describing condensed format print and contour plot program

[AAS PAPER 71-311]

23 p3725 A71-42987

Planetary quarantine constraint on 1977 Jupiter-Saturn-Pluto mission, determining fuel loading penalties, optimum biasing strategies and outer planet navigational characteristics

[AAS PAPER 71-319]

23 p3726 A71-42993

Relay data link and trajectory design integration for Viking orbiter 1975 mission

[AAS PAPER 71-320]

23 p3726 A71-42994

Bi-injection earth departure mode analysis for combined flyby/orbiter Jupiter-Saturn-Pluto and Jupiter-Uranus-Neptune Grand Tour missions

[AAS PAPER 71-322]

23 p3726 A71-42996

Branched trajectory optimization algorithm using steepest descent method applied to space shuttle vehicle mission design

[AAS PAPER 71-326]

23 p3726 A71-43000

Orbital spacecraft trajectory and attitude dynamics, using computerized state model for mission planning, orbit determination, satellite geodesy and reentry analysis

[AAS PAPER 71-344]

23 p3727 A71-43017

Grand Tour missions set optimization for 1976 to 1982, defining flight opportunity launch/arrival date space for various mission types

[AAS PAPER 71-358]

23 p3728 A71-43028

Multiple outer planets flyby opportunities during 1976-1980 Grand Tour missions launch period, presenting computer generated specific encounter dates and flyby distances

[AAS PAPER 71-359]

23 p3729 A71-43029

Earth-Jupiter-Saturn-earth trajectories, determining mission planning parameters

[AAS PAPER 71-361]

23 p3729 A71-43031

Impulsive trajectory optimization for asteroid Eros round trip sample return mission using chemical propulsion

[AAS PAPER 71-369]

23 p3730 A71-43039

Graphic mission analysis for outer planet missions, considering spacecraft and celestial bodies relative positions, sensor and spacecraft relative orientation

[AAS PAPER 71-378]

23 p3731 A71-43048

Lunar impact targeting technique improvement for Apollo 14 mission preflight analyses and flight support operations

[AAS PAPER 71-392]

23 p3732 A71-43060

MIST

Pressure wave propagation through annular and mist flow patterns, noting virtual mass effects in interphase momentum transport of rarefaction and compression waves

03 p0405 A71-14418

Post burnout heat transfer to mist flow for nuclear reactor design, using two step model

07 p1221 A71-18789

Pressure wave propagation through one and two component annular and mist flows, showing importance of inertial interphase momentum transfer

19 p3171 A71-38293

MITOCHONDRIA

African lungfish retina electron microscopy for Landolt club location, mitochondria, glycogen and microtubule content, considering relation to receptors and possible functions

01 p0009 A71-10272

Physical exercise effect on mitochondrial energy production in heart muscle and liver in rats

01 p0017 A71-11542

Glutaminase isoenzyme activators in mitochondrial brain fractions of rabbits

03 p0361 A71-13235

Bioenergetics of brain in vertebrates, concerning oxidative metabolism in neurones, glia and mitochondria structure 03 p0362 A71-13240

Cellular damage to rat mitochondria and endoplasmic reticulum by injection of radioprotectors, discussing intracellular enzymes passage into plasma 07 p1039 A71-18981

Radioprotective mercaptoethylamine (MEA) effect on aerobic resynthesis of ATP in thymus nuclei and oxidative phosphorylation in rat liver mitochondria 07 p1039 A71-18984

Mitochondrial oxidation of substrates coupled with phosphorylation studied using organelles isolated from red and white skeletal muscles of rabbit, noting enzyme activity of fatty acids 08 p1238 A71-20682

Diurnal variations of mitotic activity in thyroid epithelial cells of different follicle size 15 p2356 A71-31290

Myocardium ultrastructural and metabolic alterations in altitude acclimated rats, considering heart muscle mitochondria 16 p2529 A71-33193

Low temperature effects on succinate oxidase activity of mitochondrial membranes in hibernating squirrels 21 p3336 A71-40854

Thyroxine effects on brain glutaminase isoenzymes interaction and deamidation in mitochondrial fractions, comparing with sodium phosphate, bicarbonate and aspartate 21 p3338 A71-41069

Gangliosides inhibitory effects on active Ca ion transport in rat brain mitochondria, using succinate as respiratory substrate 21 p3338 A71-41075

Electron microscopic quantitative analysis of myocardium sections from male dogs exposed to general hypoxia, considering mitochondrion sizes, numbers and areas 23 p3634 A71-43912

MITOSIS

Cellular mitosis role in daily mitotic activity in albino rats intestinal crypts and thyroid gland 01 p0012 A71-11058

Human kidney cell generation and life cycle parameters, considering thyroxine effects 07 p1041 A71-19594

Mitotic activity of kidney undergoing compensatory hypertrophy in high mountain nonadapted rats 08 p1242 A71-21965

Mitotic response to various diets in normal and regenerating rat liver 14 p2182 A71-30069

Diurnal variations of mitotic activity in thyroid epithelial cells of different follicle size 15 p2356 A71-31290

Somatic cell mitosis control by simulated changes in electrical transmembrane potential difference 18 p2853 A71-35892

Mitosis control assuming existence of functional relationship between potential level and mitotic activity, using classical membrane potential theory 18 p2853 A71-35893

MITWA

Mitral valve muscular fibers, investigating pathological changes of myocardium of left heart ventricle 02 p0198 A71-11695

MIXED CRYSTALS

Thermal diffusion in tantalum-oxygen and columbium-oxygen mixed crystals, investigating temperature and concentration effects 16 p2599 A71-34092

Heat transfer in interstitial solid solutions, interpreting thermal diffusion measurements in transition metals mixed crystals 16 p2599 A71-34093

Simultaneous degassing and thermal diffusion phenomena in annealed tantalum-oxygen mixed crystals, investigating maximum temperature effect 16 p2599 A71-34094

MnSe-CdSe mixed crystals growth investigation by elements, binary compounds and solid solutions vapor transport properties 21 p3427 A71-40124

Spherical avalanche diodes in silicon and germanium mixed crystals, describing IR detection properties 22 p3543 A71-42125

MIXED FLOW

U MULTIPHASE FLOW

MIXING

NT DISSOLVING

NT HOMOGENIZING

NT LAMINAR MIXING

NT SIGNAL MIXING

NT SUSPENDING [MIXING]

NT TURBULENT MIXING

Solid composite propellant mixing influence on viscosity, pot life and motor reject rates based on bench scale production [AIChE PAPER 32D] 13 p2113 A71-28894

MIXING CIRCUITS

Double balanced cross coupled transistor mixer, predicting conversion gain and inter and cross modulation distortion performances 02 p0233 A71-12345

Earth station mixers design as wideband millimeter wave up- and down-converters for satellite communication systems 02 p0234 A71-12818

Operating mode of semiconductor AFC mixer of radar receiver under large signal 06 p0874 A71-17546

Wideband mixer for Intelsat 3 satellite, describing design, operation and performance 06 p0877 A71-18401

Low noise microstrip microwave mixer-preamplifier on thin polyolefin reinforced with Al, discussing design and manufacture 08 p1263 A71-20771

Wideband X band microstrip image rejection balanced mixer design 08 p1263 A71-20772

Microwave front end designs for low noise operation, discussing FET applications and mixer conversion loss reductions 11 p1731 A71-25673

Single and double balanced diode mixers characteristics comparisons for spurious response suppression, considering RF third order intercept technique 11 p1737 A71-25674

Heterodyne oscillator instability free frequency drift measurement of mixed FM signals in circuits with supplementary conversion 12 p1885 A71-26842

Measuring instrument for solar radio emission at 8 mm, using GaAs Schottky barrier diode mixer for system noise temperature reduction 14 p2239 A71-29916

Microwave frequency mixer using two inverted tunnel diodes in series connection 14 p2211 A71-30116

SHF low noise IC mixer, considering effects of series resistance and barrier capacitance in diode and internal resistance of local oscillator 16 p2548 A71-33558

UHF head for 225-400 MHz AM receiver, emphasizing choice of ring mixer and passband filter switching principle 16 p2548 A71-34124

Millimeter wave klystron single-loop phase locking using final 4th-harmonic mixer in reference chain for submillimeter laser frequency measurement 16 p2589 A71-34126

Dynamic properties of modulating and mixing nonlinear systems consisting of time dependent impedance controlled by pumping source 18 p2875 A71-35975

General purpose pulsed microwave radar receiver, describing balanced mixer and transistorized IF amplifier design and construction 18 p2887 A71-36015

Schottky barrier, point contact and Ge back diodes for microwave mixers and detectors, noting burnout characteristics 18 p2894 A71-36979

Noise temperature in microwave frequency mixers using nonlinear resistors, giving rectifier and diode loss formulas for rectangular and sinusoidal waves 19 p3027 A71-37494

MIXING LENGTH FLOW THEORY

Turbulent diffusion gas jet length in transverse flow and in stationary air medium 01 p0181 A71-11147

DA and DB white dwarf atmospheres convection effect on structure based on mixing length theory and constant flux model 04 p0658 A71-15841

Flow between parallel planes of dissimilar surface texture, obtaining mixing length models velocity profiles, skin friction coefficients and zero shear stress position 07 p1086 A71-18773

Mixing length theory of near ground Ekman boundary layer in stationary and diurnal conditions, determining surface drag and wind rotation 09 p1487 A71-22638

Numerical solution of nonuniform enthalpy mixed axisymmetric gas flow in curvilinear regions with upper boundary and discontinuity using build-up method 10 p1551 A71-24376

Shear stress and eddy viscosity distribution in Mach 20 compressible turbulent boundary layer, using mixing length flow theory 11 p1751 A71-25499

High entrainment constant area multiple nozzle ejectors with two mixing tube lengths for boundary layer control, estimating performance with analytical model [ASME PAPER 71-FE-34] 13 p2053 A71-29469

Shear stress, eddy viscosity and mixing length distributions in compressible turbulent boundary layers with air and carbon dioxide injection 14 p2228 A71-31025

Incompressible turbulent boundary layers at low Reynolds numbers, using eddy viscosity and mixing length concepts for computation 17 p2728 A71-34884

Numerical integration of turbulent boundary layer equations, using mixing length concept 18 p2902 A71-36112

Turbulent forced-convection heat transfer coefficient for supercritical fluid, extending Prandtl mixing length concept [ASME PAPER 71-HT-26] 19 p3165 A71-37996

Coaxial free mixing flow calculations, using turbulent kinetic energy method 21 p3369 A71-40958

Resonant oscillations effect on heat transfer across mixing length in cavities spanned by low speed turbulent shear layers 21 p3371 A71-41033

Incompressible turbulent boundary layer with suction and surface injection computation by implicit finite difference method and turbulent kinetic energy equation for mixing length flow 24 p3820 A71-44954

MIXTURES

NT AEROSOLS

NT AQUEOUS SOLUTIONS

NT BINARY FLUIDS

NT BINARY MIXTURES

NT COLLOIDAL PROPELLANTS

NT COLLOIDS

NT DETONABLE GAS MIXTURES

NT DISPERSIONS

NT EMULSIONS

NT EUTECTIC ALLOYS

NT EUTECTICS

NT FOG

NT GAS MIXTURES

NT LIQUID-GAS MIXTURES

NT METAL MATRIX COMPOSITES

NT NUCLEAR EMULSIONS

NT PHOTOGRAPHIC EMULSIONS

NT SMOKE

NT SOLID SOLUTIONS

NT SOLID SUSPENSIONS

NT SOLUTIONS

MOBILITY

NT ELECTRON MOBILITY

NT HOLE MOBILITY

NT IONIC MOBILITY

Crystal lattice type influence on volume and boundary diffusion mobility of iron group metals atoms 09 p1510 A71-23325

Mobility definition and measurement methods, discussing portable instrument and vibration testing application 14 p2252 A71-30056

Performance characteristics and reuse intervals of high capacity mobile radio systems with dynamic channel assignment, using computer simulations 19 p3014 A71-37216

Edge dislocations mobility in zone refined alpha Ti single crystals in bending, using etch pit techniques at 77, 200 and 300 K 21 p3404 A71-41415

MODAL RESPONSE

Rodents bimodal cochlear microphonic response to high frequencies recorded from round window membrane 01 p0016 A71-11346

Linear elastic structure statistical response characteristics relation to natural environment random pressures, considering flexural vibrations of thin cylinder for modal density 05 p0826 A71-16732

Cylindrical shell panels with free supported curved edges and arbitrary boundary conditions, investigating natural frequencies and mode shapes 07 p1213 A71-19886

Absorption peaks mode numbers and separation using magnetostatic spin waves in axially magnetic YIG rods 07 p1180 A71-20172

Critical velocity of fluid flow in cantilever tube, applying Galerkin method to modal type analysis 11 p1748 A71-25163

Rotating low aspect ratio turbomachinery blades natural frequencies and mode shapes, using finite element method for equilibrium equations eigenvalue problem [AIAA PAPER 71-374] 11 p1845 A71-25347

Real time modal purity and data quality assessment techniques 11 p1853 A71-26501

Modal characteristic pick-up system for vibration tests of rockets or aircraft on ground, using small size accelerometers with individual electronic circuit 12 p1895 A71-27719

Modal control systems with confluent eigenvalues, using system mode controllability matrix 13 p2042 A71-28701

Quandary recognition and referee strategy in digitally controlled modal survey system, noting decision making sources 14 p2208 A71-30314

Normal mode vibrations of system with trajectories of unit mass in Euclidean space, determining modal subspaces by potential function 17 p2776 A71-34295

High frequency modal response of elastic plates to impulsive line load, using Rayleigh-Lamb branch equation 18 p2983 A71-36844

Taste modalities identification by factor analysis technique based on correlation matrix between independent stimuli 21 p3341 A71-40073

Flexible rotating shafts high speed, rigid body and modal balancing machines [ASME PAPER 71-VIBR-73] 21 p3460 A71-40311
MODE [STATISTICS]

Grain size and modal analyses of lunar regoliths sampled by Apollo 11 and 12, discussing particles origin 23 p3744 A71-43654

MODE OF VIBRATION

U VIBRATION MODE

MODE SHAPES

U MODAL RESPONSE

MODE TRANSFORMERS

Uniform periodic waveguide mode coupling, obtaining mode transducer design 02 p0216 A71-12342

Baluns as electromagnetic compatibility control devices for signal and common mode currents, providing basic parameters and equivalent circuits 19 p3030 A71-38433

Thin film optical waveguide TE-TM mode converters, using gyrotropic or anisotropic substrate material 22 p3556 A71-41806

MODELS

NT AIRCRAFT MODELS

NT ASTRONOMICAL MODELS

NT ATMOSPHERIC MODELS

NT BREADBOARD MODELS

NT DIGITAL SIMULATION

NT DYNAMIC MODELS

NT ENVIRONMENT MODELS

NT LIGHTHILL GAS MODEL

NT MATHEMATICAL MODELS

NT NUCLEAR MODELS

NT REFERENCE ATMOSPHERES

NT SCALE MODELS

NT SPACECRAFT MODELS

NT THOMAS-FERMI MODEL

NT WIND TUNNEL MODELS

MODERATION [ENERGY ABSORPTION]

NT THERMALIZATION [ENERGY ABSORPTION]

MODES

NT COUPLED MODES

NT LASER MODES

NT MODES [STANDING WAVES]

NT PROPAGATION MODES

NT UNCOUPLED MODES

NT VIBRATION MODE

MODES [STANDING WAVES]

Helmholtz, half and full mode standing pressure waves for separated flow induced acoustic resonance in open cavities 15 p2391 A71-32106

MODIFIERS

U ADDITIVES

MODULATED CONTINUOUS RADIATION

Magnetoplasma modulated waves nonlinear instability, taking into account relativistic effects 07 p1171 A71-20296

Wideband communications theory applied to continuous /analog/ signals using frequency and amplitude modulation 19 p3015 A71-37254

MODULATION

NT AMPLITUDE MODULATION

NT DELTA MODULATION

NT FEEDBACK FREQUENCY MODULATION

NT FREQUENCY MODULATION

NT FREQUENCY SHIFT KEYING

NT INTERMODULATION

NT IONOSPHERIC CROSS MODULATION

NT LIGHT MODULATION

NT PHASE MODULATION

NT PHASE SHIFT KEYING

NT PULSE AMPLITUDE MODULATION

NT PULSE CODE MODULATION

NT PULSE DURATION MODULATION

NT PULSE FREQUENCY MODULATION

NT PULSE FREQUENCY MODULATION TELEMETRY

NT PULSE MODULATION

NT PULSE POSITION MODULATION

NT PULSE TIME MODULATION

NT TRAVELING WAVE MODULATION

NT ULTRASONIC LIGHT MODULATION

Laser cavity standing wave field electro-optic modulation for uniform population inversion, producing spontaneous single frequency output 05 p0764 A71-17232

Longitudinal electron oscillation suppression by beam density modulation in axially and transversely finite beam-plasma system 06 p0934 A71-17484

Hologram modulation for spatial channel selection by putting together signal hologram and carrier hologram 07 p1108 A71-19259

Low data rate m-ray frequency shift keyed /MFSK/ modulation system design 07 p1061 A71-19534

Modulated molecular beam mass and phase spectroscopy applications in hot oxygen radiative attachment, crossed beam chemical kinetics and neutrals clustering in free jets 11 p1727 A71-25228

Galactic cosmic rays solar modulation and intensity gradient in interplanetary space from satellite observation data 11 p1817 A71-25766

Nonlinear systems response to arbitrary multiple frequency inputs, deriving series expansion for nonlinear modulation products 11 p1793 A71-26424

Correlation function of modulation of radar sounding signals with nonwhite nonstationary Gaussian noise, obtaining target range and velocity maximum likelihood estimates 12 p1882 A71-27616

Book on nonlinear modulation based on optimum estimation theory covering phase synchronization, analog data transmission, digital and analog systems performance, Markov processes, etc 13 p2029 A71-28041

Reference/object wave temporal modulation effect on fringe formation in holographic interferometry 14 p2241 A71-30133

Sensing and communications technologies for short wayside headways, considering applicable equipment for personal rapid transit systems, modulation, coding and data transmission techniques 14 p2195 A71-30337

Book on detection, estimation and modulation theory, Part 3, Gaussian and radar-sonar signals in noise, covering point targets, random process and scatter channels 15 p2371 A71-31841

Electron beam modulation by laser light, considering quantum mechanical theory 17 p2753 A71-35024

High speed BPSK communication components and system aspects with V band propagating medium, considering carrier modulation and transmitted digital data reception with minimum errors 17 p2709 A71-35759

Propagation model type effect on modulation and multiple access techniques choice for regional European communication satellite system 18 p2880 A71-36550

High data rate optical communication system bit error rate determination from models for noncoherent digital baseband and subcarrier modulation formats 21 p3348 A71-40804

Electron beam modulation by laser /Schwarz-Hora effect/, investigating failure factors 21 p3394 A71-41045

Modulation instability of dispersion type NMR stabilizer of resonance conditions, determining critical frequency of self excitation and maximum amplification 22 p3519 A71-41444

Electron beam fluorescence probe with modulation technique for measuring density disturbance near sharp wedge in rarefied hypersonic flow 22 p3529 A71-42052

Mixed base modulation technique performance, considering SNR in transmission problem 22 p3512 A71-42380

Intelsat 1, 2, 3 and 4 satellite network development for world telecommunication coverage, discussing expected future replacement and modulation and multiple access technologies 23 p3643 A71-43250

Differential equation solution for plane self focusing and one dimensional self modulation of waves interacting in nonlinear media 23 p3704 A71-43408

MODULATORS

High speed small aperture electro-optic, acousto-optic and magneto-optic modulators for optical communications, considering capabilities and limitations 02 p0231 A71-12603

Optical PCM communications system with lithium tantalate traveling wave modulator capable of one gigabit/sec transmission and detection rate 02 p0215 A71-12042

Balanced modulators and multipliers, using feedback control for suppressing carrier leak 02 p0236 A71-12425

Linear low noise wideband frequency modulator for Intelsat 4 satellite telephony communication, considering channel capacity 02 p0234 A71-12819

Narrow band FM modems with high carrier frequency stability for satellite communication terminals with small dish antennas 02 p0234 A71-12820

Wideband amplitude modulator for quasi-optical waveguide channels, featuring one dimensional rotating wire grating 03 p0378 A71-13804

Chopper amplifier modulator and demodulator circuits analysis, discussing SNR performance 03 p0387 A71-13821

Input-output flow characteristics of direct and transverse fluidic impact modulators, using static model [ASME PAPER 70-WA/FLCS-2] 03 p0354 A71-14077

FM radio relay system modulation-demodulation equipment for multichannel FDM or TV signal transmission 05 p0728 A71-16146

Wideband interdigital microwave circuits using lithium niobate crystals for electro-optic modulation of light, discussing design and performance tests 05 p0762 A71-16336

Time shared FSK FM modulator using second order digital filter with one variable multiplier 05 p0725 A71-17066

Elongation characteristics of modulation type charged particle traps and analyzers, discussing ions and electrons trapping 09 p1513 A71-22668

Distortion effects in switching diode modulators due to local oscillator interference 09 p1420 A71-23681

Mode locked He-Ne laser pulse compression and expansion by electro-optic internal modulator 10 p1619 A71-23873

SHF lithium tantalum oxide optical modulator for optical detector evaluation, discussing bandwidth and phase modulation characteristics 12 p1903 A71-26790

Minimum voltages and limiting frequencies for oblique cut longitudinal octahedral crystal modulators with large electro-optic coefficients, including lithium niobates and tantalates 15 p2461 A71-32606

PSK modem for multiple access communication system with time distribution, discussing performance tests on INTELSAT 3 17 p2700 A71-34688

Quadrature phase modulator development in time division multiple access system 18 p2880 A71-36546

Rotating waveplate optical frequency shifting in lithium niobate, producing light beam with moderate requirements on modulator adjustment 20 p3204 A71-39097

Microwave waveguide semiconductor modulator with p-n-n diode as control element, taking into account semiconductor control element conductivity change along waveguide wall 20 p3206 A71-39813

Q band relative phase measurement using single sideband suppressed carrier ferrite modulator in serrodyne phase bridge 24 p3803 A71-44649

Phase sensitive magnetic semiconductor pulse width modulator with diode bridge consisting of single saturable-core choke input and transistor circuit output arms 24 p3810 A71-45155

MODULES

NT AIRLOCK MODULES

NT COMMAND MODULES

NT COMMAND SERVICE MODULES

NT ELECTRONIC MODULES

NT LANDING MODULES

NT LUNAR LANDING MODULES

NT LUNAR MODULE

NT MARS EXCURSION MODULE

NT MICROMODULES

NT SERVICE MODULES

NT SPACECRAFT MODULES

Thermionic converter integrated Cs reservoir module power efficiency and service life, considering diode technology 02 p0196 A71-12270

Design optimization of out-of-core cylindrical thermionic converter module with heat pipes and integral finned radiator 11 p1711 A71-25876

Out-of-core heat pipe heated and cooled thermionic converter module mechanical design, fabrication and subcomponent performance evaluation 11 p1715 A71-25912

Space station common module concept, discussing NASA functional program elements accommodating multidisciplinary scientific applications and technology experiment modes [AIAA PAPER 71-813] 17 p2813 A71-34728

Tubular compact air cooled thermoelectric module endurance and performance tests and computer simulation for space reactor power system 20 p3266 A71-38954

Failure analysis of memory organization in self repair memory system, using various coding and modularization techniques on subsystems
21 p3350 A71-40365

MODULI

U RATIOS

MODULUS OF ELASTICITY

High modulus graphite fiber composites, considering production, properties, utilization, availability and price/performance
[SME PAPER EM-70-114] 01 p0109 A71-11251

General solution to three dimensional problem in elasticity theory for cylindrical transverse isotropic medium, applying results to thick walled shells stress-strain
02 p0329 A71-12563

Finite elastic deformation differential operator strong ellipticity conditions, discussing dependence on material elastic moduli
03 p0501 A71-13071

Piecewise linear elastic material three dimensional stress-strain analysis for limiting surfaces between regions with different moduli
03 p0451 A71-13901

Deformation pattern, interstitial impurities and alloying elements effects on temperature dependence of elasticity modulus of Nb and alloys
04 p0613 A71-15641

Novozhilov complex transformation method extended to Timoshenko theory of elastic shells constructed with allowance for transverse shear deformation
05 p0820 A71-16187

Transverse elastic modulus and Poisson coefficient of composite materials as function of reinforcement, structure and fiber radius
05 p0771 A71-16360

Complex modulus of elasticity relation to viscoelastic cantilever beams stress or strain under forced vibration, considering fiber reinforced plastics
05 p0826 A71-16738

Composite hollow cylinders of heteromaterials materials, discussing stress-strain state
06 p0984 A71-17650

Alloy melting technique and heat treatment effects on elastic limit and modulus of elasticity
06 p0912 A71-17947

Dissolved hydrogen effects on mechanical properties, modulus of elasticity, lattice constants and X ray lines of Ti alloys, showing cold brittleness at high strain rates
07 p1130 A71-19298

Single edge notch tension Al alloy specimens mechanical compliance measurement, solving stress functions for various gage length-sample width combinations
07 p1110 A71-19469

Elastic modulus as function of chemical composition and structure of binary alloys Mo-Re and Ni-Re
07 p1141 A71-20248

Test equipment for elasticity modulus measurement of neutron irradiated materials, noting u-c nuclear fuel and alloy samples
07 p1084 A71-20356

Carbon fibers, light metal alloys and composites, studying moduli of elasticity and shear thermal variations
[PLASTICS INST. PAPER 16] 08 p1320 A71-20904

High strength and modulus continuous carbon fibers, discussing preparation and quality control
[PLASTICS INST. PAPER 5] 08 p1297 A71-20925

Amplitude dependence of Young modulus defect in metals during large stress HF oscillations
08 p1369 A71-21121

Nonshallow spherical shells of small shear modulus materials, examining boundary conditions and axisymmetric deformation
09 p1535 A71-22184

Aligned fibers reinforced material hardening rate, taking into account elastic energy and external potential due to internal stress interaction with applied stress
09 p1467 A71-22286

Quasi-static problems in nonlinear viscoelasticity theory, comparing integral operator and variable moduli methods for convergence and accuracy of successive approximations
09 p1537 A71-22513

Prolonged storage effect on polycarbonates mechanical properties, measuring tensile strength, elastic modulus, yield point and breakdown strains under uniaxial tension
09 p1483 A71-22825

Honeycomb sandwich core elastic modulus measurement under transverse compression
09 p1470 A71-22994

Rapidly quenched CuAu ordered state development on low temperature annealing, presenting Young modulus variation as function of heat treatment time
09 p1477 A71-23350

Volume, compliance and flow resistance of pulmonary vascular compartments of dogs
10 p1560 A71-24122

Thornel graphite fibers modulus of elasticity, mechanical properties, applications and price
10 p1635 A71-24773

Short carbon and glass fiber reinforced composites, calculating modulus of elasticity from mathematical model
10 p1635 A71-24806

Carbon fiber-epoxy resin composites Young modulus, thermal and electrical conductivities as function of fiber alignment and porosity
11 p1784 A71-25399

Polycrystalline NbC and TaC Young, shear and bulk moduli determination at high temperature, noting porosity and temperature effects
11 p1781 A71-26294

Hereditary elastic body model with various tensile and compressive strengths, using elasticity theory with differing moduli
12 p1982 A71-27518

Stress concentration in variable-modulus perforated plate of isotropic elastic material under hydrostatic pressure
13 p2151 A71-28142

Bending and torsional oscillations in rectangular specimens of femur and tibia, calculating elastic and shear moduli of compact bone tissues
13 p2019 A71-28658

Tungsten carbide advantages in hard metals structure, including high pressure strength, high elasticity modulus and plastic properties
14 p2255 A71-29517

Unidirectional fiber composites impact resistance, showing matrix modulus, fabrication process, fiber and void volume ratios and microresidual stress effects
14 p2264 A71-29920

Linear plastic deformation of steel under tension, investigating anisotropy in elastic modulus and strength
15 p2503 A71-31478

Polyacrylonitrile and rayon precursor graphite fibers diameter relation to Young modulus and tensile strength
15 p2438 A71-31817

Unidirectionally and cross rolled titanium alloys elastic properties anisotropy during cooling, discussing Young modulus distribution
15 p2428 A71-31857

Stress relaxation method using compliance measurement of bolted test assembly to determine initial and residual loads after exposure periods
15 p2436 A71-32505

Radiation effects on epoxy adhesive mechanical properties including compressive shear stress, modulus of elasticity and tensile strength
15 p2439 A71-32510

Fiber to matrix modulus of elasticity ratio for two dimensional plane stress composite by finite element and moire strain analyses
[SESA PAPER 1826A] 17 p2761 A71-34527

Aluminum powder filled epoxy composites, investigating particle size and filler percent effects on damping properties and elastic modulus
17 p2762 A71-34819

High modulus graphite composites application for structural weight reduction and stiffness requirement without strength loss
17 p2762 A71-35202

Inductive extensometers with spherical tips for materials testing, noting Young modulus and Poisson ratio determination
17 p2744 A71-35239

Stress-strain state of thin walled curvilinear frame-type rods of variable cross section with variable elastic moduli along length and contour
17 p2829 A71-35309

Fiber volume content, fiber-matrix bonding, heat treatment and age hardening effects on transverse modulus and tensile strength of unidirectional Al matrix fibrous composites
18 p2935 A71-36597

Temperature dependent directional differences of modulus of elasticity of Mo sheet, using resonance technique
18 p2936 A71-36711

High temperature tests of short time strength, hardness, moduli of elasticity of W-Mo alloys subject to plastic deformation and annealing
18 p2936 A71-36712

Microscopically homogeneous and isotropic two-phase composite material shear modulus formula derivation
19 p3155 A71-37481

Modulus of elasticity and Poisson ratio of composite material with anisotropic or isotropic fibers arranged in rectangular or square array
21 p3464 A71-40772

Composites and mechanical systems dynamic behavior prediction, calculating Hugoniot with effective modulus
21 p3465 A71-40792

Theoretical estimation of tensile strength, elastic modulus and deformation of cubical diamond specimens under tension and compression
22 p3565 A71-42873

Graphite high modulus fiber material tensile strength, modulus of elasticity and elongation measurement method and equipment
23 p3696 A71-42898

Magnetic field effects on complex Young and shear moduli for nonferromagnetic metals, describing experimental technique and frequency resolution criterion
23 p3689 A71-43206

Solid circular plate with diverse elastic moduli in different directions and hole at center, calculating thermoelastic stresses
23 p3777 A71-43422

Stresses and displacements in elastic half space with variable modulus of elasticity under axisymmetrical shifting load distributed along ring
23 p3778 A71-44045

Carbon fiber reinforced plastics featuring high strength and Young modulus and low density for engineering applications
24 p3840 A71-44363

Slit tube flat-to-circular transition during extension, considering mathematical model for curvature change, modulus of elasticity and Poisson ratio effects
24 p3884 A71-44959

Stress and magnetic field induced spin density wave polarization vectors rotation in Cr single crystals, accounting for Young modulus temperature and magnetic field dependence
24 p3861 A71-45131

Micrononhomogeneous elastic media with moduli as coordinate random function, investigating stress and strain tensors
24 p3849 A71-45345

Shear modulus and stress-strain relations for different plastic strain rates
24 p3886 A71-45362

MOHRE CIRCLES

U FRACTURE MECHANICS

MOIRE EFFECTS

Strain data retrieval from moire or photoelastic patterns by numerical technique based on light intensity distribution phase angle
02 p0225 A71-11703

Strain analysis by moire-rosette method, using fringe patterns from pair of crossed gratings through optical spatial filtering
03 p0423 A71-13549

Nonhomogeneous strain fields analysis by moire fringe multiplication with full field data reduction by mechanical differentiation
03 p0425 A71-13753

Beams and plates deflection optical measurement using moire gap effect generalized to include linear and rotational mismatches
[SESA PAPER 1703] 03 p0507 A71-13754

Plane nonhomogeneous strain fields deformation tensor determination by moire equations for fringe pitch and angle measurement, considering rectangular block bending
03 p0508 A71-13772

Moire contour map enhancement by removal of unwanted noncontour obscuring patterns, considering preferability of continuously moving grid to discrete translation
05 p0749 A71-16267

Elastic and plastic plane deformation photoelastic measurement at room and elevated temperatures by moire patterns, comparing performance with other methods
09 p1536 A71-22328

Shock wave free surface velocity measurement using moire method for photographic recording with image converter streak camera
09 p1444 A71-22715

Thin cracked steel plate strip necking zone relative opening displacement and strain measurements by moire method
09 p1542 A71-23540

Direct optical measurements of strains, using spatially coherent light with moire technique
10 p1611 A71-24280

Holography as quantitative tool for photoelastic measurements, using moire theory of interference phenomena
10 p1611 A71-24473

Strain concentration around holes in composite plate by moire techniques
11 p1851 A71-26389

S-shape lines of axial displacement field and interlaminar shear edge effect in laminated composites verified by moire technique
11 p1852 A71-26390

Cartesian shear and rigid rotation moire patterns by spatial filtering of superposed diffraction gratings
14 p2329 A71-30464

Moire patterns generation by two frequency image plane holographic contouring, discussing multiple source and variable refractive index techniques
15 p2405 A71-31279

Elastic materials Poisson ratio measurement by moire method in coherent and incoherent light
16 p2575 A71-32825

Shearing interferometer based on moire method using Fourier image of grating, considering applica-

- tions to phase gradient and lens aberration measurements
16 p2577 A71-33133
- Orthogonal bicolored moire fringes in mechanical interferometry, considering interpolation type determination of fractional fringe orders
[SESA PAPER 1817A] 17 p2738 A71-34548
- Moire equivalence device for simulating fringe patterns in hologram interferometry, using loci of constant pathlength
20 p3235 A71-39188
- Moire fringe method for direct determination of displacement and strain fields in two and three dimensional surfaces
21 p3377 A71-40230
- MOISTURE**
Ti hot salt stress corrosion, considering effects of oxygen, air velocity, moisture, thermal cycling, fatigue and type of salt
11 p1781 A71-26261
- MOISTURE CONTENT**
NT ATMOSPHERIC MOISTURE
Atmospheric total moisture content from Cosmos 243 satellite, describing onboard equipment calibration
01 p0074 A71-11101
- Human organ thermal properties prediction by measuring water content of equal fat/protein tissues
06 p0851 A71-17603
- Fiberglass-reinforced plastics with and without water content, studying ablation performance
06 p0915 A71-17681
- Atmospheric total moisture content from Cosmos 243 satellite, describing onboard equipment calibration
07 p1102 A71-19650
- Atmospheric moisture field radiometric microwave sounding statistical treatment, noting latitudinal dependence over oceans from Cosmos 243 satellite measurements
09 p1486 A71-22301
- Gas dynamic CW laser with supersonic hot moist carbon dioxide-nitrogen as working fluid, discussing laser gain vs water content
10 p1619 A71-23760
- High moisture content rock samples electrical conductivity and permittivity by VLF electrospectroscopic investigations based on signal phase shift
14 p2238 A71-29514
- Subsurface moisture and frost detection by capacitive measurement of ground permittivity from landed planetary probes and surface vehicles
15 p2411 A71-32473
- Nuclear magnetic resonance spectrometer for moisture content measurement of lunar and terrestrial soils and rocks
15 p2411 A71-32474
- Subsurface water detection on lunar traverse by tilt angle electromagnetic depth sounding
15 p2492 A71-32475
- Ouabain insensitive effects of metabolism on ion and water content of red blood cells
17 p2681 A71-34943
- Two dimensional supersonic moist air expansion around sharp corner, investigating water vapor condensation by homogeneous nucleation
21 p3369 A71-40952
- Latitudinal distribution of integral water drop content of clouds above Pacific, Atlantic and Indian oceans from Cosmos 243 measurements
22 p3568 A71-41653
- Venus water ice clouds existence possibility from high altitude IR spectra and ground based spectroscopic observations
22 p3603 A71-42189
- Convective cloud dissipation after rainfall, calculating temporal behavior of temperature fields, water content, moisture and air motion rate
22 p3569 A71-42847
- MOISTURE DETECTORS**
U MOISTURE METERS
MOISTURE METERS
NT HYGROMETERS
NT PSYCHROMETERS
Latitudinal distribution of integral water content of clouds in droplet form above Pacific, Atlantic and Indian oceans from Cosmos 243 measurements
12 p1924 A71-27098
- Lunar subsurface water detection from satellite in polar orbit around moon by electromagnetic measurement
15 p2492 A71-32476
- MOL (ORBITAL LABORATORIES)**
U MANNED ORBITAL LABORATORIES
MOLDING MATERIALS
Synthetic plastic materials mechanical and electrical properties for electronics industry use, emphasizing injection molded polymers, pressed molding compounds and casting resins
01 p0051 A71-10285
- Sounding rockets motors with integrally molded plastic case and nozzle, discussing cost effectiveness and demonstration tests
[AIAA PAPER 70-1386] 03 p0470 A71-13669
- Carbon fiber/carbon composites produced by moulded carbon technique, discussing mechanical properties and applications in rocket motors
[PLASTICS INST. PAPER 38] 08 p1348 A71-20914
- Polyimide system application to laminates and molding powders fabrication, exemplifying compression method and cold compaction followed by sintering
11 p1787 A71-25426
- Plastics mold design improvements, discussing steel quality, guiding/heating systems, surface finish and chrome plating
11 p1768 A71-25432
- Pyrrone foams molding, considering chemically blown and syntactic foams mechanical properties
14 p2262 A71-29650
- MOLDS**
Sandwich structures fabrication of foam core and solid polymer skin by automated injection molding
05 p0759 A71-16931
- Fluidic element fabrication techniques, discussing concrete and epoxy molds and stainless steel chemical milling
07 p1121 A71-20562
- Hydrogen discharge from Fe-C alloys in absolute suction metal mold, finding discharge decrease with increasing carbon content
18 p2926 A71-36300
- Superalloy investment casting, discussing production processes, shell molding technique, applications, cost control, solidification, ductility improvement and cooling rate
[SME PAPER CM-71-160] 18 p2927 A71-36659
- MOLECULAR ABSORPTION**
Optical /and IR/ communication systems design, considering effects of atmospheric turbulence, molecular absorption and aerosol scattering
02 p0214 A71-12023
- Carbon fiber surface reactivity relationship to various organic compounds using gas-solid chromatography, evaluating molecular absorption enthalpies
02 p0209 A71-12537
- Saturn cloud layer molecular absorption from spectral /photographic and photoelectric/ observations
11 p1827 A71-25730
- Astrophysical and aeronomic UV molecular photoabsorption cross sections, discussing experimental techniques and associated systematic and random errors
14 p2190 A71-29905
- Laser beam atmospheric monochromatic radiation attenuation isolating molecular absorption from total radiant flux attenuation
15 p2451 A71-32757
- Atmospheric molecular absorption spectra in IR region, using 15 meter multiple pass absorption cell
22 p3544 A71-42141
- MOLECULAR BEAMS**
Frequency stability of molecular beam laser with stimulated coherent emission
01 p0093 A71-10681
- Mass and phase spectrometry in modulated molecular beam experiment for neutral particles velocity measurement prior to ionization
01 p0028 A71-11303
- Ionization gate detector signal interpretation as function of reflected molecule velocity distribution, noting shutter speed errors
02 p0286 A71-12128
- Pulsed supersonic nozzle source molecular beam for shock tube target, detecting viscous effects from transient flux observation
04 p0600 A71-15596
- Supersonic molecular beams with cycling-pressure sources, investigating mass flow rate effects on skimmer interference
07 p1164 A71-19900
- Frequency stability of molecular beam laser with stimulated coherent emission
07 p1125 A71-20142
- Crossed beam model of nitrogen ion-molecular oxygen reactions in upper atmosphere as function of collision energy
08 p1251 A71-21784
- Nonresonance vibrational exchange in molecular binary harmonic and one component anharmonic oscillators with beam laser applications
10 p1622 A71-24888
- Modulated molecular beam mass and phase spectroscopy applications in hot oxygen radiative attachment, crossed beam chemical kinetics and neutrals clustering in free jets
11 p1727 A71-25228
- Reacting gases analysis by mass spectroscopy, discussing stable products microprobe and molecular beams effective samplings for free radicals and active atoms
11 p1765 A71-26278
- High energy molecular beams for collision processes investigations, discussing nozzle beam technique and experiment design
11 p1803 A71-26281
- Dissociation and particle velocity in shock heated molecular beams of oxygen or hydrogen and argon mixtures, using mass spectroscopic measurements
11 p1765 A71-26282
- Oscillations in second cavity of ammonia maser containing two resonators successively traversed by molecular beam, studying polarization and radioelectric emission
14 p2254 A71-30440
- High intensity molecular beams properties, measurement and production methods, considering kinetic energy, chemical composition and technology applications
18 p2908 A71-36438
- Molecular beam scattering at solid surfaces, outlining scattered particles angular and velocity distribution measurement
18 p2848 A71-36439
- Translational freezing in free expanding jets of Ar, nitrogen and carbon dioxide from molecular beam intensity measurements, deriving perpendicular temperature
19 p3045 A71-37882
- Emissive molecular beam masers, discussing cavity resonators, spectroscopy, amplifiers characteristics, oscillators behavior and electrostatics
20 p3247 A71-39873
- Thin single crystalline film deposition by molecular beam epitaxy of GaAs, describing surface structure observation with high energy electron diffraction
21 p3427 A71-40217
- Molecular beam extraction from equilibrium gas flows, describing shock beam formation model with associated escape probability
21 p3419 A71-40956
- Nonresonant vibrational exchange in molecular binary harmonic and one component anharmonic oscillators with beam laser applications
21 p3394 A71-41255
- Velocity dependent HD beam scattering by inert gases, measuring total effective cross section in thermal energy range
23 p3707 A71-43879
- MOLECULAR BIOLOGY**
Deleterious mutations and neutral substitutions, discussing molecular evolution model for DNA and proteins
13 p2013 A71-29096
- MOLECULAR BONDS**
U CHEMICAL BONDS
MOLECULAR CHAINS
Carbohydrate-peptide bond and residue chain structure of group blood substances, using alkali decomposition of monosaccharides
01 p0013 A71-11091
- Bond rupture and fracture in semicrystalline polymers, noting agreement with random length molecular tie chain scission model
04 p0670 A71-15388
- Bovine pituitary proteinase I action on oxidized B chain of insulin, noting preference for specific bonds
05 p0718 A71-17105
- Polymer type, temperature, crystallinity and orientation effects on fracture mode, discussing macroload carrying capacity, nylon fiber tie chains and molecular behavior
18 p2939 A71-35889
- Core binding energy difference between bridging and nonbridging oxygen atoms in silicate chain of pyroxenes, using X ray photoelectron spectra
19 p3011 A71-37415
- Internal short chain alkane populations of paraffinic hydrocarbons in tobacco teratoma and habituated tissue cultures
21 p3345 A71-40204
- MOLECULAR COLLISIONS**
Atomic and molecular collisions in gases, considering E and F regions processes, auroras and applications
01 p0129 A71-10133
- Collision induced homonuclear diatomic molecules vibrational excitation using three dimensional model, obtaining transition cross sections and relaxation rates as function of temperature
01 p0129 A71-10367
- Comparative numerical capture and experimental reaction cross sections for ion-molecule ammonia
01 p0028 A71-10476
- Laser action in visible and near IR on atomic fluorine transitions based on collisional dissociation of hydrogen fluoride
04 p0608 A71-15040
- Light emission during ion-molecule collisions, using low energy nitrogen and argon ion beams
04 p0630 A71-15655
- Isotope effects on collision dynamics of molecular hydrogen-argon ion reactions, using chemical accelerator
05 p0784 A71-15974
- Electronically excited molecule mean vibrational energy relaxation, discussing deactivation during collisions
07 p1162 A71-19132

Molecular hydrogen cations collisions with hydrogen and helium, determining dissociation cross section dependence on kinetic energy from threshold to 100 eV

07 p1163 A71-19233

Ion-molecule collision charge transfer and momentum transfer relaxation rates, using ion cyclotron resonance heterodyning method

07 p1054 A71-19371

Vibrationally excited carbon dioxide deactivation by collisions with CO, determining rate constants by laser fluorescence method

08 p1250 A71-20665

Triatomic molecules relaxation process, considering translational-vibrational energy exchange in atomic collisions and transition probabilities for carbon dioxide-helium system

08 p1337 A71-20669

Nitrogen molecule collision with metastable inert gas atoms and ions, investigating energy exchange mechanism

08 p1337 A71-20670

Born-Oppenheimer approximation for elastic and inelastic electron scattering by diatomic molecules

08 p1337 A71-20886

Electron loss and capture by hydrogen atoms, protons and negative ions during collisions between atoms and molecules in gases, interpreting cross section data

08 p1338 A71-21491

Oxygen and nitrogen molecules nonadiabatic electronic-vibrational interaction effect on vibrational relaxation during collisions with O atoms

09 p1497 A71-22530

Vibrational effects on capture cross sections and ion-molecule complexes formation based on ion-dipole collisions, noting multiple reflection probabilities and collision lifetimes

09 p1498 A71-23662

Electron exchange and nuclear symmetry for 2s and 2p collisional excitations of hydrogen by H atom based on symmetrized atomic orbitals set

10 p1644 A71-23925

Collision induced spectral cross relaxation radiative saturation and Lamb dip formation in carbon dioxide molecular lasers, using rate equations

10 p1620 A71-24151

Ammonia-parent ion reaction at low energies, comparing numerical and experimental capture cross sections

10 p1573 A71-24416

High energy molecular beams for collision processes investigations, discussing nozzle beam technique and experiment design

11 p1803 A71-26281

Molecular hydrogen cations collisions with hydrogen and helium, determining dissociation cross section dependence on kinetic energy from threshold to 100 eV

12 p1932 A71-26751

Molecular collisional analysis of normal momentum transfer from flowing rarefied gas to monocrystalline surface

12 p1934 A71-27588

Monograph on carbon dioxide laser gain observations covering spectroscopy, energy levels, radiative transitions, molecular collisions, power efficiency, etc

13 p2078 A71-28494

Collision induced hydrogen spectra for overtone absorptions by gas mixtures under temperature and density conditions matching planetary atmospheres

13 p2138 A71-28773

Neutral gas cloud expansion into vacuum explained by high altitude rocket released metal vapor molecules collisions and release mechanism characteristics

14 p2223 A71-29662

Pressure-induced absorption in planetary atmospheres from hydrogen-methane collisions, stressing resulting thermal opacity

14 p2315 A71-30659

Boltzmann equation approximate solution for molecular velocity distribution function perturbations by inelastic collisions

15 p2386 A71-31158

Motion equations for neutral matter in head atmosphere of bright comet with high density spherical source and molecular collisions

15 p2484 A71-31661

Electron loss and capture by hydrogen atoms, protons and negative ions during collisions between atoms and molecules in gases, interpreting cross section data

16 p2614 A71-33042

Effective cross sections for charged and excited particles formation from He, Ne and Ar ion collisions with CO molecules, using mass spectrometry

16 p2614 A71-33646

Upper atmosphere He, Ne, Na and K atoms collisions with molecular oxygen, determining ejected electron energy during fast Na, K, Rb and Cs ionization for meteor phenomena modeling

16 p2639 A71-33695

High resolution differential cross section measurements for nonspherical potentials and molecular scattering of nitrogen and noble gases at thermal energies

18 p2949 A71-35898

Spectral distribution moments of light scattering due to polarizability changes in colliding molecule pair

18 p2947 A71-36196

Collisional broadening of IR absorption lines in vibration-rotation bands of carbon monoxide and hydrochloric acid

19 p3106 A71-37374

Far IR collision induced spectrum in carbon dioxide, observing temperature and pressure dependence in gas phase and absorption in liquid

19 p3106 A71-38051

Light production by 2.5-490 eV helium ion collisions with nitrogen, considering 1200 and 3200 Å emission

19 p3107 A71-38055

Integrated absorption coefficient of pressure induced pure rotational and vibrational transitions in binary collisions of homonuclear diatomic molecules at high temperatures

19 p3108 A71-38719

Pressure induced hydrogen collisions vibrational spectra absorption coefficients at high temperatures and local thermodynamic equilibrium

19 p3108 A71-38720

Close coupling calculation for low energy hydrogen atom-molecule collision, discussing cross section, transition probabilities and elastic scattering

20 p3272 A71-39579

Mars ionosphere radio wave absorption integral coefficients, studying electron concentration and electron/gas molecular collisions frequency vertical profiles

20 p3297 A71-39629

Fast charged particles inelastic collisions with atoms and molecules, investigating Bethe differential cross section theory

21 p3418 A71-40675

Ion-quadrupole effects in ion-molecule collisions by numerical calculations of capture cross sections and computer-plotter studies of ion trajectories

21 p3419 A71-40906

HD rotational relaxation collision number temperature dependence calculation from excitation probability, comparing with experiment

21 p3419 A71-40911

Slow negative atomic oxygen ion production in collisions of fast protons and hydrogen atoms with oxygen molecules, measuring scattering cross sections

21 p3419 A71-41109

Chaos propagation derivation from Boltzmann equation for dilute gas with intermolecular forces and collisions in pairs

23 p3705 A71-43873

Experimental techniques for differential, total and momentum transfer electron-molecule scattering cross sections at low electron energies, discussing rotational excitation

23 p3707 A71-43899

Radiation quenching and depopulation of excited Hg atoms by collisions with ground state hydrogen molecules, using steady state flowing afterglow method

23 p3712 A71-43996

Effective excitation cross sections of molecular CO ion bands in comet tails due to He ions collisions with CO molecules, considering deviation from adiabatic hypothesis

23 p3708 A71-44314

Rotationally inelastic molecular collisions in atom rigid rotor scattering, considering infinite order approximation of generalized phase shift treatment

24 p3850 A71-44921

MOLECULAR DIFFUSION

Nb strips siliconization by silicon hydride decomposition and silicide or silicon oxidation, noting Si surface enrichment and bulk diffusion processes

02 p0272 A71-12943

Intensified molecular diffusion during turbulent mixing of supersonic slipstreams in cylindrical mixing chamber, using optical Prudnikov method

07 p1089 A71-19733

Oxygen atom deficiency and very low exospheric temperature in Mars and Venus upper atmospheres, considering photochemical processes and molecular diffusion

11 p1826 A71-25723

Toluene and aniline-methylcyclohexane and toluene-aniline nonideal liquid systems, measuring molecular diffusion coefficients as function of concentration by Savart plate birefringent interferometer

24 p3820 A71-45074

MOLECULAR DISSOCIATION

U DISSOCIATION

MOLECULAR ELECTRONICS

NT LARGE SCALE INTEGRATION

NT MEDIUM SCALE INTEGRATION

Papers on quantum electronics, Volume 1, covering carbon dioxide and YAG lasers, quantum counter action and interference holography

18 p2930 A71-36144

MOLECULAR ENERGY LEVELS

NT INTERMOLECULAR FORCES

Initial vibrational energy level distribution of hydrogen fluoride formed in reaction between atomic fluorine and molecular hydrogen, using IR chemiluminescence

03 p0375 A71-13495

Metastable radiative lifetimes of molecular states of nitrogen and CO, using time of flight and high resolution electron gun techniques

09 p1497 A71-22417

Spectroscopy and collisional transfer in methyl chloride by microwave laser double resonance, measuring population changes in various rotation vibration levels

12 p1877 A71-27004

Nitrogen dioxide ground and excited state self consistent fields energy calculations, discussing electron transitions probable assignments in spectrum

12 p1934 A71-27759

Far IR sulfur dioxide laser line prediction from transitions involving irregular Fermi interactions between molecular energy levels

15 p2422 A71-32587

Shock tube production of vibrationally excited molecules for mass spectra studies in hot gases

16 p2613 A71-32894

Conductivity measurement of shock generated nitrogen plasma in transverse magnetic field, considering vibrationally excited molecules role in electron collision frequency

16 p2616 A71-32899

Organic dye laser properties analysis using universal relation between absorption and emission spectra for solvent molecules reorientation after excitation

17 p2752 A71-34388

Vibrational population inversions due to molecular energy exchanges from rapid heating behind normal shock wave in carbon dioxide-nitrogen-helium mixtures

17 p2728 A71-34883

Oxygen molecules lower states diffuse orbitals, using self consistent fields configuration-interaction calculation method

17 p2785 A71-34948

Dynamic rate equation model of single wavelength flash lamp pumped rhodamine dye laser accounting for short molecular triplet state lifetimes

18 p2929 A71-35958

Temperature measurement by electron beam, using rarefied gas probing for determination of molecule distribution at various vibrational and rotational levels [ONERA-TP-960]

18 p2915 A71-36026

Carbon dioxide laser, discussing mixture composition, vibrational energy levels, excitation and relaxation mechanisms, output characteristics, CW and Q switching, mode locking and applications

18 p2930 A71-36147

Inverted populations of molecular vibrational states for lasers, using strongly exothermal explosion-accompanied chemical reactions

22 p3557 A71-41819

MOLECULAR EXCITATION

Collision induced homonuclear diatomic molecules vibrational excitation using three dimensional model, obtaining transition cross sections and relaxation rates as function of temperature

01 p0129 A71-10367

Vacuum UV laser emission from molecular hydrogen in Lyman band using short risetime traveling wave discharge

03 p0434 A71-13478

Single to triplet transitions of water vapor as function of scattering angle in electron impact detection

09 p1498 A71-23381

Collision excited carbon dioxide molecule vibrational relaxation rate constant based on statistical model

13 p2102 A71-27885

Tidal theory comparison with lower thermospheric wind observations, taking into consideration dissipation and excitation effects

16 p2565 A71-33736

Transversely excited carbon dioxide lasers gain measurements for linear and helical electrodes at various gas mixtures and pressures as function of time

17 p2754 A71-35404

Vibrational temperature of nitric oxide in upper atmosphere, computing collisional, radiative and chemiluminescent excitation rates

18 p2910 A71-35840

Excitation and ionization cross sections of atmospheric molecular species by low energy ions in strong auroral and man-made electric fields

19 p3055 A71-38039

Temperature dependent differential quenching rates of vibrationally excited CO fluorescence by ortho and para hydrogen, using Born-Bethe approximation

19 p3107 A71-38052

Vibrationally excited oxygen molecules formation and decomposition in upper atmosphere, calculating day and night equilibrium concentrations

19 p3057 A71-38373

Reversible electron transitions selection rule in diatomic molecules excitation by electron impact, obtaining differential cross sections

21 p3417 A71-40198

Quantum theory of molecular or atomic spontaneous emission while simultaneously undergoing stimulated emissions or absorptions 21 p3421 A71-41401

Fluorescence of iodine molecule excited at 5017 and 5145 Å by ionized Ar laser, observing magnetic depolarization /Hanle effect/ 22 p3555 A71-41623

Molecular oxygen dissociative excitation in vacuum UV by electron impact, discussing resonance triplet atomic emission cross section 23 p3706 A71-42903

Electron impact excited carbon monoxide and dioxide 1260-5000 Å spectral emission, discussing cross sections of Cameron and fourth positive bands 23 p3706 A71-42904

Carbon dioxide spectral emission at 1260-4500 Å from electron impact excitation, discussing cross sections and Mars atmosphere application 23 p3706 A71-42905

R-branch multiline performance of transversely excited pulsed HF chemical laser 23 p3688 A71-44297

Absolute transition probabilities derivation for excitation of atmospheric nitrogen molecules and positive ion systems by electrons impact from optical measurement 24 p3850 A71-44371

Werner band system and Lyman alpha radiation emission from molecular hydrogen excitation by electron impact 24 p3850 A71-44923

MOLECULAR FLOW
NT SLIP FLOW
NT TRANSITION FLOW
 Digital simulation for translational and rotational equilibrium breakdown in gaseous molecules expansions by Monte Carlo method 01 p0130 A71-10936

Normal shock wave in He, comparing measured and predicted molecular velocity distribution functions 09 p1433 A71-22857

Molecular flux distributions and capture by cryopanel in space simulation chamber using homogeneously emitting spherical gas source 09 p1428 A71-23006

Molecular incidence rate and emission over surface of cold wall and spherical test object in cylindrical space simulation chamber 15 p2393 A71-32703

Molecular jet velocity measurement, using periodic spatial variation modulation of radio frequency field 16 p2614 A71-34063

Analytical model for molecular flow of reactive gaseous species through cylindrical reactors with apertures at either end, evaluating surviving flux magnitude 17 p2695 A71-35137

Molecular chaos breakdown under shear flow, calculating thermodynamic fluctuation formula for unlimited Reynolds number increase 21 p3418 A71-40628

Cylindrical space simulation chamber with spherical test subject, deriving molecular incidence rate from integral equations with probability matrix for finite partial surfaces 24 p3816 A71-45138

MOLECULAR GASES
NT DIATOMIC GASES
NT POLAR GASES
NT POLYATOMIC GASES
 Tangential momentum transfer accommodation coefficient for gas flow based on monocrystalline molecular model of gas-solid interface 01 p0071 A71-10949

Atomic and molecular transport coefficients for various species injected into boundary layer on ablating or transpiration cooled surface 01 p0130 A71-10958

Molecular hydrogen thermodynamic properties in ideal state from spectroscopic data, using WKB method 02 p0286 A71-12185

Relaxation method for direct measurement of molecular oxygen quenching rate constants in discharge flow system 02 p0287 A71-12493

Molecular gas vibrational and rotational state equations, discussing relaxation times, sound propagation and transport processes 03 p0462 A71-14557

Shock tube measurements of vibrational energy transfer in molecular carbon dioxide-nitrogen-water system 04 p0629 A71-14693

Molecular hydrogen formation on dust grain surfaces, discussing recombination efficiency as function of surface temperature 05 p0784 A71-16205

Electron-ion recombination in dense molecular gas, presenting semiquantitative method for hydrogen, nitrogen, carbon dioxide and damp gas mixtures 05 p0785 A71-16726

Classical multiatomic gases kinetic theory, considering generalized Boltzmann equations 05 p0785 A71-16779

F region photoionization heating, investigating energy transfer from ionizing photon to neutral gas atoms and molecules 06 p0893 A71-17982

Carbon dioxide laser population inversion using chemical reaction of burning with gas combustion products of vibrationally excited polyatomic molecules 08 p1302 A71-21499

Venusian atmosphere carbon dioxide, water, molecular oxygen and nitrogen contents from Venera 5 and 6 data 09 p1523 A71-23144

Molecular gases dissociation due to pulsed carbon dioxide laser radiation, observing luminescence temporal, spatial and spectral characteristics prior to breakdown 10 p1620 A71-24040

Isotope effects in Lyman and Werner systems of molecular hydrogen, HD and molecular deuterium, calculating band strengths, oscillator strengths and Franck-Condon factors 11 p1803 A71-26072

Heat and mass transfer in monatomic molecular gases and gas mixtures, discussing energy exchange during collision and thermal diffusion effect on thermal conductivity 13 p2159 A71-28186

Neutral gas cloud expansion into vacuum explained by high altitude rocket released metal vapor molecules collisions and release mechanism characteristics 14 p2223 A71-29662

Solid helium and molecular/metallic hydrogen thermodynamic properties and phase diagrams as functions of pressures corresponding to Jupiter and Saturn 15 p2511 A71-31338

Molecular hydrogen thermodynamic properties in ideal state from spectroscopic data, using WKB method 15 p2451 A71-31493

Iodine vapor bleaching under molecular electronic-vibrational transition due to ruby laser intense monochromatic radiation 15 p2421 A71-32409

Molecular hydrogen sorption pumping by cold carbon dioxide cryodeposits, showing absorbed molecules surface diffusion into disordered frost structure 17 p2695 A71-35138

Kinetic models for gas-surface interactions, considering distribution functions of molecules at solid wall 18 p2874 A71-35900

Molecular dynamics data from neutron scattering techniques for gas mixing 18 p2949 A71-36958

Carbon dioxide laser high efficiency driven Q switching, using Stark effect in molecular gases 18 p2933 A71-37015

Interstellar dust clouds physical and chemical constitution, discussing molecular gas chemical composition and abundances 18 p2968 A71-37037

Radiation gas dynamics covering monatomic and molecular gases, chemical dissociation and vibrational relaxation 19 p3043 A71-37459

Spectroscopic analysis of continuous light emission from molecular oxygen-nitrogen mixtures in Mach 9 shock waves, stressing radiative reaction role 19 p3106 A71-37462

Translational freezing in free expanding jets of Ar, nitrogen and carbon dioxide from molecular beam intensity measurements, deriving perpendicular temperature 19 p3045 A71-37882

Thermal conductivity anomalous behavior prediction for carbon dioxide, argon, nitrogen, oxygen and methane in critical region 19 p3165 A71-37998

Vacuum UV emission features dissociative excitation by electron impact on molecular hydrogen and oxygen, measuring excitation cross sections from threshold to 350 eV 19 p3107 A71-38344

Time-of-flight measurements for relationship between velocity, mass and temperature in molecular gas motion and electron-atom collision kinematics 20 p3271 A71-38789

K-LL Auger spectra of nitrogen, oxygen, carbon monoxide, nitrogen oxide, water and carbon dioxide, using double focusing electrostatic electron spectrometer 21 p3345 A71-40235

Electronic transitions in oxygen molecule due to ion impact from kinetic energy loss spectrum 21 p3418 A71-40886

Helium, neon, nitrogen, oxygen, argon, carbon dioxide and monoxide and methane thermodynamic and transport properties calculation using computer program for state equations 21 p3351 A71-40893

Dynamic problems for molecular gases with rotational degrees of freedom, deriving hydrodynamic equations from kinetic equations integration 21 p3420 A71-41121

Molecular gas mixtures inelastic collision integral spectra, describing internal degrees of freedom with correlation functions 21 p3420 A71-41271

Gas molecular interactions, energy and momentum transfer and scattering from clean metal surfaces 22 p3577 A71-41996

Kinetic equations derivation for rarefied chemically reacting monatomic or stable molecular gases 23 p3707 A71-43924

Molecular gas dissociation in constricted DC glow discharge plasma sac /sheath boundary/, discussing characteristics and potential uses 23 p3712 A71-43931

Knudsen effusion problem in thermal molecular gas jet mixing, using moment method based on velocity distribution function 24 p3817 A71-44354

Molecular hydrogen primary ionization coefficient measurement in non-self sustained Townsend discharge, using light detection method based on radiant flux vs electron density proportionality 24 p3850 A71-44370

Atomic and molecular gases electron impact ionization, measuring secondary particle energy distribution and angular dependence 24 p3850 A71-44925

Thermomolecular pressure gradients and temperatures in flow between parallel plates for statistical gas models at arbitrary Knudsen numbers 24 p3891 A71-45242

MOLECULAR INTERACTIONS
NT MOLECULAR COLLISIONS
 Hydrogen molecule-atom short range interaction energy, calculating multicenter integrals for screening constants 02 p0286 A71-11954

Maxwellian distribution function calculation for molecules during initial phase of chemical reaction by successive approximations and Chapman-Enskog method 03 p0376 A71-14065

Complex hydrocarbon molecular formation by physical adsorption on interstellar grains in dense clouds 04 p0650 A71-15396

Molecular mechanisms of bacterial cell radiation-sensitization and protection, discussing radiation produced free radicals interactions 07 p1031 A71-18927

Oxygen ion-molecule reactions at thermal energies, using drift tube mass spectrometer 07 p1164 A71-19689

Laser applications in chemical research, exploring fast chemical processes, isotope enrichment and molecular reactions and structure observations 07 p1124 A71-19790

Beam laser operational efficiency relation to molecule /atom/ interaction in focusing system, explaining lasing power drop at large flow rates 07 p1126 A71-20186

Kinetic energy dependent charge transfer rates for ion-molecule reactions in ammonia, using cyclotron ejection and impulse methods 08 p1249 A71-20657

Gas phase ion-molecule phosphine reactions in pure and binary mixtures by ion cyclotron resonance spectroscopy, considering acidity and basicity 08 p1251 A71-21699

Partial wave method for nonspherical quantum scatterer, applying to electron elastic scattering by molecules 09 p1496 A71-22237

Half widths calculation for carbon dioxide broadened water vapor absorption lines in nu sub 2 fundamental, considering dipole-quadrupole interactions 10 p1645 A71-24966

Modulated molecular beam mass and phase spectroscopy applications in hot oxygen radiative attachment, crossed beam chemical kinetics and neutrals clustering in free jets 11 p1727 A71-25228

Rate constant temperature dependence for ozone reaction with oxygen, considering airglow features due to singlet molecular oxygen 11 p1801 A71-25370

Self consistent field /SCF/ calculations of dipyrindine glyoxal and bianthrone photoproduct molecules with triplet ground state, using unrestricted Hartree-Fock theory 11 p1727 A71-25576

Compton electrons produced ring current effects on geomagnetic fields for gamma quantum source and air molecular interactions, considering exact analytical model 11 p1817 A71-25777

Photochemical ion-molecule reactions in ionosphere by air exhaust device and RF mass spectrometer observation in geophysical rocket experiment 13 p2068 A71-28535

- Thermal unimolecular processes falloff data calculation based on Rice-Ramsperger-Kassel or Rice-Ramsperger-Kassel-Marcus theories 13 p2025 A71-29037
- Chemical reactions in electrical discharges, discussing H, O, N, halogens and free radicals, hydrides, halides and fluorinated compound synthesis and ion-molecule reactions 16 p2540 A71-32966
- Flow simulation with digital computer by Monte Carlo computation methods based on interacting molecular gas kinetics, noting application to gas flow 18 p2941 A71-36427
- Molecular dynamics data from neutron scattering techniques for gas mixing 18 p2949 A71-36958
- Turbomolecular vacuum pump impeller theoretical efficiency with allowance for diffuse law of interaction between gas molecules and interblade channel walls 20 p3183 A71-39170
- Partial wave method for nonspherical quantum scatterer, applying to electron elastic scattering by molecules 21 p3420 A71-41119
- Macromolecular binding agent effect on electrophotographic properties of high resistance layers containing photoconductive CdS 22 p3586 A71-42405
- Statistical phase space cross sections for helium ion-nitrogen molecule reactions, including dispersion and short range forces in intramolecular potential energy function 23 p3706 A71-43119
- He, HD and deuterium scattering by various gas molecules, measuring total effective cross sections for comparison with calculation 23 p3707 A71-43880
- Filler quantity and type effects on mechanical energy losses in polymers, discussing molecular interaction and chemical bond influences 23 p3697 A71-44205
- MOLECULAR IONS**
- Nighttime F region molecular ion concentrations of oxygen and nobelium and associated nightglow morphology, using numerical method for solving nonlinear equations 01 p0078 A71-11611
- Effective cross sections for molecular hydrogen positive ion formation in collision between He, Ne and Ar ions or atoms 02 p0287 A71-12503
- Valeraldehyde o-nitrophenylhydrazone mass spectrum with low intensity peak due to combined hydroxyl and water loss from molecular ion 02 p0209 A71-12573
- Imaging gas-metal surface interaction in evaporation field by ion microscopy, discussing molecular ion identification and dipole attraction due to electronic rearrangement 02 p0209 A71-12735
- Singlet-D atomic O yield per oxygen ion dissociative recombination from night airglow observations 03 p0408 A71-13382
- F I layer development at summer midday midlatitude, noting role of molecular ions composition 05 p0745 A71-17200
- Molecular N ion production, studying cross sections, collisions kinetic energies and isotopic substitution 06 p0929 A71-17407
- Indeterminacy interval reduction for ionospheric reaction rate constants by imposing supplementary condition on NO/oxygen molecular ion concentrations ratio 06 p0894 A71-18259
- Nitrogen dioxide and molecular oxygen ions densities in lower ionosphere as function of solar corpuscular radiation 06 p0895 A71-18275
- Ion cyclotron resonance application to propanol ion structure formed in double McLafferty rearrangement, demonstrating direct enol ion formation instead of by isomerization or ketonization 07 p1055 A71-19598
- Boron and carbon hydrides and carbon deuteride molecular ions radiative lifetime measurements, computing absolute oscillator strengths 08 p1250 A71-20671
- Dissociative electron attachment excess energy correlation with fragment ion translational energies, determining radical affinity 08 p1338 A71-21782
- Positive diatomic nitrogen ions dissociation during collisions with inert gas atoms, measuring mass and energy distributions from focusing parabolic spectrograph 11 p1801 A71-25227
- Nitric oxide ion two body recombination with nitrogen dioxide and trioxide molecular ions, examining ionic neutralization reactions in decaying dilute thermal plasma at 300 degrees K 11 p1801 A71-25297

- Molecular nitrogen ion potential energy curves based on valence bond method, calculating sextet and quartet states at intermediate internuclear separation distances 11 p1801 A71-25365
- Radiation from long lived ionic excited states, studying emission spectra, electron impact cross sections and positive nitric oxide ions band system 11 p1727 A71-25368
- F I layer development at summer midday midlatitude, analyzing molecular ions composition effect 13 p2059 A71-28255
- HBr positive ion formation by Ar ion beam collision with HBr, using predissociation to establish dissociation limit 13 p2026 A71-29039
- Interstellar formyl radical and carbon 13 formyl ion search in galactic radio sources 13 p2142 A71-29103
- Triatomic hydrogen positive ion surface crossing effects in chemical reactions based on potential energy surfaces calculation using diatomic-in-molecules approach 14 p2191 A71-30573
- Positive NO ion formation with excess internal energy in positive atomic oxygen ion-nitrogen collisions 16 p2538 A71-32810
- Lower thermosphere and ionosphere upper limits of positively ionized water molecules number density, considering desorption and recombination processes 16 p2571 A71-33842
- SiH molecular ion identification in solar atmosphere by solar absorption spectra 20 p3294 A71-39547
- Associative ionization and dissociative recombination cross sections of hydrogen molecular ions as function of vibrational coupling restricted to Rydberg states 20 p3272 A71-39577
- Radial distribution of electric potential in Penning discharge based on relation between sulfur hexafluoride negative ions transit time and initial energy 21 p3425 A71-41281
- Search for CH molecular ion lines in solar photospheric spectrum, discussing profiles and equivalent widths 24 p3873 A71-45144
- MOLECULAR ORBITALS**
- Chemisorption energies of organics on Pb surface by extended Hückel molecular orbital technique 07 p1055 A71-19845
- Carbon dioxide electron impact energy loss spectrum and molecular orbit calculations, discussing fourth positive bands production in Mars upper atmosphere UV daylight 15 p2398 A71-31766
- Oxygen molecules lower states diffuse orbitals, using self consistent fields configuration-interaction calculation method 17 p2785 A71-34948
- MOLECULAR OSCILLATIONS**
- Molecular gas vibrational and rotational state equations, discussing relaxation times, sound propagation and transport processes 03 p0462 A71-14557
- Oxygen molecule vibrational excitation by electron impact, measuring elastic and inelastic processes 04 p0630 A71-15653
- Shock wave propagation through converging nozzle, predicting real gas dissociation and vibrational excitation effects for comparison with shock tube measurement 05 p0735 A71-16528
- Lasers operating on rotation vibration of chemically formed carbon monoxide, discussing excitation methods 06 p0908 A71-18312
- Ar-oxygen mixture in undiluted nitrogen, discussing relaxation time change during adiabatic excitation and molecule oscillations deactivation 07 p1163 A71-19276
- Vibrationally excited carbon dioxide deactivation by collisions with CO, determining rate constants by laser fluorescence method 08 p1250 A71-20665
- Solar diatomic molecules vibrational degree of freedom model, applying Boltzmann distribution 08 p1365 A71-21773
- Ar-oxygen mixture in undiluted nitrogen, discussing relaxation time change during adiabatic excitation and molecule oscillations deactivation 14 p2276 A71-30170
- Nitrogen-carbon dioxide system molecular resonant energy exchange vibration-vibration probability measurement by shock tube and IR emission monitoring, noting temperature effects 14 p2276 A71-30399
- Similar solution of strong shock wave propagation with nonequal heat coefficients, approximating dissociation, ionization and excitation energy of molecules vibrational degrees of freedom 14 p2228 A71-30996

- Iodine vapor bleaching under molecular electronic-vibrational transition due to ruby laser intense monochromatic radiation 15 p2421 A71-32409
- Carbon monoxide gas dynamic laser oscillation generation, observing maximum power and vibrational exchange among single diatomic species states 15 p2422 A71-32583
- Complex molecules forced vibrations as material points system with quasi-elastic valence bonds 15 p2452 A71-32624
- Solar diatomic molecules vibrational degree of freedom model, applying Boltzmann distribution 15 p2495 A71-32678
- Vibrational nonequilibrium Prandtl-Meyer expansion flows, discussing vibration energy associated with change of state and hypersonic nozzle flow calculation 18 p2909 A71-36440
- MOLECULAR OSCILLATORS**
- Nonresonance vibrational exchange in molecular binary harmonic and one component anharmonic oscillators with beam laser applications 10 p1622 A71-24888
- Nonresonant vibrational exchange in molecular binary harmonic and one component anharmonic oscillators with beam laser applications 21 p3394 A71-41255
- MOLECULAR PHYSICS**
- Industrial and biological polymer compounds active surface layers, discussing thermodynamic aspects, molecular dynamics, energy conversion and boundary layer entropy 06 p0915 A71-17585
- Hydrogen recombination and molecule formation by nonactivated chemisorption on iron grains surfaces 10 p1573 A71-25006
- Quantitative analysis of secondary harmonic generation in DC polarized isotropic laser beam, emphasizing molecular mechanisms and symmetrical effects 11 p1773 A71-25566
- Computerized least squares fit of second virial coefficients vs critical temperature to Lennard-Jones potential function for hydrocarbons, halides, alcohols and cyclic compounds 13 p2103 A71-29005
- German textbook on fundamentals of thermodynamics covering energy conversion, reversible/irreversible processes, chemical/molecular thermodynamics, statistical analysis, probability theory, etc 15 p2516 A71-32767
- Shock tube spectroscopy as tool for atomic and molecular research, describing applications in chemical physics, astrophysics, gas dynamics, etc 16 p2578 A71-33152
- MOLECULAR PUMPS**
- Rotating blade/rotors and stationary/stators rows in axial flow molecular pump, deriving overall and individual transmission probabilities 09 p1455 A71-23058
- Vacuum covered gage measurements in sorption and cryogenic systems with activated pumping surfaces, concerning molecular gas flux leaving specimen 21 p3417 A71-41298
- MOLECULAR RELAXATION**
- Transport analysis of collision dominated relaxation plasma in ignited mode thermionic converter 02 p0291 A71-12237
- Nitric oxide vibrational relaxation times in Ar from IR emission measurements at high temperature 02 p0287 A71-12495
- Carbon dioxide vibrational relaxation in Ar at high temperature, using shock tube method 02 p0287 A71-12496
- Vibrational relaxation behind incident shock waves in pure nitrogen, using end wall pressure measurements 03 p0375 A71-13496
- Anharmonic oscillator diatomic molecule system, examining vibrational relaxation in expanding gas flow 03 p0460 A71-13499
- Nonequilibrium effects of vibrational relaxation on diatomic gas flow behind blast waves 03 p0342 A71-13785
- Multielectrode MHD channels, investigating relaxation effects on two dimensional current distribution and plasma properties 03 p0466 A71-14319
- Time measurements of vibration relaxation in diatomic gases excited by shock waves 04 p0568 A71-14795
- Gas dynamic coupling effect on vibrational deexcitation of carbon monoxide at 1400 to 2200 K range in shock tube 05 p0835 A71-16523
- Initial ionization, relaxation kinetics and nonequilibrium radiation behind strong shock waves in monatomic gases and air 05 p0835 A71-16524
- Sound wave damping by chemical relaxation, showing dependence on dimensionless reaction heat, equilibrium constant and Damkoehler number 05 p0717 A71-16533

German monograph on high energy propellant-oxidizer systems changes of state under high temperature conditions with chemical relaxation taken into account

05 p0795 A71-17106

Relaxation time for nitrogen molecule vibration temperature in ionosphere due to thermal electron collisions

06 p0895 A71-18274

Chemical energy conversion in lasers, discussing vibrational inversions in diatomic and multiatomic molecules and chain reactions

07 p1121 A71-19098

Electronically excited molecule mean vibrational energy relaxation, discussing deactivation during collisions

07 p1162 A71-19132

Vibrational and rotational relaxation in sulfur dioxide, measuring relaxation time as function of temperature by ultrasonic absorption

07 p1054 A71-19370

Carbon dioxide laser molecular upper level vibrational relaxation time measurement

07 p1128 A71-20527

Rotating nonvibrating diatomic low density gas molecules rotational relaxation time and viscosity, based on quantum mechanics

08 p1336 A71-20659

Triatomic molecules relaxation process, considering translational-vibrational energy exchange in atomic collisions and transition probabilities for carbon dioxide-helium system

08 p1337 A71-20669

Carbon monoxide gas phase vibrational relaxation by Fe atoms, using shock tube for determination of decomposition rate of iron carbonyl in dilute mixture with Ar

08 p1337 A71-20672

Spectral and relaxation characteristics in antiStokes two photon luminescence of polycrystalline ruby exposed to filtered light pulses

09 p1508 A71-22392

Oxygen and nitrogen molecules nonadiabatic electronic-vibrational interaction effect on vibrational relaxation during collisions with O atoms

09 p1497 A71-22530

Vibrational relaxation of CO and hydrogen atom effects in nonequilibrium nozzle flow using shock tunnel IR detection system

09 p1404 A71-23379

Gas relaxation process equations of motion based on reversibility of time, considering application to particle systems with magnetic field moments

12 p1932 A71-27206

Collision excited carbon dioxide molecule vibrational relaxation rate constant based on statistical model

13 p2102 A71-27885

Absorption gas dynamic laser operation based on polyatomic molecules vibrational relaxation process

13 p2081 A71-29347

Convectively cooled carbon dioxide-nitrogen-helium electric discharge laser theory based on excitation and relaxation processes, comparing with experiment [AIAA PAPER 71-588]

15 p2419 A71-31574

Hydrogen fluoride vibrational excitation behind incident shock waves at 1400-4100 K, describing experimental procedure and results

15 p2463 A71-31626

Exponential approximation of rotational relaxation of polar HCl and DCl at 300 and 500 K by molecular dynamics, comparing with perturbation calculations

15 p2451 A71-31673

Oxygen molecular excitation behind incident shock waves in pure oxygen and oxygen-argon and oxygen-neon mixtures, examining Schumann-Runge band system

15 p2451 A71-31674

Vibrational relaxation of CO by Fe atoms in Ar shock tube following iron pentacarbonyl decomposition

16 p2539 A71-32897

Nonequilibrium nozzle flow determination for vibrationally relaxing gas, describing sudden freeze approximation method validity

16 p2556 A71-32907

Nonequilibrium and equilibrium plasmas thermodynamic properties and molecular, atomic and ionic internal partition functions and relaxation times

16 p2617 A71-32955

Low temperature plasma reactions, discussing electron impact and collisions, ion formation, molecular excitation and thermal dissociation, vibrational relaxation, recombination, etc

16 p2539 A71-32964

Polyatomic gases thermal conductivity and rotational relaxation number from thermomolecular pressure differences across capillary tubes

17 p2785 A71-34946

Anharmonic effects in time dependent vibrational relaxation of diatomic molecules in rapidly expanding flows, considering N-CO-Ar mixtures

18 p2948 A71-35837

Carbon dioxide laser, discussing mixture composition, vibrational energy levels, excitation and relaxation mechanisms, output characteristics, CW and Q switching, mode locking and applications

18 p2930 A71-36147

Gas flows with thermodynamic relaxation, considering expanding flows in hypersonic wind tunnel nozzles

19 p3162 A71-37458

Organic dyes pulse emission spectra shifts during pumping by ruby and neodymium-glass lasers, discussing vibrational relaxations role in mechanism

19 p3072 A71-37766

Vibrational relaxation behind incident shock waves in CO based on shock tube pressure measurements at 2400-6000 K

19 p3106 A71-37880

Relaxation equations for dilute diatomic gas dissociation-recombination reactions, transforming kinetic equations to normal modes

19 p3107 A71-38079

Water vapor effect on vibrational relaxation of CO in shock tubes, measuring IR emissions

19 p3012 A71-38084

Gas relaxation process equations of motion based on reversibility of time, considering application to particle systems with magnetic field moments

19 p3108 A71-38618

Ultrasound absorption in liver tissue due to macromolecular relaxation processes

20 p3191 A71-39770

CO relaxation measurement in unsteady expansion wave, removing metal carbonyls by passing gas through liquid oxygen cooled trap

21 p3418 A71-40237

Self induced transparency in ruby attenuator, detailing phase relaxation effects at various temperatures

21 p3427 A71-40546

HD rotational relaxation collision number temperature dependence calculation from excitation probability, comparing with experiment

21 p3419 A71-40911

Semiconductor surface layer noise generation physical model with allowance for relaxation effects due to traps in space charge region

21 p3432 A71-41301

Semiconductor surface relaxation behavior with allowance for inhomogeneity and charge exchange between slow states and space charge

21 p3434 A71-41322

Gas laser power gain time dependence on molecular rotational relaxation under light pulse excitation

23 p3684 A71-43415

Hydrogen fluoride vibrational relaxation times behind incident shock waves at various temperatures

24 p3802 A71-44922

Oxygen dissociation in He, Ar, Kr and Xe gas mixtures behind incident shock waves, calculating density gradients and vibrational relaxation time

24 p3802 A71-44924

MOLECULAR ROTATION

Digital simulation for translational and rotational equilibrium breakdown in gaseous molecules expansions by Monte Carlo method

01 p0130 A71-10936

Rotational temperature and density measurements in rarefied flow over sharp leading edge flat plate, obtaining shock layer static pressure

01 p0082 A71-10955

IR microwave double resonance of ammonia during IR vibration-rotation transitions induced by pumping of nitrous oxide laser

03 p0440 A71-14198

Molecular gas vibrational and rotational state equations, discussing relaxation times, sound propagation and transport processes

03 p0462 A71-14557

Tetrahedral molecules quantum mechanical rotational partition function, nuclear spin statistical weight factors and error bounds

04 p0629 A71-14807

Lasers operating on rotation vibration of chemically formed carbon monoxide, discussing excitation methods

06 p0908 A71-18312

Vibrational and rotational relaxation in sulfur dioxide, measuring relaxation time as function of temperature by ultrasonic absorption

07 p1054 A71-19370

Diatomic molecules nonsigma states rotational excitation adiabatic theory

07 p1164 A71-19691

Sunspot molecular lines and rotational temperatures of MgH, CaH and TiO using model umbral atmospheres and photographic spectrograms

10 p1666 A71-23784

Kinetic equation for gases with rotational degrees of freedom under equality of probabilities of direct and inverse transitions and stereoisomerism of molecules

15 p2387 A71-31192

Exponential approximation of rotational relaxation of polar HCl and DCl at 300 and 500 K by molecular dynamics, comparing with perturbation calculations

15 p2451 A71-31673

Molecular rotational excitation during CO ion-Ar interactions by ion beam collision spectroscopy, observing energy loss spectra

15 p2452 A71-32551

CW gain measurements on rotation-vibration P branch transitions of CO molecular laser, calculating gas temperature, Einstein coefficient and population densities

15 p2423 A71-32609

Peak contour positions of rotation lines of hydrogen chloride as function of spectral slitwidth for wavenumber calibration of far IR spectrometers

16 p2577 A71-33134

Population inversion damping on vibrational-rotational transitions of carbon dioxide molecule during interaction with monochromatic radiation pulse, using two level model

17 p2752 A71-34387

Cylindrical nonuniform plasma with radial temperature and emitter density gradients, analyzing molecular rotational levels intensity distribution and Doppler widths

17 p2787 A71-34587

Deuterium fluoride overtone vibration-rotation chemical laser emission, studying frequency doubling and rate constant ratios

17 p2753 A71-34801

Atmospheric noise temperature variation with frequency in 2.53 mm molecular oxygen rotation line, considering Zeeman effect

19 p3048 A71-37402

Nitrous oxide internal and rotational partition functions for temperature range 200 to 350 K, using molecular constants tabulated by Pliva

19 p3106 A71-37408

Dayglow neutral and ionized diatomic nitrogen band system emission excitation mechanism from vibrational and rotational intensity distributions observations

20 p3226 A71-39829

Dynamic problems for molecular gases with rotational degrees of freedom, deriving hydrodynamic equations from kinetic equations integration

21 p3420 A71-41121

Transport properties of low density gas of rotating diatomic molecules, deriving quantum mechanical expression for relaxation time via restricted distorted wave approximation method

23 p3706 A71-42908

Gas laser power gain time dependence on molecular rotational relaxation under light pulse excitation

23 p3684 A71-43415

Translational and rotational temperature and density variations through shock waves in oxygen and nitrogen, using Monte Carlo scheme

23 p3781 A71-43444

Sgr B2 region interstellar gas microwave emission spectrum, observing inversion transitions in metastable rotational levels of ammonia

24 p3872 A71-44916

High dispersion spectroscopic observations of Venus, finding carbon dioxide band rotational temperature

24 p3873 A71-45079

MOLECULAR SIEVES

U ABSORBENTS

MOLECULAR SPECTRA

NT ELECTRONIC SPECTRA

NT RAMAN SPECTRA

NT VIBRATIONAL SPECTRA

Interstellar medium polyatomic molecules formation, destruction and excitation processes by astronomical spectroscopy and interferometry

02 p0209 A71-11867

Multiatomic molecules emission spectra excitation by superhigh frequency short duration pulsed gas discharges

02 p0286 A71-11889

German monograph on molecules in sunspots, discussing molecular absorption lines in umbral spectra recorded in 1969

04 p0643 A71-14974

Venus high resolution spectra interpretation for sub II band of carbon dioxide isotope

04 p0659 A71-15859

Continuous nitrogen and oxygen ion spectra due to photoionization and free ion transfers at high temperatures

05 p0838 A71-16788

Vacuum UV monochromators calibration by molecular branching ratio technique based on electron transition probabilities

05 p0717 A71-16907

Umbral rotational temperatures determined from equivalent widths of molecular lines

06 p0967 A71-17906

Carbon dioxide arc discharge plasma emission spectral absolute intensities under atmospheric pressure, determining molecular band contributions

07 p1162 A71-19131

Spectrographic measurements of Jovian Red Spot and Southern Tropical Zone molecular absorption bands related to cloud cover density and depth

09 p1520 A71-22839

CH molecule line formation mechanism for 4300 Å transition in solar photosphere, studying collisions with hydrogen atoms

09 p1520 A71-22843

Sunspots umbrae spectrum analysis in 4000-8000 Å region, identifying molecular absorption lines photoelectrically

10 p1666 A71-23785

Twilight airglow measurements of hydroxyl and molecular oxygen bands by balloon-borne instruments including IR grating spectrometer and filter photometers

10 p1601 A71-24400

Organic compounds astrochemistry, discussing hydroxyl absorption lines and molecular abundances in interstellar space

10 p1678 A71-24810

CO absorption spectrum in carbon dioxide atmosphere, comparing self- and nitrogen-broadened half widths

10 p1645 A71-24968

Uranus atmospheric molecular hydrogen abundance from pressure induced overtone spectra, using quadrupole moment and polarizability matrix elements theoretical values

11 p1827 A71-25731

Spectral studies on radiation from molecules, atoms and electrons, demonstrating shock tube applications in opacity measurements

11 p1764 A71-26265

Nitrogen molecular excitation by photoelectron impacts in dayglow, investigating 1 PG band emission intensity variation with solar activity

14 p2235 A71-30349

Monochromatic photometry of comets for molecular emission bands in head spectra, using wideband and narrowband filters

15 p2484 A71-31665

Continuous nitrogen and oxygen ion spectra due to photoionization and free ion transfers at high temperatures, calculating absorption coefficient

16 p2662 A71-33040

Molecular spectral coincidences of carbon monoxide and carbon dioxide IR lasers for atmospheric pollutant detection by sensing of resonant absorption, thermal emission or fluorescence

16 p2585 A71-33129

Interstellar molecular hydrogen gas near IR emission detection in dark clouds

18 p2969 A71-37042

CN radical red system molecular constants, considering degenerate perturbation effects in shifts between electronic states

19 p3106 A71-37405

Nitrous oxide internal and rotational partition functions for temperature range 200 to 350 K, using molecular constants tabulated by Pliva

19 p3106 A71-37408

Microwave spectral line receivers for radio astronomy observation of molecular clouds in interstellar space

20 p3238 A71-39401

Day airglow columnar emission rates for Lyman-Birge-Hopfield system of molecular nitrogen as function of solar zenith angle, using OGO 4 observations

20 p3231 A71-39892

Hydrogen molecule Lyman band continuous emission spectrum with fluctuations due to wave functions maxima, corresponding to transitions from vibrational levels

20 p3305 A71-39968

K-L-L Auger spectra of nitrogen, oxygen, carbon monoxide, nitrogen oxide, water and carbon dioxide, using double focusing electrostatic electron spectrometer

21 p3345 A71-40235

Fluorescence phenomena in celestial bodies, considering atomic lines and molecular bands in stellar and nebulae emissions

22 p3597 A71-41515

Microwave molecular lines of CO, CN and CS emission from infrared object IRC plus 1016

22 p3599 A71-41929

Sunspot umbrae molecular line spectra, observing equivalent widths, isotopic abundances and band intensities

22 p3602 A71-42174

Semiempirical model for molecular band mean transmission, applying to ammonia 10 and 16 micron lines

22 p3602 A71-42179

Hydrogen autoionization rates for molecular vibrational transitions near threshold, using internal conversion model

22 p3578 A71-42464

M stars atmospheric temperature determination from TiO molecular spectrum by vibrational band intensity measurement

23 p3771 A71-44307

MOLECULAR SPECTROSCOPY

NT RAMAN SPECTROSCOPY

Interstellar medium molecular composition from ground based and spaceborne UV, visible light, IR, far

IR and radio spectroscopy, discussing stellar formation

10 p1669 A71-24170

Electron spectrophotometry in molecular and solid state physics, comparing to X ray analysis

10 p1645 A71-24695

Ground state dissociation energies and long range internuclear potentials of diatomic molecules of halogens from spectroscopic vibrational spacings

11 p1728 A71-26065

IR spectrometer attachment for macromolecular investigation of polymer materials, describing constructional and operational features

15 p2383 A71-31658

Polyatomic molecule photoelectron spectroscopy, emphasizing spectra interpretation by quantum mechanical procedures

16 p2541 A71-33398

Molecular jet spectrometer with two irradiation zones, observing lines intensify

16 p2615 A71-34064

Ion cyclotron resonance spectroscopy, discussing fundamentals, instrumentation and ion-molecule chemistry applications

17 p2695 A71-35522

Effective cross section and excitation functions measurements for molecular nitrogen ion first negative system spectral bands by fast electrons

21 p3419 A71-41108

MOLECULAR STRUCTURE

Oxygen and homologous hydrocarbon mixtures detonation limits, discussing propagation, fuel molecule structure, critical temperature, initial cracking mechanism and carbonaceous solids condensation

02 p0331 A71-11957

Tetrahedral molecules quantum mechanical rotational partition function, nuclear spin statistical weight factors and error bounds

04 p0629 A71-14807

Limitations of electron and X ray microscopy concerning damage of biological molecules by observation

04 p0596 A71-15140

Dye lasers operational principles and characteristics, considering dyes molecular structure, optical pumping, continuous operation, wavelength selection and applications

05 p0761 A71-16330

Hydrocarbon fuel ignitability, investigating molecular structural characteristics and homogeneous additives effect

[WSS/CIPAPER 70-19] 06 p0943 A71-17661

Integralism in life biology, discussing reductionism and organicism at biopolymer macromolecule construction and conformational levels

06 p0852 A71-17683

Laser applications in chemical research, exploring fast chemical processes, isotope enrichment and molecular reactions and structure observations

07 p1124 A71-19790

Papers on polymers thermal stability, Volume 1, covering molecular structure, reaction kinetics, scission, thermosetting resins, etc

08 p1323 A71-21474

Gaseous 3-oxetanone ring compound, investigating IR and vibrational spectra and molecular structure

09 p1403 A71-22473

Low molecular weight liquid polybutadiene polymer flow behavior as function of shear rate, temperature, molecular structure and hydrogen bonding

09 p1403 A71-22474

Epoxy novolac resin-cured alicyclic anhydride amine-catalyzed ablative polymers molecular structure from computer correlation of analytical data

11 p1789 A71-26033

Atomic and molecular spin in cosmic medium, discussing static/dynamic orientation, resonance mechanism, hyperfine structure and magnetic sublevels

12 p1933 A71-27420

Butene hydroperoxides structure and intermolecular reactions from NMR spectra, discussing peroxide radical addition, OH group signals shifts and self association

12 p1877 A71-27751

Solid and fluid states oxalyl fluoride vibrational spectra and structure

14 p2191 A71-30575

Gradient shape influence on connectivity in two phase graded structures, considering polyphase structure of filament reinforced composites

17 p2763 A71-35226

IR and Raman vibrational spectra and structure of tetrafluorocyclobutane

17 p2695 A71-35520

Frequencies, rotational constants, molecular structure and moments of inertia of five isotopic species of vinylene carbonate from microwave spectrum analysis

19 p3011 A71-37373

Carbon dioxide lasers, covering molecular structure, IR spectra and laser transitions, population inversion mechanisms, gas discharge and longitudinal flow

20 p3243 A71-39067

MOLECULAR THEORY

Monte Carlo evaluation of molecular transport property integrals temperature dependence

06 p0917 A71-17551

Diatomic molecules nonsigma states rotational excitation adiabatic theory

07 p1164 A71-19691

Atmospheric molecular species, calculating electron impact ionization cross sections and recombination coefficients

10 p1645 A71-24970

Combustion, reaction and flame propagation during gas mixtures burning, allowing for disruption of Maxwell-Boltzmann molecular velocity distribution

13 p2162 A71-28957

Sum rule functions for expressions of atomic or molecular quantum mechanical properties

16 p0548 A71-33527

Polymer systems molecular rheology based on statistical mechanics and simplified structural models

24 p3841 A71-44644

MOLECULAR TRAJECTORIES

Ab initio calculations on trajectories and nonadiabatic transitions in reactions of hydrogen atomic ions with hydrogen molecules

18 p2949 A71-35897

MOLECULAR WEIGHT

Gel permeation chromatography for polymer molecules size /hydrodynamic volume/ separation

04 p0548 A71-15265

Microphase separation in homopolymer-block copolymer mixtures as function of composition, molecular weight and interaction parameters

17 p2695 A71-35525

MOLECULES

NT DIATOMIC MOLECULES

NT MONATOMIC MOLECULES

NT POLYATOMIC MOLECULES

NT TRIATOMIC MOLECULES

French book on macromolecular chemistry covering solid state polymers, polymerization reactions involving free radicals, linear viscoelasticity, vitreous transition of macromolecular polymers, electrical conductivity, etc

11 p1729 A71-26152

MOLIERE FORMULA

U COSMIC RAY SHOWERS

U SECONDARY COSMIC RAYS

U SPATIAL DISTRIBUTION

MOLLIER DIAGRAM

Thermodynamic properties and nozzle flow calculations for high temperature and pressure hydrogen, presenting results in Mollier diagram

24 p3887 A71-44629

MOLNIYA SATELLITES

Magnetospheric electrons and protons acceleration and slot injection between radiation belts during magnetic storms, using flux measurements onboard Molniya 1 satellite

20 p3282 A71-39738

MOLTING

Moulting of Calpodes ethlius larvae head and thorax isolated with prothoracic glands dependent on molting hormone injection

01 p0016 A71-11347

MOLYBDATES

Gadolinium molybdate neodymium ions stimulated emission, noting luminescence, absorption and spectroscopic properties

13 p2111 A71-28424

Gadolinium molybdate-neodymium ions stimulated emission, noting luminescence, absorption and spectroscopic properties

21 p3427 A71-40082

MOLYBDENUM

Langmuir S curves for W /110/-Cs and Mo /100/-Sr adsorption determined by thermionic electron emission microscope, noting minimum work function

02 p0295 A71-12203

Maximum efficiency of cylindrical thermionic converters with Mo emitter and collector over temperature range

02 p0194 A71-12224

Plastic deformation rate effect on deep drawing of sintered and vacuum melted thin sheet Mo

02 p0256 A71-12516

Temperature effect on ductility of thin sheet sintered or vacuum melted Mo during deep drawing

02 p0257 A71-12517

Longitudinal and cross rolling effects on anisotropy of mechanical properties and deep drawability of sintered thin sheet Mo

02 p0257 A71-12518

Critical ductile-brittle transition temperature and microstructure under deep drawing of sintered and vacuum melted Mo

02 p0257 A71-12519

Mo single crystals polygonization and recrystallization, examining strain rate and deformation conditions effects

02 p0266 A71-12652

Cr and Mo thin film coatings on Si-Fe, examining effect on plastic deformation and mechanical properties

02 p0266 A71-12655

Nb-Mo alloys single crystals deformed in compression, considering work hardening and slip relation to temperature, Mo content and stress level
03 p0441 A71-13313

Chromium steel surface diffusion saturation by sublimated Mo, examining process kinetics
03 p0442 A71-13400

Temperature effect on slip- and spark-induced crack propagation in polycrystalline Mo
03 p0444 A71-14317

Strain ratio measurement of pure sintered molybdenum and boron alloyed molybdenum sheets, discussing deformation anisotropy and texture
04 p0609 A71-14748

High temperature specific heat of refractory molybdenum and uranium dioxide
04 p0612 A71-14959

Tungsten, molybdenum and rhenium single crystals hemispherical emissivity at high temperatures by electron beam heating, considering grain boundary contribution
04 p0613 A71-15581

Vacuum deposited Mo and Ru films optical properties, emphasizing reflectance measurements
04 p0627 A71-15693

Mo wire annealing with degassing, investigating temperature effect on mechanical properties
04 p0616 A71-15802

High speed quenching on zone refined molybdenum, considering retained vacancies as contamination effects
05 p0765 A71-16163

Cracks nucleation by spark discharge in Mo single crystals, using optical and transmission electron microscopy
05 p0766 A71-16323

Molybdenizing effects on Cr-Ni-Ti steel strength and stability in liquid Li
05 p0768 A71-16772

Mo and W residual outgassing partial fluxes, considering process duration and impurities identification
05 p0754 A71-16947

Hydrogen and nitrogen binding states and desorption kinetics on $100/\bar{1}00$ plane of Mo, using flash mass spectrometry
06 p0865 A71-18302

Annealed Mo creep properties and long term strength, observing temperature and stress effects
07 p1130 A71-19165

Zr solid state solubility in Mo as function of quenching temperature, using optical microscopy and microhardness testing techniques
07 p1130 A71-19300

Fast neutron irradiation effects on Mo recovery stages 1 to 3 in bcc metals using electrical resistivity measurements
07 p1143 A71-20491

Fracture toughness of aluminum oxide composite containing ductile Mo fibers
08 p1304 A71-20700

Mo microstructure changes at high temperatures noting polygonization, grain migration and crack propagation during failure
08 p1305 A71-21032

W and Mo single crystals metallographic microanalysis for temperature cycles effects on microstructure
08 p1305 A71-21056

Two phase oxygen adsorption at molybdenum surface, using secondary ion-ion emission measurements
08 p1306 A71-21489

Mo single crystals dislocation velocity, discussing slip systems and stress and temperature effects
08 p1307 A71-21509

Tilt boundary intersections during creep in Mo single crystals
08 p1315 A71-21577

Mo fibers surface state and reactions under uniaxial stress from electron work function measurements
09 p1471 A71-23080

Deformed Mo single crystals, noting polygonization processes relation to recrystallization during annealing
09 p1476 A71-23318

Crystal structure alterations in work hardened surface layers of W, Nb and Mo during thermocyclic treatment, using X ray micrography
09 p1477 A71-23329

Mo high temperature melting point and electrical resistivity measurement by pulse heating method
10 p1624 A71-23912

Coarse grained recrystallized Mo ductile brittle transition temperature due to dislocation substructure and grain boundary state, noting low temperature annealing and critical straining
10 p1629 A71-25029

Thermionic emitter CVD W layer on Mo, investigating work function change due to Mo diffusion and crystal structure dependence on heat treatment
11 p1808 A71-25863

Diffusion processes in Mo-W thermionic emitters of massive couple type and piece of Mo substrate with vapor-deposited W layer respectively
11 p1709 A71-25864

Mo evaporation in vacuum, oxygen and water vapor atmospheres at high temperatures
11 p1709 A71-25865

Thermodynamic calculation of silicon chloride gas for high temperature two stage molybdenum silicification in glowing discharge under vacuum conditions
11 p1770 A71-25944

Carbon and oxygen inclusions effects on polycrystalline molybdenum rupture due to precipitation and chemisorption
11 p1781 A71-26323

Activation energy anisotropy for Mo and Nb single crystals dislocation relaxation, noting temperature dependence
12 p1917 A71-27300

Vacuum melted Ni base superalloys, determining Mo and hardener effects on gamma prime solvus temperature and solutioning rate
13 p2090 A71-29418

Mo and W single crystals mechanical properties, considering C and iron group additions influence
14 p2255 A71-29516

German monograph on Mo sheets textures and plastic anisotropy covering recrystallization processes, crystallography, etc
14 p2256 A71-29580

Temperature dependence and mechanical properties of Mo materials with various diffusive protective base coatings based on continuity and density
14 p2256 A71-29623

Structural disorientation dependent recrystallization of cold rolled and annealed Mo single crystals
14 p2258 A71-30006

W and Mo single crystals metallographic microanalysis for thermal cycling effects on microstructure
14 p2259 A71-30172

Adsorption states of Mo and Re surfaces during oxidation at low oxygen pressures and temperatures up to 2300 K, using noble gas molecular beams
14 p2190 A71-30402

Equilibria of molybdenum-nitrogen solid solutions at various temperatures
14 p2260 A71-30474

Nickel alloys susceptibility to pores formation in tungsten inert gas welding in argon-nitrogen mixture, considering influence of Cr, Mo and W
14 p2260 A71-30487

Two phase oxygen adsorption on molybdenum surface from secondary ion-ion emission
14 p2260 A71-30678

Molybdenum doped zirconium monocarbide, investigating Hall coefficient, thermal emf and resistivity measurements
15 p2460 A71-31284

Hot rolled powder metallurgy Mo, noting texture during annealing and cold rolling
15 p2425 A71-31396

Boron solubility in molybdenum, showing grain size decrease, plastic deformation change and elongation
15 p2425 A71-31399

Chromatographic separation of molybdenum, niobium and tungsten based on metal ions absorption by aluminum oxide
15 p2367 A71-31647

Optimum temperature for Zr and Mo soldering of graphite materials with formation of carbide interlayer for ensuring maximum heat resistance
15 p2439 A71-32145

Cold worked pure Mo recrystallization kinetics, indicating dependence on deformation mode and techniques
15 p2433 A71-32177

Mo sheet electron beam penetration during welding, calculating heat-affected zone temperature distribution
15 p2435 A71-32466

Microdefects of lattice structure of molybdenum plasma coatings dependent on spray gun nozzle- surface distance
15 p2437 A71-32671

Oriented Mo single crystals substructure during growth, showing crystallographic orientation
16 p2595 A71-33879

Mo single crystal growth by vacuum melting without oil vapors, noting reduced carbon content and increased ductility
16 p2595 A71-33880

Molybdenum-niobium alloys single crystals electron work function in vacuum from emission patterns and anisotropy
16 p2595 A71-33881

Molybdenum single crystals isotropic thermal conductivity, electrical resistivity and total hemispheric degree of blackness at high temperatures
16 p2595 A71-33882

Deformation conditions and annealing temperature effects on fine structure of Mo single crystals, noting polygonization
16 p2595 A71-33884

Cyclic heat treatment effect on fine structure and properties of Mo single crystals in He atmosphere
16 p2595 A71-33885

Neutron irradiated Mo single crystals polygonization after cold rolling, using X ray topology methods
16 p2596 A71-33886

Mo single crystals physicomechanical and microstructural anisotropy under tension at different tem-

peratures, noting strength and plasticity dependence on crystallographic orientation
16 p2596 A71-33888

Trace impurities effect on oxygen adsorption by Mo, using low energy electron diffraction, Auger electron spectroscopy and flash desorption mass spectrometry
17 p2694 A71-34856

Annealed Mo creep and stress rupture at high temperatures for typical deformation
17 p2760 A71-35661

German monograph on high temperature measurement of thermal and electrical conductivity of W and Mo single crystals
18 p2915 A71-35960

Molybdenum effect on morphology, size and square density of precipitating gamma particles in nickel alloys
18 p2934 A71-35991

Temperature dependent directional differences of modulus of elasticity of Mo sheet, using resonance technique
18 p2936 A71-36711

Cast electron-beam remelted Mo, investigating carbon and zirconium carbide additions effects on structure and low-temperature plasticity
18 p2937 A71-36723

Carbon impurity effects on molybdenum ingot formation, detailing crystal growth, size reduction and length
19 p3077 A71-37277

Mo and high temperature Mo alloys thermally activated deformation mechanisms from flow stress athermal component and effective stress temperature dependence observation
21 p3396 A71-40030

Thermodynamic equilibrium calculation and demonstration of Mo siliciding by circulation method in hydrogen-free gaseous medium containing silicon chlorides
21 p3390 A71-41169

Prior stressing and thermal treatments effect on shock induced substructures in polycrystalline Mo, using transmission electron microscopy
21 p3404 A71-41416

Vacuum annealing and residual gas effects on Mo single crystal dislocation structure and microhardness
23 p3692 A71-44060

Diffusive metal coatings stress-strain state effect on composite Mo material strength, deformation and creep characteristics
23 p3697 A71-44206

W and Mo thin films phase diagrams, determining surface energies and heats for transformations
24 p3860 A71-44718

W and Mo single and polycrystals structural changes by ion bombardment in Li vapor atmosphere at 1500 C, using mass spectrometer
24 p3838 A71-44862

Electron transmission microscopy of Mo single crystals irradiated with fission neutrons and defect structures prior/after postirradiation anneal
24 p3839 A71-45192

Bulk diffusion and glide and self climb mechanisms of vacancy and interstitial loop growth in Mo during neutron postirradiation annealing
24 p3839 A71-45193

Mo sheet anisotropic dynamic strain aging at high temperatures, noting plastic strain contribution to texture formation and dislocation consolidation
24 p3840 A71-45378

MOLYBDENUM ALLOYS

Ni diffusion and electric transfer in Ni-Mo alloy, using isotope tracer technique
01 p0097 A71-10043

W and W-Mo alloy creep properties during interaction with low pressure oxygen, simulating cladding-oxide fuel interaction in thermionic device
02 p0264 A71-12257

Mo-Ti-C system phase equilibria at 1400 C, considering two phase region tie lines direction by metallographic and X ray analyses
02 p0264 A71-12279

Alloying effects on room temperature mechanical properties of vacuum melted Mo-C-Ti, Mo-C-Zr and Mo-Ti-Zr under plastic deformation and recrystallization
02 p0265 A71-12520

Composition and annealing temperature effects on recrystallization of vacuum melted thin wire and rod Mo alloys
02 p0265 A71-12521

Fe-Ni-Mo alloys maraging process kinetics at various temperatures, measuring hardness, electrical resistance and lattice constants
02 p0266 A71-12653

Creep strength of Nb alloys with Mo at high temperatures in vacuum, noting Zr-C complex alloying effect
04 p0613 A71-15642

Nb-Mo alloy creep test, determining relationships between steady state creep rate, stress and Mo content
04 p0616 A71-15803

Plastic deformation and ductility of Mo alloys under various stress concentrations at room and high temperatures

05 p0765 A71-16175

Nitriding effect on hardness and wear resistance of Mo alloys

06 p0912 A71-17936

Nb-V-Mo alloys lattice structure, examining continuous solid solutions with X ray and metallographic analysis

07 p1129 A71-19144

NiMo alloy fcc disordered structure and mechanical properties correlation to domain size and orientations from thin film transmission electron microscopy

07 p1132 A71-19435

Nickel molybdenide disorder to order early transition mechanism diffraction model, using transmission electron and field ion microscopy studies

07 p1132 A71-19436

Phase equilibria of Mo-Nb-Hf alloys using metallographic durometric and X ray tests

07 p1135 A71-19614

Mechanical and plastic properties of Ni-Mo alloys subjected to hot working, determining tensile strength as function of test temperature

07 p1136 A71-19635

Phase equilibria in Zr-Mo-Re and Zr-W-Re systems, studying isothermal section diagrams via X ray and metallographic techniques

07 p1140 A71-20234

Mo-Re-Hf ternary alloys physical and mechanical properties, considering workability, electrical resistivity and expansion coefficient

07 p1140 A71-20237

Mo-Re alloy wire structure and properties, observing heat treatment effect with metallographic techniques and X ray analysis

07 p1141 A71-20242

W-Mo-Re high temperature alloys, discussing high strength, elastic properties, creep, thermal resistivity and expansion coefficient

07 p1141 A71-20243

Structure and mechanical properties of Mo alloy weld metal as function of Re concentration, using metallography, electron microscopy, X ray analysis and autoradiography

07 p1120 A71-20245

Mo-Re alloys thermal and electrical properties from X ray analysis of two phase structure

07 p1141 A71-20246

Elastic modulus as function of chemical composition and structure of binary alloys Mo-Re and Ni-Re

07 p1141 A71-20248

Dynamic strength of elastic elements from wire and tapes of Mo-Re alloy

07 p1120 A71-20249

Recrystallized and nitrided Mo alloy microstructure under plastic deformation by tension at high temperatures

08 p1305 A71-21029

Vacuum-melted and deformed Mo alloys tests, showing long term strength decrease under cyclic heating

08 p1305 A71-21030

Low alloy Mo sheet recovery and aging characteristics studied by X ray scattering

08 p1305 A71-21031

C solubility in Mo-W solid solution at various temperatures

08 p1306 A71-21063

Mo-Hf alloy dispersion hardening by internal nitriding, examining structure and high temperature mechanical behavior

08 p1311 A71-21546

Co-Ni-Cr-Mo alloys hardening mechanisms, noting martensitic transformation role

08 p1312 A71-21551

Ternary Mo-Hf-C alloys thermomechanical and mechanical property relationship, obtaining yield strength at various temperatures

08 p1313 A71-21557

Long term creep strengthening by molybdenum in untempered iron and steel

08 p1315 A71-21579

Low alloy Mo mechanical characteristics relation to structural states obtained during tensile and bending tests

08 p1316 A71-21613

Cast Mo alloy at low temperatures, investigating elasticity, plasticity and tensile strength characteristics

08 p1316 A71-21615

Ti-Mo alloys porous materials for work in hot solutions of nonoxidizing acids, discussing production technology and corrosion resistance

08 p1317 A71-21857

Molybdenum Permalloy powder cores heat treatment effects on permeability, magnetic loss and brittleness control, using metallographic techniques

09 p1466 A71-22171

Boron nitride and aluminum nitride particles behavior in Mo matrix, considering solid metallic phase formation

09 p1470 A71-23067

Ni-Mo alloys electron transfer and ion diffusion at high temperatures

09 p1471 A71-23077

Molybdenum alloy under annealing and heating by AC electric current, investigating structure change effects on strength properties

09 p1475 A71-23312

Ni-Cr-Ti-Al-Mo system equilibrium conditions, conducting phase analysis by X ray and optical and electron microscopy

10 p1627 A71-24532

Mo-Ti-C ternary alloy, examining solid state solubility, equilibrium conditions and microhardness

10 p1628 A71-24647

Mo-Fe-C ternary system, investigating various concentrations, microhardness measurements, solid state solubility and ductility

10 p1628 A71-24648

German monograph on absorbed anions effect on Ni and Ni-Mo alloys anodic behavior covering temperature dependence, electrons interaction, sulfide ions activation and magnetic properties

10 p1628 A71-24874

Mo-Re alloy single crystals asymmetric mechanical properties, discussing shear tests of Mo and Mo-Re single crystals for hard and soft flow stress planes identification

11 p1777 A71-25372

W-Mo-Ta system alloys investigated along four radial sections from tungsten corner, establishing Ta additions effect on maximal strength

11 p1782 A71-26473

Mo-Re alloy crystallographic features observation by transmission electron microscopy, noting equivalence of twin-slip and twin-twin interactions

11 p1783 A71-26477

Mo-Zr-Cr alloy samples cast annealed and quenched at 1500 C, calculating phase equilibrium diagram

12 p1918 A71-27528

Boron solubility in Mo-W solid solution, discussing microstructure, electrical and mechanical properties for range of alloying ratios

12 p1918 A71-27660

Mechanical properties of Ti-Al-Cr and Ti-Al-Cr-Mo alloys annealed below solidus temperatures

13 p2083 A71-27873

W, Mo, Ta and W-Mo alloys hardness integrity, using high temperature microhardness tester

13 p2084 A71-28113

Mechanical properties, hardness and dislocation structure of Ti bearing maraging steels, considering Mo role in strength and plastic properties improvement

13 p2086 A71-28581

Working fluid /Ar/ purity and stability effects on fatigue life and creep of Nb and Mo alloys using gas analysis, microstructure and microhardness data

14 p2256 A71-29622

Beta stabilizing Mo and Cr effects on mechanical properties of welded and heat treated Ti alloys

14 p2260 A71-30490

Porous Ti-Mo alloy materials for operation in hot solutions of nonoxidizing acids, discussing production technology and corrosion resistance

14 p2260 A71-30836

Mo alloy welding by continuous flashing method, discussing welded joints microstructure, plastic properties and strength

15 p2413 A71-31220

Mo-Ni-C ternary alloy X ray analysis, determining solidus temperature from phase diagrams

15 p2424 A71-31237

Nitrogen solubility in Ni-Mo and Ni-W melts, detailing Ti and pressure effects

15 p2424 A71-31392

Molybdenum steel annealing, noting carbide phase transformations

15 p2425 A71-31398

Co-Mo and Co-Mo-Ti stainless maraging steels tensile strength after quenching, establishing Mo and Co alloying limits

15 p2427 A71-31526

Molybdenum and tungsten alloys, detailing strengthening with hafnium carbide

15 p2428 A71-31840

Isothermal sections at 1400 C of systems niobium-titanium-boron and niobium-molybdenum-boron by X ray analysis

15 p2437 A71-32672

Mechanical and plastic properties of Ni-Mo alloys subjected to hot working, determining tensile strength as function of test temperature

16 p2593 A71-33631

Addition effects on polygonization of deformed single crystals of Mo and W with Re, using X ray analysis

16 p2596 A71-33887

Alloying elements effect on structural stability and properties of W and Mo alloys single crystals, studying thermal cycling response

16 p2596 A71-33908

Electrodeposited Ni-Mo coatings corrosion resistance improvement by heat treatment, showing crystal structure degree of perfection role

16 p2599 A71-34052

Deformation temperature effects on microstructure and mechanical properties of low alloy Mo, considering cold brittleness temperature and associated plasticity

17 p2755 A71-34418

Composite failure model tested for short term creep and rupture in Mo alloy at constant loads and 785-1400 C, considering strain hardening

17 p2834 A71-35670

Molybdenum mechanical characteristics relation to structural states obtained during tensile and bending tests

17 p2760 A71-35673

Vacuum melted Mo alloy low temperatures elasticity, plasticity and tensile strength characteristics

17 p2760 A71-35675

Deformation kinetics and failure of high melting Nb and Mo base alloys in plastic state under low cyclic fatigue

18 p2936 A71-36710

High temperature tests of short time strength, hardness, moduli of elasticity of W-Mo alloys subject to plastic deformation and annealing

18 p2936 A71-36712

Nonheat treated extruded Mo alloy under tension and vacuum conditions at various temperatures, investigating cylindrical samples dimensions effects

18 p2936 A71-36714

Mo, W and Mo-W alloys chlorination kinetics, investigating temperature and pressure effects on reaction rate from electron micrographs

18 p2938 A71-37002

High temperature strengthening of vacuum melted W-Ti alloys with Mo and Zr additions

19 p3076 A71-37267

Age hardening of Mo alloys with titanium and zirconium carbides at high temperatures after quenching

19 p3077 A71-37268

Deformation rate and temperature effects on optimum strength and ductility of die forged and extruded Mo-Ti alloys

19 p3077 A71-37269

Ni-Mo single crystals under isothermal aging, observing long range order parameter, domain size and microstrains

19 p3077 A71-37411

Mo effect on high temperature strength, heat resistance, plasticity and toughness of austenitic Cr-Mn-Ni-Al steel

19 p3077 A71-37465

Vertical phase diagrams of Ti-Al-Zr-Mo-Fe alloy system at varying Fe concentrations, showing structural hardening after quenching

19 p3078 A71-37471

Isothermal phase diagrams and composition effects on plasticity in Mo-Ti-Zr-C system in Al-rich region

19 p3078 A71-37472

Mo and high temperature Mo alloys thermally activated deformation mechanisms from flow stress athermal component and effective stress temperature dependence observation

21 p3396 A71-40030

Fine structure dislocation and phase composition of Cr-Mo steel at elevated temperature in steam pipe applications, noting recrystallization stability

23 p3690 A71-43277

Mo and Co alloying effects on high temperature chromium ball bearing steels contact strength

23 p3692 A71-44037

Cast heterophase Mo and alloys fracture strength and plastic characteristics, investigating crystal growth texture, orientation and substructure

23 p3693 A71-44215

Strain hardening effect of Ni, Mn and Mo in Cr steel after high temperature annealing

23 p3693 A71-44216

Mo alloy under impact tests, investigating notch sharpness effects on cold shortness threshold and strength

23 p3693 A71-44231

Thermodynamic properties of Ti-Mo alloys, using triple Knudsen cell technique

23 p3694 A71-44279

Mo additions to Co rich ductile permanent magnet alloys, obtaining higher coercive forces and energy products

23 p3694 A71-44283

Ti, Zr and Nb carbides alloying effects on deformed and annealed Mo alloys cellular structure and mechanical properties

24 p3836 A71-44672

MOLYBDENUM CARBIDES

Molybdenum borocarbide synthesis and properties, discussing melting temperature, electrical and heat conductivity, thermal emf, microhardness, etc

01 p0100 A71-10402

Cemented carbides based on TiC-molybdenum carbide-Ni, studying properties as function of molybdenum carbide and C contents in primary solid solution

08 p1304 A71-20994

Ti-Mo-C ternary system phase diagram

15 p2430 A71-32146

Zirconium dioxide reactions with chromium, molybdenum and tungsten carbides, studying reaction products, phase composition, sintering temperatures and chemical separation

15 p2432 A71-32166

Molybdenum hemicarbide layer as diffusion barrier between metal and disilicide, investigating system thermal stability

21 p3399 A71-40526

MOLYBDENUM COMPOUNDS

NT MOLYBDATES

NT MOLYBDENUM DISULFIDES

NT MOLYBDENUM OXIDES

Kr 85 disposition following Mo-uranium oxide cermet fuels irradiation in test chamber

02 p0296 A71-12240

Tungsten or molybdenum disulfide formation discussing tribolytic deposition process

10 p1635 A71-25010

High temperature oxidation protection of niobium by molybdenum disilicide coatings applied by hot pressing powder metallurgy method

18 p2934 A71-35952

MOLYBDENUM DISULFIDES

Solid molybdenum disulfide lubricants antifriction properties and performance under atmospheric and high vacuum conditions, noting humidity effects and composition of friction-evolved gases

01 p0106 A71-10036

Atmospheric and high vacuum performance tests of solid lubricant coatings based on molybdenum disulfide

05 p0757 A71-16174

Sliding load history effects on friction of thin burnished films of molybdenum disulfide in vacuum

[ASLE PREPRINT 70LC-18] 08 p1298 A71-21161

Molybdenite oxidation kinetics by thin layer technique with close temperature and gas composition control, measuring temperature, gas composition and particle size effects

09 p1472 A71-23128

Molybdenum disulfide bonded solid film lubricants performance characteristics, considering load, speed and temperature effects

[ASLE PREPRINT 71AM 2D-1]

13 p2076 A71-29486

Solid additives, graphite and molybdenum disulfide concentration effects on liquid lubricants and greases antiwear performance

14 p2251 A71-29827

Superconductivity in molybdenum disulfide laminate intercalated with sodium or potassium

19 p3119 A71-37842

Solid lubricant molybdenum disulfide physicochemical interaction with Ag, Ni, Fe and Co at high temperatures, using X ray structural and spectrometric analyses

23 p3697 A71-44029

Solid lubricant-epoxy compounds shear modulus measurement by cantilever beam specimens dynamic testing, calculating wear life coefficients for molybdenum disulfide in epoxy resin

[ASLE PREPRINT 71LC-1] 24 p3842 A71-45284

Humidity effects on molybdenum disulfide bonded solid film lubricant friction properties at low load and slow speed, noting mechanical escapement timers accuracy

[ASLE PREPRINT 71LC-2] 24 p3831 A71-45285

MOLYBDENUM OXIDES

Tungsten and molybdenum oxide crystals shape and size during annealing in various gas atmospheres and vacuum conditions

23 p3690 A71-43255

MOLYBDENUM SULFIDES

NT MOLYBDENUM DISULFIDES

Service life of solid molybdenum sulfide based plastic coatings with different binders under high vacuum friction investigated by mass spectroscopy

09 p1454 A71-22819

MOMENT DISTRIBUTION

Zero moments surface in problem of two immovable centers taking into account cosmic dust accumulation before binary apex moving forward with periastron of bright component

03 p0484 A71-13220

Three layer plate with metallic carrier surfaces and plastic foam filler, calculating stress state near applied concentrated moment

06 p0995 A71-17831

Flange joint moments magnitude due to bolts nonuniform tightening during assembly based on probability theory

07 p1116 A71-19359

Force moment method estimation of atmospheric circulation effect on earth polar movement

08 p1284 A71-21674

Boundary condition effects on thermomagnetic torque from moment method solution for Boltzmann equation for diatomic molecular gas in magnetic field and cylindrical geometry

09 p1502 A71-22853

Zero moment stress state realization in thin macrohomogeneous shells by selecting adequate uniform multilayer structures for reinforcement

12 p1975 A71-26963

Short open noncircular cylindrical shells supported at curvilinear ends, obtaining total values of moments

15 p2507 A71-32103

Zero moment stress state realization in thin macrohomogeneous shells by selecting adequate uniform multilayer structures for reinforcement

19 p3159 A71-38266

Airloads and moments changes of aircraft flying over trailing vortices, investigating time dependent aerodynamic forces

21 p3321 A71-40508

MOMENTS

NT BENDING MOMENTS

NT DIPOLE MOMENTS

NT DISTRIBUTION MOMENTS

NT ELECTRIC MOMENTS

NT LOADING MOMENTS

NT MAGNETIC MOMENTS

NT MEAN

NT MOMENTS OF INERTIA

NT PITCHING MOMENTS

NT ROLLING MOMENTS

NT STABILITY DERIVATIVES

NT STANDARD DEVIATION

NT TORQUE

NT VARIANCE [STATISTICS]

NT YAWING MOMENTS

Moment analysis of atomic spectral lines of Cs-Ar and Cs-He systems, using adiabatic approximation

22 p3578 A71-42462

Pseudomoments estimation of convergence rate in central limit theorem for random variables series

24 p3843 A71-44874

MOMENTS OF INERTIA

Lunar moments of inertia and density distributions, using gravitational potential and physical librations

01 p0158 A71-10772

Earth, moon and planets sizes, masses and moments of inertia determination by artificial satellites, space probes and radar observation

05 p0815 A71-17241

Long thin circular cylindrical shell circumferential wave functions reduction to beam type transverse vibration equation, including rotary inertia

06 p0984 A71-17618

Lunar bulk modulus, viscosity, inertia moments and density calculation from gravity potential values obtained by Luna 10 and Lunar Orbiter satellites

07 p1203 A71-20520

Adaptive time optimal control for inertial system with air jet attitude control

09 p1423 A71-22611

Neutron star matter equations of state involving hyperon formation effects for maximal stable mass models, tabulating moments of inertia

10 p1671 A71-24302

Tensor inertia conversion from principal to rotated coordinates system, obtaining negative products in aircraft

[DFVLR-SONDDR-111] 10 p1557 A71-24949

Variable sweep wing aircraft angular motion mathematical model, analyzing inertial moments influence on control dynamics

11 p1708 A71-25661

Disk rotating in gimbal system, describing gyroscopic moments and precession

13 p2068 A71-28632

Roll moment of inertia to static margin ratio effect on yaw of repose angle magnitude in ballistic match of projectiles

14 p2325 A71-29890

Lunar forced motions and free oscillations, considering inertia moments effects on rotational and translational movements

16 p2636 A71-33502

Transfer function and temporal behavior interrelations for linear network, characterizing circuit delay and rise time by center of gravity and inertial moment of pulse response

16 p2550 A71-34139

Rotating inertia effects on step-type MHD hydrostatic thrust bearing characteristics, discussing disk shape and operating conditions for improvement

17 p2748 A71-34641

Mass, center of gravity and moment of inertia measurements curtailment by tolerance and regression analyses and Monte Carlo method

[SAWE PAPER 883] 17 p2834 A71-35820

Center of gravity and moment of inertia measurement system based on standards of comparison principle

[SAWE PAPER 880] 17 p2835 A71-35822

Fundamental frequency of large amplitude bending vibration of elastic and isotropic rectangular plates, considering effects of transverse shear and rotary inertia

18 p2980 A71-36496

Gyroscope rotor axial moment of inertia of measurement by connection to small vibrator device

19 p3062 A71-37148

Frequencies, rotational constants, molecular structure and moments of inertia of five isotopic species of vinylene carbonate from microwave spectrum analysis

19 p3011 A71-37373

Forced axisymmetric motion of circular viscoelastic plate, including effects of rotary inertia, transverse shear and time dependent boundary conditions

19 p3157 A71-37848

Shear deformation and rotary inertia effects on flexural vibration frequencies of pretwisted, nonpretwisted and tapered cantilever beams

[ASME PAPER 71-VIBR-79] 21 p3461 A71-40316

Thin truncated conical shells axisymmetric free vibrations, considering shear deformation and rotary inertia effects

21 p3462 A71-40528

Gravitational and aerodynamic perturbation moment effects on nonsymmetric solid body rotary motion near mass center, using precession model

22 p3612 A71-42870

MOMENTUM

NT ANGULAR MOMENTUM

High energy cosmic particle interactions with LiH target, discussing relation between longitudinal and transverse momenta of generated pions

03 p0476 A71-13844

Momenta measurements of particles produced by high energy quasi-nucleon interactions of pions on photoemulsion layers, using primary particle tracks scanning

03 p0461 A71-13854

Air shower cores high transverse momenta, discussing primary particle role in core structure

04 p0640 A71-14814

Cosmic ray secondaries mean transverse momentum from muons lateral distribution measurement

04 p0640 A71-14816

Axisymmetric turbulent wakes with zero excess momentum, noting mean and pulsation velocity and Reynolds shear stresses

04 p0577 A71-15624

Weak gravitational field negative energy possibility from energy momentum leakages consideration for asymptotically flat solutions of Einstein equations

09 p1494 A71-22807

Density, momentum and electric charge measurement of nuclear interacting particles in extensive air showers, using air gap magnet spectrograph and neutron monitor

13 p2124 A71-28083

High energy cosmic muons momentum spectrum and charge ratio measurements at large zenith angles, describing magnetic spectrometer

14 p2247 A71-30601

Momentum spectrum measurement of cosmic ray muons, recording particle trajectories photographically

15 p2475 A71-31783

Cosmic ray measurements at various altitudes, describing magnet spectrograph for momentum spectra and particle identification

15 p2408 A71-31813

High energy cosmic particle interactions with LiH target, discussing relation between longitudinal and transverse momenta of generated pions

22 p3594 A71-42645

Momenta measurements of particles produced by high energy quasi-nucleon interactions of pions on photoemulsion layers, using primary particle tracks scanning

22 p3579 A71-42655

Jet mixing in cross flow at different velocity ratios and incidence angles, calculating momentum and mass flow

23 p3664 A71-43831

MOMENTUM ENERGY

U KINETIC ENERGY

MOMENTUM PRECESSION

U PRECESSION

MOMENTUM THEORY

Supersonic combustion process heat transfer, using momentum integral method for turbulent boundary layer equations

04 p0683 A71-15485

Momentum conservation in metagalactic astronomy, considering magnetoid ejection from active galactic nuclei

04 p0657 A71-15827

Submerged moving body in nonviscous incompressible fluid, evaluating finite potential flow field momentum with rigid and free far distant outer boundary

06 p0841 A71-17419

Ejector pump with gas-air jet, deriving momentum conservation equation

06 p0882 A71-18010

Turbulent boundary layer approximate analytical method based on momentum and energy integral correlations and limiting laws of friction and heat transfer

07 p1085 A71-18756

Unsteady incompressible laminar boundary layer equations, obtaining similarity solutions from momentum integral equation

07 p1093 A71-20365

Momentum thickness of boundary layer of circular cylinder in cross flow at high Reynolds numbers from static pressure and skin friction measurements

12 p1867 A71-27738

Flow momentum losses during gas mixture chemically nonequibrated expansion in nozzle
13 p2158 A71-27880

Scintillator array investigation of high transverse momenta occurrence in air showers of primary energy above 1000 TeV
13 p2124 A71-28084

Compressible turbulent boundary layers closed form solution by extending Buri momentum integral analysis of incompressible turbulent boundary layers
14 p2228 A71-31129

Energy-radiation problems in relativity theory, considering electromagnetic waves, Einstein equations, momentum tensors and moving charged particles
16 p2609 A71-33259

Multidimensional canonical formalism based on field system state description with potentials and momenta
17 p2778 A71-34635

Moller gravitational field energy-momentum pseudotensor comparison with Einstein canonical and Landau-Lipschitz pseudotensors and Mikajewitsch quasitensor, noting chronometric invariance
17 p2778 A71-34638

Effective momentum ratio for Lamb circular cylinder double vortex, Hill spherical vortex, Thomson straight line paired vortices and Helmholtz circular ring vortex
21 p3321 A71-40541

Knudsen effusion problem in thermal molecular gas jet mixing, using moment method based on velocity distribution function
24 p3817 A71-44354

MOMENTUM TRANSFER

Tangential momentum transfer accommodation coefficient for gas flow based on monocrystalline molecular model of gas-solid interface
01 p0071 A71-10949

Rotating neutron star supernova explosion without nuclear detonation, discussing rotational momentum transfer
02 p0307 A71-12089

Thermionic converter electron-cesium atom momentum transfer collision probability, considering scattering cross sections
02 p0287 A71-12227

Swirling flow in short cylindrical combustion chambers with diaphragm-free inlet section, examining momentum loss
03 p0405 A71-14382

Pressure wave propagation through annular and mist flow patterns, noting virtual mass effects in interphase momentum transport of rarefaction and compression waves
03 p0405 A71-14418

Angular momentum flux from confined gravitational radiator, using linear approximation with Landau-Lifshitz energy-momentum pseudotensor
04 p0625 A71-14731

Optimal momentum exchange desaturation in attitude control systems for orbiting spacecraft, concerning gravity gradient and disturbance torques
05 p0817 A71-16552

Gas-particle mixture cascade flow over turbine blades, considering momentum/heat transfer and particle trajectories
06 p0841 A71-17701

Ion-molecule collision charge transfer and momentum transfer relaxation rates, using ion cyclotron resonance heterodyning method
07 p1054 A71-19371

Clear air turbulence role in general atmosphere circulation, considering energy dissipation, momentum transfer and shear layer producing mesoscale processes
07 p1153 A71-20221

Turbulent transfer model in wall region, estimating mean surface renewal frequency for mass momentum and heat transfer rates and velocity, temperature and concentration profiles
07 p1092 A71-20224

Gas-particle mixture cascade flow over turbine blades, considering momentum/heat transfer and particle trajectories
07 p1017 A71-20311

Turbulent pipe flow, developing analogy between momentum and heat transfer
07 p1224 A71-20371

Spin-orbit coupling and angular momentum transfer between planets and sun by interaction with solar wind
07 p1203 A71-20522

Rotating neutron star supernova explosion without nuclear detonation, discussing rotational momentum transfer
08 p1362 A71-21139

Plane jet in counterflow with vortex shedding control, discussing solid boundary and jet momentum effects
10 p1592 A71-23980

Proton form factors and radius determination from experimental data analysis of cross sections of electron scattering by protons over wide transferred-momentum range
12 p1901 A71-27180

Molecular collisional analysis of normal momentum transfer from flowing rarefied gas to monocrystalline surface
12 p1934 A71-27588

Two phase critical flow of one component mixtures in nozzles, orifices and short tubes, considering interphase heat, mass and momentum transfer rates [ASME PAPER 70-WA/HT-5]
13 p2049 A71-28980

Internal gravity waves numerical model allowing momentum transport interaction with mean flow
14 p2269 A71-29950

Surface renewal and penetration model in heat and momentum transfer analogy for incompressible turbulent boundary layer flow
14 p2227 A71-30935

Plasma heat transport associated with matter, momentum, energy and electrical charges transfer
16 p2617 A71-32956

Momentum transfer secondary flow between rotating cylinders in terms of effective/molecular viscosity ratio as function of Taylor number
16 p2559 A71-33199

Clear air turbulence in midstratosphere, analyzing heat and momentum transports and temperature fluctuations spectra
18 p2943 A71-36008

Gravity gradient desaturation of momentum exchange attitude control system, considering control moment gyros and reaction wheels
19 p3098 A71-37185

Collisionless momentum transfer between interstreaming ions in laser produced plasma, using fast photography, shadowgraphy and electric potential probes
19 p3114 A71-38177

Pressure wave propagation through one and two component annular and mist flows, showing importance of inertial interphase momentum transfer
19 p3171 A71-38293

Atmospheric gases effective electron collision frequency calculations, using momentum transfer cross sections
20 p3271 A71-38743

Momentum transfer between gas and condensed phase in metallized solid propellant rocket motors, measuring noncontinuum and turbulence effects on sphere drag
21 p3437 A71-40861

Configuration space theory of nonrelativistic three body scattering covering transition amplitudes of three-three chemical reaction rates
22 p3577 A71-41651

High Alfvén Mach number collisionless plasma flow in weak magnetic field, investigating momentum transfer mechanisms and coupling lengths
22 p3581 A71-41890

Spacecraft pointing control system with momentum exchange controllers, considering near optimal control policy for control moment gyro system
22 p3608 A71-41966

Proton form factors and radius determination from experimental data analysis of cross sections of electron scattering by protons over wide momentum transfer range
22 p3578 A71-42454

Total and momentum transfer cross sections for low energy electron scattering by atomic and diatomic molecules
23 p3707 A71-43898

Experimental techniques for differential, total and momentum transfer electron-molecule scattering cross sections at low electron energies, discussing rotational excitation
23 p3707 A71-43899

MONATOMIC GASES

Heat transfer between rarefied monatomic gas and porous wall, examining temperature jump with model kinetic equation for Knudsen layer
01 p0179 A71-10612

Atomic and molecular transport coefficients for various species injected into boundary layer on ablating or transpiration cooled surface
01 p0130 A71-10958

Initial ionization, relaxation kinetics and nonequilibrium radiation behind strong shock waves in monatomic gases and air
05 p0835 A71-16524

Low density monatomic gases mixtures multicomponent thermal diffusion coefficients, demonstrating for heat conductivity and dissociated air equations
06 p0929 A71-18072

One component system wave propagation kinetic theory, calculating monatomic gas and plasma oscillations by discrete ordinate method
07 p1165 A71-18876

Rarefied monatomic gas flow in axisymmetric jet exhaustion into vacuum, noting expansion to low densities at thermodynamic nonequilibrium
07 p1090 A71-19894

Soviet book on thermal conductivity of monatomic and polyatomic gases and hot and cold mixtures, comparing molecular kinetic theory collision integral formulas with experimental data
08 p1375 A71-21656

Near equilibrium solutions of steady spherical expansion of monatomic gas into vacuum, using Lighthill technique for higher order analysis
09 p1430 A71-22086

Sound dispersion in monatomic gases from viewpoint of linearized hydrodynamic, Boltzmann and model equations
12 p1930 A71-27190

Heat and mass transfer in monatomic molecular gases and gas mixtures, discussing energy exchange during collision and thermal diffusion effect on thermal conductivity
13 p2159 A71-28186

Electron energy distribution function in weakly ionized monatomic gas with inelastic collisions, using differential equation asymptotic resolution techniques
13 p2106 A71-28398

Equations for radiative contribution to energy and mass transfer in monatomic and ionized gas flow in local thermodynamic nonequilibrium
14 p2338 A71-30819

Monatomic gas interaction with solid phase surface, deriving three dimensional theoretical model including hard spheres collision and surface energy
15 p2451 A71-31675

Steady state partially ionized monatomic gas expansion from sonic orifice, investigating electron-ion recombination effects on flow properties
15 p2457 A71-32101

Heat transfer through stationary monatomic rarefied gas in annular space between coaxial cylinders, using two-flow Maxwellian function for approximate molecular velocity distribution
16 p2661 A71-32832

High temperature singly and doubly ionized monatomic gas and partially dissociated and singly ionized diatomic gas, showing adiabatic and isentropic exponents relationship
16 p2662 A71-32837

Monatomic mercury gas excitation and ionization mechanisms ahead of and behind shock front, establishing electron gas heating kinetics in relaxation zone
16 p2616 A71-32902

Time dependent corrections to one component monatomic systems equilibrium rate of reactions and temperature change, using moment method for integrating nonlinear Boltzmann equation
17 p2785 A71-34945

Radiation gas dynamics covering monatomic and molecular gases, chemical dissociation and vibrational relaxation
19 p3043 A71-37459

Monatomic gas beams scattering from gas surface interface with randomly distributed energy states, confirming reciprocity or detailed balance principle
19 p3104 A71-38057

Gas nature effect on wall temperature and heat transfer in Hartmann-Sprenger tube
21 p3366 A71-40102

Radiant monatomic gas flux boundary conditions derivation, considering all points in local thermodynamic equilibrium
21 p3475 A71-40660

Helium, neon, nitrogen, oxygen, argon, carbon dioxide and monoxide and methane thermodynamic and transport properties calculation using computer program for state equations
21 p3351 A71-40893

Analytic approximation for radial integrals and electron excitation cross sections of inert gases, using atomic screening parameters
22 p3577 A71-41620

Distribution function integral representation application to steady motion of monocomponent rarefied gas containing amorphous particles, using successive approximation for kinetic equation solution
22 p3482 A71-42868

Kinetic equations derivation for rarefied chemically reacting monatomic or stable molecular gases
23 p3707 A71-43924

Atomic and molecular gases electron impact ionization, measuring secondary particle energy distribution and angular dependence
24 p3850 A71-44925

Monatomic gas flow in radiation field, noting effects on mass transfer
24 p3821 A71-45182

Ideal gases and binary monatomic gas mixtures heats of transport derivation from kinetic theory expressions for thermal transpiration
24 p3891 A71-45384

MONATOMIC MOLECULES

Nonpairwise van der Waal interactions effects on vacancy formation energies in monatomic solids, using Lorentz oscillator and two body models for comparison
08 p1344 A71-21367

Total and momentum transfer cross sections for low energy electron scattering by atomic and diatomic molecules
23 p3707 A71-43898

MONGOLIA

- Hypothetic meteorite crater in southeastern Mongolia from on-spot observation and aerial photography 07 p1098 A71-19318
- Hypothetic meteorite crater in southeastern Mongolia from on-spot observation and aerial photography 15 p2399 A71-31898

MONITORS

- Batch/Time-Sharing Monitor for achieving balance of digital computer systems efficiency and responsiveness, discussing performance modeling and empirical measurements 01 p0043 A71-10178
- Real time graphic display monitoring of time sharing computer systems operational state 01 p0046 A71-10207
- Portable direct reading spectrometer for monitoring oxygen-hydrogen containing contaminants in gas tungsten arc welding process 02 p0247 A71-11712
- Current profile monitor for scanning electron beam irradiations from accelerator, using storage oscilloscope or X-Y recorder for display 02 p0249 A71-12127
- Air pollution monitoring instrument for measuring mass concentration of aerosols and particulates in atmosphere 04 p0597 A71-15288
- Transmission impending failure detection via lubricating oil monitoring for metal particle content 04 p0532 A71-15415
- Satellite cosmic ray monitors data, examining correlation with sun to obtain interplanetary magnetic field spatial structure 06 p0951 A71-18106
- Acoustic emission monitoring system for real time detection of crack initiation and propagation in complex structure during static and fatigue tests 06 p0906 A71-18461
- TV display eye movement monitor with automatic coordinate digital printout for permanent record 07 p1053 A71-20402
- Nondestructive monitoring calibration and alignment with standard specimens conforming with metrological regulations 08 p1300 A71-21895
- German space radio monitoring service, describing facilities for receiving and evaluating 20 MHz to 1 GHz transmissions 09 p1407 A71-23046
- Optical ground contamination monitoring devices for Apollo Telescope Mount collecting time-line and integrated data [AIAA PAPER 71-458] 11 p1764 A71-26240
- Contamination degrading effects on optical surfaces, discussing application to real time monitors data analysis [AIAA PAPER 71-460] 11 p1800 A71-26242
- Global environmental monitoring system for atmosphere, oceans, land and biology, considering international cooperation 14 p2198 A71-30897
- Systematic phase variation in second harmonic of daily variation of cosmic ray intensity in one year, recorded by neutron monitor at Deep River 15 p2441 A71-31410
- Conjugate eye movement stimulator and monitor for human experimentation in closed loop, open loop and variable feedback modes of operation 17 p2693 A71-35392
- Thickness monitoring technique for thin films, using silicon solar cell mounted adjacent to substrate with iron deposition 18 p2922 A71-36591
- Broadcast sound loudness level monitor as measuring and indicating instrument, discussing technological and psychoacoustical evolution 20 p3271 A71-39763
- Operator performance improvement in monitoring automated processes by alternating displays, discussing simulated radar and sonar CRT display laboratory tests 22 p3501 A71-41636
- Radiation flaw detection by fast neutrons, monitoring thick lead plates and three-layer articles 22 p3528 A71-41761
- Decarbonization monitoring of ball bearing steel bars, describing defectoscope based on eddy current higher harmonics method 22 p3553 A71-41768
- MONKEYS**
- Vestibular nerve projection to association fields of cerebral cortex in Rhesus monkey under alpha chloralose and without anesthetic agent 04 p0537 A71-14765
- Biosatellite postflight experiment evaluating effects of forced electrolyte imbalance in Macaca nemestrina 08 p1239 A71-20821
- Biosatellite 3 monkey sleep and wake states based on visual and computer analysis of telemetered EEG data from earth orbital flight 09 p1395 A71-23242
- Carbon dioxide tolerance after hypercarbia adaptation of rhesus monkeys in upright position 09 p1395 A71-23250

- Rhesus monkeys concurrent avoidance and appetitive behavior patterns with counter discontinuities in shock proximity indicator tests 10 p1573 A71-25136
- Squirrel monkeys midbrain reticular formation direct thermal stimulation effects on physiological or behavioral thermoregulatory responses 18 p2858 A71-36860
- Macaca nemestrina monkey bone density change during Biosatellite 3 mission 21 p3330 A71-40343
- Physiological deterioration of monkey onboard Biosatellite 3 and unexpected demise, presenting collected data for response analysis 21 p3333 A71-40564
- Observing behavior in squirrel monkeys under multiple schedule of reinforcement availability 22 p3497 A71-42861

MONOCHROMATIC RADIATION

- LF spiral monochromatic wave pulse propagation from vacuum into semiinfinite semiconductor, considering bandwidth relation to electron heating 01 p0138 A71-10431
- Monochromatic light glare effect on human eye as function of wavelength, using visual threshold variation as criterion 01 p0016 A71-11389
- Monochromatic signal spectrum determination from circulating realization spectrum analysis 02 p0248 A71-11833
- Shadow and interference methods sensitivity for low density gas flows improved via monochromatic light source 02 p0248 A71-11937
- Resonant excitation of plane dielectric waveguide by plane monochromatic wave 03 p0378 A71-13798
- Plane monochromatic electromagnetic wave scattering by moving and rotating cylinder 04 p0549 A71-14612
- Soviet monograph on visible and IR waves at atmospheric propagation covering monochromatic radiation absorption and scattering, laser light beams under turbulence, etc 04 p0551 A71-14800
- Monochromatic wave propagation along cylindrical helical line, showing tubular waveguide formation from wave field and collisionless plasma interaction 04 p0633 A71-15107
- Monochromatic coronal structure in prominences, explaining light diminution by density reduction 05 p0804 A71-16027
- Pure W monochromatic emissivity measurements at 0.4 to 4 microns and at high temperatures 05 p0767 A71-16600
- Small amplitude nonlinear longitudinal plasma oscillations perturbation analysis, discussing Landau damping, monochromatic wave evolution and independent variable expansion 05 p0789 A71-16659
- Structural information propagation in optical wave fields arising in diffraction and scattering of quasi-monochromatic light by fixed objects 05 p0753 A71-16903
- Holographic interferometry application to gas dynamics, analyzing interferential patterns in monochromatic and achromatic light 05 p0695 A71-17166
- Monochromatic plasma waves excitation by electron beams, discussing nonlinear theory 06 p0936 A71-17688
- Cooperative international program of monochromatic coronal photography with interference filters for 1973-1976 06 p0968 A71-17911
- Coupling effect on monostatic-bistatic radar equivalence for monochromatic wave and short pulse scattering 07 p1060 A71-19260
- Thin polycrystalline CdTe film photovoltaic effect dependence on monochromatic light incidence angle 07 p1176 A71-19272
- Morphology and dynamics of low intensity monochromatic midlatitude auroral arcs of 6300 A /O I/, comparing results with observation during IGY 07 p1103 A71-19766
- Fourier transform hologram recording by quasi-monochromatic incoherent source, resolving bias problem at expense of resolution 08 p1290 A71-21386
- Statistics effect of quasi-monochromatic exciting radiation on generated radiation spectrum in nonlinear optics 09 p1461 A71-22396
- Planetary nebulae NGC 1535, 6572, 6543, 7662 and 7009, observing monochromatic photographs and isophotic contours 09 p1521 A71-22870
- Far field diffraction pattern of corner reflector for normally incident monochromatic light, considering polarization characteristics 10 p1640 A71-23947
- Mars monochromatic albedos, investigating longitudinal variations and opposition effects 11 p1824 A71-25707
- Holographic interferometry application to gas dynamics, analyzing interferential patterns in monochromatic and achromatic light 12 p1864 A71-27458
- Signal processing using arrays, solving for monochromatic plane wave by transforming gain equation 12 p1882 A71-27532
- Industrial polycrystalline graphite monochromatic emissivity in visible and IR spectral regions at high temperatures 13 p2090 A71-27882
- Human nervous reactions to monochromatic red, yellow green and blue light for optimal color climate in spacecraft cabins 13 p2018 A71-28411
- Fourier transform holography with partially coherent light from incoherent quasi-monochromatic source, considering bias problem 15 p2402 A71-31256
- Monochromatic photometry of comets for molecular emission bands in head spectra, using wideband and narrowband filters 15 p2484 A71-31665
- Compact monochromatic rhodamine doped polymethyl methacrylate dye laser with internal diffraction grating resonator, describing frequency selection from emission spectrum 15 p2422 A71-32585
- Small monochromatic disturbances propagation in stable ideal MHD fluid by geometric optics method, solving point source radiation at short wavelengths 15 p2459 A71-32652
- Laser beam atmospheric monochromatic radiation attenuation isolating molecular absorption from total radiant flux attenuation 15 p2451 A71-32757
- Dynamic amplification ranges of monochromatic signal by semiconductor, solid state and gas lasers in steady operation mode 17 p2750 A71-34270
- Energy balance and emission power of organic dye laser under monochromatic excitation 17 p2751 A71-34381
- Population inversion damping on vibrational-rotational transitions of carbon dioxide molecule during interaction with monochromatic radiation pulse, using two level model 17 p2752 A71-34387
- High voltage pulse shaping circuits for Kerr cell polarization shifters for modulating and deflecting monochromatic laser radiation 19 p3071 A71-37255
- Large amplitude monochromatic electron cyclotron wave broadening in plasma, producing shifted phases in finite frequency range 19 p3114 A71-37855
- Polarization ellipse and depolarization coefficients for monochromatic radio waves reflected from F 2 ionosphere using Stokes parameters 19 p3056 A71-38362
- Monochromatic radio emission from decihertz years distant stars, discussing search experiment by low noise multichannel receivers 20 p3291 A71-39319
- Submillimeter plane monochromatic waves propagation in ground layer of turbulent atmosphere, deriving received signals levels fluctuations 20 p3198 A71-39804
- Monochromatic plane electromagnetic wave reflection by electrically perfectly conducting diffraction grating 21 p3415 A71-40665
- Unidirectional gas laser amplifier using monochromatic optical pumping of coupled Doppler broadened transition 21 p3394 A71-41048
- Finite amplitude monochromatic wave self modulation in nonlinear medium, showing excitation process dependence on initial conditions 21 p3417 A71-41261
- Close binary stars monochromatic reflection effect calculation, using surface temperature distribution model 22 p3599 A71-41934
- Saturn disk monochromatic albedos observation by multicolor photoelectric photometry, comparing with Jupiter 22 p3602 A71-42178
- Plane monochromatic electromagnetic wave scattering by moving and rotating cylinder 22 p3510 A71-42252
- Monochromatic radio wave propagation in interplanetary plasma, deriving frequency spectrum and phase and amplitude fluctuations 22 p3511 A71-42302
- Monochromatic observations of coronal loop, using isophotal map from coronagraph through Fabry-Perot interferometer 23 p3768 A71-43846
- Monochromatic absorption coefficients determination for Ar heated in wall-stabilized arc at high temperatures and pressures 23 p3712 A71-43915

MONOCHROMATIZATION

Linear electron accelerator using shaping system debunching properties for minimizing electron energy differences in bunched beam

15 p2376 A71-31743

MONOCHROMATORS

OSO 4 satellite small grazing incidence monochromator as monitor for flux variations in solar He II Lyman alpha line ionizing radiation source

05 p0748 A71-16251

Vacuum UV monochromators calibration by molecular branching ratio technique based on electron transition probabilities

05 p0717 A71-16907

Solar radiation energy distribution simulated by vacuum monochromator, discussing Ar-Kr-Xe-methane mixture

09 p1513 A71-22557

Solar center-limb Fraunhofer line profile variations observed with double diffraction monochromator

09 p1524 A71-23192

Mariner 6 and 7 UV spectrometers, describing technical details, operating characteristics and calibration of planetary coronagraph and Ebert-Fastie monochromator used for Martian atmosphere analysis

11 p1766 A71-26301

UV Raman remote gas sensors incorporating laser scattered radiation with high resolution monochromator

17 p2753 A71-35292

Solar Fe XIV 5303 coronal line isolation, using solid Fabry-Perot interferometer as monochromator

18 p2966 A71-36736

Performance measurement of electrostatic spectrometers as monochromators by calculation of electron energy distribution

20 p3233 A71-38821

MONOCOQUE CYLINDERS

U CYLINDRICAL SHELLS

U MONOCOQUE STRUCTURES

MONOCOQUE STRUCTURES

Probabilistic approach to prolonged lifetime design and static strength of structures of monocoque and multispar wings, using fatigue characteristics of individual elements

16 p2657 A71-33604

MONOCRYSTALS

U SINGLE CRYSTALS

MONOCULAR VISION

Monocular and binocular vision comparison under moderate whole body Gz sinusoidal vibration stress environments

06 p0858 A71-17606

Nonius horopter theory and mathematical model, discussing binocular disparity and monocular visual direction criterion

09 p1399 A71-23016

Kundt optical illusion rule experimental testing under variable conditions with respect to monocular vision bisecting of horizontal straight lines, rectangles and squares

10 p1562 A71-24205

Human visual system gate type lateral interaction to luminous intensity, noting visual field response to monocular viewing

13 p2018 A71-28460

MONOLITHIC CIRCUITS

U INTEGRATED CIRCUITS

MONOMERS

Thermally stable polyimide graphite fiber reinforced composites from solutions of monomeric reactions, comparing amide acid prepolymers

11 p1788 A71-25560

Polymerization kinetics of nematic liquid crystal monomer in nematic and isotropic phases

11 p1728 A71-26062

Synthetic elastomers, including polymer chain growth, monomer sequence distribution, structural compatibility effects and commercial products development

18 p2939 A71-35886

MONOPLANES

NT A-7 AIRCRAFT

NT AN-24 AIRCRAFT

NT B-52 AIRCRAFT

NT B-70 AIRCRAFT

NT BAC 111 AIRCRAFT

NT BOEING 737 AIRCRAFT

NT BUCCANEER AIRCRAFT

NT C-130 AIRCRAFT

NT C-131 AIRCRAFT

NT C-135 AIRCRAFT

NT COMET 4 AIRCRAFT

NT DH 121 AIRCRAFT

NT DHC 4 AIRCRAFT

NT DO-31 AIRCRAFT

NT F-8 AIRCRAFT

NT F-28 TRANSPORT AIRCRAFT

NT F-100 AIRCRAFT

NT F-104 AIRCRAFT

NT IL-62 AIRCRAFT

NT MIRAGE 3 AIRCRAFT

NT SE-210 AIRCRAFT

NT T-33 AIRCRAFT

NT TSR-2 AIRCRAFT

NT VC-10 AIRCRAFT

NT XC-142 AIRCRAFT

MONOPOLE ANTENNAS

Microwave holography application to monopole antenna radiation field mechanism, using liquid crystals for optical reconstruction

05 p0756 A71-17231

Monopole antenna with continuous resistive loading, studying broadband characteristics over frequency range by thin film evaporation techniques

06 p0867 A71-17710

Monopole radiation on ground screens, deriving modified elevation angle to transform quasi-far zone measurements

06 p0868 A71-17716

Pulse excited finite length cylindrical monopole antenna mounted vertically on perfectly conducting ground plane, calculating near point electromagnetic fields

09 p1420 A71-23512

Electric current distributions measurement along monopole antenna in isotropic and anisotropic plasmas generated in large space chamber

17 p2716 A71-35048

Book on antenna characteristics covering tabulated data for cylindrical dipoles and monopoles, imperfectly conducting dipoles, circular loop antennas and broadside and endfire arrays

20 p3196 A71-39200

High power multielement electronically scanned array of microwave log periodic monopole antennas for ionospheric backscattering measurements

23 p3653 A71-44155

Conical monopole antenna imaging above hemispherical ground of variable radius, plotting finite screen effectiveness from analytical and numerical solutions

23 p3655 A71-44168

MONOPOLES

Electromagnetic device with superconducting elements for magnetic monopole detection in Apollo lunar samples, describing operation principle, amplifier, sample container and transport system

09 p1446 A71-22733

High energy cosmic ray components, investigating tracks and trapped magnetic monopoles

13 p2120 A71-28051

Particle motion in combined gravitational field of monopole and prolate quadrupole, deriving exact solution in Newtonian mechanics and general relativity

16 p2609 A71-33256

Heavily ionized particles search at sea level for magnetic monopoles existence evidence in highest energy cosmic rays

19 p3124 A71-37285

MONOPROPELLANTS

Monopropellant /isopropyl nitrate/ detonation limits, characteristics and properties

05 p0795 A71-16516

Monopropellant hydrazine propulsion catalysts evaluation, considering catalyst durability improvement and breakup

07 p1183 A71-19858

Fast burning rates in thin film solid composite propellants composed of McCormick-Selph 510, 164 monopropellant, oxidizer and polyvinyl chloride binder

14 p2285 A71-30730

Frequency analysis of open loop transfer function, determining combustion instability for catalytic monopropellant thrusters

14 p2286 A71-30759

Iridium-based long life hydrazine catalyst with multiple cold start capability, describing development program for substrate evaluation and physical properties and process optimization

14 p2286 A71-30761

MONOPULSE ANTENNAS

Radar target direction variation /glint/ sensed by amplitude monopulse tracking antenna receiving nonuniform waves

14 p2214 A71-30807

Dual plane monopulse multimode radar antenna feeds, determining input geometry relationship to generated modes by image method

14 p2218 A71-31065

Three-channel monopulse tracking receiver for automatic steering of satellite tracking antennas, noting gain controlled IF amplifier module

18 p2884 A71-36996

MONOPULSE RADAR

Soviet book on monopulse radar covering surveillance and target tracking systems, antennas, angular resolution, directional sensitivity, etc

01 p0038 A71-11300

Radar performance with multipath using complex angle /CA/ method for resolving low angle target, comparing S/N ratio with monopulse system without CA

07 p1058 A71-18844

Wideband microwave monopulse radar direction finding techniques, discussing concept, operation theory, characteristic equations and error analysis

07 p1059 A71-18846

Angular estimation precision in amplitude monopulse off-boresight radar, using linear approximation to error curve

09 p1405 A71-22695

Ku band monopulse receiver with electronically tunable Gunn oscillator, discussing negative resistance diodes dynamic impedance properties

16 p2547 A71-33557

Low level target locating by monopulse and conical scanning radar, solving balance equation

17 p2708 A71-35482

Radiation patterns due to four pyramidal horns used in sum and difference comparison monopulse radar from single horn pattern for design optimization

20 p3203 A71-39092

MONOSACCHARIDES

NT RIBOSE

Monosaccharides effect on catalytic synthesis of carbohydrates from formaldehyde

24 p3800 A71-44527

MONOSTABLE MULTIVIBRATORS

Monostable multivibrator tunnel diode synchronization bandwidth as function of circuit parameters and junction I-V characteristics

08 p1264 A71-21071

Integrable multivibrators insensitive to supply voltages and temperature variations, determining pulse widths from passive components

15 p2375 A71-31475

MONOTONE FUNCTIONS

Continuous monotonic nonlinear controlled systems with time dependent, phase coordinates and nonnegative parameter disturbances, considering Chetaev estimate for restricted approximate solution

06 p0879 A71-17670

Chebyshev and extremal approximations for monotonically increasing or decreasing variable

13 p2094 A71-28272

Bifurcation points in equation Au equals Mu with A as monotonic nonlinear operator and T as completely continuous nonlinear operator in real separable Hilbert space

13 p2094 A71-28274

Shock wave profile nonlinear one dimensional problems in gas dynamics, using monotonic difference scheme

18 p2907 A71-36333

Convergence theorem for singular integrands numerical quadratures, assuming domination near singularity by monotone integrable function

18 p2941 A71-36356

MONSOONS

Global monsoon atmospheric response model in geostrophic terms for heating input function parameterization, including Himalayas mountains effects

10 p1638 A71-23966

Monsoonal response of Somali Current in Indian Ocean, using spacecraft IR observations of sea surface horizontal temperature gradients

16 p2562 A71-33068

MONTE CARLO METHOD

Commercial transport aircraft maintenance simulation Monte Carlo Modeling techniques, considering application to airline operations

01 p0067 A71-10128

Computerized optimization of nonlinear dynamic control system subjected to random disturbances, using Monte Carlo method for quality functional

01 p0058 A71-10426

Digital simulation for translational and rotational equilibrium breakdown in gaseous molecules expansions by Monte Carlo method

01 p0130 A71-10936

Direct computerized simulation Monte Carlo method for numerical solution of Boltzmann equation in rarefied gas dynamics

01 p0113 A71-11472

Transparent dielectrics sheet radiation absorbance, emittance and transmittance determination by Monte Carlo method

01 p0183 A71-11591

Multiple integrals numerical evaluation techniques survey, discussing Monte Carlo, number-theoretical and functional analysis methods

02 p0276 A71-11801

Monte Carlo simulation model program, evaluating automatic test equipment design influence

03 p0381 A71-13089

Monte Carlo model of muon and active component distribution in nuclear cascade in extensive cosmic ray shower

03 p0476 A71-13849

Computerized Monte Carlo models of distributed parameter systems of partial differential equations with moving nonlinear boundaries

04 p0619 A71-15150

Monte Carlo method for ultrahigh vacuum free molecule flow transmission probability for straight tubes

05 p0785 A71-16395

Monte Carlo calculations of intrinsic radiation and blackness degree of nonisothermal cavities with non-specific temperature profile

06 p0897 A71-17529

Monte Carlo evaluation of molecular transport property integrals temperature dependence
06 p0917 A71-17551

Neutron monitors multiplicity yield function calculation, using Monte Carlo method for nucleonic cascade in atmosphere
06 p0960 A71-18165

Thermal radiation from finite cylindrical particle cloud, determining far field angular distribution by Monte Carlo method
[AIAA PAPER 71-78] 06 p1008 A71-18535

Monte Carlo technique for time domain response analysis of nonlinear structure in random pressure field with large deflection
[AIAA PAPER 71-213] 06 p1004 A71-18649

Selection index estimation from partial multivariate normal data for precision improvement, discussing procedure and Monte Carlo simulation results
07 p1147 A71-19599

Probable solar flare doses on interplanetary mission calculated by MCFLARE computer program using Monte Carlo methods
09 p1399 A71-22809

Mathematical model system analysis methods for reliability assurance, discussing worst case and Monte Carlo techniques
09 p1423 A71-23040

Fourth order partial differential equations boundary value problems solution by Monte Carlo techniques
10 p1637 A71-24601

Thermal louvers radiative heat transfer characteristics with solar irradiation effects, using Monte Carlo method
11 p1854 A71-25190

Peak structural response to nonstationary random excitations, approximating by Weibull distribution and Monte Carlo technique
[AIAA PAPER 71-347] 11 p1843 A71-25326

Hybrid computer Monte Carlo technique for simulation and optimization of system with random parameters
11 p1735 A71-25843

Two-line all-equipment test and aeronautic systems division reliability testing, analyzing by Weibull Monte Carlo simulation
12 p1909 A71-26657

Electromagnetic longitudinal cascades development numerical treatment based on Boltzmann equation, discussing Monte Carlo computing times for primary energy total electron counts
12 p1933 A71-27387

Three dimensional Monte Carlo simulation of extensive air shower development, comparing fireball and mathematical models for mean total hadronic energy spectra
12 p1951 A71-27388

Moving window and feedback integrator type scanning radar detectors performance comparison based on probability and position estimates by Monte Carlo simulation
12 p1882 A71-27441

Diffuse reflection from clouds with horizontal surface striations, using Monte Carlo method to follow photons through simplified models
13 p2056 A71-27975

Atmospheric very high energy cosmic ray propagation by three dimensional Monte Carlo simulation, employing H quantum and fireball models for multiple meson production
13 p2122 A71-28065

Extensive air showers nuclear active component energy flux lateral distribution and spectrum based on Monte Carlo simulation of elementary interactions
13 p2123 A71-28077

Air shower properties from Monte Carlo simulations, determining electron and muon numbers at sea level for primary protons and copper nuclei
13 p2124 A71-28085

Monte Carlo simulation of high energy atmospheric extensive air shower nuclear cascade based on Aleph model of nuclear interactions
13 p2125 A71-28089

Light pulses reflection from water and ice in clouds, using Monte Carlo technique for all orders of multiple scattering
13 p2031 A71-28795

Biased angle selection in Monte Carlo shielding calculations, using importance function
13 p2099 A71-29253

Reactor shielding design in U.S. based on Boltzmann transport equation solutions and Monte Carlo method
13 p2099 A71-29254

Reactor shielding problems solutions involving removal-diffusion theory, two dimensional transport theory and Monte Carlo method
13 p2099 A71-29255

Electromagnetic showers triggered in lead by 6 GeV primary cosmic ray electrons, calculating spatial distribution with Monte Carlo method
14 p2302 A71-30594

Lateral spread of nuclear-electromagnetic cascades in iron absorber from three-dimensional Monte Carlo simulation
15 p2452 A71-31810

Mathematical expectation and correlation function of combined pulse modulator by Monte Carlo method
15 p2382 A71-31983

Square cross section rectangular rotating grains dynamic behavior in magnetic fields, obtaining orientation data with Monte Carlo method
15 p2498 A71-32772

Monte Carlo Bayesian analysis technique applied to decision problem concerning population of single-use item in state of operational readiness
16 p2582 A71-33288

Autonomous unknown landmark tracking space shuttle navigation system performance assessment by digital computer program providing error analysis and Monte Carlo simulation
17 p2773 A71-35067

French monograph on system reliability of particle detection device covering methodology, functional models, Monte Carlo simulation, spectrometers and DC/DC converters
17 p2767 A71-35231

Mass, center of gravity and moment of inertia measurements curtailment by tolerance and regression analyses and Monte Carlo method
[SAWE PAPER 883] 17 p2834 A71-35820

Shock wave structure prediction by nonlinear kinetic models with Monte Carlo solutions of full Boltzmann equation
18 p2907 A71-36334

Flow simulation with digital computer by Monte Carlo computation methods based on interacting molecular gas kinetics, noting application to gas flow
18 p2941 A71-36427

Space and missile guidance performance analysis based on error sources, using Monte Carlo simulation
19 p3101 A71-37754

Air traffic congestion and delay Monte Carlo digital simulation in FORTRAN, exemplifying two-runway airport operation under instrument flight rules
19 p3041 A71-38024

Subliming nuclear microthruster design with Monte Carlo study of rarefied gas nozzle flow, noting application to spin stabilization
19 p3103 A71-38351

Monte Carlo generation method for phase-space integrals of multiperipheral models for high energies and particle multiplicities
21 p3408 A71-40850

Diffraction phenomena numerical modeling by Monte Carlo statistical analysis, using Heisenberg uncertainty principle
22 p3576 A71-42556

Monte Carlo method calculation for light pulse reflection from clouds for all orders of multiple scattering
22 p3576 A71-42562

Monte Carlo model of muon and active component distribution in nuclear cascade in extensive cosmic ray shower
22 p3595 A71-42650

Apollo command module land landing capability in case of abort after liftoff, describing Monte Carlo simulation procedure
22 p3573 A71-42776

Monte Carlo simulation of navigation and guidance for Grand Tour Jupiter-Saturn-Uranus 1977 mission, using graphics computer program [STEP VII]
[AAS PAPER 71-374] 23 p3701 A71-43044

Sequential processor performance prediction error with linear method from Monte Carlo cycle analysis of Apollo 14 early rendezvous profile
23 p3731 A71-43056

Thermal radiation hemi-ellipsoidal and hemispherical collectors efficiency characteristics from Monte Carlo simulation for focusing photon bundle trajectories
23 p3783 A71-44191

Two dimensional radiative heat transfer in absorbing-emitting medium bounded by nonisothermal gray walls from Monte Carlo simulation, showing gas emissive power distribution
23 p3784 A71-44276

MONTH
Energy considerations of satellite orbit paradox, discussing speed increase under drag, librational motion and secular month length
18 p2962 A71-36099

MONTMORILLONITE
Montmorillonite and serpentine as major crystalline constituents of Orgueil meteorite
10 p1679 A71-24983

MOODS
Affect adjective checklist assessment of mood changes as function of stress in air traffic controllers
23 p3640 A71-44240

MOON
Lunar Mach cone in flow of magnetized warm collisionless solar plasma from Explorer 35 observations
01 p0162 A71-11489

Radar astronomy principles, applications and types of measurements, discussing solar, lunar, planetary and meteor observations
02 p0313 A71-12490

Solar wind interaction with moon, using two dimensional guiding center model
02 p0303 A71-12772

Solar wind lunar impingement induction of magnetic fields used for global sounding of moon structure
03 p0486 A71-13323

Automatic solar and lunar reference guidance system with balanced photoelectric measuring equipment
04 p0591 A71-14846

Hot moon suggested from chemical and physical reasoning, discussing outer layers and surface features formation
04 p0645 A71-15138

Soviet book on planets and moon covering surfaces, atmospheres, internal structure and observation methods
04 p0657 A71-15800

Moon free libration second and third mode semiamplitudes from statistical relations
05 p0809 A71-16456

Lunar position on stellar field for ephemeris time determination, discussing planet and satellite positions with respect to astronomical constants
05 p0809 A71-16460

Lunar studies bibliography covering shape, EM properties, structure, gravitational fields, chemical composition, origin, surface features, etc
05 p0809 A71-16463

Book on geochemical exploration of moon and planets covering orbital, compositional and surface studies, Apollo missions, Lunar Receiving Laboratories and data processing
05 p0813 A71-16950

Earth, moon and planets sizes, masses and moments of inertia determination by artificial satellites, space probes and radar observation
05 p0815 A71-17241

Lunar interior electrical conductivity and temperature from various conductivity models, considering interplanetary magnetic source field
06 p0964 A71-17281

Moon shape, translational and rotational motion determination by optical tracking, discussing possible refinements as function of distance measurement accuracy
09 p1525 A71-23337

Laplace long period solar inequality effects on lunar ecliptic longitude, considering role in celestial mechanics
10 p1667 A71-23829

Quiet sun and new moon brightness temperatures simultaneous measurements as function of frequency and wavelength
12 p1969 A71-27648

Solar system space physics review covering earth atmospheric temperature, density and models, solar wind, auroras, and moon, Venus and Mars data from space missions
13 p2131 A71-27877

Bibliography on lunar and planetary subjects covering astrobology, comets, cratering, meteors temperature, structure, asteroids, tektites surface features, etc
13 p2135 A71-28293

Moon and planets - NATO Conference, University of Newcastle-upon-Tyne, England, April 1970
16 p2636 A71-33501

Lunar forced motions and free oscillations, considering inertia moments effects on rotational and translational movements
16 p2636 A71-33502

Lunar libration detection by photographing double exposure of stellar field and moon
16 p2636 A71-33503

Transportable high radiance lunar ranging laser system, describing optical equipment in ruby and Nd-glass laser experiments
18 p2883 A71-36917

Lunar electroconductivity, examining moon response to large discontinuity in interplanetary magnetic field
19 p3131 A71-37354

Ephemerides of sun, moon, planets and minor planets for October through December 1971
21 p3442 A71-40153

Terrestrial, lunar and planetary dynamical properties and internal constitution, considering data obtained from artificial satellites, lunar and planetary dynamics
22 p3607 A71-42883

Lunar physical libration effect on lunar satellite orbital elements, considering reorientation of selenographic axes fixed in true moon
[AAS PAPER 71-331] 23 p3727 A71-43004

MOON-EARTH TRAJECTORIES
Nonplanar moon-earth trajectories, determining restricted three body problem analytical solution accuracy
[AIAA PAPER 70-1060] 03 p0495 A71-14274

Analytical techniques for invariant properties of families of moon-earth trajectories
04 p0660 A71-15891

Trajectory analysis of geocentric phase and selenospheric motion of space vehicle leaving lunar surface and returning to earth atmosphere
13 p2143 A71-29209

MORL

MANNED ORBITAL RESEARCH LABORATORIES

MORPHOLOGY

NT GEOMORPHOLOGY
NT ISOMORPHISM
NT LUNG MORPHOLOGY
NT POLYMORPHISM

Morphological and histological changes in liver and kidneys of rats exposed to long term hypothermia

01 p0013 A71-11131

Al-Mg alloy oxide film morphology and composition under various oxidation conditions, using electron microscopy and diffraction

05 p0770 A71-17100

Uniaxial stress effect on morphology changes of coherent gamma prime precipitates in nickel base superalloy crystals

06 p0914 A71-18682

Stomach secretory function and histomorphological changes in dogs under stress

09 p1390 A71-22263

Composite morphology and mechanical properties relationship, considering reinforcing effect, filamentous systems, whisker growth ladder molecules synthesis and material production

10 p1635 A71-24768

Morphology, mineralogy and chemistry of Ashmore meteorite

11 p1835 A71-26482

Lunik spacecraft soil sampler landing site geological-morphological analysis from television images, indicating formation patterns similar to equatorial zone seas microrelief

12 p1966 A71-27302

Noctilucous cloud morphology and kinematics from photographic observations near Moscow

14 p2233 A71-29971

Microfossil structures from morphological alterations of proteinoid microspheres due to inclusion of organic or synthetic polyamino acids

14 p2190 A71-30178

Adrenal medulla biochemistry and morphology, discussing epinephrine synthesis control by glucocorticoid hormones

14 p2187 A71-30809

Morphological projections in astrophysics, considering single star evolution in terms of Boltzmann-Gibbs statistical mechanics

14 p2318 A71-31020

Cooling history of magma containing spherulite growth forms on basis of morphological variations in glassy and crystalline rocks

19 p3051 A71-37673

Lunik spacecraft soil sampler landing site geological-morphological analysis from TV images, indicating formation patterns similar to equatorial zone seas microrelief

19 p3145 A71-38261

Gravity influence on plant growth, lateral development, apical dominance, bud initiation, orientation and flower morphology

21 p3340 A71-39999

Carbon fibers grown on graphite by thermal decomposition of hydrocarbons, investigating external morphology and structure

21 p3406 A71-40837

Morphological relationships in solar chromospheric H alpha fine structure involving bushes, fibrils, threads and filaments

22 p3597 A71-41457

Beta eutectoid and solid solution Ti binary alloys omega phase morphology observation by transmission electron microscopy, noting elliptical and cubic types hexagonal crystal structure

22 p3562 A71-41946

Composite tissue blocks method for comparative pathomorphological investigation of radiation pathology

22 p3505 A71-42734

Morphological and cytochemical changes in red and mixed skeletal muscles of animals exposed to hypokinesia

23 p3636 A71-44237

Morphological changes in dogs brain vessels under transverse accelerations

24 p3796 A71-44546

MORPHOTROPISM

U ISOMORPHISM

MORSE POTENTIAL

Atmospheric triggered VLF emissions theory, examining magnetospheric whistler Morse pulses

23 p3643 A71-43135

Degenerate critical points Morse index type characteristics, considering maximum points of functional on surface of another

24 p3843 A71-44707

MORTALITY

Complete heart block associated with acute myocardial infarction, discussing high mortality rate and transvenous pacemaker applications

02 p0198 A71-11696

Death rates, median life span and weight in mice exposed to gamma radiation after intra-abdominal injections of cysteamine

22 p3505 A71-42712

Mortality in survivable or partially survivable U.S. Army aircraft accidents, observing death relationship to aircraft duty and seat location and type

23 p3640 A71-44248

MOS (SEMICONDUCTORS)

U METAL OXIDE SEMICONDUCTORS

MOSAICS

Side-looking airborne radars ground and slant range imagery mosaic preparation and geoscience interpretation, analyzing terrain geometry, radar shadow and layover

06 p0898 A71-17561

MOSFET

U FIELD EFFECT TRANSISTORS

MOSS (SPACE STATIONS)

U ORBITAL SPACE STATIONS

MOSSBAUER EFFECT

Mossbauer effect study of 475 C decomposition of binary Fe-Cr alloys, considering fluctuations about average composition

07 p1138 A71-19985

Mossbauer spectrometer with constant speed mechanical drive, describing special design features to avoid vibration induced lowering of spectral resolution

09 p1442 A71-22319

Nucleation, growth and spinodal decomposition during aging in Fe-Cr alloys, using Mossbauer spectroscopy

13 p2089 A71-29414

Mossbauer gamma spectrometer for operation at constant and adjustable velocities, incorporating springless vibrator and automatic zero stabilization

14 p2247 A71-30577

Apollo 11 and 12 lunar soil and rock samples abundance comparison based on Mossbauer spectroscopy

16 p2637 A71-33509

Computer interpretation of Mossbauer effect spectra with iterative, integration and comparison procedure

18 p2887 A71-36858

Mossbauer effect applications to magnetic thin films, discussing electric and magnetic hyperfine interactions and experimental difficulties

18 p2955 A71-36939

Mossbauer instrumental analysis of Apollo 12 rock and soil samples, measuring nuclear gamma resonance of iron 57

23 p3759 A71-43764

Phase analysis of Apollo 12 fines, core tube samples and rocks by Mossbauer studies, noting nearly uniform distribution of major Fe containing phases

23 p3759 A71-43765

MOT (ORBITAL TELESCOPES)

U MANNED ORBITAL TELESCOPES

MOTILITY

U LOCOMOTION

MOTION

Soviet papers on movement control covering rate regulation, human rhythms, finger coordination, etc

02 p0203 A71-12051

Human temporal performance of homogeneous discrete motor acts sequence, suggesting central nervous mechanism for movement rate generation

02 p0204 A71-12052

Human muscular control patterns during forearm precision cyclic bending on ergograph

02 p0204 A71-12053

Human discrete and continuous rhythmic movements rate control

02 p0204 A71-12054

Time interval tracking in humans during steady and transient performance of homogeneous discrete motor acts sequence

02 p0205 A71-12056

External acoustic signals for human cyclic movements temporal structure control

02 p0205 A71-12058

Biological movement control systems from structural linguistics viewpoint

02 p0206 A71-12063

Holographic images of moving objects, extending theory to objects moving with constant acceleration

08 p1291 A71-21402

MOTION AFTEREFFECTS

System with aftereffect along programmed trajectory, studying controlled motion stability and accuracy

07 p1161 A71-20269

Reduction or disappearance of visual aftereffect of movement without patterned surrounding consisting of dots, concentric circles, grid pattern or vertical bars

10 p1558 A71-23744

Instrument orientation optimization for ballistic missile applications, emphasizing acceleration induced velocity and position errors

11 p1796 A71-26410

Sound field of point acoustic stresses in arbitrary motion, investigating uniform straight line and circular motion and pure rotation effects

15 p2450 A71-32130

External oblique inguinal hernia due to acrobatic flying centrifugal accelerations, considering anatomical, clinical and medico-legal aspects

17 p2681 A71-34822

Motion measurements applications to facility design and inertial navigation hardware performance test problems concerning test platform response to ground motion, forces and disturbances

[AIAA PAPER 71-923] 19 p3102 A71-38327

Lateral accelerations effect on mice tolerance to toxic doses of aminothiols and indolylalkylamine-series radiation protection drugs

22 p3491 A71-42706

MOTION EQUATIONS

U EQUATIONS OF MOTION

MOTION PERCEPTION

U SPACE PERCEPTION

MOTION PICTURES

Left ventricular volume determination by high speed cineangiocardiology, using optical scanning and automatic data processing

02 p0203 A71-11705

Computer generated motion pictures to simulate real events, discussing design problems and airfield simulation with GPSS software package

07 p1111 A71-19511

Visual devices for training simulators, discussing film and closed circuit TV systems and components

15 p2385 A71-31889

High resolution 16mm pulse mode cine reconnaissance camera design features, discussing dynamic balance and reaction forces cancellation

17 p2746 A71-35761

Spectroheliogram Doppler movies of solar velocity fields showing oscillatory and slowly varying components

18 p2965 A71-36728

Bulk boiling studies with motion picture camera and quartz envelope of KIO 220/2500-2 tube for heat releasing surface

24 p3890 A71-45025

MOTION SICKNESS

Space mission reflex vestibular disturbance and motion sickness prevention, examining artificial gravity and drugs

02 p0198 A71-11979

Space motion sickness causes and prevention, discussing syndromes, psychophysiological factors, vestibular mechanics and adaptation

04 p0539 A71-15283

Visual analyzer functional state during latent motion sickness on rocking devices simulating moving aircraft

05 p0711 A71-17026

Target aiming function (TAF) susceptibility to vagotonic vegetative imbalance in male subjects after experimental kinetosis

07 p1047 A71-19464

Labyrinths and proprioceptors from aerospace medicine viewpoint, discussing motion sickness, spatial disorientation, manned space flight and rotation in space

08 p1244 A71-20711

Linear acceleration effects on human otolithic and vestibular apparatus, discussing vestibulovegetative motion sickness syndrome and nystagmus index activation

08 p1242 A71-21956

Modeling human disorientation and motion sickness in rotating spacecraft, stressing sensors dynamic response

[AIAA PAPER 71-870] 18 p2872 A71-36654

Vibration effects on human body, discussing neurophysiological data, safe exposure limits, therapeutic applications, motion sickness, muscular responses and biomechanical effects

21 p3342 A71-40147

Correlation coefficients between sensitivity thresholds of cupula-endolymphatic system to angular and Coriolis accelerations with human resistance to motion sickness

24 p3795 A71-44532

MOTION SICKNESS DRUGS

Unilateral labyrinthectomy model for evaluating anti-motion drug effects on vestibular function in guinea pigs

06 p0854 A71-18361

MOTION STABILITY

NT AERODYNAMIC STABILITY
NT AIRCRAFT STABILITY
NT ATTITUDE STABILITY
NT BOUNDARY LAYER STABILITY
NT DIRECTIONAL STABILITY
NT FLAME STABILITY
NT FLOW STABILITY
NT GYROSCOPIC STABILITY
NT HOVERING STABILITY
NT LATERAL STABILITY
NT LONGITUDINAL STABILITY
NT LOW SPEED STABILITY
NT MAGNETOHYDRODYNAMIC STABILITY
NT ROTARY STABILITY
NT SPACECRAFT STABILITY

Second order nonlinear control system control law derivation by Liapunov direct method, defining region of undisturbed motion asymptotic stability
01 p0058 A71-10407

Two-gyro attitude control system with conical suspension, analyzing vehicle motion asymptotic stability in circular orbit
01 p0081 A71-10634

Motion stabilization for nonlinear control systems with critical zero and imaginary roots, using Liapunov classical theory
01 p0128 A71-10667

Motion stability of satellite with rigid connection to symmetric rotors rotation axes
01 p0164 A71-11156

Perturbed motion stabilization in nonlinear control system with applicable equation containing zero root and imaginary roots
01 p0128 A71-11158

Dissipative gyroscopic system with servo link, obtaining steady motion stability
02 p0252 A71-12402

Motion stability of double-gyro inertial frame in Newtonian central force field, applying Liapunov and Chetaev methods
02 p0253 A71-12638

Nonstationary automatic control system asymptotic series solution for equations of perturbed motion, deriving unperturbed motion local stability criteria
03 p0388 A71-13287

Nonlinear stability of triangular points in restricted problem of three bodies, using second order expansions, Lie transform and multiple scale method
03 p0487 A71-13448

Heavy gyrostator motion problem, using Mozalevskaya particular solution characterized by algebraic invariant relation
03 p0458 A71-13593

Liquid filled gyroscope motion stability, examining experimental data, design and testing procedures
03 p0426 A71-13776

Heading of object moving on terrestrial sphere surface with inertial navigation aid, calculating asymptotic stability for position determination on computer
03 p0459 A71-14355

Stochastic motion stability of discrete dynamic systems involving Itô equations
04 p0625 A71-15060

Two dimensional motion stability near sun-perturbed earth-moon triangular libration points, using computerized high order treatment
04 p0653 A71-15708

Critical periodic orbits for main families and all mass ratios, considering stability in restricted problem
04 p0655 A71-15729

Stability and resonances in restricted three body problem, using method of surface-of-section
04 p0656 A71-15732

Satellite motion stability in axisymmetric field of oblique rotating planet
05 p0815 A71-16050

Axisymmetric body stationary motions around sphere, investigating secular and ordinary stability
05 p0809 A71-16473

Object motion stabilization, determining minimum control actions number for linear and nonlinear systems
05 p0782 A71-16977

Permanent motion stability of heavy body having variable mass geometry
05 p0783 A71-17038

Launch vehicle attitude control system for lateral drift minimization and prevention of structural load limit exceeding maneuvers, presenting stability analysis
06 p0979 A71-17338

Numerical and graphic drive shaft motion trajectories in dynamic gyroscopic system with four degrees of freedom
06 p0928 A71-18232

Roll resonance in reentry body motion under nonlinear pitch, damping and Magnus moments, using multiple scales method
06 p0979 A71-18508

Axisymmetric body rapid rotation under center of gravity velocity vector conditions, solving for plane gliding motion stability in air
07 p1159 A71-19354

Representative data of actual forces and moments applicable to large spacecraft attitude control system for typical crew activities obtained through simulation programs
07 p1208 A71-19866

Periodic motions stability in purely imaginary characteristic indices pairs transcendental critical case
07 p1161 A71-20266

System with aftereffect along programmed trajectory, studying controlled motion stability and accuracy
07 p1161 A71-20269

Resonances stability and development in restricted three body problem with two degrees of freedom
07 p1202 A71-20514

Gravitational stability analysis based on Boltzmann-Vlasov collisionless kinetic equation solution by trajectory integration method in plasma physics
07 p1173 A71-20531

Oscillatory systems with nonlinear elastic arresting devices, calculating dynamic characteristics and motion stability
08 p1332 A71-20687

Motion synchronization of objects with single degree of freedom and weak coupling interactions, using small parameter method
08 p1336 A71-21862

Stationary motion stability of shaft in cylindrical MHD finite length bearing, assuming incompressible lubrication and small lubrication clearance
09 p1453 A71-22139

Elastic deformable satellite motion stability in central Newtonian force field
09 p1532 A71-23134

Nonstationary automatic control system asymptotic series solution for equations of perturbed motion, deriving unperturbed motion local stability criteria
09 p1424 A71-23262

Stability of regular motions of dynamically symmetrical body with equatorial symmetry plane in Newtonian force field of spherical planet by Liapunov second method
09 p1526 A71-23346

Two-differential equations system in critical case of double zero root, deriving motion stability criteria with aid of Liapunov functions
09 p1495 A71-23430

Differential equations construction for controlled systems and controller starting from programmed motion stability requirement
09 p1495 A71-23432

Stabilized image movement control by mounting object in electric synchronous motor and rotating eccentrically
10 p1567 A71-23989

Stability and coordinate bounds of motion of linear dynamic systems over finite time intervals by solutions of differential equations
10 p1643 A71-24900

Two-degree of freedom Hamiltonian system stability and motion about equilibrium point for two-to-one commensurability
10 p1679 A71-24936

Unperturbed motion asymptotic stability and instability theorems, considering Liapunov function method
12 p1932 A71-27524

Motion stability of symmetric rotor of gyroscope with inviscid incompressible liquid filled cylindrical annular cavity around coaxial rigid rod
13 p2065 A71-27978

Stationary motions of holonomous five degree of freedom mechanical system of rod suspended homogeneous symmetrical body in central gravitational field
13 p2100 A71-28730

Positional motion rigidity of gyroscopic systems with cyclic coordinates and low spin, using Liapunov second method
13 p2069 A71-28732

Gyrostator satellite steady motion and relative position optimal stabilization by additional forces application
14 p2275 A71-30871

Motion stabilization for nonlinear control systems with zero and imaginary roots, using Liapunov classical theory
14 p2221 A71-31000

Asymptotic stability of equilibrium position of vibrating linear mechanical systems with semidefinite damping matrix applicable to satellite attitude stabilization
15 p2502 A71-31174

Equilibrium position stability of nonlinear two body satellite system in circular orbits in gravitational central force field, using linearized equations of motion
15 p2499 A71-31176

Orbital stability concept under nonperiodic motions
15 p2499 A71-31179

Nonlinear asymptotic stability of motion in critical case involving characteristic equation in first approximation with pair of imaginary roots
15 p2449 A71-31699

Aspect ratio influence on instability and non-minimum phase effects of longitudinal motion of aircraft relative to negative lift-drag expression transfer functions
16 p2523 A71-33405

Satellite motion stability in axisymmetric field of oblique rotating planet
16 p2645 A71-33454

Nonreversibility of Marachkov theorem on asymptotic stability, using scalar equation
16 p2612 A71-33595

Statistical theory of nonlinear differential equation system with discontinuous trajectory solution, deriving motion stability to first approximation using Liapunov functions
17 p2780 A71-34915

Object motion stabilization, determining minimum control actions number for linear and nonlinear systems
18 p2947 A71-36777

Motion stability for critical case of characteristic equation with purely imaginary roots, deriving solution by nonlinear mechanics asymptotic method
19 p3104 A71-38013

Bearing axis wobble for dual spin vehicle in terms of rotor static and dynamic unbalance and platform mass geometry and inertia
20 p3306 A71-39351

Motion synchronization of objects with one degree of freedom and weak coupling interactions, using small parameter method
20 p3270 A71-39361

Lagrange-Dirichlet and Routh systems stability theorems inversion, proving motion instability in case of potential energy maximum in solutions to differential equations
21 p3414 A71-40092

Soviet book on hydrodynamics of nonstationary motions of viscoplastic media covering mechanical properties of clay, mortar, cement, lubricating oil, petroleum and disperse media, etc
21 p3369 A71-40872

Relative motion interaction dynamics in rocket biaxial control with azimuth and elevation servos, using Mathieu equation and stability criterion
22 p3526 A71-41971

Altitude dynamics and motion stability analysis of gravity oriented synchronous satellite under perturbation effects of environmental forces due to sun, earth, albedo and cosmic rays
22 p3612 A71-42050

Vestibular and proprioceptive stabilization of eye movements
22 p3489 A71-42448

Motion stability analysis for force-free spinning satellites with flexible appendages by Liapunov direct method
23 p3772 A71-43018

Plane motion stability of rapidly rotating symmetric rigid body in atmosphere, deriving short-cut equations system by Bogoliubov-Zubarev method
24 p3847 A71-44416

Distant stellar satellites existence possibility based on maximum distance estimation for material particle motion stability with respect to sun or another star
24 p3870 A71-44815

Bounded circular-space three body problem, obtaining Lagrangean solutions for triangular motion configuration stability
24 p3870 A71-44816

Pneumatic hammer/self oscillation/occurrence in gas lubricated externally pressurized annular thrust bearing, comparing experimental and theoretical stability data
24 p3830 A71-44948

MOTIVATION

Conditioned reflexes in cats with mesencephalic reticular formation subject to food-signaling acoustic stimulation
01 p0007 A71-10034

Flying motivation loss, considering psychogenesis and physiological causes
05 p0715 A71-16933

Engineers time and intellectual utilization in industry dependence on local company attitudes, suggesting better management appreciation of motivation factor [ASME PAPER 70-WA/MGT-12]
07 p1225 A71-19501

Motivation principles in industry based on Maslov theory of hierarchy of needs, discussing selection of supervisory personnel
13 p2167 A71-28798

Motivations of scientists, engineers and technicians, considering changing nature of R and D projects
13 p2167 A71-28800

Air transport and travel expansion rate, discussing motivations and cost
14 p2340 A71-30159

Differentiation of hypothalamic drive and reward centers, applying electric stimulation via chronically implanted electrodes
17 p2681 A71-34944

Characteristics study of technical entrepreneurs, considering family background, education and motivation
19 p3173 A71-37631

Psychopathological causes for French Air Force flying personnel inaptitude, considering motivational problems and age factor
22 p3500 A71-41575

MOTOR SYSTEMS [BIOLOGY]

U Efferent Nervous Systems

MOTORS

NT ELECTRIC MOTORS
NT MICROMOTORS
NT SERVOMOTORS
NT SYNCHRONOUS MOTORS
NT TORQUE MOTORS

Rotary hydraulic motors dynamic behavior during pressure and fluid flow control
01 p0006 A71-10823

Gyroscopes motor couple scale factor measurement
[AGARDOGRAPH-128] 05 p0750 A71-16311

MOUNTAIN INHABITANTS

Renal oxygenation in male Peruvian natives living permanently at high altitudes, determining reduced tubular function cause

12 p1873 A71-27127

High altitude residents cardiovascular evaluations, showing right ventricular enlargement and reactive pulmonary hypertension

14 p2184 A71-30285

Ventilatory acclimatization to chronic hypoxia in high altitude natives by cerebrospinal fluid pH decrease

17 p2683 A71-35144

Urinary protein excretion rates in high altitude inhabitants, showing polycythemia effect on creatinine clearances levels

19 p3009 A71-38561

Long term effects of hypoxic stimulus suppression upon heart rate, cardiac output and pulmonary artery pressure of highlanders, observing bradycardia

23 p3631 A71-43117

Hypoxic respiratory reactions of highland natives and recently arrived residents to oxygen concentration change in inhaled mixtures

24 p3798 A71-45065

MOUNTAINS

NT HIMALAYAS

Mountain-size atmospheric eddies on leeward slope of Carpathian and Low Tatra mountains, discussing turbulence effects on air navigation

01 p0113 A71-10349

Integral equation solution for air flow over mountain system, considering boundary value problems of Helmholtz equation

07 p1149 A71-18794

Two layer structure of principle air flow over mountain system, noting effect on air waves and rotors formation in leeward region

07 p1149 A71-18795

Medical and technical aspects of air rescue and survival of astronauts in mountainous remote areas, noting dogs use for disaster victims location

22 p3482 A71-41982

Mountain induced lee waves, turbulence and wind measurements in Colorado, using aircraft flight data

22 p3569 A71-42548

MOUNTING

Strain free insulated mounting technique for semiconductors onto cold finger at liquid He 3 temperatures

02 p0294 A71-12142

Altazimuthal telescope mounting with computer controlled guidance, discussing instrumental and methodical error effects on positioning and tracking accuracy

07 p1083 A71-19348

Hybrid circuit heat sensitive semiconductor chips mounting methods for preventing thermal degradation

21 p3356 A71-40744

MOUNTS

U SUPPORTS

MOUTH

Transducer for measuring mandibular dynamic movements during speech

01 p0079 A71-10346

Prenatal exposure to hypoxia, showing prolonged suppression of labeled amino acid incorporation into developing submandibular gland and pancreas in neonatal period

07 p1042 A71-19698

MOVEMENT

U MOTION

MOVING TARGET INDICATORS

Moving target indicator detection filters with nonuniform intersperse periods, discussing design

01 p0058 A71-11575

Synthetic aperture holographic techniques in continuous wave bistatic radars for moving targets

03 p0381 A71-14477

Video MTI pulse radar Doppler filter optimum symmetrical weighting factors in clutter-plus-noise environment

07 p1059 A71-18847

Moving target indicator (MTI) performance improvement in presence of rain, chaff or other broadband clutter disturbances by adaptation for canceler setting optimization

08 p1254 A71-21338

Algorithmic analysis of detection characteristics of periodic compensation systems used in moving targets signal detection

09 p1404 A71-22153

Omnidirectional radar moving target detection from clutter, using Doppler filter system

09 p1407 A71-23047

Two-frequency moving target indicator Doppler radar system, predicting efficiency to clutter drift under stochastic echo and clutter signals

10 p1578 A71-24591

Pulse radar moving target indication and stationary targets reflection suppression, using recursive type digital filter and quadrature channels for improving signal detectability

10 p1579 A71-25068

Target movement effects on airborne coherent side-looking synthetic aperture imaging radar during scan rate and compression ratio increases

14 p2197 A71-30798

IF nonlinearities effect on Gaussian clutter rejection associated with noncoherent MTI radar receiver

17 p2708 A71-35483

Light detection and ranging (LIDAR) system in airborne and ground applications for moving target location and tracking

18 p2882 A71-36615

Moving target indicator receivers design and techniques, discussing performance limitations

20 p3200 A71-39905

Signal processing techniques for clutter suppression in moving target indicator radar

20 p3200 A71-39908

Surface based moving target indicator radar systems history, performance and problems

20 p3200 A71-39909

Digital techniques for tactical radar signal processing functions, discussing low cost integrated circuitry, moving target indicators, and analog to digital converters

21 p3348 A71-40588

MRKOS COMET

Photometry of head and tail regions of comets Kosik, Akhamarov-Iurlov-Hassel, Arend-Roland and Mrkos by equidensity method, using Sabatier effect

15 p2484 A71-31668

MTBF

Reliability of redundant repairable systems with preventive maintenance, determining mean time between failures

11 p1769 A71-25660

Statistical nature of time to complete MIL-STD-781 reliability sequential tests for military and space equipment, giving information about MTBF

12 p1908 A71-26656

Redundancy verification of parallel systems related to element MTBF and decision maker perspective involving acceptance risk of system failure

16 p2582 A71-33292

Optimum skew angle between redundant inertial systems, considering component weight, MTBF and duty cycle

17 p2773 A71-35062

Reliability engineering, reviewing MTBF, redundancy, complexity effects on failure rate, reliability prediction, repair and replacement cost and test techniques

18 p2928 A71-36806

Reliability controlled maintenance plan for avionics equipment based on mean time between failures

20 p3203 A71-39087

Relcomp conversational time-sharing computer program for rapid calculation of reliability and MTBF of systems with serial and redundant units

22 p3517 A71-42103

System quality analysis by reliability measures/mean time between failures/, using distribution free evaluation models

22 p3566 A71-42114

Optimal redundancy and availability allocation for MTBF and time to repair in multistage system, using dynamic programming

22 p3518 A71-42116

MTI RADAR

U MOVING TARGET INDICATORS

MUBIS (SCANNERS)

U MULTIPLE BEAM INTERVAL SCANNERS

MUFFLERS

Acoustic and gas dynamic characteristics of jet noise muffler, using adapters at outlet section of exhaust nozzle

15 p2469 A71-31710

Optimal design for noise attenuation by diesel engine exhaust mufflers using linearized acoustic models

20 p3268 A71-38961

Sound field measurement in circular and rectangular air duct with sound-absorbing walls (mufflers), deriving empirical formula for attenuation frequency characteristics

24 p3849 A71-45271

MULLITES

Composite Ni coatings, adding mullite crystals to enhance oxidation resistance

01 p1012 A71-10784

Ceramic particle compaction as function of size, shape, loading rate and hardness for fused alumina, magnesia and mullite

03 p0448 A71-12973

MULTICHANNEL COMMUNICATION

Ground station power control in multiple access satellite communication system

02 p0224 A71-12823

Wideband signal processing via multiple narrow band channels, discussing performance limitations due to amplitude and phase distortion and spurious outputs

04 p0555 A71-15341

FM radio relay system modulation-demodulation equipment for multichannel FDM or TV signal transmission

05 p0728 A71-16146

Multiplexed PAM signal transmission over random time multichannel and diversity systems, discussing optimization for receiver frequency response by numerical solution

[IEEE PAPER 70-TP-47-COM] 05 p0723 A71-17053

Quantized multiple access voice communications, comparing QPPM-AM and FM performances concerning transmitter power, RF bandwidth, circuit complexity, etc

[IEEE PAPER 69-TP-448-COM] 05 p0724 A71-17056

All-digital multichannel narrow band FSK data receiver with time-shared arithmetic processor, discussing prototype design and performance

[IEEE PAPER 70-TP-49-COM] 05 p0724 A71-17064

Multichannel on-line data terminals using minicomputer for communication control, error detection and data buffering

[IEEE PAPER 68-TP-448-COM] 05 p0727 A71-17068

Low distortion gain-controlled 140 MHz IF main amplifiers for 2700-channel microwave repeaters, discussing design and performance

05 p0730 A71-17069

Multichannel EEG radio telemetry for remote recording of biological activity from subjects in motion and within human body

05 p0715 A71-17110

Intelsat 3 satellite Communication, Telemetry, and Command system using transponders for multichannel voice and TV transmission

06 p0870 A71-18398

Bioelectric activity of cerebral cortex in man under neuroemotional stress, using multichannel radioelectroencephalography

06 p0856 A71-18464

Digital multiple access communications for commercial transmission via Intelsat satellites

07 p1057 A71-18817

Time division multiple access techniques for Defense Satellite Communications System

07 p1057 A71-18819

Computer controlled time division multiple access control system for U.S. Army Satellite Communication Agency, discussing tests and operational details

07 p1057 A71-18820

DCS TDM/DSCS TDMA synchronous operation, examining rate buffering, slaved clocks and constant feedback approaches

07 p1058 A71-18823

Multichannel laser telephone communication link experimental operation results in U.S.S.R.

07 p1058 A71-18838

Onboard self adaptive multichannel data reduction for redundancy by oversampling

[AIAA PAPER 71-232] 07 p1063 A71-19709

Data handling system with digital computer and multichannel scanning, processing and recording for simultaneously conducting two environmental tests of satellites

07 p1069 A71-20403

Noise rejection of two channel asynchronous storage circuit with internal detection for weak signal reception

08 p1252 A71-20734

Dual channel rotary joint combining Tm and Te modes in circular waveguide for X band antenna high average power operation

08 p1252 A71-20758

N-channel PSK/PM digital telemetry system modulation scheme for space exploration

08 p1254 A71-21315

Space-DMA or space-TDMA techniques conserving spectrum and increasing communication satellite channel capacity, discussing spot beams and switchings

08 p1254 A71-21326

HF stability audio multichannel oscillators design and operation, comparing frequency synthesizer systems for optimal circuitry characteristics

09 p1417 A71-23029

Optimal control law for regulating energy distribution of emitted radar signals in multichannel system for minimizing target search duration

10 p1579 A71-24722

Pulse radar moving target indication and stationary targets reflection suppression, using recursive type digital filter and quadrature channels for improving signal detectability

10 p1579 A71-25068

Multiplexer concentrators for data telecommunication systems with erratic information flow, concerning statistical assumptions, transient response, queueing tails and message clustering

12 p1880 A71-27072

Optimal receiver to detect multiple orthogonal signals on normal stationary noise background, assuming nonuniform a priori probability occurrence

12 p1883 A71-27618

Multichannel modular tropospheric scatter equipment as economic solution for medium range HF communication

13 p2034 A71-29317

Two cavity ring-type channel dropping filters for millimeter wave guided communication system, calculating pulse response and interchannel crosstalk characteristics

14 p2210 A71-29569

Frequency measurements of square wave signal with unknown amplitude by two mismatched channels, comparing rms error with effective estimate variance

14 p2195 A71-30106

Random multiple access technique for satellite data collection, taking advantage of frequency instability associated with oscillator circuits

14 p2199 A71-30908

Optimum power parameters and economic efficiency of Soviet communication satellite system, comparing with terrestrial multichannel communication

17 p2696 A71-34231

Satellite communication technology in next decade covering Intelsat 4 characteristics, meteorological satellites, navigation aids, multichannel telephone and TV circuits and frequency assignment

17 p2699 A71-34677

PSK modem for multiple access communication system with time distribution, discussing performance tests on INTEL SAT 3

17 p2700 A71-34688

Intelsat 4 transponder for broadband multicarrier operation with frequency and pulse modulation, considering TWT, tunnel diode amplifiers, filters, equalizers, mixers, multiplexers and antennas

17 p2705 A71-35099

Multiple access satellite digital communication system with onboard distribution center, discussing time frame synchronization methods

17 p2706 A71-35105

Multichannel PCM/PSK/PM interplex telemetry system for reducing cross modulation loss and excess carrier reference power

17 p2706 A71-35108

Satellite communication ground station center in conjunction with Intelsat 3 satellites system for transcontinental telephone links

17 p2708 A71-35508

Multiple access to communication satellites by time division multiplexing

18 p2879 A71-36544

Pulse bursts phase regulation subassembly modules, noting use for time division multiple access system control

18 p2879 A71-36545

Quadruphase mode development in time division multiple access system

18 p2880 A71-36546

Internal commutation of telephonic channels with variable destination in time division multiple access system

18 p2880 A71-36547

Time division multiple access system with narrow beam coverage

18 p2880 A71-36548

Digital speech interpolation technique application to PCM-TDMA demand assignment system, noting traffic handling capacity and cost reduction

18 p2880 A71-36549

Propagation model type effect on modulation and multiple access techniques choice for regional European communication satellite system

18 p2880 A71-36550

PSK modem for PCM-TDMA system, discussing performance tests on INTEL SAT 3

18 p2880 A71-36551

Frequency memories application to earth-satellite-aircraft UHF communications, repeater apparatus and multiple access transmission of half tone images in worldwide satellite communication

18 p2881 A71-36553

Cadence synchronization of multichannel communications systems using orthogonal signals with overlapping transmission spectra

19 p3022 A71-38493

Noise stability and rejection probability of code sequence in real multifrequency communications systems with multipositional frequency shift keying

19 p3022 A71-38495

Miniaturized multichannel FM/AM biological telemetry system for simultaneous transmission of EEGs, EMGs, EOGs and EKGs

22 p3500 A71-41574

Incoherent receiver noise stability in multichannel system with channel frequency separation, deriving formula for receiver error probability

22 p3522 A71-42314

Common channel signaling system for demand assigned multiple access satellite communication, discussing design features and applications to PCM-TDMA

22 p3514 A71-42520

Intelsat 1, 2, 3 and 4 satellite network development for world telecommunication coverage, discussing expected future replacement and modulation and multiple access technologies

23 p3643 A71-43250

Bandpass filter harmonic signal phase shift distortion effect on transient response in PSK of multichannel transmission

23 p3644 A71-43286

TV multiplexing and broadband multichannel real time telemetry data transmission without loss between Kennedy Space Center and ground station for computer operation

23 p3645 A71-43519

MULTICHANNEL RECEIVERS U MULTICHANNEL COMMUNICATION U RECEIVERS

MULTICHANNEL TRANSMITTERS U MULTICHANNEL COMMUNICATION U TRANSMITTERS

MULTILAYER INSULATION

Porous metal fiber laminar vacuum insulation, calculating steady state heat and mass transfer

01 p0179 A71-10615

Cs vapor filled cracks breakdown in thermionic trilayer insulators, calculating electron reflection and ion recombination kinetics on surfaces

02 p0232 A71-12239

Nb-sheathed insulators of three coaxial cylinders with ceramic bonding for thermionic converter, discussing pressure bonding techniques and stress relieving properties

02 p0232 A71-12248

Pressure-bonded tri-layer insulator stress analysis, using computer model for explaining alumina component fracturing during fabrication

02 p0256 A71-12249

Trilayer niobium-alumina-niobium sheath insulator thermal stability test under electrical load

02 p0232 A71-12253

Outgassing of multilayer insulation materials for use in cryogenic fuel tanks

03 p0522 A71-14441

Multilayer insulation systems for cryogenics protection aboard spacecraft, considering mechanical properties, radiation shielding, component evacuation rate and outgassing

08 p1375 A71-21748

Laser modulator with multilayer dielectric mirror coating on piezoelectric substrate, investigating vibration distribution and maximum frequency deviation

08 p1303 A71-21808

Construction and hypervelocity impact tests of penetration resistive dual bumper wall for spacecraft meteoroid protection

11 p1843 A71-25318

Multilayer insulation systems development and selection for cryogenics thermal protection on space vehicles, considering mechanical properties, radiation shielding, components, evacuation rate and outgassing

19 p3171 A71-38547

Lateral heat transfer measurements in cryogenic multilayer insulation, considering effective thermal conductivity

20 p3312 A71-39272

Low temperature thermal insulation using diffraction effects of multilayer perforated reflecting screens

22 p3622 A71-42678

MULTILAYER STRUCTURES

U LAMINATES

MULTILOOP SYSTEMS

U CASCADE CONTROL

MULTIMODE RESONATORS

Multiple region hydrogen maser using Teflon coated cylindrical vessel to reduce atom-wall collision frequency shift

01 p0096 A71-11223

Multimode power obtainable in TEM in solid laser, using convex mirror and in cavity polarization rotator

06 p0906 A71-17304

Laser modes generation in two dimensional infinitely long isotropic rod resonator, investigating emission losses and field structure

07 p1121 A71-19129

Single aperture antenna system with multimode log spiral feed

09 p1419 A71-23500

Electric and magnetic fields of fundamental modes in cylindrical and rectangular dielectric microwave resonators, classifying transmission lines connections

12 p1888 A71-27613

Double cavity tuning of Gunn oscillators at mm wavelengths achieving output power improvements

14 p2215 A71-30831

Frequency and losses differences of modes as necessary conditions for multimode lasers transverse modes self synchronization

23 p3687 A71-44176

MULTIPATH TRANSMISSION

Radio telemetry data transmission, investigating multipath propagation effects on signal to noise ratio and distortion

01 p0033 A71-10889

Laser channel multipath dispersion due to atmospheric inhomogeneities for point and nonzero-area apertures under clear weather conditions

02 p0214 A71-12034

Path intermodulation data distortion derivation from noise power ratio measurements over five tropospheric scatter paths during system acceptance tests

05 p0723 A71-17055

Wideband FSK system involving direct and reflected path transmission, predicting diversity performance from mathematical model

05 p0724 A71-17057

Group delay times criterion of multibeam propagation of ionospheric radio echoes for communications systems

06 p0869 A71-18281

Structures electromagnetic scattering and multipath transmission effects on aircraft instrument landing system localizer signals, using computer program

07 p1153 A71-18831

Satellite radio interferometer multipath reflections effect on accuracy

07 p1106 A71-18839

Unresolved radar targets or multipath distortion determination by measurement of complex indicated angle on two pulses separated by short interval

07 p1058 A71-18843

Radar performance with multipath using complex angle /CA/ method for resolving low angle target, comparing S/N ratio with monopulse system without CA

07 p1058 A71-18844

Multipath distortion and wavenumber spectrum of refractive index in radio links

07 p1060 A71-19258

Signal reflection from sporadic E layer, investigating multiplicity relationship to earth surface, ionization level, D region and nighttime absorption

07 p1100 A71-19403

Multipath effects on FM communication systems performance, using analog computer simulation

08 p1255 A71-21597

Line-of-sight radio signal transmission, investigating sea surface reflections effects on phase of arrival and coherence

09 p1409 A71-23502

Feynman path integration for multiply connected space systems of indistinguishable particles, considering bosons and fermions propagators

10 p1644 A71-24214

Radio pulses from Crab Nebula pulsar NP 0532, determining multipath scattering delay distribution function and distortion

14 p2314 A71-30641

Phase and amplitude variations of multipath fading of microwave signals relating atmospheric irregularities

19 p3015 A71-37221

Signal reflection from sporadic E layer, investigating multiplicity relationship to earth surface, ionization level, D region and nighttime absorption

19 p3053 A71-37827

Adaptive reception of weak repetitive signals on background of intense fluctuating noise, synthesizing adaptive detection system for multipath propagation and small SNR

20 p3199 A71-39809

MULTIPHASE FLOW

NT TWO PHASE FLOW

Reactant-product structure of turbulent multicomponent mixture with first order reactions at large wavenumbers

07 p1091 A71-20020

Multiphase gas flow, measuring gas concentration by laser Raman spectroscopy

09 p1464 A71-23308

Series solution for unbounded mixing of two incompressible homogeneous coaxial fluids with constant properties, using successive approximations method

11 p1748 A71-25159

Multiphase two dimensional mixing and combustion of flow fields suspended in gaseous medium for propulsion systems problems, obtaining governing equations

11 p1854 A71-25509

Impeller blade loading vorticity on stream surface of revolution for mixed flow compressor, using annular cascade theory

11 p1703 A71-25962

Three dimensional boundary layer flow and velocity profiles in mixed diffuser with equal angle walls

11 p1704 A71-25973

Reattachment angle of supersonic laminar mixed boundary layer, using revolution model with Reynolds number allowance

11 p1704 A71-26194

Turbulence level effects on mixing of three plane parallel slipstreams with equal velocities and temperature from smoke visualization

13 p2163 A71-28962

Combustion process in mixing zone of kerosene-air mixture and hot combustion products, deriving flameout time relation to characteristic temperature in mixing region

13 p2163 A71-28964

Time dependent calculation of mixed two dimensional or axisymmetric transonic flows in nozzle, writing

ing equations of motion with transformed spatial variables 18 p2906 A71-36323

Small scale flow and surface effects in multiphase media hydromechanics, obtaining entropy production in mixture for interphase transformations characterization 19 p3042 A71-37098

Combustion of homogeneous reacting gas mixture with solid or liquid fuel particles, describing motion by multiveLOCITY and multitemperature model 24 p3891 A71-45216

MULTIPLE BEAM INTERVAL SCANNERS

Colorimetry of Mars surface from dual beam area scanner, considering light and dark areas contrast during 1969 opposition 11 p1824 A71-25706

MULTIPLE DEGREES OF FREEDOM

U DEGREES OF FREEDOM

MULTIPLETS

U FINE STRUCTURE

MULTIPLEX TRANSMISSION

U MULTIPLEXING

MULTIPLEXERS

U MULTIPLEXING

MULTIPLEXING

NT FREQUENCY DIVISION MULTIPLEXING

NT TIME DIVISION MULTIPLEXING

Multiplex spectrometer for eclipse spectra photoelectric observation, using pseudorandom binary sequences as encoding pattern 03 p0424 A71-13634

Holographic multiplexing by Fresnel diffraction based on aperture field division, discussing reconstructed image quality 03 p0429 A71-14179

Multiplexed PAM signal transmission over random time multichannel and diversity systems, discussing optimization for receiver frequency response by numerical solution [IEEE PAPER 70-TP-47-COM] 05 p0723 A71-17053

Queuing model of statistical multiplexer buffer behavior for batch Poisson arrivals and single constant output, applying to time sharing computer buffer design 05 p0724 A71-17063

Hadamard-transform spectrometer experimental verification for multiplex advantage in signal to noise ratio 08 p1289 A71-21376

Multiplexer concentrators for data telecommunication systems with erratic information flow, concerning statistical assumptions, transient response, queuing tails and message clustering 12 p1880 A71-27072

Correlation-recovered adaptive majority multiplexing based on pattern recognition technique, describing prototype equipment 12 p1884 A71-27147

Optimal detection of rectangular radio signal pulse envelope distortions by multiplex fluctuations over white noise background 14 p2195 A71-30113

Recorded wave front aperture sharing technique for space division multiplexing of small holograms 14 p2242 A71-30151

Parallel pressure multiplexer and encoder for aerodynamic testing, employing zero pressure detectors coupled with IC digital electronics and reference pressure signal 14 p2222 A71-30342

Random multiple access technique for satellite data collection, taking advantage of frequency instability associated with oscillator circuits 14 p2199 A71-30908

Asynchronous digital node combination into synchronous multiplex with data traffic routing functions through switch from remote terminals 14 p2201 A71-30928

Single sideband mechanical filters for voice multiplex transmission in radio and telephone systems, discussing material characteristics 17 p2714 A71-34608

Integrated vehicular information management systems consisting of computers, multiprocessors, multiplexers, dedicated subsystem processors, sensors and effectors 17 p2743 A71-35057

Aerospace data bus for multiplexed transmission within vehicles, considering control and sequencing methods terminal concepts, capability noise reduction and reliability 17 p2712 A71-35785

Incoherent radiation distribution analysis by image multiplex coding with SNR gain applied to IR region [ONERA-TP-972] 18 p2916 A71-36031

Pattern recognition multiplex arrangement with optical relay tube and point hologram for image distribution onto spatially separated channels to obtain SNR improvement 18 p2917 A71-36054

TV multiplexing and broadband multichannel real time telemetry data transmission without loss between Kennedy Space Center and ground station for computer operation 23 p3645 A71-43519

MULTIPLICATION

Digital computer operated from remote terminal for signal analysis including Fourier transform, complex multiplication and conjugation 05 p0727 A71-17144

Gas mixture transmission function, determining multiplication method accuracy 07 p1151 A71-18910

Matrix multiplication algorithm based on degrees of freedom analysis for various transformations and spectral analysis 08 p1260 A71-21662

Periodic subtraction and multiplication systems under amplitude limitation, analyzing detection characteristics at arbitrary correlation coefficients 09 p1405 A71-22464

Algorithms for multiplication and division by different bases in residual class system 17 p2711 A71-34977

Serial binary multiplication computation speed, considering recoding algorithm with cellular array multipliers 18 p2894 A71-36829

Signed binary numbers multiplication algorithm, describing cellular arrays for twos-complements multiplication method 18 p2894 A71-36831

Cellular array for multiplication and division of two binary numbers, discussing implementation with transistor-transistor logic integrated circuits 18 p2894 A71-36833

MULTIPLIER PHOTOTUBES

U PHOTOMULTIPLIER TUBES

MULTIPLIERS

Binary cellular logic circuit array multiplication unit based on functional module concept adaptable to LSI implementation, discussing design methodology 01 p0044 A71-10185

Low power nanosecond threshold logic gates for LSI multiplier 01 p0046 A71-10208

Balanced modulators and multipliers, using feedback control for suppressing carrier leak 02 p0236 A71-12425

Stokes multipliers first approximations for outer expansions of Orr-Sommerfeld flow equation solutions 04 p0570 A71-15096

Optimal control with equality type phase operational constraints, obtaining multiplier rules for necessary conditions in maximum principle form 04 p0561 A71-15870

Transistorized four-quadrant control signals voltage multiplier, analyzing operation and circuit diagrams 06 p0879 A71-17493

Measuring transformer for AC input signal with pulse width modulated semiconductor multiplier feedback 08 p1261 A71-20737

Model of curved channel multipliers saturation gain at high applied voltages 09 p1446 A71-22736

Matrix force method for structural cut-out problems, using undetermined multipliers to incorporate modifications 09 p1540 A71-22993

Optimal control problems with phase constraints, using v technique and abstract multipliers technique 10 p1585 A71-23755

AC power meters using electronic multiplier for overcoming limitations concerning frequency ranges, response times, power factor and distortion 10 p1609 A71-23918

Large high speed binary multiplier units design 12 p1884 A71-27152

Digital multiplier based on cellular logic iterative arrays for complex numbers processing 13 p2037 A71-28470

Closed loop system analysis of triangular wave generator consisting of integrator, on-off element with hysteresis and multiplier 15 p2376 A71-32026

Transistorized analog multiplication circuit for automatic control system requiring controller input proportional to product of two values 17 p2719 A71-34787

Serial binary multiplication computation speed, considering recoding algorithm with cellular array multipliers 18 p2894 A71-36829

Signal processing circuits for 1000 MS/S optical communication link using multiplier/signal switch, bit synchronizer and data regenerator 21 p3357 A71-40807

Necessary and sufficient conditions for separating regular multiplier from matrix polynomial, presenting method for determining regular multiplier real factors 24 p3842 A71-44477

Frobenius group theorem, discussing invariant and additional Frobenius multipliers, Schmidt criteria and theorem applications 24 p3843 A71-44823

MULTIPOLAR FIELDS

Corrugated theta pinch stabilization, considering variable axial HF current and quadrupole magnetic field 03 p0464 A71-13930

International geomagnetic reference field 1965 geomagnetic potential rate of change and transformation to dipole coordinates 06 p0888 A71-17282

Plasma interchange instability in multiple magnetic field, including disturbance wavelength comparable to ion cyclotron radius 17 p2786 A71-34282

Plasma fluctuations and diffusion correlation analysis in linear octupole magnetic confinement, determining dispersion relation for interchange instability 17 p2786 A71-34283

17 p2786 A71-34283

MULTIPOLES

Circulation adjustment of n-port waveguide single junction circulator by scattering matrix eigenvalues 01 p0056 A71-11197

Stability of linear time invariant discrete systems including multiple poles 03 p0393 A71-14471

Multiparameter sensitivity functions in network theory, discussing auxiliary, adjoint and direct methods 04 p0560 A71-15148

Dipole conversion to equivalent quadrupoles and multipoles, replacing resistances by corresponding h matrices 06 p0872 A71-17373

Stability and oscillation of zero-beta magnetically confined plasmas, applying to multipole configuration 12 p1935 A71-26917

Dipole, quadrupole and octupole measurements in isolated beating hearts 13 p2016 A71-28150

Multiple EM scattering by two spheres, using multipole expansion and ray optics 17 p2701 A71-34756

Confined plasma diffusion toward current-carrying inner conductors and outer walls in multipoles 21 p3423 A71-40767

Electromagnetic scattering solutions for inhomogeneous dielectrics as power series, using multipoles for far field determination 24 p3847 A71-44427

MULTIPROGRAMMING

Multiprogrammed and time shared multiaccess digital computers operating systems design, discussing dynamic memory protection structures 01 p0043 A71-10179

Operational memory share supervisor program with storage protection feature for real time multitask digital process control and teleprocessing of electrical power utility system 01 p0043 A71-10181

Multicomputer system with preparatory and processing subsystems, discussing algorithm for distributing problems flow among processors 05 p0726 A71-17018

Optimal models for time shared computer systems with real time multiprogramming 10 p1581 A71-24727

Probabilistic cyclic queue model of overhead time and channel utilization in multiprogrammed computer systems under demand memory paging 13 p2035 A71-28973

Optimal models for time shared computer systems with real time multiprogramming 19 p3025 A71-37692

High reliability computers via multiprocessing for long duration space missions, discarding quad redundant and majority voter approaches [AAS PAPER 71-158] 19 p3152 A71-37927

MULTIROPPELLANTS

U ROCKET PROPELLANTS

MULTISPECTRAL BAND SCANNERS

Statistical methods for inventory boundary determination and data compression in automatic processing of multispectral scanner remote sensor earth observations from aircraft and spacecraft [AIAA PAPER 71-234] 07 p1068 A71-19711

Target detection improvement in reconnaissance by black and white TV system, using narrow band filters for conversion to multispectral sensor system 08 p1287 A71-21240

Bands and gray levels number selection for Mars surface multispectral imaging 09 p1447 A71-22750

Multispectral scanner and data system with 24 channels for NASA C-130 earth resources survey aircraft 18 p2920 A71-36361

Digital pattern classification of oceanographic remote sensing multispectral airborne scanner data, considering sea surface color variations 19 p3060 A71-38405

MULTISPECTRAL PHOTOGRAPHY

NT INFRARED PHOTOGRAPHY

NT RADAR PHOTOGRAPHY

Interference passband filters with wide angle lenses for multispectral photography, discussing design and applications 01 p0081 A71-10827

Earth Resources Technology Satellites /ERTS/ A and B providing one year high resolution multispectral imagery, noting data processing and distribution functions 01 p0164 A71-11436

Photographic and IR multiband spectral discrimination for rock and soil mapping from orbiting ERTS satellites [AIAA PAPER 70-303] 06 p0898 A71-17562

Crop species and soil condition computerized identification from film optical density differences, using multibase and multiemulsion photography 08 p1282 A71-21436

Apollo 9 So65 multispectral color space photography for basic land use pattern determinations 12 p1907 A71-27259

ERTS telecommunication system for space tracking and high resolution multispectral image data acquisition and commanding 14 p2199 A71-30912

Optimal sensing recording and signal processing in multispectral photography for aerial reconnaissance capability 15 p2410 A71-32470

Multispectral color aerial photography for identification of farm crops and tree species, using broadband camera filters 17 p2737 A71-34274

Remote subsurface oceanographic imagery from orbital altitudes in blue multispectral region, showing optimum filter passband 18 p2917 A71-36064

Apollo 12 multispectral lunar photography experiment using four camera configuration, verifying by ground photoelectric photometry 23 p3761 A71-43780

Crop surveys from multiband and multibase satellite photography during Apollo 9 mission, using statistical multispectral pattern recognition digital techniques 24 p3827 A71-44987

MULTISTAGE COMPRESSORS
U TURBOCOMPRESSORS

MULTISTAGE ROCKET VEHICLES
NT ASTROBEE ROCKET VEHICLES
NT DIAMANT LAUNCH VEHICLE
NT ELDO LAUNCH VEHICLE
NT KAPPA 9 ROCKET VEHICLE
NT LAMBDA ROCKET VEHICLES
NT NIKE-APACHE ROCKET VEHICLE
NT NIKE-TOMAHAWK ROCKET VEHICLE
NT RUBIS ROCKET VEHICLE
NT SATURN LAUNCH VEHICLES
NT SATURN 5 LAUNCH VEHICLES
NT SKYLARK ROCKET VEHICLE
NT THOR DELTA LAUNCH VEHICLE
NT THOR LAUNCH VEHICLES

Soviet book on rocket flight dynamics covering center of mass motion characteristics, guided missiles, external ballistics, multistage design and flight optimization 02 p0320 A71-12724

Black Brant 4 rocket second stage motor, investigating high altitude ignition problems by postflight analysis [AIAA PAPER 70-1384] 03 p0470 A71-13667

Multistage rocket propelled strategic ballistic missiles and space boosters design and trajectory optimization, using SWORD computer program 04 p0556 A71-15292

Europa 1 multistage booster rocket interstage electric circuit connection, discussing specifications and compatibility tests [DGLR-70-059] 05 p0697 A71-15955

Optimization of multistage rockets with given payload, propellants and explosive separation of stages 05 p0817 A71-16613

Space transportation system of two stage reusable space shuttle and orbit-to-orbit shuttle, supporting NASA and DOD missions 08 p1367 A71-21890

Two stage rocket trajectory optimization for prescribed flight range, maximizing hit probability for given number of launches 08 p1367 A71-22036

Multistage rockets terminal control synthesis based on linear functionals 09 p1532 A71-22660

Optimal motion of multistage body of variable mass during vertical climb with allowance for weight limitations 10 p1683 A71-24845

Analytical method for optimal rocket motors cluster arrangement in multistage spacecraft, considering horizontal trajectories rated terminal velocity performance 11 p1839 A71-26335

Two stage rocket flight optimization for minimum propellant consumption, using calculus of variations 13 p2145 A71-28734

Multistep rocket mass ratios optimization, including exhaust gas velocities, structure and efficiency 16 p2644 A71-32843

Space radio communications, considering radio links reliability between multistage launcher rocket and ground stations 17 p2696 A71-34228

Space shuttle with two stage booster and orbiter reusable vehicles, discussing performance, structural design and flight control system [AIAA PAPER 71-804] 17 p2814 A71-35431

Diamant launch vehicle multistage development for placing satellites in low perigee and high eccentricity and high and low circular orbits 22 p3610 A71-42020

Two stage reusable space shuttle system for space transportation program, discussing budget, development and testing, international cooperation and information exchange 22 p3610 A71-42022

Qualification tests for equatorial ELDO Europa Launch Site with MSRV, discussing checkout system and performance 23 p3661 A71-43474

MULTIVARIATE STATISTICAL ANALYSIS
NT CORRELATION
NT COVARIANCE
NT DISCRETE FUNCTIONS
NT ORTHOGONALITY
NT REGRESSION ANALYSIS

Selection index estimation from partial multivariate normal data for precision improvement, discussing procedure and Monte Carlo simulation results 07 p1147 A71-19599

Multivariate statistical analysis of parameters measuring reference stars effects on parallax and error estimates 21 p3444 A71-40195

Multivariable regression equations validity from dispersion analysis and limiting complexity with allowance for data sample volume 24 p3842 A71-44392

Optimum design of linear multivariate sampled data systems, using deadbeat and integral performance criteria and output response error 24 p3812 A71-44451

MULTIVIBRATORS
NT FLIP-FLOPS
NT MONOSTABLE MULTIVIBRATORS

Oscillator for guiding clock mechanism of 400 mm photographic telescope, using high stability transistorized multivibrator 04 p0591 A71-14847

Multivibrator frequency stability as function of circuit parameters, using stability/parametric errors sensitivity coefficients for general algorithm 08 p1264 A71-21072

Tunnel diode driven multivibrator, noting triggering signal amplitude and duration effects on output pulse width 11 p1740 A71-26550

MUONS

Nuclear interactions induced by cosmic ray and accelerator muons, discussing cloud chamber and nuclear emulsion data 01 p0131 A71-11412

Electric quadrupole atomic transitions in muonic PB208, charting X ray spectrum showing transitions 01 p0131 A71-11439

Monte Carlo model of muon and active component distribution in nuclear cascade in extensive cosmic ray shower 03 p0476 A71-13849

Muons spatial distribution function in mountain level extensive air showers 03 p0476 A71-13855

Extensive air shower muons at mountain levels, describing experimental procedure for fluctuation distribution 03 p0476 A71-13856

Extensive air shower muon fluctuations at mountain level, determining interaction coordinates distribution, production and energy by Monte Carlo method 03 p0477 A71-13857

Muon spatial distribution fluctuations at mountain level, using approximate methods 03 p0477 A71-13858

Extensive air shower electron photon and muon components energy spectrum at various depths 03 p0477 A71-13859

High energy muons in extensive air showers, studying spatial distribution, spectrum and electron showers by photon spark chamber telescope underground 03 p0477 A71-13860

Extensive air shower electron and muon components at mountain levels, calculating distribution functions by Monte Carlo technique 03 p0477 A71-13861

Cosmic rays intensity measurement in deep ocean with Cerenkov counter, determining Muon energy spectrum and absorption in water 03 p0477 A71-13862

Bremsstrahlung photons produced by cosmic ray muons in Fe and Pb at sea level, calculating energy spectra and angular distributions 03 p0477 A71-13863

Electromagnetic mechanism of direct muon and gamma quanta production by collision of strongly interacting particles 03 p0462 A71-13864

Extensive air showers at sea level, plotting mean numbers of muons and electrons 03 p0477 A71-13866

Underground cosmic ray showers muon pairs lateral distribution measurement 04 p0640 A71-14815

Geomagnetic field effects on cosmic radiation, determining muon component momentum distribution and charge ratio 05 p0798 A71-16219

Cosmic ray mu meson intensity power spectrum frequency dependence, comparing to interplanetary field spectra 06 p0954 A71-18125

Secondary cosmic ray spectrum latitude knee based on nucleon, proton and muon energy spectra 06 p0960 A71-18167

High energy muon flux diurnal variations related to lunar time 06 p0960 A71-18169

Muon momentum spectra and charge ratio at 60 deg in east-west plane 06 p0961 A71-18176

Muon bundles frequencies from model for propagation of various atmospheric components in combination with theoretical pion spectra 10 p1664 A71-25044

Extensive air showers and multiple muons frequencies, considering parent pions mean transverse momentum, multiplicity law form and primary cosmic ray intensity 10 p1664 A71-25046

Very high energy cosmic ray muons, discussing recent experiments with mu-meson anomalous couplings, triplets and intermediate vector bosons 11 p1815 A71-25356

Nucleon-nucleon interactions produced energetic penetrating particles /muons/ in cosmic ray showers, studying neon flash tube technique 12 p1948 A71-27186

Large air shower Cerenkov detectors system, discussing energy spectra from vertical arrays, delayed muons and radio pulse detection rates 12 p1950 A71-27384

Zenith angular air shower distribution by Monte Carlo method, discussing muons horizontal component separation from background events 12 p1951 A71-27385

High energy interactions at 10 to 12 power eV, discussing muon-poor showers, incoherent muons and horizontal air showers 12 p1933 A71-27395

Zenith angle distribution of atmospheric muons at Mt. Chacaltaya, considering differential intensity of cosmic ray mesons and horizontally incident cosmic rays 12 p1952 A71-27400

Mega showers underground, considering primary cosmic ray energies greater than 10 TeV 12 p1952 A71-27401

Cosmic ray muon flux at sea level, allowing for showers, multiple scattering, straggling, zigzag motion, detector efficiency and electronic equipment dead time 12 p1952 A71-27403

Sea level muon spectra at 83 degrees zenith angle up to 1 TeV, using Kiel spectrometer 12 p1952 A71-27404

Sea level muon spectrum measurements at 80 degrees to vertical up to 1 TeV, using Nottingham spectrometer 12 p1953 A71-27405

Muon spectra and charge ratios at sea level, analyzing by collision model and one dimensional diffusion equations 12 p1933 A71-27406

Angular distribution of muon-poor extensive air showers, considering generation by atmospheric nuclei interaction 13 p2123 A71-28073

Electron, nuclear active and muon components of extensive air showers, discussing statistical results 13 p2123 A71-28076

Particle densities and muon spectra at 100-1300 m from sea level extensive air showers axes for primary energies to 10 to 20th eV 13 p2124 A71-28086

Extensive air showers muon and electron components primary energy spectrum, using isobar and CKP formula based models 13 p2125 A71-28088

Air showers nuclear active and muon components simulation in space and time, using different shower models based on isobar-fireball concept 13 p2125 A71-28090

High energy muons measurements in extensive air showers, presenting muon densities, momenta and electric charge data obtained from spectrograph long term continuous operation 13 p2125 A71-28091

Extensive air showers muons momenta and densities from shower core spectrographic recordings 13 p2125 A71-28092

Primary cosmic rays mass composition at energy levels above 10 TeV, analyzing muons data from extensive air shower experiments 13 p2125 A71-28094

Muons arrival times distribution in extensive air showers, examining delay as function of particle production heights 13 p2126 A71-28095

Extensive air showers muon component arrival time spread and lateral density distribution 13 p2126 A71-28096

Extensive air showers muons angular distribution, considering high energy nuclear reactions 13 p2126 A71-28097

Muons lateral distribution in extensive air showers, studying density vs core distance 13 p2126 A71-28098

Muon rich showers, discussing muon density spectrum relation to primary energy spectrum 13 p2126 A71-28099

Extensive air showers muon density spectrum, describing measurement apparatus and analysis method with particular emphasis on elimination of falsifying absorber multiplication effects 13 p2126 A71-28100

Temperature effects on cosmic rays muon component variations during cold fronts passage 13 p2131 A71-29485

Plastic scintillators anomalous pulse spectra in sea level transition region attributed to EM cascades single particles /muons/ production 14 p2301 A71-30425

High energy cosmic muons momentum spectrum and charge ratio measurements at large zenith angles, describing magnetic spectrometer 14 p2247 A71-30601

Soviet book on cosmic muons and neutrinos covering anomalous and weak interactions 15 p2472 A71-31287

Cosmic rays - Conference, Budapest, August 1969, Volume 4, Muons and neutrinos techniques 15 p2474 A71-31776

Vertical muon spectra and charge ratio in energy range 30-800 GeV at sea level from Kiel cosmic ray spectrometry 15 p2474 A71-31778

Energy dependence of cosmic ray muon charge ratio at large zenith angles, using large aperture and high resolution cosmic ray momentum spectrograph 15 p2475 A71-31779

High energy muons production by cosmic rays, discussing advantages of moon based experiments over earth surface measurements 15 p2475 A71-31780

Cosmic ray muon intensity measurements in water at large depths by Cerenkov counter 15 p2475 A71-31781

Sea level high energy muon flux determination from underground burst energy spectrum measurements, using Kobayakawa-Miono formula for cascade shower fluctuation 15 p2475 A71-31782

Momentum spectrum measurement of cosmic ray muons, recording particle trajectories photographically 15 p2475 A71-31783

Muon sea level differential energy spectrum at 80 deg to vertical up to 1 TeV, using Nottingham spectrometer 15 p2475 A71-31784

Low energy muon production by neutral components of cosmic radiation at sea level, noting correlation with sidereal time 15 p2475 A71-31785

Air showers with zenith angles greater than 65 deg recorded by array comprising six scintillation counters, considering angular distribution, intensity and muon content 15 p2475 A71-31786

High energy penetrating component of cosmic radiation at mountain level recorded in underground ionization calorimeter, showing muon production in vertical and horizontal direction 15 p2476 A71-31787

Atmospheric structure effects on muons zenith angle distribution and maximum intensity direction as function of energy at two different altitudes 15 p2476 A71-31788

Energy spectrum of cosmic ray showers from high energy muon interactions with nuclear emulsion chamber 15 p2476 A71-31789

Zenith angle distribution of extremely high energy muons from bremsstrahlung showers by emulsion chamber, noting consistency with pion/kaon decay 15 p2476 A71-31790

Anomalous cosmic ray muon interactions at very high energies, using zenith angle distribution data at sea level and deep underground 15 p2476 A71-31791

Angular distribution of high energy cosmic ray muons incident at sea level at large zenith angles, investigating cascade showers initiated by muons 15 p2476 A71-31792

Ultrahigh energy muons intensity distribution as function of zenith angle at fixed slant depth of rock 15 p2476 A71-31793

Atmospheric muons anomalous zenithal distribution at extremely high energy regions 15 p2477 A71-31794

Vertical intensity of cosmic ray muons in Mont Blanc tunnel, describing apparatus and experimental site 15 p2477 A71-31795

Vertical intensity and angular distribution of cosmic ray muons from observations using scintillator neon flash tube telescopes at three depths 15 p2477 A71-31796

Sidereal anisotropy in muon signal observed by cosmic ray telescope above sea level, indicating production by neutral particle and leakage relative to anticoincidence factor 15 p2477 A71-31797

Muonic trident production by cosmic ray muons, using quantum electrodynamics methods 15 p2477 A71-31798

Cosmic ray muon-neutrinos sea level energy spectra at low energies for horizontal and vertical directions, estimating geomagnetic cut-off effects for various geomagnetic latitudes 15 p2477 A71-31799

Cosmic ray muon and neutrino measurements with deep underground scintillation detector array 15 p2477 A71-31800

Cosmic ray shower size spectrum in atmosphere for muon bremsstrahlung at large zenith angles 15 p2479 A71-31868

Underground search for cosmic ray neutrino interaction products, observing muon products 17 p2795 A71-34666

Production cross section of Lee-Wick hypothetical massive electromagnetic bosons by muons at high energy, giving Feynman diagrams 17 p2785 A71-34750

Cosmic ray muons energy loss rate measurement in Fe using Durham magnetic spectrograph 18 p2957 A71-35930

Polarization measurement of cosmic ray muons at sea level as function of energy and zenith angle 19 p3124 A71-37284

Underground interactions of primary cosmic ray produced atmospheric muon neutrinos, using large area liquid scintillation detector hodoscope 19 p3105 A71-37288

Underground muons produced by atmospheric neutrinos, noting deviation from linearity by comparing calculated and experimental muon rates 19 p3106 A71-37289

Median primary energy of underground muon telescopes response as function of depth, studying sidereal daily variation of cosmic rays 19 p3125 A71-37370

Atmospheric temperature effect on solar diurnal variation of muon component, considering asymptotic characteristics of cosmic ray anisotropy 19 p3129 A71-38378

Visual sensations produced by cosmic ray muons passing in different directions through human eyes and head 19 p3005 A71-38677

Horizontal cosmic ray muon component intensity measurement and time studies for solar and sidereal variations 20 p3277 A71-38839

Absolute measurement of vertical cosmic ray muon intensity at 3-50 GeV/c, using solid iron magnetic spectroscopy 21 p3438 A71-40587

Cosmic ray muons absolute intensity determination, using Durham vertical spectrograph 22 p3593 A71-42353

Cosmic ray muon electromagnetic interactions and energy spectrum measurements at large zenith angles at sea level 22 p3593 A71-42356

Primary and secondary cosmic ray muon variations in vertical and zenith angles, determining coupling coefficients 22 p3593 A71-42357

Muon showers underground phenomenology in terms of density spectra, shower size and radial density distributions 22 p3594 A71-42407

Sea level high energy cosmic ray muon spectra calculation based on phenomenological model of nucleon-nucleus collisions 22 p3594 A71-42408

Electromagnetic interactions of high energy cosmic ray muons from combined calorimeter-spectrograph investigation 22 p3594 A71-42409

Monte Carlo model of muon and active component distribution in nuclear cascade in extensive cosmic ray shower 22 p3595 A71-42650

Muons lateral distribution function in mountain level extensive air showers 22 p3595 A71-42656

Extensive air shower muons flux density at mountain altitudes, describing experimental procedure for fluctuation distribution 22 p3595 A71-42657

Extensive air shower muon flux density fluctuations at mountain level, determining interaction coordinates distribution, production and energy by Monte Carlo method 22 p3595 A71-42658

Muon lateral distribution fluctuations at mountain level, using approximate methods 22 p3595 A71-42659

Extensive air shower electron-photon and muon components energy spectrum at various depths 22 p3595 A71-42660

High energy muons in extensive air showers, studying spatial distribution, spectrum and electron photon showers by underground photon spark chamber telescope 22 p3595 A71-42661

Extensive air shower electron and muon components at mountain levels, calculating probability distribution functions by Monte Carlo technique 22 p3595 A71-42662

Cosmic rays intensity measurement in deep ocean with Cerenkov counter, determining muon energy spectrum and absorption in sea water 22 p3595 A71-42663

Bremsstrahlung photons produced by cosmic ray muons in Fe and Pb at sea level, calculating energy spectra and angular distributions 22 p3595 A71-42664

Electromagnetic mechanism of direct muon and photon production by collision of strongly interacting particles 22 p3579 A71-42665

Extensive air showers at sea level, plotting mean numbers and distribution functions of muons and electrons 22 p3595 A71-42667

Absolute vertical intensity measurement of cosmic ray muon energy spectrum at sea level, presenting spark chamber and absorption spectrograph data 23 p3722 A71-43876

MURRAY METEORITE

Xe and Kr isotopes gas extraction and mass spectrometer analyses of Apollo 11 lunar soil, Murray carbonaceous chondrite and atmospheric Xe 10 p1661 A71-24410

Murchison, Murray and Allende carbonaceous chondrites water extractable amino acids composition 16 p2630 A71-32950

Extraterrestrial amino acids identification in carbonaceous chondrite Murray meteorite by gas chromatographic method 19 p3132 A71-37414

MUSCLE RELAXANTS

Airway smooth muscle relaxation mechanical consequences concerning lung volumes, airway conductance, isovolume pressure flow, maximum expiratory flow volume and static lung recoil 13 p2024 A71-29497

MUSCLES

NT MYOCARDIUM

Glycogen reduction in human musculus vastus lateralis during bicycle exercise below pulse endurance limit, noting glucose infusion effect 01 p0016 A71-11400

Muscle simulation by information theory for statistical analysis of behavior based on gas thermodynamics methods, showing stress relation to motor units excitation 03 p0366 A71-12979

Muscle activity control mechanism in animals locked into external feedback loop, relating exciting stimulus to muscles stressed state 03 p0367 A71-12980

Intestinal muscle electrical behavior as series of loosely coupled oscillators, demonstrating slow wave frequency gradient and propagation velocity by computerized simulation 04 p0544 A71-15089

Carbonic acid effect on isolated skeletal muscle, discussing membrane potential and ion content measurements 05 p0710 A71-16941

Nervous and muscular elements above threshold excitation on potential subthreshold stimulation background by electronic analog model 07 p1050 A71-20114

Argyrophil sphincter formations in intraorganic vascular channels of hearing organ 08 p1243 A71-21967

Hind limb antagonistic muscles bioelectric activity dependence on animal rotation direction and head fixation 09 p1388 A71-22196

Rana temporaria isolated sciatic nerve excitation process, investigating continuous ultrasound effect 09 p1391 A71-22486

- Rats under various exercise programs, determining cardiac ventricle and gastrocnemius muscles calcium activated adenosine triphosphatase activities 09 p1400 A71-23361
- Cardiac hypertrophy in animals, discussing increased cardiac work load compensation and muscle cell alterations 10 p1565 A71-24674
- Isotonic training effects on circulation for limb muscular strength characteristics, using peak blood flow and venous compliance measurements 11 p1719 A71-26071
- Leg position effect on human calf muscle blood flow during standardized heavy rhythmic exercise 11 p1722 A71-26358
- Human transversostriated muscle plate receptors morphogenesis 12 p1872 A71-27725
- Xe 133 elimination from anterior tibial muscles in dry and water immersed sitting subjects, discussing effects of air and oxygen breathing 13 p2022 A71-29358
- Human physiological responses comparison between work with concentric and eccentric muscle contractions, observing oxygen debt in short term exercise 13 p2024 A71-29495
- Surface electromyographic recordings on biceps and peripheral muscles during sustained isometric contractions 13 p2024 A71-29499
- Pyruvate and lactate concentrations in muscle tissue and blood at rest and during exercise 14 p2187 A71-31136
- Human muscle blood flow measurement by Xe 133 clearance method during rhythmic exercise, noting work load effects 15 p2358 A71-31455
- Muscle adenosine triphosphate, creatine phosphate, adenosine diphosphate, glycogen, and lactate concentrations during intermittent exercise 15 p2358 A71-31726
- Normal muscle lactate concentration after prolonged exercise resulting in decrease in glycogen content 15 p2359 A71-31727
- Lactic and succinic acids and creatine phosphates content in rat hind leg muscles during swimming and at rest 16 p2532 A71-33897
- Calcium ions effects on electrophysiological properties of portal vein muscle cells in rats 16 p2533 A71-34109
- Temperature effects on spontaneous electrical and contractile activity of smooth muscle cells of portal vein in rats 16 p2533 A71-34110
- Reflex increase in ventilation induced by vibrations applied to cat triceps surae muscles, noting muscular and articular receptors role 17 p2678 A71-34175
- Adenosine triphosphate addition effects on heat production in intact muscular fibers by calorimetry 17 p2683 A71-35247
- Prolonged strenuous physical exercise effect on triglycerides, phospholipids and glycogen concentration in human femoral muscle 18 p2856 A71-36238
- High muscle glycogen content effect on human performance in prolonged heavy physical exercise 19 p3009 A71-38554
- Cell contacts in canine duodenal smooth muscle layers, using perfusion with glutaraldehyde fixative 20 p3187 A71-38985
- Shin muscle electrical activity during standing after 120 day bed rest hypokinesia from EMG measurement 20 p3188 A71-39230
- Active vasodilation in gracilis muscle vascular bed due to perfusion pressure changes 20 p3189 A71-39378
- Intracellular pH and carbon dioxide combining curve of muscle tissue in dogs, using DMO method 21 p3335 A71-40631
- Physiological relationship of young to old men, considering body composition, aerobic capacity and capillary-muscle fiber ratio 22 p3485 A71-41717
- Mammal extraocular muscle fiber structural and functional properties, discussing histological arrangement, fiber type classification and motor nerve endings 22 p3488 A71-42434
- Afferent oculomotor pathways to extraocular muscle nuclei, considering discrete unilateral lesion role in head posture disturbance production 22 p3488 A71-42435
- Extraocular muscle pharmacology, discussing eye twitch and tonic neuromuscular systems structure and function in frogs 22 p3488 A71-42439
- Nonactomyosin component differentiation in potassium chloride insoluble myofilaments in vertebrate smooth muscle cells 24 p3794 A71-44424
- Muscular bioelectric potential input processing into digital computer, describing amplitude, frequency and time domain analysis of electromyogram signals 24 p3801 A71-44542
- MUSCOVITE**
Muscovite mica substrate surface composition as function of preparation and processing, using Auger electron spectroscopy 06 p0941 A71-17408
- MUSCULAR FATIGUE**
Fatigue factor of lactate, ATP and creatine phosphate (CP) accumulation in working muscles during short exhaustive exercise in man 02 p0202 A71-11666
- Arterial blood and muscle lactates in cold water swimming rats indicating reduced circulation endurance factors 09 p1396 A71-23360
- Thermoelastic heat release in muscular twitch final phase, discussing energy storage as function of active or passive muscular tension 11 p1718 A71-25626
- Intense muscular work adaptation in rats, reducing biochemical and adaptive changes and enhancing anabolic processes 14 p2186 A71-30552
- Work load and maximum physical exercise duration relationship for forearm reciprocating flexion and extension, cranking of both arms and bicycle pedalling 17 p2688 A71-34359
- Muscular fatigue of healthy Bengali males with increasing work loads under varying environmental conditions, considering ventilation, heart rate and oxygen consumption 17 p2688 A71-34360
- MUSCULAR FUNCTION**
Vasodilator, oxygen, potassium and osmolality effects on exercise hyperemia in dog gracilis muscle 01 p0015 A71-11184
- Human muscular control patterns during forearm precision cyclic bending on ergograph 02 p0204 A71-12053
- Oxygen tension, blood flow, redox potential and temperature variations in cerebrum and musculus gastrocnemius of rats during high mountain adaptation 03 p0361 A71-13190
- Physical endurance and muscular activity of man as adaptation process depending on biochemical and functional changes 03 p0361 A71-13192
- Microcathodes measurement of oxygen tension on arterioles external surface in hamster cheek pouch and hamster/rat cremaster muscle for blood flow regulation mechanism 03 p0363 A71-13487
- Pulsus alternans study by noninvasive techniques for assessing cardiovascular function in hemodynamics and muscular physiology 03 p0372 A71-13492
- On-line parameter tracking algorithm, obtaining parameters in mathematical relation between full wave rectified EMG and human triceps muscle force during isometric task 03 p0374 A71-14423
- Instantaneous cardiac acceleration in man induced by voluntary muscle contraction 04 p0544 A71-15152
- Cyclic muscular voluntary movements, noting spinal segmental apparatus function 05 p0709 A71-16804
- Muscular heat production effect on contraction during cold adaptation tests 05 p0710 A71-16806
- Magnetic field effects on biological systems, discussing ergometer measurements of human subjects muscular contractions 05 p0714 A71-16896
- Hypokinesia and acceleration effects on plasma proteins displacement and bioelectric activity of striated muscles of rats 06 p0853 A71-17960
- Ischemic deafferentation of transversostriated muscle quadriceps femoris in cats contributing to hypokinesia and psychophysiological disturbances 06 p0854 A71-18362
- Carbohydrate metabolism and electrolyte changes in human muscle tissue during heavy exercise 06 p0856 A71-18387
- Subjective and electromyographic estimation of fatigue and muscle activity physiological levels, considering isometric muscle contraction task endurance 07 p1047 A71-19458
- Muscle reflex action role in contralateral remote masking at high auditory signal sound pressure levels 08 p1246 A71-20803
- Gas exchange and muscular thermoregulation activity in rats under environmental oxygen deficiency 08 p1242 A71-21963
- Rat left ventricle isolated papillary muscles contractile force in pressure chamber under high altitude adaptation 09 p1388 A71-22125
- Weightlessness effects on muscular reflexes, tonus and contractibility in Soyuz 9 astronauts 09 p1389 A71-22202
- Human electromyogram and isometric muscle tension dynamic relationship 09 p1400 A71-23363
- Structural and functional analysis of human and equine muscular drive mechanisms for extremities, deriving general rules for biomanipulators synthesis 11 p1718 A71-25619
- Thermoelastic heat release in muscular twitch final phase, discussing energy storage as function of active or passive muscular tension 11 p1718 A71-25626
- Respiratory responses and hyperventilation mechanism during static muscular work in maximal voluntary contraction, noting chemoreceptor and alarm-defense reaction 13 p2008 A71-28436
- Coronary blood flow response to acute and chronic hypoxia, observing vascular smooth muscle relaxation relation to released adenosine 14 p2184 A71-30281
- High motor stresses effects on muscle acetylcholine content, cholinesterase activity and localization, solitary contractions fusion and pessimal weakening 14 p2186 A71-30553
- Human performance after awakening at different times of night, considering reaction time and muscular coordination 15 p2362 A71-31201
- German monograph on human mental performance under simultaneous mental and above normal muscular stress involving signal response in double choice reaction problems 15 p2360 A71-32306
- German monograph on conversion of human muscular work into flywheel mechanical kinetic energy covering testing and analysis of biomechanical relationships 15 p2364 A71-32308
- Human skeletal muscle reflex and motor reactions in response to tibial nerve stimulation 15 p2360 A71-32532
- Peristaltic pumping mechanism as progressive wave train of transverse wall displacement in plane two dimensional channel 15 p2366 A71-32559
- Breathing capacity increase without rise in oxygen consumption due to active and passive muscular work and heavy energy expenditure 17 p2681 A71-34821
- Myocardial inotropism index, using left ventricle time varying pressure/volume ratio in systole 17 p2683 A71-35121
- Muscle contraction model under biological factors action, considering circular cylindrical vessel equilibrium under internal and external pressures 17 p2694 A71-35616
- Extraocular muscle structure and function, defining slow and fast motor system based on slow and fast fibers 17 p2687 A71-35801
- Eye-head coordination in monkeys by recordings from neck and eye muscles, noting central neural command role 18 p2856 A71-36232
- Human respiratory muscles electrical activity, discussing correlation analysis of interferential electromyograms from external intercostal muscles during breathing exercises 19 p3003 A71-38198
- Tissular and cellular biological resistance as indices for organism resistance to adverse effects, noting increase due to muscular training and cold adaptation 20 p3187 A71-39219
- Neosynthesized alpha-glycerophosphate and 2,3-diphosphoglycerate role in human extraocular muscle metabolism 21 p3328 A71-40099
- Vibration effects on human body, discussing neurophysiological data, safe exposure limits, therapeutic applications, motion sickness, muscular responses and biomechanical effects 21 p3342 A71-40147
- Aquanuts tremor response measurement by muscle force transducer during compression and decompression in 520-foot saturation dive, noting differences among individuals 21 p3331 A71-40350
- Humoral smooth muscle acting factor and phenylpiperazinylmethyl cyclohexanone effects on decompression sickness production and prevention in thin mice 21 p3331 A71-40352
- Mechanical properties of muscular organs, presenting mathematical model for biological fluid flow analysis 21 p3336 A71-40984
- Motor stereotype formation with different muscular loads, noting muscle electrical activity and static tension changes 21 p3337 A71-41062
- Norepinephrine induced stimulation of myocardial oxygen consumption of cat papillary muscles under afterloaded isotonic and isometric conditions 22 p3486 A71-41937

Prior muscle exertions effect on reaction time and duration of simple discrete movements, considering electromyogram frequency changes
22 p3503 A71-42194

Cat and human eye movement control system measurements, studying isolated oculomotor muscles and globe restraining tissues dynamics
22 p3489 A71-42441

Muscular work level shifts effectiveness during pedaling activity from oxygen requirement measurement, electromyograms and stress dynamograms
24 p3794 A71-44412

MUSCULAR STRENGTH

Human strength decrement and recovery for repetitive maximal muscular exertions with various intertrial intervals
04 p0540 A71-15846

Strain gage for in vivo recording of single and tetanic responses of skeletal muscles in mice during work in isometric regime
06 p0855 A71-18378

Design, construction and performance of photoelectric isometric force transducer for muscle mechanics
06 p0862 A71-18392

Alternating acceleration and increased ambient temperatures effects on time interval perception and muscular effort estimation
12 p1874 A71-27164

Reduced diaphragmatic muscle tissue resistance in rats during prolonged hypokinesia, showing sorption of basic vital neutral red stain
13 p2007 A71-28417

Maximal human anaerobic power, discussing unsplit phosphagen concentration in muscles during steady state exercise
16 p2530 A71-33247

Human muscle power fluctuations under steady state physical activity, analyzing finger flexors strength
17 p2683 A71-35172

Training cycle in altitude chamber for human adaptation to hypoxia, high temperatures and transverse myogenic loads
22 p3505 A71-42805

MUSCULAR TONUS

Human muscle hardness as isometric stress force indicator
02 p0198 A71-12065

Muscle tonus dynamics statistical analysis, obtaining destructive stereotrophic influences, therapeutic effects and control mechanisms
05 p0710 A71-16808

Weightlessness effects on muscular reflexes, tonus and contractibility in Soyuz 9 astronauts
09 p1389 A71-22202

Chemical thermoregulation muscular electricity activity during shivering and thermoregulation tonus change after cold adaptation, discussing oxygen consumption rise
10 p1564 A71-24486

Space crew members muscle tone, determining weightlessness effect by rigidity and bioelectric activity
15 p2357 A71-31317

Gas exchange, thermoregulatory muscle tone and electrical activity in rat muscles in hyperoxic atmosphere
15 p2360 A71-32533

Hypothermia effects on cat and dog vascular tonus vasomotor reflex regulation, suggesting role of inhibition due to changed afference from cooled tissues
16 p2533 A71-34111

MUSCULOSKELETAL SYSTEM

- NT BONES
- NT CEREBRUM
- NT COLLAGENS
- NT CONNECTIVE TISSUE
- NT CRANIUM
- NT FEMUR
- NT FLEXORS
- NT JOINTS [ANATOMY]
- NT KNEE [ANATOMY]
- NT MARROW
- NT MASTOIDS
- NT PELVIS
- NT SCIATIC REGION
- NT SKULL
- NT TIBIA
- NT VERTEBRAE
- NT VERTEBRAL COLUMN

Hypokinetic effect on sarcoplasmatic and myofibrillar protein composition of skeletal muscles in rats
01 p0013 A71-11130

Data processing analog for human vertical position regulation via afferent nervous system control of skeletal muscles
02 p0206 A71-12064

Healthy subjects physical training effects on blood flow and enzymatic activity in skeletal muscle
02 p0201 A71-12916

Dynamic response with feedback characterization of human musculoskeletal frameworks by linegraph-flow graph procedure
05 p0713 A71-16485

Liver and skeletal musculature morphology during hypokinesia and protein deficiency in mice
06 p0855 A71-18377

Strain gage for in vivo recording of single and tetanic responses of skeletal muscles in mice during work in isometric regime
06 p0855 A71-18378

Hyperemic skeletal muscle capillaries restricted diffusion, obtaining permeability data for chromium 51 labeled EDTA and inulin in exercising human forearm
08 p1237 A71-20677

Hypoxemia reflex neurogenic vasoconstrictor factors competition with local vasodilator mechanisms in skeletal muscle
08 p1237 A71-20680

Mitochondrial oxidation of substrates coupled with phosphorylation studied using organelles isolated from red and white skeletal muscles of rabbit, noting enzyme activity of fatty acids
08 p1238 A71-20682

Structural and functional analysis of human and equine muscular drive mechanisms for extremities, deriving general rules for biomanipulators synthesis
11 p1718 A71-25619

Temperature-respiration relations from isolated rat skeletal muscle mitochondria oxygen consumption measurements
11 p1723 A71-26408

Human skeletal muscle reflex and motor reactions in response to tibial nerve stimulation
15 p2360 A71-32532

Capillary density relationship to maximal oxygen uptake, indicating endurance training effects on human skeletal muscle
16 p2530 A71-33245

Skeletal muscles shivering thermogenesis during cold adaptation, investigating thermoregulation effects on organ and system heat production
18 p2862 A71-36895

Gas metabolism and electrical activity of skeletal muscles of rats in He/O medium at room temperature, noting rectal temperature drop
22 p3496 A71-42803

Morphological and cytochemical changes in red and mixed skeletal muscles of animals exposed to hypokinesia
23 p3636 A71-44237

MUSIC

Color and music distraction for operator in isolated environment and counteract psychophysiological activity impairment
20 p3193 A71-39225

MUTATIONS

Lethal recessive point mutation in *Drosophila melanogaster* eggs on Zond 5 spacecraft
01 p0018 A71-11552

Space flight effects on survival, mutation and cell development of *Chlorella* cells suspensions onboard Zond 5 spacecraft
01 p0019 A71-11554

Relative biological effectiveness of multicharged C ions during single irradiation of *Chlorella*, noting dose dependent mutability
06 p0854 A71-18366

PH conditional ammonia assimilation deficient mutants isolation and growth properties, studying nitrogen transport in *Hydrogenomonas cutropha*
06 p0857 A71-18672

Hydrogenomonas cutropha mutants deficient amination due to ammonia-nitrogen permeation defect
06 p0857 A71-18673

Spaceflight effects on dry crepis capillaris seeds in five day orbit, showing chromosome rearrangements and increased mutagenic sensitivity
09 p1392 A71-22563

Deleterious mutations and neutral substitutions, discussing molecular evolution model for DNA and proteins
13 p2013 A71-29096

Combined action of vibration and gamma irradiation on sporulation dynamics, survival rate and mutability of *Chlorella*
20 p3193 A71-39237

Chlorella viability and mutability aboard Soyuz and Zond spacecraft, noting trend toward growth of anomalies in autosporeulation
21 p3343 A71-40566

Lymphocyte chromosome aberrations by inhaled ozone in Chinese hamster, indicating mutagen damage
24 p3799 A71-45150

MYELIN

Lower cardiac nerve unmyelinated afferent fibers detection and functional property characteristics
15 p2362 A71-32736

MYOCARDIUM

Bioelectric potential in gap between abutting cardiac muscle cells, using differential equation for active to inactive cell transmission
01 p0025 A71-11177

Mortality of myocardial infarction patients on diet low in saturated fats and cholesterol
01 p0015 A71-11299

Mitral valve muscular fibers, investigating pathological changes of myocardium of left heart ventricle
02 p0198 A71-11695

Complete heart block associated with acute myocardial infarction, discussing high mortality rate and transvenous pacemaker applications
02 p0198 A71-11696

Coronary sclerosis morphology, discussing myocardium microcirculation disturbances
02 p0200 A71-12414

Oxygen inhalation effects on intramyocardial oxygen tension in anesthetized dogs, investigating acute myocardial infarction therapy effectiveness
02 p0202 A71-12917

Fiberoptic indicator-dilution assessment of myocardial function
03 p0362 A71-13329

Myocardial glycogen stores increase protective role in rat cardiac anoxia studied in isolated perfused heart
03 p0363 A71-13489

Clinical and hemodynamic profile of cardiogenic shock after acute myocardial infarction
04 p0541 A71-15914

Oxygen partial pressure measurements in myocardium of beating heart by miniature glass needle and surface electrodes
05 p0714 A71-16598

Autopsies compared to ECG for diagnosis accuracy for acute recurrent myocardial infarction
05 p0711 A71-16951

Myocardial infarction acute stage, noting carbohydrate metabolism disturbances
06 p0849 A71-17291

Myocardial infarction, investigating alpha-dehydroxybutyric acid dehydrogenase enzymatic activity
06 p0849 A71-17292

Myocardial infarction noting serum prealbumin changes
06 p0849 A71-17293

Ultrastructure changes of membrane and sarcoplasmic reticulum of myocardial cells in squirrels during hibernation
06 p0850 A71-17412

Cinearteriographically demonstrated coronary artery disease severity correlation with myocardial blood flow response to treadmill exercise or isoproterenol infusion
06 p0852 A71-17874

Myocardium enzyme activity after sympathetic denervation of heart in cats and mice
06 p0857 A71-18726

Acetylcholine endogenic formation in rabbit myocardium effect on ventricle rhythm guides automatic activity suppression by HF excitations
07 p1040 A71-19281

Simulated high altitude chronic hypoxia and long term sideropenic anemia adapted animals, investigating acute anoxia tolerance of myocardium
07 p1044 A71-20331

Frog ventricles myocardial fibers spontaneous activity in Ringer solution due to ion conductivity variations
08 p1239 A71-21057

Myocardial lysosomal enzymes activity in adaptation to high altitude hypoxia and during cardiac diseases, using albino rats
08 p1239 A71-21058

Myocardial depressant factor purified preparation effect on isolated perfused cat heart, studying coronary vascular, dromotropic and inotropic actions
08 p1239 A71-21176

Myocardium ultrastructure and histochemistry in dogs under hypoxic hypoxia
09 p1390 A71-22262

Excitable myocardium cell simplified model based on artificial membrane excitation phenomena, using hybrid computer complex analog section
10 p1567 A71-24166

Myocardial oxygen reduction by stimulating carotid sinus nerves and angina pectoris treatment application
11 p1718 A71-25437

Rat heart muscle series elasticity compliance, showing hypoxia effects
11 p1719 A71-25930

Digital computer analysis of orthogonal ECG and VCG from patients with myocardial infarction
12 p1875 A71-27287

Normal myocardium structure and function, discussing cardiac performance and output control
13 p2003 A71-27859

Myocardial hypertrophy, discussing various forms and mechanisms in myocardial fiber growth and eventual failure
13 p2004 A71-27863

Myocardial infarction and coronary heart disease, considering incidence, mortality and preventive measures
13 p2004 A71-27867

Myocardium cells contractile activity control with frequency dependent self regulatory mechanism
13 p2006 A71-28383

Anoxia induced ECG lesion current in conjunction with myocardial phosphocreatine collapse, discussing results with air and nitrogen ventilated guinea pigs
13 p2008 A71-28506

Myocardial ischemia and necrosis without major coronary arteries obstruction, investigating possible deranged hemoglobin, oxygen transport 14 p2185 A71-30286

Myocardial ischemia observations, utilizing morphologic and pathophysiological correlations with cinecoronary arteriography, left ventriculography and hemodynamic examination 14 p2185 A71-30287

Left ventricular posterior wall motion measurements in myocardial infarction, using ultrasonic echogram time-motion data 15 p2365 A71-32536

Atrioventricular and intraventricular conduction disturbances in acute myocardial infarction, discussing heart block 15 p2361 A71-32540

Right ventricular end-diastolic volume as index of myocardial fiber length and correlation with ventricular work at rest and exercise with and without right ventricular failure 15 p2361 A71-32541

Myocardial ischemic lesions age, discussing validity of histopathological criteria and margin of error 15 p2361 A71-32542

Spatial T-area vectors dependence on RR distances for exact examination of healthy and sick heart muscles 15 p2362 A71-32660

Myocardium ultrastructural and metabolic alterations in altitude acclimated rats, considering heart muscle mitochondria 16 p2529 A71-33193

Hypoxia effects on myocardial potassium balance in dogs during cardioaccelerator nerve and atrial stimulation 16 p2529 A71-33195

Physiologic and pathologic cardiomegaly, noting myocardial blood flow oxygen uptake and lengthening and widening of coronary vessels 16 p2531 A71-33423

Heart myocardium contractility assessment based on pressure rise rate relation to intraventricular pressure during isovolumic systole 17 p2681 A71-35039

Human ventricular activation correlation with canine model in chronic myocardial infarction 17 p2682 A71-35041

Primary cardiomyopathy, discussing obstructive and nonobstructive cases, myocardial inflammation, chronic alcoholism and age relationships 17 p2682 A71-35120

Myocardial inotropism index, using left ventricle time varying pressure/volume ratio in systole 17 p2683 A71-35121

Patients with selective cine coronary arteriography, statistically correlating vectorcardiographic diagnoses of myocardial infarcts with changes in arteries 18 p2854 A71-36139

Noradrenaline concentration in myocardium of rats subjected to high altitude hypoxia, considering heart regulation in presence of hyperfunction and hypertrophy 19 p3001 A71-37393

Canine ventricular myocardium as cardiac beta-adrenergic receptor, describing binding of norepinephrine to microsomal particles 19 p3002 A71-37900

Myocardium reactions under 2G acceleration from histological, histochemical and electron microscopic observations on rats, noting dystrophic damage level relationship to duration 20 p3189 A71-39235

Heart excitation and membrane permeability effects on two component action potentials in human atrial muscle strips, using microelectrodes 21 p3336 A71-40865

Myocardial blood flow and oxidative metabolism in cyanotic congenital heart disease patients, using lactate/pyruvate ratios and coronary sinus catheterization 22 p3484 A71-41521

Anoxia effect on laboratory animals cardiac action, discussing ECG injury current relation to myocardium phosphorylcreatine content 22 p3484 A71-41568

Antecedent clinical statistics of myocardial infarction and sudden death in actively employed middle aged men, noting cardiac rate, rhythm and conduction abnormalities 22 p3485 A71-41798

Norepinephrine induced stimulation of myocardial oxygen consumption of cat papillary muscles under after-loaded isotonic and isometric conditions 22 p3486 A71-41937

Ultrasonic evaluation of heart anatomical abnormalities in congenital and acquired heart diseases including myocardium hypertrophy and tissue degeneration 23 p3639 A71-43118

Electron microscopic quantitative analysis of myocardium sections from male dogs exposed to general hypoxia, considering mitochondrion sizes, numbers and areas 23 p3634 A71-43912

MYOELECTRICITY

Hind limb antagonistic muscles bioelectric activity dependence on animal rotation direction and head fixation 09 p1388 A71-22196

N

N-ELECTRONS

Density matrix components for multiconfiguration wave functions, constructing N electron /spin free/ Hamiltonian configuration interaction matrix 11 p1802 A71-26056

N-P JUNCTIONS

U-P-N JUNCTIONS

Neutron irradiation effects on diffusion-ion doped HF n-p-n silicon transistors of moderate power, showing radiation stability 14 p2213 A71-30625

Emitter avalanche stress on gated silicon planar n-p-n transistors, investigating degradation phenomena 19 p3034 A71-38523

Junction structures and electrical properties of silicon n-p-n transistors fabricated by various combinations of diffusion and ion implantation 21 p3354 A71-40728

Minority carriers charge distribution at boundary between neutral base and collector transition region of one dimensional n-p-n transistors 23 p3653 A71-43965

N-TYPE SEMICONDUCTORS

Hall constant and resistivity of impurity centers in seminsulating n-type GaAs during illumination and heating 01 p0138 A71-10776

Magnetic field effects on electron heating by strong electric field in n-Ge single crystals 01 p0140 A71-11459

GaAs high resistivity n-type Cr doped samples, examining field domains shape and motion by visual observation 01 p0141 A71-11467

Solid state traveling wave amplifier using thin n-type epitaxial GaAs layer 03 p0384 A71-13316

Hall effect, conductivity, thermal emf and Nerst-Ettingshausen transfer in n-type highly doped compensated GaAs 03 p0466 A71-13398

High resistance single crystal light sensitive n-type GaAs wafer for obtaining long wave photographic images via electric photosensitivity control 03 p0428 A71-13986

N-type Ge semiconductor low temperature breakdown potential dependence on neutral impurity concentration 05 p0793 A71-16420

Large optical cavity low loss n-type GaAs injection laser with reduced degradation 05 p0763 A71-16499

High Q microwave diodes on n-type germanium using carrier counterdiffusion in reducing atmosphere 06 p0873 A71-17539

Coplanar n-type GaAs Gunn effect microwave oscillators failure mechanism, suggesting role of current filament formation in thermal breakdown 06 p0874 A71-17665

Doping effect on positive Faraday rotation in n- and p-type GaAs at different impurity concentrations, noting shift of maximum to lower concentrations in p-type samples 07 p1176 A71-19227

Uniaxial compression effect on dispersion of helicon wave in n-type semiconductors, considering strain potential constants determination 07 p1176 A71-19269

Magnetoreflexion of helicon wave from n-InSb semiconductor in microwave range 07 p1176 A71-19270

N-type Si surface barriers and finishing effects on photoconductivity and photoelectric effect 07 p1179 A71-19921

N-type InSb microwave noise radiation and attendant RF current oscillations under magnetic field 07 p1180 A71-20177

Volt-ampere characteristics of dual base n-type semiconductors as function of input p-n junctions 08 p1264 A71-21070

N-type single crystal silicon semiconductor resistors with high impurity concentrations and high accuracy 09 p1414 A71-22160

Wideband UHF amplification in bulk n-type GaAs during domain generation, comparing cut-off and Gunn frequency 09 p1507 A71-22223

Hysteresis effects during retuning of n-type GaAs Gunn oscillator with bias source and RLC circuit, showing range of domain damping by low field 09 p1414 A71-22228

Degenerate n-type GaSb, calculating electron mobility dependence on impurities concentration for comparison with experiment 09 p1507 A71-22361

Stress effects on electron relaxation time anisotropies in n-type Si, using high temperature picosecondivity model for population transfer rates 09 p1508 A71-22692

Type S bulk negative differential conductivity in n-InSb at 77 K and atmospheric pressure, showing associated large current due to strong impact ionization 09 p1508 A71-22756

Epitaxial deposition of discrete separated p- and n-type silicon on single sapphire substrate, considering technique for MOS devices fabrication 09 p1509 A71-23116

Capacitance voltage measurements on interface of pyrolytically deposited n-type silicon dioxide-InAs MOS diodes as function of admittance at room and 77 K temperatures 10 p1582 A71-23774

Gammaradiation effect on electrical properties of n-type GaAs single crystals with doping impurities, calculating defect introduction rate and forbidden zone energy levels 10 p1656 A71-24141

Spatial-temporal emission of n-GaAs laser pumped by electron beam at liquid nitrogen temperatures 10 p1622 A71-24889

P-type Al-Ga-As-p-type Ga-As-n-type Ga-As single heterostructure preparation and properties, discussing effect on injection laser diode characteristics 12 p1914 A71-27027

N-type germanium Seitz coefficients relationship based on anisotropic electron scattering theory 13 p2110 A71-27958

Constant emf in bulk age and Si-N-type semiconductors under multifrequency microwave electric field 13 p2111 A71-28368

Carrier scattering related to orbiting and resonance states in screening impurity donor center of weakly doped homeopolar n-type semiconductor under injection 13 p2112 A71-28928

Radiation resistance variations of n-type and p-type silicon photocells due to formation of one or two vacancy recombination centers 15 p2461 A71-31670

IR absorption of oxygenated dislocationless phosphorus doped fast neutron irradiated n-type silicon, investigating dominant defects for different radiation dosages 17 p2790 A71-34199

Semiconductor behavior of zirconium oxide formed on Zr substrate with n-type below 685 C and p-type above 17 p2759 A71-35222

Integrated complementary MOS circuit technology, discussing low power consumption, high speed, n and p regions realization on Si plates and design parameters relations 18 p2891 A71-36562

Electron concentration and mobility of heavily doped n-type InSb single crystals at high temperatures, investigating temperature dependence of Hall coefficient 18 p2954 A71-36803

Hall effect measurements utilization for simultaneous determination of donors and acceptors concentration in semiconductors, applying to n-type silicon 19 p3118 A71-37487

High electric field Gunn effect in n-type InAs under hydrostatic pressure due to transferred carrier mechanism 20 p3275 A71-38786

Electron drag by photons during intraband light absorption by free carriers in n-Ge semiconductors 21 p3428 A71-41111

Fabrication and I-V characteristics of S-type negative resistance alloyed diodes prepared from sulfur-doped n-type Si, outlining temperature dependence of turnoff time 21 p3358 A71-41203

Spectral dependence of photon capture cross section of negative Zn center in Zn-doped n-type silicon during electron excitation to conduction band 21 p3429 A71-41206

Electron concentration and degeneracy effect on threshold photon energy for optical transitions onset from splitoff valence band to conduction band in n-type GaAs 21 p3429 A71-41211

Current-voltage characteristics of n-GaAs epitaxial structures at various temperatures, indicating use in memory devices and high power switches 21 p3430 A71-41223

Pure and doped Ge dumbbell p and n type samples at liquid helium temperatures, investigating electric breakdowns 21 p3430 A71-41224

Au-n-GaAs surface barrier diode space charge layer strong electric field effects on photoconductivity quantum efficiency 21 p3432 A71-41302

Auger recombination coefficient determination for nonequilibrium carriers in n-type InAs from photoconductivity and light absorption under laser excitation at high levels, noting electron mobility 21 p3433 A71-41310

Impurity photoconductivity spectra determination for n and p type Si crystals under 660 MeV proton irradiation

21 p3433 A71-41311

Sn-N-GaAs semiconductor surface barrier structure electrical properties measurement over wide electron density range, determining energy band diagram and current flow mechanism

21 p3433 A71-41313

Cr-doped n-type seminsulating GaAs single crystal photoconductivity measurement, noting spectral peaks dependence on temperature

21 p3434 A71-41324

Semiconducting plasma carrier density gradient instability, investigating threshold curve for n-type germanium

21 p3434 A71-41330

Carrier scattering related to orbiting and resonance states in screened field of impurity donor center in weakly doped homeopolar n-type semiconductor under injection

21 p3434 A71-41331

N-type germanium Seitz coefficients relationship based on anisotropic electron scattering theory

21 p3436 A71-41347

Te-doped n-type GaSb semiconductor negative magnetoresistance and magnetothermoelectric power dependence on longitudinal magnetic field

21 p3436 A71-41349

N-type cadmium germanium arsenide single crystal semiconductor electron and hole effective mass determination from thermoelectric power measurement

21 p3436 A71-41350

Metal film ohmic contacts to n-type GaP devices operating at high ambient temperatures

22 p3520 A71-41687

N-type In-Sb continuous coherent microwave oscillation under transverse magnetic field, discussing helical frequency instability on threshold and growing wave conditions

22 p3586 A71-42347

Bulk quantum efficiency in electron beam pumped n-type GaAs lasers at 300 K as function of impurity concentration

22 p3558 A71-42362

Low temperature investigation of microplasma breakdown in steep p-n junctions of Sb-doped n-type Ge

22 p3587 A71-42874

GaP diodes with metal-semiconductor potential barriers manufactured by chemical deposition of metal on n-GaP surface

23 p3653 A71-43960

Cryogenic n-type GaAs residual photoconductivity produced repeatedly after heating to room temperature and renewed cooling

24 p3859 A71-44463

Nonequilibrium negative bias effects on n-type metal oxide semiconductor tunnel currents

24 p3812 A71-45356

NACELLES

Airframe installation effects on underlying nacelle nozzle performance, using calibrated engines and load cells on F-106 for measurements

[AIAA PAPER 71-681] 14 p2292 A71-30745

Transonic wind tunnel testing of air intake and afterbody of double flux engine nacelle at high subsonic Mach numbers and high Reynolds numbers

[ONERA-TP-943] 18 p2956 A71-36021

NAMING

NT NORMS

NAPHTHALENE

Direct measurement of convective heat transfer coefficient by realizing proportionality to sublimation rate of naphthalene ball near body surface

04 p0545 A71-15158

Absorption spectra of benzene, naphthalene and anthracene crystals, noting resonance coupling type effect on vibrational spectrum

24 p3851 A71-45171

NAPHTHENES

Thermal stability of naphthenes up to 1000 F, considering hypersonic aircraft fuel applications

22 p3588 A71-42837

NARCOLEPSY

Rapid eye movements during nocturnal sleep of healthy human subjects, insomniacs and narcoleptics recorded on polygraphs

01 p0007 A71-10071

NARCOSIS

Alveolar nitrogen and carbon dioxide tensions changes during compressed air narcosis in constant oxygen partial pressure

08 p1239 A71-20818

NASA PROGRAMS

NT APOLLO APPLICATIONS PROGRAM

NT APOLLO PROJECT

NT CENTAUR PROJECT

NT EARTH RESOURCES PROGRAM

NT GEMINI PROJECT

NT JUPITER PROJECT

NT MARINER PROGRAM

NT MARS 69 PROJECT

NT MARS 71 PROJECT

NT ROVER PROJECT

NT SATURN PROJECT

NT SKYLAB PROGRAM

NT TEKITE PROJECT

NT VIKING MARS PROGRAM

NASA modular aerospace computer for attitude control high speed computation, describing implementation with LSI functional characters

01 p0045 A71-10198

NASA Space Documentation Service on-line information retrieval system using direct access remote consoles

01 p0183 A71-10397

NACA/NASA rotating wing aircraft research history during 1955-1970 period, discussing wind tunnel research

01 p0005 A71-11377

Power sources for future NASA programs, discussing requirements in relation to various types of space missions

03 p0351 A71-13037

Communication technology development relation to NASA programs, discussing receivers, microwave tubes, solid state transmitters, lasers, information retrieval and frequency sharing

03 p0388 A71-14412

NASA program concerning determination of RF spectrum sharing criteria and automatic data processing in aerospace systems

03 p0381 A71-14588

NASC future active role, discussing advisory capacity to Executive Branch, problems handled and space programs

04 p0689 A71-14926

OART research projects covering space shuttle, vehicle configuration, heat transfer, thermal protection, lifting bodies, electronics, power studies, etc

04 p0661 A71-14931

OART space station development, discussing long term effects, artificial gravity, environmental problems, electric power, life support, protection systems and human factors

04 p0643 A71-14932

Ossa R and D program noting budget allocations, satellite programs and international projects

04 p0690 A71-14934

NASA Office of Tracking and Data Acquisition mission support and ground and spacecraft communication networks

04 p0551 A71-14936

NASA multiple interagency interfaces, surveying work and resource integration, space programs and agency structure

04 p0690 A71-14937

NASA Office of Technology Utilization, examining publications, information sources, data processing and dissemination facilities

04 p0690 A71-14938

NASA patents and licensing policy, discussing contractor rights and invention handling

04 p0690 A71-14939

NACA/NASA rotary wing aircraft research, considering rotor loads and configurations, ground resonance, blade flutter and flapping, motion equations and VTOL

04 p0529 A71-15171

NASA program for aerospace technology application to medicine

04 p0546 A71-15281

Aerospace technology direct and derived benefits for public, discussing earth resources program, communication satellites and NASA effect on nonaerospace activities and economy

04 p0691 A71-15315

NASA satellites meteorological IR instruments, considering purpose, design, operation and performance

04 p0598 A71-15365

Planetary and interplanetary exploration missions, discussing U.S. planetary space program budgets and costs

04 p0657 A71-15818

Carbon fiber reinforced composite cryogenic fuel tanks development for post-Apollo programs, discussing fiber and resin physical properties

05 p0819 A71-15946

Post-Apollo space programs European collaboration, discussing space shuttle and space tug projects

[DGLR-70-067] 05 p0839 A71-15957

American-European space shuttle costs, comparing nonrecoverable Europa 3 with ballistic reusable devices

05 p0816 A71-16402

NASA Data Processing Facility for earth resources technology satellite telemetry

05 p0818 A71-17146

NASA bilateral and multilateral international cooperation agreements in space research, discussing political objectives, program history, regulations and procedures

06 p1010 A71-17646

Manned space flight missions in next decade, discussing potential payloads and compatibility to proposed mission structure

[AIAA PAPER 71-69] 06 p0977 A71-18527

Common module series for NASA candidate experiment program for manned space stations in 1975-1985 era, discussing configuration and subsystem design

[AIAA PAPER 71-70] 06 p0980 A71-18528

Manned flight from Montgolfier Balloon to Apollo 13, discussing future space programs including lunar base and space shuttle

07 p1195 A71-19417

ESRO/ELDO space documentation service involving NASA file remote processing and data bank for space component selection

07 p1225 A71-20001

Two stage space shuttle, discussing NASA reusable spacecraft cost reduction and technological problems

07 p1209 A71-20226

Space transportation system of two stage reusable space shuttle and orbit-to-orbit shuttle, supporting NASA and DOD missions

08 p1367 A71-21890

Space shuttle as post-Apollo key project for technology advancement, discussing predesign studies and technical problem areas in propulsion, materials, structures and avionics

09 p1531 A71-22273

NASA Earth Resources Survey Program as basis for future earth survey system combining spaceborne, airborne and ground observations

10 p1600 A71-24171

ERTS A and B projects, describing satellite communications, data handling, telemetry, tracking and command, thermal control, orbit-adjust, image processing and ground equipment

10 p1682 A71-24172

NASA aerodynamic research applicable to business aircraft concerning wind tunnel and flight tests, STOL performance and high speed cruise technology

[SAE PAPER 710378] 10 p1554 A71-24244

NASA reliability program provisions for aeronautical and space system contractors, reviewing evolution process

12 p1909 A71-26667

NASA past and future space programs, examining operations analysis problems associated with space missions planning

13 p1133 A71-28030

NASA Lewis Research Center Hg electron bombardment ion thrusters research programs

14 p2288 A71-29931

Space research impact on general economy and ecology, noting royalty-free licensing to private industry by NASA

14 p2341 A71-30257

NASA space station program, discussing relationship between space stations, Skylab and space shuttle, electric power generation, habitability, safety and communications networks

14 p2320 A71-30259

Post-Apollo program European participation, discussing need for multilateral international agreements on space shuttle, space tug and space station projects

14 p2341 A71-30262

NASA evaluation of reports on space shuttles, discussing booster and orbiter design, mission requirements, payload capabilities, reusability, etc

14 p2320 A71-30421

Biowaste resistojet propulsion system for NASA space station orbit-keeping, describing design and operation

[AIAA PAPER 71-686] 14 p2293 A71-30748

Ion thruster technology and subsystem development program status, describing design and performance characteristics

[AIAA PAPER 71-690] 14 p2293 A71-30750

NASA space station design, describing operational procedures, structure, meteoroid, thermal and radiation insulation and living quarters

15 p2498 A71-31137

Brayton space power system for NASA manned space missions, discussing control system requirements, design and performance

15 p2354 A71-32203

NASA earth resources technology satellites system, discussing ERTS A and B development, payloads and ground support systems and international aspects

16 p2630 A71-32854

International space exploration management and organization, emphasizing NASA cooperative programs

16 p2665 A71-33587

U.S. space program report to COSPAR covering organization, facilities, international activities, astronomy, lunar and planetary research, particles, fields, atmospheric, earth and life sciences

16 p2665 A71-33855

NASA space station electrical power systems discussing configurations, growth capacity, volume reliability and long term effects

[AIAA PAPER 71-825] 17 p2677 A71-34720

Lunar surface base concept synthesis, considering program objectives and hardware operational approaches

[AIAA PAPER 71-819] 17 p2723 A71-34725

Space station common module concept, discussing NASA functional program elements accommodating

multidisciplinary scientific applications and technology experiment modes
[AIAA PAPER 71-813] 17 p2813 A71-34728

Long range near-earth orbit research and applications based on NASA goals, including laboratory/observatory definition
[AIAA PAPER 71-812] 17 p2802 A71-34729

NASA space transportation system economics, discussing cost analytic considerations in comparing reusable vs expendable launch systems
[AIAA PAPER 71-806] 17 p2841 A71-34733

NASA space station navigation system, considering landmark and ground tracking, ground beacons and satellite concepts, long term effects, operational requirements and design goals
17 p2772 A71-35054

NASA ERTS program, discussing system concept automatic data processing capability, compatibility with tracking ground stations and international cooperation
17 p2805 A71-35329

NASA Scientific and Technical Information System, illustrating advantages of machine retrieval systems for legal profession
18 p2986 A71-35868

Satellite broadcasting to West African countries, discussing communications policies, NASA tracking stations in Africa and U.S.-Nigeria agreement for Comsat and Intelsat programs
18 p2987 A71-36169

NASA-SRI Round Robin Ablation Program summary, discussing dimensional analysis, Teflon, nylon and surface temperature
18 p2985 A71-36279

U.S. and U.S.S.R. space stations with European participation, discussing design, international cooperation and legal and political problems
19 p3149 A71-37305

Technical prospects of European aerospace industries participation in post-Apollo program, noting space shuttle development role
19 p3151 A71-37324

European contributions to post-Apollo space program, considering space station, space shuttle and space tug
19 p3151 A71-37325

Exploration, science and applications goals of U.S. space effort
19 p3131 A71-37326

European launcher programs and participation in post-Apollo shuttles and orbital stations development in partnership with U.S.
19 p3151 A71-37330

Balanced terrestrial and outer planets NASA solar system exploration strategy for 1970s, outlining earth based observations and flight missions program
[AAS PAPER 71-100] 19 p3140 A71-37390

NASA 12-man 10-year space station program, discussing design, information management, environmental control and life support system
19 p3153 A71-38147

NASA modular space station program, describing design and equipment
19 p3153 A71-38149

NASA space station program, discussing design, guidance, navigation, electrical power and environmental control
19 p3154 A71-38150

NASA technology utilization program, discussing technical information, spin-off benefits and various applications
19 p3173 A71-38408

NASA Stadan and Speopt optical and laser tracking sites dynamic position estimations from GEOS 1 and 2 observations, analyzing model error effects
20 p3220 A71-39662

Space shuttle impact on cost reduction in NASA space operations, considering operations costs of payloads
22 p3609 A71-41994

NASA program for lunar and planetary exploration, listing missions, instrumentation, experiments and future aims
23 p3736 A71-43498

NASA program fire safety goals, discussing development of nonflammable materials covering fibrous asbestos, glass, polyimides, Teflon, metallics and halogenated materials
[AIAA PAPER 71-1011] 24 p3841 A71-44595

Pure and pragmatic science in future NASA programs, discussing interagency cooperation, communications, ATC, education, earth resources, space science, meteorology, budgets and program management
[AIAA PAPER 71-1021] 24 p3892 A71-44599

French-American Eole project for meteorological prediction systems development, discussing balloon sounding and satellite data transmission
24 p3876 A71-45274

NATIONAL AIRSPACE UTILIZATION SYSTEM
National Airspace System air traffic control automation man machine considerations, noting controller productivity increase, input difficulties and symbology clutter
[AIAA PAPER 71-246] 07 p1049 A71-19720

Data communication role in National Airspace System, concerning radar and flight data acquisition, intersystem transfer and voice control
[AIAA PAPER 71-248] 07 p1063 A71-19722

German monograph on airport role in national economy and growth and location determination for enterprises maintaining connections with foreign countries
17 p2841 A71-34482

Airborne traffic situation display for use with national airspace/automatic radar control terminal system, using computer selected message, map and heading data
[AIAA PAPER 71-929] 19 p3097 A71-37175

NATIONAL AVIATION SYSTEM
National Aviation System stage A ATC displaying digitized radar data positions together with automatic track positions
22 p3570 A71-41634

IBM 9020 multiprocessing computer application to ATC, discussing control sectors for inflight control at air route traffic control centers in U.S.
23 p3702 A71-43888

NATIONS
Air and cosmic space common law, discussing boundaries, sovereignty over state territories and jurisprudence related to travel development
11 p1861 A71-26325

NATURAL FREQUENCIES
U RESONANT FREQUENCIES
NATURAL SATELLITES
NT LAPETUS
NT MOON
NT PHOBOS
Io Hygiea perturbation observations, determining Jupiter mass by numerical integration
01 p0155 A71-10443

Solar system origin, structure and evolution, discussing planet and satellite orbital motion, resonance effects, tides and postaccretionary changes
01 p0161 A71-11335

Numerical analysis of Hill limiting case of restricted three body problem regarding quasi-periodic, ergodic and escape orbits for natural and artificial satellites
01 p0161 A71-11380

Papers on surfaces and interiors of planets and satellites covering radio and radar observations, photometry, magnetic fields, etc
02 p0309 A71-12151

Planets and satellites masses and other dynamic parameters by numerical and analytical calculation techniques based motion and trajectory analyses
02 p0309 A71-12152

Planets and satellites diameter determination, reviewing double image technique
02 p0309 A71-12153

Galilean satellites spectral reflectivity from photometric observations during Jupiter apparitions
03 p0488 A71-13554

Accretion theory of planet and satellite formation in solar system, including earth-moon model
03 p0495 A71-14262

Absolute orbit construction for Jovian great satellites, obtaining linear equations of motion
04 p0654 A71-15714

Lunar position on stellar field for ephemeris time determination, discussing planet and satellite positions with respect to astronomical constants
05 p0809 A71-16460

Deimos photographic observations on Pulkovo normal astrophotograph during 1967 Mars opposition
07 p1194 A71-19334

Martian satellites nature and evolution, facts, theories, hypotheses and speculations
07 p1202 A71-20516

Double resonance in natural satellite motion from long period perturbation prediction
07 p1202 A71-20517

Saturn natural satellites commensurabilities evolution from analysis of libration amplitude change with time for interaction under tidal friction with planet
07 p1202 A71-20519

Jupiter decametric radiation source A position variation, considering radiation controlling influence of Jovian satellite Io
09 p1521 A71-22935

Jupiter gravitational potential mapping for Grand Tours spacecraft, discussing Jovian satellites effect on orbit and trajectory perturbations
09 p1525 A71-23222

Titan visual photometric observations, describing measurement procedures and error sources
09 p1528 A71-23549

Mimas /Saturn satellite/ perturbations effect on Cassini division in Saturn rings
10 p1673 A71-24425

Saturn satellites spectrophotometric observations at UV, visible and near IR, noting reflection spectra data
11 p1819 A71-25210

Jupiter, Saturn and Uranus satellite systems orbital radius and mass correlation, suggesting satellite orbital tidal evolution and energy dissipation at planetary atmospheric boundary layer
11 p1827 A71-25729

H and He concentrations upper limit for Titan atmosphere from molecular diffusion time constant
11 p1828 A71-25732

Planetary satellites intermediate orbits, obtaining angular orbital elements secular perturbations
12 p1964 A71-27091

Jovian atmosphere physical properties inferred from eclipses of Galilean satellites, using color photoelectric photometry
13 p2134 A71-28284

Four eclipse reappearances observations of Jovian satellite Io by area scanning photometer, considering anomalous brightening
13 p2134 A71-28285

Jupiter Galilean satellites narrowband photometric data, observing albedos, spectral reflectivity, rotational phase, and brightness variations
13 p2135 A71-28292

Outer planet large satellite steady state thermal models, indicating interiors at temperatures above ice-ammonia eutectic
14 p2318 A71-31125

Io brightness anomaly after eclipse by Jupiter
15 p2491 A71-32421

Water distribution in space, natural satellites and terrestrial planets, discussing Clarke abundance values and hydrochlorosphere concept
15 p2494 A71-32493

Planetary exploration from space, recommending flights to moons of outer planets due to possible presence of atmospheres and water ice
15 p2494 A71-32495

Ganymede thermal inertia data from simultaneous visual photometry and IR radiometry observations during 17 March 1971 eclipse
17 p2807 A71-35418

Martian satellites motion along arbitrary elliptical orbits, expressing planet gravitational potential
18 p2962 A71-36108

Jupiter Galilean satellites surface optical polarization measurement, noting bright transparent material cover possibly frost
18 p2964 A71-36290

Planetary satellites intermediate orbits, obtaining angular orbital elements secular perturbations
19 p3133 A71-37441

Jovian satellite eclipse observations, reviewing simultaneous narrow band multichannel visual and near IR studies
19 p3139 A71-37908

IR experiments planning for Outer Planets Grand Tour including investigations of planetary radiation balance and atmospheric composition and satellites composition and physical properties
[AAS PAPER 71-131] 19 p3011 A71-37920

Outer planet satellite missions for optimal imaging conditions in terms of proximity and lighting
[AAS PAPER 71-138] 19 p3140 A71-37942

Mimas-Tethys resonance motions under short period gravitational perturbations and tidal dissipation functions
20 p3286 A71-38760

Satellite capture by Jupiter, calculating satellite orbits based on apellion and perihelion conditions derived from planetary elliptical orbit three body problem
20 p3287 A71-38978

Saturn planetary system optical and radio observations during 1966, discussing Janus satellite, D ring, rarefied envelope and brightness temperature distribution
20 p3297 A71-39632

Rhea and Titan UVB photoelectric observations, obtaining light curve magnitude variation
21 p3440 A71-40056

Quantitative equivalence model in planet-satellite formation within Jupiter and Uranus systems
22 p3604 A71-42191

Mars orbiting spacecraft trajectory from spacecraft based TV pictures of Phobos and Deimos
[AAS PAPER 71-372] 23 p3730 A71-43042

To passage in front of binary star beta Scorpii on 14 May 1971, presenting satellite trajectory calculations and appulse time
23 p3733 A71-43150

IR spectral geometric albedos of Jupiter Galilean satellites, noting resemblance to spectra of frosts
24 p3871 A71-44910

Deimos and Mars photography observation by 400 mm astrophotographic camera, introducing corrections for irregularities in satellite motion and planet phase
24 p3874 A71-45177

Computer processed photographic observations of Pluto, 10 Hygiea, 433 Eros and Saturn satellites VII, VIII and IX
24 p3874 A71-45178

NAVIER-STOKES EQUATION
Spheres Oseen drag, extending Goldstein expansion for Navier-Stokes equation in powers of Reynolds number
02 p0185 A71-12380

Shear flow turbulent friction in boundary layer, deriving Navier-Stokes equation integrodifferential formulation
02 p0241 A71-12411

Plastic impact principle of hydraulic losses in turbulent viscous flow, using Navier-Stokes equation with friction term

03 p0397 A71-13006

Navier-Stokes equations numerical integration in Eulerian coordinates, applying results to compressible and incompressible fluids steady flow

[AIAA PAPER 70-2] 03 p0399 A71-13426

Turbine engine vibration dampers viscous resistance calculation based on equations of motion for incompressible and unheated Navier-Stokes liquid

03 p0470 A71-13956

Hypersonic viscous air flow past blunt bodies with radiation, obtaining solution for Navier-Stokes equations by finite difference scheme

03 p0343 A71-14062

Nonuniform flow in straight channel inlet section initiated by Fourier expandable nonuniform profile, linearizing Navier-Stokes equations about mean velocity

[ASME PAPER 70-WA/FE-27] 03 p0403 A71-14135

Navier-Stokes equations numerical solution method, considering stability and convergence of scheme and system of difference equations

03 p0452 A71-14175

Navier-Stokes equation solution in cylindrical coordinates, using finite difference scheme with brute force matrix methods

04 p0572 A71-15551

Viscous incompressible flow problems, using finite difference methods for solving Navier-Stokes equations

06 p0917 A71-17564

Stationary Navier-Stokes equations solution vorticity asymptotic behavior in three and two dimensional neighborhoods of infinity

07 p1147 A71-19640

Poiseuille pipe flow stability from finite difference equations approximation to nonlinear axisymmetric Navier-Stokes equations under stream function perturbation

07 p1094 A71-20611

Steady plane plasma shock wave structure in partially ionized and radiating gas, using Navier-Stokes equations in three fluid continuum approach

09 p1504 A71-23202

Three dimensional unsteady irrotational flow in variable cross section duct, reducing Navier-Stokes equation to Euler equation

10 p1591 A71-23850

Fractional derivatives of Navier-Stokes equations weak solutions

10 p1636 A71-23913

Recirculation patterns in coaxial steady laminar mixing of homogeneous jets in confined tube, solving Navier-Stokes equations

11 p1748 A71-25151

Bifurcation solutions of Navier-Stokes equations for time periodic motions of viscous incompressible fluid at critical Reynolds number

12 p1922 A71-26867

Steady laminar natural convective flow in concentric cylindrical annuli, using finite difference method for Navier-Stokes and energy equations solution

[ASME PAPER 70-WA/HT-9] 13 p2164 A71-28982

Numerical method for two dimensional or axisymmetric heated flows allowing for dissipation extended to viscous flow, using Navier-Stokes equations in streamwise coordinates

13 p2118 A71-29280

Convergence and accuracy of modified Gauss-Seidel finite difference scheme, calculating one dimensional Navier-Stokes shock structure

13 p2051 A71-29429

Couette flow two point boundary value problem solution using Navier-Stokes and Barnett viscous gas equations

14 p2224 A71-30185

Nonlinear dynamical evolution of two dimensional unstable shear flows, using numerical integration of time dependent incompressible Navier-Stokes equations

14 p2226 A71-30409

Steady state flow of viscous incompressible fluid, proposing difference scheme for numerical solution of Navier-Stokes equations

14 p2226 A71-30437

Laminar boundary layer of free vortex and source flow, obtaining similarity transform of Navier-Stokes equation

14 p2228 A71-31027

Two dimensional viscous incompressible fluid flow field calculation in fluidic element, giving Navier-Stokes equations solution in finite difference form

15 p2390 A71-32054

Unstable two dimensional incompressible flow and wake development, using finite difference calculations for Navier-Stokes equations

16 p2558 A71-32996

Nonlinear global strong cellular branching solutions stability of Navier-Stokes equations

16 p2558 A71-32997

Unsteady viscous flow around oscillating cylinders, calculating fluctuating lift, drag and moment effects with Navier-Stokes equations

16 p2520 A71-33098

Two dimensional laminar separation bubbles in high Reynolds number flow fields, using finite difference solutions to Navier-Stokes equations

16 p2561 A71-34165

Navier-Stokes steady nonrectilinear universal complex laminar flow, showing isochoric lamellar or plane motions of constant velocity with streamlines as concentric circles

17 p2727 A71-34695

Difference analog of nonlinear hydrodynamic boundary value problem from Navier-Stokes steady state theory

17 p2728 A71-35241

One dimensional flow with boundary layer, considering numerical solution of Navier-Stokes equation at large Reynolds number

17 p2729 A71-35466

Two dimensional steady viscous gas transonic flow Navier-Stokes equations, establishing uniqueness of solutions to boundary value problems

17 p2673 A71-35646

Droplet pairs collision efficiencies and coalescence parameters, computing flow fields from nonlinear time dependent Navier-Stokes equations

17 p2770 A71-35805

Incompressible turbulent shear boundary layer equations of motion, developing integrodifferential formulation of Navier-Stokes theory

18 p2904 A71-36184

Wave motions in viscous fluid layer in presence of surfactant elastic substances adjoining solid surface or gas, using Navier-Stokes equations

19 p3042 A71-37084

Ergodic boundary in time evolution of two dimensional incompressible Navier-Stokes equations solution at large Reynolds numbers

19 p3045 A71-37841

Vortices motion and decay, constructing asymptotic solution to Navier-Stokes equations

21 p3366 A71-40485

Two axisymmetric annular flows linear hydrodynamic stability analysis, using Navier-Stokes system

21 p3370 A71-40991

Numerically simulated turbulent velocity flow field, covering Navier-Stokes and energy conservation equations

21 p3371 A71-40996

Uniqueness theorems and boundary conditions for problem related to Navier-Stokes equations

22 p3566 A71-41514

Perturbation and projection operator algorithms for Navier-Stokes equations for incompressible flow in rectangular cavities and injection into cylindrical ducts

23 p3662 A71-43238

Kraichnan turbulence theory based on exact solution of model equations presenting strong structural similarities with turbulent Navier-Stokes equations

23 p3701 A71-43976

Navier-Stokes equations solutions for incompressible laminar viscous fluid flow produced by vortex filament placed on cone axis

23 p3664 A71-44004

Navier-Stokes equations solutions expressing flow conditions through blade cascade

24 p3817 A71-44523

Compressible viscous flow calculation, deriving finite element analog of Navier-Stokes and energy equations

24 p3818 A71-44617

Shock initiation problem collisionless solution for transport properties of gas flow, considering departure from Navier-Stokes solution

24 p3819 A71-44791

Two-dimensional asymptotic solutions to Navier-Stokes equations for weak vortex discontinuity flow with vanishing viscosity

24 p3820 A71-45060

NAVIGATION

NT AIR NAVIGATION

NT ALL-WEATHER AIR NAVIGATION

NT ASTRONAVIGATION

NT CELESTIAL NAVIGATION

NT DEAD RECKONING

NT DIGITAL NAVIGATION

NT DOPPLER NAVIGATION

NT GIMBALLLESS INERTIAL NAVIGATION

NT HYBRID NAVIGATION SYSTEMS

NT HYPERBOLIC NAVIGATION

NT INERTIAL NAVIGATION

NT INTERPLANETARY NAVIGATION

NT LORAN

NT LORAN C

NT OMEGA NAVIGATION SYSTEM

NT RADAR NAVIGATION

NT RADIO NAVIGATION

NT SPACE NAVIGATION

NT SURFACE NAVIGATION

NT TACAN

NT VHF OMNIRANGE NAVIGATION

Role of man in navigation - Conference, Colorado Springs, July 1970

01 p0122 A71-10501

Navigation, inertial guidance and position keeping

terms definitions

02 p0280 A71-12897

Navigation and communication experiment at L band on board S.S. Manhattan using ATS-5 satellite with biphasic PSK modulation of three tones for ranging

07 p1057 A71-18816

Parameter estimates effectiveness from independent discrete and continuous navigation measurements of circular orbital plane

09 p1491 A71-22543

Quasi-optimal proportional navigation, deriving feedback guidance laws for interceptor aerodynamically controlled missiles

11 p1796 A71-26409

Photography and navigation - Conference, Columbus, Ohio, May 1970

12 p1907 A71-27255

Proportional navigation for trajectory control of missile homing on target in planar pursuit

20 p3261 A71-38856

NAVIGATION AIDS

NT BEACONS

NT COMPASSES

NT GYROCOMPASSES

NT LASER ALTIMETERS

NT MAGNETIC COMPASSES

NT NAVIGATION INSTRUMENTS

NT RADAR BEACONS

NT RADIO BEACONS

NT RADIO DIRECTION FINDERS

NT SOLAR COMPASSES

Commercial and military aircraft navigator future role, considering increasing task requirement stringency and growing navigational aids availability

01 p0124 A71-10505

Airborne inertial and area navigation systems performance requirements proposed for U.S. domestic airspace, including projection through 1995

01 p0124 A71-10508

Airline experience with dual inertial systems as sole means of navigation, considering equipment reliability, cockpit design, training, etc

01 p0124 A71-10509

Star charts as orientation and navigation aids in manned space flight

01 p0125 A71-10517

Complex navigation systems training philosophy emphasizing functional approach to system and components

01 p0023 A71-10523

Air navigational training simulators, discussing navigation aids, civilian navigator use, visual simulation and land-mass radar

01 p0125 A71-10526

IFR design requirements for STOL navigation equipment from flight tests

04 p0623 A71-15424

Soviet book on inertial navigation systems covering theory, design, construction, coordinate algorithm, linear and angular accelerometers, etc

06 p0897 A71-17434

VTOL aircraft avionics systems, discussing automatic flight control and navigation systems integration

06 p0925 A71-17925

Manned aircraft crew long range navigation, discussing sensor, information processing and display systems for future commercial and military missions

07 p1157 A71-20343

VFR flying under adverse weather conditions, discussing radio navigational aid equipment and communication with ground stations

08 p1330 A71-20683

Interactive computer graphic system for compiling air navigational data on two dimensional aeronautical charts

08 p1258 A71-21236

Commercial V/STOL aircraft area navigation system requirements, discussing airborne computer, flight plan data storage and control subsystems and horizontal orientation display

10 p1639 A71-24150

Weather influence on long range radio navigation aids, considering supersonic aircraft operation and inertial navigation

10 p1640 A71-24963

Area navigation facility, discussing control and display and navigation standards

12 p1927 A71-26879

Optimum functional integration and performance requirements of navigation aids and ATC in terminal area

[SAE PAPER 710456] 13 p2098 A71-28333

Area navigation system based on radio aids by airborne receivers and sensors for aircraft movement improvement, noting advantages of pilot displays

[SAE PAPER 710457] 14 p2272 A71-30533

Control, navigation and guidance review, considering application of earth reference coordinates for aircraft, missiles and spacecraft

14 p2272 A71-30710

SK-5 air cushion vehicles evaluation including search/rescue, aids to navigation, law enforcement, safety logistics and oil pollution

[AHS PREPRINT 572] 14 p2180 A71-31113

Onboard meteorological pulse radars for cloud formations detection, navigational aids, ground reference points determination and relief surveillance
15 p2371 A71-31920

Precision area navigation system, considering position and velocity continuous measurement in three dimensional space, system components and simulation program
17 p2771 A71-34616

Satellite communication technology in next decade covering Intelsat 4 characteristics, meteorological satellites, navigation aids, multichannel telephone and TV circuits and frequency assignment
17 p2699 A71-34677

Low cost navigation equipment selection for space shuttle system updating during orbital coast, rendezvous and atmospheric flight
17 p2774 A71-35069

Military and civil aircraft navigation systems development, emphasizing self contained airborne equipment
17 p2775 A71-35374

Narita site Tokyo international airport, discussing transportation, runways, ground handling, navigation aids, lighting, etc
18 p2897 A71-35997

Aircraft onboard equipment tests in air navigation aid satellite project, estimating tracking random errors
18 p2877 A71-36509

Unified error analysis application to altimeter-aided terrestrial inertial navigation systems
[AIAA PAPER 71-901] 19 p3095 A71-37152

Motion measurements applications to facility design and inertial navigation hardware performance test problems concerning test platform response to ground motion, forces and disturbances
[AIAA PAPER 71-923] 19 p3102 A71-38327

Flashing civil aviation lights history, progress and photometric characteristics, discussing navigation and landing aids
22 p3499 A71-41489

Short haul air transportation, discussing performance requirements, community acceptance and navigation and landing aids
22 p3482 A71-42073

Book on electronic aids for navigation systems for marine and aerospace transport operation covering measuring and display instruments, radio wave properties, etc
23 p3702 A71-43225

Aeronautical radio navigation aids photo-optical calibration, describing photogrammetric procedure and ground equipment for checking out airport ILS systems
23 p3702 A71-43587

STOL aircraft system, discussing ground installations, runways, three dimensional area navigational aids, noise reduction, air traffic and short haul productivity
[AIAA PAPER 71-983] 24 p3791 A71-44579

NAVIGATION INSTRUMENTS
NT ATTITUDE INDICATORS
NT COMPASSES
NT GYRO HORIZONS
NT GYROCOMPASSES
NT MAGNETIC COMPASSES
NT SOLAR COMPASSES

Permanent magnet torque generator reaction torque effect in precision gyros and accelerometers
02 p0279 A71-12452

Analog inertial sensor digitizing methods, discussing pulse rebalancing and analog to digital conversion
02 p0279 A71-12453

STOL navigation equipment and microwave landing instruments test programs, noting data recording and flight operations
03 p0454 A71-13286

Area navigation in commuter/air taxi operations concerning airborne equipment, airport utilization and CTOL, STOL and VTOL aircraft
04 p0622 A71-14650

Dry friction autocompensation in inertial navigation accelerometers by forced rotation of platform
05 p0751 A71-16589

Aircraft navigation system requiring computer and display for approach guidance to circular orbit over fixed ground area
[AIAA PAPER 69-986] 07 p1156 A71-20305

Gyrocompass strapdown three coil synchro sensor magnetometer in conjunction with vertical gyro, eliminating azimuth detector inertial platforms
07 p1156 A71-20340

Solar aspect sensors as navigation components for rolling vehicle heading angle determination
07 p1157 A71-20415

High speed airborne scanning navigational radar antenna with matched patterns, using offset horn feed reflector and polarization modes for improved visual display
14 p2216 A71-31036

ATC system improvement, presenting data acquisition upgrading and ground automation-aircraft navigation systems interface
17 p2771 A71-34614

NASA space station navigation system, considering landmark and ground tracking, ground beacons and satellite concepts, long term effects, operational requirements and design goals
17 p2772 A71-35054

Large scale MOS IC digital VOR navigation converter, comparing accuracy, size, weight and cost with standard design
17 p2776 A71-35789

High aperture wide angle lens design for compact electro-optical systems of airborne moving map projection navigational instruments
18 p2947 A71-36605

Avionics combined display system for area navigation, discussing design, color map projection, overlays, CRT unit and viewability
21 p3413 A71-40137

Aerial photographic equipment survey, describing topographic cameras, aerial photograph orientation equipment, onboard navigation instruments and mapping survey system
21 p3380 A71-40875

Unaided, integrated and differential OMEGA radio navigation configurations, comparing accuracy and suitability for airways system operations
22 p3571 A71-42082

ATC integrated communication, navigation and identification system, discussing design, economics, technology and flexibility
22 p3571 A71-42086

NAVIGATION SATELLITES
NT EXPLORER 22 SATELLITE

Passive mode navigation satellite position fixing, using synchronous satellite and Loran type chart with correction tables
04 p0622 A71-15004

Atmospheric refraction due to ducting and trapping layers based on navigational satellite data
04 p0623 A71-15310

Satellite systems for transatlantic simultaneous air and marine navigation, traffic control and rescue, stressing technical and economical factors
06 p0925 A71-18015

Receiving equipment for navigation satellites of Naval Weapons Laboratory, considering 150 MHz channel
07 p1205 A71-19015

Celestial and satellite navigation sensitivity for Lunar roving vehicle (LRV) position fix
07 p1157 A71-20414

Electronically scanned cruciform slot-array aircraft antenna for satellite controlled navigation aid, discussing circularly polarized wave radiation
16 p2548 A71-34123

Navigation and communication satellites development for civil aviation and shipping, examining technical, organizational, operational and cost problems
17 p2771 A71-34240

Maritime operational and frequency requirements for satellite system having worldwide coverage
17 p2697 A71-34251

Civil aviation and merchant marine satellites, considering aircraft and surface vessel antenna characteristics and modulation techniques for optimum communication channel frequencies
17 p2775 A71-35582

Satellite time and frequency dissemination, discussing deficiencies of HF broadcasts for navigation and communication systems
18 p2878 A71-36530

Technical parameters and performance tradeoffs of ESRO preoperational aeronautical satellite program
19 p3153 A71-38067

Satellite navigation system for aviation and marine use, examining operational requirements, economic viability and technical solutions
22 p3570 A71-41509

Satellite navigation, surveillance and communication service requirements for maritime transportation industry, discussing initial services
22 p3572 A71-42093

Aircraft surveillance oceanic satellite systems design and reliability analysis, discussing position determination accuracy
22 p3572 A71-42094

Geostationary satellite oceanic automated ATC center design, estimating cost
22 p3572 A71-42095

Aeronautical satellite systems program planning for improved aircraft communications, ATC and other air traffic services in airspace over oceanic areas
22 p3573 A71-42096

NAVIGATORS
Man role in future navigation from SAC viewpoint, considering relationships to mission and machine
01 p0123 A71-10502

Navigator role in TACAN of reconnaissance and fighter aircraft, noting Weapon System Officer functions
01 p0123 A71-10503

Navigator role in Military Airlift Command (MAC) as navigator, weather analyst, fuel manager and flight planner
01 p0123 A71-10504

Commercial and military aircraft navigator future role, considering increasing task requirement stringency and growing navigational aids availability
01 p0124 A71-10505

Space navigator operations, procedures and computer interface and manually aided onboard Apollo cislunar navigation system possible improvement
01 p0124 A71-10510

USAF navigator training, discussing operational demands, philosophy, present and future training capabilities, etc
01 p0022 A71-10520

Aircraft navigator training, examining flight and ground trainer balance from cost effectiveness standpoint
01 p0022 A71-10521

Airborne trainer and ground simulator for undergraduate navigator training system
01 p0022 A71-10522

Complex navigation systems training philosophy emphasizing functional approach to system and components
01 p0023 A71-10523

Air navigational training simulators, discussing navigation aids, civilian navigator use, visual simulation and land-mass radar
01 p0125 A71-10526

NAVY
Naval aircraft testing, discussing weapons systems, funding commitments, outfitting schedules, time frames, contracts and management problems
07 p0108 A71-19077

U.S. Navy Satellite Navigation System error study, considering dead reckoning accuracy, random instrument errors, mathematical error model and statistical analysis procedure
08 p1331 A71-21168

NC-130 AIRCRAFT
U C-130 AIRCRAFT

NEAR INFRARED RADIATION
Organic dye lasers flash lamp pumped system for tunable coherent light production in visible and near IR spectrum
07 p1125 A71-19796

Photocathode area sensitivity contours- wavelength relationship from photomultiplier absolute intensity and near IR spectrum laser research
08 p1291 A71-21408

IR astronomical background radiation measurements at very near IR and longer wavelengths for interplanetary, galactic and intergalactic sources
10 p1677 A71-24582

Relative elevation differences on Mars surface revealed by near IR carbon dioxide bands spectroscopic observations
11 p1825 A71-25713

Photodetectors for laser applications in visible and near IR spectrum, discussing optical loss and pulse dispersion measurements
13 p0278 A71-28442

Deuterium fluoride overtone vibration-rotation chemical laser emission, studying frequency doubling and rate constant ratios
17 p2753 A71-34801

Interstellar molecular hydrogen gas near IR emission detection in dark clouds
18 p2969 A71-37042

Jovian satellite eclipse observations, reviewing simultaneous narrow band multichannel visual and near IR studies
19 p3139 A71-37908

Earth upper atmosphere outgoing thermal radiation radiance calculation in near IR spectrum
19 p3054 A71-37968

NEAR ULTRAVIOLET RADIATION
Wide angle far UV photography of Barnard Loop Nebula in Orion suggesting nebular emission intensity difference with near UV region due to interstellar dust
01 p0148 A71-10001

Near UV dye lasers, using various organic compounds as scintillators with excitation through nitrogen gas UV laser transverse pumping
04 p0606 A71-14717

Southern Milky Way isophote maps by near-UV surface photometry, showing brightest areas in Sgr/Scor, Car, Vel/Pup and Cyg
24 p3867 A71-44436

Visible and near UV spectra of vacuum Ar, Kr and Xe microwave discharge lamps with magnesium fluoride windows
24 p3849 A71-45211

NEBULAE
NT CASSIOPEIA A
NT CRAB NEBULA
NT PLANETARY NEBULAE

Wide angle far UV photography of Barnard Loop Nebula in Orion suggesting nebular emission intensity difference with near UV region due to interstellar dust
01 p0148 A71-10001

Planetesimal growth in nebulae around young stars, examining accretion and physical chemistry of solar types
01 p0157 A71-10761

Orion Nebula /NGC 1976/ physical characteristics from H alpha line radio telescopic observation, discussing energy level population, electron density, collision mechanisms, etc

02 p0308 A71-12094

Soviet papers on physics of nebulae and variable stars covering luminescence, reflecting and scattering properties, spectrophotometry, computerized simulation, etc

02 p0311 A71-12351

Optical thickness of reflecting nebula with given brightness illuminated by star, using three dimensional models

02 p0311 A71-12352

Luminescence of nebulae with C plus E spectrum, noting hydrogen emission superimposed on continuum due to reflection of stellar radiation by dust

02 p0311 A71-12353

Luminescence of optically reflecting nebulae related to shape of light scattering indicatrix of interstellar dust particles

02 p0311 A71-12355

Spherical nebula BESM-3M radiation intensity fluxes, calculating optical thickness, particle albedos and light scattering indicatrices

02 p0312 A71-12359

Computer program for processing elliptical polarization observations of nebulae and comets

02 p0251 A71-12360

Modified Fesenkov method for calculating Stokes polarization parameters applied to elliptical polarization observations of nebulae

02 p0251 A71-12361

Radio emission from small galactic nebulosities, describing position, flux densities, identification and exciting stars

05 p0811 A71-16683

Compact nebulae IC 4997, VV 8 and FG Sge observed at 3.5 and 11.0 microns, noting IR wavelength energy

05 p0812 A71-16696

Cometary nebulae and globules, discussing ionized and neutral gas densities, temperatures and morphological classifications

06 p0974 A71-18433

Gum Nebula-fossil Stromgren sphere of Vela X supernova, deriving ionization model from interstellar measurements

07 p1191 A71-18865

Dust history and physical environment near hot stars associated with nebulosity, discussing optical depths and IR energy

07 p1198 A71-19819

External galaxies radial velocity relationship to extragalactic nebulae spectral lines red shift

07 p1200 A71-20054

Orion Nebula /NGC 1976/ physical characteristics from H alpha line radio telescopic observation, discussing energy level population, electron density, collision mechanisms, etc

08 p1362 A71-21144

Evaporation of dirty ice particles surrounding early type stars, using dust grains model for explanation of anomalous reddening of Orion Nebulae

08 p1364 A71-21415

UBV colors and polarization models for reflection nebulae based on Mie scattering functions for exponential size distribution of silicate particles

09 p1517 A71-22332

German book on variable stars covering supernovae, novae, pulsating variable stars, symbiotic objects, galactic nebulae, stellar and galactic evolution, astronomical photometry, etc

10 p1675 A71-24479

Ionized gas and dust distribution in Orion nebula from Balmer line intensities photoelectric measurements

11 p1818 A71-25202

Supernova remnant HB 21 linear polarized radiation observed at 6 cm wavelength, correlating optical nebula shape with radio mapped contours

11 p1819 A71-25216

Diffuse interstellar absorption centered at 4430 A observed in reflection nebulae, using narrow band filters

11 p1831 A71-26135

Cometary nebulae and globules, discussing ionized and neutral gas densities, temperatures and morphological classifications

12 p1955 A71-26583

Light and radio emission from Orion nebula flare stars in meter waveband, discussing coherent mechanisms of plasma oscillations and gyro/synchrotron radiation amplification

15 p2485 A71-31696

Extragalactic nebulae, considering galactic formation stages and energy supply problems

15 p2486 A71-31925

Forbidden O II spectra brightness ratio measurements across Orion nebula, determining electron density variations

16 p2631 A71-33229

Analytic approximations for ionization structure of nebula photoionized by flat spectrum

16 p2632 A71-33319

Gum Nebula size, density and electron temperature data from RAE-1 and OGO-5 satellites and ground based telescopes observations, correlating with Vela X supernova outburst

17 p2806 A71-35409

Symmetrically distributed nebulae around Wolf-Rayet stars, detailing Ngc 7635 and associated star BD plus 60 deg 2522

17 p2806 A71-35410

Vela X supernova remnant blast wave model and Gum Nebula formation, discussing kinetic and rotational energy transformation into radiation

17 p2807 A71-35414

Excess intensities of diffuse cosmic X rays related to characteristic line spectrum excitation and element abundances in interstellar region and nebulae

18 p2958 A71-36761

Interstellar absorption at H alpha line wavelength in Orion nebula, obtaining contour map for comparison with radio intensity

19 p3131 A71-37230

Radio emission detection of para-formaldehyde and 2 mm formaldehyde distribution in Orion IR nebula

20 p3287 A71-39112

Formaldehyde absorption and emission lines in Orion IR nebula, indicating pumping suppression by neutral particle collisions

20 p3288 A71-39113

Gamma ray production by pulsar-emitted particles interaction with surrounding nebula matter, investigating radiation intensity time variation

20 p3279 A71-39325

Gum Nebula conceived as hydrogen gas mass ionized by UV radiation from supernova explosion related to Vela X remnant, discussing fossil Stromgren sphere model

20 p3294 A71-39572

Open stellar clusters Tr 14, 15, 16 and eta Carinae Nebula distance determination, using photoelectric and photographic photometry

21 p3441 A71-40064

Diffuse radiation field inside homogeneous spherically symmetric dust nebula from radiative transfer equation solution as expansion after Legendre polynomials

21 p3451 A71-40716

Spiral structure OB associations in outer regions of Andromeda nebula, investigating blue objects in U and B plates of Schmidt telescope

21 p3451 A71-40723

Fluorescence phenomena in celestial bodies, considering atomic lines and molecular bands in stellar and nebulae emissions

22 p3597 A71-41515

Gum Nebula ionization and heating by energetic particles from Vela X supernova

22 p3598 A71-41917

Reduced nebular helium abundances, using capture-cascade and collisional excitation calculations

23 p3733 A71-43081

NECK [ANATOMY]

Eye-head coordination in monkeys by recordings from neck and eye muscles, noting central neural command role

18 p2856 A71-36232

NEEDLES

Rayleigh scattering by obliquely oriented uniform thin cylindrical particles /needles/, using dielectric needle approximation

20 p3196 A71-39406

NEGATIVE CONDUCTANCE

Transferred electron bulk negative differential conductivity devices, analyzing combined doping and geometry effects on space charge and domain dynamics

09 p1507 A71-22250

Electron transfer bulk oscillators negative conductivity as function of geometry, field and doping nonuniformities, using computerized simulation for device frequency-voltage characteristics

09 p1417 A71-22689

Second harmonic voltage effects on quenched domain mode Gunn effect oscillator for DC to RF conversion efficiency, discussing negative device conductance at multiharmonic frequencies

09 p1417 A71-22696

Type S bulk negative differential conductivity in n-InSb at 77 K and atmospheric pressure, showing associated large current due to strong impact ionization

09 p1508 A71-22756

Semiconductor device with stable negative conductance over wide range of microwave frequencies and power levels, using transferred electron effect in epitaxial GaAs

18 p2895 A71-36985

Thermal switching and negative resistance model and measurements of amorphous semiconductor thin films of Ge, Si and chalcogenide glasses

21 p3428 A71-40741

Negative differential conductance of anthracene single crystals in electrolytes, observing N-shaped I-V characteristics

21 p3430 A71-41221

Short wavelength instabilities in collision dominated plasma confinement by rotating magnetic field, interpreting in terms of equivalent negative resistance

22 p3579 A71-41579

Photorecombination model explaining kinetics of negative photoconductivity effect during illumination of impurity region in high resistivity p-type ZnTe-CdTe single crystals at room temperatures

23 p3717 A71-43948

NEGATIVE FEEDBACK

NT SENSORY FEEDBACK

Transistor amplifiers automatic gain control open loop amplitude characteristics, discussing output level stabilization relation to signal source coupling and negative feedback

02 p0233 A71-12544

Dynamic characteristics of two degree of freedom gyroscopes with positional and integral negative feedback for simultaneous angular velocity and displacement measurement

09 p1451 A71-23171

NEGATIVE RESISTANCE CIRCUITS

Monostable multivibrator tunnel diode synchronization bandwidth as function of circuit parameters and junction I-V characteristics

08 p1264 A71-21071

Stability of RLC networks with negative resistances, applying Liapunov functions

12 p1891 A71-26998

Interdigital broadband hybrid junction transducer terminated in negative resistances for acoustic surface waves amplification

13 p2037 A71-28476

I-V characteristics and temperature responses of negative S and N-type resistances in niobium-niobium oxide-indium structures, considering use as active elements in membrane circuits

24 p3859 A71-44380

End line matching for high gain traveling wave amplifier constructed from heterogeneous transmission line with negative resistance

24 p3810 A71-45262

Joule heating effect on static negative differential resistance and switching of chalcogenide thin films

24 p3862 A71-45353

NEGATIVE RESISTANCE DEVICES

Microwave negative resistance diode avalanche region, deriving four element incremental signal model

01 p0055 A71-11168

GaAs S diodes with negative differential resistance, examining selectivity and oscillation characteristics

01 p0057 A71-11460

Packaged microwave avalanche diodes negative resistance properties three-parameter characterization at low current densities

07 p1074 A71-19125

Negative resistance diodes characteristics under laser radiation, investigating switching properties, temperature effects and noise characteristics

07 p1076 A71-19373

NbN Dayem bridge characteristics, discussing negative resistance region, self induced subharmonic current steps, temperature dependence and microwave radiation effects

07 p1079 A71-20161

Microwave amplification using negative resistance device in prototype filter equalization networks, permitting realization of wideband amplifiers for C band and superhigh frequencies

11 p1736 A71-25140

Signal stability in distributed active lines of HF semiconductor devices with negative leakage resistance

12 p1878 A71-26843

Multilayered semiconductor structures with p-n junctions, discussing I-V characteristics, noninjection component effects, carrier transport and negative resistance

13 p2111 A71-28920

Traveling wave negative resistance amplifier with corrugated surface wave structure, deriving gain equation

14 p2209 A71-29546

Physical process causing negative differential resistance segment on I-V curve of single junction transistor, describing thyristor-triggered relaxation oscillator

14 p2214 A71-30633

Ku band monopulse receiver with electronically tunable Gunn oscillator, discussing negative resistance diodes dynamic impedance properties

16 p2547 A71-33557

FM-PM conversion by frequency locking of free running Gunn oscillator

17 p2717 A71-35339

Transferred electron /Gunn/ amplifiers and oscillators for microwave applications, considering electronic and mechanical tuning over large frequency ranges

18 p2894 A71-36977

P-n-p-n quadruple layer semiconductor junction light emitting diode with negative resistance characteristics, discussing epitaxial regrowth process and applications

21 p3355 A71-40739

High Q micropower filters for VHF applications based on conditionally stable negative resistance operation, describing computer-aided design, construction and performance

21 p3361 A71-40822

Fabrication and I-V characteristics of S-type negative resistance alloyed diodes prepared from sulfur-doped n-type Si, outlining temperature dependence of turnoff time

21 p3358 A71-41203

N-type negative resistance, photoconductivity and I-V characteristics of sulfur-doped p-type Si, showing hole capture cross section dependence on electric field

21 p3429 A71-41204

Multilayered semiconductor structure with p-n junctions, discussing I-V characteristics, noninjection current component effects, carrier transport and negative resistance

21 p3433 A71-41306

Electrical properties and electroluminescence measurements for p-n junctions in Au- and Ag-doped GaP, noting negative resistance in I-V characteristics

21 p3433 A71-41312

Te-doped n-type GaSb semiconductor negative magnetoresistance and magnetothermoelectric power dependence on longitudinal magnetic field

21 p3436 A71-41349

Negative differential conductance in semiconductor containing attractive centers with Maxwellian distribution function and temperature dependence on carrier energy

21 p3436 A71-41351

Two-terminal negative resistance circuit analysis for parameters effect on linearity by parabolic relation

22 p3521 A71-42203

Negative resistance in high resistance compensated semiconductor diodes with double injection associated with diffusion growth

23 p3652 A71-43482

Design and performance of semiconductor devices with heterojunctions, covering injection laser without cooling, emission frequency converter and negative resistance triode

24 p3808 A71-44383

Noise voltage power spectrum of GaAs bulk diodes at L.F. as function of bias field approaching negative resistance region

24 p3804 A71-44992

NEODYMIUM

Continuous Nd-YAG laser welding, considering power, penetration depth and applications

01 p0087 A71-10453

Nd-glass pulsed solid state laser amplifier gain characteristics, deriving flux density and population inversion equations

02 p0261 A71-12173

Neodymium laser emission in mode locked operation, examining self focusing and modulation effect in active element

02 p0261 A71-12323

Mode locked continuously pumped Nd-YAG laser pulse shape, using optical correlation technique

02 p0262 A71-12730

Nd-YAG laser with intracavity lithium niobate phase modulator, investigating frequency sweeping/modulation/ mode operation

03 p0437 A71-13878

Nd-YAG pulsed laser, comparing Kr and Xe flash lamps for pumping performance

03 p0437 A71-13880

Nd-YAG pulsed laser mode locking with internal FM modulation

03 p0437 A71-13883

Nd glass laser radiation time and spectral structure

03 p0437 A71-13885

Vibrating mirror for continuously pumped Nd/YAG laser repetitive Q switching

03 p0438 A71-13888

Input-output properties of Nd-YAG rods in W pumped continuous lasers

04 p0606 A71-14715

Pulse repetition rate of Q switched YAG-Nd oscillator-amplifier laser systems

05 p0762 A71-16479

Nd-YAG laser branching ratios measurement for all transitions during oscillations at room temperature

05 p0764 A71-16912

High repetition rate Q switched Nd-YAG lasers, graphing theoretical Q switching from rate equations of ideal four-level laser

05 p0764 A71-17076

Neodymium glass lasers, investigating pump-induced birefringence effect on polarization and radiation distribution

06 p0907 A71-17398

Neodymium glass solid state laser transverse mode locking and capture due to active medium nonlinear properties

06 p0907 A71-17400

Nd glass traveling wave laser single frequency emission luminescence stability as function of pumping power, using dispersive ring resonator

07 p1122 A71-19136

Giant pulse amplification in Nd ion doped glass analysis using model, taking into account sublevels and multiplicity

07 p1127 A71-20387

Ce, Pr and Nd solubility in Cr, investigating temperature dependence, microhardness, deoxidation and alpha phase by X ray, metallographic and durometric analyses

07 p1144 A71-20652

Mode locked Nd-glass laser, describing dispersion and Kerr effects on pulse frequency modulation

08 p1301 A71-21125

Controllable pulse length Q switched Nd-YAG laser using lithium iodate doubling crystal

09 p1463 A71-22757

Nd-YAG laser cavity dumping for continuously pumped efficient pulsing at various repetition rates

11 p1773 A71-25797

Nd-YAG folded center lasers Q switching and cavity dumping, using fused silica and Brewster cut intracavity acousto-optic modulator

11 p1773 A71-25798

Electron and ion plasma heating by subnanosecond neodymium laser pulses, using computer calculations of hydrodynamic equations

11 p1806 A71-26089

Gadolinium molybdate neodymium ions stimulated emission, noting luminescence, absorption and spectroscopic properties

13 p2111 A71-28424

Spectral filter effects on Nd-YAG laser performance stability and output

14 p2254 A71-30155

Optimal pulsed power output of continuously pumped Q switched Nd-YAG laser as function of mode parameters

15 p2423 A71-32603

Nd-YAG laser spatial hole burning effects, considering number of oscillating modes, transverse mode degeneracy and sinusoidal phase perturbation influence

15 p2423 A71-32604

Short pulse Nd-YAG direct detection laser system for space communications, noting RF links complementation, high data rates, practical size, weight and power requirements

17 p2705 A71-35093

Emission characteristics of neodymium glass laser with polymethine dye passive shutters of finite relaxation time, investigating ultrashort pulse separation

18 p2929 A71-35985

Solid state laser with Nd ions in YAG, discussing crystal growth and structure, optical pumping continuous and Q switched operation and mode locking

18 p2930 A71-36146

Nd-YAG laser optimum single frequency output operation, discussing two-component-mode filters methods using intracavity tilted Fabry-Perot and metallic film reflector etalons

18 p2932 A71-37005

Solid state lasers, considering ruby and YAG-Nd ion materials pumped at room temperature

19 p3074 A71-38229

Lutetium effects on UV absorption strength of Nd-YAG laser materials

20 p3244 A71-39104

Gadolinium molybdate-neodymium ions stimulated emission, noting luminescence, absorption and spectroscopic properties

21 p3427 A71-40082

Lattice and grain boundary diffusion of Ce and Nd in Ni using radioactive tracer sectioning technique

21 p3598 A71-40468

Mode locked Nd-glass laser transient effects, examining pulse width limitations by side band generation

22 p3556 A71-41801

Second harmonic mode locked frequency doubled pulsed neodymium-yttrium-aluminum oxide garnet laser using single intracavity barium sodium niobate

23 p3683 A71-42957

Neodymium glass laser emission kinetics control with positive and negative feedback by introducing nonlinear media into plane-parallel resonator with two positive lenses

23 p3684 A71-43418

Nd positive ion cross section for stimulated emission with glass composition determined by laser and fluorescence measurements

23 p3685 A71-43938

NEODYMIUM ALLOYS

Nb-Ti alloy oxidation kinetics at various temperatures and pressures, noting linear patterns and oxide formation

10 p1626 A71-24403

Precipitation hardened Ti-Nb alloy, correlating room temperature tensile properties with microstructure from step aging

21 p3387 A71-40461

Nd-Bi phase diagrams from thermal differential, metallographic and X ray analyses, discussing carrier concentration and mobilities, Hall coefficients, conductivity and thermal emf

23 p3692 A71-44022

NEODYMIUM ISOTOPES

Nd 147 decay gamma-gamma directional correlations, using coaxial Ge/Li and NaI/Tl detectors in conjunction with multichannel coincidence configuration

02 p0285 A71-11646

NEON

NT NEON ISOTOPES

Solar wind elemental and isotopic He and Ne compositions from mass spectrometry of ions collected in metal foils deployed during Apollo 11 and 12 landings

01 p0146 A71-11486

Neutral Ar and Ne resonance lines Stark broadening constant from Stark width-oscillator strength product

04 p0630 A71-15651

Pressure dependent shift of He-Ne laser radiation, observing beat frequencies

07 p1123 A71-19486

Trapped solar wind He and Ne in Surveyor 3 unpainted Al tube, comparing with Apollo 11 and 12 solar wind composition

10 p1672 A71-24390

Gas rich meteorites and carbonaceous chondrites with trapped argon, noting isotopic correlation with neon

10 p1680 A71-24988

Extensive air showers multiple core and transverse momenta observations with Kiel neon hodoscope

13 p2123 A71-28075

Multiphoton ionization cross section and charge number in neon near resonance under focused laser beam

13 p2081 A71-29338

Hollow dielectric waveguide gas laser with He-Ne mixtures at 6328 A

21 p3393 A71-41040

Solar corona O VII and Ne IX helium line triplets observations, examining electron density limits

22 p3605 A71-42352

Ne ionization relaxation time behind reflected shock waves from temperature and pressure measurements of combustion driven shock tube end wall

23 p3706 A71-42909

Spatiotemporally coherent pulsed Ne and Ti vapor lasers superradiation, showing coherence time dependence on pulse length and gas pressure

23 p3683 A71-43395

Neon red lines Stark widths and shifts in function of electron and neutral Ne densities in shock tube

23 p3707 A71-43585

Nitrogen and neon cations number density time dependence during plasma decay in neon-nitrogen mixtures

23 p3711 A71-43881

Pulsed neon laser high gain oscillation at 486.1 and 434.0 nm identified as Balmer beta and gamma lines of atomic hydrogen

23 p3688 A71-44296

NEON ISOTOPES

Cosmic rays produced He, Ne and Ar isotope concentrations in iron meteorite separated phases, using Rudstam spallation model

10 p1676 A71-24506

Solid Ne isotopes specific heat at constant pressure and volume, entropy, enthalpy and Grüneisen parameters

13 p2102 A71-29481

Neutron emission yield during Pu 238 alpha particles interactions with O 18, taking into account recoil Ne isotopes

14 p2276 A71-30177

Absolute production rates of He 3 and Ne 21 in average chondrites, determining radiation ages of stony meteorites aged less than two million years

15 p2486 A71-31991

Ne 20 isotope for selective frequency absorption to obtain monofrequency radiation in He-Ne laser with naturally isotope-doped Ne as active medium

15 p2419 A71-31998

He 4 burning nucleosynthesis, noting Ne 20 buildup in massive stars

16 p2633 A71-33335

Ne 20 transition line width behavior vs pressure in He-Ne laser at 3.19 microns wavelength

17 p2752 A71-34402

Radiative width of laser transition in Ne 20 atom and line frequency shift vs pressure in dual He-Ne laser assembly effectuating atom collisions

17 p2752 A71-34403

He, Ne and Ar isotopic distribution and origin in Apollo 12 lunar samples, considering solar wind implantation

17 p2695 A71-35030

Lande g factors measurement of excited electronic states in Ne 20 II and III, using alignment of radiating particles in beam foil light source

18 p2949 A71-35978

NEON 19

U NEON ISOTOPES

NEOPLASMS

NT CANCER

NT LEUKEMIAS

NEPHANALYSIS

Soviet book on nephanalysis for synoptic forecasting covering meteorological satellite observations and network characteristics, photointerpretation, data processing, cloud identification, weather charts, etc
02 p0278 A71-12842

NEPTUNE [PLANET]

Ceres perturbation by Neptune, comparing Laplace-Neucomb and Hill methods
01 p0156 A71-10448

Pluto-Neptune system implications for solar system evolution theories, discussing deterministic and statistical models and a body problem approaches
04 p0655 A71-15726

Neptune orbital motion prediction, determining effect of variations in time and mean distance on accuracy
05 p0810 A71-16542

Pluto orbit integration over 4.5 million years by variation of parameters technique and confirming Neptune-Pluto orbital resonances
10 p1669 A71-24179

Pluto mass from reciprocal mass and density, using Neptune transit circle observations reevaluation
15 p2488 A71-32199

Uranus and Neptune microwave emission spectra and atmospheric temperatures, comparing with Jupiter and Mars
15 p2490 A71-32410

Neptune diameter and flattening, using photographic and photoelectric observations
17 p2799 A71-34477

NERNST GENERATORS

U THERMOMAGNETIC COOLING

NERNST HEAT THEOREM

NERNST-ETTINGSHAUSEN EFFECT

Hall effect, conductivity, thermal emf and Nernst-Ettingshausen transfer in n-type highly doped compensated GaAs
03 p0466 A71-13398

NERVA [ENGINE]

U NUCLEAR ENGINE FOR ROCKET VEHICLES

NERVES

Motor and sensory nerve conduction impairment in upper extremities in vibration disease
01 p0010 A71-10394

Cochlear nerve fibers two tone inhibition as signal suppressions inherent to bandpass nonlinearities, using modified analog model and mathematical analysis
05 p0712 A71-16280

Bilateral and single median nerve electrical stimulation, observing somatized cortical responses from homologous scalp derivations
05 p0706 A71-16322

Electron microscopic studies of nerve membrane fine structure, discussing cell membrane multienzyme and macromolecular energy and information transduction, protein synthesis and nucleic acids interrelations
06 p0850 A71-17500

Rana temporaria isolated sciatic nerve excitation process, investigating continuous ultrasound effect
09 p1391 A71-22486

Visual accommodation mechanism, discussing microinterval nerve interaction role
09 p1391 A71-22488

Acoustic nerve, cochlear nucleus and superior olivary complex central projection, investigating ascending auditory system organization
14 p2183 A71-30255

Vagus nerve effects on cardiac output adaptation to exercise in sympathectomized dogs
15 p2360 A71-32001

Lower cardiac nerve unmyelinated afferent fibers detection and functional property characteristics
15 p2362 A71-32736

Activation impulse blocking in nerve, using inhomogeneous LiCl electrochemical model
19 p3006 A71-37282

Weightlessness effect on vestibular apparatus from bullfrogs vestibular nerve single fibers spike train data during orbital flight
22 p3598 A71-41689

NERVOUS SYSTEM

NT AFFERENT NERVOUS SYSTEMS

NT AUTONOMIC NERVOUS SYSTEM

NT BRAIN

NT BRAIN STEM

NT CENTRAL NERVOUS SYSTEM

NT CEREBELLUM

NT CEREBRAL CORTEX

NT CEREBRUM

NT EFFERENT NERVOUS SYSTEMS

NT GANGLIA

NT HIPPOCAMPUS

NT MYELIN

NT NERVES

NT NEUROGLIA

NT NEURONS

NT PERIPHERAL NERVOUS SYSTEM

NT SPINAL CORD

NT SPINE

NT SYMPATHETIC NERVOUS SYSTEM

NT SYNAPSES

NT THALAMUS

Vasomotor reflexes latency in postganglionic cardiac and renal nerves in intact and spinalized cats, determining spinal mediation by electrophysiological methods
04 p0538 A71-15093

Nervous system activity changes relation to physical exercise type and extent, measuring visual response time
05 p0708 A71-16620

Simple nerve system receptor field organization in visual analyzer simulated by TV circuit with scanning beam controlled focusing
07 p1050 A71-20108

Nervous and muscular elements above threshold excitation on potential subthreshold stimulation background by electronic analog model
07 p1050 A71-20114

Nervous and muscular tissues excitability during subthreshold rhythmic stimulation, discussing mathematical model for compounding polarization induced electrostatic fluctuations
07 p1050 A71-20115

Human nervous system stimulus trace retention in various age groups, using skin galvanic reactions
06 p1240 A71-21788

Respiratory system self regulation and coordinational activity interference by biocontrolled stimulator incorporation into natural nerve links
10 p1567 A71-24165

Nervous system modeling, considering cybernetic brain functions, neuroheuristic programming and modes of distributed information processing pertinent to neuropsychological experiments
10 p1568 A71-24222

Information processing by living systems, considering nervous system and brain operation with emphasis on neuron structure, message coding, programming and information storage
10 p1562 A71-24223

Neurophysiological auditory information processing, considering mechanical transformation of two dimensional pressure-time signal and three dimensions for presentation to nervous system
10 p1562 A71-24228

Neural transmission to vestibular nuclei of semicircular canal response to rotational stimulation, discussing test methods and results with decerebrated or anesthetized cats
10 p1566 A71-25042

High oxygen tension during severe exercise, studying effects on humoral and nervous ventilation changes
11 p1722 A71-26363

Histamine importance in nervous system activity, discussing synaptic mediation, reception processes and pharmacological action
12 p1869 A71-26652

Nervous/cardiovascular systems and blood composition changes in moderate duration military transport flights
12 p1874 A71-27163

Cardiac output and arterial pressure control in presence or absence of functional nervous system, discussing dog experiments
13 p2003 A71-27839

Human nervous reactions to monochromatic red, yellow green and blue light for optimal color climate in spacecraft cabins
13 p2018 A71-28411

Elevated atmospheric pressure effects on human psychophysiological qualities including attention, memory and time-estimating capabilities and nervous processes equilibrium
16 p2536 A71-33578

Lateral and anterior semicircular canal neural reactions to caloric stimulation in frogs, indicating hydrodynamic interactions
16 p2532 A71-33912

Tympanic-cavity nerve plexus electric stimulation effects on cerebral blood circulation and overall arterial pressure in dogs and cats
16 p2533 A71-34108

Soviet papers on higher nervous activity physiology, Part I, Basic laws and mechanisms of conditioned reflex activity covering inhibition, and bioelectrical effects, with bibliography
17 p2684 A71-35357

Reflexes dominant in organism throughout activity or temporarily dominating reflex system directing work of nervous centers
17 p2685 A71-35363

Phrenic nerve activity correlation with ventilation in anesthetized cats, analyzing relationship between phrenic impulse rate and integrated electrical activity
20 p3192 A71-38983

Nervous system functional characteristics based on neuron structure and electrical transmission from electron microscopy, electrophysiology and biochemical analysis
21 p3329 A71-40145

Bioholographic animal information processing model, considering nervous system as diffractive medium and neural network as Fourier analyzer
21 p3380 A71-40923

Soviet book on animals morphophysiological changes in cardiovascular and nervous systems and various internal organs under RF wave exposure
21 p3344 A71-41369

Soviet book on experimental research on human higher nervous activity from growth aspect covering normal and pathological states, cerebral cortex interaction with central nervous system
21 p3339 A71-41374

Eye movement neurophysiology, discussing ocular proprioception, oculomotor muscle sensory receptor role, extraocular muscle afferent and efferent innervation and central nervous system control effect
22 p3488 A71-42433

Mammal extraocular muscle fiber structural and functional properties, discussing histological arrangement, fiber type classification and motor nerve endings
22 p3488 A71-42434

Cardiovascular system functional disorders relationship to nervous activity disturbances
24 p3795 A71-44472

NETS

NT NEURAL NETS

Numerical approximation of continuous real function in interval by polynomials using appropriate nets, estimating error
06 p0920 A71-18209

NETWORK ANALYSIS

NT CRITICAL PATH METHOD

Hybrid computer simulation program for analyzing large circuits intractable by conventional methods using PACTOLUS language
01 p0048 A71-10225

Low pass active filters with various characteristics, comparing amplitude-frequency responses
01 p0051 A71-10259

Active filters of triple layer rectangular-shaped distributed RC elements, calculating components geometric variation effect on frequency response
01 p0058 A71-10312

Computer analysis of microwave circuit parameters effects on limited space charge accumulation oscillation in CW transferred electron devices
01 p0055 A71-11169

Nonlinear networks interconnected by lossless transmission lines, deriving global asymptotic stability condition
01 p0065 A71-11574

Multiphase multivibrator with nanosecond pulse duration and parallel transistorized inductive correction, analyzing flip-flop circuit
02 p0230 A71-11831

Electronic circuit analysis using parametric reliability criteria based on progressive failures, applying statistical computerized simulation method
02 p0230 A71-11840

Steady state quantum analysis of linear distributed systems applied to attenuator, maser amplifier and multiterminal pair networks
02 p0213 A71-12017

Thevenin and Norton equivalent circuits determination using sequential method of network analysis
02 p0236 A71-12041

Computer aided network analysis for multiple project planning facilitating readjustments and budgeting
02 p0336 A71-12122

Parametric amplifier with nonlinear capacitance varying as quadratic function of voltage, deriving power gain, bandwidth and noise figure from equivalent circuit
03 p0385 A71-13270

Tunnel diode frequency multiplier circuit, analyzing harmonic I-V characteristics by equivalent network method
03 p0384 A71-13396

Computer algorithm for state variables equations used in linear and nonlinear, active and passive electronic circuits analysis
03 p0389 A71-13807

Two-terminal pair broadband matching circuits losses from method for LF series-shunt coupler with uniform scattering
03 p0386 A71-13810

Frequency response characteristics of nonlinear oscillatory circuits with inductive and complex capacitance couplings
03 p0379 A71-13812

Group delay measurements accuracy, using Nyquist method as function of FM and response characteristics of measured two-terminal pair network
03 p0386 A71-13814

Nonlinear systems near steady state oscillation transient behavior analysis by linear differential equations with periodic coefficients
03 p0451 A71-13817

Chopper amplifier modulator and demodulator circuits analysis, discussing SNR performance
03 p0387 A71-13821

Rectangular diagrams for solving linear RLC networks by digital computer graphics
03 p0390 A71-14308

Algorithm for higher order loops determination in flow graph from subgraphs of linear graph model, considering circuits with ladder/nonladder structures
03 p0382 A71-14310

Sampled data feedback control system analysis and synthesis by state variable method, discussing computer algorithms for optimal pulse control

03 p0392 A71-14409

Second order moment at output of inertialess nonlinear two terminal pair network during amplitude and phase modulation

04 p0550 A71-14620

Automatic electric network topological and electrical characteristic analysis, using mixed method for computational accuracy and speed

04 p0560 A71-14746

Multiparameter sensitivity functions in network theory, discussing auxiliary, adjoint and direct methods

04 p0560 A71-15148

Periodically reverse switched capacitor network theory, deriving equivalent resonant transfer circuit and expression for voltage transfer ratio

04 p0561 A71-15699

Feedback control circuits with delay time, examining overshoot diagrams

05 p0730 A71-16127

Synchronous digital communication system with constant clock rate established by phase locked oscillator input average, calculating two-station network dynamic stability

05 p0729 A71-17051

Postcoupled waveguide cavity Gunn effect microwave oscillator equivalent circuit analysis, using lumped constant elements

07 p1072 A71-19106

Avalanche diodes TRAPATT mode initial conditions by computer analysis

07 p1072 A71-19109

Rucker multidevice symmetrical microwave oscillator analysis, overcoming nonlinearity difficulties in eigenvector approach

07 p1073 A71-19118

Transient stabilization analysis for electronic circuits containing diverse components with variable parameters, considering active low pass filter example

07 p1078 A71-20061

Arbitrarily shaped waveguide analysis computer program EHPOL for polynomial approximation to eigenfunctions of Helmholtz equation, considering homogeneous Neumann and Dirichlet boundary conditions

08 p1261 A71-20752

Lower triangular matrices and associated foldant algorithm application to network analysis

08 p1268 A71-21271

Resistance and reactance network transfer functions determination using poles and zeros method

09 p1423 A71-22999

Noise analysis of microelectronic active RC filters by cascade of passive and active networks, considering low pass filter

10 p1582 A71-23915

Book on digital computers in engineering covering systems, man machine communication, numerical analysis, network analysis program, circuits, devices, control, etc

10 p1581 A71-24476

In-core thermionic reactor network reliability analysis, assuming component failures as equally probable stochastic events

11 p1713 A71-25893

Topological unistor graph solutions to linear equations of electronic circuits by structural conjugate numbers on digital computer

11 p1792 A71-26376

Topological methods of linear electric circuits analysis, considering Kirchhoff, Maxwell and Mason methods

11 p1743 A71-26464

Failure prevention, test discrepancy reporting and circuit analysis workshop techniques for program audits, integrating reliability managers, performers and customers

12 p1910 A71-26670

Passive two-terminal networks in rod antenna for bandwidth increase, investigating equivalent circuit on digital computer

12 p1886 A71-26987

High power multicavity klystron design, investigating cavity voltage, drift length and beam parameter effects

13 p2040 A71-29424

Transforming network conditions for two state one port terminations Q factor existence from Mobius transformations and invariance properties

14 p2209 A71-29545

Electric circuits calculation in MHD problems such as MHD channel flow, electrodynamic plasma, etc

14 p2277 A71-29558

Microwave meander line /coupled parallel commensurate conductors array/ network analysis and synthesis, using equivalent circuit transformation for computerized design

14 p2219 A71-29565

Rectangular section microstrip lumped capacitance calculation by matrix methods

14 p2210 A71-29571

TEM mode delay line microwave filters, deriving relationships between risetime, settling time, bandwidth and Q

14 p2219 A71-29601

Microwave oscillators Rieke diagram semiautomatic plotting by injection phase locking, using network analyzer for impedance measurement

14 p2211 A71-29823

German monograph on network method application for conductive and radiative energy transfer coupling problems

14 p2336 A71-30231

Linear passive network steady state FM distortion numerical calculation, applying to Chebyshev-response bandpass filter

14 p2197 A71-30806

Heat pipe application to OAO as structural isothermizer, considering overall spacecraft thermal network analysis

15 p2512 A71-31594

Fluid logic random input, irregularly activated or stochastic control network analysis, using digital control network synthesis technique /DICONESYN III/

15 p2351 A71-31685

Fluid logic circuit network analysis, utilizing classical synthesis technique with primitive flow table and maps

15 p2351 A71-31686

Linear stationary lumped-constant relaxation systems with real and positive eigenvalues and impulsive response characterizable by exponentials, evaluating error in identification

15 p2450 A71-32322

Availability and failure frequency of systems of independent repairable units, using representation by network or reliability block diagram

15 p2415 A71-32341

Computer algorithm for diode detector static and dynamic I-V characteristics calculation by trial and error process with piecewise linear approximation

16 p2546 A71-33399

Soviet book on algorithms for electronic circuit analysis covering linear and nonlinear transistor or tube circuits matrix-topological description and frequency-time domain solutions

17 p2717 A71-35219

Computer program formulation of equations of state of electronic circuits, using state variable method with mixed coordinate basis

18 p2896 A71-35883

Computer algorithm determining transfer function of linear electronic circuit in autonomous quadrupole form with zero initial conditions

18 p2887 A71-35884

Frequency domain approach for analysis of linear variable networks demonstrated by calculating system response to input

19 p3036 A71-37147

Algorithms and operator matrix language for infinite linear automata analysis, synthesis and identification

19 p3024 A71-37223

Active network analysis by topological formulation, eliminating k-trees

19 p3038 A71-38489

Computer programming for on-line correction of microwave measurements of loss and reflection effects between network analyzer and device/circuit under test

20 p3205 A71-39377

Three-pole theory of amplifiers, deriving operational resistances as function of wave resistance and control parameters by current-voltage matrices

20 p3205 A71-39467

Feedback control system with combined PFM and PDM, obtaining nonlinear discrete equivalence

21 p3360 A71-40615

Real operational amplifier analysis application to state variable filter design emphasizing high-Q HF phenomena, noting undesirable behavior by heuristic argument

21 p3360 A71-40808

Bias network analysis computer program for reliability analysis suited to failure mode, criticality, drift and catastrophic failures prediction

22 p3517 A71-42104

Two-terminal negative resistance circuit analysis for parameters effect on linearity by parabolic relation

22 p3521 A71-42203

Dummy S4 diode packages mounted in coaxial line, deriving mount-independent equivalent circuit parameters from broadband admittance measurements

22 p3521 A71-42206

Second order moment at output of inertialess nonlinear two terminal pair network during amplitude and phase modulation

22 p3510 A71-42260

Flip-flop circuits nonlinear distributed network mathematical model, investigating oscillations nonexistence

22 p3527 A71-42626

Thin film circuit microstructures and integrated microcircuits with distributed parameters, discussing analytical determination of microcell parameters

24 p3807 A71-44378

Electromagnetic fields in moving anisotropic medium, using network formulation based on radial transmission line representation

24 p3805 A71-45092

TEM mode hybrid networks analysis extension to tapered transmission lines, indicating design limitations on VSWR and isolation characteristics

24 p3816 A71-45094

NETWORK SYNTHESIS

Command system and associated algorithm for synthesis of integrated microcircuits composed of components with memories

01 p0051 A71-10090

Computer aided design system for integrated circuits including layouts and logic simulation

01 p0058 A71-10249

Nonminimal phase feedback control system synthesis by frequency methods, discussing invariance characteristics

01 p0061 A71-10709

Complex programmed control systems invariance for discrete times, synthesizing compensating filter with specific transfer function

01 p0063 A71-10725

Optimal design of toroidal inductors with DC bias without repetitive trials

01 p0053 A71-10734

Thin film lumped element microwave integrated circuits from concept to final functional devices

01 p0053 A71-10735

Thin film methods applied to microwave integrated circuits for compactness, reliability and low cost

01 p0053 A71-10736

Multielement nonperiodic antenna array synthesis for given main and diffraction lobes of radiation pattern

01 p0057 A71-11214

Moving target indicator detection filters with nonuniform interpulse periods, discussing design

01 p0058 A71-11575

MOS multiphase LSI circuits design using computer program

02 p0228 A71-11651

Frequency stability of three-loop oscillator with time lag on coupling coefficient plane used for optimal circuit configuration

02 p0230 A71-11835

Qualitative theory of unknown parameters selection electronic circuit synthesis, considering polynomial coefficients of transfer function

02 p0230 A71-11838

Active RC filters synthesis, using expanded denominator of given transfer function

02 p0230 A71-11839

Low- and high-pass active filters theory and design, describing positive and negative feedback circuits

02 p0231 A71-11863

German book on switching theory of linear microwave networks, covering waveguides for a-port network, network modeling, interconnections, etc

02 p0215 A71-12315

Noise interference problems solution by electrical and physical design action, discussing contact arc and ringing suppression

03 p0388 A71-13243

Three-stable parametrons ternary logic circuits synthesis by topological method, realizing Post algebra basic operators

03 p0382 A71-13521

Microwave bandpass filter design with couplings between nonadjacent resonant circuits for generating attenuation pole and increasing slope steepness

03 p0387 A71-13875

Computer aided design for fluidic-pneumatic sequential control circuits synthesis, discussing algorithms and computer programs [ASME PAPER 70-WA/FLCS-17]

03 p0354 A71-14090

High speed automated network design method for optimum value determination of system parameters, using sensitivity analysis and hybrid computer optimization techniques

03 p0390 A71-14305

Programming language for computerized circuit design and analysis, considering techniques for input statements translation

03 p0382 A71-14306

N-port networks interconnection by NASAP-70 transfer function capability for large scale circuit problems, considering Lammell and Cascade Parameter methods

03 p0390 A71-14309

Nonlinear control synthesis based on minimum duration of transient processes leading to system stabilization, using Pontryagin maximum principle

03 p0392 A71-14406

Time optimal control for system described by linear differential equations, discussing two-step sequential synthesis

03 p0392 A71-14407

Optimal on-off control systems with structural constraints, discussing synthesis by dynamic programming and phase plane methods

03 p0392 A71-14408

Sampled data feedback control system analysis and synthesis by state variable method, discussing computer algorithms for optimal pulse control
03 p0392 A71-14409

Nonlinear time optimal off-on feedback control system synthesis, deriving algorithms
03 p0392 A71-14410

Nonlinear stabilization systems time and energy optimal control syntheses using Pontryagin maximum principle
03 p0393 A71-14411

Regulator logic synthesis using state variable feedback for stationary linear plants
03 p0393 A71-14467

Canonical synthesis of electronic relays, considering cascade connected isolation box, analog to digital converter and switch
03 p0393 A71-14469

Rationalized design of integrated circuits for control systems, noting cost reduction and quality improvement
03 p0388 A71-14575

Actinometric network for monthly sums of overall solar radiation and earth surface radiative balance, estimating random errors mean square values
04 p0621 A71-14640

Digital measurement equipment production and circuit design principles, considering decimal memory elements in adder and divider circuits, miniaturization, reliability and integration
04 p0599 A71-15566

Laguerre networks design optimization with threshold frequency and time limit based on pulse/frequency responses energy distribution, representing low pass filters
04 p0561 A71-15700

Network synthesis of beam-forming matrices feeding linear and rectangular antenna arrays
05 p0719 A71-16145

Axissymmetric multibeam annular antenna array with interacting radiating elements synthesized by partial radiation patterns
05 p0722 A71-16867

Transistorized amplifiers synthesis with multiloop feedback
05 p0728 A71-16871

Control system synthesis and analysis, using time and frequency domain methods
06 p0878 A71-17427

Computer shift registers synthesis technique based on block buildup, estimating logic elements amount
06 p0871 A71-17521

Switched binary-weighted resistor network combined with operational amplifier to construct current-summing digital to analog converter
07 p1070 A71-18850

Soviet book on automatic control systems synthesis covering dynamic characteristics optimization, based on quality indices and computerized design
07 p1081 A71-19048

Metal ceramic microstrip L band oscillator circuit with high efficiency silicon avalanche diodes in capacitively loaded TEM coupled lines
07 p1074 A71-19122

Pulsed phase detectors for phase comparisons of pulse sequences having arbitrary frequency ratios, designing circuit to prevent false locking in AFC systems
07 p1061 A71-19509

Electronic synthesis using time structural properties of signals in radio systems
07 p1063 A71-20256

Transfer function synthesis by RC fluidic circuits, presenting transfer function element circuits analysis and experimental verification
07 p1026 A71-20570

Low pressure air jet sensing power pneumatic and fluidic circuits and interface valves for low pressure signal stepup to main line pressure, considering circuit design
07 p1030 A71-20597

Microwave circuits and components design using generalized rational function approximation in finite intervals with Zolotarev functions
08 p1252 A71-20757

Dual mode latching reciprocal ferrite microwave phase shifter, discussing operation principles, design and performance
08 p1262 A71-20764

Automated network design optimization trends and role in computer aided design of lumped-distributed and microwave networks, emphasizing adjoint network method
08 p1268 A71-20767

Microwave oscillators with Gunn effect device resonant circuit and YIG tuning, discussing design and performance
08 p1263 A71-20992

Minimum-sensitivity network synthesis using continuously equivalent transformations and weighted sum of sensitivities square magnitudes as criterion
08 p1268 A71-21272

Lossless two-port cascade network synthesis using computer-oriented technique
08 p1258 A71-21344

Bilateral switching networks synthesis by topological technique, tracing truth table optimum path by visual pattern detection
08 p1270 A71-21665

Analog information systems frequency modulators, describing network design consisting of phase shifting RC network, amplifier and inertialess resistor
09 p1415 A71-22296

Phase locked loop as versatile building block for integrated circuit design, discussing basic principles and applications in analog and digital signal processing
09 p1415 A71-22354

Electron gun synthesis by nonparaxial method, calculating beam potential distribution, trajectories and cathode geometry for cylindrical diode
09 p1415 A71-22461

Realizable method of pattern synthesis for broadside array antenna giving arbitrary current distribution
09 p1418 A71-23489

Optimum synthesis and design of distributed RC filter for oscillator feedback circuit, using calculus of variations
09 p1425 A71-23652

Reversible point integrator circuits synthesis, using AB-102 universal ALGOL computer program
10 p1581 A71-24355

Systems approximation by incontinuous orthogonal Harre functions, discussing dynamic properties and input signal synthesis with minimal errors in estimating parameters
10 p1587 A71-24741

Closed-loop nonlinear systems synthesis, using mapping in Chebyshev series converging everywhere, multidimensional linearization and Volterra singular integral equations
10 p1587 A71-24744

Digital synthesizers design and operation for radio communications, discussing reception and transmission noise performance, frequency stability and acquisition time
10 p1579 A71-24757

Linear automatic flight control systems synthesis based on transfer functions and logarithmic amplitude characteristics of open systems
10 p1588 A71-24911

Electroluminescent semiconductor diodes based on GaP and GaAlAs, discussing design, properties, uses and production
11 p1737 A71-25569

Microwave front end designs for low noise operation, discussing FET applications and mixer conversion loss reductions
11 p1731 A71-25673

Monopulse receiver design system and image band noise factors tradeoffs, discussing preselector and integrated front end trends
11 p1737 A71-25676

Logical GaAs integrated laser circuits, discussing integrated laser modules with electron-hole junctions fabricated by diffusion techniques
11 p1773 A71-25917

Total reliability requirement procedure for design, development and production of medium- and large-scale integrated circuits
12 p1884 A71-26660

Self adjusting autopilot synthesis with capability for control plant changing parameters and structural vibrations effects compensation
12 p1927 A71-26732

Design principles of complex value converters with selfbalancing circuits based on generalized graph of essential information transformations
12 p1892 A71-27024

Waveform and spectral analysis program for electronic system designs, discussing fast Fourier transform modular staging and noise control applications
12 p1884 A71-27148

Microstrip microwave circuit design by complex admittance measurement and computer modeling
12 p1892 A71-27149

Customized MOS arrays computer aided preliminary layout design methodology, using four phase clocking schemes
12 p1890 A71-27772

Engineering method for synthesizing and calculating AC correcting devices with synchronous switches, deriving equivalent transfer function
13 p2041 A71-27949

Computerized circuit design and optimization methods with allowance for constraints and error criteria
13 p2036 A71-29292

Insertion loss approach to doubly resistor terminated filters approximation-synthesis problem
14 p2209 A71-29544

Microwave meander line /coupled parallel commensurate conductors array/ network analysis and synthesis, using equivalent circuit transformation for computerized design
14 p2219 A71-29565

Nonlinear filtering synthesis of optimal receiver for pseudorandom phase shift keyed signal with arbitrary modulation angle and white noise background
14 p2195 A71-30107

Spectral theory of linear differential operators for microwave oscillatory systems synthesis from inhomogeneous line segments, determining line characteristic impedances and local reflection function
15 p2369 A71-31233

Soviet geodetic network construction and compensation, noting triangulation of first and second class in each polygon
15 p2395 A71-31464

RC analog fluidic circuits design for arbitrary transfer functions generation
15 p2351 A71-31682

Fluid logic random input, irregularly activated or stochastic control network analysis, using digital control network synthesis technique /DICONESYN III/
15 p2351 A71-31685

Fluid logic circuit network analysis, utilizing classical synthesis technique with primitive flow table and maps
15 p2351 A71-31686

Nonlinear multidimensional automatic control systems structural synthesis
15 p2379 A71-31844

Functional control system synthesis based on transition dynamics to hypersurface in form of differential equations
15 p2380 A71-31848

Mathematical theory of control systems synthesis, considering Shannon functions asymptotic behavior
15 p2442 A71-31992

Design algorithms for fluidic combinational and sequential circuits
15 p2352 A71-32068

Active all-pass networks with shaped group-frequency delay characteristics, discussing design based on automatic synthesis
15 p2372 A71-32233

Rectangular pulse formation in nonlinear homogeneously distributed systems, discussing energy conversion efficiency
15 p2382 A71-32626

Dispersionless delay line design producing signal frequency shifts for calibration tests of wideband Doppler shift measuring equipment
15 p2373 A71-32632

Parametric regeneration amplifier with capacitor modulation by signal voltage only
15 p2378 A71-32633

Unijunction transistor peak point voltage stabilization, giving formula for interbase resistance multiplier variation with temperature
15 p2378 A71-32636

Rapidly converging first order training algorithm for adaptive equalizer design in PAM signal reception, using variable step sizes for mean-square error minimization
16 p2545 A71-32821

Nonlinear filters synthesis by digital computer technique, discussing density storage and Bayes law computation problems
16 p2549 A71-33351

Lumped elements in microwave IC, considering networks design, fabrication and performance in active and passive circuits
16 p2547 A71-33552

Optimal design of logic networks in homogeneous microelectronic structures, using shortest link search and graph continuity parameters
16 p2545 A71-33704

Optimal control synthesis for saturating time-varying and stationary sampled data systems, using integral performance index and extended maximum principle
16 p2551 A71-34169

Multielement nonperiodic antenna array synthesis for given main and diffraction lobes of radiation pattern
17 p2698 A71-34265

Radio communication system optimization from viewpoints of global synthesis including economics and partial synthesis based on noise stability, precision and reliability
17 p2698 A71-34392

Logarithmic frequency characteristics in stable nonlinear pulsed systems synthesis
17 p2718 A71-34558

HF anodic oscillation tube tripler circuit optimization under constraints due to heat losses in grid electrode
17 p2714 A71-34572

Superheterodyne wideband microwave receiver requirements, design and performance
17 p2699 A71-34607

Optimal control systems synthesis with reduced sensitivity to parameter variations by trajectory sensitivity feedback with cost minimization
17 p2719 A71-34744

German monograph on plane realizations of switching circuits, covering crossover points minimization in electric lines interconnecting component parts
17 p2716 A71-34773

Circuit synthesis from unreliable functional elements through probabilistic logic, correcting codes and logic algebra functions 17 p2721 A71-34978

Nonlinear automatic control systems synthesis based on structure and parameter values selection, formulating quality criteria 17 p2783 A71-35132

Electronic circuit system for IR astronomy, describing noise figure, linearity and frequency response 17 p2744 A71-35229

Automatic electronics design, analyzing visual and graphic devices for initial data preparation, introduction, operator computer interaction and results extraction 18 p2887 A71-35878

German TDMA system based on satellite repeater, discussing network configuration, transmission parameters, control, frame/burst format and field trial 18 p2875 A71-36050

Gyrator circuit design with two antiparallel transistor amplifier stages for minimal DC current reception 18 p2888 A71-36223

Degree reduction of scattering matrix by factorization, deriving necessary and sufficient conditions by methods based on Hankel matrices and on Smith-MacMillan form 18 p2941 A71-36237

High reliability integrated complementary MOS circuit fabrication chain in Concerto satellite program, discussing technological process with account of physicochemical data 18 p2890 A71-36536

Structural synthesis of on-off servo feedback control system with combined dynamic and counterconnection braking of actuating motor within relay dead zone limits 19 p3038 A71-37776

Spacecraft electronic equipment design for reliability in long duration space missions [AAS PAPER 71-155] 19 p3153 A71-37956

Automated test capability for digital modules, describing test generation, circuit analysis and simulation programs 19 p3030 A71-38406

Basis functions for arbitrary time variable network symmetries for large scale integration, using group theory 19 p3038 A71-38488

Controller design for linear closed loop system with transport delay, discussing simplified procedure with correction by zero-pole cluster outside bandpass 19 p3040 A71-38717

Nonuniform sampling procedure for linear transversal filters synthesis, obtaining phase-sampled impulse response filters suitable for AM and FM waveforms generation and matched filtering 20 p3203 A71-38859

Third order oscillatory system optimal terminal-state control synthesis by quadratic functional minimization iterative procedure algorithm, using ODR-1204 computer program 21 p3359 A71-40164

Time optimal control synthesis for linear integration-type system described by n-order differential equations, using operational calculus 21 p3359 A71-40165

Microwave narrow bandpass filters design using microstrip lines 21 p3354 A71-40733

Fast read only memory design implemented in MOS and bipolar technology, noting low access times 21 p3355 A71-40735

Precision relaxation oscillators design and error sources, discussing miniaturization by microelectronic approaches 21 p3355 A71-40736

C-MOS integrated circuit technology emphasizing reliability, design, failure mechanisms and performance parameters [DFVLR-SONDDR-100] 21 p3355 A71-40737

Distributed active RC filters design for low pass, bandpass and biquadratic network functions, including charts for element values determination 21 p3360 A71-40809

Computerized optimal design of L band phase shift networks for broadband performance 21 p3361 A71-40816

High Q micropower filters for VHF applications based on conditionally stable negative resistance operation, describing computer-aided design, construction and performance 21 p3361 A71-40822

Adaptation algorithm for optimal synthesis of nonlinear radio reception system with additive noise 21 p3361 A71-41143

Logical GaAs integrated laser circuits, discussing integrated laser modules with diffused p-n junctions 21 p3394 A71-41228

High voltage spark generating circuit design for studying electrostatic sensitivity of electroexplosive devices, considering pyrotechnic flash charges, bridgewire detonators and electric blasting caps 22 p3587 A71-41449

Soviet book on multivariable automatic control system synthesis with adaptation to computer covering methodology, algorithms, transfer function approximation and stability problem 22 p3525 A71-41799

Linear and nonlinear models for computer aided circuit design involving Zener diodes, providing for thermal effects 22 p3524 A71-42762

Control system synthesis from transient process estimates with Liapunov functions, proposing optimality criteria based on Gaussian minimum constraint principle extension 22 p3527 A71-42855

Optimal nonlinear discrete filters with finite memory for polynomial signals, discussing synthesis with aid of minimax method 22 p3527 A71-42856

Linear dynamic system sensitivity models simplification conditions application to adaptive nonsearching system synthesis algorithms 22 p3527 A71-42857

Optimal design for minimum noise maximum gain bandwidth of lower sideband parametric up-converters 23 p3630 A71-42917

Field effect devices mathematical modeling for computer aided circuit design, using unified approach 23 p3649 A71-43069

Functional converters for logic circuits synthesis, determining mutual value order of input functions 23 p3631 A71-43830

Pneumatic passive lead networks for fluidic systems, presenting transfer functions, equivalent circuits and design information 23 p3631 A71-44096

State estimation errors in quadratic optimal control feedback gain design of stochastic linear regulator 23 p3659 A71-44100

Hybrid lumped-distributed parameter resonant LC circuit design for nuclear magnetic resonance spectrometer 23 p3661 A71-44343

Nonlinear control system optimal synthesis by statistical criteria, discussing probability and likelihood function 24 p3813 A71-44682

Statistically optimal automatic control system synthesis with phase coordinate vector 24 p3814 A71-44685

Optimal linear final parameter control synthesis for dynamic systems with given accuracy, using multivariate statistical analysis 24 p3814 A71-44690

Digital computer simulation for extremal finite network synthesis 24 p3806 A71-44715

Code conversion and coincidence circuits design for positional digital control systems with combinatorial code producing feedback elements 24 p3805 A71-45154

Series stabilization reflection type tunnel diode microwave amplifier synthesis with allowance for real circulator reactance 24 p3810 A71-45259

NETWORKS
Exact calculations of prestressed networks of arbitrary form and magnitude based on matrix displacement method 21 p3456 A71-40156

NEUMANN PROBLEM
Two dimensional mixed boundary value problems solution in elasticity theory by linear differential operators, applying to Dirichlet and Neumann problems 02 p0326 A71-12293

Neumann boundary value problem for region D Helmholtz equation, considering parameter dependence 04 p0619 A71-14649

Neumann problem for Helmholtz equation in complex configuration region, developing variational solution method 05 p0782 A71-16884

Integral equation eigenvalues extension from single to multiple interface Neumann problem 05 p0776 A71-17222

Neumann boundary value problem for Helmholtz equation in region complementary to highly jagged set in fixed surface neighborhood 08 p1325 A71-21698

Inverse diffraction of plane wave by periodic and doubly periodic arrays, calculating velocity potential and pressure distributions for Neumann and Dirichlet problems 13 p2027 A71-27905

Electric potential and current density in rotor of thin disk unipolar engine with zonal removal, formulating Neumann problem 13 p2002 A71-28930

A priori bounds on linear and nonlinear quotients of Neumann boundary value problem for uniformly elliptic difference equations over rectangular regions 14 p2265 A71-30291

Dirichlet, Neumann and mixed boundary value problems relative to wave equation for rectangle, discussing solution based on singularity theorem 14 p2266 A71-30810

Uniqueness of positive solutions to self adjoint elliptic partial differential equations with nonlinear forcing terms under Dirichlet and Neumann boundary conditions 15 p2442 A71-31872

Convergence rate for finite element method, considering Neumann problem for second-order elliptic differential equations with constant coefficients in m dimensional Euclidean space 17 p2769 A71-35688

NEURAL NETS
Sampled data feedback control systems with neural pulse frequency modulation, deriving periodic oscillations existence conditions 09 p1424 A71-23387

Computerized simulation of lateral inhibitory networks for figure aftereffects, discussing light and dark adaptation mechanism 10 p1563 A71-24232

Mean retinal threshold gradient along horizontal meridian for dark and light adapted eyes, considering dynamic neural mechanism 10 p1566 A71-24807

Grating pattern vision models, examining single neural network and multiple channel stimulus information processing 13 p2018 A71-28461

Neural network hypothesis for mechanism of backward masking and disinhibition in visual perception 17 p2684 A71-35253

Integral operating mode of nerve paths representation by linear diffusion channel with electrochemically active synapses, deriving complementary partial differential equations 19 p3001 A71-37250

Signal propagation in model neuron network in terms of differential equations system, representing retina major cell types in planar model 19 p3003 A71-38276

Bioholographic animal information processing model, considering nervous system as diffractive medium and neural network as Fourier analyzer 21 p3380 A71-40923

Oculomotor neural organization models, considering vestibular ocular reflex, saccadic eye movements and smooth pursuit systems 22 p3504 A71-42450

Brachial plexus bundle structural and histological characteristics in man and monkey, noting lack of intraneural network in monkey 23 p3634 A71-43911

NEURISTORS
Neuristor pulse propagation analysis for nonlinear distributed circuit of superconductive tunnel junction stripline 03 p0393 A71-14470

Josephson and IC type superconducting tunneling junction neuristor devices performance tests, presenting bibliography 15 p2377 A71-32317

Multijunction functional devices for operation as decade digital counter, step voltage generator, analog/digital converter, binary counter, neuristor line, etc 22 p3520 A71-41706

NEUROGLIA
Protein content in cytoplasm of neurons and glial satellite cells in supraoptical and red nuclei of white rat brains during natural and paradoxical phase deprived sleep 19 p3005 A71-38545

NEUROLOGY
Standardized EEG data recordings in Air Force neurological evaluations 02 p0208 A71-12393

Cardiovascular and biochemical effects of chronic intermittent neurogenic stimulation, noting alaphamethyltyrosine antihypertension agent 03 p0359 A71-13157

Neurological altitude decompression sickness clinical manifestations, pathophysiology, treatment by compression therapy and subsequent grand mal seizures 06 p0859 A71-17614

Neural stimuli contribution to increasing respiration and hyperpnea during exercise 06 p0862 A71-18386

Clinical aspects of aerospace neurology, considering central nervous system diseases among flying personnel 08 p1238 A71-20723

Clinical value of electroencephalogram following sleep deprivation in detecting abnormalities in neurological patients 09 p1395 A71-23248

Neural spikes and LF components separation from background noise, describing feedback amplifiers circuit 15 p2356 A71-31251

Pulmonary blood volume changes in cat due to neurogenic, pharmacological and mechanical effects on cardiovascular system, noting pulmonary function role

16 p2533 A71-34112

NEUROMUSCULAR TRANSMISSION

Neuromuscular spindles sensory information processing, determining fibers selective data transmission functions by frequency meter and model for electrical and mechanical properties

03 p0366 A71-12977

Human neuromuscular activity description by model for muscle spindles functions, considering systems parameters oscillations relation to mean muscle stress

03 p0366 A71-12978

Adaptation mechanism of human movement control as motor neuron reaction to external stimuli, considering peripheral arch, cerebrospinal canal and feedback

03 p0356 A71-12986

Ischemia effects on impulse transmission to muscle fibers in man, using single fiber electromyography

05 p0706 A71-16320

Reflex excitability of neuromuscular systems of Soyuz crewmembers during physical loads

06 p0855 A71-18372

Latency fluctuations and quantal transmitter release influence on end plate potential amplitude distribution, using frog muscle synaptic delays

07 p1045 A71-20445

Hyperthermia effects on conduction velocity of nerve fibers and peripheral motor neuron-muscular activity in man

09 p1399 A71-22924

Respiratory diaphragmatic center, investigating motor-neuron system integral activity by recording and analyzing phrenic-nerve signals in rabbits

10 p1562 A71-24164

Muscular fibers analysis for motoneuron split potentials, using needle electrode

10 p1564 A71-24484

Femoral nerve afferent muscle fibers bioelectric activity in anesthetized cats, determining effect of blood circulation level on receptors functional activity

15 p2358 A71-31323

Rat irradiated spinal cord, detailing orthodromic ventral root and monosynaptic reaction to rhythmic and increasing frequency stimulation

15 p2362 A71-32735

Afferent nerve impulse traffic from atrial A-type receptor fibers in cats in relation to heart rate control

18 p2857 A71-36688

Nervous system functional characteristics based on neuron structure and electrical transmission from electron microscopy, electrophysiology and biochemical analysis

21 p3329 A71-40145

Extraocular muscle pharmacology, discussing eye twitch and tonic neuromuscular systems structure and function in frogs

22 p3488 A71-42439

Postsynaptic potentials in adjacent synaptic regions of tonic fiber of rabbit external eye muscle

24 p3798 A71-45066

NEURON TRANSMISSION U BIOELECTRICITY NEURONS

Midbrain reticular neurons discharges in response to electrical stimulation of posterior ventral nucleus of thalamus

01 p0008 A71-10072

Neuron pairs discharge sequence temporal correlation in cats association cortex during natural sleep and wakefulness

01 p0011 A71-10849

EEG dynamics and visual cortex neuron responses in cats to conditioned optical stimulus during defensive reflex formation

01 p0011 A71-11052

Temporary connection of neurons in visual and associative cortical regions of hemispheres in cats

01 p0012 A71-11053

Respiratory neuron structure in lateral zone of medulla oblongata in cats

01 p0013 A71-11097

Neuron network modeling by stable rhythmic impulsion system, considering vestibular nystagmus

01 p0025 A71-11137

Impulsive activity of neuron populations in cerebral sections controlling psychic and motor functions in man

01 p0014 A71-11149

Rabbit hypothalamic neuron stimulation by changes in ambient temperature

03 p0361 A71-13225

Soviet book on spinal cord conducting paths electrophysiology covering anatomical and clinical data and neuron theory

03 p0364 A71-13691

Neural activities during simultaneous contrast and information processing in visual system

03 p0364 A71-14188

Ascending neuron vestibulo-ocular reflex arc, emphasizing medial longitudinal fasciculus

04 p0537 A71-14763

Impact induced closed brain injuries pathomorphology, considering dura mater, cortical contusions, neuron and glial damage, brain stem lesions and hemorrhages

04 p0537 A71-14787

Vagal sensitive neurons unitary activity, applying microelectrode technique to nodose ganglion ventral part

05 p0707 A71-16342

Retinal neurons receptive field center, examining excitation and direct inhibition interaction

05 p0707 A71-16596

Visual cortex inhibitory neurons, examining pause discharges in rabbits during light stimulation

06 p0849 A71-17383

Somatosensory and viscerosensory stimulation effects on cortex neuron amygdala complex and convergent interrelations

06 p0849 A71-17384

Antagonistic descending characteristics of medial and lateral hypothalamic nuclei on excitation of spinal cord motoneurons

06 p0856 A71-18465

Synchronous combinative time pulse polylogical structural elements for computer simulation of human neuron functions, discussing circuit design

09 p1398 A71-22271

Adrenergic neurons in intramural cardiac ganglia in rabbits, using histochemical luminescent microscopy

09 p1391 A71-22533

Ionizing radiation inhibition of spinal cord neurons ribonucleic acid synthesis and enzyme activity in mice, using autoradiographic method

09 p1393 A71-22925

Information processing by living systems, considering nervous system and brain operation with emphasis on neuron structure, message coding, programming and information storage

10 p1562 A71-24223

Mathematical neuronal model for functional learning system networks, representing brain pattern recognition, learning and size invariance mechanisms

10 p1569 A71-24233

Unanesthetized rabbits visual cortex cells neuron activity during sound-rhythmic light flashes association

12 p1871 A71-27487

Brain subcortical structure neuronal assemblies impulse activity during sleeping and dreaming in patients treated with implanted electrodes

13 p2005 A71-28378

Visual cortex neurons impulse activity and postsynaptic potential changes due to light stimuli from quasi-intracellular recordings

13 p2005 A71-28381

Humans and animals vestibular stimuli effect on external respiration function and respiration center neuron activity

13 p2007 A71-28413

S matrices application to nonlinear electric circuits and media with nonlinear permittivity coefficients, biological neurons and optical frequency integrators

14 p2220 A71-30025

Mammalian neurons, neuroendocrine transducer/pinealocytes and adrenomedullary chromaffin/and endocrine cells communication properties, noting signal transmission

14 p2182 A71-30180

Individual neurons activity during stereotaxic operations on Parkinsonism and hyperkinesia syndromes, describing microelectrodes for extracellular recording

15 p2365 A71-32535

Arterial baroreceptor reflex action in rabbits, noting central noradrenergic neuron participation

16 p2528 A71-33075

Neuron response to stimuli compared with background activity on histograms

16 p2532 A71-33898

Cochlear nucleus and posterior clivus neurons impulse activity due to tonal signals in anesthetized cats auditory system

16 p2532 A71-33899

Cat thalamus ventrolateral nucleus neuronal discharges during waking and slow and fast wave sleeps

17 p2680 A71-34689

Orientation reflexes neuronal activity due to various stimuli, noting hippocampus reaction to sound and light

17 p2685 A71-35361

Preoptic anterior hypothalamic area temperature sensitive neurons, showing integrative center for thermoregulation

18 p2859 A71-36870

Spinal cord ascending neurons temperature sensitivity, comparing data from cats experiments with hypothalamic temperature sensors sensitivity

18 p2861 A71-36894

Activity correlation of adjacent neurons of cat cerebral cortex somatosensory zone, considering distribution of same direction /cophase/ and different direction /counterphase/ of background rhythms

19 p3001 A71-37392

Signals convergence of various sensory modalities as function of impulse reactions of individual brain neurons in mammals

19 p3003 A71-38197

Protein content in cytoplasm of neurons and glial satellite cells in supraoptical and red nuclei of white rat brains during natural and paradoxical phase deprived sleep

19 p3005 A71-38545

Nervous system functional characteristics based on neuron structure and electrical transmission from electron microscopy, electrophysiology and biochemical analysis

21 p3329 A71-40145

Sensory transmission of spinal heat and cold sensitivity in ascending spinal neurons of anesthetized cats

21 p3334 A71-40630

Visual projection, magnification and retina overlap on dorsal lateral geniculate nucleus in cats measured by random scatter in receptive field

21 p3335 A71-40668

Inhibitory binocular receptive fields in dorsal nucleus of lateral geniculate body for dominant and nondominant eye in cats, using moving slit and flash spot stimulation

21 p3335 A71-40669

Posterolateral thalamus nucleus neurons response to visual, acoustic and somatic stimuli in cats with microelectrodes

22 p3490 A71-42578

Circadian rhythm in isolated Aplysia eye due to retinal neurons population interaction

23 p3633 A71-43545

Feline retinal neurons, noting span and density of branching amacrine cell protrusions and ganglion cells diversity

23 p3633 A71-43581

Receptive fields of dark adapted cats striate cortex neurons as function of barbiturate anesthetic level

23 p3634 A71-43871

Postsynaptic de- and hyperpolarization potential development mechanisms in wakeful cats cortical neurons during LF thalamic structure stimulation

24 p3797 A71-44720

NEUROPHYSIOLOGY

Movement coordination in animals during walking and running, revealing neurophysiological mechanisms of locomotion control

03 p0356 A71-12987

Neurochemical factors in auditory stimulation and susceptibility to audiogenic seizures, noting gamma-aminobutyric acid /GABA/ inhibitor

03 p0360 A71-13164

Neurophysiological aspects of human optical and acoustical perception, discussing pattern recognition and cognizance role in optical image evaluation

03 p0373 A71-14331

Visual slant averaging mechanism evidence from binocular disparator tests, considering gradient slant perception theory and neurophysiological averaging mechanism

04 p0546 A71-15170

Physiological interaction between conscious and unconscious trace processes during time count by pairing acoustic, tactile, proprioceptive and photic stimuli

06 p0850 A71-17599

Neuroelectric signal analysis using real time nerve spike recognition and separation based on nuclear instrumentation techniques

08 p1249 A71-21839

Brain cortical-subcortical functions in psychic processes, indicating developments in psychotherapy

08 p1241 A71-21940

Biosatellite 3 neurophysiological data analysis by digital computer presenting maps of parietal cortex spectra, responsive states transient changes, circadian rhythms and EEG activity

09 p1395 A71-23243

Respiratory diaphragmatic center, investigating motor-neuron system integral activity by recording and analyzing phrenic-nerve signals in rabbits

10 p1562 A71-24164

Neurophysiological auditory information processing, considering mechanical transformation of two dimensional pressure-time signal and three dimensions for presentation to nervous system

10 p1562 A71-24228

Natural sleep and wakefulness stages neurophysiology based on bioelectric activity spectral and correlation analyses

13 p2005 A71-28380

Readiness potential, vertex positive wave and contingent negative variation recordings for evaluation of neural events associated with visually stimulated perception

15 p2359 A71-31953

Psychological and neurophysiological definitions of vigilance, considering alcohol and tranquilizers effects

16 p2533 A71-34040

Soviet papers on higher nervous activity physiology, Part 1, Basic laws and mechanisms of conditioned reflex activity covering inhibition, and bioelectrical effects, with bibliography

17 p2684 A71-35357

Brain locking activity structural organization, discussing cerebral processes and control contact mechanisms activating conditioned reflexes
17 p2684 A71-35358

Higher nervous activity physiology, discussing induction, protective and conditioned inhibition mechanisms in cerebrum and electrophysiological indices
17 p2684 A71-35359

Perspiration delay times characterizing potohydrotic reflex, analyzing neurophysiological mechanism
18 p2861 A71-36885

Nervous system functional characteristics based on neuron structure and electrical transmission from electron microscopy, electrophysiology and biochemical analysis
21 p3329 A71-40145

Vibration effects on human body, discussing neurophysiological data, safe exposure limits, therapeutic applications, motion sickness, muscular responses and biomechanical effects
21 p3342 A71-40147

Neurophysiological investigation of visual tilt aftereffect, comparing judgment precision at vertical and horizontal to oblique orientation with/without gravity cue
21 p3335 A71-40671

Excitability, reactivity, adequacy, creativity and guidance at molecular, cellular, systemic and psychic levels in human biophysical neurodynamics, plotting stimulus magnitude vs response duration
21 p3344 A71-41063

Eye movement neurophysiology, discussing ocular proprioception, oculomotor muscle sensory receptor role, extraocular muscle afferent and efferent innervation and central nervous system control effect
22 p3488 A71-42433

Human ocular control system supranuclear disorder syndromes and signs in terms of physiological concepts
22 p3488 A71-42438

Human expired air toxicity effect on mice neurohumoral changes stimulating inhibitory reactions in central nervous system
22 p3506 A71-42813

Crossed retinal pathways in Siamese cats due to neuroanatomical defect impairing binocular vision and stereoscopic depth perception
23 p3633 A71-43546

Hyperoxia effects on thermoregulation and neurochemical functions, showing temperature increases in cerebrum and decreases in cortical and subcortical formations
23 p3633 A71-43582

Evoked and background activities interaction in computerized self zeroing neuron model
24 p3801 A71-44550

NEUROSCIENCE
U NEUROLOGY
NEUROSES
Psychological screening of pilot trainees, showing neurosis noncorrelation with learning ability to fly
23 p3639 A71-43221

NEUROSPORA
Neurospora germination and growth in medium of low water activity due to NaCl or nonelectrolyte addition
11 p1721 A71-26146

NEUTRAL BEAMS
NT MOLECULAR BEAMS
NT NEUTRON BEAMS
He ion beam space charge neutralization by thermal electrons injection
17 p2784 A71-34200

Relativistic neutralized cylindrical electron beam paraxial motion through uniform longitudinal magnetic field
21 p3426 A71-41289

High energy neutralized ion beam generation by focusing ultrashort laser pulses on thin foils, applying to nuclear reaction for superheavy nuclei production
22 p3555 A71-41595

NEUTRAL PARTICLES
NT FAST NEUTRONS
NT NEUTRONS
NT THERMAL NEUTRONS
Mass and phase spectrometry in modulated molecular beam experiment for neutral particles velocity measurement prior to ionization
01 p0028 A71-11303

Nuclear interactions of neutral cosmic particles with carbon target at mountain altitudes
03 p0476 A71-13848

Ion-neutral coupling in plasma acceleration revealed by velocity disparities determined spectroscopically [AIAA PAPER 70-166]
05 p0788 A71-16572

Electrostatic wave perturbation current using accelerated particles orbits in neutral sheet with electric field in plane
05 p0788 A71-16633

High energy particle interaction with magnetospheric tail neutral layer, determining limiting shape of pitch angle particle distribution
05 p0800 A71-17176

Neutral condensations and protostars in H II regions noting original density distributions
06 p0973 A71-18340

Upper atmosphere neutral component temperature measurement from thermal spread of charged particles beam
09 p1437 A71-22679

Two-wavelength interferometry of plasmas generated by Nd laser beam focalization, deriving electron and neutral particle densities
10 p1646 A71-23818

High energy particle interaction with magnetospheric tail neutral layer, determining particle pitch angle distribution limiting shape
13 p2128 A71-28233

Neutral particle gas integral kinetic equations numerical solution without integration on lag parameter
13 p1991 A71-29157

Adiabatic flow model of noiseless magnetic neutral sheet of finite width, discussing particle trajectory and charge density distribution
13 p2109 A71-29166

Supersonic plasma flow effects on neutral hydrogen, helium and charged particle density and velocity profiles in polar ionosphere
14 p2234 A71-30040

Motion equations for neutral matter in head atmosphere of bright comet with high density spherical source and molecular collisions
15 p2484 A71-31661

Density distribution of neutral matter in cometary atmosphere in transition region between hydrodynamic and free molecular flow
15 p2484 A71-31662

Low energy muon production by neutral components of cosmic radiation at sea level, noting correlation with sidereal time
15 p2475 A71-31785

Sidereal anisotropy in muon signal observed by cosmic ray telescope above sea level, indicating production by neutral particle and leakage relative to anticoincidence factor
15 p2477 A71-31797

Upper atmosphere neutral species latitudinal and seasonal distributions, using turbulent transport coefficients and photochemical reaction rate constants in finite difference solution
16 p2569 A71-33804

Neutral atmosphere density profile data from satellite-borne accelerometer experiment, observing gravity waves propagating in north-south direction at high latitudes
16 p2570 A71-33825

Bibliography on neutral atmosphere dynamics covering waves, winds, turbulence and disturbances in thermosphere and ionospheric effects
17 p2732 A71-34462

Undisturbed ionospheric ion and electron temperature warming, investigating frictional heating effect by neutral winds
19 p3048 A71-37399

Ionospheric neutral composition variations as function of height, local time and solar activity
19 p3056 A71-38356

Air shower pion/proton and neutral/charged ratios at mountain altitude, using cloud chamber, Cerenkov counter and spectrometer measurements
20 p3279 A71-39323

Neutral upper atmosphere observations, discussing lower thermospheric density and composition diurnal, seasonal and latitudinal variations and solar activity effects
20 p3220 A71-39690

Lower thermosphere and mesosphere water vapor and neutral composition spectrometric measurements, estimating hydrogen and oxygen atom recombination coefficient limits with mass analyzers
20 p3221 A71-39696

Lower thermosphere neutral composition fine structure data from rocket-borne time of flight mass spectrometer, emphasizing atomic nitrogen vertical distribution
20 p3222 A71-39697

Neutral atmospheric composition and density variations during geomagnetic disturbances fromOGO-6 satellite quadrupole mass analyzer measurements
20 p3223 A71-39711

Neutral-ionized parts interactions in upper atmosphere, discussing ionospheric plasma modulation, solar control and seasonal anomalies in lower ionosphere and ionic reactions
20 p3223 A71-39712

Ionospheric electron and neutral particle temperature average diurnal behavior from bottomside vertical soundings
20 p3225 A71-39723

Trapping of neutrals from fast atom beam impinging on molecular hydrogen influx fed electron-cyclotron plasma target
21 p3422 A71-40761

Neutral gas acceleration to high velocity at low ionization level by electromagnetic plasma gun formed unionized shock wave
21 p3423 A71-40766

High voltage source model for fast neutral particles, showing energy and yield as function of potential, pressure and magnetic field
21 p3421 A71-41295

Photoionization mass spectrometry, considering application to appearance potentials determination, ion-neutral reactions and gas analysis
22 p3537 A71-41649

Equilibrium neutral gas and plasma electron number density fluctuation determination, deriving correlation functions from Liouville equation
22 p3530 A71-41894

Nuclear interactions of neutral cosmic particles with carbon target at mountain altitudes
22 p3595 A71-42649

Relativistic electron beam propagation entering vacuum or neutral gas filled region through grounded conducting wall, using one dimensional model
23 p3713 A71-44146

NEUTRALIZERS
Parameters influence on mercury hollow cathode neutralizers for Kaufman ion thruster [AIAA PAPER 70-1090]
07 p1184 A71-19863

Ionizer, neutralizer and ion optics of cesium contact ion thruster, examining porous W materials technology [DGLR-71-033]
17 p2793 A71-35535

Hollow cathodes as main and neutralizer cathodes in Kaufman electrostatic propulsion system, discussing test installation and results [DGLR-71-045]
17 p2794 A71-35542

NEUTRINOS
Photon-neutrino coupling theory of weak interactions, noting exclusion by astrophysical data for white dwarfs
01 p0130 A71-11272

Neutrino synchrotron radiation for relativistic gas applied to white dwarfs and neutron stars
01 p0145 A71-11337

UV dwarf star evolution, using central and gap star models emphasizing photon-neutrino emission
04 p0648 A71-15250

URCA neutrino emission processes explaining anomalous isotopic heavy element abundance in solar system
04 p0651 A71-15660

Stellar free neutrino and antineutrino emission thermodynamics under hot matter neutronization and hydrodynamic stability during late evolutionary stages
06 p0974 A71-18426

Longitudinal plasmon decay in strong magnetic field into neutrino-antineutrino pair
09 p1527 A71-23533

Neutrino magnetic moment spin precession effects on solar magnetic fields, discussing electromagnetic field-charged particles interaction
09 p1528 A71-23593

Neutrino luminosity in strongly magnetized degenerate relativistic electron gas plasma from URCA energy loss rate calculations
10 p1671 A71-24303

Partial mixing effects on solar neutrino flux and stellar evolution
10 p1662 A71-24497

Cross section for electron and muon neutrino-antineutrino pair production by photons, using intermediate boson theory
11 p1802 A71-25588

Stellar free neutrino and antineutrino emission thermodynamics under hot matter neutronization and hydrodynamic stability during late evolutionary stages
12 p1954 A71-26576

Cosmic ray neutrino results from deep underground detector near Johannesburg
12 p1952 A71-27399

Solar neutrino astronomy, investigating interior central temperature, energy generation mechanism and model
13 p2142 A71-29116

Solar neutrinos and compact luminous objects, discussing unsolved problems and theoretical-observational discrepancies
14 p2309 A71-30015

Soviet book on cosmic muons and neutrinos covering anomalous and weak interactions
15 p2472 A71-31287

Cosmic rays - Conference, Budapest, August 1969, Volume 4, Muons and neutrinos techniques
15 p2474 A71-31776

Cosmic ray muon-neutrinos sea level energy spectra at low energies for horizontal and vertical directions, estimating geomagnetic cut-off effects for various geomagnetic latitudes
15 p2477 A71-31799

Cosmic ray muon and neutrino measurements with deep underground scintillation detector array
15 p2477 A71-31800

Point sources of solar neutrino radiation, explaining negative experimental results without drastic change of main assumptions concerning stellar evolution
15 p2478 A71-31801

Neutrino emission from collapsing stars, discussing possibility of detection by large mass organic scintillator
15 p2478 A71-31802

Solar neutrino detection using capture reaction in perchloroethylene medium 15 p2478 A71-31803

Main sequence stars hydrogen burning stage, examining neutrino emission and nuclear process effects in stellar evolution 16 p2625 A71-33230

Deep underground cosmic ray neutrinos interaction experiments, discussing particle motion, inelastic cross section variation, energy, mass and celestial coordinates 17 p2795 A71-34665

Underground search for cosmic ray neutrino interaction products, observing muon products 17 p2795 A71-34666

Neutron star cooling behavior models based on neutrino emission theory, explaining galactic steady state cosmic rays and pulsar radiation 18 p2959 A71-35931

Underground interactions of primary cosmic ray produced atmospheric muon neutrinos, using large area liquid scintillation detector hodoscope 19 p3105 A71-37288

Underground muons produced by atmospheric neutrinos, noting deviation from linearity by comparing calculated and experimental muon rates 19 p3106 A71-37289

NEUTRON ABSORBERS

Neutron flux perturbation by absorbing materials, considering absolute black bodies and reactor zone experimental data 04 p0629 A71-14916

NEUTRON ACTIVATION ANALYSIS

Al and Si abundances of Italian chondrites by instrumental pile neutron activation analysis 02 p0318 A71-12903

O, Si, Al and Fe abundances of Apollo 12 lunar rock 12013 from neutron activation analysis 03 p0494 A71-14218

Apollo 12 lunar rock 12013, discussing major and trace elemental abundances determination by neutron activation analysis 03 p0494 A71-14219

Surface and subsurface water analysis on moon and planets by combination neutron experiment using epithermal die-away measurements of hydrogen 15 p2411 A71-32477

Calcium, potassium and iron loss by astronauts during Apollo space missions, using instrumental neutron activation analysis 16 p2528 A71-33111

Cascade mountains volcanic ash deposits elemental abundances correlation by computerized gamma ray spectra analysis of TRIGA reactor activated glass separates 22 p3533 A71-41855

Neutron activation data on Zn, Ga, Ge, Cd, In and Ir trace elements for Apollo 12 lunar rock and soil sample 23 p3747 A71-43673

Apollo 12 specimens elemental abundance from neutron activation analysis, discussing fractional crystallization, partial melting, rare earth abundances and soil mixing model 23 p3747 A71-43674

Meteoritic material characterization from trace elements in Apollo lunar soil, core samples, breccia and anorthositic fragments by neutron activation analysis 23 p3747 A71-43678

Neutron activation analysis of Apollo 11 lunar fines, determining Pb 204, U, Bi and Tl contents 23 p3753 A71-43715

Solar protons contribution to spallogenic Mn 53 production in Apollo 12 lunar rock and soil from neutron activation analysis 23 p3755 A71-43734

NEUTRON BEAMS

Neutron radiography facility using TRIGA reactor source, discussing design and performance 13 p2044 A71-28523

German monograph on evaporation neutrons mean multiplicity for cosmic radiation energy spectrum variations measurement 18 p2958 A71-36670

NEUTRON COUNTERS

Cosmic rays neutron monitors daily data/July 1957-December 1962/, applying corrections for latitude, altitude, solar cycle phase and station efficiency 06 p0955 A71-18132

Forbush decrease rigidity dependence relation to cosmic ray solar modulation, using neutron monitors counting rate variations at different vertical cut-off rigidities 06 p0956 A71-18136

Cosmic ray intensity variations, discussing trajectory-derived cut-off rigidities for neutron monitor data analysis 06 p0959 A71-18160

High latitude neutron monitors during 15 November 1960 solar cosmic ray event, calculating asymptotic directions for protons with magnetospheric model 06 p0959 A71-18161

Cosmic ray equator position dependence on solar activity level, discussing shipborne neutron monitor observations during IGY and QSY 06 p0959 A71-18162

Neutron monitors multiplicity yield function calculation, using Monte Carlo method for nucleonic cascade in atmosphere 06 p0960 A71-18165

Latitude, mesons and radioactivity effects on planetary distribution of cosmic ray neutron component barometer coefficient during IQSY 06 p0960 A71-18166

Neutron monitor counting rate at Sanae, Antarctica, observing snow and atmospheric pressure and temperature effects 06 p0960 A71-18168

Fast neutron energy spectrum and flux, using balloon flight neutron detector with charged particle rejection scheme and pulse shape discriminator for gamma rays separation 06 p0962 A71-18178

Aircraft altitude cosmic ray intensity measurements in lower atmosphere by neutron monitor, considering long term nucleonic intensity variations 08 p1355 A71-21629

Cosmic particle gradient perpendicular to solar equator plane and semiannual cosmic ray variations, using worldwide neutron monitor network 10 p1660 A71-23839

Fast neutrons scintillation counters effectiveness, presenting calculation procedure with corrections for double carbon-hydrogen scattering and nuclear reaction effects 11 p1761 A71-25577

Magnetic cutoff variations during geomagnetic storm from counting rates of neutron monitors, noting cosmic ray intensity augmentation 14 p2298 A71-29748

Cosmic ray sidereal time period, using neutron monitors, meson telescope and various ion chambers 23 p3719 A71-43126

NEUTRON CROSS SECTIONS

Gadolinium isotopic composition and neutron capture effects in meteorites 08 p1365 A71-21693

NEUTRON DECAY

Extraterrestrial slow neutron flux and decay density, calculating spatial distribution by power function 14 p2302 A71-30592

NEUTRON DETECTORS

U NEUTRON COUNTERS

Ti-Zr-O alloys cross sections investigation by neutron and X ray diffraction, discussing stoichiometry deviation 06 p0911 A71-17382

Neutron diffraction analysis of atomic arrangements in maraging steel, discussing interatomic attractions 19 p3081 A71-37722

Neutron diffraction studies of Apollo 12 lunar samples 12070, 119, 12071, 6 and 12008, 7, observing magnetic ordering 23 p3759 A71-43761

NEUTRON DISTRIBUTION

High energy albedo neutrons energy and angular distributions, determining solar neutron flux upper limit 01 p0147 A71-11517

Neutron flux distribution in water for strong Am-Be neutron source enclosed in Be spheres, comparing calculated and measured flux distributions 11 p1797 A71-25742

NEUTRON EMISSION

Neutron emission yield during Pu 238 alpha particles interactions with O 18, taking into account recoil Ne isotopes 14 p2276 A71-30177

Tokamak T-3A plasma neutron emission, confirming thermonuclear nature of radiation 24 p3856 A71-45113

NEUTRON FLUX

U FLUX [RATE]

NEUTRON FLUX DENSITY

High energy albedo neutrons energy and angular distributions, determining solar neutron flux upper limit 01 p0147 A71-11517

Energetic solar neutrons near maximum, calculating continuous flux and proton emission from balloon measurements 02 p0302 A71-12768

Neutron flux perturbation by absorbing materials, considering absolute black bodies and reactor zone experimental data 04 p0629 A71-14916

Diurnal cosmic ray neutron variations after proton flares, comparing calculated radial and azimuthal gradients to experimental data 06 p0951 A71-18105

Cosmic ray neutron component intensity increases dependence on corpuscular stream velocity before Forbush effects 06 p0954 A71-18124

Cosmic ray multiple neutron intensities time variations measurements at Syowa Station [Antarctica], considering Forbush decrease, diurnal variations, solar protons and storm time increase 06 p0960 A71-18163

Solar proton event energy spectra based on multiplicity measurements of cosmic ray neutron intensity increases 06 p0960 A71-18164

Extraterrestrial gamma ray and neutron flux and energy spectrum at balloon altitudes over equatorial latitudes, using pulse shape discriminator during solar flare 06 p0962 A71-18177

Fast neutron energy spectrum and flux, using balloon flight neutron detector with charged particle rejection scheme and pulse shape discriminator for gamma rays separation 06 p0962 A71-18178

High energy albedo neutron production by cosmic ray collisions, investigating balloon altitude flux variations near atmospheric top 06 p0962 A71-18179

Galactic cosmic rays solar modulation effects on fast neutron flux in atmosphere 06 p0962 A71-18182

Atmospheric fast neutron flux, discussing solar proton events and Forbush decreases effects 06 p0963 A71-18183

Neutron flux distribution in water for strong Am-Be neutron source enclosed in Be spheres, comparing calculated and measured flux distributions 11 p1797 A71-25742

Particle precipitation at auroral heights, examining ground based observations evidence for existence of protons, neutrons and electrons 12 p1947 A71-26864

Ground and mountain level measurements of energy and angular distribution of high energy neutrons in lower atmosphere, using double elastic scattering with hydrogen nuclei 13 p2119 A71-27906

Solar neutron flux measurements compared to previous spark chamber scintillation experiment flown at Hyderabad, India 13 p2120 A71-27927

PAX intermediate spectrum reactor neutron and photon dose rates and fast and thermal neutron flux calculation, comparing results with experiment 13 p2099 A71-29258

Cosmic ray neutron diurnal variation phases and amplitudes from harmonic analysis of directional intensity 14 p2299 A71-29987

Atmospheric neutron data at various altitudes, relating densities, fluxes and spectra to solar activity 14 p2301 A71-30589

Extraterrestrial slow neutron flux and decay density, calculating spatial distribution by power function 14 p2302 A71-30592

Neutron flux estimate from protons number needed for white light solar flare caused by energetic particle penetration into photosphere 22 p3590 A71-41467

NEUTRON IRRADIATION

Visible and IR reflection spectra of p- and n-type GaAs under fast neutron irradiation 01 p0139 A71-10783

High temperature neutron irradiation properties of uranium oxides, carbides and nitrides coated with tungsten-rhenium 02 p0296 A71-12246

Omega West Reactor isothermal irradiation experiments, determining long term fast neutron irradiation effects on Al 995, Lucalox and yttrium oxide insulator 02 p0280 A71-12251

Absorbed dose equivalent from high energy neutrons and protons incident on tissue, using nucleon-meson cascade calculations 04 p0624 A71-14804

Neutron induced lifetime damage short term annealing dependence on minority carrier density in p-type silicon, considering majority carrier repulsion by positively charged centers 07 p1175 A71-19061

Statistical analysis of neutron induced gain degradation of silicon power transistors, determining failures distribution fit to Weibull function 07 p1070 A71-19063

Neutron radiation damage on high efficiency microwave avalanche diode sources /TRAPATT oscillators/ 07 p1071 A71-19068

Neutron irradiation induced degradation in epitaxial Gunn diode performance 07 p1071 A71-19069

GaAs transmutational doping by slow neutrons irradiation, using Cd and In screens for impurities distribution control 07 p1175 A71-19219

Test equipment for elasticity modulus measurement of neutron irradiated materials, noting u-c nuclear fuel and alloy samples 07 p1084 A71-20356

Al-Li alloy precipitation hardening after neutron irradiation, noting yield stress increase after aging at various temperatures 07 p1143 A71-20487

Fast neutron irradiation effects on Mo recovery stages 1 to 3 in bcc metals using electrical resistivity measurements 07 p1143 A71-20491

Neutron irradiation effects on Al-Mg alloys tensile properties, noting yield stress increase and appearance of Luders strain 07 p1143 A71-20492

Nuclear reaction products effect on population inversion in gas lasers, considering neutron irradiation enhancement of carbon dioxide laser output 08 p1303 A71-21668

Potassium-Argon dating analyses of neutron irradiated meteorites, discussing Chainpur chondrite chondrules gas retention ages 10 p1679 A71-24984

Black SiC varistors IV characteristics and conductivity, investigating fast neutron irradiation and isochronal annealing effects 12 p1886 A71-26898

Radiation induced visual phosphores observed by dark adapted human subjects in fast neutron, X ray and neutron pion beams at Berkeley comparative to primary cosmic ray effects 12 p1871 A71-27675

Fast neutron irradiation effect on Ni-Cr alloy electrical resistivity as function of temperature and initial composition 13 p2083 A71-27964

Multiple starlike flashes and short streaks reported by subjects exposed to neutrons under 25 mev, discussing interaction with retinal rods by proton recoils 13 p2022 A71-29353

Creep rupture strength and durability of Al, Ni and Cu irradiated by neutron flux 14 p2258 A71-30004

Neutron irradiation effects on diffusion-ion doped HF n-p-n silicon transistors of moderate power, showing radiation stability 14 p2213 A71-30625

Neutron irradiation effect on lattice parameters and distortion energy of titanium and chromium carbides, using X ray analysis 15 p2430 A71-32152

Radiation defects isochronal annealing effects on absorption spectral distribution of gallium arsenide irradiated with fast neutron flux 16 p2620 A71-33184

Neutron and gamma radiation effects on electrophysical properties of high resistivity Si single crystals grown in hydrogen atmosphere 16 p2621 A71-33186

Specific heat measurement in magnetic field for graphite under neutron irradiation at low temperatures, noting Schottky anomaly 16 p2600 A71-33379

Neutron irradiated Mo single crystals polygonization after cold rolling, using X ray topology methods 16 p2596 A71-33886

Endurance limit of construction materials under fast and thermal neutron irradiation in reactor channel 16 p2598 A71-33986

IR absorption of oxygenated dislocationless phosphorus doped fast neutron irradiated n-type silicon, investigating dominant defects for different radiation dosages 17 p2790 A71-34199

Neutron radiography and dosimetry as clinical diagnostic tool, calculating resolution through tissues for simulated human arm 17 p2693 A71-35449

Dynamic yield and absorptivity of steel during brittle fracture propagation under neutron irradiation 18 p2934 A71-35987

Neutron irradiated and unirradiated Ta sheathed BeO insulated grounded junction thermocouples drift measurement 18 p2916 A71-36046

Co 59-neutron reaction tensor spin-spin potential, using polarized targets of Ho 165 and Co 59 for nuclear spin-spin effect measurement 18 p2949 A71-36681

Neutron radiography of Apollo ordnance, describing test facility and equipment 19 p3063 A71-37449

Semiconductor neutron hardness assurance by irradiation of wafer, probe, die rejection and anneal screening technique 19 p3034 A71-38520

Chemical composition of atmospheric aerosols from Tokyo region, measuring energy spectrum of neutron irradiated specimens by gamma spectrometer 19 p3094 A71-38698

Neutron irradiation effects on radiative, nonradiative and threshold currents in epitaxial GaAs laser diodes at room temperature 20 p3275 A71-38785

Beryllium reflector plate failure in NASA Plum Brook Reactor, discussing irradiation induced mechanical and physical property changes and internal/external stress effects 21 p3414 A71-40904

Neutron irradiation effects on Si p-n junction field effect transistors I-V characteristics, charge distribution in space charge region and transconductance 22 p3586 A71-42297

Chemical agents protective properties on albino mice under gamma-neutron radiation, noting dose and composition effects 22 p3492 A71-42713

Partial body shielding effects on rats radiation sickness survival rates under gamma-neutron radiation, comparing head and belly shielding effectiveness at different intensities 22 p3492 A71-42716

Rat organs pathomorphological changes under gamma neutron irradiation with head and abdomen shielding, noting intestines early damage 22 p3493 A71-42722

Neutron bombardment effect on dislocation mobility in Ge single crystals investigated by bending and etching techniques 23 p3715 A71-43309

Neutron irradiation effects on dissociative high temperature zinc diffusion in indium and gallium arsenides 23 p3716 A71-43480

Re isotopic composition measurement in Apollo 12 rocks and regolith samples using neutron bombardment 23 p3750 A71-43697

Ar, Kr and Xe emanation during stepwise heating of lunar rocks under slow neutron irradiation in pile, using mass spectroscopy 23 p3754 A71-43726

Solar coronal heating neutron theory based on solar gamma ray flux considerations 23 p3770 A71-44014

Electron transmission microscopy of Mo single crystals irradiated with fission neutrons and defect structures prior/after postirradiation anneal 24 p3839 A71-45192

Bulk diffusion and glide and self climb mechanisms of vacancy and interstitial loop growth in Mo during neutron postirradiation annealing 24 p3839 A71-45193

NEUTRON PHYSICS

Neutron linear transport theory boundary value problems, using Green function approach 01 p0111 A71-10333

Neutron star nuclear matter superfluidity and superconductivity possibility from energy gap and critical temperature and magnetic field calculation 11 p1821 A71-25565

Thermionic reactor core design for undersea conditions based on neutron data and calculation related with diode materials 11 p1711 A71-25882

X ray telescopes and neutron cameras telephoto lenses for satellites and space stations, discussing optical design and correction methods 14 p2246 A71-30391

NEUTRON SCATTERING

Molecular dynamics data from neutron scattering techniques for gas mixing 18 p2949 A71-36958

NEUTRON SOURCES

Portable Cf 252 neutron radiographic camera, noting reactor fuel and concrete polymer content measurements 07 p1119 A71-19950

Neutron flux distribution in water for strong Am-Be neutron source enclosed in Be spheres, comparing calculated and measured flux distributions 11 p1797 A71-25742

Proton recoil measurements of PuBe neutron source spectra, using pressurized hydrogen spherical proportional counter and liquid scintillator measurements 14 p2276 A71-29918

Vacuum package with Ti bulk sublimator/ion pump combination for 150 kv neutron generator tritium decontamination 21 p3414 A71-40900

NEUTRON SPECTRA

Neutron spectra measurement in epithelial energy range by activation of threshold and resonance foils, using expansion in orthonormal polynomials 04 p0594 A71-14915

Fast neutron energy spectrum from free proton elastic scattering in emulsion plates, studying upper atmospheric altitude and latitude factors 06 p0962 A71-18180

Inelastic scattering cross sections, using measured neutron leakage spectra from thick spherical shells of Ta, W, Mo and Be 11 p1802 A71-25556

Mean neutron monitor multiplicity time variations for solar cosmic ray events and Forbush decreases with modulation spectrum allowance 11 p1816 A71-25753

Atmospheric neutron data at various altitudes, relating densities, fluxes and spectra to solar activity 14 p2301 A71-30589

Cosmic rays neutron spectrum at sea level, using charge exchange reaction 15 p2479 A71-31867

Fast neutron spectra in lead and water shielded reactor, comparing liquid scintillator measurements with discrete ordinates code calculations 16 p2606 A71-33253

NEUTRON STARS

Neutron star in accretion state, investigating generation of relativistic electrons, positrons and X ray and gamma emission 01 p0150 A71-10061

Neutrino synchrotron radiation for relativistic gas applied to white dwarfs and neutron stars 01 p0145 A71-11337

Rotating neutron star supernova explosion without nuclear detonation, discussing rotational momentum transfer 02 p0307 A71-12089

H alpha line emission in ionization zones encircling neutron stars, suggesting accretion-induced UV luminosity 02 p0308 A71-12091

Pulsars as rotating neutron stars with frozen-in magnetic field, accounting for energy and angular momentum losses due to gravitational radiation 02 p0300 A71-12473

Nonpulsing pulsar model, discussing idealized neutron star with spin axis aligned with uniform internal magnetic field 04 p0650 A71-15585

Neutron star formation, calculating reimposition mass fraction of thermonuclear supernovae explosion 05 p0811 A71-16684

Double star system with neutron star in pair with matter-losing star, discussing X ray sources variability causes 06 p0976 A71-18455

Cosmic plasma stream capture by magnetic dipole of neutron star in binary system 07 p1192 A71-19287

White dwarfs, neutron stars and black holes origin and characteristics, discussing density, mass radius, gravitation and structure 07 p1199 A71-19999

Crab Nebula pulsar characteristics, discussing neutron star hypothesis, optical counterparts, magnetic fields, mass, radius and origin 07 p1201 A71-20214

Rotating neutron star supernova explosion without nuclear detonation, discussing rotational momentum transfer 08 p1362 A71-21139

H alpha line emission in ionization zones encircling neutron stars, suggesting accretion-induced UV luminosity 08 p1362 A71-21141

Pulsars as rotating magnetic neutron stars, examining radio emission via maser amplification 08 p1363 A71-21174

Pulsar model consisting of rotating neutron star with strong magnetic field 09 p1517 A71-22337

Collapsed or neutron star companions of bright binary stars, explaining low luminosity of more massive component 10 p1665 A71-23740

Neutron star matter equations of state involving hyperon formation effects for maximal stable mass models, tabulating moments of inertia 10 p1671 A71-24302

Neutron star nuclear matter superfluidity and superconductivity possibility from energy gap and critical temperature and magnetic field calculation 11 p1821 A71-25565

Hyperon stars thermodynamics, deriving hot neutron stars equation of state with particular reference to center singularities 11 p1828 A71-25737

Neutron star formation from supernova explosion in close binary system 11 p1832 A71-26171

Binary system of neutron star paired with matter-losing star, discussing X ray emission variability causes 12 p1956 A71-26605

Periodic rotational LF synchrotron model of magnetic neutron star for pulsar radiation 12 p1947 A71-26649

Gravitational wave bursts emanating from direction of center of Milky Way Galaxy, considering pulsating neutron star as source 12 p1958 A71-26694

Relativity and neutronization effects on radial pulsations and density decrease of rotating cold white dwarfs near stability loss, using energetic method 12 p1966 A71-27236

Maximum toroidal magnetic fields of rotating neutron stars dependent on central density, using relativity corrections to plasma hydrodynamic and Maxwell equations 12 p1966 A71-27237

Galaxy nuclei and quasars model, considering supernova explosions, neutron stars matter accretion and energy radiation 12 p1968 A71-27541

Gravitational waves from rotating relativistic neutron stars /pulsars/ in far field region, assuming small velocity and spherical deformation

13 p2133 A71-27971

Pulsar nature and radiation mechanism, examining rotating neutron stars structure and atmospheric dynamics

13 p2140 A71-29041

Neutron stars origin and nature, discussing pulsars structure, mass and frequency variations

13 p2143 A71-29297

Strong magnetic fields effects on neutron stars or white dwarfs, considering Thomson scattering in fully ionized collisionless plasma

14 p2315 A71-30858

Neutron stars with pulsar characteristics in binary systems, discussing matter accretion relationship to X ray source evolution

15 p2483 A71-31342

Pulsed gamma radiation from rotating neutron star, discussing synchrotron emission mechanism based on electron pulses incident on high intensity sharply localized magnetic field

15 p2474 A71-31724

Solidification pressure of nuclear and neutron star matter, suggesting modifications to equation of state

15 p2452 A71-32548

Angular momentum of rotating Einstein-Rosen bridge, comparing neutron star models

16 p2609 A71-33262

Stability analysis of nonradial oscillations of cold nonrotating relativistic neutron stars by linearized Einstein equations with coupled gravitational waves

16 p2635 A71-33482

Soft optical, radio and X ray emission during accretion of interstellar gas by neutron star with magnetic dipole moment

17 p2800 A71-34570

Pulsars as neutron stars, explaining fast rotation by tendency to conserve angular momentum during compression

17 p2804 A71-34857

Neutron star cooling behavior models based on neutrino emission theory, explaining galactic steady state cosmic rays and pulsar radiation

18 p2959 A71-35931

Cosmic ray injection by clusters of dense magnetic neutron stars, giving particle number for Galaxy

18 p2957 A71-35962

White dwarf and neutron stars magnetic field generation, noting system in metastable Lofar state

18 p2963 A71-36242

Scorpius X-1 cocoon pulsar thermal X ray emission model, describing hot gaseous region around rotating neutron star

18 p2969 A71-37043

Temperature limit determination of rotating neutron stars based on heat dissipation due to slowing by frictional forces, noting Crab and Vela pulsars

19 p3131 A71-37337

Neutron star models based on Nemeth-Sprung equation of state, discussing dynamic stability and Crab pulsar central density

19 p3143 A71-38161

Crab Nebula optical pulse timing, noting neutron star crust rotation speedup and relaxation, eccentric planetary orbits and sinusoidal effects

20 p3302 A71-39928

Neutron star models, discussing crystalline crust, particle superfluid properties, rotational vortices and relation to Crab Nebula pulsar

20 p3304 A71-39944

Nuclear forces effects on maximum mass limit of neutron stars models using V gamma type potentials

20 p3304 A71-39945

Multiple pulsar ejection in supernova core collapse and neutron star formation energy loss

20 p3305 A71-39947

Crab Nebula pulsar magnetosphere, considering model of rotating magnetized neutron star rate of energy generation and rotation law exponent

20 p3305 A71-39948

Relativistic and Newtonian neutron star models with nuclear forces in equation of state, using unitary transformations for hard core and soft core potential

21 p3442 A71-40143

Pulsars radio wave emission characteristics, intensity variation, duration, bandwidth, similarity to space radio beacons and evidence as neutron stars

21 p3442 A71-40144

Static magnetic fields configurations of magnetic and rotating neutron stars, considering general relativistic effects

21 p3450 A71-40714

Neutron star matter equation of state and models from energy computations, discussing maximum stable mass

21 p3452 A71-41034

Period-age distribution of pulsars, using radio and optically emitting neutron star model

22 p3599 A71-41925

Low gravity field phenomena, discussing vertical jump on moon, ball trajectories launched from asteroid and voyage to neutron star

22 p3600 A71-41983

Pulsar radio emission from expanding charge sheets moving relativistically along dipolar magnetic field near neutron star polar caps, calculating energy distribution

22 p3604 A71-42336

Pulsar characteristics suppression in neutron stars of binary systems, discussing matter accretion relationship to X ray source evolution

22 p3606 A71-42617

Pulsar speedup due to neutron starquakes, deriving self gravitating elastic incompressible sphere model for time prediction

23 p3722 A71-42894

Neutron star limiting mass based on soft hadron matter resistance to gravitational collapse in stellar structural stability consideration

23 p3732 A71-43073

NEUTRON TRANSMUTATION

U NUCLEAR REACTIONS

NEUTRONS

NT FAST NEUTRONS

NT THERMAL NEUTRONS

German monograph on application of measurement principle for determination of energy of high energy neutrons in lower atmosphere

03 p0481 A71-14368

Eddington theory validity based on formulas connecting light velocity, Planck and gravitational constants and electron, proton and neutron masses

04 p0626 A71-15136

Production and annealing of defects in lithium diffused bulk silicon after irradiation with 30 MeV electrons and fission neutrons at 300 K

05 p0703 A71-16091

Neutron and gamma ray production by nuclear interactions in solar flares

06 p0961 A71-18175

Interplanetary space cosmic ray currents global survey based on neutron component measurements, noting anisotropic diffusion, inhomogeneous solar wind and Forbush effect shell model

08 p1351 A71-20966

Neutron transport equation in five dimensional tensor form, applying finite differencing by integration method via use of divergence theorem

11 p1791 A71-25741

Spherically symmetric radiative transfer problems, constructing model with neutron transport theory [ALAA PAPER 71-466]

11 p1859 A71-26247

Solar coronal heating homopolar generator model, proposing neutrons as energy source

12 p1961 A71-26877

Atmospheric neutron production by cosmic radiation over sunspot cycle, measuring energy spectrum with airplanes and balloon-borne instruments

12 p1950 A71-27382

High energy sea level cosmic ray neutrons energy spectra, noting angular distribution about zenith and attenuation length in atmosphere

13 p2120 A71-28050

Human tissues neutron induced physical doses calculation

13 p2021 A71-29260

Proposed model with neutrons as energy source for solar corona, discussing validity based on capture gamma ray flux expectation

19 p3127 A71-38009

Atmospheric neutron production by cosmic rays, calculating cadmium-indium ratio

19 p3066 A71-38379

Rapid neutron capture products evidence on peculiar A star surfaces from observation of promethium and heaviest elements abundance

24 p3865 A71-44567

NEW JERSEY

Aircraft smoke emission control, outlining legal action by New Jersey State Department of Health

08 p1380 A71-21833

NEW ZEALAND

Ionospheric drifts at 64-108 km at Birdlings Flat, New Zealand, comparing with meteor wind measurements, chemical release trails and general circulation models

09 p1440 A71-23631

NEWTON SECOND LAW

Falling body problem solution, considering curvilinear motion effects of earth rotation axis

15 p2450 A71-32039

NEWTON THEORY

Nonaffine similarity laws and transformations subject to limitations of Newtonian impact theory for two dimensional bodies, obtaining aerodynamic coefficients

01 p0002 A71-10948

Motion stability of double-gyro inertial frame in Newtonian central force field, applying Liapunov and Chetaev methods

02 p0253 A71-12638

Gyroscopic and physical pendulum stability with gimbal suspension centers moving in Newtonian central force field, using Raus method

02 p0254 A71-12639

Energy relations in physical space of general relativity theory and inertia space of Newtonian classical mechanics

03 p0458 A71-13605

Gravitational field due to point mass, proving Newton space existence

03 p0458 A71-13606

Electrical polarization of vacuum around rotating magnetic Newtonian star, evaluating electrostatic potential

04 p0643 A71-14912

Newtonian gravitational system of n mass particles, noting solutions by deterministic approach analysis and Poincare theory

04 p0652 A71-15707

Schwarz differential invariant in Kepler problem, describing point motion under Newtonian force effect

05 p0811 A71-16640

Gyrostal in circular orbit in Newtonian force field, solving for optimal rotational motion stabilization

05 p0817 A71-16997

Physics laws and simplifications, discussing Newtonian mechanics, electrodynamics, relativity, atomic physics and quantum theory

07 p1163 A71-19603

Homogeneous Newtonian cosmological model, constructing ellipsoidal velocity distributions and kinetic theory

08 p1358 A71-20932

Newtonian big bang hierarchical cosmological model, considering mean mass density dependence on volume position and size dependence on cluster order

08 p1358 A71-20933

Newton inverse square law of gravitation in solar system, considering closed orbit trajectories

08 p1363 A71-21320

Gravitational field equations in classical Newtonian mechanics within framework of macroscopic gravitation theory

09 p1523 A71-23074

Restricted three body problem with variable thrust particle motion in Newtonian field

10 p1672 A71-24337

Newtonian gravitational system n body problem infinite time approach, obtaining spatial distribution of star clusters

11 p1819 A71-25208

Earth atmospheric zonal circulation model, using hydrothermodynamic equations with Newton law for radiative heat sources

11 p1795 A71-25919

Newtonian limit of hypersonic flow over elliptic cylinder, finding standoff distance by Freeman result

12 p1863 A71-27055

Newton gravitation theory, showing extension by relativistic mass and vector gravitation potential addition

14 p2305 A71-29682

Particle motion in combined gravitational field of monopole and prolate quadrupole, deriving exact solution in Newtonian mechanics and general relativity

16 p2609 A71-33256

Nonstatic model of universe based on Newtonian cosmology, considering central body effects on interstellar dust motion

17 p2809 A71-35600

Gyrostal in circular orbit in Newtonian force field, solving for optimal rotational motion stabilization

18 p2976 A71-36797

Small bodies collisions in solar system, using Newtonian mechanics to indicate formation of meteor and asteroid streams

18 p2967 A71-36923

German monograph on static fields in general relativity theory covering covariant equilibrium conditions, two body problems, vacuum fields and Newtonian gravity principles

20 p3269 A71-39077

Earth atmospheric zonal circulation model, using hydrothermodynamic equations with Newton law for radiative heat sources

20 p3256 A71-39210

Relativistic and Newtonian neutron star models with nuclear forces in equation of state, using unitary transformations for hard core and soft core potential

21 p3442 A71-40143

Relativistic equation derivation for dynamics of point with varying rest mass from Newtonian principle

21 p3415 A71-40659

Three body problem of two heavy mass particles oscillatory motion in periodic orbits on straight line under Newtonian attraction

23 p3734 A71-43241

Newtonian analog construction, examining relativistic homogeneous anisotropic models

24 p3873 A71-45110

NEWTON-BUSEMANN LAW

Shock layer pressure distribution for axisymmetric bodies moving at supersonic velocity in gas at rest, deriving nonstationary analog of Newton-Busemann formula

22 p3481 A71-42864

NEWTON-RAPHSON METHOD

Successive approximation procedure for discrete time nonlinear systems data smoothing, developing Newton method algorithm for two point boundary value problem

02 p0277 A71-12726

Newton-Raphson method application to iterative solution of atomic excitations and radiative transfer in plasma

17 p2838 A71-35554

Laminar boundary layer flow analysis from nonlinear difference equations solution by Newton method, using block-tridiagonal factorization

18 p2905 A71-36313

Sound attenuation in lined duct, using Newton-Raphson method for complex roots of equations

18 p2947 A71-36499

Modified Newton-Raphson stiffness matrices and initial value formulations to geometrically nonlinear structural analysis for beam and plane stress triangular elements

20 p3311 A71-39870

Numerical analysis of steady state creep of simply supported circular cylindrical shells by combined Newton and finite difference methods

21 p3463 A71-40752

Spiral grooved thrust and spherical gas bearings, predicting stability and frequency response by Newton-Raphson and orthonormalization methods

22 p3551 A71-41668

NEWTONIAN FLUIDS

Three dimensional nonboundary layer laminar radially inward incompressible Newtonian fluid flow between corotating disks, using integral method [ASME PAPER 70-WA/FE-4]

03 p0402 A71-14126

Incompressible Newtonian fluid laminar flow between two surfaces of revolution rotating at various velocities about common axis

04 p0570 A71-15176

Velocity profiles of steady axial flow of homogeneous incompressible Newtonian liquid between infinitely long parallel eccentric circular cylinders

05 p0735 A71-16611

Lubricating oil thin films interfacial Newtonian fluid elastohydrodynamics, studying transient effects on contact load damping parameters

10 p1614 A71-23981

Nonlinear hydrodynamic stability of incompressible Newtonian fluid, comparing linear and energy theories

16 p2558 A71-33005

Soviet monograph on vibration method for fluid viscosity measurement covering Newtonian fluids, low and high frequency viscometers, materials coefficients, temperature and pressure factors, etc

20 p3234 A71-39146

Oscillatory modes of perturbation in onset of flow instability for Newtonian liquid between concentric rotating cylinders with transverse pressure gradient

20 p3212 A71-39484

Book on turbulence covering measurement techniques, equations of motion, Newtonian viscous fluids, Reynolds stresses, flow visualization, random processes, turbulent energy, boundary layers, etc

21 p3371 A71-41248

Plane Couette flow temperature and velocity fields for Newtonian fluid with temperature dependent viscosity under locally and temporally constant wall temperature

22 p3620 A71-41881

Flow instability due to viscosity variation in high pressure two dimensional laminar flow of Newtonian fluid between rigid parallel plates

24 p3819 A71-44945

NICHROME [TRADEMARK]

Dispersed alumina inclusions strengthening effect during nichrome alloy sintering

08 p1305 A71-21060

Nichrome powder microstructure characteristics effect on hot compaction kinetics, considering temperature, pressure and preliminary heat treatment effects

19 p3075 A71-37108

Nichrome matrix composites with W and Mo reinforcements

24 p3837 A71-44727

Heat resistant Nichrome composite alloy with tungsten filament reinforcement, discussing manufacture and mechanical properties at 1100 C

24 p3837 A71-44730

NICKEL

Ductile Ni deformation and fracture, examining simultaneous cyclic and monotonic strain effects

01 p0098 A71-10164

Composite Ni coatings, adding mullite crystals to enhance oxidation resistance

01 p0102 A71-10784

Polycrystalline Ni single and overlapping stacking faults production by tensile deformation in premicroyield region, noting stress concentration effects

02 p0268 A71-12888

Substructures and properties of Ni, Chromel A, Inconel 600 and TD-NiCr following explosive shock load deformation, using electron microscope

02 p0268 A71-12889

Ni aluminoboronizing process by circulation method, discussing thermodynamic analysis for saturation possibility and parameters experimental determination

03 p0432 A71-13961

Ni coated carbon fibers tensile properties, examining thickness, stress-strain curve, plasticity and grain size

03 p0448 A71-14185

Water impact erosion on stainless steel, Ni and Al and Ti alloys, observing impact velocity relationship with number

03 p0444 A71-14287

Liquid Fe, Co and Ni atomic distributions investigation by X ray diffraction

04 p0612 A71-15036

Powdered Ni-carbide composites compressibility, noting mixture and pressure effects on compact density

05 p0769 A71-16859

Reinforced Ni-based composites, discussing barrier coating for tungsten fibers

05 p0769 A71-16860

Ni and Ti cutting, examining wear for various microcutter refractory materials

05 p0759 A71-16862

Highly ionized line spectra of Fe, Co, Ni and Cu belonging to Na I and Mg I isoelectronic sequences

05 p0717 A71-16909

Cu and Ni electrodeless deposition on carbon fibers for composites

05 p0759 A71-16927

Proton irradiation on Fe and Ni targets, measuring spallation cross sections

07 p1158 A71-19074

Tungsten boride sintering bonds with molten Ni as function of wettability low dihedral angle, discussing cermet porosity range

07 p1130 A71-19297

Hydrogen adsorption behavior on polycrystalline nickel surfaces, using electron impact desorption flash filament with gas phase and ion spectrometer and vapor deposition

07 p1055 A71-19843

Nickel ion diffusion coefficients in high purity magnesium oxide single crystals in high temperature argon atmosphere

08 p1343 A71-20664

Portevin-Le-Chatelier effect and sharp yield point in zone refined Ni, discussing internal friction and pinning effect on dislocations by hydrogen atoms at low temperatures

08 p1310 A71-21533

Electrochemical polarization effects on Ni single crystals mechanical behavior under tensile deformation

08 p1310 A71-21539

Pure vs dispersion hardened Ni plastic deformation, noting flow stress and temperature effects on work hardening

08 p1311 A71-21544

Oscilloscopic determination conditions for Co, Ni, and Fe, giving statistical treatment of results

09 p1454 A71-22501

Ni plastic properties and creep measurement under deformation by tension at room temperature, noting effect of impurities content

09 p1473 A71-23231

Condensed state Ni and Pd atoms X ray emission spectra and electron structure

09 p1474 A71-23233

Nickel under slow loading conditions at various temperatures, examining disorientation angles of substructure

09 p1476 A71-23317

Loading rate effect on Ni creep characteristics and substructure

09 p1477 A71-23330

Arc weld metal carbon content effects on welded joints mechanical properties in Ni at low and high temperatures, noting crack reduction

09 p1479 A71-23422

Hydrogen-nickel reaction in presence of CO adsorbed gas, increasing total desorption cross section and eliminating monotonic relation between uptake and H ion current

10 p1573 A71-24540

Alumina trichite reinforcement of nickel base matrix using magnetic alignment and sintering under low pressure below melting point [ONERA-TP-911]

11 p1777 A71-25238

Monograph on plastic behavior of iron and nickel at high strain rates and at elevated temperatures, discussing thermal effect on deformation characteristics

11 p1783 A71-26489

Hot ductility correlation with microstructure from nickel softening and fracture mechanisms interaction

13 p2089 A71-29410

Nickel under diffusion controlled reactions at high temperatures, reviewing parabolic oxidation rate law

14 p2256 A71-29634

Creep rupture strength and durability of Al, Ni and Cu irradiated by neutron flux

14 p2258 A71-30004

Recrystallization nuclei linear growth rate activation energy relationship to Ni plastic deformation magnitude, temperature and purity

15 p2429 A71-31995

Plastically deformed Ni powder specimens residual microstresses as function of applied hydrostatic pressure, using X ray diffraction measurements

15 p2429 A71-31996

Nickel sponge preparation by liquid nickel sulfide reaction with NiO under reduced pressure at various temperatures

15 p2433 A71-32178

Thermal strain hardening influence on structural changes in coarse grain Ni under creep tests during heat treatment

16 p2598 A71-33990

Aluminum effect on nickel diffusion in iron from stainless and aluminum steels study

16 p2599 A71-34053

Mechanical properties, fracture and limited high temperature oxidation resistance of carbon fiber reinforced Ni composites

16 p2599 A71-34086

Low temperature tensile prestressing effect on recrystallization kinetics of polycrystalline large grain Ni by isothermal annealing method

17 p2755 A71-34194

X ray diffraction lines diffusion of deformed Ni and Nb, attributing absence to small block dispersion

17 p2755 A71-34415

Stony, stony-iron and iron meteorites magnetic properties relating susceptibility to nickel iron content

17 p2810 A71-35720

Vacuum-melted low-carbon low-manganese steel, investigating Ni and Cr additions effects on recrystallization textures

19 p3079 A71-37703

Graphite solubility in Co and Ni, discussing solution energies and entropies

19 p3081 A71-37723

Al, Cu and Ni high temperature creep noting diffusive, shear and dislocation deformation mechanisms

19 p3083 A71-38525

Book on engineering properties of Ni and Ni alloys covering Ni-Cr alloys, Ni-base superalloys, Cu-base Ni alloys, conversion factors, etc

20 p3251 A71-39199

Lattice and grain boundary diffusion of Ce and Nd in Ni using radioactive tracer sectioning technique

21 p3398 A71-40468

Oriental magnet-optic effect in nickel and ferrosilicon monocrystals, discussing anisotropy influence on frequency dependence

21 p3431 A71-41263

Vacancies production in pure Ni and V foils by bombardment with high intensity laser pulses

22 p3556 A71-41812

High purity Ni wire hardening by lucunae agglomeration during tempering, using comparative tension curves

22 p3562 A71-42245

Solar far UV Fe and Ni ion lines

23 p3723 A71-42951

Thin nickel films elastoresistance properties, examining magnetic state effects

23 p3691 A71-43361

X ray analysis of scale formation in precipitation hardened nickel, investigating thermal resistance and oxidation rates

23 p3691 A71-43520

Polycrystalline Ni preloading rate effects on dislocation structure, electrical resistance and flow stress, noting strain hardening mechanism

24 p3837 A71-44675

NICKEL ALLOYS

NT HASTELLOY [TRADEMARK]

NT INCONEL [TRADEMARK]

NT NICHROME [TRADEMARK]

NT UDIMET ALLOYS

Ni diffusion and electric transfer in Ni-Mo alloy, using isotope tracer technique

01 p0097 A71-10043

Ni base superalloys fatigue strength improvement for gas turbine engine components, discussing homogeneous deformation distribution, grain size control, etc

01 p0099 A71-10166

Fe-Ni martensite crystals microstructure, using Kossel method and electron microscopes

01 p0106 A71-10278

Intermetallic Ni-Al volume fraction dependent deformation of single crystals of binary Ni-Al system, using X ray and transmission electron microscopy

01 p0102 A71-10740

Microstructure and mechanical properties of weldable heat resistant Ni alloy containing carbon and boron

01 p0103 A71-11068

Ni and Fe alloys for tooling materials, examining die life and wear at elevated temperatures

01 p0090 A71-11266

Cu-Ni-Mn alloys hardening by heat treatment, describing various critical temperature measurement methods and micrographic analysis

01 p0105 A71-11622

Combined vacuum furnace brazing with diffusion welding for joining high strength Ni base superalloys

02 p0255 A71-11708

Ni-Al-Ti alloys strength, investigating matrix precipitate lattice parameter mismatch effects
02 p0263 A71-11865

Fe-Ni-Mo alloys managing process kinetics at various temperatures, measuring hardness, electrical resistance and lattice constants
02 p0266 A71-12653

Ni base superalloy single crystal fatigue crack propagation
02 p0268 A71-12886

Substructures and properties of Ni, Chromel A, Inconel 600 and TD-NiCr following explosive shock load deformation, using electron microscope
02 p0268 A71-12889

Solidified Ni-Mo-Al gas turbine guide vane alloy with improved melting point, creep rupture strength and structural stability
03 p0431 A71-13256

Solute core redistribution and dendritic refinement in highly undercooled Fe-Ni alloy, using metallographic and electron microprobe analyses
03 p0442 A71-13365

Ni-Ti system electrocatalysts for fuel cell and accumulator electrodes
03 p0355 A71-14318

Ni-Fe-Cr alloys microduplex structure, describing mechanical properties and workability
03 p0447 A71-14499

Presulfidized Ni alloys and Cr oxidation rates
04 p0615 A71-15787

Damage and fracture mechanisms in high temperature low cycle fatigue of cast nickel-based superalloys, noting grain boundaries oxidation role in crack nucleation and propagation
04 p0615 A71-15789

Volume diffusion role in Ni-Cr eutectic and cast alloys cellular structure growth
04 p0615 A71-15793

Age hardened Ni base material strain-age cracking phenomenon measurements, using constant strain Gleeble technique
04 p0617 A71-15912

Ti and Ni base high temperature alloys welded joints efficiency, discussing fatigue, storage, long time heat and corrosion tests
05 p0765 A71-16172

Pure Fe and Fe-Ni alloys thermal stress component temperature dependence measurement, investigating Ni addition effect on alloy softening
05 p0765 A71-16188

Nickel alloy tensile tests, investigating strain mechanisms dependence on temperature
05 p0765 A71-16189

Ni-Fe alloy films composition gradients produced by W boats evaporation, noting vapor pressures effect
05 p0791 A71-16230

Gas turbine engine Ni alloys heat resistance, examining fatigue life and creep properties at various temperatures and test durations
05 p0767 A71-16754

Fe-Ni alloy oxidations parabolic kinetics and activation energies, noting scale development as function of oxidation amount and temperature
05 p0770 A71-17098

High temperature creep comparison of single phase Fe and Ni alloys subjected to constant load tensile tests, measuring strain as function of time
06 p0911 A71-17345

Ni alloy corrosion tests, evaluating sensitization susceptibility and intergranular attack
06 p0911 A71-17414

Thoria dispersed Ni-Cr alloy hypersonic entry ablation model, accounting for Cr oxidation
[AIAA PAPER 71-34] 06 p1009 A71-18654

Stress rupture properties at elevated temperature of nickel base superalloys with varying Ti and Al additions, investigating microstructural and age hardening effects
06 p0913 A71-18676

Scanning electron microscopy for microstructures of various eutectic Ni alloys, discussing rod-plate transition
06 p0914 A71-18681

Uniaxial stress effect on morphology changes of coherent gamma prime precipitates in nickel base superalloy crystals
06 p0914 A71-18682

Ni-W eutectic alloy unidirectional solidification to obtain composite structure in Ni-W solid solution
06 p0915 A71-18689

Industrial Ni alloys and steels fatigue life by short time data extrapolation
07 p1129 A71-19152

Ni-transition element ternary alloys with bcc and fcc lattices, examining electron structure and ordering processes
07 p1163 A71-19429

TiNi antiphase boundaries direct observation using transmission electron dark field imaging technique
07 p1131 A71-19431

Kinetics of transformation to long range ordering in Ni-V as function of heat treatment
07 p1131 A71-19433

Ni-Mn, Ni-Fe and Ni-Fe-Al alloys yield behavior and microstructure as result of ordering and disordering treatments, using center annealing technique
07 p1132 A71-19434

NiMo alloy fcc disordered structure and mechanical properties correlation to domain size and orientations from thin film transmission electron microscopy
07 p1132 A71-19435

Nickel molybdenide disorder to order early transition mechanism diffraction model, using transmission electron and field ion microscopy studies
07 p1132 A71-19436

Thin nickel aluminide sheets and small particles long range ordering, discussing antiphase boundary energy effects
07 p1133 A71-19441

Mechanical properties of supersaturated Ni-Al alloys aged at 700 F, discussing composition effects on single crystals deformation and polycrystal strength variation
07 p1133 A71-19442

Ni base superalloys mechanical properties relationship to microstructure, considering precipitate dispersion and phase state effects on flow stress and creep strength
07 p1133 A71-19445

High temperature creep behavior of nickel base alloys with L12 and B2 type lattices, discussing single crystals of beta-NiAl
07 p1133 A71-19446

Ni base superalloys fatigue behavior, emphasizing role of ordered gamma prime precipitate in two phase materials
07 p1133 A71-19447

Oxidation resistant Ni-Al intermetallic compounds as protective coating for high temperature nickel base superalloys
07 p1134 A71-19448

Mechanical and plastic properties of Ni-Mo alloys subjected to hot working, determining tensile strength as function of test temperature
07 p1136 A71-19635

Hot working cast nickel based alloy for thin gage sheet, noting electroslog remelting increased temperature range
07 p1136 A71-19664

Interstitial solid solution hardening in pure Ni and Ni-C alloys, noting mechanism and C concentration effects
07 p1138 A71-19980

Aging effect on tensile mechanical properties and hardness of high purity binary Ni-Cr alloys at 290-530 C
07 p1138 A71-19986

Stress annealed Ni-base superalloy crystals, investigating orientation and applied uniaxial stress sense effect on coherent gamma prime precipitates morphology
07 p1138 A71-19987

Elastic modulus as function of chemical composition and structure of binary alloys Mo-Re and Ni-Re
07 p1141 A71-20248

Ni-Ti alloy structural modulation during aging, examining effect on yield stress by X ray diffraction and tensile tests
07 p1143 A71-20494

Microstructure and mechanical properties of weldable heat resistant Ni alloy containing carbon and boron
08 p1305 A71-21035

Stoichiometric NiAl single crystals plastic deformation study by transmission electron microscopy, determining dislocations by image matching technique
08 p1308 A71-21511

Ordered states effects on mechanical properties of Va-Co-Ni ternary alloys, considering creep behavior difference between ordered and disordered structures
08 p1309 A71-21526

Ti effects on Ni-Mo-Cr alloy strengthening, correlating microstructures and mechanical properties
08 p1311 A71-21542

Ni-Cr thoria dispersion strengthened alloys, determining texture effects on high temperature mechanical properties
08 p1311 A71-21545

Co-Ni-Cr-Mo alloys hardening mechanisms, noting martensitic transformation role
08 p1312 A71-21551

Ni superalloys plane front cast structure through controlled unidirectional solidification, discussing improved mechanical properties
08 p1314 A71-21567

Ni superalloys strengthening by body centered tetragonal gamma double prime phase precipitation, investigating various alloying components and ratios
08 p1314 A71-21568

Precipitation hardened Ni base superalloys fatigue deformation, investigating correlation between metallurgical structure characteristics and high-cycle fatigue behavior
08 p1314 A71-21570

Stoichiometric beta NiAl alloy high temperature creep behavior, presenting electron microscopic observations of deformed single crystals dislocation structures
08 p1314 A71-21571

Ni-Cr-Al alloys high temperature oxidation resistance, studying effects of Cr/Al ratio and chemical composition
08 p1315 A71-21574

Matrix stacking fault energy effects on steady state creep rate of recrystallized nickel-cobalt-aluminum oxide alloys, showing stress dependence
08 p1315 A71-21578

Gamma prime precipitate effects on flow stresses of Ni alloys single crystals at various strain rates and elevated temperatures
08 p1315 A71-21580

Stacking fault formation and mechanical twinning in Ni base superalloy during tensile deformation at high temperature
08 p1315 A71-21581

Deformation modes with associated structural defects for slip, viscous slip and climb processes in gamma prime precipitation hardened nickel based alloys
08 p1315 A71-21583

Solidification process for unidirectionally cast airfoil shaped turbine components from Ni superalloys, discussing mold withdrawal
08 p1299 A71-21682

Plasma arc welding of jet engine components of Ti and Ni alloys, comparing to gas tungsten arc and electron beam processes
08 p1299 A71-21684

Composition, microstructure, heat treatment and properties of Ni alloy with high rupture strength and hot corrosion resistance for turbine blade applications
08 p1299 A71-21687

Heat resistant Ni alloys intermetallic gamma prime phase analysis by electrolytic separation
09 p1467 A71-22322

Thermal fatigue tests of high temperature Ni and Co base alloys by fluidized bed technique
09 p1469 A71-22812

High chromium Ni-Cr alloys use and improvement, discussing refractoriness in oxidizing atmospheres and chemical corrosion in combustion products deposits
09 p1470 A71-23043

High temperature precipitation hardening of Ni-Cr alloys, discussing effect on creep rupture strength
09 p1470 A71-23044

Ni-Mo alloys electron transfer and ion diffusion at high temperatures
09 p1471 A71-23077

Al and Fe additions effect on transitional phases formation and metastable phase precipitation in Ni-Nb system, using transmission electron microscopy
09 p1471 A71-23124

Fe-Ni alloys, determining hydrogen permeability, diffusion coefficient and solubility as function of composition by electrochemical method
09 p1472 A71-23127

Directionally solidified Ni base superalloys, determining stress and temperature effect on primary creep strain
09 p1472 A71-23130

Martensitic transformation in NiAl oxidation-resistant coatings on Ni superalloys heated for 300 hr at 1093 C
09 p1472 A71-23132

High temperature Ni alloys structural stability, computing gamma prime phase coagulation and average electron vacancy number
09 p1474 A71-23289

Dispersion hardened Ni and Co alloys production by powder metallurgy, noting elastic distortion due to particle strengthened base material
09 p1474 A71-23294

High temperature austenitic steels, Ni and Co alloys machining, considering deformation resistance and strain hardening
09 p1456 A71-23297

High temperature Fe, Co and Ni alloys for gas turbine components, considering tensile and creep rupture strength increase by thermal mechanical processing
09 p1475 A71-23298

High temperature Ni and Co alloys powder metallurgy, discussing production, preparation, pressing and sintering
09 p1456 A71-23300

High temperature Ni and Co alloys for stationary gas turbines and jet engine parts, considering microstructure and mechanical behavior under stress and temperature
09 p1475 A71-23302

Steels, Ni alloys and Ti alloys deformation resistance and deformability, discussing temperature effects on forging rate
09 p1475 A71-23305

Ni-Co strained alloy, examining coercive force as function of annealing time at various temperatures
09 p1475 A71-23313

Ni-Al alloy strain hardening, observing high intensity ultrasonic irradiation effect on high temperature creep
09 p1475 A71-23315

Prediction of metals heat resistance increase by thermomechanical treatment, considering Ni-Al alloy
09 p1477 A71-23332

Ni-Cr alloys hardened by Nb and Ta, examining precipitation and plastic deformation mechanisms 09 p1479 A71-23622

Co-Cr and Ni-Cr eutectic alloys with single crystal TaC fiber reinforcement, discussing unidirectional solidification 09 p1479 A71-23623

Hot deformation of superrefractory austenitic Ni alloy, considering elastic and plastic limits 09 p1479 A71-23625

Intracrystal liquefaction in Al alloys containing Nb studied with microanalyser 09 p1480 A71-23702

Fine structure and heat resistance of thin Ni-Cr alloys specimens after prolonged exposure to high temperatures under tensile loads 09 p1480 A71-23703

Oxidation resistant high temperature Ni-Al system preparation using powder metallurgy and thermomechanical treatments without sintering 10 p1626 A71-24401

Ni-Cr-Ti-Al-Mo system equilibrium conditions, conducting phase analysis by X ray and optical and electron microscopy 10 p1627 A71-24532

German monograph on absorbed anions effect on Ni and Ni-Mo alloys anodic behavior covering temperature dependence, electrons interaction, sulfide ions activation and magnetic properties 10 p1628 A71-24874

Crystallographic relationships between Ni- and Cr-rich solid solutions, noting preferred interphase interfaces in Ni-Cr eutectic alloy 11 p1778 A71-25532

Spreading, wettability, diffusion and aggressive properties of nickel base brazing filler metals on stainless steels 11 p1769 A71-25750

Ni-based superalloy stress cycle frequency effect on elevated temperature fatigue life 11 p1779 A71-26012

TD NiC nickel based alloy high temperature oxidation control, discussing thoria dispersion effect on Ni-Cr oxidation properties 11 p1779 A71-26015

Refining process of Fe-Ni-Cu-Mn alloys, discussing aging kinetics, hardening mechanism and strength properties 11 p1781 A71-26159

Strain rate and temperature effects on flow stress of Ni-Al in polycrystalline and single crystal for activation energies and deformation volumes evaluation 11 p1782 A71-26440

Al-Ni alloys rapidly quenched from melt, determining solid solutions mechanical and microstructural properties 12 p1916 A71-26893

Predeformation effects on metastable Ni base Ti alloys precipitation aging at extrinsic stacking faults, using thin foil microscopy 12 p1916 A71-26894

Nb and Mo doped Ni-Al alloy with Ni-Nb additions, obtaining diagrams of composition versus heat resistance in high temperature bending tests 12 p1916 A71-26968

Long term aged heat resistant Ni base alloys, investigating gamma prime phase chemical composition 12 p1917 A71-27298

Nickel alloys crystallization at superhigh cooling rates by dropping liquid metals on rotating copper cylinders to obtain films 12 p1917 A71-27301

Ni-base alloys hardened by gamma prime precipitation, investigating embrittlement by oxygen [ASME PAPER 71-MET-D] 12 p1917 A71-27313

Addition effects on ordering kinetics in Ni-Mn based ternary alloys, using Rawar neutronography 12 p1918 A71-27543

Ni-Cr and Ni-W alloys high temperature strength properties, considering stacking fault energy, diffusion velocity, Young modulus and dislocation locking 12 p1919 A71-27762

Composite heat resistant Ni alloy production using refractory oxide phase dispersion hardening 13 p2083 A71-27893

Fast neutron irradiation effect on Ni-Cr alloy electrical resistivity as function of temperature and initial composition 13 p2083 A71-27964

Heat resisting Ni base alloy stress rupture strength and fatigue life, observing corrosive high temperature environment effect 13 p2084 A71-28111

High strength corrosion resistant multiphase Co-Ni-Cr-Mo alloys with fcc structure hardened to hcp by mechanical deformation 13 p2084 A71-28148

Elastic stresses during local deformation in Nb-Mo, Ni-Cr, Cu-Al and pure bcc metals, using X ray analysis 13 p2085 A71-28225

Sintering time effect on initial permeability of Ni-Fe-Cu-Mo alloy made by powder metallurgy 13 p2086 A71-28626

Postweld heat treatment cracking of high Ni alloys using mechanical testing and metallography 13 p2087 A71-29092

Oxidation and nitrogen absorption protection of Cr alloy by Ni alloy claddings applied by gas pressure bonding 13 p2087 A71-29122

Ni-Pd alloys atomic arrangements and displacements by single crystal X ray diffuse scattering, using computer simulated model 13 p2087 A71-29134

Cold rolled recrystallized Ni-Fe alloy, considering short range order structure effect on elastic limit 13 p2087 A71-29264

Ni-Ni Nb eutectic composite, investigating monotonic mechanical response, deformation and fracture mechanisms 13 p2088 A71-29401

Stage I fatigue fracture mechanism in Ni-based superalloy single crystals, observing air and vacuum effects 13 p2088 A71-29405

Gamma phase composition estimation in Ni base superalloys by phase rule principles and analytic geometry 13 p2089 A71-29407

Particle-metal matrix interface strength of dispersion strengthened Ni alloys, developing direct tensile stress measurement method 13 p2089 A71-29408

Aging behavior of Nb-containing Fe-Ni alloys, considering austenite and martensite in twinned and massive form 13 p2089 A71-29412

Vacuum melted Ni base superalloys, determining Mo and hardener effects on gamma prime solvus temperature and solutioning rate 13 p2090 A71-29418

High strength Ni base superalloy workability, investigating microstructure relation to mechanical properties 13 p2090 A71-29419

Impact strength of Cu, Cu-Ni alloy and superalloy matrices reinforced with W fibers, studying temperature, heat treatment and fiber content and toughness effects 14 p2258 A71-29919

Discontinuous phase decomposition increase in Co-Ni-Ti alloys by plastic deformation and Al additions, indicating grain boundary diffusion control 14 p2258 A71-30003

Potentiometric measurement of temperature effects on electrical resistance and Hall effect in Ni-Co alloys 14 p2259 A71-30188

Nickel alloys susceptibility to pores formation in tungsten inert gas welding in argon-nitrogen mixture, considering influence of Cr, Mo and W 14 p2260 A71-30487

Nitrogen solubility in Ni-Mo and Ni-W melts, detailing Ti and pressure effects 15 p2424 A71-31392

Fe-Ni alloys with Cr, investigating heat treatment effect on thermoelastic coefficient 15 p2426 A71-31482

Ni-Co alloys electrical resistivity dependence on temperature after mechanical and thermal treatments 15 p2429 A71-31994

Nickel and cobalt pseudobinary eutectic alloys reinforced by refractory metal monocarbides whiskers, studying mechanical properties, solidification and phase equilibria 15 p2432 A71-32169

Tensile stress and compressive effects on grain boundary precipitate morphology in Ni-base superalloy during creep 15 p2433 A71-32179

Precipitation hardenable Ni-base alloys embrittlement in high temperature oxygen atmosphere, considering intergranular crack initiation 15 p2434 A71-32257

Ni-base alloys machining, discussing special tools and manufacturing methods with special reference to machinability of Inconel 718, Rene 41 and 95 [SME PAPER MR-71-825] 15 p2416 A71-32427

Sigma phase intergranular precipitation in low carbon Ni-Co-Cr-Mo alloys, noting temperature effect on morphology 15 p2436 A71-32546

Oxidation kinetics and scale morphology of chromium oxide forming thoriated and unthoriated Ni alloys, discussing rate controlling processes effects 16 p2590 A71-32871

Single crystal Ni-base superalloy anisotropic hollow cylinder creep under biaxial loading, studying rate dependence on crystallographic axis orientation and stresses ratio 16 p2591 A71-33222

Phase diagrams of ternary systems Ta-Fe-B and Ta-Ni-B using X ray and metallographic analyses 16 p2592 A71-33575

Mechanical and plastic properties of Ni-Mo alloys subjected to hot working, determining tensile strength as function of test temperature 16 p2593 A71-33631

Heat resistant weldable dispersion hardened Ni base alloy, discussing intermetallic phase hardening 16 p2594 A71-33715

Equiaxial TiNi martensite crystal structure and internal defects investigation by electron microscopy and electron and X ray diffractions 16 p2598 A71-34045

Composition transformations at interface levels in iron-nickel alloys as function of thermal treatment, using potentiokinetic method 16 p2598 A71-34050

Recrystallization of heat treated Fe-Ni alloys microstructures after hammer hardening 16 p2598 A71-34051

Electrodeposited Ni-Mo coatings corrosion resistance improvement by heat treatment, showing crystal structure degree of perfection role 16 p2599 A71-34052

Randomly distributed domain structure of ordered Ni-Cr alloy, using electron microscopy and neutron diffraction 17 p2755 A71-34413

Fe-Ni-V-C alloy strengthening by cyclic martensitic phase transformation 17 p2756 A71-34487

Room temperature ultrasonic frequency fatigue behavior of Ni-base superalloy single crystals 17 p2756 A71-34493

Columnar grained Ni superalloy lifetimes and transverse creep ductilities enhancement and microstructural alterations due to HF additions 17 p2759 A71-35394

Gas turbine engine steels and Ni alloys heat resistance, examining fatigue life and creep properties at various temperatures and test durations 17 p2759 A71-35453

Industrial Ni alloys and steels rupture strength by short time data extrapolation 17 p2760 A71-35651

Cylindrical steel and Ni alloy specimens bearing strength in inhomogeneous stress states under cyclic elastoplastic bending and loading to failure 17 p2760 A71-35668

Molybdenum effect on morphology, size and square density of precipitating gamma particles in nickel alloys 18 p2934 A71-35991

Cutting speed, feed rate, tool geometry and other machining factors effects on surface finishes of face milled steels, titanium and nickel base alloys [SME PAPER MR-71-146] 18 p2927 A71-36663

Damping characteristics of Ni base refractory alloys at high temperatures, showing increase with cyclic strain amplitude 18 p2936 A71-36708

Nickel base alloy under axisymmetric tension compression tests, obtaining breaking load diagrams and fatigue and creep curves 18 p2937 A71-36716

Small holes effect on Ni base superalloy wrought thin sheets fatigue strength under pulsating tension load, analyzing crack initiation, propagation and critical length 18 p2938 A71-36850

Ni-Cr alloys sulfidation at 700 C from inert and radioactive marker techniques 18 p2938 A71-37003

Ni-Cr-Mo cermet alloys sinterability, physicomechanical properties and microstructure 19 p3075 A71-37109

Ni-Co alloy fine structure under plastic deformations, determining stacking fault energy effects with X ray diffraction lines 19 p3076 A71-37119

Single crystal Ni-Al solid solutions deformations, examining temperature and concentration dependence of critical cleavage stresses 19 p3076 A71-37120

Ni-Mo single crystals under isothermal aging, observing long range order parameter, domain size and microstrains 19 p3077 A71-37411

Precipitation strengthened Fe-Ni-base superalloy microstructure, investigating phase relationships 19 p3079 A71-37711

Carbon activity, free energy entropy and enthalpy in fcc solid solution of Fe-Ni-C alloy 19 p3080 A71-37714

Matrix stacking fault energy effect on tensile creep deformation modes in gamma prime precipitation hardened nickel-base alloys 19 p3080 A71-37721

Cavitation damage in water to unalloyed metals and Ni superalloy, using ultrasonic vibratory testing with magnetostrictive transducer 19 p3081 A71-37904

Ni-base heat resistant alloys loading frequency effect on fatigue resistance, noting linear relationship between creep strain and cycles to failure in logarithmic coordinates 19 p3082 A71-38348

Ni-Cr thin film resistors reliability, describing deposits on silicon dioxide, intermetallic formation and electromigration 19 p3034 A71-38515

Book on engineering properties of Ni and Ni alloys covering Ni-Cr alloys, Ni-base superalloys, Cu-base Ni alloys, conversion factors, etc

20 p3251 A71-39199

Optical constants of beta-phase NiIn, PdAl and nickel gallium aluminide, noting chemical composition and electron density effects on photon energy absorption

21 p3426 A71-40033

Composite heat resistant Ni alloy production using refractory oxide phase dispersion hardening

21 p3396 A71-40084

Intermetallic compound Ti-Ni phase transformations, relating martensite crystal structure with pre-martensitic instability

21 p3397 A71-40433

Crystallographic habit plane and martensite plate orientation in Fe-Ni and Fe-Ni-C dilute alloys

21 p3397 A71-40452

Retained lattice strain and substructure domain size effects on tensile strength at room and elevated temperature in dispersion strengthened Ni alloys

21 p3397 A71-40453

Epitaxial metal film formation on Al-Ni fibers in Al matrix during electropolishing

21 p3387 A71-40456

Ti-Ni alloy martensitic thermoelastic transformation and memory effect, using optical microscopy to examine change in lattice discontinuity

21 p3398 A71-40459

Ni-Cu alloy castings solidification experiments on catalytically clean metals to avoid heterogeneous nucleation

21 p3387 A71-40460

Solid Ni-Co and Ni-Cu alloys, investigating hydrogen nobility

21 p3398 A71-40466

Aluminum-aluminum nickelide rod eutectic composite elevated temperature stability, presenting coarsening kinetic analysis

21 p3398 A71-40469

Co-Ni alloy interdiffusion coefficient determination as function of concentration by magnetic transformation effect

21 p3399 A71-40700

Alloying effects on corrosion cracking of Cr-Ni austenitic stainless steels, testing in chloride solutions

21 p3402 A71-41094

Microstructural characteristics of Fe-Ni alloy plastic deformation at 20-500 C during cold and hot rolling, noting intergranular shear processes

21 p3402 A71-41095

Ni and Ni-base alloys gaseous carburization by circulation method, investigating gas flow velocity effect on metal diffusive saturation

21 p3389 A71-41165

Cr diffusion into Ni-Cr alloys in presence of carburized layer, noting increased diffusive mobility

21 p3390 A71-41167

Si addition effect on Ni-Cr alloy carburized layer depth, microhardness, phase structure, chemical composition and scaling resistance

21 p3390 A71-41168

Vacuum contactless metallization of carbon steels, stainless steels and nickel alloys, considering Si, Cr and Al coatings

21 p3390 A71-41172

Metallography of 700 C precipitation hardening in Fe-Ni alloy containing Be, using transmission electron microscopy

21 p3404 A71-41417

Intergranular corrosion of chromium carbide sensitized Ni base alloys, noting surface effect during solution heat treatment

22 p3560 A71-41626

Heat resistant Ni alloys hot strength level and temperature dependence as function of gamma-prime-phase particle size, discussing aging effect on creep rate

22 p3561 A71-41841

Thermoelastic coefficient development by tempering for Ni-Fe alloy containing Be

22 p3563 A71-42325

High temperature Ti-Ni alloy stacking variation stability, studying size, shear and valence electron concentration effects

22 p3586 A71-42367

Isothermal martensite transformations in Fe-Ni-Cr alloys, explaining kinetics difference in terms of elastic parameters small variations

23 p3688 A71-42925

Al-Co and Al-Ni alloy rods unidirectionally solidified, discussing compositional range in eutectic structures at high solidification rates

23 p3689 A71-43101

Nickel-chromium system powders physicochemical properties, noting use as high temperature cermet packing materials

23 p3690 A71-43256

Ni-based alloy strength characteristics dependence on heat treatment during melting and casting in vacuum and in air

23 p3691 A71-43425

Sintering of Ni based heat resistant alloy, determining phase composition, lattice constant and microhardness of compressed specimens

23 p3691 A71-43521

Heat treatment specifications selection for Ni alloy by mathematical method based on cylindrical specimens elongation under tensile loads

23 p3691 A71-43523

Cavitation damage resistance of Fe, Ni and Co alloys in liquid sodium and mercury

23 p3692 A71-43906

Electron microscopic study of antiphase domains size and shape in Ni-Mn alloy after annealing

23 p3692 A71-44009

Heat resistant Ni-base composite stiffened with W wires, investigating interaction between alloy and fibers from metallographic and X ray diffraction microscopy data

23 p3693 A71-44214

Strain hardening effect of Ni, Mn and Mo in Cr steel after high temperature annealing

23 p3693 A71-44216

Ni-Cr single crystals plastic deformation, presenting work hardening characteristics and critical resolved shear stress

23 p3694 A71-44278

Near equiatomic TiNi thermal martensite transformation premonitory events, discussing crystal structure, mechanical instability and lattice vibrations

23 p3694 A71-44280

Sodium role in accelerated oxidation behavior / sulfidation/ of Ni-base superalloys and binary alloys coated with sodium sulfate or carbonate

23 p3695 A71-44288

Ni-Co maraging steels with improved combination of mechanical and magnetic properties at elevated temperatures

24 p3836 A71-44441

Cr-Ni alloy heat treated cast specimens microstructure, metallographic, X ray and spectral investigation, noting chemical inhomogeneity

24 p3836 A71-44484

Aluminized layer phase and chemical composition of heat resistant iron and nickel alloys

24 p3837 A71-44732

Ni-base superalloys metallography, investigating catastrophic cracking in weld heat affected zones by electron microscopy

24 p3839 A71-45139

Hydrogen solubility in liquid Cr, Ni and Co alloys containing Si for various concentrations and temperatures

24 p3840 A71-45371

Ni-Zr alloy crystallization at large cooling rates obtained by melt droplets blowing with compressed He jet onto rotating Cu cylinder surface

24 p3840 A71-45374

NICKEL CADMIUM BATTERIES

Ni-Cd batteries for OAO 2 spacecraft, considering manufacturing, materials, components and tests

03 p0350 A71-13027

Chemical test method for composition analysis of Ni-Cd electrodes

03 p0374 A71-13028

Failure mechanisms and manufacturing improvement of sealed nickel cadmium batteries

14 p2181 A71-29701

High power nickel cadmium battery for geostationary communications satellites for replacement in Intelsat 4 series

18 p2852 A71-36573

NiCd battery and third electrode characteristics for different charge and discharge rates, considering end-of-charge control system optimized for satellites and manned spacecraft applications

20 p3179 A71-38904

Ni-Cd battery cell with third electrode for charge control, testing thermal and electrical performance as function of charge and discharge rate

20 p3179 A71-38905

Recoverable usable energy maximization from solar oriented spacecraft electrical power system, using silicon cell array and nickel cadmium batteries

20 p3182 A71-38956

Ni-Cd cells thermal conductivity measurements for heat balance and dissipation calculations for space vehicle power supply systems, describing experimental apparatus

20 p3184 A71-39556

NICKEL COATINGS

Oxidation resistant Ni-Al intermetallic compounds as protective coating for high temperature nickel base superalloys

07 p1134 A71-19448

Evaporated pure Ni coatings effects on carbon fiber fracture strength and microstructure at room temperature

20 p3248 A71-38815

NICKEL COMPOUNDS

NT NICKEL OXIDES

High energy long shelf life lithium-nickel sulfide batteries performance tests

03 p0351 A71-13041

Oxidation resistant Ni-Al intermetallic compounds as protective coating for high temperature nickel base superalloys

07 p1134 A71-19448

TiNi martensitic transformations-fatigue strength relation at room temperature, observing hysteresis in tensile compressive loading cycle to maximum stress

09 p1477 A71-23349

Clear taenite formation in bronzite and hypersthene chondrites studied by metallographic and electron microprobe

10 p1680 A71-24985

Nickel diffusion in intermetallic compound NiAl as function of temperature and off-stoichiometric composition, noting activation energy changes

11 p1778 A71-25562

NiGa intermetallic compound electrical transport and resistance, Hall coefficient and optical adsorption, discussing defect structure and electron scattering

14 p2260 A71-30478

Magnetostriction in cobalt and nickel-cobalt ferrites from room temperature to 300 C

15 p2426 A71-31514

NICKEL OXIDES

Gold and Aquadag contacts with single crystal nickel oxide surfaces, determining I-V characteristics

04 p0637 A71-15588

Metallic Ni trace effects on oxygen chemisorption forms on nickel oxide in various temperature regions

15 p2367 A71-31901

NICKEL PLATE

Chromium and Ni-Cr electrodeposition from amide solvent system, describing water and sulfur ligands effects on plating efficiency

22 p3554 A71-42528

NICKEL STEELS

Cr-Ni steel elastic properties under intercrystalline corrosion, examining temperature effects on internal friction, electric resistivity and vibration frequency

01 p0096 A71-10038

High strength and plasticity maraging steels of Fe-Ni-Co-Mo system, noting surface crack sensitivity in tension

01 p0103 A71-11071

Hardening effects of various Ta proportions in Fe-Ni-Ta alloys, noting austenitic nature after homogenization and quenching at high temperature

01 p0105 A71-11619

Ni maraging steel weldments stress corrosion cracking characteristics in air and pentaborane by electron microscopy

02 p0262 A71-11707

Ni maraging steel cantilever beams intergranular stress corrosion cracking in aqueous solutions, noting heat treatment effects

02 p0267 A71-12881

Intrinsic stacking fault energy temperature dependence in austenitic Fe-Cr-Ni alloys determination from dislocation mode measurements by high temperature transmission electron microscopy

07 p1138 A71-19984

Energy dissipation in heat resistant Ni steels under cyclic tension and compression at room temperature

07 p1142 A71-20479

High strength high Ni maraging steels crystal structure, alloying elements effects on mechanical properties, applications, etc

08 p1305 A71-21028

High strength and plasticity maraging steels of Fe-Ni-Co-Mo system, noting surface crack sensitivity in tension

08 p1305 A71-21036

Ni maraging steel fatigue properties in relation to Ti and Al content

08 p1312 A71-21553

Deformation-induced martensitic transformation effects on Fe-Ni-Cr-C alloy plastic behavior

08 p1313 A71-21555

Phosphorus segregation to prior austenite grain boundaries in ferrite, considering effect on Ni-Cr-C-P steel temper embrittlement

09 p1471 A71-23123

C and Ni contents effects on water quenched tempered austenitic chromium nickel-stainless steels intercrystalline corrosion

12 p1919 A71-27777

Si, Mo and Cu effects on pitting corrosion of Cr-Ni steel

13 p2082 A71-27831

Chemical composition effects on microstructure and high temperature properties of cast Cr-Ni-Al steels containing Ti, B, C and Zr

13 p2084 A71-28035

Structural evolution of Ni-Co-Mo maraging steel during martensite reversion at rapid heating, studying heating rate effect on alpha-gamma transformation

14 p2257 A71-29839

Heat treatment effect on electrochemical behavior of Ni-Co-Mo maraging steel in sulfuric acid aqueous solution, studying anodic polarization

14 p2257 A71-29840

Strengthening mechanism of Cr-Ni and Ni maraging steels related to dislocation stress field

15 p2427 A71-31524

Austenitic high nitrogen chromium-nickel steels plastic deformation and heat treatment in plasma arc furnaces 16 p2596 A71-33910

Stress corrosion cracking in Ni maraging steel in NaCl solution, using electrochemical polarization and potential analysis 18 p2934 A71-35989

Cr-Ni austenitic steels thermomechanical destabilization using cyclic strain hardening 18 p2934 A71-36173

Nickel maraging steel in NaCl solution, investigating susceptibility to stress corrosion cracking 18 p2935 A71-36595

Plastic deformation effects on austenite thermal stabilization in Fe-Ni-C alloy, considering temperature dependence 19 p3079 A71-37704

Ni-Cu-Nb age hardenable steel mechanical properties, examining hot rolling and heat treatment effects 21 p3387 A71-40455

Temperature effect on fatigue strength of Ni steel by tension-compression fatigue test at low temperatures 21 p3400 A71-40832

Ni-steels toughness improvement at cryogenic temperatures by accelerated cooling, using Charpy V-notch and static and dynamic fracture tests at 139.7-671.7 R 21 p3400 A71-40881

Strength, ductility and notch toughness research on base materials and welds of nickel maraging steel rocket motor cases 21 p3389 A71-40913

Cr and Cr-Ni ferritic and austenitic steels, investigating high temperature nitriding for intensifying nitrogen diffusion saturation 21 p3389 A71-41098

C and Ni contents effects on water quenched tempered austenitic chromium nickel-stainless steels intercrystalline corrosion 21 p3403 A71-41100

Low carbon austenitic Cr-Mn steels, noting Ni and Al combined alloying effects on structure and mechanical properties 21 p3403 A71-41101

High heat resistance of austenitic Cr-Ni-V-B steel by polygonization and recrystallization, using thermomechanical treatment 21 p3403 A71-41102

Ni-Cr-Mo-Co steel microstructures after austenitizing, quenching and tempering, correlating with mechanical properties 22 p3560 A71-41594

Crystal microstructure of strengthening precipitates in Ni maraging steel, giving electron diffraction patterns 22 p3562 A71-41949

Boron addition effects on scaling resistance of Ni-Cr steel at high temperatures 23 p3690 A71-43278

Austenitic Fe-Ni-Ti steel strengthening by precipitation hardening and subsequent aging at 600 C 23 p3690 A71-43282

Loading modes effect on stress corrosion cracking of Ni maraging steel in NaCl solution 23 p3693 A71-44074

NICKEL ZINC BATTERIES

Nickel-zinc batteries for use in hybrid heat engine/electric systems of low pollutant passenger cars, increasing service life by aerospace technology 20 p3181 A71-38936

NICOTINE

Aortic and sinus nerves afferent electric impulsion under adrenalin and nicotine, considering age peculiarities 03 p0363 A71-13522

NIGHT

Nighttime ionospheric absorption frequency dependence during solar activity cycle 07 p1100 A71-19400

Earth surface nighttime, twilight and daytime horizons visual observations by Soyuz 9 spacecraft 13 p2060 A71-28426

Electric field, atmospheric wave and other factors effects on F region storms by day and night in tables 14 p2236 A71-30941

Night rescue terminal navigation, considering design, development and tests of Limited Night Recovery System for HH-53 helicopter [AHS PREPRINT 534] 14 p2273 A71-31095

Height variations of ionospheric absorption of downgoing whistler waves during nighttime at moderate and low latitudes 15 p2369 A71-31426

Ionospheric nighttime ambient atomic oxygen concentration profiles, using nitric oxide release from sounding rockets 16 p2568 A71-33791

Nighttime ionospheric absorption frequency dependence during solar activity cycle 19 p3053 A71-37824

NIGHT AIRGLOW

U AIRGLOW
U NIGHT SKY

**NIGHT E LAYER
U E REGION
U NIGHT SKY
NIGHT F LAYER
U F REGION
U NIGHT SKY
NIGHT SKY**

Nighttime F region molecular ion concentrations of oxygen and nobelium and associated nightglow morphology, using numerical method for solving non-linear equations 01 p0078 A71-11611

Nighttime polar aurora zone during IGY and IQSY related to magnetic activity 02 p0242 A71-11759

Polar region semitransparent sporadic ionospheric layers nighttime temporal and cyclic ionization variations, determining solar activity effects and corpuscular stream densities by ionogram 02 p0243 A71-11767

Nighttime F layer true height profiles reduction from routine ionograms, discussing error corrections 03 p0408 A71-13387

Triplet O I excitation in night sky of tropical regions, using photometric measurements of line spectra 03 p0409 A71-13789

Midlatitude nighttime D region ionization source, considering precipitating energetic electrons 03 p0420 A71-14527

Nocturnal intensity and excitation temperature variation of hydroxyl vibrational rotational band in airglow 04 p0581 A71-15050

Vertical and horizontal VLF fields excited by dipoles of arbitrary orientation and elevation for nighttime ionosphere 04 p0552 A71-15216

Dawn chorus western drift and relationship to magnetic disturbances on night side 05 p0745 A71-17189

Stable midlatitude red arc in night sky south of auroral zones, reviewing observed features, ionospheric behavior and formation theories 07 p1098 A71-19322

Ring currents and polar magnetic substorms during intensive charged particle flux period in nighttime magnetosphere 07 p1101 A71-19414

Night sky H beta photometry, showing solar type spectrum at high galactic latitudes and net emission at low latitudes 08 p1350 A71-20946

Night D region ion kinetics data during thermonuclear detonation, discussing formation and conversion rates, electron concentration and recombination 08 p1278 A71-21009

Middle latitude night E region ionization, describing solar EM and corpuscular radiation absorption effects 08 p1286 A71-21853

Nighttime E layer behavior during geomagnetic storms in quiet sun years, investigating corpuscular flux effects 08 p1356 A71-21854

All-reflection optical device for stellar spectra automatic widening and concurrent night sky spectrum suppression 09 p1442 A71-22068

F 2 layer nighttime ionization at midlatitudes, investigating conjugate point effects on observation point 09 p1434 A71-22426

E region ion composition nighttime variations, examining nitrogen monoxide and oxygen ion nonequilibrium concentrations by ionic-molecular reactions 09 p1435 A71-22438

Average electron density profiles for forecasting MF sky waves field strengths, using nocturnal ionospheric measurements 10 p1575 A71-23866

Night airglow measurements over Bulgaria, showing midnight minimum, maximum between 0100 and 0200 hours local time, steady airglow periods and random fluctuations 10 p1599 A71-23877

Natural illumination and irradiance levels for photoelectric device design and specifications in nocturnal light conditions 10 p1641 A71-24056

Nighttime airflow deviations over urban areas from radar tracked tetron flights, discussing effects as function of atmospheric wind and temperature 11 p1793 A71-25377

Superfluid-helium-cooled rocket-borne far-IR radiometer for night sky radiation measurement, discussing cryogenic, optical detection and electronic systems design features and performance 12 p1903 A71-26791

Circumterrestrial meteoroid dust cloud properties based on night sky brightness photometric observation 12 p1964 A71-27090

Nocturnal large ionospheric disturbances over Ashkhabad, obtaining relationship to electron content 12 p1901 A71-27120

Midnight sector balloon measurements of X ray bremsstrahlung from electrons precipitating in auroral zone during polar magnetic substorms 13 p2119 A71-27798

Radar based values of neutral night exospheric temperature, discussing dominant effect of annual variation 13 p2055 A71-27921

Diurnal variations of loss coefficient in D region during polar cap absorption, verifying nighttime D region model by forward propagation data 13 p2059 A71-28242

Dawn chorus westward drift and relationship to polar substorm and magnetic disturbances on night side 13 p2059 A71-28246

Daytime and nighttime sporadic F layer regularities correlation with other ionospheric phenomena based on vertical sounding data 13 p2062 A71-28555

Spectral lines of O I/S₂ generated by oxygen molecule dissociative recombination in upper atmosphere observed in nightglow at geomagnetic equator with Fabry-Perot spectrometer 14 p2229 A71-29663

Gegenschein observational history and characteristic features, discussing theories regarding origin 14 p2308 A71-29904

Night sky optical emissions morphology and behavior in polar regions with emphasis on polar caps 14 p2234 A71-30045

Night sky submillimeter wave diffuse background radiation telescopic measurements above 120 km 15 p2399 A71-31827

Upper atmosphere night sky luminescence observations during IQSY, discussing correlations between night airglow, solar activity, interstellar dust disturbances and meteor phenomena 15 p2400 A71-31987

Midlatitude nighttime F region electron concentration enhancements as downward diffusion flux from protonosphere induced by ionospheric substorm associated electric fields 16 p2573 A71-33958

HF radio absorption in antarctic night ionosphere, discussing solar activity effects 17 p2733 A71-34776

Circumterrestrial meteoroid properties based on night sky brightness photometric observation 19 p3133 A71-37440

Ring currents and polar magnetic substorms during intensive charged particle flux period in nighttime magnetosphere 19 p3054 A71-37838

Nighttime D region behavior under ionization by X ray spectrum of Scorpius source 19 p3017 A71-37864

Mass spectrometric measurement of negative ion concentration in nighttime D region 19 p3128 A71-38033

Ionospheric E region nighttime model from rocket soundings, obtaining electron density profiles by Langmuir probe and wind measurements by glowing vapor release 19 p3055 A71-38036

Nighttime sporadic E layer behavior near magnetic equator, discussing occurrence frequency, seasonal variation and solar activity effects 19 p3055 A71-38037

Nighttime polar atmospheric structure and temperature variations due to gas kinetic and electron energy changes 19 p3056 A71-38361

Nighttime E region ion composition and concentration profiles, using rocket sounding 19 p3061 A71-38628

Night D region ion kinetics data during thermonuclear detonation, discussing formation and conversion rates, electron concentration and recombination 20 p3219 A71-39589

Circumterrestrial dust cloud characteristics from night sky brightness photometric measurements, noting seasonal changes 20 p3219 A71-39646

Exospheric evening temperature behavior data, using Fabry-Perot interferometer measurements of atomic oxygen line Doppler broadening 20 p3222 A71-39703

Plasmasphere evening ionization anomalies observations from spherical electrostatic analyzers onboard OV3-1 polar orbiting satellite, noting thermal plasma depletion during orbit night sector 20 p3225 A71-39741

GBR wavefield above winter nighttime ionosphere, noting latitudinal profile due to D region spatial variations and signal fading with F region structure 20 p3197 A71-39744

Night airglow oxygen Herzberg I bands covariation with O I 5577 A line, evaluating NASA 1968 airborne auroral measurements 23 p3670 A71-43186

Spread F configuration irregularities at Nairobi, investigating nocturnal and seasonal variations and magnetic and solar activity effects 23 p3672 A71-43979

- Night enhancements in 6300 Å line at Sanae related to diurnal excursion of auroral oval, observing ionospheric blackout and high energy electrons precipitation 23 p3672 A71-43980
- Night sky far IR background radiation measurements by rocket-borne superfluid HE cooled radiometer, determining average signal strength equivalency to black body temperature of 3.1 K 24 p3822 A71-44752
- ### NIGHT VISION
- Airborne night vision system performance, determining maximum range for ground target acquisition 08 p1286 A71-20692
- Vision loss from windshield tinting in night visual flying accident 08 p1247 A71-20824
- Night vision visual systems with image intensifiers, noting effect on human eye performance at low light levels 10 p1641 A71-24057
- Night vision and dark adaptation of eye, noting sunlight effects on visual acuity 13 p2017 A71-28392
- Cheyenne attack helicopter weapons system, discussing night vision capability, armament, fire control and navigation equipment integration [AHS PREPRINT 530] 14 p2178 A71-31091
- Air transport accident research in night approach simulators, noting visual information null in descent path and delay in relative motion supplement data 15 p2363 A71-31602
- Closed cycle refrigeration system for cryogenic cooling of IR illuminator in helicopter mounted U.S. Army NVASS Night Vision System for night reconnaissance 20 p3184 A71-39275
- ### NIGHTGLOW
- F region electrons heating by RF energy at or near ionospheric plasma frequency, detecting temperature changes via optical nightglow intensity variations 01 p0040 A71-11533
- Nighttime F region molecular ion concentrations of oxygen and nobelium and associated nightglow morphology, using numerical method for solving nonlinear equations 01 p0078 A71-11611
- Singlet-D atomic O yield per oxygen ion dissociative recombination from night airglow observations 03 p0408 A71-13382
- Night airglow spectral components by Cosmos 92 satellite measurements, considering UV region sources and intensity variations 03 p0417 A71-14050
- Night airglow, discussing spectrum, latitudinal dependency, diurnal variation, time and space correlations and sunspot cycle and solar activity effects 03 p0417 A71-14071
- Nightglow 6300 Å emission latitude wide enhancement at Mt. Abu, India 06 p0893 A71-17990
- Low geomagnetic latitude night airglow characteristics, using Cosmos 215 measurements in 1225 to 1350 Å range 08 p1277 A71-21008
- Nighttime ionospheric atomic nitrogen and nitric oxide production and loss mechanisms effect on nightglow continuum 09 p1441 A71-23641
- Night glow emission post twilight decay rates at different seasons by Chamberlain relation, discussing F layer ionization 09 p1441 A71-23644
- Wind transport effect on redistribution of ionization produced by geocoronal and interplanetary UV emissions in nighttime ionosphere, using electron density sounding rocket data 14 p2230 A71-29709
- IQSY night airglow from multistation photometric observation network, discussing data processing, instruments, publications and catalogs 15 p2396 A71-31609
- Rocket observation for spatial distribution of far UV nightglow at Lyman alpha and shorter wavelengths 15 p2398 A71-31764
- Night sky submillimeter wave diffuse background radiation telescopic measurements above 120 km 15 p2399 A71-31827
- Airglow research review and bibliography covering past four years observations of nightglow, twilight, dayglow and metals in upper atmosphere 17 p2732 A71-34466
- Low geomagnetic latitude night airglow characteristics, using Cosmos 215 measurements at 1225-1350 Å in oxygen spectrum 20 p3219 A71-39588
- Nighttime equatorial E region ionization and electron density gradient irregularities, noting cross field instability with rocket-borne Langmuir probes 20 p3225 A71-39727
- D region night airglow OH emissions and IR atmospheric diatomic oxygen bands excitation mechanism with aid of model involving solar photodissociation 20 p3226 A71-39831

- F region nightglow emission mechanism in terms of oxygen cations reactions with diatomic nitrogen and subsequent recombination 20 p3226 A71-39832
- Nighttime hydroxyl airglow emission intensity and excitation temperature measurements, noting seasonal and nocturnal variations 20 p3227 A71-39834
- Atomic oxygen 6300 and 5577 Å emissions nocturnal covariation from nightglow observation, considering relation to F layer height changes 23 p3667 A71-43131
- ### NIKE ROCKET VEHICLES
- NT NIKE-APACHE ROCKET VEHICLE
- NT NIKE-TOMAHAWK ROCKET VEHICLE
- ### NIKE-APACHE ROCKET VEHICLE
- Nike-Apache sounding rocket vehicle with canted fins, examining pitch-roll coupling characteristics by equilibrium and dynamic simulation methods [ALAA PAPER 70-1376] 03 p0497 A71-13659
- ### NIKE-TOMAHAWK ROCKET VEHICLE
- Life support systems test under weightlessness environment in Nike Tomahawk sounding rockets launched from Wallops Island 16 p2537 A71-33816
- ### NIMBUS SATELLITES
- NT NIMBUS 2 SATELLITE
- NT NIMBUS 3 SATELLITE
- NT NIMBUS 4 SATELLITE
- Nimbus meteorological sensor and photographic data application to geology and hydrology for repeat global and synoptic observations, terrestrial mapping and event classification 04 p0583 A71-15290
- Nimbus AVCS imagery applied to studies of bedrock geology, geomorphology and climate 04 p0597 A71-15309
- Nimbus meteorological satellite program, discussing global cloud cover mapping and automatic picture taking, radioisotopic thermoelectric generator, sounder instrumentation and remote sensors 05 p0818 A71-17133
- Nimbus 3 and 4 satellites IR grating spectrometers for remote sensing of vertical temperature and humidity profiles of stratosphere and troposphere near Philippines 05 p0818 A71-17137
- Michelson interferometer onboard Nimbus 4 satellite for recording earth IR emission spectrum 14 p2241 A71-30140
- Nimbus weather satellite with IR spectrometer, Michelson interferometer and selective chopping radiometer for atmospheric temperature remote sounding 15 p2445 A71-32295
- Nimbus 3 and 4 satellite observation data comparison with sounding rocket and rawinsondes based on temperature as function of pressure measurements 16 p2572 A71-33846
- Meteorological satellites characteristics, reviewing Tiros,ITOS, Nimbus, ATS, SMS and IGAR programs and vehicles 17 p2812 A71-34244
- Vertical temperature profiles from Nimbus 3 satellite spectral radiance measurements, stressing importance for atmospheric circulation prediction 20 p3258 A71-39666
- Nimbus B-2 satellite-borne IR spectrometer lubrication using solid film technique, discussing real time and accelerated vacuum environmental tests [ASLE PREPRINT 71LC-3] 24 p3831 A71-45286
- ### NIMBUS 2 SATELLITE
- Cloud cover areal distribution estimation model using multichannel IR radiometer data from Nimbus 2 satellite 19 p3056 A71-38267
- Nimbus 2 satellite observed 6.7 micron water vapor radiation, compared to calculated radiances 21 p3373 A71-40224
- ### NIMBUS 3 SATELLITE
- Carbon dioxide band radiances measured by Nimbus 3 satellite IR spectrometer, noting seasonal temperature changes in stratosphere due to meridional circulation 01 p0119 A71-10743
- Nimbus 3/SNAP 19 radioisotopic thermoelectric generator design and performance 05 p0780 A71-17136
- Ecological interpretation of daytime data from Nimbus 3 high resolution IR radiometer for hydrologic and plant distribution mapping 08 p1277 A71-20884
- Atmospheric ozone data in tropical regions from Nimbus 3 IR interferometer spectrometer measurements, indicating easterly jet stream existence during summer monsoon period 17 p2771 A71-35810
- Earth radiance analysis by IR interferometric spectrometer of Nimbus 3 satellite, noting cloud cover as dominant variable 18 p2912 A71-36065
- Earth IR radiance at 5-20 microns from interferometric spectrometer /IRIS/ aboard NIMBUS 3 satellite 18 p2912 A71-36101

- Orbital performance of SNAP 19 radioisotopic thermoelectric generator for nuclear power supply on Nimbus 3 observatory 20 p3266 A71-38962
- Global atmospheric ozone distribution from inverted radiance measurements by IR interferometer spectrometer onboard Nimbus 3 satellite 20 p3220 A71-39668
- Meteorological and instrumental options for atmospheric vertical temperature soundings from geosynchronous satellites, noting Nimbus 3 and ATS measurements of cloud cover and radiance levels 20 p3240 A71-39674
- Earth atmosphere radiation fields analysis from Nimbus 3 five-channel scanning radiometer measurements, determining mean planetary albedo and temperature 20 p3259 A71-39679
- Nimbus 3 satellite IR spectrometer atmospheric pressure height profiles, comparing with nearby radiosonde data 22 p3535 A71-42410
- ### NIMBUS 4 SATELLITE
- Nimbus 4 satellite telemetry information processor with data sampling and formatting flexibility 05 p0726 A71-17135
- Nimbus 4 satellite selective chopper radiometer data on IR radiation emitted by carbon dioxide, considering stratospheric warming 10 p1598 A71-23743
- Nimbus 4 Interrogation Recording and Location System meteorological experiment for tropical region upper atmosphere information 14 p2200 A71-30917
- IR atmospheric temperature profiles sounding by selective chopper radiometer launched into polar orbit on Nimbus 4 satellite 22 p3544 A71-42144
- ### NIMPH (ENGINE)
- ### NU HYDRAZINE ENGINES
- ### NIOBATES
- Lithium niobate crystal electro-optical shutter to Q switch calcium difluoride-Dy laser emitting giant pulses at high repetition rate 01 p0095 A71-11210
- Potassium niobate single crystals domain structures by interferometry, discussing surface deformations, dipole couplings and temperature dependent angles 06 p0941 A71-18039
- Temperature induced spectral line widening of trivalent positive Pr ions in lanthanum niobate crystals 09 p1507 A71-22391
- Continuously tunable stimulated far IR emission in lithium niobate with Q switched ruby laser as pumping agent, discussing power-wavelength characteristics determination 09 p1465 A71-23482
- Cylindrical lithium niobate single crystal acoustic propagation, determining speed, damping and sound reflection with He-Ne laser light scattering at hyper-sonic oscillations 13 p2080 A71-29024
- Radiation patterns from piezoelectric transducers on Y face of lithium niobate, using Green function analysis 14 p2283 A71-29795
- High coupling low diffraction loss cut for acoustic surface wave propagation on lithium niobate 14 p2283 A71-29796
- Phase holographic data storage in doped barium sodium niobate crystal, detailing decay times, energy density and diffraction efficiency 15 p2412 A71-32586
- Minimum voltages and limiting frequencies for oblique cut longitudinal octahedral crystal modulators with large electro-optic coefficients, including lithium niobates and tantalates 15 p2461 A71-32606
- Visible thermal tuning CW parametric oscillator using barium sodium niobate as nonlinear material 20 p3241 A71-38788
- Orthorhombic-tetragonal phase transition in barium sodium niobate, investigating expansion curve discontinuities due to crystallographic changes from dilatometric studies 20 p3275 A71-38816
- Rotating waveplate optical frequency shifting in lithium niobate, producing light beam with moderate requirements on modulator adjustment 20 p3204 A71-39097
- Lithium niobate hypersound attenuation and reflection coefficients frequency dependence determination by scattering laser light at hypersonic oscillations 20 p3244 A71-39162
- Voltage-polarization induced optical waveguide using electrooptical lithium niobate crystal 21 p3393 A71-41039
- Surface wave delay lines with near octave bandwidth using lithium niobate interdigital ultrasonic transducer with lumped element impedance inverter network 22 p3521 A71-42202

Laser use in computer technology, reporting lithium and barium sodium niobate single crystals capacity for data storage

23 p3686 A71-43959

He-Ne laser radiation modulator at 1.5 GHz using X and Z cut lithium niobate crystals in toroidal microwave cavity

24 p3835 A71-45265

NIOBIUM

Thermoemissive and adsorptive properties of Nb single crystals in Cs atomic beam at various temperatures

01 p0139 A71-11100

High purity Nb and Nb-O solid solution single crystals, investigating temperature dependence of yield stress

02 p0263 A71-11866

Performance tests of identical cylindrical thermionic converters with W emitters and Nb collectors, using X ray diffraction and work function measurements

02 p0193 A71-12217

Nb-sheathed insulators of three coaxial cylinders with ceramic bonding for thermionic converter, discussing pressure bonding techniques and stress relieving properties

02 p0232 A71-12248

Trilayer niobium-alumina-niobium sheath insulator thermal stability test under electrical load

02 p0232 A71-12253

Nb single crystals, examining structure in initial deformed and annealed states at various low temperatures

02 p0266 A71-12654

Niobium - Conference, Paris, October 1969

02 p0268 A71-12926

Niobium with various interstitial and substitutional type impurities, examining plastic deformation and mechanical properties at various temperatures

02 p0269 A71-12927

Niobium mechanical properties temperature dependence from plastic deformation tests, taking into account interstitial and substitutional impurity concentrations

02 p0271 A71-12936

Niobium processing methods from economic standpoint, describing pyrochlore metallurgical reduction

02 p0271 A71-12938

Pure Nb vs Nb alloy oxidation behavior, discussing oxide phases, formation temperature and exposure time

02 p0271 A71-12940

Nb strips siliconization by silicon hydride decomposition and silicide or silicon oxidation, noting Si surface enrichment and bulk diffusion processes

02 p0272 A71-12943

Nb oxidation protection by Ti or Cr modified silicide coating, noting results with various Cr-Si mixtures

02 p0272 A71-12944

Mechanical stability of self healing viscous glass layer in porous oxidation protection coating on Ni under high acceleration

02 p0272 A71-12945

Mechanical stability of liquid phase in porous oxidation protective coating on Ni turbine blades under acceleration

02 p0272 A71-12946

Structure and durability of self healing silicide based coatings for niobium oxidation protection at high temperatures

02 p0272 A71-12947

Kinetic, morphological and crystallographic effects of Nb crystals oxidation during growth at various temperatures and pressures

02 p0272 A71-12948

Corrosion rate of Nb in aqueous solutions as function of temperature, using electrochemical potential measurements

03 p0442 A71-13363

Nitriding effects on short time tensile strength, plastic properties and hardness of niobium

04 p0612 A71-15549

Ellipsometric observation of Ni optical properties changes relation to oxygen absorption, considering correctness of oxidation data

04 p0613 A71-15695

Superconducting Nb experimental tests for hypothesis concerning relations between anisotropic critical field and dislocation cell structure

07 p1138 A71-19988

Thermal recovery effects on electrical resistivity in deformed polycrystalline Nb samples tested at varying strain rates and 263-509 R temperatures

07 p1144 A71-20496

Interstitial nitrogen effects on thermally activated flow in Nb single crystals, determining yield and flow stresses and strain-rate sensitivity dependences on temperature

08 p1307 A71-21504

Nb single crystals dislocation substructure correlation with strength properties

08 p1307 A71-21508

Nb single crystals heterogeneous deformation at very low temperatures, observing jerky flow due to adiabatic temperature rise during plastic deformation

08 p1308 A71-21512

Polycrystalline Nb under plastic deformation and annealing, examining dislocation structure and mechanical properties

08 p1316 A71-21611

Crystal structure alterations in work hardened surface layers of W, Nb and Mo during thermocyclic treatment, using X ray micrography

09 p1477 A71-23329

Anomalous thermal diffusivity measurements of Hf, Nb and Zircaloy, using modulated electron beam technique

10 p1624 A71-23909

Electron beam welding of tungsten to tungsten/rhenium and tungsten/rhenium to niobium, discussing techniques for assembly of thermionic converter fuel elements

11 p1769 A71-25858

Variable spacing thermionic converter consisting of fluoride vapor deposited W emitter and Nb collector, considering cesiated work function of electrode pair

11 p1714 A71-25905

Hydrogen effects on low temperature solution strengthening and ductility of Nb-H single crystals, noting effects of normal and strain induced hydride precipitation

11 p1780 A71-26020

Stacking fault formation in Nb deformed by filing, determining coherent scattering regions with X ray diffraction

12 p1917 A71-27299

Activation energy anisotropy for Mo and Nb single crystals dislocation relaxation, noting temperature dependence

12 p1917 A71-27300

Nb single crystals structure and properties after cold rolling and annealing, determining crystallographic parameters of plastic deformation

13 p2086 A71-28579

Dielectric properties of barium titanate with Nb, noting metal oxide additives effects on conductivity

13 p2092 A71-28661

Polycrystalline Nb cyclic yield point behavior under strain softening and hardening, noting stable hysteresis loop

13 p2087 A71-29123

Matthiessen rule validity proof by Renucci method, applying to Nb-base solid solutions

13 p2087 A71-29328

Stress effects on superconductivity and dislocation cell structure in deformed niobium for compression and tension

13 p2090 A71-29416

Nb single and polycrystalline thermal conductivity/diffusivity, specific heat, electrical resistivity and monochromatic/ integrated degree of blackness at high temperatures

14 p2258 A71-30052

Fifth group transition elements V, Nb and Ta, showing most stable metal dioxide gaseous compounds

15 p2424 A71-31391

Niobium fine structure, examining annealing in vacuum effects on strength

15 p2425 A71-31400

Chromatographic separation of molybdenum, niobium and tungsten based on metal ions absorption by aluminum oxide

15 p2367 A71-31647

Oxygen adsorption kinetics at Nb single crystal surface at high temperatures and low pressures

15 p2436 A71-32547

Polyhedral Nb single crystals production from niobium pentachloride and hydrogen reaction, determining growth rate

16 p2594 A71-33877

Molybdenum-niobium alloys single crystals electron work function in vacuum from emission patterns and anisotropy

16 p2595 A71-33881

X ray diffraction lines diffusion of deformed Ni and Nb, attributing absence to small block dispersion

17 p2755 A71-34415

Niobium dislocation and electronic structure and mechanical properties after plastic deformation and annealing from electron beam studies

17 p2760 A71-35671

High temperature oxidation protection of niobium by molybdenum disilicide coatings applied by hot pressing powder metallurgy method

18 p2934 A71-35952

Variable Nb composition of meteoritic rutile grains from quantitative electron microprobe analysis

20 p3292 A71-39384

Nb nitriding kinetics and external effects observations, noting nitrogen diffusion through crystal lattices

21 p3404 A71-41163

Anomalous ultrasonic attenuation in pure superconducting Nb from pulse echo amplitude measurements

24 p3860 A71-44751

Polycrystalline Nb and Ta and Ta-on-Nb thin film thermionic emission surface barrier analysis from periodic deviations in Schottky effect

24 p3862 A71-45346

NIOBIUM ALLOYS

Nb-Fe-Al and Nb-Co-Al alloys phase equilibrium by X ray and microstructural analyses

01 p0100 A71-10417

Decomposition structure of supersaturated solid solution in Co-Nb alloy, showing beta phase transformation inhibition

01 p0101 A71-10671

Edge dislocations in deformed single crystals of Nb-Mo and Nb-Re alloys at various temperatures

01 p0101 A71-10738

Physical properties of Nb-Al-Ge alloys with maximum superconducting transition temperature close to boiling hydrogen

01 p0103 A71-11070

Nb alloys hardening due to interstitial atoms interactions with dislocations, obtaining stress-strain relationship for various impurities, precipitates, strain rates and temperature

02 p0270 A71-12929

Nb-impurity binary solid solutions, calculating interdiffusion and heterodiffusion coefficients

02 p0270 A71-12930

Nb binary solid solutions with various Ti, Mo and Zr percentages, examining structure and mechanical properties

02 p0270 A71-12931

Nb binary alloys room temperature brittleness in hydrogen atmosphere

02 p0270 A71-12932

Nb high purity binary alloys preparation and processing

02 p0270 A71-12933

Nb based refractory metal alloys, discussing phase diagrams and electromagnetic separation method

02 p0270 A71-12934

Nb alloys in hypersonic glider fabrication, discussing mechanical properties, oxidation resistance and sandwich panel design

02 p0270 A71-12935

Refractory Nb alloys with high creep strength, good ductility and moderate density, heat treatment and workability

02 p0271 A71-12937

Niobium alloys for gas turbine blades, examining working temperatures, protective coatings and ductility

02 p0271 A71-12939

Pure Nb vs Nb alloy oxidation behavior, discussing oxide phases, formation temperature and exposure time

02 p0271 A71-12940

Al based protective coatings on Nb and Nb alloys considering structure, formation and aluminate component

02 p0271 A71-12941

Niobium aluminate pest, investigating oxidation effects on Nb-Al protective coatings from 600 to 1400 C

02 p0271 A71-12942

Nb-Mo alloys single crystals deformed in compression, considering work hardening and slip relation to temperature, Mo content and stress level

03 p0441 A71-13313

Deformation pattern, interstitial impurities and alloying elements effects on temperature dependence of elasticity modulus of Nb and alloys

04 p0613 A71-15641

Creep strength of Nb alloys with Mo at high temperatures in vacuum, noting Zr-C complex alloying effect

04 p0613 A71-15642

Nb-Mo alloy creep test, determining relationships between steady state creep rate, stress and Mo content

04 p0616 A71-15803

Nb-N and Nb-Zr-N alloys phase composition, examining microconstituents at various temperatures after quenching

04 p0616 A71-15905

Nb-W-Hf-Y creep rupture properties in thermal vacuum, achieving strength improvement by pretest annealing

05 p0766 A71-16242

Precipitation reactions in concentrated Ta-Hf and Nb-Hf alloys at 600-1400 C from X ray diffraction and transmission microscopy, discussing phase relations

06 p0914 A71-18679

Nb-W single crystal deformation, discussing athermal solid solution strengthening

06 p0914 A71-18683

Nb-V-Mo alloys lattice structure, examining continuous solid solutions with X ray and metallographic analysis

07 p1129 A71-19144

Cerium effect on phase composition and mechanical properties of Nb-Al alloys, plotting isothermal cross sections

07 p1135 A71-19615

High temperature oxidation of Cr-Ti-Si coatings on Nb alloy

07 p1135 A71-19619

Time linear increase of magnetic flux flow through superconducting NbZr wall, inferring empirical critical current density model agreement with measured flow rate

07 p1179 A71-20156

Nb-Hf alloys alpha precipitation strengthening via aging at various temperatures, examining mechanical properties

08 p1312 A71-21549

Electron concentration and superconducting characteristics of Nb-Sn alloys from optical measurements

09 p1507 A71-22234

Nb alloy high temperature creep and long term strength, determining exponential relations between stress, strain rate and durability

09 p1468 A71-22628

Mo, W and Zr effects on niobium reaction with residual gases during heating in vacuum

09 p1469 A71-22846

Al and Fe additions effect on transitional phases formation and metastable phase precipitation in Ni-Nb system, using transmission electron microscopy

09 p1471 A71-23124

Intracrystalline liquifaction in Ni alloys containing Nb studied with microanalyser

09 p1480 A71-23702

Ti-Nb alloys constitution, discussing alpha-bis martensite dissolution and undercooled beta phase decomposition

10 p1623 A71-23902

Superconductivity transition of Nb-Ti solid solutions with varying Ti content, using specific heat measurements between 2.5 and 20 K

10 p1628 A71-24890

Nb-Pd system concentration profiles and thermal diffusion coefficients, investigating phase formations by electron probe microanalysis

10 p1629 A71-25035

Protective coatings of Ta, Nb and TD alloys for high performance thermal protection systems, discussing space shuttle reentry heat shield

11 p1778 A71-25554

Niobium alloys single crystals deformations, studying microyielding to macroflow transitions by dynamic microstrain technique

11 p1780 A71-26019

Al coating of Nb and Nb alloys by pack cementation, discussing coating structural states, heating cycle temperatures and growth kinetics

11 p1781 A71-26295

Nb-Ti alloys internal friction spectra due to oxygen content, applying graphical decomposition method

11 p1781 A71-26322

Equilibrium diagrams for Nb-Zr-B alloys, establishing solidus surface, Zr/B isothermal and vertical sections

11 p1782 A71-26474

Nb-V, V-Pd and Pd-Nb systems diffusion coefficient as function of concentration for equilibrium diagrams, using method of diffusion layers

11 p1782 A71-26475

Solid solution hardening in Nb alloys single crystals, explaining in terms of elastic interaction of dislocations with substitutional atoms

12 p1916 A71-26927

Nb-N and Ta-N alloys, calculating electrical resistivity and solid solutions lattice constants at various temperatures

12 p1917 A71-27295

Nb-Zr-Hf alloys superconductivity properties, determining critical current, critical magnetic field and transition temperature in cold worked and tempered samples

13 p2083 A71-27961

Nb-Ti-Zr-Hf alloys superconductivity properties, obtaining improved critical current values in tempered vs cold worked samples

13 p2083 A71-27962

Solid state solubility of B in Nb, determining binary Nb-B alloys phase diagram by microscopic, X ray and thermal analyses

13 p2085 A71-28224

Elastic stresses during local deformation in Nb-Mo, Ni-Cr, Cu-Al and pure bcc metals, using X ray analysis

13 p2085 A71-28225

Silicide coated Nb alloys for gas turbine engine components operating at temperatures above 2000 F [SAE PAPER 710460]

13 p2115 A71-28334

Superconductive Nb-Al alloy critical temperature as function of chemical composition and heat treatment

13 p2085 A71-28576

Field ion emission microscopic study of isothermal order-disorder transformation kinetics in water quenched Ni-Mo alloys

13 p2085 A71-28577

Nb and Nb alloys coating by hot-dipping in molten Al, investigating critical temperature and growth kinetics

13 p2087 A71-29121

Solution hardening and softening of single crystals, considering deformation in Nb-Mo and Nb-Re alloys

13 p2088 A71-29344

Ni-Ni Nb eutectic composite, investigating monotonic mechanical response, deformation and fracture mechanisms

13 p2088 A71-29401

Aging behavior of Nb-containing Fe-Ni alloys, considering austenite and martensite in twinned and massive form

13 p2089 A71-29412

Working fluid /Ar/ purity and stability effects on fatigue life and creep of Nb and Mo alloys using gas analysis, microstructure and microhardness data

14 p2256 A71-29622

Shape-memory effect in equiatomic Ti-Nb alloys with reversible martensitic transformation

14 p2259 A71-30392

Optimal electron beam welding of Nb alloy to bronze, showing high mechanical properties due to deep Cu diffusion

14 p2253 A71-30491

Thin sheet Nb-Zr alloy welds, detailing residual stresses in butt joints

15 p2413 A71-31204

Nb alloy ingots electron beam melting, investigating reverse zone liquation intensity and behavior dependence on melting parameters

15 p2424 A71-31241

Silicidization on Nb-Ta alloys, considering formation of niobium disilicide phase with hexagonal lattice

15 p2425 A71-31401

Cast Nb-W-Mo-Zr-C alloys heat treatment effect on microstructure and phase composition, noting ductility improvement

15 p2426 A71-31406

Nb-Re-C system, investigating polythermal NbC-Re cross section structure by metallographic chemical and X ray analyses and microhardness and melting point measurements

15 p2430 A71-32148

Niobium-zirconium system alloys Debye-Waller factor temperature and concentration dependence, noting nonmonotonities due to phonon spectra

15 p2437 A71-32625

Ti alloys argon TIG welding to Nb alloys, detailing joint impact strength, fusion zone ductility and bending tests

15 p2418 A71-32668

Isothermal sections at 1400 C of systems niobium-titanium-boron and niobium-molybdenum-boron by X ray analysis

15 p2437 A71-32672

Critical current density in niobium alloy with disperse superconducting phase as function of transverse magnetic field strength

16 p2593 A71-33653

Niobium alloy use for space shuttle thermal protection, examining oxidation and mechanical properties

17 p2757 A71-34495

Superconducting transition temperature measurement of cast and solution treated Nb-Zr alloys, substantiating dependence on density of states at Fermi surface

17 p2759 A71-35221

Consistency examination of thermal activation analysis in Nb, determining strain rate sensitivity of pure Nb and Nb-Mo single crystals subjected to compression at 178 and 273 K

17 p2759 A71-35223

Thermal and athermal yield stresses of Nb and Nb-Mo single crystals, considering strain rate sensitivity and thermal stress increase with increasing plastic strain

17 p2759 A71-35224

Deformation kinetics and failure of high melting Nb and Mo base alloys in plastic state under low cyclic fatigue

18 p2936 A71-36710

High temperature creep of niobium alloy, obtaining creep limit, microhardness and gas analysis data

18 p2936 A71-36715

Nb and Nb-Zr alloy tubular and sheet samples cyclic loading tests, determining heat treatment effects on notch sensitivity and fatigue strength

18 p2937 A71-36724

Phase transformations in superconducting Nb-Ti alloys with Zr during heating or isothermal annealing

19 p3078 A71-37469

Concentration effects of Nb and Ta on strengthening in tetrahedral section of W-Mo-Nb-Ta system at temperatures from 20 to 1100 C

19 p3078 A71-37473

Cold work peak characteristics in undeformed aged niobium-nitrogen alloys from internal friction spectrum

20 p3252 A71-39464

Grain boundary dislocations generation and motion in deformed Nb steel in relation to sliding, using electron microscope analysis

21 p3395 A71-40021

Ni-Cu-Nb age hardenable steel mechanical properties, examining hot rolling and heat treatment effects

21 p3387 A71-40455

Electron concentration and superconducting characteristics of Nb-Sn alloys from optical measurements

21 p3428 A71-41114

Superconductivity transition of Nb-Ti solid solutions with varying Ti content, using specific heat measurements at 2.5-20 K

21 p3432 A71-41266

Superhigh vacuum apparatus for creep and long term strength tests on metals at high temperatures, giving results for niobium alloys

22 p3538 A71-41699

Microstructure, yield point and creep rupture strength of Nb-Ti alloy, investigating oxygen concentration and temperature effects

22 p3563 A71-42365

Oxygen concentration and heat treatment effects on structure and mechanical properties of Nb-Zr alloys

22 p3563 A71-42366

Nitriding process on Nb alloy, presenting gas phase temperature, time and composition effects

24 p3838 A71-44894

NIOBIUM CARBIDES

Titanium and niobium monocarbides electron work function relation to homogeneity region composition, considering electron structure and thermal emission

02 p0263 A71-12199

Secondary recrystallization of Ti, Zr and Nb carbides within homogeneity ranges, determining activation energies as function of carbon deficiency in carbide lattice

04 p0609 A71-14749

Metals and alloys strengthening by in situ grown transition metal carbide fibers, noting whisker-like characteristics

08 p1315 A71-21586

Niobium carbides sintering by hot pressing at various temperatures, discussing kinetics, relative compactness and activation energy

09 p1466 A71-22163

Polycrystalline NbC and TaC Young, shear and bulk moduli determination at high temperature, noting porosity and temperature effects

11 p1781 A71-26294

Niobium and zirconium carbides enthalpy and specific heat dependence on temperature and composition

15 p2431 A71-32156

Abrasive capability, shape and strength of refractory powders of fused titanium and niobium carbides and calcium boride compared with synthetic corundum

16 p2592 A71-33574

Plastic deformation in hot compressed Ti, Zr and Nb carbides during diamond grinding, studying fine structure on diffractometer

16 p2584 A71-33896

Temperature effects on wear and failure of titanium and niobium carbides, using electron microscopy

19 p3076 A71-37114

Nonstoichiometric zirconium niobium carbide thermodynamic properties, deriving components activity equations from statistical considerations based on pairwise interaction energies

20 p3252 A71-39554

Temperature effects on niobium carbide friction process in vacuum conditions, considering surface layer microhardness and X ray and metallographic analyses

23 p3692 A71-44030

Niobium carbonitride thin film deposition temperature effects on superconducting properties, considering transition temperature and critical currents and fields

23 p3717 A71-44141

Niobium carbide film formation in pseudoliquidified layer on graphite at 3000 C in argon metal vapor mixtures with/without hydrogen

23 p3696 A71-44317

Ti, Zr and Nb carbides alloying effects on deformed and annealed Mo alloys cellular structure and mechanical properties

24 p3836 A71-44672

Titanium, niobium and tungsten carbides microhardness temperature dependence at 77-1973 K, discussing activation energy and deformation mechanism

24 p3838 A71-44741

NIOBIUM COMPOUNDS

NT NIOBATES

NT NIOBIUM CARBIDES

NT NIOBIUM OXIDES

NT NIOBIUM STANNIDES

Tantalum and niobium disilicides enthalpy and heat capacity temperature dependences

02 p0263 A71-12198

Vapor deposited niobium nitride superconducting thin films on fused silica substrates, measuring transition temperature

05 p0792 A71-16236

Superconducting niobium aluminide and niobium aluminide-Ge films formation on Nb substrate

05 p0792 A71-16238

Vanadium and niobium carbohydrides as function of C content, studying lattice constants, microhardness and electrical resistivity

06 p0912 A71-18086

Niobium nitride thin films very high critical current and field characteristics, noting deposition by sputtering

07 p1179 A71-20154

NbN Dayem bridge characteristics, discussing negative resistance region, self induced subharmonic current steps, temperature dependence and microwave radiation effects

07 p1079 A71-20161

Silicidation on Nb-Ta alloys, considering formation of niobium disilicide phase with hexagonal lattice

15 p2425 A71-31401

Tantalum and niobium disilicides enthalpy and specific heat temperature dependences in 1200-2100 K range

15 p2426 A71-31504

Titanium, vanadium and niobium carbides, investigating electronic structure effects on atomic behavior

15 p2429 A71-32140

Superconducting Nb-Sn intermetallic compound synthesis from elemental powders by converging shock waves

15 p2461 A71-32378

NIOBIUM OXIDES

Nb surface contamination by oxidation during electrolytic polishing and vacuum annealing

02 p0269 A71-12928

Niobium oxide defect structure, correlating electrical conductivity and oxygen diffusional properties with nonstoichiometry degree

05 p0770 A71-17097

Thermal diffusion in tantalum-oxygen and columbium-oxygen mixed crystals, investigating temperature and concentration effects

16 p2599 A71-34092

Tantalum and niobium ternary oxides recovery from liquid potassium solution, determining composition and crystallographic modifications by chemical and X ray diffraction analyses

20 p3194 A71-39372

NIOBIUM STANNIDES

Debye-Waller factors for Nb and Sn atoms in intermetallic niobium stannide by X ray intensity measurements on single crystal

10 p1655 A71-23770

NITRATE ESTERS

NT ISOPROPYL NITRATE

NITRATES

NT AMMONIUM NITRATES

NT CELLULOSE NITRATE

NT DINITRATES

NT HYDRAZINE NITRATE

NT HYDRAZINE NITROFORM

NT NITROGLYCERIN

NT PETN

Chlorella biomass chemical composition stability during prolonged cultivation with nitrates recycling medium

22 p3507 A71-42818

NITRIC ACID

Ballistic modification of nitric ester based propellant combustion by lead compounds, concerning burning rate-pressure relation

08 p1346 A71-20860

High density nitric acid oxidizer and unsymmetrical dimethyl hydrazine with silicone fluid additive application to Agena rocket engine for higher performance. [AIAA PAPER 71-736]

14 p2287 A71-30781

Red fuming nitric acid-sulfur dioxide as oxidizer for auxiliary ignition in liquid rocket motors

15 p2465 A71-32110

Steel joint weld decay mechanism, observing intergranular corrosion initiation and development in nitric acid solutions

15 p2417 A71-32665

NITRIC OXIDE

Rocket-borne mass spectrometer observation of NO in auroral arc

01 p0077 A71-11522

Chemiluminescent NO-O reaction spectral radiant intensity and absolute rate constant redetermination in premixed gaseous free jet and hydrogen flame atmosphere

05 p0837 A71-16568

Vertical NO profile at 100-220 km from 1968 Cosmos 224 measurement of atmospheric glow near horizon

05 p0744 A71-17186

Upper atmosphere nitric oxide density measurement by scanning UV spectrometers on Nike-Apache rockets, noting ionization consequences for D region

06 p0888 A71-17273

Aircraft gas turbine engines nitric oxide emission model, describing flow behavior and chemical processes

06 p0948 A71-18659

Nighttime ionospheric atomic nitrogen and nitric oxide production and loss mechanisms effect on nightglow continuum

09 p1441 A71-23641

Nitric oxide diurnal variation model in upper atmosphere incorporating solar flux, absorption cross sections and chemical rate constants

10 p1605 A71-24795

Nitric oxide ion two body recombination with nitrogen dioxide and trioxide molecular ions, examining ionic neutralization reactions in decaying dilute thermal plasma at 300 degrees K

11 p1801 A71-25297

Radiation from long lived ionic excited states, studying emission spectra, electron impact cross sections and positive nitric oxide ions band system

11 p1727 A71-25368

Air polluting nitric oxide and soot production by jet aircraft, discussing mixing process and atmospheric dispersion

[AIAA PAPER 70-115]

12 p1946 A71-27560

Vibrational energy transfer from excited nitrogen to CO and NO, describing flow tube measurements

12 p1934 A71-27760

Vertical NO profile at 100-220 km from 1968 Cosmos 224 measurement of atmospheric glow near horizon

13 p2059 A71-28243

Nitric oxide formation kinetics in shock induced combustion processes, considering hydrogen-oxygen-nitrogen reaction

13 p2113 A71-28616

Three body ion-neutral association reactions of NO ions with oxygen, nitrogen and carbon dioxide, noting temperature effect on rate constant

13 p2026 A71-29507

Chemical kinetic calculation of nitric oxide formation in spark ignition automobile engines and gas turbine combustors

14 p2190 A71-30454

Nitric oxide formation analytical model for gas turbine combustion chamber, considering influence of primary zone equivalence ratio, combustor residence time and initial fuel droplet size

[AIAA PAPER 71-715]

14 p2191 A71-30767

Cluster ions concentration and nitric oxide in mesosphere D region, considering electron density profiles

15 p2394 A71-31430

Turbojet engine combustor nitric oxide formation prediction based on adiabatic micromixed perfectly stirred reactor model analysis

[AIAA PAPER 71-713]

15 p2470 A71-32286

Jet engines nitric oxide air pollutant emission formation, developing gas turbine combustor models

[AIAA PAPER 71-712]

15 p2470 A71-32289

Positive NO ion formation with excess internal energy in positive atomic oxygen ion-nitrogen collisions

16 p2538 A71-32810

Ionospheric nighttime ambient atomic oxygen concentration profiles, using nitric oxide release from sounding rockets

16 p2568 A71-33791

Vibrational temperature of nitric oxide in upper atmosphere, computing collisional, radiative and chemiluminescent excitation rates

18 p2910 A71-35840

Atomic oxygen concentration from 5577 A green line emission of airglow and chemiluminescence of nitric oxide

20 p3215 A71-38739

Nitroas oxide dissociation as natural source of stratospheric nitric oxide, noting estimates use as yardstick for artificial source

23 p3642 A71-43347

NITRIDES

NT ALUMINIUM NITRIDES

NT BERYLLIUM NITRIDES

NT BORON NITRIDES

NT SILICON NITRIDES

NT TITANIUM NITRIDES

NT ZIRCONIUM NITRIDES

High temperature neutron irradiation properties of uranium oxides, carbides and nitrides coated with tungsten-rhenium

02 p0296 A71-12246

Transition metals carbides and nitrides homogeneity regions relation to nonlocalized valence electrons in lattice and configuration stabilizing ability

02 p0264 A71-12280

Vapor deposited niobium nitride superconducting thin films on fused silica substrates, measuring transition temperature

05 p0792 A71-16236

Niobium nitride thin films very high critical current and field characteristics, noting deposition by sputtering

07 p1179 A71-20154

NbN Dayem bridge characteristics, discussing negative resistance region, self induced subharmonic current steps, temperature dependence and microwave radiation effects

07 p1079 A71-20161

Ce-CeN system phase diagrams investigated by differential thermal, X ray and metallographic analysis

09 p1481 A71-22186

Disintegration energy of hard compounds/carbides, nitrides and borides/ related to wear resistance and microhardness of alloys

13 p2072 A71-27818

Transition metal carbides and nitrides ordered structures, determining C and N atoms positions with electron and neutron diffractions

16 p2597 A71-33921

Transition metals monocarbides and mononitrides electronic structure, investigating electrical, thermoelectrical and galvanomagnetic properties

16 p2597 A71-33922

Diboride-nitride system dry friction and wear resistance at room temperature

23 p3681 A71-43254

CrN discovery in iron meteorites, determining carlsbergite mineral composition by electron microprobe

23 p3770 A71-44015

Niobium carbonitride thin film deposition temperature effects on superconducting properties, considering transition temperature and critical currents and fields

23 p3717 A71-44141

NITRIDING

Cr-chromium nitride fusion phase diagram analysis, establishing nonvariant eutectic and dissociative transformations

02 p0266 A71-12673

Nitriding effects on short time tensile strength, plastic properties and hardness of niobium

04 p0612 A71-15549

Zr surface nitriding process in purified and high purity nitrogen respectively, comparing results

04 p0616 A71-15806

Nitriding effect on hardness and wear resistance of Mo alloys

06 p0912 A71-17936

Mo-Hf alloy dispersion hardening by internal nitriding, examining structure and high temperature mechanical behavior

08 p1311 A71-21546

Titanium-containing steels nitriding in ammonia, discussing hydrogen diffusion layers brittleness, cracking, peeling and thickness

12 p1919 A71-27776

Ta nitriding temperature and duration effects on tensile strength, elongation and surface hardness

15 p2424 A71-31240

Titanium-containing steels nitriding in ammonia, discussing hydrogen diffusion layers brittleness, cracking, peeling and thickness

21 p3424 A71-41097

Cr and Cr-Ni ferritic and austenitic steels, investigating high temperature nitriding for intensifying nitrogen diffusion saturation

21 p3389 A71-41098

Stainless steels nitriding in presence of halogen compounds with heat treatment, observing thermodynamic potential shift

21 p3389 A71-41099

Nb nitriding kinetics and external effects observations, noting nitrogen diffusion through crystal lattices

21 p3404 A71-41163

Alloy steels supercooled austenite nitriding in ammonia flow, examining diffusion layers by X ray analysis and hardness tests

21 p3404 A71-41164

Phase and microstructure changes during nitriding process of Fe-Ti alloys, stressing Ti concentration effect

24 p3837 A71-44733

Nitriding process on Nb alloy, presenting gas phase temperature, time and composition effects

24 p3838 A71-44894

NITRILES

NT ACRYLONITRILES

Photochemical molecular rearrangement of NN-dimethylphenylethynylamine into alpha-phenylisobutyronitrile by irradiation at 254 nm

06 p0865 A71-17548

N-t-butyliminoacetone nitrile formation by reaction between adduct from sodium bisulphite, formaldehyde, t-butylamine and potassium cyanide

06 p0865 A71-17549

NITRITES

Hemoglobin-sodium nitrite reaction in absence of oxygen, discussing methemoglobin formation by autocatalysis

03 p0363 A71-13486

NITRO COMPOUNDS

NT NITROBENZENES

NT NITROGLYCERIN

NT NITROMETHANE

NT TRINITROTOLUENE

Valeraldehyde o-nitrophenylhydrazone mass spectrum with low intensity peak due to combined hydroxyl and water loss from molecular ion

02 p0299 A71-12573

Hexanitroethane /HNE/ crystal transformation, using differential spectroscopy and X ray analysis

04 p0638 A71-15679

Burning rate of compressed charges of potassium perchlorate with lead dinitrophenolate at constant pressure

15 p2462 A71-31372

NITROAMINES

Thermal decomposition rates and explosion of dinitroxydiethyl nitramine from heat release measurements at various pressures

15 p2462 A71-31376

NITROBENZENES

NT TRINITROTOLUENE

Detonation sensitivity of ammonium nitrate containing fertilizers, compared with metadinitrobenzene in powder form

10 p1658 A71-25070

NITROCELLULOSE

U CELLULOSE NITRATE

NITROFORMS

NT HYDRAZINE NITROFORM

NITROGEN

NT LIQUID NITROGEN

NT NITROGEN ATOMS

NT NITROGEN IONS

Nitrogen inductive low pressure discharge, determining vibrational and rotational temperatures, ionization degree, electron temperature and energy balance by spectroscopic technique

02 p0286 A71-12178

Damkohler analysis of nitrogen-silica gel absorption isotherm in multimolecular range, noting vapor phase transport and absorbed phase diffusivities

03 p0517 A71-13175

Nitrogen austenite solute-solute binding energy derivation from experimental data for comparison with carbon austenite

03 p0441 A71-13314

Active nitrogen afterglow complex spectrum analysis from vacuum UV to IR, proposing energy transfer mechanism

03 p0460 A71-13352

Chemisorption and sticking probability of nitrogen on Ta films, considering relationship to temperature and pressure

03 p0441 A71-13360

Chemisorption rate and physical adsorption of nitrogen on Ta films as function of temperature

03 p0441 A71-13361

Atomic oxygen-nitrogen shock tube endothermic reaction under high translational and low vibrational energy, noting ozone loss

03 p0375 A71-13493

Vibrational relaxation behind incident shock waves in pure nitrogen, using end wall pressure measurements

03 p0375 A71-13496

Hypersonic rarefied nitrogen flow over wedge, investigating density field

04 p0570 A71-15033

Nitrogen diffusion and solubility in W, deriving expression for permeation constant

04 p0614 A71-15784

Nb-N and Nb-Zr-N alloys phase composition, examining microconstituents at various temperatures after quenching

04 p0616 A71-15905

Shock waves in nitrogen, carbon dioxide and mixtures, measuring Mach number for deviation evaluation from vibrational and dissociation equilibria

05 p0835 A71-16522

Nitrogen-alloyed austenitic steels precipitation hardening, discussing aging and strengthening rates

05 p0767 A71-16767

Continuous nitrogen and oxygen ion spectra due to photoionization and free ion transfers at high temperatures

05 p0838 A71-16788

Nitrogen chemisorption and absorption on polycrystal Ta ribbons, using static method in ultrahigh vacuum

06 p0940 A71-17298

Nitrogen chemisorption on Ta by field emission microscopy, taking into account work function changes

06 p0940 A71-17299

N and CO thermal conductivity shock tube measurements, discussing pressure distribution and high temperature effects

06 p1007 A71-18075

Relaxation time for nitrogen molecule vibration temperature in ionosphere due to thermal electron collisions

06 p0895 A71-18274

Hydrogen and nitrogen binding states and desorption kinetics on /100/ plane of Mo, using flash mass spectrometry

06 p0865 A71-18302

PH conditional ammonia assimilation deficient mutants isolation and growth properties, studying nitrogen transport in *Hydrogenomonas eutropha*

06 p0857 A71-18672

Hydrogenomonas eutropha mutants deficient amination due to ammonia-nitrogen permeation defect

06 p0857 A71-18673

Nitrogen Vegard-Kaplan and second positive band systems emission, using rocket-borne spectrometer in UV aurora

07 p1102 A71-19670

Oxygen and nitrogen metastable constituents in daytime atmosphere airglow, obtaining altitude density distributions

07 p1103 A71-19764

Hydrogen and nitrogen chemisorbed species interactions on /100/ tungsten crystals, using flash desorption methods

07 p1056 A71-19846

Free nitrogen jets ejected from small orifices, measuring acoustic emission level and spectral pattern dependence on pressure

07 p1161 A71-20058

Nitrogen molecule collision with metastable inert gas atoms and ions, investigating energy exchange mechanism

08 p1337 A71-20670

Alveolar nitrogen and carbon dioxide tensions changes during compressed air narcosis in constant oxygen partial pressure

08 p1239 A71-20818

Interstitial nitrogen effects on thermally activated flow in Nb single crystals, determining yield and flow stresses and strain-rate sensitivity dependences on temperature

08 p1307 A71-21504

Compressed nitrogen thermodynamic calculations, determining virial equation of state applicability

08 p1376 A71-21905

Metastable radiative lifetimes of molecular states of nitrogen and CO, using time of flight and high resolution electron gun techniques

09 p1497 A71-22417

Oxygen and nitrogen molecules nonadiabatic electronic-vibrational interaction effect on vibrational relaxation during collisions with O atoms

09 p1497 A71-22530

Nitrogen-oxygen and nitrogen-argon mixtures viscosity, using oscillating disk viscometer to test corresponding states principle validity

09 p1546 A71-23010

Helium and nitrogen breathing effects upon intraocular pressure during and after near vacuum exposure in anesthetized and unanesthetized dogs

09 p1400 A71-23359

Cell free extracts with high nitrogenase activity from blue green alga *Anabaena cylindrica* by sonic oscillation and French press treatment

09 p1402 A71-23475

Nitrogen molecules vibrational excitation effect on elastic collisions frequency in nitrogen plasma

10 p1646 A71-23819

Spatial distribution of aurorae in O and molecular nitrogen ion emissions

10 p1602 A71-24553

Monograph on dense gases state parameters measurement at high temperatures, applying to nitrogen

10 p1697 A71-24676

Nitrogen excitation by fast protons and electrons impact, obtaining primary collision cross sections by measurements extrapolation to zero pressure

10 p1664 A71-24793

Ionization wave varieties in nitrogen glow discharge at various pressures and current densities from phase and group velocity measurements

10 p1654 A71-24973

Positive diatomic nitrogen ions dissociation during collisions with inert gas atoms, measuring mass and energy distributions from focusing parabolic spectrograph

11 p1801 A71-25227

Molecular nitrogen ion potential energy curves based on valence bond method, calculating sextet and quartet states at intermediate internuclear separation distances

11 p1801 A71-25365

Oxygen and nitrogen thermotransport in transition metals by microindentation hardness testing for concentration determination

11 p1778 A71-25533

Upper atmospheric molecular and atomic N and O diurnal variations correlated to atmospheric heating as function of solar UV radiation from sounding rocket data

11 p1757 A71-25775

Aircraft fuel tank nitrogen inerting, fire and explosion suppression for foreign particle contamination, sludge and lacquering reduction [ASME PAPER 71-GT-45]

11 p1810 A71-25978

Nb-N and Ta-N alloys, calculating electrical resistivity and solid solutions lattice constants at various temperatures

12 p1917 A71-27295

Nonreacting and reacting ideal gases expansion between interconnected chambers, considering nitrogen and carbon dioxide simultaneous pressure measurements

12 p1877 A71-27550

Vibrational energy transfer from excited nitrogen to CO and NO, describing flow tube measurements

12 p1934 A71-27760

Ar, N and Ne partial pressure tolerance in dogs, plotting saturation curves

13 p2005 A71-28038

Oxidation and nitrogen absorption protection of Cr alloy by Ni alloy claddings applied by gas pressure bonding

13 p2087 A71-29122

Freestream density field in nonequilibrium dissociating nitrogen flow over circular cylinder, using free piston shock tunnel and optical interferometry measurements

14 p2169 A71-29884

Nitrogen molecular excitation by photoelectron impacts in dayglow, investigating 1 PG band emission intensity variation with solar activity

14 p2235 A71-30349

Nitrogen-carbon dioxide system molecular resonant energy exchange vibration-vibration probability measurement by shock tube and IR emission monitoring, noting temperature effects

14 p2276 A71-30399

Equilibria of molybdenum-nitrogen solid solutions at various temperatures

14 p2260 A71-30474

Nitrogen solubility in W at high temperature, using metal high vacuum apparatus and mass filter partial pressure measuring instrument

14 p2260 A71-30475

Nitrogen inductive low pressure discharge, determining vibrational and rotational temperatures, ionization degree, electron temperature and energy balance by spectroscopic technique

15 p2451 A71-31487

Low carbon high chromium steel, emphasizing nitrogen content effects on temper brittleness

15 p2427 A71-31529

Thermal dissociation rate of undiluted nitrogen in shock tube over 5700 to 12,000 K range, using pressure measurements

15 p2451 A71-31549

Carbonaceous chondrites total nitrogen and carbon abundances, using gas chromatography

15 p2486 A71-31990

Nitrogen beam foil spectrum analysis, calculating transitions and decay times

15 p2452 A71-32598

Fast luminous fronts /ionizing waves/ in Kanal streamer and Townsend discharges in nitrogen, discussing optical space and time resolved measurements

15 p2459 A71-32648

Hydrogen and nitrogen pores formation in welds, considering gas concentration redistribution between liquid and solid metal

15 p2417 A71-32663

Rare gas ions molecular and dissociative charge transfer reactions with nitrogen, using statistical phase-space theory of chemical reactions

16 p2538 A71-32813

Shock tube measurements of vibration-vibration energy exchange probability in nitrogen-carbon monoxide-argon mixtures

16 p2613 A71-32896

Substrate and light dependent fixation of molecular nitrogen in *Rhodospirillum rubrum* tested for nitrogenase activity by manometric measurement

16 p2527 A71-33057

Austenitic high nitrogen chromium-nickel steels plastic deformation and heat treatment in plasma arc furnaces

16 p2596 A71-33910

Nitrogen and oxygen exit rate from subcutaneous gas pockets in rats during tissue blood flow elevation due to cobalt chloride injection

17 p2678 A71-34174

Time variation of electron density and temperature in pulsed lasers operating on nitrogen band transitions, using charged particle balance equation

17 p2751 A71-34382

Carbon and nitrogen abundances in howardites, enstatite and hypersthene achondrites

17 p2800 A71-34515

German monograph on electron production effect on channel breakdown in nitrogen, showing positive space charge accumulation near anode in gas discharge

17 p2788 A71-34775

German monograph on spark discharges behavior in nitrogen, carbon dioxide and argon at excess pressure covering Toepler, Weizel-Rompe and Braginskii laws applicability

17 p2779 A71-34799

High resolution differential cross section measurements for nonspherical potentials and molecular scattering of nitrogen and noble gases at thermal energies

18 p2949 A71-35898

Carbon dioxide-helium mixture IR laser action and power gain increase by nitrogen addition

18 p2932 A71-37006

Nitrogen X ray emission K alpha band behavior in zirconium mononitride in entire range of ZrN homogeneity

19 p3083 A71-37280

Spectral measurements of nitrogen continuum radiation behind incident shocks at high speeds, suggesting free bound neutral atom-electron interactions origin

19 p3172 A71-38718

Thermospheric atomic oxygen and molecular nitrogen number densities, discussing earth atmospheric absorption of solar UV lines

20 p3214 A71-38727

Striated discharge column behavior in nitrogen with moving and stationary striations

20 p3273 A71-39046

NTWO as FORTRAN 4 family of subroutines developed on 7094-7044 system for determining thermodynamic and transport properties of nitrogen
20 p3253 A71-39268

Pulmonary nitrogen washout and carbon monoxide uptake, developing dynamic mathematical models for volume and distensibility distributions in airways and alveoli
20 p3193 A71-39441

Cold work peak characteristics in undeformed aged niobium-nitrogen alloys from internal friction spectrum
20 p3252 A71-39464

Lower thermospheric density and molecular nitrogen partial density rocket measurements, obtaining neutral gas temperature vertical distribution and ion density profile
20 p3222 A71-39699

Dayglow neutral and ionized diatomic nitrogen band system emission excitation mechanism from vibrational and rotational intensity distributions observations
20 p3226 A71-39829

F region nightglow emission mechanism in terms of oxygen cations reactions with diatomic nitrogen and subsequent recombination
20 p3226 A71-39832

Day airglow columnar emission rates for Lyman-Birge-Hopfield system of molecular nitrogen as function of solar zenith angle, using OGO 4 observations
20 p3231 A71-39892

Spiral galaxies N/O abundance gradients across disks from H II regions spectra
21 p3445 A71-40409

Reversible charge exchange reactions effects on ionization equilibrium of nitrogen in interstellar space
21 p3445 A71-40412

Nitrogen equilibrium solubility dependence on slag basicity and gas phase nitrogen/carbon monoxide contents in aluminosilicate melts
21 p3399 A71-40470

Nitrogen adsorption on single crystal W planes by flash desorption experiment, noting work function change dependence on planes
21 p3345 A71-40539

Nitrogen alloying effects on relaxation resistance of Cr-Mn austenitic steel
21 p3402 A71-41092

Cr and Cr-Ni ferritic and austenitic steels, investigating high temperature nitriding for intensifying nitrogen diffusion saturation
21 p3389 A71-41098

Nb nitriding kinetics and external effects observations, noting nitrogen diffusion through crystal lattices
21 p3404 A71-41163

Electrical conductivity and thermoelectric power measurements for polycrystalline beta-SiC heavily doped with nitrogen, estimating electron effective mass and carrier mobility at high temperatures
21 p3433 A71-41307

Upper atmospheric molecular and atomic nitrogen and oxygen diurnal variations correlated to atmospheric heating as function of solar UV radiation from sounding rocket data
22 p3532 A71-41543

German monograph on thermal equation of state for nitrogen vapor-liquid phase equilibrium covering vapor pressure and density, phase diagrams, critical temperature, etc
22 p3574 A71-41716

Hg condensation characteristics on Cs substrate in high velocity nitrogen carrier gas, formulating one dimensional flow model based on two phase three component gas dynamics
22 p3620 A71-41876

Oxygen, hydrogen and nitrogen determination in high melting point metals
22 p3563 A71-42364

Nitrogen, argon and helium viscosity measurements, obtaining density expansion by statistical analysis
22 p3621 A71-42369

Visible coherent radiation generation mechanism in ionized oxygen and nitrogen, considering free radical stabilized on discharge tube wall and metastable atom creation
23 p3706 A71-42889

Population inversion development and breakdown in active medium produced by plasma generation during disordered discharge in molecular nitrogen laser
23 p3684 A71-43406

Molecular oxygen partial pressure effect on nitrogen afterglow intensity, proposing three-body reaction kinetics
23 p3707 A71-43500

Apollo 12 samples total C and N abundances suggesting indigenous lunar material with solar wind component
23 p3750 A71-43698

Nitrogen and neon cations number density time dependence during plasma decay in neon-nitrogen mixtures
23 p3711 A71-43881

Evolutionary meaning of nitrogen and carbon sequences in Wolf-Rayet stars
23 p3770 A71-44064

Heat transfer characteristics of two phase nitrogen film boiling in tubes with tape-generated swirl flow
23 p3783 A71-44195

Temperature and electron density measurements for free jet of ionized nitrogen at atmospheric pressure by plasma spectroscopy, estimating Prandtl numbers
23 p3664 A71-44197

Absolute transition probabilities derivation for excitation of atmospheric nitrogen molecules and positive ion systems by electrons impact from optical measurement
24 p3850 A71-44371

NITROGEN ATOMS

Gas phase atomic hydrogen, nitrogen and oxygen detection by photoelectron spectroscopy of ground state, suggesting application to gas phase kinetics
04 p0548 A71-14799

Two body N atoms recombination rate coefficient, using photometric analysis
09 p1498 A71-23400

Nighttime ionospheric atomic nitrogen and nitric oxide production and loss mechanisms effect on nightglow continuum
09 p1441 A71-23641

Atomic nitrogen far UV emission excitation in auroral ionosphere due to electron impact dissociations
10 p1605 A71-24792

Atomic N and C photoionization cross sections by shock tube vacuum UV spectrometry
10 p1646 A71-24990

Lower thermosphere atomic nitrogen concentration during maximum solar activity, using rocket-borne radio frequency and time of flight mass spectrometers
16 p2572 A71-33843

Transition metal carbides and nitrides ordered structures, determining C and N atoms positions with electron and neutron diffractions
16 p2597 A71-33921

IR chemiluminescence of atomic nitrogen reaction with molecular oxygen, obtaining quantum efficiency
18 p2874 A71-35838

Excitation cross sections for resonance states by electron impact on atomic nitrogen and oxygen over aeronautical energy range
18 p2949 A71-36350

Nitrogen atoms chemiluminescent reaction spectra with carbon tetrachloride, ethylene and methylene chloride, noting application to artificial clouds formation
19 p3014 A71-38634

Lower thermosphere neutral composition fine structure data from rocket-borne time of flight mass spectrometer, emphasizing atomic nitrogen vertical distribution
20 p3222 A71-39697

NITROGEN COMPOUNDS

NT ALUMINUM NITRIDES

NT AMIDES

NT AMMONIA

NT AMMONIUM NITRATES

NT ATROPINE

NT AZIDES [INORGANIC]

NT BERYLLIUM NITRIDES

NT BORON NITRIDES

NT CELLULOSE NITRATE

NT DINITRATES

NT HYDRAZINE NITRATE

NT HYDRAZINE NITROFORM

NT HYDRAZONES

NT HYDROGEN CYANIDES

NT IMIDES

NT ISOPROPYL NITRATE

NT NICOTINE

NT NITRATES

NT NITRIC ACID

NT NITRIC OXIDE

NT NITRIDES

NT NITRITES

NT NITRO COMPOUNDS

NT NITROAMINES

NT NITROBENZENES

NT NITROGEN DIOXIDE

NT NITROGEN HYDRIDES

NT NITROGEN TETROXIDE

NT NITROGLYCERIN

NT NITROMETHANE

NT NITROUS OXIDES

NT PETN

NT PILOCARPINE

NT POLYIMIDES

NT SILICON NITRIDES

NT THURONIUM

NT THYMINE

NT TITANIUM NITRIDES

NT TRINITROTOLUENE

NT TRYPTOPHAN

NT URACIL

NT UREAS

NT ZIRCONIUM NITRIDES

Oxygen consumption by nitrogen starved nonsynchronous Chlorella culture during different assimilation of nitrogen salts in darkness and light
16 p2531 A71-33461

NITROGEN DIOXIDE

Nitrogen dioxide ground and excited state self-consistent fields energy calculations, discussing electron transitions probable assignments in spectrum
12 p1934 A71-27759

Nitrogen and sulfur dioxide reactions in isolation, determining rate by concentration measurements using light absorption technique
15 p2465 A71-32082

Mars short-wave line spectra from measurement with reflector, estimating nitrogen dioxide content in atmosphere
20 p3290 A71-39307

NITROGEN HYDRIDES

Franck-Condon factors, r-centroids and absolute band transition probabilities of NH, SiH, molecular sulfur and SO
10 p1645 A71-24544

NITROGEN IONS

Seasonal altitude variation of atomic ion-electron ratio of oxygen/nitrogen species in F1 region, comparing to radar measurements
01 p0076 A71-11507

Molecular N ion production, studying cross sections, collisions kinetic energies and isotopic substitution
06 p0929 A71-17407

Crossed beam model of nitrogen ion-molecular oxygen reactions in upper atmosphere as function of collision energy
08 p1251 A71-21784

Solar chromospheric emission line identification at 4097.3 Å, discussing N III transition
10 p1666 A71-23783

Continuous nitrogen and oxygen ion spectra due to photoionization and free ion transfers at high temperatures, calculating absorption coefficient
16 p2662 A71-33040

Auroral 4778 Å positive nitrogen ions emission relation to low energy electron precipitation, using polar orbiting Aurorae satellite photometer and particle detector data
16 p2568 A71-33794

Spectral line emission from nitrogen ions, identifying charge by Doppler shift technique application to beam foil light source
16 p2615 A71-34129

Velocity determination in hypersonic low density wind tunnel based on high energy electron beam produced nitrogen ions time of flight
17 p2670 A71-34887

Infrasonic pulsations of optical auroral luminosity in 3914 Å positive molecular nitrogen ion and 5577 Å O I emission measurement by double photometer system
19 p3048 A71-37395

Effective cross section and excitation functions measurements for molecular nitrogen ion first negative system spectral bands by fast electrons
21 p3419 A71-41108

Molecular nitrogen ions collisions with He and Xe gas atoms, discussing processes based on atomic N ion fragment velocity distribution measurements at varying electron energies
21 p3421 A71-41405

Nitrogen ions surface interactions with Al surfaces at and above earth satellite speeds, measuring normal and tangential momentum accommodation coefficients
22 p3577 A71-41980

NITROGEN OXIDES

NT NITRIC OXIDE

NT NITROGEN DIOXIDE

NT NITROGEN TETROXIDE

NT NITROUS OXIDES

Nitric oxide vibrational relaxation times in Ar from IR emission measurements at high temperature
02 p0287 A71-12495

CO laser emission lines and nitrogen oxides absorption lines spectral coincidences observations
05 p0762 A71-16339

Gaseous fuel mixtures containing nitrogen oxides, discussing combustion mechanism
09 p1403 A71-22531

Stratospheric ozone reduction through catalytic action of nitrogen oxides from SST exhaust, discussing degrading effect on atmospheric radiation shield
18 p2874 A71-36922

Earth UV dayglow observation by Aerobee rocket-borne scanning spectrometer, noting features due to atomic oxygen and nitrogen and nitrogen oxide gamma band
20 p3226 A71-39830

NITROGEN PLASMA

Nitrogen plasma flow over flat plate, comparing probe and probeless methods for boundary layer concentration profile measurement
02 p0254 A71-12648

Nitrogen plasma viscosity at atmospheric pressure, using moving sphere resistance measurement
05 p0786 A71-16225

High temperature nitrogen plasma, calculating thermodynamic and electrical parameters dependence on pressure and temperature
08 p1342 A71-21917

Nonequilibrium excitation in recombining nitrogen plasma nozzle flows
[AIAA PAPER 70-44] 09 p1498 A71-22093

Italian book on mixed plasmas equilibrium compositions and thermodynamic properties, covering numerical values tabulation for nitrogen mixtures with He, Ar and Xe
09 p1505 A71-23353

Mixed plasmas transport properties at one atmosphere and 5000-35,000 K, considering helium-nitrogen, argon-nitrogen and xenon-nitrogen plasmas
12 p1986 A71-27188

Nitrogen plasma electrical and thermal conductivities and radiative source strength at atmospheric pressure and 9,000-12,500 K, using Hall probe and optical methods
[AIAA PAPER 71-590] 15 p2454 A71-31535

Ther.e-phase plasmatrons with hot W electrodes for obtaining plasma of inert gases, nitrogen and hydrogen
15 p2457 A71-32267

Conductivity measurement of shock generated nitrogen plasma in transverse magnetic field, considering vibrationally excited molecules role in electron collision frequency
16 p2616 A71-32899

High temperature nitrogen plasma emission spectrum in 2500-5000 A range, estimating negative ion photoionization cross sections
16 p2613 A71-32900

High temperature nitrogen plasma, calculating thermodynamic and electrical parameters dependence on pressure and temperature
17 p2789 A71-35262

NITROGEN TETROXIDE

Rocket engines with nitrogen tetroxide/hydrazine injectors destructive instability due to pressure disturbances, establishing origin, propagation velocity and pops extent by streak photography
[WSS/CIPAPER 70-25] 06 p0942 A71-17653

Nitrogen tetroxide/hydrazine pulse mode rocket engines structural failure due to chemically reactive gaseous hot spots causing high pressure spiking and detonation initiation
[WSS/CIPAPER 70-24] 06 p0944 A71-17663

NITROGLYCERIN

Surface temperature discrepancy during flameless vacuum burning of trinitroglycerin gunpowder due to vaporization of volatile components
15 p2462 A71-31373

Nitroglycerin powder combustion acoustic instability, determining mean pressure and sample and combustion chamber geometry effects
17 p2840 A71-35700

NITROMETHANE

Ignition and nondetonating decomposition of liquid nitromethane explosive at 10 kbar pressure
05 p0795 A71-16517

Nitromethane detonation initiation by long duration low amplitude shock waves
07 p1182 A71-19242

Gaseous nitromethane-oxygen mixtures detonation characteristics, determining reaction time by schlieren technique
08 p1346 A71-20862

Shock compressed tetranitromethane mixtures with various benzene ethyl iodide proportions, investigating lateral discharge wave effects on detonation process structure
15 p2511 A71-31382

NITRONIUM COMPOUNDS

NT NITRONIUM PERCHLORATE

NITRONIUM PERCHLORATE

Ammonium nitrate, ammonium perchlorate and nitronium perchlorate as liquid oxidizers for hybrid propellant rocket engines, discussing oxidizer/kerosene mixing ratio
10 p1657 A71-24275

NITROUS OXIDES

Nitrous oxide tropospheric abundance from IR solar spectrum altitude variation
01 p0073 A71-10139

CW nitrous oxide laser action at 81.5 and 263.4 micrometers in optically pumped ammonia gas, measuring rotational and inversion frequencies
03 p0434 A71-13476

CW laser output in carbon dioxide and nitrous oxide induced by vibrational energy transfer from excited carbon monoxide
03 p0438 A71-13893

Coronary blood flow measurements during strenuous upright exercise, using nitrous oxide method
09 p1400 A71-23362

Thermal decomposition kinetics of nitrous oxide in shock tube, measuring IR emission behind reflected wave
16 p2539 A71-32910

Nitrous oxide internal and rotational partition functions for temperature range 20 to 350 K, using molecular constants tabulated by Pilva
19 p3106 A71-37408

High temperature oxidation of ammonia, carbon monoxide and methane by nitrous oxide in shock tubes, using optical interferometry and UV/IR emissions
19 p3012 A71-38086

High pressure transversely excited pulsed nitrous oxide laser active mode locking at subatmospheric pressures
20 p3244 A71-39101

Nitrous oxide dissociation as natural source of stratospheric nitric oxide, noting estimates use as yardstick for artificial source
23 p3642 A71-43347

NOBLE GASES

U RARE GASES

NOBLE METALS

NT GOLD

NT RUTHENIUM

NT SILVER

Stress corrosion cracking mechanism, considering anodic dissolution, local surface enrichment and hydrogen embrittlement in noble metal species
04 p0610 A71-14892

Impurity lifetime broadening due to scattering at Fermi surfaces, calculating Dingle temperature in noble metals
11 p1808 A71-26145

Bronsted relationship between adsorption heat and activation energy in electrocatalysis of purified orthophosphoric acid and phase-oxide-free noble metals
21 p3345 A71-40540

German book on metallurgy, production and application of rare metals, discussing high vacuum technology
21 p3399 A71-40783

Noble and transition metals dilute alloys electronic structure in hybridized tight binding nearly free electron representation, using Harrison-Kanamori pseudopotential theory
24 p3860 A71-45129

Noble or transition metals based dilute alloys electronic structure, describing pure metal band structure by interpolation scheme of hybridized tight binding and nearly free electron orbitals
24 p3860 A71-45130

NOCTILUCENCE

U LUMINESCENCE

NOCTILUCENT CLOUDS

Noctiluent cloud particle size composition and origin from sounding rocket flight and control collecting surfaces
02 p0246 A71-12702

Cosmic dust in mesosphere and upper atmosphere during weak noctiluent cloud from rocket collecting flight
02 p0246 A71-12703

Particle size collected on electron microscope grids attached to Luster rocket sampling surfaces during noctiluent cloud display
02 p0246 A71-12705

Photographic observation of noctiluent cloud occurrence over geographical location during sounding rocket flight
02 p0246 A71-12706

Noctiluent clouds, discussing mesosphere thermodynamics and water vapor content, solar rain, etc
03 p0414 A71-14019

Noctiluent cloud observations and research covering geographic distribution, annual and diurnal variations, kinematics, volcanic connections, cosmic dust eruptions, etc
04 p0584 A71-15677

Soviet book on noctiluent clouds covering propagation region, occurrence frequency, morphology, dynamics, color, spectrum, composition, relation to solar and ionospheric phenomena, etc
10 p1604 A71-24734

Mesospheric extraterrestrial dust and trapped water model of noctiluent cloud formation in high latitude summer conditions, using meridional trajectories
14 p2231 A71-29721

Mesospheric /noctiluent/ cloud physics - Conference, Riga, November 1968
14 p2231 A71-29955

Atmospheric and cosmic origin of noctiluent clouds, discussing solar wind effects on H, O and water vapor molecules in mesosphere and thermosphere
14 p2232 A71-29956

Noctiluent cloud formation from water vapor concentrations in mesosphere and lower thermosphere of arctic and midlatitude regions measured by rocket-borne RF mass spectrometers
14 p2232 A71-29957

Mesospheric height-temperature measurements in noctiluent cloud zone of Southern Hemisphere
14 p2232 A71-29958

MHD processes of upper atmosphere in mesospheric cloud formation, discussing solar wind-magnetic field interactions and equilibrium for Pikeler bomb
14 p2232 A71-29960

Mesospheric cloud statistics compared with 200 MHz solar radio emission during summers of 1958-1966
14 p2232 A71-29961

Spectral luminance and transmittance of noctiluent clouds for spaceborne photometric observation, using American-Swedish rocket particle experiment
14 p2232 A71-29962

Noctiluent cloud observation from space, discussing instruments, radiation spectrum, global scale formation, time dependent structures and satellite orbit requirements
14 p2232 A71-29963

Optical anomalies associated with Tungusk meteorite fall in 1908, noting volcanic activity and noctiluent cloud formations
14 p2233 A71-29964

Spatial-temporal harmonics of noctiluent cloud occurrences during IQSY with maximum displays after summer solstice in both hemispheres
14 p2233 A71-29965

Noctiluent cloud data statistical treatment by meteor observation double counting method
14 p2233 A71-29966

Noctiluent cloud incidences relation to solar activity variations, determining frequency spectrum and four year occurrence cycles
14 p2233 A71-29967

Noctiluent clouds observations and data acquisition, considering cloud amount and thickness calculations
14 p2233 A71-29969

Noctiluent cloud observations at Tomsk, Novosibirsk and other Siberian locations from 1965 to 1968
14 p2233 A71-29970

Noctiluent cloud morphology and kinematics from photographic observations near Moscow
14 p2233 A71-29971

Noctiluent clouds occurrence frequency relationship to mesospheric circulation
14 p2235 A71-30351

Mesopause thermal transitions during spring and autumn based on noctiluent cloud observations, discussing stratospheric-mesospheric coupling effects
15 p2400 A71-31988

Mesospheric noctiluent cloud formations observations from space by cosmonaut on 9 June 1970 over Arabian peninsula
15 p2496 A71-32727

Noctiluent cloud nature from cosmic dust particles collection and detection, discussing mass, absolute falling velocity and model theories
16 p2641 A71-33765

NOCTURNAL VARIATIONS

Night airglow measurements over Bulgaria, showing midnight minimum, maximum between 0100 and 0200 hours local time, steady airglow periods and random fluctuations
10 p1599 A71-23877

Electron precipitation in nocturnal E region from radiowave and rocket data, calculating ionization rates and midlatitude morphology
11 p1815 A71-25552

Upper atmosphere hydroxyl emission nocturnal average vibrational temperature correlation with molecular oxygen emission intensities
19 p3049 A71-37403

Nighttime hydroxyl airglow emission intensity and excitation temperature measurements, noting seasonal and nocturnal variations
20 p3227 A71-39834

Atomic oxygen 6300 and 5577 A emissions nocturnal covariation from nightglow observation, considering relation to F layer height changes
23 p3667 A71-43131

NODES (STANDING WAVES)

Nodal points stresses determination from finite element solved elastic problems, discussing thin disk stresses as function of mesh pattern regularity
11 p1851 A71-26312

Free vibrations of isotropic nonhomogeneous circular plates, deriving closed form expressions for nodal frequencies
12 p1983 A71-27587

NOISE [SOUND]

NT AERODYNAMIC NOISE

NT AIRCRAFT NOISE

NT ENGINE NOISE

NT JET AIRCRAFT NOISE

NT ROCKET ENGINE NOISE

NT SONIC BOOMS

NT THERMAL NOISE

Physiological effects of noise - Conference, Boston, December 1969
03 p0358 A71-13151

Sound effects on endocrine function and electrolyte excretion in animals and man, considering adenohipophyseal, neurohipophyseal and thyroid functions, diuresis and natriuresis
03 p0359 A71-13153

Endocrine and metabolic effects of noise in normal, hypertensive and psychotic subjects, considering increased corticoadrenal and adrenergic activity
03 p0359 A71-13154

Plethysmographical study of noise effects on hearing and peripheral vasoconstriction in man and animals

03 p0359 A71-13155

Quantitative relation between temporary threshold shift and peripheral circulatory effects of sound, using finger pulse amplitude strain gage

03 p0359 A71-13156

Extraauditory effects of sound on senses, concerning visual functions, nystagmus, galvanic skin response and audioanalgesic use

03 p0359 A71-13158

Audioconditioned convulsive response (ACCR)/characterization, investigating age, auditory conditioning and environmental noise effects on sound-induced seizures in mice

03 p0360 A71-13162

Impulsive sound signals perceived noisiness in anechoic chamber, investigating duration, intersignal interval, repetition and frequency effects

05 p0712 A71-16277

Aerospace environments noise effects on human physiology and speech communication

08 p1244 A71-20710

Helium-rich white dwarfs convective envelopes, acoustic noise generation and corona formation

12 p1970 A71-27746

Noise emission and acoustic efficiency in pulsating combustors, considering sound pressure level

13 p1213 A71-28618

Noise exposure index from mean sound intensity measurement, considering harmful effects on humans

13 p0201 A71-29284

Planar and nonplanar transistors noise factor dependence on signal source impedance and emitter current, considering amplification and frequency conversion application

14 p2213 A71-30628

Nonresonant noise from turbulent nonpremixed flames, discussing burner diameter, impingement angle and equivalence ratio effects on acoustic power radiated

14 p2295 A71-30779

Discrete tone noise generation by high speed fans and compressor blades, using McCune analysis for linearized three dimensional compressible flow in infinite annulus

15 p2468 A71-31555

Psychometric analysis of annoyance by wideband noise with superimposed narrow band component, using multiple regression and scaling method

19 p0308 A71-38061

Noise exposure effects on human physiological and psychological functions and performance

20 p3192 A71-38959

Book on noise effects on man covering audiometry, aural reflex, hearing damage risk, physiological responses, motor performance and speech communication

20 p3193 A71-39874

Noise sources in axial flow fans, considering radiation from turbulent boundary layers, scattering of incident turbulence and secondary flow influence

21 p3323 A71-40710

NOISE ATTENUATION

U NOISE REDUCTION

NOISE ELIMINATION

U NOISE REDUCTION

NOISE HAZARDS

U HAZARDS

U NOISE [SOUND]

NOISE INJURIES

Cochlear sensory epithelium and Corti organ degeneration after noise exposure in guinea pigs and cats, using scanning electron microscopy

02 p0199 A71-12364

Book on eye injuries covering mechanical trauma, neuro-ophthalmology, chemical, thermal, radiation, electrical and sonic injuries, etc

05 p0711 A71-17010

Nonauditory and auditory physiological effects of noise, discussing hearing conservation, noise measurement and noise hazard

11 p1726 A71-26511

Aircraft noise effect on hearing impairment of cockpit crews in civil aviation, using audiometric evaluation

19 p3008 A71-38222

NOISE INTENSITY

Human subjective responses to approaching and receding aircraft sounds during flight over stationary observer

01 p0127 A71-10345

Discrete servo position gage accuracy in presence of high uncorrelated noise level, using Markov chain

01 p0038 A71-11233

Moderate acoustic stimuli effects, discussing subjective noise ratings relation with physiological and mental state changes

02 p0208 A71-12838

Current interception in TWT electron beam affecting minimum noise factor level

03 p0386 A71-13803

Noise generation increase with unchanged mass flow rate by cone angle diffusers in jet nozzles, considering far field sound pressure level

[ASME PAPER 70-WA/GT-5] 03 p0402 A71-14117

Aircraft sound measurement standards, evaluating airport noise control and permissible levels

03 p0373 A71-14248

Low velocity and coaxial jet noise data and correlations for noise prediction of turbofan engines

05 p0796 A71-17155

Noise nuisance value index /noise pollution level/, considering aircraft and motor vehicle noise surveys and tradeoff of intensity against duration

08 p1333 A71-20802

Jet aircraft noise over residential areas, discussing actual and permissible noise levels and proposals for remedial action

08 p1230 A71-21163

F-100 pilots acute HF hearing loss due to noise ground environment and excessive in-flight noise exposure

09 p1400 A71-23249

Engine inlet noise prediction from static test and flyover data as function of time at various observer locations, examining suppression effects on total spectra

10 p1659 A71-24250

Two dimensional sound wave equation solution in terms of time retarded arguments, deriving analytical expressions for aircraft noise intensity and power

11 p1797 A71-25144

Transonic compressor shock wave noise generation and decay rates at multiple tones, using sonic boom analysis

11 p1703 A71-25953

Microwave radiometers transfer calibrations by noise injection through avalanche diode directional coupler similar to plasma tube

11 p1739 A71-26438

Noise disturbance near large airports, considering aircraft noise, public annoyance and socio-psychological conditions

12 p1875 A71-27478

Temporal and spectral stimuli combinations effects on judged noisiness of aircraft sounds by college students

12 p1868 A71-27531

Aircraft noise on and near airports and factors affecting its intensity

13 p1997 A71-29304

Optimal antennas statistical synthesis for minimum noise power for given signal gain

14 p2195 A71-30102

Atmospheric noise statistical characteristics, investigating short term variations, intensities and application to communications

14 p2237 A71-30964

Proportional fluid amplifier, measuring deflection angle, jet turbulence and noise level

15 p2390 A71-32052

Community aircraft noise intensity indexes from annoyance and physiological reaction standpoint, discussing sleep interruption, hearing loss, communication interference, etc

15 p2364 A71-32242

Radio wave propagation in ionosphere, measuring plasma frequency, cyclotron cut-off and noise level

15 p2373 A71-32443

Transistor minimum noise figure in low noise microwave amplifier circuit

15 p2378 A71-32635

Civil V/STOL aircraft projects, discussing design, lift fan engines, weights, flight performance, noise levels, safety and comfort standards

16 p2525 A71-34191

Subsonic turbulent jets acoustic emission, calculating noise intensity in far field for various Mach numbers

17 p2725 A71-34213

Frequency and level dependent discrepancy between free field and pressure thresholds at low frequencies due to physiological noise produced under earcan

17 p2681 A71-34699

Propulsion systems trends for 1980s, discussing environmental noise levels, stoichiometric gas turbine engines for military aircraft, high bypass ratio engines for V/STOL aircraft, etc

17 p2795 A71-35625

Diurnal distribution, latitudinal occurrence and intensity patterns of ELF, VLF and LF whistler-mode noise emissions from Alouette 2 satellite observation

19 p3016 A71-37364

Jet aircraft flyover noise measurement, determining average intrusion level in residential communities under approach and departure corridors

19 p2996 A71-37497

Prediction methods for human aircraft noise perception, assessing weighted sound pressure level or complex loudness-noisiness computation scales

21 p3325 A71-40866

Noy curves in perceived noise levels, noting relative noisiness dependence on relative intensities

21 p3325 A71-40867

Impurity photoconductivity, generation-recombination noise and temperature dependences of Hall coefficient and equilibrium carrier mobility in p-type cobalt-doped germanium

21 p3429 A71-41213

Unfavorable high intensity noise effects on auditory and motor analysors during space flight

22 p3495 A71-42793

Low noise IR range radiometer, including impedance matching and narrow band filtering

23 p3678 A71-43534

Fixed configuration optimal control of linear systems with state and control dependent noise

23 p3658 A71-44082

Combined heat, noise and vibration stress effects on human performance and physiological functions including heart rate, body temperature and mental arithmetic

23 p3637 A71-44247

NOISE MEASUREMENT

U ACOUSTIC MEASUREMENTS

NOISE METERS

Multichannel sound level meter capable of direct and continuous measurement and recording

18 p2897 A71-36221

Microwave acoustic delay device incorporated in phase discriminator for AFC, FM noise meters and pseudo-superheterodyne receivers

18 p2893 A71-36599

NOISE PROPAGATION

Nonlinear planar propagation of sinusoidal and band-limited noise signals in air, extending to spherical waves

05 p0784 A71-17157

Sound radiation by rotor from interaction with nonuniform flow, considering multiple blades

05 p0697 A71-17159

Far field sound radiated from steady loading of isolated subsonic rotor, noting dependence on spatial uniformity of flow entering rotor

05 p0697 A71-17160

Aerodynamic sound radiation from point force in accelerative circular motion, obtaining closed form for overall far field radiation

05 p0784 A71-17162

Fan noise random propagation and sound power in cylindrical air ducts from modal spectra and pressure measurements

10 p1596 A71-24834

Combustion generated aerodynamic noise, considering sound radiation from open turbulent flames, spectral content, power output and origin

14 p2338 A71-30780

Jet aircraft noise generation, transmission and reduction, emphasizing turbofan engine acoustics, operational characteristics and exhaust sound

15 p2349 A71-32241

Experimental research at Building Research Station on outdoor sound propagation for building design in relation to aircraft and road traffic noise

17 p2674 A71-35237

Aircraft noise propagation in city streets due to intertorn V/STOL and helicopter ports, using small scale models

20 p3178 A71-39264

Multiple pure tone and broadband noise generation in high speed turbofans, noting analytical model

20 p3277 A71-39773

NOISE REDUCTION

Coherent binary reception channels noiseproof qualities in presence of fluctuating noise and single concentrated bursts

01 p0030 A71-10473

Aladin 2 interurban Stol transport design with blown wings and jet deflection by wing flaps, emphasizing engine noise reduction

01 p0005 A71-10749

Noise reduction relationship to air transportation progress, considering cost/technology balance, quiet engine, research and development programs, etc

01 p0183 A71-10819

Flight helmet sound attenuation test, using Manikin method

01 p0026 A71-11189

Steep approach to landing for jet transport aircraft noise abatement, using ground based equipment and onboard TV display

01 p0126 A71-11311

Illiac 4 and Spectra 70 computers comparison in terms of logic circuit noise immunity and system noise sources

03 p0388 A71-13179

Noise interference problems solution by electrical and physical design action, discussing contact arc and ringing suppression

03 p0388 A71-13243

Axial flow compressors radiated sound reduction by segmented stator blades

03 p0353 A71-13283

Holographic twin image elimination by nonlinear method based on statistical differences in objects and diffraction fields

03 p0425 A71-13656

High bypass ratio jet engine noise reduction in relation to mission requirements
[ASME PAPER 76-WA/GT-13] 03 p0471 A71-14121

High bypass ratio fan engine design for low noise, discussing acoustic treatment, turbine noise and modulation tones
[ASME PAPER 70-WA/GT-14] 03 p0471 A71-14122

Large low-speed fan for low noise production, testing performance on suppression effects of acoustic treatment and exhaust jet noise
[ASME PAPER 70-WA/GT-15] 03 p0471 A71-14123

Helicopter noise minimization by various piloting maneuvers, discussing takeoff and landing, transition to forward flight, route selection, etc
04 p0531 A71-15408

Helicopter design for cabin noise level reduction
04 p0532 A71-15423

Jet noise suppressor development test techniques and facilities, discussing model tests at hydrodynamic ONERA wind tunnel
04 p0639 A71-15819

TWT noise level minimization in 8 mm band with circular spiral slow wave structure and five electrode gun
05 p0723 A71-16874

Rotating blade noise technology, discussing vehicles and components, noise nature, generation, reduction and prediction
05 p0695 A71-17158

Argon ion laser plasma tube anodic coherent oscillations and noise suppression, using secondary discharge between anode and auxiliary cathode
06 p0906 A71-17306

Pulsed phase locked automatic phase control system linear model, discussing optimal white noise filtration with integrating filter
06 p0867 A71-17377

Supersonic aircraft turbojet engine exhaust noise suppressor research program, predicting full scale noise spectra from model suppressor tests
[AIAA PAPER 68-1023] 06 p0945 A71-17693

Supersonic jet noise suppressor with tubes and shrouds, examining flow and acoustic characteristics
[AIAA PAPER 71-153] 06 p0884 A71-18595

Turbofan engine noise reduction, using acoustic liners in inlet and exhaust ducts
[AIAA PAPER 71-183] 06 p0947 A71-18622

Noise reduction in turbulent jet by repeated air injection at boundary of jet core
06 p0848 A71-18704

Electrostatic charging noise measurement, reduction and flight test verification
07 p1021 A71-19937

SST noise suppression research, discussing engine noise suppressor conceptual designs and test results with installed devices
07 p1184 A71-20302

Digital adaptive spectral filtering canceling undesired power spectra based on measured mean square values ratio and stochastic approximation methods
07 p1082 A71-20408

Aircraft optimum minimum noise takeoff profile, solving by equations of motion system for jet aircraft
08 p1331 A71-20779

Helicopter noise minimization by various piloting maneuvers, discussing takeoff and landing, transition to forward flight, route selection, etc
08 p1230 A71-21049

Jet aircraft noise over residential areas, discussing actual and permissible noise levels and proposals for remedial action
08 p1230 A71-21163

Holographic recording intermodulation noise suppression by image wave field distortion and retrieval, considering signal to noise ratio
08 p1287 A71-21187

Q-Star experimental aircraft design and acoustical characteristics to study Quiet Aircraft Technology
08 p1231 A71-21441

Noise abatement power cutback takeoff procedures, maximum altitude approaches and preferential runway systems for noise relief
08 p1232 A71-21813

Subsonic jet engine noise reduction, considering turbojets, turbofans and jet suppressors
08 p1349 A71-21814

Noise reduction at source, flight methods adjustments and airport compatible land use for jet noise abatement
08 p1378 A71-21815

Land use strategies and noise reduction by source control and flight procedures for noise exposed areas minimization
08 p1378 A71-21818

Community reactions to aircraft noise, discussing short term interim alleviation measures in airport operations and runway usage scheduling
08 p1378 A71-21819

Noise pollution control and airport noise levels abatement regulation by state government, taking into account economic and technical feasibility
08 p1379 A71-21825

Aircraft noise abatement control on international basis by setting acoustic technological capability compulsory standards of quietness
08 p1379 A71-21826

Federal legislation and regulatory activities for control and abatement of aircraft noise
08 p1379 A71-21827

Federal legislation and regulation of aircraft noise, legal rights of airport neighbors and legal aspects of compatible land use, discussing noise control efforts
08 p1379 A71-21829

Land use control in aircraft noise abatement, considering airport development and community goals
08 p1380 A71-21836

Signal fluctuation noise reduction with input screen inertia by lagging component introduction to telescopic system
08 p1294 A71-21903

Line fed microelectrode amplifier for electrophysiology, discussing noise reduction
08 p1249 A71-21974

Noise reduction in Rudd type laser velocimeter by conversion to light scattering system
09 p1453 A71-23695

Parasitic noise reduction in CW Nd-YAG laser output
10 p1620 A71-24154

Business jet aircraft noise certification, discussing test programs and cost reduction
[SAE PAPER 710384] 10 p1555 A71-24249

Receiver systems for 100 meter Effelsberg radio telescope using cryogenically cooled parametric amplifiers for receiver system noise minimization
10 p1578 A71-24510

VTOL lift fan engine design for minimum noise levels, noting silencers application
10 p1659 A71-24750

Noise reduction by antisound, using directly opposing field with identical wave geometry and reversed phase
10 p1643 A71-24948

Pulse radar moving target indication and stationary targets reflection suppression, using recursive type digital filter and quadrature channels for improving signal detectability
10 p1579 A71-25068

Single and double balanced diode mixers characteristics comparisons for spurious response suppression, considering RF third order intercept technique
11 p1737 A71-25674

Monopulse receiver design system and image band noise factors tradeoffs, discussing preselector and integrated front end trends
11 p1737 A71-25676

Large gas turbine generator sets silencing, including silencer shells and doublewall acoustical/concrete enclosures
[ASME PAPER 71-GT-26] 11 p1812 A71-25968

TWT amplifiers in radar and communication systems, investigating AM and FM noise theory and reduction
11 p1734 A71-26435

Axial flow fan noise, investigating louvers effects on sound field
12 p1945 A71-26704

Optical communication system combining heterodyne noise suppression and direct detection advantages concerning spatial coherence and wide field-of-view receiver optics
12 p1903 A71-26789

Partition walls sound insulation by porous absorbers, discussing differential equations and acoustic properties
12 p1929 A71-27062

Aircraft propulsion system testing, stressing noise reduction and inlet-engine exhaust system compatibility
[SAE PAPER 710450] 13 p2114 A71-28328

Wind noise reduction by windshields, considering effect of mean flow velocity, turbulence, flow direction, windscreen shape and size, covering material and microphone location
13 p2040 A71-29283

Operations research minimum cost model of aircraft noise abatement in airport communities
[AIAA PAPER 71-525] 14 p2339 A71-29551

Earmuff hearing protectors evaluation for attenuation of narrow band noise on experienced subjects
14 p2188 A71-30196

Noise attenuation prediction in absorbing ducts adaptable to bypass jet engines, using Morse theory
14 p2288 A71-30522

Tip turbine driven lift fan noise reduction tests, considering design parameters effects
[AIAA PAPER 71-743] 14 p2296 A71-30784

Acoustic liner design for propellant combustion instability and jet aircraft noise suppression, discussing cross flow and oscillatory pressure effects
[AIAA PAPER 71-757] 14 p2296 A71-30791

SST sonic boom minimization, discussing cross-country flight
14 p2177 A71-30820

FM threshold extension bounds during click elimination, considering pulse-averaging type discriminator
14 p2198 A71-30906

Quasi-harmonic signal suppression in theta-power amplifier as function of nonlinearity at various noise levels
15 p2375 A71-31229

Jet noise reduction by foam injection, developing mathematical model for foam behavior in sound field
[AIAA PAPER 71-734] 15 p2388 A71-31327

Commercial SST aircraft engine noise during takeoff, discussing exhaust geometries for suppression
15 p2468 A71-31595

Quiet turbfan STOL feasibility, discussing structural, propulsive and technical aspects, economy, passenger comfort and performance estimates
15 p2348 A71-31605

Curved porous wall channels for noise suppression in power plants, ventilation systems, etc
15 p2449 A71-31705

Acoustic and gas dynamic characteristics of jet noise muffler, using adapters at outlet section of exhaust nozzle
15 p2469 A71-31710

Aircraft powerplant noise test facilities and reduction, emphasizing jet acoustic Mach number, pressure and temperature ratio and exit turbulence effects
15 p2384 A71-31876

Concorde aircraft engine noise emission and reduction, examining acoustic measurements in takeoff and approach phases, reduced thrust and retractable silencer
15 p2469 A71-31877

Aircraft noise reduction criteria, examining noise measurements relation to human behavior and physical measures connection to subjective judgments
15 p2349 A71-31879

Soundproofing of air inlets and fan exhausts with reference to absorbent systems with resonant cavities, technologies, environmental conditions and material fatigue
15 p2469 A71-31880

STOL jet aircraft noise reduction by using engines with moderate dilution rate
15 p2349 A71-31882

Aircraft engine noise test methods for acoustic certification, investigating jet and compressor silencing, absorbent materials, rotor and propeller noise and psychoacoustic tests
15 p2385 A71-31890

Noise rejection in step type extremal self oscillating system with variable control period, estimating process precision
15 p2381 A71-31981

Jet aircraft noise generation, transmission and reduction, emphasizing turbofan engine acoustics, operational characteristics and exhaust sound
15 p2349 A71-32241

Community actions for jet aircraft noise reduction, discussing noise environments, nationwide goals, decision making and economic incentives
15 p2516 A71-32249

Modulator-demodulator type push-pull DC amplifier input noise reduction, using electromechanical vibrators
15 p2355 A71-32451

Low voltage signal conversion to digital code, emphasizing SNR improvement
15 p2382 A71-32452

Sonic boom phenomena, discussing supersonic flow near aircraft, atmospheric propagation, distortion, focusing, caustics, turbulence effects and reduction
15 p2350 A71-32566

French disengageable silencer for jet engine noise attenuation during aircraft takeoff
15 p2471 A71-32695

Rotorcraft and VTOL aircraft noise characteristics, noting implications of reduction to acceptable levels
16 p2523 A71-33419

Telegraphy binary data transmission through channels with frequency-selective fading, investigating noise stability improvement by programmed carrier frequency variation and receiver passband shifting
17 p2698 A71-34394

Short wave frequency-diversity radio communication systems operating at extremal frequencies of group, estimating noise reduction effectiveness
17 p2698 A71-34395

Low noise FET amplifiers for earth station radio receivers
17 p2715 A71-34687

Ground noise reduction with balancing units, discussing transmission line driving and receiving end applications
17 p2716 A71-34859

Low noise parametric amplifiers for communication satellite ground station radio receivers, considering components characteristics
17 p2709 A71-35513

Gulfstream 2 acoustics program for cabin noise level reduction, compliance with FAA takeoff and

- landing noise certification and structure qualification against sonic fatigue
[AIAA PAPER 71-783] 17 p2675 A71-35527
- Numerical methods for noise elimination from ERTS pictorial data, describing data acquisition system
18 p2886 A71-36542
- Flight dynamics for aircraft noise reduction, gust effects decrease and dynamic stability of parachute load systems
18 p2850 A71-36752
- Low noise parametric amplifier design and construction for Intelsat 4 satellite communications earth stations
19 p3027 A71-37496
- Vibration control methods, discussing oscillation and acoustic noise reduction
19 p3069 A71-37518
- Sonic boom implications and decision on acceptability with alternative policies of complete barring, controlled corridors and overflight limitations
[CASI PAPER 72/4] 19 p2996 A71-37595
- Civil aircraft future propulsion requirements, considering larger engine sizes, higher takeoff thrusts and lower noise levels
[CASI PAPER 72/10] 19 p3122 A71-37600
- Civil V/STOL aircraft engines requirements, considering noise reduction, thrust, multifunction propulsion/blowing, lift and booster fan engines
[CASI PAPER 72/19] 19 p3122 A71-38021
- Super CTOL airport planning, discussing location of runway pairs, aircraft operations, noise reduction, community relations and efficiency
19 p3041 A71-38023
- Two dimensional seismic mathematical and scale techniques appropriate to inertial navigation devices test pads noise isolation examination
[AIAA PAPER 71-912] 19 p3056 A71-38326
- Flight test measurements of shock cell noise loading of aircraft tail planes, noting alleviation by nozzle and mirror structural modifications
19 p2998 A71-38467
- Optimal design for noise attenuation by diesel engine exhaust mufflers using linearized acoustic models
20 p3268 A71-38961
- Segmented stator vanes performance in axial flow compressor, noting radiated sound reduction
20 p3175 A71-39093
- Air traffic control delays, airport airspace congestion, flyover noise reduction and performance requirements effect on airline operations economics
20 p3209 A71-39391
- Aircraft noise reduction in takeoffs/operational procedures and by land use planning
20 p3209 A71-39392
- Low noise levels of DC-10 aircraft with CF6-6D turbofan engines, discussing design, flyover tests and FAA requirements
[CASI PAPER 72/5] 20 p3178 A71-39424
- Sound absorptive materials selection for jet aircraft noise control
20 p3178 A71-39451
- Space vehicle measurements of sporadic meteor particle flux near earth, using detectors insensitive to acoustic and vibrational noise
20 p3299 A71-39648
- Structure born noise reduction by viscoelastic coatings, examining effects of thickness, density, bending and shear induced loss factors, moduli and Poisson ratio
[ASME PAPER 71-VIBR-29] 21 p3414 A71-40284
- Book on practical design for electromagnetic compatibility covering interference control, reduction, analysis, prediction and measurement, shielding problems, etc
21 p3356 A71-40779
- Inclined radial jet drive systems for noiseless gas bearings, comparing with turbine driven device
22 p3553 A71-41681
- Airport noise control regulations enforcement feasibility, noting financial burden
22 p3623 A71-41796
- Li-drifted Ge p-i-n diode for low noise IR detectors, describing spectral sensitivity and NEP value
22 p3543 A71-42127
- Aeronautics future, discussing aircraft noise reduction, computer techniques and aircraft design
22 p3482 A71-42237
- Magnetic recording of heart electrical activity by cryogenic magnetometer with two Josephson junction quantum interference reduction device
22 p3504 A71-42341
- Nonlinear filtering for noise reduction of image data by mean-squared error minimization, discussing zero memory technique
22 p3547 A71-42507
- Telemetry systems with discrete compression-expansion function, calculating noise stability improvement as compared to linear and nonlinear signal conversion operations
22 p3515 A71-42859
- Optimal design for minimum noise maximum gain bandwidth of lower sideband parametric up-converters
23 p3630 A71-42917
- Sound transmission through finite closed shells, considering statistical energy analysis, modal coupling and noise reduction
23 p3704 A71-43213
- Random amplitude bounded measurement errors, describing nonlinear filtration method of noise smoothing
24 p3813 A71-44683
- Prop rotor and lift fan VTOL aircraft ground noise level reduction, using flight trajectory management
[AIAA PAPER 71-991] 24 p3792 A71-45295
- NOISE SPECTRA**
- Area distributed incidental radio noise voltage envelope distribution functions conversion to Rayleigh distribution with range frequency relationships
01 p0037 A71-11165
- Noise stability in single-channel FM transmission system via maximum SNR obtained with optimal predistortion
02 p0212 A71-11836
- Noiselike signals frequency modulation via pseudorandom sequence, deriving relationships for spectra and combined frequency-lag/correlation functions
03 p0378 A71-13393
- Microplasma low temperature noise spectra in Si and Ge avalanche diodes
03 p0387 A71-13981
- Power train systems gear induced noise analysis, using in-flight vibration and noise measurements for comparison with calculated noise spectra
[ASME PAPER 70-WA/DGP-1] 03 p0471 A71-14137
- Heuristic flow acoustics, discussing noise frequency spectrum in reference to moving singularities
04 p0569 A71-14980
- Helicopter in-flight noise radiation pattern and spectra measurements for various operating parameters
04 p0531 A71-15406
- PSK pseudonoise/spread spectrum communication systems with SNR reduction, examining phase nonlinearities effect
05 p0725 A71-17074
- CaAs Schottky tunnel junction properties and bias independent structure evaluation by excess noise generation
06 p0940 A71-17312
- Broad spectrum pseudorandom Gaussian noise generator, describing pseudorandom binary sequence filtering technique with desirable autocorrelation properties
06 p0877 A71-17327
- Correlated noise linear filtering problem analysis, introducing concept of invariant directions for Riccati equation
06 p0877 A71-17328
- Noise stability during complex signals reception and lag measurement on fluctuating noise background
06 p0866 A71-17371
- Supersonic aircraft turbojet engine exhaust noise suppressor research program, predicting full scale noise spectra from model suppressor tests
[AIAA PAPER 68-1023] 06 p0945 A71-17693
- Noise spectra of CW hollow cathode zinc ion laser comparison with conventional discharges, noting gain per unit length on transitions
06 p0910 A71-18662
- IR system with moving space filter, calculating detector output and noise due to background radiation
07 p1058 A71-18828
- Analog to digital converter noise power generation due to quantization and saturation effects under Gaussian input
07 p1059 A71-18852
- Phase locked avalanche transit time oscillators FM noise spectra
07 p1074 A71-19124
- Noise bandwidth of optimum second order and bandpass Butterworth, Bessel and Chebyshev filters for communication and radar systems
07 p1081 A71-19539
- Ultrasonic cavitation noise spectra in liquid helium and nitrogen, comparing He I and II
07 p1160 A71-19951
- Human panel comparison of aircraft engine noise tape recordings with synthetic broadband noise approximating pure jet
09 p1398 A71-22255
- Two dimensional distribution moments of harmonic signal and normal narrow band noise mixture envelope, deriving expressions by power series expansion
09 p1404 A71-22293
- Pioneer 9 space probe electric field experiment and near earth observations of noise spectra variations related to diffusive plasma layer
09 p1529 A71-23711
- Spectrum analysis and probability distribution of burst noise pulses of silicon planar bipolar transistors consistent with Markov two state process
10 p1574 A71-23773
- Engine inlet noise prediction from static test and flyover data as function of time at various observer locations, examining suppression effects on total spectra
[SAE PAPER 710386] 10 p1659 A71-24250
- Circular subsonic free jet impinging on wall, investigating high intensity frequency noise and turbulence spectrum
10 p1594 A71-24594
- Handbook on electrical noise and electromagnetic interference specifications, Volume 1, covering noise pollution, industrial electronic equipment operation control, test plans and military standards
11 p1731 A71-25744
- Continuous cold cathode forward wave reentrant beam crossed field amplifiers with cut-off electrode, investigating AM and PM noises and phase coherence
11 p1739 A71-26434
- Noise field from subsonic air jets by velocity dependence and radiation intensity directivity determination
11 p1753 A71-26445
- Quasi-steady spectrum of hydromagnetic noise in proton belt, using random excited broad wave fields in nonisothermal magnetosphere
12 p1947 A71-26643
- Flux flow noise spectra measurement in pairs of magnetically coupled superconducting films, noting frequency response
13 p2111 A71-28502
- VLF noise spectra in earth-ionosphere cavity due to thunderstorm discharges, noting resonance level splitting by geomagnetic field
13 p2030 A71-28542
- Instantaneous frequency statistical characteristics of passive noise spectra and fluctuating signals reflected from nonpoint moving radar targets
14 p2195 A71-30111
- Complex noise emission spectra from superposition of continuous component and peaks, calculating level separations due to perfectly reflecting plane
14 p2289 A71-30523
- Man made radio noise sources frequency-distance dependence and location, noting vehicular ignition, power transmission and electrical pulsing
14 p2203 A71-30962
- Low frequency noise spectra measurement in varicaps by frequency modulation of harmonic oscillator, noting application to diode and p-n transistors
15 p2369 A71-31232
- Temperature and shock structure effects on choked jet noise characteristics, using axisymmetric convergent and convergent-divergent nozzles for radiated noise fields investigation
[AIAA PAPER 71-582] 15 p2468 A71-31570
- Noise and spectral analysis for measuring fluid flow with random temperature fluctuations by transit times
15 p2406 A71-31596
- Rotorcraft sound characteristics, discussing rotor noise spectrum, directivity, measurement and instrumentation
16 p2523 A71-33417
- Soviet book on space radio telemetry systems characteristics, design, requirements and operation conditions covering noise stability, reliability and redundant codes
17 p2699 A71-34521
- FM radio receiver SNR and noise spectra for arbitrary transmission band characteristics
17 p2701 A71-34778
- Two dimensional optical Fourier approach diagnosing interpretation-limiting pictorial noise patterns in ERTS image output
18 p2919 A71-36082
- IMPATT diode amplifiers and oscillators AM and FM noise spectra and SNR prediction for comparison with experiment
18 p2888 A71-36271
- FM noise in output spectrum of low level operating IMPATT diode microwave oscillators
19 p3029 A71-38217
- Simple source theory of aerodynamic noise, approximating relationship between radiated sound power and jet pressure spectra
19 p3124 A71-38531
- Propeller vortex noise analysis by on-line 1/3 octave band resolution, discussing characteristic results from noise measurements on various propeller configurations
21 p3325 A71-40868
- Microwave scattering noise spectrum from turbulent rocket-exhaust jet illuminated by plane wave
22 p3510 A71-42208
- Scattering from turbulent rocket-exhaust jet illuminated by focused microwave beam, calculating noise spectrum by approximate theory
22 p3510 A71-42209
- Transmission and reaction cavity stabilized Gunn microwave oscillators AM and FM noise spectra, extending calculations based on Kurokawa theory to high modulation frequencies
23 p3653 A71-43967
- Acoustic noise output from round interfering subsonic jets, considering suppressor nozzle attenuation
24 p3864 A71-44560
- Noise voltage power spectrum of GaAs bulk diodes at LF as function of bias field approaching negative resistance region
24 p3804 A71-44992

NOISE STORMS

Energetic electrons generating solar flares position relation with active regions associated with type 1 radio noise storms

12 p1953 A71-27656

Solar radio bursts and noise storms frequency band spectra, investigating warm plasma wave propagation and mode coupling theories

22 p3579 A71-41462

NOISE SUPPRESSORS

U NOISE REDUCTION

NOISE TEMPERATURE

Noise temperature measurement of mismatched cryogenic generator, using compensation method

01 p0056 A71-11198

Variable microwave thermal noise temperature standard generator with output ranging from below 40 to above 370 K

02 p0250 A71-12139

Skyнет ground stations operations and equipment, discussing receiving systems parametric amplifiers, local oscillators, demodulators, noise temperature, frequency flexibility and reliability

02 p0217 A71-12433

Skyнет and SCAT ground stations system noise temperature, considering receiver, antenna and sky sources, measurement techniques and error analysis

02 p0217 A71-12434

Gain/temperature measurement test set for earth station receiving system by radio sources program tracking unit, noting antenna power ratios determination by attenuator

02 p0222 A71-12797

Gain/temperature measurement for earth station antenna and receiving subsystem by FM method, determining Y-factor/noise power proportional increase/

02 p0222 A71-12798

Atmosphere effects on antenna noise temperature variations in G/T value for earth station performance in satellite communication system

02 p0222 A71-12799

Waveguide feeder system design for antenna receive path of Intelsat 3 satellite ground station, considering system noise temperature

02 p0223 A71-12800

Wideband low noise parametric amplifier design, discussing noise temperature improvement by refrigeration at microwave frequencies

02 p0234 A71-12815

Maintenance free cryogenic noise temperature standard for continuous microwave antenna operation independent of elevation angle

04 p0550 A71-14658

Low noise temperature high gain satellite communication antenna feeds optimal design using stepped aperture

06 p0877 A71-18395

Contour maps of antenna temperature in W31 region, discussing H I absorption features

07 p1198 A71-19816

Noise thermometry by Josephson effect, demonstrating self excitation random frequency modulation with thermal noise and thermometer having microkelvin noise temperature measurement capability

07 p1114 A71-20157

External and transistor noise temperature effects on SNR of transistorized microwave receiving antennas

09 p1417 A71-23038

V groove cathode discharge produced He plasma parameters studied for reentry electron density and temperature simulation, correlating energy flux and microwave noise emission

12 p1895 A71-27273

LF hot-electron noise during quasi-elastic scattering in semiconductor with simple band structure, evaluating convective fluctuations contribution to noise temperature

13 p2112 A71-29082

Measuring instrument for solar radio emission at 8 mm, using GaAs Schottky barrier diode mixer for system noise temperature reduction

14 p2239 A71-29916

Primary and secondary standardization and precision measurement of thermal noise power at various radio frequencies and temperatures

14 p2204 A71-30977

Deep Space Communications System low noise microwave receiver, discussing operating noise temperature calibration, error analysis and programming

15 p2372 A71-32311

Atmospheric noise temperature variation with frequency in 2.53 mm molecular oxygen rotation line, considering Zeeman effect

19 p3048 A71-37402

Noise temperature in microwave frequency mixers using nonlinear resistors, giving rectifier and diode loss formulas for rectangular and sinusoidal waves

19 p3027 A71-37494

Antennas scattering coefficients measurement by ground and atmospheric radiation, permitting antenna noise temperature components determination

20 p3205 A71-39803

Two stage decimeter wavelength quantum paramagnetic amplifier, noting noise temperature and gain

23 p3652 A71-43529

Antenna radome noise temperature under aerodynamic heating as function of losses in material, interface reflection and dielectric surfaces

23 p3647 A71-44324

Low temperature noise in p and n channel MOST amplifiers

24 p3812 A71-45361

NOISE TOLERANCE

Complex systems potential effectiveness theory, establishing reliability, noise resistance and controllability limits

01 p0065 A71-11230

Figural noise and rotation effects on visual form perception, using random and redundancy figures in figure cancellation task

01 p0026 A71-11417

Anticonvulsant drugs for counteracting noise effects on central nervous system, discussing audiogenic seizure in mice

03 p0360 A71-13163

Simulated sonic booms effects on sleeping humans, considering intensity levels, age factors, sleep stage, adaptability and housing

03 p0371 A71-13165

Sound and sonic booms effects on farm animals physiology and behavior, considering milk production, reproduction, food intake and growth rate

03 p0360 A71-13166

Impulse-noise human ear damage-risk criterion correction factor for single impulse, studying temporary threshold shift

05 p0712 A71-16284

F-100 pilots acute HF hearing loss due to noise ground environment and excessive in-flight noise exposure

09 p1400 A71-23249

Simulated sonic booms and subsonic jet aircraft noise effects on human subjects of various ages during different sleep stages

15 p2364 A71-32250

Noisy environment effects on circulatory, respiratory and metabolic parameters during physical exercise, measuring heart rate, systolic blood pressure, oxygen intake and respiratory quotient

20 p3185 A71-38889

Cortical responses of awake cat to narrow-band FM noise stimuli, proposing neuronal model

20 p3190 A71-39767

Unfavorable high intensity noise effects on auditory and motor analyzers during space flight

22 p3495 A71-42793

Psychophysiological loudness and annoyance indices application in sonic boom comfort level evaluation, pulsating noise estimation and sound insulation system effectiveness determination

24 p3799 A71-44399

Human auditory adaptation to medium intensity noise complex action under relative isolation and hypokinesia conditions from monaural hearing threshold measurement

24 p3799 A71-44400

NOMENCLATURES

Far side lunar craters nomenclature, listing names with identifying biographical data

19 p3145 A71-38271

Martian features nomenclature based on Schiaparelli application of ancient geographical and mythological

21 p3448 A71-40520

Lunar maps classification, nomenclature and scales sequence

21 p3448 A71-40549

NOMINAL VALUES

U APPROXIMATION

NOMOGRAMS

U NOMOGRAPHS

NOMOGRAPHS

Nomograms predicting transistors transition frequencies as function of geometric and physical characteristics

02 p0235 A71-12920

Nomographs for point source holographic imaging, discussing recording and reconstruction geometry

05 p0753 A71-16913

Nomograms for normal stresses and bending moments in thin circular cylindrical shell under uniformly distributed local load

08 p1374 A71-22054

Nomograms for thermoelastic stress in plate determined as function of dimensions and heat transfer

09 p1538 A71-22605

Nomograms for meteor geocentric velocity and trajectory with correction for zenith attraction and radiant

09 p1520 A71-22831

Nomogram construction for graphical solution of two body problem using radius-vector and velocity components applied to solar system

09 p1520 A71-22844

Reliability test extent, duration, confidence limits and failure rate computed by nomograms

11 p1737 A71-25623

Adhesion, recombination and electron-band curvature nomograms for space charge region in photosensitive CdS single crystals

24 p3859 A71-44388

NONADIABATIC CONDITIONS

U ADIABATIC CONDITIONS

NONADIABATIC THEORY

Nonadiabatic H-H collisions cross sections in two state time dependent impact parameter approximation, including electron exchange

08 p1337 A71-21193

Linear nonadiabatic pulsations of stellar models, discussing numerical method for eigenvalue problem

13 p2132 A71-27968

Ab initio calculations on trajectories and nonadiabatic transitions in reactions of hydrogen atoms with hydrogen molecules

18 p2949 A71-35897

Nonadiabatic effects in van der Waal line broadening, taking into account mixing between degenerate magnetic sublevels in atomic collisions

19 p3106 A71-37409

Radiation belt particles nonadiabatic changes, calculating rigidity as function of magnetic field lines

21 p3439 A71-41357

RR Lyrae stars instability strip for halo population variables, presenting linear nonadiabatic approximate pulsation calculations with emphasis on blue edges location in H-R diagram

22 p3602 A71-42171

NONAXISYMMETRY

U ASYMMETRY

NONCONDENSIBLE GASES

Noncondensable gas temperature controlled heat pipe systems design, considering working fluid, reservoir wicks and ambient thermal environment

11 p1857 A71-26211

NONCONDUCTORS

U ELECTRICAL INSULATION

NONCONSERVATIVE FORCES

Stability analysis of structural systems subject to nonconservative forces, using finite element method

05 p0829 A71-17118

Perturbed motion of class of nonconservative systems with generalized forces, discussing conditions for perturbation equations integrability

10 p1641 A71-24022

Nonconservative force system eigenvalues and eigenvectors reproduction by related conservative system

10 p1689 A71-24513

Nonconservative dynamic instability of columns under distributed tangential force, using analog computer

13 p2158 A71-29430

Continuous system nonconservative stability examined by finite element Ritz method with extended Hamilton principle

14 p2330 A71-30687

Nonconservative elastic system involving standard double pendulum model under retarded follower load, calculating damping, time delay and parameter variations effects on stability

15 p2449 A71-32012

Rods stability under nonconservative loads, applying Liapunov functions to boundary value problems

16 p2607 A71-32977

Thermoelastic stability of finitely deformed solids under nonconservative surface tractions without body force

16 p2649 A71-33009

Jet engine thrust induced nonconservative effects in aeroelastic analysis of vertical takeoff, using cantilever beam torsion and bending differential equations

16 p2650 A71-33019

Stability of linear viscoelastic systems under nonconservative forces, obtaining equations for perturbed motion for equilibrium or creep state

16 p2650 A71-33020

Cantilever column critical dynamic instability load under nonconservative follower force including thermomechanical coupling effect from boundary value problem formulation

[ASME PAPER 71-APM-L]

18 p2977 A71-36255

Boundary value problems of forced vibration of nonconservatively loaded dynamic elastic system, using William method

24 p3878 A71-44554

NONDESTRUCTIVE TESTS

NT PRELAUNCH TESTS

Nondestructive high reliability rapid comparison and identification of metals by electrical interpretation method for product variation control and laboratory unknowns determination

01 p0085 A71-10258

Ultrasonic frequency characteristics for flaw detection, discussing short and long pulses coupling to test samples

01 p0086 A71-10303

Metal flaw size measurement, discussing ultrasonic echo amplitude and defect scanning methods

01 p0086 A71-10304

Electrical resistance spot weld penetration measurement via ultrasonic method using shear waves

01 p0086 A71-10305

Ultrasonic methods for evaluating adhesive bond strength in composites, metal to metal laminates and honeycombs

01 p0086 A71-10306

Electroinductive defectoscopy using eddy currents as nondestructive materials testing method
01 p0079 A71-10335

Flaw detection system for wide Al sheets, using eddy current equipment with modulation analysis principle
01 p0087 A71-10458

Carbon-carbon composites nondestructive testing following various processing steps, discussing material variations and discrete discontinuities
01 p0090 A71-11278

Reference standards for nondestructive ultrasonic inspection for quality control
01 p0091 A71-11424

Nondestructive testing techniques for airline maintenance inspection, describing ultrasonic, eddy current, magnetic particles, and X ray methods
02 p0256 A71-12449

Carbon fiber reinforced plastics, discussing mechanical and nondestructive testing for performance factors
02 p0274 A71-12482

Nondestructive testing for reliability and lifetime of mass produced radio equipment under maximum load
02 p0257 A71-12530

Elastic bar buckling load nondestructive determination using actual boundary conditions
03 p0504 A71-13454

Nondestructive test with high resolution instrumentation for observing long thin walled cylinder lateral displacements prior to buckling under axial compression
04 p0669 A71-15297

Magnetographic defectoscopy, discussing defect field magnetic recording techniques quality
07 p1106 A71-19143

Holography and interferometry industrial applications, considering three dimensional imaging, precision distance measurement, nondestructive testing and structural strains and failures detection
07 p1113 A71-19784

Nondestructive testing in product cycle in aerospace industry
07 p1118 A71-19949

Buckling loads prediction for conservative elastic systems from vibration data by stochastic and deterministic models, providing nondestructive testing procedure
08 p1368 A71-20804

Carbon fibers and composites nondestructive testing, discussing defect detection problems in ultrasonics, X ray diffraction and X radiography methods
[PLASTICS INST. PAPER 52]
08 p1296 A71-20918

Pulsed laser schlieren system for ultrasonic wave front imaging in nondestructive testing techniques
08 p1286 A71-20949

Multielectrode ultrasonic transducer with multiplexing circuits for electronic readout scanning, discussing application in rapid inspection of plate or strip isotope heat sources
08 p1287 A71-20950

Defectoscopes with current regulation by magnetic amplifiers, describing circuitry and remanent magnetization of components with AC and rectified half wave currents
08 p1273 A71-21894

Nondestructive monitoring calibration and alignment with standard specimens conforming with metrological regulations
08 p1300 A71-21895

Electronic digital automatic defect indicator attachment to industrial echo defectoscope
08 p1300 A71-21897

Optimal time determination for using radioactive isotope as radiation source in nondestructive testing
08 p1332 A71-21898

Moving thin walled tubes surface and internal defects detection based on three dimensional thermal field surface distribution
08 p1300 A71-21899

Magnetic recording device for defect field recording by ferromagnetic tape polarization
08 p1273 A71-21900

Signaling sensitivity leveling by introduction of automatic defect indicator into defectoscope
08 p1273 A71-21904

Eddy current nondestructive tests for surface defects detection, determining optimum test parameters based on calculation
09 p1454 A71-22213

Mechanical characteristics of extruded thermally hardened aluminum alloys determined by eddy current method
09 p1468 A71-22326

Ultrasonic modulus vs strength of high modulus fiber reinforced epoxy matrix composites in nondestructive testing
09 p1484 A71-23687

Room temperature curing rubber for detection of cracks and other surface flaws in magnetic materials, revealing cracks in specimen by distinct dark lines
10 p1615 A71-24100

Photochromic paints for nondestructive testing of aerospace materials and structures
10 p1633 A71-24102

Nondestructive evaluation of ultrasonic wave propagation in adhesively bonded test specimens, using schlieren method
10 p1616 A71-24104

Metallic surfaces adhesive properties and adsorptive capacity from nondestructive testing by peeling
10 p1616 A71-24105

Relativity of nondestructive testing as related to production effort, reviewing structural adhesive bonding in U.S. for past ten years
10 p1616 A71-24106

Dynamic frequency characteristics of built-up structures by transient rapid sweep testing
11 p1841 A71-25178

Pressure vessel flaw detection at high stress and cryogenic temperatures, noting Lunar Module fuel tanks experience
[AIAA PAPER 71-336]
11 p1777 A71-25315

Nondestructive testing method obtaining relaxation modulus and accelerated degradation/stress corrosion of reinforced plastics
11 p1768 A71-25404

Representative Thornel fiber aircraft fuselage component nondestructive testing and repair, and Thornel fiber, polysulfone and polyamide-imide composites fabrication and evaluation
11 p1787 A71-25427

Gas turbine wheel design fracture mechanics, discussing buried and surface flaws analysis for rotor failure prediction applications
11 p1811 A71-25956

Pulsed laser holographic applications to aerospace components nondestructive testing, inspecting electron beam welds and internal structural flaws
[ASME PAPER 71-GT-74]
11 p1770 A71-25988

Particle impact noise detection of loose particles in electronic component cavities, discussing implementation, cost savings and reliability improvement
12 p1884 A71-26659

Nondestructive magnetic method for measuring longitudinal residual stress in outer portions of ferromagnetic cylindrical bars
12 p1974 A71-26948

Optical holographic interferometry for radial microcracks detection from bolt holes in high strength aircraft steel
[ASME PAPER 71-MET-C]
12 p1911 A71-27312

Residual stresses rapid X ray diffraction measurement, noting faster operation in go-no-go mode for nondestructive testing
12 p1912 A71-27533

Acoustic emission application to nondestructive testing of materials, manufacturing processes and structural components failures
13 p2073 A71-27939

Papers on fracture mechanics covering engineering fundamentals, environment effects, crack growth, photoelastic analysis, nondestructive testing, etc
13 p2151 A71-28212

Nondestructive testing, discussing visual, liquid penetrant, thermal, X and gamma rays, ultrasonics, magnetic, electrical and eddy currents methods
13 p2073 A71-28218

Semiquantitative X ray nondestructive analysis of metal alloys, noting critical nature of sampling
13 p2074 A71-28438

Destructive and nondestructive material testing techniques, discussing equipment design and procedures standardization
13 p2074 A71-28493

Filament wound pressure vessels and composites flaw detection nondestructive tests with X rays and thermography
14 p2262 A71-29644

Carbon-carbon spacecraft reentry heatshields evaluation and selection by nondestructive and destructive tests on flight cones
14 p2262 A71-29647

Multidirectional reinforced resin matrix composites inspection and nondestructive analysis by film/neutron radiography and X ray Vidicon
14 p2263 A71-29659

Nondestructive testing techniques for discrete local materials properties evaluation, allowing nonstatistical analysis of thermomechanical stress behavior
14 p2251 A71-29900

Holography in nondestructive materials testing, describing laser interferometry and reproduction techniques for deformation and torsional, bending, thermal and vibrational behavior
15 p2402 A71-31217

Optical techniques for holographic NDT inspection speeds increase in laminate structures flaw detectability
15 p2408 A71-31815

Graphite fiber composite structures nondestructive testing, discussing liquid penetrants, X ray radiographic sonic methods, acoustic emission and IR tests
15 p2414 A71-31816

Pulse type ultrasonic flaw detecting apparatus based on reflected echo size estimation
15 p2409 A71-32194

Lost City /Oklahoma/ and Ucera /Venezuela/ meteorites cosmogenic radionuclides data, using nondestructive analysis by gamma-gamma-coincidence counting system
15 p2489 A71-32357

Book on electromagnetic nondestructive test methods covering eddy current test, EM field theory, operation and design of sensing coils, etc
15 p2418 A71-32768

Scanning electron microscope in nondestructive testing, reviewing signal mode produced topographical data, image recording and inspection procedures
16 p2581 A71-32862

Focused ultrasonic nondestructive tests search units, describing focal distance, beam diameter and lens/crystal radius optimum ratio
16 p2581 A71-32863

Flight mission severity in cumulative damage /low cycle fatigue and creep stress rupture/ not detected by usual nondestructive testing in aircraft gas turbine industry
16 p2624 A71-33298

German monograph on correlation of Vickers and Rockwell C hardness testing methods covering indentation form measurements, deformation work, etc
17 p2739 A71-34797

Vibration response NDT for fatigue crack damage in laminated filament-reinforced epoxy composites
17 p2824 A71-34815

Hot wire and tubes nondestructive eddy current testing as cybernetic process, noting high speeds with high on-line data flow
17 p2749 A71-35494

Holography as nondestructive testing tool, considering application in vibration analysis, stress/strain measurement, bond inspection, internal flaw detection and displacement measurement
[SME PAPER IQ-71-121]
18 p2927 A71-36657

Characterization of high purity metals by residual resistivity ratio, using nondestructive eddy current decay method
18 p2938 A71-36992

Aircraft parts testing by NDT methods, considering ultrasonic system for valve defects and fluorescent particle system for crack detection
18 p2929 A71-37056

Blue edge anodize technique for revealing segregation in Ti alloys without affecting mechanical properties
18 p2938 A71-37058

Laser holographic inspection of silicon bond in pressure sensors for process control systems
19 p3068 A71-37245

Electro-optic He-Ne laser microscope for high-speed high-precision edge detection for IC masks
19 p3075 A71-38236

Acoustic emission technique for nondestructive cracking rate determination in hydrogen embrittled steel, using crack-tip stress intensity factor as critical parameter
20 p3241 A71-38773

Laser holography and interferometry in materials science, evaluating displacement and deformation within nondestructive testing
20 p3245 A71-39342

Holographic interferometry equipment design for NDT and vibrational and deformation analysis, discussing apparatus construction, optical quality and industrial applications
20 p3238 A71-39344

Nondestructive testing of carbon fiber reinforced composites with resin matrices /CFRP/, suggesting ultrasonics for void detection
21 p3387 A71-40598

Nondestructive test for fiberglass reinforced plastic tank, using percussion method
21 p3466 A71-40838

Holographic interferometry application to laser NDT of objects with nonoptical surfaces, describing techniques and industrial uses
21 p3382 A71-40939

Electroacoustic circuit of ultrasonic resonance thickness gage based on frequency dependence of piezoelectric transducer conductance in multilayered acoustic system
22 p3528 A71-41755

Ultrasonic defectoscopy of steel samples, considering grain size effects on SNR
22 p3528 A71-41757

Ultrasonic time shadow method based on defect detection by sharpness of vibration propagation time change during scanning
22 p3528 A71-41758

Differential method of ultrasonic inspection and binary comparative search heads for implementation, combining mirror shadow and echo methods features
23 p3553 A71-41760

Radiation flaw detection by fast neutrons, monitoring thick lead plates and three-layer articles
23 p3528 A71-41761

X ray monitoring process optimization with pmb-6 betatron, discussing intensifying screens thickness and composition effects on defects detectability
23 p3553 A71-41762

Multilayer printed circuit boards defects detection by temperature field monitoring 22 p3520 A71-41764

Coercive force and specimen thickness effects on outputs of meters with attached electromagnets 22 p3553 A71-41766

Decarbonization monitoring of ball bearing steel bars, describing defectoscope based on eddy current higher harmonics method 22 p3553 A71-41768

Ferromagnetic Co phase nondestructive determination in hard powdered-metal alloys by permanent magnet ponderomotive force measurement based on relationship to ferromagnetic alpha phase 22 p3561 A71-41775

Ultrasonic holography in nondestructive testing, using single transducer or separate focussed transducers for transmission and reception 22 p3541 A71-41780

Nondestructive testing evaluation of graphite epoxy composites and adhesive bonded Al composite structures using acoustical holography 22 p3554 A71-41781

Holographic ultrasonic imaging method for flow detection in aerospace materials and structures 22 p3554 A71-41782

Holographic inspection of bond between inert solid propellant grain and polymer liner, using double exposure to record surface deformation of fiberglass case 22 p3549 A71-42570

I.F eddy current bridge to measure small magnetic permeability changes in weakly ferromagnetic materials, applying to nondestructive tests of austenitic stainless steels 23 p3681 A71-43193

Holographic interferometry flow detection sensitivity on cylinders under hoop stress, comparing with strain gages 23 p3676 A71-43508

Apollo 12 returned Surveyor 3 component materials analysis for lunar exposure effects by nondestructive and destructive tests 23 p3765 A71-43811

Holographic nondestructive testing of materials, using laser for object illumination and interferometry 23 p3682 A71-43951

Optical anemometers for local nondestructive flow velocity measurements, discussing signal analysis possibilities 23 p3679 A71-43952

Basic parameters of echo and mirror shadow methods for ultrasonic defectoscopy of welded joints, considering standardization principles 24 p3829 A71-44784

Ultrasonic method for measuring poor root penetration zone width in welded T joints without reference standard, suggesting practical applications 24 p3829 A71-44785

Magnetic leakage flux method for nondestructive detection of structural defects 24 p3827 A71-45069

Aerospace industry magnetic particle inspection problem identification in complex ferromagnetic structures 24 p3831 A71-45277

Laser holographic inspection for disbands in metal/phenolic rocket nozzles of two divergent geometries, corroborating by ultrasonics and dye penetrants 24 p3829 A71-45278

Nondestructive pulse technique for quality control of electroexplosive devices, noting cost reduction 24 p3864 A71-45279

Nondestructive detection of hot corrosion-sulfidation in U.S. Navy aircraft turbine engines 24 p3865 A71-45280

Automatic eddy current system to detect fastener hole cracks consisting of scanner unit, control box, recorder and mounting hardware 24 p3831 A71-45281

Ultrasonic flow detection analytical and experimental wave propagation procedure including dynamic photoelasticity and elastic wave computer codes in nondestructive testing 24 p3831 A71-45282

NONEQUILIBRIUM CONDITIONS

Nonequilibrium electron temperature, concentration and reflection in reentry boundary layers, discussing heat transfer and ionization energy diffusion [AIAA PAPER 69-82] 07 p1015 A71-19879

Wrought high strength Al alloy nonequilibrium second phase particles formation effect on mechanical behavior during solidification 07 p1137 A71-19978

Perturbation theory of supersonic flow with nonequilibrium radiative heat transfer, investigating pressure, density, temperature and velocity as function of relaxation time 10 p1697 A71-24943

Vibrational nonequilibrium influence on IR radiative energy transfer in nongray nonisothermal gases 10 p1643 A71-24967

Kinetic processes in shock tubes, considering diagnostic techniques for monitoring time histories nonequilibrium distributions preparations 11 p1745 A71-26264

Metal particle nonequilibrium effects in mixing and combustion of ducted particle laden flow in air breathing engines [AIAA PAPER 71-722] 15 p2466 A71-32573

Jupiter atmosphere nonequilibrium radiative processes, considering energy balance and pressure and temperature conditions 16 p2637 A71-33516

I-V characteristics of compensated semiconductors during nonequilibrium carrier injection from contacts 16 p2622 A71-34028

Nonequilibrium processes, discussing chemical reactions between electronically, vibrationally, rotationally and translationally excited reagents 18 p2873 A71-35831

Radiation role in nonequilibrium boundary layer during atmospheric reentries at speeds exceeding escape velocity 21 p3368 A71-40694

Auger recombination coefficient determination for nonequilibrium carriers in n-type InAs from photoconductivity and light absorption under laser excitation at high levels, noting electron mobility 21 p3433 A71-41310

Analytical transformations of variational conditions in nonequilibrium thermodynamics, using mechanical analogies similar to d'Alembert principle 22 p3622 A71-42688

Chemical lasers diatomic and multiatomic molecules dissociation in nonequilibrium conditions, discussing vibrational energy exceeding gas temperature 24 p3834 A71-45112

Nonequilibrium negative bias effects on n-type metal oxide semiconductor tunnel currents 24 p3812 A71-45356

NONEQUILIBRIUM DRAG

U FRICTION DRAG

NONEQUILIBRIUM FLOW

Digital simulation for translational and rotational equilibrium breakdown in gaseous molecules expansions by Monte Carlo method 01 p0130 A71-10936

Ablative heat shield char layer, examining reacting nonequilibrium pyrolysis gas flow [AICHE PREPRINT 15B] 01 p0181 A71-11297

Time dependent finite difference solutions of steady state nonequilibrium quasi-one dimensional nozzle flows 03 p0400 A71-13458

Nonequilibrium effects of vibrational relaxation on diatomic gas flow behind blast waves 03 p0342 A71-13785

Shock tube diagnostics, instrumentation and rapid photography in nonequilibrium gas dynamics 04 p0565 A71-14699

German monograph on centered two dimensional nonequilibrium hypersonic expansion flow, considering real gas flow with chemical reactions 05 p0693 A71-16124

Dissociated diatomic gas nonequilibrium boundary layer flow over catalytic flat plate, examining velocity profiles, temperature and concentration 05 p0735 A71-16389

Chemical nonequilibrium effects on hypersonic, blunt body shock layers flow in reacting planetary carbon dioxide-nitrogen atmospheres [AIAA PAPER 71-35] 06 p0866 A71-18496

Inviscid air nonequilibrium shock layer properties correlation based on plenum entropy, predicting composition of downstream converging-diverging nozzle expanding air flow [AIAA PAPER 70-866] 07 p1090 A71-19905

Molecular and atomic oxygen properties in nonequilibrium flows, determining vibrational temperature and number density by electron beam fluorescence technique [AIAA PAPER 71-271] 08 p1338 A71-21997

Thin airfoils theory in nonequilibrium magnetogas dynamics with nonuniform nonequilibrium free stream, using Green function technique 09 p1383 A71-23200

Vibrational relaxation of CO and hydrogen atom effects in nonequilibrium nozzle flow using shock tunnel IR detection system 09 p1404 A71-23379

Two phase mixture nonequilibrium flow mathematical model with allowance for colliding droplets coagulation and atomization based on high speed photographic studies 10 p1551 A71-24380

Monograph on shock wave structure in nonequilibrium partially ionized gas flow covering plasma diagnostics, electron temperature, ion density, induced potential gradient, etc 13 p2048 A71-28738

Chemical nonequilibrium flows in supersonic nozzle for mixture of dissociated gases and inert diluent [ASME PAPER 71-FE-8] 13 p2166 A71-29449

Nonequilibrium modeling of pyrolysis gas products flow through char layer of ablative heat shield 14 p2334 A71-29876

Freestream density field in nonequilibrium dissociating nitrogen flow over circular cylinder, using free piston shock tunnel and optical interferometry measurements 14 p2169 A71-29884

Multicomponent gas nonequilibrium viscous flow near blunt body stagnation point, presenting shock layer parameter variations effects on heat exchange 14 p2336 A71-30224

Arc-heated nonequilibrium air expansion flow mass spectroscopic analysis, noting reservoir entropy effect [AIAA PAPER 71-621] 15 p2366 A71-31550

Multicomponent nonequilibrium air flow past axisymmetric blunt body, calculating flow distribution at various attack angles with time dependent technique [AIAA PAPER 71-595] 15 p2512 A71-31571

Nonequilibrium dissociating gas flow past blunt body using time dependent shock layer analysis 15 p2346 A71-32049

Nonequilibrium corner expansion flow of ionized argon induced by normal shock waves in hypervelocity shock tube 16 p2555 A71-32905

Heat transfer, density and pressure measurements of hypersonic two dimensional centered nonequilibrium corner expansion oxygen flow with frozen boundary in shock tunnel 16 p2555 A71-32906

Nonequilibrium nozzle flow determination for vibrationally relaxing gas, describing sudden freeze approximation method validity 16 p2556 A71-32907

Optical diagnosis and measurements for radiation from gases in nonequilibrium flow 16 p2578 A71-33153

Vibrational nonequilibrium Prandtl-Meyer expansion flows, discussing vibration energy associated with change of state and hypersonic nozzle flow calculation 18 p2909 A71-36440

Two phase nonequilibrium flow mathematical model with allowance for colliding droplets coagulation and atomization based on high speed photographic studies 24 p3790 A71-44927

Condensate particle crystallization retardation effect on energy characteristics of jet engine, calculating nonequilibrium flows of two phase combustion products in nozzle 24 p3864 A71-45004

NONEQUILIBRIUM IONIZATION

Nonequilibrium Ar-Cs plasma under rectangular pulse overvoltage, analyzing ionization and recombination kinetics 02 p0289 A71-12177

Initial ionization, relaxation kinetics and nonequilibrium radiation behind strong shock waves in monatomic gases and air 05 p0835 A71-16524

Carbon dioxide laser excitation using nonequilibrium MHD generator [AIAA PAPER 71-67] 06 p0938 A71-18526

Ionizational and electron thermal nonequilibrium effects in insulator boundary layer of potassium-seeded nitrogen MHD accelerator [AIAA PAPER 71-138] 06 p0939 A71-18581

MHD boundary layers with nonequilibrium ionization and recombination at finite rates [AIAA PAPER 71-139] 06 p0939 A71-18582

Nonequilibrium electron temperature, concentration and reflection in reentry boundary layers, discussing heat transfer and ionization energy diffusion [AIAA PAPER 69-82] 07 p1015 A71-19879

Nonequilibrium multicomponent ionization calculations for stagnation merged shock layer of hypersonic blunt body by successive accelerated replacement [AIAA PAPER 69-655] 07 p1015 A71-19890

Load currents and preionization of large nonequilibrium segmented Faraday MHD generator 09 p1386 A71-22072

Self consistent hydrodynamic heating of solid substance by laser pulse for nonequilibrium ionization 10 p1653 A71-24887

Thermal conditions in asymptotic region of atmospheric pressure Ar arc plasma, considering nonequilibrium ionization due to ambipolar diffusion 10 p1654 A71-24971

Partially ionized binary gas mixture temperature development during nonequilibrium ion formation, solving heat and ionization balance equations 13 p2062 A71-28573

Performance potential of MHD generators utilizing nonequilibrium ionization in nuclear space power systems 20 p3264 A71-38930

Self consistent hydrodynamic heating of solid substance by laser pulse for nonequilibrium ionization 21 p3424 A71-41253

Axisymmetric hypersonic flow of nonequilibrium ionized monatomic radiating inviscid gas past blunt body, using Clarke-Ferrari kinetic model 24 p3790 A71-45224

NONEQUILIBRIUM PLASMAS

Nonequilibrium plasma from pulsed discharge in crossed electric and magnetic fields 02 p0288 A71-11882

Cyclotron radiation emission and absorption in nonequilibrium plasma, deriving radiative transfer equation 03 p0465 A71-14268

LF echo oscillations in nonequilibrium plasma under low density charged particle beam 06 p0937 A71-18353

Gas laser using nonequilibrium MHD generator with He, carbon dioxide and Cs mixture [AIAA PAPER 71-68] 06 p0940 A71-18656

Nonequilibrium plasma HF conductivity, introducing dressed ion expression in terms of dielectric permittivity 07 p1165 A71-18743

Nonlinear Fokker-Planck equation solution by Mott-Smith bimodal distribution function method, investigating fully ionized nonequilibrium plasma relaxation time 07 p1171 A71-20295

Nonequilibrium population formation in dense plasma of complex composition under ionization resonance conditions 07 p1174 A71-20538

Turbulent plasmas nonequilibrium electric fields determination from hydrogen spectral lines Stark broadening 08 p1341 A71-21790

Nonequilibrium plasma molecular impurities effect on electron energy balance, considering importance in closed cycle MHD generators 08 p1342 A71-21916

Pulsed MHD generator model with nonequilibrium plasma, obtaining I-V characteristics 08 p1237 A71-21929

Nonequilibrium excitation in recombining nitrogen plasma nozzle flows [AIAA PAPER 70-44] 09 p1498 A71-22093

Radiative instability of nonequilibrium plasmas in magnetic traps, considering circularly polarized oscillations propagating along magnetic field 09 p1500 A71-22241

Cd atoms excited state populations in nonequilibrium gas discharge plasma 09 p1500 A71-22267

Steady nonlinear amplitude of electrothermal instability in nonequilibrium plasma derived by expanding electrothermal equations in terms of perturbation about equilibrium state 09 p1387 A71-23649

Preionization and velocity effects in MHD channels containing potassium seeded argon plasma at atmospheric pressure 11 p1804 A71-25488

Negative differential conductance of homogeneous nonequilibrium electronic solid-body plasma in electromagnetic field upon Cherenkov interaction 11 p1807 A71-25584

Nonequilibrium Ar-Cs plasma under rectangular pulse overvoltage, analyzing ionization and recombination kinetics 15 p2454 A71-31486

Electron density fluctuations in nonequilibrium plasma under crossed electric and magnetic fields, relating ionization instability development and background relaxation times 15 p2454 A71-31488

Nonequilibrium effects in Ar free jet plasma, using cooled Langmuir probe for electron temperature and ion density measurements through shock wave in front of blunt body [AIAA PAPER 71-591] 15 p2454 A71-31536

Ar arc plasma thermochemical nonequilibrium, using finite difference techniques for nonlinear integrodifferential equations 15 p2455 A71-31538

Resonance radiation field of positive column of low current electric arc burning in nonequilibrium Ar plasma with admixture of K, using optical probe 15 p2457 A71-32270

Steady state of nonequilibrium Ar-Cs plasma in electric field, attributing instability to plasma radiation effect 15 p2457 A71-32273

Nonequilibrium and equilibrium plasmas thermodynamic properties and molecular, atomic and ionic internal partition functions and relaxation times 16 p2617 A71-32955

Nonequilibrium plasma chemical reaction kinetics problems, discussing time dependence, dissociation and recombination theories in pulsed EM field, equations and numerical calculations 16 p2539 A71-32965

Low temperature high conductivity nonequilibrium plasma creation in MHD generators by microwave ionization 17 p2676 A71-34193

Nonequilibrium plasma molecular impurities effect on electron energy balance, noting importance in closed cycle MHD generators 17 p2789 A71-35261

Pulsed MHD generator model with nonequilibrium plasma, obtaining I-V characteristics 17 p2677 A71-35273

Interelectrode spacing effects on nonequilibrium cesium plasmas in close spaced thermionic converters 20 p3179 A71-38876

Current and potential distributions in lossless nonequilibrium MHD plasmas at high magnetic field strengths, using method of characteristics 21 p3423 A71-40946

Radiative instability of nonequilibrium plasmas in magnetic traps, considering circularly polarized oscillations propagating along magnetic field 21 p3424 A71-41130

Inhomogeneous plasma shear flow instability with ion-ion collision, using BGK model 22 p3579 A71-41581

Piezosemiconductors nonequilibrium electron plasma current oscillations under strong electric and magnetic field interactions 22 p3584 A71-41644

Spatial dispersion effect on circular polarized cyclotron radiation spontaneous emission coefficient in nonequilibrium plasma 22 p3583 A71-42326

Spectral line broadening due to radiating atom-electron gas interaction in nonequilibrium partially ionized plasma 23 p3710 A71-43392

Stratified nonequilibrium plasma ionization instability in crossed fields investigated by physical model without diffusion processes and boundary effects, considering space-time behavior of perturbation 23 p3713 A71-44152

NONEQUILIBRIUM RADIATION

Initial ionization, relaxation kinetics and nonequilibrium radiation behind strong shock waves in monatomic gases and air 05 p0835 A71-16524

Noneuclidian Geometry

U DIFFERENTIAL GEOMETRY

NONFERROUS METALS

Mathematical model for continuous elastoplastic transition stress-strain response of steels and nonferrous metals 18 p2937 A71-36835

NONFLAMMABLE MATERIALS

Nonflammable self extinguishing nontoxic fluorocarbon elastomers as adhesives and coatings for Apollo program 10 p1632 A71-24097

Nonflammable elastomeric materials and coatings for oxygen enriched atmospheres 10 p1632 A71-24098

Flame retardant silicone elastomers for use as aircraft construction materials, describing fabrication techniques, mechanical, aging and weathering properties 12 p1921 A71-27412

NASA program fire safety goals, discussing development of nonflammable materials covering fibrous asbestos, glass, polyimides, Teflon, metallics and halogenated materials [AIAA PAPER 71-1011] 24 p3841 A71-44595

NONGRAY ATMOSPHERES

Nongray equilibrium radiative heat transfer in viscous radiating shock layer around blunt body entering high temperature nonisothermal carbon dioxide-nitrogen atmosphere [AIAA PAPER 69-636] 01 p0180 A71-10938

Radiative transfer in plane layer of nongray absorbing and emitting medium bounded by black parallel plates, using rectangular model 01 p0180 A71-10945

Heat transfer in nongray radiating gas turbulent flow in circular tube 01 p0181 A71-11403

Nongray thermal radiation effect on laminar forced convection over heated horizontal flat plate, determining temperature profiles for optically thin and thick boundary layers 04 p0688 A71-15741

Nongray absorption and radiation cooling on smooth symmetric blunt bodies included in modified Maslen flow field method for radiation and large blowing [AIAA PAPER 69-637] 05 p0694 A71-16566

Vibrational nonequilibrium influence on IR radiative energy transfer in nongray nonisothermal gases 10 p1643 A71-24967

Radiative transfer in nongray gas with local molecular and slightly disturbed radiative equilibrium, deriving linearized differential equation with application to radiatively driven acoustic waves 10 p1697 A71-25065

IR radiative heat transfer in nongray nonisothermal gases, giving solutions for radiative equilibrium and combined conduction and radiation 10 p1698 A71-25094

Venus surface temperature dependence on incident solar flux based on runaway greenhouse nongray calculation, considering water vapor as IR opacity source in models 18 p2964 A71-36285

NONGRAY GAS

Electromagnetic radiation in stagnation flow region, determining temperature distribution absorption coefficient of carbon dioxide at rest between two parallel plates 22 p3621 A71-42024

Nongray radiative heat transfer in finite slab with discrete absorption coefficient and specularly and diffusely reflecting boundary surfaces of uniform temperature 24 p3886 A71-44372

NONHOMOGENEITY

U INHOMOGENEITY

NONISOTHERMAL PROCESSES

U ISOTHERMAL PROCESSES

NONISOTROPIC PLATES

U ANISOTROPIC PLATES

NONISOTROPY

U ANISOTROPY

NONLIFTING VEHICLES

U BALLISTIC VEHICLES

NONLINEAR EQUATIONS

NT CUBIC EQUATIONS

NT DUFFING DIFFERENTIAL EQUATION

NT QUADRATIC EQUATIONS

Cauchy problem for nonlinear integrodifferential equations with time lag argument, estimating iterative solution existence and uniqueness 01 p0112 A71-10491

Liapunov method applied to nonlinear differential equations for distant satellite orbit secular perturbations 01 p0156 A71-10546

Liapunov stability of neutral first order nonlinear differential equations solutions with time lag 01 p0112 A71-10655

Invariance in automatic control systems nonlinear differential equations of motion 01 p0064 A71-10730

Nonlinear space independent nuclear reactor kinetics equations, demonstrating positive periodic solutions existence 01 p0126 A71-11291

Nonlinear differential equations description in functional product form structure for digital simulation 02 p0226 A71-11781

Solar activity cycles mechanism, deriving nonlinear equations from quasisymmetric magnetic dynamo models 02 p0307 A71-12081

Mixed type nonlinear integral equations, using approximate method for numerical solutions 02 p0276 A71-12541

Self similar solutions of nonlinear partial differential equations, applying group invariance under infinitesimal transformation 03 p0449 A71-13075

Nonlinear partial differential equations solution by variable separation method [ASME PAPER 70-AUT-A] 03 p0451 A71-13713

Nonlinear partial differential equation solution for natural free-free vibrations of beam structures [ASME PAPER 70-WA/APM-55] 03 p0513 A71-14172

Nonlinear M-type traveling wave tube equations for large signal mode, discussing electron precipitation 04 p0556 A71-14623

Nonlinear thermoelasticity coupled equations, discussing stress and temperature fields in terms of material response functions 04 p0669 A71-15194

Nonlinear integrodifferential equations of heat and mass transfer problems, discussing asymptotic solution method 04 p0688 A71-15542

Nonlinear equation systems solution by epsilon algorithm based second order method 05 p0773 A71-16156

Matrix algorithms for linear and nonlinear inequalities, discussing rank generation and matrix inversion 05 p0774 A71-16398

Kincaid iterative solution for multidimensional systems of nonlinear equations, noting quadratic convergence as function of initial vectors 05 p0775 A71-17046

Wind field from macroscale atmospheric whirlpools /typhoons/ pressure fields by nonlinear hydrodynamic equations 06 p0923 A71-17514

Nonlinear singular integropartial differential equation numerical integration extension 06 p0917 A71-17553

Linear and nonlinear parabolic equations approximate solutions by Galerkin methods, leading to linear algebraic equations 06 p0917 A71-17558

Branching of periodic solutions of second order nonlinear ordinary differential equations similar to Duffing equation 06 p0918 A71-17643

Thin shallow shell theory, describing asymptotic method for nonlinear equations integration 06 p0988 A71-17776

Iteration method application to shell design nonlinear differential equations solution 06 p0988 A71-17777

Multilayer asymmetric plates deflection, stability and vibrations, deriving nonlinear bending equations with allowance for transverse shear strains 06 p0995 A71-17833

Nonlinear equations solution, considering Newton method and Henrici algorithm disadvantages and quadratic convergent procedure 06 p0919 A71-18203

Ritz-Galerkin method for solving nonlinear operator equations in Hilbert space, discussing convergence and error estimate 06 p0919 A71-18204

Iterative solution of nonlinear operator equations in Banach spaces, proving existence, uniqueness and convergence theorems 06 p0920 A71-18211

Theorems concerning relaxation in point total and single step iterative solution for Hammerstein type nonlinear equations 06 p0920 A71-18212

Matrix eigenvalue problem solution by reducing to nonlinear algebraic equations for iterative solution or integration by Runge-Kutta method 06 p0921 A71-18342

Optimal vacuum rocket trajectories over spherical earth, deriving nonlinear differential equations for position and velocity [AIAA PAPER 71-20] 06 p0976 A71-18487

Injection locked microwave oscillators nonlinear differential equation reduction to nonlinear algebraic equation, calculating AM limiting and output power increment as injected signal amplitude functions 07 p1073 A71-19113

Almost periodic solutions of two nonlinear Volterra integral equations 07 p1147 A71-19256

Nonlinear Mathieu equation response in first unstable region, comparing results to computer simulation 07 p1161 A71-19958

Two nonlinear coupled second order differential equations finite difference solution, using nonsquare and nonuniform grids for minimum error 07 p1149 A71-20612

Boundary value problem solution of nonlinear differential equation system with delayed arguments 07 p1149 A71-20644

Eigenvectors spectral structure analysis of monotonic and completely continuous nonlinear operator equations in separable real reflexive Banach space 07 p1149 A71-20646

Solar activity cycles mechanism, deriving nonlinear equations from quasi-symmetric magnetic dynamo models 08 p1362 A71-21131

Self oscillatory system behavior under sinusoidal external force, using nonlinear differential equations transformation 08 p1334 A71-21292

Complex hydrodynamic systems nonlinear differential motion equations integration, taking friction forces into account 08 p1299 A71-21620

Nonlinear MHD equations solution for laminar flow of electrically conducting fluid in cylindrical channel in traveling magnetic field 09 p1499 A71-22191

General nonlinear elasticity theory including applications, deformation laws, complex nonlinear equations solutions, equilibrium and stability problems, experimental methods and mathematical models 09 p1536 A71-22512

Lunar physical libration in longitude, considering nonlinear and dissipation terms 09 p1530 A71-23715

Arbitrary midsurface geometry thin shells nonlinear equations in terms of finite rotation vector and stress resultant tensor component 10 p1684 A71-23761

Nonlinear electrostatic theory Lagrangian analogous to gravitational Lagrangian from correspondence between Maxwell electromagnetism and Einstein gravitation 10 p1667 A71-23815

Thin spherical shell under uniform normal pressure using dynamic stability criterion and energy method for asymptotic nonlinear shell equations 10 p1685 A71-23937

Ionospheric irregularities two fluid model, using nonlinear differential equations for longitudinal waves propagating in hot collisional magnetoplasma 10 p1648 A71-24294

Sturm oscillation theorems for second order elliptic equation nonlinear partial derivatives, using linear Picone identity 11 p1791 A71-25176

Buckled rectangular panels response to random excitation via single degree of freedom nonlinear vibration equation 11 p1841 A71-25196

Elastic collapse analysis of shell structures with variable rectangular grid spacing based on modified finite difference computer program [AIAA PAPER 71-359] 11 p1844 A71-25338

Convergence rates of multistep iterative procedures for finding zero of nonlinear function defined on R to n th power 11 p1792 A71-25932

Asymptotic solution of second order nonlinear differential equation for autonomous nonlinear resonance system 11 p1743 A71-26536

Unique solution of certain classes of linear and nonlinear functional-integral equations reducible to Volterra integral equations 11 p1793 A71-26562

Transient characteristics of MOS channel transistors, solving nonlinear differential equations describing current and potential distribution 12 p1886 A71-26850

Shallow laminated shells nonlinear bending equations, using variational principle with allowance for transverse shear strain of layers 12 p1975 A71-27104

Asymptotic solutions for system of nonlinear quasilinear type differential equations for gyroscopic couplings 12 p1923 A71-27170

Nonlinear equations of motion for cylindrical elastoplastic shell under axial impact 12 p1980 A71-27452

Nonlinear elasticity displacement equations, presenting three dimensional boundary value problem formulation and solution by small parameter method 13 p2150 A71-28130

Longitudinal wave propagation in ideal elastic bar with viscous stress, calculating approximation to nonlinear wave equations 13 p2153 A71-28483

Numerical solution of nonclassical problem of calculus of variations, reducing nonlinear integral equation with Green function 13 p2095 A71-28819

Nonlinear differential equations system for one degree of freedom isochronous and anisochronous conservative oscillators resonance behavior during natural perturbation solved by coordinate transformations 14 p2265 A71-29687

Approximate method for nonlinear ordinary differential equations with variable coefficients applied to cylinder oscillation and flexible ring deformation 14 p2324 A71-29881

A priori bounds on linear and nonlinear quotients of Neumann boundary value problem for uniformly elliptic difference equations over rectangular regions 14 p2265 A71-30291

Parametric differentiation technique for axisymmetric stability of spherical shells, using Reissner nonlinear differential equations 14 p2329 A71-30506

Nonlinear ordinary first order differential equation solution for mechanical system motion, constructing asymptotic representation 14 p2266 A71-30838

Liapunov stability of neutral first order nonlinear differential equations solutions with time lag 14 p2266 A71-30989

Nonlinear hyperbolic equations integration, considering characteristic, mesh finite difference and particle in cell techniques 15 p2441 A71-31355

Averaging of nonlinear integrodifferential equations, demonstrating uniform convergence of sequence by successive approximations 15 p2442 A71-31521

Differentiability of nonlinear Volterra integral equations of second kind with convolutional weakly singular kernels 15 p2442 A71-31870

Existence and uniqueness theorem for n -point boundary value problems of nonlinear ordinary differential equations, using Polya condition 15 p2442 A71-31871

Uniqueness of positive solutions to self adjoint elliptic partial differential equations with nonlinear forcing terms under Dirichlet and Neumann boundary conditions 15 p2442 A71-31872

Plasma decay due to charged particles recombination, linearizing nonlinear equations describing diffusion of singly ionized two-component gas undergoing recombination 15 p2456 A71-31999

Nonlinear partial differential equations solution by separation of variables, obtaining reduction to ordinary nonlinear differential equations 15 p2442 A71-32251

Algorithm convergence for sparse nonlinear equations system solution with Jacobian satisfying Lipschitz condition 15 p2442 A71-32313

Forced oscillations of system governed by one dimensional nonlinear wave equations, using perturbation procedure for solutions near linear resonant frequencies 16 p2606 A71-32857

Self similar invariant group solutions to Bellman nonlinear partial differential equation for optimal correction problems of control systems motion with random disturbances 16 p2549 A71-32935

Global hydrodynamic stability theory, discussing energy methods and nonlinear Boussinesq equations for disturbed motion 16 p2558 A71-32995

Constant profile solutions stability for nonlinear wave equations with convection and dissipation 16 p2608 A71-33023

Cauchy problem for nonlinear Boltzmann equation in general relativity, utilizing energy inequalities 16 p2612 A71-34059

Numerical algorithm for Cauchy problem nonlinear partial differential integral equations solution by invariant imbedding 16 p2604 A71-34082

Nonlinear equations solution with error estimate, using iteration convergence method 16 p2604 A71-34083

Limit cycle of nonlinear oscillations of third order differential equations dependent on Euclidean phase space with central restoring control force 17 p2763 A71-34293

Generalized ordinary nonlinear differential equations, considering systems with impulses acting on surfaces 17 p2764 A71-34639

Integration method for second order nonlinear differential equation describing vibrational processes in mechanics, physics and engineering 17 p2766 A71-34913

Approximate method for solution of nonlinear equations with certain degree of freedom subjected to recall and small hereditary forces 17 p2780 A71-34916

Free and forced nonlinear oscillations differential equations approximate solution by orthogonal polynomial linearization, applying method to systems analysis near singular points 17 p2780 A71-34917

Asymptotic behavior of linear and nonlinear equations solutions 17 p2766 A71-34919

Periodic solutions of singularly perturbed hereditary systems of ordinary nonlinear integrodifferential equations 17 p2780 A71-34920

Averaging methods of nonlinear differential and integrodifferential equations with fast and slow variables over finite and infinite segments 17 p2766 A71-34923

Oscillatory systems motion by nonlinear differential equations with variable coefficients 17 p2781 A71-34924

Periodic solutions for strongly nonlinear differential system of n -coupled nonautonomous equations of Lienard and Rayleigh types 17 p2766 A71-34925

Steady oscillation frequencies in systems described by nonlinear differential equations, including external perturbations 17 p2782 A71-34931

Digital phase locked loop for FM signals demodulation, considering system nonlinear difference equation 17 p2704 A71-35084

On-off automatic control systems, using nonlinear finite difference equations for switching times and coordinate values determination 17 p2721 A71-35133

Multilayer asymmetric shallow shells with transverse shear strains, deriving finite deflection nonlinear equations 17 p2833 A71-35613

Friction forces in complex hydrodynamic systems nonlinear differential motion equations integration 17 p2749 A71-35680

Orders of convergence for iterative procedures for finding zero of nonlinear function, considering secant and Steffenson method 17 p2768 A71-35685

Bounded integral manifolds existence for perturbed system of nonlinear differential equations near critical point, periodic orbit or periodic surface 17 p2769 A71-35795

Monograph on nonlinear first order differential equations adjunction fields and solutions asymptotic behavior, seeking adjoinable solutions 18 p2940 A71-36098

Digital computers for analytic solution of second order nonlinear ordinary differential equations 18 p2884 A71-36142

Asymptotic approximations to Emden nonlinear differential equations of astrophysics for polytropic gas spheres, using multiple scale technique 18 p2941 A71-36226

Lower bound on distance between vertical asymptotes of second order differential equations solutions involving integral inequality 18 p2941 A71-36227

Laminar boundary layer flow analysis from nonlinear difference equations solution by Newton method, using block-tridiagonal factorization 18 p2905 A71-36313

Convergence of Broyden single-rank iterative solution for nonlinear equations systems involving approximation to Jacobian matrix 18 p2941 A71-36357

Asymptotic solution of nonlinear Volterra integral equation, examining nonlinear heat conduction and boundary layer heat transfer 18 p2942 A71-36747

Divergence structure nonlinear elliptic equations, demonstrating smooth solutions uniqueness of Dirichlet problem 18 p2942 A71-36816

Nonlinear eigenvalue problem solution in real Banach space, investigating continua existence and elliptic equations application 18 p2942 A71-36818

Symmetric operators family spectrum with generalized Rayleigh functional, showing analogy between linear and nonlinear theory at infinite spatial dimension 18 p2942 A71-36821

Nonlinear functional analysis - Conference, University of Wisconsin, Madison, October 1970 18 p2943 A71-36951

Functional analysis application to nonlinear integral equations, stressing Schauder fixedpoint theorem 18 p2943 A71-36952

Convergence theory for Newton-like iterative methods to solve nonlinear equations in abstract spaces, presenting error analysis 18 p2943 A71-36955

Operator solutions of nonlinear equations in linear feedback optimal control 18 p2943 A71-36956

Nonautonomous system equations of motion solution, determining conditions for nonlinearities conversion to linear equations 19 p3037 A71-37349

Nonlinear differential equations and boundary conditions describing behavior of electrically polarizable finitely deformable heat conducting continuum interacting with electric field 19 p3118 A71-37793

Transient simultaneous conductive and radiative heat transfer in plane gray layer bounded by black walls, yielding nonlinear integrodifferential equation [ASME PAPER 71-HT-22] 19 p3165 A71-37793

Critical time calculation for singularity in solutions of homogeneous nonlinear hyperbolic differential equations with smooth initial data, discussing application examples 20 p3254 A71-38790

Van der Pol equation periodic solutions using approximation scheme for all Fourier amplitudes 20 p3254 A71-38800

Nonlinear equations for traveling wave amplifiers using transverse wave interaction modes /cyclotron and synchronous electron beam waves/, calculating saturation characteristics 20 p3203 A71-39003

Nonlinear second order differential equations periodic solutions in terms of Fourier series, applying method to calculation of charged particle orbit in radial electric field 20 p3255 A71-39081

Error bounds and variational principles for nonlinear differential and integral equations, exemplifying by Liouville and Poisson-Boltzmann equations 20 p3255 A71-39496

Modified Newton-Raphson stiffness matrices and initial value formulations to geometrically nonlinear structural analysis for beam and plane stress triangular elements 20 p3311 A71-39870

Nonlinear Vlasov equation numerical integration methods, discussing Hermite expansion, characteristic function transform and truncation techniques 21 p3408 A71-40844

Vibration characteristics of cantilever beam about nonlinear equilibrium state, showing flexibility and prestressed state effect 21 p3468 A71-40968

Extracting coefficients of nonlinear differential equations from data on oscillating systems, using time derivative methods 21 p3409 A71-41015

Asymptotic behavior of nonlinear Volterra integrodifferential equation solution, noting application to nuclear reactor dynamics 21 p3409 A71-41077

Constructive existence theorem for nonlinear elliptic equation with restricted bounded domain 21 p3409 A71-41078

Nonlinear Volterra integral equation system solution using almost periodic forced oscillations 21 p3409 A71-41081

Nonlinear M-type traveling wave tube equations for large signal mode, discussing electron trajectories 22 p3521 A71-42263

Weak row sum criterion for nonlinear equation systems, applying to discrete two point boundary value problems and linear equation systems 22 p3567 A71-42374

Finite difference methods application to Euler nonlinear elliptic differential equations, using symmetric and positive Jacobian 22 p3567 A71-42375

Sturm-Liouville type nonlinear problems solution by Pruler polar coordinate technique, proving equivalency theorem for eigenvalues infinite sequence conversion 22 p3567 A71-42689

Nonautonomous nonlinear functional differential equations periodic solutions, reducing problem to existence proof of fixed point for operator in suitable space of periodic functions 22 p3567 A71-42691

Nonlinear differential equations with retarded argument, proving asymptotic and oscillatory solutions theorems 22 p3568 A71-42692

Variable structure digital control servomechanism flutter mode analysis, using nonlinear differential equation 22 p3528 A71-42878

Factor methods convergence for abstract equations with nonlinear entirely continuous operators 23 p3699 A71-43570

Cylindrical shell weakened with large circular hole, deriving nonlinear equilibrium equations in semigeodesic polar coordinates 24 p3877 A71-44479

Exact solutions of elasticity theory nonlinear differential equations by Lie group theory methods 24 p3877 A71-44480

Rotating disk creep analysis by Van Fo Fi-Ozerov nonlinear equation, obtaining numerical solution for total creep equation and time to failure for two angular velocities 24 p3882 A71-44839

Algorithm for preparation of nonlinear differential equations for simulation by analog computer in linear form 24 p3807 A71-45156

Nonlinear equations of compressible medium motion near point of contact between shock and diffraction waves 24 p3821 A71-45365

NONLINEAR FEEDBACK

Digital communication hybrid phase locked loop nonlinear feedback system with modulation and carrier components enhancing phase estimation 03 p0391 A71-14312

Plasma stabilization by nonlinear bang-bang feedback 06 p0932 A71-17459

Temporary nonlinear feedback effect on stability of triggering potential and output pulse repetition rate of transistor self relaxing blocking oscillator 09 p1424 A71-23169

Transient response and design formulas for microwave power stabilizer with nonlinear inertial feedback containing semiconductor attenuator 15 p2378 A71-31230

Control system stability with nonlinear feedback in steady equilibrium state 16 p2548 A71-32934

Cascade connection of nonlinear block and time invariant finite dimensional system, discussing stabilization by controlled state variable feedback 17 p2722 A71-35213

NONLINEAR FILTERS

Nonlinear filter construction and performance evaluation, using deterministic filter gains [ASME PAPER 70-WA/AUT-9] 03 p0387 A71-14150

Linear and nonlinear filtering, discussing theory and application in space guidance systems 07 p1081 A71-19533

PCM bit synchronization and signal detection by nonlinear filter theory, giving optimum sequential estimator 07 p1061 A71-19536

Laser operation instability with nonlinear filter, deriving electrons differential velocity distribution functions on inhomogeneous emitter 07 p1126 A71-20197

Adaptive control systems state variables and nonstationary parameters estimation in presence of random disturbance and measurement noise, using nonlinear filtering theory 09 p1423 A71-22612

Optimal nonlinear filtering, deriving algorithm based on statistical approximation of system and observer nonlinearities by second order polynomials 10 p1587 A71-24746

Gaussian processes discrimination, considering correlation functions in integral control of nonlinear filter for image recognition 13 p2039 A71-28917

Nonlinear filtering synthesis of optimal receiver for pseudorandom phase shift keyed signal with arbitrary modulation angle and white noise background 14 p2195 A71-30107

Nonlinear filters synthesis by digital computer technique, discussing density storage and Bayes law computation problems 16 p2549 A71-33351

Nonlinear gain and AM/PM conversion in FDMA communication through satellite repeater, using traveling wave tubes plus postzonal filter 17 p2703 A71-35082

Nonlinear filters performance comparison for reentry vehicle trajectory estimation from radar tracking, noting coordinate systems effect on extended Kalman filter accuracy 19 p3039 A71-38712

Single-shot joint detection-estimation for discrete and continuous data and generalization to Bayesian system identification, considering optimal nonlinear estimator realization 20 p3201 A71-38847

Bayesian estimates in nonlinear filtration of nonstationary non-Gaussian radio signals, deriving second central moments and parameter estimate errors 20 p3198 A71-39807

Nonlinear filtering for noise reduction of image data by mean-squared error minimization, discussing zero memory technique 22 p3547 A71-42507

Optimal nonlinear discrete filters with finite memory for polynomial signals, discussing synthesis with aid of minimax method 22 p3527 A71-42856

Automatic control systems optimal nonlinear digital filter design, using theoretical numerical grid 24 p3813 A71-44680

Random amplitude bounded measurement errors, describing nonlinear filtration method of noise smoothing 24 p3813 A71-44683

NONLINEAR PROGRAMMING

Parametric differentiation method for reducing structural optimization and nonlinear programming problems to solution of simultaneous nonlinear algebraic equations 01 p0174 A71-10951

Nonlinear control laws successive stochastic optimization through nonlinear and subsequent quadratic programming 03 p0392 A71-14403

Book on optimization methods covering matrix algebra, n dimensional geometry, search techniques, linear and nonlinear programming, etc 05 p0774 A71-16475

Complex zeros of complex polynomials, matrix inequalities and nonlinear programming, constructing areas intersection in complex plane defined by inequality bounds on eigenvalues of companion matrix 09 p1485 A71-22970

Man machine interactive computer graphics for design molding during evolution by computer with nonlinear programming algorithm 09 p1412 A71-23276

Search methods for nonlinear identification problems solution, evaluating and comparing nonlinear programming methods of conjugate gradients and of Davidson 12 p1892 A71-27023

Optimal nonlinear control with fixed time and compact convex target set, using gradient method 12 p1923 A71-27728

Local plastic deformation analysis of spherical and cylindrical shells subjected to yield point loads through rigid boss, using nonlinear programming 13 p2147 A71-27787

German monograph on PHENO hybrid computing elements for nonlinear operations covering ADC and DAC, level and time quantization effects on computational accuracy, etc 14 p2207 A71-30238

Elastic-plastic stiffness matrix methods, applying linear and nonlinear programming techniques to framed structures analysis 16 p2653 A71-33094

Search methods for nonlinear identification problems solution, evaluating and comparing nonlinear programming methods of conjugate gradients and of Davidson 19 p3038 A71-37693

Structural optimization problems involving vibration-weight interactions, using optimal control nonlinear programming transforms [ASME PAPER 71-VIBR-66] 21 p3460 A71-40308

Nonlinear mixed integer programming for automated design and structures optimization, describing penalty function technique and recovery scheme to satisfy integer requirements [ASME PAPER 71-VIBR-117] 21 p3350 A71-40336

Space shuttle trajectory design optimization by nonlinear programming, proposing mathematical model to handle equality and inequalities constraints 22 p3600 A71-42013

Optimal mismatched filter design for radar ranging, detection and resolution by reduction to transversal

equalizer, determining parameters by nonlinear programming 24 p3815 A71-44935

NONLINEAR SYSTEMS

Nonlinear automatic control systems steady random processes approximate analysis by integral linearization of functions and operators 01 p0058 A71-10100

Matrix perturbation methods for nonlinear perturbed systems, involving variational equations solution of regularized Keplerian motion 01 p0154 A71-10380

Polynomial finite difference description of first order nonlinear dynamic control plants with incomplete information 01 p0058 A71-10405

Second order nonlinear control system control law derivation by Liapunov direct method, defining region of undisturbed motion asymptotic stability 01 p0058 A71-10407

Computerized optimization of nonlinear dynamic control system subjected to random disturbances, using Monte Carlo method for quality functional 01 p0058 A71-10426

Nonlinear pulsed automatic control systems absolute stability with unsteady linearity by Pontryagin principle, considering forced and free motions 01 p0058 A71-10428

Nonlinear single-degree of freedom mechanical system vibration under small random perturbations 01 p0127 A71-10548

Extremal strategies of differential pursuit game for nonlinear controlled plants 01 p0128 A71-10654

Motion stabilization for nonlinear control systems with critical zero and imaginary roots, using Liapunov classical theory 01 p0128 A71-10667

Invariant automatic control structure for nonlinear plant, using inverse method 01 p0061 A71-10710

Nonlinear feedback control systems invariance, investigating coordinate and parametric disturbances compensation 01 p0063 A71-10728

Complex control nonlinear systems invariance and stability conditions, discussing harmonic balance analysis method 01 p0063 A71-10729

Continuous zonal flow nonlinear baroclinic instability, noting amplitude vacillations and flow-wave interactions 01 p0120 A71-10855

Perturbed motion stabilization in nonlinear control system with applicable equation containing zero root and imaginary roots 01 p0128 A71-11158

Nonlinear networks interconnected by lossless transmission lines, deriving global asymptotic stability condition 01 p0065 A71-11574

Nonlinear precision attitude control system stability analysis algorithm based on quadratic Liapunov function 02 p0278 A71-11648

Nonlinear closed loop-shape characteristics of vibrational mechanical systems, using forced vibration analysis 02 p0284 A71-12284

Successive approximation procedure for discrete time nonlinear systems data smoothing, developing Newton method algorithm for two point boundary value problem 02 p0277 A71-12726

Nonlinear time varying discrete feedback systems input-output properties, deriving stability criteria by generalized small gain and passivity theorems 03 p0389 A71-13327

Nonlinear system with one degree of freedom under HF and velocity dependent force, determining quasi-periodic vibrations with two frequencies by averaging method 03 p0502 A71-13406

Indirect, linear and nonlinear optimal guidance schemes from precomputed reference trajectory, using iterative techniques for boundary equations 03 p0454 A71-13449

Frequency response characteristics of nonlinear oscillatory circuits with inductive and complex capacitance couplings 03 p0379 A71-13812

Nonlinear systems near steady state oscillation transient behavior analysis by linear differential equations with periodic coefficients 03 p0451 A71-13817

First order nonlinear nonautonomous systems equivalence to second order linear autonomous systems through governing differential equations variables integral transformation 03 p0390 A71-14076

Buckled beam nonlinear vibration under harmonic excitation, solving governing partial differential equation by Galerkin and harmonic balance methods [ASME PAPER 70-WA/APM-48] 03 p0512 A71-14167

Approximate optimal control law formulation by harmonic linearization for nonlinear time invariant state regulator problem with high performance index 03 p0390 A71-14299

Soviet papers on nonlinear optimization of automatic control systems covering analysis, synthesis and stabilization problems 03 p0391 A71-14401

Nonlinear control systems optimization methods formulation according to deterministic and random disturbances and initial conditions 03 p0391 A71-14402

Nonlinear control laws successive stochastic optimization through nonlinear and subsequent quadratic programming 03 p0392 A71-14403

Nonlinear control synthesis based on minimum duration of transient processes leading to system stabilization, using Pontryagin maximum principle 03 p0392 A71-14406

Nonlinear time optimal off-on feedback control system synthesis, deriving algorithms 03 p0392 A71-14410

Nonlinear stabilization systems time and energy optimal control syntheses using Pontryagin maximum principle 03 p0393 A71-14411

Soviet book on frequency method of calculating nonlinear systems covering continuous and pulsed automatic control 03 p0393 A71-14425

Second order moment at output of inertialess nonlinear two terminal pair network during amplitude and phase modulation 04 p0550 A71-14620

Parametric resonance and first order instability region of Mathieu equation in nonlinear systems 04 p0620 A71-15737

Complete system associated with given control, discussing trajectories uniform approximation and nonlinear controllability conditions based on linear partial differential equation 04 p0620 A71-15865

Nonlinear time varying systems global and local controllability, deriving conditions related to linear systems controllability 04 p0561 A71-15867

Nonlinear systems bang-bang controllability by differential geometry approach 04 p0562 A71-15872

Oscillations of nonlinear system with conditions for main amplitude equations 05 p0780 A71-16179

Unsteady heat conductivity problems with nonlinear boundary conditions, using perturbation method 05 p0838 A71-16782

Nonlinear systems stability conditions, determining system coordinates absolute values upper bounds under initial and parametric disturbance conditions 05 p0731 A71-16792

Automatic systems design, describing optimization method for nonlinear nonstationary system acted upon by fluctuation signals and disturbances 05 p0731 A71-16793

Object motion stabilization, determining minimum control actions number for linear and nonlinear systems 05 p0782 A71-16977

Energy transfer between nonlinearly coupled oscillators described by Hamiltonian system in case of third order resonance 05 p0783 A71-16995

Direct search of performance index for optimal control of class of nonlinear distributed parameter systems 05 p0776 A71-17109

Nonlinear dynamic systems synthesis by integral linearization, obtaining gain coefficients and graphs for work reduction 05 p0732 A71-17171

Absolute stability of closed automatic control system with nonlinear components, discussing frequency criterion 05 p0732 A71-17172

Permanent magnet system as nonlinear computer problem, using Newton method and equivalent circuits with lumped parameters 05 p0705 A71-17174

Soviet book on nonlinear and parametric radio circuits covering amplification, detection, modulation, oscillation generation and frequency division, multiplication and conversion 06 p0867 A71-17441

Soviet book on Liapunov functions covering autonomous linear and nonlinear systems, asymptotic and absolute stability, etc 06 p0916 A71-17442

Soviet book on nonlinear almost-periodic oscillations covering application of integral equations method to differential equations, automatic control systems, pendulum motion, etc 06 p0926 A71-17443

Random Gaussian noise driven damped nonlinear oscillator, discussing Duffing equation, consolidated

expansions for response spectrum and common factors 06 p0926 A71-17499

Continuous monotonic nonlinear controlled systems with time dependent, phase coordinates and nonnegative parameter disturbances, considering Chetaev estimate for restricted approximate solution 06 p0879 A71-17670

Simply and multiply connected regions in nonlinear media, deriving stress concentration solutions 06 p0987 A71-17777

Unsteady heat transfer in nonlinear systems, solving hyperbolic equation by net-point method 06 p1006 A71-18000

Second order nonlinear systems with limited state variables, determining structural stability regions 06 p0928 A71-18220

Monte Carlo technique for time domain response analysis of nonlinear structure in random pressure field with large deflection [AIAA PAPER 71-213] 06 p1004 A71-18646

Stratified statistical filtering algorithm for numerical simulation of nonlinear systems behavior 07 p1081 A71-18836

Multivariate and multidimensional random processes simulation with specified cross spectral density, applying to nonlinear structural vibration analysis 07 p1161 A71-19963

Relative spectral sensitivity /amplitude frequency characteristics/ applicability to describing nonlinear systems 07 p1043 A71-20111

Nonlinear control systems with transport lag, obtaining parameter plane equations for stability analysis 07 p1082 A71-20369

Fokker-Planck boundary value solutions to transient phase error response of nonlinear phase locked tracking systems 07 p1082 A71-20428

Nonlinear absolutely stable regulator design in parameter space, using computer simplex search 08 p1324 A71-21319

Sequence solution to multidimensional time varying Fokker-Planck equation for phase locked nonlinear systems 08 p1324 A71-21342

Soviet book on nonlinear systems oscillations covering analysis methods, periodicity, mathematical models, etc 08 p1335 A71-21657

Action reproduction accuracy of nonlinear controlled systems with constraints and delays, considering stability degree 08 p1336 A71-21861

Three dimensional nonlinear heat conduction problem solving by perturbation theory and finite integral transform 08 p1377 A71-21927

Nonlinear automatic control systems stabilization by seeking Liapunov function satisfying certain integral relationships 08 p1270 A71-21977

Nonlinear automatic control system stability with random stationary parameters 08 p1271 A71-22024

Nonlinear control systems absolute instability, establishing general frequency criteria 09 p1421 A71-22117

Nonlinear control systems absolute stability range in parameter space 09 p1422 A71-22121

Nonlinear plants time optimal control 09 p1422 A71-22122

Nonlinear fluctuation-dissipation thermodynamics with time-even and time-odd parameters concerning four index relations for nonquantum Markovian case 09 p1544 A71-22366

Subharmonic forced vibrations of one degree of freedom nonlinear mechanical systems, deriving formulas for oscillation amplitude, phase shift and shape factor 09 p1536 A71-22410

Approximate optimal control synthesis, eliminating use of nonlinear functional converter for switching units design 09 p1423 A71-22607

Magnetic tape recording systems nonlinear amplitude distortion in terms of transfer function characteristics applied to analog instrumentation 09 p1449 A71-22786

Nonlinear sampled data feedback control systems periodic mode of oscillations, using state variable approach 09 p1423 A71-23033

Rectilinear trajectory optimization of second order nonlinear system, formulating existence and uniqueness theorems of optimal control 09 p1424 A71-23433

Sudden step changes in parameters of nonlinear resonance systems having several stable steady state solutions 09 p1543 A71-23612

Rumanian book on nonlinear and random vibrations covering dissipative and conservative nonlinear

mechanical systems, deterministic excitation and applications of mathematics

09 p1543 A71-23619

Algorithms for optimal control of nonlinear stochastic systems, minimizing control error variance

09 p1425 A71-23684

Nonlinear second order differential system two point boundary problems, establishing eigenvalues and associated solutions boundedness and oscillations

10 p1636 A71-24130

Soviet book on variable structure system theory covering nonlinear automatic control, stability, optimization, adaptive systems, incomplete information processes, linear filters, etc

10 p1585 A71-24147

System identification, considering input signals classification, model structure, linear/nonlinear systems identifying and on-line/real time techniques

10 p1586 A71-24736

Deterministic parameter estimation in nonlinear system near optimum feedback control by power series expansion

10 p1586 A71-24738

Dynamical nonlinear systems observability definition and necessary and sufficient criterion for checking

10 p1587 A71-24743

Closed-loop nonlinear systems synthesis, using mapping in Chebyshev series converging everywhere, multidimensional linearization and Volterra singular integral equations

10 p1587 A71-24744

Nonlinear systems parameter identification schemes using first and second order extended Kalman-Bucy linear filters and sensitivity functions, comparing performance by two examples

10 p1587 A71-24745

Penalty method and decomposition of state equations applied to nonlinear systems

10 p1637 A71-24840

Laplace transforms for nonlinear systems analysis

11 p1791 A71-25185

Microwave tunnel diode oscillator, representing nonlinear characteristics with Taylor series

11 p1737 A71-25666

Optimal characteristics for single-input single-output memoryless time invariant nonlinear dynamic systems

11 p1742 A71-25751

Laser radiation and plasma nonlinear interaction, using particle description of electron motion

11 p1806 A71-26093

Optimal reliability of system with nonlinear constraints, using mathematical model and sequential unconstrained minimization technique

11 p1771 A71-26161

Unidirectional glass fiber epoxy composite material nonlinear viscoelastic behavior, using isothermal uniaxial creep and recovery tests with thermodynamic constitutive equations

11 p1851 A71-26385

Nonlinear systems optimal control, presenting Hamilton-Jacobi equations analytical solutions for quadratic cost function minimization

11 p1742 A71-26420

Nonlinear systems response to arbitrary multiple frequency inputs, deriving series expansion for nonlinear modulation products

11 p1793 A71-26424

Nonlinear control systems dominating oscillation modes, investigating parameter variations effect by root locus technique

11 p1743 A71-26425

Soviet papers on nonlinear and microwave radio engineering systems covering antenna arrays, tunnel diode multivibrators and binary logic elements, subharmonic oscillators, etc

11 p1739 A71-26535

Asymptotic solution of second order nonlinear differential equation for autonomous nonlinear resonance system

11 p1743 A71-26536

Energy calculation for oscillatory systems with nonlinear, hysteretic and parametric elements

11 p1743 A71-26537

Nonlinear hysteretic element narrow band resonant system operating in steady state at fundamental resonance

11 p1743 A71-26538

Series resonant transistor circuit exhibiting response nonlinearity caused by conductance and charge storing capacitance of p-n junction

11 p1740 A71-26544

French monograph on nonlinear recurrences solutions and applications to sampled data systems

12 p1928 A71-26567

Nonlinear self adjusting and variable structure automatic control systems for piloted and pilotless flight vehicles, considering oscillations due to electric servosystems nonlinear characteristics

12 p1926 A71-26716

Approximate stability criteria-system parameter relationships facilitating higher order adaptive systems synthesis

12 p1890 A71-26722

Spacecraft nonlinear stabilization system phase space structure, transient processes and system stability domain, using point-to-point transformation method

12 p1972 A71-27018

Optimal control of linear and nonlinear systems with infinite degrees of freedom, deriving parabolic type partial differential equations

12 p1891 A71-27019

Automatic control systems with nonlinear hysteresis characteristics, deriving frequency conditions for absolute system stability

12 p1892 A71-27025

Nonlinear elastic shells free vibrations, obtaining phase trajectories with finite bending within Hooke's law

12 p1975 A71-27106

Asymptotic methods and Markov processes theory extension to unsteady vibration of nonlinear systems with slowly varying parameters and random perturbation

12 p1930 A71-27173

Nonlinear systems optimal control computational method, using Chebyshev algorithm

12 p1868 A71-27592

Nonlinear closed loop control system with PFM and PWM, obtaining asymptotic stability condition by Liapunov and La Salle theorems

12 p1893 A71-27726

Optimal control synthesis analog for nonlinear problem, using trial and error method based on Pontryagin maximum principle

13 p2040 A71-27834

Time optimal control problem solution for linear and nonlinear piecewise continuous systems by penalty function method

13 p2040 A71-27897

French book on practical methods for nonlinear oscillations analysis covering linear and nonlinear systems, autonomous systems, forced harmonics, nonautonomous oscillating systems, etc

13 p2041 A71-28151

Celestial mechanics and nonlinear dynamics in Poisson series, discussing Echeloned Series Processor for computer programming

13 p2034 A71-28355

Combustion chambers unstable acoustic oscillations, calculating equations for nonlinear growth and decay rate and limiting amplitude

13 p2160 A71-28613

Nonlinear sampled data control systems stabilization, eliminating intersample ripples by zero-order hold

13 p2042 A71-28702

Nonlinear multivariable sampled data systems synthesis and analysis in first harmonic approximation, introducing function arbitrary order difference

13 p2042 A71-28704

Stability criteria for nonlinear time-varying feedback systems, using passivity theorem

13 p2042 A71-28705

Output autocorrelation functions of zero memory nonlinear devices excited by signal plus Gaussian noise and interference

13 p2039 A71-28869

Nonlinear analog function generators using semiconductor junctions and combined diode-resistor network

13 p2039 A71-28914

Oscillations in system of nonlinear cubic response with narrow-band random excitation, using statistical linearization

13 p2101 A71-29077

Nonlinear differential equations system for one degree of freedom isochronous and anisochronous conservative oscillators resonance behavior during natural perturbation solved by coordinate transformations

14 p2265 A71-29687

Nonlinear damped vibratory system with two degrees of freedom excited by two external harmonic forces of different frequencies, investigating summation tones stability

14 p2322 A71-29693

Computational technique for finding bang-bang time optimal controls of nonlinear time-varying systems with bounded control function inputs

14 p2219 A71-29699

Nonlinear systems stability analysis for arbitrary disturbances, using semistochastic technique

14 p2219 A71-29735

Nonlinear control systems absolute instability, establishing general frequency criteria

14 p2219 A71-29995

Nonlinear control systems absolute stability range in parameter space, using system of inequalities

14 p2220 A71-29999

Series connected nonlinear systems time optimal control by n interval theorem or optimization with restricted phase coordinates

14 p2220 A71-30000

S matrices application to nonlinear electric circuits and media with nonlinear permittivity coefficients, biological neurons and optical frequency integrators

14 p2220 A71-30025

Gaussian input signal nonlinear sampled data systems analysis using linear components and transfer function

14 p2220 A71-30800

Extremal strategies of differential pursuit game for nonlinear controlled plants

14 p2266 A71-30988

Motion stabilization for nonlinear control systems with zero and imaginary roots, using Liapunov classical theory

14 p2221 A71-31000

Nonlinear asymptotic stability of motion in critical case involving characteristic equation in first approximation with pair of imaginary roots

15 p2449 A71-31699

Suboptimal control of nonlinear autonomous dynamical systems via linear approximation by hyperplanes

15 p2379 A71-31823

Bogoliubov averaging method application to nonlinear stochastic systems described by ordinary and partial differential equations and differential-difference equations

15 p2449 A71-31829

Zero solution stability of nonlinear system of differential equations with constantly acting perturbations

15 p2449 A71-31830

Nonlinear multidimensional automatic control systems structural synthesis

15 p2379 A71-31844

Independent noise driven nonlinear dynamic systems identification, performing linear discrete-time scalar measurements

15 p2380 A71-31934

Liapunov approach to nonlinear dynamic systems controllability, deriving conditions for linear dynamic systems

15 p2380 A71-31935

Stability criterion for cross coupled symmetrical two dimensional nonlinear control systems allowing different slopes for Popov lines

15 p2380 A71-31938

Bounded-input bounded-output stability of systems with multiplicative nonlinearity, presenting sufficient conditions in frequency domain

15 p2381 A71-31939

Nonlinear system design based on generalized Popov stability criterion

15 p2381 A71-31940

Suboptimal feedback control law for second order nonlinear systems with quadratic performance index, determining power series coefficients

15 p2381 A71-31941

Soviet book on discrete control systems covering linear and nonlinear systems synthesis and analysis, digital computer techniques, one and multidimensional pulsed systems optimization, etc

15 p2381 A71-31976

Linearly increasing input signal tracking in nonlinear control systems with pulse frequency modulation, discussing error determination, asymptotic stability and equations of motion

15 p2381 A71-31980

Input signal preservation in nonlinear dynamic system described by finite difference equation in presence of noise, deriving algorithms for discrete time computers

15 p2381 A71-31982

Optimality conditions for nonlinear distributed parameter control systems described by functionals of evolutionary and stationary equations of mathematical physics

15 p2382 A71-31993

Higher order linear and nonlinear systems equivalence from partial/ordinary differential equations

15 p2443 A71-32521

Nonoscillating and quasi-oscillating conditions of time optimal second order nonlinear control systems with piecewise-continuous right hand sides

15 p2382 A71-32620

Optimal stabilization of self adjusting control system for nonstationary plant in limited time by linear model using Lagrange multipliers

15 p2382 A71-32622

Rectangular pulse formation in nonlinear homogeneously distributed systems, discussing energy conversion efficiency

15 p2382 A71-32626

Self excited and transient oscillations parameters determination in nonlinear control systems, using control area concept

15 p2383 A71-32697

Static stability criterion dynamic extension for nonlinear continua under conservative loads, using Liapunov functions

16 p2607 A71-32980

Mathematical techniques of equilibrium states and periodic vibrations in nonlinear elastic systems illustrated by thin plate and shallow cap buckling under uniform pressure

16 p2649 A71-32998

Perturbation method for solving nonstationary heat conduction problems with nonlinear boundary conditions 16 p2662 A71-33034

Geometrically nonlinear large deflection and structural stability problems, using finite element method 16 p2653 A71-33087

Weakly nonlinear single degree of freedom cubic system under simultaneous time varying force and parametric excitation, presenting resonance frequencies classification [ASME PAPER 71-APM-24] 16 p2655 A71-33205

Controlled motion dynamics of spacecraft performing maneuvers, applying point transformation to third-order nonlinear system moving about center of mass in lateral motion 16 p2646 A71-33658

Coupled nonlinear control system optimization by noniterative perturbation method 16 p2551 A71-34170

Logarithmic frequency characteristics in stable nonlinear pulsed systems synthesis 17 p2718 A71-34558

Nonlinear optimal closed loop system control problems equivalence relations as one-to-one correspondences between Hamilton-Jacobi equations solutions 17 p2719 A71-34743

Nonlinear oscillations - Conference, Kiev, August-September 1969 17 p2779 A71-34903

Averaging method for nonlinear oscillations in celestial mechanics, radio engineering and electronics and for time lag, random forces and integrodifferential equations 17 p2779 A71-34904

Slightly nonlinear structures vibration, examining experimental means for mathematical models development and coefficients determination 17 p2779 A71-34906

Asymptotic solution for nonlinear vibrations of mechanical system with slowly varying parameters and strong resistance 17 p2779 A71-34908

Nonlinear vibrations, studying differential equations system in normal form 17 p2779 A71-34909

Statistical theory of nonlinear differential equation system with discontinuous trajectory solution, deriving motion stability to first approximation using Liapunov functions 17 p2780 A71-34915

Nonlinear differential equation system periodic functions in terms of uniformly converging periodic functions sequence 17 p2781 A71-34927

Nonlinear resonance problems analysis by averaging schemes, considering Volosov and Morgunov stability conditions 17 p2781 A71-34929

Steady oscillation frequencies in systems described by nonlinear differential equations, including external perturbations 17 p2782 A71-34931

Nonautonomous nonlinear dynamical systems with simultaneous fast and slow time response, basing analysis method on previous work of Malkin, Massera, Bogoliubov and Mitropolsky 17 p2782 A71-34932

Free and forced nonlinear oscillatory systems with harmonic perturbations, noting amplitude dependence on force frequency and friction coefficients 17 p2782 A71-34935

Nonlinear system with one degree of freedom under HF and velocity dependent forces, determining two-frequency quasi-periodic vibrations by averaging method 17 p2826 A71-35016

Soviet papers on exact analytical methods for studying nonlinear automatic control systems covering synthesis, stability, quality and dynamics problems 17 p2783 A71-35126

Parameter space sections method for nonlinear automatic control systems analysis, reducing initial system by linear transformation of variables to first and second order equations 17 p2783 A71-35127

Second order and degenerate third order nonlinear automatic control systems analysis by point mapping method, considering global stability and self oscillation mode 17 p2783 A71-35128

N-dimensional phase spaces of nonlinear nth order automatic control systems at parameter space sections /hyperplanes/, considering nonlinearities effects in servomechanisms 17 p2783 A71-35129

Frequency criteria for absolute stability of equilibrium states and processes in nonlinear automatic control systems 17 p2783 A71-35130

Nonlinear automatic control systems stability during large modulus-limited deviations based on method of sections and direct Liapunov method 17 p2783 A71-35131

Nonlinear automatic control systems synthesis based on structure and parameter values selection, formulating quality criteria 17 p2783 A71-35132

Two dimensional nonlinear discrete /pulse frequency modulation/ control system stability, using Liapunov direct method and mathematical model 17 p2721 A71-35134

Dynamic response as function of time of nonlinear nonautonomous second order control system to external disturbances, using moving phase plane method 17 p2721 A71-35135

Nonlinear automatic control systems sensitivity to changes in prescribed operating conditions and component parameters 17 p2784 A71-35136

Nonlinear feedback control system with two nonlinear memoryless energyless elements separated by linear device, discussing grapho-analytical method for self sustained oscillation determination 17 p2722 A71-35183

Optimal state regulator approximate design for nonlinear system with quadratic performance index, determining suboptimal feedback law 17 p2722 A71-35212

Cascade connection of nonlinear block and time invariant finite dimensional system, discussing stabilization by controlled state variable feedback 17 p2722 A71-35213

Soviet book on algorithms for electronic circuit analysis covering linear and nonlinear transistor or tube circuits matrix-topological description and frequency-time domain solutions 17 p2717 A71-35219

French monograph on topological classification and identification of nonlinear systems by structural decomposition method covering general systems theory fundamentals 17 p2767 A71-35230

Difference analog of nonlinear hydrodynamic boundary value problem from Navier-Stokes steady state theory 17 p2728 A71-35241

Three dimensional nonlinear heat conduction problem solving by perturbation theory and finite integral transformation method 17 p2838 A71-35271

Unstable nonlinear systems transient behavior analysis with two-time perturbation method applied to Benard and Taylor flow problems 17 p2730 A71-35797

Dynamic properties of modulating and mixing nonlinear systems consisting of time dependent impedance controlled by pumping source 18 p2875 A71-35975

Nonlinear time varying systems digital integration simulation techniques by variational equations approach, discussing accuracy, execution time and limitations 18 p2884 A71-36141

Time ordering operators applications to nonlinear unsteady systems, covering stochastic differential equations solution and phase locked loop phase error probability density calculation 18 p2940 A71-36222

Object motion stabilization, determining minimum control actions number for linear and nonlinear systems 18 p2947 A71-36777

Energy transfer between nonlinearly coupled oscillators described by Hamiltonian system in case of third order resonance 18 p2948 A71-36795

Jump phenomena of nonlinear control systems subjected to nonstationary Gaussian random inputs, using statistical linearization method 19 p3036 A71-37236

Closed loop control of nonlinear systems in potentially large neighborhood of nominal trajectory, reducing nonlinear differential equations to related canonical linear form 19 p3037 A71-37239

Nonlinear mechanical system stationary random forcing input and output response data, determining statistical linearization coefficients in Kazakov-Boon method 19 p3037 A71-37347

Nonautonomous system equations of motion solution, determining conditions for nonlinearities conversion to linear equations 19 p3037 A71-37349

Explicit procedure for discrete approximations to general nonlinear fixed-time continuous optimal control problems without intermediate trajectory constraints 19 p3037 A71-37556

Absolute instability of nonlinear control systems, applying circular criterion to systems with nonstationary nonlinearities 19 p3037 A71-37568

Spacecraft nonlinear stabilization system phase space structure, transient processes and system stability domain, using point-to-point transformation method 19 p3152 A71-37688

Automatic control systems with nonlinear hysteresis characteristics, deriving frequency conditions for absolute system stability 19 p3038 A71-37694

Computer programs for nonlinear finite element analysis with applications to large displacement and small strain problems 19 p3088 A71-38305

Electromagnetic compatibility characteristics in terms of receiver susceptibility to interference effects on selectivity and nonlinearity parameters 19 p3033 A71-38466

Nonlinear vibrating system characteristics relationship to transient process, deriving Abel integral equations for damping coefficient and restoring force 19 p3104 A71-38488

Vibrational behavior of nonlinear systems subjected to finite duration pulse excitation, transforming original differential equation into Lighthill method solvable form 20 p3267 A71-38798

Higher order approximation for normal vibration modes in nonlinear two degree of freedom systems 20 p3267 A71-38799

On-line identification for nonlinear system from noisy measurements, applying stochastic algorithm to hybrid simulation of chemical process models 20 p3207 A71-38974

Exponential absolute stability of nonlinear discrete systems of Lure type, deriving modified frequency condition 20 p3255 A71-39028

Nonlinear autonomous oscillation systems stability conditions derivation by Kamenkov method for quasi-linear systems 20 p3269 A71-39201

Action reproduction accuracy of nonlinear controlled systems with constraints and delays, estimating maximum error and stability degree 20 p3208 A71-39360

Liapunov functions application to Stability of systems described by nonlinear second-order ordinary differential equations, considering feedback control loops construction 20 p3255 A71-39499

Frequency response of nonlinear feedback control systems, using modified polar plot of open loop transfer function 20 p3208 A71-39914

Thrusting lifting orbital vehicle nonlinear longitudinal dynamics in near-circular orbit, deriving orbital elements variation behavior and angle of attack mode period and damping 21 p3454 A71-40094

Automatic computational algorithm for parameter identification of nonlinear systems, using deterministic time invariant model with memory and gain functions 21 p3407 A71-40261

Lumped parameter modeling of fluid elastic vibration response of nonlinear piston driven pneumatic-mechanical system, using finite element control volumes [ASME PAPER 71-VIBR-41] 21 p3459 A71-40299

Gradient search procedures application for nonlinear system unknown parameters identification from system dynamic response observations [ASME PAPER 71-VIBR-50] 21 p3460 A71-40299

Nonlinear autonomous systems transient response, obtaining approximate solutions by generalized averaging technique based on ultraspherical polynomial expansions 21 p3415 A71-40532

Phase-space theory of macroscopic fluctuations in nonlinear systems far from thermodynamic equilibrium, using chemical kinetics model 21 p3416 A71-40856

Nonlinear static structural mechanical problems solution, using self correcting initial value formulae 21 p3467 A71-40959

Amplitude estimates and bounds derivation for nonlinear two parameter oscillators, obtaining iterative solution for computation 21 p3358 A71-41013

Adaptation algorithm for optimal synthesis of nonlinear radio reception system with additive noise 21 p3361 A71-41143

Finite amplitude monochromatic wave self modulation in nonlinear medium, showing excitation process dependence on initial conditions 21 p3417 A71-41261

Soviet book on nonlinear sampled-data control systems with PFM and PDM covering mathematical description, transient analysis and system stability problems 22 p3526 A71-41821

Second order moment at output of inertialess nonlinear two terminal pair network during amplitude and phase modulation 22 p3510 A71-42260

Nonlinear and syllabic companded digital delta modulation systems, discussing SNR measurement and computer simulation for optimum design 22 p3514 A71-42392

Motion equations derived for slender beam transverse vibrations on continuous viscoelastic foundation, considering nonlinearities from external couplings, longitudinal displacements and curvature 22 p3617 A71-42539

Flip-flop circuits nonlinear distributed network mathematical model, investigating oscillations nonexistence 22 p3527 A71-42626

Bifurcation/branch point/ theorems and limit cycles for integral curves of hard excitation nonlinear systems 22 p3527 A71-42675

Compensator design for linear controllers for time varying nonlinear systems, using digital computer oriented approach 22 p3577 A71-42676

Thermodynamics of irreversible processes extended to nonlinear systems remote from equilibrium, considering Onsager reciprocity relations 23 p3780 A71-43104

Chebyshev polynomials computation of nonlinear oscillations of conservative autonomous system with single degree of freedom 23 p3777 A71-43493

Second order approximation algorithm for nonlinear noisy dynamical system state estimation from noise corrupted observations 23 p3656 A71-43854

Nonlinear discrete system optimal feedback controller synthesis for low sensitivity to parameter variations by difference equations quasilinearization and dynamic programming 23 p3656 A71-43855

Computer generation of sensitivity functions for nonlinear sampled data control systems, discussing simulator components and computational time economy problems 23 p3648 A71-43859

Stable feedback control of single variable nonlinear plants with arbitrary uncertainties, ensuring system error convergence to guaranteed stability 23 p3657 A71-43943

Computational method determining quadratic Liapunov functions for high order nonlinear systems 23 p3705 A71-43944

Asymptotic stability domain determination for nonlinear distributed parameter system, deriving coupling coefficients 23 p3699 A71-44079

Cost functional gradient optimization of pulse width modulated control inputs for nonlinear dynamic systems 23 p3658 A71-44088

Analytic synthesis of optimal feedback controller for nonlinear multivariable systems based on reduction to linear control problems 23 p3659 A71-44110

Suboptimal fixed point data smoothing algorithm for parameter and initial state estimation of nonlinear dynamic systems 23 p3659 A71-44113

Unknown parameter identification in nonlinear dynamic systems from state variable time history measurement 23 p3660 A71-44114

Single- and multivariable discrete nonlinear control systems with pulse amplitude modulation, deriving frequency criteria for stochastic stability in mean 24 p3812 A71-44397

Nonlinear and multivariate optimal sampled data control systems design with bounded control and state variables, using dynamic programming and divisional technique 24 p3812 A71-44452

Error evaluation of digital real time simulation of nonlinear systems 24 p3813 A71-44571

Soviet papers on nonlinear optimal control systems, discussing dynamics, adaptation, image recognition, reliability, queueing theory and random processes 24 p3813 A71-44676

Nonlinear automatic control system statistical optimization using similarity theory 24 p3813 A71-44681

Nonlinear control system optimal synthesis by statistical criteria, discussing probability and likelihood function 24 p3813 A71-44682

Statistical and combined harmonic and statistical linearization methods for piecewise-linear nonlinear system characteristics analysis 24 p3814 A71-44693

Unsteady nonlinear multidimensional feedback control systems characterized by equations in normal form for phase coordinates, investigating solutions accuracy by statistical linearization 24 p3814 A71-44694

Nonlinear stochastic systems approximate analysis based on multidimensional nonlinear transforms and distribution functions in Chebyshev-Hermite polynomials, determining dynamic accuracy 24 p3814 A71-44695

Parameters steady random variations effect on linear and nonlinear systems steady motion characteristics, using integral equation and averaging methods 24 p3815 A71-44696

Orthogonal method for studying nonlinear automatic control systems in presence of random perturbations, discussing applicability limits 24 p3815 A71-44701

Fokker-Planck-Kolmogoroff equation for radar tracking meter with nonlinear discriminator and second-order smoothing loops, obtaining steady solution by separated variables method 24 p3815 A71-44702

Unsteady random processes structural analysis application to nonlinear dynamic systems, evaluating algorithms effectiveness and improvement by self adaptive operators with finite memory 24 p3815 A71-44705

Nonlinear partial differential system analysis 24 p3843 A71-44797

Nonlinear controlled plant dynamic behavior sensitivity in parameter perturbation derived from mathematical model, applying to satellite attitude control [ASME PAPER 70-WA/AUT-5] 24 p3816 A71-45136

NONLINEARITY

Panel flutter structural nonlinearities, discussing shear flexibility, finite curvature and nonlinear inertia effects [ICAS PAPER 70-29] 03 p0501 A71-13150

General nonlinear finite deformation shell and strain membrane theories in terms of reference state quantities by direct physical derivation 03 p0502 A71-13353

Cyclic deformations and internal energy dissipation effect on hysteresis loop shape equations derivation in terms of three components including nonlinear and inelastic materials properties 03 p0502 A71-13407

Fused silica and single crystal NaCl nonlinear parameters from ultrasonic beams mixing studies 05 p0793 A71-16410

Finite difference and initial value solutions of nonlinear boundary problems for ordinary differential equations, generating algorithms by quasi-linearization method 05 p0775 A71-16646

Convection schemes finite difference formulation for nonlinear instability prevention by absolute spatial conservation rather than flux form 06 p0917 A71-17552

Nonlinear problems numerical solutions - Conference, Philadelphia, October 1968 06 p0917 A71-17563

Nonlinear boundary value problems numerical solutions using spline and Hermitian functions in Ritz-Galerkin setting 06 p0917 A71-17565

Turbine blades thermal stresses due to nonlinearities, using computerized simulation 06 p1000 A71-18003

Finite difference theory and other approximation methods convergence determination in nonlinear variational problems 06 p0919 A71-18202

Direction finding problems involving several waves of same frequency, discussing nonlinear computation methods with hybrid computers 06 p0927 A71-18205

Spacecraft structures vibration testing nonlinear effects, extending asymptotic method for transition through resonance to nonresonant regions [AIAA PAPER 71-211] 06 p1004 A71-18647

Rucker multidevice symmetrical microwave oscillator analysis, overcoming nonlinearity difficulties in eigenvector approach 07 p1073 A71-19118

Automatic test equipment for sorting large quantity resistors based on nonlinearity measurement 07 p1076 A71-19554

Conductive heat transfer with nonlinear boundary condition, reducing to linear boundary value problem through variational principle 07 p1224 A71-19902

Nonlinear effects in superconductors in electromagnetic field with constant and alternating components 07 p1181 A71-20535

Cuprous halides nonlinear properties in near and medium IR regions 08 p1302 A71-21435

Nonlinear effects of IR beam passage from continuous neodymium-yttrium garnet laser trough defocusing media 09 p1460 A71-22231

Quasi-static problems in nonlinear viscoelasticity theory, comparing integral operator and variable moduli methods for convergence and accuracy of successive approximations 09 p1537 A71-22513

Asymmetric missile nonlinear angular motion, describing quasi-linear relations for frequencies, damping rates and swerving motion amplitude [AIAA PAPER 70-534] 09 p1532 A71-22906

Finned configurations with nonlinear aerodynamic properties, obtaining solutions for angular motion at and near resonance [AIAA PAPER 70-535] 09 p1532 A71-22909

Dissipation and nonlinearity effects on linear three dimensional wave front, obtaining Burger equation for gas dynamics 09 p1433 A71-23053

Physically nonlinear theory of isotropic elastic shells and plates eliminating Love-Kirchhoff hypotheses 09 p1543 A71-23613

Numerical solution procedures evaluation for geometrically nonlinear structural analysis by direct stiffness method, noting capability of self correcting initial value formulation [AIAA PAPER 71-356] 11 p1844 A71-25335

Nonlinear physical and geometrical thermoelasticity for plane strain and stressed state at circular hole in infinite space, using approximation in Lagrangian coordinates 12 p1978 A71-27349

MHD waves nonlinear interaction in magnetosphere, calculating transverse Alfvén and magnetosonic and longitudinal acoustic wave decay instabilities 13 p2106 A71-28562

Integral transformations application to approximate elastic solutions for nonlinear hereditary media, considering elastoplastic deformations under active loads 13 p2154 A71-28649

Phase hologram nonlinearities effects, determining signal to noise power ratio in terms of Chebyshev series coefficients 13 p2069 A71-28714

Existence theorem for nonlinear boundary value problems involving two dimensional incompressible boundary layer equations 14 p2264 A71-29523

Nonlinear free oscillations, discussing linearization for nonlinear functions by weighted mean square method 14 p2325 A71-30060

Structural steady state vibration frequency response and resonance testing, investigating nonlinearity effects of large deflections 14 p2326 A71-30065

Large amplitude ion acoustic wave propagation in streaming ion plasma, noting nonlinear effect in amplitude oscillation observation 14 p2281 A71-30541

Nonlinearity effects on slow variation of small amplitude constant profile periodic sound waves propagating in radiating gas, deriving nonlinear model wave equations 16 p2607 A71-32858

Finite element analysis with material nonlinearities, defining linear incremental elastoplastic stress-strain relation 16 p2652 A71-33084

Combined finite element method and Rayleigh-Ritz procedure for geometrically nonlinear problems solution of elastic plates with arbitrary shape, boundary and load distribution 16 p2653 A71-33088

Unified finite element theory of geometrically nonlinear elasticity problems, noting restrictions applicable to different displacement formulations 16 p2653 A71-33089

IF nonlinearities effect on Gaussian clutter rejection associated with noncoherent MTI radar receiver 17 p2708 A71-35483

Nonlinearities effects on inorganic liquid laser output, investigating Raman and Brillouin scatterings and self focusing 18 p2933 A71-37012

Plastic nonlinear creep behavior theory reformulation, obtaining constitutive relations based on experimental data 19 p3084 A71-37524

Small parameter method application to quasi-linear problems solution in nonstationary heat conduction with substantial nonlinearities and weak perturbation, analyzing error 19 p3162 A71-37584

Light ponderability in gravitation theory, discussing hypothetical Freundlich effect of light velocity dependence on radiation field intensity, based on Maxwell electrodynamics nonlinear generalization 20 p3270 A71-39457

Nonlinear effects in high power Nd-YAG CW IR laser beam transmission through defocusing media 21 p3394 A71-41110

Nonlinear periodically oscillating motions in shell theory, examining buckling characteristics of thin walled structures under dynamic and shock loads action 21 p3473 A71-41152

Numerical modeling and analysis of homocentric light beams propagation in cubic and nonlinearity saturation medium, using parabolic equation approximation 21 p3417 A71-41259

Cubic nonlinearity in p-type germanium semiconductor in constant magnetic field 21 p3435 A71-41337

Response nonlinearity of multiple turn transformer type transducer for angular displacement magnitudes

conversion to electrical signals, noting relationship to turning angle and instrument dimensions
24 p3810 A71-45152

NONNEWTONIAN FLOW

Turbulent heat transfer in non-Newtonian fluid flow, considering generalized Prandtl number effect
02 p0241 A71-12642

Viscous heating and non-Newtonian behavior of incompressible steady pipe flow with variable transport properties, using perturbation method
23 p3662 A71-43370

NONNEWTONIAN FLUIDS

Non-Newtonian/second order/ fluids motion equation derivation based on statistical nonequilibrium distribution
01 p0068 A71-10026

German monograph on heat transfer in Prandtl-Eyring fluid flows through flat channels with allowance for dissipation and asymmetrical thermal boundary
02 p0241 A71-12675

Convective mass transfer, velocity and concentration fields during non-Newtonian fluid motion in circular pipe with diffusion flow at wall
04 p0579 A71-15798

Non-Newtonian liquids with arbitrary surface temperature and pressure gradients, solving dynamic and thermal boundary layers equations
06 p1006 A71-18008

Two dimensional flow of non-Newtonian fluids with rigid spherical substructure, solving linear coupled ordinary differential equations for spin and velocity field [ASME PAPER 71-APM-N]
18 p2926 A71-36257

Non-Newtonian liquids with arbitrary surface temperature and pressure gradients, solving dynamic and thermal boundary layers equations
20 p3311 A71-38975

Second order viscous liquid pulsating flow superposed on steady laminar flow through circular pipe, examining non-Newtonian effects on flow characteristics
22 p3530 A71-41562

Non-Newtonian film thickness, load capacity and maximum viscoelastic stress effect in point contact with second order fluid lubricant for slide/roll ratio [ASLE PREPRINT 71LC-16]
24 p3832 A71-45293

NONOSCILLATORY ACTION

Macroscopic derivation of Onsager relations for nonoscillatory processes with linear flow in isotropic media
18 p2852 A71-36964

NONPARAMETRIC STATISTICS

Two-sample nonparametric adaptive detection using computer test statistics selection
08 p1259 A71-21600

Signal detection in noise, investigating quantiles position optimization in nonparametric test statistics
15 p2370 A71-31588

NONREFLECTION

U ENERGY ABSORPTION

NONRELATIVISTIC MECHANICS

Configuration space theory of nonrelativistic three body scattering covering transition amplitudes of three-three chemical reaction rates
22 p3577 A71-41651

NONRESONANCE

Book on nonresonant feedback in lasers covering multimode cavity, emission spectra, generation in cloud, quasi-concentric resonator, etc
08 p1301 A71-21226

Reflection and transmission coefficients of nonresonant slots in rectangular waveguide antenna with comb type slow wave structure
19 p3019 A71-38334

NONRIGIDITY

U FLEXIBILITY

NONUNIFORM FLOW

Numerical analysis of flow field around thin airfoil in two dimensional nonuniform stream, using finite difference method
02 p0187 A71-12680

Nonuniform flow in straight channel inlet section initiated by Fourier expandable nonuniform profile, linearizing Navier-Stokes equations about mean velocity [ASME PAPER 70-WA/FE-27]
03 p0403 A71-14135

Parallel nonuniform supersonic flow of two coaxial gas jets past sphere
03 p0345 A71-14562

Nonuniform blowing and surface temperature turbulent boundary layer, investigating heat transfer
04 p0684 A71-15502

Plasmas and liquids inhomogeneous flow oscillations, determining resonance points effect on stability and oscillatory properties
05 p0790 A71-16825

Sound radiation by rotor from interaction with nonuniform flow, considering multiple blades
05 p0697 A71-17159

Nonuniform plug nozzle flow field calculated for closed wake, using flow model divided into near wake and adjacent regions [AIAA PAPER 71-41]
06 p0946 A71-18502

Incompressible fluid nonuniform turbulence statistical approach, based on finite number of equations for high order single point correlations
07 p1087 A71-18920

Continuity and balance equations of acoustic energy in nonuniform fluid flows
07 p1160 A71-19588

Thin airfoils theory in nonequilibrium magnetogasdynamics with nonuniform nonequilibrium free stream, using Green function technique
09 p1383 A71-23200

Numerical solution of nonuniform enthalpy mixed axisymmetric gas flow in curvilinear regions with upper boundary and discontinuity using build-up method
10 p1551 A71-24376

Flow in vicinity of stagnation point of sphere and cylinder during pulsating motion in nonuniform stream
12 p1897 A71-27448

Nonhomogeneous turbulent flow with magnetic field, deriving MHD turbulence model neglecting velocity correlation time
13 p2107 A71-28565

Heterogeneous fluid flow-chemical processes interaction in low density plasma flow two phase boundary layer seeding, using physicochemical model
14 p2279 A71-29878

Acoustic wave amplification and attenuation in nonhomogeneous steady flows applied to air jet discharging in organ pipe
14 p2224 A71-30208

Similarity solution of boundary layer equations for nonuniform external flow
14 p2225 A71-30217

Viscous flow fields around pointed cones at angle of attack in nonuniform supersonic flow, using axisymmetric analog for three dimensional boundary layer [AIAA PAPER 71-624]
15 p2344 A71-31552

Plasmas and liquids inhomogeneous flow oscillations, determining resonance points processes effect on stability and velocity
15 p2459 A71-32504

Steady inhomogeneous axisymmetric nozzle flow, determining pattern by simultaneous solution of radial equilibrium and continuity equations
16 p2521 A71-33614

Scalar material transport in incompressible inhomogeneous turbulent fluid based on one point correlations equations
17 p2835 A71-34211

Shock wave diffraction propagation through nonuniform fluid, noting application to two dimensional unsteady flows
18 p2907 A71-36332

Nonhomogeneous flow stratification in fluid region under thermal and gravitational forces, considering steady state and time dependent density fields
20 p3212 A71-39502

Stability problem in hydrodynamics of perturbed heterogeneous shear flow, solving initial value problem for Couette flow
20 p3213 A71-39783

Energy method application to inhomogeneous turbulent flow with large eddies as recurrent velocity field structures, considering longitudinal rolls in boundary layer wall region
21 p3370 A71-40985

Circumferentially nonuniform flow in front of axial compressor stage with stepwise two zone pressure and velocity distribution resulting in increased guide vane losses
22 p3479 A71-41845

Circumferential flow direction nonuniformity effect in front of compressor wheel on intensity spread and resonant rotor blade vibrations
22 p3615 A71-41847

NONUNIFORM MAGNETIC FIELDS

Shock wave propagation in channel with MHD interaction between compressed gas and nonuniform magnetic field
01 p0132 A71-10662

Bremsstrahlung effect on charged particle motion in nonuniform magnetic field
01 p0132 A71-10677

Nonuniform magnetic field cyclotron heating, presenting stochastic criteria in terms of Larmor rotation phase randomization
03 p0462 A71-13928

Bremsstrahlung effect on charged particle motion in nonuniform magnetic field
07 p1170 A71-20139

Charged particles acceleration in pulsed magnetic field, deriving distribution function by diffusion coefficient and turbulence spectrum determination
08 p1351 A71-20963

Charged particles velocity distribution effect on plasma flow in transverse nonuniform magnetic field, observing configuration/trajectory distortion and particle dispersion
10 p1649 A71-24319

Shock wave propagation in channel with MHD interaction between compressed gas and nonuniform magnetic field
14 p2283 A71-30995

Longitudinal magnetic field inhomogeneity influence on inhomogeneous plasma Alfvén instability, considering magnetic field pressure and trapped particles
23 p3713 A71-44151

Dense hydromagnetic plasmoid interaction with nonuniform axisymmetric magnetic field using two dimensional fully ionized two temperature model
24 p3852 A71-44487

Hydrodynamic equations for ions and electrons of ionized collision plasma in strong nonuniform magnetic field from Boltzmann kinetic equations
24 p3855 A71-44521

NONUNIFORM PLASMAS

Experimental dispersion curve for LF drift waves in inhomogeneous magnetoplasma
01 p0134 A71-11003

Two dimensional inhomogeneities effects on electrical resistance of plasma with nonuniform density in strong magnetic field
01 p0135 A71-11065

Inhomogeneous plasma oscillations excitation by high intensity electron beam, causing instability greater than hydrodynamic beam mode
02 p0288 A71-11890

Quasi-Alfvén and acoustic wave coupling in inhomogeneous stratified plasma within intense magnetic field as function of directional pressure
02 p0292 A71-12627

Microwave scattering from nonuniform plasma of low pressure mercury arc in glass tube, describing density profile
03 p0463 A71-13474

Kinetic equations derivation for computer calculation of nonuniform hydrogen plasma decay, considering hydrogen recombination, electron temperature and ambipolar diffusion
03 p0463 A71-13508

Electrode material function of electromagnetic radiation from heterogeneous plasma
03 p0466 A71-14473

Inhomogeneous magnetoplasma electrostatic LF oscillations, discussing wave modes and instability conditions
04 p0634 A71-15257

Velocity space diffusion and collision effects on fully ionized inhomogeneous plasma instability, using Fokker-Planck kinetic equation
05 p0789 A71-16654

Inhomogeneous collisionless low beta plasma drift wave instability dynamic stabilization, considering AC electric field parallel to confining field
06 p0933 A71-17474

Inhomogeneous plasma flute instability in presence of gravitational field and supported by magnetic fields
06 p0938 A71-18425

Inhomogeneous collisionless plasma stability, showing small pressure gradient effects
07 p1167 A71-19228

Finite and large pressure inhomogeneous plasma with finite electron heat conduction, calculating instability
07 p1173 A71-20534

Self and mutual admittance, isolation and radiation pattern of slots on infinite cylinder covered by inhomogeneous lossy plasma
08 p1341 A71-21886

Quasi-stationary permittivity tensor corrections for smoothly nonuniform electron plasma in absence of magnetic field, using geometrical optics methods
09 p1500 A71-22240

Interplanetary plasma electron density inhomogeneities formation explained by instability due to electron stream curvilinearity obtained from spacecraft data
09 p1518 A71-22435

Mode conversion in inhomogeneous plasma, discussing conservation laws relationships to differential equation invariants
09 p1501 A71-22535

Magnetized inhomogeneous plasma nonlinear wave coupling near hybrid resonances
09 p1503 A71-22868

Electromagnetic pulse propagation through inhomogeneous plasma, discussing electron collision frequency effects
09 p1504 A71-22987

Parametric excitation of transverse waves in inhomogeneous electron plasma driven by oscillating electric field, using multiple perturbation method
10 p1647 A71-23891

Transient electromagnetic wave propagation in lossy directionally anisotropic time varying stratified plasma, using characteristics method
10 p1648 A71-24296

Interplanetary medium small scale plasma irregularities by scintillation techniques, considering electron density deviations
10 p1674 A71-24434

Short wave HF instabilities in strongly inhomogeneous plasma with hot electrons, considering ion acoustic oscillations and electron cyclotron harmonics
10 p1650 A71-24525

Superthermal ions velocity distribution in nonisothermal plasma, comparing real velocity distribution to Maxwellian distribution 10 p1651 A71-24630

Variable density cold inhomogeneous plasma small amplitude free electrostatic oscillations investigation by Green function of differential equation 10 p1652 A71-24662

Electromagnetic wave conversion into plasma waves in cold anisotropic plasma with two dimensional inhomogeneity 10 p1654 A71-24893

Quasi-linear relaxation of ultrarelativistic electron beam in homogeneous and inhomogeneous plasmas, noting initial divergence angle threshold 10 p1654 A71-24895

Electromagnetic second harmonic wave generation in inhomogeneous magnetoactive plasma, using HF probe and horn antenna for detection 10 p1654 A71-24974

Nonuniform density cosmic plasma heating allowing energy losses by radiation and heat conduction, using filament-structured high temperature plasma region model 11 p1828 A71-25765

Inhomogeneous collisionless plasma stability, showing small pressure gradient effects 12 p1934 A71-26746

Inhomogeneous plasma, describing linear wave transformation with fourth order differential equation with variable coefficients 12 p1942 A71-27768

Microwave propagation in cylindrical waveguide containing inhomogeneous gas discharge plasma 13 p2029 A71-28363

Cylindrical microwave cavity partially containing cold nonuniform plasma enclosed by quartz tube, calculating resonant frequency by exact, multistrata and series methods 13 p2029 A71-28500

Three dimensional fields excited by arbitrarily oriented dipole in cylindrically inhomogeneous isotropic plasma, deriving closed form solution 13 p2107 A71-28786

Weak three dimensional plasma inhomogeneity effect on expression for mean force acting on plasma in HF field 13 p2108 A71-28853

Infinite radially nonuniform thin plasma cylinder wave scattering with electrical field component along inhomogeneity gradient 14 p2191 A71-29512

Soviet book on inhomogeneous plasma instabilities covering spatial gradients, charged particles collisions, temperature effects, steady electric fields and magnetic shear 14 p2279 A71-29942

Helical wave deceleration with inhomogeneous plasma approximated by anisotropically conducting plane 14 p2279 A71-30115

Electromagnetic wave energy absorption in inhomogeneous cold magnetoactive plasma cylindrical columns 15 p2455 A71-31735

Electromagnetic wave propagation along homogeneous and inhomogeneous plasma columns, establishing density distribution functions and dispersion curves 15 p2459 A71-32641

Oscillations excited by pulsed dipole antenna at upper hybrid resonance in weakly inhomogeneous plasma investigated by Wentzel-Kramer-Brillouin approximation 15 p2460 A71-32656

Magnetic drift wave instabilities in plasmas with nonuniform density and temperature gradient 16 p2572 A71-33949

Cylindrical nonuniform plasma with radial temperature and emitter density gradients, analyzing molecular rotational levels intensity distribution and Doppler widths 17 p2787 A71-34587

LF resonances for radially inhomogeneous collisionless plasma sphere impinged by plane electromagnetic waves 17 p2708 A71-35485

Inhomogeneous plasma sounding with electromagnetic waves 18 p2953 A71-37000

Hall fields effect on interaction of MHD waves in inhomogeneous plasma, considering MHD wave dispersion 19 p3109 A71-37134

Ion and electron drift waves propagation and stability in nonhomogeneous plasma containing impurity ions 19 p3115 A71-38214

Short wave HF instabilities in strongly inhomogeneous plasma with hot electrons, considering ion acoustic oscillations and electron cyclotron harmonics 19 p3116 A71-38251

Numerical procedure for electromagnetic field penetration through inhomogeneous cold plasma slab with collisions, using Riccati type differential equation 20 p3273 A71-39004

Ion-cyclotron perturbation build-up in inhomogeneous plasma, investigating ion magnetic drift instability dependence on pressure 21 p3422 A71-40760

Quasi-stationary permittivity tensor corrections for smoothly nonuniform electron plasma in absence of magnetic field, using geometrical optics methods 21 p3424 A71-41129

Magnetospheric plasma instabilities from velocity distribution anisotropies and nonuniform plasma and magnetic field distributions 21 p3374 A71-41180

Electromagnetic wave conversion into plasma waves in cold anisotropic plasma with two dimensional inhomogeneity 21 p3425 A71-41273

Weak three dimensional plasma inhomogeneity effect on average force acting on plasma in HF electric field 21 p3425 A71-41284

Nonuniform density cosmic plasma heating allowing for energy losses by radiation and heat conduction, using filament-structured high temperature plasma region model 22 p3598 A71-41533

Inhomogeneous plasma shear flow instability with ion-ion collision, using BGK model 22 p3579 A71-41581

High pressure collisional plasma instabilities caused by spatial gradients from quasi-stationary state transport equations derivation 22 p3580 A71-41585

Threshold AC electric field calculation for inhomogeneous plasma parametric instability excitation, noting role of electron plasma wave energy propagation from unstable region 22 p3582 A71-41901

Inhomogeneous high-beta collisionless plasma temperature gradient effects on ion-acoustic and Alfvénic drift instabilities 22 p3583 A71-41907

Longitudinal magnetic field inhomogeneity influence on inhomogeneous plasma Alfvén instability, considering magnetic field pressure and trapped particles 23 p3713 A71-44151

Electromagnetic pulses scattering by conducting wedge in uniaxially anisotropic plasma, obtaining electric dipole radiation fields transient time for various plasma frequencies 23 p3646 A71-44171

Radiation pattern modification factors calculation for TE excited slot antenna in ground plane covered with inhomogeneous plasma reentry sheath 23 p3646 A71-44172

Nonlinear ion acoustic soliton wave propagation and dissipation in nonhomogeneous nonisothermal weakly absorbing plasma 23 p3714 A71-44333

Microwave upper hybrid resonance absorption, emission and heating of nonuniform axially magnetized afterglow plasma column in waveguide geometry 24 p3851 A71-44430

Parametric hybrid resonance excitation of longitudinal oscillations in nonhomogeneous magnetoplasma by HF electromagnetic field 24 p3852 A71-44491

Boundary value problem of plane electromagnetic wave interaction with inhomogeneous warm plasma column, using matching method 24 p3856 A71-44794

Inhomogeneous rarefied plasma, investigating non-local, linear and nonlinear effects on electromagnetic wave reflection and transmission 24 p3857 A71-45117

Inhomogeneous high-collision finite-pressure plasma stability, finding thermal instability development under uniform temperature and arbitrary pressure 24 p3858 A71-45243

NONUNIFORMITY

Earth radiation latitude nonuniformity effect on error in onboard satellite local vertical determinations, using Cosmos satellite data 02 p0304 A71-11915

Electron transfer bulk oscillators negative conductivity as function of geometry, field and doping nonuniformities, using computerized simulation for device frequency-voltage characteristics 09 p1417 A71-22689

Earth radiation latitude nonuniformity effect on error in onboard satellite local vertical determinations, using Cosmos satellite data 13 p2133 A71-28202

Electromagnetic wave propagation in radially and axially nonuniform dielectric media, using geometric optics approximation 24 p3848 A71-44976

NONVISCOUS FLOW

U TURBULENT FLOW

NOON

Precipitation energy flux of continuous noontime aurora, using airborne ionospheric and optical measurements 13 p2054 A71-27801

F 1 layer development at summer midday midlatitude, analyzing molecular ions composition effect 13 p2059 A71-28255

NORADRENALINE

Arterial baroreceptor reflex action in rabbits, noting central noradrenergic neuron participation 16 p2528 A71-33075

Guinea pig thermoregulation of shivering and nonshivering thermogenesis, showing intrahypothalamic noradrenaline injection effects on threshold temperature elevation 18 p2862 A71-36901

Noradrenaline concentration in myocardium of rats subjected to high altitude hypoxia, considering heart regulation in presence of hyperfunction and hypertrophy 19 p3001 A71-37393

Norepinephrine induced stimulation of myocardial oxygen consumption of cat papillary muscles under afterloaded isotonic and isometric conditions 22 p3486 A71-41937

Adrenaline, noradrenaline and catecholamine excretion in railroad men during daytime and nighttime work 24 p3799 A71-45085

NOREPINEPHRINE

Brain norepinephrine synthesis pharmacological inhibition, discussing effects of ovariectomy to decrease sensitivity 09 p1391 A71-22472

L-dopa multijection timed effects on rat brain norepinephrine metabolites concentrations, observing zero time control rated modifications 09 p1393 A71-22649

Canine ventricular myocardium as cardiac beta-adrenergic receptor, describing binding of norepinephrine to microsomal particles 19 p3002 A71-37900

Circadian rhythm maturation of brain norepinephrine and serotonin in rat, relating spontaneous motor activity and sleep-wakefulness mechanism 19 p3003 A71-38071

Renin, plasma norepinephrine and epinephrine responses to work loads of various intensities, evaluating sympathetic nervous system as stimulus for secretion 19 p3008 A71-38551

NORMAL DENSITY FUNCTIONS

Gaussian probability density functions covariance matrices dimension-reducing mapping using confidence spaces 04 p0619 A71-15331

Laser irradiance pattern from aperture with truncated Gaussian field distribution, evaluating diffraction integral subject to Fresnel approximation 05 p0763 A71-16904

Complex rays for electromagnetic field construction, considering application to Gaussian laser beams 05 p0763 A71-16905

Pulsed optical parametric oscillators, investigating effects of spatially nonuniform pumping with beams having Gaussian intensity profiles 08 p1302 A71-21432

One dimensional Gaussian electrostatic wave packet nonlinear time development due to weak resonant broad beam introduction into cold uniform plasma 10 p1652 A71-24658

Weighted distribution functions of normal processes, calculating stochastic mixture components in Borel sets 10 p1637 A71-24903

Normality-independence characterization of stochastic integrals in linear processes 11 p1792 A71-26102

Power and focusing requirements in recording and reading with Gaussian laser beam in TEM mode 14 p2254 A71-30136

Signal detection on Gaussian noise background, deriving error probabilities and optimal processing algorithms 19 p3015 A71-37224

Charge neutrality in semiconductors with implanted dopant ions profiles, considering junction field penetration into Gaussian profile 19 p3118 A71-37489

Parabolic reflector aperture antennas with Gaussian distributed random phase deviations, obtaining asymptotic expansion for radiation pattern 19 p3036 A71-38605

NORMAL DISTRIBUTIONS

U NORMAL DENSITY FUNCTIONS

U NORMAL FORCE DISTRIBUTION

U FORCE DISTRIBUTION

NORMAL SHOCK WAVES

Normal shock waves in one dimensional steady flow of two phase medium, noting phase exchanges and lack of internal equilibrium 04 p0579 A71-15822

Normal shock wave stability in perfect gas with viscosity and heat conduction under arbitrary small one dimensional disturbances, formulating eigenvalue problem

07 p1224 A71-20288

Normal shock wave in He, comparing measured and predicted molecular velocity distribution functions

09 p1433 A71-22857

Emitting, absorbing and scattering gray gas flow through plane stationary normal shock wave, presenting governing equations linearized analysis

09 p1546 A71-23164

Plane normal shock wave reflection in relaxing gas for shock tube endwall upstream and downstream dynamic pressures, using method of characteristics

09 p1546 A71-23166

Highly underexpanded plasma jet structure with coaxially superimposed arc discharge, investigating stationary MHD normal shock in jet core [DFVLR-SONDR-108]

Turbulent boundary layer parameters changes across normal shock wave, integrating energy integral equation

[ASME PAPER 71-FE-16] 13 p2052 A71-29455

Dyson integral equation describing generalized field of normal waves in plane randomly inhomogeneous turbulent layer

15 p2388 A71-31513

Nonequilibrium corner expansion flow of ionized argon induced by normal shock waves in hypervelocity shock tube

16 p2555 A71-32905

Mesh method for supercritical transonic flow calculation with normal or oblique shock wave at trailing edge

17 p2674 A71-35799

Normal and oblique shock thermodynamic equilibrium state variables calculation, taking into account air dissociation and ionization

18 p2909 A71-36678

Normal shock wave propagation in nonuniform gases with arbitrary property gradients based on modified method of infinitesimal contact discontinuities

20 p3212 A71-39482

Normal shock existence in blade spacings of rotor and guide vanes of axial flow supersonic compressor as function of pressure nonuniformity

22 p3479 A71-41843

Near-normal plane shock wave reflection from rigid impermeable wall, obtaining nonstationary flow parameters in terms of Jacobi polynomials convergent series

22 p3531 A71-42865

Thermal dissociation reactions and radiation effects on flow variables in front of and behind strong normal shock, using gray gas approximation

24 p3822 A71-45368

NORMALIZING

Canonical linear Hamiltonian systems normalization algorithm, applying to restricted three body problem

05 p0810 A71-16547

NORMALIZING [STATISTICS]

Low loss cylinder loop as normalization antenna for meter waves

01 p0055 A71-11187

Soviet book on limit theorems for random walks covering random walk functionals, zero mean value, finite dispersion, sequences, normalized sums, Markov functionals, etc

07 p1148 A71-20300

Electron mass and photon wave renormalizations functional relationships, studying perturbation theory based electrodynamic divergences

07 p1162 A71-20550

Optimum normalization of computed rotation quaternions to update space vehicle orientation

12 p1923 A71-27443

Physical pendulum normalized error variance as irregularity function in excitation with narrow band frequency spectrum

13 p2065 A71-27947

NORMS

Approximate solution for equation in linear normed space by error operator norm optimization, applying to elliptical cylinder type compact sets

23 p3699 A71-43574

NORTH AMERICAN AIRCRAFT

NT B-70 AIRCRAFT

NT F-100 AIRCRAFT

NT X-15 AIRCRAFT

NORTH SEA

Sea level muon spectrum measurements at 80 degrees to vertical up to 1 TeV, using Nottingham spectrometer

12 p1953 A71-27405

NORTHERN HEMISPHERE

NT ARCTIC REGIONS

German monograph on ozone recording device and temporal and spatial variations of tropospheric ozone in Northern Hemisphere

04 p0582 A71-15100

Balloon-borne observation of X ray sources in northern sky, including Sco, Cyg and SN 1572

05 p0797 A71-15931

Northern Hemisphere midlatitude tropical weather prediction, investigating effects of tropic and southern regions by wall insertion model

07 p1152 A71-19754

Geomagnetic activity winter-summer difference in Northern and Southern Hemisphere middle latitudes

08 p1283 A71-21645

Hydrogen ion flux detected along earth magnetic force lines in Northern Hemisphere midlatitudes, determining flux magnitude

09 p1436 A71-22561

Geomagnetic and interplanetary magnetic fields, considering inverse direction of electric currents in Northern and Southern Hemispheres

11 p1757 A71-25776

Antarctic auroral ovals, determining time-longitude coordinates, statistical mean position and polewards and equatorwards boundaries for various Kp

12 p1900 A71-27056

Atmospheric energy storage and meridional transport, calculating annual cycle in Northern Hemisphere

12 p1925 A71-27193

Conjugate and closely-spaced riometer observations of auroral radio absorption, considering explanation by alternation of particle precipitation between Northern and Southern Hemispheres

14 p2192 A71-29667

Northern Hemisphere upper stratospheric temperature pressure field changes during autumn, using isobar surface charts

15 p2400 A71-31966

Northern Hemisphere upper stratosphere and lower mesosphere synoptic meteorological chart construction, using aerological network and rocket radio sounding data

15 p2400 A71-31967

Pitch distribution of protons precipitated from auroral radiation region measured by scintillation detector aboard Cosmos 261 satellite in Northern Hemisphere

17 p2731 A71-34320

Northern Hemisphere atmospheric vertical velocity computation for all seasons compatible with climatological heating functions, using time averaged thermodynamic energy equation

17 p2770 A71-34803

Seasonal variations of kinetic energy balance of mean meridional circulation in Northern Hemisphere

20 p3257 A71-39436

Geomagnetic and interplanetary magnetic fields, considering inverse direction of electric currents in Northern and Southern Hemispheres

22 p3532 A71-41544

Areal precipitation correlation with 850 mb geopotential height over Northern Hemisphere

22 p3535 A71-42414

Cumulus clouds photographs above Northern Hemisphere by meteorological satellite during active periods of earth atmospheric circulation

23 p3701 A71-44047

NOSE (ANATOMY)

Human odorant evoked response, considering stimulation of olfactory receptors and trigeminal afferences in nose

13 p2012 A71-28891

NOSE CAPS

U NOSE CONES

NOSE CONES

NT ABLATIVE NOSE CONES

NT ROCKET NOSE CONES

Transpiration cooling of reentry vehicle nosetips, noting two dimensional aspects of porous wall coolant flow and matrix-coolant energy exchange

[AIAA PAPER 69-96] 07 p1223 A71-19869

Manometric equipment arrangement in nose cone of oriented satellite with aerodynamic system stabilization

08 p1287 A71-21022

Graphite materials for nosetip/reentry applications, discussing isostatically pressed short fiber-pitch composites and binderless graphites, ablation data and NDT procedures

[AIAA PAPER 71-417] 11 p1790 A71-26341

Relaxation distance for sharp cone behavior from chemical nonequilibrium laminar boundary layer effects on simulated space shuttle configuration during reentry

13 p2146 A71-29504

Thermal stresses in multilayer anisotropic fiberglass wound conical shell under axisymmetric gradients applicable to structural missile nose cone design

14 p2330 A71-30694

Pressure and heat flux measurements at wall of nose cone in hypersonic wind tunnel flow with high generatrix enthalpy

18 p2844 A71-36182

Concorde droop nose for takeoff and landing visibility improvement, describing design and operation

19 p2997 A71-38343

Aerodynamic heating tests of cone flap reentry vehicle using temperature sensitive paint

20 p3311 A71-39197

Manometric equipment arrangement in nose cone of oriented satellite with aerodynamic system stabilization

20 p3240 A71-39602

NOSE WHEELS

Taxiing aircraft position and wheel trajectories for specific nose wheel path

02 p0187 A71-11641

Aircraft steering system design, considering oversteering effects in nose wheels, torque for reaction moment balance and tire behavior

16 p2522 A71-33225

NOSES [FOREBODIES]

NT ABLATIVE NOSE CONES

NT NOSE CONES

NT ROCKET NOSE CONES

Conical body lift/drag ratio increase by wedge shaped nose, noting applications to space vehicles entering atmosphere above escape velocity

13 p1992 A71-29183

Nonspherical nose bluntness effects on slender vehicle dynamics, considering conical geometry as approximate nose shape after ablation due to turbulent heating

[AIAA PAPER 71-931] 19 p3148 A71-37176

NOTATION

U CODING

NOTCH SENSITIVITY

Plastic zone effects on notch effect on crack initiation, analyzing ductile-brittle transition temperature relation to sample size

04 p0666 A71-14883

Linear elastic fracture mechanics in presence of notch stress concentration, considering crack formation and propagation under cyclic stresses

10 p1628 A71-24686

Wells COD /crack opening displacement/ criterion for notch root deformation and fracture measurements

16 p2591 A71-32949

Nb and Nb-Zr alloy tubular and sheet samples cyclic loading tests, determining heat treatment effects on notch sensitivity and fatigue strength

18 p2937 A71-36724

Thermal and mechanical stresses concentration near peripheral notches on ring-shaped graphite, noting notch sensitivity relationship to tip curvature and graphite grain size

23 p3698 A71-44230

NOTCH STRENGTH

High compressive residual stress and high hardness for long life fatigue strength in nonrotating bending of notched machine parts

01 p0167 A71-10171

Notched steel bars fatigue strength improvement via compressive self stresses/residual stresses/

01 p0167 A71-10172

Failure analysis of notched unidirectional composites under tensile load parallel to fiber, considering Griffith-Irwin-Orowan fracture theory applicability

[AIAA PAPER 71-369] 11 p1784 A71-25343

Vibrationally loaded hollow cylinder with slanted notch, considering fatigue strength behavior as function of rated stress state

15 p2510 A71-32738

Notch effect on stainless steel and alpha brass rods and plates ductility and fracture strength

16 p2591 A71-32947

Notched fixed-pinned columns under concentric and eccentric compressive loads, presenting failure analysis based on stress intensity concept and methods of limit analysis

18 p2983 A71-36852

Tensile properties and notch toughness of Al alloys at low temperature, considering fracture toughness and weld strength

20 p3251 A71-39266

Strength, ductility and notch toughness research on base materials and welds of nickel maraging steel rocket motor cases

21 p3389 A71-40913

NOTCH TESTS

NT CHARPY IMPACT TEST

Notched metal crack initiation, determining high cyclic loads effects by prior local plastic behavior at stress concentration

01 p0166 A71-10163

Polish book on limiting load capacity of structural elements covering notched rods and plates with hole under elastoplastic stress

02 p0330 A71-12750

Stress intensity factors of hollow notched bars and hydrogen embrittled solid specimens

[SESA PAPER 1671] 03 p0443 A71-13751

Notched tensile plate steel specimens, investigating temperature and stress state effects on nil ductility transition and fracture strength

[SESA PAPER 1735] 03 p0443 A71-13752

Photoelastoplastic analysis of creep and stress of aluminum notched bars and cracked plates under thermal cycle using epoxy resin simulation

03 p0507 A71-13757

Notched tensile tests for measuring metal ductile-brittle transition temperature, deriving proportionality law

04 p0666 A71-14877

Steels brittle fracture susceptibility by notch impact bending test, considering plastic deformation zone and crack propagation

04 p0610 A71-14889

Stress intensity factor of symmetrical notch in apex of triangular plate under concentrated loads
04 p0670 A71-15391

Single edge notch tension Al alloy specimens mechanical compliance measurement, solving stress functions for various gage length-sample width combinations
07 p1110 A71-19469

Notch geometry and temperature effects on Ti-Al-Mo-V alloy creep rupture behavior
07 p1134 A71-19470

Tensile tests of elastoplastic notched plate in plane stress
07 p1218 A71-20500

Thermal fatigue and service life of thin walled tubular pearlite steel notched specimens in various oxidizing media
10 p1626 A71-24191

Kinetic crack propagation theory of fatigue fracture toughness for notched and unnotched austempered high strength and heat treated ball bearing steels
10 p1687 A71-24307

Elastoplastic problem of stress concentration in orthotropic plate with circular notch under tension
12 p1982 A71-27517

Notch analysis of fracture, discussing elasticity theory of stress concentration and applications to brittle inhomogeneous materials and fatigue crack propagation
13 p2151 A71-28215

Stress concentration for fatigue crack propagation in smooth and notched samples under symmetrical loading
13 p2157 A71-29373

Crack initiation in Ti-refined Fe-Ni alloys, using slow bending tests of notched bar samples with various notch angles
13 p2089 A71-29411

Notched age hardening Al alloys sheets, obtaining fatigue damage test data and S-N curves
14 p2326 A71-30067

Notched unidirectional composites failure mechanics under tensile load in fiber direction, considering debonding, plasticity and strength
15 p2428 A71-31971

Fatigue S-N curves discontinuities associated with plastic yield and crack path tested on mild steel notched specimens
16 p2591 A71-33346

Neuber elastoplastic analysis of residual notch stresses for improved cumulative damage predictions applied to aluminum alloy under overload
16 p2659 A71-34012

[AIAA PAPER 71-776]

Circumferential notch effect on distribution of compressive self stresses produced by shallow skin layer expansion in round steel bars, using finite element method
17 p2819 A71-34529

Notch effect on metallographic characteristics of fatigue crack initiation and propagation in Al-Mg alloy
18 p2933 A71-35877

Creep stress and strain analysis in double edged V-shaped notched plates and circumferential V-shaped notched round bars by finite element method
21 p3400 A71-40840

Ni-steels toughness improvement at cryogenic temperatures by accelerated cooling, using Charpy V-notch and static and dynamic fracture tests at 139.7-671.7 R
21 p3400 A71-40881

Stress intensity factors determination for notched structures, using finite element technique
22 p3613 A71-41431

Plastic stress-strain history at notch roots tested in tensile steel strips under monotonic loads, verifying Hardrath-Ohman theories
22 p3615 A71-42071

Alumina, boron carbide and silicon carbide notched and unnotched impact strength tests, using drop weight technique
22 p3565 A71-42542

Mo alloy under impact tests, investigating notch sharpness effects on cold shortness threshold and strength
23 p3693 A71-44231

NOTCHED METALS
U NOTCH TESTS
NOTCHED STEEL
U NOTCH TESTS
U STEELS
NOTCHES
Elastoplastic stress analysis for samples with notches and holes under tension, discussing boundary condition calculation by finite element method
03 p0510 A71-13949

Separation controlled transonic drag-rise modification for V-shaped notches attributed to inviscid/viscid interaction controlling flow separation and reattachment
15 p2345 A71-31561

[AIAA PAPER 71-568]

NOVAE
Soviet papers on pulsating stars covering classical, dwarf and spherical component Cepheids, RV Tau and RR Lyr types, variable stars, etc
03 p0485 A71-13258

Nova-like X ray source near or in Centaurus constellation, presenting energy spectra measured by sounding rockets in Japan during August 1969
05 p0808 A71-16452

Novae, symbiotic, T Tauri, U Geminorum and UV Ceti type stars, determining mass loss rate
06 p0973 A71-18338

Book on dwarf novae covering light variations, spectra, binary systems, absolute magnitude, mass, gas streams, outburst, etc
08 p1363 A71-21165

Continuous energy distribution around light maximum of Nova Serpentis 1970 represented by yellow supergiant model, correcting observations for interstellar reddening
08 p1364 A71-21416

Stellar X ray sources as close binary stars and old novae, calculating radiation by deceleration process
09 p1528 A71-23544

Book on stellar spectroscopy for peculiar stars covering hot star spectra emission lines, novae, magnetic, metallic line and related stars
10 p1675 A71-24477

Photometric IR observations of Nova Serpentis 1970, showing visual flux decrease
14 p2303 A71-29576

Novas distance determination from estimates of envelope ejection during outburst at maximum brightness, calculating absolute magnitudes
17 p2803 A71-34838

Nova N Her 1963 brightness variations from photometric observations, interpreting data in terms of stellar evolution
17 p2803 A71-34839

Radio stars classes, discussing red dwarf flare, red supergiants, blue dwarf companion, novae, pulsars and X ray stars
21 p3448 A71-40582

Nova N Vul 1968 UVB system photoelectric observations, noting small amplitude rapid brightness variations during night
23 p3771 A71-44304

NOXIOUS MATERIALS
U CONTAMINANTS
NOZZLE COEFFICIENT
U **NOZZLE FLOW**
NOZZLE DESIGN
Low resistance nozzles for complete power compensation in rate of climb indicators
01 p0079 A71-10350

Curvature matching method for two dimensional flexible plate nozzle contour of trisonic wind tunnel, obtaining overdetermined simultaneous equations
01 p0068 A71-10970

Axisymmetric hypersonic wind tunnel nozzle design by determining inviscid contour and correcting for turbulent boundary layer growth
01 p0003 A71-11578

[AIAA PAPER 69-337]

Internal mixing scheme for continuous fuel injection in Wankel engine via swirl nozzle during intake-compression cycle
02 p0298 A71-12559

Supersonic wind tunnel design, discussing flexible nozzle flow aspects
06 p0880 A71-17700

Maximum thrust plug nozzle design for fixed inlet geometry, using calculus of variations for optimum contour determination
06 p0946 A71-18501

[AIAA PAPER 71-40]

Three dimensional/nonaxisymmetric thrust nozzle design, using calculus of variations for maximization of thrust
06 p0946 A71-18503

[AIAA PAPER 71-42]

Supersonic axisymmetric annular nozzle design, presenting analytical method for selective design optimization
06 p0946 A71-18504

[AIAA PAPER 71-43]

Axial Mach number distribution of supersonic flow in rocket nozzle with Rao optimum contour
07 p1093 A71-20366

High turbulent flow simulation in hypervelocity wind tunnel for reentry vehicles operational testing, discussing nozzle gas dynamic and mechanical design
08 p1273 A71-21982

[AIAA PAPER 71-253]

Sonic nozzle design for precise mass flow measurement, determining nozzle profile for axial velocity distribution in conformity with laminar boundary layer equations solution
10 p1597 A71-24944

Supersonic propelling nozzle optimal parameters for maximum thrust coefficient, discussing nozzle control and efficiency
12 p1865 A71-27504

Structural design effects on air driven two stage ejector supersonic propelling nozzle with conical mixing chamber
13 p2115 A71-28585

Direct Laval nozzle design problem solution using finite difference method
13 p1991 A71-29170

Gas dynamic test assemblies experiments for demonstrating theoretical basis of supersonic nozzle design with radial flow section
13 p1992 A71-29173

Convulsed nozzle extension in engine with low pressure exit seal released and blown off by venting internal pressure
14 p2292 A71-30741

[AIAA PAPER 71-677]

Dual Flex nozzle concept, discussing design equations derivation, cold flow testing, fabrication and static tests
14 p2296 A71-30843

[AIAA PAPER 71-749]

Heater and nozzle design of ONERA/SAMA hypersonic wind tunnel for supersonic combustion ramjet tests
18 p2956 A71-36017

[ONERA-TP-924]

Optimal design of rigid unadjustable contour for supersonic nozzle, taking into account aircraft flight conditions variation
20 p3176 A71-39364

Low thrust long burning solid rocket propellant motor for orbit insertion maneuvers, discussing design, static tests, nozzle composition, igniter and performance
22 p3589 A71-42016

Extendible, variable profile nozzle for various flow regimes operation, developing numerical design algorithm
24 p3821 A71-45339

NOZZLE EFFICIENCY
Nozzle performance prediction inaccuracy due to invalid drag laws, considering unresolved problem of condensed phase particle size
03 p0344 A71-14453

Circular conical diffuser inlet velocity profile effect on efficiency, presenting experimental results for different cone angles and expansion ratios
20 p3177 A71-39799

Supersonic propulsion system inlet, engine and exhaust nozzle in wind tunnel and flight tests, discussing boundary layer effects on performance
23 p3718 A71-43599

NOZZLE EXPANSION
U **GAS EXPANSION**
U **NOZZLE FLOW**
NOZZLE WALL
Nozzle wall protection against high enthalpy gas flow effects by film cooling through parietal liquid injection
01 p0143 A71-11017

Voltage distribution measurements between electrodes of MHD Faraday nozzle across ionized Ar plasma supersonic flow
01 p0136 A71-11373

Swirling flow through multiple nozzles of simulated solid propellant rocket motors, determining thrust and mass flow effects on passage
01 p0072 A71-11592

Approximate calculation for far field flow distribution of nozzle exhausting into vacuum
01 p0072 A71-11595

Time dependent finite difference solutions of steady state nonequilibrium quasi-one dimensional nozzle flows
03 p0400 A71-13458

One component two phase mixtures critical flow in nozzles, orifices and short tubes, considering interphase heat, mass and momentum transfer
03 p0520 A71-14095

[ASME PAPER 70-WA/HT-5]

Gas turbine engines nozzles flow passage cross sections area measurement, using gas flowmeter, pipes system and vacuum pump
03 p0472 A71-14260

Ionizable gas flow through two dimensional nozzle under transverse magnetic field, using quasi-one dimensional approximation
03 p0466 A71-14553

Dispersion model of turbulent mixing of isothermal and nonisothermal slipstreams of air-gasoline combustion products in nozzles
04 p0577 A71-15622

Shock wave propagation through converging nozzle, predicting real gas dissociation and vibrational excitation effects for comparison with shock tube measurement
05 p0735 A71-16528

Nozzle throat conditions at sound velocity discontinuity due to transition from one to two condensed phases during expansion
05 p0735 A71-16576

Water vapor condensation due to heterogeneous nucleation in nozzles, considering flows seeded with inorganic smoke and metallic ions
05 p0737 A71-16974

[ASME PAPER 70-FE-22]

Supersonic flow field downstream of turbofan aircraft engine fan nozzle over bodies of revolution, using boundary layer theory and method of characteristics
05 p0796 A71-17150

Nonuniform plug nozzle flow field calculated for closed wake, using flow model divided into near wake and adjacent regions
06 p0946 A71-18502

[AIAA PAPER 71-41]

Pressure distribution over blade in cascade nozzle for incompressible and compressible particulate gas flow
06 p0883 A71-18539

[AIAA PAPER 71-82]

Fully ionized quasi-one dimensional magnetic nozzle flow analysis, including effects of unequal electron and ion temperatures and electron thermal conductivity [AIAA PAPER 71-141] 06 p0939 A71-18584

Nozzle wall hypersonic boundary layers in helium tunnel, presenting skin friction measurements and heat transfer rates [AIAA PAPER 71-161] 06 p0884 A71-18603

Gas temperature in combustion chamber and jet nozzle exit, and gas jet velocity resulting from various pressures, temperatures and air excess factors combinations 06 p0948 A71-18702

Inviscid air nonequilibrium shock layer properties correlation based on plenum entropy, predicting composition of downstream converging-diverging nozzle expanding air flow [AIAA PAPER 70-866] 07 p1090 A71-19905

Axial Mach number distribution of supersonic flow in rocket nozzle with Rao optimum contour 07 p1093 A71-20366

Liquid fuel atomization spectrum in nozzles, examining proportion control of droplet size 08 p1348 A71-21262

Nonequilibrium excitation in recombining nitrogen plasma nozzle flows [AIAA PAPER 70-44] 09 p1498 A71-22093

Turbulent flow in initial section of convergent axisymmetric nozzle based on logarithmic velocity law 09 p1431 A71-22409

Numerical solution of quasi-one dimensional viscous heat conducting compressible Laval nozzle flows by time dependent finite difference scheme 09 p1545 A71-22454

Vibrational relaxation of CO and hydrogen atom effects in nonequilibrium nozzle flow using shock tunnel IR detection system 09 p1404 A71-23379

Nozzle area rated two component flow properties, combining integrated solution equations into single transcendental equation for equilibrium condensation 10 p1550 A71-24336

Flow field properties of impinging free jets from circular convergent nozzle, measuring velocity, surface pressure and momentum flux 10 p1552 A71-24616

Viscous core of incompressible swirling flow through nozzle using momentum-integral equations [AIAA PAPER 70-51] 11 p1750 A71-25468

Two dimensional analysis of isentropic perfect gas flow fields in axisymmetric nozzles for transonic two phase flow initial values, calculating particle trajectories [AIAA PAPER 69-572] 11 p1751 A71-25508

Nozzle vane air cooling system for deflector type gas turbines, estimating profile perimeter average temperature for given coolant air flow rates 11 p1856 A71-26053

High energy molecular beams for collision processes investigations, discussing nozzle beam technique and experiment design 11 p1803 A71-26281

Directional acoustic radiation from supersonic jet, discussing generation mechanism theory based on shear layer instability close to nozzle 12 p1945 A71-27221

Viscous flow in supersonic de Laval nozzle, measuring gas density and rotational temperatures by electron beam techniques [AIAA PAPER 70-810] 12 p1865 A71-27555

Viscous convergent-divergent nozzle flow slender channel approximation, discussing nozzle geometry, Reynolds number and wall temperature effects [AIAA PAPER 69-654] 12 p1865 A71-27556

Flow momentum losses during gas mixture chemically nonequilibrium expansion in nozzle 13 p2158 A71-27880

Gas flow in nozzle, stages and gas dynamic systems, discussing motion in cross sectional plane 13 p1990 A71-28588

Two phase critical flow of one component mixtures in nozzles, orifices and short tubes, considering interphase heat, mass and momentum transfer rates [ASME PAPER 70-WA/HT-5] 13 p2049 A71-28980

Transonic gas flow measurement during sudden expansion from circular nozzle into coaxial cylindrical channel, emphasizing flow attachment 13 p1993 A71-29192

Two coaxial axisymmetric subsonic gas jets of different density mixed during expulsion from convergent nozzles with high compression, using flow rate ratio 13 p2050 A71-29215

Chemical nonequilibrium flows in supersonic nozzle for mixture of dissociated gases and inert diluent [ASME PAPER 71-FE-8] 13 p2166 A71-29449

Phase changes /droplet solidification/ effect on two phase nozzle flow, considering perturbation treatment [ASME PAPER 71-FE-11] 13 p2052 A71-29452

Monograph on solid propellant rockets combustion instability covering pressure oscillations at acoustic frequencies, swirling nozzle flow, chamber pressure, etc 14 p2287 A71-29577

Spatial MHD flow in diffuser bounded by two diverging and two parallel walls, showing solutions with axial symmetry in cylindrical and spherical coordinate systems 14 p2278 A71-29605

Real gas mass flow rate computation through sonic nozzle 14 p2239 A71-29927

Methane and natural gas flow through critical flow nozzles, calculating real gas effects on mass flow rate 14 p2224 A71-29937

Pressure distribution and drag prediction over slender axisymmetric fuselages and afterbodies and exhaust nozzles at transonic Mach numbers [AIAA PAPER 71-720] 14 p2170 A71-30771

Compressible laminar plane axisymmetric boundary layer flows in Laval nozzles, studying temperature, density and velocity distribution relations 15 p2386 A71-31164

Aerodynamics of axial and axial tangential blade swirler twisted jet near nozzle, testing effectiveness of equivalent problem of heat conduction theory 15 p2388 A71-31522

Arc heated plasma expansion through nozzle, observing population inversion of neutral carbon self-absorption UV atomic line [AIAA PAPER 71-592] 15 p2454 A71-31537

Nonreacting and equilibrium chemically reacting gas turbulent boundary layer flows through hypervelocity nozzles, comparing calculation with experiment [AIAA PAPER 71-597] 15 p2512 A71-31577

Conical converging nozzle flow of perfect monatomic gas in rarefied near continuum, transition and near free molecular regimes, using finite difference methods 15 p2390 A71-32045

Thrust and flow rate control in choked convergent nozzles by potential vortex generation, verifying swirling nozzle flow analytical model 15 p2391 A71-32061

Nonequilibrium nozzle flow determination for vibrationally relaxing gas, describing sudden freeze approximation method validity 16 p2556 A71-32907

Steady inhomogeneous axisymmetric nozzle flow, determining pattern by simultaneous solution of radial equilibrium and continuity equations 16 p2521 A71-33614

Exit stream velocity increase in propulsion units by adding latent heat of vaporization by condensation in supersonic nozzle 17 p2728 A71-34882

Theoretical and photographic study of underexpanded air jets ejected simultaneously from several mutually interacting nozzles near origin 18 p2903 A71-36115

Base pressure of cluster rocket exhaust with several jets simultaneously ejecting from nozzles 18 p2903 A71-36116

Time dependent calculation of mixed two dimensional or axisymmetric transonic flows in nozzle, writing equations of motion with transformed spatial variables 18 p2906 A71-36323

Steady inviscid fluid flows in plane channel and in axially symmetric nozzle, considering external magnetic field effects with electroconductive fluid 18 p2907 A71-36327

Vibrational nonequilibrium Prandtl-Meyer expansion flows, discussing vibration energy associated with change of state and hypersonic nozzle flow calculation 18 p2909 A71-36440

Relaxation effects on velocity and temperature of solid particles in gas flows, emphasizing acoustic propagation, compression shock structure and nozzle flows 18 p2909 A71-36441

Cascade displacements and stresses in nozzle ring guide vanes with sectional diaphragm under axial and circumferential flow 18 p2980 A71-36706

Plane transonic gas flows through Laval nozzle and symmetrical wedge-shaped profile, solving boundary value problem by reduction to singular integral equation 19 p2991 A71-37101

Gas flows with thermodynamic relaxation, considering expanding flows in hypersonic wind tunnel nozzles 19 p3162 A71-37458

Inviscid swirling nozzle flow equations from Crocco relation 19 p2993 A71-37890

Subliming nuclear microthruster design with Monte Carlo study of rarefied gas nozzle flow, noting application to spin stabilization 19 p3103 A71-38351

Thermal protection of two dimensional supersonic nozzle fed with hot air by tangentially injected cold gaseous films for convergent and constant section ducts 20 p3314 A71-39415

Water tunnel study of turbulent boundary layers structure in incompressible fluid with longitudinal pressure gradient at inlet section of converging and diverging nozzles 20 p3213 A71-39789

Viscosity effect on initial part of highly underexpanded jets in Mach 1 to 5.7 nozzles for laminar, turbulent and rarefied air flows 21 p3317 A71-40079

Two phase critical flow of saturated and subcooled high pressure liquid nitrogen through convergent-divergent nozzle, comparing with water 21 p3369 A71-40894

Transonic nozzle flow with variable stagnation speed of sound across flow, deriving governing equations with stream function as independent variable 21 p3324 A71-40978

Vacuum water-air ejector with cylindrical mixing chamber and multibarrel nozzle feed, showing increased efficiency by supersonic diffuser substitution 22 p3480 A71-41852

Transverse acoustic wave amplification due to mass injection around submerged nozzle in solid propellant rocket engines, noting annular flow role 22 p3589 A71-42034

Hypersonic nozzle convergent section heat transfer optimization by Euler method, using Lagrange undetermined multiplier and pipe flow approximation 22 p3622 A71-42781

Conical nozzle roughness on heat transfer in supersonic region 22 p3622 A71-42785

Thermodynamic properties and nozzle flow calculations for high temperature and pressure hydrogen, presenting results in Mollier diagram 24 p3887 A71-44629

NOZZLE GEOMETRY

Axisymmetric hypersonic wind tunnel nozzle design by determining inviscid contour and correcting for turbulent boundary layer growth [AIAA PAPER 69-337] 01 p0003 A71-11578

Nozzle system elements size relation to passage cross section in full size two cascade and miniaturized gas turbine engine power plant 03 p0472 A71-14258

Critical nozzle pressure ratio and geometry effects on free exhaust gas jets of jet engine models [DGLR-70-055] 05 p0831 A71-15966

Exhaust nozzles configurations effect on shear jet noise based on Ribner theoretical model 05 p0735 A71-16278

Maximum thrust plug nozzle design for fixed inlet geometry, using calculus of variations for optimum contour determination [AIAA PAPER 71-40] 06 p0946 A71-18501

Three dimensional /nonaxisymmetric/ thrust nozzle design, using calculus of variations for maximization of thrust [AIAA PAPER 71-42] 06 p0946 A71-18503

Transonic gas flows in axisymmetric small throat curvature radius Laval nozzle with appreciable flow parameters variation in transverse direction 07 p1014 A71-19732

Small curvature radius/throat radius ratio supersonic nozzles mass flow rate coefficients at high Reynolds numbers, appraising isentropic flow prediction methods 07 p1015 A71-19877

Nozzle parameters effects on conical vortex heat exchanger characteristics, considering optimal area in critical cross section for maximum energy and temperature efficiency 08 p1233 A71-20835

Optimal design of rigid unadjustable contour for supersonic nozzle, taking into account vehicle flight conditions 08 p1227 A71-21865

Supersonic gas turbine nozzles with condensed particles, determining optimal contour geometries by direct variational procedures 10 p1551 A71-24379

Compressor surge effect on mixed compression inlet flow from numerical solution of one dimensional unsteady inviscid flow equations in variable area duct [AIAA PAPER 69-484] 10 p1553 A71-24855

Sonic nozzle design for precise mass flow measurement, determining nozzle profile for axial velocity distribution in conformity with laminar boundary layer equations solution 10 p1597 A71-24944

Twin spool turbojet engine dynamic response, discussing simulator predictions, digital computer control, nozzle area variations and operating trajectories [ASME PAPER 71-GT-14] 11 p1812 A71-25960

Viscous convergent-divergent nozzle flow slender channel approximation, discussing nozzle geometry, Reynolds number and wall temperature effects [AIAA PAPER 69-654] 12 p1865 A71-27556

Thermal load capacity and nozzle shape for guiding and constricting high current plasmas from electric arc data, using Ar as discharge gas 14 p2279 A71-29851

- Convulsed nozzle extension in engine with low pressure exit seal released and blown off by venting internal pressure
[AIAA PAPER 71-677] 14 p2292 A71-30741
- Two-spool turbojet engine nozzle diameter adjustment system for increasing thrust, fuel economy and reliability, describing automatic clamshell shutter control mechanism 15 p2471 A71-32527
- Geometrical parameters effect on operation of high pressure two-stage nozzle ejector with conical mixing chamber, measuring gas flow rates, total pressures and stagnation temperatures 16 p2521 A71-33612
- Gas flow behind cylindrical nozzles at roots and along periphery for narrow blades, using radial equilibrium equation 16 p2521 A71-33617
- Discharge coefficient correction factor for curvature effect on mass flow rate measurement by sonic throat for axisymmetric nozzles
[ONERA-TP-956] 18 p2915 A71-36024
- Base flow characteristics in four-nozzle rocket exhaust as functions of nozzle axis interspaces, nozzle exit section-base surface distance and Mach number 18 p2903 A71-36117
- Discharge coefficient formula for supersonic nozzles at low throat Reynolds numbers, investigating boundary layer thickness for various nozzle geometries 19 p2993 A71-37896
- Gas turbine engine adjustable nozzle ring flat arrays aerodynamic characteristics determination from profile loss factor dependence on setting angle 20 p3175 A71-39172
- Optimal design of rigid unadjustable contour for supersonic nozzle; taking into account aircraft flight conditions variation 20 p3176 A71-39364
- Two dimensional supersonic variable area nozzle geometry calculation as function of Mach number 23 p3626 A71-44071
- Extendible, variable profile nozzle for various flow regimes operation, developing numerical design algorithm 24 p3821 A71-45339
- NOZZLE THRUST COEFFICIENTS**
Proportional fluidic elements jet nozzle discharge coefficients as function of control pressure and geometrical parameters 03 p0354 A71-13959
- Supersonic propelling nozzle optimal parameters for maximum thrust coefficient, discussing nozzle control and efficiency 12 p1865 A71-27504
- Isolated axisymmetric jet engine exhaust nozzles thrust and drag predictions in sub-, trans- and supersonic flight regimes
[AIAA PAPER 71-719] 14 p2295 A71-30770
- NOZZLE WALLS**
Nozzle wall protection against high enthalpy gas flow effects by film cooling through parietal liquid injection 01 p0143 A71-11017
- Thermal boundary layer equation for sulfur hexafluoride steady arc constriction effects in nozzle throat 12 p1939 A71-27268
- Nozzle wall hypersonic turbulent boundary layers at free stream Mach number, using pitot, hot wire, wall pressure fluctuation and static pressure measurements
[AIAA PAPER 70-746] 12 p1898 A71-27558
- NOZZLES**
Plenum chamber with nozzle wind tunnel model, noting jet flow phenomena at various angles of attack 10 p1590 A71-24865
- NRX-A REACTOR**
U NUCLEAR ENGINE FOR ROCKET VEHICLES
- NUCLEAR AUXILIARY POWER UNITS**
NT SNAP 8
NT SNAP 15
NT SNAP 19
NT SNAP 21
NT SNAP 23
NT SNAP 27
- NT SPACE POWER UNIT REACTORS**
Fusion reactor applications to space propulsion and power generation, considering conversion of thermal energy of reacting plasma to electrical power and exhaust jet 15 p2447 A71-32207
- Electric power system for satellites, considering energy conversion, storage and processing from chemical, solar and nuclear sources 17 p2676 A71-34227
- NUCLEAR BINDING ENERGY**
Charged scalar static model, using dispersion theory to include two-meson effects in two nucleons binding energy at zero separation 05 p0785 A71-16449
- Post-Newtonian corrections for Maclaurin spheroids, presenting binding energy numbers 17 p2806 A71-35406
- Nuclear forces effects on maximum mass limit of neutron stars models using V gamma type potentials 20 p3304 A71-39945
- Relativistic and Newtonian neutron star models with nuclear forces in equation of state, using unitary transformations for hard core and soft core potential 21 p3442 A71-40143
- Gravitation theory within Lorentz covariant and second quantized formalism framework from gravity interaction with binding energy, discussing graviton behavior 21 p3416 A71-41035
- Filippov-Ovcharenko wave functions in form of interaction constant inverse power series for calculating two and three nucleon ground state binding energies 22 p3578 A71-42056
- NUCLEAR CAPTURE**
NT ELECTRON CAPTURE
- NUCLEAR DEFORMATION**
Predeformation effects on metastable Ni base Ti alloys precipitation aging at extrinsic stacking faults, using thin foil microscopy 12 p1916 A71-26894
- NUCLEAR ELECTRIC POWER GENERATION**
NT NUCLEAR AUXILIARY POWER UNITS
NT NUCLEAR POWER PLANTS
NT NUCLEAR POWER REACTORS
NT SNAP 8
NT SNAP 15
NT SNAP 19
NT SNAP 21
NT SNAP 23
NT SNAP 27
- NT SPACE POWER UNIT REACTORS**
Heat rejection radiator influence on space nuclear power system as function of mass/area for Brayton, Rankine, thermoelectric and thermionic conversion schemes 13 p1999 A71-28597
- Turbo-MHD cycle technology of nuclear electric power systems with high temperature reactor for space and terrestrial applications
[AIAA PAPER 71-638] 14 p2273 A71-30716
- Rankine cycle turboelectric nuclear space power conversion system with liquid K as working fluid, discussing current technology status
[GESP-623] 16 p2526 A71-33525
- Performance potential of MHD generators utilizing nonequilibrium ionization in nuclear space power systems 20 p3264 A71-38930
- NUCLEAR ELECTRIC PROPULSION**
Electric rocket propulsion systems using nuclear or solar energy and electrothermal, electromagnetic or electrostatic principle 02 p0283 A71-12309
- Nuclear electric space propulsion size and cost factors, discussing scaling laws use for size- performance relationships
[AIAA PAPER 71-193] 06 p0947 A71-18631
- NUCLEAR EMULSIONS**
High energy pN interactions, using emulsion technique in strong magnetic field 03 p0461 A71-13846
- Negative pi-NN interactions in emulsion at high energies, plotting angular distributions of secondary particles in cosmic ray showers 03 p0476 A71-13847
- Pion interactions with nucleons and nuclei in emulsions irradiated by high energy pion beams 03 p0461 A71-13852
- Positive pions coherent production by negative pions with aid of nuclear photoemulsions 03 p0461 A71-13853
- Electron photon cascades in multilayer substrate-free nuclear emulsion chamber with X ray films under lead plate 03 p0427 A71-13872
- Nuclear photoemulsions for fast neutron dosimetry, recording recoil proton tracks during elastic scattering by hydrogen nuclei 04 p0594 A71-14919
- Fast neutron energy spectrum from free proton elastic scattering in emulsion plates, studying upper atmospheric altitude and latitude factors 06 p0962 A71-18180
- Heavy cosmic rays identification by charge spectrum analysis of balloon-borne combined plastic detectors and nuclear emulsions, noting astrophysical implications 09 p1514 A71-22804
- Plasma focus hard X ray spectrum, using electron sensitive nuclear emulsions 12 p1936 A71-26920
- Nuclear emulsion produced cosmic ray jets secondaries angular distribution, primary energy and anisotropy 13 p2121 A71-28056
- Pions-photographic emulsion nuclei inelastic collisions as function of energy, comparing multiplicity, produced particles angular distribution and evaporation prongs number 13 p2121 A71-28059
- Extensive air showers hadronic component observation by nuclear emulsion chambers combined with scintillation detectors 13 p2124 A71-28080
- Cosmic radiation doses measurement on Soyuz 3 spacecraft by nuclear emulsions, giving averaged doses absorbed by various cosmonaut tissues 15 p2362 A71-31314
- Energy spectrum of cosmic ray showers from high energy muon interactions with nuclear emulsion chamber 15 p2476 A71-31790
- X ray films in emulsion chambers, discussing electron-photon cascades 22 p3550 A71-42640
- PN interactions, using emulsion technique in strong magnetic field 22 p3579 A71-42647
- Negative pi minus N and NN interactions in emulsion at high energies, plotting angular distributions of secondary particles in cosmic ray showers 22 p3594 A71-42648
- Pion interactions with nucleons and nuclei in emulsions irradiated by high energy pion beams 22 p3579 A71-42653
- Positive pions coherent production by negative pions with aid of nuclear photoemulsions 22 p3579 A71-42654
- Electron photon cascades in multilayer substrate-free nuclear emulsion chamber with X ray films under lead plate 22 p3550 A71-42673
- Cosmic radiation heavy nuclei intensity and composition measurement, treating nuclear emulsions in calcium bromide solutions 22 p3596 A71-42733
- NUCLEAR ENERGY**
Energy sources for rockets and satellites, comparing chemical, solar and nuclear supplies 02 p0282 A71-12302
- Gas lasers pumping by nuclear energy, discussing heavy particle interactions, threshold densities, population inversion, etc 06 p0909 A71-18560
- [AIAA PAPER 71-110] 06 p0909 A71-18560
- Multicharge nuclei fluxes from satellite observation, plotting energy and rigidity spectra from latitudinal dependences 08 p1350 A71-20955
- NUCLEAR ENERGY LABORATORIES**
U LABORATORIES
U NUCLEAR RESEARCH
- NUCLEAR ENGINE FOR ROCKET VEHICLES**
U-tube rocket nozzle and fuel element fabrication methods for NERVA space engine, emphasizing coating process 01 p0126 A71-10006
- NERVA XE-Prime test series, discussing computer simulation full power and high specific impulse operation and startup under varying initial conditions
[AIAA PAPER 70-709] 03 p0456 A71-14428
- Computer program for selected gases outgassing rates calculation, tabulating and plotting for NERVA fuel elements gas evaluation 09 p1492 A71-23348
- Reliability analysis as essential input in trade studies for selecting system component designs, emphasizing NERVA program 12 p1928 A71-26664
- Nuclear light bulb engine based on thermal radiation energy transfer from gaseous uranium fuel through internally cooled transparent wall to seeded hydrogen
[AIAA PAPER 71-642] 14 p2274 A71-30719
- NERVA nuclear rocket engine for space propulsion and long duration auxiliary power generation
[AIAA PAPER 71-639] 15 p2448 A71-32285
- Reusable nuclear shuttle navigation systems evaluation by mission simulation, discussing reduced NERVA cooldown thrust pulses uncertainty effects 17 p2774 A71-35075
- NERVA reactor in-flight cooldown during engine shut-down phase of reusable earth-lunar transportation vehicle, discussing coolant management considerations 23 p3703 A71-44270
- NUCLEAR EXPLOSION EFFECT**
Ballistic reentry warheads atmospheric interception, investigating defensive nuclear bursts effects 01 p0163 A71-10268
- Ionospheric and exospheric ELF magnetic waves generation by high altitude nuclear explosions, discussing hydromagnetic waves propagation 04 p0581 A71-14981
- Decay lifetimes of Starfish electrons in trapped radiation belt inner zone 08 p1356 A71-21646
- Amplitude distribution of nuclear burst electromagnetic pulse propagated through atmosphere, deriving two probability distribution functions by central limit theorem 09 p1410 A71-23524

NUCLEAR EXPLOSIONS

NT THERMONUCLEAR EXPLOSIONS

Large scale explosive driven conical shock tube nuclear air blast simulator

04 p0624 A71-14681

Transient annular structures in galaxies with nuclear explosion and fragmentation, examining radiogalaxy dynamics

04 p0655 A71-15724

Equipment survival in natural and nuclear explosion electromagnetic and particle radiation environment

19 p3027 A71-37450

NUCLEAR FISSION

Gas ionization by fission fragments emitted by spherical or cylindrical sources, deriving analytical expressions for ion distribution via diffusion model

09 p1496 A71-22358

Lexan plastic fission track analysis of uranium distribution in glassy residuum in Apollo 11 rock 10017

23 p3739 A71-43616

Superheavy elements search in lunar fine grains from Apollo 12 mission by measuring kinetic energy spectrum of nuclear fission fragments

23 p3753 A71-43718

Spontaneous fission fossil tracks of U, Pu and extinct transuranic elements in pyroxenes of Apollo 11 and 12 soil samples

23 p3764 A71-43803

NUCLEAR FORCES

U NUCLEAR BINDING ENERGY

NUCLEAR FUEL ELEMENTS

U-tube rocket nozzle and fuel element fabrication methods for NERVA space engine, emphasizing coating process

01 p0126 A71-10006

Heat conduction approximate averaging equation, determining mean unstationary temperature of arbitrary nuclear fuel element

01 p0179 A71-10617

Kr 85 disposition following Mo-uranium oxide cermet fuels irradiation in test chamber

02 p0296 A71-12240

Neutronic comparisons of design concepts for low power thermionic space power reactors based on uranium and uranium-based fuels

02 p0281 A71-12264

Computerized outgassing analyzer for nuclear rocket graphite fuel elements at various temperatures in vacuum

05 p0780 A71-16243

Computer program for selected gases outgassing rates calculation, tabulating and plotting for NERVA fuel elements gas evaluation

09 p1492 A71-23348

In-core thermionic power system for manned space station application, discussing driver fuel elements, nuclear radiation shield, heat rejection and coolant outlet temperature

11 p1710 A71-25869

Nuclear characteristics of plutonium fuel for thermoelectric generators and required shield thicknesses for sensitive radiation experiment in outer planet spacecraft

22 p3592 A71-42300

NUCLEAR FUELS

Out-of-pile experiment for measuring uranium dioxide fuel redistribution rates, determining vent hole plugging time and thermal cycling

02 p0296 A71-12247

Cobalt 60 oxides as thermionic fuels, discussing high temperature properties, fabrication and irradiation techniques

02 p0280 A71-12256

Nuclear powered long distance aircraft engines, discussing high burnup fuel, weight factors and safety problems

06 p0926 A71-17694

Ground test reactor design based on colloid fueled reactor concept

[AIAA PAPER 70-688]

07 p1158 A71-19862

Test equipment for elasticity modulus measurement of neutron irradiated materials, noting u-c nuclear fuel and alloy samples

07 p1084 A71-20356

Thermionic reactor experiment design to evaluate U-235 fueled fast spectrum core dynamic and steady state characteristics, discussing system features

11 p1710 A71-25868

Thermionic reactor parametric criticality studies, evaluating fuel element and core design variations effects

11 p1712 A71-25885

Materials technology of Ta-W-Hf clad uranium mononitride fuel for lithium cooled compact fast space power reactor, including irradiation tests

16 p2606 A71-33254

Future space flight energy requirements for onboard power supplies and propulsion, considering high temperature reactors with nuclear fuel in plasma state

19 p3122 A71-37319

Thermionic reactor technology, including insulator seal, nuclear fuel, emitter, tri-layer structure and interelectrode plasma

20 p3265 A71-38949

Lithium deuteride nuclear fuel autocatalytic burning via proton and beryllium isotope resonance in fusion chain reactions

24 p3847 A71-44497

NUCLEAR FUSION

NT CONTROLLED FUSION

Laser produced plasmas for electrical power generation and space propulsion using fusion of deuterium-tritium pellet

01 p0135 A71-11179

Book on direct energy conversion principles and methods covering fusion, fuel cells, MHD, thermoelectric, thermionic, photovoltaic, electrohydrodynamic, piezoelectric and ferroelectric power generation

01 p0006 A71-11193

Stellar nucleosynthesis processes classified into various interior nuclear reactions, discussing stellar evolution role

01 p0131 A71-11422

Plasma generation and nuclear fusion by lasers, investigating critical parameter values for heating

01 p0137 A71-11625

Models for partially mixed stars at He flash time, determining mixture degree effects, carbon production and total mass

05 p0801 A71-15932

Fusion reactor plasma feedback stabilization by nonlinear interaction of two carbon dioxide IR laser beams to produce difference frequency near hybrid resonance

06 p0931 A71-17457

Plasma physics and fusion reactor development involving electric conduction, vibration and magnetic effects, stellarator containment, etc

07 p1168 A71-19602

Red giant star s-process and subsequent delayed electron capture, accounting for large Li abundances

07 p1198 A71-19822

He shell burning termination in solar mass stars evolution to white dwarf stage

07 p1198 A71-19823

Carbon dioxide laser heterodyne plasma density length product measuring with microsecond response in Astron controlled fusion experimental area

07 p1126 A71-20166

Explosive nucleosynthesis in Galaxy, discussing carbon detonation, uniform density models, supernova rates and massive stars

09 p1521 A71-22929

Mn type peculiar A stars relative abundance from curve of growth analysis, discussing isotope shifts, nucleosynthesis, explosion reactions and structure accretion

09 p1529 A71-23596

Nucleosynthesis due to explosive burning in stellar objects for elemental synthesis

10 p1668 A71-24003

Nucleosynthesis in neutron rich supernova ejecta, performing statistical equilibrium calculations at freeze out temperature and density

10 p1670 A71-24301

Supernovae detonation model, examining nucleosynthesis for solar system abundances

10 p1675 A71-24492

Galaxies chemical evolution and aging mechanisms, considering He nucleosynthesis, galactic nuclei and clusters dense core origin

12 p1960 A71-26787

Stellar explosive nucleosynthesis and element abundances in Galactic chemical evolution

13 p2133 A71-27970

Stellar core evolution of initial mass 1.5 solar mass, starting from He-burning phase

13 p2140 A71-29013

Steady state thermonuclear fusion rockets, considering specific impulse, space propulsion and research priorities

14 p2288 A71-29929

Nuclear fusion powered pulsed space propulsion systems with laser initiation, discussing energy conversion to momentum, limitations, vehicle configuration and mission performance

[AIAA PAPER 71-636]

14 p2288 A71-30095

Economical fusion reactor requirements, considering ultrahigh temperature plasma containment for nuclei reaction and energy extraction

15 p2455 A71-31681

Fusion reactor applications to space propulsion and power generation, considering conversion of thermal energy of reacting plasma to electrical power and exhaust jet

15 p2447 A71-32207

Plasma chemistry, discussing low and high temperature plasmas, nuclear fusion reactions and chemical molecular and nuclear synthesis

16 p2539 A71-32963

Main sequence stars hydrogen burning stage, examining neutrino emission and nuclear process effects in stellar evolution

16 p2625 A71-33230

Stellar initial metal content effect on nuclear abundance distributions synthesized under explosive carbon, oxygen and silicon burning conditions

16 p2631 A71-33231

He 4 burning nucleosynthesis, noting Ne 20 buildup in massive stars

16 p2633 A71-33335

High temperature dense plasma formation by laser heating of gas target, noting fusion reaction in deuterium-tritium mixture

16 p2619 A71-33647

Laser heating of D-T plasma, deriving average equations of momentum and energy conservation with allowance for thermonuclear fusion heat

20 p3275 A71-39471

Fast hydrogen atoms penetration into fusion reactor plasma, calculating collision cross section rates coefficients

21 p3422 A71-40765

Expanding D-T plasma laser heating equations derivation, allowing for heat produced by associated thermonuclear fusion

23 p3710 A71-43320

Q values, costs, efficiencies and radioactive evaluation of D-D, D-T and D-He 3 mirror fusion plasma power systems

24 p3847 A71-44493

Lithium deuteride nuclear fuel autocatalytic burning via proton and beryllium isotope resonance in fusion chain reactions

24 p3847 A71-44497

NUCLEAR INTERACTIONS

NT ELECTRON CAPTURE

NT SPIN-ORBIT INTERACTIONS

Photon-neutrino coupling theory of weak interactions, noting exclusion by astrophysical data for white dwarfs

01 p0130 A71-11272

Soviet papers on cosmic rays and high energy nuclear interactions

01 p0145 A71-11362

High energy multiple birth inelastic interactions between cosmic ray particles and atomic nucleus targets, using Wilson chamber and ionization calorimeter

01 p0083 A71-11363

Radiation measuring instruments assembly for extensive air showers and cosmic ray particle nuclear interactions at high energies

01 p0084 A71-11367

Quasi-nucleon nuclear interactions of high energy protons in photoemulsion irradiated in pulsed magnetic field

01 p0131 A71-11368

Nuclear interactions induced by cosmic ray and accelerator muons, discussing cloud chamber and nuclear emulsion data

01 p0131 A71-11412

Nuclear interaction examination, using Wilson magnetic chamber for multiple particle production

03 p0461 A71-13836

Nuclear cascade pion energies in heavy material by Monte Carlo method, concerning cosmic ray and particle accelerator interactions

03 p0461 A71-13842

Charged particles momenta and spatial arrangement during cosmic ray particles nuclear interactions, describing recording equipment

03 p0476 A71-13845

High energy pN interactions, using emulsion technique in strong magnetic field

03 p0461 A71-13846

Negative pi-N NN interactions in emulsion at high energies, plotting angular distributions of secondary particles in cosmic ray showers

03 p0476 A71-13847

Nuclear interactions of neutral cosmic particles with carbon target at mountain altitudes

03 p0476 A71-13848

Neutron and gamma ray production by nuclear interactions in solar flares

06 p0961 A71-18175

Electron-nuclear interactions in ruby by magnetoacoustic double resonance, comparing experimental and theoretical data

07 p1181 A71-20526

Neuroelectric signal analysis using real time nerve spike recognition and separation based on nuclear instrumentation techniques

08 p1249 A71-21839

Type one fluctuations sustained by large air showers at sea level, describing simulation method for influence of first nuclear interaction altitude on shower morphology

10 p1660 A71-23853

Nuclear interactions superhigh energy measurements in cosmic particles on high mountain large sandwich assembly

10 p1662 A71-24666

Cerenkov detectors and He filled spark chambers with large interelectrode spaces in high energy nuclear interaction studies, noting cosmic ray applications

10 p1612 A71-24667

Al and Pb atoms nuclei inelastic interaction cross section with nuclear active particles, using ionization calorimeter and wide gap spark chambers

11 p1760 A71-25165

Baryon isobars average mass data in cosmic ray interactions, using particle angular measurements in backward direction of center mass system

11 p1818 A71-26427

Underground cosmic ray particles flux and nuclear interaction properties, determining integral sea level energy spectrum as function of range of particles in rock 12 p1953 A71-27407

High energy nuclear bursts without accompanying air showers, considering surviving primary protons without inelastic collision in atmosphere 13 p2121 A71-28054

Inelastic proton-proton and proton-carbon interaction cross sections, measuring proton energy with ionization calorimeter on Proton 1, 2 and 3 satellites 13 p2121 A71-28060

Fireball transverse momentum effect on angular distribution of secondary particles, considering high energy nuclear interactions 13 p2058 A71-28063

Angular distribution of muon-poor extensive air showers, considering generation by atmospheric nuclei interaction 13 p2123 A71-28073

Extensive air showers nuclear active component energy flux lateral distribution and spectrum based on Monte Carlo simulation of elementary interactions 13 p2123 A71-28077

Density, momentum and electric charge measurement of nuclear interacting particles in extensive air showers, using air gap magnet spectrograph and neutron monitor 13 p2124 A71-28083

Monte Carlo simulation of high energy atmospheric extensive air shower nuclear cascade based on Aleph model of nuclear interactions 13 p2125 A71-28089

Extensive air showers muons angular distribution, considering high energy nuclear reactions 13 p2126 A71-28097

Nucleon-nucleon and nucleon-nucleus interaction energy measuring system at mountain elevation, discussing components and design 14 p2247 A71-30600

Cosmic ray high energy pion and nucleon nuclear interaction observations, determining statistical fluctuations in secondary particles angular distribution 15 p2479 A71-32076

Collimated nuclear interactions induced by cosmic ray pions and nucleons in carbon and brass, noting energy dependence of events production frequency 17 p2796 A71-34858

Cosmic ray nuclear interactions in 10-300 GeV energy range, using balloon-borne emulsion target, spark chambers and ionization spectrometer 19 p3124 A71-37286

Underground interactions of primary cosmic ray produced atmospheric muon neutrinos, using large area liquid scintillation detector hodoscope 19 p3105 A71-37288

Nuclear interaction examination, using Wilson magnetic chamber for multiple particle production 22 p3579 A71-42637

Nuclear cascade pion energies in heavy material by Monte Carlo method, concerning cosmic ray and particle accelerator interactions 22 p3579 A71-42643

Charged particles momenta and spatial arrangement during cosmic ray particles nuclear interactions, describing recording equipment 22 p3594 A71-42646

PN interactions, using emulsion technique in strong magnetic field 22 p3579 A71-42647

Nuclear interactions of neutral cosmic particles with carbon target at mountain altitudes 22 p3595 A71-42649

NUCLEAR ISOBARS
Baryon isobars average mass data in cosmic ray interactions, using particle angular measurements in backward direction of center mass system 11 p1818 A71-26427

NUCLEAR MAGNETIC RESONANCE
NT PROTON MAGNETIC RESONANCE
NT PROTON RESONANCE
Spontaneous polarization measurement of ferroelectric Rochelle salt near Curie point, using nuclear magnetic resonance for phase transitions 04 p0637 A71-15548

Fe 57 nuclei longitudinal and transverse relaxation in yttrium iron oxide sublattices at various temperatures and magnetic field strengths 05 p0794 A71-16878

Butene hydroperoxides structure and intermolecular reactions from NMR spectra, discussing peroxide radical addition, OH group signals shifts and self association 12 p1877 A71-27751

Fluorine chemical shift tensor measurements in magnesium fluoride, using multiple pulse NMR technique 13 p2025 A71-28031

Nonmagnetic high pressure cell for pulsed and wide line nuclear magnetic resonance measurements 13 p2066 A71-28157

Temperature dependent absorption line width and secondary moments of nuclear magnetic resonance spectra of Ti-Zr-H system 14 p2258 A71-30009

Nuclear magnetic resonance spectrometer for moisture content measurement of lunar and terrestrial soils and rocks 15 p2411 A71-32474

Stress annealing effects on Al 27 NMR lineshapes in pure Al powders filled and stored at room temperature, considering residual stress 17 p2759 A71-35225

Modulation instability of dispersion type NMR stabilizer of resonance conditions, determining critical frequency of self excitation and maximum amplification 22 p3519 A71-41444

High speed gas lubricated foil supported nonmetallic rotor for nuclear magnetic resonance research 22 p3553 A71-41678

Hybrid lumped-distributed parameter resonant LC circuit design for nuclear magnetic resonance spectrometer 23 p3661 A71-44343

Enhanced low energy nuclear resonance reaction cross section estimation, finding Be 9 isotope reaction with proton for clean controlled thermionuclear reactor 24 p3847 A71-44495

NUCLEAR MODELS

Monte Carlo model of muon and active component distribution in nuclear cascade in extensive cosmic ray shower 03 p0476 A71-13849

Quark detection by telescope using production models, discussing extreme energy transfer conditions and upper production limits 12 p1952 A71-27398

Monte Carlo model of muon and active component distribution in nuclear cascade in extensive cosmic ray shower 22 p3595 A71-42650

NUCLEAR PARTICLES

NT ALPHA PARTICLES
NT ANTINEUTRINOS
NT ANTIPARTICLES
NT BETA PARTICLES
NT BOSONS
NT HYPERONS
NT MESONS
NT NUCLEONS
NT PHOTONS
NT PIONS
NT POSITRONS
Cosmic ray nuclear component during solar activity minimum, using Cerenkov counters onboard Elektron satellites 01 p0146 A71-11371

Straight and curved edges produced vidiosignal amplitude spectra discrimination in TV image scanning of nuclear particle path photographs, using filtering device 02 p0248 A71-11827

Energy spectra of ionization bursts, electromagnetic cascades and nuclear active particles at mountain altitude 03 p0476 A71-13850

Fossil nuclear charged particle tracks in lunar rock 12013 Ca-feldspar, K-feldspar and pyroxene attributed to galactic cosmic rays 03 p0494 A71-14216

Nuclear tracks high density in Apollo core small silicate crystals, discussing extralunar dust and photospheric iron-hydrogen ratio 07 p1189 A71-18740

Uncooled Si nuclear particle detector charge sensitive and pulse shaping amplifier design, discussing spacecraft instrumentation and fabrication requirements 08 p1267 A71-21848

Neutron star nuclear matter superfluidity and superconductivity possibility from energy gap and critical temperature and magnetic field calculation 11 p1821 A71-25565

Air showers nuclear active and muon components simulation in space and time, using different shower models based on isobar-fireball concept 13 p2125 A71-28090

High energy muons measurements in extensive air showers, presenting muon densities, momenta and electric charge data obtained from spectrograph long term continuous operation 13 p2125 A71-28091

Primary cosmic ray nuclear component, discussing Cosmos 163 measurements 13 p2128 A71-28547

Energy spectra of ionization bursts, electromagnetic cascades and nuclear active particles at mountain altitude 22 p3595 A71-42651

NUCLEAR PHYSICS
NT FIELD THEORY (PHYSICS)
NT PLASMA PHYSICS
NT QUANTUM THEORY
Soviet book on experimental methods in nuclear physics covering operation, structural features and application of radiation detectors 06 p0903 A71-18731

**NUCLEAR POWER
U NUCLEAR ENERGY**

**NUCLEAR POWER GENERATION
U NUCLEAR ELECTRIC POWER GENERATION**

NUCLEAR POWER PLANTS
Nuclear electric space power plant rejecting waste heat by heat pipes 01 p0126 A71-11576

Social quantitative benefit vs risk assessment of new technologies, considering atomic power safety 02 p0336 A71-12120

Energy converters for satellite nuclear power plants, discussing rotating, MHD, thermionic and thermoelectric systems 02 p0282 A71-12306

Nuclear science and power systems - IEEE Conference, New York, November 1970 08 p1267 A71-21838

Nuclear power plants safety design and evaluation via probabilistic analysis 08 p1300 A71-21852

Conceptual design of nuclear thermionic power plant for Space Base application, discussing plant efficiency, radiator area requirements, launch weight and shielding 11 p1710 A71-25871

Out of core design of reactor heated thermionic power plant for manned space station, discussing temperature distribution, shielding characteristics and power conversion 11 p1710 A71-25873

Soviet book on aircraft and rocket engines control automation, discussing nuclear power plant/fuel systems design and control simulation methods 11 p1814 A71-26403

Nuclear power station design for optimal reliability levels, noting maintainability requirements 18 p2928 A71-36807

Orbital performance of SNAP 19 radioisotopic thermoelectric generator for nuclear power supply on Nimbus 3 observatory 20 p3266 A71-38962

NUCLEAR POWER REACTORS

NT SNAP 8
NT SPACE POWER UNIT REACTORS
Ground test reactor design based on colloid fueled reactor concept 07 p1158 A71-19862

Dynamic simulation of fission product heating in reactor using multigroup Way-Wigner method 07 p1158 A71-20350

Economical fusion reactor requirements, considering ultrahigh temperature plasma containment for nuclei reaction and energy extraction 15 p2455 A71-31681

Fast neutron spectra in lead and water shielded reactor, comparing liquid scintillator measurements with discrete ordinates code calculations 16 p2606 A71-33253

Nuclear reactor Brayton cycle space power system design point characteristics, discussing cycle parameters, working fluid, turbine inlet temperature, operating pressure level, etc 20 p3262 A71-38913

Brayton cycle electric space power supply systems, describing shielded reactor and heat exchanger design 20 p3263 A71-38924

Radioisotope thermoelectric generator safety and operations considerations for users of large nuclear space power systems 20 p3264 A71-38933

Q values, costs, efficiencies and radioactive evaluation of D-D, D-T and D-He 3 mirror fusion plasma power systems 24 p3847 A71-44493

NUCLEAR POWERED SHIPS
Nuclear surface effect vehicle and subsonic aircraft for transoceanic cargo shipping, discussing mobile reactor safety tests under high speed impact conditions [AIAA PAPER 70-1221] 09 p1492 A71-22779

NUCLEAR PROPELLED AIRCRAFT
Nuclear powered long distance aircraft engines, discussing high burnup fuel, weight factors and safety problems 06 p0926 A71-17694

Nuclear surface effect vehicle and subsonic aircraft for transoceanic cargo shipping, discussing mobile reactor safety tests under high speed impact conditions [AIAA PAPER 70-1221] 09 p1492 A71-22779

Air breathing nuclear propulsion, considering reactor safety in air cushion vehicles and aircraft 14 p2273 A71-29930

NUCLEAR PROPULSION
NT NUCLEAR ELECTRIC PROPULSION
Spacecraft onboard power supply problem, discussing relative merits of electric and nuclear thermal propulsion systems 01 p0143 A71-11434

Deep space shuttles operating modes and vehicle types, considering chemical vs nuclear propulsion, direct vs near-orbit rendezvous, refueling, etc 01 p0165 A71-11593

- Thermonuclear microbombs for manned spacecraft propulsion to solar system boundary, describing system design and performance 04 p0625 A71-15647
- Air condensation onset location in supersonic nozzles for nuclear space propulsion systems, using supercooled vapor pressure measurements beyond saturation point 10 p1593 A71-24328
- Reusable Nuclear Shuttle using NERVA nuclear engines for low cost transportation to lunar and geosynchronous orbit, discussing design, operation, tests and problems 11 p1840 A71-26516
- Air breathing nuclear propulsion, considering reactor safety in air cushion vehicles and aircraft 14 p2273 A71-29930
- Nuclear fusion powered pulsed space propulsion systems with laser initiation, discussing energy conversion to momentum, limitations, vehicle configuration and mission performance [AIAA PAPER 71-636] 14 p2288 A71-30095
- Reusable nuclear shuttle design, considering various propellant tank configurations and expendable/reusable launch modes with respect to performance, development cost and cost effectiveness [AIAA PAPER 71-640] 14 p2273 A71-30717
- Nuclear space power systems computer simulation for preliminary system and mission analysis, considering Brayton, Rankine and thermionic systems [AIAA PAPER 71-689] 14 p2208 A71-30749
- Shortest transfer time interstellar propulsion systems, considering nuclear pulse and electric rockets, fusion and photon rockets, and ramjets 15 p2469 A71-31748
- Reusable nuclear shuttle concepts, performance and design requirements 17 p2813 A71-35072
- Reusable nuclear shuttle guidance and control system requirements, using nuclear engine thrust pulse train for guidance 17 p2774 A71-35073
- Navigation and guidance alternatives of reusable nuclear shuttle, stressing onboard sensors and processing systems for position and attitude determination 17 p2774 A71-35074
- Nuclear rocket propulsion for human post-Apollo space programs, including Mars exploration 19 p3131 A71-37328
- ### NUCLEAR RADIATION
- NT BETA PARTICLES
- NT FAST NEUTRONS
- NT GAMMA RAYS
- NT NEUTRON BEAMS
- NT SPALLATION
- NT THERMAL NEUTRONS
- Soviet book on experimental methods in nuclear physics covering operation, structural features and application of radiation detectors 06 p0903 A71-18731
- Nuclear and space radiation effects - NASA/IEEE Conference, University of California at San Diego, July 1970 07 p1070 A71-19051
- Nuclear radiation damage to ruby laser power output 07 p1121 A71-19067
- Transducer design selection for strain gage applications in high nuclear radiation environments based on system requirements 09 p1445 A71-22718
- Nuclear radiation shielding design for space base SNAP 8 reactor, discussing geometry constraints for lithium hydride and U loop layers model 09 p1492 A71-22808
- Nuclear component analysis of primary cosmic radiation by Cerenkov spectrometer onboard Cosmos 228 satellite 11 p1817 A71-25780
- In-core thermionic power system for manned space station application, discussing driver fuel elements, nuclear radiation shield, heat rejection and coolant outlet temperature 11 p1710 A71-25869
- Lateral spread of nuclear-electromagnetic cascades in iron absorber from three-dimensional Monte Carlo simulation 15 p2452 A71-31810
- Dispersive effect on bremsstrahlung radiation from electron atom collisions in weakly ionized plasma, using Boltzmann transport equation 15 p2456 A71-31850
- Equipment survival in natural and nuclear explosion electromagnetic and particle radiation environment 19 p3027 A71-37450
- Nuclear safety considerations for ground checkout, launch and in-orbit operations of reactors for earth orbital manned space stations 20 p3262 A71-38920
- Nuclear component analysis of primary cosmic radiation by Cerenkov spectrometer onboard Cosmos 228 satellite 22 p3591 A71-41548
- Nuclear characteristics of plutonium fuel for thermoelectric generators and required shield thicknesses for sensitive radiation experiment in outer planet spacecraft 22 p3592 A71-42300
- Wideband solid state converter circuit for quantization of signals from semiconductor nuclear radiation detectors, noting cost reduction 23 p3677 A71-43527
- Nuclear track densities in lunar core and fine samples, relating erosion history, solar activity and surface stirring 23 p3764 A71-43799
- ### NUCLEAR RADIATION SPECTROSCOPY
- Soviet book on material analysis by nuclear radiation covering heavy elements concentration in ores, radioisotope devices and gamma ray capture spectroscopy 02 p0283 A71-12721
- Magnetic Compton spectrometer for high intensity pulsed gamma ray environments and nuclear device spectral measurement 08 p1294 A71-21840
- ### NUCLEAR REACTIONS
- NT ANNIHILATION REACTIONS
- NT CONTROLLED FUSION
- NT ELECTRON CAPTURE
- NT ELECTRON SCATTERING
- NT HIGH ENERGY INTERACTIONS
- NT NEUTRON EMISSION
- NT NEUTRON SCATTERING
- NT NUCLEAR FISSION
- NT NUCLEAR FUSION
- NT NUCLEAR INTERACTIONS
- NT PHOTOPRODUCTION
- NT POSITRON ANNIHILATION
- NT PROTON SCATTERING
- NT PROTON-PROTON REACTIONS
- NT RADIOACTIVE DECAY
- NT RESONANCE SCATTERING
- NT SPALLATION
- NT SPIN-ORBIT INTERACTIONS
- NT THERMONUCLEAR REACTIONS
- Li quantitative determination in soaps and lubricants by gamma spectroscopy of nuclear reactions with alpha particles from radioactive source 01 p0106 A71-10093
- Nuclear reaction products effect on population inversion in gas lasers, considering neutron irradiation enhancement of carbon dioxide laser output 08 p1303 A71-21668
- Nuclear reactions in high temperature laboratory and stellar plasmas, discussing pinches, thermonuclear burning and star evolution 16 p2613 A71-32972
- Co 59-neutron reaction tensor spin-spin potential, using polarized targets of Ho 165 and Co 59 for nuclear spin-spin effect measurement 18 p2949 A71-36681
- Mg 24 photodisintegration rate in stellar silicon burning process, presenting reactions at low alpha particle energies 23 p3723 A71-42952
- ### NUCLEAR REACTOR CONTROL
- Enhanced low energy nuclear resonance reaction cross section estimation, finding Be 9 isotope reaction with proton for clean controlled thermonuclear reactor 24 p3847 A71-44495
- ### NUCLEAR REACTOR MATERIALS
- #### U REACTOR MATERIALS
- ### NUCLEAR REACTORS
- NT BOILING WATER REACTORS
- NT BREEDER REACTORS
- NT FAST NUCLEAR REACTORS
- NT GAS COOLED REACTORS
- NT GASEOUS FISSION REACTORS
- NT HIGH TEMPERATURE NUCLEAR REACTORS
- NT LIQUID METAL COOLED REACTORS
- NT NUCLEAR POWER REACTORS
- NT PLUM BROOK REACTOR
- NT SNAP 8
- NT SPACE POWER UNIT REACTORS
- NT THERMAL REACTORS
- NT WATER COOLED REACTORS
- Nuclear reactor kinetic differential equations, ascertaining positive bounded solutions existence 01 p0126 A71-11290
- Nonlinear space independent nuclear reactor kinetics equations, demonstrating positive periodic solutions existence 01 p0126 A71-11291
- Omega West Reactor isothermal irradiation experiments, determining long term fast neutron irradiation effects on Al 995, Lucalox and yttrium oxide insulator 02 p0280 A71-12251
- Papers on nuclear engineering for satellites and rockets covering radioisotope batteries and reactor energy sources, nuclear-electric and nuclear-thermal propulsions 02 p0281 A71-12301
- Nuclear reactors for space power supply with turboelectric, thermoelectric and thermionic converters 02 p0282 A71-12305
- Accelerometer design for nuclear reactor vibration measurements, considering environmental effects 04 p0587 A71-14824
- Post burnout heat transfer to mist flow for nuclear reactor design, using two step model 07 p1221 A71-18789
- Fusion energy technology, discussing controlled reactor construction and operation 07 p1169 A71-20000
- German monograph on thermal shock experimental analysis covering derivation of method for determining temperatures and thermal stresses in nuclear reactor structures 10 p1697 A71-25036
- Out of core design of reactor heated thermionic power plant for manned space station, discussing temperature distribution, shielding characteristics and power conversion 11 p1710 A71-25873
- BeO reflected-fast-spectrum liquid-metal-cooled thermionic reactor, discussing two dimensional transport perturbation theory computer code for temperature coefficients evaluation 11 p1712 A71-25887
- Open loop transient analysis of thermionic diode kinetics experiment with analog computer nuclear reactor simulator 11 p1797 A71-25904
- Neutron radiography facility using TRIGA reactor source, discussing design and performance 13 p2044 A71-28523
- PAX intermediate spectrum reactor neutron and photon dose rates and fast and thermal neutron flux calculation, comparing results with experiment 13 p2099 A71-29258
- Transient flow measurement with sharp-edged orifices, considering pump trip accidents simulation in water cooled nuclear reactors [ASME PAPER 71-FE-30] 13 p2053 A71-29465
- Fusion reactor applications to space propulsion and power generation, considering conversion of thermal energy of reacting plasma to electrical power and exhaust jet 15 p2447 A71-32207
- Startup testing of SNAP 8 power conversion system coupled with nuclear reactor simulator 15 p2447 A71-32217
- Out-of-core nuclear thermionic converter system design feature concerning heat pipes, vapor-cooled radiators, modularity and reliability 15 p2448 A71-32224
- Nuclear reactor design as heat source for electric power generation in space 16 p2606 A71-33249
- Reactor-shield-containment system models under impact tests, noting cracks, leaks and deformations 16 p2606 A71-33250
- Mercury properties, chemistry, safety, handling and corrosion in nuclear coolant applications 19 p3102 A71-37071
- Book on lubrication systems selection, application, handling and maintenance covering journal and thrust bearings, nuclear reactors and machine tools 19 p3069 A71-37523
- Reactor power systems for earth orbital space station, considering thermoelectric and Brayton cycle power conversion modules 20 p3262 A71-38919
- PbTe thermoelectric converter for ZrH reactor space power supply, discussing operational performance, design and materials technology 20 p3265 A71-38951
- Fast hydrogen atoms penetration into fusion reactor plasma, calculating collision cross section rates coefficients 21 p3422 A71-40765
- Asymptotic behavior of nonlinear Volterra integrodifferential equation solution, noting application to nuclear reactor dynamics 21 p3409 A71-41077
- Li-filled vacuum-deposited W heat pipes for efficient heat extraction from nuclear reactors, discussing design, fabrication and testing 23 p3682 A71-43595
- ### NUCLEAR RESEARCH
- Nuclear science and power systems - IEEE Conference, New York, November 1970 08 p1267 A71-21838
- Water radiolysis measurement in nuclear reactor tests, discussing experiment design as doubly telescoping sequences of blocks 21 p3345 A71-40202
- Nuclear test program management, considering reliability problems, delays and cost 23 p3786 A71-43462
- ### NUCLEAR RESEARCH AND TEST REACTORS
- NT HIGH TEMPERATURE NUCLEAR REACTORS
- NT PLUM BROOK REACTOR
- ### NUCLEAR ROCKET ENGINES
- Neutronic comparisons of design concepts for low power thermionic space power reactors based on uranium and uranium-based fuels 02 p0281 A71-12264

- Thermionic reactor analytical model for systems analysis, considering complex interactions between reactor physics, thermionics and thermal/hydraulics
02 p0281 A71-12265
- Thermionic performance influence on reactor design and operation, considering plant electrical ratings
02 p0281 A71-12266
- Technology gap between thermionic converter physics and reactor engineering, emphasizing language problem
02 p0281 A71-12272
- Papers on nuclear engineering for satellites and rockets covering radioisotope batteries and reactor energy sources, nuclear-electric and nuclear-thermal propulsions
02 p0281 A71-12301
- In-core thermionic reactor development for space applications
02 p0282 A71-12307
- TV broadcast satellites with in-core thermionic reactor, discussing transmitting power, design and economy
02 p0283 A71-12308
- Nuclear thermal rockets development, discussing reactor-engine tests, solid and gas cores and Saturn 5 application
02 p0283 A71-12314
- Thermionic reactor development for space applications, discussing converter fuel elements, reliability and system weight
[ASME PAPER 70-WA/ENER-13] 03 p0456 A71-14109
- Nuclear light bulb reactor and coaxial flow reactor for gas core nuclear rocket engines
[AIAA PAPER 70-708] 03 p0456 A71-14427
- Nuclear rocket nozzle cooling passages, discussing heat transfer and friction correlations for single-phase hydrogen turbulent flow
[AIAA PAPER 70-661] 03 p0456 A71-14444
- Computerized outgassing analyzer for nuclear rocket graphite fuel elements at various temperatures in vacuum
05 p0780 A71-16243
- Thermionic reactor electric propulsion for unmanned outer planets exploration, discussing spacecraft design, launch vehicle, weight factors, etc
[AIAA PAPER 70-1122] 09 p1492 A71-22914
- Thermionic reactor experiment design to evaluate U-235 fueled fast spectrum core dynamic and steady state characteristics, discussing system features
11 p1710 A71-25868
- In-core thermionic reactor flight system for space base applications, providing electric power and thermal shielding
11 p1710 A71-25870
- Thermionic reactor electric spacecraft propulsion system for unmanned outer planets missions, investigating voltage and radiator temperature effects on weight
11 p1811 A71-25872
- Nuclear thermionic systems conceptual design with converters outside reactor to reduce weight
11 p1710 A71-25874
- Driver terrestrial in-core thermionic reactor dynamic behavior, discussing computerized simulation with respect to coolant loop
11 p1711 A71-25883
- Small fast spectrum thermionic reactor experiment open loop dynamics and control, discussing nonlinear transient simulation studies on closed loop plant
11 p1712 A71-25886
- Automatic control, safety and dynamics of thermionic reactor experiment under simulated spacecraft load requirements
11 p1712 A71-25888
- Space base 100 kw thermionic reactor power plant featuring interchange core replacement package
11 p1713 A71-25895
- Externally fueled thermionic reactor power plant incorporation into unmanned ion propulsion spacecraft
11 p1811 A71-25896
- Reusable Nuclear Shuttle using NERVA nuclear engine for low cost transportation to lunar and geosynchronous orbit, discussing design, operation, tests and problems
11 p1840 A71-26516
- Two component solid gas vortex flows with end wall injection eliminating boundary layer losses for colloid core nuclear rocket engine concept
[AIAA PAPER 71-637] 14 p2273 A71-30715
- Open cycle gas core nuclear rocket engine, considering reactor critical experiments and cold and hot flow tests
[AIAA PAPER 71-641] 14 p2273 A71-30718
- Subliming nuclear microthruster design with Monte Carlo study of rarefied gas nozzle flow, noting application to spin stabilization
19 p3103 A71-38351
- Thermionic reactor technology, including insulator seal, nuclear fuel, emitter, tri-layer structure and interelectrode plasma
20 p3265 A71-38949
- Critical mass calculation for open cycle gas core rocket reactors, considering cavity size, fuel radius, reflector thickness and hydrogen bypass flow
22 p3573 A71-41637
- Volume fraction analysis of coaxial flow gas core nuclear rocket for mass flow ratios, fuel radius and density, using free jet computer code and eddy viscosity equations
22 p3573 A71-41638
- NUCLEAR SCATTERING**
NT NEUTRON SCATTERING
NT RESONANCE SCATTERING
NUCLEAR SHIELDING
U RADIATION SHIELDING
NUCLEAR SPIN
Tetrahedral molecules quantum mechanical rotational partition function, nuclear spin statistical weight factors and error bounds
04 p0629 A71-14807
- Excess Knight shift due to spin polarization in electron gas by magnetic impurity Fermi contact coupling as function of distance from nucleus
11 p1801 A71-25373
- Co 59-neutron reaction tensor spin-spin potential, using polarized targets of Ho 165 and Co 59 for nuclear spin-spin effect measurement
18 p2949 A71-36681
- NUCLEAR STRUCTURE**
Stellar nucleosynthesis processes classified into various interior nuclear reactions, discussing stellar evolution role
01 p0131 A71-11422
- DWBA optical model coupled channels comparison in 2s-1d shell for predicting proton scattering elastic cross sections
06 p0929 A71-17579
- Inelastic scattering transition densities in single particle operator reduced matrix elements between initial and final nuclear states for nucleon angular momentum calculations
14 p2276 A71-30013
- NUCLEAR SUBMARINES**
U NUCLEAR POWERED SHIPS
NUCLEAR WARHEADS
Nuclear, hydrogen/oxygen and solid propellant satellite interceptors effectiveness measurement, considering warhead kill radius, propellant weight and specific impulse
13 p2144 A71-27982
- NUCLEAR WEAPONS**
Short range air to ground attack missile system, discussing nuclear warhead, propulsion system, performance characteristics and program cost analysis
10 p1682 A71-24286
- NUCLEAR-ELECTRIC MOMENTS**
U ELECTRIC MOMENTS
NUCLEATE BOILING
NT LEIDENFROST PHENOMENON
Cryogenic fluids nucleate boiling dependence on solid surface characteristics, considering hysteresis, boiling site spreading and radiation effects
01 p0178 A71-10005
- Liquid film formation at base of bubbles and effects on heat transfer during nucleate boiling
01 p0181 A71-11404
- Explosive boiling of water and organic liquids around pulse heated Pt wire, discussing vaporization process, fluctuating nucleation and temperature behavior
02 p0331 A71-12193
- Horizontal cylindrical heaters heat transfer to pool boiling Hg at heat fluxes up to burnout
[ASME PAPER 70-HT-R] 03 p0519 A71-13698
- Liquid-vapor system in closed container, investigating transient pressure rise under heat and mass transfer interactions including incipient and nucleate boiling
04 p0687 A71-15535
- Liquid oxygen nucleate boiling in simulated reduced gravity fields, obtaining heat transfer coefficients, departure frequency and bubble growth rate
04 p0687 A71-15536
- Heat and mass transfer investigation in nucleate boiling boundary layer by salt depositions
07 p1221 A71-18787
- Vapor bubbles during nucleate boiling, deriving formation frequency relationship with departure diameter
07 p1222 A71-19197
- Explosive boiling of water and organic liquids around pulse heated Pt wire, discussing vaporization process, fluctuating nucleation and temperature behavior
15 p2512 A71-31499
- Boiling at solid heated surfaces, discussing nucleation, bubble formation, pool boiling factors, heat transfer correlation and forced convection
15 p2515 A71-32565
- Dynamic bubble growth and diameter at detachment during liquid boiling at heating surfaces, using force equilibrium, laser Mach-Zehnder interferometer and temperature measurements
16 p2663 A71-34038
- German monograph on heat transfer from vertical heating surfaces to liquids at rest in nucleate boiling, showing microstructure interaction with interfacial tension
17 p2838 A71-34852
- Boiling heat transfer to cryogenic fluids, considering pool convective, nucleate, film and forced convective subcooled boiling
19 p3162 A71-37463
- Surface heat flux for incipient boiling in liquid metal heat pipes, determining nucleation site radius upper limit in Na heat pipes
19 p3171 A71-38349
- Nucleate boiling of liquid helium I on gallium single crystal surfaces
20 p3312 A71-39282
- Large volume liquid oxygen pool boiling, investigating heat exchange coefficient dependence on flux density and pressure
23 p3705 A71-44339
- NUCLEATION**
NT CLOUD SEEDING
Liquid-phase nucleus condensation of supersaturated vapor in drawer, using statistical method
01 p0180 A71-11089
- Al alloys nucleation and precipitation hardening, examining quenching rate effects with hardness measurements and electron microscopy
04 p0613 A71-15744
- Water vapor condensation due to heterogeneous nucleation in nozzles, considering flows seeded with inorganic smoke and metallic ions
[ASME PAPER 70-FE-22] 05 p0737 A71-16974
- Al-Zn-Mg alloys, considering Cu and Cr additions effects on nucleation and incoherent precipitates formation
13 p2088 A71-29406
- Epitaxial deposition of Au on ultrahigh vacuum cleaved mica during early nucleation and growth
14 p2284 A71-30072
- High tensile strength maraging steels aging, discussing dispersed precipitates formation by homogeneous nucleation
15 p2427 A71-31525
- Statistical microstructural analysis for nucleation and growth kinetics of recrystallization nuclei of metal single crystals
17 p2755 A71-34414
- Liquid Zr drops combustion in oxygen-nitrogen atmospheres, examining critical conditions for sac formation with homogeneous bubble nucleation theory
17 p2837 A71-34511
- Tungsten-oxygen system surface reactions in vacuum, emphasizing interfacial geometry variations, faceting and oxide nucleation
17 p2694 A71-34667
- LiF and MgO high purity single crystals plastic deformation geometric characteristics, discussing nucleation probability on different slip planes
24 p3859 A71-44450
- NUCLEI**
Galactic nuclei composition of dense core with small subunits generating relativistic particles
01 p0162 A71-11421
- Mass estimation for quasars and galactic nuclei with absorption line shift into long wave region
02 p0307 A71-12090
- Mass estimation for quasars and galactic nuclei with absorption line shift into long wave region
08 p1362 A71-21140
- Beef liver cell nuclei acoustic absorption at various frequencies, determining relation to protein content
12 p1928 A71-27535
- DNA synthesis rhythm in aorta endothelial cells nuclei during direct division, noting effects of amitosis by autoradiography
12 p1872 A71-27752
- Brightness fluctuations in photometric nucleus of Ikeya-Seki comet at 29-31 March 1968
17 p2803 A71-34832
- Cloud condensation nuclei supersaturation spectrum and aerosol particle concentration variations with height
19 p3092 A71-38683
- Postflight histological analysis of turtles aboard Zond 7, noting decrease in cell nuclei size due to space flight conditions adaptation
21 p3334 A71-40568
- NUCLEI [NUCLEAR PHYSICS]**
NT ALPHA PARTICLES
NT DEUTERONS
NT HEAVY NUCLEI
Geomagnetically trapped C, N and O nuclei and alpha particles in earth outer radiation zone, noting acceleration and loss mechanisms
01 p0075 A71-11496
- Cosmic ray nuclei galactic disk confinement determination, considering particle mean age by radioactive Be10 tracer method
03 p0480 A71-14052
- Nucleus energy spectra projection from Hartree-Fock intrinsic wave functions model space, using coupled orbital matrix elements
06 p0929 A71-17578

Cosmic ray nuclei propagation through interstellar medium, solving transfer equation for simple model with allowance for boundary conditions
16 p2625 A71-33325

Statistical measurements of solar protons, alpha particles and heavier nuclei by lunar orbiting Explorer 35
16 p2628 A71-33933

Solar cosmic ray data, discussing multicharged nuclei relative abundances in photosphere and propagation models
19 p3126 A71-37625

Soyuz observation of tritium and He-3 nuclei in Al targets exposed to space radiation
20 p3280 A71-39601

High resolution time averaged energy spectrum and chemical composition of iron group cosmic ray nuclei from fossil tracks in Apollo 12 lunar rocks
23 p3764 A71-43804

Interplanetary energy spectrum of solar flare Fe nuclei from tracks in Surveyor 3 glass filter and rock 12022
23 p3765 A71-43813

NUCLEIC ACIDS

NT RIBONUCLEIC ACIDS

NT URIDYLIC ACID

SH containing radioprotectors action on nucleic acid metabolism, discussing DNA synthesis inhibitory effects
07 p1039 A71-18983

Molecular nature of circadian oscillations mechanism, suggesting nucleic acids implication
20 p3190 A71-39476

NUCLEON POTENTIAL

Nuclear soft core potential reproduction by isoscalar vector meson in nonlocal field theory of fireball in high energy cosmic ray collisions
15 p2472 A71-31151

NUCLEON-NUCLEON INTERACTIONS

Charged scalar static model, using dispersion theory to include two-meson effects in two nucleons binding energy at zero separation
05 p0785 A71-16449

Nucleon-nucleon interactions produced energetic penetrating particles /muons/ in cosmic ray showers, studying neon flash tube technique
12 p1948 A71-27186

Inelastic proton-proton and proton-carbon interaction cross sections, measuring proton energy with ionization calorimeter on Proton 1, 2 and 3 satellites
13 p2121 A71-28060

Regular multiplicities of particle production in high energy collisions and antinucleon-nucleon annihilation, comparing cosmic ray jet data and pion-nucleon difference
13 p2102 A71-28061

Nucleon-nucleon and nucleon-nucleon-interaction energy measuring system at mountain elevation, discussing components and design
14 p2247 A71-30600

Filippov-Ovcharenko wave functions in form of interaction constant inverse power series for calculating two and three nucleon ground state binding energies
22 p3578 A71-42056

NUCLEON-NUCLEON SCATTERING

Nucleon-nucleon and meson-nucleon collisions, determining secondary cosmic ray multiplicity dependence on primary particles energy spectra
13 p2121 A71-28057

NUCLEONS

Extensive atmospheric showers and energy transfer from interacting nucleons to electron photon cascades at high energy levels
01 p0146 A71-11366

Pion-nucleon interactions, determining energetically precipitated particle effects in air showers
03 p0461 A71-13841

High energy nucleon passage through lower atmosphere during chemical composition changes of primary cosmic rays, using Proton satellite observations
03 p0476 A71-13851

Pion interactions with nucleons and nuclei in emulsions irradiated by high energy pion beams
03 p0461 A71-13852

Momenta measurements of particles produced by high energy quasi-nucleon interactions of pions on photoemulsion layers, using primary particle tracks scanning
03 p0461 A71-13854

Neutron monitors multiplicity yield function calculation, using Monte Carlo method for nucleonic cascade in atmosphere
06 p0960 A71-18165

Secondary cosmic ray spectrum latitude knee based on nucleon, proton and muon energy spectra
06 p0960 A71-18167

Aircraft altitude cosmic ray intensity measurements in lower atmosphere by neutron monitor, considering long term nucleonic intensity variations
08 p1355 A71-21629

Cosmic radiation nucleonic component intensity diurnal variations relation to solar activity semiperiod
12 p1950 A71-27378

Cosmic ray jet interaction with free or quasi-free nucleons, obtaining kinematic measurement, secondary particle composition and transverse momentum
13 p2121 A71-28058

Inelastic scattering transition densities in single particle operator reduced matrix elements between initial and final nuclear states for nucleon angular momentum calculations
14 p2276 A71-30013

Cosmic ray nucleon-meson and barometric pressure data continuous recording equipment, comparing system to conventional instruments
14 p2248 A71-30602

Cosmic ray high energy pion and nucleon nuclear interaction observations, determining statistical fluctuations in secondary particles angular distribution
15 p2479 A71-32076

Primary cosmic ray nucleonic component observation by scintillator-Cerenkov telescope on OGO 3 satellite
16 p2628 A71-33932

Collimated nuclear interactions induced by cosmic ray pions and nucleons in carbon and brass, noting energy dependence of events production frequency
17 p2796 A71-34858

Pion-nucleon interactions, determining energetically precipitated particle effects in air showers
22 p3579 A71-42642

High energy nucleon passage through lower atmosphere during chemical composition changes of primary cosmic rays, using Proton satellite observations
22 p3595 A71-42652

Pion interactions with nucleons and nuclei in emulsions irradiated by high energy pion beams
22 p3579 A71-42653

Momenta measurements of particles produced by high energy quasi-nucleon interactions of pions on photoemulsion layers, using primary particle tracks scanning
22 p3579 A71-42655

NUCLEOSIDES

NT ADENINES

NT ADENOSINE DIPHOSPHATE [ADP]

NT ADENOSINE TRIPHOSPHATE [ATP]

NT ADENOSINES

Urea-inorganic phosphate mixtures as prebiotic nucleoside phosphorylating agents
07 p1055 A71-19544

Abiogenic synthesis of nucleosides, heating adenine and ribose mixture at 170 C in atmosphere of oxygen, nitrogen and carbon dioxide
21 p3346 A71-40576

Allosteric adenosine monophosphate nucleosidase stabilization by inorganic salts, substrate and essential activator, investigating enzyme inactivation mechanism in low ionic strength environments
23 p3642 A71-44268

NUCLEOSYNTHESIS

U NUCLEAR FUSION

NUCLEOTIDES

NT ADENINES

NT ADENOSINE DIPHOSPHATE [ADP]

NT ADENOSINE TRIPHOSPHATE [ATP]

NT ADENOSINES

NT PYRIDINE NUCLEOTIDES

NT URIDYLIC ACID

Biosynthesis of inosinic acid in transfer RNA in Escherichia coli by polynucleotide modification
03 p0375 A71-13173

NUCLIDES

NT ALUMINUM ISOTOPES

NT ALUMINUM 26

NT ALUMINUM 27

NT ARGON ISOTOPES

NT BERYLLIUM 7

NT BERYLLIUM 9

NT BERYLLIUM 10

NT BORON ISOTOPES

NT CADMIUM ISOTOPES

NT CALIFORNIUM ISOTOPES

NT CARBON ISOTOPES

NT CARBON 12

NT CARBON 13

NT CARBON 14

NT CERIUM ISOTOPES

NT CERIUM 144

NT CESIUM ISOTOPES

NT CESIUM VAPOR

NT CESIUM 133

NT COBALT ISOTOPES

NT COBALT 60

NT DEUTERIUM

NT HELIUM ISOTOPES

NT HYDROGEN ISOTOPES

NT IRON 57

NT ISOTOPES

NT KRYPTON ISOTOPES

NT LEAD ISOTOPES

NT LITHIUM ISOTOPES

NT LUTETIUM

NT MANGANESE ISOTOPES

NT NEODYMIUM ISOTOPES

NT NEON ISOTOPES

NT OXYGEN ISOTOPES

NT OXYGEN 18

NT PLUTONIUM

NT PLUTONIUM 238

NT POLONIUM 210

NT POTASSIUM ISOTOPES

NT RADIOACTIVE ISOTOPES

NT RADON ISOTOPES

NT RUBIDIUM ISOTOPES

NT SCANDIUM ISOTOPES

NT STRONTIUM ISOTOPES

NT TELLURIUM

NT THORIUM ISOTOPES

NT TITANIUM ISOTOPES

NT TRANSURANIUM ELEMENTS

NT TRITIUM

NT URANIUM ISOTOPES

NT URANIUM 235

NT XENON ISOTOPES

NT XENON 133

Fe meteorite Grant, measuring radial distribution of cosmogenic nuclides of K, Ca, Ti, V, Cr and Mn produced by cosmic rays
11 p1819 A71-25224

Relative abundances and mass measurements of Li, Be and B isotopes in primary cosmic rays, using balloon flown emulsion stacks
22 p3593 A71-42329

NULL REFERENCE GLIDE PATH

U GLIDE PATHS

NULL ZONES

Nulls of radiation and input impedance of flush mounted rocket antennas for telemetry and transponder systems
02 p0228 A71-11674

Geomagnetic tail structure near null sheet, indicating decrease and/or dissipation of plasma sheet particle energy density at lunar distances
06 p0893 A71-17994

Radiation nulls suppression and broadband impedance matching of infinite rectangular waveguide phased arrays, giving numerical solutions
09 p1419 A71-23494

Quantum electrodynamics on null planes in Minkowski space, discussing applications to lasers, wave packet construction, Heisenberg and Furry pictures and Compton scattering
13 p2080 A71-28998

NUMBER THEORY

NT ADDITION THEOREM

NT EXPONENTS

NT INTEGERS

NT MULTIPLICATION

NT SUBTRACTION

German monograph on Fourier coefficients of modulus forms, presenting theorem reducing infinite number of equations to limited number of equations
01 p0110 A71-10126

Multiple integrals numerical evaluation techniques survey, discussing Monte Carlo, number-theoretical and functional analysis methods
02 p0276 A71-11801

Chinese remainder theorem for noncommutative rings with divisors of zero and without two-sided unity element in number theory
18 p2976 A71-36096

NUMBERS

Dimensions in physical science, discussing fundamentals and constants in dimensional analysis, operational measurements and numerical quantities
22 p3577 A71-42677

NUMERICAL ANALYSIS

NT APPROXIMATION

NT BORN APPROXIMATION

NT BORN-OPPENHEIMER APPROXIMATION

NT CHEBYSHEV APPROXIMATION

NT DIFFERENCE EQUATIONS

NT EDDINGTON APPROXIMATION

NT ERROR ANALYSIS

NT FINITE DIFFERENCE THEORY

NT HARTREE APPROXIMATION

NT INTERPOLATION

NT ITERATION

NT ITERATIVE SOLUTION

NT LEAST SQUARES METHOD

NT MONTE CARLO METHOD

NT NEWTON-RAPHSON METHOD

NT NOMOGRAPHS

NT NUMERICAL INTEGRATION

NT OSEEN APPROXIMATION

NT PADE APPROXIMATION

NT PARTICLE IN CELL TECHNIQUE

NT RAYLEIGH-RITZ METHOD

NT RELAXATION METHOD [MATHEMATICS]

NT RITZ AVERAGING METHOD

NT RUNGE-KUTTA METHOD

NT SCHWARTZ METHOD

NT TRUNCATION ERRORS

Partial differential equations hybrid computer solution by extended space technique for overcoming slow convergence of Galerkin method
01 p0048 A71-10223

Numerical analysis of complex boundary layer at axisymmetric stagnation point with massive blowing
01 p0071 A71-10964

Numerical stress-strain calculation for design of high pressure fiberglass-reinforced plastic balloons
01 p0176 A71-11048

Plane steady boundary layer stability, describing numerical solution procedures for boundary value problem 01 p0072 A71-11292

Global atmospheric circulation numerical simulation, discussing modeling factors and applications 01 p0121 A71-11353

Numerical analysis of Hill limiting case of restricted three body problem regarding quasi-periodic, ergodic and escape orbits for natural and artificial satellites 01 p0161 A71-11380

Numerical method for stress distribution around openings in shells, using orthogonal coordinate system 02 p0321 A71-11649

French book on numerical filtering, data smoothing, parameter prediction and process identification, considering expansion, transform, least squares and Kalman methods 02 p0236 A71-11726

Planets and satellites masses and other dynamic parameters by numerical and analytical calculation techniques based motion and trajectory analyses 02 p0309 A71-12152

Nonlinear instabilities in shock wave numerical calculations, using Shuman short wave filtering operator 02 p0240 A71-12396

Mixed type nonlinear integral equations, using approximate method for numerical solutions 02 p0276 A71-12541

Numerical analysis of flow field around thin airfoil in two dimensional nonuniform stream, using finite difference method 02 p0187 A71-12680

Wing computation in steady or unsteady supersonic flow, using network, inverse discrete and numerical inversion methods [ONERA-TP-896] 03 p0339 A71-13129

Sonic boom wave pressure history prediction on arbitrarily oriented plane walls by explicit fixed mesh time dependent numerical method 03 p0349 A71-14153

Nonplanar moon-earth trajectories, determining restricted three body problem analytical solution accuracy [AIAA PAPER 70-1060] 03 p0495 A71-14274

Numerical solution of Laplace difference equations for circular and irregular annulus 04 p0619 A71-14811

Direct pointwise stress determination in twisted cracked elastic bars under torsion and longitudinal shear by numerical methods 04 p0667 A71-15180

Finite supercavitating wings numerical calculation using acceleration potential method 04 p0526 A71-15210

Heat transfer differential equations numerical solution, using latin square experimental design plans for reducing repetitions 04 p0678 A71-15461

Numerical variational analysis with weak constraint for surface analysis of severe storm gust 05 p0776 A71-16155

Variable thickness anisotropic annular plates bending on generalized elastic foundation, using numerical method 05 p0823 A71-16423

Numerical analysis of one dimensional transient temperature fields and elastic thermal stress fields, deriving equations for plate and cylinders with free edges 05 p0823 A71-16494

Cylindrical blast waves analytical solutions by combined parameter, coordinate and matched asymptotic expansions 05 p0833 A71-16504

Complex configuration solid bodies boundary value problems numerical solution algorithm using R functions 05 p0775 A71-17013

Mathematical physics multidimensional boundary value problems seminumerical solution, using differential-difference method and integral transformations 05 p0783 A71-17014

Fibrous composite materials stress and deformation analysis, using point matching numerical method and boundary point least squares method 05 p0829 A71-17119

Nonlinear problems numerical solutions - Conference, Philadelphia, October 1968 06 p0917 A71-17563

Nonlinear boundary value problems numerical solutions using spline and Hermitian functions in Ritz-Galerkin setting 06 p0917 A71-17565

Initial value problems involving linear ordinary differential equations, deriving theorems for Runge-Kutta and Adams methods effectiveness 06 p0917 A71-17566

Eccentrically reinforced cylindrical shell stability, considering numerical analysis of structurally orthotropic shell parameters 06 p0993 A71-17817

Shells of revolution of different forms, discussing numerical solution of inverse problem 06 p0995 A71-17832

Orthotropic shell with hollow elliptical paraboloid form, discussing numerical solution for normal concentrated load action 06 p0998 A71-17855

Free Lagrangian gyroscope, discussing numerical relations between precessions and nutations 06 p0899 A71-17931

Iterative methods, numerical mathematics, approximation theory - Conference, Oberwolfach, West Germany, November 1968, June and November 1969 06 p0919 A71-18201

Nonlinear equations solution, considering Newton method and Henrici algorithm disadvantages and quadratic convergent procedure 06 p0919 A71-18203

Direction finding problems involving several waves of same frequency, discussing nonlinear computation methods with hybrid computers 06 p0927 A71-18205

Dirichlet problem associated with elliptic partial differential equation, discussing integral operator methods for approximating numerical solution 06 p0920 A71-18208

Similarity methods, partial differential numerical analysis, dispersive wave and perturbation theory applications to mechanics 06 p0920 A71-18220

Inviscid mixed subsonic-supersonic gas flows with shocks, developing time dependent numerical method [AIAA PAPER 71-45] 06 p0883 A71-18506

Two dimensional turbulent boundary layer flows numerical methods with simplicity and accuracy [AIAA PAPER 71-164] 06 p0885 A71-18606

Linear systems optimal control problems numerical solution methods comparison, noting accuracy advantage of invariant imbedding technique 07 p1081 A71-18834

Chemical reaction kinetics optimal problem numerical solution based on Pontryagin maximum principle and gradient method 07 p1147 A71-19185

Low Reynolds number incompressible transient creep flow calculation by Marker-Cell numerical solution extension 07 p1094 A71-20613

Boundary layer flow with large mass injection rate, presenting numerical method with rapid convergence for increasing blowing parameter 09 p1430 A71-22108

Numerical analysis of winding and heat treatment effects on residual stress distribution in cylindrical glass fiber reinforced plastic products 09 p1482 A71-22816

Statistically indeterminate modified structures automated design reanalysis by displacement method, using matrix formulations, numerical computation and computer operations 09 p1542 A71-23282

Observation range determination numerically for cyclotron resonances of effective scattering cross section of light wave by collisionless plasma in magnetic field 10 p1646 A71-23848

Plane shock wave formation in dense Ar, using molecular dynamics numerical technique 10 p1694 A71-23953

Baroclinic instability problem analytical solutions for models with linear wind profiles, presenting growth rate variations and unstable waves phase velocity 10 p1638 A71-23962

Numerical solution of axisymmetric minimum drag bodies in hypersonic viscous gas flow, obtaining coefficient of friction by local variations method 10 p1551 A71-24370

Book on digital computers in engineering covering systems, man machine communication, numerical analysis, network analysis program, circuits, devices, control, etc 10 p1581 A71-24476

Numerical simulation of developing and decaying two dimensional isotropic turbulence consistent with Batchelor predictions 10 p1595 A71-24619

Numerical solution for planar ion sheath growth in low pressure plasma, calculating transient sheath thickness resulting from application of specific voltage waveforms 10 p1652 A71-24659

Numerical search for optimum product space as extension of Gauss-Seidel relaxation method, noting applications to partial differential equations 10 p1637 A71-24841

Atmospheric boundary layer numerical modeling, discussing subgrid scale mixing processes and parameterization 10 p1639 A71-25067

Numerical solution procedures evaluation for geometrically nonlinear structural analysis by direct stiffness method, noting capability of self correcting initial value formulation 11 p1844 A71-25335

Numerical methods solutions of implicit differential equations systems, discussing first order implicit to second order explicit systems transformation 11 p1791 A71-25640

Thermionic converter nonsaturation effect in diode I-V characteristics from computerized analysis for plasma transport phenomena and sheath-electrode-plasma interactions 11 p1713 A71-25892

Two dimensional flow in radial turbomachine bladed impeller, comparing numerical solution based on potential theory with experimental results [ASME PAPER 71-GT-20] 11 p1703 A71-25964

Numerical method for computing exact permeability/tunneling probability/ of one dimensional potential barrier 11 p1728 A71-26059

Optimal control problems, applying direct mathematical programming to linear, nonlinear, continuous and discrete time, deterministic, stochastic and distributed parameter systems 11 p1792 A71-26419

Boundary layer separation at free streamline attached to body sharp trailing edge, comparing asymptotic solution with numerical analysis of flow on flat plate 12 p1896 A71-27218

Inviscid compressible fluid jet flow, calculating instability boundaries characteristics by linear perturbation analysis and numerical solution 12 p1897 A71-27219

Electrical screening layers around charged clouds, giving numerical model for space charge accumulation, electric field distribution and forces acting on cloud droplets 12 p1925 A71-27290

Numerical solution of equations describing stress-strain state of shallow nonuniformly heated shell 12 p1979 A71-27355

Numerical solution of implicit first order ordinary differential equations with initial conditions 12 p1923 A71-27731

Numerical solution of Stefan type partial differential equations with phase variations, using nonlinear homogeneous implicit difference scheme 13 p2100 A71-27898

Linear nonadiabatic pulsations of stellar models, discussing numerical method for eigenvalue problem 13 p2132 A71-27968

Numerical solution of current distribution, wave propagation constant and propagation mode cut-off frequencies on periodic linear array 13 p2028 A71-28001

Numerical method for Mathieu equation solution applicable to ordinary and asymptotic problems 13 p2094 A71-28229

Eigenvalue, shooting and parallel shooting methods for solving Falkner-Skan boundary layer equation with positive or negative wall shear 13 p2047 A71-28230

Static problems of shells of revolution under local loads, solving by stable numerical process 13 p2152 A71-28276

Numerical solution of nonclassical problem of calculus of variations, reducing nonlinear integral equation with Green function 13 p2095 A71-28819

Numerical method for two dimensional or axisymmetric heated flows allowing for dissipation extended to viscous flow, using Navier-Stokes equations in streamwise coordinates 13 p2118 A71-29280

Numerical solution of coupled boundary layer equations describing strongly cooled turbulent flow of gas between parallel plates with property variation [ASME PAPER 71-FB-38] 13 p2166 A71-29473

Fluctuations in numerical computations of discontinuous solutions of differential equations 13 p2265 A71-29556

Numerical incremental solution of large deformation elasticity problems at finite rotations and strains 14 p2324 A71-29862

Steady state wind driven currents velocity in Lake Erie, using shallow lake level model in numerical calculation 14 p2231 A71-29935

Numerical study of three dimensional structure and energetics of unstable disturbances in pure baroclinic and barotropic zonal currents, using eigenvalue technique 14 p2269 A71-29949

Steady state flow of viscous incompressible fluid, proposing difference scheme for numerical solution of Navier-Stokes equations 14 p2226 A71-30437

Iris-type discontinuity problems in waveguides and periodic structures, investigating numerical solutions convergence 14 p2212 A71-30513

Numerical heat transfer and wall friction results, demonstrating gas transport property variation effects on three laminar flow situations 14 p2338 A71-30931

Numerical prediction of radiation patterns for antennas mounted on spacecraft, noting booms and solar cell panels effects 14 p2218 A71-31068

Numerical analysis of partial differential equations - Conference, London, June 1970 15 p2440 A71-31345

Asymptotic error expansions of differential equations approximate solutions by finite difference schemes for use as technical devices in theoretical numerical analysis

15 p2440 A71-31347

Monograph on elliptic differential equations numerical solution covering approximations, relaxation, iterative, integral equation and variational methods, and applications to boundary value problems

15 p2441 A71-31308

Numerical analysis of far field gain pattern of shielded acoustic antenna by Kirchhoff integral, assuming circular symmetry and perfectly absorbing walls

15 p2372 A71-32193

Soviet book on plane elasticity theory boundary value problems solution on digital and analog computers

15 p2508 A71-32276

Numerical analysis of accretion growing grains segregation in gravitational field with resisting gas, discussing motion equation, evaporation rate and planetary evolution

15 p2489 A71-32397

Structural strength numerical evaluation, demonstrating effectiveness of regression equations in statistical data processing

16 p2651 A71-33063

Numerical stress analysis of elastic three-dimensional fracture specimen with edge crack, using singular integral equations analogous to Green boundary formula in potential theory

16 p2655 A71-33181

Numerical evaluation for individual samples of random processes obtained from nonstationary engineering experiments

16 p2602 A71-33341

Numerical identification of linear automatic control system, starting from pulse response

16 p2549 A71-33378

Numerical algorithm for Cauchy problem nonlinear partial differential integral equations solution by invariant imbedding

16 p2604 A71-34082

Numerical method for limit analysis of axisymmetric shells of revolution, considering truncated conical shells and pressure vessels with rigid circular plates

17 p2818 A71-34400

Book on linear and ordinary celestial mechanics covering perturbed two body motion, numerical methods, canonical theory and initial value problems

17 p2799 A71-34471

Viscous incompressible flow along right angle corner, using algebraic nature of asymptotic flow field for numerical analysis boundary conditions

17 p2726 A71-34504

Numerical solution for two dimensional steady state fluid flow in square cavity by optimum time step formulation

17 p2728 A71-34880

Self similar numerical and asymptotic solutions of laminar multicomponent isothermal boundary layer equations for large blowing rates

17 p2673 A71-35633

Methods construction for initial value problem solution, using fifth and sixth order algorithms with Adams-Moulton correctors

17 p2768 A71-35686

Roundoff error reduction in numerical solution of second-order differential equation by splitting into two difference equations

17 p2769 A71-35691

Numerically stable algorithm for solving least squares problems with linear equalities and inequalities as additional constraints

17 p2769 A71-35693

Spinning centrally clamped thin shallow spherical shell free vibration numerical analysis by considering perturbation about equilibrium configuration

18 p2977 A71-36254

[ASME PAPER 71-APM-G] Fluid dynamics numerical methods - Conference, University of California at Berkeley, September 1970

18 p2904 A71-36301

Free-Lagrange method for two dimensional flow numerical simulation, covering mesh optimization and equations of motion

18 p2905 A71-36304

Transonic flow numerical analysis, discussing initial conditions and imbedded shocks choice for computation efficiency

18 p2905 A71-36307

Numerical analysis of plasma expansion confined by magnetic field, emphasizing boundary oscillation and temperature rise, based on hyperbolic and parabolic system equations

18 p2952 A71-36308

Numerical analysis of laminar recirculating flow between shrouded rotating disks for interaction between vorticity and stream function and swirl-velocity field

18 p2905 A71-36309

Numerical fluid dynamics problems in Hele-Shaw cell secondary flow, blast wave and plane jet electrostatic pinching, presenting algorithms and error estimates

18 p2905 A71-36310

Numerical solution of time dependent incompressible flow differential transport equations including turbulence effects

18 p2905 A71-36312

Small disturbance transonic flows potential equations numerical solutions, using mixed finite difference theory

18 p2844 A71-36325

Compressible three dimensional nonsimilar laminar boundary layers numerical analysis using two layer heuristic model

18 p2845 A71-36336

Numerical solution algorithm for parabolic free boundary problem in statistical decision theory, comparing convergence with asymptotic expansions

18 p2941 A71-36352

Frictionless hypersonic flow around body by time dependent numerical processes and method of characteristics

18 p2846 A71-36423

Numerical stability of extended Kantorovich method for single term variational approximation of torsional problem

18 p2980 A71-36702

Stability theorem for predictor-corrector methods for differential equations systems solution using computer

19 p3085 A71-37421

Numerical methods for unsteady compressible flows, considering method of characteristics, Lax-Wendroff and particle-in-cell method

19 p2992 A71-37456

Collisionless plasma Vlasov and Poisson equations numerical solution based on Fourier-Fourier transform, comparing with particle motion simulation

19 p3113 A71-37748

Latin square factorial design plans for reducing number of repetitions solutions of theoretical problems, noting application to differential equations numerical solution

19 p3087 A71-38290

Numerical solution of partial differential equations - Conference, University of Maryland, College Park, May 1970

19 p3087 A71-38301

Numerical analysis of plane transonic flows past shock free airfoils without boundary layer separation using inverse method of complex characteristics

19 p2994 A71-38307

Location and scale parameters estimation from ordered statistical samples with numerical applications to Gumbel and Weibull distributions

19 p3088 A71-38471

Compiler program generation for ordinary differential equations system automatic numerical solution by Taylor series method

20 p3254 A71-38754

Numerical procedure for electromagnetic field penetration through inhomogeneous cold plasma slab with collisions, using Riccati type differential equation

20 p3273 A71-39004

Creep strength extrapolation for high temperature steels, suggesting combined numerical and graphic methods

20 p3249 A71-39017

Numerical calculation of electron guns with converging spherical beams near cathode and electron-optic systems decelerating at collector

20 p3204 A71-39157

Numerical calculation of trailing vortex sheet pattern behind unstalled swept wing at low speed, obtaining downwash field

20 p3176 A71-39397

Numerical analysis of natural frequency spectrum of elastic plate free vibrations in compressible inviscid fluid

20 p3310 A71-39784

Galerkin/spectral/ method accuracy for numerical simulation of incompressible boundary flows, testing scalar-convection and Taylor-Green vortex decay problems

21 p3367 A71-40638

Elastic-plastic stress wave attenuation, applying theory of wave propagation in single crystals to flow field numerical solution

21 p3465 A71-40786

Numerical analysis for transient elastoplastic thermal stresses on turbine disks at variable rotation speeds

21 p3466 A71-40836

Projective numerical solution of integral equations arising in boundary value problems of electric and magnetic field theory

21 p3416 A71-40846

Computerized numerical optimization for Yagi-Uda antenna array gain, noting nonoptimum in standard traveling-wave design methods

21 p3349 A71-41410

Weakly ionized magnetoplasma with no axial drift, investigating collisional drift-type instability by linearized two fluid hydrodynamic numerical analysis

22 p3580 A71-41586

Numerical analysis for flexural stress pulse propagation in nonuniform elastic bars by geometric acoustics

22 p3616 A71-42213

Functional methods in numerical solution of heat transfer problems, including finite element and local variation methods

22 p3621 A71-42290

One dimensional two phase parabolic free interface/Stefan/ problem numerical solution, using method of lines to approximate partial differential equations at discrete time levels

22 p3575 A71-42294

First kind Fredholm integral equation approximation by numerical quadrature formulas plus collocation, using singular value decomposition for solution

22 p3567 A71-42296

Thin circular frame antenna input admittance computation formulas numerical results comparison, noting insignificant discrepancies

22 p3523 A71-42319

Obstruction effects in rarefied gas flow through cylindrical ducts by numerical analysis, considering specular reflection, adsorption, absorption and finite molecular mean free path

22 p3531 A71-42343

Diffraction phenomena numerical modeling by Monte Carlo statistical analysis, using Heisenberg uncertainty principle

22 p3576 A71-42556

Numerical analysis of large signal output characteristics for directly modulated GaAs junction injection lasers, investigating resonance phenomenon

23 p3683 A71-43351

Statistical modeling technique for approximate numerical solution of unsteady heat conductivity inverse problem, obtaining foam chamotte and magnesite temperature field data

23 p3782 A71-44059

Indirect numerical method for solving optimal control problems with singular arcs

23 p3658 A71-44086

Numerical solution for plane wave scattering by dielectric sheet with imbedded periodic array of conducting strips

23 p3654 A71-44164

Conical monopole antenna imaging above hemispherical ground of variable radius, plotting finite screen effectiveness from analytical and numerical solutions

23 p3655 A71-44168

Hypersonic axisymmetric slender body near wake shear layer determination by shock expansion method for numerical computation accuracy and efficiency

23 p3626 A71-44194

Numerical analysis of electromagnetic wave diffraction on inhomogeneous transmitting bodies, reducing Maxwell equations boundary value problem to differential equations solution

24 p3804 A71-44772

Numerical evaluation of structures buckling loads, considering matrix equation application to elastic stability problems

24 p3883 A71-44870

Digital computer numerical procedure to solve dynamo theory MHD equations for earth nucleus, using combination of Fourier and finite difference methods for integration

24 p3823 A71-45038

NUMERICAL CONTROL

CAMAC computer guided data acquisition system design and operation

01 p0049 A71-10260

Digital control system for azimuthal optical telescope, using invariance techniques and photoelectric system to compensate for position and program errors

01 p0081 A71-10727

Turbine and compressor blade profiles grinding, formulating mathematical rules for shaping links adaptable to programmed control

02 p0258 A71-12569

Numerical control automation in aircraft bearing production for small batch runs

04 p0603 A71-15672

Concorde airframe structures, discussing numerically controlled machining of aluminum alloy integral units

06 p0904 A71-17954

Tridea ALTAPE /automatic line tracing and programming/ system for drawing data conversion to tape for machining surfaces in direct numerical control applications

19 p3068 A71-37244

Automated electrical wire harness manufacturing for Boeing 747 aircraft, discussing development of numerical control program

21 p3386 A71-40441

Molins 24 integrated automatic complete-processing system for small light-metal parts, using numerically controlled machine tools integrated with palletized feeder system

23 p3681 A71-43473

NUMERICAL INTEGRATION

NT RUNGE-KUTTA METHOD

Atmospheric boundary layer nonlinear equations of motion numerical integration for eddies structure and wind direction and latitude effects on turbulence intensities

01 p0113 A71-10351

- Keplerian orbit numerical integration, considering Runge-Kutta method and transformations
01 p0154 A71-10377
- Numerical integration finite difference methods stabilization for perturbed Keplerian motion differential equations
01 p0154 A71-10378
- Minor planets 1969 ephemeris, considering numerical integration of celestial mechanics equations
01 p0155 A71-10438
- Cylindrical shock waves generation from instantaneous energy release along line in quiescent atmosphere studied by numerical integration of flow equations
01 p0072 A71-11471
- Multiple integrals numerical evaluation techniques survey, discussing Monte Carlo, number-theoretical and functional analysis methods
02 p0276 A71-11801
- Reference trajectory and additional phase variable methods for motion equations integration applied to vehicle in atmosphere
02 p0304 A71-11904
- Atmospheric models integration, discussing elliptic partial differential equation solution
03 p0453 A71-13326
- Navier-Stokes equations numerical integration in Eulerian coordinates, applying results to compressible and incompressible fluids steady flow
[AIAA PAPER 70-2] 03 p0399 A71-13426
- Thin shells of revolution formed of closed box sections, using numerical integration and stiffness matrix for solution
[ASME PAPER 70-PVP-12] 04 p0665 A71-14770
- Nystrom formula error estimation for numerical integration of first order differential equation, tabulating results
04 p0619 A71-15448
- Thin convex shell of evolution bounded by two parallels minimum vibration frequency using asymptotic method of integration
04 p0671 A71-15556
- Equations of motion of restricted four body problem numerically integrated for positions of three primaries
04 p0653 A71-15711
- Pseudo-problem method for errors accumulated in numerical integration computation of orbits
04 p0654 A71-15718
- Nonlinear creep problems numerical time integration solution, applying to rectangular plate
04 p0672 A71-15755
- Numerical integration of Poisson kinematic equations for direction cosines, using Runge principle for accuracy values proportional to third power of integration step
05 p0780 A71-16051
- Optimal orbital transfer problem by numerical integration of Contensou singular alternating arcs, solving second order differential system followed by quadrature
05 p0812 A71-16730
- Nonlinear singular integrodifferential equation numerical integration extension
06 p0917 A71-17553
- Numerical integration of equations of three dimensional laminar boundary layer on spreading lines
07 p1087 A71-19182
- Book on numerical solution of ordinary differential equations covering integration algorithms, Runge-Kutta, single-step, multistep, predictor-corrector and extrapolation methods
08 p1324 A71-21233
- Celestial mechanics n body equations simultaneous integration, using Taylor-Steffensen numerical method
09 p1525 A71-23335
- Supernovae light curves theory based on numerical integration of gas dynamics and radiative heat conductivity equations
09 p1528 A71-23591
- Numerical integration of perturbed linear systems of differential equations by step method comparing power series
10 p1636 A71-23960
- Numerical integration of motion equations for two layer atmospheric fronts model with baroclinicity along frontal surface separating two incompressible fluids in stable stratification
10 p1638 A71-23965
- Star orbit computation in galactic potential fields, using Hamming modified predictor corrector scheme for numerical integration
10 p1678 A71-24927
- Numerical integration of unsteady continuity equation for electron-ion gas concentration distribution in F2 region
11 p1757 A71-25770
- Automatic numerical evaluation of definite integrals of analytic functions, considering Simpson rule, Gauss quadrature, subdivision and whole interval formulas
12 p1923 A71-27732
- Reduced order numerical integration technique for plate and shell problems solution
13 p2147 A71-27791
- Reference trajectory and additional phase variable methods for motion equations integration applied to vehicle in atmosphere
13 p2133 A71-28191
- Numerical integration procedure for calculating mixed phase transformation in continuum mechanics for given volume and internal energy increments
13 p2100 A71-28232
- Algorithm for automatic closed form integration of formulas in elliptic motion arising in perturbation theories
13 p2136 A71-28358
- Neutral particle gas integral kinetic equations numerical solution without integration on lag parameter
13 p1991 A71-29157
- Elastic plastic shells of revolution deflection analysis by numerical integration with computer program
14 p2324 A71-29870
- Ekman boundary layer energy stability, determining effective Reynolds number critical value by Euler-Lagrange equations numerical integration
14 p2226 A71-30410
- Coulomb collisions in high density plasma beams from numerical integration of Fokker-Planck equation for three initial distribution functions, studying relaxation time
14 p2283 A71-30674
- Hydrometeorological fields derivatives transformation in hydrothermodynamic equations numerical integration
15 p2443 A71-31224
- Nonlinear hyperbolic equations integration, considering characteristic, mesh finite difference and particle in cell techniques
15 p2441 A71-31355
- Solar wind outflow from active regions by numerical integration of hydrodynamics equations, using corona temperature distribution
15 p2480 A71-32753
- Dynamic uncoupled thermoelasticity analysis using integration by Goodier method in five dimensional space
16 p2662 A71-33171
- Numerical integration of Poisson kinematic equations for direction cosines, using Runge principle for accuracy values proportional to third power of integration step
16 p2605 A71-33455
- Numerical integration of quasi-static system of hydrodynamic equations, considering economical production of short range high resolution meteorological forecasts
16 p2604 A71-33532
- Magnetohydrodynamic model system numerical integration as initial value problem, using finite difference scheme or differential equation conversion method
16 p2620 A71-34081
- Rigorous solution for multiple arm conical log spiral antenna by numerical solution of integral equations, considering current distribution, half power beam-width, etc
17 p2715 A71-34752
- Definite interval values calculations of integral of smooth functions, using quadrature formulas with high algebraic degree of accuracy
17 p2765 A71-34845
- Three dimensional laminar compressible boundary layer flow solution by numerical integration
17 p2728 A71-34894
- Averaging methods of nonlinear differential and integrodifferential equations with fast and slow variables over finite and infinite segments
17 p2766 A71-34923
- Direct numerical integration for equation of radiative transfer in turbid atmosphere with allowance for scattering on molecules and aerosols
17 p2736 A71-35564
- Approximate self contained numerical integration formulas for compact symmetrical regions in n dimensional Euclidean space
17 p2768 A71-35684
- Numerical integration of turbulent boundary layer equations, using mixing length concept
18 p2902 A71-36112
- Nonlinear time varying systems digital integration simulation techniques by variational equations approach, discussing accuracy, execution time and limitations
18 p2884 A71-36141
- Unstable two point boundary value problems solution by decomposition into lower order differential equations sequence for computer integration, giving illustrative examples
18 p2940 A71-36143
- Numerical integration of Euler equations for three dimensional time dependent unsteady flow by extension of method of characteristics
18 p2904 A71-36302
- Boundary conditions discretization on fluid flow moving discontinuities for analytical or numerical integration
18 p2906 A71-36315
- Generalized relaxation methods application to transonic flow problems, combining with numerical integration theory for ordinary differential equations
18 p2906 A71-36324
- Rotationally symmetric quasi-cylindrical viscous incompressible vortex flows at high swirl, discussing numerical integration with exponential functions
18 p2908 A71-36342
- Weakly singular integrals numerical compound quadrature error bound and convergence rate estimate by applying Peano theorem with modification for avoiding singularity
18 p2941 A71-36355
- Convergence theorem for singular integrands numerical quadratures, assuming domination near singularity by monotone integrable function
18 p2941 A71-36356
- Baffled piston source sound radiation impedance from numerical solution of Fredholm integral equation for vibrating disk in finite rigid concentric baffle
19 p3104 A71-37849
- Numerical integration of Schroedinger equation for spontaneous ionization of hydrogen atom in electric field
19 p3107 A71-38056
- Stellar systems existence with positive total energy, using numerical integration of equations of motion for components of Trapezium in Orion
20 p3290 A71-39300
- Numerical integration of element T (transit time through perihelion/ in perturbations of near parabolic comet orbits
20 p3291 A71-39321
- Frequency response optimization of one dimensional damped linear continuous systems, requiring initial value numerical integration of state and adjoint differential equations
[ASME PAPER 71-VIBR-1] 21 p3456 A71-40265
- Limiting polarization of radio waves emerging obliquely from ionosphere into free space, describing numerical integration method and boundary conditions
21 p3348 A71-40525
- Numerical power series integration of differential equations of special three body problem with truncation errors elimination to fifth order
21 p3450 A71-40654
- Nonlinear Vlasov equation numerical integration methods, discussing Hermite expansion, characteristic function transform and truncation techniques
21 p3408 A71-40844
- Parametric differentiation solution accuracy and stability for temperature profile and heat flux behind one dimensional hypersonic shock, including thermal radiation
21 p3409 A71-41016
- Numerical integration of unsteady continuity equation for electron-ion gas concentration distribution in F2 region
22 p3532 A71-41538
- Spalding-Patankar numerical integration for heat transfer from air cooled disk rotating near stator, considering frictional heating, disk temperature distribution and nonunity Prandtl numbers
22 p3620 A71-41878
- Three body problem involving large mass ratio by backward numerical integration in constant density resisting medium
22 p3601 A71-42164
- Differential equations system numerical integration solution global discretization error local estimation by Runge-Kutta and multistep methods
22 p3567 A71-42293
- Piecewise polynomial Taylor methods to numerically solve first order ordinary differential equations
23 p3698 A71-42901
- Lunar orbit space station lifetime, using averaged variational equations numerical integration for terrestrial, solar and lunar gravitational field effects
[AAS PAPER 71-377] 23 p3730 A71-43047
- Orbital equations of motion and associated variational equations numerical integration, calculating geopotential in terms of spherical harmonics
[AAS PAPER 71-390] 23 p3666 A71-43058
- Governing equations numerical integration for Venusian atmosphere circulation, calculating solar heating distribution in spherical polar coordinates
23 p3735 A71-43340
- Motion equations numerical integration step as function of celestial object location and velocity in interplanetary probe orbit computation
24 p3869 A71-44799
- Heat transfer with dissipation from longitudinal surface curvature, numerically integrating all equations for parameters
24 p3889 A71-44968

NUMERICAL WEATHER FORECASTING

- Atmospheric general circulation model for numerical climate digital simulation and weather forecasting, using fluid flow equations
02 p0277 A71-11808
- Numerical weather forecasting model using time dependent boundary values for restricting to acceptable error limits
04 p0622 A71-15676

Numerical variational analysis theory for weather forecasting 05 p0773 A71-16154

Vertical temperature distribution measurements by meteorological satellites distribution measurements applied to numerical weather forecasting 05 p0778 A71-17044

Lagrangian numerical forecasting barotropic global model using primitive equations with coating set of computation points 06 p0924 A71-18410

Northern Hemisphere midlatitude numerical weather prediction, investigating effects of tropic and southern regions by wall insertion model 07 p1152 A71-19754

Convective and nonconvective heat release in mesoscale parameterization improving numerical weather prediction 08 p1326 A71-21447

Diagnostic numerical model of frontal vertical circulation in atmospheric boundary layer using local parameters 08 p1326 A71-21448

Numerical weather prediction models, discussing automatic data processing meteorological parameter requirements 08 p1328 A71-21723

Weather satellite data for numerical analysis and forecasts, reconstructing geopotential field 09 p1486 A71-22300

Long range numerical weather prediction, using two level quasi-geostrophic forced general circulation model with spectral truncation 14 p2269 A71-29945

Long term atmospheric circulation prediction model, considering horizontal grid resolution effect on truncation error 14 p2269 A71-29946

Equatorial upper troposphere and lower stratosphere hurricane and wavelike motions numerical predictions, analyzing heating, friction, cloud physics and ozone dynamics 14 p2270 A71-30500

Finite difference methods application to numerical weather prediction problems, describing frontal depression growth and boundary conditions for short gravity wave suppression 15 p2443 A71-31357

Three level baroclinic model of short range large scale weather prediction at low latitudes, determining background/steering flow/ in tropical disturbances 17 p2769 A71-34300

Southern Hemisphere extended operational meteorological prediction using six level primitive equation model 20 p3256 A71-39202

Probabilistic weather forecasting for temperature and precipitation, examining feedback and prediction evaluation 20 p3256 A71-39203

Meteorological prediction from joint frequency of initial and final weather elements conditions, developing conditional probability models from bivariate normal distribution tables and Markov process 20 p3256 A71-39204

Book on numerical weather prediction covering atmospheric wave motions, scale analysis, vorticity and energy, barotropic, baroclinic and multilevel models, etc 21 p3410 A71-40780

Atmospheric circulation finite difference weather prediction model, investigating horizontal grid resolution effects 22 p3535 A71-42412

Global numerical weather prediction model, using finite difference grid and operators with smoothing techniques 22 p3568 A71-42413

Anisotropically weighted smoothing theoretical interpretation based on numerical variational analysis for upstream and downstream observations in weather forecasting 22 p3569 A71-42415

Global atmospheric research program, discussing circulation, weather forecasts, numerical modelling and observational system 23 p3701 A71-43822

Long range weather prediction based on numerical global atmospheric models, noting application to climatology 24 p3844 A71-44366

NUSSELT NUMBER

Condensate film thickness and Nusselt number on axisymmetric vertical plates and cylinders, correcting for variable gravity and body form [ASME PAPER 70-HT-P] 03 p0519 A71-13699

Laminar film condensation thickness and Nusselt number on arbitrary axisymmetric bodies in nonuniform gravity 07 p1225 A71-20655

Heat transfer to airfoil in oscillating flow at large angles of attack, showing vortex shed reattachment and Nusselt numbers increase [ASME PAPER 71-GT-18] 11 p1703 A71-25963

Heat exchange during stabilized laminar flow of incompressible liquid in circular pipe with radiative cooling, deriving temperature profile and Nusselt number dependence 13 p2046 A71-28180

Viscous dissipation effects on Nusselt number in combined free and forced convection through vertical concentric annuli 13 p2160 A71-28601

Turbulent flow in circular duct, determining asymptotic temperature profiles and Nusselt number values from Prandtl numbers and velocity distribution 16 p2554 A71-32836

French monograph on thermal microflowmeters covering anemometers, fluid mechanics, Nusselt number, thermocouple flowmeters 17 p2744 A71-35228

Finite element method application to convective heat transfer between parallel plates for arbitrary surface temperatures and Nusselt number 22 p3619 A71-41874

Heat transfer from platinum wires in He and He-air mixtures, plotting Nusselt number variation with Reynolds number for various He concentrations 22 p3620 A71-41875

Centrifugally driven thermal convection in rotating cylinder of fluid heated from above, calculating heat flux through wall and effect on Nusselt number 22 p3620 A71-41879

Heat exchange during stabilized laminar flow of incompressible liquid in circular pipe with radiative cooling, deriving temperature profile and Nusselt number dependence 24 p3888 A71-44933

NUTATION

Skyнет satellite attitude determination and adjustment by IR and solar sensors, electronics processing equipment, nutation damping and pulsed axial thrusters 02 p0320 A71-12430

Dual spin spacecraft high performance nutation damper, using wheel of uniform mass distribution 04 p0661 A71-15002

Optimal viscous damping effect of cylindrical filled fuel tanks on satellite nutations 06 p0979 A71-17417

Earth rotation polar motion dynamics, discussing wobble, drift, nutation, precession and sway 06 p0890 A71-17877

Earth mantle-inner core nutational dynamic coupling and rotation pole 24 year libration 06 p0890 A71-17883

Major earthquakes effects on earth rotation pole disturbances from latitude and time data, considering Chandler nutation excitation 06 p0891 A71-17889

Free Lagrangian gyroscope, discussing numerical relations between precessions and nutations 06 p0899 A71-17931

Semiannual nutation term determination from diurnal latitudinal observation with zenith telescope over 6 year period 07 p1194 A71-19319

Revised latitude series of nutations in Mizusawa and Paris observatories from LF noise investigations 07 p1194 A71-19329

Kimura annual Z term in latitude variations, noting agreement with semiannual solar nutation and earth tide observations 08 p1364 A71-21422

Earth tide and nutation correlation, examining internal structure 08 p1285 A71-21779

Earth free diurnal nutation frequency, examining latitude variation power spectrum 08 p1285 A71-21780

Heavy gyroscope motion in gimbal suspension for arbitrary housing gravity center, showing steady solutions with respect to nutation angle 08 p1294 A71-21870

Passive nutation damping of spin stabilized orbital satellites with mechanical and pendulum dampers involving nonlinear interaction of vibrational and rotational motions 10 p1683 A71-24562

Semipassive and active nutation dampers in orbiting dual spin spacecraft, using single axis control moment gyro 13 p2144 A71-27976

Gravity center effect on drift of gyro linear acceleration integrator on vibrating base, showing errors at frequencies near nutations 13 p2069 A71-28933

High speed spin effect on amplified or damped nutations in low friction rotary gyroscope mounted on gimbals 15 p2401 A71-31178

Semiannual nutation term determination from diurnal latitudinal observation with zenith telescope over 6 year period for earth axis 15 p2486 A71-31899

Maximum nutation-precession angles of spin stabilized satellites during extension of long flexible booms 15 p2500 A71-32046

Earth tide and nutation correlation, examining internal structure based on model with liquid center and solid inner core 15 p2401 A71-32684

Earth free diurnal nutation frequency, examining latitude variation power spectrum 15 p2401 A71-32685

Nutation damping and vibration isolation in dual spin spacecraft, using flexible dissipative coupling between platform and rotor 18 p2971 A71-36276

Parameter optimization of linear time invariant nutation damper by second Liapunov method 20 p3306 A71-38853

Heavy gyroscope motion in gimbal suspension for arbitrary housing gravity center, showing steady solutions with respect to nutation angle 20 p3238 A71-39369

Circumnutations in plants under gravitational stimulation 21 p3339 A71-39973

Nearly diurnal nutation observations from Danjon astrolabe data, comparing theoretical earth models 22 p3602 A71-42172

Canonical transformations application to spinning satellite with nutation damper [AAS PAPER 71-346] 23 p3728 A71-43019

Rotating solid body nutations damping by pendulums system oscillating in plane normal to rotation axis, deriving optimal conditions 24 p3848 A71-44855

NUTATIONAL OSCILLATION NUTATION

NUTRIENTS
Regenerated nutrients as foods for long duration space missions, discussing physicochemical methods for metabolic waste products conversion into safe synthetic nutrient compounds 01 p0026 A71-11250

Optimal mineral-organic nutrient medium and soil selection for microorganism detection on Mars 13 p2009 A71-28681

Mineral composition optimization of nutrient medium for *Hydrogenomonas*, using steepest ascent method for mathematical planning of experiments 20 p3193 A71-39236

Hydroponic plant cultivation with keramzit substrate, investigating replacement time effect and regenerative power of nutrient solution 22 p3506 A71-42816

Biologically mineralized human waste products utilization in nutrient solutions for higher and lower autotrophs cultivation 22 p3507 A71-42819

NUTRITION

Regenerated nutrients as foods for long duration space missions, discussing physicochemical methods for metabolic waste products conversion into safe synthetic nutrient compounds 01 p0026 A71-11250

Polysomal RNA disaggregation and attendant reduction in hepatic protein synthesis in rats as result of decreased feed ingestion during hypoxia 16 p2529 A71-33190

World championship gliding team medicophysiological problems during competition at Marfa, Texas, discussing climatic adaptation, nutrition, hypoxia and pilots general physical and psychomotor conditions 22 p3500 A71-41576

Hypothermia effect on brain nutritive processes and regulator activity, considering changes in brain blood supply, respiration and carbohydrate metabolism 22 p3486 A71-41940

NUTRITIONAL REQUIREMENTS NT CALORIC REQUIREMENTS

Chlorella ration effect on internal organs of protein-deficient mice compared with casein and soybean rations 01 p0025 A71-11145

Astronaut space nutrition, discussing Apollo mission short range nonregenerative mode, long range closed loop regenerative cycles and waste recycling 01 p0027 A71-11572

NUTS [FASTENERS]

Powder metallurgy parts application in aircraft, illustrating flareless-sleeve coupling nut of pressed and sintered Ti-6Al-4V alloy 10 p1618 A71-24762

NYLON [TRADEMARK]

Dynamic decelerators using nylon tricot knit fabric and high elongation suspension lines for reduced peak force parachute deployment [AIAA PAPER 70-1185] 03 p0349 A71-14273

Nylon-phenolic composites pyrolysis, deriving kinetic coefficients from thermogravimetric analysis at various heating rates 11 p1728 A71-26043

NASA-SRI Round Robin Ablation Program summary, discussing dimensional analysis, Teflon, nylon and surface temperature 18 p2985 A71-36279

Uniaxially aligned glass and carbon fiber reinforced nylon composites prepared from caprolactam by anionic polymerization 19 p3083 A71-37339

NYLON RESINS
 U POLYAMIDE RESINS
NYQUIST DIAGRAM
 Computerized design of large multivariable control systems using inverse Nyquist array method
 20 p3202 A71-38994

NYQUIST FREQUENCIES
 Group delay measurements accuracy, using Nyquist method as function of FM and response characteristics of measured two-terminal pair network
 03 p0386 A71-13814

NYSTAGMUS
 Neuron network modeling by stable rhythmic impulsion system, considering vestibular nystagmus
 01 p0025 A71-11137
 Nystagmus extinction during repeated exposures to angular accelerations in labyrinthectomized guinea pigs
 01 p0014 A71-11139
 Vestibular nystagmus and display luminance effects on hand-eye coordination in compensatory tracking of aircraft instrument
 02 p0207 A71-12381
 Extrauditory effects of sound on senses, concerning visual functions, nystagmus, galvanic skin response and audioanalgesic use
 03 p0359 A71-13158
 Astronaut visual acuity under angular acceleration, considering vestibular stimulus direction and nystagmus upheating or downbeating
 04 p0536 A71-14754
 Gravity effects on human caloric and rabbits rotational nystagmus, noting semicircular canals role
 04 p0542 A71-14757
 Gravity effects on experimental nystagmus in rabbits under electrical, rotatory and caloric vestibular stimulation, taking into account semicircular canals and otolith organs
 04 p0536 A71-14758
 Uniocular oscillopsia with vertical retinal nystagmus and internuclear ophthalmoplegia due to multiple sclerosis
 06 p0852 A71-17615
 Gastric and rectal mechanoreceptor stimulation influences on vestibular rotation nystagmus in rabbits
 06 p0856 A71-18466
 Linear acceleration effects on human otolith and vestibular apparatus, discussing vestibulovegetative motion sickness syndrome and nystagmus index activation
 08 p1242 A71-21956
 Centrifugal force effect on pigeon head nystagmus, acting on semicircular canal via otoliths or cupula
 09 p1388 A71-22123
 Coriolis effects on endolymph shift direction in semicircular canals of man under rotation with head movements in sagittal plane, involving nystagmus and illusory sensations
 09 p1392 A71-22640
 Optokinetic nystagmus device, combining TV set and bar generator with controllable frame desynchronization for moving image and electrical control of stimulus parameters
 09 p1399 A71-22973
 Phase lag in periodic Coriolis star nystagmus between Coriolis input and corresponding ocular component in cats
 10 p1559 A71-23923
 Hybrid computer program for data reduction or on-line analysis of nystagmus during closed loop experiment involving visual and/or vestibular function
 13 p2022 A71-29359
 Mathematical model for short term adaptation to vestibular stimuli, deriving transfer function relating angular velocities of nystagmus and head rotation
 14 p2182 A71-30250
 Optical tracking task performance and nystagmus during angular acceleration in yaw and pitch, comparing differences due to vertical and horizontal canal response
 16 p2535 A71-33107
 Nystagmic responses of airmen and grounded and active pilots subjected to caloric and rotational tests
 16 p2535 A71-33112
 Rotational ocular nystagmus phases induced by head rotation, developing vestibulo-ocular system mathematical model
 17 p2691 A71-35045
 Stroke number and vestibular nystagmus duration and frequency under successively increasing angular acceleration from tests on guinea pigs
 20 p3189 A71-39238
 Flying personnel equilibrium tests with pendulum armchair, investigating labyrinth reflex by induced nystagmus
 22 p3500 A71-41570
 Habituation and suppression of vestibulo-ocular vertical nystagmic responses to Coriolis stimulation in pentathlon athletes, comparing to pilots and airman trainees
 22 p3501 A71-41826
 Alcohol ingestion effects on vertigo and nystagmic vestibular responses to angular acceleration, considering visual fixation and alertness control
 22 p3501 A71-41827

Visual and vestibular analyzers interaction, noting reduction in duration of counterrotation illusion and postrotation nystagmus in humans
 22 p3505 A71-42797

O

O RING SEALS
 Flexible laminated cam ring for high speed variable displacement vane pumps
 [SAE PAPER 700792] 01 p0091 A71-11544
 High pressure and temperature seals and sealing in aircraft and spacecraft, including O rings and elastomers use
 06 p0905 A71-18056
 Elastomer O ring vacuum device for positive holding of Schumann film for precise microdensitometry during rocket flight in 7 March 1970 solar eclipse
 14 p2249 A71-30887

O STARS
 OB stars existence on utmost borders of M 31, using photometric statistics
 02 p0312 A71-12465
 Normal O, blue supergiants and brightest yellow and red supergiant massive stars, considering evolution, luminosity, lifetime mass loss, pulsational instability and supernovae
 04 p0648 A71-15248
 O-B stars velocity distribution in synthetic association, proposing method for space velocities mean value determination
 07 p1192 A71-19289
 Planetary nucleus BD plus 30.3639 degrees and Wolf-Rayet star HD 164270, comparing spectrum and ionization potential
 08 p1359 A71-20937
 O and B type stars galactic Keplerian parameters statistical distributions based on galaxy point model
 11 p1820 A71-25248
 He I lines in OB spectra, examining main sequence stars
 11 p1830 A71-26111
 Faint O-B5 type blue stars data, listing absolute spectrophotometric gradients and Balmer series discontinuities
 15 p2487 A71-32032
 Symmetrically distributed nebulae around Wolf-Rayet stars, detailing Ngc 7635 and associated star BD plus 60 deg 2522
 17 p2806 A71-35410
 H II regions near O and R stars effect on interstellar electron density in solar vicinity
 20 p3294 A71-39542
 Eclipsing binaries among Wolf-Rayet AO Casiopeia and U Geminorum stars from photometric observations
 20 p3300 A71-39821
 Space distribution of OB stars from revised Victoria H gamma spectrophotometric magnitudes by MK spectral classification
 21 p3448 A71-40594
 Spiral structure OB associations in outer regions of Andromeda nebula, investigating blue objects in U and B plates of Schmidt telescope
 21 p3451 A71-40723

OAO
 NT OAO 2
 NT OAO 3
 OAO experiments instrument packages for UV observations from orbit, discussing telescopes pointing accuracy and stability, mission objectives, etc
 05 p0755 A71-17129
 OAO for observations of stars, galaxies, planets and nebulae, discussing ground system and men and data systems integration
 05 p0734 A71-17130
 OAO simulation system including prototype spacecraft and digital computer for verifying ground system performance
 05 p0734 A71-17131
 OAO continuous observation capability, Project STAR telescopes, solar and X ray instruments and resupply missions based on space shuttle concept
 05 p0818 A71-17132
 Computer controlled ground based command and data acquisition software system for OAO-A2 spacecraft remote control stations, discussing interface with monitor and interrupt capabilities
 08 p1259 A71-21658
 Heat pipe application to OAO as structural isothermalizer, considering overall spacecraft thermal network analysis
 15 p2512 A71-31594
 Automatic data reduction system for TV images of star fields acquired from OAO
 17 p2743 A71-35009
 Stellar chromosphere characteristics from OAO observation of magnesium II emission in late type stars
 19 p3137 A71-37628
 Misalignment estimation software system /MESS/ for in-flight celestial and inertial reference attitude sensor alignment and calibration on OAO
 23 p3648 A71-43027

OAO 2
 Ni-Cd batteries for OAO 2 spacecraft, considering manufacturing, materials, components and tests
 03 p0350 A71-13027
 OAO 2 design and performance features concerning pointing accuracy and stability, command capability, data handling, thermal environment, orbit constraints, ultraviolet spectroscopy, etc
 05 p0818 A71-17128
 OAO 2 thermal test reliability analysis, using filtering process to eliminate component and subsystem level failures
 12 p1971 A71-26681

OAO 3
 Design and performance testing of arterial wick circular heat pipes for OAO-C spacecraft
 [ASME PAPER 71-AV-26] 18 p2868 A71-36393
 Gas controlled variable conductance heat pipe for OAO-C onboard processor temperature stabilization, describing thermal performance tests under simulated flight conditions
 [AIAA PAPER 71-411] 18 p2975 A71-36775

OAO-A
 U OAO

OBESITY
 Total body adipose tissue mass and composition variations, examining hyperglycemic, obese, exercised and centrifuged animals
 23 p3637 A71-44299

OBULATE SPHEROIDS
 Steady incompressible flow past oblate and prolate spheroids for Reynolds numbers up to 100, using spherical coordinates and finite difference method
 03 p0400 A71-13729
 Dicke-Goldenberg solar oblateness measurement explained by equatorial temperature excess smoothly distributed
 05 p0812 A71-16691
 Laser resonator mode representation with oblate spheroidal vector wave function through boundary value problem formulation
 08 p1301 A71-21293
 MHD oscillations of homogeneous compressible self gravitating fluid spheroid in static equilibrium with poloidal magnetic field inside and dipole field outside
 11 p1831 A71-26167
 Coma galactic cluster, investigating nuclei oblateness, diagrams and tables of variables
 12 p1962 A71-26910
 Spherical harmonic expansion of nonhomogeneous oblate spheroid mass distribution potential, giving convergence criterion
 17 p2733 A71-35029
 Solar oblateness and Li abundance interpretation by model of thermally driven turbulence terminated at rotating core surface containing partial mass
 17 p2806 A71-35385
 Elastico-viscous liquid steady secondary flow induced by oblate or prolate spheroid rotating about axis of symmetry from linear partial differential equations solution
 20 p3214 A71-39967
 Low thrust vehicle optimal takeoff calculations from orbit about oblate planet, using two variable asymptotic expansion technique
 [AAS PAPER 71-367] 23 p3729 A71-43037

OBLIQUE SHOCK WAVES
 Thermodynamic equations of state for dissociating and ionizing high temperature air applied to vertical and oblique compression shocks
 02 p0331 A71-12067
 Solar cosmic ray interaction with oblique shock wave MHD discontinuity, noting energy particle buildup and acceleration
 08 p1351 A71-20964
 Particle motion behind oblique shock wave in two phase supersonic wedge flow, deriving expressions for particle trajectories and velocity equalization time
 08 p1227 A71-21754
 Supersonic boundary layer flow profile distortion due to oblique shock during separation
 10 p1552 A71-24592
 Compressible turbulent boundary layer interaction with wedge or corner induced oblique shock waves, using transformation methods
 11 p1750 A71-25481
 Time dependent asymptotic solution for transonic flows in hyperbolic nozzle and turbine cascades with oblique shock
 11 p1704 A71-25975
 Maximum turning angle across oblique shock for fixed density ratio and for fixed upstream Mach number
 15 p2392 A71-32125
 Plane oblique shock wave diffraction on wedge moving in homogeneous gas flow at supersonic speed, reducing boundary value problem to Hilbert problem
 16 p2519 A71-32930
 Design shock wave correspondence to strong oblique shock, discussing off design behavior of caret wing
 17 p2671 A71-35280
 Mesh method for supercritical transonic flow calculation with normal or oblique shock wave at trailing edge
 17 p2674 A71-35799

Large amplitude whistler as collisionless laminar shock model, showing instability for oblique perturbation propagation 18 p2950 A71-35865

Oblique shock-combustion wave polar investigation of stationary two dimensional flow of fuel mixture in compressed gas 18 p2985 A71-36133

Normal and oblique shock thermodynamic equilibrium state variables calculation, taking into account air dissociation and ionization 18 p2909 A71-36678

Oblique shock wave incident on plane boundary of nonlinear homogeneous elastic solid, proving wave reflection pattern uniqueness 18 p2982 A71-36813

OBSERVATION

U OCCULTATION

OBSERVATION

NT SATELLITE OBSERVATION

NT VISUAL OBSERVATION

Dynamical nonlinear systems observability definition and necessary and sufficient criterion for checking 10 p1587 A71-24743

Papers on IQSY observations and bibliography covering meteorology, geomagnetism, aurora, night airglow, solar activity, cosmic rays, absorption measurements and drift observations 15 p3395 A71-31606

OBSERVATION AIRCRAFT

NT MIRAGE 3 AIRCRAFT

NT OH-6 HELICOPTER

NT TSR-2 AIRCRAFT

NT WEATHER RECONNAISSANCE AIRCRAFT

OBSERVATORIES

NT ASTRONOMICAL OBSERVATORIES

NT GEOPHYSICAL OBSERVATORIES

NT LUNAR OBSERVATORIES

NT OAO

NT OGO

NT OGO-B

NT OGO-C

NT OGO-D

NT OGO-E

NT OSO

NT OSO-E

NT OSO-F

NT OSO-G

NT OSO-3

OBSACLES

U BARRIERS

OBSSTRUCTING

U BLOCKING

OCCIPITAL LOBES

Corned-retinal potential as generator of occipital alpha rhythm in human electroencephalogram modulated at 10 Hz by tremor in extraocular muscles 21 p3329 A71-40176

Averaged potentials in vertex and occipital region of human cranium evoked by emotional visual stimuli 24 p3798 A71-45057

OCCCLUSION

Human coronary arteries fibrinolytic activity, considering histochemical and quantitative methods for arteriosclerosis and occlusion investigations 02 p0200 A71-12416

Natural or endogenous fibrinolysis and its pharmacological enhancement as possible approach to prophylaxis of vascular occlusions 02 p0200 A71-12417

Steels in stressed state, determining hydrogen saturation and occlusion 09 p1467 A71-22309

Transition metals hydrides electrical resistance calculation based on theory of hydrogen electrodiffusion /occlusion/ into incomplete d-states 09 p1473 A71-23232

OCCULTATION

NT LUNAR OCCULTATION

NT SOLAR ECLIPSES

NT STELLAR OCCULTATION

Planetary atmospheres motion effect on constant pressure surface height in radio occultation data interpretation 03 p0488 A71-13553

Atmospheric absorption models of solar X-rays at occultation times, using Solrad satellites 03 p0480 A71-14048

Planetary atmosphere Mariner spacecraft occultation experiments, showing neglect of latitudinal and longitudinal variations introduce serious errors 06 p0970 A71-17984

Beta Sco occultation by Jupiter, interpreting UV light curve 23 p3733 A71-43124

OCEAN BOTTOM

Critique of Ethiopian Afar depression formation as oceanic crust resulting from Arabia drift, considering plate tectonics analysis for bifurcated spreading zones 04 p0582 A71-15126

Marine sediment age by fission track dating of volcanic glass shards, noting agreement with K-Ar, paleomagnetic and paleontologic ages 10 p1601 A71-24430

Variable abyssal basalt populations, considering chemical analyses variations for ridges as function of ocean floor spreading rate 13 p2063 A71-29139

Bound sugar content in marine sediments by capillary gas chromatographic-mass spectrometric analysis of trimethylsilyl derivatives 19 p3055 A71-38146

OCEAN CURRENTS

Monsoonal response of Somali Current in Indian Ocean, using spacecraft IR observations of sea surface horizontal temperature gradients 16 p2562 A71-33068

Ocean layer mixing from aerial photographs using dye injections and floating cards under various wind, sea state and thermal profile conditions 22 p3569 A71-42547

OCEAN SURFACE

Soviet book on random functions theory in gravimetric observations over water covering ship dynamics, meter design, instrument damping, optimal linear filtering, etc 02 p0254 A71-12841

Extensive air showers at sea level, plotting mean numbers of muons and electrons 03 p0477 A71-13866

Atmospheric high pressure axis determination from satellite photographed sea surface sunglint reflection patterns, using model calculations 05 p0778 A71-17045

Sea surface temperature estimation by spatially scanning spaceborne systems operating in thermal IR atmospheric window spectral regions 06 p0898 A71-17560

Autocorrelation functions of anomalous gravitational and magnetic fields for ocean lines, relating Mohorovici boundary and Curie isotherm 06 p0894 A71-18268

Radar altimeter use for ocean roughness determination 07 p1095 A71-18824

Arbitrary strength and shape shock front propagation past ocean surface, calculating diffraction at interface 07 p1094 A71-20614

Tropical hurricane central pressure drop to maximal wind velocity ratio, discussing thermal to mechanical energy transfer as function of ocean surface temperature 08 p1330 A71-21873

Side-looking airborne radar /SLAR/ for sea ice identification, mapping and ship routing in Northwest Passage 09 p1439 A71-23448

Line-of-sight radio signal transmission, investigating sea surface reflections effects on phase of arrival and coherence 09 p1409 A71-23502

Infrared radiometer sea surface temperature measurements during oceanographic survey, examining inclination angle effect 09 p1440 A71-23590

Microwave emission from North Sea and North Atlantic at surface wind speeds of 5-25 m/sec, measuring brightness temperature 12 p1902 A71-27199

Mathematical model for predicting microwave signal fading characteristics due to reflections from ocean surface 15 p2368 A71-31140

Earth and ocean surface state and cloud height determination using airborne laser radar observations 16 p2568 A71-33786

Atmospheric boundary layer circulation dynamic interaction with variable depth barotropic ocean surface, studying stream function during annual cycle 16 p2605 A71-33906

Geodetic and oceanographic surface mapping by satellite radar altimeter system, discussing measurement technique, orbital parameters and data processing equipment [AIAA PAPER 71-845] 17 p2733 A71-34708

Sea surface slope distribution and wind velocity determination by sun glitter photography from synchronous satellite 17 p2734 A71-35215

Atlantic Ocean surface temperature distribution data for Gulf Stream meanders and eddies, using Ito 1 satellite direct readout IR images 17 p2734 A71-35216

Small scale turbulence structure in atmospheric boundary layers over open ocean, noting velocity derivatives probability density function lognormality 19 p3044 A71-37731

Digital pattern classification of oceanographic remote sensing multispectral airborne scanner data, considering sea surface color variations 19 p3060 A71-38405

Microwave sounding of ocean and earth surface thermal emission and atmospheric water vapor content by Cosmos 243 satellite-borne radiometers 20 p3259 A71-39672

Aeronautical satellite systems program planning for improved aircraft communications, ATC and other air traffic services in airspace over oceanic areas 22 p3573 A71-42096

Model aspects of sea echoes and clutter unsteadiness on radar 22 p3514 A71-42470

Ocean surface condition correlation to radar backscattering cross sections and wind velocity from scatterometer data 22 p3569 A71-42545

Ageostrophic deviations and advection corrections to geostrophic wind velocity and shear stresses above water surface 22 p3570 A71-42849

Gulf Stream and Middle Atlantic Bight complex synoptic sea surface temperature distribution from ITOS 1 satellite high resolution IR imagery 22 p3536 A71-42885

Ocean surface wave height /sea state/ measurement by high resolution random-signal radar based on model characterized by Poisson distributed scatterer density function 24 p3823 A71-45082

OCEANOGRAPHY

Information collection from ocean data stations networks by satellite and HF digital data communications, noting feasibility of VHF telemetry communications 01 p0037 A71-10991

Aerospace technology application to oceanic instrumentation and communication requirements 04 p0583 A71-15307

Laser light beam spread in random media, considering atmospheric and oceanographic applications 04 p0609 A71-15682

Sea morphology from satellite photographs corresponding to sun reflex zone 05 p0739 A71-16274

Microwave radiometric techniques for continuous all-weather remote sensing of sea conditions from satellites, discussing foam and surface ripple effects [AIAA PAPER 70-318] 05 p0743 A71-17101

Oceanic rise crest heat flow model, examining vertical velocity distribution of mass transport 06 p0889 A71-17635

Soviet book on physics of interaction between atmosphere and ocean covering heat transfer, wave formation, vertical mixing in upper sea layer, etc 10 p1639 A71-24671

Airborne remote sensing for oceanographic data acquisition in UV, visible, IR and microwave spectrum using reflected and emitted radiation instruments 12 p1902 A71-27260

Ocean height measurement by orbit determination from satellite altimetry, considering least squares solutions and instrument errors 13 p2066 A71-27983

Global environmental monitoring system for atmosphere, oceans, land and biology, considering international cooperation 14 p2198 A71-30897

Geodetic and oceanographic surface mapping by satellite radar altimeter system, discussing measurement technique, orbital parameters and data processing equipment [AIAA PAPER 71-845] 17 p2733 A71-34708

Remote subsurface oceanographic imagery from orbital altitudes in blue multispectral region, showing optimum filter passband 18 p2917 A71-36064

Global atmospheric research with balloons, buoys and orbiting satellites for meteorological and oceanographic data recovery 18 p2913 A71-36486

Satellite data techniques and instrumentation in earth geometry and kinetics, reviewing geopotential models, pole positions, tides, ocean physics and international cooperation 20 p3219 A71-39656

Ocean and earth tidal effect on semidiurnal lunar atmosphere tide, considering realistic model 23 p3700 A71-43339

OCEANS

NT ARCTIC OCEAN

NT ATLANTIC OCEAN

NT INDIAN OCEAN

NT PACIFIC OCEAN

Latitudinal distribution of integral water content of clouds in droplet form above Pacific, Atlantic and Indian oceans from Cosmos 243 measurements 12 p1924 A71-27098

Oceanic masses vertical gravity gradient, noting slight decrease with depth 16 p2575 A71-34065

Water vapor dimer effects on atmospheric brightness temperature in cm and mm radiometric investigations from satellites above oceans 22 p3533 A71-41654

OCTAHEDRAL RESEARCH SATELLITES

U ENVIRONMENTAL RESEARCH SATELLITES

OCTAHEDRITE

U MINERALS

OCTAVES

Multioctave microwave frequency synthesizer by subharmonic synthesis and frequency multiplication under digital programmed commands 01 p0054 A71-10972

OCULOGRAPHIC ILLUSIONS

Thresholds comparison for angular acceleration derived by subjective cupulometry and by staircase method, determining thresholds for rotation perception and oculogyral illusion

10 p1570 A71-24605

Proximal changes and stimulus patterns associated with rotation direction evoking visually perceived oscillation

10 p1570 A71-24606

Human visual geometrical illusions and figural aftereffects, determining mechanism locations for spatial patterns physical and phenomenal properties

13 p2018 A71-28464

Rotation perception in dark and oculogyral illusion, using power law to describe subjective vestibular sensation relation to angular acceleration stimulus pulses

13 p2022 A71-29327

Horizontal-vertical velocity illusions relationship, noting independent determinants

17 p2691 A71-35109

Autokinetic motion of luminous target, relating apparent visual movement to experienced displacement

17 p2694 A71-35739

Apparent movement due to closely spaced sequentially flashed dots in human peripheral field of vision, considering eye movement role

23 p3634 A71-43970

OCULOMETERS

Illumination level effect on corneo-retinal potential and electro-oculography (EOG) recording

08 p1246 A71-20812

OCULOMOTOR NERVES

Ascending neuron vestibulo-ocular reflex arc, emphasizing medial longitudinal fasciculus

04 p0537 A71-14763

Dynamic visual acuity-horizontal eye movements correlation in man and monkeys, discussing fovea, parafovea and oculomotor control

10 p1560 A71-23984

Cat single optic nerve fibers receptive field, observing functional organization and conduction velocity

13 p2008 A71-28458

Cat type I and II optic nerve fibers response to flicker stimulation, noting receptive field organization, conduction velocity and temporal and spatial information processing

13 p2008 A71-28459

Grating pattern vision models, examining single neural network and multiple channel stimulus information processing

13 p2018 A71-28461

Extraocular muscle structure and function, defining slow and fast motor system based on slow and fast fibers

17 p2687 A71-35801

Firing frequency of single trochlear nerve fibers during eye movements in alert monkey

19 p3001 A71-37413

Habituation and suppression of vestibulo-ocular vertical nystagmic responses to Coriolis stimulation in pentathlon athletes, comparing to pilots and airman trainees

22 p3501 A71-41826

Afferent oculomotor pathways to extraocular muscle nuclei, considering discrete unilateral lesion role in head posture disturbance production

22 p3488 A71-42435

Central pathway connection between vestibular and oculomotor nuclei through pons responsible for horizontal eye movements induced by visual and vestibular stimuli

22 p3488 A71-42436

Saccadic eye movement control system behavior simulation model evaluation, considering oculomotor pathways

22 p3504 A71-42443

Neural control organization in vestibulo-ocular reflex arc, considering afferent and oculomotor neural signals

22 p3490 A71-42449

Oculomotor neural organization models, considering vestibular ocular reflex, saccadic eye movements and smooth pursuit systems

22 p3504 A71-42450

Circumscribed eccentric afterimages effect on visual oculomotor control system, examining central transfer functions

23 p3635 A71-43971

ODORS

Temperature, odor mixing and stimulation frequency effects on olfactory receptor potential of fly *Lucilia sericata*

14 p2186 A71-30568

Polymer odor threshold determination for hygienic considerations in sealed/pressurized chamber construction, comparing static and dynamic methods

24 p3800 A71-44539

OFF-ON CONTROL

Optimal on-off control systems with structural constraints, discussing synthesis by dynamic programming and phase plane methods

03 p0392 A71-14408

Nonlinear time optimal off-on feedback control system synthesis, deriving algorithms

03 p0392 A71-14410

Single phase static inverter module with voltage waveform synthesis by time optimal response /bang-bang/ closed loop technique

04 p0535 A71-15287

Nonlinear systems bang-bang controllability by differential geometry approach

04 p0562 A71-15872

On-off keying system digital detection using random sampling for achieving high bit rates

05 p0725 A71-17073

Plasma stabilization by nonlinear bang-bang feedback

06 p0932 A71-17459

On-off control system with crew motion caused random disturbing torques on spacecraft, determining waiting time, jet firing frequency and fuel consumption rate

07 p1208 A71-19885

Digital on-off predictive adaptive control system feasibility analysis

07 p1082 A71-20407

Computational technique for finding bang-bang time optimal controls of nonlinear time-varying systems with bounded control function inputs

14 p2219 A71-29699

Closed loop system analysis of triangular wave generator consisting of integrator, on-off element with hysteresis and multiplier

15 p2376 A71-32026

Digital on-off follow-up system dynamics under signal time and amplitude quantization effects on transient and steady state processes, using phase-plane analysis

15 p2382 A71-32453

On-off automatic control systems, using nonlinear finite difference equations for switching times and coordinate values determination

17 p2721 A71-35133

Structural synthesis of on-off servo feedback control system with combined dynamic and counterconnection braking of actuating motor within relay dead zone limits

19 p3038 A71-37776

On-off temperature control system with distributed parameters under boundary conditions, investigating symmetric self oscillation

19 p3163 A71-37780

Singular optimal control theory generalization using appropriate transformations, considering stability results for bang-bang solutions

23 p3657 A71-43941

OGEE WINGS

U VARIABLE SWEEP WINGS

OGIVES

Side forces on ogive cylinder bodies at large incidence as function of Mach number, nose fineness and bluntness ratios for laminar and turbulent boundary layers

[AIAA PAPER 71-570] 15 p2345 A71-31563

OGO

NT OGO-B

NT OGO-C

NT OGO-D

NT OGO-E

OGO radio astronomy instrument for cosmic noise sky brightness distribution mapping by electrically short antenna ionospheric focusing

11 p1763 A71-26144

Magnetic field and electron plasma observations near dawn magnetopause by triaxial spectrometer and fluxgate magnetometer on satellite OGO 5

15 p2485 A71-31754

Neutral atmospheric composition and density variations during geomagnetic disturbances from OGO-6 satellite quadrupole mass analyzer measurements

20 p3223 A71-39711

Day airglow column emission rates for Lyman-Birge-Hopfield system of molecular nitrogen as function of solar zenith angle, using OGO 4 observations

20 p3231 A71-39892

Suprathermal electron beam induced HF wave instability in solar wind upstream from earth bow shock, interpreting OGO 5 observations

23 p3720 A71-43158

Magnetopause current layer deflection during OGO 5 crossings, noting independence on sun-earth-satellite angle

23 p3668 A71-43161

OGO 5 polar cusp observations showing dayside magnetosheath plasma penetration during magnetic storm

23 p3668 A71-43162

Interplanetary electron associations with type 3 solar bursts, using decametric OGO 3 and solar geophysical observations

23 p3721 A71-43176

OGO-B

Stable auroral red arcs on 29 September 1967, 31 October and 1 November 1968, comparing OGO 2 and OGO 4 VLF data on plasmopause crossings

15 p2397 A71-31757

OGO-2 rubidium vapor magnetometer measurements comparison with surface magnetic observatory data during geomagnetic storms, considering asymmetric ring current

16 p2572 A71-33946

OGO-C

Solar optical flares association with type 3 bursts from OGO-3 observations, suggesting temporary creation or enhancement of electron stream propagation by filament or sunspot structure change

07 p1187 A71-19724

OGO-D

Stable auroral red arcs on 29 September 1967, 31 October and 1 November 1968, comparing OGO 2 and OGO 4 VLF data on plasmopause crossings

15 p2397 A71-31757

Atomic oxygen 1304-A day airglow observed from OGO-D spacecraft, attributing subsolar emission rates to photoelectron impact excitation

16 p2574 A71-33964

OGO-E

Multiple magnetopause crossings in equatorial plane by OGO 5, showing magnetopause motion composed of two oscillations

08 p1282 A71-21631

OH-6 HELICOPTER

Rotor stability derivatives determination from instrumented OH-6A prototype helicopter wind tunnel tests, comparing data with analytical results obtained by digital computing technique

[AHS PREPRINT 543] 14 p2179 A71-31100

OHMIC DISSIPATION

Thermosphere heating due to auroral electrojets, discussing thermospheric variations and eddy viscosity

10 p1602 A71-24554

Atmospheric dynamo equations derivation based on Maxwell equations and Ohm law with anisotropic and asymmetric electric conductivity tensor for quiet geomagnetic variations explanation

20 p3217 A71-39518

Energy losses of collisional He plasma with ohmic heating in Uragan stellarator with large shear, comparing plasma lifetime to Bohm confinement time

24 p3855 A71-44664

OHMS LAW

Nonuniform conductivity effect on cosmic magnetic fields structure with zero Lorentz force, using Maxwell equations and Ohm law

14 p2274 A71-29982

Ionospheric plasma density irregularities effect on ionospheric electroconductivity, using Ohms law in Alfvén-Faelthammer form

20 p3218 A71-39521

OIL ADDITIVES

Synthesized hydrocarbon oil antiwear and extreme pressure additives effects on bearing spinning torque and endurance

06 p0904 A71-17580

OILS

NT CASTOR OIL

NT CRUDE OIL

NT LUBRICATING OILS

NT MINERAL OILS

Hydraulic servomechanism with piston-type control valve, examining oil compressibility and sustained oscillations effects on system stability

01 p0007 A71-11378

Remote sensing imaging techniques for oil pollution survey, using airborne UV, IR, color and filtered panchromatic photography

17 p2735 A71-35386

Spontaneous hot zone formation in oil flow through small pipes, showing significance in pressure losses and plain bearings calculations

19 p3046 A71-38275

Methane atmosphere polymerization by solar UV to form primordial oil slick, discussing importance to life development

22 p3535 A71-42074

OKLAHOMA

Oklahoma and Malaysia thunderstorms comparison based on weather reconnaissance aircraft measurements, considering turbulence patches

14 p2266 A71-29752

OLEFINS

U ALKENES

OLFACTORY PERCEPTION

Olfactory tract terminal distribution in prepyriform cortex

01 p0017 A71-11455

Electrophysiological studies of olfaction in vertebrates, describing role in orientation, sexual behavior and population control

08 p1241 A71-21942

Human olfactory analyzer, describing equipment for discrete delivery of successive stimuli

09 p1398 A71-22485

Organisms olfactory extraction and interpretation of low intensity chemical signals from air, outlining receptor mechanism from air physicochemistry

10 p1563 A71-24234

Human odorant evoked response, considering stimulation of olfactory receptors and trigeminal afferences in nose 13 p2012 A71-28891

Temperature, odor mixing and stimulation frequency effects on olfactory receptor potential of fly *Lucilia sericata* 14 p2186 A71-30568

Fly *Lucilia sericata* olfactory receptor and unit action potentials response to odor stimulation by homologous compounds 14 p2186 A71-30569

Human olfactory perception of inspired air composition, noting sensory differentiation improvement with subsequent exposures in space flight training 22 p3505 A71-42800

OLIVINE

Nonseparated grain low iron olivine and pyroxene in carbonaceous meteorite Orgueil, using optical and electron probe microanalysis 02 p0318 A71-12904

Cations partitioning between coexisting single and multisite phases in pyroxenes and olivines 06 p0894 A71-18236

Apollo 12 sample zoned olivines, determining Fe, Mg, Si, Ca, Mn and Cr distributions by electron probe analysis 14 p2315 A71-30865

Crystallization behavior and chemical compositions of Apollo 11 lunar basalts including olivine and silica normative varieties 16 p2637 A71-33512

Microcrater morphology in lunar soil glass, olivine and olivine, determining projectile velocity, impact angle and shape effects 18 p2961 A71-35947

Static ductile deformation in quartz, olivine, pyroxenes and plagioclase, noting plastic deformation and recovery 19 p3050 A71-37664

Aqueous etchant for charged particle tracks revelation in olivines 23 p3737 A71-43544

Minor element concentrations and population sources of Apollo 11 and 12 olivine and plagioclase, using microprobe analyses 23 p3738 A71-43614

Mineralogical and petrographic investigation of olivines, feldspars and pyroxenes in Apollo 12 fines and igneous rocks, using optical and X ray diffraction 23 p3741 A71-43631

Olivine accumulation in Apollo rock 12040 and basaltic fragments, using textural and microprobe analyses 23 p3742 A71-43644

Pyroxenes and olivines in lunar rocks from Ocean of Storms, observing plastic deformational processes since crystallization by optical, X ray and electron microprobes 23 p3744 A71-43657

OMEGA NAVIGATION SYSTEM

Omega for aircraft navigation and traffic control, discussing reliability, resolution and prediction errors 06 p0924 A71-17924

Long range hyperbolic navigation in U.S., discussing loran and Omega systems 14 p2272 A71-30711

Omega navigation application to general aviation aircraft, presenting diurnal course shift to overcome deficiencies 17 p2776 A71-35767

Integrated airborne Omega/inertial navigation systems performance prediction using statistical models for position fix errors 17 p2776 A71-35769

Unaided, integrated and differential OMEGA radio navigation configurations, comparing accuracy and suitability for airways system operations 22 p3571 A71-42082

Long distance radio navigation and tracking systems, discussing Dioscours, Loran C and Omega 24 p3845 A71-44351

OMNIDIRECTIONAL ANTENNAS

NT MONOPOLE ANTENNAS

NT TUNABLE ANTENNAS

Omnidirectional radar moving target detection from clutter, using Doppler filter system 09 p1407 A71-23047

Geometry optimization of error-free distributed nondirectional aperture array receivers, using signal detectability technique 09 p1408 A71-23491

Omnidirectional broadband telemetry antenna array for spacecraft providing near isotropic circular polarized radiation with open line microstrip feed 14 p2199 A71-30907

Optimal omnidirectional antenna array located on cylindrical head section of sounding rocket for L band telemetry 14 p2216 A71-31035

Computer program for processing of UHF radiation patterns of ESRO 4 scientific satellite omnidirectional antenna systems 14 p2217 A71-31051

Quasi-isotropic directional, omnidirectional and auxiliary antennas of Helios Solar Probe S band system, discussing design, radiation patterns, adaptability and X band measurements 14 p2217 A71-31052

Omnidirectional one slot aerial energized by dielectric waveguide for hypersonic vehicle-ground communication through ionized shock layer 18 p2887 A71-36022

VOR antenna system with Alford loops above circular conducting ground plate, investigating radiation fields 18 p2894 A71-36827

OMNIRANGE NAVIGATION

U VHF OMNIRANGE NAVIGATION

ON-LINE PROGRAMMING

On-line machine language dynamic debugger for Operating System 360, using graphic display terminal or operator typewriter 01 p0045 A71-i0193

Project DARE/Differential Analyzer Replacement/providing all-digital on-line digital simulation of dynamical systems 01 p0046 A71-10199

NASA Space Documentation Service on-line information retrieval system using direct access remote consoles 01 p0183 A71-10397

Radar reflectivity pattern calculation from cumulus cloud growth numerical model, noting similarity with radar data from on-line computer system 01 p0118 A71-10584

PERL programming language for on-line control of industrial processes and scientific experiments 01 p0051 A71-11186

Fast on-line block-diagram-based DARE II digital simulation program for use on PDP-9 computer with CRT display console 02 p0226 A71-11779

Computer controlled mass spectrometer system, processing spectral information data for on-line graphic system output 02 p0253 A71-12550

On-line parameter tracking algorithm, obtaining parameters in mathematical relation between full wave rectified EMG and human triceps muscle force during isometric task 03 p0374 A71-14423

On-line interactive graphical computer program systems for approximation problems, including least squares method 06 p0871 A71-18210

On-line computer systems performance characteristics determination through functional simulation, using FORTRAN IV program packages [AIAA PAPER 71-230] 07 p1068 A71-19708

Interactive computer graphics in cartography, considering on-line updating of digital topographic map file by human decision making 08 p1281 A71-21248

ECG signals on-line and real time monitoring mathematical, statistical and bioengineering considerations 08 p1248 A71-21330

Pattern recognition feature subset selection based on sequential decision model for on-line processes 09 p1411 A71-22624

System identification, considering input signals classification, model structure, linear/nonlinear systems identifying and on-line/real time techniques 10 p1586 A71-24736

On-line closed loop adaptive control for tracking filter with several inputs and outputs 10 p1586 A71-24739

On-line computer technique for pulmonary ventilation continuous/automatic measurement of cardiac patients exercise and work tolerances 11 p1734 A71-25255

MODAPS real time data processing system for modal vibration testing consisting of analog subsystems, digital interfaces and on-line minicomputer 11 p1746 A71-26502

Automation in cardiology, discussing analog and digital computer techniques for on-line hemodynamic analysis and collection and manipulation of cardiovascular data 13 p2016 A71-27868

Hybrid computer program for data reduction or on-line analysis of nystagmus during closed loop experiment involving visual and/or vestibular function 13 p2022 A71-29359

Photoelectric scanning photometer for visual binaries measurement, using on-line computer for data sampling and acquisition from three photon counters 14 p2246 A71-30357

On-line real time optimal control computations for aerial combat games between two aircraft, assessing airborne computer requirements 16 p2525 A71-34022

Variable star brightness measurement, using on-line electronic computer, analog to digital converter and reflector with direct current amplifying photometer 17 p2741 A71-34990

On-line identification for nonlinear system from noisy measurements, applying stochastic algorithm to hybrid simulation of chemical process models 20 p3207 A71-38974

Computer programming for on-line correction of microwave measurements of loss and reflection effects between network analyzer and device/circuit under test 20 p3205 A71-39377

On-line digital dampometer for free oscillation wind tunnel model study under varying Mach number and stagnation pressure avoiding flutter destruction 21 p3363 A71-40391

Interactive graphical computer system with remote on-line consoles for engineering problem modeling and analysis, giving illustrative examples 22 p3516 A71-41868

Computer program for on-line determination of minimal realizations of transfer function matrices, using Rosenbrock system matrix formulation 22 p3526 A71-42285

Pattern recognition problems, using on-line picture language program with flying spot scanner 22 p3519 A71-42767

ONBOARD EQUIPMENT

NT AIRBORNE EQUIPMENT

NT AIRBORNE/SPACEBORNE COMPUTERS

NT AIRCRAFT EQUIPMENT

NT SPACECRAFT ELECTRONIC EQUIPMENT

Satellite with onboard equipment for astronomical IR spectroscopy, considering stabilization accuracy and measurement duration effects on spectral resolution 01 p0163 A71-10395

Space navigator operations, procedures and computer interface and manually aided onboard Apollo cislunar navigation system possible improvement 01 p0124 A71-10510

Space vehicle onboard navigation and guidance systems capability, considering Apollo transition from direct task interaction and supervision to functional man machine communication 01 p0124 A71-10511

American ATA prototype aircraft collision avoidance equipment and proposed noncooperative system 01 p0125 A71-10753

Space shuttle integrated electronic onboard and ground reusable systems design, considering data flow management, checkout, computer decentralization, electronic switching and redundancy 02 p0231 A71-11978

Skyнет satellite mission profile, onboard equipment and control system, discussing communications, command/telemetry processing equipment, electrical power sources, and secondary propulsion 02 p0320 A71-12429

Trapped protons east-west asymmetry observations during Gemini 4 flight, using on-board high sensitivity plastic-scintillation spectrometer 03 p0479 A71-14041

Europa I third stage flight testing for onboard control system performance parameters [DGLR-70-061] 05 p0815 A71-15963

Satellite ion energy analyzer with onboard data reduction for ionospheric ion temperature and concentration measurement with high temporal resolution 05 p0755 A71-17139

Zinc-silver oxide batteries underwater and aerial applications, designing medium high rate long life cells 08 p1236 A71-21102

Space shuttle onboard vs ground checkout systems, considering vehicle autonomy and cost reduction [AIAA PAPER 71-311] 09 p1427 A71-22623

Projectiles yawing and rolling over long flight paths, describing onboard solar aspect sensor and telemetry link to ground stations [AIAA PAPER 70-538] 11 p1761 A71-25513

Flight test completed on onboard real time engine performance monitoring system, discussing thermodynamic analysis technique [ASME PAPER 71-GT-77] 11 p1813 A71-25991

Onboard aircraft refractometer design, operation and effectiveness 13 p2067 A71-28250

Onboard area navigation systems in ATC environment, discussing route structure and flight instruments [SAE PAPER 710455] 13 p2098 A71-28332

Optimality conditions for initial functions of time lag control systems onboard flight vehicles with transient response dependent on preceding trajectory coordinates 13 p2043 A71-28733

Skylab program organization and management, system design, operations and equipment 15 p2499 A71-31457

Onboard meteorological pulse radars for cloud formations detection, navigational aids, ground reference points determination and relief surveillance 15 p2371 A71-31920

Satellite communication application to maritime mobile service and position determination, discussing VHF and UHF space and shipborne equipment and modulation systems 17 p2697 A71-34241

- Traveling wave tube for reflex type amplifier on-board space communication satellite, discussing prototype reliability and performance
17 p2714 A71-34682
- Onboard orbit navigation scheme free from sensor uncertainty cause constraints, using satellite ejected from spacecraft into near orbit
17 p2772 A71-35053
- Multiple access satellite digital communication system with onboard distribution center, discussing time frame synchronization methods
17 p2706 A71-35105
- Aircraft loading system consisting of onboard weight and balance equipment and fully mechanized cargo pallet transfer, using computerized simulation model for parametric evaluation
[SAWE PAPER 900] 17 p2676 A71-35811
- Strut pressure and axle strain gage systems testing for balance and weighing onboard De Havilland C-7A aircraft
[SAWE PAPER 881] 17 p2676 A71-35827
- Scanning electron microscope examination of components and materials quality and reliability in satellite onboard equipment
18 p2890 A71-36537
- Onboard approach guidance instrument for Grand Tour to outer planets missions reducing fuel for corrective maneuvers by estimating trajectories
[AAS PAPER 71-119] 19 p3101 A71-37914
- Transient performance of phase locked loop on-board tumbling satellite, noting relation to time, SNR and fade modulation
20 p3196 A71-38871
- Two stage reusable manned space shuttle computerized onboard data management system hardware and software
[IBM-712000405] 22 p3517 A71-41977
- SkyLab program data management systems, discussing onboard data collection, transmission and ground facilities
22 p3610 A71-42007
- Planetary gravitational fields variations determination by onboard gravity gradiometer instrumentation
[AAS PAPER 71-364] 23 p3729 A71-43034
- ### ON BOARD NAVIGATION
- ### U NAVIGATION
- ### ONE DIMENSIONAL FLOW
- One dimensional motion of unsteady incompressible conducting free jet in transverse magnetic field, noting computer solution by characteristics method
01 p0133 A71-10792
- Shear wave propagation into heat conducting viscoelastic fluids, considering steady one dimensional flow stability
01 p0181 A71-11188
- One dimensional unsteady barotropic fluid flow based on Euler equations, describing rarefied plasma nonlinear motions
03 p0462 A71-13289
- Time dependent finite difference solutions of steady state nonequilibrium quasi-one dimensional nozzle flows
03 p0400 A71-13458
- Unsteady one dimensional isentropic gas flows, discussing nonlinear pressure waves geometry
03 p0405 A71-14345
- Computer solutions of one dimensional flow of constant composition and specific heat ratio fluids, using influence coefficients
03 p0405 A71-14440
- One dimensional ionized gas flow behind shock wave propagating in MGD duct
03 p0466 A71-14569
- One dimensional parallel heat transfer in rarefied gas between infinite parallel laws, using Boltzmann kinetic equation
03 p0462 A71-14570
- Incident shock tube flow interaction with one dimensional MHD channel flow
04 p0632 A71-14687
- One dimensional transient heat conduction analysis by iterative isotherm migration method, discussing boundary conditions, stability, truncation error and relative efficiency
04 p0677 A71-15452
- Nonlinear model equation for hydrodynamic perturbations, discussing solution at large Reynolds numbers for one dimensional flow
04 p0575 A71-15609
- Normal shock waves in one dimensional steady flow of two phase medium, noting phase exchanges and lack of internal equilibrium
04 p0579 A71-15822
- One dimensional unsteady flows of combustible gas mixtures with detonation waves generation, noting electromagnetic effects
05 p0833 A71-16502
- One dimensional detonation hydrodynamics of condensed high explosives and small inert particles mixtures on basis of mathematical flow model
05 p0834 A71-16518
- Transonic flow with chemical reactions, analyzing one and two dimensional problem by small perturbation method
[ONERA-Tp-749] 05 p0717 A71-16534
- One dimensional gas flow with radiative transfer, using time dependent difference scheme
05 p0735 A71-16714
- Fully ionized quasi-one dimensional magnetic nozzle flow analysis, including effects of unequal electron and ion temperatures and electron thermal conductivity
[AIAA PAPER 71-141] 06 p0939 A71-18584
- Radiation diffusion in one dimensional isothermal medium moving with constant velocity gradient, assuming complete frequency redistribution and arbitrary absorption coefficient profile
07 p1192 A71-19290
- One dimensional steady supersonic motion of partially ionized two temperature argon-caesium plasma in disk type Hall MHD generator channel
07 p1023 A71-19728
- One dimensional isentropic gas motion in acoustic wave reflection from cylindrical tube nonplane closed end under flow
08 p1276 A71-21478
- One dimensional nonstationary motion of compressible electrically conducting gas with allowance for heat conductivity and viscosity, solving MHD equations
09 p1499 A71-22129
- Positive and negative charged particle beam steady one dimensional motion analysis based on continuity, motion and Maxwell equations, allowing for electrostatic particle interactions
09 p1496 A71-22265
- MHD accelerator in pulsed mode with crossed fields, studying one dimensional steady inviscid flow
09 p1501 A71-22407
- Numerical solution of quasi-one dimensional viscous heat conducting compressible Laval nozzle flows by time dependent finite difference scheme
09 p1545 A71-22454
- One dimensional unsteady barotropic fluid flow based on Euler equations, describing rarefied plasma nonlinear motions
09 p1504 A71-23265
- Quasi-one dimensional approximation equations derivation for electrohydrodynamic channel flows with small interaction parameter, obtaining I-V characteristics
10 p1649 A71-24365
- One dimensional plane adiabatic MHD free expansion of relativistic plasma
10 p1676 A71-24495
- One dimensional Gaussian electrostatic wave packet nonlinear time development due to weak resonant broad beam introduction into cold uniform plasma
10 p1652 A71-24658
- One dimensional flow models of internal combustion engine exhaust silencers in noisy systems
11 p1810 A71-25180
- Unsteady one dimensional time-dependent diabatic gas flow equations reduced to single partial differential equation, deriving solutions for entropy distribution
13 p2158 A71-27829
- Plane one dimensional steady compressible ideally charged gas flow characteristics in electric field
13 p2107 A71-28567
- Convergence and accuracy of modified Gauss-Seidel finite difference scheme, calculating one dimensional Navier-Stokes shock structure
13 p2051 A71-29429
- Critical and near critical two phase flow in venturi tube, applying one dimensional flow equations
[ASME PAPER 71-FE-4] 13 p2051 A71-29447
- Acoustic waves reflection from nonplanar closed end of cylindrical tube with one dimensional isentropic gas flow from Riccati differential equation solution
14 p2227 A71-30665
- One dimensional two phase Stefan problem solution for melting of heated thin plate, comparing iterative methods
16 p2662 A71-33065
- Steady one dimensional MHD flow under transverse magnetic induction, determining maximum power of incompressible fluid generator
16 p2620 A71-34144
- One dimensional flow with boundary layer, considering numerical solution of Navier-Stokes equation at large Reynolds number
17 p2729 A71-35466
- Shock wave profile nonlinear one dimensional problems in gas dynamics, using monotonic difference scheme
18 p2907 A71-36333
- Computer algorithm for simulation of one dimensional unsteady compressible fluid flow in presence of area change, wall friction, heat transfer and entropy gradients
19 p3025 A71-38291
- One dimensional ambipolar diffusion parallel to magnetic field lines, considering plasma cloud imbedded in weakly ionized gas with homogeneous field
20 p3215 A71-38737
- Free vortices from slender wings, controlling strength, position, core stability and thickness on basis of one dimensional flow model
21 p3319 A71-40492
- Ideal gas and liquid droplets two phase flow continuity and motion one dimensional equations, describing relations between velocity, density, pressure and bulk component concentrations
24 p3818 A71-44709
- ### ONISOTROPY
- ### U ANISOTROPY
- ### ONISOTROPY RELATIONSHIP
- Kinetic theory of gas mixtures and thermodynamic laws of irreversible processes, deriving hydrodynamic equations and Onsager relations
01 p0130 A71-10793
- Orthogonality principle in irreversible thermodynamics, proving generalization for Onsager nonlinear symmetry relations
05 p0837 A71-16708
- Onsager relations for Soret-Dufour and diffusion coefficients in moderately dense gas mixtures based on kinetic theory, considering symmetry relations for transport properties
06 p0929 A71-18036
- Macroscopic derivation of Onsager relations for nonoscillatory processes with linear flow in isotropic media
18 p2852 A71-36964
- Crystal lattice drag by conduction electrons and Onsager relationship between electroacoustic coefficients valid for arbitrary topology of Fermi surface
21 p3428 A71-41127
- Multicomponent diffusion process calculation using eigenvalues of Onsager diffusion matrix
22 p3575 A71-42371
- Thermodynamics of irreversible processes extended to nonlinear systems remote from equilibrium, considering Onsager reciprocity relations
23 p3780 A71-43104
- ### OPACIFIERS
- Lead borosilicate glass with crystalline opacifiers, observing microstructure and reflectance
13 p2093 A71-28990
- ### OPACITY
- Opaque minerals in Apollo 12 rocks, emphasizing spinel compositions
01 p0162 A71-11426
- Three dimensional opacity function for phase objects measurements using interferometry, holography or schlieren methods
04 p0596 A71-14969
- Radiative heat transfer between opaque interacting surfaces, investigating surface roughness effects
04 p0684 A71-15513
- Ionizing plasmas partition functions, determining opacities and equations of state
08 p1359 A71-20943
- Mars UV polarization and atmospheric opacity measurements, using ground based polarimetric data at near maximum elongation
11 p1825 A71-25709
- Spectral studies on radiation from molecules, atoms and electrons, demonstrating shock tube applications in opacity measurements
11 p1764 A71-26265
- Backscattering patterns in atmospheric opacity measurements, minimizing errors due to atmospheric inhomogeneities and different stratifications
20 p3257 A71-39334
- Pulsar radiation beaming due to strong magnetic field, computing Compton scattering and opacity
20 p3285 A71-39953
- Errors resulting from linear interpolation use in opacity tables for stellar interior calculations
22 p3599 A71-41923
- Opaque minerals in Apollo 12 lunar rocks from Oceanus Procellarum by reflected light microscopy and electron microprobe analysis, including ilmenite, chromite and troilite
23 p3739 A71-43622
- Spherical stellar atmosphere radiative transfer equation, using regional averaging method with opacity dependence on layer geometrical radius
23 p3766 A71-43828
- ### OPEN CHANNEL FLOW
- Natural convective heat transfer from fin-flat in vertical rectangular arrays, comparing duct and open channel coefficients
02 p0333 A71-12605
- Turbulent pressurized and open channel flows analysis by flow visualization, using solid particles and dynamic ball rate sensors
04 p0578 A71-15627
- Longitudinal diffusivity of turbulent flows in open channels and circular pipes, discussing experiments
20 p3212 A71-39504
- Upstream influence and interfacial waves in open channel two fluid small perturbation flow
23 p3663 A71-43446
- Fluid elements streamwise dispersion in two dimensional turbulent shear open channel flow, using Markovian model for numerical simulation
24 p3817 A71-44421

OPENINGS

OPENINGS

NT APERTURES
NT IRISES [MECHANICAL APERTURES]
NT PORTS [OPENINGS]
NT SLITS
Stress intensity factors for infinite sheet rectangular cut-out with symmetrical edge internal cracks under axial tension

04 p0670 A71-15387

OPERATING SYSTEMS [COMPUTERS]

Multiprogrammed and time shared multiaccess digital computers operating systems design, discussing dynamic memory protection structures

01 p0043 A71-10179

Time sharing executive component of general purpose operating system for digital computers, discussing architecture and construction

01 p0043 A71-10180

Operational memory share supervisor program with storage protection feature for real time multitask digital process control and teleprocessing of electrical power utility system

01 p0043 A71-10181

Feedback role in mathematical operation amplifiers for analog computers

01 p0049 A71-10361

Optimal periodicity of computer systems remedial and preventive maintenance operations based on reliable operation maximum duration

01 p0049 A71-10530

Modulo value influence on computer operation reliability, allowing for supplementary verification equipment reliability

01 p0049 A71-10531

Navy avionics modular multiprocessing digital computer operating system reliability, comparing totally software and partly hardware approaches

07 p1067 A71-18833

Civil Engineering Systems Laboratory remote terminal interactive time sharing computer facility, discussing consulting engineer design office experiences and computing center management

09 p1412 A71-23277

Engineering task and computing devices cost effective matching, methodology improvements and cost penalties for less effective device spectrum utilization

09 p1412 A71-23279

MINSK 22M computer modifications, discussing peripheral switching, interrupt, timing, operation termination and storage, readout, etc

23 p3648 A71-43355

OPERATING TEMPERATURE

Solar cell array for probe mission, using optimized high temperature low resistance modules combined with mirrors of high thermal emissivity

05 p0704 A71-16096

Gas turbine engine nozzle guide vanes under pulsed thermal operation, discussing service life evaluation and increase

05 p0827 A71-16756

Soviet book on short time creep for designing structural and machine parts operating at high temperatures, analyzing stress-strain state

06 p0983 A71-17432

Long time static strength, durability and thermal stability relations determined for heat resistant alloys at operational temperatures

08 p1306 A71-21112

Thermal resistance estimation for machine parts of heat resistant alloys under real working conditions

10 p1686 A71-24190

Gas laser construction and processing techniques, considering operating temperature, cathode processing, bore design and Brewster window material

14 p2255 A71-30706

SNAP-8 mercury Rankine system performance data, investigating design change for reduced reactor operating temperatures

15 p2447 A71-32201

Gas turbine engine nozzle guide vanes under pulsed thermal operation, discussing service life evaluation and increase

17 p2832 A71-35455

Aircraft high temperature turbine engine design, reviewing technological advances coupled with laboratory engine and component tests

20 p3277 A71-39399

OPERATIONAL CALCULUS

Monograph on algebraic theory for ordinary linear time invariant difference systems covering constant shift operators, matrix formalism, operational calculus, etc

16 p2602 A71-33397

Heat conduction equation coupling to wave equation in adjacent regions from operational method solution of Volterra equation reduced problem

19 p3171 A71-38532

Step-change single blow transient temperature response synthesis by data reduction with aid of operational calculus and half-line convolution integral equation theory

20 p3314 A71-39488

Time optimal control synthesis for linear integration-type system described by n-order differential equations, using operational calculus

21 p3359 A71-40165

OPERATIONAL HAZARDS

Critique of paper on explosive hazards of large solid rocket motors, suggesting extrapolation of fractional TNT equivalent

18 p2955 A71-36284

Rockets and launch operations protection from atmospheric electricity at Kennedy Space Center, discussing current and future lightning suppression

18 p2913 A71-36451

Conditional failure density evaluation from hazard rate, considering failure time distribution function, reliability function and conditional failure distribution

21 p3408 A71-40370

OPERATIONAL PROBLEMS

Large earth station operation and maintenance for international communications, noting control consoles, static tracking, aerial flexibility, transmitter reliability, etc

02 p0224 A71-12828

Reliability and maintenance problems of U.S. Army operational environment, noting inadequate design and test criteria during development

04 p0530 A71-15402

Sand and dust effects on military helicopter flight controls and equipment service life, discussing relief program

04 p0533 A71-15430

VTOL operation under snow and ice conditions, discussing adhesion, radiation absorption and electrical properties of ice

04 p0533 A71-15437

Air-to-air, air-to-ground and USN surface-to-air guided weapons operational assessment in military environment

09 p1532 A71-22991

Operational research in designing ground-to-air launch weapons, considering model, effectiveness measure, decision and experiment

09 p1532 A71-22992

Subsonic and supersonic airline operations, restraints, considering noise, air pollution and inadequate airport facilities

12 p1927 A71-26870

Multilevel supply system operationally ready aircraft number evaluator based on item stock levels, demand rates and repair/resupply times

15 p2516 A71-32700

Optimization and operational problems of man powered aircraft, noting Kremer Competition design [ALAA PAPER 71-798]

16 p2525 A71-34023

Material properties, metallurgy, production technology and operational factors effects on machinery structural strength

23 p3779 A71-44207

OPERATIONS RESEARCH

NT CRITICAL PATH METHOD

NT DYNAMIC PROGRAMMING

NT GAME THEORY

NT LINEAR PROGRAMMING

NT MINIMAX TECHNIQUE

NT NONLINEAR PROGRAMMING

NT SADDLE POINTS [GAME THEORY]

Operational research for decision making in weapons procurement and deployment, considering military effectiveness, weapon assessment criteria, local conflict conditions, cost and operational environment

07 p1206 A71-19418

Operational research in designing ground-to-air launch weapons, considering model, effectiveness measure, decision and experiment

09 p1532 A71-22992

Operational research methods application to beam theory, deriving general deformation equation for beams with constant or variable moments of inertia and isostatic or hyperstatic systems

10 p1687 A71-24289

NASA past and future space programs, examining operations analysis problems associated with space missions planning

13 p2133 A71-28030

Processes involved in obtaining materials required for socialist organization operation, discussing operations, cost reduction by work mechanization and optimum data processing

13 p2167 A71-28492

Operations research minimum cost model of aircraft noise abatement in airport communities [ALAA PAPER 71-525]

14 p2339 A71-29551

OPERATOR PERFORMANCE

Operator behavior in man/machine system, using multidimensional manual control system model with random sampling time and information theory method

03 p0368 A71-12996

Computer operators activity analysis, suggesting computer center layout

04 p0547 A71-15847

Operator reliability control models, discussing rational work-rest schedule for man machine systems

05 p0731 A71-17017

Human operator psychophysiological characteristics as cybernetic man machine system components, emphasizing human memory activity

07 p1050 A71-20117

Excretion patterns of air traffic controllers for stress appraisal, using urinalysis

08 p1246 A71-20811

Air traffic controllers legal responsibility and disciplinary procedure, considering clearances, flight crew instructions and aircraft accidents

09 p1548 A71-22891

ATC automation system design, considering controllers decision time savings

10 p1640 A71-24271

Multiple suprathreshold visual and auditory monitoring tasks, evaluating vigilance decrement, individual differences, intertask relationships and channel capacity

12 p1874 A71-27248

Sensomotor activity tests of operator perceiving high speed stimuli in broad visual field for psychological selection of aircraft and spacecraft pilots

13 p2018 A71-28416

Performance differences between tactile and visual localization and temporal ordering ability, using sequential presentation of high rate point stimuli

15 p2363 A71-31948

Human operator work quality evaluation with EEG data based on brain electrical activity as function of central nervous system

15 p2365 A71-32530

Operator mental performance reliability prediction from heart beat rate and electromyogram

16 p2534 A71-32826

Factor analysis of phase discrimination in mental fatigue during diurnal variation of cortical functions in railroad traffic control center operators

17 p2688 A71-34362

Fatigue and stress measurement on air traffic controllers, using critical fusion frequency methods, tapping tests, self rating and urine catecholamine

17 p2688 A71-34365

Human operator models parameter estimation by stochastic approximation, considering continuous and sampled data models

19 p3007 A71-37648

Test equipment for evaluating human higher nervous activity, noting use for radiotelegraphist selection

19 p3007 A71-37775

Spacecraft manual control investigation, using human operator models described by linear transfer function with variable coefficients

20 p3193 A71-39226

ATC display device man-computer interaction faults and delays effects on operator performance

21 p3413 A71-40119

Human response time for urgent signal after operational rest, showing effect of additional activation during waiting period

21 p3337 A71-41060

Operator performance improvement in monitoring automated processes by alternating displays, discussing simulated radar and sonar CRT display laboratory tests

22 p3501 A71-41636

OPERATORS [MATHEMATICS]

Shear-invariant mean value of positive-definite operator on bicomplex group in form function of integral sequence, considering ergodic theorem

01 p0110 A71-10097

Incorrectly posed variational problems with nonlinear unbounded operators, demonstrating solution by regularization method and beta convergence

01 p0112 A71-10489

Pontryagin space and convergence of Bubnov-Galerkin method for equations with involution operators

01 p0112 A71-11092

Two dimensional mixed boundary value problems solution in elasticity theory by linear differential operators, applying to Dirichlet and Neumann problems

02 p0326 A71-12293

Nonlinear instabilities in shock wave numerical calculations, using Shuman short wave filtering operator

02 p0240 A71-12396

Finite elastic deformation differential operator strong ellipticity conditions, discussing dependence on material elastic moduli

03 p0501 A71-13071

Precommutative bounded and symmetrical unbounded operators extension to commutative bounded and self adjoint operators

04 p0618 A71-14648

Wyld diagram method extended to turbulence decay, considering operators expressed as integrals with kernels

04 p0575 A71-15604

Optimal control with equality type phase operational constraints, obtaining multiplier rules for necessary conditions in maximum principle form

04 p0561 A71-15870

- Neutral functional differential equation solution operator properties 05 p0773 A71-15972
- Structural stability of incompressible elastic rod of variable rigidity flattened along axis, reducing boundary value problem to equation with continuous operator 05 p0828 A71-16987
- Boundary value problems for singular elliptic partial differential operators, with application to region bounded by smooth manifold 06 p0916 A71-17386
- Quasi-H-analytic function classes sufficient conditions for second order linear hyperbolic type H/Hadamard/operator 06 p0918 A71-17575
- Differential operator determination in spectral analysis of inverse problem stability 06 p0865 A71-17582
- Ritz-Galerkin method for solving nonlinear operator equations in Hilbert space, discussing convergence and error estimate 06 p0919 A71-18204
- Dirichlet problem associated with elliptic partial differential equation, discussing integral operator methods for approximating numerical solution 06 p0920 A71-18208
- Unsteady motion of finite span wing in ideal incompressible liquid near solid surface by integral operator method in potential acceleration space 06 p0846 A71-18701
- Kato upper and lower bounds formula applications to Hermitian operator eigenvalues 07 p1146 A71-18748
- Soviet papers on special problems of differential equations and functions theory covering approximation, complex variables, integral operators, etc 07 p1146 A71-19038
- Eigenvectors spectral structure analysis of monotonic and completely continuous nonlinear operator equations in separable real reflexive Banach space 07 p1149 A71-20646
- Quasi-static problems in nonlinear viscoelasticity theory, comparing integral operator and variable moduli methods for convergence and accuracy of successive approximations 09 p1537 A71-22513
- Reducible parametric systems of second order linear differential equations with variable coefficients for FM or AM-FM oscillations and Riccati equations 10 p1586 A71-24712
- System identification problems, discussing approximation by polynomial integral operators, determinable classes in spectral decompositions, observation noise and stochastic systems stationary in observation time 10 p1587 A71-24742
- Structural dynamics motion matrix Newark generalized acceleration operator, Wilson averaging variant and Gurtin variational principle investigations for stability and approximation viscosity 10 p1693 A71-25050
- Satellite antenna power density contours on earth, using pattern operator for coordinate transformation 12 p1881 A71-27423
- Dirichlet problem for elliptic differential equations with lowest derivatives coefficients and leading term in Bitsadze operator, discussing reduction to singular integral equation 12 p1923 A71-27511
- Adjoint Green operator use in parabolic problems with normal boundary conditions 13 p2094 A71-27804
- Bifurcation points in equation Au equals Mu with A as monotonic nonlinear operator and T as completely continuous nonlinear operator in real separable Hilbert space 13 p2094 A71-28274
- Optimal control problems solution using linear vector space of continuous operators with constraints in Volterra integral and functional differential equations 13 p2043 A71-28829
- Differential equations analytic theory - Conference, Kalamazoo, April-May 1970 13 p2096 A71-29422
- Linear positive convolutive operators, considering convergence problem 15 p2439 A71-31144
- Difference analogs of Dirichlet problem for second order quasi-linear elliptic operators with mixed derivatives, using discretization method 15 p2442 A71-32312
- Electrodynamics Lagrangian with gauge invariant electron operator, obtaining free field nonequal time commutators and photon propagator for perturbation theory 16 p2610 A71-33269
- Monograph on algebraic theory for ordinary linear time invariant difference systems covering constant shift operators, matrix formalism, operational calculus, etc 16 p2602 A71-33397
- Matrix trace method for identities relating eigenvalues of singular ordinary differential operators and zero Bessel functions 16 p2603 A71-33593
- Uniqueness theorem for second order differential equation associated with inverse problem of spectral analysis, developing operator transformation procedure 16 p2603 A71-33890
- Self adjoint expansion of Laplace operator with point spectrum, establishing uniform convergence and Riesz summability conditions of spectral decomposition 16 p2603 A71-33999
- Nonhomogeneous media electrodynamic, solving nonstationary equations by differential operators dependent on permittivity and permeability 17 p2776 A71-34277
- Fourier coefficients and integral operators S numbers of summable functions 17 p2765 A71-34864
- Unbounded linear operator in Hilbert space, constructing characteristic function for transformation 17 p2765 A71-34865
- Functional analysis of nonlinear nonautonomous and autonomous periodic oscillations by treating equations and periodicity conditions for initial displacements and velocities as generalized operator equation 17 p2782 A71-34936
- Equilibrium strategies for linear games with quadratic costs in Hilbert space, deriving nonlinear equation in allowed operator feedback spaces 17 p2723 A71-35297
- Linear neutral differential equation uniform asymptotic stability relation to perturbed differential equation containing bounded linear operators 17 p2767 A71-35523
- Non-LTE problems computation based on integral equation approach, using discrete operator for radiative transfer equation solution 17 p2808 A71-35552
- Time ordering operators applications to nonlinear unsteady systems, covering stochastic differential equations solution and phase locked loop phase error probability density calculation 18 p2940 A71-36222
- Difference methods for hyperbolic flow equations, using third order accuracy space and time split difference operators 18 p2844 A71-36305
- Structural stability of incompressible elastic rod of variable rigidity flattened along axis, reducing boundary value problem to equation with continuous operator 18 p2982 A71-36787
- Dielectric potential operator as arbitrary bounded Lebesgue measurable set, obtaining eigenvalues and eigenfunctions spectrum 18 p2942 A71-36820
- Symmetric operators family spectrum with generalized Rayleigh functional, showing analogy between linear and nonlinear theory at infinite spatial dimension 18 p2942 A71-36821
- Nonlinear operators differentiation and integration, considering Gateaux and Frechet derivatives and Riemann integral 18 p2943 A71-36953
- Nonlinear operators properties, considering differential role in nonlinear functional analysis 18 p2943 A71-36954
- Operator solutions of nonlinear equations in linear feedback optimal control 18 p2943 A71-36956
- Algorithms and operator matrix language for infinite linear automata analysis, synthesis and identification 19 p3024 A71-37223
- Covariant definition of radius vector in Riemann space, studying position operator in general relativity theory 19 p3105 A71-38582
- Iterative finite difference solution of Laplace operator interior eigenvalues and eigenfunctions, noting convergence in application to Helmholtz equation 20 p3201 A71-38755
- F-bounded erasing operator in abstract family of language for mapping, applying to families defined by tape-bounded Turing acceptors 20 p3201 A71-38846
- Eigenfunctions of curl operator, rotationally invariant Helmholtz theorem and applications to electromagnetic theory and fluid mechanics 20 p3255 A71-39575
- Theorems on parabolic and hyperbolic differential equations solutions continuous dependence on elliptic operator coefficients, deriving proof by hypothesis of existence and uniqueness 21 p3408 A71-40651
- Cauchy problem theory covering analytic and nonanalytic functions, Gevrey function spaces, hyperbolic operators and differentiable functions spaces 22 p3566 A71-41513
- Conditions definition for nonexistence of continuous right inverse for surjective linear partial differential operators on Frechet spaces 22 p3568 A71-42693
- Factor methods convergence for abstract equations with nonlinear entirely continuous operators 23 p3699 A71-43570
- Approximate solution for equation in linear normed space by error operator norm optimization, applying to elliptical cylinder type compact sets 23 p3699 A71-43574
- Stability conditions of linear discrete system with periodic feedback from spectrum location of bounded linear operator acting in Banach space 23 p3657 A71-44078
- Biharmonic operator eigenvalues for rectangular domain, presenting bilateral a posteriori estimation methods based on discrete analysis and approximate separation of variables 24 p3842 A71-44476
- Unsteady random processes structural analysis application to nonlinear dynamic systems, evaluating algorithms effectiveness and improvement by self adaptive operators with finite memory 24 p3815 A71-44705
- Finite sigma groups complemented with quasi-permutable operators 24 p3843 A71-44796
- Orthogonality and positive operators on space of almost periodic and quasi-periodic functions, using frequency-power formulas 24 p3843 A71-44961
- OPERATORS (PERSONNEL)**
NT AIRCRAFT PILOTS
NT PILOTS (PERSONNEL)
NT TEST PILOTS
- Communication satellite systems ground stations operating personnel training, outlining basic and specialized study and on-job training program 02 p0224 A71-12826
- Psychophysiological, strict engineering-psychological and systems engineering analyses solving engineering-psychological problems in large control systems for human operators 03 p0369 A71-13001
- Body position effect on dynamic characteristics of human operator under random vibration, considering pelvis-head amplitude-frequency characteristics 04 p0543 A71-14791
- Objective monitoring of human operator, using statistical analysis of EEG based on numerical characteristics of energy spectrum 17 p2692 A71-35168
- Adaptive mathematical model of human operator during pursuit tracking, synthesizing brain in accordance with arbitrary reasonability criterion 17 p2692 A71-35169
- OPHTHALMODYNAMOMETRY**
Fluorescein permeability of hemato-ophthalmic barrier of rabbits after acceleration exposure 06 p0854 A71-18364
- OPHTHALMOLOGY**
NT EYE EXAMINATIONS
Computerization of medical records of ophthalmology clinic 02 p0206 A71-12109
- Unicocular oscillopsia with vertical retinal nystagmus and internuclear ophthalmoplegia due to multiple sclerosis 06 p0852 A71-17615
- Laser ocular effects, discussing corneal/retinal/lens lesion production, damage thresholds and application to clinical ophthalmological problems 07 p1049 A71-19792
- Aerospace ophthalmology, discussing flying personnel selection, eye anatomy, presbyopia, macular degeneration, cataracts, corneal dystrophy and glaucoma 08 p1238 A71-20721
- Stereophotogrammetric methods and instruments for studying eye anatomical-optical apparatus and pathological changes 13 p2016 A71-28012
- Holography applications in ophthalmology to determine optical constants of living eye, including retinal receptors 22 p3540 A71-41753
- Anatomic examinations and diagnostic techniques in ophthalmologic aviation medicine, discussing electronic time interval and storage measurements, cortical response, etc 23 p3631 A71-42928
- OPTICAL ABSORPTION**
U ELECTROMAGNETIC ABSORPTION
U LIGHT TRANSMISSION
OPTICAL AMPLIFIERS
U LIGHT AMPLIFIERS
OPTICAL COMMUNICATION
Carbon dioxide laser intersatellite communication systems as economical alternative to microwave and millimeter systems, noting use onboard ATS satellites 01 p0091 A71-10009
- He-Ne IR laser resonator as quadratic receiver for modulated filtered laser emission, noting strong L.F. noise 01 p0096 A71-11218
- Laser communications systems techniques, proposed designs and experiments 01 p0039 A71-11340
- Isotropic photooptical channels transfer functions analysis, using two dimensional Fourier transforms 02 p0211 A71-11829

- Image transmission in isotropic photooptical channels, examining object-image brightness relationship
02 p0211 A71-11830
- Light beam deflection due to temperature gradient in laminar gas flow in shielding pipe for laser communication, considering beam waveguide design
02 p0284 A71-11869
- Injection lasers as logic elements in optical communication systems with time division multiplexing, examining optimal switching and pulse duration reduction
02 p0259 A71-11875
- Optical communications for terrestrial and space applications, assessing state of art of optics devices, systems and theory
02 p0212 A71-12001
- Coherent optical sources in form of lasers and parametric oscillators with usable power for communications
02 p0260 A71-12002
- High speed small aperture electro-optic, acousto-optic and magneto-optic modulators for optical communications, considering capabilities and limitations
02 p0231 A71-12003
- High sensitivity photodiode, photomultiplier and photoconductive detectors characteristics for wide-band optical communication
02 p0248 A71-12005
- Optical components and technology for acquisition, tracking, transmit-beam offset and background noise discrimination functions in optical space communications
02 p0213 A71-12007
- Integrated optical communication circuit technology adaptable to batch processing, considering encapsulated planar arrays of rectangular dielectric waveguides
02 p0231 A71-12008
- Beam waveguides for optical transmission, considering cost, attenuation, dispersion and flexibility
02 p0249 A71-12009
- Clear turbulent atmosphere effects on optical transmission characteristics and communication system design
02 p0213 A71-12010
- Optical scatter channel transmission characteristics, using mathematical model consistent with radiative transfer theory and probability-computing receiver
02 p0249 A71-12012
- Background noise in optical communication system, considering direct, reflected and scattered radiation sources in atmosphere
02 p0213 A71-12015
- Free space optical channel analog and digital communication theory, considering SNR, M-ary signaling, error probabilities and information rates, etc
02 p0213 A71-12018
- Atmospheric turbulence effects reduction in optical communication by statistical communication theory, considering digital system and waveform estimation
02 p0213 A71-12019
- Direct detection, heterodyne and optimum receivers for optical scattering channels in digital communication
02 p0214 A71-12020
- Time division multiplexing methods for optical communications systems, considering error performance of digital formats used with mode-locked laser sources
02 p0214 A71-12021
- Frequency division multiplexing methods for wide-band optical communications systems, calculating approximate information capacity
02 p0214 A71-12022
- Optical /and IR/ communication systems design, considering effects of atmospheric turbulence, molecular absorption and aerosol scattering
02 p0214 A71-12023
- Ultrawide bandwidth optical data relay link between earth satellites, discussing system design concept
02 p0214 A71-12024
- Ultrawide bandwidth laboratory laser communication link for high fidelity signal transmission, discussing system configuration, components and preliminary test results
02 p0214 A71-12025
- Optical communication systems cost and weight optimization by COPTRAN program
02 p0214 A71-12028
- Operational laser communication systems performance characteristics review, considering various modulation techniques, heterodyne detection, IR applications, etc
02 p0260 A71-12030
- Optical systems using photoelectron counter system for optical signal detection and demodulation
02 p0214 A71-12031
- Laser channel multipath dispersion due to atmospheric inhomogeneities for point and non-zero-area apertures under clear weather conditions
02 p0214 A71-12034
- Optical PCM communications system with lithium tantalate traveling wave modulator capable of one gigabit/sec transmission and detection rate
02 p0215 A71-12042
- Low level optical signal transient response measuring instrument with nsec resolution and automatic photomultiplier current gain control
02 p0249 A71-12131
- Paraboloidal mirror array of spherical segments for direct detection optical receiver, discussing minimum time dispersion and blur circle
03 p0425 A71-13650
- Communication technology development relation to NASA programs, discussing receivers, microwave tubes, solid state transmitters, lasers, information retrieval and frequency sharing
03 p0388 A71-14412
- Laser communications, discussing directivity and bandwidth characteristics, receiving techniques based on photomixing /heterodyning/ and direct photodetection, modulation and signal design
04 p0550 A71-14720
- Carbon dioxide lasers for wideband data transmission in space
04 p0556 A71-15648
- Bragg diffracted light intensity increase from standing resonating acoustic wave, considering applicability for laser communication multiplexing and demultiplexing
05 p0720 A71-16269
- Optical channel capacity and laser signal distortion through turbulent atmosphere
05 p0720 A71-16288
- FM optical signals detection using Fabry-Perot interferometer with air gap between mirrors
05 p0753 A71-16875
- Structural information propagation in optical wave fields arising in diffraction and scattering of quasis-monochromatic light by fixed objects
05 p0753 A71-16903
- Optoelectronic signal transfer from rotating shafts to stationary equipment without rubbing contacts
05 p0723 A71-16973
- Photoelectron count of lognormally fading optical signal, discussing noncentral chi square random variable approximation
05 p0726 A71-17085
- Photodetector-transistor amplifier coupling for maximum SNR in optical communication systems
06 p0866 A71-17370
- Daytime pulsed optical communication within line-of-sight using GaAs IR laser
06 p0907 A71-17570
- Telecommunications by lasers, considering atmospheric propagation possibilities and limitations
06 p0869 A71-18064
- Geometrical and physical distance measurement by laser telemetry, involving time and speed factors of emission and receiver beams
06 p0869 A71-18065
- Pulse gated binary modulation /PGBM/ visible laser communications for earth orbital missions
07 p1056 A71-18810
- Single frequency carbon dioxide laser cavity length computer aided selection for reduced line competition, considering heterodyne communications systems
07 p1121 A71-18811
- Multichannel laser telephone communication link experimental operation results in U.S.S.R.
07 p1058 A71-18838
- Dielectric thin optical film waveguides excitation for integrated optical circuitry by Gaussian laser beams
07 p1123 A71-19213
- Information rates attainable in optical communication channel
07 p1110 A71-19481
- Optical phase variations on short line of sight path through turbulent atmosphere
07 p1159 A71-19512
- Single mode oversized optical waveguide fabrication and components
07 p1162 A71-20423
- Optimal recognition system for optical spatial and background inhomogeneous Gaussian signals in noise
08 p1257 A71-22022
- Multiwavelength laser beam scintillations and atmospheric turbulence spectra, investigating saturation phenomena, transverse amplitude correlation lengths and signal fluctuations receiver aperture smoothing
09 p1464 A71-22780
- Optical signal heterodyne reception, discussing reduced atmospheric distortion effects
10 p1575 A71-23812
- Binary on-off laser communication channels, calculating atmospheric turbulence effect on Poisson detection error probability
11 p1730 A71-25198
- Gunn diodes and heterojunction laser applications in optical pulse communication systems synthesis
11 p1772 A71-25235
- Optical communication system combining heterodyne noise suppression and direct detection advantages concerning spatial coherence and wide field-of-view receiver optics
12 p1903 A71-26789
- Optimal continuous recording of amplitude-phase distributions on spatial carrier frequency for light wave modulation and optical antenna simulation
12 p1878 A71-26841
- Amplitude modulated optical band signal detection, comparing optimal direct photodetection and superheterodyne receivers sensitivities
13 p0209 A71-28365
- Atmospheric laser link with automatic sensitivity control during reception, measuring detector output signal fluctuation reduction characteristics
15 p2372 A71-32319
- Optimum pulse width and information carrying capacity for dielectric single mode glass optical waveguides under distortion due to attenuation and phase velocity dispersion
16 p2541 A71-33127
- Semiconductor heterostructure junction diode lasers for operation at room temperature, discussing energy band structure and mass communications application
16 p2587 A71-33471
- He-Ne IR laser resonator as quadratic detector for modulated filtered laser radiation, noting strong I.F. noise
17 p2750 A71-34269
- Coherence properties deterioration of laser beam by atmospheric molecular scattering, considering effect on communication system performance
17 p2753 A71-34426
- Communications systems using carbon dioxide laser wave propagation, considering wave extinction by absorption and scattering, scintillations due to atmospheric turbulence, etc
17 p2700 A71-34749
- Short pulse Nd-YAG direct detection laser system for space communications, noting RF links complementation, high data rates, practical size, weight and power requirements
17 p2705 A71-35093
- Airborne vidicoder visual communication system for transmitting single frame TV information in digital form from air to ground over narrow and wideband circuits
17 p2709 A71-35760
- Fabrication technology limitations effect on use of dielectric interference filters in wide angle optical receivers
18 p2946 A71-35847
- Optical homodyne detection of light signal wave front scattered by moving surface with normally distributed roughness, calculating conditions for optimum SNR
18 p2930 A71-36058
- Precision tracking and pointing of laser beams in space for communication, discussing large space telescope /LST/ applications
18 p2920 A71-36090
- ERTS satellite-based laser communication system, calculating cloud cover effect on clear line-of-sight light transmission probability through atmosphere to ground station
18 p2876 A71-36472
- Optical wideband digital communication system performing operational space-ground link functions
18 p2878 A71-36520
- IR CdTe-HgTe detectors for laser space communications at 10.6 microns, using directivity of light waves in vacuo for wideband transmission
18 p2892 A71-36566
- Wideband fiber waveguide communication systems for optical frequencies, considering information carrying capacity limitation by components available for repeaters and terminal equipment
18 p2883 A71-36995
- Harmonically modulated reflected light signals phase shift and demodulation, assuming single scattering
19 p3018 A71-37975
- Beam pointing and tracking requirements for optical space communication system, from energy transfer considerations
19 p3018 A71-38235
- Higher order noisy optical pulse intensity correlations interpretation by statistical model, estimating spike amplitude
20 p3196 A71-39103
- Breadboard simulation model of laser space communications system consisting of carbon dioxide laser, transmitter telescope, GaAs phase modulator and attenuator
20 p3196 A71-39116
- High data rate optical communication system bit error rate determination from models for noncoherent digital baseband and subcarrier modulation formats
21 p3348 A71-40804
- Narrow beam acquisition and angle tracking for spaceborne laser communication links between low earth orbiting and synchronous satellite
21 p3348 A71-40805
- Short-pulse high-rate space digital laser communication components technology, discussing mode locked and frequency doubled Nd-YAG laser source
21 p3348 A71-40806

Signal processing circuits for 1000 MS/S optical communication link using multiplier/signal switch, bit synchronizer and data regenerator 21 p3357 A71-40807

Laser development and applications in telephone communications, manufacturing and holographic memory 21 p3393 A71-40877

Optical phase variations, temperature structure and wind velocity measurements in atmosphere using He-Ne laser beam on 70 m propagation path 22 p3509 A71-41787

Microwave biased germanium IR photoconductive detector for optical communication systems, describing operation principles, signal demodulation and performance 22 p3543 A71-42123

Quasi-optical transmission line stability improvement, investigating pulsating light beam concept 22 p3512 A71-42309

Computer technique for synthesizing binary holograms used in wave beams analysis in quasi-optical communication channels 22 p3546 A71-42320

Weakly guiding glass fiber parameters design formulas and functions for optical communication, considering propagation constant, mode delay, cladding field depth and power distribution 22 p3576 A71-42557

Experimental observation of 10.6 micron guided waves in Ge thin films, noting application to carbon dioxide laser communication 22 p3587 A71-42568

Pulsed signal secondary forward scattering in optical fiber transmission lines 23 p3646 A71-43968

OPTICAL CORRECTION PROCEDURE

Aberration analysis for manual retouching of large objective lenses, using unequal arm laser interferometer 04 p0607 A71-14867

Astronomical telescopes with Cassegrain two mirror optics, discussing optical aberrations and correction methods and modern testing procedures 10 p1612 A71-24690

Lens phase aberration correction in optical system, using holograms 11 p1766 A71-26305

Aberration reduction and optimal in-line and off-axis recording geometry in acoustical holography 12 p1904 A71-26794

Eye accommodation range limiting for increased adjustment accuracy of optico-mechanical instruments, considering spectacle lens, telescope, magnifying glass and microscope 14 p2189 A71-30416

Automatic coordinate compensation for systematic and random distortions of photographs on stereophotogrammetric devices 15 p2406 A71-31619

Aspherization coordinates and error corrections of optical systems with nonspherical surfaces by colliding beam method on digital computer 15 p2406 A71-31620

Optical center position on negative and lens distortion of satellite camera verified on zenith area photos of stellar coordinate measurements 16 p2575 A71-32835

Minimum aberrations in image wave front due to wavelength shift between recording and reconstruction beams in holography, using computer program 18 p2914 A71-35846

High resolution holographic image deblurring methods involving coherent optical analog processing and Fourier transform division filter 18 p2918 A71-36079

Computer best least square filtering and approximation by radial filter of noisy imagery using discrete array transmission from photographic film 18 p2884 A71-36081

Serial edge absolute coded and parallel alphanumeric timing on engineering sequential films, discussing frame selection, marking, offset, pull down and exposure correction 18 p2919 A71-36085

Rectilinear correction of geometric errors of images transmitted from earth resources satellites, using digital computer 18 p2886 A71-36540

Nonlinear compensation for spatial deformation in aerial photography correcting spatial phototriangulation grids 19 p3063 A71-37270

Phase and amplitude error detection in photomasks for semiconductor integrated circuits with spatial frequency coherent optical filtering 20 p3246 A71-39449

Ten cm aperture penta and roof-penta mirror assemblies for telescope internal optical alignment 22 p3549 A71-42553

OPTICAL COUPLING

Optical schemes of laser ring interferometer with selective characteristics, noting coupling via scattering at resonator optical elements 02 p0259 A71-11934

Optically coupled GaAs injection lasers emission spectra, determining maximum frequency difference in gain bandwidths for mode synchronization 03 p0435 A71-13506

Spectroscopic hole burning in coupled saturable dye-ruby lasers with frequency locking 04 p0607 A71-14725

DWBA optical model coupled channels comparison in 2s-1d shell for predicting proton scattering elastic cross sections 06 p0929 A71-17579

Unstable high speed optronic /photoelectric/ flip-flop memory elements with positive optical feedback 07 p1075 A71-19303

Combinational optic third harmonic generation enhancement by simultaneous coupled nonlinear absorption in liquid dye medium with anomalous dispersion 07 p1128 A71-20392

Variable output coupling for IR gas lasers, using Michelson interferometer with polyethylene or polypropylene beam splitter 11 p1773 A71-25805

Mutual coherence effects in time varying radiation fields on two beam interferometric optical discriminator response 11 p1800 A71-26306

Simultaneous mode locking and pulse coupling of carbon dioxide laser achieved by single internal GaAs element, discussing possible application to pulse code modulation 13 p2081 A71-29341

Continuous chemical laser, emphasizing strong coupling in cavity between radiation and chemistry [AIAA PAPER 71-574] 15 p2419 A71-31565

Optical coupling between two axes of laser light beam deflector, using reflective relay optical system for loss reduction, cost effectiveness and easy alignment 16 p2585 A71-33139

Image intensifier tube coupled to smoothing dissector to improve SNR in electronic scanning spectrometer 18 p2914 A71-35850

Optical coupling of degenerative modes in two parallel dielectric waveguides, applying to slab guides and fibers crosstalk problem 19 p3014 A71-37214

Optical dielectric slab waveguides with core thickness variations, computing crosstalk due to light scattering in terms of guided mode radiation loss 19 p3014 A71-37215

Diffraction loss equality in field distribution at confocal laser resonator mirrors with circular coupling holes 20 p3242 A71-38850

Gas laser asynchronous coupling modulation, examining dependence on lasing threshold, optical spectrum and transition line shape 20 p3199 A71-39811

OPTICAL DATA PROCESSING

Autocorrelation of weather radar precipitation patterns by incoherent optical method 01 p0030 A71-10599

Noncoherent optical analog image processing by corrective convolution integral techniques for removal of blur, defocus and noise 01 p0081 A71-10828

Coherent optical data processing system imaging qualities photographic film requirements 01 p0050 A71-10900

Electronic contour line recorder with intermittent line setting capacity and interpolation frequency regulation 01 p0083 A71-11329

Information retrieval system at Extra-terrestrial Photographic Information Center (EPIC) for identification of extraterrestrial photographs from satellites and manned space explorations 01 p0184 A71-11425

Contour signal characteristics for cloud form recognition by computer using learning algorithm and photographic data 02 p0225 A71-11691

Holographic filters for optical automatic pattern recognition systems, discussing reconnaissance target and fingerprint 02 p0247 A71-11702

Strain data retrieval from moire or photoelastic patterns by numerical technique based on light intensity distribution phase angle 02 p0225 A71-11703

Automatic pattern recognition in photographic transparencies, using diffraction pattern sampling 02 p0225 A71-11704

Information content and digital storage of aerial photography using assessing entropy of written English text 02 p0248 A71-11953

Optical systems using photoelectron counter system for optical signal detection and demodulation 02 p0214 A71-12031

Visual information industrial processing rates correction tables with digits, letters, Landholdt fringes and geometrical figures 03 p0364 A71-13525

Coherent optical data processing systems resolution testing, using multifrequency linear diffraction gratings 03 p0425 A71-13644

Holographic twin image elimination by nonlinear method based on statistical differences in objects and diffraction fields 03 p0425 A71-13656

Neurophysiological aspects of human optical and acoustical perception, discussing pattern recognition and cognizance role in optical image evaluation 03 p0373 A71-14331

Matrix addressed polarization rotating or retarding light valve arrays for optical selectors, composers and displays from nonswitching threshold materials 03 p0430 A71-14468

Semiautomatic device for vertical circle limb photographs measurement, involving beam splitting with subsequent comparison of modulated components 04 p0591 A71-14850

Semiautomatic photoelectric apparatus for limb graduations using pivoted optical arrangement, discussing accuracy, measurement rate and reliability improvement methods for similar instruments 04 p0591 A71-14852

Spatial filtering for digitally deconvolving noisy degraded image by exploiting fundamental identity between vector convolution and polynomial multiplication 04 p0627 A71-15685

Fourier transform formalism of sampling theorem in frequency domain used in coherent optical processor, obtaining multiple reproduction of space limited functions 04 p0627 A71-15686

Single and multiple exposure storage holograms with comparable diffraction efficiency 05 p0748 A71-16261

Optical fields holographic subtraction for SNR enhancement 05 p0748 A71-16262

Laser document scanner for computer entry and communications systems 05 p0762 A71-16480

Book on optical data processing covering light characteristics, Fourier transforms, spectrum analysis, photographic film, filtering, holography, etc 05 p0754 A71-17124

Multispectral and multi temporal digital imagery spatial registration using fast Fourier transform techniques, applying to earth resources satellite imagery preprocessing 05 p0756 A71-17147

Mars Mariner 6 and 7 flyby missions, discussing surface and atmospheric information and data processing techniques 06 p0965 A71-17626

Holographic optical memory and computer output applications for rapid bulk data storage, considering various laser visualization systems 06 p0908 A71-18067

Monolithic optically written and electrically read semiconductor-ferroelectric memory device employing single crystal barium titanate 07 p1067 A71-19261

Coherent optical data processing principles, discussing lens, diffraction, focused wave front, intensity vs amplitude and spectrum analyzer 07 p1067 A71-19627

Coherent optical data processing techniques, discussing diffraction phenomena, spectral analysis and holography 07 p1067 A71-19629

Coherent optical multichannel profiling correlator for increasing automatic stereocompilation speed by X parallax profiles simultaneous measure and display 07 p1114 A71-20209

Variable emission star BD plus 28.637 deg three color photographic observation data evaluation, giving light curves and H-R position 07 p1201 A71-20435

Kerr magneto-optical effect display as input to coherent optical computer, using laser lens impressed thin film matrix 08 p1258 A71-21185

Optical data storage photodetector output signal to noise and signal to background ratios, using Fourier transform amplitude and phase holograms 08 p1287 A71-21186

Natural image computer for terrain pattern recognition and delineation from aerial photographic inputs 08 p1281 A71-21255

Optical data processing by incoherent matched filtering with Fourier holograms 08 p1291 A71-21401

Automatic procedure for determining cloud motion from geosynchronous satellite pictures based on cross correlation, discussing real time operational system 08 p1327 A71-21454

Transform coding techniques using orthogonal matrices to implement bandwidth or dimensionality reduction for image processing in digital communication systems 08 p1259 A71-21591

Optical information processing systems, considering spherical lens derivation of two dimensional Fourier transform

09 p1493 A71-22776

Lens-prism model for holographic image processing in space-frequency domains with chirp signal interferometric compression

09 p1452 A71-23565

Holography utilization to data processing, discussing factors affecting recording and matched filters creation for pattern recognition

10 p1581 A71-23917

Thin holographic recording and retrieval from semipermanent optical memories

11 p1762 A71-25624

Computer program algorithm for satellite photographic observation data processing based on measurement at one station

11 p1733 A71-25833

Spatial filter synthesis for real time combined subtraction and correlation in coherent optical data processing system

12 p1905 A71-26808

Optical Fourier transformers zero order removal for low spatial frequency signal components detectability improvement

12 p1906 A71-26818

Black and white television scanning ability of color differentiation and gray tone identification by signal fluctuations in aerial imagery

12 p1907 A71-27261

Transistorized multichannel registers for optical oscillograph records, discussing frame storage and digital processing circuitry

12 p1889 A71-27755

Multichannel scaler as interface between edge scan unit and calculator to generate optical transfer functions

13 p2066 A71-28159

Optical pattern recognition by correlation measurements, detecting by zero in intensity distribution

13 p2069 A71-28715

Instant profile image correlator for coherent optical parallel processing, describing laboratory and aerial stereophotographs results

13 p2071 A71-29351

Optico-acoustic autocorrelator for linear FM signals spatial compression, discussing design and performance

14 p2194 A71-30085

Holographic techniques, optical data processing and laser properties for aerospace instrumentation

14 p2244 A71-30329

Video tape recorder /VTR/ for onboard storage of wideband analog and high rate digital sensor outputs of ERTS

14 p2249 A71-30901

Holographic lens magnification aberrations in various Fourier transform optical data storage geometries

15 p2412 A71-32592

Pulse compression and optical data correlation in side-looking radar, considering Doppler effect

15 p2374 A71-32650

Two dimensional pictorial information Fourier transform generation by coherent optics method, applying to imageries in earth sciences

17 p2737 A71-34271

Electronic multiimage processor for enhancement and interpretation of ERTS multiband remote sensor imagery data

17 p2737 A71-34273

Quantum mechanics model of optical parametric amplifier, considering performance of optical information systems

17 p2698 A71-34409

Image dissector photomultiplier for acquisition, guiding, focusing and photometric monitoring in telescope control

17 p2741 A71-34992

GALAXY machine for measuring image position and brightness and converting Schmidt telescope photographic data into computer form, outlining design and development

17 p2741 A71-34996

GALAXY measuring engine for automatic measurement of glass photographic plates taken from Schmidt telescopes, discussing performance

17 p2741 A71-34997

Automatic precise centering on photographic plate star image by movement across scanning slits for orthogonal coordinates and processing in on-line computer

17 p2742 A71-34999

High resolution microdensitometry image interpretation and manipulation by digital computer, discussing radiation coherence problems

17 p2742 A71-35002

Automatic data reduction system for TV images of star fields acquired from OAO

17 p2743 A71-35009

Automatic pattern recognition of urban development changes from aerial photographs, using computer program and nonlinear registration technique for cell pairs partitioning

17 p2711 A71-35043

Mathematical model of human visual system light adaptive signal transformation

17 p2692 A71-35171

Signal processing operation of real time optical correlator, using ultrasonic light modulators

17 p2708 A71-35484

Red blood cell image hologram reconstruction and superresolution based on coherent physical optics, using computer program

17 p2693 A71-35586

Digital processing for automatic extraction of information from reconnaissance images, discussing target and terrain configurations pattern recognition technique

17 p2747 A71-35774

Automated pattern recognition for urban texture and land use assessment by aerial photographs, using digitally scanned optical Fourier transforms

18 p2912 A71-36063

Retina photosensitive cells properties and functions compared with films photosensitive chemicals, emphasizing retinal image transformation

18 p2864 A71-36068

Sinusoidal image distributions generation by changing frequency response of optical system by exit pupil function /incoherent spatial filtering/ modification

18 p2918 A71-36073

High resolution holographic image deblurring methods involving coherent optical analog processing and Fourier transform division filter

18 p2918 A71-36079

Computer best least square filtering and approximation by radial filter of noisy imagery using discrete array transmission from photographic film

18 p2884 A71-36081

Two dimensional optical Fourier approach diagnosing interpretation-limiting pictorial noise patterns in ERTS image output

18 p2919 A71-36082

Computerized digital techniques for image motion compensation as function of additive noise level, using Fourier transform image filtering and half-tone display

18 p2919 A71-36083

Aerospace imagery enhancement for visual interpretation, considering ERTS applications

18 p2919 A71-36084

Rectilinear correction of geometric errors of images transmitted from earth resources satellites, using digital computer

18 p2886 A71-36540

ERTS-A and B pictorial data processing center, describing image processing system and available user services in terms of international participation

18 p2900 A71-36541

Numerical methods for noise elimination from ERTS pictorial data, describing data acquisition system

18 p2886 A71-36542

Electronic processing of coherent optical data for measurement and display using holography, speckle patterns, interferograms, image intensifiers and TV systems

18 p2923 A71-36608

Digital pattern classification of oceanographic remote sensing multispectral airborne scanner data, considering sea surface color variations

19 p3060 A71-38405

Walsh function imagery analysis by Hadamard-Walsh transform and eigenvector expansion technique

20 p3197 A71-39610

Picture processing using general purpose digital computer simulation for reduction of processing time and special purpose hardware investments

21 p3376 A71-40111

Tracking meteorological satellite receiving antenna orientation data computer calculation, obtaining methods for geographic picture gridding

21 p3410 A71-40824

Holographic optical memory broadband development system based on CW Ar ion laser, discussing component operating, power requirement and cost problems

21 p3380 A71-40922

Coherent optical processing system coupled to electronic readout system incorporating image orthicon TV camera, small digital computer and cell generator

21 p3381 A71-40929

Imaging with low redundancy arrays, noting holography role in image processing

22 p3538 A71-41736

Holographic image reconstruction analysis based on two beam interferometry by spatially incoherent light source, obtaining optical transfer function

22 p3539 A71-41740

Digital picture processing and holography, considering spatial filtering computer simulation and image synthesis

22 p3539 A71-41745

Computer synthesis of holograms and spatial filters for coherent optical data processing systems, noting large computational volume required for three dimensional objects

22 p3539 A71-41746

Optical information processing holographic techniques, describing random masks correlation method for pattern classification

22 p3539 A71-41747

Optical image deblurring methods, discussing coherent and incoherent optical analog, incoherent optoelectronic analog and digital computer processing

22 p3539 A71-41749

Real time coherent optical data processing, describing spatial filtering and reactive processor and image converter designs

22 p3540 A71-41750

Rotated pattern detection by optical spatial filtering with superposed holograms, obtaining optimal rotation angle for triangle with digital computer

22 p3546 A71-42475

Holography, covering thin, thick, transmission, reflection, amplitude and phase type holograms principles and applications in interferometry, microscopy, imaging, optical data processing, etc

22 p3546 A71-42476

Microwave quasi-holographic techniques, discussing synthetic aperture, chirp radar, rotating target imaging system and beam forming method

22 p3546 A71-42477

Nonlinear filtering for noise reduction of image data by mean-squared error minimization, discussing zero memory technique

22 p3547 A71-42507

Sampled video data technique with information redundancy for processing and narrow-band transmission, discussing TV display, noting applications in corporate communications and teaching

22 p3547 A71-42508

Return beam vidicon characteristics and applications for reconnaissance, optical storage and scan conversion, data and signal processing

22 p3548 A71-42509

Flat modulation transfer functions obtained by spatial filtering of high aspect ratio annular apertures images in coherent optical processor

22 p3549 A71-42552

Light pen optical writing and erasing with bistable phosphor storage tubes using screen photoconductivity

23 p3651 A71-43437

Physical and technological aspects of holographic recording including optical data processing, Fourier hologram reconstruction and random structure information determination

23 p3679 A71-43896

Radio-optics prospects in signal and information processing, image reconstruction, data transmission, computer storage, display and holographic movies and TV

23 p3681 A71-44344

Earth resources technology satellites image processing system including electron beam recorder, image corrector, electro-optical systems and digital processors as design features

24 p3825 A71-44575

Automatic resseau detection and reference ground control points for computing and correcting geometric and radiometric image for earth resource data, noting correlation with reference system

24 p3806 A71-44576

OPTICAL DENSITY

Statistical properties of multimode quantized optical fields, using density matrix in P-representation

02 p0259 A71-11932

Bone tissue optical density and blood serum and urine calcium content of Soyuz 9 crew members during and after flight

09 p1389 A71-22201

Atmospheric transmittance vertical structure, using aerosol attenuation and optical densities from aircraft sounding under cloudless conditions

11 p1795 A71-25924

Visible exhaust smoke trails from aircraft jet engines, measuring optical density by photographic photometry

13 p2114 A71-28314

Diffraction technique for three dimensional frequency spectra of photographic images using computer program based on Fourier transformation of optical density distribution

15 p2406 A71-31645

Optically dense plasma spectral characteristics, calculating reabsorbed line intensity distribution

16 p2619 A71-33707

Temperature and pressure of optically dense plasma from vaporizing wall gas discharge

19 p3110 A71-37577

Soviet book on optically dense plasma spectroscopy covering radiation reabsorption, transport equation, photon frequency, resonance energy, quantum mechanical calculations and spectral characteristics

20 p3274 A71-39145

Atmospheric transmittance vertical structure, using aerosol attenuation and optical densities from aircraft sounding under cloudless conditions

20 p3257 A71-39215

- Spectral density modulation visibility at Michelson interferometer exit illuminated with white light parallel beam
21 p3375 A71-40072
- Human eyes macular pigment optical density curves through spectral sensitivity measurements, noting differences due to race, environment, age, skin, eye and hair color
24 p3794 A71-44466
- ## OPTICAL EMISSION
- ### U LIGHT EMISSION
- ## OPTICAL EMISSION SPECTROSCOPY
- Photoelectron spectroscopy energy analyzer with spherical retarding field screen, discussing electronic circuit configuration, operational characteristics and spectral resolution
04 p0600 A71-15590
- Soviet laser spectroscopy applications including microsample chemical analysis, superhigh resolution problem, nonlinear optics devices, interferometric seismometer and air pollution analyzer
11 p1776 A71-26351
- Perseid meteors spectroscopic observations, using image orthicon technique for meteor spectral recording at luminosity thresholds below conventional spectroscopic capabilities
13 p2070 A71-29018
- Selective modulation spectroscopy by taking interference between reflected and diffracted beams of modified Michelson interferometer
14 p2241 A71-30137
- Pulsed semiconductor laser as high resolution optical range spectroscopy, noting application to Cs hyperfine absorption
15 p2421 A71-32403
- Book on interference of electromagnetic waves covering Michelson-Fizeau and Fabry-Perot interferometers, Fourier transform spectroscopy, etc
22 p3576 A71-42429
- Computer controlled image orthicon tube for low light level spectroscopy of metastable excited ions transient absorption spectra
22 p3549 A71-42558
- ## OPTICAL EQUIPMENT
- NT ASTRONOMICAL TELESCOPES
NT BAKER-NUNN CAMERA
NT BALLISTIC CAMERAS
NT CAMERAS
NT COLLIMATORS
NT DIFFRACTOMETERS
NT ELECTROPHOTOMETERS
NT ELLIPSOIDMETERS
NT EYEPIECES
NT FRAMING CAMERAS
NT GEODIMETERS
NT HELIOMETERS
NT HIGH SPEED CAMERAS
NT IMAGE CONVERTERS
NT IMAGE TUBES
NT INFRARED SPECTROMETERS
NT INFRARED SPECTROPHOTOMETERS
NT LALLEMAND CAMERAS
NT LIGHT SCATTERING METERS
NT MICRODENSITOMETERS
NT MULTISPECTRAL BAND SCANNERS
NT OPTICAL GYROSCOPES
NT OPTICAL MEASURING INSTRUMENTS
NT OPTICAL MICROSCOPES
NT OPTICAL PYROMETERS
NT OPTICAL RADAR
NT OPTICAL RANGE FINDERS
NT OPTICAL SCANNERS
NT PHOTOGRAPHIC RECTIFIERS
NT PHOTOMETERS
NT POLARIMETERS
NT POLARISCOPE
NT PRISMATIC BARS
NT PRISMS
NT PYROHELIOMETERS
NT REFLECTOMETERS
NT REFRACTOMETERS
NT SCHMIDT CAMERAS
NT SPECTROPHOTOMETERS
NT SPECTROSCOPIC TELESCOPES
NT STROBOSCOPES
NT TELEVISION CAMERAS
NT THEODOLITES
NT ULTRAVIOLET SPECTROMETERS
NT WIDE ANGLE LENSES
NT X RAY TELESCOPES
- Optical point elastohydrodynamic contact, describing optical interference system consisting of chromium plated glass plate and steel ball
01 p0087 A71-10463
- IR astronomical telescope using six independent optical systems with path and phase controls for aperture synthesis
01 p0081 A71-10829
- Czech circumzenithal instrument used with astronomical telescope for equal altitude stellar observation, discussing optical system, electronics and measurement results
01 p0082 A71-10872
- Optical communications for terrestrial and space applications, assessing state of art of optics devices, systems and theory
02 p0212 A71-12001
- Coherent optical sources in form of lasers and parametric oscillators with usable power for communications
02 p0260 A71-12002
- Optical components and technology for acquisition, tracking, transmit-beam offset and background noise discrimination functions in optical space communications
02 p0213 A71-12007
- Integrated optical communication circuit technology adaptable to batch processing, considering encapsulated planar arrays of rectangular dielectric waveguides
02 p0231 A71-12008
- Laser display technology, discussing recent systems, light beam deflectors and modulators
04 p0607 A71-14723
- High precision large optical component surface visual monitoring with aid of small size etalons
04 p0593 A71-14869
- Coherent optical system for range and azimuth ambiguity simulation in radar systems
04 p0551 A71-15010
- Second harmonic generation with focused pump beams of optimum phase mismatch and confocal parameters values for obtaining high conversion efficiency
05 p0762 A71-16337
- Holography and shapes recognition, considering optical memory, information density advantages and optical correlators
06 p0900 A71-18068
- Optical fiber index profiles for long distance light transmission, comparing single and multimode, rectangular and parabolic guides
07 p1159 A71-19174
- Low profile optical system producing annular cone of radiation from point source for high speed aircraft beacon
07 p1107 A71-19203
- Random gain statistics of avalanche diode optical detectors, analyzing simple optical binary receivers
07 p1074 A71-19216
- Radial direction shearing interferometry, considering wave front radial phase derivative display by axicon or circular grating arrangements
07 p1110 A71-19477
- Lens geometry history covering computerized design, prototype testing, optical shop aids and laser interferometry
08 p1333 A71-21177
- Optical elements aspheric testing, using computer generated synthetic holograms
08 p1290 A71-21388
- All-reflection optical device for stellar spectra automatic widening and concurrent night sky spectrum suppression
09 p1442 A71-22068
- Wave interference effects and energy transfer in coupled thin film optical waveguides
09 p1460 A71-22159
- Large aperture telescope in-orbit maintainability packaging, examining optical systems replacement tolerances and astronauts EVA mode accessibility
09 p1446 A71-22742
- Optical parametric oscillator, observing simultaneous oscillation and second harmonic and difference frequency generation
09 p1493 A71-22760
- Selective optical coatings efficiency and thermal properties under solar radiation and radiative heat exchange
09 p1510 A71-23418
- Lateral separation focus sensors for high angular resolution optical systems, reviewing autocollimating optics and operational patterns
10 p1644 A71-25090
- Vacuum UV phototube module for degradation measurement of optical components, including mirrors, windows, lenses and thermal control surfaces [AIAA PAPER 71-461]
11 p1800 A71-26243
- Spacecraft surface contamination, noting effects on thermal control and optical equipment [AIAA PAPER 71-457]
11 p1840 A71-26421
- Optical interferometer with evacuated light paths, describing operating principles, cost efficiency and compactness
14 p2238 A71-29803
- Penta prism angle reduplication by interferometric measurements
14 p2241 A71-30139
- Acoustooptic deflector modulation transfer function calculated from autocorrelation theorem
14 p2241 A71-30141
- Optical aperture configurations effect on image performance, discussing large telescope systems design criteria
14 p2242 A71-30147
- Diffracted limited achromatic doublet lenses for IR instruments, discussing applications to compact optical systems
14 p2242 A71-30148
- Optical surfaces contamination analysis by holographic interferometry, using fringe patterns for contaminant film thickness and uniformity
14 p2244 A71-30330
- Eye accommodation range limiting for increased adjustment accuracy of optico-mechanical instruments, considering spectacle lens, telescope, magnifying glass and microscope
14 p2189 A71-30416
- Image classification by optical and electro-optic processing methods for spatial signal perception and treatment in natural form
14 p2248 A71-30816
- Aspherization coordinates and error corrections of optical systems with nonspherical surfaces by colliding beam method on digital computer
15 p2406 A71-31620
- High angular resolution optical telescopes, considering mirror materials, optical coatings and pointing systems
16 p2580 A71-33739
- Airglow surveys using extended field large aperture interferometer-spectrometer with optical wedge compensators and digital recording
18 p2914 A71-35842
- Photo-optical instrumentation - Conference, Anaheim, California, September 1970
18 p2916 A71-36051
- Pattern recognition multiplex arrangement with optical relay tube and point hologram for image distribution onto spatially separated channels to obtain SNR improvement
18 p2917 A71-36054
- Image recording system low light (IR/SILL) camera design for long range attitude and events (LORAE) telescopes in short missile instrumentation
18 p2919 A71-36086
- Coherence in image plane of incoherent optical system, considering illumination conditions and component impulse response
18 p2920 A71-36104
- Optical readout system for analysis of laser Doppler velocimeter signals displayed on TV screen and recorded photographically
18 p2931 A71-36587
- Two-mirror optical system to study energy dissipation in elastic systems subjected to cyclic straining
18 p2924 A71-36727
- Outer planets Grand Tour spacecraft onboard optical guidance instruments, discussing vidicon and image dissector systems designs [AIAA PAPER 71-945]
19 p3098 A71-37186
- Star comparator automatic azimuth system using long evacuated tunnel transfer to underground inertial guidance laboratory [AIAA PAPER 71-925]
19 p3102 A71-38328
- Design considerations for bulk solid state acousto-optic devices in light diffraction and modulation applications
19 p3066 A71-38411
- Optical parametric oscillator signal wave amplitude fluctuations during nonresonant pumping, calculating damping term governing temporal behavior of deviation from stationary value
20 p3268 A71-38835
- Optical parametric oscillator pumped with laser light, calculating radiation intensity fluctuations
20 p3246 A71-39458
- Homogeneous temperature changes and radial temperature gradients effects on optical lens system, obtaining Bessel type differential equation
20 p3239 A71-39532
- Mirror meridian circle of zero expansion glass for reduction of flexure and refraction instrument errors in astrometry
20 p3240 A71-39539
- Holographic correction of lens aberration in optical system, considering turbulence effect correction
22 p3538 A71-41737
- Tunable CW optical parametric oscillator optimum operating conditions, using barium, sodium and lithium niobate crystals parametric fluorescence tuning curves for comparison
22 p3557 A71-41863
- Optical modeling of antenna radiation patterns from radio hologram of Fresnel region field
22 p3522 A71-42310
- Defocused optical system imaging properties and optical transfer function improvement by shaded aperture, discussing necessary conditions and light absorption effect
22 p3548 A71-42551
- Laser optical system for hyperballistic range hypervelocity models surface erosion measurement, describing instrumentation of front-lighted, silhouette and stereo stations
23 p3677 A71-43513
- Light modulator based on Doppler effect and diffraction, providing spatially separated beams with different wavelengths
23 p3678 A71-43535

Mach-Zehnder interferometric measurement of modulation transfer function of optical instrument disturbed by turbulent atmosphere

23 p3679 A71-43893

Optical anemometers for local nondestructive flow velocity measurements, discussing signal analysis possibilities

23 p3679 A71-43952

Incoherent light bandpass filter to amplify detail contrast of optical system

23 p3679 A71-44010

Optical system superresolution by reduction of temporal degrees of freedom using holography

24 p3824 A71-44453

OPTICAL FILTERS

NT INFRARED FILTERS

Semiautomatic electrophotometer with interference light filters for atmospheric ozone, aerosol and solar radiation recording

01 p0080 A71-10602

Interference passband filters with wide angle lenses for multispectral photography, discussing design and applications

01 p0081 A71-10827

Tunable filter reflecting telescope and accessory optics for H alpha monochromatic photography of electron corona during total eclipse

03 p0424 A71-13626

Ghost images due to reflection between interference filters and Fabry-Perot etalons during measurement of radial velocities

04 p0593 A71-14911

Spectral distribution reproduction of natural objects radiation by iodine lamp and glass filters

06 p0897 A71-17533

Coherent light photoelectric detection probability in background light passing through narrow band filter of rectangular or Lorentz frequency characteristics

07 p1059 A71-18848

Optical astronomy instrumentation automation including telescopes, computer control, filters and detectors

07 p1114 A71-20051

Single mode ruby and Nd glass lasers axial mode selection by dye filters, noting radiation spectra and spatial coherence

07 p1126 A71-20190

Image quality degradation studied with interference-polarization filter of Abastumani telescope, discussing photography of solar spectrum around H alpha line and artificial light source

07 p1115 A71-20443

Aperture concentric diffraction ring differential effects on focal irradiance, using perfect lens half-wave filter model

08 p1333 A71-21178

Multilayer interference optical minus filters low-ripple transmittance design, using equivalent layer concept

08 p1334 A71-21184

Three mirror multiple beam interferometric rejection filter for laser Raman spectroscopy

08 p1289 A71-21379

Holography utilization to data processing, discussing factors affecting recording and matched filters creation for pattern recognition

10 p1581 A71-23917

Wide field high resolution birefringent filter based on Fabry-Perot etalon and Lyot-Ohman filter, discussing limitations and applications

12 p1904 A71-26802

Spatial filter synthesis for real time combined subtraction and correlation in coherent optical data processing system

12 p1905 A71-26808

Real time holography using moving groundglass or fluorescent layer suitable for coherent matched filtering and seeing through fog

13 p2068 A71-28709

Narrow-band photometry of comet Bennett, giving intensity profiles and interference filter transmission curve

13 p2138 A71-28761

Biological tests of laser protective filters for eye as function of optical density and wavelength by sensitivity of in vivo ocular tissue response

13 p2020 A71-29035

Solid state laser with slow relaxation bleachable filter, calculating modes self synchronization probability statistics relationship to relaxation time

14 p2253 A71-30109

Spectral filter effects on Nd-YAG laser performance stability and output

14 p2254 A71-30155

Monochromatic photometry of comets for molecular emission bands in head spectra, using wideband and narrowband filters

15 p2484 A71-31665

German monograph on photographic masks as position frequency filters covering pattern recognition, transfer functions, etc

15 p2410 A71-32309

Optical filter characteristics obtainable with periodic stacks of two dielectric materials having commensurate optical thicknesses

16 p2577 A71-33128

Fabrication technology limitations effect on use of dielectric interference filters in wide angle optical receivers

18 p2946 A71-35847

Partially spatially coherent illumination influence on measurement of correlation function of two dimensional patterns, obtaining formula for optical filtering

18 p2929 A71-35973

Pseudocolor image enhancement by two-separation photographic process, considering transformation curve alterations in CIE space by changes of photographic materials, filters and exposures

18 p2918 A71-36080

Nd-YAG laser optimum single frequency output operation, discussing two-component-mode filters methods using intracavity tilted Fabry-Perot and metallic film reflector etalons

18 p2932 A71-37005

Recording device with Fourier hologram memory based on optical spatial filtration principle for identifying chemical compounds by IR absorption spectra

19 p3064 A71-37773

Holographic matched filter correlator using liquid gate precision plate holder to eliminate necessity for hologram movement

19 p3065 A71-38238

Fourier transform holograms as complex matched filter for pattern recognition and signal detection in coherent optical systems

19 p3066 A71-38239

Real time lensless holographic recognition of spatially incoherent and self luminous patterns on diffusing backgrounds using optical matched multiple filters

20 p3235 A71-39184

Atmospheric optical stability control in ozone or other selectively absorbing gases measurements, filtering out spurious scattered light from aerosol particles

20 p3257 A71-39331

Phase and amplitude error detection in photomasks for semiconductor integrated circuits with spatial frequency coherent optical filtering

20 p3246 A71-39449

Contrast level reading tests of CRT and self luminous display devices with optical filters at high ambient light for cockpit applications

21 p3376 A71-40127

Molecular iodine vapor absorption filter for stray laser light in Brillouin and Raman scattering

21 p3393 A71-41042

Solar limb high resolution photography at different H-alpha wavelengths, using tunable 1-8A and 1A Halle filters in tandem for parasitic light elimination

22 p3596 A71-41455

Rotated pattern detection by optical spatial filtering with superposed holograms, obtaining optimal rotation angle for triangle with digital computer

22 p3546 A71-42475

Compact optical Faraday rotation isolator using terbium-aluminum garnet and high field permanent magnets of rare earth alloys

22 p3559 A71-42566

Steady power pulsation measurement and operation mode theory of ruby laser with bleachable dye filters

23 p3684 A71-43416

Micrometeoroid flux determination from impact sites on Surveyor 3 TV camera optical filter surfaces, noting agreement with Pioneer, Cosmos and Pegasus spacecraft measurements

23 p3766 A71-43820

Dye laser electronic tuning by inserting calcium-molybdenum oxide acousto-optic filter into cavity

23 p3687 A71-44137

Color photography of magnetic particle and penetrant indications, discussing light sources, camera types, filter and film selection, exposure and spectral characteristics of indications

24 p3829 A71-45283

OPTICAL GENERATORS

U LASERS

OPTICAL GYROSCOPES

Ring laser coupling phenomena, presenting angular measurements for laser-gyro with Langmuir-Fizeau and Faraday effect bias

04 p0607 A71-15022

Carbon dioxide laser gyro flowing gas system, considering stability, locking frequencies and ease of construction

05 p0761 A71-16271

Carbon dioxide laser gyro with cavity configuration for polarization isotropy and enhanced competition effects, considering high gain and mechanical imperfection tolerance

05 p0761 A71-16272

High accuracy angular precession measurements with autometric gyro for satellite relativity tests, using optical system with reticle coordinates

09 p1452 A71-23595

OPTICAL HETERODYNING

Direct detection, heterodyne and optimum receivers for optical scattering channels in digital communication

02 p0214 A71-12020

Optical heterodyne receiver design, using nonlinear recursive techniques to estimate atmospheric fluctuation effects on IF signal characteristics

02 p0249 A71-12026

Operational laser communication systems performance characteristics review, considering various modulation techniques, heterodyne detection, IR applications, etc

02 p0260 A71-12030

Optical heterodyne mixing efficiency invariance to thin detector position for small frequency difference between signal and local oscillator

02 p0249 A71-12033

Sulfur hexafluoride absorption lines observation by inverted Lamb dip high resolution spectroscopy, using heterodyne methods

02 p0209 A71-12731

Stellar spectroscopy by optical heterodyning of laser and star light mixing, using He-Ne laser, high speed photocell and RF power measurement equipment

03 p0487 A71-13331

Turbulent supersonic flow measured by laser anemometry, stressing advantages over optical heterodyning

09 p1453 A71-23693

Optical signal heterodyne reception, discussing reduced atmospheric distortion effects

10 p1575 A71-23812

Sensitivity threshold of optical heterodyne receiver as function of laser amplitude spectrum, using photodetector output noise

10 p1622 A71-24882

Carbon dioxide-nitrogen-helium laser optical heterodyne experiment, obtaining various laser transitions by controlling voltage applied to PZT ceramic transducer

12 p1912 A71-26606

Optical communication system combining heterodyne noise suppression and direct detection advantages concerning spatial coherence and wide field-of-view receiver optics

12 p1903 A71-26789

High resolution holographic Fourier transform spectroscopy, discussing interferometer localized interference fringes direct recording method and heterodyning technique

12 p1905 A71-26805

Combined heterodyning, beam forming and cross correlation of broadband multichannel signal from multidimensional phased array, using coherent optical system

14 p2241 A71-30142

Signal to noise ratios for coaxial laser radar system heterodyning signal backscattered from atmospheric aerosol

16 p2541 A71-33138

Flow velocity measurement by laser differential Doppler heterodyning, obtaining SNR from frequency difference between shifted beams

18 p2914 A71-35848

Acousto-optical effects, materials and devices of laser beam control using diffraction and refraction by ultrasonic waves

18 p2932 A71-36607

Bragg imaging with optical heterodyne detection and bandpass filtering, considering resolution, SNR and dynamic range

22 p3540 A71-41777

Interfering beams amplitude modulation, applying optical heterodyne techniques

22 p3512 A71-42321

Line segment orientation visual perception relation to horizontal, vertical and oblique planes, considering induction effect susceptibility and visual illusions

01 p0010 A71-10274

Ball lightning as optical illusion resulting from positive afterimages, noting reports of energy release from ball as possible refuting evidence

10 p1599 A71-23751

Kundt optical illusion rule experimental testing under variable conditions with respect to monocular vision bisecting of horizontal straight lines, rectangles and squares

10 p1562 A71-24205

Comparative contrast and cues for illumination effects on perception of surface lightness, using target cast shadow experiments

12 p1872 A71-26613

Dynamic display of abstract visual perspective using fiber optic material as discrete lines of light-emitting elements

18 p2918 A71-36075

Zoellner illusion as function of inducing and test lines intersect angle and lines density, deriving error functions

18 p2863 A71-37019

Visual and vestibular analyzers interaction, noting reduction in duration of counterrotation illusion and postrotation nystagmus in humans

22 p3505 A71-42797

Optical images

U IMAGES

OPTICAL MASER MODULATION

U LIGHT MODULATION

OPTICAL MASERS

U LASERS

OPTICAL MEASUREMENT

NT ASTRONOMICAL PHOTOMETRY

NT COLORIMETRY

NT ELECTROPHOTOMETRY

NT PHOTOMETRY

NT POLARIMETRY

NT SPECTROPHOTOMETRY

NT STELLAR SPECTROPHOTOMETRY

NT ULTRAVIOLET PHOTOMETRY

NT VISUAL PHOTOMETRY

Meteorological, optical and coronagraphical observations of total solar eclipse of 7 March 1970

01 p0151 A71-10116

Crab pulsar optical pulses time of arrival measurements, discussing various emission mechanisms as cause for pulsar slowdown characteristics

01 p0153 A71-10363

Magnetic fields measurement in plasmas by laser scattering, discussing theory and applications

01 p0133 A71-10747

CW He-Ne laser beam scattering observation for artificial fog droplet size distribution during evolution stages

01 p0094 A71-10831

Atmospheric turbulence characteristic parameters determination by two narrow laser beams

01 p0119 A71-10833

Optical radar system absolute calibration for measuring laser irradiance backscatter function from atmosphere

01 p0094 A71-10874

Projectile velocity measurement by laser and Fabry-Perot interferometer using Doppler effect

02 p0258 A71-11657

Atmospheric refractive index average structural characteristics measurement over 25 km light propagation path, noting diurnal variation

02 p0245 A71-12011

Q switched ruby laser facility for measuring light pulse transmission spatial and temporal response through clouds

02 p0213 A71-12013

Single crystal facet angles and surface energy planes by light reflection for W emitter in vacuum, Cs and iodine

02 p0251 A71-12208

Radio sources optical position measurement on Schmidt plates

02 p0314 A71-12578

Radio sources position errors, comparing optical and radio measurements

02 p0314 A71-12579

Quasars optical positions and magnitude identification for radio sources of 4C catalog

02 p0317 A71-12862

Cladded fibers propagation modes launching coefficients evaluation by Gaussian field laser beam

03 p0433 A71-13170

Lower atmosphere vertical temperature profiles by optical refraction measurements from photographs of equally spaced illuminated targets

03 p0453 A71-13233

Fiberoptic indicator-dilution assessment of myocardial function

03 p0362 A71-13329

Strain-optical constants determination by ultrasonic technique, using Raman-Nath theory for optical diffraction produced by standing ultrasonic wave

03 p0425 A71-13716

Optical evidence of meteoric aerosols in upper atmosphere at maximum Orionids, showing double red luminosity of sky above Adi Ugru

03 p0489 A71-13750

Beams and plates deflection optical measurement using moire gap effect generalized to include linear and rotational mismatches

03 p0507 A71-13754

Laser optical field intensity correlation function determination from photoelectric counting distribution measurements

03 p0436 A71-13876

IR gas pulsed lasers continuous self mode locking, observing optical spectra with scanning Fabry-Perot interferometer

03 p0438 A71-13889

Power meter for large or divergent CW or pulsed laser beams

03 p0427 A71-13919

Alouette 2 satellite spin dynamics measurement based on telemetered optical data

03 p0379 A71-14006

Light scattering and polarization measurements in upper atmosphere by modulated searchlight, indicating dust layers

03 p0414 A71-14018

Spatial vector calculations using laser distance measurement and optical observations

03 p0380 A71-14191

Planet Mars polar and equatorial radii optical measurements comparison with radar and Mariner probes occultations results, determining optical ellipticity

03 p0493 A71-14200

Discrete radio sources precise declinations and optical identifications, using prototype space frequency interferometer

04 p0641 A71-14735

Unequal arm laser interferometer for high precision optics analysis of large astronomical devices

04 p0592 A71-14866

Radio pulsars optical counterparts, comparing absolute intensity with Crab Nebula NP 0531

05 p0802 A71-15940

Optical pulsar search, using Fourier and correlation techniques

05 p0806 A71-16207

Celestial bodies position determination, discussing optical observation, interferometry, radar, lasers and applications

05 p0811 A71-16650

Carbon dioxide refractivity measurement, determining dielectric constant, Verdet constant and Rayleigh scattering cross section by dispersion formula

05 p0717 A71-16908

Small scale isotropic turbulence intensity and refractive index measurements by optical shadow devices

06 p0897 A71-17527

Zodiacal light brightness measurement in three mutually perpendicular directions, tabulating data

06 p0966 A71-17677

Optical crossed-beam measurements of turbulence intensities in cold subsonic air jet shear layer

[AIAA PAPER 71-137] 06 p0902 A71-18580

Solid Teflon fuel pulsed plasma thruster optical measurements, showing different exhaust velocities for neutral, singly, doubly and triply ionized atoms

[AIAA PAPER 71-194] 06 p0948 A71-18632

Statistical optical measurements of solar scintillation due to atmospheric conditions

07 p1111 A71-19489

Cross and single polarized light techniques revealing coarse grained fractures cleavage facets

07 p1111 A71-19582

Gaseous plasma diagnostics by light scattering for localized minimal perturbing measurement of temperature and density parameters

07 p1172 A71-20504

Galactic optical radial velocity measurements compared to 21 cm red shifts derived velocity

08 p1357 A71-20873

Scorpius XR-1 simultaneous radio and optical measurements, discussing correlation of fluxes

08 p1360 A71-20985

Evaporated Rh films preparation at various substrate temperatures in vacuum UV, determining reflectance and optical constants

08 p1343 A71-21183

Optical elements aspheric testing, using computer generated synthetic holograms

08 p1290 A71-21388

Laser Doppler velocimeter, determining basic operational parameters including required particle density, number, type, size, output signal to noise ratio, etc

[AIAA PAPER 71-288] 08 p1304 A71-22011

Electron concentration and superconducting characteristics of Nb-Sn alloys from optical measurements

09 p1507 A71-22234

Polished surface quality control using laser divergent coherent beam

09 p1460 A71-22310

Thermal deflection tests of fused silica mirror blanks by holographic interferometry

09 p1447 A71-22745

Optical observation of structure, composition, thermal spectra and aerosol layers of giant planet atmospheres

09 p1520 A71-22827

Optical transfer function measurement and computation test applications to aerial camera wide angle lens standard design, using interlaboratory comparisons

09 p1494 A71-23001

Atmospheric Pb 210 /radium D/ aerosols concentration relationship to solar activity from measurement with blue filter

10 p1599 A71-23859

Air jet velocity and turbulence measurements by modified Doppler technique, using CW lasers

10 p1609 A71-23874

Direct optical measurements of strains, using spatially coherent light with moire technique

10 p1611 A71-24280

Space triangulation corrections of equatorial topocentric coordinates and radius vector of Jupiter in Baker-Nunn net, using Geos A satellite optical and laser observations

11 p1732 A71-25819

Ordered Ti-Al lattice parameters measurement in low and high temperature diffractometer attachment

11 p1780 A71-26023

Directional laser Doppler velocimeter measurements in perturbed circular flow, noting use in cardiovascular research

11 p1766 A71-26303

Structure constant of jet exhaust turbulence of J-57 with afterburner by laser beam probing compared with scintillation and hot-wire anemometer measurements

11 p1766 A71-26304

Fiber optics for spectroscopic illumination, discussing absolute and angular transmission measurements and optical angular transfer function calculation

12 p1905 A71-26806

Optical variation and radio spectral index statistics of extragalactic sources, including quasars from photographic monitoring with 30 inch reflector

12 p1962 A71-26932

Subsonic turbulent jet flow optical measurement by quantitative schlieren technique to overcome hot-body anemometry difficulties due to temperature and velocity fluctuations

12 p1896 A71-27215

Optical holographic interferometry for radial microcracks detection from bolt holes in high strength aircraft steel

[ASME PAPER 71-MET-C] 12 p1911 A71-27312

Spacecraft attitude measurement using spatial coherence of laser or star light beam, discussing feasibility and detection equipment

12 p1927 A71-27429

Single fiber reinforced plate initial stress distribution due to linear expansion coefficients difference between matrix and fiber, using optical polarization

13 p2091 A71-28126

Optical measurement of sprays mean droplet size, assessing operating variables effect on air-blast atomizer characteristics

13 p2117 A71-28756

Complex geometry surface light pressure momenta determination by body image projection onto photometric wedge and linear edge sliding screen procedure respectively, considering errors

13 p2071 A71-29154

Photoelectric, bolometric and photographic recording assembly for measurement of light pressure and aerodynamic forces on complex shape body in free molecular flow

13 p2071 A71-29155

Fog evolution and droplet radii spectrum determination by scattered laser beam angular distribution measurement

13 p2082 A71-29484

Planet Mercury density, discussing optical and radar measurements and theory comparison with observation

14 p2306 A71-29728

Image distortion technique for viewing deformation zones at crack tips on highly polished surface

14 p2323 A71-29849

Optical method for elastic deformations measurement of radio telescope reflector at various elevations

14 p2211 A71-29991

Spectrophotometers photometric accuracy measurement technique, using Bouguer law and optical fields superposition

14 p2240 A71-30123

Light transmission homogeneity measurements of optical materials, using Murty interferometer

14 p2242 A71-30154

Luxmeters and photoelectric receptors for illumination measurement of light beams in limited solid angle in image systems, considering automatic polar photogoniometer

14 p2246 A71-30417

Crab pulsar optical time of arrival measurements from four observatories, discussing errors in data reduction to inertial reference frame

14 p2315 A71-30658

Optical methods for measuring mechanical strain by observing shift and deformation of elemental surface areas, using holographic techniques

15 p2404 A71-31269

Binary optical detour phase holograms formation in measurements with centimeter electromagnetic waves, describing dielectric diffusers for microwaves

15 p2405 A71-31280

Optical positions of 87 identified extragalactic radio sources between declinations plus 19 and minus 80 deg, using Palomar Sky Survey plates and prints

15 p2489 A71-32398

Elastic materials Poisson ratio measurement by moire method in coherent and incoherent light

16 p2575 A71-32825

Second-order degree of coherence measurement by compact wave front shearing interferometer

16 p2577 A71-33131

Optical methods in gas dynamic research - Conference, Syracuse University, New York, May 1970

16 p2586 A71-33151

Optical diagnosis and measurements for radiation from gases in nonequilibrium flow

16 p2578 A71-33153

Optical interferometry and schlieren photography involving high power pulsed lasers, discussing applications to plasma diagnostics and holography

16 p2586 A71-33159

Pulse laser holographic interferometry for refractivity measurement, considering wave front reconstruction principles

16 p2578 A71-33160

Laser radar system for measuring atmospheric density above troposphere, discussing equipment design and construction

16 p2542 A71-33534

Optical crossed or collinear light pulse pairs for production and sounding of instantaneous processes kinetics in nanosecond and picosecond range

16 p2580 A71-33624

Two photon method of measuring ultrashort pulses and nonlinear optical effectiveness of lasers in synchronized mode

16 p2587 A71-33644

HCN laser amplifier gain measurement at IR wavelengths in gas mixtures by recording with pyroelectric receiver

17 p2750 A71-34290

Ca and Mg light emission and ionization cross section measurements at simulated meteor conditions, using photomultiplier and optical filters

17 p2798 A71-34374

Strain analysis based on thin metallic film optical measurements, determining principal strain directions from wrinkle and microfracture patterns

[SESA PAPER 1828A]

17 p2820 A71-34551

Circumterrestrial cosmic dust clouds properties determination by optical methods, using twilight observations at solar vertical symmetric points

17 p2810 A71-35725

Vortex laser Doppler velocimeter system for aircraft wake turbulence velocity profile mapping, describing optical arrangements, back and forward scattering modes and prototype design

17 p2754 A71-35756

Astigmatic image distortion in low temperature multiple reflection White cell with aluminum dewar assembly for Martian IR interpretation

18 p2914 A71-35844

Electronic processing of coherent optical data for measurement and display using holography, speckle patterns, interferograms, image intensifiers and TV systems

18 p2923 A71-36608

Laser velocimeter for wide range velocity measurement, using photodetector to observe light scattering by particles flowing across fringe pattern

18 p2932 A71-36618

OSO-6 measurements of gegenschein, comparing relative sky brightness data with ground based observations

18 p2966 A71-36766

Two phase flow model of water droplets velocity in air stream, using Fresnel biprism and laser differential scheme

19 p3072 A71-37587

Carbon dioxide laser, measuring focal length of gas defocusing lens in active medium as function of gas pressure and discharge tube diameter

19 p3073 A71-37771

Radial temperature profiles in low pressure oxygen-calcium wire diffusion flames from optical measurements based on radiative transfer equation

19 p3170 A71-38115

Transparent sample surfaces parallelism interferometric measurement using laser produced two beam nonlocalized fringes

20 p3245 A71-39181

Aspheric lenses and mirrors testing by single and double exposure two-wavelength visible light holography for obtaining interferogram

20 p3235 A71-39182

Backscattering patterns in atmospheric opacity measurements, minimizing errors due to atmospheric inhomogeneities and different stratifications

20 p3257 A71-39334

Ground based optical observation of raylike artificial auroras produced by rocket-borne accelerator generated electron beams, using image orthicon TV system

20 p3231 A71-39886

Real time mechanical strain measurement by optical correlation techniques, using coded matched-filter hologram and incoherent illumination

21 p3377 A71-40229

Free flight model accelerations, forces and trajectory measurements in short duration facilities, using optical methods and digital recording

21 p3362 A71-40383

Laser remote sensing technique for tropospheric refractivity fluctuation profile measurement with tethered balloon-borne retroreflector tracking by ground based tracker

21 p3374 A71-40977

Electron concentration and superconducting characteristics of Nb-Sn alloys from optical measurements

21 p3428 A71-41114

Optical investigation of metal-semiconductor interface blocking layer and photo-Hall effect in high resistivity crystals

21 p3433 A71-41316

Flashing lights radiation characteristics photometric measurement, discussing measuring apparatus sensitivity and errors analysis

22 p3499 A71-41496

Cylindrical plasma column light scattering diagnostics by focusing carbon diode laser beam on center

22 p3580 A71-41601

Reflected shadow method for constrained zone photoelastic observation around cracks in birefringent transparent plate under plane stress

22 p3549 A71-42555

Atmospheric self-aligning dual-scatter laser Doppler velocimeter, calculating backscattered power, range, wavelength and scatter centers number relationships

22 p3559 A71-42564

Ionospheric propagation penetrating and nonpenetrating modes full wave reflection and transmission coefficients determination for height and frequency variation by thin film optical method

23 p3643 A71-42972

Midcourse and planetary approach guidance by on-board optical measurements, noting application to earth-Mars trajectories and Grand Tour missions

[AAS PAPER 71-393]

Optical orientation determination and star pattern recognition for Skylab in solar inertial attitude by digital and hybrid stimulations

[AAS PAPER 71-397]

Reflection coefficients measurement for scanning two-mirror interferometer with absorbing Ni film matched to external medium, discussing multilayered coatings

23 p3676 A71-43399

Steady power pulsation measurement and operation mode theory of ruby laser with bleachable dye filters

23 p3684 A71-43416

Mode-locked laser ultrashort pulse duration measurement from field intensities autocorrelation functions

23 p3685 A71-43562

Collimated light beam transmission in turbulent atmosphere above ground surface, comparing measured coherence function with calculation

23 p3645 A71-43565

Aeronautical radio navigation aids photo-optical calibration, describing photogrammetric procedure and ground equipment for checking out airport ILS systems

23 p3702 A71-43587

Short range photogrammetry, describing special instrumentation problems and requirements regarding imaging precision and quality

23 p3679 A71-43591

Mach-Zehnder interferometric measurement of modulation transfer function of optical instrument disturbed by turbulent atmosphere

23 p3679 A71-43893

Supersonic Ar, He and molecular nitrogen jets, determining electron temperature and concentration and atomic state population in shock waves region by spectroscopic measurement

23 p3712 A71-43916

Light velocity measurements by optical and microwave techniques, noting electromagnetic constant error and role in distance measurement and physical theories development

24 p3827 A71-44996

OPTICAL MEASURING INSTRUMENTS

NT DIFFRACTOMETERS

NT ELECTROPHOTOMETERS

NT ELLIPSOMETERS

NT GEODIMETERS

NT INFRARED SPECTROMETERS

NT INFRARED SPECTROPHOTOMETERS

NT LIGHT SCATTERING METERS

NT MICRODENSITOMETERS

NT OCULOMETERS

NT OPTICAL PYROMETERS

NT OPTICAL RANGE FINDERS

NT OPTICAL SCANNERS

NT PHOTOGONIOMETERS

NT PHOTOMETERS

NT POLARIMETERS

NT REFLECTOMETERS

NT REFRACTOMETERS

NT SPECTROPHOTOMETERS

NT THEODOLITES

NT ULTRAVIOLET SPECTROMETERS

Low level optical signal transient response measuring instrument with nsec resolution and automatic photomultiplier current gain control

02 p0249 A71-12131

Liquefied and solidified gas IR measurements describing versatile optical cell

02 p0250 A71-12133

Echelle grating and transmission optics spectrographs using image intensifier tubes for increased sensitivity

02 p0250 A71-12138

Laser radial-shear common path interferometer for lens testing

02 p0250 A71-12144

Soviet spectral instrumentation for industry and research

02 p0254 A71-12710

Soviet optomechanical instruments for metallurgy and high temperature metallography

02 p0254 A71-12711

Optical radiation modulation and phase optical ranging, discussing theory and Soviet instrumentation

02 p0254 A71-12713

Laser image speckle interferometer design for observing vibrational modes on diffusely reflecting surfaces as alternative to holographic methods

02 p0254 A71-12718

Space communication reflector surface positioning and optical measuring techniques for best fit

02 p0234 A71-12805

Single crystal creep strain rate measurement under cryogenic temperatures by hybrid photoelectric servo system with optical extensometer avoiding physical contact with specimen

[SESA PAPER 1699]

03 p0426 A71-13759

Concave mirror interferometer for laser radiation spectra measurements, featuring piezoelectrically tuned optical system

03 p0439 A71-14000

Laser interferometry precision measurement and alignment techniques, describing application in optical lens manufacture and assembly

04 p0606 A71-14718

Laser metrology, discussing precise distance measurement techniques based on modulated CW and pulse sources, laser systems for constructional angular alignment and materials spectrography

04 p0606 A71-14719

Planned optical coincidence system for level bubble end image superimposition and transmittance to passage instrument ocular part

04 p0591 A71-14856

Astronomical spectrometers covering prism, grating, dye filter, plane Fabry-Perot, monochromator, Michelson and coherent detection laser spectrometers

04 p0593 A71-14871

Fabry-Perot etalon and focal reducer parameters for extragalactic radial velocities measurement, comparing optical mountings

04 p0593 A71-14909

Compressible flow density measurement using optical polarization interferometry with birefringent devices

04 p0601 A71-15918

Materials properties measurement by laser, describing methods for stress investigation in glass and electron density measurement in plasmas

05 p0764 A71-16969

Laser Doppler velocimeter, describing simplified stable optical arrangement

06 p0900 A71-18054

Optical system for spatially resolved measurement of extended bodies radiative emission and self absorption, describing design for measuring gas discharge plasma radiative properties

06 p0928 A71-18224

Orbital environment contamination and effect on optical instruments and astronomical experiments in Skylab Program

[AIAA PAPER 71-74]

06 p0902 A71-18531

Optical astronomy instrumentation automation including telescopes, computer control, filters and detectors

07 p1114 A71-20051

Photoelectric servosystem for three dimensional positioning of slit image, discussing system applications and accuracy

08 p1291 A71-21395

Angular resolution requirements of measurement systems and telescopes for orbital astronomy with applications to faint sources, close stars, spectroscopy, polarimetry, etc

09 p1447 A71-22747

Liquid wastes venting into space environment, producing ice particle clouds interference with spacecraft optical instruments

11 p1753 A71-26506

Spaceborne optical sensors cleanliness requirements, considering particle size distribution, shape, population densities, chemical composition and origin

[AIAA PAPER 71-471]

12 p1873 A71-26758

Interferential spectrometer with selection by amplitude modulation with double passage mirrors arrangement for obtaining double resolution

12 p1905 A71-26811

Optical synthetic aperture analogs of Covington-Drane and thin annular radio interferometers, discussing aperture resolution and spatial frequency response

14 p2238 A71-29802

Continuous burning rate measurement for metalized composite solid propellants, using optical sensor for servo tracking propellant surface

14 p2244 A71-30328

AEDC test facilities laser instrumentation for flow field diagnostics by Doppler velocimeter, holographic flow visualization and particle studies

14 p2245 A71-30332

Holographic multiple pass two-beam optical interferometer with greater sensitivity than single pass instrument/Mach-Zehnder

15 p2402 A71-31259

OMB-3P optical microbarometer for high altitude networks, discussing transmission-multiplier mechanism and instrument errors 15 p2406 A71-31468

Modified Young interferometer for measuring separation between centers of two nearly coincident slits with high resolution 16 p2577 A71-33132

Small digital computers applications to astronomical electronic instrumentation systems of microphotometry and spectroscopy 17 p2743 A71-35010

High spectral resolution image recording instrument with postrecording bandpass selection, discussing signature data base and sensor modes 18 p2917 A71-36066

Pulsed ruby laser high speed photography for accurate measurements of models contours in hypervelocity flight within aeroballistic range 18 p2923 A71-36612

Scanning densitometer for spectral transmission density continuous recording at low image contrast, discussing design and performance tests 19 p3063 A71-37248

Backscattering laser Doppler velocimeter for water flow and moving opaque object measurements, discussing velocity resolution and optical geometry 19 p3072 A71-37552

Optical cryostat suitable for Raman spectroscopy, using quartz tube optical cell and He evaporation by metal film resistor 20 p3268 A71-38833

Epoxy resin plate mechanical stress measurement under impact load, using laser light source three beam interferometric assembly with photographic recorder 22 p3555 A71-41613

Optical holographic detection and measurement of ultrasonic waves, providing practical method of investigating L.F sound waves 22 p3541 A71-41785

Atmospheric molecular absorption spectra in IR region, using 15 meter multiple pass absorption cell 22 p3544 A71-42141

Atmospheric visibility /light extinction/ measurement from modulated CW laser backscattered signal 22 p3549 A71-42565

Apparatus for optical diagnostics of helioelectrochemical conversion reaction phototransformation kinetics including diffusion coefficient measurement in liquid phase 22 p3484 A71-42845

Quasi-optical waveguide system for measuring electrical properties of dielectric and magnetic materials in submillimeter band 23 p3677 A71-43530

Short range photogrammetry, describing special instrumentation problems and requirements regarding imaging precision and quality 23 p3679 A71-43591

Red/green pigments in normal color vision, describing analytical anomaloscope for measuring protanope and deuteranope sensitivity curves 24 p3794 A71-44465

Radio-optical dispersometer for atmospheric water vapor density measurement with increased sensitivity 24 p3809 A71-44985

Low cost CW carbon dioxide laser power meter using Joule heating technique 24 p3835 A71-45213

OPTICAL METHODS
U OPTICS
OPTICAL MICROSCOPES
 Arsenic doped Si single crystal impurity segregation striae and central faceted area observations by scanned laser IR microscope 04 p0608 A71-15039

Semiconductor wafers examination with He-Ne IR laser scan microscope, producing oscilloscope shadowgraph displays of IR transmission variations in wafers 11 p1763 A71-26186

Biogenicity and significance of oldest stromatolites from optical microscopic and carbon isotopic studies 22 p3533 A71-41616

High resolution phase contrast microscope adaptation for gashight glove box use with stage and focusing knobs in box for Apollo sample microbiological examination 24 p3802 A71-45124

OPTICAL MODULATION
U LIGHT MODULATION
OPTICAL PATHS
 Optical transmission lines design techniques with thermal gas lenses, calculating system parameters by geometrical optics, wave, electrodynamic and Fourier transfer methods 04 p0628 A71-15810

System phase errors subtraction in interferometry, using modified laser unequal path interferometer and technique eliminating data reduction problem 07 p1107 A71-19210

Optical phase variations on short line of sight path through turbulent atmosphere 07 p1159 A71-19512

High resolution laser homodyne interferometer for determining small time resolved optical path length variations, using Michelson interferometer with He-Ne laser 10 p1611 A71-24507

Multipass laser interferometry sensitivity improvement for He plasma electron density determination by increasing effective path length of laser beam in medium 18 p2931 A71-36584

Geometrical optics convergence coefficient in earth ionosphere waveguide for arbitrary transmitter receiver location 19 p3017 A71-37866

Optical phase variations, temperature structure and wind velocity measurements in atmosphere using He-Ne laser beam on 70 m propagation path 22 p3509 A71-41787

OPTICAL POLARIZATION
 Multicolor polarimetry of Beta Lyrae system, discussing observations instrumentation and reduction 01 p0153 A71-10354

Holographic interferometry application to photoelasticity, discussing absolute retardation in terms of plane or circularly polarized light fringe pattern interpretation [SESA PAPER 1719] 03 p0426 A71-13767

Light scattering and polarization measurements in upper atmosphere by modulated searchlight, indicating dust layers 03 p0414 A71-14018

Matrix addressed polarization rotating or retarding light valve arrays for optical selectors, composers and displays from nonswitching threshold materials 03 p0430 A71-14468

Polarization-optical method of stress analysis problems, explaining high polymers physiomechanical properties with Boltzmann- Volterra integral equations 04 p0671 A71-15557

Compressible flow density measurement using optical polarization interferometry with birefringent devices 04 p0601 A71-15918

Neodymium glass lasers, investigating pump-induced birefringence effect on polarization and radiation distribution 06 p0907 A71-17398

Inner solar corona polarization during 22 September 1968 total eclipse based on isolines from polarimetric photographs 06 p0975 A71-18440

Cross and single polarized light techniques revealing coarse grained fractures cleavage facets 07 p1111 A71-19582

Polarizing phase shifter for quasi-optical transmission lines, describing varistor network operation 08 p1264 A71-21068

Mechanical stress amplitude measurement in optically transparent materials during HF vibrations, using polarization method 09 p1535 A71-22188

Crab Nebula emissions on 4 and 6 November 1970, observing optical circular polarization 09 p1522 A71-22981

Plane orthotropic bodies stress analysis by optical polarization method, using models consisting of anisotropic polymer plates fabricated from epoxy resins and woven fiberglass 10 p1690 A71-24573

Quantitative analysis of secondary harmonic generation in DC polarized isotropic laser beam, emphasizing molecular mechanisms and symmetrical effects 11 p1773 A71-25566

Atmospheric zero light polarization points, examining solar vertical and various almicantars, horizontal and vertical nonuniformities and albedo variations 11 p1795 A71-25925

Inner solar corona polarization during 22 September 1968 total eclipse based on isolines from polarimetric photographs 12 p1955 A71-26590

Photoelastic materials polarization characteristics analysis using Muller matrix method 12 p1976 A71-27115

Soviet book on stress analysis by optical polarization methods covering theory and practical applications to machine parts and structural components 14 p2321 A71-29528

Day sky brightness and polarization observation during total solar eclipse of 7 March 1970 14 p2309 A71-30120

Polarization Fourier spectrometer for circular dichroism spectroscopy, stressing IR application 14 p2242 A71-30156

High resolution quiescent and active solar prominences and magnetic field observations, discussing Zeeman effect and line spectrum polarization 17 p2806 A71-35393

Jupiter Galilean satellites surface optical polarization measurement, noting bright transparent material cover possibly frost 18 p2964 A71-36290

Stress wave interaction with macrocrack in elastoplastic and quasi-brittle materials, measuring stress field by optical polarization method and motion picture photography 19 p3154 A71-37086

Polarization compensator for Okayama Astrophysical Observatory solar Coude telescope, describing operational and design principles and performance characteristics 19 p3062 A71-37242

Analysis and synthesis of linear optical systems involving polarization effects by Pauli algebra of complex second order matrices 20 p3267 A71-38775

Atmospheric zero light polarization points, examining solar vertical and various almicantars, horizontal and vertical nonuniformities and albedo variations 20 p3257 A71-39216

Voltage-polarization induced optical waveguide using electrooptical lithium niobate crystal 21 p3393 A71-41039

Soviet papers on construction materials stress state dynamics, thermoelasticity and statics modeling problems, using optical polarization methods 22 p3614 A71-41609

Stress analysis of photosensitive coatings and transparent birefringent materials, applying holography to optical polarization method 22 p3537 A71-41614

Double-heterostructure injection laser radiation transverse polarization from reflectivity analysis of GaAs-air interface vs TE and ME mode incidence angle 22 p3558 A71-42201

Intensity and polarization for meteorological spherical and nonspherical particle size parameters, comparing exact Mie scattering and ray optics 23 p3704 A71-43337

Electromagnetic wave diffraction properties by ribbon metallic lattice in optically active media using Riemann-Hilbert method 24 p3804 A71-44716

Optical pulsar NP 0532 circular polarization upper limit from measurements throughout light curve 24 p3872 A71-44918

Seyfert galaxies optical polarization, investigating time and wavelength dependences by multicolor polarimetric and photometric observations 24 p3873 A71-45078

OPTICAL PROPERTIES
NT ABSORPTANCE
NT ABSORPTIVITY
NT BIREFRINGENCE
NT BRIGHTNESS
NT COLOR
NT DICHROISM
 Semiconductors optical properties, measuring Franz-Keldysh effect in specimen under strong sinusoidal electric field perpendicular to light beam direction 01 p0137 A71-10089

Imaging with partially coherent light, generalizing optical transfer function in Fresnel approximation 01 p0078 A71-10144

Atmospheric extinction coefficients dependence on wavelength, comparing theoretical prediction to observational data 01 p0119 A71-10832

Plant leaves mean effective optical constants from diffuse UV reflectance and transmittance measurements 01 p0073 A71-10834

Optical bonding agent for calcite prism on Pioneer F/G mission, emphasizing optical and mechanical properties resistance to Jupiter high energy particles 01 p0081 A71-10835

Apollo 11 lunar powder and rock samples optical properties noting similarity over Tranquility base area 02 p0305 A71-11986

Laser light frequency mixing and doubling in isotropic bodies in crossed magnetic and electric fields, examining magneto-electro-optical processes 02 p0261 A71-12171

Q switched laser wave birefringence thermal variations in liquids, calculating optical anisotropy temperature dependence 02 p0261 A71-12172

Small radio sources emission, examining correlation with optical photometric properties abnormalities 02 p0317 A71-12863

Optical plate induced helicoidal steady light field in laser cavity, imparting structure to isotropic transparent material medium 03 p0436 A71-13787

Zodiacal light theoretical models, considering interplanetary particles optics, Mie theory and multicolor polarization 03 p0491 A71-14011

Polymer materials linear photoreep characteristics description in terms of differential and integral equations, discussing relationship between optical and mechanical properties 03 p0514 A71-14357

Soviet book on optical properties of hot air covering spectral lines, radiative transfer, cross sections, pressure effects and absorptivity

03 p0460 A71-14397

Ruby and Nd-YAG laser basic mechanisms, properties and performance characteristics, discussing material problems and frequency width considerations

04 p0605 A71-14708

Glass laser types, properties and applications, noting welding and cutting, plasma generation, controlled thermonuclear reactions, neutron generation, intense short duration X ray fields, etc

04 p0605 A71-14709

Deformation monitoring of large multilens astronomical objective during assembly, using annular image reflection

04 p0593 A71-14868

BL Lacertae photometric data, noting object brightness and optical similarity to N galaxy 3C371

04 p0643 A71-15045

Ellipsometric observation of Ni optical properties changes relation to oxygen absorption, considering correctness of oxidation data

04 p0613 A71-15695

Laser rubies optical properties, considering orientation, homogeneity and inner stresses, emission in spiking and Q switched operation

05 p0761 A71-16329

Electrical, photoelectrical and optical properties of crystalline cadmium telluride-indium telluride alloys, discussing temperature dependence, spectral characteristics and photoconductivity

05 p0793 A71-16824

Optical and photoelectrical properties of thin amorphous thallium arsenic sulfide, thallium antimony sulfide and thallium bismuth sulfide films obtained by vacuum deposition

05 p0794 A71-16835

Optical systems aberrations, discussing possible deformations transfer from reflecting or refracting elements

05 p0783 A71-17032

Porphyrins optical and semiconductor properties concerning absorption, electrical conductivity and photoconductivity spectra

06 p0941 A71-17526

Optics and metrological characteristics of optimal photoelectric autocollimators

06 p0897 A71-17535

Optical properties of corundum for single and multiple layer antireflection achromatic coatings for IR below 5-6 microns

06 p0898 A71-17537

Fiber optic laser devices properties and potential applications as amplifiers, logic elements, active mode selectors and intense light sources

07 p1124 A71-19781

Amorphous semiconductors theories and models, considering structural, optical and electrical characteristics

07 p1178 A71-19847

Intermetallic III-V compound semiconducting films and layers charge carrier transport phenomena and optical properties

07 p1178 A71-19850

Age and composition effects on lunar surface processes and optical properties, explaining main albedo, maria, color contrasts and temporal changes

07 p1200 A71-20150

Cuprous halides nonlinear properties in near and medium IR regions

08 p1302 A71-21435

Secondary umkehr effect in solar UV region at twilight, proposing origin mechanism by ozone layer optical properties

08 p1357 A71-21875

Optical quasi-stellar objects searched for radio emissions, disproving previously claimed detections

09 p1518 A71-22352

Submillimeter wave extinction in clouds and fog, using spectrometric results of water optical properties

09 p1408 A71-23375

Thermal lower models in space simulation chambers, determining heat dissipation, optical efficiencies, blade geometry and solar radiation effects

11 p1854 A71-25191

Lunar surface optical properties, examining albedo, color, brightness variation and polarization

11 p1822 A71-25688

Venus atmosphere critical refraction model, examining optical effects and ray paths

11 p1823 A71-25696

Spacecraft thermal control coatings for long-duration exposure to near-earth orbital conditions, determining optical properties degradation and solar absorptance

[AIAA PAPER 71-454]

Optical ground contamination monitoring devices for Apollo Telescope Mount collecting time-line and integrated data

[AIAA PAPER 71-458]

Contamination degrading effects on optical surfaces, discussing application to real time monitors data analysis

[AIAA PAPER 71-460]

11 p1800 A71-26242

Cholesteric liquid crystal mixtures optical characteristics, measuring reflection, transmission and extinction ratio

12 p1942 A71-26800

Optical properties and relative density of lunar surface layer, deriving light reflection and scattering formulas

12 p1964 A71-27089

High temperature plasmas optical properties measurement by plasma spectroscopy, using gas driven shock tube as light source

12 p1940 A71-27276

Quasar-like N-type and Seyfert galaxies optical characteristics, discussing optical variability and radio spectrum characteristics

14 p2307 A71-29866

NiGa intermetallic compound electrical transport and resistance, Hall coefficient and optical absorption, discussing defect structure and electron scattering

14 p2260 A71-30478

Optical, mechanical, thermal and electrical properties of IR sensor materials at low operating temperatures

14 p2284 A71-30545

Optical distortion coefficients of objective for astronomical camera

14 p2250 A71-31116

Three dimensional hologram relationship to object optical properties and structure, considering hologram imaging properties

15 p2402 A71-31253

Holographic recording of optical inhomogeneities in gas flow in hypersonic wind tunnels, using Mach-Zehnder interferometer and schlieren apparatus

15 p2404 A71-31274

High directional microwave antennas optical simulation, design and measurement based on coherent optics and holography

15 p2375 A71-31282

Saturn atmospheric structure and optical properties, investigating methane absorption bands

15 p2483 A71-31337

Loading history effect on optical and mechanical properties of polymethyl methacrylate under uniaxial tension

16 p2600 A71-32815

Nonlinear optical effects associated with free holes and electrons in semiconductors, including higher harmonics generation and frequency mixing

16 p2621 A71-33375

Crystal defects and electrical and optical properties changes due to electron bombardment of semiconductors

16 p2622 A71-33622

Radio source PKS 1514-25 identification as E galaxy, investigating rapid optical variability and light curves

17 p2805 A71-35379

Gasdynamic lasers optically active medium two-fluid model, deriving solutions for CW generators and quantum amplifiers

17 p2754 A71-35397

Optical properties of metallized fluorinated ethylene propylene Teflon films with various thicknesses, discussing suitability as spacecraft thermal control surface

[ASME PAPER 71-AV-35]

18 p2869 A71-36402

Optical properties and relative density of lunar surface layer, deriving light reflection and scattering formulas

19 p3133 A71-37439

Oscillatory variation of optical length of pulsed laser resonators during lasing, testing with ruby laser in free emission mode

19 p3073 A71-37791

Calcium difluoride powder under sintering, examining optical transparency and morphological features

19 p3069 A71-38049

Optical characteristics of thermal IR scanners, using mirrors and prisms in parallel or converging ray pencils and rotating wedges

19 p3068 A71-38709

Artificial satellites optical characteristics from amateur observers, discussing brightness and absolute magnitude

20 p3305 A71-38731

Aerosol measurements over Atlantic and Indian Oceans, discussing aerosols optical thickness, effective radii, concentrations, sizes and optical properties variations with latitude and meteorological conditions

20 p3257 A71-39328

Crossbeam electric discharge convection laser, reviewing uniform and stable discharges in rectangular channel and laser optical properties

20 p3246 A71-39758

Crab Nebula optical pulse timing, noting neutron star crust rotation speedup and relaxation, eccentric planetary orbits and sinusoidal effects

20 p3302 A71-39928

Short time variability of intensity of optical pulses from pulsar NP 0532, using telescopes

20 p3303 A71-39930

Time arrival measurements of optical pulses from Crab Nebula pulsar correlated to solar system barycenter

20 p3303 A71-39931

Pulsar pulsed optical radiation search, noting dependence on determination of accurate positions by radio methods

20 p3303 A71-39938

Visible optical pulsars search with Fourier and correlation techniques in X ray sources, supernova remnants, white dwarfs, IR stars, planetary nebulae, etc

20 p3304 A71-39939

Optical constants of beta-phase NiIn, PdAl and nickel gallium aluminide, noting chemical composition and electron density effects on photon energy absorption

21 p3426 A71-40033

Optical properties of graphite-iron-silicate grain mixtures from Mie theory for spherical particles, noting models consistency with interstellar extinction and backscattering observations

21 p3444 A71-40242

Laser beam frequency mixing, discussing optical harmonics generation, light reflection/transmission and picosecond pulse measurements

21 p3392 A71-40661

Optical mixing and higher harmonics generation by free carriers in semiconductors, using carbon dioxide laser

21 p3393 A71-40663

GaAs-InAs solid solutions single crystal ingots, investigating optical absorption and reflection spectra, energy gap width and carrier mobility temperature dependence

21 p3435 A71-41335

Mica selection quality criteria for capacitors, outlining electrical, physical and optical properties standards

22 p3520 A71-41712

Galactic diffuse radiation in far UV, discussing consistency of findings on optical properties of interstellar grains

22 p3593 A71-42337

Ellipsometric determination of optical constants for weakly and strongly absorbing specimen

22 p3576 A71-42572

Saturn atmospheric structure and optical properties, investigating methane absorption bands

22 p3606 A71-42612

Insulators normalized theory application to selective transparent insulators photosynthesis operation

22 p3484 A71-42843

Nonlinear optical properties of phase matchable crystal cadmium germanium arsenide for carbon dioxide laser second harmonic generation and parametric interactions

23 p3714 A71-42960

Optical, chemical and structural properties of lunar bytownite twin from U stage, microprobe and X ray measurements

23 p3738 A71-43612

Lunar fines samples 10084,148 and 12070,98, investigating grain size, mineral and chemical composition and optical properties

23 p3744 A71-43655

Grain size distribution and optical and RF electrical properties of Apollo 12 lunar fines and core samples

23 p3759 A71-43769

Polarization characteristics, albedos and optical properties of Apollo 11 and 12 rocks, investigating wavelength dependence and proton irradiation effect

23 p3761 A71-43779

Liquid crystals structural, elastic and optical properties, noting application to measurements of temperatures, pressures and electric and magnetic fields

23 p3717 A71-43958

Objective lens with superconductive winding for high voltage electron microscope, describing optical properties and vibration reduction system

23 p3679 A71-44008

Radiation diffusion in finite thickness medium with variable optical properties, giving equations for illumination levels and excited atom density in steady state medium

24 p3833 A71-44660

Semitransparent particle model of Martian surface for reflective power at various incidence and reflection angles, discussing packing density and optical parameters

24 p3869 A71-44808

Photographic monitoring of radio sources with flat or peaked spectra, identifying as quasars or unstable galactic nuclei by optical variations

24 p3872 A71-44920

Germanium extrinsic photoconductive IR detectors with Au, Hg and Cu doping, discussing preparation and electrical and optical characteristics

24 p3860 A71-45070

Optical enhancement of photomultipliers extended to UV wavelengths, using suprasil and spectroil fused silica with high flat transmission curves as optical materials

24 p3829 A71-45212

- Hg-Te-CdTe thin films structural and optical properties, measuring absorption spectra in UV, IR and visible regions to determine Te contents effect
24 p3862 A71-45251
- OPTICAL PUMPING**
Optically pumped rubidium maser short term frequency instability caused by thermal noise and resonator temperature and pumping power fluctuation
01 p0095 A71-11211
- Carbon dioxide laser optical pumping by resonant emission from alkali metal lamp
03 p0434 A71-13290
- CW nitrous oxide laser action at 81.5 and 263.4 micrometers in optically pumped ammonia gas, measuring rotational and inversion frequencies
03 p0434 A71-13476
- Stimulated emission from stilbenyloxazole solutions under pumping by second harmonic of ruby laser, determining emission thresholds
03 p0434 A71-13502
- Organic dye laser output and service life enhancement, using filters for absorption of UV pumping radiation photodecomposition of rhodamine 6G alcohol solution
03 p0435 A71-13509
- Temperature distribution in heat conducting cylindrical laser rod at large pumping pulse repetition rates
03 p0435 A71-13512
- Tuned nitrogen laser pumped dye lasers, investigating bandwidth influence on output power
03 p0436 A71-13643
- Nd-YAG pulsed laser, comparing Kr and Xe flash lamps for pumping performance
03 p0437 A71-13880
- Semiconductor cadmium sulfide crystal structure changes during high power electron beam and optical pumping, using stimulated emission spectra measurements
03 p0439 A71-13984
- IR microwave double resonance of ammonia during IR vibration-rotation transitions induced by pumping of nitrous oxide laser
03 p0440 A71-14198
- Near UV dye lasers, using various organic compounds as scintillators with excitation through nitrogen gas UV laser transverse pumping
04 p0606 A71-14717
- Parametric laser with single mode pumping, investigating emission spectra fine structure
04 p0608 A71-15120
- High power continuously pumped Nd-YAG laser operating characteristics and design parameters
04 p0608 A71-15586
- Dye lasers operational principles and characteristics, considering dyes molecular structure, optical pumping, continuous operation, wavelength selection and applications
05 p0761 A71-16330
- Optical parametric oscillators performance improvement by nonresonant pump reflection
05 p0762 A71-16338
- Optically pumped Rb laser theory, taking into account superfine and Zeeman structure of atoms
05 p0763 A71-16872
- Traveling medium solid state lasers spike generation due to spatiotemporal fluctuations of losses and pumping
06 p0907 A71-17379
- Gas lasers pumping by nuclear energy, discussing heavy particle interactions, threshold densities, population inversion, etc
[AIAA PAPER 71-110]
06 p0909 A71-18560
- Nd and Yb ions stimulated emission from spirally wound glass fibers, comparing activator pumping energy peaks
07 p1122 A71-19135
- Nd glass traveling wave laser single frequency emission luminescence stability as function of pumping power, using dispersive ring resonator
07 p1122 A71-19136
- Q switched Nd laser pulse duration control as function of KDP crystal orientation and pumping power
07 p1122 A71-19138
- Organic dye lasers flash lamp pumped system for tunable coherent light production in visible and near IR spectrum
07 p1125 A71-19796
- Gas laser optical pumping based on photodissociation, calculating spatial temporal distributions of pump radiation absorption probability and main level population
07 p1125 A71-19806
- Organic dye lasers lasing conditions calculation for constant emission frequency from nonstationary emission kinetics analysis
07 p1125 A71-19807
- Optically pumped pulsed ruby laser welding unit, noting joining and hole drilling problems
07 p1119 A71-19968
- Singly resonant optical parametric oscillator allowable pump bandwidth
07 p1126 A71-20179
- Stimulated emission wavelength tuning from GaAs and CdSe electron beam pumping laser crystals as function of time and current
07 p1128 A71-20393
- YAG-Nd laser rods CW pumping by cooled and room temperature GaAsP diodes, determining threshold temperature dependence
07 p1129 A71-20621
- Gas dynamic lasers design and operation, discussing pumping techniques, waste energy removal and mode control
08 p1301 A71-20693
- Carbon dioxide-nitrogen CW laser AC excitation in optical cavity, considering power output
08 p1301 A71-20997
- Optical pumping efficiency in ruby laser for different rod cross sections
08 p1301 A71-21220
- Light-microwave signal relation in optical pumping and detection in Rb atomic oscillator
08 p1289 A71-21273
- Pulsed optical parametric oscillators, investigating effects of spatially nonuniform pumping with beams having Gaussian intensity profiles
08 p1302 A71-21432
- Electron beam pumped CdS laser, investigating output pulse time duration based on laser oscillation quenching model
08 p1302 A71-21433
- Spectral properties of solid state laser with cavity lengthened by optical delay line
08 p1303 A71-21954
- Wide angle high gain image amplification by organic dye solution lasers using rhodamine or fluorescein disodium salt
09 p1463 A71-22752
- Carbon dioxide laser optical pumping by resonant emission from alkali metal lamp
09 p1464 A71-23266
- Continuously pumped Q switched neodymium doped YAG laser micromachining tool for resistor trimming, resonator/filter frequency tuning and diode/transistor vaporizing
09 p1457 A71-23402
- Continuously tunable stimulated far IR emission in lithium niobate with Q switched ruby laser as pumping agent, discussing power-wavelength characteristics determination
09 p1465 A71-23482
- Organic lasers with xanthene dyes solutions, investigating triplet states molecular population effect on output energy characteristics in pumping
10 p1620 A71-24344
- Pulse rate and pumping power effects on emission spectra and I-V characteristics of multielement GaS injection lasers
10 p1622 A71-24884
- Time delay in pulsed optical carbon dioxide laser pumping mechanism in high current gaseous discharge
11 p1773 A71-25796
- Nd-YAG laser cavity dumping for continuously pumped efficient pulsing at various repetition rates
11 p1773 A71-25797
- Nitrogen laser pumped cresyl violet dye laser output increase through excitation transfer from added intermediary dye
11 p1773 A71-25926
- GaAs multiple beam injection laser amplifier avoiding light flux saturation by periodic signal release
12 p1913 A71-26852
- Population inversion in Cs133 ground state hyperfine levels, using CW GaAs laser at 77 K for optical pumping
12 p1913 A71-26977
- Thermal transient effects in optically pumped pulsed lasers, presenting approximate calculation of temperature distribution and laser rod distortion effect on collimated light beam
12 p1914 A71-26979
- Traveling medium solid state lasers spike generation due to spatiotemporal fluctuations of losses and pumping
12 p1915 A71-27459
- Optical losses and quantum efficiencies of electron beam pumped CdS lasers, determining extinction coefficient from dependence of threshold current on resonator length
12 p1915 A71-27639
- Carbon dioxide laser pulse shape, duration and power dependence on repetition rate during continuous pumping
13 p2077 A71-28366
- High intensity tunable InSb spin flip stimulated Raman scattering from pulsed high pressure carbon dioxide laser radiation pumping
13 p2081 A71-29336
- German monograph on application of theory of optical pumping with crossed light beams to magnetic fields vector measurement
14 p2242 A71-30230
- Gas laser birefringence observation in active elements under pumping action, using light beam components polarization intensity measurements
14 p2255 A71-30586
- Optically pumped magnetometers for earth and interplanetary magnetic fields measurement, using Zeeman effect
15 p2405 A71-31409
- Self induced second order mode locking optical pulsing of double heterostructure stripe geometry junction lasers operating continuously at room temperature
15 p2421 A71-32388
- Rhodamine 6 G in ethanol partial mode locked dye laser picosecond pulses, using pulsed nitrogen laser pumping
15 p2422 A71-32580
- Optimal pulsed power output of continuously pumped Q switched Nd-YAG laser as function of mode parameters
15 p2423 A71-32603
- High voltage power supply for optically pumped solid state lasers, including water cooling of ruby and discharge tube jacket
16 p2585 A71-33074
- Krypton arc lamps of high conversion efficiency for optical pumping of neodymium lasers, setting lamp and Nd-YAG rod in prolate ellipsoidal cavity
16 p2585 A71-33140
- High average power flash lamp pumped pulsed dye laser development and application in atmospheric sodium probing
16 p2586 A71-33148
- Flash lamp pumped pulsed dye lasers using triplet quenchers cycloheptatriene and cyclooctatetraene with 600 microsec emission times in rhodolane
16 p2589 A71-34122
- Parametric microwave amplifier feasibility with laser pumped electro-optical crystal as nonlinear element
16 p2589 A71-34135
- Optically pumped rubidium maser short term frequency instability caused by thermal noise and resonator temperature and pumping power fluctuations
17 p2750 A71-34262
- Optical parametric oscillation internal to laser cavity, including temporal response effects of laser population inversion
17 p2751 A71-34377
- Energy balance and emission power of organic dye laser under nonmonochromatic excitation
17 p2751 A71-34381
- Optical pumping and detection of spin polarized electrons created in p-type GaSb conduction band by excitation with light
17 p2791 A71-35583
- Dynamic rate equation model of single wavelength flash lamp pumped rhodamine dye laser accounting for short molecular triplet state lifetimes
18 p2929 A71-35958
- Solid state laser with Nd ions in YAG, discussing crystal growth and structure, optical pumping continuous and Q switched operation and mode locking
18 p2930 A71-36146
- Dye lasers developments and applications, including flash lamp pumps, frequency narrowing and tuning and picosecond pulse mode locking
18 p2931 A71-36602
- Thermal effects of continuously tungsten iodine lamp pumped Nd-YAG laser, measuring rod temperature distribution by microprobe beam
18 p2932 A71-37009
- Tuning range extension of doubly resonant lithium iodate parametric oscillator by upconversion, using simultaneous pumping by single ruby laser beam
19 p3071 A71-37477
- Ring laser formed by single mode light guiding thin film, using nitrogen laser for pump source
19 p3071 A71-37478
- IR pumped stimulated light emission in semiconductors, noting upconversion due to energy transfer between impurity ions
19 p3071 A71-37479
- Organic dyes pulse emission spectra shifts during pumping by ruby and neodymium-glass lasers, discussing vibrational relaxations role in mechanism
19 p3072 A71-37766
- Crystal laser pyrotechnic illumination lamps with noncompacted explosive mixture, noting Nd ion doped calcium tungstate and YAG laser tests
19 p3073 A71-37788
- Solid state lasers, considering ruby and YAG-Nd ion materials pumped at room temperature
19 p3074 A71-38229
- Optical parametric oscillator signal wave amplitude fluctuations during nonresonant pumping, calculating damping term governing temporal behavior of deviation from stationary value
20 p3268 A71-38835
- Platelet lasers optically pumped by pulsed xenon laser, investigating single mode operation, threshold-temperature curves, efficiency and gain spatial inhomogeneity
20 p3243 A71-39006
- Spontaneous emission decreases at CdS and GaAs lasing onset observed visually in internal reflection cavity under electron beam pumping
20 p3243 A71-39007

- Elliptical laser illuminator pumping efficiency dependence on light source focal displacement, using optical systems image forming theory 20 p3243 A71-39075
- Optical parametric oscillator pumped with laser light, calculating radiation intensity fluctuations 20 p3246 A71-39458
- Laser dye cell optical quality dependence on light pumping and liquid dye flow velocity, using schlieren method 20 p3246 A71-39489
- Elliptical cylinder pump cavity design for solid state laser with ideal beam geometry 20 p3246 A71-39493
- Millimeter and submillimeter laser action in symmetric tip molecules optically pumped via parallel absorption bands 20 p3246 A71-39759
- Repetitively pulsed flashlamp pumped dye laser, noting high average outputs in red end of spectrum with rhodamine B 20 p3246 A71-39760
- Unidirectional gas laser amplifier using monochromatic optical pumping of coupled Doppler broadened transition 21 p3394 A71-41048
- Waveguide structure effect on electron beam pumped GaAs laser characteristics, considering diffraction losses and laser threshold reduction 21 p3394 A71-41233
- Room temperature visible surface laser action in praseodymium chloride and bromide, obtaining optical pumping into upper laser level by wavelength tunable dye laser 22 p3556 A71-41802
- Nonstationary laser generation of organic dyes in picosecond optical pumping, considering kinetic and spectrum nonstationarity 22 p3557 A71-41815
- Kinetic theory of optically pumped gas, incorporating atomic line radiation effects on spatial and time evolution of velocity distribution 22 p3530 A71-41888
- Electrical CO laser performance prediction from pumping mechanism based on vibrational energy exchange under thermal nonequilibrium conditions 23 p3683 A71-42954
- Laser pumped solid state masers operational characteristics, describing spontaneous emission noise 23 p3683 A71-43084
- Explosion-pumped gas dynamic carbon dioxide laser, obtaining high pulse energy by common hydrocarbon fuels 23 p3687 A71-44135
- Gallium arsenide phosphide electroluminescent junction diode pumped Nd-YAG laser room temperature CW and pulsed outputs 23 p3687 A71-44139
- OPTICAL PYROMETERS**
- Electrical conductivity of pyrographite at high temperatures along and across deposition plane, using optical pyrometer measurements 17 p2761 A71-34304
- OPTICAL RADAR**
- Lidar observation of clear atmospheric structure including lee wave clouds, turbulence, stratification in trade wind inversion layer, etc 01 p0118 A71-10583
- Optical radar system absolute calibration for measuring laser irradiance backscatter function from atmosphere 01 p0094 A71-10874
- Q switched ruby laser-Raman radar for real time air pollution probe 02 p0213 A71-12014
- Coherent laser synthetic aperture radar at microwave frequencies for airborne ground point target mapping 02 p0215 A71-12044
- Doubly scattered radiation magnitude as function of heights and aerosol concentrations for bistatic laser radar 04 p0609 A71-15761
- Atmospheric aerosol vertical distribution by lidar system, describing ruby Q switched giant pulse laser design and operation 05 p0720 A71-16221
- Atmospheric aerosol vertical distribution by lidar system, discussing backscatter function, relative humidity, wind velocity, visibility, etc 05 p0720 A71-16222
- Lidar observations of visually clear troposphere compared with simultaneous rawinsonde data for relationship between lidar echoes and atmospheric winds aloft 05 p0721 A71-16670
- Upper atmosphere investigation by ground based pulsed laser radar 06 p0910 A71-18719
- Integrated electro-optical microwave radar and laser /lidar systems for earth oriented, environmental and domestic applications 07 p1095 A71-18827
- Tropospheric temperature and aerosol to molecule ratio measurements by optical radar to determine relative concentrations and scattering cross section contributions 07 p1153 A71-20007
- Lidar wavelength optimization for Raman scatter atmospheric studies, taking into account aerosol and weak signal statistical effects 08 p1254 A71-21458
- Upper atmospheric composition by nitrogen molecules radiative transition analysis, using laser resonance backscattering effect 09 p1436 A71-22581
- Optical distance correction for fluctuating atmospheric index of refraction in long base line measurements using Lidar with Q switched ruby laser 09 p1495 A71-23451
- Tropospheric temperature and aerosol/molecule ratio determination by optical radar measurements, using Doppler broadening in spectral analysis of laser radar echoes 09 p1466 A71-23628
- Cloud base height estimation methods involving vertical radar, laser, stereotelemeter and ceilograph measurements with instrument error analyses 10 p1639 A71-25100
- Threshold and power relations for optical radars in pure and turbid atmospheres, determining visibility range for object detection 13 p2027 A71-27856
- Signal to noise ratios for coaxial laser radar system heterodyning signal backscattered from atmospheric aerosol 16 p2541 A71-33138
- Laser radar system for measuring atmospheric density above troposphere, discussing equipment design and construction 16 p2542 A71-33534
- Laser radar investigation of upper atmosphere dust layer, obtaining evidence for Silverberg cometary micrometeoroid shower hypothesis 16 p2641 A71-33760
- Earth and ocean surface state and cloud height determination using airborne laser radar observations 16 p2568 A71-33786
- Lidar soundings of troposphere, investigating multilayer echo structure of haze layers, clouds and rainstorms 17 p2770 A71-34706
- Upper atmosphere density observation by Q switched ruby laser radar 17 p2753 A71-34748
- Backscattered laser radar pulses and downward IR flux enhancements in clear air around small cumulus clouds, discussing hygroscopic aerosols for increased radiance 17 p2707 A71-35381
- Lidar observations of artificial warm fog seeding operations, analyzing spatial and temporal variations 17 p2770 A71-35741
- Aerosol size distribution from lidar light scattering polarization properties, constructing inversion model 17 p2770 A71-35806
- Linearly polarized lidar light scattering in spherically symmetrical uniformly distributed cloud water drops, investigating multiple backscattering effects on depolarization 17 p2770 A71-35807
- Light detection and ranging (LIDAR) system in airborne and ground applications for moving target location and tracking 18 p2882 A71-36615
- Lower atmospheric multiple wavelength laser radar data compared to clear atmosphere model and radiosonde measurements, discussing mixing layer location 18 p2882 A71-36617
- Optical radar aircraft tracking and position system, using IR Q switched flash pumped Nd-YAG laser transmitter and pulse receiver with magnetic tape recorder and real time computer 18 p2900 A71-36905
- Satellite docking systems, discussing laser radar feasibility and device design 19 p3149 A71-37307
- Combined lidar and radiometric techniques for high layer cumulus and cirrus clouds IR emissivity determination 19 p3089 A71-37501
- Laser radar observation of comet Bennett dust at 40-90 km, deducing particle size from rate of descent 19 p3142 A71-38041
- Atmospheric optical transmission coefficient measurements using steerable laser radar system 21 p3372 A71-40040
- GaAs injection laser radar for measuring cloud height, determining required laser output power as function of state of atmosphere and receiver sensitivity 21 p3394 A71-41238
- Emitted signal delay time effect on operational precision of semiconductor laser radar for measuring lower cloud boundary heights 21 p3394 A71-41239
- Laser radar for lower cloud boundary measurements, using information theory for potentials evaluation 22 p3550 A71-42850
- Resonance scattering laser radar for atmospheric pollution detection, discussing Rayleigh and Mie scattered light suppression 24 p3803 A71-44570
- Optimum signal processing for distance measurement with lasers, considering propagation, detection and measure process statistical properties, optical radar and sine wave modulation 24 p3834 A71-45206
- OPTICAL RANGE FINDERS**
- NT LASER RANGE FINDERS**
- Short pulse optical tracking systems ranging error, analyzing effects of tracker, target and propagating medium characteristics 02 p0214 A71-12029
- Optical radiation modulation and phase optical ranging, discussing theory and Soviet instrumentation 02 p0254 A71-12713
- Q switched ruby laser ranging system of tracking station for use with retroreflecting satellites 03 p0379 A71-14007
- European ground stations geodetic surveys by laser range measurements and photographic observations of satellites with reflectors 03 p0413 A71-14008
- High power pulsed laser applications, considering satellite orbit determination, distant satellite ranging and precise triggering of high voltage spark gaps 07 p1124 A71-19780
- Pulsed optical range finders, predicting transmitter pulse waveshape effects on calibration, precision and efficiency by probability density function 12 p1903 A71-26792
- Distance determination accuracy improvement by OTD double image range finder 15 p2405 A71-31467
- Transportable high radiance lunar ranging laser system, describing optical equipment in ruby and Nd-glass laser experiments 18 p2883 A71-36917
- OPTICAL REFLECTION**
- Visible and IR reflection spectra of p- and n-type GaAs under fast neutron irradiation 01 p0139 A71-10783
- Light echo obtained via giant laser pulse peak overlapping in space and time 01 p0095 A71-11034
- Luminescence of optically reflecting nebulas related to shape of light scattering indicatrix of interstellar dust particles 02 p0311 A71-12355
- Optical parametric oscillators performance improvement by nonresonant pump reflection 05 p0762 A71-16338
- Human eye optical performance, noting retina anatomy and physiology, visual acuity, resolving power and reflectometry 05 p0713 A71-16482
- Oblique incidence effect on reflection and absorption of laser light by solid surrounded by plasma in vacuum 07 p1166 A71-18886
- Venusian atmospheric cloud cover, determining nature of particles by optical reflective properties 07 p1191 A71-18907
- Ion implantation lattice damage effects in crystalline silicon with allowance for optical reflectivity, considering annealing temperature and amorphous layer formation 07 p1175 A71-19062
- Light pulses reflection from water and ice in clouds, using Monte Carlo technique for all orders of multiple scattering 13 p0231 A71-28795
- Spectral dependence of GaAs-CdSe alloys optical reflection coefficient 17 p2790 A71-34203
- Apollo 11 and 12 lunar landings, discussing retrieved lunar material, seismographs, solar wind and light reflector for measuring earth-moon distance 18 p2959 A71-35906
- Laser beam reflection from arbitrary geometric surface, considering reverse problem of response of flat or curved mirror to incident collimated light 18 p2929 A71-36055
- Semitransparent particle model of Martian surface for reflective power at various incidence and reflection angles, discussing packing density and optical parameters 24 p3869 A71-44808
- OPTICAL RESONANCE**
- Carbon dioxide laser optical pumping by resonant emission from alkali metal lamp 03 p0434 A71-13290
- IR microwave double resonance of ammonia during IR vibration-rotation transitions induced by pumping of nitrous oxide laser 03 p0440 A71-14198

CW Nd-YAG laser response to sinusoidal cavity perturbation, observing resonance modes
05 p0761 A71-16332

Optical hyperfine splitting of Rb resonance lines of atomic beam light source, using Fabry-Perot interferometer
07 p1111 A71-19488

Ring laser beat frequency response near parametric resonance
07 p1125 A71-19810

Singly resonant optical parametric oscillator allowable pump bandwidth
07 p1126 A71-20179

Carbon dioxide laser IR pulse transmission under moderate pressure conditions using four state model of molecular laser passive Q switching and double resonance
07 p1128 A71-20391

Carbon dioxide laser optical pumping by resonant emission from alkali metal lamp
09 p1464 A71-23266

High altitude low latitude aurora, observing intense spectral bands and lines and excitation due to optical resonance, atom- and molecule- electron collisions
09 p1441 A71-23643

Resonant excitation of thin film dielectric optical waveguide through supercritical layer by limited light beam with arbitrary amplitude-phase distribution
15 p2375 A71-31227

He-Ne lasers stimulated emission, studying optical resonant cavities and discharge tubes construction
15 p2422 A71-32572

Doubly resonant optical parametric oscillator frequency instabilities and threshold, studying non-resonant mode feedback effects
15 p2423 A71-32605

Resonant energy exchanges between gaseous media and externally applied radiation fields from wavelength-tunable lasers
16 p2586 A71-33164

Spectroscopic measurement of vacuum UV radiation from shock heated krypton plasma, noting self reversed resonance lines indicating cold boundary layer
17 p2787 A71-34589

Picosecond duration coherent light pulse propagation in resonant medium, discussing basic equation, self induced transparency, Bloch equations, soluble model and higher conservation laws
17 p2754 A71-35375

Carbon dioxide laser signatures prediction from multiple application of optical resonant equation by computer program, studying line competition effects
20 p3247 A71-39771

Transversally excited and atmospheric carbon dioxide laser, measuring time behavior of refraction index profile and lensing effects on resonator
21 p3392 A71-40547

Traveling wave power resonances in ring laser with nonlinearly absorbing cell, noting role of absorbing component lamb saturation
21 p3394 A71-41257

OPTICAL RESONATORS
U LASERS
OPTICAL SCANNERS
NT FLYING SPOT SCANNERS
NT MULTISPECTRAL BAND SCANNERS
Queueing model for analyzing video scan converter
01 p0047 A71-10215

IR flying spot telescope with CW laser beam scanning and target motion sensing capabilities
01 p0081 A71-10830

Left ventricular volume determination by high speed cineangiography, using optical scanning and automatic data processing
02 p0203 A71-11705

Straight and curved edges produced vidiosignal amplitude spectra discrimination in TV image scanning of nuclear particle path photographs, using filtering device
02 p0248 A71-11827

Limited scanning function of optical system consisting of He-Ne laser and Fabry-Perot interferometers with small effective apertures
03 p0435 A71-13514

Laser document scanner for computer entry and communications systems
05 p0762 A71-16480

Air bearings design for laser scanner high speed rotating mirror in vacuum, describing static and dynamic tests for rotor inversion point
07 p1117 A71-19506

[ASME PAPER 70-LUB-15]
Design and operation of scanning laser based on exciting electron beam directional variation, discussing laser characteristics for various operating modes
12 p1913 A71-26851

High resolution Fabry-Perot spectrometer with stepwise automatic scanning, discussing reproducibility, flexibility and stability
12 p1908 A71-27672

Photoelectric scanning photometer for visual binaries measurement, using on-line computer for data sampling and acquisition from three photon counters
14 p2246 A71-30357

Flying spot scanner electron optical systems for reading data from photographic film for studies of recognition algorithms, image simulation and automatic particle track measurements
15 p2409 A71-32191

Thermal imaging devices scanning systems for producing television-like images, noting alternate line scanning
15 p2412 A71-32759

Diffraction limited circular holographic determination of Airy radius by photoelectric scanning of image irradiance
16 p2577 A71-33143

Rapid photoelectric spectrum scanning techniques using multichannel analyzer and triggering mechanism
17 p2741 A71-34991

Scanning densitometer for spectral transmission density continuous recording at low image contrast, discussing design and performance tests
19 p3063 A71-37248

Stable auroral red arc excitation observations by HF radar scattering, scanning photometers and Alouette 1 satellite, noting local electron concentration increase
19 p3054 A71-38034

Display system for scanning medical thermometer covering temperature range 28.0-37.4 C with 0.2 C accuracy, using liquid nitrogen cooled indium antimonide photoresistive detector
22 p3545 A71-42149

Return beam vidicon characteristics and applications for reconnaissance, optical storage and scan conversion, data and signal processing
22 p3548 A71-42509

Diffuse object scanned illumination hologram recording, discussing intermodulation flare light elimination for speed and reconstruction efficiency
22 p3549 A71-42561

Absolute spectral energy distribution and K-corrections for giant elliptical galaxies from scanner observations
23 p3722 A71-42936

Hologram recording by optical wave field scanning with arbitrary aperture and point source at center of entrance pupil and photoreceiver
23 p3675 A71-43398

ITOS meteorological satellite scanning radiometer using point detector optical system for earth imaging
23 p3676 A71-43511

Intercavity scanning for mode selection of carbon dioxide laser in transversely degenerate resonator by localized electron-beam-trigger excitation
23 p3687 A71-44132

OPTICAL SENSORS
U OPTICAL MEASURING INSTRUMENTS
OPTICAL SIGNALS
U OPTICAL COMMUNICATION
OPTICAL SPECTRUM
U LIGHT [VISIBLE RADIATION]
OPTICAL THICKNESS
Threshold currents of injection lasers with heterojunctions providing correction for optical thickness in terms of electromagnetic theory
01 p0094 A71-10779

Optically thin medium convective instability, examining radiant pressure and magnetic field effects
01 p0158 A71-10804

Electric conductivity dependence on optical depth in photospheres of spectral type F, G and K stars for different gravitational acceleration values on surface
01 p0159 A71-10866

Solar active regions lambda 10 830 line from photometric observations, determining optical thickness, Doppler width and radiation source activity
02 p0306 A71-12080

Comet head physical processes, discussing atomic and molecular distributions, gas ejection velocity and temperature, UV optical thickness, photodissociation, etc
02 p0308 A71-12097

Optical thickness of reflecting nebula with given brightness illuminated by star, using three dimensional models
02 p0311 A71-12352

Spherical nebula BESM-3M radiation intensity fluxes, calculating optical thickness, particle albedos and light scattering indicatrices
02 p0312 A71-12359

Carbon monoxide fundamental band spectral absorptivity distributions at various high temperatures and optical densities
04 p0549 A71-15512

Axisymmetrical, optically thick nonNewtonian, power law boundary layer with injection and suction, obtaining similarity transformations for simultaneous convection and radiation
04 p0685 A71-15516

Solar Lyman alpha radiation absorption by molecular oxygen, examining optical thickness with Inter-cosmos-1 satellite
05 p0807 A71-16214

Optically thick clouds reflected light radiance and polarization for haze and nimbostratus models
05 p0781 A71-16252

Vertical behavior of stratospheric optical thickness and dispersion coefficient in red region of spectrum from photometric analysis of Soyuz 3 photographs of daytime horizon
05 p0742 A71-16839

Thin gas optical limit isothermal curves, discussing Planck mean emission coefficients
07 p1222 A71-18993

Thermal Ar plasma with gas additives as standard intensity light source of optically thick spectral lines, using interpolation and Kirchhoff-Planck function
07 p1168 A71-19323

Dust history and physical environment near hot stars associated with nebulosity, discussing optical depths and IR energy
07 p1198 A71-19819

Solar active regions lambda 10 830 line from photometric observations, determining optical thickness, Doppler width and radiation source activity
08 p1361 A71-21130

Comet head physical processes, discussing atomic and molecular distributions, gas ejection velocity and temperature, UV optical thickness, photodissociation, etc
08 p1362 A71-21147

Fraunhofer line profiles, determining optical depth at various points in photosphere
09 p1524 A71-23191

Emission line profile and source function in finite optical thickness plane layer, using matrix equation
09 p1525 A71-23195

Sunspot umbra empirical model, deriving temperature and optical depth relationship from IR continuous limb darkening
10 p1666 A71-23787

Martian studies during opposition, discussing atmosphere, optical thickness, pressure, brightness phase dependencies over land and sea, crust material and dust clouds
10 p1677 A71-24584

Inviscid flow distribution of high temperature jet of optically thick radiating gas exhausting from two-dimensional nozzle into low temperature quiescent medium
10 p1552 A71-24588

Galactic radio source Sagittarius optically thick component evidence based on flux density measurement
12 p1956 A71-26612

Mars atmosphere optical thickness by polarimetric/ground and spacecraft/ observations, considering light areas roughness /smoothness/ factor variation with wavelength
12 p1964 A71-27086

Saturn, Titan and ring IR photometric observations, examining brightness temperature albedos, optical thickness and individual particles
13 p2134 A71-28283

Gray air flow in turbulent optically thin boundary layer, determining radiant energy transport by Patankar-Spalding finite difference procedure
14 p2338 A71-30932

Albedo-optical thickness relation in photometry of gas and dust comets
15 p2484 A71-31663

Photon dwell time in one dimensionally isotropically scattering medium, assuming absorbed state as arbitrary function of optical thickness
15 p2492 A71-32460

Optical filter characteristics obtainable with periodic stacks of two dielectric materials having commensurate optical thicknesses
16 p2577 A71-33128

Saturn radio emission and brightness temperature measurements, determining rings optical thickness upper limit
16 p2639 A71-33692

Homogeneous spherical hot hydrogen plasma cloud at various temperatures and optical depths, presenting electron scattering effects on optical and X ray spectral emission
18 p2951 A71-36012

Mars atmosphere optical thickness by polarimetric/ground and spacecraft/ observations, considering light areas roughness /smoothness/ factor variation with wavelength
19 p3133 A71-37436

Resonance broadening measurements of alkali metals, giving relation between optically thick and thin full widths for Lorentzian and Gaussian line shapes
19 p3105 A71-38721

Aerosol measurements over Atlantic and Indian Oceans, discussing aerosols optical thickness, effective radii, concentrations, sizes and optical properties variations with latitude and meteorological conditions
20 p3257 A71-39328

Linear system model for multiple scattering light transmission through optically thick clouds, calculating optical effects by four dimensional linear superposition integral
22 p3575 A71-41789

Isotropic light scattering in unsteady plane layer of finite optical thickness, obtaining reflection and transmission coefficients for radiative transfer
22 p3607 A71-42869

He ionization and excitation in optically thick solar prominences, considering recombination excitation for observed triplet-level populations at 5000-10,000 K electron temperature

24 p3869 A71-44805

OPTICAL TRACKING

Optical components and technology for acquisition, tracking, transmit-beam offset and background noise discrimination functions in optical space communications

02 p0213 A71-12007

Short pulse optical tracking systems ranging error, analyzing effects of tracker, target and propagating medium characteristics

02 p0214 A71-12029

Differential radiometer with ultranarrow interference filter for daytime tracking of high altitude chemical vapor trails

03 p0424 A71-13636

Transportable photoelectric satellite tracking system with 4-axis support for Schmidt-Cassegrain telescope, discussing field testing results

03 p0397 A71-14004

Precise radio sources positions by Schmidt telescope and AGK 3 reference frame, noting comparison with optical positions

04 p0644 A71-15048

Orbital solutions based on critical optical tracking and Doppler observations, comparing with GEOS 1 and 2 satellite orbits

04 p0553 A71-15305

Intercept Ground Optical Recording telescope and Mobile Optical Tracking System for electro-optical photography, discussing measurement and system errors and CAMDAT computer program

04 p0554 A71-15320

Altazimuth telescope mounting with computer controlled guidance, discussing instrumental and methodical error effects on positioning and tracking accuracy

07 p1083 A71-19348

Moon shape, translational and rotational motion determination by optical tracking, discussing possible refinements as function of distance measurement accuracy

09 p1525 A71-23337

High accuracy deflector and diffraction sensors for optical tracking systems, noting dependence on ultrasonic frequency

10 p1610 A71-24169

Predictive stochastic optimal control model for saccadic eye movements in visual target tracking based on target motion estimate

11 p1723 A71-25142

Automatic telescope guidance system for faint light source tracking, using cumulative photocurrent mismatch signal storage

14 p2271 A71-29994

Optical tracking task performance and nystagmus during angular acceleration in yaw and pitch, comparing differences due to vertical and horizontal canal response

16 p2535 A71-33107

Optical telescopes automatic electronic control by positioning mechanical axis to specified coordinates and tracking guide star

17 p2740 A71-34983

Q switched laser range finders, discussing programmed ephemeris guided, divergence data utilizing and semiautomatic tracking systems with emphasis on target acquisition

[ONERA-TP-964] 18 p2945 A71-36029

Optical tracking systems - Conference, El Paso, Texas, January 1971

18 p2882 A71-36902

Optical tracking system for high angular acceleration missile flights, using movable mirrors with motion picture camera interfaced with computer

18 p2900 A71-36906

Optical target detection and position error signal system for boost phase missiles, using TV with digital computer controlled dual tracking electronics

18 p2883 A71-36911

Human performance in optical high inertia tracking system interface, considering proprioceptive feedback, display magnification, control dynamics view field and anticipatory processes effects

18 p2873 A71-36912

Direct digital control technology for optical tracking systems, discussing advantage and deficiencies

18 p2883 A71-36913

Image dissectors in optical tracking applications, discussing design, operation, SNR performance, tracking modes, relative merits and disadvantages

18 p2883 A71-36915

Beam pointing and tracking requirements for optical space communication system, from energy transfer considerations

19 p3018 A71-38235

Apollo range instrumentation aircraft, describing C-135A modification with airborne lightweight optical tracking systems

19 p3022 A71-38546

NASA Stadan and Speopt optical and laser tracking sites dynamic position estimations from GEOS 1 and 2 observations, analyzing model error effects

20 p3220 A71-39662

Pagosa satellite optical tracking experiment, discussing camera, point image quality and quartz clocks rms error

21 p3347 A71-40260

Laser remote sensing technique for tropospheric refractivity fluctuation profile measurement with tethered balloon-borne retroreflector tracking by ground based tracker

21 p3374 A71-40977

Optical spacecraft tracking, using pulsed ruby lasers at Baker-Nunn camera stations of Smithsonian Astrophysical Observatory for retroreflector-equipped satellites ranges

21 p3349 A71-41404

Flashing lights vision threshold systematic variations, using quadrant adaptometer for continuous tracking of sensitivity fluctuations

22 p3500 A71-41498

Human eye-tracking phase lags representation by time delays depending on target motion class

22 p3490 A71-42451

Onboard optical tracking effectiveness for Grand Tour deep space navigation, considering star-planet angles, plane diameter angles and natural satellite observations

[AAS PAPER 71-394] 23 p3732 A71-43062

Adaptive random search optimization of optical tracking self organizing feedback control system under inherent coupling signals

23 p3657 A71-43942

OPTICAL TRANSITION

Nd-YAG laser branching ratios measurement for all transitions during oscillations at room temperature

05 p0764 A71-16912

CW electric discharge mixing chemical lasers, identifying molecular transitions responsible for radiations from output spectral distribution measurements

[AIAA PAPER 71-216] 06 p0909 A71-18652

X ray emission from optical and inner shell transitions of multiply ionized Cu, Fe, and Ti in low pressure discharge dense plasma

09 p1501 A71-22414

Upper atmospheric composition by nitrogen molecules radiative transition analysis, using laser resonance backscattering effect

09 p1436 A71-22581

Intense superradiant emission in HF and DF molecules high gain IR transitions, examining spectral distributions with pneumatically tuned Fabry-Perot interferometer

09 p1498 A71-23478

Pulsed output, delay time and rotational-vibrational transitions of high pressure transverse discharge CO laser

15 p2424 A71-32613

Ba atoms excitation and optical transitions line broadening by collisions with Ar atoms behind shock waves, using atomic absorption spectroscopy

16 p2613 A71-32889

Coherent electromagnetic excitation of optical transition levels by fluorescence measurement, obtaining dipole moment and relaxation times

18 p2929 A71-35903

Electron concentration and degeneracy effect on threshold photon energy for optical transitions onset from splitoff valence band to conduction band in n-type GaAs

21 p3429 A71-41211

Transition selection with adjustable outcoupling for laser device applied to carbon dioxide

23 p3688 A71-44294

OPTICS

Quantum optics - NATO Conference, Musselburgh, Scotland, July 1969

04 p0607 A71-14803

Papers on optics, Volume 8, covering synthetic apertures, light beating spectroscopy, multilayer antireflection coatings, interference microscopy, photoelectron counting, human eye performance, laser light, etc

05 p0713 A71-16481

Book on visual perception covering physics of light, rods and cones, color vision, brightness psychophysiology, stimulus generalization, etc

06 p0850 A71-17409

Optical systems with large aberration, deriving merit function expressed as quadratic form of aberration coefficients

08 p1333 A71-21179

Light rays bundle compression devices performance based on phase space treatment using Liouville theorem, comparing linear tapers and lenses performance to compressor with graded refractive index distribution

08 p1335 A71-21373

Laser applications in physics research, discussing nonlinear optics and spectroscopy, time and distance measurements and Raman and Rayleigh light scattering

09 p1462 A71-22585

Magnetoacoustic wave propagation in magnetic plasma traps by geometrical optics methods, considering annular traps existence

10 p1651 A71-24638

German monograph on holographic method to increase effective aperture in optical imaging covering optical systems resolving power increase holography, etc

10 p1613 A71-24875

Nonstatic random isotropic medium geometrical optics, considering refractive index temporal fluctuation [ONERA-TP-970]

12 p1929 A71-26822

Nonlinear optics classical macroscopic treatment with Maxwell equations

13 p2078 A71-28517

Optical effects observation by air traveler during takeoff, including haze or cloud droplet scattering, halos, shock wave shadows, shallow watercolors and twilight wedge

13 p2022 A71-29350

Acoustooptic deflector modulation transfer function calculated from autocorrelation theorem

14 p2241 A71-30141

Multiple EM scattering by two spheres, using multiple expansion and ray optics

17 p2701 A71-34756

Astronomical Cassegrain echelle spectrograph, discussing optical and mechanical design and aberration effects

22 p3542 A71-41933

OPTIMAL CONTROL

NT TIME OPTIMAL CONTROL

Complex optimal control problems solution using iterative decomposition algorithms

01 p0111 A71-10319

Computerized optimization of nonlinear dynamic control system subjected to random disturbances, using Monte Carlo method for quality functional

01 p0058 A71-10426

Power gyrostabilizer optimal controlling section with random base frame oscillations, solving filtration problem as function of platform structure by Wiener method

01 p0079 A71-10427

Optimal multipulse compensation for dynamic system external disturbances by minimax differential game approach, restricting impulse number and magnitude

01 p0059 A71-10429

Themis project automatic navigation program, examining optimum stochastic feedback error analysis and sensitivity algorithms

01 p0125 A71-10525

Optimal periodicity of computer systems remedial and preventive maintenance operations based on reliable operation maximum duration

01 p0049 A71-10530

Optimal automatic systems statistical theory in relation to sensitivity, identification, invariance and control object dynamic characteristics

01 p0060 A71-10705

Optimal synthesis of selective multidimensional invariant control systems applied to turboprop engine with differential reductor

01 p0062 A71-10718

Gaussian message optimal transmission through channel with white Gaussian noise in presence of total feedback

01 p0064 A71-11152

Regular optimal motion problem for nonlinear controls reduced to degenerate problem for solving optimal control of solid rotating body angular velocity

01 p0065 A71-11234

Single channel step-type extremal systems with inertial control plants, proposing automatic optimizer

01 p0065 A71-11235

Axisymmetric spacecraft fuel optimal reorientation control by reaction jets determined using Pontryagin maximum principle

01 p0165 A71-11586

Adaptive optimal electromagnetic and acoustic detection antenna synthesis, considering signal direction and spatial noise structure

02 p0229 A71-11716

Inverse problems for parameters and optimal heat transfer model in thermophysical processes

02 p0331 A71-11731

Digital optimal feedback control device, discussing design requirements, algorithm, block diagram, flow chart and measurement results

02 p0236 A71-12150

Optimal control of exhaust velocity for plane motion of variable mass point along trajectory under gravitational and resisting forces

02 p0284 A71-12292

Optimal control synthesis for inertialless plant with feedback based on parameter estimation

02 p0236 A71-12622

Book on optimal control theory covering dynamic programming, calculus of variations, Pontryagin maximum principle and iterative techniques

02 p0236 A71-12773

Communication satellite ground station steerable antenna autotracking, evaluating on-line optimal search techniques by digital simulation

02 p0222 A71-12791

Minimization of unconstrained function of several variables by gradient dependent techniques, discussing applications to boundary value problems in optimal control

[AIAA PAPER 69-951] 03 p0450 A71-13444

Neighboring optimum feedback guidance to motivate min-distance lookup parameter determined by minimizing metric function of perturbed state and reference trajectory

[AIAA PAPER 69-888] 03 p0454 A71-13446

Indirect, linear and nonlinear optimal guidance schemes from precomputed reference trajectory, using iterative techniques for boundary equations

03 p0454 A71-13449

Stochastic stability for optimum systems with general search control law for boundary parameters under vector stochastic differential equation

03 p0389 A71-13518

Spacecraft attitude suboptimal control by orthogonal set of amplitude limited PWM reaction control jets, presenting spacecraft controlled motion computer simulation

[AIAA PAPER 70-997] 03 p0499 A71-13722

Pontryagin maximum principle applied to optimal control of standing TE wave electric field strength in microwave gyrotron

03 p0386 A71-13813

Optimal piecewise constant control of continuous time systems with time varying delay, deriving restrictive condition on Hamiltonian integrated between switching instants

03 p0389 A71-14075

Satellite optimal guidance, discussing gyroscope application for stabilization and orientation control

03 p0500 A71-14227

Approximate optimal control law formulation by harmonic linearization for nonlinear time invariant state regulator problem with high performance index

03 p0390 A71-14299

Linear optimal control systems with penalty on state and control vector sensitivities, avoiding mathematical difficulties

03 p0391 A71-14313

Variable inertia rotating rigid body stabilization by nonlinear optimal control problem, using Hamilton-Jacobi and Riccati equations

03 p0391 A71-14314

Random parameter plant control, considering recursion formulas, optimal strategy and computerized simulation

03 p0391 A71-14379

Soviet papers on nonlinear optimization of automatic control systems covering analysis, synthesis and stabilization problems

03 p0391 A71-14401

Nonlinear control systems optimization methods formulation according to deterministic and random disturbances and initial conditions

03 p0391 A71-14402

Nonlinear control laws successive stochastic optimization through nonlinear and subsequent quadratic programming

03 p0392 A71-14403

Optimal controller analytical design procedures using dynamic programming and Liapunov function

03 p0392 A71-14404

Two controlled motions rendezvous problems treated as game between partners using quality criterion as payoff, deriving optimal strategies

03 p0392 A71-14405

Optimal on-off control systems with structural constraints, discussing synthesis by dynamic programming and phase plane methods

03 p0392 A71-14408

Sampled data feedback control system analysis and synthesis by state variable method, discussing computer algorithms for optimal pulse control

03 p0392 A71-14409

Optimal model of pressurization system for liquid propellant on Surveyor lunar landing spacecraft

03 p0472 A71-14447

Aerial photography, discussing optimal exposure selection and control to obtain maximum number of fine details

04 p0585 A71-14642

Spinning aerospace vehicle optimal attitude control system by minimizing reaction fuel, noting application of Pontryagin maximum principle

04 p0623 A71-15143

Computerized Monte Carlo models of distributed parameter systems of partial differential equations with moving nonlinear boundaries

04 p0619 A71-15150

Feedback control system parameters optimization by target model method, with automatic pilot example

04 p0560 A71-15205

Rotorcraft ideal height-velocity boundary and critical decision point height prediction, discussing pilots optimal control under emergency conditions

04 p0527 A71-15414

Control system problems with state space constraints, deriving sufficient conditions for optimality

04 p0561 A71-15868

Optimal control with equality type phase operatorial constraints, obtaining multiplier rules for necessary conditions in maximum principle form

04 p0561 A71-15870

Continuous time stochastic optimal control systems necessary and sufficient dynamic programming conditions for optimality

04 p0562 A71-15871

Rocket optimum control synthesis for powered flight phase, determining angle of attack for transfer to maximum velocity by Cauchy problem

05 p0779 A71-16038

Optimal momentum exchange desaturation in attitude control systems for orbiting spacecraft, concerning gravity gradient and disturbance torques

05 p0817 A71-16552

Optimal synthesis of rational composite system for gyrostabilizer stabilization

05 p0751 A71-16588

Optimal control systems, using vector analysis in definition of envelope contact test

05 p0774 A71-16644

Object motion stabilization, determining minimum control actions number for linear and nonlinear systems

05 p0782 A71-16977

Controlled objects convergence game, constructing optimal minimax pursuer strategy

05 p0782 A71-16979

Initial conditions selection for optimal control of systems with time lag

05 p0782 A71-16982

Optimal solutions to control problem with bounded coordinates

05 p0731 A71-17016

Optimal control system design quality, using generalized performance characteristics as principal parameter

05 p0732 A71-17022

Optimal control problems for functional extremization, developing modified quasi-linearization algorithm

05 p0776 A71-17089

Direct search of performance index for optimal control of class of nonlinear distributed parameter systems

05 p0776 A71-17109

Suboptimal control of linear time invariant systems subject to structure constraints and combination of measurable/nonmeasurable states

06 p0878 A71-17330

Noninferior set for static optimization of systems with vector valued objective function using dual linear inequality

06 p0878 A71-17333

Plant parameter variations in linear optimal control systems along stability ray

06 p0878 A71-17334

Soviet monograph on differential games of encounter of motions covering optimal control, rendezvous, pursuit, evasion, extremal guidance, etc

06 p0926 A71-17438

Invariant control system with optimum gain and time lag adjustment for compensating parameter changes under random disturbance

06 p0879 A71-17519

Optimal control epsilon technique solution for capture conditions in pursuit and evasion problems

06 p0918 A71-17597

State space constrained linear optimal control systems, using cutting plane algorithm for convex programs in Banach spaces

06 p0918 A71-17598

Continuous monotonic nonlinear controlled systems with time dependent, phase coordinates and nonnegative parameter disturbances, considering Chetaev estimate for restricted approximate solution

06 p0879 A71-17670

Optimal process control with various delay times, discussing maximum principle variant and calculus of variations

06 p0879 A71-17671

Sensitivity analysis and optimal control theory used to design optimal gust alleviation systems, discussing gain and gear ratios

06 p0848 A71-18483

[AIAA PAPER 71-9] Hypersonic body optimum lift control during atmospheric entry, taking into account drag coefficients and density

06 p0842 A71-18488

[AIAA PAPER 71-21] Minimum propellant deterministic guidance law for bounded-thrust constant jet exhaust velocity spacecraft, using neighboring extremal theory

06 p0978 A71-18568

[AIAA PAPER 71-118] Boundary condition iteration methods in chemical process plant optimal design and control, considering simplicity and ease of programming, computation time and storage requirements

07 p1054 A71-18800

Linear systems optimal control problems numerical solution methods comparison, noting accuracy advantage of invariant imbedding technique

07 p1081 A71-18834

Optimal control for distributed parameter system described by linear hyperbolic partial differential equation, deriving existence theorem and cost function

07 p1147 A71-19471

Noninferior performance index vectors in multicriteria optimal control theory

07 p1147 A71-19472

Saturn launch vehicle navigation, guidance and control system, discussing optimal system design for flight path optimization

07 p1155 A71-19527

Optimal solution existence theorem for control system described by linear hyperbolic partial differential equation

07 p1148 A71-19770

Optimal control sufficient conditions with state and control constraints

07 p1082 A71-19771

Catastrophic error propagation and minimum weight codewords in convolutional codes

07 p1069 A71-20417

Book on stochastic processes covering random events, Markov chains, fixed terminal time, discounted cost problem, optimal control and stability theory

08 p1268 A71-21310

Aircraft collision avoidance dynamical system, determining barriers between possible capture regions by optimal control problem solution

08 p1331 A71-21322

Earth-moon libration point space station optimal control, considering restricted four body problem

08 p1363 A71-21323

Numerical results for optimal trajectory control and filtering using Kalaba method

08 p1269 A71-21327

Optimal air traffic control coordinating flow and holding patterns of aircraft landing in single runway using linear-quadratic technique

08 p1332 A71-21335

Moving target indicator (MTI) performance improvement in presence of rain, chaff or other broadband clutter disturbances by adaptation for canceler setting optimization

08 p1254 A71-21338

Optimal phased array radar pulse scheduling multiple transmissions and receptions in minimum time, using integer programming

08 p1254 A71-21339

Optimal algorithmic coordination of spaceborne computer-transmitter coupling, using SIMSCRIPT language simulation

08 p1259 A71-21599

Optimal asymptotic stability laws of control systems with unstable plant, using piecewise coordinate functions

08 p1270 A71-21949

Optimal recognition system for optical spatial and background inhomogeneous Gaussian signals in noise

08 p1257 A71-22022

Optimal variational control with frequency and time coupling concerning dynamic precision of linear systems

08 p1271 A71-22023

Supersonic airplane minimum time turns at constant altitude, determining thrust, bank angle and angle of attack programs with optimal control theory

08 p1232 A71-22032

Linear optimal stochastic control systems described by covariance matrix correlating errors and estimates of state variables, analyzing instability under parameter variations

09 p1421 A71-22076

[AIAA PAPER 70-36] Linear one dimensional systems with infinite degrees of freedom, examining optimal constrained control

09 p1421 A71-22118

Self adaptive systems with dynamic characteristics stabilization, obtaining algorithm for adaptive loop optimization

09 p1422 A71-22120

Linear processes optimal sampled data controls, noting effect of sampling on closed loop system and cost asymptotic behavior

09 p1422 A71-22281

Linear optimal stochastic regulator control, using system output instantaneous feedback with minimum quadratic performance measure

09 p1422 A71-22283

Mathematical model for optimal control of spacecraft reentry into atmosphere

09 p1519 A71-22558

Spacecraft optimal impulsive braking by onboard engine to ensure maximum angle of atmospheric reentry

09 p1519 A71-22567

Optimal control theory application to environmental control of confined spaces and life support systems, considering algorithm of Pontryagin principle

09 p1423 A71-22588

Approximate optimal control synthesis, eliminating use of nonlinear functional converter for switching units design

09 p1423 A71-22607

Optimal orientation control of axisymmetric rotating space vehicle, using cyclic sliding mode theory

09 p1532 A71-22659

Book on matrix methods in stability theory covering matrix algebra, Liapunov theory and functions, stability matrices properties and optimal control theory applications

09 p1539 A71-22872

Control systems optimization via heuristic approach based on Pontryagin maximum principle and pseudotrajectory concept

09 p1423 A71-22968

Computer algorithm for optimal linear impulse corrections to satellite orbit under inequality type constraints

09 p1424 A71-23135

Optimal control of composite spacecraft propulsion system incorporating high thrust-weight ratio chemical engine and low thrust ion engine

09 p1512 A71-23138

Rectilinear trajectory optimization of second order nonlinear system, formulating existence and uniqueness theorems of optimal control

09 p1424 A71-23433

Linear one dimensional system with infinite degrees of freedom, discussing optimal control by Fredholm integral equation

09 p1424 A71-23457

State regulator optimal control problem error bounds, using finite dimensional piecewise polynomial approximations

09 p1424 A71-23466

Optimal control theory of systems with time and state variables dependent coefficients, considering systems described by measure delay-differential equations

09 p1486 A71-23468

Distributed parameter control systems optimality conditions, using Pontryagin maximum principle

09 p1425 A71-23469

Algorithms for optimal control of nonlinear stochastic systems, minimizing control error variance

09 p1425 A71-23684

Optimal control problems with phase constraints, using v technique and abstract multipliers technique

10 p1585 A71-23755

Soviet book on variable structure system theory covering nonlinear automatic control, stability, optimization, adaptive systems, incomplete information processes, linear filters, etc

10 p1585 A71-24147

Aircraft motion and traffic control at air corridors intersections for minimum flight schedule deviation under random disturbance due to weather, using statistical simulation

10 p1639 A71-24158

Soft lunar landing powered descent optimal control for cost functional minimization, considering linear analytic approach with fuel consumption reduction

10 p1682 A71-24330

Trans-Mars launch window problem, discussing minimum delta-V three-impulse noncoplanar transfer from circular parking orbit onto asymptotic velocity vector

10 p1671 A71-24331

Autonomous dynamic systems optimal control problems solution by reduction to operator equation, using Pontryagin maximum principle

10 p1636 A71-24352

Nonlinear satellite system attitude control for minimum fuel consumption, deriving linear programming algorithm based on optimal control theory

10 p1683 A71-24522

Detection characteristics of optimal interperiod processing radar pulse systems for arbitrary correlation of signal and noise fluctuations

10 p1578 A71-24710

Optimal reception of Markov radio signals with intrapulse FM, using nonlinear filtration theory

10 p1578 A71-24711

Optimal two stage signal search in frequency vs arrival time indeterminacy plane of communication system

10 p1579 A71-24714

Optimal control stabilization under continuous small disturbances applied to aircraft stability in horizontal flight under vertical gust loads

10 p1586 A71-24726

Deterministic parameter estimation in nonlinear system near optimum feedback control by power series expansion

10 p1586 A71-24738

Optimal nonlinear filtering, deriving algorithm based on statistical approximation of system and observer nonlinearities by second order polynomials

10 p1587 A71-24746

Control optimization methods - Conference, Novosibirsk, U.S.S.R., June 1968

10 p1637 A71-24839

Numerical search for optimum product space as extension of Gauss-Seidel relaxation method, noting applications to partial differential equations

10 p1637 A71-24841

Krylov-Bogoliubov averaging method in optimal satellite motion programming of transfer orbit and low thrust correction

10 p1587 A71-24843

Optimal stochastic orbit transfer strategy solution by dynamic programming algorithm

10 p1678 A71-24844

Optimal motion of multistage body of variable mass during vertical climb with allowance for weight limitations

10 p1683 A71-24845

Control parameter optimization of dynamic system for single and series maneuvers

10 p1637 A71-24846

Optimal thrust programming for rocket near spherical planet, transfer between circular orbits and lunar landing at predicted point

10 p1683 A71-24847

Constrained gain problem optimality conditions, presenting algorithm for optimal gains and application to aircraft control problems

10 p1588 A71-24859

Optimal stochastic control and gust alleviation for jet aircraft response for flight through turbulent upwash field

10 p1557 A71-24870

Correlation estimates and optimal detector for incomplete a priori information signal reception on random and white noise background

10 p1579 A71-24878

Q factor of control systems as mathematical expectation of functional on input signal set with prescribed probabilistic measure and random initial conditions

10 p1588 A71-24904

Linear discrete time stochastic system with unknown gain parameters, interpreting open loop feedback optimal control identifier and controller equations

11 p1741 A71-25361

Optimal characteristics for single-input single-output memoryless time invariant nonlinear dynamic systems

11 p1742 A71-25751

Conflicting and relaxed minimax controls for Weierstrass E condition or Pontryagin maximum principle

11 p1792 A71-25752

Dynamic optimization with constrained state and control vectors, solving problems by hybrid method with partial derivatives

11 p1735 A71-25842

Delay compensation in flip-flop element of optimal relay system with self oscillations, using optimal control algorithm constructed by phase space method

11 p1742 A71-26095

Soviet book on optimal, multiply connected and adaptive control systems covering variational methods, dynamic programming, functional analysis and statistical methods

11 p1742 A71-26098

Manned space station optimal thermal control design, investigating heat pipe and semipassive/air cooled concepts

[AIAA PAPER 71-431]

11 p1838 A71-26220

Quasi-optimal proportional navigation, deriving feedback guidance laws for interceptor aerodynamically controlled missiles

11 p1796 A71-26409

Fluid interface Rayleigh-Taylor type instability, considering control as optimal regulator problem

11 p1742 A71-26413

Optimal fixed dimensionality dynamic compensator design for linear time-invariant closed-loop system based on quadratic cost and gain criteria

11 p1742 A71-26414

Optimal control problems, applying direct mathematical programming to linear, nonlinear, continuous and discrete time, deterministic, stochastic and distributed parameter systems

11 p1792 A71-26419

Nonlinear systems optimal control, presenting Hamilton-Jacobi equations analytical solutions for quadratic cost function minimization

11 p1742 A71-26420

Optimal control of material point motion in thin spherical layer of central gravitational field, solving by approximation

12 p1957 A71-26631

Optimal flight of material point in central field of forces subject to controlled small thrust

12 p1957 A71-26632

Game theory application to spacecraft reentry problem, obtaining optimal control algorithms

12 p1972 A71-27017

Optimal control of linear and nonlinear systems with infinite degrees of freedom, deriving parabolic type partial differential equations

12 p1891 A71-27019

Optimal impulse correction of linear dynamic system motion based on system phase coordinates

statistical information, taking into account correction finite accuracy and power expenditure

12 p1892 A71-27021

Satellite pitching oscillations optimal stabilization, obtaining approximate solution for finite time

12 p1972 A71-27026

Minimum error pre- and post-filtered sampled signals for pulse modulation and data compression optimization

12 p1879 A71-27070

Optimal stabilization system synthesis for multidimensional linear control plant in presence of random perturbation

12 p1892 A71-27176

Optimal output regulator for linear time invariant systems with reference vector and quadratic cost functional

12 p1893 A71-27430

Optimally controlled boundary layer equations reduction to ordinary differential equations

12 p1898 A71-27490

Nonlinear systems optimal control computational method, using Chebyshev algorithm

12 p1868 A71-27592

Optimal receiver to detect multiple orthogonal signals on normal stationary noise background, assuming nonuniform a priori probability occurrence

12 p1883 A71-27618

Optimal control synthesis analog for nonlinear problem, using trial and error method based on Pontryagin maximum principle

13 p2040 A71-27834

Optimal control systems with discontinuities in right members of differential equations, considering solution to Cauchy problem

13 p2040 A71-27896

Controllability and optimal control for linear system with discontinuous restriction on control function

13 p2041 A71-28009

Linear optimal control system quality functional, deriving sensitivity upper estimate

13 p2041 A71-28635

Optimal control systems design with random parameters and initial state, considering open loop and feedback correction terms

13 p2042 A71-28708

Optimal control synthesis of one dimensional stochastic heat and mass transfer processes with distributed parameters

13 p2161 A71-28727

Optimal control of oscillations of electrically conducting fluid by magnetic field in plane channel with free boundaries, using dynamic programming

13 p2107 A71-28728

Optimal linear feedback for systems governed by differential operational equations, considering stochastic control and cost function

13 p2095 A71-28814

Relaxation methods application to optimal control of systems described by equations with partial derivatives, studying minimizing sequences

13 p2043 A71-28817

Optimal symmetric minimum-impulse rendezvous between close near-circular noncoplanar orbits

13 p2139 A71-28820

Satellite launcher flight plan maximizing mass in orbit or apogee for rocket trajectories optimal control

13 p2139 A71-28827

Optimal control problems solution using linear vector space of continuous operators with constraints in Volterra integral and functional differential equations

13 p2043 A71-28829

Optimal thermonuclear plasma confinement considering external electromagnetic field as control variable, based on Boltzmann-Vlasov model

13 p2107 A71-28832

Optimal quick response control synthesis for hydraulic drive with throttle, using two step phase space method

13 p2002 A71-28937

Vibration absorbers optimization for multiple degree of freedom systems with random excitations, applying optimal control theory in frequency domain

13 p2158 A71-29427

Respiratory air flow optimal regulation hypothesis, testing analytic prediction model results with experiment under stress and rest conditions

13 p2023 A71-29491

Approximate methods for optimal control problems solution in terms of functionals differentiable only with respect to direction

14 p2265 A71-29554

Infimum principle for dynamic optimal control with nonscalar valued cost criteria, rederiving Kalman-Bucy filter

14 p2219 A71-29627

Adaptive controller consisting of real time identifier and minimum variance regulator approached through stochastic optimal control theory

14 p2219 A71-29696

Linear one dimensional systems with infinite degrees of freedom, examining optimal constrained control

14 p2219 A71-29996

Self adaptive systems with dynamic characteristics stabilization, obtaining algorithm for adaptive loop optimization 14 p2220 A71-29998

Flight vehicle equations of motion for computer simulation, calculating optimal servosystem parameters and optimal range control by hybrid computer scheme 14 p2319 A71-30001

Optimal control and tracking problems duality in cases of bounded coordinates and continuously acting perturbations respectively 14 p2220 A71-30870

Gyrostatt satellite steady motion and relative position optimal stabilization by additional forces application 14 p2275 A71-30871

Optimal terminal control stochastic synthesis for linear systems by Bellman second order nonlinear partial differential equations 14 p2220 A71-30872

Extremal strategies of differential pursuit game for nonlinear controlled plants 14 p2266 A71-30988

Ritz-Trefftz algorithm application to optimal state regulator problem computer processing to improve speed of solution and storage requirements 15 p2374 A71-31182

Quality degradation and sensitivity standard of plant parameter definition accuracy in optimal open control system 15 p2379 A71-31520

Suboptimal control of nonlinear autonomous dynamical systems via linear approximation by hyperplanes 15 p2379 A71-31823

Russian papers on complex control systems covering hierarchical structures, automatic, optimal, self adaptive, multidimensional and nonlinear systems analysis and synthesis 15 p2379 A71-31842

Necessary and sufficient conditions for optimality for singular control problems with totally singular extremal path 15 p2380 A71-31900

Iterative technique for state and control-constrained linear optimal control problems with strictly convex cost functions 15 p2380 A71-31936

Optimal tracking of goal seeking vehicles, evaluating Luenberger formulation for tracking error sensitivity 15 p2380 A71-31937

Suboptimal feedback control law for second order nonlinear systems with quadratic performance index, determining power series coefficients 15 p2381 A71-31941

Discrete control system optimization in terms of power requirements minimization, using Pontryagin maximum principle 15 p2381 A71-31977

Optimality conditions for nonlinear distributed parameter control systems described by functionals of evolutionary and stationary equations of mathematical physics 15 p2382 A71-31993

Optimal trajectory analysis for constant thrust optimal-coast minimum propellant control of rocket powered space vehicle 15 p2488 A71-32091

Linear closed loop optimal intercept guidance law compensating for short range tactical missile time lag, guidance command saturation and target acceleration 15 p2446 A71-32113

Optimal phase trajectories of coordinates of electrodynamic vibration test stand, analyzing motion of moving part and optimal control signal along coil 15 p2353 A71-32190

Mathematical models to optimize successive fault finding programs in complex control systems with/without recovery 15 p2382 A71-32618

Optimal discrete time detection of radar signal parameters in nonGaussian correlated and noncorrelated noise, using Markov model 15 p2373 A71-32619

Self similar invariant group solutions to Bellman nonlinear partial differential equation for optimal correction problems of control systems motion with random disturbances 16 p2549 A71-32935

Suboptimization of closed loop adaptive systems by simple dual control method, using dynamic programming 16 p2549 A71-33353

Optimal control of distributed parameter systems described by integral and partial differential equations, providing theory and bibliography 16 p2549 A71-33354

Dynamically symmetrical satellite optimal transfer into steady axial rotation state with simultaneous alignment of symmetry axis, considering control jets moments 16 p2605 A71-33441

Aircraft optimum control synthesis for powered flight phase, determining angle of attack for transfer to maximum velocity by Cauchy problem 16 p2523 A71-33442

Pontryagin maximum principle application to optimal control problems with phase coordinate constraints, noting existence theorem validity 16 p2550 A71-33592

High order optimality conditions of singular controls, considering Pontryagin maximum principle, Bellman dynamic programming and functional analysis 16 p2550 A71-33701

Optimal control algorithm for spacecraft descent in atmosphere at speed near escape velocity, using game theory 16 p2646 A71-33702

Multidimensional control system transmission matrix optimization in presence of random signals and noise 16 p2550 A71-33717

Closed linear systems optimal stabilization, determining transfer function from Wiener Hopf equation 16 p2550 A71-33900

On-line real time optimal control computations for aerial combat games between two aircraft, assessing airborne computer requirements 16 p2525 A71-34022

Optimal control synthesis for saturating time-varying and stationary sampled data systems, using integral performance index and extended maximum principle 16 p2551 A71-34169

Coupled nonlinear control system optimization by noniterative perturbation method 16 p2551 A71-34170

Calculus of variations application to optimal control theory, outlining method for optimal control problems transformation into equivalent classical Lagrange problems 17 p2764 A71-34443

Accelerated procedures for Markov chain model optimal control problems solution with computation time advantage over usual dynamic programming 17 p2719 A71-34737

Distributed parameter systems described by parabolic differential equations in Hilbert space, discussing existence of optimal control based on quadratic cost criteria 17 p2719 A71-34738

Optimal structure and parameter adaptive estimation for continuous and discrete data Gaussian process models with linear dynamics 17 p2719 A71-34739

Linear time-invariant dynamic feedback system suboptimal control by lower order generalized aggregated model for reducing computational complexity 17 p2719 A71-34740

Linear system optimal stochastic control and observation strategies simultaneous determination with quadratic cost by dynamic programming 17 p2719 A71-34742

Nonlinear optimal closed loop system control problems equivalence relations as one-to-one correspondences between Hamilton-Jacobi equations solutions 17 p2719 A71-34743

Optimal control systems synthesis with reduced sensitivity to parameter variations by trajectory sensitivity feedback with cost minimization 17 p2719 A71-34744

Optimum pulse transmission through thin exponentially inhomogeneous plasma region for maximum amplitude signal reception, using matched filter theory 17 p2788 A71-34768

German monograph on plane realizations of switching circuits, covering crossover points minimization in electric lines interconnecting component parts 17 p2716 A71-34773

Infinite-time linear dynamic system suboptimal control derivation from lower dimension models, exemplifying by flexible-bodied rocket vehicle pitch plane dynamics 17 p2720 A71-34871

Distributed parameter system measurement optimization devices location for error estimation cost minimization by disturbances statistical characteristics and boundary conditions 17 p2722 A71-35211

Optimal state regulator approximate design for nonlinear system with quadratic performance index, determining suboptimal feedback law 17 p2722 A71-35212

Optimal control of plant with varying parameters, obtaining suboptimal systems with feedback loops 17 p2722 A71-35214

Continuity and smoothness properties of piecewise optimal control at junction between singular and nonsingular subarcs, developing necessary conditions 17 p2723 A71-35296

Optimal maneuvers of axisymmetrical rotating satellite, minimizing orbital transfer 17 p2815 A71-35603

Economic acceptability, structure and decomposition of multilevel optimal control for complex systems 18 p2896 A71-35916

Optimality conditions for trajectory in Banach space, considering generalized controls 18 p2896 A71-36188

Linear systems with constant inputs optimal with respect to infinite terminal time quadratic performance, using Riccati equation 18 p2896 A71-36236

Object motion stabilization, determining minimum control actions number for linear and nonlinear systems 18 p2947 A71-36777

Controlled objects convergence game, constructing optimal minimax pursuer strategy 18 p2948 A71-36779

Initial conditions selection for optimal control of systems with time lag 18 p2948 A71-36782

Computer designed optimal or suboptimal feedback controllers, considering least-pth and minimax cost functions 18 p2886 A71-36832

Operator solutions of nonlinear equations in linear feedback optimal control 18 p2943 A71-36956

Conflict rendezvous, pursuit and deviation game problems, obtaining optimal control strategies approximation by continuous functions 19 p3103 A71-37104

Optimal lateral guidance switching thresholds for low L/D shuttle vehicle entry, using optimal stochastic control theory for problem formulation in conjunction with dynamic programming 19 p3096 A71-37164

Interceptor aircraft optimal nonlinear command guidance scheme for reduction of airborne computation load with forward prediction of interceptor and target state vectors 19 p3096 A71-37166

Reentry glider approximate optimal atmospheric entry trajectories for maximizing function of terminal velocity, altitude, flight path and heading angle under terminal nonlinear constraints 19 p3096 A71-37168

Three dimensional hypervelocity reentry trajectories, using aerodynamic lift and vehicle bank angle as optimal control parameter 19 p3096 A71-37169

Optimized momentum and attitude control system /MACS/ for Skylab class space stations employing control moment gyro and reaction jet elements 19 p3098 A71-37183

Kalman filter for computerized optimal SRAM air to surface missile alignment, discussing design, digital simulation and flight tests 19 p3098 A71-37189

Aircraft control design by implicit model-following technique with optimal feedback sampled data and continuous control algorithm, exemplifying STOL aircraft landing approach control 19 p2995 A71-37197

Optimal Kalman filter gyro drift rate mathematical models for limiting inertial navigation errors 19 p3100 A71-37212

Specific optimal techniques in control and estimation, emphasizing fixed configuration optimization with time variant parameters and two point boundary value problem 19 p3036 A71-37237

Optimal control of linear time varying neutral system, solving differential equations set 19 p3037 A71-37238

Asymptotic optimal rank criterion for noncoherent detection of fluctuating radar signal in noise of unknown intensity 19 p3015 A71-37253

Boundary value problems solution in optimal control theory, discussing gradient descent method in state space 19 p3037 A71-37534

Optimization problems for control processes described by ordinary differential equations, solving by variational methods 19 p3086 A71-37555

Explicit procedure for discrete approximations to general nonlinear fixed-time continuous optimal control problems without intermediate trajectory constraints 19 p3037 A71-37556

Balance function concept extension to optimal control problem for finding numerical iterative solutions, considering low thrust orbit transfer problem 19 p3037 A71-37557

Optimality of Contensou singular alternating arcs in time-free central-field orbital transfer problem, using succession of infinitely small impulses 19 p3134 A71-37558

High order optimality conditions, considering multidimensional control and transformation in space of states 19 p3037 A71-37567

Game theory application to spacecraft reentry problem, obtaining optimal control algorithms 19 p3152 A71-37687

Optimal impulse correction of linear dynamic system motion based on system phase coordinates statistical information, taking into account correction finite accuracy and power expenditure

19 p3037 A71-37690

Satellite pitching oscillations optimal stabilization, obtaining approximate solution for finite time

19 p3152 A71-37695

Optimality in classification of stochastic processes in recognition system, using predicting filter rms error as discriminating function

19 p3038 A71-37779

Minimum mass design of two dimensional plate-like structure with free vibration fundamental frequency or aeroelastic constraints, using optimal theory for extremum

19 p3158 A71-37877

Filter design for optimal transient performance, comparing with steady state frequency response

19 p3038 A71-38487

Optimal zero-memory regulator for linear system with stochastic jump parameters, considering Bayes and minimax controllers

19 p3039 A71-38711

Optimal control with minimax cost for systems of n first-order state equations with performance measured by Chebyshev type functional over state trajectory

19 p3039 A71-38716

Comments on optimum bandwidth of low pass RC filter for pulse signal detection in nonstationary noise

20 p3203 A71-38867

NiCd battery and third electrode characteristics for different charge and discharge rates, considering end-of-charge control system optimized for satellites and manned spacecraft applications

20 p3179 A71-38904

Suboptimal design of closed loop least upper bound fuel control for dynamic systems, minimizing fuel consumption on basis of fixed ultimate error

20 p3206 A71-38971

Simultaneous identification and feedback control optimization using predictor updating scheme

20 p3206 A71-38972

Interaction measure for optimal multivariable feedback control system design for complex blending processes, noting paradoxical solution

20 p3207 A71-38993

Suboptimal control with nearly isocost surfaces involving plants subject to large set point changes

20 p3207 A71-38996

Model following technique for optimal control applied to hovering motion of CH-3 helicopter

20 p3178 A71-39000

Spacecraft reentry into random medium atmosphere, determining optimal control procedure for prescribed arrival region and time with simulation equation

20 p3269 A71-39123

Spacecraft interplanetary guidance trajectory correction, deriving algorithm for optimal accuracy and minimum fuel expenditure

20 p3288 A71-39124

Flight mechanics of point with limited power propulsion system and energy storage unit, investigating variational maximum payload problem with singular control optimization

20 p3288 A71-39125

Third order oscillatory system optimal terminal-state control synthesis by quadratic functional minimization iterative procedure algorithm, using ODRA-1204 computer program

21 p3359 A71-40164

Optimal tracking feedback filter for closed loop systems with irrational transfer function, using heuristic method

21 p3359 A71-40251

Optimal control laws existence for stochastic systems with minimized cost functional, considering trajectory information for controller decisions

21 p3360 A71-40254

Optimal trajectories and controls for dynamic systems modeled by coupled rigid bodies, applying to systems of robots and all-terrain vehicles [ASME PAPER 71-VIBR-82]

21 p3414 A71-40318

Optimal numerical solutions of linear control systems with quadratic integral form, using dynamic programming, successive optimization and algorithm-aided dynamic programming

21 p3360 A71-40617

Linear multivariate sampled-data control systems optimal design based on deadbeat performance

21 p3360 A71-40618

Dual stochastic relations of optimal control and minimal error observation under random noise, using programming method

21 p3361 A71-41136

Controllability and optimal control for linear system with discontinuous restriction on control function

21 p3361 A71-41137

Stochastic optimal control of discrete processes with random disturbances

21 p3361 A71-41139

Graph-analytical method of determining optimal adjustment of real differentiating units and components

introduced into single loop automatic control system with time lag

22 p3525 A71-41440

Optimal control of linear systems with distributed parameters, using hyperbolic type equation

22 p3526 A71-41909

Spacecraft pointing control system with momentum exchange controllers, considering near optimal control policy for control moment gyro system

22 p3608 A71-41966

Space shuttle trajectory design optimization by nonlinear programming, proposing mathematical model to handle equality and inequalities constants

22 p3600 A71-42013

Spinning and dual spin spacecraft angular momentum and axis control, investigating optimal fuel and small angle reorientation techniques

22 p3611 A71-42045

French monograph on extrapolation type extremal control systems speed and stability performance improvement based on Jacob step duration modulation method

22 p3526 A71-42067

Book on dynamic programming application to optimal control covering discrete random processes, continuous deterministic and stochastic processes, etc

22 p3567 A71-42428

Probabilistic system observation at random times, calculating Markov renewal processes optimal long run control

22 p3527 A71-42628

Discrete system high order optimality sufficient conditions and methods for singular and nonsingular controls study

22 p3527 A71-42854

Control system synthesis from transient process estimates with Liapunov functions, proposing optimality criteria based on Gaussian minimum constraint principle extension

22 p3527 A71-42855

Optimal lift control of hypersonic lifting body during atmospheric entry by singular perturbation method [AAS PAPER 71-366]

23 p3773 A71-43036

Helicopter optimal autorotation landing parameters for touchdown at zero speed, including rotor rpm drop due to flow separation on blades

23 p3627 A71-43090

Closed phase lock loop FM demodulator design, determining resonant frequency parameters, attenuation factor and low pass filter elements

23 p3650 A71-43094

Gyrocompass with optimal error correction under rapid acceleration change

23 p3675 A71-43297

Optimal control of self excited vibration of high speed rotor with thrust magnetic bearing, using analog simulation

23 p3681 A71-43311

Distributed parameter system optimal feedback control with quadratic performance indices dependence on discrete point states, applying to uniform bar temperature control

23 p3656 A71-43853

Nonlinear discrete system optimal feedback controller synthesis for low sensitivity to parameter variations by difference equations quasilinearization and dynamic programming

23 p3656 A71-43855

Valentine technique difficulty in testing stationary solution for control optimality, discussing overcoming method for problem of sounding rocket thrust control in vacuo

23 p3773 A71-43856

Deterministic system optimal control with single control and several cost functionals by Pontryagin maximum principle

23 p3656 A71-43858

Necessary and sufficient conditions for optimal control problems equivalence, considering time functions for disturbing influence of external forces

23 p3656 A71-43861

Singular optimal control theory generalization using appropriate transformations, considering stability results for bang-bang solutions

23 p3657 A71-43941

Adaptive random search optimization of optical tracking self organizing feedback control system under inherent coupling signals

23 p3657 A71-43942

Error insensitive proportional integral derivative (P-I-D) tracking controller design using optimal linear regulator theory

23 p3657 A71-43946

Riccati equation reduction for optimal control of linear quadratic distributed parameter systems applied to temperature and heat flow regulation

23 p3653 A71-43969

Minimum order state vector reconstruction linear filters for constant plants optimal control, applying to aircraft flight multiple control-point problem

23 p3657 A71-44077

Parameter sensitivity reduction in linear optimal feedback control systems based on two degree of freedom structure

23 p3658 A71-44080

Fixed configuration optimal control of linear systems with state and control dependent noise

23 p3658 A71-44082

Linear constrained optimal filtering by multistage linear transformations using Kalman-Bucy estimates and Lagrange multipliers

23 p3658 A71-44084

Gradient algorithm for optimal trajectory control with inequality and singular arcs, using nonlinear programming and Euler-Lagrange equations

23 p3658 A71-44085

Indirect numerical method for solving optimal control problems with singular arcs

23 p3658 A71-44086

Optimal control of time delay systems described by linear differential difference equations

23 p3658 A71-44087

Cost functional gradient optimization of pulse width modulated control inputs for nonlinear dynamic systems

23 p3658 A71-44088

Optimal inner product angular momentum controllers, analyzing performance criteria and feedback control laws

23 p3658 A71-44090

Linear regression optimal filtering application to aircraft target tracking

23 p3659 A71-44094

Maximally achievable accuracy of linear optimal regulators and filters

23 p3659 A71-44099

State estimation errors in quadratic optimal control feedback gain design of stochastic linear regulator

23 p3659 A71-44100

Space vehicle low thrust minimum terminal variance guidance problem reduced to stochastic bang-bang optimal control system

23 p3702 A71-44101

Stochastic optimal control theory application to airplane rescheduling model, obtaining dynamic programming algorithm for optimal landing and takeoff rules

23 p3702 A71-44104

Computer-aided decision algorithm for ATC problem in near terminal area, emphasizing scheduling and holding strategies

23 p3703 A71-44105

Analytic synthesis of optimal feedback controller for nonlinear multivariable systems based on reduction to linear control problems

23 p3659 A71-44110

Jump type behavioral uncertainties in stochastic optimal control problems, considering control of spinning spacecraft

23 p3659 A71-44112

Suboptimal feedback link estimation algorithms for stochastic control, comparing with separation principle

23 p3660 A71-44118

Linear dynamic systems suboptimal control determination from lower dimension models, characterizing system and model outputs as Hilbert space elements

23 p3660 A71-44121

Nonlinear and multivariate optimal sampled data control systems design with bounded control and state variables, using dynamic programming and divisional technique

24 p3812 A71-44452

Trends in automatic control field in last two decades, emphasizing optimal control and performance criteria selection

24 p3813 A71-44591

Modified perturbation method for solving optimal control boundary value problems with state variable inequality constraints, noting application to reentry trajectories

24 p3876 A71-44608

Matched asymptotic solutions for optimum lift controlled atmospheric entry of hypersonic lifting vehicles

24 p3876 A71-44609

Suboptimal control laws calculation, using functional form of variables for algorithm

24 p3813 A71-44615

Soviet papers on nonlinear optimal control systems, discussing dynamics, adaptation, image recognition, reliability, queueing theory and random processes

24 p3813 A71-44676

Statistically optimal linear systems characteristics under unsteady input signal, noting relation between error components

24 p3813 A71-44679

Automatic control systems optimal nonlinear digital filter design, using theoretical numerical grid

24 p3813 A71-44680

Nonlinear automatic control system statistical optimization using similarity theory

24 p3813 A71-44681

Nonlinear control system optimal synthesis by statistical criteria, discussing probability and likelihood function

24 p3813 A71-44682

Linear system under state dependent random noise, obtaining optimal steady control

24 p3814 A71-44684

Statistically optimal automatic control system synthesis with phase coordinate vector
24 p3814 A71-44685

Linear control system optimal weighting function determination from maximum probability for system error
24 p3814 A71-44687

Stochastic process optimal control in presence of constraints, solving two-point boundary value problem by successive approximation method
24 p3814 A71-44688

Accuracy analysis of statistically optimal dynamic system with modulus bounded control for discrete and continuous information input, using Fokker-Planck-Kolmogoroff equation
24 p3814 A71-44689

Statistical optimization of spherical gyroscope regarded as servocontrol system under random perturbation, using measured values of relative angles between sphere and inner gimbal
24 p3825 A71-44691

Optimal dynamic accuracy of control systems with random signals and parameter oscillations, using sensitivity theory
24 p3815 A71-44697

Optimal stochastic control law derivation for linear regulator with quadratic performance criterion from limiting form of transfer function
24 p3816 A71-45134

Spacecraft motion stabilization about mass center and optimal angular velocity control using minimax technique
24 p3846 A71-45308

Second order differential guidance game, formulating strategy for optimal feedback control
24 p3849 A71-45338

OPTIMIZATION

NT FLIGHT OPTIMIZATION
NT OPTIMAL CONTROL
NT TIME OPTIMAL CONTROL
NT TRAJECTORY OPTIMIZATION

Optimal prediction of stochastic differential equation solution with Gaussian member and small nonlinearity
01 p0110 A71-10098

Jet pump optimization for incompressible flow, considering friction losses, nonuniform densities and diffuser losses for overall energy conversion efficiency
01 p0085 A71-10105

Cylindrical shells and circular plates optimal limiting and adaptable loads calculation by Pontryagin maximum principle
01 p0170 A71-10639

Quadratically convergent algorithms for function minimization tested by numerical examples
01 p0112 A71-10847

Parametric differentiation method for reducing structural optimization and nonlinear programming problems to solution of simultaneous nonlinear algebraic equations
01 p0174 A71-10951

Conjugate direction minimization procedure based on sequences and inferred second partial derivative matrix inverse
01 p0112 A71-10962

Book on approximate methods in optimization problems covering nonlinear extremum, functional analysis, algorithms, optimal control theory and finite dimensional spaces
01 p0113 A71-11323

Thrust-minus-drag optimization by base bleed and/or boattailing, using computer program
01 p0004 A71-11589

Cardiovascular system blood flow mathematical model parameter optimization by simulation on hybrid computer, using OPTTRAN program
02 p0203 A71-11807

Optimal quantum receiver mathematical specification derivation for M-ary digital signal detection
02 p0215 A71-12036

Maximum power transfer theorem generalization for n-terminal pair network containing sources
02 p0236 A71-12043

Gradient /steepest ascent/ methods for differential equation systems optimization, discussing convergence acceleration and nonlinear programming
02 p0277 A71-12729

Elastic column optimization, examining material distribution for minimum volume without buckling
03 p0501 A71-13023

High speed homopolar alternators as static frequency converter supplies, optimizing design parameters by computer geometric programming
03 p0352 A71-13052

Dynamic polysystems stability and optimization, discussing minimality and recurrence in state space set
03 p0450 A71-13120

Minimization of unconstrained function of several variables by gradient dependent techniques, discussing applications to boundary value problems in optimal control
03 p0450 A71-13444

[AIAA PAPER 69-951]

Linear control systems searchless automatic optimization on basis of ideal reviewing model
03 p0389 A71-13519

Truss systems optimal structural design, noting elastic-plastic stability conditions
03 p0509 A71-13897

Flat cooling wall optimum thickness for minimum steady state temperature at point exposed to local heating
03 p0520 A71-13955

Convex Taylor series truncations minimization by iterative method based on approximating initial functional
03 p0452 A71-14058

Iterative functional minimization methods using Lagrange multipliers, examining convergence
03 p0452 A71-14059

Optimal design of rotating disks of nonuniform thickness with integral shafts, using two and three dimensional numerical analysis for stress distribution [ASME PAPER 70-WA/DE-6]
03 p0511 A71-14141

Hydrazine-oxygen fuel cells energy costs minimization by optimizing diaphragm thickness, hydrazine concentration and load
03 p0355 A71-14321

Optimal synthesis of antenna array radiation patterns with minimum square deviation from zero in sidelobe
04 p0557 A71-14629

Signal optimization for binary data transmission system with noiseless feedback channel, considering receiver signal energy and structure
04 p0560 A71-14743

Optimum synthesis of mechanical systems using effort functions
04 p0625 A71-15061

Optimal and nonoptimal signal reception under conditions of incomplete a priori information based on approximation by Markov processes in white noise
05 p0730 A71-16000

Optimal design of low noise multistage microwave oscillator, discussing quartz master oscillator frequency effects
05 p0727 A71-16001

Markov process optimal stoppage, using strongly supermedian functions
05 p0773 A71-16157

Linear, nonlinear and stochastic real control systems optimization by numerical techniques, considering gradient methods and linear programming
05 p0730 A71-16250

Second harmonic generation with focused pump beams of optimum phase mismatch and confocal parameters values for obtaining high conversion efficiency
05 p0762 A71-16337

Single mass vibrational impact system optimal periodic motions, analyzing vibrorams productivity optimization via analog of sphere bouncing down staircase
05 p0821 A71-16358

Orthotropic sandwich and homogeneous single layer circular cylindrical shells optimal design
05 p0822 A71-16419

Book on optimization methods covering matrix algebra, n dimensional geometry, search techniques, linear and nonlinear programming, etc
05 p0774 A71-16475

Linear programming application to optimum structural design, noting savings in design and price
05 p0825 A71-16610

Optimization of multistage rockets with given payload, propellants and explosive separation of stages
05 p0817 A71-16613

Extremals optimal endpoints, obtaining necessary and sufficient conditions by method based on dichotomy concept
05 p0774 A71-16645

Automatic systems design, describing optimization method for nonlinear nonstationary system acted upon by fluctuation signals and disturbances
05 p0731 A71-16793

Optimal quasi-regular signal detection on amplitude and frequency modulated noise background
05 p0723 A71-17020

Multiplexed PAM signal transmission over random time multichannel and diversity systems, discussing optimization for receiver frequency response by numerical solution [IEEE PAPER 70-TP-47-COM]
05 p0723 A71-17053

Squaring loops for establishing coherent carrier reference for bi-phase PSK modulation, deriving optimal presquaring filter
05 p0730 A71-17075

Radar receiver dynamic range centering for log-normal target statistics for minimum probability of signal exclusion
05 p0725 A71-17084

Structural optimization by concave and piecewise linear programmings, discussing mathematical foundation and iterative method efficiency
05 p0829 A71-17121

Permanent magnet optimal size selection from initial operating point on demagnetization curve
05 p0705 A71-17173

Optimal design with geometric constraints for simply supported Tresca plastic disk and cantilever plate under concentrated force
05 p0830 A71-17223

Haunched beam design optimization for lightest weight, analyzing failure modes under assumption of elastically rigid perfectly plastic material
06 p0981 A71-17301

Positive-negative feedback control system optimum switching conditions, deriving simple algebraic formula for nth order system switching equation coefficients
06 p0878 A71-17339

Soviet book on radar signal processing optimization covering detection and measurement, electronic analog and discrete digital filters design, etc
06 p0867 A71-17445

Optimum design of dominant type adaptive control systems with large parameter variations, using fourth order approximation
06 p0878 A71-17449

Optimality criteria for communication systems, considering data transmission rate
06 p0867 A71-17496

Analog to digital conversion mathematical model, considering comparators dynamic properties effects on optimal algorithms selection
06 p0871 A71-17523

Analog to digital converter optimal algorithm for detecting and correcting errors caused by pulsed noise at input
06 p0871 A71-17524

Lubrication considerations concerning mechanical and service variables for obtaining optimum gear performance under severe operating conditions
06 p0904 A71-17576

Doubly shunt loaded short slot antenna, determining optimum capacitive loadings for enhanced radiation or improved directivity
06 p0876 A71-17740

Complex supply system large quantity data handling and cost savings through optimum planning of storage points and transport using linear separable programming
06 p1010 A71-17746

Variational methods application to optimal heating of thin elastic shells, using elastic-energy functional minimization as optimality criterion
06 p1006 A71-17767

Optimal parameter selection for thin walled shell structures, using mathematical programming
06 p0989 A71-17781

Cost-optimal zero moment shell geometry, developing digital computer algorithm with dynamic programming
06 p0992 A71-17804

Reinforced zero moment minimum weight shells strength analysis and optimal design algorithms, using discrete calculation scheme
06 p0998 A71-17854

Plate and shell designs, considering thin walled structures optimization for minimum weight, volume and cost vs maximum stresses
06 p0998 A71-17858

Low noise temperature high gain satellite communication antenna feeds optimal design using step-tapered aperture
06 p0877 A71-18395

Maximum thrust plug nozzle design for fixed inlet geometry, using calculus of variations for optimum contour determination [AIAA PAPER 71-40]
06 p0946 A71-18501

Three dimensional /nonaxisymmetric/ thrust nozzle design, using calculus of variations for maximization of thrust [AIAA PAPER 71-42]
06 p0946 A71-18503

He-Cd laser output description by rate equations, investigating saturation effects, discharge processes and optimization
06 p0910 A71-18666

Mathematical model of small scale versatile aircraft component production process, developing computer production optimization algorithm
06 p0906 A71-18715

Soviet book on automatic control systems synthesis covering dynamic characteristics optimization, based on quality indices and computerized design
07 p1081 A71-19048

Minimization with superlinear convergence based on second derivative matrix successive approximation scheme
07 p1146 A71-19176

Optimal algorithm for searching minimum of single variable convex function
07 p1146 A71-19177

Chemical reaction kinetics optimal problem numerical solution based on Pontryagin maximum principle and gradient method
07 p1147 A71-19185

Metal cutting on lathes, discussing machining conditions optimization based on productivity and cost criteria and linear programming solution
07 p1117 A71-19367

Optimal structural design for nonconservative elastic stability of cantilever column, obtaining critical load

07 p1212 A71-19473

Optimum transmitted data volume, orientation accuracy and size of narrow beam parabolic spacecraft antennas, defining optimum parabola for approximate radiation pattern

07 p1078 A71-19871

Satellite communication system parameters optimization based on economical and technical constraints, applying to Intelsat 3

07 p1063 A71-20040

Optimum AM reticle-detector models, discussing image resolution, electrical bandwidth and detection problems

07 p1115 A71-20368

Turbulence amplifier optimal dimensioning for maximum fan-out factor and minimal signal transport time

07 p1024 A71-20554

Elastoplastic arresting device, predicting mass impact effect for optimal design in terms of deformation or contact time

08 p1367 A71-20688

Automated network design optimization trends and role in computer aided design of lumped-distributed and microwave networks, emphasizing adjoint network method

08 p1268 A71-20767

Aircraft optimum minimum noise takeoff profile, solving by equations of motion system for jet aircraft

08 p1331 A71-20779

Optimal thin walled structures design, using discrete matrix methods for computer programming

08 p1368 A71-20791

Trajectory measurement program optimization, constructing algorithm for variational problems

08 p1360 A71-21001

Trajectory measurement optimal program, using least squares method

08 p1360 A71-21002

Minimum-sensitivity network synthesis using continuously equivalent transformations and weighted sum of sensitivities square magnitudes as criterion

08 p1268 A71-21272

Fabry-Perot resonator with anisotropic medium, deriving reflection mirror shape for optimizing diffraction loss and resonant conditions for extraordinary waves

08 p1289 A71-21284

Hybrid phase locked loop for deriving phase error estimate from carrier and information components, discussing system parameters optimization for performance

08 p1270 A71-21353

Lidar wavelength optimization for Raman scatter atmospheric studies, taking into account aerosol and weak signal statistical effects

08 p1254 A71-21458

Optimal detector parameters for stochastic signals in noise, discussing analytic and simulation studies of adaptive techniques of pattern recognition

08 p1259 A71-21594

Adaptive array processor analysis and optimum design for passive detection of sonar type directional stochastic signals

08 p1256 A71-21602

Optimum antenna array processing design for target detection in nonuniform clutter background, using decision-theoretic processor with digital computer

08 p1256 A71-21604

Soviet book on research and design work optimization and automation based on mathematical methods and computer techniques

08 p1299 A71-21650

Optimal time determination for using radioactive isotope as radiation source in nondestructive testing

08 p1332 A71-21898

Optimal error correcting code structure selection for binary data transmission systems synchronization, using criterion of minimum false detection probability

08 p1260 A71-21979

Frequency signal structure selection to ensure maximum information capacity for given SNR at receiver output in discrete information transmission

08 p1257 A71-21980

Planar microwave array antenna for scan requirement, discussing tilt angle and element arrangement optimization

08 p1229 A71-22030

Direct search algorithm for automated optimum structural design with spiral stiffened cylindrical shell application

09 p1533 A71-22077

Sounding rocket design parameters optimization, investigating apogee-payload relations, thrust as function of time, total weight, maximum altitude and acceleration

09 p1531 A71-22127

Optimal inlet parameters of MHD generator channel employing kerosene-gaseous oxygen combustion products

09 p1386 A71-22136

Optimal phase regulated AFC system for PM signal filtration in presence of internal noise

09 p1404 A71-22155

Single gap klystron output resonator optimization, showing maximum electronic efficiency during bunched beam excitation

09 p1414 A71-22220

Klystron output resonator efficiency optimization under excitation of plasma with Pi-shaped charge concentration based on performance analysis as function of plasma width

09 p1415 A71-22360

Semiconductor integrated circuit fabrication optimization, considering defect density, component number, crystal size and cost analysis

09 p1416 A71-22490

Positive curvature type shallow shells computation for optimum efficiency and minimum material expenditure by dimensionless modeling method

09 p1537 A71-22517

Closed spherical shell, calculating optimal internal temperature fields for keeping thermal stresses at low level under local axisymmetric heating

09 p1537 A71-22520

Optimum test logic and constraint network for space shuttle program

[AIAA PAPER 71-309]

09 p1531 A71-22621

Reactor shield weight optimization using FASTER-III Monte Carlo computer program for neutron and gamma ray transport

09 p1539 A71-22810

Optimal design parameters in minimization of reinforcement elements weight in cylindrical glass fiber reinforced orthotropic plastic shells under axial compression

09 p1539 A71-22826

Structural design optimization in rheology, classifying various objectives and constraints

09 p1540 A71-23086

Optimization of slot angle, slot positioning and flow quantity affecting boundary layer control in energy transfer over airfoil profiles

09 p1383 A71-23201

Hall MHD generator duct optimization, using digital calculation for Carter integral minimum for size under required power output

09 p1512 A71-23441

Geometry optimization of error-free distributed nondirectional aperture array receivers, using signal detectability technique

09 p1408 A71-23491

Arbitrary antenna arrays of not necessarily identical elements, deriving maximum realizable gain under impedance matching, and applying to spaced circular arrays

09 p1419 A71-23508

Optimum synthesis and design of distributed RC filter for oscillator feedback circuit, using calculus of variations

09 p1425 A71-23652

Iterative computation of variational optimization problems by analog computers with digital logic control/hybrid computers

09 p1413 A71-23665

Growth minimization of nonzero elements in sparse matrix during reduction to Hessenberg triangular form by Gaussian similarity transformations

10 p1635 A71-23775

Design optimization of aircraft starting and generating systems, identifying information required and system analysis methods

[SAE PAPER 710392]

10 p1558 A71-24256

Positive signal optimal detection system in unsteady non-Gaussian noise

10 p1577 A71-24282

Computerized interactive scheduling system for modeling, optimization and priority requirements for NASA manned space flight network

10 p1581 A71-24297

German book on optimization for variational problems with ordinary differential equations as secondary conditions

10 p1636 A71-24480

Optimal prestressing against buckling of structures with reserve capacity, using energy methods of structural analysis

10 p1689 A71-24514

Optimal models for time shared computer systems with real time multiprogramming

10 p1581 A71-24727

Systems approximation by incontinuous orthogonal Harre functions, discussing dynamic properties and input signal synthesis with minimal errors in estimating parameters

10 p1587 A71-24741

Multistage two player zero-sum games with state determined by difference equations, deriving optimal strategy pair satisfying saddle point condition

10 p1637 A71-24842

Flight path optimization with multiple time scales, discussing decoupling of high order three dimensional aircraft flight problem into several low order problems

10 p1556 A71-24858

Optimum one term series solution for multidimensional heat conduction problem with initial profiles

10 p1698 A71-25086

Threshold-extension phase-lock demodulator design for optimizing satellite communication ground station systems, using FM carriers

10 p1580 A71-25106

Ionized argon laser optimum performance, comparing master oscillator power amplifier configuration to simple oscillator

11 p1772 A71-25141

Weight minimization of semiinfinite flat sandwich panel at constant dynamic pressure in supersonic flow subject to flutter constraint, using finite element model

[AIAA PAPER 71-330]

11 p1842 A71-25310

Automated optimal weight fully stressed large scale structural design of aircraft, using matrix-mathematical programming technique

[AIAA PAPER 71-361]

11 p1844 A71-25340

Stability analysis and design optimization with dynamics and aeroelasticity constraints for helicopter rotor blade minimum weight with bending torsion flutter and favorable frequency placements

[AIAA PAPER 71-388]

11 p1846 A71-25352

Scalar Gaussian channel information optimal input capacity as function of random variable, assuming finite number of values for amplitude and variance constraints

11 p1730 A71-25374

Spacecraft structures weight optimization based on fracture mechanics and reliability cost constraints applied to pressure vessel design

11 p1847 A71-25464

Optimum buckling load of cylindrical shells under lateral pressure using Rayleigh-Ritz method

11 p1848 A71-25484

Inequality constraints in primer optimal N impulse solutions, introducing penalty function and its gradient with respect to control variables

11 p1791 A71-25497

Lunar flying vehicle propulsion system optimization, discussing weight, performance, engine life, reliability, etc

[AIAA PAPER 70-605]

11 p1810 A71-25504

System design and optimization computer subroutines based on biological mutation and selection principles, using random number generator

11 p1734 A71-25639

Shear deformation effect on optimal design of elastic beams, considering rectangular cross section circular ring by Timoshenko beam theory

11 p1849 A71-25677

Optimal elastic beam structural design for given deflection in presence of body forces, considering rod under centrifugal loads

11 p1849 A71-25680

Optimal synchronous plane accuracy for space triangulation as function of geometrical position of artificial satellite relative to earth sphericity

11 p1758 A71-25812

Relativistic effects and optimization in Doppler geodetic measurements, using model computations for satellite azimuth-elevation relation

11 p1732 A71-25832

Parameter optimization in linear control systems subject to random disturbances, using hybrid computer

11 p1735 A71-25840

Direct impulse response method application to function optimization, using high speed hybrid computer

11 p1735 A71-25841

Hybrid computer Monte Carlo technique for simulation and optimization of system with random parameters

11 p1735 A71-25843

Hybrid computer operating system for piloted aircraft simulation and optimization studies

11 p1736 A71-25853

Design optimization of out-of-core cylindrical thermionic converter module with heat pipes and integral finned radiator

11 p1711 A71-25876

Quasi-vacuum mode thermionic converter for space and remote terrestrial power supplies, describing computer codes for design optimization

11 p1713 A71-25899

Optimum calibration of turbine flow sensors AC voltage signals with volume proportional frequency by weighted least squares techniques

11 p1762 A71-25934

Optimal reliability of system with nonlinear constraints, using mathematical model and sequential unconstrained minimization technique

11 p1771 A71-26161

Optimal blowing wall jet prediction for suppressing separation from high lift aerofoils with incomplete mixing of upstream boundary layer

11 p1704 A71-26196

Space shuttle thermal protection system optimal weight by numerical parameterization, discussing temperature constraints and material rearrangement effects

[AIAA PAPER 71-444]

11 p1839 A71-26229

Radio interference suppression rules optimization, using mathematical model to characterize interference voltage, antenna sensitivity and radio transmitter field strength

11 p1733 A71-26339

Instrument orientation optimization for ballistic missile applications, emphasizing acceleration induced velocity and position errors

11 p1796 A71-26410

P-n junction controlled discrete microwave commutation diodes performance calculation and design optimization

11 p1741 A71-26554

Optimal measurement programs for instrument controlled spacecraft trajectory sections, using maximum likelihood method

12 p1957 A71-26630

Product quality characterization, using Harrington dimensionless scale of desirability as optimization criterion

12 p1988 A71-26709

Extremal experiment planning for optimal search, defining intuitive acceptance of solutions during non-formal stages

12 p1988 A71-26710

Experiment planning in electronic component design and microelectronics, using mathematical theory for optimal strategies

12 p1885 A71-26712

Boundary layer suction optimization to achieve normal velocity component distribution for local Reynolds number equal to critical value at transition point

12 p1896 A71-26973

Data transmission with redundancy, discussing optimum data compressing encoding of correlated source signals through linear transformation

12 p1883 A71-27009

Filament winding techniques for glass fiber reinforced plastics, discussing processes, configurations and materials for achieving optimum strength

12 p1920 A71-27011

Average risk minimization based on empirical data, showing relationship of problem to uniform convergence of averages toward expectation value

12 p1892 A71-27020

Wall-stabilized arc column optimization from energy balance solutions, considering temperature and pressure effects on Ar arcs

12 p1939 A71-27275

Thin shallow annular radiating fins for heat removal from sphere or polyhedron with isothermal surfaces, determining optimal weight and geometrical parameters

12 p1986 A71-27331

Adaptive array antennas with control loop, deriving noise expression for maximizing signal to noise ratio

12 p1881 A71-27426

Kalman filtering for complex systems, deriving algorithms for dynamic modeling and bias errors effects in discrete-time state optimum estimation

12 p1893 A71-27435

Modulation cancellation altimeter error analysis and performance optimization

12 p1908 A71-27437

Optimum normalization of computed rotation quaternions to update space vehicle orientation

12 p1923 A71-27443

Statically determinate beams optimal design, considering displacement and stress constraints in optimality conditions derivation

12 p1983 A71-27596

Parameters optimization for increasing tuning range of resonator with contactless piston based on numerical solution of transcendental equation

12 p1889 A71-27623

Minimization algorithms unified derivation, using Hessian matrix inverse

12 p1923 A71-27727

Steepest gradient method for optimum structural design, using search for unconstrained maximum or minimum of function with many independent variables

12 p1247 A71-27789

Minimization of convex functions without derivative calculation, proving superlinear convergence

13 p2094 A71-27895

Optimization of military VTOL aircraft secondary power systems, considering alternate power source for aircraft hydraulics, pneumatic drives, etc

13 p1998 A71-28326

Optimization of time intervals of conveyor harvestings and harvested age of oxygen producing plants for life support system

13 p2017 A71-28406

Microwave power transmission from orbiting solar power station to earth, discussing design optimization problems

13 p1999 A71-28666

Optimization - Conference, Nice, June-July 1969

13 p2043 A71-28811

Identification by minimization of Gaussian-Markovian representation of stochastic process, considering positive linear systems and algorithm for matrix calculation

13 p2043 A71-28818

Accelerated gradient projection algorithm for non-linear constraints, examining terminal phase convergence and compatibility with Davidson process

13 p2043 A71-28821

Dual methods for calculating minimum of convex function on intersection of convexes, considering reflexive Banach space and normalized vector space

13 p2095 A71-28822

Minimization of functions with unconstrained variables, using memory gradient method

13 p2095 A71-28826

Optimization of nonclassical equations of state systems, considering concepts of adjoint and Hamiltonian states

13 p2043 A71-28830

Metal removal rate optimization in electro-discharge machining process, considering governing parameters of relaxation circuit

13 p2075 A71-28947

Optimal penetration effect on peripheral gas flow temperature field at outlet of turbine combustion chamber with circular flame tubes

13 p2118 A71-28971

Optimal shape of single radiative cooling elements without self irradiation relative to cross sections and linear generatrices of radiator

13 p2165 A71-29179

Optimization algorithm for multielement support structure exhibiting minimum deformation energy, comparing Lagrange conditional search method

13 p2101 A71-29186

Wing thickness optimal distribution for minimum wave drag in supersonic flow at zero angle of attack for given planform, using Ritz method at lower Mach numbers

13 p1994 A71-29222

Analytic optimization of Cassegrain antennas of revolution used in satellite telecommunications

13 p2033 A71-29241

Computerized circuit design and optimization methods with allowance for constraints and error criteria

13 p2036 A71-29292

Optimal structural design of minimum weight trusses and beam cross sections for given load using computerized nonlinear programming method

14 p2321 A71-29541

Algorithm for calculating optimal covering of regions in plane, assembling computer program

14 p2264 A71-29552

Minimization of convex maxmin functions, obtaining formula for derivative with respect to direction

14 p2265 A71-29553

Quasi-optimum frequency measurement with linearly dispersive delay line, introducing variance factor for real-ideal systems comparison

14 p2192 A71-29806

Heat and mass transfer optimization in hydrogen-oxygen fuel cells with ion exchange membrane

14 p2181 A71-30050

Transfer function optimization for linear tracking filter model with controlled resonant frequency, analyzing noise band performance

14 p2194 A71-30089

One dimensional optimum design lubrication treatment as imbeddings of nonlocal optimization problems

14 p2252 A71-30097

Design interface requirements for optimal aircraft engine condition monitoring system, using parameter, vibration, oil, borescope and radiography analysis

14 p2289 A71-30531

Exponentially varying thickness thin plate volume minimization for simultaneous stress and deflection constraints under axisymmetric load, using digital computer

14 p2330 A71-30691

Pulse-burst radar design optimization and performance comparison with low and high pulse repetition frequency Doppler radar

14 p2197 A71-30797

Optimal linear filter gain relation to feedback difference, using Riccati matrix differential equation

14 p2220 A71-30808

Optimal omnidirectional antenna array located on cylindrical head section of sounding rocket for L band telemetry

14 p2216 A71-31035

Chebyshev antenna array optimum spacing derivation for beamwidth decrease without sidelobe level increase

15 p2368 A71-31142

Differential equation systems optimal scaling for analog computer, proposing amplitude and time scaling factors and disposition parameters with linear programming

15 p2440 A71-31155

One variable unimodal function minimization, describing adaptive algorithm with iterative four point interpolation process

15 p2440 A71-31156

Optimum configuration/cost design of computer graphics systems, using mathematical model involving response time prediction by queueing analysis

15 p2374 A71-31181

Optimal Bayesian system for simultaneous discrimination and parameter estimation of several signals in noise background

15 p2370 A71-31585

Asymptotically optimal rank algorithms for signal resolution at phase and amplitude detectors outputs

15 p2370 A71-31587

Signal detection in noise, investigating quantiles position optimization in nonparametric test statistics

15 p2370 A71-31588

Cost optimization for solar generator thermobatteries by selecting temperature, contact resistance, material parameters and fabrication technology

15 p2351 A71-31671

Series and parallel complex systems reliability maximization by allocating optimum numbers of stocked spare parts

15 p2415 A71-32343

Optimal sensing recording and signal processing in multispectral photography for aerial reconnaissance capability

15 p2410 A71-32470

Transistor minimum noise figure in low noise microwave amplifier circuit

15 p2378 A71-32635

Hamilton-Jacobi equation application to forces selection for mechanical systems asymptotic stabilization, minimizing functional by Euler-Lagrange equations

16 p2602 A71-32814

Optimal structural design for nonconservative systems under buckling, noting application to minimal weight nonprismatic elastic bar shape determination

16 p2649 A71-33012

Life cycle cost optimization of STOL aircraft and tracked air cushion vehicles for operating transportation system

16 p2522 A71-33306

Optimal design of logic networks in homogeneous microelectronic structures, using shortest link search and graph continuity parameters

16 p2545 A71-33704

Constrained optimization problems solution combining modified pattern search methods and polynomial constraints in aircraft design parameters selection

16 p2603 A71-33721

Optimization and operational problems of man powered aircraft, noting Kremer Competition design

16 p2525 A71-34023

Optimality condition for statically indeterminate beams minimum deflection design, using principle of stationary mutual complementary energy

16 p2661 A71-34148

Optimal radiative capacity of star shaped radiator with mirror reflecting surfaces for vacuum cooling of elongated finned bodies

17 p2836 A71-34311

Radio communication system optimization from viewpoints of global synthesis including economics and partial synthesis based on noise stability, precision and reliability

17 p2698 A71-34392

Optimal parameters of Fabry-Perot etalon for error minimization in Doppler and dispersion portions determination of Voigt profile width

17 p2737 A71-34410

Cooling fin shape optimization for minimum volume, considering convective and radiative heat exchange for assumed temperature distribution

17 p2837 A71-34442

Space shuttle cost effectiveness and utilization analyzed for system-level requirements to maximize economic benefits

17 p2813 A71-34730

Worst case criterion for finite circular antenna aperture illuminations effectiveness comparison and optimization in synthesizing ideal radiation pattern

17 p2715 A71-34763

Differential equations optimization method based on auxiliary functional and minimization at simple structure manifold

17 p2765 A71-34849

Aircraft structural parameters optimization satisfying flutter velocity constraint and minimum mass, applying to box beam design

17 p2825 A71-34874

Redundant information optimizer design, using nonlinear elements

17 p2720 A71-34957

Filament wound shell of revolution optimum configuration, deriving equations for orthotropic filament axes coincidence with principal stress trajectories

17 p2830 A71-35317

Dynamic programming to design beams and plates under steady creep with minimum weight, applying to cantilever beam

17 p2832 A71-35505

RF ion thruster /RIT-10/ optimization, investigating energy balance and plasma diagnostics

17 p2794 A71-35547

Optimal design of axisymmetrical annular plate and cylindrical and spherical shells by maximum principle

17 p2833 A71-35621

- Random access signaling system application to aircraft control, discussing signal redundancy requirement for access capability optimization based on radio environment model 17 p2747 A71-35783
- Book on optimum structural design covering single element optimizations, load transmission, slender columns, cost-weight tradeoffs and statically indeterminate structures 18 p2977 A71-36249
- Free-Lagrange method for two dimensional flow numerical simulation, covering mesh optimization and equations of motion 18 p2905 A71-36304
- Nuclear power station design for optimal reliability levels, noting maintainability requirements 18 p2928 A71-36807
- MHD generator duct external loop electric current maximization by working material resistivity tensor optimal distribution 19 p3108 A71-37102
- Three dimensional minimum fuel turns for supersonic aircraft by energy state approximation [AIAA PAPER 71-913] 19 p3096 A71-37163
- Lifting entry and terminal phase system optimization for 1975 Mars Viking lander, considering graphical tradeoff approach including design parameter and atmosphere model variations 19 p3148 A71-37171 [AIAA PAPER 71-922]
- Signal detection on Gaussian noise background, deriving error probabilities and optimal processing algorithms 19 p3015 A71-37224
- Specific optimal techniques in control and estimation, emphasizing fixed configuration optimization with time variant parameters and two point boundary value problem 19 p3036 A71-37237
- Set covering algorithm based on single branch search coupled with linear programming and suboptimization techniques 19 p3025 A71-37546
- Linear programs optimality conditions, using differential calculus approach to classical optimization theory in Danzig simplex algorithm development 19 p3086 A71-37548
- Modified linear programming algorithm for columnar methods in mathematical programming applicable to decomposition principle, concave maximization and Lagrange multipliers search 19 p3086 A71-37549
- High order optimality conditions, considering multidimensional control and transformation in space of states 19 p3037 A71-37567
- Economically optimal operation of circuits protecting object subject to stationary random process, determining object malfunction intensity 19 p3025 A71-37572
- Optimal investment model for R and D project evaluation and selection, using discrete cash flow and linear programming techniques 19 p3173 A71-37630
- Average risk minimization based on empirical data, showing relationship of problem to uniform convergence of averages toward expectation value 19 p3037 A71-37689
- Optimal models for time shared computer systems with real time multiprogramming 19 p3025 A71-37692
- Simulation model for optimal cost time-independent component replacement of complex system subject to probabilistic deterioration 19 p3069 A71-38288
- Splitting-up method with variational optimization for time independent nonstationary hydrodynamic transfer equations for use in meteorology, oceanology, etc 19 p3088 A71-38310
- Optimality criterion for convergence of iterative solution of linear time optimal problem in reflexive Banach space 19 p3088 A71-38414
- Antenna linear array power pattern synthesis, determining optimum nonnegative harmonic approximation to given function in Gauss/weighted least-mean-square/ and Chebyshev senses 19 p3021 A71-38472
- Criterion selection and minimum margin search for optimization of complex electronic circuit parameters described by mathematical models 19 p3039 A71-38503
- Systems oriented components selection optimization technique by reliability/quality levels, considering repair and failure cost, storage time and mission duty cycle 19 p3034 A71-38518
- Constrained optimization of array antennas performance for obtaining radiation pattern with desired sidelobe levels 19 p3023 A71-38591
- Quadrifilar helix antenna pitch angle and ground plane size optimization based on beam pattern data 19 p3036 A71-38603
- Aerodynamic control surfaces optimal location for flexible aircraft disturbed by random wind gusts, using matrix minimum principle and calculus of variations 19 p2998 A71-38713
- Centrifugal blowers optimum blade number for maximum efficiency, discussing design measures for shock and friction loss minimization 20 p3277 A71-38750
- Single-shot joint detection-estimation for discrete and continuous data and generalization to Bayesian system identification, considering optimal nonlinear estimator realization 20 p3201 A71-38847
- Parameter optimization of linear time invariant nutation damper by second Liapunov method 20 p3306 A71-38853
- Grand tour missions radioisotope thermoelectric generator power source, presenting optimization technique for hot thermocouple junction operation 20 p3264 A71-38932
- High speed wind tunnels air heating system optimization, considering pebble bed air heater for intermittent operations 20 p3209 A71-39086
- Radiation patterns due to four pyramidal horns used in sum and difference comparison monopulse radar from single horn pattern for design optimization 20 p3203 A71-39092
- Trajectory measurement method optimization determined by algorithm, applying to radial velocities of artificial satellite orbit around Mars 20 p3294 A71-39581
- Trajectory measurement optimal program, using least squares method 20 p3294 A71-39582
- Necessary conditions of optimality for control problems with state variable inequality constraints, using separating hyperplane theorem 21 p3359 A71-40207
- Frequency response optimization of one dimensional damped linear continuous systems, requiring initial value numerical integration of state and adjoint differential equations 21 p3456 A71-40265
- [ASME PAPER 71-VIBR-1] Mechanical elements and systems optimal design, discussing variational and programming techniques application to machine elements design optimization [ASME PAPER 71-VIBR-62] 21 p3385 A71-40306
- Structural optimization problems involving vibration-weight interactions, using optimal control nonlinear programming transforms [ASME PAPER 71-VIBR-66] 21 p3460 A71-40308
- Linear multidegree of freedom shock isolation system optimum design, masses, spring and damping coefficients, using mathematical programming [ASME PAPER 71-VIBR-81] 21 p3461 A71-40317
- Dual variational formulation for rigid plastic structure minimum cost design, applying to sandwich and fiber-reinforced plates [ASME PAPER 71-VIBR-110] 21 p3462 A71-40333
- Nonlinear mixed integer programming for automated design and structures optimization, describing penalty function technique and recovery scheme to satisfy integer requirements [ASME PAPER 71-VIBR-117] 21 p3350 A71-40336
- Computational algorithms for solving unconstrained and constrained optimization problems [ASME PAPER 71-VIBR-118] 21 p3407 A71-40337
- Hybrid electromechanical analog computer real time simulation technique for optimizing vibration response of two degree of freedom system with impact damper [ASME PAPER 71-VIBR-119] 21 p3350 A71-40338
- Radiative-conductive heat transfer systems optimum thermal design, using nonlinear programming with mathematical model based on nodal analysis [ASME PAPER 71-VIBR-120] 21 p3474 A71-40339
- Direct search penalty function algorithm for treating general mathematical programming form of optimal design problem [ASME PAPER 71-VIBR-121] 21 p3350 A71-40340
- Optimal design for system reliability and maintainability, using dynamic programming model 21 p3407 A71-40363
- Monograph on satellite airport system modeling for large metropolitan areas covering systems analysis methodology and computer algorithms for optimization [SU-TR-71-1] 21 p3365 A71-40799
- Computerized optimal design of L band phase shift networks for broadband performance 21 p3361 A71-40816
- Redundancy optimization of series-parallel k-out-of-n systems for maximum reliability subject to multiple cost constraints 21 p3388 A71-40878
- Optimal design procedure as experimental design finite decision problem, using Bayes and minimax techniques 21 p3408 A71-40879
- Holographic process theoretical and experimental optimization, considering object/reference beam ratio and photographic emulsion thickness effects 21 p3380 A71-40924
- Sonic boom minimization including front and rear shocks, exemplifying by SST aircraft 21 p3324 A71-40972
- Elastic trusses optimal design under multiple mechanical constraint conditions, describing steepest descent method with constraint error compensation 21 p3470 A71-41021
- Computerized numerical optimization for Yagi-Uda antenna array gain, noting nonoptimum in standard traveling-wave design methods 21 p3349 A71-41410
- Perturbation procedure application to linear and circular antenna array directivity optimization by phase adjustments under uniform amplitude excitation 21 p3359 A71-41412
- Electronic and electrical systems optimization effectiveness through generation of statistical priorities 22 p3525 A71-41438
- Centrally-fed circular inherently-compensated aerostatic gas thrust bearing flow behavior in inlet region, obtaining graphs for design optimization 22 p3551 A71-41663
- Design parameters optimization for flat spiral coils printed on dielectric substrates based on equivalent circuit analysis, emphasizing coil shape effects on Q and inductance 22 p3520 A71-41715
- Computerized reliability optimization system program for electronic equipment design and management methods to achieve high reliability and low cost 22 p3517 A71-42105
- Computerized system redundancy optimization formulation as zero-one type variables integer programming problem, obtaining algorithmic solution for maximum reliability 22 p3517 A71-42106
- Optimal redundancy and availability allocation for MTBF and time to repair in multistage system, using dynamic programming 22 p3518 A71-42116
- Fast Fourier transform calculating discrete Fourier transform, considering optimized algorithm for digital computers 22 p3566 A71-42249
- Optimal synthesis of antenna array radiation patterns with minimum square deviation from zero in sidelobe 22 p3510 A71-42269
- Galerkin approximation for boundary value problem finite difference scheme optimization by interpolation in Hilbert subspace 22 p3566 A71-42292
- Design and performance optimization of series mode step recovery diode frequency multipliers, using computer aided analysis 22 p3523 A71-42358
- Projection type 3-D display lenticular lens sheet optimum design and depth resolution 22 p3549 A71-42560
- Optimal and nonoptimal signal reception under conditions of incomplete a priori information based on approximation by Markov processes in white noise 22 p3527 A71-42749
- Optimal design of low noise multistage microwave oscillator, discussing quartz master oscillator frequency effects 22 p3524 A71-42750
- Hypersonic nozzle convergent section heat transfer optimization by Euler method, using Lagrange undetermined multiplier and pipe flow approximation 22 p3622 A71-42781
- Optimal nonlinear discrete filters with finite memory for polynomial signals, discussing synthesis with aid of minimax method 22 p3527 A71-42856
- Optimal design for minimum noise maximum gain bandwidth of lower sideband parametric up-converters 23 p3630 A71-42917
- Space shuttle optimal design problem, applying accelerated gradient parameter optimization technique [AAS PAPER 71-329] 23 p3727 A71-43002
- Microwave bipolar transistors computer aided design, describing optimization and synthesis procedures and RF performance 23 p3649 A71-43067
- Boundary displacement conditions in linear elasticity with friction, using minimization of nondifferentiable convex functional and variational inequalities 23 p3775 A71-43239
- Primary sensor transfer function selection to minimize rms error in information transmission over telemetry channel for subsequent digital processing 23 p3648 A71-43294
- Optimal gyroscopic servosystems feasibility analysis, using approximation technique for finite memory optimal filter transfer function 23 p3675 A71-43296
- Approximate solution for equation in linear normed space by error operator norm optimization, applying to elliptical cylinder type compact sets 23 p3699 A71-43574

- Minimal partial realizations of linear input/output map, discussing significance in regard to adaptive dynamics identification procedures 23 p3661 A71-44190
- Optimum design of linear multivariate sampled data systems, using deadbeat and integral performance criteria and output response error 24 p3812 A71-44451
- Flexible ram air inflated keel and leading edge parawing design optimization for increased stability and reliability, introducing semirigid member concept [AIAA PAPER 71-986] 24 p3791 A71-44582
- N-step conjugate gradient minimization algorithm for nonquadratic functions, giving numerical example of application to double precision arithmetic 24 p3842 A71-44623
- Thermally loaded rod structures optimization, presenting method for estimating canonical equations influence parameters 24 p3842 A71-44642
- Dynamic system optimal weighting function determination, using variational methods for statistical criteria 24 p3813 A71-44677
- Optimal strategies in search of function global maximum 24 p3843 A71-44770
- Optimum synthesis of spatial four-link chain mechanism with pressure angles deviating least from zero degrees for force transmission 24 p3848 A71-44900
- Optimal mismatched filter design for radar ranging, detection and resolution by reduction to transversal equalizer, determining parameters by nonlinear programming 24 p3815 A71-44935
- Position line location determination by discrepancy moduli sum minimization algorithm 24 p3846 A71-45161
- Optimum signal processing for distance measurement with lasers, considering propagation, detection and measure process statistical properties, optical radar and sine wave modulation 24 p3834 A71-45206
- OPTIMUM CONTROL**
- U OPTIMAL CONTROL**
- OPTIMUM THRUST PROGRAMMING**
- U THRUST PROGRAMMING**
- OR-GATES**
- U GATES (CIRCUITS)**
- ORBIT CALCULATION**
- Computer program for orbital elements of spectroscopic binaries and probable error computation 01 p0152 A71-10352
- Orbital elements of spectroscopic binary Zeta Scuti by computer program and spectrograph observations, tabulating results 01 p0152 A71-10353
- Satellites initial circular orbit determination from incomplete observations 01 p0155 A71-10444
- Planetary satellites intermediate orbits calculation in three dimensional Hill problem, allowing for solar disturbances 01 p0156 A71-10447
- Kalman optimal linear filter application to near earth satellite orbit calculation based on earth radar observations 01 p0156 A71-10518
- Orbital coordinates for body moving along parabola with small perihelion distance calculated for ephemeride 01 p0157 A71-10607
- Linear algorithms for determining spacecraft relative orbital state using angle data with digital computer 01 p0163 A71-11588
- Planets and satellites masses and other dynamic parameters by numerical and analytical calculation techniques based motion and trajectory analyses 02 p0309 A71-12152
- High drag satellite 1968-59A orbits from optical and radar observations, obtaining rotational speed of upper atmosphere 03 p0407 A71-13305
- Mathematical model for determining thrust interplanetary spacecraft orbit, considering time history of position, velocity and thrust acceleration [AIAA PAPER 69-901] 03 p0487 A71-13451
- Hyperbolic, elliptical and parabolic heliocentric motion, determining location of body in orbit with unitary method 03 p0493 A71-14194
- Planetary system effects on long period comets orbital characteristics, presenting eccentricities and reciprocal semimajor axes calculations 04 p0642 A71-14738
- Orbit determination accuracy using synchronous satellite system for tracking near earth spacecraft 04 p0553 A71-15312
- Absolute orbit construction for Jovian great satellites, obtaining linear equations of motion 04 p0654 A71-15714
- Pseudo-problem method for errors accumulated in numerical integration computation of orbits 04 p0654 A71-15718
- Periodic orbits in general three body problem with nonzero angular momenta 04 p0656 A71-15730
- Restricted three body problem of asteroid orbital motion in solar and Jupiter field in three dimensional space 04 p0656 A71-15734
- Neptune orbital motion prediction, determining effect of variations in time and mean distance on accuracy 05 p0810 A71-16542
- Mars 1971 orbiter mission, investigating orbit determination accuracy during approach phase [AIAA PAPER 71-189] 06 p0978 A71-18627
- Earth based orbit determination for Mars orbiting spacecraft, comparing batch and sequential tracking filter data processing methods [AIAA PAPER 71-119] 06 p0978 A71-18657
- Space vehicle landing trajectories calculation from visual and radio observations of orbital parameters 07 p1196 A71-19495
- Spacecraft orbital elements determination, using statistical analysis in processing observed motion data 08 p1360 A71-21005
- Satellite geodesy, discussing reference orbits calculation, gravity field spherical harmonics, station positions, etc 08 p1285 A71-21800
- Parameter estimates effectiveness from independent discrete and continuous navigation measurements of circular orbital plane 09 p1491 A71-22543
- Minimal characteristic velocity of single impulse transfer between coplanar elliptical orbits with allowance for thrust action finite time 09 p1519 A71-22544
- Intermediate orbit calculation, allowing for spacecraft large gravitational perturbation during motion near planetary sphere of influence 09 p1519 A71-22663
- Satellite path geometry along Keplerian elliptical orbit, taking earth flattening into consideration 09 p1520 A71-22664
- Intermediate elliptical orbits for planetary satellites with small inclination to equatorial plane 09 p1520 A71-22671
- Manual onboard orbit determination assuming electronic equipment failure, discussing geometric in-plane orbital parameters and safe orbit check [AIAA PAPER 70-159] 09 p1521 A71-22910
- Computer algorithm for optimal linear impulse corrections to satellite orbit under inequality type constraints 09 p1424 A71-23135
- Asteroids or comets orbital elements calculation, using initial heliocentric position and velocity as zero time orbital elements 10 p1668 A71-24023
- Pluto orbit integration over 4.5 million years by variation of parameters technique and confirming Neptune-Pluto orbital resonances 10 p1669 A71-24179
- Star orbit computation in galactic potential fields, using Hamming modified predictor corrector scheme for numerical integration 10 p1678 A71-24927
- Algorithms for close earth satellite orbit calculation developed by numerical integration methods, discussing solution efficiency [AIAA PAPER 69-948] 11 p1820 A71-25463
- Topocentric satellite trajectory approximation along circular orbit by n-degree equation, using coordinate-time relation 11 p1829 A71-25809
- Satellite orbit elements over short time intervals from basic and asynchronous observations, using rectangular geocentric coordinates 11 p1829 A71-25810
- PERLO program for analysis of satellite orbital period changes to determine celestial equator crossings from sequence of positions 11 p1829 A71-25825
- Lozinskii method orbit periods, comparing with quasi-draconic orbit periods from subsatellite point method 11 p1732 A71-25827
- Photographic quasi-draconic period measurements from satellite transit across topocentric celestial equator tested on Echo 2 and Pages A 11 p1732 A71-25828
- Ocean height measurement by orbit determination from satellite altimetry, considering least squares solutions and instrument errors 13 p2066 A71-27983
- German monograph on linear theory of optimization problems for low thrust rockets covering orbital calculations, flight characteristics and Coast Arc problem 14 p2319 A71-30233
- Orbit computation and measurement errors of visual binaries by wire micrometer distance method 14 p2312 A71-30372
- Artificial earth satellites initial elliptical orbit calculation, discussing function minimization for optical radar and laser observation 15 p2481 A71-31301
- Comet and asteroid orbits tangential approximation, determining minimal distances and velocities as function of orbital elements 15 p2482 A71-31303
- Goddard trajectory determination system, discussing attitude dynamics, data preparation, differential correction and orbit information 15 p2495 A71-32645
- Papers on mathematical methods in astrodynamics and celestial mechanics for earth-moon trajectories computation, satellite orbit determination and three body problem 16 p2630 A71-33056
- Elliptic restricted three body problem, calculating fictitious retrograde Jovian satellites orbits in rotating-pulsating axes for sun-Jupiter case 16 p2633 A71-33337
- Comet Honda 1968 c, determining osculatrix hyperbolic orbit from osculating elements 16 p2634 A71-33426
- Stellar movement in Galactic field, discussing observational and mathematical techniques for stellar orbits and velocities determination 17 p2801 A71-34697
- Optimality of Contensou singular alternating arcs in time-free central-field orbital transfer problem, using succession of infinitely small impulses 19 p3134 A71-37558
- Navigation error sources and orbit determination accuracies for Jupiter planetary encounter, using earth based radio tracking data [AAS PAPER 71-118] 19 p3101 A71-37937
- Orbit computation and tracking system for Iris satellite using differential correction program 19 p3142 A71-38066
- Satellite capture by Jupiter, calculating satellite orbits based on aphelion and perihelion conditions derived from planetary elliptical orbit three body problem 20 p3287 A71-38978
- Spacecraft orbital elements determination, using statistical analysis in processing observed motion data 20 p3294 A71-39585
- Two dimensional elliptic restricted three body problem, considering regularization mechanism and periodic collision orbits 21 p3441 A71-40095
- Herrick-Gibbs preliminary orbit determination method in matrix form for spacecraft extended to process greater than three inertial position vectors [AAS PAPER 71-317] 23 p3725 A71-42991
- Orbital spacecraft trajectory and attitude dynamics, using computerized state model for mission planning, orbit determination, satellite geodesy and reentry analysis [AAS PAPER 71-344] 23 p3727 A71-43017
- Artificial satellite lunar orbit calculation, representing unmodeled accelerations by first order Gauss-Markov sequence with time correlated and random components 23 p3730 A71-43041
- Mars surface cartography and orbit determination using TV data from Mars orbiting spacecraft [AAS PAPER 71-373] 23 p3730 A71-43043
- Long term orbit calculation by superposition of gravity and drag perturbations, taking into account solar and geomagnetic induced density variations [AAS PAPER 71-376] 23 p3730 A71-43046
- Mariner 9 Mars 71 mission orbit determination, trajectory and maneuver strategy for near earth, cruise, planetary approach and satellite phases, using in-flight tracking data [AAS PAPER 71-391] 23 p3732 A71-43059
- Upper atmosphere rotation rate decrease at altitudes above 350 km, determining zonal wind variations by satellite orbits analysis from Hewitt camera observations 23 p3667 A71-43140
- Floccule theory three dimensional planetary formation model of collapsing cloud leading to nonplanar system with protoplanets in retrograde orbits 23 p3769 A71-43991
- Transplutonian planet dynamical search through numerical integration of outer planets orbits 24 p3868 A71-44440
- Motion equations numerical integration step as function of celestial object location and velocity in interplanetary probe orbit computation 24 p3869 A71-44799
- Orbital elements of Encke comet from 1953-1954, 1957, 1960-1961 and 1963-1964 apparitions, finding secular acceleration coefficient 24 p3874 A71-45176
- Near circular orbit elements determination as functions of spacecraft initial speed and coordinates deviation by mathematical expectation procedure 24 p3876 A71-45317
- ORBIT DECAY**
- Exact expression for minimum range sensitivity deorbit from elliptical orbits for ballistic atmospheric entry vehicle, considering retrovelocity 07 p1199 A71-19873

ORBIT EQUATIONS

Artificial earth satellite orbital decay rate measurement for upper atmosphere density data, using combined directional observations and orbit data
19 p3048 A71-37394

ORBIT EQUATIONS

U ORBITAL MECHANICS

ORBIT PERTURBATION

NT SATELLITE PERTURBATION

Numerical integration finite difference methods stabilization for perturbed Keplerian motion differential equations
01 p0154 A71-10378

Hansen method for partial anomalies applied to orbit perturbation equations
01 p0155 A71-10439

Ceres perturbation by Neptune, comparing Laplace-Newcomb and Hill methods
01 p0156 A71-10448

Canonical transformations for method of variations applied to differential equations describing satellite orbit perturbations
01 p0156 A71-10544

Liapunov method applied to nonlinear differential equations for distant satellite orbit secular perturbations
01 p0156 A71-10546

Juno absolute perturbations due to large planets, using Hill method with digital computer
01 p0156 A71-10549

Satellite orbit perturbations by solar radiation pressure, considering earth shadow in homogeneous field and long term effects
02 p0313 A71-12491

Computerized simulation of disturbance torques of spin stabilized spacecraft in near earth orbit
03 p0500 A71-14433

Orbit evolution of small mass near earth-moon system, noting solar perturbations and equations of motion
04 p0653 A71-15709

Critical periodic orbits for main families and all mass ratios, considering stability in restricted problem
04 p0655 A71-15729

Satellite motion in orbits with semilatus rectum of 1/6 equatorial radius of oblate planet, discussing errors outside planetary radius
04 p0656 A71-15735

Satellite motion stability in axisymmetric field of oblique rotating planet
05 p0815 A71-16050

Lunar satellite motion semianalytic solution, considering perturbative effects due to gravitational fields, solar radiation pressure and libration
05 p0809 A71-16541

Electric microthrusters for geostationary satellites orbit corrections, discussing orbital perturbations and operational characteristics of ammonia electrothermal and ion thrusters
07 p1207 A71-19528

Spacecraft single parameter orbital correction, considering correction impulse error effects and error minimization
07 p1155 A71-19530

Satellite orbital motion, discussing idealized perturbations limiting problem from point mass
08 p1360 A71-21004

Intermediate orbit calculation, allowing for spacecraft large gravitational perturbation during motion near planetary sphere of influence
09 p1519 A71-22663

Satellite path geometry along Keplerian elliptical orbit, taking earth flattening into consideration
09 p1520 A71-22664

Jupiter gravitational potential mapping for Grand Tours spacecraft, discussing Jovian satellites effect on orbit and trajectory perturbations
09 p1525 A71-23222

Secular perturbations of Leonid meteor shower via Gauss-Halphen-Goriachev method, indicating applicability to variations of meteor streams orbital elements
09 p1526 A71-23343

Nonperiodic orbit behavior in highly perturbed dynamic systems, examining invariant curve evolution
10 p1669 A71-24178

Pluto orbit integration over 4.5 million years by variation of parameters technique and confirming Neptune-Pluto orbital resonances
10 p1669 A71-24179

Collinear libration centers of spacecraft motion in sun perturbed three dimensional earth-moon system
10 p1671 A71-24329

Mimas /Saturn satellite/ perturbations effect on Cassini division in Saturn rings
10 p1673 A71-24425

Earth oblateness and air drag effects on satellite trajectories by asymptotic method of nonlinear mechanics, obtaining closed form solutions for first order approximation
10 p1678 A71-24928

Artificial lunar satellites orbits, examining disturbing functions expansions due to nonsphericity of primary body and disturbing point mass body actions
10 p1679 A71-24931

Asteroid ring origin, discussing osculating and corresponding secular orbital elements of mother planet
11 p1820 A71-25245

Drag-free satellite design and propulsion requirements, noting orbit perturbation mechanisms
11 p1838 A71-25522

[AIAA PAPER 70-1145]
Lunar motion theory, discussing radial perturbation, variation, parallactic and annual inequalities, secular acceleration and evection
11 p1822 A71-25684

Satellite orbit period variation data for PERLO program visual observations, calculating topocentric celestial equator transits
11 p1732 A71-25826

Planetary satellites intermediate orbits, obtaining angular orbital elements secular perturbations
12 p1964 A71-27091

Orbital space stations and spacecraft courses, determining orbit precession and perturbation
12 p1968 A71-27628

Spacecraft intermediate orbit osculating elements first order secular disturbances due to atmospheric resistance
13 p2132 A71-27936

Short term interval satellite orbit perturbations, computing direct solar radiation pressure effects with computer program
13 p2137 A71-28477

Optimal two impulse minimum thrust transfer of particle between coplanar circular orbits under perturbations in flight plane
14 p2310 A71-30187

Orbital stability concept under nonperiodic motions
15 p2499 A71-31179

Daniel 1909 IV comet orbit evolution, discussing capture by Jupiter, asteroid collision, brightness, orbit perturbation and nongravitational force effects
15 p2481 A71-31298

Radar ranging experiment onboard Jupiter orbiter, concerning perturbations, gravitational harmonics and short arc orbit determination
15 p2487 A71-32041

Lost City meteorite secular and encounter perturbation effects on orbital evolution, interpreting short lived cosmic radiogenic isotopes formation
15 p2489 A71-32359

Satellite orbital elements perturbations, examining resonance due to earth geopotential
15 p2495 A71-32683

Satellite motion stability in axisymmetric field of oblique rotating planet
16 p2645 A71-33454

Asteroids 457-Allegbania, 649-Josepha, 1038-Tuckia, 1161-Thessalia, 1162-Larissa and 1297-Quadea orbital elements and ephemerides, taking into account planetary perturbations
17 p2809 A71-35581

Planetary satellites intermediate orbits, obtaining angular orbital elements secular perturbations
19 p3133 A71-37441

Black holes in binary star systems from orbital eccentricity observations
19 p3142 A71-38006

Numerical integration of element T /transit time through perihelion/ in perturbations of near parabolic comet orbits
20 p3291 A71-39321

Satellite orbital motion, discussing idealized perturbations limiting problem from point mass
20 p3294 A71-39584

Five outer planets orbital perturbations by four inner planets, comparing second differentials with disturbing force numerical values
21 p3441 A71-40096

Outer planets masses determination from orbit perturbations analysis and optical observations
23 p3725 A71-42988

[AAS PAPER 71-312]
Artificial lunar satellite motion in gravitational fields of nonspherical moon, earth and sun, deriving orbit perturbations
24 p3874 A71-45174

ORBITAL ASSEMBLY

Space station assembly in earth orbit, providing low transportation costs, modular elements return and incremental growth
18 p2974 A71-36485

ORBITAL ELEMENTS

Computer program for orbital elements of spectroscopic binaries and probable error computation
01 p0152 A71-10352

Orbital elements of spectroscopic binary Zeta Scuti by computer program and spectrograph observations, tabulating results
01 p0152 A71-10353

Comet Tempel-Tuttle elements, discussing association with Leonids meteor shower
01 p0159 A71-10808

Geopotential coefficient recovery, using resonant satellite orbits long arc elements
02 p0245 A71-11995

Sunspot cycle period relationship to planetary orbital periods
03 p0493 A71-14210

Micrometeorites orbital elements, evaluating cosmic dust experiment data from Pioneer 8
03 p0496 A71-14500

AG Vir /HD 104350/ orbital element variations and light curve distortions, using least squares method
04 p0651 A71-15600

Satellite orbital elements perturbation due to tesser and sectorial harmonics of earth gravitational potential
06 p0976 A71-18400

Geodetic satellite transmissions for ionospheric research, discussing orbital elements and frequency data
07 p1095 A71-19000

Faint meteor orbit characteristics, observing distribution, eccentricities, dimensions and inclination to ecliptic plane
07 p1194 A71-19300

Space vehicle landing trajectories calculation from visual and radio observations of orbital parameters
07 p1196 A71-19400

Light and radial velocity curves of binary HD 175514, obtaining spectroscopic and photometric orbital elements
07 p1204 A71-20600

Spacecraft orbital elements determination, using statistical analysis in processing observed motion data
08 p1360 A71-21000

Satellite orbital elements, examining resonance due to earth potential
08 p1366 A71-21700

Optimal trajectory measurement program for orbital parameter determination, assuming random errors and nondegenerate weighting matrix of normal equations
09 p1519 A71-22500

Orbital elements of small high velocity meteor determined by oblique radio sounding
09 p1520 A71-22800

Planetary rotational and translational motion interaction in Einstein gravitation theory, describing orbital elements secular disturbances in two body problem
09 p1526 A71-23300

Satellite orbital period variation under earth gravitational potential tesser and sectorial harmonics
09 p1526 A71-23300

Secular perturbations of Leonid meteor shower via Gauss-Halphen-Goriachev method, indicating applicability to variations of meteor streams orbital elements
09 p1526 A71-23300

Approximate determination of 44 minor planets orbits, tabulating orbital elements
09 p1526 A71-23300

Observations distribution influence on accuracy of almost circular planetary orbits determining elements considering geocentric distances and ecliptic longitudes and latitudes
09 p1526 A71-23300

WX Cep eclipsing system photoelectric components computed in standard UVB colors, obtaining orbital elements
09 p1527 A71-23500

Mission objectives and orbit parameters of Azur satellite, considering satellite control and data transmission as function of ground support system
10 p1589 A71-23900

Asteroids or comets orbital elements calculation using initial heliocentric position and velocity as zero time orbital elements
10 p1668 A71-24000

Star catalogue systematic error corrections from minor planet photographic observations and orbital elements determination
10 p1670 A71-24100

Asteroid ring origin, discussing osculating and corresponding secular orbital elements of mother planet
11 p1820 A71-25200

Meteoroids orbital elements statistically compared to asteroids
11 p1820 A71-25200

O and B type stars galactic Keplerian parameters statistical distributions based on galaxy point model
11 p1820 A71-25200

Satellite orbit elements over short time intervals from basic and asynchronous observations, using rectangular geocentric coordinates
11 p1829 A71-25800

Quasi-draconic and draconic orbital periods of earth satellites, showing ascending and descending pass variations
11 p1829 A71-25800

Comet orbits correction, including differential coefficients perturbations based on Kulikov equation for difference between computed and true radius vector
11 p1833 A71-26300

Meteor streams dynamic properties, computing mean orbit elements with statistical mathematical model
11 p1835 A71-26400

Satellite orbital elements perturbation due to tesser and sectorial harmonics of earth gravitational potential
12 p1955 A71-26600

- Spacecraft intermediate orbit osculating elements first order secular disturbances due to atmospheric resistance
13 p2132 A71-27936
- Hill-Brown differential equations for satellite coordinates transformed for integration with analytical programming language
13 p2135 A71-28352
- Orbital elements and corrected light curve of eclipsing variable star Z Vulpeculae, using FORTRAN 4 program
13 p2137 A71-28513
- Optimal transfers in central gravitational field, using perturbation formulas of osculating Keplerian orbit elements and corresponding linearized equations
13 p2139 A71-28825
- Point motion in axisymmetrical planet equatorial plane gravitational field, taking into account orbital elliptical elements osculation
14 p2310 A71-30186
- Instrumentation and orbital parameters of meteorological satellites observing winds, tropical circulations, heat budget, hydrology and ocean surfaces
14 p2270 A71-30498
- Absolute magnitudes of 1965-1969 comets, including orbit elements, perihelion coordinates and maximum values of reduced head diameter and tail length
15 p2483 A71-31339
- European electric propulsion systems for flight trajectories within low gravity fields and orbital parameter attitude control and correction
15 p2469 A71-31730
- Faint meteor orbit characteristics, observing distribution, eccentricities, dimensions and inclinations to ecliptic plane
15 p2486 A71-31896
- Satellite orbital elements perturbations, examining resonance due to earth geopotential
15 p2495 A71-32683
- Circular orbit patterns for continuous whole earth surface coverage with five satellites
16 p2630 A71-32840
- European meteorological satellite system, discussing measurement program, data management, orbital parameters and stability, satellite positioning and instrumentation
16 p2644 A71-32844
- Comet Honda 1968 c, determining osculatrix hyperbolic orbit from osculating elements
16 p2634 A71-33426
- Computer model of eclipsing binary stars tested with photometric B and Y observations and orbital elements of RU Ursae Minoris
16 p2635 A71-33436
- Geminid meteoroid dust particles detection, determining velocity and orbital elements from OGO 3 flux measurements
16 p2640 A71-33741
- Upper atmosphere rotational speed variations from measurements of orbital inclination of satellites
16 p2569 A71-33807
- Lunar gravity field global model from moon orbiters secular and long period trends, noting large anomaly on far side
16 p2642 A71-33815
- Very long baseline interferometry of radio emissions from geostationary satellites, determining orbital elements and inertial position
16 p2544 A71-33845
- Orbital elements determination for Osumi Japanese satellite, describing trajectory correction for atmospheric effect
17 p2802 A71-34746
- Asteroids 457-Alleghania, 649-Josepha, 1038-Tuckia, 1161-Thessalia, 1162-Larissa and 1297-Quadea orbital elements and ephemerides, taking into account planetary perturbations
17 p2809 A71-35581
- Book on astrodynamics covering n body equations of motion, orbital elements, differential corrections, time of flight, ballistic missiles and interplanetary transport
18 p2963 A71-36248
- Spectroscopic binary star system with orbital eccentricities less than 5 percent, discussing elliptical or circular orbit possibility
18 p2971 A71-37068
- On-line radar tracking of six orbital elements of thrust maneuvering spacecraft, obtaining discrete nonlinear measurement and dynamical equations
19 p3095 A71-37153
- Numerical integration of element T /transit time through perihelion/ in perturbations of near parabolic comet orbits
20 p3291 A71-39321
- One way UHF clock synchronization, using geostationary communication satellites with propagation delays calculated from orbital elements
20 p3239 A71-39460
- Spacecraft orbital elements determination, using statistical analysis in processing observed motion data
20 p3294 A71-39585
- Orbital elements of W Ursae Majoris systems, considering radial velocity curves, spectroscopic orbital solution, spectral peculiarities and spectrophotometry
20 p3300 A71-39820
- Light curve and orbital elements of eclipsing binary star V 539 Arae
21 p3440 A71-40058
- Thrusting lifting orbital vehicle nonlinear longitudinal dynamics in near-circular orbit, deriving orbital elements variation behavior and angle of attack mode period and damping
21 p3454 A71-40094
- Global lunar gravity field from weighted least squares analysis of Lunar Orbiters elements, deriving zonal and sectorial harmonics from libration data
21 p3443 A71-40183
- Absolute magnitudes of 1965-1969 comets, including orbit elements, perihelion coordinates and maximum values of reduced head diameter and tail length
22 p3606 A71-42614
- Lunar physical libration effect on lunar satellite orbital elements, considering reorientation of selenographic axes fixed in true moon
23 p3727 A71-43004
- Cometary nucleus disintegration rate as function of orbital elements, calculating lifetimes for Encke and Halley type comets
23 p3772 A71-44313
- Orbital elements of Encke comet from 1953-1954, 1957, 1960-1961 and 1963-1964 apparitions, finding secular acceleration coefficient
24 p3874 A71-45176
- Near circular orbit elements determination as functions of spacecraft initial speed and coordinates deviation by mathematical expectation procedure
24 p3876 A71-45317
- ORBITAL LAUNCHING**
Symphonie Franco-German satellite telecommunication system, describing orbital launching operations
11 p1840 A71-26523
- ORBITAL MECHANICS**
NT KEPLER LAWS
Krylov-Bogoliubov integration theory for first-order perturbation analysis of multidimensional harmonic oscillator applied to body motion in earth gravity
01 p0151 A71-10113
- Asteroids, comets and meteor dynamics in solar system, examining motion and orbital evolution by computer techniques
01 p0155 A71-10437
- Hansen method for partial anomalies applied to orbit perturbation equations
01 p0155 A71-10439
- Hilda minor planet group and Thule motion, examining real orbit relation to Schwarzschild type periodic orbits
01 p0155 A71-10441
- Two fixed centers problem generalization for case of material point attracted to coordinates origin by force proportional to radius
01 p0155 A71-10445
- Juno absolute perturbations due to large planets, using Hill method with digital computer
01 p0156 A71-10549
- Numerical analysis of Hill limiting case of restricted three body problem regarding quasi-periodic, ergodic and escape orbits for natural and artificial satellites
01 p0161 A71-11380
- Solid body motion kinematics about fixed point for Euler-Poisson equations
03 p0458 A71-13594
- Sun and planet system relative motion, using equations of invariant mechanics
03 p0492 A71-14190
- Orbital solutions based on critical optical tracking and Doppler observations, comparing with GEOS 1 and 2 satellite orbits
04 p0553 A71-15305
- Periodic orbits, stability and resonances - Conference, Sao Paulo, Brazil, September 1969
04 p0651 A71-15701
- Orbit evolution of small mass near earth-moon system, noting solar perturbations and equations of motion
04 p0653 A71-15709
- Equations of motion of restricted four body problem numerically integrated for positions of three primaries
04 p0653 A71-15711
- Collision periodic orbit sets in restricted n body problem for various mass ratios
04 p0654 A71-15715
- Periodic orbits representation in trigonometric series with numerical coefficients and truncation for applications
04 p0654 A71-15716
- Two dynamic systems on borderline of wildness, assuming one moving in oblate planet field
04 p0655 A71-15721
- Long period comets orbital orientations and perihelion distances, discussing Oort evolutionary theory modification
04 p0659 A71-15858
- General elliptic three body problem, discussing triangular Lagrangian point stability
05 p0809 A71-16472
- Axisymmetric body stationary motions around sphere, investigating secular and ordinary stability
05 p0809 A71-16473
- Book on geochemical exploration of moon and planets covering orbital, compositional and surface studies, Apollo missions, Lunar Receiving Laboratories and data processing
05 p0813 A71-16950
- Equilibrium points and periodic orbits, using qualitative theory of autonomous functional differential equations
06 p0927 A71-17639
- Nearly parabolic comets orbital orientation relation to sun peculiar motion direction, noting repulsive particles capture mechanism
06 p0976 A71-18449
- Mars 1971 orbiter mission, investigating orbit determination accuracy during approach phase
06 p0978 A71-18627
- Faint meteor orbit characteristics, observing distribution, eccentricities, dimensions and inclinations to ecliptic plane
07 p1194 A71-19316
- Mercury spin orbit resonance probability computation, making a priori assumptions for long term orbital variations, tidal torque and equatorial asymmetry
07 p1203 A71-20521
- Angular velocity and momentum vector evolution of isolated bodies in solar system, considering models to trace rotational motion evolution
07 p1203 A71-20525
- Periodic comets Giacobini-Zinner and Borrelly motions, determining orbits with nonNewtonian motion equations and three orthogonal nongravitational terms
08 p1358 A71-20877
- Satellite orbital motion, discussing idealized perturbations limiting problem from point mass
08 p1360 A71-21004
- Newton inverse square law of gravitation in solar system, considering closed orbit trajectories
08 p1363 A71-21320
- Linear coupling between orbital and attitude motions of rigid body, deriving 12th order six degrees of freedom linearized motion equation
09 p1516 A71-22173
- Coplanar transfer orbits optimal trajectories in central Newtonian gravitational field, using Krotov sufficient criteria
09 p1519 A71-22566
- Nomogram construction for graphical solution of two body problem using radius-vector and velocity components applied to solar system
09 p1520 A71-22844
- Media resistance effects on three body problem three dimensional periodic orbits, discussing implications to solar system formation from surrounding nebula
09 p1527 A71-23534
- Ceres and Pallas orbital commensurability, considering resonance effects
09 p1527 A71-23537
- Nonperiodic orbit behavior in highly perturbed dynamic systems, examining invariant curve evolution
10 p1669 A71-24178
- Orbital analysis of two body problem with slowly decreasing mass, constructing limited time interval approximate solutions for three distinct phase domains
10 p1676 A71-24523
- Two-degree of freedom Hamiltonian system stability and motion about equilibrium point for two-to-one commensurability
10 p1679 A71-24936
- Jupiter, Saturn and Uranus satellite systems orbital radius and mass correlation, suggesting satellite orbital tidal evolution and energy dissipation at planetary atmospheric boundary layer
11 p1827 A71-25729
- NonKeplerian intermediate orbit of artificial earth satellite motion with account of zonal harmonics, using fixed centers
11 p1829 A71-25807
- Satellite orbit period variation data for PERLO program visual observations, calculating topocentric celestial equator transits
11 p1732 A71-25826
- Lunar ephemeris, examining orbit with Delaunay theory
11 p1831 A71-26136
- Analytical lunar ephemeris, comparing variational and parallactic inequalities with various theories
11 p1831 A71-26137
- Dynamic systems with singular trajectories, analyzing orbital stability in locally compact space
11 p1799 A71-26157
- Meteor streams dynamic properties, computing mean orbit elements with statistical mathematical model
11 p1835 A71-26458
- Nearly parabolic comets orbital orientation relation to sun peculiar motion direction, noting repulsive particles capture mechanism
12 p1955 A71-26599

Stellar orbits for nearby stars, examining short arc statistics and galactic field models

12 p1959 A71-26781

Orbital flight time in terms of isochronism kinematic theory, discussing Lambert and Hamilton hodographic representations

13 p2135 A71-28351

Artificial satellites eccentric orbits commensurable with earth rotation, noting resonance effects of geopotential

13 p2135 A71-28354

Tumbling triaxial satellite in elliptical orbit about spherical planet, determining resonant and nonresonant gravity gradient perturbations

13 p2145 A71-28356

Optimal transfers in central gravitational field, using perturbation formulas of osculating Keplerian orbit elements and corresponding linearized equations

13 p2139 A71-28825

Fuel optimal noncoplanar orbital transfers of thrust limited rocket

13 p2139 A71-28828

Gravity field determination from satellite orbit analysis, using surface gravity and astrogodetic data

14 p2131 A71-30488

Orbital stability concept under nonperiodic motions

15 p2499 A71-31179

Soviet papers on irregular forces of cometary motion, emphasizing Daniel comet-asteroid collisions, orbit evolution, brightness, orbital distances, etc

15 p2481 A71-31297

Daniel 1909 IV comet orbit evolution, discussing capture by Jupiter, asteroid collision, brightness, orbit perturbation and nongravitational force effects

15 p2481 A71-31298

Simplified H. A. Newton formula applied to two zero-mass bodies rectilinear motion, using time coordinates power series

15 p2481 A71-31300

Faint meteor orbit characteristics, observing distribution, eccentricities, dimensions and inclinations to ecliptic plane

15 p2486 A71-31896

Goddard trajectory determination system, discussing attitude dynamics, data preparation, differential correction and orbit information

15 p2495 A71-32645

Elliptic restricted three body problem, calculating fictitious retrograde Jovian satellites orbits in rotating-pulsating axes for sun-Jupiter case

16 p2633 A71-33337

Comet origin hypotheses, examining orbit axes and perihelions distribution

16 p2639 A71-33693

Orbital elements oscillations in celestial mechanics two body problem with slowly decreasing mass described by nonlinear nonautonomous differential equations system, obtaining approximate solutions

17 p2804 A71-34912

Outer planets missions combined zodiacal experiment, examining meteoric, asteroidal and satellite particles distribution and orbits

19 p3064 A71-37919

Navigation, orbit and trajectory analysis of 1979 Jupiter-Uranus-Neptune Grand Tour mission, assuming deep space network tracking

19 p3101 A71-37936

Elliptic parameters of osculating orbits in two body problem with variable mass

20 p3267 A71-38791

Two body orbits problem concerning satellite flightpath transfer possibility to orbit touching cyclic or elliptical trajectories

20 p3287 A71-38849

Liapunov stability of rigorous particular solutions /corresponding to libration points/ of three body problem, determining motions of satellite influenced by two spherical bodies

20 p3291 A71-39315

Satellite orbital motion, discussing idealized perturbations limiting problem from point mass

20 p3294 A71-39584

Two dimensional elliptic restricted three body problem, considering regularization mechanism and periodic collision orbits

21 p3441 A71-40095

Five outer planets orbital perturbations by four inner planets, comparing second differentials with disturbing force numerical values

21 p3441 A71-40096

Icarus photographic observations, determining general relativity effects on orbital motion

21 p3443 A71-40187

Orbital transfer time equation reformulation, discussing various orbit constraints accommodation and rapid convergence in rendezvous orbit iterative determination

23 p3727 A71-43008

Orbital equations of motion and associated variational equations numerical integration, calculating geopotential in terms of spherical harmonics

23 p3666 A71-43058

First order variational equations of Hamiltonian systems with two degrees of freedom for symmetric periodic orbit

23 p3699 A71-43240

Three body problem of two heavy mass particles oscillatory motion in periodic orbits on straight line under Newtonian attraction

23 p3734 A71-43241

Gravitational system dynamics, discussing massive-light star mixtures with collisions and systems with equal mass objects

24 p3869 A71-44803

ORBITAL MOTION

U ORBITS

ORBITAL POSITION ESTIMATION

Solar radiation pressure acceleration effects on flat satellite in earth synchronous orbit, examining orbital shift and counteracting thrust velocity applications

10 p1671 A71-24333

Topocentric satellite trajectory approximation along circular orbit by n-degree equation, using coordinate-time relation

11 p1829 A71-25809

Orbit computation and tracking system for Iris satellite using differential correction program

19 p3142 A71-38066

Batch and sequential consider filters data processing methods for Mars orbiting spacecraft state estimation, investigating error sources

23 p3731 A71-43055

ORBITAL RENDEZVOUS

NT EARTH ORBITAL RENDEZVOUS

NT LUNAR ORBITAL RENDEZVOUS

Spacecraft navigation, guidance and control for manual rendezvous with orbiting target, examining error sources perturbing effects

01 p0022 A71-10513

Artificial satellites rendezvous, describing common Kepler ellipse in central body field with positioning after time delay

03 p0500 A71-14389

Two impulse rendezvous between coplanar circular planetary orbits, considering mono-impulsive interception /flyby/ problem for optimality

05 p0812 A71-16731

Satellite rendezvous programmed control with allowance for thrust limitation by free trajectories method, determining impulse duration, magnitude and time

09 p1531 A71-22571

Minimum propellant optimal rendezvous maneuver of two cosmic vehicles on circular orbits, considering tracking vehicle motion equations

10 p1672 A71-24335

Optimal symmetric minimum-impulse rendezvous between close near-circular noncoplanar orbits

13 p2139 A71-28820

Approximate multi-impulse large amplitude optimal rendezvous between neighboring elliptical orbits

17 p2807 A71-35472

Orbit-to-orbit shuttles as earth capture systems for round trip planetary missions, using hyperbolic rendezvous technique with returning interplanetary spacecraft

22 p3600 A71-41954

Orbital transfer time equation reformulation, discussing various orbit constraints accommodation and rapid convergence in rendezvous orbit iterative determination

23 p3727 A71-43008

Fuel optimal transfer from circular orbit space station to rendezvous with vehicles in different circular orbits

23 p3729 A71-43035

ORBITAL SIMULATORS

U SPACE SIMULATORS

ORBITAL SPACE STATIONS

NT EOSS

NT ORBITAL WORKSHOPS

Manned space station research capabilities in earth orbital environment for agravic force field, hard vacuum, cosmic radiation and spatial disposition

02 p0237 A71-11685

Orbital space stations for earth studies, considering atmospheric, hydrological and meteorological observations, astronomy, medico-biological and technological experiments and interplanetary spacecraft bases construction

03 p0497 A71-13418

Skylab earth-orbiting manned space station attitude and pointing control systems design

04 p0623 A71-15323

Manned artificial satellites, discussing problems of orbiting and interplanetary space stations with reference to U.S./U.S.S.R. future projects

05 p0816 A71-16195

Earth resources coverage capabilities of manned orbital space station, comparing to remote measurement requirements

06 p0980 A71-18532

Computer requirements of self contained guidance, navigation and control system onboard manned orbital space station

07 p1155 A71-19702

Atmospheric seal leakage control tests for long orbital lifetime space station designs, discussing vacuum chamber monitored pressure shell penetrations

11 p1836 A71-25316

Logistics system for synchronous orbit space stations supply, discussing parking to synchronous orbit transfer of reusable and disposable logistics vehicles

11 p1838 A71-25530

Out of core design of reactor heated thermionic power plant for manned space station, discussing temperature distribution, shielding characteristics and power conversion

11 p1710 A71-25872

Manned space station optimal thermal control design, investigating heat pipe and semipassive/active cooled concepts

11 p1838 A71-26220

Aerial and orbital remote sensing of water quality considering waste materials effect on coastal marine environment

11 p1760 A71-26593

Semielastic body rotational stability, investigating elastic coupling effects on controllability of rotating space stations in earth orbit

12 p1973 A71-27590

Orbital space stations and spacecraft courses, determining orbit precession and perturbation

12 p1968 A71-27628

Orbital space stations for earth studies, considering atmospheric, hydrological and meteorological observations, astronomy, medico-biological and technological experiments and interplanetary spacecraft bases construction

14 p2319 A71-29695

Permanent orbital space station design proposal for launch in latter 1970s, discussing systems concepts and configurations

14 p2320 A71-30422

Biowaste resistojet propulsion system for NASA space station orbit-keeping, describing design and operation

14 p2293 A71-30748

Eight channel micropowered miniature biomedical PAM/FM telemetry system for implantation into research subjects aboard orbiting space station

14 p2189 A71-30930

Environmental thermal control/life support systems for manned space station, discussing maintenance, weight, power and volume

17 p2690 A71-34719

NASA space station electrical power systems discussing configurations, growth capacity, volume, reliability and long term effects

17 p2677 A71-34720

NASA space station navigation system, considering landmark and ground tracking, ground beacons and satellite concepts, long term effects, operation requirements and design goals

17 p2772 A71-35054

Atomic clocks on manned space stations, discussing stability in aerospace environment, techniques for earth based timer calibration, reference device, maintenance and corrections

17 p2743 A71-35056

Single sortie or clustered mode orbital space stations systems safety, noting effects on operations, configurations and design

17 p2814 A71-35423

Computer simulation model for experimental data in post-Skylab space station design

18 p2973 A71-36458

Weightlessness simulation for orbital man machine experimentation, discussing teterboard and cargo transfer examples

18 p2871 A71-36643

Salut 1/Soyuz 10 mission, discussing configuration, size orbits and docking procedure

18 p2975 A71-36685

Orbiting stations and space shuttles - Conference, Rome, April 1971

19 p3149 A71-37301

Space station biological/medical laboratories, discussing physiology, pathology, hematological, static and dynamic equilibrium, neuropsychic, dietetic, radiobiological, hygiene and prophylaxis departments

19 p3006 A71-37308

Space and orbital laboratories construction and operation legitimacy problem covering satellites, stations and space transport concepts and international management

19 p3151 A71-37323

European launcher programs and participation in post-Apollo shuttles and orbital stations development in partnership with U.S.

19 p3151 A71-37330

Space transportation orbiter design covering thermal protection, aerodynamics and cross range problems during earth reentry

22 p3609 A71-41979

Manned orbital operations economy for space station utilization, discussing laboratory equipment, on-orbit supervision, maintenance and remote communications limitations

22 p3611 A71-42030

Mission analysis aspects of space shuttle operations between earth orbit station and lunar orbit station

23 p3724 A71-42977

Lunar orbit space station lifetime, using averaged variational equations numerical integration for terrestrial, solar and lunar gravitational field effects [AAS PAPER 71-377] 23 p3730 A71-43047

ORBITAL TRANSFER
U TRANSFER ORBITS
ORBITAL VELOCITY
 Radio meteor orbit velocity and radiant measurements by pulse diffraction technique 09 p1520 A71-22829
 Nomograms for meteor geocentric velocity and trajectory with correction for zenith attraction and radiant 09 p1520 A71-22831
 Artificial satellite orbital velocity tangential component time variation from variational calculus direction law 10 p1674 A71-24441
 Long period gravitational radiation detection, using relative velocity discrepancies of earth and Mariner 6 and 7 10 p1664 A71-25007
 Restricted four body problem, obtaining graphs for Hill surface of zero relative velocity 13 p2137 A71-28478
 White dwarfs production in small mass binary systems, deriving formulas for final mass and orbital velocity with application to blue stragglers 19 p3143 A71-38160

ORBITAL WORKERS
 Apollo Telescope Mount for high resolution solar observation and manned instruments evaluation in space environment, discussing attitude and pointing control systems 15 p2500 A71-31458
 Orbital Earth Resources Experiment Package sensor components, functions and crew tasks for operation 15 p2500 A71-31459

ORBITAL WORKSHOPS
 Skylab design and mission objectives, describing attitude control, MDA, quarters, Apollo telescope mount and proposed experiments 02 p0321 A71-12738
 High voltage power supply for NASA orbital gravity substitute electrostatic workbench, including abnormal load and oxygen environment tests 03 p0394 A71-13050
 Skylab program, describing equipment based on Saturn 5 workshop experiments and objectives 07 p1206 A71-19088
 Skylab workshop as orbital manned platform for scientific investigation, discussing system design details and technical evaluation 10 p1682 A71-24276
 Orbital Earth Resources Experiment Package sensor components, functions and crew tasks for operation 15 p2500 A71-31459
 Skylab as orbital factory, worksite and observatory for experiments in science, technology, materials science and manufacturing 15 p2500 A71-31460
 Manufacturing processes in orbital workshop, considering metal and optical lenses casting crystal growth and gravity lack effects 16 p2606 A71-32856
 Skylab habitability considerations in Orbital Workshop design, discussing waste management, food management and sleeping compartments [AIAA PAPER 71-872] 18 p2870 A71-36628
 Skylab electrical power system located on Orbital Workshop and Airlock Module and on ATM, discussing capabilities, characteristics and limitations 20 p3179 A71-38903
 Hot spots and voltage breakdowns due to open or shadowed solar cells, studying effect in orbital workshop array 20 p3182 A71-38945

ORBITALS
 NT ELECTRON ORBITALS
 NT MOLECULAR ORBITALS

ORBITER PROJECT
 NT LUNAR ORBITER
 Outer planets combined orbiter/flyby missions, investigating single launch feasibility with INT-20/Centaur launch vehicle [AAS PAPER 71-114] 19 p3140 A71-37935
 Planetary quarantine constraints for Mariner Mars 1971 orbiter missions, considering heliocentric and areocentric phases [AAS PAPER 71-318] 23 p3725 A71-42992

ORBITING ASTRONOMICAL OBSERVATORY
 U OAO

ORBITING GEOPHYSICAL OBSERVATORY
 U OGO

ORBITING SATELLITES
 U ARTIFICIAL SATELLITES
 ORBITING SOLAR OBSERVATORY
 U OSO

ORBITS
 NT APOGEES
 NT CIRCULAR ORBITS
 NT EARTH ORBITS
 NT ECCENTRIC ORBITS

NT ELLIPTICAL ORBITS
 NT EQUATORIAL ORBITS
 NT INTERPLANETARY TRANSFER ORBITS
 NT LUNAR ORBITS
 NT PARKING ORBITS
 NT PERIGEEES
 NT PERIHELIONS
 NT PLANETARY ORBITS
 NT POLAR ORBITS
 NT SATELLITE ORBITS
 NT SOLAR ORBITS
 NT SPACECRAFT ORBITS
 NT STATIONARY ORBITS
 NT TRANSFER ORBITS
 NT TROJAN ORBITS
 Hamiltonian systems properties in relation to Poicare function and canonical variables in bilinear form, discussing periodic orbits 01 p0128 A71-10668
 Limiting bounds determination for existence of periodic orbits near known existing periodic orbit, presenting linear perturbation analysis 04 p0654 A71-15717
 Periodic orbit families in planar Pythagorean three body problem 04 p0656 A71-15731
 Hamiltonian systems properties in relation to Poicare function and canonical variables in bilinear form, discussing periodic orbits 14 p2276 A71-31001
 Plane photogravitational restricted circular three body problem symmetrical periodic orbits closing on rotating plane after revolutions 15 p2483 A71-31340
 Periodic orbits around Lagrange libration points of restricted three body problem disturbed by gravitational and radiative influences 17 p2809 A71-35599
 Plane photogravitational restricted circular three body problem symmetrical periodic orbits closing on rotating plane after revolutions 22 p3606 A71-42615

ORDER-STOICHIOMETRY TRANSFORMATIONS
 Near stoichiometric binary alloys atomic ordering parameters quantization by field ion micrography, using direct counting and optical transformation techniques 02 p0297 A71-12736
 Alpha titanium-oxygen solid solutions surface structure, using low energy electron diffraction for determination of order-disorder transition and superlattice reflections 04 p0610 A71-14895
 Ordered intermetallic CsCl compounds thermodynamic properties determination, noting linear relationship between intrinsic disorder and formation heat 07 p1131 A71-19428
 Binary A15 phases transition elements compositional variations effects on atomic ordering 07 p1163 A71-19430
 Critical temperature short to long range ordering mechanism theories, discussing lattice type, transition continuity and spinodal decomposition factors 07 p1131 A71-19432
 Kinetics of transformation to long range ordering in Ni-V as function of heat treatment 07 p1131 A71-19433
 Ni-Mn, Ni-Fe and Ni-Fe-Al alloys yield behavior and microstructure as result of ordering and disordering treatments, using center annealing technique 07 p1132 A71-19434
 NiMo alloy fcc disordered structure and mechanical properties correlation to domain size and orientations from thin film transmission electron microscopy 07 p1132 A71-19435
 Nickel molybdenide disorder to order early transition mechanism diffraction model, using transmission electron and field ion microscopy studies 07 p1132 A71-19436
 Mg-Cd single crystals deformation by prismatic slip as function of testing temperature and state of order 07 p1132 A71-19437
 Atomic ordered alloy compressive strengthening for fcc and bcc lattices in terms of yielding, work hardening and no hardening stages 07 p1132 A71-19438
 Alloy matrix short range ordered particle microstructures and properties, correlating electron diffraction and field ion microscopy studies 07 p1132 A71-19439
 Alloy strengthening by ordered precipitates, predicting antiphase boundary energy from flow stress vs particle size plots 07 p1132 A71-19440
 Thin nickel aluminide sheets and small particles long range ordering, discussing antiphase boundary energy effects 07 p1133 A71-19441
 Disordered materials electronic structure, discussing crystal types, amorphous semiconductors and Mott-CFO model 08 p1343 A71-21173

Crystal lattice disordered systems, calculating electronic density of states by overlap integral transformation 08 p1344 A71-21364
 Ordered states effects on mechanical properties of Va-Co-Ni ternary alloys, considering creep behavior difference between ordered and disordered structures 08 p1309 A71-21526
 Amorphous semiconductors for memory and logic devices, using reversible structural transformations between disordered and ordered states 09 p1509 A71-23114
 Rapidly quenched CuAu ordered state development on low temperature annealing, presenting Young modulus variation as function of heat treatment time 09 p1477 A71-23350
 Superconducting alloys order parameter spatial variation and resonance scattering near nonmagnetic impurity at critical temperature, using Heinrich perturbation theory expansion solutions 12 p1942 A71-26744
 Addition effects on ordering kinetics in Ni-Mn based ternary alloys, using Rawar neutronography 12 p1918 A71-27543
 Field ion emission microscopic study of isothermal order-disorder transformation kinetics in water quenched Ni-Mo alloys 13 p2085 A71-28577
 Ordered structure recovery in Fe-Co-V alloy from elasticity limit behavior, studying duration effect on mechanical properties of strain hardened samples 16 p2591 A71-33370
 Ammonium chloride specific heat measurement near order-disorder transition, comparing results to Ising model behavior 17 p2791 A71-35743
 Diffusion controlled order-disorder transformations kinetics, considering internal strain and gradient energy 21 p3397 A71-40431
 Space charge density and carrier mobility in disordered regions of p-n microjunctions 23 p3717 A71-43486

ORDINATES
U COORDINATES
ORDNANCE

External store surface pressure distributions during captive flight aboard F-4B aircraft, considering carrying aircraft effects on flow field about airborne ordnance [AIAA PAPER 71-295] 08 p1232 A71-22015
 Neutron radiography of Apollo ordnance, describing test facility and equipment 19 p3063 A71-37449

ORES
U MINERALS
ORGANIC CHEMISTRY

Photosynthesis models, discussing photoenergetics of molecular systems 02 p0201 A71-12714
 German papers on plasma physics, metal corrosion, organic chemistry, molecular biology, etc 07 p1160 A71-19601
 Computerized method of interpreting low resolution mass spectra in organic chemical analysis, describing inference maker program applications and results 09 p1403 A71-22471

ORGANIC COMPOUNDS

NT ACETIC ACID
 NT ADENINES
 NT ADENOSINE DIPHOSPHATE [ADP]
 NT ADENOSINE TRIPHOSPHATE [ATP]
 NT ADENOSINES
 NT AMINO ACIDS
 NT ASPARTATES
 NT ASPARTIC ACID
 NT CARBON TETRAFLUORIDE
 NT CASTOR OIL
 NT CHOLINE
 NT CYSTEINE
 NT FATS
 NT FATTY ACIDS
 NT FLUORINE ORGANIC COMPOUNDS
 NT FLUOROAMINES
 NT FLUOROCARBONS
 NT FLUOROHYDROCARBONS
 NT GLUTAMIC ACID
 NT GLUTAMINE
 NT GLYCINE
 NT HISTIDINE
 NT IODOACETIC ACID
 NT METHIONINE
 NT NUCLEOTIDES
 NT ORGANIC LIQUIDS
 NT OXIDASE
 NT PHENYLALANINE
 NT PYRIDINE NUCLEOTIDES
 NT THYROXINE
 NT TRYPTOPHAN
 NT URIDYLIC ACID

Antifurcation effects of heteroorganic compounds in medium-distillation hydrocarbon fuels for rocket engines 01 p0141 A71-11108

Polyatomic organic adsorbates effect on field emission total energy distribution from W and Mo surfaces, discussing electronic and phononic spectra 02 p0297 A71-12733

Carbon kinetic isotope fractionation into carbon dioxide and organic compounds in meteorite-like Fischer-Tropsch reaction with nickel-iron or magnetite catalyst 03 p0483 A71-13013

Organic compounds carbon K emission spectra, using light element X ray spectrometer for aliphatic, aromatic and partly ionic substances spectral analysis 03 p0375 A71-13200

Organic compounds oxidation inhibition by polycyclic aromatic hydrocarbons, analyzing peroxide radicals charge transfer complex stability 05 p0716 A71-16382

Stereoisomeric organic structures in animate nature and life origin on earth 06 p0857 A71-18725

Sulfur containing organic chelating compounds as radiation protective agents 07 p1034 A71-18941

Organic free radical radioprotective and radiosensitizing effect, reporting Chinese hamster cell line survival characteristics after treatment 07 p1035 A71-18949

Organic free radical photographic films for biomedical microimager 07 p1110 A71-19475

Flame resistant properties of phosphorus containing organic and inorganic high polymers 07 p1145 A71-19841

Chemisorption energies of organics on Pb surface by extended Hückel molecular orbital technique 07 p1055 A71-19845

Frequency and spectral composition effect of incident radiation on stimulated Raman scattering of organic compounds, using ruby laser harmonic emission 09 p1461 A71-22395

Organic compounds biosynthesis in simulated Mars atmosphere, using UV irradiation for photocatalytic production from CO and water mixtures 09 p1403 A71-22647

Orgueil carbonaceous chondrite organic matter, detecting homologous compounds, optically active species, isotopes, bacteria and organized elements 10 p1565 A71-24612

Organic compounds astrochemistry, discussing hydroxyl absorption lines and molecular abundances in interstellar space 10 p1678 A71-24810

Cement systems based on metal oxides and organic compounds, stressing acidity factor for organic component selection 13 p2090 A71-28007

Hydrocarbons, amino acids and large molecule organic compounds formation in chondrite meteorites by abiogenic reactions 13 p2010 A71-28692

Chondrites bibliography and review, considering classification, metamorphism, ages and thermal history, achondrites and organic compounds 17 p2798 A71-34454

Quantum mechanical considerations underlying calculations of two-photon transition probabilities, discussing experiments on semiconductors, ionic crystals and organic compounds 18 p2930 A71-36241

Permeability and porosity of Precambrian Onverwacht cherts and other low permeability rocks, discussing geological origin of rock-contained organic compounds 18 p2913 A71-36768

Maximum bubble pressure automatic capillary electrometer for salt solutions and organic compounds electroosorption, comparing with Lippmann instrument and capacitance bridge 22 p3548 A71-42529

Urine preservatives for urine water recovery system, noting ammonia and organic compound contents in condensate 22 p3506 A71-42809

Solar system organic compounds detection and evolution, considering element, isotope and pigment composition, optical activity and polymerization 22 p3496 A71-42824

Apollo 12 lunar surface samples analysis for organic compounds by mass spectroscopy and pyrolysis-gas chromatography 23 p3756 A71-43741

Volatilizable organic polymers and hydrocarbons in Apollo 12 lunar core samples 12025 and 12028, using mass spectrometric analysis 23 p3756 A71-43742

Tektite organic constituents evidence from high temperature mass spectrometry, investigating relation to formation process and terrestrial contamination 23 p3769 A71-43926

Crack propagation kinetics in organic glass subjected to monotonically increasing tension perpendicular to crack plane, examining crack contour prior to spontaneous rupture 24 p3883 A71-44858

ORGANIC COOLANTS

Life tests and properties of organic working fluids heat pipes for electronic component cooling [AIAA PAPER 71-408] 11 p1856 A71-26203

High flash point polyalkylene glycol base synthetic quenchants for high strength alloy heat treatment, noting application to aluminum, titanium and steel parts 13 p2073 A71-28144

ORGANIC FLUORINE COMPOUNDS

U FLUORINE ORGANIC COMPOUNDS

ORGANIC LASERS

Stimulated emission from stilbenylloxazole solutions under pumping by second harmonic of ruby laser, determining emission thresholds 03 p0434 A71-13502

Organic dye laser output and service life enhancement, using filters for absorption of UV pumping radiation photodecomposition of rhodamine 6G alcohol solution 03 p0435 A71-13509

Tuned nitrogen laser pumped dye lasers, investigating bandwidth influence on output power 03 p0436 A71-13643

Long pulse rhodamine 6G flash lamp-pumped circulating dye laser with cyclooctatetraene cycloheptatriene as triplet state quenchers, testing performance 03 p0437 A71-13884

Organic lasers using fluorescent dye in liquid solution or polymer, discussing gain and output performance, tuning, mode locking and CW operation 04 p0605 A71-14710

Near UV dye lasers, using various organic compounds as scintillators with excitation through nitrogen gas UV laser transverse pumping 04 p0606 A71-14717

Spectroscopic hole burning in coupled saturable dye-ruby lasers with frequency locking 04 p0607 A71-14725

Dye lasers operational principles and characteristics, considering dyes molecular structure, optical pumping, continuous operation, wavelength selection and applications 05 p0761 A71-16330

Time dependent Q switched energy storage of trifluoromethanodimethane photodissociation laser 06 p0910 A71-18661

IR difference frequency generation using tunable dye laser 06 p0910 A71-18663

Emission frequency tunable organic dye laser development and construction 07 p1123 A71-19239

Organic dye lasers flash lamp pumped system for tunable coherent light production in visible and near IR spectrum 07 p1125 A71-19796

Organic dye lasers lasing conditions calculation for constant emission frequency from nonstationary emission kinetics analysis 07 p1125 A71-19807

Laser excited atoms quenching by iodine molecules from light pulse induced photodissociation of perfluoropropyl iodide active media 07 p1126 A71-20195

Organic scintillators as active laser materials, discussing absorption, oscillation and emission spectra and luminescence quantum yield 09 p1461 A71-22386

Wide angle high gain image amplification by organic dye solution lasers using rhodamine or fluorescein sodium salt 09 p1463 A71-22752

Organic lasers with xanthene dyes solutions, investigating triplet states molecular population effect on output energy characteristics in pumping 10 p1620 A71-24344

Tunable organic dye laser with dispersion prism for increased radiation spectral density and luminescence band smooth frequency control 12 p1912 A71-26757

Light combination scattering in organic liquids, measuring frequency dependence with dye laser technique 13 p2080 A71-29021

Broadly tunable liquid dye laser action with narrow line output through use of distributed feedback obtained by spatial modulation of gain and refractive index 13 p2081 A71-29339

Absorption spectra enhancement by organic dye laser quenching, considering applications for absorbing species spectroscopic detection 13 p2082 A71-29439

Flashtube pumped rhodamine 6G dye laser with four prism tuner, giving reflection losses equations and performance characteristics 14 p2254 A71-30135

Pulsed nitrogen-pumped dye laser output spectral narrowing by injection of argon laser monochromatic radiation into cavity 15 p2420 A71-32382

Rhodamine 6 G in ethanol partial mode locked dye laser picosecond pulses, using pulsed nitrogen laser pumping 15 p2422 A71-32580

Ruby laser pumped tunable organic dye laser to excite atomic flame fluorescence of 5535.5 A barium resonance line, obtaining intensity vs concentration 15 p2422 A71-32582

Compact monochromatic rhodamine doped polymethyl methacrylate dye laser with internal diffraction grating resonator, describing frequency selection from emission spectrum 15 p2422 A71-32585

Continuously tunable pulsed UV source using broadband dye laser emission input to rotatable KDP crystal 16 p2586 A71-33141

High average power flash lamp pumped pulsed dye laser development and application in atmospheric sodium probing 16 p2586 A71-33148

Rhodamine, sodium fluorescein and cyanine dyes for liquid lasers, investigating electroluminescence by polarography 16 p2587 A71-33382

Flash lamp pumped pulsed dye laser using triplet quenchers cycloheptatriene and cyclooctatetraene with 600 microsec emission times in rhodamine 16 p2589 A71-34122

Energy balance and emission power of organic dye laser under nonmonochromatic excitation 17 p2751 A71-34381

Organic dye laser properties analysis using universal relation between absorption and emission spectra for solvent molecules reorientation after excitation 17 p2752 A71-34388

Dynamic rate equation model of single wavelength flash lamp pumped rhodamine dye laser accounting for short molecular triplet state lifetimes 18 p2929 A71-35958

Dye lasers developments and applications, including flash lamp pumps, frequency narrowing and tuning and picosecond pulse mode locking 18 p2931 A71-36602

Papers on semiconductor, carbon dioxide and dye lasers 20 p3243 A71-39065

Dye laser physics and technology development, discussing dye selection for frequency and cavity parameter variation tuning of lasing wavelength 20 p3243 A71-39068

Laser dye cell optical quality dependence on light pumping and liquid dye flow velocity, using schlieren method 20 p3246 A71-39489

Repetitively pulsed flashlamp pumped dye laser, noting high average outputs in red end of spectrum with rhodamine B 20 p3246 A71-39760

High resolution spectroscopy of Na D resonance lines in saturated absorption with repetitively pulsed tunable dye laser 21 p3391 A71-40199

Nonstationary laser generation of organic dyes in picosecond optical pumping, considering kinetic and spectrum nonstationarity 22 p3557 A71-41815

Liquid laser output wavelength dependence on rhodamine dye concentration, comparing experimental data with Stepanov theory 23 p3684 A71-43417

Mode locked CW dye laser operation, describing output stability and pulse rate and widths 23 p3687 A71-44133

CW dye laser mode locking with lithium niobate phase modulator, observing 500 psec pulse generation 23 p3687 A71-44134

Dye laser electronic tuning by inserting calcium-molybdenum oxide acousto-optic filter into cavity 23 p3687 A71-44137

ORGANIC LIQUIDS

Nonlinear light absorption in organic dyes liquid solutions 01 p0095 A71-11028

Explosive boiling of water and organic liquids around pulse heated Pt wire, discussing vaporization process, fluctuating nucleation and temperature behavior 02 p0331 A71-12193

Reciprocating organic single cylinder Rankine cycle engine using thiophene working fluid 03 p0351 A71-13034

Pure hydrocarbon droplets heating, expansion, vapor phase fuel storage and gasification in oxidizing gas at elevated pressures, using high speed cinematography 06 p1007 A71-18300

Ti stress corrosion in organic liquids, considering intergranular and transgranular failure 11 p1781 A71-26262

Light combination scattering in organic liquids, measuring frequency dependence with dye laser technique 13 p2080 A71-29021

Explosive boiling of water and organic liquids around pulse heated Pt wire, discussing vaporization process, fluctuating nucleation and temperature behavior 15 p2512 A71-31499

ORGANIC MATERIALS

Organic thin film layer semiconductors photoconductivity, developing semiempirical theory of pulse formation

06 p0941 A71-17735

Organo-ceramic composites for thermal protection of aerospace vehicles, discussing heat sink property

09 p1483 A71-23206

High modulus organic fiber for aerospace use, considering fiber-epoxy composite mechanical and physical properties

14 p2263 A71-29658

Physicochemical properties and applications of lubricant materials based on organic compounds, discussing developments in inorganic lubricants

16 p2600 A71-32839

Nitrogen atoms chemiluminescent reaction spectra with carbon tetrachloride, ethylene and methylene chloride, noting application to artificial clouds formation

19 p3014 A71-38634

Early solar system organic matter origin, discussing amino acid synthesis from CO, H and ammonia reaction with N, alumina or clay catalysts

23 p3633 A71-43244

Prebiotic organic matter in solar system, investigating contamination free amino acid catalytic synthesis from deuterated reactants

23 p3633 A71-43245

Development and performance characteristic of batteries including Zn and Mg dry cells, metal air, organic electrolytic, organic cathode and secondary systems

24 p3793 A71-45133

ORGANIC NITRATES

NT CELLULOSE NITRATE

NT HYDRAZINE NITROFORM

NT NITROGLYCERIN

NT PETN

ORGANIC PHOSPHORUS COMPOUNDS

NT URIDYLIC ACID

Foamy properties at various temperatures of nonaqueous hydroliquids based on petroleum fractions and organic silicon and phosphorus oligomers

01 p0088 A71-11107

Altitude acclimatization of albino rats and guinea pigs, measuring chronic and acute hypoxia effect on oxygen affinity and red cell 2,3 diphosphoglycerate concentration

10 p1558 A71-23894

Vitamin B6 protection against asymmetrical dimethylhydrazine poisoning, administering B6 alone and with cortical phospholipids in mice

10 p1572 A71-24979

Organic phosphate compounds effects on oxygen affinity and intracellular pH of human erythrocytes

18 p2857 A71-36691

Phosphoenolpyruvate as enzyme inhibitor of phosphoribulokinase in *Pseudomonas facilis* with respect to ribulose-5-phosphate and ATP

20 p3185 A71-38820

Chronic hypercapnia effects on oxygen affinity and 2,3-diphosphoglycerate in red cell from tests on guinea pigs

20 p3189 A71-39440

Neosynthesized alpha-glycerophosphate and 2,3-diphosphoglycerate role in human extraocular muscle metabolism

21 p3328 A71-40099

Halophilic bacteria electron transport chain, studying protein, phospholipids, flavoproteins and cytochromes sedimentation properties by electron microscopy and light scattering technique

21 p3334 A71-40593

Organophosphate pesticide poisoning implication in aircraft crash of duster pilot from cholinesterase activity drop evidence

23 p3641 A71-44249

ORGANIC SEMICONDUCTORS

Photoelectron emission of organic semiconductors, considering molecular and defect photoionization and exciton collisions

03 p0467 A71-13399

ORGANIC SILICON COMPOUNDS

Foamy properties at various temperatures of nonaqueous hydroliquids based on petroleum fractions and organic silicon and phosphorus oligomers

01 p0088 A71-11107

ORGANISMS

Organic thermoregulator control signal generation as function of body peripheral to central temperature ratios, using skin temperature rise measurements

10 p1564 A71-24485

Papers on gravitation effects on properties and behavior of living matter

21 p3326 A71-39969

Plants and animals reactions to environment gravitational component, showing organisms perception of accelerating force

21 p3326 A71-39970

Living organisms life-sustaining possibility under simulated Martian temperature, humidity and atmospheric composition conditions, emphasizing unicellular organisms radiation resistance

21 p3334 A71-40572

ORGANIZATIONS

Organization size in relation to staff personnel percentage, comparing various models

06 p1010 A71-18011

ORGANOMETALLIC COMPOUNDS

NT CARBOXYHEMOGLOBIN

NT CHLOROPHYLLS

NT HEMOGLOBIN

NT OXYHEMOGLOBIN

Thermal expansion of dilute binary composites concerning ceramic-glass, glass-metal, metal-metal and organic-metal systems

03 p0449 A71-14458

ORGANS

NT BLADDER

NT ESOPHAGUS

NT KIDNEYS

NT LIVER

NT LUNGS

NT PITUITARY GLAND

NT SPLEEN

NT STOMACH

Chlorella ration effect on internal organs of protein-deficient mice compared with casein and soybean rations

01 p0025 A71-11145

Long term hypoxia effects on granuloma and various organs in rats, noting collagen and noncollagenous proteins formation stimulation and/or inhibition

05 p0706 A71-16293

Cerebral cortex regulation of internal organ functions, examining neural and neurohumoral channels, hormones and vascular changes

05 p0709 A71-16802

Human organ thermal properties prediction by measuring water content of equal fat/protein tissues

06 p0851 A71-17603

Acute hydrazine hydrate poisoning morphological effects on internal organs and blood in guinea pigs, noting pronounced changes in liver and kidneys

09 p1393 A71-22921

Human inner organic system simulation by digital computer, using overall quantitative heuristic model

12 p1876 A71-27742

Dipeptidyl aminopeptidase I /cathepsin C/ properties, subcellular localization and polypeptide degradation in rat liver and bovine spleen and pituitary glands

13 p2025 A71-28179

Turtles organs and tissues responses during Zond 5 and 7 lunar probes circumlunar flight

16 p2532 A71-33678

Hyperoxic medium effects on experimental animal cells, tissues and organs morphology, infrastructure and histochemistry

22 p3495 A71-42801

ORGUEIL METEORITE

Primordial trapped planetary noble gases and solar isotopic ratios in separated meteoritic minerals from Orgueil carbonaceous chondrite

02 p0318 A71-12901

Nonseparated grain low iron olivine and pyroxene in carbonaceous meteorite Orgueil, using optical and electron probe microanalysis

02 p0318 A71-12904

Magnetite particles in Orgueil meteorite, discussing high symmetry morphology and generation

03 p0487 A71-13333

Orgueil carbonaceous chondrite organic matter, detecting homologous compounds, optically active species, isotopes, bacteria and organized elements

10 p1565 A71-24612

Montmorillonite and serpentine as major crystalline constituents of Orgueil meteorite

10 p1679 A71-24983

ORIENTATION

Line segment orientation visual perception relation to horizontal, vertical and oblique planes, considering induction effect susceptibility and visual illusions

01 p0010 A71-10274

Polar auroral arc orientations spatial and diurnal distribution and morphological characteristics for grouping into four types, discussing aurora borealis

05 p0744 A71-17188

Preferable orientation of physical galactic pairs, obtaining equatorial plane inclinations and great axes positional angles distribution

06 p0974 A71-18432

Stress annealed Ni-base superalloy crystals, investigating orientation and applied uniaxial stress sense effect on coherent gamma prime precipitates morphology

07 p1138 A71-19987

Aerial photographs orientation point location, relating measurement weight of transverse parallax

09 p1451 A71-23178

Macroscopic working model for CVD tungsten assuming change of substrate work function and preferential crystal orientation by impurity adsorbed molecules

11 p1808 A71-25861

Auroral arc orientation spatial and diurnal distribution, location and morphological characteristics, grouping into four types

13 p2059 A71-28245

Square cross section rectangular rotating grains dynamic behavior in magnetic fields, obtaining orientation data with Monte Carlo method

15 p2498 A71-32772

Semicircular canal and otolithic organ function in free swimming fish angular orientation behavior

21 p3328 A71-39996

Angular momentum vector orientation of reentry vehicle at end of spin-up, using helioid precession concept to characterize rotational motion during constant thrust

22 p3611 A71-42029

Graphic mission analysis for outer planet missions, considering spacecraft and celestial bodies relative positions, sensor and spacecraft relative orientation

[AAS PAPER 71-378] 23 p3731 A71-43048

Three-legged slewing about nonorthogonal axes, solving single-axis reorientations by two successive rotations about arbitrary fixed lines

[AAS PAPER 71-389] 23 p3773 A71-43057

Lunar surface orientation of whole Apollo 12 rocks, considering microcraters distribution

23 p3765 A71-43806

ORIFICE FLOW

Finite amplitude sound interaction with Helmholtz resonator, attributing losses to viscous damping and orifice jet flow kinetic energy dissipation

03 p0456 A71-13279

One component two phase mixtures critical flow in nozzles, orifices and short tubes, considering interphase heat, mass and momentum transfer

[ASME PAPER 70-WA/HT-5] 03 p0520 A71-14095

Contraction coefficient of orifice for subsonic and supersonic flows, including velocity-of-approach and compressibility effects upstream and downstream

[ASME PAPER 70-WA/FM-1] 03 p0402 A71-14103

Flow coefficient equations of square edged orifices, comparing graphically computed and test values

[ASME PAPER 70-WA/FM-2] 03 p0402 A71-14104

Compressible subsonic and supercritical flows, developing flowmeter orifice expansion factors

[ASME PAPER 70-WA/FM-3] 03 p0402 A71-14105

Fluid transmission lines terminated by orifice with nonlinear pressure flow characteristics, calculating harmonic distortion frequency response by perturbation method

[ASME PAPER 70-WA/FE-6] 03 p0402 A71-14128

Free nitrogen jets ejected from small orifices, measuring acoustic emission level and spectral pattern dependence on pressure

07 p1161 A71-20058

Hydrodynamic model of human red blood cell rotation in flow toward sizing orifice, predicting volume distribution

07 p1045 A71-20446

Back pressure sensor improvement, discussing orifice square law relationship between pressure and flow

07 p1094 A71-20608

Velocity distribution measurement of Cs gas flow from orifice in near-free molecule regime, using apparatus based on time of flight method

09 p1432 A71-22682

Computer programmable flow coefficient formulas for standard constrictions, orifice gages and Venturi nozzles

10 p1595 A71-24640

Pressure orifices inclination in low density flow from experiments with cooled flat plate model in hypersonic low density wind tunnel

11 p1751 A71-25490

Turbulent vortex rings motion empirical model, deriving equations valid at large distances from discharging orifice

11 p1751 A71-25498

Sharp circular edged orifice dynamic characteristics under high amplitude periodic fluid flow conditions, discussing hydraulic resistance coefficients

12 p1898 A71-27506

Two phase critical flow of one component mixtures in nozzles, orifices and short tubes, considering interphase heat, mass and momentum transfer rates

[ASME PAPER 70-WA/HT-5] 13 p2049 A71-28980

Steady state partially ionized monatomic gas expansion from sonic orifice, investigating electron-ion recombination effects on flow properties

15 p2457 A71-32101

Solid disk supported above flat plate by thin layer of gas flowing from central orifice, studying vertical motion equilibrium and dynamic data

[ASME PAPER 71-APM-3] 16 p2559 A71-33220

Rarefied gas flow characteristics through pipe orifice in intermediate range of rarefaction between free molecular flow and continuum flow

18 p2849 A71-37023

Pressure wave interaction with orifices inside ducts, calculating reflection and transmission characteristics relationship to orifice geometry and initial steady flow conditions

19 p3044 A71-37642

ORIFICES

Traveling shock waves interaction with orifice inside ducts, noting anomalous phenomena probably due to unsteady boundary layer growth or time lag

10 p1596 A71-24923

Rocket engine propellant injectors with noncircular orifice geometry, presenting experimental spray patterns and predicted performance for noncircular and circular orifice configurations 11 p1810 A71-25520

Errors due to air flow pulsation in orifice meters, discussing various diameter ratios 12 p1906 A71-26872

Automated orifice drilling optimal treatment routines, including proper timing and adequate total depth allowance 13 p2074 A71-28941

Transient flow measurement with sharp-edged orifices, considering pump trip accidents simulation in water cooled nuclear reactors [ASME PAPER 71-FE-30] 13 p2053 A71-29465

ORION CONSTELLATION

Wide angle far UV photography of Barnard Loop Nebula in Orion suggesting nebular emission intensity difference with near UV region due to interstellar dust 01 p0148 A71-10001

Orion Nebula (NGC 1976) physical characteristics from H alpha line radio telescopic observation, discussing energy level population, electron density, collision mechanisms, etc 02 p0308 A71-12094

Orion Nebula (NGC 1976) physical characteristics from H alpha line radio telescopic observation, discussing energy level population, electron density, collision mechanisms, etc 08 p1362 A71-21144

Evaporation of dirty ice particles surrounding early type stars, using dust grains model for explanation of anomalous reddening of Orion Nebulae 08 p1364 A71-21415

Multicolor photographic photometry of flare stars in Orion aggregate based on two UBV photoelectric sequences 10 p1680 A71-25061

Ionized gas and dust distribution in Orion nebula from Balmer line intensities photoelectric measurements 11 p1818 A71-25202

Light and radio emission from Orion nebula flare stars in meter waveband, discussing coherent mechanisms of plasma oscillations and gyro/synchrotron radiation amplification 15 p2485 A71-31696

Forbidden O II spectra brightness ratio measurements across Orion nebula, determining electron density variations 16 p2631 A71-33229

Interstellar absorption at H alpha line wavelength in Orion nebula, obtaining contour map for comparison with radio intensity 19 p1313 A71-37230

Formaldehyde absorption and emission lines in Orion IR nebula, indicating pumping suppression by neutral particle collisions 20 p3288 A71-39113

Stellar systems existence with positive total energy, using numerical integration of equations of motion for components of Trapezium in Orion 20 p3290 A71-39300

Methyl alcohol transitions in Orion at 1 cm noting emission source coincidence with IR nebula 21 p3447 A71-40445

Orion constellation hot stars UV spectra observation by photography from stratospheric balloon gondola using geomagnetic field for stabilization 23 p3735 A71-43249

ORIONID METEORIDS

Optical evidence of meteoric aerosols in upper atmosphere at maximum Orionids, showing double red luminosity of sky above Adi Ugrí 03 p0489 A71-13750

Upper atmospheric ion composition during Orionid meteor shower activity by rocket-borne RF mass spectrometer 09 p1437 A71-22680

Meteoric aerosols optical manifestation from photometric measurements on stratospheric balloons, demonstrating Orionids effects on twilight sky brightness 12 p1960 A71-26832

Orionid and Leonid meteor trains, determining diffusion coefficient from isophotes variation 12 p1965 A71-27230

Orionid and Leonid meteor trains, determining diffusion coefficient from isophotes variation 19 p3132 A71-37382

ORNITHOPTER AIRCRAFT

U RESEARCH AIRCRAFT

OROGRAPHY

Mesoscale orographic inhomogeneities in vertical air flows past surfaces, noting leeward air waves and upper/lower boundary layers 07 p1149 A71-18793

Orography, cloudiness and surface temperature effects in six-layer global atmospheric circulation model, giving January simulation data 17 p2770 A71-35804

ORTHICES

U ASTRONOMICAL MODELS

ORTHICONS

NT IMAGE ORTHICONS

Closed system for air cooling of image converter tubes and superorthicons for wear light flux, using refrigerator or dry ice 01 p0080 A71-10622

ORTHO HYDROGEN

Temperature dependent differential quenching rates of vibrationally excited CO fluorescence by ortho and para hydrogen, using Born-Bethe approximation 19 p3107 A71-38052

Thermal conductivities of pure and mixed ortho- and parahydrogen and/or deuterium at temperatures with no molecular internal energy exchange 24 p3850 A71-44553

ORTHOGONAL FUNCTIONS

NT WALSH FUNCTION

Orthogonal polynomials method for integral equations solution in two dimensional mixed boundary value problems of elasticity theory 01 p0171 A71-10660

Numerical method for stress distribution around openings in shells, using orthogonal coordinate system 02 p0321 A71-11649

Biorthogonal relation for bending of uniformly loaded clamped sector plates with boundary functions along curved edge 02 p0327 A71-12397

F 2 region critical frequency diurnal variation forecasting, using series expansion of natural orthogonal components 06 p0895 A71-18276

Counting rate source encoding algorithm with orthogonal functions in space experiment data processing before telemetering to ground 08 p1259 A71-21592

Orthogonal signal analysis and synthesis with Walsh functions, giving practical implementations of required operations 09 p1406 A71-23030

Systems approximation by incontinuous orthogonal Harre functions, discussing dynamic properties and input signal synthesis with minimal errors in estimating parameters 10 p1587 A71-24741

Atmospheric thermal sounding problem, using regularization and statistical methods and expanding by empirical orthogonal functions 11 p1795 A71-25920

Walsh orthogonal functions application in signal processing and as carrier waves in telemetry data transfer systems 14 p2199 A71-30909

Orthogonal polynomials method for integral equations solution in two dimensional mixed boundary value problems of elasticity theory 14 p2333 A71-30994

Bubnov-Galerkin method convergence prediction, discussing J spaces and orthonormal bases 15 p2439 A71-31154

Free and forced nonlinear oscillations differential equations approximated solution by orthogonal polynomial linearization, applying method to systems analysis near singular points 17 p2780 A71-34917

Optimum and suboptimum decision rules for two-channel deep space telemetry system with modulation consisting of PM with two orthogonal phase functions 17 p2704 A71-35088

Atmospheric thermal sounding problem, using regularization and statistical methods and expanding by empirical orthogonal functions 20 p3256 A71-39211

Walsh functions in image processing, rotational feature selection and pattern recognition, defining set of orthogonal transformations 20 p3255 A71-39611

Periodic functions complete orthogonal sequences class as linear combinations of Fourier expansions, obtaining convergence theorem 21 p3410 A71-41083

ORTHOGONAL MULTIPLEXING THEORY

Optimal receiver to detect multiple orthogonal signals on normal stationary noise background, assuming nonuniform a priori probability occurrence 12 p1883 A71-27618

ORTHOGONALITY

Orthogonality principle in irreversible thermodynamics, proving generalization for Onsager nonlinear symmetry relations 05 p0837 A71-16708

Elastic deformation of strip, rectangular annulus and cylinder with homogeneous displacement boundary conditions, deriving orthogonality relations for expanded eigenvectors 05 p0828 A71-16993

Orthogonal transforms and feature selection using pattern, Harr, Walsh, Fourier and Karhunen-Loeve spaces for providing efficient classification algorithms in pattern recognition 08 p1258 A71-21354

Temperature distribution in composite media sections involving solid interfacial sources, using Vodicica orthogonality equations 10 p1697 A71-24694

X ray astronomy orthogonal mirror telescopes, noting collecting efficiency, angular resolution and focusing 11 p1766 A71-26307

Elastic deformation of strip, rectangular annulus and cylinder with homogeneous displacement boundary conditions, deriving orthogonality relations for expanded eigenvectors 18 p2982 A71-36793

Orthogonality and positive operators on space of almost periodic and quasi-periodic functions, using frequency-power formulas 24 p3843 A71-44961

ORTHONORMAL FUNCTIONS

Boundary value problems solution for second order finite difference equations, applying second order orthonormal polynomials and related functions 17 p2764 A71-34843

Orthonormal series expansion for features generation with predetermined properties, applying to handwritten numerals recognition 22 p3515 A71-41512

Spiral grooved thrust and spherical gas bearings, predicting stability and frequency response by Newton-Raphson and orthonormalization methods 22 p3551 A71-41668

ORTHOPEDICS

Aircrew static reach reduction caused by upper and lower limb orthopedic disabilities 12 p1876 A71-27632

ORTHOPHOTOGRAPHY

Stereo-orthophoto mapping system design and operation 06 p0901 A71-18289

Terrain altitude evaluation in orthoprojectors, using off-line systems for contour lines approximation 06 p0901 A71-18290

ORTHOSTATIC TOLERANCE

Sight of body and active locomotion effects on perceptual adaptation to tilted vision in male subjects 01 p0010 A71-10398

External respiration, gas exchange and energy expenditures during orthostatic tests involving immersion experiment 01 p0014 A71-11136

Human orthostatic tolerance measurement via leg and lower body negative pressure, discussing heart rate and stroke volume variations 04 p0543 A71-15052

Soyuz 9 astronaut vertical posture control after 18 day orbital flight, considering cardiovascular disturbances caused by reduced muscle tone and changed interaction between analyzers 09 p1389 A71-22203

Soyuz 9 spacecraft astronauts cardiovascular and respiratory systems responses to orthostatic effect after 18-day orbital flight from EKG measurements and sphygmography 09 p1389 A71-22208

Afferent mechanisms of orthostasis in space flight, discussing plasma fluid volume reduction and cardiovascular adjustments on passive tilting [AIAA PAPER 71-883] 18 p2856 A71-36634

Astronaut orthostatic tolerance loss due to weightlessness, describing compensation by periodic lower body negative pressure [AIAA PAPER 71-859] 18 p2872 A71-36648

Plasma renin activity in hypertonic and normotonic persons exposed to exogenous stress, comparing with measurements at rest and in orthostasis 20 p3185 A71-38893

Motor and vestibular analyzers and frontal hypothalamus role in gravitational loads compensation during orthostasis, noting respiration, arterial pressure and brain bioelectric activity changes 20 p3188 A71-39223

Human orthostatic and vestibular stability responses to weightlessness during extended space flights noting acceleration tolerance, physical efficiency, infection resistance and medication sensitivity 22 p3495 A71-42790

ORTHOTROPIC CYLINDERS

Orthotropic cylindrical shell stress distribution near axial line crack, formulating problem as system of singular integral equations 01 p0167 A71-10175

Naturally twisted and orthotropic cylindrical beam bending by transverse load 04 p0673 A71-15886

Stress analysis of orthotropic twisted bars under tension applied at ends 06 p0985 A71-17747

Equilibrium stability of orthotropic cylindrical shell under longitudinal compression, discussing critical stresses 06 p0986 A71-17762

Thin single layer orthotropic circular cylindrical shell shear coupled traveling wave reflections, determining stresses in terms of particle velocities 07 p1216 A71-20134

Longitudinal, flexural and elastic waves propagation in infinite orthotropic circular cylinders 11 p1850 A71-26176

Transversally isotropic sphere and orthotropic cylinder in symmetrical temperature field, calculating thermal stress equations

12 p1975 A71-27112

Thermal stresses in anisotropic infinite elastic orthotropic laminated cylinder with arbitrary number of layers under axisymmetric heating

16 p2657 A71-33599

Orthotropic bar under compression loads, calculating Eulerian values for critical force

17 p2817 A71-34335

Pure and transverse bending of orthotropic cylindrical shell wound with elastic glass plastic filaments, presenting stress-strain diagrams under tension and compression

17 p2830 A71-35318

Three dimensional orthotropic elastic cylinders symmetric deformations under external loads, calculating stress-strain state with approximate method

19 p3155 A71-37528

Stability formula for critical pressure in cylindrical shells orthotropically reinforced by closely spaced eccentric ribs

22 p3616 A71-42487

Free elastic vibrations and waves in laminated orthotropic circular cylinders

24 p3878 A71-44561

ORTHOTROPIC PLATES

Thin elastic orthotropic plate in finite difference formulation, determining natural vibration mode and instability by summary representation method

01 p0168 A71-10410

Contact problems of orthotropic fiberglass-reinforced plastic plate with low shear rigidity

01 p0169 A71-10498

Orthotropic annular plates buckling, using finite difference equations and Vianello-Stodola iterative method

01 p0174 A71-10968

Corrugated membrane of nonuniform profile calculated as variable thickness orthotropic plate, considering corrugations deformation due to bending

02 p0329 A71-12640

Starting functions solutions for axially symmetric orthotropic annular plates

02 p0329 A71-12689

Elastic plate plane stress analysis by Euler variational method for arbitrary geometric shapes and loading, obtaining isotropic and orthotropic solutions

02 p0330 A71-12747

Book on laminated plate theory covering anisotropic continua, bending, orthotropic plates, energy equations, etc

02 p0330 A71-12844

Mechanical model for orthotropic elastoplastic plates with clamped torsion susceptible ribs

03 p0504 A71-13528

Rectangular and circular thin orthotropic plates thermal buckling approximate solution using Rayleigh-Ritz energy method

05 p0819 A71-15978

Uniform thin orthotropic skew flat plates free undamped vibration based on classical plate theory, using Rayleigh-Ritz method

05 p0820 A71-15987

Orthotropic plate dynamics, examining plane vibrations with group theory approximate equations

06 p0993 A71-17818

Free flexural vibrations of orthotropic rectangular plates subjected to large amplitude free or forced oscillations, using von Karman nonlinear equations

08 p1370 A71-21307

Laminated orthotropic plates under transverse loading, developing Navier type solution for Stavsky generalized stress function equation

09 p1534 A71-22101

Soviet book on problems in anisotropic body elasticity theory, covering orthotropic beams and plates torsion, bending, vibration, stability and boundary value problems, etc

09 p1542 A71-23438

Book on elastic plate theory covering bending and transverse shear effects, boundary problems, rectangular isotropic, structurally orthotropic, circular and annular plates under various loads

09 p1544 A71-23701

Flexural vibration analysis of rectangular isotropic and orthotropic polygonal elastic plates with constant or variable thickness, considering mass distribution and boundary conditions

10 p1625 A71-24019

Plane orthotropic bodies stress analysis by optical polarization method, using models consisting of anisotropic polymer plates fabricated from epoxy resins and woven fiberglass

10 p1690 A71-24573

Elastic properties of bonded orthotropic layer plates, finding good agreement with fiberglass reinforced plastic laminates

11 p1851 A71-26199

Thermal stresses in circular plate with cylindrical orthotropy and reinforced edge, determining temperature and stress distributions

12 p1979 A71-27356

Elastoplastic problem of stress concentration in orthotropic plate with circular notch under tension

12 p1982 A71-27517

Vibration transversely isotropic orthotropic plates, presenting approximate nonlinear dynamic theory

13 p2153 A71-28482

Nonlinear vibrations of clamped and edge supported laminated orthotropic plates, obtaining nonlinear equations of motion solutions by Ritz-Galerkin method

14 p2327 A71-30206

Elastic properties of orthotropic composite disks of fiber-reinforced materials, comparing actual stress in composite with permissible stress of fiber and matrix

14 p2329 A71-30472

German monograph on orthotropic plate equations derivation by kinematics and statics in general coordinates and elasticity relation

15 p2509 A71-32304

Method of producing transparent model composite materials for photo-orthotropic-elastic studies, allowing preparation of larger laminates

17 p2820 A71-34540

Axisymmetric nonlinear buckling equations for composite thin circular elastic plates of isotropic or orthotropic layers under radial compression

17 p2821 A71-34580

Orthotropic laminated plates dynamic response to impulse loads, detailing flexural wave propagation

17 p2823 A71-34809

Optimal design of locally orthotropic elastic flat bodies of fiber reinforced plastics or metals

17 p2763 A71-35620

Orthotropic annular plate plastic flow law, establishing yield conditions with plane stress-strain state equations

19 p3155 A71-37527

Stress analysis of rotating orthotropic disks mounted on elastic shafts, obtaining closed form solution for governing differential equations

20 p3308 A71-39088

Five-layer rectangular sandwich plate containing two soft orthotropic cores and three plate stiff isotropic layers

[ASME PAPER 71-VIBR-48] 21 p3459 A71-40297

Flexural vibration of rectangular orthotropic plates under in-plane hydrostatic forces

21 p3464 A71-40768

Nominal stress prediction for plastic tensile instability occurrence in flat orthotropic sheet loaded by biaxial stress system, considering localized and diffuse necking

21 p3469 A71-41005

Rectangular laminated orthotropic plates natural vibrations analysis, using extended Ritz technique

21 p3471 A71-41024

Buckling thermal gradients for rotating orthotropic annular plates under edge pull load

22 p3619 A71-42842

ORTHOTROPIC SHELLS

NT CYLINDRICAL SHELLS

Thermoelastic stresses in closed laminar orthotropic shells of revolution subjected to axisymmetric loads and temperature gradients

02 p0322 A71-11735

Laminar orthotropic cylindrical shell stress state under inversely symmetrical loading

02 p0322 A71-11737

Axisymmetric and unsymmetric free vibrations of orthotropic sandwich cylindrical or conical shells under various boundary conditions

02 p0325 A71-11999

Bending of thin elastic orthotropic shallow shells, taking into account large deflections, temperature distribution and material nonuniformities

02 p0325 A71-12288

Laminated cylindrical shells of orthotropic layers, deriving linear theory and equations of motion

03 p0504 A71-13430

Thin elastic orthotropic oval cylindrical shells nonlinear flexural vibration based on assumed modes, using Galerkin method

05 p0819 A71-15979

Orthotropic cylindrical shell stability under variable compression loads, considering glass fiber reinforced plastic tube

05 p0822 A71-16368

Moment loads and stress functions of orthotropic laminar shells with low shear rigidity

05 p0822 A71-16371

Orthotropic sandwich and homogeneous single layer circular cylindrical shells optimal design

05 p0822 A71-16419

Thin orthotropic shallow elastic shells with initial defects, analyzing critical pressure states

06 p0982 A71-17355

Circular cylindrical orthotropic fiberglass-reinforced shell buckling under longitudinal impact, assuming initial surface imperfections

06 p0985 A71-17684

Local distributed load effects on bending of fiberglass reinforced plastic laminar orthotropic cylindrical shell

06 p0986 A71-17761

Orthotropic shallow shells nonlinear theory, examining inverse bending problems

06 p0988 A71-17778

Eccentrically reinforced cylindrical shell stability, considering numerical analysis of structurally orthotropic shell parameters

06 p0993 A71-17817

Thin orthotropic shells thermocreeep in variable temperature field reduced to integration of linear partial differential equation system

06 p0997 A71-17852

Orthotropic shell with hollow elliptical paraboloid form, discussing numerical solution for normal concentrated load action

06 p0998 A71-17855

Asymmetric three layer cylindrical shells with orthotropic layers under deflection due to high temperature, deriving differential bending equations

07 p1217 A71-20456

Shallow orthotropic cylindrical shells with weak anisotropy, deriving equations for stress concentration at circular hole

07 p1217 A71-20457

Stability characteristics of glass fiber reinforced plastic orthotropic cylindrical shell with elastic filler under torsion

09 p1539 A71-22821

Optimal design parameters in minimization of reinforcement elements weight in cylindrical glass fiber reinforced orthotropic plastic shells under axial compression

09 p1539 A71-22826

Orthotropic shells of revolution with concentrated masses and oscillator inclusions and reinforced by stringers and ribs, calculating free vibration by Ritz method

10 p1690 A71-24570

Heterogeneous orthotropic cylindrical shells, calculating free natural vibration frequency spectra from refined equations of motion in Love and Donnell type theories

11 p1841 A71-25184

Orthotropic conical shell subjected to torsion, using Ritz approximate energy method for linear stability problem solution

11 p1848 A71-25618

Heat generation in hinged orthotropic viscoelastic cylindrical shells under transverse vibrations and cyclic surface load

12 p1978 A71-27343

Initial thermal stresses effect on natural vibrations of orthotropic cylindrical shells

12 p1979 A71-27360

Buckling of eccentrically stiffened multilayered circular cylindrical shells with different orthotropic moduli in tension and compression

12 p1982 A71-27572

Shear strength effect on axisymmetrical stress-strain state of orthotropic cylindrical shell subjected to nonuniform surface heating

13 p2148 A71-27825

Radial free vibration frequency of pressurized orthotropic shells with bending terms

14 p2325 A71-29886

Stability of structurally orthotropic stringer reinforced cylindrical shell closed by spherical or plane bottoms under uniform external pressure

14 p2333 A71-30892

Orthotropic layered cylindrical shells, deriving equations of motion for rotationally symmetric vibration

15 p2509 A71-32513

Buckling and postbuckling loads of initially imperfect orthotropic cylindrical shells under axial compression and internal pressure, using potential energy principle

16 p2651 A71-33025

Filament wound shell of revolution optimum configuration, deriving equations for orthotropic filament axes coincidence with principal stress trajectories

17 p2830 A71-35317

Variable thickness thin orthotropic spherical shell with hole, calculating stressed state with successive approximation technique

19 p3155 A71-37533

Interlaminar shear stress and midsurface displacement of thin orthotropic laminated cylindrical shells, using linear deformation theory

21 p3470 A71-41018

Orthotropic shells of revolution limit analysis, considering yield conditions and flow rules

22 p3614 A71-41605

Variational stress-strain equation for flexible shallow orthotropic multilayer shells with large deflections under normal pressure and contour loading

23 p3778 A71-44040

Stress-strain state of hinged thin multilayer orthotropic cylindrical shells with parameters variable with respect to directrix

24 p3881 A71-44828

ORTHOTROPISM

Unidirectional fiber reinforced orthotropic composite materials elastic constants calculation as function of two isotropic components characteristics

06 p1001 A71-18309

Failure theory for anisotropic homogeneous materials, discussing interaction factor, resistance, orthotropy and planar stress

07 p1214 A71-20011

Adhesive bonded joints mechanical behavior relation to materials, processes and experimental techniques, developing statistical analysis and formulas for orthotropic-elastic joints

10 p1614 A71-24087

Unbounded orthotropic body with two internal coaxial elliptical cuts, calculating elastic equilibrium

13 p2156 A71-29068

Mechanics of laminated filamentary composite orthotropic material used for cover skin in advanced aircraft component design

15 p2507 A71-32109

Orthotropic semiinfinite elastic solid under plane strain, calculating thermal stresses in terms of Green functions

[ASME PAPER 71-APM-18] 16 p2655 A71-33211

Orthotropic thin walled bars with rigidly connected rectangular elements, applying displacement under torsion with allowance for shear to H beam

17 p2823 A71-34782

Transverse waves propagation in vibrating orthotropic rectangular beams, noting inexact information regarding shear distribution

20 p3307 A71-39037

Three dimensional solution for statics and dynamics of homogeneous plates, laminates and orthotropic materials in series form, noting Mindlin analysis

21 p3456 A71-40262

OSCILLATING CYLINDERS

Circular cylindrical shell with trapezoidal stringers reinforcement system along length, calculating strain during oscillation

03 p0514 A71-14359

Hypersonic flow past freely vibrating hemisphere-cylinder-cone, noting Reynolds and Mach numbers dependence and conical stabilizer aperture angle

03 p0345 A71-14571

Thin cylindrical shell in ideal compressible fluid, calculating longitudinal resonance waves for acoustic excitation

06 p0985 A71-17755

Thin circular cylindrical shell thermoelastic vibrations, deriving differential equations of motion with allowance for shear, rotary and translational inertia

06 p0996 A71-17840

Torsional oscillation of hollow isotropic elastic cylinder encased in thin elastic shell, deriving representation satisfying equation of motion and initial and boundary conditions

09 p1539 A71-22918

Spring supported circular cylinder stability in wake flow of similar cylinder at various spacings using quasi-static aerodynamic derivatives and flutter theory

09 p1539 A71-22942

Vibrating cylindrical shell with circular plate, discussing bending moments, deflections and frequencies from Lagrangian

09 p1540 A71-23056

Cylinder vibration due to wake force in wind tunnel, discussing self exciting force induction

09 p1540 A71-23057

Elastic cylindrical shells oscillations and stability in inviscid incompressible liquid flow, reducing problem to integro-differential equation by Fourier integral transformation

10 p1688 A71-24357

Infinitely small flexural oscillations of initially stretched incompressible elastic circular cylinder, showing stretch effect on wave propagation velocity

10 p1689 A71-24521

Natural vibration analysis method for circular cylindrical shell based on three dimensional theory of elasticity and energy principle, discussing boundary conditions effect

11 p1852 A71-26405

Oscillation and stability of free composite body with elastically suspended masses, simulating liquid sloshing in cavity by equivalent mechanical model

14 p2321 A71-29537

Horizontal conducting fluid cylinder ultrasonic oscillations in crossed electric and magnetic fields, obtaining boundary value problem

14 p2278 A71-29614

Approximate method for nonlinear ordinary differential equations with variable coefficients applied to cylinder oscillation and flexible ring deformation

14 p2324 A71-29881

Stokes second problem solution, obtaining transient and steady state fluid flow pattern near cylinder executing harmonic rotational oscillations around axis

15 p2393 A71-32263

Unsteady viscous flow around oscillating cylinders, calculating fluctuating lift, drag and moment effects with Navier-Stokes equations

16 p2520 A71-33098

Oscillating circular cylinder wake fluctuating velocity measurement at low Reynolds numbers, using hot-wire anemometer

[ASME PAPER 71-APM-33] 16 p2520 A71-33196

Wake formation behind circular cylinders undergoing self excited and forced transverse oscillations

[ASME PAPER 71-VIBR-25] 21 p3458 A71-40282

Finite cylinder forced longitudinal axisymmetric vibrations with prescribed surface stresses, reducing problem to quasi-regular infinite system of linear algebraic equations

24 p3880 A71-44723

OSCILLATING FLOW

Hydraulic servomechanism with piston-type control valve, examining oil compressibility and sustained oscillations effects on system stability

01 p0007 A71-11378

Liquid sloshing frequencies in partially filled arbitrarily shaped vertical container

03 p0398 A71-13113

Cavity fluid oscillation near convecting field, calculating onset velocity as hydrodynamic stability problem

03 p0399 A71-13438

Boundary layer flow field exposed to oscillating stream, determining third term of Fourier series expansion

03 p0405 A71-14295

Gas flow past straight airfoil, analyzing damped natural oscillations

03 p0345 A71-14561

Two phase mixtures thermally induced flow oscillations, discussing scaling criteria, phase change numbers and stability boundaries

04 p0687 A71-15532

Plasmas and liquids inhomogeneous flow oscillations, determining resonance points effect on stability and oscillatory properties

05 p0790 A71-16825

Vertical circular cylindrical tank with shallow spherical shell bottom filled partially by ideal incompressible liquid, calculating joint oscillations

06 p0994 A71-17826

MHD oscillating flow along infinite unagnetized conducting plane porous wall, deriving temperature field in boundary layer

06 p0937 A71-18231

Wind tunnel experiments on vortex shedding from circular cylinders in oscillating free stream

07 p1090 A71-19908

Rocket fuel lines disruptive cavitation oscillations, considering rocket body mechanical vibrations and fuel line oscillation frequency characteristics

08 p1366 A71-21753

Concentration profile in incompressible viscous fluid flow across plane plate in oscillating motion, considering gravity diffusion

09 p1434 A71-23729

Single jet oscillations excitation of two resonant tubes, observing air motion with wool threads and stroboscopic lighting

10 p1591 A71-23823

Velocity distributions in axisymmetric air jets submerged in coaxial oscillating stream measured by hot-wire anemometer

11 p1748 A71-25156

Heat transfer to airfoil in oscillating flow at large angles of attack, showing vortex shed reattachment and Nusselt numbers increase

[ASME PAPER 71-GT-18] 11 p1703 A71-25963

Photospheric layers supergranular motion and oscillations as function of solar atmosphere height and sun position, investigating velocity fields two dimensional structure

12 p1970 A71-27701

Quasi-axisymmetric and superposed fine fluctuating structure of ideal incompressible vortex flows in axial flow turbines, assuming infinite mutual blade proximity

12 p1866 A71-27714

Propagation of 26-month oscillations in meridional component of wind velocity in stratosphere at extraequatorial latitudes from hydrothermodynamic equations solution

13 p2057 A71-28021

Nonzonal atmospheric motion effects on meteorological elements 26-month oscillations stability in equatorial zone from linear hydrothermodynamic equations

13 p2057 A71-28022

Laminar boundary layer separation by free stream with large amplitude oscillating velocity, using multiple hot-wire anemometer arrays

13 p2050 A71-29247

Numerical technique for two dimensional non-similar unsteady laminar boundary layer in oscillatory flow by integral matrix method

[ASME PAPER 71-FE-10] 13 p2052 A71-29451

True time averaged oscillating pressure measurements and testing in turbomachinery, including hydraulic, mechanical and evaluation methods

[ASME PAPER 71-FE-28] 13 p1995 A71-29464

Gas-filled spherical cavity in infinite compressible liquid, deriving radial oscillations by numerical solution

14 p2225 A71-30229

Velocity profiles of oscillating flow in wake of blunt based body, using finite difference solutions of vorticity transport and Poisson equations

[AIAA PAPER 71-603] 15 p2345 A71-31579

Incompressible laminar boundary layer on flat plate, calculating flow oscillation effect on time-mean heat transfer

15 p2513 A71-31929

Plasmas and liquids inhomogeneous flow oscillations, determining resonance points processes effect on stability and velocity

15 p2459 A71-32504

Incompressible viscous fluid flow between disks oscillating about state of rigid rotation, studying spin-up time effects

16 p2607 A71-32861

Isoperimetric problem upper bounds for fundamental frequencies in free oscillations of incompressible fluid in container

16 p2559 A71-33483

Liquid flow about oscillating flat plates, determining drag coefficient relationships to low Reynolds number and period parameter from graphical representation

18 p2902 A71-36033

Circular cylinder resistance in oscillating stream of second order fluid, calculating flow distribution

18 p2843 A71-36042

Kernel function for nonplanar oscillating surfaces in supersonic flow, using finite element method for interfering configurations

19 p2991 A71-37295

Unsteady burning rate response of condensed phase fuel plate adjacent to reacting gaseous boundary layer with oscillating external flow

19 p3123 A71-38095

Slide valve slot fluid flow oscillation frequency range estimate for quasi-stationarity

20 p3183 A71-39168

Oscillatory modes of perturbation in onset of flow instability for Newtonian liquid between concentric rotating cylinders with transverse pressure gradient

20 p3212 A71-39484

Second order viscous liquid pulsating flow superposed on steady laminar flow through circular pipe, examining non-Newtonian effects on flow characteristics

22 p3530 A71-41562

Oscillatory free convection laminar boundary flow from semiinfinite vertical flat plate, investigating surface temperature variations as distance function from leading edge

22 p3619 A71-41602

Velocity profiles of heavy viscous fluid free oscillatory motion in U-tube by hot-wire anemometry

22 p3531 A71-42242

Dynamic coupling response between convectively controlled burning process and nonsteady flow field with pressure, density and gas velocity periodic variations

23 p3782 A71-43593

Rocket fuel lines disruptive cavitation oscillations, considering rocket body mechanical vibrations and fuel line oscillation frequency characteristics

24 p3876 A71-44926

Perturbations generated by two dimensional supersonic channel flows with walls oscillating with harmonic time dependence and small pressure amplitude computed, using linearized method of characteristics

24 p3819 A71-44951

Unsteady gas pulsations in compliant tube, predicting pressure amplitude extremum as function of mean flow by linear theory with frictional effect

24 p3820 A71-45073

OSCILLATION DAMPERS

Shock absorber selection for reducing one dimensional oscillations of elastic linearly damped body on supporting base

01 p0127 A71-10633

Surface oscillations energy and attenuation in damped spectral region of semibounded degenerate electron plasma

02 p0288 A71-11630

Vibration dampers optimization, considering viscous and inelastic resistance effect on sensitivity of harmonically moving system response

03 p0503 A71-13409

Dual spin spacecraft high performance nutation damper, using wheel of uniform mass distribution

04 p0661 A71-15002

Oscillatory systems with nonlinear elastic arresting devices, calculating dynamic characteristics and motion stability

08 p1332 A71-20687

Magnetic damper motions in rapidly spinning satellite

09 p1533 A71-23140

Linear damping in piston type liquid damped accelerometers, using porous glass materials

09 p1451 A71-23173

Light aircraft longitudinal stability control systems, discussing downspring and bobweight effects on flight characteristics

10 p1555 A71-24252

- Linearized equations of motion for stability of dual spin satellite composed of platform, rotor, platform mounted damper and rotor mounted damper
11 p1837 A71-25514
- Semipassive and active nutation dampers in orbiting dual spin spacecraft, using single axis control moment gyro
13 p2144 A71-27976
- Acoustic absorbers for combustion instability prevention, discussing design theory and experimental results
[AIAA PAPER 71-699] 14 p2294 A71-30758
- Angular accelerometer with paddle torsion damper, comparing sensitivity with ordinary inertial instrument
17 p2739 A71-34562
- Vibration dampers optimization, considering viscous and inelastic resistance effect and sensitivity of harmonically moving system response
17 p2826 A71-35018
- German monograph on field effect transistors as controllable resistors with applications in adjustable amplifiers and dampers, covering nonlinear harmonic distortion and control dynamics
18 p2887 A71-35961
- Vibration control methods, discussing oscillation and acoustic noise reduction
19 p3069 A71-37518
- Vibrating systems behavior under combined parametric excitation and self oscillation mechanism, investigating damping and generation control
19 p3155 A71-37526
- Parameter optimization of linear time invariant nutation damper by second Liapunov method
20 p3306 A71-38853
- Damped isolation and undamped vibration absorber model for dynamic control, discussing frequency response and tuning and damping performance
[ASME PAPER 71-VIBR-45] 21 p3459 A71-40294
- High load structural dampers evaluation under linear or sinusoidal /triangular/ displacement control with constant speed testing machines
[ASME PAPER 71-VIBR-46] 21 p3459 A71-40295
- On-line digital dampometer for free oscillation wind tunnel model study under varying Mach number and stagnation pressure avoiding flutter destruction
21 p3363 A71-40391
- Instrument servomechanisms with spring-coupled inertial dampers, evaluating dimensional design parameters from analytical root locus
21 p3326 A71-40616
- Canonical transformations application to spinning satellite with nutation damper
[AAS PAPER 71-346] 23 p3728 A71-43019
- OSCILLATIONS**
NT ELECTRON OSCILLATIONS
NT H WAVES
NT HARMONIC OSCILLATION
NT MOLECULAR OSCILLATIONS
NT NONOSCILLATORY ACTION
NT PLASMA OSCILLATIONS
NT PRESSURE OSCILLATIONS
NT SELF OSCILLATION
NT STABLE OSCILLATIONS
NT TRANSIENT OSCILLATIONS
NT TRANSVERSE OSCILLATION
NT UNDAMPED OSCILLATIONS
NT WING OSCILLATIONS
- Saturn V second stage longitudinal oscillation from structure and propulsion system interaction examined by transfer function simulator subroutine /TRANSIM/ computer program
02 p0318 A71-11788
- Giant pulse laser emission stabilization, describing technique for eliminating short time oscillations in subnanosecond range
02 p0261 A71-12321
- Aircraft propulsive thrust moment effect on phugoid motion, examining angle of attack and flight path variations with resulting instability
03 p0347 A71-13340
- Limit cycle oscillations in satellite attitude control system, producing control moment by pulse modulated controller
03 p0499 A71-14074
- Oscillations of nonlinear system with conditions for main amplitude equations
05 p0780 A71-16179
- Detonation wave with finite reaction velocity interaction with rarefaction wave from behind, noting oscillations development associated with attenuation
05 p0834 A71-16511
- Perturbation method in nonlinear oscillations theory, using asymptotic recurrence formulas based on Lie transform
05 p0774 A71-16544
- Oscillation application to steady current in MHD generator to stabilize electrothermal instability
05 p0791 A71-16938
- Dynamic systems oscillation period doubling in presence of C bifurcations
05 p0782 A71-16985
- Soviet book on nonlinear almost-periodic oscillations covering application of integral equations method to differential equations, automatic control systems, pendulum motion, etc
06 p0926 A71-17443
- Hafnium droplets burning in ultrapure oxygen at various pressures, considering combustion induced natural mode periodic oscillations
[WSS/CIPAPER 70-14] 06 p0942 A71-17654
- Decaying oscillations of sensitive element in ground based gyrocompasses with suspension system permitting Euler angle and translational displacement
07 p1108 A71-19304
- Multimass system oscillations due to viscous friction factor and kinematic random disturbances, considering dynamic behavior of wheeled vehicle on rough roadbed
07 p1162 A71-20469
- Multiple magnetopause crossings in equatorial plane byOGO 5, showing magnetopause motion composed of two oscillations
08 p1282 A71-21631
- Soviet book on nonlinear systems oscillations covering analysis methods, periodicity, mathematical models, etc
08 p1335 A71-21657
- Polarization of LF oscillation branch of uniaxial ferrites in noncollinear phases analyzed by four column matrix, considering magnetic moments terminal points
09 p1507 A71-22291
- Pendulum oscillations under impact force in low resistance medium
09 p1494 A71-22875
- Spectral distributions of absorption cross sections of IR radiation by quasi-local oscillations
09 p1494 A71-22885
- Sampled data feedback control systems with neural pulse frequency modulation, deriving periodic oscillations existence conditions
09 p1424 A71-23387
- Body profile low frequency oscillations in transonic gas flow, investigating nonlinear differential equation boundary value problem by approximation method
10 p1550 A71-24363
- Proximal changes and stimulus patterns associated with rotation direction evoking visually perceived oscillation
10 p1570 A71-24606
- Sturm oscillation theorems for second order elliptic equation nonlinear partial derivatives, using linear Picone identity
11 p1791 A71-25176
- Free solid body carrying heavy pendulum, calculating oscillations as function of geometrical and inertial characteristics during motion under tangential force
12 p1929 A71-27117
- Sharp circular edged orifice dynamic characteristics under high amplitude periodic fluid flow conditions, discussing hydraulic resistance coefficients
12 p1898 A71-27506
- Hydrodynamic wave modes calculation for solar atmospheric model with ionization effects, noting trapped resonant gravity waves calculation agreement with observed oscillations
12 p1969 A71-27647
- Gunn diode operation at below threshold bias voltage, investigating microwave oscillations amplification
13 p2036 A71-27953
- French book on practical methods for nonlinear oscillations analysis covering linear and nonlinear systems, autonomous systems, forced harmonics, nonautonomous oscillating systems, etc
13 p2041 A71-28151
- Oscillations in system of nonlinear cubic response with narrow-band random excitation, using statistical linearization
13 p2101 A71-29077
- Singly ionized magnesium CW laser oscillation in He-Mg discharge at micron wavelengths with possible extension to visible and UV spectrum
15 p2420 A71-32386
- Nonoscillating and quasi-oscillating conditions of time optimal second order nonlinear control systems with piecewise-continuous right hand sides
15 p2382 A71-32620
- Magnetoelastic oscillations of thin conducting plate in magnetic field, solving electrodynamic equations
16 p2647 A71-32928
- Oscillatory systems motion by nonlinear differential equations with variable coefficients
17 p2781 A71-34924
- Functional analysis of nonlinear nonautonomous and autonomous periodic oscillations by treating equations and periodicity conditions for initial displacements and velocities as generalized operator equation
17 p2782 A71-34936
- Phugoid motion at constant angle of attack without thrust line displacement from aircraft center of gravity, noting longitudinal stability
21 p3324 A71-40168
- Signal quantization induced low amplitude oscillations in digital control systems, discussing relationship to digital controller programming form
21 p3361 A71-40980
- Second order rotational effects on stellar nonradial oscillations by perturbation method, taking into account equilibrium configuration distortion by coordinates transformation
22 p3602 A71-42173
- Angle of attack instrumentation for evaluating aircraft lift performance and phugoid oscillations
23 p3628 A71-43382
- Chebyshev polynomials computation of nonlinear oscillations of conservative autonomous system with single degree of freedom
23 p3777 A71-43493
- OSCILLATORS**
NT CRYSTAL OSCILLATORS
NT GYROSCOPIC PENDULUMS
NT HARMONIC OSCILLATORS
NT MECHANICAL OSCILLATORS
NT MICROWAVE OSCILLATORS
NT MOLECULAR OSCILLATORS
NT PENDULUMS
NT PHANTASTRONS
NT RELAXATION OSCILLATORS
NT SYNCHRONIZED OSCILLATORS
NT VACUUM TUBE OSCILLATORS
- Constant bandwidth FM subcarrier oscillators signal preemphasis for FM and PM transmitters
01 p0033 A71-10897
- Varactor-tuned Gunn diode oscillators, discussing computerized design, circuit analysis and device characteristics
01 p0054 A71-10974
- Upper frequency limit to mechanical tuning range of waveguide-mounted transferred electron oscillators due to transverse resonance
01 p0055 A71-11173
- Frequency stability of three-loop oscillator with time lag on coupling coefficient plane used for optimal circuit configuration
02 p0230 A71-11835
- Phase meter channels correlation effect on mean phase difference measurements accuracy in heterodyne oscillators
02 p0212 A71-11837
- Self excited cavity oscillators with tunnel and parametric diodes and nonequilibrium medium, noting single and multimodes, energy capabilities and frequency interactions
02 p0231 A71-11874
- Phase and amplitude fluctuations in oscillator circuits, determining power spectrum, disturbing voltage and current sources and step and impulse functions
03 p0383 A71-13168
- Frequency response characteristics of nonlinear oscillator circuits with inductive and complex capacitance couplings
03 p0379 A71-13812
- Transistorized displacement meter with variable frequency oscillator and inductive transducer as sensing element
03 p0387 A71-13816
- Fluidic acoustic signal detector for output determination of HF fluid oscillators, discussing performance, constant loading effect and signal amplitude
[ASME PAPER 70-WA/FLCS-7] 03 p0428 A71-14083
- Fluoroc oscillators as sensors for carbon dioxide concentration detection in exhaled breathing gases, noting frequency dependence on gas properties
[ASME PAPER 70-WA/FLCS-10] 03 p0372 A71-14086
- Gunn oscillator frequency characteristics vs displacement voltage in low Q factor resonance circuits
04 p0557 A71-14634
- Oscillator for guiding clock mechanism of 400 mm photographic telescope, using high stability transistorized multivibrator
04 p0591 A71-14847
- Automatic amplitude control of transistorized quartz clock master oscillator
04 p0592 A71-14860
- Linear theory of acoustoelectric oscillator with sandwiched piezoelectric plate accounting for mode enhancement and quenching
04 p0558 A71-15146
- Determinate phases formation mechanisms in unbalanced parametric oscillators, considering periodic shunting and bias modulation methods for oscillator starting
05 p0727 A71-16004
- Oscillator signal frequency instability relationship with spectral purity based on thermal noise effects
[ONERA-TP-912] 05 p0722 A71-16706
- Energy transfer between nonlinearly coupled oscillators described by Hamiltonian system in case of third order resonance
05 p0783 A71-16995
- Oscillatory systems slow monotonic motion due to carrying elements performing HF low amplitude relative oscillations
06 p0897 A71-17364
- Random Gaussian noise driven damped nonlinear oscillator, discussing Duffing equation, consolidated

expansions for response spectrum and common factors 06 p0926 A71-17499

Transferred electron devices (TED), reviewing physics of transferred electron effect, theory and design of amplifiers and oscillators 07 p1072 A71-19102

Compact microwave circuits for high efficiency operation of high power transferred electron oscillators 07 p1072 A71-19107

Thermal noise perturbed oscillator RF spectrum determination from frequency instability in time domain [ONERA-TP-927] 07 p1075 A71-19265

Hydrogen and deuterium oscillator strengths and transition probabilities for Lyman and Werner system individual bands by electronic dipole moment functions 07 p1164 A71-20019

Transistorized ultrasonic oscillator active conductances and other circuit parameters effects on self oscillation frequency stability 07 p1078 A71-20060

Monostable fluidic feedback oscillator analysis, using mathematical models describing function, feedback control theory and analog computer simulation to determine oscillation frequency 07 p1027 A71-20577

External feedback fluidic oscillators design and analysis using branched pneumatic transmission line arrangements 07 p1027 A71-20578

Volume variations detection by Hartmann air jet fluidic oscillator 07 p1030 A71-20602

Hysteresis effects during retuning of n-type GaAs Gunn oscillator with bias source and RLC circuit, showing range of domain damping by low field 09 p1414 A71-22228

Magnetically coupled tunnel diode oscillator with square loop core, calculating leakage and source inductances effect on switching pattern [IEEE PAPER 11.4] 09 p1416 A71-22593

HF stability audio multichannel oscillators design and operation, comparing frequency synthesizer systems for optimal circuitry characteristics 09 p1417 A71-23029

Stable single mode cavity resonators of high Fresnel number with increased fundamental transverse mode for carbon dioxide laser oscillators 09 p1466 A71-23727

Ionized argon laser optimum performance, comparing master oscillator power amplifier configuration to simple oscillator 11 p1772 A71-25141

Microwave tunnel diode oscillator, representing nonlinear characteristics with Taylor series 11 p1737 A71-25666

Tunable Gunn oscillator obtained by semiconductor surface loading, discussing oscillation frequency as function of anode to edge distance 11 p1738 A71-26365

InP pulsed and CW millimeter wave oscillators at frequencies above 30 GHz 11 p1739 A71-26367

IMPATT oscillators noise properties at large RF amplitudes, deriving expression for noise current as function of threshold current 11 p1733 A71-26369

Short term frequency stability of precision oscillators and frequency generators, discussing conversion from frequency to time domain and among time domain measures 11 p1739 A71-26422

Cavity controlled Gunn effect oscillators FM-current noise ratio, studying device current and domain capacitance as functions of carrier concentration and GaAs layer internal field 11 p1739 A71-26437

Energy calculation for oscillatory systems with nonlinear, hysteretic and parametric elements 11 p1743 A71-26537

Nonlinear hysteretic element narrow band resonant system operating in steady state at fundamental resonance 11 p1743 A71-26538

Equilibrium energy distribution in system of nonlinearly coupled oscillators 12 p1930 A71-27168

Nonlinear differential equations system for one degree of freedom isochronous and anisochronous conservative oscillators resonance behavior during natural perturbation solved by coordinate transformations 14 p2265 A71-29687

Automatic amplitude control dynamic performance of system with oscillating frequency determination by ring gain bandpass behavior 14 p2210 A71-29809

Passage through resonance of linear oscillator with slowly varying frequency, matching inner and outer asymptotic expansions 14 p2274 A71-29861

Two loop parametrically coupled oscillatory amplifier with unlimited degrees of freedom, investigating segment of long line loaded at one end with periodically varying capacitance 14 p2211 A71-30083

Random multiple access technique for satellite data collection, taking advantage of frequency instability associated with oscillator circuits 14 p2199 A71-30908

Jet edge tone sensor and internal feedback fluidic oscillator for temperature measurement, using dependence of sound speed in gas 15 p2352 A71-32065

Doubly resonant optical parametric oscillator frequency instabilities and threshold, studying non-resonant mode feedback effects 15 p2423 A71-32605

FM-PM conversion by frequency locking of free running Gunn oscillator 17 p2717 A71-35339

Self consistent one dimensional large signal analysis of Read type IMPATT diode oscillator, taking into account device-circuit interaction 18 p2888 A71-36130

Random noise effects on oscillator short term frequency stability and velocity measurement by Doppler effect 18 p2879 A71-36531

Energy transfer between nonlinearly coupled oscillators described by Hamiltonian system in case of third order resonance 18 p2948 A71-36795

Ultrashort pulse formation in short pulse stimulated Raman oscillator, achieving partial group velocity matching 19 p3071 A71-37475

Combustion oscillator for MHD energy conversion, using products flow modulation by traveling pressure wave 19 p2998 A71-38099

Dual input null networks application in RC feedback oscillators, examining frequency stability 20 p3206 A71-39915

Gunn effect devices properties and applications, discussing microwave energy sources tunable and local oscillators, parametric amplifier pumps and radar transmitters 21 p3357 A71-40819

Amplitude estimates and bounds derivation for nonlinear two parameter oscillators, obtaining iterative solution for computation 21 p3358 A71-41013

Gunn oscillator frequency characteristics vs displacement voltage in low Q factor resonance circuits 22 p3521 A71-42274

Determinate phases formation mechanisms in unbalanced parametric oscillators, considering periodic shunting and bias modulation methods for oscillator starting 22 p3524 A71-42753

Radio astronomic intercontinental base interferometry, discussing independent local oscillators requirements and atomic clock frequency standards 23 p3674 A71-43087

Current controlled diodes used as voltage variable capacitors in oscillators 23 p3652 A71-43832

OSCILLOGRAMS

U OSCILLOGRAPHS

OSCILLOGRAPHIS

Unsteady scattering patterns analysis, determining atmospheric extinction coefficient by reflected light oscillograms, formulas or signal amplitude time recording 09 p1487 A71-22385

Oscillographic determination conditions for Co, Ni, and Fe, giving statistical treatment of results 09 p1454 A71-22501

Piezoelectric transducer/oscillograph technique for simultaneously rating fuels knock properties and detonation intensity 13 p2113 A71-28228

Monograph on oscillographic high accuracy technique for phase angle measurement covering applications for harmonic generator phase control 14 p2243 A71-30237

Open singing flame from propane-butane and oxygen jet mixture, constructing oscillogram model of sound emission 17 p2839 A71-35696

Contactless oscillography of static and kinetic moments of friction in ball bearings in aggressive gas media, discussing experimental assembly design 22 p3529 A71-42489

Antenna impedance measurements using frequency sweep generator and oscillograph 24 p3810 A71-45127

OSCILLOSCOPES

Real time oscilloscope observation of ultrafast photodiode response to mode locked laser pulses 03 p0438 A71-13886

Boxcar integrator attachment for oscilloscopes, improving S/N ratio of repetitive signal 03 p0427 A71-13918

LF oscilloscope display of periodic subnanosecond optical pulses from mode locked lasers 05 p0761 A71-16334

Oscilloscope and automatically tuned superheterodyne receiver panoramic display units for 10 kHz-60 MHz, considering design, circuits, performance and mechanical arrangement 21 p3353 A71-40518

OSCULATORY INTERPOLATION

U ORBIT CALCULATION

U ORBIT PERTURBATION

OSEEN APPROXIMATION

Spheres Oseen drag, extending Goldstein expansion for Navier-Stokes equation in powers of Reynolds number 02 p0185 A71-12380

Numerical calculation of Oseen hydrodynamic fields around sphere in unbounded fluid for various Reynolds numbers, obtaining flow velocity and drag 10 p1592 A71-23935

Soviet book on MHD flow of incompressible electrically conducting fluid past bodies covering inviscid flows and viscous flows of Stokes and Oseen type 10 p1596 A71-24669

Steady Oseen flow past semiinfinite flat plate with force singularity, deriving integral equation solution 12 p1896 A71-26938

Time dependent analysis of swirling flow boundary layers in rotating container using modified Oseen method 21 p3367 A71-40639

Laminar viscous flow past semiinfinite flat plate to second Oseen type approximation, obtaining shear stress on plate 21 p3368 A71-40707

OSMIUM

Re and Os abundance and meteoritic contamination levels in Apollo 11 and 12 rocks, fines and breccia 23 p3750 A71-43696

OSMIUM ALLOYS

Intermediary eutectic phase in Ti-Os equilibrium diagram based on microstructural, X ray and differential thermal analyses 19 p3078 A71-37467

OSMOSIS

Emotionally induced osmotic pressure and thirst increase of rats during stress, noting eating behavior 02 p0201 A71-12875

Renal function osmoregulation in Soyuz crew members 06 p0854 A71-18370

Decompression urticaria response in subjects after inert gas breathing at constant ambient pressure, noting osmosis mechanism 08 p1246 A71-20813

Internal osmotic balance and stress induced body fluid osmolality changes due to food or water deprivation, reporting on experimental results with rats 08 p1240 A71-21750

Blood plasma hyperosmolality and pulmonary vascular resistance in cats, infusing hyperosmolar solutions of sodium chloride, mannitol, urea, glucose, thiourea and ethylene glycol 09 p1396 A71-23258

Body fluid osmolality control of food intake initiation in rehydrated rats injected with hypertonic sodium chloride solution 11 p1719 A71-26073

Capillary and electro-osmotic flow pumping in heat pipes, discussing capacity increase [AIAA PAPER 71-423] 11 p1857 A71-26214

Reverse osmosis application to wash water recovery in manned space mission life support systems, emphasizing membranes development [ASME PAPER 71-AV-1] 18 p2864 A71-36368

Potassium concentrations and osmolality levels changes effects on vascular resistance in subcutaneous adipose tissue blood flow 20 p3189 A71-39379

OSMOTIC PRESSURE

U OSMOSIS

OSO

NT OSO-E

NT OSO-F

NT OSO-G

NT OSO-3

OSO satellites observations, studying X ray flare phases, temperatures and spectra 17 p2808 A71-35521

Far UV solar spectra observations, using OSO-2, 4, 5 and 6 spectroheliograms 19 p3136 A71-37614

Trap states existence in OSO type satellites, considering damping mechanism and computer results 23 p3773 A71-44092

OSO-E

Solar Lyman alpha emission line monitoring by OSO 5 satellite during 1969, noting solar activity effects 16 p2643 A71-33938

Lightning observation by OSO-E satellite, suggesting maximum thunderstorm incidence over North Atlantic Ocean 19 p3061 A71-38675

OSO-F

OSO-6 measurements of gegenschein, comparing relative sky brightness data with ground based observations 18 p2966 A71-36766

OSO-G

OSO-G satellite instrumentation for solar and celestial X ray detection, exploring spectral distribution, temporal intensity variations, sources and atmospheric albedo 13 p2070 A71-29135

OSO-3

Hard solar X-ray spectra measurements, reinterpreting OSO 3 scintillation counter response due to pulse pile-up 02 p0302 A71-12766

Diffuse cosmic X ray observations, discussing balloon and OSO-3 data 09 p1514 A71-22934

OSO-4

OSO 4 satellite small grazing incidence monochromator as monitor for flux variations in solar He II Lyman alpha line ionizing radiation source 05 p0748 A71-16251

OTOLARYNGOLOGY

Physiopathological and otolaryngological repercussions of supersonic flight on SST passengers 03 p0371 A71-13098

Soyuz 9 spacecraft astronauts otorhinolaryngological organs response to 18-day orbital flight, observing pathological changes from clinical post flight examination 09 p1389 A71-22207

OTOLITH ORGANS

Extraterrestrial vestibular research, discussing geocentric and heliocentric otolithic regulation and gravitation theory 04 p0542 A71-14759

Ocular counter-rolling as otolith organ function indicator 04 p0542 A71-14761

Labyrinth destruction, Meniere disease, labyrinthectomy and vestibular neuritis effects on eyes counter-rolling, discussing otolith organ damage determination 04 p0537 A71-14762

Sodium bicarbonate intravenous effects on cat and rabbit otolithic reactions to accelerations and motion 06 p0861 A71-18375

Linear acceleration effects on human otolithic and vestibular apparatus, discussing vestibulovegetative motion sickness syndrome and nystagmus index activation 08 p1242 A71-21956

Centrifugal force effect on pigeon head nystagmus, acting on semicircular canal via otoliths or cupula 09 p1388 A71-22123

Semicircular canal influence on otolith reactions in pigeons, noting caudal and rostral shifts evoking levator and depressor coccygei contractions during horizontal acceleration 09 p1390 A71-22214

Functional anatomy of vertebrate gravity receptor system in spatial orientation, discussing otolith organs, sensory cells and hair cell topography in elasmobranch labyrinth 21 p3327 A71-39994

Semicircular canal and otolithic organ function in free swimming fish angular orientation behavior 21 p3328 A71-39996

OUTER PLANET MISSIONS

U GRAND TOURS

OUTER PLANET SPACECRAFT

U OUTER PLANETS EXPLORERS

OUTER PLANETS EXPLORERS

Unmanned scientific missions to outer planets in late 1970s, discussing instruments requirements, flight paths, spacecraft designs and payloads 04 p0649 A71-15347

Thermionic reactor electric propulsion for unmanned outer planets exploration, discussing spacecraft design, launch vehicle, weight factors, etc [AIAA PAPER 70-1122] 09 p1492 A71-22914

Thermionic reactor electric spacecraft propulsion system for unmanned outer planets missions, investigating voltage and radiator temperature effects on weight 11 p1811 A71-25872

Radioisotope thermionic power supply for unmanned electric propulsion missions to outer planets, using 69 modules consisting of thermionic converter and emitter heat pipe 11 p1811 A71-25897

High energy fast Grand Tour multiplanet flyby missions to outer planets omitting Jupiter, noting identical arrival date at Neptune 12 p1958 A71-26697

Pioneer F spacecraft investigation of Jupiter regions and outer interplanetary space, discussing design, communication system and possible future missions 12 p1973 A71-27603

Jupiter, Saturn, Uranus and Neptune space missions, discussing acceleration constraints, time, radio 12 p1973 A71-27603

communication, navigation and control of grand tour spacecraft 13 p2141 A71-29085

Spacecraft system design with long life reliability for outer planet exploration missions 17 p2814 A71-35428

Outer planets Grand Tour spacecraft onboard optical guidance instruments, discussing vidicon and image disector systems designs [AIAA PAPER 71-945] 19 p3098 A71-37186

Jupiter orbiters and probes noting objectives, spacecraft design and mission descriptions [AAS PAPER 71-103] 19 p3152 A71-37905

Pioneer Jupiter probe missions as precursor to subsequent outer planets exploration, discussing primary objective of asteroid belt and Jupiter radiation belt hazards evaluation [AAS PAPER 71-111] 19 p3152 A71-37911

Shuttle/Centaur injection stage, considering application to comet rendezvous mission via Jovian powered swingby [AAS PAPER 71-113] 19 p3139 A71-37912

Onboard approach guidance instrument for Grand Tour to outer planets missions reducing fuel for corrective maneuvers by estimating trajectories [AAS PAPER 71-119] 19 p3101 A71-37914

Onboard silicon detector TV guidance sensor for establishing outer planet mission spacecraft orientation with precise targeting, based on patched conic trajectory simulation [AAS PAPER 71-120] 19 p3101 A71-37915

Terminal guidance sensing from spinning spacecraft in swingby mission to outer planets [AAS PAPER 71-121] 19 p3101 A71-37916

Planetary quarantine constraint effect on multiple outer planet missions, considering navigation error sources and midcourse maneuvers [AAS PAPER 71-122] 19 p3002 A71-37917

Magnetic field measurements on Outer Planets Grand Tour to yield solar system origin and evolution and interstellar medium data [AAS PAPER 71-123] 19 p3139 A71-37918

Outer planets missions combined zodiacal experiment, examining meteoric, asteroidal and satellite particles distribution and orbits [AAS PAPER 71-127] 19 p3064 A71-37919

IR experiments planning for Outer Planets Grand Tour including investigations of planetary radiation balance and atmospheric composition and satellites composition and physical properties [AAS PAPER 71-131] 19 p3011 A71-37920

Mission analysis for multi-planet flyby and major satellites close encounter to determine solar system planetary evolution data, presenting Grand Tour trajectory parameters [AAS PAPER 71-137] 19 p3139 A71-37922

Grand Tour spacecraft configuration design involving system requirements, communications, power, guidance, etc [AAS PAPER 71-149] 19 p3152 A71-37924

Skewed and orthogonal redundant reaction wheels comparison for outer planet exploration spacecraft attitude control based on reliability analysis [AAS PAPER 71-157] 19 p3101 A71-37926

Balanced terrestrial and outer planets NASA solar system exploration strategy for 1970s, outlining earth based observations and flight missions program [AAS PAPER 71-100] 19 p3140 A71-37930

Pioneer F/G spacecraft Jupiter missions, trajectories and objectives with relation to outer system [AAS PAPER 71-101] 19 p3140 A71-37931

Multipoint gravity assist grand tours in outer solar system, discussing launch opportunities and mission effects on spacecraft design [AAS PAPER 71-102] 19 p3140 A71-37932

Outer planet exploration spacecraft subsystems reliability and ten year flight requirements for planet orbiting and flyby missions [AAS PAPER 71-112] 19 p3140 A71-37934

Outer planets combined orbiter/flyby missions, investigating single launch feasibility with INT-20/Centaur launch vehicle [AAS PAPER 71-114] 19 p3140 A71-37935

Navigation error sources and orbit determination accuracies for Jupiter planetary encounter, using earth based radio tracking data [AAS PAPER 71-118] 19 p3101 A71-37937

Plasma ion and electron distribution functions measurement on outer planet missions [AAS PAPER 71-124] 19 p3114 A71-37938

Plasma wave instrument for measuring AC electrical and magnetic field levels in outer planets missions [AAS PAPER 71-125] 19 p3064 A71-37939

Cosmic rays and solar energetic particles properties near earth and requirements on measurement during outer planets missions [AAS PAPER 71-126] 19 p3127 A71-37940

Outer planet satellite missions for optimal imaging conditions in terms of proximity and lighting [AAS PAPER 71-138] 19 p3140 A71-37942

Outer planets atmospheric entry vehicles at atmospheric heating, discussing shock and boundary layer physical and chemical effects [AAS PAPER 71-144] 19 p3163 A71-37947

Graphitic ablative heat shield fractions and forebody configurations for probe entry into atmospheres of Saturn, Uranus and Neptune [AAS PAPER 71-145] 19 p3141 A71-37948

Jupiter entry probe integration on TOPS and Pioneer outer planet spacecraft for flyby missions, discussing design feasibility and spacecraft modification requirements [AAS PAPER 71-153] 19 p3153 A71-37955

Parts qualification and acceptance for outer planet mission spacecraft, minimizing random and wear-out failures to meet weight and other constraints [AAS PAPER 71-161] 19 p3153 A71-37958

Multihundred watt radioisotope thermoelectric generator for JPL outer planet missions, discussing vacuum/xenon filled performance and response to thermal/electrical transients 20 p3263 A71-38926

Performance tests of high temperature silicon-germanium alloy thermoelectric generator for outer planet mission spacecraft 20 p3264 A71-38928

Dust environment estimation in asteroid belt during trans-Martian spacecraft missions, considering cosmological, dynamical and observational evidence 20 p3297 A71-39633

Outer planet explorers design for Grand Tour mission, discussing launch parameters, flight paths, environmental hazards, communications, ground control, navigation and power generation 22 p3601 A71-42028

Radiation effects on components of science instruments used on outer planets Grand Tour mission 22 p3574 A71-42299

Nuclear characteristics of plutonium fuel for thermoelectric generators and required shield thicknesses for sensitive radiation experiment in outer planet spacecraft 22 p3592 A71-42300

Planetary quarantine constraint on 1977 Jupiter-Saturn-Pluto mission, determining fuel loading penalties, optimum biasing strategies and outer planet navigational characteristics [AAS PAPER 71-319] 23 p3726 A71-42993

Bi-injection earth departure mode analysis for combined flyby/orbiter Jupiter-Saturn-Pluto and Jupiter-Uranus-Neptune Grand Tour missions [AAS PAPER 71-322] 23 p3726 A71-42996

Multiple outer planets flyby opportunities during 1976-1980 Grand Tour missions launch period, presenting computer generated specific encounter dates and flyby distances [AAS PAPER 71-359] 23 p3729 A71-43029

Graphic mission analysis for outer planet missions, considering spacecraft and celestial bodies relative positions, sensor and spacecraft relative orientation [AAS PAPER 71-378] 23 p3731 A71-43048

Solar system escape trajectory analysis for Jupiter-Saturn-Pluto and Jupiter-Uranus-Neptune Grand Tour missions, presenting flyby characteristics and heliocentric postencounter directions [AAS PAPER 71-383] 23 p3731 A71-43053

OUTER RADIATION BELT

Geomagnetically trapped C, N and O nuclei and alpha particles in earth outer radiation zone, noting acceleration and loss mechanisms 01 p0075 A71-11496

Directional differential energy spectra for proton intensities in outer radiation zone near magnetic equator from satellite observations 06 p0949 A71-17261

Magnetospheric convection and polar wind influence on outer radiation belt energetic electron loss, subjecting previously large fluxes of lower energy electrons to trapping limit 07 p1186 A71-19661

Earth outer radiation belt electrons intensity, differential energy spectra and radial diffusion during maximum solar activity 10 p1663 A71-24783

Geomagnetically trapped protons differential energy spectrum in Van Allen inner and outer radiation belts over various energies, using thin solid state detector 10 p1663 A71-24784

Outer radiation belt energetic electron flux intensity correlation with auroral activity and Kp index 11 p1816 A71-25760

Cyclotron instability of outer radiation belt under growing waves self modulation conditions, describing discrete signals production by continuous excitation 13 p2128 A71-28171

Electron and proton precipitation observations in auroral, polar cap and outer radiation zones by electrostatic analyzers on earth satellite Injun 5 15 p2397 A71-37156

Outer radiation belt energetic electron flux intensity correlation with auroral activity and Kp index 22 p3591 A71-41528

Outer radiation belt parameters dependence on interplanetary magnetic field sectorial structure and solar wind velocity 24 p3866 A71-45039

OUTGASSING

Outgassing of multilayer insulation materials for use in cryogenic fuel tanks

03 p0522 A71-14441

Computerized outgassing analyzer for nuclear rocket graphite fuel elements at various temperatures in vacuum

05 p0780 A71-16243

Mo and W residual outgassing partial fluxes, considering process duration and impurities identification

05 p0754 A71-16947

Gas pressure conversion for spacecraft outgassing products investigation by mass spectrometer analysis, noting plastic decomposition products calibration

07 p1023 A71-20067

Hydrogen outgassing from proton irradiated aluminum samples, determining gas evolution and blister formation during annealing

07 p1139 A71-20173

ESRO 1 satellites space simulation chamber tests for residual gas effects, measuring spacecraft outgassing rate

09 p1533 A71-23732

Transient pressures in spacecraft and volume compartments with outgassing for ambient pressure decrease and low pressures unattainable with large chambers

11 p1840 A71-26398

Thermal analysis-quadrupole mass spectrometric analyses on inorganic released gases of Apollo 11 and 12 samples and synthetic lunar analogs

23 p3750 A71-43699

Active and inert gases released by crushing Apollo 11 and 12 samples at room temperature and by low temperature heating

23 p3751 A71-43701

OUTPUT

NT LASER OUTPUTS

NT MASER OUTPUTS

Matched filter output response computation for combined Barker codes, considering Doppler mismatch

04 p0551 A71-15013

OV-1 SATELLITES

High drag satellite 1968-59A orbits from optical and radar observations, obtaining rotational speed of upper atmosphere

03 p0407 A71-13305

Subprotonospheric and ion cyclotron whistlers generated by same lightning discharge observed by OV1-10 satellite

06 p0869 A71-17995

OV-3 SATELLITES

Semiannual atmospheric density variation measurements by OV3-6 satellite

16 p2570 A71-33821

OVENS

Reflecting oven for very high temperatures under gas pressure, describing apparatus, heat source and possible contamination

10 p1613 A71-25040

OVERCAST

U CLOUD COVER

OVERESTIMATION

U ESTIMATING

OVEREXPOSURE

U RADIATION DOSAGE

OVERPRESSURE

Plane compression waves propagation into constant state nonviscous fluid, considering shock formation of pressure pulses and overpressure as function of time

07 p1091 A71-19961

Wind tunnel stability tests of wing with different blowing nozzle arrangements on bottom overpressure surface at 18 and 30 m/sec air speeds

09 p1384 A71-23663

Sonic booms loudness as function of peak overpressures and rise times, using semiempirical formulae

21 p3325 A71-40530

OVERTONES

U HARMONICS

OVERVOLTAGE

Nonequilibrium Ar-Cs plasma under rectangular pulse overvoltage, analyzing ionization and recombination kinetics

02 p0289 A71-12177

Oxygen reduction on Teflon bonded Pt electrodes, eliminating concentrated overvoltage

02 p0210 A71-12955

Nonequilibrium Ar-Cs plasma under rectangular pulse overvoltage, analyzing ionization and recombination kinetics

15 p2454 A71-31486

OXALIC ACID

Solid and fluid states oxalyl fluoride vibrational spectra and structure

14 p2191 A71-30575

OXAMIC ACIDS

IR spectra of oxamide and dithiooxamide, studying Raman spectrum in LF range

23 p3642 A71-43825

OXAZOLE

Emission spectra of solutions of oxazole and adiazole derivatives and of tetraphenylbutadiene as effective active media for liquid phase lasers

11 p1774 A71-26001

OXIDASE

Low temperature effects on succinate oxidase activity of mitochondrial membranes in hibernating squirrels

21 p3336 A71-40854

OXIDATION

NT ELECTROCHEMICAL OXIDATION

Double beam monochromatic differential cinespectrophotometer for recording oxidation/reduction reactions in intercellular pigments

01 p0021 A71-10243

Initial surface superheating effects on high temperature oxidation of titanium in oxygen or dynamic air atmosphere

01 p0101 A71-10672

Oxygen diffusion coefficient during metal Ti/oxidation in unsteady high temperature region, allowing for interfacial phase boundary shift

01 p0101 A71-10673

Redox estimation from natural phase Eu ion concentrations in rocks

01 p0029 A71-11428

Austenitic Cr-Ni-Nb stabilized steel, evaluating high temperature oxidation and creep process interaction

01 p0104 A71-11603

Carbon fiber surface treatment for reinforced plastic composites interlaminar strength increase, using wet oxidation process based on hypochlorous acid

02 p0274 A71-12485

Nb surface contamination by oxidation during electrolytic polishing and vacuum annealing

02 p0269 A71-12928

Pure Nb vs Nb alloy oxidation behavior, discussing oxide phases, formation temperature and exposure time

02 p0271 A71-12940

Kinetic, morphological and crystallographic effects of Nb crystals oxidation during growth at various temperatures and pressures

02 p0272 A71-12948

Surface oxidation kinetics of iron by solid electrolyte techniques, comparing weight gain method

03 p0374 A71-13122

Vaporization chemistry in C, Si, Cr, Mo and Nb high temperature oxidation, using thermodynamic diagrams

03 p0374 A71-13123

Soviet book on oxidation in Ti and Ti alloys covering physical, chemical and crystallographic characteristics of Ti-O system, Ti component manufacture, etc

04 p0612 A71-15374

Ellipsometric observation of Ni optical properties changes relation to oxygen absorption, considering correctness of oxidation data

04 p0613 A71-15695

Presulfidized Ni alloys and Cr oxidation rates

04 p0615 A71-15787

Fe-Ni alloy oxidations parabolic kinetics and activation energies, noting scale development as function of oxidation amount and temperature

05 p0770 A71-17098

Single layer graphite oxidation kinetics evaluated by electron microscopy, discussing removal rate

06 p0915 A71-17302

Ti alloy deformation through surface oxidation at elevated temperature, considering lattice parameter and alpha concentration effects

06 p0913 A71-18677

Rats and mice blood redox potentials injected with cystamine, investigating increased radioprotection

07 p1039 A71-18980

Vitamin K3 effect on redox equilibria in red cell, discussing radiosensitizer mechanism

07 p1039 A71-18985

Zirconium droplet combustion in oxygen-rare gas mixtures, observing transient burning phenomena, oxidation conditions and luminosity-time records

07 p1223 A71-19623

Oxidative and hydrolytic enzymes localization in rhesus monkey brain, investigating glutaraldehyde fixation effect with histochemistry

07 p1042 A71-20017

Co oxidation rate measurements over temperature range 475-1325 C at various oxygen pressures, determining oxide formation kinetic law and activation energy

07 p1139 A71-20225

Phase equilibria, microstructure and physical properties of high temperature vacuum sintered oxygen deficient zirconia and thorium

08 p1304 A71-20697

MnO oxidation reduction kinetics measurement in carbon monoxide/dioxide atmospheres by gravimetry and electrical conductivity

08 p1318 A71-20698

X ray analysis of oxide film structure, oxygen concentration and residual stresses at surface of oxidized Ti and Ti alloy

08 p1317 A71-21760

Oxidation/vaporization kinetics of chromium oxide hot pressed and sintered pellets

09 p1480 A71-22113

Mo, W and Zr effects on niobium reaction with residual gases during heating in vacuum

09 p1469 A71-22846

Molybdenite oxidation kinetics by thin layer technique with close temperature and gas composition control, measuring temperature, gas composition and particle size effects

09 p1472 A71-23128

Nb-Ti alloy oxidation kinetics at various temperatures and pressures, noting linear patterns and oxide formation

10 p1626 A71-24403

Reaction rate controlling mechanisms in shock wave initiated oxidation of formaldehyde

13 p2113 A71-28617

Atomic Ba excitation, ionization and oxidation during release in sunlight at high altitudes

13 p2026 A71-29038

Nickel under diffusion controlled reactions at high temperatures, reviewing parabolic oxidation rate law

14 p2256 A71-29634

Hypersonic flight load bearing refractory alloy control surface protective coatings, emphasizing oxidation screening tests

14 p2262 A71-29646

Zirconium oxidation kinetics at 500-1200 C under low oxygen pressure

14 p2257 A71-29843

Adsorption states of Mo and Re surfaces during oxidation at low oxygen pressures and temperatures up to 2300 K, using noble gas molecular beams

14 p2190 A71-30402

Metals bulk ignition temperature in oxygen atmospheres, emphasizing preignition surface oxidation effects

14 p2337 A71-30456

Methane high temperature oxidation in steady flow system, predicting change rate of species concentrations and gas properties during reaction

14 p2285 A71-30457

Oxidation kinetics of pure Al in dry oxygen as function of pressure and temperature, using manometric method

15 p2426 A71-31408

Ternary Co-Cr-Al alloy oxidation data, detailing kinetics, products, mechanisms, resistance behavior and rate

16 p2589 A71-32870

Oxidation kinetics and scale morphology of chromium oxide forming thoria and unthoria Ni alloys, discussing rate controlling processes effects

16 p2590 A71-32871

Prealloyed Al powder liquid phase sintering without precompacting, discussing oxidation and density control

18 p2928 A71-36667

High temperature oxidation of ammonia, carbon monoxide and methane by nitrous oxide in shock tubes, using optical interferometry and UV/IR emissions

19 p3012 A71-38086

Slow and explosive gas phase oxidation of carbon suboxide and monoxide over various pressure and temperature ranges, noting branching reactions

19 p3167 A71-38088

Calculation method for standard potentials and enthalpies of metals during oxidation and chlorination, representing molar functions dependence on temperature

19 p3082 A71-38153

Ta-W polycrystals and single crystals oxidation at 850-1100 C, noting anisotropic scale-fracture morphologies

20 p3252 A71-39373

Oxygen diffusion coefficient during metal/titanium/oxidation in unsteady high temperature region, allowing for interfacial phase boundary shift

21 p3401 A71-41054

Quasi-equilibrium prediction of rate of volatilization/erosion/ of solid tungsten by reaction with gaseous oxygen at high temperature and low pressure

21 p3404 A71-41419

Two temperature region oxidation of zirconium diboride, showing formation of continuous surface film and quadratic crystallized discontinuous layer

22 p3563 A71-42246

Monocrystalline and polycrystalline Ta-Hf oxidation at 750-1050 C, noting orientation

22 p3563 A71-42363

Oxidation of water in regeneration under spacecraft conditions, measuring organic impurities degree of oxidation in inhabited cabin atmospheric vapor condensates

22 p3506 A71-42814

X ray analysis of scale formation in precipitation hardened nickel, investigating thermal resistance and oxidation rates

23 p3691 A71-43520

Oxidation state of iron and cation distribution over M1 and M2 sites in clinopyroxenes from Apollo 12 by Mossbauer absorption spectroscopy, noting cooling history

23 p3738 A71-43609

Magnetic properties of glass spherules from Apollo 11 and 12 fines, determining oxidation effect

23 p3762 A71-43791

OXIDATION RESISTANCE

Composite Ni coatings, adding mullite crystals to enhance oxidation resistance

01 p0102 A71-10784

Nb alloys in hypersonic glider fabrication, discussing mechanical properties, oxidation resistance and sandwich panel design

02 p0270 A71-12935

Niobium aluminate pest, investigating oxidation effects on Nb-Al protective coatings from 600 to 1400 C

02 p0271 A71-12942

Nb oxidation protection by Ti or Cr modified silicide coating, noting results with various Cr-Si mixtures

02 p0272 A71-12944

Mechanical stability of self healing viscous glass layer in porous oxidation protection coating on Ni under high acceleration

02 p0272 A71-12945

Mechanical stability of liquid phase in porous oxidation protective coating on Ni turbine blades under acceleration

02 p0272 A71-12946

Structure and durability of self healing silicide based coatings for niobium oxidation protection at high temperatures

02 p0272 A71-12947

Organic compounds oxidation inhibition by polycyclic aromatic hydrocarbons, analyzing peroxide radicals charge transfer complex stability

05 p0716 A71-16382

Protective oxide formation on single phased Cu-Al-Si alloys during high temperature oxidation

05 p0770 A71-17099

Oxidation resistance of silica gel lubricants, noting optimum diphenyl amine inhibitor

06 p0916 A71-18470

Oxidation resistant Ni-Al intermetallic compounds as protective coating for high temperature nickel base superalloys

07 p1134 A71-19448

High temperature oxidation of Cr-Ti-Si coatings on Nb alloy

07 p1135 A71-19619

Multisample test equipment for steels and alloys oxidation resistance at high temperatures in corrosive gaseous atmospheres

08 p1292 A71-21440

High temperature alloys oxidation resistance and strength characteristics, considering influence of various alloying compositions via use of oxide mapping method

08 p1314 A71-21573

Ni-Cr-Al alloys high temperature oxidation resistance, studying effects of Cr/Al ratio and chemical composition

08 p1315 A71-21574

Al-Mg alloy oxidation, observing Be, B, Mo and Zr addition effects

09 p1468 A71-22656

High chromium Ni-Cr alloys use and improvement, discussing refractoriness in oxidizing atmospheres and chemical corrosion in combustion products deposits

09 p1470 A71-23043

Martensitic transformation in NiAl oxidation-resistant coatings on Ni superalloys heated for 300 hr at 1093 C

09 p1472 A71-23132

High temperature turbine parts protective coatings, discussing aluminum diffusion prevention and crack and oxidation resistance

09 p1456 A71-23290

High temperature oxidation protective coatings behavior, emphasizing jet engine applications

09 p1483 A71-23296

Graphite fiber reinforced ablative composites fabricated into rocket propulsion test units for oxidative liquid high temperature and pressure environments

09 p1459 A71-23685

Comparative isothermal oxidation of Fe-Cr-Al, Ni-Cr-Al and Co-Cr-Al alloys with protective scales

10 p1624 A71-23971

Manganese and silicon effects on oxidation and scale mechanisms of Co-Cr alloys, using thermogravimetric, metallographic and microprobe techniques

10 p1625 A71-23973

Thermal fatigue and service life of thin walled tubular pearlite steel notched specimens in various oxidizing media

10 p1626 A71-24191

Oxidation resistant high temperature Ni-Al system preparation using powder metallurgy and thermomechanical treatments without sintering

10 p1626 A71-24401

ABM control surfaces active oxidation protection, using ammonia as reactive coolant injected through porous W wall matrix

[AIAA PAPER 71-391] 11 p1837 A71-25353

Al anodizing processes, stressing modern theory of anodic oxidation and anodized Al corrosion

11 p1779 A71-26000

TD NiCr nickel based alloy high temperature oxidation control, discussing thoria dispersion effect on Ni-Cr oxidation properties

11 p1779 A71-26015

Oxidation and nitrogen absorption protection of Cr alloy by Ni alloy claddings applied by gas pressure bonding

13 p2087 A71-29122

High density polyethylene composition oxidation rates and photodegradation resistance data, using IR spectroscopy

14 p2261 A71-29641

Ternary Co-Cr-Al alloy oxidation resistant composition selection, using oxide maps superimposed on phase diagram

16 p2590 A71-32872

Mechanical properties, fracture and limited high temperature oxidation resistance of carbon fiber reinforced Ni composites

16 p2599 A71-34086

Niobium alloy use for space shuttle thermal protection, examining oxidation and mechanical properties

17 p2757 A71-34495

High temperature oxidation protection of niobium by molybdenum disulfide coatings applied by hot pressing powder metallurgy method

18 p2934 A71-35952

Thermal stability and oxidation and corrosion resistance of lubricating oil based on trimethyl propane ester

[ONERA-TP-930] 18 p2939 A71-36016

Chromium sesquioxide instability towards oxygen at high temperature, using spring thermobalance

18 p2937 A71-36763

Refractory diborides in oxidizing environments, considering mechanical strength, thermal stability, oxidation resistance, heat conductivity, thermal expansion, specific heat and electrical resistance

21 p3405 A71-40138

Oxidation resistance and scale fracture healing by Al additions to Co-Cr alloys at high temperatures, using electron probe and scanning electron microscope analyses

21 p3405 A71-41420

Sodium role in accelerated oxidation behavior /sulfidation/ of Ni-base superalloys and binary alloys coated with sodium sulfate or carbonate

23 p3695 A71-44288

Steel silicification in liquid media for high temperature oxidation resistance improvement

24 p3829 A71-44731

Free radical induced high temperature oxidation degradation curtailment of polyphenyl ethers by oxides, hydroxides and carbonates of alkali metals and Ba

[ASLE PREPRINT 71LC-11] 24 p3842 A71-45290

OXIDES

NT ALUMINUM OXIDES

NT ANHYDRIDES

NT BARIUM OXIDES

NT BERYLLIUM OXIDES

NT BISMUTH OXIDES

NT CALCIUM OXIDES

NT CARBON DIOXIDE

NT CARBON MONOXIDE

NT CHLORINE OXIDES

NT CHROMITES

NT CHROMIUM OXIDES

NT COBALT OXIDES

NT COESITE

NT COPPER OXIDES

NT ENSTATITE

NT HAFNIUM OXIDES

NT HEAVY WATER

NT HYDROGEN PEROXIDE

NT ILMENITE

NT INORGANIC PEROXIDES

NT IRON OXIDES

NT LANTHANUM OXIDES

NT LEAD OXIDES

NT LITHIUM OXIDES

NT MAGNESIUM OXIDES

NT MAGNETITE

NT MANGANESE OXIDES

NT MERCURY OXIDES

NT METAL OXIDES

NT MOLYBDENUM OXIDES

NT MUSCOVITE

NT NICKEL OXIDES

NT NIOBIUM OXIDES

NT NITRIC OXIDE

NT NITROGEN DIOXIDE

NT NITROGEN OXIDES

NT NITROGEN TETROXIDE

NT NITROUS OXIDES

NT PEROXIDES

NT PHOSPHORUS OXIDES

NT POTASSIUM OXIDES

NT PYROXENES

NT QUARTZ

NT RUTILE

NT SAPPHIRE

NT SCANDIUM OXIDES

NT SILICON DIOXIDE

NT SILICON OXIDES

NT SILVER OXIDES

NT SODIUM PEROXIDES

NT SULFUR OXIDES

NT TANTALUM OXIDES

NT THORIUM OXIDES

NT TIN OXIDES

NT TITANIUM OXIDES

NT TUNGSTEN OXIDES

NT URANIUM OXIDES

NT VANADIUM OXIDES

NT YTTRIUM OXIDES

NT ZINC OXIDES

NT ZIRCONIUM OXIDES

Soviet book on oxide and silicate materials chemistry and technology covering corrosion, thermophysical properties shear stress, drying, etc

02 p0272 A71-11825

Oxide bronzes as oxygen reduction catalysts in batteries and fuel cells, considering effects of varying compositions and crystal faces

03 p0374 A71-13054

Apollo 11 and 12 lunar rock opaque oxides differences in titanium contents

05 p0807 A71-16298

Thin oxide films on solution grown single crystals of cubic beta-silicon carbide, discussing physical and electronic properties measurements

07 p1177 A71-19571

Oxide films effect on heat resistant steels hydrogen permeability, using mass spectrometer

07 p1136 A71-19920

Carbon suboxide polymers formation in Martian atmosphere, examining carbon monoxide photolysis and radiolysis processes enhanced by solar ionizing radiation

15 p2491 A71-32420

Energy spectrum parameters from Burstein-Moss effect observation in thin CdO layers, explaining absorption edge shape at various electron concentrations

16 p2622 A71-34029

Slow and explosive gas phase oxidation of carbon suboxide and monoxide over various pressure and temperature ranges, noting branching reactions

19 p3167 A71-38088

OXIDIZERS

NT LIQUID OXIDIZERS

NT LIQUID OXYGEN

NT ROCKET OXIDIZERS

Diffusion controlled combustion of liquid fuel droplet in oxygen-steam oxidizer mixture

03 p0468 A71-13996

Jet engine liquid fuel wall layer combustion stimulation by repeated oxidizer injection into supersonic section of nozzle

03 p0472 A71-14256

Flame propagation along interface between fuel slab /polymers, aluminum and tungsten powders/ and oxidizer slab /inorganic salts and oxides/

03 p0521 A71-14278

Heterogeneous detonation propagation in mixture of liquid fuel droplets suspended in gaseous oxidizer, discussing droplets disintegration time and shock wave parameters

10 p1698 A71-25124

Fast burning rates in thin film solid composite propellants composed of McCormick-Selph 510, 164 monopropellant, oxidizer and polyvinyl chloride binder

[AIAA PAPER 71-655] 14 p2285 A71-30730

High density nitric acid oxidizer and unsymmetrical dimethyl hydrazine with silicone fluid additive application to Agena rocket engine for higher performance

[AIAA PAPER 71-736] 14 p2287 A71-30781

Al and Mg powder dispersed in solid ammonium perchlorate oxidizer, investigating various combustion mechanisms

19 p3120 A71-38120

Shock tube investigation of solid polymeric hydrocarbon fuel ignition in hot oxidizing gas stream

19 p3121 A71-38124

OXYACETYLENE

CH free radicals detection in oxyacetylene flame magnetic resonance absorption spectrum by IR water vapor laser

15 p2420 A71-32380

OXYGEN

NT HIGH PRESSURE OXYGEN

NT LIQUID OXYGEN

NT OXYGEN ATOMS

NT OXYGEN ISOTOPES

NT OXYGEN 18

NT OZONE

Initial surface superheating effects on high temperature oxidation of titanium in oxygen or dynamic air atmosphere

01 p0101 A71-10672

Relaxation method for direct measurement of molecular oxygen quenching rate constants in discharge flow system

02 p0287 A71-12493

Oxygen reduction on Teflon bonded Pt electrodes, eliminating concentrated overvoltage

02 p0210 A71-12955

Mixed venous oxygen tension oxide determination by nitrogen-carbon rebreathing method, considering pulmonary blood flow and oxygen carrying capacity

03 p0360 A71-13182

Chemisorption layer kinetics of oxygen on thin Ta films at room temperature and low pressures

03 p0441 A71-13359

Earth atmosphere origin, discussing oxygen and carbon dioxide balance

03 p0409 A71-13697

Hydrogen-oxygen induction period kinetics behind shock waves, monitoring OH concentration by UV line absorption method

03 p0376 A71-14276

Alpha titanium-oxygen solid solutions surface structure, using low energy electron diffraction for determination of order-disorder transition and superlattice reflections

04 p0610 A71-14895

Ultrahigh vacuum deposited Ni, Fe, W and Mo films, determining molecular oxygen adsorption efficiencies

04 p0636 A71-15015

Oxygen molecule vibrational excitation by electron impact, measuring elastic and inelastic processes

04 p0630 A71-15653

Oxygen solubility and activity in Fe-Al and Fe-Ti melts, using neutron activation analysis

04 p0614 A71-15785

Solar Lyman alpha radiation absorption by molecular oxygen, examining optical thickness with Intercoms-1 satellite

05 p0807 A71-16214

Density and compressibility of oxygen in critical region, using capacitance measurements

05 p0781 A71-16703

Continuous nitrogen and oxygen ion spectra due to photoionization and free ion transfers at high temperatures

05 p0838 A71-16788

Niobium oxide defect structure, correlating electrical conductivity and oxygen diffusional properties with nonstoichiometry degree

05 p0770 A71-17097

Atmospheric absorption by oxygen, determining metastable molecules absorption cross section at 1095 Å

06 p0888 A71-17290

Apollo 11 flight glass basalt, determining crystallization sequence and phase assemblage of high Ti specimens as oxygen fugacity function

06 p0970 A71-18235

Atmospheric oxygen absorption spectra fluctuations related to presence or absence of jet stream

07 p1151 A71-18912

DNA modification in *Escherichia coli* exposed to X rays and sensitized by triacetoneamine N-oxyl and oxygen

07 p1033 A71-18939

Ar-oxygen mixture in undiluted nitrogen, discussing relaxation time change during adiabatic excitation and molecule oscillations deactivation

07 p1163 A71-19276

Time-altitude diurnal variations in molecular and atomic oxygen concentrations at 65-200 km from continuity equations

07 p1099 A71-19391

Atmospheric oxygen evolution and stability, discussing effects of photosynthesis inhibition, hydrogen passage and burial carbon

07 p1102 A71-19540

Flame retardant effects on smoke density and oxygen index of polystyrene, acrylonitrile-butadiene-styrene (ABS) and polyester systems

07 p1144 A71-19572

Oxygen effect on mechanical properties of Ti alloys with V and V-Al content, showing strengthening up to 400°C

07 p1136 A71-19631

D region oxygen photoionization rates decrease due to carbon dioxide absorption

07 p1103 A71-19673

Oxygen and nitrogen metastable constituents in daytime atmosphere airglow, obtaining altitude density distributions

07 p1103 A71-19764

Oxygen molecules photolysis at 1849 and 1931 Å, investigating ozone formation quantum yield

08 p1337 A71-20663

IR laser action at 2-3 microns by low pressure discharge and gas mixtures containing molecular oxygen and sulfur dioxide

08 p1301 A71-21190

Oxygen-kerosene fuel combustion products, calculating thermal and physical constants

08 p1346 A71-21263

Two phase oxygen adsorption at molybdenum surface, using secondary ion-ion emission measurements

08 p1306 A71-21489

Crossed beam model of nitrogen ion-molecular oxygen reactions in upper atmosphere as function of collision energy

08 p1251 A71-21784

Diurnal variation symmetry of upper atmosphere molecular oxygen concentration in terms of ozone photodissociation

09 p1435 A71-22446

Oxygen and nitrogen molecules nonadiabatic electronic-vibrational interaction effect on vibrational relaxation during collisions with O atoms

09 p1497 A71-22530

Nitrogen-oxygen and nitrogen-argon mixtures viscosity, using oscillating disk viscometer to test corresponding states principle validity

09 p1546 A71-23010

Quenching rates for oxygen during 1470 Å pulse photolysis in carbon dioxide, nitrogen and helium mixtures

09 p1404 A71-23382

O I and II resonance transitions radiative lifetimes in vacuum UV, using beam foil method

10 p1676 A71-24501

Spatial distribution of auroras in O and molecular nitrogen ion emissions

10 p1602 A71-24553

Rate constant temperature dependence for ozone reaction with oxygen, considering airglow features due to singlet molecular oxygen

11 p1801 A71-25370

Oxygen and nitrogen thermotransport in transition metals by microindention hardness testing for concentration determination

11 p1778 A71-25333

Upper atmospheric molecular and atomic N and O diurnal variations correlated to atmospheric heating as function of solar UV radiation from sounding rocket data

11 p1757 A71-25775

Mo evaporation in vacuum, oxygen and water vapor atmospheres at high temperatures

11 p1709 A71-25865

Shock induced combustion by firing spheres or cone cylinders into air- or oxygen-hydrogen mixtures, taking shadow photographs of resulting disturbances

11 p1860 A71-26268

Dissociation and particle velocity in shock heated molecular beams of oxygen or hydrogen and argon mixtures, using mass spectroscopic measurements

11 p1765 A71-26282

Carbon and oxygen inclusions effects on polycrystalline molybdenum rupture due to precipitation and chemisorption

11 p1781 A71-26323

Equilibrium compositions and thermodynamic properties tabulated for argon-oxygen plasmas at 0.01 to 10 atm and up to 35,000 K

12 p1986 A71-27187

Ni-base alloys hardened by gamma prime precipitation, investigating embrittlement by oxygen [ASME PAPER 71-MET-D]

12 p1917 A71-27313

Functional-biochemical shifts in rats central nervous system during initial stage of increased oxygen pressure exposure

13 p2002 A71-27810

Mechanical properties of welded joints in Ti alloys with high oxygen content

13 p2072 A71-27875

Thermal ion-atom charge transfer effects on ionization equilibrium of interstellar oxygen in H I regions, using Bahcall-Wolf orbiting approximation

13 p2132 A71-27966

UV photolysis of ozone in presence of molecular oxygen, discussing energy exchange reaction with molecular oxygen

13 p2025 A71-28350

Inhomogeneous atmosphere transmission functions, noting Lindholm line shift in O absorption spectra effects

13 p2063 A71-29019

Equilibrium temperatures, pressures and oxygen fugacities of equilibrated chondrites in meteorites

13 p2141 A71-29098

Ar-oxygen mixture in undiluted nitrogen, discussing relaxation time change during adiabatic excitation and molecule oscillations deactivation

14 p2276 A71-30170

Flash points, fire points and impact sensitivity of materials under gaseous oxygen pneumatic and mechanical impact

14 p2222 A71-30550

Two phase oxygen adsorption on molybdenum surface from secondary ion-ion emission

14 p2260 A71-30678

Gaseous oxygen/hydrogen injector element modeling based on composition profile measurements for cold flows

14 p2291 A71-30738

Low pressure gaseous hydrogen/gaseous oxygen APS rocket engines operating with propellant stored

as liquids and fed to thruster without pressure augmentation [AIAA PAPER 71-738]

15 p2467 A71-31326

Viscosity of dissociating oxygen, carbon-air and argon plasmas at high temperature range, including error estimates and expansion up to 12,000 K

15 p2512 A71-31502

High chromium low carbon steel, detailing oxygen content effects on high temperature reduction in intercrystalline corrosion and grain growth

15 p2427 A71-31528

Solar UV radiation atmospheric absorption during IQSY by ion chamber measurements, considering upper atmosphere oxygen concentration

15 p2396 A71-31616

Oxygen molecular excitation behind incident shock waves in pure oxygen and oxygen-argon and oxygen-neon mixtures, examining Schumann-Runge band system

15 p2451 A71-31674

Jet fuel dissolved oxygen concentration effects on plunger antiwear properties

15 p2464 A71-31677

Metallic Ni trace effects on oxygen chemisorption forms on nickel oxide in various temperature regions

15 p2367 A71-31901

Flammability limits measurement of hydrogen-oxygen mixtures containing fluorocarbon diluents

15 p2465 A71-32086

Stoichiometric hydrogen-carbon monoxide-oxygen mixtures detonation wave propagation at critical Mach number, noting explosion limit chemical kinetics role

15 p2465 A71-32088

Thermodynamic properties of dilute solutions of oxygen in liquid Fe-Co and Fe-Ni binary mixtures, obtaining Gibbs energy variation with temperature

15 p2432 A71-32174

Precipitation hardenable Ni-base alloys embrittlement in high temperature oxygen atmosphere, considering intergranular crack initiation

15 p2434 A71-32257

Oxygen adsorption kinetics at Nb single crystal surface at high temperatures and low pressures

15 p2436 A71-32547

High power carbon disulfide-oxygen combustion pulsed laser, discussing foreign gases effects on performance and energy transfer mechanism

16 p2586 A71-33165

Sputtered tantalum films oxygen content determination by anodization current efficiency measurements

16 p2621 A71-33187

Oxygen effect on mechanical properties of Ti alloys with V and V-Al content, showing strengthening up to 400°C

16 p2593 A71-33627

Nitrogen and oxygen exit rate from subcutaneous gas pockets in rats during tissue blood flow elevation due to cobalt chloride injection

17 p2678 A71-34174

Tungsten-oxygen system surface reactions in vacuum, emphasizing interfacial geometry variations, faceting and oxide nucleation

17 p2694 A71-34667

Trace impurities effect on oxygen adsorption by Mo, using low energy electron diffraction, Auger electron spectroscopy and flash desorption mass spectrometry

17 p2694 A71-34856

Oxygen molecules lower states diffuse orbitals, using self consistent fields configuration-interaction calculation method

17 p2785 A71-34948

Oxygen sorption rate by Ti at low pressure from measurement in stainless steel ultrahigh vacuum chamber

17 p2695 A71-35139

IR chemiluminescence of atomic nitrogen reaction with molecular oxygen, obtaining quantum efficiency

18 p2874 A71-35838

Oxygen adsorption study on polycrystalline W through work function variation and adhesion coefficient measurements, using mass spectrometry

18 p2874 A71-35974

Mars, Venus and earth atmospheres, considering abundance of volatiles such as carbon dioxide, water, oxygen, nitrogen, argon, carbon monoxide, chlorine and fluorine

18 p2968 A71-37032

Time-altitude diurnal variations in molecular and atomic oxygen concentrations at 65-200 km from continuity equations

19 p3053 A71-37815

Hydrogen-oxygen reaction sensitized by ammonia, comparing with nitrogen dioxide and nitrosyl chloride activators

19 p3012 A71-38081

Oxygen contamination effect on GaP solar cell electroluminescence and photoluminescence characteristics from electrical and mass spectroscopic analysis data

19 p2998 A71-38143

Vibrationally excited oxygen molecules formation and decomposition in upper atmosphere, calculating day and night equilibrium concentrations

19 p3057 A71-38373

Oxygen enhanced sublimation of p-type PbTe thermoelectric materials in isothermal and ingradient testing of couples

20 p3266 A71-38953

Upper atmospheric anomalous molecular oxygen distribution, discussing turbulent theory with autocorrelation of density fluctuations

20 p3222 A71-39701

H, He and O ion fluxes along exospheric magnetic field lines, determining flux energy and direction from RF mass spectrometer measurements onboard Elektron 4 satellite

20 p3226 A71-39742

F region nightglow emission mechanism in terms of oxygen cations reactions with diatomic nitrogen and subsequent recombination

20 p3226 A71-39832

Spiral galaxies N/O abundance gradients across disks from H II regions spectra

21 p3445 A71-40409

Strain hardened zirconium alpha tensile stress analysis, explaining inelastic phenomena by dislocation motion blocking with oxygen in lattice structure

21 p3397 A71-40432

Electronic transitions in oxygen molecule due to ion impact from kinetic energy loss spectrum

21 p3418 A71-40886

Oxygen effects on SiC electrical properties by comparison of photoluminescence spectra of alpha-SiC crystals grown by sublimation in Ar atmosphere

21 p3436 A71-41348

Upper atmospheric molecular and atomic nitrogen and oxygen diurnal variations correlated to atmospheric heating as function of solar UV radiation from sounding rocket data

22 p3532 A71-41543

LEED studies of oxygen adsorption on (111) and (110) surfaces of Al single crystals

22 p3561 A71-41730

Criticism of paper on spallation cross section for Be 10 production from oxygen high energy fragmentation in meteorites

22 p3508 A71-42350

Solar corona O VII and Ne IX helium line triplets observations, examining electron density limits

22 p3605 A71-42352

Oxygen, hydrogen and nitrogen determination in high melting point metals

22 p3563 A71-42364

Visible coherent radiation generation mechanism in ionized oxygen and nitrogen, considering free radical stabilized on discharge tube wall and metastable atom creation

23 p3706 A71-42889

Oxygen interaction with polycrystalline W, calculating sticking probabilities and desorption spectra at various temperatures

23 p3641 A71-42906

Reduced oxygen effect on structure and mechanical, technological and corrosive properties of stainless steel melted in open and vacuum furnaces

23 p3690 A71-43279

Molecular oxygen partial pressure effect on nitrogen afterglow intensity, proposing three-body reaction kinetics

23 p3707 A71-43500

Unpaired electrons and oxygen adsorptive capacity of clean lunar rock and soil surfaces, noting decrease of uptake rate at one monolayer coverage

23 p3764 A71-43798

Electron transfer cross sections for low energy negative oxygen ion collisions with oxygen molecules measured by single-collision beam technique

23 p3707 A71-43930

Oxygen dissociation in He, Ar, Kr and Xe gas mixtures behind incident shock waves, calculating density gradients and vibrational relaxation time

24 p3802 A71-44924

Molecular oxygen dissociation rate constant determination during interaction with He atoms in cylindrical shock tube

24 p3850 A71-45056

Oxygen viscosity variation under strong magnetic field, comparing angular dependence of Senftleben effect

24 p3802 A71-45116

Quartz crystal mass monitor study of monolayer oxygen adsorption on Al films, noting surface roughness variation with deposition temperature

24 p3803 A71-45348

OXYGEN ANALYZERS

Gas concentration determination for mixture by UV energy absorption measured in terms of photomultiplier tube output current, describing oxygen sensor

08 p1287 A71-20987

Laser spectral-isotopic determination of oxygen content in metals, noting analysis variant dependence on metal purity

17 p2751 A71-34384

OXYGEN ATOMS

Photodissociation produced O(3P) atoms detection and reaction rate measurements by resonance fluorescence scattering

01 p0130 A71-10369

Seasonal altitude variation of atomic ion-electron ratio of oxygen/nitrogen species in F1 region, comparing to radar measurements

01 p0076 A71-11507

Metastable atomic oxygen ion production in F region plasma due to photoionization by solar XUV radiation

03 p0462 A71-13271

Singlet-D atomic O yield per oxygen ion dissociative recombination from night airglow observations

03 p0408 A71-13382

Atomic oxygen-nitrogen shock tube endothermic reaction under high translational and low vibrational energy, noting ozone loss

03 p0375 A71-13493

Gas phase atomic hydrogen, nitrogen and oxygen detection by photoelectron spectroscopy of ground state, suggesting application to gas phase kinetics

04 p0548 A71-17499

Angular distribution of atomic oxygen ions produced by electron bombardment of oxygen, showing electron energy dependence

04 p0631 A71-15657

Chemiluminescent NO-O reaction spectral radiant intensity and absolute rate constant redetermination in premixed gaseous free jet and hydrogen flame atmosphere

05 p0837 A71-16568

Geomagnetic activity effects on atomic oxygen emissions in green and red light, noting radiant intensity, strong dispersion, local and planetary Kp indices

07 p1101 A71-19413

Molecular and atomic oxygen properties in nonequilibrium flows, determining vibrational temperature and number density by electron beam fluorescence technique

08 p1338 A71-21997

Slow negative atomic oxygen ion production in collisions between fast protons or hydrogen atoms and gas molecules

09 p1496 A71-22230

Oxygen and nitrogen molecules nonadiabatic electronic-vibrational interaction effect on vibrational relaxation during collisions with O atoms

09 p1497 A71-22530

Atomic oxygen and carbon dioxide measurement in lower thermosphere by mass spectroscopy

10 p1606 A71-24803

D region atomic oxygen measurement via Nike Cajun sounding rocket flight

13 p2056 A71-27932

German monograph on bimolecular reactions of H and O atoms in shock waves with hydrogen peroxide and dioxide and nitrous oxide

13 p2102 A71-28881

Oxygen /super 1S/ effective lifetime measurements in pulsating aurora, discussing mechanisms, quenching coefficients and heights

15 p2397 A71-31762

Ionospheric nighttime ambient atomic oxygen concentration profiles, using nitric oxide release from sounding rockets

16 p2568 A71-33791

Chemical trimethyl aluminum releases in lower thermosphere for temperature, density, winds, turbulence, diffusion coefficients and atomic oxygen content measurements

16 p2568 A71-33792

Atomic oxygen 1304-A day airglow observed fromOGO-D spacecraft, attributing subsolar emission rates to photoelectron impact excitation

16 p2574 A71-33964

Ionospheric atomic oxygen concentration estimates from radar backscatter and rocket probe measurements of electron and ion temperatures and concentration

16 p2574 A71-33965

Time of flight energy spectra of high lying and Rydberg metastable atoms by electron impact dissociation of molecular oxygen, noting atmospheric applications

16 p2614 A71-34043

Excitation cross sections for resonance states by electron impact on atomic nitrogen and oxygen over aeronautical energy range

18 p2949 A71-36350

Core binding energy difference between bridging and nonbridging oxygen atoms in silicate chain of pyroxenes, using X ray photoelectron spectra

19 p3011 A71-37415

Geomagnetic activity effects on atomic oxygen emissions in green and red light, noting radiant intensity, strong dispersion, local and planetary Kp indices

19 p3054 A71-37837

Reactions of H and O with hydrogen peroxide and water in discharge flow systems, measuring rate coefficients

19 p3012 A71-38083

Thermospheric atomic oxygen and molecular nitrogen number densities, discussing earth atmospheric absorption of solar UV lines

20 p3214 A71-38727

Atomic oxygen concentration from 5577 A green line emission of airglow and chemiluminescence of nitric oxide

20 p3215 A71-38739

OXYGEN CONSUMPTION

Midlatitude lower thermosphere atomic and molecular oxygen rocket measurements, presenting concentration and vertical distribution data

20 p3222 A71-39700

Earth UV dayglow observation by Aerobee rocket-borne scanning spectrometer, noting features due to atomic oxygen and nitrogen and nitrogen oxide gamma band

20 p3226 A71-39830

Slow negative atomic oxygen ion production in collisions of fast protons and hydrogen atoms with oxygen molecules, measuring scattering cross sections

21 p3419 A71-41109

Molecular oxygen dissociative excitation in vacuum UV by electron impact, discussing resonance triplet atomic emission cross section

23 p3706 A71-42903

Atomic oxygen 6300 and 5577 A emissions nocturnal covariation from nightglow observation, considering relation to F layer height changes

23 p3667 A71-43131

Atomic oxygen and hydrogen identification in Mars upper atmospheric emission spectra by Mariner UV spectrometer, inferring carbon monoxide presence by self absorption

23 p3735 A71-43330

OXYGEN BREATHING

Cardiovascular and ventilatory responses to room air and pure oxygen breathing under various exercise work load conditions

01 p0016 A71-11407

Oxygen inhalation effects on intramyocardial oxygen tension in anesthetized dogs, investigating acute myocardial infarction therapy effectiveness

02 p0202 A71-12917

Electrochemical aircrew oxygen breathing systems, considering water electrolysis and oxygen separation and concentration from air

04 p0543 A71-15056

Oxygen respiration effect on self stimulation and emotional reactions in rabbits during hypothalamus electrical stimulation

06 p0855 A71-18376

Altitude range for supplemental aircraft continuous flow, diluter and pressure demand oxygen systems, discussing regulations and pressure breathing

08 p1244 A71-20714

Oxygen vs air in treatment of divers with decompression sickness

08 p1242 A71-21957

Heart, lungs and erythropoiesis optimum functional parameters mathematical model based on oxygen transport minimum losses

09 p1388 A71-22126

Pathological effects of pure oxygen on animal organism at atmospheric pressure, noting perivascular edema, diapedesis hemorrhages, respiratory and metabolic disorders

09 p1392 A71-22641

Succinic dehydrogenase activity inhibition and pentobarbital sodium protection of lung tissue in mouse breathing oxygen at atmospheric pressure

11 p1721 A71-26125

Human heart rate, minute ventilation and oxygen uptake measurement during treadmill and track running at three speeds

12 p1874 A71-27134

Pulmonary oxygen toxicity, considering composition of endobronchial saline extracts of rats and edema development

13 p2015 A71-29362

Pulmonary oxygen toxicity development rate and effects on lung volume and alveolar-arterial gas exchange during oxygen breathing

13 p2024 A71-29501

Alveolar arterial oxygen pressure gradient derivation as sum of shunt, ventilation/perfusion inequalities and membrane and airway diffusions

15 p2363 A71-31444

Oxygen pulmonary diffusion capacity estimation by rebreathing procedure based on gas-blood partial oxygen-pressure equilibration

17 p2678 A71-34173

Advantages and drawbacks of pure oxygen and oxygen-nitrogen space breathing, considering decompression sickness in Apollo missions

18 p2863 A71-35907

Pulmonary antibacterial defenses with pure oxygen breathing mice, noting inhibition of early interpulmonary clearance of Staphylococcus aureus and enhanced clearance of Klebsiella pneumoniae

22 p3487 A71-42241

OXYGEN COMPOUNDS

Magnesium vapor-oxygen low pressure diffusion flames temperature profile measurement, using subminiature thermocouple

15 p2464 A71-31631

OXYGEN CONSUMPTION

Pt electrode oxygen diffusion and consumption systematic errors effect on oxygen partial pressure measurement in perfused tissues

01 p0021 A71-10073

Resting oxygen consumption in exercise-trained and nontrained normal, hypophysectomized and thyroidectomized rats

01 p0016 A71-11408

Oxygen uptake kinetics in human submaximal exercise during work load transitions and work-rest cycle
02 p0202 A71-11663

Oxygen debt after steady state work in submaximal physical exercise
02 p0202 A71-11668

Alpha and beta receptor blocking drugs effects on oxygen consumption of methemoglobin-containing erythrocytes and hemolysates
03 p0363 A71-13483

Diurnal variations due to actual heat output, oxygen consumption and carbon dioxide production in rats undergoing eating habit changes
04 p0539 A71-15157

CO pulmonary diffusing capacity rebreathing measurements at rest and while exercising, noting relationship to oxygen consumption
04 p0545 A71-15162

Physical fitness in prolonged muscular work tolerance evaluation by oxygen consumption for 170 beat/min heart rate, considering age, sex and occupation
05 p0708 A71-16614

Oxygen intake, ventilation and heart rate during various intensity and duration tests
05 p0708 A71-16615

Human valvular heart disease, examining work load effects on oxygen demand
06 p0849 A71-17294

Oxygen consumption and carbonic acid output in hypothermic rats cooled under diethyl ether anesthesia, investigating physiological indices during hypothermia
06 p0852 A71-17667

Oxygen transport and consumption, ventilation and cardiac index in natives and sojourners at high altitudes
06 p0853 A71-18060

Circadian patterns of deer mice oxygen consumption in constant dark and thermally neutral zone
06 p0856 A71-18381

Hypoxic and hypercapnic ventilatory control and oxygen uptake in athletes, noting chemoreceptor function
06 p0862 A71-18384

Human work capacity measurements by graded step test and bicycle ergometer, considering heart rate and oxygen uptake
07 p1046 A71-19457

Rate constant for oxygen uptake exponential increase during low intensity exercise by algebraic solution
07 p1052 A71-20336

Furosemide effect on physical work capacity, studying recovery pulse response, oxygen extraction during exercise and altitude acclimatized subjects oxygen uptake
09 p1394 A71-23237

Human steady and unsteady state treadmill exercise, comparing cardiac output, heart rate and oxygen uptake interrelationships
09 p1401 A71-23367

High altitude submaximal and maximal work by humans, noting time required for steady state oxygen consumption, ventilation and heart rate
09 p1401 A71-23368

Age effect on pulmonary circulation in normal subjects, measuring oxygen consumption, cardiac output and pulmonary arterial pressure by floated catheter technique
10 p1561 A71-24129

Chemical thermoregulation muscular electricity activity during shivering and thermoregulation tonus change after cold adaptation, discussing oxygen consumption rise
10 p1564 A71-24486

Myocardial oxygen reduction by stimulating carotid sinus nerves and angina pectoris treatment application
11 p1718 A71-25437

Porous structure effects in oxygen consuming cathode, discussing electrode thickness, effective pore diameter, pressure difference and electrode performance
11 p1709 A71-25553

Temperature-respiration relations from isolated rat skeletal muscle mitochondria oxygen consumption measurements
11 p1723 A71-26408

Alveolar gas exchanges and cardiovascular functions during breath holding with air, determining resting oxygen consumption
12 p1870 A71-27135

Equipment for prolonged measurement of oxygen consumption, respiratory quotient and insensitive perspiration in man, noting cost reduction and operation simplification
13 p2021 A71-29316

Oxygen dissociation curve shift, hemoglobin affinity and diphosphoglycerate concentration in blood of acidotic and normal subjects at altitude
13 p2016 A71-29494

Human physiological responses comparison between work with concentric and eccentric muscle contractions, observing oxygen debt in short term exercise
13 p2024 A71-29495

Trained college and recreational swimmers cardiac output and maximum oxygen consumption during tethered swimming and treadmill running
13 p2024 A71-29496

Metabolic, ventilator and cardiovascular response during free swimming and treadmill walking, relating oxygen consumption to work intensity
13 p2024 A71-29500

Maximum oxygen uptake prediction by stepwise regression technique from data collected during sub-maximum treadmill work
16 p2530 A71-33241

Physical exercise oxygen uptake and debt in dogs at ground level and high altitude, investigating beta adrenergic blocking agent effects
16 p2530 A71-33242

Trained young runners maximum oxygen consumption rate at sea level and high altitude
16 p2530 A71-33244

Capillary density relationship to maximal oxygen uptake, indicating endurance training effects on human skeletal muscle
16 p2530 A71-33245

Maximal human anaerobic power, discussing unsplit phosphagen concentration in muscles during steady state exercise
16 p2530 A71-33247

Oxygen consumption by nitrogen starved nonsynchronous *Chlorella* culture during different assimilation of nitrogen salts in darkness and light
16 p2531 A71-33461

Factors affecting tissue oxygen supply in old people, showing capillary circulation disturbance role in hypoxia development during aging
17 p2679 A71-34220

Increased oxygen concentrations effect on mice pulmonary tissues during prolonged exposure
17 p2679 A71-34222

Circulatory fatigue during shift work, determining pulse rate/oxygen intake at two different loads on bicycle ergometer
17 p2687 A71-34358

Muscular fatigue of healthy Bengali males with increasing work loads under varying environmental conditions, considering ventilation, heart rate and oxygen consumption
17 p2688 A71-34360

Sympathetic nervous system in short term adaptation to cold, observing oxygen consumption, urinary noradrenaline proportion and excretion
17 p2681 A71-34698

Breathing capacity increase without rise in oxygen consumption due to active and passive muscular work and heavy energy expenditure
17 p2681 A71-34821

Lactic acid production rate in human blood during supramaximal exercise, noting relationship to oxygen consumption
17 p2685 A71-35366

Oxygen intake relation to anaerobic component of work during submaximal exercise on bicycle ergometer by young and older men
17 p2686 A71-35435

Maximum oxygen uptake measurement by two techniques, calculating heart rate
19 p3008 A71-38553

Heart maximal aerobic and anaerobic power and stroke volume, discussing cardiac output and blood oxygen capacity measurements in subalpine population subjects
20 p3185 A71-38887

World champion marathon runner metabolic responses during submaximal and maximal treadmill running, recording oxygen consumption, heart rate and lactic acid
20 p3185 A71-38890

Postexercise elevated tissue temperatures contributions to oxygen consumption in rats, suggesting hypothalamic adjustment
20 p3186 A71-38981

Power derived from aerobic, lactic acid and alactacid energy sources during human muscular work under normoxic and hypoxic conditions, noting oxygen consumption
22 p3485 A71-41721

Norepinephrine induced stimulation of myocardial oxygen consumption of cat papillary muscles under afterloaded isotonic and isometric conditions
22 p3486 A71-41937

Muscular work level shifts effectiveness during pedaling activity from oxygen requirement measurement, electromyograms and stress dynamograms
24 p3794 A71-44412

Hypokinesia effects on gas exchange and oxygen consumption in rats, noting weight losses
24 p3795 A71-44526

OXYGEN DEFICIENCY

U HYPOXIA

OXYGEN DETECTORS

U OXYGEN ANALYZERS

OXYGEN FLUORIDES

Oxygen difluoride/diborane propellant thrust chamber and injector technology, discussing engine duty cycles and performance
[AIAA PAPER 70-717] 07 p1183 A71-18890

Initial reaction rates of oxygen difluoride with diborane related to reactant concentration and temperature
09 p1510 A71-22071

OXYGEN ISOTOPES

NT OXYGEN 18

Oxygen isotope fractionation in Apollo 12 rocks and soils, noting plagioclase ilmenite isotopic temperature
23 p3751 A71-43704

Apollo 11 and 12 lunar samples O 18/O 16, Si 30/Si 28, D/H and C 13/C 12 ratio determination, examining whole rocks, breccias, soils, plagioclases and fines
23 p3751 A71-43705

OXYGEN METABOLISM

Oxygen uptake by hemoglobin solution, considering diffusion rate and chemical reaction by mathematical model numerical solution
03 p0360 A71-13180

Chronic hypercapnia oxygen dissociation curves and red cell cation exchange in rats, considering compensated/uncompensated phases of respiratory acidosis
03 p0360 A71-13181

Bioenergetics of brain in vertebrates, concerning oxidative metabolism in neurones, glia and mitochondria structure
03 p0362 A71-13240

Myocardial glycogen stores increase protective role in rat cardiac anoxia studied in isolated perfused heart
03 p0363 A71-13489

Oxygen balance of intact and denervated dog spleen during asphyxia, distinguishing splenic contraction and metabolic rate-storage capacity ratio
04 p0538 A71-15087

Cerebral oxygenation and metabolism during progressive hyperthermia
04 p0538 A71-15092

Spacecraft cabin rare gas-oxygen atmosphere decompression effects on animal metabolic rates
06 p0853 A71-17956

Metabolic effects of sulphur containing cysteamine, cystamine and cysteine radioprotective drugs on oxygen uptake in rats
07 p1039 A71-18982

Arterial oxygen, carbon dioxide tension, pH and lactic acid changes during rapid descent from altitude to sea level in deep mine
07 p1052 A71-20334

Cardiac output variations in regulation of arterial oxygen transport during hypoxia
08 p1241 A71-21939

Altitude acclimatization of albino rats and guinea pigs, measuring chronic and acute hypoxia effect on oxygen affinity and red cell 2,3 diphosphoglycerate concentration
10 p1558 A71-23894

High altitude aerobic working capacity limitations, examining oxygen transport system and circulator factors
14 p2183 A71-30276

High altitude acclimatized humans, noting decreased coronary blood flow and increased oxygen extraction
14 p2184 A71-30283

Human hypoxic ventilatory drive data for high altitude breathing, noting motivation reduction inversely related to time and altitude
14 p2185 A71-30288

Microbiological respirometer for oxidative metabolism for plants and small animals, considering manned space flight applications
14 p2189 A71-30344

Dietary antioxidant vitamin level effects on fine structure of proximal convoluted tubules in rats, studying changes due to oxygen toxicity
16 p2528 A71-33116

Myocardium ultrastructural and metabolic alterations in altitude acclimated rats, considering heart muscle mitochondria
16 p2529 A71-33193

Physiologic and pathologic cardiomegaly, noting myocardial blood flow oxygen uptake and lengthening and widening of coronary vessels
16 p2531 A71-33423

Oxygen metabolic rate in isolated canine lungs at various static inflation levels and cyclic ventilation, examining mechanical deformation effects
17 p2683 A71-35145

Organic phosphate compounds effects on oxygen affinity and intracellular pH of human erythrocytes
18 p2857 A71-36691

Regional cerebral blood flow, tissue oxygen, EEG activity and behavioral reaction at high pressure
19 p3009 A71-38557

Oxygen uptake kinetics by hemoglobin layers, using Hill advancing front equation
19 p3010 A71-38567

Daily endurance exercise influence on key tissues resting aerobic metabolism, using Warburg technique to determine rats heart, skeletal muscle and liver tissue oxygen consumption
20 p3185 A71-38886

Bed rest effects on human hemodynamic and gaseous metabolism, observing increased cardiac output

and decreased oxygen consumption and carbon dioxide production

20 p3188 A71-39231

Chronic acceleration effects on animals, considering growth rate, food intake, oxygen metabolism and life expectancy

21 p3328 A71-40003

Myocardial blood flow and oxidative metabolism in cyanotic congenital heart disease patients, using lactate/pyruvate ratios and coronary sinus catheterization

22 p3484 A71-41521

Respiratory function and gas metabolism shift under high transverse accelerations in reclined centrifuged subjects

22 p3495 A71-42795

Gas metabolism and electrical activity of skeletal muscles of rats in He/O medium at room temperature, noting rectal temperature drop

22 p3496 A71-42803

OXYGEN PRODUCTION

Electrochemical aircrew oxygen breathing systems, considering water electrolysis and oxygen separation and concentration from air

04 p0543 A71-15056

Fick diffusion model for Haxo-Blinks electrochemical determination of photosynthetic oxygen evolution

04 p0546 A71-15169

Chlorates use in breathable oxygen production for aircrews

06 p0860 A71-18193

Commercial business and utility aircraft chemical oxygen generators to satisfy FAA requirements, discussing weight, size and maintenance savings and increased safety

[SAE PAPER 710390]

10 p1558 A71-24254

Optimization of time intervals of conveyor harvestings and harvested age of oxygen producing plants for life support system

13 p2017 A71-28406

Oxygen generation system for 90-day space station simulator, considering carbon dioxide removal and reduction and water electrolysis

[ASME PAPER 71-AV-18]

18 p2867 A71-36385

Saturating flash delayed luminescence from chloroplasts, considering relationship to oxygen evolution

24 p3799 A71-45382

OXYGEN RECOMBINATION

Cooled porous plug burner for flame recombination of oxygen and hydrogen, noting boiling water reactor off-gas application

03 p0517 A71-13367

Singlet-D atomic O yield per oxygen ion dissociative recombination from night airglow observations

03 p0408 A71-13382

Air and oxygen electron-ion recombination coefficients, considering plasma deionization rate

05 p0756 A71-17208

Sealed secondary Ag cells, controlling H and O recombination by auxiliary electrode

08 p1236 A71-21106

Dissociative recombination source of atomic oxygen green line excitation in day airglow, considering differential photoelectron flux

13 p2055 A71-27919

Air and oxygen electron-ion recombination coefficients, considering plasma deionization rate

13 p2067 A71-28263

Spectral lines of O I/S/ generated by oxygen molecule dissociative recombination in upper atmosphere observed in nightglow at geomagnetic equator with Fabry-Perot spectrometer

14 p2229 A71-29663

Oxygen dissociation and recombination rate constants at high temperatures from gas density interferometric measurement in relaxation zone of normal shock waves

15 p2367 A71-32570

Hydrogen oxygen recombination rate constants from hydroxyl radical decay measurements in shock tube steady expansion

16 p2539 A71-32908

Impact ionization cross section measurements for multielectron-oxygen ion reaction, using crossed beams

22 p3578 A71-42421

OXYGEN REGULATORS

Continuous flow oxygen regulators construction, performance and testing SAE standard, covering automatic, adjustable and preset types

[SAE-AS-1197]

07 p1049 A71-19648

OXYGEN SENSORS

U OXYGEN ANALYZERS

OXYGEN SPECTRA

Total free electron energy disparity with energy radiated in forbidden O I lines in supernova spectra explained by nova luminescence formation

01 p0151 A71-10067

Lyman alpha and O I 1304 A airglow depressions over poles from OGO 4 satellite observations

01 p0076 A71-11503

Altitude distribution of oxygen in atmosphere with eddy diffusion allowance from ARCAS 2 rocket photometric observations

01 p0077 A71-11528

Triplet O I excitation in night sky of tropical regions, using photometric measurements of line spectra

03 p0409 A71-13789

Solar activity effects on day airglow atomic oxygen red line, calculating production rates for photodissociation, dissociative recombination and electron impact excitation

03 p0418 A71-14265

O I 1304-A airglow, observing conjugate excitation with OGO 4 spacecraft

06 p0888 A71-17279

Solar X-ray resonance, intercombination and forbidden lines variations of O VII emission

06 p0968 A71-17910

Geomagnetic activity effects on atomic oxygen emissions in green and red light, noting radiant intensity, strong dispersion, local and planetary Kp indices

07 p1101 A71-19413

Oxygen ion-molecule reactions at thermal energies, using drift tube mass spectrometer

07 p1164 A71-19689

Morphology and dynamics of low intensity monochromatic midlatitude auroral arcs of 6300 A /O I/, comparing results with observation during IGY

07 p1103 A71-19766

Lambda 6300 A /OI/ airglow excitation by soft electron fluxes

07 p1103 A71-20006

Low geomagnetic latitude night airglow characteristics, using Cosmos 215 measurements in 1225 to 1350 A range

08 p1277 A71-21008

Total free electron energy disparity with energy radiated in forbidden O I lines in supernova spectra explained by nova luminescence formation

09 p1525 A71-23260

Ice, solid carbon dioxide and alcohols oxygen K spectra from long wave X ray spectroscopy

09 p1498 A71-23479

Auroral pulsation analysis from rocket soundings, investigating oxygen green linear excitation sources

11 p1753 A71-25549

Oxygen red-green line emission intensity in quiet auroral arc, using rocket-borne photometers

11 p1754 A71-25551

Predawn enhancement structure of oxygen red line airglow at 6300 A from time-latitude isophote diagrams, discussing F region photoelectrons recombination role

11 p1755 A71-25611

UV airglow in 1304 A line of oxygen from Cosmos 215 satellite observation

12 p1899 A71-26638

Dissociative recombination source of atomic oxygen green line excitation in day airglow, considering differential photoelectron flux

13 p2055 A71-27919

Photodissociative excitation of atomic oxygen dayglow emission, considering electron impact and dissociative recombination

13 p2056 A71-27933

Spectral lines of O I/S/ generated by oxygen molecule dissociative recombination in upper atmosphere observed in nightglow at geomagnetic equator with Fabry-Perot spectrometer

14 p2229 A71-29663

Upper atmosphere temperature measurements using red emission Doppler contour width data of atomic oxygen at 6300 A

14 p2229 A71-29673

Continuous nitrogen and oxygen ion spectra due to photoionization and free ion transfers at high temperatures, calculating absorption coefficient

16 p2662 A71-33040

Ion beam-foil produced oxygen spectra in wavelength range between 450 and 2200 A, determining mean radiative lives of O I - O VI excitation levels

16 p2529 A71-33183

Forbidden O II spectra brightness ratio measurements across Orion nebula, determining electron density variations

16 p2631 A71-33229

Altitude variation of forbidden line of 5577 A and 3914 A auroral emissions intensities ratio from rocket sounding

16 p2566 A71-33748

Molecular oxygen densities at 80-160 km by rocket sounding with absorption of solar Lyman alpha line and C IV doublet at 1550 A

16 p2574 A71-33966

Solar activity and intensity ratios of O VII X-ray coronal emission lines, giving upper bound on electron density

18 p2965 A71-36734

Infrasonic pulsations of optical auroral luminosity in 3914 A positive molecular nitrogen ion and 5577 A O I emission measurement by double photometer system

19 p3048 A71-37395

Atmospheric noise temperature variation with frequency in 2.53 mm molecular oxygen rotation line, considering Zeeman effect

19 p3048 A71-37402

Upper atmosphere hydroxyl emission nocturnal average vibrational temperature correlation with molecular oxygen emission intensities

19 p3049 A71-37403

Geomagnetic activity effects on atomic oxygen emissions in green and red light, noting radiant intensity, strong dispersion, local and planetary Kp indices

19 p3054 A71-37837

Oxygen telluric lines contours shape analysis, allowing for atmospheric nonisothermicity and inhomogeneity

19 p3090 A71-37978

Dumb-bell Nebula forbidden O III line profiles observation with two-etalon scanning Fabry-Perot

19 p3144 A71-38171

Low geomagnetic latitude night airglow characteristics, using Cosmos 215 measurements at 1225-1350 A in oxygen spectrum

20 p3219 A71-39588

Dayglow emissions for OH, molecular oxygen, sodium, lithium, potassium, atomic oxygen and nitrogen, considering height profiles and diurnal variations

20 p3226 A71-39828

D region night airglow OH emissions and IR atmospheric diatomic oxygen bands excitation mechanism with aid of model involving solar photodissociation

20 p3226 A71-39831

Atomic oxygen 6300 and 5577 A emissions nocturnal covariation from nightglow observation, considering relation to F layer height changes

23 p3667 A71-43131

Photoelectron impact vs dissociative excitation cross sections of atomic oxygen resonance radiation in terrestrial airglow

23 p3669 A71-43171

Night airglow oxygen Herzberg I bands covariation with O I 5577 A line, evaluating NASA 1968 airborne auroral measurements

23 p3670 A71-43186

Oxygen Schumann-Runge bands system from photographic and photoelectric spectra recording for arc jet heated air and oxygen-noble gas mixtures [AVERL-RR-354]

24 p3850 A71-45088

OXYGEN SUPPLY EQUIPMENT

Electrochemical aircrew oxygen breathing systems, considering water electrolysis and oxygen separation and concentration from air

04 p0543 A71-15056

Apollo 13 in flight emergencies and countermeasures, discussing fire in Service Module oxygen tank causes and effects on spacecraft systems and solutions

07 p1206 A71-19087

Commercial business and utility aircraft chemical oxygen generators to satisfy FAA requirements, discussing weight, size and maintenance savings and increased safety

[SAE PAPER 710390]

10 p1558 A71-24254

Solid electrolyte oxygen generator electrolysis test module with improved ceramic to ceramic and metal seals, electrode and grid design, discussing performance tests

[ASME PAPER 71-AV-8]

18 p2866 A71-36375

Zero-gravity circulating water electrolysis system prototype design for metabolic and leakage makeup oxygen supply in 12-man space station regenerative life support system

[ASME PAPER 71-AV-20]

18 p2867 A71-36387

Water vapor electrolysis for oxygen generation and humidity control in long term manned space flight

[ASME PAPER 71-AV-24]

18 p2868 A71-36391

Closed-loop solid electrolyte oxygen regeneration life support system, discussing 180-day life test

[ASME PAPER 71-AV-32]

18 p2869 A71-36399

Oxygen supply to air transported patients by chemical compounds, suggesting use of permanganates and chlorates

22 p3500 A71-41571

Spacecraft closed loop oxygen recovery system using electrochemical carbon dioxide concentrator, Sabatier reactor and water electrolysis subsystem

22 p3503 A71-42017

High altitude decompression disorders prevention in humans by increasing pressure level in oxygen equipment assembly

24 p3795 A71-44474

OXYGEN SYSTEMS

U OXYGEN SUPPLY EQUIPMENT

OXYGEN TENSION

NT HYPOXEMIA

Pt electrode oxygen diffusion and consumption systematic errors effect on oxygen partial pressure measurement in perfused tissues

01 p0021 A71-10073

Oxygen inhalation effects on intramyocardial oxygen tension in anesthetized dogs, investigating acute myocardial infarction therapy effectiveness

02 p2022 A71-12917

Oxygen tension, blood flow, redox potential and temperature variations in cerebrum and musculus gastrocnemius of rats during high mountain adaptation

03 p0361 A71-13190

Microcathodes measurement of oxygen tension on arterioles external surface in hamster cheek pouch and hamster/rat cremaster muscle for blood flow regulation mechanism

03 p0363 A71-13487

Human alveolar-arterial oxygen pressure differences, investigating inert gas effects

04 p0540 A71-15576

Oxygen partial pressure measurements in myocardium of beating heart by miniature glass needle and surface electrodes

05 p0714 A71-16598

Middle cerebral artery occlusion effect on cortical blood flow, tissue oxygen pressure and acid base equilibrium in animals under extended ligations

05 p0708 A71-16617

Training effect on oxygen tension dynamics in rats brain cortex under progressive high altitude hypoxia conditions, noting adaptation influence on motor activity and survival rate

06 p0850 A71-17394

Pt electrode response time during unsteady oxygen partial pressures measurement

06 p0860 A71-18323

Oxygen tension in skin and kidneys using chronoamperometric measurements

06 p0857 A71-18724

Electrical conductivity measurement for thorium oxide at 1000-1600 C and at low oxygen partial pressures, discussing Seebeck coefficient behavior

07 p1177 A71-19569

Carbohydrate ingestion produced respiratory gas exchange ratio and alveolar ventilation effects on arterial oxygen tension in normal men

07 p1052 A71-20333

Polarographic blood oxygen measurement by principle of oxygen liberation into physical solution by potassium ferricyanide

07 p1053 A71-20337

Alveolar nitrogen and carbon dioxide tensions changes during compressed air narcosis in constant oxygen partial pressure

08 p1239 A71-20818

Oxygen tension effect on pulmonary diffusion capacity and postnatal lung growth in rats under hypoxic, normoxic and hyperoxic atmospheres

10 p1559 A71-23899

High oxygen tension during severe exercise, studying effects on humoral and nervous ventilation changes

11 p1722 A71-26363

Partial oxygen tension in blood and biological fluids measurement with enclosed electrode polarographic sensor

12 p1876 A71-27744

Low alloy alpha Ti alloy ignition during breaking in oxygen containing gases, considering partial oxygen pressure and tensile loads

13 p2082 A71-27815

Spleen role as erythrocytic depot in reticulocytic reaction to acute hypoxia in splenectomized dogs inhaling air with reduced partial oxygen pressure

13 p2007 A71-28418

Oxygen exposure effect on food consumption/utilization efficiency, growth and biochemical parameters

13 p2015 A71-29360

Lung diffusing capacity for oxygen during exercise and alveolar hypoxia measured without blood samples by ear oximeter

13 p2023 A71-29492

High altitude pulmonary edema syndrome, investigating increased alveolar-arterial oxygen gradients of humans during treadmill exercise

14 p2184 A71-30279

Chronic hypoxia effects on blood oxygen and carbon dioxide tensions and pH changes in unanesthetized chickens at high altitude compared to sea level control

14 p2186 A71-30565

Arterial or venous blood oxygen tension continuous measurement, describing electrode cuvette design with response time of less than 3 sec

16 p2535 A71-33248

Oxygen pulmonary diffusion capacity estimation by rebreathing procedure based on gas-blood partial-oxygen-pressure equilibration

17 p2678 A71-34173

Venous and arterial blood gases in hibernating and normothermic ground squirrels, showing venous oxygen and carbon dioxide partial pressures reduction in hibernation

17 p2681 A71-34941

Dynamic characteristics of arterial oxygen tension response to supine submaximal leg exercise in man from harmonic analysis

18 p2856 A71-36239

Copper on copper friction coefficient dependence on oxygen pressure, investigating exoelectron emission from differently oxidized copper surface layers

18 p2928 A71-36750

Exercise temperature plateau shift and sweat rate during moderate CO poisoning associated with resetting of thermoregulating centers by low oxygen tensions

18 p2861 A71-36886

Alveolar-arterial oxygen pressure difference during controlled hyperventilation and posthyperventilatory phase

19 p3003 A71-38200

Diffusion component of alveolar-arterial oxygen pressure differences in man at rest and during exercise

19 p3009 A71-38556

Chronic hypercapnia effects on oxygen affinity and 2,3-diphosphoglycerate in red cell from tests on guinea pigs

20 p3189 A71-39440

Inspired oxygen concentrations effects on arterial and mixed venous pH, carbon dioxide uptake and oxygen partial pressure in normal subjects

20 p3189 A71-39442

Human expiratory oxygen and carbon dioxide partial pressure and dissociation curves for intrapulmonary gas mixing, using mass spectrometry

21 p3328 A71-40098

Frequency analysis of blood circulation rhythms and oxygen tension fluctuations in cerebra of rabbits, cats, monkeys and men

22 p3490 A71-42580

Radiation effects on rats peripheral blood state in low pressure environment with sea level value oxygen tension

22 p3494 A71-42732

Respiratory carbon dioxide and oxygen partial pressure effects on intraocular and blood pressure in rabbits under Somnifen narcosis

24 p3793 A71-44368

Oxygen tension distribution in cats glomus caroticum under influence of varying arterial oxygen partial pressure, using platinum microelectrodes

24 p3796 A71-44562

OXYGEN TOXICITY

U HYPEROXIA

OXYGEN 18

Apollo 12 lunar rock 12013 oxygen 18 and silicon 30 ratios, comparing to terrestrial basalts and gabbros, Apollo 11 rocks and oceanic rhyolite obsidians

03 p0495 A71-14225

Oxygen diffusion in monoclinic zirconia as function of equivalent pressure, using oxygen 18 gas-solid exchange techniques

05 p0769 A71-17096

Neutron emission yield during Pu 238 alpha particles interactions with O 18, taking into account recoil Ne isotopes

14 p2276 A71-30177

Radio telescopic search for extraterrestrial oxygen 18 containing water microwave emission, suggesting water vapor maser pumping mechanism dependence on isotopic species

21 p3444 A71-40223

OXYGENATION

Free radical activity in white mice tissues under hyperbaric oxygenation, examining antioxidants effects

01 p0012 A71-11075

Cerebral oxygenation and metabolism during progressive hyperthermia

04 p0538 A71-15092

Renal oxygenation in male Peruvian natives living permanently at high altitudes, determining reduced tubular function cause

12 p1873 A71-27127

Proton release association with whole blood oxygenation at constant plasma pH and carbon dioxide partial pressure, using alkaline titration

13 p2007 A71-28433

OXYHEMOGLOBIN

Myocardial ischemia and necrosis without major coronary arteries obstruction, investigating possible deranged hemoglobin-oxygen transport

14 p2185 A71-30286

OZONE

High altitude aircraft effects on stratospheric ozone due to added water vapor, discussing effects on solar energy transmission, surface temperature and weather

01 p0120 A71-11341

Ozone atmospheric concentration, dissociation in SST air conditioning systems and biochemical poisoning

03 p0358 A71-13096

Stratospheric ozone, comparing observations to numerical models of formation, distribution and destruction

04 p0582 A71-15071

Ozone in Mars solid carbon dioxide polar cap, using UV reflection-absorption spectra

04 p0661 A71-15897

Vertical atmospheric ozone distribution from inversion of spectral UV radiation, comparing results with statistical method

05 p0742 A71-16671

Polar region atmospheric ozone density profile measurements, using rocket sounding

05 p0743 A71-17007

Vibrationally excited ground state hydroxyl in fast flow system, considering mean radiative lifetime and reaction rate with ozone

08 p1250 A71-20662

Oxygen molecules photolysis at 1849 and 1931 A, investigating ozone formation quantum yield

08 p1337 A71-20663

Upper atmosphere hydroxyl emission mechanism, discussing absorption band, energy balance, atomic hydrogen and ozone in lower thermosphere and nitrogen oxides

08 p1277 A71-21006

Diurnal variation symmetry of upper atmosphere molecular oxygen concentration in terms of ozone photodissociation

09 p1435 A71-22446

Low temperature laboratory measurements of ozone absorption coefficients for atmospheric standards, using Dobson spectrophotometer and quartz iodine source

09 p1438 A71-23026

Umkehr inversion system for vertical ozone distribution observation, calculating error due to ignorance of temperature dependence of ozone absorption

09 p1489 A71-23447

Ozone distribution measurements in mesosphere and stratosphere by rocket during seasonal ionospheric disturbance and solar eclipse

09 p1490 A71-23562

Rate constant temperature dependence for ozone reaction with oxygen, considering airglow features due to singlet molecular oxygen

11 p1801 A71-25370

Vertical ozone distribution estimation by umkehr observations, discussing optimum statistical inversion technique application

11 p1794 A71-25387

Thermosphere daily variations consisting of diurnal oscillations excited by ozone and EUV heating

12 p1925 A71-27729

Flash UV photolysis of ozone/water vapor mixtures, noting OH radical nonreaction with ozone

13 p2025 A71-28349

UV photolysis of ozone in presence of molecular oxygen, discussing energy exchange reaction with molecular oxygen

13 p2025 A71-28350

Stratospheric circulation, investigating ozone heating role in temperature field formation by numerical experiment

15 p2399 A71-31963

Sunlight photodetachment rates and energy dependent cross sections for ozone ions, using photon beam excitation in buffer gas

16 p2574 A71-33962

Atmospheric ozone data in tropical regions from Nimbus 3 IR interferometer spectrometer measurements, indicating easterly jet stream existence during summer monsoon period

17 p2771 A71-35810

Vibrationally excited hydroxyl formation by atomic hydrogen reaction with ozone, using Fourier transform spectroscopy

18 p2874 A71-35833

Reaction rate of vibrationally excited hydroxyl with ozone, obtaining hydroxyl emission spectra by Fourier transform spectroscopy

18 p2874 A71-35836

Stratospheric ozone reduction through catalytic action of nitrogen oxides from SST exhaust, discussing degrading effect on atmospheric radiation shield

18 p2874 A71-36922

Rabbit tolerance to pulmonary edema by lung exposure to low ozone dosage

19 p3009 A71-38558

Low ozone dosage exposure effects on rabbit lung endogenous defense mechanisms

19 p3009 A71-38559

Upper atmosphere hydroxyl emission mechanism, discussing absorption band, energy balance, atomic hydrogen and ozone in lower thermosphere and nitrogen oxides

20 p3218 A71-39586

Mesosphere and stratosphere ozone vertical density distribution from sounding rocket data, considering photochemical theory and hydrogenic reductions

20 p3221 A71-39694

High altitude aerosol layer effects on atmospheric UV albedo, correcting ozone scale height spaceborne measurements

20 p3221 A71-39695

Seasonal variations in vertical distribution of ozone at high latitudes, using Murgatroyd model of looped meridional atmospheric circulation

21 p3375 A71-41395

Ozone concentration measurements near sunrise by balloon-borne electrochemical ozonesonde, noting scattered radiation effect

23 p3667 A71-43074

Hydroxyl emission of upper atmosphere, considering atomic hydrogen and ozone near thermosphere base

23 p3673 A71-43982

Vertical equatorial ozone distribution, incorporating oxygen hydrogen reactions and diffuse and advective transport in time dependent meridional model
23 p3673 A71-43987

Lymphocyte chromosome aberrations by inhaled ozone in Chinese hamster, indicating mutagen damage
24 p3799 A71-45150

OZONOMETRY

Semiautomatic electrophotometer with interference light filters for atmospheric ozone, aerosol and solar radiation recording
01 p0080 A71-10602

Umkehr technique vs Mast-Brewer sondes for ozone vertical distributions
01 p0073 A71-10857

Global ozone distribution from inverted radiance measurements by IR interferometer spectrometer /IRIS/ on Nimbus 3 satellite
01 p0074 A71-11249

German monograph on ozone recording device and temporal and spatial variations of tropospheric ozone in Northern Hemisphere
04 p0582 A71-15100

Ozone flux measurement in atmospheric surface layer by profile method as function of destruction coefficient, friction velocity and concentration
09 p1438 A71-23023

German monograph on ozone determination from sky radiance, considering Rayleigh and Mie scattering
17 p2733 A71-34794

Soviet papers on actinometry, atmospheric optics and ozonometry, covering atmospheric ozone contents measurement techniques, radiation balance, atmospheric spectral transmissivity, etc
20 p3257 A71-39326

Circumsolar scattered radiation effects on ozonometer reading accuracy, taking into account effect of sun angular altitude under cloudless conditions
20 p3237 A71-39329

Atmospheric optical stability control in ozone or other selectively absorbing gases measurements, filtering out spurious scattered light from aerosol particles
20 p3257 A71-39331

Wide passband techniques for atmospheric total ozone content measurements, discussing choice of ozonometer characteristics and filter parameters
20 p3238 A71-39335

Global atmospheric ozone distribution from inverted radiance measurements by IR interferometer spectrometer onboard Nimbus 3 satellite
20 p3220 A71-39668

Brewer bubbler as continuous surface ozone sensor, measuring ozone vertical distribution in atmosphere
21 p3377 A71-40181

OZONOSPHERE

Ozone screening heights from sunrise effects on D region VLF wave reflection
02 p0212 A71-11968

Atmospheric reflection latitude and angular dependence on wavelengths from satellite UV measurements, noting ozone content seasonal variation of ozonosphere
03 p0413 A71-14010

Secondary umkehr effect in solar UV region at twilight, proposing origin mechanism by ozone layer optical properties
08 p1357 A71-21875

Diurnal correlation between cosmic ray meson intensity and atmospheric ozone content on magnetically undisturbed days
14 p2231 A71-29723

Atmospheric total ozone increase during 1960s, investigating possibility due to southward air flow in troposphere and low stratosphere
19 p3047 A71-37298

P

P BAND

Projectile P band FM/FM telemetry system for in-barrel data acquisition
01 p0034 A71-10912

P-channel MOSFET tetrodes static and dynamic characteristics compared to conventional MOS triode, considering transfer and gate threshold voltage
02 p0229 A71-11811

P WAVES

Earth and planetary surface soil dielectric constants and conductivity determination based on p-wave velocity data correlation
05 p0743 A71-17142

P-I-N DIODES

U DIODES
U P-I-N JUNCTIONS

P-I-N JUNCTIONS

End layers role in forward I-V characteristics of P-I-N power diodes, ensuring minority carrier current continuity
02 p0235 A71-12919

Microwave diode technology, discussing Schottky barrier, p-i-n junction, varactor, tunnel, bulk effect and avalanche diodes performance and applications
08 p1266 A71-21622

P-i-n avalanche diode trapped plasma avalanche triggered transit /TRAPATT/ oscillations characteristics and voltage waveform under square wave driving current, using computer program
12 p1887 A71-27046

Microstrip p-i-n diode controlled L band digital phase shifter for aircraft-satellite communication
14 p2217 A71-31055

Computer aided design of P-I-N diodes equipped S band phase shifter for phased array antennas, discussing optimization problems
15 p2375 A71-31414

Li-drifted Ge p-i-n diode for low noise IR detectors, describing spectral sensitivity and NEP value
22 p3543 A71-42127

Impedance and capacitance frequency dependence of p-i-n junction diodes at microwave frequencies with high injection levels
23 p3650 A71-43308

Operational principles and circuit diagram of transistorized preamplifier for Si p-i-n gamma quanta radiant flux detector, noting noise properties and possible improvements
24 p3810 A71-45151

P-N JUNCTIONS

I-V characteristics of low and high resistance p/SiC-n/CdS/ junctions prepared by different methods
01 p0139 A71-11116

GaAs strongly doped p-n junctions, examining I-V characteristics changes under electron bombardment and mixed reactor field irradiation
01 p0140 A71-11458

Magnetoconcentrating effect in diodes with hemispherical p-n junction and semiorganic base in longitudinal magnetic field
01 p0057 A71-11461

Alloyed p-n junction diode with deep impurities, discussing barrier capacitance frequency dependence
01 p0057 A71-11462

P-n junction formation in zinc mercury telluride samples, using heat treatment to control carrier concentration
01 p0140 A71-11464

CdS-CuS n-p junction solar converters, noting long-wave sensitivity dependence on light extrinsic absorption
02 p0190 A71-11896

Si diffusion p-n junctions at high injection levels in strong electric fields, discussing I-V characteristics, minority carrier lifetime, barrier capacitance, etc
03 p0384 A71-13374

Polarization of spontaneous emission in Zn-doped GaAs p-n junctions as function of electric field strength
03 p0467 A71-13985

Multilayer structures dynamic phenomena during switching, examining similarity theory with simple p-n junctions
03 p0388 A71-14387

N-p Si solar cells controlled lifetime doping effects on electrical performance
05 p0700 A71-16063

Ti-Ag contact N-P and P-N single crystal Si solar cells electrical and mechanical performance characteristics
05 p0700 A71-16069

N-p Si solar cells, investigating mechanism of low energy proton irradiation damage to back contacts
05 p0702 A71-16084

Lithium-containing p-n solar cells photovoltaic performance and stability tests at room temperature
05 p0703 A71-16090

Thermal resistance of thermal p-n junction semiconductor microwave limiter diodes in continuous and pulsed mode operation
06 p0873 A71-17543

MOS transistors and bipolar microcircuits mobile charge density, observing p-n junction effects
07 p1079 A71-20175

Volt-ampere characteristics of dual base n-type semiconductors as function of input p-n junctions
08 p1264 A71-21070

Planar-epitaxial IC resistors p-n junction parasitic effects on cut-off frequency, obtaining design formulas for capacitance and geometry
08 p1264 A71-21074

Light emission of microplasmas and mesoplasmas in silicon p-n junctions, determining spectral distribution
09 p1507 A71-22190

Forward biased asymmetric p-n junction diodes with arbitrary impurity distributions, measuring minority carrier lifetimes by refined step recovery technique
09 p1414 A71-22248

I-V and capacitance characteristics of silicon diodes prepared by diffusive melting, considering recombination processes in p-n junctions
09 p1414 A71-22290

GaAs lasers p-n junction active region thickness from minority carrier mobility and spontaneous emission measurements in threshold current determination
09 p1460 A71-22305

High temperature ultraminiature pressure transducers, reviewing p-n junctions thermal limitations and thermal properties of dielectric oxides used with solid state epitaxially grown sensors
09 p1448 A71-22772

Single crystal indium gallium phosphide p-n junction preparation by epitaxial vapor phase growth technique, determining energy gap dependence on alloy composition
09 p1510 A71-23121

P-n junctions formation in p-silicon irradiated by alpha particles
10 p1656 A71-24145

Series resonant transistor circuit exhibiting response nonlinearity caused by conductance and charge storing capacitance of p-n junction
11 p1740 A71-26544

P-n junction controlled discrete microwave commutation diodes performance calculation and design optimization
11 p1741 A71-26554

Photocurrent frequency dependence in thin-base silicon photodiodes for carrier optical generation behind p-n junction and depleted region
12 p1886 A71-26848

Accuracy requirements on crystal orientation for p-n junction laser with tilted mirrors and various resonator lengths concerning output vs current characteristics
12 p1914 A71-27095

I-V characteristics and electrical properties of n-p silicon solar cells at low temperature and low illumination intensities
12 p1869 A71-27434

Nonlinear planar transistor model, analyzing majority carrier current flow fields in base due to injection of emitter and collector p-n junctions
12 p1888 A71-27612

Junction conversion and fabrication of Hg-Cd-Te n-p photovoltaic detectors by proton bombardment
13 p2066 A71-28043

Transverse mode locking effect on radiation intensity of injection semiconductor laser as function of time and p-n junction refractivity
13 p2077 A71-28172

Multilayered semiconductor structures with p-n junctions, discussing I-V characteristics, noninjection component effects, carrier transport and negative resistance
13 p2111 A71-28920

Semiconductor thermoelectric battery p-n cell elements joining with mercury amalgam for commutating
14 p2181 A71-29953

Poisson equation for space charge layer of reverse-biased p-n junction in p-n-p structure with allowance for two types of moving current carriers
16 p2546 A71-33495

Low noise operation of CW devices with GaAs vapor grown p-n junctions, observing optimum AM SNR of minus 140 dB
17 p2713 A71-34445

Si p-n junctions microplasmas I-V characteristics, discussing avalanche breakdown, temperature dependence and light emission
18 p2953 A71-35872

Localized deformation effect on common-emitter transistor current gain, giving equations system defining band diagram configuration of p-n junction in thermal equilibrium
19 p3027 A71-37490

Relaxation time model of solid state diodes based on equations for electrons of given energy, including p-n junction and tunnel diodes
19 p3027 A71-37495

Theoretical model of excess surface current in p-n junctions, based on surface-controlled tetrode transistor experiment for bipolar transistors I-V characteristics explanation
19 p3029 A71-38142

Semiconductor lasers, noting AlGaAs-GaAs p-n heterojunction structure contribution to room temperature efficiency of diode lasers
19 p3074 A71-38230

P-n-p-n quadruple layer semiconductor junction light emitting diode with negative resistance characteristics, discussing epitaxial regrowth process and applications
21 p3355 A71-40739

Semiconductor surface state effects on p-n junction photodiode frequency characteristics under short and open circuit conditions, noting nonequilibrium capacitance during illumination
21 p3358 A71-41215

Electrical, photoelectric and electroluminescent properties of reverse biased GaP p-n structures at room temperature, considering isolated microplasmas
21 p3430 A71-41217

Logical GaAs integrated laser circuits, discussing integrated laser modules with diffused p-n junctions
21 p3394 A71-41228

Multilayered semiconductor structure with p-n junctions, discussing I-V characteristics, noninjection current component effects, carrier transport and negative resistance

21 p3433 A71-41306

Electrical properties and electroluminescence measurements for p-n junctions in Au- and Ag-doped GaP, noting negative resistance in I-V characteristics

21 p3433 A71-41312

Photocurrent for two stage transition in space charge layer in p-n junctions of germanium with radiation defects

21 p3435 A71-41333

Si Pt-n-p transit time microwave diode source noise measurement, noting low noise characteristics and suitability for local oscillator applications

21 p3359 A71-41413

Emitter-base junction degradation by avalanche breakdown in planar transistors with low doped/epitaxial base region

22 p3520 A71-41682

Temperature dependent threshold current density and doping gradient at p-n junction in epitaxial GaAs injection laser diodes

22 p3555 A71-41686

Neutron irradiation effects on Si p-n junction field effect transistors I-V characteristics, charge distribution in space charge region and transconductance

22 p3586 A71-42297

Low temperature investigation of microplasma breakdown in steep p-n junctions of Sb-doped n-type Ge

22 p3587 A71-42874

Large photomagnetic effect in semiconductor films using multilayered Cd-Te p-n microjunctions

23 p3716 A71-43484

Electron energy spectrum in periodic semiconductor structures of super thin p-n junction layers

23 p3716 A71-43485

Space charge density and carrier mobility in disordered regions of p-n microjunctions

23 p3717 A71-43486

High power semiconductor devices in pulsed operation mode for transient thermal resistance and p-n junction temperature estimation

23 p3652 A71-43584

Indium gallium phosphide p-n junction laser operation at 4.2 and 77 K, considering threshold currents magnitude

23 p3687 A71-44138

Kinetic parameters and conditions for optimal epitaxial growth of GaAs from liquid phase, observing solution cooling rate effect on p-n junction quality

24 p3808 A71-44724

P-N-P JUNCTIONS

Temperature dependence of current gain in p-n-p transistors due to increased surface recombination rate

14 p2213 A71-370623

P-N-P-N JUNCTIONS

Switched power limitation in p-n-p-n devices turned off by control current pulse, discussing thermal signal level

11 p1808 A71-25916

Thyristors junction area current rise time extension, discussing emitter field regional delay times as function of p-n-p-n structural properties

12 p1886 A71-26849

Switching on p-n-p-n structure under high injection level in both bases, noting current concentration and voltage steady state buildup

16 p2546 A71-33496

Switched power limitation due to thermal processes in p-n-p-n devices turned off by gate current pulse

21 p3430 A71-41219

Reduced switch-off time high voltage p-n-p-n structures using diode blocking coincident with thyristor collector junction

23 p3716 A71-43483

One dimensional diffusion model for on state propagation along p-n-p-n structure, determining propagation velocity as function of structural parameters and current density

24 p3859 A71-44462

P-TYPE SEMICONDUCTORS

Free hole drag in p-type Ge by photons in optical transitions between valence band subbands, examining magnetic field effects

02 p0296 A71-12613

Tunneling in boron doped p-type silicon metal-semiconductor and MIS tunnel junctions

04 p0636 A71-14973

Impurity effects of annealing of radiation defects in p-type silicon, considering annealing temperature

04 p0636 A71-15037

P-type aluminum gallium arsenide phosphide growth on gallium arsenide phosphide from solution, noting lattice match preservation and heterostructure junction devices

04 p0608 A71-15041

Amorphous Se p-type conductivity, discussing temperature and crystalline phase dependence

05 p0792 A71-16379

Dynamic stabilization of helical and sausage instabilities of p-indium antimonide electron-hole plasmas, using Ioffe type RF energized magnetic quadrupoles

06 p0935 A71-17489

Neutron induced lifetime damage short term annealing dependence on minority carrier density in p-type silicon, considering majority carrier repulsion by positively charged centers

07 p1175 A71-19061

Doping effect on positive Faraday rotation in n- and p-type GaAs at different impurity concentrations, noting shift of maximum to lower concentrations in p-type samples

07 p1176 A71-19227

Optical absorption spectra in Cu-doped p-type GaAs samples

07 p1177 A71-19498

Gamma ray spectrometers made from high purity p-type Ge crystal, observing performance

08 p1345 A71-21843

Gate voltage drift in enhanced p-channel MIS transistors having either pure silicon dioxide insulation or silicon dioxide with silicon nitride

09 p1413 A71-22156

Epitaxial deposition of discrete separated p- and n-type silicon on single sapphire substrate, considering technique for MOS devices fabrication

09 p1509 A71-23116

MOS transistors on P substrates, investigating ionizing radiation effects on I-V characteristics

12 p1885 A71-26830

Gamma irradiation effect on conductivity of varistors made of p-type black SiC

12 p1886 A71-26897

P-type Al-Ga-As-p-type Ga-As-n-type Ga-As single heterostructure preparation and properties, discussing effect on injection laser diode characteristics

12 p1914 A71-27027

P-type gallium selenide crystals impurity photoconductivity measurements by Q switched ruby laser

13 p2077 A71-27959

Capacitance/voltage characteristics of MOS capacitors before/after 25 MeV proton irradiation

14 p2210 A71-29797

Radiation resistance variations of n-type and p-type silicon photocells due to formation of one or two vacancy recombination centers

15 p2461 A71-31670

Diffusive p-type Si valve photocells, investigating barrier capacitance

17 p2713 A71-34565

Magnetostriction and magnetoelastic quantum oscillations in p-PbTe, using thermodynamic derivatives of Lifshitz-Kosevich expression for oscillatory part of electronic free energy

17 p2791 A71-34860

Semiconductor behavior of zirconium oxide formed on Zr substrate with n-type below 685 C and p-type above

17 p2759 A71-35222

Optical pumping and detection of spin polarized electrons created in p-type GaSb conduction band by excitation with light

17 p2791 A71-35583

Integrated complementary MOS circuit technology, discussing low power consumption, high speed, n and p regions realization on Si plates and design parameters relations

18 p2891 A71-36562

Heavily Ge doped p-InSb photoelectric and electric properties, showing impurity concentration effects

19 p3120 A71-38526

Oxygen enhanced sublimation of p-type PbTe thermoelectric materials in isothermal and ingradient testing of couples

20 p3266 A71-38953

N-type negative resistance, photoconductivity and I-V characteristics of sulfur-doped p-type Si, showing hole capture cross section dependence on electric field

21 p3429 A71-41204

Impurity photoconductivity, generation-recombination noise and temperature dependences of Hall coefficient and equilibrium carrier mobility in p-type cobalt-doped germanium

21 p3429 A71-41213

Pure and doped Ge dumbbell p and n type samples at liquid helium temperatures, investigating electric breakdown

21 p3430 A71-41224

Cyclotron absorption and resonance spectra of hot electrons in p-type InSb samples cut from single crystals containing different amounts of impurities

21 p3430 A71-41226

Coherent stimulated recombination radiation emission by p-type cadmium silicon arsenide single crystals in liquid nitrogen cryostat under various pumping levels

21 p3431 A71-41229

Impurity photoconductivity spectra determination for n and p type Si crystals under 660 MeV proton irradiation

21 p3433 A71-41311

Cubic nonlinearity in p-type germanium semiconductor in constant magnetic field

21 p3435 A71-41337

P-type germanium photon drag detectors with carbon dioxide lasers, discussing response speed and sensitivity

22 p3543 A71-42129

Illumination effects on drain current for p channel enhancement type MOS transistor, attributing photoresponse to electron excitation in conduction band

22 p3523 A71-42481

Photorecombination model explaining kinetics of negative photoconductivity effect during illumination of impurity region in high resistivity p-type ZnTe-CdTe single crystals at room temperatures

23 p3717 A71-43948

Two component 1/f noise measurements in p-channel MOS transistors

24 p3812 A71-45352

PACIFIC ISLANDS

NT JAPAN

NT NEW ZEALAND

NT PHILIPPINES

Manua Islands/Samoa/ lavas chemical composition, geology and probable history

18 p2911 A71-35887

PACIFIC OCEAN

Spectral statistics of seasonal tropospheric wave disturbances in tropical Western Pacific, observing synoptic and planetary scale wind field

21 p3374 A71-41177

Latitudinal distribution of integral water drop content of clouds above Pacific, Atlantic and Indian oceans from Cosmos 243 measurements

22 p3568 A71-41653

PACKAGES

NT APOLLO LUNAR SURFACE EXPERIMENTS PACKAGE

PACKAGING

NT ELECTRONIC PACKAGING

Si solar cell cover glass assembly and packaging improvements using Teflon

05 p0702 A71-16079

PACKING DENSITY

Combined continuity and force equations for sound attenuation as function of thermal and viscous losses in liquid gases, taking into account fcc and bcc packing

06 p0927 A71-17569

Steady multifiber winding process conditions in compact glass fiber packing for glass fiber reinforced plastic tubes

09 p1482 A71-22817

Electron microscope investigation of packing defect energy effect on structure of crystal dislocations in hardened metals during annealing and deformation

09 p1473 A71-23226

Semitransparent particle model of Martian surface for reflective power at various incidence and reflection angles, discussing packing density and optical parameters

24 p3869 A71-44808

PACKINGS [SEALS]

Elastomeric seals for aircraft fastener countersinks, providing corrosion protection to static metal surface treatments and organic coatings

10 p1633 A71-24118

Rotational effects on laminar subsonic compressible viscous flow across shaft face seals, noting leakage rates and pressure profiles

14 p2251 A71-29936

PADE APPROXIMATION

Pade fractions use in calculation of axisymmetric flow of perfect gas past blunt body of revolution, obtaining stream function Taylor expansion terms

15 p3246 A71-32122

PAGEOS SATELLITE

Pageos 1 balloon satellite rotation observation over two years, determining period as time function

03 p0379 A71-14005

Spin dynamics and deformation measurements on PAGEOS balloon satellite by photoelectric photometry, noting solar radiation pressure torque

11 p1761 A71-25546

Photographic observations of Pageos satellite during 1968 with PO-2 camera

14 p2250 A71-31118

Trace length analysis of Pageos and Echo 2 satellites by camera observations

14 p2318 A71-31119

Pageos spacecraft orbital acceleration prediction by radiation pressure perturbation theory accounting for anisotropic scattering of solar spectra from rotating ellipsoidal body

16 p2641 A71-33772

Pageos satellite optical tracking experiment, discussing camera, point image quality and quartz clocks rms error

21 p3347 A71-40260

PAIN SENSITIVITY

Anatomical load sensing method, determining torso pain thresholds by sensitivity tests [SESA PAPER 1823A]

17 p2689 A71-34539

PAINTS

Far IR cryogenic black paints absorptive throughout IR with surface stability at liquid He temperature and resistance to abrasion and flaking

08 p1335 A71-21383

Underfilm in high humidity environments corrosion of Al alloys coated with paint films, using pH indicating dyes
[NACE PAPER 19] 09 p1469 A71-22888

Photochromic paints for nondestructive testing of aerospace materials and structures
10 p1633 A71-24102

Paint absorbance values effect on passive thermal control system primary component, using calibrated computer satellite model
[AIAA PAPER 71-455] 11 p1859 A71-26238

Space stable thermal control coatings, noting reflectance optical spectroscopy of zinc oxide based paints and zinc orthotitanate
11 p1747 A71-26520

Space radiation environmental effects on reactively encapsulated zinc orthotitanates and paints
[AIAA PAPER 71-449] 12 p1920 A71-26762

Aircraft personnel radiation hazards from radioactive luminous paint on instrument dials, signs and operational elements
13 p2021 A71-29145

Aerodynamic heating tests of cone flap reentry vehicle using temperature sensitive paint
20 p3311 A71-39197

Apollo 12 returned Surveyor 3 surface sampler examination for micrometeorite pits and soil, glassy spheres and other granular materials adhesion to paint
23 p3766 A71-43817

PAIR PRODUCTION

Electron-positron pair production during focusing of laser radiation in dense plasma
01 p0135 A71-11094

Bogoliubov electronic excitations anomalous scattering and tunneling in superconductor intermediate state, noting pair production one direction step function changes
07 p1181 A71-20207

Electron-positron pair production during focusing of laser radiation in dense plasma
08 p1342 A71-21952

Longitudinal plasmon decay in strong magnetic field into neutrino-antineutrino pair
09 p1527 A71-23533

Cross section for electron and muon neutrino-antineutrino pair production by photons, using intermediate boson theory
11 p1802 A71-25588

Preferential pairing detection in Cds at 4.2 K through electron radiation damage of donor-acceptor pair green edge emission, discussing resulting wavelength shift
14 p2284 A71-29818

Ion pairing study in unresolved metal hyperfine splitting spectral region, using electron spin resonance line shape analysis
21 p3345 A71-40372

PALEOMAGNETISM

Ancient geomagnetic intensity in Japan by comparing natural remanent magnetization with known thermomagnetic magnetization induction, using stepwise heating method on antique pottery
04 p0582 A71-15127

Geomagnetic field intensity during past 2000 years from global data, noting cyclic variations
05 p0745 A71-17193

Geomagnetic reversals in volcanic flows, computing paleomagnetic pole positions similar to Tertiary rocks
10 p1601 A71-24397

Central Colorado basaltic lava flows tertiary paleomagnetic transition zone data, illustrating whole rock K-Ar dating difficulties
18 p2911 A71-35949

PALEONTOLOGY

Rotaformidae of upper cretaceous Nassellariina /radiolaria/ from Great Valley Sequence, California Coast Ranges
07 p1104 A71-20013

Supernova explosion or solar outburst theory of climatic effects on mass extinction of organisms at Cretaceous-Tertiary boundary
10 p1673 A71-24422

PALLADIUM

Benzoylformic and alpha-acetamidoacrylic acid hydrogenation, using modified ion exchange resin-palladium catalysts
03 p0375 A71-13199

Condensed state Ni and Pd atoms X ray emission spectra and electron structure
09 p1474 A71-23233

Platinum, palladium and gold detection in silver assay buttons by atomic absorption spectrophotometry
15 p2367 A71-31649

Hydrogen content effect on annealing and work hardened palladium wire tensile properties, determining yield/tensile stress and elongation
20 p3247 A71-38765

PALLADIUM ALLOYS

Resistance thermometer using amorphous Pd-Si-Cr alloy for enhancing sensitivity at cryogenic temperatures
09 p1444 A71-22714

Nb-Pd system concentration profiles and thermal diffusion coefficients, investigating phase formations by electron probe microanalysis
10 p1629 A71-25035

Nb-V, V-Pd and Pd-Nb systems diffusion coefficient as function of concentration for equilibrium diagrams, using method of diffusion layers
11 p1782 A71-26475

Ni-Pd alloys atomic arrangements and displacements by single crystal X ray diffuse scattering, using computer simulated model
13 p2087 A71-29134

Optical constants of beta-phase NiIn, PdAl and nickel gallium aluminide, noting chemical composition and electron density effects on photon energy absorption
21 p3426 A71-40033

Rh and Ag-Pd alloys magnetic susceptibility, investigating hydrostatic pressure effects
21 p3432 A71-41269

PALMGREN-MINER RULE

Miner theory of fatigue damage mechanism, considering validity and limitations
04 p0666 A71-14879

PAM [MODULATION]

U PULSE AMPLITUDE MODULATION

PANAVIA MILITARY AIRCRAFT

Panavia 200 multipurpose military aircraft, describing variable geometry design concept, performance characteristics, engines, armament and electronics
24 p3792 A71-44766

PANCREAS

Prenatal exposure to hypoxia, showing prolonged suppression of labeled amino acid incorporation into developing submandibular gland and pancreas in neonatal period
07 p1042 A71-19698

Pancreas pathomorphology under acute hyperthermia in animals, showing hemodynamic changes of vessel dilatation and intravascular leukocytosis
08 p1243 A71-21968

PANEL FLUTTER

Skew panels with in-plane forces under yawed supersonic flow, calculating flutter by matrix displacement methods
01 p0173 A71-10939

Critical velocity and elastic panel flutter stabilization in magnetohydrodynamic flow by distributed magnetic field control
02 p0293 A71-12628

Panel flutter structural nonlinearities, discussing shear flexibility, finite curvature and nonlinear inertia effects
[ICAS PAPER 70-29] 03 p0501 A71-13150

Panel with segment-wise constant mass distribution structural optimization design, considering flutter
05 p0824 A71-16577

Rectangular panel acoustic response by variational finite element method, including radiated sound field effects on structural vibration
06 p0984 A71-17622

Flutter analysis of stressed flat simply supported skew panels in supersonic flow, using small deflection thin plate theory
08 p1370 A71-21302

Nonlinear panel flutter analysis and response under random excitation or nonlinear aerodynamic loading, using Rayleigh-Ritz approximation to Hamilton variational principle
09 p1534 A71-22080

Cylindrical panel vibration in supersonic flow under random effects, calculating stress-strain statistical properties as function of incident flow velocity
10 p1690 A71-24572

Cylindrical shells panel flutter analysis for internal stress and supersonic flow, considering still air buckling data useful for determining buckling loads
[AIAA PAPER 71-328] 11 p1842 A71-25308

Weight minimization of semiinfinite flat sandwich panel at constant dynamic pressure in supersonic flow subject to flutter constraint, using finite element model
[AIAA PAPER 71-330] 11 p1842 A71-25310

Flutter analysis of clamped thin skew panels with midplane forces in supersonic flow, using Galerkin method
12 p1974 A71-26766

Computer program for aerodynamic forces on flexible plate undergoing transient motion in shear flow, applying to panel flutter
12 p1866 A71-27559

Supersonic flutter analysis of clamped skew panels with in-plane forces by Galerkin method, using two dimensional static approximation for aerodynamic loading
14 p2177 A71-30607

Structural and inertial nonlinearities influence on flat or curved panel flutter
14 p2331 A71-30825

Integrally stiffened five bay panel, calculating free vibration and random response to jet noise excitation
[AIAA PAPER 71-585] 15 p2504 A71-31532

Probability theory of stresses during random vibrations of flat panel in acoustic field of jet engine exhaust
15 p2504 A71-31704

Aeroelastic stability of flat plates and shells, considering panel flutter
16 p2648 A71-32987

Liapunov functions applications, discussing panel flutter, Couette flow and feedback control
16 p2607 A71-32994

Thin elastic shallow cylindrical panel in steady conducting supersonic gas flow, detailing magnetic field effects on static and dynamic stability and flutter
17 p2816 A71-34326

Nonlinear flutter of hinged closed cylindrical shells in supersonic gas flow, comparing with wind tunnel tests on panels
21 p3473 A71-41155

Edge supported cylindrically curved panels flutter, investigating in-plane boundary conditions and geometry effects on natural frequency
22 p3616 A71-42216

PANELS

NT CURVED PANELS

NT RECTANGULAR PANELS

NT WING PANELS

Stiffened integrally formed panel stability evaluation based on compression structural efficiency and manufacturing costs
[AIAA PAPER 69-760] 02 p0329 A71-12686

Graphite/epoxy composite structural spacecraft panels, discussing design analysis and fabrication procedure
04 p0618 A71-15344

Sandwich panels with conical shell or elongated honeycomb fillers, calculating stability and elastic properties
06 p0986 A71-17757

Ribbed aluminum panels airborne sound transmission loss, evaluating structural damping effects
08 p1231 A71-21431

Structural panel under acoustic loading by supersonic convected turbulence, deriving responses with finite Fourier transforms
15 p2507 A71-32131

Stiffened panel acoustically induced stress estimation using experimentally determined random S-N curves with various structural parameters
17 p2826 A71-35033

Integrally stiffened panels with bonding material across stringer tops, calculating vibration damping characteristics
17 p2826 A71-35034

Center cracked tension panels residual strength evaluation and prediction, deriving analysis technique based on stress intensity factor
17 p2827 A71-35155

Aircraft structural panels under cyclic static loads, examining fatigue life with probability theory, statistics and regression analysis
17 p2829 A71-35312

Composite panel of ten-ply unidirectional boron/epoxy laminate adhesively bonded to Al face sheets, discussing ultrasonic inspection technique
17 p2749 A71-35495

Panels and cassettes mechanical design for Camac modular construction of electronic analog and digital measuring instruments based on integrated circuits
19 p3029 A71-38065

PANORAMIC SCANNING

Photogrammetric coordinate relation of points on lunar surface and stereopanoramas of scanning photographs by Luna 9 and 13 orbiters
15 p2406 A71-31618

Oscilloscope and automatically tuned superheterodyne receiver panoramic display units for 10 kHz-60 MHz, considering design, circuits, performance and mechanical arrangement
21 p3353 A71-40518

PAPER CHROMATOGRAPHY

Paper chromatography combination with diminutophenyl amino acids mass spectrometry for analyzing purine and pyrimidine bases
06 p0865 A71-17574

Dipeptides separation and identification by column and paper chromatography for elution times prediction and sequence studies
08 p1251 A71-21688

Human lens fluorescent pigment O-beta-D-glucoside of L-3-hydroxykynurenine, discussing preparation, electrophoresis and paper chromatograms
11 p1718 A71-25634

Chromatographic paper extraction of residual thiosulfate in processed photographic film
19 p3062 A71-37247

PAPERS

Carbon fiber cladding paper for corrosion resistant asbestos laminates, discussing short fibers orientation and acid solutions effects on flexural strength and weight
12 p1921 A71-27014

PAPILLAE

Norepinephrine induced stimulation of myocardial oxygen consumption of cat papillary muscles under afterloaded isotonic and isometric conditions
22 p3486 A71-41937

PARA HYDROGEN

Temperature dependent differential quenching rates of vibrationally excited CO fluorescence by ortho and para hydrogen, using Born-Bethe approximation
19 p3107 A71-38052

Thermal conductivities of pure and mixed ortho- and parahydrogen and/or deuterium at temperatures with no molecular internal energy exchange
24 p3850 A71-44553

PARABOLIC ANTENNAS

Skyнет system small communications terminal specifications and equipment for ship to shore telegraphic traffic, considering small dish antenna for shipboard installation
02 p0217 A71-12436

Test terminal for Skyнет satellite communications, describing parabolic antenna, computer, receiver system, calibration program, etc
02 p0218 A71-12441

Hybrid mode flare feed horns for parabolic antennas, discussing horn parameters and angular aperture effects on gain factor or aperture transmission efficiency
02 p0234 A71-12807

Monograph on dual beam parabolic antennas in radio astronomy covering atmospheric effects, EM surface current density and scalar aperture field, etc
07 p1077 A71-19725

Optimum transmitted data volume, orientation accuracy and size of narrow beam parabolic spacecraft antennas, defining optimum parabola for approximate radiation pattern
07 p1078 A71-19871

ATS F and G, discussing communications experimental program with deployable 30 ft parabolic antenna
08 p1366 A71-21368

Efficiency evaluation of large parabolic antenna reflector by frequency scaling
09 p1409 A71-23496

Parabolic antenna instantaneous phase center calculations, using radiation patterns from aperture field and current distribution methods
10 p1582 A71-23807

Lightweight parabolic antenna model with inflated Mylar tube torus and central mast interconnected by wires, discussing construction, performance tests and tradeoffs
11 p1736 A71-25273

Large steerable radio telescope with equatorially mounted parabolic cylinder for lunar occultation, pulsar and scintillation observations
12 p1894 A71-26930

Multimode coaxial feed with circular cross section waveguide and concentric ring shaped radiator for parabolic antennas
16 p2546 A71-33480

Polarization structure of parabolic reflector antennas circular radiation by geometrical diffraction theory of spherical edge waves
17 p2697 A71-34256

Fixed multiple beam toroidal reflector antenna operating above 12 GHz, analyzing 10 by 15 ft scaled model parabolic torus
17 p2704 A71-35091

Composite ATS 6 and 7 satellite antenna feed capable of illuminating large space-deployable parabolic antenna
17 p2716 A71-35096

Filled aperture antennas for radio astronomy, considering mm wave observations, parabolic cylinder antennas and active/passive control of antenna surfaces
18 p2901 A71-37036

PARABOLIC BODIES

Orthotropic shell with hollow elliptical paraboloid form, discussing numerical solution for normal concentrated load action
06 p0998 A71-17855

Influence coefficients closed forms for one and two sheet hyperboloids and ellipsoidal and paraboloidal shells under axisymmetrical edge loads
06 p1002 A71-18413

Thin paraboloidal shells of revolution under external hydrostatic pressure loading, analyzing free vibrations by finite element method
06 p1004 A71-18650

Laminar incompressible boundary layer flow over thin Joukowski, parabolic and slender wedge airfoils, using small perturbation and quasi-similar theories
10 p1549 A71-23957

Edge loading effects on shallow hyperbolic paraboloid shell elastic damping, discussing flat plate theory analog solution
10 p1686 A71-23995

Spherical and paraboloid shells of revolution internal and external forces correlation, considering boundary value problem differential solution
10 p1686 A71-23996

Incompressible laminar boundary layer flow over parabolas and paraboloids, comparing results by local truncation methods with results by finite difference method
10 p1594 A71-24524

Lenslike media with parabolic index profiles, deriving equivalent transformation theorem for distributed optical systems design
12 p1928 A71-26810

Clamped and hinged spherical and paraboloidal shell caps elastic stability tests under external pressure loading, determining critical pressure
14 p2323 A71-29846

Incompressible laminar boundary layer on parabolic profile at angle of attack, noting singularity in all vanishing shear stress/separation/points
16 p2520 A71-33198

Viscous incompressible fluid flow downstream of paraboloid of revolution described by matching boundary layer approximations to potential flow solutions
17 p2727 A71-34673

Asymptotic solution of viscous incompressible flow past uniformly heated paraboloid of revolution with constant surface temperature
17 p2730 A71-35800

Paraboloidal shells of revolution inextensional vibrations comparison to Sanders theory, using finite element method
21 p3471 A71-41030

PARABOLIC DIFFERENTIAL EQUATIONS

Elliptic boundary value methods applied to parabolic initial boundary problems
01 p0111 A71-10320

Bubnov-Galerkin approximation method, reducing Cauchy problem for parabolic equations to ordinary differential system
01 p0111 A71-10436

Initial Dirichlet boundary value problem parabolic and elliptic equations of order 2b, discussing existence and uniqueness proofs
02 p0276 A71-12532

Boundary value problem for pluriparabolic differential equations
03 p0451 A71-13965

Cauchy problem for parabolic system with discontinuous coefficients
05 p0775 A71-17034

Algorithm for solving parabolic and elliptic partial differential equations with computing time, storage requirement and programming ease advantages
05 p0776 A71-17221

Linear and nonlinear parabolic equations approximate solutions by Galerkin methods, leading to linear algebraic equations
06 p0917 A71-17558

Parabolic equation for plate unsteady thermal conductivity during nonuniform heating, analyzing finite difference solution accuracy
06 p1006 A71-18007

Adjoint Green operator use in parabolic problems with normal boundary conditions
13 p2094 A71-27804

Parabolic systems solutions asymptotic behavior with dissipation in half space greater than zero, considering Cauchy problem
13 p2094 A71-27805

Time dependent problems involving parabolic and hyperbolic differential equations, discussing formulation for approximate solution by Galerkin methods
14 p2265 A71-30294

Hydrodynamic stability, determining velocity field bounds in laminar boundary layer by Nagumo-Westphal theory of parabolic differential operators [DFVLR-SONDDR-131]
16 p2557 A71-32982

Distributed parameter systems described by parabolic differential equations in Hilbert space, discussing existence of optimal control based on quadratic cost criteria
17 p2719 A71-34738

Hyperbolic and parabolic system three dimensional boundary layer equations, discussing characteristics and subcharacteristics roles in influence and dependence zones determination
18 p2902 A71-36039

Linear functional equations bounded solutions stability by reflexive Banach space mapping, applying to elliptical and parabolic differential equations ill-posed problems
18 p2941 A71-36351

Alternating-direction Galerkin methods application to parabolic and hyperbolic differential equations for obtaining efficient iterative solution of heat equation on rectangle
19 p3087 A71-38305

Theorems on parabolic and hyperbolic differential equations solutions continuous dependence on elliptic operator coefficients, deriving proof by hypothesis of existence and uniqueness
21 p3408 A71-40651

Integral and pointwise estimates of insulated cylinder temperature field spatial decay for semilinear parabolic equations
21 p3473 A71-41186

Numerical modeling and analysis of homocentric light beams propagation in cubic and nonlinearity saturation medium, using parabolic equation approximation
21 p3417 A71-41259

Stability of finite difference approximation to mixed initial boundary value problems for linear parabolic system of equations
22 p3567 A71-42295

Asymptotic expansion method for hyperbolic and parabolic differential equations fundamental solutions featuring validity near surface and in interior of characteristic conoid
23 p3698 A71-43096

Validity proof of asymptotic methods in one dimensional dynamic systems described by hyperbolic and parabolic differential equations
24 p3844 A71-45063

PARABOLIC FLIGHT

Orbital coordinates for body moving along parabola with small perihelion distance calculated for ephemeride
01 p0157 A71-10607

Transient heart rate response to square wave breathing in man under zero G parabolic flight
22 p3501 A71-41828

Two step spacecraft reentry guidance involving skip trajectory at parabolic speeds, proposing algorithm for running coordinate and speed vector components values
24 p3846 A71-45301

Spacecraft roll stabilization during parabolic earth atmosphere reentry, developing single parameter multistep algorithm
24 p3846 A71-45302

Parabolic velocity atmospheric reentry navigation algorithm for spacecraft control, demonstrating guidance accuracy to landing point
24 p3846 A71-45304

PARABOLIC REFLECTORS

NT PARABOLOID MIRRORS

L and S band paraboloidal dish antenna stellar calibration technique using absolute flux density from Cassiopeia A or Cygnus A
01 p0032 A71-10888

Unfurlable spacecraft antenna design and electrical characteristics, using Gregorian geometry with conical main and parabolic subreflector
02 p0232 A71-12324

Cassegrain antenna equivalent parabolic reflector concept for feeds near focus
02 p0233 A71-12424

Computer program description of radiation pattern of imperfect paraboloidal reflectors by transforming numerically expressed phase variations in plane electromagnetic wave
04 p0552 A71-15021

Directional antenna with parabolic reflector for missile tracking in telemetry band, considering radiation diagrams and design approach
07 p1078 A71-20012

Equatorially mounted parabolic reflector radio telescope, discussing structural design, mechanical drives and electronic control system
08 p1271 A71-21152

Circularly polarized parabolic reflector UHF antenna with helical feed for direct TV reception from satellite, discussing design and performance
09 p1417 A71-23034

Double curved reflectors assembly methods for rotating search radar antennas, considering parabolic and elliptic strip shapes for sidelobe suppression modification
09 p1409 A71-23495

Efficiency evaluation of large parabolic antenna reflector by frequency scaling
09 p1409 A71-23496

Max Planck Institute 100 m radio telescope at Bonn with all motions fully controllable, describing foundation constructional details, reflector structure and positioning gear
14 p2214 A71-30813

Radiation pattern of linear radiator mounted at quarter-wavelength in front of cylindrical parabolic reflector, discussing calculation procedure based on half-wavelength dipole near field
15 p2369 A71-31415

Wide angle microwave antenna radiation beam steering with fixed parabolic reflectors, using adaptive primary feed for intercepted field spatial Fourier transformation
17 p2708 A71-35493

Second Pleumeur-Bodou /France/ ground station for Telstar satellite communication, discussing equipment specifications, Cassegrain antenna and parabolic reflector
17 p2708 A71-35509

Pleumeur-Bodou /France/ ground station steerable parabolic reflector Cassegrain antenna for communication satellites, discussing specifications and radioelectric and mechanical characteristics
17 p2717 A71-35510

Wide angle paraboloid reflector electromagnetic field intensity distribution measurements in focal region

19 p3035 A71-38601

Parabolic reflector aperture antennas with Gaussian distributed random phase deviations, obtaining asymptotic expansion for radiation pattern

19 p3036 A71-38605

Broadband helical antenna feeds for millimeter wave parabolic reflectors and lenses, determining beamwidths and polarizations as functions of helix parameters and frequency

21 p3359 A71-41408

Circularly polarized parabolic SHF antenna with plane and parabolic reflectors, testing radiation pattern performance

22 p3515 A71-42521

PARABOLIC VELOCITY U ESCAPE VELOCITY PARABOLIC MIRRORS

Polarization structure of paraboloid mirror antennas circular emission by geometrical diffraction theory of spherical edge waves

01 p0056 A71-11204

Paraboloid mirror array of spherical segments for direct detection optical receiver, discussing minimum time dispersion and blur circle

03 p0425 A71-13650

Paraboloidal, hyperboloidal and flattened spheroidal telescope mirrors testing with optical compensation lenses by Foucault shadow and Ronchi methods

07 p1116 A71-20641

Parabolic radio telescope phase errors for field distribution, compensating for mirror system mass deformations

08 p1266 A71-21468

Parabolic two-mirror antenna design with one small mirror for diffraction fringe effects correction

14 p2196 A71-30637

PARABOLOIDS U PARABOLIC BODIES PARACHUTE DESCENT

Venera-borne gas analyzers for parachute descent probing of Venus atmosphere, describing design and operation

02 p0248 A71-11916

Military parachutists physiological and force field responses to aerospace recovery environment, using multichannel FM/FM telemetry for heart rates

02 p0207 A71-12389

Para-plane type parachute design with pilot chute controlled reefing for long range target

05 p0696 A71-16129

Parachute ejectable rocket-borne instrument package with telemetry system for lower ionosphere measurements, describing electrical and mechanical design and operation

07 p1208 A71-19803

Two stage parachute system RESY for water and land recovery of sounding rocket payloads

09 p1533 A71-23599

Gliding guided ribbon parachute for transonic speed deployment, investigating turn capability, opening reliability, structural integrity and effective drag

10 p1557 A71-24868

Venera-borne gas analyzers for parachute descent probing of Venus atmospheric composition, describing design and operation

13 p2067 A71-28203

Dimensionless products associated with scale factor effects of parachute critical opening /squidding/ velocity

19 p2996 A71-37293

Hematological characteristics of emotional stresses during parachute jump, studying leucocyte, erythrocyte and eosinophil populations changes

24 p3800 A71-44413

Flight dynamics of noise optimal flight profiles for V/STOL aircraft, minimization of gust effects on aircraft and nonlinear dynamic stability of parachute-load systems

24 p3792 A71-44761

PARACHUTE FABRICS

Dynamic decelerators using nylon tricot knit fabric and high elongation suspension lines for reduced peak force parachute deployment

03 p0349 A71-14273

PARACHUTES

NT DRAG CHUTES NT RECOVERY PARACHUTES NT RIBBON PARACHUTES

Para-plane type parachute design with pilot chute controlled reefing for long range target

05 p0696 A71-16129

Aerodynamic decelerator technology, emphasizing ribbon parachutes and flexible wings

06 p0846 A71-17692

Parachute weight, configuration and strength correlations for tradeoffs and design

07 p1017 A71-18900

Low speed wind tunnel stability tests of small guide surface, slotted solid, ring slot, cross and streamer decelerators, considering parachutes and drag measurement

07 p1022 A71-20310

Stokes flow parachute extremely lightweight decelerator for increasing altitude and rocket-borne radiosondes atmospheric data sampling quality

11 p1707 A71-25277

Parachutes for low density atmospheres, describing low and high altitude test results

11 p1707 A71-25525

West German parachute research, discussing stretching/filling shock, fabric material properties and static stability

15 p2350 A71-32373

Woomera /Australia/ meteorological rocket firings, using temperature and wind profiles to assess sensors and parachutes performance

20 p3221 A71-39691

PARACHUTING U PARACHUTE DESCENT PARADOXES

Energy considerations of satellite orbit paradox, discussing speed increase under drag, librational motion and secular month length

18 p2962 A71-36099

PARAFFINS

Internal short chain alkane populations of paraffinic hydrocarbons in tobacco teratoma and habituated tissue cultures

21 p3345 A71-40204

PARAGLIDERS

NT FLEXIBLE WINGS NT PARAWINGS

Flexible ram air inflated keel and leading edge parawing design optimization for increased stability and reliability, introducing semirigid member concept

24 p3791 A71-44582

PARALLAX

NT SOLAR PARALLAX

Limited parallax holograms of silhouetted objects for bandwidth reduction properties, considering suitability for viewing with extended incoherent sources

03 p0425 A71-13655

Coherent optical multichannel profiling correlator for increasing automatic stereocompilation speed by X parallax profiles simultaneous measure and display

07 p1114 A71-20209

Aerial photographs orientation point location, relating measurement weight of transverse parallax

09 p1451 A71-23178

Parallax errors in drawing contour lines on universal stereograph due to aerial photographic images brightness difference

13 p2070 A71-29083

Double stars astrometry, discussing proper motions, parallaxes and mass ratios of visual binaries

14 p2310 A71-30359

Stellar masses calculation, using dynamical parallaxes, Kepler third law and mass-luminosity relation

14 p2311 A71-30362

Visual binary stars spectroscopic observations, discussing spectra, luminosity, parallax and radial velocities of mass center and individual stars

14 p2311 A71-30365

Visual double stars spectroscopy, discussing stellar mass and parallax determination

14 p2311 A71-30367

White dwarf discovery method and properties, discussing color, spectra, parallaxes, luminosities, masses, red shifts, cluster and frequency distribution

14 p2316 A71-31005

Red subluminoous stars, presenting catalog identification, proper motions, spectral type, photometric parallax, tangential velocity, UB_V photometry, etc

14 p2316 A71-31006

Trigonometric white dwarf star parallax measurements, using astrometric reflector to derive H-R diagram

14 p2316 A71-31007

Secular parallaxes of reference stars by photometric distances and relative proper motions of open clusters at low galactic latitude

15 p2483 A71-31341

Position, parallax, distance, visual apparent and absolute magnitude, spectrum and visual luminosity tables for nearby stars

18 p2968 A71-37030

Binary stars survey at Nice observatory, presenting expression for probable period and parallax of newly discovered binaries

19 p3143 A71-38156

Multivariate statistical analysis of parameters measuring reference stars effects on parallax and error estimates

21 p3444 A71-40195

Secular parallaxes of reference stars by photometric distances and relative proper motions of open clusters at low galactic latitude

22 p3606 A71-42616

PARALLEL PLATES

Radiative transfer in plane layer of nongray absorbing and emitting medium bounded by black parallel plates, using rectangular model

01 p0180 A71-10945

Interference patterns obtained in transmitted light, determining surface parallelism of thin plates transparent in IR region using carbon dioxide laser

02 p0259 A71-11936

PARALLEL PROCESSING [COMPUTERS]

Rarefied gas linearized Poiseuille flow between parallel plates, using variational methods for Boltzmann equation

03 p0398 A71-13102

Radiation heat transfer from parallel plates with grooved surfaces for direction dependent radiation properties

03 p0521 A71-14293

One dimensional steady heat transfer in rarefied gas between infinite parallel laws, using Boltzmann kinetic equation

03 p0462 A71-14570

Thermal radiation absorbing and emitting medium in flow between parallel plates, examining heat transfer for simultaneous radiation and convection

04 p0685 A71-15517

Wall stability of parallel elastic plate duct in contact with inviscid compressible liquid flow

04 p0573 A71-15563

Minimum image size in parallel plate electrostatic spectrograph under focusing with small angular aberrations

04 p0600 A71-15593

Laminar flow heat transfer between plane parallel plates under generalized Graetz conditions, retaining longitudinal conduction term

06 p1007 A71-18306

Parallel plate plasma accelerator energy deposition, considering kinetic and thermal modes based on flow velocity, temperature and Mach number measurements

06 p0939 A71-18635

Cavitation flow of fluid with free surface past flat plate between parallel walls

07 p1092 A71-20081

Finite element solution of plane Poiseuille rarefied gas flow between parallel infinite plates

07 p1093 A71-20284

Rarefied gases heat transfer and density distribution between parallel plates at different temperatures

09 p1432 A71-22854

Rarefied gas thermal creep flow between parallel plates, using Boltzmann equation relaxation model for all Knudsen numbers

09 p1433 A71-23055

Capillary pressure and contact angle drop of two fluid flow separated by parallel plate interface

11 p1750 A71-25443

Lateral heat transfer along parallel conducting and radiating plates spaced by absorbing and isotropically scattering dielectric

11 p1788 A71-25524

Fredholm equation solution for radiative transfer between parallel plate configuration at midpoint

13 p2159 A71-27981

Heat flux between parallel plates in rarefied gas at various temperature ratios and Knudsen numbers, using Monte Carlo method

13 p2165 A71-29226

Numerical solution of coupled boundary layer equations describing strongly cooled turbulent flow of gas between parallel plates with property variation

13 p2166 A71-29473

Laminar incompressible fully developed pulsating flow between parallel flat plates effects on local time-average heat flux

14 p2334 A71-29603

Slip flow development in parallel plate channel entrance, discussing center line velocity and excess pressure distributions

15 p2393 A71-32262

H wave propagation in waveguide consisting of two parallel plates with longitudinal rectangular grooves, determining electric and magnetic fields by reduction method

19 p3019 A71-38331

Laminar-turbulent inverse transition in divergent radial flow between two parallel flat disks

21 p3366 A71-40101

Finite element method application to convective heat transfer between parallel planes for arbitrary surface temperatures and Nusselt number

22 p3619 A71-41874

Conductive heat transfer and temperature jump in polyatomic gas between parallel plates evaluated by variational principle based on linearized integro-differential equation

24 p3889 A71-44969

Microstrip line on silicon-silicon oxide system, investigating propagation modes and fringing effect by parallel-plate waveguide model

24 p3809 A71-45091

PARALLEL PROCESSING [COMPUTERS]

Navy avionic modular multiprocessing digital computer operating system reliability, comparing totally software and partly hardware approaches

07 p1067 A71-18833

Instant profile image correlator for coherent optical parallel processing, describing laboratory and aerial stereophotographs results

13 p2071 A71-29351

PARALLELEPIPEDS

Boundary value problems solution of Helmholtz and Poisson equations for parallelepiped, applying to elasticity theory

02 p0328 A71-12542

Rectangular parallelepiped and solid cylinder temperature distributions under time dependent ambient heating or cooling, solving thermal conductivity equation

02 p0333 A71-12647

Triple integrals approximation using cubature formulas symmetrical with respect to parallelepiped center

06 p0921 A71-18344

Base pressure measurement behind wedge-parallelepiped and cone-cylinder models of variable geometry

13 p2049 A71-29199

PARALYSIS

Chronic inability of succinate for protection against paralysis of rats exposed to hyperbaric oxygen toxicity, correlating thermocontrol response

11 p1720 A71-26124

PARAMAGNETIC AMPLIFIERS

U MASERS

PARAMAGNETIC RESONANCE

NT ELECTRON

PARAMAGNETIC

RESONANCE

PARAMAGNETISM

Macroscopic model of impurity electron centers for strong exchange interactions in ferromagnetic and paramagnetic semiconductors

09 p1508 A71-22880

Coulomb impurity centers in paramagnetics and ferromagnetics at Curie temperature with spin-electron exchange interaction

09 p1508 A71-22881

Low pressure paramagnetic regime axially symmetric hydromagnetic equilibria with spherical plasma-vacuum interfaces, extending solution to high pressure diamagnetic regime

13 p2104 A71-27843

Tunnelling conductance anomaly in metal-insulator-metal junctions containing paramagnetic impurities, analyzing I-V characteristics during switching effect

18 p2954 A71-36802

Single crystal vanadium carbide magnetic susceptibility decrease with increasing carbon content attributed to orbital paramagnetism

21 p3395 A71-40025

Paramagnetic cycles for low temperature superconducting magnet cooling, discussing refrigerator, cryogenic pumps, regenerators and adjustable heat source and sink

21 p3476 A71-40898

Magnetostriction in antiferromagnetic, spin flopped and paramagnetic phases of hydrated cesium manganese trichloride, studying volume changes and thermal expansion near phase transition

22 p3585 A71-41885

Millimeter and submillimeter wave radiation detection by paramagnetic materials, noting noise equivalent power dependence on various parameters

23 p3717 A71-44293

PARAMECIA

Cosmic and telluric radiation biological effects on paramecia, discussing relationship between dosage and growth rate

16 p2532 A71-33757

PARAMETERIZATION

Parametric differentiation method for reducing structural optimization and nonlinear programming problems to solution of simultaneous nonlinear algebraic equations

01 p0174 A71-10951

Switching bipolar transistor dynamic model equivalent circuit diagram characterization by parameters

02 p0228 A71-11655

Weakly differentiable functional systems related to analytic functions with parametric representation via Stieltjes integral, discussing range theorems

02 p0276 A71-11724

Optimal control synthesis for inertialess plant with feedback based on parameter estimation

02 p0236 A71-12622

Theoretical frameworks for testing relativistic gravity, using presence of metric and gravitational response equation from Dicke approach as postulates of parameterized postNewtonian formalism

07 p1190 A71-18859

Parameterized postNewtonian formalism for perfect fluids applied to Nordvedt effect in relativistic gravity

07 p1190 A71-18860

Parasitic reactances in Gunn effect device packages from microwave equivalent circuit parameters

07 p1072 A71-19104

Packaged microwave avalanche diodes negative resistance properties three-parameter characterization at low current densities

07 p1074 A71-19125

Comparison of experimental and gas dynamic fluid parameter jumps across earth bow shock, suggesting

reappraisal of gas dynamic analog from satellite observation

07 p1103 A71-19678

Multivibrator frequency stability as function of circuit parameters, using stability/parametric errors sensitivity coefficients for general algorithm

08 p1264 A71-21072

Fredholm integral equations solutions in atmospheric optics, proposing algorithm for optimal parameter regularization values

09 p1487 A71-22378

Metal-oxide-metal tunnel diode properties, discussing parametric effects on small and large signals detector operation

09 p1416 A71-22684

Dynamic control plants parametric identification theory for linear and nonlinear systems

09 p1423 A71-22874

Rational scale selection for theoretical and experimental graphs, investigating slopes and angles between line segments for various parameters

09 p1439 A71-23347

British Aircraft Corporation Numerical Master Geometry system using parameter surface mathematics and digital computer

10 p1580 A71-23759

Global monsoon atmospheric response model in geostrophic terms for heating input function parameterization, including Himalayas mountains effects

10 p1638 A71-23966

Collisional plasma background influence on classification of two stream instability, considering lines of equal asymptotic growth rates in parameter space

10 p1651 A71-24635

Reducible parametric systems of second order linear differential equations with variable coefficients for FM or AM-FM oscillations and Riccati equations

10 p1586 A71-24712

Parameter estimation - Conference, Prague, June 1970

10 p1586 A71-24735

Deterministic parameter estimation in nonlinear system near optimum feedback control by power series expansion

10 p1586 A71-24738

Second order system with structure perturbation affected parameter value, studying identification and autoadaptation by sign functions

10 p1586 A71-24740

Atmospheric boundary layer numerical modeling, discussing subgrid scale mixing processes and parameterization

10 p1639 A71-25067

Parameter optimization in linear control systems subject to random disturbances, using hybrid computer

11 p1735 A71-25840

Space shuttle thermal protection system optimal weight by numerical parameterization, discussing temperature constraints and material rearrangement effects

11 p1839 A71-26229

Nonlinear control systems dominating oscillation modes, investigating parameter variations effect by root locus technique

11 p1743 A71-26425

Equations system describing parametric distribution of ionized plasma in thermionic converter gap, discussing current density effects on low voltage arc discharge

12 p1938 A71-27210

Iteration parameters ordering in Chebyshev cyclic iteration method

14 p2265 A71-29557

French monograph on algorithms for parameters estimation for adaptive identification in real time of linear processes perturbed by related noise

17 p2767 A71-35232

Equations system describing parametric distribution of ionized plasma in thermionic converter gap, discussing current density effects on low voltage arc discharge

19 p3000 A71-38622

Automatic computational algorithm for parameter identification of nonlinear systems, using deterministic time invariant model with memory and gain functions

21 p3407 A71-40261

Heat transfer with dissipation from longitudinal surface curvature, numerically integrating all equations for parameters

24 p3889 A71-44968

Minimal order linear time-invariant systems description by smallest possible number of parameters, deriving differential or difference equations based on input/output parameters

24 p3816 A71-45122

[DFVLR-SONDDR-135]

PARAMETERS

U INDEPENDENT VARIABLES

PARAMETRIC AMPLIFIERS

Book on numerical method for coupled modes in plasmas, elastic media and parametric amplifiers covering differential equations, recursive functions, wave propagation and iterative calculations

01 p0111 A71-10356

Broadband cooled parametric amplifier with low noise for satellite communications ground station, discussing performance at room and cryogenic temperatures

01 p0053 A71-10799

Coherent optical sources in form of lasers and parametric oscillators with usable power for communications

02 p0260 A71-12002

Skyнет ground stations operations and equipment, discussing receiving systems parametric amplifiers, local oscillators, demodulators, noise temperature, frequency flexibility and reliability

02 p0217 A71-12433

Two stage parametric SHF amplifier for Skyнет V Naval receiver system

02 p0234 A71-12812

Remotely controlled room temperature microwave parametric amplifier design for shipboard satellite telegraphy terminal

02 p0234 A71-12813

Uncooled low noise microwave parametric amplifier for small receiving earth stations, describing three stage design, gain and bandwidth

02 p0234 A71-12814

Wideband low noise parametric amplifier design, discussing noise temperature improvement by refrigeration at microwave frequencies

02 p0234 A71-12815

Optimal gain tuning elements of cryogenically cooled parametric amplifiers

02 p0235 A71-12833

Nondegenerate parametric amplifiers above X band for satellite communication systems, discussing circuitry, varactors, diode packaging and solid state pump sources improvements

02 p0235 A71-12906

Parametric amplifier with nonlinear capacitance varying as quadratic function of voltage, deriving power gain, bandwidth and noise figure from equivalent circuit

03 p0383 A71-13270

Optical signal amplifiers operational principles, discussing parametric, semiconductor laser, and solid state amplifiers and amplifiers using gas in Fabry-Perot resonator

04 p0608 A71-15079

Multiparameter sensitivity functions in network theory, discussing auxiliary, adjoint and direct methods

04 p0560 A71-15148

Determinate phases formation mechanisms in unbalanced parametric oscillators, considering periodic shunting and bias modulation methods for oscillator starting

05 p0727 A71-16004

Optical parametric oscillators performance improvement by nonresonant pump reflection

05 p0762 A71-16338

Soviet book on nonlinear and parametric radio circuits covering amplification, detection, modulation, oscillation generation and frequency division, multiplication and conversion

06 p0867 A71-17441

Self pumped parametric amplification and oscillation of Gunn effect diodes

07 p1075 A71-19262

Singly resonant optical parametric oscillator allowable pump bandwidth

07 p1126 A71-20179

K band double-tuned nondegenerate parametric amplifier using single-packaged GaAs varactor diode, discussing design and performance

08 p1262 A71-20763

Wide band low noise millimeter wave parametric amplification using wafer varactor diodes with Schottky barrier junctions

08 p1263 A71-20769

K band cryogenically cooled wideband /600 MHz/ low noise parametric amplifier for millimeter wave satellite communication earth terminals, discussing design

08 p1263 A71-20770

Pulsed optical parametric oscillators, investigating effects of spatially nonuniform pumping with beams having Gaussian intensity profiles

08 p1302 A71-21432

Frequency characteristics calculation of regenerative two cavity microwave bandpass amplifiers, applying to parametric and quantum amplifiers and underexcited microwave relaxation oscillators

09 p1413 A71-22157

Autoparametric oscillator with tunnel diode and variable capacitors, considering effective frequency range extension

09 p1414 A71-22258

Optical parametric oscillator, observing simultaneous oscillation and second harmonic and difference frequency generation

09 p1493 A71-22760

Receiver systems for 100 meter Effelsberg radio telescope using cryogenically cooled parametric amplifiers for receiver system noise minimization

10 p1578 A71-24510

Ground stations for communication satellites, discussing radio transmitter and receiver systems using low noise parametric amplifiers at low temperatures and extended demodulator threshold

10 p1590 A71-25101

Communication satellite ground station radio receiver and transmitter systems including parametric amplifier and phase lock demodulators applications

10 p1590 A71-25102

Parametric amplifier design and construction for communication satellite ground station, discussing noise temperature, distortions, bandwidth and antenna gain

10 p1580 A71-25105

Book on radio astronomy instruments and observations covering high sensitivity radiometers, masers, parametric amplifiers, radio telescope design, radio spectrometers, parabolic reflectors, etc

11 p1737 A71-25359

Junction diameter reduction approaches for low noise generation, using Schottky diode parameters

11 p1737 A71-25675

Computer synthesis of nondegenerate parametric amplifiers with single mesh filter for maximum flat or Chebyshev frequency response applicable to quantum devices

12 p1886 A71-26844

Circuit design of double balanced parametric amplifiers regarding low cost and least degradation performance limits

13 p2039 A71-28906

Integrated S band microstrip parametric amplifier modules with self contained Gunn effect pump oscillator for space flight applications

14 p2210 A71-29570

Two loop parametrically coupled oscillatory amplifier with unlimited degrees of freedom, investigating segment of long line loaded at one end with periodically varying capacitance

14 p2211 A71-30083

Parametric amplification of two laser waves with amplitude and phase modulation under exponential signal growth applied to Raman scattering in picosecond pulse field

15 p2418 A71-31188

High gain parametric generation of coherent light in ammonium dihydrogen phosphate crystal continuously tunable across visible spectrum with UV harmonic of Nd-YAG laser

15 p2420 A71-32383

Doubly resonant optical parametric oscillator frequency instabilities and threshold, studying nonresonant mode feedback effects

15 p2423 A71-32605

Gain improvement in TWT parametric amplifiers based on slow space charge waves interaction with slow wave structure field by electron beam modulation

15 p2378 A71-32629

Parametric regeneration amplifier with capacitor modulation by signal voltage only

15 p2378 A71-32633

Parametric microwave amplifier feasibility with laser pumped electro-optical crystal as nonlinear element

16 p2589 A71-34135

Optical parametric oscillation internal to laser cavity, including temporal response effects of laser population inversion

17 p2751 A71-34377

Quantum mechanics model of optical parametric amplifier, considering performance of optical information systems

17 p2698 A71-34409

Low noise parametric amplifiers for communication satellite ground station radio receivers, considering components characteristics

17 p2709 A71-35513

Parametric amplifiers for ground station low-noise receivers in communication satellite systems, considering frequency range extension effect on noise temperature and passband requirements

18 p2890 A71-36557

Parametric resonant circuit with low pumping frequency and transfer function variation according to arbitrary complex periodic law

18 p2896 A71-36623

Tuning range extension of doubly resonant lithium iodate parametric oscillator by upconversion, using simultaneous pumping by single ruby laser beam

19 p3071 A71-37477

Low noise parametric amplifier design and construction for Intelsat 4 satellite communications earth stations

19 p3027 A71-37496

Vibrating systems behavior under combined parametric excitation and self oscillation mechanism, investigating damping and generation control

19 p3155 A71-37526

Visible thermal tuning CW parametric oscillator using barium sodium niobate as nonlinear material

20 p3241 A71-38788

Optical parametric oscillator signal wave amplitude fluctuations during nonresonant pumping, calculating

damping term governing temporal behavior of deviation from stationary value

20 p3268 A71-38835

Fluctuations in parametrically excited subharmonic oscillator, deriving steady state probability distribution for amplitude and phase transitions analogous to Brownian motion of particle in potential well

20 p3203 A71-39094

Optical parametric oscillator pumped with laser light, calculating radiation intensity fluctuations

20 p3246 A71-39458

Three-frequency parametric traveling wave amplifier amplification and conversion factors calculation by numerical method with allowance for fast and slow space charge wave effects

20 p3206 A71-39812

Gunn effect devices properties and applications, discussing microwave energy sources tunable and local oscillators, parametric amplifier pumps and radar transmitters

21 p3357 A71-40819

Sound waves interaction in piezoelectric semiconductors under pumping, deriving basic equations for parametric amplification investigation

21 p3430 A71-41216

Extinguishing parametric vibrations, changing equivalent natural frequency from resonant state by supplementary load

21 p3473 A71-41368

Tunable CW optical parametric oscillator optimum operating conditions, using barium, sodium and lithium niobate crystals parametric fluorescence tuning curves for comparison

22 p3557 A71-41863

Determinate phases formation mechanisms in unbalanced parametric oscillators, considering periodic shunting and bias modulation methods for oscillator starting

22 p3524 A71-42753

Optimal design for minimum noise maximum gain bandwidth of lower sideband parametric up-converters

23 p3630 A71-42917

PARAMETRIC DIODES

Self excited cavity oscillators with tunnel and parametric diodes and nonequilibrium medium, noting single and multimodes, energy capabilities and frequency interactions

02 p0231 A71-11874

Superhigh multiplicity wideband tunable parametric diode frequency multipliers for decimeter range

06 p0873 A71-17542

Optoelectronic elements for information system applications, discussing photomultipliers, photodiodes, photoresistors, avalanche and photoparametric diodes response and bandwidth characteristics

17 p2752 A71-34391

PARAMETRIC FREQUENCY CONVERTERS

FM demodulator system with parametric tracking filters for threshold improvement, discussing reception performance

08 p1265 A71-21279

Single diode microwave circuit for simultaneous function as frequency doubler and parametric up-converter

12 p1887 A71-26999

Parametric up-converters for low noise broadband microwave receivers, discussing electronically tunable pump frequency accuracy and stability

17 p2714 A71-34606

Neodymium-yttrium-aluminate laser for high average power operation and second harmonic and parametric generation

17 p2753 A71-34802

Optimal design for minimum noise maximum gain bandwidth of lower sideband parametric up-converters

23 p3630 A71-42917

PARAMETRIC OSCILLATORS

U PARAMETRIC AMPLIFIERS

PARAMETREONS

Three-stable parametrons ternary logic circuits synthesis by topological method, realizing Post algebra basic operators

03 p0382 A71-13521

Single circuit parametric oscillator with balance modulated pumping voltage envelope as periodic function satisfying Dirichlet condition

11 p1740 A71-26539

Subharmonic quadrature components in parametron with balance modulated pumping voltage

11 p1740 A71-26540

Analog to digital converters employing subharmonic oscillator phase as recording medium, discussing parametron application as phase comparator

11 p1743 A71-26541

PARANASAL SINUSES

Röntgenological analysis of paranasal sinuses in civil aviators, studying facial cavities infection

13 p2023 A71-29367

PARAWINGS

Statics and aerodynamics of lifting decelerators /parawings and sailwings/ at supersonic and hypersonic speeds

01 p0002 A71-10927

PARTIAL DIFFERENTIAL EQUATIONS

Para-plane type parachute design with pilot chute controlled reefing for long range target

05 p0696 A71-16129

PARITY

Majority logic decoding for primitive polynomial and dual codes, discussing nonorthogonal parity-check sums formation methods and Euclidean geometry maximality

14 p2207 A71-30011

PARKING

Airport facilities operational planning, discussing computer simulation parking systems and arrivals building

19 p3041 A71-38026

Unassisted aircraft parking system /Accu-Park/, discussing equipment design safety and accuracy

21 p3325 A71-41247

PARKING ORBITS

Trans-Mars launch window problem, discussing minimum delta-V three-impulse noncoplanar transfer from circular parking orbit onto asymptotic velocity vector

10 p1671 A71-24331

Saturn S-4B continuous vent system for propellant tanks during parking orbit to prevent excessive pressure, requiring liquid settling with auxiliary ullaging rockets

18 p2973 A71-36453

PARKINSON DISEASE

Individual neurons activity during stereotaxic operations on Parkinsonism and hyperkinesia syndromes, describing microelectrodes for extracellular recording

15 p2365 A71-32535

Stop test method to study acceleration in movement control processes in man, considering elbow joint movements in normal and pathological tremors in Parkinson disease afflicted subjects

19 p3007 A71-37569

PARTIAL DIFFERENTIAL EQUATIONS

NT BIHARMONIC EQUATIONS

NT BURGER EQUATION

NT ELLIPTIC DIFFERENTIAL EQUATIONS

NT FOKKER-PLANCK EQUATION

NT GAUSS EQUATION

Q approach to problem solving applied to partial derivatives determination on digital computer, discussing approach structure and characteristics

01 p0048 A71-10221

Partial differential equations hybrid computer solution by extended space technique for overcoming slow convergence of Galerkin method

01 p0048 A71-10223

Partial differential equations finite difference approximation, applying convergence theorems with probabilistic method

01 p0111 A71-10318

Transform for hydrogen ion exchange perturbation problem, involving first order partial differential equations and method of characteristics

01 p0130 A71-10368

Cauchy problem for nonlinear integrodifferential equations with time lag argument, estimating iterative solution existence and uniqueness

01 p0112 A71-10491

Computer source code generation for symbolic partial differentiation program for continuous system digital simulation

02 p0226 A71-11778

Weak periodic solutions of hyperbolic partial differential equation with quadratic dissipative term for biharmonic waves

02 p0276 A71-12000

Partial differential equations solving device for analog computers

03 p0381 A71-13004

Self similar solutions of nonlinear partial differential equations, applying group invariance under infinitesimal transformation

03 p0449 A71-13075

Partial differential equation approximate solution by matrix transformation, reducing boundary or mixed problem to n independent linear ordinary differential equations

03 p0449 A71-13117

Nonlinear partial differential equations solution by variable separation method

03 p0451 A71-13713

Nonlinear partial differential equation solution for natural free-free vibrations of beam structures

03 p0513 A71-14172

Computerized Monte Carlo models of distributed parameter systems of partial differential equations with moving nonlinear boundaries

04 p0619 A71-15150

Complete system associated with given control, discussing trajectories uniform approximation and nonlinear controllability conditions based on linear partial differential equation

04 p0620 A71-15865

Adiabatic invariant of nonlinear periodic wave described by partial differential equations in weakly inhomogeneous medium

05 p0780 A71-16177

Singly curved rectangular plate free vibration characteristics obtained by partial differential equations of motion

05 p0825 A71-16605

German monograph on hot-wire anemometry in fluidics, taking into account partial differential equation solution for temporal and spatial temperature distribution along wire

05 p0753 A71-16899

Linear boundary value problem for first order partial differential equations of composite type with two real characteristics, deriving index formula

05 p0775 A71-17015

Partial differential equations approximate solution using Hermitian functions and collocation for improved numerical accuracy

05 p0776 A71-17220

Partial differential equations mixed boundary value problems with unsteadiness over part of boundary reduced to Cauchy problem

06 p0916 A71-17385

Nonlinear singular integropartial differential equation numerical integration extension

06 p0917 A71-17553

Similarity methods, partial differential numerical analysis, dispersive wave and perturbation theory applications to mechanics

06 p0920 A71-18220

Polyvibrating equation boundary value problem solution in Fourier series form, obtaining Green function

06 p0928 A71-18226

Optimal control for distributed parameter system described by linear hyperbolic partial differential equation, deriving existence theorem and cost function

07 p1147 A71-19471

Optimal solution existence theorem for control system described by linear hyperbolic partial differential equation

07 p1148 A71-19770

Partial differential equation solution for aircraft hydraulic lines flexural vibration by Bubnov-Galerkin method, reducing to Duffing equation analysis

08 p1286 A71-20783

Second order hyperbolic partial differential equation in canonical form solution by iterative method

09 p1485 A71-22277

Mechanical systems partial differential equations solution through reduction to infinite systems of ordinary differential equations, considering Cauchy problem power series solution

09 p1492 A71-22523

Linear theory of weakly perturbed supersonic plane axisymmetric flows of gas-particles mixture, deriving partial differential equation for perturbation potential

10 p1551 A71-24373

Fourth order partial differential equations boundary value problems solution by Monte Carlo techniques

10 p1637 A71-24601

Numerical search for optimum product space as extension of Gauss-Seidel relaxation method, noting applications to partial differential equations

10 p1637 A71-24841

Existence proof of periodic solutions to second order partial differential equations with imaginary roots

12 p1923 A71-27240

Numerical solution of Stefan type partial differential equations with phase variations, using nonlinear homogeneous implicit difference scheme

13 p2100 A71-27898

Relaxation methods application to optimal control of systems described by equations with partial derivatives, studying minimizing sequences

13 p2043 A71-28817

Linear control of systems governed by second order equations, discussing games in operational partial differential equations

13 p2095 A71-28823

Simultaneous partial differential equations, applying to one directional diffusion in finite porous slab accompanied by chemical reaction

13 p2025 A71-29011

Stress tensor components partial differential equations solution by method of characteristics, using isochromatic fringes

14 p2328 A71-30377

Optimal terminal control stochastic synthesis for linear systems by Bellman second order nonlinear partial differential equations

14 p2220 A71-30872

Numerical analysis of partial differential equations - Conference, London, June 1970

15 p2440 A71-31345

Variational principles and finite element method in partial differential equations, emphasizing basis functions fundamental to Galerkin procedure

15 p2441 A71-31351

Time dependent partial differential equations solutions, considering hopscotch class algorithms, Galerkin type methods and finite difference schemes

15 p2441 A71-31352

Constant density and viscosity fluid steady plane two dimensional flow under no external forces, deriving partial differential equations for vorticity, energy and pressure

15 p2389 A71-31728

Nonlinear partial differential equations solution by separation of variables, obtaining reduction to ordinary nonlinear differential equations

15 p2442 A71-32251

Higher order linear and nonlinear systems equivalence from partial/ordinary differential equations

15 p2443 A71-32521

Self similar invariant group solutions to Bellman nonlinear partial differential equation for optimal correction problems of control systems motion with random disturbances

16 p2549 A71-32935

Joule heating and winds in upper atmosphere due to geomagnetic disturbances at 140 km altitude, deriving set of nonlinear partial differential equations

16 p2564 A71-33726

Existence and uniqueness of generalized weak solution to problem of coupling unsteady partial differential equations

16 p2603 A71-34000

Laplace transform application to linear system of partial differential, integrodifferential and difference equations with periodic and quasi-periodic coefficients

17 p2780 A71-34911

Partial differential equations governing second order correlation functions for velocity and magnetic field in isotropic conducting turbulent flow

17 p2789 A71-35443

Global convergence of iterative schemes by Newton-Gauss-Seidel method, considering discrete approximations of elliptic partial differential equations

17 p2769 A71-35689

Dissipative wave motion asymptotic theory, considering initial boundary value problems for linear partial differential equations

18 p2910 A71-36819

Integral operating mode of nerve paths representation by linear diffusion channel with electrochemically active synapses, deriving complementary partial differential equations

19 p3001 A71-37250

Mixed problem for hyperbolic type linear non-homogeneous second order partial differential equation with delayed arguments, obtaining asymptotic solution for derived Cauchy problem

19 p3086 A71-38011

Solution of higher order linear partial differential equations with variable coefficients, using functions of multidimensional matrices

19 p3086 A71-38012

Hybrid computer continuous space methods for time dependent partial differential equations involving solution of sequence of two point boundary value problems

19 p3025 A71-38292

Numerical solution of partial differential equations - Conference, University of Maryland, College Park, May 1970

19 p3087 A71-38301

Continuity equation properties for incoherent fluid, obtaining linear partial differential equation

19 p3105 A71-38584

Linear theory of weakly perturbed supersonic plane axisymmetric flows of gas-particles mixture, deriving partial differential equation for perturbation potential

20 p3175 A71-38898

Small perturbations of stationary parallel flow with relaxation, considering boundary conditions around slender wings, partial differential equations and similarity law

20 p3213 A71-39569

Symbolic ALGOL programming of partial differential equations applied to three dimensional MHD runs

21 p3351 A71-40847

One dimensional two phase parabolic free interface/Stefan problem numerical solution, using method of lines to approximate partial differential equations at discrete time levels

22 p3575 A71-42294

Conditions definition for nonexistence of continuous right inverse for surjective linear partial differential operators on Frechet spaces

22 p3568 A71-42693

Dual control theory for distributed systems with time lag described by partial differential equations, considering controller and algorithms synthesis

24 p3814 A71-44686

Nonlinear partial differential system analysis

24 p3843 A71-44797

PARTIAL PRESSURE

NT HYPOXEMIA

NT OXYGEN TENSION

Human blood gases continuous measurement in vivo by mass spectrography, considering arterial nitrogen washout and cerebral blood flow determination

01 p0021 A71-10237

Output properties of electrically pulsed carbon dioxide laser as functions of partial gas pressure and discharge voltage

01 p0092 A71-10372

Alveolar air samples of human subjects at various altitudes, determining gas composition and partial pressure

12 p1876 A71-27658

Ar, N and Ne partial pressure tolerance in dogs, plotting saturation curves

13 p2005 A71-28038

Alveolar and arterial carbon dioxide partial pressure during rebreathing experiments at rest

13 p2007 A71-28435

Venous and arterial blood gases in hibernating and normothermic ground squirrels, showing venous oxygen and carbon dioxide partial pressures reduction in hibernation

17 p2681 A71-34941

Coronary blood flow at increased arterial carbonic acid partial pressure, noting induced hypercapnia

21 p3335 A71-40633

PARTICLE ACCELERATION

Electrons motion across gas plasma magnetic field under stochastic electric field, noting accelerating effect

01 p0135 A71-11032

Particle acceleration by coherent electrostatic wave propagation through plasma, producing monoenergetic particle beam

01 p0131 A71-11513

Meteor particle speed and size estimation using accelerated glass microsphere bombardment in plasmod

02 p0304 A71-11914

Solar proton and electron events from viewpoint of particle acceleration and magnetic field configuration in active region

03 p0478 A71-14036

Soviet book on cosmic ray physics covering high energy particles interactions, origin, acceleration mechanism, etc

03 p0481 A71-14424

Energetic electron magnetospheric motion and acceleration during substorms, examining fault line existence at near local midnight

03 p0419 A71-14519

Quasi-steady coaxial MPD arcs characteristics, studying Ar ion velocities, electrostatic ion acceleration mechanism and arc voltage gradient

[ALAA PAPER 70-165] 05 p0795 A71-16573

Electrostatic wave perturbation current using accelerated particles orbits in neutral sheet with electric field in plane

05 p0788 A71-16633

Double sheath model between two plasmas, taking into account reflected and accelerated particles initial velocities

05 p0790 A71-16727

Collective longitudinal space charge waves in trapped relativistic one dimensional plasma, calculating inhibition/enhancement of cosmic ray Fermi acceleration

05 p0791 A71-16940

Charged particle acceleration by electrical mechanism in magnetosphere, evaluating particle flux penetration into ionosphere

05 p0800 A71-17177

Short duration proton energy increases observation by Explorer 34, considering interpretation as acceleration associated interplanetary shocks

06 p0949 A71-17254

Electrostatic fields parallel to geomagnetic field role in charged particles acceleration mechanism to auroral energies, considering electron and proton precipitation

06 p0893 A71-17989

Extended stellar atmospheres production mechanism involving outward acceleration of material in rarefaction wave following shock wave arrival at atmosphere edge

06 p0976 A71-18472

Computational model for post acceleration propagation of solar flare charged particles

07 p1185 A71-19652

Charged particles acceleration in pulsed magnetic field, deriving distribution function by diffusion coefficient and turbulence spectrum determination

08 p1351 A71-20963

Solar cosmic ray interaction with oblique shock wave MHD discontinuity, noting energy particle buildup and acceleration

08 p1351 A71-20964

High energy electron background flux in F 2 layer, discussing grouped particle acceleration

08 p1354 A71-21012

Deceleration of low energy cosmic rays in solar wind involving Fermi acceleration by MHD waves and adiabatic energy change

09 p1514 A71-22802

Stochastic particle acceleration in random electromagnetic field determination by turbulent plasma motion in external homogeneous magnetic field

10 p1655 A71-25075

Solar flare two stage particle acceleration from X-ray burst observations, discussing induced electric field and Fermi mechanism

12 p1946 A71-26624

Cosmic rays origin from pulsar model with particles accelerated by magnetic dipole radiation, producing equal energy spectrum

12 p1948 A71-27365

Pulsar electrodynamics, considering oblique rotator with dense magnetosphere to supply particles for Gunn-Ostriker mechanism

12 p1968 A71-27539

Meteor particle speed and size estimation using accelerated glass microsphere bombardment in plasmoid

13 p2133 A71-28201

Charged particles acceleration by electric field in magnetosphere, evaluating injected particles flux into ionosphere under quiet conditions

13 p2128 A71-28234

Absolute spectra above atmosphere and magnetosphere and of particles accelerated in solar atmosphere during solar flare of 23 February 1956

13 p2128 A71-28253

Nonthermal X rays and 10-100 KeV electron acceleration and emission from solar flares, using spacecraft observations

13 p2129 A71-29056

Solar cosmic ray acceleration and propagation from time variation and heliocentric distance dependence of relative abundance of protons to helium nuclei

13 p2129 A71-29058

Test particle uniform acceleration motion in curved space-time, requiring torsion free and constant curvature particle world line

14 p2274 A71-29575

Forward/reverse drift pair bursts relation to decimeter type 3 solar radio emission, postulating existence of electron acceleration sources in upper corona

15 p2485 A71-31714

Cosmic ray particles acceleration in pulsar strong electromagnetic fields, investigating refractive index effects

15 p2473 A71-31717

Crab nebula pulsar model, discussing charged particles acceleration to relativistic energies by intense LF electromagnetic wave

16 p2632 A71-33236

Magnetic stars as cosmic ray generators, considering interstellar gas particle acceleration by EM forces produced by rotating stellar magnetic field

16 p2625 A71-33324

Cosmic rays lifetime in Galaxy in presence of particle acceleration in interstellar space

16 p2626 A71-33463

Ions acceleration during current passage through plasma, discussing maximum energies, threshold current and electron beam flux density

17 p2787 A71-34284

Solar flare X-ray origin model, discussing charged particle acceleration to relativistic energies, ambient gas heating and thermal and nonthermal X rays

18 p2958 A71-36740

Particle acceleration in solar flares, examining current layer generation in magnetic field above bipolar spot group

19 p3126 A71-37520

Matter effluence forming comet Bennett 1969 i tail, calculating particle ejection acceleration as function of intrinsic anomaly of nucleus

19 p3138 A71-37783

Charged particle acceleration by nonstationary sinusoidal electric fields in earth magnetosphere based on mathematical model

19 p3129 A71-38377

High energy electron background flux in F 2 layer, discussing grouped particle acceleration

20 p3280 A71-39592

Magnetospheric electrons and protons acceleration and slot injection between radiation belts during magnetic storms, using flux measurements onboard Molniya 1 satellite

20 p3282 A71-39738

Large and small scale auroral formation dynamics, covering precipitating electron and proton acceleration and plasma instabilities role

20 p3229 A71-39860

Neutral gas acceleration to high velocity at low ionization level by electromagnetic plasma gun formed ionized shock wave

21 p3423 A71-40766

Charged particles acceleration in homogeneous magnetic field varying periodically with time /Alfven magnetic pumping/

21 p3424 A71-41117

Electron acceleration and solar flare triggering due to quasi-static electric field caused by gas motion near photosphere

22 p3590 A71-41466

Stochastic ion acceleration in excitation of LF oscillations in second regime of intense pulsed plasma beam discharge

22 p3577 A71-41814

Solar wind velocity increase by magnetic field energy conversion to kinetic energy, constructing steady state MHD one fluid model

23 p3719 A71-42949

Metagalactic X ray and cosmic electrons power spectra explanation by electron acceleration and scattering in turbulent plasma with frozen-in magnetic field

24 p3865 A71-44568

PARTICLE ACCELERATORS

NT BETATRONS

NT CYCLOTRONS

NT ELECTRON ACCELERATORS

NT ION ACCELERATORS

NT LINEAR ACCELERATORS

NT SYNCHROTRONS

NT VAN DE GRAAFF ACCELERATORS

Nuclear cascade pion energies in heavy material by Monte Carlo method, concerning cosmic ray and particle accelerator interactions

03 p0461 A71-13842

High velocity microparticle simulation techniques for studying properties, dynamics and origin of micrometeoroids, considering accelerators and impact results

[AIAA PAPER 70-30] 09 p1425 A71-22099

Broadband multicavity multimegawatt klystron design for superpower amplifiers in radars and particle accelerators

11 p1734 A71-26433

Two temperature model of cosmic ray high energy jets, predicting one particle accelerator momentum spectra

12 p1951 A71-27397

Nuclear cascade pion energies in heavy material by Monte Carlo method, concerning cosmic ray and particle accelerator interactions

22 p3579 A71-42643

PARTICLE BEAMS

NT ATOMIC BEAMS

NT ELECTRON BEAMS

NT ION BEAMS

NT MOLECULAR BEAMS

NT NEUTRAL BEAMS

NT NEUTRON BEAMS

NT PION BEAMS

NT PROTON BEAMS

Particle acceleration by coherent electrostatic wave propagation through plasma, producing monoenergetic particle beam

01 p0131 A71-11513

Charged particle beam interaction with electrostatic surface waves in plasma layer

06 p0929 A71-17317

LF echo oscillations in nonequilibrium plasma under low density charged particle beam

06 p0937 A71-18353

HF plasma instabilities driving mechanisms and distribution types, considering beam plasma computer simulation example

07 p1173 A71-20508

Positive and negative charged particle beam steady one dimensional motion analysis based on continuity, motion and Maxwell equations, allowing for electrostatic particle interactions

09 p1496 A71-22265

Automatic control application to liquid metal and semiconductor materials, plasma flows, charged particle beams and similar media interacting with magnetic fields

12 p1936 A71-26972

Particle flux, energy storage and beam loading effects on superconducting traveling and standing wave resonators in linear accelerators

16 p2587 A71-33494

Mathematical model of arc Pioneer 6/7 plasma probe electrostatic analyzer responding to monoenergetic unidirectional charged particle beam

18 p2952 A71-36583

Plasma cyclotron wave excitation with charged particle beam, determining unstable oscillations frequency range and spatial and time development with nonlinear analysis

19 p3111 A71-37633

Plasma resonator excitation by Cerenkov emission from density modulated uncompensated charged particle beam

24 p3854 A71-44512

PARTICLE CLOUDS

U CLOUDS

PARTICLE COLLISIONS

Auroral electrojet electric fields from plasma electron density and collision frequency profiles measurements via Black Brant rockets variable frequency impedance probes

01 p0075 A71-11332

Effective cross sections for molecular hydrogen positive ion formation in collision between He, Ne and Ar ions or atoms

02 p0287 A71-12503

Thermal DC noise generated in plasma at electron-ion collisions, using quantum mechanics for noise frequencies in EM radiation RF spectra

03 p0463 A71-13345

Slow positive ion and electron production in collisions of protons and hydrogen atoms with gases of planetary atmospheres

03 p0460 A71-13494

Inelastic particle collisions with energies exceeding 10 to the 13th eV, considering cosmic rays, nucleons and hadrons

03 p0475 A71-13837

Electromagnetic mechanism of direct muon and gamma quanta production by collision of strongly interacting particles

03 p0462 A71-13864

Sodium atom excitation by high energy particle collisions behind shock waves, measuring electron and vibrational temperatures

03 p0376 A71-13992

Electromagnetic wave absorption in steady state cosmology, considering particle collision and radiation damping effects in plasma model

05 p0806 A71-16167

Electromagnetic wave absorption in Einstein-de Sitter cosmology, considering collision and radiation damping effects for radiated angular frequencies

05 p0806 A71-16168

Ion-neutral coupling in plasma acceleration revealed by velocity disparities determined spectroscopically [AIAA PAPER 70-166]

05 p0788 A71-16572

Hard-sphere gas three-particle collision integrals, using binary collision expansion

05 p0785 A71-16704

Cold bounded nonuniform magnetoplasma harmonic generations model for small collision frequencies

07 p1166 A71-18889

Plasma concentration and heavy particle-electron collision frequency in open cylindrical cutoff resonator based on frequency shift and passband broadening data

07 p1171 A71-20184

Linear and nonlinear collisional processes in uniform weakly interacting plasma near equilibrium in absence of external magnetic field, using quantum mechanics treatment

09 p1503 A71-22864

Negative pion capture in nuclei, examining charged particle emission energy spectra

10 p1644 A71-24538

Collisional plasma background influence on classification of two stream instability, considering lines of equal asymptotic growth rates in parameter space

10 p1651 A71-24635

Micrometeoroid detector design for hypervelocity particle impacts, discussing solar radiation pressure effects on satellite measurements

11 p1761 A71-25544

Plasma in strong electric and magnetic field with allowance for inelastic electron collisions with neutral particles, showing resonant oscillations from Born approximation

12 p1937 A71-27183

Muon spectra and charge ratios at sea level, analyzing by collision model and one dimensional diffusion equations

12 p1933 A71-27406

Two phase supersonic barotropic flow with solid particles around thin profile with allowance for elastic particle collisions

12 p1864 A71-27450

Nucleon-nucleon and meson-nucleon collisions, determining secondary cosmic ray multiplicity dependence on primary particles energy spectra

13 p2121 A71-28057

Particle collisions effects on whistler ray paths, considering penetration through lower boundary of ionosphere

14 p2193 A71-29917

Soviet book on inhomogeneous plasma instabilities covering spatial gradients, charged particles collisions, temperature effects, steady electric fields and magnetic shear

14 p2279 A71-29942

RF power absorption of uniform hot ion-electron plasma column, considering collision effects and EM radiation

14 p2281 A71-30556

Nonlinear Fokker-Planck equation numerical tests for collision effects on self consistent field first order component and plasma electron distribution function perturbation

15 p2453 A71-31146

Nuclear soft core potential reproduction by isoscalar vector meson in nonlocal field theory of fireball in high energy cosmic ray collisions

15 p2472 A71-31151

Carbon dioxide laser flow-through discharge, measuring electron density and collision rates with heavy particles as function of tube parameters

15 p2419 A71-31741

Synchronous and oscillatory energy gain with electron-wave resonance time in collision magnetospheric plasma

15 p2371 A71-32024

Particle collision effects on electrostatic probe electron or ion current collection in transition regime as function of relative thermal energy

15 p2409 A71-32107

Molecular rotational excitation during CO ion-Ar interactions by ion beam collision spectroscopy, observing energy loss spectra

15 p2452 A71-32551

Plasma generation by photon irradiation, radiolytic mechanism and high energy particle bombardment, discussing ionized media chemical reactions

16 p2540 A71-32971

Collision integral for classical electron plasma, concerning Born-Bogoliubov-Green-Kirkwood-Yvon equations for long range interaction potential and motions of multiple particles

16 p2619 A71-33650

Collision rates in photon and relativistic particle gases, noting importance for cosmic radio and X ray sources processes calculations

18 p2949 A71-36100

Fireball model of meson production in high energy nucleons collisions

18 p2949 A71-36210

Collisions or weak turbulence caused noise effects on broadening of echo pulses in magnetically trapped particles, using propagator formalism

19 p3113 A71-37746

Binary elastic collision integral between particles of disparate mass, determining angular momentum form of Boltzmann equation for Lorentz mixtures

19 p3115 A71-38210

Cloud particle electrification mechanism with allowance for secondary collisions between particles

19 p3092 A71-38685

Time-of-flight measurements for relationship between velocity, mass and temperature in molecular gas motion and electron-atom collision kinematics

20 p3271 A71-38789

Fast charged particles inelastic collisions with atoms and molecules, investigating Bethe differential cross section theory

21 p3418 A71-40675

Long wavelength ion acoustic instability of two temperature collisional fully ionized plasma with heat transfer, noting additional destabilizing currents

21 p3422 A71-40708

Particle model measurements of collision and heating times in two dimensional thermal computer plasma

21 p3423 A71-40843

Gas molecular interactions, energy and momentum transfer and scattering from clean metal surfaces

22 p3577 A71-41996

Sea level high energy cosmic ray muon spectra calculation based on phenomenological model of nucleon-nucleus collisions

22 p3594 A71-42408

Plasma in strong electric and magnetic field with allowance for inelastic electron collisions with neutral particles, showing resonant oscillations from Born approximation

22 p3584 A71-42460

Inelastic particle collisions with energies exceeding 10 to 13th eV, considering cosmic rays, nucleons and hadrons

22 p3594 A71-42638

Electromagnetic mechanism of direct muon and photon production by collision of strongly interacting particles

22 p3579 A71-42665

Fully ionized plasma particle collision effects on surface oscillation stability

23 p3711 A71-43558

Particle collisions and relativistic effects on electromagnetic wave propagation within plasma in direction normal to external magnetic field near gyrofrequencies

23 p3645 A71-43559

Apollo 12 returned Surveyor 3 samples examination for meteoroid and lunar ejecta impacts evidence by optical and electron microscopy

23 p3766 A71-43819

Statistical system formation in fast hadrons collision process and multiple hadron production

24 p3851 A71-45170

PARTICLE COUNTERS

U RADIATION COUNTERS

PARTICLE DECAY

U RADIOACTIVE DECAY

PARTICLE DENSITY (CONCENTRATION)

NT ELECTRON DENSITY (CONCENTRATION)

NT ELECTRON DENSITY PROFILES

NT ELECTRON DISTRIBUTION

NT ION DENSITY (CONCENTRATION)

NT IONOSPHERIC ELECTRON DENSITY

NT IONOSPHERIC ION DENSITY

NT MAGNETOSPHERIC ELECTRON DENSITY

NT MAGNETOSPHERIC ION DENSITY

NT MAGNETOSPHERIC PROTON DENSITY

NT PLASMA DENSITY

NT PROTON DENSITY (CONCENTRATION)

Parabolic particle distribution stability in plasmoids in guiding magnetic field under diffusion due to electron-ion collisions

01 p0133 A71-10680

Similar gas discharges for carbon dioxide lasers, including thermal effects and particle distributions over energy levels

01 p0093 A71-10682

Low energy particle environment at synchronous altitude during magnetically quiet times from ATS 5 auroral particles experiment

01 p0147 A71-11497

Space charge problem for thermionic converter emitter sheath for electrons and ions with half-Maxwellian distribution

02 p0291 A71-12234

Total particle number changes, evaluating approximate methods for transition effect calculation

03 p0426 A71-13870

Aerosols in stratosphere, describing physical appearance, size distribution and concentration

03 p0418 A71-14206

Carbide particles mean interparticle spacing and low alloyed steels dislocation density determination by planar and volume methods for metal matrix

04 p0612 A71-15076

Solar wind plasma power spectra noting frequency dependence, particle density and speed and interplanetary magnetic fields

05 p0802 A71-15942

Planetary nebulae and H II region dust density perturbation e-folding time, examining Lyman continuum radiation

05 p0812 A71-16689

Heliocentric cosmic ray particle density gradient production of north-south streaming in interplanetary magnetic sector, using neutron monitor

06 p0953 A71-18116

Nuclear tracks high density in Apollo core small silicate crystals, discussing extralunar dust and photospheric iron-hydrogen ratio

07 p1189 A71-18740

Plasma produced by pulsating fast electron beam, observing electron temperature and charged particle concentration

07 p1167 A71-19232

Parabolic particle distribution stability in plasmoids in guiding magnetic field under diffusion due to electron-ion collisions

07 p1170 A71-20141

Similar gas discharges for carbon dioxide lasers, including thermal effects and particle distributions over energy levels

07 p1125 A71-20143

Interstellar dust density, constructing cosmological model with gravitational equations

08 p1366 A71-21785

Sporadic meteoroid particles in ionospheric spatial density determined from kinetic energy measurements

09 p1519 A71-22562

Spatially uniform dense partially ionized plasmas asymptotic thermochemical relaxation processes due to heavy particle density, temperature or superimposed electric field changes

09 p1502 A71-22859

Concentration profile in incompressible viscous fluid flow across plane plate in oscillating motion, considering gravity diffusion

09 p1434 A71-23729

Mesosphere charged particles concentration and mobility measurements, using rocket-borne aspiration probes

10 p1604 A71-24705

Plasma production by pulsating fast electron beam, observing electron temperature and charged particle concentration

12 p1934 A71-26750

Monodispersed particle semiinfinite atmosphere, calculating invariance principles of diffused radiation based on Mie theory

12 p1960 A71-26823

Vacuum merging speed and magnetospheric cross tail electric field inverse proportionality to plasma sheet particle concentration

13 p2056 A71-27934

Muons lateral distribution in extensive air showers, studying density vs core distance

13 p2126 A71-28098

Cosmic ray muon intensity measurements in water at large depths by Cerenkov counter

15 p2475 A71-31781

Atmospheric structure effects on muons zenith angle distribution and maximum intensity direction as function of energy at two different altitudes

15 p2476 A71-31788

Density distribution of plasmaspheric particles in equatorial plane via model of plasmasphere streaming, noting current system production in lower ionosphere

16 p2562 A71-32806

Diffuse skylight measurement for atmospheric dust particle concentration, considering sunlight scattering by air molecules and aerosol layers

16 p2567 A71-33767

Cometal dust polydispersion, showing particle distribution near nuclei similar to meteor streams

17 p2803 A71-34829

Outer planets missions combined zodiacal experiment, examining meteoric, asteroidal and satellite particles distribution and orbits

[AAS PAPER 71-127] 19 p3064 A71-37919

Ice particles initial concentration effect on coagulation growth kinetics, considering distribution function variation with time

19 p3095 A71-38705

D region ionization by solar corpuscular streams, considering formation of charged particle concentration profiles

20 p3216 A71-39141

Aerosol measurements over Atlantic and Indian Oceans, discussing aerosols optical thickness, effective radii, concentrations, sizes and optical properties variations with latitude and meteorological conditions

20 p3257 A71-39328

Gas-solid particles flow pseudofluid equations, discussing difference of species and partial density and various flow phases

21 p3365 A71-40018

Sea level high energy cosmic ray muon spectra calculation based on phenomenological model of nucleon-nucleus collisions

22 p3594 A71-42408

Total particle number changes, evaluating approximate methods for transition effect calculation

22 p3550 A71-42671

PARTICLE DETECTORS

U RADIATION COUNTERS

PARTICLE DIFFUSION

NT ELECTRON DIFFUSION

Monograph on particle diffusion losses in contact ionization plasmas under Q machine conditions covering collisionless theory, thermalization, alkali metals, ion recombination, etc

01 p0131 A71-10102

Energetic relativistic particles diffusion from radio galaxies

01 p0161 A71-11384

Decaying helium gas plasma particles diffusion across magnetic fields by combined microwave and Langmuir electron density probes, considering instabilities

03 p0463 A71-13470

Asymmetrical cosmic ray showers kinematic interpretation by heuristic model, discussing particle dispersion angular distribution

03 p0476 A71-13843

Cosmic ray particles diffusion with simultaneous energy transport, using leakage lifetime approximation

05 p0798 A71-16448

Solar flare event of 28 January 1967, observing parent flare location, particle fluxes and diffusion and spectral exponent

06 p0957 A71-18143

Relativistic velocity particles diffusion in cloud of scattering centers in centrifugal motion from Boltzmann equation solution by method of extensions

06 p0963 A71-18229

Diffusion coefficient estimation for energetic charged particles across magnetic fields from mathematical model

07 p1186 A71-19662

Particle diffusion modulation by simultaneous VLF and ULF electromagnetic waves during rocket experiment

07 p1062 A71-19680

Discrete particles dispersion effects on polycrystals mechanical properties, examining various models

08 p1311 A71-21540

Gas ionization by fission fragments emitted by spherical or cylindrical sources, deriving analytical expressions for ion distribution via diffusion model

09 p1496 A71-22358

Crystal lattice type influence on volume and boundary diffusion mobility of iron group metals atoms

09 p1510 A71-23325

Geomagnetically trapped particles radial diffusion across L shells, considering influence on steady state structure and dynamics of radiation belts

09 p1514 A71-23460

Transverse spatial particle diffusion in plasma under random oscillations, examining interaction between collisionless plasma and longitudinal wave

10 p1649 A71-24318

Interplanetary magnetic field irregularities and solar proton diffusion mean free path during 25 February 1969 event

10 p1677 A71-24556

Cosmic ray diffusion from discrete sources in random galactic location, studying chemical constituents anisotropy and age with scattering model

12 p1948 A71-27367

Monoenergetic beam relaxation dynamics in plasma, describing oscillation excitation and diffusion allowing for instability

12 p1942 A71-27769

Cosmic ray components atmospheric diffusion and production based on H quantum, two fireball and alpha model

13 p2122 A71-28064

Solar flare cosmic ray propagation, investigating bounded interplanetary diffusion medium effects

13 p2130 A71-29060

Nonequatorial charged particle radial diffusion in asymmetric magnetosphere by third adiabatic invariant violation, using Kosik model

14 p2235 A71-30347

Thermal electron density fluctuations in weakly ionized gas from viewpoint of particle diffusion in single charged particle phase space, considering incoherent scattering

15 p2458 A71-32392

Main sequence A and early F stars with shallow convective envelopes, investigating particle diffusion effects on element abundance data

18 p2960 A71-35939

Asymmetrical cosmic ray showers kinematic interpretation by heuristic model, discussing particle dispersion angular distribution

22 p3594 A71-42644

Cosmic ray solar diurnal variation anomaly at 1954 minimum, discussing diffusion and scattering in interplanetary medium

23 p3720 A71-43136

Shock-heated Mg/MgO particle dispersion, postulating kinetic mechanism consistent with spectrometric observations

24 p3863 A71-44940

Upper atmosphere minor component distribution rearrangement, investigating transition time to diffusion equilibrium

24 p3823 A71-45031

PARTICLE EMISSION

NT ELECTRON EMISSION

NT FIELD EMISSION

NT ION EMISSION

NT NEUTRON EMISSION

NT PHOTOELECTRIC EMISSION

NT SECONDARY EMISSION

Pulsed coaxial plasma accelerator, measuring longitudinal gas pressure distribution, particle emission and magnetic fields characteristics under various operating conditions

08 p1341 A71-21498

Negative pion capture in nuclei, examining charged particle emission energy spectra

10 p1644 A71-24538

Cometary atmosphere photometric data, determining particle distribution and ejection rate, temperature, molecular lifetime, acceleration and emission velocity

11 p1821 A71-25542

Molecular incidence rate and emission over surface of cold wall and spherical test object in cylindrical space simulation chamber

15 p2393 A71-32703

Pulsed coaxial plasma accelerator, measuring longitudinal gas pressure distribution, particle emission and magnetic fields characteristics under various operating conditions

16 p2618 A71-33046

Carbon and methyl radical formation, studying emission intensities and chemi-ionization rates in hydrogen-oxygen flames with hydrocarbons

19 p3013 A71-38090

HF gravitational radiation due to quantum transitions, studying absorption, emission and sources

21 p3439 A71-40612

Book on high power laser radiation covering heating, melting, vaporization, particle emission, plasma production, gas and transparent material breakdown and biological effects

22 p3558 A71-42426

PARTICLE ENERGY

NT ELECTRON ENERGY

NT ELECTRON STATES

NT PROTON ENERGY

Electron photon cascade energy measurement by photomonitoring blackened spots on X ray films

01 p0084 A71-11369

Energetic relativistic particles diffusion from radio galaxies

01 p0161 A71-11384

Miniature multigrid probes for measuring energy spectra of charged particles and absolute plasma densities, comparing results to microwave measurements

02 p0247 A71-11637

Proton 4 satellite high and superhigh energy cosmic ray spectrometer, discussing principles of operation and parameters

03 p0426 A71-13833

Inelastic particle collisions with energies exceeding 10 to the 13th eV, considering cosmic rays, nucleons and hadrons

03 p0475 A71-13837

High energy muons in extensive air showers, studying spatial distribution, spectrum and electron showers by photon spark chamber telescope underground

03 p0477 A71-13860

Carbon/oxygen and nitrogen/oxygen ratios in cosmic rays, considering energy dependence interstellar ionization loss and necessity for two component source model

03 p0480 A71-14051

German monograph on application of measurement principle for determination of energy of high energy neutrons in lower atmosphere

03 p0481 A71-14368

Differential energy losses of alpha particles traversing materials in superconducting and normal states

03 p0468 A71-14414

Energetic proton bursts in magnetotail, examining flow direction and intensity, spectral energies and origin

03 p0482 A71-14517

Low energy particle variable flux measurement in midlatitude ionosphere, using rocket-borne thin window proportional counters

03 p0421 A71-14539

Auroral ionosphere, examining low energy proton fluxes parallel to geomagnetic field lines of force

05 p0738 A71-16160

Electrostatic fields parallel to geomagnetic field role in charged particles acceleration mechanism to auroral energies, considering electron and proton precipitation

06 p0893 A71-17989

Energetic solar wind particles, discussing interplanetary magnetic field curvature and gradient effects

06 p0956 A71-18142

Diffusion coefficient estimation for energetic charged particles across magnetic fields from mathematical model

07 p1186 A71-19662

Dawn to dusk magnetospheric electric field effect on energetic stably trapped particle drift shell pitch angle degeneracy

07 p1103 A71-19675

Ionospheric low energy electron and proton fluxes near equator from Isis 1 satellite soft particle spectrometer observations, considering energy spectra and pitch angle distribution

07 p1187 A71-19679

Solar cosmic ray interaction with oblique shock wave MHD discontinuity, noting energy particle buildup and acceleration

08 p1351 A71-20964

Satellite-borne spectrometer for low energy ion measurement

09 p1436 A71-22554

Upper atmosphere neutral component temperature measurement from thermal spread of charged particles beam

09 p1437 A71-22679

Polar caps energetic particle environment involving solar flare proton and electron fluxes

10 p1600 A71-24309

Very high energy cosmic ray muons, discussing recent experiments with mu-meson anomalous couplings, triplets and intermediate vector bosons

11 p1815 A71-25356

Field aligned anisotropy for auroral ionospheric energetic ions, calculating pitchangle distributions

12 p1899 A71-26885

Energetic charged particle motion in magnetosphere, considering radiation belt dynamics

12 p1949 A71-27372

Shower size distributions of accompanying energetic protons at mountain altitude as function of released energy

12 p1951 A71-27392

Magnetic dipole field second invariant and drift frequency in terms of pitch angle and energy from analytical approximation to trapped charged particle bounce period

13 p2055 A71-27925

High energy sea level cosmic ray neutrons energy spectra, noting angular distribution about zenith and attenuation length in atmosphere

13 p2120 A71-28050

High energy cosmic ray components, investigating tracks and trapped magnetic monopoles

13 p2120 A71-28051

Cosmic ray jet interaction with free or quasi-free nucleons, obtaining kinematic measurement, secondary particle composition and transverse momentum

13 p2121 A71-28058

Cosmic ray energetic spectrum variation from observed latitudinal effects during 1954-1962 solar activity cycle

13 p2129 A71-28551

Interstellar grain temperatures, considering radiant energy distribution and optical properties effects

14 p2305 A71-29679

Cosmic ray telescopes with scintillation and Cerenkov counters for 2 to 8 BeV energy range, describing structural details and operational specifications

14 p2247 A71-30597

Large volume Cerenkov detector design for cosmic ray energy total absorption spectrometer measurements

14 p2247 A71-30599

High energy cosmic muons momentum spectrum and charge ratio measurements at large zenith angles, describing magnetic spectrometer

14 p2247 A71-30601

Atmospheric cosmic ray propagation based on phenomenological model of hadron-nucleus collisions, predicting sea level nucleon, pion and muon energy spectra and ionization profile

15 p2474 A71-31732

Sea level high energy muon flux determination from underground burst energy spectrum measurements, using Kobayakawa-Miomo formula for cascade shower fluctuation

15 p2475 A71-31782

Muon sea level differential energy spectrum at 80 deg to vertical up to 1 TeV, using Nottingham spectrometer

15 p2475 A71-31784

Atmospheric structure effects on muons zenith angle distribution and maximum intensity direction as function of energy at two different altitudes

15 p2476 A71-31788

Zenith angle distribution of extremely high energy muons from bremsstrahlung showers by emulsion chamber, noting consistency with pion/kaon decay

15 p2476 A71-31790

Angular distribution of high energy cosmic ray muons incident at sea level at large zenith angles, investigating cascade showers initiated by muons

15 p2476 A71-31792

Cosmic ray measurements at various altitudes, describing magnet spectrograph for momentum spectra and particle identification

15 p2408 A71-31813

Collimated nuclear interactions induced by cosmic ray pions and nucleons in carbon and brass, noting energy dependence of events production frequency

17 p2796 A71-34858

Cosmic ray muons energy loss rate measurement in Fe using Durham magnetic spectrograph

18 p2957 A71-35930

Polarization measurement of cosmic ray muons at sea level as function of energy and zenith angle

19 p3124 A71-37284

Ion-exosphere in open magnetic field, calculating number density, pitch, moment and energy flux distribution from simple mathematical model

19 p3138 A71-37737

Proposed model with neutrons as energy source for solar corona, discussing validity based on capture gamma ray flux expectation

19 p3127 A71-38009

Solar effects contradictory relationships with earth atmosphere, discussing geomagnetic disturbance, annual variations, stratospheric transport and high energy particles

19 p3128 A71-38354

Polar cap absorption event, investigating solar high energy protons precipitation effects

19 p3129 A71-38360

Fast charged particle flux measurement in inner radiation belt by Cosmos 137 satellite in January-February 1967

20 p3278 A71-39140

Charged particle motion in constant magnetic field under random electric field, deriving maximum energy and diffusion coefficient

20 p3269 A71-39163

Pioneer 8 and 9 micrometeorite measurements of particles kinetic energy, momentum, velocity and direction, correlating measured particle flux rates with predictions based on zodiacal light

20 p3297 A71-39634

Ionospheric electron and neutral particle temperature average diurnal behavior from bottomside vertical soundings

20 p3225 A71-39723

Finite amplitude entropic waves with propagated acoustic radiation-fluid particle motion energy coupling, using thermodynamic J function methods

20 p3315 A71-39772

Low energy auroral particle measurements from polar satellites, obtaining electron and proton precipitations location, and angular and energy distributions

20 p3228 A71-39847

Low energy solar particle observation by widely separated Mariner and Explorer spacecraft, noting flare-associated and nonflare intensity peak correlation with sun

20 p3284 A71-39876

Radio pulses from pulsars, noting relativistic energy of particles from volume emissivity and surface flux density

20 p3305 A71-39950

Ionization amplitude calculation method, using extrapolation from complex energies approach

21 p3418 A71-40249

Fast hydrogen atoms penetration into fusion reactor plasma, calculating collision cross section rates coefficients

21 p3422 A71-40765

Electron concentration and degeneracy effect on threshold photon energy for optical transitions onset from splitoff valence band to conduction band in n-type GaAs

21 p3429 A71-41211

Electroabsorption spectra of cadmium telluride at photon energies smaller than forbidden band width, observing energy levels

21 p3429 A71-41212

High energy neutralized ion beam generation by focusing ultrashort laser pulses on thin foils, applying to nuclear reaction for superheavy nuclei production

22 p3555 A71-41595

Gum Nebula ionization and heating by energetic particles from Vela X supernova

22 p3598 A71-41917

Proton 4 satellite high and superhigh energy cosmic ray spectrometer, discussing operational principles and parameters

22 p3594 A71-42634

Inelastic particle collisions with energies exceeding 10 to 13th eV, considering cosmic rays, nucleons and hadrons

22 p3594 A71-42638

High energy muons in extensive air showers, studying spatial distribution, spectrum and electron photon showers by underground photon spark chamber telescope

22 p3595 A71-42661

Mg 24 photodisintegration rate in stellar silicon burning process, presenting reactions at low alpha particle energies

23 p3723 A71-42952

Underground meson telescope coupling functions calculations, using effective primary threshold energy

23 p3720 A71-43152

Solar high energy particles directional and temporal properties, investigating single encounter model with propagating interplanetary shock waves

23 p3720 A71-43153

High energy particle environment model at synchronous altitudes during quiet geomagnetic periods from satellite observation, establishing outer radiation belt distribution function

23 p3722 A71-43978

Multispecies high temperature Tokamak plasma heating by energetic particle injection, using Balescu-Lenard kinetic equation

24 p3852 A71-44490

Craters produced by high speed hardened spherical particles, investigating depth and diameter relationship to impact speed

24 p3885 A71-45324

PARTICLE FLUX

U FLUX [RATE]

PARTICLE FLUX DENSITY

NT ELECTRON FLUX DENSITY

NT NEUTRON FLUX DENSITY

NT PROTON FLUX DENSITY

Transformation properties of radiation field and electromagnetic energy fluxes of relativistic charged particles in magnetic field

02 p0312 A71-12362

Upper atmosphere micrometeorite research with sounding rockets, considering interplanetary particle flux

03 p0485 A71-13250

Extensive air shower muons at mountain levels, describing experimental procedure for fluctuation distribution

03 p0476 A71-13856

Zodiacal light interpretation based on ground-based, satellite and deep space probe Helios observations, considering particle flux measurements

03 p0491 A71-14012

Picogram dust particle flux measurements in selenocentric cislunar and interplanetary space by Mariner 4, OGO 3 and Explorer 35

03 p0491 A71-14014

Cosmic dust fluxes determination by rocket-borne micrometeorite experiments, using piezoelectric acoustic type impact detectors

03 p0492 A71-14017

Low energy particle variable flux measurement in midlatitude ionosphere, using rocket-borne thin window proportional counters

03 p0421 A71-14539

Charged particle acceleration by electrical mechanism in magnetosphere, evaluating particle flux penetration into ionosphere

05 p0800 A71-17177

Particle flux toward charged plate /plane probe/ moving relative to plasma

05 p0814 A71-17181

Absolute particle spectra above atmosphere and magnetosphere during solar flare of 23 February 1956

05 p0800 A71-17198

Plasma confinement in Tokamak, calculating particle and heat fluxes due to conductivity current and electric field

06 p0930 A71-17405

Geomagnetic tail structure near null sheet, indicating decrease and/or dissipation of plasma sheet particle energy density at lunar distances

06 p0893 A71-17994

Quiet time fluxes and differential energy spectra of protons and alpha particles at 2-20 MeV measured by cosmic ray detectors on OGO-3

06 p0954 A71-18127

Solar flare event of 28 January 1967, observing parent flare location, particle fluxes and diffusion and spectral exponent

06 p0957 A71-18143

Magnetic storm of 31 October 1968, observing charged particle increase at geomagnetic equator

06 p0961 A71-18172

Temporal intensity variations of geomagnetically trapped solar alpha particles from Injun 5 observations

08 p1356 A71-21644

Low energy cosmic ray H 2 and He 3 nuclei intensities /1967-1968/ from Pioneer 8 and IMP 4 measurements

09 p1512 A71-22336

Stochastic scattering process charged particle flux by Lagrange expansion based on Fokker-Planck equation

09 p1529 A71-23594

Cosmic ray muon flux at sea level, allowing for showers, multiple scattering, straggling, zigzag motion, detector efficiency and electronic equipment dead time

12 p1952 A71-27403

Underground cosmic ray particles flux and nuclear interaction properties, determining integral sea level energy spectrum as function of range of particles in rock

12 p1953 A71-27407

Quark flux and generation cross sections above atmosphere from Proton 3 satellite elementary particle spectrometer data

13 p2121 A71-28053

Cosmic hadron flux measurements and energy spectra at various altitudes in atmosphere, using calorimeters

13 p2122 A71-28066

Power law dependence of lateral distribution function and core location of showers detected by Haverah Park array

13 p2122 A71-28068

Density, momentum and electric charge measurement of nuclear interacting particles in extensive air showers, using air gap magnet spectrograph and neutron monitor

13 p2124 A71-28083

Particle densities and muon spectra at 100-1300 m from sea level extensive air showers axes for primary energies to 10 to 20th eV

13 p2124 A71-28086

Density spectrum of cosmic ray showers, discussing altitude effects, structure function and transition

13 p2125 A71-28087

Extensive air showers muons momenta and densities from shower core spectrographic recordings

13 p2125 A71-28092

Extensive air showers muon density spectrum, describing measurement apparatus and analysis method with particular emphasis on elimination of falsifying absorber multiplication effects

13 p2126 A71-28100

Charged particles acceleration by electric field in magnetosphere, evaluating injected particles flux into ionosphere under quiet conditions

13 p2128 A71-28234

Particle flux toward charged metal plate /flat probe/ moving relative to plasma

13 p2134 A71-28238

Absolute spectra above atmosphere and magnetosphere and of particles accelerated in solar atmosphere during solar flare of 23 February 1956

13 p2128 A71-28253

Longitudinal variations of inner radiation belt particle flux density at low altitudes from Proton 2 satellite data

13 p2128 A71-28548

OGO 4 satellite micrometeoroid flux detection, emphasizing noise control procedures for data correlation

13 p2145 A71-28700

Terrestrial influx of small meteoric particles, discussing data uncertainties

14 p2307 A71-29902

Low energy precipitating auroral particle fluxes over magnetic poles delineating polar cap, noting electron precipitated flux

14 p2299 A71-30030

High latitude regions of low energy electron precipitation from OGO 4 satellite auroral particle experiment

14 p2300 A71-30032

Sea level high energy muon flux determination from underground burst energy spectrum measurements, using Kobayakawa-Miono formula for cascade shower fluctuation

15 p2475 A71-31782

Particle flux, energy storage and beam loading effects on superconducting traveling and standing wave resonators in linear accelerators

16 p2587 A71-33494

Geminid meteoroid dust particles detection, determining velocity and orbital elements from OGO 3 flux measurements

16 p2640 A71-33741

Solar particle flux profile and low latitude cut-off observation by low altitude satellite during March 1969 to July 1970 events

16 p2628 A71-33936

Micrometeoroids bibliography and review, considering ground based photometry and scattering theory, satellite flux measurements, particle collection and craters

17 p2798 A71-34456

Galactic clusters evolution in universe with zero rest mass particles, showing size dependence on cosmic dust energy density

18 p2969 A71-37040

Satellites interaction with ionosphere, concerning applications to particle density, electric field, flux and drag measurements

19 p2992 A71-37560

Fast charged particle flux measurement in inner radiation belt by Cosmos 137 satellite in January-February 1967

20 p3278 A71-39140

Pioneer 8 and 9 micrometeorite measurements of particles kinetic energy, momentum, velocity and direction, correlating measured particle flux rates with predictions based on zodiacal light

20 p3297 A71-39634

Zodiacal light lines in interplanetary dust particle flux diagram, suggesting agreement with micrometeorite data

20 p3298 A71-39636

Galactic cosmic rays and interplanetary magnetic field flux measurements onboard Venera 4 space probe, noting lack of correspondence with Forbush decrease

20 p3282 A71-39737

H, He and O ion fluxes along exospheric magnetic field lines, determining flux energy and direction from RF mass spectrometer measurements onboard Elektron 4 satellite

20 p3226 A71-39742

High latitude auroral particle precipitation patterns and connections to plasma sheet, ring current, cusp and radiation belt sources, using rocket and satellite observations

21 p3439 A71-41179

Galactic cosmic rays solar modulation and particle intensity gradient in interplanetary space from satellite observation data

22 p3591 A71-41534

Extensive air shower muons flux density at mountain altitudes, describing experimental procedure for fluctuation distribution

22 p3595 A71-42657

Extensive air shower muon flux density fluctuations at mountain level, determining interaction coordinates distribution, production and energy by Monte Carlo method

22 p3595 A71-42658

Cosmic radiation heavy nuclei intensity and composition measurement, treating nuclear emulsions in calcium bromide solutions

22 p3596 A71-42733

Intensity and polarization for meteorological spherical and nonspherical particle size parameters, comparing exact Mie scattering and ray optics

23 p3704 A71-43337

Coulomb interaction effect between charged traps in amorphous semiconductor, noting state density reduction at Fermi energy

23 p3715 A71-43472

Micrometeoroid flux determination from impact sites on Surveyor 3 TV camera optical filter surfaces, noting agreement with Pioneer, Cosmos and Pegasus spacecraft measurements

23 p3766 A71-43820

Absolute vertical intensity measurement of cosmic ray muon energy spectrum at sea level, presenting spark chamber and absorption spectrograph data

23 p3722 A71-43876

Pulsar high energy cosmic ray periodic flux detection with favorable interstellar magnetic field configuration along line of sight

24 p3865 A71-44569

High energy gamma quanta flux measurements in primary cosmic rays, using Cosmos 208 satellite data

24 p3866 A71-45026

PARTICLE IN CELL TECHNIQUE

Nonlinear hyperbolic equations integration, considering characteristic, mesh finite difference and particle in cell techniques

15 p2441 A71-31355

Limits theorems of occupancy problem, concerning asymptotic behavior of random particle distribution to fixed cell with equal probabilities

17 p2764 A71-34574

PARTICLE INTENSITY

Heavy cosmic ray nuclei intensity and energy spectra, investigating solar modulation effects

06 p0954 A71-18129

Forbush decreases and long term cosmic ray particle intensity changes, investigating spectral variations

06 p0956 A71-18137

Solar flare induced cosmic ray intensity increases registered by high latitude neutron monitors and Explorer 35 satellite, presenting intensity time profiles analyses

06 p0957 A71-18146

Solar flare associated increases in cosmic ray intensity during November 1968-April 1969, correcting anisotropic peak and decay rates to standard barometric coefficients

06 p0957 A71-18148

Cosmic ray intensity variations, discussing trajectory-derived cut-off rigidities for neutron monitor data analysis

06 p0959 A71-18160

Primary cosmic ray variations energy spectra on rising and declining solar activity arm, analyzing stratospheric particle intensities

08 p1353 A71-20980

Zenith angle distribution of atmospheric muons at Mt. Chacaltaya, considering differential intensity of cosmic ray mesons and horizontally incident cosmic rays

12 p1952 A71-27400

Ultrahigh energy muons intensity distribution as function of zenith angle at fixed slant depth of rock

15 p2476 A71-31793

Vertical intensity of cosmic ray muons in Mont Blanc tunnel, describing apparatus and experimental noise

15 p2477 A71-31795

Vertical intensity and angular distribution of cosmic ray muons from observations using scintillator neon flash tube telescopes at three depths

15 p2477 A71-31796

Horizontal cosmic ray muon component intensity measurement and time studies for solar and sidereal variations

20 p3277 A71-38839

Electron flux time dependence, observing flare increases, Forbush decreases, counting rate changes and intensity variations

20 p3281 A71-39733

PARTICLE INTERACTIONS

NT ELECTRON CAPTURE

NT ION ATOM INTERACTIONS

NT MOLECULAR COLLISIONS

NT MOLECULAR INTERACTIONS

NT NUCLEAR INTERACTIONS

NT SPIN-ORBIT INTERACTIONS

Vibrational degrees of freedom effects on capture cross sections and ion-molecule complexes formation in ion-dipole collisions

01 p0130 A71-10477

Semiautomatic stereophotographic processing of particle interaction data from Wilson chamber

01 p0083 A71-11364

Extensive atmospheric showers and energy transfer from interacting nucleons to electron photon cascades at high energy levels

01 p0146 A71-11366

Equilibrium, highly imperfect, partially ionized Hg and Li vapor plasmas, examining charged and neutral particle interaction forming charged clusters

02 p0292 A71-12617

High energy interaction multiperipheral theories, examining inelastic events

03 p0461 A71-13834

Strong cosmic ray interactions, considering meson production in accelerators

03 p0475 A71-13835

Extensive air shower experiments, considering origin, particle interactions and detectors

03 p0475 A71-13838

Pion-nucleon interactions, determining energetically precipitated particle effects in air showers

03 p0461 A71-13841

Monte Carlo model of muon and active component distribution in nuclear cascade in extensive cosmic ray shower

03 p0476 A71-13849

Pion interactions with nucleons and nuclei in emulsions irradiated by high energy pion beams

03 p0461 A71-13852

Momenta measurements of particles produced by high energy quasi-nucleon interactions of pions on photoemulsion layers, using primary particle tracks scanning

03 p0461 A71-13854

Extensive air shower muon fluctuations at mountain level, determining interaction coordinates distribution, production and energy by Monte Carlo method

03 p0477 A71-13857

Solar wind microscopic structure, examining interplanetary wave-particle interactions

03 p0480 A71-14068

Soviet book on cosmic ray physics covering high energy particles interactions, origin, acceleration mechanism, etc

03 p0481 A71-14424

Charged particles-noble gases interactions with resultant vacuum UV radiation, considering conservation of energy principle and Jesse effect

04 p0630 A71-15652

Extragalactic radio sources relativistic electrons interaction with cosmic black body radiation, noting effect on sources lifetime and X ray background

04 p0641 A71-15838

Quark fusion in quasi-stellar objects, deriving approximate formula for efficiency of converting rest mass into photons

05 p0785 A71-16686

Quasi-means definition and auxiliary system introduction for models including negative four-fermion

interaction, solving limiting expressions problem for free energy

05 p0775 A71-16865

Anomalous Cu concentration profile due to migrating Cu ions-GaAs crystal defects interaction

05 p0794 A71-16877

Photoemulsions densitometric characteristics for protonogram analysis, during fast charged particle interaction with single crystals

05 p0754 A71-17031

High energy particle interaction with magnetospheric tail neutral layer, determining limiting shape of pitch angle particle distribution

05 p0800 A71-17176

Classical many component plasma dynamics with collective particle interactions in self consistent longitudinal electric field, deriving complex wave equations

06 p0937 A71-18062

Positive and negative charged particle beam steady one dimensional motion analysis based on continuity, motion and Maxwell equations, allowing for electrostatic particle interactions

09 p1496 A71-22265

Charge source density during interaction between atmosphere and electron/proton fluxes at prescribed boundary parameters

09 p1513 A71-22675

Cosmic rays observations, using particle interaction with interstellar gas and magnetic fields

09 p1515 A71-23536

Electron-electron interaction effects on electronic states density in electron gas impurity bands, using matrix method

10 p1644 A71-23772

Feynman path integration for multiply connected space systems of indistinguishable particles, considering bosons and fermions propagators

10 p1644 A71-24214

Radiation and gas-dust interactions, examining dispersion relation and instability for cosmological models

10 p1675 A71-24490

Electric charge of interacting cosmic ray particles at sea level by experimental arrangement of flash tubes, and scintillation and proportional counters

10 p1664 A71-25043

Cs thermoelectric power near critical temperature and pressure, determining dense plasma electron-neutral elements interaction effects

11 p1715 A71-26153

Longitudinal plasma layer waves kinetic theory, considering particles specular reflection from layer boundaries

12 p1937 A71-27203

Cosmic rays resonant interaction with hydromagnetic waves, determining turbulent source for confining high energy radiation to Galactic disk

12 p1948 A71-27366

Particle interaction with wedge surface in supersonic two phase flow, determining incidence coordinates and collision frequency as function of initial conditions

12 p1866 A71-27665

Ionospheric wave/particle interactions under controlled electron beam energy and flux conditions, using Aerobee rocket for experimental investigation

12 p1902 A71-27668

Cosmic ray jet interaction with free or quasi-free nucleons, obtaining kinematic measurement, secondary particle composition and transverse momentum

13 p2121 A71-28058

High energy particle interaction with magnetospheric tail neutral layer, determining particle pitch angle distribution limiting shape

13 p2128 A71-28233

Massive body gravitational to inertial mass ratio from equilibrium assembly model of particle interactions

13 p2139 A71-28997

Hadron matter thermodynamical properties at high temperatures, developing dual resonance dynamic model of high energy particle interactions

14 p2304 A71-29597

Neutron emission yield during Pu 238 alpha particles interactions with O 18, taking into account recoil Ne isotopes

14 p2276 A71-30177

Three particle elastic scattering amplitudes calculation using local Yukawa potentials

14 p2277 A71-30862

Tensional thermoelasticity theory of continuum media, analyzing material particle interactions by stress tensor and equations of motion

17 p2815 A71-34187

Deep underground cosmic ray neutrinos interaction experiments, discussing particle motion, inelastic cross section variation, energy, mass and celestial coordinates

17 p2795 A71-34665

Underground search for cosmic ray neutrino interaction products, observing muon products

17 p2795 A71-34666

German monograph on self consistent ring current models of geomagnetic field interaction with charged particles

17 p2733 A71-34789

Pulsar radiation generation by charged particles nonlinear Thomson scattering of strong LF electromagnetic wave and nonthermal radio emission

18 p2960 A71-35940

Charged particles elastic interaction and recombination in low temperature weakly ionized potassium plasma

19 p3109 A71-37135

Nonthermal electrons interaction with electron plasma oscillations and HF transverse waves in upstream solar wind

19 p3125 A71-37353

Cs and Hg vapors compressibility factor in supercritical range as function of density, considering charged particles and atoms polarization interactions in ionized metal vapors

19 p3111 A71-37590

Debye potential well formation in collisionless current carrying plasma, noting wave-particle resonant interaction role

19 p3115 A71-38216

Solid cylindrical particles interaction under entrainment in pipe by viscous incompressible fluid, obtaining numerical solution by reduction to flow past moving body

19 p3046 A71-38418

Longitudinal plasma sheath waves kinetic theory, considering particles specular reflection from sheath boundaries

19 p3116 A71-38615

Cosmos satellite data on mainland China thermonuclear explosion of 27 December 1968, observing radiation effects on particles in natural radiation belts

20 p3278 A71-39128

Gamma ray production by pulsar-emitted particles interaction with surrounding nebula matter, investigating radiation intensity time variation

20 p3279 A71-39325

Book on cosmic gamma rays covering secondary particle decay, electron-positron annihilation, proton-antiproton interactions, galactic radiation and cosmology

21 p3438 A71-40450

Exchange interaction in excitons for arbitrary band structure of semiconductors in effective mass approximation allowing correction

21 p3431 A71-41262

High energy interaction multiperipheral theories, examining inelastic events

22 p3578 A71-42635

Strong cosmic ray interactions and meson production in accelerators

22 p3594 A71-42636

Extensive air shower experiments, considering origin, particle interactions and detectors

22 p3594 A71-42639

Pion-nucleon interactions, determining energetically precipitated particle effects in air showers

22 p3579 A71-42642

Monte Carlo model of muon and active component distribution in nuclear cascade in extensive cosmic ray shower

22 p3595 A71-42650

Pion interactions with nucleons and nuclei in emulsions irradiated by high energy pion beams

22 p3579 A71-42653

Extensive air shower muon flux density fluctuations at mountain level, determining interaction coordinates distribution, production and energy by Monte Carlo method

22 p3595 A71-42658

Triggered whistler emissions in magnetosphere, considering nonlinear interaction between whistler wave and resonating particles

23 p3643 A71-43175

Quasar and pulsar gamma ray absorption by critical energy collisions with low energy photons

24 p3866 A71-44917

Particle interaction with wedge surface in supersonic two phase flow, determining incidence coordinates and collision frequency as function of initial conditions

24 p3790 A71-44930

Auroral charged particle fluxes electrodynamic interaction with atmosphere, determining ion formation rate and electron concentration and conductivity

24 p3866 A71-45032

PARTICLE MASS

NT ELECTRON MASS

Spectrograph design for simultaneous measurement of velocity spectra and charge-to-mass ratios of ions, using magnetic and electric fields deflection effects

02 p0249 A71-12126

Eddington theory validity based on formulas connecting light velocity, Planck and gravitational constants and electron, proton and neutron masses

04 p0626 A71-15136

Baryon isobars average mass data in cosmic ray interactions, using particle angular measurements in backward direction of center mass system

11 p1818 A71-26427

Primary cosmic rays mass composition at energy levels above 10 TeV, analyzing muons data from extensive air shower experiments

13 p2125 A71-28094

Very low mass gravitationally collapsed objects, formed as fluctuation effects in early universe

14 p2307 A71-29865

Mass and mobility measurements for small ions in air by Pu bombardment in closed chamber at low pressure

16 p2614 A71-33380

Noctilucous cloud nature from cosmic dust particles collection and detection, discussing mass, absolute falling velocity and model theories

16 p2641 A71-33765

Galactic clusters evolution in universe with zero rest mass particles, showing size dependence on cosmic dust energy density

18 p2969 A71-37040

Heat and fictitious forces in variable rest mass relativistic particle dynamics for thermal energy conservation laws interpretation

19 p3162 A71-37641

Binary elastic collision integral between particles of disparate mass, determining angular momentum form of Boltzmann equation for Lorentz mixtures

19 p3115 A71-38210

Mass of virtual particle responsible for gravitation of vacuum and expansion of universe, considering correspondence to red shift in quasar spectra

19 p3146 A71-38644

Ionospheric low hybrid resonance measurements by rocket-borne quadrupole probe, deriving electron density and effective ion mass along trajectory

20 p3224 A71-39722

Photon mass terrestrial and extraterrestrial limit measurements, discussing speed of light frequency dependence, Coulomb law analog in magnetostatics energy conservation, etc

21 p3418 A71-40674

Exchange interaction in excitons for arbitrary band structure of semiconductors in effective mass approximation allowing correction

21 p3431 A71-41262

Electromagnetic radiation active gravitational mass relationship to particle mass from decay of particle into two radiation pulses

21 p3417 A71-41402

Relative abundances and mass measurements of Li, Be and B isotopes in primary cosmic rays, using balloon flown emulsion stacks

22 p3593 A71-42329

PARTICLE MOTION

Monograph on nonlinear theory of one dimensional homogeneous collisionless plasma resonance covering charged particle motion in sinusoidal and standing potential waves

01 p0131 A71-10101

Charged particle motion in magnetic dipole field, investigating singularity and topological flow nature

01 p0127 A71-10382

Dynamic problems linear variational equations associated with one and two particle motion in force field

01 p0111 A71-10385

Bremsstrahlung effect on charged particle motion in nonuniform magnetic field

01 p0132 A71-10677

Laser heated surface layer fragmentation taking into account particles dispersion due to vaporization, reactive force and mechanical recoil moment

01 p0070 A71-10796

Charged particle motion in self consistent continuous wave spectrum from Vlasov and Poisson equations solution

02 p0289 A71-11955

Optimal control of exhaust velocity for plane motion of variable mass point along trajectory under gravitational and resisting forces

02 p0284 A71-12292

Spherical particle motion investigation in plane Couette flow, predicting critical Reynolds number for transition to turbulent flow

03 p0398 A71-13112

Asymmetrical cosmic ray showers kinematic interpretation by heuristic model, discussing particle dispersion angular distribution

03 p0476 A71-13843

Lateral drift of solid particles suspended in plane supersonic gas flow along wall with recess step, using successive approximation for equations

03 p0404 A71-14255

Dynamic problems of two dimensions with semisurface of section, examining charged particles motion in axisymmetric magnetic field

04 p0627 A71-15706

Particle nonlinear motion near equatorial libration points in restricted three body problem [AIAA PAPER 70-98]

05 p0810 A71-16553

Electric field strength in earth ionosphere and magnetosphere during irregular motion of fast ions and electrons

06 p0894 A71-18253

Particle motion in gravitational field for disk-like configurations, solving kinetic equation for quadratic potential

07 p1192 A71-19286

Bremsstrahlung effect on charged particle motion in nonuniform magnetic field

07 p1170 A71-20139

Planetary diurnal rotation, discussing motion of small particle in solar and planet gravitational fields

07 p1201 A71-20437

Night D region ion kinetics data during thermonuclear detonation, discussing formation and conversion rates, electron concentration and recombination

08 p1278 A71-21009

Dynamo theory for electric current variations in magnetosphere-ionosphere interactions, discussing electrostatic fields mapping and plasma particle drift motion production

08 p1279 A71-21213

Particle motion behind oblique shock wave in two phase supersonic wedge flow, deriving expressions for particle trajectories and velocity equalization time

08 p1227 A71-21754

Positive and negative charged particle beam steady one dimensional motion analysis based on continuity, motion and Maxwell equations, allowing for electrostatic particle interactions

09 p1496 A71-22265

Near earth motion equations for electrically charged dust particles in gravitating dipole magnetic fields, using zero-relative-velocity surfaces and energy integral

09 p1437 A71-22832

Cerenkov energy losses of rigid cylindrical uniformly charged bunch moving at constant speed through homogeneous isotropic dispersive dielectric

09 p1498 A71-23574

Restricted three body problem with variable thrust particle motion in Newtonian field

10 p1672 A71-24337

Mesosphere charged particles concentration and mobility measurements, using rocket-borne aspiration probes

10 p1604 A71-24705

Atmospheric vertical particle motion inside convective storms observed by airborne pulse Doppler radar techniques

11 p1794 A71-25378

Charge particle motion and radiation in strong plane and spherical electromagnetic waves with nonthermal astrophysical applications

12 p1877 A71-26616

Optimal control of material point motion in thin spherical layer of central gravitational field, solving by approximation

12 p1957 A71-26631

Optimal flight of material point in central field of forces subject to controlled small thrust

12 p1957 A71-26632

Collisionless motion of solar wind ions in helical magnetic field, giving transfer function of charged particles

12 p1947 A71-26636

Energetic charged particle motion in magnetosphere, considering radiation belt dynamics

12 p1949 A71-27372

Kinetic equations for particle motion in gravitational fields, discussing stellar configurations evolution

13 p2100 A71-27973

Quarks search near extensive air shower cores, discussing apparatus and results for detection of long delayed particles

13 p2120 A71-28052

Plasma electron and proton motion in equatorial plane of magnetosphere under geomagnetic disturbance generated electric field

13 p2060 A71-28530

Quasi-unsteady approximation of mutual hydrodynamic drift velocity of aerosol particles in high power sound field

13 p2101 A71-28849

Equations of motion of infinitesimal particles attracted by Newtonian gravitation of two mutual revolving masses in circular orbits

13 p2101 A71-29114

Small spherical solid or liquid particles deceleration, melting and shattering due to spherical and conical bodies in compressible hypersonic shock layer flow field

[AIAA PAPER 69-712]

14 p2334 A71-29873

Trapped charged particle cyclotron, bounce and drift motion in distorted geomagnetic field

14 p2300 A71-30033

Point motion in axisymmetrical planet equatorial plane gravitational field, taking into account orbital elliptical elements osculation

14 p2310 A71-30186

Optimal two impulse minimum thrust transfer of particle between coplanar circular orbits under perturbations in flight plane

14 p2310 A71-30187

German monograph on particle motion in symmetric rotation flow velocity covering potential vorticity, track curves, resistance laws, transition region, drag and pressure effects

14 p2170 A71-30234

Geomagnetic pulsation effect on charged particles motion, based on Mead magnetosphere analytic model, using Parker perturbation method

14 p2235 A71-30346

Particle displacements during resonance motion of shear and compression waves in linearly viscoelastic flat plate of finite thickness

14 p2332 A71-30851

Guiding center equations for charged particle motion and statistical fluctuations of plasma in magnetic field, using Krylov-Bogoliubov transformation

15 p2458 A71-32393

Particle motion in combined gravitational field of monopole and prolate quadrupole, deriving exact solution in Newtonian mechanics and general relativity

16 p2609 A71-33256

Spinning and point particles motion from Einstein equations based on covariance with general coordinate transformations

16 p2610 A71-33270

Collision integral for classical electron plasma, concerning Born-Bogoliubov-Green-Kirkwood-Yvon equations for long range interaction potential and motions of multiple particles

16 p2619 A71-33650

Geminid meteoroid dust particles detection, determining velocity and orbital elements from OGO 3 flux measurements

16 p2640 A71-33741

Noctilucous cloud nature from cosmic dust particles collection and detection, discussing mass, absolute falling velocity and model theories

16 p2641 A71-33765

Astronomical photography of solar eclipse of 7 March 1970 from two locations indicating negative evidence of bulk particle movements above 20 km/sec related to cosmic rays

16 p2642 A71-33810

Heat and mass transfer during deposition on heated surfaces in nonisothermal gas flow with suspended solid particles, using motion of continuous Newtonian medium

17 p2836 A71-34305

Particle gyration in homogeneous magnetic field and perpendicularly propagating electrostatic wave, calculating wave-particle energy transfer and wave-amplitude limiting effects

18 p2950 A71-35862

Nondeveloping synoptic weather systems description by isentropic structural analysis, studying particle motion and dynamic behavior using models

18 p2944 A71-36219

Simply supported Bernoulli-Euler beam resting on elastic foundation and carrying equally spaced moving mass particles, calculating lateral response dynamic stability by Galerkin method [ASME PAPER 71-APM-M]

18 p2978 A71-36256

Plasma heating and compression with nonadiabatic charged particle motion in uniform magnetic field

19 p3109 A71-37137

High temperature gas dispersed Al particle flow, investigating electrical conductivity and radiation properties

19 p3161 A71-37265

Collisionless plasma Vlasov and Poisson equations numerical solution based on Fourier-Fourier transform, comparing with particle motion simulation

19 p3113 A71-37748

Electron density inhomogeneity behavior, examining thermal electron motion and collisionless plasma initial condition effects

19 p3114 A71-37857

Dimensional analysis of wear by solid particle impact in fluid flows in pumps and ducts

19 p3046 A71-38273

Charged particle motion in constant magnetic field under random electric field, deriving maximum energy and diffusion coefficient

20 p3269 A71-39163

Night D region ion kinetics data during thermonuclear detonation, discussing formation and conversion rates, electron concentration and recombination

20 p3219 A71-39589

Finite amplitude entropic waves with propagated acoustic radiation-fluid particle motion energy coupling, using thermodynamic χ function methods

20 p3315 A71-39772

Radiation belt particles nonadiabatic changes, calculating rigidity as function of magnetic field lines

21 p3439 A71-41357

Asymmetrical cosmic ray showers kinematic interpretation by heuristic model, discussing particle dispersion angular distribution

22 p3594 A71-42644

Three body problem of two heavy mass particles oscillatory motion in periodic orbits on straight line under Newtonian attraction

23 p3734 A71-43241

Longitudinal ambipolar sound instability effect on duration of plasma particle motion to wall across magnetic field, using phase method

23 p3709 A71-43263

Relativistic electron beam propagation entering vacuum or neutral gas filled region through grounded conducting wall, using one dimensional model

23 p3713 A71-44146

Plasma spraying steel coating process, establishing regularity of particle flight velocity variation with distance from burner nozzle

24 p3829 A71-44737

Distant stellar satellites existence possibility based on maximum distance estimation for material particle motion stability with respect to sun or another star

24 p3870 A71-44815

Auroral plasma particle discharge during motion in strong magnetic field, discussing magnetospheric instability due to temperature anisotropy

24 p3867 A71-45309

PARTICLE PRODUCTION

Neutron star in accretion state, investigating generation of relativistic electrons, positrons and X ray and gamma emission

01 p0150 A71-10061

Strong cosmic ray interactions, considering meson production in accelerators

03 p0475 A71-13835

Nuclear interaction examination, using Wilson magnetic chamber for multiple particle production

03 p0461 A71-13836

Positive pions coherent production by negative pions with aid of nuclear photoemulsions

03 p0461 A71-13853

Momenta measurements of particles produced by high energy quasi-nucleon interactions of pions on photoemulsion layers, using primary particle tracks scanning

03 p0461 A71-13854

Ionospheric electron production, slowing down and disappearance processes, considering collisions with atmospheric constituents

03 p0417 A71-14072

Neutron and gamma ray production by nuclear interactions in solar flares

06 p0961 A71-18175

Particle production near Kasner singularity in anisotropic cosmological model

07 p1162 A71-19217

E layer critical frequencies and sporadic E layer boundary frequencies interrelationship, assuming equal electron production rates

10 p1599 A71-23876

Lunar soil particle production, noting radiation erosion effects

10 p1673 A71-24414

Midlatitude ionosphere electron production rates during quiet solar activity, deriving seasonally varying electron density profiles

11 p1755 A71-25609

Meteorological, geomagnetic and extraterrestrial variations of cosmic ray layer electron production rate in lower D region

11 p1816 A71-25610

Nucleon-nucleon interactions produced energetic penetrating particles /muons/ in cosmic ray showers, studying neon flash tube technique

12 p1948 A71-27186

Intense solar microwave burst indication of high energy electron production, discussing synchrotron radiation, interplanetary medium particle propagation and cosmic ray modulation

12 p1950 A71-27381

Atmospheric neutron production by cosmic radiation over sunspot cycle, measuring energy spectrum with airplanes and balloon-borne instruments

12 p1950 A71-27382

Proton-proton interactions at 70-600 GeV in Echo Lake cosmic ray experiment, discussing multiplicity, prongs, hadron flux and ionization calorimeter

12 p1933 A71-27391

Quark detection by telescope using production models, discussing extreme energy transfer conditions and upper production limits

12 p1952 A71-27398

Fireball model at various energies, describing multiple meson production at very high energy

13 p2058 A71-28049

Quark flux and generation cross sections above atmosphere from Proton 3 satellite elementary particle spectrometer data

13 p2121 A71-28053

Regular multiplicities of particle production in high energy collisions and antinucleon-nucleon annihilation, comparing cosmic ray jet data and pion-nucleon difference

13 p2102 A71-28061

Cosmic ray components atmospheric diffusion and production based on H quantum, two fireball and alph model

13 p2122 A71-28064

Air shower properties from Monte Carlo simulations, determining electron and muon numbers at sea level for primary protons and copper nuclei

13 p2124 A71-28085

Muons arrival times distribution in extensive air showers, examining delay as function of particle production heights

13 p2126 A71-28095

Plastic scintillators anomalous pulse spectra in sea level transition region attributed to EM cascades single particles /muons/ production

14 p2301 A71-30425

Interstellar gas heating by soft X rays and cosmic rays for electron production, calculating heating rate with Boltzmann equation and Monte Carlo method

14 p2302 A71-30642

Electron production by proton impact on nitrogen, oxygen, neon and argon, measuring cross sections angular and energy distribution by electrostatic analysis and electron counting

14 p2277 A71-30660

Flat plate electrostatic probe for ionization rate measurements behind reflected shock waves, monitoring time evolution of electron production

14 p2248 A71-30884

High energy muons production by cosmic rays, discussing advantages of moon based experiments over earth surface measurements

15 p2475 A71-31780

Low energy muon production by neutral components of cosmic radiation at sea level, noting correlation with sidereal time

15 p2475 A71-31785

High energy penetrating component of cosmic radiation at mountain level recorded in underground ionization calorimeter, showing muon production in vertical and horizontal direction

15 p2476 A71-31787

Muonic trident production by cosmic ray muons, using quantum electrodynamics methods

15 p2477 A71-31798

Production cross section of Lee-Wick hypothetical massive electromagnetic bosons by muons at high energy, giving Feynman diagrams

17 p2785 A71-34750

German monograph on electron production effect on channel breakdown in nitrogen, showing positive space charge accumulation near anode in gas discharge

17 p2788 A71-34775

Lyman alpha resonant radiation in regions distant from cometary tails due to additional atomic hydrogen production from dust particles

17 p2809 A71-35595

Fireball model of meson production in high energy nucleons collisions

18 p2949 A71-36210

Energy requirements for antihydrogen production in interstellar photonic drives, discussing feasibility

18 p2956 A71-36683

Ion charge composition in plasma-electron beam system in strong longitudinal magnetic field, noting multiply charged ions production under high temperature conditions

19 p3109 A71-37132

Underground interactions of primary cosmic ray produced atmospheric muon neutrinos, using large area liquid scintillation detector hodoscope

19 p3105 A71-37288

Underground muons produced by atmospheric neutrinos, noting deviation from linearity by comparing calculated and experimental muon rates

19 p3106 A71-37289

Atmospheric neutron production by cosmic rays, calculating cadmium-indium ratio

19 p3066 A71-38379

Foillless diode for production of high power relativistic electron beams, using multicathode system

20 p3202 A71-38831

Ion and electron production rate during PCA event, computing electron/ion density, differential proton flux spectrum and ion production rate

20 p3225 A71-39729

Dayglow and twilight emission data, discussing atomic excitation mechanisms, particle production rates, height profiles and temporal variations

20 p3227 A71-39835

Strong cosmic ray interactions and meson production in accelerators

22 p3594 A71-42636

Nuclear interaction examination, using Wilson magnetic chamber for multiple particle production

22 p3579 A71-42637

Positive pions coherent production by negative pions with aid of nuclear photoemulsions

22 p3579 A71-42654

Momenta measurements of particles produced by high energy quasi-nucleon interactions of pions on photoemulsion layers, using primary particle tracks scanning

22 p3579 A71-42655

Electromagnetic mechanism of direct muon and photon production by collision of strongly interacting particles

22 p3579 A71-42665

Radio absorption in lower ionosphere, determining vertical distribution of electron density and production rates from solar protons energy spectrum

24 p3867 A71-45041

Statistical system formation in fast hadrons collision process and multiple hadron production

24 p3851 A71-45170

PARTICLE SIZE DISTRIBUTION

CW He-Ne laser beam scattering observation for artificial fog droplet size distribution during evolution stages

01 p0094 A71-10831

Combustion residues particle size and distribution during rocket plume impingement on Al surface

01 p0183 A71-11594

Noctilucent cloud particle size composition and origin from sounding rocket flight and control collecting surfaces

02 p0246 A71-12702

Particle size collected on electron microscope grids attached to Luster rocket sampling surfaces during noctilucent cloud display

02 p0246 A71-12705

Condensed metal particle size distribution measurement at ambient conditions by photography using electron microscope

02 p0333 A71-12854

Limiting temperature and size conditions for aluminum particle ignition in mixtures of oxygen with argon and nitrogen

03 p0468 A71-13990

Cosmic dust size distribution measurement by electron microscopic examination of in-flight shadowed substrates during particle collection on ESSO rocket

03 p0491 A71-14015

Lunar surface structure, discussing soil grain size-albedo relationship

03 p0492 A71-14054

Aerosols in stratosphere, describing physical appearance, size distribution and concentration

03 p0418 A71-14206

Ultrafine grain metals strength properties at cryogenic temperatures and near melting point, discussing grain boundaries

03 p0446 A71-14487

Holographic measurement of moving cloud droplets size distribution from aircraft using Q switched ruby laser

04 p0596 A71-14968

Cloud drop size distribution from spectral transmission measurements, using spectroradiometer

04 p0621 A71-15073

Rushing effects on fractional composition and quality of sponge titanium, including optimum end size of pieces

04 p0616 A71-15825

Apollo 11 lunar soil size distribution, examining deficiency in material finer than 15 micrometers

05 p0807 A71-16215

Adaptive algorithms in particle size and form distribution control, using scanning light beam

06 p0872 A71-18699

Alloy strengthening by ordered precipitates, predicting antiphase boundary energy from flow stress vs particle size plots

07 p1132 A71-19440

Thin nickel aluminide sheets and small particles long range ordering, discussing antiphase boundary energy effects

07 p1133 A71-19441

Al particle size and filler volume optimization effects on epoxy composite dynamic response

07 p1139 A71-20136

Hydrodynamic model of human red blood cell rotation in flow toward sizing orifice, predicting volume distribution

07 p1045 A71-20446

Bcc metals slip band formation, investigating deformation and friction behavior

08 p1308 A71-21515

UVB colors and polarization models for reflection nebulae based on Mie scattering functions for exponential size distribution of silicate particles

09 p1517 A71-22332

Agglomeration process of dust particles growth in primordial solar nebula, considering early evolutionary phase of nearly free contraction and later phase with nebula flattening into gaseous disk rotating about protosun

09 p1523 A71-23045

Granulometric composition effects on stainless steel powders bulk weight, friability and compactability, taking into account particle shape

09 p1470 A71-23062

Shape and size variations of dispersed particles of Ta, Zr, La and Y in tungsten during sintering

10 p1624 A71-23904

Lunar surface polarimetric properties, discussing grain size effect on normal albedo and polarization maximum degree

10 p1674 A71-24436

Spaceborne optical sensors cleanliness requirements, considering particle size distribution, shape, population densities, chemical composition and origin [AIAA PAPER 71-471]

12 p1873 A71-26758

Lunar crust regolith thermophysical properties concerning particle size and mass, specific heat and ther-

mal conductivity from Luna 16 automatic station sampler

12 p1963 A71-26964

Venus polarimetric observational data comparison with polarization characteristics of radiation scattered at gamma-distribution particle sizes, determining refractivity and particle radius

12 p1964 A71-27088

Aerosol power law distribution exponent and particle limiting radii from turbid atmosphere outgoing visible radiation polarization high altitude measurements

13 p2063 A71-29111

Holography background, classification and application to microscopy, particle size analysis, interferometry, optical elements and data storage

13 p2071 A71-29349

Altitude size distribution of atmospheric aerosol from sky radiance measurements in sun aureole region, calculating sunlight forward single scattering

14 p2310 A71-30125

Single and multibeam holography application to size, trajectory, distribution, population density and velocity measurements of water and electric arc welding sprays droplets

14 p2243 A71-30299

Ignition initiation, burning time and particle size distribution determination for dispersed Mg and Al particles in condensed system

14 p2337 A71-30615

Particle size effect on self ignition temperature of powdered Al-Mg alloys

14 p2285 A71-30621

Udimet 700 superalloy gamma prime precipitate particle size, volume fraction and chemical composition as function of time and temperature

15 p2433 A71-32176

Acoustic damping of small amplitude waves by non-burning particles in T burners and rocket motors, noting propellant seeding with zirconium oxide [AIAA PAPER 71-633]

15 p2471 A71-32574

Fog drop size distribution measurement with laser hologram camera

16 p2604 A71-33535

Convective mass or heat transfer to or from uniform or size distributed drops, bubbles or solid particles at high Peclet and low particle Reynolds numbers

17 p2837 A71-34690

Aluminum powder filled epoxy composites, investigating particle size and filler percent effects on damping properties and elastic modulus

17 p2762 A71-34819

Aerosol size distribution from lidar light scattering polarization properties, constructing inversion model

17 p2770 A71-35806

Venus polarimetric observational data comparison with polarization characteristics of radiation scattered at gamma-distribution particle sizes, determining refractivity and particle radius

19 p3133 A71-37438

Particle size-frequency distributions of volcanic pyroclastic tuffs for transport and deposit evaluation

19 p3051 A71-37672

Lunar crust regolith thermophysical properties concerning particle size and mass, specific heat and thermal conductivity from Luna 16 automatic station sampler

19 p3144 A71-38259

Fog droplet size spectral distribution from artificial fog induced He-Ne laser beam scatter, using five photometers for angular distribution measurements

19 p3091 A71-38657

Chemical composition and size distribution of particulate matter in solid propellant combustor of boron loaded rocket motor

21 p3436 A71-40944

Heat resistant Ni alloys hot strength level and temperature dependence as function of gamma-prime-phase particle size, discussing aging effect on creep rate

22 p3561 A71-41841

Size distribution and concentration of magnetic spherules in troposphere from electron and optical microscopy

23 p3665 A71-42965

Epoxy-alumina trihydrate composite system fracture energy data, noting interdependence of surface topography, phase dispersion volume fraction, particle size and spacing

23 p3696 A71-43102

Intensity and polarization for meteorological spherical and nonspherical particle size parameters, comparing exact Mie scattering and ray optics

23 p3704 A71-43337

Electro-optical techniques for particle size measurements from aircraft, noting imaging techniques superiority for nonaerosol and large particles

23 p3677 A71-43514

Petrography, mineral composition and grain size distribution of Apollo 12 lunar fines

23 p3743 A71-43649

Size distribution, composition and history of regolith fines at Apollo 12 site

23 p3743 A71-43651

Grain size and modal analyses of lunar regoliths sampled by Apollo 11 and 12, discussing particles origin

23 p3744 A71-43654

Apollo 12 fines sample 12057,72 particle size distribution determination procedure, discussing characteristic shapes, glassy agglomerates, smooth opaque particles and volume

23 p3757 A71-43752

Glass spherical particles formation mechanisms for lunar surface, discussing size limitation factors

23 p3757 A71-43753

Particle size and shape distributions of Apollo 12 lunar fines by computer evaluation of scanning electron microscope images

23 p3758 A71-43755

Grain size distribution and optical and RF electrical properties of Apollo 12 lunar fines and core samples

23 p3759 A71-43769

PARTICLE SPIN

NT ELECTRON SPIN

General relativity theory quantization, admitting kink states with fermion-like properties and spin

08 p1335 A71-21362

Atom rigid rotor problem, applying generalized phase shift rotational excitation treatment in lowest approximation

12 p1932 A71-26949

PARTICLE TELESCOPES

Cosmic ray telescopes geometric factor determination, taking into account particle incidence angle

06 p0898 A71-17705

Cosmic ray solar modulation anisotropy during 23 March 1966, 25 May 1967 and 26 January 1968 events in preForbush phase, evaluating multidirectional meson observations

06 p0956 A71-18138

Antimatter search in primary cosmic rays by balloon-borne cosmic ray telescope formed from gas Cerenkov detector combined with scintillator elements

10 p1659 A71-23748

Cosmic ray anisotropies perpendicular to ecliptic plane from underground muon telescopes in New Mexico and Bolivia

12 p1967 A71-27380

Quark detection by telescope using production models, discussing extreme energy transfer conditions and upper production limits

12 p1952 A71-27398

Quarks search in cosmic rays at sea level and mountain altitude, using telescope with plastic scintillation counters and wire spark chambers

13 p1212 A71-28055

Cosmic ray telescopes with scintillation and Cerenkov counters for 2 to 8 BeV energy range, describing structural details and operational specifications

14 p2247 A71-30597

Sidereal anisotropy in muon signal observed by cosmic ray telescope above sea level, indicating production by neutral particle and leakage relative to anticoincidence factor

15 p2477 A71-31797

Satellite-borne semiconductor telescope for relativistic heavy primary cosmic rays identification, increasing resolving power by minimum pulse selection method

15 p2407 A71-31806

Calculation method for zenith and azimuth directional sensitivity characteristics of cylindrical cosmic ray telescopes with circular recording surfaces

17 p2746 A71-35650

Median primary energy of underground muon telescopes response as function of depth, studying sidereal daily variation of cosmic rays

19 p3125 A71-37370

Cosmic ray sidereal time period, using neutron monitors, meson telescope and various ion chambers

23 p3719 A71-43126

Underground meson telescope coupling functions calculations, using effective primary threshold energy

23 p3720 A71-43152

PARTICLE THEORY

Relativistic kinetic theory of particles with magnetic dipole moment in external EM field, deriving transport equations for distribution function

03 p0463 A71-13425

Laser radiation and plasma nonlinear interaction, using particle description of electron motion

11 p1806 A71-26093

Elementary particle recombination probabilities on solid body surface, using reactive gas model in form of quantum mechanics three body problem

12 p1934 A71-27546

Lift and particle displacement around lifting body with stream function as fluid motion equation integral

12 p1866 A71-27577

Kinetic theory of gases in general relativity, including model of matter particle structure

16 p2610 A71-33267

Soviet papers on gravitation and elementary particle theory covering unified and quantum field theories,

geometrical models, mass spectrum, internal space, etc

17 p2777 A71-34626

Heat and fictitious forces in variable rest mass relativistic particle dynamics for thermal energy conservation laws interpretation

19 p3162 A71-37641

Monte Carlo generation method for phase-space integrals of multiperipheral models for high energies and particle multiplicities

21 p3408 A71-40850

PARTICLE TRACKS

U PARTICLE TRAJECTORIES

PARTICLE TRAJECTORIES

NT ELECTRON TRAJECTORIES

Fossil nuclear charged particle tracks in lunar rock 12013 Ca-feldspar, K-feldspar and pyroxene attributed to galactic cosmic rays

03 p0494 A71-14216

Low energy cosmic ray propagation anisotropies in interplanetary medium examined by unidirectional detectors on geostationary satellites

03 p0482 A71-14543

Heavy cosmic particle dosage measurement by chemical etching of particle tracks on Apollo astronauts plastic helmets

04 p0543 A71-14822

Charged particle trajectory under dipole magnetic field, deriving Stoermer orbit existence and uniqueness proof

04 p0625 A71-15081

Gas-particle mixture cascade flow over turbine blades, considering momentum/heat transfer and particle trajectories

06 p0841 A71-17701

Whistler wave packet propagating in ambient magnetic field direction, computing nonlinear particle trajectories

06 p0869 A71-17987

Diurnal intensity variations of high energy galactic cosmic rays, taking into account particle trajectories in sectorial interplanetary magnetic field

06 p0952 A71-18115

Nuclear tracks high density in Apollo core small silicate crystals, discussing extralunar dust and photospheric iron-hydrogen ratio

07 p1189 A71-18740

Plastic track detectors calibration for heavy charged particles in cosmic ray experiments, considering track etching rates as function of particle charge and velocity

07 p1113 A71-20042

Heavy ion track registration in nonconductor minerals, discussing radiation damage and atomic species along trajectory

07 p1158 A71-20270

Spark discharge enhancement of heavy ion track etching in Lexan polycarbonate

07 p1114 A71-20271

Heavy ion tracks in silicate minerals, using thermal annealing to identify origins

07 p1158 A71-20273

Gas-particle mixture cascade flow over turbine blades, considering momentum/heat transfer and particle trajectories

07 p1017 A71-20311

Galactic primary cosmic rays nuclei tracks in meteorite olivine, studying intensity of VH and VVH groups

08 p1351 A71-20961

Laser Doppler velocimetric technique for supersonic flow particle trajectory and density measurements, noting particle lag

08 p1303 A71-22010

Solar particle tracks in clear filter glass from Surveyor 3 spacecraft, comparing with lunar rocks track results

09 p1529 A71-23655

Gas rich Kapoeta howardite composition, evolution, high particle fossil track densities and normal track rich crystals spatial relations

10 p1672 A71-24392

Heavy cosmic ray nuclei track counts in plastics, examining Apollo mission 8 and 12 helmets

10 p1665 A71-25121

Iron nuclei emission during 1967-1969 solar flares from spacecraft window and lunar camera lens etched tracks, discussing Fe/He ratio and lunar soil densities

11 p1815 A71-25299

Centrifugal particle separation limit in free vortex, stressing particle interference with vortex flow and viscous effects

11 p1750 A71-25467

Two dimensional analysis of isentropic perfect gas flow fields in axisymmetric nozzles for transonic two phase flow initial values, calculating particle trajectories

11 p1751 A71-25508

Baryon isobars average mass data in cosmic ray interactions, using particle angular measurements in backward direction of center mass system

11 p1818 A71-26427

Cosmic ray particles propagation anisotropies in model magnetosphere, suggesting detection interplanetary medium with geostationary satellites 12 p1950 A71-27377

High energy cosmic ray components, investigating tracks and trapped magnetic monopoles 13 p2120 A71-28051

Adiabatic flow model of noiseless magnetic neutral sheet of finite width, discussing particle trajectory and charge density distribution 13 p2109 A71-29166

Momentum spectrum measurement of cosmic ray muons, recording particle trajectories photographically 15 p2475 A71-31783

Balloon-borne magnetic spectrograph for primary cosmic ray particle trajectory and rigidities measurement 15 p2407 A71-31812

Mass transfer in close binaries, determining gaseous ring formation conditions and properties from ejected particle trajectories computation 17 p2809 A71-35594

Straight-line orbit approximation for plasma response function in system with periodic particle orbits 19 p3113 A71-37750

Electric fields for solid and liquid fuels dispersion and trajectory manipulation of charged particles to control mixing with air, vaporization and burning 19 p3171 A71-38193

Solar proton trajectories calculations in Williams-Mead geomagnetic field model, showing longitude difference in tail region 20 p3216 A71-38747

Ion-quadrupole effects in ion-molecule collisions by numerical calculations of capture cross sections and computer-plotter studies of ion trajectories 21 p3419 A71-40906

Aqueous etchant for charged particle tracks revelation in olivines 23 p3737 A71-43544

Lexan plastic fission track analysis of uranium distribution in glassy residuum in Apollo 11 rock 10017 23 p3739 A71-43616

Lunar rocks 12040 and 12013 and anorthosites, determining U-Th distributions with induced fission track maps 23 p3752 A71-43712

Lunar atmosphere as source of lunar surface gaseous elements, calculating ions trajectory and impact energy as function of interplanetary magnetic field strength 23 p3754 A71-43728

Nuclear track densities in lunar core and fine samples, relating erosion history, solar activity and surface stirring 23 p3764 A71-43799

Solar and galactic iron group cosmic ray track distributions in Apollo 12 lunar rocks, investigating surface residence times 23 p3764 A71-43800

Primary cosmic ray and spallation track density distribution in Apollo 12 deep core soil samples 23 p3764 A71-43801

Spontaneous fission fossil tracks of U, Pu and extinct transuranic elements in pyroxenes of Apollo 11 and 12 soil samples 23 p3764 A71-43803

Interplanetary energy spectrum of solar flare Fe nuclei from tracks in Surveyor 3 glass filter and rock 12022 23 p3765 A71-43813

Liquid particles motion over variable profile turbine rotor blade edge, concave and fanning surfaces as function of Coriolis and centrifugal force 24 p3819 A71-44932

PARTICLES

NT AEROSOLS

NT ALPHA PARTICLES

NT ANIONS

NT ANTINEUTRINOS

NT ANTIPARTICLES

NT ARGON PLASMA

NT BETA PARTICLES

NT BOSONS

NT CATIONS

NT CESIUM PLASMA

NT CHARGED PARTICLES

NT COLD PLASMAS

NT COLLISIONLESS PLASMAS

NT CONDUCTION ELECTRONS

NT CORPUSCULAR RADIATION

NT COSMIC PLASMA

NT CYCLOTRON RADIATION

NT DEUTERIUM PLASMA

NT DEUTERONS

NT DROPS [LIQUIDS]

NT ELECTRON BEAMS

NT ELECTRON PLASMA

NT ELECTRON PRECIPITATION

NT ELECTRON RADIATION

NT ELECTRONS

NT ELEMENTARY PARTICLES

NT FAST NEUTRONS

NT FERMIONS

NT FERRIC ION

NT FINES

NT FOG

NT FREE ELECTRONS

NT HADRONS

NT HIGH ENERGY ELECTRONS

NT HOT ELECTRONS

NT HYPERONS

NT INNER RADIATION BELT

NT ION CYCLOTRON RADIATION

NT MAGNETICALLY TRAPPED PARTICLES

NT MANGANESE IONS

NT MESONS

NT METAL IONS

NT METAL PARTICLES

NT MICROPARTICLES

NT MIST

NT N ELECTRONS

NT NEUTRAL PARTICLES

NT NEUTRINOS

NT NEUTRONS

NT NUCLEAR PARTICLES

NT NUCLEONS

NT OUTER RADIATION BELT

NT PHOTOELECTRONS

NT PHOTONS

NT PIONS

NT POLARONS

NT POSITRONS

NT POWDER [PARTICLES]

NT POWDERED ALUMINUM

NT PRIMARY COSMIC RAYS

NT PROTON BELTS

NT PROTONS

NT QUARKS

NT RADIATION BELTS

NT RAINDROPS

NT RECOIL PROTONS

NT RELATIVISTIC PARTICLES

NT SOLAR CORPUSCULAR RADIATION

NT SOLAR COSMIC RAYS

NT SOLAR PROTONS

NT SOOT

NT STELLAR WINDS

NT TACHYONS

NT THERMAL NEUTRONS

NT TRAPPED PARTICLES

PARTICULATE FILTERS

U FLUID FILTERS

PARTITIONS [MATHEMATICS]

High electron temperature H and He I and II, calculating partition functions 01 p0158 A71-10806

Ionizing plasmas partition functions, determining opacities and equations of state 08 p1359 A71-20943

Algorithm determining sequential machine error partition representing inessential errors 14 p2206 A71-29521

Nitrous oxide internal and rotational partition functions for temperature range 200 to 350 K, using molecular constants tabulated by Pliva 19 p3106 A71-37408

Partitioning method for Reissner shell theory equations, constructing rod system 24 p3877 A71-44407

PARTITIONS [STRUCTURES]

Aerospace digital computer partitioning based on MOS MSI technology using functional building blocks /FBB/ 03 p0384 A71-13281

Rare earth, alkali and alkaline earth elements content of phenocrysts and acidic igneous magma 23 p3734 A71-43246

PARTS

U COMPONENTS

PASSBANDS

U BANDPASS FILTERS

U BANDWIDTH

PASSENGER AIRCRAFT

NT A-300 AIRCRAFT

NT BAC 111 AIRCRAFT

NT BO-105 HELICOPTER

NT BOEING 737 AIRCRAFT

NT BOEING 747 AIRCRAFT

NT BOEING 7207 AIRCRAFT

NT CH-3 HELICOPTER

NT CH-46 HELICOPTER

NT CH-47 HELICOPTER

NT CH-54 HELICOPTER

NT COMET 4 AIRCRAFT

NT DC 10 AIRCRAFT

NT DH 121 AIRCRAFT

NT EUROPEAN AIRBUS

NT F-28 TRANSPORT AIRCRAFT

NT H-53 HELICOPTER

NT H-56 HELICOPTER

NT IL-62 AIRCRAFT

NT L-1011 AIRCRAFT

NT SE-210 AIRCRAFT

NT TU-134 AIRCRAFT

NT TU-144 AIRCRAFT

NT VC-10 AIRCRAFT

NT YAK 40 AIRCRAFT

VC 400 tilt wing VTOL cargo and passenger transport aircraft, discussing component and system development and testing phase 01 p0004 A71-10466

Aviation accidents liability limitation by treaty and statute for passengers personal injury or death, discussing Warsaw Convention revisions 03 p0523 A71-12966

ATC regulations considered for Concorde introduction to passenger service, discussing landing and takeoff characteristics 11 p1706 A71-25232

Passenger aircraft structures accelerated testing for safety and fatigue durability under operational conditions, describing tests, planning and evaluation 12 p1974 A71-26946

Fuselage influence on total aircraft drag in subsonic passenger aircraft, considering high aspect ratio cylindrical fuselages 14 p2177 A71-30821

European Airbus automatic pilot and flight control system, including computers in electromechanical subassemblies 15 p2446 A71-31914

Soviet book on subsonic gas turbine passenger planes power supply systems covering Boeing 747, short haul aircraft, DC-10, L-1011, etc 17 p2677 A71-34472

Lockheed L-1011 passenger jumbo jet layout, ground handling and servicing 18 p2849 A71-35995

Passenger travel demand model for STOL transportation in underdeveloped areas 18 p2987 A71-36348

Mercury short range passenger aircraft design conception, analyzing cost 19 p2997 A71-38242

Mil Mi-12 Soviet giant rigid rotor helicopter with 30,000 kg load or 250 passenger capacity 20 p3178 A71-39375

PASSENGERS

Seasonal distribution of air transportation requirements and utilization rate of transport capacity in passenger traffic 19 p3173 A71-38221

Airport design for passenger and baggage handling efficiency, considering choice between continuous and batching type intra-airport transit system 22 p3529 A71-42072

PASSIVATION

U PASSIVITY

PASSIVE SATELLITES

NT BEACON SATELLITES

NT ECHO 1 SATELLITE

NT ECHO 2 SATELLITE

NT EXPLORER 22 SATELLITE

NT PAGEOS SATELLITE

Passive mode navigation satellite position fixing, using synchronous satellite and Loran type chart with correction tables 04 p0622 A71-15004

PASSIVITY

Stability criteria for nonlinear time-varying feedback systems, using passivity theorem 13 p2042 A71-28705

PASTES

Sandwich structure cores of foamglass granulate filled unsaturated polyester paste, discussing development of highly thixotropic paste mixtures 01 p0172 A71-10699

Thermal conductivity coefficients of heat conducting pastes in transistor application 08 p1318 A71-20845

PATCHING

U MAINTENANCE

PATENT APPLICATIONS

Technological forecasting by evaluating patent significance, applying to earth moving equipment development 02 p0335 A71-11858

Quantitative and qualitative philosophical aspects of measure and forecasting applied to patent handling 02 p0336 A71-11861

Industrial ownership in R and D markets, considering customer and supplier objectives compatibility in patent rights clauses 23 p3786 A71-43465

PATENTS

Industrial innovations legal protection, discussing patents, registered designs, copyright and trademarks 01 p0183 A71-10756

NASA patents and licensing policy, discussing contractor rights and invention handling 04 p0690 A71-14939

PATHOGENESIS

Flight concomitant pathogenetic effects on urinary tract conditions, noting kidney descent, inflammatory episodes and calculosis 10 p1566 A71-24977

Extrinsic factors in pathogenesis of congenital heart diseases, considering morphogenetic processes in heart and great vessels development 13 p2002 A71-27811

PATHOLOGICAL EFFECTS

Motor and sensory nerve conduction impairment in upper extremities in vibration disease

01 p0010 A71-10394

Continuous and intermittent effect of carbon tetrachloride breathing on pathomorphological and histochemical structure of liver in test animals

01 p0013 A71-11129

Statistical analysis of airline flight crew psychological unfitness

01 p0028 A71-11598

Physiopathological and otolaryngological repercussions of supersonic flight on SST passengers

03 p0371 A71-13098

Pancreas pathomorphology under acute hyperthermia in animals, showing hemodynamic changes of vessel dilatation and intravascular leukocytosis

08 p1243 A71-21968

Soyuz 9 spacecraft astronauts otorhinolaryngological organs response to 18-day orbital flight, observing pathological changes from clinical post flight examination

09 p1389 A71-22207

Pathological effects of pure oxygen on animal organism at atmospheric pressure, noting perivascular edema, diapedesis hemorrhages, respiratory and metabolic disorders

09 p1392 A71-22641

Acute hydrazine hydrate poisoning morphological effects on internal organs and blood in guinea pigs, noting pronounced changes in liver and kidneys

09 p1393 A71-22921

Physical and physiopathological effects of high altitude supersonic flight in TF-104G aircraft told by flight surgeon

10 p1572 A71-24980

Pathophysiological aspects of microwave irradiation, considering thermal response of human and animal organisms to electromagnetic radiation exposure

10 p1573 A71-25079

Stereophotogrammetric methods and instruments for studying eye anatomical-optical apparatus and pathological changes

13 p2016 A71-28012

Myocardial ischemic lesions age, discussing validity of histopathological criteria and margin of error

15 p2361 A71-32542

Acute fatal nontraumatic collapse during physical work and sports due to pathological processes

18 p2855 A71-36214

Stop test method to study acceleration in movement control processes in man, considering elbow joint movements in normal and pathological tremors in Parkinson disease afflicted subjects

19 p3007 A71-37569

Flashing light stimuli application to clinical instrument design for detection and quantitative assessment of early pathological visual loss based on minimum discernible luminance difference

22 p3498 A71-41482

Pathomorphological and histochemical changes in rat lungs, liver, heart, diaphragm and adrenal glands from acceleration and cysteamine caused tissue oxygen deficiency

22 p3491 A71-42703

High energy proton irradiation of rats with partial shielding of abdominal region, observing pathomorphological changes in myocardium, nervous system and radiosensitive organs

22 p3493 A71-42721

Hyperoxia pathological effects on albino rats subcutaneous connective tissue, noting oxidizing enzyme activity depression and cellular metabolism suppression

22 p3496 A71-42802

PATHOLOGY

NT HUMAN PATHOLOGY

German book on clinical pathophysiology of respiration covering respiratory physiology, pulmonary gas exchange, respiratory control, hypoxia, hyperoxia, pressure breathing, etc

09 p1394 A71-23069

Primary cardiomyopathy, discussing obstructive and nonobstructive cases, myocardial inflammation, chronic alcoholism and age relationships

17 p2682 A71-35120

Soviet book on experimental research on human higher nervous activity from growth aspect covering normal and pathological states, cerebral cortex interaction with central nervous system

21 p3339 A71-41374

Composite tissue blocks method for comparative pathomorphological investigation of radiation pathology

22 p3505 A71-42734

PATIENTS

Aerial transportation of patients, potential hazards due to motion sickness, decreased atmospheric pressure and oxygen tension, fatigue, inactivity and dehydration

08 p1245 A71-20726

Oxygen supply to air transported patients by chemical compounds, suggesting use of permanganates and chlorates

22 p3500 A71-41571

Sick and injured transportation aboard regular airliners, considering pathological and psychological contraindications

22 p3500 A71-41572

PATTERN DISTRIBUTION

U DISTRIBUTION (PROPERTY)

PATTERN RECOGNITION

NT CHARACTER RECOGNITION

Telemetry decommutation system using linguistic and statistical methods in pattern recognition

01 p0036 A71-10989

Contour signal characteristics for cloud form recognition by computer using learning algorithm and photographic data

02 p0225 A71-11691

Pattern recognition - Conference, New York City, June 1969

02 p0225 A71-11701

Holographic filters for optical automatic pattern recognition systems, discussing reconnaissance target and fingerprint

02 p0247 A71-11702

Automatic pattern recognition in photographic transparencies, using diffraction pattern sampling

02 p0225 A71-11704

Radio electronic equipment components reliability, using image recognition theory

03 p0384 A71-13422

Automatic determination of linear pattern recognition and evaluation functions, computing coefficients for half space problem

03 p0450 A71-13621

Neurophysiological aspects of human optical and acoustical perception, discussing pattern recognition and cognizance role in optical image evaluation

03 p0373 A71-14331

Linear pattern classifiers design, using error correction and least mean square adaptive algorithms

03 p0383 A71-14480

Pattern classification algorithms using potential functions to construct discriminant functions from sample points set

03 p0383 A71-14481

Arbitrary patterns recognition by parallel processing, deriving mathematical instructions for signal processing based on statistical communication theory

05 p0726 A71-16391

Image recognition process based on binary digit codes descriptions, developing algorithm for minimal system of characteristics

05 p0726 A71-17019

Automatic pattern recognition, discussing texture as discriminant of crops on radar imagery

05 p0743 A71-17145

Visual pattern perception learning, recognition upon subsequent encountering and unfavorable conditions

05 p0716 A71-17243

Coded recording technique for microfilming daily aerological data, decoding by computer in rapid and compact search and recognition procedure

06 p0922 A71-17503

Saccadic eye movements saccades during pattern perception under poor visibility

06 p0859 A71-17962

Holography and shapes recognition, considering optical memory, information density advantages and optical correlators

06 p0900 A71-18068

Matched spatial filters for holographic image recognition in biological studies

06 p0903 A71-18695

ECG beat-to-beat variation reduction using digital computer wave recognition

07 p1049 A71-19839

Perceptron learning systems with cross connections in single functional elements class, discussing visual patterns training schemes

07 p1068 A71-20103

Two dimensional adaptive pattern-recognizing model of human operator in visual-manual compensatory tracking task

07 p1053 A71-20406

Horizontally and vertically polarized sferic signals from lightning discharges by airborne instrumentation, using pattern recognition approach

08 p1325 A71-20883

Natural image computer for terrain pattern recognition and delineation from aerial photographic inputs

08 p1281 A71-21255

Orthogonal transforms and feature selection using pattern, Harr, Walsh, Fourier and Karhunen-Loeve spaces for providing efficient classification algorithms in pattern recognition

08 p1258 A71-21354

Automatic adaptive pattern recognition in photomapping

08 p1259 A71-21438

Computer pattern recognition technique for determining cloud motions in real time from ATS satellite photographs

08 p1326 A71-21453

Optimal detector parameters for stochastic signals in noise, discussing analytic and simulation studies of adaptive techniques of pattern recognition

08 p1259 A71-21594

Clustering and decision making with interactive a priori problem knowledge insertion in subcategory mean vectors and covariance matrices form for pattern recognition and learning

08 p1260 A71-21664

Pattern recognition feature subset selection based on sequential decision model for on-line processes

09 p1411 A71-22624

Time series analysis techniques concerning correlation, auto and cross power spectral density, amplitude and period histograms, real time pattern recognition and filtering

09 p1405 A71-22783

Holography utilization to data processing, discussing factors affecting recording and matched filters creation for pattern recognition

10 p1581 A71-23917

Theory of form based on geometric probabilities, leading to two dimensional retinal type computer programmed to exhibit elementary form perception aspects

10 p1567 A71-23997

Pattern recognition systems, considering receptor, preprocessing and decision making stages

10 p1568 A71-24225

Mathematical neuronal model for functional learning system networks, representing brain pattern recognition, learning and size invariance mechanisms

10 p1569 A71-24233

Proximal changes and stimulus patterns associated with rotation direction evoking visually perceived oscillation

10 p1570 A71-24606

Algorithm for using presence indicator context and test for target recognition system, discussing simulation technique for use without hardware target recognizer

11 p1734 A71-25143

Venus cloud pattern contrast, using photoelectric scans with narrow band interference filter sequences

11 p1824 A71-25702

Book on color and pattern vision physiology covering retinal induction, electrical excitation of eye, optical illusion, figural aftereffect, movement sensation, etc

12 p1870 A71-26769

Correlation-recovered adaptive majority multiplexing based on pattern recognition technique, describing prototype equipment

12 p1884 A71-27147

Algorithm for subclass identification in image recognition

13 p2034 A71-27835

Grating pattern vision models, examining single neural network and multiple channel stimulus information processing

13 p2018 A71-28461

Spatio-temporal patterns in visual contrast sensitivity, noting exaggerated eye movements effects

13 p2018 A71-28462

Optical pattern recognition by correlation measurements, detecting by zero in intensity distribution

13 p2069 A71-28715

Behavioral effects of electrically induced EEG abnormalities in inferotemporal and occipital cortex in monkeys on visual pattern discrimination and successive spatial reversals

13 p2011 A71-28806

Visual evoked cortical response in man related to rate, spatial frequency and wavelength of alternating barred pattern with background illumination

13 p2012 A71-28888

Gaussian processes discrimination, considering correlation functions in integral control of nonlinear filter for image recognition

13 p2039 A71-28917

Intramodal and crossmodal sensory transfer of visual and auditory temporal patterns in normal young adults

13 p2022 A71-29326

Noisy image visual discrimination and detection, investigating Bayes criterion ideal statistical method validity for pattern recognition

14 p2197 A71-30815

Image classification by optical and electro-optic processing methods for spatial signal perception and treatment in natural form

14 p2248 A71-30816

German monograph on photographic masks as position frequency filters covering pattern recognition, transfer functions, etc

15 p2410 A71-32309

Pattern recognition machine construction for written alphanumeric symbols and human voice identification, providing bibliography

15 p2372 A71-32316

SkyLab earth resources experimental equipment, describing sensing and recording instrumentation for electromagnetic spectral pattern recognition studies [AIAA PAPER 71-841] 17 p2739 A71-34712

Automatic pattern recognition of urban development changes from aerial photographs, using computer program and nonlinear registration technique for cell pairs partitioning 17 p2711 A71-35043

Two dimensional adaptive model of human operator control in visual-manual compensatory tracking task using pattern recognition 17 p2691 A71-35046

Recognition response time experiments for word number effects in target set, discussing familiarity judgment and response decision 17 p2683 A71-35250

Stimulus familiarization effects on visual selection patterns during exposure to banal and incongruous paired stimuli 17 p2683 A71-35251

Human visual depth impression by gradient patterns, discussing experimental verification for hypothesis concerning perceptual economy principle 17 p2684 A71-35252

Digital processing for automatic extraction of information from reconnaissance images, discussing target and terrain configurations pattern recognition technique 17 p2747 A71-35774

Pattern recognition techniques application to metallurgical data analysis, discussing spatial filtering and classification process 17 p2749 A71-35791

Psychological correlates of pattern identification tasks and invariance of pattern recognition under rotation, using Kabrisky model of human visual system 17 p2694 A71-35792

Human visual system biological model for pattern recognition based on spatial filtering covering Fourier transform modification for application to discrete case 17 p2694 A71-35793

Pattern recognition multiplex arrangement with optical relay tube and point hologram for image distribution onto spatially separated channels to obtain SNR improvement 18 p2917 A71-36054

Holographic interferometry for speckle pattern interpretation in metrology, using video techniques 18 p2917 A71-36056

Automated pattern recognition for urban texture and land use assessment by aerial photographs, using digitally scanned optical Fourier transforms 18 p2912 A71-36063

Prisoner dilemma game matrix, noting response patterns to various formats 18 p2863 A71-37017

Fourier transform holograms as complex matched filter for pattern recognition and signal detection in coherent optical systems 19 p3066 A71-38239

Digital pattern classification of oceanographic remote sensing multispectral airborne scanner data, considering sea surface color variations 19 p3060 A71-38405

Mathematical feature selection transformations by multidimensional rotations, considering character recognition experiment 19 p3026 A71-38490

Real time lensless holographic recognition of spatially incoherent and self luminous patterns on diffusing backgrounds using optical matched multiple filters 20 p3235 A71-39184

Walsh functions in image processing, rotational feature selection and pattern recognition, defining set of orthogonal transformations 20 p3255 A71-39611

Orthonormal series expansion for features generation with predetermined properties, applying to handwritten numerals recognition 22 p3515 A71-41512

Fingerprint identification by holographic correlator pattern recognition techniques, discussing reconstructed image visual observation and photoelectric measurement 22 p3539 A71-41748

Pattern recognition technique for system error analysis, applying to inertial guidance system test 22 p3566 A71-42110

Versional eye movement control system models, considering dual mode control, intermittency, plant dynamics and pattern recognition 22 p3489 A71-42444

Rotated pattern detection by optical spatial filtering with superposed holograms, obtaining optimal rotation angle for triangle with digital computer 22 p3546 A71-42475

Pattern recognition problems, using on-line picture language program with flying spot scanner 22 p3519 A71-42767

Optical orientation determination and star pattern recognition for Skylab in solar inertial attitude by digital and hybrid simulations [AAS PAPER 71-397] 23 p3732 A71-43065

Scanpaths in saccadic eye movements during pattern vision and recognition 23 p3635 A71-43973

Potential function, permissible transformations, geometrical, linguistic, optimal statistical and heuristic methods for pattern recognition, discussing unifying approach based on invariant decision functions 24 p3812 A71-44391

Crop surveys from multiband and multiscale satellite photography during Apollo 9 mission, using statistical multispectral pattern recognition digital techniques 24 p3827 A71-44987

PATTERN REGISTRATION

Spatial and temporal patterned light flashes effects on dark adapted subjects, discussing cortical response changes in contrast depth 10 p1565 A71-24680

Optical information processing holographic techniques, describing random masks correlation method for pattern classification 22 p3539 A71-41747

PATTERNS

Pattern classification as linear programming problem, presenting optimal algorithm 09 p1412 A71-22969

PAULI EXCLUSION PRINCIPLE

Solid glyoxal Raman spectrum data, showing operativity of mutual exclusion principle by IR comparison to Raman bands 18 p2873 A71-35830

PAVEMENTS

Aircraft pavement design - Conference, London, November 1970 02 p0237 A71-12162

Transport aircraft tire pressure and multiwheeled landing gear limitations regarding pavement design 02 p0189 A71-12163

Aircraft multiwheel undercarriage effect on rigid and flexible pavements, examining failure modes 02 p0189 A71-12164

Municipal airport rigid pavements design considering supporting effects of soil subgrade, asphaltic concrete subbase and pavement strength 02 p0237 A71-12165

Flexible pavements design for giant transports considering load repetitions, total systems, environmental effects, etc 02 p0238 A71-12166

Rigid and flexible pavement design and construction in Europe, discussing unreinforced and crack reinforced slabs and CBR method 02 p0238 A71-12167

Aircraft pavements in UK, discussing reinforced and unreinforced concrete, tar-bound bases and surface coatings 02 p0238 A71-12168

Aircraft pavements design and construction problems regarding adverse soil conditions 02 p0238 A71-12170

Airport pavement design principles, considering imposed stresses at flight operation areas, runways, taxiways, apron and waiting position overrun areas, shoulders and strips 13 p2045 A71-29311

Asphalt pavement design for heavy multiwheel aircraft, using BISTRO computer program 18 p2897 A71-36000

Systems approach to airfield pavement for future aircraft, integrating design, construction, operation and maintenance 18 p2897 A71-36346

PAYLOAD MASS RATIO

Nuclear powered long distance aircraft engines, discussing high burnup fuel, weight factors and safety problems 06 p0926 A71-17694

PAYLOADS

High acceleration resistant electronic trigger fuse for in-flight gun launched projectile payloads ignition and ejection [AIAA PAPER 70-1389] 03 p0468 A71-13671

Europa 2 booster payload increase by using beryllium-containing solid fuels in perigee and apogee stages 05 p0815 A71-15969

Electric propulsion spacecraft mission performance scaling laws for invariant trajectory, obtaining optimum gross payload over wide range of system input parameters [AIAA PAPER 71-160] 06 p0981 A71-18602

Optimal low thrust power plant for spacecraft payload-maneuver tradeoff 09 p1512 A71-23139

Sounding rockets, outlining experimental missions, design and payload varieties, auxiliary systems and electronic equipment 15 p2499 A71-31213

Dachs three axis payload stabilization and attitude control system for spectroscopic comet observation 15 p2499 A71-31218

Solar electric propulsion and transfer system for higher payloads of SECOM communication satellites, using Europa 2 launcher 16 p2644 A71-32855

High energy solid propellants use in Europa 2 launch vehicle perigee-apogee motor, considering synchronous satellite payload increase 16 p2645 A71-33365

Launch vehicles for space telecommunications applications, considering payload capacity for missions involving earth resources, radio and visual astronomy and meteorology 17 p2811 A71-34226

Space shuttle applications and utilization, discussing payloads, performance modes, Mission Support Module, ancillary equipment, system interfaces and related profiles [AIAA PAPER 71-816] 17 p2812 A71-34726

Payload cost and response time reductions for shuttleborne space experiments, examining NASA Ames airborne research program management technique [AIAA PAPER 71-808] 17 p2813 A71-34731

Space shuttle economic and design impact on satellite payloads, noting variations in flight frequency and cost, hardware and performance [AIAA PAPER 71-807] 17 p2813 A71-34732

On-orbit payload handling for space shuttles, including manipulator arms for drawing docking vehicles together, closed circuit TV and airlocking [AIAA PAPER 71-811] 17 p2814 A71-35427

Europa 3 two stage vehicle characteristics, outlining electrical system configuration and payload capacity 18 p2971 A71-35927

Electronic time delay fuses with high-g components for gun launched projectiles for placing payloads at high altitudes 18 p2851 A71-36281

Integrated system for precision attitude determination and pointing control of spacecraft gimbaled payloads [AIAA PAPER 71-962] 19 p3099 A71-37203

Variable geometry B-1A bomber aircraft, discussing size, payloads, speed, altitude range and runway takeoff 19 p2996 A71-37516

Space tug optimal round trip trajectories for payload earth escape injection missions, obtaining boundary value problem solution by Newton-Raphson iteration technique 21 p3452 A71-40908

Space shuttle impact on cost reduction in NASA space operations, considering operations costs of payloads 22 p3609 A71-41994

Spacecraft and payload design under influence of space shuttle availability, discussing program cost savings 22 p3610 A71-42003

Earth orbit shuttle payload increase, discussing refueling and auxiliary hydrogen tank concept [AAS PAPER 71-302] 23 p3772 A71-42978

Solar electric propulsion application to Halley Comet flythrough and rendezvous missions, describing trajectory characteristics and payload capabilities [AAS PAPER 71-363] 23 p3729 A71-43033

PCM [MODULATION]

U PULSE CODE MODULATION

PCM TELEMETRY

PCM telemetry data transmission bit error probability confidence intervals upper bounds based on Markov chain model analysis 01 p0032 A71-10877

PCM telemetry signal encoding, investigating aliasing and pulse width errors dependence on frequency band occupied by bandpass signal 01 p0032 A71-10881

PCM telemetry receiving stations testing, comparing bit error probabilities of coherent and noncoherent methods of synchronizing pseudonoise sequences 01 p0033 A71-10890

PCM telemetry bit synchronizer/signal conditioner, discussing bit acquisition, error and slippage rates 01 p0053 A71-10907

S band PCM telemetry system using frequency diversity for spin stabilized high velocity blunt nosed reentry vehicle signal reception 01 p0163 A71-10980

Small Astronomy Satellite PCM/PM telemetry transmitting split phase encoded data at 136 MHz 01 p0036 A71-10987

SkyNet telemetry and command stations configuration and equipment functions, discussing antenna subsystem parabolic reflector and positioning, PCM demodulation and computer systems 02 p0217 A71-12431

PCM telemetry bit error probability confidence intervals and Bayesian posterior distributions derivation, using statistical method 04 p0554 A71-15327

Balloon X ray astronomy techniques and observations, noting collimated scintillation counter instrumentation and PCM telemetry 16 p2641 A71-33754

Multichannel PCM/PSK/PM interplex telemetry system for reducing cross modulation loss and excess carrier reference power 17 p2706 A71-35108

PDM [MODULATION]

U PULSE DURATION MODULATION

PDP COMPUTERS

NT PDP 8 COMPUTER

Cost effective general purpose minicomputer PDP-11/45 design and technology using Schottky TTL/MSI, semiconductor memories, multiple buses, microprogramming and floating point units

22 p3519 A71-42761

PDP 8 COMPUTER

High speed real time interpretive language for biological calculations with PDP-8 computer

01 p0049 A71-10244

PEAKS

FORTAN 4 computer program for gamma ray energy spectra, determining peak locations, peak areas and elemental abundances

11 p1729 A71-26069

PEARSON DISTRIBUTIONS

Astronomical observations weighted estimation based on smoothing Pearson curves empirical distribution

23 p3771 A71-44257

PECLET NUMBER

Heat transfer in cylindrical cavity with circulating flow as function of time and Peclet number

10 p1696 A71-24615

Heat transfer at high Peclet number from sphere freely rotating in shear flow field at low Reynolds numbers

10 p1697 A71-24621

Exact method for low Peclet number thermal entry region heat transfer in channel flow, considering transverse nonuniformity of fluid velocity and axial conduction

13 p2164 A71-29009

PEDALS

Foot operation of pedals, investigating speed and accuracy of lower leg motion in different directions

18 p2873 A71-36972

PEDOLOGY

U SOIL SCIENCE

PEELING

Structural film adhesives peel-thickness correlation and cure rate study by torsion pendulum

10 p1614 A71-24074

Metallic surfaces adhesive properties and adsorptive capacity from nondestructive testing by peeling

10 p1616 A71-24105

Shelf stable two component urethane adhesives with prepolymer reactive silane coupling agents for high peel strength retention in humid environment

14 p2261 A71-29637

PEENING

Peen forming of large complex parts from sheet and plate, illustrating dihedral break in airplane wing skin

01 p0091 A71-11550

Explosive peening effects on weld fatigue in Ni maraging steel, Fortiwell and Al-Zn-Mg alloy

23 p3682 A71-43877

PELLETS

InAs-AlAs pseudobinary system solidus boundary determination from pellet phase diagram

08 p1344 A71-21472

PELTIER EFFECTS

High density DC effects on displacement of solid GaAs-liquid metal interface, considering Peltier effect and dislocation density

08 p1344 A71-21444

PELVIS

Visual contrast sensitivity and fundus oculi pattern changes due to accelerations in pelvis-head axis

12 p1870 A71-27165

PENALTIES

Penalty method and decomposition of state equations applied to nonlinear systems

10 p1637 A71-24840

PENDULOUS GYROSCOPES

U GYROSCOPIC PENDULUMS

PENDULUMS

NT GYROSCOPIC PENDULUMS

Pendulum clock with contactless drive for isochronal autooscillation period, outlining pulse amplitude and duration stabilization

04 p0592 A71-14863

Null shift errors of compensated electromechanical pendulum accelerometers during random vibration of base

07 p1108 A71-19308

Navigational precision timing from earth rotation based pendulum to atomic second based quartz oscillator clocks

07 p1156 A71-20341

Horizontal pendulum angular velocity and motion due to harmonic vibrations at base

07 p1162 A71-20651

Torsional pendulum behavior variations during solar eclipse of 7 March 1970

09 p1493 A71-22805

Pendulum oscillations under impact force in low resistance medium

09 p1494 A71-22875

Torsion pendulum for measuring internal friction and shear modulus of refractory metals and alloys

09 p1452 A71-23333

Velocity measurements for slowly moving pendulum bob with incandescent filament lamp, detecting

Doppler shifted beam interference beat frequency with photomultiplier

10 p1574 A71-23738

Free solid body carrying heavy pendulum, calculating oscillations as function of geometrical and inertial characteristics during motion under tangential force

12 p1929 A71-27117

Hipp pendulum controller electromechanical clock, considering dry and viscous friction dynamic models

12 p1932 A71-27525

Physical pendulum normalized error variance as irregularity function in excitation with narrow band frequency spectrum

13 p2065 A71-27947

Nonconservative elastic system involving standard double pendulum model under retarded follower load, calculating damping, time delay and parameter variations effects on stability

15 p2449 A71-32012

Subharmonic oscillations excited by horizontal vibrations of mathematical pendulum suspension

16 p2607 A71-32936

Compound pendulum in artificial satellite for establishing attitude reference or detecting rotation rate variations

17 p2813 A71-34870

Force and heat transfer measurement in hypersonic flows of low gas density, using electromagnetic balances for horizontal and vertical forces and pendulum method for measuring resistance

18 p2921 A71-36416

Instrumentation and techniques of torsional pendulum and braid analyses, studying trace moisture and cure cycle effects on thermomechanical spectra of polymeric materials

18 p2939 A71-36596

Free falling spheres rocking/lateral motions, deriving nonlinear damped pendulum equation with motion coupling expressed as Reynolds number dependent phase shift effect

21 p3416 A71-40953

PENETRANTS

Radioisotopes technical applications in industrial and aerospace sciences, discussing radioactive gas penetrants, radiation interaction and geometrical measurements

03 p0455 A71-13533

PENETRATING PARTICLES

U CORPUSCULAR RADIATION

PENETRATION

Electron beam welding penetration depth, using constant melt temperature boundary interface

[ASME PAPER 70-WA/HT-2] 03 p0432 A71-14094

Turbulent heat and mass exchange intensity at gas screen, investigating nonisothermality and wall penetrability effects

04 p0683 A71-15497

Electron beam welding, calculating penetration depth from mathematical model

[ASME PAPER 70-WA/HT-2] 13 p2075 A71-28978

PENETRATION BALLISTICS

U TERMINAL BALLISTICS

PENTROMETERS

Cone penetration resistance tests on granular lunar soil simulants for in-place shear strength and packing characteristics under various gravity conditions

23 p3757 A71-43751

PENICILLIN

Cysteamine and penicillamine effects on copper ion charge transfer, using electron spin resonance and optical absorption measurements

07 p1033 A71-18935

PENNING DISCHARGE

Radial distribution of electric potential in Penning discharge based on relation between sulfur hexafluoride negative ions transit time and initial energy

13 p2107 A71-28852

Stoletov constant for gas mixture, discussing average avalanche energy at reduced electric field with maximum ionization coefficient and Penning effect for Ne-Ar

13 p2103 A71-29081

Radial distribution of electric potential in Penning discharge based on relation between sulfur hexafluoride negative ions transit time and initial energy

21 p3425 A71-41281

PENNING EFFECT

Cs plasma thermionic diode, using Penning effect for ionization rate increase via Hg or Cd seeding

05 p0705 A71-16170

He-Zn vapor lasers excitation mechanism, presenting Penning and charge transfer cross sections

06 p0910 A71-18670

He-Zn ion laser, considering charge exchange and Penning collisions as primary excitation sources of Zn II levels

11 p1773 A71-25927

Cd ion laser with He-Ne, suggesting Cd ion excitation by Penning process

18 p2929 A71-35981

He-Cd CW laser transitions, describing charge exchange and Penning ionization-excitation processes

21 p3393 A71-41038

Penning process for small ionization probability per atomic collision, obtaining ion production constant relationship to temperature

21 p3420 A71-41252

PENNING GAGES

Magnetic field effect on emission spectrum and intensity at electron cyclotron frequency harmonics from PIG Reflex discharge, discussing electron oscillations excitation in plasma

12 p1938 A71-27214

Magnetic field effect on emission spectrum and intensity at electron cyclotron frequency harmonics from PIG Reflex discharge, discussing electron oscillations excitation in plasma

19 p3117 A71-38626

PENS

Pen actuators prototype models for fast response graphic recording instruments, using DC servomotors or galvanometers

09 p1452 A71-23386

PENTACHLORIDES

U CHLORIDES

PENTARYTHRITOL TETRANITRATE

U PETN

PENTOBARBITAL SODIUM

Succinic dehydrogenase activity inhibition and pentobarbital sodium protection of lung tissue in mouse breathing oxygen at atmospheric pressure

11 p1721 A71-26125

PENTOSE

NT RIBOSE

Pentose breakdown photosensitivity from UV irradiation in presence of minerals, considering prebiological period carbohydrates evolution and interaction with purines and pyrimidines

01 p0029 A71-11561

Photocatalytic stimulation of UV radiation photolysis of amino acids and pentoses in aqueous solutions by metal oxide sols

21 p3345 A71-40574

PENUMBRAE

Sunspot penumbra displacements, emphasizing fine structure elements velocity and directional motion

14 p2308 A71-29972

Sunspot umbrae and penumbrae, plotting period and amplitude curves for oscillatory velocity field

15 p2497 A71-32744

PEPSIN

Pilot nervous-emotional state during flight conditions determined from uropepsin excreted in urine

05 p0711 A71-17028

Immunochemical investigation of dogfish pepsinogens A, C and D, determining characteristics in terms of immunodiffusion, immuno-electrophoresis, complement fixation and enzymic activity inhibition

13 p2015 A71-29480

Dog uropepsin excretion dynamics under extremal flight conditions, detailing hypoxia, high temperature radical accelerations and impact G forces effects

15 p2358 A71-31322

PEPTIDES

Carbohydrate-peptide bond and residue chain structure of group blood substances, using alkali decomposition of monosaccharides

01 p0013 A71-11091

Dipeptides separation and identification by column and paper chromatography for elution times prediction and sequence studies

08 p1251 A71-21688

Dipeptidyl aminopeptidase I/cathepsin C/ properties, subcellular localization and polypeptide degradation in rat liver and bovine spleen and pituitary glands

13 p2025 A71-28179

Proteinoids self assembly into primitive cell from observations of polypeptide generation during amino acid heating

14 p2190 A71-30179

Peptides formation from glycine in presence of trimetaphosphate, investigating mechanism

21 p3345 A71-40175

Polymerized and hydrolyzed polypeptides from condensed amino acid adenylates for prebiological synthesis model

22 p3508 A71-42232

UV radiation effect on amino acids and peptides in different gas atmospheres in presence of salts and metal oxides

22 p3496 A71-42829

PERCENTAGE

U RATIOS

PERCEPTION

NT AUDITORY PERCEPTION

NT AUTOKINESIS

NT BINAURAL HEARING

NT CONSCIOUSNESS

NT CRITICAL FLICKER FUSION

NT OLFACTORY PERCEPTION

NT PAIN SENSITIVITY

NT PROPRIOCEPTION

NT SENSORY PERCEPTION

NT SPACE PERCEPTION

NT TACTILE DISCRIMINATION

NT TASTE

NT VERTICAL PERCEPTION

NT VIBRATION PERCEPTION

NT VISUAL DISCRIMINATION
NT VISUAL PERCEPTION
Gestalt psychology perceptual organization, analyzing contextual background and residual stimuli, interaction concepts, configurational principles and organismic factors
07 p1042 A71-19696
Biological memory and perception processes electronic simulation by keyboard structure reenacting word reception, storage and delivery
07 p1051 A71-20118

PERCEPTORS
U SELF ORGANIZING SYSTEMS

PERCHLORATES
NT AMMONIUM PERCHLORATES
NT HYDROXYLAMMONIUM PERCHLORATES
NT NITRONIUM PERCHLORATE
NT POTASSIUM PERCHLORATES
Crystal lattice energies of solvation of alkali metal perchlorate in water
22 p3508 A71-42530

PERCHLORIC ACID
Chromium oxide electric conductivity activation energy and active oxygen, discussing perchloric acid and ammonium perchlorate vapors effect
07 p1182 A71-19247
Anodic dissolution of aluminum bicrystals in electrolytes containing perchloric acid during electropolishing, showing anisotropic layer existence
16 p2592 A71-33371
Perchloric acid reactivity with respect to hydrogen, methane, ethane and ethylene by flow method, using twin concentric jet reactor of Pyrex glass
17 p2792 A71-35709
Perchloric acid catalytic pyrolysis relationship to ammonium perchlorate decomposition and combustion from electric conductivity measurements, IR spectroscopy, chemical and thermal analysis
19 p3120 A71-38119

PERCUSSION
Nondestructive test for fiberglass reinforced plastic tank, using percussion method
21 p3466 A71-40838

PERFECT GAS
U IDEAL GAS

PERFLUORO COMPOUNDS
Perfluorinated monocarboxylic fatty acids additives for controlling lubricating oils spreading on metals and antifriction properties improvement
15 p2438 A71-31680
Perfluoropolyether fluid lubricant physical and chemical properties at high and low temperatures, explaining metals effects on thermal stability by topochemical reaction mechanism
19 p3083 A71-37424

PERFORATED PLATES
Isotropic nonlinearly elastic plate weakened by doubly periodic reinforced curvilinear holes, calculating stress-strain state by Cauchy integrals
01 p0168 A71-10412
Elastic plane with hypertrochoid hole under axial tension, determining stress concentration at hole boundary due to irregularities
01 p0168 A71-10424
Boundary value problems in thermoelastic equilibrium of unbounded isotropic plate with slits and foreign circular inclusion
01 p0170 A71-10643
Thermal stress concentration around hole in edge-heated elastic strip, using quasi-static formulation
02 p0322 A71-11732
Two dimensional stressed state of isotropic plate with elastically reinforced elliptical hole under biaxial tension
02 p0326 A71-12290
Stress concentration at free and reinforced curvilinear holes with random surface roughness applied to plane under hydrostatic tension
02 p0326 A71-12291
Polish book on limiting load capacity of structural elements covering notched rods and plates with hole under elastoplastic stress
02 p0330 A71-12750
Stress-strain state of plate made from highly elastic polymer containing circular and elliptical holes
03 p0506 A71-13602
Distance dependent stress concentration of isotropic plate with two elliptical holes under tension of opposed point forces
03 p0506 A71-13603
Stress distribution around elliptical hole in thin flat rectangular elastic plate under axial in-plane edge loads
[ASME PAPER 70-DE-M] 03 p0506 A71-13705
Hollow annular inserts for stress concentration and alternating stress range reduction around holes in thin flat plates, taking friction coefficient into account
[ASME PAPER 70-DE-L] 03 p0506 A71-13706
Flat sheet under uniform radial tension, varying thickness reinforcement around hole for high stress concentration avoidance
03 p0513 A71-14238

Discrete vortex formation above perforated flat plate in wind tunnel, examining unsteady boundary layer
03 p0345 A71-14568
Shallow spherical shells with periodically spaced holes, discussing stress analysis by least squares method for curved perforated plates
[ASME PAPER 70-PVP-11] 04 p0665 A71-14771
Central hole effect on flat metal sheet fatigue under tension-compression load cycles, noting application to aircraft materials
04 p0670 A71-15389
Soviet book on perforated plates and shells covering strength, rigidity, lattice tension and bending, stress and strain states, boundary value problems, etc
04 p0671 A71-15398
German monograph on stress distribution around cutouts in disks, plates and cylindrical shells
05 p0820 A71-16121
Rectangular thin elastic plate with circular holes under heat flow, solving thermoelastic problem by point matching
05 p0823 A71-16492
Thick plate with circular holes of various sizes, studying stress-strain state
05 p0828 A71-16890
Stress concentration in planar rectangular shallow shells and plates with polygonal holes
07 p1218 A71-20470
Hardened plasticity zone around circular hole in creep deformed plane under normal forces, determining stress-strain relation and time dependent variations
07 p1219 A71-20647
Elastic and elastic-plastic surface strain fields around skewed circular holes in flat plate under uniaxial tension
08 p1372 A71-21654
Stressed state in region of strain raisers around holes in plate subjected to two axial tension associated with plastic yield
08 p1372 A71-21703
Stress analysis of anisotropic plate with square holes under tension, using small parameter method
08 p1374 A71-21947
Elastic plate with circular hole, solving contact problem in elasticity theory with integrodifferential equation
09 p1535 A71-22181
Fatigue crack propagation rate in steel alloys with holes as stress concentrators related to duration of various development phases
09 p1538 A71-22597
Dynamic plastic bending theory of thin circular annular plate with central hole under uniform impulse
10 p1689 A71-24519
Strain concentration around holes in composite plate by moire techniques
11 p1851 A71-26389
Temperature and membrane thermal stress distribution in finite rectangular plate with insulated circular hole, considering steady state heat conduction equation
11 p1852 A71-26404
Wake flow behind two dimensional perforated plates normal to air stream, measuring drag, shedding, velocity and turbulence at Reynolds number 25,000-90,000
11 p1705 A71-26449
Anisotropic plate with curvilinear holes, noting stress concentrations
12 p1975 A71-27110
Stress concentrations over smooth perimeters of curvilinear holes in infinite isotropic plates subjected to loads
12 p1984 A71-27694
Stress concentration in variable-modulus perforated plate of isotropic elastic material under hydrostatic pressure
13 p2151 A71-28142
Thermoelastic stress analysis of circular perforated plate under point heat source
14 p2326 A71-30195
Dislocation stress analysis in infinite elastic plate with two circular holes under arbitrary steady temperature field
14 p2332 A71-30850
Stress analysis of nonlinearly elastic plate with ring reinforced circular hole
14 p2332 A71-30854
Stress-strain measurements in inelastic elements by photoelastic, laser, memory, load and plane deformation methods, considering plate with circular hole
14 p2333 A71-30894
Dynamic response and perforation of thin plates subjected to projectile impact, measuring plastic deformation, dynamic strain and displacement with high speed camera
15 p2503 A71-31422
Sound passage through rigid screen of arbitrary wave thickness with apertures, using linear algebraic equations
15 p2449 A71-31709

Elastoplastic analysis by matrix displacement method, discussing perforated plate under tension and bar thermal stress due to rapid heating
16 p2652 A71-33085
Circular plate deflection weakened by hole and under constant external pressure, obtaining successive approximation method solution convergence
17 p2816 A71-34329
Stress-strain state of homogeneous and inhomogeneous cylinders and disks with central axial curvilinear hole under internal pressure and thermal loads
17 p2816 A71-34331
Multicomponent system of elastic plate with hole and built-in viscous-fluid-filled syphon bellows, calculating oscillation by asymptotic methods
17 p2777 A71-34423
Elastoplastic strain distribution in bent circular Al plate with central hole under concentrated load, giving moire patterns and stress-strain diagram
[SESA PAPER 1822] 17 p2820 A71-34542
Propagating crack arrest capability of circular hole in plate, studying dynamic stress intensity and concentration factors changes
[SESA PAPER 1827A] 17 p2820 A71-34546
Metal strips with holes under tensile loads, determining plastic region boundaries with photoelastic method
17 p2821 A71-34592
Thermoelastic Cosserat plate with insulated un-stressed circular hole under uniform temperature gradient at infinity
17 p2822 A71-34675
Generalized periodic problem of infinite isotropic plate of constant thickness with periodically arranged groups of holes, determining stress-strain state
17 p2833 A71-35611
Photoelastic analysis of maximum stress in wide plate with asymmetrically reinforced circular hole under tension, noting effects of rounded corner at hole edge
18 p2984 A71-37022
Elastic circular plate with hole traversed by tube filled with viscous fluid, studying system motion
19 p3043 A71-37539
Displacement in circular plate with radial slit under transverse forces
19 p3156 A71-37796
Stress distribution in cylindrical bodies in internal contact, considering thick elastic plate with elastic disk fitted tightly into hole
19 p3160 A71-38482
Variable thickness plate under cylindrical bending, considering stress concentration around circular hole
19 p3160 A71-38542
Infinite elastic plate forcing by time varying radial pressure in circular hole at center
20 p3309 A71-39563
Thermal stresses in infinite elastic plate with circular hole and single heat source, considering steady state heat conduction
21 p3464 A71-40753
Stress concentration near holes in high modulus epoxy resin polymer thin plates under pressure wave loads
22 p3614 A71-41611
Low temperature thermal insulation using diffraction effects of multilayer perforated reflecting screens
22 p3622 A71-42678
Solid circular plate with diverse elastic moduli in different directions and hole at center, calculating thermoelastic stresses
23 p3777 A71-43422
Nonlinear geometry effects on stress concentration in elastic plates weakened by two circular holes, using complex potential approximations
23 p3778 A71-44041
Thermoelasticity, thermal conductivity and stress distributions in plates with two circular holes under constant contour temperatures, using complex variables theory
23 p3778 A71-44042
Edge supported anisotropic elliptic plate with hole under bending by constant lateral edge load, presenting stress-strain state
24 p3882 A71-44837
Stress-strain state of nonlinearly elastic reinforced polymer plate with circular hole, deriving stress tensor components and first approximation solution for pure bending
24 p3882 A71-44838
Mixed boundary elasticity solutions for plane with cut on real axis, using Riemann surface
24 p3885 A71-45102
Glass multichannel perforated plate manufacture technology, discussing drawing and hollow fiber techniques
24 p3832 A71-45335

PERFORATED SHELLS
Spherical shell stressed state weakened by holes, investigating shear deformation effect
12 p1975 A71-27107
Spherical shallow shell with hole, noting natural vibration frequency
12 p1975 A71-27108

Stress concentration at circular hole in conical shell, using Bubnov-Galerkin method in conjunction with linear thin shell theory

13 p2150 A71-28135

Thin walled cylindrical elastic shell with rectangular holes at equal intervals along straight line, deriving boundary conditions expression by R-functions

14 p2326 A71-30190

Circular cylindrical shell with elliptic hole, calculating stress concentration around hole under torsion

15 p2506 A71-32014

Stress distribution in cylindrical shell with two unequal diametrically opposite reinforced circular holes under internal pressure

16 p2661 A71-34159

Conical shell with circular hole, determining stress function and normal deflection in torsion

17 p2817 A71-34338

Variable thickness thin orthotropic spherical shell with hole, calculating stressed state with successive approximation technique

19 p3155 A71-37533

Stress concentration formulas for elliptical hole in spherical shell with or without cap

19 p3156 A71-37540

Thin shallow spherical shell weakened by circular hole, calculating stressed state from boundary value problem solution

20 p3308 A71-39165

Membrane and bending stresses analysis around elliptic hole in long thin circular cylindrical shell, using perturbation technique

20 p3309 A71-39776

Natural frequencies and vibration modes of perforated cylindrical, conical and spherical shells of revolution, using Ritz method

22 p3617 A71-42488

Cylindrical shell weakened with large circular hole, deriving nonlinear equilibrium equations in semigeodesic polar coordinates

24 p3877 A71-44479

Cylindrical shell with elliptical hole, calculating elastic stress concentration due to axial tension based on shallow shell theory

24 p3879 A71-44625

Equivalent stiffening of circular hole in convex shell of revolution by short shell under symmetric and antisymmetric loads

24 p3882 A71-44845

PERFORATION

Perforated thick shallow spherical shell, solving boundary value problem for external loads

02 p0329 A71-12671

PERFORMANCE

Optimal control system design quality, using generalized performance characteristics as principal parameter

05 p0732 A71-17022

Direct search of performance index for optimal control of class of nonlinear distributed parameter systems

05 p0776 A71-17109

Noninferior performance index vectors in multicriteria optimal control theory

07 p1147 A71-19472

Finite wall conductance effect on performance /pressure and load capacity/ of MHD hydrostatic thrust bearings

07 p1117 A71-19503

On-line computer systems performance characteristics determination through functional simulation, using FORTRAN IV program packages

07 p1068 A71-19708

Primary and secondary silver oxide-zinc cells performance capability

08 p1235 A71-21098

Hybrid phase locked loop for deriving phase error estimate from carrier and information components, discussing system parameters optimization for performance

08 p1270 A71-21353

One dimensional steady state performance characteristics of thermomagnetic generators and refrigerators in dimensionless form

09 p1387 A71-23647

Reynolds number effects on centrifugal compressor performance characteristics, discussing power losses in compressor, impeller and diffuser stages and compressor adiabatic efficiency

11 p1703 A71-25967

Monograph on tolerance effects and performance degradation in microwave aerials covering axial displacement, active array, radiation pattern prediction and mutual coupling

13 p2037 A71-28495

PERFORMANCE CHARACTERISTICS

U PERFORMANCE

PERFORMANCE DECREMENT

U PERFORMANCE

PERFORMANCE PREDICTION

NT PREDICTION ANALYSIS TECHNIQUES

Materials and welded joints brittle fracture resistance estimation from impact bending tests

01 p0085 A71-10084

Cassegrain system far field radiation pattern and gain loss prediction for beam steering by subreflector tilting

02 p0222 A71-12793

Shaped dual reflector antenna gain prediction based on feedhorn radiation pattern and system geometry

02 p0233 A71-12795

Earth station antennas structural parameters and performance prediction, considering autotrack loop stability optimization by multiple lag compensation using single axis model

02 p0223 A71-12803

STOL future performance and safety level, considering current jet aircraft fatal accident record and proportional perpetuation, airworthiness and operational considerations

03 p0347 A71-13568

Polymeric materials plastic deformation properties during service and storage, discussing prediction and testing methods

03 p0448 A71-14300

Motor design parameters effects on solid propellant extinguishment predicted from mathematical combustion model

03 p0469 A71-14442

Nozzle performance prediction inaccuracy due to invalid drag laws, considering unresolved problem of condensed phase particle size

03 p0344 A71-14453

Space transportation system performance risks due to design parameter uncertainties, presenting analysis method for tradeoff studies based on figure of merit calculation

04 p0663 A71-15335

Implosion driven hypervelocity launcher performance prediction, considering loss mechanisms, hydrodynamic calculations and shock phenomena

05 p0733 A71-16505

Carbon and metal film resistors stability, presenting service life characteristics prediction method for arbitrary electric loads and time

05 p0728 A71-16774

Computer systems performance simulation, discussing data collection and preparation and language selection

05 p0727 A71-17048

Adaptive/self synchronizing PSK receivers with common power and bandwidth, discussing analytical and numerical investigations of performance characteristics

05 p0723 A71-17054

Wideband FSK system involving direct and reflected path transmission, predicting diversity performance from mathematical model

05 p0724 A71-17057

Logic circuitry materials physical properties changes effects on performance-controlling parameters at low temperatures

05 p0732 A71-17077

Lubrication considerations concerning mechanical and service variables for obtaining optimum gear performance under severe operating conditions

06 p0904 A71-17576

Night carrier landing final approach glide slope altitude, lateral and sink rate pilot errors prediction, using linear regression model

06 p0858 A71-17602

Linear dynamic object output reaction prediction by Kalman method constructed model

06 p0879 A71-17673

Spacecraft phased arrays design, considering solid state amplifiers effect on total array performance and transistors and varactors output power efficiency

07 p1069 A71-18813

Large signal oscillation mode model for GaAs devices operational prediction, including space charge and intervalley transfer time effects

07 p1070 A71-18867

Electronic equipment reliability prediction, considering confidence limits

07 p1077 A71-19564

Series connected three level perceptron type learning system with sensory, association and response units, establishing performance selection and prediction parameters

07 p1068 A71-20102

Multistage axial flow turbine off-design performance prediction, exploring inlet temperature and pressure and exit pressure variation effects

07 p1184 A71-20199

Heterojunctions with II-VI compound semiconductors, evaluating electro-optical performance

07 p1181 A71-20409

Four-cavity elliptic waveguide microwave bandpass filter design and performance prediction from mathematical model

08 p1262 A71-20762

Bipolar silicon microwave transistors process technology improvements related to extensions of frequency, power handling or low noise performance

08 p1263 A71-20991

Blowout characteristics prediction analysis for safety fuses with current limiting feature

08 p1233 A71-21075

FM demodulator system with parametric tracking filters for threshold improvement, discussing reception performance

08 p1265 A71-21279

Moving target indicator /MTI/ performance improvement in presence of rain, chaff or other broadband clutter disturbances by adaptation for canceler setting optimization

08 p1254 A71-21338

Maneuvering vehicles behavior model selection for real time Kalman filter tracking algorithm, based on accuracy predictions and empirical performance

08 p1270 A71-21349

Satellite carrier tracking and phase lock carrier loops, evaluating lock and reacquisition performance loss by linear model and Monte Carlo digital simulation

08 p1270 A71-21352

Multipath effects on FM communication systems performance, using analog computer simulation

08 p1255 A71-21597

Single and dual channel weak signal adaptive detectors theoretical performance under statistically undefined noise background

08 p1256 A71-21601

Metal parts fatigue life prediction by eddy current method, using experimental relationship between disbalance voltage and stress cycle number

08 p1300 A71-21893

High speed aircraft external store separation testing and prediction techniques, considering flow field survey, dynamically similar drop models and captive trajectory methods

08 p1229 A71-22014

Flight time, path and fuel consumption in climb at constant radius turn, variable or constant velocity and constant engine power, deriving approximate simple formulas

08 p1232 A71-22050

Elastic and plastic plane deformation photoelastic measurement at room and elevated temperatures by moire patterns, comparing performance with other methods

09 p1536 A71-22328

Klystron output resonator efficiency optimization under excitation of plasma with Pi-shaped charge concentration based on performance analysis as function of plasma width

09 p1415 A71-22360

Information specialists performance prediction, discussing multiple discriminate analysis of selected variables

09 p1548 A71-22479

Prediction of metals heat resistance increase by thermomechanical treatment, considering Ni-Al alloy

09 p1477 A71-23332

Helicopter vibrational behavior prediction in flight with known aerodynamic loads, using branch modes method

09 p1385 A71-23606

Centrifugal compressor fluid dynamics, discussing unresolved problems governing design and performance prediction

10 p1550 A71-24216

Two-frequency moving target indicator Doppler radar system, predicting efficiency to clutter drift under stochastic echo and clutter signals

10 p1578 A71-24591

Nonlinear systems parameter identification schemes using first and second order extended Kalman-Bucy linear filters and sensitivity functions, comparing performance by two examples

10 p1587 A71-24745

Model concepts and mathematical methods for planned economy conditions and goals representation, considering prediction reliability

11 p1860 A71-25257

Validity range of response prediction methods for large flexible aircraft to continuous atmospheric turbulence, discussing power spectral densities and fatigue life

11 p1707 A71-25321

Fiber reinforced composites, predicting mechanical properties, stress-strain behavior, interface failure, creep and fatigue by mathematical model

11 p1849 A71-25655

Thermionic converters performance in ignited mode from transport equations for diffusion region, determining electron concentration, potential and temperature

11 p1711 A71-25879

Thermionic converter nonsaturation effect in diode I-V characteristics from computerized analysis for plasma transport phenomena and sheath-electrode-plasma interactions

11 p1713 A71-25892

Gas turbine exhaust silencer performance prediction by transmission line theory, considering LF requirements effect on size and cost

11 p1811 A71-25954

Steady transonic flow through two dimensional gas turbine cascades predicted with time dependent formulation of flow equations, giving airfoil surface pressure distributions

11 p1704 A71-25996

Epoxy resin heat shield performance prediction based on chemical structure relation to ablative properties, discussing thermal degradation mechanism and char forming reactions

11 p1855 A71-26038

Performance prediction of fixed wing leading edges radiative, ablative and active cooling thermal protection systems and system weights comparison for space shuttle entry mission

[AIAA PAPER 71-445] 11 p1839 A71-26230

P-n junction controlled discrete microwave commutation diodes performance calculation and design optimization

11 p1741 A71-26554

Decimeter range diode commutation devices, calculating speed, wideband capability, noise level and maximum power

11 p1741 A71-26555

Pulsed optical range finders, predicting transmitter pulse waveshape effects on calibration, precision and efficiency by probability density function

12 p1903 A71-26792

Response strategies in two-choice reaction task with continuous cost for time, confirming fast-guess model prediction

12 p1873 A71-27008

Helicopter blades inherent vibration damping, comparing theoretical and semiempirical predictions to experimental results

12 p1976 A71-27123

Modulation cancellation altimeter error analysis and performance optimization

12 p1908 A71-27437

Moving window and feedback integrator type scanning radar detectors performance comparison based on probability and position estimates by Monte Carlo simulation

12 p1882 A71-27441

Burst-like signal detectability evaluation in terms of optimum detector performance and probability theory

12 p1882 A71-27442

Klystron power conversion efficiency augmentation by electrostatic depressed collector design, presenting performance prediction calculation method

12 p1889 A71-27734

Data correlation and effectiveness prediction from film cooling injection geometries, considering finitely thick slot lip and boundary layers

13 p2161 A71-28751

Graphical method for predicting intermodulation components and spurious responses

13 p2038 A71-28867

German monograph on game theory and planning techniques for aircraft evaluation

13 p1996 A71-28880

Quantitative performance evaluation of man machine systems in stochastic environments, deriving simulation algorithm

13 p2021 A71-29286

Pulsed GaAs point contact diodes quick response performance, obtaining contact electrical characteristics and Schottky-type rectifying barriers by half period currents

14 p2211 A71-30093

Liquid hydrogen fueled space vehicle fluorine-hydrogen main tank injection pressurization system performance prediction by computerized analysis

[AIAA PAPER 71-645] 14 p2290 A71-30722

Acoustic linings for attenuation of fan generated noise in turbofan engines, considering interaction between analytical lining performance prediction and flow duct testing

14 p2295 A71-30778

Pulse-burst radar design optimization and performance comparison with low and high pulse repetition frequency Doppler radar

14 p2197 A71-30797

Digital wire line system data bus design, calculating transmission performance of noise environment shielded twisted pair cable by linear filter model

14 p2198 A71-30904

Tape recorder equalization techniques effects on attainable bit error probability in digital communication, considering asymptotic prediction recording PCM/FM

14 p2249 A71-30918

Performance predictions for Viterbi decoding algorithm by simulation on UNIVAC 1108

14 p2200 A71-30922

Miniature 20-watt CW TWT with samarium cobalt focusing magnets for fitting X-band waveguide, comparing performance, size and weight with conventional design

15 p2375 A71-31206

Axial flow steam and gas turbines performance estimations over ranges of loading, velocity/blade ratio, Reynolds number and aspect ratio

15 p2469 A71-31733

Bridge-feedback amplifier constant-temperature hot-wire anemometer static and dynamic response determination

15 p2408 A71-31931

Electrically-heated Brayton power conversion system, comparing performance tests with prediction

15 p2354 A71-32212

Hybrid thermocouple with PbTe and SiGe thermoelectric materials, discussing development status and performance prediction

15 p2355 A71-32225

Ferromagnetic shields effectiveness against magnetic fields, permitting solutions to nonlinear shielding problems

15 p2377 A71-32369

Arbitrary shape pulsed AM systems prediction technique improvement, using time-domain signal

15 p2373 A71-32371

Operator mental performance reliability prediction from heart beat rate and electromyogram

16 p2534 A71-32826

Machine structural elements endurance margin prediction from limited tests, proposing statistical method of integral estimates and tolerance factors

16 p2651 A71-33064

Structural reliability predictions using finite element stress program and partial derivative method involving finite approximations

16 p2583 A71-33294

Unmanned spacecraft first day failures, discussing launch environment, duration tests in simulated space and performance improvement

16 p2645 A71-33296

Fault tree, failure mode and effect analysis, prediction apportionment and assessment, discussing system effectiveness

16 p2664 A71-33317

Human performance reliability data system using taxonomic structure for classifying behavioral studies and predicting man-machine performance

16 p2536 A71-33318

Elliptical and circular orbit satellite injection capabilities of Europa 2 launch vehicle, considering geostationary orbit and launcher performance

16 p2645 A71-33364

Materials and welded joints low temperature operation reliability prediction by estimating brittle fracture resistance from impact bending tests

16 p2584 A71-33640

Quadrupole mass spectrometer ultimate characteristics concerning resolution, range, recording speed, working pressure and sensitivity

17 p2737 A71-34288

Short wave frequency-diversity radio communication systems operating at extremal frequencies of group, estimating noise reduction effectiveness

17 p2698 A71-34395

Rotating inertia effects on step-type MHD hydrostatic thrust bearing characteristics, discussing disk shape and operating conditions for improvement

17 p2748 A71-34641

German monograph on extrapolation procedure based on Taylor series expansion and on algorithm for identification and prediction of eye pursuit movements

17 p2690 A71-34790

Space shuttle guidance, evaluating performance of strapdown and gimbal systems by nominal and abort trajectories

17 p2773 A71-35061

Electromagnetic coupling measurement between two antennas in cluttered communications system, emphasizing scale model prediction technique

17 p2703 A71-35078

SPADE system digital channel unit applicability to services other than voice transmission, discussing narrow- and wide-band data transmissions and bit-error-rate performance

17 p2706 A71-35104

Error sampled discrete continuous feedback control system performance, comparing adaptive and periodic sampling methods

17 p2722 A71-35184

Fatigue life prediction for structure undergoing random steady Gaussian centered process, determining statistics of absolute maximums

17 p2832 A71-35471

Integrated airborne Omega/inertial navigation systems performance prediction using statistical models for position fix errors

17 p2776 A71-35769

Aerial cameras performance prediction by computer simulation technique with random number generation

18 p2917 A71-36069

Gyro drift rate acceptance test design to reflect system performance, using Bayes philosophy for derivation of test cost, product yield and quality

[AIAA PAPER 71-968] 19 p3068 A71-37209

Space and missile guidance performance analysis based on error sources, using Monte Carlo simulation

19 p3101 A71-37754

On-design performance characteristics of radial gas turbines, investigating blade geometry, rotor losses and pressure ratio effects

19 p3123 A71-38269

Performance prediction model for electromagnetic compatibility of ATC radar beacon system, testing interrogator-transponder links along air route

19 p3102 A71-38435

Radar antenna interference determination based on model using electrical and physical characteristics of

reflector type antenna for statistical gain distribution prediction

19 p3021 A71-38458

Broadband antenna twist reflector with wire grids, deriving design formulas and theoretical performance in terms of polarization attenuation

19 p3036 A71-38606

Long life performance predictions for lead telluride and silicon germanium radioisotope thermoelectric generators for deep space missions

20 p3263 A71-38925

Long life radioisotope thermoelectric generator, discussing mathematical model to simulate expected performance profiles

20 p3266 A71-38958

Variable thickness ice film water-to-cryogen heat exchanger design, presenting mathematical model for performance calculation by modified integration digital analog simulator computer program

20 p3314 A71-39291

Fast time digital computer simulation model for evaluation of man-machine interface /display/ problem of ATC system including personnel and equipment

21 p3412 A71-40112

Composites and mechanical systems dynamic behavior prediction, calculating Hugoniot with effective modulus

21 p3465 A71-40792

Color defective vision and aviation color signal light flashes recognition, indicating Farnsworth Lantern performance prediction test superiority

22 p3499 A71-41490

Steels fatigue behavior and cumulative damage effect prediction under strain controlled conditions, comparing with experimental data

22 p3559 A71-41593

Performance levels prediction for airborne solid state phased array radar transmission sources, considering TRAPATT devices

22 p3509 A71-41630

Hemispherical and spherical pressurized gas bearing design with narrow circumferential feed slot as laminar flow restrictors, predicting static load performance

22 p3551 A71-41667

Computer-aided statistical analysis correlation method for prediction of electronic circuit component part variability effects on performance and reliability

22 p3517 A71-42102

Electric circuit component failure prediction and probability distribution in troubleshooting search

23 p3638 A71-42900

Electrical CO laser performance prediction from pumping mechanism based on vibrational energy exchange under thermal nonequilibrium conditions

23 p3683 A71-42954

FET nonlinear and cross modulation characteristics, basing performance prediction on power series approximation to measured LF transfer characteristics

23 p3649 A71-43068

Performance prediction and evaluation of propulsion-augmented high lift systems for STOL aircraft, considering weight, thrust and wing loading

[AIAA PAPER 71-990] 24 p3791 A71-44585

Open cylindrical thermosiphon for laminar flow, predicting heat transfer performance by finite difference solution for comparison with Lighthill analysis

24 p3889 A71-44973

PERFORMANCE TESTS

Batch/Time-Sharing Monitor for achieving balance of digital computer systems efficiency and responsiveness, discussing performance modeling and empirical measurements

01 p0043 A71-10178

Electrical fault location and detection techniques for cellular logic circuit arrays fabricated with LSI procedures

01 p0044 A71-10184

Pad relocation technique by DC wafer probe tests for interconnecting LSI arrays of imperfect yield

01 p0044 A71-10186

Inertial navigation system augmented by digital distance measuring equipment in FAA flight inspection aircraft for performance evaluation

01 p0124 A71-10507

Instrumentation System Margin Analysis Program /ISMAP/ for ICBM telemetry data acquisition systems performance tests

01 p0032 A71-10882

PCM telemetry receiving stations testing, comparing bit error probabilities of coherent and noncoherent methods of synchronizing pseudonoise sequences

01 p0033 A71-10890

Notch power ratio noise tests on magnetic tape recorder/reproducer using direct recording in baseband

01 p0034 A71-10910

Aircraft high temperature polyimide hydraulic actuator rod seals, discussing design and performance tests

[SAE PAPER 700790] 01 p0091 A71-11543

Microelectronic remanent type /latching/ circulating, switching and phase-shifting microwave devices design and performance

02 p0228 A71-11654

Digital simulation computer program in FORTRAN IV for radar systems performance evaluation in various environments

02 p0211 A71-11796

Basic and special field effect transistor design and operation, discussing performance and fabrication

02 p0229 A71-11810

Medium speed data transmission systems tested for quality and functional characteristics

02 p0228 A71-11819

Ultrawide bandwidth laboratory laser communication link for high fidelity signal transmission, discussing system configuration, components and preliminary test results

02 p0214 A71-12025

Miniature centrifugal pump for circulating liquid He in flow loop, testing performance

02 p0255 A71-12129

Mechanical transducers for generating and detecting second sound in He isotopes at millidegree temperatures, discussing construction and performance

02 p0250 A71-12135

Thermionic converter with single crystal 110 W emitter surfaces and Nb collector, measuring I-V performance

02 p0193 A71-12212

Thermionic converter tests, discussing W emitter with Nb and Mo-on-Nb collectors, surface and electrode combinations

02 p0193 A71-12214

Thermionic converter with oriented W electrodes, discussing computerized data acquisition system for mapping I-V performance

02 p0193 A71-12215

Performance tests of identical cylindrical thermionic converters with W emitters and Nb collectors, using X ray diffraction and work function measurements

02 p0193 A71-12217

Long term stability and post test analysis of vapor deposited W emitters in high performance cylindrical thermionic converters

02 p0193 A71-12218

Low temperature cylindrical thermionic converters with CVD Re electrodes, discussing design, fabrication and performance

02 p0193 A71-12219

Sirene 311 cylindrical thermionic converter in pile life testing in Triton swimming pool nuclear reactor

02 p0193 A71-12220

Cylindrical thermionic converter for Incore Thermionic Reactor, discussing diodes engineering problems and performance test for lifetime

02 p0194 A71-12221

Isothermal irradiators of neon filled stainless steel heat pipes with Na as working fluid, discussing laboratory and reactor feasibility tests

02 p0280 A71-12250

Thermionic Diode Kinetics Experiment analog simulation results concerning coupling, burnout, startup, etc

02 p0196 A71-12259

Low power thermionic reactors, comparing four types design, characteristics and performance estimates for power plants

02 p0281 A71-12263

Thermionic performance influence on reactor design and operation, considering plant electrical ratings

02 p0281 A71-12266

Externally pressurized gas thrust bearings, examining performance and pressure distribution in film

02 p0256 A71-12412

Skyнет types 3 and 4 ground stations performance, discussing antenna gain, FM carrier to noise ratio, channel capacity, error rates and system reliability

02 p0217 A71-12438

Transmitter system for Skyнет spacecraft performance tests using calibrated automatic level control and microwave calorimeters

02 p0218 A71-12442

Microwave radiometry for earth terminal and communication satellite performance measurements, including gain, tracking, noise temperature, radome attenuation, power and transfer characteristics

02 p0218 A71-12446

Hydrazine-hydrogen peroxide fuel cells coulombic efficiency measurement

02 p0197 A71-12960

Zinc-mercuric oxide cells with self supporting anodes of controlled porosity for improving low temperature performance

03 p0351 A71-13039

Zinc air battery, evaluating materials capable of peroxide decomposition as low cost oxygen electrodes

03 p0351 A71-13040

High energy long shelf life lithium-nickel sulfide batteries performance tests

03 p0351 A71-13041

High voltage DC power supplies for aerospace detectors operation, considering different resonant configurations for performance

03 p0352 A71-13051

Alkaline fuel cells electrochemical regeneration for controlling carbonate concentration in electrolyte for performance improvement

03 p0353 A71-13057

Noncircular cross section static pressure probes theoretically insensitive to pitch, yaw and Mach number, testing performance

03 p0341 A71-13730

Elevated temperature strain gages using capacitance changes as indication, discussing design and response tests

03 p0426 A71-13770

Bonded and weldable strain gages for aircraft flight loads measurements at high temperatures, discussing installation, calibration and performance tests

03 p0426 A71-13781

Sealed-off carbon dioxide laser power output and efficiency test during continuous operation over one year

03 p0438 A71-13894

Transportable photoelectric satellite tracking system with 4-axis support for Schmidt-Cassegrain telescope, discussing field testing results

03 p0397 A71-14004

Nonvented vortex fluid amplifier receiver tubes flow and performance characteristics [ASME PAPER 70-WA/FLCS-18]

03 p0354 A71-14091

Large low-speed fan for low noise production, testing performance on suppression effects of acoustic treatment and exhaust jet noise

03 p0471 A71-14123

Nonlinear filter construction and performance evaluation, using deterministic filter gains [ASME PAPER 70-WA/AUT-9]

03 p0387 A71-14150

Ni-Cr foil resistance strain gages for high temperature operation, discussing performance test data

03 p0430 A71-14327

Ablative materials performance in high radiative heat flux environments produced by CW carbon dioxide laser

03 p0449 A71-14437

High performance shock tube driving techniques, determining effectiveness and flow properties predictability

04 p0564 A71-14669

Shock tubes with linear explosive driver for helium and air, determining performance by high speed camera measurements

04 p0565 A71-14680

Organic lasers using fluorescent dye in liquid solution or polymer, discussing gain and output performance, tuning, mode locking and CW operation

04 p0605 A71-14710

Performance tests for guidance accuracy and tracking smoothness of Crimean Astrophysical Observatory radio telescope, discussing pointing and tracking errors

04 p0565 A71-14849

Modified constant temperature hot-wire anemometer for extended bandwidth operation, discussing improved frequency response test

04 p0596 A71-14971

Silicon and gallium arsenide photovoltaic solar cells, examining performance at high illumination intensities

04 p0535 A71-15006

Data system environment simulator /DASYS/ for real time test bed capability for software development and testing

04 p0556 A71-15294

Aerospace systems instrumentation magnetic tape standardization and testing

04 p0597 A71-15298

Telemetry systems prelaunch calibration tests, considering bit error rate, intermodulation distortion and antenna tracking

04 p0554 A71-15317

Europa 1 multistage booster rocket interstage electric circuit connection, discussing specifications and compatibility tests [DGLR-70-059]

05 p0697 A71-15955

Europa 1 third stage flight testing for onboard control system performance parameters [DGLR-70-061]

05 p0815 A71-15963

CdS solar cells thermal stability and performance, discussing satellite applications

05 p0699 A71-16056

Electroformed Al contact solar cells without soldering, investigating process parameters effects on performance

05 p0699 A71-16062

N-p Si solar cells controlled lifetime doping effects on electrical performance

05 p0700 A71-16063

Si solar cells with titanium oxide antireflection coatings, discussing environmental test results

05 p0700 A71-16064

Si solar cells with antireflection titanium dioxide layer, comparing performance with conventional adhesive cover system

05 p0700 A71-16065

Si solar cells spectral responses at low temperatures

05 p0701 A71-16072

Si solar cell low temperature low solar illumination intensity I-V performance deficiencies, considering corrective design modifications

05 p0701 A71-16073

Si solar cell performance improvement from use of achromatic antireflective coatings

05 p0701 A71-16077

CdS solar cells performance under simulated synchronous orbit conditions, describing test equipment

05 p0702 A71-16081

Si solar cells electrical performance tests, considering 1 MeV electron irradiation effect on efficiency

05 p0702 A71-16082

Lithium-containing p-n solar cells photovoltaic performance and stability tests at room temperature

05 p0703 A71-16090

Pulsed xenon solar simulator system for testing single and group cells and panels for flight spacecraft programs

05 p0733 A71-16098

Atmospheric and high vacuum performance tests of solid lubricant coatings based on molybdenum disulfide

05 p0757 A71-16174

Papers on inertial component testing including equipment, costs, etc

05 p0749 A71-16301

Gyroscope reliable performance life testing economic justification, noting cost lowering by deficient gyro rejection

05 p0749 A71-16304

Inertial gyro testing, measuring coefficients for performance model equation

05 p0750 A71-16306

Inertial quality accelerometer tests, including mathematical models and error analysis

05 p0750 A71-16307

Inertial instruments system-level tests under final use environment, discussing cost reduction

05 p0750 A71-16308

Gyro testing in UK, discussing equipment, methods, errors, etc

05 p0750 A71-16309

Gyroscopes diagnostic tests for design shortcomings, discussing spin-axis ball and gas bearings, spin-motor reaction torque, flotation fluid and ligament creep

05 p0750 A71-16310

Gyros and accelerometers with hydrostatic gas bearings, discussing design and adjustments, drift measurement methods and environmental tests

05 p0751 A71-16314

Wideband interdigital microwave circuits using lithium niobate crystals for electro-optic modulation of light, discussing design and performance tests

05 p0762 A71-16336

GaAs FET design and performance, discussing fabrication techniques and scattering and noise parameter measurements

05 p0729 A71-16916

OA0 simulation system including prototype spacecraft and digital computer for verifying ground system performance

05 p0734 A71-17131

Rh alloys thermodynamic reactions with fluorinating agents including fluorine, bromine, pentafluoride and chlorine trifluoride

06 p0904 A71-17949

Rubber seals performance testing, discussing measuring methods

06 p0905 A71-18216

Performance characteristics of horizontal and vertical stabilizers at medium Reynolds number from wind tunnel measurements, considering air foil and flap effects

06 p0842 A71-18249

Intelsat 3 global satellite communication system design and performance

06 p0870 A71-18393

Wideband mixer for Intelsat 3 satellite, describing design, operation and performance

06 p0877 A71-18401

Intelsat 3 satellite reliability program, discussing test procedures, redundancy, tradeoff against weight, etc

06 p0877 A71-18404

Oil diffusion pumped space simulation vacuum chamber performance improvement methods including water vapor and carbon dioxide desorption, Ti sublimation pumping and 20 K cryopumping

06 p0881 A71-18462

Negatively charged conical electrostatic probe characteristics determination in supersonic plasma stream, using shock tube

06 p0939 A71-18586

Electron bombardment ion thruster using hollow cathode and two-grid ion accelerating geometry, discussing performance tests

06 p0947 A71-18600

Light emitting diodes performance comparison under electron irradiation effect in space environment

07 p1071 A71-19070

Plane discrete fluidic switching element external static characteristics tests in relay and trigger modes

07 p1023 A71-19362

ESRO 2 satellite program reliability prediction and procedures in design and manufacture, defects during development and tests and performance in orbit

07 p1207 A71-19552

Automatic test equipment for sorting large quantity resistors based on nonlinearity measurement

07 p1076 A71-19554

Terrain-following radar for TSR-2 aircraft, discussing reliability trials and improvement

07 p1062 A71-19557

Planar transistors operating conditions effects on current gain degradation following emitter-base reverse biasing

07 p1076 A71-19560

GaAs-GaAsP heterostructure injection lasers performance tests

[ECS PAPER 71] 07 p1123 A71-19570

Communication satellite station at Fucino /Italy/, testing receiving and transmitting equipment transmission quality

07 p1063 A71-20041

Low aspect ratio compressor blade cascade performance at blade span center, discussing pressure loss, angle of attack and staggering

07 p1017 A71-20624

Airborne night vision system performance, determining maximum range for ground target acquisition

08 p1286 A71-20692

Slot transmission line bandpass and bandstop filters and hybrid couplers for microwave IC applications, presenting experimental performance data

08 p1262 A71-20761

Dual mode latching reciprocal ferrite microwave phase shifter, discussing operation principles, design and performance

08 p1262 A71-20764

Filament wound carbon fiber reinforced plastics components fabrication and performance tests [PLASTICS INST. PAPER 47]

08 p1296 A71-20902

Microwave oscillators with Gunn effect device resonant circuit and YIG tuning, discussing design and performance

08 p1263 A71-20992

Airline collision avoidance system test and evaluation program, considering range, rate and altitude accuracy, communications reliability, synchronization and system integration with air traffic control

08 p1331 A71-21167

Microwave multistage transistor amplifier with IC configuration, discussing design and performance

08 p1265 A71-21287

Performance test methods and equipment for aircraft avionics and weapons systems, discussing computer integration with radar and phototeodolite range instrumentation system

08 p1260 A71-21660

Meteorological equipment development and test program, discussing technical objectives, feasibility and user requirements

08 p1330 A71-21736

Fabry-Perot interferometer for dielectrics permittivity and loss measurements in millimeter and submillimeter ranges, discussing design, tests and accuracy

08 p1294 A71-21806

Gamma ray spectrometers made from high purity p-type Ge crystal, observing performance

08 p1345 A71-21843

Satellite-borne Ge radiation detectors, investigating design criteria and performance at elevated temperatures

08 p1267 A71-21847

Fatigue life gages performance test using calibration program for cryogenic temperature applications

09 p1444 A71-22716

High temperature dynamic strain gage test equipment for evaluating precision, life and environmental limitations

09 p1445 A71-22719

Extensometer for evaluating remote reading strain gage performance at high and rapidly changing temperatures

09 p1445 A71-22720

Alloy and heat treatment effect on Ti bondability for adhesive bonded aircraft structure, using annealed and aged Ti-6Al-4V and Ti-6Al-6V-2Sn alloys for testing

10 p1615 A71-24093

Fabricated product test program design for meeting customer specifications, outlining routine tests for preimpregnated film adhesive materials

10 p1516 A71-24107

Human time estimation tests, describing methods of reproduction, verbal estimation and production in randomized blocks of trials

10 p1562 A71-24207

Trisomic wind tunnel calibration tests results including second throat effects, Mach number and static pressure distributions, flow inclination and aerodynamic characteristics

10 p1590 A71-24819

Lightweight parabolic antenna model with inflated Mylar tube torus and central mast interconnected by wires, discussing construction, performance tests and tradeoffs

[AIAA PAPER 71-397] 11 p1736 A71-25273

Mechanical properties and performance characteristics comparison of syntactic foams fabricated by conventional mixing or vacuum impregnation, including filler packing factors

11 p1784 A71-25394

Breakdown voltage and high power tests for pressure bonded collector sheath tubes with cracked alumina insulators and flowing liquid metal coolant

11 p1709 A71-25859

Liquid metal cooled, fast spectrum thermionic reactor experiment design based on Fast Reactor Core Test Facility use for dynamic and steady state characteristics determination

11 p1710 A71-25867

In-pile tests of multicell thermionic converter with Mo- and W-based alloy cathodes, noting output electric power dependence on internal heat release

11 p1711 A71-25877

Computer aided performance mapping of fixed spaced planar diode with etched Re emitter and Nb collector over wide operating temperature range

11 p1737 A71-25907

Long term performance stability of two unfueled out-of-pile thermionic converters

11 p1714 A71-25908

Double ended full length external fuel thermionic converter, describing component fabrication, assembly sequence, joining methods, vacuum test procedures and converter load control

11 p1715 A71-25910

Out-of-core heat pipe heated and cooled thermionic converter module mechanical design, fabrication and subcomponent performance evaluation

11 p1715 A71-25912

Resin systems for ablative composites, correlating hyperthermal performance characteristics via thermogravimetric, mechanical flexural and ablation tests

11 p1789 A71-26039

Long life vacuum tests of dry and wet lubricated slip ring systems for power and signal transfer, discussing wear, noise and contact resistance

11 p1771 A71-26050

Grooved Al heat pipes experimental performance in moderate temperature for space vehicle applications [AIAA PAPER 71-409]

11 p1856 A71-26204

Two-line all-equipment test and aeronautics systems division reliability testing, analyzing by Weibull Monte Carlo simulation

12 p1909 A71-26657

High resolution far IR interferometer in Michelson configuration for measuring gas optical properties in symmetric or asymmetric operation mode, testing performance

12 p1904 A71-26799

High energy hydrogen-oxygen launch vehicle thermal insulation system, discussing closed cell rigid polyvinyl chloride foam mechanical characteristics, use and tests

12 p1985 A71-26835

Performance testing of fluorosilicone hydraulic fluid in high temperature supersonic aircraft piston pumps

12 p1921 A71-27040

Large system performance test resources allocation priorities determination methodology using decision theory, discussing extensive and diminutive forms

12 p1895 A71-27438

CF6 turbofan engine development, discussing performance and endurance tests and design changes for reliable low cost operation

13 p2114 A71-28308

Airline engine performance testing from operator perspective, using automated test cell data acquisition system

13 p2044 A71-28329

Measurement errors in testing single stage air driven axial flow compressors and turbines

13 p2115 A71-28582

Wind tunnel tests of geometrically compatible airfoils for variable chord sailplane

13 p1994 A71-29257

Acquisition system consisting of positioning of local station burst signal in time slot for PCM-TDMA satellite communication system, discussing design and performance tests

13 p2034 A71-29393

Pressure recovery performance of straight-wall two dimensional diffusers with subsonic air-water mixtures, studying gas volume flow ratio and diffuser geometry effects

13 p2052 A71-29458

High entrainment constant area multiple nozzle ejectors with two mixing tube lengths for boundary layer control, estimating performance with analytical model

13 p2053 A71-29469

Molybdenum disulfide bonded solid film lubricants performance characteristics, considering load, speed and temperature effects [ASLE PREPRINT 71AM 2D-1]

13 p2076 A71-29486

Axial flow turbines comparative performance tests under steady and pulse flow conditions for turbocharger application

14 p2169 A71-29819

Performance tests of electron bombardment ion thruster, using xenon, krypton argon, neon, nitrogen, helium and carbon dioxide

14 p2287 A71-29922

Airframe installation effects on underwing nacelle nozzle performance, using calibrated engines and load cells on F-106 for measurements

[AIAA PAPER 71-681] 14 p2292 A71-30745

Radiation cooled MPD thruster with permanent and superconducting magnets, describing test facilities and measurement techniques for performance tests

[AIAA PAPER 71-696] 14 p2293 A71-30755

Multimission strategic aircraft installation effects testing in propulsion and aerodynamic wind tunnels, yielding flowfield definition, inlet internal performance, drag, forebody shape and orientation [AIAA PAPER 71-759]

14 p2171 A71-30792

Field testing for radio telemetry receiving systems calibration, including tape recorder degradation effects during data processing

14 p2198 A71-30903

Digital communication system frame synchronizer performance analysis, using mean time formula and state transition matrices

14 p2201 A71-30925

Alphanumeric display devices with liquid crystal and dynamic light scattering for low voltage, power, cost and fabrication advantages, testing performance

14 p2249 A71-31029

SK-5 air cushion vehicles evaluation including search/rescue, aids to navigation, law enforcement, safety logistics and oil pollution

[AHS PREPRINT 572] 14 p2180 A71-31113

Model 6A geodimeter /photometric range finders/ laboratory and field tests

15 p2405 A71-31466

Heat transfer surfaces performance measurements, considering tube bundles with fluid flow perpendicular to tube generatrices

[HEAT EXCH. CONF. PAPER 25] 15 p2383 A71-31639

Single phase and evaporative systems for liquid cooling high temperature gas turbine rotor blades, reviewing heat transfer performance evaluation

15 p2469 A71-31734

SYDAC ILS systems flight tests

15 p2446 A71-31911

Performance test facility for pulsed axial flow gas turbine of turbocharger unit on large diesel engines

15 p2469 A71-31943

Gundefender earplug evaluation tests, using temporary threshold shift reduction and modified rhyme techniques for speech intelligibility measurement in noise

15 p2364 A71-32196

Brayton space power system for NASA manned space missions, discussing control system requirements, design and performance

15 p2354 A71-32203

Brayton power system electrical subsystem and component performance tests, discussing engine control package, DC supply, inverters and instrumentation

15 p2354 A71-32204

SNAP 8 turbine-alternator as nuclear-electric space power converter, discussing rotating machinery components design and 10,000 hr endurance testing results

15 p2447 A71-32208

Electrically-heated Brayton power conversion system, comparing performance tests with prediction

15 p2354 A71-32212

Performance tests of two identical Brayton cycle heat exchanger units consisting of recuperator, heat sink exchanger and ducting in combination with turbine

15 p2355 A71-32213

Tantalum/stainless steel mercury boilers for SNAP 8, evaluating performance

15 p2448 A71-32219

Hot performance tests of three identical Brayton rotating units on gas bearings

15 p2355 A71-32226

Josephson and IC type superconducting tunneling junction neuron devices performance tests, presenting bibliography

15 p2377 A71-32317

Jet engine high pressure turbine high temperature alloy blades and vanes grinding operation, discussing testing, operating conditions and coolant application [SME PAPER MR-71-802]

15 p2416 A71-32432

Series and bypass fluidic pressure regulators, discussing component selection, performance details, sensing circuits, feedback amplifier and flow controller

16 p2579 A71-33526

Mental load physiological parameters determination by binary choice task, noting changes in heart and respiratory rates and systolic and diastolic pressure

17 p2688 A71-34364

Soviet book on microwave quantum amplifiers covering traveling wave and multicavity masers calculation, design, tests, applications and basic components

17 p2753 A71-34474

PSK modem for multiple access communication system with time distribution, discussing performance tests on INTELSAT 3

17 p2700 A71-34688

GALAXY measuring engine for automatic measurement of glass photographic plates taken from Schmidt telescopes, discussing performance

17 p2741 A71-34997

Intelsat 4 communication system simulation by transponder engineering model to test performance objective concerning baseband distortion and intermodulation

17 p2705 A71-35102

Radio controlled small aircraft as measurement platform for meteorological sensors, discussing development and performance from field tests

17 p2675 A71-35334

FSK L-level or duobinary system performance evaluation under intersymbol interference, using limiter-discriminator without postdetection filter as detector

17 p2707 A71-35479

Herringbone grooved gas lubricated journal bearing load capacity, attitude angle and power loss measurements

17 p2749 A71-35487

Performance evaluation of variable geometry external fuel tank prototypes by static structural tests, wind tunnel tests and flight tests on F-111 aircraft

[AIAA PAPER 71-763] 17 p2675 A71-35533

Ion microthruster for satellite orbit and position corrections, describing optimum performance characteristics and test facility

[DGLR 71-032] 17 p2795 A71-35548

Life support water management subsystem 4-man 90-day test in space station simulator with closed water and oxygen loops and no resupply

[ASME PAPER 71-AV-6] 18 p2865 A71-36373

Solid electrolyte oxygen generator electrolysis test module with improved ceramic to ceramic and metal seals, electrode and grid design, discussing performance tests

[ASME PAPER 71-AV-8] 18 p2866 A71-36375

Design and performance testing of arterial wick circular heat pipes for OAO-C spacecraft

[ASME PAPER 71-AV-26] 18 p2868 A71-36393

Closed-loop solid electrolyte oxygen regeneration life support system, discussing 180-day life test

[ASME PAPER 71-AV-32] 18 p2869 A71-36399

Space station regenerative life support system 90-day manned test in simulator, discussing objectives, facilities and procedures

[ASME PAPER 71-AV-38] 18 p2870 A71-36405

Space shuttle facilities planning, discussing vehicles, overall assembly flow, manufacturing, tests and operations

18 p2926 A71-36478

PSK modem for PCM-TDMA system, discussing performance tests on INTELSAT 3

18 p2880 A71-36551

Manned earth-orbital missions performance assessment experiments, studying effects of artificial and zero gravity spacecraft environments on humans

[AIAA PAPER 71-891] 18 p2857 A71-36641

Performance limitation of simplified radio-inertial lateral control guidance system subject to stochastic gusts for automatic landing

[AIAA PAPER 71-957] 19 p3099 A71-37198

K band satellite transmit/receive frequency converters, describing design features and performance tests under simulated environmental conditions

19 p3028 A71-37697

Polymer materials strength and lifetime prediction under natural conditions from mathematical model based on laboratory accelerated test data

19 p3084 A71-37781

Motion measurements applications to facility design and inertial navigation hardware performance test problems concerning test platform response to ground motion, forces and disturbances

[AIAA PAPER 71-923] 19 p3102 A71-38327

Transistor circuit driven hydrogen-oxygen fuel cell, testing internal impedance effect on power supply noise for comparison with lumped parameter model

19 p3000 A71-38463

Integrated circuit life testing, comparing functional and pin-to-pin screening data

19 p3034 A71-38516

Sealed and vented fusing devices, testing vacuum effects on performance at high and low temperatures

19 p3035 A71-38536

Nonlinear filters performance comparison for reentry vehicle trajectory estimation from radar tracking, noting coordinate systems effect on extended Kalman filter accuracy

19 p3039 A71-38712

Performance measurement of electrostatic spectrometers as monochromators by calculation of electron energy distribution

20 p3233 A71-38821

Transient performance of phase locked loop on-board tumbling satellite, noting relation to time, SNR and fade modulation

20 p3196 A71-38871

Ni-Cd battery cell with third electrode for charge control, testing thermal and electrical performance as function of charge and discharge rate

20 p3179 A71-38905

Automated endurance testing of 2-15 kW Brayton power conversion system, using rotating unit, heat exchanger, electronic voltage regulator, parasitic speed control

20 p3180 A71-38907

Component performance of three loop Rankine cycle test rig using lithium, potassium and NaK-78 as working fluids

20 p3263 A71-38923

Multihundred watt radioisotope thermoelectric generator for spacecraft power supply, discussing system design, performance and safety requirements

20 p3263 A71-38927

Performance tests of high temperature silicon-germanium alloy thermoelectric generator for outer planet mission spacecraft

20 p3264 A71-38928

High voltage solid state electrolytic cell battery with Li anodes, testing storage and discharge characteristics

20 p3181 A71-38935

Tubular compact air cooled thermoelectric module endurance and performance tests and computer simulation for space reactor power system

20 p3266 A71-38954

Long term performance of lead telluride thermoelectric generators tested under SNAP 21, 23A and 27 programs

20 p3266 A71-38955

Orbital electric power system performance simulation for analysis of solar array/battery lock-up, comparing graphical and computer techniques

20 p3183 A71-38957

Orbital performance of SNAP 19 radioisotopic thermoelectric generator for nuclear power supply on Nimbus 3 observatory

20 p3266 A71-38962

SNAP 19 TAGS thermoelectric generator life tests at high temperature in Ar, predicting long term performance including thermoelectric material and isotope fuel decay effects

20 p3266 A71-38963

High resolution gas discharge plasma display panel, discussing design, capabilities and performance

20 p3233 A71-39061

GaAs solar batteries for spacecraft power supplies, comparing effectiveness with Si cells for optimum utilization

20 p3183 A71-39133

Ultrasonic radar simulator to produce data for radar system performance evaluation, describing automated short range and manual long range systems

20 p3196 A71-39376

Coaxial cable antenna lead with shield or external conductor in form of slotted corrugated metal foil, testing performance

20 p3197 A71-39469

Remote image-forming sensors on satellites and aircraft, considering resolving power, contrast rendition, dynamic range, SNR, sensitivity, and reliability as performance measures

20 p3240 A71-39608

Woomera /Australia/ meteorological rocket firings, using temperature and wind profiles to assess sensors and parachutes performance

20 p3221 A71-39691

Computerized touch display for ATC tasks compared to conventional keyboard tabular display performance

21 p3413 A71-40114

Vibration isolation system performance under transient conditions, deriving equations of motion with and without inertia torque effect

[ASME PAPER 71-VIBR-33] 21 p3458 A71-40287

Independent sideband transmitter checkout and maintenance for maximum communication circuit performance

21 p3353 A71-40519

Plastic encapsulated IC reliability tests, relating results to failure mechanism

21 p3356 A71-40747

LSI logic arrays testing problems minimization by test procedures based on circuit design characteristics and MOS structure properties

21 p3356 A71-40803

Hybrid integrated wideband linear microwave power amplifiers for S and C bands, discussing construction and performance

21 p3357 A71-40817

Valves and regulators development and testing for liquid hydrogen propellant tank pressurization system

22 p3588 A71-41503

Externally pressurized air lubricated bearing boring spindle performance tests, considering circular accuracy, maintenance, tool life and cost effectiveness

22 p3552 A71-41675

Mobile concept and automated checkout applications in Apollo/Saturn 5 Launch Complex 39, discussing performance

22 p3611 A71-42044

Pyroelectric IR detectors performance, investigating strontium barium nitrate, lithium sulphate and triglycine sulfate materials effects on frequency range and sensitivity

22 p3542 A71-42122

Rollin InSb hot electron bolometer performance and calibration

22 p3543 A71-42124

Agusta helicopter design and testing criteria, discussing four-blade rotor, fuselage and radio navigation equipment

22 p3482 A71-42224

Takeoff and landing performance evaluation for commercial STOL aircraft, noting high bypass ratio turbofans and high lift systems use

22 p3483 A71-42286

Mixed base modulation technique performance, considering SNR in transmission problem

22 p3512 A71-42380

GaAs LSA mode V band oscillator CW and pulsed operations power and efficiency limitations

23 p3649 A71-42915

High power hydrogen thyatron grid-anode structure without gradient grids, discussing design and performance tests

23 p3649 A71-42916

Aircraft permanent magnetic fields strength variation, observing magnetic anomaly detection equipment performance degradation

23 p3674 A71-42923

Qualification tests for equatorial ELDO Europa Launch Site with MSRV, discussing checkout system and performance

23 p3661 A71-43474

Precision calibration system with adjustable temperature extended radiance source for long wavelength IR radiometer, discussing performance tests

23 p3676 A71-43512

Li-filled vacuum-deposited W heat pipes for efficient heat extraction from nuclear reactors, discussing design, fabrication and testing

23 p3682 A71-43595

Fraunhofer diffraction apparatus design based on He-Ne laser, testing performance in distorted point lattices photography

23 p3686 A71-43956

Single channel electron multiplier manufacture and performances, discussing test equipment and procedures

24 p3811 A71-45331

Aviation fuels lubricating characteristics, discussing refining methods, viscosity, service performance and load testing

24 p3864 A71-45383

PERFUSION

U DIFFUSION

PERIDOTITE

NT ENSTATITE

NT OLIVINE

NT PYROXENES

NT SERPENTINE

PERIGES

Precambrian and Cambrian stromatolites used for determination of nearest lunar approach to earth

04 p0583 A71-15141

Artificial earth satellite orbit perigee motion, calculating perturbation effect due to gravitational and magnetic fields on orientation and rotation

09 p1523 A71-23150

High energy solid propellants use in Europa 2 launch vehicle perigee-apogee motor, considering synchronous satellite payload increase

16 p2645 A71-33365

PERIHELIONS

Orbital coordinates for body moving along parabola with small perihelion distance calculated for ephemeride

01 p0157 A71-10607

Relativistic correction for planet perihelion rotation within Einstein gravitation theory, using proper magnitudes in terms of chromometric invariants

01 p0159 A71-10920

Mars yellow clouds extent during near perihelion apparitions since 1877, considering dust storm origin in Southern Hemisphere

09 p1520 A71-22698

Absolute magnitudes of 1965-1969 comets, including orbit elements, perihelion coordinates and maximum values of reduced head diameter and tail length

15 p2483 A71-31339

Comet origin hypotheses, examining orbit axes and perihelions distribution

16 p2639 A71-33693

Action-at-a-distance theory of gravitation generalized to tensor interactions of all orders, considering special relativity demands and perihelion advance of Mercury

17 p2797 A71-34368

Space-time model of torsion tensor effect on geodetic lines under Schwarzschild metric, evaluating orbital perihelion motion of planets and light ray bending
18 p2967 A71-36826

Numerical integration of element T /transit time through perihelion/ in perturbations of near parabolic comet orbits
20 p3291 A71-39321

PERIOD EQUATIONS

U PERIODIC FUNCTIONS

PERIODIC FUNCTIONS

NT SINE SERIES

NT TRIGONOMETRIC FUNCTIONS

Nonlinear space independent nuclear reactor kinetics equations, demonstrating positive periodic solutions existence
01 p0126 A71-11291

Pole Chandler motion, discussing residual deviations distributions in Jeffreys and Arato- Kolmogorov models
02 p0309 A71-12105

Fourier series in almost periodic Bohr functions, examining uniform convergence definitiveness
03 p0450 A71-13294

Characteristic exponents for linear differential equations with periodic coefficients, using recurrence multipliers suitable for computer
03 p0451 A71-13786

Branching of periodic solutions of second order nonlinear ordinary differential equations similar to Duffing equation
06 p0918 A71-17643

Almost periodic solutions of two nonlinear Volterra integral equations
07 p1147 A71-19256

Periodic motions stability in purely imaginary characteristic indices pairs transcendental critical case
07 p1161 A71-20266

Conservative systems of differential equations with single degree of freedom, considering periodic solutions existence, determination and stability
09 p1495 A71-23436

Quasi-draconic and draconic orbital periods of earth satellites, showing ascending and descending passage variations
11 p1829 A71-25811

Single circuit parametric oscillator with balance modulated pumping voltage envelope as periodic function satisfying Dirichlet condition
11 p1740 A71-26539

Existence proof of periodic solutions to second order partial differential equations with imaginary roots
12 p1923 A71-27240

Critique on pulsar distance estimates based on dispersion measure, introducing period luminosity function
13 p2137 A71-28592

Stability of governing parameters critical values /Taylor, Rayleigh or Reynolds numbers/ and periodic solutions in fluid mechanics
16 p2558 A71-33002

Periodic or almost periodic small combination vibrations onset conditions by integral equations method and averaging principle
17 p2779 A71-34910

Periodic surface concept application to restricted three body problem of dynamical systems through averaging method, presenting stability theorem
17 p2804 A71-34918

Periodic solutions of singularly perturbed hereditary systems of ordinary nonlinear integrodifferential equations
17 p2780 A71-34920

Periodic solutions for strongly nonlinear differential system of n-coupled nonautonomous equations of Lienard and Rayleigh types
17 p2766 A71-34925

Nonlinear differential equation system periodic solutions in terms of uniformly converging periodic functions sequence
17 p2781 A71-34927

Linear differential equations system with periodic coefficients, determining solutions by stationary components matrix location on complex plane
17 p2766 A71-34933

Periodic solutions existence for autonomous system of ordinary differential equations, modifying parameter functionalization of vector fields in phase spaces
17 p2766 A71-34934

Time delayed systems periodic and quasi-periodic solutions
17 p2782 A71-34937

Van der Pol equation periodic solutions using approximation scheme for all Fourier amplitudes
20 p3254 A71-38800

Nonlinear second order differential equations periodic solutions in terms of Fourier series, applying method to calculation of charged particle orbit in radial electric field
20 p3255 A71-39081

Existence theorem of quasi-periodic solutions with two degrees of freedom for planar three body problem
21 p3441 A71-40093

Periodic functions complete orthogonal sequences class as linear combinations of Fourier expansions, obtaining convergence theorem
21 p3410 A71-41083

Analog data computation with hybrid and logic operational elements, applying to periodic function arithmetic mean determination and transistor characteristics representation
22 p3518 A71-42430

Nonautonomous nonlinear functional differential equations periodic solutions, reducing problem to existence proof of fixed point for operator in suitable space of periodic functions
22 p3567 A71-42691

Periodic solutions to Hamiltonian systems with convex potential, considering application to n-body problem
22 p3568 A71-42694

Conservative Hamiltonian systems with infinitely deep potential wells, obtaining periodic solutions with variational technique
23 p3698 A71-43005

Orthogonality and positive operators on space of almost periodic and quasi-periodic functions, using frequency-power formulas
24 p3843 A71-44961

PERIODIC ORBITS

U ORBITS

PERIODIC OSCILLATIONS

U OSCILLATIONS

PERIODIC PROCESSES

U CYCLES

PERIODIC VARIATIONS

NT ALTERNATIONS

NT ANNUAL VARIATIONS

NT DIURNAL VARIATIONS

NT NOCTURNAL VARIATIONS

Pulsars periods distribution at different galactic latitudes
01 p0161 A71-11339

Mammal species body temperature during 24 hr periodic light cycle, using statistical data analysis
01 p0020 A71-11570

Coherent light wave propagation in two level system, discussing wave periodicity, deviation from sinusoidal form, interaction with medium and energy loss and gain effects
02 p0215 A71-12319

Soft solar X-ray flares six minute periodicity from satellite observation
02 p0300 A71-12472

Pulsar pulse arrival times measurement for general relativity theory test, determining positions and period change rates
02 p0315 A71-12660

Scorpius X-1 high energy X ray flux variations from balloon-borne scanner data
02 p0301 A71-12661

Solar activity long term variations in 11 year cycle maxima, noting preferred locations on disk
02 p0315 A71-12695

Satellite tracking by radio direction finder, noting periodic azimuth deviations related to ionospheric Faraday effect
03 p0377 A71-13169

Wolf numbers monthly fluctuations, giving histogram of fluctuation amplitude distribution
03 p0484 A71-13211

Semiregular and irregular variable stars spatial densities and distributions, amplitudes and periods
03 p0486 A71-13268

Jupiter details rotational periods variations, characterizing dynamic properties of atmosphere upper layers
03 p0490 A71-13940

Earth instantaneous rotation pole coordinates, calculating yearly and Chandler motions
03 p0492 A71-14192

Lunar and solar periodic magnetic variations, using time series analysis based on discrete Fourier transforms for frequency spectrum lines
04 p0582 A71-15097

Magnetic stars with brightness variations in visual and blue light, noting method for period determination
04 p0650 A71-15397

Periodic orbits representation in trigonometric series with numerical coefficients and truncation for applications
04 p0654 A71-15716

Linearized shock waves and periodic disturbances propagation by discrete ordinates method in planar radiative gas dynamics
04 p0689 A71-15742

Saturn satellite Iapetus periodic light variation curve explanation in terms of meteoroids impact erosion
04 p0660 A71-15861

Soviet book on nonlinear almost-periodic oscillations covering application of integral equations method to differential equations, automatic control systems, pendulum motion, etc
06 p0926 A71-17443

Planetary atmosphere Mariner spacecraft occultation experiments, showing neglect of latitudinal and longitudinal variations introduce serious errors
06 p0970 A71-17984

Homogeneous isotropic layers stack on rigid base with periodically varying elasticity parameters, calculating equilibrium under normal distributed load
07 p1217 A71-20460

Periodic nonstationary random process spectral representation derivation by applying Loeve harmonizability theorem
08 p1334 A71-21298

Periodic subtraction and multiplication systems under amplitude limitation, analyzing detection characteristics at arbitrary correlation coefficients
09 p1405 A71-22464

Individual M-type red supergiants luminosity, masses and periodicities based on cluster membership and pulsational Q value
10 p1674 A71-24433

Higher approximations of spherical harmonic method and moment method applied to propagation of periodic disturbances in radiating gas
10 p1696 A71-24545

Streamwise vortices of distinct periodicity in laminar transitional turbulent reattaching flows over wide Mach number range
11 p1751 A71-25496

Partly time invariant and periodically time varying gain equations based on Banach algebras spectral mapping theorem and higher order circle criteria
11 p1742 A71-26411

Periodic variations in circular polarization of continuum radiation of white dwarf G195-19 from 3800 to 5400 A
12 p1956 A71-26610

Cepheids period and luminosity relation, using Kraft method
12 p1962 A71-26906

Rigidity dependence of Forbush decreases and 11 year variation in cosmic ray intensity at Calgary and Sulphur Mountain and other neutron monitor stations
12 p1949 A71-27374

Lower ionospheric plasma frequencies height determination for actual motions, relating periodic variations to spatial electron density structure
13 p0209 A71-28003

Propagation of 26-month oscillations in meridional component of wind velocity in stratosphere at extraequatorial latitudes from hydrothermodynamic equations solution
13 p0207 A71-28021

Cosmic ray density distribution inside modulating spherical cone over long-lived solar wind regions, noting modulation depth quasi-periodic variation
13 p1219 A71-28550

Crab Nebula pulsar NP0532 radio observations, noting long term slowing down and irregular perturbations in periodicity
13 p1237 A71-28591

Long term pulsar intensity observations, noting periodic variations and power spectrum analysis
13 p1243 A71-29270

Periodic disturbances propagation in radiating gray gas, using singular eigenfunction expansions
13 p1265 A71-29356

Galactic dynamo generated magnetic field periodic modes based on mathematical model involving cyclonic turbulence and nonuniform rotation of gaseous disk
14 p2203 A71-29591

Quasi-biennial oscillation in low latitude geomagnetic Sq field, showing larger amplitude under equatorial electrojet by harmonic analysis
14 p2231 A71-29719

Multiple periodicity of Cygnus X-1 X ray emission from rocket sounding
14 p2302 A71-30653

Plane horizontal fluid film convective stability with free boundaries in vertical circular cylinder for periodic modulation of vertical temperature gradient or gravitational field
14 p2338 A71-30873

Atmospheric noise statistical characteristics, investigating short term variations, intensities and application to communications
14 p2237 A71-30964

Gunpowder mean burning rate at constant pressure with periodic variation of heat influx into flame zone
15 p2462 A71-31374

Zenomagnetic core-mantle coupling and fluctuations in period of rotation of Jupiter Great Red Spot
16 p2637 A71-33515

Periodic solar flare X-ray emission, presenting time separation from Vela 5 and 6 scintillation detectors
16 p2629 A71-34078

Nonlinear differential equation system periodic solutions in terms of uniformly converging periodic functions sequence
17 p2781 A71-34927

Plane Poiseuille flow stability evaluation for finite amplitude periodic disturbances, using harmonic analysis
17 p2729 A71-35389

Equations of multiple periodic motions, considering quantification of parameters with Hamilton-Jacobi equation
18 p2948 A71-36947

- Discrete galactic and extragalactic radio sources observations at 3.3 mm, detailing flux and variability measurements 18 p2970 A71-37067
- Binary stars survey at Nice observatory, presenting expression for probable period and parallax of newly discovered binaries 19 p3143 A71-38156
- Forbush decreases comparison with 11 year cosmic ray intensity variation, examining rigidity dependence and modulation functions 20 p3277 A71-38742
- Dispersion equation determining periodic structures natural modes propagation constants, using induced electromotive and magnetomotive forces method 20 p3198 A71-39806
- Short time variability of intensity of optical pulses from pulsar NP 0532, using telescopes 20 p3303 A71-39930
- RR Lyrae variables period-frequency distribution in Oosterhoff types I and II globular clusters, interpreting in terms of pulsation theory 21 p3445 A71-40413
- Climatic changes periodicity in Italy, considering cause by sirocco enhancement 21 p3411 A71-40827
- UK 5 spacecraft experiments in X ray astronomy, investigating spatial distribution and energy spectra of emissions in space, polarization and pulsar periodicities 22 p3610 A71-42015
- Periodic variations in amount of dark material present in Jupiter atmospheric belts, noting uncorrelation with solar activity 22 p3603 A71-42182
- Three body problem of two heavy mass particles oscillatory motion in periodic orbits on straight line under Newtonian attraction 23 p3734 A71-43241
- Atmospheric wind velocity time variations at 80-100 km altitudes from ionospheric drift data, finding planetary oscillation periodicities relationship to solar activity cycle 24 p3822 A71-44349
- PERIODICITY**
U PERIODIC VARIATIONS
PERIODICITY [BIOLOGY]
U RHYTHM [BIOLOGY]
PERIPHERAL CIRCULATION
 Cutaneous blood flow in anesthetized pig forelimb modified by brain temperature changes 02 p0197 A71-11671
- Quantitative relation between temporary threshold shift and peripheral circulatory effects of sound, using finger pulse amplitude strain gage 03 p0359 A71-13156
- Asphyxia induced changes in regional cutaneous and visceral sympathetic activity in anesthetized rabbits, noting relationship with ear blood flow increase 06 p0854 A71-18324
- Venomotor responses of forearm and hand veins to rapid changes in skin temperature in exercising man 06 p0861 A71-18382
- Venomotor responses of forearm veins to local and remote thermal stimuli to skin in exercising man 06 p0862 A71-18383
- Amino-ethyl-S-2-isothiuronium radio protective dose effects on enzyme activity, cardiovascular changes, blood transaminases concentration, bone marrow and peripheral circulation 07 p1040 A71-18986
- Cystamine effects on lymphocytes chromosomal aberrations in human peripheral blood during local fractionated gamma irradiation 08 p1240 A71-21797
- Vascular effector structure in orientation reaction of peripheral vessels to sound, using plethysmogram and rheoencephalogram indications 08 p1242 A71-21962
- Cardiac output in relation to peripheral resistance in borderline hypertension 09 p1392 A71-22591
- Closed steady streamline creeping flow in cylindrical cavity applied to bubble or plug train in pulmonary and peripheral capillaries 10 p1571 A71-24614
- Age, obliterating arteriopathy and peripheral arterial sclerosis effects on rheographic wave propagation speed to lower limbs 10 p1566 A71-24976
- Dogs peripheral blood reaction to complex action of transverse accelerations and gamma irradiation 22 p3494 A71-42727
- Vibration influence on peripheral blood reaction to gamma radiation in dogs, using clinico-hematological indices 22 p3494 A71-42728
- Radiation effects on rats peripheral blood state in low pressure environment with sea level value oxygen tension 22 p3494 A71-42732
- Arterial blood pressure spontaneous fluctuations due to cutaneous circulation adjustments by thermoregulatory system 23 p3632 A71-43142

PERIPHERAL JET FLOW

- Optimal penetration effect on peripheral gas flow temperature field at outlet of turbine combustion chamber with circular flame tubes 13 p2118 A71-28971
- Critical forward speed effects on two dimensional peripheral jet ground effect support systems, comparing theoretical analysis with wind tunnel model data [AIAA PAPER 71-908] 19 p2995 A71-37159
- PERIPHERAL NERVOUS SYSTEM**
 Adaptation mechanism of human movement control as motor neuron reaction to external stimuli, considering peripheral arch, cerebrospinal canal and feedback 03 p0356 A71-12986
- Hyperthermia effects on conduction velocity of nerve fibers and peripheral motor neuron-muscular activity in man 09 p1399 A71-22924
- Organic thermoregulator control signal generation as function of body peripheral to central temperature ratios, using skin temperature rise measurements 10 p1564 A71-24485
- Cochlear/vestibular apparatus, ganglion cells, spinal roots and nerve trunk damage from ionizing radiation based on neural elements transirradiation in neoplasms 10 p1566 A71-25039

PERIPHERIES**U BOUNDARIES****PERITONEUM**

- Hypertensive effects and tissue metal levels due to Cd, Hg and Zn intraperitoneal injection in rats 09 p1397 A71-23543
- Peritoneal macrophagocytic ingestive capacity decrease in mice under hypobaric hypoxia, indicating infection susceptibility in altitude environments 22 p3486 A71-41832

PERMALLOYS [TRADEMARK]

- Mass fabrication of three hole integrated Permalloy sheet magnetic memories 01 p0047 A71-10212
- Supercritical Permalloy thin films thickness effect on magnetic domain structure 06 p0941 A71-17401
- Molybdenum Permalloy powder cores heat treatment effects on permeability, magnetic loss and brittleness control, using metallographic techniques 09 p1466 A71-22171
- Conductivity in microwave Permalloy thin films without external magnetic field comparing Fuchs-Sondheimer theory 10 p1656 A71-24213
- Bloch-wall Permalloy films coercive force effects on low frequency creep, using high resolution Bitter pattern observation technique 15 p2461 A71-32003
- Coupling effects between two Permalloy films for different interface treatments, using standing spin wave resonances 18 p2955 A71-36941
- Transcritical Permalloy thin film domain structure, investigating external field effect on powder depositions and proposing model 18 p2955 A71-36942
- Evaporated Permalloy films deposition temperature measurement by vacuum evaporated Chromel-constantan thin film thermocouple, noting temperature difference between film and glass substrate 21 p3384 A71-40220

PERMANGANATES

- Oxygen supply to air transported patients by chemical compounds, suggesting use of permanganates and chlorates 22 p3500 A71-41571

PERMEABILITY**NT DIELECTRIC PERMEABILITY**

- Gas permeable dispersion layer between impermeable solid wall and high temperature gas flow, calculating dimensionless heat flux equations 02 p0332 A71-12200
- Cr-Ni stainless steel tensile and compressive stresses effect on hydrogen permeability at elevated temperatures 06 p0912 A71-17946
- Oxide films effect on heat resistant steels hydrogen permeability, using mass spectrometer 07 p1136 A71-19920
- Hyperemic skeletal muscle capillaries restricted diffusion, obtaining permeability data for chromium 51 labeled EDTA and inulin in exercising human forearm 08 p1237 A71-20677
- Molybdenum Permalloy powder cores heat treatment effects on permeability, magnetic loss and brittleness control, using metallographic techniques 09 p1466 A71-22171
- Fe-Ni alloys, determining hydrogen permeability, diffusion coefficient and solubility as function of composition by electrochemical method 09 p1472 A71-23127
- Numerical method for computing exact permeability/tunneling probability/ of one dimensional potential barrier 11 p1728 A71-26059

Longitudinal and transverse differential permeabilities of discrete regions in thin ferromagnetic films, accounting for material inhomogeneities 11 p1809 A71-26546

Sintering time effect on initial permeability of Ni-Fe-Cu-Mo alloy made by powder metallurgy 13 p2086 A71-28626

Gas permeable dispersion layer between impermeable solid wall and high temperature gas flow, solving dimensionless heat flux equations 15 p2512 A71-31505

Gas permeability of polymeric foils reduction by vapor metallization in vacuum, noting dependence on surface state, diffusion layer and macroporosity 16 p2601 A71-33684

Permeability and porosity of Precambrian Onverwacht cherts and other low permeability rocks, discussing geological origin of rock-contained organic compounds 18 p2913 A71-36768

Porous materials prepared from electrolytic Cr powder, noting high permeability and strength and filter applications 23 p3689 A71-43252

Mn-Zn ferrite for pulse transformers, discussing permeability and temperature range 23 p3650 A71-43348

Slip, surface permeability and temperature gradient effects on surface friction and heat transfer in boundary layer near cylinder critical point 24 p3887 A71-44743

PERMITTIVITY

- Complex permittivity of spherical conducting particles in dielectric host medium, showing dependence of real and imaginary parts 13 p2038 A71-28611
- High moisture content rock samples electrical conductivity and permittivity by VLF electrospectroscopic investigations based on signal phase shift 14 p2238 A71-29514
- Arbitrarily dimensioned microwave dielectric modules complex permittivity calculation 14 p2212 A71-30511
- Plane uniform waves reflected from layer with random permittivity inhomogeneities, determining distribution function and scattered wave propagation direction 16 p2543 A71-33568
- Microwave receiving and transmitting antennas proximity effects on permittivity measurements of dielectric layer 17 p2697 A71-34258
- Narrow flare angle low permittivity conical dielectric waveguide antenna, examining radiation patterns and propagation characteristics by approximate theory 20 p3196 A71-39380
- Quasi-stationary permittivity tensor corrections for smoothly nonuniform electron plasma in absence of magnetic field, using geometrical optics methods 21 p3424 A71-41129
- Dielectric conductivity, relative permittivity and loss tangent of Apollo 11 and 12 rock samples 23 p3762 A71-43787
- Temperature and frequency effects on permittivity and dielectric loss angle tangent in glasses and pyroceramics 24 p3859 A71-44379
- Permittivity increase in fluor-substituted barium titanate solid solutions for ceramic capacitor microminiaturization 24 p3859 A71-44387
- Nonmagnetic dielectric artificial birefringence determination, using permittivity additivity with bivalent symmetrical tensor 24 p3877 A71-44408
- Diffraction angular microwave beam scattering in fluctuating dense plasma, determining spatial scale of turbulence and permittivity 24 p3853 A71-44506
- Electromagnetic scattering of plane wave obliquely incident on infinitely long circular cylinder with radially varying permittivity and permeability 24 p3805 A71-45179
- PEROVSKITES**
 Perovskite crystals phase transition with unit cells atom displacement, considering permittivity anomalies, structure and free energy expansion coefficients 01 p0138 A71-10430
- Ionic conduction in perovskite-type oxide solid solution, discussing application to high temperature hydrogen oxygen fuel cells 18 p2852 A71-36966
- PEROXIDES**
NT HYDROGEN PEROXIDE
NT INORGANIC PEROXIDES
NT SODIUM PEROXIDES
 Organic compounds oxidation inhibition by polycyclic aromatic hydrocarbons, analyzing peroxide radicals charge transfer complex stability 05 p0716 A71-16382
- Silyl peroxides as promotion agents for polymeric materials adhesion to solid substrates and for cross-linking polyethylene to other polymers 10 p1633 A71-24109

Butene hydroperoxides structure and intermolecular reactions from NMR spectra, discussing peroxide radical addition, OH group signals shifts and self association 12 p1877 A71-27751

Peroxide-alkaline polishing solution for GaAs, evaluating optical quality, surface damage, polishing rate and metallic contact resistance 18 p2955 A71-37004

PERSEID METEORIODS

Meteor telescopic observations during Perseid stream activity, determining radiants, stellar magnitudes, length and velocity 12 p1961 A71-26905

Perseid meteors spectroscopic observations, using image orthicon technique for meteor spectral recording at luminosity thresholds below conventional spectroscopic capabilities 13 p2070 A71-29018

PERSONALITY

Soviet book on psychology and outer space covering astronaut experiences and emotions during training and flights, daily routine, equipment, food, habits and personal characteristics 21 p3336 A71-40876

PERSONALITY TESTS

Psychometric measurements approaches for pilot training questionnaires, considering personality traits standard model 10 p1559 A71-23929

Human vigilance performance and personality traits characterization by EEG alpha frequencies, correlating rest and task period recordings 15 p2359 A71-31954

Three phase code transformation task reliability and correlation, representing general/factor analytic intellectual abilities and personality characteristics 20 p3192 A71-39073

PERSONNEL

NT AIRCRAFT PILOTS

NT ASTRONAUTS

NT COSMONAUTS

NT FLIGHT CREWS

NT FLIGHT SURGEONS

NT FLYING PERSONNEL

NT GROUND CREWS

NT NAVIGATORS

NT OPERATORS [PERSONNEL]

NT ORBITAL WORKERS

NT PILOTS [PERSONNEL]

NT SCIENTISTS

NT SPACECREWS

NT TEST PILOTS

PERSONNEL DEVELOPMENT

Engineering management, discussing technical men work effort, time/intellectual changes, performance measurements, motivational factors and relationship to company 13 p2167 A71-28799

Personnel training in airline operations technology at Friedrich List Transportation Institute for aircraft pilots, flight safety engineers and systems engineers 13 p2021 A71-29143

Characteristics study of technical entrepreneurs, considering family background, education and motivation 19 p3173 A71-37631

Psychological training for personality development of aircraft stewardesses for conscious passenger relation establishment 19 p3008 A71-38224

PERSONNEL MANAGEMENT

Social factors of labor organization and control in scientific teams for industry 02 p0335 A71-11856

Mathematical model for optimizing observational data sampling and working time losses by scientific research personnel 02 p0336 A71-11859

Organization size in relation to staff personnel percentage, comparing various models 06 p1010 A71-18011

Engineers time and intellectual utilization in industry dependence on local company attitudes, suggesting better management appreciation of motivation factor [ASME PAPER 70-WA/PGT-12] 07 p1225 A71-19501

Information specialists performance prediction, discussing multiple discriminate analysis of selected variables 09 p1548 A71-22479

Military pilot handling characteristics, discussing combat operations, accident prevention and blind landing 22 p3504 A71-42239

PERSONNEL SELECTION

NT PILOT SELECTION

Personnel selection for emotionally and physically taxing situations by studying physiological responses to anticipated stressors and stress recovery 06 p0851 A71-17607

Psychological aspects influencing aircrewman capacity to perform useful work, detailing selection, training, operational environment and global factors 08 p1245 A71-20724

Astronaut selection and training, considering acceleration, hypoxia, weightlessness and temperature variation tolerance 12 p1873 A71-26951

Motivation principles in industry based on Maslow theory of hierarchy of needs, discussing selection of supervisory personnel 13 p2167 A71-28798

Psychological tests for aerial photograph interpreter selection and performance prediction 16 p2534 A71-32829

Soviet book on space biology and medicine covering cosmonaut selection and training, flight safety, normal life support factors, interplanetary space sojourn, etc 17 p2689 A71-34475

Tektite II program of underwater research as future manned space flight operations model, discussing mission structure, crew selection and communications [AIAA PAPER 71-828] 17 p2690 A71-34718

Test equipment for evaluating human higher nervous activity, noting use for radiotelegraphist selection 19 p3007 A71-37775

Program management techniques, discussing organization, planning, systems engineering and personnel selection 23 p3785 A71-43453

Project management methods oversophistication, discussing French space activity and managerial apprenticeship 23 p3785 A71-43454

PERSONNEL SUBSYSTEMS

Industrial project management executive work team for space programs, emphasizing responsibilities of prime contractor 23 p3786 A71-43461

PERSPIRATION

Sweating responses in men during intermittent hard treadmill work, considering regulation by skin/core temperatures, neuromuscular reflexes and vein/muscle thermoreceptors 04 p0544 A71-15151

Equipment for prolonged measurement of oxygen consumption, respiratory quotient and insensitive perspiration in man, noting cost reduction and operation simplification 13 p2021 A71-29316

Heat acclimatization effects on sweat Na concentration over wide sweat rates range, discussing possible mechanisms 13 p2024 A71-29498

Carbon dioxide elimination across human skin, investigating perspiration effects 14 p2186 A71-30567

Human sweating regulation at rest, evaluating thermal inputs effects on thermoregulatory center and internal hypothalamic and skin temperatures 17 p2683 A71-35146

Skin temperature and perspiration role in metabolic heat elimination, considering evaporation coefficient relationship to convection coefficient 18 p2859 A71-36873

Sweat and time constant response of human thermostat to linear gradient heat load, using analog computer experiment 18 p2859 A71-36874

Temperature regulation during exercise by proportional control, investigating skin temperature effect on set point temperature, sweat rate and skin thermal conductance 18 p2860 A71-36879

Physiological control of local sweating rate 18 p2860 A71-36884

Perspiration delay times characterizing potohydrotic reflex, analyzing neurophysiological mechanism 18 p2861 A71-36885

Exercise temperature plateau shift and sweat rate during moderate CO poisoning associated with resetting of thermoregulating centers by low oxygen tensions 18 p2861 A71-36886

Pilocarpine induced synchronous sweat expulsions, noting frequency linear dependence on ambient temperature with and without generalized sweating 18 p2861 A71-36889

Time constant for perspiration onset in humans exposed to stepwise increase in external heat load 18 p2862 A71-36897

PERT

Skynet project UK and U.S. cooperation, discussing system scope, coordination, contract placing and PERT critical path analysis in management planning 02 p0337 A71-12427

PERTURBATION

NT ORBIT PERTURBATION

NT SATELLITE PERTURBATION

Canonical theory of dynamics, examining independent variable transformations for perturbed two body problem 01 p0154 A71-10379

Nonlinear single-degree of freedom mechanical system vibration under small random perturbations 01 p0127 A71-10548

Perturbed magnetic surfaces topology in quadrupole, estimating local imperfections size for plasma control 10 p1652 A71-24661

Second order system with structure perturbation affected parameter value, studying identification and autoadaptation by sign functions 10 p1586 A71-24740

Retroversion from preferred eigenvalues to determine compatible structural characteristics, deducing design changes in model configurations from perturbations imposed [AIAA PAPER 71-345] 11 p1843 A71-25324

Tangential body forces and pressure perturbation interactions in thin liquid film, considering destabilizing effect impairing film cooling efficiency 11 p1751 A71-25491

Line shifts in first overtone band of DF perturbed by HF, studying pressure induced transitions and partial pressures 11 p1729 A71-26139

Asymptotic methods and Markov processes theory extension to unsteady vibration of nonlinear systems with slowly varying parameters and random perturbation 12 p1930 A71-27173

Aerodynamic perturbation due to single hot-wire probes, comparing with evaluations derived from potential flow scheme [ASME PAPER 71-APM-T] 18 p2904 A71-36262

Three degree of freedom perturbed two body problem, applying theory of redundant variables to Lagrangian equations of motion 19 p3143 A71-38163

Mesoscale perturbations in wind velocity field in jet streams, interpreting data in terms of hydrodynamic stability theory 21 p3412 A71-41392

GaAs lasers filamentary coupling, investigating various mode perturbations in temporal output 22 p3558 A71-42346

PETURBATION THEORY

Krylov-Bogoliubov integration theory for first-order perturbation analysis of multidimensional harmonic oscillator applied to body motion in earth gravity 01 p0151 A71-10113

Transform for hydrogen ion exchange perturbation problem, involving first order partial differential equations and method of characteristics 01 p0130 A71-10368

Matrix perturbation methods for nonlinear perturbed systems, involving variational equations solution of regularized Keplerian motion 01 p0154 A71-10380

Local invariants under axial rotation, deriving recurrence relations for time series expansions and perturbation methods 01 p0154 A71-10387

Space navigation variation problem, examining perturbation differential equation for semimajor axis and eccentricity and momentum and eccentric anomaly relationship 01 p0122 A71-10389

Lipschitz functional differential equations systems uniform asymptotic stability under diminishing perturbations 01 p0111 A71-10470

Perturbation theory of Hookes law model for He atom, obtaining ground state energy through third order 02 p0287 A71-12494

Plasma echo oscillations superposition of consecutive perturbations separated by intervals greater than characteristic decay time 02 p0291 A71-12508

Heat transfer analysis literature survey, including bibliography of perturbation, asymptotic and integral equations methods 02 p0333 A71-12650

Nonstationary automatic control system asymptotic series solution for equations of perturbed motion, deriving unperturbed motion local stability criteria 03 p0388 A71-13287

Turbulent plasma correlation functions for decay and nondecay spectra, deriving descriptive equations by perturbation theory series summation 03 p0464 A71-13932

Couette flow stability between coaxial rotating cylinders, calculating eigenvector in first approximation small perturbation equations 03 p0404 A71-14231

Dynamic response of linear systems with parameters subjected to step perturbations, obtaining quasi-linear mathematical model describing parameter-perturbation transmission path 03 p0394 A71-14483

Perturbation method in microwave electromagnetic field pattern determination and resonator design 04 p0586 A71-14657

Shock wave stability with respect to infinitesimal disturbances, using Burger and Korteweg-de Vries equations via Liapunov method application 04 p0570 A71-15080

Laminar flow stability and transition to turbulent flow, giving nonlinear theory for perturbations development

04 p0574 A71-15602

Nonlinear model equation for hydrodynamic perturbations, discussing solution at large Reynolds numbers for one dimensional flow

04 p0575 A71-15609

Two dimensional motion stability near sun-perturbed earth-moon triangular libration points, using computerized high order treatment

04 p0653 A71-15708

Limiting bounds determination for existence of periodic orbits near known existing periodic orbit, presenting linear perturbation analysis

04 p0654 A71-15717

Hori and Deprit perturbation theories comparison based on Poisson brackets, giving computer program determining functions through sixth order for equivalence proof

04 p0660 A71-15889

Perturbation theory diagrammatic version for describing lattice vibrations effect on scattering cross sections of low energy electrons from single crystal solid surfaces

05 p0792 A71-16316

Perturbations effect on tube flow and density variations due to noninstantaneous shock wave formation

05 p0836 A71-16529

Perturbation method in nonlinear oscillations theory, using asymptotic recurrence formulas based on Lie transform

05 p0774 A71-16544

Perturbation theory using Lie transforms, discussing reformulation leading to algorithm

05 p0774 A71-16545

Perturbation theory of celestial mechanics, using expansions of negative powers of mutual distances between two bodies

05 p0810 A71-16546

Small amplitude nonlinear longitudinal plasma oscillations perturbation analysis, discussing Landau damping, monochromatic wave evolution and independent variable expansion

05 p0789 A71-16659

Unsteady heat conductivity problems with nonlinear boundary conditions, using perturbation method

05 p0838 A71-16782

German monograph on shock wave diffraction wedge angular changes in ideal gas region, comparing experimental with perturbation theoretical results

05 p0737 A71-17107

Power series uniformization by transformations of perturbation functions irregular part, considering compatibility problem

06 p0919 A71-18197

Similarity methods, partial differential numerical analysis, dispersive wave and perturbation theory applications to mechanics

06 p0920 A71-18220

Perturbation growth in free particle expanding Universe with critical density, considering Newton gravitation theory

06 p0974 A71-18427

On-off control system with crew motion caused random disturbing torques on spacecraft, determining waiting time, jet firing frequency and fuel consumption rate

07 p1208 A71-19885

Dynamic system stability criterion under constantly acting perturbations over finite time interval

07 p1161 A71-20267

Cylindrical viscous jet surrounded by flowing gas, investigating flow stability by linear perturbation theory

07 p1093 A71-20281

Double resonance in natural satellite motion from long period perturbation prediction

07 p1202 A71-20517

Electron mass and photon wave renormalizations functional relationships, studying perturbation theory based electrodynamic divergences

07 p1162 A71-20550

Physically nonlinear bodies of revolution, investigating stress-strain state by small parameter and perturbation methods

07 p1219 A71-20650

Perturbation theory for reduced density matrices representable as functions of independent parameters

08 p1332 A71-20660

Three body problem stability investigation, using Liapunov perturbation function

08 p1361 A71-21052

Three dimensional nonlinear heat conduction problem solving by perturbation theory and finite integral transform

08 p1377 A71-21927

Dynamic systems toroidal manifolds disturbance, discussing invariant torus preservation

08 p1336 A71-22017

Random gravitational encounter effects of passing stars on dynamical evolution of spherically symmetric stellar system, using modified Monte Carlo method

09 p1517 A71-22330

Compressible boundary layer separation near zero skin friction by Kaplun perturbation technique, studying nonlinear integral equation with Abel kernel

09 p1432 A71-22455

Motion perturbation equations for guided space vehicles, allowing for sloshing liquid propellant viscosity effects

09 p1532 A71-22657

Nonstationary automatic control system asymptotic series solution for equations of perturbed motion, deriving unperturbed motion local stability criteria

09 p1424 A71-23262

Planetary motion mutual perturbation, presenting method for expansion of disturbing function

09 p1525 A71-23334

Differential equations system theorems for conditions of solution stability in presence of large initial perturbation

09 p1495 A71-23429

Rotating self gravitating axisymmetric fluid mass structure steady state equations, examining Clairaut theory asymptotic nature

09 p1527 A71-23532

Steady nonlinear amplitude of electrothermal instability in nonequilibrium plasma derived by expanding electrothermal equations in terms of perturbation about equilibrium state

09 p1387 A71-23649

Nonlinear stability of incompressible laminar flows involving perturbation in Banach space

10 p1591 A71-23914

Singular perturbation problems for linear second order elliptic equation, obtaining asymptotic approximations for simple unbounded regions with free boundary layer terms

10 p1636 A71-23934

Unsteady low Mach number flow calculation by singular perturbation method with matched asymptotic expansions, considering application to aerodynamic noise

10 p1549 A71-23936

Numerical integration of perturbed linear systems of differential equations by step method comparing power series

10 p1636 A71-23960

Perturbed motion of class of nonconservative systems with generalized forces, discussing conditions for perturbation equations integrability

10 p1641 A71-24022

Linear theory of weakly perturbed supersonic plane axisymmetric flows of gas-particles mixture, deriving partial differential equation for perturbation potential

10 p1551 A71-24373

Analytical lunar ephemeris main problem solution by canonical perturbation theory based on Lie transforms and echeloned series processing

10 p1674 A71-24431

Phythan perturbation theory for stationary homogeneous turbulence of incompressible fluid

10 p1594 A71-24511

Nonuniform transonic shear compressible flow past symmetric airfoil, using linearized small disturbance theory

10 p1552 A71-24761

Canonical perturbation theory formulation applied to Poincare-von Zeipel method

10 p1679 A71-24935

Perturbation theory of supersonic flow with nonequilibrium radiative heat transfer, investigating pressure, density, temperature and velocity as function of relaxation time

10 p1697 A71-24943

Acoustic and shock waves propagation in quasi-steady supersonic flow in duct with varying cross section

10 p1598 A71-25083

Gravitational radiation damping of slowly moving systems, discussing treatment as singular perturbation problem with approximation solution by method of matched asymptotic expansions

11 p1797 A71-25139

Earth-moon distance perturbations from anisotropic gravitational mass effect

11 p1819 A71-25209

Ammonium perchlorate deflagrations, determining intrinsic stability of one dimensional burning configuration based on flame structure modeling [AIAA PAPER 70-123]

11 p1809 A71-25455

Second and higher order perturbation theory for two body trajectories, using recursive formulas [AIAA PAPER 70-1056]

11 p1820 A71-25459

BeO reflected-fast-spectrum liquid-metal-cooled thermionic reactor, discussing two dimensional transport perturbation theory computer code for temperature coefficients evaluation

11 p1712 A71-25887

Atmospheric wave dynamics in equatorial region, obtaining approximate solution with Coriolis force within perturbation theory

11 p1795 A71-25921

Coupled and uncoupled versions of Hartree-Fock theory, calculating atomic system linear response to external time dependent perturbation and Green function

11 p1802 A71-26057

Rayleigh-Schrodinger perturbation energies for ground state of two electron atomic Hooke's law model through tenth order

11 p1803 A71-26151

Bogoliubov generalization principle applicability conditions for second order hyperbolic equations with functionally perturbed argument, using Wendroff-Bellman lemma

11 p1792 A71-26154

Comet orbits correction, including differential coefficients perturbations based on Kulikov equation for difference between computed and true radius vector

11 p1833 A71-26328

Perturbation growth in free particle expanding universe with critical density, considering Newton gravitation theory

12 p1954 A71-26577

Gravitational lunar theory high order solution for geophysical relevance, discussing perturbation methods and computer analyzed ephemeris time

12 p1961 A71-26837

Steady supersonic isoelectric flow of thermally and calorically perfect gas past circular cones at zero angle of attack, using dimensional perturbation method

12 p1863 A71-26939

Gravitational field quantum fluctuations role in general theory of relativity and cosmological model

12 p1965 A71-27179

Inviscid compressible fluid jet flow, calculating instability boundaries characteristics by linear perturbation analysis and numerical solution

12 p1897 A71-27219

Statistical space density and velocity perturbations of galaxies relative to origin of rotation in range of Friedman cosmological model

12 p1966 A71-27235

Kane-Mindlin differential equations solved by perturbation techniques for free extensional vibrations in elastic plates

12 p1981 A71-27483

Zerilli equation solutions for even-parity gravitational perturbations on Schwarzschild geometry, considering gravitational collapse and black hole effects

13 p2133 A71-27972

Rapid differential rotation in completely degenerate white dwarfs, using perturbation method

13 p2135 A71-28300

Algorithm for automatic closed form integration of formulas in elliptic motion arising in perturbation theories

13 p2136 A71-28358

Constant space curvature perturbations, considering density, rotational and propagation of gravitational waves with Lipschitz method

13 p2137 A71-28479

Necessary and sufficient global stability criteria for axisymmetric perturbations of stellar dynamic disk models of galaxies

13 p2138 A71-28775

Optimal transfers in central gravitational field, using perturbation formulas of osculating Keplerian orbit elements and corresponding linearized equations

13 p2139 A71-28825

Fluctuations of Gaussian light beams due to turbulence in lenslike medium, using perturbation method

13 p2102 A71-29388

Phase changes /droplet solidification/ effect on two phase nozzle flow, considering perturbation treatment [ASME PAPER 71-FE-11]

13 p2052 A71-29452

Nonlinear systems stability analysis for arbitrary disturbances, using semistochastic technique

14 p2219 A71-29735

TM, TE and combination cavity modes choice for plasma column electron density distribution determination by perturbation methods

14 p2279 A71-29859

Three body problem stability investigation, using Liapunov perturbation function

14 p2310 A71-30169

Nonlinear vibration of changing boundaries structures, approximating boundary values by perturbation technique

14 p2331 A71-30699

Nonstationary perturbation propagation in gaseous medium with irreversible internal process /chemical reactions or excitations with one degree of freedom of molecules/

14 p2338 A71-30823

Perturbed motion linear equations of body rigidly coupled to thin walled elastic shell partially filled with heavy compressible fluid

14 p2227 A71-30867

External field perturbations by local inhomogeneities in elastic medium, deriving expressions for interaction energy and forces between defects

14 p2332 A71-30869

Optimal control and tracking problems quality in cases of bounded coordinates and continuously acting perturbations respectively

14 p2220 A71-30870

Boltzmann equation approximate solution for molecular velocity distribution function perturbations by inelastic collisions

15 p2386 A71-31158

Nonlinear asymptotic stability of motion in critical case involving characteristic equation in first approximation with pair of imaginary roots

15 p2449 A71-31699

Zero solution stability of nonlinear system of differential equations with constantly acting perturbations

15 p2449 A71-31830

Forced oscillations of system governed by one dimensional nonlinear wave equations, using perturbation procedure for solutions near linear resonant frequencies

16 p2606 A71-32857

Bifurcating systems analysis in structural stability problems, discussing perturbation patterns in nonlinear branching theory

16 p2650 A71-33018

Perturbation method for solving nonstationary heat conduction problems with nonlinear boundary conditions

16 p2662 A71-33034

Wave fronts in Einstein-Maxwell theory, showing perturbation propagation along background space-time metric field

16 p2609 A71-33261

Electrodynamics Lagrangian with gauge invariant electron operator, obtaining free field nonequal time commutators and photon propagator for perturbation theory

16 p2610 A71-33269

Spiral structure of Galaxy, using perturbation method for analysis of steady state interstellar gas with differential rotation due to coupling with stellar gas

16 p2643 A71-34069

Dynamic cryptodeterministic linear systems with random initial state, calculating stochastic response by perturbation scheme

16 p2660 A71-34072

Diffusion flame theoretical model characterization as singular perturbation problem

16 p2664 A71-34073

Laminar boundary layer past continuous moving surface with constant wall velocity, deriving perturbation solution in terms of Green function

16 p2560 A71-34074

Coupled nonlinear control system optimization by noniterative perturbation method

16 p2551 A71-34170

Limit cycle of nonlinear oscillations of third order differential equations dependent on Euclidean phase space with central restoring control force

17 p2763 A71-34293

German book on satellite geodesy covering two body problem, perturbation theory, earth gravitational field, gravitational effects of sun and moon, radiation pressure, etc

17 p2799 A71-34470

Book on linear and ordinary celestial mechanics covering perturbed two body motion, numerical methods, canonical theory and initial value problems

17 p2799 A71-34471

Periodic solutions of singularly perturbed hereditary systems of ordinary nonlinear integrodifferential equations

17 p2780 A71-34920

Perturbation theory of invariant manifolds of dynamic systems based on Green function, deriving new existence theorems

17 p2781 A71-34930

French monograph on algorithms for parameters estimation for adaptive identification in real time of linear processes perturbed by related noise

17 p2767 A71-35232

Three dimensional nonlinear heat conduction problem solving by perturbation theory and finite integral transformation method

17 p2838 A71-35271

Singular perturbation theory for finite rate chemical kinetics effect on regression rate of seminfinit flat fuel plate in gas oxidizer stream

17 p2792 A71-35796

Unstable nonlinear systems transient behavior analysis with two-time perturbation method applied to Bernard and Taylor flow problems

17 p2730 A71-35797

Sequence of double exposure holograms corresponding to repetition laser to study objects undergoing perturbation

18 p2916 A71-36045

Mach number effects on flow field in gas bearings at high subsonic and supersonic tangential speeds based on perturbation theory

18 p2926 A71-36263

Heuristic approaches for generating perturbations to automatically evaluate partial derivatives for interplanetary space missions

19 p3135 A71-37561

Small parameter method application to quasi-linear problems solution in nonstationary heat conduction with substantial nonlinearities and weak perturbation, analyzing error

19 p3162 A71-37584

Automated algebraic manipulation in celestial mechanics, discussing use of Poisson series in perturbation theory problem

19 p3088 A71-38400

Linear theory of weakly perturbed supersonic plane axisymmetric flows of gas-particles mixture, deriving partial differential equation for perturbation potential

20 p3175 A71-38898

Gas resonant oscillations in closed end tube, describing time-periodic motion by perturbation method with Mach number as flow parameter

20 p3211 A71-39078

Atmospheric wave dynamics in equatorial region, obtaining approximate solution with Coriolis force within perturbation theory

20 p3256 A71-39212

Modified asymptotic perturbation expansion method application to free flow rotation effect on boundary layer for hypersonic flow about blunt body

20 p3177 A71-39483

Lame equation perturbation solution and applications to problems involving elliptic cones or infinite sectors

20 p3177 A71-39497

Delta wing problem reduction to Laplace equation solution, using perturbation technique to solve Lame equation resulting from elliptic conal coordinates transformation

20 p3177 A71-39498

Steady and unsteady flow work and energy loss relationships expressed in integral form representing perturbation kinetic energy, internal energy and pressure work

21 p3317 A71-40011

Computer implementation for Hansen theory of general perturbations, constructing program based on automatic Poisson series processor

21 p3445 A71-40257

Perturbation study of subharmonic rotor instability due to elastic symmetry, obtaining equations of motion

21 p3385 A71-40302

Perturbation velocity of laminar wake downstream of two dimensional body in boundary layer, considering transition behind trip wire

21 p3322 A71-40640

Perturbation procedure application to linear and circular antenna array directivity optimization by phase adjustments under uniform amplitude excitation

21 p3359 A71-41412

Electron-electron correlation effects in photoabsorption induced double electron ejection process, using many body perturbation theory

22 p3577 A71-41628

Homogeneous positive plasma column perturbation analysis in axial magnetic field, deriving model for ionization waves dispersion characteristics

22 p3582 A71-41898

Second order rotational effects on stellar nonradial oscillations by perturbation method, taking into account equilibrium configuration distortion by coordinates transformation

22 p3602 A71-42173

Regular and singular perturbation solutions for beam bending under axial forces and shaft warping in torsion

22 p3616 A71-42214

Gravitational field quantum fluctuations role in general theory of relativity and cosmological models

22 p3605 A71-42453

Perturbation method in transition effect theory for electron photon cascades in extensive air showers

22 p3596 A71-42672

Local dynamical system behavior in perturbed Tikhonov space, showing fundamental cycle periods continuous variations

22 p3568 A71-42695

Optimal lift control of hypersonic lifting body during atmospheric entry by singular perturbation method

23 p3773 A71-43036

Modified perturbation method for solving optimal control boundary value problems with state variable inequality constraints, noting application to reentry trajectories

24 p3876 A71-44608

Orthogonal method for studying nonlinear automatic control systems in presence of random perturbations, discussing applicability limits

24 p3815 A71-44701

Kruskal transformation canonization of perturbed periodic systems with Hamiltonian

24 p3843 A71-44789

Classical Poincare-von Zeipel canonical perturbation theory extension to adiabatically perturbed systems with slow dependence on time or dynamic variables

24 p3848 A71-44790

Cavity cross sections perturbed motion equations

24 p3819 A71-44840

Flat diffusion flame structure experimental investigation on Parker-Wolfhard burner, comparing results with perturbation solutions theoretical predictions

24 p3888 A71-44939

Finite plane strain inflation of compressible hollow circular cylinder, using perturbation method for nonlinear boundary value problem

24 p3884 A71-44955

Nonlinear controlled plant dynamic behavior sensitivity in parameter perturbation derived from mathematical model, applying to satellite attitude control

[ASME PAPER 70-WA/AUT-5] 24 p3816 A71-45136

PERVEANCE

Computer design of magnetron gun forming electron beam of specific perveance and oscillatory energy in converging magnetic field

03 p0385 A71-13796

Periodic electrostatic focusing of high perveance electron beams for high power klystrons

19 p3028 A71-37696

Electron guns perveance increase by transverse and longitudinal charge compression, reviewing beam formation theory

20 p3204 A71-39154

High perveance three electrode electron gun with longitudinal compression, examining beam profiles and radial current density distributions

20 p3204 A71-39161

High vacuum ion source classification according to ionization technique, using perveance and current flow parameters

22 p3589 A71-42055

PETN

Casing material effects on velocity of low speed phase prior to detonation onset of high density PETN, testing steel, Plexiglas, Duralumin and brass

15 p2511 A71-31390

PETROGRAPHY

Mesosiderites silicate textures and compositions and metal-silicate relationships from mineralogical, petrographical and chemical data

10 p1602 A71-24504

Petrography, chemistry and mineralogy of El Paso meteorite

11 p1835 A71-26481

Chemical analysis and petrography of Murchison meteorite compared to Murray meteorite

11 p1836 A71-26483

Petrographic study of Allende carbonaceous chondrite by high voltage transmission electron microscopy, comparing substructure with terrestrial rocks

14 p2308 A71-29912

Lost City /Oklahoma/ meteorite classification as type H5 chondrite based on bulk chemical composition, mineralogy and petrography

15 p2489 A71-32356

Remote sensing for geologic problems, using side-looking radar for fracture and fault detection and IR images for limestone, dolomite and granite discrimination

18 p2911 A71-35890

Australian Liverpool and Strang way craters as probable meteoritic impact origin from topographic and petrographic data

19 p3049 A71-37653

Charlevoix structure impactite description, discussing meteoritic impact origin from petrographic and chemical data

19 p3049 A71-37656

Detritus and breccias occurrence, composition, shock metamorphism, ejection mode and deposition at terrestrial small impact crater formations based on petrographic observation

19 p3051 A71-37667

Comparative electron petrography and chemical analysis of Apollo 11 and 12 and terrestrial rocks, noting pyroxene, plagioclase, ilmenite and cristobalite

23 p3738 A71-43608

Luminescence petrography of Apollo 12 lunar igneous rocks, comparing to meteorites and terrestrial basalts

23 p3740 A71-43624

Petrography and mineral composition of Apollo 12 crystalline rocks

23 p3740 A71-43629

Apollo 11 and 12 lunar rocks and soil chemical composition, considering petrogenesis and major and trace elements abundance

23 p3741 A71-43635

Apollo 11 and 12 crystalline rocks petrographical analysis and textural-mineralogical-chemical group classification, considering local stratigraphy reconstruction

23 p3742 A71-43638

Petrography, mineral composition and grain size distribution of Apollo 12 lunar fines

23 p3743 A71-43649

Regular particle morphology and petrostatistics in Apollo 11 and 12 lunar fines and conglomerates, using phase contrast and scanning microscopes

23 p3758 A71-43757

Lunar origin hypothesis, discussing Apollo 11 crystalline rocks nature and basalts petrogenesis

23 p3770 A71-44075

PETROLEUM

U CRUDE OIL

PETROLOGY

NT PETROGRAPHY

Redox estimation from natural phase Eu ion concentrations in rocks

01 p0029 A71-11428

Apollo 11 basalts chemistry and petrogenesis by partial melting, considering implications for lunar origin theories

02 p0305 A71-11981

Apollo 11 crystalline igneous rocks mineralogy and petrology, suggesting origin from pyroxenite mantle melting

02 p0305 A71-11982

Apollo 11 lunar soil sample derived from basaltic and anorthositic rocks, considering basalt origin by melting due to internal radioactive heating

02 p0305 A71-11983

Surveyor lunar probes alpha scattering chemical analysis technique tested on rocks of known composition

02 p0305 A71-11984

Petrographic microscope and electron microprobe analysis of Apollo 12 rock 12013, noting biminerale composition with dominant potassic feldspar plus silica

03 p0493 A71-14214

Apollo 12 lunar rock 12013 petrologic and mineralogical characteristics, discussing data on isotopic Xe and Gd composition

03 p0494 A71-14217

Volcanic petrochemical differences of Ethiopian rift and plateaus

09 p1436 A71-22645

Kaersutite amphibole formation from pargasite amphibole interaction with basanite, discussing Fe, Ti, K, Mg, Si, Na and Cr contents

10 p1601 A71-24415

Apollo 11 sample basalts lunar interior origin assumption from comparison with terrestrial massif anorthositic series, using chemical and petrographic analyses

11 p1834 A71-26452

Mineralogy, petrology, chemistry and microstructure of Valdinizza meteorite

11 p1835 A71-26480

Lunar anorthositic comparison with terrestrial igneous rocks, discussing petrogenetic schemes based on models

12 p1958 A71-26693

Lunar samples mineralogy, petrology and geochemistry, considering lunar surface processes, cosmic ray flux and solar wind

12 p1967 A71-27414

Mineralogical, petrological and chemical features of four Apollo 12 lunar microgabbros

23 p3740 A71-43625

Apollo 12 crystalline rocks mineralogy, petrology and chemical composition, considering magmatic origin

23 p3740 A71-43626

Mineralogy and petrology of Apollo 12 igneous rocks 12004, 12008, 12009 and 12022, noting ilmenite, olivine and spinel content and metal grains composition

23 p3740 A71-43627

Mineralogy, petrology and chemical composition of Apollo 12 rocks and fines

23 p3740 A71-43628

Apollo 12 lunar rocks and fines mineralogy and petrology, using optical and electron microscopy, electron and X ray diffraction and electron probe microanalysis

23 p3741 A71-43630

Petrology of Apollo 11 and 12 rock samples with silicate melt inclusions, discussing terrestrial equivalents

23 p3742 A71-43641

Apollo 12 basalts petrology and petrogenesis, studying crystallization sequences

23 p3743 A71-43646

Petrogenesis and crystallization of prothyperserene basalts in lunar maria lava lakes, deducing eruption temperatures

23 p3743 A71-43647

Apollo 11 and 12 unshocked and shocked microbreccias petrology, noting shock compression and shock welding

23 p3745 A71-43658

Critique of paper on Apollo 11 ilmenite basalts petrology and lunar bodies origin and form

23 p3769 A71-43886

PFM [MODULATION]

U PULSE FREQUENCY MODULATION

PH

Electronic instrumentation for monitoring intragastric pH, temperature, motility and electrical activity

01 p0023 A71-10887

Arterial oxygen, carbon dioxide tension, pH and lactic acid changes during rapid descent from altitude to sea level in deep mine

07 p1052 A71-20334

Mean whole body intracellular pH and buffer capacity for arterial carbon dioxide tension in ventilated dogs

10 p1558 A71-23896

Body temperature effects on intracellular carbon dioxide dissociation, pH and buffer capacity in hypothermic and hyperthermic dogs

10 p1559 A71-23897

Proton release association with whole blood oxygenation at constant plasma pH and carbon dioxide partial pressure, using alkaline titration

13 p2007 A71-28433

Respiratory acid-base disturbances, studying deviations of bicarbonate ion vs pH pathway followed by buffered solution on carbon dioxide titration

13 p2007 A71-28434

Oxygen dissociation curve shift, hemoglobin affinity and diphosphoglycerate concentration in blood of acidotic and normal subjects at altitude

13 p2016 A71-29494

Human erythrocyte 2, 3-diphosphoglycerate concentration elevation effects on glycolytic metabolism and intracellular pH

16 p2533 A71-34090

Solution chemistry at stress corrosion crack tips in Al alloys, considering factors affecting pH change with time of initially acidic NaCl solutions

17 p2755 A71-34439

Ventilatory acclimatization to chronic hypoxia in high altitude natives by cerebrospinal fluid pH decrease

17 p2683 A71-35144

Organic phosphate compounds effects on oxygen affinity and intracellular pH of human erythrocytes

18 p2857 A71-36691

Inspired oxygen concentrations effects on arterial and mixed venous pH, carbon dioxide uptake and oxygen partial pressure in normal subjects

20 p3189 A71-39442

Intracellular pH and carbon dioxide combining curve of muscle tissue in dogs, using DMO method

21 p3335 A71-40631

Electron transport chain of extremely halophilic bacteria, investigating cytochrome oxidase activity dependence on pH

23 p3633 A71-43525

PH FACTOR

High yield strength steel stress corrosion crack tip electrochemical and pH potential conditions, using AgCl reference electrode

07 p1137 A71-19973

Al alloys and steel, determining potential and pH changes during stress corrosion crack propagation by microelectrode technique

11 p1783 A71-26497

Chronic hypoxia effects on blood oxygen and carbon dioxide tensions and pH changes in unanesthetized chickens at high altitude compared to sea level control

14 p2186 A71-30565

Human blood pH and gas composition regulation mechanism under response to carbon dioxide partial pressure changes in inhaled air

15 p2357 A71-31316

PHANTASTRONS

Linear sawtooth voltage phantastron type generator, presenting operation time diagrams and circuit advantages

12 p1906 A71-26900

Stable oscillation development time in phantastron oscillator, using linearization of nonlinear term

14 p2211 A71-30114

PHANTOM AIRCRAFT

NT F-4 AIRCRAFT

Phantom and Buccaneer aircraft boundary layer control, examining lift from trailing and leading edges

06 p0847 A71-17953

PHARMACOLOGY

Natural or endogenous fibrinolysis and its pharmacological enhancement as possible approach to prophylaxis of vascular occlusions

02 p0200 A71-12417

Telemetric techniques for pharmacological effects of body temperature, motor activity and food and fluid intake on rat brain, describing recording and monitoring equipment

05 p0716 A71-17112

Laboratory and clinical investigations of radiosensitization of cells and viruses by halogenated pyrimidine analogs

07 p1032 A71-18929

Radiosensitizing effect of iodine compounds in dilute solution on Ehrlich ascites tumor cells and SH enzymes

07 p1036 A71-18957

Aminoethylisothiuronium and methoxy-tryptamine synergism quantitative analysis by pharmacological methods of radioprotective effect in X irradiated mice

07 p1038 A71-18971

6-azauridine effect on radiation induced inhibition of Yoshida sarcomas, Ehrlich carcinomas, benzopyrene-induced carcinomas and spontaneous mammary carcinomas growth and transplantability

07 p1039 A71-18978

Chlorophenoxyisobutyric acid action on human cholesterol metabolism, suggesting cholesterol synthesis inhibition

07 p1044 A71-20353

Brain norepinephrine synthesis pharmacological inhibition, discussing effects of ovariectomy to decrease sensitivity

09 p1391 A71-22472

Furosemide effect on physical work capacity, studying recovery pulse response, oxygen extraction during exercise and altitude acclimatized subjects oxygen uptake

09 p1394 A71-23237

Histamine importance in nervous system activity, discussing synaptic mediation, reception processes and pharmacological action

12 p1869 A71-26652

Pulmonary blood volume changes in cat due to neurogenic, pharmacological and mechanical effects on cardiovascular system, noting pulmonary function role

16 p2533 A71-34112

Isoproterenol, atrial pacing, ouabain and methoxamine effects on dogs during experimental cardiac tamponade, observing arterial pressure, cardiac output and heart rate changes

20 p3186 A71-38968

Extraocular muscle pharmacology, discussing eye twitch and tonic neuromuscular systems structure and function in frogs

22 p3488 A71-42439

Medical preparations use and avoidance by spacecraft and aircraft crew members, discussing aftereffects, allergies and health requirements

22 p3491 A71-42705

Caffeine, ephyllin, cordiamin, morphine, calcium chloride, adrenaline and mesaton effects on organism physiology during hypothermia

23 p3492 A71-42709

Prophylactic medication for radiation damage treatment, covering toxicity, pharmacological properties, metabolism, dosage and physiological action

22 p3505 A71-42711

Reactivity changes to pharmacocchemical preparations under total proton and gamma ray irradiation of abdomen and head shielded rats

22 p3492 A71-42717

PHARYNX

Streptococcal flora in pharynx of men during prolonged enclosure noting concomitant hemolytic microbes

06 p0854 A71-18369

Pharyngeal streptococcal flora of men confined in sealed chamber, observing microbial transfer

24 p3800 A71-44530

PHASE ANGLE

U PHASE SHIFT

PHASE CHANGES

U PHASE TRANSFORMATIONS

PHASE COHERENCE

Phase-coherent communication systems with phase locked loops for data detector synchronization, calculating noisy timing effects on detection efficiency

05 p0724 A71-17059

Laser beam propagation through atmosphere, measuring phase variation dependence on turbulent temperature structure for comparison with prediction

07 p1123 A71-19574

Line-of-sight radio signal transmission, investigating sea surface reflections effects on phase of arrival and coherence

09 p1409 A71-23502

Receiving system for phase measurement on coherent signals from satellites, discussing frequency conversion through phase locked filter

13 p2033 A71-29275

Phase holographic data storage in doped barium sodium niobate crystal, detailing decay times, energy density and diffraction efficiency

15 p2412 A71-32586

Pulsed ruby laser holography improvement by coherence length increase with temperature controlled multitelons and beam uniformity through ruby crystals improvement

21 p3393 A71-40925

Superradiant laser stationary characteristics description by Fokker-Planck equation for classical distribution function, taking into account phase destroying effects

21 p3421 A71-41398

Millimeter wave holographic imaging for concealed weapon detection by phase-only hologram, discussing recording and reconstruction systems configurations

22 p3546 A71-42485

PHASE CONTRAST

Wind tunnel hypersonic flow visualization by schlieren and phase contrast methods at low volumetric mass

11 p1764 A71-26273

Photoactivated electric field effects in nematic liquid crystals for recording real time transparent phase holograms

23 p3674 A71-42955

High resolution phase contrast microscope adaptation for gastight glove box use with stage and focusing knobs in box for Apollo sample microbiological examination

24 p3802 A71-45124

PHASE CONTROL

Varicap loop circuits for controllable IF phase corrector with independent delay suitable for automatic control

01 p0054 A71-11083

Widely separated microwave oscillators phase synchronization via satellite transponder

02 p0216 A71-12330

Ionospheric and tropospheric effects on differential phase path in very long baseline interferometry, using ray tracing computer program

02 p0251 A71-12331

Automatic phase control system with separating capacitance containing low and high frequency electric filters

06 p0866 A71-17375

Regenerative transfer amplifiers normalized reactive parameters effects on phase linearity

06 p0872 A71-17376

Pulsed phase locked automatic phase control system linear model, discussing optimal white noise filtration with integrating filter

06 p0867 A71-17377

Time varying multivariable system transformation to phase variable canonical form

08 p1324 A71-21329

Phase regulated AFC system design for millimeter and submillimeter wave backward wave tubes

08 p1267 A71-21805

Dynamic frequency and phase characteristics of oscillatory circuit dependent linearly on time variable capacitance

10 p1643 A71-24907

Interaural phase angle control, using equal masker/signal narrow noise bands and phase shifting network between channels

12 p1871 A71-27534

Book on thyristor phase-controlled converters and cycloconverters covering operation, control and performance

13 p1998 A71-27941

Continuous relative phase control between reference and object beams in holographic interferometry

13 p2066 A71-28161

Computer phase hologram synthesis simplified modification, using EM field vector transformation for points

13 p2070 A71-29029

Steady state analysis of phase controlled parasitic current, discussing reduction of alternator apparent power requirements and harmonic distortion

15 p2355 A71-32218

Pulse bursts phase regulation subassembly modules, noting use for time division multiple access system control

18 p2879 A71-36545

Phase control circuits used in frequency division and multiplication, noting applications as filters and demodulators

20 p3208 A71-39433

Perturbation procedure application to linear and circular antenna array directivity optimization by phase adjustments under uniform amplitude excitation

21 p3359 A71-41412

German monograph on analysis and design of digital microwave phase shifters for phase controlled antennas covering admittance loaded lines, transmission and reflection behavior

23 p3649 A71-42999

Binary parabolic phase coded waveform generation from analog signals by pi-quantization

23 p3645 A71-43440

Multimode different-phase discharge carbon dioxide laser output power characteristics as function of discharge current and number of modes

23 p3686 A71-44000

Wideband phase-matched carbon dioxide laser second harmonic generation in GaAs thin film waveguide through dielectric dispersion

23 p3687 A71-44136

PHASE DEMODULATORS

Noise stability of synchronous phase demodulator in satellite and tropospheric communications, considering threshold characteristics

09 p1413 A71-22146

PHASE DETECTORS

Holographic interferometry with both beams traversing transparent object, providing variable sensitivity and directional phase detection

03 p0425 A71-13654

X band radar system to compare electrical lengths in 100 m range with 10 to minus 6 accuracy, noting applications in geodetic and radio waves phase fluctuation measurements

07 p1075 A71-19345

Pulsed phase detectors for phase comparisons of pulse sequences having arbitrary frequency ratios, designing circuit to prevent false locking in AFC systems

07 p1061 A71-19509

Phase measurement at millimeter wavelengths in free space, using reference signal and interference pattern of slowly varying electric field

13 p2030 A71-28609

Microwave phase discriminators sensitivity and linearity performance improvement, noting diode detectors nonideal nature

13 p2038 A71-28779

Phase locked AFC system, calculating phase detector response effects on dynamic properties

15 p2370 A71-31592

Rapid response multiple phase detector for balancing of AC digital bridge networks

17 p2718 A71-35712

Shock wave attenuation in two diaphragm tube, obtaining velocity profiles with microwave phase detector system

23 p3674 A71-43086

PHASE DEVIATION

Proton Flare Project 1969 observation of VLF radio wave propagation, detecting sudden phase anomaly events due to solar activity

01 p0144 A71-10288

Annular solar eclipse effects on VLF transmissions phase delay

02 p0212 A71-11969

Large signal mode tunnel diode amplifier amplitude and phase characteristics by computer study

04 p0556 A71-14622

Phase fluctuations in nonautonomous reflex klystron oscillators due to shot noise in electron beams

04 p0557 A71-14624

Microwave phase measuring system using programmable digital dividing circuits, considering application to plasma diagnostics

04 p0586 A71-14655

Partially coherent laser beam phase fluctuations using reversing-front interferometer for time integrated irradiance measurement, considering atmospheric turbulence effects

04 p0627 A71-15683

PSK pseudonoise/spread spectrum communication systems with SNR reduction, examining phase nonlinearities effect

05 p0725 A71-17074

Telephone channel phase-frequency distortions effects on discrete signal transmission quality from phase-delay-time frequency characteristics criterion

08 p1253 A71-20774

Solid state laser oscillation transient features analysis by dynamic rate equations, taking into account electric field phase variations in mode locking

08 p1301 A71-21277

Coherent optical target recognition through phase distorting medium, using holography, Fourier transform and autocorrelation functions

08 p1335 A71-21377

Laser radiation amplitude and phase fluctuations in complex media, using interferometry

09 p1459 A71-22143

He-Ne ring laser in locking range, studying opposing waves amplitude and phase differences dependence on cavity rotation and oscillation frequency tuning

09 p1461 A71-22382

Negative sudden phase anomalies, related signal strength enhancements and short wave fadeouts, considering maximum flux density of solar X-ray flares

10 p1575 A71-23883

Nonlinear dynamic systems phase coordinate variations statistical characteristics, describing data reduction method

11 p1798 A71-25662

Amplitude-phase distortions of optical beam during nonlinear amplification in carbon dioxide laser with periodic correction

12 p1913 A71-26846

Fluctuation power spectra of CW phase path HF sounders in ionosphere compared with Vaisala frequency curve for upper atmosphere monitoring

14 p2230 A71-29717

VLF signal propagation during low and high solar activity, discussing equipment precision, diurnal and seasonal phase variations and phase anomalies correlation

14 p2204 A71-30973

Systematic phase variation in second harmonic of daily variation of cosmic ray intensity in one year, recorded by neutron monitor at Deep River

15 p2441 A71-31410

VLF radio signals phase anomalies due to solar X-ray flares, monitoring by detectors onboard OSO-4 satellite

15 p2369 A71-31434

Amplifier effects on phase distortion of pulse signals passing through power amplifier stages of coherent pulse communication systems

19 p3015 A71-37257

Message distortions analysis in PCM communications systems due to phase fluctuations of synchronization signal

19 p3022 A71-38494

Parabolic reflector aperture antennas with Gaussian distributed random phase deviations, obtaining asymptotic expansion for radiation pattern

19 p3036 A71-38605

Optical phase variations, temperature structure and wind velocity measurements in atmosphere using He-Ne laser beam on 70 m propagation path

22 p3509 A71-41787

Large signal mode tunnel diode amplifier amplitude and phase characteristics by computer study

22 p3521 A71-42262

Quantum phase fluctuations in IR gas lasers, noting nearly Lorentzian power spectrum with bandwidth inversely proportional to output power

23 p3688 A71-44269

Phase discontinuity transmitter-receiver system for VLF/LF time signals

24 p3804 A71-44997

PHASE DIAGRAMS

Nb-Fe-Al and Nb-Co-Al alloys phase equilibrium by X ray and microstructural analyses

01 p0100 A71-10417

Cr-Tb alloys phase transformations and diagrams dependence on temperature and composition, using physicochemical analysis

01 p0100 A71-10418

Ti-Al-V alloy transformations under continuous cooling, using TTT diagram to describe kinetics

01 p0105 A71-11618

In-Bi alloys electrical conductivity measurement for compositions covering characteristic points of phase diagram at temperatures from liquidus line to 850 C

02 p0294 A71-11895

Mo-Ti-Cr system phase equilibria at 1400 C, considering two phase region tie lines direction by metallographic and X ray analyses

02 p0264 A71-12279

Cr-chromium nitride fusion phase diagram analysis, establishing nonvariant eutectic and dissociative transformations

02 p0266 A71-12673

Stainless steel sputter deposits equilibrium phases, determining deposition temperature ranges for austenite and ferrite formation

02 p0267 A71-12884

Nb based refractory metal alloys, discussing phase diagrams and electromagnetic separation method

02 p0270 A71-12934

Zr-Ga phase diagram eutectoid region metallographic analysis, discussing solubility, reactions and compound formation

04 p0614 A71-15779

Ti-Ir alloy equilibrium diagram in entire concentration range, emphasizing phase stabilization at room temperature

04 p0616 A71-15805

Nb-N and Nb-Zr-N alloys phase composition, examining microconstituents at various temperatures after quenching

04 p0616 A71-15905

Powdered W, Mo, Nb and Ta sulfides and compacts thermal vacuum behavior, examining phase compositions and transformations

05 p0769 A71-16861

Alloys constitution research, discussing experimental methods in phase diagram investigations of multicomponent systems

06 p0910 A71-17340

TiNi antiphase boundaries direct observation using transmission electron dark field imaging technique

07 p1131 A71-19431

Computer calculation of phase diagrams from thermochemical data for Cr-Mo and Mg-Cd systems

07 p1054 A71-19519

Phase equilibria of Mo-Nb-Hf alloys using metallographic durometric and X ray tests

07 p1135 A71-19614

X ray Debye chambers and diffractometer cameras for high temperature investigations of metal systems phase equilibrium

07 p1112 A71-19620

Equilibrium diagrams of Re with W, Mo, Co, Ni, discussing high strength system elastic components with torsional support applications

07 p1140 A71-20232

Phase equilibria in Zr-Mo-Re and Zr-W-Re systems, studying isothermal section diagrams via X ray and metallographic techniques

07 p1140 A71-20234

W-Re-Ir ternary system phase diagrams, studying physicochemical properties via X ray and metallographic techniques

07 p1140 A71-20235

Phase equilibria, microstructure and physical properties of high temperature vacuum sintered oxygen deficient zirconia and thoria

08 p1304 A71-20697

InAs-AlAs pseudobinary system solidus boundary determination from pellet phase diagram

08 p1344 A71-21472

Co-Cr-W alloy systems equilibrium and precipitation effects, investigating microstructural properties at elevated temperatures

08 p1314 A71-21569

Ternary systems Hf-W-B, Hf-Re-B and Nb-Re-B isothermal sections phase diagrams at high temperature, using X ray analysis

08 p1317 A71-21858

Ce-CeN system phase diagrams investigated by differential thermal, X ray and metallographic analysis

09 p1481 A71-22186

V-Mn-B, Mo-Mn-B and W-Mn-B systems phase equilibria, describing diagrams isothermal sections at specific temperature

09 p1470 A71-23065

Thermal, microstructural and X ray analyses of Al-Ti alloys phase diagrams, measuring hardness and conductivity

09 p1480 A71-23704

Phase diagram isothermal cross sections of Ti-Zr-Nb alloys for various temperatures and heating periods by X ray and microstructural analysis

09 p1480 A71-23705

Phase diagram of Ti-Ta-Mo alloy system, obtaining solubility and electrical conductivity for various cross sections

09 p1480 A71-23706

Machine tool friction slides dynamics simulation for phase diagrams analysis, using Szoke model

10 p1614 A71-23994

Ni-Cr-Ti-Al-Mo system equilibrium conditions, conducting phase analysis by X ray and optical and electron microscopy

10 p1627 A71-24532

Book on computer calculation of phase diagrams covering quantitative computation of phase equilibrium and lattice stability parameters of refractory metal systems

11 p1777 A71-25197

Monovariant eutectic Co-Cr-C ternary systems, determining pseudobinary and near-pseudobinary phases by differential thermal and microprobe analyses and optical microscopy

11 p1780 A71-26025

Ti-Zr alloy phase diagram from vacuum melting, using high purity wafers and apparatus similar to McQuillan

11 p1780 A71-26028

W-Mo-Ta system alloys investigated along four radial sections from tungsten corner, establishing Ta additions effect on maximal strength

11 p1782 A71-26473

Equilibrium diagrams for Nb-Zr-B alloys, establishing solidus surface, Zr/B isothermal and vertical sections

11 p1782 A71-26474

Mo-Zr-Cr alloy samples cast annealed and quenched at 1500 C, calculating phase equilibrium diagram

12 p1918 A71-27528

Time optimal control system design with lag, determining phase coordinate prediction unit structure

13 p2041 A71-27944

Ti-Co-B and Ti-Re-B systems diagrams of isothermal sections at 800 and 1400 C

13 p2083 A71-28008

Solid state solubility of B in Nb, determining binary Nb-B alloy's phase diagram by microscopic, X ray and thermal analyses

13 p2085 A71-28224

Hf-W-B, Hf-Re-B and Nb-Re-B ternary systems isothermal phase diagrams at high temperature, using X ray analysis

14 p2261 A71-30837

Mo-Ni-C ternary alloy X ray analysis, determining solidus temperature from phase diagrams

15 p2424 A71-31237

Solid helium and molecular/metallic hydrogen thermodynamic properties and phase diagrams as functions of pressures corresponding to Jupiter and Saturn interiors

15 p2511 A71-31338

Microstructure and mechanical properties of Ti-rich alloys of Ti-W system, constructing phase diagram

15 p2425 A71-31402

Magnesium corner of Mg-Li-Sn system phase diagram, detecting two invariant transformations in Mg-rich alloys

15 p2425 A71-31403

Al-Zn-Mg-Li solid solutions isothermal phase diagrams, obtaining Al-rich alloys phase compositions for quenching and aging temperatures

15 p2426 A71-31405

Solidus-liquidus surfaces and isothermal phase diagrams of quaternary system of Cr with Ti, Zr, Nb and Ta, showing Laves phase interactions and continuous solid solutions

15 p2426 A71-31407

Interferometric holograms of vibrating body via numerical analysis of oscillations amplitude and phases

15 p2406 A71-31706

Ti-Mo-C ternary system phase diagram

15 p2430 A71-32146

Ta-V-C ternary system solidus surface and equilibrium diagram determination by metallographic techniques and X ray and thermal analyses

15 p2430 A71-32147

Isothermal sections at 1400 C of systems niobium-titanium-boron and niobium-molybdenum-boron by X ray analysis

15 p2437 A71-32672

Ternary Co-Cr-Al alloy oxidation resistant composition selection, using oxide maps superimposed on phase diagram

16 p2590 A71-32872

Zinc arsenide-zinc telluride ternary system phase diagram investigation by X ray, differential thermal

and microstructural analyses and microhardness measurements

16 p2621 A71-33564

Si-B-C alloy phase diagram near SiC-B cross section, noting B solubility limit, microhardness and electrical resistivity

16 p2592 A71-33565

Phase diagrams of ternary systems Ta-Fe-B and Ta-Ni-B using X ray and metallographic analyses

16 p2592 A71-33575

Bismuthide chemistry research, presenting equilibrium diagrams with all elements

16 p2622 A71-33923

Ternary systems chemical composition of contacting and equilibrium states due to directional flow in multicomponent diffusion layer, noting relationship to phase diagrams

16 p2541 A71-33929

Iron based Cr-Co-Mo alloys equilibrium diagrams and phase transformations at various temperatures, emphasizing intermetallic compounds effects on mechanical properties

17 p2758 A71-35148

Beta Ti-Pu solid solution, constructing diffusion phase diagrams from electron beam microprobe analysis and autoradiography

18 p2935 A71-36174

Ti-W-B, Hf-Ta-B and Ta-W-B alloys isothermal phase diagrams at 1400 C, using X ray analysis and metallographic techniques

19 p3076 A71-37112

Phase diagram of Ti-Cr alloys for temperatures from 800 to 1600 C

19 p3077 A71-37466

Intermediary eutectic delta phase in Ti-Os equilibrium diagram based on microstructural, X ray and differential thermal analyses

19 p3078 A71-37467

Phase equilibria of Al-Mg-Li-Mn system in Al-rich region, noting composition effects on mechanical properties

19 p3078 A71-37470

Vertical phase diagrams of Ti-Al-Zr-Mo-Fe alloy system at varying Fe concentrations, showing structural hardening after quenching

19 p3078 A71-37471

Isothermal phase diagrams and composition effects on plasticity in Mo-Ti-Zr-C system in Al-rich region

19 p3078 A71-37472

Concentration effects of Nb and Ta on strengthening in tetrahedral section of W-Mo-Nb-Ta system at temperatures from 20 to 1100 C

19 p3078 A71-37473

Zirconium oxide-lanthanum oxide systems near melting point, plotting solidification and phase diagrams

20 p3254 A71-39962

German monograph on thermal equation of state for nitrogen vapor-liquid phase equilibrium covering vapor pressure and density, phase diagrams, critical temperature, etc

22 p3574 A71-41716

Solid helium and molecular metallic hydrogen thermodynamic properties and phase diagrams as functions of pressures corresponding to Jupiter and Saturn interiors

22 p3606 A71-42613

Co-Mn binary alloy phase diagram redetermination, noting sigma phase formation after heavy deformation

23 p3689 A71-42933

Stepping electromotor in self commutation mode with local feedback, examining dynamics with phase plane method

23 p3655 A71-43293

Equilibrium phase relations in lunar rocks and synthesized analogs, determining liquidus and solidus temperatures

23 p3742 A71-43640

Nd-Bi phase diagrams from thermal differential, metallographic and X ray analyses, discussing carrier concentration and mobilities, Hall coefficients, conductivity and thermal emf

23 p3692 A71-44022

Copper-indium-tellurides homogeneity region components solubility in different cross sections of concentration triangle at room temperature

23 p3717 A71-44023

W and Mo thin films phase diagrams, determining surface energies and heats for transformations

24 p3860 A71-44718

InTc thin films with 60-75 percent Te content, investigating phase composition and physical properties

24 p3862 A71-45250

TiTe thin films phase composition and structural properties as functions of component contents, deposition conditions and annealing parameters, using X ray diffractometer and IR microscope

24 p3862 A71-45252

PHASE ERROR

Long period variable stars cumulative error increase for larger period variability

01 p0150 A71-10059

Shaped dual reflector system phase errors due to feedhorn or subreflector axial displacement, examining effects on gain and secondary radiation pattern

02 p0222 A71-12796

CW sounding for HF adaptive control for data transmission with ionospheric phase error

04 p0552 A71-15145

Absolute value type early-late gate bit synchronizer steady state phase noise performance evaluation by Fokker-Planck method

05 p0730 A71-19060

System phase errors subtraction in interferometry, using modified laser unequal path interferometer and technique eliminating data reduction problem

07 p1107 A71-19210

Aperture antennas gain loss due to aperture phase errors

07 p1075 A71-19268

Microwave dual mode reciprocal ferrite phasers, deriving insertion phase variations as function of ambient temperature and high average power heating

08 p1262 A71-20760

Eigenfunction expansions of reduced nonGaussian phase error transition probability density function for first order tracking loop, analyzing spectral properties of Fokker-Planck equation

08 p1324 A71-21341

Hybrid phase locked loop for deriving phase error estimate from carrier and information components, discussing system parameters optimization for performance

08 p1270 A71-21353

Parabolic radio telescope phase errors for field distribution, compensating for mirror system mass deformations

08 p1266 A71-21468

High Q factor rotor systems applications in dielectrics electromagnetic viscosity measurement and radio transmitters with low oscillation phase drift

09 p1492 A71-22363

Aperture zoning methods for reducing phase errors on radiation patterns of equidistant dimensional arrays with traveling wave slotted waveguide elements

11 p1738 A71-26346

Slip vs static error offset for first and passive second order phase locked loop as function of signal to noise ratio via computer simulation

12 p1892 A71-27073

Phase and amplitude error detection in photomasks for semiconductor integrated circuits with spatial frequency coherent optical filtering

20 p3246 A71-39449

Phase aberrations in Bragg imaging for sound components projecting out of plane normal to light beam

22 p3540 A71-41778

PHASE FADING

U FADING

PHASE LOCK DEMODULATORS

Tan-lock type compared to other phase demodulators in communication signal processing system, describing basic loop configuration

03 p0377 A71-13242

Threshold carrier to noise ratio for phase lock demodulators, using computerized prediction model

10 p1574 A71-23764

Tracking loops coherent reference signal with data aided demodulator, using power in modulation and carrier

12 p1879 A71-27071

Probability density function of optimum phase locked loop synchronizer of sinusoidal signal with white Gaussian noise in partially coherent receiver

20 p3195 A71-38858

Closed phase lock loop FM demodulator design, determining resonant frequency parameters, attenuation factor and low pass filter elements

23 p3650 A71-43094

PHASE LOCKED SYSTEMS

Oscillator frequency synchronization by injection locking, considering nonlinear oscillation model

02 p0230 A71-11818

Digital communication hybrid phase locked loop nonlinear feedback system with modulation and carrier components enhancing phase estimation

03 p0391 A71-14312

Phase locked AFC theory, analyzing equation by bifurcation methods

05 p0731 A71-16984

Synchronous digital communication system with each station clock rate established by phase locked oscillator input average, calculating two-station network dynamic stability

05 p0729 A71-17051

Phase-coherent communication systems with phase locked loops for data detector synchronization, calculating noisy timing effects on detection efficiency

05 p0724 A71-17059

Sampled phase lock loop filter for tracking short pulses, deriving frequency stability criterion and margin

05 p0725 A71-17080

Pulsed phase locked automatic phase control system linear model, discussing optimal white noise filtration with integrating filter

06 p0867 A71-17377

Phase locked automatic direction finder /ADF/ flight test results, indicating signal to noise threshold reduction by coherent detection

07 p1057 A71-18815
Phase locked avalanche transit time oscillators FM noise spectra

07 p1074 A71-19124
Injection phase locked oscillator as input microwave limiting amplifier for noise measuring microwave discriminator

07 p1074 A71-19126
Frequency modulation technique based on injection phase locking theory applied to microwave oscillator Q measurement

07 p1074 A71-19127
Pulsed phase detectors for phase comparisons of pulse sequences having arbitrary frequency ratios, designing circuit to prevent false locking in AFC systems

07 p1061 A71-19509
Fokker-Planck boundary value solutions to transient phase error response of nonlinear phase locked tracking systems

07 p1082 A71-20428
IMPATT and Gunn microwave oscillators injection phase locking, discussing stationary state synchronization theory and phase vs frequency deviation measurements

08 p1263 A71-20990
Eigenfunction expansions of reduced nonGaussian phase error transition probability density function for first order tracking loop, analyzing spectral properties of Fokker-Planck equation

08 p1324 A71-21341
Sequence solution to multidimensional time varying Fokker-Planck equation for phase locked nonlinear systems

08 p1324 A71-21342
First order digital phase locked loops analysis for single channel command system, using random walk techniques

08 p1270 A71-21351
Satellite carrier tracking and phase lock carrier loops, evaluating lock and reacquisition performance loss by linear model and Monte Carlo digital simulation

08 p1270 A71-21352
Hybrid phase locked loop for deriving phase error estimate from carrier and information components, discussing system parameters optimization for performance

08 p1270 A71-21353
Phase locked loop as versatile building block for integrated circuit design, discussing basic principles and applications in analog and digital signal processing

09 p1415 A71-22354
CW X band frequency-locked Gunn oscillators as frequency demodulator with millivolt range detection sensitivity

09 p1421 A71-23720
Frequency counted measurements and phase locking to noisy oscillators, showing counted frequency method sample variance slow convergence to actual variance

10 p1574 A71-23763
IMPATT diode oscillators noise and injection phase locking, discussing theoretical refinements of original simple model by Read

10 p1584 A71-24818
Communication satellite ground station radio receiver and transmitter systems including parametric amplifier and phase lock demodulators applications

10 p1590 A71-25102
Threshold-extension phase-lock demodulator design for optimizing satellite communication ground station systems, using FM carriers

10 p1580 A71-25106
Nonlinear photoelectric electron emission due to picosecond mode locked laser pulse irradiation

11 p1776 A71-26426
Slip vs static error offset for first and passive second order phase locked loop as function of signal to noise ratio via computer simulation

12 p1892 A71-27073
Time optimal phase locked AFC system synthesis based on Pontryagin maximum principle, comparing computerized and experimental transient response

12 p1882 A71-27514
Phase locked loop model configuration derivation to yield same locking signatures as driven oscillators with FM feedback

13 p2037 A71-28605
Nd-YAG laser operation with simultaneous intracavity frequency doubling and mode locking, observing mode-locked pulse lengthening and circulating power decrease

13 p2081 A71-29335
Simultaneous mode locking and pulse coupling of carbon dioxide laser achieved by single internal GaAs element, discussing possible application to pulse code modulation

13 p2081 A71-29341
Transmitter clock phase lock loop for PCM-TDMA satellite communication system, applying to control system design having time lag

Locking in time of phase locked loop with sawtooth comparator for synchronizing two oscillators

14 p2210 A71-29808
Microwave oscillators Rieke diagram semiautomatic plotting by injection phase locking, using network analyzer for impedance measurement

14 p2211 A71-29823
Gated phase locked loop system characteristics based on sampled data model, comparing with continuous loop operation

14 p2214 A71-30795
Sampled data delay-lock loop for tracking biphasic modulated pulsed-envelope RF signal arrival time

14 p2197 A71-30796
Lock-lock loop technique with pulsed oscillator for feedback frequency demodulation and tracking filter operation

14 p2220 A71-30920
Phase locked AFC system, calculating phase detector response effects on dynamic properties

15 p2370 A71-31592
Millimeter wave klystron single-loop phase locking using final 4th-harmonic mixer in reference chain for submillimeter laser frequency measurement

16 p2589 A71-34126
Controllable phase locked frequency splitting in two-frequency lasers by anisotropic or nonreciprocal resonator elements

17 p2751 A71-34380
Digital phase locked loop for FM signals demodulation, considering system nonlinear difference equation

17 p2704 A71-35084
Time ordering operators applications to nonlinear unsteady systems, covering stochastic differential equations solution and phase locked loop phase error probability density calculation

18 p2940 A71-36222
Phase locked AFC theory, analyzing equation by bifurcation methods

18 p2896 A71-36784
Phase locked loop oscillator applications in communication and instrumentation, discussing tracking receivers, FM and FSK detection, laser modes, pulse width modulation, etc

18 p2884 A71-36997
Phase locked loop models with off-tuned binary PSK interfering signal and angle modulated signal and noise at input, noting performance degradation

19 p3020 A71-38429
Hybrid microelectronics IC S band double conversion phase locked receiver, discussing fabrication, process requirements and component selection criteria

19 p3035 A71-38538
Transient performance of phase locked loop on-board tumbling satellite, noting relation to time, SNR and fade modulation

20 p3196 A71-38871
Millimeter wave klystrons phase locking to HCN far IR laser line via harmonic mixing in Si and metal-oxide-metal Josephson point contacts

22 p3555 A71-41599
Mode locked Nd-glass laser transient effects, examining pulse width limitations by side band generation

22 p3556 A71-41801
Mode locked transversely excited atmospheric carbon dioxide laser with Ge ultrasonic diffraction cell active loss modulator generating 10.6 micron wavelength pulses

22 p3557 A71-42132
IR ring laser rotation sensor, describing design principles for alignment and eliminating locking phenomenon

22 p3557 A71-42153
Estimation-correlation principle application to harmonic signal receiver with unknown carrier frequency, using searching phase locked AFC circuit as estimation unit

22 p3512 A71-42313
Combined injection locking with indirect synchronization for FM signals in noisy environment with allowance for bias oscillator LF time constant effect

22 p3514 A71-42393
Gas ring laser lock-in-zone, showing dependence on resonator mirror curvature radius and mode competition between oppositely directed waves

23 p3683 A71-43393
CW dye laser mode locking with lithium niobate phase modulator, observing 500 psec pulse generation

23 p3687 A71-44134
Joint phase locked and delay tracking system dynamics for pseudorandom radio signal detection

23 p3646 A71-44267
Transverse mode locking by cylindrically symmetric laser, noting time varying spot size with spacing frequency

23 p3688 A71-44295

PHASE MODULATION

NT PHASE SHIFT KEYING

Constant bandwidth FM subcarrier oscillators signal preemphasis for FM and PM transmitters

01 p0033 A71-10897

Single sideband phase modulation compared with conventional PM or FM effect on spectrum conservation

01 p0037 A71-11164
Spacecraft signal amplitude and phase modulation and fault diagnosis by VLF analysis

02 p0218 A71-12447
Carbon dioxide laser stable mode locking with resonated internal electro-optic phase modulator driven at frequencies near axial mode interval

03 p0434 A71-13481
Second order moment at output of inertially nonlinear two terminal pair network during amplitude and phase modulation

04 p0550 A71-14620
Phase modulation drift of radio emission from pulsar MP 0031-07

05 p0801 A71-15927
Transistorized transmitters constant phase low distortion AM system based on Chireix method, generating AM from two push-pull phase modulated signals

05 p0720 A71-16392
Sequence spectrum of phase modulated discrete signal for frequency division multiplex filters

07 p1064 A71-20264
Suppressed RF carrier tracking for two channel interplex phase modulated telemetry

07 p1066 A71-20427
Computation of IF filter characteristics effect on angle modulation distortion

07 p1082 A71-20429
N-channel PSK/PM digital telemetry system modulation scheme for space exploration

08 p1254 A71-21315
Optimal phase regulated AFC system for FM signal filtration in presence of internal noise

09 p1404 A71-22155
Phase velocity modulated backward wave antenna with slow wave structure, consisting of dipoles spaced along antenna length

09 p1415 A71-22295
Combination frequency spectra asymmetry in bounded plasma column resulting from HF AM and PM wave interactions

10 p1651 A71-24637
Measuring technique for short term laser beam propagation direction fluctuations, discussing atmospheric turbulence effect on initial modulation phase distribution

11 p1774 A71-26047
Time variation in phase transitions at output of arbitrary band limiting channel in differential phase modulation system, using calculation method

11 p1733 A71-26340
SHF lithium tantalum oxide optical modulator for optical detector evaluation, discussing bandwidth and phase modulation characteristics

12 p1903 A71-26790
Digital data recording system based on multiple beam interference pattern photography, using optical phase modulation

12 p1905 A71-26807
Phase modulation application to interferometers for submillimeter waves exceeding 10 microns

12 p1905 A71-26817
Optimal continuous recording of amplitude-phase distributions on spatial carrier frequency for light wave modulation and optical antenna simulation

12 p1878 A71-26841
Gain and noise characteristics of reactive phase/amplitude modulation ferrite amplifier as function of pumping power and resonator coupling

12 p1886 A71-26845
Phase controlled linear FM pulse generation by digital square wave carrier phase modulation, using parabolic function generator

12 p1879 A71-26995
Carrier suppression in angle modulated transponding telemetry by first order stationary stochastic processes

12 p1880 A71-27074
Mathematical model for harmonic emission spectrum in FM and PM communication transmitters modulated by random signal

13 p2032 A71-28875
Phase modulation theory for two-beam far IR Michelson interferometers, discussing application to Fourier transform spectrometry

14 p2238 A71-29741
Phase modulation in far IR interferometers applied to Fourier spectrometry and metrology, obtaining modulus, phase, absorption and refraction spectra

14 p2238 A71-29742
Phase modulation in far IR interferometers applied to laser refraction measurements in solids and organic liquids

14 p2238 A71-29743
Sampled data delay-lock loop for tracking biphasic modulated pulsed-envelope RF signal arrival time

14 p2197 A71-30796
Parametric amplification of two laser waves with amplitude and phase modulation under exponential

signal growth applied to Raman scattering in picosecond pulse field

15 p2418 A71-31188

Mode locking with internal phase modulation observed in He-Se ion laser emitting on many transitions in visible region

15 p2419 A71-31750

Error probability and reception stability in synchronous detection of phase manipulated signals with additive Gaussian noise at multiplied carrier frequency

16 p2542 A71-33498

Nonlinear gain and AM/PM conversion in FDMA communication through satellite repeater, using traveling wave tubes plus postzonal filter

17 p2703 A71-35082

Optimum and suboptimum decision rules for two-channel deep space telemetry system with modulation consisting of PM with two orthogonal phase functions

17 p2704 A71-35088

FM-PM conversion by frequency locking of free running Gunn oscillator

17 p2717 A71-35339

Quadruphase modem development in time division multiple access system

18 p2880 A71-36546

Relaxation processes in Michelson interferometer as integral part of carbon dioxide laser cavity in phase Q switching regime

19 p3071 A71-37389

Combined AM/PM digital data transmission, using error rate and communication efficiency in bits per cycle of bandwidth vs average SNR as performance criteria

21 p3349 A71-41197

Pulsars properties, examining pulse profile and duration, subpulse phase modulation and polarization

22 p3598 A71-41918

Invariant detection law for signals with singular phase difference modulation, considering application to-signal fading

22 p3510 A71-42256

Second order moment at output of inertialess nonlinear two terminal pair network during amplitude and phase modulation

22 p3510 A71-42260

Pulse shape of mode locked frequency doubled Nd-YAG laser, using single crystal for second harmonic generation and phase modulation

22 p3558 A71-42348

Binary coding and phase displacement modulation of digital data in radio transmission

22 p3514 A71-42471

Signal AM-PM conversion by locking oscillator with single external injection

22 p3523 A71-42480

Elastic surface waves bi-phase modulated encoding and decoding at 10 Mbit/sec using Y-cut quartz

23 p3645 A71-43436

Holographic method for investigating piston type oscillations with phase modulated reference light beam

24 p3829 A71-45270

PHASE RULE

Gamma phase composition estimation in Ni base superalloys by phase rule principles and analytic geometry

13 p2089 A71-29407

PHASE SHIFT

Oxygen diffusion coefficient during metal Ti/ oxidation in unsteady high temperature region, allowing for interfacial phase boundary shift

01 p0101 A71-10673

Variational bounds on phase shifts for electromagnetic wave scattering by dielectric obstacles in waveguides

01 p0056 A71-11199

Strain data retrieval from moire or photoelastic patterns by numerical technique based on light intensity distribution phase angle

02 p0225 A71-11703

Phase meter channels correlation effect on mean phase difference measurements accuracy in heterodyne oscillators

02 p0212 A71-11837

Signal sources output impedance matching effect on phase difference measurement accuracy

02 p0212 A71-11842

Cepheid radius-temperature variation functions phase shift

02 p0308 A71-12101

Internal friction measurement under hydrostatic pressure, describing apparatus to determine phase angle between stress and strain

02 p0255 A71-12132

Optimum frequency channels and delay estimates in very long baseline interferometry with large bandwidth for fringe and phase measurements

02 p0216 A71-12329

Phase and amplitude fluctuations in oscillator circuits, determining power spectrum, disturbing voltage and current sources and step and impulse functions

03 p0383 A71-13168

Long baseline radio interferometry, discussing phase difference measurement principles in terms of signal characteristics and wave forms, astronomy and geodesy applications

03 p0484 A71-13244

Mode locked pulsed lasers statistical amplitude and phase variations effects on time dependent output intensity and nonlinear optical processes efficiency

03 p0437 A71-13881

Small phase differences amplification in holographic interferometry, using nonlinear development of recordings

03 p0429 A71-14182

He-Ne laser self-locked or mode-locked with Ne absorption cell, investigating phase relationships between modes

03 p0440 A71-14183

Photometric observations of lunar surface regions, noting color variations with phase change

05 p0809 A71-16461

Transionospheric ranging error correction by second difference of phase shift method

06 p0867 A71-17714

Phase shift measurement by digital encoding via time interval, angle of rotation and voltage conversions

06 p0876 A71-18076

Finite amplitude helical instability effect on microwave beam phase propagated through plasma column

07 p1166 A71-18888

Second difference of phase shift method for measuring ionospheric electron density

07 p1096 A71-19013

Second order phase path differences for Faraday rotation and dispersive Doppler shift in transionospheric propagation

07 p1097 A71-19027

Pulkovo radio telescope reflector adjustment by phase comparator, using centimeter wave transmitting-receiving antenna for sun, moon and Venus observations

07 p1083 A71-19344

Optical phase variations on short line of sight path through turbulent atmosphere

07 p1159 A71-19512

Bandlimiting effects on PCM/split phase signal detection

07 p1066 A71-20431

Fluidic Helmholtz resonator for FM signal analysis, showing instantaneous phase difference between input and output pressures

07 p1026 A71-20568

Short-slot waveguide latching ferrite switch structure, operation principle, phase constants calculation and isolation characteristics

08 p1262 A71-20756

Phase quantization theoretical derivation, applying mathematical technique used in signal processing nonlinear problems

08 p1291 A71-21403

Phase quantization in holograms, presenting experimental verification of Goodman and Silvestri theory

08 p1291 A71-21404

Gravitational field effect on phase difference of moving waves and polarization in rotating ring laser

09 p1462 A71-22398

Bounded electromagnetic wave propagation in randomly inhomogeneous medium, calculating correlation in amplitude and phase fluctuations

09 p1407 A71-23109

Line-of-sight radio signal transmission, investigating sea surface reflections effects on phase of arrival and coherence

09 p1409 A71-23502

Signal mean and noise variance as direct functions of phase angle between signal component passed by bandpass limiter and coherent reference

10 p1582 A71-23765

Phase lag in periodic Coriolis star nystagmus between Coriolis input and corresponding ocular component in cats

10 p1559 A71-23923

Phase and frequency instabilities in electromagnetic wave propagation - NATO/AGARD Conference, Ankara, Turkey, October 1967

10 p1576 A71-24185

Time variation in phase transitions at output of arbitrary band limiting channel in differential phase modulation system, using calculation method

11 p1733 A71-26340

Positron-hydrogen scattering below positronium pickup threshold by Hylleraas bound technique, discussing phase shifts and linear parameters

11 p1803 A71-26372

Line formation effective pressure from Venus atmosphere spectra, discussing phase angle variations

11 p1835 A71-26457

Parabolic approximation of total Mars brightness phase dependence observations, using statistical analysis

12 p1955 A71-26596

Two beam interferometry, measuring phase shift and dispersion at slit by channeled spectra

12 p1904 A71-26797

Quasi-stationary three dimensional array excitation by large phase shift calculated for circular conducting elements

12 p1885 A71-26840

Atom rigid rotor problem, applying generalized phase shift rotational excitation treatment in lowest approximation

12 p1932 A71-26949

Nonlinear elastic shells free vibrations, obtaining phase trajectories with finite bending within Hooke's law

12 p1975 A71-27106

Radiation intensity spatial dependence on laser polarization, giving three dimensional model for wave function phase calculation

13 p2077 A71-28046

Lower ionosphere magnetic fields generated by three dimensional Alfvén waves, examining amplitude and phase spatial distribution and frequency dependence

13 p2059 A71-28254

Strip array excitation by field with large phase shift per period, deriving approximate solution from averaged boundary conditions

13 p2029 A71-28361

Electromagnetic field amplitude and phase scattering diagrams analysis for shape information capacity

13 p2029 A71-28369

Inhomogeneous atmosphere transmission functions, noting Lindholm line shift in O absorption spectra effects

13 p2063 A71-29019

Transverse spatial diffusion of phase-dispersed pulses, showing effects on dechirped pulse duration, output beam cross section and two-photon fluorescence display

13 p2081 A71-29332

Monograph on oscillographic high accuracy technique for phase angle measurement covering applications for harmonic generator phase control

14 p2243 A71-30237

Microwave oscillations small phase difference variation measurement, using polarization effects

14 p2196 A71-30636

X band focused beam interferometer for plasma phase shift measurement independent of propagation path attenuation over 30 dB dynamic range

14 p2214 A71-30804

Radio frequency measurements below 30 GHz, considering power, impedance, phase shift, voltage and current data

14 p2205 A71-30981

Acoustic wave after passage through turbulent wake, measuring phase fluctuations

15 p2387 A71-31169

Lateral shearing interferometry sensitivity improvement by amplifying phase difference with nonlinear holograms

15 p2403 A71-31260

EEG phase relations measurement technique, using small digital computer for frequency components separation and EEG activity phases comparison between electrodes

15 p2363 A71-31959

Russell law validity of planet brightness dependence on phase integral, discussing backscattering surface and thick atmospheres effects

15 p2491 A71-32425

Rayleigh scattering planetary atmosphere radiative transfer equation, calculating phase curves for flux and polarization

15 p2498 A71-32778

Phase object visualization by Hilbert transformation, noting image properties evolution as function of various experimental parameters

18 p2947 A71-36043

Adhesively bonded structures inspection by laser holography, producing diffraction pattern recording of amplitude and phase shift

18 p2925 A71-37057

Large amplitude monochromatic electron cyclotron wave broadening in plasma, producing shifted phases in finite frequency range

19 p3114 A71-37855

Harmonically modulated reflected light signals phase shift and demodulation, assuming single scattering

19 p3018 A71-37975

Short path VLF phase and amplitude measurements during stratospheric warming in February 1969, discussing D region electron density changes

19 p3018 A71-38040

Atomic hydrogen maser wall shift elimination by operating at temperature to obtain zero average phase shift per atomic collision

21 p3391 A71-40201

Self induced transparency in ruby attenuator, detailing phase relaxation effects at various temperatures

21 p3427 A71-40546

Oxygen diffusion coefficient during metal/titanium/oxidation in unsteady high temperature region, allowing for interfacial phase boundary shift

21 p3401 A71-41054

Nonlinear hologram application to interferometry, discussing phase difference amplification

22 p3539 A71-41744

Phase distribution randomization in switched antenna array, noting radiation pattern sidelobe compensation application

22 p3522 A71-42312

Dynamic frequency and phase response of digital communications system of synchronized oscillators from time-incremental computer simulation

22 p3523 A71-42376

Human eye-tracking phase lags representation by time delays depending on target motion class

22 p3490 A71-42451

Sporadic E layer thickness measurement by Phase Ionosonde, measuring phase advance on F region echoes

23 p3666 A71-42975

Low frequency phase method application to fast electron processes and characteristic relaxation times in quick response Ge and Si junction diodes

23 p3650 A71-43307

Traveling wave laser emission phase and amplitude fluctuations and spectral line width determination from single-mode distributed parameter model

23 p3685 A71-43563

Q band relative phase measurement using single sideband suppressed carrier ferrite modulator in serrodyne phase bridge

24 p3803 A71-44649

Rotationally inelastic molecular collisions in atom rigid rotor scattering, considering infinite order approximation of generalized phase shift treatment

24 p3850 A71-44921

PHASE SHIFT CIRCUITS

NT CIRCULATORS [PHASE SHIFT CIRCUITS]

Microelectronic remanent type /latching/ circulating, switching and phase-shifting microwave devices design and performance

02 p0228 A71-11654

Phased array radar systems accuracy increase, using ferrite core magnetic flux feedback for phase shifter control

02 p0215 A71-12174

Phased arrays sidelobe reduction by digital phase shifters, considering scan angle and phase quantization step size

06 p0875 A71-17711

Optimal nonreciprocal waveguide phase shifters using ferrites with rectangular hysteresis loop, considering electromagnetic wave propagation

07 p1079 A71-20074

Microwave dual mode reciprocal ferrite phase shifters, deriving insertion phase variations as function of ambient temperature and high average power heating

08 p1262 A71-20760

Dual mode latching reciprocal ferrite microwave phase shifter, discussing operation principles, design and performance

08 p1262 A71-20764

Ferrite microstrip microwave phase shifters with transverse and longitudinal magnetization, calculating diamagnetic and permeability tensor effects

08 p1263 A71-20768

Polarizing phase shifter for quasi-optical transmission lines, describing varistor network operation

08 p1264 A71-21068

Analog information systems frequency modulators, describing network design consisting of phase shifting RC network, amplifier and inertialess resistor

09 p1415 A71-22296

Linear frequency beam scanning array antenna excited by individual phase shifter, studying rectangular waveguide in magnetic field plane

11 p1741 A71-26552

Cylindrical waveguide with three differential phase shift sections, deriving microwave output magnitude and polarization for comparison with ferrite experiment

13 p2037 A71-28604

Microstrip p-i-n diode controlled L band digital phase shifter for aircraft-satellite communication

14 p2217 A71-31055

Computer aided design of P-I-N diodes equipped S band phase shifter for phased array antennas, discussing optimization problems

15 p2375 A71-31414

Ninety degree phase shifter and frequency multiplier for square waves

15 p2376 A71-32025

High power microwave phase shifter, using beryllium oxide filler ceramic dielectrics to obtain thermal coupling between ferrite element and waveguide wall

17 p2713 A71-34396

Continuously variable microwave stripline phase shifter with linear shift vs frequency by dielectric constant variation

18 p2889 A71-36272

Computerized optimal design of L band phase shift networks for broadband performance

21 p3361 A71-40816

Ferrite and dielectric element waveguide phase shifters with rectangular hysteresis loop, deriving differential phase and attenuation constants for wave propagation

22 p3512 A71-42308

Frequency conversion /division, multiplication and shifting/ application to multistable phase-frequency elements design

22 p3524 A71-42573

German monograph on analysis and design of digital microwave phase shifters for phase controlled antennas covering admittance loaded lines, transmission and reflection behavior

23 p3649 A71-42999

PHASE SHIFT KEYING

Differential PSK signal detection, using decoding circuit with uncontrolled oscillator

01 p0031 A71-10822

Invariant detection law for signals with single phase differential keying, considering application to signal fading

04 p0550 A71-14616

Adaptive/self synchronizing PSK receivers with common power and bandwidth, discussing analytical and numerical investigations of performance characteristics

05 p0723 A71-17054

PSK pseudonoise/spread spectrum communication systems with SNR reduction, examining phase nonlinearities effect

05 p0725 A71-17074

Squaring loops for establishing coherent carrier reference for bi-phase PSK modulation, deriving optimal presquaring filter

05 p0730 A71-17075

Navigation and communication experiment at L band on board S.S. Manhattan using ATS-5 satellite with biphasic PSK modulation of three tones for ranging

07 p1057 A71-18816

N-channel PSK/PM digital telemetry system modulation scheme for space exploration

08 p1254 A71-21315

Wideband subcarrier frequencies demodulation technique for uncoded or coded PSK telemetry over large input SNR range for deep space interplanetary communication

08 p1254 A71-21316

Binary pseudorandom codes sequences correlation properties in PSK telemetry

09 p1404 A71-22154

Synthesizing antenna arrays perpendicular to conducting screen by PSK signal theory, discussing optimal binary phasing and radiation patterns numerical data

14 p2211 A71-30104

Nonlinear filtering synthesis of optimal receiver for pseudorandom phase shift keyed signal with arbitrary modulation angle and white noise background

14 p2195 A71-30107

PSK modem for multiple access communication system with time distribution, discussing performance tests on INTEL SAT 3

17 p2700 A71-34688

Bandlimiting effects on coherent detection of PSK, ASK and FSK signals in presence of white Gaussian noise, using SNR as performance criterion

17 p2704 A71-35085

FDMA single channel per carrier satellite communication system voice processing and modulation techniques, discussing analog frequency modulation and phase shift keying

17 p2704 A71-35086

PSK signals time division multiplexing and frequency multiplexed subcarrier systems equivalence and efficiency for digital communications

17 p2706 A71-35107

Multichannel PCM/PSK/PM interplex telemetry system for reducing cross modulation loss and excess carrier reference power

17 p2706 A71-35108

Computer simulation of error probability performances of binary coherent PSK system under thermal noise and intersymbol and interchannel radio interferences effects

17 p2707 A71-35476

Binary differentially coherent PSK modulated PCM radio link performance under noise and intersymbol and interchannel interferences effects, deriving error probability

17 p2707 A71-35477

Binary and quaternary PSK systems performance with intersymbol, interchannel and cochannel interferences and fading

17 p2707 A71-35478

High speed BPSK communication components and system aspects with V band propagating medium, considering carrier modulation and transmitted digital data reception with minimum errors

17 p2709 A71-35759

PSK modem for PCM-TDMA system, discussing performance tests on INTEL SAT 3

18 p2880 A71-36551

Short wave radio signal analyzer for joint distribution of phase and amplitude probabilities and PSK communications noise stability in ionosphere

19 p3028 A71-37784

PHASE TRANSFORMATIONS

Phase locked loop models with off-tuned binary PSK interfering signal and angle modulated signal and noise at input, noting performance degradation

19 p3020 A71-38429

Bandpass filter harmonic signal phase shift distortion effect on transient response in PSK of multichannel transmission

23 p3644 A71-43286

Multiple mismatch reflection and mode conversion echo effect on error rate in guided millimeter wave phase shift keying systems

24 p3804 A71-44989

PHASE SWITCHING INTERFEROMETERS

Laser radial-shear common path interferometer for lens testing

02 p0250 A71-12144

Broadband phase switch designs for high sensitivity RF and microwave interferometry at low signal power levels

12 p1889 A71-27698

PHASE TRANSFORMATIONS

NT ARC MELTING

NT BOILING

NT EVAPORATION

NT FILM BOILING

NT FLASHING [VAPORIZING]

NT FREEZING

NT FUSION [MELTING]

NT LEIDENFROST PHENOMENON

NT LIQUEFACTION

NT MELTING

NT NUCLEATE BOILING

NT PROPELLANT EVAPORATION

NT SUBLIMATION

NT TRANSPIRATION

NT VACUUM MELTING

NT VAPORIZING

NT VIBRATIONAL FREEZING

Cr-Tb alloys phase transformations and diagrams dependence on temperature and composition, using physicochemical analysis

01 p0100 A71-10418

Perovskite crystals phase transition with unit cells atom displacement, considering permittivity anomalies, structure and free energy expansion coefficients

01 p0138 A71-10430

Periodically modulated phase structure transformations in decomposition of Cu-Ti and Cu-Ti-Al alloys during aging at different temperatures

01 p0101 A71-10670

Decomposition structure of supersaturated solid solution in Co-Nb alloy, showing beta phase transformation inhibition

01 p0101 A71-10671

Plastic deformation and phase transformation in textured austenitic stainless steel, considering stacking fault energy contribution

01 p0101 A71-10737

Acoustic attenuation in condensing vapor, using continuumlike formulation allowing for phase exchange process

01 p0182 A71-11470

Ti-Al-V alloy transformations under continuous cooling, using TTT diagram to describe kinetics

01 p0105 A71-11618

Time, temperature and transformation curves for Ti alloy by dilatometry, hardness measurements, X rays and micrography, discussing martensite and beta-alpha transformations

01 p0105 A71-11620

A-B-A block copolymers statistical thermodynamics, describing postulated microstructure theoretical model for phase transition prediction

02 p0273 A71-12450

Alpha and beta Ti alloys metastable phases decomposition behavior, using electrical resistance measurements and X ray analysis

02 p0266 A71-12651

Titanium dichromide phase modifications under hardening at various temperatures, using thermal and X ray analysis

02 p0266 A71-12674

Fermion system phase transition model thermodynamic behavior near critical point region for various interactions

03 p0456 A71-13350

Variational methods applied to shells transition into plastic state during cylindrical bending, giving critical load formulas

03 p0509 A71-13873

Cu and Al bronze civil transformation kinetics, using electron photoemission microscopy

03 p0444 A71-14337

Transient heat transfer in fins undergoing phase transformation, obtaining approximate solution to temperature distribution and interface motion by perturbation technique

04 p0678 A71-15457

Heat transfer through phase change in metallic heat carrier exposed to strong centrifugation encountered in turbine blades

04 p0639 A71-15462

Spontaneous polarization measurement of ferroelectric Rochelle salt near Curie point, using nuclear magnetic resonance for phase transitions

04 p0637 A71-15548

Near equiatomic Ta-Ru alloys phase transformations by resistance and susceptibility changes and X ray powder patterns of cooled structure

04 p0614 A71-15777

Low carbon Mn-Mo-Ni steel dilatometric measurements with RPI Gleeble machine, examining bainitic transformation

04 p0617 A71-15913

Potentiokinetic study of anodic polarization in maraging Fe alloys, considering relationship to structural transformations during tempering

05 p0765 A71-16200

Reflection point slide velocity of traveling F region ionospheric disturbance by receivers amplitude focusing and echo phase path changes

05 p0741 A71-16440

Nozzle throat conditions at sound velocity discontinuity due to transition from one to two condensed phases during expansion

05 p0735 A71-16576

Ti alloys beta phase solid solution decomposition during cooling and plastic deformation at low temperatures

05 p0767 A71-16770

Austenite-martensite transformation effects on Fe-Ni-Co alloys low temperature thermal conductivity

05 p0768 A71-16771

Phase transitions effect on cloud turbulence behavior from relaxation time, energy and temperature dissipation and supersaturation spectral density

07 p1150 A71-18799

Gas-particle mixtures weak disturbances, applying linearized hydromechanic and phase transformation kinetic equations

07 p1088 A71-19191

High carbon Cr and Mn steels martensitic transformation points, ascertaining short range order occurrence by electron microscopic study

07 p1130 A71-19278

Stability of slowly rotating stars with phase transition in center, determining critical density jump for stability loss

07 p1193 A71-19296

Ordered phases precipitation in ternary and quaternary ferritic alloys, investigating morphology, structure, distribution, coarsening kinetics and mechanical properties

07 p1133 A71-19443

Ni base superalloys mechanical properties relationship to microstructure, considering precipitate dispersion and phase state effects on flow stress and creep strength

07 p1133 A71-19445

Ni base superalloys fatigue behavior, emphasizing role of ordered gamma prime precipitate in two phase materials

07 p1133 A71-19447

Soviet papers on phase transformations covering Mo-Nb-Hf, Nb-Al, Fe-Cr-Zr systems, rhenium steels, Bi-Sn alloys, etc

07 p1135 A71-19612

Cerium effect on phase composition and mechanical properties of Nb-Al alloys, plotting isothermal cross sections

07 p1135 A71-19615

Spinodal decay of supersaturated solid solutions with nonenergetic phase nucleus formation

07 p1135 A71-19616

Phase transformations during tempering of rhenium steels using X ray, dilatometric and conductivity measurements

07 p1135 A71-19617

Phase change solidification phenomena in n-hexadecane for spacecraft thermal control systems, considering two or three dimensional models

07 p1223 A71-19876

Rayleigh and phase change instability for olivine-spinel mantle convection

07 p1105 A71-20450

Fe-S condensates structure and phase transformations during heating, noting importance for antifission materials synthesis

08 p1322 A71-21062

Martensitic transformation-induced plasticity in austenitic Fe alloys, examining strain rate and chemical composition effects

08 p1312 A71-21554

Deformation-induced martensitic transformation effects on Fe-Ni-Cr-C alloy plastic behavior

08 p1313 A71-21555

Fe-Ni-Co alloy strengthening by martensite to austenite transformation taking into account microstructure

08 p1313 A71-21556

Phase transitions possibility in nonideal multiply ionized plasma, analyzing equation of state and ionization equilibrium equation for various ionization multiplicities

09 p1500 A71-22244

Heat resistant Ni alloys intermetallic gamma prime phase analysis by electrolytic separation

09 p1467 A71-22322

Martensitic transformation of Fe-Ni-Si alloys under tensile plastic strains at 233-373 K

09 p1469 A71-22849

Complex alloying of structural steels, stressing structural changes, electron interactions and phase transition changes

09 p1470 A71-23075

Al and Fe additions effect on transitional phases formation and metastable phase precipitation in Ni-Nb system, using transmission electron microscopy

09 p1471 A71-23124

Martensitic transformation in NiAl oxidation-resistant coatings on Ni superalloys heated for 300 hr at 1093 C

09 p1472 A71-23132

Hf alloys containing transition metals, discussing phase transformations and solid solutions

09 p1473 A71-23225

Temperature and pressure effects on phase transformations, structural changes and related processes in metals, comparing thermographic and calorimetric methods

09 p1547 A71-23227

Al-Co alloys, investigating Al and Co intermediate phases formation effect on X ray emission K spectra

09 p1474 A71-23234

High temperature Ni alloys structural stability, computing gamma prime phase coagulation and average electron vacancy number

09 p1474 A71-23289

TiNi martensitic transformations-fatigue strength relation at room temperature, observing hysteresis in tensile compressive loading cycle to maximum stress

09 p1477 A71-23349

Ti-Nb alloys constitution, discussing alpha-bis martensite dissolution and undercooled beta phase decomposition

10 p1623 A71-23902

Ti thermal conductivity, electrical resistivity and total emittance at high temperatures in ultrahigh vacuum, discussing phase transformation effect

10 p1624 A71-23910

Isothermal transformation of metastable beta Ti-Mo alloys, considering contraction start point coincidence with point of quenched omega transformation to aged omega in TTT diagram

10 p1625 A71-24006

Gas phase ignition of solid propellants involving gas phase variable density for constant density based equations by Howarth transformation

10 p1695 A71-24332

Cu-Ti-Al system intermediate phases crystallization from melt in large concentration areas, discussing four-phase reactions

10 p1627 A71-24597

Steel structural transformations under arc melting, cooling and electroslag remelting, noting delta ferrite precipitation with hot stage microscope

11 p1776 A71-25168

Crystallographic relationships between Ni- and Cr-rich solid solutions, noting preferred interphase interfaces in Ni-Cr eutectic alloy

11 p1778 A71-25532

Magnetostriction in hydrated cesium manganese chloride, examining dimensional changes as function of magnetic field and temperature through antiferromagnetic, spin flopped and paramagnetic phases

11 p1807 A71-25559

Fast heated titanium-vanadium martensite beta-phase transformations comparison with slow heated structures

11 p1782 A71-26472

Ti-V alloys, observing as-quenched omega phase and transition to aged form by selected-area diffraction and dark-field electron microscopy

11 p1783 A71-26479

Solid propellant combustion stability theory for two dimensional disturbances, considering process as elastic body transformation into gaseous combustion products

13 p2159 A71-28138

Alloying elements isomorphic and valence-electron localization effects on Ti alpha/beta transformation temperature

13 p2085 A71-28223

Numerical integration procedure for calculating mixed phase transformation in continuum mechanics for given volume and internal energy increments

13 p2100 A71-28232

Fe/Ti pair diffusion coefficients at various temperatures, showing thin central and two single phase zone formations

13 p2087 A71-29263

Structural evolution of Ni-Co-Mo maraging steel during martensite reversion at rapid heating, studying heating rate effect on alpha-gamma transformation

14 p2257 A71-29839

Discontinuous phase decomposition increase in Co-Ni-Ti alloys by plastic deformation and Al additions, indicating grain boundary diffusion control

14 p2258 A71-30003

Shape-memory effect in equiatomic Ti-Nb alloys with reversible martensitic transformation

14 p2259 A71-30392

Al-Li alloys precipitation characteristics and time-temperature-transformation curves after solution treatment, water quenching and aging

14 p2259 A71-30393

Thermal emission analysis method for studying phase transformations and chemical conversion kinetics in multicomponent systems, applying to liquid evaporation rate measurement

14 p2338 A71-30618

Molten Co-Cr alloy structural transitions at increasing temperatures, relating to change in solid state with increasing Cr content

15 p2425 A71-31393

Molybdenum steel annealing, noting carbide phase transformations

15 p2425 A71-31398

Magnesium corner of Mg-Li-Sn system phase diagram, detecting two invariant transformations in Mg-rich alloys

15 p2425 A71-31403

Ti-Al-V alloys heat resistance relationship to phase structure from bending test at high temperature

15 p2426 A71-31404

High density degenerate stellar plasma analysis, obtaining phase transition thresholds, elementary particle stability, thermal energy density and interaction model

15 p2487 A71-32038

Rare earth metals di- and sesquicarbides physical characteristics, establishing changing properties patterns during phase transitions

15 p2461 A71-32153

Rhenium tellurides phase transformation during decomposition in Ar

16 p2621 A71-33566

Deformable thermally work hardenable Al-Mg-Li alloy, detailing phase composition changes during aging

16 p2594 A71-33711

Temperature dependent electron structure model of free energy decomposition of beta phase in Ti alloys

16 p2599 A71-34085

Fe-Ni-V-C alloy strengthening by cyclic martensitic phase transformation

17 p2756 A71-34487

Vibrational stress induced phase transitions in strontium titanate near transition temperature, using soft mode Raman scattering

17 p2791 A71-34949

Iron based Cr-Co-Mo alloys equilibrium diagrams and phase transformations at various temperatures, emphasizing intermetallic compounds effects on mechanical properties

17 p2758 A71-35148

Superconducting phase transition temperature measurements as function of magnetic field in thin film hollow Al and In cylinders

17 p2791 A71-35742

Molybdenum effect on morphology, size and square density of precipitating gamma particles in nickel alloys

18 p2934 A71-35991

Space shuttle aerothermodynamics, discussing heat transfer measurements, phase change patterns, electron beam flow visualization and boundary layer transition

18 p2847 A71-36430

Small scale flow and surface effects in multiphase media hydromechanics, obtaining entropy production in mixture for interphase transformations characterization

19 p3042 A71-37098

Beryllium impurities effects on ductile-brittle transition temperature, investigating fracture characteristics deformation mechanism

19 p3076 A71-37121

Phase transformations in superconducting Nb-Ti alloys with Zr during heating or isothermal annealing

19 p3078 A71-37469

Martensite-type omega phase formation in Ti alloys during grinding by abrasive wheels and tapes, noting dependence on plastic deformation

19 p3078 A71-37474

Shock wave data for Bamle elastic in 60-480 kb range, considering Hugoniot limit and phase transition produced shock front

19 p3050 A71-37663

Interstitial solute thermomigration of C in Ti, V, Fe, Co, Ni and Pd, using radioactive tracer technique

19 p3079 A71-37710

Variable thermal conductance wall based on working fluid evaporation and condensation [ASME PAPER 71-HT-39]

19 p3166 A71-38001

Droplet clouds microstructure and phase state occurrence as function of temperature, size distribution and water content based on experimental data

19 p3091 A71-38680

Orthorhombic-tetragonal phase transition in barium sodium niobate, investigating expansion curve discontinuities due to crystallographic changes from dilatometric studies

20 p3275 A71-38816

Lithium magnesium zinc silicates crystallization phase equilibria, noting temperature effects, structure, melting and solubility

20 p3253 A71-38818

Pure Fe phase transformation plasticity as function of material, stress, temperature interval and change rate, cycle number and experiment duration

21 p3396 A71-40028

Intermetallic compound Ti-Ni phase transformations, relating martensite crystal structure with pre-martensitic instability

21 p3397 A71-40433

Fe-C alloys martensitic transformation, investigating high quench rate effects

21 p3397 A71-40451

Crystallographic habit plane and martensite plate orientation in Fe-Ni and Fe-Ni-C dilute alloys

21 p3397 A71-40452

Ti-Ni alloy martensitic thermoelastic transformation and memory effect, using optical microscopy to examine change in lattice discontinuity

21 p3398 A71-40459

Optical phonons and temperature dependent phase transitions in paraelectric antimony and ferroelectric sulfonide semiconductors, using polarized IR and Raman spectra measurements

21 p3428 A71-40775

Iron response to dynamic loads, discussing pressure induced phase changes, constitutive equation relationship to dislocation processes and dynamic fracture criteria

21 p3399 A71-40789

Alloying elements effects on martensite decomposition and carbide phase formation during tempering of chromium steels

21 p3401 A71-41085

High strength steel structural transformations under arc melting, cooling and electroslag remelting, noting delta ferrite precipitation with hot stage microscope

21 p3402 A71-41089

Phase transitions possibility in nonideal multiply ionized plasma, analyzing equations of state and ionization equilibrium equation for various ionization multiplicities

21 p3424 A71-41133

Turbulence energy balance and temperature pulsations in free atmosphere in presence of water phase transformation in clouds of given microstructure

21 p3412 A71-41394

Transformation zones of Ti alloy in isothermal conditions after tempering, showing martensite decomposition and omega phase detection by hardness measurements

22 p3560 A71-41624

Magnetostriiction in antiferromagnetic, spin flopped and paramagnetic phases of hydrated cesium manganese trichloride, studying volume changes and thermal expansion near phase transition

22 p3585 A71-41885

Metastable beta type Ti binary alloys isothermal transformation microstructure observation by microscopic and X ray diffraction methods

22 p3562 A71-41947

Tempering anomalies of austenitic stainless steels partially transformed into martensite, using dilatometry, resistivity and internal friction measurements

22 p3562 A71-42244

Carbon effects on fracture phenomena in martensitic transformation of steels under heat and thermomechanical treatments

22 p3563 A71-42322

Isothermal martensite transformations in Fe-Ni-Cr alloys, explaining kinetics difference in terms of elastic parameters small variations

23 p3688 A71-42925

WC and TiC-Co solid solution phase after sintering inhomogeneous structure, investigating grain growth and phase decomposition behavior at various temperatures

23 p3689 A71-43103

Phase transformations and mechanical properties of heat resistant martensitic stainless steel during precipitation aging at prolonged high temperature exposures

23 p3690 A71-43280

High temperature phase transition and composition of Apollo 12 pigeonite/augite clinopyroxene crystal rock 12021 from X ray diffraction

23 p3738 A71-43607

Near equiatomic TiNi thermal martensite transformation premonitory events, discussing crystal structure, mechanical instability and lattice vibrations

23 p3694 A71-44280

Co-Ni-Ti alloy intermittent decomposition kinetics observation by light and electron microscopy, noting finely divided phase coagulation

24 p3836 A71-44670

Phase and microstructure changes during nitriding process of Fe-Ti alloys, stressing Ti concentration effect

24 p3837 A71-44733

Alloying elements effects on high-carbon steels phase transformation under shock loading to form martensite-austenitic structure

24 p3840 A71-45376

Diffusion acceleration in bcc Ti due to imperfections of fine structure created during polymorphous transformation

24 p3840 A71-45379

PHASE VELOCITY

Stacked dipole antenna arrays with modulated phase velocity, comparing measured and calculated radiation patterns

01 p0052 A71-10474

Regionalized models for earth with oceanic, shield or tectonic crust and upper mantle, taking phase velocities into consideration

02 p0245 A71-11992

Attenuation and phase velocities of ELF slow tail atmospherics for easterly and westerly nighttime propagation over Pacific Ocean

04 p0552 A71-15217

Electromagnetic waves phase velocity in helical waveguides in magnetodielectric medium with cylindrical void interspace

05 p0722 A71-16827

Wave buildup in weakly turbulent plasma, noting epithelial pulse background effect on phase velocity

06 p0936 A71-17664

Wave number/phase velocity spectrum of wall pressure measurements beneath two dimensional turbulent boundary layer

06 p0882 A71-18317

Heuristic method for phase velocities and growth rates of ion and electron plasma oscillations generalized to multicomponent plasmas

07 p1166 A71-18887

Phase velocities and vertical amplitude profile of nonsingular mesoscale gravity waves produced in stratified jet flows by floating and deflecting earth rotation forces

11 p1793 A71-25171

Earth-ionosphere spherical waveguide, calculating mean and differential phase velocities and field amplitude of low frequency waves

11 p1731 A71-25774

Mesoscale gravity waves and jet stream stability in temperature-stratified atmosphere with small wave perturbations, estimating wave phase velocities and amplitude functions

12 p1924 A71-26736

Phase velocity for three dimensional structures of impedance elements, using approximate solution methods and dispersion equation

14 p2194 A71-30080

Laminated plate flexural mode free vibration analysis by asymptotic method, obtaining phase velocity for comparison with experiment

14 p2330 A71-30684

Electrodeless AC plasma accelerator /traveling wave pump/ using coil assembly to produce variable phase velocity and eliminate end effects

15 p2457 A71-32102

Traveling ionospheric disturbances dynamic properties, calculating horizontal phase velocity from triangulation data

16 p2568 A71-33783

Single and double pass traveling wave electro-optic light modulator phase retardation transient response calculation

20 p2325 A71-39180

Compressible circular free jet instability allowing for turbulent boundary layer thickness, considering influence of axisymmetry on spatial growth rate and disturbance phase velocity

21 p3365 A71-40013

Earth-ionosphere spherical waveguide, calculating mean and differential phase velocities and field amplitude of LF waves

22 p3509 A71-41542

Ionospheric geomagnetic field effect on ELF/VLF radio propagation

23 p3643 A71-42967

Ion acoustic waves dispersion relation, presenting attenuation and phase velocity tables

23 p3667 A71-43138

Nonlinear stabilization of beam instability in plasma with comparable phase velocity, electron capture and decay effects

23 p3709 A71-43264

Frequency shift in air-coupled surface waves during Saturn 5 launches, computing apparent phase velocity experienced by ground

23 p3672 A71-43883

Stability of dissipative shear flow of inviscid incompressible electrically conductive fluid in presence of magnetic field, deriving instability modes phase velocity limiting conditions from MHD equations

24 p3855 A71-44645

VLF day and night waveguide modes attenuation coefficients and phase velocities, using moving secondary source formed by mode conversion at sunrise and sunset shadow line

24 p3803 A71-44650

Long distance atmospherics propagation in earth-ionosphere waveguide, obtaining phase velocities and damping factors

24 p3804 A71-45030

PHASE-SPACE INTEGRAL

Limit cycle of nonlinear oscillations of third order differential equations dependent on Euclidean phase space with central restoring control force

17 p2763 A71-34293

Monte Carlo generation method for phase-space integrals of multiperipheral models for high energies and particle multiplicities

21 p3408 A71-40850

Phase-space theory of macroscopic fluctuations in nonlinear systems far from thermodynamic equilibrium, using chemical kinetics model

21 p3416 A71-40856

Bifurcation /branch point/ theorems and limit cycles for integral curves of hard excitation nonlinear systems

22 p3527 A71-42675

Phase integral correction for reflected radio wave absorption in ionosphere, comparing with ray theory

23 p3643 A71-42969

Stellar density function outside symmetry plane of galactic phase-space model

24 p3868 A71-44461

PHASED ARRAYS

Phased array radar systems accuracy increase, using ferrite core magnetic flux feedback for phase shifter control

02 p0215 A71-12174

Horn antennas phase centers calculation by vector method from far field expressions

06 p0867 A71-17708

Phased arrays sidelobe reduction by digital phase shifters, considering scan angle and phase quantization step size

06 p0875 A71-17711

Phased arrays sidelobe reduction through reflection lobe dispersion

06 p0875 A71-17718

Phased array antenna element with circular polarization by superposition of complementary dipole and slot, achieving equal E- and H-plane patterns

06 p0875 A71-17719

Phase grating lobes redistribution by aperiodic phased array of line sources with linear variation of element lengths and linear amplitude weighting

06 p0875 A71-17722

Airborne X band reflect phased array radar antenna design for simultaneous functions including large volume search, target attack with general surveillance and low altitude assist

06 p0876 A71-18096

Spacecraft phased arrays design, considering solid state amplifiers effect on total array performance and transistors and varactors output power efficiency

07 p1069 A71-18813

Gain and radiation properties of phased array antenna with dielectric, using integral method

07 p1078 A71-20070

Optimal phased array radar pulse scheduling multiple transmissions and receptions in minimum time, using integer programming

08 p1254 A71-21339

Linear phased antenna arrays, calculating influence of interaction between radiating elements on radiation pattern

09 p1404 A71-22225

Radiation nulls suppression and broadband impedance matching of infinite rectangular waveguide phased arrays, giving numerical solutions

09 p1419 A71-23494

Electric field bounds over phased array antenna aperture, discussing use in predicting array power handling capability

09 p1419 A71-23504

Simulated far field patterns of linear and phased arrays without radiation coupling by hybrid analog computer

11 p1735 A71-25851

Computerized design of optimally efficient dual-series feed microwave networks for waveguide phased arrays

14 p2209 A71-29566

Combined heterodyning, beam forming and cross correlation of broadband multichannel signal from multidimensional phased array, using coherent optical system

14 p2241 A71-30142

Airborne phased array using computer control for beam steering, investigating row-and-column logic effects on beam shaping and stabilization

14 p2209 A71-31045

High speed electronic phase and frequency scanned linear, static fed and monopulse arrays element and angular error analysis

14 p2205 A71-31049

Aircraft phased arrays for L-band ATC satellite system application, alleviating problems of power budget and vulnerability to multipath and interference

14 p2217 A71-31054

Tape helix radiators for spacecraft phased antenna arrays, analyzing performance for proposed L band system

14 p2217 A71-31057

Computer aided design of P-I-N diodes equipped S band phase shifter for phased array antennas, discussing optimization problems

15 p2375 A71-31414

S-band hybrid microwave IC module for phased arrays, presenting mechanical and electrical design details and performance test data

16 p2547 A71-33554

Phased array pulsed X band microstrip Gunn diode transmitters with temperature stabilization at 9.4 GHz

16 p2547 A71-33555

Infrared and thermal evaluation of tactical aircraft phased array radar antenna design with cooling air distribution for steady state operating temperature maintenance

21 p3352 A71-40434

Performance levels prediction for airborne solid state phased array radar transmission sources, considering TRAPATT devices

22 p3509 A71-41630

Waveguide simulator study of blindness/resonance or surface wave/ effect in phased array antennas

22 p3509 A71-41631

Plated through holes interconnection in nine layer phased array antenna printed circuit board, using numerically controlled drilling and plastic encased preform solder system

22 p3525 A71-42765

Real time interactive simulation of multifunction phased array radar, using digital computer links

23 p3648 A71-44272

PHASED LOCKED SYSTEMS

Locking characteristics of automatic phase control circuits in noisy environment

03 p0391 A71-14311

PHENOLIC RESINS

Thermal conductivity prediction during ablation of phenolic-carbon and phenolic-graphic composites for heating and cooling conditions

[AIAA PAPER 71-380] 11 p1783 A71-25304
Nylon-phenolic composites pyrolysis, deriving kinetic coefficients from thermogravimetric analysis at various heating rates

11 p1728 A71-26043

Pyrolysis-gas chromatography locating degradation front in phenolic ablative plastics, giving percent phenolic resin vs distance normal to surface

11 p1728 A71-26044

Stress wave propagation in quartz-phenolic composite, measuring particle velocity by velocity interferometer

17 p2762 A71-35207

Optical transmission in unexposed phenolic resin base laminates with silica cloth reinforcements, studying stabilization treatments, pyrolysis and incident radiation spectral distribution

17 p2838 A71-35473

Spray foam insulation for Saturn S-2 stage, consisting of phenolic honeycomb core composite purged with helium

20 p3312 A71-39270

PHENOLS

NT BISPHENOLS

Dinitrophenol inhibition of rejoining of X ray induced DNA breaks by L cells

07 p1045 A71-20447

Ablative polymers synthesis from formaldehyde, phenols and ethers reaction products, discussing char yield, thermally stable fillers incorporation and thermogravimetric analysis

11 p1855 A71-26034

Phenol furfuraldehyde-ammonium perchlorate solid propellant combustion, investigating burning rate

12 p1944 A71-26742

Preservative phenol derivative effects on toxic gas evolution from stored urine in sealed vessels

22 p3506 A71-42808

PHENOMENOLOGY

Physics and phenomenology of radiation field in spectral lines, considering radiation transfer with optical depth effects and kinetic energy transformation into radiation

18 p2968 A71-37035

Muon showers underground phenomenology in terms of density spectra, shower size and radial density distributions

22 p3594 A71-42407

PHENYLALANINE

Sexual behavior of male cats after parachlorophenylalanine injections, noting unchanged or diminished performance and serotonin lowering in brain

02 p0199 A71-12365

Chemoautotrophic Thiobacillus neapolitanus growth inhibition by histidine, methionine, phenylalanine and threonine under imbalance conditions

04 p0537 A71-14776

High resolution X ray diffraction patterns of yeast phenylalanyl transfer RNA crystals, discussing double helical regional distribution characteristics

11 p1727 A71-25834

Quantitative determination of phenylalanine in serum by gas-liquid chromatographic analysis method

13 p2026 A71-29477

Brain polysomes disaggregation and tryptophan elevation in immature rats and adult animals after L-dopa administration

20 p3186 A71-38979

PHENYLS

NT POLYPHENYLS

Phenylalkylcarbinol steric purity determination from asymmetric secondary alcohol derivatives separation by gas chromatographic resolution

09 p1403 A71-22478

Phenylated imide-quinoxaline copolymers, describing synthesis and thermal and solubility properties

11 p1787 A71-25425

Paraterphenyl coated photomultiplier as detector in far UV spectra, detailing efficiency range and sensitivity

17 p2745 A71-35589

Lithium iodide and tetramethyl ammonium iodide additions effect on radical exchange between phenyl lithium and bromobenzene in diethyl ether

19 p3011 A71-37391

Phenylpropargylene and phenylethynyl nitrene intermediacy, abstracting hydrogen to produce benzylacetylene, phenylallene and 1-methyl-2-phenylacetylene

22 p3508 A71-42886

PHILIPPINES

Capelinhos and Taal volcanoes base surges and deposits

19 p3051 A71-37670

PHILOSOPHY

NT PARADOXES

Mathematics role in human activities relating to technology and pure thinking, discussing computer technology, cybernetics and mathematical models

01 p0112 A71-11159

Quantitative and qualitative philosophical aspects of measure and forecasting applied to patent handling

02 p0336 A71-11861

PHOBOS

Deimos and Phobos position measurements by photographic observations, including refractor and astrophot errors

07 p1194 A71-19333

Deimos and Phobos photographic observations with light reducing slit attenuator diaphragm on refractometer

07 p1195 A71-19335

Phobos and Deimos missions, examining lander and lander/orbiter configurations and Titan-Centaur and space shuttle-Centaur launch systems

17 p2802 A71-34716

Mars orbiting spacecraft trajectory from spacecraft based TV pictures of Phobos and Deimos

23 p3730 A71-43042

Mars physicochemistry, discussing Wright effect/blue veil, atmosphere, polar cap migration, Phobos acceleration and relief inversion darkening

23 p3736 A71-43360

PHONEMES

Auditory illusions, investigating phonemic restorations, verbal transformations and perceptual organization

07 p1051 A71-20212

PHONETICS

Healthy subject speech speed effect on phonation phase length, noting relation to normal articulator phase

16 p2531 A71-33462

PHONOCARDIOGRAMS

U PHONOCARDIOGRAPHY

Phonocardiography

Maximal treadmill stress test correlation with postexercise phonocardiogram, ECG and double master test in normal subjects, discussing third and fourth heart sound incidence

15 p2361 A71-32538

Heart sounds duration, intervals and Q-I lengths, studying displacement, velocity, acceleration tracings and filtration

18 p2854 A71-36140

Phonocardiograph design and calibration for accurate measuring and recording of cardiac vibration displacements, velocities and accelerations

19 p3005 A71-37231

First heart sound changes, discussing sound vibration and transmission and cardiac function

19 p3000 A71-37232

Second heart sound changes due to position and magnitude variations of aortic or pulmonary component

19 p3001 A71-37233

Frequency phonocardiography technique for heart sounds and murmurs registration, producing analog voltage proportional to frequency by zero crossing detector

19 p3006 A71-37234

Diastolic heart sounds and filling waves in coronary artery disease, relating graphic abnormalities and clinical, arteriographic and hemodynamic findings

19 p3002 A71-37550

Frequency distribution of heart sounds in precordium, studying slope of attenuation and relative peaking

20 p3185 A71-38803

Jet and turbulence mechanism of vascular murmurs associated with stenosis for minimum flow Reynolds numbers, using aorta orifice plates in dogs

21 p3336 A71-40864

Midsystolic clicks and papillary muscle dysfunction evidence in arteriosclerotic heart disease from ECG, carotid pulse tracing and phonocardiography

23 p3635 A71-44126

Early systolic clicks shown due to mitral valve prolapse by phonocardiography, cardiac catheterization and angiography

23 p3635 A71-44127

PHONONS

Inelastic scattering by impurities and phonons in metals, determining energy level structure from non-linear corrections to Ohm law

02 p0297 A71-12615

Phonon-magnon absorption bands temperature dependences in Ni, Co and Li ferrimagnetic spinels, giving graphical data for Curie points

04 p0637 A71-15106

Phonon distribution function kinetic equation solution, determining two dimensional lattice heat conductivity

05 p0794 A71-16876

Crystal dislocation dynamics at high strain rates, investigating viscous phonon drag

08 p1371 A71-21563

Phonon excitations radiated from thermal source in He II below 0.3 K, using carbon film detectors

09 p1497 A71-22418

Diffusion-ion capture and heat transfer by phonons in solid and liquid metals

09 p1494 A71-22882

High purity GaAs transverse magnetophonon amplitudes, investigating magnetic field dependence and Landau level collision broadening

10 p1621 A71-24537

Background phonon X ray and gamma quanta intensities dependence on solar activity from Geiger counter recordings in outer space

16 p2626 A71-33675

Nonlinear optics of combination scattering of IR laser radiation in crystals and statistical frequency mixing-multiplication of polarons and longitudinal phonons

16 p2588 A71-33997

Low temperature phonon assisted edge emission bands in pure cadmium sulfide crystals

20 p3276 A71-39008

Raman tensor, scattering efficiency and line widths in semiconductors due to optical phonons, discussing electro-optical coefficients

21 p3427 A71-40662

Optical phonons and temperature dependent phase transitions in paraelectric antimony and ferroelectric sulfonide semiconductors, using polarized IR and Raman spectra measurements

21 p3428 A71-40775

PHOSPHATES

NT ADENINES

NT ADENOSINE DIPHOSPHATE [ADP]

NT ADENOSINE TRIPHOSPHATE [ATP]

NT ADENOSINES

NT AMMONIUM PHOSPHATES

NT CALCIUM PHOSPHATES

NT DIPHOSPHATES

NT INDIUM PHOSPHATES

NT NUCLEOTIDES

NT POTASSIUM PHOSPHATES

NT PYRIDINE NUCLEOTIDES

NT URIDYLIC ACID

Urea-inorganic phosphate mixtures as prebiotic nucleoside phosphorylating agents

07 p1055 A71-19544

Lactic and succinic acids and creatine phosphates content in rat hind leg muscles during swimming and at rest

16 p2532 A71-33897

Peptides formation from glycine in presence of trimetaphosphate, investigating mechanism

21 p3345 A71-40175

Allosteric adenosine monophosphate nucleosidase stabilization by inorganic salts, substrate and essential activator, investigating enzyme inactivation mechanism in low ionic strength environments

23 p3642 A71-44268

PHOSPHENE

Radiation induced visual phosphenes observed by dark adapted human subjects in fast neutron, X ray and positive pion beams at Berkeley comparative to primary cosmic ray effects

12 p1871 A71-27675

Threshold electrical phosphene dependence on impulse duration and stimulation frequency in subjects adapted to darkness

19 p3002 A71-37444

PHOSPHIDES

NT BORON PHOSPHIDES

NT GALLIUM PHOSPHIDES

NT INDIUM PHOSPHIDES

PHOSPHINES

Gas phase ion-molecule phosphine reactions in pure and binary mixtures by ion cyclotron resonance spectroscopy, considering acidity and basicity

08 p1251 A71-21699

PHOSPHORIC ACID

Phosphoric acid corrosion resistant alloys for electrolyte fuel cells, discussing materials selection and optimization

03 p0440 A71-13055

Bronsted relationship between adsorption heat and activation energy in electrocatalysis of purified orthophosphoric acid and phase-oxide-free noble metals

21 p3345 A71-40540

PHOSPHORS

Organic and inorganic phosphors for monochromatic laser illuminated black and white and color displays

05 p0760 A71-16258

Current-sensitive single-gun polychromatic CRT phosphor screen operational characteristics

14 p2215 A71-31032

Luminescence quenching in Hg tube activated Zn-Cu phosphors under action of ruby laser red light

17 p2752 A71-34404

PHOSPHORUS

Phosphorus segregation to prior austenite grain boundaries in ferrite, considering effect on Ni-Cr-C-P steel temper embrittlement

09 p1471 A71-23123

Thermoluminescent phosphorus films irradiation by electrons with energies up to 15 keV in vacuum chamber

12 p1942 A71-26648

Boron or phosphorus doping of silicon, noting microhardness increase and friction coefficient reduction

12 p1911 A71-26820

Hypoxic hypoxia and hypercapnia effect on calcium, inorganic phosphorus and total protein in rats blood during hypodynamic syndrome

15 p2356 A71-31306

Mineralogy, chemistry and origin of KREEP/potassium, rare earth element and phosphorus/ component in Apollo 12 soil and breccia samples from Ocean of Storms

23 p3741 A71-43632

PHOSPHORUS COMPOUNDS

NT ADENINES

NT ADENOSINE DIPHOSPHATE [ADP]

NT ADENOSINE TRIPHOSPHATE [ATP]

NT ADENOSINES

NT AMMONIUM PHOSPHATES

NT BORON PHOSPHIDES

NT CALCIUM PHOSPHATES

NT DIPHOSPHATES

NT GALLIUM PHOSPHIDES

NT INDIUM PHOSPHATES

NT INDIUM PHOSPHIDES

NT NUCLEOTIDES

NT ORGANIC PHOSPHORUS COMPOUNDS

NT PHOSPHATES

NT PHOSPHINES

NT PHOSPHORIC ACID

NT PHOSPHORUS OXIDES

NT POTASSIUM PHOSPHATES

NT PYRIDINE NUCLEOTIDES

NT URIDYLIC ACID

Phospholipid composition of lipid extracts of hypothalamo-neurohypophyseal system of cattle

03 p0362 A71-13237

Phospholipid dynamics of blood entering and leaving brain during unilateral desympathectomy in dogs

03 p0362 A71-13238

Flame resistant properties of phosphorus containing organic and inorganic high polymers

07 p1145 A71-19841

Laser parameters of Nd-doped hydrated phosphorus oxychloride-stannic chloride liquid system compared with YAG and Nd-doped glass, studying optical evolution and losses

13 p2078 A71-28400

Maximal human anaerobic power, discussing unsplit phosphagen concentration in muscles during steady state exercise

16 p2530 A71-33247

Human erythrocyte 2, 3-diphosphoglycerate concentration elevation effects on glycolytic metabolism and intracellular pH

16 p2533 A71-34090

Prolonged strenuous physical exercise effect on triglycerides, phospholipids and glycogen concentration in human femoral muscle

18 p2856 A71-36238

PHOSPHORUS METABOLISM

Human erythrocytes phosphate metabolism in hyperthermia

05 p0711 A71-16944

Neosynthesized alpha-glycerophosphate and 2,3-diphosphoglycerate role in human extraocular muscle metabolism

21 p3328 A71-40099

Differential lipid and phospholipid composition of white matter in brain, cervical, thoracic and lumbosacral sections of spinal cord and sciatic nerve in dogs

21 p3338 A71-41074

PHOSPHORUS OXIDES

Flatband voltage stabilization of metal-glass-oxide-silicon systems for phosphosilicate glass

22 p3587 A71-42532

PHOSPHORYLATION

Radioprotective mercaptoethylamine /MEA/ effect on aerobic resynthesis of ATP in thymus nuclei and oxidative phosphorylation in rat liver mitochondria

07 p1039 A71-18984

Urea-inorganic phosphate mixtures as prebiotic nucleoside phosphorylating agents

07 p1055 A71-19544

PHOTICS

Photoc stimulation at South Pole by EEG, showing no brain stress, undue tension nor anxiety during hypobaric hypoxia acclimatization

06 p0851 A71-17608

PHOTOABSORPTION

High power carbon dioxide laser radiation absorption on vaporized and heated quartz

02 p0260 A71-11944

Luminescence excitation in chelates under pulsed ruby and neodymium laser radiation action, examining two photon absorption mechanism

07 p1122 A71-19130

Astrophysical and aeronomic UV molecular photoabsorption cross sections, discussing experimental techniques and associated systematic and random errors

14 p2190 A71-29905

Electron-electron correlation effects in photoabsorption induced double electron ejection process, using many body perturbation theory

22 p3577 A71-41628

PHOTOCATHODES

Photocatheter technology based on GaAs/Cs photocathodes

03 p0468 A71-14466

Photocathode area sensitivity contours- wavelength relationship from photomultiplier absolute intensity and near IR spectrum laser research

08 p1291 A71-21408

Electron emitter photomultipliers and photocathodes for low light level and scintillation counter applications, using negative electron affinity

23 p3651 A71-43432

PHOTOCELLS

U PHOTOELECTRIC CELLS

PHOTOCHEMICAL REACTIONS

NT PHOTOCROMISM

NT PHOTODECOMPOSITION

NT PHOTOLYSIS

NT PHOTOSYNTHESIS

NT RADIOLYSIS

Self-sustaining coacervates photochemical formation, discussing enzyme-like properties and abiogenesis

01 p0017 A71-11453

Photochemistry, diffusion and escape of atomic and molecular hydrogen on Mars, noting water vapor spectroscopy consistent with temperature profiles

01 p0162 A71-11488

Pure carbon dioxide planetary atmospheres, calculating photochemical instability from atmospheric model

03 p0377 A71-14549

Isolated tobacco chloroplasts disintegration, measuring simultaneous particle size and photochemical reduction rate changes by electron microscopy

04 p0539 A71-15269

Photochemical molecular rearrangement of NN-dimethylphenylethynylamine into alpha-phenylisobutyronitrile by irradiation at 254 nm

06 p0865 A71-17548

Carbon dioxide and carbon monoxide atmospheric distribution dependence on combined effects of photochemical production, loss and transport in mesosphere and upper stratosphere

06 p0893 A71-17980

Rhodopsin dissociation and retina photochemical and bioelectrical processes after light flashes of various intensity

09 p1172 A71-22124

Self consistent field /SCF/ calculations of dipyrindine glyoxal and bianthrone photoproduct molecules with triplet ground state, using unrestricted Hartree-Fock theory

11 p1727 A71-25576

Oxygen atom deficiency and very low exospheric temperature in Mars and Venus upper atmospheres, considering photochemical processes and molecular diffusion

11 p1826 A71-25723

Photochemical ion-molecule reactions in ionosphere by air exhaust device and RF mass spectrometer observation in geophysical rocket experiment

13 p2068 A71-28535

Photochemical machining, describing parts design, line width and corner radii relation to metal thickness and base materials

15 p2416 A71-32428

Photochemical machining applied to thin complex flat metal parts manufacture, discussing tooling,

prototype, production costs and dimensional requirements

[SME PAPER MR-71-813] 15 p2416 A71-32430

Photoreduction regulation in Rhodospirillum rubrum by ammonium chloride, discussing nitrogen fixation and protein metabolism

16 p2527 A71-33058

Gas exchange metabolic fluctuations of nitrogen fixation, hydrogen evolution and photoreduction in Rhodospirillum rubrum as function of culture conditions and age

16 p2528 A71-33059

Ion formation in photochemically initiated combustion of acetylene-oxygen-nitric oxide mixtures, measuring carbon, CH and OH emission spectra and ion current time change

19 p3013 A71-38091

UV photochemistry of lower Jovian clouds, using experimental simulation

21 p3447 A71-40427

Photochemical mechanism of atomic carbon production in Mars and Venus atmospheres, comparing dayglow emissions with Mariner results

23 p3734 A71-43157

Carbon dioxide photolysis at 1740-2100 A applied to photochemistry of Mars lower atmosphere

23 p3641 A71-43327

Venusian photochemistry, discussing hydrogen source from HCl, loss of water in relation to HCl, carbon dioxide stability and COS and hydrogen sulfide in visible clouds

23 p3736 A71-43341

PHOTOCHEMISTRY

U PHOTOCHEMICAL REACTIONS

PHOTOCROMISM

Real time large scale display system with information image projection on reversible photochromic emulsion via IR laser

02 p0249 A71-12072

Photochromic calcium fluoride preparation by rare earth additive coloration techniques

09 p1509 A71-23120

Photochromic paints for nondestructive testing of aerospace materials and structures

10 p1633 A71-24102

Light line and dark photochromic film large scale display devices, using neodymium and UV lasers for film bleaching and darkening respectively

14 p2249 A71-31031

Photochromic glass activation process for recording three dimensional holograms, using radiation with maximum spectral brightness coincidence with absorption band edge

19 p3064 A71-37772

PHOTOCONDUCTIVITY

Field effect photocurrent maximum in thin film semiconductors below Debye radius associating hole capture by recombination centers

01 p0139 A71-10781

High sensitivity photodiode, photomultiplier and photoconductive detectors characteristics for wide-band optical communication

02 p0248 A71-12005

Organic thin film layer semiconductors photoconductivity, developing semiempirical theory of pulse formation

06 p0941 A71-17735

Traveling wave phototube for demodulating pulse amplitude modulated laser emission, investigating equivalent resistance

06 p0900 A71-18184

N-type Si surface barriers and finishing effects on photoconductivity and photoelectric effect

07 p1179 A71-19921

Cu doped GaAs electron radiative capture mechanisms based on photoconductivity and photoluminescence dependence on temperature and excitation intensity

10 p1657 A71-24324

P-type gallium selenide crystals impurity photoconductivity measurements by Q switched ruby laser

13 p2077 A71-27959

Thermal suppression of photoconductivity in crystals with two impurity types, showing carrier concentration decrease in conduction band in narrow temperature range

13 p2112 A71-28924

In situ double exposure differential interferometry, using photoconductive thermoplastic sandwich in place of film, allowing second hologram inscription

14 p2242 A71-30153

Transient photoconductivity measurements of room temperature electron mobility in deuterated anthracene single crystals, discussing isotope effect

20 p3194 A71-39348

Microwave photoconductivity of boron single crystals under pulsed illumination, determining temperature effects on carrier mobility, recombination coefficients and relaxation times

21 p3428 A71-41202

N-type negative resistance, photoconductivity and I-V characteristics of sulfur-doped p-type Si, showing hole capture cross section dependence on electric field

21 p3429 A71-41204

- Impurity photoconductivity, generation-recombination noise and temperature dependences of Hall coefficient and equilibrium carrier mobility in p-type cobalt-doped germanium 21 p3429 A71-41213
- Activator Mn impurity effect of carrier redistribution and partial photoionization of photoconductivity spectra of ZnS single crystals 21 p3430 A71-41218
- Au-n-GaAs surface barrier diode space charge layer strong electric field effects on photoconductivity quantum efficiency 21 p3432 A71-41302
- Thermal suppression of photoconductivity in crystals with two impurity types, showing carrier concentration decrease in conduction band in narrow temperature range 21 p3434 A71-41320
- Cr-doped n-type semiinsulating GaAs single crystal photoconductivity measurement, noting spectral peaks dependence on temperature 21 p3434 A71-41324
- Lead oxide pigment photoconductivity, investigating surface processes effects on spectral sensitivity and absorption spectrum 21 p3434 A71-41329
- Photoelectric properties of gold doped germanium semiconductor structures, investigating long wavelength background illumination effect on nonequilibrium conductivity 21 p3435 A71-41336
- Gallium selenide excitation by ruby laser radiation, investigating impurity photoconductivity dependence on radiation intensity 21 p3395 A71-41352
- Electron transitions between excited states of donors in Ge, investigating photoconductivity in 500-1300 micron band 22 p3585 A71-41817
- Microwave biased germanium IR photoconductive detector for optical communication systems, describing operation principles, signal demodulation and performance 22 p3543 A71-42123
- Photorecombination model explaining kinetics of negative photoconductivity effect during illumination of impurity region in high resistivity p-type ZnTe-CdTe single crystals at room temperatures 23 p3717 A71-43948
- Cryogenic n-type GaAs residual photoconductivity produced repeatedly after heating to room temperature and renewed cooling 24 p3859 A71-44463
- PHOTOCONDUCTORS**
- Solid state receiver for IR, using microwave biased Ge photoconductor 02 p0231 A71-12027
- Photoresist for hologram recording and diffraction gratings formation, using Ar laser output 03 p0425 A71-13640
- Vibration simulation of elastohysteretic systems on analog computers using photocurrent-voltage relationship of polycrystalline photoresistors 16 p2658 A71-33978
- Multielement IR photoconductive detector arrays of InSb and mercury cadmium telluride operating at cryogenic temperatures 18 p2923 A71-36606
- Macromolecular binding agent effect on electrophotographic properties of high resistance layers containing photoconductive CdS 22 p3586 A71-42405
- Photoconductive CdS disintegration effect on heterophase electrophotographic layer electric and photoelectric properties, noting optimal properties relationship to grain diameter 22 p3586 A71-42406
- Germanium extrinsic photoconductive IR detectors with Au, Hg and Cu doping, discussing preparation and electrical and optical characteristics 24 p3860 A71-45070
- PHOTOCURRENTS**
- U ELECTRIC CURRENT
- U PHOTOELECTRIC EMISSION
- PHOTODECOMPOSITION**
- Bleached hologram lifetime extension, decreasing light induced decay rate by gelatin hardening 12 p1905 A71-26815
- Formaldehyde vapor photodecomposition modes by end product analysis, utilizing mixed isotope, radical scavenger, inert gas pressurization and lamp intensity attenuation 12 p1877 A71-27758
- High density polyethylene composition oxidation rates and photodegradation resistance data, using IR spectroscopy 14 p2261 A71-29641
- Mg 24 photodisintegration rate in stellar silicon burning process, presenting reactions at low alpha particle energies 23 p3723 A71-42952

PHOTODETACHMENT

Sunlight photodetachment rates and energy dependent cross sections for ozone ions, using photon beam excitation in buffer gas 16 p2574 A71-33962

PHOTODETECTORS**U PHOTOMETERS****PHOTODIODES**

- Silicon avalanche photodiode detectors for near IR laser pulse receivers, discussing quantum efficiencies, internal gains and room temperature responsivities 01 p0092 A71-10011
- High sensitivity photodiode, photomultiplier and photoconductive detectors characteristics for wide-band optical communication 02 p0248 A71-12005
- IR photodiode heterodyne dependence, deriving noise equivalent power, conversion gain, frequency response, local oscillator power and IF amplifier noise factor 02 p0249 A71-12035
- Real time oscilloscope observation of ultrafast photodiode response to mode locked laser pulses 03 p0438 A71-13886
- Converter-indicator direct digital readout design, using photodiodes for LSI VOR area navigation display systems low power operation 09 p1491 A71-22610
- Photocurrent frequency dependence in thin-base silicon photodiodes for carrier optical generation behind p-n junction and depleted region 12 p1886 A71-26848
- Output power stabilization of He-Ne laser, using vacuum photodiodes or semiconductor diodes for discharge current regulation 12 p1915 A71-27733
- Junction conversion and fabrication of Hg-Cd-Te n-p photovoltaic detectors by proton bombardment 13 p2066 A71-28043
- Semiconductor materials technologies, discussing optoelectronic and microwave components, photodiode arrays, HF diodes and transistors and IC Doppler radar units 13 p2111 A71-28908
- Optoelectronic elements for information system applications, discussing photomultipliers, photodiodes, photoresistors, avalanche and photoparametric diodes response and bandwidth characteristics 17 p2752 A71-34391
- P-n-p-n quadruple layer semiconductor junction light emitting diode with negative resistance characteristics, discussing epitaxial regrowth process and applications 21 p3355 A71-40739
- Semiconductor surface state effects on p-n junction photodiode frequency characteristics under short and open circuit conditions, noting nonequilibrium capacitance during illumination 21 p3358 A71-42125
- Avalanche Si photodiode current pulse formation frequency governing mechanism, considering roles of free carriers and electron tunneling 21 p3358 A71-41344
- High intensity light sources hazards analysis, discussing thermal detectors and vacuum and semiconductor photodiodes for pulsed laser outputs measurement 22 p3541 A71-41795
- Diffused slice Pb-Sn-Te photodiode arrays for IR detection and thermal imaging, evaporating Pb-Sn contacts onto n and p type surfaces 22 p3543 A71-42130
- Injection laser range finder with avalanche photodiode for Mars rover obstacle sensing, discussing range data processing methods 22 p3529 A71-42772

PHOTODISSOCIATION

- Photodissociation produced O/P3/ atoms detection and reaction rate measurements by resonance fluorescence scattering 01 p0130 A71-10369
- Mars atmosphere carbon dioxide photodissociation via pressure independent one step process 03 p0497 A71-14548
- Carbon dioxide and carbon monoxide atmospheric distribution dependence on combined effects of photochemical production, loss and transport in mesosphere and upper stratosphere 06 p0893 A71-17980
- Time dependent Q switched energy storage of trifluoromethanediode photodissociation laser 06 p0910 A71-18661
- Gas laser optical pumping based on photodissociation, calculating spatial temporal distributions of pump radiation absorption probability and main level population 07 p1125 A71-19806
- Laser excited atoms quenching by iodine molecules from light pulse induced photodissociation of perfluoropropyl iodide active media 07 p1126 A71-20195
- Diurnal variation symmetry of upper atmosphere molecular oxygen concentration in terms of ozone photodissociation 09 p1435 A71-22446

Iodine photodissociation laser kinetic model for pumping, radiative and collisional processes, predicting reactant pressure and flashlamp parameters 11 p1773 A71-25795

Photodissociative excitation of atomic oxygen dayglow emission, considering electron impact and dissociative recombination 13 p2056 A71-27933

Carbon dioxide photodissociation in vacuum UV, using time-of-flight spectroscopy and metastable photofragment detection by electron emission from metal surfaces 14 p2190 A71-30571

H atoms generation by photodissociation of molecules evaporated from cometary core, basing analysis on hydrogen atmosphere line spectra 20 p3293 A71-39538

Zero field hyperfine splitting in carbon trifluorobromide photodissociation laser emission 21 p3391 A71-40215

PHOTOELASTIC ANALYSIS**NT PHOTOGRAMMETRY**

- Photoelastic analysis using stress freezing to evaluate closure and precataphoric crack extension in plates under cylindrical bending 01 p0167 A71-10295
- Strain data retrieval from moire or photoelastic patterns by numerical technique based on light intensity distribution phase angle 02 p0225 A71-11703
- Polymer binder effect photoviscoelastic stress analysis near discontinuous reinforcing fibers, comparing results with finite element method for time dependence [SESA PAPER 1630] 03 p0507 A71-13755
- Photoelastic analysis of creep and stress of aluminum notched bars and cracked plates under thermal cycle using epoxy resin simulation 03 p0507 A71-13757
- Photoelastic study of stress wave propagation in composites under fiber matrix strip directed impulsive loading with exploding wire [SESA PAPER 1708] 03 p0507 A71-13758
- Orthotropic photoelastic analysis of residual stresses in filament-wound composite ring structures, comparing with boring-out and cut-through methods 03 p0508 A71-13773
- Stress analysis of DC 10 nose landing gear unit, using photoelastic coating technique 04 p0534 A71-15669
- Principal stresses separation method combining conventional isoclinic parameter and isochromatic fringe order measurements and scattered light method 05 p0822 A71-16373
- Photoelastic model stress analysis by holographic interferometry and automatic measurement of light shapes, discussing slicing technique 05 p0752 A71-16733
- Electron beam drilled workpieces, investigating residual stresses origin and character with photoelastic measurement 06 p0905 A71-18092
- HF dynamic elastic deformation observation and measurement, including photoelastic method for transient phenomena 06 p1003 A71-18422
- Photoelastic fringe patterns in double exposure holography interferometric technique for stress wave analysis 07 p1209 A71-19044
- Displacement function and principal stress differences in transverse plane of symmetry of axially symmetric photoelastic body 08 p1372 A71-21653
- Elastic and plastic plane deformation photoelastic measurement at room and elevated temperatures by moire patterns, comparing performance with other methods 09 p1536 A71-22328
- Fringe interpretation in stress-holo- interferometry, emphasizing isopachic-isochromatic interaction effects in photoelastic analysis [SESA PAPER 1642] 09 p1542 A71-23538
- Cruciform biaxial fatigue under alternate tensile and compressive forces, using finite element analysis and photoelastic-coating techniques 10 p1685 A71-23941
- Photometric method for birefringence parameters determination in photoelastic stress distribution measurements, using proposed photosensitivity calibration standards 10 p1611 A71-24354
- Holography as quantitative tool for photoelastic measurements, using moire theory of interference phenomena 10 p1611 A71-24473
- Plane orthotropic bodies stress analysis by optical polarization method, using models consisting of anisotropic polymer plates fabricated from epoxy resins and woven fiberglass 10 p1690 A71-24573
- Simultaneous determination of first and second mode photoelastic maximum shear stress intensity patterns of epoxy model, using computer plotted ellipses 10 p1694 A71-25060

Slip front mechanisms in clamped or bolted double lap joints from photoelastic analysis of stress environments, discussing fretting fatigue
[AIAA PAPER 71-370] 11 p1845 A71-25344

Papers on fracture mechanics covering engineering fundamentals, environment effects, crack growth, photoelastic analysis, nondestructive testing, etc
13 p2151 A71-28212

Two and three dimensional static and dynamic photoelasticity and birefringent coating techniques applications in linear fracture mechanics
13 p2152 A71-28217

Jupiter circularly polarized visible light measurements, using photoelastic polarimeter
14 p2306 A71-29729

Holographic interferometer for photoelastic stress analysis, eliminating isochromatic pattern interference from isopachic interferogram by double pass object beam and optical rotator
14 p2239 A71-29845

Photoelastic stress analysis, examining light transformations in plane and circular polariscopes by light ellipse method
14 p2323 A71-29848

Vibrating cantilever beam dynamic stress photoelastic determination based on photomechanics and optic-stress laws
14 p2324 A71-29850

Photoelastic analysis of oil film effects on rolling/sliding contact stresses of plastic and glass cylinders on steel ring, showing discrepancy with Hertzian distribution
15 p2414 A71-31946

Photoelastic determination of stress distribution in thin square plates subjected to gravitational forces multiplied by immersion in Hg
16 p2647 A71-32824

Structural elements residual, principal and total stress determination, using photoelastic coating method
16 p2651 A71-33061

Stress difference elasticity equations from photoelastic data and first stress invariant
[SESA PAPER 1780] 17 p2819 A71-34530

Gross static material elastic constants for layered composite materials, using photoelastic models
[SESA PAPER 1845A] 17 p2761 A71-34531

Holographic interferometer for photoelastic stress analysis by simultaneous acquisition of isochromatic and isopachic fringe patterns without mutual interference, providing increased sensitivity
[SESA PAPER 1792] 17 p2738 A71-34532

Photoelastic determination of crack tip stress intensity factors for various specimen geometries and loading conditions
[SESA PAPER 1825A] 17 p2819 A71-34535

Method of producing transparent model composite materials for photo-orthotropic-elastic studies, allowing preparation of larger laminates
17 p2820 A71-34540

Holography applications to complete stress analysis of three dimensional photoelastic models, using double exposure in conjunction with immersion tank
[SESA PAPER 1852] 17 p2738 A71-34541

Precatastrophic extension effects on local stresses in cracked plates under bending fields, using stress freezing and slicing for photoelastic experiments
[SESA PAPER 1820] 17 p2820 A71-34549

Crack wave loading, investigating dynamic stress intensity factor and time response with photoelastic technique
[SESA PAPER 1835] 17 p2820 A71-34550

Service failure prediction by photoelastic methods, discussing failure sources and analysis techniques
17 p2820 A71-34554

Dynamic polariscopes for birefringent materials stress wave low cost analysis
18 p2923 A71-36611

Photoelastic analysis of cylindrical shells of revolution with one hemispheric closed end and reinforcing flanges at opposite end rim, examining boundary conditions effects
18 p2981 A71-36718

Photoelastic analysis of maximum stress in wide plate with asymmetrically reinforced circular hole under tension, noting effects of rounded corner at hole edge
18 p2984 A71-37022

Stress wave interaction with macrocrack in elastoplastic and quasi-brittle materials, measuring stress field by optical polarization method and motion picture photography
19 p3154 A71-37086

Holographic interferometry application to photoelasticity, interpreting fringe patterns for two dimensional stress analysis
20 p3238 A71-39345

Holographic interferometry application to photoelasticity, discussing relationship between isochromatic and isopachic fringes and fringe families separation method
21 p3456 A71-40228

Dynamic photoelasticity for stress wave propagation in anisotropic fiber reinforced composites, using birefringent models and pulsed ruby laser beam
21 p3471 A71-41027

Reflected shadow method for constrained zone photoelastic observation around cracks in birefringent transparent plate under plane stress
22 p3549 A71-42555

Optically active material photoelastic properties utilization for residual stress distribution determination in machine elements after lathe working
22 p3617 A71-42575

Boundary retardation with respect to fringes in scattered light photoelasticity, using quarter wave plate
24 p3881 A71-44776

Photoelastic analysis of thermal stresses in polyurethane rubber ring reinforced polymers, cermets and rubber-metal composites
24 p3883 A71-44895

PHOTOELASTIC MATERIALS
Photoelastic compensator of urethane rubber, describing construction and applications
01 p0082 A71-11009

Stress separation data for axisymmetric and three dimensional data from frozen stress photoelastic model slices
01 p0174 A71-11010

Photoelastic materials polarization characteristics analysis using Muller matrix method
12 p1976 A71-27115

Principal stresses separation in nitrocellulose transparent material with photoelastoplastic properties, using scattered light method
14 p2322 A71-29700

Elastic stress waves propagation in photoelastic layered composite materials, indicating wave front steady state
17 p2824 A71-34816

PHOTOELASTIC STRESS MEASUREMENT
U PHOTOELASTIC ANALYSIS
PHOTOELASTICITY
NT PHOTOVISCOELASTICITY
Holographic interferometry application to photoelasticity, discussing absolute retardation in terms of plane or circularly polarized light fringe pattern interpretation
[SESA PAPER 1719] 03 p0426 A71-13767

Exploding wires in photoelastic specimens, examining axially symmetric cylindrical stress wave front with high speed photographs
[SESA PAPER 1656] 03 p0459 A71-13769

Photoelasticity application for stress-strain state determination around bores made by electron beam, using epoxy models for internal stress distribution
03 p0429 A71-14272

Two and three dimensional photoelasticity, discussing theory and procedures in stress analysis
06 p1001 A71-18063

Image scale of photoelastic device model and negative in photographic camera
07 p1116 A71-20544

Photoelasticity methods applied to model of beam of revolution under simple torsion constructed by stress freezing technique
10 p1684 A71-23837

Two and three dimensional static and dynamic photoelasticity and birefringent coating techniques applications in linear fracture mechanics
13 p2152 A71-28217

Stress state determination in birefringent elastic material for plane dynamic problems by photoelasticimetric and interferometric techniques
21 p3376 A71-40103

Holographic interferometry application to photoelasticity, discussing relationship between isochromatic and isopachic fringes and fringe families separation method
21 p3456 A71-40228

Ultrasonic flaw detection analytical and experimental wave propagation procedure including dynamic photoelasticity and elastic wave computer codes in nondestructive testing
24 p3831 A71-45282

PHOTOELECTRIC CELLS
Stellar spectroscopy by optical heterodyning of laser and star light mixing, using He-Ne laser, high speed photocell and RF power measurement equipment
03 p0487 A71-13331

Stellar photoelectric servo guide with photon counting in mismatch sensor for telescope positioning
04 p0590 A71-14845

Natural illumination and irradiance levels for photoelectric device design and specifications in nocturnal light conditions
10 p1641 A71-24056

Radiation resistance variations of n-type and p-type silicon photocells due to formation of one or two vacancy recombination centers
15 p2461 A71-31670

Reliability analysis of solar thermoelectric generator module as function of individual photocells, circuit design and redundancy
15 p2351 A71-31672

Selenium photocell photovoltaic effect, observing recombination and generation processes in space charge region
16 p2623 A71-34046

Diffusive p-type Si valve photocells, investigating barrier capacitance
17 p2713 A71-34565

Telecommunication satellites photoelectric power systems, discussing solar generators with silicon cells
18 p2851 A71-36572

Beam splitting photocell for pulsed laser power and energy measurement
19 p3072 A71-37551

Solar to electric energy conversion efficiency and electrical properties of photoconverters using compressed sintered CdS
24 p3808 A71-44390

PHOTOELECTRIC EFFECT
NT PHOTOIONIZATION
Semiconductor photoelectric sensor for monitoring laser emission energy in conjunction with memory oscillograph or single pulse peak voltmeter
01 p0093 A71-10623

Automatic solar and lunar reference guidance system with balanced photoelectric measuring equipment
04 p0591 A71-14846

High speed measurements of thermophysical properties at high temperatures, including photoelectric and photographic methods
04 p0595 A71-14957

Copper sulfide-cadmium disulfide heterojunctions photocapacitance effects, discussing current generating mechanism and modulation by trapped charge with heat treatment effects taken into account
05 p0699 A71-16054

Optics and metrological characteristics of optimal photoelectric autocollimators
06 p0897 A71-17535

Sensitivity threshold measurement of photoelectric shadow instrument with test adapter simulating periodic input signal
06 p0898 A71-17536

Design, construction and performance of photoelectric isometric force transducer for muscle mechanics
06 p0862 A71-18392

N-type Si surface barriers and finishing effects on photoconductor and photoelectric effect
07 p1179 A71-19921

Higher order laser light coherence effects on photoelectron distribution detected by third order photoeffect
12 p1913 A71-26961

Optimal radiant source power for photoelectric two axis autocollimation angle trackers, considering detector threshold sensitivity
19 p3067 A71-38659

Photoeffect efficiency of solar energy converters based on semiconductor cadmium sulfide-copper sulfide heterojunctions
22 p3483 A71-42536

Photoactivated electric field effects in nematic liquid crystals for recording real time transparent phase holograms
23 p3674 A71-42955

Waveguide system for measuring semiconductor electrical and photoelectric properties at SHF, observing temperature effects
23 p3652 A71-43531

Solar spectrum photoelectric recording instrument signal ratio accuracy, discussing divider circuit analysis
23 p3681 A71-44312

PHOTOELECTRIC EMISSION
Anomalous temperature dependent silver halides photoemission related to lattice vibrationally dependent hybridization of valence states
01 p0137 A71-10148

Photocathode technology based on GaAs/Cs photocathodes
03 p0468 A71-14466

Time lag between actual and measured stellar transit times based on photocurrent expansion into Fourier series
04 p0598 A71-15380

KCl films exciton-induced photoemission, discussing mechanism of photoelectron emission rise with time under steady UV radiation
09 p1508 A71-22685

Plasma immersed photoemitting plate surface potential distribution, discussing electron/photoelectron temperatures and number densities
10 p1653 A71-24800

Emission spectra, wavelengths and photoelectric intensities of triply-ionized gadolinium, using hollow cathode source with Czerny-Turner vacuum spectrograph
11 p1801 A71-25137

Venus cloud pattern contrast, using photoelectric scans with narrow band interference filter sequences
11 p1824 A71-25702

Nonlinear photoelectric electron emission due to picosecond mode locked laser pulse irradiation
11 p1776 A71-26426

Photocurrent frequency dependence in thin-base silicon photodiodes for carrier optical generation behind p-n junction and depleted region
12 p1886 A71-26848

Lunar occultation photoelectric observations, emphasizing double star nature 14 p2306 A71-29685

GaAs solar cells photoelectric energy characteristics as function of light flux, comparing with Si cells 14 p2181 A71-29952

Photoelectric system for recording Raman spectra with He-Ne laser excitation source suitable for liquid, solution, crystal and powder and depolarization measurements 17 p2751 A71-34383

Neptune diameter and flattening, using photographic and photoelectric observations 17 p2799 A71-34477

UV photoemission measurements on hexagonal ZnO cleaved in vacuum, determining Zn 3d states location 17 p2791 A71-34854

Photoelectric astrometry to determine stellar position, noting application to binary stars 17 p2741 A71-34995

Planetary nebulae helium/hydrogen and nitrogen/oxygen abundance ratios from photoelectric observations, taking into account temperature fluctuations and collisional excitation effects 21 p3446 A71-40416

Tellurium concentrations and photocurrent spectra in Te-doped InSb single crystal samples, determining Te diffusion after annealing 21 p3430 A71-41225

Photocurrent for two stage transition in space charge layer in p-n junctions of germanium with radiation defects 21 p3435 A71-41333

Cl abundance in sun, discussing low noise photoelectric scan 23 p3767 A71-43833

Photoelectric localization of features via optical signal modulation, noting sensitivity dependence on illumination type 23 p3679 A71-43895

Surface potential barrier models for thermionic and photoelectric emissions from semiconductors in Schottky deviation region 24 p3862 A71-45350

PHOTOELECTRIC GENERATORS

Copper sulfide-cadmium sulfide heterojunctions photocapacitance effects, discussing current generating mechanism and modulation by trapped charge with heat treatment effects taken into account 05 p0699 A71-16054

PHOTOELECTRIC MATERIALS

Homogeneous and inhomogeneous photoelectric semiconductors, examining photomagnetic, photomechanic, photovoltaic and Dember effects 03 p0468 A71-14303

Electrical, photoelectric and electroluminescent properties of reverse biased GaP p-n structures at room temperature, considering isolated microplasmas 21 p3430 A71-41217

Photoelectric properties of gold doped germanium semiconductor structures, investigating long wavelength background illumination effect on nonequilibrium conductivity 21 p3435 A71-41336

PHOTOELECTRIC PHOTOMETRY U ELECTROPHOTOMETERS

PHOTOELECTRICITY

Laser optical field intensity correlation function determination from photoelectric counting distribution measurements 03 p0436 A71-13876

Photoelectric measurements of four comets, discussing instrumental data transformations to international UVB system 03 p0490 A71-13943

Duplex telescope system design and functions for photoelectrical stellar brightness measurements 04 p0588 A71-14829

Stellar transit time recording by photoelectric instruments, discussing time constant and slit characteristics 04 p0598 A71-15377

Time lag between actual and measured stellar transit times by photoelectric recording instruments, noting atmospheric, spectral and instrumental factors 04 p0598 A71-15378

Photoelectronic stellar transit instrument lens with increased spherical aberration based on light beam passage analysis 04 p0598 A71-15379

Stellar transit time photoelectric instruments time lag measurements by variable flux light source 04 p0599 A71-15382

Precision systems oscillations measurement by transistorized two channel photoelectric image converter, discussing circuit diagram 05 p0751 A71-16356

Photoelectrical and thermoelectrical properties of CdS, CdS-CdSe and CdSe single crystals epitaxial films 05 p0793 A71-16823

Electrical, photoelectrical and optical properties of crystalline cadmium telluride-indium telluride alloys, discussing temperature dependence, spectral characteristics and photoconductivity 05 p0793 A71-16824

Optical and photoelectrical properties of thin amorphous thallium arsenic sulfide, thallium antimony sulfide and thallium bismuth sulfide films obtained by vacuum deposition 05 p0794 A71-16835

Pi2 geomagnetic pulsation polarization characteristic observations, using photoelectric fluxmeters 05 p0747 A71-17213

Precise Brorfelde transit circle reading by photoelectric scanning, determining diameter and group corrections 06 p0899 A71-17967

Silicon dioxide space charge distribution dependence on photojected currents in MOS structures, showing charge effects on I-V characteristics 07 p1174 A71-19055

Unstable high speed optronic /photoelectric/ flip-flop memory elements with positive optical feedback 07 p1075 A71-19303

Soviet papers on solid state electronics problems covering semiconductor photoelectric, magnetic, surface properties, autoemission, photoemission, etc 07 p1178 A71-19917

Eclipsing variable binary system RR Centauri observed photoelectrically in yellow and blue light 08 p1357 A71-20875

Planetary nebulae central stars power spectra and HF stellar oscillation observations, using photoelectric time series data 08 p1359 A71-20938

Papers on photoelectronic imaging devices covering radiometry, photometry, vision, electro-optical system evaluation, etc 10 p1609 A71-24055

Electro-optical systems in photoelectronic imaging devices, discussing electron gun, electrostatic focusing lens, spherical aberration, magnetic field computation and ray tracing 10 p1609 A71-24058

Photoelectric imaging devices resolution performance, considering modulation transfer function and measurement methods 10 p1610 A71-24060

Pi2 geomagnetic micropulsation polarization characteristics, using photoelectric fluxmeters 13 p2060 A71-28268

Visual binary star observations by Lallemand electronic camera and photo-electronic image devices 14 p2311 A71-30363

Heavily Ge doped p-InSb photoelectric and electric properties, showing impurity concentration effects 19 p3120 A71-38526

Lunar dust potential as function of solar wind flux and particle photoefficiency 20 p3298 A71-39639

Fingerprint identification by holographic correlator pattern recognition techniques, discussing reconstructed image visual observation and photoelectric measurement 22 p3539 A71-41748

Photoconductive CdS disintegration effect on heterophase electrophotographic layer electric and photoelectric properties, noting optimal properties relationship to grain diameter 22 p3586 A71-42406

Odessa observatory automatic film winding photoelectric system, discussing construction and accuracy 23 p3680 A71-44266

PHOTOELECTROMAGNETIC DETECTORS

U RADIATION MEASURING INSTRUMENTS

PHOTOELECTRONICS

U ELECTRONICS

U PHOTOELECTRICITY

PHOTOELECTRONS

Photoelectron fluxes and energy spectra in ionosphere for predawn and sunlit atmospheres, taking into account elastic and inelastic collisions 01 p0147 A71-11506

Photoionization coefficients and photoelectron impact excitation efficiencies in daytime ionosphere, noting role in dayglow 01 p0077 A71-11515

Ionospheric photoelectron exchange at magnetic conjugates, considering electron density and impact ionization by inelastic collisions 03 p0408 A71-13381

Photoelectron emission of organic semiconductors, considering molecular and defect photoionization and exciton collisions 03 p0467 A71-13399

Photoelectron spectroscopy energy analyzer with spherical retarding field screen, discussing electronic circuit configuration, operational characteristics and spectral resolution 04 p0600 A71-15590

Single mode laser light modulation by low amplitude LF sinusoidal wave, considering photoelectron distributions 05 p0760 A71-16161

Papers on optics, Volume 8, covering synthetic apertures, light beating spectroscopy, multilayer antireflection coatings, interference microscopy, photoelectron counting, human eye performance, laser light, etc 05 p0713 A71-16481

Photoelectron count of logarithmically fading optical signal, discussing noncentral chi square random variable approximation 05 p0726 A71-17085

Photoelectron counting distribution for random medium passage scintillated stochastic light, considering low level amplitude stabilized and chaotic radiation transmission through turbulent atmosphere 07 p1159 A71-19513

Satellite studies of geoeactive particles and photoelectrons, including interactions with earth atmosphere 09 p1436 A71-22552

Satellite-borne spectrometer for low energy electrons measurement, describing virgin photoelectrons equilibrium energy spectrum for different latitudes and pitch angles 09 p1436 A71-22553

KCl films exciton-induced photoemission, discussing mechanism of photoelectron emission rise with time under steady UV radiation 09 p1508 A71-22685

Photoelectron noise limited low light level imaging sensors, investigating resolving power, signal degradation and camera tube performance 10 p1610 A71-24061

Photoelectron energy loss rate to ambient electrons in thermal plasma, noting geomagnetic field influence 10 p1662 A71-24558

Asymptotic expression for low energy photoelectron energy loss to ambient thermal electrons 10 p1662 A71-24559

Photoelectron sheath and electric field around spacecraft in interplanetary space, considering typical sheath profiles and tenuous ambient plasma effects 10 p1678 A71-24799

Predawn enhancement structure of oxygen red line airglow at 6300 A from time-latitude isophote diagrams, discussing F region photoelectrons recombination role 11 p1755 A71-25611

Higher order laser light coherence effects on photoelectron distribution detected by third order photoeffect 12 p1913 A71-26961

Dissociative recombination source of atomic oxygen green line excitation in day airglow, considering differential photoelectron flux 13 p2055 A71-27919

Nitrogen molecular excitation by photoelectron impacts in dayglow, investigating 1 PG band emission intensity variation with solar activity 14 p2235 A71-30349

Photomultiplier tube operation in terms of photoelectron counting photometry, examining emitted signal statistical properties 15 p2408 A71-31832

Ejected photoelectron count probability distribution due to periodic irradiance modulation of amplitude stabilized light beam 15 p2452 A71-32595

Polyatomic molecule photoelectron spectroscopy, emphasizing spectra interpretation by quantum mechanical procedures 16 p2541 A71-33398

Escaping photoelectrons effect on polar wind exospheric model, suggesting kinetic pressure predominance at very high altitudes 16 p2569 A71-33814

Conjugate photoelectrons existence from rocket measurements during total solar eclipse of 7 March 1970 16 p2570 A71-33823

Atomic oxygen 1304-A day airglow observed fromOGO-D spacecraft, attributing subsolar emission rates to photoelectron impact excitation 16 p2574 A71-33964

F region plasma phenomena discoveries by U.S. researchers /1967-1970/, considering thermal structure, ion composition, conjugate photoelectrons effects, wind effects, etc 17 p2732 A71-34465

Spatial coherence measurement for two points of pseudothermal light source by comparing photocathode luminous intensity probability density and photoelectron distribution moments 17 p2754 A71-35585

Jovian magnetospheric plasma densities, discussing roles of centrifugal ejection, solar wind plasma injection and photoelectron diffusion 18 p2964 A71-36291

Core binding energy difference between bridging and nonbridging oxygen atoms in silicate chain of pyroxenes, using X ray photoelectron spectra 19 p3011 A71-37415

Dispersive photoelectron spectrometers, considering entrance area and solid angle product /etendue/ 19 p3063 A71-37553

Photoelectron flux and energy spectra effects on ionospheric phenomena, examining sunlit and predawn atmospheric models 20 p3225 A71-39726

Superthermal electrons energy spectra and pitch angle distribution, presenting photoelectron flux recordings by Cosmos 261 satellite 20 p3282 A71-39740

Photoelectron impact vs dissociative excitation cross sections of atomic oxygen resonance radiation in terrestrial airglow 23 p3669 A71-43171

Daytime photoelectron energy distribution and electron gas heating in F region as function of height and solar cycle variations 23 p3673 A71-44003

PHOTOEMISSION

U PHOTOELECTRIC EMISSION

PHOTOEMISSIVITY

U EMISSIVITY

U PHOTOELECTRIC EMISSION

PHOTOEMITTERS

U PHOTOELECTRIC MATERIALS

PHOTOGEOLGY

Pseudo radar imagery by high contrast aerial photography at low sun angles for aiding geological analysis 04 p0598 A71-15370

PHOTOGNOMIOMETERS

Luxmeters and photoelectric receptors for illumination measurement of light beams in limited solid angle in image systems, considering automatic polar photogoniometer 14 p2246 A71-30417

PHOTOGRAMMETRY

Celestial body gravitational field from satellite photogrammetry 01 p0083 A71-11326

Photogrammetry in precision three dimensional X ray stereoradiography, comparing doses with Kymography, Tomography and Sierescopy 02 p0203 A71-11951

Stereophotogrammetric system for human motion measurement, describing design and operation 04 p0547 A71-15844

Astronautical TV camera and photogrammetric systems use on manned and unmanned lunar probes, discussing applications to earth surface surveys 06 p0901 A71-18287

Close range photogrammetry with simple cameras, using calibration device and digital data processing 06 p0901 A71-18288

Automatic coordinate measuring and recording devices for photogrammetric restitution equipment 06 p0901 A71-18293

Photogrammetric data digitization system with terrain model measurement and mapping capability 06 p0901 A71-18294

Photogrammetry and aerial photography - Conference, Denver, October 1970 08 p1280 A71-21239

Aerial photographs point marking by Markov instrument, discussing high precision stereophotogrammetric equipment for photogrammetric work and physical marking 09 p1451 A71-23177

Photogrammetry - Conference, Washington, D.C., March 1971 09 p1438 A71-23207

Hologram mensuration, discussing photogrammetric stereo model differences, close range objects, pointing, geometric fidelity, computerized plate analysis and reconstruction shift 12 p1907 A71-27262

Stereophotogrammetric methods and instruments for studying eye anatomical-optical apparatus and pathological changes 13 p2016 A71-28012

Anblock method adjusted photogrammetric strips and blocks accuracy, examining errors by model coordinates covariance matrix 13 p2062 A71-28904

Lunar mapping metric camera subsystems stellar calibration for photography maximum usability in photogrammetric data reduction 13 p2071 A71-29348

Photogrammetric coordinate relation of points on lunar surface and stereopanoramas of scanning photographs by Luna 9 and 13 orbiters 15 p2406 A71-31618

Automatic coordinate compensation for systematic and random distortions of photographs on stereophotogrammetric devices 15 p2406 A71-31619

Photogrammetric three dimensional digitizer for automatically measuring and recording automotive models dimensions 17 p2744 A71-35288

Stellar calibration of lunar mapping camera for precision metric photography and time correlated postflight attitude determination 18 p2925 A71-36916

Photogrammetric instruments digital servo, using printed disk DC motor drive, incremental measure-

ment, nonlinear feedback and digital integrated circuit logic 20 p3233 A71-38829

Stereophotogrammetric measurement of body and limb volume changes after prolonged space mission 22 p3502 A71-41861

Lower atmosphere wind and cloud velocity measurements by combined stereophotogrammetry and balloon visual observation 22 p3542 A71-41862

Photogrammetry of moving objects - Conference, Saint-Mande, France, September 1970 23 p3678 A71-43586

Aeronautical radio navigation aids photo-optical calibration, describing photogrammetric procedure and ground equipment for checking out airport ILS systems 23 p3702 A71-43587

Photogrammetric recording of helicopter rotor induced aerodynamic effects using wind tunnel test smoke visualization technique 23 p3678 A71-43588

Objects motion analysis by dynamical photogrammetric methods, integrating optical image points differential motion for trajectory equations 23 p3678 A71-43589

Stationary or moving objects spatial coordinates determination by three and four dimensional terrestrial photogrammetry, using phototheodolite stereophotographic pictures 23 p3671 A71-43590

Short range photogrammetry, describing special instrumentation problems and requirements regarding imaging precision and quality 23 p3679 A71-43591

Photogrammetry of moving objects - Conference, Saint Mande, France, September 1970, Part 3 24 p3825 A71-44753

Photogrammetric flow rate determination in centrifugal pump impeller, using rotating camera 24 p3825 A71-44754

Stereophotogrammetric measurements of displacements and strains in Al membrane during explosive forming 24 p3825 A71-44755

Spatial photogrammetric restitution of terrestrial photographs using projective transformations 24 p3825 A71-44756

Ultrarapid motion photogrammetry using three dimensional holography with pulsed laser recording 24 p3825 A71-44757

Objects in motion measurement by photogrammetry in Japan noting surf, rocket tracking, snow, roof deformation, avalanches, car collisions, water and air turbulence applications 24 p3826 A71-44758

Photogrammetry of objects in motion, discussing variable time equipment, picture taking methods, applications and accuracy 24 p3826 A71-44759

PHOTOGRAPH INTERPRETATION

U PHOTOINTERPRETATION

PHOTOGRAPHIC EMULSIONS

NT NUCLEAR EMULSIONS

Quasi-nucleon nuclear interactions of high energy protons in photoemulsion irradiated in pulsed magnetic field 01 p0131 A71-11368

Photoresist for hologram recording and diffraction gratings formation, using Ar laser output 03 p0425 A71-13640

Photographic gelatin microimpurities quantitative analysis and removal techniques 04 p0585 A71-14645

Photoemulsions densitometric characteristics for protonogram analysis, during fast charged particle interaction with single crystals 05 p0754 A71-17031

Holography development, discussing three dimensional images, fine grain recording emulsions and beam switching during reconstruction 06 p0897 A71-17369

Telescope star photographic magnitude perception maximum capacity, considering effective or equivalent quantum yield and photoemulsion sensitivity 07 p1109 A71-19346

Photographic emulsion model for signal to average noise irradiance ratio analysis in hologram reconstruction 08 p1287 A71-21188

Photographic materials holographic exposure index improvement due to increased sensitometric speed and macroscopic transfer characteristics 08 p1290 A71-21385

TV and silver halide emulsion application to planetary photography from space orbit, providing film system immediate information storage and high resolution 09 p1447 A71-22746

Folded all-reflecting Schmidt camera UV image converter system for space astronomy applications, discussing pressure sensitivity effects on UV direct recording emulsion 09 p1447 A71-22751

Pions-photographic emulsion nuclei inelastic collisions as function of energy, comparing multiplicity, produced particles angular distribution and evaporation prongs number 13 p2121 A71-28059

Reversal processing technique for producing high diffraction efficiency, low noise and good light stability phase holograms on silver halide emulsions 13 p2068 A71-28713

High quality hologram copies, using photosensitive emulsion layer technique 13 p2070 A71-29027

Photographic emulsion thickness variation effect on wave front recording and reconstruction on holographic plate 14 p2241 A71-30132

Two interferograms holographic laser recording on same emulsion by double exposure with ruby and harmonic wavelengths 15 p2454 A71-31277

Spectroscopic plate emulsion with excellent signal to noise characteristics, investigating baking time response in controlled nitrogen atmosphere 16 p2577 A71-33137

Medium energy electrons action on photographic emulsions, assuming volume element behavior not totally opaque 18 p2916 A71-36044

Pseudocolor image enhancement by two-separation photographic process, considering transformation curve alterations in CIE space by changes of photographic materials, filters and exposures 18 p2918 A71-36080

Controlled photographic emulsion study of cosmic ray showers with electron photon components 19 p3124 A71-37261

Holographic process theoretical and experimental optimization, considering object/reference beam ratio and photographic emulsion thickness effects 21 p3380 A71-40924

Exposing light and resulting density distribution and granularity in lower photographic emulsion layer, investigating modulation transfer function and power spectrum 22 p3538 A71-41733

Latent photographic image formation mechanism, explaining neutral atoms drift towards negatively charged center with surrounding polarized silver atoms 23 p3678 A71-43580

Laser light action in photosensitive materials, comparing development techniques 23 p3686 A71-44057

PHOTOGRAPHIC EQUIPMENT

NT BAKER-NUNN CAMERA

NT BALLISTIC CAMERAS

NT CAMERAS

NT FRAMING CAMERAS

NT HIGH SPEED CAMERAS

NT LALLEMAND CAMERAS

NT PHOTOGRAPHIC RECTIFIERS

NT SCHMIDT CAMERAS

NT TELEVISION CAMERAS

Photographic materials in holography, examining resolving power dependence on size and on angle between reference and signal light beams 07 p1108 A71-19238

High speed photographic assembly with turbine drive for continuous recording and frame photography 10 p1613 A71-24872

Photographic materials in holography, examining resolving power dependence on size and angle between reference and signal light beams 12 p1903 A71-26756

Apollo lunar and Skylab photographic systems, discussing topographic, panoramic, metric, stellar and multispectral cameras and instrumentation 12 p1907 A71-27257

German monograph on photographic masks as position frequency filters covering pattern recognition, transfer functions, etc 15 p2410 A71-32309

Photo-optical instrumentation - Conference, Anaheim, California, September 1970 18 p2916 A71-36051

Stellar proper motions in photographic zenith tubes programs for time service clocks correction, examining catalogs used for astronomical data processing 18 p2962 A71-36110

Aerial photographic equipment survey, describing topographic cameras, aerial photograph orientation equipment, onboard navigation instruments and mapping survey system 21 p3380 A71-40875

Fraunhofer diffraction apparatus design based on He-Ne laser, testing performance in distorted point lattices photography 23 p3686 A71-43956

Photogrammetry of objects in motion, discussing variable time equipment, picture taking methods, applications and accuracy 24 p3826 A71-44759

PHOTOGRAPHIC FILM

NT MICROFILMS

Coherent optical data processing system imaging qualities photographic film requirements

01 p0050 A71-10900

Electron photon cascade energy measurement by photometering blackened spots on X ray films

01 p0084 A71-11369

X ray films in emulsion chambers, discussing electron-photon cascades

03 p0426 A71-13839

Electron photon cascades in multilayer substrate-free nuclear emulsion chamber with X ray films under lead plate

03 p0427 A71-13872

Photographic material information capacity in holography

04 p0585 A71-14643

Aerial photographic film color separation tests

04 p0585 A71-14644

Hologram formation in gelatin, photopolymeric and photochromic materials for high diffraction efficiency, in-place real-time processing and erasability

04 p0596 A71-15167

Book on optical data processing covering light characteristics, Fourier transforms, spectrum analysis, photographic film, filtering, holography, etc

05 p0754 A71-17124

Organic free radical photographic films for biomedical microimaging

07 p1110 A71-19475

Light effect on dielectric constant of thin hardened dichromated gelatin films for holographic recordings

07 p1110 A71-19482

Aerial color negative system for processing Ektachrome aero film type 8442 to obtain negative transparency with fourfold effective film speed increase

08 p1288 A71-21261

Radiant flux diffraction effectiveness of amplitude holograms with allowance for nonlinearity of photo-material

09 p1442 A71-22400

High temperature measurement by photographic technique using radiation-sensitive color film for unpredictable exposure conditions

09 p1444 A71-22712

Photographic materials characteristic curve description by sensitometric parameters including contrast, hardness and refinement

11 p1767 A71-26468

Camera shutter spatial frequency spectrum and components light scattering effects on negatives quality based on composite image representation systems theory

11 p1767 A71-26469

Visual flight simulation devices, considering high resolution photographic films and digital memories

13 p2046 A71-29483

Hologram size and film type limitations effects on resolution of reconstructed image in edgeline holography

14 p2241 A71-30131

Image spatial frequency content of speckle patterns on illuminated diffuse screen and photographic film by optical Fourier analysis

14 p2242 A71-30152

In situ double exposure differential interferometry, using photoconductive thermoplastic sandwich in place of film, allowing second hologram inscription

14 p2242 A71-30153

Elastomer O ring vacuum device for positive holding of Schumann film for precise microdensitometry during rocket flight in 7 March 1970 solar eclipse

14 p2249 A71-30887

Light line and dark photochromic film large scale display devices, using neodymium and UV lasers for film bleaching and darkening respectively

14 p2249 A71-31031

Flying spot scanner electron optical systems for reading data from photographic film for studies of recognition algorithms, image simulation and automatic particle track measurements

15 p2409 A71-32191

GALAXY measuring engine for automatic measurement of glass photographic plates taken from Schmidt telescopes, discussing performance

17 p2741 A71-34997

Automatic precise centering on photographic plate star image by movement across scanning slits for orthogonal coordinates and processing in on-line computer

17 p2742 A71-34999

Stellar spectrograms digital filtering for SNR improvement from photographic plate with line widths larger than granulation noise mean period

17 p2743 A71-35008

Holographic diffraction gratings on plane or concave spherical surface photographic plate, investigating interference fringes and aberration properties

17 p2745 A71-35588

Flat field condensing system for illuminating film projected on screen using Hg-Xe short arc lamp

18 p2918 A71-36071

Computer best least square filtering and approximation by radial filter of noisy imagery using discrete array transmission from photographic film

18 p2884 A71-36081

Serial edge absolute coded and parallel alphanumeric timing on engineering sequential films, discussing frame selection, marking, offset, pull down and exposure correction

18 p2919 A71-36085

Chromatographic paper extraction of residual thiosulfate in processed photographic film

19 p3062 A71-37247

Nonlinear compensation for film deformation in aerial photography correcting spatial phototriangulation grids

19 p3063 A71-37270

IR holography with cholesteric liquid crystals as recording medium and carbon dioxide laser as light source, discussing demagnification and image reconstruction

21 p3379 A71-40703

Vesicular photographic film mechanics, sensitometry and densitometry

22 p3548 A71-42513

X ray films in emulsion chambers, discussing electron-photon cascades

22 p3550 A71-42640

Electron photon cascades in multilayer substrate-free nuclear emulsion chamber with X ray films under lead plate

22 p3550 A71-42673

Analytical function approximation of photofilm characteristic curves, noting validity for all exposure times

23 p3680 A71-44055

Odessa observatory automatic film winding photoelectric system, discussing construction and accuracy

23 p3680 A71-44266

PHOTOGRAPHIC MEASUREMENT

Photographic measuring method for angular misalignment associated with broken ball bearing

01 p0086 A71-10296

Electron photon cascade energy measurement by photometering blackened spots on X ray films

01 p0084 A71-11369

Photographic and photoelectric photometry of asteroids, discussing luminescence, reflectivities, light curves, colors and phase variations observations

02 p0310 A71-12157

Solar general magnetic field determination by measuring visually small displacements on photographic plate

02 p0316 A71-12752

European ground stations geodetic surveys by laser range measurements and photographic observations of satellites with reflectors

03 p0413 A71-14008

High speed measurements of thermophysical properties at high temperatures, including photoelectric and photographic methods

04 p0595 A71-14957

High current free-burning arc characteristics in air at various pressures, examining dimensions from photographs

04 p0676 A71-15031

Error estimates for turbulent flow characteristics determination by visualization and solid particle photography

04 p0573 A71-15562

Gegenschein photographic and photoelectric scan observations, considering origin in light reflection from interplanetary dust outside earth orbit

04 p0659 A71-15853

In-plane surface displacement measurement by double exposure speckle photography

05 p0747 A71-16191

Deimos photographic observations on Pulkovo normal astrophotograph during 1967 Mars opposition

07 p1194 A71-19334

TV spectrophotometer with photographic and photoelectric measurement techniques advantages for measuring astronomical telescope spectral passbands

07 p1109 A71-19349

Holography and interferometry industrial applications, considering three dimensional imaging, precision distance measurement, nondestructive testing and structural strains and failures detection

07 p1113 A71-19784

High temperature measurement by photographic technique using radiation-sensitive color film for unpredictable exposure conditions

09 p1444 A71-22712

Shock wave free surface velocity measurement using moire method for photographic recording with image converter streak camera

09 p1444 A71-22715

Star catalogue systematic error corrections from minor planet photographic observations and orbital elements determination

10 p1670 A71-24180

Mercury transit across solar disk on 9 May 1970, using photographic micromasurements

10 p1677 A71-24587

Polar substorm energy from auroral region size and brightness photographic observations, discussing total flux dependence on magnetic field disturbance intensity

10 p1606 A71-24917

Photographic quasi-draconitic period measurements from satellite transit across topocentric celestial equator tested on Echo 2 and Pageos A

11 p1732 A71-25828

Direction of chord in space from synchronous photographic satellite observations, considering optimum satellite altitude

12 p1900 A71-26969

Atmospheric currents and turbulence determination from meteor trail photographic observations

12 p1901 A71-27075

Translation of geodetic geographical coordinates and ellipsoidal altitudes by synchronous photographic satellite observations and satellite-distance measurements from two ground stations

12 p1903 A71-27753

Vibration analysis by holography, discussing recording media, maximum light utilization, stroboscopic and time-averaged techniques and alterations in sensitivity

13 p2067 A71-28396

Hollow cone water spray from pressure jet swirl atomizer into uniform air stream, observing drop velocities and trajectories by high speed photography

13 p2049 A71-28753

Narrow-band photometry of comet Bennett, giving intensity profiles and interference filter transmission curve

13 p2138 A71-28761

Nucleus brightness of comet Ikeya-Seki from plates in photographic and photovisual spectral regions, indicating relation to solar rotation

15 p2484 A71-31667

Photometry of head and tail regions of comets Kosik, Akhmarov-Iurlov-Hassel, Arend-Roland and Mrkos by equidensity method, using Sabatier effect

15 p2484 A71-31668

Optical center position on negative and lens distortion of satellite camera verified on zenith area photos of stellar coordinate measurements

16 p2575 A71-32835

Fog drop size distribution measurement with laser hologram camera

16 p2604 A71-33535

Multispectral color aerial photography for identification of farm crops and tree species, using broadband camera filters

17 p2737 A71-34274

Strain rate effects on composite material tensile and flexural properties measured by load sensors and streak photography

17 p2737 A71-34345

Neptune diameter and flattening, using photographic and photoelectric observations

17 p2799 A71-34477

Computer controlled encoding device with laser flying spot scanning for automatic photographic image measurement

17 p2741 A71-34998

Remote sensing imaging techniques for oil pollution survey, using airborne UV, IR, color and filtered panchromatic photography

17 p2735 A71-35386

Pulsed ruby laser high speed photography for accurate measurements of models contours in hypervelocity flight within aeroballistic range

18 p2923 A71-36612

Brightness profiles of earth daytime horizon from Soyuz spacecraft photographic photometry, deriving atmospheric scattering coefficient relation to optical thickness vertical distribution

19 p3054 A71-37967

Stellar proper motion measurement by densitometer automatic scanning of star plates pairs, assessing accuracy

20 p3239 A71-39529

Ballistic measurement system for photographing satellites, illustrating minimum brightness relation to satellite distance

20 p3240 A71-39536

Photometric determination of solar granulation rms intensity fluctuation, using ground telescope

22 p3596 A71-41453

Isotopic X ray photography application to welded joint flaw detection in atomic power plant with radiation background

22 p3540 A71-41763

Artificial illumination for Venus surface pictures from landed space vehicle

22 p3608 A71-41953

PHOTOGRAPHIC PROCESSING

Double beam microphotometer for simultaneous measurement of negatives, reducing processing time and density fluctuations

02 p0251 A71-12358

Mariner near encounter pictures with maximum discriminability, applying algorithms for contrast and resolution enhancement and noise removal

06 p0898 A71-17634

Aerial color negative system for processing Ektachrome aero film type 8442 to obtain negative transparency with fourfold effective film speed increase

08 p1288 A71-21261

Reversal processing technique for producing high diffraction efficiency, low noise and good light stability phase holograms on silver halide emulsions 13 p2068 A71-28713

Reversal bleaching process for low flare light and high diffraction efficiencies and SNR in holograms 14 p2241 A71-30134

Light line and dark photochromic film large scale display devices, using neodymium and UV lasers for film bleaching and darkening respectively 14 p2249 A71-31031

Phase and amplitude error detection in photomasks for semiconductor integrated circuits with spatial frequency coherent optical filtering 20 p3246 A71-39449

Laser light action in photosensitive materials, comparing development techniques 23 p3686 A71-44057

PHOTOGRAPHIC RECORDING

Transonic flow through planar cylinder lattices, discussing flow pattern visualization and recording techniques by high speed camera 01 p0001 A71-10108

Fluid jets disintegration into uniform droplets with and without satellite formation, using stroboscopic photography 03 p0399 A71-13292

Small phase differences amplification in holographic interferometry, using nonlinear development of recordings 03 p0429 A71-14182

Mechanical vibrations recording and measurement by photographing motions of points and lines on tested surface 03 p0430 A71-14330

Intercept Ground Optical Recording telescope and Mobile Optical Tracking System for electro-optical photography, discussing measurement and system errors and CAMDAT computer program 04 p0554 A71-15320

Surface roughness determination by spatially coherent laser light speckles correlation and spectral distribution on film records 04 p0609 A71-15689

Holography applications, recording and reconstructing three dimensional objects by split laser beam interference technique 05 p0747 A71-16194

Hologram recording material characterization concerning maximum diffraction, linearity and sensitivity 07 p1110 A71-19483

Image scale of photoelastic device model and negative in photographic camera 07 p1116 A71-20544

Phototechnology for phase holograms recording and information storage in hardened gelatin 07 p1116 A71-20620

Automatic record of terrain profiles from stereoscopic aerial photographs by intersection of ray traces 08 p1288 A71-21252

Holographic recording media low signal energy densities comparison, determining peak values of diffraction efficiency and normal contrast ratio divided by signal beam exposure 08 p1290 A71-21389

Wideband photographic signal recording by modulated laser beams, discussing performance characteristics in terms of signal to noise ratio and laser power 09 p1460 A71-22355

Shock wave free surface velocity measurement using moire method for photographic recording with image converter streak camera 09 p1444 A71-22715

Fluid jets disintegration into uniform droplets with and without satellite formation, using stroboscopic photography 09 p1434 A71-23267

Ultrarapid holographic recording in IR light at 1.06 micron 10 p1608 A71-23838

Recording and interpretation of aerial photographs applied to geomorphology 10 p1599 A71-23872

Holography utilization to data processing, discussing factors affecting recording and matched filters creation for pattern recognition 10 p1581 A71-23917

Photomaterial nonlinear effects on contour distortion in holographic recording of Fourier image slit for graphic memory use 10 p1612 A71-24716

Holographic image recording and reconstruction in two and three dimensions, including light wavelike nature, Huygens principle, wavefront reproduction and spectral composition 10 p1613 A71-24849

High speed photographic assembly with turbine drive for continuous recording and frame photography 10 p1613 A71-24872

Photographic study of burning metallized composite propellant, noting burning rate augmentation by heat transfer from alumina particles retained on propellant surface 11 p1809 A71-25502

Holography principles development, history, wave field recording, processing and reconstructing techniques for image quality improvement, laser applications, etc 11 p1767 A71-26352

Plane and three dimensional dynamic holograms recording in bleachable dyes, using ruby laser with gallium chloride phthalocyanin in chlorobenzene as Q switch 11 p1767 A71-26356

Digital data recording system based on multiple beam interference pattern photography, using optical phase modulation 12 p1905 A71-26807

Vibration analysis by holography, discussing recording media, maximum light utilization, stroboscopic and time-averaged techniques and alterations in sensitivity 13 p2067 A71-28396

Plane wave holographic recording and reconstruction, investigating effects of photosensitive medium as three dimensional diffractive pupil 13 p2068 A71-28711

Automated data acquisition and analysis during cardiac catheterization, using photokymographic and analog magnetic tape recording system in conjunction with digital computer 13 p2020 A71-29003

Power and focusing requirements in recording and reading with Gaussian laser beam in TEM mode 14 p2254 A71-30136

Momentum spectrum measurement of cosmic ray muons, recording particle trajectories photographically 15 p2475 A71-31783

Optimal sensing recording and signal processing in multispectral photography for aerial reconnaissance capability 15 p2410 A71-32470

Continuous holographic recording of wave front temporal variations for nonstationary processes 15 p2413 A71-32788

Three dimensional hologram recording and reconstruction, discussing image geometry, reference beam intensity, size finiteness, transition limits and photosensitive materials 16 p2580 A71-33623

Plane and three dimensional dynamic holograms recording in bleachable dyes, using ruby laser with gallium chloride phthalocyanin in chlorobenzene as Q switch 17 p2745 A71-35507

Photopolymer recording materials fixing by flashing holograms with Xe light or deactivating catalyst with thermal methods 17 p2745 A71-35591

Time resolution enhancement in laser photography, recording fast events with long pulse length laser without auxiliary shutters 18 p2914 A71-35851

Pseudocolor image enhancement by two-separation photographic process, considering transformation curve alterations in CIE space by changes of photographic materials, filters and exposures 18 p2918 A71-36080

Optical readout system for analysis of laser Doppler velocimeter signals displayed on TV screen and recorded photographically 18 p2931 A71-36587

Image intensifiers for color conversion, image deflection and scanning, shuttering and recording, defining information gain criterion for comparison with unaided photography 18 p2925 A71-36907

High quality continuous tone micromachining and image recording on metal thin films by low power pulsed gas laser heating 19 p3071 A71-37213

Scanning densitometer for spectral transmission density continuous recording at low image contrast, discussing design and performance tests 19 p3063 A71-37248

Photochromic glass activation process for recording three dimensional holograms, using radiation with maximum spectral brightness coincidence with absorption band edge 19 p3064 A71-37772

Recording device with Fourier hologram memory based on optical spatial filtration principle for identifying chemical compounds by IR absorption spectra 19 p3064 A71-37773

Ultrafast camera with picosecond framing times for photographic measurement of light pulses 20 p3235 A71-39189

Pre- or postexposure effect in holographic recording and reconstruction in reference to object beam intensity ratio 20 p3236 A71-39193

Photographic phase holograms including printout effect, bleaching, conversion with iodine compound and light stability 20 p3236 A71-39195

Real time multitrack half tone recorder for displaying three dimensional information on instantaneous blood velocity measurement by Doppler effect 21 p3377 A71-40132

Binary computer holograms construction, discussing two and three dimensional objects, wave propagation, plotter instrumentation, photographic reduction and diffusers 21 p3380 A71-40921

High resolution portable hologram recording camera with pulsed ruby laser light source and rechargeable storage batteries as self contained power supply 21 p3380 A71-40926

Photopolymer holography systems and holograms fixing techniques, discussing polymer films image storing and fixing processes 21 p3381 A71-40927

Photographically recorded image enhancement, discussing filtering, SNR and film grain noise 21 p3382 A71-40936

Delta wing shock envelope visualization at hypersonic speed, obtaining flow field photographs by vapor screen technique 21 p3324 A71-40973

Pre- and post-exposure recording in holographic measurement of high object velocities for enhanced image reconstruction 22 p3537 A71-41597

Millimeter wave holographic imaging for concealed weapon detection by phase-only hologram, discussing recording and reconstruction systems configurations 22 p3546 A71-42485

Diffuse object scanned illumination hologram recording, discussing intermodulation flare light elimination for speed and reconstruction efficiency 22 p3549 A71-42561

Hologram recording by optical wave field scanning with arbitrary aperture and point source at center of entrance pupil and photoreceiver 23 p3675 A71-43398

Photographic recording for graduated circle readings during stellar observation, discussing method, errors and system 23 p3680 A71-44264

Goloseyev Wanshaff vertical circle photographic device, discussing photomicroscopes and automatic control unit 23 p3680 A71-44265

Photogrammetry of objects in motion, discussing variable time equipment, picture taking methods, applications and accuracy 24 p3826 A71-44759

Stellar UV cut-off by statospheric nacelle recorded on photographic film by Schmidt telescope fitted with objective prism, widening spectrum by scanning 24 p3875 A71-45272

PHOTOGRAPHIC RECORDING INSTRUMENTS

U OPTICAL MEASURING INSTRUMENTS

U PHOTOGRAPHIC RECORDING

U RECORDING INSTRUMENTS

PHOTOGRAPHIC RECTIFIERS

Astrophotographs reduction for wide angle negatives, using linear and eight constants method 04 p0599 A71-15559

Global lunar map coordinate grid from spaceborne photography and rectification on spherical screen, noting rays and maria 20 p3296 A71-39621

PHOTOGRAPHIC TRACKING

Camera focal distance, optical center position and distortion determination of Zeiss Astrographic objective by moving star pairs method 03 p0428 A71-13941

Artificial satellite photographic tracking, discussing Baker-Nunn cameras, international projects and future research 03 p0455 A71-14070

Dynamics and thermodynamics of water and oxygen particles ejected into space by Apollo during translunar flight, using ground based photographic observations [AIAA PAPER 71-474] 11 p1833 A71-26254

Photographic observations of Pageos satellite during 1968 with PO-2 camera 14 p2250 A71-31118

Trace length analysis of Pageos and Echo 2 satellites by camera observations 14 p2318 A71-31119

Camera vibration, and refraction anomaly effects on error of designated position for star or satellite 14 p2250 A71-31120

Coordinate measurement accuracy for star and satellite photographic observation using Zeiss Ascorecord 14 p2250 A71-31121

Photographic and laser observations during passage of satellite for determination of distance between observer and earth rotational axis 14 p2250 A71-31123

Mercury transit across solar disk, discussing visual and photographic observations with Repsold and sun refractors and coronagraphs 17 p2809 A71-35579

Optical tracking system for high angular acceleration missile flights, using movable mirrors with motion picture camera interfaced with computer 18 p2900 A71-36906

Objects in motion measurement by photogrammetry in Japan noting surf, rocket tracking, snow, roof

deformation, avalanches, car collisions, water and air turbulence applications

24 p3826 A71-44758

PHOTOGRAPHS

NT CLOUD PHOTOGRAPHS
NT LUNAR PHOTOGRAPHS
NT MOTION PICTURES

Picture transmission by Fourier transform based data reduction system, considering law of module probability and spatial distribution, statistical analysis and degradation

05 p0722 A71-16746

Photoemulsions densitometric characteristics for protonogram analysis, during fast charged particle interaction with single crystals

05 p0754 A71-17031

Vibration modes of objects and light scattering from rough surfaces, using laser speckle changes

11 p1776 A71-26138

High resolution full spatial frequency range optical image by incoherent superposition of low resolution partial frequency range component photographs, using optical aperture synthesis

22 p3538 A71-41735

PHOTOGRAPHY

NT AERIAL PHOTOGRAPHY
NT ALL SKY PHOTOGRAPHY
NT ASTRONOMICAL PHOTOGRAPHY
NT CHRONOPHOTOGRAPHY
NT CINEMATOPHOTOGRAPHY
NT CLOUD PHOTOGRAPHY
NT COLOR PHOTOGRAPHY
NT ELECTRO-OPTICAL PHOTOGRAPHY
NT ELECTRON PHOTOGRAPHY
NT FRACTOGRAPHY
NT FRAME PHOTOGRAPHY
NT HOLOGRAPHY
NT INFRARED IMAGERY
NT INFRARED PHOTOGRAPHY
NT LUNAR PHOTOGRAPHY
NT METRIC PHOTOGRAPHY
NT MULTISPECTRAL PHOTOGRAPHY
NT ORTHOPHOTOGRAPHY
NT PHOTOMICROGRAPHY
NT RADAR PHOTOGRAPHY
NT ROCKET-BORNE PHOTOGRAPHY
NT SATELLITE-BORNE PHOTOGRAPHY
NT SCHLIEREN PHOTOGRAPHY
NT SHADOWGRAPH PHOTOGRAPHY
NT SPACEBORNE PHOTOGRAPHY
NT STEREOPHOTOGRAPHY
NT ULTRAVIOLET PHOTOGRAPHY
NT ULTRAVIOLET PHOTOMETRY
NT UNDERWATER PHOTOGRAPHY

Multiple exposure holographic interferometer for static and dynamic photomechanics

03 p0422 A71-13171

Image polarity in holography and carrier frequency photography

04 p0601 A71-15696

Submerged arc welding process, observing arc motion and metal transfer with X ray high speed photography

06 p0905 A71-18090

Gamma radiation influence on photochemical effect in GaP and GaAs single crystals, using microhardness tester

10 p1656 A71-24143

Photography and navigation - Conference, Columbus, Ohio, May 1970

12 p1907 A71-27255

Inertial-inertial beam stabilization application for image surface mechanical coupling to instrument /photography/ and uncoupled surface /eye/

14 p2242 A71-30146

Diffraction technique for three dimensional frequency spectra of photographic images using computer program based on Fourier transformation of optical density distribution

15 p2406 A71-31645

Photosystem resolution of coherent laser illuminated objects, discussing experimental investigation of image quality dependence on relative aperture

19 p3073 A71-38194

PHOTOINTERPRETATION

Bibliography of bibliographies, manuals and books covering photointerpretation and remote sensing

01 p0084 A71-11379

Remote sensing systems for vegetation analysis, discussing machine-aided photointerpretation methods for data analysis

01 p0084 A71-11590

Automatic pattern recognition in photographic transparencies, using diffraction pattern sampling

02 p0225 A71-11704

Information content and digital storage of aerial photography using assessing entropy of written English text

02 p0248 A71-11953

Semiautomatic device for vertical circle, limb photographs measurement, involving beam splitting with subsequent comparison of modulated components

04 p0591 A71-14850

Mars Mariner 6 and 7 flyby missions, discussing surface and atmospheric information and data processing techniques

06 p0965 A71-17626

Mars surface TV pictures from Mariner 6 and 7, including cratered and uncratered terrains, light and dark markings and south polar cap

06 p0965 A71-17628

Photointerpretation automation, discussing computer pattern input system, image scanning and correlation, optical image transformations, trainable logic techniques, etc

06 p0900 A71-18095

Inner solar corona polarization during 22 September 1968 total eclipse based on isolines from polarimetric photographs

06 p0975 A71-18440

Weather radar plan position indicator automatic film reading for digital mapping of rainfall intensity, discussing raindrop sizing

08 p1286 A71-20690

Image specifications and data interpretation techniques for regional resource survey using small scale aerial and space photography

08 p1288 A71-21245

Natural image computer for terrain pattern recognition and delineation from aerial photographic inputs

08 p1281 A71-21255

Aerial photographic block aerotriangulation error analysis, discussing block configuration, perimeter and vertical controls, premarking, overlapping, etc

08 p1288 A71-21260

Crop species and soil condition computerized identification from film optical density differences, using multibase and multiemulsion photography

08 p1282 A71-21436

Air-photo interpretation to inventory kind of cattle-raising operation practiced on farms of southern Ontario

08 p1282 A71-21437

Automatic adaptive pattern recognition in photomapping

08 p1259 A71-21438

Venus photographs analysis during synoptic periods, noting inconclusive results on cloud layer and planetary surface structures

09 p1521 A71-22845

Aerial photographs point marking by Markov instrument, discussing high precision stereophotogrammetric equipment for photogrammetric work and physical marking

09 p1451 A71-23177

Fringe interpretation in stress-holo- interferometry, emphasizing isopachic-isochromatic interaction effects in photoelastic analysis

[SESA PAPER 1642] 09 p1542 A71-23538

Recording and interpretation of aerial photographs applied to geomorphology

10 p1599 A71-23872

Algorithm for using presence indicator context and test for target recognition system, discussing simulation technique for use without hardware target recognizer

11 p1734 A71-25143

Inner solar corona polarization during 22 September 1968 total eclipse based on isolines from polarimetric photographs

12 p1955 A71-26590

Statistical diameter size distribution of random circles on plane or spheres in space from satellite and aircraft measurements for aerial and cloud photography

12 p1929 A71-27100

Photography date effects on intensive study sites airphoto interpretations, using color and color-IR films

12 p1907 A71-27258

Parallax errors in drawing contour lines on universal stereograph due to aerial photographic images brightness difference

13 p2070 A71-29083

Dwelling unit estimation with color IR photos, applying aerial photointerpretation to urban analysis

13 p2064 A71-29396

Satellite IR photography, discussing camera systems, photointerpretation, applications in glaciology, hydrology, oceanography, geology, volcanology and environmental protection

15 p2408 A71-31835

Psychological tests for aerial photograph interpreter selection and performance prediction

16 p2534 A71-32829

Electronic multiimage processor for enhancement and interpretation of ERTS multiband remote sensor imagery data

17 p2737 A71-34273

Lunar Apennine-Hadley region geological implications from high resolution earth-based radar map and Lunar Orbiter photography

20 p3287 A71-38977

Cloud amount and cloud cover interpretation from satellite data compared with ground, noting radiometric limitations

20 p3258 A71-39549

Earth surface effective temperature map from meteorological satellites IR imagery interpretation

20 p3260 A71-39686

Earth surface characteristics relationship to meteorological elements based on interpretation of color space photographs from automated Zond 7 station

20 p3260 A71-39687

Statistical diameter size distribution of random circles on plane or spheres in space from satellite and aircraft measurements for aerial and cloud photography

22 p3537 A71-41655

PHOTOIONIZATION

Photoionization coefficients and photoelectron impact excitation efficiencies in daytime ionosphere, noting role in dayglow

01 p0077 A71-11515

Metastable atomic oxygen ion production in F region plasma due to photoionization by solar XUV radiation

03 p0462 A71-13271

Photoelectron emission of organic semiconductors, considering molecular and defect photoionization and exciton collisions

03 p0467 A71-13399

Intergalactic gas photoionization by quasars UV radiation, using Friedman cosmological model

05 p0805 A71-16111

Rare gases interaction with focused multimode Q switched laser beam, measuring orders of nonlinearity and multiphoton ionization probabilities

05 p0761 A71-16335

Continuous nitrogen and oxygen ion spectra due to photoionization and free ion transfers at high temperatures

05 p0838 A71-16788

Cross sections for fluorescence production in carbon dioxide photoionization by 58.4 nm radiation, deriving emission spectra

06 p0963 A71-17255

Solar stimulated X ray fluorescence by photoelectric ionization in upper atmosphere, discussing effects on X ray astronomy experiments

06 p0949 A71-17268

F region photoionization heating, investigating energy transfer from ionizing photon to neutral gas atoms and molecules

06 p0893 A71-17982

UV absorption line spectra from HI regions, evaluating X ray and photoionization heating models

07 p1190 A71-18853

Photoionization cross section in resonance continuum of CI, using wall stabilized argon arc

07 p1111 A71-19487

D region oxygen photoionization rates decrease due to carbon dioxide absorption

07 p1103 A71-19673

Hydrogen and helium photoionization, calculating total cross section and transitions for soft X ray region

08 p1350 A71-20948

Atomic N and C photoionization cross sections by shock tube vacuum UV spectrometry

10 p1646 A71-24990

Li photoionization cross sections determined from spectral intensity measurements as function of threshold wavelength, discussing radiative electron-ion recombination into first excited state

10 p1646 A71-24992

Atomic Ba excitation, ionization and oxidation during release in sunlight at high altitudes

13 p2026 A71-29038

Shock front electron number density profile due to ground state precursor atoms photoionization, assuming LTE in heated gas

15 p2392 A71-32120

High temperature nitrogen plasma emission spectrum in 2500-5000 A range, estimating negative ion photoionization cross sections

16 p2613 A71-32900

Continuous nitrogen and oxygen ion spectra due to photoionization and free ion transfers at high temperatures, calculating absorption coefficient

16 p2662 A71-33040

Analytic approximations for ionization structure of nebula photoionized by flat spectrum

16 p2632 A71-33319

Hydrated electrons photoexcitation by giant pulse Q-switched ruby laser, investigating absorptivity over wide range of light intensities

17 p2753 A71-34950

Potassium photoionization cross section, including spin-orbit interaction, orientation of photoejected electrons and dipole transition moment correction due to core polarization

21 p3417 A71-40197

Activator Mn impurity effect of carrier redistribution and partial photoionization of photoconductivity spectra of ZnS single crystals

21 p3430 A71-41218

Photoionization mass spectrometry, considering application to appearance potentials determination, ion-neutral reactions and gas analysis

22 p3537 A71-41649

- Interstellar He photoionization effect on solar wind abundance 23 p3721 A71-43182
- PHOTOLUMINESCENCE**
NT X RAY FLUORESCENCE
 Black and white and multicolor laser display systems with monochromatic or bichromatic source, using photoluminescent materials and acousto-optic deflectors and modulators 05 p0760 A71-16259
 Daytime near horizon atmospheric luminescence measurement by Cosmos 224 satellite, discussing contributions of nitrogen and aerosol and Rayleigh scatterings 09 p1435 A71-22432
 Cu doped GaAs electron radiative capture mechanisms based on photoconductivity and photoluminescence dependence on temperature and excitation intensity 10 p1657 A71-24324
 Oxygen contamination effect on GaP solar cell electroluminescence and photoluminescence characteristics from electrical and mass spectroscopic analysis data 19 p2998 A71-38143
 Temperature dependence of impurity photoluminescence of Cr-doped GaAs single crystals, measuring activation energy 21 p3430 A71-41214
 Oxygen effects on SiC electrical properties by comparison of photoluminescence spectra of alpha-SiC crystals grown by sublimation in Ar atmosphere 21 p3436 A71-41348
 Silicon carbide single crystal photoluminescence under pulsed ruby laser light irradiation at 77 K, discussing radiative recombination of excitons 24 p3833 A71-44666
- PHOTOLYSIS**
NT RADIOLYSIS
 Hydrogen fluoride elimination chemical laser from difluoromethylamine using temperatures below 268 K and flash photolysis 07 p1123 A71-19372
 Intermediates structure and IR spectrum in OH reaction with CO by vacuum UV photolysis, studying refractive product absorptions and valence force potentials 08 p1336 A71-20661
 Oxygen molecules photolysis at 1849 and 1931 Å, investigating ozone formation quantum yield 08 p1337 A71-20663
 Quantum yield of carbon dioxide photolysis at 1470 Å concerning Mars and Venus atmospheres 09 p1403 A71-23377
 Atomic and molecular hydrogen yields of propyne photolysis at 1470 Å Xe resonance line 09 p1403 A71-23378
 Quenching rates for oxygen during 1470 Å pulse photolysis in carbon dioxide, nitrogen and helium mixtures 09 p1404 A71-23382
 Photolysis of HCl photosensitized evolution from dichlorobutane in solution by aliphatic ketones 11 p1728 A71-25937
 Quadrupole mass spectrometry in studies of heterogeneous and flash photolytic reactions and unstable intermediates detection 11 p1765 A71-26279
 Quantitative UV radiative transfer and photolysis in model Jupiter atmosphere, considering coloration by ammonia and hydrogen sulfide gases in cloud region 11 p1834 A71-26455
 Flash photolysis produced methyl and methylene radical transitions maximum extinction coefficients and oscillator strength in vacuum UV 12 p1876 A71-26788
 Flash UV photolysis of ozone/water vapor mixtures, noting OH radical nonreaction with ozone 13 p2025 A71-28349
 UV photolysis of ozone in presence of molecular oxygen, discussing energy exchange reaction with molecular oxygen 13 p2025 A71-28350
 Rhodopsin kinetics mathematical analysis by cyclic five-component model, applying to flash and extended photolysis in rat retina 17 p2680 A71-34653
 Photolysis of metarhodopsin I, discussing rate and extent of conversion to rhodopsin 17 p2680 A71-34654
 Pulsed chain reaction chemical lasers using flash photolysis of hydrogen-fluorine-helium mixtures 17 p2754 A71-35750
 Human cone visual pigments kinetic equation testing by comparing photolysis rate at equilibrium to regeneration rates 18 p2854 A71-36001
 Flash photolysis produced gaseous carbon difluoride IR spectrum analysis by rapid scan IR spectroscopy 19 p3011 A71-38053
 Flash photolysis initiated gaseous explosions detonation effects, observing ionization and radical emission spectra, absorption intensities and induction periods 19 p3169 A71-38110
 Pulsed laser emission chemically pumped by exothermic chain reaction between hydrogen and fluorine mixed with He initiated by flash photolysis 21 p3391 A71-40238
 Photocatalytic stimulation of UV radiation photolysis of amino acids and pentoses in aqueous solutions by metal oxide sols 21 p3345 A71-40574
 Carbon dioxide photolysis at 1849 Å and various pressures, suggesting gas dissociation at wavelengths with appreciable absorption 23 p3641 A71-43328
- PHOTOMAGNETIC EFFECTS**
 Transverse parity photomagnetic effect during intense illumination in isotropic semiconductor crystals with relaxation time independent of energy 05 p0794 A71-17041
 Bipolar photomagnetic effect relation to nonheating electric field in semiconductors with isotropic holes and multivalley electrons, obtaining surface intervalley relaxation rates 10 p1656 A71-24320
 Photomagnetic effect in ferric borate, noting photoinduced change, radiation sensitivity and temperature effects 12 p1943 A71-26857
 Large photomagnetic effect in semiconductor films using multilayered Cd-Te p-n microjunctions 23 p3716 A71-43484
- PHOTOMECHANICS**
U PHOTOGRAPHY
U PRINTING
PHOTOMETERS
NT ELECTROPHOTOMETERS
NT ULTRAVIOLET SPECTROMETERS
 High sensitivity photodiode, photomultiplier and photoconductive detectors characteristics for wide-band optical communication 02 p0248 A71-12005
 Low brightness spacecraft photometer calibration using moonlight earth radiance as reference 02 p0249 A71-12075
 Double beam microphotometer for simultaneous measurement of negatives, reducing processing time and density fluctuations 02 p0251 A71-12358
 Iris microphotometer based on slot type instrument, discussing design and operational characteristics 04 p0590 A71-14839
 Iris photometer for star observations, discussing automatic compensation for plate background 04 p0590 A71-14840
 Photodetector triggered single pulse selection from mode locked ruby laser 04 p0608 A71-15595
 Photodetector-transistor amplifier coupling for maximum SNR in optical communication systems 06 p0866 A71-17370
 Photometric attenuator with linear birefringent polarizers, describing construction and calibration 07 p1110 A71-19468
 Photoelectron counting distribution for random medium passage scintillated stochastic light, considering low level amplitude stabilized and chaotic radiation transmission through turbulent atmosphere 07 p1159 A71-19513
 Optical data storage photodetector output signal to noise and signal to background ratios, using Fourier transform amplitude and phase holograms 08 p1287 A71-21186
 Photodetector frequency response measurement, using beat light signals from mixed single mode He-Ne lasers 09 p1460 A71-22227
 Photon counting stellar photometer for UVB spectra, describing operation and block diagram 09 p1451 A71-23187
 Sensitivity threshold of optical heterodyne receiver as function of laser amplitude spectrum, using photodetector output noise 10 p1622 A71-24882
 Refraction correction in photometer with cylindrical light scattering cell and detectors, describing experimental testing by mathematical and geometrical analysis 11 p1799 A71-26063
 Auroral spectroscopy, considering grating spectrometers, Fabry-Perot and Michelson spectrometers, filter photometers, etc 13 p2058 A71-28039
 Amplitude modulated optical band signal detection, comparing optimal direct photodetector and superheterodyne receivers sensitivities 13 p2029 A71-28365
 Photodetectors for laser applications in visible and near IR spectrum, discussing optical loss and pulse dispersion measurements 13 p2078 A71-28442
 Computer installations on photometric telescope control system for astronomical observations 17 p2711 A71-34981
- Digitized microphotometer for star image and stellar spectra detection, describing design, operational principles and applications 17 p2742 A71-35001
 Microphotometer digital data processing at Canadian astrophysical observatory 17 p2743 A71-35007
 IR astronomy review covering semiconductor detectors and astronomical radiation sources including thermal and nonthermal sources 18 p2959 A71-35909
 Autoexposure system for tracking telescopes, describing photometer and camera shuttle automatic control subsystems 18 p2919 A71-36088
 Laser velocimeter for wide range velocity measurement, using photodetector to observe light scattering by particles flowing across fringe pattern 18 p2932 A71-36618
 Thermal, pyroelectric and photoelectric detectors for middle IR wavelength range 19 p3064 A71-38064
 Schottky barrier diodes as photodetectors in hot electron mode, deriving ballistic transport model for scattering mechanisms effects 20 p2326 A71-39191
 Statistical analysis of microphotometer scan of solar granulation photographs blurring during partial eclipse of 20 May 1966, correcting image for atmospheric and instrument effects 21 p3439 A71-40053
 High capacity holographic storage system including frequency doubled Nd-YAG laser, Si integrated photodetector array and digital light deflector 22 p3540 A71-41754
 Semiconductor diode image tube system as digital multichannel photometer, noting cost, weight and size advantages over photomultiplier tube array with pulse counting electronics 22 p3541 A71-41793
 Weak modulated signal sensitivity of photodetectors with strong background as function of bias voltage and illumination power 23 p3678 A71-43533
 Electronic optical astronomy, describing image detectors and computer controlled microphotometers and telescope setting systems 23 p3678 A71-43542
 He-Ne laser coherent radiation photodetection by variable diaphragm photomultiplier, analyzing photocurrent spectra as function of diaphragms aperture size and shape 23 p3687 A71-44175
- PHOTOMETRY**
NT ASTRONOMICAL PHOTOMETRY
NT ELECTROPHOTOMETRY
NT SPECTROPHOTOMETRY
NT STELLAR SPECTROPHOTOMETRY
NT ULTRAVIOLET PHOTOMETRY
NT VISUAL PHOTOMETRY
 Photometric observations of lunar surface regions, noting color variations with phase change 05 p0809 A71-16461
 Automatic cytophotometric techniques including microphotometer, ultramicrospectrophotograph, radiographic analyzer, microinterferometers, cytofluorometer and differential microfluorometers 06 p0864 A71-18693
 Cytophotometric method using digital computer program and scanning microscope 06 p0864 A71-18694
 Uranus physically self consistent atmosphere model based on spectroscopic, photometric and radio observational data 07 p1198 A71-19828
 Full photographic spectral range spaceborne cameras photometric calibration, involving determination of absolute magnitude and illuminance spatial variation in image plane 09 p1447 A71-22744
 Photometric method for birefringence parameters determination in photoelastic stress distribution measurements, using proposed photosensitivity calibration standards 10 p1611 A71-24354
 Meteoric aerosols optical manifestation from photometric measurements on stratospheric balloons, demonstrating Orionids effects on twilight sky brightness 12 p1960 A71-26832
 Photometric analysis of manned spacecraft twilight brightness photographs for spherical atmosphere in single scattering approximation 12 p1901 A71-27103
 Spectral luminance and transmittance of noctilucent clouds for spaceborne photometric observation, using American-Swedish rocket particle experiment 14 p2232 A71-29962
 Spectrophotometers photometric accuracy measurement technique, using Bouguer law and optical fields superposition 14 p2240 A71-30123
 Supplementary tables to SI nomenclature for radiometry and photometry including photon flux 14 p2242 A71-30157

IQSY night airglow from multistation photometric observation network, discussing data processing, instruments, publications and catalogs

15 p2396 A71-31609

Reagents for photometric determination of rare earth elements of yttrium subgroup in binary mixtures with La or Ce

15 p2367 A71-31646

Gray tone differences between undisturbed lunar surface and darker ejecta around Surveyor 1 footpads based on footprint photometry and albedo

15 p2493 A71-32482

Gaseous chromium carbonyl or aqueous chromium salt spray additives behavior photometric investigations in premixed hydrogen-oxygen-nitrogen flames

16 p2540 A71-33374

Height resolved atmospheric turbulence properties from photometric measurements of airglow intensity fluctuations, discussing detection, separation from noise and statistical analysis

20 p3227 A71-39837

Flashing civil aviation lights history, progress and photometric characteristics, discussing navigation and landing aids

22 p3499 A71-41489

Flashing lights radiation characteristics photometric measurement, discussing measuring apparatus sensitivity and errors analysis

22 p3499 A71-41496

Limited interval definitions of photometric functions of lunar crater walls by photography from orbiting Apollo 11

22 p3603 A71-42187

PHOTOMICROGRAPHY

Electron microscope micrographs enhancement by holographic image deblurring

04 p0596 A71-15135

Organic free radical photographic films for biomedical microimaging

07 p1110 A71-19475

Microradiographic and acoustic evaluation of fracture in boron filament aluminum matrix composite under tensile stress

19 p3081 A71-37903

Goloseyev Wanshaff vertical circle photographic device, discussing photomicroscopes and automatic control unit

23 p3680 A71-44265

PHOTOMULTIPLIER TUBES

High sensitivity photodiode, photomultiplier and photoconductive detectors characteristics for wide-band optical communication

02 p0248 A71-12005

Dynamic cross-field photomultiplier sampling function characteristics measurement using self-mode-locked He-Ne pulsed laser

02 p0248 A71-12006

Low level optical signal transient response measuring instrument with nsec resolution and automatic photomultiplier current gain control

02 p0249 A71-12131

Eclipse photon counting for solar atmosphere height determination, describing spectrograph-photomultiplier apparatus

03 p0424 A71-13632

Stellar spectrometers design features and performance with photomultipliers, emphasizing sensitivity

04 p0589 A71-14834

Electron accelerator with broad stable beam for calibration of spectrometers and channel electron multipliers

04 p0599 A71-15587

Helical channel multipliers encapsulation for space flight applications

04 p0600 A71-15597

Pulkovo observatory six channel two slit single photomultiplier rotating photographic plate magnetograph, for solar spectra polarization and radial velocities observation

07 p1109 A71-19337

Photocathode area sensitivity contours-wavelength relationship from photomultiplier absolute intensity and near IR spectrum laser research

08 p1291 A71-21408

Ion acoustic waves propagation and structure measurements with metal electrode technique and continuous channel electron multiplier in plasma wind tunnel

10 p1611 A71-24517

Quantum counting efficiency of commercial photomultiplier at 0328 Å by direct measurements, including signal and background dependence

11 p1766 A71-26300

Sapphire windowed argon filled tungsten ribbon filament lamp in vacuum UV for application in photomultiplier quantum efficiency calibration

12 p1904 A71-26801

Versatile pulse amplifier for use with scintillation counters, surface barrier detectors, proportional counters or channel electron multipliers

13 p2067 A71-28163

Experimental solar blind photomultipliers for stellar photometry above earth atmosphere at 1450-2800 Å, giving spectral response and quantum efficiency

14 p2240 A71-30122

Time coordinate compensator for time variable spectrometers operating on long plastic scintillators with two terminal photomultipliers

14 p2247 A71-30579

Digital nonregular pulse counter, determining noise characteristics of photomultipliers in single pulse recording mode

14 p2213 A71-30580

Photomultiplier tube operation in terms of photoelectron counting photometry, examining emitted signal statistical properties

15 p2408 A71-31832

Critique on photomultiplier tube for photon counting, considering pulse height distribution, SNR and electron collection efficiency errors

16 p2578 A71-33146

Temperature effects on photoelectric photometry, considering photomultiplier tube and electronics as black box with photons and electric pulses

16 p2548 A71-34097

Optoelectronic elements for information system applications, discussing photomultipliers, photodiodes, photoresistors, avalanche and photoparametric diodes response and bandwidth characteristics

17 p2752 A71-34391

Image dissector photomultiplier for acquisition, guiding, focusing and photometric monitoring in telescope control

17 p2741 A71-34992

Paraterphenyl coated photomultiplier as detector in far UV spectra, detailing efficiency range and sensitivity

17 p2745 A71-35589

Electron emitter photomultipliers and photocathodes for low light level and scintillation counter applications, using negative electron affinity

23 p3651 A71-43432

Illumination wavelength effect and supply voltage dependence of photomultiplier area sensitivity map

23 p3676 A71-43505

He-Ne laser coherent radiation photodetection by variable diaphragm photomultiplier, analyzing photocurrent spectra as function of diaphragms aperture size and shape

23 p3687 A71-44175

Optical enhancement of photomultipliers extended to UV wavelengths, using suprasil and spectroil fused silica with high flat transmission curves as optical materials

24 p3829 A71-45212

Channel electron multiplier principles and characteristics, discussing secondary electron production probability during electron irradiation of surface in vacuum

24 p3811 A71-45326

Surface electronic conductivity in oxide glasses for microchannel electron multipliers, noting heat treatment and chemical composition effects

24 p3862 A71-45327

Computer model of microchannel electron multiplier plates in imaging devices using Monte Carlo method

24 p3811 A71-45328

Electron multiplier pulse height distribution for single electron input, investigating relative variance correlation with statistical fluctuations of gain

24 p3811 A71-45329

Current and charge saturation effects on channel electron multipliers in continuous and pulse operation

24 p3811 A71-45330

Single channel electron multiplier manufacture and performances, discussing test equipment and procedures

24 p3811 A71-45331

Mullard channel electron multipliers applications to space research, scientific instruments, vacuum devices and mass spectrometers

24 p3811 A71-45332

Single channel electron multiplier applications to sounding rockets, orbital satellites and deep space probes, discussing fatigue effects, ultrahigh vacuum environments and UV and X ray studies

24 p3811 A71-45333

Microchannel plate/compact array of channel electron multipliers/amplifying electron beam containing spatial information, discussing material and technological considerations in plate construction

24 p3811 A71-45334

Microchannel plates detection efficiency for 2-150 keV electrons from C 14 pellet and electron gun

24 p3829 A71-45336

Photoelectric tubes microchannel plates degassing during bake-out or during operation by electron bombardment, discussing desorption elimination by multiplier treatment before tube sealing

24 p3811 A71-45337

PHOTON ABSORPTION

U ELECTROMAGNETIC ABSORPTION

PHOTON BEAMS

NT LIGHT BEAMS

Steady state photon transfer through homogeneous semimfinite isothermal atmosphere with two level atoms, deriving linear integral equation for escape probability distribution

10 p1643 A71-24964

Multiphoton ionization cross section and charge number in neon near resonance under focused laser beam

13 p2081 A71-29338

Sunlight photodetachment rates and energy dependent cross sections for ozone ions, using photon beam excitation in buffer gas

16 p2574 A71-33962

Temporal distribution of photons radiated by He-Ne laser operating in five modes

17 p2750 A71-34202

PHOTON DENSITY

Earth atmosphere X ray absorption, determining photon flux, energy and angular distribution as function of altitude by Monte Carlo method

02 p0299 A71-11776

Eclipse photon counting for solar atmosphere height determination, describing spectrograph-photomultiplier apparatus

03 p0424 A71-13632

Stratospheric soft photon anomalous fluxes associated with May 1967 solar cosmic ray bursts

06 p0959 A71-18157

Detectable information rate changes of photon counter with finite observation time and background noise

08 p1289 A71-21286

Approximate photocount statistics for superposition of coherent and chaotic radiation of Gaussian, triangular, square and Lorentzian shaped spectra

09 p1462 A71-22686

Photon intensities of UV spectral lines from energetic magnetically confined vacuum carbon arc, using monochromator double ion chamber detector system

09 p1502 A71-22813

Polar cap atomic processes stimulated by photons, electrons and protons, considering particle morphology

10 p1661 A71-24311

Supplementary tables to SI nomenclature for radiometry and photometry including photon flux

14 p2242 A71-30157

Collision rates in photon and relativistic particle gases, noting importance for cosmic radio and X ray sources processes calculations

18 p2949 A71-36100

Virgo XR-1 X rays observation with rocket-borne proportional counters, noting photo index or bremsstrahlung temperature consistency with spectrum

18 p2959 A71-37050

PHOTON-ELECTRON INTERACTION

Electron entrainment by photons during intraband light absorption by free carriers in Ge semiconductors

09 p1507 A71-22232

Cross section for electron and muon neutrino-antineutrino pair production by photons, using intermediate boson theory

11 p1802 A71-25588

Deuterium gas breakdown by ruby laser, using quantum kinetic equation for electron interactions with molecules and photon field

12 p1915 A71-27284

Compton synchrotron spectra of gamma rays produced in Crab Nebula by photons scattered by relativistic electrons, assuming magnetic field due to pulsar

18 p2963 A71-36154

Quantum mechanical considerations underlying calculations of two-photon transition probabilities, discussing experiments on semiconductors, ionic crystals and organic compounds

18 p2930 A71-36241

Electron drag by photons during intraband light absorption by free carriers in n-Ge semiconductors

21 p3428 A71-41111

Urbach absorption-photon energy law for excitons in AII-BVI semiconductors

23 p3716 A71-43481

PHOTONIC PROPULSION

Shortest transfer time interstellar propulsion systems, considering nuclear pulse and electric rockets, fusion and photon rockets, and ramjets

15 p2469 A71-31748

Energy requirements for antihydrogen production in interstellar photonic drives, discussing feasibility

18 p2956 A71-36683

PHOTONS

Laser oscillation buildup from quantum noise, deriving equations of motion for moments of photon distribution and time dependence

01 p0094 A71-10826

Galactic interstellar grains alignment by starlight, noting photon intrinsic angular momentum role

01 p0159 A71-10865

Photon-neutrino coupling theory of weak interactions, noting exclusion by astrophysical data for white dwarfs

01 p0130 A71-11272

Turbulent plasma radio emission theory of photon production and transport, considering application to quasars

02 p0292 A71-12587

Free hole drag in p-type Ge by photons in optical transitions between valence band subbands, examining magnetic field effects 02 p0296 A71-12613

Cosmic photons Planck constant, considering photon absorption dependence on variations of spin angular momentum 03 p0473 A71-13562

Expanding universe adiabatic density fluctuation evolution, describing photon distribution function collision equation for plasma recombination 05 p0801 A71-15929

Quark fusion in quasi-stellar objects, deriving approximate formula for efficiency of converting rest mass into photons 05 p0785 A71-16686

Photoemulsions densitometric characteristics for protonogram analysis, during fast charged particle interaction with single crystals 05 p0754 A71-17031

F region photoionization heating, investigating energy transfer from ionizing photon to neutral gas atoms and molecules 06 p0893 A71-17982

Electron mass and photon wave renormalizations functional relationships, studying perturbation theory based electrodynamic divergences 07 p1162 A71-20550

Photon emission from electron moving in field of two plane electromagnetic waves with different frequencies and propagating in same direction 09 p1460 A71-22364

Spectral and relaxation characteristics in antiStokes two photon luminescence of polycrystalline ruby exposed to filtered light pulses 09 p1508 A71-22392

Photon counting stellar photometer for UV spectra, describing operation and block diagram 09 p1451 A71-23187

Semiconductor zinc selenide and zinc cadmium selenide crystals two photon absorption coefficients, noting forbidden bandwidth relation 13 p2077 A71-27954

Diffuse reflection from clouds with horizontal surface striations, using Monte Carlo method to follow photons through simplified models 13 p2056 A71-27975

Angular distribution of muon-poor extensive air showers, considering generation by atmospheric nuclei interaction 13 p2123 A71-28073

PAX intermediate spectrum reactor neutron and photon dose rates and fast and thermal neutron flux calculation, comparing results with experiment 13 p2099 A71-29258

Electron velocity, spin, energy and mass derivation based on consideration as negative component of photon 13 p2103 A71-29277

Pulsar signature on diffuse X ray background, converting fraction of luminosity into k series photons 14 p2297 A71-29584

Transparency of extragalactic space to very high energy photons, considering background gamma rays effects 15 p2472 A71-31198

Interferometric observation of photon fluctuation during Fraunhofer diffraction by small round hole, considering light granular structure at low intensities 15 p2421 A71-32405

Photon dwell time in one dimensionally isotropically scattering medium, assuming absorbed state as arbitrary function of optical thickness 15 p2492 A71-32460

Galaxy formation in expanding universe, discussing primordial plasma and photon gas turbulent medium for magnetic field amplification by dynamo mechanism 16 p2625 A71-33052

Critique on photomultiplier tube for photon counting, considering pulse height distribution, SNR and electron collection efficiency errors 16 p2578 A71-33146

Electrodynamics Lagrangian with gauge invariant electron operator, obtaining free field nonequal time commutators and photon propagator for perturbation theory 16 p2610 A71-33269

Two photon method of measuring ultrashort pulses and nonlinear optical effectiveness of lasers in synchronized mode 16 p2587 A71-33644

Secondary electrons and photons energy spectra and depth dependence in upper atmosphere from numerical solution of one dimensional transport equations 16 p2628 A71-33937

Temperature effects on photoelectric photometry, considering photomultiplier tube and electronics as black box with photons and electric pulses 16 p2548 A71-34097

Image amplifier camera resolution as function of light level based on photon statistics and cathode quantum efficiency 17 p2746 A71-35762

Critique of Woodward-Young hypothesis of frequency dependence of light velocity in gravitational fields based on variable stars observations, considering photon rest mass 20 p3286 A71-38836

Photon mass terrestrial and extraterrestrial limit measurements, discussing speed of light frequency dependence, Coulomb law analog in magnetostatics energy conservation, etc 21 p3418 A71-40674

Computer algorithms for gamma algebra of electromagnetic form factors in terms of Chebyshev polynomials with photon 4-momentum 21 p3415 A71-40842

Electron concentration and degeneracy effect on threshold photon energy for optical transitions onset from splitoff valence band to conduction band in n-type GaAs 21 p3429 A71-41211

Electroabsorption spectra of cadmium telluride at photon energies smaller than forbidden band width, observing energy levels 21 p3429 A71-41212

Electromagnetic wave dispersion in interstellar plasma, noting indistinguishable form from natural dispersion of photons with nonzero rest mass 22 p3574 A71-41598

P-type germanium photon drag detectors with carbon dioxide lasers, discussing response speed and sensitivity 22 p3543 A71-42129

Quantum fluctuations in gas laser radiation, obtaining photon diffusion coefficients for traveling and standing waves 22 p3558 A71-42456

Bremsstrahlung photons produced by cosmic ray muons in Fe and Pb at sea level, calculating energy spectra and angular distributions 22 p3595 A71-42664

Electromagnetic mechanism of direct muon and photon production by collision of strongly interacting particles 22 p3579 A71-42665

Temperature effects on long wavelength photon frequency and linewidth in diamond, using Raman scattering techniques 23 p3715 A71-43471

Quasar and pulsar gamma ray absorption by critical energy collisions with low energy photons 24 p3866 A71-44917

PHOTOPIEZOELECTRICITY

U PHOTOELECTRICITY
U PIEZOELECTRICITY

PHOTOPRODUCTION

Organic compounds biosynthesis in simulated Mars atmosphere, using UV irradiation for photocatalytic production from CO and water mixtures 09 p1403 A71-22647

Self consistent field (SCF) calculations of dipyrindine glyoxal and bianthrone photoproduct molecules with triplet ground state, using unrestricted Hartree-Fock theory 11 p1727 A71-25576

Long wavelength UV photoproduction of amino acids on primitive earth, using hydrogen sulfide as photon acceptor 18 p2855 A71-36229

Charged pions differential photoproduction cross section description by theoretical model 22 p3578 A71-42060

PHOTORECEPTORS

Vitamin A initial uptake site and intracellular transport pathway in snails photoreceptors 01 p0009 A71-10230

Visual cells outer segments structure and retinal photoreception characteristics, describing open thermodynamic system 01 p0009 A71-10231

Light pulse generator for amplitude-frequency analysis of photoreceptors, using wideband modulated semiconductor injection laser emission 01 p0093 A71-10624

Retinal neurons receptive field center, examining excitation and direct inhibitory interaction 05 p0707 A71-16596

Retinal electronic model with about 700 photoreceptors and output cells and new interconnections technique 05 p0715 A71-17079

Vertebrate retina receptive field structure, suggesting interaction between receptor, horizontal and bipolar cells 07 p1046 A71-20623

Carotenoid depleted Drosophila circadian rhythm and visual receptors photosensitivity, discussing photopigment effects 09 p1394 A71-23160

Luxmeters and photoelectric receptors for illumination measurement of light beams in limited solid angle in image systems, considering automatic polar photogoniometer 14 p2246 A71-30417

PHOTORECONNAISSANCE

Electronic imaging devices specifications, emphasizing real time reconnaissance systems performance requirements 10 p1609 A71-24059

High resolution 16mm pulse mode cine reconnaissance camera design features, discussing dynamic balance and reaction forces cancellation 17 p2746 A71-35761

Digital processing for automatic extraction of information from reconnaissance images, discussing target and terrain configurations pattern recognition technique 17 p2747 A71-35774

Monograph on satellite-borne orbital photographic imaging techniques application to natural resources survey, discussing remote areas geomorphological and geological reconnaissance maps preparation 18 p2915 A71-35905

BITSIM computer simulation technique for application to real time airborne photoreconnaissance imagery data transmission system design and performance analysis 18 p2917 A71-36070

Wideband stabilizer design for high acuity aerial reconnaissance camera to obtain high degree of attenuation to roll and pitch rotational motion inputs 18 p2919 A71-36087

PHOTOREDUCTION

U PHOTOCHEMICAL REACTIONS
U REDUCTION [CHEMISTRY]

PHOTOSENSITIVITY

U PHOTOCONDUCTIVITY

PHOTORESISTORS

U PHOTOCONDUCTORS

PHOTOSENSITIVITY

NT LIGHT ADAPTATION
NT PHOTOTROPISM

Cats photopic and scotopic spectral sensitivity functions from dark adaptation curves, using behavioral tracking procedure 01 p0009 A71-10232

Pentose breakdown photosensitivity from UV irradiation in presence of minerals, considering prebiological period carbohydrates evolution and interaction with purines and pyrimidines 01 p0029 A71-11561

CdS-CuS n-p junction solar converters, noting long-wave sensitivity dependence on light extrinsic absorption 02 p0190 A71-11896

High resistance single crystal light sensitive n-type GaAs wafer for obtaining long wave photographic images via electric photosensitivity control 03 p0428 A71-13986

Hill reaction of disintegrating chloroplasts in vitro, investigating transient color sensitivity /red-blue effect/ 04 p0539 A71-15270

CdS single crystals treatment in salt melts to obtain given conductivity and photosensitivity, discussing LiCl, Ag, Cu, Na, Cd and In concentration effects 05 p0793 A71-16822

Telescope star photographic magnitude perception maximum capacity, considering effective or equivalent quantum yield and photoemulsion sensitivity 07 p1109 A71-19346

Light effect on dielectric constant of thin hardened dichromated gelatin films for holographic recordings 07 p1110 A71-19482

Photocathode area sensitivity contours- wavelength relationship from photomultiplier absolute intensity and near IR spectrum laser research 08 p1291 A71-21408

Photoperiodic effects on insect brain circadian clock control, investigating eclosion cycle initiation, stimulant hormone release and termination as functions of dark phase 09 p1392 A71-22648

Carotenoid depleted Drosophila circadian rhythm and visual receptors photosensitivity, discussing photopigment effects 09 p1394 A71-23160

Three-beam holographic interferometry featuring sensitivity increase and aberrations compensation 10 p1611 A71-24345

Photolysis of HCl photosensitized evolution from dichlorobutane in solution by aliphatic ketones 11 p1728 A71-25937

Photographic materials characteristic curve description by sensitometric parameters including contrast, hardness and refinement 11 p1767 A71-26468

Laser interference patterns recorded on photosensitive surface of test sample before and after deformation, considering irregularly shaped objects with rough surfaces 13 p2067 A71-28441

Thyroidectomized vitamin A deficient rats, noting visual sensitivity loss not correlated to thyroid 13 p2008 A71-28455

Small spotted dogfish shark epiphysis cerebri, determining light sensitivity and properties 13 p2008 A71-28456

Dark adapted albino rats behavioral assessment, measuring absolute visual thresholds to white and colored light

13 p2008 A71-28457

Spatio-temporal patterns in visual contrast sensitivity, noting exaggerated eye movements effects

13 p2018 A71-28462

Plane wave holographic recording and reconstruction, investigating effects of photosensitive medium as three dimensional diffractive pupil

13 p2068 A71-28711

High quality hologram copies, using photosensitive emulsion layer technique

13 p2070 A71-29027

Antimony trisulfide semiconductor films, noting chemical composition effects on photosensitive properties

15 p2461 A71-31286

Spectral sensitivities of discrete slow potentials and threshold level nerve spikes in *Limulus* ommatidium as function of hyperpolarizing current

16 p2527 A71-32869

Spectroscopic plate emulsion with excellent signal to noise characteristics, investigating baking time response in controlled nitrogen atmosphere

16 p2577 A71-33137

Volume hologram formation in photopolymer materials with bright low noise images, considering sensitivity, spatial frequency response, particle scattering noise and nonlinearities

16 p2577 A71-33144

Human visual system differential luminance sensitivity tests using simultaneous stimuli in yes-no procedure

17 p2684 A71-35256

Static converters of computer graphic information using photoreceivers with linearly decreasing and increasing spatial sensitivity

18 p2884 A71-35882

Retina photosensitive cells properties and functions compared with films photosensitive chemicals, emphasizing retinal image transformation

18 p2864 A71-36068

Multicolor images with volume dielectric holograms in photopolymer materials, reconstructing complex three dimensional images with high resolution in white light

20 p3236 A71-39192

Optically sensitive epoxy resin based high polymers under pulsed loads, observing deformation and mechanical displacement with high speed photography

22 p3614 A71-41610

Duralumin rods deformation and stress propagation study under dynamic pulse loads, using photosensitive epoxy coatings and high speed photography

22 p3537 A71-41612

Stress analysis of photosensitive coatings and transparent birefringent materials, applying holography to optical polarization method

22 p3537 A71-41614

Photosensitive epoxy resin coating light path propagation variation measurements, using continuous radiation gas laser and Fabry-Perot interferometers

22 p3555 A71-41615

Illumination effects on drain current for p channel enhancement type MOS transistor, attributing photoresponse to electron excitation in conduction band

22 p3523 A71-42481

Illumination wavelength effect and supply voltage dependence of photomultiplier area sensitivity map

23 p3676 A71-43505

Nondiffusion theory for I-V characteristics of monopolar and quasi-monopolar photosensitive semiconductors with various carrier injection levels

24 p3859 A71-44385

Adhesion, recombination and electron-band curvature nomograms for space charge region in photosensitive CdS single crystals

24 p3859 A71-44388

PHOTOSENSORS

U PHOTOELECTRICITY

U RADIATION MEASURING INSTRUMENTS

PHOTOSPHERE

Solar photospheric spectrum, investigating deuterium abundance relative to hydrogen

01 p0157 A71-10762

Electric conductivity dependence on optical depth in photospheres of spectral type F, G and K stars for different gravitational acceleration values on surface

01 p0159 A71-10866

Sunspot and photosphere electric conductivity relationships based on Michard, Mattig and Fricke-Elsasser models

01 p0159 A71-10867

Photosphere and facula turbulent velocities and damping constants from Ni and Fe IR lines analysis

02 p0306 A71-12079

Photospheric magnetic field direction autocorrelation showing differential and rigid rotation properties at various heliographic latitudes

02 p0316 A71-12751

Solar faculae semiempirical models, cospatial with strong photospheric magnetic fields constructed from continuum observations

02 p0316 A71-12757

Solar photosphere temperature constancy in thin CO layer from equivalent spectral line width determination

03 p0484 A71-13208

MHD parameters in photospheric plasmas of giant and dwarf stars, noting electric conductivity, Joule dissipation, Reynold and Lundquist numbers

03 p0490 A71-13938

Sunspots visual observations in 1969, giving Wolf numbers and rotational means by Carrington elements

04 p0644 A71-15070

Subphotospheric trapped standing acoustic wave mechanism of 5 minute oscillations on solar surface

05 p0801 A71-15936

Photospheric and interplanetary magnetic field polarity and magnitude comparison, using Explorer observations

05 p0802 A71-16012

Eu II and La II line profiles in sunspots and undisturbed photosphere

05 p0803 A71-16022

White light flares due to photosphere heating by flux of energetic ions and electrons impinging from above

05 p0797 A71-16028

Solar photosphere oscillations, suggesting convection zone acting as resonant cavity

06 p0971 A71-18243

Solar photosphere macroturbulence effects on Fraunhofer lines and central intensities of various absorption lines

06 p0975 A71-18443

Electron scattering effect on emission and absorption lines in stellar atmosphere, considering primary radiation sources uniform distribution and photosphere radiation transmission through electron atmosphere

07 p1192 A71-19291

Photosphere and facula turbulent velocities and damping constants from Ni and Fe IR lines analysis

08 p1361 A71-21129

Coronal magnetic field geometry maps, using high altitude photospheric field measurements for correlations with active sun

08 p1363 A71-21154

Solar photosphere facula, applying Schuster-Schwarzschild model for molecular lines and bedding level of carbon hydride

08 p1365 A71-21772

CH molecule line formation mechanism for 4300 A transition in solar photosphere, studying collisions with hydrogen atoms

09 p1520 A71-22843

Fraunhofer line profiles, determining optical depth at various points in photosphere

09 p1524 A71-23191

Solar photosphere turbulent velocity, taking into account instrumental profile effects

09 p1524 A71-23193

Solar granular or convective motion velocities vs photospheric oscillations for Doppler shifts in line spectra

10 p1665 A71-23776

Empirical solar photosphere continuum models, calculating temperature distribution for absolute intensities at center and limb darkening ratios

10 p1666 A71-23779

Brightness temperature from solar UV continuum in 1680 to 600 A in photosphere-chromosphere transition model

10 p1666 A71-23780

Turbulent photosphere and chromosphere, investigating finite resistivity effects on solar flare phenomena

11 p1832 A71-26173

Solar photosphere macroturbulence effects on Fraunhofer lines and central intensities of various absorption lines

12 p1955 A71-26593

Solar photosphere vibrational temperature determination, using Franck-Condon factor with equivalent line widths for five CN vibrational bands

12 p1963 A71-27081

Active unperturbed solar photosphere, determining variations in spectral line profiles

12 p1963 A71-27082

Photospheric layers supergranular motion and oscillations as function of solar atmosphere height and sun position, investigating velocity fields two dimensional structure

12 p1970 A71-27701

Continuous emission in solar flare spectra from spectroheliographic data, suggesting photospheric origin

13 p2129 A71-29052

Sunspot deep subphotospheric layer structure, noting evolution, velocity field, visibility and model formulation

13 p2142 A71-29115

Solar active regions velocity field at different levels, discussing transition region from photosphere to chromosphere

14 p2308 A71-29973

Solar active region photospheric radial velocity field time variations, using magnetograph in Fe I line

14 p2308 A71-29977

Unipolar sunspot magnetic field and electric currents, comparing chromosphere and photosphere total field vector

14 p2298 A71-29978

Solar photosphere and faculae temperature, gas/electron pressures, density and turbulence velocity from Schuster-Schwarzschild model

15 p2495 A71-32677

Solar atmospheric model, calculating shock wave dissipation in chromosphere for photosphere central iron line intensity correlation with magnetic field intensity

15 p2497 A71-32746

Sunspot convective heat transfer in terms of magnetic field convection theory, considering motion in photosphere

17 p2802 A71-34826

Solar photospheric velocity field measurements, using balloon-borne sodium resonance cell with diffraction limited telescope

18 p2965 A71-36729

Solar photosphere vibrational temperature determination, using Franck-Condon factor with equivalent line widths for five CN vibrational bands

19 p1333 A71-37431

Active unperturbed solar photosphere, determining variations in spectral line profiles

19 p1333 A71-37432

Solar photosphere and low chromosphere models temperature-height profile

19 p1335 A71-37609

Solar photosphere iron abundance data from Fraunhofer spectrum and EUV line measurements

19 p1335 A71-37610

Solar cosmic ray data, discussing multicharged nuclei relative abundances in photosphere and propagation models

19 p1326 A71-37625

Solar and stellar chromospheres and coronas production based on turbulence in granulation, photospheric mechanical flux and supergranular network magnetic field structures

19 p1336 A71-37626

Harvard-Smithsonian reference atmosphere model of solar atmosphere, combining photosphere and quiet lower chromosphere

19 p1446 A71-38660

MHD models of photospheric layers of sunspots emphasizing magnetic forces distribution

20 p3292 A71-39444

Electron acceleration and solar flare triggering due to quasi-static electric field caused by gas motion near photosphere

22 p3590 A71-41466

Neutron flux estimate from protons number needed for white light solar flare caused by energetic particle penetration into photosphere

22 p3590 A71-41467

Radiation attenuation effect on solar photosphere turbulence determination by Goldberg-Unno method

23 p3772 A71-44311

Electric conductivity correlation between solar faculae and Bilderberg model of photosphere and chromosphere

24 p3868 A71-44458

Scattered light effect on measured facula-to-photosphere contrast, leading to hotter average facula model

24 p3868 A71-44460

PHOTOSTRESSES

Metal strips with holes under tensile loads, determining plastic region boundaries with photostress method

17 p2821 A71-34592

PHOTOSYNTHESIS

Low compensation point species capacity for carbon dioxide fixation, suggesting reduced photorespiration role

02 p0201 A71-12475

Photosynthesis models, discussing photoenergetics of molecular systems

02 p0201 A71-12714

Fick diffusion model for Haxo-Blinks electrochemical determination of photosynthetic oxygen evolution

04 p0546 A71-15169

Unicellular algae photosynthesis measurement by radiometric methods under optimum and equalized conditions of light, temperature and carbon dioxide supply

05 p0714 A71-16815

Atmospheric oxygen evolution and stability, discussing effects of photosynthesis inhibition, hydrogen passage and burial carbon

07 p1102 A71-19540

Q switched ruby laser emission effect on long wave pigment system of photosynthesizing organisms

11 p1774 A71-26006

Autotrophic cultivation of cereals with high photosynthetic activity under intensive illumination as biological components in life support systems

13 p2017 A71-28405

Substrate and light dependent fixation of molecular nitrogen in *Rhodospirillum rubrum* tested for nitrogenase activity by manometric measurement

16 p2527 A71-33057

Insulators normalized theory application to selective transparent insulators photosynthesis operation 22 p3484 A71-42843

PHOTOTHERMOTROPISM
 U ANISOTROPY
 U PHOTOTROPISM
 U TEMPERATURE EFFECTS

PHOTOTROPISM
 Ruby laser passive Q switching by phototropic thin film shutter, outlining advantages over bleachable dyes 07 p1122 A71-19140
 Spectral sensitivity by stimulus control and presentation in barred pattern alternatives and photopic system monitoring by visual evoked responses 10 p1560 A71-23986
 Lettuce seedlings growth reduction and geotropic and phototropic behavior modification by 3-prime chlorophenyl 3-methoxy phthalide, noting gravity response elimination through action on statolith 23 p3639 A71-43143

PHOTOTUBES
 NT PHOTOMULTIPLIER TUBES

PHOTOVISCOELASTICITY
 Polymer binder effect photoviscoelastic stress analysis near discontinuous reinforcing fibers, comparing results with finite element method for time dependence [SESA PAPER 1630] 03 p0507 A71-13755

PHOTOVOLTAGES
 Surface state energy positions determination in high-energy gap semiconductors by photovoltage spectral distribution 14 p2284 A71-30404

PHOTOVOLTAIC CELLS
 Silicon and gallium arsenide photovoltaic solar cells, examining performance at high illumination intensities 04 p0535 A71-15006
 Si solar cells lightweight economical deployable arrays, discussing temperature performance, assembly, coverslips, interconnection, stowage and telescopic mast and ends 05 p0704 A71-16099
 Si solar cell technology, discussing contacts, low temperature performance and conversion efficiency 05 p0757 A71-16103
 Curve power factors and radiation induced changes in silicon photovoltaic solar cells, considering junction depth, bulk resistivity, temperature and illuminating light intensity 17 p2677 A71-35049
 Copper sulfide-cadmium sulfide photovoltaic solar cell electronic processes observation at heterojunction, noting electron trapping and hole injection roles in long term stability 19 p3119 A71-38140

PHOTOVOLTAIC EFFECT
 Lithium-containing p-n solar cells photovoltaic performance and stability tests at room temperature 05 p0703 A71-16090
 CdTe thin film anomalous photovoltaic effect and piezoeffect dependence on real state 07 p1176 A71-19271
 Thin polycrystalline CdTe film photovoltaic effect dependence on monochromatic light incidence angle 07 p1176 A71-19272
 Cadmium telluride epitaxial films on potassium bromide, investigating external gases effects on photovoltaic properties 07 p1179 A71-19919
 Selenium photocell photovoltaic effect, observing recombination and generation processes in space charge region 16 p2623 A71-34046
 Photovoltaic and electron-voltaic properties of diffused and Schottky barrier GaAs diodes, considering irradiance in 0.001-10,000 microwatt/sq cm range 19 p3027 A71-37484

PHTHALATES
 Lettuce seedlings growth reduction and geotropic and phototropic behavior modification by 3-prime chlorophenyl 3-methoxy phthalide, noting gravity response elimination through action on statolith 23 p3639 A71-43143

PHTHALOCYANIN
 Ruby laser Q switching by hydrogen and copper phthalocyanin vapors, obtaining nanosecond single pulses with high power density 19 p3072 A71-37768

PHUGOID OSCILLATIONS
 U OSCILLATIONS
 U OSCILLATORS
 U PITCH [INCLINATION]

PHYLLQUINONE
 Vitamin K3 effect on redox equilibria in red cell, discussing radiosensitizer mechanism 07 p1039 A71-18985

PHYSICAL CHEMISTRY
 W-Re-Ir ternary system phase diagrams, studying physicochemical properties via X ray and metallographic techniques 07 p1140 A71-20235
 Potential foods synthesis for long duration space missions by physicochemical methods, discussing

regeneration of carbohydrates from metabolic waste carbon dioxide and electrolytic byproduct hydrogen 07 p1056 A71-20375
 Soviet book on fuel burning process physicochemical fundamentals covering combustion gases thermophysical and thermochemical characteristics, methane, formaldehyde and carbon monoxide combustion reaction kinetics, etc 20 p3194 A71-39089
 Physical chemistry of Aouellou impact crater glass, suggesting meteoritic origin of tektites 21 p3450 A71-40647
 Solid lubricant molybdenum disulfide physicochemical interaction with Ag, Ni, Fe and Co at high temperatures, using X ray structural and spectrometric analyses 23 p3697 A71-44029

PHYSICAL CONSTANTS TESTING REACTOR
 U WATER COOLED REACTORS

PHYSICAL ENDURANCE
 U PHYSICAL FITNESS

PHYSICAL EXAMINATIONS
 Coronary artery heart disease detection in aircraft pilots to age 45 during physical examinations 02 p0208 A71-12392
 Flight surgeons guidance criteria for flying personnel, detailing individual areas examination, documentation and clinical findings 08 p1245 A71-20719
 Soyuz 9 cosmonauts postflight clinical examination, noting muscle pain, eyelid edema, leg muscle atrophy, etc 09 p1389 A71-22200
 Laser thermal/photochemical burns and electric shock prevention by preemployment/regular physical examinations and safety requirement education 09 p1402 A71-23412
 Aircraft pilot physical examination for regression curves on near vision and eye accommodation, noting age effect 17 p2692 A71-35197

PHYSICAL EXERCISE
 Glycogen reduction in human musculus vastus lateralis during bicycle exercise below pulse endurance limit, noting glucose infusion effect 01 p0016 A71-11400
 Resting oxygen consumption in exercise-trained and nontrained normal, hypophysectomized and thyroidectomized rats 01 p0016 A71-11408
 Human skin blood flow and venous tone in middle finger and forearm during leg muscle exercise to exhaustion 01 p0016 A71-11410
 Physical exercise effect on mitochondrial energy production in heart muscle and liver in rats 01 p0017 A71-11542
 Physical exercises to increase cosmonaut space environment tolerance, discussing effects of acceleration, altitude and hypoxia 01 p0027 A71-11556
 Oxygen uptake kinetics in human submaximal exercise during work load transitions and work-rest cycle 02 p0202 A71-11663
 Fatigue factor of lactate, ATP and creatine phosphate (CP) accumulation in working muscles during short exhaustive exercise in man 02 p0202 A71-11666
 Oxygen debt after steady state work in submaximal physical exercise 02 p0202 A71-11668
 Human muscle hardness as isometric stress force indicator 02 p0198 A71-12065
 Healthy subjects physical training effects on blood flow and enzymatic activity in skeletal muscle 02 p0201 A71-12916
 Positive effect of physical training on heat endurance of man 03 p0361 A71-13193
 Submaximal exercise ECG test in screening high risk populations for occult ischemic heart disease 03 p0372 A71-13491
 Tidal volume and respiratory rate changes at start and end of exercise, considering ventilation control and neurogenic respiratory reflexes 04 p0545 A71-15161
 Nervous system activity changes relation to physical exercise type and extent, measuring visual response time 05 p0708 A71-16620
 Human physical exercise with stepwise increasing load noting working capacity, cardiovascular and respiratory system performance and blood composition interrelations 05 p0709 A71-16805
 Cinearteriographically demonstrated coronary artery disease severity correlation with myocardial blood flow response to treadmill exercise or isoproterenol infusion 06 p0852 A71-17874
 Human body thermography for studying physiological changes due to exercise, anoxia or accelerations 06 p0860 A71-18189

Aircrews coronary insufficiency diagnosis via electrocardiographic modifications after exertion, observing ischemia 06 p0860 A71-18192
 Venomotor responses of forearm and hand veins to rapid changes in skin temperature in exercising man 06 p0861 A71-18382
 Venomotor responses of forearm veins to local and remote thermal stimuli to skin in exercising man 06 p0862 A71-18383
 Hypoxic and hypercapnic ventilatory control and oxygen uptake in athletes, noting chemoreceptor function 06 p0862 A71-18384
 Neural stimuli contribution to increasing respiration and hyperpnea during exercise 06 p0862 A71-18386
 Cardiac output during submaximal bicycle exercise in children and teen-agers, discussing oxygen transport function of blood 06 p0857 A71-18722
 Respiratory rate and cardiac responses to exercise in man 07 p1052 A71-20326
 Control and prolonged exercised rats adrenal and plasma catecholamine, corticosterone and epinephrine level comparisons using fluorometric analysis 07 p1044 A71-20330
 Rate constant for oxygen uptake exponential increase during low intensity exercise by algebraic solution 07 p1052 A71-20336
 Barometric pressure and exercise effects on erythropoietin titer in normal and hypoxic rat plasma, noting lactic acid concentration and acid base balance changes 08 p1237 A71-20676
 Acceleration tolerance improvement in human subjects by gymnastics, games, athletics and aviation pilot training 09 p1399 A71-22920
 Central nervous system responsiveness changes after exhausting physical exercise, giving electroencephalogram and sensorimotor reaction records 11 p1719 A71-25668
 Leg position effect on human calf muscle blood flow during standardized heavy rhythmic exercise 11 p1722 A71-26358
 Ventilation and heart rate responses to muscular exercise by work load ramp function changes studies 11 p1722 A71-26359
 Cardiovascular system response to swimming exercise by dogs, measuring left ventricular internal diameter and pressure, cardiac output and heart rate 12 p1873 A71-27130
 Human heart rate, minute ventilation and oxygen uptake measurement during treadmill and track running at three speeds 12 p1874 A71-27134
 Sitting and supine position effect on exercise tolerance, heart rate, systolic pressure and respiration rate in male subjects with coronary insufficiency, noting onset of angina pectoris 13 p2014 A71-29303
 Diastolic and mean blood pressure responses to exercise after beta-adrenergic blockade in normal and labile hypertensive subjects, using Trasacor 13 p2014 A71-29320
 Position, exercise and lung volume effects on healthy males pulmonary diffusing capacity for CO at rest and during exercise 13 p2015 A71-29493
 Human physiological responses comparison between work with concentric and eccentric muscle contractions, observing oxygen debt in short term exercise 13 p2024 A71-29495
 Trained college and recreational swimmers cardiac output and maximum oxygen consumption during tethered swimming and treadmill running 13 p2024 A71-29496
 Pyruvate and lactate concentrations in muscle tissue and blood at rest and during exercise 14 p2187 A71-31136
 Regulation patterns of external respiration rate in man during physical exertion, showing load dependent pulmonary ventilation in accord with minimum energy expenditure principle 15 p2358 A71-31321
 Computer quantitation of ST segment response to graded exercise in untrained and trained subjects, continuously recording amplitude of selected points on ECG waveform 15 p2358 A71-31452
 Lowered cardiac output and arterial pressure response to exercise after autonomic heart blockade in man, noting retained work capacity 15 p2358 A71-31454
 Human muscle blood flow measurement by Xe 133 clearance method during rhythmic exercise, noting work load effects 15 p2358 A71-31455

Muscle adenosine triphosphate, creatine phosphate, adenosine diphosphate, glycogen, and lactate concentrations during intermittent exercise

15 p2358 A71-31726

Normal muscle lactate concentration after prolonged exercise resulting in decrease in glycogen content

15 p2359 A71-31727

Vagus nerve effects on cardiac output adaptation to exercise in sympathectomized dogs

15 p2360 A71-32001

Maximal treadmill stress test correlation with postexercise phonocardiogram, ECG and double master test in normal subjects, discussing third and fourth heart sound incidence

15 p2361 A71-32538

Right ventricular end-diastolic volume as index of myocardial fiber length and correlation with ventricular work at rest and exercise with and without right ventricular failure

15 p2361 A71-32541

Human body water metabolism during acute high altitude exposure with heavy physical activity and high food intakes

16 p2530 A71-33240

Physical exercise oxygen uptake and debt in dogs at ground level and high altitude, investigating beta adrenergic blocking agent effects

16 p2530 A71-33242

Human body temperature regulation under various hydration regimes during exercise, noting changes related to sweating

16 p2530 A71-33243

Work load and maximum physical exercise duration relationship for forearm reciprocating flexion and extension, cranking of both arms and bicycle pedalling

17 p2688 A71-34359

Lactic acid production rate in human blood during supramaximal exercise, noting relationship to oxygen consumption

17 p2685 A71-35366

Human thermoregulator set point under physical exercise, using behavioral indicator

17 p2686 A71-35388

Human power output during short duration exercise, relating to body size and composition

17 p2686 A71-35434

Oxygen intake relation to anaerobic component of work during submaximal exercise on bicycle ergometer by young and older men

17 p2686 A71-35435

Human violent exercise burst effect on cognitive task, noting mild hypoxia irrelevance to skills decrements

17 p2686 A71-35436

Coagulation and fibrinolysis changes after physical exercise in males with atherosclerosis, noting fibrinolytic response differences with age

18 p2853 A71-35918

Acute fatal nontraumatic collapse during physical work and sports due to pathological processes

18 p2855 A71-36214

Acute renal failure due to heat stress and physical exercise, noting discrepancy between physiological alterations and histopathological abnormalities

18 p2855 A71-36218

Prolonged strenuous physical exercise effect on triglycerides, phospholipids and glycogen concentration in human femoral muscle

18 p2856 A71-36238

Dynamic characteristics of arterial oxygen tension response to supine submaximal leg exercise in man from harmonic analysis

18 p2856 A71-36239

Dynamic characteristics of arterial blood pressure responses to sinusoidal work load in man from harmonic analysis

18 p2856 A71-36240

Human adaptation to high altitude, considering effects of physical preconditioning, exercise, high carbohydrate diets and normal food intake maintenance

18 p2859 A71-36867

Temperature regulation during exercise by proportional control, investigating skin temperature effect on set point temperature, sweat rate and skin thermal conductance

18 p2860 A71-36879

Exercise temperature plateau shift and sweat rate during moderate CO poisoning associated with resetting of thermoregulating centers by low oxygen tensions

18 p2861 A71-36886

Fatigue effects on standing broad jump and other body movements patterns

18 p2873 A71-36975

Exercise-induced human protein catabolism not due to caloric deficit

19 p3008 A71-38552

High muscle glycogen content effect on human performance in prolonged heavy physical exercise

19 p3009 A71-38554

Noisy environment effects on circulatory, respiratory and metabolic parameters during physical exercise,

measuring heart rate, systolic blood pressure, oxygen intake and respiratory quotient

20 p3185 A71-38889

Heart rate variation during and after muscular exercise, discussing correlated measurements of rectal and mean skin temperatures, blood lactate, pyruvate and glucose

20 p3185 A71-38891

Polycythemia and altitude hypoxia effects on rats heart and sea level exercise tolerance

20 p3186 A71-38980

Amino acid levels in fasted and fed rats plasma, liver, muscle and kidney during and after exercise, noting glutamine decrease in liver tissue

20 p3186 A71-38982

Physicotechnical and biomedical aspects of human efficiency under weightlessness, discussing physical exercise role in adaptation

20 p3192 A71-39217

Resting and postexercise apexcardiogram correlation with maximal treadmill stress test, noting mean a-wave ratios

21 p3332 A71-40406

Trace processes as basis for efficiency change during exercise and active rest

21 p3337 A71-41061

Motor stereotype formation with different muscular loads, noting muscle electrical activity and static tension changes

21 p3337 A71-41062

Prior muscle exertions effect on reaction time and duration of simple discrete movements, considering electromyogram frequency changes

22 p3503 A71-42194

Prolonged bed rest effects on EEG sleep patterns in young healthy subjects with and without exercise

23 p3631 A71-43109

Dynamic characteristics of human respiratory and circulatory adaptation to muscular exercise, using systems analysis approach

23 p3634 A71-43905

Preclinical coronary heart disease detection by near maximal treadmill exercise ECG

23 p3636 A71-44129

Total body adipose tissue mass and composition variations, examining hyperglycemic, obese, exercised and centrifuged animals

23 p3637 A71-44299

PHYSICAL FACTORS

Experiences of living on moon, discussing effects on task performance and physical movements and observations of lunar surface, lighting and color

20 p3295 A71-39614

PHYSICAL FITNESS

Physical endurance and muscular activity of man as adaptation process depending on biochemical and functional changes

03 p0361 A71-13192

Optic analyzer dark adaptation dynamics during spatial body position changes, observing restoration speed dependence on physical training

03 p0364 A71-13523

Long term human biomedical and behavioral characteristics research, examining enhanced physiological fitness in space

04 p0543 A71-14933

Physical fitness in prolonged muscular work tolerance evaluation by oxygen consumption for 170 beat/min heart rate, considering age, sex and occupation

05 p0708 A71-16614

Personnel selection for emotionally and physically taxing situations by studying physiological responses to anticipated stressors and stress recovery

06 p0851 A71-17607

Preventive and clinical medicine effect on aircrew health maintenance

08 p1245 A71-20725

Tarahumara Indian runners cardiovascular system physical conditioning for endurance extremes

08 p1240 A71-21887

Quick-check audiometry reliability for testing hearing ability according to fitness regulations, comparing to complete tone and speech audiometry

14 p2188 A71-29821

Skylab habitability facilities for astronaut work effectiveness and physical well being

15 p2363 A71-31456

Physical fitness relation to flight requirements, pilot performance and age, considering muscular strength, cardio-respiratory capacity, body weight and mental aspects

16 p2528 A71-33114

Trained young runners maximum oxygen consumption rate at sea level and high altitude

16 p2530 A71-33244

Capillary density relationship to maximal oxygen uptake, indicating endurance training effects on human skeletal muscle

16 p2530 A71-33245

Physical training effects on human plasma glutamic-oxalacetic transaminase, creatine phosphokinase and lactic dehydrogenase enzyme levels

17 p2683 A71-35143

Spine radiological examination for helicopter pilot fitness determination, discussing spinal weakness symptoms, special exercises, medical examinations and vibration reducing seat construction

22 p3500 A71-41578

Cumulative /chronic/ and acute skill fatigue and physical fitness in aircrews, considering relationship to pilot error accidents

23 p3639 A71-43390

PHYSICAL OPTICS

Electromagnetic wave glancing incidence on ideally conducting screen of infinitely thin strips by geometrical optics approximation

04 p0625 A71-14646

Nonlinear materials and optics, second harmonic generation, optical parametric oscillators and IR converters

04 p0635 A71-14721

Soviet book on optics of scattering media covering visible radiation transfer in water, atmosphere, powders, tissues, dyes, inhomogeneous systems and photometry

04 p0626 A71-15224

Small wavelength wave optics of media with inhomogeneous refractivity developed from geometric optics, representing probability amplitude of classical ray by wave function

07 p1110 A71-19476

Statistics effect of quasi-monochromatic exciting radiation on generated radiation spectrum in nonlinear optics

09 p1461 A71-22396

Applied optics, reviewing homogeneous and inhomogeneous optical conversion elements, fiber and Fresnel optics, lens properties, programmed optical reliefs, holography, etc

15 p2410 A71-32299

Harmonic analysis of signal processing radar antennas spatial filtering process, noting application to physical optics theory

20 p3200 A71-39903

PHYSICAL PROPERTIES

Soviet bibliography concerning lunar surface physical properties, covering ground and orbiters observations data

01 p0148 A71-10045

Physical properties of Nb-Al-Ge alloys with maximum superconducting transition temperature close to boiling hydrogen

01 p0103 A71-11070

Be mechanical and physical properties, corrosion behavior, toxicity, fabrication and application as aircraft and spacecraft structural material

01 p0104 A71-11539

Saturn rings physical properties concerning optical thickness, particle features, albedo and mass

02 p0310 A71-12158

Apollo 11 and 12 lunar rocks physical and mechanical properties and chemical composition compared with terrestrial rocks

03 p0487 A71-13421

Single crystal indium gallium phosphide solid solution synthesis, discussing crystallophysical and electrophysical properties

03 p0467 A71-13424

Physical, chemical and electrical properties of silicon nitride thin films deposited pyrolytically on Si substrates, analyzing deposition process effects

03 p0468 A71-14001

Polarization-optical method of stress analysis problems, explaining high polymers physicochemical properties with Boltzmann-Volterra integral equations

04 p0671 A71-15557

Ferromagnetic dielectric composites physicochemical properties, considering thermal conductivity, density, linear expansion, resistivity, thermal stability and magnetic permeability

04 p0618 A71-15570

Titanium alloys for drop and press forged airframe, engine, rocket and spacecraft components, presenting physical and mechanical properties for various alloys and applications

05 p0757 A71-16136

Aging process effects on thermoelectric semiconductors physical stability for cryogenic applications

05 p0793 A71-16799

Stainless steel physicochemical properties stability, discussing equipment for industrial materials testing under various environmental and loading conditions

05 p0769 A71-16897

Logic circuitry materials physical properties changes effects on performance-controlling parameters at low temperatures

05 p0732 A71-17077

Soviet lunar surface rocks physical properties ground observation including colorimetry, spectrophotometry and polarimetry

07 p1193 A71-19311

Plastics for long life microcircuit encapsulation, investigating materials properties and failure mechanisms for device reliability assessment

07 p1077 A71-10661

Thin oxide films on solution grown single crystals of cubic betasilicon carbide, discussing physical and electronic properties measurements

07 p1177 A71-19571

Refractory metals and alloys fabrication and mechanical and physical properties at high temperatures

07 p1134 A71-19581

Re intermetallic compounds structure and physical properties, examining chemical reactivity with transition metals as function of elements periodic table position

07 p1140 A71-20236

Mo-Re-Hf ternary alloys physical and mechanical properties, considering workability, electrical resistivity and expansion coefficient

07 p1140 A71-20237

Soviet bibliography concerning lunar surface physical properties, covering ground and orbiters observations data

08 p1360 A71-21039

Silver oxides crystal structures and physical and electrochemical properties

08 p1234 A71-21084

Elastic ultrasonic vibrations effects on metals and alloys microstructure and elastic and nonelastic properties

09 p1477 A71-23326

Physical properties, structure and sintering of refractory oxides of rare earth elements and actinides, including chromia

09 p1478 A71-23399

Physical properties of Cs discharge plasma with incandescent electrode, considering Cs atoms ionization near cathode by thermal electrons accelerated by potential jump

10 p1650 A71-24528

Pyrolytic graphite, discussing fabrication by chemical vapor deposition process, mechanical and physical properties, residual stresses, applications in reentry vehicle heat shields, rocket nozzle throats, etc

11 p1789 A71-25743

Thermionic converters surface physics theory, discussing work functions, desorption energy and rates relationship to atomic and crystallographic properties

11 p1711 A71-25878

High performance ablative composites thermal physical characteristics from differential equations, describing thermochemical ablation-in-depth and boundary layer transport processes

11 p1856 A71-26041

Solar wind-Mercury interaction, discussing planet physical properties, magnetized wind parameters and bow shock wave existence

13 p2120 A71-27924

Filament reinforced composite materials, considering spacecraft and missile applications mechanical and physical properties

13 p2144 A71-28166

Jovian atmosphere physical properties inferred from eclipses of Galilean satellites, using color photoelectric photometry

13 p2134 A71-28284

Electrical and physical nature of microbial membranes implicated in aircraft fuel quantity probe malfunction

[SAE PAPER 710439]

13 p2113 A71-28321

Refractory materials production using chemical deposits from gaseous phase, discussing mechanical, physical and thermal properties of obtained coatings

13 p2074 A71-28526

Soviet book on experimental aerodynamics covering wind tunnels, shock tubes, liquid and gas physical properties, flow parameter measurement equipment, etc

14 p2221 A71-29524

High modulus organic fiber for aerospace use, considering fiber-epoxy composite mechanical and physical properties

14 p2263 A71-29658

Physicochemical properties of powdered Al and Al-Mg-Zn alloy combustion products from chemical, electron microscopic and X ray analysis

14 p2191 A71-30617

Low flame temperature propellants, investigating temperature and humidity aging effects on physical and ballistic properties

[AIAA PAPER 71-664]

14 p2286 A71-30732

Physical characteristics of comet Encke from visual observations, indicating nucleus of porous refractory material and ice structure

15 p2484 A71-31664

Soviet lunar surface rocks physical properties ground observation including colorimetry, spectrophotometry and polarimetry

15 p2485 A71-31891

D-transition metal carbides properties based on electron configuration localization model

15 p2429 A71-32138

Titanium, vanadium and niobium carbohydrides, investigating electronic structure effects on atomic behavior

15 p2429 A71-32140

Ti, Zr, Nb, Cr, Mo and W carbides compaction, investigating effects of compression, duration, pressing number, moisture and plasticizer contents and stress distribution

15 p2415 A71-32141

Rare earth metals di- and sesqui-carbides physical characteristics, establishing changing properties patterns during phase transitions

15 p2461 A71-32153

Transition metals classification according to effect on structure and physical properties of deformable Al alloys

15 p2434 A71-32331

Physicochemical properties and applications of lubricant materials based on organic compounds, discussing developments in inorganic lubricants

16 p2600 A71-32839

Heat transfer and drag calculations in longitudinal turbulent air flow around plate with constant or variable physical properties

16 p2662 A71-33036

Mo single crystals physicochemical and microstructural anisotropy under tension at different temperatures, noting strength and plasticity dependence on crystallographic orientation

16 p2596 A71-33888

Cuban tektite classification based on age, discussing physical properties and chemical composition

17 p2797 A71-34275

Lunik 16 soil samples physical properties, rock types, chemical analysis, mineral composition and petrology, comparing to Apollo project

17 p2805 A71-35332

Ni-Cr-Mo cermet alloys sinterability, physicochemical properties and microstructure

19 p3075 A71-37109

Physicochemical properties of cermet sintered thermoelectric materials, considering n- and p-type samples of Si-Ge alloys

19 p3075 A71-37111

Perfluoropolyether fluid lubricant physical and chemical properties at high and low temperatures, explaining metals effects on thermal stability by topochemical reaction mechanism

19 p3083 A71-37424

Circumterrestrial meteoroid properties based on night sky brightness photometric observation

19 p3133 A71-37440

Carbon and noncarbon polymers based high temperature elastomeric materials chemical structure and physical properties

19 p3085 A71-38068

Physical, chemical, mineralogical and biological analysis of Apollo 14 lunar rocks and fines

19 p3144 A71-38179

Physical properties of Cs discharge plasma with incandescent electrode, considering Cs atoms ionization near cathode by thermal electrons accelerated by potential jump

19 p3116 A71-38255

Hydraulic servo equipment filtration systems design, discussing contamination effects and servo components physical characteristics effects on tolerance level

19 p2999 A71-38320

Luna 16 automatic probe drilling experiment, obtaining lunar rocks physicochemical properties for comparison with terrestrial rocks

20 p3209 A71-39131

Book on engineering properties of Ni and Ni alloys covering Ni-Cr alloys, Ni-base superalloys, Cu-base Ni alloys, conversion factors, etc

20 p3251 A71-39199

Mica selection quality criteria for capacitors, outlining electrical, physical and optical properties standards

22 p3520 A71-41712

Ultrasonics use in physiological and pathophysiological experiments on human organism, considering ultrasonic vibration physical properties

22 p3502 A71-41941

Physical and mechanical properties of controlled flow vacuum cured glass reinforced polyimide prepreg laminates

22 p3565 A71-42595

Transition metal physicochemical properties explanation by many-electron effects in Hubbard model

23 p3714 A71-42932

Synthetic fibers and plastics development, chemical composition, physical and mechanical properties, production growth rates and applications

23 p3696 A71-43107

Nickel-chromium system powders physicochemical properties, noting use as high temperature cermet packing materials

23 p3690 A71-43256

Physical properties, mineralogy and chemical composition of lunar regolith sample returned by unmanned Lunik 16 probe

23 p3737 A71-43602

Morphological, physical and chemical characteristics of basaltic and anorthositic glassy spheroids in Apollo 12 lunar fines

23 p3746 A71-43666

Physical characterization of Apollo 11 and 12 lunar fines and glasses by diffuse reflectance, Raman and X ray spectroscopy and thermally stimulated currents

23 p3760 A71-43773

Polyethylene coating physicochemical properties under Uv radiation, discussing density and modulus of elasticity, internal stresses, microcrack formation and preventive heat treatment

23 p3697 A71-44032

Vacuum and inert gas TOR-1 device for studying physical properties of lunar soil and terrestrial analogs

24 p3828 A71-45104

InTe thin films formation, growth kinetics and physical properties, determining vapor deposited film thickness dependence on glass substrate temperature

24 p3861 A71-45249

InTe thin films with 60-75 percent Te content, investigating phase composition and physical properties

24 p3862 A71-45250

PHYSICAL WORK

Human cardiovascular control system model by analog computer program for various work loads up to submaximal, estimating correspondence to real life

03 p0368 A71-12995

Flat products skin milling work determination from microgrid deformation graphs, using continuum mechanics equations

04 p0602 A71-14607

Sweating responses in men during intermittent hand treadmill work, considering regulation by skin/core temperatures, neuromuscular reflexes and vein/muscle thermoreceptors

04 p0544 A71-15151

Blood plasma nonesterified fatty acids mobilization in relation to work load severity during and after prolonged exercise in men

04 p0544 A71-15154

Previous heavy work effect on central hemodynamics and autonomic nervous system, discussing ensuing heart rate changes

04 p0545 A71-15156

Respiratory features for conscious or unconscious warning of impending exhaustion, noting work load-performance decrement relation

04 p0545 A71-15159

Human strength decrement and recovery for repetitive maximal muscular exertions with various intertrial intervals

04 p0540 A71-15846

Circulatory response to beta adrenergic blockade during muscular work, causing reduction in cardiac frequency, exercise tolerance and oxygen consumption

05 p0709 A71-16622

Chemical energy conversion into mechanical work, examining irreversible mixing, Van Hoff box and Carnot cycle

05 p0717 A71-16785

Water cooled head cap for heat stress amelioration in subjects working in warm environments

06 p0859 A71-17611

Strain gage for in vivo recording of single and tetanic responses of skeletal muscles in mice during work in isometric regime

06 p0855 A71-18378

Bicycle ergometer workout effects on serum proteins, noting intravascular redistribution, tissue damage and membrane permeability

07 p1052 A71-20328

Visceral system regulation processes investigation in human organism during manual labor and environmental adaptation, using multichannel biotelemetry and computer processing

08 p1241 A71-21941

Furosemide effect on physical work capacity, studying recovery pulse response, oxygen extraction during exercise and altitude acclimatized subjects oxygen uptake

09 p1394 A71-23237

High altitude submaximal and maximal work by humans, noting time required for steady state oxygen consumption, ventilation and heart rate

09 p1401 A71-23368

Proprioceptive thermoregulatory mechanism of sweat secretion during positive and negative work in man

09 p1401 A71-23369

Electronic ergometer calibration equipment and errors at high work loads

09 p1401 A71-23373

Cardiac hypertrophy in animals, discussing increased cardiac work load compensation and muscle cell alterations

10 p1565 A71-24674

Transient dynamics of ventilation and heart rate following positive and negative sustained step changes in work load initiated from different load levels

11 p1722 A71-26357

Cardiovascular responses to submaximum and maximum effort cycling and running on bicycle ergometer and motor driven treadmill, using carbon dioxide rebreathing method

12 p1873 A71-27128

Respiratory responses and hyperventilation mechanism during static muscular work in maximal voluntary contraction, noting chemoreceptor and alarm-defense reaction

13 p2008 A71-28436

Human physiological responses comparison between work with concentric and eccentric muscle contractions, observing oxygen debt in short term exercise

13 p2024 A71-29495

High altitude aerobic working capacity limitations, examining oxygen transport system and circulator factors

14 p2183 A71-30276

Intense muscular work adaptation in rats, reducing biochemical and adaptive changes and enhancing anabolic processes

14 p2186 A71-30552

German monograph on conversion of human muscular work into flywheel mechanical kinetic energy covering testing and analysis of biomechanical relationships

15 p2364 A71-32308

Chemical energy conversion into mechanical work, examining irreversible mixing, vant Hoff box and Carnot cycle

16 p2540 A71-33037

Maximum oxygen uptake prediction by stepwise regression technique from data collected during sub-maximum treadmill work

16 p2530 A71-33241

Muscular fatigue of healthy Bengali males with increasing work loads under varying environmental conditions, considering ventilation, heart rate and oxygen consumption

17 p2688 A71-34360

Breathing capacity increase without rise in oxygen consumption due to active and passive muscular work and heavy energy expenditure

17 p2681 A71-34821

Human muscle power fluctuations under steady state physical activity, analyzing finger flexors strength

17 p2683 A71-35172

Acute fatal nontraumatic collapse during physical work and sports due to pathological processes

18 p2855 A71-36214

Acute fatal nontraumatic collapse during physical exertion due to circulatory diseases

18 p2855 A71-36215

Sudden death during physical exertion due to congenital anomalies of coronary arteries

18 p2855 A71-36217

Chill level index for skin temperature effects on rate of evaporative heat loss and thermal information to central controller during heavy work

18 p2860 A71-36876

Renin, plasma norepinephrine and epinephrine responses to work loads of various intensities, evaluating sympathetic nervous system as stimulus for secretion

19 p3008 A71-38551

Two stage rotor-piston vacuum pump, determining minimum work of gas compression

20 p3183 A71-39171

Power derived from aerobic, lactic acid and alactacid energy sources during human muscular work under normoxic and hypoxic conditions, noting oxygen consumption

22 p3485 A71-41721

Free fatty acids reduced availability effects on physical working capacity in normal man

22 p3485 A71-41722

Muscular work level shifts effectiveness during pedaling activity from oxygen requirement measurement, electromyograms and stress dynamograms

24 p3794 A71-44412

PHYSICS

Physics and astrophysics problem areas justifying intensified research

11 p1799 A71-25918

Physics and astrophysics problem areas justifying intensified research, discussing superconductivity, relativity, neutron stars, gravitational waves, etc

22 p3576 A71-42620

Cosmic ray physics - Conference, Leningrad, October 1969

22 p3594 A71-42633

Digital computer applications to physics problems, giving examples of plasma research and methane molecule properties determination based on quantum mechanics

24 p3847 A71-44355

Physics and technology discoveries utilization in industrial control, considering semiconductors, thin films, lasers, holography, cryogenics, etc

24 p3827 A71-45071

PHYSIOGRAPHY

U GEOMORPHOLOGY

PHYSIOLOGICAL DEFENSES

Direct and reverse conditioned connections including defense reflexes, response to indifferent stimuli and electrophysiological manifestations

17 p2685 A71-35360

Tissular and cellular biological resistance as indices for organism resistance to adverse effects, noting increase due to muscular training and cold adaptation

20 p3187 A71-39219

Microflora simplification effects on immunocompetent organism systems, observing shifts in guinea pigs lymphoid tissue with limited flora

21 p3332 A71-40555

PHYSIOLOGICAL EFFECTS

NT HEMODYNAMIC RESPONSES

NT PHYSIOLOGICAL RESPONSES

Behaviorally induced hypertension in squirrel monkey following conditioned key-pressing response schedules

01 p0015 A71-11330

Glycogen reduction in human musculus vastus lateralis during bicycle exercise below pulse endurance limit, noting glucose infusion effect

01 p0016 A71-11400

Physiological effects of heat exchange between human organism and ambient medium by evaporation, radiation, conduction and convection

01 p0028 A71-11597

Moderate acoustic stimuli effects, discussing subjective noise ratings relation with physiological and mental state changes

02 p0208 A71-12838

Microwave effects on living creatures, considering thermal and nonthermal effects on individual body organs and systems, permanent changes and protective measures

02 p0208 A71-12845

Medicophysiological problems in Concorde SST relative to altitude and speed, noting risks of cosmic radiation, ozone in atmosphere, decompression, wing loss and high temperatures

03 p0371 A71-13093

Physiological effects of noise - Conference, Boston, December 1969

03 p0358 A71-13151

Sound effects on endocrine function and electrolyte excretion in animals and man, considering adenohipophyseal, neurohipophyseal and thyroid functions, diuresis and natriuresis

03 p0359 A71-13153

Endocrine and metabolic effects of noise in normal, hypertensive and psychotic subjects, considering increased corticoadrenal and adrenergic activity

03 p0359 A71-13154

Quantitative relation between temporary threshold shift and peripheral circulatory effects of sound, using finger pulse amplitude strain gage

03 p0359 A71-13156

Sound and sonic booms effects on farm animals physiology and behavior, considering milk production, reproduction, food intake and growth rate

03 p0360 A71-13166

X ray effects on dogs with and without UV preexposure, determining blood protein and chemical composition, hemoglobin content and thermostability

03 p0364 A71-13524

Local cooling effects on responsiveness of muscular and cutaneous arteries and veins in dogs, noting blood flow redistribution

04 p0538 A71-15091

Blood plasma nonesterified fatty acids mobilization in relation to work load severity during and after prolonged exercise in men

04 p0544 A71-15154

Adverse physiological effects of downwash on man, considering tissue damage, hypothermia, dust and sound pressure effects

04 p0546 A71-15411

High environmental carbon dioxide effects on cardiac depression and respiratory rate in rhesus monkeys and chimpanzees

06 p0851 A71-17612

Spacecraft cabin rare gas-oxygen atmosphere decompression effects on animal metabolic rates

06 p0853 A71-17956

Human body thermography for studying physiological changes due to exercise, anoxia or accelerations

06 p0860 A71-18189

Thermal shock physiological effects, determining skin-air convective heat exchange coefficient

06 p0860 A71-18190

Clinical, physiological and metabolic changes in human body during 120 day bed rest

06 p0855 A71-18371

Laser ocular effects, discussing corneal/retinal/lens lesion production, damage thresholds and application to clinical ophthalmological problems

07 p1049 A71-19792

Physiological characteristics in llamas pulmonary circulation at sea level and changes after 5 and 10 weeks at 3,420 m above sea level, noting arterial hypertension

08 p1237 A71-20678

Radial, angular and transverse accelerations physiological effects, discussing physiological acceleration systems, symptoms, human centrifuging, etc

08 p1244 A71-20708

Vibration and buffeting effects on man, discussing aerospace environments, biomechanics, human tolerances and performance, etc

08 p1244 A71-20709

Aerospace environments noise effects on human physiology and speech communication

08 p1244 A71-20710

Neuroendocrine and metabolic responses to rotating workshift schedules, using urinalysis to assess physiological disturbances and adaptive changes

08 p1239 A71-20817

Physiological effects of cooling measured by men wearing air and water cooling garment under external heat loads or large metabolic heat

08 p1248 A71-21232

Sonic boom effects on human physiology and behavior and structures, based on theoretical studies and simulators

08 p1232 A71-21812

Human gastrointestinal tract functional disturbances after prolonged work in UHF field

08 p1249 A71-21955

Hypothalamus supraoptic nucleus morphological changes in rats under prolonged transverse acceleration

09 p1388 A71-22195

Electroencephalogram alterations in dogs and monkeys during bromotrifluoromethane exposure, correlating brain wave patterns with CNS depression [AMRL-TR-69-14]

09 p1398 A71-22475

Atmospheric ions effects on human visual performance, taking into account ozone concentration and humidity

09 p1493 A71-22741

Cardiovascular functional reactions in pilot trainees during training flights, presenting case histories

10 p1570 A71-24341

Flight concomitant pathogenetic effects on urinary tract conditions, noting kidney descent, inflammatory episodes and calculosis

10 p1566 A71-24977

Physical and physiopathological effects of high altitude supersonic flight in TF-104G aircraft told by flight surgeon

10 p1572 A71-24980

Prolonged perceptual deprivation effects on behavioral, physiological and chemical reactions, discussing EEG mean frequency changes

11 p1724 A71-25362

Physiological and biochemical changes arising in allergic reactions and hypothalamic neurohumoral regulation disorders role, comparing with diencephalic syndromes

11 p1718 A71-25667

Secretory function intensity of salivary glands, liver and stomach of animals and humans with different water-salt metabolism conditions

11 p1719 A71-25669

Nonauditory and auditory physiological effects of noise, discussing hearing conservation, noise measurement and noise hazard

11 p1726 A71-26511

Serotonin role in central nervous system activity, stressing sleep/wakefulness cycle regulation

12 p1869 A71-26651

Human blood cholinergic complex during various physiological states, noting nonmediator action of acetylcholine

13 p2006 A71-28384

Ionized air exposure effects on acetylcholine content and cholinesterase activity in mice, noting cholinergic and serotonergic interaction

13 p2006 A71-28404

Large subsonic jet aircraft civil pilots performance under physiological and psychological stresses induced during severe atmospheric turbulence

14 p2188 A71-29783

Skin temperature sensitivity factors, discussing neural correlates of thermal sensation and skin receptors causing thermal stimulation sensitivity

14 p2183 A71-30253

Endolymph and perilymph fluid systems pathophysiology from induced and spontaneous disorders changes observed in inner ear

14 p2183 A71-30254

Hypokinesia effect on formation and elimination of ketones, aldehydes, carbon monoxide and ammonia in rats

15 p2356 A71-31305

Peripheral blood and bone marrow morphological composition in dogs subjected to chronic and repeated gamma irradiation

15 p2357 A71-31308

Cellular respiration and high altitude adaptation effect on cytochrome content and on oxidation and oxidative phosphorylation parameters of brain homogenates in rats

15 p2357 A71-31310

DC magnetic field effect on organism sympathoadrenal system, noting hypokinesia reduction of noradrenalin in hypothalamus and myocardium

15 p2357 A71-31311

Amytetravite and ATP effect on hemopoiesis of dogs subjected to chronic and repeated gamma irradiation 15 p2357 A71-31312

Simulated sonic booms and subsonic jet aircraft noise effects on human subjects of various ages during different sleep stages 15 p2364 A71-32250

Dietary antioxidant vitamin level effects on fine structure of proximal convoluted tubules in rats, studying changes due to oxygen toxicity 16 p2528 A71-33116

French shock tube test facility for reproducing and investigating effects of sonic booms on vision and physiological processes 16 p2552 A71-33350

Frequency and level dependent discrepancy between free field and pressure thresholds at low frequencies due to physiological noise produced under earcap 17 p2681 A71-34699

Lactic acid production rate in human blood during supramaximal exercise, noting relationship to oxygen consumption 17 p2685 A71-35366

Multiple positive off effects in human electroretinogram, recording rhythmic wavelets due to intense stimuli with averaging computer and short time constant amplifier 17 p2687 A71-35802

Laser-induced retinal damage model based on energy interaction modes, including thermal and acoustic transients, vaporization and dielectric breakdown 18 p2863 A71-35955

Astronaut orthostatic tolerance loss due to weightlessness, describing compensation by periodic lower body negative pressure [AIAA PAPER 71-859] 18 p2872 A71-36648

Organic phosphate compounds effects on oxygen affinity and intracellular pH of human erythrocytes 18 p2857 A71-36691

Physiological strains due to industrial heat stress, investigating heart rate and body temperature 18 p2860 A71-36882

Physiological control of local sweating rate 18 p2860 A71-36884

Fatigue effects on standing broad jump and other body movements patterns 18 p2873 A71-36975

Dietary effects of formose sugars ingestion, investigating toxic mechanisms involved 19 p3011 A71-37573

Book on biological effects of radiation covering ionizing radiation properties and effects at molecular, cellular and tissue levels 19 p3002 A71-38048

Exercise-induced human protein catabolism not due to caloric deficit 19 p3008 A71-38552

Low ozone dosage exposure effects on rabbit lung endogenous defense mechanisms 19 p3009 A71-38559

Urinary protein excretion rates in high altitude inhabitants, showing polycythemia effect on creatinine clearances levels 19 p3009 A71-38561

High altitude exposure effects on concentration and total quantity of electrolytes in human serum and extracellular space 19 p3009 A71-38562

Vestibular apparatus effect on brain stem somatic activity 21 p3328 A71-39998

Transport aircrew sleep patterns effects on fatigue and sleep disturbances, discussing physiologic debt and stresses 21 p3342 A71-40341

Aircraft noise effects on hearing acuity and perceptual and intellectual judgment tasks 21 p3342 A71-40351

Gangliosides and cerebroside content in rat brain under normal conditions, during hypoxia and under small X ray doses action 21 p3337 A71-41057

World championship gliding team medicophysiological problems during competition at Marfa, Texas, discussing climatic adaptation, nutrition, hypoxia and pilots general physical and psychomotor conditions 22 p3500 A71-41576

Water immersion effect on plasma renin activity, urinary aldosterone excretion and renal sodium and potassium handling in normal man 22 p3485 A71-41720

Beta-aminoethylthiophosphoric acid monosodium salt effect on mice stability to lateral accelerations 22 p3491 A71-42701

Sympathomimetic amines effects on central nervous system reflex activity of irradiated and desympathized animals 22 p3492 A71-42708

Gastrointestinal tract reactions to atropine sulfate, acetylcholine and carbacholine in rats after acceleration exposures, using roentgenograms 22 p3495 A71-42796

Physiological effects on rats of argon substitution for nitrogen in hermetically sealed chambers under conditions of anoxia and high carbon dioxide concentration 22 p3505 A71-42804

Physiological effects on mice of air pollution with gaseous toxic substances from urine and feces, noting increased respiration rate and choline esterase activity 22 p3506 A71-42807

Sparrows pinealectomy effect on circadian rhythms of body temperature in light and darkness from radio telemetric monitoring 23 p3633 A71-43547

Morphological and cytochemical changes in red and mixed skeletal muscles of animals exposed to hypokinesia 23 p3636 A71-44237

Posture and lower body negative pressure effects on human heart rate and blood pressure 23 p3636 A71-44241

Biorhythms and related physiological and psychic disturbances, stressing importance in aerospace medicine 23 p3637 A71-44245

Combined heat, noise and vibration stress effects on human performance and physiological functions including heart rate, body temperature and mental arithmetic 23 p3637 A71-44247

Rat thyroid gland changes during acclimatization to simulated high altitude environments, observing high hormone stimulation 23 p3637 A71-44300

Hematological characteristics of emotional stresses during parachute jump, studying leucocyte, erythrocyte and eosinophil populations changes 24 p3795 A71-44526

Hypokinesia effects on gas exchange and oxygen consumption in rats, noting weight losses 24 p3796 A71-44536

Minute blood and stroke volumes dynamics during prolonged hypokinesia by acetylene method 24 p3796 A71-44546

Morphological changes in dogs brain vessels under transverse accelerations 24 p3796 A71-44546

PHYSIOLOGICAL FACTORS

NT PHYSICAL FACTORS
Flying motivation loss, considering psychogenesis and physiological causes 05 p0715 A71-16933

Subjective and electromyographic estimation of fatigue and muscle activity physiological levels, considering isometric muscle contraction task endurance 07 p1047 A71-19458

Human work load assessments by time study of officers and physiologists, noting disagreeing values 07 p1047 A71-19466

Physiological aspects of aircraft accident investigation, considering pilot errors 08 p1247 A71-20825

Orbiting Biosatellite 3 monkey environmental and physiological parameters circadian rhythms, investigating desynchronization or arrhythmia 09 p1395 A71-23241

Speech processing and recognition, considering progressive data reduction by ear and physiological limitations imposed information rate time variation 10 p1568 A71-24230

Medical physiological requirements of angular velocity and g level for artificial gravity creation by rotating space vehicle, considering human tolerances and vehicle design 18 p2870 A71-36627

Shower habitability requirements for adequate cleansing of body and hair to satisfy physiological, psychological and social needs of crew members on long space missions 18 p2870 A71-36629

Heat removal from space suit, discussing anatomic and physiological features suitable for cooling 20 p3188 A71-39224

Physiological factors in fatal aircraft accidents, discussing pilot incapacitation and transient functional disturbances 22 p3502 A71-41834

Physiological systems connected with sensory perception of equilibrium and orientation on ground and in air, discussing pilot training and selection 23 p3632 A71-43148

PHYSIOLOGICAL INDEXES

U PHYSIOLOGICAL TESTS

PHYSIOLOGICAL RESPONSES

NT HEMODYNAMIC RESPONSES

Stimulus transretinal velocity effects on human torsional eye movements 01 p0009 A71-10236

Orientation reflex in healthy and nervous human subjects from peripheral vessels blood pressure fluctuations in response to acoustic signals 01 p0012 A71-11055

Slow cortical potentials associated with human motor and mental acts differentiated via spatial distribution 01 p0015 A71-11220

Rodents bimodal cochlear microphonic response to high frequencies recorded from round window membrane 01 p0017 A71-11542

Physical exercise effect on mitochondrial energy production in heart muscle and liver in rats 01 p0020 A71-11567

Circadian rhythm in dermestid beetles *Trogoderma glabrum* Herbst as response to compulsory constant light and temperature conditions 02 p0202 A71-11667

Human thermoregulatory response to ambient temperature variations, considering deep body and skin temperature interrelations 02 p0202 A71-11667

Sexual behavior of male cats after parachlorophenylalanine injections, noting unchanged or diminished performance and serotonin lowering in brain 02 p0199 A71-12365

Eye movements frequency and slow phase displacement in response to optokinetic stimulation of parrots and cats 02 p0199 A71-12385

Military parachutists physiological and force field responses to aerospace recovery environment, using multichannel FM/FM telemetry for heart rates 02 p0207 A71-12389

Arterial sclerosis and stenosis physical factors, discussing connective and vascular tissue adaptive responses to mechanical stresses 02 p0200 A71-12415

Skin temperature and metabolism changes magnitude, duration and variability in unacclimatized male subjects during cold stress 02 p0208 A71-12836

Healthy subjects physical training effects on blood flow and enzymatic activity in skeletal muscle 02 p0201 A71-12916

Biological and medical cybernetics approach to closed systems construction for continuous automatic monitoring and control of human physiological processes under harmful conditions 03 p0368 A71-13000

Biotelemetry in aviation medicine, discussing telemetric methods and applications for continuous observation of physiological processes under environmental exercise and stress conditions 03 p0370 A71-13063

Audioconditioned convulsive response [ACCR/ characterization, investigating age, auditory conditioning and environmental noise effects on sound-induced seizures in mice 03 p0360 A71-13162

Anticonvulsant drugs for counteracting noise effects on central nervous system, discussing audiogenic seizure in mice 03 p0360 A71-13163

Physiological and psychological human responses to sonic booms in France, UK and U.S. considered as acceptability criteria 03 p0371 A71-13167

Oxygen tension, blood flow, redox potential and temperature variations in cerebrum and musculus gastrocnemius of rats during high mountain adaptation 03 p0361 A71-13190

Frog eye response to UV light stimulation, investigating sensitivity from electroretinogram 03 p0363 A71-13484

Human left ventricle mathematical models, determining physiological response oriented mechanical parameters with diagnostic significance [ASME PAPER 70-WA/BHF-14] 03 p0373 A71-14112

Elasmobranch fish labyrinth electrophysiology, analyzing semicircular canals linear acceleration response 04 p0536 A71-14755

Angiotensin I infusion effect on intrarenal blood flow distribution, using krypton 85 method and autoradiography 04 p0538 A71-15088

Human legs thermal response during cooling for refrigeration anesthesia, deriving analytical model for temperature level prediction as function of time 04 p0545 A71-15160

Conditioned reflex gas exchange shifts in persons under repeated local thermal stimuli 04 p0540 A71-15572

Acoustic intensity and exposure time duration for threshold lesion in cat brain 05 p0712 A71-16283

Hippocampal, neocortical and somatic effects of HF electrical stimulation of mesencephalic reticular formation during different stages of sleep in cats 05 p0707 A71-16424

Nervous system activity changes relation to physical exercise type and extent, measuring visual response time 05 p0708 A71-16620

Circulatory response to beta adrenergic blockade during muscular work, causing reduction in cardiac 05 p0708 A71-16620

frequency, exercise tolerance and oxygen consumption

05 p0709 A71-16622

Parafoveal sensitivity disruption /flash blindness/ due to retinal location and high intensity short duration adapting flash

06 p0851 A71-17605

Personnel selection for emotionally and physically taxing situations by studying physiological responses to anticipated stressors and stress recovery

06 p0851 A71-17607

Neurological altitude decompression sickness clinical manifestations, pathophysiology, treatment by compression therapy and subsequent grand mal seizures

06 p0859 A71-17614

Electroencephalographic and motor effects of electrically stimulated reinforcing and negative subcortical structures in sleeping cats

06 p0852 A71-17669

Reflex excitability of neuromuscular systems of Soyuz crewmembers during physical loads

06 p0855 A71-18372

Time constant for collateral ventilation in human, dog and pig lungs under various physiological conditions

06 p0856 A71-18385

Cardiovascular, respiratory and thermoregulatory mechanisms in aqualung diver drillers

06 p0864 A71-18721

X ray influence on protein and mineral content of blood serum in dogs

06 p0858 A71-18728

Hypoxia protection against ionizing irradiation by anaerobic glycolysis stimulation, lactic acid increase and blood glucose level elevation

07 p1037 A71-18966

Pilot physiological responses as indicators of pitch motion cues effect on flight simulator fidelity

07 p1047 A71-19465

Hyperresponsiveness in hibernating mammals, discussing responsiveness increase with body temperature decrease as compensating mechanism for sensitivity loss

07 p1041 A71-19524

Perceived and responded to discriminative stimuli identification in probability learning, using parameter free model of event pattern association strength

07 p1049 A71-19775

Bicycle ergometer workout effects on serum proteins, noting intravascular redistribution, tissue damage and membrane permeability

07 p1052 A71-20328

Carbohydrate ingestion produced respiratory gas exchange ratio and alveolar ventilation effects on arterial oxygen tension in normal men

07 p1052 A71-20333

Intrareversal times for figures eliciting and not eliciting apparent depth in flat drawings

07 p1045 A71-20383

Sleep period time displacement effect on sleep using EEG recordings

08 p1239 A71-20816

Mechanical, physiological and psychological responses of man to sinusoidal whole body vibration

08 p1248 A71-21230

Central nervous system functions under high oxygen concentrations at normal and elevated pressures

08 p1241 A71-21938

Bone tissue optical density and blood serum and urine calcium content of Soyuz 9 crew members during and after flight

09 p1389 A71-22201

Soyuz 9 spacecraft astronauts space flight effect on digestive system enzyme secretion function based on pre- and post-flight examinations

09 p1389 A71-22206

Soyuz 9 spacecraft astronauts otorhinolaryngological organs response to 18-day orbital flight, observing pathological changes from clinical post flight examination

09 p1389 A71-22207

Soyuz 9 spacecraft astronauts cardiovascular and respiratory systems responses to orthostatic effect after 18-day orbital flight from EKG measurements and sphygmography

09 p1389 A71-22208

Soyuz 9 spacecraft simulator prolonged confinement effect on human cardiovascular system functional state

09 p1390 A71-22209

Humans and animals acute hypoxia effects on EEG pattern and behavioral reactions

09 p1390 A71-22210

Cerebral lipid fractions, examining relation between physiological functions and metabolism

09 p1391 A71-22481

Decompression sickness physical and physiological aspects, discussing gas transport quantification, inert gas elimination and metabolic gas exchange in recompression therapy, work performance, etc

09 p1394 A71-23236

Furosemide effect on physical work capacity, studying recovery pulse response, oxygen extraction during exercise and altitude acclimatized subjects oxygen uptake

09 p1394 A71-23237

Monkey physiological responses from lift-off to orbital insertion, showing EEG and EMG arousal reactions, motion sickness development, cardiovascular and respiratory changes

09 p1394 A71-23239

Biosatellite 3 monkey sleep and wake states based on visual and computer analysis of telemetered EEG data from earth orbital flight

09 p1395 A71-23242

Biosatellite 3 neurophysiological data analysis by digital computer presenting maps of parietal cortex spectra, responsive states transient changes, circadian rhythms and EEG activity

09 p1395 A71-23243

Skin cooling effect on awake exercising dog ventilation, noting carbon dioxide response curve, arterial partial pressure and hyperpnea

09 p1396 A71-23366

Prolonged hyperoxia effects on lipid synthesis in rat liver and adipose tissue slices

10 p1559 A71-23969

Prolonged hypoxia, hypercapnia and combination effects on rats circulating red cell volume

10 p1559 A71-23970

Contour density effects on evoked critical response, discussing improved photopic visibility, spatial summation area and retina interaction

10 p1559 A71-23983

Spectral sensitivity by stimulus control and presentation in barred pattern alternatives and photopic system monitoring by visual evoked responses

10 p1560 A71-23986

Pulmonary vasoconstrictor response to temperature dependent acute hypoxia, using isolated rat lungs with heparinized homologous blood under constant volume pulsatile inflow

10 p1561 A71-24124

Vestibular system functions physical analog model, predicting responses to motion inputs and possible problems for flight situations

10 p1569 A71-24237

Circannual biological clock operation without environmental signals based on squirrel hibernation and bird migration studies

10 p1563 A71-24298

Nitrogen, helium, argon and neon containing atmospheres relation to altitude decompression of rats, noting interspecies comparison of metabolic effects

10 p1570 A71-24610

Long term zero gravity effects on mammal physiologic rhythms characteristics, studying rats in biosatellite orbits

10 p1565 A71-24611

Human visual system response to moving spatially periodic stimuli, developing mathematical model for motion perception

10 p1572 A71-24999

Pathophysiological aspects of microwave irradiation, considering thermal response of human and animal organisms to electromagnetic radiation exposure

10 p1573 A71-25079

Central nervous system responsiveness changes after exhausting physical exercise, giving electroencephalogram and sensomotor reaction records

11 p1719 A71-25668

Thermal environment effect on human skin temperature and final temperature and tolerance time prediction from early exposure

11 p1725 A71-26117

Retinal sine wave flicker transient response obtained with circular uniform field and counterphase grating targets

11 p1799 A71-26141

Human heart beat phase frequency changes after acoustic stimulation during natural sleep from EEG, EKG, EMG of musculus hypoglossus and eye motions

11 p1721 A71-26292

Body temperature regulation and heat dissipation responses during continuous and intermittent exercise in man

11 p1721 A71-26354

Transient dynamics of ventilation and heart rate following positive and negative sustained step changes in work load initiated from different load levels

11 p1722 A71-26357

Ventilation and heart rate responses to muscular exercise by work load ramp function changes studies

11 p1722 A71-26359

Subsonic jet aircraft noise and simulated sonic booms awakening effects on human sleep

11 p1726 A71-26510

Dynamics of increasing organism resistance to hypoxia, considering reactions occurring in various tissues during adaptation

12 p1869 A71-26653

Book on color and pattern vision physiology covering retinal induction, electrical excitation of eye, optical illusion, figural aftereffect, movement sensation, etc

12 p1870 A71-26769

Cardiovascular responses to submaximum and maximum effort cycling and running on bicycle ergometer and motor driven treadmill, using carbon dioxide rebreathing method

12 p1873 A71-27128

Human heart rate, minute ventilation and oxygen uptake measurement during treadmill and track running at three speeds

12 p1874 A71-27134

Anesthetized cats visual cortex responses to prolonged light stimuli, studying dependence on photopic retina cone and rod apparatus

12 p1871 A71-27489

EEG examination of healthy aircrew for high performance aircraft flying fitness evaluation, stressing hyperventilation factor importance

12 p1876 A71-27631

Benzodiazepine series tranquilizers effect on mice resistance to hypoxia and lifetime, noting diazepam as most effective

12 p1872 A71-27722

Direct electrical stimulation of musculus tensor tympani on click elicited responses in cochlea and cochlear nucleus

13 p2003 A71-27832

Somatosensory cortical and cuneate evoked responses and EEG amplitude/frequency changes due to hypovolemic shock

13 p2003 A71-27836

Ventricular septal defect, discussing incidence, human physiological responses, morbidity and mortality in various age groups

13 p2004 A71-27862

Diurnal rhythms of human physiological functions and performance during frequently alternating sleep-work cycles

13 p2006 A71-28410

Exhaled air microimpurities composition of humans exposed to stress effects including bed rest, starvation, lyophilized diet feeding, high temperature and humidity

13 p2007 A71-28412

Somatic and autonomic responses in vestibular tolerance of human subjects, using Coriolis acceleration test

13 p2007 A71-28414

Cat type I and II optic nerve fibers response to flicker stimulation, noting receptive field organization, conduction velocity and temporal and spatial information processing

13 p2008 A71-28459

Human visual system gate type lateral interaction to luminous intensity, noting visual field response to monocular viewing

13 p2018 A71-28460

Grating pattern vision models, examining single neural network and multiple channel stimulus information processing

13 p2018 A71-28461

Soviet book on vestibular reactions covering functional relationship between stimulus parameters and labyrinth nonauditory part, adaptation to Coriolis forces and response to ionizing radiation

13 p2008 A71-28672

Local cutaneous heat regulation in man, using thermocouple method in analyzing response to constant temperature thermode application to small skin surface

13 p2014 A71-29314

Microwave exposure effects on organisms and biological functions responses and thermal stresses as function of specific frequencies, power density and environmental temperature

13 p2021 A71-29325

Hypercapnia in rat, measuring carbon dioxide concentration effect on tidal and minute volumes, respiratory rate, pH depression, blood gases, hematocrit and percent oxyhemoglobin saturation

13 p2015 A71-29364

Position, exercise and lung volume effects on healthy males pulmonary diffusing capacity for CO at rest and during exercise

13 p2015 A71-29493

Human physiological responses comparison between work with concentric and eccentric muscle contractions, observing oxygen debt in short term exercise

13 p2024 A71-29495

Airway smooth muscle relaxation mechanical consequences concerning lung volumes, airway conductance, isovolume pressure flow, maximum expiratory flow volume and static lung recoil

13 p2024 A71-29497

Heat acclimatization effects on sweat Na concentration over wide sweat rates range, discussing possible mechanisms

13 p2024 A71-29498

Surface electromyographic recordings on biceps and peripheral muscles during sustained isometric contractions

13 p2024 A71-29499

Computer quantitation of ST segment response to graded exercise in untrained and trained subjects, con-

tinuously recording amplitude of selected points on ECG waveform

15 p2358 A71-31452

Cortical and subcortical electrical activity during electrically and drug induced convulsive seizures in cats, correlating with spinal monosynaptic reflex variations

15 p2359 A71-31957

Human skeletal muscle reflex and motor reactions in response to tibial nerve stimulation

15 p2360 A71-32532

Nystagmic responses of airmen and grounded and active pilots subjected to caloric and rotational tests

16 p2355 A71-33112

Myocardium ultrastructural and metabolic alterations in altitude acclimated rats, considering heart muscle mitochondria

16 p2529 A71-33193

Human body water metabolism during acute high altitude exposure with heavy physical activity and high food intakes

16 p2530 A71-33240

Maximum oxygen uptake prediction by stepwise regression technique from data collected during sub-maximum treadmill work

16 p2530 A71-33241

Cardiovascular responses to hypothalamic, spinal cord and stellate ganglion stimulation as function of intensity, pulse duration and frequency in cats

16 p2531 A71-33367

Healthy subject speech speed effect on phonation phase length, noting relation to normal articulator phase

16 p2531 A71-33462

Elevated atmospheric pressure effects on human psychophysiological qualities including attention, memory and time-estimating capabilities and nervous processes equilibrium

16 p2536 A71-33578

Cardiovascular and respiratory systems, motor and muscular activity, metabolism and body energetics functional changes due to prolonged weightlessness

16 p2531 A71-33676

Pyridoxine and serotonin metabolism changes and vestibular disorders observation in space flight

16 p2532 A71-33677

Turtles organs and tissues responses during Zond 5 and 7 lunar probes circumlunar flight

16 p2532 A71-33678

Neuron response to stimuli compared with background activity on histograms

16 p2532 A71-33898

Functional systems changes in intact and anesthetized rats during increasing hypoxia in decompression chamber

16 p2532 A71-33911

Spontaneous deep sighing breath physiological regulation in rats as lung inflation response due to vagally mediated mechanoreflex

17 p2679 A71-34176

Human visual evoked cortical potential spectral sensitivity measurement, comparing results with psychophysical data

17 p2680 A71-34652

Rhodopsin kinetics mathematical analysis by cyclic five-component model, applying to flash and extended photolysis in rat retina

17 p2680 A71-34653

Photolysis of metarhodopsin I, discussing rate and extent of conversion to rhodopsin

17 p2680 A71-34654

Human visual perception response to brightness under sinusoidal current, suggesting interaction with retinal neural structures

17 p2680 A71-34656

Cat pupillary system static and dynamic response determination under light and electrical stimulation, using TV pupillometer and on-line computer

17 p2691 A71-35044

Physiological tests for psychic stress effects on aircraft pilot tracking performance, respiration and heart rate

17 p2693 A71-35199

Deep cerebral structures and cortex electrical activity in apes, noting biopotentials during orientation/defense reactions and light signals responses

17 p2683 A71-35246

Human central fovea theoretical model for target stimuli threshold detection performance prediction

17 p2693 A71-35325

Direct and reverse conditioned connections including defense reflexes, response to indifferent stimuli and electrophysiological manifestations

17 p2685 A71-35360

Reaction times distributions in visual or auditory mode single and multiple motor response units

17 p2686 A71-35433

Human violent exercise burst effect on cognitive task, noting mild hypoxia irrelevance to skills decrements

17 p2686 A71-35436

Physiological mechanisms of human auditory attention, measuring changes in cerebral cortex averaged evoked potential and cochlear nerve response

17 p2693 A71-35575

Microwave radiation biological effects review and bibliography covering protein activity, genetic, central nervous system and cardiovascular effects

18 p2864 A71-35956

Acute renal failure due to heat stress and physical exercise, noting discrepancy between physiological alterations and histopathological abnormalities

18 p2855 A71-36218

Dynamic characteristics of arterial oxygen tension response to supine submaximal leg exercise in man from harmonic analysis

18 p2856 A71-36239

Dynamic characteristics of arterial blood pressure responses to sinusoidal work load in man from harmonic analysis

18 p2856 A71-36240

Human physiological responses to rotating environment, evaluating heart rates, blood pressure, pulmonary functions, visual observations and vital capacities [AIAA PAPER 71-890]

18 p2856 A71-36639

Structural development in rat bone under earth gravity, hypergravity and simulated weightlessness, discussing physical dimensions, density, rigidity, microhardness and ash content

[AIAA PAPER 71-895]

18 p2856 A71-36640

Squirrel monkeys midbrain reticular formation direct thermal stimulation effects on physiological or behavioral thermoregulatory responses

18 p2858 A71-36860

Human sweat gland duct filling and skin epidermal hydration behavior by analysis of time delays between seat emergence and steady state, using electrical stimulation

18 p2858 A71-36865

Hypothalamic unit activity relation to thermoregulation, investigating preoptic area response to local and peripheral temperature changes

18 p2859 A71-36869

Male and female physiological responses to heat stress, discussing sweating, skin and body temperature, heart rate and metabolism

18 p2859 A71-36871

Impulse skin temperature encoding in primate cutaneous thermoreceptors in dynamic thermal conditions

18 p2860 A71-36877

Brain temperature change effects on cardiovascular responses, examining heart rate and systemic arterial blood pressure

18 p2860 A71-36880

Perspiration delay times characterizing potohydrotic reflex, analyzing neurophysiological mechanism

18 p2861 A71-36885

Exercise temperature plateau shift and sweat rate during moderate CO poisoning associated with resetting of thermoregulating centers by low oxygen tensions

18 p2861 A71-36886

Cats preoptic and skin temperature change effects on posterior hypothalamic neurons

18 p2861 A71-36888

Squirrel monkey physiological and behavioral thermoregulation elements interrelationships, considering mean skin and medial preoptic hypothalamic temperatures

18 p2862 A71-36896

Functional relation of primary responses and unit spike activity at subcortical visual centers in cats

19 p3001 A71-37443

Positive and negative deflections in human electroretinogram off response to stimuli

19 p3007 A71-38058

Visually evoked cerebral cortex responses to on- and off-set of patterned light and contour density and sharpness in humans

19 p3004 A71-38282

Renin, plasma norepinephrine and epinephrine responses to work loads of various intensities, evaluating sympathetic nervous system as stimulus for secretion

19 p3008 A71-38551

Physiological responses of burro *Equus asinus* to oxygen lack in mountain altitudes, studying red blood cell and plasma volumes

19 p3005 A71-38560

Pigeon acclimatization response to simulated high altitude, determining body weights, hematocrit ratios, hemoglobin concentrations and plasma and blood volumes

19 p3005 A71-38563

Surround luminance effect on relative perceptual latency of response, using test stimuli confined to rod free area of fovea

20 p3184 A71-38774

Cholesterol and esterified cholesterol distribution in human skin from analysis on fat, epidermis, cotium, subcutaneous tissue and serum by chromatographic/colorimetric methods

20 p3185 A71-38892

Plasma renin activity in hypertonic and normotonic persons exposed to exogenous stress, comparing with measurements at rest and in orthostasis

20 p3185 A71-38893

Noise exposure effects on human physiological and psychological functions and performance

20 p3192 A71-38959

Brain polysomes disaggregation and tryptophan elevation in immature rats and adult animals after L-dopa administration

20 p3186 A71-38979

Mammalian cells cultivation at suboptimal temperatures, considering reproduction and cytophysiological changes

20 p3188 A71-39220

Astronaut chromosome aberrations, presenting peripheral blood leukocytes cytogenetic tests for pre and post space flight

20 p3188 A71-39227

Human retinal blood circulation changes and vision disturbance under transversely directed acceleration, using dark chamber teleophthalmoscopy

20 p3188 A71-39228

Nasal vascular system reactions during 120-day bed rest hypokinesia under drug affected metabolism

20 p3188 A71-39229

Stagnant asphyxia in cat carotid body during abrupt blood pressure drop by simultaneous carotid artery clamping and tap opening

20 p3190 A71-39443

Instrumental learning of cardiovascular and visceral responses and behavioral, physiological and biochemical consequences in relation to psychosomatic therapy

20 p3190 A71-39548

Cortical responses of awake cat to narrow-band FM noise stimuli, proposing neuronal model

20 p3190 A71-39767

Intracochlear electric potential of anesthetized cats recorded with potassium filled glass micropipets, determining magnitude and phase of responses

20 p3191 A71-39768

Book on noise effects on man covering audiometry, aural reflex, hearing damage risk, physiological responses, motor performance and speech communication

20 p3193 A71-39874

Gravity receptor evolution in invertebrates, considering cilia role in reception and transduction into responses

21 p3327 A71-39991

Animals physiological responses to gravity chronic acceleration

21 p3328 A71-40002

Taste modalities identification by factor analysis technique based on correlation matrix between independent stimuli

21 p3341 A71-40073

Human blood pressure in brachial artery during spontaneous night sleep, recording EEG, EKG and horizontal eye movements

21 p3329 A71-40185

Macaca nemestrina monkey bone density change during Biosatellite 3 mission

21 p3330 A71-40343

Decompression sickness, investigating surface excursion diving and selection of limb bends vs CNS symptoms by tests on goats

21 p3330 A71-40344

Normal females electrophysiological changes during sensory isolation of water tank variety from EEG, EMG, EOG, EKG and electrodermal measurements, considering cortical activities reduction

21 p3330 A71-40346

Hyperbaric normoxic breathing helium, nitrogen and neon gas mixture effects on EEG and reaction time in man

21 p3342 A71-40347

Altitude and cold acclimatization effects on human basal heart rate, blood pressure, respiration and breath-holding

21 p3330 A71-40349

Aquanuts tremor response measurement by muscle force transducer during compression and decompression in 520-foot saturation dive, noting differences among individuals

21 p3331 A71-40350

Human vascular and extravascular fluid changes during six days bedrest based on fluid volume and ideal body weight from individual heights

21 p3331 A71-40354

Physiological responses to head and neck vs trunk and leg cooling under hyperthermic stress

21 p3331 A71-40356

Physiological deterioration of monkey onboard Biosatellite 3 and unexpected demise, presenting collected data for response analysis

21 p3333 A71-40564

Radioprotectants effects on mice and guinea pigs physiological reactions to back-to-chest transverse accelerations

21 p3336 A71-41053

Soviet book on animals morphophysiological changes in cardiovascular and nervous systems and various internal organs under RF wave exposure

21 p3344 A71-41369

Blind goldfish gravity reference response under linear accelerations on motor car and parallel swing from movie camera recording

22 p3487 A71-42228

- Hyperoxic medium effects on experimental animal cells, tissues and organs morphology, infrastructure and histochemistry
22 p3495 A71-42801
- Animal tolerance to carbon monoxide, nitrogen oxide, triethylamine and freon-12 toxic effects after adaptation to hypoxia from tests on albino mice
22 p3496 A71-42810
- Human expired air toxicity effect on mice neurohumoral changes stimulating inhibitory reactions in central nervous system
22 p3506 A71-42813
- Auditory stimulus conditioning of human skin resistance responses on escape-avoidance schedule
22 p3497 A71-42862
- Dynamic characteristics of human respiratory and circulatory adaptation to muscular exercise, using systems analysis approach
23 p3634 A71-43905
- Low grade hypoxia effects on human physiological responses and performance in vigilance/display monitoring tasks
23 p3636 A71-44238
- Preoptic and environmental temperature effects on hibernator thermoregulatory responses, noting changes in metabolic rates
23 p3637 A71-44301
- Psychophysiological loudness and annoyance indices application in sonic boom comfort level evaluation, pulsating noise estimation and sound insulation system effectiveness determination
24 p3799 A71-44399
- High blood pressure and age effect on human baroreflex arc controlling pulse interval sensitivity, showing systolic pressure response to phenylephrine intravenous injection
24 p3794 A71-44434
- Stabilographic indices and excitability curves of vestibular response to galvanic currents, using van Egmond cupulometry method
24 p3796 A71-44544
- Simultaneous recordings of ERG and visually evoked cortical potential to stimuli of differing luminance and pattern, comparing spatial frequency characteristics
24 p3801 A71-44977
- PHYSIOLOGICAL TELEMETRY**
U BIOTELEMETRY
PHYSIOLOGICAL TESTS
NT CARBOXYHEMOGLOBIN TEST
NT VESTIBULAR TESTS
Biotelemetry data acquisition and electrode technology, discussing physiological measurements and pickup techniques for conversion into electrical signals
03 p0369 A71-13060
- Oxygen intake, ventilation and heart rate during various intensity and duration tests
05 p0708 A71-16615
- Oxygen consumption and carbonic acid output in hypothermic rats cooled under diethyl ether anesthesia, investigating physiological indices during hypothermia
06 p0852 A71-17667
- K, Na, Ca and I electrolytes content in thyroid gland and blood during experimental hypothyroidism in rabbits
06 p0852 A71-17668
- Automated vision tester for evaluating space environment effects and multiphasic health screening
07 p1046 A71-18805
- Somatic concentration and brief sensory deprivation effects on rod and frame and embedded figures test performance
07 p1045 A71-20382
- Informative precordial palpation taking into account location, timing, duration and amplitude
08 p1241 A71-21889
- Electroencephalophone for stereophonic display of four channel EEG physiological signals from skull quadrants
09 p1397 A71-22252
- Information support system for physiological studies of human performance, including indexing approach for references categorization, microfiche file and data bank
11 p1860 A71-25253
- Left ventricular enlargements, comparing vectorcardiographic spatial magnitude and electrocardiographic precordial QRS voltage measurements
11 p1725 A71-26428
- Dipole, quadrupole and octapole measurements in isolated beating hearts
13 p2016 A71-28150
- Physical fitness relation to flight requirements, pilot performance and age, considering muscular strength, cardio-respiratory capacity, body weight and mental aspects
16 p2528 A71-33114
- Human motor control behavior sampling hypothesis of open loop system at voluntary effort initiation, discussing validity based on ankle rotation physiological test
17 p2690 A71-34741
- Antiexposure suits physiological evaluation for subjective comfortableness, oral and skin temperatures and pulse rate, determining optimum environmental temperature
17 p2692 A71-35195
- Flying personnel equilibrium tests with pendulum armchair, investigating labyrinth reflex by induced nystagmus
22 p3500 A71-41570
- Ultrasonics use in physiological and pathophysiological experiments on human organism, considering ultrasonic vibration physical properties
22 p3502 A71-41941
- Controlled caloric stimulation of labyrinths in man by water at various temperatures
22 p3504 A71-42583
- Solute diffusion coefficients dependence on proteins concentrations in human plasma from experiment, presenting equation for prediction
23 p3637 A71-44253
- Biological effects of ionizing radiation and non-radiative factors on radiation damage from satellite space flight tests on dogs and plants
24 p3798 A71-44891
- PHYSIOLOGY**
NT BODY COMPOSITION [BIOLOGY]
NT ELECTROPHYSIOLOGY
NT HEMATOPOIETIC SYSTEM
NT NEUROPHYSIOLOGY
NT PSYCHOPHYSIOLOGY
NT RESPIRATORY PHYSIOLOGY
Eight channel physiological data scanning and timing control, sequential conversion, printing and punching
05 p0714 A71-16923
- Book on clinical physiology techniques and anesthesiology measurements covering electronics, ECG analysis, blood pressure measurement, cardiac function, respiratory mechanics, etc
09 p1398 A71-22459
- Soviet book on aviation medicine covering human anatomy and physiology, atmospheric physics, flight effects, respiratory systems, crew diets, etc
14 p2188 A71-29943
- Papers on anatomy and mechanisms of mammalian sensory systems including vision, audition and touch
14 p2183 A71-30251
- PICKLING**
U CHEMICAL CLEANING
PICTURE TUBES
Astronomical telescope efficiency improvement, using TV kinescope equipment with superorthicons and videofrequency amplifiers
04 p0589 A71-14832
- Kinescope light characteristics nonlinearity effect of television system penetrating ability for image reproduction of faint stars
07 p1115 A71-20444
- PICTURES**
U PHOTOGRAPHS
PIEZOELECTRIC CRYSTALS
Transverse surface wave propagation in piezosemiconducting body with electron damping, formulating boundary conditions
01 p0140 A71-11287
- Lamb wave interaction with current carriers in cubic symmetry piezosemiconductors, obtaining amplification factor
06 p0942 A71-18352
- Ionizing radiation effect on piezoelectric properties of quartz plates, covering X rays, gamma rays, electrons, protons and alpha particles
10 p1656 A71-24146
- Transverse excitation of elastic ultrasonic waves in CdS piezoelectric plates, considering conductivity effect on damping
12 p1944 A71-27544
- Simplified characteristic equation for plane piezoelectric vibrations of lithium niobate and lithium tantalate crystals, using perturbation methods
15 p2461 A71-31701
- Slow wideband excitation of ultrasonic waves with piezoelectric crystal delay line subject to microwave radiation
19 p3015 A71-37251
- Papers on ultrasonic transducer materials covering magnetostrictive metals and alloys and piezoelectric crystals and ceramics
20 p3236 A71-39253
- Piezoelectric crystals and ceramics for acoustic power detectors and radiators, considering crystal symmetry and coupling factor effect on piezoelectricity
20 p3253 A71-39255
- Surface acoustic waves in layered substructure of piezoelectric epitaxial film of cadmium sulfide on germanium substrate
21 p3429 A71-41208
- HF electric signal detection, using acoustoelectric surface wave field in piezo semiconducting crystal
21 p3436 A71-41363
- Elastic plates radial vibrations excited by piezoelectric elements, investigating electromechanical coupling coefficient and ultrasonic radiation constants
21 p3473 A71-41365
- Piezosemiconductors nonequilibrium electron plasma current oscillations under strong electric and magnetic field interactions
22 p3584 A71-41644
- Transverse surface wave amplification in piezosemiconductors, considering cases of total or drift current in thin near-surface semiconducting layer
22 p3585 A71-41707
- PIEZOELECTRIC GAGES**
Stress dynamics of optimum high speed piezoelectric pressure probes utilizing backing rod material
03 p0427 A71-13913
- Piezoelectric and capacitive transducer pressure measurements in low pressure fluidic elements
07 p1026 A71-20571
- Laser pulse shape, beam modulation and power fluctuation quality control measurements, using non-selective, thermally stable piezoelectric sensor with low time constant
15 p2421 A71-32456
- Piezoelectric probe for pressure measurement in plasma behind shock front, discussing design and measuring circuit
24 p3825 A71-44750
- PIEZOELECTRIC TRANSDUCERS**
NT PIEZOELECTRIC GAGES
Touch sensitive X-Y position encoder for computer display input using surface wave piezoelectric transducer
01 p0047 A71-10214
- Piezoelectric transducer voltage-displacement response characteristics under connection with interferometric device, considering linearity and repeatability
01 p0079 A71-10311
- Interdigital Rayleigh wave transducer on piezoelectric ceramics with comb-to-comb polarization
01 p0055 A71-11174
- Engine vibration high temperature transducer, discussing piezoelectric materials properties and design considerations relative to temperature, pressure, acoustic noise, humidity environment
02 p0255 A71-12911
- Interdigital converter for excitation and reception of acoustic surface waves on piezoelectric materials in bandpass filter design
03 p0388 A71-14574
- Linear theory of acoustoelectric oscillator with sandwiched piezoelectric plate accounting for mode enhancement and quenching
04 p0558 A71-15146
- Piezoelectric ceramic transducer vibration measurement under mechanical loading, noting displacement as function of thickness and time
04 p0601 A71-15835
- Piezoelectric transducer echo signals spectral analysis, taking into account electrical load and electromechanical coupling degree
08 p1294 A71-21896
- Piezoelectric accelerometers for high temperature vibration measurements, examining materials critical characteristics, design minimal weights and vibration system test methods
09 p1443 A71-22707
- Differential charge amplifier design using ferromagnetic high signal bandwidth isolation with grounded input transducer and output load
09 p1417 A71-22782
- Frequency characteristics determination of fixed piezoaccelerometers, using three mass equivalent system
09 p1450 A71-22797
- Amplitude-frequency characteristics of physically similar piezoelectric accelerometer converters
09 p1450 A71-22798
- Equivalent electrical circuits of interdigital transducers for piezoelectric generation and detection of ultrasonic Rayleigh waves
09 p1420 A71-23680
- Piezotron accelerometer for vibration measurement, combining quartz sensing element with subminiature solid state electrostatic amplifier
11 p1767 A71-26442
- Piezoelectric transducer/oscillograph technique for simultaneously rating fuels knock properties and detonation intensity
13 p2113 A71-28228
- Equivalent circuit for interdigital piezoelectric Rayleigh wave transducer
13 p2037 A71-28472
- Piezoelectric substrate dependent differences between in-line and crossed field three port circuit models for interdigital surface wave transducers
13 p2038 A71-28612
- Ultrasonic field distribution patterns from metallic and ceramic concave spherical reflectors under excitation by single or multiple piezoelectric elements
13 p2101 A71-29267
- Radiation patterns from piezoelectric transducers on Y face of lithium niobate, using Green function analysis
14 p2283 A71-29795
- Unsteady force and pressure measurements by molecular and parametric transducers including strain

gauge, drag, moment and piezoelectric balance instruments
15 p2411 A71-32563

Composite piezoelectric transducer subjected to current flow in semiconducting boundary layer under polarization gradient, determining mechanical response by Laplace transform
17 p2739 A71-34669

Weber antenna sensitivity for short pulses of gravitational radiation, giving limit for connection coefficient of piezotransducer with detector
18 p2946 A71-35979

Static and transient pressure measurement in turbulent boundary layers, using transducer with piezoelectric sensing element
20 p3233 A71-38822

Solid state linear array piezoelectric hydroacoustic image transducer for underwater viewing in turbid oceanic environments
20 p3233 A71-38828

Piezoelectric transducer materials and techniques for ultrasonic devices, covering delay lines, light deflectors and modulator operating above 100 MHz
20 p3237 A71-39256

Multilayer microwave semiconducting film piezoelectric acoustic transducer loss and frequency response derivation from electromechanical power conversion theory
20 p3240 A71-39764

Handwritten graphical data computer input device with pen position coordinate measurement from acoustic signal propagation delay time in piezoelectric solid plate
21 p3376 A71-40122

Transient calibration method for piezoelectric accelerometer in high g-level range [ASME PAPER 71-VIB-43]
21 p3377 A71-40293

Electroacoustic circuit of ultrasonic resonance thickness gage based on frequency dependence of piezoelectric transducer conductance in multilayered acoustic system
22 p3528 A71-41755

Ultrasonic inspection apparatus for defects detection in metal pipes, using immersion echo mode with two piezoelectric scanning heads rotating about pipe
22 p3529 A71-41774

PIEZOELECTRICITY

Microwave emission from InSb due to sound amplification by piezoelectric electron-phonon coupling at low magnetic fields
01 p0052 A71-10321

YIG with thin piezosemiconductor coating, investigating transverse surface wave amplification and velocity
01 p0140 A71-11288

Mechanical characteristics of generalized Rayleigh waves in piezosemiconductors of cubic symmetry, deriving amplification and damping factors for zero diffusion coefficient
02 p0294 A71-11894

Semiconductor developments, discussing field effect transistors, MOS, microwave components, piezoelectric effects, optoelectronics and galvanomagnetism
03 p0384 A71-13534

Poling techniques modifications for piezoelectric activity enhancement in bulk polymers, considering arcing minimization, AC field superimposition and repeated cycling of process
03 p0448 A71-13721

Piezoelectric surface waves physical characteristics, examining excitation relationship to construction of microwave devices
04 p0550 A71-14742

CdTe thin film anomalous photovoltaic effect and piezoelectric dependence on real state
07 p1176 A71-19271

Ultrasonic surface wave generation by infinite interdigital electrode array on piezoelectric material, predicting behavior from equivalent circuit by variational principle
17 p2717 A71-35491

Sound waves interaction in piezoelectric semiconductors under pumping, deriving basic equations for parametric amplification investigation
21 p3430 A71-41216

PIEZORESISTIVE TRANSDUCERS

NT PIEZOELECTRIC GAGES

Solid propellants stress measurement using piezoresistive transducer
03 p0501 A71-13172

Stress effects on electron relaxation time anisotropies in n-type Si, using high temperature piezoresistivity model for population transfer rates
09 p1508 A71-22692

Transient ground motion velocity measurement system, using piezoresistive acceleration transducers, electronic integrator and digital zeroing circuit
14 p2245 A71-30340

PIGEONS

Pigeon vestibular apparatus fluids and structures physical properties, detailing specific gravity and viscosity of endolymph, perilymph and cupola
14 p2185 A71-30467

PIGMENTS

NT CAROTENE

NT CHLOROPHYLLS

NT CYTOCHROMES

Salmonid fishes from Great Britain and southern Germany, analyzing visual pigments and liver retinols
01 p0008 A71-10229

Double beam monochromatic differential cinespectrophotometer for recording oxidation/ reduction reactions in intercellular pigments
01 p0021 A71-10243

Rudd vision mechanism, considering daylight effect on spectral sensitivity and visual pigment retinal extract proportions
01 p0009 A71-10271

Apollo 11 lunar samples effect on terrestrial microorganisms, noting pigment production effects of Fe leaching from bulk fines and core samples
10 p1566 A71-23747

Q switched ruby laser emission effect on long wave pigment system of photosynthesizing organisms
11 p1774 A71-26006

Surface roughness and surface area effect on UV stability of zinc orthotitanate pigments, using electron microscopy and BET nitrogen adsorption [ALAA PAPER 71-451]
11 p1790 A71-26235

Human color vision investigation by psychophysical methods, discussing spectral sensitivity, pigment absorption and defective color vision as function of stimulus wavelength
12 p1873 A71-26863

Centrally parietal chromatophore in green coccal algae, noting individual cell division and total number increase throughout ontogeny
16 p2531 A71-33465

Lead oxide pigment photoconductivity, investigating surface processes effects on spectral sensitivity and absorption spectrum
21 p3434 A71-41329

Porphyrin-like pigments in Apollo 12 lunar soil sample 12023, using spectral analysis involving fluorescence, absorption and magnetic circular dichroism spectrometry
23 p3756 A71-43739

Visual pigments in color blind subjects, using retinal densitometry
24 p3794 A71-44464

Red/green pigments in normal color vision, describing analytical anomaloscope for measuring protanopia and deuteranopia sensitivity curves
24 p3794 A71-44465

Human eyes macular pigment optical density curves through spectral sensitivity measurements, noting differences due to race, environment, age, skin, eye and hair color
24 p3794 A71-44466

PILOCARPINE

Pilocarpine induced synchronous sweat expulsions, noting frequency linear dependence on ambient temperature with and without generalized sweating
18 p2861 A71-36889

PILOT ERROR

In-flight EEG recordings telemetry for pilot aptitude testing, showing pilot error relationship to brain oversteering
03 p0370 A71-13067

Cockpit simulator motion effects on ILS approach pilot guidance errors, using Erdmann model [DGLR-70-071]
05 p0779 A71-15956

Night carrier landing final approach glide slope altitude, lateral and sink rate pilot errors prediction, using linear regression model
06 p0858 A71-17602

Physiological aspects of aircraft accident investigation, considering pilot errors
08 p1247 A71-20825

Aircraft spin tests preparation and evaluation, describing pilot errors
15 p2348 A71-31462

Epidemiology statistics of USAF spatial disorientation aircraft accidents, noting pilot training, flight environment and indoctrination remedy programs
21 p3342 A71-40359

Physiological factors in fatal aircraft accidents, discussing pilot incapacitation and transient functional disturbances
22 p3502 A71-41834

Corporate aircraft pilot ground and flight phase training, errors and accidents
23 p3629 A71-43388

Cumulative /chronic/ and acute skill fatigue and physical fitness in aircrews, considering relationship to pilot error accidents
23 p3639 A71-43390

PILOT PERFORMANCE

Flight simulators pilot performance monitoring and recording, discussing multichannel data acquisition and use in specific training tasks performance evaluations
01 p0066 A71-10021

Avionics system maximizing pilot chances of surviving mission and destroying selected target by removing mental limitations
01 p0124 A71-10506

Electronic control indicator for human pilot capability enhancement using color coded cathode ray display, presenting information from seven different instruments
01 p0081 A71-10750

Aircraft flying qualities research program, discussing navy test pilot evaluations and longitudinal handling characteristics for simulated carrier landing task [ALAA PAPER 69-897]
02 p0189 A71-12678

Weather effects on pilot performance
03 p0369 A71-13021

In-flight ECG telemetry for aircraft pilots diagnostics, discussing characteristic recordings and measuring probes development for simultaneous parameters transmission
03 p0370 A71-13062

Superior jet pilots social, military and flying case histories, noting predominance of firstborn children with close father-son relationships
03 p0371 A71-13325

Helicopter noise minimization by various piloting maneuvers, discussing takeoff and landing, transition to forward flight, route selection, etc
04 p0531 A71-15408

Rotorcraft ideal height-velocity boundary and critical decision point height prediction, discussing pilots optimal control under emergency conditions
04 p0527 A71-15414

Pilot performance under helicopter cabin high temperature and humidity
04 p0547 A71-15422

VTOL handling qualities criteria for civil IFR qualifications, taking into account pilot abilities
04 p0533 A71-15427

V/STOL spray generation tests concerning pilot visibility impairment in low altitude overwater hover
04 p0534 A71-15444

Pilot nervous-emotional state during flight conditions determined from uropepsin excreted in urine
05 p0711 A71-17028

Frequency and amplitude during longitudinal control surface pumping by pilots in precise flight path handling for aircraft design [ALAA PAPER 70-567]
06 p0847 A71-17699

Pilot physiological responses as indicators of pitch motion cues effect on flight simulator fidelity
07 p1047 A71-19465

U.S. domestic ATC airspace enroute and terminal area navigation system effects on pilot workload, projecting future FAA requirements
07 p1157 A71-20347

Pilot visual perception time of instrument readings after viewing external features and landmarks
07 p1053 A71-20540

Glider flight in thermal air currents, discussing aircraft behavior, pilot sensory perceptions and reactions and use of variometers for ascent rate determination
08 p1230 A71-20685

Preventive and clinical medicine effect on aircrew health maintenance
08 p1245 A71-20725

Pilot vision during final approach and landing in turbojet transport operations
08 p1247 A71-20826

Helicopter noise minimization by various piloting maneuvers, discussing takeoff and landing, transition to forward flight, route selection, etc
08 p1230 A71-21049

Electroluminescent aircraft instrument lighting effects on pilots dark adaptation taking into account color, panel legibility, scotopic sensitivity and acuity
08 p1248 A71-21229

Pilots hypoxic hypoxia occurrence and treatment
08 p1249 A71-21959

Optokinetic and vestibular effects on human operator reliability in aircraft control systems
09 p1399 A71-22681

Navy pilots performance improvement through symbolic flight displays
09 p1453 A71-23675

Jet pilots flight stresses assessment via biotelemetric transmission of pulse rate, respiratory rate, electrocardiographic data, flight altitude and velocity
10 p1567 A71-23880

Influence sources affecting self organization of man machine systems, discussing human pilot model
10 p1571 A71-24760

Psychophysical evaluation of glide slope detection accuracy by diamond vs square shape in runway centerline stripping as aircraft landing aid
12 p1875 A71-27252

Midair collisions analysis for civil-military integrated ATC air space, discussing near miss volume, random heading aircraft density and pilots evasive action vs avoidance percentages
12 p1927 A71-27599

Aircrew static reach reduction caused by upper and lower limb orthopedic disabilities
12 p1876 A71-27632

Jet fighter pilot blackout episode report, correlating laboratory data with flight profile and events sequence
12 p1871 A71-27634

Automatic landing systems independent monitor for L-1011 aircraft, providing pilot confidence under reduced visibilities
[SAE PAPER 71-0443] 13 p2098 A71-28324

V/STOL and supersonic commercial aircraft developments, comparing man and machine performance as information processing systems for aircraft control and navigation 13 p2018 A71-28486

Functional diagnostics in aerospace medicine for evaluating pilot ability and flight stresses 13 p2018 A71-28488

Toxicological evaluation of CO in humans and other mammals, considering pilot performance prediction for aircraft environment 13 p2012 A71-28902

Case histories of pilot failure during training or operational flight due to cerebral cortical dysfunction 13 p2023 A71-29365

Atmospheric turbulence induced aircraft vibrations effects on aircrew performance, discussing physiological and psychological responses 14 p2187 A71-29778

Low altitude turbulence simulation in piloted flight simulators, discussing turbulence induced aircraft disturbances and effects on pilot 14 p2188 A71-29781

Commercial aircraft piloting in atmospheric turbulence, discussing aircraft characteristics, instrumentation, flying procedures, pilot training and kinesthetic cues 14 p2173 A71-29782

Large subsonic jet aircraft civil pilots performance under physiological and psychological stresses induced during severe atmospheric turbulence 14 p2188 A71-29783

Controlled aircraft motion under strict kinematic constraints in terms of simple subsystems, noting pilots role in Newmark theory 14 p2177 A71-31024

EEG and derivative spectral characteristics evaluation in determining pilot mental activity during flight 15 p2362 A71-31250

Hemodynamic changes in healthy pilots with excess weight investigated by mechanocardiograph, showing decreased cardiac output, left ventricle strength and volume rate 15 p2357 A71-31319

Air transport accident research in night approach simulators, noting visual information null in descent path and delay in relative motion supplement data 15 p2363 A71-31602

Pilots illusory attitude perception causes, suggesting psychological and medical remedies 16 p2534 A71-32830

Young pilot performance in emergency situations including communication system failure and other equipment breakdowns, noting emotional reactions 16 p2534 A71-32831

Nystagmic responses of airmen and grounded and active pilots subjected to caloric and rotational tests 16 p2535 A71-33112

Physical fitness relation to flight requirements, pilot performance and age, considering muscular strength, cardio-respiratory capacity, body weight and mental aspects 16 p2528 A71-33114

Epidemiological statistics for age specific incidence rate of serious in-flight pilot failure, considering fatal and nonfatal causes 16 p2535 A71-33121

Pilot psychic states in flight, including preliminary demobilization, drowsiness, stunning, euphoria and phobias 16 p2536 A71-33576

Soviet book on aircraft automatic control systems covering linear theory, design, autopilot, man machine performance, operation modes, etc 17 p2771 A71-34473

Psychosociological and medical evaluation of private pilots to promote flight safety 17 p2690 A71-34824

Physiological tests for psychic stress effects on aircraft pilot tracking performance, respiration and heart rate 17 p2693 A71-35199

Aircraft accident litigation related to wake turbulence concerning pilot or air traffic controller faults 17 p2842 A71-35387

Eye-point-of-regard system including eye and head movements devices and analog computer for pilot scanning and display research 18 p2864 A71-36091

Pilot workload reduction in steep approach landing of light aircraft from flight test data analysis [AIAA PAPER 71-904] 19 p3095 A71-37155

Automation in third generation ATC requiring distributed management and spacing functions delegation to pilot [CASI PAPER 72/15] 19 p3100 A71-37602

Literature survey of nervous-emotional stress effects on pilot during flight, discussing premature fatigue, cardiovascular disorders, psychic disturbances and circadian rhythms 19 p3002 A71-37763

Air safety standards and objectives, discussing human factors as accident causes, piloting aids and management 20 p3178 A71-39395

One man Jaguar aircraft navigation, weapon aiming system and pilot operational tasks, noting inertial platform alignment, displays and target attack modes 20 p3261 A71-39825

Sleep related fatigue in pilot performance and flight safety, considering sleep lack and disruption and irregular duty patterns 21 p3343 A71-40590

Simulated airline pilot cerebral incapacitation etiology, incidence and detection, noting unimpaired crew members conduct and reaction times during approach for landing 22 p3501 A71-41824

In-flight study of work/rest cycle effects on double crew performance and fatigue in flying transport missions 22 p3501 A71-41829

Pilot EEG, behavioral and subjective correlates of natural and drug induced sleep at atypical hours, using calculation and vigilance tests 22 p3502 A71-41835

Military pilot handling characteristics, discussing combat operations, accident prevention and blind landing 22 p3504 A71-42239

Aircraft pilots and astronauts relationship with environment, considering weightlessness, emotional reactions, cabin pressure and temperature control and space survival and rescue 23 p3639 A71-43223

Circadian rhythm relation to aircraft pilot safe performance 23 p3632 A71-43232

Aircraft accelerate-stop factors and regulations, pilot reaction times and accidents during takeoff 23 p3628 A71-43380

Stereoacuity role in pilot ability to land aircraft at minima, questioning adequacy of Verhoeff depth perception test administration conditions 23 p3637 A71-44244

Organophosphate pesticide poisoning implication in aircraft crash of duster pilot from cholinesterase activity drop evidence 23 p3641 A71-44249

Automatic flight control systems, discussing pilot as systems manager or retained in control loop 24 p3845 A71-44454

American development in automatic flight control, noting FAA requirements, pilot involvement and visibility enhancement 24 p3846 A71-44455

Emotional stress of pilots in difficult flight conditions, noting pulse rate increase and biopotentials amplitude changes 24 p3800 A71-44473

PILOT SELECTION

In-flight EEG recordings telemetry for pilot aptitude testing, showing pilot error relationship to brain oversteering 03 p0370 A71-13067

Civil aviation medicine practice, discussing airman certification for flight fitness, government legislation, accidents and carrier operations 08 p1245 A71-20728

Cosmonauts selection with regard to psychological and physical fitness, discussing clinical examination, hospital tests and training 09 p1397 A71-22192

Psychological selection of pupil pilots, discussing statistical correlations between values of some single parameters of Zulliger test and instructional data 10 p1572 A71-24981

Sensomotor activity tests of operator perceiving high speed stimuli in broad visual field for psychological selection of aircraft and spacecraft pilots 13 p2018 A71-28416

Lower extremity Army aviator amputees retention on flight status regarding service need, amputation and prosthetic fit, age, career, hours flown and time in military 16 p2535 A71-33120

Medical rejection statistics of applicants for BEA/BOAC pilot training, considering ophthalmic, ear, nose, throat and general health condition 22 p3501 A71-41823

EEG characteristics of cadets and flying personnel, noting spike wave paroxysmal screening and epilepsy detection 22 p3502 A71-41836

Anatomic examinations and diagnostic techniques in ophthalmologic aviation medicine, discussing electronic time interval and storage measurements, cortical response, etc 23 p3631 A71-42928

Physiological systems connected with sensory perception of equilibrium and orientation on ground and in air, discussing pilot training and selection 23 p3632 A71-43148

Psychological screening of pilot trainees, showing neurosis noncorrelation with learning ability to fly 23 p3639 A71-43221

Psychological screening of pilot trainees, investigating Minnesota Multiphasic Personality Inventory test data correlation with learning ability to fly 23 p3639 A71-43222

Corporate aircraft 1970 accident statistics analysis stressing pilot selection, training and supervision 23 p3628 A71-43227

PILOT TRAINING

Airline flight simulators and associated pilot training equipment, discussing improvements in flying control systems, computers, visual systems and power supplies 01 p0066 A71-10013

Flight simulators pilot performance monitoring and recording, discussing multichannel data acquisition and use in specific training tasks performance evaluations 01 p0066 A71-10021

Pilot training flight simulators without visual or motion cues, discussing validity for aircraft handling qualities assessment and pilot role in simulation process [DGLR-70-070] 05 p0733 A71-15968

Link 747 simulator design and operation, describing cockpit layout, motion picture system and malfunction insertion and display unit 06 p0881 A71-18665

Coriolis vestibular reaction testing of pilot trainees, evaluating brief vestibular disorientation test validity and reliability at 10 and 15 rpm test conditions 08 p1247 A71-20823

Acceleration tolerance improvement in human subjects by gymnastics, games, athletics and aviation pilot training 09 p1399 A71-22920

Psychometric measurements approaches for pilot training questionnaires, considering personality traits standard model 10 p1559 A71-23929

Cardiovascular functional reactions in pilot trainees during training flights, presenting case histories 10 p1570 A71-24341

Ground based flight equipment evaluation in routine primary pilot training 12 p1875 A71-27249

Jet pilots training technologies, discussing multimedia instruction, psychological stress reduction, self study, airborne video application and simulation [SAE PAPER 71-0477] 13 p2017 A71-28342

Airline pilot training specific behavioral objective concept, noting introduction with Boeing 744 [SAE PAPER 71-0479] 13 p2017 A71-28344

Flight training program for twin-engine transition, using commercially available training device [SAE PAPER 71-0480] 13 p2017 A71-28345

DC 10 flight crew individualized ground training program, emphasizing hands-on equipment and instruction hardware [SAE PAPER 71-0472] 14 p2176 A71-30538

Head- or helmet-mounted display/control system in V/STOL aircraft for pilot workload and training reduction [AHS PREPRINT 532] 14 p2189 A71-31093

Aircraft-simulating cockpit procedure trainer statistical data and development problems concerning safety, economy and efficiency performance 15 p2384 A71-31883

Pilot training efficiency increase through advanced simulation technology utilization, discussing computerized flight simulators, CRT display systems and automated briefings 15 p2384 A71-31886

Aircraft accidents due to engine-out simulation, discussing human factors, minimum control speed certification requirements and pilot flight training procedures [AIAA PAPER 71-793] 16 p2525 A71-34025

Category II operations at various airports, considering all-weather landing requirements of airborne equipment, maintenance standards, pilot training, etc [SAE PAPER 71-0442] 17 p2674 A71-34499

Aircraft pilot learning process with C-8 trainer, determining effective evaluation indexes including error ratio, control numbers, pulse rate and reaction time 17 p2692 A71-35196

Aircraft pilots anthropometric survey for human factors engineering, discussing measurement techniques and arrangements for training 17 p2692 A71-35198

Link 747 simulator with six degrees of motion system for engineers and pilot training 18 p2900 A71-36970

Boeing 747 digital computer type flight simulator with four degrees of movement for engineer and pilot training 18 p2901 A71-36971

Adaptive technique feasibility for flight simulator training of pilots 18 p2873 A71-36974

Medical rejection statistics of applicants for BEA/BOAC pilot training, considering ophthalmic, ear, nose, throat and general health condition 22 p3501 A71-41823

- Psychophysiological and conversion mechanisms as unconscious expression of student pilot motivation decrease for further flight training, presenting case histories
22 p3502 A71-41837
- Physiological systems connected with sensory perception of equilibrium and orientation on ground and in air, discussing pilot training and selection
23 p3632 A71-43148
- Serotonin metabolism of helicopter pilots, showing effects of emotional factors due to flight inexperience
23 p3632 A71-43220
- Corporate aircraft 1970 accident statistics analysis stressing pilot selection, training and supervision
23 p3628 A71-43227
- Airlines procedures in conducting pilot training programs within ICAO recommendations and German regulations
23 p3639 A71-43230
- Corporate aircraft pilot ground and flight phase training, errors and accidents
23 p3629 A71-43388

PILOTED CENTRIFUGES
U HUMAN CENTRIFUGES
PILOTLESS AIRCRAFT
NT DRONE AIRCRAFT

- Remotely piloted vehicles development and limitations, considering air superiority, weapons delivery, sensors and survivability
18 p2849 A71-35899

PILOTS [PERSONNEL]
NT AIRCRAFT PILOTS
NT TEST PILOTS

- Optimal preflight feeding for pilots, discussing protein content and vitamin enrichment
01 p0024 A71-11109
- Aircraft instrumentation deficiencies from pilot viewpoint, proposing pilot designed display
[AIAA PAPER 71-787] 16 p2537 A71-34017
- World championship gliding team medicophysiological problems during competition at Marfa, Texas, discussing climatic adaptation, nutrition, hypoxia and pilots general physical and psychomotor conditions
22 p3500 A71-41576
- Military pilot handling characteristics, discussing combat operations, accident prevention and blind landing
22 p3504 A71-42239

PINCH EFFECT
NT PLASMA PINCH
NT THETA PINCH

- Pinch effect in nondegenerate intrinsic inhomogeneous semiconductors under nonuniform spatial volume recombination, resulting in nonlinear I-V characteristics
10 p1656 A71-24321

PINEAL GLAND

- Pineal gland endocrine functions, discussing melatonin synthesis and secretion in response to environmental illumination
05 p0712 A71-17108
- Small spotted dogfish shark epiphysis cerebri, determining light sensitivity and properties
13 p2008 A71-28456
- Biosynthesis control of melatonin and other methoxyindoles in mammalian pineal organ
14 p2182 A71-29631
- Sparrows pinealectomy effect on circadian rhythms of body temperature in light and darkness from radio telemetric monitoring
23 p3633 A71-43547

PINHOLES

- Ruby watch jewels as pinhole diaphragms in laser beam broadening systems, determining optimal size
16 p2588 A71-34102

PINS

- Service life of pin jointed connections with elastoplastic strains in bore walls
04 p0602 A71-14606

PION BEAMS

- Negative pion elastic scattering differential cross section measurements from 1.71 to 5.53 GeV/c, using zero gradient synchrotron beam on liquid hydrogen target
02 p0286 A71-11647
- Radiation induced visual phosphores observed by dark adapted human subjects in fast neutron, X ray and positive pion beams at Berkeley comparative to primary cosmic ray effects
12 p1871 A71-27675
- Pion beam dosimetry with silicon detectors and plastic scintillators, presenting depth dose and isodose distributions and differential range curves
24 p3799 A71-44359

PIONEER SPACE PROBES

- NT PIONEER 6 SPACE PROBE**
NT PIONEER 7 SPACE PROBE
NT PIONEER 8 SPACE PROBE
NT PIONEER 9 SPACE PROBE
- Optical bonding agent for calcite prism on Pioneer F/G mission, emphasizing optical and mechanical properties resistance to Jupiter high energy particles
01 p0081 A71-10835

- Pioneer spacecraft flight missions, discussing interplanetary, solar-earth and deep space observations
01 p0160 A71-10990

- Corotating solar wind electron number density from sun orbiting Pioneer spacecraft radio propagation measurements
07 p1189 A71-20320

- Pioneer F spacecraft investigation of Jupiter regions and outer interplanetary space, discussing design, communication system and possible future missions
12 p1973 A71-27603

- Solar flare radiation data from Pioneer spacecraft, detailing anisotropy, heliocentric longitude gradients, decay time constants and energy spectra
15 p2480 A71-32752

- Mathematical model of arc Pioneer 6/7 plasma probe electrostatic analyzer responding to monoenergetic unidirectional charged particle beam
18 p2952 A71-36583

- Pioneer Jupiter probe missions as precursor to subsequent outer planets exploration, discussing primary objective of asteroid belt and Jupiter radiation belt hazards evaluation
[AAS PAPER 71-111] 19 p3152 A71-37911

- Pioneer F and G spacecraft Jupiter flyby postencounter mission options ranging from solar system escape to high-inclination low-perihelion trajectories
[AAS PAPER 71-136] 19 p3139 A71-37921

- Pioneer F/G spacecraft Jupiter missions, trajectories and objectives with relation to outer system
[AAS PAPER 71-101] 19 p3140 A71-37931

- Jupiter entry probe integration on TOPS and Pioneer outer planet spacecraft for flyby missions, discussing design feasibility and spacecraft modification requirements
[AAS PAPER 71-153] 19 p3153 A71-37955

- Solar wind formation of heliosphere, discussing solar wind-interstellar medium interaction region probes by Pioneers F and G
[AAS PAPER 71-165] 19 p3141 A71-37962

- Pioneer Jupiter spacecraft, noting low weight, radioisotope thermoelectric generators and gyroscopic stabilization by spinning with antenna pointed at earth
[AAS PAPER 71-167] 19 p3141 A71-37964

- Pioneer 8 and 9 micrometeorite measurements of particles kinetic energy, momentum, velocity and direction, correlating measured particle flux rates with predictions based on zodiacal light
20 p3297 A71-39634

PIONEER 6 SPACE PROBE

- Interplanetary magnetic field power spectra fluctuation measurements by Pioneer 6 satellite
06 p0956 A71-18141

- Jupiter grand tour mission, discussing objectives and technical aspects of unmanned Pioneer F and G vehicle
18 p2965 A71-36684

- Radioisotope thermoelectric generators integration for Pioneer 6/7 program, discussing design requirements
[AAS PAPER 71-150] 19 p3103 A71-37952

PIONEER 7 SPACE PROBE

- Pressure conditions across distant magnetopause from interplanetary magnetic field measurements, comparing Pioneer 7 plasma data with Explorer 33 distant geomagnetic tail field magnitudes
08 p1285 A71-21692

- Solar wind compressed magnetic field in sunward magnetosphere and extended geomagnetic tail observation by Pioneer 7 spacecraft
14 p2234 A71-30028

- Jupiter grand tour mission, discussing objectives and technical aspects of unmanned Pioneer F and G vehicle
18 p2965 A71-36684

- Radioisotope thermoelectric generators integration for Pioneer 6/7 program, discussing design requirements
[AAS PAPER 71-150] 19 p3103 A71-37952

PIONEER 8 SPACE PROBE

- Micrometeorites orbital elements, evaluating cosmic dust experiment data from Pioneer 8
03 p0496 A71-14505

- Galactic cosmic ray proton and He nuclei spectra measurements aboard Pioneer 8 spacecraft over large energy range, considering solar modulation parameters
08 p1355 A71-21626

- Qualitative micrometeoroid model for predicting results of in situ experiments, considering correlation to Pioneer 8 and 9 results
20 p3300 A71-39654

PIONEER 9 SPACE PROBE

- Pioneer 9 space probe electric field experiment and near earth observations of noise spectra variations related to diffusive plasma layer
09 p1529 A71-23711

- Pioneer 9 interplanetary observations, presenting deep space data for solar rotations and radial gradient in VLF electric field behavior
13 p2064 A71-29163

- Qualitative micrometeoroid model for predicting results of in situ experiments, considering correlation to Pioneer 8 and 9 results
20 p3300 A71-39654

PIONS

- Pion-nucleon interactions, determining energetically precipitated particle effects in air showers
03 p0461 A71-13841

- Nuclear cascade pion energies in heavy material by Monte Carlo method, concerning cosmic ray and particle accelerator interactions
03 p0461 A71-13842

- High energy cosmic particle interactions with LiH target, discussing relation between longitudinal and transverse momenta of generated pions
03 p0476 A71-13844

- Pion interactions with nucleons and nuclei in emulsions irradiated by high energy pion beams
03 p0461 A71-13852

- Positive pions coherent production by negative pions with aid of nuclear photoemulsions
03 p0461 A71-13853

- Momenta measurements of particles produced by high energy quasi-nucleon interactions of pions on photoemulsion layers, using primary particle tracks scanning
03 p0461 A71-13854

- Atmospheric high energy gamma rays, pion production and electron energy spectra over Hyderabad, using stack nuclear emulsions
07 p1189 A71-20497

- Negative pion capture in nuclei, examining charged particle emission energy spectra
10 p1644 A71-24538

- Muon bundles frequencies from model for propagation of various atmospheric components in combination with theoretical pion spectra
10 p1664 A71-25044

- Extensive air showers and multiple muons frequencies, considering parent pions mean transverse momentum, multiplicity law form and primary cosmic ray intensity
10 p1664 A71-25046

- Neutral pion decay and galactic gamma radiation from demodulated cosmic ray spectrum, discussing neutral pion meson production
11 p1815 A71-25593

- Pions-photographic emulsion nuclei inelastic collisions as function of energy, comparing multiplicity, produced particles angular distribution and evaporation prongs number
13 p2121 A71-28059

- Cosmic ray high energy pion and nucleon nuclear interaction observations, determining statistical fluctuations in secondary particles angular distribution
15 p2479 A71-32076

- Collimated nuclear interactions induced by cosmic ray pions and nucleons in carbon and brass, noting energy dependence of events production frequency
17 p2796 A71-34858

- Air shower pion/proton and neutral/charged ratios at mountain altitude, using cloud chamber, Cerenkov counter and spectrometer measurements
20 p3279 A71-39323

- Charged pions differential photoproduction cross section description by theoretical model
22 p3578 A71-42060

- Pion-nucleon interactions, determining energetically precipitated particle effects in air showers
22 p3579 A71-42642

- Nuclear cascade pion energies in heavy material by Monte Carlo method, concerning cosmic ray and particle accelerator interactions
22 p3579 A71-42643

- High energy cosmic particle interactions with LiH target, discussing relation between longitudinal and transverse momenta of generated pions
22 p3594 A71-42645

- Pion interactions with nucleons and nuclei in emulsions irradiated by high energy pion beams
22 p3579 A71-42653

- Positive pions coherent production by negative pions with aid of nuclear photoemulsions
22 p3579 A71-42654

- Momenta measurements of particles produced by high energy quasi-nucleon interactions of pions on photoemulsion layers, using primary particle tracks scanning
22 p3579 A71-42655

PIPE FLOW

- Inviscid fluid flow in cylindrical channel excited by internal hydrodynamic energy source, calculating velocity and density distribution
01 p0071 A71-11045

- Rotating inviscid incompressible fluids in tubes, investigating axisymmetric nonlinear waves motion in relation to vortex breakdown
01 p0072 A71-11224

- Heat transfer in nongray radiating gas turbulent flow in circular tube
01 p0181 A71-11403

- Pipe bends effects on heat transfer coefficient of turbulent forced convection
02 p0330 A71-11650

- Unsteady convective heat transfer in pipes in presence of heat flux density and flow rate aperiodic variations
02 p0331 A71-11885

Circular pipe gas laminar flow at constant wall temperature, determining heat exchange and drag by motion and energy equations integration in boundary layer approximations

02 p0240 A71-12192

Initial phase of unsteady laminar flow from cylindrical vessel through circular cylindrical tube

03 p0398 A71-13105

Iron corrosion product deposition on pipe wall from aqueous stream dependent on shear rate, using radioactive tracer technique

03 p0442 A71-13368

Turbulent fluid flow through pipe, measuring circumferential velocity component close to wall by electrochemical techniques

03 p0400 A71-13733

Steady incompressible laminar pipe flow within porous wall cylinder, determining velocity, pressure distribution and shear stress
[ASME PAPER 70-WA/FLCS-3]

03 p0401 A71-14079

One component two phase mixtures critical flow in nozzles, orifices and short tubes, considering interphase heat, mass and momentum transfer
[ASME PAPER 70-WA/HT-5]

03 p0520 A71-14095

Rarefied gas flow through long square tubes, solving continuum differential equation with noncontinuum slip boundary conditions

Air jet mixing with low velocity stream in constant diameter pipe, measuring flow characteristics for non-separating conditions
[ASME PAPER 70-WA/PID-1]

03 p0402 A71-14098

Downstream heat transfer and wall friction predictions for quasi-developed strongly heated turbulent pipe flow, using mixing length model
[ASME PAPER 70-HT-8]

03 p0405 A71-14294

Heat transfer and pressure drop in air flowing in square tube with two dimensional discrete turbulence promoters applied to opposite walls

04 p0675 A71-14781

Nonlinear two dimensional free boundary problem of axisymmetric fluid flow in tubes with surface solidification, obtaining numerical solution based on finite difference equations

04 p0677 A71-15454

Laminar turbulent tube flow heat transfer, investigating internal radiation exchange and wall heat conduction and generation effects

04 p0685 A71-15519

Subcooled nitrogen tube flow film boiling, investigating heat transfer and hydraulic resistance

04 p0687 A71-15530

Multitube condensers of various geometries, investigating tube flow stability, distribution and gravitational effects

04 p0688 A71-15538

Closed system of differential equations derived for kinematic characteristics of turbulent flow in pressurized smooth pipe

04 p0575 A71-15608

Laminar to turbulent transition in pipes, using scattered light method

04 p0578 A71-15635

Convective mass transfer, velocity and concentration fields during nonNewtonian fluid motion in circular pipe with diffusion flow at wall

04 p0579 A71-15798

Monte Carlo method for ultrahigh vacuum free molecule flow transmission probability for straight tubes

05 p0785 A71-16395

Laminar or turbulent chemically reacting gas mixture flow in circular tube, examining heat transfer with enthalpy equation

05 p0838 A71-16791

Variable viscosity fluid laminar flow, measuring tube resistance at critical Reynolds numbers as function of energy dissipation

05 p0737 A71-17037

Viscous fluid laminar periodic flow in constant cross section circular pipe, noting Kelvin functions, flow profile, wall forces and Reynolds number

06 p0881 A71-17411

Forced convective heat transfer in laminar flow fluid of vanishing viscosity in constant wall temperature pipe, discussing velocity distribution effects

06 p0882 A71-18073

Laminar flow heat transfer in circular pipes, solving for Graetz equation eigenvalues and eigenfunctions

06 p1007 A71-18304

Laminar flow heat transfer in circular pipes, including longitudinal conduction term in Graetz problem

06 p1007 A71-18305

Incompressible unsteady viscous fluid flow through circular cross section curved pipe, noting centrifugal effects in interior

06 p0882 A71-18316

Large diameter tube high Reynolds number air flow temperature profiles, using chromel-alumel thermocouple

07 p1220 A71-18762

Turbulent diffusion coefficients in isothermal and nonisothermal pipe flow, comparing with Bory and Taylor theories

07 p1222 A71-18994

Compressibility effect on turbulent pipe flow shear stress distribution, presenting high subsonic Mach number theoretical results from Kjellstrom-Hedberg momentum equation integration

07 p1088 A71-19423

Viscous incompressible slow unsteady flow through circular tube with small axial roughness, obtaining velocity components by integral transform technique

07 p1092 A71-20093

Turbulent pipe, channel and plane Couette flow by Prandtl model equations, comparing with experimental data

07 p1092 A71-20278

Boundary layer separation in unsteady pipe flow, examining velocity profiles under influence of periodic pressure fluctuations

07 p1093 A71-20280

Stability of two concentrically flowing fluids in straight circular tube, investigating axisymmetric and asymmetric disturbances by small perturbation method

07 p1093 A71-20282

Turbulent pipe flow, developing analogy between momentum and heat transfer

07 p1224 A71-20371

Jet pipe valve characteristics, discussing pressure and flow recovery for various loads, nozzle diameter ratios and spacings

07 p1025 A71-20559

Poiseuille pipe flow stability from finite difference equations approximation to nonlinear axisymmetric Navier-Stokes equations under stream function perturbation

07 p1094 A71-20611

Time estimation for plasma front propagation in quartz glass circular pipes without imposition of axial magnetic field

08 p1338 A71-20829

Acoustical response of closed flue pipe as function of blowing pressure and air jet turbulence level

08 p1276 A71-21766

Equations of motion for Poiseuille flow in circular tubes, solving Gromeko problem with integral Laplace transforms and Bubnov-Galerkin method

08 p1277 A71-21935

Inviscid incompressible vortex-free axisymmetric pipe flow near arbitrary shape body symmetrically located near axis

09 p1431 A71-22180

Pipe flow turbulent friction, describing pressure drop measurements and flow visualization studies on wall roughness effects

09 p1431 A71-22275

Turbulent hot gas motion in round pipes from semiempirical turbulence theory, accounting for energy dissipation and thermodynamic parameter variability

09 p1431 A71-22370

Incompressible flow stability to axisymmetric disturbances in circular pipe

09 p1434 A71-23165

One component two phase flow in tubes with increasing pressure gradient, investigating flow choking and correlating measurements with analytical results

09 p1434 A71-23464

Turbulent flows in diverging cylindrical tube, observing stationary and traveling vortex breakdowns

10 p1592 A71-23952

Flow visualization and velocity measurements in repeatedly branching tube systems representative of human lung, estimating viscous dissipation and pressure drop

10 p1571 A71-24625

Pipe flow hot wire measurements at turbulence onset Reynolds numbers, exhibiting axisymmetric laminar velocity profile distortion

11 p1748 A71-25155

Viscous liquid unsteady flow in long circular tube as function of mean velocity distribution, discussing radial flow and pressure distribution

11 p1749 A71-25268

Hydrodynamic flow of conducting viscous incompressible fluid in rotating straight annular pipe under constant pressure gradient

11 p1804 A71-25433

Resistance and heat transfer coefficients in hydrodynamically and thermally developed MHD pipe flow

12 p1941 A71-27740

Laminar flow breakdown in circular tubes, noting disturbance level effect on intermittent flow parameters and turbulent zone length distribution

13 p2046 A71-27827

Heat exchange during stabilized laminar flow of incompressible liquid in circular pipe with radiative cooling, deriving temperature profile and Nusselt number dependence

13 p2046 A71-28180

Local and mean heat transfer at initial thermal segment for stabilized turbulent air flow in circular tubes and rectangular channels

13 p2159 A71-28419

Pipe gas flow with heated solid particles injection, presenting flow equations numerical solution by digital computer

13 p2166 A71-29460

Gromeka-Beltrami ideal incompressible fluid flow in semiminfinite circular cylindrical tube

14 p2225 A71-30221

Circular pipe gas laminar flow at constant wall temperature, determining heat exchange and drag by motion and energy equations integration in boundary layer approximations

15 p2388 A71-31498

Heat transfer surfaces performance measurements, considering tube bundles with fluid flow perpendicular to tube generatrices
[HEAT EXCH. CONF. PAPER 25]

15 p2383 A71-31639

Tube or duct confined submerged turbulent jet exit cone angle calculation for various expansion area ratios

15 p2390 A71-32016

Random turbulent signals from hot wires across pipe flow, studying form, skewness and flatness factors

15 p2391 A71-32108

Air-water flow pressure loss and phase distribution in tube with wire coil swirl generators
[GESP-449]

15 p2354 A71-32209

German monograph on viscous fluids heat transfer in pipes covering Prandtl number dependence, turbulent boundary layer flow and transition areas

15 p2514 A71-32375

Shock wave attenuation along uniform perforated tube, considering rarefaction and compression waves in resulting unsteady flow

16 p2554 A71-32883

Temporal and spatial flow velocity profiles produced by shock tube generated pressure wave propagation in open-end pipe

16 p2556 A71-32921

Pipe Poiseuille flow instability with respect to finite amplitude disturbances, calculating Reynolds stress by linear wall mode

16 p2558 A71-33021

Laminar or turbulent chemically reacting gas mixture flow in circular tube, examining heat transfer with enthalpy equation

16 p2662 A71-33041

High temperature high Mach number expansion tube flows, determining impurities by time integrated spectroscopic measurements

16 p2551 A71-33155

Transverse magnetic field influence on heat transfer of conductive fluid/mercury/ in electrically insulated pipe subjected to uniform heat flux

17 p2788 A71-34660

Mass transfer in turbulent flow region downstream of circular pipe sudden enlargement for high Schmidt numbers, using diffusion controlled electrolysis technique

17 p2837 A71-34692

Eddy viscosity model for turbulent pipe flow, yielding velocity distribution, shear, energy production and viscous dissipation rate

17 p2728 A71-34881

Hydrodynamically stabilized turbulent viscous incompressible fluid flow in circular tube, examining unsteady convective heat transfer by numerical methods

17 p2729 A71-35267

Tubular models sealed at one end with cavity facing oncoming steady gas flow, measuring increased stagnation temperature associated with shock wave formation

17 p2672 A71-35628

Quasi-stationary viscous incompressible liquid flow in porous tube with deforming wall

17 p2694 A71-35641

Surface renewal and penetration heat transfer model for turbulent flow in smooth and rough tubes

18 p2986 A71-36593

Rarefied gas flow characteristics through pipe orifice in intermediate range of rarefaction between free molecular flow and continuum flow

18 p2849 A71-37023

Turbulent rotating tube flows kinematic similarities, deriving heat and mass transfer, swirl damping and axial and rotational velocity profile

19 p3043 A71-37127

Air flow in pipe with double screw thread, calculating tangential forces and turbulent viscosity coefficient along isochats

19 p3043 A71-37266

Heat transfer and drag during air laminar flow in circular pipe with constant heat flux density at wall

19 p3044 A71-37585

Heat transfer due to combined free and forced convection in horizontal isothermal tube flow
[ASME PAPER 71-HT-3]

19 p3163 A71-37981

Gravity effect on developing laminar flow with forced convection in vertical isothermal tube, in

investigating velocity and temperature profiles and heat transfer rate
[ASME PAPER 71-HT-6] 19 p3164 A71-37983

Gas and surface temperature distributions for laminar flow in circular tube, considering conduction, convection and radiation effects
[ASME PAPER 71-HT-17] 19 p3164 A71-37988

Hydrogen near-critical point flow in heated cylindrical tube, measuring flow parameters radial profiles by combination pitot tube/thermopile/hot-wire sensor probe
[ASME PAPER 71-HT-25] 19 p3165 A71-37995

Turbulent pipe flow dissipation rate, presenting turbulence energy diffusion and stress components spectral distribution measurements
19 p3045 A71-38201

Spontaneous hot zone formation in oil flow through small pipes, showing significance in pressure losses and plain bearings calculations
19 p3046 A71-38275

Solid cylindrical particles interaction under entrainment in pipe by viscous incompressible fluid, obtaining numerical solution by reduction to flow past moving body
19 p3046 A71-38418

Gas resonant oscillations in closed end tube, describing time-periodic motion by perturbation method with Mach number as flow parameter
20 p3211 A71-39078

Blower suction line random vibrations due to distributed random pressure, investigating various isolation arrangements for vibration reduction
20 p3308 A71-39085

Longitudinal diffusivity of turbulent flows in open channels and circular pipes, discussing experiments
20 p3212 A71-39504

Flow induced flutter and buckling instability of elastic tube with displacement spring support
[ASME PAPER 71-VIBR-39] 21 p3459 A71-40289

Hot-wire anemometer measurement of free oscillation damping of viscous and sluggish fluid in U tube, determining velocity distribution
21 p3366 A71-40512

Laminar and rotationally symmetrical flow of viscous incompressible fluid in circular pipe of constant temperature, considering inlet swirl effects and heat transfer to wall
21 p3368 A71-40756

Second order viscous liquid pulsating flow superposed on steady laminar flow through circular pipe, examining non-Newtonian effects on flow characteristics
22 p3530 A71-41562

Turbulent flow of incompressible fluid in rough pipe, determining skin friction coefficient variation with Reynolds number
22 p3531 A71-42291

Hypersonic nozzle convergent section heat transfer optimization by Euler method, using Lagrange undetermined multiplier and pipe flow approximation
22 p3622 A71-42781

Hydrodynamic model of momentum, heat and mass transport for turbulent flow in straight circular pipes, tabulating velocity profiles and eddy diffusivity
23 p3780 A71-43091

Viscous heating and non-Newtonian behavior of incompressible steady pipe flow with variable transport properties, using perturbation method
23 p3662 A71-43370

Fluid flow friction and combined free and forced convective heat transfer characteristics in rotating curved circular tube, using finite difference scheme and iterative solution
23 p3783 A71-44192

Gas concentration measurement at wall with argon and helium injection at pipe entrance, investigating protecting film cooling efficiency
24 p3819 A71-44929

Heat exchange during stabilized laminar flow of incompressible liquid in circular pipe with radiative cooling, deriving temperature profile and Nusselt number dependence
24 p3888 A71-44933

Computer program for recirculating fluid flows applied to concentration curves obtained by gas injection on pipe center line with fully developed turbulent flow
24 p3820 A71-44956

Dynamics of pipelines with nonstationary fluid flow, deriving equations for dynamic instability regions and for resonant vibration amplitudes
24 p3884 A71-45014

Unsteady gas pulsations in compliant tube, predicting pressure amplitude extremum as function of mean flow by linear theory with frictional effect
24 p3820 A71-45073

PIPLINES

Rocket body longitudinal autooscillation modes, taking into account pipeline fluid discontinuous cavitation oscillations
16 p2644 A71-32834

LF axisymmetric vibrations of spherical completely filled tank with free liquid surface in upper tank and pipeline
16 p2657 A71-33602

Constant stiffness beam-columns analysis in pressure piping systems calculations for nuclear industry, using initial parameter method
19 p3102 A71-37073

Dynamics of pipelines with nonstationary fluid flow, deriving equations for dynamic instability regions and for resonant vibration amplitudes
24 p3884 A71-45014

PIPER AIRCRAFT

Piper Cherokee aircraft air conditioning system, discussing various operating principles, design criteria, power drain, effects on aircraft performance and weight, system serviceability and control
[SAE PAPER 710391] 10 p1558 A71-24255

PIPES [TUBES]

NT GAS PIPES

Deformation and strength of pipes manufactured from oriented glass fiber reinforced plastics under axial tension
01 p0177 A71-11237

Petroleum mechanical engineering and pressure vessels and piping - ASME Conference, Denver, September 1970
04 p0665 A71-14767

Magnetic pulse technique connecting Al pipe with steel pipe, determining mechanical and physical parameters
06 p0906 A71-18713

Elastoplastic tubular rods rotation under constant bending moments, solving for large rotational angles
07 p2122 A71-19352

Optimal heat resistance, mechanical properties and microstructure of steam pipe Cr-Mo-V steel
07 p1135 A71-19618

Partial differential equation solution for aircraft hydraulic lines flexural vibration by Bubnov-Galerkin method, reducing to Duffing equation analysis
08 p1286 A71-20783

Metal pipes coaxial welding by detonation, estimating energy conversion
08 p1300 A71-21910

Limit load carrying capacity of thin walled tube under combined forces, including pressure effects by variational method of plasticity theory
10 p1688 A71-24384

Approximate solution for limit load carrying capacity of thin walled tube under combined loadings, deriving formulas describing boundary surface
10 p1688 A71-24385

Lightweight parabolic antenna model with inflated Mylar tube torus and central mast interconnected by wires, discussing construction, performance tests and tradeoffs
[AIAA PAPER 71-397] 11 p1736 A71-25273

Fiberglass reinforced plastic rocket launcher tubes with internal helical rails to impart spin to missiles, discussing design, fabrication and testing
11 p1786 A71-25419

Minimum strength of groove and fillet welded joints in heat treated Al alloy tubular members
11 p1769 A71-25745

Rectilinear piping system with steady liquid flow, investigating free vibration damping, steady-state amplitudes and stability
12 p1975 A71-27113

Arc melter using Pyrex pipe cross for controlled atmosphere chamber, incorporating Ar jet into electrode holder for dynamic flushing and rapid quenching
13 p2044 A71-28154

Shock produced stress relaxation in thin walled Al tubes, comparing strain-time profiles with thin shell theory
16 p2647 A71-32923

Low thermal flux lightweight glass fiber composite tubing for cryogenic propulsion plumbing systems
17 p2762 A71-35206

Book on external corrosion and deposits on boiler tubes and gas turbine blades covering mineral matter in fuels, oxidation, additives, etc
18 p2935 A71-36247

Gripping method for short length tubing during high temperature tensile tests
19 p3069 A71-38139

Fiber reinforced tube under lateral compression between two flat dies, determining finite deformation from nonlinear elastic and elastoplastic shearing response analysis
20 p3311 A71-39966

Karman vortex street induced fluctuating lift forces on tube bundles as function of steady pressure drag coefficient and Strouhal number
[ASME PAPER 71-VIBR-13] 21 p3457 A71-40275

Initial conditions influence on transfer matrices of real zero leakage hydraulic tubing
21 p3326 A71-40595

German monograph on creep buckling tests of finned and unfinned thin walled pipes of heat resistant breeder reactor cladding materials
21 p3464 A71-40781

Ultrasonic inspection apparatus for defects detection in metal pipes, using immersion echo mode with two piezoelectric scanning heads rotating about pipe
22 p3529 A71-41774

Surveyor 3 unpainted Al tubing examination by replication electron microscopy for surface damage due to particle impact and ion bombardment in lunar environment
23 p3766 A71-43821

Heat generating granular layer tube, obtaining temperature distribution across cross section and boundary conditions
23 p3719 A71-44338

Cross section behavior of tube under plastic bending based on hollow rod treatment
24 p3883 A71-44848

Thin walled tube under combined bending and torsion, considering stress distribution and curvature behavior
24 p3883 A71-44892

Slit tube flat-to-circular transition during extension, considering mathematical model for curvature change, modulus of elasticity and Poisson ratio effects
24 p3884 A71-44959

PISTON ENGINES

NT DIESEL ENGINES

Air cooled opposed 4, 6 and 8 cylinder light aircraft engines with or without turbosupercharging, considering horsepower improvement and torsional vibration control
[SAE PAPER 700205] 01 p0142 A71-10129

Reciprocating organic single cylinder Rankine cycle engine using thiophene working fluid
03 p0351 A71-13034

Book on fixed and rotary winged aircraft air cooled piston engine design, performance and maintenance in business and military operators manual terminology
05 p0796 A71-17125

Gasoline icing inhibitors effect on light aircraft piston engine carburetor icing
[SAE PAPER 710371] 10 p1658 A71-24240

Light aircraft piston engines design and maintenance, discussing engine design features, materials, lubrication, controlled flight operation and maintenance techniques
[SAE PAPER 710381] 10 p1658 A71-24246

Piston engine crankshafts load and strength specification, treating axial force as resultant of gas force and inertial force
11 p1851 A71-26200

Antwear property assessment of piston engine and aviation jet fuels under point contact conditions, recommending ball and cylinder test technique
17 p2792 A71-34447

Shuttle convective heat transfer involving similar axial temperature gradients in piston and cylinder, calculating interaction with wall conduction by finite difference computer program
20 p3312 A71-39281

Torsional natural frequencies in coupled turbine and reciprocating engine system driving common propeller, using matrix techniques
[ASME PAPER 71-VIBR-83] 21 p3461 A71-40319

PISTON THEORY

Free piston shock drivers concerning plateau pressure reduction
04 p0564 A71-14674

Compression waves produced in viscous heat conducting gas by impulsive one dimensional piston start and by wall temperature change
05 p0831 A71-16477

Beam pattern near vibrating piston near sound field, discussing boundary between far field
07 p1113 A71-19953

Linear damping in piston type liquid damped accelerometers, using porous glass materials
09 p1451 A71-23173

Hydrodynamic forces on pistons in sharp-edged spool valves with double throttling gaps at Reynolds numbers from 60 to 240
09 p1434 A71-23664

Free piston shock tube with air driver producing strong waves at speeds corresponding to gas effects
17 p2724 A71-34892

Plane unsteady gas flow under action of dihedral angle shaped piston traveling at constant velocity
19 p3042 A71-37080

Two and three dimensional pistons motion in stationary gas, calculating potential flow characteristics near weak discontinuities as function of piston geometry and acceleration
19 p3043 A71-37099

Baffled piston source sound radiation impedance from numerical solution of Fredholm integral equation for vibrating disk in finite rigid concentric baffle
19 p3104 A71-37849

Lumped parameter modeling of fluid elastic vibration response of nonlinear piston driven pneumatic-mechanical system, using finite element control volumes
[ASME PAPER 71-VIBR-41] 21 p3459 A71-40291

Self similar solutions for ideal gas flow driven by piston ahead of shock propagating in medium at rest with power law density distribution
23 p3719 A71-44143

Laminar heat transfer losses effects on piston gas heater performance, computing heat transfer rate and thermal boundary layer thickness
24 p3887 A71-44603

PISTONS

NT MAGNETIC PISTONS

Hydraulic system axial- and radial-piston pumps design and operation principles, considering cost reduction

01 p0006 A71-10817

Piston expulsion seals for storable fueled and ready liquid rockets

06 p0905 A71-18218

Far field sound radiation pattern from vibrating circular piston set in nonrigid baffle for sonar detectors

11 p1798 A71-25186

Differential circuit for bilateral stopping control of double action piston cylinders, discussing solenoids valves operation

11 p1716 A71-26324

Parameters optimization for increasing tuning range of resonator with contactless piston based on numerical solution of transcendental equation

12 p1889 A71-27623

Contactless piston resonator ensuring one parallel resonance in tuning range, using quadrupole theory

19 p3030 A71-38341

Two stage rotor-piston vacuum pump, determining minimum work of gas compression

20 p3183 A71-39171

PITCH

Human voice imitation of tonal signals pitch interval

02 p0206 A71-12061

Multiple pure tone and broadband noise generation in high speed turbofans, noting analytical model

20 p3277 A71-39773

PITCH [INCLINATION]

Cholesteric liquid crystal pitch from IR transmission measurements

02 p0209 A71-12572

Aircraft propulsive thrust moment effect on phugoid motion, examining angle of attack and flight path variations with resulting instability

03 p0347 A71-13340

Anomalous low magnetospheric He alpha/proton flux ratio in terms of electrostatic radial diffusion taking into account charge exchange and pitch angle loss processes

06 p0964 A71-17284

Pitch angle distribution of protons and helium ions in magnetosphere from numerical solution of Fokker-Planck equation

06 p0964 A71-17285

Pilot physiological responses as indicators of pitch motion cues effect on flight simulator fidelity

07 p1047 A71-19465

Dawn to dusk magnetospheric electric field effect on energetic stably trapped particle drift shell pitch angle degeneracy

07 p1103 A71-19675

Light general aviation airplanes flying qualities in-flight simulation, considering longitudinal short period frequency and damping, pitch control sensitivity and lift curve slope

10 p1554 A71-24242

Equation error approach to parameter identification in third order pitch plane dynamics for high performance aerodynamically controlled aerospace vehicle

11 p1742 A71-26418

Field aligned anisotropy for auroral ionospheric energetic ions, calculating pitchangle distributions

12 p1899 A71-26885

Airfoils unsteady stall by testing two dimensional model in harmonic pitching oscillation for helicopter rotor blades characteristics

12 p1866 A71-27609

Magnetic dipole field second invariant and drift frequency in terms of pitch angle and energy from analytical approximation to trapped charged particle bounce period

13 p2055 A71-27925

Aircraft flight characteristics dependence on angle of attack, roll and pitch

13 p1997 A71-29043

Propeller vortex theory, calculating vortex streets pitch distributions and wake configuration

14 p2170 A71-30443

Handling qualities and control sensitivity of high performance helicopters, considering pitch and collective control

14 p2179 A71-31099

Flexible blades cascade at various pitch angles and Reynolds numbers

15 p2343 A71-31203

Pitch angle diffusion of electrons in postbreakup auroral glow, measuring electron intensities by Petrel sounding rocket

15 p2394 A71-31423

Pitch distribution of protons precipitated from auroral radiation region measured by scintillation detector aboard Cosmos 261 satellite in Northern Hemisphere

17 p2731 A71-34320

Magnetic activity effect on pitch angle distribution of low energy auroral electrons from ESRO 1A measurements

19 p3060 A71-38575

Quadrifilar helix antenna pitch angle and ground plane size optimization based on beam pattern data

19 p3036 A71-38603

German monograph on electron flux properties in polar atmosphere, discussing pitch angle distribution, energy spectrum and relation to geomagnetic field disturbances

19 p3130 A71-38646

Superthermal electrons energy spectra and pitch angle distribution, presenting photoelectron flux recordings by Cosmos 261 satellite

20 p3282 A71-39740

Phugoid motion at constant angle of attack without thrust line displacement from aircraft center of gravity, noting longitudinal stability

21 p3324 A71-40168

Equatorial proton and electron pitch angle distributions in loss cone and at large angles from geostationary ATS 5 satellite observation

23 p3720 A71-43165

Angle of attack instrumentation for evaluating aircraft lift performance and phugoid oscillations

23 p3628 A71-43382

Flow models for turbomachinery, averaging equations for flow through blade cascades across pitch

23 p3627 A71-44348

PITCH [MATERIAL]

Tensile, shear, bulk density and electrical properties of pitch based strain graphitized glassy carbon fibers [PLASTICS INST. PAPER 13]

08 p1319 A71-20897

Hollow carbon microspheres from pitch material, emphasizing applications in porous composites

14 p2263 A71-29657

PITCH ANGLES

U PITCH [INCLINATION]

PITCH ATTITUDE CONTROL

U LONGITUDINAL CONTROL

PITCHING MOMENTS

Pitching stability derivatives of sharp oscillating wedges at zero incidence in viscous hypersonic flow from perturbation method, including thickness and wave reflection effects

14 p2171 A71-31023

PITOT STATIC TUBES

U PITOT TUBES

U SPEED INDICATORS

PITOT TUBES

Pitot type intake inlet additive drag in terms of capture area ratio, static and total pressure coefficients

02 p0187 A71-12688

Supersonic pitot fluidistor in bistable mode, investigating improved pressure and flow recovery at large expansion ratios

07 p1029 A71-20591

Turbulent boundary layer skin friction measurement by dual pitot tube, taking into account mean velocity profile

08 p1275 A71-21309

Fast miniature shielded pitot pressure transducer for spatial resolution of flow details

09 p1453 A71-23728

Maximum velocity position in turbulent shear flow for differential pressure effect between double pitot tubes, using inductance type transducer

11 p1767 A71-26313

Nozzle wall hypersonic turbulent boundary layers at free stream Mach number, using pitot, hot wire, wall pressure fluctuation and static pressure measurements [AIAA PAPER 70-746]

12 p1898 A71-27558

Aerodynamic probes for determining flow state of high enthalpy hypersonic flow fields, considering pitot pressure, total enthalpy and current density

18 p2921 A71-36414

Pitot and static pressure measurement in low density hypersonic flows, considering thermal transpiration, gas nonequilibrium near measurement cavity and nature of inlet geometry

18 p2921 A71-36415

Pitot tube interaction with subsonic rarefied gas flow, considering impact pressure

21 p3323 A71-40695

Aircraft pitot static systems design with removable drain plug, noting line installation problems

23 p3675 A71-43387

Two dimensional potential flow model of Pitot static probe and subsonic free jet interaction, using conformal mapping and hodograph method

24 p3817 A71-44589

PITTING

Lubricant and ball steel effects on fatigue life /pit formation after repeated stress cycles/

[ASME PAPER 70-LUB-16]

07 p1118 A71-19507

Artificial corrosion pits effect on fatigue durability of smooth samples and aircraft duraluminum skin elements

13 p1995 A71-27819

Si, Mo and Cu effects on pitting corrosion of Cr-Ni steel

13 p2082 A71-27831

Metallographic examination of inorganic, metal plated and intermetallic coatings on martensitic stainless steels for pitting and surface corrosion prevention

19 p3081 A71-37902

PITUITARY GLAND

Phospholipid composition of lipid extracts of hypothalamo-neurohypophyseal system of cattle

03 p0362 A71-13237

Stress and behavior regulation, investigating pituitary-adrenal system operation

07 p1043 A71-20213

Brain monoamines localization and metabolism and endocrine function, discussing pituitary secretion and neurotransmitter input

23 p3637 A71-44274

PITUITARY HORMONES

Bovine pituitary proteinase I action on oxidized B chain of insulin, noting preference for specific bonds

05 p0718 A71-17105

PIVOTED WING AIRCRAFT

U TILT WING AIRCRAFT

PIVOTS

Odessa observatory meridian circle pivot irregularities effects determination on horizontal axis inclination and azimuth, using Challis method

23 p3680 A71-44263

PL/I

MESY systems programming with PL/I, comparing with ALGOL and FORTRAN

19 p3025 A71-37422

PLAGES [FACULAE]

U FACULAE

PLAN POSITION INDICATORS

Weather radar plan position indicator automatic film reading for digital mapping of rainfall intensity, discussing raindrop sizing

08 p1286 A71-20690

ATC height and plan position indicator composite picture display system design and operation, combining functions of primary and secondary surveillance radars

21 p3413 A71-40128

Radar observation of convective process in clear air, presenting turret top cell contour tracings from PPI sequence

23 p3700 A71-43088

PLANAR STRUCTURES

German monograph on field equations solution for Cosserat continua in planar strip type regions covering stress analysis

03 p0515 A71-14370

Plane or axisymmetric revolution geometry elasticity problems using finite element method and Fourier series

06 p1002 A71-18421

Planar-epitaxial IC resistors p-n junction parasitic effects on cut-off frequency, obtaining design formulas for capacitance and geometry

08 p1264 A71-21074

Elastic and plastic plane deformation photoelastic measurement at room and elevated temperatures by moire patterns, comparing performance with other methods

09 p1536 A71-22328

Handbook on radar cross sections, Volume 2, covering scattering from planar surfaces, complex bodies, rough surfaces, ionized media, plasmas, radar targets and various objects

11 p1733 A71-26009

Uniformly and nonuniformly spaced circular cylinders contacting two planes, calculating conductive heat transfer coefficient under vacuum conditions [AIAA PAPER 71-436]

11 p1858 A71-26224

Edge geometries and aperture distributions of physically realizable planar antennas

13 p2027 A71-27989

Optimized thin walled elements in elastic planar frame structures minimum weight design

14 p2324 A71-29872

Extended flat body thermal conductivity determination by local heating at constant heater helix temperature

14 p2338 A71-30622

Silicon planar transistors at low injection levels, showing current transfer function temperature dependence

14 p2213 A71-30624

Planar and nonplanar transistors noise factor dependence on signal source impedance and emitter current, considering amplification and frequency conversion application

14 p2213 A71-30628

Work hardening material planar frame inelastic load deformation and buckling, using finite difference method and variational principle

14 p2330 A71-30693

German monograph on plane, arbitrarily curved and bending resistant trusses calculations allowing for elastic and plastic deformation

17 p2823 A71-34800

Complex wave structure development upon under-expanded jet impact on plane obstruction at small incidence angles, determining gas dynamics parameters of supersonic jet

18 p2903 A71-36120

Microwave planar Gunn oscillators performance in X band, giving pulsed and CW I-V characteristics

23 p3649 A71-42913

Computer acquired I-V characteristics of thermionic fixed spaced planar diodes
23 p3630 A71-43596

PLANCKS CONSTANT

Cosmic photons Planck constant, considering photon absorption dependence on variations of spin angular momentum
03 p0473 A71-13562

Planck formula correction for small cavity black body radiation, considering application to far IR standard sources
04 p0676 A71-14955

Thin gas optical limit isothermal curves, discussing Planck mean emission coefficients
07 p1222 A71-18993

Observational test of Planck constant variation on cosmic scale in terms of radiation absorption by interstellar and intergalactic gases
11 p1832 A71-26183

Gray radiative transfer equations, bridging Planck and Rosseland mean absorption coefficients
17 p2839 A71-35557

PLANE WAVES

Plane acoustic wave diffraction by dense periodic grating, using crimped surface scattering with Neumann and mixed boundary conditions
01 p0128 A71-11120

Plane acoustic wave diffraction and acting force on sphere in low viscosity medium, obtaining asymptotic formulas for pressure, velocity and intensity
01 p0128 A71-11123

Monograph on plane shock wave interactions covering supersonically moving two dimensional thin airfoils, slender bodies of revolution and thin wings
01 p0003 A71-11227

Ionospheric columnar electron content perturbation by plane atmospheric waves
01 p0077 A71-11509

Electromagnetic wave Poynting vector trajectories in absorbing inhomogeneous media, discussing reversibility and energy propagation of spherical and plane structures
02 p0210 A71-11631

Antenna polar diagrams short range measurement, using far field approximation for incident plane waves source and radio star or satellite
02 p0223 A71-12801

Two dimensional diffraction of plane wave by perfectly conducting wedge using straightforward scattering approach
03 p0456 A71-13347

Plane straight shock wave stability in inviscid compressible medium, discussing gas dynamic equation discontinuous solution
03 p0401 A71-13967

Plane acoustic wave diffraction at thin semiinfinite elastic plate, reducing to Riemann boundary problems for Helmholtz equation in half space
03 p0459 A71-14061

Plane shock wave propagation in polytropic gas of variable density, using successive approximation technique
03 p0345 A71-14558

Plane electromagnetic wave diffraction on infinite system of parallel metallic strips, determining natural frequencies
04 p0549 A71-14611

Plane monochromatic electromagnetic wave scattering by moving and rotating cylinder
04 p0549 A71-14612

Absorption coefficient of plane wave scattering by thin spherical resistive shell for broadband RF radiation monitoring
04 p0558 A71-15149

Acoustic plane waves transient interaction with cylindrical elastic shell, using Volterra integral equations
04 p0668 A71-15189

Plane wave propagation in layer direction in fiber reinforced viscoelastic materials
04 p0669 A71-15202

Transient pulse plane wave reflection from ionospheric model with linear electron density profile
04 p0553 A71-15218

Kirchhoff integral evaluation for Gaussian incident field in Fresnel diffraction from plane wave beams truncated by circular apertures
04 p0627 A71-15688

Plane wave diffraction by double grating of thin cylindrical, determining field polarization in directions parallel and perpendicular to axis
05 p0718 A71-15995

Far field characteristics for diffraction of plane harmonic electromagnetic wave obliquely incident on rectangular wedge in uniaxially anisotropic medium
05 p0781 A71-16414

Plane electromagnetic wave inhomogeneous diffraction field from multilayer metal band gratings
05 p0722 A71-16829

German monograph on vibration fields representation by superposition of planar waves with complex wave vectors, considering convergent series of Hankel and Bessel functions
05 p0782 A71-16898

Plane EM waves at two dimensional periodic media boundary, obtaining reflection and refraction for harmonics
05 p0723 A71-17029

Nonlinear planar propagation of sinusoidal and band-limited noise signals in air, extending to spherical waves
05 p0784 A71-17157

Shock heating effects due to compression and plastic dissipation on basis of finite one dimensional waves in strain rate sensitive elastic viscoplastic solids
05 p0830 A71-17238

Elastic shells under pressure wave loads, examining front discontinuities induced by plane and axisymmetrical wave deformation
06 p0992 A71-17807

Plane sound waves incident on flat plate airfoils lattice, obtaining transmitted and reflected pressure amplitudes
[AIAA PAPER 71-181]
06 p0885 A71-18620

Monograph on optical imaging of ultrasonic fields by acoustic Bragg diffraction covering heuristic plane wave and ray approach scattered fields
07 p1111 A71-19575

Obliquely incident p-polarized plane electromagnetic wave interaction with hot plasma half space, using linearized relativistic Vlasov equation and Laplace transform technique
07 p1171 A71-20292

Plane electromagnetic wave propagation and reflection in presence of substances with arbitrary complex permittivity
07 p1066 A71-20543

Plane, steady state MHD shock wave structure in infinitely conducting fluid under magnetic field perpendicular to shock velocity, introducing quadratic artificial viscosity factor
07 p1174 A71-20616

Field intensity of plane electromagnetic wave diffracted at conducting sphere
08 p1252 A71-20735

Plane light wave interactions with moving dispersive dielectric medium, considering electron UV or ion IR resonant oscillation in regions of anomalous dispersion
08 p1253 A71-21278

IR laser propagation through fog with droplet vaporization, assuming incident electromagnetic radiation as plane harmonic wave
08 p1302 A71-21392

HF backscattering by plane electromagnetic wave at oblique incidence from perfectly conducting right circular cone, applying geometrical theory of diffraction
08 p1257 A71-21884

Electromagnetic wave propagation through bounded time-space periodic cold plasma under plane wave incidence, calculating transmitted and reflected components
09 p1503 A71-22986

Plane TM wave scattering by systems of two parallel conducting elliptical cylinders, metal tapes and combinations
09 p1407 A71-23106

Scattering structures of two parallel elliptical cylinders, tapes or combinations, deriving surface current density distribution under plane TM wave excitation
09 p1407 A71-23107

Electric field equations of plane EM wave diffraction at lattice of conducting cylinders, using Hankel function
09 p1408 A71-23113

Emitting, absorbing and scattering gray gas flow through plane stationary normal shock wave, presenting governing equations linearized analysis
09 p1546 A71-23164

Gas dynamic solutions of plane shock wave propagation in moving medium, considering conservation laws
09 p1525 A71-23198

Steady plane plasma shock wave structure in partially ionized and radiating gas, using Navier-Stokes equations in three fluid continuum approach
09 p1504 A71-23202

Plane electromagnetic wave scattering, arbitrarily polarized and normally impinging on wedge tapered absorbing structure
09 p1409 A71-23501

Ideal reflector simulation of periodically supported infinite plane metallic wire gratings with rectangular mesh showing small sag
09 p1409 A71-23503

Plane electromagnetic wave reflection from conducting convex cylinder in radially inhomogeneous absorbing medium, deriving equations for beam trajectories calculation
10 p1574 A71-23805

Plane shock wave formation in dense Ar, using molecular dynamics numerical technique
10 p1694 A71-23953

Plane stationary shock wave propagation through one component vapor-liquid mixture, calculating profile and mixture parameters under evaporation and condensation
10 p1593 A71-24348

Magnetic field effects on plane wave propagation in plasma, reducing motion data problem to vectorial differential equation with mean electronic velocity as only unknown
11 p1804 A71-25174

Homogeneous Gaussian beam propagation in inhomogeneous negative absorption media, noting amplification of plane wave
11 p1798 A71-25665

Phase and log amplitude spectral and angular covariance of scintillation for propagation of two differing plane waves in randomly inhomogeneous medium
11 p1800 A71-26297

Charge particle motion and radiation in strong plane and spherical electromagnetic waves with nonthermal astrophysical applications
12 p1877 A71-26616

Elastic plane shear wave diffraction on elliptical cylinders in half space, using elliptical wave function series and linear algebraic equations
12 p1978 A71-27332

Signal processing using arrays, solving for monochromatic plane wave by transforming gain equation
12 p1882 A71-27532

Plane traveling electromagnetic wave existence, propagation and refraction in nonlinear dispersive nonmagnetic isotropic lossless medium
13 p2027 A71-27899

Uniform asymptotic diffraction of plane wave from ideally reflecting cylinder, using parabolic equation method
13 p2027 A71-27900

Inverse diffraction of plane wave by periodic and doubly periodic arrays, calculating velocity potential and pressure distributions for Neumann and Dirichlet problems
13 p2027 A71-27905

Electromagnetic wave diffraction by ideally conducting wedge of finite radius, deriving asymptotic formula for plane wave scattering
13 p2029 A71-28360

HF diffraction of plane electromagnetic waves by ideally conducting iris diaphragm, developing boundary value problem asymptotic solution
13 p2029 A71-28448

Plane longitudinal stress waves propagation in plane-parallel viscoelastic partition of finite thickness dividing two linear half spaces with different elastic properties
13 p2155 A71-28655

Plane wave holographic recording and reconstruction, investigating effects of photosensitive medium as three dimensional diffractive pupil
13 p2068 A71-28711

Dynamic damping of plane one dimensional unsteady stress wave passing through viscoelastic layer separating linearly elastic half spaces
13 p2155 A71-28848

Harmonic pressure generator design based on plane sound waves principle
13 p2071 A71-29293

Reflection, diffraction and transmission of plane microwave incident on conducting screen perforated periodically with circular holes, using transmission line analysis and dipole moments method
14 p2192 A71-29568

Plane electromagnetic waves diffraction by moving periodic metal strip gratings, taking into account relativistic effects
14 p0000 A71-30076

Plane wave and virtual image reconstruction from three dimensional holograms
14 p2248 A71-30676

Small caliber smoothbore powder sabot guns generating planar shock wave in solids, using streak camera monitoring of impact and recoil velocities
14 p2223 A71-30885

Asymptotic intensity fluctuations of plane light wave propagating in turbulent medium, using parabolic equation and Markov model
15 p2387 A71-31190

Missile circumferential current density for plane wave electromagnetic field illumination, using Kao shadowing theory
15 p2372 A71-32367

Magnetospheric resonator properties bounded by ionosphere/earth system lines of force, examining nonuniform plane wave generation and standing wave pulsation period
15 p2401 A71-32731

Approximation analysis for laminar two dimensional boundary layer behind plane shock wave moving over infinite flat plate
16 p2556 A71-32914

Plane oblique shock wave diffraction on wedge moving in homogeneous gas flow at supersonic speed, reducing boundary value problem to Hilbert problem
16 p2519 A71-32930

Low density plasma in magnetic field, investigating existence possibilities of stationary isothermal jump and plane wave periodic solution
16 p2618 A71-33044

Plane and cylindrical waves three dimensional propagation, investigating finite electrical fluid conductivity and radiation effects in MGD flow
16 p2618 A71-33172

Plane electromagnetic wave diffraction on ideally conducting convex body of large electrical dimensions, obtaining Maxwell equations asymptotic solution
16 p2542 A71-33485

Plane uniform waves reflected from layer with random permittivity inhomogeneities, determining distribution function and scattered wave propagation direction
16 p2543 A71-33568

Dynamical thermal expansion effect on plane elastic-plastic stress wave propagation, using classical heat conduction equation
17 p2819 A71-34507

Impulsive time variation plane wave reflection from ionospheric sech squared electron density profile, comparing full wave and WKB solutions
17 p2701 A71-34769

Transverse wave structure of two-dimensional detonation waves propagating in narrow channel, considering longitudinal instabilities
17 p2841 A71-35708

Energy momentum stress tensors for harmonic oscillator model, calculating energetic interaction with plane gravitational wave of same frequency
18 p2946 A71-35982

Test facility for thermal diffusivity measurements in solids by method of plane temperature waves using periodic optical heating at 1500 K
19 p3063 A71-37589

Continuum mechanical approach to velocity dispersion of longitudinal plane waves in elastic solid containing dislocations
19 p3118 A71-37794

Plane electromagnetic wave diffraction by dense periodic array with Dirichlet and mixed boundary conditions, determining solution asymptotic behavior
19 p3104 A71-38416

Plane electromagnetic wave diffraction by circular cylinder with longitudinal slot, determining scattered field by Riemann-Hilbert method
19 p3020 A71-38417

Free space diffraction of E-polarized plane electromagnetic wave by slit in thick conducting screen, deriving approximate solution from Wiener Hopf equation by matrix techniques
19 p3023 A71-38592

Monostatic plane wave scattering by semiinfinite perfectly conducting wedge with rounded edge for line source excitation in far field
19 p3023 A71-38593

Electromagnetic plane wave monostatic scattering incident to thin circular metallic disk, calculating spectral and transient response from far field amplitude and phase data
19 p3036 A71-38608

Soviet book on unsteady motions of continuous media covering gas dynamics, thermodynamics, shock and plane detonation waves, three dimensional gas motions, etc
20 p3211 A71-39144

Thermoelastic plane harmonic and Rayleigh surface waves in elastic solids with thermal relaxation, using Maxwell heat conduction equation
20 p3310 A71-39779

Superposed plastic deformation and plane wave propagation in elastic-plastic media applied to circular bar twisting
20 p3310 A71-39780

Submillimeter plane monochromatic waves propagation in ground layer of turbulent atmosphere, deriving received signals levels fluctuations
20 p3198 A71-39804

Plane sound waves transmission and reflection through finite plates single cascade by Wiener Hopf technique
21 p3437 A71-40537

Plane waves propagation in viscoelastic body representing parallel union of Kelvin and Maxwell bodies in magneto-thermal field
21 p3463 A71-40577

Monochromatic plane electromagnetic wave reflection by electrically perfectly conducting diffraction grating
21 p3415 A71-40665

Plane acoustic wave transmission problem through finite chord plate array in subsonic gas flow, using factorization method in diffraction theory
21 p3322 A71-40686

Fiber reinforced elastic materials steady state plane wave propagation by modeling constituents as continua undergoing individual motions
21 p3469 A71-41004

Plane wave propagation following thin elastic rectangular plate impact against smooth rigid obstacle, using difference scheme
22 p3531 A71-41910

One dimensional propagation and multiple reflection of plane thermoelastic wave in Lamé elastic isotropic plate with finite heat transmission
22 p3615 A71-41911

Microwave scattering noise spectrum from turbulent rocket-exhaust jet illuminated by plane wave
22 p3510 A71-42208

Plane electromagnetic wave diffraction by infinite system of parallel metallic strips, determining natural frequencies and eigenfunctions
22 p3510 A71-42251

Plane monochromatic electromagnetic wave scattering by moving and rotating cylinder
22 p3510 A71-42252

Plane electromagnetic wave diffraction on periodic arbitrary profile array, presenting near and far field asymptotic characteristics
22 p3511 A71-42306

Plane wave diffraction by double grating of thin circular cylinders, determining field polarization in directions parallel and perpendicular to axis
22 p3515 A71-42744

Near-normal plane shock wave reflection from rigid impermeable wall, obtaining nonstationary flow parameters in terms of Jacobi polynomials convergent series
22 p3531 A71-42865

Plane electromagnetic waves reflection and transmission at boundary of semiinfinite magnetolectric medium
23 p3642 A71-42918

Infinite plane elastic wave reflection and refraction coefficients at fluid-solid interface, noting reflected beam lateral displacement at critical angles
23 p3703 A71-43202

Boundary value problem for plane wave scattering by spherical cap, obtaining scattering cross section for Helmholtz resonator and hemispherical shell
23 p3703 A71-43208

Plane superconic ionizing shock wave in magnetic field under small wave plane perturbation from equilibrium position, calculating stability from linearized equations
23 p3663 A71-43575

Numerical solution for plane wave scattering by dielectric sheet with imbedded periodic array of conducting strips
23 p3654 A71-44164

Absorption cross section for plane electromagnetic wave in circular plasma cylinder in constant magnetic field, assuming small Larmor radius
23 p3714 A71-44328

Plane electromagnetic wave diffraction by infinitely conducting grating at nonorthogonal incidence angles, using conformal mapping technique
24 p3847 A71-44357

Convolution integral equation unique solution in second kind Fredholm equation form, applying to plane polarized electromagnetic wave diffraction on infinitely thin band
24 p3804 A71-44769

Boundary value problem of plane electromagnetic wave interaction with inhomogeneous warm plasma column, using matching method
24 p3856 A71-44794

Plane TEM wave propagation in free space using rectangular waveguide partially filled with two dielectric slabs
24 p3809 A71-45093

Electromagnetic scattering of plane wave obliquely incident on infinitely long circular cylinder with radially varying permittivity and permeability
24 p3805 A71-45179

Linearly polarized plane electromagnetic wave scattering by radially inhomogeneous spherical shell, presenting boundary value problems solutions and approximations
24 p3805 A71-45184

PLANET EPHEMERIDES

Minor planets 1969 ephemeris, considering numerical integration of celestial mechanics equations
01 p0155 A71-10438

Mars photographic positions on double short focus astrograph with random error for ascent and declination
07 p1194 A71-19332

Lunar ephemeris and astrometric corrections from occultation observations, noting FK4 equinox location
08 p1357 A71-20876

Asteroids photographic observations for catalog of faint stars positions orientation, correcting observation times to ephemeris time
09 p1525 A71-23338

Analytical lunar ephemeris main problem solution by canonical perturbation theory based on Lie transforms and echeloned series processing
10 p1674 A71-24431

Lunar ephemeris, examining orbit with Delaunay theory
11 p1831 A71-26136

Analytical lunar ephemeris, comparing variational and parallax inequalities with various theories
11 p1831 A71-26137

Gravitational lunar theory high order solution for geophysical relevance, discussing perturbation methods and computer analyzed ephemeris time
12 p1961 A71-26837

Venus Schroter effect, noting phase deviations from ephemeris values
13 p2136 A71-28387

Asteroids 457-Alleghania, 649-Josepha, 1038-Tuckia, 1161-Thessalia, 1162-Larissa and 1297-Quadea orbital elements and ephemerides, taking into account planetary perturbations
17 p2809 A71-35581

Apollo type asteroid with high orbital eccentricity and inclination and rough elongated shape, noting ephemerides
21 p3443 A71-40188

Asteroid 1967 observation and ephemeris activity, surveying 1966-1967 literature
24 p3874 A71-45172

PLANET ORIGINS

U PLANETARY EVOLUTION PLANETARIUMS

Planetaria as celestial navigation instruction aids, discussing astronomical simulation capabilities, celestial coordinate systems, special effect projectors, etc
01 p0022 A71-10519

Planetarium use in teaching celestial navigation and space sky simulation
07 p1157 A71-20345

PLANETARY ATMOSPHERES

NT JUPITER ATMOSPHERE

NT MARS ATMOSPHERE

Planetary scale Rossby waves, examining vertical structure for zonal flow blocking and polar stratosphere warming
01 p0120 A71-10860

Absorption line formation in scattering planetary atmospheres with cloud particles
01 p0162 A71-11420

Reflecting and scattering models of line formation in planetary atmospheres allowing for inhomogeneously distributed gas and particles and for anisotropic scattering phase function
03 p0486 A71-13320

Slow positive ion and electron production in collisions of protons and hydrogen atoms with gases of planetary atmospheres
03 p0460 A71-13494

Planetary atmosphere circulation kinetic energy, energy transformation and driving temperature gradients, using similarity, dimensional and thermodynamic approaches
03 p0488 A71-13551

Planetary atmospheres motion effect on constant pressure surface height in radio occultation data interpretation
03 p0488 A71-13553

Convective velocity and temperature scales deduced numerically and observationally for unstable planetary boundary layer and for turbulent Rayleigh convection
03 p0453 A71-13613

Pure carbon dioxide planetary atmospheres, calculating photochemical instability from atmospheric model
03 p0377 A71-14549

Mercurian atmosphere models, discussing replenishing processes involving chemical reactions in thin and thick models
04 p0650 A71-15583

Soviet book on planets and moon covering surfaces, atmospheres, internal structure and observation methods
04 p0657 A71-15800

Planetary atmospheres ionosphere formation by cosmic rays, examining ionization of various gases
05 p0799 A71-16817

Planetary boundary layer forecast model, determining horizontal and vertical wind components, temperature, pressure and moisture with numerical variational objective analysis
05 p0778 A71-17049

Planetary atmosphere Mariner spacecraft occultation experiments, showing neglect of latitudinal and longitudinal variations introduce serious errors
06 p0970 A71-17984

Chemical nonequilibrium effects on hypersonic, blunt body shock layers flow in reacting planetary carbon dioxide-nitrogen atmospheres
06 p0866 A71-18496

[AIAA PAPER 71-35]

Planetary atmospheres radiant energy fluxes, developing validity of isolated line approximation in finite spectral intervals
07 p1191 A71-18908

Planetary atmospheres structure and dynamics, discussing composition and vertical temperature profile models
07 p1191 A71-18915

Polarized light multiple scattering in planetary atmospheres, applying extended doubling method to realistic simulations with allowance for radiation polarization and azimuth dependence
07 p1153 A71-19759

Space environment and operations from medical viewpoint, discussing gravitation, magnetic fields, particle rays, planetary atmospheres, etc
08 p1357 A71-20703

Optical observation of structure, composition, thermal spectra and aerosol layers of giant planet atmospheres
09 p1520 A71-22827

Quantum yield of carbon dioxide photolysis at 1470 Å concerning Mars and Venus atmospheres

09 p1403 A71-23377

Skipping entry trajectories up to fifth extremal points in planetary atmosphere, using matched asymptotic solution

11 p1837 A71-25483

Planetary atmospheres - Conference, Marfa, Texas, October 1969

11 p1823 A71-25690

Wind speed and potential temperature vertical profile in day/night planetary atmospheres estimated by similarity theory of boundary layer parameters

11 p1826 A71-25719

Dynamics of planetary atmospheres large scale motions, using similarity theory and dimensional analysis methods for atmospheric circulation characteristics calculation

11 p1826 A71-25720

Hydrogen-helium gas mixtures high pressure phase behavior, considering solidified gas core under Jupiter and Jovian planets atmospheres

11 p1827 A71-25728

Jupiter, Saturn and Uranus satellite systems orbital radius and mass correlation, suggesting satellite orbital evolution and energy dissipation at planetary atmospheric boundary layer

11 p1827 A71-25729

Saturn cloud layer molecular absorption from spectral/photographic and photoelectric observations

11 p1827 A71-25730

Uranus atmospheric molecular hydrogen abundance from pressure induced overtone spectra, using quadrupole moment and polarizability matrix elements theoretical values

11 p1827 A71-25731

Alpha particle gas densitometric response to planet atmospheric density profiles in terms of radioactive source energy distribution, considering contoured baffle models

11 p1763 A71-26079

Thermal control, pressure survival and structural tradeoffs of Jovian atmospheric probe for mission parametric studies

[AIAA PAPER 71-482]

11 p1839 A71-26257

Long time planetary atmosphere motions, investigating sideband resonance mechanism in Rossby wave packet interactions with weak shear zonal flow

12 p1925 A71-27195

Uranus radio emission measurements at 8.22 mm wavelength, noting brightness temperature and atmospheric properties

12 p1965 A71-27226

Inhomogeneous planetary atmosphere resonantly scattered sunlight, calculating intensities with frequency redistribution functions

13 p2100 A71-28346

Collision induced hydrogen spectra for overtone absorptions by gas mixtures under temperature and density conditions matching planetary atmospheres

13 p2138 A71-28773

Solar wind interaction with planetary atmospheres, discussing various models relationship to observational data

14 p2298 A71-29908

Pressure-induced absorption in planetary atmospheres from hydrogen-methane collisions, stressing resulting thermal opacity

14 p2315 A71-30659

Saturn atmospheric structure and optical properties, investigating methane absorption bands

15 p2483 A71-31337

Uranus and Neptune microwave emission spectra and atmospheric temperatures, comparing with Jupiter and Mars

15 p2490 A71-32410

Planetary exploration from space, recommending flights to moons of outer planets due to possible presence of atmospheres and water ice

15 p2494 A71-32495

Rayleigh scattering planetary atmosphere radiative transfer equation, calculating phase curves for flux and polarization

15 p2498 A71-32778

Mathematical theory of planetary atmosphere oscillations, considering coriolis, magnetic and viscous forces effects

16 p2561 A71-32804

Polarized light multiple scattering in homogeneous plane parallel planetary atmospheres, considering Rayleigh scattering, test models and phase function obtained by neglecting polarization

16 p2632 A71-33320

Reflection and transmission on plane parallel layers of planetary atmospheres with strongly anisotropic scattering, examining three eigenvalue problems

17 p2736 A71-35567

Absorption spectra formation by diffuse reflection from semiinfinite plane parallel scattering planetary atmosphere, using asymptotic expressions for higher order scattering

17 p2736 A71-35568

Planetary atmospheres composition from ground based IR spectroscopy, including multiple scattering, cloud layers, line formation and absorption

17 p2808 A71-35570

Variational principle with reflectivity extremum for inhomogeneous planetary atmospheric line spectra profile calculation from radiative transfer equation

18 p2964 A71-36286

Gas flow energy transport, discussing thermal radiation, radiant flux density, planetary atmosphere entry, thermodynamic equilibrium and differential approximations

18 p2847 A71-36426

Greenhouse effect in gray planetary atmosphere, showing thermal radiation generation and scattering with principles of invariance

18 p2970 A71-37049

Uranus radio emission measurements at 8.22 mm wavelength, noting brightness temperature and atmospheric properties

19 p3132 A71-37378

Thermal radio emission of Jovian planets atmospheres, deriving brightness temperature

[AAS PAPER 71-109]

19 p3139 A71-37909

IR experiments planning for Outer Planets Grand Tour including investigations of planetary radiation balance and atmospheric composition and satellites composition and physical properties

[AAS PAPER 71-131]

19 p3011 A71-37920

Outer planets atmospheric entry vehicles atmospheric heating, discussing shock and boundary layer physical and chemical effects

[AAS PAPER 71-144]

19 p3163 A71-37947

Ionization rates induced by solar flares charged particles in planetary atmospheres

19 p3142 A71-38047

Spacecraft entry into planetary atmosphere, considering heating, deceleration and landing

20 p3305 A71-38814

Saturn atmospheric structure and optical properties, investigating methane absorption bands

22 p3606 A71-42612

Laboratory analog simulation of absorption line spectra in cloudy planetary atmospheres, comparing with computational model based on plane parallel atmosphere

23 p3700 A71-43075

Planetary atmospheric motions, discussing solar radiation, internal heat sources, planetary rotation and magnetic field effects

23 p3672 A71-43891

PLANETARY COMPOSITION

Meteorites and earth core composition and models for terrestrial planets internal constitution

02 p0310 A71-12159

Jupiter model construction from improved state equation, considering chemical composition, contraction and rotation

02 p0314 A71-12589

Earth interior structure, composition and evolution, using seismic, ultrasonic, shock wave and petrological data

09 p1438 A71-23159

Pluto iron richness from analysis of similarities between Pluto spectra and Fe bearing terrestrial silicate crystals

10 p1673 A71-24426

Spectroscopic search for water on Mars during 1963-1970, summarizing conclusions concerning quantity and variations with location, season and from year to year

11 p1826 A71-25715

Liquid water natural occurrence on Martian surface, considering possibility of ice melting by sunlight or other heat sources

11 p1826 A71-25718

Jupiter occultation of beta Scorpii on 13 May 1971, determining hydrogen/helium ratio

12 p1961 A71-26876

Spectral analysis methods for detection of water on celestial bodies, considering possible abundance on planets and stars

12 p1962 A71-26956

Jupiter and Saturn magnetic field differences, considering metallic interior models

14 p2304 A71-29599

Mars IR spectral geometric albedo of bright and dark regions for surface composition model

15 p2491 A71-32419

Crustal and meteoritic abundances of elements and water, considering chondritic and achondritic composition

19 p3055 A71-38145

Heavy rare gases adsorption on terrigenous sediments, comparing earth atmospheric composition with meteoritic planetary primordial component

20 p3194 A71-39385

Saturn internal constitution, discussing Ramsey theory of planetary interior composition of hydrogen-helium mixture

22 p3596 A71-41450

PLANETARY ENTRY

U ATMOSPHERIC ENTRY

PLANETARY ENVIRONMENTS

NT JUPITER ATMOSPHERE

NT MARS ATMOSPHERE

NT MARS ENVIRONMENT

NT PLANETARY ATMOSPHERES

Jupiter Great Red Spot continuous changes on basis of observational records of South Equatorial Belt disturbances

04 p0643 A71-15000

Venus life forms, describing algae grown in pure carbon dioxide under pressure in acidic nutrient media at high temperatures

11 p1724 A71-25701

Existence conditions for liquid water on Mars, considering freezing depression, condensation, capillary evaporation and permafrost melting

15 p2494 A71-32492

Jupiter orbiter missions, considering satellite emphasis and planetary environment and planetology missions

[AAS PAPER 71-140]

19 p3140 A71-37923

Infusoria adaptation ability to extreme environmental conditions with emphasis on Mars surface

22 p3496 A71-42825

PLANETARY EVOLUTION

Planetesimal growth in nebulae around young stars, examining accretion and physical chemistry of solar types

01 p0157 A71-10761

Solar system origin, structure and evolution, discussing planet and satellite orbital motion, resonance effects, tides and postaccretional changes

01 p0161 A71-11335

Primordial trapped planetary noble gases and solar isotopic ratios in separated meteoritic minerals from Orgueil carbonaceous chondrite

02 p0318 A71-12901

Earth atmosphere origin, discussing oxygen and carbon dioxide balance

03 p0409 A71-13697

Accretion theory of planet and satellite formation in solar system, including earth-moon model

03 p0495 A71-14262

Martian satellites nature and evolution, facts, theories, hypotheses and speculations

07 p1202 A71-20516

Saturn natural satellites commensurabilities evolution from analysis of libration amplitude change with time for interaction under tidal friction with planet

07 p1202 A71-20519

Earth interior structure, composition and evolution, using seismic, ultrasonic, shock wave and petrological data

09 p1438 A71-23159

Earth and meteorites evolution, discussing material transport between lower and upper mantles and crust based on model of trace elements

11 p1820 A71-25226

Asteroid ring origin, discussing osculating and corresponding secular orbital elements of mother planet

11 p1820 A71-25245

Planetary condensation under conditions of Woollson solar system origin capture theory

11 p1820 A71-25296

Planetary formation, obtaining retrograde orbit probability and distances and masses expectation by stochastic model

11 p1830 A71-26110

Planetary system formation, examining particulate matter aggregation within dust cloud and gas around sun by computer simulation

14 p1835 A71-26459

Venus retrograde rotation, showing consistency with Laplacian theory of cosmology and Fesenko theory

12 p1961 A71-26901

Hydrodynamic model of coalescing meteors substantiating cosmogonic Laplace-Schmidt hypotheses of solar system planetary formation from cosmic dust

13 p2131 A71-27892

Planetary mass distribution, considering accretional theory of gas condensation into particles and particle accretion by growing embryo

14 p2312 A71-30389

Numerical analysis of accretion growing grains segregation in gravitational field with resisting gas, discussing motion equation, evaporation rate and planetary evolution

15 p2489 A71-32397

Lunar and Martian cratering possibility by cometary icy blocks based on sonic impact fluidation experiments

16 p2636 A71-33508

Planetary dynamics bibliography and review, considering range determination and ephemerides, general relativity, tidal evolution and lunar orbit, solar system commensurabilities, etc

17 p2798 A71-34457

Mission analysis for multi-planet flyby and major satellites close encounter to determine solar system planetary evolution data, presenting Grand Tour trajectory parameters

[AAS PAPER 71-137]

19 p3139 A71-37922

Missions beyond solar system for studying origin and evolution of life, planets and stars

19 p3141 A71-37960

- Hydrodynamic model of adhering meteors substantiating cosmogonic Laplace-Schmidt hypotheses of solar system planetary formation from cosmic dust
21 p3441 A71-40076
- Quantitative equivalence model in planet-satellite formation within Jupiter and Uranus systems
22 p3604 A71-42191
- Planetary formation from sun ejected charged bodies captured in orbit due to electromagnetic effects, considering Sarvajna model
22 p3604 A71-42334
- Floccule theory three dimensional planetary formation model of collapsing cloud leading to nonplanar system with protoplanets in retrograde orbits
23 p3769 A71-43991
- Lunar evolution theory, discussing terrestrial cluster dynamics during earth accumulation
24 p3870 A71-44811
- Asteroid belt structure by statistical methods, discussing asteroidal zones and agreement with Kuiper hypothesis and protoplanet theory
24 p3874 A71-45173
- PLANETARY EXPLORATION**
U SPACE EXPLORATION
PLANETARY EXPLORER
U OUTER PLANETS EXPLORERS
PLANETARY GRAVITATION
Earth spherical and ellipsoidal gravity potential coefficients association using Lane orthogonal function properties
01 p0155 A71-10388
- Rocket probe with constant tangential acceleration in planetary gravitational field, investigating flight direction
03 p0495 A71-14388
- Planetary system effects on long period comets orbital characteristics, presenting eccentricities and reciprocal semimajor axes calculations
04 p0642 A71-14738
- Jupiter and Saturn gravitational moments calculation procedure based on planetary density angular distribution
08 p1361 A71-21054
- Intermediate orbit calculation, allowing for spacecraft large gravitational perturbation during motion near planetary sphere of influence
09 p1519 A71-22663
- Spacecraft motion during flight toward planet, including trajectory correction energy loss, autonomous angular measurements and attractive forces
13 p2146 A71-29237
- Jupiter and Saturn gravitational moments calculation procedure based on planetary density angular distribution
14 p2310 A71-30167
- Point motion in axisymmetrical planet equatorial plane gravitational field, taking into account orbital elliptic elements osculation
14 p2310 A71-30186
- Radar ranging experiment onboard Jupiter orbiter, concerning perturbations, gravitational harmonics and short arc orbit determination
15 p2487 A71-32041
- Planet density distribution, deriving successive approximations for equilibrium figure equations for gravitational potential and level surfaces
15 p2495 A71-32680
- Martian satellites motion along arbitrary elliptical orbits, expressing planet gravitational potential
18 p2962 A71-36108
- Gravitational fields of giant planets in hydrostatic equilibrium, solving equations for linear and quadratic density distributions
20 p3290 A71-39310
- Gravity coefficients of geopotential expansion in ellipsoidal harmonics via Lane functions, noting application to earth, Jupiter and Saturn
23 p3666 A71-43011
- Covariance analysis of Mars gravity harmonics, ephemeris and radiation pressure from Mariner 1971 range and Doppler radar tracking data
23 p3727 A71-43016
- Planetary gravitational fields variations determination by onboard gravity gradiometer instrumentation
23 p3729 A71-43034
- Planetary tidal forces correlation with solar activity distribution, observing Ca flocculi spectrum
23 p3768 A71-43851
- PLANETARY LANDING**
Heat sterilizable remotely activated silver zinc battery for energy source of planetary lander capsule
03 p0352 A71-13043
- Mars lander deorbit trajectory sensitivity analysis for fixed flight path and communications angles at atmospheric entry, comparing with Monte Carlo simulation
06 p0978 A71-18628
- Impact resistant power packages for unmanned planetary probe landers, discussing radioisotope thermionic multiconverter array optimal configuration
11 p1713 A71-25898
- High thrust throttleable monopropellant hydrazine catalytic reactors for planetary landing vehicles, con-

- sidering engine designs, dynamic characteristics and response to commanded duty cycles
14 p2294 A71-30762
- German book on models and constructions for interplanetary space flights covering Helios project, grand tour, Mars landing, planetary exploration, etc
16 p2645 A71-33523
- PLANETARY LONGITUDE**
U PLANET EPHEMERIDES
PLANETARY MAGNETIC FIELDS
Turbulent diffusion role in magnetic fields origin in sun, planets and galactic gaseous disk
01 p0162 A71-11419
- Earth and Jupiter magnetic fields relationship to core motional induction
02 p0310 A71-12160
- Magnetometers for space research, discussing instrumentation, spacecraft response, data, earth orbit, lunar, planetary and interplanetary measurements
05 p0748 A71-16228
- Jupiter and Saturn magnetosphere calculations, considering solar wind characteristics and planetary magnetic fields
06 p0977 A71-18494
- Jupiter magnetic field geometry related to Io modulated Jovian decametric radio emission
12 p1956 A71-26620
- Jupiter and Saturn magnetic field differences, considering metallic interior models
14 p2304 A71-29599
- Simultaneous two magnetometer measurements of weak magnetic fields in interplanetary space, near moon and planets by satellites in presence of spacecraft field
15 p2406 A71-31753
- Zenomagnetic core-mantle coupling and fluctuations in period of rotation of Jupiter Great Red Spot
16 p2637 A71-33515
- Jupiter radio observations, measuring nonthermal emission, magnetic field and trapped radiation belts
19 p3140 A71-37933
- Jupiter and Saturn IR radiation sources, radio emission storms, magnetic fields, life existence, Grand Tour missions, etc
21 p3442 A71-40150
- Mars mass, dimensions, configuration, internal structure, magnetic field, color evolution, surface properties, atmospheric parameters, etc
21 p3452 A71-40885
- PLANETARY MASS**
Io Hygiea perturbation observations, determining Jupiter mass by numerical integration
01 p0155 A71-10443
- Earth rotation axis and mass center position determination, using earth-moon laser ranging data
01 p0161 A71-11383
- Planets and satellites masses and other dynamic parameters by numerical and analytical calculation techniques based motion and trajectory analyses
02 p0309 A71-12152
- Satellite dynamics applications in determination of atmospheric drag, earth and moon gravitational fields and Mars and Venus mass from trajectory construction
03 p0491 A71-14003
- Minor celestial objects for determining Jupiter mass, noting problem geometry, nodal points and orbit correction
04 p0653 A71-15712
- Earth, moon and planets sizes, masses and moments of inertia determination by artificial satellites, space probes and radar observation
05 p0815 A71-17241
- Inner and outer planets groups mass and mean density, considering terrestrial seismic data and lunar, Venus, Mars and Mercury structural models
08 p1358 A71-20888
- Planetary mass system as pulsar timing error sources, noting change in barycenter of solar system
10 p1675 A71-24493
- Jupiter, Saturn and Uranus satellite systems orbital radius and mass correlation, suggesting satellite orbital tidal evolution and energy dissipation at planetary atmospheric boundary layer
11 p1827 A71-25729
- Planet Mercury density, discussing optical and radar measurements and theory comparison with observation
14 p2306 A71-29728
- Planetary mass distribution, considering accretional theory of gas condensation into particles and particle accretion by growing embryo
14 p2312 A71-30389
- Daniel comet minimum distance distributions between asteroids, determining minor planet masses
15 p2482 A71-31302
- Pales /49/ orbit motion analysis for Jupiter mass, noting discrepancies between old and new observations
15 p2488 A71-32198
- Pluto mass from reciprocal mass and density, using Neptune transit circle observations reevaluation
15 p2488 A71-32199

- Saturn and Jupiter mass determination from Schwassmann-Wachmann 1 comet motion observations, using perturbation program based on Schubart-Stumpf n-body integration program
18 p2970 A71-37062
- Planets masses based on observational or analytical methods, discussing systematic errors effects
19 p3339 A71-37907
- Mars mass, dimensions, configuration, internal structure, magnetic field, color evolution, surface properties, atmospheric parameters, etc
21 p3452 A71-40885
- Outer planets masses determination from orbit perturbations analysis and optical observations
23 p3725 A71-42988
- PLANETARY MOTION**
U SOLAR ORBITS
PLANETARY NEBULAE
Planetary nebulae and scattered stellar cluster visible coincident distribution near galactic center
02 p0308 A71-12103
- Planetary nebula NGC 7027 mapping at 11.1 cm, examining structure, ionized H mass and electron density
02 p0317 A71-12869
- Planetary nebulae radio spectra observations by Jodrell Bank interferometer and total power instruments, using variable radius spherical shell model for flux density
04 p0658 A71-15836
- Planetary nebulae and H II region dust density perturbation e-folding time, examining Lyman continuum radiation
05 p0812 A71-16689
- Planetary nebulae continuous UV spectrum, discussing glow process, electron temperature and density and Balmer discontinuity
06 p0974 A71-18434
- Planetary nebulae upper distance limits by photometry, including mean nebular parameters and extinction coefficients in galaxy dust model
07 p1191 A71-18999
- Planetary nebulae NGC 6572, NGC 7009, NGC 7027 IR line emission, examining fine structure for Ne II, Cl IV, S IV and Ar III
07 p1199 A71-19836
- Planetary nucleus BD plus 30.3639 degrees and Wolf-Rayet star HD 164270, comparing spectrum and ionization potential
08 p1359 A71-20937
- Planetary nebulae central stars power spectra and HF stellar oscillation observations, using photoelectric time series data
08 p1359 A71-20938
- Planetary nebulae NGC 1535, 6572, 6543, 7662 and 7009, observing monochromatic photographs and isophotic contours
09 p1521 A71-22870
- Planetary nebulae central stars extended atmospheres, calculating gray and nongray models under hydrostatic, radiative and LTE
11 p1818 A71-25203
- Planetary nebulae mass ejection by radiation pressure, describing mathematical models for time independent outflowing envelopes
11 p1821 A71-25537
- Planetary nebulae continuous UV spectrum, discussing glow process, electron temperature and density and Balmer discontinuity
12 p1955 A71-26584
- Strong planetary nebulae measurement at short centimeter wavelengths, observing flux densities and thermal spectra
13 p2138 A71-28760
- Planetary nebulae observations in radio spectrum, determining interstellar extinction, electron temperature recombination theory and models
14 p2312 A71-30388
- Planetary nebula NGC 7009 narrow band filter photographs and spectra, detailing emission lines, intensity and velocity variations and model
14 p2313 A71-30430
- Anomalous OH emission in direction of planetary nebula NGC 2438 and optically radio-weak galactic nebulae S 247, S 269, IC 2162 and NGC 2264
14 p2313 A71-30431
- H85 alpha recombination line in planetary nebula NGC 7027, considering IR physical parameters consistent with radio observations
14 p2313 A71-30432
- Galactic nebula YM 29 radiometric observations showing thermal source, mass and Balmer line fluxes comparable to planetary nebula
14 p2314 A71-30643
- Monograph on planetary nebulae covering structure, luminosity, spectra, origin, chemical composition, temperature, magnetic fields, etc
15 p2481 A71-31148
- Galactic discrete X ray sources identification with black nebulae, H II regions, close binary stars, Wolf-Rayet stars and planetary nebulae
15 p2482 A71-31330

Planetary nebulae nuclei colorimetric, photographic and brightness data, listing temperatures, absolute values and bolometric corrections

15 p2487 A71-32034

H beta fluxes of planetary nebulae along southern Milky Way from photoelectric telescope

17 p2809 A71-35593

Planetary nebulae central stars, considering elementary stellar evolution theory, globular cluster stars and ejection mechanism

18 p2968 A71-37031

Dumb-bell Nebula forbidden O III line profiles observation with two-etalon scanning Fabry-Perot

19 p3144 A71-38171

Electron temperature and density vs ionization potential in bright planetary gaseous nebulae, using forbidden emission line intensity ratios and level populations

21 p3440 A71-40059

Photoelectric and photographic spectrophotometric observations of relatively bright moderate excitation planetary nebula NGC 6826, obtaining electron density and ion concentration

21 p3446 A71-40415

Planetary nebulae helium/hydrogen and nitrogen/oxygen abundance ratios from photoelectric observations, taking into account temperature fluctuations and collisional excitation effects

21 p3446 A71-40416

Young dust-filled planetary nebulae models with hot central stellar black body radiation, evaluating IR radiation absorption and reradiation in H I region

21 p3446 A71-40417

Planetary nebulae microwave radiation emission survey by Algonquin Radio Observatory, determining flux densities

23 p3769 A71-43988

PLANETARY ORBITS

Minor planet distribution in asteroid belt central area, noting inclination angle, eccentricity, ascending node and perihelion longitude

01 p0155 A71-10442

Juno absolute perturbations due to large planets, using Hill method with digital computer

01 p0156 A71-10549

Planets and satellites masses and other dynamic parameters by numerical and analytical calculation techniques based on motion and trajectory analyses

02 p0309 A71-12152

Long period effects in motion of Chicago and Thule, noting commensurability with Jupiter orbit

04 p0652 A71-15705

Two impulse rendezvous between coplanar circular planetary orbits, considering mono-impulsive interception/flyby/ problem for optimality

05 p0812 A71-16731

Earth based orbit determination for Mars orbiting spacecraft, comparing batch and sequential tracking filter data processing methods

[AIAA PAPER 71-119]

06 p0978 A71-18657

Double resonance in natural satellite motion from long period perturbation prediction

07 p1202 A71-20517

Saturn natural satellites commensurabilities evolution from analysis of libration amplitude change with time for interaction under tidal friction with planet

07 p1202 A71-20519

Intermediate elliptical orbits for planetary satellites with small inclination to equatorial plane

09 p1520 A71-22671

Approximate determination of 44 minor planets orbits, tabulating orbital elements

09 p1526 A71-23344

Observations distribution influence on accuracy of almost circular planetary orbits determining elements, considering geocentric distances and ecliptic longitudes and latitudes

09 p1526 A71-23345

Pluto orbit integration over 4.5 million years by variation of parameters technique and confirming Neptune-Pluto orbital resonances

10 p1669 A71-24179

Planetary satellites intermediate orbits, obtaining angular orbital elements secular perturbations

12 p1964 A71-27091

Point motion in axisymmetrical planet equatorial plane gravitational field, taking into account orbital elliptical elements osculation

14 p2310 A71-30186

Pales /49/ orbit motion analysis for Jupiter mass, noting discrepancies between old and new observations

15 p2488 A71-32198

Pluto mass from reciprocal mass and density, using Neptune transit circle observations reevaluation

15 p2488 A71-32199

Gravity decrease effects on planetary orbits, considering two bodies in circular and elliptical orbits and many bodies solar system with interaction between planets

16 p2631 A71-33167

Elliptic restricted three body problem, calculating fictitious retrograde Jovian satellites orbits in rotating-pulsating axes for sun-Jupiter case

16 p2633 A71-33337

Heliocentric energy per mass changes in close planetary encounters, noting relation to cometary and asteroidal material evolution

17 p2811 A71-35744

Planetary satellites intermediate orbits, obtaining angular orbital elements secular perturbations

19 p3133 A71-37441

Jupiter orbiters and probes noting objectives, spacecraft design and mission description

[AAS PAPER 71-103]

19 p3152 A71-37905

Jupiter orbiter missions, considering satellite emphasis and planetary environment and planetology missions

[AAS PAPER 71-140]

19 p3140 A71-37923

Outer planet exploration spacecraft subsystems reliability and ten year flight requirements for planet orbiting and flyby missions

[AAS PAPER 71-112]

19 p3140 A71-37934

Planetary capture in restricted three body problem and bridge formation between galaxies

20 p3286 A71-38761

Five outer planets orbital perturbations by four inner planets, comparing second differentials with disturbing force numerical values

21 p3441 A71-40096

Probe for circular polar Mercury orbit, obtaining missions values

22 p3600 A71-42010

Trajectory aiming plane in optimum satellite orbit selection for planetary flyby and orbiter missions

[AAS PAPER 71-305]

23 p3724 A71-42981

Bi-injection earth departure mode analysis for combined flyby/orbiter Jupiter-Saturn-Pluto and Jupiter-Uranus-Neptune Grand Tour missions

[AAS PAPER 71-322]

23 p3726 A71-42996

Actual navigation dispersions, estimation uncertainties and resultant Mars orbit insertion statistical delta V requirements for six Mars approach angles in 1977 Mars window

[AAS PAPER 71-323]

23 p3726 A71-42997

Low thrust vehicle optimal takeoff calculations from orbit about oblate planet, using two variable asymptotic expansion technique

[AAS PAPER 71-367]

23 p3729 A71-43037

Batch and sequential consider filters data processing methods for Mars orbiting spacecraft state estimation, investigating error sources

[AAS PAPER 71-385]

23 p3731 A71-43055

Transplutonian planet dynamical search through numerical integration of outer planets orbits

24 p3868 A71-44440

Mars orbiters and Kepler laws, discussing planetary motion, satellite orbits and orbital characteristics

24 p3875 A71-45268

PLANETARY QUARANTINE

Planetary quarantine including background, program evolution, sterilization technology and contamination sources

16 p2537 A71-33744

Planetary quarantine analysis for unmanned Mars orbiter, considering accidental spacecraft impact, loose particles and gases used for attitude control and pressurization

16 p2537 A71-33799

Planetary quarantine constraint effect on multiple outer planet missions, considering navigation error sources and midcourse maneuvers

[AAS PAPER 71-122]

19 p3002 A71-37917

Planetary quarantine constraints for Mariner Mars 1971 orbiter missions, considering heliocentric and areocentric phases

[AAS PAPER 71-318]

23 p3725 A71-42992

Planetary quarantine constraint on 1977 Jupiter-Saturn-Pluto mission, determining fuel loading penalties, optimum biasing strategies and outer planet navigational characteristics

[AAS PAPER 71-319]

23 p3726 A71-42993

PLANETARY RADIATION

International joint optical and radio astronomical observations on Saturn rings and disk /1966/

01 p0149 A71-10046

Optical bonding agent for calcite prism on Pioneer F/G mission, emphasizing optical and mechanical properties resistance to Jupiter high energy particles

01 p0081 A71-10835

Planetary and lunar thermal radio emission and brightness temperature measurements using sensitive receivers and large aperture radio telescopes

02 p0309 A71-12155

Very long baseline interferometry /VLBI/ of Jupiter decametric bursts at HF

02 p0310 A71-12326

Frequency and phase analyses of cross correlated signals from very long baseline interferometry of decametric radiation from Jupiter

02 p0310 A71-12333

Venus spectra 10488 A carbon dioxide band from high dispersion spectroscopy

03 p0488 A71-13556

Martian dayglow spectrum, examining excitation processes for carbon monoxide Cameron bands

03 p0497 A71-14544

L.F. radio emission from Jupiter at 3-8 MHz

04 p0641 A71-14737

Mars atmospheric water vapor detection during Southern Hemisphere spring and summer season

04 p0645 A71-15139

Saturn millimeter wave spectrum and brightness temperature measurements, showing ammonia absorption characteristics in atmosphere

04 p0659 A71-15851

Venus high resolution spectra interpretation for sub II band of carbon dioxide isotope

04 p0659 A71-15859

Mars, Jupiter, Saturn and Uranus millimeter wave radiation brightness temperatures, considering search for variations with time or phase angle

04 p0660 A71-15860

Latitude, mesons and radioactivity effects on planetary distribution of cosmic ray neutron component barometer coefficient during IQSY

06 p0960 A71-18166

Statistical analysis for parabolic approximation of phase dependence observations of integral Mars brightness

06 p0975 A71-18446

Alfven waves and magnetosonic radiation by rotating magnetic stars and planets

07 p1193 A71-19293

Theoretical submillimeter spectrum of Venusian radiation, determining brightness temperature

07 p1193 A71-19313

Martian radio emission measurements at millimeter wavelength and surface thermal and electric parameters estimation

07 p1193 A71-19314

Radio telescope measurements of circular polarization and total flux of Jupiter at 13.1 cm wavelength

08 p1357 A71-20871

International joint optical and radio astronomical observations on Saturn rings and disk /1966/

08 p1361 A71-21040

Uranus radio emission model, considering presence of gaseous ammonia at saturation pressure in atmosphere

09 p1519 A71-22526

Jupiter decametric radiation source A position variation, considering radiation controlling influence of Jovian satellite Io

09 p1521 A71-22935

Pluto iron richness from analysis of similarities between Pluto spectra and Fe bearing terrestrial silicate crystals

10 p1673 A71-24426

IR polarization of Venus, providing Venus atmosphere effective particle size estimate

10 p1675 A71-24489

Jupiter far IR emission spectra models, examining atmospheric composition, temperature and structure

11 p1821 A71-25538

Venus atmosphere composition and structure from microwave spectrum, noting surface pressure and temperature and water vapor

11 p1823 A71-25694

Venus atmosphere spectra, emphasizing line and continuum absorption coefficients relative to scattering

11 p1823 A71-25697

Venus, Mars, Jupiter and lunar thermal emission data in 7-25 micron region

11 p1824 A71-25698

Venus thermal radiation limb darkening measurements, indicating complex atmospheric structure

11 p1824 A71-25699

Mars monochromatic albedos, investigating longitudinal variations and opposition effects

11 p1824 A71-25707

Mars UV polarization and atmospheric opacity measurements, using ground based polarimetric data at near maximum elongation

11 p1825 A71-25709

Jupiter color variations observation by multicolor photoelectric photometry, noting consistency with activity in Jovian atmosphere

11 p1827 A71-25725

Mars 1969 opposition effects, describing Syrtis Major, Arabia and disk brightness, color and spectrum

11 p1835 A71-26456

Line formation effective pressure from Venus atmosphere spectra, discussing phase angle variations

11 p1835 A71-26457

Parabolic approximation of total Mars brightness phase dependence observations, using statistical analysis

12 p1955 A71-26596

Jupiter magnetic field geometry related to Io modulated Jovian decametric radio emission

12 p1956 A71-26620

Mars regolith carbon dioxide, water and Kr adsorption, explaining diurnal brightness phenomena

12 p1961 A71-26875

Jupiter upper atmosphere extreme UV dayglow, involving resonant scattering and fluorescence of incident solar flux

12 p1961 A71-26888

Venus polarimetric observational data comparison with polarization characteristics of radiation scattered

at gamma-distribution particle sizes, determining refractivity and particle radius

12 p1964 A71-27088

Martian continents, seas and polar caps spectrum analysis, noting spectral reflectivity and brightness distributions

12 p1965 A71-27225

Uranus radio emission measurements at 8.22 mm wavelength, noting brightness temperature and atmospheric properties

12 p1965 A71-27226

Jovian radio source angular diameter measurement by radio interferometry

12 p1967 A71-27310

Planetary disks brightness temperature measurement using 22 m radio telescope with indium antimonide detector at 1.4 mm

13 p2141 A71-29102

Saturn polarimetric observation, noting rings polarization Stokes parameters, methane absorption bands and continuous spectrum

15 p2482 A71-31336

Solar wind velocity and Io phase relationship during decametric radio bursts from Jupiter, indicating plasmasphere existence

15 p2474 A71-31723

Theoretical submillimeter spectrum of Venusian radiation, determining brightness temperature

15 p2486 A71-31893

Martian radio emission measurements at millimeter wavelength and surface thermal and electric parameters estimation

15 p2486 A71-31894

Uranus radio emission measurement at 8.22 mm, obtaining brightness temperature

15 p2490 A71-32412

Mars and Jupiter radio emission at 2.3 mm and 8.15 mm, determining brightness temperature and electrical and thermal waves soil penetration depth ratio

15 p2490 A71-32413

Mars microwave brightness temperature measurements, defining planetary spectra

15 p2490 A71-32415

Russell law validity of planet brightness dependence on phase integral, discussing backscattering surface and thick atmospheres effects

15 p2491 A71-32425

Jupiter radio spectrum decametric component observations, emphasizing core and mantle rotation under coupled torsional oscillations

16 p2637 A71-33514

Saturn radio emission and brightness temperature measurements, determining rings optical thickness upper limit

16 p2639 A71-33692

Mars atmosphere high resolution line spectra, calculating carbon dioxide abundance, rotational temperature and surface pressure

17 p2800 A71-34588

Scattered light circular polarization data from Jupiter and other planets indicating nonmagnetic origin

17 p2805 A71-35377

Uranus radio emission model, indicating presence of gaseous ammonia at saturation pressure

17 p2807 A71-35501

Variational principle with reflectivity extremum for inhomogeneous planetary atmospheric line spectra profile calculation from radiative transfer equation

18 p2964 A71-36286

Jupiter Red Spot and other photographic features in 1969-1970, noting 90-day oscillation in longitude and south tropical zone disturbance

18 p2964 A71-36289

Venus L alpha emission, negating deuterium origin

18 p2970 A71-37055

Martian continents, seas and polar caps spectrum analysis, noting spectral reflectivity and brightness distributions

19 p3132 A71-37377

Uranus radio emission measurements at 8.22 mm wavelength, noting brightness temperature and atmospheric properties

19 p3132 A71-37378

Venus polarimetric observational data comparison with polarization characteristics of radiation scattered at gamma-distribution particle sizes, determining refractivity and particle radius

19 p3133 A71-37438

Thermal radio emission of Jovian planets atmospheres, deriving brightness temperature

[AAS PAPER 71-109] 19 p3139 A71-37909

IR experiments planning for Outer Planets Grand Tour including investigations of planetary radiation balance and atmospheric composition and satellites composition and physical properties

[AAS PAPER 71-131] 19 p3011 A71-37920

Jupiter radio observations, measuring nonthermal emission, magnetic field and trapped radiation belts

[AAS PAPER 71-108] 19 p3140 A71-37933

Planetary LF radio emission experiments on Grand Tours, discussing models and spectrum, polarization, position and time variation measurements

[AAS PAPER 71-168] 19 p3141 A71-37965

Mars short-wave line spectra from measurement with reflector, estimating nitrogen dioxide content in atmosphere

20 p3290 A71-39307

Jovian planets methane and ammonium absorption bands spectrophotometric investigation, noting Saturn spectral variations

20 p3290 A71-39311

Saturn planetary system optical and radio observations during 1966, discussing Janus satellite, D ring, rarefied envelope and brightness temperature distribution

20 p3297 A71-39632

Planetary, stellar, galactic, sky and extragalactic UV radiation from OAO-2 spectrophotometric observations, noting interstellar extinction curves

20 p3300 A71-39747

Radio telescopic observations of Jupiter, Venus and radio source 3 C 273 at 2 and 8 mm wavelengths, determining brightness temperatures and radiation flux densities

21 p3445 A71-40258

Planetary luminosity correlated with solar activity, discussing far UV and solar wind particle interactions with atmosphere

22 p3591 A71-41472

Mars IR spectra with Connes-type interferometer, noting atmospheric absorption and albedo drop due to surface water

22 p3602 A71-42176

Saturn disk monochromatic albedos observation by multicolor photoelectric photometry, comparing with Jupiter

22 p3602 A71-42178

Radiative heat transfer from lunar and Mercurian surfaces during eclipse

22 p3603 A71-42188

Venus water ice clouds existence possibility from high altitude IR spectra and ground based spectroscopic observations

22 p3603 A71-42189

Saturn polarimetric observation, noting rings polarization, Stokes parameters, methane absorption bands and continuous spectrum

22 p3606 A71-42611

Ashen light over Venus nocturnal hemisphere due to reflected earthlight and starlight

23 p3733 A71-43128

Jovian geometric albedo at 1800-1950 A decrease explained as absorption by gaseous and solid ammonia in cubic crystal form

23 p3736 A71-43345

Cyclotron magnetoacoustic wave generation by planets and binary stars in circular orbits, deriving interstellar gas density variations

24 p3869 A71-44804

High dispersion spectroscopic observations of Venus, finding carbon dioxide band rotational temperature

24 p3873 A71-45079

PLANETARY ROTATION

Earth and Jupiter magnetic fields relationship to core motional induction

02 p0310 A71-12160

Jupiter model construction from improved state equation, considering chemical composition, contraction and rotation

02 p0314 A71-12589

Jupiter details rotational periods variations, characterizing dynamic properties of atmosphere upper layers

03 p0490 A71-13940

Venus low retrograde spin rate explained as result of capture of moonlike object from retrograde orbit, transforming planet rotational energy into heat

04 p0642 A71-14823

Gravitational and tidal torque effects on Mercury spin rate as model of passage through resonance

04 p0657 A71-15738

High resolution spectroscopy of rotating planets, discussing improvement principles

07 p1107 A71-19204

Planetary diurnal rotation, discussing motion of small particle in solar and planet gravitational fields

07 p1201 A71-20437

Planetary rotation classical and radio measurement effects on physics of planetary interiors, discussing Jupiter rotation, terrestrial planets composition and earth and moon palaeorotation

07 p1203 A71-20524

Angular velocity and momentum vector evolution of isolated bodies in solar system, considering models to trace rotational motion evolution

07 p1203 A71-20525

Planet rotation vector determination, using satellite stellar observations and planetary surface reference points

08 p1365 A71-21776

Differential rotation in sun, giant planets and upper atmospheres of earth and Venus, attributing solar rotation to tides caused by planets

09 p1522 A71-22961

Planetary rotational and translational motion interrelation in Einstein gravitation theory, describing or-

bital elements secular disturbances in two body problem

09 p1526 A71-23339

Lunar libration presented as general rotation of solid body in external force field

11 p1822 A71-25685

Venus retrograde rotation, showing consistency with Laplacian theory of cosmology and Fesenko theory

12 p1961 A71-26901

Jupiter rotation from Jovian decametric emission data

13 p2135 A71-28347

Venus rotation observations during 1964 eastern spring elongation, noting weather period and wind velocities

13 p2136 A71-28386

Planet intrinsic rotation vector determination, using satellite stellar observations and planetary surface reference points

15 p2495 A71-32681

Jupiter radio spectrum decametric component observations, emphasizing core and mantle rotation under coupled torsional oscillations

16 p2637 A71-33514

Zenomagnetic core-mantle coupling and fluctuations in period of rotation of Jupiter Great Red Spot

16 p2637 A71-33515

Planetary dynamics bibliography and review, considering range determination and ephemerides, general relativity, tidal evolution and lunar orbit, solar system commensurabilities, etc

17 p2798 A71-34457

Planetary atmospheric motions, discussing solar radiation, internal heat sources, planetary rotation and magnetic field effects

23 p3672 A71-43891

PLANETARY SATELLITES

U NATURAL SATELLITES

PLANETARY SPACE FLIGHT

U INTERPLANETARY FLIGHT

PLANETARY SPACECRAFT

U INTERPLANETARY SPACECRAFT

PLANETARY SURFACES

NT MARS SURFACE

Mercury planet average dark side temperature indicating top surface layer similarity with moon

01 p0148 A71-10004

Papers on surfaces and interiors of planets and satellites covering radio and radar observations, photometry, magnetic fields, etc

02 p0309 A71-12151

Radar observation of planetary surface characteristics, emphasizing albedo, surface roughness and differentiation

02 p0309 A71-12154

Planetary surfaces photometry, discussing parameters, phase laws, albedos, spectral reflectivities, phase function theory and light scattering

02 p0309 A71-12156

Radar interferometric mapping of Venus surface reflectivity in polarized mode at 70 cm wavelength

03 p0490 A71-13782

Venus surface alteration for human habitation

04 p0539 A71-15346

Soviet book on planets and moon covering surfaces, atmospheres, internal structure and observation methods

04 p0657 A71-15800

Earth and planetary surface soil dielectric constants and conductivity determination based on p-wave velocity data correlation

05 p0743 A71-17142

Escape mechanisms examined to explain liquid water absence on Venus surface, considering hot acidic hydrosphere consequences for biological activity

06 p0968 A71-17955

Jupiter surface features motions and changes, discussing planetary fine structure

06 p0971 A71-18247

Radar scattering law derivation method for small regions of Venus surface, synthesizing CW spectra

08 p1357 A71-20872

Planet rotation vector determination, using satellite stellar observations and planetary surface reference points

08 p1365 A71-21776

Planetary surface smoothness factor determination by disk brightness, Mars red light and phase curves methods, indicating superiority of visual observation

09 p1520 A71-22828

Venus maps from high resolution radio telescope observations, investigating surface pressure/temperature, planetary atmosphere and water vapor presence

11 p1830 A71-26109

Subsurface moisture and frost detection by capacitive measurement of ground permittivity from landed planetary probes and surface vehicles

15 p2411 A71-32473

Surface and subsurface water analysis on moon and planets by combination neutron experiment using epithermal die-away measurements of hydrogen

15 p2411 A71-32477

- Planet density distribution, deriving successive approximations for equilibrium figure equations for gravitational potential and level surfaces
15 p2495 A71-32680
- Planet intrinsic rotation vector determination, using satellite stellar observations and planetary surface reference points
15 p2495 A71-32681
- Jupiter systematic visual observations during 1968-1969 apparition, noting Red Spot conspicuousness, south temperate zone white spots, etc
16 p2635 A71-33429
- Spores released from solids interiors by aeolian erosion on planetary surface, noting application to microbes in planetary quarantine
16 p2537 A71-33796
- Bibliography and review of solar system bodies surfaces, considering remote sensing at UV, optical, IR, microwave and radio wavelengths, in situ lunar measurement and surface exploration
17 p2798 A71-34458
- Position determination on planetary surface from gravity and star line-of-sight direction measurements, presenting numerical results for Apollo lunar landing missions
[AIAA PAPER 71-900] 19 p3095 A71-37151
- Planetary and lunar meteorite craters classification according to radius logarithm to base ten, covering diameter size from 2 microns to 2000 km
21 p3444 A71-40206
- Artificial illumination for Venus surface pictures from landed space vehicle
22 p3608 A71-41953
- Circularly polarized ultrashort radio wave reflection from lunar and planetary surfaces, determining angular scattering spectrum
24 p3805 A71-45313
- PLANETARY TEMPERATURE**
Martian environment simulator chamber for pressure, visible light, biological objectives UV irradiation and daily temperature cycle
01 p0068 A71-11559
- Mariner 5 Venus exospheric Lyman alpha measurements for dayside temperature value, using molecular hydrogen photodissociation model
11 p1823 A71-25692
- Venus water, discussing polar seas, acidity, temperature, wind patterns and clouds
11 p1824 A71-25700
- Jupiter equatorial belt effective temperature during 1965 apparition from limb darkening profile observation
11 p1827 A71-25726
- Venus maps from high resolution radio telescope observations, investigating surface pressure/temperature, planetary atmosphere and water vapor presence
11 p1830 A71-26109
- Mercury, Mars, Venus, Jupiter and Saturn temperatures at 9.55 mm wavelength, calibrating antenna gain with radio sources
15 p2490 A71-32414
- Venus surface temperature dependence on incident solar flux based on runaway greenhouse nongray calculation, considering water vapor as IR opacity source in models
18 p2964 A71-36285
- Solar cycle variation of planetary exospheric temperature from heat balance equation solution
19 p3131 A71-37334
- Earth atmosphere radiation fields analysis from Nimbus 3 five-channel scanning radiometer measurements, determining mean planetary albedo and temperature
20 p3259 A71-39679
- Jupiter disk temperature measurement at eight frequencies in 20.5-35.5 GHz range, comparing with saturated ammonia model calculations
22 p3599 A71-41922
- Enthalpy change between atmospheric carbon dioxide and Venus surface rocks for damping short term lower atmosphere temperature excursions
23 p3736 A71-43344
- Mars surface soil thermophysical properties, temperature and thermal emission from Mariner spacecraft IR radiometer data, correlating with visual images
24 p3867 A71-44439
- PLANETOCENTRIC COORDINATES**
NT GEOCENTRIC COORDINATES
Minor planet Icarus earth approach observations with reflector and TV camera, determining spherical coordinates by comparison with reference stars
14 p2309 A71-29993
- PLANETOLOGY**
Papers on surfaces and interiors of planets and satellites covering radio and radar observations, photometry, magnetic fields, etc
02 p0309 A71-12151
- Saturn rings physical properties concerning optical thickness, particle features, albedo and mass
02 p0310 A71-12158
- Planetary nebula NGC 7027 mapping at 11.1 cm, examining structure, ionized H mass and electron density
02 p0317 A71-12869
- Mercury microwave and IR observations interpreted for thermophysical models for planetary subsurface, discussing rotation and heating
03 p0492 A71-14069
- Planet Mars polar and equatorial radii optical measurements comparison with radar and Mariner probes occultations results, determining optical ellipticity
03 p0493 A71-14200
- Hot moon suggested from chemical and physical reasoning, discussing outer layers and surface features formation
04 p0645 A71-15138
- Soviet book on planets and moon covering surfaces, atmospheres, internal structure and observation methods
04 p0657 A71-15800
- Venus atmosphere and lithosphere thermochemical composition, examining various models
06 p0966 A71-17898
- Martian satellites nature and evolution, facts, theories, hypotheses and speculations
07 p1202 A71-20516
- Cassini second and third laws generalization to energy extremes, discussing Mercury shape
07 p1203 A71-20523
- Planetary rotation classical and radio measurement effects on physics of planetary interiors, discussing Jupiter rotation, terrestrial planets composition and earth and moon palaeorotation
07 p1203 A71-20524
- Inner and outer planets groups mass and mean density, considering terrestrial seismic data and lunar, Venus, Mars and Mercury structural models
08 p1358 A71-20888
- Planet density distributions, deriving successive approximations for equilibrium figure equations
08 p1365 A71-21775
- Selenodesy and planetary geodesy of moon, inner and outer planets, including sun-planet mass ratios
08 p1366 A71-21798
- Mercury drawings from refractor observations /1964-1967/ 09 p1520 A71-22834
- Venus motion, mass, dimensions, shape, topography and atmosphere
09 p1520 A71-22835
- Papers on geological problems in lunar and planetary research covering sensing techniques, phenomenology, exploration methods, etc
15 p2492 A71-32469
- Planetary exploration from space, recommending flights to moons of outer planets due to possible presence of atmospheres and water ice
15 p2494 A71-32495
- Planetological terminology for geological processes and features of earth, moon and planets
15 p2516 A71-32499
- Sulfur effervescing molten slag/gas systems causing planetary vulcanism, examining patterns on earth, moon and Mars
15 p2496 A71-32708
- Moon and planets - NATO Conference, University of Newcastle-upon-Tyne, England, April 1970
16 p2636 A71-33501
- Venus planetology missions, discussing objectives, experimental packages, payloads, costs and entry/lander configurations
17 p2802 A71-34717
- Book on space science covering celestial coordinates, time and mechanics, planetary atmospheres and interiors, comets, meteors, stellar structure, etc
18 p2963 A71-36246
- Impact craters crustal thickness and forms relationship to changing physical state of planetary surface during once-molten cooling
19 p3051 A71-37669
- Jupiter orbiter missions, considering satellite emphasis and planetary environment and planetology missions
19 p3140 A71-37923
- Soviet papers on terrestrial planets, discussing Mercury, Venus and Mars atmosphere, surface, internal structure and physical conditions
21 p3452 A71-40882
- Mercury visual, radar and radio data, describing rotation, temperature, surface properties, subsurface layers and atmospheric model
21 p3452 A71-40883
- Venus survey, discussing mass, radius, rotation, internal structure, magnetic field, radiation belts, surface properties, atmospheric composition, cloud layer, etc
21 p3452 A71-40884
- Mars mass, dimensions, configuration, internal structure, magnetic field, color evolution, surface properties, atmospheric parameters, etc
21 p3452 A71-40885
- Mars physicochemistry, discussing Wright effect /blue veil/, atmosphere, polar cap migration, Phobos acceleration and relief inversion darkening
23 p3736 A71-43360
- PLANETS**
NT EARTH [PLANET]
NT JUPITER [PLANET]
NT MARS [PLANET]
NT MERCURY [PLANET]
- NT NEPTUNE [PLANET]**
NT PLUTO [PLANET]
NT SATURN [PLANET]
NT URANUS [PLANET]
NT VENUS [PLANET]
- Solar activity cycles correlation with planets positions over ecliptic
01 p0149 A71-10053
- Planets and satellites diameter determination, reviewing double image technique
02 p0309 A71-12153
- Radar astronomy principles, applications and types of measurements, discussing solar, lunar, planetary and meteor observations
02 p0313 A71-12490
- Solar activity cycles correlation with planets positions over ecliptic
08 p1361 A71-21047
- Crab Nebula pulsar NP 0532, discussing possible planetary system existence
09 p1522 A71-22975
- Astronomical methods for determination of distances to planets, stars and galaxies, considering human distance perception
12 p1962 A71-26955
- Dark companions and extrasolar planetary system detection, discussing characteristic colorimetric signature method
13 p2134 A71-28291
- Bibliography on lunar and planetary subjects covering astrobology, comets, cratering, meteors temperature, structure, asteroids, tektites surface features, etc
13 p2135 A71-28293
- Outer planet large satellite steady state thermal models, indicating interiors at temperatures above ice-ammonia eutectic
14 p2318 A71-31125
- Water distribution in space, natural satellites and terrestrial planets, discussing Clarke abundance values and hydrochlorosphere concept
15 p2494 A71-32493
- Intra-Mercurial planets and comets discovered during solar eclipses, discussing size, orbital eccentricity, albedo and equilibrium temperature
16 p2642 A71-33830
- Ephemerides of sun, moon, planets and minor planets for October through December 1971
21 p3442 A71-40153
- Terrestrial, lunar and planetary dynamical properties and internal constitution, considering data obtained from artificial satellites, lunar and planetary dynamics
22 p3607 A71-4288
- NASA program for lunar and planetary exploration, listing missions, instrumentation, experiments and future aims
23 p3736 A71-43498
- PLANFORMS**
NT CARET WINGS
NT DELTA WINGS
NT INFINITE SPAN WINGS
NT RECTANGULAR PANELS
NT RECTANGULAR PLANFORMS
NT RECTANGULAR PLATES
NT RECTANGULAR WINGS
NT SWEPTBACK WINGS
NT VARIABLE SWEEP WINGS
NT WING PLANFORMS
- PLANIMETRY**
U AREA
U DIMENSIONAL MEASUREMENT
- PLANNING**
NT AIRPORT PLANNING
NT MISSION PLANNING
NT PRODUCTION PLANNING
NT PROJECT PLANNING
NT URBAN PLANNING
- PLANOTRONS**
NT CATHODE RAY TUBES
High efficiency and power long life cross field amplifier generator for solar energy conversion in space into microwave, discussing magnetron and amplitron
13 p2000 A71-28668
- Amplitron effects on phase distortion of pulse signals passing through power amplifier stages of coherent pulse communication systems
19 p3015 A71-37257
- PLANT ROOTS**
Hormone movement in geotropism, discussing supraoptimal auxin content and indoleacetic acid in wheat roots
21 p3340 A71-39981
- PLANTS [BOTANY]**
NT ALGAE
NT ANABAENA
NT AUTOTROPHS
NT BACILLUS
NT BACTERIA
NT BLUE GREEN ALGAE
NT CHLORELLA
NT ESCHERICHIA
NT FOLLAGE
NT FUNGI
NT GRASSES
NT HYDROGENOMONAS
NT KLEBSIELLA

NT LEAVES
 NT MICROCYSTIS
 NT NEUROSPORA
 NT PORPHYRA
 NT PSEUDOMONAS
 NT SPORES
 NT STAPHYLOCOCCUS
 NT STEAROTHERMOPHILUS
 NT STREPTOCOCCUS
 NT STREPTOMYCETES
 NT TOBACCO
 NT TREES [PLANTS]
 NT YEAST

Low compensation point species capacity for carbon dioxide fixation, suggesting reduced photorespiration role

02 p0201 A71-12475
 Botanical quarantine studies on Apollo 11 and 12 lunar soil samples effects on terrestrial plants, indicating absence of disease generating agents

04 p0539 A71-15393
 Horizontal clinostat rotation rate for optimal and acceptable weightlessness simulation in plants, comparing with wheat seedlings growth in Biosatellite 2

05 p0712 A71-16150
 Ecological interpretation of daytime data from Nimbus 3 high resolution IR radiometer for hydrologic and plant distribution mapping

08 p1277 A71-20884
 Circumlar space flight effects on spiderwort, dry seeds and onion bulbs germinating capacity, growth stimulation and chromosome rearrangements

08 p0527 A71-21025
 Activated charcoal effects moss development alterations on artificial agar substrate

11 p1721 A71-26319
 Optimization of time intervals of conveyor harvestings and harvested age of oxygen producing plants for life support system

13 p2017 A71-28406
 Circadian rhythm of leaves of Phaseolus angularis plants in controlled carbon dioxide and humidity environment

13 p2015 A71-29475
 Endogenous short period rhythms in rotational movements of unifoliate leaves of Phaseolus angularis Wight grown under controlled environmental conditions

13 p2015 A71-29476
 Hawaiian silversword seed germination and inhibition showing extraordinary heat sensitivity

16 p2527 A71-33049
 Biological experiments on plants, animals and bacteria aboard Zond 5, 6 and 7 space probes

20 p3187 A71-39134
 Circumlar space flight effects on spiderwort, dry seeds and onion bulbs germinating capacity, growth stimulation and chromosome rearrangements

20 p3193 A71-39605
 Plants and animals reactions to environment gravitational component, showing organisms perception of accelerating force

21 p3326 A71-39970
 Gravitational and other forces involved in equilibrium of growing plants, showing gravity sensing ability lower limit existence

21 p3339 A71-39971
 Circumnutations in plants under gravitational stimulation

21 p3339 A71-39973
 Geotropic stimulus in plants, describing method to test correlations between microscopically visible cell particles and geotropic bending direction

21 p3339 A71-39974
 Gravity receptors in lower plants including Phycomyces sporangiophores and Chara rhizoids

21 p3339 A71-39975
 Gravity receptors in Phycomyces sporangiophores, considering transient and long term geotropic responses

21 p3339 A71-39976
 Gravity susception by higher plants, proving starch statolith hypothesis

21 p3339 A71-39977
 Gravity susception by higher plants, analyzing geotonic data for georeception theories

21 p3340 A71-39978
 Arguments against statolith theory of gravitational perception in plants

21 p3340 A71-39979
 Auxin transport and geotropic response of roots and shoots, discussing plant growth mechanisms under stimulation-inhibition conditions

21 p3340 A71-39980
 Linkage mechanism between gravity perceptrors and auxin redistribution causing differential growth and geotropic curvatures in plants

21 p3340 A71-39983
 Geoelectric effects on plants geotropic reaction chain, discussing hormone auxin asymmetric distribution due to gravity

21 p3340 A71-39984
 Simultaneous measurement of transverse and longitudinal bioelectric potential differences in plants

without direct contact with tissues, using vibrating reed electrometer

21 p3375 A71-39985
 External indole-3-acetic acid effect on elongation and geotropic bending of Avena coleoptiles related to auxin induced electrical responses

21 p3340 A71-39986
 Gravity influence on plant growth, lateral development, apical dominance, bud initiation, orientation and flower morphology

21 p3340 A71-39999
 Geopinnastic bending of Fritillaria Meleagris axes as prototype of geoinduced plagiotropic growth

21 p3341 A71-40000
 Wheat seedling responses to chronic acceleration, considering total height, coleoptile diameter, root length, sensitivity to growth retardation and histological changes

21 p3341 A71-40001
 Plants behavioral reactions to continuous gravitational field directional reorientation by clinostat, discussing gravity compensation effects on tropism and forces required for geotropic response

21 p3341 A71-40004
 Gravity effects on auxin transport, growth and foliage spread of green plants for efficient radiation capture, using horizontal clinostat experiments

21 p3341 A71-40005
 Pinto beans circadian leaf movements in simulated weightless environment, relating rotational treatment time to rhythm phase

21 p3341 A71-40006
 Gravity responses and geotropic behavior at ontogenetic stages of higher green plants, noting tendril movement under mechanical stimulation

21 p3341 A71-40008
 Internal short chain alkane populations of paraffinic hydrocarbons in tobacco teratoma and habituated tissue cultures

21 p3345 A71-40204
 Hydroponic plant cultivation with keramzit substrate, investigating replacement time effect and regenerative power of nutrient solution

22 p3506 A71-42816

PLANTS [INDUSTRIES]

U INDUSTRIAL PLANTS

PLASMA ACCELERATION

Artificial solar wind production by plasma electrodynamic acceleration, investigating simulated earth-wind interaction

01 p0160 A71-11067
 Ion-neutral coupling in plasma acceleration revealed by velocity disparities determined spectroscopically [AIAA PAPER 70-166]

05 p0788 A71-16572
 Plasma jet two stage acceleration in coaxial systems, superposing additional discharge current

07 p1167 A71-19234
 Pulsed coaxial plasma accelerator, measuring longitudinal gas pressure distribution, particle emission and magnetic fields characteristics under various operating conditions

08 p1341 A71-21498
 Plasma jet two stage acceleration in coaxial systems, superposing additional discharge current

12 p1934 A71-26752
 Current distribution effect on stability of exploding and collapsing accelerated cylindrical plasma shell in axial and azimuthal magnetic field

12 p1935 A71-26765
 Equations system describing plasmoid acceleration process in coaxial injector with inductive energy storage

12 p1938 A71-27205
 Plasma acceleration in injector with inductive energy storage, discussing arc discharge circuit opening time effect

13 p2108 A71-28856
 Electric circuits calculation in MHD problems such as MHD channel flow, electrodynamic plasma, etc

14 p2277 A71-29558
 Pulsed coaxial plasma accelerator, measuring longitudinal gas pressure distribution, particle emission and magnetic fields characteristics under various operating conditions

16 p2618 A71-33046
 Plasma jet formation within high pressure discharges in air at atmospheric pressure, discussing electrode configuration, current density and accelerating magnetic field strength

17 p2787 A71-34285
 Coaxial electrodynamic plasma acceleration, investigating triple electron and ion recombinations effects

19 p3108 A71-37129
 Solar wind acceleration due to Alfvén wave pressure gradient, taking into account coronal parameters of temperature, magnetic field and energy density

19 p3128 A71-38162
 Equations system describing plasmoid acceleration process in coaxial injector with inductive energy storage

19 p3117 A71-38617

Plasma acceleration in inductive energy storage inductor, discussing arc discharge circuit opening time effect

21 p3426 A71-41291
 Plasma acceleration of low pressure toroidal gas discharge, measuring plasma velocity as function of radial magnetic field for different pressures

23 p3711 A71-43874

PLASMA ACCELERATORS

NT COAXIAL PLASMA ACCELERATORS

Dielectrics erosion under pulsed electric discharge in conical plasma accelerator, varying capacitance and inductance for evaporated mass relation to current strength

04 p0631 A71-14597
 Plasma accelerator self ionizing current free stable radiative shock wave structure in hydrogen, using time resolved spectroscopic measurements

04 p0548 A71-14696
 Book on ion propulsion covering technology, performance, accelerator design, propellant feed and control, etc

04 p0638 A71-14797
 Plasmoid mass and velocity distribution in pulsed plasma accelerators, using mass spectrometers and platinum thermal probe

04 p0634 A71-15111
 Electrodynamical plasma accelerator with single phase salient pole magnetoelectric generator and storage condenser, giving component characteristics and transient processes equations systems

04 p0535 A71-15812
 Quasi-steady coaxial MPD arcs characteristics, studying Ar ion velocities, electrostatic ion acceleration mechanism and arc voltage gradient

05 p0795 A71-16573
 Ionizational and electron thermal nonequilibrium effects in insulator boundary layer of potassium-seeded nitrogen MHD accelerator

06 p0939 A71-18581
 Parallel plate plasma accelerator energy deposition, considering kinetic and thermal modes based on flow velocity, temperature and Mach number measurements

06 p0939 A71-18635
 Quasi-steady MPD accelerators current conduction and power loss mechanism investigation through local anode fall voltage and current density measurements at different arc current levels

06 p0939 A71-18636
 Conical metal core electrode erosion rates in pulsed plasma accelerators with refractory dielectric chamber

08 p1340 A71-21484
 Pulsed plasma accelerator energy balance determination by spectroscopic measurement

09 p1498 A71-22100
 MHD accelerator in pulsed mode with crossed fields, studying one dimensional steady inviscid flow

09 p1501 A71-22407
 Aerodynamic probe measurements for plasma jets produced by electrothermal and Hall current accelerators

11 p1764 A71-26275
 Restricted set of correlated measurements with inductive theta pinch in MHD plasma accelerators, determining electromagnetic field structure and electron density distribution

11 p1766 A71-26288
 High velocity plasma jet accelerator operation, plotting heat and electromagnetic forces vs air current, mass flow rate and nozzle diameter

11 p1807 A71-26289
 Plasma accelerator central electrode erosion and heat flux, describing measurement techniques and results

14 p2280 A71-30266
 Two lens high current plasma accelerator with closed electron drift, using crossed electric and magnetic fields

14 p2282 A71-30664
 Conical metal core electrode erosion rates in pulsed plasma accelerators with refractory dielectric chamber

14 p2282 A71-30671
 Inductive impulsive plasma accelerator current sheet electron density determination by electron probe and laser light scattering

15 p2455 A71-31545
 Electrodeless AC plasma accelerator /traveling wave pump/ using coil assembly to produce variable phase velocity and eliminate end effects

15 p2457 A71-32102
 Steady and unsteady modes of electric arc combustion in Ar and Ar-Cs flows produced by plasma accelerator in closed glass contour

15 p2457 A71-32269
 Energy transfer to MPD quasi-steady accelerator having electrolytic capacitors with large series resistance, integrating transmission line equations with Runge-Kutta method

17 p2794 A71-35539
 Ribbed surface electrode effects in plasma accelerator producing high speed monoenergetic blobs

19 p3108 A71-37091

- Traveling wave plasma accelerator, discussing use for spacecraft propulsion 19 p3122 A71-37321
- Pulsed erosion accelerators plasmoid discontinuities in structure streak photographs for various electrode configurations and pressures 19 p3116 A71-38253
- PLASMA ARC SPRAYING**
U PLASMA SPRAYING
PLASMA ARC WELDING
 High speed light gage Al welding, discussing plasma arc system 01 p0087 A71-10454
- Superalloy turbine engine guide vane thermal fatigue cracks repair by plasma arc fusion method 03 p0432 A71-13257
- Plasma arc welding of jet engine components of Ti and Ni alloys, comparing to gas tungsten arc and electron beam processes 08 p1299 A71-21684
- PLASMA ARCS**
U PLASMA JETS
PLASMA CHEMISTRY
 Physical chemistry of arc plasma, considering radial distribution, spectral density and energy relations for spectrochemical applications 03 p0465 A71-13973
- Space research goals emphasizing solar system formation, and plasma physics and chemistry 14 p2310 A71-30197
- Plasma chemistry, discussing low and high temperature plasmas, nuclear fusion reactions and chemical molecular and nuclear synthesis 16 p2539 A71-32963
- Nonequilibrium plasma chemical reaction kinetics problems, discussing time dependence, dissociation and recombination theories in pulsed EM field, equations and numerical calculations 16 p2539 A71-32965
- Plasma jet chemical reactions, discussing temperature and quenching effects, molecular and gas decomposition and endothermic compounds formation 16 p2540 A71-32967
- Low temperature plasma chemical processes, investigating molecular and atomic ionization, reactions under equilibrium and nonequilibrium conditions and specific energy production 16 p2540 A71-32968
- PLASMA CLOUDS**
 Cross field instability effect on weakly ionized plasmas with ionization density gradients under crossed electric and magnetic fields, using linear analysis 08 p1339 A71-21207
- Electric field, neutral wind velocities and ion collision frequency from artificial ionic clouds motion and deformation in ionospheric E and F regions 10 p1602 A71-24549
- Magnetic field aligned currents during 18 March 1969 substorms, observing electric field by Ba plasma cloud motion for magnetic perturbation field 10 p1677 A71-24789
- Barium ion cloud experiments for ionospheric vapor release determination from Rubis Rocket trajectory visible markings 11 p1755 A71-25643
- Electron scattering effects on spectral emission at optical and X ray wavelengths for homogeneous spherical ionized hydrogen plasma cloud, discussing radiation transfer 14 p2297 A71-29592
- Massive rotating plasma cloud contraction with magnetic field perpendicular to rotation axis, causing magneto-rotational explosions 14 p2312 A71-30386
- Magnetospheric plasma clouds equatorial observation by ATS 5 satellite, revealing plasma injection during substorms and dispersion by earth magnetic and electric fields 15 p2397 A71-31755
- Homogeneous spherical hot hydrogen plasma cloud at various temperatures and optical depths, presenting electron scattering effects on optical and X ray spectral emission 18 p2951 A71-36012
- Dissipative plasma instability in lower E region investigation by alkali plasma clouds injection, observing irregular echo behavior by coherent pulse Doppler radar 19 p3110 A71-37365
- One dimensional ambipolar diffusion parallel to magnetic field lines, considering plasma cloud imbedded in weakly ionized gas with homogeneous field 20 p3215 A71-38737
- PLASMA COMPOSITION**
 Structure and propagation of large amplitude modulated isolated compression waves in cold three component plasma with negatively charged ions 01 p0132 A71-10676
- Solar wind ion abundances from satellite observation, discussing energy spectra, particle distributions, etc 01 p0147 A71-11518
- Solar wind ion energy per charge spectra, comparing to Vela 3A observations for composition 01 p0148 A71-11519
- Solar wind plasma composition and dynamics, discussing element and ion abundances, solar activity effects, plasma stability, etc 02 p0300 A71-12374
- Collisional effects on Taylor and Kelvin instabilities in composite medium, considering longitudinal wave propagation mode 05 p0788 A71-16627
- Photoresonant cesium plasma ionization, discussing pumping spectra, electron gas, molecular-atomic ion ratio and dynamics 06 p0936 A71-17591
- Snowplow theory modification for plasma temperature, ion population and release time prediction, noting agreement with plasma rail gun data 07 p1165 A71-18879
- Carbon dioxide dissociation plasma composition as function of gas mixture, flow rate, pressure and discharge current in sealed and flow-through laser systems 07 p1122 A71-19134
- Structure and propagation of large amplitude modulated isolated compression waves in cold three component plasma with negatively charged ions 07 p1170 A71-20138
- Nonequilibrium population formation in dense plasma of complex composition under ionization resonance conditions 07 p1174 A71-20538
- Homogeneous equilibrium low temperature dense helium plasma ionization composition and radiative energy losses, calculating ionization potential 09 p1501 A71-22380
- Italian book on mixed plasmas equilibrium compositions and thermodynamic properties, covering numerical values tabulation for nitrogen mixtures with He, Ar and Xe 09 p1505 A71-23353
- Hypervelocity impact produced metallic plasmas equilibrium composition and radiation, calculating radiative energy as function of wavelength and internal partition functions 11 p1804 A71-25510
- Equilibrium compositions and thermodynamic properties tabulated for argon-oxygen plasmas at 0.01 to 10 atm and up to 35,000 K 12 p1986 A71-27187
- Ionospheric anisotropic plasma with mixture of different ions, deriving refractivity at whistler frequencies 13 p2058 A71-28027
- Ion charge composition in plasma-electron beam system in strong longitudinal magnetic field, noting multiply charged ions production under high temperature conditions 19 p3109 A71-37132
- PLASMA CONDUCTIVITY**
 Electric current carrying plasma with finite and anisotropic conductivity in longitudinal magnetic field, determining equilibrium and stability 01 p0132 A71-10173
- Slowly varying plane flows of highly conducting inviscid quasi-neutral gas plasma in channel with solid metallic walls as electrodes 01 p0133 A71-10790
- Shock tube generated Ar plasma electric conductivity augmentation by electrical discharge through supersonic plasma flow in Faraday tube 01 p0134 A71-10998
- Two dimensional inhomogeneities effects on electrical resistance of plasma with nonuniform density in strong magnetic field 01 p0135 A71-11065
- Quark regions in massive stars internal structure, discussing plasma superconductivity and spectral line emission 01 p0160 A71-11112
- Longitudinal electrical and thermal conductivities of fully ionized plasma in strong external magnetic field 01 p0136 A71-11473
- Multicomponent plasma electrical and thermal conductivities from quantum mechanical scattering cross sections 02 p0289 A71-12176
- High voltage solar cell array operation for satellite in ionosphere, discussing plasma leakage current minimization by electrical insulation 05 p0703 A71-16094
- Incompressible inviscid perfectly conducting cylindrical plasma stability against azimuthal disturbance in monotonic decreasing magnetic field with constant pitch, using energy principle 05 p0787 A71-16478
- Partially ionized Hg plasma electrical conductivity at various pressures and temperatures 05 p0790 A71-16787
- Plasma confinement in Tokamak, calculating particle and heat fluxes due to conductivity current and electric field 06 p0930 A71-17405
- Nonequilibrium plasma HF conductivity, introducing dressed ion expression in terms of dielectric permittivity 07 p1165 A71-18743
- Magnetospheric Debye radius, critical electric field voltage and normal and anomalous conductivities from low energy plasma concentration and temperature measurements 07 p1098 A71-19377
- Current carrying plasma in toroidal trap, studying instability and equilibrium due to captured and escaping particles 08 p1339 A71-21476
- Pulsed discharge path in He at 100 atm and air at atmospheric pressures, determining electrical conductivity dependence on discharge time by high speed photography 08 p1341 A71-21497
- Conductivity measurement of hot ion hydrogen plasma for runaway electric field, comparing Spitzer and Buneman formulas 09 p1502 A71-22860
- Weakly turbulent plasmas static electric conductivity derivation from kinetic equation for linear response to one-particle distribution function 09 p1503 A71-22861
- Electron collision frequency energy dependence influence on electrical conductivity of weakly ionized plasmas, considering Taylor series expansion around probable plasma electron velocity 10 p1623 A71-23875
- Helical motions with vorticity-velocity and conduction current-free force magnetic vectors parallelisms 11 p1804 A71-25177
- Electron hole n-p plasma conductivity in cylindrical germanium specimens as function of current produced azimuthal magnetic field 12 p1936 A71-27036
- Wide range nonimmersive RF coil with marginal oscillator for plasma electrical conductivity measurements tested for simulated reentry vehicle 12 p1908 A71-27285
- Acoustic instability of plasma with current under ionizational equilibrium and moderate neutral gas pressures 13 p2105 A71-27878
- Hydrodynamic instabilities of MHD plasma with current, using two fluid model in crossed magnetic-electric fields 13 p2105 A71-27879
- Electrode nonlinear current distribution in plasma with anisotropic conductivity, noting Hall parameter effect on electric field structure 13 p2107 A71-28566
- Conductivity tensor of turbulent plasma from coherent response to external test wave, introducing effective collision frequencies 13 p2109 A71-29244
- Equilibrium of current carrying plasma in toroidal system, studying instabilities due to trapped and slowly drifting particles 14 p2282 A71-30662
- Multicomponent plasma electrical and thermal conductivities from Debye potential quantum mechanical scattering cross sections 15 p2454 A71-31485
- Nitrogen plasma electrical and thermal conductivities and radiative source strength at atmospheric pressure and 9,000-12,500 K, using Hall probe and optical methods 15 p2454 A71-31535
- [AIAA PAPER 71-590]
 Coaxial type MHD generator with steady magnetic field and plasma consisting of inert gases and ionizable alkali metal additives, obtaining electrical conductivity 15 p2355 A71-32268
- Conductivity measurement of shock generated nitrogen plasma in transverse magnetic field, considering vibrationally excited molecules role in electron collision frequency 16 p2616 A71-32899
- Partially ionized Hg plasma electrical conductivity at various pressures and temperatures 16 p2618 A71-33039
- Plasma conductivity frequencies, including electromagnetic wave propagation in alternating field and scattered light intensities 17 p2786 A71-34276
- Intense pulsed electron beam formation during current flow through plasma 17 p2786 A71-34279
- Bulk semiconductor microwave control components, considering dielectric and conductive properties of plasma state 18 p2894 A71-36980
- Polooidal Hall current calculation in hydrodynamic approximation for stationary weakly interacting and conducting cylindrical plasma flow with uniform transverse flow parameter distribution 19 p3109 A71-37138
- Magnetospheric Debye radius, critical electric field voltage and normal and anomalous conductivities from low energy plasma concentration and temperature measurements 19 p3052 A71-37802

Magnetosphere neutral layer plasma conductivity determination from model of linear magnetic dipole in conducting fluid flow

20 p3216 A71-39138

Electron gas in constant crossed E and H fields, deriving nonlinear conductivity theory

21 p3424 A71-41260

Spectra and correlation functions for ion sound turbulence, calculating anomalous resistivity for plasma in external electric field

22 p3579 A71-41582

Transverse current conduction through MHD generator seeded hot plasma flow, showing Joule heating dominance in cathode boundary layer due to thermal instability

22 p3584 A71-42596

Plasma conductivity dependence on electron velocity distribution function in distorted Maxwellian form

23 p3709 A71-43259

German monograph on experimental determination of noble gas plasma conductivity under normal pressure in high temperature range, covering measurements under electric arc conditions

23 p3711 A71-43475

Dense low temperature Ar and Hg plasmas, observing correlation between electrical conductivity and optical emission

23 p3712 A71-43914

Ar-K and He-R plasma conductivity measurement at atmospheric pressure from equilibrium to nonequilibrium conditions, using electrostatic probes

23 p3714 A71-44275

Ohmic discharge plasma resistance, temperature and oscillations in weak electric fields under electron beam excitation in Sirius stellarator

24 p3854 A71-44518

PLASMA CONFINEMENT

U PLASMA CONTROL

PLASMA CONTROL

Thermal insulation and confinement of resistance heated He plasma in Uranus stellarator with large shear

01 p0132 A71-10678

Q switched laser irradiated solid lithium hydride particle plasma formation and heating, determining optimal conditions

01 p0096 A71-11482

Magnetic field confinement of ionized plasmas generated by laser-irradiated lithium hydride solid particle

01 p0137 A71-11483

Surface oscillations energy and attenuation in damped spectral region of semibounded degenerate electron plasma

02 p0288 A71-11630

Stability of finite pressure plasma trapped by magnetic field, discussing trapped particle effects

03 p0463 A71-13296

Plasma confinement in Tokamak, calculating particle and heat fluxes due to conductivity current and electric field

06 p0930 A71-17405

Feedback and dynamic control of plasmas - Conference, Princeton, June 1970, Volume 1

06 p0931 A71-17451

Plasma stabilization, considering feedback loop system with Maxwell-Vlasov equations

06 p0931 A71-17452

Plasma confinement in specified bounded spatial domain by feedback control localized to outer shell

06 p0931 A71-17453

Plasma stability criterion for feedback systems limitations, noting geometrical and electronic effects on phase and amplitude

06 p0931 A71-17454

Plasma feedback system boundary conditions, describing electrical properties, dispersion relation and mode interaction

06 p0931 A71-17455

Plasma stabilization, discussing external feedback system model

06 p0931 A71-17456

Fusion reactor plasma feedback stabilization by nonlinear interaction of two carbon dioxide IR laser beams to produce difference frequency near hybrid resonance

06 p0931 A71-17457

MHD continua z-theta pinch stabilization, discussing analytical models for determining feedback spatial and temporal resolution

06 p0931 A71-17458

Plasma stabilization by nonlinear bang-bang feedback

06 p0932 A71-17459

Videotype sampling in electromechanical equilibria feedback stabilization of hydromagnetically contained plasmas

06 p0932 A71-17460

Cylindrical plasma Kruskal-Shafranov modes, examining active feedback stabilization

06 p0932 A71-17461

Tokamak copper shell as feedback control device for toroidal plasma, considering stabilization of thermal instability

06 p0932 A71-17462

High-beta sharp-boundaried stellarator plasma column feedback stabilization with helical fields

06 p0932 A71-17463

Drift type plasma instabilities, discussing feedback stabilization and remote sensing

06 p0932 A71-17465

Plasma LF instabilities, observing temporal growth and effect on confinement by switching feedback control off

06 p0932 A71-17466

Q-machine with boundary segments to provide passive feedback for reducing Kelvin-Helmholtz instability and plasma losses

06 p0933 A71-17467

Plasma transverse Kelvin-Helmholtz instability, describing stabilization by feedback controlled electron sink

06 p0933 A71-17468

Electron-hole plasmas feedback stabilization, considering instability coefficients measurement

06 p0933 A71-17470

Dynamic plasma stabilization, discussing closed and open loop approaches

06 p0933 A71-17472

Magnetically confined plasma dynamic stabilization, using HF potential

06 p0933 A71-17473

Inhomogeneous collisionless low beta plasma drift wave instability dynamic stabilization, considering AC electric field parallel to confining field

06 p0933 A71-17474

Dynamic stabilization of drift dissipative instability by inhomogeneous RF electric field parallel to magnetic field

06 p0934 A71-17475

HF stabilization of plasma instabilities, noting electrostatic instability suppression by ordinary and helicon type waves

06 p0934 A71-17476

Electron-ion collision effects on parametric instability growth rate in plasma dynamic stabilization

06 p0934 A71-17477

Dynamic stabilization of high-beta plasmas with sharp boundary, illustrating model effect on stability by numerical calculation

06 p0934 A71-17478

MHD dynamic stabilization, deriving stability conditions from periodic solutions of time dependent equations in Eulerian form

06 p0934 A71-17479

Dynamic stabilization of instability in bumpy theta pinch by generalization of energy principle

06 p0934 A71-17480

Dynamic stabilization of two stream ion instability in collisionless plasma

06 p0934 A71-17483

Longitudinal electron oscillation suppression by beam density modulation in axially and transversely finite beam-plasma system

06 p0934 A71-17484

Hot electron plasma confinement in cusped magnetic field, considering production in electron cyclotron resonance region by pulsed microwaves

06 p0935 A71-17491

Low pressure toroidal plasma confinement with flow in axially symmetric configurations, using numerical model

06 p0935 A71-17554

Confinement and loss mechanisms of ohmically heated plasma in stellarator

06 p0937 A71-18351

Steady state current-free magnetized plasma generation by microwave discharge, using feedback control to reduce power fluctuations

06 p0938 A71-18458

Magnetically confined laser produced plasma radial oscillations, deriving equation of motion for expanding boundary

[ALAA PAPER 71-108]

06 p0938 A71-18558

Transverse velocity shear effects on low-beta resistive plasma LF stability in uniform magnetic field

07 p1166 A71-18882

Plasma containment in adiabatic magnetic traps, discussing particles, Coulomb collisions, instabilities, cyclotron resonance masers, Van Allen belts, etc

07 p1166 A71-19097

Low temperature confined cesium plasma, observing ion-acoustic oscillation excitation effects on transfer process and ionization

07 p1167 A71-19236

Plasma heated by cyclotron resonance using waveguide method, considering properties, confinement conditions and instabilities

07 p1170 A71-20182

Plasma instabilities and mode stabilization, discussing density-gradient-driven drift waves in collision-dominated regime

07 p1173 A71-20510

Plasma HF heating boundaries by magnetic traps, noting diamagnetic effects due to ion and electron heating

08 p1339 A71-21480

HF wave absorption in Ar plasma, observing production in open magnetic trap

08 p1339 A71-21481

Plasma ions lifetime and energy spectra in quadrupole magnetic trap as function of energy and time

08 p1340 A71-21483

Ionization instabilities feedback suppression in magnetized nonisothermal plasma

08 p1342 A71-21932

Radiative instability of nonequilibrium plasmas in magnetic traps, considering circularly polarized oscillations propagating along magnetic field

09 p1500 A71-22241

Confined plasma drift instability universal eigenmode stabilization by magnetic field shear

09 p1500 A71-22246

Stability of finite pressure plasma trapped by magnetic field, discussing trapped particle effects

09 p1504 A71-23269

Plasma confinement in Heliotron magnetic field discussing equilibrium and stability problems

09 p1505 A71-23442

Magnetic mirror confined microwave heated plasmas stability based on uniform collisionless plasma model

10 p1651 A71-24632

Plasma feedback stabilization, investigating flute instabilities

10 p1651 A71-24633

Magnetoacoustic wave propagation in magnetic plasma traps by geometrical optics methods, considering annular traps existence

10 p1651 A71-24638

Magnetic mirror confined plasma diagnostics, considering hot electron density, X ray pulse height and synchrotron radiation measurement techniques

10 p1651 A71-24651

Bounce effects in negative mass instability of plasma in short mirror magnetic bottle with ion cyclotron frequency dispersion

10 p1652 A71-24652

Perturbed magnetic surfaces topology in quadrupole, estimating local imperfections size for plasma control

10 p1652 A71-24661

Low temperature confined Cs plasma, observing ion-acoustic oscillation excitation effects on transfer process and ionization

12 p1935 A71-26754

Stability and oscillation of zero-beta magnetically confined plasmas, applying to multipole configuration

12 p1935 A71-26917

Bounded low pressure plasma oscillation frequency dependence on discharge chamber length, constant/variable potentials longitudinal profiles and density distribution

12 p1936 A71-27037

Cross field magnetic discharge stabilization of plasma column in flowing CW electrically initiated chemical laser

12 p1940 A71-27278

Plasma ion waves external control with HF fields in subthreshold regime

13 p2104 A71-27845

Paired comparison tests of relative signal detected by capacitive and floating Langmuir probes in steady state turbulent plasma confined in magnetic mirror geometry

13 p2066 A71-28155

Optimal thermonuclear plasma confinement considering external electromagnetic field as control variable, based on Boltzmann-Vlasov model

13 p2107 A71-28832

Wave propagation near upper hybrid frequency in mirror-confined hot electron unstable plasma

13 p2109 A71-29242

Plasma ion-sound instability feedback stabilization with remote modulated source at electron cyclotron resonance frequency

13 p2109 A71-29245

Thermal load capacity and nozzle shape for guiding and constricting high current plasmas from electric arc data, using Ar as discharge gas

14 p2279 A71-29851

Afterglow plasma drift-dissipative instability stabilization by RF magnetic and electric fields

14 p2280 A71-30504

Ion-acoustic oscillations excitation in rarefied plasma layers confined by external high frequency TE wave electromagnetic field

14 p2281 A71-30555

Theorem proving impossibility of stabilizing unstable MHD configuration with nondissipative plasma in vacuum surrounded by superconducting wall by means of finite electrical conductivity wall

14 p2282 A71-30557

Equilibrium of current carrying plasma in toroidal system, studying instabilities due to trapped and slowly drifting particles

14 p2282 A71-30662

- Hydrogen plasma HF heating boundaries by magnetic traps, noting diamagnetic effects due to ion and electron heating
14 p2282 A71-30667
- Limiting frequency for Ar plasma absorption of HF waves, observing plasma production in open magnetic mirror configuration
14 p2282 A71-30668
- Plasma ions lifetime and energy spectra in quadrupole magnetic trap as function of energy and time
14 p2282 A71-30670
- Coronal flare onset, examining dynamic processes of plasma compression with longitudinal magnetic field
15 p2482 A71-31335
- Magnetic cut-off system reducing length of high density jet flows from plasma guns, using axially asymmetric field configurations
15 p2455 A71-31644
- Economical fusion reactor requirements, considering ultrahigh temperature plasma containment for nuclei reaction and energy extraction
15 p2455 A71-31681
- Magnetoelectrostatic containment ion thruster, considering adaptation for Hg operation based on discharge chamber loss comparison with Cs [AIAA PAPER 71-692]
15 p2470 A71-32288
- Feedback stabilization of linear distributive systems in form of second-order evolutionary equation in Hilbert space, applying to plasma stabilization
16 p2618 A71-33006
- Ohmically heated collision plasma confinement in Uranian racetrack stellarator with large shear, describing magnetic field topography effects and plasma lifetime
17 p2785 A71-34196
- Equilibrium state linear theta pinch plasma confinement dependence on magnetic force lines curvature radius
17 p2786 A71-34278
- Moving plasma beam capture by transverse magnetic field due to polarization space charges electrostatic separation
17 p2786 A71-34280
- Magnetic properties of contained plasma, discussing equilibrium equations and pressure profiles
17 p2788 A71-35025
- Ionization instabilities suppression in magnetized nonisothermal plasma by feedback control
17 p2789 A71-35276
- Mirror-contained collisional plasmas, deriving wave reflection and absorption from equilibrium density and temperature profile equations
18 p2950 A71-35860
- Numerical analysis of plasma expansion confined by magnetic field, emphasizing boundary oscillation and temperature rise, based on hyperbolic and parabolic system equations
18 p2952 A71-36308
- Swept Langmuir probe with sweep speeds greater than 150 V/microsec, considering electron cyclotron resonance heated hydrogen plasma confined in toroidal quadrupole
18 p2952 A71-36582
- Weakly ionized gas plasma confined by cylindrical electrodes and dielectric fronts, calculating rotational movement behavior in transverse electric and longitudinal magnetic fields
18 p2952 A71-36943
- Plasma confinement in injector-diverter system of stellarator, measuring radial density distribution
19 p3109 A71-37131
- Plasma guns hot and cold plasma separation, describing diverter operation principles
19 p3112 A71-37639
- Finite-beta stabilization of collisionless trapped particle mode in toroidal plasma confinement devices, using magnetic well dug by plasma diamagnetism
19 p3112 A71-37742
- Gas concentration, field frequency and applied power level for control over electron temperature and emission spectra in microwave gas discharge plasma
19 p3113 A71-37764
- Tokamak T-3A device plasma electron temperature measurements, using Thomson scattering with electric, microwave, laser and diamagnetic data
19 p3113 A71-37854
- Electron beam for determining plasma potential and charge density as function of radius of inertially confined tenuous plasma cylinder
20 p3273 A71-39009
- High current pulsed electron beams formation in bounded plasma due to changes in current, ohmic resistance and potential difference in electrode gap
20 p3274 A71-39159
- Confined plasma diffusion toward current-carrying inner conductors and outer walls in multipoles
21 p3423 A71-40767
- Radiative instability of nonequilibrium plasmas in magnetic traps, considering circularly polarized oscillations propagating along magnetic field
21 p3424 A71-41130
- Confined plasma drift instability universal eigenmode stabilization by magnetic field shear
21 p3424 A71-41135
- Surface waves at Fermi electron plasma boundary, using kinetic theory of plasma electromagnetic oscillations
21 p3425 A71-41278
- Electron beam heating of cold plasma in magnetic trap as function of plasma density, showing two stream instability due to Cerenkov effect
21 p3425 A71-41285
- Short wavelength instabilities in collision dominated plasma confinement by rotating magnetic field, interpreting in terms of equivalent negative resistance
22 p3579 A71-41579
- Plasma confinement in bounded systems, considering externally induced field HF pressure effect on plasma density distribution
22 p3580 A71-41600
- Electrostatic mode wave equations for low beta plasma microinstabilities in axisymmetric magnetic mirror machines, including effects of particle cyclotron, bouncing and drift motions
22 p3582 A71-41902
- Electron distributions in afterglow of hot electron mirror contained plasma as function of time, using bremsstrahlung spectra measurement
22 p3582 A71-41903
- Coronal flare onset, examining dynamic processes of plasma compression with longitudinal magnetic field
22 p3606 A71-42610
- F layer perturbations by intense vertically upward radio waves for aeronomy and plasma control studies
23 p3671 A71-43543
- Stationary stable cellular pattern onset relationship to plasma confinement in single ended Q machine
23 p3713 A71-44153
- Off-resonance electron heating by microwaves in mirror contained high beta plasmas
24 p3852 A71-44486
- Magnetosonic wave excitation and electron heating in magnetically confined hydrogen plasma hybrid resonance region
24 p3853 A71-44502
- PLASMA CYLINDERS**
- Axisymmetric bulge region formed in long uniform plasma column by reduction of external magnetic field
01 p0134 A71-11004
- Trapped LF ion wave propagation along warm plasma cylinder imbedded in dielectric, obtaining dispersion relation
01 p0136 A71-11476
- Argon plasma column inductive discharge parameters at atmospheric pressure from radial temperature distribution measurements
02 p0290 A71-12181
- Ignited mode theory applied to wide-spaced thermionic diodes, verifying LTE plasma column development
02 p0291 A71-12233
- Resonance excitation of high amplitude waves in plasma cylinder by HF azimuthal axially periodic current flowing through coil encircling plasma
02 p0291 A71-12504
- Incompressible inviscid perfectly conducting cylindrical plasma stability against azimuthal disturbance in monotonic decreasing magnetic field with constant pitch, using energy principle
05 p0787 A71-16478
- Cylindrical plasma Kruskal-Shafranov modes, examining active feedback stabilization
06 p0932 A71-17461
- High-beta sharp-boundaried stellarator plasma column feedback stabilization with helical fields
06 p0932 A71-17463
- Multimode ionization wave growth and saturation in finite length positive plasma column of gas discharge, investigating feedback and external driving signal effects
06 p0933 A71-17469
- Plasma stabilization in screw pinch, using combined inertial forces and dynamic shear in diffuse column
06 p0935 A71-17487
- Dynamic stabilization of MHD instabilities in high beta plasma column, using superposed fluids parametric resonance model
06 p0935 A71-17488
- Plasmasphere total columnar electron content up to plasmopause, describing various measurement methods
07 p1096 A71-19006
- Columnar electron content measurements by geostationary satellites, discussing research in developing countries for cost reduction
07 p1096 A71-19007
- Sawtooth structure of convective plasma column in sulfur hexafluoride at cross flow Mach numbers, using thermionic rail accelerator
09 p1498 A71-22096
- Trapezoidal and Killian distributions profile parameters at S band in plasma column, noting electron density
09 p1501 A71-22306
- LF electrostatic waves axisymmetric and nonaxisymmetric propagation modes in weakly ionized plasma column under weak magnetic field
09 p1504 A71-23051
- Heated mirrors and hot plasma column effects on diffraction losses and power output of gas lasers
10 p1623 A71-25093
- Current distribution effect on stability of exploding and collapsing accelerated cylindrical plasma shell in axial and azimuthal magnetic field
12 p1935 A71-26765
- Electron electrostatic or space charge oscillations in nonneutral plasma columns with cylindrical symmetry around axial magnetic field
13 p2104 A71-27848
- Self- and mutual admittances for axial rectangular slots in inhomogeneous cylindrical plasma layer, giving coupled radial transmission line model for propagation
13 p2105 A71-28002
- Electromagnetic radiation from stationary electric dipole imbedded in plasma column moving in axial direction
13 p2110 A71-29389
- Infinite radially nonuniform thin plasma cylinder wave scattering with electrical field component along inhomogeneity gradient
14 p2191 A71-29512
- TM, TE and combination cavity modes choice for plasma column electron density distribution determination by perturbation methods
14 p2279 A71-29859
- Electron beam instability in cylindrical magnetically confined plasma column, calculating quasi-static oscillations spatial growth increments
14 p2279 A71-30090
- Thermalization and diffusion of electron cloud injected into afterglow cylindrical plasma, calculating steady state distribution as function of position and velocity
14 p2280 A71-30175
- RF power absorption of uniform hot ion-electron plasma column, considering collision effects and EM radiation
14 p2281 A71-30556
- Dynamic stabilization of plasma column drift dissipative instability by inhomogeneous RF electric field, using two fluid macroscopic equations
14 p2196 A71-30560
- Argon plasma column inductive discharge parameters at atmospheric pressure from radial temperature distribution measurements
15 p2454 A71-31489
- Electromagnetic wave energy absorption in inhomogeneous cold magnetoactive plasma cylindrical columns
15 p2455 A71-31735
- Refraction and absorption length of coherent laser radiation propagating in high temperature cylindrical plasma column
15 p2458 A71-32390
- Electromagnetic wave propagation along homogeneous and inhomogeneous plasma columns, establishing density distribution functions and dispersion curves
15 p2459 A71-32641
- Geomagnetic tail natural oscillations, applying model of plasma cylinder with free boundary immersed in interplanetary medium
16 p2564 A71-33673
- Wavelike ionospheric undulations of total columnar electron content and of true height of bottomside plasma frequencies before and during solar eclipse of 7 March 1970
16 p2565 A71-33738
- Cylindrical nonuniform plasma with radial temperature and emitter density gradients, analyzing molecular rotational levels intensity distribution and Doppler widths
17 p2787 A71-34587
- Two-stream instability for magnetically confined pure electron gas column resulting from surface wave interaction
18 p2950 A71-35864
- Electron wave coupling in plasma column, determining exact resonance and field configurations of frequencies
19 p3111 A71-37635
- Thermal motion effects on space charge waves propagation along plasma columns in weak magnetic field, comparing measured wavelength/frequency relationship with theoretical prediction
20 p3273 A71-38879
- Electron beam for determining plasma potential and charge density as function of radius of inertially confined tenuous plasma cylinder
20 p3273 A71-39009
- Striated discharge column behavior in nitrogen with moving and stationary striations
20 p3273 A71-39046
- Plasma layer effect on natural oscillations of magnetosphere tail, using infinite plasma cylinder model immersed in interplanetary plasma
20 p3216 A71-39137
- Cylindrical plasma column light scattering diagnostics by focusing carbon diode laser beam on center
22 p3580 A71-41601

Homogeneous positive plasma column perturbation analysis in axial magnetic field, deriving model for ionization waves dispersion characteristics
22 p3582 A71-41898

Absorption cross section for plane electromagnetic wave in circular plasma cylinder in constant magnetic field, assuming small Larmor radius
23 p3714 A71-44328

Lower hybrid frequency heating and wave absorption efficiency in inhomogeneous HF cylindrical plasma
24 p3852 A71-44492

Refraction of electromagnetic wave with electric field perpendicular to applied magnetic field in anisotropic plasma cylinder cross section
24 p3858 A71-45236

Weakly damped Alfvén ion-cyclotron waves and fast magnetoacoustic waves in infinite plasma cylinder inserted into current bearing finite coil
24 p3858 A71-45245

PLASMA DECAY

HF oscillations excitation in decaying plasma-electron beam system, noting Coulomb collisions and nonlinear effects role
02 p0288 A71-11632

Decaying helium gas plasma particles diffusion across magnetic fields by combined microwave and Langmuir electron density probes, considering instabilities
03 p0463 A71-13470

Kinetic equations derivation for computer calculation of nonuniform hydrogen plasma decay, considering hydrogen recombination, electron temperature and ambipolar diffusion
03 p0463 A71-13508

Turbulent plasma correlation functions for decay and nondecay spectra, deriving descriptive equations by perturbation theory series summation
03 p0464 A71-13932

Molecular ion recombination coefficient of decaying plasma formed by UV irradiation of Cs vapor in inert gas, using microwave diagnostic method
04 p0634 A71-15115

High temperature laboratory plasmas diagnostics, noting time resolution for growth and decay mechanisms
06 p0896 A71-17297

Computer simulation of strongly ionized potassium and hydrogen plasmas relaxation during rapid electrode cooling by He atoms, noting population inversions
08 p1342 A71-21913

Longitudinal plasmon decay in strong magnetic field into neutrino-antineutrino pair
09 p1527 A71-23533

Plasma decay turbulence in spatially homogeneous ensemble of undamped dispersive waves in macroscopic and Vlasov terms, using time asymptotic perturbation method
10 p1647 A71-23887

Metastable atom destruction, collision-radiative recombination and electron heating in low temperature decaying helium plasmas, using spectroscopic resonance line measurements
10 p1654 A71-24896

Nitric oxide ion two body recombination with nitrogen dioxide and trioxide molecular ions, examining ionic neutralization reactions in decaying dilute thermal plasma at 300 degrees K
11 p1801 A71-25297

German monograph on time dependent gas temperature in decaying plasmas, using frequencies of standing acoustic wave stimulated by pulsed discharges in rarefied gases
13 p2110 A71-29423

Plasma decay due to charged particles recombination, linearizing nonlinear equations describing diffusion of singly ionized two-component gas undergoing recombination
15 p2456 A71-31999

Cesium spectral lines luminescence and population during helium-cesium discharge plasma decay
15 p2458 A71-32407

Photoresonance cesium plasma development and decay, determining density spatial-temporal behavior and recombination and polar diffusion coefficients by probe measurements
17 p2787 A71-34287

Computer simulation of strongly ionized potassium and hydrogen plasmas relaxation during rapid electrode cooling by He atoms, noting population inversions
17 p2788 A71-35257

Decay instability at ion-sound frequency induced by large amplitude Bernstein mode wave in plasma
18 p2951 A71-35929

Metastable atom destruction, collision-radiative recombination and electron heating in low temperature decaying helium plasmas, using spectroscopic resonance line measurements
21 p3425 A71-41276

Low temperature investigation of microplasma breakdown in steep p-n junctions of Sb-doped n-type Ge
22 p3587 A71-42874

Weakly ionized decaying plasma potential fluctuations and instability in magnetic field, using electrostatic probes
23 p3709 A71-43262

Nonlinear stabilization of beam instability in plasma with comparable phase velocity, electron capture and decay effects
23 p3709 A71-43264

Nitrogen and neon cations number density time dependence during plasma decay in neon-nitrogen mixtures
23 p3711 A71-43881

PLASMA DENSITY

Dense plasma high current density effects on low voltage arc in thermionic converter
01 p0005 A71-10159

Pulsed Ar ion laser plasma electron density and temperature, discussing Tonks-Langmuir free fall model validity
01 p0096 A71-11623

Miniature multigrid probes for measuring energy spectra of charged particles and absolute plasma densities, comparing results to microwave measurements
02 p0247 A71-11637

Electron density fluctuations in nonstationary plasma under crossed electric and magnetic fields, relating times of instability development and background relaxation
02 p0289 A71-12179

Fast electron elastic and inelastic scattering Ar plasma at large Rutherford cross section, obtaining charged particle density
02 p0291 A71-12317

Nitrogen plasma flow over flat plate, comparing probe and probeless methods for boundary layer concentration profile measurement
02 p0254 A71-12648

Comparative simultaneous ionospheric temperature and plasma concentration by Explorer 31 probes and ground based radar measurements
03 p0407 A71-13311

Microwave scattering from nonuniform plasma of low pressure mercury arc in glass tube, describing density profile
03 p0463 A71-13474

Neutral atoms collision effects on partially ionized plasmadynamic stability, considering fluid medium model with one dimensional density gradient
03 p0464 A71-13927

Polar orbiting satellite observed transient plasma density enhancements relation to geomagnetic activity
03 p0417 A71-14042

Thermal magnetospheric plasma densities from hydromagnetic whistlers dispersion characteristics by normalized dispersion curve method
03 p0419 A71-14521

Collisionless plasma density measurement by spherical probe, considering probe to Debye radius ratio
04 p0635 A71-15260

Jupiter rotating inner magnetosphere plasma density distribution, using Lorentz term in force balance equation
05 p0810 A71-16631

Collisionless plasma density determination valid for probe/Debye radii finite ratio, using positive ion current-voltage characteristics
06 p0936 A71-17680

Magnetospheric plasma concentration from geomagnetic pulsations periods
06 p0894 A71-18270

Radial density distribution in plasmoid and radial expansion of plasmoid investigated by microwave measurements
06 p0940 A71-18703

Plasma density irregularities in solar wind, showing wavelength dependence of interplanetary scintillation inconsistent with magnetic variations
07 p1184 A71-18862

Carbon dioxide laser heterodyne plasma density length product measuring with microsecond response in Astron controlled fusion experimental area
07 p1126 A71-20166

Plasma concentration and heavy particle-electron collision frequency in open cylindrical cutoff resonator based on frequency shift and passband broadening data
07 p1171 A71-20184

Coulomb collisions in high density plasma beams, examining relaxation time
08 p1340 A71-21486

Low density plasma in magnetic field, investigating existence possibilities of stationary isothermal jump and plane wave periodic solution
08 p1340 A71-21493

Midlatitude VLF discrete emissions generation regions location by dispersion analysis of ground station observations, determining plasma density along path for events
08 p1282 A71-21634

Homogeneous equilibrium low temperature dense helium plasma ionization composition and radiative energy losses, calculating ionization potential
09 p1501 A71-22380

Solar wind flux correlation with earth EM field pulsations, noting flare-generated shock front effects on magnetosphere
09 p1513 A71-22422

Meteor trails isotropic diffusion in presence of moving point source of ionization with variable intensity, calculating plasma density on and near trajectory
09 p1518 A71-22447

Spatially uniform dense partially ionized plasmas asymptotic thermochemical relaxation processes due to heavy particle density, temperature or superimposed electric field changes
09 p1502 A71-22859

Weakly ionized plasma density fluctuations and diffusion from kinetic equations for electron-space density cross correlation, assuming BGK model
09 p1503 A71-22867

LF plasma beam density oscillation spectra from microwave emission amplitude modulation
10 p1648 A71-24316

Flute oscillations stability in low density plasmas within strong magnetic field of mirror geometry, calculating unstable oscillation spectrum by Galerkin method
10 p1650 A71-24526

Steady state streaming of cold magnetospheric plasma in magnetic equatorial plane near plasmapause
10 p1650 A71-24557

Variable density cold inhomogeneous plasma small amplitude free electrostatic oscillations investigation by Green function of differential equation
10 p1652 A71-24662

Plasma immersed photoemitting plate surface potential distribution, discussing electron/photoelectron temperatures and number densities
10 p1653 A71-24800

Measured and calculated comparison of thermionic converter cesium plasma electron densities, using rate equations taking into account collision, diffusion and photoabsorption processes
11 p1712 A71-25889

High density and temperature plasmas produced by laser pulse heating massive solid targets, discussing interaction processes
11 p1807 A71-26094

Cs thermoelectric power near critical temperature and pressure, determining dense plasma electron-neutral elements interaction effects
11 p1715 A71-26153

Discrete ionospheric model of supersonic two dimensional low density plasma flow past large bodies, using quasi-neutrality condition
13 p1990 A71-28532

Magnetospheric model calculation for self oscillation period and amplitude dependence on longitude and plasma density estimation from observed geomagnetic pulsation period
14 p2228 A71-29531

German monograph on drift waves in plasma with density gradient covering LF electrostatic disturbances in low density plasma
14 p2277 A71-29581

TM, TE and combination cavity modes choice for plasma column electron density distribution determination by perturbation methods
14 p2279 A71-29859

Spectral lines self reversal effects on plasma temperature and density measurement in MHD duct boundary layer
14 p2279 A71-30046

HF modulated transverse electromagnetic wave penetration into plasma with negative dielectric constant, noting plasma density fluctuations and electroacoustic wave formation
14 p2281 A71-30542

Unstable collisional drift waves in high density ionized Li arc plasma, possibly causing anomalous losses and fluctuations
14 p2281 A71-30544

Hydrogen plasma transport in linear magnetic quadrupole field, studying polarization potential and density distribution
14 p2282 A71-30669

Coulomb collisions in high density plasma beams from numerical integration of Fokker-Planck equation for three initial distribution functions, studying relaxation time
14 p2283 A71-30674

Satellite measurements of cold plasma density and plasmapause in magnetosphere, comparing Whistler, Langmuir probe and ion trap data
14 p2237 A71-30951

Electron density fluctuations in nonequilibrium plasma under crossed electric and magnetic fields, relating ionization instability development and background relaxation times
15 p2454 A71-31488

Radio sources 3C 48, 3C 144, 3C 161, 3C 273 and 3C 298 scintillations by interplanetary plasma at 60 MHz, determining electron density fluctuations
15 p2487 A71-32033

High density degenerate stellar plasma analysis, obtaining phase transition thresholds, elementary parti-

cle stability, thermal energy density and interaction model 15 p2487 A71-32038

Microwave probing of electron number density and collision frequency in slightly ionized plasmas 15 p2458 A71-32395

Pinch devices under laser heating, determining plasma density and temperature and confining magnetic field strength with thermodynamic model 15 p2458 A71-32396

Axisymmetrical dense plasma, calculating radiation intensity radial distribution with approximate method 15 p2459 A71-32458

Electromagnetic wave propagation along homogeneous and inhomogeneous plasma columns, establishing density distribution functions and dispersion curves 15 p2459 A71-32641

Highly ionized plasma column anomalous microwave absorption near critical density as function of plasma frequency 16 p2619 A71-33176

High temperature dense plasma formation by laser heating of gas target, noting fusion reaction in deuterium-tritium mixture 16 p2619 A71-33647

Electron-ion recombination and ambipolar diffusion disruption of electron density in cryogenic helium plasma, using cavity resonator measurements 16 p2619 A71-33648

Magnetic drift wave instabilities in plasmas with nonuniform density and temperature gradient 16 p2572 A71-33949

Photoresonance cesium plasma development and decay, determining density spatial-temporal behavior and recombination and polar diffusion coefficients by probe measurements 17 p2787 A71-34287

Microfield double probe for plasma density and electron temperature determination, studying random signals crossed spectrum 17 p2789 A71-35350

Continuous flush electrostatic probe for weakly ionized flowing gas surface density gradient and charged particle free stream density determination, obtaining I-V characteristics 18 p2950 A71-35858

Mirror-contained collisional plasmas, deriving wave reflection and absorption from equilibrium density and temperature profile equations 18 p2950 A71-35860

Explosive instability effect on plasma distribution function, field energy level and time response 18 p2950 A71-35863

Jovian magnetospheric plasma densities, discussing roles of centrifugal ejection, solar wind plasma injection and photoelectron diffusion 18 p2964 A71-36291

Solar wind plasma density and flow speed semiannual variations from Vela 3 and 4 satellite observations, noting dependence on heliographic latitude 19 p3124 A71-37351

Second order MHD equations for density fluctuations driven by Alfvén waves with relation to solar wind 19 p3110 A71-37352

Spatial distribution, ion density and space potential measurements in plasma boundary layer at conducting sphere 19 p3112 A71-37738

Low density plasma electron velocity distribution deviation due to Maxwellian photon radiation resulting from inelastic collisions with atoms 19 p3112 A71-37739

Density fluctuation dispersal in uniform magnetoplasma, obtaining expressions for Fourier-Laplace transforms of perturbed density, potential field and flux distribution 19 p3113 A71-37745

Dense plasma focus conjectured as short finite two dimensional Z pinch forming near or at end of coaxial plasma accelerator 19 p3116 A71-38248

Solar coronal X ray spectrum calculation of high-temperature low-density plasma, considering line emission from electron collisional excitation and radiation 20 p3278 A71-39058

Ionospheric plasma density irregularities effect on ionospheric electroconductivity, using Ohms law in Alfvén-Faethammer form 20 p3218 A71-39521

HF plasma heating in Tokamak torus device by magnetosonic wave energy absorption in high density region via Buchsbaum hybrid resonance 21 p3422 A71-40764

Electron beam heating of cold plasma in magnetic trap as function of plasma density, showing two stream instability due to Cerenkov effect 21 p3425 A71-41285

Semiconducting plasma carrier density gradient instability, investigating threshold curve for n-type germanium 21 p3434 A71-41330

Plasma flow around disk in single ended Q machine with magnetic field parallel to flow velocity, measuring density profile for wake structure 22 p3580 A71-41587

Plasma confinement in bounded systems, considering externally induced field HF pressure effect on plasma density distribution 22 p3580 A71-41600

Equilibrium neutral gas and plasma electron number density fluctuation determination, deriving correlation functions from Liouville equation 22 p3530 A71-41894

Coulomb interactions within dense Boltzmann plasma in transition from ideal to nonideal state, proposing effective Coulomb pair cross section concept 23 p3712 A71-43913

Dense hydromagnetic plasmoid interaction with nonuniform axisymmetric magnetic field using two dimensional fully ionized two temperature model 24 p3852 A71-44487

Transverse instability of charged particle beam in segmented linear accelerators due to beam encounter with wall 24 p3855 A71-44522

Ram current effect in sounding rockets for plasma ion density measurement 24 p3822 A71-44793

PLASMA DIAGNOSTICS

Plasma potential measurement in closed magnetic trap /stellarator/ by electron emitting electrostatic probe 01 p0133 A71-10679

Open barrel shaped resonators in plasma diagnostics, using waveguide concepts 01 p0133 A71-10683

Magnetic fields measurement in plasmas by laser scattering, discussing theory and applications 01 p0133 A71-10747

Shock tube generated Xe plasma electron density measurements by spectroscopy and laser interferometry, deriving ionization relaxation time 01 p0134 A71-10995

Electron density profiles in ruby laser generated Xe plasma, using differential interferometry 01 p0134 A71-10996

High impedance electric probes and floating double probes for plasma stream electric field, potential, density and temperature 01 p0134 A71-11002

Quasi-transverse extraordinary wave interaction with density fluctuations in inhomogeneous magnetized plasma, using modulation measurement for instability diagnosis 01 p0136 A71-11440

Magnetic flux transfer measurement at hyperbolic neutral point resulting in plasma compression 01 p0136 A71-11474

Arc discharge plasma response to turbulent gas flow covering wide range of Reynolds numbers measured with Langmuir probes 01 p0136 A71-11479

Electron concentration distribution over plasma discharge cross section, using interferometry 02 p0288 A71-11887

Dense Li plasma pulsed power discharge temperature, structure, propagation velocity and emission characteristics 02 p0290 A71-12183

Capillary plasma heating source processes, using textolite and fiberglass-reinforced textolite dielectric discharge chambers 02 p0292 A71-12556

Nitrogen plasma flow over flat plate, comparing probe and probeless methods for boundary layer concentration profile measurement 02 p0254 A71-12648

Spherical and cylindrical electrostatic probes for point ion density measurements in continuum flowing plasmas in hypersonic wake, discussing shock tube program for calibration 03 p0423 A71-13441

Collisionless electrostatic single and double probe measurements for electron temperature and number density, making algebraic fit for numerical analysis results 03 p0423 A71-13442

Microwave interferometer for low density electron laboratory plasmas 03 p0428 A71-13926

IR Q switched gas laser with Michelson interferometer for plasma diagnostics, describing equipment operation 03 p0439 A71-14056

Microwave phase measuring system using programmable digital dividing circuits, considering application to plasma diagnostics 04 p0586 A71-14655

Locally slowly varying magnetoplasma, determining electron concentration and collision frequency by wave propagation experiment 04 p0633 A71-15034

High temperature plasma electron density and ion signal intensity measuring apparatus for reaction rate evaluation 04 p0600 A71-15591

Plasma temperature measurement in local thermodynamic equilibrium using total continuum emitted during seeding with hydrogen 05 p0786 A71-16171

Temperature measurements for xenon plasma diagnostics in high output pulsed mode 05 p0786 A71-16223

Plasma temperature determination in Hg high pressure discharge with TII addition 05 p0786 A71-16224

Nitrogen plasma viscosity at atmospheric pressure, using moving sphere resistance measurement 05 p0786 A71-16225

Plasma diagnostics with focussed laser beams, discussing localized electron density determination 05 p0787 A71-16331

H-He partially ionized plasma bremsstrahlung, radiative and dielectronic recombination, discrete levels excitation and collisional ionization 05 p0787 A71-16489

Particle flux toward charged plate /plane probe/ moving relative to plasma 05 p0814 A71-17181

High temperature laboratory plasmas diagnostics, noting time resolution for growth and decay mechanisms 06 p0896 A71-17297

Electron temperature and concentration profiles behind shock front from IR emission and absorption simultaneous measurement, applying method to xenon ionization and recombination processes 06 p0936 A71-17594

Laser produced plasma temperature measurements using X ray detectors 06 p0938 A71-18459

Laser produced plasma expansion into vacuum, discussing ion energy angular distributions measurement 06 p0938 A71-18460

Negatively charged conical electrostatic probe characteristics determination in supersonic plasma stream, using shock tube [AIAA PAPER 71-143] 06 p0939 A71-18586

Radial density distribution in plasmoid and radial expansion of plasmoid investigated by microwave measurements 06 p0940 A71-18703

Current sheet collapse phase in dense deuterium plasma focus gun heating, using streak photography and X ray and neutron measuring techniques 07 p1165 A71-18877

Ion collection by spherical and cylindrical probes in collisional He plasma, comparing saturation current measurements with transitional regime probe theories 07 p1169 A71-19909

Plasma potential measurement in closed magnetic trap /stellarator/ by electron emitting electrostatic probe 07 p1170 A71-20140

Open barrel shaped resonators in plasma diagnostics, using waveguide concepts 07 p1170 A71-20145

Carbon dioxide laser heterodyne plasma density length product measuring with microsecond response in Astron controlled fusion experimental area 07 p1126 A71-20166

Self similar laser produced plasma examination, using irradiated multilayer targets and spectrum analysis 07 p1170 A71-20169

Plasma waves and echoes characteristics and diagnostics, emphasizing longitudinal waves 07 p1172 A71-20502

Microwave scattering from gaseous plasmas, discussing EM waves, fluctuation and diagnostics problems 07 p1172 A71-20503

Gaseous plasma diagnostics by light scattering for localized minimal perturbing measurement of temperature and density parameters 07 p1172 A71-20504

Atomic processes in plasmas including excitation, deexcitation, ionization, recombination, charge transfer, free-free transitions and spectral line broadening for theta pinch parameters determination 07 p1172 A71-20505

Hot plasma production by strong shock wave heating, using EM shock tubes under laboratory controlled conditions 07 p1172 A71-20506

Collisionless shock waves generation in theta pinches, plasma formation, experimental devices, diagnostic methods and magnetic probes 07 p1172 A71-20507

High beta plasmas instabilities, discussing collisionless bounce model of theta pinch and diagnostic measurements 07 p1173 A71-20511

Cathode material ions acceleration during pulsed discharge in vacuum, discussing experimental investigation results

08 p1341 A71-21496

Pulsed coaxial plasma accelerator, measuring longitudinal gas pressure distribution, particle emission and magnetic fields characteristics under various operating conditions

08 p1341 A71-21498

Turbulent plasmas nonequilibrium electric fields determination from hydrogen spectral lines Stark broadening

08 p1341 A71-21790

High pressure electrodeless HF gas discharge plasmas, investigating effects of external magnetic field, gas and pressure on discharge rotation frequency

08 p1342 A71-21915

Simultaneous plasma internal energy, temperature and volume determination based on energy balance analysis during pulsed heating

08 p1342 A71-21928

Flush-mounted electrostatic probe for plasma properties measurement, calculating negative ions effect on I-V characteristics

09 p1442 A71-22073

Holographic spectrum analyzer for plasma diagnostics in microwave band, deriving formulas for emission spectrum based on interference patterns intensities in waveguide

09 p1499 A71-22150

Plasma electron temperature measurement from scattering indicatrix of laser radiation

09 p1501 A71-22394

Electron-ion plasma in HF electric and constant magnetic field, determining relaxation times and collision frequency for temperature compensation

09 p1502 A71-22539

Plasma flame temperature and flow characteristics in plasma jet transfer-type metal cutters from spectroscopic measurement and high speed streak camera photography

09 p1454 A71-23032

Xe flash tube discharge saturable absorption effects, using YAG-Nd laser radiation for plasma attenuation measurements

09 p1465 A71-23484

Pioneer 9 space probe electric field experiment and near earth observations of noise spectra variations related to diffusive plasma layer

09 p1529 A71-23711

Magnetic mass spectrometer for ionosphere composition measurements permitting single spectrum analysis of plasma of negative and positive ions

10 p1608 A71-23817

Two-wavelength interferometry of plasmas generated by Nd laser beam focalization, deriving electron and neutral particle densities

10 p1646 A71-23818

Dense hot plasma generation by laser beam focusing on gas or solid targets, discussing experimental setups, diagnostic methods and ionization theories

10 p1647 A71-23920

Soviet papers on low temperature plasma physics covering production and diagnostic techniques, electrokinetic and optical characteristics, electromagnetic and shock effects, metal plasmas, etc

10 p1648 A71-24188

Electromagnetic second harmonic wave generation in inhomogeneous magnetoactive plasma, using HF probe and horn antenna for detection

10 p1654 A71-24974

Flush mounted electrostatic probes behavior under different flow regimes, studying bias, area, geometry and position effects on collected current density

11 p1743 A71-25148

Book on high temperature plasma diagnostics methods covering measurement errors, holographic interferometers and light scattering

11 p1804 A71-25280

Long period, pearls and irregular geomagnetic pulsations for plasma diagnostics in magnetosphere

11 p1756 A71-25647

Transient ion sheath effects on spherical metallic plasma probe complex admittance at different frequencies, comparing numerical results with experiment

11 p1805 A71-25803

Plasma anode tube in metal-ceramic envelope with improved capabilities for electron emission studies, considering movable Langmuir probe

11 p1806 A71-25902

Thomson light diffusion in laser diagnostics, deducing electron density/temperature and ion temperature

11 p1776 A71-26274

Aerodynamic probe measurements for plasma jets produced by electrothermal and Hall current accelerators

11 p1764 A71-26275

Plasma diagnostics covering magnetic, electron beam, electrostatic, laser, holography, interferometry, Thomson scattering, microwave and electroacoustic techniques

11 p1766 A71-26287

Plasma electron density measurements by carbon dioxide laser as function of discharge current, using interferometry and scattering methods

12 p1912 A71-26573

Holographic interferometry method application to plasma electron concentration measurements

12 p1906 A71-27211

Electron energy distribution functions in carbon dioxide laser plasmas, using Langmuir probes

12 p1940 A71-27280

Plasma refractive index and electron density measurements by He-Ne vernier interferometric laser

12 p1940 A71-27282

Pulsed MPD arc experiment, determining voltage characteristics and rotating current spokes occurrence and behavior

12 p1941 A71-27567

Local electron density measurements in low beta plasmas, using nonlinear electromagnetic wave mixing under synchronism condition

13 p2104 A71-27849

Cold plasma convection production by ion driven LF drift instability, noting tokamaks and stellarators stabilization

13 p2104 A71-27850

Electric field angular distribution of short radio frequency probe in warm anisotropic plasma under magnetic field

13 p2104 A71-27852

Electron density distribution determination from microwave resonant frequencies of parallel plate cavity containing cold, collisionless, isotropic plasma

13 p2105 A71-27994

Subnanosecond interferograms with high spatial resolution of plasma filaments in ruby laser produced spark

13 p2077 A71-28047

Particle flux toward charged metal plate /flat probe/ moving relative to plasma

13 p2134 A71-28238

Monograph on shock wave structure in nonequilibrium partially ionized gas flow covering plasma diagnostics, electron temperature, ion density, induced potential gradient, etc

13 p2048 A71-28738

Improved accuracy electron temperature Langmuir probe by eliminating geomagnetic field, rocket velocity and random noise effects

14 p2238 A71-29532

Ion and electron probe currents correlation for justification of electrostatic probes use for turbulent plasma diagnostics

14 p2280 A71-30174

Two-wavelength holographic interferometry for phase objects dispersion characteristics, noting plasma diagnostics application

14 p2248 A71-30675

Electromagnetic radiation scattering detection limits for plasma diagnostics, considering plasma properties effect on satellites aperture broadening in spectrum

14 p2283 A71-30677

X band focused beam interferometer for plasma phase shift measurement independent of propagation path attenuation over 30 dB dynamic range

14 p2214 A71-30804

Stable plasma resonance behavior, calculating small signal and nonlinear responses for theory verification and diagnostic techniques

14 p2283 A71-30948

Mass spectrometric investigation of high power laser beam plasma on solid target, determining multicharged ion yield, energy, angular distribution and recombination effect

15 p2418 A71-31191

Plasma physics measurement objectives in terms of deviations from thermodynamic equilibrium, discussing relationship between measuring device calibration and experimental data interpretation

15 p2453 A71-31200

Dense Li plasma pulsed power discharge temperature, structure, propagation velocity and emission characteristics

15 p2454 A71-31491

Supersonic arc-heated Ar flow, measuring heavy particle temperature and velocity and electron density profiles by pressure scanned Fabry-Perot interferometer [AIAA PAPER 71-589]

15 p2454 A71-31534

Superhigh frequency microwave absorption region localization in collisionless plasmas by plasma parameters measurement in toroidal magnetic field

15 p2370 A71-31737

Ionization profiles of shock heated argon with impurities, using microwave and pulsed Langmuir probe measurements

16 p2616 A71-32912

Plasma local thermodynamic equilibrium relation to continuum, molecular band, atomic lines intensity and absorption line reversal/equivalent widths measurements

16 p2617 A71-32959

Microwave and laser diagnostics of plasmas based on interaction with electromagnetic fields

16 p2617 A71-32960

Electrical plasma probes, discussing ion-surface effects, geometry, cleaning procedures, collisionless regime and electron/ion current

16 p2617 A71-32961

Ion mass spectrometry in plasma analysis, reviewing complex ionized gaseous media investigations and specific reactions

16 p2576 A71-32962

Pulsed coaxial plasma accelerator, measuring longitudinal gas pressure distribution, particle emission and magnetic fields characteristics under various operating conditions

16 p2618 A71-33045

Plasma temperature determination errors from relative gf-values, noting effects on absolute transition probabilities

16 p2618 A71-33111

Optical interferometry and schlieren photography involving high power pulsed lasers, discussing applications to plasma diagnostics and holography

16 p2586 A71-33159

Low density plasma diagnostics using Thomson scattering of laser light

16 p2618 A71-33161

Rarefied plasma flow generation by Q-switched laser pulse focusing on solid target, measuring plasma properties with Langmuir probes and microwave interferometers

16 p2586 A71-33162

Collisionless turbulent plasmas nonequilibrium electric fields determination from hydrogen spectral lines Stark broadening

16 p2619 A71-33549

Simultaneous plasma internal energy, temperature and volume determination based on energy balance analysis during pulsed heating

17 p2789 A71-35272

RF ion thruster /RIT-10/ optimization, investigating energy balance and plasma diagnostics [DGLR-71-041]

17 p2794 A71-35547

Continuous flush electrostatic probe for weakly ionized flowing gas surface density gradient and charged particle free stream density determination, obtaining I-V characteristics

18 p2950 A71-35858

Flow processes around body of hypersonic velocity studying plasma diagnostics in ionized wake

18 p2952 A71-36421

Mathematical model of arc Pioneer 6/7 plasma probe electrostatic analyzer responding to monoenergetic unidirectional charged particle beam

18 p2952 A71-36588

Multipass laser interferometry sensitivity improvement for He plasma electron density determination by increasing effective path length of laser beam in medium

18 p2931 A71-36588

Charged particles transport in thermionic converter near-emitter profiles, determining potential and electron density profiles

18 p2953 A71-36968

Inhomogeneous plasma sounding with electromagnetic waves

18 p2953 A71-37006

Rotating magnetic field plasma pinch, discussing streak and framing photography, electron line density profiles, magnetic probes and ion and electron temperature measurements

19 p3111 A71-37631

Plasma potential differential measuring method using emitting and cold probes for simultaneous current data

19 p3112 A71-37634

Spatial distribution, ion density and space potential measurements in plasma boundary layer at conducting sphere

19 p3112 A71-37738

Langmuir probe and microwave measurements of density, velocity and electron and ion temperatures in streaming plasmas generated by focused laser pulse

19 p3112 A71-37748

Plasma diagnostics based on IR continuum intensity due to bremsstrahlung emission from plasma

19 p3113 A71-37767

Tokamak T-3A device plasma electron temperature measurements, using Thomson scattering with electric, microwave, laser and diamagnetic data

19 p3113 A71-37854

Papers on plasma physics covering optical refractivity, deep space measurements, whistlers as diagnostic tools in space plasma, radio wave scattering from ionosphere, etc

19 p3115 A71-38243

Plasma optical refractivity, considering gas laser interferometry and holographic phase measurements

19 p3116 A71-38244

Deep space plasma measurement techniques by instruments on earth satellites

19 p3116 A71-38244

Whistlers as diagnostic tools in space plasma, measuring electron densities at large distances in earth outer atmosphere within magnetosphere

19 p3116 A71-38244

Radio wave scattering from ionosphere, considering plasma experiments in E and F region
19 p3018 A71-38247

Pulsed erosion accelerators plasmod discontinuities in structure streak photographs for various electrode configurations and pressures
19 p3116 A71-38253

Holographic interferometry method application to plasma electron concentration measurements
19 p3067 A71-38623

Dynamic pressure measurement method and apparatus for anode center of heavy current electric arcs in plasmas, applying to plasma welding arcs
20 p3274 A71-39047

Magnetospheric plasma convection electric field double-probe measurement at high latitude by Injun-5 satellite, noting east-west velocity reversals or discontinuities at auroral zone
20 p3230 A71-39882

Magnetospheric plasma observation by Sirio 1 satellite, measuring protons, electrons and magnetic field with sensors
20 p3307 A71-39959

Plasma losses in high current plasma configuration due to inverse skin effect by observation for discharge regimes in theta pinch, zeta and Tokamak systems
21 p3422 A71-40763

Three frame pulsed holographic interferometry of plasma radial density profiles and helical displacement for use with theta pinch device
21 p3423 A71-40937

Probe size and orientation effects in turbulent plasma flow diagnostics, considering electrostatic probes frequency filtering and wake effects
21 p3423 A71-40979

Element and isotope separation effects under centripetal acceleration in rotating plasma, using mass spectrometric diagnostics
22 p3580 A71-41584

Plasma flow around disk in single ended Q machine with magnetic field parallel to flow velocity, measuring density profile for wake structure
22 p3580 A71-41587

Slow toroidal theta-Z pinch experiment, describing measurements temperature distribution with emphasis on transitions between stable and unstable states
22 p3580 A71-41588

Enhanced scattering signal observation at electrostatic plasma wave frequency by focusing Q switched laser beam on hydrogen plasma
22 p3580 A71-41596

Cylindrical plasma column light scattering diagnostics by focusing carbon diode laser beam on center
22 p3580 A71-41601

Diagnostics of Ar free jet expansion from high pressure inductive arc source into low density wind tunnel, observing background gas effects
22 p3583 A71-42048

German monograph on experimental determination of noble gas plasma conductivity under normal pressure in high temperature range, covering measurements under electric arc conditions
23 p3711 A71-43475

Coulomb interactions within dense Boltzmann plasma in transition from ideal to nonideal state, proposing effective Coulomb pair cross section concept
23 p3712 A71-43913

Ar-K and He-R plasma conductivity measurement at atmospheric pressure from equilibrium to nonequilibrium conditions, using electrostatic probes
23 p3714 A71-44275

Harmonic analysis applicability to amplitude-frequency characteristics of plasma current fluctuations, governing spectral characteristics determination accuracy by passband filter delineation precision
24 p3851 A71-44394

PLASMA DIFFUSION

Electron cyclotron drift instability shown by numerical simulation as cause for anomalous plasma diffusion and heating
01 p0132 A71-10147

Parabolic particle distribution stability in plasmoids in guiding magnetic field under diffusion due to electron-ion collisions
01 p0133 A71-10680

Experimental dispersion curve for LF drift waves in inhomogeneous magnetoplasma
01 p0134 A71-11003

Analog device for harmonic functions modeling and electron plasma dispersion function computation
01 p0135 A71-11078

Decaying helium gas plasma particles diffusion across magnetic fields by combined microwave and Langmuir electron density probes, considering instabilities
03 p0463 A71-13470

Plasma rotation effects on toroidal systems diffusion, considering pressure gradient, rotational velocity, transverse electric field and path lengths
03 p0464 A71-13931

Laser torch plasma dispersion gas dynamics from motion and kinetics of ionization processes
05 p0760 A71-16181

Velocity space diffusion and collision effects on fully ionized inhomogeneous plasma instability, using Fokker-Planck kinetic equation
05 p0789 A71-16654

Parabolic particle distribution stability in plasmoids in guiding magnetic field under diffusion due to electron-ion collisions
07 p1170 A71-20141

Powerful laser beam and material interaction, investigating gas dynamics of plasma heating and dispersion
07 p1127 A71-20254

Meteor trails isotropic diffusion in presence of moving point source of ionization with variable intensity, calculating plasma density on and near trajectory
09 p1518 A71-22447

Weakly ionized plasma density fluctuations and diffusion from kinetic equations for electron-space density cross correlation, assuming BGK model
09 p1503 A71-22863

Collisionless plasma steady flow past thin symmetrical semiinfinite wedge, considering dispersion due to finite Larmor radius
09 p1504 A71-23052

Electromagnetic waves reflection and transmission from weakly ionized moving plasma, noting dependence on medium velocity and nonlinearity effect
09 p1505 A71-23519

Pioneer 9 space probe electric field experiment and near earth observations of noise spectra variations related to diffusive plasma layer
09 p1529 A71-23711

Hall current effects on plasma screw pinch stability, obtaining dispersion relation from perturbations characteristic equations
10 p1647 A71-23889

Anomalous dispersion and instability in solar wind plasma with thermal anisotropy and high beta ratio, applying magnetosonic wave-particle interactions
11 p1816 A71-25754

Polar H ion plasma escape from ionosphere into magnetospheric tail effect on plasmopause formation, using hydrodynamic approximation
11 p1756 A71-25756

Thermionic converters performance in ignited mode from transport equations for diffusion region, determining electron concentration, potential and temperature
11 p1711 A71-25879

Diffusion measurement of highly ionized thermal Cs plasma in magnetic field by Langmuir probe, determining density profile
13 p2106 A71-28450

Diffusion and acoustic ion waves in weakly ionized plasma as function of exciting/collision frequency ratio
13 p2110 A71-29372

Holographic investigation of laser sparks in hydrogen and helium, determining electron concentration spatial distribution and plasma dispersion dynamics
15 p2419 A71-31738

Dispersive effect on bremsstrahlung radiation from electron atom collisions in weakly ionized plasma, using Boltzmann transport equation
15 p2456 A71-31850

Plasma mobility, diffusion, electron energy distribution, surface phenomena, elastic collisions, charge transfer, etc
16 p2617 A71-32954

Quasi-neutral inhomogeneity /particle cloud/ in collisionless hot or cold plasmas without magnetic field
16 p2619 A71-33521

Plasma fluctuations and diffusion correlation analysis in linear octupole magnetic confinement, determining dispersion relation for interchange instability
17 p2786 A71-34283

Equilibrium diffusion of rotating plasma in toroidal systems, deriving two fluid hydrodynamic equations with allowance for ion temperature perturbation
19 p3109 A71-37140

Transverse waves and electromagnetic instabilities propagating along magnetic field in homogeneous plasma, discussing ions and electrons energy losses and plasma dispersion
19 p3114 A71-38206

Confined plasma diffusion toward current-carrying inner conductors and outer walls in multipoles
21 p3423 A71-40767

Stationary toroidal plasma under external magnetic field, investigating classical resistive diffusion velocity with one fluid MHD equations
23 p3713 A71-44147

Plasma diffusion lifetime and electron concentration measurements in Tokamak-3 by pulsed neutral hydrogen injection and microwave multichord probing
24 p3852 A71-44488

Hydrogen plasma generation by microwave field in magnetic-mirror device due to electron cyclotron resonance, measuring transverse diffusion coefficient dependence on magnetic field
24 p3858 A71-45235

PLASMA DIODES

Feedback instability of LF oscillations in high pressure plasma diode
01 p0133 A71-10685

Cs plasma thermionic diode, using Penning effect for ionization rate increase via Hg or Cd seeding
05 p0705 A71-16170

Feedback instability of LF oscillations in high pressure plasma diode
07 p1170 A71-20147

Spectral emission and level populations of diffusion and principal series lines of cesium vapor in 5 mm discharge plasma diode with hot cathode
12 p1941 A71-27549

Thermionic converters experimental testing, developing kinetic theory of plasma diodes in steady state Knudsen model for uniform potential distribution
19 p2999 A71-38256

Weakly ionized cesium plasmas produced in sealed diodes, examining LF instabilities with fluid equations
23 p3708 A71-43083

I-V characteristics of plasma varactor formed near central or external conductor surface during coaxial line filling with plasma
23 p3651 A71-43403

Spectroscopic analysis of pulsed gas discharge in crossed electric and magnetic fields of gas magnetron diode in 3100-4660 Å wavelength range
23 p3712 A71-43933

Plane collisionless plasma diode between two hot emitters, considering potential distributions
24 p3808 A71-44551

PLASMA DISCHARGES

U PLASMA JETS

PLASMA DISPERSION

U PLASMA DIFFUSION

PLASMA DYNAMICS

Plasma motion in magnetosphere under undisturbed geomagnetic conditions, taking solar wind into account
02 p0244 A71-11919

Transport analysis of collision dominated relaxation plasma in ignited mode thermionic converter
02 p0291 A71-12237

Thermomagnetic gas torque within kinetic theory framework for collinear static and alternating magnetic fields
02 p0291 A71-12316

Solar wind plasma composition and dynamics, discussing element and ion abundances, solar activity effects, plasma stability, etc
02 p0300 A71-12374

Anisotropic plasma discontinuities in solar wind, noting shock misidentification
03 p0463 A71-13307

Moving plasma hydrodynamic equations of motion, continuity and energy in axially symmetric coordinate system
03 p0464 A71-13904

Neutral atoms collision effects on partially ionized plasmadynamic stability, considering fluid medium model with one dimensional density gradient
03 p0464 A71-13927

Isonospheric plasma drift from spinning rocket shadow effect, using retarding potential analyzer
03 p0416 A71-14034

Global stability of closed plasma configurations relation to dynamical principle of least constraint and space-time and gage symmetries of flow fields
05 p0789 A71-16651

Lagrangian methods yielding relativistically covariant formalism for wave packets in weakly inhomogeneous and time dependent plasma dynamics, obtaining motion equations from Euler-Lagrange equations
05 p0789 A71-16657

Plasma stabilization in screw pinch, using combined inertial forces and dynamic shear in diffuse column
06 p0935 A71-17487

Photoresonant cesium plasma ionization, discussing pumping spectra, electron gas, molecular-atomic ion ratio and dynamics
06 p0936 A71-17591

Classical many component plasma dynamics with collective particle interactions in self consistent longitudinal electric field, deriving complex wave equations
06 p0937 A71-18062

Cosmic plasma dynamics collective phenomena, investigating models, instabilities, nonlinear interactions, wave transformations, turbulence, cosmic rays and radiative acceleration
06 p0972 A71-18330

Nanosecond laser produced lithium hydride spherical plasma expansion model, taking into account three body and radiative recombinations
06 p0938 A71-18457

Snowplow theory modification for plasma temperature, ion population and release time prediction, noting agreement with plasma rail gun data
07 p1165 A71-18879

Macroscopic dynamics of many-component plasmas in electromagnetic fields, discussing formula-

tion in scalar complex wave equations containing pressure and electromagnetic potentials

07 p1168 A71-19688

Effective electric field formulation of kinetic theory of classical Coulomb plasmas, computing wavevectors

07 p1169 A71-19994

Papers on plasma physics experimental methods covering waves, echoes, scattering, diagnostics, heating by shock waves, stabilities, etc

07 p1172 A71-20501

Plasma sheet convection velocities from electron flux measurements at synchronous altitude, noting flux increase time dependence on energy

08 p1339 A71-21216

Electromagnetic waves reflection and transmission from weakly ionized moving plasma, noting dependence on medium velocity and nonlinearity effect

09 p1505 A71-23519

Charged particles velocity distribution effect on plasma flow in transverse nonuniform magnetic field, observing configuration/trajectory distortion and particle dispersion

10 p1649 A71-24319

Magnetic field effects on plane wave propagation in plasma, reducing motion data problem to vectorial differential equation with mean electronic velocity as only unknown

11 p1804 A71-25174

Net fusion energy from laser heated deuterium-tritium particles dependent on plasma temperature, electrical energy and electron-ion thermalization through collisions

11 p1805 A71-25799

One dimensional charged particle continuity equation solution in low energy neutral plasma with current flows

11 p1804 A71-26374

Monograph on marginal stability analysis of MHD instabilities by force free magnetic fields in plasma-vacuum systems covering gravitational, pinch and shearless models

12 p1934 A71-26569

Galactic and plasma dynamics similarities, considering collisionless and collisional relaxation of stellar systems, stability problems, etc

12 p1960 A71-26782

Ionospheric plasma drift from rockets wake measurements at high latitude, discussing plasma rarefaction

12 p1899 A71-26889

Computer simulated semiinfinite uniform plasma expansion in vacuum, showing inapplicability of thermal velocity burst ion model

13 p2104 A71-27846

Plasma motion in magnetosphere under undisturbed geomagnetic conditions, taking into account solar wind

13 p2058 A71-28206

Plasma electron and proton motion in equatorial plane of magnetosphere under geomagnetic disturbance generated electric field

13 p2060 A71-28530

Plasmoid ejection during flare and condensation by radiative instability, interpreting Simple 3 solar radio bursts in terms of thermal emission

13 p2129 A71-29054

Polar ionospheric plasma transport, predicting ion density profiles from ionospheric processes models consistent with polar wind theory

14 p2234 A71-30039

German monograph on shock waves in anisotropic plasma covering parameters derivation based on kinetic plasma theory and experimental verification possibilities

14 p2280 A71-30235

Motion and collision of plasma blobs generated by giant pulse ruby laser irradiation on lithium plate

15 p2455 A71-31643

Low temperature plasma reactions, discussing electron impact and collisions, ion formation, molecular excitation and thermal dissociation, vibrational relaxation, recombination, etc

16 p2539 A71-32964

Plasma interchange instability in multipole magnetic field, including disturbance wavelength comparable to ion cyclotron radius

17 p2786 A71-34282

Energy transfer to MPD quasi-steady accelerator having electrolytic capacitors with large series resistance, integrating transmission line equations with Runge-Kutta method

17 p2794 A71-35539

Hydrodynamic equations for anisotropic plasma in magnetic fields, considering collisionless and collisional transport effects

19 p3111 A71-37634

Straight-line orbit approximation for plasma response function in system with periodic particle orbits

19 p3113 A71-37750

Charged particles interaction with geomagnetic field, discussing plasma equations of motion, ionospheric current induction, transition layer and magnetotail rotation

20 p3216 A71-39118

Plasma transport processes role in E region from midlatitude nocturnal and auroral ionospheric models in terms of transport equations

20 p3232 A71-39893

Magnetospheric plasma instabilities from velocity distribution anisotropies and nonuniform plasma and magnetic field distributions

21 p3374 A71-41180

Weakly ionized magnetoplasma with no axial drift, investigating collisional drift-type instability by linearized two fluid hydrodynamic numerical analysis

22 p3580 A71-41586

Spatially separated plasma beams of different temperatures, determining amplified wave instability boundaries and growth increments by quasi-hydrodynamic approximation

23 p3711 A71-43557

Wave field pulsations induced electron scattering as factor modifying excited plasma electron distribution function

24 p3855 A71-44668

PLASMA ELECTRODES

Electrode material function of electromagnetic radiation from heterogeneous plasma

03 p0466 A71-14473

Kinetic theory calculation of partially ionized plasma near-electrode electron temperature profiles

06 p0939 A71-18583

Oxide hollow cathode ion thruster power conditioner, evaluating electrical efficiency, weight, reliability integration and testing

06 p0947 A71-18601

Physical properties of Cs discharge plasma with incandescent electrode, considering Cs atoms ionization near cathode by thermal electrons accelerated by potential jump

10 p1650 A71-24528

Closed form formula for plasma thrust from arc jets with self induced magnetic fields, predicting electrode erosion and entrainment

11 p1810 A71-25457

Thermionic energy converter, calculating behavior of transition regions between collisionless region adjacent to electrodes and plasmas

11 p1712 A71-25890

Plasma anode tube in metal-ceramic envelope with improved capabilities for electron emission studies, considering movable Langmuir probe

11 p1806 A71-25902

Electrode nonlinear current distribution in plasma with anisotropic conductivity, noting Hall parameter effect on electric field structure

13 p2107 A71-28566

Plasma accelerator central electrode erosion and heat flux, describing measurement techniques and results

14 p2280 A71-30266

Three-phase plasmatrons with hot W electrodes for obtaining plasma of inert gases, nitrogen and hydrogen

15 p2457 A71-32267

Compressible electrically conducting gas boundary layer on MHD channel electrode, deriving equations for ambipolar region with finite ionization and recombination rates

17 p2790 A71-35644

Ribbed surface electrode effects in plasma accelerator producing high speed monoenergetic blobs

19 p3108 A71-37091

Pulsed erosion accelerators plasmoid discontinuities in structure streak photographs for various electrode configurations and pressures

19 p3116 A71-38253

Physical properties of Cs discharge plasma with incandescent electrode, considering Cs atoms ionization near cathode by thermal electrons accelerated by potential jump

19 p3116 A71-38255

Interelectrode spacing effects on nonequilibrium cesium plasmas in close spaced thermionic converters

20 p3179 A71-38876

Free electron distribution function, atomic level population and ionization rate in low voltage arc near electrodes

23 p3709 A71-43266

Electrode region in plasma with alkali metal admixture, discussing potential drop, thermionic emission, Schottky effect, diffusion, recombination and bulk and surface ionization

24 p3857 A71-45215

PLASMA ENGINES

Arc oscillation spectra in MPD thruster operation at low magnetic field

01 p0142 A71-10959

MPD thruster, discussing electrodes, coaxial magnetic nozzle, accelerator and tests

02 p0283 A71-12311

LES 6 satellite solid Teflon pulsed plasma thruster performance, determining energy balance thrust and circuit parameters

[AIAA PAPER 70-179]

03 p0472 A71-14429

Dynamic I-V characteristics of megawatt pulsed MPD-arc plasma thruster under various axial magnetic fields given for Ar and hydrogen propellants

[AIAA PAPER 70-164]

Solid Teflon fuel pulsed plasma thruster optical measurements, showing different exhaust velocities for neutral, singly, doubly and triply ionized atoms

[AIAA PAPER 71-194]

Pulsed megawatt MPD arc thruster exhaust pressure measurements, discussing time dependence, peak dynamic and static pressures, etc

[AIAA PAPER 71-196]

Low power MPD arc thruster performance with downstream cathode, using Xe propellant

[AIAA PAPER 70-1084]

Auxiliary propulsion system using low power MPD thrusters, discussing feasibility of thrust vectoring with skewed magnetic coil arrangement

[AIAA PAPER 71-695]

Radiation cooled MPD thruster with permanent and superconducting magnets, describing test facilities and measurement techniques for performance tests

[AIAA PAPER 71-696]

Pulsed plasma rail mercury propellant thruster for satellite attitude control, measuring thrust and exhaust velocity with balance and Langmuir probe respectively

18 p2956 A71-36243

Pulsed plasma thrusters, propellants, trigger and feed systems developments for long life secondary spacecraft propulsion

22 p3588 A71-41975

Quasi-steady MPD thrusters performance correlation with structural and operational parameters

22 p3589 A71-42040

PLASMA FLOW

U MAGNETOHYDRODYNAMIC FLOW

PLASMA FLUX MEASUREMENTS

Auroral electrojet electric fields from plasma electron density and collision frequency profiles measurements via Black Brant rockets variable frequency impedance probes

01 p0075 A71-11332

Plasma with oriented charged particle fluxes macroscopic parameter measurement by multigrid probes facing and reversed to drift, noting graphical data processing

07 p1171 A71-20183

Plasma fluxes transport in vacuum chamber by quadrupole magnetic field, studying H plasmoids motion

08 p1340 A71-21482

Preferred orientations of rotational and tangential discontinuities in solar wind from Mariner 5 data

08 p1356 A71-21642

Langmuir probe measurement of ionization density of Ar plasma jet, suggesting electron-ion recombination in probe vicinity

17 p2789 A71-35338

Density fluctuation dispersal in uniform magnetoplasma, obtaining expressions for Fourier-Laplace transforms of perturbed density, potential field and flux distribution

19 p3113 A71-37745

PLASMA FREQUENCIES

F region electrons heating by RF energy at or near ionospheric plasma frequency, detecting temperature changes via optical nightglow intensity variations

01 p0040 A71-11533

Electron density and collision frequency in plasma under RF modulation, solving energy balance equation

05 p0787 A71-16290

Plasma coated spherical antenna radiation, discussing hot and cold plasmas frequency and electroacoustic wave effects

06 p0875 A71-17730

Topside sounders received frequencies of oblique echoes at plasma resonance, using WKB technique

07 p1168 A71-19676

Plasma frequency resonance time duration-local electron cyclotron frequency relationship by oblique echo model

07 p1168 A71-19681

HF plasma instabilities driving mechanisms and distribution types, considering beam plasma computer simulation example

07 p1173 A71-20508

Noncollisional plasma LF instabilities, discussing flute-like, drift wave and trapped particle modes from spatially confined plasma Vlasov equation

07 p1173 A71-20509

Plasma HF heating boundaries by magnetic traps, noting diamagnetic effects due to ion and electron heating

08 p1339 A71-21480

High pressure electrodeless HF gas discharge plasmas, investigating effects of external magnetic field, gas and pressure on discharge rotation frequency

08 p1342 A71-21915

Microwave noise emission in He negative glow plasma frequency range, discussing high energy electron densities near cathode

09 p1502 A71-22694

Charged conductors in homogeneous collisionless magnetoelectric plasma at hybrid frequencies, investigating antenna array quasi-electrostatic field one dimensional structure

10 p1582 A71-23809

LF plasma beam density oscillation spectra from microwave emission amplitude modulation
10 p1648 A71-24316

Electromagnetic extraordinary wave propagation in toroidal plasma with sheared magnetic field, discussing ordinary component generation at upper hybrid frequency
10 p1650 A71-24629

Lower ionospheric plasma frequencies height determination for actual motions, relating periodic variations to spatial electron density structure
13 p2029 A71-28003

Diffusion and acoustic ion waves in weakly ionized plasma as function of exciting/collision frequency ratio
13 p2110 A71-29372

Ionospheric propagation, considering traveling disturbances, sporadic E phenomena, plasma frequency distributions and D region parameters
14 p2202 A71-30950

Radio wave propagation in ionosphere, measuring plasma frequency, cyclotron cut-off and noise level
15 p2373 A71-32443

Highly ionized plasma column anomalous microwave absorption near critical density as function of plasma frequency
16 p2619 A71-33176

Total electron content and F region plasma frequencies height during magnetic storm of 8 March 1970
16 p2563 A71-33393

Wavelike ionospheric undulations of total columnar electron content and of true height of bottomside plasma frequencies before and during solar eclipse of 7 March 1970
16 p2565 A71-33738

Steady LF geomagnetic pulsations, deriving dispersion equation relating plasma electron frequency, hot ion velocity and particle radii and drift frequencies
17 p2735 A71-35243

High pressure electrodeless HF gas discharge plasmas, investigating effects of external magnetic field, gas and pressure on discharge rotation frequency
17 p2789 A71-35260

Type 3 solar radio burst instantaneous emission frequency relationship to local plasma frequency in region with subrelativistic particles
18 p2958 A71-36742

Plasma cyclotron wave excitation with charged particle beam, determining unstable oscillations frequency range and spatial and time development with nonlinear analysis
19 p3111 A71-37633

Electron wave coupling in plasma column, determining exact resonance and field configurations of frequencies
19 p3111 A71-37635

Electrostatic plasma instabilities under HF alternating electric field oscillating at plasma frequency
22 p3584 A71-42465

Weakly ionized cesium plasmas produced in sealed diodes, examining LF instabilities with fluid equations
23 p3708 A71-43083

Sound waves propagation in fully ionized gas, considering electron plasma frequency
23 p3705 A71-44001

Nonlinear sum and difference frequency and second harmonic generations of current density in homogeneous magnetoplasma by nonuniform microwave electric fields
23 p3712 A71-44002

Magnetic energy pumping into plasma by slowly modulating plasmon frequency-dependent external magnetic field
24 p3851 A71-44485

PLASMA GENERATION

U PLASMA GENERATORS

PLASMA GENERATORS

NT PLASMA GUNS

NT PLASMATRONS

Shock tube generated Xe plasma electron density measurements by spectroscopy and laser interferometry, deriving ionization relaxation time
01 p0134 A71-10995

Electron density profiles in ruby laser generated Xe plasma, using differential interferometry
01 p0134 A71-10996

Shock generated Ar plasma emission spectrum intensity measurements, describing fast-response spectrometer sensitivity calibration method
01 p0134 A71-10997

Shock tube generated Ar plasma electric conductivity augmentation by electrical discharge through super-sonic plasma flow in Faraday tube
01 p0134 A71-10998

Laser produced plasmas for electrical power generation and space propulsion using fusion of deuterium-tritium pellet
01 p0135 A71-11179

Q switched laser irradiated solid lithium hydride particle plasma formation and heating, determining optimal conditions
01 p0096 A71-11482

Magnetic field confinement of ionized plasmas generated by laser-irradiated lithium hydride solid particle
01 p0137 A71-11483

Plasma generation and nuclear fusion by lasers, investigating critical parameter values for heating
01 p0137 A71-11625

Nonequilibrium plasma from pulsed discharge in crossed electric and magnetic fields
02 p0288 A71-11882

Relativistic self confined electron beam produced plasmas, measuring electron density profile by multiple pass Mach-Zehnder laser illuminated interferometer
02 p0289 A71-11946

Plasma generators for spectrochemical analysis, discussing properties and design
03 p0465 A71-13969

Steady high power plasma flows using three phase AC generator
04 p0632 A71-14794

Subnanosecond laser pulses interaction with thin Ni foil targets leading to energetic pulsed plasma beam production
04 p0608 A71-15134

High temperature laboratory plasmas diagnostics, noting time resolution for growth and decay mechanisms
06 p0896 A71-17297

Hot electron plasma confinement in cusped magnetic field, considering production in electron cyclotron resonance region by pulsed microwaves
06 p0935 A71-17491

Nanosecond laser produced lithium hydride spherical plasma expansion model, taking into account three body and radiative recombinations
06 p0938 A71-18457

Plasma produced by pulsating fast electron beam, observing electron temperature and charged particle concentration
07 p1167 A71-19232

Microwave plasma device development, noting beam plasma amplifiers and quiescent source
07 p1167 A71-19257

Plasma produced by focused Q switched ruby laser beam, considering use for minimum ignition energy measurement
07 p1123 A71-19577

Self similar laser produced plasma examination, using irradiated multilayer targets and spectrum analysis
07 p1170 A71-20169

Ion source emitter plasma column generated by electron beam injection through gas filled chamber, compensating ion space charge with fast discharge electrons
07 p1170 A71-20180

Plasma formation from transition metal target under monopulse laser radiation, noting absorbed surface density energy role in onset
07 p1171 A71-20191

Cs ion beam space charge and current neutralization by electron capture for partially ionized plasma formation, investigating longitudinal electrostatic wave excitation
07 p1171 A71-20193

Collisionless shock waves generation in theta pinches, plasma formation, experimental devices, diagnostic methods and magnetic probes
07 p1172 A71-20507

High microwave power for studying interactions in high concentration linear Ar discharge plasma waveguide in magnetic field
08 p1339 A71-21479

HF wave absorption in Ar plasma, observing production in open magnetic trap
08 p1339 A71-21481

Energetic highly ionized plasma production by pulsed laser heating of lithium hydride pellets
09 p1503 A71-22867

Dense hot plasma generation by laser beam focusing on gas or solid targets, discussing experimental setups, diagnostic methods and ionization theories
10 p1647 A71-23920

Soviet papers on low temperature plasma physics covering production and diagnostic techniques, electrokinetic and optical characteristics, electromagnetic and shock effects, metal plasmas, etc
10 p1648 A71-24188

Hydrodynamic model for heating of pulsed laser produced plasma generated at plane solid target, deriving electron temperature and ion expansion energy
10 p1621 A71-24673

Laser pulse produced energetic ion and plasma measurements fore and aft side of targets including Al and Au foils
11 p1775 A71-26084

Gas dynamics models for plasma production by irradiating solids with laser beams, taking into account spatial inhomogeneity of absorption process
11 p1775 A71-26090

Expanding laser generated plasma self similarity model from hydrodynamic equations, describing thermokinetic properties
11 p1806 A71-26092

High density and temperature plasmas produced by laser pulse heating massive solid targets, discussing interaction processes
11 p1807 A71-26094

Spontaneous magnetic fields in laser produced plasmas explained as thermoelectric currents
11 p1807 A71-26406

Plasma production by pulsating fast electron beam, observing electron temperature and charged particle concentration
12 p1934 A71-26750

Synthesized plasma of interpenetrating positive and negative ion beams, investigating oscillation amplification conditions
12 p1941 A71-27766

RF discharge quasi-homogeneous plasma device for measuring antenna impedance and sheath effects
13 p2105 A71-27996

Interferometric studies of focused Nd laser radiation interaction with thin graphite absorbing surface layer, discussing time behavior of plasma expansion and density distribution
13 p2078 A71-28446

High microwave power for studying interactions in high density linear Ar discharge plasma waveguide in magnetic field
14 p2282 A71-30666

Limiting frequency for Ar plasma absorption of HF waves, observing plasma production in open magnetic mirror configuration
14 p2282 A71-30668

Motion and collision of plasma blobs generated by giant pulse ruby laser irradiation on lithium plate
15 p2455 A71-31643

Electrochemical plasma production based on cathodic hydrogen combustion using giant condenser batteries for energy storage and quick release, applying to space propulsion technology
15 p2456 A71-31833

Plasma as fourth state of matter, including high temperature behavior, radiation emission, applied electric/magnetic fields effects and laboratory generation
16 p2617 A71-32953

Flame, laser and shock wave plasma generation, considering afterglows, ionized gas flows and high temperature effects
16 p2617 A71-32958

Shock wave generated plasmas elementary reactions, discussing shock tubes and noble and diatomic gases chemionization
16 p2540 A71-32970

Plasma generation by photon irradiation, radiolytic mechanism and high energy particle bombardment, discussing ionized media chemical reactions
16 p2540 A71-32971

Rarefied plasma flow generation by Q-switched laser pulse focusing on solid target, measuring plasma properties with Langmuir probes and microwave interferometers
16 p2586 A71-33162

High temperature dense plasma formation by laser heating of gas target, noting fusion reaction in deuterium-tritium mixture
16 p2619 A71-33647

Ultrafast laser pulses, revealing fluorescence decay, stimulated Raman scattering and plasma formation transient details
16 p2588 A71-33873

Low temperature high conductivity nonequilibrium plasma creation in MHD generators by microwave ionization
17 p2676 A71-34193

Thermal flux model of lithium plasma source at various temperatures and pressures, using arc channel model with conducting cross section
17 p2787 A71-34303

Thermal electrodeless plasma generation below RF range through magnetic induction heating, applying to argon glow and arc discharges
17 p2788 A71-34869

Electric current distributions measurement along monopole antenna in isotropic and anisotropic plasmas generated in large space chamber
17 p2716 A71-35048

Low voltage arc discharge development in cesium vapor with glowing spherical plasma cluster formation in electrode gap
19 p3109 A71-37136

Mass spectrometric investigation of plasma created in atomization of Ni and Y ferrites by laser radiation
19 p3110 A71-37142

Laser pulse heated target with thermal plasma production, obtaining target surface temperature as function of time and vaporization rate
20 p3242 A71-38845

Microwave plasma generation in magnetic field, detecting expansion related to electron cyclotron frequency harmonics
21 p3426 A71-41287

Book on high power laser radiation covering heating, melting, vaporization, particle emission, plasma production, gas and transparent material breakdown and biological effects
22 p3558 A71-42426

Operating characteristics of arc plasma generator with film and water cooling protected anode
22 p3484 A71-42784

Initial development period of low voltage arc discharge in cesium vapor leading to quasi-neutral plasma formation
23 p3710 A71-43269

Population inversion development and breakdown in active medium produced by plasma generation during pulsed discharge in molecular nitrogen laser
23 p3684 A71-43406

Interferometric fringes from study of gas plasma produced by ruby laser pulses, using Nd glass laser for heating
23 p3710 A71-43409

Plasma generation with transversely excited high pressure carbon dioxide laser and solid targets, describing optical emission spectral characteristics
23 p3712 A71-43932

Nd glass laser system with Pockels cell Q switched oscillator for producing highly ionized plasmas
23 p3686 A71-43954

Laser pulse produced plasma in freely expanding high density nitrogen gas jets, measuring electron temperature and light-plasma interaction time
23 p3687 A71-44140

Langmuir electron oscillation excitation by ion beam at velocity exceeding average electron thermal velocity in plasma formed by residual gas ionization
24 p3858 A71-45234

Hydrogen plasma generation by microwave field in magnetic-mirror device due to electron cyclotron resonance, measuring transverse diffusion coefficient dependence on magnetic field
24 p3858 A71-45235

PLASMA GUNS

Current sheet collapse phase in dense deuterium plasma focus gun heating, using streak photography and X ray and neutron measuring techniques
07 p1165 A71-18877

Dynamics of focusing electric discharges generated by coaxial plasma gun illuminated by ruby laser beam, using schlieren photography
10 p1653 A71-24758

Magnetic field generation from coaxial plasma gun, discussing mechanism in terms of azimuthal plasma mass motion imparted during initial gas discharge
14 p2281 A71-30543

Magnetic cut-off system reducing length of high density jet flows from plasma guns, using axially asymmetric field configurations
15 p2455 A71-31644

Plasma guns hot and cold plasma separation, describing diverter operation principles
19 p3112 A71-37639

Space propulsion by plasma deflagration gun, measuring specific impulse by piezoelectric probe and pendulum methods
19 p3122 A71-37871

Neutral gas acceleration to high velocity at low ionization level by electromagnetic plasma gun formed unionized shock wave
21 p3423 A71-40766

PLASMA HEATING

Electrostatic vibrations from turbulent plasma heating on basis of Stark broadening of hydrogen spectral lines, obtaining electric field strength
01 p0131 A71-10069

Electron cyclotron drift instability shown by numerical simulation as cause for anomalous plasma diffusion and heating
01 p0132 A71-10147

Thermal insulation and confinement of resistance heated He plasma in Uranan stellarator with large shear
01 p0132 A71-10678

Power transfer in plasma heating with combined RF and steady magnetic fields
01 p0137 A71-11481

Q switched laser irradiated solid lithium hydride particle plasma formation and heating, determining optimal conditions
01 p0096 A71-11482

Beam current instability and plasma heating by electron beam generated in linear discharge, discussing electron beam-cold plasma interactions
02 p0291 A71-12501

Capillary plasma heating source processes, using textolite and fiberglass-reinforced textolite dielectric discharge chambers
02 p0292 A71-12556

Plasma column ohmic and collisional heating by RF electromagnetic field, deriving energy transfer expressions
03 p0464 A71-13550

Nonuniform magnetic field cyclotron heating, presenting stochastic criteria in terms of Larmor rotation phase randomization
03 p0462 A71-13928

High Mach number collisionless shock waves in low density argon plasma, measuring electron heating and shock thickness
04 p0631 A71-14685

Hydrogen plasma turbulent heating, simulating ion-acoustic instability
05 p0786 A71-16226

Electron heating in weakly ionized plasma by magnetic perturbation
05 p0787 A71-16291

Energy deposition by MHD into supersonic argon plasma flow in shock tube
05 p0787 A71-16537

Current-interchange instability in plasma turbulent heating by current
06 p0930 A71-17395

Plasma electron cyclotron heating, observing wave excitation at 100 MHz and decay after initial wave
06 p0930 A71-17396

Plasma satellites near He I forbidden lines during turbulent heating
06 p0936 A71-17592

Self similar thermal wave in two-temperature plasma under laser heating for different pulse duration and energy absorption values
06 p0936 A71-17689

Energetic lifetime, equilibrium and thermal insulation of ohmically heated plasma in stellarator
06 p0937 A71-18350

Confinement and loss mechanisms of ohmically heated plasma in stellarator
06 p0937 A71-18351

Current sheet collapse phase in dense deuterium plasma focus gun heating, using streak photography and X ray and neutron measuring techniques
07 p1165 A71-18877

One dimensional laser heating of stationary plasma for application to controlled thermonuclear reactions
07 p1165 A71-18880

Plasma heated by cyclotron resonance using waveguide method, considering properties, confinement conditions and instabilities
07 p1170 A71-20182

Powerful laser beam and material interaction, investigating gas dynamics of plasma heating and dispersion
07 p1127 A71-20254

Hot plasma production by strong shock wave heating, using EM shock tubes under laboratory controlled conditions
07 p1172 A71-20506

Plasma HF heating boundaries by magnetic traps, noting diamagnetic effects due to ion and electron heating
08 p1339 A71-21480

High enthalpy electric arc plasma jet heaters for simulating entries in hydrogen rich Jovian atmosphere [AIAA PAPER 71-263]
08 p1274 A71-21989

Hot Cs plasma parametric resonance in variable electric field related to plasma heating
09 p1499 A71-22229

Plasma electrons heating by interaction with ultrashort laser pulses, considering hard bremsstrahlung generation
09 p1460 A71-22245

Thermal expansion of gas breakdown plasma in argon under heating by high voltage transient pumped carbon dioxide laser
09 p1463 A71-22761

Electrostatic vibrations from turbulent plasma heating on basis of Stark broadening of hydrogen spectral lines, obtaining electric field strength
09 p1504 A71-23264

Magnetic mirror confined microwave heated plasmas stability based on uniform collisionless plasma model
10 p1651 A71-24632

Hydrodynamic model for heating of pulsed laser produced plasma generated at plane solid target, deriving electron temperature and ion expansion energy
10 p1621 A71-24673

Turbulent plasma heating in current sheet between opposed magnetic fields
10 p1653 A71-24891

Metastable atom destruction, collision-radiative recombination and electron heating in low temperature decaying helium plasmas, using spectroscopic resonance line measurements
10 p1654 A71-24896

Nonuniform density cosmic plasma heating allowing energy losses by radiation and heat conduction, using filament-structured high temperature plasma region model
11 p1828 A71-25765

Electron and ion plasma heating by subnanosecond neodymium laser pulses, using computer calculations of hydrodynamic equations
11 p1806 A71-26089

Anomalous resistance and turbulent heating of strongly nonisothermal plasma in strong magnetic field due to electron scattering by ion-acoustic turbulent pulsations beats
12 p1936 A71-27032

Plasma turbulent electron and ion heating by large amplitude whistler resonant excitation, investigating mechanisms
12 p1937 A71-27182

Ion beams heating by ion-ion two stream instability perpendicular to magnetic field with cold electron background
13 p2104 A71-27851

Thermalization processes in earth bow shock with emphasis on ion heating, using electromagnetic dispersion relation for ion-ion streaming instability
13 p2054 A71-27908

Anomalous microwave energy dissipation and electron heating in collisionless plasma without decay at high collision frequencies
14 p2281 A71-30539

Hydrogen plasma HF heating boundaries by magnetic traps, noting diamagnetic effects due to ion and electron heating
14 p2282 A71-30667

Arc heated plasma expansion through nozzle, observing population inversion of neutral carbon self-absorption UV atomic line [AIAA PAPER 71-592]
15 p2454 A71-31537

Resonant plasma heating at electron cyclotron frequency second harmonic, studying interactions with microwave electromagnetic radiation in adiabatic trap
15 p2455 A71-31736

Combustion flame plasma reactions, considering collisional and chemical ionization, ion decay, electron temperatures and additives
16 p2540 A71-32969

Theta pinch deuterium plasma heating by carbon dioxide laser as function of pulse duration and energy
16 p2587 A71-33188

Ohmically heated collision plasma confinement in Uranan racetrack stellarator with large shear, describing magnetic field topography effects and plasma lifetime
17 p2785 A71-34196

Axisymmetric blunted body heating by high temperature plasma flow as function of geometry, pressure and stagnation enthalpy
17 p2669 A71-34207

Thermal electrodeless plasma generation below RF range through magnetic induction heating, applying to argon glow and arc discharges
17 p2788 A71-34869

Anomalous microwave heating of electrons in magnetized plasma, showing resonances dependence on magnetic fields and charged particles concentration
17 p2790 A71-35735

Swept Langmuir probe with sweep speeds greater than 150 V/microsec, considering electron cyclotron resonance heated hydrogen plasma confined in toroidal quadrupole
18 p2952 A71-36582

Plasma heating and compression with nonadiabatic charged particle motion in uniform magnetic field
19 p3109 A71-37137

Laser heating of D-T plasma, deriving average equations of momentum and energy conservation with allowance for thermonuclear fusion heat
20 p3275 A71-39471

Stochastic model for electron-cyclotron plasma heating by high power microwaves in magnetic mirror
21 p3422 A71-40762

HF plasma heating in Tokamak torus device by magnetosonic wave energy absorption in high density region via Buchsbaum hybrid resonance
21 p3422 A71-40764

Highly ionized hot Cs plasma parametric resonance in alternating electric field related to plasma heating
21 p3424 A71-41107

Electrons heating by matter interaction with ultrashort laser pulses, considering hard bremsstrahlung generation
21 p3394 A71-41134

Turbulent plasma heating in current sheet between opposed magnetic fields
21 p3424 A71-41270

Metastable atom destruction, collision-radiative recombination and electron heating in low temperature decaying helium plasmas, using spectroscopic resonance line measurements
21 p3425 A71-41276

Electron beam heating of cold plasma in magnetic trap as function of plasma density, showing two stream instability due to Cerenkov effect
21 p3425 A71-41285

D-T plasma cumulation laser heating problem, considering similarity theory for electron conductivity and bremsstrahlung
21 p3395 A71-41360

Cumulation-laser plasma heating analysis, considering average value theory
21 p3395 A71-41362

Nonuniform density cosmic plasma heating allowing for energy losses by radiation and heat conduction, using filament-structured high temperature plasma region model
22 p3598 A71-41533

Dense plasma heating by electron beam in magnetic trap as function of cyclotron frequency and field strength, noting strong microwave emission
22 p3583 A71-42064

- Plasma turbulent electron and ion heating by large amplitude whistler resonant excitation, investigating mechanisms 22 p3583 A71-42459
- Statistical HF electron heating at oscillating plasma boundary with acceleration of double Langmuir layer 23 p3709 A71-43260
- Acoustic instability of Joule heated nonisothermal electron plasma 23 p3709 A71-43261
- Expanding D-T plasma laser heating equations derivation, allowing for heat produced by associated thermonuclear fusion 23 p3710 A71-43320
- Interferometric fringes from study of gas plasma produced by ruby laser pulses, using Nd glass laser for heating 23 p3710 A71-43409
- Microwave upper hybrid resonance absorption, emission and heating of nonuniform axially magnetized afterglow plasma column in waveguide geometry 24 p3851 A71-44430
- Off-resonance electron heating by microwaves in mirror contained high beta plasmas 24 p3852 A71-44486
- Multispecies high temperature Tokamak plasma heating by energetic particle injection, using Balescu-Lenard kinetic equation 24 p3852 A71-44490
- Lower hybrid frequency heating and wave absorption efficiency in inhomogeneous HF cylindrical plasma 24 p3852 A71-44492
- Energy losses of collisional He plasma with ohmic heating in Uragan stellarator with large shear, comparing plasma lifetime to Bohm confinement time 24 p3855 A71-44664
- Low temperature plasma radiation flux heated absorbing fluid, investigating convective heat transfer to semitransparent wall 24 p3856 A71-44893
- PLASMA INSTABILITY**
U MAGNETOHYDRODYNAMIC STABILITY
PLASMA INTERACTIONS
NT PLASMA-ELECTROMAGNETIC INTERACTION
 Mathematical model for interaction between solar wind and interstellar gas 01 p0144 A71-10066
- VHF radiation from plasma during electron beam interaction with fast magnetoacoustic wave stimulated by external spatially periodic currents 01 p0132 A71-10155
- Solar wind injection into magnetosphere, noting effects of magnetopause outward velocity and electric field strength 01 p0146 A71-11452
- Nonlinear electrostatic vibrations in colliding antiparallel flows of rarefied plasma 02 p0289 A71-11928
- Solar wind interaction with moon, using two dimensional guiding center model 02 p0303 A71-12772
- Boundary position and thickness between geomagnetic field and solar wind plasma, simulating interaction with magnetosphere 03 p0473 A71-13107
- Thermal DC noise generated in plasma at electron-ion collisions, using quantum mechanics for noise frequencies in EM radiation RF spectra 03 p0463 A71-13345
- Carbon dioxide laser plasma lensing effect used as mirror curvature compensation for maximum output power 03 p0436 A71-13641
- Incident shock tube flow interaction with one dimensional MHD channel flow 04 p0632 A71-14687
- High temperature plasma electron density and ion signal intensity measuring apparatus for reaction rate evaluation 04 p0600 A71-15591
- Fully ionized hydrogen cosmic plasma interaction with surrounding neutral gas, noting minimum temperature and power input 05 p0810 A71-16637
- Plasma feedback system boundary conditions, describing electrical properties, dispersion relation and mode interaction 06 p0931 A71-17455
- Cosmic plasma dynamics collective phenomena, investigating models, instabilities, nonlinear interactions, wave transformations, turbulence, cosmic rays and radiative acceleration 06 p0972 A71-18330
- Recombination frequency spectrum asymmetry in interaction between high and low frequency plasma oscillations, noting role of Doppler effect 08 p1340 A71-21495
- Magnetic disturbances caused by magnetosphere-solar wind filamentary inhomogeneity interaction observed by Pioneer 6 09 p1513 A71-22560
- Linear and nonlinear collisional processes in uniform weakly interacting plasma near equilibrium in absence of external magnetic field, using quantum mechanics treatment 09 p1503 A71-22864
- Mathematical model for interaction between solar wind and interstellar gas 09 p1514 A71-23259
- Solar wind simulation for interaction with lunar magnetic field, discussing particle shadowing effects generation of electric fields 09 p1514 A71-23310
- Plasma intrusion into simulated magnetosphere compared with satellite observations, discussing spatial distribution and interplanetary magnetic field effects 09 p1529 A71-23707
- Nonhomogeneous plane parallel cold plasma flows in external magnetic field, deriving energy transfer between two sliding plasmas 10 p1651 A71-24634
- Combination frequency spectra asymmetry in bounded plasma column resulting from HF AM and PM wave interactions 10 p1651 A71-24637
- Atmospheric electrical structure control by lower ionosphere force, considering interaction between neutral atmosphere tidal circulations and ionospheric plasma in presence of geomagnetic field 10 p1604 A71-24702
- Solar wind-magnetosphere interaction modes from Explorer 33 and 35 interplanetary plasma and magnetic field data 10 p1663 A71-24780
- Photoelectron sheath and electric field around spacecraft in interplanetary space, considering typical sheath profiles and tenuous ambient plasma effects 10 p1678 A71-24799
- Papers on electronics and electron physics, Volume 29, covering plasma-RF field interactions, cluster ions formation and electron beams energy distribution 11 p1802 A71-25628
- Nonlinear beam plasma interactions theory review, using plasma column circuit equation models 11 p1805 A71-25629
- Laser-blowoff metal plasma interaction with strong transverse magnetic field, observing velocity reduction due to inhibited ambipolar electron-ion energy transfer 11 p1805 A71-25794
- Laser radiation and plasma nonlinear interaction, using particle description of electron motion 11 p1806 A71-26093
- High density and temperature plasmas produced by laser pulse heating massive solid targets, discussing interaction processes 11 p1807 A71-26094
- Small amplitude oscillations in system of relativistic electron beam penetrated plasma, calculating dispersion curves 12 p1936 A71-26919
- MHD wave coupling in homogeneous plasma in field dependent on single coordinate, obtaining modified Alfvén and acoustic waves stability conditions 13 p2106 A71-28498
- Interplanetary magnetic field angular gradient and sectorial effects on solar wind, discussing wind velocity 13 p2128 A71-28527
- Energy transport mechanisms of rapid diamagnetism decay in plasma stream collisions, using two fluid shock front model 13 p2110 A71-29371
- Polar magnetic disturbances, discussing correlation with interplanetary magnetic field and interaction effects between solar wind and magnetosphere 14 p2231 A71-29907
- Solar wind interaction with planetary atmospheres, discussing various models relationship to observational data 14 p2298 A71-29908
- Coaxial plasma beam polarization interaction in toroidal magnetic field with diverter, showing axial stream trapping in hollow plasma cylinder 15 p2453 A71-31244
- Asymmetries in magnetospheric shock layer due to upstream interplanetary magnetic field, considering forward stagnation region of solar wind-magnetosphere interaction 15 p2395 A71-31546
- [AIAA PAPER 71-610] Plasma induced random noise and striation oscillations in carbon dioxide lasers as function of operational parameters 15 p2423 A71-32608
- Combination frequency spectrum asymmetry in interaction between high and low frequency plasma oscillations, noting Doppler effect role 16 p2618 A71-33045
- Plasma beams injection into toroidal magnetic field along gradient or radius, using polarizational interaction 17 p2786 A71-34281
- Stationary plasma flow interaction with axisymmetric spatially periodic magnetic field in presence of Hall effect, determining electric currents structure 19 p3109 A71-37139
- Magnetic field aligned electric field production by hot magnetospheric plasma interaction with cold ionosphere 19 p3048 A71-37401
- Solar wind MHD interaction with magnetosphere, taking into account photospheric origin, velocity in interplanetary space and Parker theory 19 p3126 A71-37460
- Satellites interaction with ionosphere, concerning applications to particle density, electric field, flux and drag measurements 19 p2992 A71-37560
- Collisionless momentum transfer between interstreaming ions in laser produced plasma, using fast photography, shadowgraphy and electric potential probes 19 p3114 A71-38177
- Debye potential well formation in collisionless current carrying plasma, noting wave-particle resonant interaction role 19 p3115 A71-38216
- Interplanetary plasma and magnetic field interaction with earth magnetosphere using spacecraft measurements during storms 19 p3145 A71-38272
- Astronomical models of solar wind interaction with interstellar medium, determining magnetic field effects on shock wave 20 p3278 A71-39139
- Nonisothermal plasma longitudinal ion acoustic and Langmuir oscillations phase and amplitude interactions, estimating energy transfer and turbulence criteria 24 p3853 A71-44509
- Rarefied theta pinch plasma collective interactions, examining kinetic instability, electron energy distribution, anisotropy, suprathermal microwave emission, cyclotron harmonics and oscillations 24 p3854 A71-44513
- Thermal and nonequilibrium microwave emission from colliding plasma beams in transverse magnetic mirror field 24 p3854 A71-44517
- PLASMA JET SYNTHESIS**
 Plasma jet chemical reactions, discussing temperature and quenching effects, molecular and gas decomposition and endothermic compounds formation 16 p2540 A71-32967
- Plasma jet formation within high pressure discharges in air at atmospheric pressure, discussing electrode configuration, current density and accelerating magnetic field strength 17 p2787 A71-34285
- PLASMA JET WIND TUNNELS**
 Heat flux measurement in high pressure arc heated wind tunnel flow by swept null point calorimetry, describing calorimeter configurations and test results [AIAA PAPER 71-428] 11 p1763 A71-26217
- High enthalpy plasma jet wind tunnels, considering arc heaters and simulation range extension to higher adiabatic static pressures to avoid nonequilibrium expansion in nozzle 18 p2898 A71-36413
- Plasma wind tunnels for high enthalpy flows of low density, considering plasma arc heaters and expansion nozzles with diffusers 19 p3040 A71-37461
- PLASMA JETS**
 Dense plasma high current density effects on low voltage arc in thermionic converter 01 p0005 A71-10159
- Saha equilibrium deviations in wall stabilized rare gas arc plasmas under normal pressure, describing numerical method for temperature and density distributions evaluation 01 p0133 A71-10746
- Arc oscillation spectra in MPD thruster operation at low magnetic field 01 p0142 A71-10959
- Electron concentration distribution over plasma discharge cross section, using interferometry 02 p0288 A71-11887
- Atomic and ion temperatures in Ar plasma low pressure discharge in metallic tubes with conducting walls 02 p0259 A71-11931
- Plasma jet electron temperature and distribution behind pulsed coaxial accelerator exit section 02 p0290 A71-12182
- Discharge current oscillations attributed to acoustic wave excitation by Q switched carbon dioxide laser 02 p0261 A71-12341
- Analytical sensitivity and reproducibility in plasma jet excitation for spectrochemical applications 03 p0465 A71-13970
- Aerosol powder suspensions for spectrochemical objectives in plasma jets 03 p0465 A71-13971
- Physical chemistry of arc plasma, considering radial distribution, spectral density and energy relations for spectrochemical applications 03 p0465 A71-13973

Ar-Ag arc, microwave discharge and plasma torch techniques in emission spectroscopy of trace elements in biological materials

03 p0377 A71-14421

Argon plasma jet local thermodynamic equilibrium at various electron densities, examining Boltzmann excitation and ionization temperatures

04 p0633 A71-14902

Laminar boundary layer on porous plane situated in plasma jet, examining transfer phenomena with chemical reaction

04 p0572 A71-15507

Quasi-steady coaxial MPD arcs characteristics, studying Ar ion velocities, electrostatic ion acceleration mechanism and arc voltage gradient

[AIAA PAPER 70-165]

05 p0795 A71-16573

Plasma jet radial velocity distribution measurement by probe technique, calculating current density from azimuthal magnetic field via Maxwell equation

[DFVLR-SONDDR-88]

05 p0788 A71-16643

Solid metal plates breakdown mechanism at high temperatures and supersonic plasma jet action

05 p0768 A71-16778

Plasma torch stagnation point heat transfer measurements, using heat pipe calorimetry

[AIAA PAPER 71-81]

06 p0902 A71-18538

Underexpanded plasma jet supersonic outflow simulation, using laser irradiation of absorbent target materials

07 p1166 A71-19133

Plasma jet two stage acceleration in coaxial systems, superposing additional discharge current

07 p1167 A71-19234

Weakly ionized gas discharge three dimensional unsteady motion of viscous incompressible gas discharge plasma in homopolar device curvilinear channel, emphasizing secondary overflow during acceleration

07 p1167 A71-19235

Flame stabilization by plasma jets increasing electrical input power

07 p1168 A71-19579

Electron density profiles in supersonic plasma jet, using immersed microwave probe

[AIAA PAPER 71-272]

08 p1342 A71-21998

Sawtooth structure of convective plasma column in sulfur hexafluoride at cross flow Mach numbers, using thermionic rail accelerator

09 p1498 A71-22096

X ray emission from optical and inner shell transitions of multiply ionized Cu, Fe, and Ti in low pressure discharge dense plasma

09 p1501 A71-22414

Plasma flame temperature and flow characteristics in plasma jet transfer-type metal cutters from spectroscopic measurement and high speed streak camera photography

09 p1454 A71-23032

Physical properties of Cs discharge plasma with incandescent electrode, considering Cs atoms ionization near cathode by thermal electrons accelerated by potential jump

10 p1650 A71-24528

Highly underexpanded plasma jet structure with coaxially superimposed arc discharge, investigating stationary MHD normal shock in jet core

[DFVLR-SONDDR-108]

10 p1650 A71-24600

Thermal conditions in asymptotic region of atmospheric pressure Ar arc plasma, considering nonequilibrium ionization due to ambipolar diffusion

10 p1654 A71-24971

Closed form formula for plasma thrust from arc jets with self induced magnetic fields, predicting electrode erosion and entrainment

11 p1810 A71-25457

Carbon dioxide plasma discharge current changes from Q switched laser irradiation, studying excitation and relaxation mechanisms

11 p1774 A71-25933

Aerodynamic probe measurements for plasma jets produced by electrothermal and Hall current accelerators

11 p1764 A71-26275

High velocity plasma jet accelerator operation, plotting heat and electromagnetic forces vs air current, mass flow rate and nozzle diameter

11 p1807 A71-26289

Plasma jet two stage acceleration in coaxial systems, superposing additional discharge current

12 p1934 A71-26752

DC vacuum arc ion currents between copper electrodes, discussing wall geometry, plasma ionization, starvation phenomena and anode spot formation

12 p1939 A71-27269

Plasma jet drift stabilization in toroidal magnetic field with divertor producing 180 degree field line rotation

12 p1941 A71-27548

Pulsed MPD arc experiment, determining voltage characteristics and rotating current spokes occurrence and behavior

12 p1941 A71-27567

Rotating spole in unstable pulsed MPD arc, noting rotation frequency and resemblance to plasma rotation

[AIAA PAPER 69-234]

12 p1941 A71-27568

Electron energy distribution in plasma discharge of Hg electron bombardment ion engines, using Langmuir probe

13 p2114 A71-27985

Fast plasma ions energy distributions in toroidal accelerators with quasi-stationary discharge

13 p2108 A71-28854

Nonlinear skin effects in gas discharge plasma during electromagnetic wave propagation with dissipation, obtaining wave amplitude and carrier temperature dependence on reflection parameters

13 p2108 A71-29042

Argon plasma jet velocity distribution at MHD channel exit with magnetic quadrupole, using calorimetric plasma velocity measurements and Doppler shift observations

14 p2278 A71-29611

German monograph on hot machining of high temperature steels by flame heating with propane-oxygen and plasma arc burners

14 p2252 A71-30232

Azimuthal current growth and microwave radiation in theta pinch hydrogen plasma discharge from sensitive superheterodyne receivers

14 p2282 A71-30663

High microwave power for studying interactions in high density linear Ar discharge plasma waveguide in magnetic field

14 p2282 A71-30666

Plasma jet electron temperature and distribution behind pulsed coaxial electromagnetic accelerator exit section, studying time variation

15 p2454 A71-31490

Nonequilibrium effects in Ar free jet plasma, using cooled Langmuir probe for electron temperature and ion density measurements through shock wave in front of blunt body

[AIAA PAPER 71-591]

15 p2454 A71-31536

Ar arc plasma thermochemical nonequilibrium, using finite difference techniques for nonlinear integrodifferential equations

15 p2455 A71-31538

Magnetic cut-off system reducing length of high density jet flows from plasma guns, using axially asymmetric field configurations

15 p2455 A71-31644

Thermal stability test assembly for refractory materials cylindrical specimens, using argon plasma jet

15 p2385 A71-32238

Soviet papers on gas discharge plasmas and strong magnetic fields covering plasmatrons, MHD generators, electric arc combustion, etc

15 p2457 A71-32266

Cesium spectral lines luminescence and population during helium-cesium discharge plasma decay

15 p2458 A71-32407

Energy necessary to produce beam ion in plasma discharge of Hg electron bombardment ion source

16 p2623 A71-32841

Electrical discharge plasmas, investigating electron multiplication, secondary processes, Paschen law, pressure effects and formation time lag

16 p2617 A71-32957

Solid metal plates erosion mechanism at high temperatures under supersonic plasma jet action, noting dependence on specific heat and latent heat of fusion

16 p2591 A71-33030

Rotating arc plasma jet exhaust flow pattern visualization, using bifocal lens system and photographic flash technique in particle track photography

16 p2579 A71-33339

He-Ne laser emission and discharge plasma parameters, detailing variable magnetic field effects on modulation

17 p2752 A71-34389

Transverse magnetic field effects on Ar cross flow arc in constant velocity mainstream

17 p2788 A71-34868

Langmuir probe measurement of ionization density of Ar plasma jet, suggesting electron-ion recombination in probe vicinity

17 p2789 A71-35338

Hydrazine formation from ammonia in constricted plasma discharge using electron source in selected high energy range

18 p2955 A71-35968

Gas and electron temperature and thermal nonequilibrium in argon plasma jet from electrodeless induction discharge

19 p3111 A71-37578

Diagnostic He-Ne laser interferometer for measuring electron concentration in cross section of argon plasma jet

19 p3073 A71-37786

Physical properties of Cs discharge plasma with incandescent electrode, considering Cs atoms ionization near cathode by thermal electrons accelerated by potential jump

19 p3116 A71-38255

Monograph on electron drift rate measurement in low pressure arc discharge using microwave dragging technique

19 p3116 A71-38549

Positive ion composition of collision dominated weakly ionized HF hydrogen plasma discharge, measuring abundance ratio as function of extraction voltage and gas density

20 p3275 A71-39429

Acoustic pulse excited ionization waves and wakes measurement in glow discharge plasma, giving phenomenological explanation

21 p3421 A71-40089

LF oscillations excitation and resonance amplification in mercury vapor plasma discharge

21 p3425 A71-41283

Hot plasma fast ions energy distributions in toroidal accelerators with quasi-stationary discharge

21 p3426 A71-41286

Plasma anodization of Si in positive column of DC oxygen glow discharge, considering silicon dioxide growth rate in negative glow, Faraday dark space and anode fall

22 p3581 A71-41809

Diagnostics of Ar free jet expansion from high pressure inductive arc source into low density wind tunnel, observing background gas effects

22 p3583 A71-42048

Strong current z discharge collisionless plasma, investigating ions distribution functions fine structure

23 p3708 A71-42890

Plasma jet injection stoppage and reflection in strong transverse magnetic field, considering instability due to flow interactions

23 p3709 A71-43265

Coalescence /collapse/ of overlapping spectral lines due to nonadiabatic broadening for Stark structure of hydrogen and helium lines in discharge plasma

23 p3707 A71-43407

Cesium ion sampling measurements in DC and RF plasma discharges, using mass spectrometry

24 p3851 A71-44429

Electron temperature and density oscillations in beam plasma discharge, using light intensity spectroscopic observations

24 p3854 A71-44516

High current pulsed arc in hydrogen plasma at 400 atm, showing instability with rising pressure and arc length

24 p3854 A71-44519

Dense discharge plasma temperature and ionization distributions in He, H and Ar, investigating pulsed arc emission dependence on current and pressure

24 p3855 A71-44520

Electron temperature and density of HF inductive discharge in hydrogen plasma

24 p3855 A71-44524

PLASMA LAYERS

Quasi-Alfven and acoustic wave coupling in inhomogeneous stratified plasma within intense magnetic field as function of directional pressure

02 p0292 A71-12627

Warm continuously stratified electron plasma fields behavior in coupling region excited by incident electron-acoustic wave

02 p0293 A71-12742

Magnetotail energetic electron event simultaneous observations by Vela 3A and Imp 3 satellites, evaluating plasma sheet boundary motion hypotheses

03 p0421 A71-14545

Magnetotail plasma sheet electron and proton energy spectra and angular distribution over auroral zone, comparing Vela satellite and rocket measurements

06 p0887 A71-17260

Charged particle beam interaction with electrostatic surface waves in plasma layer

06 p0929 A71-17317

Plasma coated spherical antenna radiation, discussing hot and cold plasmas frequency and electroacoustic wave effects

06 p0875 A71-17730

Spherical antenna covered by lossy hot plasma layer, calculating radiation power

06 p0869 A71-18018

Energetic electrons in magnetospheric tail plasma sheet, investigating flux time profiles and correlation with local magnetic fields from Imp 3 satellite observation data

07 p1186 A71-19658

Plasma configurations kinetic description by differential equations based on Vlasov and Maxwell equations, obtaining boundary layer distribution between plasma and magnetic field

08 p1340 A71-21492

Pioneer 9 space probe electric field experiment and near earth observations of noise spectra variations related to diffusive plasma layer

09 p1529 A71-23711

Plasma sheet proton ring current, trapping boundary and plasmopause interrelations near magnetic equator and local midnight by satellite-borne analyzer array

10 p1605 A71-24781

Longitudinal plasma layer waves kinetic theory, considering particles specular reflection from layer boundaries

12 p1937 A71-27203

- Hydromagnetic wave coupled solar wind-plasma sheet effects on resonant oscillations of geomagnetic tail, using two dimensional model 13 p2119 A71-27910
 - States stabilization in low density plasma layer in ion-accelerating constant external electric field 13 p2108 A71-28857
 - Magnetoactive plasma layer in strong constant magnetic field, computing dispersion equation for large amplitude thermomagnetic wave propagation 15 p2456 A71-31745
 - Plasma configurations kinetic description by differential equations based on Vlasov and Maxwell equations, obtaining boundary layer distribution between plasma and magnetic field 16 p2618 A71-33043
 - Time variations of magnetotail plasma sheet from electron energy spectral measurements on Vela satellites 16 p2629 A71-33945
 - Van Allen radiation belts and plasma sheet energy loss control, using cold plasma injection 16 p2629 A71-33976
 - Plane plasma layer stabilization by force-free magnetic field 17 p2789 A71-35342
 - Reflection and transmission coefficients for electromagnetic propagation across magnetic field in parabolic plasma layer, determining EM-plasma wave conversion efficiency 19 p3014 A71-37079
 - Spatial distribution, ion density and space potential measurements in plasma boundary layer at conducting sphere 19 p3112 A71-37738
 - Plasma layer effect on natural oscillations of magnetosphere tail, using infinite plasma cylinder model immersed in interplanetary plasma 20 p3216 A71-39137
 - Magnetotail plasma sheet variations association with auroral display features during substorms from all sky photography 20 p3230 A71-39880
 - German monograph on plasma layer temperature distribution in optical resonator covering spectral distribution of thermal radiation 21 p3379 A71-40749
 - Electromagnetic HF wave field pressure effects on slow transverse magnetic wave propagation along plasma layer, noting dispersion equations difference from linear theory 21 p3426 A71-41400
 - Geomagnetic Pi 2 pulsations association with magnetic storm onset in quiet conditions, discussing plasma sheet and pause theories 22 p3535 A71-42051
 - I-V characteristics of weakly ionized cold plasma plane layer with electron-atom collisions 22 p3584 A71-42875
 - Low energy particle plasma sheet and convection electric field distributions over auroral zones and polar caps from satellite Injun 5 observation 23 p3669 A71-43168
 - Statistical HF electron heating at oscillating plasma boundary with acceleration of double Langmuir layer 23 p3709 A71-43260
 - Stratified nonequilibrium plasma ionization instability in crossed fields investigated by physical model without diffusion processes and boundary effects, considering space-time behavior of perturbation 23 p3713 A71-44152
- PLASMA LIFETIME**
- Energetic lifetime, equilibrium and thermal insulation of ohmically heated plasma in stellarator 06 p0937 A71-18350
 - Plasma ions lifetime and energy spectra in quadrupole magnetic trap as function of energy and time 08 p1340 A71-21483
 - Plasma ions lifetime and energy spectra in quadrupole magnetic trap as function of energy and time 14 p2282 A71-30670
 - Ohmically heated collision plasma confinement in Uragan racetrack stellarator with large shear, describing magnetic field topology effects and plasma lifetime 17 p2785 A71-34196
 - Longitudinal ambipolar sound instability effect on duration of plasma particle motion to wall across magnetic field, using phase method 23 p3709 A71-43263
 - Plasma diffusion lifetime and electron concentration measurements in Tokamak-3 by pulsed neutral hydrogen injection and microwave multichord probing 24 p3852 A71-44488
 - Energy losses of collisional He plasma with ohmic heating in Uragan stellarator with large shear, comparing plasma lifetime to Bohm confinement time 24 p3855 A71-44664
- PLASMA LOSS**
- Monograph on particle diffusion losses in contact ionization plasmas under Q machine conditions covering collisionless theory, thermalization, alkali metals, ion recombination, etc 01 p0131 A71-10102
 - End loss elimination in MHD induction generators via nonconducting baffles and end coils 01 p0143 A71-10965
 - Q-machine with boundary segments to provide passive feedback for reducing Kelvin-Helmholtz instability and plasma losses 06 p0933 A71-17467
 - Dynamic control of steady state plasma loss in cusped magnetic field, considering density and electron and ion temperatures 06 p0935 A71-17490
 - Confinement and loss mechanisms of ohmically heated plasma in stellarator 06 p0937 A71-18351
 - Plasma ordinary wave mode electromagnetic cyclotron instability, discussing Dory-Guest-Harris type loss cone distributions 21 p3421 A71-40627
 - Plasma losses in high current plasma configuration due to inverse skin effect by observation for discharge regimes in theta pinch, zeta and Tokamak systems 21 p3422 A71-40763
- PLASMA OSCILLATIONS**
- Feedback instability of LF oscillations in high pressure plasma diode 01 p0133 A71-10685
 - Arc oscillation spectra in MPD thruster operation at low magnetic field 01 p0142 A71-10959
 - Longitudinal oscillations excitation by transverse electromagnetic wave in collision-magnetized plasma, noting LF wave buildup 01 p0134 A71-11030
 - Microwave signal scattering by LF oscillations in electrodeless induction discharge plasma 01 p0135 A71-11031
 - HF and LF spatial echo plasma oscillations associated with wave transformations produced by external perturbations 01 p0135 A71-11033
 - Self similar unsteady waves in cold plasma containing magnetic field, determining plasma oscillations 01 p0135 A71-11095
 - Surface oscillations energy and attenuation in damped spectral region of semibounded degenerate electron plasma 02 p0288 A71-11630
 - Regular and stochastic oscillations in plasma beam discharge produced by beam instability from observing time dependent variations in spectral line luminescence intensities 02 p0288 A71-11634
 - Inhomogeneous plasma oscillations excitation by high intensity electron beam, causing instability greater than hydrodynamic beam mode 02 p0288 A71-11890
 - Discharge current oscillations attributed to acoustic wave excitation by Q switched carbon dioxide laser 02 p0261 A71-12341
 - Plasma echo oscillations superposition of consecutive perturbations separated by intervals greater than characteristic decay time 02 p0291 A71-12508
 - Monograph on corrections to Holtsmark continuum model for plasma fluctuations covering probability distributions, quantum mechanical corrections for hot plasmas, etc 02 p0293 A71-12843
 - Satellite topside sounders oblique echoes, investigating upper hybrid resonance with WKB technique 03 p0420 A71-14531
 - Two stream electron plasma with Coulomb particle collisions, considering autooscillations and nonlinear friction characteristic 04 p0633 A71-15109
 - Inhomogeneous magnetoplasma electrostatic LF oscillations, discussing wave modes and instability conditions 04 p0634 A71-15257
 - Plasma oscillations excitation in ion sheath by electron beam, presenting frequency and amplitude variations as functions of discharge current and target bias voltage 04 p0634 A71-15259
 - Small amplitude nonlinear longitudinal plasma oscillations perturbation analysis, discussing Landau damping, monochromatic wave evolution and independent variable expansion 05 p0789 A71-16659
 - Plasmas and liquids inhomogeneous flow oscillations, determining resonance points effect on stability and oscillatory properties 05 p0790 A71-16825
 - Density thresholds for anisotropy and loss-cone instabilities onset in hot electron plasmas as function of frequency, wavelength and propagation direction of oscillations 05 p0790 A71-16937
 - Argon ion laser plasma tube anodic coherent oscillations and noise suppression, using secondary discharge between anode and auxiliary cathode 06 p0906 A71-17306
 - Solar photosphere oscillations, suggesting convection zone acting as resonant cavity 06 p0971 A71-18243
 - LF echo oscillations in nonequilibrium plasma under low density charged particle beam 06 p0937 A71-18353
 - Surface wave conversion to longitudinal oscillations near strong discontinuity in resonant cold magnetoactive plasma 06 p0937 A71-18355
 - Magnetically confined laser produced plasma radial oscillations, deriving equation of motion for expanding boundary [AIAA PAPER 71-108] 06 p0938 A71-18558
 - One component system wave propagation kinetic theory, calculating monatomic gas and plasma oscillations by discrete ordinate method 07 p1165 A71-18876
 - Heuristic method for phase velocities and growth rates of ion and electron plasma oscillations generalized to multicomponent plasmas 07 p1166 A71-18887
 - Plasma nonlinear drift oscillation instabilities, discussing plasma interaction with HF electromagnetic fields 07 p1167 A71-19229
 - Plasma instabilities under radial magnetic field effect across homogeneous field, considering oscillation modes 07 p1167 A71-19231
 - Low temperature confined cesium plasma, observing ion-acoustic oscillation excitation effects on transfer process and ionization 07 p1167 A71-19236
 - Feedback instability of LF oscillations in high pressure plasma diode 07 p1170 A71-20147
 - Nonlinear collisionless magnetoplasma waves and ionospheric irregularities electric field intensity, defining nonlinear oscillations domain by pseudopotential well 08 p1339 A71-21206
 - Plane light wave interactions with moving dielectric medium, considering electron UV or ion resonant oscillation in regions of anomalous dispersion 08 p1253 A71-21278
 - Recombination frequency spectrum asymmetry in interaction between high and low frequency plasma oscillations, noting role of Doppler effect 08 p1340 A71-21495
 - Self similar unsteady waves in cold plasma containing magnetic field, determining plasma oscillations 08 p1342 A71-21953
 - Natural potential and nonpotential electron oscillations excitation in plasma by transverse wave field, determining wave amplitude threshold and excitation instability 09 p1500 A71-22239
 - Radiative instability of nonequilibrium plasmas in magnetic traps, considering circularly polarized oscillations propagating along magnetic field 09 p1500 A71-22241
 - Nonisothermal plasma ion acoustic oscillations spectral energy density in electromagnetic wave field, calculating HF conductivity and absorption coefficient 09 p1500 A71-22243
 - MHD wave propagation in magnetoplasma perturbed by LF magnetoacoustic waves, considering wave scattering and polarization 09 p1505 A71-23566
 - Unstable electron plasma oscillations quasi-linear theory, discussing improper treatment of perturbed electron distribution for damped waves leading to negative diffusion coefficient 10 p1647 A71-23893
 - Soviet book on homogeneous plasma instabilities covering oscillations, magnetic effects, particle velocities, Landau damping, dielectric permittivity, electron fluxes and ion-cyclotron instabilities 10 p1648 A71-24016
 - LF plasma beam density oscillation spectra from microwave emission amplitude modulation 10 p1649 A71-24316
 - Transverse spatial particle diffusion in plasma under random oscillations, examining interaction between collisionless plasma and longitudinal wave 10 p1649 A71-24318
 - Short wave HF instabilities in strongly inhomogeneous plasma with hot electrons, considering ion acoustic oscillations and electron cyclotron harmonics 10 p1650 A71-24525
 - Flute oscillations stability in low density plasma within strong magnetic field of mirror geometry, calculating unstable oscillation spectrum by Galerkin method 10 p1650 A71-24526
 - Electron beam relaxation in plasma, discussing experimental studies of oscillation amplitude and beam electrons energy distribution relationships during predominantly longitudinal plasma oscillation excitation 10 p1650 A71-24627

Variable density cold inhomogeneous plasma small amplitude free electrostatic oscillations investigation by Green function of differential equation

10 p1652 A71-24662

Microwave signal attenuation in LF oscillation beam plasma discharge, comparing to braking cyclotron absorption effect

10 p1653 A71-24880

Plasma nonlinear drift oscillation instabilities, discussing plasma interaction with HF electromagnetic fields

12 p1934 A71-26747

Plasma instabilities under radial magnetic field effects across homogeneous field, considering oscillation modes

12 p1934 A71-26749

Low temperature confined Cs plasma, observing ion-acoustic oscillation excitation effects on transfer process and ionization

12 p1935 A71-26754

Stability and oscillation of zero-beta magnetically confined plasmas, applying to multipole configuration

12 p1935 A71-26917

Small amplitude oscillations in system of relativistic electron beam penetrated plasma, calculating dispersion curves

12 p1936 A71-26919

Short wave ion-cyclotron plasma oscillations excitation by electrons drifting in magnetic field for wavelength much less than ion Larmor radius

12 p1936 A71-27033

Potential and nonpotential equation for Alfvén waves and ion cyclotron oscillations in low density nonisothermal plasma

12 p1936 A71-27035

Bounded low pressure plasma oscillation frequency dependence on discharge chamber length, constant/variable potentials longitudinal profiles and density distribution

12 p1936 A71-27037

Plasma in strong electric and magnetic field with allowance for inelastic electron collisions with neutral particles, showing resonant oscillations from Born approximation

12 p1937 A71-27183

Hot plasma oscillations analysis for instabilities as function of magnetic viscosity and heat fluxes, using inertial waves dispersion equations

12 p1937 A71-27202

Synthesized plasma of interpenetrating positive and negative ion beams, investigating oscillation amplification conditions

12 p1941 A71-27766

Monoenergetic beam relaxation dynamics in plasma, describing oscillation excitation and diffusion allowing for instability

12 p1942 A71-27769

Statistical analysis of random oscillations excited in electron beam-plasma system based on signal recording data

13 p2106 A71-28364

Optimal control of oscillations of electrically conducting fluid by magnetic field in plane channel with free boundaries, using dynamic programming

13 p2107 A71-28728

Electron beam instability in cylindrical magnetically confined plasma column, calculating quasi-static oscillations spatial growth increments

14 p2279 A71-30090

Large amplitude ion acoustic wave propagation in streaming ion plasma, noting nonlinear effect in amplitude oscillation observation

14 p2281 A71-30541

Ion-acoustic oscillations excitation in rarefied plasma layers confined by external high frequency TE wave electromagnetic field

14 p2281 A71-30555

Ion beam collisionless relaxation in hot electron plasma, observing oscillation spectra and velocity distributions

15 p2453 A71-31245

Light and radio emission from Orion nebula flare stars in meter waveband, discussing coherent mechanisms of plasma oscillations and gyro/synchrotron radiation amplification

15 p2485 A71-31696

Guiding center equations for charged particle motion and statistical fluctuations of plasma in magnetic field, using Krylov-Bogoliubov transformation

15 p2458 A71-32393

Plasmas and liquids inhomogeneous flow oscillations, determining resonance points processes effect on stability and velocity

15 p2459 A71-32504

Ion motion effect on first order oscillations in infinite homogeneous two-component cold plasma in constant magnetic field and circularly polarized external field

15 p2459 A71-32651

Oscillations excited by pulsed dipole antenna at upper hybrid resonance in weakly inhomogeneous plasma investigated by Wentzel-Kramer-Brillouin approximation

15 p2460 A71-32656

Plasma oscillations growth rates for symmetrical double-humped velocity distributions, comparing with distribution functions without infinite tails

15 p2460 A71-32657

Plasma-electron beam system relaxation oscillations due to threshold excitation of transverse ionic oscillations by HF vibrations

15 p2460 A71-32706

HF magnetic field effects on LF plasma instability and oscillation spectrum

16 p2615 A71-32794

Combination frequency spectrum asymmetry in interaction between high and low frequency plasma oscillations, noting Doppler effect role

16 p2618 A71-33045

Temporal echo oscillations in collisionless relativistic electron plasma

17 p2786 A71-34198

Plasma fluctuations and diffusion correlation analysis in linear octupole magnetic confinement, determining dispersion relation for interchange instability

17 p2786 A71-34283

Numerical analysis of plasma expansion confined by magnetic field, emphasizing boundary oscillation and temperature rise, based on hyperbolic and parabolic system equations

18 p2952 A71-36308

Parametric plasma instability in HF electric field and constant magnetic field, noting longitudinal plasma oscillations growth

19 p3108 A71-37130

Nonthermal electrons interaction with electron plasma oscillations and HF transverse waves in upstream solar wind

19 p3125 A71-37353

Stark contours of hydrogen spectral lines in turbulent plasma with high noise level due to HF Langmuir oscillations

19 p3110 A71-37388

Plasma cyclotron wave excitation with charged particle beam, determining unstable oscillations frequency range and spatial and time development with nonlinear analysis

19 p3111 A71-37633

Electrical microwave probe for measuring HF potential oscillations in low temperature plasma

19 p3064 A71-37787

Short wave HF instabilities in strongly inhomogeneous plasma with hot electrons, considering ion acoustic oscillations and electron cyclotron harmonics

19 p3116 A71-38251

Ion acoustic instability in ionosphere in presence of fast particles inhomogeneity, estimating ions and electrons drift velocities

19 p3129 A71-38366

Hot plasma oscillations analysis for instabilities as function of magnetic viscosity and heat fluxes, using inertial waves dispersion equations

19 p3116 A71-38614

VLF plasma oscillations in spherical magnetized cold cathode DC discharge, determining frequency relationship to current/voltage, gas pressure, magnetic field strength and cathode diameter

20 p3273 A71-38880

Electrostatic oscillations excitation in magnetized homogeneous plasma by electromagnetic waves nonlinear interactions, deriving expression for induced fluctuations spectral density

20 p3273 A71-38966

Plasma layer effect on natural oscillations of magnetosphere tail, using infinite plasma cylinder model immersed in interplanetary plasma

20 p3216 A71-39137

Nonlinear Landau damping proposed as explanation for electron plasma oscillations amplification by plasma wave amplitude increase

20 p3274 A71-39349

Ion-cyclotron perturbation build-up in inhomogeneous plasma, investigating ion magnetic drift instability dependence on pressure

21 p3422 A71-40760

Natural potential and nonpotential electron oscillations excitation in plasma by transverse wave field, determining wave amplitude threshold and excitation instability

21 p3424 A71-41125

Radiative instability of nonequilibrium plasmas in magnetic traps, considering circularly polarized oscillations propagating along magnetic field

21 p3424 A71-41130

Nonisothermal turbulent plasma ion acoustic oscillations spectral energy density in electromagnetic wave field, calculating HF conductivity and absorption coefficient

21 p3424 A71-41132

Surface waves at Fermi electron plasma boundary, using kinetic theory of plasma electromagnetic oscillations

21 p3425 A71-41278

LF oscillations excitation and resonance amplification in mercury vapor plasma discharge

21 p3425 A71-41283

Oscillations in He, Ne and Ar glow discharges, obtaining I-V characteristics

21 p3426 A71-41290

Piezosemiconductors nonequilibrium electron plasma current oscillations under strong electric and magnetic field interactions

22 p3584 A71-41644

Electron beam interaction with plasma in ion sources with oscillating electrons, noting increased ion current

22 p3580 A71-41645

Kinetic equations for phase space cross correlation functions of electron density fluctuations in magnetized weakly ionized plasma, using relaxation model

22 p3581 A71-41895

Homogeneous positive plasma column perturbation analysis in axial magnetic field, deriving model for ionization waves dispersion characteristics

22 p3582 A71-41898

Electron beam-plasma system oscillation spectrum control through modulation by external HF signal, discussing theory and experimental verification

22 p3583 A71-42317

Longitudinal electron oscillations damping in ionized plasma, obtaining wave dispersion relation from BGK model

22 p3583 A71-42372

Plasma in strong electric and magnetic field with allowance for inelastic electron collisions with neutral particles, showing resonant oscillations from Born approximation

22 p3584 A71-42460

Statistical HF electron heating at oscillating plasma boundary with acceleration of double Langmuir layer

23 p3709 A71-43260

Conversion effectiveness of oscillations induced by electron beam in bounded anisotropic plasma into electromagnetic emission

23 p3710 A71-43275

Fully ionized plasma particle collision effects on surface oscillation stability

23 p3711 A71-43558

Strong magnetic field effects on acoustic oscillations and instability in stationary inhomogeneous low temperature plasma flow in crossed fields

23 p3712 A71-43917

Parametric hybrid resonance excitation of longitudinal oscillations in nonhomogeneous magnetoplasma by HF electromagnetic field

24 p3852 A71-44491

External, HF, traveling wave field interactions with homogeneous electron plasma longitudinal oscillations under magnetic field

24 p3853 A71-44503

Plasma LF oscillations in Sirius stellarator, showing fundamental frequency dependence on density temperature and magnetic field strength

24 p3853 A71-44504

Raman microwave scattering on Langmuir oscillations, showing suprathermal emission origin in theta pinch plasma

24 p3853 A71-44505

Electron temperature and density oscillations in beam plasma discharge, using light intensity spectroscopic observations

24 p3854 A71-44516

Ohmic discharge plasma resistance, temperature and oscillations in weak electric fields under electron beam excitation in Sirius stellarator

24 p3854 A71-44518

Plasma perturbations in curved magnetic field due to electron thermal conductivity finiteness

24 p3856 A71-45053

Electron beam and plasma nonlinear interactions, noting scattering zone, amplitude oscillation maximum, longitudinal velocity and relaxation patterns

24 p3856 A71-45097

Stepwise ionization effects on ionic wave propagation and oscillation stability in inert gas DC discharges

24 p3857 A71-45230

Spark source generated electron beam interaction with plasma in uniform magnetic field, estimating HF longitudinal oscillation power

24 p3857 A71-45233

Subharmonic frequency division for neon discharge plasma oscillations under resonance due to nonuniform electric field

24 p3858 A71-45263

PLASMA PERTURBATION

U PLASMA OSCILLATIONS

PLASMA PHYSICS

Argon ion CW lasers, discussing design, inverse population, plasma, radiative transition probabilities, pumping, frequency spectra and active medium

01 p0092 A71-10145

Electrons motion across gas plasma magnetic field under stochastic electric field, noting accelerating effect

01 p0135 A71-11032

Plasma electric field effects on atomic spectral line shape by plasma kinetic theory

01 p0130 A71-11349

Magnetic probes effectiveness study of electron heating behind shock wave front in plasma, measuring electron temperature

02 p0288 A71-11636

Nonideal plasma thermodynamics data, discussing particle interactions, Coulomb potential, stability, etc

02 p0288 A71-11888

German monograph on helicon resonances in low pressure plasmas, examining HF discharge with applied external static cross magnetic field

04 p0633 A71-14975

Plasma echo and spin echo holophones for electrical signals temporal sequence recording and cued playback, noting human brain memory function analogy

05 p0787 A71-16451

Electron-hole plasma in current carrying wire azimuthal magnetic field, noting electric field intensity by hydrodynamic approximation

05 p0790 A71-16880

Electron scattering out of electron beam in beam plasma, presenting evidence for nonlinear effective inverse mean free path

06 p0935 A71-17485

Dynamic stabilization of MHD instabilities in high beta plasma column, using superposed fluids parametric resonance model

06 p0935 A71-17488

Plasma physics, obtaining very high temperatures and electron/ion densities by power laser heating

06 p0908 A71-18066

Signal cross correlation processing in unstable and turbulent plasmas, comparing correlational and spectral analyses of plasma dispersion and transfer function measurements

06 p0938 A71-18456

Space station plasma physics experiments, investigating electron and ion wakes, resonance, VLF electromagnetic energy propagation and magnetospheric phenomena

[AIAA PAPER 71-71]

06 p0938 A71-18529

German papers on plasma physics, metal corrosion, organic chemistry, molecular biology, etc

07 p1160 A71-19601

Plasma physics and fusion reactor development involving electric conduction, vibration and magnetic effects, stellarator containment, etc

07 p1168 A71-19602

Cosmological plasma physics, considering matter, antimatter, electrodynamics, ambiplasma, annihilation and heavy nuclei

07 p1196 A71-19649

Plasma refractive index effects in pulsed HCN lasers, calculating stable cavity mirror curvatures constriction as function of electron density by ray matrix approach

07 p1124 A71-19795

Self consistent Darwin model for slow wave electromagnetic plasma simulation

07 p1172 A71-20297

Papers on plasma physics experimental methods covering waves, echoes, scattering, diagnostics, heating by shock waves, stabilities, etc

07 p1172 A71-20501

Gravitational stability analysis based on Boltzmann-Vlasov collisionless kinetic equation solution by trajectory integration method in plasma physics

07 p1173 A71-20531

Nonideal plasma thermodynamically complete equation of state based on shock wave experiments

07 p1173 A71-20533

Book on gaseous ionization and plasma electronics covering atomic structure, electron emission, charged particle behavior, self sustaining discharge and breakdown mechanisms

08 p1341 A71-21700

Book on plasma physics, Volume 1, covering electromagnetic fields, fluid mechanics and theory, mathematical analysis and thermodynamics

08 p1341 A71-21892

Fluctuations effect on MHD shock wave propagating in plasma perpendicular to external magnetic field, obtaining field amplitude distribution function

09 p1500 A71-22242

Phase transitions possibility in nonideal multiply ionized plasma, analyzing equation of state and ionization equilibrium equation for various ionization multiplicities

09 p1500 A71-22244

Electromagnetic and electrostatic waves direct nonlinear coupling in plasma, describing experimental measurements of interacting waves frequency, wavelength, field configuration and power levels

09 p1504 A71-23254

Soviet papers on low temperature plasma physics covering production and diagnostic techniques, electrodynamics and optical characteristics, electromagnetic and shock effects, metal plasmas, etc

10 p1648 A71-24188

Polarized radiation transfer in collective plasma, analyzing proper modes phase correlation effects by Liouville equation perturbation technique

10 p1654 A71-24996

Transverse EM field in plasma, deriving closed equation for distribution function

11 p1804 A71-25500

Laser interaction and related plasma phenomena - U.S. Army Conference, Hartford, June 1969

11 p1775 A71-26080

Kinetic and ionization phenomena in Q switched laser produced plasmas, considering gas dynamic

plasma parameters /velocity, density distribution, pressure and temperature/

11 p1806 A71-26086

Single isolated solid particle irradiation in vacuum, using electrical suspension system with electric field produced by six electrodes on solid cube surface

11 p1806 A71-26087

Spherical plasma ball thermokinetic expansion model, considering solid state laser irradiation

11 p1806 A71-26091

Anisotropic instability in velocity distribution of ions in plasmas under external RF electric field

12 p1934 A71-26572

Ion temperature measurement for plasma focus, using laser light scattering

13 p2079 A71-28673

Laser light enhanced scattering by optical mixing of beams in plasma

13 p2079 A71-28797

Weak three dimensional plasma inhomogeneity effect on expression for mean force acting on plasma in HF field

13 p2108 A71-28853

Overcharging effects on ion source with volume ionization, considering two dimensional ionization chamber model with lengthwise distributed neutral plasma component

13 p2109 A71-29202

Kinetic theory of two dimensional boundary layer between plasma and magnetic field, using computer for vector potential differential equations solution

13 p2109 A71-29214

Helical wave deceleration with inhomogeneous plasma approximated by anisotropically conducting plane

14 p2279 A71-30115

Space research goals emphasizing solar system formation, and plasma physics and chemistry

14 p2310 A71-30197

Cold cathode pulsed gas laser construction with glass plasma tube allowing operation with oxygen and variety gases

14 p2255 A71-30882

Plasma physics measurement objectives in terms of deviations from thermodynamic equilibrium, discussing relationship between measuring device calibration and experimental data interpretation

15 p2453 A71-31200

Nonlinear and linear plasma properties influence on nonstationary processes in channeling arc core

15 p2455 A71-31740

Structural stability for two beam plasma model with proportional controller using distributed feedback

15 p2456 A71-31846

Book on chemical reactions under plasma conditions covering thermodynamics, equilibrium states, transport properties and experimental production

16 p2617 A71-32952

Nonequilibrium and equilibrium plasmas thermodynamic properties and molecular, atomic and ionic internal partition functions and relaxation times

16 p2617 A71-32955

Plasma heat transport associated with matter, momentum, energy and electrical charges transfer

16 p2617 A71-32956

Ions acceleration during current passage through plasma, discussing maximum energies, threshold current and electron beam flux density

17 p2787 A71-34284

Optimum pulse transmission through thin exponentially inhomogeneous plasma region for maximum amplitude signal reception, using matched filter theory

17 p2788 A71-34768

Particle gyration in homogeneous magnetic field and perpendicularly propagating electrostatic wave, calculating wave-particle energy transfer and wave-amplitude limiting effects

18 p2950 A71-35862

Ion accelerating system for minimum angular ion beam divergence with plasma ions ejection from source through slits in electrodes

19 p3109 A71-37133

Electric field fluctuations in magnetospheric plasma at multiples of local electron gyrofrequency due to plasma instability

19 p3048 A71-37368

Low density plasma electron velocity distribution deviation due to Maxwellian photon radiation resulting from inelastic collisions with atoms

19 p3112 A71-37739

Finite Larmor radius equations for collisionless plasmas in magnetic fields, noting application to axisymmetric systems stability

19 p3115 A71-38209

Papers on plasma physics covering optical refractivity, deep space measurements, whistlers as diagnostic tools in space plasma, radio wave scattering from ionosphere, etc

19 p3115 A71-38243

Two dimensional magnetospheric model, investigating magnetic line dipole field confinement in empty cavity by tail-like infinitely conducting plasma at constant pressure

20 p3286 A71-38732

Fluctuations effect on MHD shock wave propagating in plasma perpendicular to external magnetic field, obtaining field amplitude distribution function

21 p3424 A71-41131

Phase transitions possibility in nonideal multiply ionized plasma, analyzing equations of state and ionization equilibrium equation for various ionization multiplicities

21 p3424 A71-41133

Weak three dimensional plasma inhomogeneity effect on average force acting on plasma in HF electric field

21 p3425 A71-41284

Electrodynamics of turbulently moving electrically conducting medium, allowing for Hall effect

21 p3453 A71-41356

Rotating plasma theory and devices, noting applications to fusion, cosmic physics and technical systems

24 p3852 A71-44494

Equilibrium plasma in perfectly conducting rigid wall with closed magnetic field lines, deriving necessary conditions for MHD stability

24 p3852 A71-44496

Soviet papers on plasma physics and controlled thermonuclear synthesis problems covering interactions with charged particle beams, stability, HF properties, etc

24 p3853 A71-44501

Dense discharge plasma temperature and ionization distributions in He, H and Ar, investigating pulsed arc emission dependence on current and pressure

24 p3855 A71-44520

Space plasma physics, considering solar system origin

24 p3874 A71-45169

Electrode region in plasma with alkali metal admixture, discussing potential drop, thermionic emission, Schottky effect, diffusion, recombination and bulk and surface ionization

24 p3857 A71-45215

PLASMA PINCH

NT THETA PINCH

Magnetic flux transfer measurement at hyperbolic neutral point resulting in plasma compression

01 p0136 A71-11474

Dynamic stabilization of MHD instability of low current z-pinch by HF quadrupole and oscillating magnetic fields

06 p0935 A71-17486

Plasma stabilization in screw pinch, using combined inertial forces and dynamic shear in diffuse column

06 p0935 A71-17487

Hall current effects on plasma screw pinch stability, obtaining dispersion relation from perturbations characteristic equations

10 p1647 A71-23889

Pooidal magnetic field measurements in toroidal pinch by Thomson scattered carbon dioxide laser beam

10 p1651 A71-24631

High intensity vacuum UV solar simulator, using high pressure jet pinched xenon arc lamp with magnesium fluoride envelope

11 p1747 A71-26515

High beta diffuse plasma pinch configurations, deriving stability requirement hydromagnetic energy principle

14 p2281 A71-30540

Pinch devices under laser heating, determining plasma density and temperature and confining magnetic field strength with thermodynamic model

15 p2458 A71-32396

Nuclear reactions in high temperature laboratory and stellar plasmas, discussing pinches, thermonuclear burning and star evolution

16 p2613 A71-32972

Rotating magnetic field plasma pinch, discussing streak and framing photography, electron line density profiles, magnetic probes and ion and electron temperature measurements

19 p3111 A71-37632

Marginal stabilization of MHD instabilities of linear pinch by force free magnetic fields, comparing with energy method

20 p3275 A71-39462

Shearless magnetic fields discontinuities in marginal stabilization of MHD instabilities for constant pinch force free fields, including toroidal effects

20 p3275 A71-39463

Deuterium Balmer line intensities and overpopulation measurements relationship to thermal equilibrium in pinch discharges

21 p3421 A71-40142

Plasma losses in high current plasma configuration due to inverse skin effect by observation for discharge regimes in theta pinch, zeta and Tokamak systems

21 p3422 A71-40763

Plasma/magnetic field pressure ratio and inductance per unit length in Tokamak plasma pinch with arbitrary cross section

22 p3579 A71-41583

PLASMA POTENTIALS

- Plasma potential measurement in closed magnetic trap /stellarator/ by electron emitting electrostatic probe
01 p0133 A71-10679
- Capacitive and floating Langmuir probes paired comparison measurements of electrostatic potential fluctuations spectrum in steady state turbulent magnetically confined plasma
03 p0430 A71-14416
- Magnetically confined plasma dynamic stabilization, using HF potential
06 p0933 A71-17473
- Plasma potential measurement in closed magnetic trap /stellarator/ by electron emitting electrostatic probe
07 p1170 A71-20140
- Spatial potential measurements in magnetized non-Maxwellian hydrogen plasma, using Zaitsev-Mnev method
07 p1171 A71-20192
- Natural potential and nonpotential electron oscillations excitation in plasma by transverse wave field, determining wave amplitude threshold and excitation instability
09 p1500 A71-22239
- Two group model of stationary plasma flow in magnetosphere with space charges due to inertia drift and forbidden regions
09 p1529 A71-23710
- Monoenergetic beam relaxation dynamics in plasma, describing oscillation excitation and diffusion allowing for instability
12 p1942 A71-27769
- Radial distribution of electric potential in Penning discharge based on relation between sulfur hexafluoride negative ions transit time and initial energy
13 p2107 A71-28852
- Potential measurements in collisionless plasma sheath of conducting plate, evaluating electrostatic vs emissive and floating emissive probes
15 p2458 A71-32391
- Collision integral for classical electron plasma, concerning Born-Bogoliubov-Green-Kirkwood-Yvon equations for long range interaction potential and motions of multiple particles
16 p2619 A71-33650
- Plasma potentials spatial distribution measurement, describing switching circuit and probe design
16 p2620 A71-33905
- Nonisothermal collisionless low beta plasma with electron temperature greater than ion, investigating low frequency potential modes for Kelvin-Helmholtz instability
16 p2620 A71-34167
- Plasma potential differential measuring method, using emitting and cold probes for simultaneous current data
19 p3112 A71-37638
- Electrical microwave probe for measuring HF potential oscillations in low temperature plasma
19 p3064 A71-37787
- Debye potential well formation in collisionless current carrying plasma, noting wave-particle resonant interaction role
19 p3115 A71-38216
- Plasma sheath formation near absorbing wall, calculating electric potential and current variations in space and time
19 p3117 A71-38723
- Electron beam for determining plasma potential and charge density as function of radius of inertially confined tenuous plasma cylinder
20 p3273 A71-39009
- Natural potential and nonpotential electron oscillations excitation in plasma by transverse wave field, determining wave amplitude threshold and excitation instability
21 p3424 A71-41125
- Radial distribution of electric potential in Penning discharge based on relation between sulfur hexafluoride negative ions transit time and initial energy
21 p3425 A71-41281
- Electron plasma waves and free streaming bursts response to fast rising voltage step in low density cylindrical plasma in strong magnetic field
22 p3582 A71-41899
- Weakly ionized decaying plasma potential fluctuations and instability in magnetic field, using electrostatic probes
23 p3709 A71-43262
- Plane collisionless plasma diode between two hot emitters, considering potential distributions
24 p3808 A71-44551

PLASMA POWER SOURCES

NT PLASMA ENGINES

PLASMA PROBES

NT ELECTROSTATIC PROBES

- High impedance electric probes and floating double probes for plasma stream electric field, potential, density and temperature
01 p0134 A71-11002

- Miniature multigrid probes for measuring energy spectra of charged particles and absolute plasma densities, comparing results to microwave measurements
02 p0247 A71-11637
- Small size calorimetric probe for measuring enthalpy, temperature and pressure in high velocity dense plasma flow
02 p0290 A71-12194
- Collisionless plasma density measurement by spherical probe, considering probe to Debye radius ratio
04 p0635 A71-15260
- Particle flux toward charged plate /plane probe/ moving relative to plasma
05 p0814 A71-17181
- Double probe technique for electric field measurements in magnetoplasma
06 p0936 A71-17703
- Plasma electron temperature probes, investigating electron heating effects
07 p1112 A71-19765
- Ion collection by spherical and cylindrical probes in collisional He plasma, comparing saturation current measurements with transitional regime probe theories
07 p1169 A71-19909
- Plasma with oriented charged particle fluxes macroscopic parameter measurement by multigrid probes facing and reversed to drift, noting graphical data processing
07 p1171 A71-20183
- Ion currents to cylindrical electrodes in mobility dominated plasma flow from thin sheath theory involving convection currents
09 p1505 A71-23374
- Integral electron flux and current in retarding-potential plasma probes, considering application to nonconcave geometry and spacecraft probes
11 p1805 A71-25615
- Transient ion sheath effects on spherical metallic plasma probe complex admittance at different frequencies, comparing numerical results with experiment
11 p1805 A71-25803
- Particle flux toward charged metal plate /flat probe/ moving relative to plasma
13 p2134 A71-28238
- Small size calorimetric probe for measuring enthalpy, temperature and pressure in high velocity dense plasma flow
15 p2454 A71-31500
- Electrical plasma probes, discussing ion-surface effects, geometry, cleaning procedures, collisionless regime and electron/ion current
16 p2617 A71-32961
- Plasma potentials spatial distribution measurement, describing switching circuit and probe design
16 p2620 A71-33905
- Microfield double probe for plasma density and electron temperature determination, studying random signals crossed spectrum
17 p2789 A71-35350
- Positive biased ionospheric probes in steady state plasma flow, presenting self consistent parameter computation
18 p2915 A71-36013
- [ONERA-TP-935] Quadrupole probe for measuring magnetospheric electric currents, noting transfer impedance dependence on probe motion relative to ambient plasma
18 p2912 A71-36198
- Plasma potential differential measuring method, using emitting and cold probes for simultaneous current data
19 p3112 A71-37638
- Collisionless plasma shock front microstructure, examining isomagnetic discontinuity with high spatial resolution probes
19 p3045 A71-37853
- Plasma ion and electron distribution functions measurement on outer planet missions
19 p3114 A71-37938
- Upper ionospheric plasma measurements by gyro plasma probe equipped Lambda rocket, deducing electron density profile from plasma resonance effects
20 p3224 A71-39721
- Cooled spherical electrostatic probe idealized theory in quiescent continuum slightly ionized chemically frozen gas, interpreting plasma measurements
21 p3423 A71-40947
- Probe size and orientation effects in turbulent plasma flow diagnostics, considering electrostatic probes frequency filtering and wake effects
21 p3423 A71-40979
- Stochastic properties of probe particle motion in Lorentz plasma, considering interactions and friction and diffusion coefficients
24 p3854 A71-44511
- Piezoelectric probe for pressure measurement in plasma behind shock front, discussing design and measuring circuit
24 p3825 A71-44750

PLASMA PROPULSION

- Pulsed plasma thruster system as secondary propulsion unit for spacecraft attitude, station and trajectory control
04 p0638 A71-15325

- Electron bombardment mercury ion thruster plasma properties and performance, computing ion beam current, discharge losses and propellant utilization efficiency
07 p1184 A71-19881
- [AIAA PAPER 69-256] Auxiliary propulsion system using low power MPD thrusters, discussing feasibility of thrust vectoring with skewed magnetic coil arrangement
14 p2293 A71-30754
- [AIAA PAPER 71-695] Electrochemical plasma production based on cathodic hydrogen combustion using giant condenser batteries for energy storage and quick release, applying to space propulsion technology
15 p2456 A71-31833
- Fusion reactor applications to space propulsion and power generation, considering conversion of thermal energy of reacting plasma to electrical power and exhaust jet
15 p2447 A71-32207

PLASMA RADIATION

- Magnetic field generation during radiation era, discussing generating mechanism by angular momentum transfer between ion and electron-photon gases in expanding plasma
01 p0148 A71-10024
- Rayleigh-Gans-Born approximation application to thermal radiation of reflecting convex plasma sphere, cylinder and ellipsoid
02 p0288 A71-11633
- Regular and stochastic oscillations in plasma beam discharge produced by beam instability from observing time dependent variations in spectral line luminescence intensities
02 p0288 A71-11634
- Thermionic converter spectroscopic measurements in several regions of I-V characteristics, noting plasma radiation intensity periodic waveform
02 p0195 A71-12238
- Theta pinch plasma enhanced radiation at far IR wavelengths, observing emission exceeding thermal bremsstrahlung
03 p0465 A71-14189
- Cyclotron radiation emission and absorption in nonequilibrium plasma, deriving radiative transfer equation
03 p0465 A71-14268
- Electrode material function of electromagnetic radiation from heterogeneous plasma
03 p0466 A71-14473
- Charged particle power radiation in homogeneous magnetoplasma
05 p0790 A71-16660
- Stark broadening of hydrogen lines in plasma, noting role of amplitude modulation and nonadiabaticity
06 p0930 A71-17406
- Optical system for spatially resolved measurement of extended bodies radiative emission and self absorption, describing design for measuring gas discharge plasma radiative properties
06 p0928 A71-18224
- Magnetic stars models on possibility of rotational deceleration by hydromagnetic waves radiation without mass loss
07 p1190 A71-18857
- Spectrograms of potassium and iron ions radiated by laser plasma
09 p1462 A71-22403
- X ray emission from optical and inner shell transitions of multiply ionized Cu, Fe, and Ti in low pressure discharge dense plasma
09 p1501 A71-22414
- Electron collisional-radiative ionization and recombination rate coefficients, using hydrogenic plasma model with resonance radiation trapping
10 p1653 A71-24672
- Hypervelocity impact produced metallic plasmas equilibrium composition and radiation, calculating radiative energy as function of wavelength and internal partition functions
11 p1804 A71-25510
- Plasma plate under vacuum conditions, examining transient radiation and spatial dispersion
12 p1937 A71-27118
- Low temperature plasma radiation transfer equation, computing problems with absorption coefficient accounting for re-emission
14 p2280 A71-30168
- Azimuthal current growth and microwave radiation in theta pinch hydrogen plasma discharge from sensitive superhetrodyne receivers
14 p2282 A71-30663
- Nitrogen plasma electrical and thermal conductivities and radiative source strength at atmospheric pressure and 9,000-12,500 K, using Hall probe and optical methods
15 p2454 A71-31535
- [AIAA PAPER 71-590] Resonance radiation field of positive column of low current electric arc burning in nonequilibrium Ar plasma with admixture of K, using optical probe
15 p2457 A71-32270
- Axissymmetrical dense plasma, calculating radiation intensity radial distribution with approximate method
15 p2459 A71-32458

- High temperature nitrogen plasma emission spectrum in 2500-5000 Å range, estimating negative ion photoionization cross sections 16 p2613 A71-32900
- Plasma as fourth state of matter, including high temperature behavior, radiation emission, applied electric/magnetic fields effects and laboratory generation 16 p2617 A71-32953
- Cold plasma flow rate determination from emission inhomogeneities, using time of flight method and high speed streak photography for instantaneous velocity measurements 17 p2787 A71-34286
- Spectroscopic measurement of vacuum UV radiation from shock heated krypton plasma, noting self reversed resonance lines indicating cold boundary layer 17 p2787 A71-34589
- Newton-Raphson method application to iterative solution of atomic excitations and radiative transfer in plasma 17 p2838 A71-35554
- Bounded nonthermal plasma radiation temperature variations relationship to electron velocity distribution functions 19 p3113 A71-37747
- Gas concentration, field frequency and applied power level for control over electron temperature and emission spectra in microwave gas discharge plasma 19 p3113 A71-37764
- Plasma diagnostics based on IR continuum intensity due to bremsstrahlung emission from plasma 19 p3113 A71-37765
- Plasma radiation effects in gas tube electric arc heating, obtaining temperature and heat flux profiles and I-V characteristics from energy transport mathematical model [ASME PAPER 71-HT-18] 19 p3164 A71-37989
- Unified linear theory for MHD waves in weakly ionized radiating plasma, deriving two-fluid model set of equations corresponding to magnetoacoustic, thermal, electrothermal and ionization rate waves 21 p3423 A71-40945
- Periodic current pulse and superradiant radiation pulsing in DC excited xenon plasma with increased cathode-anode capacitance 21 p3424 A71-41046
- Spectral line intensity measurement errors due to electron-temperature fluctuations averaging in continuous plasma sources 22 p3581 A71-41790
- Hydrogen plasma Balmer spectrum measurement for emission coefficients, comparing results with theories 22 p3583 A71-42373
- Dense low temperature Ar and Hg plasmas, observing correlation between electrical conductivity and optical emission 23 p3712 A71-43914
- Plasma generation with transversely excited high pressure carbon dioxide laser and solid targets, describing optical emission spectral characteristics 23 p3712 A71-43932
- Spectroscopic analysis of pulsed gas discharge in crossed electric and magnetic fields of gas magnetron diode in 3100-4660 Å wavelength range 23 p3712 A71-43933
- Millimeter band plasma microwave radiation receivers for emission measurement, presenting schematic diagrams for superheterodyne 24 p3825 A71-44507
- Thermal and nonequilibrium microwave emission from colliding plasma beams in transverse magnetic mirror field 24 p3854 A71-44517
- Solar coronal plasma radiative capacity and temperature structure from cooling function in thermal balance equation 24 p3869 A71-44806
- Low temperature plasma radiation flux heated absorbing fluid, investigating convective heat transfer to semitransparent wall 24 p3856 A71-44893
- Tokamak T-3A plasma neutron emission, confirming thermonuclear nature of radiation 24 p3856 A71-45113
- Microwave radiation intensity and spectral frequencies of Knudsen discharge in cesium plasma 24 p3858 A71-45244
- PLASMA RESONANCE**
- Monograph on nonlinear theory of one dimensional homogeneous collisionless plasma resonance covering charged particle motion in sinusoidal and standing potential waves 01 p0131 A71-10101
- Nonlinear resonance excitation of ion acoustic plasma waves by weak external electric field, using partial differential equations 01 p0134 A71-11027
- Topside ionosphere plasma resonance due to electrostatic wave echoes, comparing electron temperature dependent beat pattern with ray tracing calculations 03 p0421 A71-14540
- German monograph on helicon resonances in low pressure plasmas, examining HF discharge with applied external static cross magnetic field 04 p0633 A71-14975
- Magnetoplasma electric and magnetic resonances by Voigt configuration, noting similarity to single particle scattering and particle size dependence 05 p0787 A71-16497
- Electron plasma in strong HF electric field, investigating possibility of parametric resonance 06 p0930 A71-17403
- Antenna radiation in isotropic plasma near resonance 06 p0937 A71-18311
- Surface wave conversion to longitudinal oscillations near strong discontinuity in resonant cold magnetoactive plasma 06 p0937 A71-18355
- Space station plasma physics experiments, investigating electron and ion wakes, resonance, VLF electromagnetic energy propagation and magnetospheric phenomena [AIAA PAPER 71-71] 06 p0938 A71-18529
- Topside sounders received frequencies of oblique echoes at plasma resonance, using WKB technique 07 p1168 A71-19676
- Plasma frequency resonance time duration-local electron cyclotron frequency relationship by oblique echo model 07 p1168 A71-19681
- Hydromagnetic wave propagation with coupled isotropic and guided modes, obtaining steady state solution with toroidal, plasma resonance induced period dependent reflecting barrier 07 p1197 A71-19767
- Nonequilibrium population formation in dense plasma of complex composition under ionization resonance conditions 07 p1174 A71-20538
- Hot Cs plasma parametric resonance in variable electric field related to plasma heating 09 p1499 A71-22229
- Magnetized inhomogeneous plasma nonlinear wave coupling near hybrid resonances 09 p1503 A71-22868
- Pseudoacoustic energy flux influence on accessibility of ground emitted wave to plasma resonance in F region, using adiabatic approximation with scalar pressure 10 p1602 A71-24465
- Nonlinear theory of ion-sound plasma turbulence for strong wave-particle interaction near resonance 12 p1935 A71-26915
- Magnetoactive spatially homogeneous plasma parallel and perpendicular waves derivation from hydrodynamic equations in quasi-linear approximation, noting resonances and nonlinear effects 12 p1937 A71-27181
- Plasma in strong electric and magnetic field with allowance for inelastic electron collisions with neutral particles, showing resonant oscillations from Born approximation 12 p1937 A71-27183
- Ionospheric electron resonance observation by sounders aboard rocket and satellites 14 p2202 A71-30947
- Stable plasma resonance behavior, calculating small signal and nonlinear responses for theory verification and diagnostic techniques 14 p2283 A71-30948
- Resonant plasma heating at electron cyclotron frequency second harmonic, studying interactions with microwave electromagnetic radiation in adiabatic trap 15 p2455 A71-31736
- Warm plasmas impedances and power transfer near lower hybrid resonance, including electron pressure effects in full electromagnetic treatment 15 p2456 A71-31923
- Synchronous and oscillatory energy gain with electron-wave resonance time in collision magnetospheric plasma 15 p2371 A71-32024
- Photoresonance cesium plasma development and decay, determining density spatial-temporal behavior and recombination and polar diffusion coefficients by probe measurements 17 p2787 A71-34287
- LF resonances for radially inhomogeneous collisionless plasma sphere impinged by plane electromagnetic waves 17 p2708 A71-35485
- Anomalous microwave heating of electrons in magnetized plasma, showing resonances dependence on magnetic fields and charged particles concentration 17 p2790 A71-35735
- Electron wave coupling in plasma column, determining exact resonance and field configurations of frequencies 19 p3111 A71-37635
- Upper ionospheric plasma measurements by gyro plasma probe equipped Lambda rocket, deducing electron density profile from plasma resonance effects 20 p3224 A71-39721
- Highly ionized hot Cs plasma parametric resonance in alternating electric field related to plasma heating 21 p3424 A71-41107
- Magnetoactive spatially homogeneous plasma parallel and perpendicular waves derivation from hydrodynamic equations in quasi-linear approximation, noting resonances and nonlinear effects 22 p3583 A71-42458
- Plasma in strong electric and magnetic field with allowance for inelastic electron collisions with neutral particles, showing resonant oscillations from Born approximation 22 p3584 A71-42460
- Off-resonance electron heating by microwaves in mirror contained high beta plasmas 24 p3852 A71-44486
- Parametric hybrid resonance excitation of longitudinal oscillations in nonhomogeneous magnetoplasma by HF electromagnetic field 24 p3852 A71-44491
- Magnetosonic wave excitation and electron heating in magnetically confined hydrogen plasma hybrid resonance region 24 p3853 A71-44502
- Plasma resonator excitation by Cerenkov emission from density modulated uncompensated charged particle beam 24 p3854 A71-44512
- Subharmonic frequency division for neon discharge plasma oscillations under resonance due to nonuniform electric field 24 p3858 A71-45263
- PLASMA RINGS**
- U TOROIDAL PLASMAS**
- PLASMA ROCKETS**
- U PLASMA ENGINES**
- PLASMA SHEATHS**
- Sunward magnetosheath magnetic field fluctuations, noting power levels spatial variations, transverse shock aligned fields and longitudinal waves 01 p0075 A71-11493
- Cylindrical electric dipole antenna in magnetoactive ionospheric plasma, noting ion sheath effect on input impedance and active length 02 p0212 A71-11873
- Flat plate ion density probe with convection and ion production in electric sheath, comparing to shock waves in air 04 p0632 A71-14706
- Double sheath model between two plasmas, taking into account reflected and accelerated particles initial velocities 05 p0790 A71-16727
- Magnetic field effects on collisionless plasma sheath near planar electrode, solving electric and magnetic potentials nonlinear differential equations by numerical scheme 07 p1171 A71-20290
- Self and mutual admittance, isolation and radiation pattern of slots on infinite cylinder covered by inhomogeneous lossy plasma 08 p1341 A71-21886
- Ion currents to cylindrical electrodes in mobility dominated plasma flow from thin sheath theory involving convection currents 09 p1505 A71-23374
- Numerical solution for planar ion sheath growth in low pressure plasma, calculating transient sheath thickness resulting from application of specific voltage waveforms 10 p1652 A71-24659
- Shot noise effect on ambient plasma magnetosphere electric field measurements with Langmuir and double probes for electron density and temperature 11 p1756 A71-25644
- Thermionic converter electrostatic sheath analysis, using discontinuous distribution functions for emitted, plasma and trapped particles, and computer program 11 p1713 A71-25891
- Wire grid simulation of electron density, transmission and reflection of lossless and lossy reentry plasma sheath under microwave radiation at X and K bands 12 p1935 A71-26767
- Spherical free-molecular electrostatic probe surrounded by finite sheath, calculating I-V characteristic saturation current regimes 15 p2409 A71-32100
- Potential measurements in collisionless plasma sheath of conducting plate, evaluating electrostatic vs emissive and floating emissive probes 15 p2458 A71-32391
- Thermal X ray sources associated with rotating collapsed stars with surrounding plasma shells, discussing plasma density profile and electron distribution in stellar magnetosphere 15 p2497 A71-32762
- Slot antennas electromagnetic radiation patterns in conducting ground plane coated with moving isotropic cold plasma sheath 17 p2701 A71-34758
- Digital simulation of pseudowaves and plasma sheath formation about grid by computer solution of

ion Vlasov equation for ion distribution function time evolution 19 p3113 A71-37749

Longitudinal plasma sheath waves kinetic theory, considering particles specular reflection from sheath boundaries 19 p3116 A71-38615

Plasma sheath formation near absorbing wall, calculating electric potential and current variations in space and time 19 p3117 A71-38723

OGO 5 polar cusp observations showing dayside magnetosheath plasma penetration during magnetic storm 23 p3668 A71-43162

Molecular gas dissociation in constricted DC glow discharge plasma sac/sheath boundary, discussing characteristics and potential uses 23 p3712 A71-43931

Radiation pattern modification factors calculation for TE excited slot antenna in ground plane covered with inhomogeneous plasma reentry sheath 23 p3646 A71-44172

Ion current sheath-convection effects with flush mounted electrostatic probes in high pressure flowing plasmas 24 p3826 A71-44792

PLASMA SLABS

Geomagnetic tail structure near null sheet, indicating decrease and/or dissipation of plasma sheet particle energy density at lunar distances 06 p0893 A71-17994

Compressible isotropic plasma slab effect on magnetic dipole radiation pattern, using reciprocity theorem 08 p1253 A71-21274

Kinetic theory of electromagnetic waves obliquely incident upon plasma slab considered as boundary value problem 09 p1409 A71-23499

Reciprocity theorem for magnetostatic modes, considering arbitrary plane slab within magnetoplasma with parameter variation in direction normal to horizontal plane of stratification 10 p1577 A71-24293

Vacuum merging speed and magnetospheric cross tail electric field inverse proportionality to plasma sheet particle concentration 13 p2056 A71-27934

Third harmonic component generation in reflected and transmitted waves from magnetoplasma slab, using Boltzmann transport equation and Maxwell equation 13 p2109 A71-29243

Numerical procedure for electromagnetic field penetration through inhomogeneous cold plasma slab with collisions, using Riccati type differential equation 20 p3273 A71-39004

Electromagnetic wave transmission through conducting plasma slab, reducing nonlocal wave interaction two point boundary value problem to Cauchy system 20 p3274 A71-39080

Point source radiation in stratified waveguide system with magnetoplasma slab, evaluating transverse field by Fourier integral representation 24 p3857 A71-45181

PLASMA SOUND WAVES

U MAGNETOHYDRODYNAMIC WAVES

U PLASMA WAVES

PLASMA SPECTRA

Shock generated Ar plasma emission spectrum intensity measurements, describing fast-response spectrometer sensitivity calibration method 01 p0134 A71-10997

Turbulent plasma correlation functions for decay and nondecay spectra, deriving descriptive equations by perturbation theory series summation 03 p0464 A71-13932

MHD parameters in photospheric plasmas of giant and dwarf stars, noting electric conductivity, Joule dissipation, Reynold and Lundquist numbers 03 p0490 A71-13938

Capacitive and floating Langmuir probes paired comparison measurements of electrostatic potential fluctuations spectrum in steady state turbulent magnetically confined plasma 03 p0430 A71-14416

Spectroscopic studies of helium-hydrogen plasmas in first reflected shock region in electromagnetic T-tube 04 p0631 A71-14684

Solar wind plasma power spectra noting frequency dependence, particle density and speed and interplanetary magnetic fields 05 p0802 A71-15942

Quasi-linear equations consequences in discrete spectra and damped electron plasma waves, discussing conservation laws relation to resonance approximation 05 p0789 A71-16652

Plasma satellites near He I forbidden lines during turbulent heating 06 p0936 A71-17592

Carbon dioxide arc discharge plasma emission spectral absolute intensities under atmospheric pressure, determining molecular band contributions 07 p1162 A71-19131

Magnetic mass spectrometer for ionosphere composition measurements permitting single spectrum analysis of plasma of negative and positive ions 10 p1608 A71-23817

Plasma focus hard X ray spectrum, using electron sensitive nuclear emulsions 12 p1936 A71-26920

Electron energy distribution for spectroscopic determination in hollow cathode discharge helium-mercury plasma based on Druyvesteyn function 12 p1937 A71-27050

High temperature plasmas optical properties measurement by plasma spectroscopy, using gas driven shock tube as light source 12 p1940 A71-27276

Magnetospheric two component plasma model, considering thermal and suprathermal spectra 13 p2060 A71-28432

Hydrogen plasma internal magnetic field determination, using spectral characteristic measurements due to level intersection 13 p2108 A71-29030

Electromagnetic radiation scattering detection limits for plasma diagnostics, considering plasma properties effect on satellites aperture broadening in spectrum 14 p2283 A71-30677

Plasma local thermodynamic equilibrium relation to continuum, molecular band, atomic lines intensity and absorption line reversal/equivalent widths measurements 16 p2617 A71-32959

Optically dense plasma spectral characteristics, calculating reabsorbed line intensity distribution 16 p2619 A71-33707

Homogeneous spherical hot hydrogen plasma cloud at various temperatures and optical depths, presenting electron scattering effects on optical and X ray spectral emission 18 p2951 A71-36012

Soviet book on optically dense plasma spectroscopy covering radiation absorption, transport equation, photon frequency, resonance energy, quantum mechanical calculations and spectral characteristics 20 p3274 A71-39145

Electron beam-plasma system oscillation spectrum control through modulation by external HF signal, discussing theory and experimental verification 22 p3583 A71-42317

Incoherent scatter observations of ion concentration and plasma line in F1 region 23 p3670 A71-43188

Millimeter band plasma microwave radiation receivers for emission measurement, presenting schematic diagrams for superheterodyne 24 p3825 A71-44507

PLASMA SPRAYING

Metal matrix composites formation methods, emphasizing diffusion bonding and plasma spray deposition [SME PAPER EM-70-124] 01 p0090 A71-11265

Reflectance restoration of proton and UV degraded spacecraft thermal control coatings by low temperature oxygen plasma treatment applied to Surveyor 3 [AIAA PAPER 71-463] 11 p1800 A71-26244

Low cost metal matrix composite fabrication, discussing plasma spraying and continuous casting 14 p2263 A71-29655

Flame or plasma sprayed ceramic coating porosity estimation, using statistical distribution of breakdown voltage in coating 15 p2438 A71-31285

Microdefects of lattice structure of molybdenum plasma coatings dependent on spray gun nozzle-surface distance 15 p2437 A71-32671

Plasma spraying steel coating process, establishing regularity of particle flight velocity variation with distance from burner nozzle 24 p3829 A71-44737

Plasma metal coating facility, noting antifriction and mechanical properties 24 p3816 A71-44864

PLASMA STABILITY

U MAGNETOHYDRODYNAMIC STABILITY

PLASMA TEMPERATURE

Electron temperature determination in low density helium plasma 01 p0134 A71-11005

Pulsed Ar ion laser plasma electron density and temperature, discussing Tonks-Langmuir free fall model validity 01 p0096 A71-11623

Spatial-temporal distribution of laser spark plasma electron density and temperature based on holographic interferometry 02 p0258 A71-11639

Atomic and ion temperatures in Ar plasma low pressure discharge in metallic tubes with conducting walls 02 p0259 A71-11931

Argon plasma column inductive discharge parameters at atmospheric pressure from radial temperature distribution measurements 02 p0290 A71-12181

Small size calorimetric probe for measuring enthalpy, temperature and pressure in high velocity dense plasma flow 02 p0290 A71-12194

Three component two temperature plasma model of thermionic converter, including volume ionization-recombination processes 02 p0194 A71-12225

Air plasmas temperature measurements behind reflected shock wave, examining radiative cooling effects and total radiant energy 04 p0632 A71-14704

Electromagnetic instability of counterstreaming electron plasmas with anisotropic temperatures, using Vlasov equation 04 p0633 A71-15032

Plasma temperature measurement in local thermodynamic equilibrium using total continuum emitted during seeding with hydrogen 05 p0786 A71-16171

Plasma temperature determination in Hg high pressure discharge with TII addition 05 p0786 A71-16224

Fully ionized hydrogen cosmic plasma interaction with surrounding neutral gas, noting minimum temperature and power input 05 p0810 A71-16637

Plasma boundary layer temperature distribution near conducting surfaces by measuring current voltage characteristics 05 p0790 A71-16776

Self similar thermal wave in two-temperature plasma under laser heating for different pulse duration and energy absorption values 06 p0936 A71-17689

Cooling models for flare produced plasmas in solar corona, considering collisional, radiative and conductive mechanisms 06 p0968 A71-17913

Laser produced plasma temperature measurements using X ray detectors 06 p0938 A71-18459

Snowplow theory modification for plasma temperature, ion population and release time prediction, noting agreement with plasma rail gun data 07 p1165 A71-18879

Plasma electron temperature probes, investigating electron heating effects 07 p1112 A71-19765

Low density plasma flow past bodies, measuring disturbed zone velocity, density and temperature distributions by Langmuir probes 07 p1173 A71-20528

Simultaneous plasma internal energy, temperature and volume determination based on energy balance analysis during pulsed heating 08 p1342 A71-21928

Electron-ion plasma in HF electric and constant magnetic field, determining relaxation times and collision frequency for temperature compensation 09 p1502 A71-22539

Controlled thermonuclear reactions produced by exposing LiD target to short pulses of Nd-glass laser, measuring neutrons number and plasma temperature 10 p1620 A71-24208

Plasma immersed photoemitting plate surface potential distribution, discussing electron/photoelectron temperatures and number densities 10 p1653 A71-24800

Flame plasma temperature determination by microwave attenuation measurements, discussing measured values comparison with predictions by thermal ionization equation 11 p1804 A71-25193

High density and temperature plasmas produced by laser pulse heating massive solid targets, discussing interaction processes 11 p1807 A71-26094

Rarefied collisionless plasma, obtaining hydrodynamic equations for magnetic viscosity and thermal conductivity 13 p2106 A71-28564

Collisionless heat propagation along plasma magnetic field, showing relation to ion sound velocity 13 p2107 A71-28568

Soviet book on inhomogeneous plasma instabilities covering spatial gradients, charged particles collisions, temperature effects, steady electric fields and magnetic shear 14 p2279 A71-29942

Spectral lines self reversal effects on plasma temperature and density measurement in MHD duct boundary layer 14 p2279 A71-30046

Argon plasma column inductive discharge parameters at atmospheric pressure from radial temperature distribution measurements 15 p2454 A71-31489

Small size calorimetric probe for measuring enthalpy, temperature and pressure in high velocity dense plasma flow

15 p2454 A71-31500

Finite ion temperature effect on large amplitude magnetosonic disturbances and collisionless shock waves formation in plasmas, using one dimensional macroparticle code

15 p2458 A71-32394

Pinch devices under laser heating, determining plasma density and temperature and confining magnetic field strength with thermodynamic model

15 p2458 A71-32396

Helium plasma afterglow at low temperatures, describing triatomic ion recombination and dissociation

15 p2460 A71-32730

Low density collisionally ionized plasma at equilibrium, calculating permitted, forbidden and semiforbidden radiative cooling coefficients

15 p2460 A71-32776

Plasma boundary layer temperature distribution near conducting surfaces from I-V characteristics of ~~the gap~~

16 p2618 A71-33028

Plasma temperature determination errors from relative gf-values, noting effects on absolute transition probabilities

16 p2618 A71-33154

Low latitude topside plasma temperature, electron content and ion production/loss rates during sunspot minimum to maximum

17 p2731 A71-34316

Simultaneous plasma internal energy, temperature and volume determination based on energy balance analysis during pulsed heating

17 p2789 A71-35272

Mirror-contained collisional plasmas, deriving wave reflection and absorption from equilibrium density and temperature profile equations

18 p2950 A71-35860

Numerical analysis of plasma expansion confined by magnetic field, emphasizing boundary oscillation and temperature rise, based on hyperbolic and parabolic system equations

18 p2952 A71-36308

Reentry plasmas ionization and microwave and optical radiation properties, considering radar echo, electromagnetic scattering, thermal equilibrium and ablation products

18 p2952 A71-36422

Temperature and pressure of optically dense plasma from vaporizing wall gas discharge

19 p3110 A71-37577

Gas and electron temperature and thermal nonequilibrium in argon plasma jet from electrodeless induction discharge

19 p3111 A71-37578

Bounded nonthermal plasma radiation temperature variations relationship to electron velocity distribution functions

19 p3113 A71-37747

Long wavelength ion acoustic instability of two temperature collisional fully ionized plasma with heat transfer, noting additional destabilizing currents

21 p3422 A71-40708

German monograph on plasma layer temperature distribution in optical resonator covering spectral distribution of thermal radiation

21 p3379 A71-40749

Particle model measurements of collision and heating times in two dimensional thermal computer plasma

21 p3423 A71-40843

Helium plasma afterglow at low temperatures, describing triatomic ion recombination and dissociation

23 p3710 A71-43301

Spatially separated plasma beams of different temperatures, determining amplified wave instability boundaries and growth increments by quasi-hydrodynamic approximation

23 p3711 A71-43557

Dense hydromagnetic plasmoid interaction with nonuniform axisymmetric magnetic field using two dimensional fully ionized two temperature model

24 p3852 A71-44487

Ohmic discharge plasma resistance, temperature and oscillations in weak electric fields under electron beam excitation in Sirius stellarator

24 p3854 A71-44518

Solar coronal plasma radiative capacity and temperature structure from cooling function in thermal balance equation

24 p3869 A71-44806

Zero temperature relativistic plasma ground state energy calculation using Fermi momentum and Green function

24 p3857 A71-45115

PLASMA THEORY

U PLASMA PHYSICS

PLASMA TURBULENCE

Electrostatic vibrations from turbulent plasma heating on basis of Stark broadening of hydrogen spectral lines, obtaining electric field strength

01 p0131 A71-10069

Microwave scattering from plasma fluctuations produced by forcing gas in turbulent flow through discharge tube, investigating frequency spectrum broadening

01 p0136 A71-11480

Turbulent plasma radio emission theory of photon production and transport, considering application to quasars

02 p0292 A71-12587

Relativistic electron spectra of cosmic rays accelerated by plasma turbulence, examining singularity in solution

03 p0483 A71-13202

Turbulent plasma correlation functions for decay and nondecay spectra, deriving descriptive equations by perturbation theory series summation

03 p0464 A71-13932

High beta plasma, calculating turbulence for fast shock propagating perpendicular to magnetic field

03 p0496 A71-14514

Strong turbulence theory of ionospheric cross field instability of weakly ionized plasma

03 p0420 A71-14533

Interstellar gas small scale irregularities in electron density, considering nonlinear processes in plasmas causing turbulence in spectrum

05 p0805 A71-16113

Expanding universe magnetic field origin, examining Batchelor condition for spontaneous appearance in turbulent conducting fluid motion

05 p0809 A71-16470

Current-interchange instability in plasma turbulent heating by current

06 p0930 A71-17395

Nonlinear interaction between waves with random phases in magnetoactive plasma of solid body, discussing weak turbulence theory

06 p0930 A71-17404

Wave buildup in weakly turbulent plasma, noting epithermal pulse background effect on phase velocity

06 p0936 A71-17664

H lines Stark broadening in turbulent plasma, considering Langmuir vibrations monadiabatic action and energy density

07 p1168 A71-19277

Turbulent plasma flame incoherent scatter calculation by modified first order Born approximation, considering attenuation due to absorption and scatter by energy conservation

07 p1171 A71-20294

Low density plasma flow past bodies, measuring disturbed zone velocity, density and temperature distributions by Langmuir probes

07 p1173 A71-20528

Turbulent plasmas nonequilibrium electric fields determination from hydrogen spectral lines Stark broadening

08 p1341 A71-21790

Nonisothermal plasma ion acoustic oscillations spectral energy density in electromagnetic wave field, calculating HF conductivity and absorption coefficient

09 p1500 A71-22243

Interplanetary plasma disturbances in Venus proximity from Venera measurements

09 p1520 A71-22669

Weakly turbulent plasmas static electric conductivity derivation from kinetic equation for linear response to one-particle distribution function

09 p1503 A71-22861

Electrostatic vibrations from turbulent plasma heating on basis of Stark broadening of hydrogen spectral lines, obtaining electric field strength

09 p1504 A71-23264

Weak turbulence analysis of Maxwellian plasma waves nonlinear interactions effects on two stream instability with Gaussian momentum distribution

10 p1647 A71-23886

Plasma decay turbulence in spatially homogeneous ensemble of undamped dispersive waves in macroscopic and Vlasov terms, using time asymptotic perturbation method

10 p1647 A71-23887

Shock and turbulent ray interactions of plasma streams with neutral gas cloud, noting comet tail similarity

10 p1652 A71-24653

High beta turbulent plasmas radiation scattering due to magnetic field strength and direction fluctuations from optical Faraday rotation observation

10 p1652 A71-24660

Turbulent plasma heating in current sheet between opposed magnetic fields

10 p1653 A71-24891

Stochastic particle acceleration in random electromagnetic field determination by turbulent plasma motion in external homogeneous magnetic field

10 p1655 A71-25075

Nonlinear theory of ion-sound plasma turbulence for strong wave-particle interaction near resonance

12 p1935 A71-26915

Solar corona plasma turbulence spectra, evaluating radar echo structure

12 p1963 A71-27080

Plasma turbulent electron and ion heating by large amplitude whistler resonant excitation, investigating mechanisms

12 p1937 A71-27182

Anomalous resistivity due to weak electrostatic turbulence in plasma, discussing applications to perpendicular collisionless shock experiments

12 p1940 A71-27418

Paired comparison tests of relative signal detected by capacitive and floating Langmuir probes in steady state turbulent plasma confined in magnetic mirror geometry

13 p2066 A71-28155

Magnetic pumping of collisionless turbulent plasma with I.F. Alfvén and magnetosonic waves, assuming high initial plasmon energy

13 p2105 A71-28175

Conductivity tensor of turbulent plasma from coherent response to external test wave, introducing effective collision frequencies

13 p2109 A71-29244

H lines Stark broadening in turbulent plasma, considering Langmuir vibrations nonadiabatic action and energy density

14 p2280 A71-30171

Ion and electron probe currents correlation for justification of electrostatic probes use for turbulent plasma diagnostics

14 p2280 A71-30174

Coronal emission from turbulent plasma excited by shock wave, discussing relation to type 2 radio bursts

15 p2473 A71-31719

Galaxy formation in expanding universe, discussing primordial plasma and photon gas turbulent medium for magnetic field amplification by dynamo mechanism

16 p2625 A71-33052

Collisionless turbulent plasmas nonequilibrium electric fields determination from hydrogen spectral lines Stark broadening

16 p2619 A71-33549

Transverse shock waves fine structure and saturation of ion-acoustic turbulence in collisionless plasma, using magnetic field probe and MHD equations

16 p2619 A71-33649

Solar wind turbulence spectrum from Mariner 6 and 7 space probe radar measurements, using differenced range vs integrated Doppler technique

16 p2627 A71-33728

Stark contours of hydrogen spectral lines in turbulent plasmas with high noise level due to HF Langmuir oscillations

19 p3110 A71-37388

Solar corona plasma turbulence spectra, evaluating radar echo structure

19 p3133 A71-37430

Electromagnetic wave scattering from turbulent plasma at 31 GHz, determining cross section dependence on bistatic angle and electron density

19 p3017 A71-37868

High frequency plasma turbulence in solar flares due to nonlinear conversion of ion-acoustic plasmons to Langmuir plasmons

20 p3279 A71-39304

Solar wind origin in active regions by radar exploration, noting signal backscattering from coronal plasma turbulent pulsations

20 p3281 A71-39732

Probe size and orientation effects in turbulent plasma flow diagnostics, considering electrostatic probes frequency filtering and wake effects

21 p3423 A71-40979

Nonisothermal turbulent plasma ion acoustic oscillations spectral energy density in electromagnetic wave field, calculating HF conductivity and absorption coefficient

21 p3424 A71-41132

Turbulent plasma heating in current sheet between opposed magnetic fields

21 p3424 A71-41270

Plasma turbulent electron and ion heating by large amplitude whistler resonant excitation, investigating mechanisms

22 p3583 A71-42459

High Mach number turbulent magnetosonic shocks generation by driving reflecting piston into plasma, simulating by electromagnetic particle code

23 p3708 A71-42893

Large scale electron-neutral and neutral-neutral correlation effects on turbulent weakly ionized plasma electromagnetic scattering cross section

23 p3711 A71-43524

Diffraction angular microwave beam scattering in fluctuating dense plasma, determining spatial scale of turbulence and permittivity

24 p3853 A71-44506

Nonisothermal plasma longitudinal ion acoustic and Langmuir oscillations phase and amplitude interactions, estimating energy transfer and turbulence criteria

24 p3853 A71-44509

Metagalactic X ray and cosmic electrons power spectra explanation by electron acceleration and scat-

tering in turbulent plasma with frozen-in magnetic field

24 p3865 A71-44568

MHD wave spectrum relaxation during wave-plasma interactions in weakly turbulent plasma, treating associated triplason processes as elementary events

24 p3855 A71-44661

PLASMA WAVES

NT ELECTROSTATIC WAVES

Collisionless shock waves in magnetized plasma as function of Alfvén-Mach number, measuring electron temperature jump on wave front spectroscopically

01 p0132 A71-10153

Book on numerical method for coupled modes in plasmas, elastic media and parametric amplifiers covering differential equations, recursive functions, wave propagation and iterative calculations

01 p0111 A71-10356

Structure and propagation of large amplitude modulated isolated compression waves in cold three component plasma with negatively charged ions

01 p0132 A71-10676

Nonlinear resonance excitation of ion acoustic plasma waves by weak external electric field, using partial differential equations

01 p0134 A71-11027

Self similar unsteady waves in cold plasma containing magnetic field, determining plasma oscillations

01 p0135 A71-11095

Quasi-transverse extraordinary wave interaction with density fluctuations in inhomogeneous magnetized plasma, using modulation measurement for instability diagnosis

01 p0136 A71-11440

Transverse wave instability of unmagnetized collisionless plasma subjected to shear flow

01 p0136 A71-11477

Weak nonlinear ion-acoustic shock waves in cold ion-warm electrons plasma, using nonlinear perturbation method

02 p0288 A71-11868

Charged particle motion in self consistent continuous wave spectrum from Vlasov and Poisson equations solution

02 p0289 A71-11955

Resonance excitation of high amplitude waves in plasma cylinder by HF azimuthal axially periodic current flowing through coil encircling plasma

02 p0291 A71-12504

Coupled wave equations for magnetoplasma with anisotropic pressure

03 p0463 A71-13346

Electron plasma waves one dimensional quasi-linear instability with allowance for spontaneous emission

03 p0464 A71-13929

Dispersion relation for LF quasi-static ion acoustic waves in finite geometry plasma

03 p0464 A71-13933

Large amplitude upstream wave solar wind event of 10 March 1968 with suprathermal protons, correlating magnetometer plasma probe and Lepede proton data

03 p0482 A71-14550

Locally slowly varying magnetoplasma, determining electron concentration and collision frequency by wave propagation experiment

04 p0633 A71-15034

Wave kinetics in anisotropic plasma of weakly damped magnetosonic vibrations, using Lagrangians of three and four wave interactions

04 p0633 A71-15108

Ion acoustic waves in streaming ion plasma, discussing wave modes and energy exchange

04 p0634 A71-15258

Coherent emission mechanisms for pulsar models, discussing plasma wave conversion into radio emission

04 p0650 A71-15582

Nonlinear interaction between three longitudinal plasma waves, calculating dissipation effect on coupling coefficients

04 p0635 A71-15902

Refractive index equation for oblique wave propagation in inhomogeneous compressible electron plasmas

05 p0786 A71-16287

Hydrodynamic model describing intermediate stages of propagation of plasma shock wave created by laser light focusing

05 p0787 A71-16333

Solar wind upstream waves ahead of earth bow shock by dual satellite observations

05 p0741 A71-16629

Quasi-linear equations consequences in discrete spectra and damped electron plasma waves, discussing conservation laws relation to resonance approximation

05 p0789 A71-16652

Weakly ionized magnetoplasma waves and instabilities due to effects of electrons parallel, Hall and diamagnetic drifts relative to ions

05 p0789 A71-16653

Collisionless plasma shock longitudinal wave propagation perpendicular to magnetic field, demon-

strating ion acoustic/electron Bernstein modes instability

05 p0789 A71-16655

Collision effects on temporal plasma wave echoes, using free particle model

05 p0790 A71-16661

Acoustic and surface plasma waves in superconducting semiconductor metal films and laminates

05 p0793 A71-16826

Supraluminous waves modes in field free two component anisotropic plasma by linearized relativistic Vlasov equation

05 p0791 A71-16939

Collective longitudinal space charge waves in trapped relativistic one dimensional plasma, calculating inhibition/enhancement of cosmic ray Fermi acceleration

05 p0791 A71-16940

Plasma electron cyclotron heating, observing wave excitation at 100 MHz and decay after initial wave

06 p0930 A71-17396

Nonlinear interaction between waves with random phases in magnetoactive plasma of solid body, discussing weak turbulence theory

06 p0930 A71-17404

Wave buildup in weakly turbulent plasma, noting epithermal pulse background effect on phase velocity

06 p0936 A71-17664

Monochromatic plasma waves excitation by electron beams, discussing nonlinear theory

06 p0936 A71-17688

Electromagnetic wave trapping by nonlinear resonant interactions involving ion sound wave and two electromagnetic waves in isotropic plasma

06 p0869 A71-17988

One component system wave propagation kinetic theory, calculating monatomic gas and plasma oscillations by discrete ordinate method

07 p1165 A71-18876

Unstable electrostatic waves propagating in uniform infinite plasma with weak beam, Fourier transforming space dependent variables

07 p1166 A71-18881

Collisional drift plasma wave instability nonlinear analysis, calculating wave amplitude as function of magnetic field based on two fluid theory

07 p1166 A71-18883

Extraordinary waves propagating perpendicularly to uniform magnetic field in hot electron plasma, discussing wave interaction

07 p1166 A71-18884

Magnetoactive cold plasma wave interaction theory, investigating energy transfer

07 p1167 A71-19230

Structure and propagation of large amplitude modulated isolated compression waves in cold three component plasma with negatively charged ions

07 p1170 A71-20138

Plasma waves and echoes characteristics and diagnostics, emphasizing longitudinal waves

07 p1172 A71-20502

Microwave scattering from gaseous plasmas, discussing EM waves, fluctuation and diagnostics problems

07 p1172 A71-20503

Plasma instabilities and mode stabilization, discussing density-gradient-driven drift waves in collision-dominated regime

07 p1173 A71-20510

Time estimation for plasma front propagation in quartz glass circular pipes without imposition of axial magnetic field

08 p1338 A71-20829

Solar burst theories, considering type 3 radiation source model for determination of lower corona plasma waves energy densities

08 p1358 A71-20889

Artificial solar wind experiments, describing interaction between hydrogen plasma shock wave and simulated geomagnetic field

08 p1354 A71-21010

Nonlinear collisionless magnetoplasma waves and ionospheric irregularities electric field intensity, defining nonlinear oscillations domain by pseudopotential well

08 p1339 A71-21206

Low density plasma in magnetic field, investigating existence possibilities of stationary isothermal jump and plane wave periodic solution

08 p1340 A71-21493

Longitudinal electron plasma waves generated by electron beam-plasma interactions, discussing simultaneous radiation and incoherent microwave scatter measurements in relation to theory

08 p1341 A71-21746

Type 2 and 3 solar radio burst model, examining exciting agent as electron bunch emitting electron plasma waves

08 p1356 A71-21756

Self similar unsteady waves in cold plasma containing magnetic field, determining plasma oscillations

08 p1342 A71-21953

Ion acoustic and helicon waves nonlinear interactions in plasma, evaluating whistler buildup rate

09 p1501 A71-22536

One dimensional plasma wave nonlinear dispersion relation, stability and harmonic generation from statistical properties of trapped particle orbits in random potential

09 p1503 A71-22862

Magnetized inhomogeneous plasma nonlinear wave coupling near hybrid resonances

09 p1503 A71-22868

Compton scattering of relativistic electrons in cosmic plasma waves as source of HF radio emission from metagalactic objects

09 p1521 A71-22926

Steady plane plasma shock wave structure in partially ionized and radiating gas, using Navier-Stokes equations in three fluid continuum approach

09 p1504 A71-23202

Magnetoionic theory for drifting plasma whistler mode propagation, deriving magnetic field effects on imaginary and real parts of complex refractivity

09 p1505 A71-23385

Weak turbulence analysis of Maxwellian plasma waves nonlinear interactions effects on two stream instability with Gaussian momentum distribution

10 p1647 A71-23886

Electrostatic waves high order interaction in collisionless plasma, deriving coupling constants from energy conservation and invariance under time reversal

10 p1647 A71-23888

Parametric excitation of transverse waves in inhomogeneous electron plasma driven by oscillating electric field, using multimode perturbation method

10 p1647 A71-23891

Ion acoustic waves propagation and structure measurements with metal electrode technique and continuous channel electron multiplier in plasma wind tunnel

10 p1611 A71-24517

Strong interaction between plasma forward wave and electron beam slow wave at equal densities, causing double stream instability nonlinear limitations

10 p1651 A71-24636

Electromagnetic wave conversion into plasma waves in cold anisotropic plasma with two dimensional inhomogeneity

10 p1654 A71-24893

Pulsed magnetic piston produced shock waves propagation along field in collisionless hydrogen plasma

10 p1654 A71-24894

Electromagnetic second harmonic wave generation in inhomogeneous magnetoactive plasma, using HF probe and horn antenna for detection

10 p1654 A71-24974

Nonlinear beam plasma interactions theory review, using plasma column circuit equation models

11 p1805 A71-25629

Magnetoactive cold electron plasma wave interaction theory, investigating energy transfer

12 p1934 A71-26748

Drift waves dynamic stabilization in collisionless plasma, considering AC electric field effects on low frequency instabilities

12 p1935 A71-26914

Double structured perpendicular magnetoplasma shock waves possessing precursor foot due to ion reflection from resistive shock front

12 p1936 A71-26918

Magnetoactive spatially homogeneous plasma parallel and perpendicular waves derivation from hydrodynamic equations in quasi-linear approximation, noting resonances and nonlinear effects

12 p1937 A71-27181

Longitudinal plasma layer waves kinetic theory, considering particles specular reflection from layer boundaries

12 p1937 A71-27203

Inhomogeneous plasma, describing linear wave transformation with fourth order differential equation with variable coefficients

12 p1942 A71-27768

Similarities between ion waves in plasmas and gravity waves in incompressible fluid /steady water flow with allowance for surface tension/

13 p2046 A71-27844

Plasma ion waves external control with HF fields in subthreshold regime

13 p2104 A71-27845

Stability of trapped particle equilibrium, considering contribution to plasma wave dispersion

13 p2104 A71-27847

Topside ionospheric instabilities of electrostatic ion acoustic and ion cyclotron waves to field aligned currents in single and multilayer plasmas

13 p2054 A71-27917

Isomagnetic potential discontinuity of electrostatic character in collisionless plasma shock waves, studying Mach number effect

13 p2105 A71-28169

Collisionless plasma thermal shock wave, showing heat in electron component transportable along magnetic field at lower rates than thermal velocity

13 p2106 A71-28425

Solar and geophysical morphology of radio burst of active sun, treating bremsstrahlung, gyro, synchrotron and Cerenkov radiation and plasma waves

13 p2137 A71-28514

Book on shock waves in collisionless plasmas covering basic equations and classification of shock structures, magnetosonic waves, shocks and solitons, electrostatic shocks and solitons, etc
13 p2108 A71-28896

German monograph on drift waves in plasma with density gradient covering LF electrostatic disturbances in low density plasma
14 p2277 A71-29581

Resonant dipole antenna with feed points immersed in weakly ionized plasma, investigating performance under electro-acoustic and electromagnetic wave excitation
14 p2193 A71-29858

Collisionless plasmas stationary flow hydrodynamic equations applied to plasma waves analysis
14 p2280 A71-30211

German monograph on shock waves in anisotropic plasma covering parameters derivation based on kinetic plasma theory and experimental verification possibilities
14 p2280 A71-30235

Soviet monograph on wave propagation in cold and hot magnetoplasmas covering particle collisions, plasma control and instability and plasma-particle interactions
14 p2280 A71-30246

Longitudinal waves correlation damping in high temperature plasma under magnetic field, calculating dielectric constant by quantum statistical method
14 p2280 A71-30450

Monograph on instabilities in ion beam-plasma system covering surface wave propagation, magnetic effect and ion cyclotron radiation characteristics
14 p2281 A71-30507

Large amplitude ion acoustic wave propagation in streaming ion plasma, noting nonlinear effect in amplitude oscillation observation
14 p2281 A71-30541

Longitudinal ionic wave excitation by grid in collisionless Q machine plasma
15 p2456 A71-31820

Matrix solution for wave equation with mode coupling of VLF and ELF radio waves in horizontally stratified layer of anisotropic ionosphere plasma
15 p2373 A71-32444

Collisionless small amplitude shocks in plasmas, considering wave dispersion and critical Mach number effects
15 p2459 A71-32561

Nonlinear interaction between three resonant modified ordinary electromagnetic waves propagating perpendicular to static magnetic field in homogeneous electron plasma, studying relativistic effects
15 p2460 A71-32655

Magnetic stabilization of transverse plasma instabilities, considering waves propagating transversely to plasma direction in presence of uniform external magnetic field
15 p2460 A71-32658

Low density plasma in magnetic field, investigating existence possibilities of stationary isothermal jump and plane wave periodic solution
16 p2618 A71-33044

Plasma energy cumulation by concentric spherical and cylindrical waves, calculating stability limit by integral solution
16 p2619 A71-33355

Visible spectrum electromagnetic waves propagation in plasma, emphasizing parametric coupling
16 p2620 A71-34136

Plasma conductivity frequencies, including electromagnetic wave propagation in alternating field and scattered light intensities
17 p2786 A71-34276

Mirror-contained collisional plasmas, deriving wave reflection and absorption from equilibrium density and temperature profile equations
18 p2950 A71-35860

Bernstein mode wave instability growth rate in collisionless shocks propagating perpendicular to magnetic field, including pressure gradient effects
18 p2950 A71-35928

Decay instability at ion-sound frequency induced by large amplitude Bernstein mode wave in plasma
18 p2951 A71-35929

Reflection and transmission coefficients for electromagnetic propagation across magnetic field in parabolic plasma layer, determining EM-plasma wave conversion efficiency
19 p3014 A71-37079

Plasma cyclotron wave excitation with charged particle beam, determining unstable oscillations frequency range and spatial and time development with nonlinear analysis
19 p3111 A71-37633

Electron wave coupling in plasma column, determining exact resonance and field configurations of frequencies
19 p3111 A71-37635

Surface wave patterns created by constant velocity pressure point on inviscid plasma bounded by magnetic field
19 p3111 A71-37637

Digital simulation of pseudowaves and plasma sheath formation about grid by computer solution of ion Vlasov equation for ion distribution function time evolution
19 p3113 A71-37749

Large amplitude monochromatic electron cyclotron wave broadening in plasma, producing shifted phases in finite frequency range
19 p3114 A71-37855

Modulated electron beam interaction with plasma, showing amplitude growth and traveling wave profile distortion
19 p3114 A71-37856

Plasma wave instrument for measuring AC electrical and magnetic field levels in outer planets missions [AAS PAPER 71-125]
19 p3064 A71-37939

Longitudinal plasma sheath waves kinetic theory, considering particles specular reflection from sheath boundaries
19 p3116 A71-38615

Pressure anisotropy effects on plasma wave coupling and modification for dispersion in collisionless beam-plasma systems
20 p3273 A71-39045

Uniform magnetic field effects on beam-plasma waves, using scalar pressure hypothesis
20 p3274 A71-39049

Nonlinear Landau damping proposed as explanation for electron plasma oscillations amplification by plasma wave amplitude increase
20 p3274 A71-39349

Artificial solar wind experiments, describing interaction between hydrogen plasma shock wave and simulated geomagnetic field
20 p3279 A71-39590

Collisionless plasma thermal shock wave, showing heat in electron component transportable along magnetic field at lower rates than thermal velocity
21 p3421 A71-40083

Plasma ordinary wave mode electromagnetic cyclotron instability, discussing Dory-Guest-Harris type loss cone distributions
21 p3421 A71-40627

Unified linear theory for MHD waves in weakly ionized radiating plasma, deriving two-fluid model set of equations corresponding to magnetoacoustic, thermal, electrothermal and ionization rate waves
21 p3423 A71-40945

Electromagnetic wave conversion into plasma waves in cold anisotropic plasma with two dimensional inhomogeneity
21 p3425 A71-41273

Pulsed magnetic piston produced shock waves propagation along field in collisionless plasma
21 p3425 A71-41274

Quasi-static surface waves in Fermi electron plasma with Maxwellian electron velocity distribution
21 p3425 A71-41277

Plasma shock wave propagation along weak magnetic field, considering energy dissipation
21 p3425 A71-41279

Sound waves excitation and amplification in weakly ionized plasma within alternating electric field
21 p3425 A71-41282

Solar radio bursts and noise storms frequency band spectra, investigating warm plasma wave propagation and mode coupling theories
22 p3579 A71-41462

Short wavelength instabilities in collision dominated plasma confinement by rotating magnetic field, interpreting in terms of equivalent negative resistance
22 p3579 A71-41579

Acoustic wave detection in K-seeded methane-oxygen flame plasma, using I-V characteristic modulation of fixed electrostatic probe
22 p3580 A71-41622

LF waves and instabilities on positive column in magnetic field, comparing three theories for helical modes for He at low pressures
22 p3582 A71-41897

Electron plasma waves and free streaming bursts response to fast rising voltage step in low density cylindrical plasma in strong magnetic field
22 p3582 A71-41899

Kinetic wave equation matrix elements for three resonantly coupled electrostatic plasma waves noting application to electron plasma coupling with ion sound waves
22 p3582 A71-41900

Threshold AC electric field calculation for inhomogeneous plasma parametric instability excitation, noting role of electron plasma wave energy propagation from unstable region
22 p3582 A71-41901

Electrostatic mode wave equations for low beta plasma microinstabilities in axisymmetric magnetic mirror machines, including effects of particle cyclotron, bouncing and drift motions
22 p3582 A71-41902

LF wave propagation in weakly ionized plasma under magnetic field, observing forward and backward waves dispersions near cathode
22 p3582 A71-41905

Stochastic ion acceleration by relativistic electron beam in plasma traveling waves with different phase velocities
22 p3578 A71-42065

Resonant coupling of two electron plasma waves with ion sound wave at large electron Larmor radii under weak magnetic field
22 p3583 A71-42418

Magnetoactive spatially homogeneous plasma parallel and perpendicular waves derivation from hydrodynamic equations in quasi-linear approximation, noting resonances and nonlinear effects
22 p3583 A71-42458

Exact test particle propagator of Lenard-Bernstein equation for magnetoplasma, applying to transverse plasma echoes
22 p3584 A71-42466

Nonlinear effects on spatial growth of cesium plasma wave excited by electron beam of varying density and velocity
22 p3584 A71-42535

Magnetic drift waves near proton cyclotron frequency, noting magnetic field gradient role in plasma instability
23 p3709 A71-43181

Wave phenomena in space chamber rarefied plasma, clarifying spontaneously excited noise wave properties by passive experiment
23 p3710 A71-43365

Spatially separated plasma beams of different temperatures, determining amplified wave instability boundaries and growth increments by quasi-hydrodynamic approximation
23 p3711 A71-43557

Particle collisions and relativistic effects on electromagnetic wave propagation within plasma in direction normal to external magnetic field near gyrofrequencies
23 p3645 A71-43559

Wide wavelength parametric plasma instability in constant magnetic and weak HF electric fields above ion gyroscopic frequency
23 p3714 A71-44327

Nonlinear ion acoustic soliton wave propagation and dissipation in nonhomogeneous nonisothermal weakly absorbing plasma
23 p3714 A71-44333

Electrostatic waves nonlinear interactions in uniform plasma in presence of external constant magnetic field, deriving coupling coefficients by coupled mode theory
24 p3858 A71-45276

PLASMA-ELECTROMAGNETIC INTERACTION
Longitudinal oscillations excitation by transverse electromagnetic wave in collision-magnetized plasma, noting LF wave buildup
01 p0134 A71-11030

Electron-positron pair production during focusing of laser radiation in dense plasma
01 p0135 A71-11094

Particle acceleration by coherent electrostatic wave propagation through plasma, producing monoenergetic particle beam
01 p0131 A71-11513

Solar coronal plasma electromagnetic wave amplification, discussing maser action effect on radar echoes
02 p0306 A71-12078

Electron velocity distribution in fully ionized plasma under crossed electric and magnetic fields, assuming Fokker-Planck expression for Lorentz gas
02 p0293 A71-12743

Far field diffraction of unidirectional surface wave by conducting rectangular wedge in cold anisotropic plasma, showing frequency dependent transmission coefficient
03 p0465 A71-13953

Electromagnetic wave propagation along conducting wire in magnetoplasma
03 p0381 A71-14472

Strong turbulence theory of ionospheric cross field instability of weakly ionized plasma
03 p0420 A71-14533

Beam-plasma mechanism of very long delayed radio echoes from ionosphere
03 p0381 A71-14552

Electromagnetic wave generation by interaction in plasma stream resonator, considering Coulomb friction and boundary reflection coefficients
04 p0633 A71-15110

Short dipole antenna impedance in warm isotropic plasma using Vlasov theory
04 p0553 A71-15221

Electromagnetic instability growth in counterstreaming nonrelativistic plasmas, comparing electrostatic rate
05 p0788 A71-16601

Magnetospheric sudden impulses amplitude and rise time distributions observation byOGO 3 and 5 satellites
06 p0889 A71-17686

Nonsteady third harmonic generation due to plasma interaction with microwave
06 p0937 A71-18041

Antenna radiation in isotropic plasma near resonance 06 p0937 A71-18311

Oblique incidence effect on reflection and absorption of laser light by solid surrounded by plasma in vacuum 07 p1166 A71-18886

Plasma nonlinear drift oscillation instabilities, discussing plasma interaction with HF electromagnetic fields 07 p1167 A71-19229

Maximum ponderomotive force on laser produced plasmas, using wave equation in linear critical layer 07 p1171 A71-20291

Obliquely incident p-polarized plane electromagnetic wave interaction with hot plasma half space, using linearized relativistic Vlasov equation and Laplace transform technique 07 p1171 A71-20292

Coupled electroacoustic and electromagnetic wave propagation in inhomogeneous compressible and lossy plasma 07 p1065 A71-20324

Microwave scattering from gaseous plasmas, discussing EM waves, fluctuation and diagnostics problems 07 p1172 A71-20503

Solar coronal plasma electromagnetic wave amplification, discussing maser action effect on radar echoes 08 p1361 A71-21128

Compressible isotropic plasma slab effect on magnetic dipole radiation pattern, using reciprocity theorem 08 p1253 A71-21274

Electromagnetic wave scattering by perfectly conducting cylinder in anisotropic plasma with external magnetic field, deriving radiation pattern from asymptotic expression 08 p1253 A71-21295

Plasma configurations kinetic description by differential equations based on Vlasov and Maxwell equations, obtaining boundary layer distribution between plasma and magnetic field 08 p1340 A71-21492

Low density plasma in magnetic field, investigating existence possibilities of stationary isothermal jump and plane wave periodic solution 08 p1340 A71-21493

Incompressible equilibrium plasma ellipsoid stability in electromagnetic traveling wave field 08 p1341 A71-21500

Electron-positron pair production during focusing of laser radiation in dense plasma 08 p1342 A71-21952

Naturally generated electromagnetic waves interaction with electron flux in magnetoplasma, noting gyroresonance 09 p1501 A71-22304

Klystron output resonator efficiency optimization under excitation of plasma with Pi-shaped charge concentration based on performance analysis as function of plasma width 09 p1415 A71-22360

Solar wind flux correlation with earth EM field pulsations, noting flare-generated shock front effects on magnetosphere 09 p1513 A71-22422

Electromagnetic HF potential effect on reflection of waves obliquely incident on plasma with gas kinetic pressure nonlinearity 09 p1406 A71-22886

Electromagnetic wave propagation through bounded time-space periodic cold plasma under plane wave incidence, calculating transmitted and reflected components 09 p1503 A71-22986

Plasma flow interaction with nozzle-shaped magnetic field generated by current loop with strong Hall effect 09 p1504 A71-23309

Transient electromagnetic wave propagation in lossy directionally anisotropic time varying stratified plasma, using characteristics method 10 p1648 A71-24296

Shock wave propagation in electronically excited hot plasma in electromagnetic field, assuming negligible electron-ion collisions 10 p1653 A71-24828

Microwave signal attenuation in LF oscillation beam plasma discharge, comparing to braking cyclotron absorption effect 10 p1653 A71-24880

Fully ionized gas under electric and magnetic fields, calculating electron velocity distribution and runaway rate as function of time from Boltzmann equation 10 p1654 A71-24975

Strong cylindrical and spherical electromagnetic wave propagation in plasmas, calculating amplitude and electron temperature 11 p1805 A71-25768

Plasma nonlinear drift oscillation instabilities, discussing plasma interaction with HF electromagnetic fields 12 p1934 A71-26747

Wire grid simulation of electron density, transmission and reflection of lossless and lossy reentry plasma sheath under microwave radiation at X and K bands 12 p1935 A71-26767

Transverse electromagnetic wave penetration in semibounded plasma with specular electron reflection 12 p1878 A71-26958

Plasma turbulent electron and ion heating by large amplitude whistler resonant excitation, investigating mechanisms 12 p1937 A71-27182

Plasma in strong electric and magnetic field with allowance for inelastic electron collisions with neutral particles, showing resonant oscillations from Born approximation 12 p1937 A71-27183

Semiconductor or gas-discharge two-component plasmas, calculating permittivity variation due to carrier heating and diffusion during strong plane monochromatic, electromagnetic wave propagation 12 p1937 A71-27184

Local electron density measurements in low beta plasmas, using nonlinear electromagnetic wave mixing under synchronism condition 13 p2104 A71-27849

Self trapping of intense microwave signal penetrating dense transcritical plasma 13 p2105 A71-28174

Solar wind deflection due to permanent lunar surface magnetism 13 p2129 A71-28780

Electromagnetic wave reflection from interface between moving and stationary electron plasma, giving boundary conditions at velocity discontinuity surface 13 p2108 A71-28855

Conjugate duct irregularities in magnetosphere involving interchange of plasma tubes by spatially varying electric fields, applying to spread F formation 14 p2230 A71-29714

HF modulated transverse electromagnetic wave penetration into plasma with negative dielectric constant, noting plasma density fluctuations and electroacoustic wave formation 14 p2281 A71-30542

Far zone field and radiated power equations for corner driven traveling wave loop antenna in warm plasma, comparing data for Ariel 3 satellite 14 p2283 A71-31040

Electromagnetic wave energy absorption in inhomogeneous cold magnetoactive plasma cylindrical columns 15 p2455 A71-31735

Resonant plasma heating at electron cyclotron frequency second harmonic, studying interactions with microwave electromagnetic radiation in adiabatic trap 15 p2455 A71-31736

Superhigh frequency microwave absorption region localization in collisionless plasmas by plasma parameters measurement in toroidal magnetic field 15 p2370 A71-31737

Synchronous and oscillatory energy gain with electron-wave resonance time in collision magnetospheric plasma 15 p2371 A71-32024

Refraction and absorption length of coherent laser radiation propagating in high temperature cylindrical plasma column 15 p2458 A71-32390

Fast argon plasma flow interaction with strong magnetic fields, describing ionization relaxation phenomena behind magnetically reflected shock fronts 16 p2615 A71-32898

Microwave and laser diagnostics of plasmas based on interaction with electromagnetic fields 16 p2617 A71-32960

Plasma configurations kinetic description by differential equations based on Vlasov and Maxwell equations, obtaining boundary layer distribution between plasma and magnetic field 16 p2618 A71-33043

Low density plasma in magnetic field, investigating existence possibilities of stationary isothermal jump and plane wave periodic solution 16 p2618 A71-33044

Incompressible equilibrium plasma ellipsoid stability in electromagnetic traveling wave field 16 p2618 A71-33048

Neutral current sheets in slow moving plasma with frozen-in magnetic field with null force line 16 p2638 A71-33651

Electric current distributions measurement along monopole antenna in isotropic and anisotropic plasmas generated in large space chamber 17 p2716 A71-35048

Homogeneous infinite weakly ionized plasma dielectric permittivity tensor in crossed electric and magnetic field 17 p2790 A71-35444

LF resonances for radially inhomogeneous collisionless plasma sphere impinged by plane electromagnetic waves 17 p2708 A71-35485

Coupled longitudinal-transverse wave modifications of electrostatic dispersion relation with ion gyrofrequency instabilities in magnetized plasma 18 p2950 A71-35866

Harmonic generation due to strong microwaves nonlinear mixing in He plasma, noting resonances at fundamental frequencies 18 p2951 A71-35932

Thermal self focusing of pulsed millimeter waves transmitted through cylindrical plasma, observing power dependence and beam asymmetry 18 p2951 A71-35986

Asteroid magnetospheres effects on magnetic moments and whistler mode noise propagation in solar wind 18 p2964 A71-36292

Magnetopause current layer equilibrium based on numerical solution of uniform magnetic field confinement by warm plasma with net parallel velocity 19 p3132 A71-37355

Electromagnetic wave propagation through magnetoplasma disturbed by acoustic wave, calculating transmitted and reflected waves amplitude modulation 19 p3110 A71-37480

Transient RF pulse dispersion along plasma loaded coaxial gas discharge, noting group delay 20 p3272 A71-38783

Numerical procedure for electromagnetic field penetration through inhomogeneous cold plasma slab with collisions, using Riccati type differential equation 20 p3273 A71-39004

Linear antenna in anisotropic plasma, calculating reactance change with surrounding dielectric layer thickness with allowance for ion depletion 20 p3204 A71-39142

Auroral radio reflections mechanism in terms of auroral plasma instability processes, identifying ion acoustic wave characteristics among other echo components 20 p3199 A71-39852

Electromagnetic wave reflection from interface between moving and stationary electron plasmas, giving boundary conditions at velocity discontinuity surface 21 p3426 A71-41288

Strong cylindrical and spherical electromagnetic wave propagation in plasmas, calculating amplitude and electron temperature 22 p3579 A71-41536

Electromagnetic wave dispersion in interstellar plasma, noting indistinguishable form from natural dispersion of photons with nonzero rest mass 22 p3574 A71-41598

Piezosemiconductors nonequilibrium electron plasma current oscillations under strong electric and magnetic field interactions 22 p3584 A71-41644

Monochromatic radio wave propagation in interplanetary plasma, deriving frequency spectrum and phase and amplitude fluctuations 22 p3511 A71-42302

Plasma turbulent electron and ion heating by large amplitude whistler resonant excitation, investigating mechanisms 22 p3583 A71-42459

Plasma in strong electric and magnetic field with allowance for inelastic electron collisions with neutral particles, showing resonant oscillations from Born approximation 22 p3584 A71-42460

Semiconductor or gas-discharge two-component plasmas, calculating permittivity variation due to carrier heating and diffusion during strong plane monochromatic electromagnetic wave propagation 22 p3584 A71-42461

Electrostatic plasma instabilities under HF alternating electric field oscillating at plasma frequency 22 p3584 A71-42465

Steady state transition layer between cold solar plasma flow and geomagnetic field in one dimensional model 22 p3536 A71-42622

Millimeter transverse electric wave diffraction by spherical plasma, interpreting interferometric measurements of electron density 23 p3708 A71-43085

Plasma jet injection stoppage and reflection in strong transverse magnetic field, considering instability due to flow interactions 23 p3709 A71-43265

Electron periodic energization by magnetospheric RF wave propagation, examining cyclotron resonant interaction 23 p3644 A71-43321

F layer perturbations by intense vertically upward radio waves for aeronomy and plasma control studies 23 p3671 A71-43543

Nonlinear sum and difference frequency and second harmonic generations of current density in homogeneous

ous magnetoplasma by nonuniform microwave electric fields

23 p3712 A71-44002

Laser pulse produced plasma in freely expanding high density nitrogen gas jets, measuring electron temperature and light-plasma interaction time

23 p3687 A71-44140

Magnetic modulation observation in plasma light scattering spectra experiments, noting dependence on angle between scattering and magnetic field vectors

23 p3713 A71-44150

Radiation pattern modification factors calculation for TE excited slot antenna in ground plane covered with inhomogeneous plasma reentry sheath

23 p3646 A71-44172

Wide wavelength parametric plasma instability in constant magnetic and weak HF electric fields above ion gyroscopic frequency

23 p3714 A71-44327

Absorption cross section for plane electromagnetic wave in circular plasma cylinder in constant magnetic field, assuming small Larmor radius

23 p3714 A71-44328

Dense hydromagnetic plasmoid interaction with nonuniform axisymmetric magnetic field using two dimensional fully ionized two temperature model

24 p3852 A71-44487

Supersonic plasma flow interaction with mirror field studied by changing ion-ion collision mean free path in BSG-1A device

24 p3852 A71-44489

Parametric hybrid resonance excitation of longitudinal oscillations in nonhomogeneous magnetoplasma by HF electromagnetic field

24 p3852 A71-44491

Lower hybrid frequency heating and wave absorption efficiency in inhomogeneous HF cylindrical plasma

24 p3852 A71-44492

RF power absorption by magnetized uniform hot electron-ion plasma column submitted to TE and TM waves

24 p3852 A71-44498

External, HF, traveling wave field interactions with homogeneous electron plasma longitudinal oscillations under magnetic field

24 p3853 A71-44503

Diffraction angular microwave beam scattering in fluctuating dense plasma, determining spatial scale of turbulence and permittivity

24 p3853 A71-44506

MHD wave spectrum relaxation during wave-plasma interactions in weakly turbulent plasma, treating associated triplasmon processes as elementary events

24 p3855 A71-44661

Boundary value problem of plane electromagnetic wave interaction with inhomogeneous warm plasma column, using matching method

24 p3856 A71-44794

Inhomogeneous rarefied plasma, investigating non-local, linear and nonlinear effects on electromagnetic wave reflection and transmission

24 p3857 A71-45117

Linear transformation and absorption of electromagnetic waves in plasma

24 p3857 A71-45167

Refraction of electromagnetic wave with electric field perpendicular to applied magnetic field in anisotropic plasma cylinder cross section

24 p3858 A71-45236

Subharmonic frequency division for neon discharge plasma oscillations under resonance due to nonuniform electric field

24 p3858 A71-45263

Auroral plasma particle discharge during motion in strong magnetic field, discussing magnetospheric instability due to temperature anisotropy

24 p3867 A71-45309

Radio wave propagation characteristics in Venusian atmosphere and interplanetary plasma from Venera 7 probe data

24 p3805 A71-45312

PLASMA-PARTICLE INTERACTIONS

Electron beam nonlinear interaction with plasma, considering electrostatic wave propagation, instability and dispersion equation

01 p0135 A71-11209

Stability analysis of magnetosphere whistler amplification, discussing energetic electron interaction with background plasma

01 p0038 A71-11308

HF oscillations excitation in decaying plasma-electron beam system, noting Coulomb collisions and nonlinear effects role

02 p0288 A71-11632

Inhomogeneous plasma oscillations excitation by high intensity electron beam, causing instability greater than hydrodynamic beam mode

02 p0288 A71-11890

Relativistic self confined electron beam produced plasmas, measuring electron density profile by multiple pass Mach-Zehnder laser illuminated interferometer

02 p0289 A71-11946

Beam current instability and plasma heating by electron beam generated in linear discharge, discussing electron beam-cold plasma interactions

02 p0291 A71-12501

Quasi-neutral electron beam instabilities in plasmas within longitudinal magnetic field with ion compensated space charge

02 p0291 A71-12546

Nonlinear stabilization of beam instability during electron beam interaction with decay plasma, determining distribution function in damping dynamics of HF vibrations

02 p0292 A71-12610

Electrons longitudinal and transverse energy distribution in beam during cyclotron interaction with magnetoactive plasma waveguide

02 p0292 A71-12611

Plasma oscillations excitation in ion sheath by electron beam, presenting frequency and amplitude variations as functions of discharge current and target bias voltage

04 p0634 A71-15259

Single pulse relativistic electron beam passage through plasma, calculating induced current density in axial direction

04 p0635 A71-15371

Ion-neutral coupling in plasma acceleration revealed by velocity disparities determined spectroscopically [AIAA PAPER 70-166]

05 p0788 A71-16572

Weakly ionized magnetoplasma waves and instabilities due to effects of electrons parallel, Hall and diamagnetic drifts relative to ions

05 p0789 A71-16653

Charged particle beam interaction with electrostatic surface waves in plasma layer

06 p0929 A71-17317

Longitudinal electron oscillation suppression by beam density modulation in axially and transversely finite beam-plasma system

06 p0934 A71-17484

LF echo oscillations in nonequilibrium plasma under low density charged particle beam

06 p0937 A71-18353

Multiple speed flow onset and energy distribution in nonlinear electron beam-plasma interaction

06 p0937 A71-18354

Coulomb collisions effect on instability of cold and warm monoenergetic electron beams in plasma

07 p1166 A71-18885

Plasma-electron beam interaction instability transition from absolute to convective in hydrogen tube system at various pressures, considering electron collision effects

07 p1170 A71-20181

Longitudinal electron plasma waves generated by electron beam-plasma interactions, discussing simultaneous radiation and incoherent microwave scatter measurements in relation to theory

08 p1341 A71-21746

Relativistic electron beam instability and mean free path in dense plasma target, using Vlasov equation

09 p1500 A71-22238

Electron gun diode design for beam-collisionless plasma interaction nonlinear evolution, studying delta function beam velocity distribution

09 p1502 A71-22754

Transverse spatial particle diffusion in plasma under random oscillations, examining interaction between collisionless plasma and longitudinal wave

10 p1649 A71-24318

Strong interaction between plasma forward wave and electron beam slow wave at equal densities, causing double stream instability nonlinear limitations

10 p1651 A71-24636

Shock and turbulent ray interactions of plasma streams with neutral gas cloud, noting comet tail similarity

10 p1652 A71-24653

Ion beam deceleration and effective energy transfer to plasma at nonisothermal acoustic velocities in presence of ion acoustic instability

10 p1653 A71-24892

Quasi-linear relaxation of ultrarelativistic electron beam in homogeneous and inhomogeneous plasmas, noting initial divergence angle threshold

10 p1654 A71-24895

Thermionic converter nonsaturation effect in diode I-V characteristics from computerized analysis for plasma transport phenomena and sheath-electrode-plasma interactions

11 p1713 A71-25892

Nonlinear explosive ion beam-plasma interaction, discussing coupling coefficients and Landau damping

12 p1935 A71-26912

Low density plasma-double gridded antenna system for ion and electron signal propagation studies, observing multiple reflections of acoustic and ballistic pulses and bulk phenomenon

12 p1935 A71-26913

Nonlinear theory of ion-sound plasma turbulence for strong wave-particle interaction near resonance

12 p1935 A71-26915

Linear longitudinal ion wave instabilities in electrostatic shock in plasma by double humped/bump in tail/velocity distribution

12 p1935 A71-26916

PLASMA-PARTICLE INTERACTIONS

Statistical analysis of random oscillations excited in electron beam-plasma system based on signal recording data

13 p2106 A71-28364

Charged particles magnetic scattering on cyclotron instability waves of radiation belt plasma, estimating proton relaxation time

13 p2129 A71-28552

Electron beam instability in cylindrical magnetically confined plasma column, calculating quasi-static oscillations spatial growth increments

14 p2279 A71-30090

Dispersive effect on bremsstrahlung radiation from electron atom collisions in weakly ionized plasma, using Boltzmann transport equation

15 p2456 A71-31850

Plasma decay due to charged particles recombination, linearizing nonlinear equations describing diffusion of singly ionized two-component gas undergoing recombination

15 p2456 A71-31999

Quasi-neutral electron beam instabilities in plasmas within longitudinal magnetic field with ion compensated space charge

15 p2459 A71-32502

Plasma-electron beam system relaxation oscillations due to threshold excitation of transverse ionic oscillations by HF vibrations

15 p2460 A71-32706

Modulated relativistic electron beams interaction with plasma, investigating coherent energy loss

15 p2460 A71-32789

Collision integral for classical electron plasma, concerning Born-Bogoliubov-Green-Kirkwood-Yvon equations for long range interaction potential and motions of multiple particles

16 p2619 A71-33650

Electron beam nonlinear interaction with plasma, considering electrostatic wave propagation, instability and dispersion equation

17 p2786 A71-34261

Modulated electron beam interaction with plasma, showing amplitude growth and traveling wave profile distortion

19 p3114 A71-37856

Cyclotron resonance energization of trapped electrons in magnetosphere from plasma pseudopotential shape calculation, noting geophysical effect

19 p3117 A71-38724

Intense relativistic electron beam propagation in drift tube with neutral gas and plasma background, determining front velocity and energy transport

20 p3272 A71-38784

Electron oscillation induced longitudinal standing wave excitation and suppression in beam-plasma system by passing electron beam through axially bounded plasma

20 p3275 A71-39864

Artificial auroral experiment by Aerobee rocket-borne electron accelerator generated monoenergetic electron beam injection onto magnetospheric field

20 p3231 A71-39885

Trapping of neutrals from fast atom beam impinging on molecular hydrogen influx fed electron-cyclotron plasma target

21 p3422 A71-40761

Relativistic electron beam instability and mean free path in dense plasma target, using Vlasov equation

21 p3424 A71-41124

Ion beam deceleration and effective energy transfer to plasma at nonisothermal acoustic velocities in presence of ion acoustic instability

21 p3425 A71-41272

Quasi-linear relaxation of ultrarelativistic electron beam in homogeneous and inhomogeneous plasmas, noting initial divergence angle threshold

21 p3425 A71-41275

Electron beam interaction with plasma in ion sources with oscillating electrons, noting increased ion current

22 p3580 A71-41645

Rotational energy electron beam-plasma interactions in static magnetic field, showing exponential saturated intensity variation

22 p3582 A71-41906

Nonlinear electron beam bunching in zero temperature plasma during modulation by two frequencies, using klystron model

22 p3583 A71-42265

Nonlinear effects on spatial growth of cesium plasma wave excited by electron beam of varying density and velocity

22 p3584 A71-42535

I-V characteristics of weakly ionized cold plasma plane layer with electron-atom collisions

22 p3584 A71-42875

Nonlinear stabilization of beam instability in plasma with comparable phase velocity, electron capture and decay effects

23 p3709 A71-43264

Spectral line broadening due to radiating atom-electron gas interaction in nonequilibrium partially ionized plasma

23 p3710 A71-43392

Asymptotic expressions for electromagnetic field and currents induced in unbounded dense plasma by relativistic electron beam passage

23 p3711 A71-43410

Fine structure of energy distribution function for electron beam interacting with plasma

23 p3711 A71-43411

Large scale electron-neutral and neutral-neutral correlation effects on turbulent weakly ionized plasma electromagnetic scattering cross section

23 p3711 A71-43524

Multispecies high temperature Tokamak plasma heating by energetic particle injection, using Balescu-Lenard kinetic equation

24 p3852 A71-44490

Electron motion in plasma under stochastic electric field, emphasizing distribution function dependence on velocity and time

24 p3853 A71-44510

Stochastic properties of probe particle motion in Lorentz plasma, considering interactions and friction and diffusion coefficients

24 p3854 A71-44511

Plasma resonator excitation by Cerenkov emission from density modulated uncompensated charged particle beam

24 p3854 A71-44512

Injected ion beam interaction with hot plasma in cylindrical magnetic mirror, noting acoustic frequency oscillation heating effect

24 p3854 A71-44514

Temporal electron and ion temperature behavior for pulsed beam-plasma discharge interaction in probkotron mirror-like device

24 p3854 A71-44515

Artificial magnetosphere interaction with 8 keV electrons in hydrogen plasma beam simulating solar wind, noting penetration caused by boundary instability

24 p3823 A71-45043

Electron beam and plasma nonlinear interactions, noting scattering zone, amplitude oscillation maximum, longitudinal velocity and relaxation patterns

24 p3856 A71-45097

Charged particles effect on plasma negative ions, examining Stark effect in energy level

24 p3857 A71-45114

Spark source generated electron beam interaction with plasma in uniform magnetic field, estimating HF longitudinal oscillation power

24 p3857 A71-45233

Langmuir electron oscillation excitation by ion beam at velocity exceeding average electron thermal velocity in plasma formed by residual gas ionization

24 p3858 A71-45234

PLASMAGUIDES

Plasma beam systems dispersion equation with allowance for electron collisions with heavy particles

01 p0132 A71-10154

Bounded plasma wave interaction matrix elements calculation from orthogonal system formation by normal waveguide modes

02 p0289 A71-11891

Electrons longitudinal and transverse energy distribution in beam during cyclotron interaction with magnetoactive plasma waveguide

02 p0292 A71-12611

Slow electromagnetic wave propagation in plasma waveguide with inhomogeneous electron concentration, considering interaction with electron beam

04 p0634 A71-15112

Dispersion equations of plane parallel waveguide filled with hot magnetized plasma, using linear approximation

09 p1503 A71-22883

Microwave propagation in cylindrical waveguide containing inhomogeneous gas discharge plasma

13 p2029 A71-28363

Circular thin glass tube waveguide containing cold cylindrically stratified plasma, calculating electromagnetic wave propagation

13 p2029 A71-28499

Microwave upper hybrid resonance absorption, emission and heating of nonuniform axially magnetized afterglow plasma column in waveguide geometry

24 p3851 A71-44340

Electromagnetic wave amplification using coaxial line matching with plasma waveguide by charged particle beam

24 p3853 A71-44508

PLASMAUSE

Pc I micropulsation source region relation to plasmopause, using amplitude and polarization measurements

06 p0964 A71-17263

Alfven irregularities near plasmopause, discussing significance in relation to geomagnetic micropulsations based on OGO-3 and ground station observations correlation

07 p1104 A71-20008

Magnetospheric electric fields properties via simultaneous balloon flights between plasmopause and

polar cap, indicating fields and bulk plasma flow turbulence

08 p1282 A71-21632

Geomagnetic distributions of VLF hiss intensity and drifting frequency bursts near inner boundary of plasmopause on middle latitudes

09 p1411 A71-23634

Plasma sheet proton ring current, trapping boundary and plasmopause interrelations near magnetic equator and local midnight by satellite-borne analyzer array

10 p1605 A71-24781

Polar H ion plasma escape from ionosphere into magnetospheric tail effect on plasmopause formation, using hydrodynamic approximation

11 p1756 A71-25756

Magnetospheric location of SAR-ac field lines, discussing proximity to plasmopause, electron trough and ring current

13 p2055 A71-27918

Satellite measurements of cold plasma density and plasmopause in magnetosphere, comparing Whistler, Langmuir probe and ion trap data

14 p2237 A71-30951

Stable auroral red arcs on 29 September 1967, 31 October and 1 November 1968, comparing OGO 2 and OGO 4 VLF data on plasmopause crossings

15 p2397 A71-31757

Stable auroral red arcs generation at plasmopause from ion cyclotron wave turbulent dissipation of ring current proton energy

16 p2572 A71-33947

Plasmopause position during stormtime increase in trapped energetic electrons, measuring near prime geomagnetic meridian by whistler techniques

16 p2629 A71-33969

Bibliography on magnetosphere covering structure, magnetopause, geomagnetic tail, plasma sheet, convection plasmopause, storm and substorms, ring current and energetic particles

17 p2732 A71-34468

French monograph on ULF geomagnetic field variations covering plasmopause, geomagnetic pulsations, WKB limit and magnetospheric density

17 p2735 A71-35248

Precipitating protons measurement in 2.5-200 KeV energy range by OV1-15 satellite, comparing spatial distribution with plasmopause profile

19 p3125 A71-37358

Plasmopause Alfven, ion-acoustic, electron and ion drift wave modes coupling, calculating instability condition and growth rate

19 p3110 A71-37371

Geomagnetic micropulsation periods variation with latitude and plasmopause presence, calculating uncoupled toroidal and poloidal modes eigenperiods of hydromagnetic waves

20 p3215 A71-38735

Time dependent plasmopause motion after increase and decrease in magnetic activity based on analytical model of plasma flow

20 p3232 A71-39897

Geomagnetic Pi 2 pulsations association with magnetic storm onset in quiet conditions, discussing plasma sheet and pause theories

22 p3535 A71-42051

Earth corotating plasma tail evidence in plasmopause variations from high resolution proton distribution data obtained by Ogo 4 satellite during magnetic storm

23 p3668 A71-43166

PLASMAS (PHYSICS)

NT ARGON PLASMA

NT BETA PARTICLES

NT CESIUM PLASMA

NT COLD PLASMAS

NT COLLISIONLESS PLASMAS

NT COSMIC PLASMA

NT DEUTERIUM PLASMA

NT ELECTRON PLASMA

NT HELIUM PLASMA

NT HIGH TEMPERATURE PLASMAS

NT HYDROGEN PLASMA

NT METALLIC PLASMAS

NT MICROPLASMAS

NT NITROGEN PLASMA

NT NONEQUILIBRIUM PLASMAS

NT NONUNIFORM PLASMAS

NT RAREFIED PLASMAS

NT RELATIVISTIC PLASMAS

NT ROTATING PLASMAS

NT STELLAR WINDS

NT THERMAL PLASMAS

Parabolic particle distribution stability in plasmoids in guiding magnetic field under diffusion due to electron-ion collisions

01 p0133 A71-10680

Experimental dispersion curve for LF drift waves in inhomogeneous magnetoplasma

01 p0134 A71-11003

Multicomponent gaseous mixtures and plasmas transport analysis improved formalism consisting of N moment Boltzmann equation and N parameter distribution function representation

02 p0290 A71-12229

Dense plasma cluster charge exchange in supersonic Mg jet, examining pair collision model, particle scattering, target thickness and Q switching

02 p0292 A71-12614

Equilibrium, highly imperfect, partially ionized Hg and Li vapor plasmas, examining charged and neutral particle interaction forming charged clusters

02 p0292 A71-12617

Partially ionized bounded plasma LF natural oscillations due to ionization processes, ambipolar diffusion and charged particles recombination at walls

02 p0292 A71-12619

High beta plasma, calculating turbulence for fast shock propagating perpendicular to magnetic field

03 p0496 A71-14514

High density atmospheric pressure plasma ionization measurement by negatively pulsed Langmuir probe, showing agreement with space charge controlled sheath expansion model

04 p0586 A71-16660

Wave kinetics in anisotropic plasma of weakly damped magnetosonic vibrations, using Lagrangians of three and four wave interactions

04 p0633 A71-15108

Plasmoid mass and velocity distribution in pulsed plasma accelerators, using mass spectrometers and platinum thermal probe

04 p0634 A71-15111

Magnetoplasma electric and magnetic resonances by Voigt configuration, noting similarity to single particle scattering and particle size dependence

05 p0787 A71-16497

Charged particle power radiation in homogeneous magnetoplasma

05 p0790 A71-16660

Auroral phenomena, using dimensional analysis to examine MHD equations for fields and plasmas in magnetosphere

06 p0888 A71-17286

Diffusion coefficient and thermal conductivity dependence on plasma parameters in Tokamak installation

06 p0930 A71-17397

Drift wave instability suppression by homogeneous RF electric field in DC discharge diffused plasma

06 p0934 A71-17482

Plane grid condenser movement through magnetized plasma, calculating resistance by quasi-hydrodynamic approximation for plasma dielectric tensor

06 p0936 A71-17731

Kinetic theory calculation of partially ionized plasma near-electrode electron temperature profiles [AIAA PAPER 71-140]

06 p0939 A71-18583

Parabolic particle distribution stability in plasmoids in guiding magnetic field under diffusion due to electron-ion collisions

07 p1170 A71-20141

Magnetoplasma modulated waves nonlinear instability, taking into account relativistic effects

07 p1171 A71-20296

Input impedance of cylindrical and helical antennas in cold lossy magnetoplasma, discussing sensitivity to current distribution

07 p1065 A71-20323

Ionizing plasmas partition functions, determining opacities and equations of state

08 p1359 A71-20943

Critique on existence of one hundred million degree K solar flare plasma

08 p1350 A71-20944

Microwaves anomalous skin effect in high density gaseous magnetoplasma, comparing experimental electromagnetic field penetration increase due to thermal electron motion with theoretical prediction

09 p1502 A71-22800

Electromagnetic transient signal nonlinear dispersion in homogeneous isotropic partially ionized plasma medium

09 p1505 A71-23520

Reciprocity theorem for magnetoelectric modes, considering arbitrary plane slab within magnetoplasma with parameter variation in direction normal to horizontal plane of stratification

10 p1577 A71-24293

Correction factors for small values of logarithm of Debye length ratio to mean impact parameter in electrical conductivity of fully ionized plasmas

12 p1936 A71-26950

Anomalous resistance and turbulent heating of strongly nonisothermal plasma in strong magnetic field due to electron scattering by ion-acoustic turbulent pulsations beats

12 p1936 A71-27032

P-i-n avalanche diode trapped plasma avalanche triggered transit (TRAPATT) oscillations characteristics and voltage waveform under square wave driving current, using computer program

12 p1887 A71-27046

Si p-n-n junction avalanche diode, investigating experimental evidence of microwave generation at subharmonics of transit time excitation and trapped-plasma mode

12 p1887 A71-27047

Weakly ionized plasma instabilities in high frequency field exceeding electron collision frequency, considering waves parametric excitations

12 p1937 A71-27204

Equations system describing parametric distribution of ionized plasma in thermionic converter gap, discussing current density effects on low voltage arc discharge

12 p1938 A71-27210

Semiconductors high carrier densities at low temperatures, showing possible soft plasma branch and electron sound

12 p1944 A71-27770

Nonlinear interaction between three weakly coupled waves with well defined phases in dissipative media /fluids, plasmas or crystals/

13 p2106 A71-28453

Self modulation of amplitude modulated electromagnetic wave propagation in magnetoplasmas, considering interaction effects for ordinary and extraordinary propagation modes

13 p2107 A71-28787

Glow discharge, ion and excited state properties of laser plasmas, including CW conditions for argon

14 p2253 A71-29542

Xe plasma flash tubes with very low discharge current magnetic field for spectroscopic and laser applications in presence of Zeeman effect

14 p2243 A71-30272

Electron gyro and synchrotron radiation from vacuum and isotropic plasma, deriving approximate general formula for power spectrum and polarization

14 p2282 A71-30661

Plasma state and IV characteristics of thermionic converter, discussing cathode emitting area increases and patchiness effects

14 p2182 A71-30680

Relativistic electron beams in plasma, considering electrostatic instability conditions and critical currents

15 p2453 A71-31235

Electron hole plasma in plate shaped semiconductor under rapidly increasing external magnetic field, examining density

15 p2453 A71-31247

Magnetized plasma and vacuum plane interface, deriving dispersion equation for electromagnetic surface waves propagating at arbitrary angles

15 p2456 A71-31744

Magnetoplasma reflection coefficient for nonzero angle of incidence in Voigt configuration in superconducting coil, calculating effective intervening mass

17 p2789 A71-35348

Homogeneous infinite weakly ionized plasma dielectric permittivity tensor in crossed electric and magnetic field

17 p2790 A71-35444

Finite beta microinstabilities inherent in magnetic mirror confined plasmas, considering wave propagation across magnetic field at multiples of ion cyclotron frequency

18 p2950 A71-35861

Feed point axial displacement effects on radiation resistance and patterns of dipole antenna in weakly ionized plasma

18 p2875 A71-35971

One-dimensional numerical model of nonisothermal plasma, showing soliton separation from leading front by ion-acoustic shock waves after reversal stage

19 p3042 A71-37076

Plasma drift cyclotron instability feedback stabilization, using immersed modulated electron sources

19 p3111 A71-37636

Surface wave patterns created by constant velocity pressure point on inviscid plasma bounded by magnetic field

19 p3111 A71-37637

Fully ionized plasma expansion from spherical source into vacuum, deriving equations of motion and collision integrals

19 p3115 A71-38212

Partially ionized plasma expansion from spherical source into vacuum, obtaining equations of motion, collision integrals and recombination rate coefficient

19 p3115 A71-38213

Weakly ionized plasma instabilities in high frequency field exceeding electron collision frequency, considering waves parametric excitations

19 p3117 A71-38616

Equations system describing parametric distribution of ionized plasma in thermionic converter gap, discussing current density effects on low voltage arc discharge

19 p3000 A71-38622

Stability conditions for square wave sustaining voltage, including complex rectangular waveforms with pulsed discharges in plasma display

20 p3233 A71-39060

High resolution gas discharge plasma display panel, discussing design, capabilities and performance

20 p3233 A71-39061

Halos around black holes, showing luminosities caused by synchrotron radiation of magnetized plasma

20 p3289 A71-39295

AC plasma panel /gas discharge matrix/ display, discussing operation principles, static and switching characteristics and driving circuitry

21 p3352 A71-40120

Stochastic ion acceleration in excitation of LF oscillations in second regime of intense pulsed plasma beam discharge

22 p3577 A71-41814

Light spark plasma in gas cloud, considering directed ejection to vacuum chamber and fireball acceleration

22 p3581 A71-41816

High beta laser produced spherical plasma expansion in background magnetic field and ambient plasma, treating electrons as inertialess fluid

22 p3581 A71-41891

Dynamical formation and structure of plasma focus, using two dimensional numerical fluid model

22 p3581 A71-41892

Ionospheric small scale electron content irregularities and electrostatic plasma instabilities correlated with electrojet current intensity

22 p3535 A71-42223

Electron velocity distribution relaxation in time dependent weakly ionized plasma within electric field, solving Boltzmann equation

23 p3708 A71-43151

Hydrodynamic equations for ions and electrons of ionized collision plasma in strong nonuniform magnetic field from Boltzmann kinetic equations

24 p3855 A71-44521

PLASMATRONS

Single chamber plasmatron with rising arc I-V characteristics, obtaining electrical and thermal properties in dimensionless form

05 p0790 A71-16844

Soviet papers on gas discharge plasmas and strong magnetic fields covering plasmatrons, MHD generators, electric arc combustion, etc

15 p2457 A71-32266

Three-phase plasmatrons with hot W electrodes for obtaining plasma of inert gases, nitrogen and hydrogen

15 p2457 A71-32267

PLASMOIDS

U PLASMAS [PHYSICS]

PLASMONS

Longitudinal plasmon decay in strong magnetic field into neutrino-antineutrino pair

09 p1527 A71-23533

Magnetic pumping of collisionless turbulent plasma with LF Alfvén and magnetosonic waves, assuming high initial plasmon energy

13 p2105 A71-28175

Linear and nonlinear two-stream instability under relative motion between cold plasma components from Hamiltonian derivation for plasmons

19 p3112 A71-37744

High frequency plasma turbulence in solar flares due to nonlinear conversion of ion-acoustic plasmons to Langmuir plasmons

20 p3279 A71-39304

Plasmaron coupling and laser emission in optically excited Ag-doped cadmium tin diphosphide

21 p3391 A71-40200

Magnetic energy pumping into plasma by slowly modulating plasmon frequency-dependent external magnetic field

24 p3851 A71-44485

PLASTIC AIRCRAFT STRUCTURES

Polyimide/boron reinforced plastic structures fabrication, discussing use in leading edges

[SME PAPER EM-70-133] 01 p0090 A71-11263

Nonmetallic aircraft construction materials, discussing wood epoxy and polyester resins

02 p0273 A71-12299

High strength polyimide resin composites, discussing commercial and aerospace applications, chemistry, void content, volatiles and moisture absorption

02 p0274 A71-12487

Carbon fiber-epoxy resin composites in aircraft industry, examining fatigue life, cost, specific moduli and mechanical properties

02 p0275 A71-12488

Carbon fibers for low weight aircraft plastic structural materials

06 p0915 A71-17743

Lightning protection for nonmetallic helicopter rotor blades

07 p1021 A71-19939

Composite plastic aircraft structures lightning protection, considering hazard to composite materials and use of metal filled or plasma sprayed coatings and metal foil coverings

07 p1021 A71-19943

Boron-epoxy structural skins design for F-14 honeycomb horizontal stabilizer, using computer program

11 p1786 A71-25420

Graphite-epoxy composite skins for commercial aircraft flight spoiler, discussing multiangle ply design and fabrication

12 p1921 A71-27413

PLASTIC ANISOTROPY

NT ELASTIC ANISOTROPY

PLASTIC DEFORMATION

Anisotropic plasticity theories for metals predicting load-deformation relations [ASME PAPER 70-WA/APM-17]

03 p0443 A71-14154

Plasticity theory isotropic and anisotropic yield conditions for various stresses

04 p0672 A71-15774

Plastic anisotropy in bcc metal crystals, measuring flow strength for various plane strain compression states

08 p1308 A71-21513

PLASTIC COATINGS

Service life of solid molybdenum sulfide based plastic coatings with different binders under high vacuum friction investigated by mass spectroscopy

09 p1454 A71-22819

Subsonic velocities erosion behavior of polymeric coatings and composites, considering void content and reinforcement influence on composite structure

09 p1483 A71-23425

Polyurethane coatings development for subsonic rain erosion protection for aircraft structures, using whirling arm apparatus with simulated rainfall

10 p1632 A71-24101

Plastic encapsulation for microcircuits including packaging, failure mechanisms, military qualifications and economic factors

19 p3033 A71-38508

Duralumin rods deformation and stress propagation study under dynamic pulse loads, using photosensitive epoxy coatings and high speed photography

22 p3377 A71-41612

Stress analysis of photosensitive coatings and transparent birefringent materials, applying holography to optical polarization method

22 p3537 A71-41614

Photosensitive epoxy resin coating light path propagation variation measurements, using continuous radiation gas laser and Fabry-Perot interferometers

22 p3555 A71-41615

Polyethylene coating physicochemical properties under Uv radiation, discussing density and modulus of elasticity, internal stresses, microcrack formation and preventive heat treatment

23 p3697 A71-44032

Polyethylene coated machine steel fatigue strength in air, 3 percent NaCl bath and molecular sulfuric acid solution

24 p3841 A71-44865

PLASTIC DEFORMATION

Cracked metals brittle fracture statistical analysis, discussing plastic deformation under load

01 p0166 A71-10080

Metal fatigue relationship to cyclic plastic deformation resistance, considering fracture behavior, stress-strain curve, hardening and ductility

01 p0098 A71-10162

Plastic deformation and phase transformation in textured austenitic stainless steel, considering stacking fault energy contribution

01 p0101 A71-10737

Impulsively loaded rigid plastic continua deformation lower bounds calculation, considering beams and plates

01 p0173 A71-10943

Load deflection relations for rigid plastic cylindrical shells beyond incipient collapse load

01 p0175 A71-11011

Fe-Ti alloys at large plastic elongations, investigating strain hardening behavior

01 p0105 A71-11604

Ferritic steel with 17 percent Cr, examining dynamic behavior under high speed tension test regarding heterogeneity of plastic deformation, stress peak, etc

01 p0105 A71-11616

Iron single crystal wavy slip pattern of plastic deformation under tension at room temperature, noting relation between yield point and crystal orientation

01 p0105 A71-11621

Clamped rectangular metal plates dynamic plastic behavior under uniformly distributed impulsive velocities

02 p0321 A71-11678

Plastic deformation continuum model, including first and second strain gradients

02 p0321 A71-11679

Simple variable loading and unloading in theory of small elastoplastic deformation under nonuniform heating for residual stress-strain determination

02 p0323 A71-11739

Thin cylindrical work hardening shell under nonuniform heating and external stresses, determining elastoplastic deformation by flow theory

02 p0323 A71-11744

Disk elongation plastic deformation, determining elastoplastic stressed state for inhomogeneous thermal cycles

02 p0323 A71-11748

Polycrystalline material nonisothermal plastic deformation, using model based on metals and alloys properties and microstructure

02 p0324 A71-11749

Metal hardening under cyclic thermal loads, determining deformation, breakdown, creep and stress-strain relation 02 p0324 A71-11752

Spherical shell plastic deformations under internal pressure, discussing stress instability condition 02 p0325 A71-12123

Zinc single crystals plastic deformation and dislocations movement enhancement under pulsating direct current, noting stress peaks-voltage relationship 02 p0296 A71-12297

Convex functions theory of rigid perfectly plastic structures, formulating strain rate and stress fields relation in subgradients 02 p0326 A71-12339

Soviet papers on plastic deformation of high melting metals and alloys covering tungsten, molybdenum, titanium and stainless steels 02 p0264 A71-12511

Plastic deformation rate effect on deep drawing of sintered and vacuum melted thin sheet Mo 02 p0256 A71-12516

Alloying effects on room temperature mechanical properties of vacuum melted Mo-C-Ti, Mo-C-Zr and Mo-Ti-Zr under plastic deformation and recrystallization 02 p0265 A71-12520

Reduction-elongation relation in plastic deformation of tensile test samples of Ti alloys subject to thermomechanical treatment 02 p0265 A71-12523

Temperature and plastic deformation rate effects on plasticity and strength of cast iron, Ti and steels 02 p0257 A71-12525

Superficial residual stresses measurement in plastic region by Hertzian hardness method, considering indentation by ball and proportionality to load variations 02 p0328 A71-12535

Groove depth /residual deformation/ in vibrational rolling of Ti cylindrical samples, considering impression force, cylinder and steel spheres diameters 02 p0258 A71-12641

Cr and Mo thin film coatings on Si-Fe, examining effect on plastic deformation and mechanical properties 02 p0266 A71-12655

Niobium with various interstitial and substitutional type impurities, examining plastic deformation and mechanical properties at various temperatures 02 p0269 A71-12927

Niobium mechanical properties temperature dependence from plastic deformation tests, taking into account interstitial and substitutional impurity concentrations 02 p0271 A71-12936

Deformed metals stage I recovery, considering plastic deformation microscopic description, defect creation, interstitials and experimental methods 03 p0441 A71-13348

Marguerre equations for deflection and buckling of partially and fully loaded spherical caps, noting inaccuracy of finite difference approximation 03 p0503 A71-13428

Variational methods applied to shells transition into plastic state during cylindrical bending, giving critical load formulas 03 p0509 A71-13873

Beam structures plastic shakedown sufficient conditions derivation in terms of bending moments 03 p0510 A71-13947

Stereophotogrammetric measurement of plastic deformations of circular Al membrane loaded by pressure pulse, using high speed cameras 03 p0428 A71-13948

Polymeric materials plastic deformation properties during service and storage, discussing prediction and testing methods 03 p0448 A71-14300

Stress development in elastic plate with crack under edge loads, estimating plastic zone size at crack ends 03 p0514 A71-14361

Plastic zone near crack end under forces causing plane deformation, calculating stress-strain state by finite element method 03 p0515 A71-14363

Plastic flow rates in materials under complex loads producing constant stress intensity, considering plastic deformation 03 p0515 A71-14364

Thick strips widening by rolling, deriving formula for maximum widening from plastic deformation process description by displacement-rate fields 04 p0602 A71-14608

Metallic components strain localization and concentration factors under high pressures or temperatures involving plastic strain, noting static and cyclic load effects 04 p0666 A71-14882

Steels brittle fracture susceptibility by notch impact bending test, considering plastic deformation zone and crack propagation 04 p0610 A71-14889

Plastic wave propagation of combined stresses due to longitudinal impact of pretorqued tube 04 p0668 A71-15190

Energy dissipation during torsional and flexural vibrations of steel and duralumin specimens subjected to plastic deformation, accounting for discrepancies due to methodical errors 04 p0671 A71-15640

Tensile-compressive yield strengths of wrought Mg alloy, noting plastic deformation by slip on basal plane 04 p0614 A71-15786

Deformation time and displacement bound theorems for impulsive loading of plastic and viscoplastic materials 04 p0673 A71-15883

Thick walled noncircular cylinders shape showing full plasticization at collapse 04 p0673 A71-15885

Strengthening curve determination by tensile tests for plastic yield limit, strength and elongation at rupture 04 p0673 A71-15898

Plastic deformation and ductility of Mo alloys under various stress concentrations at room and high temperatures 05 p0765 A71-16175

Ti alloys beta phase solid solution decomposition during cooling and plastic deformation at low temperatures 05 p0767 A71-16770

Self-consistent polycrystalline model for combined stress state time dependent creep, examining flow potential existence 05 p0830 A71-17236

Iron meteorites microstructure investigation by light and transmission electron microscopy, determining plastic deformation and cooling rate from thermomechanical history 06 p0964 A71-17343

Cylindrical shell reinforced by transverse ribs under hydrostatic pressure, determining elastoplastic deformation 06 p0988 A71-17774

Plates and shells stability under plastic deformations at subcritical strains, using three dimensional linearized equations 06 p0989 A71-17787

Elastoplastic conical shells strain under longitudinal impact by large rigid body, analyzing plastic bending 06 p0996 A71-17842

Thin plate impact and plastic nonpenetrating deformation by blunt projectiles 07 p1209 A71-19045

Crystalline materials plastic deformation and dynamic yield stress based on elastic shock wave damping 07 p1210 A71-19151

Refractory alloys elastoplastic deformation under cyclic loading, deriving thermal fatigue equations 07 p1129 A71-19155

Plastic deformation of circular plates and shells from material with different yield and strengthening moduli in tension and compression 07 p1211 A71-19164

Atomic ordered alloy compressive strengthening for fcc and bcc lattices in terms of yielding, work hardening and no hardening stages 07 p1132 A71-19438

Binary Ti-Al and ternary Ti-Al-X alloys precipitation strengthening, investigating structure, mechanical properties and deformation behavior 07 p1133 A71-19444

Figural change perception in apparent motion, considering resolving capabilities and visual stimuli for plastic deformation and shape rotation 07 p1048 A71-19516

Thin spherical roller supported domes stability and axisymmetric deformation under apex point loads, investigating plastic buckling and inelastic strain effects 07 p1216 A71-20222

Recrystallized and nitrided Mo alloy microstructure under plastic deformation by tension at high temperatures 08 p1305 A71-21029

Bcc metals plastic deformation, discussing active slip systems, stress asymmetry, dislocation dynamics, interstitial and substitutional alloys, defect configurations, etc 08 p1307 A71-21502

Stoichiometric NiAl single crystals plastic deformation study by transmission electron microscopy, determining dislocations by image matching technique 08 p1308 A71-21511

Nb single crystals heterogeneous deformation at very low temperatures, observing jerky flow due to adiabatic temperature rise during plastic deformation 08 p1308 A71-21512

Luders bands motion in steel and iron, studying plastic zone velocity dependence on stress, composition, grain size, dislocation substructure and temperature 08 p1308 A71-21517

Magnesium indium alloys single crystal plastic deformation, investigating basal and prismatic slip at various temperatures 08 p1309 A71-21528

Pure vs dispersion hardened Ni plastic deformation, noting flow stress and temperature effects on work hardening 08 p1311 A71-21544

Crystalline solids strain rate effects due to simultaneous operation of plastic deformation mechanisms including diffusion controlled creep and dislocation-drag processes 08 p1371 A71-21560

Deformation modes with associated structural defects for slip, viscous slip and climb processes in gamma prime precipitation hardened nickel based alloys 08 p1315 A71-21583

Fracture kinetics, emphasizing plastic deformation, dislocation and diffusion micromechanics, point defects effects and microcrack formation 08 p1371 A71-21606

Cylindrical steel specimens bearing strength under cyclic elastoplastic deformation, investigating stress redistribution effects 08 p1316 A71-21607

Polycrystalline Nb under plastic deformation and annealing, examining dislocation structure and mechanical properties 08 p1316 A71-21611

Stressed state in region of strain raisers /round holes/ in plate subjected to two axial tension associated with plastic yield 08 p1372 A71-21703

Soviet papers on physics of metals and metallography covering residual stresses, energy dissipation after plastic deformation, heat treatment, etc 08 p1317 A71-21759

Sponge iron sintered powder compacts deformation behavior from uniaxial compression tests, proposing plasticity prediction criteria 09 p1466 A71-22169

True torsional stress at plastic strain onset determination in terms of elasticity theory 09 p1536 A71-22323

Elastic and plastic plane deformation photoelastic measurement at room and elevated temperatures by moire patterns, comparing performance with other methods 09 p1536 A71-22328

Plastic strains buildup during thermal cycling, establishing relation between strain interval and cycles number to failure for strain hardening materials 09 p1538 A71-22599

Martensitic transformation of Fe-Ni-Si alloys under tensile plastic strains at 233-373 K 09 p1469 A71-22849

Metallic polycrystalline materials volume changes in plastic deformation from measurements on steel elongation and cross section diameter reduction 09 p1540 A71-22997

Ni plastic properties and creep measurement under deformation by tension at room temperature, noting effect of impurities content 09 p1473 A71-23231

Cr specimens containing Y, investigating microscopic breakdown at high temperatures as function of deformation during vacuum rolling 09 p1474 A71-23235

Ni-Cr alloys hardened by Nb and Ta, examining precipitation and plastic deformation mechanisms 09 p1479 A71-23622

Hot deformation of superrefractory austenitic Ni alloy, considering elastic and plastic limits 09 p1479 A71-23625

Ferrous and nonferrous sheet metals neck formation prevention for increasing elongation in tensile tests, using continuous plastic bending method 09 p1479 A71-23697

Perfectly plastic and viscoplastic materials relation between permanent deflection and response time in boundary value problems 10 p1684 A71-23931

Aluminum-epoxy joints stress corrosion cracking inhibition and crack tip plastic deformation by scanning electron microscopy 10 p1615 A71-24091

Steel sheet specimens under temperature and stress cycles, studying creep, plastic deformation and service life 10 p1686 A71-24189

Deformability and strength of soft fiber reinforced plastics under biaxial tension, determining low temperature critical tensile stresses and elongation ratios 10 p1634 A71-24194

Dynamic plastic bending theory of thin circular annular plate with central hole under uniform impulse 10 p1689 A71-24519

Physical model describing mechanism of recording through surface corrugation of thermoplastic viscofluid layer by electron beam 10 p1613 A71-24873

Fiber reinforced plastics /epoxy resins/ electrical effects association with deformation and failure 10 p1635 A71-25013

Jetting collision effect on structural changes at interface between Ti and steel in explosive bonding, considering plastic deformation and residual stresses 10 p1629 A71-25030

Elastic-plastic fracture behavior engineering model based on surface flaw severity by crack length dimensions measurements
[AIAA PAPER 71-71] 11 p1845 A71-25345

Nonhomogeneous variable diameter rods plastic torsion, deriving stress function and distribution
11 p1848 A71-25620

Incremental plastic analysis under large displacement and physical instabilizing effects, using finite element models and quadratic programming
11 p1849 A71-25679

Plastic spherical shell containing cylindrical section under Tresca yield conditions, obtaining upper critical load limits
11 p1850 A71-25943

High strain rate effects on Al single crystals deformation, presenting overall and local strain and lattice rotation measurements in impact tested specimens
11 p1779 A71-26014

Plastic deformation of elliptic inclusion in plane strain of infinite plate, using viscoelastic analogy
11 p1852 A71-26395

Monograph on turbine blade fir tree roots, calculating stress-strain state of long term static strength under elastic and elastoplastic deformation and unsteady creep
11 p1852 A71-26400

Plastic deformation and aging effects on fatigue characteristics of steels until rupture under cyclic loads
12 p1916 A71-26945

Soviet book on spherical bottoms weakened by openings covering shell stress/strain, elastic-plastic deformations, reinforcing elements and composite materials
12 p1977 A71-27293

Fiberglass reinforced plastic structural elements heat induced deformation and carrying capacity due to material macroinhomogeneity and rigidities asymmetry
12 p1921 A71-27346

Small deformation theory of thermoplasticity with medium mechanical characteristics dependent on temperature, noting use in nonmechanical structural transformations and radioactive irradiation
12 p1978 A71-27348

Static and dynamic stress analysis and limiting loads of plastic shells and plates with temperature field in structural element, using deformation theory
12 p1979 A71-27350

Nonisothermal plasticity and creep models, stressing real materials deformation micromechanism theories
12 p1979 A71-27354

Inhomogeneous microstructure elastoplastic medium, examining strain and work in plastic deformation
12 p1982 A71-27516

Shells of revolution plastic deformation problem, applying rigid viscoplastic strain hardenable material model
12 p1984 A71-27686

Local plastic deformation analysis of spherical and cylindrical shells subjected to yield point loads through rigid boss, using nonlinear programming
13 p2147 A71-27787

Refractory and structural steels and Al alloys, obtaining low cyclic plastic deformation and breaking stress curves
13 p2148 A71-28116

Refractory steels plastic deformation characteristics under isothermal creep
13 p2084 A71-28125

High strength alloys fatigue in terms of irreversible microplastic deformations accumulations, discussing fatigue crack mechanisms and cyclic straining effects on bulk properties
13 p2152 A71-28219

Plastic deformation and alloying effect of small additions of interstitial elements on decomposition of metastable beta phase
13 p2086 A71-28580

Grain boundary precipitation in austenitic steels during creep deformation and ordinary aging treatment
13 p2086 A71-28623

Strain and strain rate effect on flow stress and microstructure of Al-Cu eutectic alloy during superplastic deformation, deriving stress-strain diagrams
13 p2086 A71-28624

Stress-strain state of annular billet under local plastic bending by forces in cross sectional plane
13 p2154 A71-28646

Integral transformations application to approximate elastic solutions for nonlinear hereditary media, considering elastoplastic deformations under active loads
13 p2154 A71-28649

Nonlinear heredity theory related to Volterra-Frechet heredity theory under uniaxial tension, giving expression for polymers deformation relaxation processes
13 p2092 A71-28650

Complex loading history effect on elastoplastic deformation trajectories delay trail characteristic angles and length variation, determining plastic strain vector components in Euclidean space
13 p2155 A71-28652

Carbon steel fatigue crack tip plastic zone substructure by X ray microbeam technique, determining dislocation density, stress intensity and crack propagation rate interrelationships
13 p2155 A71-28789

Plastic deformation of aluminum oxide by indentation and abrasion at room temperature, using transmission electron microscopy
13 p2093 A71-28989

Circular elastic ideally plastic plate deformation due to circumferentially distributed rectangular pulse loading
13 p2156 A71-29075

Elastic deformation and plastic buckling of rectangular column with initial deflection under axial compression
13 p2157 A71-29287

Be sheet plastic bend ductility and yield strength, considering purity and processing effects
13 p2088 A71-29403

Structural stability in tension and strength tests of thin walled tubes at various stress and strain intensities based on loss of resistance to plastic deformation
14 p2321 A71-29620

Cyclic strain effects on creep for steel at elevated temperatures, discussing overload frequency effects on plastic strain buildup
14 p2256 A71-29626

Plastic strain development at fatigue crack tip in mild carbon and stainless austenitic steels from electron and optical microscopy
14 p2257 A71-29841

Elastic plastic shells of revolution deflection analysis by numerical integration with computer program
14 p2324 A71-29870

Creep-fatigue analysis by strain range partitioning, considering metals inelastic deformation at high temperature due to plastic flow
14 p2325 A71-29923

Discontinuous phase decomposition increase in Co-Ni-Ti alloys by plastic deformation and Al additions, indicating grain boundary diffusion control
14 p2258 A71-30003

Thermally activated plastic deformation of metals at low temperatures, determining stress flow, creep properties and upper yield limit
14 p2258 A71-30007

Work hardening material planar frame inelastic load deformation and buckling, using finite difference method and variational principle
14 p2330 A71-30693

Flexible spherical domes elastic-plastic deformation, using variational equation and iterative algorithm
14 p2331 A71-30840

Plastic deformation work derivation, taking into account deviation from similarity of stress deviators
15 p2501 A71-31150

Boron solubility in molybdenum, showing grain size decrease, plastic deformation change and elongation
15 p2425 A71-31399

Dynamic response and perforation of thin plates subjected to projectile impact, measuring plastic deformation, dynamic strain and displacement with high speed camera
15 p2503 A71-31422

Linear plastic deformation of steel under tension, investigating anisotropy in elastic modulus and strength
15 p2503 A71-31478

Metal specific work breakdown during crack propagation, investigating thermal effect of plastic deformation with thermocouples
15 p2413 A71-31479

Deformation work for strained copper during tensile testing until fracture as function of slenderness in neck
15 p2427 A71-31700

Stress distribution during plastic deformation of steel turbine disk from hardness measurements
15 p2505 A71-31863

Al and Cu dynamic plastic deformation at elevated temperatures, discussing relationship between strain rate sensitivity and activation energy
15 p2428 A71-31972

Elastic-plastic mechanics of steady crack growth under antiplane shear, discussing residual stress effect, plastic zones shape and strain distribution
15 p2428 A71-31974

Flow velocity field in main plastic deformation zone during orthogonal cutting from continuity equation
15 p2415 A71-31986

Recrystallization nuclei linear growth rate activation energy relationship to Ni plastic deformation magnitude, temperature and purity
15 p2429 A71-31995

Plastically deformed Ni powder specimens residual microstresses as function of applied hydrostatic pressure, using X ray diffraction measurements
15 p2429 A71-31996

Arbitrarily shaped thin shell elastic-plastic deformation transient response prediction, using improved finite difference method
15 p2505 A71-32008

Combined mechanical and cyclic thermal stresses effect on plastic deformation buildup in E1435 alloy preceding breakdown
15 p2433 A71-32236

Structural inhomogeneity effect on fatigue strength of Al alloys, considering microstructure qualitative estimation on basis of microplastic deformation
15 p2434 A71-32330

Transition metals classification according to effect on structure and physical properties of deformable Al alloys
15 p2434 A71-32331

Plastic strain range-fatigue life behavior as two slope relationship, considering low cycle fatigue laws in terms of crack propagation mode change
15 p2436 A71-32508

Inductor winding dependent magnetic pulse deformation of cylindrical blanks allowing for mutual electromagnetic and mechanical coupling
15 p2417 A71-32525

Yield condition and stability of elastoplastic bodies with large deformations, using Gibbs method of thermodynamics
16 p2650 A71-33015

Structural instability due to cyclic strain accumulation, using plastic deformation constitutive relation with stress tensor and elastic effects
16 p2650 A71-33016

Iron single crystals plastic deformation under tension, studying ductile/brittle fractures mechanisms and transition temperature
16 p2591 A71-33369

Cracked metals brittle fracture statistical analysis, discussing plastic deformation under loading
16 p2658 A71-33636

Cobalt and lanthanum with face and body centered lattices, studying plastic deformation during allotropic transformations under sliding friction and gripping
16 p2584 A71-33895

Plastic deformation in hot compressed Ti, Zr and Nb carbides during diamond grinding, studying fine structure on diffractometer
16 p2584 A71-33896

Austenitic high nitrogen chromium-nickel steels plastic deformation and heat treatment in plasma arc furnaces
16 p2596 A71-33910

Thermal polymorphous metals and alloys crystal structure, discussing plastic deformation due to formation of cubic lattice and metallic bonds
16 p2597 A71-33915

Plastic deformation, creep rupture strength, endurance limit and service life of prestressed strain hardenable material
16 p2659 A71-33985

Stress-strain dependence on surface deflection and nonlinearity during bending of elliptic flat plate under plastic deformation
16 p2659 A71-33994

Viscoplastic elastic medium behavioral relations, considering instantaneous and nonretarded plastic deformation
16 p2660 A71-34066

Large plastic strains in fiber in sheet bending for wide angle range, using Hill theory
17 p2816 A71-34298

Limit analysis of dissipation power and collapse load of rigid perfectly plastic continua with piecewise linear yield surface, using linear programming
17 p2816 A71-34324

Storing and plastic deformation effects on artificial aging of Al-Zn-Mg alloy, using thin foil electron microscopy and hardness measurements
17 p2755 A71-34417

Deformation temperature effects on microstructure and mechanical properties of low alloy Mo, considering cold brittleness temperature and associated plasticity
17 p2755 A71-34418

Dugdale mathematical model for cylindrical bending of thin plates, finding resulting plastic zone dependence on applied moment and normal coordinate [SESA PAPER 1854A]
17 p2819 A71-34538

Metal strips with holes under tensile loads, determining plastic region boundaries with photostress method
17 p2821 A71-34592

German monograph on plane, arbitrarily curved and bending resistant trusses calculations allowing for elastic and plastic deformation
17 p2823 A71-34800

Thermal and athermal yield stresses of Nb and Nb-Mo single crystals, considering strain rate sensitivity and thermal stress increase with increasing plastic strain
17 p2759 A71-35224

Plastic deformation and embrittlement due to stress raisers in steel cylinders from high speed tensile tests at low temperatures
17 p2832 A71-35462

Stress variation with varying plastic deformation rate and temperature in tantalum carbide between 1200 and 2200 C
17 p2760 A71-35550

Refractory alloys elastoplastic deformation under cyclic loading, deriving thermal fatigue equations
17 p2760 A71-35653

Plastic deformation of circular plates and shells of material with different yield and hardening moduli in

tension and compression from creep theory relationships

17 p2834 A71-35660

Fracture kinetics, emphasizing plastic deformation, dislocation and diffusion micromechanics, point defects effects, microcrack formation and interstitial mechanisms

17 p2834 A71-35667

Niobium dislocation and electronic structure and mechanical properties after plastic deformation and annealing from electron beam studies

17 p2760 A71-35671

Creep rate enhancement by additional microplastic deformation in refractory alloys during thermal cycling

17 p2761 A71-35678

High rate quasi-static dynamic pressure deformation hardening of magnesium single crystals

18 p2934 A71-35990

Plastic deformation resistance of rough metal surfaces under heavy loads, discussing mechanical contact changes due to asperities reactions as coherent block

18 p2926 A71-36186

Viscoplastic elastic medium behavior, breaking down elastoplastic deformation into plastic and elastic deformations

18 p2977 A71-36187

Incompressible fiber reinforced composite materials finite plane deformation continuum theory and stress analysis without restriction concerning elasticity, plasticity or viscoelasticity behavior

18 p2978 A71-36264

Axisymmetric plastic deformation of imperfection sensitive spherical shell after elastic buckling, considering load carrying capacity

18 p2978 A71-36266

Deformation kinetics and failure of high melting Nb and Mo base alloys in plastic state under low cyclic fatigue

18 p2936 A71-36710

High temperature tests of short time strength, hardness, moduli of elasticity of W-Mo alloys subject to plastic deformation and annealing

18 p2936 A71-36712

Strain rate dependence of shear stress, plastic cross-slip and stacking fault energy of Al single crystals at 77 K

18 p2937 A71-36749

Dynamic loading of cantilever beams by magnetomotive and explosive loads and high bullet speed impact, noting elastic and plastic deformation modes

18 p2981 A71-36770

Mathematical model of hemispherical inclusion in elastic half space for estimating plastic deformation

18 p2937 A71-36772

Plastic zones and stable crack growth at notches in thin high strength sheet alloys, using replication technique

18 p2938 A71-36853

High purity metals residual electrical resistivity, observing impurities, vacancies, dislocations, plastic strain and polyisotropy effects

19 p3076 A71-37115

Ni-Co alloy fine structure under plastic deformations, determining stacking fault energy effects with X ray diffraction lines

19 p3076 A71-37119

Plastic deformation and fracture of beta Ti alloy under tensile tests at room and low temperatures

19 p3077 A71-37464

Martensite-type omega phase formation in Ti alloys during grinding by abrasive wheels and tapes, noting dependence on plastic deformation

19 p3078 A71-37474

Static ductile deformation in quartz, olivine, pyroxenes and plagioclase, noting plastic deformation and recovery

19 p3050 A71-37664

Plastic deformation effects on austenite thermal stabilization in Fe-Ni-C alloy, considering temperature dependence

19 p3079 A71-37704

Simple structures large elastic-plastic transient deformations, using finite element method

19 p3157 A71-37874

Pressure pulse shape effect on final plastic deformation of simply supported thin circular plate

19 p3158 A71-38181

Finite strain theory for elastic-plastic deformation, considering isothermal shear of neo-Hookean material before yielding and during elastic unloading

20 p3267 A71-38794

Creep test and long time strength results extrapolation, determining accumulation of plastic deformation and creep fracture effects

20 p3250 A71-39020

Nonlinear behavior of compressed elastic and elastoplastic rods in presence of large deformations, determining bearing capacity by step method

20 p3269 A71-39164

Finite elastoplastic deformation thermodynamic theory based on isotropic work hardening, excluding

Bauschinger effect or localized modification of yield surface due to plastic flow

20 p3308 A71-39486

Superposed plastic deformation and plane wave propagation in elastic-plastic media applied to circular bar twisting

20 p3310 A71-39780

Stress-strain curves of dual slip orientation in Ge single crystals deformed in compression, using interference, optical and electron microscopy

21 p3397 A71-40457

Plastic wave propagation along rods and through slabs, describing finite deformation elastic-plastic theory

21 p3464 A71-40785

Macroscopic residual stress and strain measurement and crack tip substructure, discussing crystal plastic deformation effect on fatigue crack propagation

21 p3466 A71-40831

Nonablating inelastic deformable material surface interaction with external supersonic turbulent boundary layer, observing crosshatch patterns

21 p3323 A71-40941

Semiinfinite rods in maximal plastic deformation, observing impulse and energy constraint distinction

21 p3467 A71-40961

Metal deformation processing in solid mechanics, discussing plastic idealization for viscous behavior theorems, Ekstein paradox, free surface problems and incremental forging

21 p3389 A71-40983

Microstructural characteristics of Fe-Ni alloy plastic deformation at 20-500 C during cold and hot rolling, noting intergranular shear processes

21 p3402 A71-41095

Design and technological calculations in machine building, analyzing flow, creep and elastoplastic deformation theories

21 p3472 A71-41144

Half space with periodic continuous distributed dislocations and plastic distortions, calculating stress fields and free surface orientation with cartesian coordinate system

22 p3613 A71-41432

Lower bound deformation theorem for rigid plastic continua and structures under impulsive loading, using kinematically admissible velocity field

22 p3614 A71-41608

Hold time effects on plastic deformation and fracture in high temperature low cycle metal fatigue

22 p3561 A71-41942

Superplasticity and materials forming methods for metal alloys, considering reformation speed increase by finer grained and stable alloys development

22 p3563 A71-42323

Automatic measurement of materials nonlinear deformation, considering Morrow mechanical strain gage for plastic deformation

23 p3774 A71-42895

Loading cycles dependence of energy dissipation and plastic deformation during fatigue tests, using Fourier series

23 p3774 A71-42897

Increased microplastic deformation resistance, relaxation stability and aging of beryllium by cyclic heat treatment

23 p3690 A71-43281

Plastic shells under finite bending, deriving large deflection theory from nonlinear continuum mechanics by yield criterion Lagrangian formulation

23 p3775 A71-43317

Plastic buckling stability of hinged arches for perfect and imperfect structures with linear work hardening stress-strain behavior

23 p3776 A71-43372

Polycrystalline body macrohomogeneous plastic deformation, deriving basic postulates for slippage and plane relationships to tangential stress and shear strength dependence on elastic deformation

23 p3777 A71-43576

Pyroxenes and olivines in lunar rocks from Ocean of Storms, observing plastic deformational processes since crystallization by optical, X ray and electron microprobes

23 p3744 A71-43657

Load stress pulse shape and frequency effects on macroscopic dislocations during plastic deformation of crystalline materials

23 p3777 A71-43875

Rough spheres, cylinders and annuli in contact, determining surface roughness and waviness effects on surface geometry under elastic and plastic deformations

23 p3682 A71-43928

Fine structure at crack tip expanding in ideally elastoplastic material in plane deformation state and plane stressed state

23 p3778 A71-44061

Soviet book on elastoplastic deformations of plates and cylindrical shells made of low strain hardening materials, covering strength and stability calculations

23 p3779 A71-44186

Ni-Cr single crystals plastic deformation, presenting work hardening characteristics and critical resolved shear stress

23 p3694 A71-44278

Stable austenitic stainless steels and fcc metals plastic deformation flow curve model, presenting stress-strain relation

23 p3695 A71-44284

Swaged high purity fine grained Ti stress-strain behavior below 424 K, emphasizing mechanical twinning in plastic deformation

23 p3695 A71-44289

LiF and MgO high purity single crystals plastic deformation geometric characteristics, discussing nucleation probability on different slip planes

24 p3859 A71-44450

Deformations and stresses in elastoplastic half space indented by rigid sphere, using finite element method

24 p3879 A71-44631

Recrystallized metalceramic W plastic deformation effects on brittleness temperature threshold, revealing relationship to impurity segregations at grain boundaries

24 p3837 A71-44674

Three dimensional incompressible anisotropic body with small deformations, calculating elastic stability theory with variational principle

24 p3880 A71-44708

Cross section behavior of tube under plastic bending based on hollow rod treatment

24 p3883 A71-44848

Metal cylindrical shells plastic collapse under axial compression, deriving theoretical load/deflection relationship

24 p3883 A71-44875

Previous plastic loading deformation effect on contact area, print number, size distribution and thermal conductivity for flat surfaces

24 p3830 A71-44943

Plastic deformation of solid body in terms of slip dislocations displacement rate

24 p3885 A71-45052

Elastoplastic deformation of Zn single crystals under uniaxial tensile loads, noting critical stresses relationship to current pulses

24 p3838 A71-45100

Surface oxide, organic and lead film effects on friction and plastic deformation of Zn single crystal during sliding

24 p3839 A71-45288

Shear modulus and stress-strain relations for different plastic strain rates

24 p3886 A71-45362

Mo sheet anisotropic dynamic strain aging at high temperatures, noting plastic strain contribution to texture formation and dislocation consolidation

24 p3840 A71-45378

PLASTIC FILMS

U POLYMERIC FILMS

PLASTIC FLOW

NT TRESCA FLOW

Elastoplastic constitutive laws with nonassociated flow laws and work hardening, nonhardening and softening behavior

01 p0174 A71-10999

Quenched Al-Mg alloys, investigating dislocation mechanisms for plastic flow by creep tests at various temperatures

01 p0105 A71-11605

Plastic flow of metal during rolling in T groove, determining particle velocity and strain energy distributions

02 p0257 A71-12565

Plastic flow rates in materials under complex loads producing constant stress intensity, considering plastic deformation

03 p0515 A71-14364

Anomalous dynamic strain aging in supersaturated Al-Cu, Al-Mg and Al-Zn alloy sheet and wire, discussing activation energies and volumes for plastic flow

08 p1310 A71-21534

Creep-fatigue analysis by strain range partitioning, considering metals inelastic deformation at high temperature due to plastic flow

14 p2325 A71-29923

Guinier-Preston zone size and volume fraction effects on polycrystalline Al-Zn alloys yield strength, discussing precipitation strengthening and thermally activated plastic flow

15 p2433 A71-32182

Impulsively loaded expanding cylindrical shell transient elastic-plastic response, using linearized assumption on plastic flow behavior

17 p2821 A71-34577

Orthotropic annular plate plastic flow law, establishing yield conditions with plane stress-strain state equations

19 p3155 A71-37527

Displacement fields for two dimensional minimum weight frames for load dispositions analogous to perfectly plastic plane flow in metal working

21 p3391 A71-41428

Second order theory of plane plastic flow, investigating characteristic slip lines of perturbed velocity field and stress equations 23 p3774 A71-43144

Stable austenitic stainless steels and fcc metals plastic deformation flow curve model, presenting stress-strain relation 23 p3695 A71-44284

PLASTIC MATERIALS

U PLASTICS

PLASTIC MEMORY

Variable elasticity algorithm for axial flow turbine disks with allowance for plasticity, creep and loading history 12 p1979 A71-27351

Shape-memory effect in equiatomic Ti-Nb alloys with reversible martensitic transformation 14 p2259 A71-30392

Isotropic materials with memory, discussing induced birefringence theory to account for memory and nonlinearity effects in dielectric properties dependence on deformation history 19 p3118 A71-37525

Ti-Ni alloy martensitic thermoelastic transformation and memory effect, using optical microscopy to examine change in lattice discontinuity 21 p3398 A71-40459

Plastic stress-strain history at notch roots tested in tensile steel strips under monotonic loads, verifying Hardrath-Ohman theories 22 p3615 A71-42071

PLASTIC PROPELLANTS

Flame propagation along interface between fuel slab /polymers, aluminum and tungsten powders/ and oxidizer slab /inorganic salts and oxides/ 03 p0521 A71-14278

Compositional and oxidizer particle size effects on combustion instability of plastic propellant based on ammonium perchlorate and polyisobutene [AIAA PAPER 69-478] 11 p1809 A71-25454

Burning rate of Al particles suspended in polymer propellant gas flow with inorganic oxidizers 14 p2285 A71-30620

Shock tube investigation of solid polymeric hydrocarbon fuel ignition in hot oxidizing gas stream 19 p3121 A71-38124

Radiative ignition of polymeric fuels /polystyrene and epoxy/ in oxygen/nitrogen mixtures 19 p3121 A71-38125

PLASTIC PROPERTIES

NT ELASTOPLASTICITY

NT THERMOPLASTICITY

NT VISCOPLASTICITY

NT YIELD POINT

Notched metal crack initiation, determining high cyclic loads effects by prior local plastic behavior at stress concentration 01 p0166 A71-10163

Splat cooled hypoeutectic Al-Cu alloy superplasticity, using tensile tests and electron microscopy 01 p0100 A71-10280

Weight allowance in optimal design of plastic structures under creep 01 p0170 A71-10641

Successive approximations method for boundary value problems in plasticity theory of continuous media under complex loading 01 p0171 A71-10652

I-beam plastic moment under shear force, using empirical curve for interaction between bending moment and shear force 01 p0174 A71-11000

Fatigue effects on metallic materials elastoviscoplasticity properties 01 p0175 A71-11025

High strength and plasticity maraging steels of Fe-Ni-Co-Mo system, noting surface crack sensitivity in tension 01 p0103 A71-11071

Lower bound load carrying capacity of thin walled structures of rods, plates and shells with statistical stable stress field, using plasticity theory 02 p0326 A71-12296

Strain rate effects on plastic properties of various metals and alloys 02 p0265 A71-12568

Plasticity theory simplified via revision based on thermodynamics 03 p0501 A71-13109

Elastic and perfectly plastic plane stress problems yield point load lower bounds by finite element method, considering weakened slabs 03 p0505 A71-13541

Rigid-perfectly plastic model for real materials behavior, considering modification for strain hardening and elastic effects under various load conditions 03 p0509 A71-13780

Finite element program for structural design and stress analysis, introducing creep and plasticity into strain equations [ASME PAPER 70-WA/DE-4] 03 p0511 A71-14140

Superplastic alloys fabrication and applications, discussing grain size and surface area roles 03 p0516 A71-14498

Plastic zone effects on notch effect on crack initiation, analyzing ductile-brittle transition temperature relation to sample size 04 p0666 A71-14883

Rigid cellular plastics mechanical properties based on model assuming pentagonal dodecahedron cell form 04 p0667 A71-14894

Nitriding effects on short time tensile strength, plastic properties and hardness of niobium 04 p0612 A71-15549

Plasticity theory isotropic and anisotropic yield conditions for various stresses 04 p0672 A71-15774

Heat, solution and cooling treatment of Ti-Al-V-Sn alloy for high strength and plastic properties 05 p0765 A71-16199

Solid deformable body combined brittle and plastic elements model for strain analysis 05 p0827 A71-16758

Machine components resistance to low temperature failure, considering threaded joints, gears and shafts for strength and plasticity characteristics 05 p0827 A71-16764

Beta stabilizers effects on Ti strength, plasticity and stress concentration sensitivity at low temperatures 05 p0767 A71-16766

Composite materials plasticity limit calculation using variational principles 05 p0773 A71-16992

Optimal design with geometric constraints for simply supported Tresca plastic disk and cantilever plate under concentrated force 05 p0830 A71-17223

Strain hardened plastic cylindrical shells, investigating load bearing capacity 06 p0994 A71-17822

Physical analogy treating low cycle metal fatigue relation to stress growth in plastic region, discussing cracking mechanisms 07 p1211 A71-19166

Mechanical and plastic properties of Ni-Mo alloys subjected to hot working, determining tensile strength as function of test temperature 07 p1136 A71-19635

W-Re alloy microstructure creep, long term strength and plastic properties as function of temperature, using electron microscopy 07 p1141 A71-20241

Hardened plasticity zone around circular hole in creep deformed plane under normal forces, determining stress-strain relation and time dependent variations 07 p1219 A71-20647

Tall thin strip rolling in ribbed grooves, determining critical area reductions causing plastic stability loss 08 p1295 A71-20841

High strength and plasticity maraging steels of Fe-Ni-Co-Mo system, noting surface crack sensitivity in tension 08 p1305 A71-21036

Superconducting transition effects on metal and alloy single and polycrystals plasticity 08 p1344 A71-21520

Martensitic transformation-induced plasticity in austenitic Fe alloys, examining strain rate and chemical composition effects 08 p1312 A71-21554

Deformation-induced martensitic transformation effects on Fe-Ni-Cr-C alloy plastic behavior 08 p1313 A71-21555

Hot extruded W-Cu pseudoalloys under tension and compression, determining impact strength and plasticity 08 p1316 A71-21614

Cast Mo alloy at low temperatures, investigating elasticity, plasticity and tensile strength characteristics 08 p1316 A71-21615

Nonlinear elastoplastic ring buckling under compression 09 p1534 A71-22145

Plasticity zone changes near circular hole, examining material structure inhomogeneity effects in presence of creep 09 p1535 A71-22183

Soviet book on metal alloys plasticity gaps covering crystallization, thermomechanical treatment, heat induced brittleness zones formation, etc 09 p1472 A71-23161

Ni plastic properties and creep measurement under deformation by tension at room temperature, noting effect of impurities content 09 p1473 A71-23231

Cr plastic properties, investigating recovery and recrystallization effects from La and Y additions 09 p1476 A71-23316

Variational formulation for minimum weight of structures with given yield stress, considering homogeneous isotropic material, plasticity condition and collapse mechanism 10 p1685 A71-23977

Low temperature plasticity of Al alloy thin walled tubular specimens under axial tension and internal pressure 10 p1626 A71-24193

Metal strip with circular hole under tension, calculating plastic strain and stress concentration coefficients 10 p1687 A71-24199

Macroscopic and microscopic plastic zones ahead of propagating fatigue crack on surface and inside of specimen as function of load cycles 10 p1626 A71-24306

Monograph on plastic behavior of iron and nickel at high strain rates and at elevated temperatures, discussing thermal effect on deformation characteristics 11 p1783 A71-26489

Physically nonlinear bent rod, deriving strain method equations for plasticity with hardening according to broken line law 12 p1978 A71-27336

Fiber reinforced composite materials plastic behavior shear stress theory, determining yield criteria and plastic strain rates associated with various failure modes 12 p1984 A71-27773

Tensile strength and plasticity of hot rolled maraging steel at low temperatures 13 p2082 A71-27869

Approximate limiting loads with minimum yield stress for axisymmetric rigid-plastic body of arbitrary shape, using computerized static equilibrium method 13 p2150 A71-28137

Crack growth and fracture mechanics, discussing linear stress field and plasticity analyses for three dimensional and dynamic problems 13 p2151 A71-28213

Solids continuum mechanics and fracture criteria, emphasizing intermixed elastic, plastic or viscoelastic types materials behavior idealization 13 p2151 A71-28214

Cylindrical shell laminar plastic structure effect on stability under hydrostatic pressure, applying Kirchhoff-Love hypothesis 13 p2155 A71-28654

Dynamically loaded rigid plastic bodies, solving limiting equilibrium problems by extremal principles 13 p2156 A71-29065

Biaxial plastic extension stability of anisotropic sheets and cylindrical shells, using Hill plasticity theory of orthotropic materials 13 p2156 A71-29074

Tungsten carbide advantages in hard metals structure, including high pressure strength, high elasticity modulus and plastic properties 14 p2255 A71-29517

German monograph on Mo sheets textures and plastic anisotropy covering recrystallization processes, crystallography, etc 14 p2256 A71-29580

Composite materials elastic-plastic behavior under uniaxial loading, determining stress-strain relationships by dislocation theory 14 p2321 A71-29688

Plasticity theory for materials with different mechanical properties in tension and compression, deriving yield criteria and flow rules by tensorial expansions 14 p2322 A71-29736

Three dimensional elastic plastic solid, calculating stress and deformation with finite difference procedure 14 p2322 A71-29737

Statically determinate plane strains in plastic solids, establishing geometrical relations between constant normal-shear stresses and principal directions curves 14 p2323 A71-29816

Incompressible plastic shells behavior, discussing deformation, energy dissipation rate, equilibrium equations and boundary conditions 14 p2328 A71-30380

Complex media and plasticity theory deformation models based on central friction mechanism, discussing elastic spring analog 14 p2332 A71-30879

Superplastic metal alloys microstructure, development history and shaping technology, noting Zn-Al alloy for auto bodies fabrication 15 p2429 A71-32004

Strength, plastic properties, electrical conductivity and fine structure associated with decomposition kinetics of Al alloy supersaturated solid solution 15 p2435 A71-32333

Ultrahigh magnesium based alloys classification by Li content, noting lattices, structural composition, specific weight, plastic properties and impact strength 15 p2435 A71-32336

Plastic structures buckling and instability phenomena, using elementary models with limited number of degrees of freedom and associated yield profiles 16 p2649 A71-32999

Mechanical and plastic properties of Ni-Mo alloys subjected to hot working, determining tensile strength as function of test temperature 16 p2593 A71-33631

Cold hardened Cr-Si steels strength/plasticity thermal dependence and brittleness from short torsion and 16 p2593 A71-33631

compression tests, identifying low temperature failure mechanisms

16 p2593 A71-33638

Idealized model for anisotropy of metals inelastic characteristics due to plastic prestraining, demonstrating applicability to polycrystalline materials

16 p2659 A71-33989

German monograph on characteristics and upper and lower bound methods in plastic layer theory, deriving static and kinematic equations

17 p2748 A71-34798

Two phase fiber reinforced composites under poliaxial stresses, predicting plastic behavior by deformation theory

17 p2823 A71-34810

Soviet monograph on plasticity and strength of solid bodies at low temperatures covering solidifying gases, static tests, dynamic properties and creep

17 p2724 A71-35186

Rigid plastic framed structures minimum weight design and analysis formulation by network-topological approach based on yielding concept

17 p2831 A71-35356

Combined brittle and plastic elements model for strain analysis of nonelastic deformed solid

17 p2832 A71-35457

Beta stabilizers effects on Ti base binary alloys strength, plasticity and stress concentration sensitivity at low temperatures

17 p2760 A71-35465

Physical analysis treating low cycle metal fatigue relation to stress growth in plastic region, discussing cracking mechanisms

17 p2834 A71-35662

Vacuum melted Mo alloy low temperatures elasticity, plasticity and tensile strength characteristics

17 p2760 A71-35675

Carbon effects on strength, ductility, brittle transition and plastic strains of tungsten at high temperatures

18 p2936 A71-36713

Cast electron-beam remelted Mo, investigating carbon and zirconium carbide additions effects on structure and low-temperature plasticity

18 p2937 A71-36723

Composite materials plasticity limit calculation using variational principles

18 p2940 A71-36792

Isothermal phase diagrams and composition effects on plasticity in Mo-Ti-Zr-C system in Al-rich region

19 p3078 A71-37472

Plastic nonlinear creep behavior theory reformulation, obtaining constitutive relations based on experimental data

19 p3084 A71-37524

Plasticity with noncoincident yield and loading surfaces, noting isothermal isotropic hardening

20 p3309 A71-39565

Pure Fe phase transformation plasticity as function of material, stress, temperature interval and change rate, cycle number and experiment duration

21 p3396 A71-40028

Metal deformation processing in solid mechanics, discussing plastic idealization for viscous behavior theorems, Ekstein paradox, free surface problems and incremental forging

21 p3389 A71-40983

Nominal stress prediction for plastic tensile instability occurrence in flat orthotropic sheet loaded by biaxial stress system, considering localized and diffuse necking

21 p3469 A71-41005

Soviet book on mathematical plasticity theory covering stress/strain flow and deformation, stress/strain tensors statistical averaging methods and hardening conditions

21 p3473 A71-41370

Testing machine stiffness determination during strain rate variation and stress relaxation tests for metallic and nonmetallic engineering materials plastic properties assessment

22 p3559 A71-41589

Superplasticity and materials forming methods for metal alloys, considering reformation speed increase by finer grained and stable alloys development

22 p3563 A71-42323

Cast tetraphase Mo and alloys fracture strength and plastic characteristics, investigating crystal growth texture, orientation and substructure

23 p3693 A71-44215

Inelastic transverse strain coefficient and Poisson ratio dependences on plastic and brittle properties

23 p3780 A71-44227

Width/thickness ratio effect on steel, brass and molybdenum sheet specimens plasticity and deformation under tension at room temperature

23 p3694 A71-44233

Metal cored cylindrical plastic shells response to transient external pressures, considering failure modes

24 p3878 A71-44610

Strength and plasticity characteristics of hardened multilayer structural steels, investigating layer thickness effect

24 p3837 A71-44729

PLASTIC YIELDING

U PLASTIC DEFORMATION

PLASTICITY

U PLASTIC PROPERTIES

PLASTICS

NT ACRYLIC RESINS

NT EPOXY RESINS

NT NYLON [TRADEMARK]

NT PHENOLIC RESINS

NT POLYAMIDE RESINS

NT POLYBUTADIENE

NT POLYESTER RESINS

NT POLYETHER RESINS

NT POLYETHYLENES

NT POLYMETHYL METHACRYLATE

NT POLYPROPYLENE

NT POLYSTYRENE

NT POLYTETRAFLUOROETHYLENE

NT POLYVINYL CHLORIDE

NT REINFORCED PLASTICS

NT SYNTHETIC RESINS

NT TEFLON [TRADEMARK]

NT THERMOPLASTIC RESINS

NT THERMOSETTING RESINS

NT VINYL COPOLYMERS

Synthetic plastic materials mechanical and electrical properties for electronics industry use, emphasizing injection molded polymers, pressed molding compounds and casting resins

01 p0051 A71-10285

Plastic low emittance Au coating for spacecraft, controlling thickness via electron bombardment method

01 p0109 A71-11271

Soviet book on engineering theory of ideally plastic thin shells covering elastoplastic equilibrium, bearing capacity, material anisotropy, etc

02 p0324 A71-11850

Crack initiation and propagation in fracture of plastic materials

03 p0516 A71-14580

Rigid cellular plastics mechanical properties based on model assuming pentagonal dodecahedron cell form

04 p0667 A71-14894

Test stand for endurance and creep testing of plastics, glazed ceramics and other brittle materials

04 p0567 A71-15645

Shearing strength of and lubrication effect on metal-plastic adhesion bond, using solid rotating indenter technique

05 p0759 A71-16363

Creep testing machine for plastics and composites

05 p0772 A71-16929

Plastics thermal decomposition, investigating combustion products and toxicity

06 p0916 A71-18089

Plastics for long life microcircuit encapsulation, investigating materials properties and failure mechanisms for device reliability assessment

07 p1077 A71-19561

Plastics for long life microcircuit encapsulation, investigating water absorption and resin-to-lead adhesion effects on reliability

07 p1077 A71-19562

Flame retardant effects on smoke density and oxygen index of polystyrene, acrylonitrile-butadiene-styrene (ABS) and polyester systems

07 p1144 A71-19572

Plastic track detectors calibration for heavy charged particles in cosmic ray experiments, considering track etching rates as function of particle charge and velocity

07 p1113 A71-20042

Plastics and metals as construction materials in aircraft, missile and rocket design

07 p1215 A71-20044

Etchant type, concentration and temperature effect on various plastics track etching ratio and sensitivity

07 p1145 A71-20272

Elastic characteristics of graphite plastics and graphite materials impregnated with synthetic resins, considering aging effect on elastic modulus

09 p1483 A71-22824

Dielectric constant and loss tangent measurements at 60 and 90 GHz for Teflon, polystyrene and Lucite sheets, using Fabry-Perot interferometer

09 p1418 A71-23415

Plastics as potting compounds in military aircraft electrical systems, investigating resistance to reversion and hydrolytic stability

10 p1633 A71-24115

Heat resistant plastics, considering thermal endurance characteristics and use of high strength fillers in aerospace industry

10 p1634 A71-24580

Heavy cosmic ray nuclei track counts in plastics, examining Apollo mission 8 and 12 helmets

10 p1665 A71-25121

Ablative plastics - ACS Conference, San Francisco, March-April 1968

11 p1789 A71-26029

High heating rate thermogravimetric analyzer for ablative plastics, predicting response with semiempirical analytical model

11 p1744 A71-26042

Rigid plastic media dynamic model, showing yielding time delay effect on residual deflection as function of load duration

12 p1982 A71-27515

High temperature plastic lubricants thermal stability, discussing thickening agent-dispersed medium interaction effects

12 p1922 A71-27663

Failure analysis of plastic materials susceptible to cyclic strain hardening under thermal load

13 p2148 A71-28114

Plastics contact strength test apparatus, describing wear test machine for contact load resistance of epoxides used in automobile engine bearings

15 p2383 A71-31656

Total inelastic energy dissipation in structure of creeping plastic material under variable repeated loading and shakedown

[ASME PAPER 71-APM-C] 18 p2977 A71-36252

Synthetic materials technology development, discussing macromolecular materials synthesizing methods and properties

19 p3085 A71-38144

Aerothermodynamics and scale modeling techniques for prediction of plastic burning rates, using Spalding mass transfer theory and dimensional analysis

19 p3171 A71-38250

Reliable plastic encapsulated semiconductor devices design, production and evaluation, noting application to IC

19 p3033 A71-38509

Surface cover materials thermal radiation characteristics and radiation resistance of plastics and solar cells, discussing friction in vacuum and spacecraft surface contamination by outgassing

20 p3210 A71-39453

Dual variational formulation for rigid plastic structure minimum cost design, applying to sandwich and fiber-reinforced plates

[ASME PAPER 71-VIBR-110] 21 p3462 A71-40333

Plastic encapsulated IC reliability tests, relating results to failure mechanism

21 p3356 A71-40747

Flexible polyurethane foam plastics under high rate loading, investigating strain rate and structural parameters effects on mechanical properties

22 p3565 A71-41592

Synthetic fibers and plastics development, chemical composition, physical and mechanical properties, production growth rates and applications

23 p3696 A71-43107

Strength and deformation characteristics of glass plastic under torsional and compressive shear loads, investigating temperature effects on elastic modulus

23 p3697 A71-44204

Plastic strain hardening media stress-strain relations, discussing rheology, temperature effects, isotropy postulate and deformation processes

24 p3876 A71-44401

Rigidly plastic shell theory Lagrangian formulation for moderately large deflections, defining kinematic and dynamic tensors for field equations

24 p3880 A71-44640

PLASTISOLS

NT SMOKE

PLATE [METAL]

U METAL PLATES

PLATE THEORY

Shell theory of anisotropic shells and plates with low shear rigidity, using Timoshenko-type model

01 p0169 A71-10497

Contact problems of orthotropic fiberglass-reinforced plastic plate with low shear rigidity

01 p0169 A71-10498

Stability theory of plates beyond elastic limit, discussing elimination of stress variations discontinuity at interface between plastic loading and unloading zones

01 p0170 A71-10648

Variable thickness circular plate uniformly clamped along edge, calculating critical force from eigenfunctions and eigenvalues of equation with one independent variable

01 p0171 A71-10650

Buckling under compressive loads of incompressible neo-Hookean plates

01 p0171 A71-10659

Flutter analysis of plates with inplane boundary support flexibility exposed to transverse pressure loading or buckled by uniform thermal expansion

01 p0173 A71-10940

Stress-strain state of thin circular plate with variable thickness along circumference under bending due to uniformly distributed load, using small p

02 p0326 A71-12289

Two dimensional stressed state of isotropic plate with elastically reinforced elliptical hole under biaxial tension

02 p0326 A71-12290

Biorthogonal relation for bending of uniformly loaded clamped sector plates with boundary functions along curved edge

02 p0327 A71-12397

German monograph on polygonal thin plates calculation by differential equations method for two dimensional boundary value problems solution

02 p0327 A71-12399

Corrugated membrane of nonuniform profile calculated as variable thickness orthotropic plate, considering corrugations deformation due to bending

02 p0329 A71-12640

Modal coupling in thermally stressed plates, obtaining solution for frequencies and stiffness

02 p0329 A71-12685

Starting functions solutions for axially symmetric orthotropic annular plates

02 p0329 A71-12689

Book on laminated plate theory covering anisotropic continua, bending, orthotropic plates, energy equations, etc

02 p0330 A71-12844

Load limit surfaces for composite plates with long elastic plastic fibers site bonded or imbedded in low strength matrix

03 p0504 A71-13429

Distance dependent stress concentration of isotropic plate with two elliptical holes under tension of opposed point forces

03 p0506 A71-13603

Laminated plates two dimensional theory, discussing equations of motion, stress-strain relations, harmonic wave propagation, etc [ASME PAPER 70-WA/APM-25]

03 p0512 A71-14157

Book on flat plate stability covering initial buckling stresses, compressive and shear loads, holes, various reinforcements and shapes, sandwiching, etc

04 p0667 A71-15074

Stress intensity factor of symmetrical notch in apex of triangular plate under concentrated loads

04 p0670 A71-15391

Uniform thin orthotropic skew flat plates free undamped vibration based on classical plate theory, using Rayleigh-Ritz method

05 p0820 A71-15987

Dynamic thermoelastic response of rapidly heated plate elements, developing variational principle

05 p0824 A71-16560

Stress-strain state in elasticity theory of three layer symmetrical plate

05 p0828 A71-16986

Cosserat surfaces and variable thickness elastic plates linear isothermal theory, deriving constitutive equations corresponding to isotropic three dimensional plate bending and stretching

05 p0831 A71-17250

Thickness variation law for plates and shells with minimal elastic strain energy

06 p0982 A71-17358

Shell and plate theory - Conference, Dnepropetrovsk, U.S.S.R., September 1969

06 p0985 A71-17751

Reinforced plate and shell theory, taking into account ribs arbitrary direction and contour profile

06 p0985 A71-17753

Supercritical behavior of metallic plates, using nonlinear equilibrium and strain compatibility equations

06 p0987 A71-17765

Applicability limits of equations of theory of three-layer plates and shells of asymmetric structure

06 p0987 A71-17766

Stress-strain state of isotropic three-layer plates and shells with rigid and light weight fillers, noting weakening by curvilinear holes

06 p0987 A71-17769

Plates and shells under concentrated loads, determining stress-strain state

06 p0988 A71-17773

Equilibrium equations for flexible plates and shells with nonlinear terms in one dimensional case

06 p0989 A71-17782

Static and kinematic adaptability of plates and shells under progressive structural failure

06 p0989 A71-17784

Plates and shells stability under plastic deformations at subcritical strains, using three dimensional linearized equations

06 p0989 A71-17787

Thermoelastic equilibrium of multiply connected plate during convective heat exchange

06 p0989 A71-17788

Orthotropic plate dynamics, examining plane vibrations with group theory approximate equations

06 p0993 A71-17818

Multilayer asymmetric plates deflection, stability and vibrations, deriving nonlinear bending equations with allowance for transverse shear strains

06 p0995 A71-17833

Multilayer plates and shells, considering bending, stability, boundary layer stress state, rigid filters theory and local strength

06 p0998 A71-17857

Stress concentration at holes in plates and shells with multiply connected regions

06 p0999 A71-17863

Deformation theory of dynamic bending, buckling and stability of plates and shells beyond elastic limit

06 p0999 A71-17865

Thermoelasticity, mechanical and thermal processes in deformation of elastic plates and shells

06 p0999 A71-17866

Triple integral equations solution based on analytic functions theory, applying to stress-strain state in plate with two equal collinear cracks

06 p1002 A71-18346

Stress-strain state of three-layer polymer plate having different thicknesses, Poisson coefficients and creep functions

06 p1005 A71-18707

Stress wave propagation in plates from explosive loading, discussing wave front interaction and scab formation

07 p1215 A71-20091

Tensile tests of elastoplastic notched plate in plane stress

07 p1218 A71-20500

Resistive network computation in plate and shell dynamics, exemplifying skew plate under central concentrated load

08 p1370 A71-21303

Elastic plate with circular hole, solving contact problem in elasticity theory with integrodifferential equation

09 p1535 A71-22181

Unknowns elimination from partial linear equations system with constant coefficients, applying to differential equations for bending transversely isotropic plate under normal external load

09 p1535 A71-22257

Mathematical model for calculating plates of variable thickness referred to curvilinear triorthogonal coordinate system

09 p1536 A71-22411

Rumanian book on stress computation in theory of cylindrical median surface plates with arbitrary section and minimal area

09 p1536 A71-22420

Theory of plates under finite initial elastic deformation, applying to rectangular plate stability under compressions in two mutually perpendicular directions

09 p1537 A71-22521

Infinite isotropic plate weakened by cracks along circular arcs, calculating stress-strain state and critical loads

09 p1538 A71-22524

Physically nonlinear theory of isotropic elastic shells and plates eliminating Love-Kirchhoff hypothesis

09 p1543 A71-23613

Book on elastic plate theory covering bending and transverse shear effects, boundary problems, rectangular isotropic, structurally orthotropic, circular and annular plates under various loads

09 p1544 A71-23701

Nonconforming displacement triangular finite element derivation for plate bending problems, considering constant bending moment element

10 p1685 A71-23939

Thin simply supported polygonal and rhombic plates critical hydrostatic buckling loads and free vibration frequency calculation by conformal mapping and power series expansion

10 p1686 A71-24018

Flexural vibration analysis of rectangular isotropic and orthotropic polygonal elastic plates with constant or variable thickness, considering mass distribution and boundary conditions

10 p1625 A71-24019

Temperature stress distribution in infinite plate with time varying heat transfer coefficient

10 p1687 A71-24197

Limiting equilibrium of thin rigid plastic plate with piecewise smooth contour under skew symmetric load

10 p1690 A71-24568

Polygonal elastic plates natural frequencies investigation by conformal mapping and variational method, transforming holomorphic function into equivalent problem of circular boundary plate

10 p1691 A71-24813

Plate thickness effect on stress distribution around crack, using three dimensional elasticity equations

10 p1693 A71-25055

Plastic deformation of elliptic inclusion in plane strain of infinite plate, using viscoelastic analogy

11 p1852 A71-26395

Dynamic programming for designing beams and plates under steady creep with minimum weight, discussing cantilever beam optimization

11 p1853 A71-26564

Bending problems of elastoplastic plate rigidly clamped over edges, deriving theorems on existence, uniqueness and convergence of approximate solutions

12 p1974 A71-26962

Static and dynamic stress analysis and limiting loads of plastic shells and plates with temperature field in structural element, using deformation theory

12 p1979 A71-27350

Steady thermoelastic equilibrium of infinite isotropic plate containing imbedded circular inclusion with cuts along circumference

12 p1984 A71-27693

Minimum volume design of sandwich axisymmetric plates obeying Mises criterion, using calculus of variations

13 p2146 A71-27782

Reduced order numerical integration technique for plate and shell problems solution

13 p2147 A71-27791

Approximate determination of first characteristic root of equation for plate, hollow sphere and hollow cylinder, using variational method for heat conduction problem

13 p2159 A71-28184

Thermal stresses in infinite viscoelastic plate due to external heat source

13 p2152 A71-28278

Vibration transversely isotropic orthotropic plates, presenting approximate nonlinear dynamic theory

13 p2153 A71-28482

Circular elastic ideally plastic plate deformation due to circumferentially distributed rectangular pulse loading

13 p2156 A71-29075

Instability limit curves for twisted square metal plates under vertical loads with transition from antielastic to synelastic deformation

13 p2158 A71-29431

Nonlinear stability of saddle-like deformed circular and square flat plates and shallow shells under transverse loadings

14 p2322 A71-29692

Elastic stability and buckling behavior of transversely isotropic rectangular Mindlin plate under initial stress and displacement

14 p2324 A71-29871

Multiple Fourier method for plate bending compared with least squares and boundary collocation solutions

14 p2325 A71-29888

Axisymmetric vibrations of heterogeneous isotropic composite clamped circular plates based on Kirchhoff theory

14 p2327 A71-30205

Thermoelastic shells and plates approximate linear theory, detailing uniqueness theorem for initial mixed boundary value problem

14 p2329 A71-30446

Convergent finite element equations for dynamic stability of plates dependent on vibration and buckling modes

14 p2331 A71-30696

Simply supported skew plates buckling under uniform in-plane stresses, obtaining numerical results for various ratios and angles

14 p2331 A71-30698

Strength analysis of shells of revolution and plates under axisymmetrical loads for rigidly plastic material with Tresca yield condition

14 p2332 A71-30849

Soviet papers on three dimensional structures covering strength and stability of compound curvature shells, bodies of revolution and multilayer plates

14 p2332 A71-30888

Buckling under compressive loads of incompressible neo-Hookean plates for homogeneous initial deformation, using variational principle

14 p2333 A71-30993

Plates analysis under static and dynamic loads based on finite difference, lattice analogs, mathematically consistent lumped parameters and finite element models

15 p2503 A71-31438

Soviet book on multilayered media elasticity theory three dimensional problems covering Fourier and Hankel integral transformations, compression, bending, normal and tangential loads, etc

15 p2506 A71-32020

Monograph on rectangular shear elastic plates stability covering Cosserat plane, stress functions, buckling conditions, compressive forces and two dimensional equations

15 p2509 A71-32302

German monograph on orthotropic plate equations derivation by kinematics and statics in general coordinates and elasticity relation

15 p2509 A71-32304

Aeroelastic stability of flat plates and shells, considering panel flutter

16 p2648 A71-32987

Thin plates and shallow shells stability, investigating weak solutions of wall displacement differential equations

16 p2649 A71-32993

Thin plate theory approach with discrete triangular approximation of moment and displacement surfaces for plate bending analysis

16 p2652 A71-33081

Hydrodynamic and plate structural analysis by finite element method, discussing diffusion, oil films and element couplings

16 p2654 A71-33096

Strain energy and stability of nonlinear plate and shell bending under Love-Kirchhoff hypothesis, using three dimensional elasticity theory

17 p2815 A71-34296

Precatastrophic extension effects on local stresses in cracked plates under bending fields, using stress freezing and slicing for photoelastic experiments [SESA PAPER 1820] 17 p2820 A71-34549

Annular plate stability and postbuckling behavior in steady plane axisymmetric temperature field 17 p2822 A71-34598

German monograph on corner singularities in oblique plates calculated with aid of displacement and stress functions, covering bending theory 17 p2823 A71-34796

Rectangular flexible plate displacement theory, solving boundary value problems with fractional step method 17 p2824 A71-34848

Finite element procedure for plate large deflection by considering effects of element membrane forces due to initial deflection and bending on stiffness matrices 17 p2825 A71-34872

Microcracks analysis by micropolar continua theory, presenting solution for circular hole in infinite plate 17 p2832 A71-35421

Generalized periodic problem of infinite isotropic plate of constant thickness with periodically arranged groups of holes, determining stress-strain state 17 p2833 A71-35611

Clamped rectangular plate buckling under uniaxial and biaxial compression, obtaining critical loads for various aspect ratios 18 p2979 A71-36360

Finite difference approximation for discrete eigenvalues of clamped plate, using operator and perturbation technique 18 p2980 A71-36701

Stress-strain state in elasticity theory of three layer symmetrical plate 18 p2982 A71-36786

Wrinkled flat membranes analogy to very thin plates in flexure 18 p2982 A71-36836

Circular inclusion effects in infinite viscoelastic plate under monotonically increasing uniaxial tension, considering stress distribution 19 p3157 A71-37798

Wave propagation in three layered plates, giving frequency spectrum 19 p3158 A71-37884

Shallow lattice shell equations approximated by generalization of asymptotic theories for lattice-type disks and plates 19 p3158 A71-38151

Pressure pulse shape effect on final plastic deformation of simply supported thin circular plate 19 p3158 A71-38181

Nonassociated constitutive equations for rigid viscoplastic plates and thin rotationally symmetric shells under dynamic loading with Huber-Mises yield condition 20 p3310 A71-39777

Approximate theory for vibration of nonhomogeneous anisotropic layered plates using asymptotic integration of elasticity equations 20 p3310 A71-39782

Three dimensional solution for statics and dynamics of homogeneous plates, laminates and orthotropic materials in series form, noting Mindlin analysis 21 p3456 A71-40262

Peak resonant response of thin rectangular plate with elastic edge restraint under concentrated load [ASME PAPER 71-VIBR-6] 21 p3456 A71-40269

Transfer matrix and finite element combination technique for plates and shells vibration analysis [ASME PAPER 71-VIBR-85] 21 p3461 A71-40321

Flexural vibration of rectangular orthotropic plates under in-plane hydrostatic forces 21 p3464 A71-40768

Bending of semiinfinite rectangular plates clamped at long edges 21 p3464 A71-40770

Thin elastic plate under dynamic loading, applying asymptotic expansion techniques to three dimensional dynamic elasticity theory 22 p3613 A71-41435

Finite element method for stress intensity factors calculation in cracked plates under bending 22 p3614 A71-41639

Holographic interferometry application to plate Poisson ratio determination and bending vibration analysis 22 p3539 A71-41741

Thin elastic elliptic plate stress analysis by approximate solution for rectangular plate and parallelepiped equilibrium problems 22 p3616 A71-42212

Finite plates coincidence effect occurrence with sound waves, examining backing cavity and incidence angle influence 22 p3576 A71-42538

Forced vibration of internally damped circular and annular plates with clamped boundaries, obtaining driving point and transfer impedances and force transmissibility 23 p3775 A71-43204

Soviet book on computerized finite difference solutions for physically nonlinear plates and shells covering material anisotropy, creep, thermal, radiative and cyclic load effects 23 p3779 A71-44184

Soviet book on elastoplastic deformations of plates and cylindrical shells made of low strain hardening materials, covering strength and stability calculations 23 p3779 A71-44186

Stiffness matrix algorithm for triangular plate bending elements using hierarchy of interpolation polynomials 24 p3879 A71-44637

Hermite polynomials application to stiffness matrix determination in plate finite element method for disk under plane stress, presenting digital computer program flow diagram 24 p3880 A71-44641

Thermal stresses produced by steady heat flow in two layer plate simply supported at contour 24 p3886 A71-45363

PLATEAUS

Volcanic petrochemical differences of Ethiopian rift and plateaus 09 p1436 A71-22645

PLATES

Covering plate steady state response to acoustic vibrations in viscoelastic half space, calculating interface displacement frequency spectra under zero shear stress assumption 03 p0459 A71-13719

Plate critical surface temperature in case of stabilization by supersonic boundary layer cooling 05 p0695 A71-16852

Continuous flow past plate located perpendicular to wall with inviscid incompressible fluid having linear variation of velocity with height 08 p1227 A71-20828

Compressible viscous gas supersonic flow, observing near wake region behind perpendicular trailing face of plate with motion, state, energy and continuity equations 13 p2047 A71-28421

Heat exchange and temperature distribution between two liquids divided by plate, discussing possible errors 14 p2335 A71-30048

Plate temperature field and stress distribution under thermal pulses, evaluating critical heat load for damage 14 p2325 A71-30049

Plate excitation by supersonic turbulent and shock boundary layers, measuring wall pressure fluctuation and panel displacement 15 p2507 A71-32132

Stress distribution in plates and tubes bonded by stepped joints, assuming generalized plane stress 17 p2824 A71-34814

PLATES (STRUCTURAL MEMBERS)

NT ANISOTROPIC PLATES

NT ANNULAR PLATES

NT CANTILEVER PLATES

NT CIRCULAR PLATES

NT CORRUGATED PLATES

NT ELASTIC PLATES

NT END PLATES

NT ORTHOTROPIC PLATES

NT PERFORATED PLATES

NT POROUS PLATES

NT REINFORCED PLATES

Two concentric circular arc parallel cracks interaction in infinite plate under tension, calculating crack tip stress intensity factor based on elastostatics theory 01 p0167 A71-10174

Photoelastic analysis using stress freezing to evaluate closure and precatastrophic crack extension in plates under cylindrical bending 01 p0167 A71-10295

Impulsively loaded rigid plastic continua deformation lower bounds calculation, considering beams and plates 01 p0173 A71-10943

Beams and plates deflection optical measurement using moire gap effect generalized to include linear and rotational mismatches 03 p0507 A71-13754

[SESA PAPER 1703]

Mathematical stress wave model for sandwich plates under high velocity impact, considering structural multiple reflections and various material combinations [SESA PAPER 1653] 03 p0508 A71-13774

Shells and plate disk structures elastoplasticity analysis problems, considering limit loads, large deflections, boundary state theory, optical design, etc 03 p0510 A71-13944

Polish book on impact in discrete mechanical systems covering beams, curved rods, plates, nonlinear damping, numerical analysis, subjected to shock loading 03 p0513 A71-14297

Computation scheme for hinged plate systems subject to arbitrarily oriented loads based on two layer flexible base model 04 p0664 A71-14601

Papers on structural mechanics covering plates and shells buckling and vibration behavior 05 p0819 A71-15977

Thick plate with circular holes of various sizes, studying stress-strain state 05 p0828 A71-16890

Forced vibrations of three layer plates and shells made from physically nonlinear materials, deriving nonlinear equations with allowance for rigid filler tangential displacement 06 p0991 A71-17797

Nonstationary temperature fields and thermal stresses in plates and shells for discontinuous boundary conditions 06 p0991 A71-17799

Three layer plate with metallic carrier surfaces and plastic foam filler, calculating stress state near applied concentrated moment 06 p0995 A71-17831

Boundary layer construction near free edge of laminar plates by asymptotic integration of three dimensional equations of elasticity theory 06 p0997 A71-17849

Complex form plates bending and oscillations under various boundary conditions, discussing procedure for coordinate sequences construction 06 p0997 A71-17853

Plate and shell designs, considering thin walled structures optimization for minimum weight, volume and cost vs maximum stresses 06 p0998 A71-17858

Brittle plates with statistically distributed cracks, examining limiting equilibrium under tension and compression 06 p1000 A71-17941

Parabolic equation for plate unsteady thermal conductivity under nonuniform heating, analyzing finite difference solution accuracy 06 p1006 A71-18007

Electromagnetic induction in plate with two dimensional conductivity distribution for case of E polarization, representing field by Green functions 06 p0928 A71-18264

Bending stiffness matrix for sandwich folded plate, reproducing core shearing deformations 08 p1367 A71-20748

Multilayer plate vibrations calculated with allowance for energy dissipation in material, deriving equations of motion 09 p1538 A71-22602

Nomograms for thermoelastic stress in plate determined as function of dimensions and heat transfer 09 p1538 A71-22605

Geometric dispersion of dilatational stress wave propagating in laminated plate composite, comparing transmitted wave forms to code calculations 09 p1538 A71-22687

Bending analysis of clamped and simply supported isotropic skew plates under uniformly distributed load 09 p1540 A71-22995

Plane sandwich plates in supersonic gas flow, investigating aeroelastic stability, transverse shear flexibility and axial loads 09 p1543 A71-23609

Multilayer sandwich plates with transverse shear resistant inner layers and bending and twisting moment resistant outer layers, calculating critical buckling loads by finite elements 10 p1686 A71-24020

Nonlinear forced vibrations of aeroelastic plate in two dimensional supersonic flow under harmonic pressure near critical Mach number 10 p1690 A71-24643

Arbitrary plates and axisymmetric bodies creep analysis by finite element method 10 p1691 A71-24820

Asymmetrical three layer plate with filler under impact loading, examining material and layer thickness effects on deformation 12 p1975 A71-27111

Plate and acoustic finite elements simulation of window-room system coupled transient response to sonic booms, discussing equations of motion and cavity depth effect 12 p1981 A71-27481

Computer program for aerodynamic forces on flexible plate undergoing transient motion in shear flow, applying to panel flutter 12 p1866 A71-27559

Flutter of buckled plate exposed to static pressure differential and streamwise applied in-plane load, comparing experimental results with stability boundary calculations 12 p1983 A71-27584

Stress concentration due to holes and other stress raisers in plates and shells, taking into account transverse shear strains effects 13 p2149 A71-28127

Eigenvalue problems in theory of sandwich plates with rigid cores, obtaining solutions by Galerkin method 14 p2322 A71-29734

Time independent three dimensional streaming secondary motion due to vibrating flexible plate 14 p2325 A71-30061

Simply supported normal mode plate time response to traveling wave at oblique incidence, using numerical analysis

14 p2326 A71-30068

Bending equations solution for arbitrarily shaped quadrilateral plates with simply supported edges, using finite difference method

14 p2329 A71-30485

Stress-strain state of finite length elastic rod free of bending moments and coupled to seminfinit plate

14 p2332 A71-30868

Equilibrium stability of rods, shells and plates during creep due to applied load

14 p2333 A71-30893

Brittle plates with stochastic distribution of cracks under biaxial tensile-compressive stresses, obtaining critical load

15 p2504 A71-31853

Curved sandwich plate strain and kinetic energy expression derivation for use with finite element displacement method

15 p2508 A71-32136

Crack interaction effect along straight line on critical equilibrium and fracture of plate relative to cross-piece length

16 p2658 A71-33685

Thermoelastic critical equilibrium of plate with rectilinear crack under heat transfer from edge surface and tensile stress

16 p2658 A71-33686

Complex form plates with energy sources in combined cooling system, calculating temperature field

17 p2836 A71-34422

Oriented glass fiber-plastics plates and shells design, noting zero moment stress shells and filament overwrapped metallic pressure vessels

17 p2830 A71-35315

Minimum mass design of two dimensional plate-like structure with free vibration fundamental frequency or aeroelastic constraints, using optimal theory for extremum

19 p3158 A71-37877

Universal dispersion curve for steady state sinusoidal flexural wave propagation in plates and bars, using Poisson ratio as single parameter

21 p3463 A71-40535

High precision displacement functions for finite element models of rotational shell and plate bending problems

21 p3470 A71-41019

Reflected shadow method for constrained zone photoelastic observation around cracks in birefringent transparent plate under plane stress

22 p3549 A71-42555

Local elastic buckling of component plate elements of single-cell simply supported folded plate structures under uniform transverse loads

22 p3618 A71-42585

Dynamic three dimensional stress distribution near crack tip in finite plate, using finite difference scheme

23 p3776 A71-43376

Thermoviscoelastic problem for semiinfinite plate, determining temperature field and stresses permitting heat propagation

23 p3780 A71-44223

Natural vibrations of complex shape plates with clamped edge on resilient base, deriving approximate solution via R functions

24 p3877 A71-44481

Stress field due to two rigid circular disk inclusions in isotropic homogeneous infinite plate

24 p3879 A71-44627

Global-local finite element combined Ritz methods for beam and plate vibration analysis

24 p3880 A71-44638

Nonhomogeneous plate under pulsating and uniformly distributed loads, considering dynamic elasticity problem

24 p3880 A71-44712

PLATFORMS

Motion platform systems evolution for flight research and training simulation

15 p2384 A71-31887

PLATING

NT NICKEL PLATE

Solid metal lubricant films bonding by ion plating using diode method, noting interface type and structure examination by electron microscopy

01 p0087 A71-10483

Cr and V diffusion plating influence on principal characteristics of highly alloyed martensitic and carbon steels

12 p1912 A71-27690

Bimetallic plated high strength steel, noting transition zone effects on mechanical properties

23 p3692 A71-44026

PLATINUM

Quasi-spherical divergent shock waves produced by Pt wire explosion in air

02 p0332 A71-12336

Oxygen reduction on Teflon bonded Pt electrodes, eliminating concentrated overvoltage

02 p0210 A71-12955

Hydrogen and carbon monoxide coadsorption on platinum single crystal surface, examining interactions

and species formation by thermal flash and electron impact techniques in ultrahigh vacuum

07 p1055 A71-19844

Quenched and aged Pt, investigating secondary defects for vacancies clustering modes by transmission electron and field-ion microscopy

11 p1779 A71-26016

Platinum, palladium and gold detection in silver assay buttons by atomic absorption spectrophotometry

15 p2367 A71-31649

Platinum resistance thermometers calibration normalized in resistance-difference ratios

18 p2916 A71-36047

Thermodynamic measurement of cryogenic temperatures based on gases at low pressures or platinum electrical resistance

20 p3270 A71-39243

Si Pt-n-p transit time microwave diode source noise measurement, noting low noise characteristics and suitability for local oscillator applications

21 p3359 A71-41413

Heat transfer from platinum wires in He and He-air mixtures, plotting Nusselt number variation with Reynolds number for various He concentrations

22 p3620 A71-41875

PLATINUM COMPOUNDS

Platinoid boride production, determining reaction sintering temperature with thermal metallographic and X ray analysis

24 p3838 A71-44735

PLAYBACKS

Plasma echo and spin echo holophones for electrical signals temporal sequence recording and cued playback, noting human brain memory function analogy

05 p0787 A71-16451

PLENUM CHAMBERS

Plenum chamber with nozzle wind tunnel model, noting jet flow phenomena at various angles of attack

10 p1590 A71-24865

Supersonic staggered gutter colander combustion system for plenum chamber burning on high bypass Pegasus turbofan engine of Harrier VTOL aircraft, noting performance improvement

13 p2116 A71-28743

Electrically excited gas dynamic CO laser using glow discharge in supersonic nozzle plenum

23 p3683 A71-42958

PLETHYSMOGRAPHY

Total impedance plethysmography boundary value problems, developing computer program based on Jacobi iterative method

03 p0367 A71-12993

Plethysmographical study of noise effects on hearing and peripheral vasoconstriction in man and animals

03 p0359 A71-13155

Four-electrode impedance plethysmograph system for evaluating conduction variations of upper and lower body segments relative to blood volume displacement

06 p0853 A71-17958

Photoplethysmographic analysis of pulse wave velocity in healthy subjects and in patients with hypertension, heart disease, diabetes and anemia

22 p3490 A71-42518

PLEURAE

Dogs intrapleural and intrasophageal pressures dependence on head positions

19 p3010 A71-38564

PLEXIGLASS [TRADEMARK]

U POLYMETHYL METHACRYLATE

PLOTTERS

NT X-Y PLOTTERS

Automatic cartography, using plotting machine digital output via attached shaft encoders

06 p0895 A71-18292

Cost effective high speed projectile trajectory plotting system for gunnery range instrumentation, applying to aircraft path recording during automatic landing control

18 p2924 A71-36613

Autoplotter for radar echoes on CRT screen, using video tape recorder for ship navigation use

19 p3017 A71-37700

Binary computer holograms construction, discussing two and three dimensional objects, wave propagation, plotter instrumentation, photographic reduction and diffusers

21 p3380 A71-40921

PLOTTING

Two shaft turbojet engine parameter plot techniques effectiveness, varying low pressure cascade rpm or nozzle system passage cross sections

03 p0472 A71-14259

PLOTTING INSTRUMENTS

U PLOTTERS

PLSS

U PORTABLE LIFE SUPPORT SYSTEMS

PLUG NOZZLES

Maximum thrust plug nozzle design for fixed inlet geometry, using calculus of variations for optimum contour determination

06 p0946 A71-18501

Nonuniform plug nozzle flow field calculated for closed wake, using flow model divided into near wake and adjacent regions

[AIAA PAPER 71-41]

06 p0946 A71-18502

PLUGGING

Plug-in relay hazards and minimization for aircraft flight safety applications

13 p2001 A71-28841

PLUGS

Liquid He containment in space zero-g environment, proposing use of high thermal conductivity porous plug operating in superfluid regime

20 p3184 A71-39280

PLUM BROOK REACTOR

Beryllium reflector plate failure in NASA Plum Brook Reactor, discussing irradiation induced mechanical and physical property changes and internal/external stress effects

21 p3414 A71-40904

PLUMBANE

U LEAD COMPOUNDS

U METAL HYDRIDES

PLUMES

NT ROCKET EXHAUST

Forced plume entrainment of turbulent buoyant jet in stratified fluid as function of Reynolds, similarity and Froude numbers

02 p0278 A71-12704

Jet plume in subsonic cross flow, calculating counter-rotating vortices as function of distance along trajectory from semiempirical model

07 p1090 A71-19901

Two and three dimensional thermals and steady and starting plumes convective fluid motion formulas, using vorticity integration method

07 p1104 A71-20223

Mach disk in underexpanded exhaust plume predicted by dividing flow field into subregions

09 p1382 A71-22097

Inviscid model for flow field within plumes of two-dimensional underexpanded jets calculated by time dependent finite difference method

11 p1853 A71-25160

Electron and laser pulse plumes, using thermomechanical shock wave theory

13 p2079 A71-28768

Carbon dioxide free jet plumes issuing from supersonic nozzle into high vacuum, measuring densities and temperature

13 p2026 A71-29355

Flow field calculation in intermediate altitude rocket exhaust plumes by modified Lagrangian finite difference technique

22 p3590 A71-42774

PLUNGERS

Jet fuel dissolved oxygen concentration effects on plunger antiwear properties

15 p2464 A71-31677

PLUTO [PLANET]

Pluto-Neptune system implications for solar system evolution theories, discussing deterministic and statistical models and n body problem approaches

04 p0655 A71-15726

Pluto orbit integration over 4.5 million years by variation of parameters technique and confirming Neptune-Pluto orbital resonances

10 p1669 A71-24179

Pluto iron richness from analysis of similarities between Pluto spectra and Fe bearing terrestrial silicate crystals

10 p1673 A71-24426

Pluto mass from reciprocal mass and density, using Neptune transit circle observations reevaluation

15 p2488 A71-32199

Computer processed photographic observations of Pluto, 10 Hygiea, 433 Eros and Saturn satellites VII, VIII and IX

24 p3874 A71-45178

PLUTONIUM

NT PLUTONIUM 238

Plutonium in peculiar A stars surfaces as nuclear cosmochronology for determination of r process nuclei age, considering emission line spectra obscurement

05 p0808 A71-16413

Nuclear characteristics of plutonium fuel for thermoelectric generators and required shield thicknesses for sensitive radiation experiment in outer planet spacecraft

22 p3592 A71-42300

PLUTONIUM ALLOYS

Beta Ti-Pu solid solution, constructing diffusion phase diagrams from electron beam microprobe analysis and autoradiography

18 p2935 A71-36174

PLUTONIUM ISOTOPES

NT PLUTONIUM 238

PLUTONIUM 238

Neutron emission yield during Pu 238 alpha particles interactions with O 18, taking into account recoil Ne isotopes

14 p2276 A71-30177

PLUVIOGRAPHS

U RAIN GAGES

U RECORDING INSTRUMENTS

PNEUMATIC CIRCUITS

Book on fluid power circuits and systems covering switching theory, closed loop systems, pneumatic circuits, servo systems and pressure control

02 p0190 A71-11871

Blocked and series connected pneumatic fluidic transmission lines, determining amplitude frequency response

07 p1026 A71-20566

Beam deflection fluidic circuit design by linear static matching method, considering servoamplifier feedback control system

07 p1026 A71-20569

Moving part pneumatic logic element static and dynamic characteristics, determining air flow rate and output pressure

07 p1027 A71-20574

Missile fluidic attitude control system, discussing integrator, transducer amplifiers and circuits

07 p1028 A71-20583

Low pressure air jet sensing power pneumatic and fluidic circuits and interface valves for low pressure signal stepup to main line pressure, considering circuit design

07 p1030 A71-20597

Pneumatic resistance transducer for fluidic measurement of mechanical quantities

07 p1030 A71-20598

Book on fluidics components and circuits covering fluid logic devices, fluid mechanics, analog devices, moving and nonmoving part digital devices, switching elements, etc

09 p1386 A71-22070

Control and instrumentation fluidics, describing equipment, circuits and applications to jet engine controls, missile guidance, flight control, ordnance and machine tool control

09 p1386 A71-22775

High pressure pneumatic lines dynamics, considering equation of state for real gas with given compressibility function

16 p2527 A71-33618

Pneumatic isolation system for inertial instrument testing, using computer simulation model to evaluate physical parameter variation effect on pad suspension dynamic behavior

[AIAA PAPER 71-910]

19 p3040 A71-37161

Pneumatic passive lead networks for fluidic systems, presenting transfer functions, equivalent circuits and design information

23 p3631 A71-44096

PNEUMATIC CONTROL

Computer aided design for fluidic-pneumatic sequential control circuits synthesis, discussing algorithms and computer programs

[ASME PAPER 70-WA/FLCS-17]

03 p0354 A71-14090

Moving parts pneumatic control, discussing valves adaptation to control language and functional requirements

07 p1023 A71-19996

Fluidic pneumatic control system compensator for digital signal processing

07 p1026 A71-20567

Moving part digital pneumatic logic system, using elements molded into rubber sheet between two rigid flat plates

07 p1027 A71-20575

Digital fluidic metering system for composition control of liquid batch mixing from circuit design to final product

07 p1028 A71-20581

Pneumatic and hydraulic fluidic power control systems, discussing moving part position servos and cold gas reaction systems

07 p1028 A71-20585

Fluidic pressure ratio control for vertical takeoff aircraft lift engine fuel system, describing breadboard circuit, test bed and flight standard

07 p1028 A71-20587

PNEUMATIC EQUIPMENT

NT PNEUMATIC CIRCUITS

Oleopneumatic accumulators in gearboxes for rationalizing installed power

07 p1023 A71-20004

External feedback fluidic oscillators design and analysis using branched pneumatic transmission line arrangements

07 p1027 A71-20578

Pneumatic membrane logic elements on basis of figure of merit characterizing usability in system engineering

11 p1709 A71-25570

Electropneumatic transducer system linearization, matching nonlinearities in EM and pneumatic subsystems

13 p1999 A71-28638

Atomization drop size distributions in sprays from convergent pneumatic nozzles for molten wax and polyethylene mixtures

13 p2049 A71-29007

Fluidic devices with combined pneumatic and hydraulic components, describing jet-siphon liquid

flow frequency transducer with pneumatic pulse counting device

15 p2353 A71-32071

Aerospace pneumatic and fluidic developments, discussing high speed and response air motors, control functions, thrust reverser actuator and various drive systems

18 p2851 A71-36208

Lumped parameter modeling of fluid elastic vibration response of nonlinear piston driven pneumatic-mechanical system, using finite element control volumes

[ASME PAPER 71-VIBR-41] 21 p3459 A71-40291

Automatic control theory application to pneumatic self vibration /hammer/ occurrence criteria derivation for externally-pressurized gas-lubricated thrust collar bearings

22 p3551 A71-41660

PNEUMATIC PROBES

Vortex type pneumatic angular rate sensor with vanes and hydrodynamic viscous coupling, determining differential pressure outputs

15 p2352 A71-32063

Constant speed vortex rate sensor, calculating angular momentum dissipation due to shear stresses and response to step signal input

15 p2352 A71-32064

PNEUMATIC RESET

U PNEUMATIC CONTROL

PNEUMATICS

Transfer function system relating cornering force and aligning torque of rolling pneumatic aircraft tire to yaw angle and lateral displacement

21 p3324 A71-40167

PNEUMONIA

Hypobaric pressure and hypoxic or hyperoxic atmospheres effect on mice resistance to pneumococcal pneumonia

02 p0199 A71-12382

Cold environment exposure effect on mouse resistance to infection with Klebsiella pneumoniae

16 p2528 A71-33115

POCKELS EFFECT

U BIREFRINGENCE

PODS [EXTERNAL STORES]

Fighter F-14 podded engine high variable sweep wing design including nozzle, nacelle, fuselage shift, aspect ratio and lift control improvements

16 p2526 A71-34152

POGO EFFECTS

Dynamic stability analysis, ground testing and corrective accumulator devices for POGO oscillations in space booster structure

22 p3609 A71-41992

POIKILOthermia

NT FROGS

NT SNAKES

NT TURTLES

POINCARÉ PROBLEM

Poincaré hydrodynamic analogy in celestial mechanics, relating differential equations for dynamic systems with two degrees of freedom and two and three dimensional flow

01 p0154 A71-10383

Curved space-time mathematical structure /quasi-groups/, investigating 10-parametric classes of coordinate systems and Poincaré groups

08 p1334 A71-21358

Conformal transformation of multiply connected plane domain of Poincaré standardization

17 p2672 A71-35469

POINCARÉ SPHERES

Closed invariant sets of smooth flow on compact manifold involving homoclinic or heteroclinic point theory of Poincaré

06 p0918 A71-17640

Flow patterns on Poincaré sphere as aid to qualitative study of polarization and intensity of quasi-stationary laser mode in anisotropic resonator

20 p3243 A71-39095

POINT DEFECTS

NT FRENKEL DEFECTS

NT VACANCIES [CRYSTAL DEFECTS]

Variant function describing long term fatigue strength under complex loads in determining given material damage point during breakdown

01 p0169 A71-10494

Differential equations derivation for metal fatigue point defect colonies concentration changes, discussing diffusion and dislocation interactions

06 p1002 A71-18418

Solid solution hardening theories, discussing point obstacles random distribution effect on strength and superposition of multiple hardening mechanisms

08 p1309 A71-21522

Fracture kinetics, emphasizing plastic deformation, dislocation and diffusion micromechanics, point defects effects and microcrack formation

08 p1371 A71-21606

Point defects and fine precipitates effects on fatigue strength of high strength alloys, exhibiting higher fatigue strength in isothermally aged samples

10 p1625 A71-24009

Probability of quasi-chemical reactions between point defects in semiconductors due to ionizing radiation

10 p1655 A71-24139

Lead zirconate-titanate point defects crystal chemistry, interpreting sintering and grain growth behavior

13 p2093 A71-28992

Point defects relation to thermoelectric emission at high temperatures in yttrium oxide

15 p2462 A71-32714

Electromagnetic absorption cross sections from wave function of free carriers in semiconductors with point defects

16 p2623 A71-34031

Mechanical interactions of point defects in homogeneous isotropic continuous elastic media, deriving interaction energy from Siems multipole forces analysis

17 p2831 A71-35395

POINT IMPACT

Optical point elastohydrodynamic contact, describing optical interference system consisting of chromium plated glass plate and steel ball

01 p0087 A71-10463

Stress and contact time calculation for impact of spheres on finite thickness elastic plate overlying rigid foundation

21 p3472 A71-41031

POINT MATCHING METHOD [MATHEMATICS]

U BOUNDARY VALUE PROBLEMS

POINT SOURCES

Point source acoustic radiation field in presence of absorbing plane, presenting solutions and approximations based on plane wave reflection and modified image method

03 p0456 A71-13276

Gravitational field due to point mass, proving Newton space existence

03 p0458 A71-13606

Two point resolution in Fourier holography with partially coherent recording and illuminating light

03 p0429 A71-14180

Shock waves and chemical reactions due to plane, cylindrical and spherical point explosions in combustible gaseous mixtures

05 p0833 A71-16503

Nomographs for point source holographic imaging, discussing recording and reconstruction geometry

05 p0753 A71-16913

Aerodynamic sound radiation from point force in accelerative circular motion, obtaining closed form for overall far field radiation

05 p0784 A71-17162

Low profile optical system producing annular cone of radiation from point source for high speed aircraft beacon

07 p1107 A71-19203

Modified double point source differential shear interferometer for neutral reference light beam, using pinhole stop

07 p1110 A71-19478

Sound field due to point source inside absorbent lined enclosure for anechoic chamber performance prediction

07 p1160 A71-19587

Pulse propagation from time-step point force at surface of transversely isotropic elastic half space, obtaining solutions by integral transforms

08 p1371 A71-21428

Human visual analyzer excitability shifts due to short duration point light stimuli

08 p1243 A71-21972

Meteor trails isotropic diffusion in presence of moving point source of ionization with variable intensity, calculating plasma density on and near trajectory

09 p1518 A71-22447

Loci of perceived, equi-, half- and double distance in stereoscopic vision with point source stimuli relative to Vieth-Müller circle

09 p1394 A71-23014

Contour map of galactic radio emission in Cassiopeia and Cepheus region, noting discrete sources

11 p1831 A71-26132

Sound radiation from time varying point force in accelerative motion, applying to fan or helicopter rotor noise at subsonic tip speeds

12 p1867 A71-26702

Diffraction of spherical wave on triangular prism, using reduction by group theory of point sources

12 p1878 A71-26838

Direction finder for point source signals from two simultaneous transmitters

14 p2210 A71-29810

HF response of point excited cylindrical shell, converting normal-mode series to integral representation with Watson transformation

14 p2327 A71-30201

Point sources of solar neutrino radiation, explaining negative experimental results without drastic change of main assumptions concerning stellar evolution

15 p2478 A71-31801

High energy cosmic gamma ray point sources identification near galactic plane from balloon flights data 15 p2478 A71-31826

Random time variation in sound radiation far field of point sources in subsonic circular rotational motion 15 p2450 A71-32129

Sound field of point acoustic stresses in arbitrary motion, investigating uniform straight line and circular motion and pure rotation effects 15 p2450 A71-32130

Small monochromatic disturbances propagation in stable ideal MHD fluid by geometric optics method, solving point source radiation at short wavelengths 15 p2459 A71-32652

Earth masses substitution by nearly minimum number of point sources of gravity anomalies 17 p2734 A71-35188

Closed form solution for quasi-static thermal stress field due to moving point heat source in circular disk, noting application to welding problems 21 p3467 A71-40966

Field ion current angular distribution for large point emitter potentials as function of emitter geometry 22 p3578 A71-42057

Far field radiation patterns of axially oriented point current sources in presence of dielectric circular cylinders, developing solutions via plane wave scattering 23 p3654 A71-44160

Point source average signal reflection from conductive plane in random oscillation 23 p3654 A71-44163

Acoustical harmonic point source in motion relative to surrounding fluid, using Fourier integrals for mathematical representation 24 p3847 A71-44418

Point source radiation in stratified waveguide system with magnetoplasma slab, evaluating transverse field by Fourier integral representation 24 p3857 A71-45181

POINT TO POINT COMMUNICATIONS

Intercontinental point to point radio communication, discussing Hertzian beam /radio relay links/ and satellite communication comparison with underground and submarine cables 19 p3016 A71-37343

Broadband point-to-point communication satellite systems for 1970s, discussing R and D effort, economics and international and domestic applications 20 p3197 A71-39606

POINTING CONTROL SYSTEMS

Soviet radio telescope tracking control system, describing feedback sensors, digital computer, servomotors, actuators and control panels 04 p0565 A71-14848

Performance tests for guidance accuracy and tracking smoothness of Crimean Astrophysical Observatory radio telescope, discussing pointing and tracking errors 04 p0565 A71-14849

Skylab earth-orbiting manned space station attitude and pointing control systems design 04 p0623 A71-15323

OA0 2 design and performance features concerning pointing accuracy and stability, command capability, data handling, thermal environment, orbit constraints, ultraviolet spectroscopy, etc 05 p0818 A71-17128

Space station experiments fine pointing and stability, discussing attached or coorbiting free flying mode with zero G conditions [AIAA PAPER 71-62] 06 p0980 A71-18521

Passive airborne computer augmented aircraft antenna pointing control system for communication satellites tracking [AIAA PAPER 71-233] 07 p1077 A71-19710

Automatic telescope guidance system for faint light source tracking, using cumulative photocurrent mismatch signal storage 14 p2271 A71-29994

Apollo Telescope Mount for high resolution solar observation and manned instruments evaluation in space environment, discussing attitude and pointing control systems 15 p2500 A71-31458

Control moment gyro for attitude pointing control system of Skylab space station 17 p2743 A71-35063

Precision tracking and pointing of laser beams in space for communication, discussing large space telescope /LST/ applications 18 p2920 A71-36090

Synchronous three-axes stabilized communication satellites attitude control system with double gimbaled reaction wheel control actuator, obtaining 0.1 degree pointing accuracy with pitch and roll sensors [AIAA PAPER 71-949] 19 p3098 A71-37190

Sight line autopilot (SLAP) for side-firing aircraft pointing accuracy improvement, using optimal regulator theory to generate control gains 19 p3099 A71-37201

Integrated system for precision attitude determination and pointing control of spacecraft gimbaled payloads [AIAA PAPER 71-962] 19 p3099 A71-37203

Spacecraft pointing control system with momentum exchange controllers, considering near optimal control policy for control moment gyro system 22 p3608 A71-41966

Large telescope design - Conference, Geneva, March 1971, covering telescope projects, optical properties, mountings and control and drive systems 22 p3542 A71-42120

POINTS [MATHEMATICS]

NT FIXED POINTS [MATHEMATICS]

Triangulation position fix techniques employing lines of bearing, n-locus, least square fits and resection by intersection method 02 p0280 A71-12900

Nonlinear stability of triangular points in restricted problem of three bodies, using second order expansions, Lie transform and multiple scale method 03 p0487 A71-13448

Neron-Tate height fine structure of points on Abelian manifolds, considering canonical bounded and diophantine problems 06 p0917 A71-17571

Closed invariant sets of smooth flow on compact manifold involving homoclinic or heteroclinic point theory of Poincare 06 p0918 A71-17640

Lunar surface mass distribution, using dynamic point mass solution 09 p1530 A71-23717

Stationary points of functional corresponding to boundary value problem with free boundary 12 p1930 A71-27167

Invariant imbedding for two point boundary value problems for difference equations, noting conversion to initial value problem 17 p2764 A71-34519

Flight mechanics of point with limited power propulsion system and energy storage unit, investigating variational maximum payload problem with singular control optimization 20 p3288 A71-39125

Stationary signal space topology concept in special relativity, considering points neighborhoods as independent of signal sending time 21 p3346 A71-40091

Relativistic equation derivation for dynamics of point with varying rest mass from Newtonian principle 21 p3415 A71-40659

One and two dimensional function values calculation for curve systems by continued fraction interpolation from point grids, using computer program 22 p3518 A71-42394

Degenerate critical points Morse index type characteristics, considering maximum points of functional on surface of another 24 p3843 A71-44707

POISEUILLE FLOW

U LAMINAR FLOW

POISONING

Intrarenal vascular pattern in carbon dioxide death of rhesus monkeys and dogs, observing sympathetic vasoconstriction 06 p0851 A71-17610

Pargyline behavioral effects in primates, concerning therapeutic use for decabranic intoxication 08 p1239 A71-20819

Acute hydrazine hydrate poisoning morphological effects on internal organs and blood in guinea pigs, noting pronounced changes in liver and kidneys 09 p1393 A71-22921

POISONING [REACTION INHIBITION]

Organophosphate pesticide poisoning implication in aircraft crash of duster pilot from cholinesterase activity drop evidence 23 p3641 A71-44249

POISONING [TOXICOLOGY]

U TOXIC DISEASES

POISONS

NT ENDOTOXINS

NT URETHANES

POISSON FUNCTIONALS

Queueing model of statistical multiplexer buffer behavior for batch Poisson arrivals and single constant output, applying to time sharing computer buffer design 05 p0724 A71-17063

Threshold distribution of time intervals between atmospheric contradicting Poisson law 09 p1435 A71-22445

Distribution functions of initial and established intervals of stochastic and Poisson sequences in automatic control, reliability and communications theories 10 p1588 A71-24902

Bayesian modeling of nonstationary Poisson process with probabilistic lambda in time 11 p1791 A71-25252

Large scale clustering of galaxies and galactic clusters, comparing observed and Poisson distributions 13 p2138 A71-28759

Gaussian and Poisson noise and SNR effects on subjective image quality rating, using transparency aerial scenes 20 p3235 A71-39190

POISSON EQUATION

Charged particle motion in self consistent continuous wave spectrum from Vlasov and Poisson equations solution 02 p0289 A71-11955

Boundary value problems solution of Helmholtz and Poisson equations for parallelepiped, applying to elasticity theory 02 p0328 A71-12542

Soviet monograph on universal program for finite difference solution of Dirichlet problem of Poisson equation with enhanced accuracy formulas 04 p0619 A71-15450

Numerical integration of Poisson kinematic equations for direction cosines, using Runge principle for accuracy values proportional to third power of integration step 05 p0780 A71-16051

Poisson-Boltzmann equation solution for potential of charged sphere with radius not larger than Debye radius 05 p0781 A71-16383

Infinite universe compatibility with gravity potential satisfying Poisson equation, avoiding cosmological difficulties by universal gravitational field sources and sinks introduction 10 p1681 A71-25074

Flat galaxies dynamics via linearized Vlasov equation integration and Poisson equation exact solution 14 p2303 A71-29590

Numerical integration of Poisson kinematic equations for direction cosines, using Runge principle for accuracy values proportional to third power of integration step 16 p2605 A71-33455

Poisson equation for space charge layer of reverse-biased p-n junction in p-n-p-n structure with allowance for two types of moving current carriers 16 p2546 A71-33495

Thermoelectric and thermomagnetic phenomena in semiconductors with impurity ions, solving electric conductivity and diffusion and Poisson equations for weak magnetic fields 16 p2622 A71-34027

Vlasov-Poisson equations of collisionless plasma flow around conducting cylinder without magnetic effects, using nonrestrictive hybrid simulation techniques [ONERA-TP-958] 18 p2951 A71-36025

Influence coefficient matrix method for discretized Poisson equation solution 18 p2905 A71-36306

Collisionless plasma Vlasov and Poisson equations numerical solution based on Fourier-Fourier transform, comparing with particle motion simulation 19 p3113 A71-37748

POISSON PROCESS

U POISSON DENSITY FUNCTIONS

U STOCHASTIC PROCESSES

POISSON RATIO

Transverse elastic modulus and Poisson coefficient of composite materials as function of reinforcement, structure and fiber radius 05 p0771 A71-16360

Soviet monograph on refractory materials elasticity at high temperatures covering elastic and shear modulus, Poisson coefficient and resonance methods 05 p0766 A71-16400

Elastic materials Poisson ratio measurement by moire method in coherent and incoherent light 16 p2575 A71-32825

Inductive extensometers with spherical tips for materials testing, noting Young modulus and Poisson ratio determination 17 p2744 A71-35239

UV Cet and YZ CMi star flare activity data, noting Poisson distribution of time sequence 19 p3134 A71-37510

Harmonic excitation response of masses on elastic half space, considering Poisson ratio effect, vibration amplitudes and resonant frequencies [ASME PAPER 71-VIBR-59] 21 p3460 A71-40304

Universal dispersion curve for steady state sinusoidal flexural wave propagation in plates and bars, using Poisson ratio as single parameter 21 p3463 A71-40535

Modulus of elasticity and Poisson ratio of composite material with anisotropic or isotropic fibers arranged in rectangular or square array 21 p3464 A71-40772

Holographic interferometry application to plate Poisson ratio determination and bending vibration analysis 22 p3539 A71-41741

Elastic surface wave amplitude and propagation velocity in lunar rocks, calculating Poisson ratio 23 p3761 A71-43784

Inelastic transverse strain coefficient and Poisson ratio dependences on plastic and brittle properties 23 p3780 A71-44227

Slit tube flat-to-circular transition during extension, considering mathematical model for curvature change, modulus of elasticity and Poisson ratio effects 24 p3884 A71-44959

POLAR AURORAS

U AURORAS

POLAR CAP ABSORPTION

Black Brant rocket measurement of PCA event at Churchill, Canada on 19 November 1968, discussing electron density and alpha particle and proton flux
03 p0417 A71-14038

PCA ionization, using range-energy ratio of solar cosmic rays penetrating spirally into polar atmosphere for electron production rate determination
05 p0742 A71-16812

Diurnal variations of loss factor in D region during polar cap absorption, verifying nighttime D region model by forward propagation data
05 p0744 A71-17185

Time dependence of atmospheric ionization at polar cap absorption event, obtaining relativistic and non-relativistic solar cosmic rays ionization equations
11 p1734 A71-25586

Diurnal variations of loss coefficient in D region during polar cap absorption, verifying nighttime D region model by forward propagation data
13 p2059 A71-28242

Geomagnetic tail influence on polar ionosphere proton and electron precipitation, considering ionospheric ionization and polar cap absorption
14 p2300 A71-30034

Day and nighttime effective electron loss rate measurement in D region during polar cap absorption events, using rocket-borne spectrometers and Faraday rotation
16 p2573 A71-33961

Ionospheric electron concentration and proton flux rocket-borne measurements during nighttime PCA event, discussing atomic oxygen role in recombination processes
16 p2575 A71-33974

Equatorial and precipitating solar proton fluxes interrelationship in magnetosphere from riometer absorption in auroral and polar cap regions
19 p3125 A71-37360

Polar cap absorption event, investigating solar high energy protons precipitation effects
19 p3129 A71-38360

Ion and electron production rate during PCA event, computing electron/ion density, differential proton flux spectrum and ion production rate
20 p3225 A71-39729

PCA due to solar proton event, measuring electron/ion densities and temperatures, proton/electron energy flux spectrum, Lyman alpha radiation and X rays
20 p3281 A71-39730

ELF and VLF emissions during PCA, correlating data with particle and photometer recordings from ground based, satellite and rocket-borne observations
20 p3229 A71-39856

POLAR CAPS

Carbon dioxide clathrate in Martian ice cap suggested from hydrate stability relative to solid phase and water ice as function of temperature
01 p0148 A71-10002

Proton Flare Project 1969 observation of polar cap ionospheric disturbance due to proton event by VLF propagation phase measurement
01 p0073 A71-10289

SD geomagnetic variations and electron jet spread over polar cap stream during solar cycle
02 p0243 A71-11763

Upper ionosphere electron concentration enhancement in polar cap from satellite probe measurements
03 p0408 A71-13385

Martian north polar cap observations, discussing physical aspects and seasonal regression curves
03 p0489 A71-13560

Thermogravimetric analysis of goethite-rich sample of Mars type limonite, considering sorption process relation to Mars environment and polar caps
04 p0644 A71-15131

Mars surface TV pictures from Mariner 6 and 7, including cratered and uncratered terrains, light and dark markings and south polar cap
06 p0965 A71-17628

Cosmic rays transient north-south polar asymmetry, confirming time lag between Forbush decrease onsets
06 p0956 A71-18140

Solar flares of 25-27 February 1969 effects on polar cap and interplanetary space flux rates, confirming magnetospheric modulation of proton density peaks
06 p0958 A71-18151

Solar proton event on 9 June 1968 observed at polar caps by ESRO 2 satellite, noting flux profile structure
06 p0958 A71-18154

Magnetospheric electric fields properties via simultaneous balloon flights between plasmapause and polar cap, indicating fields and bulk plasma flow turbulence
08 p1282 A71-21632

Light ion flow from polar caps in hydrodynamic and evaporative forms, noting pressure gradient force, exospheric electric field and realistic boundary conditions
09 p1440 A71-23459

Mars observations at August 1971 opposition, discussing dark spots, polar cap and darkening, atmosphere, etc
10 p1670 A71-24277

Polar cap as distinct geophysical entity, considering open magnetic field lines for connectedness to interplanetary plasma and particle input to lower latitudes
10 p1600 A71-24308

Polar caps energetic particle environment involving solar flare proton and electron fluxes
10 p1600 A71-24309

Polar cap cosmic radiation intensity measurement for deducing electromagnetic conditions near earth and in interplanetary space
10 p1661 A71-24310

Polar cap atomic processes stimulated by photons, electrons and protons, considering particle morphology
10 p1661 A71-24311

Polar cap lower ionosphere mapping by solar and magnetospheric charged particles, considering disturbances in polar regions
10 p1661 A71-24312

Solar particle effects on polar cap VLF radio propagation along polar and transpolar paths, considering short term phase effects
10 p1577 A71-24313

Polar caps magnetic field variations, considering relationship to auroral phenomenon and ionospheric conductivity variations
10 p1600 A71-24314

Low energy precipitating auroral particle fluxes over magnetic poles delineating polar cap, noting electron precipitated flux
14 p2299 A71-30030

Low energy electron precipitation effects on upper atmosphere based on polar cap and auroral oval electron spectrum comparison
14 p2300 A71-30035

Spread F ionospheric electron density irregularities and satellite scintillation over polar cap
14 p2300 A71-30043

Night sky optical emissions morphology and behavior in polar regions with emphasis on polar caps
14 p2234 A71-30045

QSY data analysis of pulse reflection measurements from midlatitude station, determining polar cap and auroral absorption
15 p2396 A71-31611

Electron and proton precipitation observations in auroral, polar cap and outer radiation zones by electrostatic analyzers on earth satellite Injun 5
15 p2397 A71-31756

Thermospheric convective instability as interpretation of north polar cap high speed winds observed by satellite at 200 km altitude during magnetic storm of May 1967
16 p2572 A71-33847

Solar protons penetration over polar cap during 25 February 1969 event from particle and magnetic field measurements inside and outside magnetosphere by satellites
16 p2628 A71-33934

Energetic solar protons asymmetric access to north south polar caps by satellite observation during 24 January 1969 event
16 p2628 A71-33935

Energetic electrons, protons and alpha particle measurements by Azur satellite over polar cap and in radiation belt during March 1970 solar particle event
19 p3126 A71-37419

Annual heat balance in Martian northern polar cap, considering atmospheric, ground and solar heat flux absorbed by snow
20 p3290 A71-39309

Solar proton enhancement over auroral zone observed aboard near earth polar orbiting ESRO 2 satellite
20 p3282 A71-39735

Auroral morphology, covering static and dynamic ovals, polar cap and dayside auroras, auroral zones, substorms and electron precipitation
20 p3227 A71-39838

Polar cap magnetic variation mechanism based on electric field aligned continuity of Hall current auroral electrojets, noting ionospheric electron density gradients effects
20 p3230 A71-39862

Polar cap electric field and relationship to magnetic disturbances from measurements on Ba ion clouds released by rockets
20 p3230 A71-39883

Martian polar caps heat balance, noting albedo differences due to irregularities in solid carbon dioxide cover
22 p3603 A71-42190

Localized abnormal geomagnetic disturbance near polar cap and simultaneous ionospheric variation during auroral zone weak magnetic activity periods
22 p3536 A71-42625

Low energy particle plasma sheet and convection electric field distributions over auroral zones and polar caps from satellite Injun 5 observation
23 p3669 A71-43168

Precipitation measurements in polar cap electron aurora, discussing neutral point entry, acceleration mechanisms, flux, pitch angle and magnetospheric models
23 p3669 A71-43169

Mars physicochemistry, discussing Wright effect (blue veil), atmosphere, polar cap migration, Phobos acceleration and relief inversion darkening
23 p3736 A71-43360

Mars telescopic observations, emphasizing south polar cap prominences around edge
24 p3872 A71-44999

POLAR COORDINATES

Numerical integration for continuously thrusting spacecraft optimal trajectory, considering rectangular Cartesian and polar cylindrical coordinates characteristics
07 p1191 A71-18891

Singularities in linear elliptic partial differential equations, considering Cartesian and cylindrical polar coordinate problems
15 p2440 A71-31348

Frequency response of nonlinear feedback control systems, using modified polar plot of open loop transfer function
20 p3208 A71-39914

Sturm-Liouville type nonlinear problems solution by Prufer polar coordinate technique, proving equivalency theorem for eigenvalues infinite sequence conversion
22 p3567 A71-42689

Theta /north-south/ component in spherical polar coordinates of interplanetary magnetic field from Explorer 33 and 35 measurements
23 p3734 A71-43155

Governing equations numerical integration for Venusian atmosphere circulation, calculating solar heating distribution in spherical polar coordinates
23 p3735 A71-43340

POLAR GASES

Exponential approximation of rotational relaxation of polar HCl and DCl at 300 and 500 K by molecular dynamics, comparing with perturbation calculations
15 p2451 A71-31673

POLAR IONOSPHERE BEACON

U BEACON SATELLITES

POLAR METEOROLOGY

Commercial aviation stratospheric water vapor injections influence on radiation budget, ozone, polar night cloudiness and potential climatic effects
08 p2186 A71-21822

Nighttime polar atmospheric structure and temperature variations due to gas kinetic and electron energy changes
19 p3056 A71-38361

Polar mesosphere internal gravity waves generation and propagation, using temperature and wind profiles from rocket granade method
20 p3221 A71-39693

Magnetosphere-ionosphere electric coupling for polar magnetic disturbances and auroral break-up origin, discussing thermal particles precipitation due to transient electric field
21 p3375 A71-41354

POLAR ORBITS

Gyroscopic precession effects in earth polar orbital satellite experiments for Einstein general relativity tests
02 p0312 A71-12369

Ionospheric electron mean content by polar satellites, using combination of Doppler differential and Faraday rotation hybrid methods
07 p1206 A71-19032

Meteorological satellites remote sensing advanced instruments and techniques, discussing retrograde polar and synchronous satellite orbits
08 p3666 A71-21744

German low attitude polar orbiting research satellite AZUR orbital characteristics and bearing on auroral zone substorm phenomena
12 p1899 A71-26833

Lunar exploration system based on modified earth-orbit space station in polar lunar orbit as remote sensor platform and lander deployment base
18 p2972 A71-36443

Dynamic derivation of surface layer representation of lunar gravitational field from Doppler observations on polar and equatorial lunar orbiters
21 p3449 A71-40643

Probe for circular polar Mercury orbit, obtaining missions values
22 p3600 A71-42010

POLAR REGIONS

NT ANTARCTIC REGIONS

NT ARCTIC REGIONS

Power spectra and cross spectra of surface pressure variations in polar regions compared to solar emission, noting Antarctic-Arctic relationship
01 p0119 A71-10741

Lyman alpha and O I 1304 A airglow depressions over poles from OGO 4 satellite observations
01 p0076 A71-11503

Polar magnetic substorms perturbation pattern westward motion related to ionospheric current lengthening

01 p0077 A71-11512

Soviet papers on polar ionosphere covering auroras, magnetic activity, ionospheric disturbances during solar activity, auroral radio wave absorption, etc

02 p0241 A71-11756

Visual, photographic and photoelectric observations of polar auroras and hydrogen emission at conjugate points

02 p0242 A71-11757

Diurnal variations of polar aurora-magnetic activities correlation at high latitudes

02 p0242 A71-11758

Nighttime polar aurora zone during IGY and IQSY related to magnetic activity

02 p0242 A71-11759

Regularities of polar auroras and ionospheric disturbances during solar cycle with decreased low energy corpuscular flux

02 p0242 A71-11760

Polar aurora pulsations of 4-12 sec intensity with associated cosmic radio noise absorption, using photometric measurements

02 p0242 A71-11761

Polar region semitransparent sporadic ionospheric layers nighttime temporal and cyclic ionization variations, determining solar activity effects and corpuscular stream densities by ionogram

02 p0243 A71-11767

Polar ionospheric auroral zone ionization, obtaining ion production function for single electron and proton flux

02 p0244 A71-11772

Atmospheric circulation and earth rotational energy contribution to energy release by intense polar auroras, noting ionospheric current subsonic heating and oxygen emission

02 p0244 A71-11909

Polar orbiting satellite observed transient plasma density enhancements relation to geomagnetic activity

03 p0417 A71-14042

Planet Mars polar and equatorial radii optical measurements comparison with radar and Mariner probes occultations results, determining optical ellipticity

03 p0493 A71-14200

Suprathermal electron flux and temperature in 5-200 eV range at high latitude with Explorer 31 potential analyzer

03 p0420 A71-14528

Ionospheric current system in polar E region, using earth surface equivalence model

04 p0584 A71-15547

Polar chorus background hiss generation, investigating VLF wave characteristics responsible for harder electron precipitation from magnetosphere

05 p0743 A71-17004

Average electron density profiles for quiet and disturbed topside ionosphere at high latitudes, tabulating profile numbers

05 p0743 A71-17005

Polar auroras emission bursts at 6300 and 5577 A, noting diurnal variation with electrophotometer

05 p0746 A71-17209

Solar polar magnetic field simultaneous measurements at Crimea and Mount Wilson from magnetographs

06 p0967 A71-17901

F layer absence and nonuniform horizontal electron concentration of nighttime ionosphere at high latitudes, using Alouette 1 sounding

06 p0894 A71-18258

Aurora polaris activity appearance frequency mean annual values cycle curves

07 p1101 A71-19411

Ring currents and polar magnetic substorms during intensive charged particle flux period in nighttime magnetosphere

07 p1101 A71-19414

Polar magnetic disturbances in electrojet, studying Hall conductivity, electric field behavior and auroral ionosphere ionization

07 p1101 A71-19415

Pc 3-4 period range geomagnetic micropulsations simultaneous recordings at Canadian stations spanning auroral and polar regions

07 p1102 A71-19665

High latitude E region plasma irregularities based on wind velocity shear fields

07 p1153 A71-19760

Polar E region equivalent current system, determining height direction and width

08 p1279 A71-21209

Polar substorms electric current systems and magnetic effect below and above ionosphere

08 p1279 A71-21211

Ionospheric radio wave absorption above polar aurora during solar activity minimum, discussing diurnal and annual behavior

09 p1435 A71-22429

Polar ionosphere ion composition measurement by meteorological rocket-borne RF mass spectrometer

09 p1435 A71-22444

High latitude magnetosphere structure, using two dipole model

09 p1437 A71-22665

French Geole spatial system utilization in polar zones, combining satellite with ground beacons, telemetry ground receiving station and computer

10 p1599 A71-23860

Scintillation effects on synchronous satellite signal fading observed through polar ionosphere

10 p1577 A71-24315

Collisionless ion exosphere kinetic and hydrodynamic models comparison for polar wind supersonic flow characteristics

10 p1605 A71-24796

Polar substorm energy from auroral region size and brightness photographic observations, discussing total flux dependence on magnetic field disturbance intensity

10 p1606 A71-24917

DP 2 fluctuations and polar substorm activity morphological distinctions, using worldwide magnetograms

11 p1753 A71-25545

A type red aurora in polar region accompanied by sporadic F 2 layer

11 p1754 A71-25608

High latitude F region electron density irregularity measurements, using rocket-borne impedance probe

11 p1755 A71-25617

Polar H ion plasma escape from ionosphere into magnetospheric tail effect on plasmopause formation, using hydrodynamic approximation

11 p1756 A71-25756

Latitudinal profiles of geomagnetic H and Z components due to return current of auroral zone electrojet during polar substorms

11 p1756 A71-25757

Atmospheric circulation and earth rotational energy contribution to energy release by intense polar auroras, noting ionospheric current subsonic heating and oxygen emission

13 p2058 A71-28196

Polar auroras emission bursts at 6300 and 5577 A, noting diurnal variation with electrophotometer

13 p2060 A71-28264

Polar magnetic disturbances, discussing correlation with interplanetary magnetic field and interaction effects between solar wind and magnetosphere

14 p2231 A71-29907

Polar ionosphere and magnetospheric processes - Conference, Kjeller, Norway, April 1969

14 p2299 A71-30027

High latitude measurements of low energy electron precipitation by Auroral 1 satellite, explaining anomalous high level F region ionization near dark pole

14 p2299 A71-30031

High latitude regions of low energy electron precipitation from OGO 4 satellite auroral particle experiment

14 p2300 A71-30032

LF whistler mode radio noise emissions observations in polar regions with Alouette 2, noting association with energetic particles influx into ionosphere

14 p2300 A71-30036

Suprathermal electron temperature and ion composition as function of geomagnetic latitude in polar ionosphere, using Explorer 31 mass spectrometer measurements

14 p2234 A71-30037

Physical processes and variations in polar F region, discussing solar photoionization, particle ionization, thermal expansion, electric fields, neutral air winds, ion drag, etc

14 p2234 A71-30038

Polar ionospheric plasma transport, predicting ion density profiles from ionospheric processes models consistent with polar wind theory

14 p2234 A71-30039

Supersonic plasma flow effects on neutral hydrogen, helium and charged particle density and velocity profiles in polar ionosphere

14 p2234 A71-30040

Upper F region transpolar plasma distribution from Alouette 1 data, relating results to satellite measurements of magnetospheric low energy charged particles

14 p2234 A71-30041

High latitude upper ionospheric structures and plasma flow in magnetosphere from Alouette/ISIS topside sounders, noting solar UV and particle ionization sources

14 p2234 A71-30042

Diurnal variations of electron number density against height in lower ionosphere over Resolute Bay, relating to solar proton events

14 p2300 A71-30044

Night sky optical emissions morphology and behavior in polar regions with emphasis on polar caps

14 p2234 A71-30045

Electron flux rigidities in polar aurora region, using stratospheric nighttime X ray and cosmic radio noise absorption measurements

14 p2302 A71-30595

Magnetometer network operation during IQSY, establishing Sq variations in polar regions on quiet days and nature of geomagnetic disturbances

15 p2396 A71-31607

Topside ionosphere structure in high latitudes, discussing electron density profile, corpuscular radiation ionizing effects, polar peak and trough

15 p2400 A71-32349

Proton measurements in ring current by OGO-3 satellite compared with geomagnetic field data at low and high latitudes

16 p2626 A71-33663

Upper atmosphere heating at high latitudes, analyzing air density variations from Molniya 1K satellite observations over 2 year period

16 p2565 A71-33740

Northern high latitude electron trapping boundary position diurnal, seasonal and geomagnetic Kp variations based on ESRO 1/Aurora polar satellite observations

16 p2627 A71-33753

Mass spectroscopy of upper atmosphere neutral composition at equatorial, middle and polar latitudes from meteorological rockets

16 p2566 A71-33758

Electron and proton precipitation, studying effects at high latitudes on 2 February 1969 magnetic storm

16 p2627 A71-33795

Neutral atmosphere density profile data from satellite-borne accelerometer experiment, observing gravity waves propagating in north-south direction at high latitudes

16 p2570 A71-33825

Mode conversion and auroral effects observations on polar VLF propagation path, noting seasonal and solar cycle variations

17 p2731 A71-34319

High latitude sudden impulses, calculating transverse hydromagnetic waves propagation from magnetosphere equatorial plane

17 p2733 A71-34777

German monograph on determination of instantaneous position of polar electrojet for rocket launching parameters computation

18 p2911 A71-35920

German monograph on three component magnetometer for position determination of polar electrojet by sounding rocket

18 p2915 A71-35921

Plasma in dayside polar magnetosphere, analyzing Imp 5 and other earth satellites measurements data

19 p3047 A71-37357

Aurora Polaris activity appearance frequency mean annual values cycle curves

19 p3054 A71-37835

Ring currents and polar magnetic substorms during intensive charged particle flux period in nighttime magnetosphere

19 p3054 A71-37838

Polar magnetic disturbances in electrojet, studying Hall conductivity, electric field behavior and auroral ionosphere ionization

19 p3054 A71-37839

Magnetic perturbations in near polar region and morning-night sectors of auroral oval as function of current sources and modulation by universal time

19 p3059 A71-38397

German monograph on electron flux properties in polar atmosphere, discussing pitch angle distribution, energy spectrum and relation to geomagnetic field disturbances

19 p3130 A71-38646

Venusian polar tropopause and cloud layer from IR spectral recording in carbon dioxide band near inferior conjunction for crescent regions

20 p3290 A71-39306

Circadian rhythms of human renal excretions in polar, temperate and equatorial regions

20 p3190 A71-39477

Elemental abundance ratio patterns in microscopic spherules collected from atmosphere and polar snows, comparing to terrestrial and lunar rocks

20 p3298 A71-39638

Low energy electron and proton precipitation pattern in northern polar region, using low orbit satellite-borne spectrometer

20 p3281 A71-39728

High latitude VLF radio emissions rate of occurrence at all magnetic times, noting diurnal variations

20 p3198 A71-39745

Low energy auroral particle measurements from polar satellites, obtaining electron and proton precipitations location, and angular and energy distributions

20 p3228 A71-39847

Radio and optical aurora correlation and control by polar electrojet, using VHF backscatter and geomagnetic recordings

20 p3229 A71-39853

Auroral ELF and VLF emission at high latitudes, discussing chorus and hiss generation regions and noise mechanism

20 p3229 A71-39854

- Infrasonic waves correlation to supersonic auroral motions and polar electrojet during substorm periods
20 p3229 A71-39859
- Polar ionospheric ion density enhancement correlation to low energy electron precipitation from observations by polar satellite
20 p3231 A71-39888
- Broadband electrostatic VLF wave observation in polar magnetosphere by OV3-3 satellite, noting emission power spectra density relationship to frequency
20 p3199 A71-39889
- VLF ion wave instabilities in polar wind based on plasma kinetic theory, comparing with electrostatic wave observation by OV3-3 satellite
20 p3231 A71-39890
- Height variations of Venusian cloud tops at planet equatorial and polar regions
21 p3449 A71-40608
- High latitude auroral particle precipitation patterns and connections to plasma sheet, ring current, cusp and radiation belt sources, using rocket and satellite observations
21 p3439 A71-41179
- Seasonal variations in vertical distribution of ozone at high latitudes, using Murgatroyd model of looped meridional atmospheric circulation
21 p3375 A71-41395
- Interplanetary magnetic sector polarity effects on polar geomagnetic field diurnal variation
22 p3604 A71-42221
- OGO 5 polar cusp observations showing dayside magnetosheath plasma penetration during magnetic storm
23 p3668 A71-43162
- Comparative north and south polar F layer electron density dependence on universal time and latitude, using ionosonde data
23 p3669 A71-43172
- Periodic and isolated /nonperiodic/ ionospheric electron content fluctuations showing noon and midnight peaks and winter increase at high latitudes
23 p3670 A71-43180
- Geophysical data analysis for high latitude negative geomagnetic disturbances revealing geomagnetic pulsations during auroral arcs passage
24 p3823 A71-45037
- POLAR SUBSTORMS**
- Auroral zone X ray events due to electron precipitation, considering relationship to polar magnetic substorms
13 p2119 A71-27797
- Temporal and spatial relations between impulsive Pi bursts near midnight at polar substorms onset and IPDP micropulsation events in afternoon-evening hours
16 p2573 A71-33952
- Large scale traveling ionospheric disturbances at midlatitudes related to polar substorms on statistical basis
16 p2573 A71-33955
- Polar substorms relation to interplanetary magnetic field from IMP 3 satellite magnetic measurements
19 p3132 A71-37396
- Ionospheric model for magnetic perturbation field global distribution during polar magnetic substorm, considering ground level geomagnetic effects from Birkeland and Pedersen currents
20 p3229 A71-39857
- Noon-midnight high latitude proton trapping and precipitation boundary variations associated with polar magnetic substorms observed by ESRO IA satellite
23 p3719 A71-43127
- IGY interplanetary field independent storm sudden commencement triggered magnetospheric polar substorms, indicating sympathetic flare analogy
23 p3668 A71-43164
- Polar electrojet development during polar magnetic substorms, considering current intensification at northern and/or southern borders
23 p3668 A71-43167
- Magnetotail magnetic fluctuation observation during polar magnetic substorms, noting localized character
23 p3669 A71-43178
- Vela 4A and 4B satellite observation of impulsive energetic electron fluxes in distant magnetotail associated with magnetospheric polar substorms
23 p3670 A71-43184
- Geomagnetic bay-like disturbances formation and decay during multiple midlatitude 6300 Å auroral arc after magnetic storm, observing time variation of current system pattern
23 p3672 A71-43981
- POLARIMETERS**
- Artificial Ba clouds resonance radiation, measuring polarization with photoelectric polarimeter
01 p0075 A71-11333
- Automated precision polarimeter for HF-VHF range
04 p0586 A71-14654
- Flare star light polarization parameters measurement, describing polarimeter design
15 p2487 A71-32036

- Homologous solar microwave bursts from different active centers recorded with 7 GHz polarimeter
18 p2957 A71-35964
- Taurus X-1 X ray emission polarization from rocket-borne polarimeter measurements, utilizing incoherent scattering
20 p3302 A71-39921
- Polarimeter for simultaneous determination of Stokes parameters, analyzing electric signal in frequency and phase
22 p3537 A71-41474
- POLARIMETRY**
- Linearly polarized light measurements of solar spectral lines Zeeman effects, describing calibration method based on Fraunhofer lines broadening due to magnetic fields
04 p0642 A71-14903
- Lunar surface polarimetric properties, discussing invariance of polarization curves
06 p0969 A71-17968
- Low elevation polarimetric recordings of 136.44 MHz transmission from Early Bird geostationary satellite
07 p1206 A71-19022
- Soviet lunar surface rocks physical properties ground observation including colorimetry, spectrophotometry and polarimetry
07 p1193 A71-19311
- Polarimetric measurements of solar X-ray flares by Intercoms 1 satellite
08 p1354 A71-21013
- Lunar surface polarimetric properties, discussing grain size effect on normal albedo and polarization maximum degree
10 p1674 A71-24436
- Mars UV polarization and atmospheric opacity measurements, using ground based polarimetric data at near maximum elongation
11 p1825 A71-25709
- Mars atmosphere optical thickness by polarimetric /ground and spacecraft/ observations, considering light areas roughness /smoothness/ factor variation with wavelength
12 p1964 A71-27086
- Venus polarimetric observational data comparison with polarization characteristics of radiation scattered at gamma-distribution particle sizes, determining refractivity and particle radius
12 p1964 A71-27088
- Jupiter circularly polarized visible light measurements, using photoelastic polarimeter
14 p2306 A71-29729
- Saturn polarimetric observation, noting rings polarization Stokes parameters, methane absorption bands and continuous spectrum
15 p2482 A71-31336
- Soviet lunar surface rocks physical properties ground observation including colorimetry, spectrophotometry and polarimetry
15 p2485 A71-31891
- Star EV Lac polarimetric observations during flare, using Cassegrainian reflector
15 p2487 A71-32031
- Polarimetric observations of Venus during 1969 inferior conjunction, showing no evident halo effect due to hexagonal ice crystals
15 p2491 A71-32424
- Lunar surface anomalous brightness during 26 March 1970 photometric and polarimetric observations, discussing possible correlation to solar activity
17 p2797 A71-34183
- Mars atmosphere optical thickness by polarimetric /ground and spacecraft/ observations, considering light areas roughness /smoothness/ factor variation with wavelength
19 p3133 A71-37436
- Venus polarimetric observational data comparison with polarization characteristics of radiation scattered at gamma-distribution particle sizes, determining refractivity and particle radius
19 p3133 A71-37438
- Polarimetric measurements of solar X-ray flares by Intercoms 1 satellite
20 p3280 A71-39593
- Pulse, nebula and wisp component in photometric and polarimetric observations of Crab pulsar
20 p3303 A71-39932
- Comet Bennett 1969i nucleus light polarimetric observations, noting vibration direction
21 p3440 A71-40060
- Astronomical polarimetry at 5 and 10 microns for intensity measurements of IR sources
22 p3545 A71-42147
- Saturn polarimetric observation, noting rings polarization, Stokes parameters, methane absorption bands and continuous spectrum
22 p3606 A71-42611
- POLARISCOPES**
- Biaxial crystals utilization in polarized interferometers, noting Wollaston prisms useful beam aperture and Savart polariscopes streak linearity domain
07 p1109 A71-19453

- Photoelastic stress analysis, examining light transformations in plane and circular polariscopes by light ellipse method
14 p2323 A71-29848
- Dynamic polariscopes for birefringent materials stress wave low cost analysis
18 p2923 A71-36611
- POLARITY**
- Solar magnetic field polarity mapping from H-alpha filtergrams, using magnetic configurations in flare location and time forecasting
02 p0316 A71-12696
- Photospheric and interplanetary magnetic field polarity and magnitude comparison, using Explorer observations
05 p0802 A71-16012
- Polarity pattern of interplanetary magnetic field near solar maximum, using poloidal model
05 p0803 A71-16017
- Electric currents in undisturbed magnetospheric tail, discussing interplanetary magnetic field polarity effect and neutral sheet characteristics
08 p1280 A71-21214
- Related solar active regions during 14 January-1 June 1969, associating largest flares with inverted polarity
22 p3597 A71-41460
- Interplanetary magnetic sector polarity effects on polar geomagnetic field diurnal variation
22 p3604 A71-42221
- POLARIZATION [CHARGE SEPARATION]**
- NT DIELECTRIC POLARIZATION**
- NT ELECTROLYTIC POLARIZATION**
- Polarization influence on transition effect behavior in avalanche transition between media, discussing critical energies
03 p0478 A71-13869
- Spontaneous polarization measurement of ferroelectric Rochelle salt near Curie point, using nuclear magnetic resonance for phase transitions
04 p0637 A71-15548
- Potentiokinetic study of anodic polarization in maraging Fe alloys, considering relationship to structural transformations during tempering
05 p0765 A71-16200
- Al electrodes in molten salt electrolytes, investigating electrochemical kinetics by polarization measurements
08 p1250 A71-21470
- Electrochemical polarization effects on Ni single crystals mechanical behavior under tensile deformation
08 p1310 A71-21539
- Reaction dynamics for CO ion plus deuterium to yield COD ion plus D, noting polarization forces role
09 p1497 A71-22702
- Ionospheric drift mechanism in midlatitude F region, discussing ground level magnetic field, E region side effects, horizontal winds and polarization fields
11 p1753 A71-25550
- Neutral winds produced vertical ion drift toward electric polarization in equatorial F region, discussing field discharge through E region and atmospheric superrotation effects
12 p1900 A71-26890
- Ionospheric currents due to electric polarization field transfer from magnetosphere under quiet and disturbed conditions, using Ba ion cloud and geomagnetic measurements
14 p2230 A71-29715
- Charge generating mechanism based on charge separation from falling precipitation particles effect on thunderstorm electrification
14 p2269 A71-29951
- Na and K transition oscillator strengths, noting core polarization effects on mathematical model
16 p2615 A71-34088
- Signal waves amplifier in medium of high nonlinear electric polarization, considering reflected waves effect on amplification
16 p2544 A71-34131
- Moving plasma beam capture by transverse magnetic field due to polarization space charges electrostatic separation
17 p2786 A71-34280
- Plasma beams injection into toroidal magnetic field along gradient or radius, using polarizational interaction
17 p2786 A71-34281
- Composite piezoelectric transducer subjected to current flow in semiconducting boundary layer under polarization gradient, determining mechanical response by Laplace transform
17 p2739 A71-34669
- Crevice effect at stress corrosion crack apex during cathodic polarization of Ti-Al-Mo-V alloy in sulfuric acid, potassium bromide and iodide and methanol solutions
17 p2761 A71-35733
- Electric charge generation in storm clouds, considering water droplets, ice crystals and air movements role in precipitation and charge separation mechanism
20 p3256 A71-39071

Potassium photoionization cross section, including spin-orbit interaction, orientation of photoejected electrons and dipole transition moment correction due to core polarization

21 p3417 A71-40197

Polarization influence on transition effect behavior in avalanche transition between media, discussing critical energies

22 p3595 A71-42670

POLARIZATION (SPIN ALIGNMENT)

Excess Knight shift due to spin polarization in electron gas by magnetic impurity Fermi contact coupling as function of distance from nucleus

11 p1801 A71-25373

Optical pumping and detection of spin polarized electrons created in p-type GaSb conduction band by excitation with light

17 p2791 A71-35583

Polarization measurement of cosmic ray muons at sea level as function of energy and zenith angle

19 p3124 A71-37284

Soft galactic X rays role in interstellar grains alignment, taking into account interstellar absorption

19 p3124 A71-37336

POLARIZATION (WAVES)

NT CIRCULAR POLARIZATION

NT ELLIPTICAL POLARIZATION

Moving type IV solar bursts polarization and rapid fadeout, discussing relativistic electrons synchrotron radiation intensity

01 p0152 A71-10331

Classification of electromagnetic wave scattering fluctuating objects from statistical scattering matrices, obtaining incident wave polarization

01 p0038 A71-11208

Diffraction properties of three dimensional asymmetric gratings for reflected and transmitted E-polarized waves

01 p0038 A71-11215

Artificial Ba clouds resonance radiation, measuring polarization with photoelectric polarimeter

01 p0075 A71-11333

Polarization and sky radiance data before, during and after 7 March 1970 solar eclipse

03 p0425 A71-13688

Polarization control of emission from cross-shaped slots on square and circular waveguide walls via phase and amplitude adjustment

03 p0386 A71-13809

Reflected electromagnetic wave polarization parameters, obtaining correlation functions for radar echoes

04 p0557 A71-14632

High red shift quasars linear polarization, examining absorption lines and depolarization due to Faraday rotation

04 p0649 A71-15272

Crab Nebula pulsar pulses polarization using polarimeter feed in Mark I telescope comparison to analysis by integration and photographic recording

04 p0649 A71-15274

Solar corona isophotes ellipticity and equal polarization curves during 7 March 1970 eclipse, using isodensitometric and polarimetric techniques

04 p0651 A71-15666

Plane wave diffraction by double grating of thin circular cylinders, determining field polarization in directions parallel and perpendicular to axis

05 p0718 A71-15995

Angular distribution and polarization of solar X-ray bremsstrahlung, taking into account magnetic field effects

05 p0000 A71-16032

Radar echo signal amplitude probability distribution during fully polarizational reception

05 p0723 A71-16873

Radio wave ionospheric heating effect on absorption of probing waves of different polarization

06 p0888 A71-17289

Pulsar MP 0628 meter wave radiation, noting linear polarization and frequency dependence of pulse rate

06 p0965 A71-17387

High power light beams attenuator usable as polarizing and depolarizing device, describing design for efficiency and elimination of beam shifting

06 p0908 A71-18081

Polarization splitting of EW and NS Alfvén oscillations in axisymmetric magnetosphere

06 p0894 A71-18269

Galactic magnetic field observation, investigating cluster polarization, Zeeman effect, pulsar rotation and signal dispersion, interstellar cloud elongation and models

06 p0972 A71-18331

Pulkovo observatory six channel two slit single photomultiplier rotating photographic plate magnetograph, for solar spectra polarization and radial velocities observation

07 p1109 A71-19337

Geomagnetic quiet field and terrestrial currents diurnal variations, discussing interrelations and vector polarization

07 p1104 A71-20047

UBV colors and polarization models for reflection nebulae based on Mie scattering functions for exponential size distribution of silicate particles

09 p1517 A71-22332

Gravitational field effect on phase difference of moving waves and polarization in rotating ring laser

09 p1462 A71-22398

Average radar backscattering cross section calculation for conducting obstacles for arbitrary transmitter and receiver antenna polarizations, obtaining results for straight wires, circular loops and helices

09 p1410 A71-23516

MHD wave propagation in magnetoplasma perturbed by LF magnetoacoustic waves, considering wave scattering and polarization

09 p1505 A71-23566

Crab Nebula pulsar magnetic field structure, discussing linear polarization modifications and wisps

10 p1668 A71-23870

Polarization distortion of partially polarized wave emission and reception by two channel horn antennas, noting radio astronomy, radar and optics applications

10 p1584 A71-24876

Mars UV polarization and atmospheric opacity measurements, using ground based polarimetric data at near maximum elongation

11 p1825 A71-25709

Longitudinal magnetic field effect on output power, polarization and lasing frequency of He-Ne laser operating at 0.63 micron wavelength

11 p1774 A71-26003

Book on phenomenological theory of radar targets covering wave polarization and antennas, single, statistical independent and distributed targets, decomposition theorems and surface scattering

12 p1877 A71-26568

Time dependent variation of IR polarization of eta Carinae and VY Canis Majoris with separation of interstellar scattering by associated nebula

12 p1956 A71-26611

Interstellar dust, investigating starlight reddening by extinction, galactic light, IR star observations and polarization

12 p1959 A71-26775

E- and H-polarized waves diffraction on three antenna arrays crossing at arbitrary angles

12 p1882 A71-27615

Polarization behavior of radio waves propagating through magnetoionic medium near and across transversal point of magnetic field

13 p2028 A71-27997

Inverted combination light scattering in liquid and solid crystals, showing polarization effects on absorption coefficient

13 p2101 A71-29020

Normal albedo and polarization maximum degree wavelength dependence from terrestrial volcanic pulverized samples

14 p2305 A71-29677

Pulsar MP 0628 meter wave radiation, noting linear polarization and frequency dependence of pulse rate

14 p2310 A71-30166

Oscillations in second cavity of ammonia maser containing two resonators successively traversed by molecular beam, studying polarization and radioelectric emission

14 p2254 A71-30440

Transmission loss measurements at HF over 960 km temperate latitude path for wave polarization calculations and ionospheric absorption estimation

14 p2196 A71-30468

Antenna and radome constructions/shape effects on minimizing cross polarization produced by flat, cylindrical, conical and paraboloidal randoms in linear and circular beams

14 p2216 A71-31039

Coaxial plasma beam polarization interaction in toroidal magnetic field with diverter, showing axial stream trapping in hollow plasma cylinder

15 p2453 A71-31244

Telemetry polarization diversity combiners for data dropout elimination, considering input signal characteristics and propagation

15 p2370 A71-31642

Mu, VV, ST and RW Cephei cold supergiants polarization data, noting spectral dependence

15 p2487 A71-32030

Laser light pulses in anisotropic crystal, investigating nonlinear thermal rotation of polarization plane

16 p2587 A71-33570

Faraday rotation of satellite signals across transverse region, considering sudden jumps at transverse point in lower and topside ionosphere

16 p2544 A71-33959

Classification reliability of electromagnetic wave scattering fluctuating objects from statistical scattering matrices, obtaining incident wave polarization

17 p2698 A71-34260

Measuring apparatus for envelope distortion of transmitted high-energy transversely polarized pulses through ionizable or partially ionized gas

18 p2952 A71-36589

Polarization direction finder determining electromagnetic waves azimuth on basis of field intensity vectors

19 p3014 A71-37074

VLF wave excitation, noting ratios between vertically and horizontally polarized sources

19 p3024 A71-38613

Flow patterns on Poincare sphere as aid to qualitative study of polarization and intensity of quasi-stationary laser mode in anisotropic resonator

20 p3243 A71-39095

Electro-optic mode locking of dual polarization carbon dioxide laser using intracavity birefringence modulation

20 p3244 A71-39096

Polarization flip with hysteresis effect at zero magnetic field in CW far IR HCN laser

20 p3244 A71-39098

Linear polarization of pulsar PSR 22 18 plus 47 radio emission pulses, attributing periodic fine structure of spectrum to rotation of polarization plane in interstellar medium

20 p3291 A71-39316

Structure and polarization differences of strong pulses from pulsar NP 0532, showing discontinuous frequency spectrum

20 p3302 A71-39926

Polarization characteristics of pulsars, considering angular position changes due to interstellar magnetic field using Faraday rotation measurements

20 p3303 A71-39935

Limiting polarization of radio waves emerging obliquely from ionosphere into free space, describing numerical integration method and boundary conditions

21 p3348 A71-40525

UK 5 spacecraft experiments in X ray astronomy, investigating spatial distribution and energy spectra of emissions in space, polarization and pulsar periodicities

22 p3610 A71-42015

Reflected electromagnetic wave polarization parameters, obtaining correlation functions for radar echoes

22 p3510 A71-42272

Wave polarization and midpath ground reflection effects on power loss of two hop radio signal propagation through ionosphere

22 p3511 A71-42280

Plane wave diffraction by double grating of thin circular cylinders, determining field polarization in directions parallel and perpendicular to axis

22 p3515 A71-42744

Polarized solar radio emission at millimeter wavelength in active regions associated with sunspot magnetic fields

23 p3733 A71-43125

Pulsar radio pulse shape and structure, discussing pulse widths and polarization angle change

23 p3769 A71-43989

Transmission coefficient calculations for infinite grating of conducting circular cylinders, considering parallel and perpendicular polarizations

23 p3655 A71-44170

Plane electromagnetic wave diffraction on dense periodic array at conducting screen, showing far field asymptotic behavior for E and H polarization

23 p3647 A71-44331

POLARIZATION CHARACTERISTICS

Kamchatka volcanic mantles and lunar surface radiation polarization characteristics similarities

01 p0149 A71-10049

Ap-type magnetic stars wavelength dependent polarization, discussing polarimetric observations in different spectrum regions

01 p0153 A71-10355

Polarization structure of paraboloid mirror antennas circular emission by geometrical diffraction theory of spherical edge waves

01 p0056 A71-11204

Stationary waves produced by earth bow shock, calculating cyclotron radiation amplitude and polarization characteristics by thin current sheet model

01 p0075 A71-11490

Modified Fesenkov method for calculating Stokes polarization parameters applied to elliptical polarization observations of nebulae

02 p0251 A71-12361

Precision measurement of satellite microwave flux and polarization at ground, involving Skyenet tests

02 p0218 A71-12444

Antenna array radar reflector for simulating objects with given polarization characteristics during radar equipment tuning and calibrating

02 p0233 A71-12634

Polarization characteristics of dual rod ruby laser emission, determining phase coincidence and energy output

03 p0434 A71-13503

Single mode polarization in simple gas laser for long path difference Michelson interferometry

03 p0436 A71-13653

Oppositely polarized maximal magnetic field strengths in sunspot regions during proton flares

03 p0478 A71-13937

Polarization of spontaneous emission in Zn-doped GaAs p-n junctions as function of electric field strength 03 p0467 A71-13985

Zodiacal light theoretical models, considering interplanetary particles optics, Mie theory and multicolor polarization 03 p0491 A71-14011

Vestibular sensory epithelial cells form and organization, discussing morphological polarization 04 p0536 A71-14760

Electrical polarization of vacuum around rotating magnetic Newtonian star, evaluating electrostatic potential 04 p0643 A71-14912

Average radar cross section relative values for echoes from rain, considering horizontal, vertical and circular polarization in various sea states 04 p0551 A71-15008

Mars and Mercury polarization measurements, investigating Rayleigh scattering in atmospheres 05 p0806 A71-16204

Carbon dioxide laser gyro with cavity configuration for polarization isotropy and enhanced competition effects, considering high gain and mechanical imperfection tolerance 05 p0761 A71-16272

Pc 1 micropulsation source region relation to plasmopause, using amplitude and polarization measurements 06 p0964 A71-17263

Lunar surface polarimetric properties, discussing invariance of polarization curves 06 p0969 A71-17968

Diurnal variations in polarization axis direction of Pc 1 pulsations 06 p0895 A71-18282

Pulverized volcanogenic products and chemicals polarizing properties determination, applying to lunar surface layer 07 p1107 A71-19201

Magnetic hologram reconstruction process, discussing diffracted field, polarization properties and efficiency [IEEE PAPER 8.2] 07 p1112 A71-19610

Electron and proton whistlers polarization reversal and mode coupling, explaining magnetic latitude dependence 07 p1062 A71-19667

Radiation transport equations for stellar atmosphere model with variable depth magnetic field, considering absorption line formation and polarization characteristics 07 p1205 A71-20637

Kamchatka volcanic mantles and lunar surface radiation polarization characteristics similarities 08 p1361 A71-21043

Fluoride overcoated Al reflectance measurements and polarization effects at various angles of incidence, noting utilization in vacuum UV instrumentation 08 p1335 A71-21381

Statistical analysis of center-limb variations of intensity, spectrum and polarization of solar microwave impulsive bursts 08 p1364 A71-21419

Polarization characteristics of 42 MHz oblique backscatter from breakup auroras 08 p1272 A71-21639

Magnetic recording device for defect field recording by ferromagnetic tape polarization 08 p1273 A71-21900

Polarization of LF oscillation branch of uniaxial ferrites in noncollinear phases analyzed by four column matrix, considering magnetic moments terminal points 09 p1507 A71-22291

Statistical properties of radio communication system polarization reception coefficient as function of receiving antenna and signal polarization characteristics 09 p1405 A71-22294

Ring laser active medium polarization characteristics in strong field, taking into account spatial modulation of population 09 p1461 A71-22365

Polarization of short period oscillations Pc2-Pc4 dependence on time of day, oscillation type and geoelectromagnetic field activity 09 p1436 A71-22449

Far field diffraction pattern of corner reflector for normally incident monochromatic light, considering polarization characteristics 10 p1640 A71-23947

Lunar surface electromagnetic sounding, presenting analysis of radiation fields and polarization characteristics for magnetic dipole situated on layered half space 10 p1576 A71-24054

Single-mode He-Ne laser, investigating longitudinal magnetic field effect on output amplitude, frequency and polarization characteristics 10 p1620 A71-24343

Lunar surface polarimetric properties, discussing grain size effect on normal albedo and polarization maximum degree 10 p1674 A71-24436

Diffuse interstellar bands polarization and extinction based on silicate and graphite grain composition and sizes 10 p1675 A71-24469

IR polarization of Venus, providing Venus atmosphere effective particle size estimate 10 p1675 A71-24489

Photoelastic materials polarization characteristics analysis using Muller matrix method 12 p1976 A71-27115

Geomagnetic effects on radio signals mechanism in extensive air showers, discussing scintillators array for east-west to north-south ratio polarization measurements 12 p1967 A71-27390

Solar type 3 radio bursts polarization measurement by recording and subsequent digital processing 12 p1969 A71-27653

Solar corona high radial and tangential polarization during 7 March 1970 eclipse from photographs with neutral density filter and rotating linear polaroid sectors 12 p1970 A71-27705

Radiation intensity spatial dependence on laser polarization, giving three dimensional model for wave function phase calculation 13 p2077 A71-28046

Extensive air showers radio wave emission based on cascade theory, determining polarization characteristics 13 p2127 A71-28103

Pi2 geomagnetic micropulsation polarization characteristics, using photoelectric fluxmeters 13 p2060 A71-28268

Cylindrical waveguide with three differential phase shift sections, deriving microwave output magnitude and polarization for comparison with ferrite experiment 13 p2037 A71-28604

Quasars circular polarization measurements at 21 cm, noting synchrotron self absorption 14 p2307 A71-29867

Microwave oscillations small phase difference variation measurement, using polarization effects 14 p2196 A71-30636

Electron gyro and synchrotron radiation from vacuum and isotropic plasma, deriving approximate general formula for power spectrum and polarization 14 p2282 A71-30661

Hydrogen plasma transport in linear magnetic quadrupole field, studying polarization potential and density distribution 14 p2282 A71-30669

Harmonic type 3 solar bursts radioheliographic observations, discussing polarization characteristics 15 p2473 A71-31691

Long period quasi-monochromatic geomagnetic micropulsations amplitude spectra and polarization as function of geomagnetic latitude 15 p2397 A71-31760

Flare star light polarization parameters measurement, describing polarimeter design 15 p2487 A71-32036

Solar corona photometric intensity and polarization measurements during 1970 solar eclipse 16 p2580 A71-33819

Polarization structure of parabolic reflector antennas circular radiation by geometrical diffraction theory of spherical edge waves 17 p2697 A71-34256

Free-free bremsstrahlung emission in anisotropic hot electron plasma in magnetic mirror, measuring polarization by Compton scattering 17 p2788 A71-34853

Pulsar polarization characteristics and pulse profile observations in 250-450 MHz range 17 p2807 A71-35417

Inhomogeneous synchrotron source model calculation for correlation between linear and circular polarization, comparing with quasars observation 18 p2963 A71-36157

Telescopic phase retardation effect on polarization in Zeeman split Fraunhofer line, discussing consequence for solar magnetic field determination 18 p2965 A71-36732

Polarization characteristics of solar coude telescope and Littrow spectrograph at Okayama Astrophysical Laboratory 19 p3062 A71-37241

Brightness and polarization of solar corona at total eclipse on 12 November 1966 from polarographic observations 19 p3131 A71-37243

Neodymium-glass lasers active elements thermal-stress-induced birefringence effects on energetic and polarization characteristics 19 p3072 A71-37767

Comet Bennett 1969 head and tail polarization distribution data, using triple astrophotograph 19 p3145 A71-38524

Broadband antenna twist reflector with wire grids, deriving design formulas and theoretical performance in terms of polarization attenuation 19 p3036 A71-38606

Atomic level interference and hyperfine splitting effects on angular and polarization distributions of resonantly scattered light in magnetic field 21 p3420 A71-41120

Polarization and pulse profiles of pulsars at 410 and 1665 MHz, indicating radiation originating close to star surface 21 p3453 A71-41244

Broadband helical antenna feeds for millimeter wave parabolic reflectors and lenses, determining beamwidths and polarizations as functions of helix parameters and frequency 21 p3359 A71-41408

Photoelectric polarization curve, reflectivity and absolute diameter of Vesta, comparing with Lyot curve 22 p3602 A71-42177

Linearly and circularly polarized electromagnetic field effective scattering surfaces relationships determination as value proportional to reflected and transmitted rms flux density ratio 23 p3644 A71-43285

Polarization characteristics, albedos and optical properties of Apollo 11 and 12 rocks, investigating wavelength dependence and proton irradiation effect 23 p3761 A71-43779

Type 3 solar radio bursts polarization characteristics distribution, determining Faraday rotation dispersion effect by trial and error technique 23 p3768 A71-43850

Mode changing in pulsar radiation, observing intensity profiles and polarization characteristics 23 p3769 A71-43995

Log spiral antenna with selectable polarization, showing electric field radiation patterns 23 p3654 A71-44165

Polarization transforming feed horns for rapid scan X-band radar antenna, allowing transmission in various polarization modes and parallel and orthogonal polarized return reception 23 p3655 A71-44167

POLARIZATION CHARTS

U GRAPHS [CHARTS]

U POLARIZATION [WAVES]

POLARIZED ELECTROMAGNETIC RADIATION

NT POLARIZED LIGHT

NT SYNCHROTRON RADIATION

High luminosity red variable star radiation, examining degrees of intrinsic polarization 01 p0150 A71-10056

Oblique reflection of horizontally and vertically polarized electromagnetic waves from isotropic media with limiting Epstein stratifications 01 p0031 A71-10775

Short wave signal polarization fading minimization by dispersed reception of circularly polarized components, discussing power gain relation to antenna configuration 02 p0219 A71-12543

Spatial distribution and polarization of radio emission from extensive air showers, using Geiger and scintillation counters, muon detectors and antennae 03 p0477 A71-13865

Field of determinate signal with normal noise, considering representation as superposition of two circularly polarized components of directly opposite rotation 05 p0719 A71-16010

Solar disk computed continuum and estimated line polarizations compared to BCA photosphere values, discussing metal abundances 05 p0803 A71-16019

Pulsar 150 MHz radiation linear polarization measurements, correlating interstellar Faraday rotation with determinations from neighboring extragalactic radio sources 06 p0971 A71-18242

Linearly polarized CW signal transmission through near solar corona, measuring Faraday rotation 07 p1191 A71-19030

Polarization of thunderstorm IF electromagnetic noise, taking into account earth electrical conductivity under detector 07 p1063 A71-19758

Obliquely incident p-polarized plane electromagnetic wave interaction with hot plasma half space, using linearized relativistic Vlasov equation and Laplace transform technique 07 p1171 A71-20292

Functional method application to ultrarelativistic particles in external fields quantum electrodynamics, discussing electromagnetic field superposition 07 p1162 A71-20549

Horizontally and vertically polarized sferic signals from lightning discharges by airborne instrumentation, using pattern recognition approach 08 p1325 A71-20883

Plane electromagnetic wave scattering, arbitrarily polarized and normally impinging on wedge tapered absorbing structure 09 p1409 A71-23501

Air showers emitted radio pulses polarization, noting inconsistency with geomagnetic origin 13 p2127 A71-28102

Frequency composition in glass laser with Fabry-Perot resonator producing polarized radiation components, discussing transverse modes selection 15 p2420 A71-32000

Diffraction properties of three dimensional asymmetric arrays for reflected and transmitted H- and E-polarized waves 17 p2698 A71-34266

Free space diffraction of E-polarized plane electromagnetic wave by slit in thick conducting screen, deriving approximate solution from Wiener Hopf equation by matrix techniques 19 p3023 A71-38592

Electromagnetic wave arbitrary incidence on conducting circular disk for polarization parallel and perpendicular to incidence plane, calculating backscattering cross section for comparison with measurement 20 p3194 A71-38840

Polarized plane electromagnetic waves oblique specular reflection from discretely layered lunar models based on Apollo 11 and 12 data, determining near-surface layers electrical properties 21 p3450 A71-40644

Pulsars properties, examining pulse profile and duration, subpulse phase modulation and polarization 22 p3598 A71-41918

Brightness and polarization distributions for supernova remnants IC443 and Puppis A, considering magnetic field orientation and thermal radio emission 22 p3606 A71-42601

Lateral distribution and polarization of radio emission from extensive air showers, using Geiger and scintillation counters, muon detectors and antennae 22 p3595 A71-42666

Deterministic signal with normal noise, considering field representation as superposition of two circularly polarized components of directly opposite rotation 22 p3515 A71-42758

Convolution integral equation unique solution in second kind Fredholm equation form, applying to plane polarized electromagnetic wave diffraction on infinitely thin band 24 p3804 A71-44769

Linearly polarized plane electromagnetic wave scattering by radially inhomogeneous spherical shell, presenting boundary value problems solutions and approximations 24 p3805 A71-45184

POLARIZED LIGHT

Zodiacal light polarized component observation at ecliptic longitudes and latitudes compared to zodiacal cloud model 01 p0158 A71-10773

Matrix method for multiple scattering extended to polarized light 03 p0458 A71-13611

Astronomical objects light polarization recording on magnetic video tape, providing digitized data for computer input 03 p0424 A71-13631

Matrix addressed polarization rotating or retarding light valve arrays for optical selectors, compositors and displays from nonswitching threshold materials 03 p0430 A71-14468

Linearly polarized light measurements of solar spectral lines Zeeman effects, describing calibration method based on Fraunhofer lines broadening due to magnetic fields 04 p0642 A71-14903

Optically thick clouds reflected light radiance and polarization for haze and nimbostratus models 05 p0781 A71-16252

Light attenuation and depolarization measurements on glass fibers in index matching oil 07 p1159 A71-19212

Biaxial crystals utilization in polarized interferometers, noting Wollaston prisms useful beam aperture and Savart polariscopes streak linearity domain 07 p1109 A71-19453

Handedness formula for elliptical polarization after specular metallic reflection of linearly polarized light 07 p1111 A71-19485

Polarized light multiple scattering in planetary atmospheres, applying extended doubling method to realistic simulations with allowance for radiation polarization and azimuth dependence 07 p1153 A71-19759

Magnetic white dwarf G195-19 circularly polarized light, confirming handedness and approximate magnitude 07 p1199 A71-19833

Polarization of sunlight multiply scattered by atmosphere and cloud particles of Venus from UV to IR 07 p1204 A71-20622

Martian atmosphere Mie scattering analysis, using limonite and bulk solid carbon dioxide complex refractivity to interpret polarization effects 11 p1825 A71-25708

Fe ion photodetachment cross section polarization dependence on a sites in YIG-Si to explain photoinduced uniaxial anisotropy, using crystal field theory 12 p1943 A71-26858

Comet Bennett light polarization data, determining color index and chemical composition 12 p1965 A71-27227

Skylight polarization dispersion in relation to multiple scattering in molecular atmosphere 13 p2063 A71-29110

Aerosol power law distribution exponent and particle limiting radii from turbid atmosphere outgoing visible radiation polarization high altitude measurements 13 p2063 A71-29111

Jupiter circularly polarized visible light measurements, using photoelastic polarimeter 14 p2306 A71-29729

Gas laser birefringence observation in active elements under pumping action, using light beam components polarization intensity measurements 14 p2255 A71-30586

Star EV Lac polarimetric observations during flare, using Cassegrainian reflector 15 p2487 A71-32031

Flare star light polarization parameters measurement, describing polarimeter design 15 p2487 A71-32036

Polarized light multiple scattering in homogeneous plane parallel planetary atmospheres, considering Rayleigh scattering, test models and phase function obtained by neglecting polarization 16 p2632 A71-33320

Scattered light circular polarization data from Jupiter and other planets indicating nonmagnetic origin 17 p2805 A71-35377

Doubling method application to multiple scattering of polarized light, studying Venus visible disk reflection of sunlight 17 p2784 A71-35569

Aerosol size distribution from lidar light scattering polarization properties, constructing inversion model 17 p2770 A71-35806

Linearly polarized lidar light scattering in spherically symmetrical uniformly distributed cloud water drops, investigating multiple backscattering effects on depolarization 17 p2770 A71-35807

Comet Bennet light polarization data, determining color index and chemical composition 19 p3132 A71-37379

Wave reconstruction from gaseous flow hologram analysis with differential interferometry in polarized light and schlieren techniques with phase filter defocusing 20 p3239 A71-39461

Comet Bennett 1969i nucleus light polarimetric observations, noting vibration direction 21 p3440 A71-40060

Current-optical effects of anisotropic absorption of polarized and unpolarized light in rarefied cosmic media 24 p3860 A71-45106

POLARIZED RADIATION

NT POLARIZED ELECTROMAGNETIC RADIATION

NT POLARIZED LIGHT

NT SYNCHROTRON RADIATION

Galactic soft X rays role in interstellar dust grains alignment producing starlight polarization 01 p0145 A71-11344

Neodymium glass laser with intracavity emission polarization, determining thermally induced double refraction effect on energy characteristics 03 p0435 A71-13505

Emission kinetics for linearly polarized waves from composite ruby laser, describing pumping power effects 03 p0435 A71-13513

K corona radially and tangentially polarized components color differences from 7 March 1970 eclipse photographs analysis 03 p0489 A71-13628

Pulsar NP 0532 average polarization absence due to Crab Nebula depolarization or unpolarized radiation on emission 04 p0643 A71-15047

Gas laser radiation depolarization coefficient as function of radiation energy, cavity anisotropy and operating transition type 06 p0907 A71-17595

Fraunhofer line resonance polarization from solar spectral bands statistical analysis, noting collisional depolarization 06 p0969 A71-17973

Polarization fluctuations of radio waves reflected from ionosphere E and F layers, describing radio polarimeter and preliminary measurement results 07 p1061 A71-19384

Resonance line radiation polarization of potassium and cesium isotopes excited by electron impact 09 p1496 A71-22187

Polarized radiation transfer in collective plasma, analyzing proper modes phase correlation effects by Liouville equation perturbation technique 10 p1654 A71-24996

Supernova remnant HB 21 linear polarized radiation observed at 6 cm wavelength, correlating optical nebula shape with radio mapped contours 11 p1819 A71-25216

Extragalactic radio sources total and linearly polarized radiation one dimensional distributions, not-

ing spectral variations, magnetic fields and rotation measurements 11 p1830 A71-26131

Water and ice cloud discrimination by angular distribution measurement of various polarization parameters of scattered laser beam radiation, using Mie theory 11 p1776 A71-26298

Polarization Fourier spectrometer for circular dichroism spectroscopy, stressing IR application 14 p2242 A71-30156

Omnidirectional broadband telemetry antenna array for spacecraft providing near isotropic circular polarized radiation with open line microstrip feed 14 p2199 A71-30907

Semiinfinite atmospheric multiple conservative Rayleigh scattering, describing polarized radiation transfer 15 p2449 A71-31333

Polarized meandering type 4 burst of solar flare from 80 MHz radioheliographic observations, noting association with plasmoids containing synchrotron emitting relativistic electrons 15 p2473 A71-31695

Rayleigh scattering planetary atmosphere radiative transfer equation, calculating phase curves for flux and polarization 15 p2498 A71-32778

Outer corona polarization determination from airborne photographic observations in March solar eclipse, presenting preliminary results of photometric data reduction 16 p2642 A71-33803

Time dependent multiple backscattering of pulsed light for linearly polarized incident radiation 17 p2709 A71-35809

Polarized solar millimeter emission associated with sunspot magnetic field compatible with multiple sources from chromosphere 18 p2966 A71-36762

Polarization fluctuations of radio waves reflected from ionosphere E and F layers, describing radio polarimeter and preliminary measurement results 19 p3017 A71-37809

Taurus X-1 X ray emission polarization from rocket-borne polarimeter measurements, utilizing incoherent scattering 20 p3302 A71-39921

Extragalactic radio sources polarized radiation intensity statistical analysis, calculating magnetic field scale 22 p3602 A71-42175

Semiinfinite atmospheric multiple conservative Rayleigh scattering, describing polarized radiation transfer 22 p3576 A71-42608

Mode changing in pulsar radiation, observing intensity profiles and polarization characteristics 23 p3769 A71-43995

POLARIZERS

Commercially produced metallic wire gratings reflection spectra measurement, determining use as high performance filters and light polarizers in far IR region 03 p0457 A71-13507

Photometric attenuator with linear birefringent polarizers, describing construction and calibration 07 p1110 A71-19468

Freestanding wire grid manufacture of polarizing films for submillimeter interferometry 08 p1291 A71-21405

High voltage pulse shaping circuits for Kerr cell polarization shifters for modulating and deflecting monochromatic laser radiation 19 p3071 A71-37255

POLAROGRAPHS

U POLAROGRAPHY

POLAROGRAPHY

Polarographic blood oxygen measurement by principle of oxygen liberation into physical solution by potassium ferricyanide 07 p1053 A71-20337

Oscillopolarographic determination conditions for Co, Ni, and Fe, giving statistical treatment of results 09 p1454 A71-22501

Polarographic measurements of secondary Couette flow between coaxial cylinders for diffusion coefficient effects on mean friction factor, using wall flush microelectrodes 10 p1592 A71-23978

Rhodamine, sodium fluorescein and cyanocyanine dyes for liquid lasers, investigating electroluminescence by polarography 16 p2587 A71-33382

POLARONS

Two center bound polaron in rutile single crystal, studying dielectric behavior in applied magnetic field 08 p1345 A71-21690

Nonlinear optics of combination scattering of IR laser radiation in crystals and statistical frequency mixing-multiplication of polarons and longitudinal phonons 16 p2588 A71-33997

POLES

- Astronomically determined latitude, longitude and azimuth reduction to common epoch, discussing secular nonperiodic pole motion due to crust drift
03 p0484 A71-13217
- Poling techniques modifications for piezoelectric activity enhancement in bulk polymers, considering arcing minimization, AC field superimposition and repeated cycling of process
03 p0448 A71-13721

POLICIES

- Sonic boom implications and decision on acceptability with alternative policies of complete barring, controlled corridors and overflight limitations [CASI PAPER 72/4]
19 p2996 A71-37595

POLISHED METALS

U METAL POLISHING

POLISHING

NT ELECTROPOLISHING

NT METAL POLISHING

- Polished surface quality control using laser divergent coherent beam
09 p1460 A71-22310

- Milling, band grinding, final manual polishing and tumbler polishing effect on fatigue life and surface finish of steel compressor blades
12 p1912 A71-27680

- Peroxide-alkaline polishing solution for GaAs, evaluating optical quality, surface damage, polishing rate and metallic contact resistance
18 p2955 A71-37004

POLITICS

- NASA bilateral and multilateral international cooperation agreements in space research, discussing political objectives, program history, regulations and procedures
06 p1010 A71-17646

- Aerospace business future, discussing political, military and social factors effect
17 p2841 A71-34575

POLLUTANTS

U CONTAMINANTS

POLLUTION

NT AIR POLLUTION

NT ENVIRONMENT POLLUTION

NT THERMAL POLLUTION

NT WATER POLLUTION

- Everyday antipollution policy in electromagnetic compatibility, concerning social, medical, commercial, industrial, scientific and national defense aspects
19 p3021 A71-38431

- Low cost Ti substitutions for Ni and alloys in corrosion resistant applications, prosthetic devices and pollution control equipment
20 p3251 A71-39339

POLONIUM

NT POLONIUM 210

POLONIUM ISOTOPES

NT POLONIUM 210

POLONIUM 210

- Alpha radioactivity in Surveyor 3 camera visor, calculating upper limit of Po 210 at equilibrium of Oceanus Procellarum
23 p3765 A71-43812

POLYACRYLATES

U ACRYLIC RESINS

POLYAMIDE RESINS

NT NYLON [TRADEMARK]

- Low temperature curing nylon epoxy adhesive, discussing high peel strengths
10 p1630 A71-24070

- Fatigue failure of polyamide filaments from optical and electron microscopic observations, describing crack initiation and propagation
16 p2600 A71-32817

- Polyamides reinforced with finely chopped glass fiber, noting mechanical strength, Martens yield temperature and heat stability
19 p3085 A71-38476

POLYATOMIC GASES

NT DIATOMIC GASES

- Kinetic equation for rarefied polyatomic gases derived from Liouville equation
02 p0286 A71-11883

- Polyatomic gases thermal conductivity coefficient, examining magnetic field effect
06 p1005 A71-17316

- Soviet book on thermal conductivity of monatomic and polyatomic gases and hot and cold mixtures, comparing molecular kinetic theory collision integral formulas with experimental data
08 p1375 A71-21656

- Classical polyatomic gases kinetic theory, considering generalized Boltzmann equation solution
16 p2614 A71-33031

- Carbon dioxide laser population inversion based on chemical combustion reaction producing gas of vibrationally excited polyatomic molecules
16 p2585 A71-33047

- Polyatomic gases thermal conductivity and rotational relaxation number from thermomolecular pressure differences across capillary tubes
17 p2785 A71-34946

- Macroscopic values of energy exchange between polyatomic gas and solid wall, considering heat transfer rate and wall temperature change
23 p3781 A71-43105

- Conductive heat transfer and temperature jump in polyatomic gas between parallel plates evaluated by variational principle based on linearized integro-differential equation
24 p3889 A71-44969

POLYATOMIC MOLECULES

NT DIATOMIC MOLECULES

NT TRIATOMIC MOLECULES

- Interstellar medium polyatomic molecules formation, destruction and excitation processes by astronomical spectroscopy and interferometry
02 p0209 A71-11867

- Multiatomic molecules emission spectra excitation by superhigh frequency short duration pulsed gas discharges
02 p0286 A71-11889

- Polyatomic organic adsorbates effect on field emission total energy distribution from W and Mo surfaces, discussing electronic and phononic spectra
02 p0297 A71-12733

- Absorption gas dynamic laser operation based on polyatomic molecules vibrational relaxation process
13 p2081 A71-29347

- Polyatomic molecule photoelectron spectroscopy, emphasizing spectra interpretation by quantum mechanical procedures
16 p2541 A71-33398

- Chemical lasers diatomic and multiatomic molecules dissociation in nonequilibrium conditions, discussing vibrational energy exceeding gas temperature
24 p3834 A71-45112

POLYBENZIMIDAZOLE

- Flammability and heat transfer characteristics of flame retardant cotton, Nomex and polybenzimidazole (PBI) protective fabrics
07 p1145 A71-19573

POLYBUTADIENE

- Low molecular weight liquid polybutadiene polymer flow behavior as function of shear rate, temperature, molecular structure and hydrogen bonding
09 p1403 A71-22474

- Crystallites in hydrogenated hydroxy terminated polybutadiene from polarized light examination, viscosity-temperature curve discontinuity and elastomer modulus-temperature curve
10 p1573 A71-25126

- Electrical properties, chemical resistance and reinforced plastics applications of telechelic ultrahigh vinyl polybutadiene resins
11 p1786 A71-25422

- Solid propellants based on low cost hydroxyl terminated polybutadiene binders meeting burning rate, mechanical properties and processing requirements for large booster motors [AIAA PAPER 71-708]
14 p2286 A71-30764

POLYCARBONATES

NT LEXAN [TRADEMARK]

- Prolonged storage effect on polycarbonates mechanical properties, measuring tensile strength, elastic modulus, yield point and breakdown strains under uniaxial tension
09 p1483 A71-22825

- Polycarbonates transparency applications in aircraft windshield design, discussing heat resistance, mechanical, chemical and optical properties
20 p3253 A71-38751

POLYCRYSTALS

- Polycrystalline semiconductors Hall effect by grain structure model for low and high resistivity boundaries, giving vapor deposited cadmium selenide film data
01 p0137 A71-10283

- Polycrystalline material nonisothermal plastic deformation, using model based on metals and alloys properties and microstructure
02 p0324 A71-11749

- Homogeneous and composite polycrystalline materials macroscopic thermoelastic characteristics determination based on structural model
02 p0324 A71-11750

- Anisotropic polycrystalline carbon fiber tensile strength and bending behavior, interpreting inelastic characteristics from single filament experiments
02 p0273 A71-11945

- Creep failure model, using wedge crack nucleation in polycrystalline materials due to grain boundary sliding
02 p0329 A71-12716

- Polycrystalline Zr extremely low temperature tensile deformation, discussing prestraining effects, stress-displacement relations, strain distribution, twinning, etc
02 p0267 A71-12878

- Polycrystalline Ni single and overlapping stacking faults production by tensile deformation in premicroyield region, noting stress concentration effects
02 p0268 A71-12888

- Rare earth polycrystalline powders luminescence stimulation by ruby laser radiation, discussing two

- photon mechanism, luminous intensities relations and UV radiation
03 p0435 A71-13510

- Grain boundary sliding on Mg-Al alloy polycrystalline specimens measured at successive strains during creep under 2800 psi stress
03 p0443 A71-14184

- Submicron sectioning apparatus for studying slow carbon self diffusion in dense polycrystalline tungsten carbide
03 p0429 A71-14187

- Temperature effect on slip- and spark-induced crack propagation in polycrystalline Mo
03 p0444 A71-14317

- Pressure and strain rate effects on polycrystalline Be shear strength, determining activation energy for dislocation motion
03 p0445 A71-14463

- Transport mechanism for holes in polycrystalline Ge films based on Matthiessen rule, considering surface scattering and dislocation
03 p0468 A71-14464

- Intergranular failure modes in polycrystalline metals and alloys, discussing boundary sliding, cracking and structure
03 p0447 A71-14496

- German monograph on polycrystalline ferrites studies with quasi-optical resonators in mm wave range
05 p0791 A71-16125

- Pure polycrystalline Al under uniaxial tension, noting vacancy rupture mechanism
06 p1000 A71-17940

- Polycrystalline semiconductors grain boundaries effect on conductivity, Hall mobility and current carriers concentration
06 p0942 A71-18187

- Structure changes of Al single and polycrystals with initial cube orientation under cold rolling
06 p0913 A71-18420

- Mechanical properties of supersaturated Ni-Al alloys aged at 700 F, discussing composition effects on single crystals deformation and polycrystal strength variation
07 p1133 A71-19442

- Uniaxial elastic stresses effect on ferromagnetic resonance parameters in polycrystalline ferrites
07 p1177 A71-19497

- Hydrogen adsorption behavior on polycrystalline nickel surfaces, using electron impact desorption flash filament with gas phase and ion spectrometer and vapor deposition
07 p1055 A71-19843

- Hydrostatic pressure effects on Al polycrystals stress-strain behavior at room temperature, using magnetostriuctive load cell
07 p1143 A71-20490

- Thermal recovery effects on electrical resistivity in deformed polycrystalline Nb samples tested at varying strain rates and 263-509 R temperatures
07 p1144 A71-20496

- Light transmitting vacuum deposited NaF polycrystal for IR measurements
08 p1343 A71-21288

- GaAs-InAs type single crystals, polycrystals and epitaxial films solid solutions, studying optical, electrical and luminescent properties
08 p1344 A71-21443

- Discrete particles dispersion effects on polycrystals mechanical properties, examining various models
08 p1311 A71-21540

- Polycrystalline Nb under plastic deformation and annealing, examining dislocation structure and mechanical properties
08 p1316 A71-21611

- Ultrasonic effects on dislocations and grain boundaries in vacuum annealed polycrystalline Al specimens
09 p1467 A71-22288

- Spectral and relaxation characteristics in antiStokes two photon luminescence of polycrystalline ruby exposed to filtered light pulses
09 p1508 A71-22392

- Measuring instrument for amorphous and polycrystalline materials resistivity and Seebeck coefficient as function of temperature and pressure
09 p1446 A71-22737

- Metallic polycrystalline materials volume changes in plastic deformation from measurements on steel elongation and cross section diameter reduction
09 p1540 A71-22997

- Discrete phase vs binder strength of inorganic brittle polycrystalline powder metallurgy materials, including alumina and magnesia
09 p1483 A71-23398

- Strain hardening and grain size effects on early fatigue damage of polycrystalline metal under fluctuating stress, using micromechanics theory
10 p1685 A71-23933

- Fiber textures formation in polycrystalline Zr from cold forging and cold drawing, observing fully developed recrystallization
10 p1629 A71-25028

- Carbon and oxygen inclusions effects on polycrystalline molybdenum rupture due to precipitation and chemisorption
11 p1781 A71-26323

Polycrystalline copper and magnetic films thin intermediate layers, showing prevention of epitaxial growth

12 p1943 A71-26855

Industrial polycrystalline graphites monochromatic emissivity in visible and IR spectral regions at high temperatures

13 p2090 A71-27882

Polycrystalline pure Al and Al-Mg alloy strength, investigating temperature and strain rate effects

13 p2084 A71-28112

Elastically and plastically anisotropic single crystals randomly oriented in polycrystalline aggregate, noting initial yield surface in fcc lattice

13 p2155 A71-29063

Polycrystalline Nb cyclic yield point behavior under strain softening and hardening, noting stable hysteresis loop

13 p2087 A71-29123

Polycrystalline Hf under tension at various temperatures, determining H effects on fracture, operative deformation modes and hydride habit planes

13 p2090 A71-29417

Nb single and polycrystalline thermal conductivity/diffusivity, specific heat, electrical resistivity and monochromatic/ integrated degree of blackness at high temperatures

14 p2258 A71-30052

Single crystal and polycrystalline alumina specimens strengthening by annealing with various metal oxide powders

15 p2438 A71-31975

Polycrystalline graphite total creep time dependent effects based on mathematical model of nonlinear hereditary theory

16 p2600 A71-32799

Surface deformation in polycrystalline Al samples produced by ultrasound generated cyclic stresses, examining slip bands formation by electron microscope

16 p2591 A71-33224

Constant load tensile creep tests on polycrystalline ceramics, determining high density alumina applied stress and strain rate

16 p2553 A71-33384

Idealized model for anisotropy of metals inelastic characteristics due to plastic prestraining, demonstrating applicability to polycrystalline materials

16 p2659 A71-33989

Oxygen adsorption study on polycrystalline W through work function variation and adhesion coefficient measurements, using mass spectrometry

18 p2874 A71-35974

LF ferromagnetic resonance in anisotropic polycrystalline thin magnetic films, noting dependence on magnetization inhomogeneity

18 p2955 A71-36940

Gaseous and solid polycrystalline HNCs and DNCs IR and Raman spectra, studying LF of lattice vibrations

19 p3118 A71-37649

Polycrystalline barium titanates solid solutions with fluorine displacement of oxygen atoms, observing IR absorption spectra

20 p3276 A71-39151

Ta-W polycrystals and single crystals oxidation at 850-1100 C, noting anisotropic scale-fracture morphologies

20 p3252 A71-39373

Strain rate and temperature effects on polycrystalline Al-Mg alloy strength, considering deformation mechanism

21 p3400 A71-40834

Grain scattering in unstable spin wave region of parametrically excited magnons in polycrystalline YIG

21 p3428 A71-41047

Longitudinal and transverse magnetostriction of polycrystalline iron garnets containing Gd, Tb, Dy and Ho in high magnetic fields

21 p3428 A71-41116

Prior stressing and thermal treatments effect on shock induced substructures in polycrystalline Mo, using transmission electron microscopy

21 p3404 A71-41416

Metallic polycrystal deformation equations, obtaining creep, Norton law dependences and thermally dissipated energy

22 p3560 A71-41606

Monocrystalline and polycrystalline Ta-Hf oxidation at 750-1050 C, noting orientation

22 p3563 A71-42363

Pure Al annealed polycrystal electron microscopic observation for fatigue deformation at room and elevated temperatures, noting dislocation loop role in crack initiation and propagation

22 p3564 A71-42497

Oxygen interaction with polycrystalline W, calculating sticking probabilities and desorption spectra at various temperatures

23 p3641 A71-42906

Corrosive oxide layer formation kinetics during interaction of oxygen with polycrystalline W at 500-1000 K, using desorption mass spectrometry

23 p3641 A71-42907

Ferromagnetic electron spin resonance spectra of Apollo 11 lunar samples, using model for polycrystalline spectra simulation

23 p3734 A71-43242

Polycrystalline body macrohomogeneous plastic deformation, deriving basic postulates for slippage and plane relationships to tangential stress and shear strength dependence on elastic deformation

23 p3777 A71-43576

Polycrystals thermoelastic characteristics, determining thermal expansion and conductivity macroscopic coefficients

24 p3840 A71-44402

W and Mo single and polycrystals structural changes by ion bombardment in Li vapor atmosphere at 1500 C, using mass spectrometer

24 p3838 A71-44862

POLYCYTHEMIA

Ventilatory control in acute hypoxia, detailing polycythemia effects on respiratory chemoreceptor sensitivity

14 p2185 A71-30289

Urinary protein excretion rates in high altitude inhabitants, showing polycythemia effect on creatinine clearances levels

19 p3009 A71-38561

Polycythemia and altitude hypoxia effects on rats heart and sea level exercise tolerance

20 p3186 A71-38980

Erythropoietic activity dosage in polycythemic mice after intermittent hypobaric hypoxia

23 p3632 A71-43216

Hypobaric hypoxia effect on polycythemic mice erythropoietic hyperactivity, evaluating iron content in peripheral erythrocytes

23 p3632 A71-43217

POLYESTER RESINS

Sandwich structure cores of foamglass granulate filled unsaturated polyester paste, discussing development of highly thixotropic paste mixtures

01 p0172 A71-10699

Nonmetallic aircraft construction materials, discussing wood epoxy and polyester resins

02 p0273 A71-12299

Glass reinforced polyester laminates under static and repeated loading, investigating resin flexibility effects on fatigue strength

02 p0274 A71-12479

Fire retardant glass reinforced polyester resins optimum formulation, examining burning properties, volatility, extinction time and flame propagation

02 p0274 A71-12483

Flame propagation and inhibition in polymers and unsaturated polyester resins, considering component and composition effect on flammability

02 p0275 A71-12492

Polyester resin model fatigue crack closure, determining residual stress distribution and crack opening and closing force by photoelastic research

04 p0670 A71-15390

Interfacial bonding effect on fracture toughness of glass sphere filled epoxy and polyester resins, using tapered cleavage specimen

11 p1846 A71-25413

Winding equipment for continuous production of large diameter cylindrical filaments of reinforcing materials and polyester resins

11 p1768 A71-25418

Research bibliography on resins and additives covering polyesters, epoxies and new polymers with improved corrosion, fire and heat resistance

11 p1788 A71-25431

Tensile strength and fracture toughness of carbon fiber polyester composites, using mechanical testing and scanning electron microscopy

13 p2092 A71-28625

Epoxy and unsaturated polyester resin compounds for embedding glass fibers in fiberglass-reinforced plastics

15 p2439 A71-32737

POLYESTERS

Lowered ignition temperature and fire propagation of polyester containing bromides

07 p1182 A71-19243

Carbon fiber and carbon fiber-polyester composites chemical resistance to acid and alkaline solutions at various concentrations and temperatures [PLASTICS INST. PAPER 32]

08 p1320 A71-20903

Impact composite materials with reactive resins as binders for polyester fabric, determining peel resistance, tensile shear strength and high temperature aging effect

11 p1786 A71-25416

Fatigue strength of polyester laminates reinforced with glass cloth and mats

14 p2264 A71-30484

POLYETHER RESINS

NT POLYMETHYL METHACRYLATE

Rolling ball fatigue and lubrication with fluorinated polyethers at cryogenic temperatures compared to superperformed mineral oil

01 p0107 A71-10484

Perfluoropolyether fluid lubricant physical and chemical properties at high and low temperatures, explaining metals effects on thermal stability by topochemical reaction mechanism

19 p3083 A71-37424

POLYETHYLENES

Isotactic polypropylene and high pressure polyethylene in contact with steel, examining temperature effect on friction and adhesion

01 p0106 A71-10299

Semipermeable polyethylene grafted membranes/separators/ for extended cycle life in silver zinc cells

08 p2135 A71-21094

Polyethylene plastic packet with chemical pellets, describing welding, cutting and small hole punching by CW carbon dioxide laser

09 p1458 A71-23410

High density polyethylene composition oxidation rates and photodegradation resistance data, using IR spectroscopy

14 p2261 A71-29641

Polyethylene, polypropylene and copolymers sliding friction viscoelastic nature, obtaining relationship between sliding force, adhesional bond shear strength and contact area

19 p3068 A71-37425

Spherulitic linear polyethylene rod cold drawing, observing fibrous structure formation by light and electron microscopy and X ray scattering

19 p3084 A71-37650

Laser illuminated Mach-Zehnder interferometer system including high speed cameras for studying flame propagation among polythene particles suspended in air

19 p3064 A71-38063

Polyethylene coating physicomechanical properties under UV radiation, discussing density and modulus of elasticity, internal stresses, microcrack formation and preventive heat treatment

23 p3697 A71-44032

Polyethylene coated machine steel fatigue strength in air, 3 percent NaCl bath and molecular sulfuric acid solution

24 p3841 A71-44865

POLYMERIZATION

Mo single crystals polymerization and recrystallization, examining strain rate and deformation conditions effects

02 p0266 A71-12652

Deformed Mo single crystals, noting polymerization processes relation to recrystallization during annealing

09 p1476 A71-23318

Polymerization and recrystallization processes in Fe-Cr alloy, using electron diffraction and microscopy

09 p1476 A71-23322

Subgrain growth kinetics for tungsten deformed by rolling and polymerizing annealing, using metallography, X ray microradiography and crystal spectroscopy

09 p1476 A71-23324

Aluminum single crystals tensile deformation and annealing to produce polymerized substructure

15 p2432 A71-32172

Deformation conditions and annealing temperature effects on fine structure of Mo single crystals, noting polymerization

16 p2595 A71-33884

Neutron irradiated Mo single crystals polymerization after cold rolling, using X ray topology methods

16 p2596 A71-33886

Addition effects on polymerization of deformed single crystals of Mo and W with Re, using X ray analysis

16 p2596 A71-33887

High heat resistance of austenitic Cr-Ni-V-B steel by polymerization and recrystallization, using thermomechanical treatment

21 p3403 A71-41102

POLYGONS

NT HEXAGONS

NT RECTANGLES

NT TRAPEZOIDS

NT TRIANGLES

Matrix force analysis, discussing methods for expressing elastic behavior of semimonocoque polygon membrane and isotropic polygon bending elements

16 p2652 A71-33082

POLYHEDRONS

NT PARALLELEPIPEDS

NT RHOMBOHEDRONS

NT TETRAHEDRONS

Radiative cooling system for nearly spherical or polyhedral bodies using radially attached diverging conical elements

17 p2836 A71-34307

POLYIMIDE RESINS

High strength polyimide resin composites, discussing commercial and aerospace applications, chemistry, void content, volatiles and moisture absorption

02 p0274 A71-12487

Heat resistant extended life carbon fiber/polyimide resin composites, noting aerospace applications [PLASTICS INST. PAPER 34]

08 p1321 A71-20920

Long term oxidative aging effects on interlaminar shear strength retention of low void graphite/ boron reinforced polyimide resin composites

11 p1785 A71-25410

Thermally stable polyimide graphite fiber reinforced composites from solutions of monomeric reactions, comparing amide acid prepolymers

11 p1788 A71-25560

POLYIMIDES

Polyimide/boron reinforced plastic structures fabrication, discussing use in leading edges

[SME PAPER EM-70-133] 01 p0090 A71-11263

Aircraft high temperature polyimide hydraulic actuator rod seals, discussing design and performance tests

[SAE PAPER 700790] 01 p0091 A71-11543

Polyimide system application to laminates and molding powders fabrication, exemplifying compression method and cold compaction followed by sintering

11 p1787 A71-25426

Polyimide plastics, considering mechanical properties high temperature applications and cost effectiveness

13 p2091 A71-28165

Physical and mechanical properties of controlled flow vacuum cured glass reinforced polyimide prepreg laminates

22 p3565 A71-42595

POLYMER CHEMISTRY

Gel permeation chromatography for polymer molecules size /hydrodynamic volume/ separation

04 p0548 A71-15265

Papers on polymers thermal stability, Volume 1, covering molecular structure, reaction kinetics, scission, thermosetting resins, etc

08 p1323 A71-21474

Thermally stable fibers fabricability and properties relation to polymer chemical structure and tensile strength

09 p1481 A71-22247

Silyl peroxides as promotion agents for polymeric materials adhesion to solid substrates and for cross-linking polyethylene to other polymers

10 p1633 A71-24109

Epoxy novolac resin-cured alicyclic anhydride amine-catalyzed ablative polymers molecular structure from computer correlation of analytical data

11 p1789 A71-26033

Ablative polymers synthesis from formaldehyde, phenols and ethers reaction products, discussing char yield, thermally stable fillers incorporation and thermogravimetric analysis

11 p1855 A71-26034

Polymeric ablation materials testing in arc image furnace over various temperatures, pressures and thermal flux

11 p1790 A71-26045

French book on macromolecular chemistry covering solid state polymers, polymerization reactions involving free radicals, linear viscoelasticity, vitreous transition of macromolecular polymers, electrical conductivity, etc

11 p1729 A71-26152

Synthetic elastomers, including polymer chain growth, monomer sequence distribution, structural compatibility effects and commercial products development

18 p2939 A71-35886

Polymer thermal degradation theory of pressure sensitive hybrid combustion, calculating linear regression rates

19 p3170 A71-38123

POLYMER PHYSICS

Polyethyl methacrylate lifetime under simultaneous mechanical stresses and ionizing radiation

01 p0106 A71-10044

Isotactic polypropylene and high pressure polyethylene in contact with steel, examining temperature effect on friction and adhesion

01 p0106 A71-10299

High temperature pyrolysis molding, discussing covalent organic bonds breakage and subsequent structural rearrangement of crosslinked polymer network

01 p0107 A71-10459

Bond rupture and fracture in semicrystalline polymers, noting agreement with random length molecular tie chain scission model

04 p0670 A71-15388

Industrial and biological polymer compounds active surface layers, discussing thermodynamic aspects, molecular dynamics, energy conversion and boundary layer entropy

06 p0915 A71-17585

Static friction in steel-polymer couples under vacuum, considering temperature, contact time, normal load and physicochemical properties effects

09 p1454 A71-22818

Fracture mechanics and time dependent strength of elastic or viscoelastic solids adhesively jointed by soft polymeric bonding layer

11 p1851 A71-26383

Low ductility materials, considering applications to stress analysis, failure criteria, fatigue, physical metallurgy and polymer mechanics

14 p2251 A71-29893

Atomic bond rupture and molecular mechanisms of polymer fracture, using EPR spectroscopy

16 p2600 A71-32944

Polymer type, temperature, crystallinity and orientation effects on fracture mode, discussing macroload carrying capacity, nylon fiber tie chains and molecular behavior

18 p2939 A71-35889

Polymer systems molecular rheology based on statistical mechanics and simplified structural models

24 p3841 A71-44644

POLYMERIC FILMS

Hologram formation in gelatin, photopolymeric and photochromic materials for high diffraction efficiency, in-place real-time processing and erasability

04 p0596 A71-15167

Electron, proton and UV irradiation effects on CdS solar cell protective plastic films with or without adhesive coatings, measuring transmission changes

05 p0771 A71-16087

Polybenzothiazole as solid film formulations binder for friction wear improvements, noting thermal and oxidative stability, toughness, adhesive properties and handling ease

05 p0772 A71-16375

Low energy proton irradiation induced thin polymer contaminant films effect on far UV reflecting mirrors reflectance and scattered light

08 p1290 A71-21382

Polyethylene plastic packet with chemical pellets, describing welding, cutting and small hole punching by CW carbon dioxide laser

09 p1458 A71-23410

B and C polymer laminated film composites efficiency for stability designed structures, considering weight reduction by planar reinforcements

[AIAA PAPER 71-353] 11 p1783 A71-25331

In situ double exposure differential interferometry, using photoconductive thermoplastic sandwich in place of film, allowing second hologram inscription

14 p2242 A71-30153

Gas permeability of polymeric foils reduction by vapor metallization in vacuum, noting dependence on surface state, diffusion layer and macroporosity

16 p2601 A71-33684

Closed cycle life support water electrolysis system using solid plastic sheet electrolyte /ion exchange membrane/ of sulfonated perfluoro polymer

[ASME PAPER 71-AV-9] 18 p2866 A71-36376

Optical properties of metallized fluorinated ethylene propylene Teflon films with various thicknesses, discussing suitability as spacecraft thermal control surface

[ASME PAPER 71-AV-35] 18 p2869 A71-36402

Photopolymer holography systems and holograms fixing techniques, discussing polymer films image storing and fixing processes

21 p3381 A71-40927

POLYMERIZATION

NT VINYL COPOLYMERS

Cellulose application as zinc silver oxide battery separator, considering chemical stability, cellophane properties, polymerization and crystallinity

08 p1234 A71-21093

Polymerization kinetics of nematic liquid crystal monomer in nematic and isotropic phases

11 p1728 A71-26062

French book on macromolecular chemistry covering solid state polymers, polymerization reactions involving free radicals, linear viscoelasticity, vitreous transition of macromolecular polymers, electrical conductivity, etc

11 p1729 A71-26152

Polyester formation by *Escherichia coli* ribosome catalyzed alpha-hydroxy acid incorporation into polymer chain

17 p2686 A71-35574

Methane atmosphere polymerization by solar UV to form primordial oil slick, discussing importance to life development

22 p3535 A71-42074

Polymerized and hydrolyzed polypeptides from condensed amino acid adenylates for prebiological synthesis model

22 p3508 A71-42232

Solar system organic compounds detection and evolution, considering element, isotope and pigment composition, optical activity and polymerization

22 p3496 A71-42824

POLYMERS

Sanitary, chemical and toxic properties of polymeric materials in isolation chamber with contaminated outgassing atmosphere at moderate temperature

01 p0024 A71-11128

Flame propagation and inhibition in polymers and unsaturated polyester resins, considering component and composition effect on flammability

02 p0275 A71-12492

Stress-strain state of plate made from highly elastic polymer containing circular and elliptical holes

03 p0506 A71-13602

Poling techniques modifications for piezoelectric activity enhancement in bulk polymers, considering arcing minimization, AC field superimposition and repeated cycling of process

03 p0448 A71-13721

Polymeric materials plastic deformation properties during service and storage, discussing prediction and testing methods

03 p0448 A71-14300

Polymer materials linear photocreep characteristics description in terms of differential and integral equations, discussing relationship between optical and mechanical properties

03 p0514 A71-14357

Polymer neck autooscillatory expansion under drawing as result of interaction between elastic deformation and heat release during orientational transformation

03 p0448 A71-14362

Clear potting polymers, investigating temperature and ionizing particle irradiation effects on properties

04 p0618 A71-14898

Combined deformation of reinforcing elements and polymer binder in monodirectional composite structure, determining stress distribution

06 p0915 A71-17380

Integratism in life biology, discussing reductionism and organicism at biopolymer macromolecule construction and conformational levels

06 p0852 A71-17683

Cured thermosetting polymers, investigating water effect on microstructure and mechanical properties

06 p0916 A71-17945

Metal gluing with synthetic polymer based adhesives, discussing history, technology and high temperature resistance

06 p0905 A71-18093

Stress-strain state of three-layer polymer plate having different thicknesses, Poisson coefficients and creep functions

06 p1005 A71-18707

Carbon fiber reinforced polymers for self lubricating materials applications, discussing friction and wear characteristics under fresh and sea water, alcohols, mineral oils, etc

[PLASTICS INST. PAPER 31]

08 p1319 A71-20896

Polymeric materials for silver zinc battery separators, discussing porous and solvent-type pore free membranes

08 p1234 A71-21091

Polymer adhesive protective coatings for improving fatigue resistance of butt and lap welded joints in thin Al sheet construction

09 p1478 A71-23355

Polyblends and composites - Conference, New York, June 1969

10 p1634 A71-24767

Elastic plastic wave cancellation in energy absorbing materials, considering polymer group efficiency for shock mitigation from weight and volume standpoint

[AIAA PAPER 71-350] 11 p1843 A71-25329

Longitudinal tensile strength of unidirectional fibrous glass/polymeric matrix composites under high loading rates

11 p1785 A71-25405

Research bibliography on resins and additives covering polyesters, epoxies and new polymers with improved corrosion, fire and heat resistance

11 p1788 A71-25431

Ablative polymers for thermal protection of aerodynamic surfaces, propulsion structures and ground equipment, discussing energy absorption of various polymeric materials

11 p1789 A71-26030

Combined deformation of reinforcing elements and polymer binder in monodirectional composite structure, determining stress distribution

12 p1921 A71-27462

Electron paramagnetic resonance atomic scale stress analysis of high polymer fibers and rubber, measuring chain scission and bond rupture for different loading histories

13 p2091 A71-28440

Nonlinear heredity theory related to Volterra-Freschet heredity theory under uniaxial tension, giving expression for polymers deformation relaxation processes

13 p2092 A71-28650

Dipolar charge density of electret formed by polar polymers above critical temperature under dielectric polarization with quenching

14 p2181 A71-29747

Linear viscoelastic analysis of two dimensional plane stress model of polyphase composite material with rigid inclusions and voids and polymeric binder

14 p2323 A71-29836

IR spectrometer attachment for macromolecular investigation of polymer materials, describing constructional and operational features

15 p2383 A71-31658

Carbon suboxide polymers formation in Martian atmosphere, examining carbon monoxide photolysis and

radiolysis processes enhanced by solar ionizing radiation 15 p2491 A71-32420

Volume hologram formation in photopolymer materials with bright low noise images, considering sensitivity, spatial frequency response, particle scattering noise and nonlinearities 16 p2577 A71-33144

Transparent polymer dielectric luminescence and destruction under Q switched laser radiation with subthreshold power and picosecond pulses 16 p2588 A71-33652

Polymers mechanical losses temperature-frequency dependence, using nonlinear viscoelastic theory 16 p2602 A71-33982

Microphase separation in homopolymer-block copolymer mixtures as function of composition, molecular weight and interaction parameters 17 p2695 A71-35525

Photopolymer recording materials fixing by flashing holograms with Xe light or deactivating catalyst with thermal methods 17 p2745 A71-35591

Instrumentation and techniques of torsional pendulum and braid analyses, studying trace moisture and cure cycle effects on thermomechanical spectra of polymeric materials 18 p2939 A71-36596

Polymer materials strength and lifetime prediction under natural conditions from mathematical model based on laboratory accelerated test data 19 p3084 A71-37781

Inorganic polymers and glasses at high temperatures, detecting LF internal friction 19 p3084 A71-38050

Carbon and noncarbon polymers based high temperature elastomeric materials chemical structure and physical properties 19 p3085 A71-38068

Multicolor images with volume dielectric holograms in photopolymer materials, reconstructing complex three dimensional images with high resolution in white light 20 p3236 A71-39192

Metal and polymer matrix materials research based on stringent requirements for thermal reactors, jet engines and space vehicles, discussing tests and analysis methods 21 p3401 A71-40901

Mechanical properties of various polymeric solids under compressive loading cycles of 100 microsec duration and under steady state compressive loads 21 p3406 A71-41427

Polymer materials for aerospace construction, considering behavior in cryogenic and high temperature environments 22 p3564 A71-41510

Optically sensitive epoxy resin based high polymers under pulsed loads, observing deformation and mechanical displacement with high speed photography 22 p3614 A71-41610

Stress concentration near holes in high modulus epoxy resin polymer thin plates under pressure wave loads 22 p3614 A71-41611

Electronic double differentiator for producing spectroscopic absorption curves second derivatives, considering application to polymers IR examination 22 p3545 A71-42154

Radiation dose effects on polymer strain magnitude under critical cyclic loading 23 p3697 A71-44033

Filler quantity and type effects on mechanical energy losses in polymers, discussing molecular interaction and chemical bond influences 23 p3697 A71-44205

Polymer odor threshold determination for hygienic considerations in sealed/pressurized chamber construction, comparing static and dynamic methods 24 p3800 A71-44539

POLYMETHYL METHACRYLATE

Polymethyl methacrylate lifetime under simultaneous mechanical stresses and ionizing radiation 01 p0106 A71-10044

Through-thickness fatigue crack growth in polymethyl methacrylate sheets, observing stress intensity factor range, frequency and mean effects [SESA PAPER 177] 03 p0448 A71-13771

Pressure effect on combustion rate of model mixtures of ammonium perchlorate with polystyrene and polymethyl methacrylate 03 p0468 A71-13989

Aluminum addition effect on combustion rate of mixtures of ammonium perchlorate with polymethyl methacrylate at different temperatures 03 p0520 A71-13995

Thin Al and plexiglass sheets biaxial stress field effect on fatigue and fracture [ASME PAPER 70-PVP-17] 04 p0665 A71-14768

Structural damage by laser radiation in polymethyl methacrylate, using polarized light microscopy 05 p0772 A71-16370

High energy electron penetration and scattering in solids, obtaining beam density profiles by polymethyl methacrylate resist exposure 06 p0940 A71-17305

Kaolin and quartz powder additions effect on glass-like polymethyl methacrylate specific heat, thermal conductivity and diffusivity 07 p1144 A71-18922

Strain field measurement near crack tip in polymethyl methacrylate by holographic interferometry 07 p1209 A71-19043

Quartz, organic glass and plexiglass luminescence under giant pulse ruby laser radiation 15 p2422 A71-32462

Compact monochromatic rhodamine doped polymethyl methacrylate dye laser with internal diffraction grating resonator, describing frequency selection from emission spectrum 15 p2422 A71-32585

Loading history effect on optical and mechanical properties of polymethyl methacrylate under uniaxial tension 16 p2600 A71-32815

Critical induced acceleration for shock propagation as function of strain in polymethyl methacrylate [ASME PAPER 71-APM-14] 16 p2600 A71-33213

Polymethyl methacrylate lifetime tested in water and heptane, showing increase with orientation degree 16 p2601 A71-33683

Surface cracking resistance of polymethyl methacrylate glass in vacuum, air and nitrogen, noting humidity effect 16 p2601 A71-33690

Holographic fiber optics image-guiding structures preparation in sensitized polymethyl methacrylate cast sheet by refractive index gratings pair recording 18 p2946 A71-35852

Linear viscoelastic stress-strain-time relations for polymethyl methacrylate and epoxy resin 23 p3696 A71-43375

Polymethyl methacrylate samples resistance to crack propagation, detailing modulus of cohesion effects 24 p3841 A71-45050

POLYMORPHISM

Human gamma globulin polymorphism, discussing characteristics, statistical distribution and potential utilization for gene frequency studies in paternity serology 05 p0710 A71-16943

Dissimilar metals welding, emphasizing melting point, linear expansion coefficient, thermal conductivity, electrical resistivity and polymorphic transformation 13 p2072 A71-27887

Thermal polymorphous metals and alloys crystal structure, discussing plastic deformation due to formation of cubic lattice and metallic bonds 16 p2597 A71-33915

Titanium dihydride room temperature polymorphic transition from fcc to body centered tetragonal, noting different transition temperatures 22 p3563 A71-42368

POLYNOMIALS

NT HERMITIAN POLYNOMIAL

Polynomial finite difference description of first order nonlinear dynamic control plants with incomplete information 01 p0058 A71-10405

Orthogonal polynomials method for integral equations solution in two dimensional mixed boundary value problems of elasticity theory 01 p0171 A71-10660

Polynomial microwave frequency filter composed of random symmetric components of randomly selected circuit 01 p0057 A71-11217

Qualitative theory of unknown parameters selection electronic circuit synthesis, considering polynomial coefficients of transfer function 02 p0230 A71-11838

Real polynomial quadratic divisors determination with maximum accuracy in floating point arithmetic, using Bairstow method algorithm 03 p0450 A71-13118

Heavy gyrostat equations of motion having fixed point and zero momentum integral constant, obtaining polynomial solutions 03 p0457 A71-13585

Numerical approximation of continuous real function in interval by polynomials using appropriate nets, estimating error 06 p0920 A71-18209

Analytic function steady approximation with aid of polynomials in given region, considering Dirichlet series 07 p1146 A71-19042

Optimal synthesis of linear equidistant antenna arrays with sum and difference radiation patterns, using orthogonal polynomials 07 p1078 A71-20069

Finite difference description for dynamic control plants with unknown disturbances based on integral 01 p0106 A71-10299

transformation and extrapolation, applying to automatic control systems synthesis 08 p1270 A71-21975

Complex zeros of complex polynomials, matrix inequalities and nonlinear programming, constructing areas intersection in complex plane defined by inequality bounds on eigenvalues of companion matrix 09 p1485 A71-22970

Amplitude characteristic polynomial Chebyshev approximation by linear phase nonrecursive digital filter transfer function 09 p1417 A71-23037

Polynomial approximation of current along thin isolated asymmetrical cylindrical dipoles 09 p1419 A71-23506

System identification problems, discussing approximation by polynomial integral operators, determinable classes in spectral decompositions, observation noise and stochastic systems stationary in observation time 10 p1587 A71-24742

Optimal nonlinear filtering, deriving algorithm based on statistical approximation of system and observer nonlinearities by second order polynomials 10 p1587 A71-24746

Majority logic decoding for primitive polynomial and dual codes, discussing nonorthogonal parity-check sums formation methods and Euclidean geometry maximality 14 p2207 A71-30011

Orthogonal polynomials method for integral equations solution in two dimensional mixed boundary value problems of elasticity theory 14 p2333 A71-30994

Geophysical map preparation by automatic procedure using polynomial representation of fields in iteration process 16 p2563 A71-33460

Constrained optimization problems solution combining modified pattern search methods and polynomial constraints in aircraft design parameters selection 16 p2603 A71-33721

Polynomial fitting for information compression of Wild BC-4 satellite photographs, comparing short arc with geometric compensation methods 16 p2581 A71-34041

Polynomial microwave frequency filters composed of random symmetric components of randomly selected circuit 17 p2718 A71-34268

Boundary value problems solution for second order finite difference equations, applying second order orthonormal polynomials and related functions 17 p2764 A71-34843

Rotating shaft critical speed determination as root of polynomial from frequency equation /characteristic determinant/ without iterative search [ASME PAPER 71-VIBR-53] 21 p3385 A71-40300

Nonlinear autonomous systems transient response, obtaining approximate solutions by generalized averaging technique based on ultraspherical polynomial expansions 21 p3415 A71-40532

Extreme eigenvalues of Toeplitz matrices associated with Laguerre and Jacobi polynomials, using finite difference operators 21 p3410 A71-41084

Complex solutions blocking in sectoral second order differential equations with polynomials, involving conformal mapping 21 p3410 A71-41191

Piecewise polynomial Taylor methods to numerically solve first order ordinary differential equations 23 p3698 A71-42901

Polynomial equation roots determination, analyzing floating point arithmetic errors 23 p3698 A71-43097

Average number of real roots of polynomials consisting of independent random quantities with identical distribution 23 p3699 A71-43571

Necessary and sufficient conditions for separating regular multiplier from matrix polynomial, presenting method for determining regular multiplier real factors 24 p3842 A71-44477

POLYPHENYL ETHER

Free radical induced high temperature oxidation degradation curtailment of polyphenyl ethers by oxides, hydroxides and carbonates of alkali metals and Ba [ASLE PREPRINT 71LC-11] 24 p3842 A71-45290

POLYPHENYLS

Polyphenylene thermal degradation and curing, discussing pyrolytic effects of chlorine and polynuclear structure 11 p1855 A71-26035

Thermosetting polyphenylene resins synthesis and use in reinforced ablative composites, discussing polymerization and curing 11 p1789 A71-26036

POLYPROPYLENE

Isotactic polypropylene and high pressure polyethylene in contact with steel, examining temperature effect on friction and adhesion 01 p0106 A71-10299

Filler and reinforcing agent effects on polypropylene rigidity, tensile strength and creep resistance at elevated temperatures [PLASTICS INST. PAPER 11]

09 p1481 A71-22342

Stress-time superposition creep data for unfilled and coupled glass reinforced polypropylene at 23-80 C

14 p2264 A71-29835

Polyethylene, polypropylene and copolymers sliding friction viscoelastic nature, obtaining relationship between sliding force, adhesion bond shear strength and contact area

19 p3068 A71-37425

POLYSACCHARIDES

NT CELLULOSE

NT GLYCOSIDES

Mucopolysaccharide content and composition of fatty streaks in young male aortas, discussing atherosclerosis effects

18 p2854 A71-35919

POLYSTYRENE

Pressure effect on combustion rate of model mixtures of ammonium perchlorate with polystyrene and polymethyl methacrylate

03 p0468 A71-13989

High temperature decomposition kinetics in vacuum of mixed ammonium perchlorate-polystyrene solid fuel, using time of flight mass spectrometer

03 p0469 A71-13997

Spark ignition of polystyrene suspensions during free fall in air, investigating ignition mechanism by high speed photography

12 p1986 A71-26967

Luneberg lens fabrication technique using thin insulated Al slivers embedded in low density polystyrene foam

14 p2205 A71-31059

Microcrater morphology in soda-lime-silica glass by polystyrene spheres, detailing shape, density, velocity and incidence angle effects

18 p2961 A71-35948

Radiative ignition of polymeric fuels/polystyrene and epoxy in oxygen/nitrogen mixtures

19 p3121 A71-38125

POLYSULFIDES

Outdoor five year aging tests on polysulfide and silicone adhesive sealants under semiarid, marine and high humidity environments

10 p1634 A71-24119

POLYTETRAFLUOROETHYLENE

Friction coefficient in antifriction polytetrafluoroethylene compounds with lead, bronze or graphite

02 p0275 A71-12600

Carbon fiber and carbon fiber-polytetrafluoroethylene composites high temperature mechanical properties [PLASTICS INST. PAPER 35]

08 p1319 A71-20899

Mechanical property modifications of polytetrafluoroethylene by filler additions, noting improved wear resistance [PLASTICS INST. PAPER 13]

09 p1482 A71-22346

POLYTROPES

Polytrope solar wind equations, expressing distance and flow velocity as functions of mass density

01 p0147 A71-11510

Plane shock wave propagation in polytropic gas of variable density, using successive approximation technique

03 p0345 A71-14558

Polytropic gas spheres gravitational instability under external pressure, obtaining critical masses and densities

05 p0813 A71-17091

Polytropic models second order pulsations, evaluating stellar pulsational stability and thermal imbalance

08 p1359 A71-20941

Rapidly rotating polytropes in post-Newtonian approximation to general relativity

22 p3604 A71-42327

Polooidal magnetic field effects on polytrope oscillation modes, using second order tensor virial equations

24 p3871 A71-44909

POLYTROPIC PROCESSES

Earth atmosphere polytropic equilibrium model density distribution and effective size and mass, taking into account gravitational interactions

07 p1152 A71-19375

Plane unsteady polytropic MHD flow equations reduced to time independent system, using complex variable techniques

11 p1804 A71-25439

Small amplitude resonant thermal acoustic oscillations of inviscid polytropic gas contained in finite length tube

11 p1798 A71-25446

Polytropic process description for gas flow by introducing resistance and heat transfer coefficients

24 p3820 A71-45020

POLYURETHANE FOAM

Nonsupporting aerodynamic foam material thermal insulation system with reliability for cryogenic rocket

propellant tank, considering polyurethane and polyvinylchloride

01 p0164 A71-11541

Book on foam polyurethanes synthesis and use in flight vehicles

09 p1455 A71-23162

Polyurethane foam effects on fuel contamination during installation for fuel system fire and explosion protection

[ASME PAPER 71-GT-54]

11 p1708 A71-25981

Maximum acoustic attenuation in lead-wool-polyurethane and nickel-Cerrobend composites for different compositions, frequencies and pressures

18 p2948 A71-36933

Flexible polyurethane foam plastics under high rate loading, investigating strain rate and structural parameters effects on mechanical properties

22 p3565 A71-41592

POLYURETHANE RESINS

Vibrational damping, composition and structural design of cast polyurethane elastomers for Poseidon missile launch tube liner

08 p1367 A71-20694

Polyurethane structural adhesives with excellent tensile shear and T-peel strengths at cryogenic temperatures, long pot lives and good processing characteristics

10 p1630 A71-24068

Structural bonding with polyurethane adhesives in missile systems

10 p1615 A71-24094

Polyurethane coatings development for subsonic rain erosion protection for aircraft structures, using whirling arm apparatus with simulated rainfall

10 p1632 A71-24101

Photoelastic analysis of thermal stresses in polyurethane rubber ring reinforced polymers, cermet and rubber-metal composites

24 p3883 A71-44895

POLYVINYL CHLORIDE

Nonsupporting aerodynamic foam material thermal insulation system with reliability for cryogenic rocket propellant tank, considering polyurethane and polyvinylchloride

01 p0164 A71-11541

Polyvinyl chloride nonlinear viscoelastic behavior by multiple integral representation, determining kernel functions for mixed time parameters from tension/torsion creep experiments

[ASME PAPER 70-WA/APM-21]

03 p0512 A71-14156

High energy hydrogen-oxygen launch vehicle thermal insulation system, discussing closed cell rigid polyvinyl chloride foam mechanical characteristics, use and tests

12 p1985 A71-26835

EPR spectra and spin-lattice relaxation time in coal pitch and polyvinyl chloride during low temperature carbonization

17 p2763 A71-35245

Polyvinyl chloride foam insulation system for liquid hydrogen-liquid oxygen space vehicles tested under groundhold and simulated flight conditions

20 p3253 A71-39269

PONDEROMOTIVE FORCES

Maximum ponderomotive force on laser produced plasmas, using wave equation in linear critical layer

07 p1171 A71-20291

Self magnetic field effect on I-V characteristics of Cs-Ba thermionic converter, noting effects of pressure differential due to ponderomotive forces action

21 p3326 A71-41294

Ferromagnetic Co phase nondestructive determination in hard powdered-metal alloys by permanent magnet ponderomotive force measurement based on relationship to ferromagnetic alpha phase

22 p3561 A71-41775

PONTYAGIN PRINCIPLE

Nonlinear pulsed automatic control systems absolute stability with unsteady linearity by Pontryagin principle, considering forced and free motions

01 p0058 A71-10428

Cylindrical shells and circular plates optimal limiting and adaptable loads calculation by Pontryagin maximum principle

01 p0170 A71-10639

Pontryagin space and convergence of Bubnov-Galerkin method for equations with involution operators

01 p0112 A71-11092

Book on optimal control theory covering dynamic programming, calculus of variations, Pontryagin maximum principle and iterative techniques

02 p0236 A71-12773

Pontryagin maximum principle applied to optimal control of standing TE wave electric field strength in microwave gyromonotron

03 p0386 A71-13813

Nonlinear control synthesis based on minimum duration of transient processes leading to system stabilization, using Pontryagin maximum principle

03 p0392 A71-14406

Nonlinear stabilization systems time and energy optimal control syntheses using Pontryagin maximum principle

03 p0393 A71-14411

Spinning aerospace vehicle optimal attitude control system by minimizing reaction fuel, noting application of Pontryagin maximum principle

04 p0623 A71-15143

Trajectory optimization, using Pontryagin maximum principle for differential inclusions

07 p1146 A71-19178

Chemical reaction kinetics optimal problem numerical solution based on Pontryagin maximum principle and gradient method

07 p1147 A71-19185

Optimal control theory application to environmental control of confined spaces and life support systems, considering algorithm of Pontryagin principle

09 p1423 A71-22588

Distributed parameter control systems optimality conditions, using Pontryagin maximum principle

09 p1425 A71-23469

Search scanning system synthesis based on forces optimal distribution over investigated field, using Pontryagin maximum principle

10 p1586 A71-24167

Autonomous dynamic systems optimal control problems solution by reduction to operator equation, using Pontryagin maximum principle

10 p1636 A71-24352

Conflicting and relaxed minimax controls for Weierstrass E condition or Pontryagin maximum principle

11 p1792 A71-25752

Time optimal phase locked AFC system synthesis based on Pontryagin maximum principle, comparing computerized and experimental transient response

12 p1882 A71-27514

Optimal control synthesis analog for nonlinear problem, using trial and error method based on Pontryagin maximum principle

13 p2040 A71-27834

Discrete control system optimization in terms of power requirements minimization, using Pontryagin maximum principle

15 p2381 A71-31977

Pontryagin maximum principle application to optimal control problems with phase coordinate constraints, noting existence theorem validity

16 p2550 A71-33592

High order optimality conditions of singular controls, considering Pontryagin maximum principle, Bellman dynamic programming and functional analysis

16 p2550 A71-33701

Second variation for general space trajectories in terms of pseudo-Hamiltonian of Pontryagin, applying to singular arc optimality in space vehicle escape maneuver

23 p3768 A71-43857

Deterministic system optimal control with single control and several cost functionals by Pontryagin maximum principle

23 p3656 A71-43858

POPULATION INVERSION

Argon ion CW lasers, discussing design, inverse population, plasma, radiative transition probabilities, pumping, frequency spectra and active medium

01 p0092 A71-10145

CO chemical laser power output augmentation by selective depopulation of CO lower vibrational levels by energy transfer to added gases

02 p0262 A71-12709

High power carbon dioxide electric discharge mixing laser with vibrationally excited nitrogen providing population inversion

03 p0434 A71-13480

Helium effects on dissociation and population inversion dynamics in pulsed carbon dioxide lasers

04 p0605 A71-14628

Population inversions in shock induced dissociation of alkali halides in 2000 to 7000 K range, considering rate constants and molecular relaxation

04 p0629 A71-14694

Operational characteristics, spectroscopy and inversion mechanisms of noble gas ion lasers in light of plasma theories and atomic data

05 p0763 A71-16551

Laser cavity standing wave field electro-optic modulation for uniform population inversion, producing spontaneous single frequency output

05 p0764 A71-17232

Explosion products population inversion by combining vibrational chemical excitation with thermal ignition

06 p0865 A71-17402

Chemical energy conversion in lasers, discussing vibrational inversions in diatomic and multiatomic molecules and chain reactions

07 p1121 A71-19098

Flow-through carbon dioxide lasers population inversion relation to individual gas components and electron velocity distribution functions

07 p1126 A71-20187

Recombination emission by atoms or radicals used with population for inversion thermal gas laser production

07 p1128 A71-20529

Carbon dioxide laser population inversion using chemical reaction of burning with gas combustion products of vibrationally excited polyatomic molecules

08 p1302 A71-21499

Nuclear reaction products effect on population inversion in gas lasers, considering neutron irradiation enhancement of carbon dioxide laser output

08 p1303 A71-21668

Computer simulation of strongly ionized potassium and hydrogen plasmas relaxation during rapid electrode cooling by He atoms, noting population inversions

08 p1342 A71-21913

Helium role in populating upper levels of cadmium gas laser in discharge tube

09 p1462 A71-22401

Stress effects on electron relaxation time anisotropies in n-type Si, using high temperature piezoresistivity model for population transfer rates

09 p1508 A71-22692

Einstein relations for stimulated luminescence, and application to high pressure chemical laser power gain and population inversion calculation

12 p1913 A71-26966

Population inversion in CsI33 ground state hyperfine levels, using CW GaAs laser at 77 K for optical pumping

12 p1913 A71-26977

Laser designs with thermal pumping, obtaining electron states phototransition probability, cooling rates for population inversion and laser action threshold for diatomic gas molecules

12 p1914 A71-27029

Spectral emission and level populations of diffusion and principal series lines of cesium vapor in 5 mm discharge plasma diode with hot cathode

12 p1941 A71-27549

Cavity mirror transmittance variation effect on output power and pulse length of single-pulse Nd-doped glass laser with nonuniform inverted population distribution

13 p2077 A71-27855

Arc heated plasma expansion through nozzle, observing population inversion of neutral carbon self-absorption UV atomic line

15 p2454 A71-31537

CW gain measurements on rotation-vibration P branch transitions of CO molecular laser, calculating gas temperature, Einstein coefficient and population densities

15 p2423 A71-32609

Carbon dioxide laser population inversion based on chemical combustion reaction producing gas of vibrationally excited polyatomic molecules

16 p2585 A71-33047

Optical parametric oscillation internal to laser cavity, including temporal response effects of laser population inversion

17 p2751 A71-34377

Population inversion damping on vibrational-rotational transitions of carbon dioxide molecule during interaction with monochromatic radiation pulse, using two level model

17 p2752 A71-34387

Vibrational population inversions due to molecular energy exchanges from rapid heating behind normal shock wave in carbon dioxide-nitrogen-helium mixtures

17 p2728 A71-34883

Computer simulation of strongly ionized potassium and hydrogen plasmas relaxation during rapid electrode cooling by He atoms, noting population inversions

17 p2788 A71-35257

Operating characteristics of Q switched CO-He laser, discussing energy transfer processes leading to population inversion

18 p2929 A71-35835

Self pulsing in homogeneously broadened oscillator, using materials with short recovery time for appreciable inverted population density modulation

18 p2929 A71-35901

Gas dissociation in carbon dioxide laser by IR absorption method, investigating role in population inversion

18 p2932 A71-37008

Einstein relations for stimulated luminescence, and application to high pressure chemical laser power gain and population inversion calculation

19 p3075 A71-38265

Carbon dioxide lasers, covering molecular structure, IR spectra and laser transitions, population inversion mechanisms, gas discharge and longitudinal flow

20 p3243 A71-39067

Carbon dioxide, nitrogen and water vapor hot mixture expansion through Laval nozzle, showing population inversion on carbon dioxide laser transition

22 p3556 A71-41726

Inverted populations of molecular vibrational states for lasers, using strongly exothermal explosion-accompanied chemical reactions

22 p3557 A71-41819

Helium effects on dissociation and population inversion dynamics in pulsed carbon dioxide lasers

22 p3558 A71-42268

Population inversion development and breakdown in active medium produced by plasma generation during pulsed discharge in molecular nitrogen laser

23 p3684 A71-43406

Traveling wave laser with confocal, plane and semiconcentric resonators, calculating emission field spatial-temporal structure and inversion distribution

23 p3685 A71-43561

POPULATION THEORY

Gas laser optical pumping based on photodissociation, calculating spatial temporal distributions of pump radiation absorption probability and main level population

07 p1125 A71-19806

Biomathematical model and least square estimation from time series data of discrete particle population in stochastic compartmental system

14 p2265 A71-30181

POPULATIONS

Dwelling unit estimation with color IR photos, applying aerial photointerpretation to urban analysis

13 p2064 A71-29396

PORCELAIN

Ti dioxide-opacified porcelain enamel reflectance spectra analysis, deriving scattering cross sections and dispersed particle sizes and distribution

09 p1480 A71-22116

PORES

U POROSITY

POROSITY

NT MICROPOROSITY

TiC and ZrC samples with different porosities, examining bending strength at various temperatures

01 p0102 A71-10786

Au plated contacts deterioration by pore corrosion, noting resistance relation to basis or underplated metals porosity

01 p0102 A71-10800

Doped W wire core porosity and anomalous recrystallization behavior microstructural observation by electron microscopy

02 p0268 A71-12890

Porosity in gas tungsten arc aluminum weldments and elimination by hydrogen reduction

07 p1119 A71-19969

Semiconductor thermoelectric materials intercrystalline boundaries porosity effects on electrical and thermal conductivity

09 p1506 A71-22162

Mercury intrusion porosimetry application to pore size and shape measurements for porous solids, discussing solid and air compressibilities, surface tension, contact angle, etc

09 p1453 A71-22168

Al-Mg alloy positional welding for porosity elimination

09 p1457 A71-23356

Nickel alloys susceptibility to pores formation in tungsten inert gas welding in argon-nitrogen mixture, considering influence of Cr, Mo and W

14 p2260 A71-30487

Flame or plasma sprayed ceramic coating porosity estimation, using statistical distribution of breakdown voltage in coating

15 p2438 A71-31285

Hydrogen and nitrogen pores formation in welds, considering gas concentration redistribution between liquid and solid metal

15 p2417 A71-32663

Permeability and porosity of Precambrian Onverwacht cherts and other low permeability rocks, discussing geological origin of rock-contained organic compounds

18 p2913 A71-36768

Shock metamorphism of Coconino sandstone at Meteor Crater /Arizona/, examining porosity role in rock compression and in high pressure phases formation

19 p3050 A71-37659

Flow induced vibration suppression by perforated concentric shroud around circular cylinder, investigating porosity and shroud/cylinder diameter ratio effects

21 p3458 A71-40283

Apollo 12 basalts porosity and volume compressibility under hydrostatic pressure

23 p3759 A71-43768

Brittle ceramic materials strength, showing porosity effect dependence on Weibull homogeneity parameter value

23 p3698 A71-44225

Total-to-open porosity ratio for carbide-iron type materials sintering, noting relative density and chemical composition effects

24 p3838 A71-44736

POROUS BOUNDARY LAYER CONTROL

Minimum suction rate preventing laminar boundary layer separation from curvilinear porous surface in jet flow

02 p0186 A71-12553

Two dimensional test facility in blowdown wind tunnel transonic section, discussing porous sidewall boundary layer control effects on airfoils geometric characteristics

[AIAA PAPER 71-293]

09 p1428 A71-22957

Boundary layer approximation for isothermal turbulent plane semibounded jet expanding over porous surface, deriving friction stresses and flow velocity in skin and stream regions

20 p3214 A71-39795

POROUS MATERIALS

Porous metal fiber laminar vacuum insulation, calculating steady state heat and mass transfer

01 p0179 A71-10615

Porous Ti thermal and electrical properties from room to high temperatures

01 p0102 A71-10785

Fuel cell electrodes preparation by sputtering thin Ta and Pt layers on porous Vycor

03 p0353 A71-13056

Blunt body nose protection from radiation-convective heat transfer, using porous injection of radiation absorbing substance

04 p0685 A71-15518

Sponge titanium quality improvement involving chlorination, tetrachloride purity, magnesium and thermal reduction

04 p0616 A71-15824

Rushing effects on fractional composition and quality of sponge titanium, including optimum end size of pieces

04 p0616 A71-15825

Accelerating flame front generation and propagation controlling mechanism in porous propellant

[AIAA PAPER 71-210]

06 p0948 A71-18646

Polymeric materials for silver zinc battery separators, discussing porous and solvent-type pore free membranes

08 p1234 A71-21091

Ti-Mo alloys porous materials for work in hot solutions of nonoxidizing acids, discussing production technology and corrosion resistance

08 p1317 A71-21857

Mercury intrusion porosimetry application to pore size and shape measurements for porous solids, discussing solid and air compressibilities, surface tension, contact angle, etc

09 p1453 A71-22168

Sponge iron sintered powder compacts deformation behavior from uniaxial compression tests, proposing plasticity prediction criteria

09 p1466 A71-22169

Liquid-solid interface phenomena during sintering and porous materials impregnation by liquid metals, using spherical and nonspherical particle models

09 p1457 A71-23391

Binary phase systems stress analytic method for water saturated elastic porous medium

10 p685 A71-39993

Porous structure effects in oxygen consuming cathode, discussing electrode thickness, effective pore diameter, pressure difference and electrode performance

11 p1709 A71-25553

Partition walls sound insulation by porous absorbers, discussing differential equations and acoustic properties

12 p1929 A71-27062

Gas flow heat loss through porous metals, deriving hydraulic resistance and heat release coefficients

13 p2165 A71-29218

Porous glass hyperfiltration membranes stabilization by aluminum chloride solution, noting retreatment need

13 p2026 A71-29377

Porous carbon and graphite substrates chemical vapor deposition carbon infiltration process, discussing isothermal and thermal and pressure gradients techniques

14 p2262 A71-29652

Hollow carbon microspheres from pitch material, emphasizing applications in porous composites

14 p2263 A71-29657

Porous Ti-Mo alloy materials for operation in hot solutions of nonoxidizing acids, discussing production technology and corrosion resistance

14 p2260 A71-30836

Explosives in porous state under impact loads, obtaining adiabats, compressibility and temperatures

15 p2511 A71-31384

Porous refractory materials for thermochemical protection against high temperature plasma flow, discussing effectiveness in erosive wear reduction

15 p2432 A71-32164

Coolant thermophysical properties effect on heat transfer intensity in porous metals, analyzing differential equations

17 p2835 A71-34204

High porosity carbon-graphite materials thermal and electrical conductivities at high temperatures by potentiometric method 17 p2761 A71-34208

Ionizer, neutralizer and ion optics of cesium contact ion thruster, examining porous W materials technology [DGLR-71-033] 17 p2793 A71-35535

Sealing porous metal castings and powdered parts, discussing impregnation by vacuum-pressure and internal circulatory methods and sealant types 18 p2928 A71-36838

Diaplectic glass formation by experimental shock loading of orthoclase in porous mixtures 19 p3084 A71-37662

Counterflow methane diffusion flames structure in forward stagnation region of porous cylinder, measuring velocity, temperature, concentration, reaction rate and heat release rate profiles 19 p3168 A71-38108

Porous material slab pyrolysis, studying density and thermal conductivity changes and reaction kinetics 19 p3170 A71-38117

Strain rate dependent constitutive relation for shock propagation in porous materials, discussing relaxation time 21 p3465 A71-40794

Computationally convenient equation of state describing porous materials shock response 21 p3466 A71-40795

Porous Cu and W shock loading properties, discussing principal Hugoniot data for P alpha dynamic response model 21 p3466 A71-40796

Porous materials prepared from electrolytic Cr powder, noting high permeability and strength and filter applications 23 p3689 A71-43252

Temperature field measurements above porous surface during ice-water sublimation into vacuum, showing discontinuities due to external heat and mass transfer 23 p3784 A71-44340

Porous fiber reinforced composite low density heat insulating materials thermal conductivity measurements, showing energy transport by heat transfer mechanisms 23 p3784 A71-44341

Flow and strain analysis and engineering design of porous cylindrical gas film foil bearing at low pressures 24 p3830 A71-44944

Pressure distribution in narrow porous metal bearings solved with Bessel functions in cylindrical coordinates, finding lower load capacity 24 p3830 A71-44950

Heat transfer in transpiration cooled porous heat sources, deriving dimensionless temperature profiles 24 p3891 A71-45185

Gas accumulation mechanisms in porous lunar surface layer, discussing ground samples from Sea of Tranquility 24 p3875 A71-45189

POROUS PLATES

Laminar boundary layer on porous plane plate situated in plasma jet, examining transfer phenomena with chemical reaction 04 p0572 A71-15507

Air injection into turbulent boundary layer flow through porous plate, examining heat transfer and shielding efficiency 05 p0838 A71-16783

Plane incompressible MHD boundary layer on porous plate, considering heat and mass transfer in blowing or suction velocity distribution 06 p0936 A71-17736

Turbulent boundary layer on porous plate with suction and heating, measuring mean velocity and temperature profiles at various locations along wall as function of suction rate 07 p1219 A71-18759

Fluid inertia effect on porous thrust plate, using mathematical model for prediction [ASME PAPER 70-LUB-18] 07 p1088 A71-19625

Viscous conducting fluid MHD fluctuating flow over porous flat plate with time dependent suction, determining skin friction and transient velocity profiles 07 p1169 A71-20028

Uniform magnetic field effect on rarefied gas slip flow over porous flat plate for skin friction response, using velocity and temperature fields equations 10 p1649 A71-24407

Steady two dimensional MHD laminar flow between two parallel circular porous disks in transverse magnetic field, determining velocity, pressure and shear stress distribution 10 p1649 A71-24408

Velocity, temperature and concentration profiles correlation for compressible turbulent boundary layer along porous flat plate, with carbon dioxide injection, discussing cooling applications 10 p1598 A71-25095

Laminar source flow between rotating parallel porous disks with equal suction/injection rates solved for infinite radius series, discussing radial velocity and shear stress distributions 12 p1896 A71-27052

Plane Couette flow with suction/injection at stationary plate, obtaining motion and continuity equations, pressure distribution and friction coefficient 13 p2047 A71-28520

Compressible laminar boundary layer flow over semiinfinite isothermal porous flat plate in nearly quasi-steady motion, considering skin friction and heat transfer 13 p2048 A71-28600

Simultaneous partial differential equations, applying to one directional diffusion in finite porous slab accompanied by chemical reaction 13 p2025 A71-29011

Viscous gas flow past semiinfinite porous plate with gas injection or suction and identical composition in outer flow 14 p2224 A71-30002

Incompressible laminar skin friction calculation on porous plate by Karman-Pohlhausen method, considering surface blowing 15 p2392 A71-32118

Gas cooled porous plate unsteady temperature field during high temperature action, considering thermoradiative, convective and mixed radiative-convective heat transfer 16 p2662 A71-32833

Air injection into turbulent boundary layer flow through porous plate, examining heat transfer and shielding efficiency 16 p2662 A71-33035

Heat and mass transfer through porous plate into turbulent two dimensional incompressible boundary layer, using Van Driest damped mixing length [ASME PAPER 71-HT-10] 19 p3045 A71-37986

Fuel rich premixed hydrogen-oxygen flame stabilization on cooled porous plate burners at 10 mm Hg 19 p3168 A71-38107

Pressure sensors thermal protection by porous Zr disk as heat shield, considering acoustic transparency, linearity, transient response and air flow resistance [ONERA-TP-957] 22 p3547 A71-42501

POROUS WALLS

Heat transfer between rarefied monatomic gas and porous wall, examining temperature jump with model kinetic equation for Knudsen layer 01 p0179 A71-10612

Gas and fluid flow through flat and cylindrical porous cermets walls, determining permeation energy loss and radial flow hydraulic resistance 02 p0240 A71-12277

Turbulent flow near porous wall with pressure gradient, calculating velocity and shear distribution by modified Van Driest theory 03 p0399 A71-13432

Heat exchange in dissociating partly ionized gas flow over critical point on permeable surface with injection into laminar boundary layer 03 p0342 A71-13748

Steady incompressible laminar pipe flow within porous wall cylinder, determining velocity, pressure distribution and shear stress [ASME PAPER 70-WA/FLCS-3] 03 p0401 A71-14079

Turbulent heat and mass exchange intensity at gas screen, investigating nonisothermality and wall penetrability effects 04 p0683 A71-15497

Supersonic compressible turbulent boundary layer on porous cylinder with air injected through wall, investigating heat transfer 04 p0571 A71-15498

Aqueous acid solution turbulent boundary layer characteristics during alkali solution injection through porous surface in presence of positive pressure gradient 04 p0576 A71-15614

MHD oscillating flow along infinite unmagnetized conducting plane porous wall, deriving temperature field in boundary layer 06 p0937 A71-18231

Tilting pad hydrodynamic and porous hydrostatic gas lubricated journal bearings for miniature cryogenic turbomachinery [ASLE PREPRINT 70LC-10] 08 p1298 A71-21158

Incompressible inviscid fluid flow in presence of two homogeneous porous layers, examining hydrodynamic instability 10 p1591 A71-23754

MHD effects on transpiration cooled Couette flow through porous wall, considering magnetic drag produced pressure differential and shear recovery rates 10 p1649 A71-24404

ABM control surfaces active oxidation protection, using ammonia as reactive coolant injected through porous W wall matrix [AIAA PAPER 71-391] 11 p1837 A71-25353

Partition walls sound insulation by porous absorbers, discussing differential equations and acoustic properties 12 p1929 A71-27062

Laminar boundary layer equations integration for jet propagating along porous surface, determining transverse velocity component effect 12 p1896 A71-27114

Heat exchange at large Prandtl numbers near porous flat wall with liquid injection, calculating Stanton number 13 p2046 A71-28181

Supersonic flow around porous-wall conical body with uniform gas injection through wall, deriving equations for pressure at contact surface 13 p1990 A71-28182

Entrance region laminar flow development under suction or blowing at porous inner wall in concentric annular duct 13 p2160 A71-28602

Radiant heat transfer measurements on sintered gauzes, considering mathematical model of porous wall with sweat cooling 13 p2161 A71-28750

Curved porous wall channels for noise suppression in power plants, ventilation systems, etc 15 p2449 A71-31705

Radiation source consisting of porous wall heated internally by hot gas, noting application as high altitude or space flare 17 p2728 A71-34888

Interior region of incompressible turbulent boundary layer with pressure gradient on permeable wall, discussing local similitude hypothesis 17 p2729 A71-35346

Quasi-stationary viscous incompressible liquid flow in porous tube with deforming wall 17 p2694 A71-35641

MHD equations of motion solved for conducting fluid interaction with electromagnetic field in porous media in range of Darcy law 18 p2953 A71-36948

Plane Couette-Poiseuille flow stability between porous walls with fluid injection and suction causing uniform crossflow 19 p3044 A71-37728

Unsteady viscous compressible flow through straight channel with flat porous walls under time varying pressure 21 p3367 A71-40591

Plain externally pressurized thrust air bearings with porous inserts and high supply pressures, comparing with discrete orifice feed 22 p3553 A71-41679

Steady laminar viscous hydromagnetic flow in annulus with porous walls of different permeability, giving wall friction coefficients and velocity distribution 23 p3708 A71-43099

Heat and mass transfer in binary laminar boundary layer with free convection on vertical porous surface, integrating momentum and energy equations for upper limits 24 p3887 A71-44744

Compressible gas flow in two dimensional porous wall, calculating heat transfer and mass flow by conformal mapping for Laplace equation solution 24 p3889 A71-44972

PORPHYRA

Rare earth, alkali and alkaline earth elements content of phenocrysts and acidic igneous magma 23 p3734 A71-43246

PORPHYRINS

NT CHLOROPHYLLS

Porphyryns and amino acids chemical bonding under geochemically plausible conditions, considering diagenesis of biogenic compounds and life processes prebiotic chemical evolution 02 p0198 A71-12047

Porphyryns optical and semiconductor properties concerning absorption, electrical conductivity and photoconductivity spectra 06 p0941 A71-17526

Hematoporphyrin chlorhydrate radioprotective effects on mice, removing, weighing and fixing spleens for hematopoietic colonies count 07 p1036 A71-18960

Biochemical luminescence reaction for ferro-porphyrin proteins determination in extraterrestrial life detection 13 p2009 A71-28684

Porphyry-like pigments in Apollo 12 lunar soil sample 12023, using spectral analysis involving fluorescence, absorption and magnetic circular dichroism spectrometry 23 p3756 A71-43739

Apollo 12 lunar surface fines examination noting absence of porphyryns 23 p3756 A71-43740

PORTABLE EQUIPMENT

Lunar communications relay unit, discussing system design, capability and tradeoffs 01 p0035 A71-10919

Portable direct reading spectrometer for monitoring oxygen-hydrogen containing contaminants in gas tungsten arc welding process
02 p0247 A71-11712

Skyнет type 3 and 4 transportable ground stations, describing antenna, radio cabin with IF and control equipment and channeling cabin with baseband equipment
02 p0217 A71-12437

High efficiency spherical reflector antennas with scanning and multiple feed properties for communication satellite portable earth stations
02 p0233 A71-12792

Skyнет satellites earth stations design, structure, transportation and erection ease, considering operational and stowed position survivability in high velocity winds
02 p0223 A71-12804

Transportable photoelectric satellite tracking system with 4-axis support for Schmidt-Cassegrain telescope, discussing field testing results
03 p0397 A71-14004

Portable photoelectric recorder for solar limb vibration frequency spectrum and amplitude measurements
04 p0590 A71-14844

Thermoconductometric portable hydrogen analyzer for air around industrial centers, using bridge tungsten sensor network
04 p0601 A71-15675

Portable Cf 252 neutron radiographic camera, noting reactor fuel and concrete polymer content measurements
07 p1119 A71-19950

Rail track roughness and irregularities evaluation by railcar vibration measurements, using portable LF low amplitude acceleration measuring and recording system
[AIAA PAPER 71-384] 11 p1845 A71-25349

Total emittance measurements by portable IR reflectometer, tabulating nongray error effects
13 p2159 A71-27979

Gunn effect diode in portable Doppler radar, describing electron transfer, negative resistance and domains formation and propagation
13 p2040 A71-29238

Mobility definition and measurement methods, discussing portable instrument and vibration testing application
14 p2252 A71-30056

Low cost go/no-go portable aircraft engine tester connected to engine mounted sensors
14 p2221 A71-30327

Satellite telecommunication systems, considering standard and small transportable ground stations and Intelsat system
17 p2696 A71-34233

Portable self contained Imacon image converter high speed camera system capable of framing and streak operation
18 p2924 A71-36614

Transportable high radiance lunar ranging laser system, describing optical equipment in ruby and Nd-glass laser experiments
18 p2883 A71-36917

Portable run-of-wind recorder featuring variable gear changes to facilitate range adjustments
18 p2925 A71-36960

High resolution portable hologram recording camera with pulsed ruby laser light source and rechargeable storage batteries as self contained power supply
21 p3380 A71-40926

Mobile monitoring and testing meteorological laboratory design and equipment for automated station network, considering pressure sensors, thermohygrostat and wind measurement
21 p3365 A71-41381

PORTABLE LIFE SUPPORT SYSTEMS
Advanced regenerative portable life support system concept analysis for long duration and multiple extravehicular activity
[ASME PAPER 71-AV-10] 18 p2866 A71-36377

PORTS [OPENINGS]
Internally ported vortex amplifier, presenting dynamic equivalent circuit with transfer functions
07 p1025 A71-20555

Static pressure port errors in hypersonic turbulent flow, using approximate shear layer momentum balance for pressure increase derivation
[AIAA PAPER 71-270] 08 p1228 A71-21996

POSITION
S-wave elastic positron-hydrogen scattering in ionization region, estimating error in extrapolated t matrix from complex energy
19 p3106 A71-37375

POSITION [LOCATION]
NT SOLAR POSITION
Visual threshold dependence on retinal location for various colors under conditions of scotopic, mesopic and photopic adaptation
01 p0009 A71-10233

Disordered materials electronic structure band states localization, examining mobility edges
01 p0140 A71-11441

Radio sources position measurement with three-element interferometer by self calibrating technique
02 p0314 A71-12577

Radio sources optical position measurement on Schmidt plates
02 p0314 A71-12578

Pulsar pulse arrival times measurement for general relativity theory test, determining positions and period change rates
02 p0315 A71-12660

Lagrange points role in three body problem, discussing applications to space probe positioning
02 p0316 A71-12739

Triangulation position fix techniques employing lines of bearing, n-locus, least square fits and resection by intersection method
02 p0280 A71-12900

Cosmic ray nuclei galactic disk confinement determination, considering particle mean age by radioactive Be10 tracer method
03 p0480 A71-14052

Minor planets precise position tabulations, correcting previously published data
03 p0493 A71-14195

Passive mode navigation satellite position fixing, using synchronous satellite and Loran type chart with correction tables
04 p0622 A71-15004

Balloon position determination in Venusian atmosphere, using ranging measurement and radiated signal polarization
04 p0623 A71-15014

Lunar position on stellar field for ephemeris time determination, discussing planet and satellite positions with respect to astronomical constants
05 p0809 A71-16460

Celestial bodies position determination, discussing optical observation, interferometry, radar, lasers and applications
05 p0811 A71-16650

Radio emission from small galactic nebulosities, describing position, flux densities, identification and exciting stars
05 p0811 A71-16683

X ray sources identification and position measurements near galactic center on basis of rocket experiments
05 p0814 A71-17234

Pulsar data tabulation of positions, dispersion measures, and class I pulse periods and widths
06 p0966 A71-17676

Computer program for determining roving vehicle position and heading on lunar surface by landmarks
08 p1332 A71-21348

Suzuki-Sato-Seki and other 1970 comets, discussing position observation and ephemeris calculation
09 p1516 A71-22069

Aerial photographs orientation point location, relating measurement weight of transverse parallax
09 p1451 A71-23178

Simulated artificial satellite position determination, using experienced and inexperienced observers
09 p1528 A71-23547

Fog droplet and rain effects on propagation of echo location signals from bats
10 p1638 A71-24423

Cygnus X-1 and X-2 X ray source location from Uhuru satellite measurements
11 p1814 A71-25213

Eccentric satellite observation, considering geodesic determination of coordinate difference between observation station and reference point
11 p1732 A71-25818

Radio source and associated elliptical galaxy major axes position angles correlation
13 p2135 A71-28299

Locating neutral layer and critical curvature radius in aircraft components waffle panels under elastoplastic bending
13 p2074 A71-28940

Distant artificial cosmic objects coordinate determination by image converter/closed TV system screen photography and TV observations of space probes
14 p2309 A71-29992

Thunderstorms and lightning flashes location determination by ground based and satellite measurements of disturbance induced RF noise, using atmospheric spectral characteristics for range estimating methods
14 p2203 A71-30958

Positions and flux densities of radio sources from Fourth Cambridge catalog by pencil beam measurements at 408 MHz, using Molonglo telescope
15 p2485 A71-31697

Optical positions of 87 identified extragalactic radio sources between declinations plus 19 and minus 80 deg, using Palomar Sky Survey plates and prints
15 p2489 A71-32398

Autonomous location determination for rotating dynamic plant with inertial platform by constructing finite rotation vector
17 p2775 A71-35601

X ray source Cygnus X-1 location measurement by balloon, noting agreement with Uhuru data
18 p2959 A71-37052

X ray source Cygnus X-1 position determination by Aerobee rocket-borne rotating modulation collimator
18 p2970 A71-37053

Position determination on planetary surface from gravity and star line-of-sight direction measurements, presenting numerical results for Apollo lunar landing missions
[AIAA PAPER 71-900] 19 p3095 A71-37151

Geometrical optics convergence coefficient in earth ionosphere waveguide for arbitrary transmitter receiver location
19 p3017 A71-37866

NASA Staden and Speopt optical and laser tracking sites dynamic position estimations from GEOS 1 and 2 observations, analyzing model error effects
20 p3220 A71-39662

Geodetic locations of Doppler satellite observing stations consistent with CIO pole and astronomical determinations
[AAS PAPER 71-341] 23 p3666 A71-43014

X ray sources pulsation limits and locations determination by rocket-borne rotating modulation collimator
24 p3866 A71-44914

Eclipsing variables period change dependence on spherical coordinate of stellar position in sky from O-C diagrams
24 p3873 A71-45080

Position line location determination by discrepancy moduli sum minimization algorithm
24 p3846 A71-45161

Selenodetic catalog centers mutual positions determination from lunar near side hypsometric charts
24 p3875 A71-45316

POSITION ERRORS
Short pulse optical tracking systems ranging error, analyzing effects of tracker, target and propagating medium characteristics
02 p0214 A71-12029

Radio sources position errors, comparing optical and radio measurements
02 p0314 A71-12579

Orbiting vehicle state variables at ballistic transfer termination for known injection errors, calculating fuel consumption for final adjustments
03 p0485 A71-13249

Heading of object moving on terrestrial sphere surface with inertial navigation aid, calculating asymptotic stability for position determination on computer
03 p0459 A71-14355

Hybrid computer simulation of three degree of freedom surface to air missile trajectory, obtaining cluster of points for position errors
04 p0642 A71-14798

Range and range rate measurement errors between ground station and artificial satellite, investigating atmospheric refraction effects
04 p0661 A71-15003

Geodetic survey adjustment and accuracy improvement using satellite radar range and ballistic camera data
04 p0583 A71-15302

Geodetic position rapid determination accuracy by Doppler satellite observation
04 p0583 A71-15304

Mars photographic positions on double short focus astrophotograph with random error for ascent and declination
07 p1194 A71-19332

Deimos and Phobos position measurements by photographic observations, including refractor and astrophotograph errors
07 p1194 A71-19333

Altazimuthal telescope mounting with computer controlled guidance, discussing instrumental and methodical error effects on positioning and tracking accuracy
07 p1083 A71-19348

Celestial and satellite navigation sensitivity for Lunar roving vehicle (L/RV) position fix
07 p1157 A71-20414

Longitudinal direction positioning error effects on grating lobe field deviation and reduction in uniform linear arrays
08 p1257 A71-21885

Instrument orientation optimization for ballistic missile applications, emphasizing acceleration induced velocity and position errors
11 p1796 A71-26410

Moving window and feedback integrator type scanning radar detectors performance comparison based on probability and position estimates by Monte Carlo simulation
12 p1882 A71-27441

Observation errors in double star studies, considering inclusion of corrections in Central Catalog
14 p2311 A71-30370

Combined inertial and instrument landing aircraft navigation systems with reduced cross runway position and velocity errors, using optimal linear estimation
14 p2272 A71-30606

Camera vibration, and refraction anomaly effects on error of designated position for star or satellite
14 p2250 A71-31120

Stereoscopic effects and apparent shape or position of moving objects at relativistic speeds under binocular observation 16 p2535 A71-33166

Schmidt telescope as astrometric instrument, comparing mean error with catalog positions 16 p2578 A71-33322

Correction method for satellite radio tracking errors due to VHF refraction in atmosphere 16 p2543 A71-33832

Integrated airborne Omega/inertial navigation systems performance prediction using statistical models for position fix errors 17 p2776 A71-35769

Radio tracking of aircraft by two geostationary satellites, discussing measurement, navigation and position errors 18 p2945 A71-36508

Aircraft position errors computation for ATC mathematical surveillance models, estimating collision risk [AIAA PAPER 71-927] 19 p3097 A71-37173

Visual target pursuit tracking test confirming error amending by central mechanism without sensory feedback 19 p3007 A71-37545

Radio sources position data table based on high accuracy telescope observation including calibration uncertainties and measurement random errors 19 p3142 A71-38008

POSITION INDICATORS

NT PLAN POSITION INDICATORS

NT RADIO DIRECTION FINDERS

NT SPACECRAFT POSITION INDICATORS

LOLA /Location and Orientation of Lunar Astronauts/ system using RF ranging and solar sensor, discussing configuration, operation, accuracy and electronics 04 p0623 A71-15303

Ultrasonic position sensor for automatic control, using short pulses for azimuth and range resolution 06 p0896 A71-17321

Fluidic noncontact position sensor, investigating flapper insertion effect on laminar jet flow 07 p1030 A71-20599

Fluidic coincidence position sensors, using wall attachment amplifiers and nozzle displacement 07 p1030 A71-20601

Selenographic position determination method based on stellar observations 09 p1530 A71-23714

Magnetometer for indicating position of constant level meteorological balloons provided with solar sensors 10 p1612 A71-24759

Precision area navigation system, considering position and velocity continuous measurement in three dimensional space, system components and simulation program 17 p2771 A71-34616

GALAXY machine for measuring image position and brightness and converting Schmidt telescope photographic data into computer form, outlining design and development 17 p2741 A71-34996

POSITION SERVOS

U SERVO MOTORS

POSITIONING

Space communication reflector surface positioning and optical measuring techniques for best fit 02 p0234 A71-12805

Al-Mg alloy positional welding for porosity elimination 09 p1457 A71-23356

Ion microthruster for satellite orbit and position corrections, describing optimum performance characteristics and test facility [DGLR-71-032] 17 p2795 A71-35548

Dynamic positioning stationkeeping and stability criteria for formation flight systems extended to helicopter and V/STOL transports 18 p2849 A71-35923

Dogs intrapleural and intraesophageal pressures dependence on head positions 19 p3010 A71-38564

Aircraft lateral dynamics effect on positioning accuracy along straight flight path, using Loran C data 20 p3261 A71-38864

POSITIONING DEVICES [MACHINERY]

NT BOOMS [EQUIPMENT]

NT CAMS

He-Ne laser as detectors in mine boring, quality/compensational control, data collection/reduction and positioning accuracies 09 p1458 A71-23409

Max Planck Institute 100 m radio telescope at Bonn with all motions fully controllable, describing foundation constructional details, reflector structure and positioning gear 14 p2214 A71-30813

High angular resolution optical telescopes, considering mirror materials, optical coatings and pointing systems 16 p2580 A71-33739

Optical telescopes automatic electronic control by positioning mechanical axis to specified coordinates and tracking guide star 17 p2740 A71-34983

Digital computer process controller for telescope with driving system consisting of single worm wheels for tracking and slewing 17 p2740 A71-34985

Automatic star follower for camera by optically splitting stellar image and measuring radial displacement by comparing signals 17 p2740 A71-34987

Skylab pointing and control system using control moment gyros and cold gas reaction thruster system to provide attitude control 17 p2813 A71-35064

Precision tracking and pointing of laser beams in space for communication, discussing large space telescope /LST/ applications 18 p2920 A71-36090

POSITIVE FEEDBACK

Regenerative feedback amplifier with maximally flat amplitude-frequency response 04 p0556 A71-14621

Regenerative transfer amplifiers normalized reactive parameters effects on phase linearity 06 p0872 A71-17376

Unstable high speed optronic /photoelectric/ flip-flop memory elements with positive optical feedback 07 p1075 A71-19303

Frequency characteristics calculation of regenerative two cavity microwave bandpass amplifiers, applying to parametric and quantum amplifiers and underexcited microwave relaxation oscillators 09 p1413 A71-22157

Superregenerative linear mode amplification in Q switched He-Xe laser as function of resonator phase, length and signal angle 10 p1621 A71-24713

Differential phase frequency characteristics of low noise or tunnel diode regenerative amplifiers 11 p1738 A71-25941

Parametric regeneration amplifier with capacitor modulation by signal voltage only 15 p2378 A71-32633

Differential phase frequency characteristics of low noise or tunnel diode regenerative amplifiers 20 p3205 A71-39261

Regenerative feedback amplifier with maximally flat amplitude-frequency response 22 p3521 A71-42261

Dynamic active element model of electroluminescent image converter with positive optical feedback, using voltage-brightness approximation 24 p3808 A71-44389

Regenerative nonlinear RC amplifier oscillations due to series opposed varicap diode capacitance 24 p3810 A71-45261

POSITRON ANNIHILATION

Annihilation quanta detector and positron source for gas density measurement, noting sensitivity, counting interval and Be covering thickness 07 p1164 A71-20178

Positron annihilation rates in lanthanum hydrides of various composition 09 p1506 A71-22148

Low energy gamma ray measurements by balloon flights, detecting peak energy due to electron-positron annihilation 15 p2479 A71-32077

POSITRONIUM

Positron-hydrogen scattering below positronium pickup threshold by Hylleraas bound technique, discussing phase shifts and linear parameters 11 p1803 A71-26372

POSITRONS

Electron-positron pair production during focusing of laser radiation in dense plasma 01 p0135 A71-11094

Supernovae positrons and low energy cosmic rays flux, determining ejected matter plasma properties 01 p0145 A71-11338

Electron-positron pair production during focusing of laser radiation in dense plasma 08 p1342 A71-21952

Positron-hydrogen scattering below positronium pickup threshold by Hylleraas bound technique, discussing phase shifts and linear parameters 11 p1803 A71-26372

S wave scattering from H and He positron systems at low energies, applying Kohn and Harris variational methods 11 p1803 A71-26373

POSTERIOR SECTIONS

Posterolateral thalamus nucleus neurons response to visual, acoustic and somatic stimuli in cats with microelectrodes 22 p3490 A71-42578

POSTFLIGHT ANALYSIS

Postflight analysis including six degree of freedom trajectory digital simulation of Aerobee 350 sounding rocket behavior under large thrust misalignment [AIAA PAPER 70-1380] 03 p0498 A71-13663

MITOL problem-oriented compiler language for real time and postflight telemetry data processing 04 p0556 A71-15295

Skin tissues autmicroflora composition and natural immunity indices changes after 18 day orbital flight from microbiological and immunological examinations 09 p1389 A71-22204

Postflight histological analysis of turtles aboard Zond 7, noting decrease in cell nuclei size due to space flight conditions adaptation 21 p3334 A71-40568

POSTULATES

U AXIOMS

POSTURE

Coronary hemodynamic responses to postural changes in hemorrhaged dogs involving head-up and head-down tilts 11 p1720 A71-26114

Joint action of various afferents in regulation of human posture, considering appropriate differential reactions 13 p2003 A71-27833

Posture and lower body negative pressure effects on human heart rate and blood pressure 23 p3636 A71-44241

POTABLE LIQUIDS

NT POTABLE WATER

POTABLE WATER

Feeding systems, potable water and waste disposal in space cabins 08 p1245 A71-20730

Automated self sterilizing breadboard unit for potable water reclamation from urine by electrolysis-electrodialysis for long term space missions [ASME PAPER 71-AV-11] 18 p2866 A71-36378

POTASSIUM

NT LIQUID POTASSIUM

NT POTASSIUM ISOTOPES

Potassium vapor emission spectrum fine structure in high power ruby laser field, noting dependence on vapor pressure 02 p0262 A71-12612

Apollo 11 igneous rocks potassium content vs irradiation exposure age, comparing lunar geology models 06 p0966 A71-17897

K-U abundance systematics in Apollo 11 and 12 lunar rock suites and earth crust 06 p0968 A71-17961

Ehrlich ascites tumor cell membrane potassium and electrophoretic mobility loss, investigating radiation effects under radiosensitizing and radioprotecting drugs 07 p1036 A71-18956

MHD generator with Ar-K plasma, examining electrical insulation behavior 08 p1237 A71-21930

Preionization and velocity effects in MHD channels containing potassium seeded argon plasma at atmospheric pressure 11 p1804 A71-25488

Apollo 11 and 12 lunar samples compared with deep earth rocks, noting potassium-uranium ratio 14 p2318 A71-31126

Three stage potassium vapor turbine for space systems electric power generation, discussing erosion and endurance tests 15 p2415 A71-32214

Resonance radiation field of positive column of low current electric arc burning in nonequilibrium Ar plasma with admixture of K, using optical probe 15 p2457 A71-32270

Hypoxia effects on myocardial potassium balance in dogs during cardioaccelerator nerve and atrial stimulation 16 p2529 A71-33195

Temperature stabilization with self controlled water and radiation cooled heat pipes using argon in addition to K heat transfer medium 16 p2663 A71-34039

Na and K transition oscillator strengths, noting core polarization effects on mathematical model 16 p2615 A71-34088

Vapor bubble growth on heated surface with random temperature distribution and liquid microfilm for water and boiling potassium 17 p2836 A71-34306

Potassium-argon age determination for shock-metamorphosed anorthosites of Manicouagan-Mushalagan Lakes structure 19 p3049 A71-37657

K-Ar dating of shock metamorphosed rocks from Brent impact crater /Ontario, Canada/ 19 p3050 A71-37658

Potassium concentrations and osmolality levels changes effects on vascular resistance in subcutaneous adipose tissue blood flow 20 p3189 A71-39379

Potassium photoionization cross section, including spin-orbit interaction, orientation of photoejected electrons and dipole transition moment correction due to core polarization 21 p3417 A71-40197

Fission track and K-Ar ages of coexisting minerals in drill core from heat-flow boreholes in western central Sierra Nevada batholith 21 p3374 A71-40649

Mineralogy, chemistry and origin of KREEP /potassium, rare earth element and phosphorus/ component in Apollo 12 soil and breccia samples from Ocean of Storms 23 p3741 A71-43632

Ar-K and He-R plasma conductivity measurement at atmospheric pressure from equilibrium to nonequilibrium conditions, using electrostatic probes 23 p3714 A71-44275

Residual resistance measurements for studying recovery of high purity potassium wires deformed at/below 4.2 K, discussing anomalous difference with sodium 24 p3861 A71-45195

POTASSIUM ALLOYS
NaK lubricated segmented hydrodynamic fluid film tilting pad type journal bearings and Kingsbury type self aligning thrust bearings 15 p2447 A71-32210

POTASSIUM BROMIDES
Cadmium telluride epitaxial films on potassium bromide, investigating external gases effects on photovoltaic properties 07 p1179 A71-19919

Shock wave splitting in KBr, determining shock profiles and velocities by electromagnetic method 15 p2463 A71-31385

POTASSIUM CHLORIDES
Sm double plus ion sites distribution in KCl by spectroscopy 09 p1506 A71-22147

KCl films exciton-induced photoemission, discussing mechanism of photoelectron emission rise with time under steady UV radiation 09 p1508 A71-22685

Liquid KCl and LiF surface films effect on combustion rate of ammonium perchlorate mixtures with polystyrene or polymethyl methacrylate for various initial temperatures 15 p2462 A71-31371

Optical absorption and electron spin resonance in KCl with and without KOH, noting F band existence 21 p3414 A71-40070

Trapped hydrogen atoms detection in proton irradiated KCl and NaCl single crystals at 77 K, using electron paramagnetic resonance spectroscopy 24 p3802 A71-44425

POTASSIUM COMPOUNDS
NT POTASSIUM BROMIDES
NT POTASSIUM CHLORIDES
NT POTASSIUM HYDROXIDES
NT POTASSIUM OXIDES
NT POTASSIUM PERCHLORATES
NT POTASSIUM PHOSPHATES
Potassium niobate single crystals domain structures by interferometry, discussing surface deformations, dipole couplings and temperature dependent angles 06 p0941 A71-18039

POTASSIUM HYDROXIDES
Hydrazine concentration measurement in potassium hydroxide, describing instrument design and operation 06 p0900 A71-18014

Optical absorption and electron spin resonance in KCl with and without KOH, noting F band existence 21 p3414 A71-40070

POTASSIUM ISOTOPES
Resonance line radiation polarization of potassium and cesium isotopes excited by electron impact 09 p1496 A71-22187

K-Ar age measurement by optimizing integrated neutron flux and sample size parameters, using graphical method 10 p1601 A71-24411

K-Ar isotope ages of whole sample and feldspar concentrate from apollo 11 lunar rock 10003 16 p2633 A71-33349

POTASSIUM OXIDES
Respiratory gas reaction mechanism on potassium superoxide in closed circuit breathing apparatus 13 p2021 A71-29113

POTASSIUM PERCHLORATES
Burning rate of compressed charges of potassium perchlorate with lead dinitrophenolate at constant pressure 15 p2462 A71-31372

Combustion model of solid composite propellants containing monopropellant oxidizers ammonium perchlorate, cyclotetramethylene-tetranitramine and potassium perchlorate 19 p3121 A71-38122

POTASSIUM PHOSPHATES
Contact electro-optic KDP crystal shutters for Q switching ruby laser 06 p0907 A71-17530

Q switched Nd laser pulse duration control as function of KDP crystal orientation and pumping power 07 p1122 A71-19138

Coated abrasive grinding of Ti alloys using water, various soluble cutting oils and inorganic phosphate solutions as coolants and lubricants 11 p1771 A71-26142

Lossless KDP Pockels cell modulator for high power laser Q switching based on tuned face electro-optical crystal 12 p1905 A71-26813

Surface/volume damage induced by Nd-YAG laser irradiation to LiNbO₃ and KDP crystals in frequency doublers and Pockels cells, using scanning electron micrographs 17 p2790 A71-34376

POTENTIAL ENERGY
NT BIOELECTRIC POTENTIAL
NT CONTACT POTENTIALS
NT COULOMB POTENTIAL
NT ELECTRIC POTENTIAL
NT GEOPOTENTIAL HEIGHT
NT IONIZATION POTENTIALS
NT LOW VOLTAGE
NT PHOTOVOLTAGES
NT PLASMA POTENTIALS
NT SPIKE POTENTIALS
Kinetic energy and available potential energy balance in atmospheric stationary disturbances /standing waves/, using atmospheric flow statistics 01 p0119 A71-10853

Atomic system ground state energy upper bound, considering internuclear distances and removal of restriction for negative definite potential energy operator 04 p0630 A71-15268

Muscular fibers analysis for motoneuron split potentials, using needle electrode 10 p1564 A71-24484

Molecular nitrogen ion potential energy curves based on valence bond method, calculating sextet and quartet states at intermediate internuclear separation distances 11 p1801 A71-25365

Computerized least squares fit of second virial coefficients vs critical temperature to Lennard-Jones potential function for hydrocarbons, halides, alcohols and cyclic compounds 13 p2103 A71-29005

Langer transformation effects on radial equation for internuclear potential curves calculation by Rydberg-Klein-Rees method 14 p2277 A71-30572

Triatomic hydrogen positive ion surface crossing effects in chemical reactions based on potential energy surfaces calculation using diatomics-in-molecules approach 14 p2191 A71-30573

Potential energy minimization for elastic elements with integral loads applied to bending of bar and wedge, using variational method 16 p2659 A71-33995

Stressed state of nonuniformly heated thermoelastic flexible plates with variable elastic parameters, using integral principle of minimum total potential energy 17 p2829 A71-35310

Nonempirical LCAO-SCF-MO method for potential energy surface for ground state of linear helium-hydrogen ion system 19 p3117 A71-37332

Lagrange-Dirichlet and Routh systems stability theorems inversion, proving motion instability in case of potential energy maximum in solutions to differential equations 21 p3414 A71-40092

Cyclic discrete holonomic mechanical systems Liapunov stability analysis, developing matrix formalism for kinetic energy, Routhian, Hamiltonian and dynamic potential energy quadratic approximation 21 p3454 A71-40097

Micropolar continuum, potential energy, stresses and constitutive relations for buckling of large rectangular grid frameworks under axial load 21 p3469 A71-41009

Atomic model potentials for spectroscopic and scattering data, using perturbation theory 22 p3578 A71-42420

Statistical phase space cross sections for helium ion-nitrogen molecule reactions, including dispersion and short range forces in intramolecular potential energy function 23 p3706 A71-43119

POTENTIAL FIELDS
Electric potential and field distribution in dielectric plate insert of rectangular waveguide calculated by net point method using computer program 01 p0051 A71-10149

Pursuit game strategy based on Hamilton-Jacobi formalism, considering internal and external potential fields, optimum trajectories and gravitational and electromagnetic fields 03 p0483 A71-13116

Finite supercavitating wings numerical calculation using acceleration potential method 04 p0526 A71-15210

Resonance phenomena in spiral galaxies, determining stellar orbits, potential and distribution functions 04 p0655 A71-15725

Voltage distribution in transistor base for forward and reverse biases, discussing nonuniform potential distribution 05 p0728 A71-16007

Electrochemical metal machining tool profile two dimensional steady state problem, solving for cathode surface changes as function of interelectrode potential 08 p1296 A71-20854

Translation-rotation motion of elongated body in Vinti potential field 10 p1667 A71-23814

Infinite universe compatibility with gravity potential satisfying Poisson equation, avoiding cosmological difficulties by universal gravitational field sources and sinks introduction 10 p1681 A71-25074

Distinctive visual evoked response potential field patterns resulting from human retina stimulation, using electrode array on occipital scalp 13 p2012 A71-28893

EM field and wave propagation in static and spherical gravitation, obtaining modified Debye potentials and amplitude and eikonal equations 13 p2139 A71-28999

Pressure, velocity and potential distribution of flow around arbitrarily shaped body of revolution during arbitrary motion in perfect liquid 13 p1992 A71-29187

Acoustic tone radiation from subsonic rotor near potential field by interaction with nonuniform inlet flow based on Lighthill aerodynamic sound equation 14 p2225 A71-30210

Normal terrestrial gravitational field potential, taking into account second order variables and distances from earth ellipsoid 16 p2563 A71-33466

Reflex klystron repeller space analysis of potential distribution, electron trajectories, transit time and admittance, taking into account space charge effect 17 p2713 A71-34432

Charged particles transport in thermionic converter near-emitter plasma, determining potential and electron density profiles 18 p2953 A71-36968

Density fluctuation dispersal in uniform magnetoplasma, obtaining expressions for Fourier-Laplace transforms of perturbed density, potential field and flux distribution 19 p3113 A71-37745

Thermionic converters experimental testing, developing kinetic theory of plasma diodes in steady state Knudsen mode for uniform potential distribution 19 p2999 A71-38256

Fluctuations in parametrically excited subharmonic oscillator, deriving steady state probability distribution for amplitude and phase transitions analogous to Brownian motion of particle in potential well 20 p3203 A71-39094

Nuclear forces effects on maximum mass limit of neutron stars models using V gamma type potentials 20 p3304 A71-39945

Voltage distribution in transistor base for forward and reverse biases, discussing nonuniform potential distribution 22 p3524 A71-42756

Conservative Hamiltonian systems with infinitely deep potential wells, obtaining periodic solutions with variational technique 23 p3698 A71-43005

Helmholtz vorticity equation application for indirect determination of inaccessible area geopotential field from satellite data 23 p3700 A71-43305

Magnetic induction by HF current passing over conducting torus enclosed by larger torus, obtaining vector potential, current density and inductance expressions 24 p3857 A71-45232

POTENTIAL FLOW
Plane linear cascades of thin curved profiles, obtaining potential flow velocities and lifting force on leading edge 01 p0001 A71-10339

Two dimensional potential flow theory for incompressible unsteady flow about multiple lifting bodies in small amplitude motion 01 p0071 A71-10929

Hess solution for heavy body rotating about fixed point, considering cavities filled with ideal incompressible fluid in turbulent and irrotational motion and linear invariant relation 03 p0458 A71-13591

Flat plate wake displacement sources in potential flow, considering high Reynolds numbers outside boundary layer 05 p0695 A71-16960

Inlet turbulence interaction with rotor potential flow as noise source in axial flow fans, developing expression for sound power radiated 05 p0738 A71-17163

Self-consistent polycrystalline model for combined stress state time dependent creep, examining flow potential existence 05 p0830 A71-17236

Submerged moving body in nonviscous incompressible fluid, evaluating finite potential flow field momentum with rigid and free far distant outer boundary 06 p0841 A71-17419

Monograph on transonic shock free potential flow around quasi-elliptical airfoil sections, investigating flow stability under unsteady disturbances

07 p1015 A71-19773

Ideal fluid jets theory, discussing cavitation flows calculation, jet flow and plane steady potential incompressible fluid flow

07 p1091 A71-20080

Potential flow past cylinder with sources and sinks singularities, deriving formulas for aerodynamic characteristics of infinite span wings with boundary layer control

08 p1227 A71-20777

Steady nonrotational flow around rectilinear profile in finite width uniform current in linear theory, calculating fluid exerted forces

10 p1549 A71-23822

Three dimensional unsteady irrotational flow in variable cross section duct, reducing Navier-Stokes equation to Euler equation

10 p1591 A71-23850

Low speed airfoil characteristics calculation by digital computer, using Theodorsen conformal transformation method for potential flow pressure distribution

[SAE PAPER 710389] 10 p1550 A71-24253

Integral equation for solving potential incompressible fluid flow past blade cascade on axisymmetric current surface in variable thickness layer

10 p1593 A71-24369

Ideal incompressible holomorphic fluid plane irrotational motion velocity due to deformable constant area airfoil displacement

10 p1594 A71-24453

Critical speeds for inviscid compressible potential flow past thin elastic cylindrical shells, using long wave approximation

10 p1689 A71-24565

Entrainment induced potential flow near free jets, using equivalent sink distribution derived from known boundary layer solutions

10 p1596 A71-24937

Airfoil profiles coupling method for determining complex potential of two dimensional ideal incompressible fluid flow due to arbitrary airfoil section movement near rectilinear wall

10 p1597 A71-25015

Inviscid incompressible two dimensional jet deflection by various dimension segments, investigating potential flow with Schwarz-Christoffel transformation and free streamline theory

11 p1753 A71-26444

Hydrodynamic analogy for postulates in special relativity theory, analyzing steady and potential flow of inviscid compressible medium for Chaplygin gas with unreal time

12 p1932 A71-27547

Potential flow of incompressible inviscid liquid film along inclined semiinfinite flat plate for large Froude number values, using matched asymptotic expansions method

13 p2047 A71-28485

Plane stationary constant-vorticity incompressible flow region surrounded by potential flow, determining two dimensional velocity distribution by numerical calculation

13 p2050 A71-29220

Two dimensional transonic potential flow near convex corner

14 p2225 A71-30215

Two dimensional subsonic irrotational isentropic flow around thick profiles, using coordinate perturbation method

15 p2343 A71-31167

Supersonic potential flow at large distance from slender body of revolution at angle of attack, deriving nonlinear partial differential equations system

15 p2343 A71-31170

Compressible transonic flow about two dimensional airfoils, developing inviscid nonlinear potential equations by relaxation procedures

[AIAA PAPER 71-569] 15 p2345 A71-31562

Fluid jets along curved or straight walls with non-zero external potential flow, analyzing Coanda effect

15 p2390 A71-32055

Potential vortex with turbulent viscous core and axial velocity excess or deficiency, using integral method with quasi-cylindrical flow approximations to describe core flow

[AIAA PAPER 71-615] 15 p2393 A71-32278

German monograph on incompressible potential flow field calculation about thick rectangular wings with control surfaces and ground effects

15 p2347 A71-32307

Finite element method application to potential flow field problems governed by Laplace equation in fluid mechanics, developing computer program

[ASME PAPER 71-APM-22] 16 p2520 A71-33207

Viscous fluid flow velocities instantaneous potential based on continuous medium, energy conservation and classic kinetic matter theories

16 p2560 A71-34055

Viscous incompressible fluid flow downstream of paraboloid of revolution described by matching boundary layer approximations to potential flow solutions

17 p2727 A71-34673

Steady incompressible flow with potential vortex over flat surface under suction

17 p2670 A71-34889

Two dimensional steady potential incompressible flow past elastic expandable gas filled envelope fastened to edge of plate normal to flow

17 p2730 A71-35640

Aerodynamic perturbation due to single hot-wire probes, comparing with evaluations derived from potential flow scheme

[ASME PAPER 71-APM-T] 18 p2904 A71-36262

Laminar boundary layer structure under semi-infinite potential vortex maintained in incompressible steady flow by appropriate conditions at infinity

18 p2906 A71-36317

Small disturbance transonic flows potential equations numerical solutions, using mixed finite difference theory

18 p2844 A71-36325

High subsonic potential flow calculation past circular cylinder by integral relations method

18 p2844 A71-36326

Subcritical nonlinear potential flows over two dimensional subsonic airfoils by multistrip method of integral relations

18 p2845 A71-36330

Two and three dimensional pistons motion in stationary gas, calculating potential flow characteristics near weak discontinuities as function of piston geometry and acceleration

19 p3043 A71-37099

Relativistic hydrodynamic solution for gravitational interaction of vortex and potential motion of homogeneous medium

19 p3134 A71-37515

Curvature effect on heat and mass transfer from isothermal sphere in potential flow

[ASME PAPER 71-HT-7] 19 p3164 A71-37984

Potential flow and laminar boundary layer separation about profiled circular disks, calculating streamlines

20 p3175 A71-39029

Two dimensional jet flapped symmetric wing in subsonic flow, assuming irrotational flow inside jet bounded by vortex sheets

21 p3318 A71-40172

Spanwise lift distribution over wings and wake formation in thin airfoils of finite aspect ratio in linear subsonic potential flow

21 p3319 A71-40495

Straight line vortices in uniform two dimensional straining field, detailing irrotational strain and simple shear

21 p3320 A71-40501

Plane steady irrotational flow of ideal compressible fluid around jet profile, obtaining Kutta-Joukowski theorem

21 p3322 A71-40580

Incompressible potential cascade flow interaction, presenting approximate method based on blade profile flow expression by power series with distance between cascades as parameter

21 p3322 A71-40685

Potential flow with free surface, comparing finite element and finite difference methods for liquid sloshing problem

21 p3369 A71-40974

Laminar incompressible plane wall jet, calculating flow characteristics for potential core region with integral method

21 p3370 A71-40988

Numerical computation of potential vortex induced laminar boundary layer on circular disks, using two layer asymptotic expansion

22 p3530 A71-41886

Potential two and three dimensional flows past body in presence of rigid wall, using matched asymptotic expansions

23 p3625 A71-43369

Two dimensional potential flow model of Pitot static probe and subsonic free jet interaction, using conformal mapping and hodograph method

[AIAA PAPER 71-998] 24 p3817 A71-44589

Small perturbation development of plane potential motion of ideal incompressible fluid in elliptical region, confirming instability

24 p3821 A71-45219

POTENTIAL GRADIENTS

Magnetoresistance of coil surrounded electromagnetic mechanisms air gaps, noting potential distribution at pole aperture axis

05 p0705 A71-17175

Solar flares effect on potential gradient and air-earth current characteristics, suggesting solar triggered increase in thunderstorm frequency

13 p2130 A71-29107

Atmospheric potential gradient measurements during solar eclipse of 7 March 1970, using airborne and ground observations

17 p2731 A71-34321

Cross power spectral analysis of atmospheric electric potential gradient relation to meteorological parameters, noting diurnal variations

18 p2944 A71-36010

Plane collisionless plasma diode between two hot emitters, considering potential distributions

24 p3808 A71-44551

POTENTIAL PROBLEMS U POTENTIAL THEORY POTENTIAL THEORY

Electromagnetic potentials and Lorentz relation in anisotropic medium, considering Bromwich function and plane wave propagation

02 p0211 A71-11719

Vibrational transition matrix elements for diatomic molecules, using semiempirical Cashion method for potential functions

03 p0460 A71-13497

Axisymmetrical potential theory for two spherical circular disks system, using X-analytic functions for reducing to Fredholm equation

06 p0928 A71-18345

Macroscopic dynamics of many-component plasmas in electromagnetic fields, discussing formulation in scalar complex wave equations containing pressure and electromagnetic potentials

07 p1168 A71-19688

Komkov class of boundary value problems and associated variational principles, discussing necessary conditions for basic functional or potential extremal behavior

08 p1323 A71-20878

Helmholtz and relativistic electrodynamics, discussing kinetic interaction potential using Lorentz invariance

10 p1644 A71-25110

Spherical shell potential extension to shells of differing diameters for intermolecular forces in globular molecules, considering binary gaseous mixtures

11 p1801 A71-25369

Numerical method for computing exact permeability/tunneling probability/ of one dimensional potential barrier

11 p1728 A71-26059

Stellar mass relativistic integral theorems and upper and lower bounds for gravitational potential theory

11 p1830 A71-26106

Solid profile wing motion near solid wall or free surface, using acceleration potential method

12 p1863 A71-27174

Potential theory mixed inverse problem and uniqueness theorem concerning body shape and density determination from external potential of bulk masses

12 p1931 A71-27510

Internal potential of heterogeneous ellipsoids for even and odd power variation of density with coordinates, using depolarization factors

14 p2304 A71-29600

Stokes flow equations solutions existence and completeness, considering vector and scalar potentials

14 p2224 A71-30094

Numerical stress analysis of elastic three-dimensional fracture specimen with edge crack, using singular integral equations analogous to Green boundary formula in potential theory

16 p2655 A71-33181

Geodetic boundary value problem reformulation, using measured gravity values on known earth surface and potential theory

16 p2563 A71-33476

Multidimensional canonical formalism based on field system state description with potentials and momenta

17 p2778 A71-34635

Runner and cavitation characteristics of hydraulic machine with finite blade number and ideal frictionless incompressible working fluid determination by potential theory

17 p2727 A71-34668

Circular symmetry stressed state for flat disk with flat circular crack, detailing potential and elasticity theories

17 p2824 A71-34844

Feinman integral definition and relation to Schroedinger equation for square summable potentials with lower bound

17 p2765 A71-34866

Spherical harmonic expansion of nonhomogeneous oblate spheroid mass distribution potential, giving convergence criterion

17 p2733 A71-35029

Bounded system gravitational fields Debye potentials, using linearized gravitation theory field equations in form similar to Maxwell equations

17 p2784 A71-35341

Co 59-neutron reaction tensor spin-spin potential, using polarized targets of Ho 165 and Co 59 for nuclear spin-spin effect measurement

18 p2949 A71-36681

Dielectric potential operator as arbitrary bounded Lebesgue measurable set, obtaining eigenvalues and eigenfunctions spectrum

18 p2942 A71-36820

Potential function transformation under coordinate rotations, deriving coefficients for Laplace equation series expansion

19 p3138 A71-37755

Cosserat continuum elastic tensor potentials applied to Kirchhoff theory of wave diffraction
20 p3269 A71-39033

Electrical resistivity of structural metal crystal defects in terms of Ziman-Harrison pseudopotential theory
21 p3395 A71-40023

Multibeam holographic interference Gabor theory construction, using variational principle and potential theory
21 p3379 A71-40626

Multibeam holographic interferometry, using variational principle and potential theory
22 p3574 A71-41786

Relativistic gravitation theory, using Lorentz invariant scalar potential and gravitational metric
22 p3575 A71-42355

Periodic solutions to Hamiltonian systems with convex potential, considering application to n-body problem
22 p3568 A71-42694

Lifting configurations unsteady air loads prediction, investigating loading singularities in linearized potential theory
22 p3481 A71-42832

Noble and transition metals dilute alloys electronic structure in hybridized tight binding nearly free electron representation, using Harrison-Kanamori pseudopotential theory
24 p3860 A71-45129

POTENTIOMETERS [INSTRUMENTS]

Solar magnetograph with potentiometers, recording magnetic fields, emission and absorption lines, radial velocity and brightness
04 p0589 A71-14836

Electron beams formation and focusing, including current density distributions, electronic potentiometer recording, parameters and comparison with simulation data
20 p3204 A71-39160

POTENTIOMETERS [RESISTORS]

German monograph on field effect transistors as controllable resistors with applications in adjustable amplifiers and dampers, covering nonlinear harmonic distortion and control dynamics
18 p2887 A71-35961

POTENTIOMETRIC ANALYSIS

Potentiometric measurement of temperature effects on electrical resistance and Hall effect in Ni-Co alloys
14 p2259 A71-30188

Aircraft turbine oils acid number potentiometric determination, discussing automatic titration procedure and apparatus and solvents influence on titration curve and inflection point
18 p2940 A71-36680

POTENTIOMETRY

U POTENTIOMETRIC ANALYSIS

POTTING COMPOUNDS

Clear potting polymers, investigating temperature and ionizing particle irradiation effects on properties
04 p0618 A71-14898

Adhesives in Apollo command, service and lunar modules primary load carrying structures, electrical potting and sealing medium
10 p1630 A71-24067

Plastics as potting compounds in military aircraft electrical systems, investigating resistance to reversion and hydrolytic stability
10 p1633 A71-24115

Electrical potting compounds reversion problems on Air Force aircraft, discussing inherent properties and environmental effects on polyester urethane and polyacrylate compounds deterioration
10 p1633 A71-24116

Potting compounds service life estimation based on accelerated hydrolytic reversion data at high temperatures and humidities
10 p1633 A71-24117

POWDER [PARTICLES]

NT FINES

NT METAL POWDER

NT POWDERED ALUMINUM

Thermal conductivity and diffusivity determination of powders by introducing dispersed metal particles
01 p0182 A71-11447

Ceramic particle compaction as function of size, shape, loading rate and hardness for fused alumina, magnesia and mullite
03 p0448 A71-12973

Aerosol powder suspensions for spectrochemical objectives in plasma jets
03 p0465 A71-13971

Tubular powder channel gas velocity distribution and pressure buildup during burning
04 p0638 A71-15680

Powder combustion unsteady processes equations, taking into account nonadiabatic flame front and chemical reactions incompleteness
06 p1005 A71-17389

Kaolin and quartz powder additions effect on glass-like polymethyl methacrylate specific heat, thermal conductivity and diffusivity
07 p1144 A71-18922

Commercial sodium bicarbonate powder for methane air diffusion flames extinction, noting particle surface areas
07 p1182 A71-19248

Powder form structural adhesives for cost reduction and increased productivity
10 p1614 A71-24066

Detonation sensitivity of ammonium nitrate containing fertilizers, compared with metadinitrobenzene in powder form
10 p1658 A71-25070

Polyimide system application to laminates and molding powders fabrication, exemplifying compression method and cold compaction followed by sintering
11 p1787 A71-25426

Monolayer submicron self supporting particle film samples preparation for sintering by transmission electron microscopy
11 p1763 A71-26150

Measuring system for 180 degree Raman scattering in single crystals, powders, liquids and strongly absorbing solutions
12 p1915 A71-27673

Pipe gas flow with heated solid particles injection, presenting flow equations numerical solution by digital computer
13 p2166 A71-29460

Combination light scattering in liquids, single crystal and crystal powders, employing long lived argon laser with internal mirrors and large diameter capillaries
14 p2255 A71-30585

Vibrational combustion study of powder, using Helmholtz resonators with connected auxiliary combustion chamber
17 p2839 A71-35697

Cylindrical shaped powder samples vibrational combustion, observing acoustic instability with high speed motion picture photography
17 p2839 A71-35698

Cylindrical powder samples combustion stability, noting gaseous and condensed phase interaction effects on sound emission
17 p2840 A71-35699

Nitroglycerin powder combustion acoustic instability, determining mean pressure and sample and combustion chamber geometry effects
17 p2840 A71-35700

Self excitation and amplitude limitation of powder vibratory combustion, considering pressure and sample length effects
17 p2840 A71-35701

Internal ballistics equations of powder solid fuel rocket motor treated as homogeneous chemical reactor
24 p3890 A71-45107

Self similar solution for unsteady powder combustion rate with decreasing pressure, generalizing to rate dependence on pressure and initial temperature
24 p3891 A71-45217

POWDER METALLURGY

Precalloyed hot formed Cr-Ni-Mo and Ni-Mo steels manufactured from powders, considering toughness, tensile properties, fatigue and impact strength
01 p0100 A71-10464

Tensile and stress rupture tests of Co base alloy bars extruded from prealloyed powders made by Ar gas atomization
01 p0100 A71-10480

Cr-alloyed Fe powders fine crystalline structure from X ray analysis
01 p0102 A71-10789

Isostatic pressing for large complex metal powder parts, comparing with die-compacting
01 p0088 A71-10814

Powder metallurgy for fine grain metals and alloys, discussing grain size-mechanical properties relationship
03 p0446 A71-14490

Thermal conductivity and emittance of arc cast and powdered W at 1800-2800 K
04 p0612 A71-15579

Powdered Ni-carbide composites compressibility, noting mixture and pressure effects on compact density
05 p0769 A71-16859

Ti-Be composites produced by powder coextrusion, discussing microprobe studies to determine microstructure thermal stability
05 p0000 A71-17104

[AIME PAPER F-70-3]

Metal powders sintering computer simulated dynamic volume diffusion model based on Laplace equation, comparing calculated growth rates with electron microscope data
06 p0903 A71-17344

Heat treatment and deformation effects on blended metal powder compacts homogenization, using mathematical model
07 p1137 A71-19976

Solid solution reactions analysis for W/TiC powder formation
08 p1304 A71-20993

Zinc electrodes manufacturing processes, describing materials used in electrodeposition and pressed

powder methods, quality control procedures and Zn-Ag batteries electrical characteristics
08 p1297 A71-21088

Ti alloy powders and Ti-base refractory compounds production from Ti alloys wastes
08 p1317 A71-21856

Dispersion hardened Ni and Co alloys production by powder metallurgy, noting elastic distortion due to particle strengthened base material
09 p1474 A71-23294

High temperature Ni and Co alloys powder metallurgy, discussing production, preparation, pressing and sintering
09 p1456 A71-23300

Soviet papers on powder metallurgy covering metal powder fabrication, forming and sintering techniques and materials for friction, antifriction, and heat resistant applications
09 p1478 A71-23388

Thermal reduction methods for refractory metal powders of W, Mo, Zr, V, Hf, Nb, Ta and Ti
09 p1457 A71-23389

Cermet antifriction and friction powder metallurgy sintered materials for working at high temperatures without lubricants, in vacuum and inert gases
09 p1483 A71-23392

Iron base, white cast iron and high alloy powder metallurgy products for antifriction bearing elements
09 p1478 A71-23393

Refractory oxygenless powder metallurgy products in high temperature technology, considering covalent bond formation
09 p1478 A71-23395

Sintering and pressing techniques for compact semifinished products of refractory metal powders including W, Mo, Ta, Nb, Zr and Ti
09 p1457 A71-23396

Discrete phase vs binder strength of inorganic brittle polycrystalline powder metallurgy materials, including alumina and magnesia
09 p1483 A71-23398

Strengthening processes in precipitation hardened and dispersion hardened alloys produced by powder metallurgy
10 p1614 A71-23903

Oxidation resistant high temperature Ni-Al system preparation using powder metallurgy and thermomechanical treatments without sintering
10 p1626 A71-24401

Powder metallurgy parts application in aircraft, illustrating flareless-sleeve coupling nut of pressed and sintered Ti-6Al-4V alloy
10 p1618 A71-24762

Powder metallurgy superalloy parts, discussing production methods and mechanical properties comparison with conventional process products
10 p1618 A71-24763

Spark sintering powder metallurgy using alternating and direct current plus pressure, discussing use in Be components production for aerospace applications
10 p1618 A71-24765

Powders and torch techniques for brazing, including Mn-Ni-Co, Cu-Mn-Ni, Zr-Ti-Be, Ti-Cu-Ni and Zr-Be alloys
11 p1769 A71-25746

Sintering time effect on initial permeability of Ni-Fe-Cu-Mo alloy made by powder metallurgy
13 p2086 A71-28626

Ti alloy powders and Ti-based refractory compounds production from Ti alloy scrap, describing electrorefining, hydrogenation and carbidization processing
14 p2260 A71-30835

Comparative creep rupture properties of tungsten-rhenium consolidated by arc melting and powder metallurgy, considering rupture life and rupture ductility
15 p2427 A71-31818

Creep rupture properties of W-Re arc melted and powder metallurgy materials at 1650 and 2200 C as function of time, void and grain size
15 p2428 A71-31819

Optimum sintering temperature, bulk composition and gas medium effects on structure and mechanical properties of silicon nitride and silicon carbide materials
15 p2437 A71-32670

Structural shapes extrusion technique with superalloy powders, noting fine grain, chemical homogeneity and elevated temperature mechanical properties
16 p2592 A71-33540

[ASM PAPER W71-5.4]

Pressure distribution during cold rolling of metallic powders of stainless steels, iron, titanium and copper, using dynamometer mounted in roll
19 p3075 A71-37107

Nichrome powder microstructure characteristics effect on hot compaction kinetics, considering temperature, pressure and preliminary heat treatment effects
19 p3075 A71-37108

Sintered metals and powder metallurgy technology, discussing methods and materials available to widen applications
22 p3562 A71-42225

- Solid powder metallurgy tungsten alloys, determining scale factor effect on bending strength and fatigue limit
23 p3693 A71-44226
- POWDERED ALUMINUM**
Limiting temperature and size conditions for aluminum particle ignition in mixtures of oxygen with argon and nitrogen
03 p0468 A71-13990
AL particle size and filler volume optimization effects on epoxy composite dynamic response
07 p1139 A71-20136
Al particle burning in oxygen and water vapor, examining surface oxide film role in ignition mechanism
08 p1376 A71-21908
Burning mechanism of condensed ballistite compositions with metallic particles of aluminum, magnesium and ammonium perchlorate
08 p1376 A71-21912
Al particles combustion kinetics in propellant flames, showing gas composition and pressure effects on burning rate
15 p2464 A71-31633
[WSS/CJ PAPER 71-24]
Aluminum powder filled epoxy composites, investigating particle size and filler percent effects on damping properties and elastic modulus
17 p2762 A71-34819
High temperature gas dispersed Al particle flow, investigating electrical conductivity and radiation properties
19 p3161 A71-37265
Aluminum particles ignition by focused laser flux in controlled oxygen-Argon environment, observing by cinephotomicrography throughout entire burning time
19 p3169 A71-38114
Al and Mg powder dispersed in solid ammonium perchlorate oxidizer, investigating various combustion mechanisms
19 p3120 A71-38120
Gortler-Taylor vortices visualization in liquids between rotating concentric cylinders using pulverized aluminum
20 p3213 A71-39781
Crystal Al powder electrolytic production in inert atmosphere, discussing fractional composition, current efficiency, gravimetric density and particle morphology
24 p3837 A71-44734
- POWDERED METALS**
U METAL POWDER
POWDER
Power meter for large or divergent CW or pulsed laser beams
03 p0427 A71-13919
- POWER AMPLIFIERS**
Push-pull power amplifiers with class B complementary transistors, describing driver stage
02 p0229 A71-11693
Communication satellite earth station technology, considering steerable antenna subsystems, high power amplifiers, terminal equipment and frequency bands allocation
02 p0222 A71-12787
Broadband hybrid UHF integrated power amplifiers providing high output, noting integration techniques, design, fabrication and characterization
04 p0559 A71-15876
Silicon junction avalanche diodes as S band oscillators and amplifiers, presenting peak power efficiency and gain data
05 p0729 A71-16921
Electron tubes for radars, discussing history and development of magnetrons, Thomson-CSF display tube and power amplifiers
06 p0874 A71-17568
Power amplification with anomalous mode Si p-n-n mesa structure avalanche diodes under input driving power at system resonance frequency
07 p1073 A71-19116
Charge sensitive low power amplifier and fast coincidence system for solid state detectors and random counting rates in Skylab application
08 p1267 A71-21849
Ionized argon laser optimum performance, comparing master oscillator power amplifier configuration to simple oscillator
11 p1772 A71-25141
LF transistor power amplifier protection from power overloads in case of short circuit at output
12 p1889 A71-27625
Power amplifier klystron self excitation in linear electron accelerators, describing tunable driver circuit with quartz reference oscillator
12 p1889 A71-27754
Quasi-harmonic signal suppression in theta-power amplifier as function of nonlinearity at various noise levels
15 p2375 A71-31229
Emission transistor for Eole balloon transmitter power amplifier, discussing trouble-free emission, high output, wide temperature range, lightweight and reliability features
18 p2891 A71-36563

- High power microwave CW tubes and power amplifier requirements for communication satellites
18 p2892 A71-36571
Silicon microwave transistors frequency response theory, considering application as small-signal and power amplifiers
18 p2894 A71-36978
Amplifon effects on phase distortion of pulse signals passing through power amplifier stages of coherent pulse communication systems
19 p3015 A71-37257
Microwave transistor amplifier dynamic range performance, comparing low noise and high power capabilities with traveling wave tubes
19 p3029 A71-38295
Linearization techniques for multiple signal interference reduction in broadband transistor power amplifiers in 225-400 MHz range
19 p3030 A71-38434
Unidirectional regenerative ring carbon dioxide laser power amplifier tests for below and above threshold operations, noting saturation role in performance
20 p3242 A71-38843
Hybrid integrated wideband linear microwave power amplifiers for S and C bands, discussing construction and performance
21 p3357 A71-40817
Emitter-base W metallized contacts RF power transistors for improved hot spotting and breakdown reliability, comparing with Al
23 p3651 A71-43441

POWER CONDITIONING

- Iterative graphical method for broadband N way TEM mode power divider design, using Smith chart
01 p0055 A71-11194
Cs vapor thermionic diodes with low temperature dual mode characteristics applicable as switching elements in DC to AC power conditioner
02 p0196 A71-12267
Spacecraft electric power transformation and control techniques enhancement, using DC to DC converter, voltage converter/regulator and solar array reorientation system
03 p0352 A71-13049
Oxide hollow cathode ion thruster power conditioner, evaluating electrical efficiency, weight, reliability integration and testing
06 p0947 A71-18601
[AIAA PAPER 71-159]
SERT 2 power conditioning, describing operating requirements, components construction, overload protection, system performance, etc
09 p1511 A71-22900
Hollow cathode ion thruster and lightweight power conditioner of solar-electric propulsion system for unmanned deep space probes
09 p1511 A71-22904
[AIAA PAPER 70-648]
ESKA-18P electrostatic ion propulsion system control characteristics and power conditioning, describing pulse width modulated power supply unit
17 p2794 A71-35543
[DGLR-71-029]
Thyristor power conditioning application to high voltage DC electric power system, presenting SST aircraft sample load profiles
17 p2678 A71-35770
Power conditioning electronics for integrally regulated and controlled high voltage solar array spacecraft power system, increasing reliability and reducing weight
20 p3181 A71-38942

POWER CONVERSION**U ELECTRIC GENERATORS****POWER DENSITY****U FLUX DENSITY****POWER EFFICIENCY**

- Flame-fired thermionic diode service life, output power and voltage efficiency and weight reduction
02 p0196 A71-12269
Thermionic converter integrated Cs reservoir module power efficiency and service life, considering diode technology
02 p0196 A71-12270
Liquid Cs graphite integral reservoir effect on thermionic converter performance
02 p0196 A71-12271
Ground station power control in multiple access satellite communication system
02 p0224 A71-12823
Sealed-off carbon dioxide laser power output and efficiency test during continuous operation over one year
03 p0438 A71-13894
Hydrazine-oxygen fuel cells energy costs minimization by optimizing diaphragm thickness, hydrazine concentration and load
03 p0355 A71-14321
Carbon dioxide laser output power and efficiency as function of tube length, discussing bore diameter and cavity insertion losses effects
04 p0606 A71-14716
Electric discharge carbon dioxide lasers, obtaining increased power output with convective cooling process
06 p0909 A71-18522
[AIAA PAPER 71-63]

Digital computer program for optimum design of narrow band klystron, discussing beam interception and power conversion efficiency
08 p1261 A71-20742

Maximum efficiency of turbine for driving auxiliary equipment, noting design constraints
08 p1349 A71-22046

Power augmented lift STOL aircraft operating costs reduction by channel wing concept, discussing aerodynamic theory and structural applications to high lift flaps aircraft
09 p1385 A71-22592

Hall MHD generator duct optimization, using digital calculation for Carter integral minimum for size under required power output
09 p1512 A71-23441

Lossless radiating antenna element efficiency in circular cylindrical arrays of identical elements, relating to reflection coefficient
09 p1419 A71-23505

High pressure ratio centrifugal compressors for small gas turbine engines, investigating power and specific fuel consumption variation with pressure and temperature
10 p1658 A71-24218

Hybrid M-type microwave oscillators including backward and traveling wave tubes with crossed fields in large amplitude mode, considering power efficiency and frequency control
12 p1888 A71-27620

Klystron power conversion efficiency augmentation by electrostatic depressed collector design, presenting performance prediction calculation method
12 p1889 A71-27734

Transferred electron microwave oscillators high efficiency operation mode with more severe limitation than limited space charge accumulation mode
14 p2215 A71-30826

Power output of stable sealed off CO lasers with semiconfocal cavities and totally reflecting spherical and dielectrically coated flat mirrors
15 p2420 A71-32387

Microwave Gunn diodes I-V characteristics as function of carrier concentration and power efficiency
17 p2713 A71-34264

High power efficiency solid state UHF sources, comparing Gunn and avalanche diodes performance
17 p2715 A71-34685

Nonplanar dipole antenna with arbitrarily displaced feedpoints, considering far field radiation patterns, radiation resistance, power gain, effective aperture and efficiency
18 p2887 A71-36014

Satellite telecommunications problems, discussing frequency assignment and power efficiency
18 p2877 A71-36515

Microwave avalanche diodes, considering drift velocity and power efficiency limitations of IMPATT mode
18 p2894 A71-36976

Harmonic extraction from high power efficiency avalanche diodes, discussing circuit in terms of multiple reflection triggering process
18 p2895 A71-36983

High-power high-efficiency CW X band Gunn oscillators on diamond heat sinks, noting operation in waveguide cavities
19 p3029 A71-38219

Line source excitation for maximum aperture efficiency with given sidelobe level
19 p3035 A71-38596

Brayton cycle power conversion system using He-Xe gas mixture, discussing compressor net engine and turbine static efficiencies
20 p3180 A71-38908

Semiconductor lasers, discussing laser action concepts, optical waveguiding, power conversion efficiency, thermal properties, reliability, crystal imperfections, GaAs laser properties, transient phenomena, etc
20 p3243 A71-39066

Maximum efficiency of 10-20 W output semiconductor amplifier at 2.3 GHz, discussing possible replacement of vacuum tubes
20 p3205 A71-39456

X band GaAs diffused IMPATT diodes for high CW efficiencies
22 p3523 A71-42483

GaAs LSA mode V band oscillator CW and pulsed operations power and efficiency limitations
23 p3649 A71-42915

Q values, costs, efficiencies and radioactive evaluation of D-D, D-T and D-He 3 mirror fusion plasma power systems
24 p3847 A71-44493

Compressors and turbines centripetal stages operational characteristics, investigating airflow rate and pressure ratio effects on power
24 p3790 A71-45380

Transonic airfoil cascade analytical design, determining efficiency from velocity distribution
24 p3791 A71-45381

POWER GAIN

- Transverse gain inhomogeneity effect on monopulse duration and development in multimode spherical laser resonator 01 p0094 A71-11026
- Gain measurement on pulsed radiation from high voltage discharges in mixtures of carbon dioxide, nitrogen and helium 01 p0096 A71-11423
- Antenna gain, transmission efficiency and receiving cross sections in dissipative isotropic medium 01 p0041 A71-11614
- Nd-glass pulsed solid state laser amplifier gain characteristics, deriving flux density and population inversion equations 02 p0261 A71-12173
- Wellenweber antennas characteristics, calculating input and mutual impedances, total field radiated and power gain 02 p0232 A71-12343
- CO chemical laser power output augmentation by selective depopulation of CO lower vibrational levels by energy transfer to added gases 02 p0262 A71-12709
- Shaped dual reflector antenna gain prediction based on feedhorn radiation pattern and system geometry 02 p0233 A71-12795
- Hybrid mode flare feed horns for parabolic antennas, discussing horn parameters and angular aperture effects on gain factor or aperture transmission efficiency 02 p0234 A71-12807
- Parametric amplifier with nonlinear capacitance varying as quadratic function of voltage, deriving power gain, bandwidth and noise figure from equivalent circuit 03 p0383 A71-13270
- Atmospheric pressure pulsed carbon dioxide laser, investigating gain, peak power and pulse duration as function of gas pressure and discharge voltage 03 p0440 A71-14461
- C band field effect transistor amplifiers with stable power gain, discussing circuit analysis, design parameters and test results 05 p0729 A71-16917
- Multimode power obtainable in TEM in solid laser, using convex mirror and in cavity polarization rotator 06 p0906 A71-17304
- Low noise temperature high gain satellite-communication antenna feeds optimal design using tapered aperture 06 p0877 A71-18395
- Semiconductor laser threshold current temperature dependence, considering maximum power gain and compensation techniques 06 p0908 A71-18424
- Statistical analysis of neutron induced gain degradation of silicon power transistors, determining failures distribution fit to Weibull function 07 p1070 A71-19063
- Gas laser gain and loss coefficients measurement, using resonator staged calibrator plate for optimal and nonoptimal conditions 07 p1122 A71-19139
- Random gain statistics of avalanche diode optical detectors, analyzing simple optical binary receivers 07 p1074 A71-19216
- Aperture antennas gain loss due to aperture phase errors 07 p1075 A71-19268
- Arbitrary antenna arrays of not necessarily identical elements, deriving maximum realizable gain under impedance matching, and applying to spaced circular arrays 09 p1419 A71-23508
- Waves arrival directional fluctuations effect on power gain of horizontal rhombic antennas for high frequencies and various antenna and wave parameters 09 p1420 A71-23676
- Einstein relations for stimulated luminescence, and application to high pressure chemical laser power gain and population inversion calculation 12 p1913 A71-26966
- Traveling wave tube magnetic field focusing and accelerating voltage effects on power output 12 p1889 A71-27627
- Threshold and power relations for optical radars in pure and turbid atmospheres, determining visibility range for object detection 13 p2027 A71-27856
- Power gain of Q-band GaAs FET with Schottky-barrier gate, giving amplifier and oscillator designs 14 p2210 A71-29800
- Power gain distribution in Ne-He laser cuvettes at 0.63 and 3.39 microns wavelength, noting current density dependent laser power gain shifts 17 p2752 A71-34405
- Transversely excited carbon dioxide lasers gain measurements for linear and helical electrodes at various gas mixtures and pressures as function of time 17 p2754 A71-35404
- Nonplanar dipole antenna with transversely displaced feed points, considering effects on far field

radiation patterns, radiation resistance, power gain, effective aperture and efficiency 18 p2887 A71-35970

Nonplanar dipole antenna with arbitrarily displaced feedpoints, considering far field radiation patterns, radiation resistance, power gain, effective aperture and efficiency 18 p2887 A71-36014

Low noise microwave transistor, describing geometry and diffusions optimization, power gain, reliability and base resistance 18 p2892 A71-36564

Gain and stability of MOS transistor small signal amplifier as function of frequency, using lumped element equivalent circuit 19 p3028 A71-37563

Liquid Xe filled single wire proportional and multiple wire ionization chambers, measuring gain and time/spatial resolution properties 19 p3065 A71-38178

Integral equation for determination of nonuniform gain profile effect on resonant modes of ion laser cavity, considering ring modes at high current densities 19 p3074 A71-38228

Einstein relations for stimulated luminescence, and application to high pressure chemical laser power gain and population inversion calculation 19 p3075 A71-38265

Time resolved gain measurements of pulsed two level laser system, using computer for curve analysis 20 p3245 A71-39179

Radiation resistance, power gain, effective aperture and efficiency of modified log periodic dipole antenna 21 p3352 A71-40378

Computerized numerical optimization for Yagi-Uda antenna array gain, noting nonoptimum in standard traveling-wave design methods 21 p3349 A71-41410

Laser amplifier with range variable automatic gain control in Fabry-Perot cavity with allowance for oscillation 22 p3556 A71-41807

Geometrical-optical approximation for residue series of obstacle /terminal/ gain in radio wave propagation over inhomogeneous earth 22 p3511 A71-42281

Early effect incorporation in Ebers-Moll simulation model for junction transistor large signal behavior to obtain current gain and conductance dependence on voltage 22 p3523 A71-42484

Gas laser power gain time dependence on molecular rotational relaxation under light pulse excitation 23 p3684 A71-43415

Frequency and power limits of field effect triodes, noting application to gridistor for millimeter waves 23 p3653 A71-43950

Single mode output power multiplication in standard commercial He-Ne laser with cavity extension and etalon 24 p3835 A71-45214

POWER GENERATORS

U ELECTRIC GENERATORS

POWER LIMITERS

Incore thermionic cell power output limitation and thermal/electrical data determination at steady state operation, considering temperature distribution 11 p1713 A71-25894

POWER LINES

AC superconducting cables design for utilities underground power transmission lines, discussing superconductor and cryogenic envelope configuration and characteristics 07 p1024 A71-20159

Power line and signal line transients in digital systems 13 p2032 A71-28863

POWER PLANTS

Cost optimization for solar generator thermobatteries by selecting temperature, contact resistance, material parameters and fabrication technology 15 p2351 A71-31671

Curved porous wall channels for noise suppression in power plants, ventilation systems, etc 15 p2449 A71-31705

Liapunov direct method for transient multimachine power-system stability analysis using multivariable control modeling 20 p3207 A71-38991

Creep fracture of Cr-Mo-V steel after operational heat treatment and power plant operation, noting intercrystalline and transcrystalline fracture 20 p3249 A71-39016

POWER REACTORS

Incore thermionic diode reactor stability review and evaluation, discussing reactivity feedback mechanisms, analytical models and results 02 p0280 A71-12260

Hydride thermionic reactor system transient behavior dynamic mathematical model and digital simulation 02 p0281 A71-12262

Low power thermionic reactors, comparing four types design, characteristics and performance estimates for power plants 02 p0281 A71-12263

Reactor powered Brayton cycle power conversion system, evaluating performance at different turbine inlet temperatures and power levels by computer simulation 20 p3262 A71-38914

POWER SERIES

NT TAYLOR SERIES

Perturbation theory of celestial mechanics, using expansions of negative powers of mutual distances between two bodies 05 p0810 A71-16546

Power series uniformization by transformations of perturbation functions irregular part, considering compatibility problem 06 p0919 A71-18197

Inhomogeneous heat transfer lines analysis by matrix method in form of power converging series by Laplace operator 07 p1221 A71-18925

Hypersonic strong interaction flow over inclined surface, using asymptotic expansion in powers of hypersonic interaction parameter for boundary layer equations reduction 09 p1382 A71-22109

Series inverse in powers of time and radius of convergence for universal form of Kepler equation, discussing recursion formulas for coefficients 09 p1516 A71-22174

Finite length rotating cylinder, calculating axisymmetric creep under thermal effects in power series from theory of small elastoplastic deformation 09 p1537 A71-22516

Mechanical systems partial differential equations solution through reduction to infinite systems of ordinary differential equations, considering Cauchy problem power series solution 09 p1492 A71-22523

Lagrange implicit functions generalization to n dimensions, developing inversion as power series 10 p1637 A71-24933

Magnetic corrections to Boltzmann distribution function by power expansion, determining current density in system of free electrons accelerated by crossed electric and magnetic fields -13 p2109 A71-29288

Simplified H. A. Newton formula applied to two zero-mass bodies rectilinear motion, using time coordinates power series 15 p2481 A71-31300

Suboptimal feedback control law for second order nonlinear systems with quadratic performance index, determining power series coefficients 15 p2381 A71-31941

Temperature distribution along short heated wire cooled by flowing liquid with parabolic velocity distribution, using power series for differential equation solution 21 p3378 A71-40581

Numerical power series integration of differential equations of special three body problem with truncation errors elimination to fifth order 21 p3450 A71-40654

Filipov-Ovcharenko wave functions in form of interaction constant inverse power series for calculating two and three nucleon ground state binding energies 22 p3578 A71-42056

Electromagnetic scattering solutions for inhomogeneous dielectrics as power series, using multipoles for far field determination 24 p3847 A71-44427

Power series analysis of circular cylindrical shells stability under biaxial compression, expressing critical loadings 24 p3878 A71-44612

POWER SPECTRA

Frequency-wavenumber power spectrum estimators probability distribution, using Gaussian distribution probability density function 02 p0215 A71-12046

Phase and amplitude fluctuations in oscillator circuits, determining power spectrum, disturbing voltage and current sources and step and impulse functions 03 p0383 A71-13168

Solar wind plasma power spectra noting frequency dependence, particle density and speed and interplanetary magnetic fields 05 p0802 A71-15942

W, Nb, Mo and Ta spectral radiative power at wavelengths from 0.66 to 5.12 mu at various high temperatures 05 p0768 A71-16780

Power spectra of cosmic ray intensity variations at ground and atmospheric pressure oscillations 06 p0950 A71-17979

Cosmic ray mu meson intensity power spectrum frequency dependence, comparing to interplanetary field spectra 06 p0954 A71-18125

Interplanetary magnetic field power spectra fluctuation measurements by Pioneer 6 satellite 06 p0956 A71-18141

- Power spectrum analysis of ELDO Europa 1 third stage thrust phase vibrations, using digital filters
07 p1208 A71-19804
- Planetary nebulae central stars power spectra and HF stellar oscillation observations, using photoelectric time series data
08 p1359 A71-20938
- Earth free diurnal nutation frequency, examining latitude variation power spectrum
08 p1285 A71-21780
- Time series analysis techniques concerning correlation, auto and cross power spectral density, amplitude and period histograms, real time pattern recognition and filtering
09 p1405 A71-22783
- Power spectral density /PSD/ analysis of multilevel binary coded signals for high density PCM recording
09 p1412 A71-22784
- Solar radio bursts power spectra associated with proton events, noting extension to millimeter waves
09 p1514 A71-22933
- Power spectra and electrostatic mechanism of thunder from intercloud and cloud to ground lightning using analog and digital methods
09 p1489 A71-23444
- Micropulsations power spectrum from magnetospheric model based on transient current sheets, approximating background frequency dependence and daytime/nighttime spectral line widths
09 p1441 A71-23638
- Complex and envelope covariance for Rician fading communication channel, deriving equation for unsymmetric power spectrum
10 p1574 A71-23767
- Power density spectrum of longitudinal velocity fluctuations in pretransition pulsed boundary layer
10 p1591 A71-23836
- Cygnus A two component radio source scintillations power spectrum observation by dipole array
10 p1678 A71-24804
- Mean and fluctuating forces on flat plates normal to turbulent flow, giving power spectral density measurements of drag fluctuating component
10 p1598 A71-25085
- Power spectrum symmetry effect on radar signal correlation function and bandwidth
10 p1580 A71-25107
- Power spectral density analysis of aircraft structural response to taxiing produced random vibrations involving landing gear orifice damping and Coulomb friction
11 p1708 A71-26311
- Power law dependence of lateral distribution function and core location of showers detected by Haverah Park array
13 p2122 A71-28068
- Monograph on carbon dioxide laser gain observations covering spectroscopy, energy levels, radiative transitions, molecular collisions, power efficiency, etc
13 p2078 A71-28494
- Transversely excited atmospheric pressure carbon dioxide laser operation at 9.6 microns, describing proper gas mixture for power adjustment
13 p2079 A71-28674
- Long term pulsar intensity observations, noting periodic variations and power spectrum analysis
13 p2143 A71-29270
- Pulsating aurora observations, noting light intensity, diurnal variations and power spectra
14 p2229 A71-29671
- Fluctuation power spectra of CW phase path HF sounders in ionosphere compared with Vaisala frequency curve for upper atmosphere monitoring
14 p2230 A71-29717
- Extreme turbulence measurement during low level flights of Mirage A3-76 fighter aircraft, determining true gust velocities and power spectral energy distributions
14 p2267 A71-29756
- Discrete gust and power spectrum models of atmospheric turbulence, considering energy distribution effect on aircraft dynamic response
14 p2174 A71-29790
- Electron gyro and synchrotron radiation from vacuum and isotropic plasma, deriving approximate general formula for power spectrum and polarization
14 p2282 A71-30661
- Radio frequency measurements below 30 GHz, considering power, impedance, phase shift, voltage and current data
14 p2205 A71-30981
- HF stellar radiation oscillations based on photoelectric monitoring of southern white dwarfs power spectra
14 p2317 A71-31010
- Pc micropulsations spectra fine structure and diurnal variations, analyzing rubidium magnetometer recordings by power spectral density method
15 p2394 A71-31425
- Local time variations of power spectra of magnetospheric electric field from balloon flight data
15 p2397 A71-31758
- Solar eclipse on 7 March 1970, determining midlatitude geomagnetic pulsations with dynamic power spectral analysis
15 p2397 A71-31761

Simplified EEG time domain procedure, using method of period analytic estimates of power spectrum moments
15 p2364 A71-31960

Laser pulse shape, beam modulation and power fluctuation quality control measurements, using non-selective, thermally stable piezoelectric sensor with low time constant
15 p2421 A71-32456

Earth free diurnal nutation frequency, examining latitude variation power spectrum
15 p2401 A71-32685

W, Nb, Mo and Ta spectral emissive power at wavelengths from 0.66 to 5.12 μ at various high temperatures
16 p2591 A71-33032

Resistojet power and specific impulse performance, investigating biowaste derived propellant chemical nonequilibrium effects
17 p2696 A71-35534
[AIAA PAPER 71-688]

Cross power spectral analysis of atmospheric electric potential gradient relation to meteorological parameters, noting diurnal variations
18 p2944 A71-36010

Simple source theory of aerodynamic noise, approximating relationship between radiated sound power and jet pressure spectra
19 p3124 A71-38531

Power spectral analyses of auroral light and X ray pulsations, discussing damping due to velocity dispersions of electrons with various energies
21 p3373 A71-40069

Solar atmosphere oscillatory component observations at 3 mm wavelengths with two radio telescopes, obtaining power spectra
21 p3447 A71-40424

Structural vibrations excited by spatially and temporally random pressure loading, discussing power spectra and vibration measurement
21 p3467 A71-40912

Exposing light and resulting density distribution and granularity in lower photographic emulsion layer, investigating modulation transfer function and power spectrum
22 p3538 A71-41733

Power spectral density of N-ary orthogonal continuous phase FSK waveforms for ELF/VLF communications
22 p3513 A71-42385

Random fluctuating longitudinal pressure gradient effect on steady incompressible channel flow for arbitrary power spectrum and probability density
23 p3664 A71-43597

Lunar electrical conductivity profile from joint power spectral density analysis of Apollo 12 and Explorer 35 magnetometer data
23 p3762 A71-43790

Power spectrum analysis of solar granular intensity fluctuations and velocities, noting asymmetry behavior of Ba II line in individual convection cells
23 p3767 A71-43834

Quantum phase fluctuations in IR gas lasers, noting nearly Lorentzian power spectrum with bandwidth inversely proportional to output power
23 p3688 A71-44269

Metagalactic X ray and cosmic electrons power spectra explanation by electron acceleration and scattering in turbulent plasma with frozen-in magnetic field
24 p3865 A71-44568

POWER SUPPLIES

Electrochemical machining package consisting of machine tool, electrolyte system and power supply
[SME PAPER MR-70-512] 01 p0090 A71-11268

Electric power supplies for communication satellite earth stations, considering methods for power availability and stability
02 p0222 A71-12788

Power sources - Conference, Atlantic City, May 1970
03 p0349 A71-13026

High voltage DC power supplies for aerospace detectors operation, considering different resonant configurations for performance
03 p0352 A71-13051

High speed homopolar alternators as static frequency converter supplies, optimizing design parameters by computer geometric programming
03 p0352 A71-13052

ECG miniaturized single channel biotelemetry transmitter, discussing lightweight design and power supply
10 p1570 A71-24487

Impact resistant power packages for unmanned planetary probe landers, discussing radioisotope thermionic multiconverter array optimal configuration
11 p1713 A71-25898

Quasi-vacuum mode thermionic converter for space and remote terrestrial power supplies, describing computer codes for design optimization
11 p1713 A71-25899

Book on solid state power supplies covering transistorized DC/DC converters and DC/AC inverters, oscillators, power amplifiers, transformers, inductors, magnetic amplifiers, voltage regulators, etc
14 p2182 A71-30857

Optimum power parameters and economic efficiency of Soviet communication satellite system, comparing with terrestrial multichannel communication
17 p2696 A71-34231

Soviet book on subsonic gas turbine passenger planes power supply systems covering Boeing 747, short haul aircraft, DC-10, L-1011, etc
17 p2677 A71-34472

Transistor circuit driven hydrogen-oxygen fuel cell, testing internal impedance effect on power supply noise for comparison with lumped parameter model
19 p3000 A71-38463

Monograph on strong signal behavior of control systems containing multiphase rectifier, covering stability of high power sources
19 p3039 A71-38550

Electrical subsystem of 2-15 kW Brayton power conversion system consisting of speed controller, alternator voltage regulator, DC power supply, etc
20 p3180 A71-38910

Single phase stable frequency AC current power supplies, using stable master oscillator and asynchronous generator
24 p3793 A71-44717

POWER SUPPLY CIRCUITS

Iterative graphical method for broadband N way TEM mode power divider design, using Smith chart
01 p0055 A71-11194

AAP electrical power system simulation for Skylab earth orbit missions, taking environmental effects into account
02 p0190 A71-11795

High power regulated energy transfer by inductor-transformers with single and multiple stages using trapezoidal current waveshapes
03 p0352 A71-13048

Symphonic communication satellite power supply system voltage control, discussing controlled system properties based on closed circuit frequency characteristics
10 p1683 A71-24642

Analog computer power relay analysis simulating flux, coil current, moving mass motion and magnetic and spring forces as function of time
13 p2001 A71-28839

Circuit design of double balanced parametric amplifiers regarding low cost and least degradation performance limits
13 p2039 A71-28906

Modulated power control for fusion welding, considering modification to conventional magnetic amplifier controlled power sources
13 p2076 A71-29093

Book on solid state power supplies covering transistorized DC/DC converters and DC/AC inverters, oscillators, power amplifiers, transformers, inductors, magnetic amplifiers, voltage regulators, etc
14 p2182 A71-30857

Transistorized long time delay relay for power supply circuits with constant function on reenergization after interruption
15 p2376 A71-32021

High voltage power supply for optically pumped solid state lasers, including water cooling of ruby and discharge tube jacket
16 p2585 A71-33074

Spurious effects on stabilizing circuits with loaded Zener diodes for reference voltage source
18 p2893 A71-36800

Microelectronics high power hybrid circuit design, discussing application of packaging techniques to 10 Amp series regulator
21 p3353 A71-40440

Timer devices and applications, discussing timing and power functions, switching cycles, mechanisms, ratings and life/cost evaluation
21 p3379 A71-40672

POWER TRANSMISSION

Power train systems gear induced noise analysis, using in-flight vibration and noise measurements for comparison with calculated noise spectra
[ASME PAPER 70-WA/DGP-1] 03 p0471 A71-14137

High power continuous and pulsed coherent radiation generation by gas lasers, discussing transmission by proton generators and transforming engines
[AIAA PAPER 71-106] 06 p0946 A71-18557

Long life vacuum tests of dry and wet lubricated slip ring systems for power and signal transfer, discussing wear, noise and contact resistance
11 p1771 A71-26050

Y-shaped microwave power splitter, using dielectric wedge partially extending into rectangular metallic waveguide
11 p1733 A71-26349

Helicopter power transmission failure modes, presenting field experiences correlation with conventional design stress analysis and bench test data
[SAE PAPER 71-0454] 13 p2074 A71-28331

Microwave power transmission from orbiting solar power station to earth, discussing design optimization problems
13 p1999 A71-28666

Microwave power transmission for supplying electric power to space station complex for performing scientific experiments over long periods in earth orbits
13 p2000 A71-28667

Microwave power transmission from satellite solar energy station to earth, discussing atmospheric attenuation mechanisms and wavelength and power density optimization

13 p2000 A71-28670

Powered landing gear wheel system requirements for parking and taxiing of commercial jet transport airplanes

[SAE PAPER 710446]

14 p2176 A71-30530

Strain gage torgometer as primary power indicating instrument in helicopter transmission systems, providing advantages for helicopter designer and operator

[AHS PREPRINT 563]

14 p2250 A71-31110

Tapered roller bearing lubrication, considering application to CH-47 Boeing helicopter transmission

17 p2749 A71-35300

Hydrostatic power transmission systems classifications, considering transformation, transport and accumulation of energies /mass, heat, optical, chemical, pneumatic, hydraulic, etc/

18 p2850 A71-36202

Power by wire actuators and fly by wire flight controls, discussing systems configuration, reliability, economy and durability

20 p3183 A71-39150

POYNTING THEOREM

Electromagnetic wave Poynting vector trajectories in absorbing inhomogeneous media, discussing reversibility and energy propagation of spherical and plane structures

02 p0210 A71-11631

POYNTING-ROBERTSON EFFECT

VLF Poynting flux measurement technique on Juno 5 satellite using one electric and one magnetic antenna, discussing magnetic orientation errors effects

07 p1062 A71-19668

PPI [POSITION INDICATORS]

U PLAN POSITION INDICATORS

PPM [MODULATION]

U PULSE POSITION MODULATION

PRACTICES

U PROCEDURES

PRANDTL NUMBER

Turbulent heat transfer in nonNewtonian fluid flow, considering generalized Prandtl number effect

02 p0241 A71-12642

Coolants Prandtl number effect on pressure drop, heat transfer and friction of rough surfaces

04 p0675 A71-14779

Prandtl number measurement in turbulent thermal boundary layer along flat plate with stepwise wall temperature variation

04 p0680 A71-15477

Heat transfer from finite flat plate in channel flow for vanishing Prandtl number, using Fourier transform and Wiener-Hopf technique

[DFVLR-SONDDR-98]

05 p0837 A71-16710

Hydromagnetic boundary layer free convection past vertical flat plate, discussing flow rates, temperature profiles and skin friction for high and low Prandtl numbers

07 p1165 A71-18744

Heat exchange in turbulent flow at large Prandtl numbers, using Van Driest formula

07 p1223 A71-19747

Asymptotic far field velocity component in Prandtl boundary layer equations for steady laminar two dimensional flow past rigid body

09 p1486 A71-23578

Heterogeneous chemical reaction for visualization of wall streamlines on moving obstacle, discussing boundary layer structure at large Prandtl and Schmidt numbers

10 p1591 A71-23835

Low Prandtl number laminar compressible boundary layer flow over flat plate, obtaining recovery temperature profile and heat transfer by matched asymptotic expansions method

10 p1597 A71-25066

Smooth annuli correlation equation for friction factor, discussing Prandtl turbulence based Spalding inner velocity profile modification

12 p1896 A71-27053

Heat exchange at large Prandtl numbers near porous flat wall with liquid injection, calculating Stanton number

13 p2046 A71-28181

Thermal turbulence at infinite Prandtl number of horizontally infinite fluid layer heated from below, using Boussinesq equations

13 p2162 A71-28776

German monograph on viscous fluids heat transfer in pipes covering Prandtl number dependence, turbulent boundary layer flow and transition areas

15 p2514 A71-32375

Heat transfer in wall region of steady turbulent flow at large Prandtl numbers, plotting temperature distribution curves

17 p2728 A71-35119

Prandtl three dimensional boundary layer equations in orthogonal curvilinear coordinates, applying implicit finite difference scheme to solution

18 p2906 A71-36318

Laminar free convection from line heat source for Prandtl number 2 based on differential equation solution

20 p3314 A71-39491

Temperature and electron density measurements for free jet of ionized nitrogen at atmospheric pressure by plasma spectroscopy, estimating Prandtl numbers

23 p3664 A71-44197

High Prandtl /Schmidt/ number fluids turbulent flow temperature profile derivation by turbulent transport mathematical model

23 p3664 A71-44199

Vertical laminar natural convection boundary layer stability during thermal expansion at large Prandtl number

24 p3886 A71-44422

PRANDTL-MEYER EXPANSION

NT THERMAL BUCKLING

Vibrational nonequilibrium Prandtl-Meyer expansion flows, discussing vibration energy associated with change of state and hypersonic nozzle flow calculation

18 p2909 A71-36440

Fundamental derivative /gamma/ and other thermodynamic variables in gas dynamics, considering transonic passage variation, Prandtl-Meyer wave, adiabatic flow and nonlinear wave propagation

22 p3530 A71-41887

Ideal compressible fluid plane unsteady vortex-free selfsimilar flow, obtaining particular solutions families similar to Riemann waves and Prandtl-Meyer flows

22 p3532 A71-42866

PRASEODYMIUM

Ce, Pr and Nd solubility in Cr, investigating temperature dependence, microhardness, deoxidation and alpha phase by X ray, metallographic and durometric analyses

07 p1144 A71-20652

Temperature induced spectral line widening of trivalent positive Pr ions in lanthanum niobate crystals

09 p1507 A71-22391

Room temperature visible surface laser action in praseodymium chloride and bromide, obtaining optical pumping into upper laser level by wavelength tunable dye laser

22 p3556 A71-41802

PREAMPLIFIERS

Low noise microstrip microwave mixer-preamplifier on thin polyolefin reinforced with Al, discussing design and manufacture

08 p1263 A71-20771

Microwave MESFET HF circuits, discussing noise factor advantage over bipolar transistors in low noise preamplifiers

21 p3355 A71-40743

Radio pulse synchronous detection with wideband preamplifier, evaluating frequency mismatch effects on signal distortion by transient response analysis

23 p3644 A71-43287

Operational principles and circuit diagram of transistorized preamplifier for Si p-i-n gamma quanta radiant flux detector, noting noise properties and possible improvements

24 p3810 A71-45151

PRECAMBRIAN PERIOD

Precambrian and Cambrian stromatolites used for determination of nearest lunar approach to earth

04 p0583 A71-15141

Carbonaceous chondrite and Precambrian chert amino acids detection, using simultaneous optical configuration determination and gas chromatography

09 p1393 A71-22984

Permeability and porosity of Precambrian Onverwacht cherts and other low permeability rocks, discussing geological origin of rock-contained organic compounds

18 p2913 A71-36768

Blue-green algae survival or growth ability tests under simulated Precambrian atmospheric conditions

22 p3487 A71-42230

PRECAUTIONS

U ACCIDENT PREVENTION

PRECESSION

NT LARMOR PRECESSION

NT PROTON PRECESSION

Lunar tides and precession effects on model earth fluid core dynamics

02 p0245 A71-11994

Pole Chandler motion, discussing residual deviations distributions in Jeffreys and Arato-Kolmogorov models

02 p0309 A71-12105

Gyroscopic precession effects in earth polar orbital satellite experiments for Einstein general relativity tests

02 p0312 A71-12369

Tied aether existence hypothesis determination, comparing gyrocompass precessional couple at earth surface and at 3300 m depth for negative results

03 p0456 A71-13358

Precession equations of gyroscope onboard near earth satellite, comparing Schiff and Brans-Dicke theories

05 p0781 A71-16488

Earth rotation polar motion dynamics, discussing wobble, drift, nutation, precession and sway

06 p0890 A71-17877

Chandler wobble seismic excitation by dislocations elasticity theory, discussing pole path changes-earthquake correlation

06 p0891 A71-17886

Earthquakes association with Chandler wobble from ILS-IPMS polar data

06 p0891 A71-17888

Earth core-mantle coupling as energy source for mantle wobble, taking into account precession cross coupling

06 p0891 A71-17890

Free Lagrangian gyroscope, discussing numerical relations between precessions and nutations

06 p0899 A71-17931

Two-body satellite of axisymmetric rigid bodies interconnected by lossy universal joint, calculating transient oscillation damping of forced precession under external torque

07 p1205 A71-18895

Single rotor gyrocompass dynamics under LF three component linear vibration of base, using precessional equations

07 p1108 A71-19305

Orbiting gyroscope de Sitter precession in different versions of Brans-Dicke theory, discussing term arising from anomalous scalar force in equations of motion

07 p1160 A71-19550

Earth poles motion, measurement methods and possible causes due to earth core and mantle effects on earth rotation

09 p1434 A71-22057

Maximum deviations of corrected uniaxial gyrostatilizer under disturbances on stabilization and precession axes with modulus constraints

09 p1450 A71-22796

Forced rotation influence of gimbal suspension on astatic gyroscope motion with respect to inertial coordinates, demonstrating pseudoregular precession

09 p1451 A71-23172

High accuracy angular precession measurements with automatic gyro for satellite relativity tests, using optical system with reticle coordinates

09 p1452 A71-23595

Longitude precessional constant determined by long baseline interferometry through dynamical behavior observation of earth orbiting or interplanetary artificial spacecraft

10 p1674 A71-24437

Precessional equation of gyroscopic systems with rigid structural elements connected by single degree of freedom axial hinges

10 p1611 A71-24577

Newcomb precession constant accuracy, noting stellar motion analogies and analytic effects on earth polar secular motion

12 p1901 A71-27092

Orbital space stations and spacecraft courses, determining orbit precession and perturbation

12 p1968 A71-27628

Disk rotating in gimbal system, describing gyroscopic moments and precession

13 p2068 A71-28632

Maximum nutation-precession angles of spin stabilized satellites during extension of long flexible booms

15 p2500 A71-32046

Energy dissipation measurement in liquid filled spinning precessing spherical cavity by gimbaled mechanism

[ASME PAPER 71-APM-4]

16 p2644 A71-33219

Newcomb precession determination from Bradley stars proper motions, evaluating neglect of galactic rotation

18 p2961 A71-35942

Rigid sphere and concentric shells models approximation to turbulent motion in liquid-filled precessing spherical cavity

[ASME PAPER 71-APM-Y]

18 p2904 A71-36265

Correction values to centennial precession, using stellar proper motions

18 p2970 A71-37063

Active precession control devices for spin stabilized spacecraft, noting energy dissipation effect

[AIAA PAPER 71-952]

19 p3148 A71-37193

Newcomb precession constant accuracy, noting stellar motion analogies and analytic effects on earth polar secular motion

19 p3049 A71-37442

Angular momentum vector orientation of reentry vehicle at end of spin-up, using helicoid precession concept to characterize rotational motion during constant thrust

22 p3611 A71-42029

Gravitational and aerodynamic perturbation moment effects on nonsymmetric solid body rotary motion near mass center, using precession model

22 p3612 A71-42870

Liquid flow rate measurement by determining fall time of emf generated in sensor coil by fluid nuclei precessing freely in magnetic field

23 p3678 A71-43536

- Cayley-Klein parameters application to quasi-precessional motion of satellite with multiple rotors, using perturbation method 24 p3848 A71-44830
- Precession rate of balanced gyroscope in Cardan suspension with elastic gimbal couplings 24 p3826 A71-44833

PRECIOUS METALS

U NOBLE METALS

PRECIPITATION [CHEMISTRY]

- Titanium carbide ingots production for laminar and flake precipitation of graphite, using electric arc furnace with consumable electrode 02 p0238 A71-12281

- Precipitation reactions in concentrated Ta-Hf and Nb-Hf alloys at 600-1400 C from X ray diffraction and transmission microscopy, discussing phase relations 06 p0914 A71-18679

- Stress annealed Ni-base superalloy crystals, investigating orientation and applied uniaxial stress sense effect on coherent gamma prime precipitates morphology 07 p1138 A71-19987

- Gamma prime precipitate effects on flow stresses of Ni alloys single crystals at various strain rates and elevated temperatures 08 p1315 A71-21580

- Chemical precipitation techniques for dispersion hardened high temperature alloys, considering Co, Ni, Cr, Mo and W multicomponent alloys 09 p1455 A71-23285

- Point defects and fine precipitates effects on fatigue strength of high strength alloys, exhibiting higher fatigue strength in isothermally aged samples 10 p1625 A71-24009

- Stress-strain curve and single crystal dislocation structure of Al alloys with coherent precipitates, noting screw dislocations predominance 10 p1629 A71-25033

- Crystal imperfections effect on MC carbide precipitation on coherent twin boundaries and regions close to grain boundaries in austenitic steels, using electron microscopy 11 p1780 A71-26027

- Metal carbide grain boundary precipitates effect on austenitic stainless steels high temperature fatigue fracture behavior 11 p1782 A71-26439

- Grain boundary precipitation in austenitic steels during creep deformation and ordinary aging treatment 13 p2086 A71-28623

- Al-Zn-Mg alloys, considering Cu and Cr additions effects on nucleation and incoherent precipitates formation 13 p2088 A71-29406

- Precipitation kinetics and austenite formation during aging of Fe-Ni-Mo and Fe-Ni-Co-Mo maraging alloys from dilatometry, electrical resistivity measurement and electron microscopy 14 p2257 A71-29838

- Al-Li alloys precipitation characteristics and time-temperature-transformation curves after solution treatment, water quenching and aging 14 p2259 A71-30393

- Stable eta phase precipitation at dislocations in Al-Zn alloy, using X ray diffraction and electron microscopy 14 p2260 A71-30477

- High tensile strength maraging steels aging, discussing dispersed precipitates formation by homogeneous nucleation 15 p2427 A71-31525

- Udimet 700 superalloy gamma prime precipitate particle size, volume fraction and chemical composition as function of time and temperature 15 p2433 A71-32176

- Sigma phase intergranular precipitation in low carbon Ni-Co-Cr-Mo alloys, noting temperature effect on morphology 15 p2436 A71-32546

- Iron precipitation rate from supersaturated Al alloy solid solution in structures with low and high dislocation densities 19 p3079 A71-37702

- Hydraulic fluids contribution to system contamination, discussing precipitate formation due to reaction with water, filtration inability and contaminant elimination 19 p2999 A71-38323

- Polar cap absorption event, investigating solar high energy protons precipitation effects 19 p3129 A71-38360

PRECIPITATION [METEOROLOGY]

- NT DEW
NT HAIL
NT RAIN
NT SNOW

- Radar attenuation along slant paths due to precipitation, comparing ATS-5 direct measurements with calculations based on backscatter and sky temperature measurements 01 p0030 A71-10579

- Radar precipitation measurement accuracy improvement, using various Z-R relationships for correlation of radar data and rainfall rates 01 p0117 A71-10581

- Cloud and precipitation boundaries in convective storms studied by stereophotogrammetry and radar, discussing radar echo motion within cloud envelope 01 p0118 A71-10586

- Digital range-bin integrator for precipitation echoes, using static shift registers as memory element 01 p0049 A71-10592

- Autocorrelation of weather radar precipitation patterns by incoherent optical method 01 p0030 A71-10599

- Annual and diurnal variations of temperature inversion over antarctic plateau, discussing wind field structure and ice crystal precipitation 05 p0778 A71-17043

- Space charge effects on fog precipitation, taking droplet size into account 05 p0779 A71-17141

- Spatial correlations between inside cumulus cloud conditions and precipitation onset and intensity for modification experiments from aircraft penetration measurements 08 p1326 A71-21450

- Areal precipitation quantitative radar measurements, describing signal processing and digital system for contour mapped displays and numerical summaries 08 p1257 A71-21738

- Electromagnetic interference, discussing man-made, inherent and natural types including atmospheric electrical disturbance, precipitation static, sunspots, etc 12 p1879 A71-27059

- Conjugate and closely-spaced riometer observations of auroral radio absorption, considering explanation by alternation of particle precipitation between Northern and Southern Hemispheres 14 p2192 A71-29667

- Nonadiabatic convection parameters calculation allowing for vertical wind shear, determining effect on thunderstorm maximum possible duration, gusts and precipitation quantity 15 p2444 A71-31361

- Martian blue haze clearings and flash phenomena meteorological mechanism, considering atmospheric clearing due to water precipitation 18 p2966 A71-36767

- Precipitation formation and regulation from supercooled and frontal clouds, noting crystalline cloud seeding effects 19 p3092 A71-36869

- Hail precipitation process from cumulonimbus clouds based on aircraft and ground observations 19 p3093 A71-36892

- Tropical cumulus clouds seeding experiments with silver iodide smoke, discussing cloud growth and precipitation increase 19 p3093 A71-36893

- Electric charge generation in storm clouds, considering water droplets, ice crystals and air movements role in precipitation and charge separation mechanism 20 p3256 A71-39071

- Probabilistic weather forecasting for temperature and precipitation, examining feedback and prediction evaluation 20 p3256 A71-39203

- Unified international scaling for annual and seasonal precipitations measured by national gages, comparing U.S.S.R. and U.S. reduction coefficients 21 p3383 A71-41377

- Error factors of seasonal precipitation measurements by total precipitation gages 21 p3383 A71-41378

- Areal precipitation correlation with 850 mb geopotential height over Northern Hemisphere 22 p3535 A71-42414

- Weather and climate modification, reviewing techniques for meteorological processes control, cloud and precipitation modification, ascending flow stimulation, etc 23 p3701 A71-43450

- Radio echoes from clouds and precipitation, determining detection threshold, station potential and statistical distribution numerical characteristics 24 p3844 A71-44879

- Atmospheric attenuation effects on cloud and precipitation radar reflection coefficient 24 p3845 A71-44880

- Cloud and precipitation effects on radio echoes intensity measurement, discussing pulse dimensions influence on average signal magnitude 24 p3845 A71-44881

- Laser IR radiation attenuation in atmospheric precipitation, considering snow, rain and drizzle 24 p3835 A71-45255

PRECIPITATION HARDENING

NT MARAGING

- Al alloys nucleation and precipitation hardening, examining quenching rate effects with hardness measurements and electron microscopy 04 p0613 A71-15744

- Al alloys grain boundary precipitation pattern relationship to stress corrosion sensitivity 04 p0613 A71-15746

- Sulfide precipitates shape preservation in high strength low alloy hot rolled steel sheets, discussing effects of various additive elements 04 p0614 A71-15782

- Age hardened Ni base material strain-age cracking phenomenon measurements, using constant strain Gleeble technique 04 p0617 A71-15912

- German monograph on Co-free heat resistant austenitic steel alloys precipitation hardening and creep strength properties as function of chemical composition 05 p0764 A71-15973

- Nitrogen-alloyed austenitic steels precipitation hardening, discussing aging and strengthening rates 05 p0767 A71-16767

- Fiber composites reinforcement obtained in oriented solidification by structural precipitation hardening of matrix [ONERA-TP-920] 06 p0913 A71-18094

- Stress rupture properties at elevated temperature of nickel base superalloys with varying Ti and Al additions, investigating microstructural and age hardening effects 06 p0913 A71-18676

- Uniaxial stress effect on morphology changes of coherent gamma prime precipitates in nickel base superalloy crystals 06 p0914 A71-18682

- Alloy strengthening by ordered precipitates, predicting antiphase boundary energy from flow stress vs particle size plots 07 p1132 A71-19440

- Ordered phases precipitation in ternary and quaternary ferritic alloys, investigating morphology, structure, distribution, coarsening kinetics and mechanical properties 07 p1133 A71-19443

- Binary Ti-Al and ternary Ti-Al-X alloys precipitation strengthening, investigating structure, mechanical properties and deformation behavior 07 p1133 A71-19444

- Ni base superalloys mechanical properties relationship to microstructure, considering precipitate dispersion and phase state effects on flow stress and creep strength 07 p1133 A71-19445

- Ni base superalloys fatigue behavior, emphasizing role of ordered gamma prime precipitate in two phase materials 07 p1133 A71-19447

- Al-Li alloy precipitation hardening after neutron irradiation, noting yield stress increase after aging at various temperatures 07 p1143 A71-20487

- Neutron irradiation effects on Al-Mg alloys tensile properties, noting yield stress increase and appearance of Luders strain 07 p1143 A71-20492

- Maraging steels precipitation hardening due to alloying with Si, obtaining improved strength with satisfactory plasticity 08 p1305 A71-21026

- Pure vs dispersion hardened Ni plastic deformation, noting flow stress and temperature effects on work hardening 08 p1311 A71-21544

- Ni-Cr thoria dispersion strengthened alloys, determining texture effects on high temperature mechanical properties 08 p1311 A71-21545

- Mo-Hf alloy dispersion hardening by internal nitriding, examining structure and high temperature mechanical behavior 08 p1311 A71-21546

- Al-Cu precipitation hardened alloys, determining microstructure effects on fatigue life and flow stress 08 p1312 A71-21547

- Mg-Y alloy age hardening due to coherent metastable phase precipitation 08 p1312 A71-21548

- Nb-Hf alloys alpha precipitation strengthening via aging at various temperatures, examining mechanical properties 08 p1312 A71-21549

- High strength martensite beta Ti alloy microstructure, discussing ductility and age hardening 08 p1312 A71-21552

- Ni superalloys strengthening by body centered tetragonal gamma double prime phase precipitation, investigating various alloying components and ratios 08 p1314 A71-21568

- Precipitation hardened Ni base superalloys fatigue deformation, investigating correlation between metallurgical structure characteristics and high-cycle fatigue behavior 08 p1314 A71-21570

- Paired dislocations after high temperature deformation in precipitation hardened Co-Ti alloy 08 p1315 A71-21582

Tensile data for dispersion hardened iron containing thorium spherulites analyzed in terms of Orowan theory, considering bcc materials yield strength

09 p1466 A71-22172

Discontinuous decomposition and aging kinetics of supersaturated solid solutions of tungsten in cobalt, comparing to precipitation theories

09 p1469 A71-22848

High temperature precipitation hardening of Ni-Cr alloys, discussing effect on creep rupture strength

09 p1470 A71-23044

Al and Fe additions effect on transitional phases formation and metastable phase precipitation in Ni-Nb system, using transmission electron microscopy

09 p1471 A71-23124

Chemical precipitation techniques for dispersion hardened high temperature alloys, considering Co, Ni, Cr, Mo and W multicomponent alloys

09 p1455 A71-23285

Dispersion hardened Ni and Co alloys production by powder metallurgy, noting elastic distortion due to particle strengthened base material

09 p1474 A71-23294

Thorium containing Ni and Co base powders reduction in hydrogen atmosphere for precipitation hardened materials production, determining optimal thermodynamic and reaction kinetic factors

09 p1475 A71-23306

Yield strength theories of heterophase systems with precipitates surrounded by elastic strain fields, considering dislocation precipitation interaction mechanism

09 p1510 A71-23321

Cold prestraining effect on steady state creep strength and rate of precipitation hardened heat resistant steel

09 p1477 A71-23331

Heat resistant dispersion strengthened and fiber reinforced metal matrix superalloys for high temperature applications, considering superstrength alloys development

09 p1478 A71-23397

Ni-Cr alloys hardened by Nb and Ta, examining precipitation and plastic deformation mechanisms

09 p1479 A71-23622

Strengthening processes in precipitation hardened and dispersion hardened alloys produced by powder metallurgy

10 p1614 A71-23903

Zr effect on Ti-Mo beta alloy stability, considering Zr suppression and retardation of omega precipitation on basis of TTT diagram and tensile tests

10 p1625 A71-24007

Al-Cu alloys recrystallization and age hardening irregularities, discussing inhomogeneous and anisotropic effects on ideal characteristics

10 p1628 A71-24823

High strength stainless steel dislocation structure and mechanical properties, discussing tempering, tensile strength, precipitation hardening and temperature effects

11 p1776 A71-25167

Steel structural transformations under arc melting, cooling and electroslag remelting, noting delta ferrite precipitation with hot stage microscope

11 p1776 A71-25168

Intermetallic compound precipitation processes in Ti-Cu alloys for high yield strengths, using electron microscopy

11 p1779 A71-26017

Hydrogen effects on low temperature solution strengthening and ductility of Nb-H single crystals, noting effects of normal and strain induced hydride precipitation

11 p1780 A71-26020

All-beta Ti alloy Ti-V-Cr-Al, testing dynamic behavior of strain aging during stress relaxation period

11 p1780 A71-26026

Atomic bond strength of solid solution hardening as function of composition for calcium/strontium difluorides, using vibrational IR and laser Raman spectra

12 p1877 A71-26804

Predeformation effects on metastable Ni base Ti alloys precipitation aging at extrinsic stacking faults, using thin foil microscopy

12 p1916 A71-26894

High chromium hot corrosion resistant superalloys in sheet form, noting precipitation hardening and creep resistance equivalent to Nimonic alloys

12 p1916 A71-26922

Ni-base alloys hardened by gamma prime precipitation, investigating embrittlement by oxygen [ASME PAPER 71-MET-D]

12 p1917 A71-27313

Composite heat resistant Ni alloy production using refractory oxide phase dispersion hardening

13 p2083 A71-27893

Explosive and isostatic forming effects on commercial precipitation-hardenable Al-Cu alloy microstructure, tensile properties and fatigue life

15 p2433 A71-32180

Guinier-Preston zone size and volume fraction effects on polycrystalline Al-Zn alloys yield strength,

discussing precipitation strengthening and thermally activated plastic flow

15 p2433 A71-32182

Dispersion hardened Co strength and plasticity temperature dependence, determining Ti and Nb carbides additives effects

15 p2434 A71-32237

Precipitation hardenable Ni-base alloys embrittlement in high temperature oxygen atmosphere, considering intergranular crack initiation

15 p2434 A71-32257

Age hardenable Inconel X-750 superalloy mechanical response to tensile loads for identifying microstructural changes due to deformation

15 p2437 A71-32616

Heat resistant weldable dispersion hardened Ni base alloy, discussing intermetallic phase hardening

16 p2594 A71-33715

Tensile properties, plane strain fracture toughness and stress corrosion threshold of high strength precipitation hardening stainless steels

17 p2755 A71-34438

Ti alloys metastable omega phase precipitation effect on mechanical properties, using thin film microscopy

17 p2756 A71-34492

Wrought precipitation hardened Co-base alloy, investigating Ti and Al additives effects on tensile and stress rupture strengths, microstructure and fabricability

17 p2758 A71-35147

Environment and frequency effects on fatigue properties of age hardening Al-Cu-Mg alloy

18 p2933 A71-35876

Molybdenum effect on morphology, size and square density of precipitating gamma particles in nickel alloys

18 p2934 A71-35991

Fiber volume content, fiber-matrix bonding, heat treatment and age hardening effects on transverse modulus and tensile strength of unidirectional Al matrix fibrous composites

18 p2935 A71-36597

Age hardening of Mo alloys with titanium and zirconium carbides at high temperatures after quenching

19 p3077 A71-37268

Precipitation strengthened Fe-Ni-base superalloy microstructure, investigating phase relationships

19 p3079 A71-37711

Matrix stacking fault energy effect on tensile creep deformation modes in gamma prime precipitation hardened nickel-base alloys

19 p3080 A71-37721

Recovery creep properties and intercrystalline fracture in precipitation hardened alloys heat treated on relative stable conditions

20 p3250 A71-39024

Composite heat resistant Ni alloy production using refractory oxide phase dispersion hardening

21 p3396 A71-40084

Retained lattice strain and substructure domain size effects on tensile strength at room and elevated temperature in dispersion strengthened Ni alloys

21 p3397 A71-40453

Precipitation hardened Ti-Nb alloy, correlating room temperature tensile properties with microstructure from step aging

21 p3387 A71-40461

Hardness, internal friction, microstress, martensite lattice and density changes during aging of precipitation hardening Fe-Cr-Ni steel, using dilatometric and X ray analysis

21 p3402 A71-41086

High strength stainless steel dislocation structure and mechanical properties, discussing tempering, tensile strength, precipitation hardening and temperature effects

21 p3402 A71-41088

High strength steel structural transformations under arc melting, cooling and electroslag remelting, noting delta ferrite precipitation with hot stage microscope

21 p3402 A71-41089

Alloying effects on crack propagation resistance of precipitation hardening austenitic steel

21 p3402 A71-41091

Metallography of 700 C precipitation hardening in Fe-Ni alloy containing Be, using transmission electron microscopy

21 p3404 A71-41417

Crystal microstructure of strengthening precipitates in Ni maraging steel, giving electron diffraction patterns

22 p3562 A71-41949

Phase transformations and mechanical properties of heat resistant martensitic stainless steel during precipitation aging at prolonged high temperature exposures

23 p3690 A71-43280

Austenitic Fe-Ni-Ti steel strengthening by precipitation hardening and subsequent aging at 600 C

23 p3690 A71-43282

Weakly diffracted beam observation of small quenching vacancy loops and Guinier-Preston

precipitate zones in Al and Al-Cu, using transmission electron microscopy

23 p3691 A71-43359

X ray analysis of scale formation in precipitation hardened nickel, investigating thermal resistance and oxidation rates

23 p3691 A71-43520

Precipitation hardenable Cr-Cu liquid phase sintered powder composite, showing matrix properties variations

23 p3695 A71-44291

Age hardenable Mg-Y alloys, investigating impurity phase in solution heat treatment

23 p3696 A71-44292

Metal hardening by dispersion of spherical ordered and coherent precipitates from statistical theory

24 p3861 A71-45196

Mo sheet anisotropic dynamic strain aging at high temperatures, noting plastic strain contribution to texture formation and dislocation consolidation

24 p3840 A71-45378

PREDICTION PARTICLE MEASUREMENT

Alloy strengthening by ordered precipitates, predicting antiphase boundary energy from flow stress vs particle size plots

07 p1132 A71-19440

Charge generating mechanism based on charge separation from falling precipitation particles effect on thunderstorm electrification

14 p2269 A71-29951

Droplet size and concentration in gas stream, discussing measurement error analysis and recording medium calibration procedure

16 p2663 A71-33363

Auroral electrons and protons precipitation patterns from ESR 1A northern polar cap observations, identifying electron energy zones

19 p3060 A71-38574

Water aerosol flux interaction and drop capture with particles of solid reagent, considering agaroid films and precipitation on thin wires

19 p3094 A71-38699

Electrooptical measurement of high altitude rain cloud droplets size, shape and distribution

23 p3676 A71-43507

PREDICTION

Precision timing system implementation and operation, considering synchronization maintenance by flying cesium beam clocks, satellite, VLF and LF techniques

03 p0429 A71-14270

PREDICTION ANALYSIS TECHNIQUES

Optimal prediction of stochastic differential equation solution with Gaussian member and small non-linearity

01 p0110 A71-10098

Reliability prediction method effectiveness for control plant with efficiency represented by canonical forms

01 p0064 A71-10924

Parameter estimation of mixed autoregressive moving-average /ARMA/ time series using output data

06 p0878 A71-17332

Dynamic digital predictive compensation learning control systems with time delay transform identification by template matching technique

06 p0878 A71-17336

Digital on-off predictive adaptive control system feasibility analysis

07 p1082 A71-20407

Regular and stochastic algorithms for efficiency estimation of adaptive predicting filters

08 p1260 A71-22021

Selection of uncorrelated measurement composition ensuring optimal accuracy of space vehicle trajectory

09 p1519 A71-22541

Parameter estimates effectiveness from independent discrete and continuous navigation measurements of circular orbital plane

09 p1491 A71-22543

Solid propellant instantaneous burning rates prediction methods based on flame structure model and steady state burning data as functions of pressure and initial temperature

09 p1510 A71-22905

Prediction analysis of downstream effectiveness in high speed laminar boundary layer for reentry vehicular surfaces film cooling, using reference enthalpy method

11 p1752 A71-26216

Failure prediction from interval data for reliability and inventory problems, considering irregular inspection and manufacture for aging in calendar time

12 p1911 A71-26687

German monograph on spacecraft systems launch readiness prediction covering reliability requirements, configuration analysis, tradeoffs, failure analysis, mathematical techniques, etc

13 p2146 A71-29482

Numerical prediction of radiation patterns for antennas mounted on spacecraft, noting booms and solar cell panels effects

14 p2218 A71-31068

Synthesis method for combining individual part repair time distributions for maintainability prediction using computer

16 p2552 A71-33301

Linear dynamic system recursive state estimation for set-membership description of uncertainty under unknown input disturbances and observation errors

17 p2718 A71-34734

Interceptor aircraft optimal nonlinear command guidance scheme for reduction of airborne computation load with forward prediction of interceptor and target state vectors

[AIAA PAPER 71-916] 19 p3096 A71-37166

Computerized automatic estimation techniques application to real time aircraft tracking in ATC system design

[AIAA PAPER 71-926] 19 p3096 A71-37172

Optimality in classification of stochastic processes in recognition system, using predicting filter rms error as discriminating function

19 p3038 A71-37779

Polymer materials strength and lifetime prediction under natural conditions from mathematical model based on laboratory accelerated test data

19 p3084 A71-37781

Aerothermodynamics and scale modeling techniques for prediction of plastic burning rates, using Spalding mass transfer theory and dimensional analysis

19 p3171 A71-38250

Performance prediction model for electromagnetic compatibility of ATC radar beacon system, testing interrogator-transponder links along air route

19 p3102 A71-38435

Computer-aided statistical analysis correlation method for prediction of electronic circuit component part variability effects on performance and reliability

22 p3517 A71-42102

Second order approximation algorithm for nonlinear noisy dynamical system state estimation from noise corrupted observations

23 p3656 A71-43854

Laminar boundary layer transition prediction techniques, evaluating empirical formulations and Schlichting-Tollmien stability methods

[AIAA PAPER 71-985] 24 p3817 A71-44581

Discrete parameter covariance stationary stochastic process in rotation sampling, deriving minimum variance unbiased linear population mean estimator by constrained optimization procedure

24 p3844 A71-45132

PREDICTIONS

NT IMPACT PREDICTION

NT LINEAR PREDICTION

NT PERFORMANCE PREDICTION

Optimization of linear tracking strategies, considering time independent and translation invariant N point predictor

15 p2379 A71-31411

Predictor-corrector algorithms with identical regions of absolute or relative stability

17 p2769 A71-35690

PREDICTORS

U PREDICTIONS

PREFLIGHT TESTS

Qualification tests for equatorial ELDO Europa Launch Site with MSRV, discussing checkout system and performance

23 p3661 A71-43474

PREFLIGHT ANALYSIS

Preflight balance analysis of dual spin satellites, discussing error sources

[SAWE PAPER 882] 17 p2815 A71-35821

Mission analysis aspects of space shuttle operations between earth orbit station and lunar orbit station

[AAS PAPER 71-301] 23 p3724 A71-42977

Graphic mission analysis for outer planet missions, considering spacecraft and celestial bodies relative positions, sensor and spacecraft relative orientation

[AAS PAPER 71-378] 23 p3731 A71-43048

Lunar impact targeting technique improvement for Apollo 14 mission preflight analyses and flight support operations

[AAS PAPER 71-392] 23 p3732 A71-43060

PREFLIGHT OPERATIONS

Optimal preflight feeding for pilots, discussing protein content and vitamin enrichment

01 p0024 A71-11109

PREFORMS

Forgeability and tensile properties of spark sintered unstrained Ti-Al-V preforms from prealloyed powders in uncontrolled atmosphere

13 p2084 A71-28147

PREGNANCY

Glucose intestinal absorption, blood glucose and hematocrit in hamsters, relating physiologic modifications to pregnancy

02 p0201 A71-12608

PREHEATERS

U HEATING EQUIPMENT

PREHEATING

U HEATING

PREIMPREGNATION

Composite fiber-reinforced structures fabrication methods

[SME PAPER EM-70-112] 01 p0089 A71-11256

Single ply sandwich composite prepregs for use with honeycomb reinforcement, noting one step curing for light weight structural panels

10 p1630 A71-24065

Fabricated product test program design for meeting customer specifications, outlining routine tests for preimpregnated film adhesive materials

10 p1616 A71-24107

Epoxy resin in fiber reinforced composite prepregs, characterizing by thermomechanical analysis and gel permeation chromatography

11 p1786 A71-25411

Physical and mechanical properties of controlled flow vacuum cured glass reinforced polyimide prepreg laminates

22 p3565 A71-42595

PRELAUNCH PROBLEMS

Direct in-orbit alignment of integrated optical strap-down inertial guidance system for space application, considering self contained prelaunch alignment and calibration

17 p2774 A71-35071

PRELAUNCH TESTS

Telemetry systems prelaunch calibration tests, considering bit error rate, intermodulation distortion and antenna tracking

04 p0554 A71-15317

Thermal/vacuum space simulation assembly level testing for prelaunch confidence of Mariner spacecraft

12 p1893 A71-26680

Space station facilities and launch and prelaunch operations at Kennedy Space Center, discussing statistical analysis for activity optimization and integrated mission management concept

18 p2899 A71-36474

Skylab checkout and launch facilities and operations, describing modifications required for Apollo lunar missions facilities utilization at Cape Kennedy

18 p2899 A71-36476

Apollo/Saturn 5 propulsion system design, development, testing and integration

22 p3589 A71-42026

PRELOADING

U PRESTRESSING

PREMATURE OPERATION

Premature scheduled maintenance, providing model for duplication between repair and overhaul/replacement cost

16 p2552 A71-33313

PREMIXED FLAMES

Supersonic inviscid flow fields associated with conical premixed flame sheet

03 p0521 A71-14242

Premixed laminar flames in flow fields, amplifying fluid mechanical disturbances including vibratory motion and overall feedback loop

06 p1007 A71-18221

Back mixing effects on hydrocarbons combustion, comparing well-stirred reactor with flat flame soot yields

07 p1181 A71-19240

Post reaction zone properties of premixed fuel rich propane-oxygen flames on torch, measuring temperature, composition and hydroxyl radicals

08 p1345 A71-20858

HCN, acetylene and ethylene formation by propane in mixed jet staged flames

08 p1346 A71-20861

Combustion kinetics of premixed laminar graphite dust-oxygen-nitrogen flames with/without hydrocarbon

08 p1346 A71-20866

Heat fluxes from premixed methane-oxygen and propane-oxygen flames measurement by transient calorimetric method, comparing forward stagnation point results with calculated values

10 p1695 A71-24049

One dimensional premixed turbulent flame energy equation as function of heat release rate curve, temperature, velocity, composition and density

12 p1985 A71-26741

Flame quenching device for distances determination by burning premixed laminar propane-air at atmospheric pressures between nonparallel walls

15 p2385 A71-32089

Nonpremixed and premixed combustion theory in laminar flows, considering diffusion flame- reaction time ratio and activation energy effects

15 p2515 A71-32564

Gaseous chromium carbonyl or aqueous chromium salt spray additives behavior photometric investigations in premixed hydrogen-oxygen-nitrogen flames

16 p2540 A71-33374

Metal additives catalytic effects on premixed hydrogen-oxygen-nitrogen flames free radical recombination rates, discussing heterogeneous and homogeneous schemes

19 p3012 A71-38082

Negative ion and compound formation in premixed fuel-rich laminar atmospheric pressure hydrogen-oxygen-nitrogen flames with molybdenum and potassium atoms

19 p3167 A71-38092

Combustion driven acoustic oscillations in gas fired burner of premixed methane, nitrogen and oxygen, noting mixture ratio and flow rate effects

19 p3123 A71-38098

Area measurement on steady, fluctuating, turbulent and expanding premixed flames, using saturation current method

19 p3168 A71-38103

Fuel rich premixed hydrogen-oxygen flame stabilization on cooled porous plate burners at 10 mm Hg

19 p3168 A71-38107

Aerodynamic combustion noise generation from premixed or diffusion open turbulent flames, using fluid mechanics and Lighthill method

23 p3781 A71-43448

PREPARATION

NT PRESTRESSING

NT PRETREATMENT

PREPOLYMERS

NT DIMERS

Thermally stable polyimide graphite fiber reinforced composites from solutions of monomeric reactions, comparing amide acid prepolymers

11 p1788 A71-25560

PRESELECTORS

U PREAMPLIFIERS

PRESERVATIVES

Preservative phenol derivative effects on toxic gas evolution from stored urine in sealed vessels

22 p3506 A71-42808

Urine preservatives for urine water recovery system, noting ammonia and organic compound contents in condensate

22 p3506 A71-42809

PRESINTERING

U SINTERING

PRESSES

Vertical hydraulic press for metal extrusion at temperatures from 4 to 77 K, discussing design

08 p1299 A71-21809

PRESSING [FORMING]

NT BLANKING [CUTTING]

NT COINING

NT STAMPING

Isostatic pressing for large complex metal powder parts, comparing with die-compacting

01 p0088 A71-10814

Titanium, Inconel and stainless steel alloys deep drawing press loads under various lubrication and temperature conditions, considering work hardening, friction and anisotropic coefficients

[ASME PAPER 70-WA/PROD-26] 03 p0433 A71-14114

Titanium alloys for drop and press forged airframe, engine, rocket and spacecraft components, presenting physical and mechanical properties for various alloys and applications

05 p0757 A71-16136

Sintering and pressing techniques for compact semifinished products of refractory metal powders including W, Mo, Ta, Nb, Zr and Ti

09 p1457 A71-23396

Precision forging and pressing of Al alloy and Ti alloy parts of aircraft structures at cost effective prices

09 p1459 A71-23691

Three dimensional isostatic pressing process, discussing equipment, tooling and forging preforms and finished parts production

10 p1618 A71-24764

Unsteady press forging process in dies with material extrusion through plane strained slot, describing deformation stages, slip line patterns and hodographs

16 p2581 A71-32818

PRESSORS

U VASOCONSTRICTOR DRUGS

PRESSURE

NT ATMOSPHERIC PRESSURE

NT BASE PRESSURE

NT BLOOD PRESSURE

NT CRITICAL PRESSURE

NT DENSIFICATION

NT DIFFERENTIAL PRESSURE

NT DYNAMIC PRESSURE

NT ELECTRON PRESSURE

NT GAS PRESSURE

NT HIGH ALTITUDE PRESSURE

NT HIGH PRESSURE

NT HIGH VACUUM

NT HYDROSTATIC PRESSURE

NT HYPERTENSION

NT HYPOTENSION

NT HYPOXEMIA

NT ILLUMINANCE

NT IMPACT LOADS

NT INLET PRESSURE

NT INTERNAL PRESSURE

NT INTRACRANIAL PRESSURE

NT INTRAOCULAR PRESSURE

NT ISOSTATIC PRESSURE

NT LOW PRESSURE

NT LUMENS

NT LUMINANCE
 NT LUMINOUS INTENSITY
 NT MIDDLE EAR PRESSURE
 NT OVERPRESSURE
 NT OXYGEN TENSION
 NT PARTIAL PRESSURE
 NT RADIATION PRESSURE
 NT SOUND PRESSURE
 NT STAGNATION PRESSURE
 NT STATIC PRESSURE
 NT SUPERCRITICAL PRESSURES
 NT SYSTOLIC PRESSURE
 NT THRUST CHAMBER PRESSURE
 NT TRANSIENT PRESSURES
 NT ULTRAHIGH VACUUM
 NT VACUUM
 NT VAPOR PRESSURE
 NT WALL PRESSURE
 NT WATER PRESSURE
 NT WIND PRESSURE

PRESSURE BREATHING
 Respiratory mechanics and ventilatory response to carbon dioxide during positive pressure breathing in conscious man 06 p0861 A71-18379
 Altitude range for supplemental aircraft continuous flow, diluter and pressure demand oxygen systems, discussing regulations and pressure breathing 08 p1244 A71-20714
 German book on clinical pathophysiology of respiration covering respiratory physiology, pulmonary gas exchange, respiratory control, hypoxia, hyperoxia, pressure breathing, etc 09 p1394 A71-23069

PRESSURE CABINS
 U PRESSURIZED CABINS

PRESSURE CHAMBERS
 NT HYPERBARIC CHAMBERS
 NT VACUUM CHAMBERS
 Martian environment simulator chamber for pressure, visible light, biological objectives UV irradiation and daily temperature cycle 01 p0068 A71-11559
 Ti alloy research, describing transparent atmosphere chamber design and dilatometer control modifications 04 p0604 A71-15908
 Rabbits and humans behavioral reactions and EEG changes relation to hypoxia in pressure chamber 12 p1871 A71-27488
 Artificial respiration in elevated gas pressure chamber to revive organism after clinical death by rapid decompression 12 p1876 A71-27745
 Harmonic pressure generator design based on plane sound waves principle 13 p2071 A71-29293
 Local shielding chambers for welding circumferential and longitudinal seams in Ti alloys with minimum residual oxygen concentrations 14 p2253 A71-30489
 Intermittent hypersonic wind tunnels, considering pressure and vacuum storage, blowdown tunnels and pressure tubes 18 p2897 A71-36409
 Spectroscopic study of imploding shock waves in hemispherical chamber filled with oxygen-hydrogen-helium mixture at high pressure 19 p3163 A71-37735

PRESSURE COEFFICIENT
 U AERODYNAMIC COEFFICIENTS

PRESSURE DISTRIBUTION
 Aerodynamic theory of pressure field induced on lifting surface by isotropic atmospheric turbulence, considering transfer function of Concorde aircraft [ICAS PAPER 70-30] 01 p0002 A71-11019
 Pressure distributions prediction on blunt bodies at angle of attack, considering bodies of revolution and large angle cones 01 p0004 A71-11580
 Externally pressurized gas thrust bearings, examining performance and pressure distribution in film 02 p0256 A71-12412
 Infinite MHD journal bearing with electrically conducting fluid lubricant in radial magnetic field, obtaining pressure distribution, load capacity and driving torque 02 p0258 A71-12601
 Sweptback turboblades in parallel wall channel, investigating thickness, camber and leading edge curvature effects on flow and pressure distributions and vortex movement 02 p0186 A71-12606
 Steady incompressible laminar pipe flow within porous wall cylinder, determining velocity, pressure distribution and shear stress [ASME PAPER 70-WA/FLCS-3] 03 p0401 A71-14079
 Structural vibration response to nonhomogeneous random pressure fields based on homogeneous field theory [ASME PAPER 70-WA/DE-11] 03 p0511 A71-14145
 Aerodynamic forces on control surfaces in subsonic range, investigating pressure distribution on harmonically oscillating wing 03 p0344 A71-14347

Pressure boundary layer profile numerical solution for transient and steady hydrodynamic gas film under high speed and small trailing edge thickness 04 p0570 A71-15178
 Modified buried collector gauge performance over He pressure range, determining sensitivity dependence on filament geometry 05 p0748 A71-16231
 Strong shock wave Mach reflection, determining pressure and temperature at wedge surface by shock tube experiment 05 p0835 A71-16526
 Gas phase reactions near solid-gas interface of deflagrating double base propellant causing abrupt changes in burning rate-pressure curve [AIAA PAPER 70-124] 05 p0837 A71-16571
 Wind field from macroscale atmospheric whirlpools /typhoons/ pressure fields by nonlinear hydrodynamic equations 06 p0923 A71-17514
 Stainless steel shells under uniform external pressure and constrained deformation, noting critical load increase 06 p0986 A71-17760
 Ground effects on pressure distribution on slender wing bodies with low aspect ratio and thick cross sections 06 p0842 A71-18047
 Solid propellant rocket chamber unstable motion, discussing pressure and velocity coupling 06 p0946 A71-18297
 Pressure distribution singularity at tip of thin lifting parabolic wing in subsonic flow [AIAA PAPER 71-10] 06 p0842 A71-18484
 Pressure distribution over blade in cascade nozzle for incompressible and compressible particulate gas flow [AIAA PAPER 71-82] 06 p0883 A71-18539
 Airflows in two dimensional nonuniformly sheared slipstreams, predicting pressure distribution from mathematical model for comparison with measurement [AIAA PAPER 71-94] 06 p0843 A71-18549
 Far field sonic boom pressure profiles simulation by methane-oxygen mixture detonation in balloons [AIAA PAPER 71-186] 06 p0886 A71-18625
 Monte Carlo technique for time domain response analysis of nonlinear structure in random pressure field with large deflection [AIAA PAPER 71-213] 06 p1004 A71-18649
 Caret wing serial tests in Mach 8 to 15 hypersonic flow, including three component force, spanwise direction pressure distribution and shock wave angular measurements by flow visualization 07 p1016 A71-20015
 Inverse boundary value problems in hydroaeromechanics, involving profile construction from given velocity or pressure distribution and supersonic flow boundaries determination 07 p1091 A71-20078
 Rock forming monomineralic aggregates thermal conductivity at ordinary temperature and pressure in relation to density, crystal structure and chemical composition 07 p1105 A71-20448
 Boundary layer pressure distributions for supersonic fluidics bistable devices 07 p1029 A71-20589
 Gas turbine rotor axial load determination, using static pressure distribution 08 p1348 A71-21268
 Jet propulsion optimization by exergy and anergy for minimum total cost flux by varying unit compressor pressure ratio 08 p1348 A71-21300
 Pressure conditions across distant magnetopause from interplanetary magnetic field measurements, comparing Pioneer 7 plasma data with Explorer 33 distant geomagnetic tail field magnitudes 08 p1285 A71-21692
 Surface station pressure reduction to sea level, determining differential expression by least squares method 08 p1329 A71-21727
 Surface heating and pressure distribution on Lunar Module from rocket exhaust plume impingement tests in vacuum [AIAA PAPER 71-256] 08 p1377 A71-21985
 External store surface pressure distributions during captive flight aboard F-4B aircraft, considering carrying aircraft effects on flow field about airborne ordnance [AIAA PAPER 71-295] 08 p1232 A71-22015
 Temperature and pressure discontinuity stresses in compact heat exchangers, considering tubes as elastic foundation underneath tube plate 08 p1374 A71-22034
 Three dimensional laminar boundary layer on cone at incidence in supersonic flow evaluated by pressure distribution technique, comparing heat transfer, Pitot probe measurements, etc [AIAA PAPER 70-48] 09 p1381 A71-22088
 Surface pressure field sampled natural functions statistical stability, taking into account eigenvalue magnitudes and rate of decrease 09 p1487 A71-22303

Electrohydrodynamic flow in plane channel with conducting walls and axial emitter electrode, determining velocity and pressure profiles distortion 09 p1502 A71-22538
 Detonation products expansion in vacuum, measuring gas flow speeds and pressure profiles far from charge 09 p1545 A71-22690
 Pressure distribution on arbitrary finite symmetrical wings with rounded leading edges at zero incidence in subsonic flow 09 p1383 A71-22945
 Incompressible viscous fluid nonsteady three dimensional flow, obtaining velocity field and pressure distribution in boundary layer 09 p1433 A71-23092
 Two dimensional incompressible laminar boundary layer with longitudinal surface curvature, examining equations with particular attention to pressure boundary conditions and pressure gradient formulation 09 p1433 A71-23098
 Supersonic flow separation around cross shaped horizontal tail plane with subsonic leading edge, obtaining pressure distribution and aerodynamic characteristics 09 p1384 A71-23608
 Mach cones reflection at thin wing subsonic leading edges in supersonic flow, considering axial disturbance velocity and pressure distributions 09 p1384 A71-23616
 Balance equation solution in spherical coordinate form, applying vector alterations to geostrophic wind field from pressure-height observations grid point analysis 10 p1638 A71-23964
 Low speed airfoil characteristics calculation by digital computer, using Theodorsen conformal transformation method for potential flow pressure distribution [SAE PAPER 710389] 10 p1550 A71-24253
 Short N wave refraction and diffraction by gas-filled soap bubble, discussing measurements to explain peaking and rounding in sonic boom pressure signature 10 p1642 A71-24811
 Velocity and static pressure redistribution in distorted flow field upstream of axial flow compressors [AIAA PAPER 69-485] 10 p1553 A71-24856
 Propeller blade profile thickness distribution for given pressure distribution, deriving integral equation with singular kernel function via source-sink and vorticity distribution linearized theory 10 p1553 A71-24945
 Viscous liquid unsteady flow in long circular tube as function of mean velocity distribution, discussing radial flow and pressure distribution 11 p1749 A71-25268
 Collocation method predicting oscillatory subsonic pressure distributions on interfering parallel lifting surfaces, considering approach more economical than finite element method [AIAA PAPER 71-329] 11 p1701 A71-25309
 Semiinfinite crack perpendicular to elastic half plane surface under pressure distribution on faces or remote loading, obtaining fracture mechanics solution with Wiener-Hopf method 11 p1847 A71-25444
 Reentry vehicles configuration lift and drag coefficients in hypersonic flow from pressure distribution and balance measurements, comparing with isolated cone data 11 p1702 A71-25487
 High subsonic flow two dimensional turbine cascade design by approximate hodograph method, noting pressure distribution measurements [ASME PAPER 71-GT-34] 11 p1704 A71-25971
 Glass fiber rotor blades design with longitudinal pressure tappings for cascade wind tunnel and turbomachinery flow research applications 11 p1772 A71-26316
 Bending stress in conical shell subjected to thermal and pressure loadings with uniform spatial distribution, using perturbation method 12 p1983 A71-27594
 Superpressurization mechanism in hollow cathode active zone, calculating upstream pressure variation as function of discharge current 13 p2106 A71-28399
 Plane Couette flow with suction/injection at stationary plate, obtaining motion and continuity equations, pressure distribution and friction coefficient 13 p2047 A71-28520
 Air inlet for simulation of shock wave separated flow in supersonic diffusers, deriving pressure variation profile along free boundary 13 p1992 A71-29175
 Pressure, velocity and potential distribution of flow around arbitrarily shaped body of revolution during arbitrary motion in perfect liquid 13 p1992 A71-29187
 Error in determining pressure and loading distribution on surface of slender bodies of revolution 13 p1994 A71-29323

Liquid-vapor interactions in constant area steam-water condensing ejector mixing section, measuring axial static and stagnation pressure profiles [ASME PAPER 71-FE-21] 13 p2052 A71-29459

Curved wall jet pressure distribution numerical calculation for given velocity profiles 14 p2328 A71-30306

Sound radiation and pressure fields inside vibrating turbomachine blades, using miniaturized microphones and compact capacitive detectors 14 p2288 A71-30517

Pressure distribution and drag prediction over slender axisymmetric fuselages and afterbodies and exhaust nozzles at transonic Mach numbers [AIAA PAPER 71-720] 14 p2170 A71-30771

Retreating blade stall experiments on model helicopter rotor, considering series of pressure distribution and boundary layer events [AHS PREPRINT 521] 14 p2172 A71-31087

Space shuttle vehicle models, calculating surface flow patterns and pressure and aerodynamic heating distributions for comparison with test data [AIAA PAPER 71-594] 15 p2343 A71-31539

Flat plate span effects on ramp induced adiabatic laminar boundary layer separation at supersonic and hypersonic speeds, measuring surface pressure distribution [AIAA PAPER 71-559] 15 p2344 A71-31557

Turbulent mixing between parallel incompressible air streams, using statistical investigation of pressure and velocity fields [AIAA PAPER 71-613] 15 p2389 A71-31582

Pressure fluctuations in acoustic field of boundary layer under slot suction, considering vortex formation and separation on edges 15 p2389 A71-31713

DC equivalent circuit, describing pressure and flow distribution at input ports of fluidic line branchings 15 p2352 A71-32067

Pressure and velocity distributions in gas filled cavity undergoing resonant acoustic oscillations due to heat addition 15 p2392 A71-32126

Slip flow development in parallel plate channel entrance, discussing center line velocity and excess pressure distributions 15 p2393 A71-32262

Pressure histories due to weak shock wave propagation through dividing flow junction, describing wave decay in side branch duct 16 p2555 A71-32887

Approximate calculation of pressure distribution, separation points and drag on circular cylinder in viscous liquid flow, using ideal fluid jet model 16 p2560 A71-33597

Jet induced secondary flow interaction with circular plate, showing ring vortex effects on pressure distribution 17 p2669 A71-34334

Polyatomic gases thermal conductivity and rotational relaxation number from thermomolecular pressure differences across capillary tubes 17 p2785 A71-34946

Magnetic properties of contained plasma, discussing equilibrium equations and pressure profiles 17 p2788 A71-35025

Wall pressure spectra and rms wall pressure levels measurements in subsonic separated flows, postulating model for pressure fluctuation estimation 17 p2728 A71-35037

Monograph on dynamic viscous pressure interaction in hypersonic flow covering boundary layer effect on oscillating body steady pressure distribution in continuum hypersonic flow 17 p2671 A71-35217

Stagnation pressure changes in unsteady flow downstream of turbomachine blades with fluctuating circulation related to vortex sheets 17 p2671 A71-35279

Flow distribution behind laminar boundary layer separation point in supersonic flow, calculating plateau region pressure 17 p2672 A71-35629

Turbulent boundary layer interaction with supersonic outer flow behind step, calculating pressure distribution, momentum thickness and friction 17 p2672 A71-35631

Supersonic flow past V-shaped wings with leading edges, applying method of establishment to space variable for pressure distribution 17 p2673 A71-35647

Transient laminar two dimensional boundary layer induced pressures due to suddenly accelerated hypersonic semiinfinite flat plate 18 p2901 A71-35856

Siren wail in turbine axial stage due to nonuniform pressure fields behind blade cascades 18 p2843 A71-36180

Turbulent flow of air film between rotating circular and stationary plane surfaces, determining pressure distributions, inertial forces effects and velocity profiles 18 p2926 A71-36185

Stratospheric pressure surfaces height over polar, middle and tropical latitudes as function of long term solar activity 18 p2944 A71-36220

Pressure distribution over deflected flap as function of boundary layer separation, flap geometry, Reynolds number and Mach number 18 p2972 A71-36435

Gas flow through hypersonic conical nozzle in shock-gun tunnel, measuring pressure ratio and Mach number distributions at test section 18 p2849 A71-37024

Pressure distribution during cold rolling of metallic powders of stainless steels, iron, titanium and copper, using dynamometer mounted in roll 19 p3075 A71-37107

Radiation heat transfer volume interchange factors approximation for gases with nonuniform temperature, composition or pressure, comparing with exact numerical computations 19 p3164 A71-37990

Elastic field and stress distribution in composite circular rotating disk under constant normal pressure 19 p3159 A71-38187

Alveolar-arterial oxygen pressure difference during controlled hyperventilation and posthyperventilatory phase 19 p3003 A71-38200

Simple source theory of aerodynamic noise, approximating relationship between radiated sound power and jet pressure spectra 19 p3124 A71-38531

Blower suction line random vibrations due to distributed random pressure, investigating various isolation arrangements for vibration reduction 20 p3308 A71-39085

Intraocular pressure distribution of healthy mental workers in 25-40 years age range, noting symmetry 20 p3189 A71-39234

Turbulent boundary layer response to step change in surface roughness, discussing wind tunnel measurements of pressure and velocity profiles 20 p3212 A71-39505

Two dimensional flow over two dimensional finite wing without correction for downwash, assuming known pressure distribution 21 p3318 A71-40173

Quasi-static pressure characteristics of gas lubricated thrust bearing with shrouded Rayleigh step pads, solving nonlinear equation of motion [ASME PAPER 71-VIBR-75] 21 p3385 A71-40313

Uniform inlet flow inside centrifugal turbomachinery diffusers with flat parallel side walls, measuring pressure distribution and boundary layer velocity profiles 21 p3323 A71-40757

Flap span length effects on boundary layer separation, giving streamline pressure distributions 21 p3323 A71-40967

Jet flaps application to autogyro rotor, using pressure jump for air centrifugation 21 p3324 A71-41399

Normal shock existence in blade spacings of rotor and guide vanes of axial flow supersonic compressor as function of pressure nonuniformity 22 p3479 A71-41843

Circumferentially nonuniform flow in front of axial compressor stage with stepwise two zone pressure and velocity distribution resulting in increased guide vane losses 22 p3479 A71-41845

Centrifugal pump pressure characteristics calculation by pressure quality coefficient dependence on relative flow rate, assuming arbitrary number of blades 22 p3554 A71-41848

Heat transfer and pressure distribution on biconic and hemispherical geometries with sharp and blunt noses in Mach 15-20 flow 22 p3480 A71-41964

Heat transfer and pressure distribution of cone shaped model at different angles of attack in hypersonic flow simulating reentry flight in wind tunnel 22 p3480 A71-41965

Nimbus 3 satellite IR spectrometer atmospheric pressure height profiles, comparing with nearby radiosonde data 22 p3535 A71-42410

Shock layer pressure distribution for axisymmetric bodies moving at supersonic velocity in gas at rest, deriving nonstationary analog of Newton-Busemann formula 22 p3481 A71-42864

Laminar convective heat transfer from rotating isothermal disk in uniform forced stream, using pressure distribution measurements 23 p3781 A71-43314

Geometrically nonlinear integral solutions to equilibrium equations of curvilinear beam under uniform pressure, using Weierstrass functions 24 p3883 A71-44850

Pressure distribution in narrow porous metal bearings solved with Bessel functions in cylindrical coordinates, finding lower load capacity 24 p3830 A71-44950

PRESSURE DRAG

NT INTERFERENCE DRAG
NT WAVE DRAG

Pitot type intake inlet additive drag in terms of capture area ratio, static and total pressure coefficients 02 p0187 A71-12688

Pressure drag and cross flow force coefficients of inclined circular cylinder in supercritical flow 09 p3182 A71-22098

Karman vortex street geometry calculation for single circular cylinder, using pressure drag coefficient, Strouhal number and Krounauer criterion [ASME PAPER 71-VIBR-11] 21 p3457 A71-40273

Karman vortex street induced fluctuating lift forces on single circular cylinder, deriving relationship between lift coefficient and steady state pressure drag coefficient [ASME PAPER 71-VIBR-12] 21 p3457 A71-40274

Karman vortex street induced fluctuating lift forces on tube bundles as function of steady pressure drag coefficient and Strouhal number [ASME PAPER 71-VIBR-13] 21 p3457 A71-40275

PRESSURE DROP

Shock wave dynamic behavior in shock tube under variable diaphragm opening time for high pressure gas flow into lower pressure section 03 p0472 A71-14261

Coolants Prandtl number effect on pressure drop, heat transfer and friction of rough surfaces 04 p0675 A71-14779

Heat transfer and pressure drop in air flowing in square tube with two dimensional discrete turbulence promoters applied to opposite walls 04 p0675 A71-14781

Heat transfer in exchangers with forced laminar or turbulent flows with linear pressure drop and exponential thermal flux distribution 04 p0688 A71-15740

Aerodynamic seals theoretical analysis and experimental test results, considering pressure ratios, pressure recovery coefficients and pump efficiency 07 p1117 A71-19422

Static fluid logic elements, discussing short circuit during switchover, snap action, pressure loss and circuit examples 07 p1027 A71-20573

Flow visualization and velocity measurements in repeatedly branching tube systems representative of human lung, estimating viscous dissipation and pressure drop 10 p1571 A71-24625

Capillary pressure and contact angle drop of two fluid flow separated by parallel plate interface 11 p1750 A71-25443

Aircraft crew without pressure suits, noting abrupt ambient pressure drop tolerance in trained and untrained subjects 12 p1876 A71-27659

Heat pipes design and applications, examining pressure losses in steam and liquid phases and capillarity and gravity effects [HEAT EXCH. CONF. PAPER 23] 15 p2513 A71-31637

Heat transfer and pressure drop characteristics of He in two phase and supercritical flow, calculating He heat exchangers for superconductive devices [HEAT EXCH. CONF. PAPER 24] 15 p2513 A71-31638

Air-water flow pressure loss and phase distribution in tube with wire coil swirl generators [GESP-449] 15 p2354 A71-32209

Heat transfer, fluid flow and pressure loss, noting application to cryogenic heat exchangers and process plants 20 p3312 A71-39245

PRESSURE EFFECTS

Shock wave diffraction at sharp edges, discussing physical principles, angle and pressure ratio effects 01 p0001 A71-10109

Guinea pigs head and eye movements produced by vestibular apparatus stimulation via static pressure changes 01 p0010 A71-10347

Output properties of electrically pulsed carbon dioxide laser as functions of partial gas pressure and discharge voltage 01 p0092 A71-10372

Optically thin medium convective instability, examining radiant pressure and magnetic field effects 01 p0158 A71-10804

Flutter analysis of plates with inplane boundary support flexibility exposed to transverse pressure loading or buckled by uniform thermal expansion 01 p0173 A71-10940

Plane diffuser cascade losses at low main stream pressures, discussing Reynolds number role 01 p0003 A71-11062

Carbon dioxide IR absorption bands at elevated pressures, deriving transmission function 01 p0130 A71-11104

Liquid volume deformation effect on hydraulic drive under continuous or jumpwise pressure 01 p0007 A71-11243

Laser vs electron beam welding, examining high and partial vacuum and atmospheric pressure environ-

- ments, penetration and ionization and dissociation processes
[SME PAPER MR-70-523] 01 p0090 A71-11269
Simply supported cylindrical shell buckling under linearly varying lateral pressure 01 p0178 A71-11399
Magnesium particle combustion in rarefied air at various pressures 01 p0182 A71-11444
Gravitational fields and atmospheric pressure effects on soils subjected to static and dynamic loading, using aircraft parabolic gravity simulation [AIAA PAPER 69-1009] 01 p0068 A71-11581
Gaseous atmospheres environmental effects on metal mechanical properties at high temperatures, discussing failure mode with crack growth rate dependence on pressure 02 p0263 A71-11864
Visual images induced in aircraft crew members, during pressure chamber experiments, discussing latent period and persistence of sequences 02 p0198 A71-11899
Circular cone with cross shaped wings in supersonic flow, determining flow characteristics, velocities and pressure 02 p0185 A71-11958
Hypobaric pressure and hypoxic or hyperoxic atmospheres effect on mice resistance to pneumococcal pneumonia 02 p0199 A71-12382
Prebuckling deformations influence on circular cylindrical shell buckling under external pressure, applying Galerkin method to Donnell equations 02 p0329 A71-12602
Quasi-Alfven and acoustic wave coupling in inhomogeneous stratified plasma within intense magnetic field as function of directional pressure 02 p0292 A71-12627
Supersonic underexpanded jet-plane obstacle flow interaction patterns, discussing pressure and distance effects 02 p0186 A71-12643
Incompressible fluid filled circular cylindrical shells loaded by pressure ring at center, obtaining yield point load 03 p0500 A71-13022
Stability of finite pressure plasma trapped by magnetic field, discussing trapped particle effects 03 p0463 A71-13296
Pressure effect on combustion rate of model mixtures of ammonium perchlorate with polystyrene and polymethyl methacrylate 03 p0468 A71-13989
Intraluminal pressure effect on stress concentration and deformation of arterial wall in relation to atherosclerosis, using finite element method [ASME PAPER 70-WA/BHF-15] 03 p0373 A71-14113
Thin walled circular cylindrical shells creep buckling under radial pressure and thermal gradients [ASME PAPER 70-WA/APM-8] 03 p0512 A71-14152
Accelerated cavitation damage in Na, examining pressure and temperature effects 03 p0443 A71-14286
Soviet book on optical properties of hot air covering spectral lines, radiative transfer, cross sections, pressure effects and absorptivity 03 p0460 A71-14397
Pressure and strain rate effects on polycrystalline Be shear strength, determining activation energy for dislocation motion 03 p0445 A71-14463
High density atmospheric pressure plasma ionization measurement by negatively pulsed Langmuir probe, showing agreement with space charge controlled sheath expansion model 04 p0586 A71-14660
High current free-burning arc characteristics in air at various pressures, examining dimensions from photographs 04 p0676 A71-15031
Human orthostatic tolerance measurement via leg and lower body negative pressure, discussing heart rate and stroke volume variations 04 p0543 A71-15052
Pressure-temperature equivalences in elasticity problems, considering applications to case bonded solid propellant rocket grains 04 p0638 A71-15197
Eccentrically stiffened thin spherical shell instability under uniform external pressure 04 p0669 A71-15199
Stellar structure theory, examining particle aggregates gravitational and pressure forces, energy flow, generation and opacity and equations of state 04 p0648 A71-15246
Pressure effects on calibration characteristics of hot-film anemometers, discussing heat loss from sensing element 04 p0601 A71-15765
Pressure and temperature variation effects on vibratory cavitation damage tests conducted in water 04 p0604 A71-15767
Interstellar gas cloud equilibrium and gravitational stability, examining evaporation, condensation, thermal balance and pressure 04 p0658 A71-15837
Liquid fuel drop evaporation under pressure on hot surface, measuring lifetime and transient interface temperature at subcritical and supercritical conditions 04 p0689 A71-15919
Transient response of solid propellant combustion to pressure variations and sudden depressurization 05 p0795 A71-16540
Circular cylindrical shells buckling with different elastic moduli in tension and compression under arbitrary axial and lateral pressure 05 p0823 A71-16558
Internal combustion engine exhaust system sound radiation, discussing pressure wave effects, energy flux and boundary conditions 05 p0796 A71-16604
Ionization gage with ion current linear dependence on pressure at room temperature 05 p0753 A71-16945
Polytropic gas spheres gravitational instability under external pressure, obtaining critical masses and densities 05 p0813 A71-17091
Aerodynamic sound generation dependence on convective derivative of hydrodynamic pressure within turbulence source region 05 p0784 A71-17154
Thin elastic shallow spherical dome nonlinear motion under uniformly distributed external pressure 06 p0982 A71-17360
Rocket engines with nitrogen tetroxide/hydrazine injectors destructive instability due to pressure disturbances, establishing origin, propagations velocity and pops extent by streak photography [WSS/CI PAPER 70-25] 06 p0942 A71-17653
Shallow spherical shells stability under constant external pressure 06 p0987 A71-17768
Smooth cylindrical shell stability, considering internal pressure effect on critical axial stresses 06 p0993 A71-17819
Cylindrical anisotropic shells transient deformation processes under external pressure, discussing equations of motion integration 06 p0996 A71-17838
Cylindrical shell stability under arbitrary external pressure, discussing forces and displacements of precritical stressed state 06 p0997 A71-17848
Pure hydrocarbon droplets heating, expansion, vapor phase fuel storage and gasification in oxidizing gas at elevated pressures, using high speed cinematography 06 p1007 A71-18300
Solid propellant engine structural analysis, examining transient thermal loading and internal pressure effects [AIAA PAPER 71-115] 06 p1003 A71-18565
Nonlinear finite difference computer program applied to elliptic cylinder collapse under uniform external pressure, comparing with theoretical bifurcation buckling [AIAA PAPER 71-146] 06 p1003 A71-18589
Pulsed laser emissions in carbon dioxide under high pressure, discussing onset inversion and pulse duration 07 p1121 A71-19128
Calcite and aragonite high pressure Raman line spectra comparisons, testing structural identification theory 07 p1034 A71-19369
Pressure dependent shift of He-Ne laser radiation, observing beat frequencies 07 p1123 A71-19486
Reaction heat for flameless combustion of double-base propellant using differential scanning calorimetry and thermogravimetric analysis, noting pressure effects [AIAA PAPER 70-125] 07 p1183 A71-19898
Free nitrogen jets ejected from small orifices, measuring acoustic emission level and spectral pattern dependence on pressure 07 p1161 A71-20058
Plasma-electron beam interaction instability transition from absolute to convective in hydrogen tube system at various pressures, considering electron collision effects 07 p1170 A71-20181
Multistage axial flow turbine off-design performance prediction, exploring inlet temperature and pressure and exit pressure variation effects [ASME PAPER 70-PWR-2] 07 p1184 A71-20199
Stiffened long cylinder with time variable thickness and strengthening thin shell system elastic displacements due to nonstationary vibrations and nonuniform pressure distribution 07 p1217 A71-20459
Gas bubble growth and dissolution due to pressure fluctuations in turbulent diffusion liquid flow 07 p1094 A71-20475
Hydrostatic pressure effects on Al polycrystals stress-strain behavior at room temperature, using magnetostriuctive load cell 07 p1143 A71-20490
Finite and large pressure inhomogeneous plasma with finite electron heat conduction, calculating instability 07 p1173 A71-20534
Jet reattachment to adjacent flat plate, investigating back pressure effects 07 p1094 A71-20606
Pressure and gas composition effects on sodium acetate-C 14 incorporation into liver lipids, indicating metabolic relationships to decompression sickness 08 p1238 A71-20814
Pressure increase, dry air consumption and power requirements effects of water quantity fed into centrifugal compressor 08 p1347 A71-20833
Carbon dioxide IR absorption bands at elevated pressures, deriving transmission function 08 p1337 A71-20848
Ethylene diffusion flame radiation measurements, determining pressure effects and contributory ratio of carbon particles and gaseous radiation 08 p1346 A71-20859
High temperature nitrogen plasma, calculating thermodynamic and electrical parameters dependence on pressure and temperature 08 p1342 A71-21917
Ultrasound propagation velocity dependence on high pressure and temperature in carbon dioxide, considering Rao rule applicability to highly compressed gases 09 p1492 A71-22529
Measuring instrument for amorphous and polycrystalline materials resistivity and Seebeck coefficient as function of temperature and pressure 09 p1446 A71-22737
Folded all-reflecting Schmidt camera UV image converter system for space astronomy applications, discussing pressure sensitivity effects on UV direct recording emulsion 09 p1447 A71-22751
Clamped shallow spherical caps under uniform pressure, computing axisymmetric buckling 09 p1541 A71-23091
Temperature and pressure effects on phase transformations, structural changes and related processes in metals, comparing thermographic and calorimetric methods 09 p1547 A71-23227
Stability of finite pressure plasma trapped by magnetic field, discussing trapped particle effects 09 p1504 A71-23269
Pulmonary arterial blood flow regulation by hydrostatic pressure in low resistance circulatory system 10 p1561 A71-24127
Ultrasonic cleaning by cavitation disintegration of highly adhesive surface coatings, discussing cleansing liquid, field parameters and external static pressure effects on process efficiency 10 p1617 A71-24135
Cross-excited electrically pulsed carbon dioxide laser investigating self mode locking as function of cavity length, operating pressure and bleachable absorber sulfur hexafluoride 10 p1620 A71-24152
High pressure ratio centrifugal compressors for small gas turbine engines, investigating power and specific fuel consumption variation with pressure and temperature 10 p1658 A71-24218
Limit load carrying capacity of thin walled tube under combined forces, including pressure effects by variational method of plasticity theory 10 p1688 A71-24384
Nb-Ti alloy oxidation kinetics at various temperatures and pressures, noting linear patterns and oxide formation 10 p1626 A71-24403
Axisymmetric snap-through of shallow clamped spherical caps under uniform pressure, revealing existence of higher modes as isolated closed loops from approximate solution 10 p1689 A71-24518
Nitrogen, helium, argon and neon containing atmospheres relation to altitude decompression of rats, noting interspecies comparison of metabolic effects 10 p1570 A71-24610
Nonlinear stability analysis of inviscid and viscous liquid film adjacent to compressible gas flow, using gravity and pressure perturbation models 10 p1595 A71-24620
Inhomogeneous collisionless plasma instabilities under dense blanket of neutral gas, investigating Alfven type oscillation 10 p1650 A71-24628
Light scattering from gas thermal fluctuations, deriving density-density correlation function over various pressures 10 p1642 A71-24836
Aerodynamic infrasound, considering atmospheric pressure variations in seconds to minutes period range 10 p1596 A71-24915

Ionization wave varieties in nitrogen glow discharge at various pressures and current densities from phase and group velocity measurements

10 p1654 A71-24973

Structures dynamic loading and damage by sonic booms, discussing structural response prediction by boom pressure wave model

10 p1693 A71-25052

In-plane boundary conditions influence on clamped conical shells buckling under external pressure, using displacement method based on Donnell stability equations

11 p1841 A71-25158

Normal shock wave acceleration of water droplets by external pressure, observing distortion and breakup through shadowgraph techniques

[AIAA PAPER 71-325]

11 p1749 A71-25305

Venus life forms, describing algae grown in pure carbon dioxide under pressure in acidic nutrient media at high temperatures

11 p1724 A71-25701

Transient pressures in spacecraft and volume compartments with outgassing for ambient pressure decrease and low pressures unattainable with large chambers

11 p1840 A71-26398

Lunar surface properties, noting shock effects from impact induced pressures and temperatures

11 p1834 A71-26453

Line formation effective pressure from Venus atmosphere spectra, discussing phase angle variations

11 p1835 A71-26457

Pressure effects on human ventilation and gas exchange, determining stratified inhomogeneity during deep diving

12 p1873 A71-27126

Wall-stabilized arc column optimization from energy balance solutions, considering temperature and pressure effects on Ar arcs

12 p1939 A71-27275

Turbomachine blade cascades in supersonic flow, noting wave configurations, entropy and counter pressure variations

12 p1864 A71-27475

Pressure and wall temperature gradients effects on equilibrium enthalpy profiles and heat transfer coefficients of incompressible turbulent boundary layers, using eddy conductivity model

[AIAA PAPER 69-689]

12 p1986 A71-27553

Abdominal pressure decrease resulting in transpulmonary pressure cranio-caudal gradient increase under gravitational effect simulation

13 p2008 A71-28437

Short term interval satellite orbit perturbations, computing direct solar radiation pressure effects with computer program

13 p2137 A71-28477

Liquid and gaseous Hg thermoelectric power measurements at sub and supercritical temperatures and various pressures

13 p2000 A71-28676

Distant geomagnetic tail longitudinal magnetic field gradient model based on pressure balance between internal field and solar wind, discussing tail flux content

13 p2064 A71-29162

Axissymmetrical snap buckling of clamped shallow spherical shell with initial deformation under external pressure, using energy method

14 p2322 A71-29689

Systemic arterial blood pressure response to chronic high altitude and hypoxia effects

14 p2184 A71-30280

Closed membrane shell of revolution finite creep due to uniform pressure, applying large deformation incremental theory

14 p2328 A71-30396

Incident sonic boom shock wave reflection factors off smooth surface, discussing pressure rise and flight near threshold Mach number

14 p2177 A71-30610

Pressure-induced absorption in planetary atmospheres from hydrogen-methane collisions, stressing resulting thermal opacity

14 p2315 A71-30659

Stability of structurally orthotropic stringer reinforced cylindrical shell closed by spherical or plane bottoms under uniform external pressure

14 p2333 A71-30892

Solid helium and molecular/metallic hydrogen thermodynamic properties and phase diagrams as functions of pressures corresponding to Jupiter and Saturn

15 p2511 A71-31338

Thermal decomposition rates and explosion of dinitroxydiethyl nitramine from heat release measurements at various pressures

15 p2462 A71-31376

Oxidation kinetics of pure Al in dry oxygen as function of pressure and temperature, using manometric method

15 p2426 A71-31408

Boron combustion characteristics as function of temperature, pressure and gaseous fuel mixture ratio, using color photography

[WSS/CI PAPER 71-19]

15 p2464 A71-31628

Warm plasmas impedances and power transfer near lower hybrid resonance, including electron pressure effects in full electromagnetic treatment

15 p2456 A71-31923

Spherical caps under step pressure loading, noting elastic damping effects on dynamic stability

15 p2506 A71-32093

Ammonium perchlorates deflagration rate at 20-100 atm, assessing relative roles of exothermic condensed phase and gas phase reactions by mathematical model

15 p2465 A71-32099

Compact pulsed carbon dioxide laser with uniform volume excitation, obtaining output energy as function of discharge voltage, gas composition and pressure

15 p2424 A71-32698

Electrical discharge plasmas, investigating electron multiplication, secondary processes, Paschen law, pressure effects and formation time lag

16 p2617 A71-32957

Stress field in elastic strip of finite width under pressure applied to faces of symmetrically situated Griffith crack

16 p2654 A71-33170

Biological effects of inert gases in elevated pressure respiratory mixtures on human central nervous system

16 p2536 A71-33577

Elevated atmospheric pressure effects on human psychophysiological qualities including attention, memory and time-estimating capabilities and nervous processes equilibrium

16 p2536 A71-33578

Escaping photoelectrons effect on polar wind exospheric model, suggesting kinetic pressure predominance at very high altitudes

16 p2569 A71-33814

Nimbus 3 and 4 satellite observation data comparison with sounding rocket and rawinsondes based on temperature as function of pressure measurements

16 p2572 A71-33846

Pressure ratios and surface effects on regenerative heat exchanger in Brayton gas turbine cycles with intercooling or reheating

16 p2663 A71-34037

Moment state stability of elastic hinged cylindrical shell and closed ring under pressure and concentrated load, using nonlinear equilibrium theory

16 p2660 A71-34114

Circular plate deflection weakened by hole and under constant external pressure, obtaining successive approximation method solution convergence

17 p2816 A71-34329

Incompressible materials weak compressibility effect in elastic theory, deriving displacement equation with average pressure function for any Poisson coefficient values

17 p2818 A71-34350

Ne 20 transition line width behavior vs pressure in He-Ne laser at 3.19 microns wavelength

17 p2752 A71-34402

Radiative width of laser transition in Ne 20 atom and line frequency shift vs pressure in dual He-Ne laser assembly effectuating atom collisions

17 p2752 A71-34403

Sound velocity in real gases as function of pressure and temperature, deriving by van Isterbeek result generalization for higher pressures

17 p2783 A71-35038

Monograph on dynamic viscous pressure interaction in hypersonic flow covering boundary layer effect on oscillating body unsteady pressure distribution in continuum hypersonic flow

17 p2671 A71-35217

High pressure electrodeless HF gas discharge plasmas, investigating effects of external magnetic field, gas and pressure on discharge rotation frequency

17 p2789 A71-35260

High temperature nitrogen plasma, calculating thermodynamic and electrical parameters dependence on pressure and temperature

17 p2789 A71-35262

Temperature and pressure effects on viscosity and thermal conductivity of dissociating air at high temperatures

17 p2785 A71-35277

Thin elastic spherical shells reinforced by stringers and frames and loaded by internal or external uniform pressure, calculating by energy method

17 p2829 A71-35311

Isotropic circular cylindrical shell stability with longitudinal hinges under uniform external pressure, determining critical load

17 p2831 A71-35322

Sympathetic response in renal and splanchnic nerves to elevated fall and rise of arterial blood pressure in anesthetized rabbits, investigating baroreceptor reflex effect

17 p2685 A71-35367

Transversely excited carbon dioxide lasers gain measurements for linear and helical electrodes at various gas mixtures and pressures as function of time

17 p2754 A71-35404

Ultrasound propagation velocity dependence on high pressure and temperature in carbon dioxide, con-

sidering Rao rule applicability to highly compressed gases

17 p2784 A71-35506

Muscle contraction model under biological factors action, considering circular cylindrical vessel equilibrium under internal and external pressures

17 p2694 A71-35616

Nitroglycerin powder combustion acoustic instability, determining mean pressure and sample and combustion chamber geometry effects

17 p2840 A71-35700

Self excitation and amplitude limitation of powder vibratory combustion, considering pressure and sample length effects

17 p2840 A71-35701

Large scale atmospheric turbulence, considering anisotropy, thermal stratification, pressure and Coriolis forces effects

18 p2944 A71-36009

Fluid amplifier digital elements dynamic switching, noting back pressure effects

18 p2851 A71-36207

Astronaut orthostatic tolerance loss due to weightlessness, describing compensation by periodic lower body negative pressure

18 p2872 A71-36648

Copper on copper friction coefficient dependence on oxygen pressure, investigating exoelectron emission from differently oxidized copper surface layers

18 p2928 A71-36750

Elastic buckling load of cylindrical shells with dimple imperfections under external pressure, applying perturbation expansion to Karman-Donnell equations

18 p2982 A71-36839

Mo, W and Mo-W alloys chlorination kinetics, investigating temperature and pressure effects on reaction rate from electron micrographs

18 p2938 A71-37002

Light elements thermodynamic state variables at high pressure, calculating electron density distribution as function of ion configuration with linear response theory

18 p2970 A71-37047

Vacuum deposited thin Cr films on glass, investigating substrate temperature and inert gas pressure effects on texture

19 p3076 A71-37117

Carbon dioxide laser, measuring focal length of gas defocusing lens in active medium as function of gas pressure and discharge tube diameter

19 p3073 A71-37771

Longitudinal edge stiffness and internal pressure effects on buckling and initial postbuckling behavior of axially compressed stringer reinforced cylindrical panels, discussing imperfection sensitivity

19 p3157 A71-37873

Atmospheric pressure and temperature inhomogeneities effects on thermal radiation transmission function of water vapor

19 p3090 A71-37973

Far IR collision induced spectrum in carbon dioxide, observing temperature and pressure dependence in gas phase and absorption in liquid

19 p3106 A71-38051

Slow and explosive gas phase oxidation of carbon suboxide and monoxide over various pressure and temperature ranges, noting branching reactions

19 p3167 A71-38088

Photographic study of acceleration and pressure effects on Al agglomerates and combustion processes on solid propellant surface, describing pit growth by combustion model

19 p3120 A71-38121

Polymer thermal degradation theory of pressure sensitive hybrid combustion, calculating linear regression rates

19 p3170 A71-38123

Pulsed erosion accelerators plasmoid discontinuities in structure streak photographs for various electrode configurations and pressures

19 p3116 A71-38253

On-design performance characteristics of radial gas turbines, investigating blade geometry, rotor losses and pressure ratio effects

19 p3123 A71-38269

Hypergolic rocket propellant system gas phase ignition, measuring ambient pressure, flow parameters and propellant temperature effects on delay characteristics

19 p3123 A71-38297

Circular planform punch pressure on elastic half space, solving system of two dimensional dual integral equations

19 p3160 A71-38478

Regional cerebral blood flow, tissue oxygen, EEG activity and behavioral reaction at high pressure

19 p3009 A71-38557

Integrated absorption coefficient of pressure induced pure rotational and vibrational transitions in binary collisions of homonuclear diatomic molecules at high temperatures

19 p3108 A71-38719

Pressure induced hydrogen collisions vibrational spectra absorption coefficients at high temperatures and local thermodynamic equilibrium

19 p3108 A71-38720

Rechargeable cylindrical hydrogen-oxygen fuel cell for synchronous satellites, determining energy density as function of current, pressure and electrolytes with computer model

20 p3182 A71-38947

Pressure anisotropy effects on plasma wave coupling and modification for dispersion in collisionless beam-plasma systems

20 p3273 A71-39045

Uniform magnetic field effects on beam-plasma waves, using scalar pressure hypothesis

20 p3274 A71-39049

Collision effects on line shapes using quantum mechanical description of atomic center of mass motion, considering pressure effects in gas lasers

20 p3271 A71-39069

High power continuous electron-optical beam formation in electron gun, determining cathode and leakage current and I-V characteristics as function of pressure

20 p3204 A71-39158

Corresponding states fluids film boiling with cylindrical heaters, studying pressure and diameter effects

20 p3312 A71-39283

Pressure, subcooling and diameter effects on heat transfer and circumferential flow transition of thin wire film boiling of liquid nitrogen in pool

20 p3313 A71-39284

Heat transfer rate correlation with local surface pressure for blunt cones at angle of attack

20 p3176 A71-39355

Active vasodilation in gracilis muscle vascular bed due to perfusion pressure changes

20 p3189 A71-39378

Infinite elastic plate forcing by time varying radial pressure in circular hole at center

20 p3309 A71-39563

Internal pressure deformed star shaped crack, calculating stress intensity factor, crack energy and normal displacement

20 p3310 A71-39866

Physical determinants of gravity receptor mechanisms, discussing hydrostatic stress effects on membranes and gravity influence on enzymatic transport

21 p3339 A71-39972

Mathematical model for studying solar radiation pressure effects on artificial satellite motion

21 p3438 A71-40104

Hyperbaric normoxic breathing helium, nitrogen and neon gas mixture effects on EEG and reaction time in man

21 p3342 A71-40347

Aquanuts tremor response measurement by muscle force transducer during compression and decompression in 520-foot saturation dive, noting differences among individuals

21 p3331 A71-40350

Outwardly propagating coronal Alfvén waves pressure exertion on solar wind, using one fluid polytrope model

21 p3438 A71-40423

Sonic booms loudness as function of peak overpressures and rise times, using semiempirical formulae

21 p3325 A71-40530

Ion-cyclotron perturbation build-up in inhomogeneous plasma, investigating ion magnetic drift instability dependence on pressure

21 p3422 A71-40760

Iron response to dynamic loads, discussing pressure induced phase changes, constitutive equation relationship to dislocation processes and dynamic fracture criteria

21 p3399 A71-40789

Heat transfer from incandescent platinum wires in saturated liquid nitrogen, examining film boiling from atmospheric to critical pressure

21 p3476 A71-40899

Structural vibrations excited by spatially and temporally random pressure loading, discussing power spectra and vibration measurement

21 p3467 A71-40912

Stress-strain state of rotating viscoelastic hollow cylinder with mobile inner boundary under internal pressure and temperature effects

21 p3472 A71-41145

Temperature, magnetic field and pressure dependence of electrical conductivity, thermal emf, Hall effect and transverse Nernst-Ettingshausen effect in indium-doped lead telluride

21 p3429 A71-41210

Ge and Si point contact semiconductor diodes anisotropic deformation, investigating pressure effects on current and negative resistance in forward branch of I-V characteristics

21 p3430 A71-41222

Rh and Ag-Pd alloys magnetic susceptibility, investigating hydrostatic pressure effects

21 p3432 A71-41269

Self magnetic field effect on I-V characteristics of Cs-Ba thermionic converter, noting effects of pressure differential due to ponderomotive forces action

21 p3326 A71-41294

Cyclotron resonance measurement for holes in uniaxially compressed Si, determining pressure and temperature effects on relative half width of hole line by relaxation time

21 p3433 A71-41309

Electromagnetic HF wave field pressure effects on slow transverse magnetic wave propagation along plasma layer, noting dispersion equations difference from linear theory

21 p3426 A71-41400

Plasma confinement in bounded systems, considering externally induced field HF pressure effect on plasma density distribution

22 p3580 A71-41600

Pressure dependent absorption of carbon dioxide laser by boron chloride, considering saturation and line overlapping effects

22 p3556 A71-41805

Solid propellant rocket motor stable operation region, describing propellant response function to pressure and velocity fluctuations

[ONERA-TP-1016] 22 p3588 A71-41956

Alouette and Isis satellites flight data comparison with attitude and spin dynamics theory, considering solar radiation pressure and gravitation and magnetic field effects

22 p3609 A71-41997

Coupled librational dynamics of gravity oriented cylindrical satellite, calculating solar radiation pressure effects on attitude control behavior

22 p3611 A71-42042

Exothermic decomposition reaction and sublimation mechanism of ammonium perchlorate burning, showing pressure dependence of burning rate

22 p3587 A71-42100

Air pressure effects on absorption dependence at IR wavelengths, using water vapor transmittance windows

22 p3511 A71-42303

Solid helium and molecular metallic hydrogen thermodynamic properties and phase diagrams as functions of pressures corresponding to Jupiter and Saturn interiors

22 p3606 A71-42613

Radiation effects on rats peripheral blood state in low pressure environment with sea level value oxygen tension

22 p3494 A71-42732

Mathematical model of solar radiation pressure force and torque acting on spacecraft surface intercepting solar photon stream

[AAS PAPER 71-352] 23 p3728 A71-43024

Plastic work hardening produced by pressure application to spherical cavity surface in infinite elastoplastic medium, considering spherical elastic wave attenuation

23 p3775 A71-43147

Sporadic E layer ionization relation to thundersquall surface pressure disturbance, considering gravity wave propagation

23 p3670 A71-43322

Carbon dioxide photolysis at 1849 Å and various pressures, suggesting gas dissociation at wavelengths with appreciable absorption

23 p3641 A71-43328

Molecular oxygen partial pressure effect on nitrogen afterglow intensity, proposing three-body reaction kinetics

23 p3707 A71-43500

Dynamic coupling response between convectively controlled burning process and nonsteady flow field with pressure, density and gas velocity periodic variations

23 p3782 A71-43593

Random fluctuating longitudinal pressure gradient effect on steady incompressible channel flow for arbitrary power spectrum and probability density

23 p3664 A71-43597

Apollo 12 basalts porosity and volume compressibility under hydrostatic pressure

23 p3759 A71-43768

Elastic wave velocities in Apollo 12 rocks 12052 and 12065 at high pressures, noting basalt-like composition and crystal structure

23 p3761 A71-43783

Longitudinal magnetic field inhomogeneity influence on inhomogeneous plasma Alfvén instability, considering magnetic field pressure and trapped particles

23 p3713 A71-44151

Posture and lower body negative pressure effects on human heart rate and blood pressure

23 p3636 A71-44241

Large volume liquid oxygen pool boiling, investigating heat exchange coefficient dependence on flux density and pressure

23 p3705 A71-44339

Respiratory carbon dioxide and oxygen partial pressure effects on intraocular and blood pressure in rabbits under Somnifen narcosis

24 p3793 A71-44368

Gas lasers application to length measurement technology, discussing temperature, air pressure and vibration effects on laser frequency stabilization

24 p3833 A71-44449

High altitude decompression disorders prevention in humans by increasing pressure level in oxygen equipment assembly

24 p3795 A71-44474

Dense discharge plasma temperature and ionization distributions in He, H and Ar, investigating pulsed arc emission dependence on current and pressure

24 p3855 A71-44520

Metal cored cylindrical plastic shells response to transient external pressures, considering failure modes

24 p3878 A71-44610

Stability under uniform external pressure of closed spherical shell with axisymmetric initial imperfection in equatorial region, using finite difference technique

24 p3883 A71-44853

Seizing of flat and flat/spherical steel samples pairs in vacuum as function of temperature, pressure and time of contact, using compression-tension machine

24 p3838 A71-44857

Liquid properties and ambient pressure effects on cavitation erosion in thin film

24 p3819 A71-44946

Pressure and flow direction defects behind Mach reflected shock near three shock intersection, considering steady flow theoretical model

24 p3820 A71-44953

Thermal contact resistance of adhesive joints as function of adhesive solidification pressure and temperature and of joint surface physicochemical and geometrical parameters

24 p3831 A71-45024

Pressure effects on Fermi surface of metals, examining crystal lattice parameters influence on electrons energy spectrum

24 p3839 A71-45168

Self similar solution for unsteady powder combustion rate with decreasing pressure, generalizing to rate dependence on pressure and initial temperature

24 p3891 A71-45217

Inhomogeneous high-collision finite-pressure plasma stability, finding thermal instability development under uniform temperature and arbitrary pressure

24 p3858 A71-45243

PRESSURE FIELDS

U PRESSURE DISTRIBUTION

PRESSURE GAGES

NT BAROMETERS

NT IONIZATION GAGES

NT KNUDSEN GAGES

NT MANOMETERS

NT PENNING GAGES

NT PIEZOELECTRIC GAGES

NT VACUUM GAGES

Static pressure measuring instruments operating principles and characteristics

09 p1448 A71-22768

In situ metal-gas secondary standard assembly for ultrahigh vacuum gage calibration, using repeatable pressure generation from binary erbium-hydrogen system

17 p2744 A71-35140

PRESSURE GAUGES

U PRESSURE GAGES

PRESSURE GRADIENTS

Orientation reflex in healthy and nervous human subjects from peripheral vessels blood pressure fluctuations in response to acoustic signals

01 p0012 A71-11055

Turbulent flow near porous wall with pressure gradient, calculating velocity and shear distribution by modified Van Driest theory

03 p0399 A71-13432

Stresses and deformation in circular matrix subject to internal pressure gradients, assuming cylindrical anisotropy on macroscopic scale

03 p0504 A71-13463

Laminar shock induced boundary layers, examining velocity, pressure gradients and enthalpy

03 p0400 A71-13739

Mean velocity profile measurements in turbulent wake behind single or parallel arbitrarily spaced and sized cylinders with adverse pressure gradient

03 p0403 A71-14131

Bulk solids melting on inclined plane heated surface, investigating heat transfer and mass flow rates, fluid driving force and pressure gradient

04 p0678 A71-15456

Pressure gradients and slot Reynolds number effects on impervious wall film cooling effectiveness in constant density flow

04 p0680 A71-15474

Turbulent compressible two dimensional boundary layer flows with heat transfer, pressure gradients and wall blowing or suction

04 p0681 A71-15482

Aqueous acid solution turbulent boundary layer characteristics during alkali solution injection through porous surface in presence of positive pressure gradient

04 p0576 A71-15614

Velocity distribution equation for steady incompressible two dimensional turbulent flow, taking pressure gradients and surface roughness effects into account

04 p0578 A71-15764

Incompressible fluid boundary layer with negative pressure gradient near separation point, discussing stability characteristics and velocity profiles

05 p0736 A71-16847

Plane incompressible boundary layer stability in presence of pressure gradient and suction

05 p0736 A71-16851

NonNewtonian liquids with arbitrary surface temperature and pressure gradients, solving dynamic and thermal boundary layers equations

06 p1006 A71-18008

Laminar incompressible flow heat transfer in inlet between parallel plates at constant temperature, considering pressure gradient effect on boundary layer velocity profile

[AIAA PAPER 71-36] 06 p1008 A71-18497

High subsonic jet near-field acoustic energy flux distribution calculation from pressure gradient measurements

[AIAA PAPER 71-155] 06 p0884 A71-18597

Supersonic turbulent boundary layer measurements in moderate adverse pressure gradient region along two dimensional ramp model

[AIAA PAPER 71-162] 06 p0884 A71-18604

Nonadiabatic compressible turbulent boundary layer heat transfer to rough surfaces under arbitrary pressure gradient

[AIAA PAPER 71-166] 06 p0885 A71-18608

Heat transfer in turbulent boundary layer for arbitrary surface temperature with fluid injection and pressure gradient

07 p1220 A71-18765

Positive pressure gradient turbulent boundary layer local characteristics in plane diffuser, using Reynolds stress change equations

07 p1086 A71-18770

Inhomogeneous collisionless plasma stability, showing small pressure gradient effects

07 p1167 A71-19228

Tropical hurricane central pressure drop to maximal wind velocity ratio, discussing thermal to mechanical energy transfer as function of ocean surface temperature

08 p1330 A71-21873

Pressure gradient and roughness effects on laminar, transition and turbulent boundary layer in hypersonic shock tunnel

08 p1377 A71-22031

Light ion flow from polar caps in hydrodynamic and evaporative forms, noting pressure gradient force, exospheric electric field and realistic boundary conditions

09 p1440 A71-23459

Mathematical model for secondary flow in turbulent boundary layer in corners and salients, confirming existence of transversal pressure gradient variation

10 p1592 A71-23979

Compressible flow in two dimensional boundary layers in arbitrary pressure gradient, using turbulent energy equation for skin frictions and free stream Mach numbers

10 p1598 A71-25082

Inhomogeneous collisionless plasma stability, showing small pressure gradient effects

12 p1934 A71-26746

Laminar boundary layer equations for rotating plate with surface of arbitrary curvilinear shape, determining external flow pressure gradient leading to separation

12 p1865 A71-27502

Flutter of buckled plate exposed to static pressure differential and streamwise applied in-plane load, comparing experimental results with stability boundary calculations

12 p1983 A71-27584

Turbulent boundary layer friction and heat transfer under longitudinal pressure gradient

13 p2048 A71-28590

Critical overexpanded jet conditions of gas ejector at large pressure gradients based on supersonic compressed layer theory

13 p1993 A71-29213

Turbulent wall jets in presence of main flow longitudinal pressure gradient, using approximate integral method

13 p2050 A71-29225

Turbulent gas flow through duct with alternating pressure gradient, considering heat transfer and frictional resistance

13 p2166 A71-29370

Stationary Gaussian Markovian form randomly fluctuating pressure gradient effects on steady incompressible channel flow velocity

14 p2223 A71-29924

Gas pressure gradient and transmittance of sunspots, obtaining contours of D2 Na I and 5173 A Mg I lines

14 p2309 A71-29983

Approximate calculation of turbulent boundary layers with adverse pressure gradient, using empirical

auxiliary and momentum integral equations and skin friction formula

14 p2226 A71-30400

Book on pressure losses in ducted flows covering subsonic flow in straight or curved ducts, constrictions flow characteristics, etc

15 p2386 A71-31149

Alveolar-arterial oxygen pressure gradient derivation as sum of shunt, ventilation/perfusion inequalities and membrane and airway diffusions

15 p2363 A71-31444

Shock and pressure gradient induced turbulent transonic flow separation, using two dimensional circular arc model for flow field investigation

[AIAA PAPER 71-565] 15 p2344 A71-31559

Turbulent wall jet with initial boundary layer, calculating growth and separation in arbitrary pressure gradient by integral method

[AIAA PAPER 71-612] 15 p2389 A71-31581

Integral analysis of incompressible turbulent boundary layer with mass transfer and pressure gradient, including Stevenson velocity profiles and skin friction law

[ASME PAPER 71-APM-2] 16 p2559 A71-33221

Viscous stresses distribution in isothermal incompressible turbulent boundary layer with positive pressure gradient by diffusers in open jet wind tunnel

17 p2725 A71-34209

German monograph on pressure changes as boundary layer effect in tube wind tunnels covering test equipment and experimental design, Becker theory, pipe flow, etc

17 p2670 A71-34792

Interior region of incompressible turbulent boundary layer with pressure gradient on permeable wall, discussing local similitude hypothesis

17 p2729 A71-35346

Bernstein mode wave instability growth rate in collisionless shocks propagating perpendicular to magnetic field, including pressure gradient effects

18 p2950 A71-35928

Pressure change accompanying mixing of two ideal gases, assuming constant specific heats

18 p2904 A71-36280

Adverse pressure gradient effects on compressible turbulent boundary layer flow in parallel duct at Mach 4 and high Reynolds number

18 p2904 A71-36297

Two dimensional turbulent boundary layer in incompressible fluid on smooth and rough impermeable wall surfaces under arbitrary pressure gradients

19 p3042 A71-37088

Solar wind acceleration due to Alfvén wave pressure gradient, taking into account coronal parameters of temperature, magnetic field and energy density

19 p3128 A71-38162

Dogs intrapleural and intraesophageal pressures dependence on head positions

19 p3010 A71-38564

Non-Newtonian liquids with arbitrary surface temperature and pressure gradients, solving dynamic and thermal boundary layers equations

20 p3311 A71-38975

Incompressible turbulent boundary layer with pressure gradients, calculating Clauser equilibrium model and flow with constant wall shear stress

20 p3210 A71-39030

Water tunnel study of turbulent boundary layers structure in incompressible fluid with longitudinal pressure gradient at inlet section of converging and diverging nozzles

20 p3213 A71-39789

Plane equilibrium turbulent boundary layer with longitudinal pressure gradient

20 p3214 A71-39791

Higher pressure ratios trend in aircraft gas turbines leading to higher exit temperatures from compressor, noting real gas effects

21 p3437 A71-40170

Supersonic and hypersonic viscous gas flows with boundary layer induced pressure gradients, investigating disturbance upstream propagation by asymptotic theory

21 p3322 A71-40680

Unsteady pressure gradient reduction effect on airfoil dynamic stall delay

22 p3481 A71-42841

Thermomolecular pressure gradients and temperatures in flow between parallel planes for statistical gas models at arbitrary Knudsen numbers

24 p3891 A71-45242

PRESSURE MEASUREMENTS

Medium length journal bearing pressure profiles, deriving ordinary differential equation for load capacity

01 p0086 A71-10300

Small size calorimetric probe for measuring enthalpy, temperature and pressure in high velocity dense plasma flow

02 p0290 A71-12194

Mountainous region vertical air flow research, describing superpressure balloon and precise pressure radiosonde system

02 p0189 A71-12420

Metal shaping process during angle steel ream-type rolling, determining metal particles velocity fields, strain energy and total metal pressure on rollers

02 p0257 A71-12566

Noncircular cross section static pressure probes theoretically insensitive to pitch, yaw and Mach number, testing performance

03 p0341 A71-13730

Boeing 747 flight loads measurements, describing aircraft instrumentation with strain gages and pressure pickups

03 p0348 A71-13766

Simple pressure selector switch for measurement up to 40 input pressures

06 p0900 A71-18055

Wave number/phase velocity spectrum of wall pressure measurements beneath two dimensional turbulent boundary layer

06 p0882 A71-18317

Pt electrode response time during unsteady oxygen partial pressures measurement

06 p0860 A71-18323

Finite amplitude waves from supersonic jet, discussing pressure fluctuations measurement for explaining wave patterns visible on spark shadowgraphs

[AIAA PAPER 71-151] 06 p0845 A71-18593

Sonic boom problem, investigating pressure signature of large models in supersonic wind tunnels

[AIAA PAPER 71-184] 06 p0886 A71-18623

Pulsed megawatt MPD arc thruster exhaust pressure measurements, discussing time dependence, peak dynamic and static pressures, etc

[AIAA PAPER 71-196] 06 p0948 A71-18634

Static pressure measurements near oblique shock waves using short probe, evaluating readings accuracy

07 p1090 A71-19911

Fluidic/electronic pressure ratio computer prototype, using two free jets interaction for instrument error reduction

07 p1031 A71-20603

Automatic system for indirect blood pressure measurement in carotid compression test, discussing applications

08 p1247 A71-20827

Turbulent boundary layer pressure fluctuations in-flight measurements on Boeing 737 aircraft, obtaining power spectral densities and RMS pressure fluctuations for various Mach numbers

08 p1231 A71-21426

Static pressure port errors in hypersonic turbulent flow, using approximate shear layer momentum balance for pressure increase derivation

[AIAA PAPER 71-270] 08 p1228 A71-21996

Static pressure measuring instruments operating principles and characteristics

09 p1448 A71-22768

Dynamic pressure primary standard in terms of mass, time, length and temperature, describing phenomenon selection, error analysis and physical and mathematical models

09 p1448 A71-22769

Blood pressure measurement by catheter gages, analyzing error due to wave reflection at catheter tip

09 p1399 A71-22972

Transthoracic measurements of left and right ventricular systolic pressures in anesthetized mice, using fiber optics and strain gage manometer techniques

09 p1401 A71-23371

Venus atmospheric temperature and pressure measurements during and after Venera 7 soft landing

09 p1528 A71-23560

Supersonic and subsonic jets coexistence in rectilinear constant section duct, characterizing flow boundaries by pressure readings and Schlieren flow visualization

09 p1384 A71-23605

Vapor pressure measurements of mineral oils for hydraulic power systems, using transpiration method

09 p1484 A71-23666

MHD Hg flow between concentric cylinders with nonconductive walls, comparing pressure loss and voltage measurements with theoretical predictions for large Hartmann numbers

10 p1647 A71-23862

Carbon dioxide tension in pulmonary arterial blood before/during prolonged rebreathing in oxygen mixtures at rest and exercise

10 p1558 A71-23895

Cold cathode ionization gages dynamic pressure response as function of gas pulse mean speed and gas type, using magnetron test measurements

10 p1610 A71-24182

Mediastinum effect on human esophageal pressure and lung compliance measurements

10 p1565 A71-24678

Rocket propellant performance improvement with boron, giving boiling temperature vs pressure and calculation methods for combustion products composition

11 p1809 A71-25573

Mars surface pressure and elevation differences determined by spectroscopic observation of carbon dioxide band

11 p1825 A71-25714

Blood pressure measurement with Doppler ultrasonic flowmeter, providing sensitive and accurate noninvasive approach for continuous measurement of systemic arterial pressure

12 p1874 A71-27139

Arterial tonometry for atraumatic measurement of arterial blood pressure, considering transient effects of drugs or physiological interventions

12 p1874 A71-27140

Large axial compressor flow straightening stator blades unsteady pressure measurements with short response time detectors

12 p1945 A71-27469

Nonreacting and reacting ideal gases expansion between interconnected chambers, considering nitrogen and carbon dioxide simultaneous pressure measurements

12 p1877 A71-27550

Mechanical sterilization and cleansing of Goldmann applanation tonometer prisms contaminated with coliphage, comparing with germicidal immersion

13 p2020 A71-29036

Base pressure measurement behind wedge-parallelepipeds and cone-cylinder models of variable geometry

13 p2049 A71-29199

True time averaged oscillating pressure measurements and testing in turbomachinery, including hydraulic, mechanical and evaluation methods

[ASME PAPER 71-FE-28] 13 p1995 A71-29464

Fluctuating pressure measurement in mixing zone of axisymmetric jet, using total head and static probes coupled to 1/8 inch microphone

[ASME PAPER 71-FE-31] 13 p2053 A71-29466

Miniature transducers design and fabrication for fluctuating pressure measurements in jet engine testing, noting frequency response and power dissipation

14 p2244 A71-30324

Fluctuating pressure measurements in jet engine testing, using miniature transducers with calibration and data acquisition equipment

14 p2244 A71-30325

Cosmic ray nucleon-meson and barometric pressure data continuous recording equipment, comparing system to conventional instruments

14 p2248 A71-30602

Supersonic hydrogen combustion in vitiated air stream with stepped wall injection, considering temperature, pressure and composition measurements

[AIAA PAPER 71-721] 14 p2286 A71-30772

Hertzian radiometry experimental aspects covering background and medium temperature measurements, sky radiometry and absorbing gas total pressure measurements

14 p2204 A71-30969

Small size calorimetric probe for measuring enthalpy, temperature and pressure in high velocity dense plasma flow

15 p2454 A71-31500

Sonic boom pressure signature laboratory scale measurement after modification by traveling through air jet turbulence, comparing with statistical prediction

[AIAA PAPER 71-618] 15 p2388 A71-31547

Sonic boom wave interaction with topographic models, measuring surface pressure time history

[AIAA PAPER 71-619] 15 p2389 A71-31548

Low density hypersonic flow on flat plate, discussing surface pressure measuring techniques

[AIAA PAPER 71-606] 15 p2346 A71-31580

Unsteady force and pressure measurements by molecular and parametric transducers including strain gage, drag, moment and piezoelectric balance instruments

15 p2411 A71-32563

Turbulent boundary layer growth over flat plate and compression corner model in hypersonic gun tunnels, measuring pressure and heat transfer rate distributions

16 p2554 A71-32880

Shock wave propagation in ducts and cavities of different shapes and cross sections, compensating errors in recorded signals for shock tube pressure measuring equipment development

16 p2555 A71-32885

Plane shock front collapse through logarithmic spiral contraction, obtaining pressure and temperature conditions downstream of front

16 p2556 A71-32919

Geometrical parameters effect on operation of high pressure two-stage nozzle ejector with conical mixing chamber, measuring gas flow rates, total pressures and stagnation temperatures

16 p2521 A71-33612

Wall pressure spectra and rms wall pressure levels measurements in subsonic separated flows, postulating model for pressure fluctuation estimation

17 p2728 A71-35037

Preencapsulated strain gage measurement during water pressure tests on site built vessels

17 p2744 A71-35238

Pressure and heat flux measurements at wall of nose cone in hypersonic wind tunnel flow with high generatrix enthalpy

18 p2844 A71-36182

Pitot and static pressure measurement in low density hypersonic flows, considering thermal transpiration, gas nonequilibrium near measurement cavity and nature of inlet geometry

18 p2921 A71-36415

Vibratory flame propagation and pressure measurements in short closed tubes and vessels, using high speed schlieren cinematography and quartz piezoelectric transducer

19 p3167 A71-38097

Ignition delays of propane-oxygen-argon mixtures in shock tubes from pressure and heat flux measurements in reflected region

19 p3169 A71-38109

Autoclave chronic catheter system and restraining box for blood sampling and pressure measurement for hibernating marmots

19 p3010 A71-38568

Pressure, time and attenuation measurements of high explosive driven air shock in steel pipe, comparing with numerical simulation

20 p3208 A71-38787

Static and transient pressure measurement in turbulent boundary layers, using transducer with piezoelectric sensing element

20 p3233 A71-38822

Dynamic pressure measurement method and apparatus for anode center of heavy current electric arcs in plasmas, applying to plasma welding arcs

20 p3274 A71-39047

Venera 7 satellite data during descent through Venus atmosphere and activity after soft landing on 15 December 1970, noting temperature and pressure measurements

20 p3289 A71-39130

Light pressure measurement acting on Echo 1 satellite, considering integral reflection coefficient

20 p3306 A71-39132

Blunt planetary entry probe full scale flight test base pressure measurements, noting insensitivity to angle of attack variations up to 10 degrees

20 p3176 A71-39353

Transient pressure, temperature and density measurement of dense hot gas

21 p3364 A71-40402

Baric levels determination for weather forecasting from statistical analysis of atmospheric numerical model

21 p3410 A71-40823

Plasma/magnetic field pressure ratio and inductance per unit length in Tokamak plasma pinch with arbitrary cross section

22 p3579 A71-41583

Unbounded turbulent jet transducer element fluidic sensors, measuring ambient velocity and density from pressure data

22 p3531 A71-42768

Transient pressure measurement in plasma exhaust flow of 500 microsec duration, discussing discharge temporal behavior and cold gas pressure front existence

23 p3711 A71-43598

Pressure histories from densification and relaxation measurements on lunar glass and synthetic samples, investigating refractive index changes after annealing

23 p3758 A71-43760

Liquid crystals structural, elastic and optical properties, noting application to measurements of temperatures, pressures and electric and magnetic fields

23 p3717 A71-43958

Piezoelectric probe for pressure measurement in plasma behind shock front, discussing design and measuring circuit

24 p3825 A71-44750

Pressure and mass velocity profiles behind two dimensional shock wave generation on Al flat plates explosive surface

24 p3839 A71-45228

PRESSURE MICROPHONES

U MICROPHONES

PRESSURE OSCILLATIONS

Supersonic and transonic flow including effects of pressure oscillations within cavity, predicting rectangular cavities drag from mathematical model

01 p0002 A71-10931

Pressure fluctuations on fixed blades of axial flow compressor, determining sensor dynamic characteristics

01 p0003 A71-11024

Semiannual atmospheric wind and pressure oscillations relation to seasonal meridional baric systems displacements, considering cosinusoidal wave motion variations between Northern and Southern Hemispheres

04 p0621 A71-14639

Turbulent fluid flow past surfaces, calculating pressure pulsations at boundary layer

04 p0576 A71-15612

Turbulent pressure pulsations at surface of floating body of revolution moving unsteadily in sea water during boundary layer development

04 p0576 A71-15613

Microsensor measurement of spatial correlation between pressure fluctuations of turbulent boundary layer

04 p0600 A71-15636

Sporadic E layer structure and disturbances from pulsed radio signal measurement, noting correlation to pressure oscillation at ground level

04 p0584 A71-15757

Turbulent boundary layer wall pressure fluctuations on hydrodynamically smooth and rough surfaces, investigating eddies, space-time decay rate and flow structure

05 p0736 A71-16961

Power spectra of cosmic ray intensity variations at ground and atmospheric pressure oscillations

06 p0950 A71-17979

Finite amplitude waves from supersonic jet, discussing pressure fluctuations measurement for explaining wave patterns visible on spark shadowgraphs

06 p0645 A71-18593

Boundary layer separation in unsteady pipe flow, examining velocity profiles under influence of periodic pressure fluctuations

07 p1093 A71-20280

Atmospheric pressure pulsation time spectra on earth surface as function of stratification conditions

08 p1286 A71-21876

Liquid fuel rocket combustor longitudinal pressure oscillations nonlinear analysis, using multiple scales technique

09 p1544 A71-22107

Turbulent incompressible air flow in-stream static pressure fluctuations measurement, describing bleed type pressure transducer theory, design and operational characteristics

10 p1611 A71-24516

Soviet book on nonstationary waves covering gravity waves development, moving periodic pressure systems, seismic disturbances and nonhomogeneous ideal liquids

10 p1595 A71-24650

Cavitation in liquids with dissolved gases by acoustic wave induced oscillating pressure, discussing gas bubble formation through rectified diffusion process

10 p1597 A71-24942

Tangential body forces and pressure perturbation interactions in thin liquid film, considering destabilizing effect impairing film cooling efficiency

11 p1751 A71-25491

Wind resonance in ionosphere under pressure fluctuations, noting turbulent friction factor above 110 km

13 p2060 A71-28533

Fluctuating pressure measurement in mixing zone of axisymmetric jet, using total head and static probes coupled to 1/8 inch microphone

[ASME PAPER 71-FE-31] 13 p2053 A71-29466

Monograph on solid propellant rockets combustion instability covering pressure oscillations at acoustic frequencies, swirling nozzle flow, chamber pressure, etc

14 p2287 A71-29577

Fan-produced sound pressure fluctuation in very low speed subsonic wind tunnel test stream, noting resulting anemometer calibration errors

14 p2275 A71-30526

Comparative variable area, pulsed and modified T burners for testing oscillatory combustion and stability of propellants containing aluminum

14 p2289 A71-30714

Turbopropulsion systems thrust augmentor combustion instability, discussing physical causes due to various pressure oscillation modes

14 p2293 A71-30756

Turbojet and turbopump augmentors combustion instability, discussing pressure oscillations elimination by screech liner and flameholder design

14 p2294 A71-30757

Combustion instability with wave motion coupling in solid propellant rocket motors due to energy gain and loss mechanisms within chamber

14 p2296 A71-30787

Missile component vibration environments generation by Minuteman 2 and 3 third stage motors solid propellant oscillatory burning

14 p2296 A71-30790

Solid propellant rocket engines combustion instability, reexamining Culick analysis of longitudinal oscillations with pressure and velocity coupling

15 p2467 A71-31473

Vibratory stresses in heat exchangers due to pressure pulsation induced acoustic resonances, calculating flow pulsations from Karman vortex streets

15 p2513 A71-31635

Acoustic radiation of supersonic jet toward nozzle exit section, plotting pressure pulsations vs active/passive pressure ratio

18 p2903 A71-36122

Inlet turbulent pressure data scaling hypothesis, investigating Reynolds number effect

18 p2956 A71-36774

In-flight noise radiation by wing-mounted jet engines on aircraft fuselage based on correlation with turbulent boundary layer pressure fluctuations

19 p2997 A71-37846

Solid propellant combustion pressure oscillations amplification, developing mathematical model as function of reaction rate constant, chamber pressure, frequency and solid properties

19 p3123 A71-38096

Combustion driven acoustic oscillations in gas fired burner of premixed methane, nitrogen and oxygen, noting mixture ratio and flow rate effects

19 p3123 A71-38098

Atmospheric pressure pulsation time spectra on earth surface as function of stratification conditions

19 p3060 A71-38469

Holographic investigation of acoustical fields, describing shadowgraph recording apparatus for sound pressure amplitude distribution

20 p2322 A71-38811

Unsteady gas pulsations in compliant tube, predicting pressure amplitude extremum as function of mean flow by linear theory with frictional effect

24 p3820 A71-45073

PRESSURE PROBES

U PRESSURE SENSORS

PRESSURE PULSES

Acoustic velocity in water, examining air bubble effects on pressure pulse attenuation

03 p0459 A71-13720

Launching intermediate velocity thin plastic sheets for short duration pressure pulse studies of dynamic materials properties

03 p0427 A71-13916

Stereophotogrammetric measurement of plastic deformations of circular Al membrane loaded by pressure pulse, using high speed cameras

03 p0428 A71-13948

Fuel rod bundle boundary layer in longitudinal fluid flow, investigating turbulent temperature and pressure pulsations

04 p0684 A71-15504

Statistical characteristics of pulsation pressure on surface in turbulent boundary layer of incompressible fluid, discussing effects near smooth flat wall

04 p0575 A71-15607

Plane compression waves propagation into constant state nonviscous fluid, considering shock formation of pressure pulses and overpressure as function of time

07 p1091 A71-19961

Stress waves in elastic spherical shell due to external pressure pulse, approximating near field by saddle point technique

07 p1215 A71-20097

Transient stresses in heat shield generated by short duration pressure pulses, using method of characteristics for interface stresses

11 p1844 A71-25330

Longitudinal space-time correlation function of turbulent near wall pressure pulsations with hydrodynamic wavelength exceeding boundary layer thickness at streamlined model

13 p2049 A71-28846

Baroreflex regulation of pulse interval during bicycling exercise, using systolic pressure-pulse relation to express reflex sensitivity

13 p2012 A71-28951

Pulsed T-burner testing of oscillatory combustion and droplet damping of aluminized solid propellants as function of frequency and sample properties

14 p2289 A71-30713

Error analysis of Corcos hypothesis concerning cross spectra of pseudoacoustic LF turbulent pressure pulsations on flat plate

15 p2389 A71-31708

Surface wave patterns created by constant velocity pressure point on inviscid plasma bounded by magnetic field

19 p3111 A71-37637

Pressure pulse shape effect on final plastic deformation of simply supported thin circular plate

19 p3158 A71-38181

Rectangular plate under lateral and inplane pressure pulses, examining transient response with Mathieu equation

21 p3471 A71-41023

PRESSURE RECOVERY

Flow and dynamic pressure recovery in wall-attachment fluid amplifiers, considering large scale flip-flop

[ASME PAPER 70-WA/FLCS-9]

03 p0354 A71-14085

Cone shaped diffusers effectiveness, noting inlet conditions effect on pressure recovery coefficient

05 p0694 A71-16750

Conical diffusers swirling inlet flow effects on pressure recovery and outlet flow profile

06 p0883 A71-18541

Aerodynamic seals theoretical analysis and experimental test results, considering pressure ratios, pressure recovery coefficients and pump efficiency

07 p1117 A71-19422

Jet pipe valve characteristics, discussing pressure and flow recovery for various loads, nozzle diameter ratios and spacings

07 p1025 A71-20559

Supersonic fluidic bistable switch, developing improved pressure recovery

07 p1029 A71-20590

Supersonic pitot fluidistor in bistable mode, investigating improved pressure and flow recovery at large expansion ratios

07 p1029 A71-20591

Static pressure recovery and core region velocity profile in rectangular wall diffusers with uniform shear flow

[ASME PAPER 71-GT-5]

11 p1751 A71-25951

Truncated conical diffusers with various geometrical configurations and incompressible inlet flow conditions, noting reduced pressure recovery

13 p2047 A71-28468

Pressure recovery performance of straight-wall two dimensional diffusers with subsonic air-water mixtures, studying gas volume flow ratio and diffuser geometry effects

[ASME PAPER 71-FE-20]

13 p2052 A71-29458

Short conical diffusers with radial splitters for flow stabilization with high pressure recovery performance

14 p2225 A71-30304

Submerged free air jet with laminar parabolic profile, investigating pressure recovery characteristics for various tube diameters, spacing and Reynolds number

15 p2389 A71-31683

FLE-251 fluidic NOR gate impact modulator developing equivalent circuit model for pressure gain recovery and cut-off, output capacitance and step response

15 p2351 A71-31684

Conical diffusers outlet flow profile and performance, investigating swirling inlet flow effects on pressure recovery

21 p3323 A71-40950

PRESSURE REDUCTION

NT EXPLOSIVE DECOMPRESSION

Free piston shock drivers concerning plateau pressure reduction

04 p0564 A71-14674

Dynamic pressure reduction method errors in vacuum gages calibration

05 p0754 A71-16949

Carboxyhemoglobin changes in circulating blood volume during lower body negative pressure exposure

06 p0854 A71-18363

Composite propellant transient burning rates continuous measurement during rapid depressurization

[AIAA PAPER 71-173]

06 p0944 A71-18612

Chronic hypoxia effects on capillary development during high altitude exposure in decompression chamber and maintenance at sea level

08 p1237 A71-20679

Surface station pressure reduction to sea level, determining differential expression by least squares method

08 p1329 A71-21727

Accelerated testing of jet fuel containment sealant, using reduced pressure and hybrid fluorocarbon silicone

10 p1632 A71-24083

Composite propellant flame temperature and emission spectra during depressurization by rarefaction waves, using rapid scanning spectrometer

[AIAA PAPER 70-663]

12 p1945 A71-27564

Artificial respiration in elevated gas pressure chamber to revive organism after clinical death by rapid decompression

12 p1876 A71-27745

Depressurization extinguishment of composite solid propellants for thrust termination, considering flame structure, surface characteristics and restart capability

[DFVLR-SONDDR-129]

13 p2113 A71-28615

Simply supported nearly circular cylindrical shell, calculating nonlinear damped dynamic response due to exponentially decaying radial pressure

14 p2330 A71-30688

Nickel sponge preparation by liquid nickel sulfide reaction with NiO under reduced pressure at various temperatures

15 p2433 A71-32178

Solid propellants extinguishment by depressurization, using transient flame model

[AIAA PAPER 71-631]

15 p2466 A71-32283

Functional systems changes in intact and anesthetized rats during increasing hypoxia in decompression chamber

16 p2532 A71-33911

Spontaneous hot zone formation in oil flow through small pipes, showing significance in pressure losses and plain bearings calculations

19 p3046 A71-38275

Unsteady pressure gradient reduction effect on air-foil dynamic stall delay

22 p3481 A71-42841

Vortice generation in laminar boundary layer of water flow under hydraulic pressure reduction, proposing mathematical model

23 p3662 A71-43315

PRESSURE REGULATORS

Book on fluid power circuits and systems covering switching theory, closed loop systems, pneumatic circuits, servo systems and pressure control

02 p0190 A71-11871

Fluidic instrument pressure regulator, noting pressure sensing circuit, confined jet amplifier and control valve

[ASME PAPER 70-WA/FLCS-4]

03 p0428 A71-14080

German monograph on loss estimation for non-steady gasdynamic duct-drum pressure exchangers, discussing design and optimization problems

04 p0568 A71-14925

Pressure regulator design and construction, using high pressure fluidic proportional chain

07 p1027 A71-20580

Series and bypass fluidic pressure regulators, discussing component selection, performance details, sensing circuits, feedback amplifier and flow controller

16 p2579 A71-33526

Valves and regulators development and testing for liquid hydrogen propellant tank pressurization system

22 p3588 A71-41503

Passive gas flow control with compensation for ambient temperature and supply pressure variations, using choked orifice with area variation linearly proportional to diaphragm deflection

[ASME PAPER 70-WA/AUT-14]

24 p3828 A71-45137

PRESSURE SENSORS

Intracranial pressure measurement by miniature transducer with modifications for baseline reading and calibration checking throughout implantation period, giving circuit diagram

01 p0021 A71-10241

Sinusoidal pressure generator for determining frequency response of small pressure transducers, pressure probes and characteristics of small diameter infinite lines

01 p0067 A71-10478

Accelerometers and dynamic pressure transducers calibration, using laser interferometer system

01 p0082 A71-10862

Temperature compensated semiconductor transducers for dynamic pressure measurements, using Si Zener diodes

01 p0057 A71-11289

Noncircular cross section static pressure probes theoretically insensitive to pitch, yaw and Mach number, testing performance

03 p0341 A71-13730

Stress dynamics of optimum high speed piezoelectric pressure probes utilizing backing rod material

03 p0427 A71-13913

Two-wire IC pressure transducer bridge circuit performance features based on circuit analysis

04 p0561 A71-15594

Microsensor measurement of spatial correlation between pressure fluctuations of turbulent boundary layer

04 p0600 A71-15636

Static pressure measurements near oblique shock waves using short probe, evaluating readings accuracy

07 p1090 A71-19911

Piezoelectric and capacitive transducer pressure measurements in low pressure fluidic elements

07 p1026 A71-20571

High performance fighter aircraft engine pressure ratio and turbine inlet temperature measurement, using fluidic sensors

07 p1028 A71-20586

Fluidic ambient velocity and pressure measurement sensors, using unbounded turbulent jets

07 p1029 A71-20595

Back pressure sensor improvement, discussing orifice square law relationship between pressure and flow

07 p1094 A71-20608

Transients estimation for measuring lines of LF pressure sensors, taking into account hydraulic resistance in inlet channel

08 p1286 A71-20834

High altitude radiosonde thermometer and pressure sensor construction, discussing radiation error and wire lag

08 p1293 A71-21740

Miniature pressure transducer with extended temperature capability, discussing design and operation

09 p1445 A71-22723

High temperature ultraminiature pressure transducers, reviewing p-n junctions thermal limitations and thermal properties of dielectric oxides used with solid state epitaxially grown sensors

09 p1448 A71-22772

In-flight profile drag measurement of gliders with total and static pressure sensors in boundary layer wake, using moments method

09 p1384 A71-23667

Fast miniature shielded pitot pressure transducer for spatial resolution of flow details

09 p1453 A71-23728

Turbulent incompressible air flow in-stream static pressure fluctuations measurement, describing bleed

type pressure transducer theory, design and operational characteristics

10 p1611 A71-24516

Cam profile selection for adjustment in computing-resolving unit of aneroid sensors of altimeters

13 p2069 A71-28938

High altitude balloons pressure-altitude transducer assembly, discussing electronic circuitry, calibration and temperature and vibration effects

14 p2240 A71-30070

Altitude-airspeed and Mach number pressure transducer with diaphragm free of temperature and vibration effects

14 p2243 A71-30322

Miniature transducers design and fabrication for fluctuating pressure measurements in jet engine testing, noting frequency response and power dissipation

14 p2244 A71-30324

Fluctuating pressure measurements in jet engine testing, using miniature transducers with calibration and data acquisition equipment

14 p2244 A71-30325

Miniature pressure transducers for wind tunnel aircraft models buffet phenomena measurements, discussing calibration, frequency and pressure range, sensitivity and accuracy

14 p2245 A71-30335

Miniature integrated sensor pressure transducers for inlet air flow distortion and buffet studies of wind tunnel models

14 p2245 A71-30336

Parallel pressure multiplexer and encoder for aerodynamic testing, employing zero pressure detectors coupled with IC digital electronics and reference pressure signal

14 p2222 A71-30342

Total and vapor pressure sensing and hybrid analog/digital electronic controller for multiburn cryogenic spacecraft propulsion pressurization [AIAA PAPER 71-647]

14 p2290 A71-30724

Shock wave attenuation in perforated duct, using pressure transducers and schlieren photography

16 p2554 A71-32884

Laser holographic inspection of silicon bond in pressure sensors for process control systems

19 p3068 A71-37245

Pressure sensors thermal protection by porous Zr disk as heat shield, considering acoustic transparency, linearity, transient response and air flow resistance [ONERA-TP-957]

22 p3547 A71-42501

Fluid amplifiers theory and use as temperature and pressure sensors, discussing applications in chemical and ammunition industries and jet aircraft control [IEEE PAPER 70-TP-120-IGA]

23 p3630 A71-42921

PRESSURE SUITS

NT SPACE SUITS

Analytic functions approximation in complex regions with aid of different systems of functions

07 p1146 A71-19041

Pressure suit assemblies /PSA/ reference for aerospace and environmental control engineers [SAE-AIR-1103]

07 p1049 A71-19641

Emergency backup /secondary pressurization/ devices for aerospace crew and passenger safety and comfort, considering high altitude pressure suits

08 p1244 A71-20716

Reevaluation of emergency pressurization requirements for brief flights over 50,000 feet, considering pressure suit requirement

08 p1247 A71-20822

Anthropometry for aircraft cockpit and pressure suit design compatible with mission requirements

11 p1724 A71-26115

PRESSURE TRANSDUCERS

U PRESSURE SENSORS

PRESSURE VESSEL DESIGN

Petroleum mechanical engineering and pressure vessels and piping - ASME Conference, Denver, September 1970

04 p0665 A71-14767

Ellipsoidal pressure vessel heads failure mode analysis, considering buckling under internal pressure and design formula with safety factors [ASME PAPER 70-PVP-26]

04 p0665 A71-14769

Fiber reinforced cryogenic pressure vessels design, manufacture and testing for space and terrestrial applications, comparing glass fibers to carbon fibers

04 p0618 A71-15650

Weight-optimal cylindrical shells of revolution with uniform strength edge reinforcement, discussing pressure vessel design

06 p0982 A71-17356

Aboveground liquid storage tanks design with fiberglass-reinforced composites based on pressure vessels requirements - [DFVLR-SONDDR-93]

13 p2157 A71-29307

PRESSURE VESSELS

Cryogenic pressure vessels carrying capacity, discussing loading types, materials properties, thermal effects, etc

01 p0097 A71-10077

Energy accumulation effects on pressure vessels strength and failure mode, examining crack propagation and arrest

03 p0517 A71-14586

Pressurized isotropic viscoelastic hollow cylinder bonded to elastic casing, analyzing stress during finite deformation

04 p0668 A71-15191

Carbon fiber evaluation of structural reinforcement potentialities for rocket motor cases and pressure vessels filament winding [PLASTICS INST. PAPER 48]

08 p1297 A71-20924

Pressure vessel method improvement by electronic equipment application in determining data characteristics for propellant powders ballistic properties

10 p1696 A71-24447

Pressure vessel flaw detection at high stress and cryogenic temperatures, noting Lunar Module fuel tanks experience [AIAA PAPER 71-336]

11 p1777 A71-25315

Atmospheric seal leakage control tests for long orbital lifetime space station designs, discussing vacuum chamber monitored pressure shell penetrations [AIAA PAPER 71-337]

11 p1836 A71-25316

Spacecraft structures weight optimization based on fracture mechanics and reliability cost constraints applied to pressure vessel design

11 p1847 A71-25464

Filament wound pressure vessels and composites flaw detection nondestructive tests with X rays and thermography

14 p2262 A71-29644

Aerospace pressure vessels delayed time failure, discussing flaws growth rate in context of linear elastic crack tip stress intensity factors

14 p2325 A71-29898

Cryogenic pressure vessels carrying capacity, discussing loading types, materials properties, thermal effects, etc

16 p2593 A71-33633

Numerical method for limit analysis of axisymmetric shells of revolution, considering truncated conical shells and pressure vessels with rigid circular plates

17 p2818 A71-34400

Preencapsulated strain gage measurement during water pressure tests on site built vessels

17 p2744 A71-35238

Viking Mars spacecraft pressure vessel design, incorporating linear elastic fracture mechanics for long life

18 p2979 A71-36487

PRESSURE WAVES

U ELASTIC WAVES

PRESSURE WELDING

NT DIFFUSION WELDING

NT EXPLOSIVE WELDING

NT ULTRASONIC WELDING

Comparative review of friction welding mechanisms, including inertia and metallurgical aspects

[SME PAPER AD-70-574]

07 p1121 A71-20548

Forge phase rigid and plastic region model of friction welding, deriving interfacial dispersion parameter of weld quality optimization

09 p1459 A71-23456

Air cooled turbine blades activated diffusion brazing and gas pressure welding, using composite finned configuration model

[ASME PAPER 71-GT-32]

11 p1770 A71-25969

Jet engine components inertia welding, discussing process, equipment, low weight-cost advantage and mechanical properties reproducibility [ASME PAPER 71-GT-33]

11 p1770 A71-25970

Soviet book on microwelding by pressure covering semiconductor-metal bonding, ultrasonic soldering and thermal processes

23 p3682 A71-44125

PRESSURIZED CABINS

Aeromedical requirements, control limitations and hazards of aircraft pressure cabins and rapid decompression

08 p1244 A71-20715

Emergency backup /secondary pressurization/ devices for aerospace crew and passenger safety and comfort, considering high altitude pressure suits

08 p1244 A71-20716

Fluidic cabin pressure automatic control systems for military and civil aircraft, discussing design, operation and performance

14 p2182 A71-30308

Polymer odor threshold determination for hygienic considerations in sealed/pressurized chamber construction, comparing static and dynamic methods

24 p3800 A71-44539

PRESSURIZING

NT FUEL TANK PRESSURIZATION

Dynamic response of pressurized thin circular cylindrical shells under moving loads [AIAA PAPER 71-175]

06 p1004 A71-18614

Total and vapor pressure sensing and hybrid analog/digital electronic controller for multiburn cryogenic spacecraft propulsion pressurization [AIAA PAPER 71-647]

14 p2290 A71-30724

PRESTON TUBES

U PITOT TUBES

U SPEED INDICATORS

PRETRAINING

U PRESTRESSING

PRESTRESSING

Thermal stresses on curved surface of initially stressed circular cylinder with smooth rigid insulated cover

01 p0172 A71-10839

Thermally induced preload changes in roller bearings due to temperature gradients measured, using strain gage bridges and thermocouples

01 p0088 A71-11006

Thermal prestress effect on natural vibrations of hinge supported isotropic cylindrical shell, integrating equations of motion by Bubnov-Galerkin method

02 p0322 A71-11738

Circular shallow prestressed arches with fixed ends, considering initial thrust effect on snap buckling

03 p0505 A71-13545

Elastic straightening of slightly curved shell and significantly curved beam, considering prestressed structural stiffness

04 p0672 A71-15771

Nonelastic unloading microstrains in Cu crystals after stage II macroscopic pretraining, discussing stresses action on dislocations

09 p1468 A71-22700

Cold pretraining effect on steady state creep strength and rate of precipitation hardened heat resistant steel

09 p1477 A71-23331

Vibrational characteristics of pretwisted cantilever beams with uniform rectangular cross section, investigating slenderness ratio effect on natural frequencies

09 p1543 A71-23661

Prior deformation and subsequent annealing influence on fatigue response of coarse grained alpha Ti, evaluating relative effects of dislocation locking and mechanical twinning

10 p1626 A71-24445

Optimal prestressing against buckling of structures with reserve capacity, using energy methods of structural analysis

10 p1689 A71-24514

Prestress vibration hardening of shells of revolution for circumferential 0 and 1 wave number, using VALORS and BALORS programs

11 p1848 A71-25486

Coupled natural frequencies in rectangular cross section pretwisted cantilever beams flexural vibrations

15 p2503 A71-31442

Prestressing of two layer fiberglass-reinforced plastic cylindrical shell under internal pressure

16 p2657 A71-33410

Initial strains effect on propagation rate of elastic waves, applying finite deformation theory

16 p2658 A71-33902

Plastic deformation, creep rupture strength, endurance limit and service life of prestressed strain hardenable material

16 p2659 A71-33985

Idealized model for anisotropy of metals inelastic characteristics due to plastic pretraining, demonstrating applicability to polycrystalline materials

16 p2659 A71-33989

Low temperature tensile prestressing effect on recrystallization kinetics of polycrystalline large grain Ni by isothermal annealings method

17 p2755 A71-34194

Prestrain directional effects in steel tension and compression test specimens, noting Bauschinger and work hardening effects

18 p2937 A71-36834

Prestressed thin shells elastic deformation, using Kirchhoff hypothesis of shell theory

19 p3154 A71-37072

Prestressing effect on yield surfaces of Al and Cu thin walled tubes

19 p3079 A71-37705

Creep tests effect on Cr-Mo-V steels mechanical properties during alternating stress fatigue testing, considering preliminary static prestressing

20 p3250 A71-39023

Exact calculations of prestressed networks of arbitrary form and magnitude based on matrix displacement method

21 p3456 A71-40156

Vibration characteristics of cantilever beam about nonlinear equilibrium state, showing flexibility and prestressed state effect

21 p3468 A71-40968

Prior stressing and thermal treatments effect on shock induced substructures in polycrystalline Mo, using transmission electron microscopy

21 p3404 A71-41416

Frequency and buckling stability eigenvalue evaluation for anisotropic circular cylindrical shells under nonuniform lateral prestress

22 p3615 A71-42210

Polycrystalline Ni preloading rate effects on dislocation structure, electrical resistance and flow stress, noting strain hardening mechanism
24 p3837 A71-44675

Prestraining effect on D16 duraluminum corrosion fatigue and tensile strengths
24 p3838 A71-44856

PRETESTS

U TESTS

PRETREATMENT

NT PRESTRESSING

Acute mountain sickness due to oxygen deficiency, discussing control by acetazolamide, placebo or furosemide pretreatment
06 p0851 A71-17613

PRETWISTING

U PRESTRESSING

U TWISTING

PREVENTION

NT ACCIDENT PREVENTION
NT CORROSION PREVENTION
NT FIRE PREVENTION
NT ICE PREVENTION

PRIMARY BATTERIES

NT ALKALINE BATTERIES
NT MAGNESIUM CELLS
NT METAL AIR BATTERIES
NT NICKEL ZINC BATTERIES
NT THERMAL BATTERIES
NT ZINC-OXYGEN BATTERIES

PRIMARY COSMIC RAYS

NT SOLAR COSMIC RAYS

High energy nucleon passage through lower atmosphere during chemical composition changes of primary cosmic rays, using Proton satellite observations
03 p0476 A71-13851

Primary cosmic ray electrons intensity energy spectrum data, suggesting plots based on electron energy to positive gamma power
03 p0482 A71-14542

Primary cosmic rays heavy ion tracks from balloon-borne emulsion
04 p0641 A71-15368

Primary cosmic ray solar modulation calculations using Trilling formula for response functions and upper limiting rigidity to diurnal variation
06 p0953 A71-18119

Primary cosmic ray electrons energy spectrum measurement at Fort Churchill, examining geomagnetic cut-off rigidity daily variations
06 p0959 A71-18159

Large Z primary cosmic rays charge spectra, using semiautomatic photometer
08 p1350 A71-20953

Primary gamma radiation flux measurement, using spark chamber on satellite
08 p1350 A71-20954

Galactic primary cosmic rays nuclei tracks in meteorite olivine, studying intensity of VH and VVH groups
08 p1351 A71-20961

Primary cosmic ray variations energy spectra on rising and declining solar activity arm, analyzing stratospheric particle intensities
08 p1353 A71-20980

Primary cosmic gamma-quanta fluxes measured using telescope consisting of Cerenkov counters
09 p1513 A71-22556

Antimatter body size determination, using primary high energy cosmic ray flux
09 p1515 A71-23535

Antimatter search in primary cosmic rays by balloon-borne cosmic ray telescope formed from gas Cerenkov detector combined with scintillator elements
10 p1659 A71-23748

Type I fluctuations experienced by extensive air showers generated by protons or heavy nuclei, discussing effect on primary cosmic ray energy determination
10 p1661 A71-23858

Microcraters on Apollo 12 crystalline rocks and breccia surfaces attributed to primary cosmic particles
10 p1673 A71-24427

Planetary distribution of primary cosmic rays and residual charged particles over atmosphere from Cosmos 208 and 228 satellite data
11 p1816 A71-25761

Nuclear component analysis of primary cosmic radiation by Cerenkov spectrometer onboard Cosmos 228 satellite
11 p1817 A71-25780

Cosmic IR sources model based on assumption of cosmic ray particles emitting galactic sources surrounded by dust shells absorbing and reemitting energy
12 p1947 A71-26933

Light flashes in eyes of dark adapted Apollo astronauts, considering Cerenkov radiation effects from primary cosmic ray single charged particles on retinal elements
12 p1933 A71-27383

TeV hadrons lateral energy distributions in air shower cores from Ne hodoscope measurements for

fluctuations between primary energy and shower size, discussing French alpine scintillators array
12 p1951 A71-27386

Electromagnetic longitudinal cascades development numerical treatment based on Boltzmann equation, discussing Monte Carlo computing times for primary energy total electron counts
12 p1933 A71-27387

Surviving high energy primary protons of cosmic ray nuclear bursts in atmosphere without air shower at Chacaltaya
12 p1933 A71-27393

Muon showers underground, considering primary cosmic ray energies greater than 10 TeV
12 p1952 A71-27401

Nuclear emulsion produced cosmic ray jets secondary angular distribution, primary energy and anisotropy
13 p2121 A71-28056

Nucleon-nucleon and meson-nucleon collisions, determining secondary cosmic ray multiplicity dependence on primary particles energy spectra
13 p2121 A71-28057

Extensive air shower size measurements, relating energy spectra to primary energies up to 10 million TeV by calorimetric method
13 p2122 A71-28069

Atmospheric scintillation light detection from air shower, determining interaction mean free path of .1-10 million TeV primary particles
13 p2122 A71-28070

Scintillator array investigation of high transverse momenta occurrence in air showers of primary energy above 1000 TeV
13 p2124 A71-28084

Air shower properties from Monte Carlo simulations, determining electron and muon numbers at sea level for primary protons and copper nuclei
13 p2124 A71-28085

Particle densities and muon spectra at 100-1300 m from sea level extensive air showers axes for primary energies to 10 to 20th eV
13 p2124 A71-28086

Primary cosmic rays mass composition at energy levels above 10 TeV, analyzing muons data from extensive air shower experiments
13 p2125 A71-28094

Muon rich showers, discussing muon density spectrum relation to primary energy spectrum
13 p2126 A71-28099

Primary cosmic ray nuclear component, discussing Cosmos 163 measurements
13 p2128 A71-28547

Primary cosmic rays spectrum and intensity data in 4 to 10 BeV range, evaluating albedo particle effects
14 p2301 A71-30590

Electromagnetic showers triggered in lead by 6 GeV primary cosmic ray electrons, calculating spatial distribution with Monte Carlo method
14 p2302 A71-30594

Primary cosmic ray electron energy and intensity measuring equipment, using Cerenkov and scintillation counters, spark chamber, lead absorber and photorecorder
14 p2247 A71-30598

Electromagnetic showers in lead, using 20 GeV primary cosmic ray electrons to calculate spatial evolution
14 p2302 A71-30603

High energy primary cosmic ray program of Goddard Space Flight Center involving charge composition and energy spectra studies in balloon and satellite experiments
15 p2478 A71-31804

Satellite-borne semiconductor telescope for relativistic heavy primary cosmic rays identification, increasing resolving power by minimum pulse selection method
15 p2407 A71-31806

Mean and standard deviation of fraction of total primary cosmic ray energy losses not measurable by ionization spectrometers
15 p2407 A71-31809

Balloon-borne ionization spectrometer for high energy cosmic ray measurement, discussing calibration and accuracy
15 p2407 A71-31811

Balloon-borne magnetic spectrograph for primary cosmic ray particle trajectory and rigidities measurement
15 p2407 A71-31812

Primary cosmic ray nucleonic component observation by scintillator-Cerenkov telescope on OGO 3 satellite
16 p2628 A71-33932

Underground interactions of primary cosmic ray produced atmospheric muon neutrinos, using large area liquid scintillation detector hodoscope
19 p3105 A71-37288

Primary cosmic ray proton energy spectrum in 50 GeV to 300 TeV range, using Proton 1, 2 and 3 satellite-borne counters
19 p3128 A71-38352

Primary cosmic rays high energy gamma ray intensity spectrometric measurements onboard Cosmos 208 satellite, allowing for charged particles effects
20 p3283 A71-39753

High energy cosmic ray spectrometer onboard Proton 4, discussing ionization calorimeter, nuclear targets, particle charge and radiation detectors and primary measurements
20 p3283 A71-39755

Relativistic primary cosmic rays chemical composition between Be and Fe from charge spectrum obtained with Cerenkov counters
20 p3284 A71-39756

Planetary distribution of primary cosmic rays and residual charged particles over atmosphere from Cosmos 208 and 228 satellite data
22 p3591 A71-41529

Nuclear component analysis of primary cosmic radiation by Cerenkov spectrometer onboard Cosmos 228 satellite
22 p3591 A71-41548

Upper atmospheric primary cosmic ray layer ionization, considering secondary particles, X rays, neutrons, tritons and mesons as ionizing agents
22 p3591 A71-41647

Relative abundances and mass measurements of Li, Be and B isotopes in primary cosmic rays, using balloon flown emulsion stacks
22 p3593 A71-42329

Relative abundances and mass measurements of Li and B isotopes in primary low energy cosmic rays
22 p3593 A71-42339

Primary and secondary cosmic ray muon variations in vertical and zenith angles, determining coupling coefficients
22 p3593 A71-42357

High energy nucleon passage through lower atmosphere during chemical composition changes of primary cosmic rays, using Proton satellite observations
22 p3595 A71-42652

Ultrahigh energy electrons and gamma quanta in ground produced by primary cosmic rays, plotting mean free path vs energy
22 p3595 A71-42669

Underground meson telescope coupling functions calculations, using effective primary threshold energy
23 p3720 A71-43152

Primary cosmic ray and spallation track density distribution in Apollo 12 deep core soil samples
23 p3764 A71-43801

Low energy primary cosmic gamma ray measurements for spectrum latitude dependence and time variations near earth by Cosmos satellite scintillation spectrometer
24 p3865 A71-44564

Pulsar high energy cosmic ray periodic flux detection with favorable interstellar magnetic field configuration along line of sight
24 p3865 A71-44569

High energy gamma quanta flux measurements in primary cosmic rays, using Cosmos 208 satellite data
24 p3866 A71-45026

PRIMATES

NT CHIMPANZEES

Primate restraint harness of nylon jacket and cotton cot on aluminum frame padded seat for bone resorption and calcium metabolism studies
09 p1398 A71-22476

Impulse skin temperature encoding in primate cutaneous thermoreceptors in dynamic thermal conditions
18 p2860 A71-36877

PRIMERS (COATINGS)

Metal-metal bonded structures corrosion resistance improvement by use of primers or Al alloy honeycomb core
10 p1626 A71-24110

Adhesive primers corrosion resistance test methods, noting aircraft design implications
10 p1633 A71-24112

PRINCETON SAILINGS

U SAILINGS

PRINTED CIRCUITS

NT LARGE SCALE INTEGRATION

NT MEDIUM SCALE INTEGRATION

Glass substrates for thin film circuits compared to other materials for properties and suitability, emphasizing surface properties
02 p0230 A71-11816

Masking techniques for printed and thin film circuits and semiconductor devices fabrication
05 p0759 A71-16775

Basket wound and printed circuit moving coil electric and servomotors design characteristics
13 p2000 A71-28794

Electron-optical system with electro- and magneto-static lenses, ensuring large image reduction for producing printed microcircuits
16 p2579 A71-33500

Hybrid circuits thick film technology, discussing printed circuits fabrication processes and electrical and mechanical properties
18 p2888 A71-36224

Commercial production of high reliability components in plane transistors, bipolar integrated circuits and printed circuits technologies

18 p2889 A71-36535

Low power nonpulsating arithmetic unit of 16 bit integer numbers for spaceborne applications, using module printed circuit cards

18 p2886 A71-36570

Complex electronic modules automatic checkout, discussing processing time and cost reduction for large printed circuit logic boards test and diagnostic programs

[ASME PAPER 71-VIBR-115] 21 p3362 A71-40335
Multilayer printed circuit board development, design and production for high reliability and cost effectiveness, emphasizing multidisciplinary communication

21 p3352 A71-40436

Design parameters optimization for flat spiral coils printed on dielectric substrates based on equivalent circuit analysis, emphasizing coil shape effects on Q and inductance

22 p3520 A71-41715

Multilayer printed circuit boards defects detection by temperature field monitoring

22 p3520 A71-41764

Plated through holes interconnection in nine layer phased array antenna printed circuit board, using numerically controlled drilling and plastic encased preform solder system

22 p3525 A71-42765

Printed circuit board components and connections survival under severe vibration and G forces, considering resonant frequency, mounting methods and lead wire strain relief

23 p3652 A71-43538

PRINTED RESISTORS

Ni-Cr thin film resistors reliability, describing deposits on silicon dioxide, intermetallic formation and electromigration

19 p3034 A71-38515

PRINTERS

NT PRINTERS [DATA PROCESSING]

PRINTERS [DATA PROCESSING]

TV display eye movement monitor with automatic coordinate digital printout for permanent record

07 p1053 A71-20402

PRINTING

NT LITHOGRAPHY

Multiple exposure holographic interferometer for static and dynamic photomechanics

03 p0422 A71-13171

High speed magnetic printing apparatus for digital computers, discussing ferrographic process

03 p0382 A71-13819

Standard printing color identification system for DOD mapping, charting and geodesy services standardization

08 p1281 A71-21259

PRIORITIES

Parallel and standby redundancy systems with priority or noninstantaneous switchover, applying renewal theory integral equation

11 p1772 A71-26163

Electronic and electrical systems optimization effectiveness through generation of statistical priorities

22 p3525 A71-41438

PRISMATIC BARS

Test equipment for damping ability of vibration absorbing coatings on prismatic rods under pure bending, using electromagnetic vibration induction system and optical recorder

03 p0396 A71-13417

Thin walled prismatic body resistance to torque by extension of solution for rectangular bars, considering shearing stresses and transverse forces

03 p0505 A71-13542

Euler buckling of hinged slender prismatic bars of rectangular and elliptic cross sections with shear and transverse stress allowance

10 p1685 A71-23959

Hydrostatic extrusion, emphasizing prismatic products fabrication from industrial metals and alloys

14 p2252 A71-30469

Weak discontinuity unloading wave propagation in semiinfinite slender prismatic bar of elastoplastic material

16 p2656 A71-33356

Large deflections of thin piecewise prismatic elastic bars by electronic analog computer simulation

16 p2661 A71-34117

Square cross section prismatic bars transient creep analysis based on strain, time and combined hardening theories

17 p2815 A71-34188

Rectangular composite prismatic bar with T shaped cross section, calculating torsion with summary representation method

17 p2824 A71-34847

Low rigidity stretched prismatic beam bending under tension by force couple

17 p2831 A71-35345

Zero moment reinforced prismatic shells of rectangular cross section with arbitrary load distribution

21 p3472 A71-41146

Elastic stability of prismatic and cantilever bars in torsion

21 p3472 A71-41150

Function construction procedure for ring-shaped structure conformal mapping onto doubly connected regions with simple contours, applying to prismatic rod torsion problem

23 p3776 A71-43419

Algorithm for pure torsion of doubly connected square profile prismatic bars with hole, using R functions and variational technique

24 p3881 A71-44834

PRISMS

NT PRISMATIC BARS

Optical bonding agent for calcite prism on Pioneer F/G mission, emphasizing optical and mechanical properties resistance to Jupiter high energy particles

01 p0081 A71-10835

Gravitational anomaly distributions of rectangular prismatic bodies, using tables

04 p0581 A71-15069

Beam-combining prism/magnifier eyepiece configuration with miniature CRT for superimposing magnified virtual image upon user visual field

04 p0597 A71-15362

Beam splitter prisms with dielectric multilayer coatings

06 p0907 A71-17534

Parallel light beam triangular path interferometer with linear compressive shear effect for flow measurement applications, describing prism system and interference patterns

12 p1905 A71-26816

Diffraction of spherical wave on triangular prism, using reduction by group theory of point sources

12 p1878 A71-26838

Mechanical sterilization and cleansing of Goldmann applanation tonometer prisms contaminated with coliphage, comparing with germicidal immersion

13 p2020 A71-29036

Penta prism angle reduplication by interferometric measurements

14 p2241 A71-30139

PRIVATE AIRCRAFT

U GENERAL AVIATION AIRCRAFT

PRIVATE AVIATION

U CIVIL AVIATION

U GENERAL AVIATION AIRCRAFT

PROBABILITY

U PROBABILITY THEORY

PROBABILITY DENSITY FUNCTIONS

NT NORMAL DENSITY FUNCTIONS

NT PEARSON DISTRIBUTIONS

NT RAYLEIGH DISTRIBUTION

NT WEIBULL DENSITY FUNCTIONS

Frequency-wavenumber power spectrum estimators probability distribution, using Gaussian distribution probability density function

02 p0215 A71-12046

Eigenfunction expansions of reduced nonGaussian phase error transition probability density function for first order tracking loop, analyzing spectral properties of Fokker-Planck equation

08 p1324 A71-21341

Distribution curves of F 2 critical frequency variations, considering probability density functions interpretation via asymmetric model

11 p1757 A71-25771

Amplitude-quantized random noise contaminated unknown signal sample, deriving conditional probability density function of combined output error and signal confidence interval

12 p1880 A71-27157

Nonparametric Bayes risk estimation for measurement classification, using nearest neighbor error rate and Parzen probability density function estimators

16 p2602 A71-32822

Digital generation algorithm for random number sequences with specified autocorrelation and probability density function, illustrating computation accuracy and versatility

17 p2719 A71-34745

Probability density function for parameter of exponential measurement model based on structural inference theory, developing prediction densities as life test inferences

17 p2768 A71-35537

Time ordering operators applications to nonlinear unsteady systems, covering stochastic differential equations solution and phase locked loop phase error probability density calculation

18 p2940 A71-36222

Recurrent procedure for probability characteristics analysis of stationary random process, using density functions and Euler equations

19 p3085 A71-37146

Small scale turbulence structure in atmospheric boundary layers over open ocean, noting velocity derivatives probability density function lognormality

19 p3044 A71-37731

Probability density function of optimum phase locked loop synchronizer of sinusoidal signal with white Gaussian noise in partially coherent receiver

20 p3195 A71-38858

Doppler tracking radar systems, obtaining probability density function of Doppler signal amplitude

20 p3200 A71-39907

Distribution curves of F 2 critical frequency variations, considering probability density functions interpretation via asymmetric model

22 p3532 A71-41539

Probability density and distribution functions of clock amplitudes for rectangular IF, determining frequency modulation effect

22 p3513 A71-42386

Random fluctuating longitudinal pressure gradient effect on steady incompressible channel flow for arbitrary power spectrum and probability density

23 p3664 A71-43597

Random processes overshoots, determining probability distributions of overshoot duration and time of first attainment of given level for random sequences

24 p3815 A71-44703

Galactic stochastic magnetic field lines, deriving dynamic equation for probability density function

24 p3871 A71-44902

PROBABILITY DISTRIBUTION FUNCTIONS

Frequency-wavenumber power spectrum estimators probability distribution, using Gaussian distribution probability density function

02 p0215 A71-12046

Statistical analysis of digital data transmission time error distributions in Polish post office and railroad communications network

03 p0380 A71-14375

Randomly used shared communication channels capacity, calculating probability function dependence on frequency assignment policy

05 p0721 A71-16467

Elastic medium residual microstresses probability distribution, noting microdistortion tensor linear and transverse components and tangential and normal stresses relation

06 p1002 A71-18417

Atmospheric turbulence steady random process correlation function, spectral density and probability distribution based on aircraft measurements

07 p1150 A71-18797

Amplitude distribution of nuclear burst electromagnetic pulse propagated through atmosphere, deriving two probability distribution functions by central limit theorem

09 p1410 A71-23524

Steady state photon transfer through homogeneous semiinfinite isothermal atmosphere with two level atoms, deriving linear integral equation for escape probability distribution

10 p1643 A71-24964

Radio noise amplitude probability distribution, considering RMS voltage, average voltage and average logarithm of voltage

13 p2031 A71-28861

Biased angle selection in Monte Carlo shielding calculations, using importance function

13 p2099 A71-29253

Output probability distributions and covariance functions of nonlinear transformations of Gaussian stochastic processes occurring in signal detection and control theory

15 p2379 A71-31822

Ejected photoelectron count probability distribution due to periodic irradiance modulation of amplitude stabilized light beam

15 p2452 A71-32595

Cost distribution theory for various costs of failure, using probability distribution functions for modeling maintainability and reliability

16 p2583 A71-33305

Exact confidence intervals for probability and sampling quantiles of random quantity from beta distribution law

17 p2763 A71-34302

Limits theorems of occupancy problem, concerning asymptotic behavior of random particle distribution to fixed cell with equal probabilities

17 p2764 A71-34574

Recurrent procedure for probability characteristics analysis of stationary random process, using density functions and Euler equations

19 p3085 A71-37146

Fluctuations in parametrically excited subharmonic oscillator, deriving steady state probability distribution for amplitude and phase transitions analogous to Brownian motion of particle in potential well

20 p3203 A71-39094

Statistical fatigue life models, surveying failure probability distributions in reliability studies

22 p3566 A71-42117

Hazard rate functions of systems with identically distributed subsystem failure times in sequential or simultaneous operation

22 p3566 A71-42118

Gaussian errors effect in maximal ratio diversity combiner weighting factors on probability distribution of output SNR

22 p3513 A71-42384

- Probability density and distribution functions of click amplitudes for rectangular IF, determining frequency modulation effect 22 p3513 A71-42386
- Extensive air shower electron and muon components at mountain levels, calculating probability distribution functions by Monte Carlo technique 22 p3595 A71-42662
- Electric circuit component failure prediction and probabilistic distribution in troubleshooting search 23 p3638 A71-42900
- Damped exponential cosine probability distribution function for clipped waveforms of voiced speech signal 23 p3645 A71-43439
- Random processes overshoots, determining probability distributions of overshoot duration and time of first attainment of given level for random sequences 24 p3815 A71-44703

PROBABILITY THEORY

- Solution search strategy optimization by analytic graphic techniques for problem with several approaches involving Bernoulli type trials 01 p0110 A71-10088
- Partial differential equations finite difference approximation, applying convergence theorems with probabilistic method 01 p0111 A71-10318
- Probability method for gyroscope instrumental errors associated with inaccurate fabrication and components assembly, classifying external moments 01 p0800 A71-10534
- ATC system improvement by procedural changes, applying probability concepts to flight safety 02 p0278 A71-11699
- Monograph on visibility of satellite in elliptic orbit covering probabilistic aspects, communication, navigation, weather, reconnaissance and scientific satellites 02 p0319 A71-11970
- Optical scatter channel transmission characteristics, using mathematical model consistent with radiative transfer theory and probability-computing receiver 02 p0249 A71-12012
- Radar signal probability ratio over finite interval 02 p0219 A71-12620
- Maximum likelihood estimation algorithm for arrival direction of narrowband signal under correlated noise 04 p0550 A71-14618
- Increase approximation of estimation errors covariance between discrete measurements due to random forcing function uncertainty 04 p0561 A71-15869
- Random graphs probabilistic characteristics, deriving algorithms for graph connectivity probability estimation 05 p0731 A71-16795
- One dimensional Markovian process residence probability in region with variable boundaries 05 p0732 A71-17021
- Extraterrestrial civilizations, discussing probability theory and radio communication 06 p0852 A71-17739
- Soviet papers on statistical and probabilistic weather forecasting covering computerization problems, atmospheric circulation, correlation methods, etc 07 p1150 A71-18870
- Probabilistic weather forecasts reliability estimation 07 p1150 A71-18871
- Admissible translations of probability measures on sigma algebra of Borel sets of Hilbert space 07 p1147 A71-19200
- Bit error probability estimation from sync word error rate data 07 p1062 A71-19538
- Three element model for choice behavior binary prediction consisting of logical, experiential and error components 07 p1048 A71-19595
- Probability theory for viable microorganism exposure in fractured contaminated solid, using quantum response model 07 p1048 A71-19600
- Perceived and responded to discriminative stimuli identification in probability learning, using parameter free model of event pattern association strength 07 p1049 A71-19775
- Gas laser optical pumping based on photodissociation, calculating spatial temporal distributions of pump radiation absorption probability and main level population 07 p1125 A71-19806
- Lightning stroke probability model for point selection on aerospace vehicles 07 p1020 A71-19928
- Two phase mixture spark ignition dynamics, investigating probabilistic character and ignition energy 07 p1224 A71-20068
- Complex human memory processes large scale simulation/cybernetic modeling/ based on information handling probability and retrieval 07 p1050 A71-20105

- Mercury spin orbit resonance probability computation, making a priori assumptions for long term orbital variations, tidal torque and equatorial asymmetry 07 p1203 A71-20521
- Book on probability theory and applications covering stable distributions, renewal theory, large numbers laws, central limit theorem, Markov processes, random walks, etc 08 p1325 A71-21655
- Probabilistic estimate of aerodynamic imbalance of aircraft gas turbine rotors due to production errors in compressor blade angle 08 p1349 A71-22045
- Shaped beam radiation patterns synthesis by iterative sampling method with line sources or uniformly spaced antenna arrays 09 p1409 A71-23493
- Theory of form based on geometric probabilities, leading to two dimensional retinal type computer programmed to exhibit elementary form perception aspects 10 p1567 A71-23997
- Meteor trails ionization probability determination based on data since 1948, comparing results of theoretical, semiempirical, experimental and simulation method 10 p1669 A71-24031
- Probability of quasi-chemical reactions between point defects in semiconductors due to ionizing radiation 10 p1655 A71-24139
- Signals temporal uncertainty and sensory modality influence on watchkeeping performance, discussing signal density effect on pulses duration increments detection 10 p1568 A71-24183
- Uncertainty factors in management decisions and operations optimization in international air transportation industry 10 p1698 A71-24265
- Structural inference theory applied to stochastic processes class characterized by gamma-distributed interarrival times, deriving conditional probability mass function for process counting variable 11 p1791 A71-25251
- Second order probabilities and strictly proper scoring rules in weather forecasting, discussing subjective judgment role in forecasting processes 11 p1793 A71-25376
- Misconceptions and distortions in n dimensional covariance matrices interpretation regarding probability confidence levels to error ellipsoid and hyperellipsoid 11 p1791 A71-25485
- Fatigue failure probabilistic model under variable amplitude loading, considering relation between safety factor and fatigue failure probability 11 p1848 A71-25492
- Probability theory application to entropy and conductivity matrices 12 p1986 A71-26960
- Statistical estimation techniques for error probability of digital communication systems 12 p1880 A71-27145
- Burst-like signal detectability evaluation in terms of optimum detector performance and probability theory 12 p1882 A71-27442
- Probability characteristics of glass/epoxy plastics mechanical properties, considering tangential and axial tensile and bending strength, modulus of elasticity, buckling and compression strength 13 p2092 A71-28653
- Probabilistic cyclic queue model of overhead time and channel utilization in multiprogrammed computer systems under demand memory paging 13 p2035 A71-28973
- Closed-loop control of discrete time systems with uncertainty, discussing minimax reachability of target sets and tubes 14 p2219 A71-29698
- Book on dynamic probabilistic systems, Volume 1, covering Markov models, linear processes, systems analysis, statistics, recurrent events, population models, time variations, etc 15 p2440 A71-31196
- Book on dynamic probabilistic systems, Volume 2, covering semi-Markov and decision processes 15 p2440 A71-31197
- Probabilistic methods for solving ATC and navigation problems, considering stochastic processes theory 15 p2445 A71-31463
- German textbook on fundamentals of thermodynamics covering energy conversion, reversible/irreversible processes, chemical/molecular thermodynamics, statistical analysis, probability theory, etc 15 p2516 A71-32767
- Human inferences based on partially reliable reports, studying likelihood ratio estimates and probabilistic relations in nature 16 p2534 A71-33103
- Stationary narrow band Gaussian vibration excursion probability based on Markov point process [ASME PAPER 71-APM-19] 16 p2655 A71-33210

- Hybrid computer use for dynamic system probabilistic modeling, determining hydraulic actuator output statistics 16 p2549 A71-33295
- Information model for simulating systems reliability estimates uncertainty, noting state transition matrix, methodology and sensitivity analysis of effectiveness 16 p2583 A71-33304
- Probabilistic approach to prolonged lifetime design and static strength of structures of monocoque and multispar wings, using fatigue characteristics of individual elements 16 p2657 A71-33604
- Kolmogoroff differential equations for probabilities of system states, showing validity for Markovian random processes and processes with aftereffects 16 p2603 A71-33891
- Uniform convergence of frequencies of events in independent tests sequence to probabilities of occurrence 17 p2764 A71-34573
- Linear dynamic system recursive state estimation for set-membership description of uncertainty under unknown input disturbances and observation errors 17 p2718 A71-34734
- Additional redundancy in information transmission systems with feedback to reduce error probability due to incorrect addressing 17 p2702 A71-34975
- Upper bound on error probability due to intersymbol interference for correlated and uncorrelated digital signals, presenting examples for data communication systems 17 p2703 A71-35077
- Measurement uncertainty effects in linear multistage games, considering state variables construction from player measurement sequences 17 p2767 A71-35298
- Computer simulation of error probability performances of binary coherent PSK system under thermal noise and intersymbol and interchannel radio interferences effects 17 p2707 A71-35476
- Binary differentially coherent PSK modulated PCM radio link performance under noise and intersymbol and interchannel interferences effects, deriving error probability 17 p2707 A71-35477
- German monograph on nonlinear distortion correction of binary bipolar signals in Gaussian noise covering receiver, decision theory and error probabilities 18 p2874 A71-35959
- Beam column with probabilistic material and geometric properties, axial loads and boundary conditions, obtaining free vibration and natural frequency stochastic equations 18 p2979 A71-36358
- Adaptive frequency selection for reduction of effects of noise differing irregularly from useful pulse signals, estimating error probabilities 18 p2882 A71-36622
- Image parameters identification and estimation problems /in learning without teacher/, deriving error variance lower bounds and spurious solution probabilities 19 p3024 A71-37225
- Helium-like ion forbidden line emission and transition probabilities, deriving solar densities in active regions 19 p3136 A71-37621
- S-N curve and structural failure probability due to combined random and primary loads based on mathematical model 19 p3157 A71-37847
- Probabilistic weather forecasting for temperature and precipitation, examining feedback and prediction evaluation 20 p3256 A71-39203
- Meteorological prediction from joint frequency of initial and final weather elements conditions, developing conditional probability models from bivariate normal distribution tables and Markov process 20 p3256 A71-39204
- Thermodynamics and statistical mechanics of low temperature physics, including entropy, probability, energy spectra and gas liquefaction 20 p3270 A71-39240
- Binary systems formation probability during triple encounters, considering random initial conditions 20 p3290 A71-39301
- Cumulative probability of target detection for pulse surveillance radars, relating target cross section, velocity and radar frame 20 p3199 A71-39901
- Probabilistic behavior of repairable two-state systems, assuming reliability measurability by operating time 21 p3407 A71-40362
- Generalized reliability function for systems of arbitrary configurations, using path enumeration approach based on probability theory 21 p3407 A71-40369

Molecular beam extraction from equilibrium gas flows, describing shock beam formation model with associated escape probability 21 p3419 A71-40956

Probability approach to visual effectiveness of signal flashing lights, showing graphically Broca-Sulzer effect 22 p3498 A71-41485

Error probability during diversity reception under random radio noise 22 p3510 A71-42253

Signal design and error rate of impulse noise channel, analyzing error probability of smear-desmear and standard data channels through Rice integral evaluation 22 p3513 A71-42381

Two dimensional probabilistic images generation and statistical characteristics determination, noting application to psychophysiological experiments 22 p3518 A71-42422

Exact test particle propagator of Lenard-Bernstein equation for magnetoplasma, applying to transverse plasma echoes 22 p3584 A71-42466

Single channel queueing system with Poisson input and waiting time dependent mass servicing time, deriving arrival number probabilities generating function 22 p3527 A71-42491

Probabilistic system observation at random times, calculating Markov renewal processes optimal long run control 22 p3527 A71-42628

Actual navigation dispersions, estimation uncertainties and resultant Mars orbit insertion statistical delta V requirements for six Mars approach angles in 1977 Mars window [AAS PAPER 71-323] 23 p3726 A71-42997

Probabilistic analysis of random pulse signal gating on time selective zero lag converter with rectangular pulse input 23 p3647 A71-44322

Waiting time distribution in computer controlled queueing system with Poisson input, deriving formulas on basis of total probability and Markov chain theory 24 p3806 A71-44654

Nonlinear control system optimal synthesis by statistical criteria, discussing probability and likelihood function 24 p3813 A71-44682

Linear control system optimal weighting function determination from maximum probability for system output 24 p3814 A71-44687

Cylindrical space simulation chamber with spherical test subject, deriving molecular incidence rate from integral equations with probability matrix for finite partial surfaces 24 p3816 A71-45138

Near circular orbit elements determination as functions of spacecraft initial speed and coordinates deviation by mathematical expectation procedure 24 p3876 A71-45317

PROBES

High input impedance wideband frequency measurement probe with bipolar and unipolar transistor circuits 01 p0051 A71-10284

Mechanized ultrasonic inspection probes with high stable dynamic acoustic coupling coefficient, high sensitivity and wear resistance and low coupling fluid expenditure 09 p1450 A71-22897

HF rake probes with high temperature integrated sensor for inflight aircraft engine intake air flow distortion measurements 14 p2243 A71-30321

Aerodynamic probes for determining flow state of high enthalpy hypersonic flow fields, considering pitot pressure, total enthalpy and current density 18 p2921 A71-36414

PROBLEM SOLVING

NT ASYMPTOTIC METHODS

NT ITERATIVE SOLUTION

NT THEOREM PROVING

Solution search strategy optimization by analytic graphic techniques for problem with several approaches involving Bernoulli type trials 01 p0110 A71-10088

Q approach to problem solving applied to partial derivatives determination on digital computer, discussing approach structure and characteristics 01 p0048 A71-10221

Initial value or boundary value problems in mathematical physics, solving by process of condition elimination 05 p0780 A71-16178

Neumann problem for Helmholtz equation in complex configuration region, developing variational solution method 05 p0782 A71-16884

Thermoelasticity equations solutions for special cases 09 p1535 A71-22259

Human operators performance under control problem programs, determining training and fatigue effects 09 p1398 A71-22483

Boundary value problem for Laplace equations, noting conditions for convergence of solutions sequence 17 p2765 A71-34867

Generalized finite Hankel transform method for engineering problems with complicated boundary conditions 20 p3255 A71-39034

Strategies and tactics for industrial R and D problems selection and solution for products innovation, noting element of chance 24 p3891 A71-44364

PROCEDURES

NT FINITE ELEMENT METHOD

NT OPTICAL CORRECTION PROCEDURE

Standard equipment and procedures for aircraft gas turbine engine exhaust smoke measurement [ASME PAPER 71-GT-88] 11 p1813 A71-25995

PROCESSORS [COMPUTERS]

U CENTRAL PROCESSING UNITS

U COMPUTERS

PROCUREMENT

NT GOVERNMENT PROCUREMENT

Flight simulators procurement and commissioning, discussing difficulties due to different aircraft configurations, advantages of equipment and procedures standardization, etc 01 p0066 A71-10015

Risk assessment associated with reliability demonstration testing, considering fixed price procurement and cost effectiveness 12 p1910 A71-26677

Cost effectiveness of reliability screening program from parts procurement through system test, using experience with attack radar for F-111 aircraft 12 p1885 A71-26683

Government and public agencies procurement policy evolution from legal obligations to economic impact consideration 23 p3786 A71-43464

PROCUREMENT MANAGEMENT

Shillelagh missile reliability program development, deployment using part qualification levels and fly-before-buy procurement 12 p1885 A71-26684

PRODUCT DESIGN

U PRODUCT DEVELOPMENT

PRODUCT DEVELOPMENT

NT WEAPONS DEVELOPMENT

Search procedures selection from heuristic methods of solving design development problems by computer 01 p0087 A71-10408

Technological forecasting by evaluating patent significance, applying to earth moving equipment development 02 p0335 A71-11858

Long term planning of technological and scientific development of machine design and construction on national industrial and enterprise levels 02 p0336 A71-11860

M49 Larzac turbopfan engine, describing design, development, performance data, manufacturing techniques, operation and maintenance 02 p0299 A71-12607

Black Brant 3B sounding rocket design and development, discussing payload capability, static and dynamic stability, flight and ground handling loads [AIAA PAPER 70-1396] 03 p0499 A71-13677

Turbomachinery R and D to improve components and engine performance 03 p0470 A71-13824

BD-1 Yankee aircraft development, design and construction 07 p1018 A71-19084

Microwave plasma device development, noting beam plasma amplifiers and quiescent source 07 p1167 A71-19257

Tools production and shaping for extrusion of light metal profiles 10 p1619 A71-25032

Glass fiber reinforced plastics reinforcement techniques, emphasizing E glass filament manufacture, properties, advantages and products 11 p1788 A71-25653

Vertical straight lift turbojet engine design and development, presenting component materials properties/weights, endurance tests and performance data [ASME PAPER 71-GT-75] 11 p1813 A71-25989

Air Force development programs with graphite reinforced composites, discussing matrix materials and cost and weight savings [ASME PAPER 71-DE-13] 12 p1921 A71-27323

Olympus 593 pure jet twin shaft engine development program for Concorde, discussing engine evolution, design considerations and flight development [SAE PAPER 710422] 13 p2114 A71-28309

Commercial aircraft powerplant development, discussing engine and components test programs and techniques [SAE PAPER 710449] 13 p2114 A71-28327

DC-10 wide body tri-jet aircraft design and development, considering sizing, number of engines and thrust optimization and selection of cruise, approach and stall speeds [AIAA PAPER 71-780] 17 p2674 A71-34525

Phonocardiograph design and calibration for accurate measuring and recording of cardiac vibration displacements, velocities and accelerations 19 p3005 A71-37231

Electronic component products improvement history, discussing electron tubes, future trends and reliability 19 p3027 A71-37345

Synthetic materials technology development, discussing macromolecular materials synthesizing methods and properties 19 p3085 A71-38144

Gas lasers, discussing engineering developments for size and cost reduction, reliability, long life and high power 19 p3074 A71-38227

European research, development and production of solar cells, discussing Intelsat 4 program applications 20 p3179 A71-38851

Low cost high performance rate gas bearing gyroscope development, emphasizing large scale production and overall instrument design optimization 22 p3551 A71-41664

Synthetic fibers and plastics development, chemical composition, physical and mechanical properties, production growth rates and applications 23 p3696 A71-43107

Strategies and tactics for industrial R and D problems selection and solution for products innovation, noting element of chance 24 p3891 A71-44364

NASA program fire safety goals, discussing development of nonflammable materials covering fibrous asbestos, glass, polyimides, Teflon, metallics and halogenated materials [AIAA PAPER 71-1011] 24 p3841 A71-44595

PRODUCTION ENGINEERING

NT PRODUCTION PLANNING

Automated machinery for reinforced plastic structural products manufacture by filament winding [SME PAPER EM-70-135] 01 p0089 A71-11261

Aircraft assembly accuracy parameters, using holes as reference points 02 p0257 A71-12564

Bench-line product assembly analysis, calculating rhythm, cycle and required number of workers 02 p0257 A71-12567

Niobium processing methods from economic standpoint, describing pyrochlore metallurgical reduction 02 p0271 A71-12938

Soviet book on aircraft construction technology covering parts fabrication, protective coatings, production automation, etc 03 p0433 A71-14399

Group and form classification of production errors and tolerances in aircraft construction 04 p0602 A71-14610

Numerical control automation in aircraft bearing production for small batch runs 04 p0603 A71-15672

Solar cell module joints welding technology development under ESO sponsorship, emphasizing resistance welding and process optimization 05 p0704 A71-16095

Aerospace industry engineering company management and marketing, discussing corporate strategy, production control, market analysis and professionally trained managers 05 p0840 A71-17148

Sheet blanks shaping into conical products by rolling, discussing stress-strain state in blank and time dependent rolling process 06 p0906 A71-18711

Mathematical model of small scale versatile aircraft component production process, developing computer production optimization algorithm 06 p0906 A71-18715

Quality management planning for 1970s, discussing reliability, maintainability and production quality programs 07 p1225 A71-19558

Nondestructive testing in product cycle in aerospace industry 07 p1118 A71-19949

Map preparation techniques and cartographic design for cost reduction and production speeding 08 p1280 A71-21247

Ti alloy powders and Ti-base refractory compounds production from Ti alloys wastes 08 p1317 A71-21856

Ti-Mo alloys porous materials for work in hot solutions of nonoxidizing acids, discussing production technology and corrosion resistance 08 p1317 A71-21857

Steady multifiber winding process conditions in compact glass fiber packing for glass fiber reinforced plastic tubes 09 p1482 A71-22817

High temperature steel and alloys metallurgical processes for stationary and aircraft gas turbine engine components, discussing production-quality control-research interrelationship

09 p1456 A71-23301

Quality assurance in Ti and Ti alloys processing, discussing smelting, ingot homogenization staging, costs and facilities

09 p1456 A71-23303

Carbon dioxide production laser for automatic resistors trimming without current carrying capability reduction, noting accuracy, flexibility and speed

09 p1465 A71-23405

Processing variables effects on epoxy adhesive joints fracture toughness and crack extension resistance

10 p1632 A71-24089

Contoured silicone internal pressure bag mandrels for helicopter rotor blades fabrication

10 p1615 A71-24096

Relativity of nondestructive testing as related to production effort, reviewing structural adhesive bonding in U.S. for past ten years

10 p1616 A71-24106

Brittle materials ultrasonic machining, discussing abrasive particle shape, size, temperature and pressure effects on process accuracy, speed, quality and efficiency

10 p1617 A71-24133

Ultrasonic cleaning by cavitation disintegration of highly adhesive surface coatings, discussing cleansing liquid, field parameters and external static pressure effects on process efficiency

10 p1617 A71-24135

Powder metallurgy superalloy parts, discussing production methods and mechanical properties comparison with conventional process products

10 p1618 A71-24763

Three dimensional isostatic pressing process, discussing equipment, tooling and forging preforms and finished parts production

10 p1618 A71-24764

Spark sintering powder metallurgy using alternating and direct current plus pressure, discussing use in Be components production for aerospace applications

10 p1618 A71-24765

Refractory metals and alloys products fabrication for aerospace applications, discussing hydrostatic bulge forming and aluminide coating in Nb alloy nozzle extension production

10 p1618 A71-24766

Space shuttle vehicles and assembly flow manufacturing, development and operations requirements, including ground rules, verification test facilities, cost reduction and interrelationships

[AIAA PAPER 71-316]

10 p1590 A71-24831

Tools production and shaping for extrusion of light metal profiles

10 p1619 A71-25032

SVAM glass reinforced plastics production and properties, discussing drawing, coating and forming oriented laminate on drum

11 p1784 A71-25396

Winding equipment for continuous production of large diameter cylindrical filaments of reinforcing materials and polyester resins

11 p1768 A71-25418

Plastics mold design improvements, discussing steel quality, guiding/heating systems, surface finish and chrome plating

11 p1768 A71-25432

Electroluminescent semiconductor diodes based on GaP and GaAlAs, discussing design, properties, uses and production

11 p1737 A71-25569

Electron beam welding machine reducing number of fabrication variables during final assembly procedure in thermionic converters fabrication, discussing UHV systems

11 p1709 A71-25866

Metal matrix composite fabrication procedures for gas turbine engine fan blades, stressing diffusion bonding process susceptibility to blades volume producibility

[ASME PAPER 71-GT-46]

11 p1770 A71-25979

Total reliability requirement procedure for design, development and production of medium- and large-scale integrated circuits

12 p1884 A71-26660

Optimal reliability proposals for industry competitive posture improvement in difficult market environment, recommending military electronics reliability standards specification

12 p1909 A71-26669

Reliability assurance in product manufacturing, discussing specific tasks during design, preproduction and production phases

12 p1910 A71-26672

Filament winding techniques for glass fiber reinforced plastics, discussing processes, configurations and materials for achieving optimum strength

12 p1920 A71-27011

Human position in socialist productive system, examining pedagogical aspects of leadership

13 p2019 A71-28491

Book on electron beam welding covering generation and control, thermal effects, techniques and equipment, metallurgical and mechanical properties, etc

13 p2074 A71-28736

Book on fusion welding covering workshop problems, production processes, miniature casting and resistance welding techniques

13 p2076 A71-29444

Advanced plastic composites fabrication and processing techniques, using resins, reinforcements and fillers

14 p2263 A71-29653

Complex structural aircraft components manufacture, using group technology principle based on subdivision of parts classes

14 p2252 A71-30267

Ti alloy powders and Ti-based refractory compounds production from Ti alloy scrap, describing electrorefining, hydrogenation and carbidization processing

14 p2260 A71-30835

Porous Ti-Mo alloy materials for operation in hot solutions of nonoxidizing acids, discussing production technology and corrosion resistance

14 p2260 A71-30836

Cost optimization for solar generator thermobatteries by selecting temperature, contact resistance, material parameters and fabrication technology

15 p2351 A71-31671

Titanium carbide based cermet materials with alloy steel binder, investigating production conditions, hardness, machining and quenching properties

15 p2429 A71-32139

Truncated sequential test for production models based on preproduction testing with allowance for unequal sample sizes

15 p2416 A71-32344

Multilevel supply system operationally ready aircraft number evaluator based on item stock levels, demand rates and repair/resupply times

15 p2516 A71-32700

Aircraft industrial cleaning agents, processes and techniques applied to components in course of manufacturing and assembly phases, emphasizing emulsion and alkaline methods

[ASM PAPER C70-4.3]

16 p2584 A71-33542

Production efficiency prerequisites in extruded Al alloy products manufacture, discussing billet material and processing conditions effects

16 p2584 A71-34091

Modular manufacturing for F-14 aircraft at low cost using end product configuration reducing final assembly

16 p2585 A71-34157

Commercial production of high reliability components in plane transistors, bipolar integrated circuits and printed circuits technologies

18 p2889 A71-36535

Communication satellite components reliability assurance method, discussing production and qualification tests

18 p2890 A71-36538

Aircraft jet engine application of electric discharge machining for repetitive continuous production, considering automated closed cycle equipment

[SME PAPER MR-71-143]

18 p2927 A71-36658

Semifinished product production technology influence on heat resistant alloys mechanical properties, considering forging, rolling, casting, melting, diffusion welding and powder metallurgy

18 p2937 A71-36725

Scanning electron microscope for poor metallization detection in manufacturing cycle of semiconductor devices

19 p3034 A71-38519

Multilayer printed circuit board development, design and production for high reliability and cost effectiveness, emphasizing multidisciplinary communication

21 p3352 A71-40436

Beam-lead technology application to complementary MOS IC processing

21 p3357 A71-40814

Masking techniques in monolithic IC production in microelectronics, emphasizing contactless, lens, holographic and electron beam projection methods

22 p3525 A71-41713

Active digital and proportional fluidic devices design and manufacture including turbulence, wall-attachment, focused jet, beam deflection and vortex amplifiers

22 p3483 A71-42783

Quality control organization in British spacecraft projects, discussing material selection system and subsystem tests, process engineering and inspector training

23 p3681 A71-43470

Molins 24 integrated automatic complete-processing system for small light-metal parts, using numerically controlled machine tools integrated with palletized feeder system

23 p3681 A71-43473

Material properties, metallurgy, production technology and operational factors effects on machinery structural strength

23 p3779 A71-44207

PRODUCTION MANAGEMENT

Control reliability in automated system of discrete production management

17 p2721 A71-34961

PRODUCTION METHODS

U PRODUCTION ENGINEERING

PRODUCTION PLANNING

Production startups deviation from increased productivity anticipation patterns, noting management actions minimizing losses

05 p0840 A71-16742

Service support for hardware engineering models from breadboard to preproduction stages, determining spare parts location, quantity and cost requirements

09 p1430 A71-23477

System effectiveness tasks of producibility analysis, maintainability evaluation and tradeoff studies

16 p2664 A71-33316

PRODUCTIVITY

Production startups deviation from increased productivity anticipation patterns, noting management actions minimizing losses

05 p0840 A71-16742

Powder form structural adhesives for cost reduction and increased productivity

10 p1614 A71-24066

Commercial spinoff from government sponsored R and D, considering productivity and industry benefits

14 p2342 A71-31133

Negotiations of BEA/BOAC productivity agreements in aircraft industry

18 p2926 A71-35924

Astronaut teleoperators use for space operations cost reduction and future experiments productivity increase

22 p3503 A71-42033

Defense and aerospace industry demand cyclical variations effect on productivity growth and cost

22 p3624 A71-42525

PRODUCTS

Product test duration and extent from reliability theory viewpoint

05 p0759 A71-16725

PROFICIENCY MEASUREMENT

U HUMAN PERFORMANCE

U PERFORMANCE TESTS

PROFILES

Plane linear cascades of thin curved profiles, obtaining potential flow velocities and lifting force on leading edge

01 p0001 A71-10339

Steady nonrotational flow around rectilinear profile in finite width uniform current in linear theory, calculating fluid exerted forces

10 p1549 A71-23822

Body profile low frequency oscillations in transonic gas flow, investigating nonlinear differential equation boundary value problem by approximation method

10 p1550 A71-24363

Transonic gas flow around profile, proving uniqueness of Frankl solution

13 p1993 A71-29221

PROGNOSIS

Meteor-reflected radio wave propagation diurnal and annual variations prognosis, discussing indispensability of incident meteor particle velocity and density distributions

10 p1669 A71-24034

PROGRAM MANAGEMENT

U PROJECT MANAGEMENT

PROGRAMMED INSTRUCTION

Differential equations of thermodynamics presentation to engineering students in form suitable for programmed study

03 p0518 A71-13526

PROGRAMMING

NT QUADRATIC PROGRAMMING

Space vehicle trajectories, discussing programming method to control motion for prescribed boundary conditions

03 p0495 A71-14236

Optimal control problems, applying direct mathematical programming to linear, nonlinear, continuous and discrete time, deterministic, stochastic and distributed parameter systems

11 p1792 A71-26419

Convergence characteristics of sequential and combined conjugate gradient restoration algorithms for mathematical programming, studying constrained function minimization

17 p2764 A71-34520

Soviet papers on mathematic methods application in programming covering optimal control, game theory, impact problems, thermoelastic waves, etc

22 p3526 A71-41908

Computerized system redundancy optimization formulation as zero-one type variables integer programming problem, obtaining algorithmic solution for maximum reliability

22 p3517 A71-42106

PROGRAMMING (SCHEDULING)

NT THRUST PROGRAMMING

Electron beam welding system, discussing solid state controls, programmed operation and type and thickness of welded materials

01 p0087 A71-10451

Linear system programmed maxmin transfer time problem solvability, investigating control process theory with time inversion
12 p1931 A71-27523

PROGRAMS

NT APOLLO APPLICATIONS PROGRAM
NT APOLLO PROJECT
NT CENTAUR PROJECT
NT COMSAT PROGRAM
NT DEFENSE PROGRAM
NT EARTH RESOURCES PROGRAM
NT EUROPEAN SPACE PROGRAMS
NT GEMINI PROJECT
NT JUPITER PROJECT
NT LUNAR PROGRAMS
NT MARINER PROGRAM
NT MARS 69 PROJECT
NT MARS 71 PROJECT
NT NASA PROGRAMS
NT ROVER PROJECT
NT SATURN PROJECT
NT SKYLAB PROGRAM
NT SPACE PROGRAMS
NT TEKTITE PROJECT
NT U.S.S.R. SPACE PROGRAM

PROJECT MANAGEMENT

Error model and digital computer simulation programs for technical management of missile development and testing
01 p0068 A71-10883

Data transmission/acquisition/processing systems engineering project management using digital simulation models
01 p0184 A71-10885

Rational structure selection for scientific research organizations, using systems analysis
02 p0335 A71-11855

Computer aided network analysis for multiple project planning facilitating readjustments and budgeting
02 p0336 A71-12122

Skyнет project UK and U.S. cooperation, discussing system scope, coordination, contract placing and PERT critical path analysis in management planning
02 p0337 A71-12427

Radio frequency interference project control responsibilities and teamwork, noting communication transmitter design example
03 p0383 A71-13177

Defense and space programs management systems, discussing structured activities planning for efficient resources use
[ASME PAPER 70-WA/MGT-5] 03 p0524 A71-14097

NASA multiple interagency interfaces, surveying work and resource integration, space programs and agency structure
04 p0690 A71-14937

Aerospace systems project management using graphic networking critical path method for planning and control
04 p0691 A71-15293

U.S.-Europe cooperative space programs survey and experience from project management with ESRO-1 satellite
04 p0692 A71-15349

Europa 3 experimental preparatory program, discussing hardware development and project management planning and control
[DGLR-70-064] 05 p0839 A71-15949

R and D management decision making process structural model, discussing technological forecasting based on organized technical information, quantized judgments, optimum resource allocation and hybrid technique
05 p0840 A71-16744

F-15 air superiority fighter, describing military requirements, program management and procedures in terms of speed, maneuverability, acceleration and weaponry
07 p1018 A71-19078

Integrated project information and simulation system for management of aerospace vehicle development, discussing simulation models application
[AIAA PAPER 71-238] 07 p1225 A71-19714

Power spectrum in project management of matrix organizations involving support personnel cooperation
07 p1225 A71-20014

Civil Engineering Systems Laboratory remote terminal interactive time sharing computer facility, discussing consulting engineer design office experiences and computing center management
09 p1412 A71-23277

Research and development project funds allocation, developing mathematical dynamic modeling method for cost management
10 p1699 A71-24539

Failure prevention, test discrepancy reporting and circuit analysis workshop techniques for program audits, integrating reliability managers, performers and customers
12 p1910 A71-26670

Statistical decision theory in reliability and project management, discussing Venus probe loss
12 p1911 A71-26690

Aircraft industry materials development, discussing innovations in governmental programs management, procurement specifications and Department of Defense contracting procedures
12 p1918 A71-27677

Costs-reliability relationships in helicopter development testing and demonstration, emphasizing decision making in program management
[SAE PAPER 710452] 13 p2167 A71-28330

Logistics planning as integral part of phased program planning process, considering preliminary analysis, definition, design, development, fabrication, test and operations phases
13 p2167 A71-28895

Organization and funding criterion of unsuccessful R and D projects, considering project abandonment or failure
14 p2340 A71-29854

Mathematical programming models for resource allocation and project selection decision in R and D
14 p2340 A71-29855

Satellite auxiliary electric propulsion systems survey for program managers and systems engineers, considering cost and component reliability
[AIAA PAPER 71-685] 14 p2292 A71-30747

Criteria for converting aeronautical project operational targets into actual requirements and technical specifications, emphasizing cost effectiveness
14 p2177 A71-30824

Skylab program organization and management, system design, operations and equipment
15 p2499 A71-31457

Safety engineers integration into overall system through basic development programs, involving management, manufacturing, testing and integrated logistic support
16 p2664 A71-33309

Earth remote sensing in Brazil, discussing program organization and data acquisition related to NASA environmental resources technology satellites
16 p2570 A71-33826

Earth orbital space stations modular design, discussing space shuttle use, crew training and program management
[AIAA PAPER 71-824] 17 p2812 A71-34721

Administrative techniques of cost/weight tradeoff program for jet transport airplane
[SAWE PAPER 899] 17 p2750 A71-35812

Reliability in key project decision making, including failure mode/effect analyses, design tradeoff, baseline meetings, hardware storage and data bases
18 p2926 A71-36491

Parallel strategies effectiveness in R and D projects, discussing learning rate as critical parameter in project management decision making process
19 p3173 A71-37629

Optimal investment model for R and D project evaluation and selection, using discrete cash flow and linear programming techniques
19 p3173 A71-37630

International cooperation in aerospace projects, discussing Concorde program organization
22 p3623 A71-42011

Economic analysis effect on R and D projects choice, assessing Space Shuttle system
22 p3624 A71-42526

Space program management - Conference, Paris and Neuilly-sur-Seine, February 1970
23 p3784 A71-43451

Large project management model, presenting schematic diagrams for nature and interrelation of functions
23 p3784 A71-43452

Program management techniques, discussing organization, planning, systems engineering and personnel selection
23 p3785 A71-43453

Project management methods oversophistication, discussing French space activity and managerial apprenticeship
23 p3785 A71-43454

International HEOS project organization, discussing communication, task delegation, decision making and structure
23 p3785 A71-43455

Organization problems of research laboratory for space astronomy experiments, delineating roles of chief scientist, project manager and technical services
23 p3785 A71-43456

Management information techniques, discussing project reports, meetings, decision process, work breakdown, planning schedules and computerization
23 p3785 A71-43457

Space project management techniques under European conditions, covering requirements, style, motivations, concepts and rules
23 p3785 A71-43458

Industrial project management, defining functions and responsibilities of program director, contractor, subcontractor and manufacturer
23 p3785 A71-43460

Industrial project management executive work team for space programs, emphasizing responsibilities of prime contractor
23 p3786 A71-43461

Nuclear test program management, considering reliability problems, delays and cost
23 p3786 A71-43462

Multinational consortiums of industrial firms from member states for ESRO satellite programs
23 p3786 A71-43463

Project management by contractual procedures for ELDO space research
23 p3786 A71-43466

Project management quality control factors learned from Diamant A satellite launching vehicle and French military programs
23 p3786 A71-43469

Quality control organization in British spacecraft projects, discussing material selection system and subsystem tests, process engineering and inspector training
23 p3681 A71-43470

NASA NHB reliability engineering provisions for aeronautical and space system contractors, considering criteria for program management, system engineering, manufacturing and facilities
23 p3682 A71-43497

Technology transfer management, distinguishing between active and passive pursuit of technology, catalyst and vertical and horizontal transfer
[AIAA PAPER 71-1008] 24 p3891 A71-44593

PROJECT PLANNING

Canadian program of remote sensing for gathering information on earth resources and environment
16 p2566 A71-33749

PROJECTED AREAS

U AREA

U PROJECTIVE GEOMETRY

PROJECTILE CRATERING

Thin plate impact and plastic nonperforating deformation by blunt projectiles
07 p1209 A71-19045

Spherical head projectiles collision with hemispherical shells and square plates with and without protective covering, calculating stress distribution
12 p1976 A71-27160

Combat aircraft vulnerability to projectile impact predicted by model giving target penetration, damage size and structural response
[AIAA PAPER 71-777] 16 p2660 A71-34013

Microcrater morphology in lunar soil glass, oligoclase and olivine, determining projectile velocity, impact angle and shape effects
18 p2961 A71-35947

Microcrater morphology in soda-lime-silica glass by polystyrene spheres, detailing shape, density, velocity and incidence angle effects
18 p2961 A71-35948

Craters produced by oblique trajectory missile impact, suggesting crater dimension dependence on target material and missile kinetic energy
19 p3156 A71-37683

Double frustum phenomenon in mushrooming of cylindrical Al projectiles upon high speed impact with hardened steel anvil
21 p3474 A71-41424

Craters produced by high speed hardened spherical particles, investigating depth and diameter relationship to impact speed
24 p3885 A71-45324

PROJECTILE PENETRATION

U TERMINAL BALLISTICS

PROJECTILES

NT HYPERVELOCITY PROJECTILES

NT SABOT PROJECTILES

Projectile P band FM/FM telemetry system for in-barrel data acquisition
01 p0034 A71-10912

Projectile velocity measurement by laser and Fabry-Perot interferometer using Doppler effect
02 p0258 A71-11657

Ballistic projectile velocity measurement using condenser charged thin wire circuit
03 p0422 A71-13273

Projectile entry into water vertically from air, predicting cavity shape as function of time based on hydraulic flow model
[ASME PAPER 70-WA/FE-8] 03 p0402 A71-14129

Trajectories prediction for subsonic spin stabilized projectiles via water tunnel tests, considering blunt nose and tail and rounded nose right circular cylinders
[AIAA PAPER 71-296] 08 p1275 A71-22016

Projectiles yawing and rolling over long flight paths, describing onboard solar aspect sensor and telemetry link to ground stations
[AIAA PAPER 70-538] 11 p1761 A71-25513

Hybrid simulation to increase hit possibility of rocket fired from military tanks at moving targets
11 p1735 A71-25848

Roll moment of inertia to static margin ratio effect on yaw of repose angle magnitude in ballistic match of projectiles
14 p2325 A71-29890

Dynamic response and perforation of thin plates subjected to projectile impact, measuring plastic deformation, dynamic strain and displacement with high speed camera
15 p2503 A71-31422

Electronic time delay fuses with high-g components for gun launched projectiles for placing payloads at high altitudes

18 p2851 A71-36281

PROJECTION

Pseudocylindrical, polyconical pseudocylindrical secant and tangential, isoparametric nonorthogonal cartographic projections

03 p0418 A71-14351

Terrain altitude evaluation in orthoprojections, using off-line systems for contour lines approximation

06 p0901 A71-18290

PROJECTIVE DIFFERENTIAL GEOMETRY

U DIFFERENTIAL GEOMETRY

U PROJECTIVE GEOMETRY

PROJECTIVE GEOMETRY

NT MERCATOR PROJECTION

Meteorological uses of stereographic horizon map projection, permitting placement of map center at any point on earth

16 p2564 A71-33538

Linear, affine and projective coordinate transformation from one mapping plane to another with quick maximum error estimation

17 p2734 A71-35187

PROJECTORS

Real time large scale display system with information image projection on reversible photochromic emulsion via IR laser

02 p0249 A71-12072

Flat field condensing system for illuminating film projected on screen using Hg-Xe short arc lamp

18 p2918 A71-36071

High aperture wide angle lens design for compact electro-optical systems of airborne moving map projection navigational instruments

18 p2947 A71-36605

PROJECTS

NT APOLLO PROJECT

NT CENTAUR PROJECT

NT GEMINI PROJECT

NT JUPITER PROJECT

NT MARS 69 PROJECT

NT MARS 71 PROJECT

NT ORBITER PROJECT

NT ROVER PROJECT

NT SATURN PROJECT

NT THEMIS PROJECT

PROLATE SPHEROIDS

Steady incompressible flow past oblate and prolate spheroids for Reynolds numbers up to 100, using spherical coordinates and finite difference method

03 p0400 A71-13729

Microwave biological exposure systems implementation in limited space, describing focused prolate spheroid, absorber-lined horn and compact range illumination system

11 p1723 A71-25288

Elastico-viscous liquid steady secondary flow induced by oblate or prolate spheroid rotating about axis of symmetry from linear partial differential equations solution

20 p3214 A71-39967

PROMETHIUM

Rapid neutron capture products evidence on peculiar A star surfaces from observation of promethium and heaviest elements abundance

24 p3865 A71-44567

PROMINENCES

NT SOLAR PROMINENCES

PROPAGATION

Cosmic ray anisotropy fluctuation and propagation function dimensionality relationship, demonstrating essentially one dimensional propagation

02 p0300 A71-12370

Measuring technique for short term laser beam propagation direction fluctuations, discussing atmospheric turbulence effect on initial modulation phase distribution

11 p1774 A71-26047

Cosmic ray nuclei propagation through interstellar medium, solving transfer equation for simple model with allowance for boundary conditions

16 p2625 A71-33325

PROPAGATION [EXTENSION]

NT CRACK PROPAGATION

NT FLAME PROPAGATION

Chaos propagation derivation from Boltzmann equation for dilute gas with intermolecular forces and collisions in pairs

23 p3705 A71-43873

PROPAGATION MODES

Round dielectric waveguides dominant mode radiation losses calculation

01 p0052 A71-10467

EM wave propagation along radially inhomogeneous dielectric cylinders, considering permittivity variation

01 p0037 A71-11170

Wave dispersion and evanescent modes in rectangular waveguides filled with transversely inhomogeneous dielectric rod

01 p0056 A71-11196

Slow mode shocks in interplanetary space detected by Mariner 5 spacecraft 3.5 and 27 million km from earth

01 p0148 A71-11527

Bounded plasma wave interaction matrix elements calculation from orthogonal system formation by normal waveguide modes

02 p0289 A71-11891

Uniform periodic waveguide mode coupling, obtaining mode transducer design

02 p0216 A71-12342

Cladded fibers propagation modes launching coefficients evaluation by Gaussian field laser beam

03 p0433 A71-13170

Propagation modes and circularly polarized wave production in circular waveguides with anisotropic walls

03 p0384 A71-13317

Collisional effects on Taylor and Kelvin instabilities in composite medium, considering longitudinal wave propagation mode

05 p0788 A71-16627

Supraluminous waves modes in field free two component anisotropic plasma by linearized relativistic Vlasov equation

05 p0791 A71-16939

Multimode power obtainable in TEM in solid laser, using convex mirror and in cavity polarization rotator

06 p0906 A71-17304

Solar particles propagation to earth during solar proton event of 25 February 1969, discussing local interplanetary field

06 p0958 A71-18150

Low energy solar and galactic cosmic ray propagation in interplanetary medium from Zond 3 and Venus 2-4 space probes measurements

06 p0958 A71-18152

Propagation modes involved in HF or VHF reception at ground station of beyond-horizon satellite transmission

07 p1097 A71-19024

Radio wave propagation at frequencies near proton gyrofrequency in horizontally stratified ionosphere, taking into account intermode coupling

07 p1102 A71-19666

Hydromagnetic wave propagation with coupled isotropic and guided modes, obtaining steady state solution with toroidal, plasma resonance induced period dependent reflecting barrier

07 p1197 A71-19767

Single mode oversize optical waveguide fabrication and components

07 p1162 A71-20423

Infinitely long dielectric rod waveguide HE sub 11 surface wave mode launching efficiency, using Fourier integral

08 p1262 A71-20754

Dual channel rotary joint combining Tm and Te modes in circular waveguide for X band antenna high average power operation

08 p1252 A71-20758

LF electrostatic wave axisymmetric and nonaxisymmetric propagation modes in weakly ionized plasma column under weak magnetic field

09 p1504 A71-23051

Magnetoionic theory for drifting plasma whistler mode propagation, deriving magnetic field effects on imaginary and real parts of complex refractivity

09 p1505 A71-23385

Multimode slow wave planar spiral antenna design and radiation field characteristics

09 p1420 A71-23510

VLF electromagnetic propagation, calculating mode conversion efficiency at solar terminator on angle based on flat model with finite wall conductivities

09 p1411 A71-23576

Asymptotic solution for conical horn modes, comparing with exact solution for eigenfunctions and eigenvalues

09 p1420 A71-23677

Phase and frequency instabilities in electromagnetic wave propagation - NATO/AGARD Conference, Ankara, Turkey, October 1967

10 p1576 A71-24185

Wideband gas discharge duplexer as transmitter receiver microwave antenna switch in H₀₁/mode circular waveguide

10 p1584 A71-24720

Coupled vacuum mode equations modified for cylindrical stratification for calculation of propagation characteristics of earth-ionosphere waveguide

11 p1731 A71-25664

Electric and magnetic fields of fundamental modes in cylindrical and rectangular dielectric microwave resonators, classifying transmission lines connections

12 p1888 A71-27613

Hydrodynamic wave modes calculation for solar atmospheric model with ionization effects, noting trapped resonant gravity waves calculation agreement with observed oscillations

12 p1969 A71-27647

Numerical solution of current distribution, wave propagation constant and propagation mode cut-off frequencies on periodic linear array

13 p2028 A71-28001

Circular waveguides containing pure dielectrics, examining propagation mode inversion criteria via TE and TM characteristic equations

13 p2037 A71-28606

Propagation constant relation to frequency for waveguide filled with simple moving medium, presenting dispersion curves set

13 p2030 A71-28607

Self modulation of amplitude modulated electromagnetic wave propagation in magnetoplasmas, considering interaction effects for ordinary and extraordinary propagation modes

13 p2107 A71-28787

Solar flare cosmic ray propagation, investigating bounded interplanetary diffusion medium effects

13 p2130 A71-29060

Simply supported normal mode plate time response to traveling wave at oblique incidence, using numerical analysis

14 p2326 A71-30068

Beamguides with inhomogeneities regulated for constant radiation losses of waves-analogs of modes

14 p2211 A71-30077

Power and focusing requirements in recording and reading with Gaussian laser beam in TEM mode

14 p2254 A71-30136

Dielectric loaded waveguides electromagnetic fields solution by finite element method for cutoff modes determination

14 p2212 A71-30509

Hydromagnetic approximation of ELF propagation modes and emission in magnetosphere, using satellite and ground based observations

14 p2202 A71-30953

Dual plane monopulse multimode radar antenna feeds, determining input geometry relationship to generated modes by image method

14 p2218 A71-31065

Modal interference spacing in frequency range 13.6-22.3 kHz during sunrise transitions on middle latitude east-west propagation paths

15 p2369 A71-31432

Acoustic propagation in rigid wall rectangular duct with uniform flow, calculating higher mode energy transmission properties

15 p2392 A71-32195

Plastic strain range-fatigue life behavior as two slope relationship, considering low cycle fatigue laws in terms of crack propagation mode change

15 p2436 A71-32508

Multimode coaxial feed with circular cross section waveguide and concentric ring shaped radiator for parabolic antennas

16 p2546 A71-33480

Normal angle determination by rocket observations for whistler mode waves propagation through magnetosphere and ionosphere from conjugate VLF ground station signals

16 p2569 A71-33805

Centimeter TEM waves excitation in Fabry-Perot cavity of cyclotron resonance maser by helical electron beam

17 p2750 A71-34263

Mode conversion and auroral effects observations on polar VLF propagation path, noting seasonal and solar cycle variations

17 p2731 A71-34319

TE modes propagation in rectangular guide partially filled with dielectric slab, considering two waveguides junction equivalent circuit

17 p2708 A71-35481

Bernstein mode wave instability growth rate in collisionless shocks propagating perpendicular to magnetic field, including pressure gradient effects

18 p2950 A71-35928

Decay instability at ion-sound frequency induced by large amplitude Bernstein mode wave in plasma

18 p2951 A71-35929

Optical coupling of degenerative modes in two parallel dielectric waveguides, applying to slab guides and fibers crosstalk problem

19 p3014 A71-37214

Geomagnetic micropulsation periods variation with latitude and plasmapause presence, calculating uncoupled toroidal and poloidal modes eigenperiods of hydromagnetic waves

20 p3215 A71-38735

Laser beam spatial coherence properties dependence on transverse mode structure for given longitudinal mode

20 p3245 A71-39350

Acoustic signal pressure mode propagation velocity in infinite rectangular hard-walled duct with steady flow, noting Doppler effect

20 p3271 A71-39765

Dispersion equation determining periodic structures natural modes propagation constants, using induced electromotive and magnetomotive forces method

20 p3198 A71-39806

Pulsed ruby laser transmission and reflection holography in single transverse and axial electromagnetic mode, stressing safety aspects

22 p3556 A71-41743

- LF waves and instabilities on positive column in magnetic field, comparing three theories for helical modes for He at low pressures 22 p3582 A71-41897
- Electromagnetic wave propagation and radiation pattern of circular corrugated waveguide antenna feeds, considering unity azimuthally dependent modes 22 p3511 A71-42278
- Field configuration of TM mode in elliptical waveguide, showing inaccuracy of microwave theory 22 p3522 A71-42279
- Ionspheric HF wave ordinary (O) and extraordinary (E) modes coupling effect on satellite signal Faraday rotation 23 p3642 A71-42964
- Ionspheric propagation penetrating and nonpenetrating modes full wave reflection and transmission coefficients determination for height and frequency variation by thin film optical method 23 p3643 A71-42972
- Low latitude whistler propagation characteristics associated with magnetic storms in March 1970 at Sugadaira (Japan) 23 p3644 A71-43364
- Low loss microwave iris-loaded circular TE mode waveguide delay line for pulse compression at X band 23 p3653 A71-43963
- Critical frequencies of higher order modes in circular waveguides with arbitrary thick dielectric sleeve 23 p3647 A71-44319
- Open waveguide field expansion in orthogonal wave system with proper and improper modes 23 p3647 A71-44332
- Spectral representation and propagation mode of microwave transmission line on circular waveguides at great distance 24 p3803 A71-44361
- High order transverse cavity mode selection and propagation in homojunction and heterojunction GaAs injection lasers, using five layer dielectric model 24 p3832 A71-44432
- Spinning acoustic modes transmission and backscatter in nonuniform long cylindrical ducts with throat 24 p3848 A71-44556
- VLF day and night waveguide modes attenuation coefficients and phase velocities, using moving secondary source formed by mode conversion at sunrise and sunset shadow line 24 p3803 A71-44650
- Microstrip line on silicon-silicon oxide system, investigating propagation modes and fringing effect by parallel-plate waveguide model 24 p3809 A71-45091
- PROPAGATION VELOCITY**
- Mathematical model for laser-induced supersonic crack propagation in crystals with weak cleavage planes 01 p0092 A71-10293
- Detonation propagation velocity through tubes with walls coated with thin fuel film, using turbulent boundary layer theory 01 p0181 A71-11305
- Oxygen and homologous hydrocarbon mixtures detonation limits, discussing propagation, fuel molecule structure, critical temperature, initial cracking mechanism and carbonaceous solids condensation 02 p0331 A71-11957
- Transient creep propagation velocity in dead annealed thin walled Al alloy tubes, using constitutive equation for mean stress-strain-time relationship 03 p0508 A71-13761
- Gaseous explosives free detonation waves for hydrogen-oxygen, noting propagation velocity deficit and detonability limit 05 p0834 A71-16512
- Gaseous mixtures turbulent combustion, considering turbulent flame propagation velocity 05 p0836 A71-16536
- Brittle fracture propagation velocity and branching, using high speed photography, electrical and ultrasonic methods 06 p0981 A71-17296
- Rocket engines with nitrogen tetroxide/hydrazine injectors destructive instability due to pressure disturbances, establishing origin, propagation velocity and pops extent by streak photography [WSS/CI PAPER 70-25] 06 p0942 A71-17653
- Time estimation for plasma front propagation in quartz glass circular pipes without imposition of axial magnetic field 08 p1338 A71-20829
- Elastic waves in isotropic body, calculating initial deformation effect on propagation rate based on finite deformation theory 09 p1537 A71-22515
- Ultrasound propagation velocity dependence on high pressure and temperature in carbon dioxide, considering Rao rule applicability to highly compressed gases 09 p1492 A71-22529
- Fatigue crack propagation rate in sheet alloys with holes as stress concentrators related to duration of various development phases 09 p1538 A71-22597
- Reflected radiative shock wave propagation velocity under transverse magnetic field, taking into account radiation pressure and energy 09 p1506 A71-23588
- Age, obliterating arteriopathy and peripheral arterial sclerosis effects on rheographic wave propagation speed to lower limbs 10 p1566 A71-24976
- Lower earth mantle shear velocity models derivation and core radius estimation based on S travel times observation 11 p1760 A71-26060
- Rayleigh wave propagation along edge of thin plate, calculating velocity dependence on frequency 12 p1929 A71-26929
- Surface wave velocity at interface between liquid He 4 and saturated vapor 13 p2101 A71-28769
- Laminar flame speeds in chlorine-fluorine mixtures, predicting low temperature isothermal rates and spontaneous ignition limits 15 p2465 A71-32090
- Tunguska explosion of 30 June 1908, determining air waves propagation velocity 16 p2639 A71-33696
- Initial strains effect on propagation rate of elastic waves, applying finite deformation theory 16 p2658 A71-33902
- Stress wave propagation in quartz-phenolic composite, measuring particle velocity by velocity interferometer 17 p2762 A71-35207
- Ultrasound propagation velocity dependence on high pressure and temperature in carbon dioxide, considering Rao rule applicability to highly compressed gases 17 p2784 A71-35506
- Finiteness of deformations and convective terms effect on medium velocity in terms of displacements on shock wave propagation in three dimensional elastic medium 18 p2982 A71-36788
- Seismic wave velocity measurements in pahoehoe basal flows in lava beds, comparing with laboratory dilatational velocities 19 p3052 A71-37685
- Detonation propagation through tubes with thin fuel film coated walls, obtaining heat transfer coefficients, friction, evaporation rate, reaction zone length and propagation velocity 19 p3171 A71-38129
- Intense relativistic electron beam propagation in drift tube with neutral gas and plasma background, determining front velocity and energy transport 20 p3272 A71-38784
- Acoustic signal pressure mode propagation velocity in infinite rectangular hard-walled duct with steady flow, noting Doppler effect 20 p3271 A71-39765
- Weak discontinuities propagation speeds, equations and eigenvectors in uniform collisionless plasma 21 p3421 A71-40209
- Quantitative schlieren system for shock wave velocity, density ratio and relaxation time measurements, discussing electro-optical modification and calibration technique 21 p3364 A71-40404
- High performance electric arc driven shock tube for shock velocities to 45 km/sec and test times over 4 microseconds, using 80/20 helium-hydrogen mixture 21 p3365 A71-40975
- Ultrasonic time shadow method based on defect detection by sharpness of vibration propagation time change during scanning 22 p3528 A71-41758
- Steady laminar flame propagation speed prediction computation, applying to hydrazine decomposition 22 p3621 A71-42098
- Flexural wave propagation in thin curved rod oscillating in plane, calculating frequency and velocity from boundary conditions according to Saint Venant 22 p3617 A71-42574
- Crack model with strain rate dependent yield stress, calculating stress intensity factor variation with fracture propagation velocity 23 p3774 A71-43145
- Frequency dependence of Rayleigh wave propagation velocity along rough surfaces, based on smooth surface mass loading 23 p3703 A71-43203
- Elastic wave velocities in Apollo 12 rocks 12052 and 12065 at high pressures, noting basalt-like composition and crystal structure 23 p3761 A71-43783
- Elastic surface wave amplitude and propagation velocity in lunar rocks, calculating Poisson ratio 23 p3761 A71-43784
- One dimensional diffusion model for on state propagation along p-n-p-n structure, determining propagation velocity as function of structural parameters and current density 24 p3859 A71-44462
- Crack propagation kinetics in organic glass subjected to monotonically increasing tension perpendicular to crack plane, examining crack contour prior to spontaneous rupture 24 p3883 A71-44858
- PROPAGATORS**
- U PROPAGATION**
- PROPANE**
- Post reaction zone properties of premixed fuel rich propane-oxygen flames on torch, measuring temperature, composition and hydroxyl radicals 08 p1345 A71-20858
- Multiple port baffles tests using stoichiometric propane-air mixtures 13 p2116 A71-28746
- Spacecraft propane boiler system, obtaining heat transfer behavior under simulated aerospace conditions 14 p2319 A71-29726
- Esters synthesis from cyclic trimethylolpropane butyral and monobasic saturated acids mixtures 15 p2438 A71-31679
- Hydrogen bromide effect on argon diluted propane-oxygen flame structure 19 p3167 A71-38100
- Buoyant centrifugal force effect on combustion of homogeneous propane-air mixtures at stoichiometric proportions, using steel pipe as centrifuge 19 p3167 A71-38101
- PROPELLANT ADDITIVES**
- NT PROPELLANT BINDERS**
- Aluminum addition effect on combustion rate of mixtures of ammonium perchlorate with polymethyl methacrylate at different temperatures 03 p0520 A71-13995
- Hydrocarbon fuel ignitability, investigating molecular structural characteristics and homogeneous additives effect [WSS/CI PAPER 70-19] 06 p0943 A71-17661
- Monopropellant hydrazine propulsion catalysts evaluation, considering catalyst durability improvement and breakup 07 p1183 A71-19858
- Ballistic modification of nitric ester based propellant combustion by lead compounds, concerning burning rate-pressure relation 08 p1346 A71-20860
- High density nitric acid oxidizer and unsymmetrical dimethyl hydrazine with silicone fluid additive application to Agena rocket engine for higher performance [AIAA PAPER 71-736] 14 p2287 A71-30781
- Hydrazine-hydrazine azide blending for propellant performance improvement and freezing point reduction, presenting engine test data 22 p3588 A71-42778
- PROPELLANT BINDERS**
- Composite solid propellant binders thermal decomposition investigation by differential scanning calorimetry method, discussing kinetic data relevance to solid propellant combustion 10 p1657 A71-24046
- Low modulus solid propellants family for low thrust-to-mass ratio fully case bonded end-burning motors, using polymer network theory for binder formulation [AIAA PAPER 71-654] 14 p2285 A71-30729
- Solid propellants based on low cost hydroxyl terminated polybutadiene binders meeting burning rate, mechanical properties and processing requirements for large booster motors [AIAA PAPER 71-708] 14 p2286 A71-30764
- Ammonium perchlorate based solid propellants combustion, assuming pyrolysis of solid binder 17 p2792 A71-35549
- PROPELLANT CHEMISTRY**
- Bora-Sond rocket for upper atmosphere low cost sounding, describing propulsion system design and chemistry [AIAA PAPER 70-1388] 05 p0816 A71-16417
- PROPELLANT COMBUSTION**
- NT SOLID PROPELLANT IGNITION**
- Gas dynamics of fuel boundary layer combustion and surface pyrolysis in hybrid rocket motors 01 p0178 A71-10131
- Bipropellant droplet supercritical steady combustion temperature measurements in zero gravity near critical point, comparing high and low pressures models for ambient gas solubility 01 p0141 A71-11309
- Erosive burning resulting from nonplanar surface structure of solid propellant 02 p0334 A71-12858
- Propellant low temperature preignition reactions during simulated engine shutdown conditions, discussing IR spectroscopic observation method 02 p0298 A71-12861
- AP composite solid propellant combustion model based on multiple flame structure surrounding individual oxidizer crystals 03 p0469 A71-13440

Pressure effect on combustion rate of model mixtures of ammonium perchlorate with polystyrene and polymethyl methacrylate 03 p0468 A71-13989

Rocket propellants and gun powders performance calculation, using FORTRAN IV program 04 p0637 A71-15678

Tubular powder channel gas velocity distribution and pressure buildup during burning 04 p0638 A71-15680

Gas dynamic analysis of hybrid boundary layer combustion with nonequilibrium surface pyrolysis, using Rayleigh analogy 05 p0837 A71-16539

Transient response of solid propellant combustion to pressure variations and sudden depressurization 05 p0795 A71-16540

Stability criteria for longitudinal combustion instability tested for generality using data from various solid propellant formulations [AIAA PAPER 69-480] 05 p0837 A71-16569

Gas phase reactions near solid-gas interface of deflagrating double base propellant causing abrupt changes in burning rate-pressure curve [AIAA PAPER 70-124] 05 p0837 A71-16571

One dimensional kinetic calculations for hydrogen fluorine rocket nozzles compared to firing data, discussing Cl addition effect on performance [WSS/CI PAPER 70-21] 06 p0943 A71-17656

Liquid hypergolic propellants heat and gas release determination by calorimetric and PVT measurements, using impinging free jets for propellant mixing [WSS/CI PAPER 70-26] 06 p0943 A71-17658
Cellulose, explosives and propellants thermal surface ignition, using heat transport and chemical kinetic equations 06 p0944 A71-18298

Composite propellant transient burning rates continuous measurement during rapid depressurization [AIAA PAPER 71-173] 06 p0944 A71-18612

Electric field effects on burning rates of composite metallized solid propellant containing ammonium perchlorate [AIAA PAPER 71-174] 06 p0947 A71-18613

Solid propellant combustion instability, considering burning propellant mass flux response to periodic thermal radiation [AIAA PAPER 71-209] 06 p0948 A71-18645

Reaction heat for flameless combustion of double-base propellant using differential scanning calorimetry and thermogravimetric analysis, noting pressure effects [AIAA PAPER 70-125] 07 p1183 A71-19898

Ballistic modification of nitric ester based propellant combustion by lead compounds, concerning burning rate-pressure relation 08 p1346 A71-20860

Flame structure in laminar condensed systems, noting burning rate dependence on pressure and specimen layer thickness, composition and mechanical condition 08 p1376 A71-21906

Solid propellant instantaneous burning rates prediction methods based on flame structure model and steady state burning data as functions of pressure and initial temperature [AIAA PAPER 70-667] 09 p1510 A71-22905

Burning rate temperature sensitivity of composite solid propellants, using granular diffusion flame model 09 p1510 A71-22911

Combustion rate of pure ammonium perchlorate propellants derived from ablation theory 10 p1657 A71-23905

Pressure vessel method improvement by electronic equipment application in determining data characteristics for propellant powders ballistic properties 10 p1696 A71-24447

Erosive burning of composite propellants based on ammonium perchlorate, studying oxidizer grain size effect 10 p1658 A71-25122

Compositional and oxidizer particle size effects on combustion instability of plastic propellant based on ammonium perchlorate and polyisobutene [AIAA PAPER 69-478] 11 p1809 A71-25454

Ammonium perchlorate deflagrations, determining intrinsic stability of one dimensional burning configuration based on flame structure modeling [AIAA PAPER 70-123] 11 p1809 A71-25455

Photographic study of burning metallized composite propellant, noting burning rate augmentation by heat transfer from alumina particles retained on propellant surface [AIAA PAPER 69-173] 11 p1809 A71-25502

Regeneratively cooled stainless steel thrust chamber failure related to internal carburization by fuel decomposition and propellant combustion 11 p1810 A71-25505

Aircraft fuel tank nitrogen inerting, fire and explosion suppression for foreign particle contamination, sludge and lacquer reduction [ASME PAPER 71-GT-45] 11 p1810 A71-25978

Solid propellant burning surface irradiance measurement, using optical lightpipe and radiation detector [AIAA PAPER 71-469] 11 p1859 A71-26250

Phenol furfuraldehyde-ammonium perchlorate solid propellant combustion, investigating burning rate 12 p1944 A71-26742

Combustion chamber design with flame stabilizers, deriving gas flow, energy conservation equations and propellant combustion rates 13 p2163 A71-28967

Continuous burning rate measurement for metallized composite solid propellants, using optical sensor for servo tracking propellant surface 14 p2244 A71-30328

Throttleable bipropellant rocket engine, discussing cryogenic and space storable propellants and injection system optimization based on combustion mechanism photographic observation [AIAA PAPER 71-740] 14 p2296 A71-30783

Combustion instability with wave motion coupling in solid propellant rocket motors due to energy gain and loss mechanisms within chamber [AIAA PAPER 71-753] 14 p2296 A71-30787

Minuteman 2 third stage rocket engine instrumentation performance evaluation for oscillatory combustion characteristics analysis [AIAA PAPER 71-755] 14 p2248 A71-30789

Missile component vibration environments generation by Minuteman 2 and 3 third stage motors solid propellant oscillatory burning [AIAA PAPER 71-756] 14 p2296 A71-30790

Acoustic liner design for propellant combustion instability and jet aircraft noise suppression, discussing cross flow and oscillatory pressure effects [AIAA PAPER 71-757] 14 p2296 A71-30791

Surface temperature discrepancy during flameless vacuum burning of trinitroglycerin gunpowder due to vaporization of volatile components 15 p2462 A71-31373

Gunpowder mean burning rate at constant pressure with periodic variation of heat influx into flame zone 15 p2462 A71-31374

Gunpowder unsteady burning as closed dynamic system, studying frequency characteristics and transient processes 15 p2462 A71-31375

Inflammability, burning rates and exothermal decomposition of compact hydroxylamine and hydrazine sulfate and chloride with/without copper chloride additions, plotting pressure variations curves 15 p2463 A71-31377

Burning gunpowder temperature measurement in gaseous phase, describing thermocouple method 15 p2463 A71-31388

Al particles combustion kinetics in propellant flames, showing gas composition and pressure effects on burning rate [WSS/CI PAPER 71-24] 15 p2464 A71-31633

Solid propellants extinguishment by depressurization, using transient flame model [AIAA PAPER 71-631] 15 p2466 A71-32283

Acoustic damping of small amplitude waves by non-burning particles in T burners and rocket motors, noting propellant seeding with zirconium oxide [AIAA PAPER 71-633] 15 p2471 A71-32574

Catalytic role in ammonium perchlorate solid rocket propellants ignition and combustion 17 p2792 A71-34434

Ammonium perchlorate based solid propellants combustion, assuming pyrolysis of solid binder 17 p2792 A71-35549

Solid propellant combustion pressure oscillations amplification, developing mathematical model as function of reaction rate constant, chamber pressure, frequency and solid properties 19 p3123 A71-38096

Deflagration behavior of pure and isomorphously doped ammonium perchlorate, using cinephotomicrography of burning samples and scanning electron microscopy of quenched samples 19 p3120 A71-38118

Perchloric acid catalytic pyrolysis relationship to ammonium perchlorate decomposition and combustion from electric conductivity measurements, IR spectroscopy, chemical and thermal analysis 19 p3120 A71-38119

Photographic study of acceleration and pressure effects on Al agglomerates and combustion processes on solid propellant surface, describing pit growth by combustion model 19 p3120 A71-38121

Combustion model of solid composite propellants containing monopropellant oxidizers ammonium perchlorate, cyclotetramethylene-tetranitramine and potassium perchlorate 19 p3121 A71-38122

Burn time and acceleration effects on molten metallic material chemical composition near burning surface of aluminized composite solid propellant 19 p3121 A71-38298

Acceleration dependent burning rate increases of aluminized composite solid propellants induced by combined erosive and acceleration 21 p3436 A71-40943

Q-switched ruby laser holographic interferometry for hypergolic flame combustion recording 22 p3539 A71-41742

Small hybrid rocket engine using aromatic amines mixture as fuel and nitric acid as oxidizer, discussing regression rate relations and internal ballistics design 22 p3589 A71-42019

Hybrid rocket /Barbarella I/ design, tests, engine, feed system oxidizer tank, fairings fins, propellants and launch facilities 22 p3589 A71-42049

Shock wave initiation of hydrogen-oxygen at 1200-1800 K, using UV absorption spectroscopy in shock tube studies 22 p3587 A71-42097

Solid propellant combustion simplified laminar flame theory, calculating pressure effect on burning rate, surface energy loss and temperature effects 24 p3888 A71-44938

PROPELLANT DECOMPOSITION

High temperature decomposition kinetics in vacuum of mixed ammonium perchlorate-polystyrene solid fuel, using time of flight mass spectrometer 03 p0469 A71-13997

Mass spectrometric technique for investigation of hydrazine catalytic decomposition on heated platinum at low pressure, considering advantages of quadrupole spectrometer 11 p1765 A71-26280

Thermal decomposition rates and explosion of dinitroxydiethyl nitramine from heat release measurements at various pressures 15 p2462 A71-31376

Inflammability, burning rates and exothermal decomposition of compact hydroxylamine and hydrazine sulfate and chloride with/without copper chloride additions, plotting pressure variations curves 15 p2463 A71-31377

Low temperature condensed phase ammonium perchlorate decomposition effects on ballistic and postheat sterilization properties of CTPB propellant [AIAA PAPER 71-717] 15 p2465 A71-32282

Radiation induced etch-pit dislocations and thermal decomposition kinetics in ammonium perchlorate crystals 18 p2955 A71-35967

Perchloric acid catalytic pyrolysis relationship to ammonium perchlorate decomposition and combustion from electric conductivity measurements, IR spectroscopy, chemical and thermal analysis 19 p3120 A71-38119

Exothermic decomposition reaction and sublimation mechanism of ammonium perchlorate burning, showing pressure dependence of burning rate 22 p3587 A71-42100

Carbonyl fluoride thermal decomposition in excess Ar behind incident and reflected shock waves, analyzing reaction rate variation with temperature and total pressure 24 p3802 A71-44941

PROPELLANT EVAPORATION

Liquid fuel droplet transient evaporation in high temperature environment, examining vaporization process with coupled heat and mass transfer [AIAA PAPER 71-126] 06 p1008 A71-18570

Fuel evaporation in combustion chambers L-shaped and annular vaporizers, determining operational parameters effect on evaporation ratio 10 p1658 A71-25123

Surface temperature discrepancy during flameless vacuum burning of trinitroglycerin gunpowder due to vaporization of volatile components 15 p2462 A71-31373

Individual liquid fuel droplets ignition factors, introducing heating-up and evaporation delay 15 p2516 A71-32709

PROPELLANT GRAINS

Nonlinear elastic effect on stress concentration of incased tubular solid propellant grain 03 p0504 A71-13462

Burning rate manual determination for solid propellant rocket motors with sliverless grains 03 p0522 A71-14451

Pressure-temperature equivalences in elasticity problems, considering applications to case bonded solid propellant rocket grains 04 p0638 A71-15197

Stress concentration at interface between bonding agent and fuel element in solid propellant grain 05 p0000 A71-15981

Accelerating flame front generation and propagation controlling mechanism in porous propellant [AIAA PAPER 71-210] 06 p0948 A71-18646

Erosive burning of composite propellants based on ammonium perchlorate, studying oxidizer grain size effect 10 p1658 A71-25122

PROPELLANT OXIDIZERS

U ROCKET OXIDIZERS

PROPELLANT PROPERTIES

Book on aviation fuels covering gasoline and turbine fuel properties, handling problems and future fuels 03 p0469 A71-14298

Liquid rocket propellants characteristics study for explosive yield prediction, using mathematical model and critical mass method

- 04 p0637 A71-15345
- Solid composite propellant mixing influence on viscosity, pot life and motor reject rates based on bench scale production [AICHE PAPER 32D] 13 p2113 A71-28894
- Low modulus solid propellants family for low thrust-to-mass ratio fully case bonded end-burning motors, using polymer network theory for binder formulation [AIAA PAPER 71-654] 14 p2285 A71-30729
- Low temperature condensed phase ammonium perchlorate decomposition effects on ballistic and postheat sterilization properties of CTPB propellant [AIAA PAPER 71-717] 15 p2465 A71-32282
- Hydrazine-hydrazine azide blending for propellant performance improvement and freezing point reduction, presenting engine test data 22 p3588 A71-42778

PROPELLANT SPRAYS

- Liquid fuel droplets in heterogeneous detonation of dilute sprays, noting deformation and fragmentation in reaction zone 07 p1222 A71-19189
- Rocket engine propellant injectors with noncircular orifice geometry, presenting experimental spray patterns and predicted performance for noncircular and circular orifice configurations 11 p1810 A71-25520
- Gas turbine engine combustion chamber start-up and burning performance, considering air injection and propellant atomization 13 p2117 A71-28968
- Gas turbine engine startup igniter with modified propellant atomizer enhanced by air injection 13 p2118 A71-28969
- Cold flow analysis of liquid propellant sprays from rocket engine injectors, relating propellant mixing and combustion performance 15 p2465 A71-32044

PROPELLANT STORAGE

- Piston expulsion seals for storable fueled and ready liquid rockets 06 p0905 A71-18218
- Jet fuels thermal stability and corrosive properties during prolonged storage 07 p1182 A71-19492
- Combustion research laboratory at Purdue University consisting of buildings, housing test cells, data acquisition system, propellant storage and instrument service area 09 p1427 A71-22727
- Superinsulation for long term storage of cryogenic propellants in space tanks using double aluminized Mylar with Dacron needles 09 p1546 A71-23009
- Mixed ullage heating, convection and conduction models of thermal stratification of cryogenic propellants stored in low gravity environment 11 p1810 A71-26507
- Launch facility requirements for liquid fluorine upper stage, considering propellant storage and transfer, vapor disposal, leak detection, spills, aborts and range safety 18 p2898 A71-36457
- Capacitance measurement technique for density and mass flow measurements for hydrogen slush storage and transfer 20 p3237 A71-39276

PROPELLANT TANKS

- Thermodynamic similarity laws for rocket fuel tanks with cryogenic propellants, using dimensional analysis for unsteady temperature distributions 02 p0332 A71-12526
- Spacecraft propellant tank development from Al alloy providing excellent weldability, propellant compatibility and strength to weight ratio 07 p1116 A71-18899
- Structural materials criteria for cryogenic propellant tanks, discussing chosen alloy composition, heat treatment and general properties 07 p1118 A71-19802
- Computerized sloshing frequencies of tilting two dimensional tank of flat free surfaces with respect to effective gravity 11 p1752 A71-26198
- LF vibration qualification tests for Mariner Mars 1971 propellant tanks 11 p1746 A71-26494
- Cryogenic propellant tank thermal insulation system based on polypropylene oxide, polyurethane polyvinylchloride and polymethacrylimide foams, discussing design, technology and model tests 12 p1985 A71-26834
- Rotational stability of spin stabilized satellite with liquid filled propellant tanks, investigating viscous effects on motion coupling between rigid body and liquid 15 p2499 A71-31175
- Liquid hydrogen rocket propellant tanks insulation problems in space shuttle and orbiter 15 p2499 A71-31216

- Reusable space shuttle optimization, discussing earth-to-orbit transportation, economic aspects, booster vehicles design, propellant cryogenic tanks and thermal protection [AIAA PAPER 71-805] 17 p2814 A71-35430
- Saturn S-4B continuous vent system for propellant tanks during parking orbit to prevent excessive pressure, requiring liquid settling with auxiliary ullaging rockets 18 p2973 A71-36453
- Zero-g propellant tank quantity gaging methods, suggesting large cryogenic propellant tanks for space shuttle orbiter stage 18 p2922 A71-36455

PROPELLANT TESTS

- Combustion instability data with same solid propellants by T-burner and L super asterisk burner, discussing theoretical models of transient combustion 05 p0837 A71-16570
- Replica technique facilitating investigation of quenched solid propellant sandwich sample characteristics 08 p1271 A71-20868
- Pressure vessel method improvement by electronic equipment application in determining data characteristics for propellant powders ballistic properties 10 p1696 A71-24447
- Pulsed T-burner testing of oscillatory combustion and droplet damping of aluminized solid propellants as function of frequency and sample properties [AIAA PAPER 71-634] 14 p2289 A71-30713
- Comparative variable area, pulsed and modified T burners for testing oscillatory combustion and stability of propellants containing aluminum [AIAA PAPER 71-635] 14 p2289 A71-30714
- Low flame temperature propellants, investigating temperature and humidity aging effects on physical and ballistic properties [AIAA PAPER 71-664] 14 p2286 A71-30732
- Ignition and combustion tests of storable boron/magnesium/hexane slurry injected directly in high speed air stream [AIAA PAPER 71-723] 14 p2286 A71-30773

PROPELLANT TRANSFER

- Saturn 5 S-2 stage propellant feedlines and V-2 engines simulating structural longitudinal oscillation by analog computer [AIAA PAPER 70-626] 03 p0472 A71-14430
- Spacecraft propellant expulsion systems, comparing capillary with conventional techniques [AIAA PAPER 70-685] 07 p1183 A71-19856
- Hydrogen slush storage and transfer density and flow measuring instrumentation, emphasizing capacitance measurement [NAS PAPER M-2] 08 p1292 A71-21695
- Soviet book on liquid propellant rocket engines non-stationary operation covering dynamic processes, transient conditions, component elements, fuel delivery, etc 10 p1659 A71-24649
- Space shuttle operation phases hazards, emphasizing propellant loading, fire suppression systems, survival equipment and self contained life support devices 17 p2813 A71-34784
- Centaur/shuttle integration and operations, considering ground tanking modes and in-flight propellant transfer 18 p2973 A71-36477
- Capacitance measurement technique for density and mass flow measurements for hydrogen slush storage and transfer 20 p3237 A71-39276

PROPELLANTS

- NT CASE BONDED PROPELLANTS
- NT COLLOIDAL PROPELLANTS
- NT COMPOSITE PROPELLANTS
- NT CRYOGENIC ROCKET PROPELLANTS
- NT DOUBLE BASE PROPELLANTS
- NT GASEOUS ROCKET PROPELLANTS
- NT GUN PROPELLANTS
- NT HIGH ENERGY PROPELLANTS
- NT HYBRID PROPELLANTS
- NT HYDRAZINE NITROFORM
- NT HYPERGOLIC ROCKET PROPELLANTS
- NT LIQUID ROCKET PROPELLANTS
- NT METAL PROPELLANTS
- NT MONOPROPELLANTS
- NT PLASTIC PROPELLANTS
- NT ROCKET PROPELLANTS
- NT SLURRY PROPELLANTS
- NT SOLID PROPELLANTS
- NT SOLID ROCKET PROPELLANTS
- German monograph on high energy propellant-oxidizer systems changes of state under high temperature conditions with chemical relaxation taken into account 05 p0795 A71-17106

PROPELLER BLADES

- Density gradient visualization with schlieren optical system, discussing propeller aerodynamics 10 p1616 A71-24103
- Propeller blade profile thickness distribution for given pressure distribution, deriving integral equation

- with singular kernel function via source-sink and vorticity distribution linearized theory 10 p1553 A71-24945
- Aerodynamic design of VTOL propellers, demonstrating possibility of cyclic control of XC-142 experimental propeller [DGLR-71-017] 15 p2347 A71-32784
- Propeller blade structures for high speed tilt wing turboprop V-STOL aircraft, considering materials selection, weight control, cyclic pitch control, noise reduction, etc [DGLR-71-018] 15 p2350 A71-32785
- Dirichlet problem in hodograph plane of compressible fluid flow from aircraft, helicopter blades or turbine blade airfoils 17 p2672 A71-35470

PROPELLER DRIVE

NT HELICOPTER PROPELLER DRIVE

PROPELLER EFFICIENCY

- Propeller driven VTOL aircraft performance improvement, comparing variable camber/diameter counterrotating and blowing device equipped propellers [DGLR-71-023] 15 p2350 A71-32786

PROPELLER FANS

- Prop-fan propulsion system for V-STOL short haul transport aircraft, discussing performance, noise and weight characteristics [SAE PAPER 710470] 13 p2115 A71-28338
- Noise research facility for fan and multistage compressor sound radiation, discussing anechoic chamber, power drive, test control, recording and real time analysis system 16 p2553 A71-33418

PROPELLER SLIPSTREAMS

- VTOL aircraft wing-propeller interaction, using mean flow deflection angle in lift and drag characteristics prediction 04 p0526 A71-14988
- Aerodynamics of wing immersed in propeller slipstreams, presenting calculation method for lift, drag, pitching moment, normal force distribution and wake characteristics [DGLR-70-057] 05 p0693 A71-15947
- Wing flap slipstream deflection correction method for evaluation of propeller power effect on lift and drag coefficients of Arava twin engine STOL aircraft 11 p1706 A71-25164
- Propeller vortex theory, calculating vortex streets pitch distributions and wake configuration 14 p2170 A71-30443
- Interference analysis of wing with overlapping multipropellers in uniform velocity stream confined in elliptical cross section cylinder [AIAA PAPER 71-614] 15 p2346 A71-31583

PROPELLER SYNCHRONIZERS

U PROPELLERS

U SYNCHRONIZERS

PROPELLERS

- NT PROPELLER FANS
- NT SHROUDED PROPELLERS
- NT TILTED PROPELLERS
- Soviet book on aircraft power plant systems and devices covering layout, engine attachment, propellers, control, fuel and oil systems, fire fighting, monitoring, etc 02 p0299 A71-12722
- Experimental arrangement for delay times in propeller/rpm controller system 08 p1271 A71-20832
- Biological oscillating propulsion systems, investigating plate propeller, boundary layer control, low drag fuselage shapes and VTOL engine installations 10 p1569 A71-24235
- Low disk-loading propotor application to propeller and fanjet STOL and fanjet VTOL short haul aircraft [AIAA PAPER 71-781] 17 p2674 A71-34481
- Propeller vortex noise analysis by on-line 1/3 octave band resolution, discussing characteristic results from noise measurements on various propeller configurations 21 p3325 A71-40868

PROPHYLAXIS

- Natural or endogenous fibrinolysis and its pharmacological enhancement as possible approach to prophylaxis of vascular occlusions 02 p0200 A71-12417
- Prophylactic radiation protection through lipid toxicants reduction in white rats tissues by high efficiency chemical radioprotectors 06 p0849 A71-17391
- Radiation sickness prophylaxis chemical compounds, discussing protection mechanisms, radical inactivation and afflicted cell recovery 22 p3505 A71-42710
- Prophylactic medication for radiation damage treatment, covering toxicity, pharmacological properties, metabolism, dosage and physiological action 22 p3505 A71-42711

PROPORTIONAL CONTROL

- Automatic temperature monitor and proportional solid state DC controller for electrophysiological use 01 p0022 A71-10247

Proportional fluidic elements jet nozzle discharge coefficients as function of control pressure and geometrical parameters

03 p0354 A71-13959

High gain proportional fluid amplifier, examining defined region geometry with flow visualization and quantitative data

[ASME PAPER 70-WA/FLCS-12]

03 p0354 A71-14087

Proportional navigation vs optimally evasive constant speed target in two dimensions, considering lateral acceleration and time constraints in pursuer control

03 p0455 A71-14438

Eigen proportional control method for second order system with time varying parameters, applying to aircraft autopilot systems

06 p0925 A71-18308

Large model fluid proportional amplifier, investigating optimum static and dynamic pressure gain by methodological and transmission line approach

07 p1025 A71-20558

Fluidic proportional amplifier circuit with two bistable element stages, using pulse width modulation techniques

07 p1027 A71-20579

Pressure regulator design and construction, using high pressure fluidic proportional chain

07 p1027 A71-20580

Liquid fuel atomization spectrum in nozzles, examining proportion control of droplet size

08 p1348 A71-21262

Proportional fluidic element static characteristics, calculating main jet interaction with control jet

09 p1386 A71-22655

Quasi-optimal proportional navigation, deriving feedback guidance laws for interceptor aerodynamically controlled missiles

11 p1796 A71-26409

Structural stability for two beam plasma model with proportional controller using distributed feedback

15 p2456 A71-31846

Proportional fluid amplifier, measuring deflection angle, jet turbulence and noise level

15 p2390 A71-32052

Facility for signal noise measurement in proportional fluidic amplifiers, discussing stored sweep spectra interpretation

15 p2351 A71-32053

Transistorized analog multiplication circuit for automatic control system requiring controller input proportional to product of two values

17 p2719 A71-34787

Modal control for linear multivariable time-invariant systems incorporating multiloop single input proportional controllers

18 p2896 A71-36235

Proportional navigation for trajectory control of missile homing on target in planar pursuit

20 p3261 A71-38856

Active digital and proportional fluidic devices design and manufacture including turbulence, wall-attachment, focused jet, beam deflection and vortex amplifiers

22 p3483 A71-42783

PROPORTIONAL COUNTERS

Low energy particle variable flux measurement in midlatitude ionosphere, using rocket-borne thin window proportional counters

03 p0421 A71-14539

Gas proportional counting system gain stabilization, using feedback loop radioactive X ray emitter and correction signal

06 p0901 A71-18225

X ray source in Perseus region, studying Aerobee rocket proportional counters measurements

09 p1512 A71-22348

Versatile pulse amplifier for use with scintillation counters, surface barrier detectors, proportional counters or channel electron multipliers

13 p2067 A71-28163

Cosmic X ray background observations, using rocket-borne proportional counter

13 p2131 A71-29269

Proportional counters design for ionizing radiation detection, examining cosmic ray meson component

15 p2408 A71-31814

Liquid Xe filled single wire proportional and multiple wire ionization chambers, measuring gain and time/spatial resolution properties

19 p3065 A71-38178

Laser beam ionization of gold investigated by proportional electron counter

21 p3392 A71-40516

Cosmic soft X rays in energy range 0.14-7 keV from rocket soundings with thin polypropylene window proportional counters, covering field of view in Cygnus-Cassiopeia region

22 p3593 A71-42330

PROPORTIONAL LIMIT

Deformation fatigue theory extended to tests at stresses below elastic limit, explaining cyclic loading frequency effect on fatigue life

12 p1984 A71-27681

Linear plastic deformation of steel under tension, investigating anisotropy in elastic modulus and strength

15 p2503 A71-31478

PROPRIOCEPTION

NT AUTOKINESIS

Ocular pursuit movement evocation by visual and proprioceptive stimulation

01 p0009 A71-10235

Proprioception role in perception of arm bending and extension during weightlessness and accelerations in aircraft flight along parabolic trajectory

01 p0014 A71-11143

Human performance in optical high inertia tracking system interface, considering proprioceptive feedback, display magnification, control dynamics view field and anticipatory processes effects

18 p2873 A71-36912

Eye movement neurophysiology, discussing ocular proprioception, oculomotor muscle sensory receptor role, extraocular muscle afferent and efferent innervation and central nervous system control effect

22 p3488 A71-42433

Vestibular and proprioceptive stabilization of eye movements

22 p3489 A71-42448

PROPRIOCEPTORS

Labyrinths and proprioceptors from aerospace medicine viewpoint, discussing motion sickness, spatial disorientation, manned space flight and rotation in space

08 p1244 A71-20711

Proprioceptive thermoregulatory mechanism of sweat secretion during positive and negative work in man

09 p1401 A71-23369

Reflex mechanisms and programmed command in insect flight stabilization, discussing gravity proprioceptors, wind sensing and optomotor control

21 p3326 A71-39987

Proprioceptive gravity perception in Hymenoptera, noting joint located hair plates and constant angle space orientation in dark

21 p3327 A71-39989

PROPULSION

NT AUXILIARY PROPULSION

NT CHEMICAL PROPULSION

NT ELECTRIC PROPULSION

NT ELECTROMAGNETIC PROPULSION

NT ELECTROSTATIC PROPULSION

NT ION PROPULSION

NT JET PROPULSION

NT LOW THRUST PROPULSION

NT MARINE PROPULSION

NT NUCLEAR ELECTRIC PROPULSION

NT NUCLEAR PROPULSION

NT PHOTONIC PROPULSION

NT PLASMA PROPULSION

NT SOLAR PROPULSION

NT SPACECRAFT PROPULSION

Experimental techniques in propulsion and energetics research - NATO/AGARD Conference, Munich, September 1967

11 p1764 A71-26263

PROPULSION CALCULATIONS

U MATHEMATICAL MODELS

U PROPULSION

PROPULSION SYSTEM CONFIGURATIONS

NT DESCENT PROPULSION SYSTEMS

German monograph on systems analysis of future jet and fan propulsion systems for VTOL commercial aircraft weight and cost reduction

01 p0142 A71-10115

Auxiliary propulsion devices for satellite stabilization, discussing monopropellant, bipropellant, post-combustion, hydrazine plenum, electrical, plasma jet, ion and colloid systems

02 p0299 A71-12749

V/STOL aircraft in civil air transportation, discussing safety, reliability, maintainability and propulsion system concepts

03 p0348 A71-13576

Astrobree D low cost high performance sounding rocket with long duration radial burning propulsion system for D region and meteorological research

03 p0498 A71-13670

Aircraft propulsion, discussing piston, turbojet, turboprop and turbofan engines in terms of thrust to weight ratio, specific fuel consumption and propulsive efficiency

04 p0638 A71-14977

Composite propulsion systems including Turbo-Ram-Scramjet, Ejector Ramjet, Hyperjet and Biliquid Ramjet Rocket

04 p0638 A71-15285

Bora-Sond rocket for upper atmosphere low cost sounding, describing propulsion system design and chemistry

05 p0816 A71-16417

Ground effect vehicles limiting volumetric dissipations from air cushion and propulsion systems with fluid boundary by Coanda effect

07 p1019 A71-19923

Lift fan propulsion for civil VTOL transports, considering applicability, attitude control, system design, fan transition and cross flow noise

07 p1022 A71-20373

Composite rocket cum hypersonic airbreathing propulsion reducing space exploration program cost

08 p1348 A71-21301

Air cushion vehicle technology, considering economics, propulsion, structures, controllability, flexible skirt systems and R and D

08 p1231 A71-21713

Electric propulsion systems integration into SERT 2 spacecraft, discussing launch imposed environment, thrust vector control, thruster breakdown, power conditioning, etc

[AIAA PAPER 70-1123]

09 p1511 A71-22898

Biological oscillating propulsion systems, investigating plate propeller, boundary layer control, low drag fuselage shapes and VTOL engine installations

10 p1569 A71-24235

SIRIO satellite project, discussing orbital dynamics, propulsion system, attitude control, onboard and ground electronic equipment

10 p1682 A71-24272

Aladin 2 French STOL project, consisting of suitably flapped wings with multiple propulsion units with fishtail exhaust nozzles inside rectangular ejectors

10 p1556 A71-24283

Space shuttle main, auxiliary and air breathing propulsion systems, describing various design concepts

10 p1682 A71-24284

Propulsion system and fuel regulator design effect on thrust change during air ejection for VTOL aircraft stabilization in hovering flight

10 p1659 A71-24753

Supersonic transport inlet-engine-airframe compatibility programs, noting exhaust nozzle installation effects, distortions and noise

10 p1659 A71-24854

Helicopter jet propulsion systems, considering turbocompressors, gas generators, turbine air jet systems, pulsed jet engines, ramjet engines and rocket engines

11 p1706 A71-25259

Lightweight high performance regenerative gas turbine designs for aircraft propulsion, comparing various compressor, turbine, combustor and recuperator arrangements

[ASME PAPER 71-GT-67]

11 p1812 A71-25983

Ablative thermal insulation materials testing for naval missile propulsion system application

11 p1789 A71-26032

Convertible fan/shaft engine for V/STOL tactical and transport aircraft, detailing mechanical arrangement, design and performance

11 p1813 A71-26054

Analytical method for optimal rocket motors cluster arrangement in multistage spacecraft, considering horizontal trajectories rated terminal velocity performance

11 p1839 A71-26335

Space shuttle propulsion systems, describing main engine prototype designs, booster attitude and docking control systems

12 p1946 A71-27606

Prop-fan propulsion system for V/STOL short haul transport aircraft, discussing performance, noise and weight characteristics

[SAE PAPER 710470]

13 p2115 A71-28338

Propulsion, guidance and stability of ground effect vehicle with perimetric Coanda fluid boundary

13 p1997 A71-29308

Nuclear fusion powered pulsed space propulsion systems with laser initiation, discussing energy conversion to momentum, limitations, vehicle configuration and mission performance

[AIAA PAPER 71-636]

14 p2288 A71-30095

Wind tunnel force test program design for jet aircraft configurations, including propulsion system simulation

14 p2176 A71-30605

VTOL turboshaft engine powered propulsion system development, detailing design requirements, program planning, component research and system integration

[AHS PREPRINT 562]

14 p2297 A71-31109

STOL commercial aircraft propulsion systems, considering two stream augmentor wing engine and high bypass ratio three stream engine

[AIAA PAPER 71-746]

15 p2467 A71-31325

European electric propulsion systems for flight trajectories within low gravity fields and orbital parameter attitude control and correction

15 p2469 A71-31730

Composite materials fabrication primary and secondary aerospace and aeropropulsion structural components

[SME PAPER EM-71-710]

15 p2416 A71-32343

Propulsion system design and performance requirements for space shuttle booster and orbiter vehicle,

- considering low cost, long life, reliability, safety and minimum maintenance
[AIAA PAPER 71-657] 15 p2471 A71-32577
- Propeller blade structures for high speed tilt wing turboprop V/STOL aircraft, considering materials selection, weight control, cyclic pitch control, noise reduction, etc
[DGLR 71-018] 15 p2350 A71-32785
- Gas turbine design advances for helicopter powerplants, illustrating by Turbomeca engines
16 p2624 A71-33416
- VTOL transport optimal airframe/propulsion systems design, discussing thrust requirements, performance, control, cruise functions, fuel consumption and fan characteristics
[AIAA PAPER 71-744] 17 p2792 A71-34225
- Supersonic aircraft propulsion by external heat addition, discussing numerical method for suitable caret wing design
17 p2793 A71-35398
- Lunik 16 and 17 automatic lunar landing stations and Lunokhod-1 lunar surface vehicle, describing propulsion systems, control elements and scientific equipment
17 p2724 A71-35401
- Solar electric propulsion system design for interplanetary spacecraft, describing Hg bombardment ion engine
17 p2794 A71-35546
- Space shuttle auxiliary propulsion subsystems for attitude control, orbit maneuvering and power supply, discussing design requirements with emphasis on fail-operational and fail-safe criteria
[AIAA PAPER 71-661] 17 p2795 A71-35624
- Propulsion systems trends for 1980s, discussing environmental noise levels, stoichiometric gas turbine engines for military aircraft, high bypass ratio engines for V/STOL aircraft, etc
17 p2795 A71-35625
- Mixed mode propulsion system for optimization of reusable space shuttle, discussing one-stage-to-orbit vehicle advantages and feasibility
19 p3121 A71-37126
- Space transport rendezvous and docking techniques, emphasizing guidance, propulsion system configuration and sensors
19 p3149 A71-37306
- Civil aircraft future propulsion requirements, considering larger engine sizes, higher takeoff thrusts and lower noise levels
[CASI PAPER 72/10] 19 p3122 A71-37600
- Attitude control propulsion system for booster and orbiter of space shuttle in European participation package
21 p3454 A71-40159
- Cold gas rocket propulsion systems design parameters, determining performance and weight formulae
21 p3437 A71-41050
- Book on aircraft propulsion covering design, dynamics, control, installation, gas turbine, ramjet, rocket and piston engines, compressors, combustion and energy cycles, etc
22 p3589 A71-42427
- PROPULSION SYSTEM PERFORMANCE**
- Hybrid rocket propulsion engine combustion efficiency, burnout patterns and operating conditions, using nitric acid oxidizer
02 p0298 A71-12070
- Air transportation reliability through turbojet engine performance monitoring
02 p0298 A71-12368
- M49 Larzac turbofan engine, describing design, development, performance data, manufacturing techniques, operation and maintenance
02 p0299 A71-12607
- Electric propulsion in space, emphasizing rocket performance relation to exhaust velocity, propellant consumption, thrust duration and payload capability
03 p0469 A71-13285
- FOILAC solid propellant rocket motors for high thrust short action time propulsion, reviewing development status and performance
[AIAA PAPER 70-1385] 03 p0470 A71-13668
- LES 6 satellite solid Teflon pulsed plasma thruster performance, determining energy balance thrust and circuit parameters
[AIAA PAPER 70-179] 03 p0472 A71-14429
- Book on ion propulsion covering technology, performance, accelerator design, propellant feed and control, etc
04 p0638 A71-14797
- Inertial and semiinertial propulsion systems output power and efficiency, taking into account continuous kinetic and potential energy buildup and fuel release
06 p0979 A71-17583
- Nuclear electric space propulsion size and cost factors, discussing scaling laws use for size-performance relationships
[AIAA PAPER 71-193] 06 p0947 A71-18631
- Spacecraft high performance resistojet engines, discussing design criteria for high temperature long term operation with minimum thermal losses
[AIAA PAPER 71-195] 06 p0948 A71-18633
- Oxygen difluoride/diborane propellant thrust chamber and injector technology, discussing engine duty cycles and performance
[AIAA PAPER 70-717] 07 p1183 A71-18890
- Resistojet design criteria for performance modeling of ammonia propellant thrusters and manned space stations using biowaste propellants
[AIAA PAPER 70-211] 07 p1183 A71-18898
- Aerospace Recommended Practice for gas turbine engine steady state performance presentation for digital computer programs, describing engine type, operating and control characteristics
[SAE-ARP-681B] 07 p1183 A71-19647
- Colloid microthruster system life test, discussing design and steady state performance
[AIAA PAPER 70-1110] 07 p1184 A71-19864
- Space shuttle safety, discussing rocket engine durability, turbine life, flaw detection, radiation hazards, etc
[AIAA PAPER 71-302] 09 p1511 A71-22616
- SERT 2 spacecraft ion thruster ground tests and flight operation, tabulating performance data
[AIAA PAPER 70-1125] 09 p1511 A71-22899
- Low power MPD arc thruster performance with downstream cathode, using Xe propellant
[AIAA PAPER 70-1084] 09 p1511 A71-22903
- Optimal low thrust power plant for spacecraft payload-maneuver tradeoff
09 p1512 A71-23139
- VTOL heat engine and propulsion system design and performance, citing Pegasus jet lift engine as compromise between takeoff and cruise function
10 p1659 A71-24751
- Supersonic compressor performance, discussing shock and dump losses and wave structure model errors
10 p1553 A71-24869
- Stable limit cycles and triggering limits of first radial mode in nonlinearly unstable liquid propellant rocket motors, using wave equation and Galerkin method
11 p1836 A71-25162
- Lunar flying vehicle propulsion system optimization, discussing weight, performance, engine life, reliability, etc
[AIAA PAPER 70-605] 11 p1810 A71-25504
- Drag-free satellite design and propulsion requirements, noting orbit perturbation mechanisms
[AIAA PAPER 70-1145] 11 p1838 A71-25522
- Out-of-core thermionic converter system using heat pipes as electrical resistive elements, discussing design and performance
11 p1710 A71-25875
- Thrust measurement of aircraft and rocket propulsion systems, comparing cost and characteristics of mechanical, electrical and hydraulic systems
12 p1894 A71-26991
- Air transport propulsion systems, discussing aircraft operating economics with reference to weight, size, powerplant efficiency, noise and air pollution
12 p1946 A71-27542
- CF6 turbofan engine development, discussing performance and endurance tests and design changes for reliable low cost operation
[SAE PAPER 710421] 13 p2114 A71-28308
- Aircraft propulsion system testing, stressing noise reduction and inlet-engine exhaust system compatibility
[SAE PAPER 710450] 13 p2114 A71-28328
- Thrust measurement of aircraft propulsion systems, considering hydraulic piston device, edge clearance, oil quantity and calibration
14 p2251 A71-29860
- Direct digital control and data acquisition system for propulsion research testing, transmitting data over differential signal pairs to remote test cell
14 p2208 A71-30316
- V/STOL propulsion units lift ratings based on aircraft system requirements
[SAE PAPER 710471] 14 p2176 A71-30537
- Airframe installation effects on underwing nacelle nozzle performance, using calibrated engines and load cells on F-106 for measurements
[AIAA PAPER 71-681] 14 p2292 A71-30745
- Ion thruster technology and subsystem development program status, describing design and performance characteristics
[AIAA PAPER 71-690] 14 p2293 A71-30750
- High thrust density colloid emitting source development as basic microthruster for electrostatic propulsion systems
[AIAA PAPER 71-694] 14 p2293 A71-30753
- Radiation cooled MPD thruster with permanent and superconducting magnets, describing test facilities and measurement techniques for performance tests
[AIAA PAPER 71-696] 14 p2293 A71-30755
- Multimission strategic aircraft installation effects testing in propulsion and aerodynamic wind tunnels, yielding flowfield definition, inlet internal performance, drag, forebody shape and orientation
[AIAA PAPER 71-759] 14 p2171 A71-30792
- Space shuttle engine design based on reusable XLR129 rocket engine, presenting performance data
15 p2467 A71-31469
- High performance superheated subliming solid ammonium carbamate thruster using resistojet technology for specific impulse increase
[WSS/CI PAPER 70-210] 15 p2469 A71-32048
- High performance low cost space shuttle propulsion systems airbreathing engines, attitude control thruster and orbital maneuvering
[AIAA PAPER 71-656] 15 p2470 A71-32292
- Biowaste resistojet engine design and performance for various propellants and propellant mixtures
[AIAA PAPER 71-687] 15 p2470 A71-32293
- Propulsion system design and performance requirements for space shuttle booster and orbiter vehicle, considering low cost, long life, reliability, safety and minimum maintenance
[AIAA PAPER 71-657] 15 p2471 A71-32577
- Maximum temperature engine concept, definition and application to future aircraft propulsion system performance
[SAE PAPER 710461] 17 p2792 A71-34498
- Exit stream velocity increase in propulsion units by adding latent heat of vaporization by condensation in supersonic nozzle
17 p2728 A71-34882
- Performance characteristics of jet engines equipped with afterburner, discussing combustion, flame stabilization, outlet nozzle regulation and operational cost
17 p2793 A71-35439
- Electron bombardment mercury ion rocket engine, considering mass flow rate and magnetic field strength effect on performance
17 p2794 A71-35540
- V/STOL aircraft with vectored thrust propulsion systems, noting weight and center of gravity lift-thrust relationship changes effect on performance
[SAWE PAPER 894] 17 p2676 A71-35817
- Civil aircraft future propulsion requirements, considering larger engine sizes, higher takeoff thrusts and lower noise levels
[CASI PAPER 72/10] 19 p3122 A71-37600
- Ultraplannary probes for exploration beyond solar system, discussing heliosphere, cometary, interstellar and stellar mission categories propulsion system selection
[AAS PAPER 71-164] 19 p3141 A71-37961
- Flight mechanics of point with limited power propulsion system and energy storage unit, investigating variational maximum payload problem with singular control optimization
20 p3288 A71-39125
- Apollo/Saturn 5 propulsion system design, development, testing and integration
22 p3589 A71-42026
- Solar electric multimission spacecraft effects on low thrust performance by characteristic surface representation
[AAS PAPER 71-324] 23 p3772 A71-42998
- Supersonic propulsion system inlet, engine and exhaust nozzle in wind tunnel and flight tests, discussing boundary layer effects on performance
23 p3718 A71-43599
- PROPULSIVE EFFICIENCY**
- NT PROPELLER EFFICIENCY**
- Air cooled opposed 4, 6 and 8 cylinder light aircraft engines with or without turbosupercharging, considering horsepower improvement and torsional vibration control
[SAE PAPER 700205] 01 p0142 A71-10129
- Submillipound mercury electron bombardment ion thruster efficiency, noting cathode pole piece, baffle position and geometry influence on ion chamber performance
[AIAA PAPER 70-616] 01 p0143 A71-11577
- Thrust equation, control volume and propulsive efficiency for rockets and air breathing jets from energy conservation principle
02 p0299 A71-12681
- Aircraft propulsion, discussing piston, turbojet, turboprop and turbofan engines in terms of thrust to weight ratio, specific fuel consumption and propulsive efficiency
04 p0638 A71-14977
- Inertial and semiinertial propulsion systems output power and efficiency, taking into account continuous kinetic and potential energy buildup and fuel release
06 p0979 A71-17583
- Electron bombardment mercury ion thruster plasma properties and performance, computing ion beam current, discharge losses and propellant utilization efficiency
[AIAA PAPER 69-256] 07 p1184 A71-19881
- Two-spool turbojet engine nozzle diameter adjustment system for increasing thrust, fuel economy and reliability, describing automatic clamshell shutter control mechanism
15 p2471 A71-32527
- Turbojet engines thrust and fuel economy improvement by gas-air jet mixing, discussing efficiency increase and noise reduction
15 p2472 A71-32717
- Multistep rocket mass ratios optimization, including exhaust gas velocities, structure and efficiency
16 p2644 A71-32843

Cold gas rocket propulsion systems design parameters, determining performance and weight formulae
21 p3437 A71-41050

PROPYL COMPOUNDS

Ion cyclotron resonance application to propanol ion structure formed in double McLafferty rearrangement, demonstrating direct enol ion formation instead of by isomerization or ketonization
07 p1055 A71-19598

PROPYLENE

Ions association constant with water in propylene carbonate from proton magnetic resonance measurements
13 p2026 A71-29040

Liquefied gas solutions of methane in carbon tetrafluoride and propylene, calculating pressure and temperature dependence of density
15 p2462 A71-31246

Shock tube isomerization of cyclopropane to propylene as model system for small ring compounds, noting rate constants
19 p3010 A71-37272

Fluorinated ethylene propylene covers for silicon solar cells, describing processing parameters effects on optical and electrical characteristics
20 p3182 A71-38944

PROSTHETIC DEVICES

NT ARTIFICIAL EARS

Hybrid computer simulation for cardio-circulatory assist device, discussing atrium to aorta and ventricle to aorta optimal output, time tension index and flow control
07 p1048 A71-19584

Biped locomotion machines dynamic analysis and synthesis by minimum energy criteria for prosthetic-orthotic equipment design and human locomotion analysis
09 p1399 A71-22971

Mechanical impedance measurement of artificial and human mastoids for bone vibrator calibration as function of frequency
11 p1725 A71-26189

Lower extremity Army aviator amputee retention on flight status regarding service need, amputation and prosthetic fit, age, career, hours flown and time in military
16 p2535 A71-33120

Low cost Ti substitutions for Ni and alloys in corrosion resistant applications, prosthetic devices and pollution control equipment
20 p3251 A71-39339

PROTECTION

NT ACCELERATION PROTECTION

NT CIRCUIT PROTECTION

NT CORROSION PREVENTION

NT EYE PROTECTION

NT METEOROID PROTECTION

NT RADIATION PROTECTION

NT RADIATION SHIELDING

NT SOLAR RADIATION SHIELDING

NT THERMAL PROTECTION

Materials and construction techniques in lightning protection for aircraft and helicopters
07 p1020 A71-19930

Lightning protection for nonmetallic helicopter rotor blades
07 p1021 A71-19939

Lightning protection for dielectric composites, analyzing damage from shock waves, vaporization pressure, magnetic forces and burning
07 p1021 A71-19942

Ground space facilities protection from lightning and electromagnetic interference
07 p1084 A71-19947

PROTECTIVE CLOTHING

NT HELMETS

NT PRESSURE SUITS

NT SPACE SUITS

Antihat protective clothing effectiveness for aircraft crews, discussing outer coating reflectivity and emissivity, insulating layer and internal surface
05 p0715 A71-16934

Flight personnel green protection system from nuclear weapons high intensity thermal effects
06 p0858 A71-17609

Water cooled head cap for heat stress amelioration in subjects working in warm environments
06 p0859 A71-17611

Water cooled garments, discussing human thermoregulation, developments and current suits
06 p0859 A71-17957

Flammability and heat transfer characteristics of flame retardant cotton, Nomex and polybenzimidazole (PBI) protective fabrics
07 p1145 A71-19573

Astronaut protection from solar flare high energy protons, discussing spacecraft orientation and solid, electrostatic, magnetic and plasma shielding
13 p2021 A71-29252

Fire fighter protective clothing, considering efficiency as function of garment weight and heat stress loading
17 p2690 A71-34785

Cold climate clothed human windchill tables, considering various heat transfer modes and skin temperature
20 p3192 A71-39205

Heat acclimatization by evaporative cooling prevention in men wearing vapor barrier suits, considering body temperature and heart and sweat rates
21 p3331 A71-40355

PROTECTIVE COATINGS

NT ANODIC COATINGS

NT CERAMIC COATINGS

NT PRIMERS [COATINGS]

U-tube rocket nozzle and fuel element fabrication methods for NERVA space engine, emphasizing coating process
01 p0126 A71-10006

Diffusion boride protective coatings on Nb, Ta, Mo and W against carbon diffusion from carburizing agents
01 p0100 A71-10401

Composite Ni coatings, adding mullite crystals to enhance oxidation resistance
01 p0102 A71-10784

High voltage thermionic module eliminating power conditioning and multiple units series connection, discussing design and coating technologies
02 p0195 A71-12244

Niobium alloys for gas turbine blades, examining working temperatures, protective coatings and ductility
02 p0271 A71-12939

Al based protective coatings on Nb and Nb alloys considering structure, formation and aluminide component
02 p0271 A71-12941

Niobium aluminide pest, investigating oxidation effects on Nb-Al protective coatings from 600 to 1400 C
02 p0271 A71-12942

Nb oxidation protection by Ti or Cr modified silicide coating, noting results with various Cr-Si mixtures
02 p0272 A71-12944

Mechanical stability of self healing viscous glass layer in porous oxidation protection coating on Ni under high acceleration
02 p0272 A71-12945

Mechanical stability of liquid phase in porous oxidation protective coating on Ni turbine blades under acceleration
02 p0272 A71-12946

Structure and durability of self healing silicide based coatings for niobium oxidation protection at high temperatures
02 p0272 A71-12947

Soviet book on aircraft construction technology covering parts fabrication, protective coatings, production automation, etc
03 p0433 A71-14399

Vacuum UV degradation of thermal control coatings on ATS-1 satellite, comparing with laboratory simulation
04 p0618 A71-14896

Heat transfer boundary conditions determination in studying heat protective coatings effectiveness, discussing measurement methods for stagnation temperatures and heat fluxes from exhaust gases
04 p0618 A71-15643

Low stress integral coverslips deposition by high vacuum ion beam sputtering for solar cell manufacturing cost reduction
05 p0702 A71-16078

Electron, proton and UV irradiation effects on CdS solar cell protective plastic films with or without adhesive coatings, measuring transmission changes
05 p0771 A71-16087

Protective oxide formation on single phased Cu-Al-Si alloys during high temperature oxidation
05 p0770 A71-17099

Temperature profile similarity and thermal protective coating thickness for single reentered spacecraft [AIAA PAPER 71-37]
06 p0916 A71-18498

Stainless steel coatings vacuum deposition on Ti alloy plates, considering product cryogenic and mechanical properties
07 p1118 A71-19853

Composite plastic aircraft structures lightning protection, considering hazard to composite materials and use of metal filled or plasma sprayed coatings and metal foil coverings
07 p1021 A71-19943

Lightning protective coatings for boron and graphite fiber reinforced plastics
07 p1021 A71-19944

Si solar cells transparent radiation protective coatings stability and degree of blackness, discussing UV irradiation and proton and electron bombardment
08 p1287 A71-21024

Aluminum high temperature resistant diffusion type coatings structure and chemical composition, outlining turbine blades testing for thermal shock, oxidation and sulfur and sea salt corrosion
09 p1474 A71-23287

High temperature turbine parts protective coatings, discussing aluminum diffusion prevention and crack and oxidation resistance
09 p1456 A71-23290

High temperature oxidation protective coatings behavior, emphasizing jet engine applications
09 p1483 A71-23296

Polymer adhesive protective coatings for improving fatigue resistance of butt and lap welded joints in thin Al sheet construction
09 p1478 A71-23355

Nonflammable self extinguishing nontoxic fluorocarbon elastomers as adhesives and coatings for Apollo program
10 p1632 A71-24097

Nonflammable elastomeric materials and coatings for oxygen enriched atmospheres
10 p1632 A71-24098

Polyurethane coatings development for subsonic rain erosion protection for aircraft structures, using whirling arm apparatus with simulated rainfall
10 p1632 A71-24101

Elastomeric seals for aircraft fastener countersinks, providing corrosion protection to static metal surface treatments and organic coatings
10 p1633 A71-24118

Protective coatings of Ta, Nb and Ti alloys for high performance thermal protection systems, discussing space shuttle reentry heat shield
11 p1778 A71-25554

Superalloy dispersion strengthened and fused sulfur silicide coatings for aircraft gas turbine engines and space shuttle heat shields
11 p1778 A71-25555

Thermal control coating materials, measuring separate and combined electron and UV radiation effects on reflectance and emittance in vacuum
11 p1800 A71-26519

Space stable thermal control coatings, noting reflectance optical spectroscopy of zinc oxide based paints and zinc orthotitanate
11 p1747 A71-26520

Spherical head projectiles collision with hemispherical shells and square plates with and without protective covering, calculating stress distribution
12 p1976 A71-27160

Silicide coated Nb alloys for gas turbine engine components operating at temperatures above 2000 F [SAE PAPER 710460]
13 p2115 A71-28334

Temperature dependence and mechanical properties of Mo materials with various diffusive protective base coatings based on continuity and density
14 p2256 A71-29623

Materials and processing methods for rain erosion resistant ceramic coated plastic structures for supersonic aircraft, considering fiberglass reinforced polyimide radomes with alumina coating
14 p2262 A71-29645

Hypersonic flight load bearing refractory alloy control surface protective coatings, emphasizing oxidation screening tests
14 p2262 A71-29646

Surfacing materials based on transition metal borides with boron carbide additions, testing brittleness, hardness and abrasive wear resistance
15 p2431 A71-32163

High temperature oxidation protection of niobium by molybdenum disilicide coatings applied by hot pressing powder metallurgy method
18 p2934 A71-35952

Metallographic examination of inorganic, metal plated and intermetallic coatings on martensitic stainless steels for pitting and surface corrosion prevention
19 p3081 A71-37902

Si solar cells transparent radiation protective coatings stability and degree of blackness, discussing UV irradiation and proton and electron bombardment
20 p3240 A71-39604

PROTECTORS

NT EAR PROTECTORS

PROTEIN METABOLISM

NT LIPID METABOLISM

Blood cholesterol and protein fraction concentrations in pathogenesis of hypothalamic atherosclerosis patients
02 p0201 A71-12531

Long term hypoxia effects on granuloma and various organs in rats, noting collagen and noncollagenous proteins formation stimulation and/or inhibition
05 p0706 A71-16293

Decaborane effects on amino acid metabolic patterns of various rat tissues, considering holoenzyme inactivation
05 p0706 A71-16294

Liver and skeletal musculature morphology during hypokinesia and protein deficiency in mice
06 p0855 A71-18377

Bicycle ergometer workout effects on serum proteins, noting intravascular redistribution, tissue damage and membrane permeability
07 p1052 A71-20328

Division cycle of *Myxococcus xanthus*, considering kinetics of cell growth and protein synthesis
09 p1396 A71-23473

Photoreduction regulation in *Rhodospirillum rubrum* by ammonium chloride, discussing nitrogen fixation and protein metabolism

16 p2527 A71-33058

Polysomal RNA disaggregation and attendant reduction in hepatic protein synthesis in rats as result of decreased feed ingestion during hypoxia

16 p2529 A71-33190

Urinary metabolites relationship to fatigue, considering excretion of proteins, electrolytes, simple organic compounds and hormones

17 p2679 A71-34357

Chlorella extracellular metabolites, identifying indole nature biologically active substances

19 p3004 A71-38544

Protein content in cytoplasm of neurons and glial satellite cells in supraoptical and red nuclei of white rat brains during natural and paradoxical phase deprived sleep

19 p3005 A71-38545

Exercise-induced human protein catabolism not due to caloric deficit

19 p3008 A71-38552

Urinary protein excretion rates in high altitude inhabitants, showing polycythemia effect on creatinine clearances levels

19 p3009 A71-38561

Cerebral gamma-aminobutyric acid metabolism and hyperbaric oxygen induced seizures in chicks during brain development, noting increased membrane permeability

20 p3186 A71-38970

PROTEINOIDS

Microfossil structures from morphological alterations of proteinoid microspheres due to inclusion of organic or synthetic polyamino acids

14 p2190 A71-30178

Proteinoids self assembly into primitive cell from observations of polypeptide generation during amino acid heating

14 p2190 A71-30179

PROTEINS

NT ADENINES
NT ADENOSINE DIPHOSPHATE [ADP]
NT ADENOSINE TRIPHOSPHATE [ATP]
NT ADENOSINES
NT ALBUMINS
NT ASPARTATES
NT CARBOXYHEMOGLOBIN
NT COENZYMES
NT ELASTIN
NT FIBRIN
NT GAMMA GLOBULIN
NT GLOBULINS
NT NUCLEOTIDES
NT OXIDASE
NT OXYHEMOGLOBIN
NT PEPTIDES
NT PROTEINOIDS
NT PYRIDINE NUCLEOTIDES
NT URIDYLIC ACID

Hypokinetic effect on sarcoplasmic and myofibrillar protein composition of skeletal muscles in rats

01 p0013 A71-11130

Chlorella ration effect on internal organs of protein-deficient mice compared with casein and soybean rations

01 p0025 A71-11145

Space diets for maximum energy consisting of fats and proteins from biological systems and carbohydrates from chemical systems

01 p0027 A71-11573

Polymorphic nucleus leukocytes pyrogenic protein fraction effects on rabbits hypothalamus thermal control structures

05 p0707 A71-16386

Computer applications in analysis of biological structures, considering tissues, cells, chromosomes, proteins and lipids

06 p0863 A71-18691

Human crystalline lens protein and lipid discussing cholesterol accumulation with age

09 p1390 A71-22421

Proteins hydrolysis, investigating temperature effect on reaction, determining optimum conditions for maximum amino acids yields

11 p1728 A71-26066

Lipid, protein and carbohydrate concentrations in *Chlorella* biomass from pyrolysis and aluminogel column chromatography

13 p2017 A71-28407

Biochemical luminescence reaction for ferroporphyrin proteins determination in extraterrestrial life detection

13 p2009 A71-28684

Mars physical conditions compared to earth, simulating Martian conditions and low temperature and UV effects on proteins

13 p2009 A71-28688

Deleterious mutations and neutral substitutions, discussing molecular evolution model for DNA and proteins

13 p2013 A71-29096

Nonproteins detection in presence of protein amino acids with Beckman analyzer chromatograms

13 p2026 A71-29478

Hypoxic hypoxia and hypercapnia effect on calcium, inorganic phosphorus and total protein in rats blood during hypodynamic syndrome

15 p2356 A71-31306

Anabaena cylindrica alga chromosomes protein components, noting histone absence

16 p2536 A71-33359

Rhodopsin kinetics mathematical analysis by cyclic five-component model, applying to flash and extended photolysis in rat retina

17 p2680 A71-34653

Photolysis of metarhodopsin I, discussing rate and extent of conversion to rhodopsin

17 p2680 A71-34654

Halophilic bacteria electron transport chain, studying protein, phospholipids, flavoproteins and cytochromes sedimentation properties by electron microscopy and light scattering technique

21 p3334 A71-40593

Coronary dilating substances of low molecular weight separated through dialysis from hypothalamus protein carriers

21 p3338 A71-41072

Solute diffusion coefficients dependence on proteins concentrations in human plasma from experiment, presenting equation for prediction

23 p3637 A71-44253

PROTON BEAMS

Cross sections of metastable H formation by charge transfer of hydrogen ion beam on helium, argon, nitrogen and oxygen targets

11 p1803 A71-26371

Auroral radio noise from electrostatic oscillations excited by fast proton beams

19 p3018 A71-38046

PROTON BELTS

Trapped protons east-west asymmetry observations during Gemini 4 flight, using on-board high sensitivity plastic-scintillation spectrometer

03 p0479 A71-14041

Equatorial proton belt radial profile analysis by satellite electron distribution data

08 p1351 A71-20962

Cyclotron instability of high energy protons in magnetosphere with refraction of growing Alfvén waves

09 p1435 A71-22437

Quasi-steady spectrum of hydromagnetic noise in proton belt, using random excited broad wave fields in nonisothermal magnetosphere

12 p1947 A71-26643

Geomagnetic Pc-1 type micropulsations appearance and development due to proton belt cyclotron instability

14 p2301 A71-30350

Solar wind proton penetration through earth magnetosphere, taking into account drift, force lines curvature and nonstationary plasma boundary

19 p3129 A71-38376

Noon-midnight high latitude proton trapping and precipitation boundary variations associated with polar magnetic substorms observed by ESR0 1A satellite

23 p3719 A71-43127

PROTON DAMAGE

LES 6 synchronous orbit solar cells experiments, determining various type cells degradation due to low energy proton damage

05 p0702 A71-16085

Silicon solar cells radiation damage from low energy protons, discussing current degradation as function of exposed area and particle energy

16 p2621 A71-33414

PROTON DENSITY [CONCENTRATION]

Directional differential energy spectra for proton intensities in outer radiation zone near magnetic equator from satellite observations

06 p0949 A71-17261

Polar cap atomic processes stimulated by photons, electrons and protons, considering particle morphology

10 p1661 A71-24311

Earth corotating plasma tail evidence in plasmopause variations from high resolution proton distribution data obtained by Ogo 4 satellite during magnetic storm

23 p3668 A71-43166

PROTON ENERGY

Solar energetic protons measurements by ESR0 1 satellite following flare of 18 November 1968, noting cut-off latitude over northern polar cap

03 p0478 A71-14039

Electron and proton energy measurements by near-polar orbit ESR0 1 satellite, noting anisotropy and isotropy near and in proton zones

03 p0479 A71-14040

Simple two fluid solar wind speed and proton temperature model, discussing nonthermal energy dissipation

03 p0481 A71-14504

Auroral zone electron and proton energy spectra measurements, using sounding rockets with electrostatic analyzers

03 p0419 A71-14524

Short duration proton energy increases observation by Explorer 34, considering interpretation as acceleration associated interplanetary shocks

06 p0949 A71-17254

Magnetotail plasma sheet electron and proton energy spectra and angular distribution over auroral zone, comparing Vela satellite and rocket measurements

06 p0887 A71-17260

Directional differential energy spectra for proton intensities in outer radiation zone near magnetic equator from satellite observations

06 p0949 A71-17261

Periodic drift echoes in magnetospheric energetic proton fluxes from satellite observation

06 p0950 A71-17283

Low energy protons radial gradient in interplanetary space measured with intercalibrated solid state detectors on Venus bound Mariner 5 and earth orbiting Explorer 33

06 p0952 A71-18113

Zond 4 and 5 space probes proton flux measurements at 1.5-50 MeV, describing instrument equipment used and results obtained

06 p0953 A71-18120

Fine structure of geomagnetic Pc 1 micropulsations by cyclotron instability due to anisotropic energetic proton velocity

06 p0895 A71-18283

Proton flux range between solar wind and cosmic radiation protons energy by spacecraft observation

08 p1350 A71-20952

ATS-5 satellite-borne auroral electron and proton energy spectrum measuring instrument using cylindrical coordinate electrostatic analyzer

08 p1294 A71-21845

Satellite-borne scintillation spectrometers for medium and high energy electron and proton measurements

09 p1513 A71-22555

Midlatitude upper atmospheric low energy proton intensity obtained from meteorological rocket data

09 p1513 A71-22579

Proton energy change effects on charged particles propagating in interplanetary space, using low energy solar flare proton fluxes observations

09 p1514 A71-22801

Satellite instruments to measure intensity and energy spectrum of high energy electrons and protons

10 p1683 A71-24464

Interplanetary space low energy cosmic ray protons steady state anisotropy based on radial gradient model of outward convection at solar wind speeds

10 p1663 A71-24777

Geomagnetically trapped protons differential energy spectrum in Van Allen inner and outer radiation belts over various energies, using thin solid state detector

10 p1663 A71-24784

Surviving high energy primary protons of cosmic ray nuclear bursts in atmosphere without air shower at Chacaltaya

12 p1933 A71-27393

Inelastic proton-proton and proton-carbon interaction cross sections, measuring proton energy with ionization calorimeter on Proton 1, 2 and 3 satellites

13 p1212 A71-28060

Proton recoil measurements of PuBe neutron source spectra, using pressurized hydrogen spherical proportional counter and liquid scintillator measurements

14 p2276 A71-29918

Proton flux measuring spectrometer with automatic tracking of distribution maxima over energy range from 0.15 to 4 keV

14 p2247 A71-30578

Thermal properties of solar wind plasma, determining electron and proton temperature distributions, proton heating rate, electron thermal conductivity and energy exchange rates

15 p2480 A71-32754

Energetic solar protons asymmetric access to north south polar caps by satellite observation during 24 January 1969 event

16 p2628 A71-33935

Stable auroral red arcs generation at plasmopause from ion cyclotron wave turbulent dissipation of ring current proton energy

16 p2572 A71-33947

Radiation belt proton intensities and energy spectra measurements by Azur satellite solid state detector telescope with energy level discrimination electronics

19 p3125 A71-37417

Auroral zone proton measurements during slowly varying cosmic noise absorption, obtaining energy spectrum by rocket soundings

19 p3125 A71-37418

Energetic electrons, protons and alpha particle measurements by Azur satellite over polar cap and in radiation belt during March 1970 solar particle event

19 p3126 A71-37419

Primary cosmic ray proton energy spectrum in 50 GeV to 300 TeV range, using Proton 1, 2 and 3 satellite-borne counters
19 p3128 A71-38352

Magnetospheric high energy protons relaxation due to interaction with Alfvén waves, presenting Einstein-Kolmogoroff equation numerical solution for particle momentum distribution function
20 p3278 A71-39074

PCA due to solar proton event, measuring electron-ion densities and temperatures, proton/electron energy flux spectrum, Lyman alpha radiation and X rays
20 p3281 A71-39730

Solar high energy cosmic ray proton burst observations, examining maximum flux delay time with Venus 6 satellite
20 p3281 A71-39730

Midlatitude ionosphere and magnetosphere thermal protons dynamic behavior, investigating magnetic storm effects
23 p3720 A71-43129

Enhanced low energy nuclear resonance reaction cross section estimation, finding Be 9 isotope reaction with proton for clean controlled thermonuclear reactor
24 p3847 A71-44495

Suprathermal proton bremsstrahlung cross section calculation, using Weizsacker-Williams method
24 p3865 A71-44905

PROTON FLUX DENSITY

Proton fluxes at 300 keV associated with propagating interplanetary shock waves, noting alpha particle enhancement
01 p0146 A71-11487

Directed proton fluxes measurements in bow shock, magnetosheath and solar wind by OGO 5 satellite ion spectrometer
01 p0147 A71-11491

Polar ionospheric auroral zone ionization, obtaining ion production function for single electron and proton flux
02 p0244 A71-11772

Energetic solar neutrons near maximum, calculating continuous flux and proton emission from balloon measurements
02 p0302 A71-12768

Solar proton flares, coronal radio diameter and cosmic radiation intensity relationship
03 p0473 A71-13788

Black Brant rocket measurement of PCA event at Churchill, Canada on 19 November 1968, discussing electron density and alpha particle and proton flux
03 p0417 A71-14038

Energetic proton bursts in magnetotail, examining flux direction and intensity, spectral energies and origin
03 p0482 A71-14517

Auroral ionosphere, examining low energy proton fluxes parallel to geomagnetic field lines of force
05 p0738 A71-16160

Proton whistlers damping compared to predictions by cyclotron damping theory, discussing proton density
06 p0949 A71-17262

Zond 4 and 5 space probes proton flux measurements at 1.5-50 MeV, describing instrument equipment used and results obtained
06 p0953 A71-18120

Quiet time fluxes and differential energy spectra of protons and alpha particles at 2-20 MeV measured by cosmic ray detectors on OGO-3
06 p0954 A71-18127

Cosmic rays anomalous diurnal variations, describing proton excess flux from direction outside geomagnetic field
06 p0956 A71-18139

Solar flares of 25-27 February 1969 effects on polar cap and interplanetary space flux rates, confirming magnetospheric modulation of proton density peaks
06 p0958 A71-18151

Solar proton event on 9 June 1968 observed at polar caps by ESO 2 satellite, noting flux profile structure
06 p0958 A71-18154

Solar flare on 9 June 1968, observing proton energy spectra and flux variation with time profiles
06 p0958 A71-18155

Particle flux energy spectra and time dependence of 25 February 1969 solar proton event
06 p0959 A71-18156

Low energy electron and proton fluxes observation by Isis 1 satellite, concluding solar wind penetration to low altitudes through magnetopause cusp
07 p1186 A71-19659

Magnetopause electric field accounting for ATS 5 energetic proton and electron flux measurements, comparing to various models
07 p1186 A71-19660

Ionospheric low energy electron and proton fluxes near equator from Isis 1 satellite soft particle spectrometer observations, considering energy spectra and pitch angle distribution
07 p1187 A71-19679

Proton flux range between solar wind and cosmic radiation protons energy by spacecraft observation
08 p1350 A71-20952

Midlatitude upper atmospheric low energy proton intensity obtained from meteorological rocket data
09 p1513 A71-22579

Charge source density during interaction between atmosphere and electron/proton fluxes at prescribed boundary parameters
09 p1513 A71-22675

Proton energy change effects on charged particles propagating in interplanetary space, using low energy solar flare proton fluxes observations
09 p1514 A71-22801

Altitude spectrum of ion formation in interaction of proton flux with atmosphere, using Bragg dissipation function
09 p1514 A71-23153

Solar cycle time variations in trapped radiation belt proton flux, deriving proton transport equation from Boltzmann equation
10 p1663 A71-24785

Comparative proton flux and Pc-1 pulsations from Explorer 26 satellite and ground observations
11 p1756 A71-25648

Shower size distributions of accompanying energetic protons at mountain altitude as function of released energy
12 p1951 A71-27392

Solar proton anisotropy measurements, discussing flux directional distribution
14 p2297 A71-29670

Low energy electron and proton fluxes in geomagnetic tail of equatorial magnetosphere forming plasma sheet related to auroral oval
14 p2299 A71-30029

Proton flux measuring spectrometer with automatic tracking of distribution maxima over energy range from 0.15 to 4 keV
14 p2247 A71-30578

Proton measurements in ring current by OGO-3 satellite compared with geomagnetic field data at low and high latitudes
16 p2626 A71-33663

Ionospheric electron concentration and proton flux rocket-borne measurements during nighttime PCA event, discussing atomic oxygen role in recombination processes
16 p2575 A71-33974

Precipitating protons measurement in 2.5-200 KeV energy range by OV1-15 satellite, comparing spatial distribution with plasmopause profile
19 p3125 A71-37358

Electron and proton fluxes intercorrelation in recovery phase of auroral substorm
19 p3125 A71-37362

Radiation belt proton intensities and energy spectra measurements by Azur satellite solid state detector telescope with energy level discrimination electronics
19 p3125 A71-37417

Radionuclides depth distribution gradient in lunar samples, suggesting solar proton medium flux constancy over last million years
19 p3127 A71-38004

Ion and electron production rate during PCA event, computing electron/ion density, differential proton flux spectrum and ion production rate
20 p3225 A71-39729

Solar proton enhancement over auroral zone observed aboard near earth polar orbiting ESO 2 satellite
20 p3282 A71-39735

Solar proton events intensity forecasts using time parameters of microwave bursts
22 p3590 A71-41465

Solar proton flux from 7 July 1966 flare observation via Proton 3 satellite, obtaining cosmic rays integral spectra
22 p3591 A71-41549

PROTON IMPACT

Lunar atomic hydrogen atmosphere from solar wind proton bombardment, considering detection by scattered Lyman alpha radiation measurements
04 p0659 A71-15854

Inelastic ionization cross sections for protonic and atomic hydrogen collisions with atomic and molecular gases in 0.5 keV to 5 MeV energy range
06 p0928 A71-17266

Cross sections for simultaneous ionization and charge transfer in fast proton-helium atom collisions, using Born approximation
09 p1497 A71-22416

Nitrogen excitation by fast protons and electrons impact, obtaining primary collision cross sections by measurements extrapolation to zero pressure
10 p1664 A71-24793

Dust particle angular momentum orientation in comet tails through bombardment by solar wind protons, noting role in scattered light polarization
11 p1832 A71-26182

Electron production by proton impact on nitrogen, oxygen, neon and argon, measuring cross sections angular and energy distribution by electrostatic analysis and electron counting
14 p2277 A71-30660

Si solar cells transparent radiation protective coatings stability and degree of blackness, discussing UV irradiation and proton and electron bombardment
20 p3240 A71-39604

Glauber scattering amplitudes for atomic hydrogen excitation by electrons or protons, presenting closed form expressions requiring no numerical integration
21 p3420 A71-41195

PROTON IRRADIATION

Quasi-nucleon nuclear interactions of high energy protons in photoemulsion irradiated in pulsed magnetic field
01 p0131 A71-11368

Absorbed dose equivalent from high energy neutrons and protons incident on tissue, using nucleon-meson cascade calculations
04 p0624 A71-14804

N-p Si solar cells, investigating mechanism of low energy proton irradiation damage to back contacts
05 p0702 A71-16084

Electron, proton and UV irradiation effects on CdS solar cell protective plastic films with or without adhesive coatings, measuring transmission changes
05 p0771 A71-16087

Shielding effectiveness of different body portions during repeated proton irradiation on dogs
06 p0861 A71-18360

Electron-proton radiation effects on scintillating materials in space environment chamber, evaluating background light degradation of active source monitoring
07 p1175 A71-19066

Si surface barrier radiation detectors depletion region low energy proton irradiation damage determination from capacitance-voltage curves and capacitance recovery techniques
07 p1071 A71-19071

Low energy proton irradiation damage to ATS and Intelsat satellites Si solar cells junction properties
07 p1022 A71-19072

Proton irradiation on Fe and Ni targets, measuring spallation cross sections
07 p1158 A71-19074

Ce 138 excited states identification in beta decay spectra of Pr 138m and Pr 138 sources, using proton target bombardment
07 p1163 A71-19547

Hydrogen outgassing from proton irradiated aluminum samples, determining gas evolution and blister formation during annealing
07 p1139 A71-20173

Low energy proton irradiation induced thin polymer contaminant films effect on far UV reflecting mirrors reflectance and scattered light
08 p1290 A71-21382

Renal anatomical pathology in dogs long after high energy proton irradiation, noting similarity to natural aging
09 p1388 A71-22194

Electron emission from He ion by proton bombardment, calculating double differential cross sections relative to ejection energy and angle
09 p1497 A71-22415

Radiation defects distribution in Si irradiated by protons, deuterons and alpha particles
10 p1655 A71-24140

Reflectance restoration of proton and UV degraded spacecraft thermal control coatings by low temperature oxygen plasma treatment applied to Surveyor 3 [AIAA PAPER 71-463]
11 p1800 A71-26244

Junction conversion and fabrication of Hg-Cd-Te n-p photovoltaic detectors by proton bombardment
13 p2066 A71-28043

Capacitance/voltage characteristics of MOS capacitors before/after 25 MeV proton irradiation
14 p2210 A71-29797

Impurity photoconductivity spectra determination for n and p type Si crystals under 660 MeV proton irradiation
21 p3433 A71-41311

Low temperature proton irradiation damage and recovery in discontinuous Ta films sputtered in oxygen and nitrogen
22 p3585 A71-41804

Optical line spectrum and ionization equilibria of hard UV radiation and energetic proton heated hydrogen, helium, nitrogen, oxygen and neon
22 p3601 A71-42160

Reactivity changes to pharmacocochemical preparations under total proton and gamma ray irradiation of abdomen and head shielded rats
22 p3492 A71-42717

High energy proton irradiation of rats with partial shielding of abdominal region, observing pathomorphological changes in myocardium, nervous system and radiosensitive organs
22 p3493 A71-42721

Lunar fines luminescence emission spectra in visible and near IR region under proton and electron excitations, discussing cause and plagioclase distribution
23 p3760 A71-43777

Proton irradiation damage on lunar surface, considering solar wind sputtering, reduction, chemical bond breakage and electron paramagnetic resonance
24 p3867 A71-44423

Trapped hydrogen atoms detection in proton irradiated KCl and NaCl single crystals at 77 K, using electron paramagnetic resonance spectroscopy
24 p3802 A71-44425

CNES hypotheses and methods determining current delivered by solar generator of FR 1 satellite, discussing electrical performance due to electron and proton irradiation 24 p3793 A71-44760

PROTON MAGNETIC RESONANCE
Ions association constant with water in propylene carbonate from proton magnetic resonance measurements 13 p2026 A71-29040

Magnetic drift waves near proton cyclotron frequency, noting magnetic field gradient role in plasma instability 23 p3709 A71-43181

PROTON PRECESSION
Time dependence of signal emf induced in toroidal proton precession magnetometer sensor with elliptical cross section 14 p2246 A71-30481

German monograph on calibrating induction coil and proton precession magnetometers for polar electrojet rocket experiments 18 p2915 A71-35922

PROTON PRECIPITATION
Electrostatic fields parallel to geomagnetic field role in charged particles acceleration mechanism to auroral energies, considering electron and proton precipitation 06 p0893 A71-17989

Energetic electron and proton precipitation measurements by sounding rocket-borne particle detectors in pulsating aurora 07 p1186 A71-19669

Auroral electron and proton precipitation patterns observed at Fort Churchill, discussing particle energies 08 p1282 A71-21636

Particle precipitation at auroral heights, examining ground based observations evidence for existence of protons, neutrons and electrons 12 p1947 A71-26864

Ring current as source region for proton auroras, calculating energetic proton lifetimes for model magnetosphere 13 p2064 A71-29167

Geomagnetic tail influence on polar ionosphere proton and electron precipitation, considering ionospheric ionization and polar cap absorption 14 p2300 A71-30034

Electron and proton precipitation observations in auroral, polar cap and outer radiation zones by electrostatic analyzers on earth satellite Injun 5 15 p2397 A71-31756

Lyman alpha emission cross sections for collisions of hydrogen ion and atom beams with thin target nitrogen and oxygen relevant to proton auroral analysis 15 p2397 A71-31763

Electron and proton precipitation, studying effects at high latitudes on 2 February 1969 magnetic storm 16 p2627 A71-33795

Pitch distribution of protons precipitated from auroral radiation region measured by scintillation detector aboard Cosmos 261 satellite in Northern Hemisphere 17 p2731 A71-34320

Precipitating protons measurement in 2.5-200 KeV energy range by OVI-15 satellite, comparing spatial distribution with plasmopause profile 19 p3125 A71-37358

Diurnal variations in equatorial and precipitating low energy solar proton-produced gamma rays in magnetosphere 19 p3125 A71-37359

Equatorial and precipitating solar proton fluxes interrelationship in magnetosphere from riometer absorption in auroral and polar cap regions 19 p3125 A71-37360

Magnetospheric current effects on geomagnetic field structure, noting electron and proton precipitation into auroral zone 19 p3059 A71-38396

Auroral luminosity patterns over northern Scandinavia based on ESRO all-sky camera recordings, noting relationship to electron and proton precipitation 19 p3060 A71-38573

Auroral electrons and protons precipitation patterns from ESRO 1A northern polar cap observations, identifying electron energy zones 19 p3060 A71-38574

Low energy electron and proton precipitation pattern in northern polar region, using low orbit satellite-borne spectrometer 20 p3281 A71-39728

Proton auroras ionization and excitation cross sections of atmospheric constituents by energetic hydrogen ions and atoms, presenting recent measurements and H emission laboratory results 20 p3228 A71-39845

Auroral electron and proton precipitation patterns, noting LF radio noise emissions relationship to low energy electron flux through Cerenkov process 20 p3228 A71-39846

Low energy auroral particle measurements from polar satellites, obtaining electron and proton

precipitations location, and angular and energy distributions 20 p3228 A71-39847

Auroral electron and proton precipitation patterns, measuring airglow emissions 20 p3284 A71-39848

Large and small scale auroral formation dynamics, covering precipitating electron and proton acceleration and plasma instabilities role 20 p3229 A71-39860

Proton precipitation satellite observation, comparing with simultaneous ground based measurement of auroral radar echoes 20 p3285 A71-39887

Magnetospheric plasma observation by Sirio 1 satellite, measuring protons, electrons and magnetic field with sensors 20 p3307 A71-39959

High latitude auroral particle precipitation patterns and connections to plasma sheet, ring current, cusp and radiation belt sources, using rocket and satellite observations 21 p3439 A71-41179

Noon-midnight high latitude proton trapping and precipitation boundary variations associated with polar magnetic substorms observed by ESRO 1A satellite 23 p3719 A71-43127

PROTON PROTUBERANCES
Solar proton and electron events from viewpoint of particle acceleration and magnetic field configuration in active region 03 p0478 A71-14036

PROTON RESONANCE
Auroral protons and substorm resonance concept, eliminating discrepancy between hydrogen emission spectroscopic and direct measurements 09 p1513 A71-22674

Resonant proton drift in asymmetric rotating magnetosphere, discussing flow from boundary or tail to auroral zone 13 p2128 A71-28235

Magnetospheric electric field dynamics, examining resonant protons role in magnetic storms 19 p3127 A71-37760

PROTON SATELLITES
NT PROTON 1 SATELLITE
NT PROTON 2 SATELLITE
NT PROTON 4 SATELLITE

PROTON SCATTERING
Inelastic scattering of protons from In 115, using proton beam cyclotron 01 p0130 A71-10482

Slow positive ion and electron production in collisions of protons and hydrogen atoms with gases of planetary atmospheres 03 p0460 A71-13494

DWBA optical model coupled channels comparison in 2s-1d shell for predicting proton scattering elastic cross sections 06 p0929 A71-17579

Fast neutron energy spectrum from free proton elastic scattering in emulsion plates, studying upper atmospheric altitude and latitude factors 06 p0962 A71-18180

Interplanetary magnetic field irregularities and solar proton diffusion mean free path during 25 February 1969 event 10 p1677 A71-24556

Unaccompanied hadron vs primary proton spectra in atmosphere and proton-air inelastic cross sections above 500 GeV from cosmic ray measurements 12 p1951 A71-27394

Charged particles magnetic scattering on cyclotron instability waves of radiation belt plasma, estimating proton relaxation time 13 p2129 A71-28552

Glauber approximations for elastic and inelastic scattering of protons by ground state hydrogen atoms, comparing with measurements 20 p3272 A71-39578

High energy proton spallation cross sections for several radionuclides from Ti targets, discussing application to lunar materials and meteorites analysis 23 p3706 A71-43199

High energy proton spallation cross sections for several radionuclides from Fe targets, discussing application to beam monitoring and meteoritic studies 23 p3706 A71-43200

PROTON TELESCOPES
U PARTICLE TELESCOPES

PROTON 1 SATELLITE
Electron flux and energy spectra measurements at 200-600 km altitude by Cerenkov counters onboard Proton 1 and 2 19 p3129 A71-38375

PROTON 2 SATELLITE
Atmospheric density variations determination from Proton 2 braking data for aerodynamic drag coefficient, constructing model for rarefied gas flow-satellite interaction 05 p0804 A71-16043

Atmospheric excess radiation flux azimuthal asymmetry in equatorial region, discussing angular intensity distribution data from Proton 2 Cerenkov counter 08 p1354 A71-21011

Atmospheric density variations determination from Proton 2 braking data for aerodynamic drag coefficient, constructing model for rarefied gas flow-satellite interaction 16 p2635 A71-33447

Electron flux and energy spectra measurements at 200-600 km altitude by Cerenkov counters onboard Proton 1 and 2 19 p3129 A71-38375

Atmospheric excess radiation flux azimuthal asymmetry in equatorial region, discussing angular intensity distribution data from Proton 2 Cerenkov counter 20 p3279 A71-39591

PROTON 4 SATELLITE
Proton 4 satellite high and superhigh energy cosmic ray spectrometer, discussing principles of operation and parameters 03 p0426 A71-13833

High energy cosmic ray spectrometer onboard Proton 4, discussing ionization calorimeter, nuclear targets, particle charge and radiation detectors and primary measurements 20 p3283 A71-39755

Proton 4 satellite high and superhigh energy cosmic ray spectrometer, discussing operational principles and parameters 22 p3594 A71-42634

PROTON-PROTON REACTIONS
Strongly magnetized relativistic degenerate electron gas proton-proton reaction rates and electron capture over various temperatures, densities and magnetic field strengths 10 p1661 A71-24305

Proton-proton interactions at 70-600 GeV in Echo Lake cosmic ray experiment, discussing multiplicity, prongs, hadron flux and ionization calorimeter 12 p1933 A71-27391

PROTONS
NT RECOIL PROTONS
NT SOLAR PROTONS

Interstellar H I region Lyman alpha production by suprathermal protons, determining temperature and ionization equilibrium 04 p0640 A71-14873

Eddington theory validity based on formulas connecting light velocity, Planck and gravitational constants and electron, proton and neutron masses 04 p0626 A71-15136

Resonant proton drift in axisymmetric rotating magnetosphere, discussing flow from boundary or tail to auroral region 05 p0800 A71-17178

Pitch angle distribution of protons and helium ions in magnetosphere from numerical solution of Fokker-Planck equation 06 p0964 A71-17285

Subprotonospheric and ion cyclotron whistlers generated by same lightning discharge observed by OVI-10 satellite 06 p0869 A71-17995

Galactic cosmic ray proton and He spectrum measurements in 1968 compared to electron spectra, explaining solar modulation features by models incorporating energy loss effects 06 p0952 A71-18112

Secondary cosmic ray spectrum latitude knee based on nucleon, proton and muon energy spectra 06 p0960 A71-18167

Electron and proton whistlers polarization reversal and mode coupling, explaining magnetic latitude dependence 07 p1062 A71-19667

Galactic cosmic ray proton and He nuclei spectra measurements aboard Pioneer 8 spacecraft over large energy range, considering solar modulation parameters 08 p1355 A71-21626

Type I fluctuations experienced by extensive air showers generated by protons or heavy nuclei, discussing effect on primary cosmic ray energy determination 10 p1661 A71-23858

Magnetospheric numerical model with two-monoenergetic-component proton distribution function, examining ring current belt formation causing inflation 10 p1663 A71-24782

Proton form factors and radius determination from experimental data analysis of cross sections of electron scattering by protons over wide transferred-momentum range 12 p1901 A71-27180

High energy nuclear bursts without accompanying air showers, considering surviving primary protons without inelastic collision in atmosphere 13 p2121 A71-28054

Proton release association with whole blood oxygenation at constant plasma pH and carbon dioxide partial pressure, using alkaline titration 13 p2007 A71-28433

- Solar wind modulation effects on galactic protons and cosmic rays, using radial magnetic field mathematical model and Monte Carlo method
17 p2795 A71-34373
- Air shower pion/proton and neutral/charged ratios at mountain altitude, using cloud chamber, Cerenkov counter and spectrometer measurements
20 p3279 A71-39323
- Auroral substorm model refinements for proton aurora by classifying substorms according to intensity or magnitude
20 p3284 A71-39858
- Trapped protons flux vs L profile measurement on-board sounding rocket near equator, comparing results with calculation from neutron albedo source and atmospheric losses
20 p3284 A71-39881
- Proton form factors and radius determination from experimental data analysis of cross sections of electron scattering by protons over wide momentum transfer range
22 p3578 A71-42454
- Equatorial proton and electron pitch angle distributions in loss cone and at large angles from geostationary ATS 5 satellite observation
23 p3720 A71-43165
- Proton recording equipment onboard automatic interplanetary stations Zond 4 and 5 at 1.5-50 MeV using silicon drift counters
23 p3675 A71-43274
- Nonadiabatic and atmosphere induced energy losses as causes of proton capture in geomagnetic field
24 p3867 A71-45320

PROTOPLASM

- Soviet monograph on coacervates and protoplasm covering colloidal-chemical properties, enzyme catalysts and multiphase cell and organism simulation
21 p3336 A71-40870

PROTOSTARS

- NT T TAURI STARS
Neutral condensations and protostars in H II regions noting original density distributions
06 p0973 A71-18340
- Protosun and primordial solar nebula evolution based on dust particles behavior
11 p1819 A71-25221
- Prestellar evolution, discussing interstellar medium, star development phases, cloud formation, gravitational/thermal instability and protostars
12 p1960 A71-26783

PROTOTYPES

- Missile prototype reliability prediction, using reliability theory concepts in establishing computation and test programs without damage probability determination
02 p0298 A71-12366
- Pilot vacuum pump with piston-rotor compression action to enhance pumping performance, comparing to single stage pumps
22 p3554 A71-42490

PROTOZOA

- NT PARAMEDIA
Hypoxia effects on organism resistance and immunobiological reactivity, noting bacterial and protozoa infections aggravation
13 p2006 A71-28401
- Infusoria adaptation ability to extreme environmental conditions with emphasis on Mars surface
22 p3496 A71-42825

PROTUBERANCES

- NT PROTON PROTUBERANCES

PROVING

- NT THEOREM PROVING

PROXIMITY

- Microwave receiving and transmitting antennas proximity effects on permittivity measurements of dielectric layer
01 p0057 A71-11206
- Proximal changes and stimulus patterns associated with rotation direction evoking visually perceived oscillation
10 p1570 A71-24606
- Microwave receiving and transmitting antennas proximity effects on permittivity measurements of dielectric layer
17 p2697 A71-34258

PSEUDOMONAS

- Phosphoenolpyruvate as enzyme inhibitor of phosphoribulokinase in *Pseudomonas facilis* with respect to ribulose-5-phosphate and ATP
20 p3185 A71-38820

PSEUDONOISE

- PCM telemetry receiving stations testing, comparing bit error probabilities of coherent and noncoherent methods of synchronizing pseudonoise sequences
01 p0033 A71-10890
- Noiselike signals frequency modulation via pseudorandom sequence, deriving relationships for spectra and combined frequency-lag correlation functions
03 p0378 A71-13393
- Coherent communication link pseudonoise synchronization error due to white Gaussian noise and amplitude jitter produced by reference carrier phase error, discussing digital simulation
05 p0725 A71-17072

PSEUDORANDOM SEQUENCES

- Reception and transmission of reduced sidelobe pseudorandom FM signals using quaternary S-sequence synthesis
01 p0037 A71-11082
- Filter output voltage in pseudorandom signals correlation processing, using Duhamel integral
03 p0378 A71-13392
- Multiplex spectrometer for eclipse spectra photoelectric observation, using pseudorandom binary sequences as encoding pattern
03 p0424 A71-13634
- Uniform frequency distribution pseudorandom digital sequences, using shift register generator
04 p0560 A71-14745
- Subsequences of pseudorandom sequences for correlation detection, discussing algorithms for weight distribution moments determination
05 p0724 A71-17062
- Binary pseudorandom codes sequences correlation properties in PSK telemetry
09 p1404 A71-22154
- Interference threshold probabilities of pseudorandom frequency hopped signals in conventional spread spectrum communications relative to Gaussian receiver bandwidth
12 p1881 A71-27428
- Pseudorandom binary codes for improved microwave antenna range measurements by suppressing unwanted reflections
15 p2373 A71-32370
- Binary sequences generated by conventional pseudorandom shift register sequences for communication and system identification
18 p2881 A71-36568

PSYCHIATRY

- Aerospace psychiatry, discussing relationships between personality patterns and environmental factors, adaptability to occupational situations in combat flying and space activities
08 p1238 A71-20722
- Pilot psychic states in flight, including preliminary demobilization, drowsiness, stunning, euphoria and phobias
16 p2536 A71-33576

PSYCHOACOUSTICS

- Broadcast sound loudness level monitor as measuring and indicating instrument, discussing technological and psychoacoustical evolution
20 p3271 A71-39763

PSYCHOLOGICAL EFFECTS

- NT ILLUSIONS
NT OCULOGRAPHIC ILLUSIONS
Human subjective responses to approaching and receding aircraft sounds during flight over stationary observer
01 p0127 A71-10345
- Moderate acoustic stimuli effects, discussing subjective noise ratings relation with physiological and mental state changes
02 p0208 A71-12838
- Physiological and psychological human responses to sonic booms in France, UK and U.S. considered as acceptability criteria
03 p0371 A71-13167
- Mechanical, physiological and psychological responses of man to sinusoidal whole body vibration
08 p1248 A71-21230
- Psychoreactive action caused by flying accident in group, discussing repercussions in civil and military aviation fields
10 p1572 A71-24982
- Noise disturbance near large airports, considering aircraft noise, public annoyance and socio-psychological conditions
12 p1875 A71-27478
- Psychobiological effects of prolonged bed rest in young healthy volunteers from EEG recording, psychological testing and psychomotor performance
13 p2022 A71-29363
- Large subsonic jet aircraft civil pilots performance under physiological and psychological stresses induced during severe atmospheric turbulence
14 p2188 A71-29783
- Young pilot performance in emergency situations including communication system failure and other equipment breakdowns, noting emotional reactions
16 p2534 A71-32831
- Pilot psychic states in flight, including preliminary demobilization, drowsiness, stunning, euphoria and phobias
16 p2536 A71-33576
- Elevated atmospheric pressure effects on human psychophysiological qualities including attention, memory and time-estimating capabilities and nervous processes equilibrium
16 p2536 A71-33578
- Visual evoked potentials and cortical recovery cycle data for normal and psychiatric subjects of various ages
17 p2682 A71-35113
- Zoellner illusion as function of inducing and test lines intersect angle and lines density, deriving error functions
18 p2863 A71-37019

SUBJECT INDEX

- Noise exposure effects on human physiological and psychological functions and performance
20 p3192 A71-38959
- Long term exposure to electric shock and associated stimuli on squirrel monkeys, considering aggressive and manual responses
20 p3187 A71-39070
- Apparent motion effects associated with stationary flashing lights configurations, noting frequency response characteristics analogous to real motion effects in human visual system model
22 p3498 A71-41487
- Presentation modality as encoding variable in short term memory, obtaining mean recall score as function of trials
23 p3639 A71-43113
- Observer psychological response to air defense oriented visual information displays
23 p3640 A71-43904
- Affect adjective checklist assessment of mood changes as function of stress in air traffic controllers
23 p3640 A71-44240
- Biorhythms and related physiological and psychic disturbances, stressing importance in aerospace medicine
23 p3637 A71-44245
- Averaged potentials in vertex and occipital region of human cranium evoked by emotional visual stimuli
24 p3798 A71-45057
- PSYCHOLOGICAL FACTORS
Behaviorally induced hypertension in squirrel monkey following conditioned key-pressing response schedules
01 p0015 A71-11330
- Statistical analysis of airline flight crew psychological unfitness
01 p0028 A71-11598
- Flying motivation loss, considering psychogenesis and physiological causes
05 p0715 A71-16933
- Pilot nervous-emotional state during flight conditions determined from uropepsin excreted in urine
05 p0711 A71-17028
- Complex psychomotor task time duration relation to subtask performance and psychological measures
07 p1047 A71-19459
- Psychopathology identification by manifest phenotypic behavior, discussing syndrome identification, misperceptions and distorted impressions
07 p1042 A71-19697
- Psychological aspects influencing aircrewman capacity to perform useful work, detailing selection, training, operational environment and global factors
08 p1245 A71-20724
- Visual recognition process for simple achromatic image confined within simultaneous-perception viewing angles, deriving hypothetical model based on psychological factors
10 p1567 A71-24162
- Motivation principles in industry based on Maslow theory of hierarchy of needs, discussing selection of supervisory personnel
13 p2167 A71-28798
- Motivations of scientists, engineers and technicians, considering changing nature of R and D projects
13 p2167 A71-28800
- Shower habitability requirements for adequate cleansing of body and hair to satisfy physiological, psychological and social needs of crew members on long space missions
[AIAA PAPER 71-873]
18 p2870 A71-36629
- Psychological training for personality development of aircraft stewardesses for conscious passenger relation establishment
19 p3008 A71-38224
- Soviet book on psychology and outer space covering astronaut experiences and emotions during training and flights, daily routine, equipment, food, habits and personal characteristics
21 p3336 A71-40876
- Sick and injured transportation aboard regular airliners, considering pathological and psychological contraindications
22 p3500 A71-41572
- Psychopathological causes for French Air Force flying personnel inaptitude, considering motivational problems and age factor
22 p3500 A71-41575
- Human adaptive behavior under psychological stress of astronauts tasks posture-motor characteristics, discussing stabilographic platform test results
22 p3503 A71-42041
- Short term central fatigue as causal factor of delayed psychological refractory period in multiple choice visual signal tasks
23 p3634 A71-43864
- PSYCHOLOGICAL INDEXES
U PSYCHOLOGICAL TESTS
PSYCHOLOGICAL TESTS
Visual slant averaging mechanism evidence from binocular disparator tests, considering gradient slant perception theory and neurophysiological averaging mechanism
04 p0546 A71-15170

Psychometric measurements approaches for pilot training questionnaires, considering personality traits standard model

10 p1559 A71-23929

Pretask instructions effect on vigilance task performance, measuring time related signal detection correct and incorrect response percentages

10 p1571 A71-24808

Psychological selection of pupil pilots, discussing statistical correlations between values of some single parameters of Zulliger test and instructional data

10 p1572 A71-24981

Rhesus monkeys concurrent avoidance and appetitive behavior patterns with counter discontinuities in shock proximity indicator tests

10 p1573 A71-25136

Multiple suprathreshold visual and auditory monitoring tasks, evaluating vigilance decrement, individual differences, intertask relationships and channel capacity

12 p1874 A71-27248

Sensomotor activity tests of operator perceiving high speed stimuli in broad visual field for psychological selection of aircraft and spacecraft pilots

13 p2018 A71-28416

Psychological tests for aerial photograph interpreter selection and performance prediction

16 p2534 A71-32829

Psychosociological and medical evaluation of private pilots to promote flight safety

17 p2690 A71-34824

Recognition response time experiments for word number effects in target set, discussing familiarity judgment and response decision

17 p2683 A71-35250

Stimulus familiarization effects on visual selection patterns during exposure to banal and incongruous paired stimuli

17 p2683 A71-35251

Human visual depth impression by gradient patterns, discussing experimental verification for hypothesis concerning perceptual economy principle

17 p2684 A71-35252

Risk additivity in portfolios from experiments on accommodation role in binocular rivalry control

17 p2684 A71-35254

Human visual system differential luminance sensitivity tests using simultaneous stimuli in yes-no procedure

17 p2684 A71-35256

Autokinetic motion of luminous target, relating apparent visual movement to experienced displacement

17 p2694 A71-35739

Human performance in rotating environment, discussing Stromberg Dexterity, pursuit rotor, mental arithmetic, verbal learning and NAMI Ataxia tests

18 p2871 A71-36637

Artificial gravity selection by rats in centrifugal acceleration fields superimposed on weightlessness during sounding rocket flights

18 p2857 A71-36646

Fear measurement and mastery, investigating relationship between experience and electrodermal arousal in responses to stimulus words of varying relevance

18 p2862 A71-36944

Time duration judgment under visual stimulus, noting numerosity effects

18 p2863 A71-37018

Mental work capacity investigation methodology, including Kekchev, Kosilov, Zinchenko, Pratushevich and Kraepelin tests

19 p3006 A71-37446

Test equipment for evaluating human higher nervous activity, noting use for radiotelegraphist selection

19 p3007 A71-37775

Computer generated buffered displays for psychological experiments involving interception, tracking, steering, memory and calculation tasks

21 p3341 A71-40136

Flashing lights attention attraction classification based on experimental results conversion into psychometric scale

22 p3498 A71-41486

Pilot EEG, behavioral and subjective correlates of natural and drug induced sleep at atypical hours, using calculation and vigilance tests

22 p3502 A71-41835

Psychophysiological and conversion mechanisms as unconscious expression of student pilot motivation decrease for further flight training, presenting case histories

22 p3502 A71-41837

Visual stimulus control removal and restoration in rhesus monkeys, analyzing test errors

22 p3497 A71-42860

Psychological screening of pilot trainees, showing neurosis noncorrelation with learning ability to fly

23 p3639 A71-43221

Psychological screening of pilot trainees, investigating Minnesota Multiphasic Personality Inventory test data correlation with learning ability to fly

23 p3639 A71-43222

Human visual system color and edge-sensitive channels confirmation by psychological tests of tuning for orientation

23 p3640 A71-43548

Stereoacuity role in pilot ability to land aircraft at minima, questioning adequacy of Verhoeff depth perception test administration conditions

23 p3637 A71-44244

Psychophysiological loudness and annoyance indices application in sonic boom comfort level evaluation, pulsating noise estimation and sound insulation system effectiveness determination

24 p3799 A71-44399

PSYCHOLOGY

NT MILITARY PSYCHOLOGY

NT PSYCHOACOUSTICS

NT PSYCHOPHYSICS

Perception - Conference, New York, October 1970

07 p1042 A71-19694

Gestalt psychology perceptual organization, analyzing contextual background and residual stimuli, interaction concepts, configurational principles and organismic factors

07 p1042 A71-19696

Psychological and neurophysiological definitions of vigilance, considering alcohol and tranquilizers effects

16 p2533 A71-34040

Psychological correlates of pattern identification tasks and invariance of pattern recognition under rotation, using Kabrisky model of human visual system

17 p2694 A71-35792

Human factors engineering, discussing industrial, engineering and experimental psychology, human relations, research on attention, perceptual motor skills and control systems laboratory

18 p2864 A71-36296

PSYCHOMETRICS

Input-output transformations for judgments of area of circles and paired weights, using nonmetric scaling

05 p0713 A71-16548

Relevant cue placement effects in concept identification tasks employing enforced verbal encoding

07 p1048 A71-19514

Computer aided statistical model of visual evoked potential in man as normality criterion for pathological indicator

09 p1397 A71-22253

Psychometric measurements approaches for pilot training questionnaires, considering personality traits standard model

10 p1559 A71-23929

Psychometric analysis of annoyance by wideband noise with superimposed narrow band component, using multiple regression and scaling method

19 p3008 A71-38061

Flashing lights attention attraction classification based on experimental results conversion into psychometric scale

22 p3498 A71-41486

PSYCHOMOTOR PERFORMANCE

NT PSYCHOSOMATICS

Proprioception role in perception of arm bending and extension during weightlessness and accelerations in aircraft flight along parabolic trajectory

01 p0014 A71-11143

Impulsive activity of neuron populations in cerebral sections controlling psychic and motor functions in man

01 p0014 A71-11149

Slow cortical potentials associated with human motor and mental acts differentiated via spatial distribution

01 p0015 A71-11220

Information feedback distortion and countertraining effects on learning and performance in lever displacement-target test

01 p0026 A71-11415

Figural noise and rotation effects on visual form perception, using random and redundancy figures in figure cancellation task

01 p0026 A71-11417

Vestibular nystagmus and display luminance effects on hand-eye coordination in compensatory tracking of aircraft instrument

02 p0207 A71-12381

Reward magnitude effects on runway performance of rats with intertrial feeding

03 p0372 A71-13693

Pursuit tracking skill acquisition in humans, considering sex, initial ability, age, aptitude and proficiency levels and psychomotor performances

05 p0713 A71-16549

Complex psychomotor task time duration relation to subtask performance and psychological measures

07 p1047 A71-19459

Hypoxia from aerospace medicine viewpoint, discussing respiration physiology, oxygen transport, altitude effects, psychomotor functions, etc

08 p1238 A71-20705

CO exposure effects on human psychomotor performance for blood carboxyhemoglobin saturation levels, using sleep monitored EEG methods

11 p1726 A71-26509

Psychobiological effects of prolonged bed rest in young healthy volunteers from EEG recording, psychological testing and psychomotor performance

13 p2022 A71-29363

Human factors engineering, discussing industrial, engineering and experimental psychology, human relations, research on attention, perceptual motor skills and control systems laboratory

18 p2864 A71-36296

Human psychomotor performance measurements in rotating environments, using Langley complex coordinator and decision response time devices

19 p3006 A71-37275

Human EEG changes and motor analyzer activity during mental visualization of motions

19 p3002 A71-37445

Conditioned motor reactions characterizing higher nervous activity, using logokinetic method

19 p3006 A71-37447

Computer generated buffered displays for psychological experiments involving interception, tracking, steering, memory and calculation tasks

21 p3341 A71-40136

Human perceptual motor skill development in tracking performance, using feedback control system gain and effective time delay as measures

21 p3343 A71-40909

Human adaptive behavior under psychological stress of astronauts tasks posture-motor characteristics, discussing stabilographic platform test results

22 p3503 A71-42041

Healthy males immersion in water containing NaCl, determining modified gravitational field effect on motor functions

22 p3505 A71-42792

Alpha activity parameters during human performance of motor tasks with open and closed eyes

23 p3631 A71-43108

PSYCHOPHYSICS

NT PSYCHOACOUSTICS

World four dimensional and space three dimensional characters and psychophysical sensations dependence on Weber-Fechner law and tritstimulus principle in psychology

09 p1530 A71-23730

Thresholds comparison for angular acceleration derived by subjective cupulometry and by staircase method, determining thresholds for rotation perception and oculogyral illusion

10 p1570 A71-24605

Human color vision investigation by psychophysical methods, discussing spectral sensitivity, pigment absorption and defective color vision as function of stimulus wavelength

12 p1873 A71-26863

Ergonomic evaluation of flight crew working conditions from viewpoint of static and dynamic adaptation of aircraft system design to human psychophysical capabilities

19 p3007 A71-38016

PSYCHOPHYSIOLOGY

Psychophysiological, strict engineering-psychological and systems engineering analyses, solving engineering-psychological problems in large control systems for human operators

03 p0369 A71-13001

Book on visual perception covering physics of light, rods and cones, color vision, brightness psychophysiology, stimulus generalization, etc

06 p0850 A71-17409

Mean period spontaneous EEG as psychophysiological characteristics of higher nervous activity in human individuals

06 p0858 A71-17600

Human operator psychophysiological analysis by memory-activity interdependence simulation, noting buffer memory, reflex system and habit acquisition

07 p1050 A71-20107

Psychological aspects influencing aircrewman capacity to perform useful work, detailing selection, training, operational environment and global factors

08 p1245 A71-20724

Psychobiological stress of prolonged weightlessness/bed rest/ in man in terms of adaptive homeostatic state and decreased sensory-motor-muscular input

11 p1725 A71-26120

Color and music distraction for operator in isolated environment and counteract psychophysiological activity impairment

20 p3193 A71-39225

Psychophysiological reactions to understimulation and overstimulation, noting catecholamine output, heart rate and performance efficiency in humans

21 p3329 A71-40177

Psychophysiological and conversion mechanisms as unconscious expression of student pilot motivation decrease for further flight training, presenting case histories

22 p3502 A71-41837

Two dimensional probabilistic images generation and statistical characteristics determination, noting application to psychophysiological experiments

22 p3518 A71-42422

Psychophysiological loudness and annoyance indices application in sonic boom comfort level evaluation, pulsating noise estimation and sound insulation system effectiveness determination
24 p3799 A71-44399

PSYCHOSES

NT SCHIZOPHRENIA

Endocrine and metabolic effects of noise in normal, hypertensive and psychotic subjects, considering increased corticoadrenal and adrenergic activity
03 p0359 A71-13154

Psychopathology identification by manifest phenotypic behavior, discussing syndrome identification, misperceptions and distorted impressions
07 p1042 A71-19697

PSYCHOSOMATICS

Instrumental learning of cardiovascular and visceral responses and behavioral, physiological and biochemical consequences in relation to psychosomatic therapy
20 p3190 A71-39548

PSYCHOTHERAPY

Brain cortical-subcortical functions in psychic processes, indicating developments in psychotherapy
08 p1241 A71-21940

PSYCHROMETERS

Mean dry bulb temperature estimation during daylight hours by subtracting proportion of average daily range from daily maxima average
18 p2944 A71-36961

PSYCHROPHILES

Thermophilic, mesophilic and psychrophilic anaerobes fatty acid composition, discussing results obtained by mass spectral analysis
15 p2360 A71-32050

PTM [MODULATION]

U PULSE TIME MODULATION

PUBLICATIONS

U DOCUMENTS

PULMONARY CIRCULATION

Direct continuous radiotelemetry of blood pressure measurements taken from aorta, pulmonary artery and inside heart during normal activity of test subjects
03 p0371 A71-13070

Mixed venous oxygen tension oxide determination by nitrogen-carbon rebreathing method, considering pulmonary blood flow and oxygen carrying capacity
03 p0360 A71-13182

Pulmonary gas exchange relation to cyclical pattern of ventilatory flow, considering alveolar dead space and metabolic and respiratory rate effects
03 p0361 A71-13183

CO pulmonary diffusing capacity rebreathing measurements at rest and while exercising, noting relationship to oxygen consumption
04 p0545 A71-15162

Main pulmonary artery velocity profiles in dogs and man, using thin-film resistance anemometer
05 p0706 A71-16324

Lung volume direction and change rate effects on pulmonary vascular conductance and arterial flow in isolated dog lung lobe
05 p0711 A71-16952

Right and left ventricular systolic time intervals from high fidelity pulmonary arterial pulse wave measurements
06 p0852 A71-17875

Acute pulmonary embolism diagnoses, using vasculature angiography
07 p1042 A71-19838

Physiological characteristics in llamas pulmonary circulation at sea level and changes after 5 and 10 weeks at 3,420 m above sea level, noting arterial hypertension
08 p1237 A71-20678

Premature pulmonary valve closure due to severe mitral insufficiency by left atrial V wave retrograde transmission
08 p1240 A71-21888

Excitation-contraction coupling of papillary muscles from hypertrophied right ventricles of cats with pulmonary artery artificial stenosis
09 p1395 A71-23257

Blood plasma hyperosmolality and pulmonary vascular resistance in cats, infusing hyperosmolar solutions of sodium chloride, mannitol, urea, glucose, thiourea and ethylene glycol
09 p1396 A71-23258

Book on gravity and acceleration effects on lungs covering breathing mechanics, ventilation distribution, blood flow, gas exchange, arterial oxygen saturation and pulmonary shunting
[AGARDOGRAPH-133] 09 p1402 A71-23620

Pulmonary circulation - Conference, Prague, June 1969
10 p1560 A71-24121

Volume, compliance and flow resistance of pulmonary vascular compartments of dogs
10 p1560 A71-24122

Stroke-pulmonary blood volume relation and vascular recruitment and distensibility in dogs, allowing independent control of flow, heart rate and left atrial pressure
10 p1561 A71-24123

Gradual unilateral hypoxia effects on pulmonary blood flow partition, noting interaction with hypercapnia
10 p1561 A71-24125

Regional pulmonary vasomotor activity in sitting man, determining pulmonary flow distribution with Xe 133 technique
10 p1561 A71-24126

Pulmonary arterial blood flow regulation by hydrostatic pressure in low resistance circulatory system
10 p1561 A71-24127

Aging effects on blood pressure-flow relations and cardiac output/ventricular end diastolic pressure, discussing pulmonary vascular bed capacity dependence on increasing flow during supine exercise
10 p1561 A71-24128

Age effect on pulmonary circulation in normal subjects, measuring oxygen consumption, cardiac output and pulmonary arterial pressure by floated catheter technique
10 p1561 A71-24129

Closed steady streamline creeping flow in cylindrical cavity applied to bubble or plug train in pulmonary and peripheral capillaries
10 p1571 A71-24614

Pulmonary arterial system impedance and transmission properties, noting hypoxia and serotonin infusion vasoconstrictor effects
11 p1719 A71-25929

Hypertensive heart and pulmonary vascular disease, examining chronic alveolar hypoxia effects
11 p1719 A71-25931

Human heart rate, minute ventilation and oxygen uptake measurement during treadmill and track running at three speeds
12 p1874 A71-27134

Pulmonary circulation regulating factors, examining heart disease effects on lung capillary blood flow
13 p2003 A71-27861

High altitude pulmonary edema in unacclimatized humans, discussing symptoms, etiology incidence and prevention
14 p2183 A71-30277

High altitude blood coagulation, determining hypercoagulability relationship to altered pulmonary hemodynamics
14 p2183 A71-30278

High altitude pulmonary edema syndrome, investigating increased alveolar-arterial oxygen gradients of humans during treadmill exercise
14 p2184 A71-30279

High altitude residents cardiovascular evaluations, showing right ventricular enlargement and reactive pulmonary hypertension
14 p2184 A71-30285

Vago sympathetic nerve trunk stimulation effects on pulmonary blood volume changes magnitudes and pattern in isolated perfused lungs
14 p2187 A71-31135

Validity and reproducibility of cardiac output determination by thermolulution, using dual thermistor catheter introduced in pulmonary artery
16 p2531 A71-33366

Pulmonary blood volume changes in cat due to neurogenic, pharmacological and mechanical effects on cardiovascular system, noting pulmonary function role
16 p2533 A71-34112

M-cholinergic and adrenergic subcortical structures blockage effects on blood flow rate in dog pulmonary circulation system
16 p2534 A71-34113

Automatic regulation of volumetric blood flow rate during artificial blood circulation, using electromechanical system for controlling arterial pump of cardiopulmonary machine
19 p3010 A71-38641

Right and left heart and pulmonary blood volume determination, using radiocardiograms and analog computer analysis
20 p3191 A71-38801

Analog computer analysis of radiocardiograms, determining cardiac function and pulmonary blood volume
20 p3191 A71-38802

Pulmonary nitrogen washout and carbon monoxide uptake, developing dynamic mathematical models for volume and distensibility distributions in airways and alveoli
20 p3193 A71-39441

Pulmonary circulation pressure and flow telemetry of free ranging intact animals, describing instrumentation and technique for transduction and transmission
23 p3640 A71-44243

Pulmonary blood flow and carbon monoxide diffusing capacity uneven distribution measurements, determining body position effects
24 p3798 A71-44782

PULMONARY FUNCTIONS

Human gas metabolism under rarefied atmosphere via gas chromatography, discussing pulmonary ventilation determination and exhaled samples collection equipment
01 p0025 A71-11142

Lung volume direction and change rate effects on pulmonary vascular conductance and arterial flow in isolated dog lung lobe
05 p0711 A71-16952

Air blast effects on pulmonary ventilation, gas exchange, venous-arterial shunt and blood gas parameters
06 p0851 A71-17601

Lipid peroxidation in pulmonary hyperoxia, noting effects of hyperbaric oxygen, ascorbic acid and ferrous iron
06 p0851 A71-17604

Right and left ventricular systolic time intervals from high fidelity pulmonary arterial pulse wave measurements
06 p0852 A71-17875

Respiratory mechanics and ventilatory response to carbon dioxide during positive pressure breathing in conscious man
06 p0861 A71-18379

Time constant for collateral ventilation in human, dog and pig lungs under various physiological conditions
06 p0856 A71-18385

Oxygen tension effect on pulmonary diffusion capacity and postnatal lung growth in rats under hypoxic, normoxic and hyperoxic atmospheres
10 p1559 A71-23899

Pulmonary vasoconstrictor response to temperature dependent acute hypoxia, using isolated rat lungs with heparinized homologous blood under constant volume pulsatile inflow
10 p1561 A71-24124

On-line computer technique for pulmonary ventilation continuous/automatic measurement of cardiac patients exercise and work tolerances
11 p1734 A71-25255

Alveolar air samples of human subjects at various altitudes, determining gas composition and partial pressure
12 p1876 A71-27658

Abdominal pressure decrease resulting in transpulmonary pressure cranio-caudal gradient increase under gravitational effect simulation
13 p2008 A71-28437

Pulmonary oxygen toxicity, considering composition of endobronchial saline extracts of rats and edema development
13 p2015 A71-29362

Lung diffusing capacity for oxygen during exercise and alveolar hypoxia measured without blood samples by ear oximeter
13 p2023 A71-29492

Position, exercise and lung volume effects on healthy males pulmonary diffusing capacity for CO at rest and during exercise
13 p2015 A71-29493

Airway smooth muscle relaxation mechanical consequences concerning lung volumes, airway conductance, isovolume pressure flow, maximum expiratory flow volume and static lung recoil
13 p2024 A71-29497

Pulmonary oxygen toxicity development rate and effects on lung volume and alveolar-arterial gas exchange during oxygen breathing
13 p2024 A71-29501

Human hypoxic ventilatory drive data for high altitude breathing, noting motivation reduction inversely related to time and altitude
14 p2185 A71-30288

Ventilatory control in acute hypoxia, detailing polycythemia effects on respiratory chemoreceptor sensitivity
14 p2185 A71-30289

Regulation patterns of external respiration rate in man during physical exertion, showing load dependent pulmonary ventilation in accord with minimum energy expenditure principle
15 p2358 A71-31321

Diaphragm mechanics, discussing thoracic pressure-lung volume and air flow relationships of respiratory system during electrophrenic stimulation in men and cats
16 p2530 A71-33239

Pulmonary blood volume changes in cat due to neurogenic, pharmacological and mechanical effects on cardiovascular system, noting pulmonary function role
16 p2533 A71-34112

Oxygen pulmonary diffusion capacity estimation by rebreathing procedure based on gas-blood partial oxygen-pressure equilibration
17 p2678 A71-34173

Human physiological responses to rotating environment, evaluating heart rates, blood pressure, pulmonary functions, visual observations and vital capacities [ALAA PAPER 71-890]
18 p2856 A71-36639

Pulmonary diastolic pressure relation to left ventricle and atrium of patient with diagnostic heart catheterization at rest
19 p3004 A71-38296

Rabbit tolerance to pulmonary edema by lung exposure to low ozone dosage
19 p3009 A71-38558

- Low ozone dosage exposure effects on rabbit lung endogenous defense mechanisms 19 p3009 A71-38559
- Respiratory reflex mechanism of deep breath occurrence after period of airway occlusion in rabbits related to stimulation of vagal receptors 20 p3187 A71-39040
- Inspired oxygen concentrations effects on arterial and mixed venous pH, carbon dioxide uptake and oxygen partial pressure in normal subjects 20 p3189 A71-39442
- Human expiratory oxygen and carbon dioxide partial pressure and dissociation curves for intrapulmonary gas mixing, using mass spectrometry 21 p3328 A71-40098
- Pulmonary dissipation of gas emboli produced by oxygen, nitrogen and carbon dioxide intravenous injection in unanesthetized sheep with chronically implanted ultrasonic Doppler flow probes 21 p3330 A71-40342
- Pulmonary antibacterial defenses with pure oxygen breathing mice, noting inhibition of early interpulmonary clearance of *Staphylococcus aureus* and enhanced clearance of *Klebsiella pneumoniae* 22 p3487 A71-42241
- Respiratory function and gas metabolism shift under high transverse accelerations in reclined centrifuged subjects 22 p3495 A71-42795
- Pulmonary carbon monoxide diffusing capacity of sea level and high altitude dwellers at various altitudes, noting early postnatal lung growth effects 24 p3797 A71-44778
- PULMONARY LESIONS**
- Generalized hyperoxia and local effects of oxygen on lungs in etiology of pulmonary damage due to oxygen, noting nitrogen and carbon monoxide effects 08 p1237 A71-20681
- Succinic dehydrogenase activity inhibition and pentobarbital sodium protection of lung tissue in mouse breathing oxygen at atmospheric pressure 11 p1721 A71-26125
- PULSARS**
- Crab pulsar optical pulses time of arrival measurements, discussing various emission mechanisms as cause for pulsar slowdown characteristics 01 p0153 A71-10363
- Pulsar distances tabulation, discussing possible IR emission 01 p0153 A71-10365
- Pulsars characteristics including rotation periods, age, magnetic field strength, gravitational fields and translational motion 01 p0160 A71-11066
- Pulsars periods distribution at different galactic latitudes 01 p0161 A71-11339
- Pulsars as rotating neutron stars with frozen-in magnetic field, accounting for energy and angular momentum losses due to gravitational radiation 02 p0300 A71-12473
- Vela pulsar optical emission identification using phase selective image tube photographs 02 p0315 A71-12658
- Vela pulsar optical emission identification by photoelectric measurements 02 p0315 A71-12659
- Pulsar pulse arrival times measurement for general relativity theory test, determining positions and period change rates 02 p0315 A71-12660
- Gas heating near quasars, Seyfert galaxies nuclei and pulsars by induced Compton effect 02 p0317 A71-12872
- Pulsar radio signal characteristics, examining pulse profiles, nulls interstellar scintillation and optical and X ray bursts 02 p0318 A71-12914
- Pulsar PSR 1237 plus 25, noting correlated subpulse structure with Fourier analysis method 02 p0318 A71-12951
- Physical processes in galactic and extragalactic sources of nonthermal radio emission, assuming pulsars as principal magnetic field and cosmic rays sources 03 p0483 A71-13201
- Small angular diameter radio source in central Crab Nebula association with pulsar NP 0532 based on spectra and pulse duration 03 p0483 A71-13203
- Pulsar radio wave generation, discussing emission theory and frequency independence of beam width and polarization 03 p0493 A71-14208
- Pulsar free rotational dynamics accounting for amplitude and time variations in signals, considering nonrigidity and viscosity effects 03 p0493 A71-14211
- Runaway pulsar formation and ejection in supernova collapse, fragmentation, condensation, radiation and disruption 04 p0643 A71-15046
- Pulsar NP 0532 average polarization absence due to Crab Nebula depolarization or unpolarized radiation on emission 04 p0643 A71-15047
- Pulsar radiation intensity time variations at radio frequencies, noting observations of CP 1133 04 p0649 A71-15273
- Crab Nebula pulsar radio pulses polarization using polarimeter feed in Mark I telescope comparison to analysis by integration and photographic recording 04 p0649 A71-15274
- Coherent emission mechanisms for pulsar models, discussing plasma wave conversion into radio emission 04 p0650 A71-15582
- Nonpulsing pulsar model, discussing idealized neutron star with spin axis aligned with uniform internal magnetic field 04 p0650 A71-15585
- Crab Nebula pulsar NP 0532, examining radio pulse shapes, flux densities and dispersion 05 p0800 A71-15926
- Phase modulation drift of radio emission from pulsar MP 0031-07 05 p0801 A71-15927
- Extragalactic pulsars visible and X ray detection and luminosity 05 p0801 A71-15928
- Pulsars CP 0328, CP 0834, CP 1133 and CP 1919 radio spectra, examining interstellar scintillation model, transverse velocities and line widths 05 p0802 A71-15939
- Radio pulsars optical counterparts, comparing absolute intensity with Crab Nebula NP 0531 05 p0802 A71-15940
- Pulsars relationship to very high energy cosmic ray electron propagation, examining far IR background and radiation sources 05 p0797 A71-15941
- Pulsar number-period distribution, using oblique rotator model under electromagnetic and gravitational torque effects 05 p0804 A71-16106
- Crab Nebula pulsar NP 0532 light flash arrival times, suggesting oscillations due to growing amplitude instabilities 05 p0806 A71-16201
- Optical pulsar search, using Fourier and correlation techniques 05 p0806 A71-16207
- Interstellar scintillation index and fading time of pulsar signals at 2388 MHz 05 p0807 A71-16208
- Pulsars optical and X ray luminosity secular decrease, examining emission close to velocity of light radius 05 p0807 A71-16209
- Pulsar PSR 1237 plus 25 pulse sequence change, examining profile at 318 MHz 05 p0807 A71-16213
- Crab pulsar magnetic field structure measurements, using optical wavelengths linear polarization 05 p0808 A71-16454
- Crab Nebula pulsar PSR 0531 plus 21 at 410-1664 MHz, noting mean pulse profiles and spectral indices 05 p0812 A71-16697
- Quasi-stellar radio sources similarity to pulsars based on similar characteristics 05 p0814 A71-17235
- Pulsar MP 0628 meter wave radiation, noting linear polarization and frequency dependence of pulse rate 06 p0965 A71-17387
- Pulsar data tabulation of positions, dispersion measures, and class I pulse periods and widths 06 p0966 A71-17676
- HF modulation of optical, X ray and gamma radiation of Crab pulsar, discussing radiation production mechanisms 06 p0970 A71-18033
- Pulsar 150 MHz radiation linear polarization measurements, correlating interstellar Faraday rotation with determinations from neighboring extragalactic radio sources 06 p0971 A71-18242
- Galactic magnetic field observation, investigating cluster polarization, Zeeman effect, pulsar rotation and signal dispersion, interstellar cloud elongation and models 06 p0972 A71-18331
- Maserlike pulsar radiation mechanism using Coulomb bremsstrahlung near strong quantizing magnetic field 07 p1190 A71-18858
- Precursor pulse disappearance of Crab Nebula pulsar NP 0532 at 606 MHz 07 p1190 A71-18864
- Electromagnetic radiation pumping by stimulated Compton scattering near pulsars, determining secondary emission frequencies from energy and momentum conservation laws 07 p1192 A71-19292
- X ray observations of NP0532 and other radio pulsars and galactic X ray sources 07 p1200 A71-20052
- Crab Nebula pulsar characteristics, discussing neutron star hypothesis, optical counterparts, magnetic fields, mass, radius and origin 07 p1201 A71-20214
- Radiotelescopic observations of period and declination of pulsar Mp 0450 in South India 07 p1201 A71-20499
- Long term fluctuations in pulsar radiation intensity due to interstellar scintillation 08 p1359 A71-20935
- Crab Nebula and pulsar NP 0532 X ray spectra discussing pulse profile, emission and interstellar absorption 08 p1353 A71-20984
- Pulsars as rotating magnetic neutron stars, examining radio emission via maser amplification 08 p1363 A71-21174
- Pulsar model consisting of rotating neutron star with strong magnetic field 09 p1517 A71-22337
- Pulsar association with supernova remnants as energy source for supernova explosions, considering Crab Nebula, Vela X, Cas A and eta Car observations 09 p1518 A71-22350
- Crab Nebula pulsar NP 0532, discussing possible planetary system existence 09 p1522 A71-22975
- Pulsar radiation circular polarization component Stokes parameter, noting average value different from zero 09 p1522 A71-22978
- Crab Nebula pulsar magnetic field structure, discussing linear polarization modifications and wisps 10 p1668 A71-23870
- Pulsar dispersion measures for spatial distributions above galactic plane, determining mean interstellar electron density of local spiral arm 10 p1671 A71-24304
- Planetary mass system as pulsar timing error sources, noting change in barycenter of solar system 10 p1675 A71-24493
- Pulsar oblique magnetic rotator model, noting large amplitude EM traveling wave effects on electron motion 10 p1679 A71-24956
- Pulsar CP 0328 data at 1420 MHz, examining mean intensity and long term fluctuation due to interstellar scintillations 10 p1680 A71-25008
- Pulsar mechanism relation to solar cycle mechanism, discussing magnetic flux correlation to period 10 p1681 A71-25073
- Southern galactic plane search for high dispersion pulsars, giving calibration data for Molonglo searches 11 p1820 A71-25295
- Periodic rotational LF synchrotron model of magnetic neutron star for pulsar radiation 12 p1947 A71-26649
- Pulsars CP 0950 and CP 1133, examining pulse spectra characteristics in 83-111 MHz frequency range 12 p1963 A71-27076
- Relativity and neutronization effects on radial pulsations and density decrease of rotating cold white dwarfs near stability loss, using energetic method 12 p1966 A71-27236
- Maximum toroidal magnetic fields of rotating neutron stars dependent on central density, using relativity corrections to plasma hydrodynamic and Maxwell equations 12 p1966 A71-27237
- Cosmic rays origin from pulsar model with particles accelerated by magnetic dipole radiation, producing equal energy spectrum 12 p1948 A71-27365
- Pulsar electrodynamics, considering oblique rotator with dense magnetosphere to supply particles for Gunn-Ostriker mechanism 12 p1968 A71-27539
- Gravitational waves from rotating relativistic neutron stars (pulsars) in far field region, assuming small velocity and spherical deformation 13 p2133 A71-27971
- Crab Nebula pulsar NP0532 radio observations, noting long term slowing down and irregular perturbations in periodicity 13 p2137 A71-28591
- Critique on pulsar distance estimates based on dispersion measure, introducing period luminosity function 13 p2137 A71-28592
- Rotating Jacobi ellipsoid evolution by gravitational waves emission, discussing triaxial nonaxisymmetrical configurations for rapidly rotating pulsars 13 p2140 A71-29000
- Pulsar nature and radiation mechanism, examining rotating neutron stars structure and atmospheric dynamics 13 p2140 A71-29041
- Pulsar CP 0834 pulse energy fluctuations spectra secondary periodicities fluctuations from radioheliographic observation 13 p2141 A71-29099

Long term pulsar intensity observations, noting periodic variations and power spectrum analysis 13 p2143 A71-29270

Neutron stars origin and nature, discussing pulsars structure, mass and frequency variations 13 p2143 A71-29297

Pulsar cosmic rays emission mechanisms, noting high energy particle, X and gamma rays direction 13 p2131 A71-29298

Pulsar signature on diffuse X ray background, converting fraction of luminosity into k series photons 14 p2297 A71-29584

Pulsar MP 0628 meter wave radiation, noting linear polarization and frequency dependence of pulse rate 14 p2310 A71-30166

Pulsar oblique rotator model wobble and alignment time scales, considering Crab and Vela pulsars precession damping mechanism by internal friction of crust 14 p2313 A71-30428

Pulsars origin from type 2 supernovae, deriving characteristics of exploding massive stars 14 p2313 A71-30436

Radio pulses from Crab Nebula pulsar NP 0532, determining multipath scattering delay distribution function and distortion 14 p2314 A71-30641

Pulsars 0527 and 0531 as remnants of binary star supernova explosion, considering mass exchange and measured proper motion of 0531 and Crab Nebula 14 p2315 A71-30657

Crab pulsar optical time of arrival measurements from four observatories, discussing errors in data reduction to inertial reference frame 14 p2315 A71-30658

Neutron stars with pulsar characteristics in binary systems, discussing matter accretion relationship to X ray source evolution 15 p2483 A71-31342

Cosmic ray particles acceleration in pulsar strong electromagnetic fields, investigating refractive index effects 15 p2473 A71-31717

High energy pulsed gamma rays detection from pulsars emission based on time averaged phase histograms 15 p2479 A71-31838

Crab pulsar frequency increase associated with nebula activity surge 15 p2494 A71-32549

Crab nebula pulsar model, discussing charged particles acceleration to relativistic energies by intense LF electromagnetic wave 16 p2632 A71-33236

Pulsating gamma ray flux from pulsar NP 0532 in energy range from 250 keV to 2.3 MeV 16 p2626 A71-33389

Rotation measure and intrinsic angle of Crab pulsar emission, discussing optical and radio radiation origin 16 p2634 A71-33390

Crab Nebula pulsar rotation and magnetic axes disposition from pulse shape and polarization data at optical and radio wavelengths 16 p2634 A71-33391

Supernovae outburst remnant radio emission from Crab Nebula, discussing synchrotron mechanism and connection with pulsars 16 p2635 A71-33472

Exploding universe phenomena, considering supernovae, exploding galaxies, Crab Nebula, pulsars, quasars and radio galaxies 16 p2643 A71-34036

Pulsar emission data, presenting average phase shapes and pulse to pulse intensity fluctuations 17 p2797 A71-34372

Pulsars as neutron stars, explaining fast rotation by tendency to conserve angular momentum during compression 17 p2804 A71-34857

Gamma rays in Crab Nebula pulsar, considering synchrotron radiation and inverse Compton scattering as production mechanisms 17 p2796 A71-35335

Pulsar polarization characteristics and pulse profile observations in 250-450 MHz range 17 p2807 A71-35417

Neutron star cooling behavior models based on neutrino emission theory, explaining galactic steady state cosmic rays and pulsar radiation 18 p2959 A71-35931

Pulsar radiation generation by charged particles nonlinear Thomson scattering of strong LF electromagnetic wave and nonthermal radio emission 18 p2960 A71-35940

Cyg X-1 X ray pulsar age determination and emission model speculations based on observation data for supernova remnant and radio counterpart absence explanation 18 p2962 A71-36151

Compton synchrotron spectra of gamma rays produced in Crab Nebula by photons scattered by relativistic electrons, assuming magnetic field due to pulsar 18 p2963 A71-36154

Pulsed X ray emission from NP 0532 at 20-200 keV measured by balloon flown sun sensor controlled azimuth stabilized detectors 18 p2958 A71-36760

Coherent neutral sheet radiation from pulsars, examining relationship between pulsation-driving energy source and mechanisms for pulsed emission 18 p2958 A71-36928

Scorpius X-1 cocoon pulsar thermal X ray emission model, describing hot gaseous region around rotating neutron star 18 p2969 A71-37043

Temperature limit determination of rotating neutron stars based on heat dissipation due to slowing by frictional forces, noting Crab and Vela pulsars 19 p3131 A71-37337

Pulsed emission of hard X rays from Crab Nebula pulsar NP 0532, using balloon-borne telescope 19 p3124 A71-37338

Pulsars CP 0950 and CP 1133, examining pulse spectra characteristics in 83-111 MHz frequency range 19 p3133 A71-37426

Pulsars electromagnetic radiation, considering bunch of relativistic charged particles 19 p3134 A71-37513

Crab Nebula pulsar timing measurement leading to model involving inflation of closed magnetosphere with explosively released plasma 19 p3142 A71-38007

Neutron star models based on Nemeth-Sprung equation of state, discussing dynamic stability and Crab pulsar central density 19 p3143 A71-38161

Short term timing stability of Crab pulsar clock from telescope observations at 256 and 405 MHz 19 p3144 A71-38173

Pulsar periods change rate and radio luminosity decay, discussing magnetic field braking 20 p3286 A71-38762

Crab pulsar NP 0532 low energy gamma radiation emission data, observing flux ratios and pulsations 20 p3278 A71-39109

Crab pulsar observations analysis by means of nonaligning or stabilized oblique rotator, discussing starquake theory and stressed magnetic field instability as alternative interpretations 20 p3288 A71-39115

Gas heating by LF radiation due to Compton scattering near quasars, Seyfert galaxies nuclei and pulsars 20 p3289 A71-39293

Linear polarization of pulsar PSR 22 18 plus 47 radio emission pulses, attributing periodic fine structure of spectrum to rotation of polarization plane in interstellar medium 20 p3291 A71-39316

Gamma ray production by pulsar-emitted particles interaction with surrounding nebula matter, investigating radiation intensity time variation 20 p3279 A71-39325

Critique of Smith oblique rotator model for Crab pulsar radiation, concerning observation of optical pulse position angle variation and interpulse offset location 20 p3279 A71-39402

Hard X ray pulsations limits in higher energy range from Cyg X-1, comparing with Crab Nebula pulsar 20 p3279 A71-39407

Negative search for radio pulsar near Cyg X-1 or associated variable radio source, using fast holding algorithm 20 p3292 A71-39408

Crab Nebula pulsar NP 0532 pulsed gamma emission from balloon flight measurements with spark chamber equipped gamma ray telescope 20 p3283 A71-39754

Crab Nebula and pulsar gamma ray emission from synchrotron or inverse Compton mechanism 20 p3301 A71-39919

Crab Nebula pulsar radio properties, observing energy release due to increase in period, multipath propagation effects, intensity and time dependence 20 p3302 A71-39923

Identity relation of LF compact source to Crab pulsar NP 0532 with respect to interstellar scattering 20 p3302 A71-39924

Radio pulse shapes from NP 0531 observed with swept frequency machine, showing broadening due to interstellar scattering 20 p3302 A71-39925

Structure and polarization differences of strong pulses from pulsar NP 0532, showing discontinuous frequency spectrum 20 p3302 A71-39926

Time variable dispersion of Crab Nebula pulsar, showing coincidence with occultation by solar corona 20 p3302 A71-39927

Crab Nebula optical pulse timing, noting neutron star crust rotation speedup and relaxation, eccentric planetary orbits and sinusoidal effects 20 p3302 A71-39928

Crab Nebula pulsar timing observations, correcting arrival times to solar system barycenter and dispersion effect 20 p3302 A71-39929

Short time variability of intensity of optical pulses from pulsar NP 0532, using telescopes 20 p3303 A71-39930

Time arrival measurements of optical pulses from Crab Nebula pulsar correlated to solar system barycenter 20 p3303 A71-39931

Pulsars luminosity, z-distance and period distribution in Galaxy, comparing supernova remnants 20 p3303 A71-39933

Comparative properties of pulsars, discussing Crab Nebula pulsar period, outside radio band emission, amplitude variations and interpulse intensity 20 p3303 A71-39934

Polarization characteristics of pulsars, considering angular position changes due to interstellar magnetic field using Faraday rotation measurements 20 p3303 A71-39935

Timing measurements of pulsar NP 0527 relating frequency, position and transverse velocity with NP 0532, excluding origin in supernova explosion 20 p3303 A71-39936

Vela pulsar interstellar scattering, studying pulse broadening, rotation measure and radiation origin near magnetic pole 20 p3303 A71-39937

Pulsar pulsed optical radiation search, noting dependence on determination of accurate positions by radio methods 20 p3303 A71-39938

Visible optical pulsars search with Fourier and correlation techniques in X ray sources, supernova remnants, white dwarfs, IR stars, planetary nebulae, etc 20 p3304 A71-39939

Observation probability of orbital motion and mass transfer of pulsars in close binary systems, excluding supernova explosion origin for runaway velocities 20 p3304 A71-39943

Supermassive pulsar model of quasars periodicity and luminosity for Kelvin-Helmholtz contraction, concerning gravitational-rotational energy transformation 20 p3304 A71-39946

Multiple pulsar ejection in supernova core collapse and neutron star formation energy loss 20 p3305 A71-39947

Crab Nebula pulsar magnetosphere, considering model of rotating magnetized neutron star rate of energy generation and rotation law exponent 20 p3305 A71-39948

Pulsar radio emission via maser amplification, presenting model based on electrons behavior in intense magnetic field 20 p3285 A71-39949

Radio pulses from pulsars, noting relativistic energy of particles from volume emissivity and surface flux density 20 p3305 A71-39950

Radio pulses from pulsars based on model of coherent synchrotron radiation from magnetosphere trapped charged particles 20 p3285 A71-39951

Pulsar radiation from oscillating interface with steady current sheet between rotating radiating magnetic dipole and external plasma 20 p3285 A71-39952

Pulsar radiation beaming due to strong magnetic field, computing Compton scattering and opacity 20 p3285 A71-39953

Crab Nebula pulsar and extra emission from collapsed star magnetosphere, accounting for physical characteristics with nonthermal plasma mechanism 20 p3285 A71-39954

Pulsars radio wave emission characteristics, intensity variation, duration, bandwidth, similarity to space radio beacons and evidence as neutron stars 21 p3442 A71-40144

Radio stars classes, discussing red dwarf flare, red supergiants, blue dwarf companion, novae, pulsars and X ray stars 21 p3448 A71-40582

Polarization and pulse profiles of pulsars at 410 and 1665 MHz, indicating radiation originating close to star surface 21 p3453 A71-41244

Pulsars properties, examining pulse profile and duration, subpulse phase modulation and polarization 22 p3598 A71-41918

Period-age distribution of pulsars, using radio and optically emitting neutron star model 22 p3599 A71-41925

UK 5 spacecraft experiments in X ray astronomy, investigating spatial distribution and energy spectra of emissions in space, polarization and pulsar periodicities 22 p3610 A71-42015

Balloon obtained Crab pulsar gamma ray emission data searched for pulsation above 50 MeV 22 p3592 A71-42220

Pulsar radio emission from expanding charge sheets moving relativistically along dipolar magnetic field near neutron star polar caps, calculating energy distribution 22 p3604 A71-42336

Cosmic rays origin, discussing nuclear, electron and electromagnetic components, supernovae, pulsars, white dwarfs and gas motions in Galactic Center 22 p3594 A71-42550

Southern pulsars pulse energy flux average nightly values at 80 MHz 22 p3606 A71-42602

Pulsar characteristics suppression in neutron stars of binary systems, discussing matter accretion relationship to X ray source evolution 22 p3606 A71-42617

Pulsar speedup due to neutron starquakes, deriving self gravitating elastic incompressible sphere model for time prediction 23 p3722 A71-42894

Pulsar radio pulse shape and structure, discussing pulse widths and polarization angle change 23 p3769 A71-43989

Mode changing in pulsar radiation, observing intensity profiles and polarization characteristics 23 p3769 A71-43995

Tables of Crab Nebula pulsar radio pulse arrival times at Arecibo observatory 24 p3867 A71-44435

Pulsar 0833-45 LF radiation spectrum decrease explained by pulse broadening due to interstellar scattering 24 p3868 A71-44565

Pulsar high energy cosmic ray periodic flux detection with favorable interstellar magnetic field configuration along line of sight 24 p3865 A71-44569

Pulsar CP 0950 radio emission intensity variation measurement, using dispersion removal technique for interstellar medium signal distortion 24 p3871 A71-44903

Quasar and pulsar gamma ray absorption by critical energy collisions with low energy photons 24 p3866 A71-44917

Optical pulsar NP 0532 circular polarization upper limit from measurements throughout light curve 24 p3872 A71-44918

Pulsar JP 1933 distance lower limit from 21 cm absorption and galactic rotation model, noting scintillation parameters consistency with observations in thin screen model 24 p3873 A71-45141

PULSATING FLOW
U UNSTEADY FLOW
PULSE AMPLITUDE
 Light echo obtained via giant laser pulse peak overlapping in space and time 01 p0095 A71-11034

Pulse rise, fall times and peak current values in sawtooth-voltage generator relaxation circuits with avalanche transistors 03 p0387 A71-13998

Self giant pulsed operation of ruby and Nd-YAG lasers obtained by mirror misalignment 04 p0606 A71-14714

Pendulum clock with contactless drive for isochronal autooscillation period, outlining pulse amplitude and duration stabilization 04 p0592 A71-14863

Nonuniform feed effects on height of electrospar surface machining microsperties, investigating linear elliptical interpolator pulse sequence 08 p1296 A71-20851

ELF atmospheric pulse trains recordings at widely separated stations for spectral amplitude ratio differentials, using lightning and ionospheric heating mechanisms 09 p1489 A71-23445

Random response of stationary linear system to pulse noise in time with independent amplitudes 10 p1588 A71-24901

Auroral pulsation analysis from rocket soundings, investigating oxygen green linear excitation sources 11 p1753 A71-25549

Output pulse amplitude from lithium-drifted detector-amplifier combination under conditions of carrier diffusion and bulk and surface recombination 11 p1802 A71-25804

Air shower radio pulse amplitude variations with zenith and azimuth angle, distance from shower axis and primary energy, examining frequency spectrum characteristics 13 p2127 A71-28105

Angular momentum influence on linear axisymmetric motions of centrally condensed bodies, considering finite amplitude pulsations of rapidly rotating columns 15 p2481 A71-31202

Pc-type micropulsation amplitude variation correlation at separate places up to 10,000 km distances, suggesting pi-type as cause 15 p2395 A71-31435

Large amplitude periodic X ray pulsations from Centaurus X-3, observing abrupt source intensity and pulse rate changes 17 p2798 A71-34375

Optimum pulse transmission through thin exponentially inhomogeneous plasma region for maximum amplitude signal reception, using matched filter theory 17 p2788 A71-34768

Computer controlled pulse counting technique application to astronomical photoelectric photometry for improved telescope efficiency 17 p2740 A71-34989

Structure and polarization differences of strong pulses from pulsar NP 0532, showing discontinuous frequency spectrum 20 p3302 A71-39926

Comparative properties of pulsars, discussing Crab Nebula pulsar period, outside radio band emission, amplitude variations and interpulse intensity 20 p3303 A71-39934

Nanosecond solid dielectric discharger fired by Q switched ruby laser for commutation of coaxial line forming high amplitude voltage pulses 24 p3835 A71-45238

Electron multiplier pulse height distribution for single electron input, investigating relative variance correlation with statistical fluctuations of gain 24 p3811 A71-45329

PULSE AMPLITUDE MODULATION
 Multiplexed PAM signal transmission over random time multichannel and diversity systems, discussing optimization for receiver frequency response by numerical solution [IEEE PAPER 70-TP-47-COM] 05 p0723 A71-17053

Traveling wave phototube for demodulating pulse amplitude modulated laser emission, investigating equivalent resistance 06 p0900 A71-18184

PAM/FM radio telemetry coder including electronic commutator for sampling and sequential time control, discussing design, operation, performance and reliability 06 p0870 A71-18399

Eight channel micropowered miniature biomedical PAM/FM telemetry system for implantation in research subjects aboard orbiting space station 14 p2189 A71-30930

PAM data transmission systems timing recovery, discussing maximum likelihood estimation method for timing parameter from random data 15 p2377 A71-32314

Arbitrary shape pulsed AM systems prediction technique improvement, using time-domain signal 15 p2373 A71-32371

Rapidly converging first order training algorithm for adaptive equalizer design in PAM signal reception, using variable step sizes for mean-square error minimization 16 p2545 A71-32821

PAM signal transmission through statistically rough waveguide, calculating wall roughness effects on transient response by multiple scattering theory 23 p3645 A71-43566

Single- and multivariable discrete nonlinear control systems with pulse amplitude modulation, deriving frequency criteria for stochastic stability in mean 24 p3812 A71-44397

PULSE CODE MODULATION
NT DELTA MODULATION
 NRZ PCM signal conditioning, bit and group synchronization and decommutation techniques 01 p0034 A71-10901

Optical PCM communications system with lithium tantalate traveling wave modulator capable of one gigabit/sec transmission and detection rate 02 p0215 A71-12042

Gigabit PCM data communications system using functional circuits with microstrip interconnect 05 p0719 A71-16152

Band limiting effects on PCM/split phase signal detection, considering signal to noise ratio degradation 07 p1061 A71-19263

PCM bit synchronization and signal detection by nonlinear filter theory, giving optimum sequential estimator 07 p1061 A71-19536

Bandlimiting effects on PCM/split phase signal detection 07 p1066 A71-20431

Long distance PCM-AM pulse regenerator for 4 GHz band and millimeter wave communication 08 p1265 A71-21285

PCM TV photographic data communication for grand tour of outer planets, emphasizing adaptive information-preserving data compression system for optimal performance 08 p1254 A71-21346

PCM signal encoding redundancy reduction using discrete code transformation, considering telephony implementation 08 p1255 A71-21593

Power spectral density /PSD/ analysis of multilevel binary coded signals for high density PCM recording 09 p1412 A71-22784

Acquisition system consisting of positioning of local station burst signal in time slot for PCM-TDMA satellite communication system, discussing design and performance tests 13 p2034 A71-29393

Concorde SST flight test equipment installation with PCM recording and visual instruments 14 p2174 A71-30055

Error estimates in transmission of pulse code telemetering signals by nonredundant binary code through asymmetric channel 16 p2543 A71-33706

Transmission performance of thin route satellite communication system for northern Canada, comparing FM, PCM and delta modulation techniques 17 p2703 A71-35081

Comparison of demand assignment multiple access/modulation techniques for satellite communication using high quality telephone channels 17 p2706 A71-35103

Binary differentially coherent PSK modulated PCM radio link performance under noise and intersymbol and interchannel interferences effects, deriving error probability 17 p2707 A71-35477

Range and range rate measuring equipment for PCM-TDMA satellite communications system data feed and orbit observation 18 p2879 A71-36533

Digital speech interpolation technique application to PCM-TDMA demand assignment system, noting traffic handling capacity and cost reduction 18 p2880 A71-36549

PSK modem for PCM-TDMA system, discussing performance tests on INTELSTAT 3 18 p2880 A71-36551

Message distortions analysis in PCM communications systems due to phase fluctuations of synchronization signal 19 p3022 A71-38494

Critique of paper on additional signal power for optimum performance of PCM binary signal detection under channel band limiting effect in white noise 20 p3196 A71-38870

Signal to quantizing noise ratios for differential PCM systems used to encode analog signals from Markov processes into digital form 22 p3514 A71-42391

Common channel signaling system for demand assigned multiple access satellite communication, discussing design features and applications to PCM-TDMA 22 p3514 A71-42520

Pulse code modulation systems measurement techniques, deriving diagrams with preset limit patterns incorporated 23 p3652 A71-43925

PULSE COMMUNICATION
 Information collection from ocean data stations networks by satellite and HF digital data communications, noting feasibility of VHF telemetry communications 01 p0037 A71-10991

Wall loss influence on energy flow center velocity of rectangular carrier pulses in circular waveguide for long distance transfer 01 p0056 A71-11195

Atmospheric turbulence effects reduction in optical communication by statistical communication theory, considering digital system and waveform estimation 02 p0213 A71-12019

Direct detection, heterodyne and optimum receivers for optical scattering channels in digital communication 02 p0214 A71-12020

Digital communication hybrid phase locked loop nonlinear feedback system with modulation and carrier components enhancing phase estimation 03 p0391 A71-14312

Signal parameter estimation during pulse sequence reception on background of nonstationary additive noise 04 p0549 A71-14614

Synchronous digital communication system with each station clock rate established by phase locked oscillator input average, calculating two-station network dynamic stability 05 p0729 A71-17051

Daytime pulsed optical communication within line-of-sight using GaAs IR laser 06 p0907 A71-17570

Digital multiple access communications for commercial transmission via Intelsat satellites 07 p1057 A71-18817

Optimum low pass filter bandwidth for pulse detection in exponential noise, using two dimensional spectrum 07 p1059 A71-18849

Binary signal parameters estimation mixed with Gaussian noise, using method of moments 07 p1065 A71-20420

Laboratory test set for integration of data compression and error correction encoding of digital communications system 07 p1065 A71-20424

Transform coding techniques using orthogonal matrices to implement bandwidth or dimensionality reduction for image processing in digital communications systems 08 p1259 A71-21591

Unique word detection in digital burst communication, determining effects on voice quality from analytic study and digital simulation 08 p1255 A71-21595

Gunn diodes and heterojunction laser applications in optical pulse communication systems synthesis

11 p1772 A71-25235

Gram-Charlier error probabilities of digital satellite communication systems due to intersymbol interference and additive noise applied to Chebyshev, Gaussian and cutoff filters

12 p1879 A71-27069

Statistical estimation techniques for error probability of digital communication systems

12 p1880 A71-27145

Stretch technique for pulse time transformation including signal slowdown, speedup or time reversal performed within window with duration determined by time-bandwidth product

12 p1881 A71-27427

Two cavity ring-type channel dropping filters for millimeter wave guided communication system, calculating pulse response and interchannel crosstalk characteristics

14 p2210 A71-29569

Heuristic signal design for digital communication over fast-fading Gaussian channels, stressing nonorthogonal signaling schemes

14 p2193 A71-30010

Two theorems on minimax transversal filter equalization at receiver for digital communication systems distortion reduction

14 p2193 A71-30012

Digital communication system frame synchronizer performance analysis, using mean time formula and state transition matrices

14 p2201 A71-30925

Binary pulse sequences correlation and synchronization, developing effectiveness criteria with two stage measures

14 p2201 A71-30927

Noise stability at reduced peak signal power of PTM-AM communications using wideband linearly frequency modulated carrier pulses

15 p2368 A71-31228

Solar system interstellar communication with Galaxy, discussing information transmission, coding decoding, recording, display, pulse use and economics

15 p2371 A71-31747

Pulse detection equipment by peak voltage and current value sampling, using avalanche transistors

15 p2377 A71-32324

Phased array pulsed X band microstrip Gunn diode transmitters with temperature stabilization at 9.4 GHz

16 p2547 A71-33555

Long distance FM signal pulse propagation and maximum compression synthesis in dispersive media, using asymptotic theory for mathematical treatment

17 p2701 A71-34761

Upper bound on error probability due to intersymbol interference for correlated and uncorrelated digital signals, presenting examples for data communication systems

17 p2703 A71-35077

PSK signals time division multiplexing and frequency multiplexed subcarrier systems equivalence and efficiency for digital communications

17 p2706 A71-35107

Synchronization of high-speed digital data communication systems with continent-wide interconnected switching centers, discussing elastic storage buffering to compensate for transmission time delay variations

17 p2712 A71-35784

Digital filtering in PCM communication systems with active repeater satellites and space vehicle telemetry

18 p2881 A71-36569

Amplitude distribution of pulse train with given constant pulse durations in communication channels

18 p2882 A71-36621

Adaptive frequency selection for reduction of effects of noise differing irregularly from useful pulse signals, estimating error probabilities

18 p2882 A71-36622

Automatic equalizer with fast startup time for digital communication systems including partial response and single subband Nyquist systems

19 p3026 A71-37220

Probability error calculation for digital signals contaminated by intersymbol interference and additive Gaussian noise

19 p3015 A71-37222

Amplifier effects on phase distortion of pulse signals passing through power amplifier stages of coherent pulse communication systems

19 p3015 A71-37257

Wideband spectrum utilization above 10 GHz for high rate digital communications and ecology monitoring of sea state, earth surface contour and atmospheric pollutants

19 p3020 A71-38407

Message distortions analysis in PCM communications systems due to phase fluctuations of synchronization signal

19 p3022 A71-38494

Capacitive memory storage for filtration of repetitive pulse radio signals mixed with additive noise

19 p3022 A71-38500

Transient RF pulse dispersion along plasma loaded coaxial gas discharge, noting group delay

20 p3272 A71-38783

Short-pulse high-rate space digital laser communication components technology, discussing mode locked and frequency doubled Nd-YAG laser source

21 p3348 A71-40806

Signal parameter estimation during pulse sequence reception on background of nonstationary additive noise

22 p3510 A71-42254

Dynamic frequency and phase response of digital communications system of synchronized oscillators from time-incremental computer simulation

22 p3523 A71-42376

Bit synchronization in high SNR digital communication system, using Kalman filtering algorithm

22 p3513 A71-42383

Radio pulse synchronous detection with wideband preamplifier, evaluating frequency mismatch effects on signal distortion by transient response analysis

23 p3644 A71-43287

Mn-Zn ferrite for pulse transformers, discussing permeability and temperature range

23 p3650 A71-43348

Probabilistic analysis of random pulse signal gating on time selective zero lag converter with rectangular pulse input

23 p3647 A71-44322

Binary nonconsecutive one code for time-tag data compression in digital communication, noting transmission power and bandwidth requirements reduction

24 p3803 A71-44651

PULSE COMPRESSION

Weather radar resolution enhancement by pulse compression system for signal bandwidth increase by phase coding

01 p0030 A71-10597

Holographic amplitude modulation procedure for pulse compression in synthetic aperture radar

02 p0215 A71-12037

Frequency modulation and compression of ultrashort light pulses by optical Kerr effect

04 p0552 A71-15035

Mode locked He-Ne laser pulse compression and expansion by electro-optic internal modulator

10 p1619 A71-23873

Low power vertical-incidence solid state pulse compression FM ionosonde

14 p2246 A71-30480

Pulse compression and optical data correlation in side-looking radar, considering Doppler effect

15 p2374 A71-32650

Long distance FM signal pulse propagation and maximum compression synthesis in dispersive media, using asymptotic theory for mathematical treatment

17 p2701 A71-34761

Pulse compression circuit techniques combined with radar system philosophy for signal encoding application to pulse radar

20 p3201 A71-39911

Pulse compression dispersive filters for signal processing

20 p3206 A71-39912

Swept frequency or chirp signals for data transmission and pulse compression, considering long range air ground communication in HF band

22 p3510 A71-42277

Low loss microwave iris-loaded circular TE mode waveguide delay line for pulse compression at X band

23 p3653 A71-43963

PULSE DIFFRACTION

Radio meteor orbit velocity and radiant measurements by pulse diffraction technique

09 p1520 A71-22829

Radar equipment for meteor velocity and radiants measurement at VHF by pulse diffraction method

19 p3067 A71-38635

PULSE DOPPLER RADAR

NT MONOPULSE RADAR

NT PULSE RADAR

Severe thunderstorm warning by single pulse Doppler radar plan shear indicator

01 p0117 A71-10572

Constant false alarm rate /CFAR/ operation of airborne pulse Doppler radar in nonhomogeneous and point clutter, using similar critical region test

07 p1065 A71-20421

Atmospheric vertical particle motion inside convective storms observed by airborne pulse Doppler radar techniques

11 p1794 A71-25378

Electromagnetic compatibility performance of pulse Doppler radar receivers, considering CW or synchronous pulse interference

19 p3020 A71-38430

Optical correlation for surveillance and pulse Doppler radar receivers signal processing

20 p3200 A71-39910

Book on pulse, CW, Doppler, pulse Doppler and space radar theory, operation and maintenance, describing equipment, tracking and siting

22 p3509 A71-41621

PULSE DURATION

Ultrasonic frequency characteristics for flaw detection, discussing short and long pulses coupling to test samples

01 p0086 A71-10303

Transverse gain inhomogeneity effect on monopulse duration and development in multimode spherical laser resonator

01 p0094 A71-11026

Multiphase multivibrator with nanosecond pulse duration and parallel transistorized inductive correction, analyzing flip-flop circuit

02 p0230 A71-11831

Giant pulses composed of shorter pulse trains obtained in Q switched carbon dioxide laser with transverse modes

02 p0259 A71-11880

Multiatomic molecules emission spectra excitation by superhigh frequency short duration pulsed gas discharges

02 p0286 A71-11889

Cavity resonator length effect on lasing threshold, output energy, pulse power and duration and spectral width of hybrid single pulse mode laser with passive Q switch

02 p0259 A71-11933

Short pulse optical tracking systems ranging error, analyzing effects of tracker, target and propagating medium characteristics

02 p0214 A71-12029

Small angular diameter radio source in central Crab Nebula association with pulsar NP 0532 based on spectra and pulse duration

03 p0483 A71-13203

Long pulse rhodamine 6G flash lamp-pumped circulating dye laser with cyclooctatetraene cycloheptatriene as triplet state quenchers, testing performance

03 p0437 A71-13884

Nd glass laser radiation time and spectral structure

03 p0437 A71-13885

Electron beam welding and boring, considering temperature distribution relation to pulse duration

03 p0433 A71-14271

Atmospheric pressure pulsed carbon dioxide laser, investigating gain, peak power and pulse duration as function of gas pressure and discharge voltage

03 p0440 A71-14461

Laser technology, discussing short duration pulse generation

04 p0606 A71-14713

Frequency modulation and compression of ultrashort light pulses by optical Kerr effect

04 p0552 A71-15035

Active directional nanosecond pulse filter design based on hybrid technique, using metal semiconductor field effect transistors /MESFET/

04 p0559 A71-15698

Crab Nebula pulsar NP 0532, examining radio pulse shapes, flux densities and dispersion

05 p0800 A71-15926

Laser beam modulation by nanosecond rise time mechanical chopper for rectangular variable duration pulses, considering use in fluorescence lifetimes measurement, photomultipliers and photodiodes

05 p0761 A71-16270

LF oscilloscope display of periodic subnanosecond optical pulses from mode locked lasers

05 p0761 A71-16334

Pulse transmission mode Q switched neodymium laser, discussing pulse duration

05 p0762 A71-16374

Mode locked high pressure carbon dioxide lasers subnanosecond pulse widths measurement based on photon flux and fast shutter in semiconductor

06 p0907 A71-17310

Ultrafast Q switched laser induced shock waves in solids, discussing model for picosecond impulse

06 p0907 A71-17311

Pulsar data tabulation of positions, dispersion measures, and class I pulse periods and widths

06 p0966 A71-17676

Q switched Nd laser pulse duration control as function of KDP crystal orientation and pumping power

07 p1122 A71-19138

Mode locked picosecond laser pulse duration measurement by beat frequency detection

07 p1123 A71-19211

Stimulated thermal Rayleigh scattering with picosecond pulses, discussing contributory processes

07 p1164 A71-19779

Light pulses from tandem bisected GaAs lasers nonuniform excitation, determining width by intensity correlation in lithium iodate crystal

07 p1126 A71-20167

High energy narrow pulsewidth HF chemical laser emission from transverse multiple electrode nitrogen fluoride and nitric tetrafluoride discharge

07 p1128 A71-20397

Statistical scatter of pulse duration in relaxation oscillator with common-emitter coupling concerning mass production

08 p1261 A71-20739

Electron beam pumped CdS laser, investigating output pulse time duration based on laser oscillation quenching model

08 p1302 A71-21433

Pulse rise time effect on nanosecond magnetic thin film switching with flux reversal and stray field interaction

09 p1508 A71-22704

Controllable pulse length Q switched Nd-YAG laser using lithium iodate doubling crystal

09 p1463 A71-22757

Coupled fiber lasers maximum energy transfer between passive conductors, determining minimum pulse duration

09 p1464 A71-23112

Ionospheric dispersion of FM electromagnetic pulse, examining distortion of amplitude, pulse length and modulation in terms of integrated electron density along transmission path

09 p1410 A71-23523

Metallic target in radiation damage from focused ruby laser beams as function of energy and luminous pulse duration

09 p1465 A71-23563

Foveal vision absolute thresholds for various duration light pulses and flash pairs at different separations

10 p1560 A71-23992

High pressure laser action in gas mixtures with pulsed transverse excitation, observing molecular and atomic transitions

10 p1620 A71-24045

C and higher band pulse modulated signal generation with nanosecond duration, using TEM- mode pulse-forming network

10 p1577 A71-24211

Electron and ion plasma heating by subnanosecond neodymium laser pulses, using computer calculations of hydrodynamic equations

11 p1806 A71-26089

Tunnel diode driven multivibrator, noting triggering signal amplitude and duration effects on output pulse width

11 p1740 A71-26550

Pulsars CP 0950 and CP 1133, examining pulse spectra characteristics in 83-111 MHz frequency range

12 p1963 A71-27076

Cavity mirror transmittance variation effect on output power and pulse length of single-pulse Nd-doped glass laser with nonuniform inverted population distribution

13 p2077 A71-27855

Energy level threshold gradients for steady and unsteady lasing in four-level lasers, obtaining power output and pulse duration

13 p2077 A71-28153

Subpicosecond structure and frequency sweep observation results of single pulse of Nd-glass laser, considering explanation by mode locking theory

13 p2079 A71-28712

Ultrashort optical pulse propagation through two level attenuating or amplifying atomic medium

13 p2080 A71-29136

Transverse spatial diffusion of phase-dispersed pulses, showing effects on dechirped pulse duration, output beam cross section and two-photon fluorescence display

13 p2081 A71-29332

Argon ion laser mode locking in UV lines with intracavity acousto-optic modulator, describing pulse duration and average power

15 p2423 A71-32588

Cavity loss dependent erbium glass laser line oscillations in lower threshold region under Q switch and long pulse conditions

15 p2424 A71-32612

Optimum pulse width and information carrying capacity for dielectric single mode glass optical waveguides under distortion due to attenuation and phase velocity dispersion

16 p2541 A71-33127

Theta pinch deuterium plasma heating by carbon dioxide laser as function of pulse duration and energy

16 p2587 A71-33188

Short light pulse evolution from noise, considering time dependence of pulse duration and peak intensity

16 p2589 A71-34137

Intense pulsed electron beam formation during current flow through plasma

17 p2786 A71-34279

Picosecond duration coherent light pulse propagation in resonant medium, discussing basic equation, self induced transparency, Bloch equations, soluble model and higher conservation laws

17 p2754 A71-35375

Weber antenna sensitivity for short pulses of gravitational radiation, giving limit for connection coefficient of piezotransducer with detector

18 p2946 A71-35979

Amplitude distribution of pulse train with given constant pulse durations in communication channels

18 p2882 A71-36621

Pulsars CP 0950 and CP 1133, examining pulse spectra characteristics in 83-111 MHz frequency range

19 p3133 A71-37426

Ultrashort pulse formation in short pulse stimulated Raman oscillator, achieving partial group velocity matching

19 p3071 A71-37475

Ruby laser Q switching by hydrogen and copper phthalocyanin vapors, obtaining nanosecond single pulses with high power density

19 p3072 A71-37768

Vibrational behavior of nonlinear systems subjected to finite duration pulse excitation, transforming original differential equation into Lighthill method solvable form

20 p3267 A71-38798

Ultrafast camera with picosecond framing times for photographic measurement of light pulses

20 p3235 A71-39189

Radio pulse shapes from NP 0531 observed with swept frequency machine, showing broadening due to interstellar scattering

20 p3302 A71-39925

Pulsars radio wave emission characteristics, intensity variation, duration, bandwidth, similarity to space radio beacons and evidence as neutron stars

21 p3442 A71-40144

Nanosecond ruby laser pulse generation using electro-optic shutter switching circuit external to Q-spoiled cavity

21 p3391 A71-40179

Nonlinear absorption in transparent semiconductors of picosecond light pulses from Nd laser with locked modes

21 p3431 A71-41256

Absolute foveal thresholds as function of flashes pulse length and null period

22 p3497 A71-41480

Pulsars properties, examining pulse profile and duration, subpulse phase modulation and polarization

22 p3598 A71-41918

Nonlinear losses in ultrashort light pulse generators and amplifiers, attributing to self focusing of laser radiation in active and optical media

22 p3558 A71-42457

Pulse duration of atmospheric radio noise bursts at 3 MHz from lightning flashes, considering effect on data communication

23 p3643 A71-42970

Second harmonic aperture in ultrashort pulses length measurement by mixing two AM light beams in nonlinear crystals

23 p3683 A71-43397

Mode-locked laser ultrashort pulse duration measurement from field intensities autocorrelation functions

23 p3685 A71-43562

Pulsar radio pulse shape and structure, discussing pulse widths and polarization angle change

23 p3769 A71-43989

CW dye laser mode locking with lithium niobate phase modulator, observing 500 psec pulse generation

23 p3687 A71-44134

Self focusing in gas breakdown produced by nanosecond laser pulses, using schlieren photography and laser light forward transmission measurements

24 p3832 A71-44358

Pulsar 0833-45 LF radiation spectrum decrease explained by pulse broadening due to interstellar scattering

24 p3868 A71-44565

Carbon dioxide-helium-nitrogen laser with nonlinearly absorbing cell, presenting emission pulse duration and rate

24 p3834 A71-45111

PULSE DURATION MODULATION

First and second order lag system frequency response to pulse width modulated input signals [ASME PAPER 70-WA/AUT-8] 03 p0380 A71-14149

Satellite voice communication by suppressed clock pulse duration modulation technique, using optimum digital modulation and processing for maximum traffic and cost effectiveness

04 p0555 A71-15340

Static friction influence on readings of gyrotachometer with pulse width modulated torque sensor current

07 p1108 A71-19306

Chirped optical pulses nature, properties, generation and applications in pulse shape measurement in nonlinear wave propagation, ultrashort pulse generation and adiabatic population inversions

07 p1160 A71-19778

Pulse width controlled, regulated DC-DC converter with passive low pass filtering, discussing open loop transfer functions, stability analysis and linear models

07 p1024 A71-20413

Fluidic proportional amplifier circuit with two bistable element stages, using pulse width modulation techniques

07 p1027 A71-20579

Measuring transformer for AC input signal with pulse width modulated semiconductor multiplier feedback

08 p1261 A71-20737

PULSE FREQUENCY MODULATION

Nonlinear closed loop control system with PFM and PWM, obtaining asymptotic stability condition by Liapunov and La Salle theorems

12 p1893 A71-27726

Pulse width modulation controlled DC motors, deriving formulas for speed and torque characteristics

13 p1999 A71-28630

Fluidic servo amplifier operation by PWM mode with PD computation and ripple removal circuit

15 p2352 A71-32069

Pulse width modulated output voltage analysis in autonomous inverters, using Fourier series and digital computer

15 p2353 A71-32078

Dynamic stability and reliability analysis of pulse width modulated control systems by point-to-point mapping method

15 p2382 A71-32621

N-order continuous linear automatic control system compensation method, using model of sampled systems with duration modulation

16 p2549 A71-33377

Feedback control system with combined PFM and PDM, obtaining nonlinear discrete equivalence

21 p3360 A71-40615

Soviet book on nonlinear sampled-data control systems with PFM and PDM covering mathematical description, transient analysis and system stability problems

22 p3526 A71-41821

Cost functional gradient optimization of pulse width modulated control inputs for nonlinear dynamic systems

23 p3658 A71-44088

Phase sensitive magnetic semiconductor pulse width modulator with diode bridge consisting of single saturable-core choke input and transistor circuit output arms

24 p3810 A71-45155

PULSE FREQUENCY MODULATION

Transient response of pulse frequency modulation automatic control systems for zero or nonzero initial conditions, using signal Laplace transforms

01 p0059 A71-10528

Neural pulse frequency modulation model limitations and modification for error sampled control system stability analysis

01 p0038 A71-11312

Pulse frequency modulated pulsed control systems, deriving sufficient conditions for limit boundedness/dissipativity

02 p0236 A71-12621

Neural pulse frequency modulated error sampled control system stability, considering model limitations and modifications

03 p0390 A71-14307

Mode locked Nd-glass laser, describing dispersion and Kerr effects on pulse frequency modulation

08 p1301 A71-21125

Pulse frequency modulation feedback system nonlinear discrete equivalence, investigating stability by Liapunov method

09 p1422 A71-22280

Sampled data feedback control systems with neural pulse frequency modulation, deriving periodic oscillations existence conditions

09 p1424 A71-23387

Optimal reception of Markov radio signals with intrapulse FM, using nonlinear filtration theory

10 p1578 A71-24711

Phase controlled linear FM pulse generation by digital square wave carrier phase modulation, using parabolic function generator

12 p1879 A71-26995

Current controlled unstable pulse oscillator, discussing depletion layer transistors and upper frequency limit as function of thermal loads and switching times

12 p1887 A71-27043

Nonlinear closed loop control system with PFM and PWM, obtaining asymptotic stability condition by Liapunov and La Salle theorems

12 p1893 A71-27726

Pulse frequency modulated control systems stability analysis by Liapunov method, introducing discrete correction into modulation law

15 p2381 A71-31979

Linearly increasing input signal tracking in nonlinear control systems with pulse frequency modulation, discussing error determination, asymptotic stability and equations of motion

15 p2381 A71-31980

Long distance FM signal pulse propagation and maximum compression synthesis in dispersive media, using asymptotic theory for mathematical treatment

17 p2701 A71-34761

Two dimensional nonlinear discrete/pulse frequency modulation/control system stability, using Liapunov direct method and mathematical model

17 p2721 A71-35134

Transmission characteristics of communication systems with incoherent carriers through fading and nonfading media, showing advantage of PFM-AM with clipped noise carrier

20 p3201 A71-39913

- Feedback control system with combined PFM and PDM, obtaining nonlinear discrete equivalence 21 p3360 A71-40615
- Soviet book on nonlinear sampled-data control systems with PFM and PDM covering mathematical description, transient analysis and system stability problems 22 p3526 A71-41821
- Sampled data control systems with pulse frequency modulation and time lag element, determining error response 22 p3527 A71-42493
- Comparative qualitative simulation of pulse frequency modulation control with/without error signal derivatives 23 p3656 A71-43867
- PULSE FREQUENCY MODULATION TELEMETRY**
Eight channel micropowered miniature biomedical PAM/FM telemetry system for implantation in research subjects aboard orbiting space station 14 p2189 A71-30930
- PULSE GENERATORS**
Start-stop pulse generator for gas laser in quasi-steady monoimpulse mode with given emission duration 01 p0093 A71-10621
- Light pulse generator for amplitude-frequency analysis of photoreceivers, using wideband modulated semiconductor injection laser emission 01 p0093 A71-10624
- Laser technology, discussing short duration pulse generation 04 p0606 A71-14713
- High power pulsed electron beam generator, using distilled water as dielectric and multiblade cathode electron gun 06 p0876 A71-18077
- Long distance PCM-AM pulse regenerator for 4 GHz band and millimeter wave communication 08 p1265 A71-21285
- Programmable solid state pulse generator for charge-sensitive amplifier excitation at high pulse repetition rates, discussing circuit elements and applications 08 p1267 A71-21850
- Pulsed plasma accelerator energy balance determination by spectroscopic measurement 09 p1498 A71-22100
- Single mode laser pumping generator of stimulated Brillouin scattering pulse in water 09 p1462 A71-22399
- Nonstationary stress modeling in aircraft structures using random pulse generator applied to jet landing gear break strut fatigue test 10 p1692 A71-24954
- Phase controlled linear FM pulse generation by digital square wave carrier phase modulation, using parabolic function generator 12 p1879 A71-26995
- Versatile pulse amplifier for use with scintillation counters, surface barrier detectors, proportional counters or channel electron multipliers 13 p2067 A71-28163
- High speed rotating optical attenuator for sub-second sawtooth radiance pulse generation for detection, cooling or heating experiments 19 p3063 A71-37249
- Nanosecond ruby laser pulse generation using electro-optic shutter switching circuit external to Q-spilled cavity 21 p3391 A71-40179
- Massive main sequence stars pulsation kinetics, examining amplitude growth, time scale ratios and evolutionary stabilization 22 p3596 A71-41447
- Nonlinear losses in ultrashort light pulse generators and amplifiers, attributing to self focusing of laser radiation in active and optical media 22 p3558 A71-42457
- Circuit generating short rectangular current pulses for pumping semiconductor lasers 23 p3685 A71-43528
- Solid state lasers, discussing ruby lasers application for welding and drilling, mode coupling of glass lasers and extremely short pulses generation 23 p3685 A71-43953
- PULSE HEATING**
Transient heat conduction in dual-layer insulated plate exposed to pulse heating, discussing temperature response [AIAA PAPER 70-14] 03 p0522 A71-14439
- Production welding and annealing, investigating low heat input, intermetallics formation, atmospheric contamination, hot short cracking, speed and cost 09 p1458 A71-23408
- Mo high temperature melting point and electrical resistivity measurement by pulse heating method 10 p1624 A71-23912
- Computerized use of transient thermal resistance and power pulses superposition to calculate instantaneous transistor junction temperatures for various pulse conditions 13 p2038 A71-28770
- Thermoelastic stress generation in Cu and Ta samples by linear accelerator produced monochromatic MeV electron pulses, comparing measurements with wave theory predictions 15 p2414 A71-31973
- Surface melting, spallation and stress response prediction for metals under pulsed electron beam heating, using one dimensional finite difference computer program 15 p2390 A71-32005
- Pulsed electron beam heating of metals, determining surface melting, spallation and induced stresses with one dimensional computer programs 15 p2429 A71-32006
- High speed system for thermophysical properties measurement of electrical conductors above 2000 K in subsecond experiments 19 p3062 A71-37246
- PULSE HEIGHT**
U PULSE AMPLITUDE
PULSE MODULATION
NT DELTA MODULATION
NT PULSE AMPLITUDE MODULATION
NT PULSE CODE MODULATION
NT PULSE DURATION MODULATION
NT PULSE FREQUENCY MODULATION
NT PULSE FREQUENCY MODULATION TELEMETRY
NT PULSE POSITION MODULATION
NT PULSE TIME MODULATION
Small Astronomy Satellite PCM/PM telemetry transmitting split phase encoded data at 136 MHz 01 p0036 A71-10987
- Semiconductor lasers direct amplitude, pulse and frequency modulation methods, comparing advantages and limitations 02 p0260 A71-12004
- Analog inertial sensor digitizing methods, discussing pulse rebalancing and analog to digital conversion 02 p0279 A71-12453
- Limit cycle oscillations in satellite attitude control system, producing control moment by pulse modulated controller 03 p0499 A71-14074
- Transient waveform distortion of arbitrarily modulated signal propagating through ideal waveguide 04 p0553 A71-15219
- Elastic wave properties and technological applications, discussing acoustic delay, compression and filtering electric signals 05 p0722 A71-16745
- Giant pulse amplification in Nd ion doped glass analysis using model, taking into account sublevels and multiplicity 07 p1127 A71-20387
- Nd-glass laser amplified mode locked pulse measurements, noting signal to noise ratio above 10,000 07 p1129 A71-20617
- Solid state pulse modulated radioonde for meteorological data transmission in digital form, using MOS integrated circuits 10 p1583 A71-24052
- C and higher band pulse modulated signal generation with nanosecond duration, using TEM- mode pulse-forming network 10 p1577 A71-24211
- Nd-YAG folded center lasers Q switching and cavity dumping, using fused silica and Brewster cut intracavity acousto-optic modulator 11 p1773 A71-25798
- Minimum error pre- and post-filtered sampled signals for pulse modulation and data compression optimization 12 p1879 A71-27070
- Mathematical expectation and correlation function of combined pulse modulator by Monte Carlo method 15 p2382 A71-31983
- Laser pulse shape, beam modulation and power fluctuation quality control measurements, using non-selective, thermally stable piezoelectric sensor with low time constant 15 p2421 A71-32456
- Intelsat 4 transponder for broadband multicarrier operation with frequency and pulse modulation, considering TWT, tunnel diode amplifiers, filters, equalizers, mixers, multiplexers and antennas 17 p2705 A71-35099
- Multichannel PCM/PSK/PM interplex telemetry system for reducing cross modulation loss and excess carrier reference power 17 p2706 A71-35108
- High voltage pulse shaping circuits for Kerr cell polarization shifters for modulating and deflecting monochromatic laser radiation 19 p3071 A71-37255
- Comments on optimum bandwidth of low pass RC filter for pulse signal detection in nonstationary noise 20 p3203 A71-38867
- Incoherent carrier communications system, obtaining message SNR of 60-70 dB for analog signals with compound pulse modulation and carrier clipping 21 p3347 A71-40375
- Unmodulated and step-modulated HF pulse signal envelope calculation and diagram plotting 23 p3644 A71-43319
- Pulsed modulation of continuous laser resonator Q factor, recording output on oscillograph 24 p3834 A71-45045
- PULSE POSITION MODULATION**
Quantized multiple access voice communications, comparing QPPM-AM and FM performances concerning transmitter power, RF bandwidth, circuit complexity, etc [IEEE PAPER 69-TP-448-COM] 05 p0724 A71-17056
- Temporal registration efficiency of rectangular pulse by position of front at ideal band filter output 07 p1064 A71-20259
- PULSE RADAR**
NT MONOPULSE RADAR
Instantaneous radar pulse frequency measurement for microwave bands, discussing multiplexed filters, wideband discriminators, dissipative frequency sensitive attenuators and band division receivers 04 p0555 A71-15360
- Air traffic control radar separation by pulse repetition frequency discrimination for double and triple stagger configurations 05 p0720 A71-16347
- Doppler pulse radar signal reception, calculating noise signal optimal relationship for comparison with adapted filtration technique 05 p0722 A71-16707
- S band pulsed cotal radar transponder for ground base Centaur rocket trajectory tracking from takeoff to splashdown 06 p0870 A71-18475
- Unresolved radar targets or multipath distortion determination by measurement of complex indicated angle on two pulses separated by short interval 07 p1058 A71-18843
- Video MTI pulse radar Doppler filter optimum symmetrical weighting factors in clutter-plus noise environment 07 p1059 A71-18847
- X band gas tube attenuator for ruby maser saturation protection in pulsed high power radar 07 p1070 A71-18866
- Coupling effect on monostatic-bistatic radar equivalence for monochromatic wave and short pulse scattering 07 p1060 A71-19260
- Optimal phased array radar pulse scheduling multiple transmissions and receptions in minimum time, using integer programming 08 p1254 A71-21339
- Detection characteristics of optimal interperiod processing radar pulse systems for arbitrary correlation of signal and noise fluctuations 10 p1578 A71-24710
- Pulse radar moving target indication and stationary targets reflection suppression, using recursive type digital filter and quadrature channels for improving signal detectability 10 p1579 A71-25068
- Pulse-burst radar design optimization and performance comparison with low and high pulse repetition frequency Doppler radar 14 p2197 A71-30797
- Onboard meteorological pulse radars for cloud formations detection, navigational aids, ground reference points determination and relief surveillance 15 p2371 A71-31920
- Varactor tuned FM pulsed Gunn oscillator for testing X band delay lines for pulse compression radar 16 p2546 A71-33415
- Magnetically conjugate range-time observations of E region radio aurora by pulsed VHF radar echoes 16 p2875 A71-35963
- General purpose pulsed microwave radar receiver, describing balanced mixer and transistorized IF amplifier design and construction 18 p2887 A71-36015
- Resolution and clutter performance of simultaneous Doppler and acceleration measurement with coherent pulse trains 20 p3195 A71-38855
- Doppler distortions of clutter and resolution performance of pulse trains with large time bandwidth products 20 p3195 A71-38861
- Cumulative probability of target detection for pulse surveillance radars, relating target cross section, velocity and radar frame 20 p3199 A71-39901
- Pulse compression circuit techniques combined with radar system philosophy for signal encoding application to pulse radar 20 p3201 A71-39911
- Book on pulse, CW, Doppler, pulse Doppler and space radar theory, operation and maintenance, describing equipment, tracking and siting 22 p3509 A71-41621
- Airborne radar sea return averaged pulse shape measurements over various water surfaces, noting clear distinction between specular and scattered reflection components 24 p3824 A71-45083

PULSE RATE

Lithium niobate crystal electro-optical shutter to Q switch calcium difluoride-Dy laser emitting giant pulses at high repetition rate

01 p0095 A71-11210

Temperature distribution in heat conducting cylindrical laser rod at large pumping pulse repetition rates

03 p0435 A71-13512

Reactive Q switching in carbon dioxide multimode multipass laser with movable end mirror, measuring pulse rates and amplitudes

03 p0438 A71-13892

Huffman /impulse-equivalent/ pulse sequence design, examining energy distribution form control of signal in time-frequency plane

04 p0551 A71-15005

Catheter-flush system for continuous monitoring of central arterial pulse waveform and pressure

04 p0545 A71-15165

Pulsar PSR 1237 plus 25 pulse sequence change, examining profile at 318 MHz

05 p0807 A71-16213

Pulse repetition rate of Q switched YAG-Nd oscillator-amplifier laser systems

05 p0762 A71-16479

Pulsar MP 0628 meter wave radiation, noting linear polarization and frequency dependence of pulse rate

06 p0965 A71-17387

Carotid pulse wave slope variations in normal subjects, aortic valvular diseases and hypertrophic sub-aortic stenosis

09 p1392 A71-22590

Uncooled GaAs injection laser with high pulse repetition rate, discussing structural features and current-power characteristics

10 p1619 A71-23811

Jet pilots flight stresses assessment via biotelemetric transmission of pulse rate, respiratory rate, electrocardiographic data, flight altitude and velocity

10 p1567 A71-23880

Pulse rate and pumping power effects on emission spectra and I-V characteristics of multielement GaAs injection lasers

10 p1622 A71-24884

Pulse wave velocity measurements in human veins by transcutaneous ultrasonic flow detectors, noting respiration and Valsalva effects

12 p1874 A71-27136

Alpha radiation machmeter with semiconductor pulse detectors, discussing supersonic regime effects on rate variations

12 p1908 A71-27607

Carbon dioxide laser pulse shape, duration and power dependence on repetition rate during continuous pumping

13 p2077 A71-28366

Pulsar MP 0628 meter wave radiation, noting linear polarization and frequency dependence of pulse rate

14 p2310 A71-30166

Triangular pulse shaper using transistors and dynistors, obtaining pulse duration, rise time and maximum repetition frequency

14 p2213 A71-30581

High speed pulse response and power-delay product of planar Gunn diodes, noting delay time and power delay product

14 p2215 A71-30834

Truncated pulse signal height distributions of atmospheric sources

14 p2203 A71-30960

Pulse frequency behavior during acquisition of perceptual and motor skills with particular attention to rest periods

15 p2362 A71-31195

Crab pulsar frequency increase associated with nebula activity surge

15 p2494 A71-32549

Circulatory fatigue during shift work, determining pulse rate/oxygen intake at two different loads on bicycle ergometer

17 p2687 A71-34358

Pulsar emission data, presenting average phase shapes and pulse to pulse intensity fluctuations

17 p2797 A71-34372

Pc 3 and 4 micropulsations period structure data, observing multiple frequencies during magnetically active times

19 p3048 A71-37397

Avalanche Si photodiode current pulse formation frequency governing mechanism, considering roles of free carriers and electron tunneling

21 p3358 A71-41344

Radar echoes maximal intensity measurements from meteorological formations, describing pulse by pulse recording system

24 p3826 A71-44883

Carbon dioxide-helium-nitrogen laser with nonlinearly absorbing cell, presenting emission pulse duration and rate

24 p3834 A71-45111

PULSE RECORDERS

U COUNTERS

PULSE TIME MODULATION

NT PULSE DURATION MODULATION

NT PULSE POSITION MODULATION

Noise stability at reduced peak signal power of PTM-AM communications using wideband linearly frequency modulated carrier pulses

15 p2368 A71-31228

PULSE WIDTH

U PULSE DURATION

PULSE WIDTH MODULATION

U PULSE DURATION MODULATION

PULSED JET ENGINES

LES 6 satellite solid Teflon pulsed plasma thruster performance, determining energy balance thrust and circuit parameters

[ALAA PAPER 70-179] 03 p0472 A71-14429

Dynamic I-V characteristics of megawatt pulsed MPD-arc plasma thruster under various axial magnetic fields given for Ar and hydrogen propellants

[ALAA PAPER 70-164] 05 p0796 A71-16574

Solid Teflon fuel pulsed plasma thruster optical measurements, showing different exhaust velocities for neutral, singly, doubly and triply ionized atoms

[ALAA PAPER 71-194] 06 p0948 A71-18632

Pulsed megawatt MPD arc thruster exhaust pressure measurements, discussing time dependence, peak dynamic and static pressures, etc

[ALAA PAPER 71-196] 06 p0948 A71-18634

Pulsed plasma rail mercury propellant thruster for satellite attitude control, measuring thrust and exhaust velocity with balance and Langmuir probe respectively

18 p2956 A71-36243

Pulsed plasma thrusters, propellants, trigger and feed systems developments for long life secondary spacecraft propulsion

22 p3588 A71-41975

PULSED LASERS

NT Q SWITCHED LASERS

Silicon avalanche photodiode detectors for near IR laser pulse receivers, discussing quantum efficiencies, internal gains and room temperature responsivities

01 p0092 A71-10011

Pulsed hydrogen fluoride gas laser output line spectral distribution, describing experimental setup and measurements

01 p0092 A71-10371

Output properties of electrically pulsed carbon dioxide laser as functions of partial gas pressure and discharge voltage

01 p0092 A71-10372

Light echo obtained via giant laser pulse peak overlapping in space and time

01 p0095 A71-11034

Pulsed laser emissions in atmosphere, noting backscattered light spatial and temporal structure under various meteorological conditions

01 p0120 A71-11105

Surface destruction of glass dielectric by pulsed laser beam, considering plasma clouds, shock waves, ablation and crack formation

02 p0258 A71-11640

Self locked He-Cd 114 laser pulse velocity behavior, discussing stability

02 p0260 A71-11948

Dynamic cross-field photomultiplier sampling function characteristics measurement using self-mode-locked He-Ne pulsed laser

02 p0248 A71-12006

Atmospheric pressure pulsed carbon dioxide lasers electrical excitation using double transverse discharge technique

02 p0260 A71-12130

Nd-glass pulsed solid state laser amplifier gain characteristics, deriving flux density and population inversion equations

02 p0261 A71-12173

Giant pulse laser emission stabilization, describing technique for eliminating short time oscillations in subnanosecond range

02 p0261 A71-12321

Mode locked continuously pumped Nd-YAG laser pulse shape, using optical correlation technique

02 p0262 A71-12730

Vacuum UV laser emission from molecular hydrogen in Lyman band using short risetime traveling wave discharge

03 p0434 A71-13478

Temperature distribution in heat conducting cylindrical laser rod at large pumping pulse repetition rates

03 p0435 A71-13512

Nd-YAG pulsed laser, comparing Kr and Xe flash lamps for pumping performance

03 p0437 A71-13880

Mode locked pulsed lasers statistical amplitude and phase variations effects on time dependent output intensity and nonlinear optical processes efficiency

03 p0437 A71-13881

Homogeneously broadened pulsed laser mode locking with internal frequency or amplitude modulation

03 p0437 A71-13882

Nd-YAG pulsed laser mode locking with internal FM modulation

03 p0437 A71-13883

Long pulse rhodamine 6G flash lamp-pumped circulating dye laser with cyclooctatetraene cycloheptatriene as triplet state quenchers, testing performance

03 p0437 A71-13884

Real time oscilloscope observation of ultrafast photodiode response to mode locked laser pulses

03 p0438 A71-13886

IR gas pulsed lasers continuous self mode locking, observing optical spectra with scanning Fabry-Perot interferometer

03 p0438 A71-13889

Pulsed laser threshold measurements in YAG activated by Ho, Er and Tm isotopes, noting temperature dependence

03 p0438 A71-13890

Real time analysis and display of pulsed laser propagation data in rectangular X-Y field

03 p0427 A71-13920

Quantitative spectrographic microanalysis using laser pulse vaporization and spark discharge

03 p0438 A71-13975

Atmospheric pressure pulsed carbon dioxide laser, investigating gain, peak power and pulse duration as function of gas pressure and discharge voltage

03 p0440 A71-14461

Helium effects on dissociation and population inversion dynamics in pulsed carbon dioxide lasers

04 p0605 A71-14628

Laser technology, discussing short duration pulse generation

04 p0606 A71-14713

Self giant pulsed operation of ruby and Nd-YAG lasers obtained by mirror misalignment

04 p0606 A71-14714

Thermal conductivity determination for materials by pulsed laser or flash lamp energy absorption

04 p0595 A71-14961

Subnanosecond laser pulses interaction with thin Ni foil targets leading to energetic pulsed plasma beam production

04 p0608 A71-15134

Pulsed laser holography, discussing illumination source and holocameras for high contrast recording with Q switched ruby lasers

04 p0597 A71-15363

Photodetector triggered single pulse selection from mode locked ruby laser

04 p0608 A71-15595

LF oscilloscope display of periodic subnanosecond optical pulses from mode locked lasers

05 p0761 A71-16334

Homogeneous pulsed laser with intracavity FM modulator, predicting modulation frequency detuning effect on mode locking behavior

05 p0762 A71-16340

Spontaneous mode locking in high pressure carbon dioxide laser with nanosecond pulse separations

05 p0763 A71-16496

Double pulse laser holographic interferometry for large noisy vibrating subjects, including demonstration on Al plate

05 p0751 A71-16580

Mode locked high pressure carbon dioxide lasers subnanosecond pulse widths measurement based on photon flux and fast shutter in semiconductor

06 p0907 A71-17310

Pulsed carbon dioxide laser amplifier, examining spatial and temporal refractive index variations with interferometric measurements

06 p0910 A71-18667

Multipass carbon dioxide pulsed laser mode competition and self locking

06 p0910 A71-18668

Upper atmosphere investigation by ground based pulsed laser radar

06 p0910 A71-18719

Pulse gated binary modulation /PGBM/ visible laser communications for earth orbital missions

07 p1056 A71-18810

Pulsed laser emissions in carbon dioxide under high pressure, discussing onset inversion and pulse duration

07 p1121 A71-19128

Luminescence excitation in chelates under pulsed ruby and neodymium laser radiation action, examining two photon absorption mechanism

07 p1122 A71-19130

Chirped optical pulses nature, properties, generation and applications in pulse shape measurement in nonlinear wave propagation, ultrashort pulse generation and adiabatic population inversions

07 p1160 A71-19778

High power pulsed laser applications, considering satellite orbit determination, distant satellite ranging and precise triggering of high voltage spark gaps

07 p1124 A71-19780

Pulsed laser holography physical principles and applications in stress and vibration analysis, flow pattern visualization, biophysical and medical research

07 p1113 A71-19783

Plasma refractive index effects in pulsed HCN lasers, calculating stable cavity mirror curvatures constriction as function of electron density by ray matrix approach

07 p1124 A71-19795

Optically pumped pulsed ruby laser welding unit, noting joining and hole drilling problems

07 p1119 A71-19968

Erbium ions stimulated emission, spectroscopic properties, pulsed laser action and absorption spectra in yttrium orthoaluminate

07 p1126 A71-20165

Light pulses from tandem bisected GaAs lasers nonuniform excitation, determining width by intensity correlation in lithium iodate crystal

07 p1126 A71-20167

Pulsed ruby laser radiation energy characteristics relation to crystal temperature distribution, thermal deformation and compensating lens focal length

07 p1126 A71-20188

Single mode ruby and Nd glass lasers axial mode selection by dye filters, noting radiation spectra and spatial coherence

07 p1126 A71-20190

Partial mode locking in picosecond self pulsing GaAs injection lasers

07 p1128 A71-20394

Mode locked pulsing from carbon dioxide-nitrogen-helium multipass laser by cavity end reflector sinusoidal modulation along axis

07 p1128 A71-20395

Carbon dioxide laser IR pulses self focusing in liquid carbon disulfide, calculating nonlinear refractive index

07 p1128 A71-20396

Nd-glass laser amplified mode locked pulse measurements, noting signal to noise ratio above 10,000

07 p1129 A71-20617

Nitrogen-carbon dioxide electric discharge mixing laser /EDML/ used as pulse amplifier, using high flow rate for waste heat removal

07 p1129 A71-20618

Sparks induced in gases by transversely excited atmospheric pressure carbon dioxide IR pulsed lasers, observing plasma filament forward propagation

07 p1129 A71-20619

Pulsed laser emissions in atmosphere, noting backscattered light spatial and temporal structure under various meteorological conditions

08 p1325 A71-20849

Pulsed laser schlieren system for ultrasonic wave front imaging in nondestructive testing techniques

08 p1286 A71-20949

Mode locked Nd-glass laser, describing dispersion and Kerr effects on pulse frequency modulation

08 p1301 A71-21125

Gaussian shaped laser pulse holographic brightness analysis, presenting theoretical and experimental holographic coherence length curves for Q switched laser oscillator and amplifier system

08 p1290 A71-21390

Near Gaussian intensity distributions from multimode high power pulsed ruby lasers, using rotating diffuser

08 p1302 A71-21407

Pulsed optical parametric oscillators, investigating effects of spatially nonuniform pumping with beams having Gaussian intensity profiles

08 p1302 A71-21432

Electron beam pumped CdS laser, investigating output pulse time duration based on laser oscillation quenching model

08 p1302 A71-21433

Single longitudinal mode operation and mode locking of pulsed high pressure transversely excited carbon dioxide laser by saturable absorbers

09 p1463 A71-22758

Spectral mode, band to band carrier decay, pulsed and CW operation of laser quality In-Ga-P

09 p1463 A71-22765

Energetic highly ionized plasma production by pulsed laser heating of lithium hydride pellets

09 p1503 A71-22867

Infrared laser output from giant pulse laser beam photoexcited alkali metal vapors, assuming buffer gas collisional mechanism

09 p1464 A71-23380

Long pulse glass laser welder-driller, determining mean energy densities and spot sizes

09 p1464 A71-23404

Spontaneous self locking axial modes in transversely excited high pressure carbon dioxide laser of helical geometry, measuring emission pulses in MW power range

09 p1465 A71-23483

Laser fluid flow velocimeter pulse output resolution approximation, using spectrum analyzer or discriminator measurements

09 p1453 A71-23726

Uncooled GaAs injection laser with high pulse repetition rate, discussing structural features and current-power characteristics

10 p1619 A71-23811

Spectral bandwidth of Q switched giant pulse laser as function of single pass gain, optical switch and resonator loss

10 p1619 A71-23955

Molecular gases dissociation due to pulsed carbon dioxide laser radiation, observing luminescence temporal, spatial and spectral characteristics prior to breakdown

10 p1620 A71-24040

NASA pulsed laser ranging systems for scientific satellite tracking, determining accuracy by trajectory and long arc orbital comparison

10 p1576 A71-24051

Cross-excited electrically pulsed carbon dioxide laser investigating self mode locking as function of cavity length, operating pressure and bleachable absorber sulfur hexafluoride

10 p1620 A71-24152

Pulsed HF chemical laser output as function of fluorine source, flow rate and output coupling

10 p1620 A71-24153

Controlled thermonuclear reactions produced by exposing LiD target to short pulses of Nd-glass laser, measuring neutrons number and plasma temperature

10 p1620 A71-24208

Atmospheric pressure carbon dioxide laser electrode design for uniform pulse excitation discharge

10 p1621 A71-24508

Hydrodynamic model for heating of pulsed laser produced plasma generated at plane solid target, deriving electron temperature and ion expansion energy

10 p1621 A71-24673

Emission dynamics of pulsed laser with optical delay line in resonator

10 p1622 A71-24885

Self consistent hydrodynamic heating of solid substance by laser pulse for nonequilibrium ionization

10 p1653 A71-24887

Pulsed ion laser electron density measurement by cavity method in S band, evaluating relaxation time

10 p1623 A71-25021

Gunn diodes and heterojunction laser applications in optical pulse communication systems synthesis

11 p1772 A71-25235

Time delay in pulsed optical carbon dioxide laser pumping mechanism in high current gaseous discharge

11 p1773 A71-25796

Nd-YAG laser cavity dumping for continuously pumped efficient pulsing at various repetition rates

11 p1773 A71-25797

Pulsed laser holographic applications to aerospace components nondestructive testing, inspecting electron beam welds and internal structural flaws

11 p1770 A71-25988

Laser pulse produced energetic ion and plasma measurements fore and aft side of targets including Al and Au foils

11 p1775 A71-26084

High density and temperature plasmas produced by laser pulse heating massive solid targets, discussing interaction processes

11 p1807 A71-26094

Nonlinear photoelectric electron emission due to picosecond mode locked laser pulse irradiation

11 p1776 A71-26426

Capacitor discharge excited atmospheric pressure carbon dioxide-nitrogen-helium pulsed IR laser, investigating laser output dependence on gas flow and electrical parameters

12 p1913 A71-26976

Thermal transient effects in optically pumped pulsed lasers, presenting approximate calculation of temperature distribution and laser rod distortion effect on collimated light beam

12 p1914 A71-26979

Transversely excited atmospheric pressure carbon dioxide lasers, considering multimewatt laser pulse generation

12 p1914 A71-27279

Barium titanate pyroelectric receivers for giant pulse laser emission measurements

12 p1915 A71-27756

Cavity mirror transmittance variation effect on output power and pulse length of single-pulse Nd-doped glass laser with nonuniform inverted population distribution

13 p2077 A71-27855

Carbon dioxide laser pulse shape, duration and power dependence on repetition rate during continuous pumping

13 p2077 A71-28366

Subpicosecond structure and frequency sweep observation results of single pulse of Nd-glass laser, considering explanation by mode locking theory

13 p2079 A71-28712

Electron and laser pulse plumes, using thermomechanical shock wave theory

13 p2079 A71-28768

Frequency and temperature variations of active diode region in pulsed GaAs laser, using Fabry-Perot interferometer

13 p2079 A71-28923

Pulsed Xe ion laser properties, considering emission divergence, coherence and cross section

13 p2080 A71-29028

Transverse spatial diffusion of phase-dispersed pulses, showing effects on dechirped pulse duration, output beam cross section and two-photon fluorescence display

13 p2081 A71-29332

Nd-YAG laser operation with simultaneous intracavity frequency doubling and mode locking, ob-

serving mode-locked pulse lengthening and circulating power decrease

13 p2081 A71-29335

Simultaneous mode locking and pulse coupling of carbon dioxide laser achieved by single internal GaAs element, discussing possible application to pulse code modulation

13 p2081 A71-29341

Airborne equipment for CAT detection ahead of aircraft, considering pulsed Doppler laser and IR detectors

14 p2268 A71-29765

Pulsed atmospheric pressure carbon dioxide laser output pulse characteristics and self mode locking

14 p2253 A71-29799

Cadmium sulfide pulsed laser spectrum analysis, discussing output stabilization by mode selection and electron beam scanning

14 p2253 A71-30092

CW 28 micron signal resonant regenerative amplification in pulsed water vapor laser, showing pulse to pulse frequency coherence

14 p2255 A71-30832

Cold cathode pulsed gas laser construction with glass plasma tube allowing operation with oxygen and variety gases

14 p2255 A71-30882

Parametric amplification of two laser waves with amplitude and phase modulation under exponential signal growth applied to Raman scattering in picosecond pulse field

15 p2418 A71-31188

Pulsed lasers coherence measurements by holographic techniques, considering high fraction of near field pattern with appreciable coherence

15 p2419 A71-31255

Pulsed gas dynamic laser for radiation generation at high power levels, using shock tube

[AIAA PAPER 71-572]

Motion and collision of plasma blobs generated by giant pulse ruby laser irradiation on lithium plate

15 p2455 A71-31643

Ultrasonic effects on synchronization of ruby laser radiation, investigating emission pulse structure and peak sequence

15 p2419 A71-31712

Pulsed nitrogen-pumped dye laser output spectral narrowing by injection of argon laser monochromatic radiation into cavity

15 p2420 A71-32382

Self induced second order mode locking optical pulsing of double heterostructure stripe geometry junction lasers operating continuously at room temperature

15 p2421 A71-32388

Pulsed semiconductor laser as high resolution optical range spectroscopy, noting application to Cs hyperfine absorption

15 p2421 A71-32403

Thermomechanical damage by pulsed lasers in metals, discussing energy deposition and stress wave generation for optimal fracture conditions

15 p2422 A71-32555

Rhodamine 6 G in ethanol partial mode locked dye laser picosecond pulses, using pulsed nitrogen laser pumping

15 p2422 A71-32580

Multiple laser cavities in single lasing medium, describing spatial separation of single giant pulses

15 p2422 A71-32584

Pulsed output, delay time and rotational-vibrational transitions of high pressure transverse discharge CO laser

15 p2424 A71-32613

Compact pulsed carbon dioxide laser with uniform volume excitation, obtaining output energy as function of discharge voltage, gas composition and pressure

15 p2424 A71-32698

Giant pulse ruby laser, using potassium dihydrophosphate crystals linear electro-optical effect for Q modulation

15 p2424 A71-32758

Pulsed laser double exposure holographic interferometry for measuring transverse wave propagation in beams

15 p2413 A71-32790

Electron density gradient and radial compression waves in pulsed IR laser gas discharge tube

16 p2585 A71-32795

High average power flash lamp pumped pulsed dye laser development and application in atmospheric sodium probing

16 p2586 A71-33148

Optical interferometry and schlieren photography involving high power pulsed lasers, discussing applications to plasma diagnostics and holography

16 p2586 A71-33159

Pulse laser holographic interferometry for refractivity measurement, considering wave front reconstruction principles

16 p2578 A71-33160

High power carbon disulfide-oxygen combustion pulsed laser, discussing foreign gases effects on performance and energy transfer mechanism

16 p2586 A71-33165

Luminous pulse production by internally modulated Ar laser, observing overall modes amplitudes 16 p2587 A71-33381

Two photon method of measuring ultrashort pulses and nonlinear optical effectiveness of lasers in synchronized mode 16 p2587 A71-33644

Ultrafast laser pulses, revealing fluorescence decay, stimulated Raman scattering and plasma formation transient details 16 p2588 A71-33873

Mode locked laser pulse signal recovery from time integrated correlation functions of arbitrary order, including field amplitude fluctuations 16 p2588 A71-34075

Flash lamp pumped pulsed dye lasers using triplet quenchers cycloheptatriene and cyclooctatetraene with 600 microsec emission times in rhodamine 16 p2589 A71-34122

Transversely excited atmospheric pressure pulsed carbon dioxide laser with helical electrode, discussing diverging lens effect due to cavity transverse electric discharges 17 p2750 A71-34370

Time variation of electron density and temperature in pulsed lasers operating on nitrogen band transitions, using charged particle balance equation 17 p2751 A71-34382

Pulsed emission and modulation of output power of He-Ne laser at 0.63 and 1.15 micron wavelengths as function of external longitudinal magnetic field 17 p2751 A71-34385

Book on optical holography covering basic concepts, Fourier transform, propagation and diffraction, pulsed lasers, interferometry, geometric analysis of point source hologram, etc 17 p2738 A71-34450

Short pulse Nd-YAG direct detection laser system for space communications, noting RF links complementation, high data rates, practical size, weight and power requirements 17 p2705 A71-35093

Holography with single transverse longitudinal mode pulsed ruby laser, emphasizing carrier frequency shift as limiting factor on depth of field 17 p2745 A71-35587

Pulsed chain reaction chemical lasers using flash photolysis of hydrogen-fluorine-helium mixtures 17 p2754 A71-35750

Time resolution enhancement in laser photography, recording fast events with long pulse length laser without auxiliary shutters 18 p2914 A71-35851

Self pulsing in homogeneously broadened oscillator, using materials with short recovery time for appreciable inverted population density modulation 18 p2929 A71-35901

Emission characteristics of neodymium glass laser with polymethine dye passive shutters of finite relaxation time, investigating ultrashort pulse separation 18 p2929 A71-35985

Double exposure pulsed laser holographic interferometry application to transverse wave propagation in Al plate 18 p2977 A71-36233

Dye lasers developments and applications, including flash lamp pumps, frequency narrowing and tuning and picosecond pulse mode locking 18 p2931 A71-36602

High power GaAs injection laser diodes characteristics and array module design for pulsed operation, using confinement junction formation and reflective end coating 18 p2931 A71-36604

Pulsed ruby laser high speed photography for accurate measurements of models contours in hypervelocity flight within aeroballistic range 18 p2923 A71-36612

Reflection, material and resonator losses correlation in solid state lasers, investigating pulse power in Q switched operation 18 p2932 A71-36801

Pulsed combustion heated carbon dioxide gas dynamic laser with expansion separation, showing composition and stagnation pressure dependent gain and energy variations 19 p3071 A71-37144

Beam splitting photocell for pulsed laser power and energy measurement 19 p3072 A71-37551

Oscillatory variation of optical length of pulsed laser resonators during lasing, testing with ruby laser in free emission mode 19 p3073 A71-37791

High repetition line selectable compact electrically pulsed hydrogen fluoride lasers operating on sulfur fluoride and hydrogen mixture 20 p3242 A71-38825

Platelet lasers optically pumped by pulsed xenon laser, investigating single mode operation, threshold-temperature curves, efficiency and gain spatial inhomogeneity 20 p3243 A71-39006

High pressure transversely excited pulsed nitrous oxide laser active mode locking at subatmospheric pressures 20 p3244 A71-39101

Pulsed laser oscillation from F atoms in mixed helium-fluorine gases using electric discharge excitation 20 p3244 A71-39107

Dual beam pulsed gas laser magnetic resonance spectrometer for magneto-optic studies of solids in far IR frequencies 20 p3244 A71-39177

Time resolved gain measurements of pulsed two level laser system, using computer for curve analysis 20 p3245 A71-39179

Pulsed ruby laser holographic instrumentation for materials tests, detailing reflected wave front complex amplitude characterization 20 p3245 A71-39347

Pulsed Nd laser source mass spectroscopy application to geological material analysis, tabulating assessed limits of detection for various elements 20 p3245 A71-39422

Repetitively pulsed flashlamp pumped dye laser, noting high average outputs in red end of spectrum with rhodamine B 20 p3246 A71-39760

Radial energy contours of pulsed ruby laser beam in direct determination of thermal conductivity by flash technique, using heat flux transducer 21 p3391 A71-40180

High resolution spectroscopy of Na D resonance lines in saturated absorption with repetitively pulsed tunable dye laser 21 p3391 A71-40199

Pulsed laser emission chemically pumped by exothermic chain reaction between hydrogen and fluorine mixed with He initiated by flash photolysis 21 p3391 A71-40238

Pulsed argon ion laser data, presenting excitation mechanisms and time resolved gain measurements 21 p3392 A71-40625

Pulsed ruby laser holography improvement by coherence length increase with temperature controlled multitelons and beam uniformity through ruby crystals improvement 21 p3393 A71-40925

High resolution portable hologram recording camera with pulsed ruby laser light source and rechargeable storage batteries as self contained power supply 21 p3380 A71-40926

Electrons heating by matter interaction with ultrashort laser pulses, considering hard bremsstrahlung generation 21 p3394 A71-41134

Self consistent hydrodynamic heating of solid substance by laser pulse for nonequilibrium ionization 21 p3424 A71-41253

CdS crystals faces damage caused by picosecond light pulses from free oscillating Nd-glass laser 21 p3432 A71-41305

Frequency and temperature variation with time in active region of pulsed GaAs laser diode, using Fabry-Perot interferometer 21 p3394 A71-41318

Optical spacecraft tracking, using pulsed ruby lasers at Baker-Nunn camera stations of Smithsonian Astrophysical Observatory for retroreflector-equipped satellites ranges 21 p3349 A71-41404

High energy neutralized ion beam generation by focusing ultrashort laser pulses on thin foils, applying to nuclear reaction for superheavy nuclei production 22 p3555 A71-41595

Pulsed ruby laser transmission and reflection holography in single transverse and axial electromagnetic mode, stressing safety aspects 22 p3556 A71-41743

High intensity light sources hazards analysis, discussing thermal detectors and vacuum and semiconductor photodiodes for pulsed laser outputs measurement 22 p3541 A71-41795

Vacancies production in pure Ni and V foils by bombardment with high intensity laser pulses 22 p3556 A71-41812

Mode locked transversely excited atmospheric carbon dioxide laser with Ge ultrasonic diffraction cell active loss modulator generating 10.6 micron wavelength pulses 22 p3557 A71-42132

Pulsed atmospheric pressure carbon dioxide laser, studying pulse power and shape as functions of energy storage capacitor value, charging voltage and gas composition 22 p3557 A71-42159

Helium effects on dissociation and population inversion dynamics in pulsed carbon dioxide lasers 22 p3558 A71-42268

Pulse shape of mode locked frequency doubled Nd-YAG laser, using single crystal for second harmonic generation and phase modulation 22 p3558 A71-42348

Heating dynamics of transparent dielectrics exposed to pulsed laser beam operating in free laser mode 23 p3683 A71-43270

Spatiotemporally coherent pulsed Ne and Ti vapor lasers superradiation, showing coherence time dependence on pulse length and gas pressure 23 p3683 A71-43395

Interferometric fringes from study of gas plasma produced by ruby laser pulses, using Nd glass laser for heating 23 p3710 A71-43409

Mode-locked laser ultrashort pulse duration measurement from field intensities autocorrelation functions 23 p3685 A71-43562

Spectral properties and tunability of far IR from ZnTe and lithium niobate crystals from difference-frequency mixing of mode-locked Nd glass laser pulses 23 p3686 A71-43997

N-hexane-air mixture ignition by giant pulse laser beam, analyzing probability and development time to formation of measurable nucleus 23 p3686 A71-43998

Mode locked CW dye laser operation, describing output stability and pulse rate and widths 23 p3687 A71-44133

CW dye laser mode locking with lithium niobate phase modulator, observing 500 psec pulse generation 23 p3687 A71-44134

Explosion-pumped gas dynamic carbon dioxide laser, obtaining high pulse energy by common hydrocarbon fuels 23 p3687 A71-44135

Laser pulse produced plasma in freely expanding high density nitrogen gas jets, measuring electron temperature and light-plasma interaction time 23 p3687 A71-44140

Pulsed neon laser high gain oscillation at 486.1 and 434.0 nm identified as Balmer beta and gamma lines of atomic hydrogen 23 p3688 A71-44296

R-branch multiline performance of transversely excited pulsed HF chemical laser 23 p3688 A71-44297

Self focusing in gas breakdown produced by nanosecond laser pulses, using schlieren photography and laser light forward transmission measurements 24 p3832 A71-44358

Ultrarapid motion photogrammetry using three dimensional holography with pulsed laser recording 24 p3825 A71-44757

Liquid-state pulsed laser active element lens parameters effects on output radiation divergence 24 p3835 A71-45240

PULSED RADIATION

NT ELECTROMAGNETIC PULSES

Crab pulsar optical pulses time of arrival measurements, discussing various emission mechanisms as cause for pulsar slowdown characteristics 01 p0153 A71-10363

Gain measurement on pulsed radiation from high voltage discharges in mixtures of carbon dioxide, nitrogen and helium 01 p0096 A71-11423

Q switched ruby laser facility for measuring light pulse transmission spatial and temporal response through clouds 02 p0213 A71-12013

Unstable massive main sequence stars nonlinear pulsation, using small amplitude tests of approximation technique 05 p0806 A71-16202

High power continuous and pulsed coherent radiation generation by gas lasers, discussing transmission by proton generators and transforming engines [AIAA PAPER 71-106] 06 p0946 A71-18557

GaAs lasers self-induced pulses signal structure, measuring pulse width, repetition rate and amplitude fluctuations 06 p0910 A71-18671

Carbon dioxide laser IR pulse transmission under moderate pressure conditions using four state model of molecular laser passive Q switching and double resonance 07 p1128 A71-20391

Coherent radiative phenomena with nontrivial zero-pi pulses propagation behavior in attenuating media 08 p1334 A71-21194

Pulse propagation from time-step point force at surface of transversely isotropic elastic half space, obtaining solutions by integral transforms 08 p1371 A71-21428

Pulsed radio wave interactions with various lower ionosphere models, estimating cross modulation by computer calculation for comparison with measurements 09 p1405 A71-22443

Pulsed optical range finders, predicting transmitter pulse waveshape effects on calibration, precision and efficiency by probability density function 12 p1903 A71-26792

Low density plasma-double gridded antenna system for ion and electron signal propagation studies, observing multiple reflections of acoustic and ballistic pulses and bulk phenomenon

12 p1935 A71-26913

Radio pulses at 2 MHz from cosmic ray air showers, using high speed digital techniques in statistical data analysis

12 p1948 A71-26936

Ion sources designs involving high energy electron beam injections, discussing input power continuous and pulsed modes optimal efficiencies

12 p1940 A71-27507

Simultaneous equatorial ionospheric absorption measurements at different longitudinal locations, using pulse reflection technique at 2.0-7.5 MHz

12 p1902 A71-27671

Extensive cosmic rays high and low frequency radio pulses investigation, using plastic scintillator triggered receivers

13 p2127 A71-28107

Gated light pulse technique for multiple-pass interferometry

13 p2067 A71-28444

Pulsating aurora observations, noting light intensity, diurnal variations and power spectra

14 p2229 A71-29671

Pulsed gamma radiation from rotating neutron star, discussing synchrotron emission mechanism based on electron pulses incident on high intensity sharply localized magnetic field

15 p2474 A71-31724

Auroral 1.2-4 second periodicity X ray pulsations during magnetic storms, using omnidirectional detector at balloon altitude

15 p2474 A71-31775

High energy pulsed gamma rays detection from pulsars emission based on time averaged phase histograms

15 p2479 A71-31838

Continuously tunable pulsed UV source using broadband dye laser emission input to rotatable KDP crystal

16 p2586 A71-33141

Two frequency ultrasonic flaw detector for determination of defects opening widths, examining ultrasonic pulse transmission through thin air layers

16 p2580 A71-33562

Laser light pulses in anisotropic crystal, investigating nonlinear thermal rotation of polarization plane

16 p2587 A71-33570

Optical crossed or collinear light pulse pairs for production and sounding of instantaneous processes kinetics in nanosecond and picosecond range

16 p2580 A71-33624

Short narrow light pulse reflection from thick turbid medium with strong anisotropic scattering, obtaining backscattering signal power from unsteady transport equation solution

16 p2544 A71-34105

Galactic center isolated radio pulse search at 151.5 MHz, correlating with Weber gravitational events

17 p2805 A71-35378

Pulsar polarization characteristics and pulse profile observations in 250-450 MHz range

17 p2807 A71-35417

Time dependent multiple backscattering of pulsed light for linearly polarized incident radiation

17 p2709 A71-35809

Thermal self focusing of pulsed millimeter waves transmitted through cylindrical plasma, observing power dependence and beam asymmetry

18 p2951 A71-35986

High efficiency avalanche diode microwave oscillator design guidelines based on oscillation mode theory, covering CW and pulsed operations

18 p2888 A71-36131

Automatic fringe counting pulsed ultrasonic interferometer for transit time measurement, using phase sensitive multiple echo detection

18 p2922 A71-36586

Coherent neutral sheet radiation from pulsars, examining relationship between pulsation-driving energy source and mechanisms for pulsed emission

18 p2958 A71-36928

High speed rotating optical attenuator for sub-second sawtooth radiance pulse generation for detection, cooling or heating experiments

19 p3063 A71-37249

Pulsed gamma radiation detection from Crab Nebula by balloon-borne telescope

19 p3124 A71-37333

Pulsed emission of hard X rays from Crab Nebula pulsar NP 0532, using balloon-borne telescope

19 p3124 A71-37338

Infrasound pulsations of optical auroral luminosity in 3914 A positive molecular nitrogen ion and 5577 A O I emission measurement by double photometer system

19 p3048 A71-37395

Organic dyes pulse emission spectra shifts during pumping by ruby and neodymium-glass lasers, discussing vibrational relaxations role in mechanism

19 p3072 A71-37766

High peak power microwave oscillators, discussing pulsed limited space charge accumulation and TRAPATT diodes pulsed radiation sources performance

19 p3029 A71-38294

Auroral pulsations physical correlation with cosmic noise absorption, using statistical correlation analysis

20 p3215 A71-38734

Auroral zone ionosphere time lag observations, noting delay in cosmic noise absorption pulsations to fast bremsstrahlung X rays, luminosity and micropulsations

20 p3215 A71-38740

Higher order noisy optical pulse intensity correlations interpretation by statistical model, estimating spike amplitude

20 p3196 A71-39103

Cygnus X-1 X ray data with temporal resolution, examining pulsations and flare activity

20 p3278 A71-39110

Cygnus XR-1 X ray intensity fluctuations, discussing time scales and periodicities

20 p3278 A71-39111

Critique of quasar model of independent random pulse emitting sources conglomeration from incompatibility with light curve

20 p3289 A71-39294

Pulsar pulsed optical radiation search, noting dependence on determination of accurate positions by radio methods

20 p3303 A71-39938

Power spectral analyses of auroral light and X ray pulsations, discussing damping due to velocity dispersions of electrons with various energies

21 p3373 A71-40069

Periodic current pulse and superradiant radiation pulsing in DC excited xenon plasma with increased cathode-anode capacitance

21 p3424 A71-41046

Massive main sequence stars pulsation kinetics, examining amplitude growth, time scale ratios and evolutionary stabilization

22 p3596 A71-41447

Absolute foveal thresholds as function of flashes pulse length and null period

22 p3497 A71-41480

Flashing lights radiation characteristics photometric measurement, discussing measuring apparatus sensitivity and errors analysis

22 p3499 A71-41496

Circinus pulsating X ray source spectrum analysis, considering bremsstrahlung and black body models

22 p3592 A71-41928

Low cost two channel pulse counter (RUFAS) for astronomical photoelectric occultation observations, describing resolution, data output and computer interfacing

22 p3542 A71-41932

Quasi-optical transmission line stability improvement, investigating pulsating light beam concept

22 p3512 A71-42309

Monte Carlo method calculation for light pulse reflection from clouds for all orders of multiple scattering

22 p3576 A71-42562

Southern pulsars pulse energy flux average nightly values at 80 MHz

22 p3606 A71-42602

Atmospheric triggered VLF emissions theory, examining magnetospheric whistler Morse pulses

23 p3643 A71-43135

Radiant heat flux measurement during pulsed processes from surface in high temperature emitting gas, using thin film sensor with small time constant

23 p3782 A71-43922

Pulsed signal secondary forward scattering in optical fiber transmission lines

23 p3646 A71-43968

Pulsar radio pulse shape and structure, discussing pulse widths and polarization angle change

23 p3769 A71-43989

Extensive air shower radio pulse emission by geomagnetic charge separation mechanism, using antenna and scintillation counters arrays

23 p3646 A71-44012

X ray sources pulsation limits and locations determination by rocket-borne rotating modulation collimator

24 p3866 A71-44914

Dielectrics breakdown under ultrashort neodymium laser pulses at fundamental and second harmonic frequencies

24 p3834 A71-45120

PULSES

NT ELECTRIC PULSES
NT ELECTROMAGNETIC PULSES
NT GEOMAGNETIC MICROPULSATIONS
NT GEOMAGNETIC PULSATIONS
NT MICROPULSATIONS

Transistor collector pulse response characteristics measurement at high voltages in avalanche multiplication region, considering dissipated power curve

01 p0051 A71-10282

Numerical analysis for flexural stress pulse propagation in nonuniform elastic bars by geometric acoustics

22 p3616 A71-42213

Load stress pulse shape and frequency effects on macroscopic dislocations during plastic deformation of crystalline materials

23 p3777 A71-43875

PULVERIZING

U GRINDING [COMMINUTION]

PUMP IMPELLERS

Impeller radial forces in volute casing centrifugal pumps, using potential theory

03 p0431 A71-13145

Experimental materials for axial flow vane pumps operating under cavitation conditions, considering separated flow around impeller blades

20 p3241 A71-39169

Turbomolecular vacuum pump impeller theoretical efficiency with allowance for diffuse law of interaction between gas molecules and interblade channel walls

20 p3183 A71-39170

Flow rate and heating analysis of centrifugal pumps with variable cross section impeller blade ring inlet

22 p3554 A71-41850

Photogrammetric flow rate determination in centrifugal pump impeller, using rotating camera

24 p3825 A71-44754

PUMPING

YIG C band microwave amplifier using longitudinal pumping, comparing to other systems

02 p0228 A71-11692

Capillary and electro-osmotic flow pumping in heat pipes, discussing capacity increase

11 p1857 A71-26214

Peristaltic pumping mechanism as progressive wave train of transverse wall displacement in plane two dimensional channel

15 p2366 A71-32559

PUMPS

NT AXIAL FLOW PUMPS
NT CENTRIFUGAL PUMPS
NT CONDENSATION PUMPS
NT DIFFUSION PUMPS
NT ELECTROMAGNETIC PUMPS
NT FUEL PUMPS
NT ION PUMPS
NT JET PUMPS
NT MOLECULAR PUMPS
NT RAMS (PUMPS)
NT TURBINE PUMPS
NT VACUUM PUMPS

Hydraulic vane pumps, including variable displacement, double and compound pumps

01 p0006 A71-10815

Hydraulic system axial- and radial-piston pumps design and operation principles, considering cost reduction

01 p0006 A71-10817

Aircraft gear pumps bearing elements design for increasing service life

08 p1295 A71-20793

Performance testing of fluorosilicone hydraulic fluid in high temperature supersonic aircraft piston pumps

12 p1921 A71-27040

PUNCHED TAPES

Fluidic 8 track punched tape reader, discussing design simplicity, flexibility, accuracy, wear and long life operation

07 p1025 A71-20560

PUNCHES

Circular planform punch pressure on elastic half space, solving system of two dimensional dual integral equations

19 p3160 A71-38478

PUPIL SIZE

Pupil neurological control system for reaction to light and accommodation process by statistical eye noise analysis and microelectrode recordings of brain stem neurons

03 p0367 A71-12985

Pupil size effect on dynamics of pupillary movements, considering reactions to light and darkness

13 p2013 A71-29032

Pupil size influence on surface area and radius of inner/pupillary/ and outer/ciliary/iris ring

13 p2013 A71-29034

PUPILLOMETRY

Commercial airline pilots alertness tests, using IR pupillometry

04 p0543 A71-15051

Human afterimage and pupillary activity in darkness after strong light exposure, noting dependence on stimulus intensity and duration

13 p2018 A71-28463

Pupil size influence on surface area and radius of inner/pupillary/ and outer/ciliary/iris ring

13 p2013 A71-29034

Eye pupil response during short term memory task, noting postsignal cycle of dilation-constriction

23 p3638 A71-43112

PUPILS

Mathematical model for eye crystalline lens accommodation control interaction with pupil, deriving dynamic equations from human/cat experiments with/without neurological control

03 p0356 A71-12984

Cat pupillary system static and dynamic response determination under light and electrical stimulation, using TV pupilometer and on-line computer

17 p2691 A71-35044

PURGING

Continuous impurities purging from hydrogen oxygen fuel cells gas compartments, describing operation mode and design techniques

21 p3326 A71-41250

PURIFICATION

NT AIR PURIFICATION

Gas-metal reactions in refractory metals purification, discussing reaction kinetics, thermodynamic equilibria and dissolved gases induced mechanical properties changes

22 p3564 A71-42423

PURIFIERS

U PURIFICATION

PURINES

NT ADENINES

Pentose breakdown photosensitivity from UV irradiation in presence of minerals, considering prebiological period carbohydrates evolution and interaction with purines and pyrimidines

01 p0029 A71-11561

Paper chromatography combination with dinitrophenyl amino acids mass spectrometry for analyzing purine and pyrimidine bases

06 p0865 A71-17574

Purine and pyrimidine derivatives of cattle hypothalamus determined by gel filtration and subsequent spectral analysis and chromatography

21 p3338 A71-41071

PURITY

Real time modal purity and data quality assessment techniques

11 p1853 A71-26501

Metallic materials static to dynamic transition in creep noting temperature and purity effects

13 p2084 A71-28110

Be sheet plastic bend ductility and yield strength, considering purity and processing effects

13 p2088 A71-29403

PURSUIT TRACKING

Ocular pursuit movement evocation by visual and proprioceptive stimulation

01 p0009 A71-10235

Extremal strategies of differential pursuit game for nonlinear controlled plants

01 p0128 A71-10654

Pursuit game strategy based on Hamilton-Jacobi formalism, considering internal and external potential fields, optimum trajectories and gravitational and electromagnetic fields

03 p0483 A71-13116

Proportional navigation vs optimally evasive constant speed target in two dimensions, considering lateral acceleration and time constraints in pursuer control

03 p0455 A71-14438

Pursuit tracking skill acquisition in humans, considering sex, initial ability, age, aptitude and proficiency levels and psychomotor performances

05 p0713 A71-16549

Efficient evasion strategies for vehicle pursuit-evasion games with imperfect information, using computer solution

06 p0846 A71-17331

Soviet monograph on differential games of encounter of motions covering optimal control, rendezvous, pursuit, evasion, extremal guidance, etc

06 p0926 A71-17438

Optimal control epsilon technique solution for capture conditions in pursuit and evasion problems

06 p0918 A71-17597

Capture and control of derelict spacecraft drifting through gravitational field of solar system by pursuit craft

06 p0927 A71-17642

Pursuit and evasion games, proving existence and approximation theorems

06 p0921 A71-18238

Human performance in pursuit tracking task with realistic structured and blank backgrounds

07 p1047 A71-19460

Human performance in continuous pursuit tracking with temporary target obscurations, noting positional and velocity control systems

07 p1047 A71-19461

Two body pursuit problem minimax and optimum absorption time control algorithm

07 p1082 A71-20642

Extremal strategies of differential pursuit game for nonlinear controlled plants

14 p2266 A71-30988

Optimization of linear tracking strategies, considering time independent and translation invariant N point predictor

15 p2379 A71-31411

Adaptive mathematical model of human operator during pursuit tracking, synthesizing brain in accordance with arbitrary reasonability criterion

17 p2692 A71-35169

Visual target pursuit tracking test confirming error amending by central mechanism without sensory feedback

19 p3007 A71-37545

Unmanned spacecraft pursuit of evading manned vehicle by game theory, assuming full information availability to both players

19 p3038 A71-38014

Rapid saccadic and smooth pursuit tracking eye movement systems characteristics

22 p3489 A71-42445

PUSH-PULL AMPLIFIERS

Push-pull power amplifiers with class B complementary transistors, describing driver stage

02 p0229 A71-11693

Modulator-demodulator type push-pull DC amplifier input noise reduction, using electromechanical vibrators

15 p2355 A71-32451

PWM [MODULATION]

U PULSE DURATION MODULATION

PYRAMIDAL BODIES

Aerodynamic characteristics of conical and pyramidal configurations with various planforms by slender body theory, replacing three dimensional flow by two dimensional flow

08 p1227 A71-20776

German monograph on three dimensional steady hypersonic flow of perfect gas past pyramid shaped bodies of rhombic planform

21 p3323 A71-40774

PYRAZINES

NT AZINES

NT CYANURATES

PYREX [TRADEMARK]

U BOROSILICATE GLASS

PYRIDINE NUCLEOTIDES

Pyridine nucleotide concentration in cerebral hemispheres of rats under hyperoxia

09 p1391 A71-22534

PYRIDINES

Self consistent field /SCF/ calculations of dipyrindine glyoxal and bianthrone photoproduct molecules with triplet ground state, using unrestricted Hartree-Fock theory

11 p1727 A71-25576

PYRIDOXINE

Vitamin B6 protection against asymmetrical dimethylhydrazine poisoning, administering B6 alone and with cortical phospholipids in mice

10 p1572 A71-24979

Dietary pyridoxal deficiency causing amino acid content reduction in liver, kidney, brain and heart tissues

13 p2003 A71-27837

Pyridoxine and serotonin metabolism changes and vestibular disorders observation in space flight

16 p2532 A71-33677

PYRIMIDINES

NT MITOCHONDRIA

NT THYMIDINE

NT THYMINE

NT URACIL

Pentose breakdown photosensitivity from UV irradiation in presence of minerals, considering prebiological period carbohydrates evolution and interaction with purines and pyrimidines

01 p0029 A71-11561

Paper chromatography combination with dinitrophenyl amino acids mass spectrometry for analyzing purine and pyrimidine bases

06 p0865 A71-17574

Laboratory and clinical investigations of radiosensitization of cells and viruses by halogenated pyrimidine analogs

07 p1032 A71-18929

Tumor DNA increase of halogenated pyrimidines incorporation compared to normal tissue DNA, discussing intraarterial infusion of radiosensitizing agents

07 p1040 A71-18989

Purine and pyrimidine derivatives of cattle hypothalamus determined by gel filtration and subsequent spectral analysis and chromatography

21 p3338 A71-41071

PYROELECTRICITY

Barium titanate pyroelectric receivers for giant pulse laser emission measurements

12 p1915 A71-27756

Thermal, pyroelectric and photoelectric detectors for middle IR wavelength range

19 p3064 A71-38064

Pyroelectric IR detectors performance, investigating strontium barium nitrate, lithium sulphate and triglycine sulfate materials effects on frequency range and sensitivity

22 p3542 A71-42122

Pyroelectric detector linear arrays for IR thermal imaging at room temperature

22 p3543 A71-42131

Pyroelectric, pneumatic and thermocouple detectors comparison, discussing IR detectors availability for use in spectrophotometers in 2-20 micron region

22 p3544 A71-42142

PYROGRAPHALLOY

U COMPOSITE MATERIALS

U PYROLYTIC GRAPHITE

U REFRACTORY MATERIALS

PYROHELIOMETERS

Circumsolar radiation and atmospheric turbidity effects on readings of compensation type pyroheliometers with allowance for receiver sensitivity

21 p3384 A71-41382

Compensation type reference pyroheliometer design and calibration, considering accuracy, constant characteristics and turbidity effects

21 p3384 A71-41383

PYROLYSIS

Gas dynamics of fuel boundary layer combustion and surface pyrolysis in hybrid rocket motors

01 p0178 A71-10131

Reaction mechanism for ammonium nitrate thermal decomposition, discussing chloride catalytic effects

01 p0141 A71-10344

Pyrolyzing vinyl polymers thermal degradation kinetics, deriving surface regression rates relationship to temperature

01 p0109 A71-10935

Ablative heat shield char layer, examining reacting nonequilibrium pyrolysis gas flow

01 p0181 A71-11297

High temperature decomposition kinetics in vacuum of mixed ammonium perchlorate-polystyrene solid fuel, using time of flight mass spectrometer

03 p0469 A71-13997

Gas dynamic analysis of hybrid boundary layer combustion with nonequilibrium surface pyrolysis, using Rayleigh analogy

05 p0837 A71-16539

Acetylene pyrolysis kinetics, considering isothermal vs adiabatic conditions and surface catalyzed vs homogeneous gaseous

06 p0943 A71-17660

Plastics thermal decomposition, investigating combustion products and toxicity

06 p0916 A71-18089

Radiation effects on thermal decomposition induction period in ammonium perchlorate and other pseudostable inorganic solids

06 p0944 A71-18301

Epitaxial boron phosphides single crystals growth, using thermal decomposition and reduction for deposition on hexagonal silicon carbide substrates basal plane

07 p1180 A71-20174

Methyl radicals reactions produced by azomethane or ethane pyrolysis in reflected shock waves, describing chain reaction mechanism

08 p1250 A71-20668

Silver oxides stability, considering solubility, reduction by hydrogen and thermal decomposition

08 p1234 A71-21085

Composite solid propellant binders thermal decomposition investigation by differential scanning calorimetry method, discussing kinetic data relevance to solid propellant combustion

10 p1657 A71-24046

Hydrocarbons pyrolysis in Knudsen cells at low pressures, using mass spectrometry to study reactions and products

11 p1727 A71-25229

Polyphenylene thermal degradation and curing, discussing pyrolytic effects of chlorine and polynuclear structure

11 p1855 A71-26035

Nylon-phenolic composites pyrolysis, deriving kinetic coefficients from thermogravimetric analysis at various heating rates

11 p1728 A71-26043

Pyrolysis-gas chromatography locating degradation front in phenolic ablative plastics, giving percent phenolic resin vs distance normal to surface

11 p1728 A71-26044

German monograph on gaseous detonations stability covering carbon dioxide thermal decomposition, initial temperature/pressure, reflected shock waves and water adsorption

13 p2049 A71-28878

Carbon/graphite cloth reinforced aromatic/heterocyclic resins ablative composites pyrolysis kinetics by computer code analysis

14 p2262 A71-29649

Nonequilibrium modeling of pyrolysis gas products flow through char layer of ablative heat shield

14 p2334 A71-29876

Thermal decomposition rates and explosion of dinitroxydiethyl nitramine from heat release measurements at various pressures

15 p2462 A71-31376

ClF diluted solutions in Ne, investigating thermal decomposition mechanism behind shock waves by mass spectroscopy

15 p2367 A71-31874

Thermal decomposition kinetics of nitrous oxide in shock tube, measuring IR emission behind reflected wave 16 p2539 A71-32910

Sodium superoxide isothermal decomposition, detailing metallic oxide effects with differential thermal analysis, thermogravimetry and differential thermogravimetry 17 p2694 A71-34672

Ammonium perchlorate based solid propellants combustion, assuming pyrolysis of solid binder 17 p2792 A71-35549

Radiation induced etch-pit dislocations and thermal decomposition kinetics in ammonium perchlorate crystals 18 p2955 A71-35967

Dissociation reaction in presence of halogen atoms produced in shock wave by thermal decomposition of hydrogen fluoride 19 p3012 A71-38085

Porous material slab pyrolysis, studying density and thermal conductivity changes and reaction kinetics 19 p3170 A71-38117

Perchloric acid catalytic pyrolysis relationship to ammonium perchlorate decomposition and combustion from electric conductivity measurements, IR spectroscopy, chemical and thermal analysis 19 p3120 A71-38119

Carbon fibers grown on graphite by thermal decomposition of hydrocarbons, investigating external morphology and structure 21 p3406 A71-40837

Apollo 12 lunar surface samples analysis for organic compounds by mass spectroscopy and pyrolysis-gas chromatography 23 p3756 A71-43741

PYROLYTIC GRAPHITE

Pyrolysis products of polyacrylonitrile fibers in low pressure apparatus, using mass spectrometer [PLASTICS INST. PAPER 4] 08 p1250 A71-20926

Highly ordered pressure-annealed pyrolytic graphite majority carrier electrons and holes locations in Brillouin zone from measurements in magnetic fields 08 p1344 A71-21363

Pyrolytic graphite hemispherical emissivity measurement on surface parallel and perpendicular to deposition surface at 1200-2300 K 08 p1323 A71-21921

Stress equations for thin pyrolytic graphite shells with thermal allowance 09 p1534 A71-22095

Pyrolytic graphite microcalorimeter for X ray absorbed dose measurement, exploiting for calibration self heating 10 p1608 A71-23742

Thermal conductivity prediction during ablation of phenolic-carbon and phenolic-graphic composites for heating and cooling conditions [AIAA PAPER 71-380] 11 p1783 A71-25304

Pyrolytic graphite, discussing fabrication by chemical vapor deposition process, mechanical and physical properties, residual stresses, applications in reentry vehicle heat shields, rocket nozzle throats, etc 11 p1789 A71-25743

Pyrolytic graphite heat conductivity coefficients in direction perpendicular to deposition surface at high temperatures 13 p2090 A71-27883

Radioisotope heat sources protection from reentry ablation and thermal stress with outer anisotropic pyrolytic graphite shield 13 p2099 A71-29259

Electrical conductivity of pyrographite at high temperatures along and across deposition plane, using optical pyrometer measurements 17 p2761 A71-34304

Pyrolytic graphite hemispherical emissivity measurement on surface parallel and perpendicular to deposition surface at 1200-2300 K 17 p2763 A71-35265

Analog analysis of shape history of ablating graphite nose tips of reentry vehicle, eliminating geometrical instabilities 18 p2984 A71-35953

PYROLYTIC MATERIALS

NT PYROLYTIC GRAPHITE

Beryllium hydride pyrolytic decomposition kinetics noting temperature range, time distribution, linear growth rate and X ray irradiation 07 p1182 A71-19241

PYROMETERS

NT RADIATION PYROMETERS

NT THERMOCOUPLE PYROMETERS

PYROMETRY

U TEMPERATURE MEASUREMENT

PYROPHORIC MATERIALS

Pyrophoric materials literature, discussing nature, behavior, production, safe handling and fire control 13 p2158 A71-27854

PYROPHYLLITE

Van der Waal bound lamellar solids interlayer binding energy computational model, discussing talc and pyrophyllite equilibrium stacking arrangements and force constants 10 p1573 A71-24541

PYROTECHNICS

Crystal laser pyrotechnic illumination lamps with noncompacted explosive mixture, noting Nd ion doped calcium tungstate and YAG laser tests 19 p3073 A71-37788

PYROXENES

NT ENSTATITE

Nonseparated grain low iron olivine and pyroxene in carbonaceous meteorite Orgueil, using optical and electron probe microanalysis 02 p0318 A71-12904

Cations partitioning between coexisting single and multisite phases in pyroxenes and olivines 06 p0894 A71-18236

Apollo 12 clinopyroxenes exsolution and epitaxy by electron microprobe and single crystal X ray diffraction 10 p1672 A71-24391

Apollo 12 soils composition and derivation, finding feldspathic orthopyroxene rich rock and chemically comparable glass fragments 10 p1672 A71-24393

Core binding energy difference between bridging and nonbridging oxygen atoms in silicate chain of pyroxenes, using X ray photoelectron spectra 19 p3011 A71-37415

Static ductile deformation in quartz, olivine, pyroxenes and plagioclase, noting plastic deformation and recovery 19 p3050 A71-37664

Fe content of clinopyroxene in basalt-basaltic andesite-andesite-laitite of Mogollon Plateau (New Mexico) 20 p3216 A71-39386

High temperature phase transition and composition of Apollo 12 pigeonite/augite clinopyroxene crystal rock 12021 from X ray diffraction 23 p3738 A71-43607

Oxidation state of iron and cation distribution over M1 and M2 sites in clinopyroxenes from Apollo 12 by Mossbauer absorption spectroscopy, noting cooling history 23 p3738 A71-43609

Exsolution lamellae structure of Lunar pyroxenes from Apollo 12 samples, using electron microscopy and diffraction 23 p3738 A71-43610

Mineralogical and petrographic investigation of olivines, feldspars and pyroxenes in Apollo 12 fines and igneous rocks, using optical and X ray diffraction 23 p3741 A71-43631

Pyroxenes morphological significance in Apollo 12 lunar igneous rock samples petrogenesis, analyzing crystallization process history 23 p3742 A71-43642

Clinopyroxene crystallization histories of Apollo 12 porphyritic basalt rocks 12021 and 12052 from Oceanus Procellarum 23 p3742 A71-43643

Pyroxenes and olivines in lunar rocks from Ocean of Storms, observing plastic deformational processes since crystallization by optical, X ray and electron microprobes 23 p3744 A71-43657

Spontaneous fission fossil tracks of U, Pu and extinct transuranic elements in pyroxenes of Apollo 11 and 12 soil samples 23 p3764 A71-43803

PYROXYLIN

U CELLULOSE NITRATE

PYRRHOTITE

NT TROILITE

PYRROLES

NT INDOLES

NT TRYPTOPHAN

PYRRONES (TRADEMARK)

High temperature pyrrones molding, discussing covalent organic bonds breakage and subsequent structural rearrangement of crosslinked polymer network 01 p0107 A71-10459

Imide-pyrone copolymers preparation by solution polymerization, considering base/acid degradation resistance and thermal stability in air and vacuum 04 p0549 A71-15749

Pyrone foams molding, considering chemically blown and syntactic foams mechanical properties 14 p2262 A71-29650

PYRUVATES

Pyruvate and lactate concentrations in muscle tissue and blood at rest and during exercise 14 p2187 A71-31136

Heart rate variation during and after muscular exercise, discussing correlated measurements of rectal and mean skin temperatures, blood lactate, pyruvate and glucose 20 p3185 A71-38891

ing collisionless theory, thermalization, alkali metals, ion recombination, etc 01 p0131 A71-10102

Collisional drift instability remote feedback suppression in Q machine Cs plasma by microwave modulation at upper hybrid frequency 06 p0932 A71-17464

Q-machine with boundary segments to provide passive feedback for reducing Kelvin-Helmholtz instability and plasma losses 06 p0933 A71-17467

Longitudinal ionic wave excitation by grid in collisionless Q machine plasma 15 p2456 A71-31820

Stationary collisional shock observation in continuous supersonic plasma wind tunnel involving Q device modified into magnetic de Laval nozzle 21 p3426 A71-41403

Plasma flow around disk in single ended Q machine with magnetic field parallel to flow velocity, measuring density profile for wake structure 22 p3580 A71-41587

Stationary stable cellular pattern onset relationship to plasma confinement in single ended Q machine 23 p3713 A71-44153

Q FACTORS

Gunn oscillator frequency characteristics vs displacement voltage in low Q factor resonance circuits 04 p0557 A71-14634

High Q microwave diodes on n-type germanium using carrier counterdiffusion in reducing atmosphere 06 p0873 A71-17539

Frequency modulation technique based on injection phase locking theory applied to microwave oscillator Q measurement 07 p1074 A71-19127

Superconducting microstrip microwave resonators with high Q, using vacuum deposited lead on alumina substrate 07 p1079 A71-20162

High Q factor rotor systems applications in dielectrics electromagnetic viscosity measurement and radio transmitters with low oscillation phase drift 09 p1492 A71-22363

Optical resonators with anisotropic elements, altering natural oscillations Q factor and spectrum 09 p1461 A71-22384

Microwave resonator Q factor and coupling and matching characteristics measurement using line probe with AM and FM signals 10 p1584 A71-24724

Q factor of control systems as mathematical expectation of functional on input signal set with prescribed probabilistic measure and random initial conditions 10 p1588 A71-24904

Linear optimal control system quality functional, deriving sensitivity upper estimate 13 p2041 A71-28635

Transforming network conditions for two state one port terminations Q factor existence from Mobius transformations and invariance properties 14 p2209 A71-29545

Microwave resonator Q factor measurement by reflection coefficient method, using swept signal generator to eliminate incidental FM problem 15 p2376 A71-32310

Inductive voltage divider bridge network for ferrite coils inductance and Q measurements 17 p2723 A71-35713

Real operational amplifier analysis application to state variable filter design emphasizing high-Q HF phenomena, noting undesirable behavior by heuristic argument 21 p3360 A71-40808

High Q micropower filters for VHF applications based on conditionally stable negative resistance operation, describing computer-aided design, construction and performance 21 p3361 A71-40822

Stability and quality diagrams of linear discrete automatic control systems with time constant parameters 21 p3361 A71-41142

Apollo 11, 12 and 14 lunar seismometer results suggesting lunar material Q factors up to 3000 21 p3453 A71-41407

Tapered distributed RC low pass network configuration with voltage-controlled sources for sensitivity reduction low and high Q factors 21 p3361 A71-41409

Design parameters optimization for flat spiral coils printed on dielectric substrates based on equivalent circuit analysis, emphasizing coil shape effects on Q and inductance 22 p3520 A71-41715

System quality analysis by reliability measures /mean time between failures/, using distribution free evaluation models 22 p3566 A71-42114

Gunn oscillator frequency characteristics vs displacement voltage in low Q factor resonance circuits 22 p3521 A71-42274

Gunn oscillator frequency stabilization at minus 10 to 60 C by high Q single tuned oscillator circuit, considering requirements for 20 GHz radio relay system 23 p3651 A71-43438

Q

Q DEVICES

Monograph on particle diffusion losses in contact ionization plasmas under Q machine conditions cover-

- HF and LF transistors suitability for integrated high Q LC circuits, studying inductivity, Q and component frequency dependence 24 p3807 A71-44377
- Pulsed modulation of continuous laser resonator Q factor, recording output on oscillograph 24 p3834 A71-45045
- SHF resonator small resonant frequency shift and Q factor changes measurement based on FM signal envelope shape analysis 24 p3858 A71-45237
- Q SWITCHED LASERS**
- Spark discharge ignition in air by Q switched ruby laser 01 p0093 A71-10684
- Pulse transmission control equipment for Q switched ruby laser output 01 p0095 A71-11171
- Lithium niobate crystal electro-optical shutter to Q switch calcium difluoride-Dy laser emitting giant pulses at high repetition rate 01 p0095 A71-11210
- Q switched monomode ruby laser coherence length measurements, using holography at various beam intensities 01 p0096 A71-11374
- Giant pulses composed of shorter pulse trains obtained in Q switched carbon dioxide laser with transverse modes 02 p0259 A71-11880
- Cavity resonator length effect on lasing threshold, output energy, pulse power and duration and spectral width of giant single pulse mode laser with passive Q switch 02 p0259 A71-11933
- Q switched ruby laser facility for measuring light pulse transmission spatial and temporal response through clouds 02 p0213 A71-12013
- Q switched ruby laser-Raman radar for real time air pollution probe 02 p0213 A71-12014
- Q switched laser wave birefringence thermal variations in liquids, calculating optical anisotropy temperature dependence 02 p0261 A71-12172
- Discharge current oscillations attributed to acoustic wave excitation by Q switched carbon dioxide laser 02 p0261 A71-12341
- Constant dispersion rotating grating Q switch for carbon dioxide laser with simultaneous band selection and cavity adjustment 03 p0436 A71-13652
- Vibrating mirror for continuously pumped ND/YAG laser repetitive Q switching 03 p0438 A71-13888
- Single mode locked Nd-glass laser pulse time synchronization with Q switched ruby laser 03 p0438 A71-13891
- Reactive Q switching in carbon dioxide multimode multipass laser with movable end mirror, measuring pulse rates and amplitudes 03 p0438 A71-13892
- Q switched ruby laser ranging system of tracking station for use with retroreflecting satellites 03 p0379 A71-14007
- IR Q switched gas laser with Michelson interferometer for plasma diagnostics, describing equipment operation 03 p0439 A71-14056
- Hologram and optical elements insertion in Q switched laser for generation switching, using YAG /Nd/ basic laser 03 p0439 A71-14176
- Atmospheric air breakdown by mode-locked Q switched laser pulse train, investigating threshold electric field dependence on characteristic diffusion length 03 p0440 A71-14178
- IR lasers, discussing carbon dioxide CW and Q-switched operation and semiconductor lasers 04 p0606 A71-14712
- Carbon dioxide laser with simultaneous active rotating mirror Q switch and passive absorbing gas cell 05 p0760 A71-16256
- Rare gases interaction with focused multimode Q switched laser beam, measuring orders of nonlinearity and multiphoton ionization probabilities 05 p0761 A71-16335
- Pulse transmission mode Q switched neodymium laser, discussing pulse duration 05 p0762 A71-16374
- Pulse repetition rate of Q switched YAG-Nd oscillator-amplifier laser systems 05 p0762 A71-16479
- High repetition rate Q switched Nd-YAG lasers, graphing theoretical Q switching from rate equations of ideal four-level laser 05 p0764 A71-17076
- Ultrafast Q switched laser induced shock waves in solids, discussing model for picosecond impulse 06 p0907 A71-17311
- Contact electro-optic KDP crystal shutters for Q switching ruby laser 06 p0907 A71-17530
- Ruby Q switched lasers with modular electro-optic shutters for low insertion loss and high optical radiation resistance 06 p0908 A71-18303
- Time dependent Q switched energy storage of trifluoromethane photodissociation laser 06 p0910 A71-18661
- Q switched Nd laser pulse duration control as function of KDP crystal orientation and pumping power 07 p1122 A71-19138
- Ruby laser passive Q switching by phototropic thin film shutter, outlining advantages over bleachable dyes 07 p1122 A71-19140
- Plasma produced by focused Q switched ruby laser beam, considering use for minimum ignition energy measurement 07 p1123 A71-19577
- Emission of ruby laser with resonator containing passive Q switch solution and lenses, investigating regular self oscillation region 07 p1125 A71-19811
- Carbon dioxide lasers passive Q switching by saturable absorbers, using four state kinetic model 07 p1128 A71-20390
- Carbon dioxide laser IR pulse transmission under moderate pressure conditions using four state model of molecular laser passive Q switching and double resonance 07 p1128 A71-20391
- Gaussian shaped laser pulse holographic brightness analysis, presenting theoretical and experimental holographic coherence length curves for Q switched laser oscillator and amplifier system 08 p1290 A71-21390
- Doppler effect mechanism for laser Q switching with rotating mirror, noting pulse width dependence on wavelength 08 p1302 A71-21434
- Controllable pulse length Q switched Nd-YAG laser using lithium iodate doubling crystal 09 p1463 A71-22757
- Continuously pumped Q switched neodymium doped YAG laser micromachining tool for resistor trimming, resonator/filter frequency tuning and diode/transistor vaporizing 09 p1457 A71-23402
- Q switched and continuous laser collimated radiation exposure limits for eye cornea and skin, discussing environmental contamination 09 p1402 A71-23414
- Spectral bandwidth of Q switched giant pulse laser as function of single pass gain, optical switch and resonator loss 10 p1619 A71-23955
- Superregenerative linear mode amplification in Q switched He-Xe laser as function of resonator phase, length and signal angle 10 p1621 A71-24713
- Amplitude characteristics of Q switched He-Xe laser at 3.5 microns, using rotating reflection prism and velocity equations 10 p1621 A71-24715
- Microwave frequency sound generation in solids with Q switched ruby laser 10 p1621 A71-24838
- Q switched ruby laser time dependent spectrum analysis by high speed camera with Fabry-Perot interferometer, noting holographic interferometry application 10 p1622 A71-24962
- Carbon dioxide laser design and characteristics, discussing lasing action, spectral properties of continuous and Q switching output power 10 p1623 A71-25089
- Nd-YAG folded center lasers Q switching and cavity dumping, using fused silica and Brewster cut intracavity acousto-optic modulator 11 p1773 A71-25798
- Carbon dioxide plasma discharge current changes from Q switched laser irradiation, studying excitation and relaxation mechanisms 11 p1774 A71-25933
- Q switched ruby laser emission effect on long wave pigment system of photosynthesizing organisms 11 p1774 A71-26006
- Kinetic and ionization phenomena in Q switched laser produced plasmas, considering gas dynamic plasma parameters /velocity, density distribution, pressure and temperature/ 11 p1806 A71-26086
- Plane and three dimensional dynamic holograms recording in bleachable dyes, using ruby laser with gallium chloride phthalocyanin in chlorobenzene as Q switch 11 p1767 A71-26565
- Lossless KDP Pockels cell modulator for high power laser Q switching based on tuned face electro-optical crystal 12 p1905 A71-26813
- P-type gallium selenide crystals impurity photoconductivity measurements by Q switched ruby laser 13 p2077 A71-27959
- Repetitive passive Q switching of single frequency carbon dioxide laser with intracavity saturable absorber, developing nonlinear model 15 p2423 A71-32602
- Optimal pulsed power output of continuously pumped Q switched Nd-YAG laser as function of mode parameters 15 p2423 A71-32603
- Cavity loss dependent erbium glass laser line oscillations in lower threshold region under Q switch and long pulse conditions 15 p2424 A71-32612
- Giant pulse ruby laser, using potassium dihydrophosphate crystals linear electro-optical effect for Q modulation 15 p2424 A71-32758
- Stark effect saturable absorber modulation of passively Q switched carbon dioxide laser, using difluoroethane, difluoroethylene, methyl fluoroform, trichloroethylene and vinyl chloride 16 p2586 A71-33147
- Rarefied plasma flow generation by Q-switched laser pulse focusing on solid target, measuring plasma properties with Langmuir probes and microwave interferometers 16 p2586 A71-33162
- Three dimensional hologram recording, showing He-Ne laser reconstruction of Q switched ruby laser hologram image of mosquito flight 16 p2579 A71-33528
- Self focusing effect of Q switched single mode ruby laser emission in CdS crystal, noting 60 kW minimum threshold power 16 p2588 A71-33645
- Transparent polymer dielectric luminescence and destruction under Q switched laser radiation with subthreshold power and picosecond pulses 16 p2588 A71-33652
- Balance equations expansion for giant-pulse Q switched laser model, considering output intensity 16 p2589 A71-34138
- Upper atmosphere density observation by Q switched ruby laser radar 17 p2753 A71-34748
- Hydrated electrons photoexcitation by giant pulse Q-switched ruby laser, investigating absorptivity over wide range of light intensities 17 p2753 A71-34950
- Plane and three dimensional dynamic holograms recording in bleachable dyes, using ruby laser with gallium chloride phthalocyanin in chlorobenzene as Q switch 17 p2745 A71-35507
- High coherence Q switched spatially filtered Nd-glass laser operating in fundamental mode for high power 17 p2754 A71-35747
- Operating characteristics of Q switched CO-He laser, discussing energy transfer processes leading to population inversion 18 p2929 A71-35835
- Q switched laser range finders, discussing programmed ephemeris guided, divergence data utilizing and semiautomatic tracking systems with emphasis on target acquisition [ONERA-TP-964] 18 p2945 A71-36029
- Q switched ruby laser holography, using controlled multimode emission for contour recordings of reflected light scenes 18 p2920 A71-36102
- Solid state laser with Nd ions in YAG, discussing crystal growth and structure, optical pumping continuous and Q switched operation and mode locking 18 p2930 A71-36146
- Carbon dioxide laser, discussing mixture composition, vibrational energy levels, excitation and relaxation mechanisms, output characteristics, CW and Q switching, mode locking and applications 18 p2930 A71-36147
- Reflection, material and resonator losses correlation in solid state lasers, investigating pulse power in Q switched operation 18 p2932 A71-36801
- Optical radar aircraft tracking and position system, using IR Q switched flash pumped Nd-YAG laser transmitter and pulse receiver with magnetic tape recorder and real time computer 18 p2900 A71-36905
- Carbon dioxide laser high efficiency driven Q switching, using Stark effect in molecular gases 18 p2933 A71-37015
- Relaxation processes in Michelson interferometer as integral part of carbon dioxide laser cavity in phase Q switching regime 19 p3071 A71-37389
- Ruby laser Q switching by hydrogen and copper phthalocyanin vapors, obtaining nanosecond single pulses with high power density 19 p3072 A71-37768
- Low vibrational level CO transitions of flowing electrochemically excited liquid nitrogen cooled helium-air-methane-carbon monoxide laser in Q switched operation 20 p3244 A71-39100

Spatially periodic inhibition of gold vapor condensation by intense optical standing wave using Q switched laser radiation

20 p3245 A71-39403

High efficiency room temperature lasing operation assisted by energy transfer in holmium doped yttrium lithium fluoride

20 p3247 A71-39761

Nanosecond ruby laser pulse generation using electro-optic shutter switching circuit external to Q-spoiled cavity

21 p3391 A71-40179

Enhanced scattering signal observation at electrostatic plasma wave frequency by focusing Q switched laser beam on hydrogen plasma

22 p3580 A71-41596

Q-switched ruby laser holographic interferometry for hypergolic flame combustion recording

22 p3539 A71-41742

Characteristic energies of exponential band tails in GaAs junction lasers from wavelength shift with cavity Q and spontaneous emission line width

22 p3558 A71-42360

Optical second harmonic generation in excised tissues by Q switched ruby laser irradiation, observing narrow band emission line in collagenous tissues

22 p3559 A71-42567

Single mode ruby laser spatiotemporal coherence characteristics with emission moment controlled by Q switch operating on modulated ultrasonic traveling waves

23 p3683 A71-43394

Nd glass laser system with Pockels cell Q switched oscillator for producing highly ionized plasmas

23 p3686 A71-43954

Q switched inorganic Nd liquid laser oscillator, noting output capability

23 p3686 A71-43957

Nanosecond solid dielectric discharger fired by Q switched ruby laser for commutation of coaxial line forming high amplitude voltage pulses

24 p3835 A71-45238

Q VALUES

Distribution laws of statistical Q characteristics and of junction capacitance of varicaps

11 p1740 A71-26542

Sobolev function Q in radiative transfer, using invariant imbedding approach for integral equation transform

19 p3133 A71-37506

Ionospheric heating Q calculation of electron gas, evaluating heat inflow at various altitudes

20 p3281 A71-39725

Q values, costs, efficiencies and radioactive evaluation of D-D, D-T and D-He 3 mirror fusion plasma power systems

24 p3847 A71-44493

QSO [RADIO SOURCES]

U QUASARS

QUADRATIC EQUATIONS

Nonlinear quadratic elasticity theory of isotropic tube and hollow shell under small linear deformations, obtaining stress-strain relation

02 p0326 A71-12294

Real polynomial quadratic divisors determination with maximum accuracy in floating point arithmetic, using Bairstow method algorithm

03 p0450 A71-13118

Flat triangular elements for shell analysis, describing membrane and bending displacements by identical quadratic polynomials [AIAA PAPER 71-114]

06 p1003 A71-18564

Nonlinear proportional navigation guided homing missile and minimum time to turn, developing quadratic equation with close larger positive root approximation

07 p1156 A71-19878

Nonlinear systems optimal control, presenting Hamilton-Jacobi equations analytical solutions for quadratic cost function minimization

11 p1742 A71-26420

Structural properties of equilibrium solutions of quadratic matrix equation, using variational interpretation of associated Riccati equation, transform techniques and Parseval formula

13 p2095 A71-28815

Optimal numerical solutions of linear control systems with quadratic integral form, using dynamic programming, successive optimization and algorithm-aided dynamic programming

21 p3360 A71-40617

Computational method determining quadratic Liapunov functions for high order nonlinear systems

23 p3705 A71-43944

Integral quadratic control quality estimates in terms of system coefficients with allowance for system oscillation characteristics

24 p3812 A71-44483

QUADRATIC PROGRAMMING

Nonlinear control laws successive stochastic optimization through nonlinear and subsequent quadratic programming

03 p0392 A71-14403

Incremental plastic analysis under large displacement and physical instabilizing effects, using finite element models and quadratic programming

11 p1849 A71-25679

Third order oscillatory system optimal terminal-state control synthesis by quadratic functional minimization iterative procedure algorithm, using ODR-1204 computer program

21 p3359 A71-40164

Linear elastic structures analysis by quadratic programming, considering equilibrium equations for forces at joints

22 p3618 A71-42589

QUADRATURE APPROXIMATION

U QUADRATURES

QUADRATURES

Laminar boundary layer convective heat transfer with constant wall temperature, using Gaussian quadrature formulas

02 p0332 A71-12394

Transient heat flow mean and first moments prediction by discontinuous linear or quadratic trial functions and variations

05 p0831 A71-16491

Subharmonic quadrature components in parametron with balance modulated pumping voltage

11 p1740 A71-26540

Automatic numerical evaluation of definite integrals of analytic functions, considering Simpson rule, Gauss quadrature, subdivision and whole interval formulas

12 p1923 A71-27732

German monograph on Fourier-Chebyshev approximation of primary functions, giving quadrature method

17 p2764 A71-34484

Definite interval values calculations of integral of smooth functions, using quadrature formulas with high algebraic degree of accuracy

17 p2765 A71-34845

Weakly singular integrals numerical compound quadrature error bound and convergence rate estimate by applying Peano theorem with modification for avoiding singularity

18 p2941 A71-36355

Convergence theorem for singular integrands numerical quadratures, assuming domination near singularity by monotone integrable function

18 p2941 A71-36356

Quadrature formula for Cauchy integrals

19 p3086 A71-37883

First kind Fredholm integral equation approximation by numerical quadrature formulas plus collocation, using singular value decomposition for solution

22 p3567 A71-42296

Quadrature errors in satellite geodesy via geopotential simple layer model, investigating different size surface elements and methods of subdivision [AAS PAPER 71-340]

23 p3666 A71-43013

QUADRUPOLE LENSES

U MAGNETIC LENSES

QUADRUPOLE NETWORKS

Optimum L shaped quadrupole filter for controlled valve voltage inverters

15 p2353 A71-32079

QUADRUPOLES

Electric quadrupole atomic transitions in muonic PB208, charting X ray spectrum showing transitions

01 p0131 A71-11439

Solar magnetic field variation observation, revealing sun as quadrupole magnetic rotator

04 p0657 A71-15828

Relativity and solar quadrupole moment effects in time delay measurements of signal traveling from earth to artificial satellites

05 p0808 A71-16446

Dipole conversion to equivalent quadrupoles and multipoles, replacing resistances by corresponding h matrices

06 p0872 A71-17373

Quadrupole interaction in crystals of diamond-like semiconductors gallium telluride and indium telluride

07 p1177 A71-19275

Frequency generators using RC /RL/ designs with odd selective quadrupole element numbers as converters

07 p1078 A71-20062

Geomagnetic quadrupole field secular oscillation causing earth rotation change, discussing earth core induced velocity field and field attenuation

10 p1603 A71-24599

Perturbed magnetic surfaces topology in quadrupole, estimating local imperfections size for plasma control

10 p1652 A71-24661

Theoretical and experimental performance studies of quadrupole mass analyzers with round and hyperbolic field forming surfaces, noting resolving power superiority of hyperbolic rods

11 p1760 A71-25219

Quadrupole mass spectrometry in studies of heterogeneous and flash photolytic reactions and unstable intermediates detection

11 p1765 A71-26279

Dipole, quadrupole and octapole measurements in isolated beating hearts

13 p2016 A71-28150

Dense interstellar cloud radio recombination lines in H I regions, calculating quadrupole effects on line splitting

15 p2498 A71-32771

Particle motion in combined gravitational field of monopole and prolate quadrupole, deriving exact solution in Newtonian mechanics and general relativity

16 p2609 A71-33256

Quadrupole mass spectrometer ultimate characteristics concerning resolution, range, recording speed, working pressure and sensitivity

17 p2737 A71-34288

Computer algorithm determining transfer function of linear electronic circuit in autonomous quadrupole form with zero initial conditions

18 p2887 A71-35884

Weber antenna sensitivity for short pulses of gravitational radiation, giving limit for connection coefficient of piezotransducer with detector

18 p2946 A71-35979

Quadrupole probe for measuring magnetospheric electric currents, noting transfer impedance dependence on probe motion relative to ambient plasma

18 p2912 A71-36198

Swept Langmuir probe with sweep speeds greater than 150 V/microsec, considering electron cyclotron resonance heated hydrogen plasma confined in toroidal quadrupole

18 p2952 A71-36582

Ionospheric low hybrid resonance measurements by rocket-borne quadrupole probe, deriving electron density and effective ion mass along trajectory

20 p3224 A71-39722

Ion-quadrupole effects in ion-molecule collisions by numerical calculations of capture cross sections and computer-plotter studies of ion trajectories

21 p3419 A71-40906

Thermal analysis-quadrupole mass spectrometric analyses on inorganic released gases of Apollo 11 and 12 samples and synthetic lunar analogs

23 p3750 A71-43699

QUALITY CONTROL

Nondestructive high reliability rapid comparison and identification of metals by electrical interpretation method for product variation control and laboratory unknowns determination

01 p0085 A71-10258

Fiberglass reinforced plastics heavy duty structural parts quality control, discussing strength parameters, safety coefficients, testing methods, etc

01 p0088 A71-10689

Reference standards for nondestructive ultrasonic inspection for quality control

01 p0091 A71-11424

Soviet book on bolting and coupling elements threads used in aircraft industry covering configurations selection, cutting, tolerance requirements and quality control

02 p0258 A71-12723

Aviation products liability and warranty law, noting reliability trends and quality control methods

03 p0523 A71-12971

Apollo Applications Program command and service module test requirements to achieve reliable hardware for extended missions [AIAA PAPER 70-378]

03 p0500 A71-14436

Deformation monitoring of large multilens astronomical objective during assembly, using annular image reflection

04 p0593 A71-14868

Product test duration and extent from reliability theory viewpoint

05 p0759 A71-16725

Corrosion damage relationship to military aircraft accidents, discussing quality control, material selection and manufacturing processes

06 p0911 A71-17415

MIL-STD-414 sampling procedures and tables for inspection by variables for percent defective

06 p0905 A71-18059

Intelsat 3 satellite mechanical and electronic components fabrication, emphasizing quality and reliability assurance procedures and assembly techniques

06 p0905 A71-18403

ESRO 2 satellite program reliability prediction and procedures in design and manufacture, defects during development and tests and performance in orbit

07 p1207 A71-19552

Metal film resistors rapid evaluation method including thermal, load and shock tests devised by British electronic component manufacturers

07 p1076 A71-19553

Quality management planning for 1970s, discussing reliability, maintainability and production quality programs

07 p1225 A71-19558

Satellite electronic equipment reliability engineering, considering circuit and system design, components screening, assembly and test procedures and quality assurance plans

07 p1207 A71-19563

High strength and modulus continuous carbon fibers, discussing preparation and quality control [PLASTICS INST. PAPER 5] 08 p1297 A71-20925

Quality control for Minuteman zinc silver oxide battery production 08 p1298 A71-21109

Primitive centralized quality control program model applicable to Department of Commerce environmental sciences 08 p1329 A71-21728

Meteorological data quality control, discussing inconsistencies, data interrelationships and frequency distribution 08 p1329 A71-21729

Quality control role in meteorological instruments maintenance 08 p1329 A71-21730

Defective resistors physical processes during thermal control method, appraising quality from surface temperature distribution 08 p1300 A71-21901

Polished surface quality control using laser divergent coherent beam 09 p1460 A71-22310

IC quality control by temperature fields contactless measurement, using microthermographs 09 p1450 A71-22894

Mathematical model system analysis methods for reliability assurance, discussing worst case and Monte Carlo techniques 09 p1423 A71-23040

High temperature steel and alloys metallurgical processes for stationary and aircraft gas turbine engine components, discussing production-quality control-research interrelationship 09 p1456 A71-23301

Quality assurance in Ti and Ti alloys processing, discussing smelting, ingot homogenization staging, costs and facilities 09 p1456 A71-23303

He-Ne laser as detectors in mine boring, quality/compensational control, data collection/reduction and positioning accuracies 09 p1458 A71-23409

Fabricated product test program design for meeting customer specifications, outlining routine tests for preimpregnated film adhesive materials 10 p1616 A71-24107

Brittle materials ultrasonic machining, discussing abrasive particle shape, size, temperature and pressure effects on process accuracy, speed, quality and efficiency 10 p1617 A71-24133

Deferred state sampling plans using accept/reject decisions dependent on future lot disposition according to quality drift 12 p1909 A71-26661

Reliability assurance in product manufacturing, discussing specific tasks during design, preproduction and production phases 12 p1910 A71-26672

Product quality characterization, using Harrington dimensionless scale of desirability as optimization criterion 12 p1988 A71-26709

Traversing Infrared Inspection System for C-5 aircraft fail-safe strap panels of bonded Ti-Al laminates, discussing design and application [ASME PAPER 71-DE-37] 12 p1911 A71-27327

Transistor resistances difference measurement under reversed polarities during quality control testing 14 p2214 A71-30635

Truncated sequential test for production models based on preproduction testing with allowance for unequal sample sizes 15 p2416 A71-32344

Laser pulse shape, beam modulation and power fluctuation quality control measurements, using non-selective, thermally stable piezoelectric sensor with low time constant 15 p2421 A71-32456

Producer risk determination and tables for Method 4 maintainability demonstration plan of MIL-STD-471 16 p2583 A71-33303

Gallium antimonide synthesis without antimony evaporation stoichiometry disturbances, describing zone refining procedures and quality control 16 p2621 A71-33473

Scanning electron microscope examination of components and materials quality and reliability in satellite onboard equipment 18 p2890 A71-36537

Adhesively bonded structures inspection by laser holography, producing diffraction pattern recording of amplitude and phase shift 18 p2925 A71-37057

Parts qualification and acceptance for outer planet mission spacecraft, minimizing random and wear-out failures to meet weight and other constraints [AAS PAPER 71-161] 19 p3153 A71-37958

Characteristic smooth test bar ductility correlation and prediction in high temperature creep rupture tests, noting application to material quality control 19 p3082 A71-38138

Aerial and satellite environmental water quality control surveillance, discussing remote sensing techniques and objectives 19 p3059 A71-38402

Systems oriented components selection optimization technique by reliability/quality levels, considering repair and failure cost, storage time and mission duty cycle 19 p3034 A71-38518

Scanning electron microscope for poor metallization detection in manufacturing cycle of semiconductor devices 19 p3034 A71-38519

Cost effectiveness screening program for integrated circuits, considering four stages of life cycle 20 p3202 A71-38753

Semiconductor components reliability assurance under assumption of failure rate decrease with time for IC quality and performance improvement 21 p3356 A71-40746

Spacecraft tape recorder design for five years minimum continuous unattended reliable operation, describing quality control and environmental/life testing procedures 22 p3608 A71-41507

Dielectric articles thickness and flaw control by microwave magic tee junction waveguide, describing instrument design and operating characteristics 22 p3521 A71-41772

Quality control for space programs hardware suppliers, discussing contractual aspects 23 p3786 A71-43468

Project management quality control factors learned from Diamant A satellite launching vehicle and French military programs 23 p3786 A71-43469

Quality control organization in British spacecraft projects, discussing material selection system and subsystem tests, process engineering and inspector training 23 p3681 A71-43470

NASA NHB reliability engineering provisions for aeronautical and space system contractors, considering criteria for program management, system engineering, manufacturing and facilities 23 p3682 A71-43497

Nondestructive pulse technique for quality control of electroexplosive devices, noting cost reduction 24 p3864 A71-45279

QUALITY FACTORS
U Q FACTORS

QUANTITATIVE ANALYSIS
Near stoichiometric binary alloys atomic ordering parameters quantization by field ion microscopy, using direct counting and optical transformation techniques 02 p0297 A71-12736

Quantitative spectrographic microanalysis using laser pulse vaporization and spark discharge 03 p0438 A71-13975

Photographic gelatin microimpurities quantitative analysis and removal techniques 04 p0585 A71-14645

Carbon dioxide laser performance quantitative analysis, considering electron to optical energy conversion via electric discharge in carbon dioxide-nitrogen-helium mixture 09 p1465 A71-23481

Quantitative gas liquid chromatography analysis of amino acids in biological materials, discussing ion exchange techniques 11 p1729 A71-26068

Quantitative determination of phenylalanine in serum by gas-liquid chromatographic analysis method 13 p2026 A71-29477

Variable Nb composition of meteoritic rutile grains from quantitative electron microprobe analysis 20 p3292 A71-39384

Ti alloy microarea alloying element concentration quantitative analysis by EPMA program, obtaining working curves for Al, Fe, Cr, Mo and V 22 p3561 A71-41944

QUANTIZATION
U MEASUREMENT

QUANTIZER
U COUNTERS

QUANTUM AMPLIFIERS
Semiconductor quantum amplifier dynamic range in steady operation mode, analyzing monochromatic signal gain 01 p0096 A71-11219

Frequency characteristics calculation of regenerative two cavity microwave bandpass amplifiers, applying to parametric and quantum amplifiers and underexcited microwave relaxation oscillators 09 p1413 A71-22157

Optimal location of nonreciprocal disk shaped YIG element of traveling wave quantum ruby paramagnetic amplifier for weak magnetic field levels 10 p1585 A71-24883

Computer synthesis of nondegenerate parametric amplifiers with single mesh filter for maximum flat or Chebyshev frequency response applicable to quantum devices 12 p1886 A71-26844

Gasdynamic lasers optically active medium two-fluid model, deriving solutions for CW generators and quantum amplifiers 17 p2754 A71-35397

Two stage decimeter wavelength quantum paramagnetic amplifier, noting noise temperature and gain 23 p3652 A71-43529

QUANTUM COUNTERS
Quantum counting efficiency of commercial photomultiplier at 0328 A by direct measurements, including signal and background dependence 11 p1766 A71-26300

Papers on quantum electronics, Volume 1, covering carbon dioxide and YAG lasers, quantum counter action and interference holography 18 p2930 A71-36144

Quantum counter action in various media including trivalent and divalent rare earth ions, Fe group transition metal ions, semiconductors and gases 18 p2930 A71-36145

QUANTUM ELECTRODYNAMICS
Functional method application to ultrarelativistic particles in external fields quantum electrodynamics, discussing electromagnetic field superposition 07 p1162 A71-20549

Electron mass and photon wave renormalizations functional relationships, studying perturbation theory based electrodynamic divergences 07 p1162 A71-20550

Quantum electrodynamic analysis of relaxation processes in two level laser 11 p1774 A71-26005

Quantum electrodynamics on null planes in Minkowski space, discussing applications to lasers, wave packet construction, Heisenberg and Furry pictures and Compton scattering 13 p2080 A71-28998

Magnetostriiction and magnetoelastic quantum oscillations in p-PbTe, using thermodynamic derivatives of Lifshitz-Kosevich expression for oscillatory part of electronic free energy 17 p2791 A71-34860

QUANTUM GENERATORS
U STIMULATED EMISSION DEVICES

QUANTUM MECHANICS
NT PAULI EXCLUSION PRINCIPLE
NT QUANTUM ELECTRODYNAMICS

Quasi-classical equations of relativistic quantum mechanics, considering Klein-Gordon equation 01 p0129 A71-11293

Quantum mechanical communication theory of optimal receivers, using statistical detection and estimation theory 02 p0213 A71-12016

Tetrahedral molecules quantum mechanical rotational partition function, nuclear spin statistical weight factors and error bounds 04 p0629 A71-14807

Laser light statistical properties including Fokker-Planck equation, photoelectron counting distributions and quantum mechanical equation from Weidlich and Haake theory 05 p0762 A71-16483

Macroscopic dynamics of many-component plasmas in electromagnetic fields, discussing formulation in scalar complex wave equations containing pressure and electromagnetic potentials 07 p1168 A71-19688

Ionized gases quantum transport cross sections and collision integrals, considering energy and temperature ranges for attractive and repulsive screened Coulomb potentials 07 p1224 A71-20283

Rotating nonvibrating diatomic low density gas molecules rotational relaxation time and viscosity, based on quantum mechanics 08 p1336 A71-20659

Quantum mechanical relation for magnetized electron gas in constant magnetic field and thermal equilibrium 08 p1337 A71-21192

Phase quantization theoretical derivation, applying mathematical technique used in signal processing nonlinear problems 08 p1291 A71-21403

Phase quantization in holograms, presenting experimental verification of Goodman and Silvestri theory 08 p1291 A71-21404

Quantum mechanical theory of nonrelativistic fast electron backscattering from continuous media, considering scattering cross sections 09 p1496 A71-22236

Linear and nonlinear collisional processes in uniform weakly interacting plasma near equilibrium in absence of external magnetic field, using quantum mechanics treatment 09 p1503 A71-22864

Pair correlation function for gaseous hydrogen at low density and temperature from quantum mechanical calculation, using Lennard-Jones potential 11 p1801 A71-25367

Collision effects on atomic spectral line profiles, using quantum mechanical description of atomic center-of-mass motion with particular application to lasers 11 p1803 A71-26147

- Cloud height distribution pattern, developing analogy between diffusion and quantum motions 12 p1924 A71-26737
- Polyatomic molecule photoelectron spectroscopy, emphasizing spectra interpretation by quantum mechanical procedures 16 p2541 A71-33398
- Sum rule functions for expressions of atomic or molecular quantum mechanical properties 16 p2603 A71-33527
- Quantum mechanics model of optical parametric amplifier, considering performance of optical information systems 17 p2698 A71-34409
- Electron beam modulation by laser light, considering quantum mechanical theory 17 p2753 A71-35024
- Quantum mechanical considerations underlying calculations of two-photon transition probabilities, discussing experiments on semiconductors, ionic crystals and organic compounds 18 p2930 A71-36241
- Quantum mechanics axiom system construction from physical theories, using imbedding operation 19 p3103 A71-37276
- German monograph on comparison between quantum mechanical approximate methods through projection of approximated eigenfunctions covering Schroedinger equation, wave functions, Born-Oppenheimer approximation, etc 20 p3271 A71-39042
- Collision effects on line shapes using quantum mechanical description of atomic center of mass motion, considering pressure effects in gas lasers 20 p3271 A71-39069
- Quantum mechanical theory of nonrelativistic fast electron backscattering from continuous media, considering scattering cross sections 21 p3419 A71-41118
- Electron production cross sections in inelastic atomic collisions, evaluating classical scaling law and quantum mechanical statistical methods against experimental results [AIAA PAPER 71-995] 24 p3850 A71-44587
- QUANTUM NUMBERS**
- Diatomic molecular autoionization model, calculating limit of high vibrational and electronic principal quantum numbers 07 p1164 A71-19687
- Interstellar H II regions high quantum number recombination line measurements, indicating Stark broadening 13 p2143 A71-29268
- Nonthermal electron population of energy levels in cool dense helium afterglow for small principal quantum number, using Saha equation and optical spectroscopy techniques 16 p2620 A71-34044
- QUANTUM STATISTICS**
- Laser light statistical properties, emphasizing time evolution of density matrix equation 01 p0094 A71-10811
- Laser oscillation buildup from quantum noise, deriving equations of motion for moments of photon distribution and time dependence 01 p0094 A71-10826
- Quantum statistical analogy between laser threshold region and second order phase transition of ferromagnets 03 p0440 A71-14197
- Quasi-static surface waves in Fermi electron plasma with Maxwellian electron velocity distribution 21 p3425 A71-41277
- Surface waves at Fermi electron plasma boundary, using kinetic theory of plasma electromagnetic oscillations 21 p3425 A71-41278
- QUANTUM THEORY**
- Motion equations of spherical gyroscope in gravitational field of larger mass derived from Gupta quantum theory of gravitation 01 p0161 A71-11274
- Book on uncertainties of relativity and quantum theories covering potential energy, atomic clocks, coordinates and frames of reference, Doppler effect, gravity red shift, gravistatics, etc 02 p0284 A71-11843
- Steady state quantum analysis of linear distributed systems applied to attenuator, maser amplifier and multiterminal-pair networks 02 p0213 A71-12017
- Simple gases and liquids thermodynamic properties, calculating isotopic effects by corresponding states law with quantum corrections 02 p0331 A71-12187
- Quantum diffusion in scattering medium with absorption as sequence of random events 02 p0311 A71-12354
- Quantum theory for spontaneous parametric light scattering, determining photon spectral distribution 02 p0285 A71-12506
- Quantum optics - NATO Conference, Musselburgh, Scotland, July 1969 04 p0607 A71-14803

- Stark induced quantum beats in H Ly alpha emission, using beam foil excited hydrogen 05 p0785 A71-16701
- Electron-ion recombination in dense molecular gas, presenting semiquantitative method for hydrogen, nitrogen, carbon dioxide and damp gas mixtures 05 p0785 A71-16726
- Physics laws and simplifications, discussing Newtonian mechanics, electrodynamics, relativity, atomic physics and quantum theory 07 p1163 A71-19603
- Soviet papers on quantum radio physics covering injection lasers, high intensity beam and material interactions and laser dynamics 07 p1126 A71-20251
- Oxygen molecules photolysis at 1849 and 1931 A, investigating ozone formation quantum yield 08 p1337 A71-20663
- Partial wave method for nonspherical quantum scatterer, applying to electron elastic scattering by molecules 09 p1496 A71-22237
- Relativity - Conference, Cincinnati, June 1969 11 p1798 A71-25279
- Zero point fluctuations measurement standards for thermal and quantum noise, considering microwave network analytic application 11 p1733 A71-26366
- Closed universes quantization and gravitational field in general relativity, emphasizing superspace concept and finite-dimensional model quantum theories construction 13 p2100 A71-28395
- Raman effect quantum theory, considering light scattering about atomic system 13 p2078 A71-28449
- Intense magnetic fields in astrophysics, emphasizing flux conservation law and quantum effects 13 p2144 A71-29436
- Laser quantum theoretical analysis, considering atomic thermal motion, photon emission and absorption induced recoil effects on lasing threshold and operating frequency 14 p2253 A71-29574
- Experimental solar blind photomultipliers for stellar photometry above earth atmosphere at 1450-2800 A, giving spectral response and quantum efficiency 14 p2240 A71-30122
- Quantum-theoretical transport equation for dilute gases with internal degrees of freedom, generalizing for arbitrary spacing between internal energy levels 14 p2275 A71-30449
- Electromagnetic and gravitational waves scattering by static gravitational field, comparing classical general relativistic and quantum field theoretic results 14 p2275 A71-30861
- Laser action internal differential quantum yield estimation using GaAs injection lasers near field emission patterns 15 p2422 A71-32461
- Canonical quantization, discussing Schroedinger equation, Hamilton-Jacobi theory, Feynman integrals and sandwich conjecture 16 p2609 A71-33258
- Classical gravitational field equations modification for virtual quantized matter, taking into account additional mass due to attractive forces 16 p2610 A71-33271
- Image amplifier camera resolution as function of light level based on photon statistics and cathode quantum efficiency 17 p2746 A71-35762
- Equations of multiple periodic motions, considering quantification of parameters with Hamilton-Jacobi equation 18 p2948 A71-36947
- Coherent optical fields properties, discussing equivalence of quantum and classical descriptions 18 p2932 A71-36959
- HF gravitational radiation due to quantum transitions, studying absorption, emission and sources 21 p3439 A71-40612
- Gravitation theory within Lorentz covariant and second quantized formalism framework from gravity interaction with binding energy, discussing graviton behavior 21 p3416 A71-41035
- Partial wave method for nonspherical quantum scatterer, applying to electron elastic scattering by molecules 21 p3420 A71-41119
- Electron beam modulation at optical frequencies, calculating excited radiation characteristics with quantum theory 21 p3420 A71-41254
- Quantum theory of molecular or atomic spontaneous emission while simultaneously undergoing stimulated emissions or absorptions 21 p3421 A71-41401
- Quantum fluctuations in gas laser radiation, obtaining photon diffusion coefficients for traveling and standing waves 22 p3558 A71-42456

- Vacuum symmetry and asymmetry, analyzing physical meaning of Dirac vacuum in quantum field theory 22 p3577 A71-42853
- Quantum phase fluctuations in IR gas lasers, noting nearly Lorentzian power spectrum with bandwidth inversely proportional to output power 23 p3688 A71-44269
- QUARKS**
- Quark regions in massive stars internal structure, discussing plasma superconductivity and spectral line emission 01 p0160 A71-11112
- Quark fusion in quasi-stellar objects, deriving approximate formula for efficiency of converting rest mass into photons 05 p0785 A71-16686
- Quark flux measurement by simulating fractional charge particle pulses, testing calibration procedures by comparing simulated and genuine quarklike events 10 p1613 A71-24957
- Relativistic quarks in cosmic rays at sea level and at mountain altitude, estimating production cross section vs absorption mean free path and mass 11 p1815 A71-25589
- Penetrating particle observations on showers produced at 70 mwe underground, revealing weakly ionized group in quark flux contradiction 12 p1951 A71-27396
- Quark detection by telescope using production models, discussing extreme energy transfer conditions and upper production limits 12 p1952 A71-27398
- Quarks search near extensive air shower cores, discussing apparatus and results for detection of long delayed particles 13 p2120 A71-28052
- Quark flux and generation cross sections above atmosphere from Proton 3 satellite elementary particle spectrometer data 13 p2121 A71-28053
- Quarks search in cosmic rays at sea level and mountain altitude, using telescope with plastic scintillation counters and wire spark chambers 13 p2121 A71-28055
- Apollo 11 and 12 fines analysis, observing no quarks 23 p3765 A71-43809
- QUARTZ**
- NT COESITE**
- High quality quartz single crystal synthesis by hydrothermal recrystallization in autoclave 02 p0229 A71-11718
- High power carbon dioxide laser radiation absorption on vaporized and heated quartz 02 p0260 A71-11944
- Small tissue equivalent ionization chamber quartz fiber electrometer dosimeter system, for use as space qualified radiation detection instruments 02 p0250 A71-12136
- Heat transfer to walls of quartz discharge tube in Ne, Ar and Xe, measuring integral energy flux 02 p0290 A71-12191
- Electronic frequency divider with discrete correction of negative quartz clock rate 04 p0592 A71-14859
- Automatic amplitude control of transistorized quartz clock master oscillator 04 p0592 A71-14860
- Quartz magnetometer design and operation for simultaneous geomagnetic field declination and horizontal component measurements 05 p0756 A71-17216
- Quartz magnetic variometer allowing simultaneous recording of magnetic field variations and suspension axis inclination changes 06 p0901 A71-18285
- Quartz astatic galvanometer resistant to geomagnetic field variations, vibrations or microseismic noise 06 p0901 A71-18286
- Kaolin and quartz powder additions effect on glasslike polymethyl methacrylate specific heat, thermal conductivity and diffusivity 07 p1144 A71-18922
- Ionizing radiation effect on piezoelectric properties of quartz plates, covering X rays, gamma rays, electrons, protons and alpha particles 10 p1656 A71-24146
- Thermosensitive quartz anemometer operating in vibrational mode, discussing design and applications in low airflow velocity measurement 12 p1906 A71-26826
- Single loop quartz vacuum tube oscillators, calculating oscillation spectral line width due to thermal and shot noise and circuit parameters fluctuations 12 p1889 A71-27622
- Quartz magnetometer design and operation for simultaneous geomagnetic field declination and horizontal component measurements 13 p2067 A71-28270
- Cylindrical microwave cavity partially containing cold nonuniform plasma enclosed by quartz tube, calculating resonant frequency by exact, multistrata and series methods 13 p2029 A71-28500

- Field components, frequency, quality and filling factors effects of storage quartz bulbs in master microwave cavities 14 p2254 A71-30563
- Quartz, organic glass and plexiglass luminescence under giant pulse ruby laser radiation 15 p2422 A71-32462
- Stress wave propagation in quartz-phenolic composite, measuring particle velocity by velocity interferometer 17 p2762 A71-35207
- Static ductile deformation in quartz, olivine, pyroxenes and plagioclase, noting plastic deformation and recovery 19 p3050 A71-37664
- Coupled resonator AT cut quartz crystal bandpass filter design in ladder configuration with low sensitivity and simple manufacturing methods 21 p3360 A71-40810
- UV and IR transmissivity and absorption coefficients of fused quartz between room temperature and 1500 C 22 p3565 A71-42559
- QUARTZ CRYSTALS**
- Quartz clock nonsystematic and frequency fluctuation statistical properties compared with GBR radio station 04 p0600 A71-15664
- High vacuum calibration of cryogenic quartz crystal for atmospheric density 07 p1113 A71-19852
- QUARTZ LAMPS**
- Aircraft flash light designs, discussing tandem oscillating lights, fixed lamp rotating reflectors and lamps, xenon flashtube, quartz-iodine lamp and flash frequencies 22 p3483 A71-41494
- QUARTZ TRANSDUCERS**
- Piezotron accelerometer for vibration measurement, combining quartz sensing element with subminiature solid state electrostatic amplifier 11 p1767 A71-26442
- QUASARS**
- Energy spectra of expanding relativistic particle clouds producing quasar and Seyfert galaxy nuclei outbursts 02 p0307 A71-12082
- Mass estimation for quasars and galactic nuclei with absorption line shift into long wave region 02 p0307 A71-12090
- Quasars spatial distribution and luminosity functions based on red shift observation 02 p0314 A71-12576
- Turbulent plasma radio emission theory of photon production and transport, considering application to quasars 02 p0292 A71-12587
- Quasars optical positions and magnitude identification for radio sources of 4C catalog 02 p0317 A71-12862
- Quasars PKS 2345-16 and NRAO 512 optical flares photometric observation 02 p0317 A71-12864
- Gas heating near quasars, Seyfert galaxies nuclei and pulsars by induced Compton effect 02 p0317 A71-12872
- Compton scattering in quasars, discussing gamma rays effects on core chemical abundances 03 p0481 A71-14266
- High red shift quasars linear polarization, examining absorption lines and depolarization due to Faraday rotation 04 p0649 A71-15272
- Multiple absorption red shifts in quasars, discussing measured properties and negative clues 04 p0650 A71-15584
- High galactic latitude faint blue stars from Tonantzintla and Asiago catalogs, finding quasars and subwarps by spectroscopy and UVB photoelectric photometry 04 p0651 A71-15659
- Quasars as images of Seyfert galaxies nuclei resulting from gravitational lens mechanism 04 p0658 A71-15829
- Intergalactic gas photoionization by quasars UV radiation, using Friedman cosmological model 05 p0805 A71-16111
- Quasars radio spectra in 1-5 GHz frequency range, examining emission from expanding clouds due to synchrotron radiation with self absorption 05 p0805 A71-16112
- Hot stars, supergiants and quasars extended and expanding atmospheres, examining resonance line profile formation by coherent scattering 05 p0806 A71-16203
- Quasars primordial He abundance, discussing relation to galactic evolution 05 p0808 A71-16406
- Quasars spectrophotometry data, obtaining physical conditions, abundances and electron temperature 05 p0811 A71-16685
- Quark fusion in quasi-stellar objects, deriving approximate formula for efficiency of converting rest mass into photons 05 p0785 A71-16686
- Quasi-stellar radio sources similarity to pulsars based on similar characteristics 05 p0814 A71-17235
- Ionized gas galactic cluster stabilization model construction, considering ionizing radiation enhanced cosmic flux and quasar PKS 1116 plus 12 absorption spectrum 07 p1198 A71-19830
- Quasars red shift and absorption lines observations, discussing distance measurement, brightness and intergalactic matter 07 p1200 A71-20211
- Cosmic objects and phenomena research, considering matter and galaxy compacting and dispersing processes, red shift, quasars, etc 08 p1358 A71-20890
- Quasars radio structures observations in S band, using NRAO interferometer 08 p1358 A71-20934
- Energy spectra of expanding relativistic particle clouds producing quasar and Seyfert galaxy nuclei outbursts 08 p1362 A71-21132
- Mass estimation for quasars and galactic nuclei with absorption line shift into long wave region 08 p1362 A71-21140
- Modulation of long scale time variations of quasi-stellar radio sources and Seyfert galaxies due to intergalactic scintillations 08 p1364 A71-21414
- Expanding source model verification for radio outbursts in quasars and Seyfert galaxy nuclei 08 p1365 A71-21424
- Radio source OZ-252 radiant flux density spectrographic observation, noting quasi-stellar object emission spectra 09 p1516 A71-22065
- Optical quasi-stellar objects searched for radio emissions, disproving previously claimed detections 09 p1518 A71-22352
- Variable stars, quasars and X ray source ScoXR-1 UVB light photoelectric data, examining optical emissions and brightness variations 09 p1524 A71-23186
- Quasar radio emission fine structure measurements by very long baseline interferometry, using Goldstone Mars antenna and Haystack radio telescope 10 p1671 A71-24325
- Quasars or blue stars possibility of radio sources usually identified with galaxies 10 p1674 A71-24448
- Quasar 3C 147 angular structure observations, using long baseline interferometer 11 p1830 A71-26113
- Quasar evolution, considering cosmological red shifts 12 p1958 A71-26695
- Optical variation and radio spectral index statistics of extragalactic sources, including quasars from photographic monitoring with 30 inch reflector 12 p1962 A71-26932
- Quasars and X ray sources, observing UVB magnitude variation with photoelectric data 12 p1963 A71-27077
- Optical luminosity function and space density of quasars from 4C and Parker survey, assuming cosmological red shifts 12 p1966 A71-27233
- Galaxy nuclei and quasars model, considering supernova explosions, neutron stars matter accretion and energy radiation 12 p1968 A71-27541
- Universe global structure and quasar frequency distribution based on red shifts and cosmological interpretations 12 p1968 A71-27642
- Galactic structure and spectra, examining universe expansion, Hubble law and quasar distances 13 p2142 A71-29129
- Matter density in universe, comparing delayed galactic growth with observed radio sources and quasars 14 p2305 A71-29675
- Quasar-like N-type and Seyfert galaxies optical characteristics, discussing optical variability and radio spectrum characteristics 14 p2307 A71-29866
- Quasars circular polarization measurements at 21 cm, noting synchrotron self absorption 14 p2307 A71-29867
- Large and small red shift quasars relative probability correlation with cataloged galaxies clusters direction 14 p2315 A71-30656
- Quasars as nuclei of nascent galaxies, proposing protogalaxy model from spectroscopic or color observations 15 p2482 A71-31328
- Quasar mass lower limit estimation from emission and absorption red shift data 15 p2483 A71-31368
- Rapidly rotating early stars and quasars, determining magnetic field generation by turbulent dynamo mechanism 15 p2485 A71-31725
- Quasar 3C 48 observations at 408 MHz, noting scintillations due to interplanetary plasma inhomogeneities 15 p2487 A71-32035
- Long baseline radio interferometers, considering quasars, interstellar masers, geodesy and geology applications 15 p2412 A71-32705
- Bright quasi-stellar radio sources B2 1215 plus 30 and ON231, discussing positions and spectrum 16 p2634 A71-33401
- Exploding universe phenomena, considering supernovae, exploding galaxies, Crab Nebula, pulsars, quasars and radio galaxies 16 p2643 A71-34036
- Quasi-stellar objects, investigating velocity dispersion, column densities and abundance of Mg and Fe in absorbing region by Stromgren method of line pairs 17 p2797 A71-34371
- Quasar internal kinematics and fine structure rapid time variations from radio interferometry 17 p2799 A71-34502
- Quasars as proto-blackholes in galactic nuclei blackhole model, discussing lifetimes, dust and IR radiation using models 17 p2811 A71-35745
- Statistical analysis of radio structure of quasars, considering red shift and anisotropy in angular size distribution 17 p2811 A71-35746
- Upper limits to quasars masses with optical emission lines inside radio sources, using method independent of red shift composition 18 p2961 A71-35965
- Inhomogeneous synchrotron source model calculation for correlation between linear and circular polarization, comparing with quasars observation 18 p2963 A71-36157
- Synchrotron radiation reabsorption in inhomogeneous sources, considering IR spectra of quasars and galactic nuclei 18 p2963 A71-36158
- Kinematic illusions in connection with retardation effects involving extragalactic sources with varying microwave output, noting occurrence in quasar 3C 279 18 p2925 A71-36924
- Quasars and X ray sources, observing UVB magnitude variation with photoelectric data 19 p3133 A71-37427
- Quasar red shifts distribution, indicating discretization in form of geometrical series 19 p3142 A71-38154
- Mass of virtual particle responsible for gravitation of vacuum and expansion of universe, considering correspondence to red shift in quasar spectra 19 p3146 A71-38644
- Gas heating by LF radiation due to Compton scattering near quasars, Seyfert galaxies nuclei and pulsars 20 p3289 A71-39293
- Critique of quasar model of independent random pulse emitting sources conglomeration from incompatibility with light curve 20 p3289 A71-39294
- Supermassive pulsar model of quasars periodicity and luminosity for Kelvin-Helmholtz contraction, concerning gravitational-rotational energy transformation 20 p3304 A71-39946
- Double radio emission sources during occultation period, noting structure, angular size components, positional errors and association to quasars 21 p3443 A71-40189
- Galaxy active nucleus and quasar fragmentation based on model of rotating supermassive star releasing thermal radiation 21 p3449 A71-40610
- Quasar brightness estimates on celestial photographs, noting variability on time scale 21 p3451 A71-40722
- Quasars emission line red shifts distribution observations, evaluating selection effects 22 p3605 A71-42351
- Quasars as nuclei of nascent galaxies, proposing test of protogalaxy model from spectroscopic or color observations 22 p3606 A71-42603
- Book on cosmology covering stars, galaxies, radio galaxies, universe models, quasars, expansion, intergalactic matter and microwave radiation 22 p3607 A71-42773
- Quasars light curves and intensity-time tables 23 p3769 A71-43993
- Quasar and pulsar gamma ray absorption by critical energy collisions with low energy photons 24 p3866 A71-44917
- Photographic monitoring of radio sources with flat or peaked spectra, identifying as quasars or unstable galactic nuclei by optical variations 24 p3872 A71-44920
- QUASI-STEADY STATES**
- Intrinsic helical and quasi-rigid hydrodynamic motions of incompressible, ideal and viscous fluids, using mobile frame method 11 p1804 A71-25175

Initial value problem in quasi-static thermoelasticity, using heat equation and Somiglian tensor 15 p2504 A71-31698

Energy transfer to MPD quasi-steady accelerator having electrolytic capacitors with large series resistance, integrating transmission line equations with Runge-Kutta method [DGLR-71-037] 17 p2794 A71-35539

QUASI-STEELAR RADIO SOURCES

U QUASARS

QUASILINEARITY

U NONLINEARITY

QUATERNARY ALLOYS

Heat, solution and cooling treatment of Ti-Al-V-Sn alloy for high strength and plastic properties 05 p0765 A71-16199

Nb-W-Hf-Y creep rupture properties in thermal vacuum, achieving strength improvement by pretest annealing 05 p0766 A71-16242

Ordered phases precipitation in ternary and quaternary ferritic alloys, investigating morphology, structure, distribution, coarsening kinetics and mechanical properties 07 p1133 A71-19443

Notch geometry and temperature effects on Ti-Al-Mo-V alloy creep rupture behavior 07 p1134 A71-19470

Ti-Al-Mo-V alloy stress corrosion cracking, using controlled potential technique in aqueous and methanol environments with and without halogen ions 11 p1777 A71-25448

Nb-Ti-Zr-Hf alloys superconductivity properties, obtaining improved critical current values in tempered vs cold worked samples 13 p2083 A71-27962

High strength corrosion resistant multiphase Co-Ni-Cr-Mo alloys with fcc structure hardened to hcp by mechanical deformation 13 p2084 A71-28148

Solidus-liquidus surfaces and isothermal phase diagrams of quaternary system of Cr with Ti, Zr, Nb and Ta, showing Laves phase interactions and continuous solid solutions 15 p2426 A71-31407

Phase equilibria of Al-Mg-Li-Mn system in Al-rich region, noting composition effects on mechanical properties 19 p3078 A71-37470

QUATERNIONS

Solid body finite rotation theory involving formal operations on quaternions 10 p1642 A71-24576

Optimum normalization of computed rotation quaternions to update space vehicle orientation 12 p1923 A71-27443

Quaternion representation of successive rotations in space vehicle control, locating final position of coordinate frame with respect to original position 17 p2773 A71-35066

QUENCHING

Laser excited atoms quenching by iodine molecules from light pulse induced photodissociation of perfluoropropyl iodide active media 07 p1126 A71-20195

Quenching rates for oxygen during 1470 A pulse photolysis in carbon dioxide, nitrogen and helium mixtures 09 p1404 A71-23382

Temperature dependent differential quenching rates of vibrationally excited CO fluorescence by ortho and para hydrogen, using Born-Bethe approximation 19 p3107 A71-38052

Partial quenching of radiation from ionized inert gases during bases irradiation by IR produced with carbon dioxide lasers 22 p3581 A71-41808

QUENCHING (COOLING)

Hot forming/die quenching of aluminum and titanium alloy integrally stiffened panels [SME PAPER EM-70-178] 01 p0089 A71-11259

Quenched Al-Mg alloys, investigating dislocation mechanisms for plastic flow by creep tests at various temperatures 04 p0613 A71-15744

Al alloys nucleation and precipitation hardening, examining quenching rate effects with hardness measurements and electron microscopy 01 p0105 A71-11605

High speed quenching on zone refined molybdenum, considering retained vacancies as contamination effects 05 p0765 A71-16163

Structural elements carrying capacity increase by strain hardening and nonuniform quenching 05 p0826 A71-16752

Zr solid state solubility in Mo as function of quenching temperature, using optical microscopy and microhardness testing techniques 07 p1130 A71-19300

Amorphous semiconducting thin films quenching fabrication techniques and electrical properties 07 p1181 A71-20410

Loop patterns of secondary defect structures in quenched Al based alloys interpreted in terms of internal stress and stacking fault energy 08 p1310 A71-21531

WC-Co system binder phase composition and properties, studying W content as function of initial carbide grain size, Co content, sintering and quenching time 09 p1466 A71-22170

Rapidly quenched CuAu ordered state development on low temperature annealing, presenting Young modulus variation as function of heat treatment time 09 p1477 A71-23350

Stress and structure effects on creep rate of two austenitic steels in quenched state, considering decorated stacking faults 09 p1479 A71-23624

Al alloys microstructure and mechanical properties after rapid solidification, considering rapid quenching techniques and resulting metastable variations 10 p1627 A71-24596

Rapid melt quenching in Al alloys metastably extended supersaturated solid solutions, discussing strengthening mechanisms, high temperature decomposition and powder metallurgy utilization 10 p1628 A71-25027

Quenched and aged Pt, investigating secondary defects for vacancies clustering modes by transmission electron and field-ion microscopy 11 p1779 A71-26016

Al-Zn-Mg-Cu alloys, investigating minor elements Cr, Mn and Zr effects on quench sensitivity 11 p1780 A71-26018

Cr and Zr additives influence on Al-Zn-Mg-Cu alloys quench sensitivity, discussing mechanical properties and electron microscopic investigation of microstructural characteristics 11 p1780 A71-26021

Ti-V alloys, observing as-quenched omega phase and transition to aged form by selected-area diffraction and dark-field electron microscopy 11 p1783 A71-26479

Al-Ni alloys rapidly quenched from melt, determining solid solutions mechanical and microstructural properties 12 p1916 A71-26893

Mechanical properties and heat treatment of Ti-V and Ti-V-Al alloys in quenched and quenched-aged states 13 p2083 A71-28772

High flash point polyalkylene glycol base synthetic quenchants for high strength alloy heat treatment, noting application to aluminum, titanium and steel parts 13 p2073 A71-28144

Field ion emission microscopic study of isothermal order-disorder transformation kinetics in water quenched Ni-Mo alloys 13 p2085 A71-28577

Stress relief cracking in Cr-Mo steel, considering correlation with embrittlement of water quenched base metal tempered at low temperature 13 p2086 A71-29091

Al-Mg-Si alloy development with low quenching sensitivity and high tensile strength 14 p2259 A71-30471

Al-Zn-Mg-Li solid solutions isothermal phase diagrams, obtaining Al-rich alloys phase compositions for quenching and aging temperatures 15 p2426 A71-31405

Co-Mo and Co-Mo-Ti stainless maraging steels tensile strength after quenching, establishing Mo and Co alloying limits 15 p2427 A71-31526

Flame quenching device for distances determination by burning premixed laminar propane-air at atmospheric pressures between nonparallel walls 15 p2385 A71-32089

Thin thermally insulating film on metallic sample, showing vapor layer elimination during liquid nitrogen quenching 18 p2934 A71-36172

Mechanical properties of carburized cermet steel with hypereutectic structure after water quenching and tempering at 300 C 19 p3076 A71-37113

Chromium stainless steels fine structure, noting quenching and tempering temperatures effects 19 p3076 A71-37118

GaAs laser diode junction temperature measurement methods for verification of stimulated emission quenching due to heating 19 p3074 A71-38231

Formation and interdependence of quenched induced defect structure in Al-Zn, discussing nucleated loops and screw dislocation developed helical dislocations 20 p3249 A71-39001

Fe-C alloys martensitic transformation, investigating high quench rate effects 21 p3397 A71-40451

Quenching effects on glazed and unglazed alumina rods in various media, noting improved flexural and tensile strength, thermal shock resistance and impact resistance 22 p3565 A71-42342

Weakly diffracted beam observation of small quenching vacancy loops and Guinier-Preston precipitate zones in Al and Al-Cu, using transmission electron microscopy 23 p3691 A71-43359

QUEUEING THEORY

Queueing model for analyzing video scan converter 01 p0047 A71-10215

Queueing model of statistical multiplexer buffer behavior for batch Poisson arrivals and single constant output, applying to time sharing computer buffer design 05 p0724 A71-17063

Probabilistic cyclic queue model of overhead time and channel utilization in multiprogrammed computer systems under demand memory paging 13 p2035 A71-28973

Queueing theory approach to communication satellite network design, applying to ocean air traffic control and worldwide military broadcast systems 17 p2721 A71-35106

Single channel queueing system with Poisson input and waiting time dependent mass servicing time, deriving arrival number probabilities generating function 22 p3527 A71-42491

Feedback controlled computerized queueing system, deriving generating functions for system state probabilities corresponding to different service time types 24 p3806 A71-44653

Waiting time distribution in computer controlled queueing system with Poisson input, deriving formulas on basis of total probability and Markov chain theory 24 p3806 A71-44654

Summation theory of random number of independent random variables relation to queueing and reliability theories 24 p3843 A71-44873

Algorithm for rational function incomplete decomposition into partial fractions 20 p3255 A71-39490

R

RABBITS

Amino acid content alteration in internal organs in rabbits under HF electromagnetic and ultrasound oscillations 04 p0547 A71-15573

Respiratory diaphragmatic center, investigating motor-neuron system integral activity by recording and analyzing phrenic-nerve signals in rabbits 10 p1562 A71-24164

RACON BEACONS

U RADAR BEACONS

RADAR

NT COHERENT RADAR

NT CONTINUOUS WAVE RADAR

NT DOPPLER RADAR

NT METEOROLOGICAL RADAR

NT MONOPULSE RADAR

NT MOVING TARGET INDICATORS

NT OPTICAL RADAR

NT PULSE DOPPLER RADAR

NT PULSE RADAR

NT RADAR MEASUREMENT

NT RANGE AND RANGE RATE TRACKING

NT SATELLITE-BORNE RADAR

NT SEARCH RADAR

NT SECONDARY RADAR

NT SIDE-LOOKING RADAR

NT SURVEILLANCE RADAR

NT TRACKING RADAR

Holographic amplitude modulation procedure for pulse compression in synthetic aperture radar 02 p0215 A71-12037

Telecommunication developments covering coaxial cables, waveguides, error elimination, information theory, sound transmission and radars 19 p3016 A71-37340

RADAR ALTIMETERS

U RADIO ALTIMETERS

RADAR ANTENNAS

Soviet book on monopulse radar covering surveillance and target tracking systems, antennas, angular resolution, directional sensitivity, etc 01 p0038 A71-11300

Soviet book on antenna radomes of flight vehicles covering electromagnetic wave transmission through dielectric media, fabrication, construction materials, etc 01 p0057 A71-11322

Phased array radar systems accuracy increase, using ferrite core magnetic flux feedback for phase shifter control 02 p0215 A71-12174

Wideband radar array antenna system with suppressed grating lobes 06 p0867 A71-17712

Airborne X band reflect phased array radar antenna design for simultaneous functions including large 06 p0867 A71-17712

volume search, target attack with general surveillance and low altitude assist

06 p0876 A71-18096

Beam scanning radar antenna, deriving optimum field distributions in aperture

08 p1266 A71-21462

Envelopes of antenna beams produced by variation of one antenna dimension in radar system

09 p1406 A71-23031

Double curved reflectors assembly methods for rotating search radar antennas, considering parabolic and elliptic strip shapes for sidelobe suppression modification

09 p1409 A71-23495

Radiation patterns of radar antennas with single near field cylindrical obstructions, considering directional S band antenna

09 p1420 A71-23678

Static wind loading on large radar antenna structures from wind tunnel tests, considering forces and moments reduction by perforated reflectors and shallow curved cover

10 p1591 A71-23757

Book on phenomenological theory of radar targets covering wave polarization and antennas, single, statistical independent and distributed targets, decomposition theorems and surface scattering

12 p1877 A71-26568

Reinforced plastics components in supersonic transport nose radome and missile radar antennas, discussing molding, sandwich materials and computer controlled spraying techniques

12 p1887 A71-27016

Radar target direction variation /glint/ sensed by amplitude monopulse tracking antenna receiving nonuniform waves

14 p2214 A71-30807

High speed airborne scanning navigational radar antenna with matched patterns, using offset horn fed reflector and polarization modes for improved visual display

14 p2216 A71-31036

Microwave wideband and multiband radome design for strength, environmental and electrical requirements, achieving transmission efficiencies with dielectric and wall thickness selection

14 p2216 A71-31037

Antenna and radome constructions/shape effects on minimizing cross polarization produced by flat, cylindrical, conical and paraboloidal randoms in linear and circular beams

14 p2216 A71-31039

Structural design, mechanical stability and aircraft compatibility for airborne side-looking radar antennas, using end fed slotted waveguide arrays

14 p2205 A71-31041

Dual plane monopulse multimode radar antenna feeds, determining input geometry relationship to generated modes by image method

14 p2218 A71-31065

Slotted waveguide arrays in precision Doppler radar antennas, correlating predicted and actual performance

14 p2206 A71-31073

Radar antenna interference determination based on model using electrical and physical characteristics of reflector type antenna for statistical gain distribution prediction

19 p3021 A71-38458

Harmonic analysis of signal processing radar antennas spatial filtering process, noting application to physical optics theory

20 p3200 A71-39903

Infrared and thermal evaluation of tactical aircraft phased array radar antenna design with cooling air distribution for steady state operating temperature maintenance

21 p3352 A71-40434

Polarization transforming feed horns for rapid scan X-band radar antenna, allowing transmission in various polarization modes and parallel and orthogonal-polarized return reception

23 p3655 A71-44167

Antenna radome noise temperature under aerodynamic heating as function of losses in material, interface reflection and dielectric surfaces

23 p3647 A71-44324

Circular aperture illuminations for high beam efficiency and low sidelobes in search radar antenna applications, using Fredholm integral equation

24 p3809 A71-44990

RADAR APPROACH CONTROL

Airborne radar as helicopter approach aid

04 p0624 A71-15425

V/STOL microwave scanning beam approach and landing system, describing ground and airborne station equipment and operation

08 p1332 A71-21680

RADAR ASTRONOMY

Radar observation of planetary surface characteristics, emphasizing albedo, surface roughness and differentiation

02 p0309 A71-12154

Radar astronomy principles, applications and types of measurements, discussing solar, lunar, planetary and meteor observations

02 p0313 A71-12490

Venus planetary science, discussing radar and space probe measurements as basis for different atmospheric models

05 p0814 A71-17226

Lunar radar reflectivity mapping at 7.5 m wavelength for maria and highlands echo powers, using interferometric techniques

11 p1834 A71-26451

Mars surface harmonics and continental drift from radar and spectroscopic topographic height determination

16 p2638 A71-33519

Radar observation of lunar distance, motion and surface statistical nature, noting enhanced reflectivity associated with craters

17 p2804 A71-35178

RADAR ATTENUATION

Reflectivity and attenuation observations of hail and radar bright band during storms, discussing rain effects

01 p0115 A71-10554

Radar attenuation along slant paths due to precipitation, comparing ATS-5 direct measurements with calculations based on backscatter and sky temperature measurements

01 p0030 A71-10579

Auroral absorption of HF radar waves over high latitude ionospheric paths

01 p0041 A71-11610

Dry radar reflectivity and attenuation due to wet ice spheres exponential distributions, noting hail detection procedures

11 p1794 A71-25379

Airborne Doppler velocity sensors, considering hydrometeors effects on HF signal attenuation and reflection

17 p2747 A71-35768

Terrain and atmospheric parameters affecting radar system design at microwave frequencies, discussing radar backscatter cross section and attenuation

20 p3200 A71-39904

RADAR BACKSCATTER

U BACKSCATTERING

U RADAR SCATTERING

RADAR BEACONS

Radarscope net for target azimuth and distance and for direct altitude readout through beacon numerics

13 p2033 A71-28886

Performance prediction model for electromagnetic compatibility of ATC radar beacon system, testing interrogator-transponder links along air route

19 p3102 A71-38435

RADAR BEAMS

Optimal control law for regulating energy distribution of emitted radar signals in multichannel system for minimizing target search duration

10 p1579 A71-24722

Vertical plane dual beam properties of doubly curved shaped reflector, considering surveillance radar antenna modification to improve performance with ground clutter

13 p2028 A71-27990

Point target horizontal speed determination with circular beam radar for measuring signal intensity and range, noting application to insects in atmospheric waves

17 p2706 A71-35122

Remote double resonance coupling of radar energy to ionospheric irregularities by sweeping radar modulation frequency through whole range

18 p2914 A71-36929

RADAR CHAFF

U CHAFF

RADAR CORNER REFLECTORS

Trihedral metallic post corner reflector for radar echo enhancement, reflecting same sense rotation as incident circularly polarized signal

04 p0559 A71-15879

Luneberg lens antenna theory and gain for communication satellite radio links, discussing shielding from hostile space environment

10 p1583 A71-24450

Multiple planar Luneberg lens circular array for airborne electronically scanned X band narrow beam antenna mounted under aircraft nose or fuselage

14 p2216 A71-31038

Missile system passive radar echo enhancement, discussing dielectric enhancers comprising antennas and corner reflectors

14 p2206 A71-31070

RADAR CROSS SECTIONS

Average radar cross section relative values for echoes from rain, considering horizontal, vertical and circular polarization in various sea states

04 p0551 A71-15008

Rain and drizzle millimeter wave attenuation and radar scattering cross section calculation

05 p0718 A71-15988

Terrain backscatter characteristics in EHF band, establishing average radar cross sections for various incidence angles

06 p0867 A71-17713

Average radar backscattering cross section calculation for conducting obstacles for arbitrary transmitter and receiver antenna polarizations, obtaining results for straight wires, circular loops and helices

09 p1410 A71-23516

Thin metallic disk radar cross sections for near resonance frequencies backscatter, comparing experimental and computer results

09 p1410 A71-23518

Handbook on radar cross section, Volume 1, covering scattering theory, edge/tip diffraction, creeping/traveling waves and various geometric shapes

11 p1733 A71-26008

Handbook on radar cross sections, Volume 2, covering scattering from planar surfaces, complex bodies, rough surfaces, ionized media, plasmas, radar targets and various objects

11 p1733 A71-26009

Radar cross section data analysis, considering economical approximation techniques in HF and LF ranges

12 p1882 A71-27440

Electromagnetic wave multiple scattering by colinear spheres, computing radar cross sections with recursion relation for computer solution

17 p2701 A71-34757

Bistatic radar frequency spectra and cross sections dependence on surface scattering laws, studying echo bandwidth

17 p2702 A71-35026

Bistatic radar scattering cross section from slightly rough perfectly conducting infinite surface, using Fourier transform

19 p3024 A71-38609

Cumulative probability of target detection for pulse surveillance radars, relating target cross section, velocity and radar frame

20 p3199 A71-39901

Terrain and atmospheric parameters affecting radar system design at microwave frequencies, discussing radar backscatter cross section and attenuation

20 p3200 A71-39904

Rain and drizzle submillimeter wave attenuation and radar scattering cross section calculation

22 p3515 A71-42737

RADAR DATA

Automatic aerological ground station with processing and transmission facilities for radio probe and radar data

01 p0029 A71-10360

Clear air convective process, examining dynamic model with radar patterns

01 p0116 A71-10562

Radar reflectivity pattern calculation from cumulus cloud growth numerical model, noting similarity with radar data from on-line computer system

01 p0118 A71-10584

Storm reflectivity models using weather radar and surface rainfall data correlations

01 p0118 A71-10585

Weather radar automatic data processing system for digitizing echo reflectivity by Video Integrator and Processor

01 p0050 A71-10594

Computerized acquisition and processing of radar precipitation signals and lightning data

01 p0050 A71-10595

Radar weather echo data processing by digital computer, providing economical means for analyzing large quantities of data

01 p0050 A71-10596

Acquisition and processing of aircraft search radar data obtained by track-while-scan technique, using off-line digital computer

01 p0040 A71-11392

Radar information digital extractors for processing signals from airborne transponder

03 p0382 A71-13570

Data communication role in National Airspace System, concerning radar and flight data acquisition, intersystem transfer and voice control [AIAA PAPER 71-248]

07 p1063 A71-19722

Analog surveillance radar signal analysis by digital storage and evaluation methods

08 p1252 A71-20745

Radar cross section data analysis, considering economical approximation techniques in HF and LF ranges

12 p1882 A71-27440

Discretization interval in discrete analog filters for optimal processing of complex radar signals, estimating systematic errors

14 p2194 A71-30081

Real time radar instrumentation data processing and control system, discussing computer selection, software requirements and configuration, etc

14 p2196 A71-30338

Digital techniques for tactical radar signal processing functions, discussing low cost integrated

- circuitry, moving target indicators, and analog to digital converters. 21 p3348 A71-40588
- National Aviation System stage A ATC displaying digitized radar data positions together with automatic track positions 22 p3570 A71-41634
- Soviet papers on radar meteorology covering formations classification, signal intensity measurement, detection probability, efficiency and errors 24 p3844 A71-44876
- Meteorological formation classification problems from radar data, discussing optimal solution with discrete selection space 24 p3844 A71-44877
- RADAR DETECTION**
- Hail detection by dual wavelength radar overcoming prior limitations, discussing equipment design and technique limitations 01 p0115 A71-10552
- Hail cells aloft interactions and radar detectability inferred from surface data, giving statistically random model 01 p0115 A71-10553
- Mesoscale meteorological structure during radar CAT detection at Wallops Island during January-March 1968 and 1969 01 p0116 A71-10568
- Snow storms wind field and turbulent region detection, using Doppler VAD pattern and mapping 01 p0117 A71-10576
- Optimal detection of narrow band signal with random phase and arrival time in radar or sonar, using nonlinear adaptive filter 02 p0211 A71-11720
- Radar detection problem, using pseudo Bayes techniques to determine likelihood ratio computational algorithms for stochastic process 04 p0551 A71-15007
- Radar detection ranges on nonfading targets as function of sea state in marine environment 05 p0723 A71-16972
- Radar altimeter use for ocean roughness determination 07 p1095 A71-18824
- Airborne severe storm surveillance, including radar detection hurricane model 07 p1058 A71-18826
- Double threshold detection radar performance, defining M out of N algorithm for nonfluctuating target and false alarm cases 07 p1058 A71-18841
- Radar performance with multipath using complex angle /CA/ method for resolving low angle target, comparing S/N ratio with monopulse system without CA 07 p1058 A71-18844
- Atmospheric turbulence measurement and detection using non-Doppler radar 07 p1058 A71-18845
- Video MTI pulse radar Doppler filter optimum symmetrical weighting factors in clutter-plus-noise environment 07 p1059 A71-18847
- Frequency agile waveforms effects on detection and tracking radars performance, decorrelating distributed clutter echoes 08 p1253 A71-20798
- Detection characteristics of optimal interperiod processing radar pulse systems for arbitrary correlation of signal and noise fluctuations 10 p1578 A71-24710
- Optimal control law for regulating energy distribution of emitted radar signals in multichannel system for minimizing target search duration 10 p1579 A71-24722
- Pulse radar moving target indication and stationary targets reflection suppression, using recursive type digital filter and quadrature channels for improving signal detectability 10 p1579 A71-25068
- Power spectrum symmetry effect on radar signal correlation function and bandwidth 10 p1580 A71-25107
- Moving window and feedback integrator type scanning radar detectors performance comparison based on probability and position estimates by Monte Carlo simulation 12 p1882 A71-27441
- Threshold and power relations for optical radars in pure and turbid atmospheres, determining visibility range for object detection 13 p2027 A71-27856
- Optimal correlating detector of fluctuating two frequency radar signals in unknown random noise 14 p2195 A71-30112
- Radar target detection in nonGaussian sea clutter, calculating trimmed-mean detector performance under Rayleigh fluctuation 14 p2197 A71-30805
- Airborne ECM receiver, determining conditions for detecting victim radar signal before signal reflection from aircraft 15 p2368 A71-31207

- Passive and active radar detection theory and practice, considering advances in sensors, signal generators, processors and filters 15 p2371 A71-31907
- Civil and military aviation operational problems, including cloud masses and CAT detection, landing aids and radar navigation 15 p2446 A71-31917
- Optimal discrete time detection of radar signal parameters in nonGaussian correlated and noncorrelated noise, using Markov model 15 p2373 A71-32619
- Two stage noncoherent rank detector of fluctuating radar signals in noise with unknown distribution 15 p2373 A71-32630
- Comparative detection performance of Siebert and Dicke-fix constant false alarm rate /CFAR/ radar detectors for signals in Gaussian noise 20 p3195 A71-38866
- Cumulative probability of target detection for pulse surveillance radars, relating target cross section, velocity and radar frame 20 p3199 A71-39901
- Surface based moving target indicator radar systems history, performance and problems 20 p3200 A71-39909
- Time resolved tropospheric scatter layers from simultaneous bistatic and monostatic radar detection 23 p3646 A71-44174
- Optimal mismatched filter design for radar ranging, detection and resolution by reduction to transversal equalizer, determining parameters by nonlinear programming 24 p3815 A71-44935

RADAR DIRECTION FINDERS**U RADIO DIRECTION FINDERS****RADAR DISPLAYS****U RADARSOPES****RADAR ECHOES****NT CLUTTER****NT LUNAR RADAR ECHOES****NT VENUS RADAR ECHOES**

- Quantization in data transmission and extraction, considering analog signals transmission in digital form and radar echoes recognition by digital integration systems 01 p0029 A71-10307
- Cloud and precipitation boundaries in convective storms studied by stereophotogrammetry and radar, discussing radar echo motion within cloud envelope 01 p0118 A71-10586
- In- and outflow fields in hurricane Debbie, using airborne radar echoes and ATS 3 satellite pictures 01 p0118 A71-10589
- Weather radar echoes quantization following detection, discussing subsequent digital processing 01 p0049 A71-10591
- Digital range-bin integrator for precipitation echoes, using static shift registers as memory element 01 p0049 A71-10592
- Weather radar automatic data processing system for digitizing echo reflectivity by Video Integrator and Processor 01 p0050 A71-10594
- Radar weather echo data processing by digital computer, providing economical means for analyzing large quantities of data 01 p0050 A71-10596
- Weather radar signals decorrelation times due to vertical wind shear and azimuth scanning 01 p0030 A71-10598
- Remote sea state information acquisition system using video attachment to radar for sea return spectrum recording and analysis 01 p0031 A71-10600
- Atmospheric interaction layer large recombination coefficient existence possibility according to corpuscular model of radar head echo 01 p0159 A71-10871
- Echoing area relation to radar range resolution cell size and aircraft dimensions, using mathematical model 02 p0210 A71-11643
- Solar coronal plasma electromagnetic wave amplification, discussing maser action effect on radar echoes 02 p0306 A71-12078
- Bremsstrahlung X rays-radar echoes relation in southern auroral zone, discussing electron precipitation role 03 p0408 A71-13388
- Reflected electromagnetic wave polarization parameters, obtaining correlation functions for radar echoes 04 p0557 A71-14632
- Average radar cross section relative values for echoes from rain, considering horizontal, vertical and circular polarization in various sea states 04 p0551 A71-15008
- Trihedral metallic post corner reflector for radar echo enhancement, reflecting same sense rotation as incident circularly polarized signal 04 p0559 A71-15879

- Gravitational constant time variation based on planetary radar echo time delay in comparison with atomic time, discussing accuracy limits 05 p0807 A71-16227
- Lidar observations of visually clear troposphere compared with simultaneous rawinsonde data for relationship between lidar echoes and atmospheric winds aloft 05 p0721 A71-16670
- Radar echo signal amplitude probability distribution during fully polarizational reception 05 p0723 A71-16873
- Vertical air motions velocity in rainfall from Doppler spectrum total radar reflectivity and median velocity 07 p1150 A71-18798
- Solar coronal plasma electromagnetic wave amplification, discussing maser action effect on radar echoes 08 p1361 A71-21128
- Woodward ambiguity function generalization for case of radar signal reflection from rapidly fluctuating target, mixed with white Gaussian noise 09 p1404 A71-22292
- Dry radar reflectivity and attenuation due to wet ice spheres exponential distributions, noting hail detection procedures 11 p1794 A71-25379
- High sensitivity S band meteorological radar detecting clear air echoes from low horizontal layers and high altitude turbulence 12 p1880 A71-27156
- Variable target reflectivity effect on weather radar measurements, using extended echo fluctuation theory for average and maximum signals 13 p2031 A71-28723
- Missile system passive radar echo enhancement, discussing dielectric enhancers comprising antennas and corner reflectors 14 p2206 A71-31070
- Lidar soundings of troposphere, investigating multilayer echo structure of haze layers, clouds and rainstorms 17 p2770 A71-34706
- Bistatic radar frequency spectra and cross sections dependence on surface scattering laws, studying echo bandwidth 17 p2702 A71-35026
- Automatic classification of targets characterized by radar returns at discrete set of frequencies in Rayleigh region and first resonance range 17 p2747 A71-35773
- Magnetically conjugate range-time observations of E region radio aurora by pulsed VHF radar echoes 18 p2875 A71-35963
- Dissipative plasma instability in lower E region investigation by alkali plasma clouds injection, observing irregular echo behavior by coherent pulse Doppler radar 19 p3110 A71-37365
- Autoplotter for radar echoes on CRT screen, using video tape recorder for ship navigation use 19 p3017 A71-37700
- Radar measurements of vertical structure and motion trajectories of cumulus-rain clouds, studying vertical flows velocities and radar echo characteristics 19 p3094 A71-38701
- Proton precipitation satellite observation, comparing with simultaneous ground based measurement of auroral radar echoes 20 p3285 A71-39887
- Radar data video extractor adaptive threshold device synthesis criteria to quantize echoes for ensuring constant false alarm rate and target visibility 22 p3508 A71-41525
- Reflected electromagnetic wave polarization parameters, obtaining correlation functions for radar echoes 22 p3510 A71-42272
- Parasitic radar echoes of meteorological, ground and sea origin 22 p3514 A71-42468
- Amplitude prediction for terrestrial radar echoes from ground using topographical data 22 p3514 A71-42469
- Model aspects of sea echoes and clutter unsteadiness on radar 22 p3514 A71-42470
- Polarization transforming feed horns for rapid scan X-band radar antenna, allowing transmission in various polarization modes and parallel and orthogonal-polarized return reception 23 p3655 A71-44167
- Upwind/downwind differential Doppler spectra of radar sea echo for P, L and C bands 23 p3646 A71-44173
- Atmospheric attenuation effects on cloud and precipitation radar reflection coefficient 24 p3845 A71-44880
- Radar echoes maximal intensity measurements from meteorological formations, describing pulse by pulse recording system 24 p3826 A71-44883
- Airborne radar sea return averaged pulse shape measurements over various water surfaces, noting

clear distinction between specular and scattered reflection components
24 p3824 A71-45083

RADAR EQUIPMENT

NT PLAN POSITION INDICATORS
NT RADAR ANTENNAS
NT RADAR BEACONS
NT RADAR CORNER REFLECTORS
NT RADAR FILTERS
NT RADAR RECEIVERS
NT RADAR REFLECTORS
NT RADARSCOPES

Remote sea state information acquisition system using video attachment to radar for sea return spectrum recording and analysis

01 p0031 A71-10600

Digital simulation computer program in FORTRAN IV for radar systems performance evaluation in various environments

02 p0211 A71-11796

Radar information digital extractors for processing signals from airborne transponder

03 p0382 A71-13570

Deception repeaters for erroneous information transmission to radar, considering echo signal level, burnthrough, target size, sensitivity, gain and bandwidth

04 p0555 A71-15359

Electron tubes for radars, discussing history and development of magnetrons, Thomson-CSF display tube and power amplifiers

06 p0874 A71-17568

S band pulsed cotal radar transponder for ground base Centaur rocket trajectory tracking from takeoff to splashdown

06 p0870 A71-18475

Terrain-following radar for TSR-2 aircraft, discussing reliability trials and improvement

07 p1062 A71-19557

Multiradar tracking system with monoradar units interconnected by central digital computers for wide airspace surveillance

08 p1255 A71-21598

Radar analog simulators for Polish air traffic controllers training, describing optical and electronic equipment

09 p1428 A71-22950

Computerized finite element techniques for stress and structural analysis for space communication and radar applications

10 p1684 A71-23756

Broadband multicavity multimegawatt klystron design for superpower amplifiers in radars and particle accelerators

11 p1734 A71-26433

Cost effectiveness of reliability screening program from parts procurement through system test, using experience with attack radar for F-111 aircraft

12 p1885 A71-26683

Radar duct surface interference phenomena and focusing effects on radar beam energy propagation

14 p2201 A71-30936

Passive and active radar detection theory and practice, considering advances in sensors, signal generators, processors and filters

15 p2371 A71-31907

Helicopter radar equipment for obstacle avoidance in all-weather low altitude flight, describing components installation, cockpit display and controls

15 p2446 A71-31919

Airborne traffic situation display for use with national airspace/automatic radar control terminal system, using computer selected message, map and heading data

19 p3097 A71-37175

[AIAA PAPER 71-929]
Radar equipment for meteor velocity and radiants measurement at VHF by pulse diffraction method

19 p3067 A71-38635

Ultrasonic radar simulator to produce data for radar system performance evaluation, describing automated short range and manual long range systems

20 p3196 A71-39376

Gunn effect devices properties and applications, discussing microwave energy sources tunable and local oscillators, parametric amplifier pumps and radar transmitters

21 p3357 A71-40819

Radar data video extractor adaptive threshold device synthesis criteria to quantize echoes for ensuring constant false alarm rate and target visibility

22 p3508 A71-41525

Book on pulse, CW, Doppler, pulse Doppler and space radar theory, operation and maintenance, describing equipment, tracking and siting

22 p3509 A71-41621

Radar systems performance constraints, discussing environmental effects, carrier frequency, aerial directivity, clutter echoes, transmitter power, etc

22 p3509 A71-42199

Solid state airborne weather radar for civil aviation, discussing design, weight and power requirement reduction

23 p3647 A71-44273

RADAR FILTERS

Moving target indicator detection filters with nonuniform interpulse periods, discussing design

01 p0058 A71-11575

Video MTI pulse radar Doppler filter optimum symmetrical weighting factors in clutter-plus-noise environment

07 p1059 A71-18847

Noise bandwidth of optimum second order and bandpass Butterworth, Bessel and Chebyshev filters for communication and radar systems

07 p1081 A71-19539

Clutter signals simulation with predetermined auto- and cross correlation, describing mathematical method for filter weighting function

16 p2541 A71-33424

Optimal mismatched filter design for radar ranging, detection and resolution by reduction to transversal equalizer, determining parameters by nonlinear programming

24 p3815 A71-44935

RADAR IMAGERY

Spatial and temporal structure in turbulent breakdown of shear flows in stably stratified atmosphere from radar images of vertical cross sections

01 p1116 A71-10569

Side-looking airborne radar (SLAR) imagery and site selection for soil pattern topography

02 p0244 A71-11952

Synthetic endfire hologram radar for small target and clear air turbulence detection

03 p0381 A71-14476

Pseudo radar imagery by high contrast aerial photography at low sun angles for aiding geological analysis

04 p0598 A71-15370

Automatic pattern recognition, discussing texture as discriminant of crops on radar imagery

05 p0743 A71-17145

Side-looking airborne radars ground and slant range imagery mosaic preparation and geoscience interpretation, analyzing terrain geometry, radar shadow and layover

06 p0898 A71-17561

Department of Defense data processing equipment for all weather airborne terrain imaging radar mapping

08 p1288 A71-21250

Cumulative frequency curves of terrain slopes by radar shadow frequency method

09 p1439 A71-23216

Vegetation penetration with K-band side-looking airborne imaging radars, noting multifrequency multipolarization system application for terrain reconnaissance

18 p2875 A71-36365

Side-looking airborne radars and image recording scanners design for geoscience applications, discussing gray scale improvement, multispectral sensing, target discrimination, etc

18 p2875 A71-36366

Active synthetic aperture coherent imaging technique to fill and double diameter of sparsely sampled aperture array

22 p3574 A71-41783

RADAR MAPS

NT RADAR IMAGERY

Radar interferometric mapping of Venus surface reflectivity in polarized mode at 70 cm wavelength

03 p0490 A71-13782

Onboard air navigation computers direct correction by mapping radar, calculating position by region overflown image/measured geographic features comparison

06 p0925 A71-17952

Mapping by position data extraction from airborne high resolution side-looking radar

06 p0869 A71-18295

Cumulative frequency curves of terrain slopes by radar shadow frequency method

09 p1439 A71-23216

Lunar Apennine-Hadley region geological implications from high resolution earth-based radar map and Lunar Orbiter photography

20 p3287 A71-38977

Radar Meteor 50 PPI taken pictures concerning Adriatic regions meteorologic situations

21 p3411 A71-40828

RADAR MEASUREMENT

Reflectivity and attenuation observations of hail and radar bright band during storms, discussing rain effects

01 p0115 A71-10554

Free fall speed characteristics of simulated hailstones measured by tracking radar, discussing roughness effects on speed and drag

01 p0115 A71-10556

Radar and air flow structure of Alberta hailstorms from radiosonde data, aircraft measured cloud base updrafts and weak echo region concept

01 p0115 A71-10558

Surface and aircraft radar observations of updrafts within weak echo region of Alberta hailstorm,

discussing adiabatic flow breakdown into turbulent flow

01 p0115 A71-10559

Clear air radar structures temperature, wind components and true gust velocities combined with radar data for observed traveling wave features

01 p0030 A71-10560

Land breeze fronts observed by X and S band radars at Wallops Island

01 p0116 A71-10563

Breaking waves and resulting CAT characteristics from ultrahigh resolution FM-CW radar observation, using model of unstable waves at sheared inversion layer

01 p0116 A71-10565

CAT radar observation from instrumented and uninstrumented jet fighter flights, analyzing data statistically for spatial correspondence of ground and airborne observations

01 p0116 A71-10566

Thin CAT layer detection in lower stratosphere by L band radar complemented by radiosonde and U-2 aircraft probes

01 p0116 A71-10567

CAT layer simultaneous radar and instrumented aircraft observations, noting eddy dissipation rate computation from radar reflectivity measurement

01 p0116 A71-10570

Dual Doppler radar method of convective storms observation, noting optimization via COPLAN scanning

01 p0117 A71-10574

Snowflakes melting region radar observation, discussing fall speed, reflectivity profile, particle size distribution, Doppler characteristics, etc

01 p0117 A71-10575

Lower atmosphere turbulence model derivation from data obtained by Doppler radar windfield measurements in snowfall environment

01 p0117 A71-10578

Radar precipitation measurement accuracy improvement, using various Z-R relationships for correlation of radar data and rainfall rates

01 p0117 A71-10581

Meteorological radar rainfall estimates comparison with dispersed tipping bucket gage measurements during storms

01 p0118 A71-10582

Cloud and precipitation boundaries in convective storms studied by stereophotogrammetry and radar, discussing radar echo motion within cloud envelope

01 p0118 A71-10586

Anticyclonic eddy formation and emergence within severe thunderstorm observed by radar and surface data, noting wave development along pseudocold front

01 p0118 A71-10588

Radar observation of planetary surface characteristics, emphasizing albedo, surface roughness and differentiation

02 p0309 A71-12154

Neutral atmospheric wind measurements at 75-110 km by radar observation of meteor trail drift, discussing diurnal variations

03 p0407 A71-13308

Comparative simultaneous ionospheric temperature and plasma concentration by Explorer 31 probes and ground based radar measurements

03 p0407 A71-13311

VHF radar measurements of scattering by field aligned irregularities associated with equatorial spread F

03 p0420 A71-14532

Clear air turbulence due to large amplitude Kelvin-Helmholtz billows, noting simultaneous measurements by instrumented aircraft and radar

04 p0621 A71-15043

Seasonal and year-to-year crop radar sensing in agriculture for socioeconomic applications

07 p1095 A71-18825

X band radar system to compare electrical lengths in 100 m range with 10 to minus 6 accuracy, noting applications in geodetic and radio waves phase fluctuation measurements

07 p1075 A71-19345

Areal precipitation quantitative radar measurements, describing signal processing and digital system for contour mapped displays and numerical summaries

08 p1257 A71-21738

Meteor observations by radar, determining number, range, velocity, deceleration, duration, radiants, orbits and densities

09 p1517 A71-22212

Meteor trails azimuth angle measurement by radar interferometry, describing system advantages with respect to receiver noise, angular resolution and calibration

10 p1576 A71-24053

Solar corona plasma turbulence spectra, evaluating radar echo structure

12 p1963 A71-27080

Radar based values of neutral night exospheric temperature, discussing dominant effect of annual variation

13 p2055 A71-27921

Wind profile data in Cape Kennedy area from FPS-16 radar/Jimsphere master tapes 13 p2098 A71-29346

Meteorological tower high resolution CW-FM radar measurements for studies of temperature inversions, waves, thermal plumes and convection in atmospheric boundary layer 14 p2192 A71-29707

Planet Mercury density, discussing optical and radar measurements and theory comparison with observation 14 p2306 A71-29728

Large amplitude formations and turbulence in Kelvin-Helmholtz instability, comparing with radar observations 14 p2267 A71-29760

High power 10 cm radar as CAT detector, comparing with radar and aircraft data coincident in space and time 14 p2267 A71-29761

Wind profile determinations at 90-100 km from meteor trail drift and ionosphere inhomogeneity radar data, noting semidiurnal harmonics in wind components 15 p2395 A71-31450

Laser radar system using retroreflector on lunar surface for measurement of distance between earth and moon 16 p2543 A71-33811

Geomagnetic equatorial ionospheric ion temperature, comparing incoherent scatter radar and OGO-D retarding potential analyzer values 16 p2573 A71-33956

Ionospheric atomic oxygen concentration estimates from radar backscatter and rocket probe measurements of electron and ion temperatures and concentration 16 p2574 A71-33965

Radar observation of lunar distance, motion and surface statistical nature, noting enhanced reflectivity associated with craters 17 p2804 A71-35178

Tropospheric stratification structure from high resolution FM/CW radar sounder, comparing with internal gravity wave atmospheric models 17 p2771 A71-35808

Lower atmospheric multiple wavelength laser radar data compared to clear atmosphere model and radiosonde measurements, discussing mixing layer location 18 p2882 A71-36617

Solar corona plasma turbulence spectra, evaluating radar echo structure 19 p3133 A71-37430

Laser radar observation of comet Bennett dust at 40-90 km, deducing particle size from rate of descent 19 p3142 A71-38041

Power density prediction based on electromagnetic compatibility analysis of radar environments, comparing predicted propagation losses with measurements 19 p3021 A71-38455

Radar measurements of vertical structure and motion trajectories of cumulus-rain clouds, studying vertical flows velocities and radar echo characteristics 19 p3094 A71-38701

Automated meteorological radar information operation methods for cloud fields, discussing data analysis and processing 19 p3094 A71-38702

Simultaneous radar and instrumented aircraft observations in clear air turbulent layer for eddy dissipation rates calculation 20 p3256 A71-39207

Proton precipitation satellite observation, comparing with simultaneous ground based measurement of auroral radar echoes 20 p3285 A71-39887

Radar determination of reference change related to sudden acceleration, deducing Galilean-accelerated reference transition in two dimensional space-time 21 p3415 A71-40513

Emitted signal delay time effect on operational precision of semiconductor laser radar for measuring lower cloud boundary heights 21 p3394 A71-41239

Detailed wind velocities and temperature profile measurements by FPS-14 radar/Jimsphere technique for space vehicle and SST applications 22 p3569 A71-42543

Radar vs visual observation of cloudiness and hazardous weather phenomena, emphasizing storm warnings 24 p3845 A71-44885

Ocean surface wave height /sea state/ measurement by high resolution random-signal radar based on model characterized by Poisson distributed scatterer density function 24 p3823 A71-45082

RADAR NAVIGATION

ATC automated systems, discussing National Airspace System En Route Stage A and Advanced Radar Terminal System [AJAA PAPER 71-244] 07 p1156 A71-19719

Terrain following radar for airborne guidance of low flying military aircraft 12 p1927 A71-26881

Radar avoidance action logic for converging aircraft safe passage, discussing near miss and collision situations 12 p1927 A71-27600

Air navigation techniques history, considering radio, radar, loran Doppler and inertial navigation 14 p2272 A71-30712

Radio and radar air navigation for civil aviation, discussing Doppler effect, inertia and satellite systems 19 p3100 A71-37344

RADAR OBSERVATION

U RADAR TRACKING

RADAR PHOTOGRAPHY

Electron attachment rate determination by combined photographic and radar observation of meteors 13 p2137 A71-28545

Small meteor bodies fragmentation, using radar diffractional pictures 16 p2639 A71-33697

Radar Meteor 50 PPI taken pictures concerning Adriatic regions meteorologic situations 21 p3411 A71-40828

RADAR RANGE

Geodetic survey adjustment and accuracy improvement using satellite radar range and ballistic camera data 04 p0583 A71-15302

Radar detection ranges on nonfading targets as function of sea state in marine environment 05 p0723 A71-16972

Meteor trails distance determination by radar pulses reflection observation, estimating reflected signal delay dispersion and plotting mean square errors 10 p1576 A71-24037

Suboptimal estimation of remaining flight distance of aircraft at each radar range measurement by limited state recursive estimators 11 p1741 A71-25489

Radar ranging experiment onboard Jupiter orbiter, concerning perturbations, gravitational harmonics and short arc orbit determination 15 p2487 A71-32041

Three dimensional ATC radar supporting simultaneous range, azimuth and elevation information for indefinite number of targets by continuous searching 15 p2371 A71-32167

Mars motion 1751-1969, comparing Clemence theory and Newcomb Tables of sun with meridian and radar ranging Mars observations 19 p3144 A71-38166

Optimal mismatched filter design for radar ranging, detection and resolution by reduction to transversal equalizer, determining parameters by nonlinear programming 24 p3815 A71-44935

RADAR RECEIVERS

Radar receiver dynamic range centering for log-normal target statistics for minimum probability of signal exclusion 05 p0725 A71-17084

Operating mode of semiconductor AFC mixer of radar receiver under large signal 06 p0874 A71-17546

Noise effects on characteristics of automatic radar rangefinder with logarithmic receiver, showing discrimination curve deformation with increasing SNR 09 p1415 A71-22297

Airborne ECM receiver, determining conditions for detecting victim radar signal before signal reflection from aircraft 15 p2368 A71-31207

L band microwave IC front end for identification friend or foe (IFF) receiver, noting environmental and filtering requirements 16 p2547 A71-33556

Ku band monopulse receiver with electronically tunable Gunn oscillator, discussing negative resistance diodes dynamic impedance properties 16 p2547 A71-33557

IF nonlinearities effect on Gaussian clutter rejection associated with noncoherent MTI radar receiver 17 p2708 A71-35483

General purpose pulsed microwave radar receiver, describing balanced mixer and transistorized IF amplifier design and construction 18 p2887 A71-36015

Electromagnetic compatibility performance of pulse Doppler radar receivers, considering CW or synchronous pulse interference 19 p3020 A71-38430

Moving target indicator receivers design and techniques, discussing performance limitations 20 p3200 A71-39905

Optical correlation for surveillance and pulse Doppler radar receivers signal processing 20 p3200 A71-39910

RADAR RECEPTION

Radar signal probability ratio over finite interval 02 p0219 A71-12620

Radar station-satellite contact times using horizon crossing, lunar occultation and keyhole constraints 02 p0280 A71-12898

Shading reflector transverse motion effect on radar signal spectrum based on geometric optics approximation 05 p0719 A71-15999

Doppler pulse radar signal reception, calculating noise signal optimal relationship for comparison with adapted filtration technique 05 p0722 A71-16707

Asymptotic optimal rank criterion for noncoherent detection of fluctuating radar signal in noise of unknown intensity 19 p3015 A71-37253

Signal processing techniques for clutter suppression in moving target indicator radar 20 p3200 A71-39908

Shading reflector transverse motion effect on radar signal spectrum based on geometric optics approximation 22 p3515 A71-42748

RADAR REFLECTIONS

U RADAR ECHOES

RADAR REFLECTORS

Antenna array radar reflector for simulating objects with given polarization characteristics during radar equipment tuning and calibrating 02 p0233 A71-12634

Shading reflector transverse motion effect on radar signal spectrum based on geometric optics approximation 05 p0719 A71-15999

Radar target optimal detection algorithms in cloud of passive reflectors, noting space surveillance regularities 05 p0722 A71-16870

Vertical plane dual beam properties of doubly curved shaped reflector, considering surveillance radar antenna modification to improve performance with ground clutter 13 p2028 A71-27990

Shading reflector transverse motion effect on radar signal spectrum based on geometric optics approximation 22 p3515 A71-42748

RADAR RESOLUTION

Weather radar resolution enhancement by pulse compression system for signal bandwidth increase by phase coding 01 p0030 A71-10597

Echoing area relation to radar range resolution cell size and aircraft dimensions, using mathematical model 02 p0210 A71-11643

Air traffic control radar separation by pulse repetition frequency discrimination for double and triple stagger configurations 05 p0720 A71-16347

Uniqueness theorem for sources of electromagnetic fields expressible as magnitude integrable functions of time, considering implications for antenna aperture limitations on radar resolution 06 p0868 A71-17729

Iterative method for good aperiodic binary sequences in radar range resolution 07 p1148 A71-19769

High sensitivity S band meteorological radar detecting clear air echoes from low horizontal layers and high altitude turbulence 12 p1880 A71-27156

Correlation function of modulation of radar sounding signals with nonwhite nonstationary Gaussian noise, obtaining target range and velocity maximum likelihood estimates 12 p1882 A71-27616

Resolution and clutter performance of simultaneous Doppler and acceleration measurement with coherent pulse trains 20 p3195 A71-38855

Doppler distortions of clutter and resolution performance of pulse trains with large time bandwidth products 20 p3195 A71-38861

Radar resolution performance for targets with range acceleration, determining matched filter or correlation radar effects 20 p3195 A71-38868

Radar systems performance constraints, discussing environmental effects, carrier frequency, aerial directivity, clutter echoes, transmitter power, etc 22 p3509 A71-42199

Optimal mismatched filter design for radar ranging, detection and resolution by reduction to transversal equalizer, determining parameters by nonlinear programming 24 p3815 A71-44935

RADAR SCANNING

Acquisition and processing of aircraft search radar data obtained by track-while-scan technique, using off-line digital computer 01 p0040 A71-11392

Stochastic model for analysis of track-while-scan technique for aircraft search radar, based on Kalman filter theory 01 p0065 A71-11393

Cartographic characteristics and applications of airborne radar sensors, stressing synthetic aperture radar and electronic techniques and equipment 09 p1452 A71-23219

Thunderstorms environment analysis from radar and aircraft scanings, determining cumulonimbus

- cloud air kinematic properties for three dimensional circulation model
09 p1488 A71-23252
- Moving window and feedback integrator type scanning radar detectors performance comparison based on probability and position estimates by Monte Carlo simulation
12 p1882 A71-27441
- Space shuttle scanning beam landing guidance system, discussing accuracy in penetration, alignment, flare out and touchdown maneuvers and trajectories
17 p2773 A71-35068
- Low level target locating by monopulse and conical scanning radar, solving balance equation
17 p2708 A71-35482
- Real time interactive simulation of multifunction phased array radar, using digital computer links
23 p3648 A71-44272
- ### RADAR SCATTERING
- Radar reflectivities in South Dakota hailshafts from hailstone momentum data, applying microwave scattering theory
01 p0115 A71-10557
- Radar reflectivity pattern calculation from cumulus cloud growth numerical model, noting similarity with radar data from on-line computer system
01 p0118 A71-10584
- Radar scattering from turbulent underdense ionized wakes, showing relationship between Doppler spectrum and wake characteristics
04 p0551 A71-15011
- Radar target backscattering characteristics description using scattering matrix invariants
04 p0619 A71-15329
- Coupling effect on monostatic-bistatic radar equivalence for monochromatic wave and short pulse scattering
07 p1060 A71-19260
- Radar scattering law derivation method for small regions of Venus surface, synthesizing CW spectra
08 p1357 A71-20872
- Average radar backscattering cross section calculation for conducting obstacles for arbitrary transmitter and receiver antenna polarizations, obtaining results for straight wires, circular loops and helices
09 p1410 A71-23516
- Radar backscattering from thin metallic conductive films, giving results for Al and Ni from anechoic chamber measurements
09 p1410 A71-23517
- Radar incoherent scatter technique for ionospheric propagation forecasting, using nocturnal and diurnal electron density profiles measurements
10 p1575 A71-23867
- Covariance matrix of coordinate fluctuations of instantaneous radar center of reflection from set of scatterers
10 p1578 A71-24709
- Handbook on radar cross section, Volume 1, covering scattering theory, edge/tip diffraction, creeping/traveling waves and various geometric shapes
11 p1733 A71-26008
- Handbook on radar cross sections, Volume 2, covering scattering from planar surfaces, complex bodies, rough surfaces, ionized media, plasmas, radar targets and various objects
11 p1733 A71-26009
- Book on phenomenological theory of radar targets covering wave polarization and antennas, single, statistical independent and distributed targets, decomposition theorems and surface scattering
12 p1877 A71-26568
- Electromagnetic wave scattering from rough surfaces, discussing radar return differences for different polarizations
14 p2203 A71-30968
- Bistatic radar frequency spectra and cross sections dependence on surface scattering laws, studying echo bandwidth
17 p2702 A71-35026
- Stable auroral red arc excitation observations by HF radar scattering, scanning photometers and Alouette 1 satellite, noting local electron concentration increase
19 p3054 A71-38034
- Bistatic radar scattering cross section from slightly rough perfectly conducting infinite surface, using Fourier transform
19 p3024 A71-38609
- Cumulonimbus cloud hail danger, precipitation and water content measurements with scattering and attenuation of centimeter radar waves, including automated echo subtraction device
19 p3094 A71-38700
- Inverse scattering at low frequencies, estimating target diameter for various shapes
20 p3195 A71-38869
- Solar wind origin in active regions by radar exploration, noting signal backscattering from coronal plasma turbulent pulsations
20 p3281 A71-39732
- Ocean surface condition correlation to radar backscattering cross sections and wind velocity from scatterometer data
22 p3569 A71-42545
- ### RADAR SIGNATURES
- Midlatitude ionospheric signatures from narrow beam HF radar backscatter sounder, discussing diurnal and seasonal occurrences
13 p2031 A71-28782
- ### RADAR TARGETS
- Radar energy loss estimate over space targets, considering various energy distributions in given search volume, target acquisition probability, signal to noise ratio, etc
02 p0212 A71-11879
- Coherent laser synthetic aperture radar at microwave frequencies for airborne ground point target mapping
02 p0215 A71-12044
- Radar target optimal detection algorithms in cloud of passive reflectors, noting space surveillance regularities
05 p0722 A71-16870
- Radar detection ranges on nonfading targets as function of sea state in marine environment
05 p0723 A71-16972
- Double threshold detection radar performance, defining M out of N algorithm for nonfluctuating target and false alarm cases
07 p1058 A71-18841
- Fluctuating radar target detection in clutter by sidelobe blanking system, discussing false alarm adaptive threshold procedure
07 p1154 A71-18842
- Unresolved radar targets or multipath distortion determination by measurement of complex indicated angle on two pulses separated by short interval
07 p1058 A71-18843
- Woodward ambiguity function generalization for case of radar signal reflection from rapidly fluctuating target, mixed with white Gaussian noise
09 p1404 A71-22292
- Ground based coherent radar synthetic aperture procedure against uniform velocity targets, discussing airborne holographic synthetic gain applications to stationary antennas
09 p1405 A71-22697
- Omnidirectional radar moving target detection from clutter, using Doppler filter system
09 p1407 A71-23047
- Book on phenomenological theory of radar targets covering wave polarization and antennas, single, statistical independent and distributed targets, decomposition theorems and surface scattering
12 p1877 A71-26568
- Correlation function of modulation of radar sounding signals with nonwhite nonstationary Gaussian noise, obtaining target range and velocity maximum likelihood estimates
12 p1882 A71-27616
- Signals single set synthesis for simultaneous target information transmission and range and velocity measurement
12 p1883 A71-27617
- Variable target reflectivity effect on weather radar measurements, using extended echo fluctuation theory for average and maximum signals
13 p2031 A71-28723
- Target trajectory detector optimization, using surveillance radar data and Markovian chain apparatus
13 p2033 A71-28993
- Quasi-point type radar target angular motion simulation by controlling electromagnetic wave phase front in receiving field
14 p2193 A71-29825
- Instantaneous frequency statistical characteristics of passive noise spectra and fluctuating signals reflected from nonpoint moving radar targets
14 p2195 A71-30111
- Electromagnetic inverse scattering model of electrical radius of conducting spherical radar target employing expansion of scattered field in vector wave functions
14 p2196 A71-30564
- Target movement effects on airborne coherent sidelooking synthetic aperture imaging radar during scan rate and compression ratio increases
14 p2197 A71-30798
- Radar target detection in nonGaussian sea clutter, calculating trimmed-mean detector performance under Rayleigh fluctuation
14 p2197 A71-30805
- Radar target direction variation /glint/ sensed by amplitude monopulse tracking antenna receiving nonuniform waves
14 p2214 A71-30807
- Meteorologic bistatic radar equation for randomly distributed targets, applying to raindrops, refractivity perturbations, etc
14 p2197 A71-30830
- Three dimensional ATC radar supplying simultaneous range, azimuth and elevation information for indefinite number of targets by continuous searching
15 p2371 A71-32167
- Point target horizontal speed determination with circular beam radar for measuring signal intensity and range, noting application to insects in atmospheric waves
17 p2706 A71-35122
- Radar glint reduction by diversity techniques, indicating tracking improvement by error signal choice
19 p3022 A71-38587
- Radar resolution performance for targets with range acceleration, determining matched filter or correlation radar effects
20 p3195 A71-38868
- Inverse scattering at low frequencies, estimating target diameter for various shapes
20 p3195 A71-38869
- Binary moving-window integrator radar target azimuth measurement error determination, presenting target detection probability curves obtained by digital simulation
21 p3348 A71-40725
- ### RADAR TRACKING
- Meteor population radar observation data at Antarctica station, noting monthly variations
01 p0149 A71-10054
- Radar tracking systems stretcher detector circuit output signal amplitude and spectral distribution analysis
01 p0029 A71-10308
- Stochastic model for analysis of track-while-scan technique for aircraft search radar, based on Kalman filter theory
01 p0065 A71-11393
- Statistical connection strategies for automatic multiradar air traffic surveillance using track computer
03 p0380 A71-14395
- Synthetic aperture holographic techniques in continuous wave bistatic radars for moving targets
03 p0381 A71-14477
- German monograph on digital simulation system for ergonomic investigation of radar observation problems covering flight plan data with density variation
04 p0551 A71-14900
- Hurricane Gladys structure and dynamics observations by Apollo 7 spacecraft, satellites and radar, noting large cloud feature
05 p0777 A71-16662
- S band pulsed cotal radar transponder for ground base Centaur rocket trajectory tracking from takeoff to splashdown
06 p0870 A71-18475
- SAGE/Buic vs Kalman filters for aircraft tracking, determining accuracy by radar model [AIAA PAPER 71-58]
06 p0925 A71-18517
- Meteor population radar observation data at Antarctica station, noting monthly variations
08 p1361 A71-21048
- Multiradar tracking system with monoradar units interconnected by central digital computers for wide airspace surveillance
08 p1255 A71-21598
- Meteor observations by radar, determining number, range, velocity, deceleration, duration, radiants, orbits and densities
09 p1517 A71-22212
- Woodward ambiguity function generalization for case of radar signal reflection from rapidly fluctuating target, mixed with white Gaussian noise
09 p1404 A71-22292
- Upper atmosphere wind measurement by meteor trails radar sounding, discussing seasonal variations, amplitudes and phases of harmonic components
09 p1487 A71-22302
- High order conditional algebraic equations in determination from azimuthal radar observation sporadic meteor density distribution over celestial sphere, discussing solution procedure and convergence
10 p1576 A71-24030
- Wind velocity data processing technique for azimuthal radar observations in meteor zone, using least squares method
10 p1600 A71-24035
- Atmospheric turbulence parameters determination from radar meteor observation, calculating antenna radiation patterns effect on error
10 p1583 A71-24036
- Sounding rocket flight accurate trajectory data, determining cost effective radar tracking system
10 p1610 A71-24149
- Vertical air motions measurement by balloon radar tracking, discussing method of radar noise error reduction by ascent rate smoothing technique
11 p1794 A71-25385
- Electron attachment rate determination by combined photographic and radar observation of meteors
13 p1317 A71-28545
- Space trajectory radars for measurements on military firing ranges and civil space centers, using microelectronics for data processing
16 p2544 A71-34098
- Low level target locating by monopulse and conical scanning radar, solving balance equation
17 p2708 A71-35482
- Optical radar aircraft tracking and position system, using IR Q switched flash pumped Nd-YAG laser transmitter and pulse receiver with magnetic tape recorder and real time computer
18 p2900 A71-36905

- Computer-based aircraft tracking with aid of twin radar air traffic control system, discussing components and operation 18 p2883 A71-36993
- On-line radar tracking of six orbital elements of thrust maneuvering spacecraft, obtaining discrete non-linear measurement and dynamical equations [AIAA PAPER 71-902] 19 p3095 A71-37153
- Radar returns from convective fields and cells in visually clear atmosphere explained by thermal effects and air motion 19 p3090 A71-37753
- Antenna azimuthal radiation patterns and meteor radial distribution effects on wind velocity measurement by radar observation of meteor trains 19 p3145 A71-38372
- Radar glint reduction by diversity techniques, indicating tracking improvement by error signal choice 19 p3022 A71-38587
- Nonlinear filters performance comparison for reentry vehicle trajectory estimation from radar tracking, noting coordinate systems effect on extended Kalman filter accuracy 19 p3039 A71-38712
- Book on pulse, CW, Doppler, pulse Doppler and space radar theory, operation and maintenance, describing equipment, tracking and siting 22 p3509 A71-41621
- Radar observation of convective process in clear air, presenting turreted top cell contour tracings from PPI sequence 23 p3700 A71-43088
- Fokker-Planck-Kolmogoroff equation for radar tracking meter with nonlinear discriminator and second-order smoothing loops, obtaining steady solution by separated variables method 24 p3815 A71-44702
- RADAR TRANSMISSION**
- Soviet book on radar signal processing optimization covering detection and measurement, electronic analog and discrete digital filters design, etc 06 p0867 A71-17445
- Optimal phased array radar pulse scheduling multiple transmissions and receptions in minimum time, using integer programming 08 p1254 A71-21339
- Book on detection, estimation and modulation theory, Part 3, Gaussian and radar-sonar signals in noise, covering point targets, random process and scatter channels 15 p2371 A71-31841
- Performance levels prediction for airborne solid state phased array radar transmission sources, considering TRAPATT devices 22 p3509 A71-41630
- Model aspects of sea echoes and clutter unsteadiness on radar 22 p3514 A71-42470
- RADARSCOPES**
- NT PLAN POSITION INDICATORS**
- Radarscope net for target azimuth and distance and for direct altitude readout through beacon numerics 13 p2033 A71-28886
- ATC radar display systems mapping techniques using vectors and optical projections 14 p2271 A71-30014
- ATC display devices with computer-derived alphanumeric labels on radar screen, examining feasibility and effectiveness 21 p3413 A71-40118
- RADIAL DISTRIBUTION**
- Radially loaded bearings rolling on flat track, determining slip-stick areas and creep conditions 01 p0086 A71-10298
- Laser radial-shear common path interferometer for lens testing 02 p0250 A71-12144
- Direction indicating color schlieren system displaying radial refractive index gradients, comparing with knife edge monochrome image resolution 03 p0423 A71-13459
- Underground cosmic ray showers muon pairs lateral distribution measurement 04 p0640 A71-14815
- Cylindrical electromagnetic wave amplification in TWT with radial line and diverging electron flux 05 p0727 A71-16003
- Low energy protons radial gradient in interplanetary space measured with intercalibrated solid state detectors on Venus bound Mariner 5 and earth orbiting Explorer 33 06 p0952 A71-18113
- Radial microdistribution of absorbed dose in heavy charged particle track, allowing for delta electron emission 06 p0963 A71-18365
- Radial density distribution in plasmoid and radial expansion of plasmoid investigated by microwave measurements 06 p0940 A71-18703
- Plasma instabilities under radial magnetic field effect across homogeneous field, considering oscillation modes 07 p1167 A71-19231
- Saturn rings radial structure model featuring purely gravitational forces association with primary and perturbers, using planar restricted three body problem formalism 07 p1202 A71-20518
- Equatorial proton belt radial profile analysis by satellite electron distribution data 08 p1351 A71-20962
- Radio meteor orbit velocity and radiant measurements by pulse diffraction technique 09 p1520 A71-22829
- Hypothetical geocentric/interplanetary dust cloud concentration detection possibility by earth shadow 10 p1601 A71-24449
- Fe meteorite Grant, measuring radial distribution of cosmogenic nuclides of K, Ca, Ti, V, Cr and Mn produced by cosmic rays 11 p1819 A71-25224
- Radial load effects along length of hinged cylindrical shell for maximum displacement positions, using trigonometric Fourier series 11 p1850 A71-25942
- Plasma instabilities under radial magnetic field effects across homogeneous field, considering oscillation modes 12 p1934 A71-26749
- Radial distribution of electric potential in Penning discharge based on relation between sulfur hexafluoride negative ions transit time and initial energy 13 p2107 A71-28852
- Gas particle radial reflection model application to hypersonic nearly-free molecular flow about convex bodies, solving steady state problem 13 p1991 A71-29153
- Pioneer 9 interplanetary observations, presenting deep space data for solar rotations and radial gradient in VLF electric field behavior 13 p2064 A71-29163
- Modular digital TDM switch for radially distributed clock synchronization, discussing design and control 13 p2034 A71-29318
- Axisymmetrical dense plasma, calculating radiation intensity radial distribution with approximate method 15 p2459 A71-32458
- Electrical conductivity of lunar rock, considering radial variation of bulk composition with oxygen loss in outer layers due to thermal cycles and vacuum 16 p2634 A71-33388
- Stresses in smooth circular cylindrical shell under radial local load applied on small area 17 p2828 A71-35303
- Plasma confinement in injector-diverter system of stellarator, measuring radial density distribution 19 p3109 A71-37131
- Radial temperature profiles of long induction discharge in argon at atmospheric pressure 19 p3111 A71-37579
- Hydrogen near-critical point flow in heated cylindrical tube, measuring flow parameters radial profiles by combination pitot tube/thermopile/hot-wire sensor probe [ASME PAPER 71-HT-25] 19 p3165 A71-37995
- RF magnetic field radial distribution measurement in thermal argon induction plasma flame 20 p3273 A71-38841
- Electric discharge carbon dioxide laser gas temperature, electron and current densities radial distribution from mathematical model 20 p3242 A71-38844
- High pervance three electrode electron gun with longitudinal compression, examining beam profiles and radial current density distributions 20 p3204 A71-39161
- Radial distribution of electric potential in Penning discharge based on relation between sulfur hexafluoride negative ions transit time and initial energy 21 p3425 A71-41281
- Radial electric field and electrostatic potential in solar wind from two fluid model 22 p3592 A71-41921
- Dynamic model for Saturn rings radial structure, considering outside composition material, Titan perturbation effect and particle space density 22 p3603 A71-42186
- Muon showers underground phenomenology in terms of density spectra, shower size and radial density distributions 22 p3594 A71-42407
- Cylindrical electromagnetic wave amplification in TWT with radial line and diverging electron flux 22 p3524 A71-42752
- Temperature field profiling along radius in front of gas turbine stage, applying to regeneratively cooled turbine engine 24 p3864 A71-45011
- RADIAL FLOW**
- Compressible flow similarity parameters, establishing dimensionless relations for radial turbomachines design 03 p0343 A71-13830
- Three dimensional nonboundary layer laminar radially inward incompressible Newtonian fluid flow between corotating disks, using integral method [ASME PAPER 70-WA/FE-4] 03 p0402 A71-14126

Anomalous low magnetospheric He alpha/proton flux ratio in terms of electrostatic radial diffusion taking into account charge exchange and pitch angle loss processes 06 p0964 A71-17284

Gas turbine cascade radial gap inverse heat transfer, calculating release coefficients 06 p1006 A71-18002

Magnetically confined laser produced plasma radial oscillations, deriving equation of motion for expanding boundary [AIAA PAPER 71-108] 06 p0938 A71-18558

Two axisymmetric jets impingement in fluid amplifiers, discussing velocity profiles of radial jet 07 p1029 A71-20592

Radial flow energy losses in rotating cylindrical cascade of inward-flow turbine wheel, determining profile losses and exit blade angle 08 p1349 A71-22044

Axial-radial and radial compressor stage optimum exit blade angle, considering flow rate control by variable pitch nozzle guide vanes 08 p1230 A71-22049

Unsteady inward and outward velocities of subsonic radial air flow between two disks, using hot-wire anemometer and cylindrical wave equation 10 p1550 A71-24000

High pressure ratio radial outflow compressor analysis, design, construction and testing 10 p1550 A71-24217

Galactic wind as steady radial perfect gas flow from stars and central gravitating source 11 p1818 A71-25207

Viscous liquid unsteady flow in long circular tube as function of mean velocity distribution, discussing radial flow and pressure distribution 11 p1749 A71-25268

Flow variation effect on velocity and flow angle distribution at exit of shrouded radial flow impeller with backward swept blades, using streamline curvature method [ASME PAPER 71-GT-15] 11 p1703 A71-25961

Two dimensional flow in radial turbomachine bladed impeller, comparing numerical solution based on potential theory with experimental results [ASME PAPER 71-GT-20] 11 p1703 A71-25964

Quasi-three dimensional method for radial flow compressor blade loadings computation, presenting combined meridional plane and blade to blade solutions for adaptation to computer [ASME PAPER 71-GT-60] 11 p1704 A71-25982

Gas dynamic test assemblies experiments for demonstrating theoretical basis of supersonic nozzle design with radial flow section 13 p1992 A71-29173

Nondimensional entrance loss equation for radial turbulent flows without swirl between parallel disks 14 p2226 A71-30415

Incompressible laminar flow between rotating and stationary disks with small gap width and radial mass flow, using Navier-Stokes and continuity equations 15 p2387 A71-31168

Gas flow behind cylindrical nozzles at roots and along periphery for narrow blades, using radial equilibrium equation 16 p2521 A71-33617

Laminar flow in incompressible fluid between rotating disk and fixed wall at small distances with radial mass stream, using finite difference method for Navier-Stokes equations 17 p2726 A71-34581

On-design performance characteristics of radial gas turbines, investigating blade geometry, rotor losses and pressure ratio effects 19 p3123 A71-38269

Motor starting techniques for 2-15 kW Brayton space power system with turbine driven radial flow compressor and Lundell type alternator 20 p3180 A71-38911

Laminar-turbulent inverse transition in divergent radial flow between two parallel flat disks 21 p3366 A71-40101

Radially symmetric shocked flows computation method, using momentum equation in conservation form in original Cartesian coordinates 21 p3368 A71-40848

Inclined radial jet drive systems for noiseless gas bearings, comparing with turbine drive device 22 p3553 A71-41681

Flow acceleration coefficient effect at inlet on centrifugal compressor wheel characteristics during axial-radial rotation 23 p3626 A71-43553

RADIAL VELOCITY

Stellar distances inaccuracy effects on kinematical parameters estimation from radial velocities 04 p0643 A71-14907

Fabry-Perot etalon and focal reducer parameters for extragalactic radial velocities measurement, comparing optical mountings 04 p0593 A71-14909

Thermal variations of all-glass and air-gap Fabry-Perot etalons for radial velocities measurement, discussing resolution 04 p0593 A71-14910

Ghost images due to reflection between interference filters and Fabry-Perot etalons during measurement of radial velocities

04 p0593 A71-14911

Stellar radial velocity measurements using Doppler shifted absorption lines, discussing cluster stars

04 p0646 A71-15227

Binary star radial velocity measurement, discussing formation, evolution, motion frequency and H-R diagram

04 p0647 A71-15242

White dwarf data, examining continuous energy distribution, degenerate star theory, mass-radius relation, spectra, radial velocities and Einstein shift

04 p0648 A71-15244

OH absorption line measurements for longitude range near galactic center, suggesting existence of radial velocity gradient

04 p0657 A71-15760

Plasma jet radial velocity distribution measurement by probe technique, calculating current density from azimuthal magnetic field via Maxwell equation [DPVLR-SONDDR-88]

05 p0788 A71-16643

Galaxy cluster expansion theory, noting dispersion in radial velocities of members

05 p0812 A71-16694

Changing rotational velocity recording device for vestibular apparatus tests, examining stimulus reaction speed

05 p0714 A71-16810

Atlas of 21 cm H I emission line profiles of outer part of Galaxy in Galactic anticenter region, plotting brightness temperature vs radial velocity

06 p0964 A71-17348

Double galaxies mass distribution from pair components motion dependence on radial velocity

06 p0966 A71-17750

Radial velocity distribution-magnetic fields connection in solar atmosphere active and quiet regions

06 p0975 A71-18437

Pulkovo observatory six channel two slit single photomultiplier rotating photographic plate magnetograph, for solar spectra polarization and radial velocities observation

07 p1109 A71-19337

Sunspot observations on 3 July and 14 September 1967, examining transverse magnetic field distribution and radial gas velocities and motion with magnetograph

07 p1195 A71-19338

External galaxies radial velocity relationship to extragalactic nebulae spectral lines red shift

07 p1200 A71-20054

Light and radial velocity curves of binary HD 175514, obtaining spectroscopic and photometric orbital elements

07 p1204 A71-20633

Solar disk active region gas development radial velocities on two levels /4 July 1966/, using double magnetograph

07 p1205 A71-20636

Galactic optical radial velocity measurements compared to 21 cm red shifts derived velocity

08 p1357 A71-20873

Zeta Aurigae chromospheric lines observed radial velocities mean variations, taking into account H ion gas acceleration, K star mass ejection and rotation

08 p1364 A71-21417

Quasi-radial hypervelocity approximation of rotating azimuthally dependent solar wind under magnetic field

09 p1515 A71-23709

Sunspot group magnetic field distribution and radial velocities, investigated at H alpha and 6302.499 A atmospheric levels

10 p1666 A71-23788

RR Lyrae type variable star statistical population indices evaluation based on space and radial velocities and position

11 p1820 A71-25247

Atmospheric wind velocity radial components measurements for meteor drift as function of wind direction, using transmitter and receiver antennas synchronized orientation method

11 p1758 A71-25791

Radial velocity fields-magnetic fields relationship in solar atmosphere active and quiet regions

12 p1955 A71-26587

Hercules galaxies cluster rotation, determining radial velocities, axis position angle and center position

12 p1962 A71-26911

Laminar source flow between rotating parallel porous disks with equal suction/injection rates solved for infinite radius series, discussing radial velocity and shear stress distributions

12 p1896 A71-27052

Nonlinear limit rotation velocity and circulation induced by wheel in axial flow turbomachine for incompressible ideal fluid, using iterative numerical algorithm [ONERA-TP-946]

12 p1866 A71-27715

Solar active region photospheric radial velocity field time variations, using magnetograph in Fe I line

14 p2308 A71-29977

Visual binary stars spectroscopic observations, discussing spectra, luminosity, parallax and radial velocities of mass center and individual stars

14 p2311 A71-30365

Radial velocity differences between components of close visual binary stars by spectroscopic and oscilloscopic measurements

14 p2311 A71-30366

Visual binaries high resolution spectroscopy, obtaining radial velocity changes with Coude spectrograph

14 p2311 A71-30368

White dwarfs from Catalog of Nearby Stars, indicating radial and tangential velocities, proper motions, positions luminosity and UVB spectra

14 p2317 A71-31009

Galactic clusters characteristics tabulation and statistical analysis, calculating dimensions, luminosity and radial velocities dispersion

17 p2804 A71-34841

Solar atmosphere mean radial velocity relation to low excitation potential based on Fraunhofer lines blue shifts observations

17 p2808 A71-35576

Supermassive double galaxy spectrographic and photometric data for cluster Abell 1775, showing radial velocity difference, visual magnitude and mass estimates

18 p2969 A71-37041

Wavelength table for determination of stellar radial velocities in spectral classes F6-M2, including Hyades cluster and Coma Berenices

19 p3144 A71-38168

Hydroxyl emission at T Tauri stars positions in Taurus-Auriga region, discussing radial velocities of stars and dust clouds

19 p3144 A71-38172

Orbital elements of W Ursae Majoris systems, considering radial velocity curves, spectroscopic orbital solution, spectral peculiarities and spectrophotometry

20 p3300 A71-39820

Radio observation for radial velocities in center region of Perseus cluster of galaxies

21 p3445 A71-40408

Spectroscopic radial velocity study of Algol eclipsing variable stars, deriving masses and apsidal motion evidence in short period orbit

21 p3446 A71-40418

B star in galactic north pole region, noting high radial velocity

21 p3448 A71-40517

Atmospheric wind velocity radial components measurements for meteor drift as function of wind direction, using transmitter and receiver antennas synchronized orientation method

22 p3533 A71-41559

H II regions kinematic properties in Large Magellanic Cloud, presenting emission line profiles and radial velocities

23 p3723 A71-42939

RADIANCE

Laser data on coherence and radiance, deriving from manufacturer specifications for application selection

02 p0261 A71-12325

Polarization and sky radiance data before, during and after 7 March 1970 solar eclipse

03 p0425 A71-13688

Mutual information between radiance of incoherently radiating object plane and field of observing system aperture, obtaining Shannon type formula

04 p0627 A71-15684

Optically thick clouds reflected light radiance and polarization for haze and nimbostratus models

05 p0781 A71-16252

Strongly coherent Nd doped glass laser development by decreasing cavity Fresnel number, discussing maximized radiance and infrared output

09 p1465 A71-23564

Graphite arc radiance temperature measurements with submillisecond resolution, using high speed photoelectric and photographic pyrometers

12 p1905 A71-26812

Earth radiance analysis by IR interferometric spectrometer of Nimbus 3 satellite, noting cloud cover as dominant variable

18 p2912 A71-36065

Earth IR radiance at 5-20 microns from interferometric spectrometer /IRIS/ aboard NIMBUS 3 satellite

18 p2912 A71-36101

Earth upper atmosphere outgoing thermal radiation radiance calculation in near IR spectrum

19 p3054 A71-37968

Global atmospheric ozone distribution from inverted radiance measurements by IR interferometer spectrometer onboard Nimbus 3 satellite

20 p3220 A71-39668

Nimbus 2 satellite observed 6.7 micron water vapor radiation, compared to calculated radiances

21 p3373 A71-40224

RADIANT COOLING

Tropical storms and cyclones development numerical simulation with ten-level model, considering radiational cooling and physical parameters effects

03 p0453 A71-14202

Nongray absorption and radiation cooling on smooth symmetric blunt bodies included in modified Maslen flow field method for radiation and large blowing

[AIAA PAPER 69-637]

05 p0694 A71-16566

Evolutionary cooling sequences and lifetimes for low mass white dwarfs in Hyades cluster, considering near surface convection in models with hydrogen envelopes

07 p1190 A71-18856

Optimal shape of single radiative cooling elements without self irradiation relative to cross sections and linear generatrices of radiator

13 p2165 A71-29179

Low density collisionally ionized plasma at equilibrium, calculating permitted, forbidden and semiforbidden radiative cooling coefficients

15 p2460 A71-32776

Radiative cooling system for nearly spherical or polyhedral bodies using radially attached diverging conical elements

17 p2836 A71-34307

Aerodynamic heating of reentry vehicle, suggesting shielding by radiative cooling

18 p2848 A71-36432

Heat shields for space applications, reviewing heat sinks, double wall cooling techniques and radiative, transpiration and ablation cooling systems

18 p2848 A71-36433

Generalized radiation cooling of convex solid, demonstrating existence of unique stable positive solution to boundary value problem related to temperature distribution

21 p3477 A71-41184

Thermal radiative cooling system characteristics determination allowing surface material thermal conductivity and blackness degree dependence on temperature

23 p3782 A71-43919

Space vehicle radiative cooling system rib temperature field calculation, taking into account material heat conductivity temperature dependence

24 p3889 A71-45023

RADIANT FLUX DENSITY

NT ELECTRON FLUX DENSITY

NT ILLUMINANCE

NT IRRADIANCE

NT LUMENS

NT LUMINANCE

NT LUMINOUS INTENSITY

NT NEUTRON FLUX DENSITY

NT PARTICLE FLUX DENSITY

NT PROTON FLUX DENSITY

NT RADIANCE

NT SOLAR CONSTANT

NT SOLAR FLUX DENSITY

Radiometric temperature measurement via source radiated power/photon flux ratio, using Planck equation variation

01 p0178 A71-10140

Galactic EM energy radiation, discussing flux upper limits in Low model

01 p0153 A71-10364

Laser light statistical properties, emphasizing time evolution of density matrix equation

01 p0094 A71-10811

Limb flares relationships to solar soft X ray bursts intensity growth phase

01 p0144 A71-10868

Solar hard X ray absorption in D region, calculating integral flux radiation

01 p0145 A71-11076

Supernovae positrons and low energy cosmic rays flux, determining ejected matter plasma properties

01 p0145 A71-11338

Diffuse galactic X ray background intensity as function of galactic scattering and discrete sources

01 p0145 A71-11345

He-Ne discharge regular oscillations effect on laser output power

02 p0259 A71-11930

Solar cell array for high radiation intensity application in Helios solar probe

02 p0191 A71-12068

Long wave radiation fluxes calculation in troposphere based on principal radiant heat transfer components separation

02 p0277 A71-12117

Spherical nebula BESM-3M radiation intensity fluxes, calculating optical thickness, particle albedos and light scattering indicatrices

02 p0312 A71-12359

Solar flare classification based on X ray intensity, offering geophysical significance advantages [AIAA PAPER 70-1370]

02 p0301 A71-12697

Hydrogen Lyman alpha radiation intensity and atmospheric absorption before and during solar eclipse of 20 May 1966, considering D region ion production

03 p0407 A71-13376

Solrad 8 satellite monitoring of Lyman alpha and UV radiation, discussing flux variation at 1080-1350 Å 03 p0479 A71-14043

Forbush decreases vertical cutoff rigidity dependence, comparing cosmic ray intensities from Pioneer 8 detector and ground based neutron monitors 03 p0481 A71-14501

Cosmic ray data, showing perpendicular density gradient to ecliptic plane 03 p0482 A71-14547

Radiation intensity produced by inverse Compton effect between solar flux and Van Allen belt trapped high energy electrons 04 p0640 A71-14875

Intensity correlation functions as parameters for cosmic radiation activity 04 p0640 A71-15086

Pulsar radiation intensity time variations at radio frequencies, noting observations of CP 1133 04 p0649 A71-15273

Crab Nebula pulsar NP 0532, examining radio pulse shapes, flux densities and dispersion 05 p0800 A71-15926

Gamma radiation flux distribution and spectral composition by satellite observation, analyzing background effects 05 p0798 A71-16047

Near space annihilation gamma radiation intensity and spectral energy composition by satellite observation, considering possible antimatter nature of comets and meteor streams 05 p0798 A71-16048

Si solar cell low temperature low solar illumination intensity I-V performance deficiencies, considering corrective design modifications 05 p0701 A71-16073

Helios solar probe satellite solar array techniques for high temperature and illumination intensity 05 p0702 A71-16080

X ray source Sco X-1 gamma radiation due to Compton synchrotron process, comparing flux observation for synchrotron origin validity 05 p0799 A71-16476

Chemiluminescent NO-O reaction spectral radiant intensity and absolute rate constant redetermination in premixed gaseous free jet and hydrogen flame atmosphere 05 p0837 A71-16568

Forbush midlatitude microdecreases effects on diurnal cosmic ray intensity, using neutron monitor 05 p0799 A71-16624

H II regions compact radiation sources flux densities observation at centimeter wavelengths 05 p0812 A71-16690

North Galactic Pole soft X ray flux measurements, using Teflon windowed proportional counter 05 p0799 A71-16699

W, Nb, Mo and Ta spectral radiative power at wavelengths from 0.66 to 5.12 μm at various high temperatures 05 p0768 A71-16780

Semidiurnal variation of galactic cosmic ray intensity, using neutron and meson monitor data 05 p0800 A71-17008

Atmospheric path effects on spectral radiance intensity in remote airborne multispectral sensors 06 p0898 A71-17559

Absolute intensities measurement method for spectrum of solar disk center at 2962-4087 Å 06 p0967 A71-17902

Interplanetary cosmic ray gradients and anisotropies from Pioneer 8 probe 06 p0952 A71-18111

Solar cosmic ray intensity yearly variation by pressure corrected neutron monitor, discussing atmospheric temperature effects, coronal emission heliolatitude distribution and annual wave amplitude 06 p0953 A71-18117

Solar activity correlation with cosmic ray intensity and solar wind properties, analyzing hysteresis diagrams for wind modulation characteristics dependence on heliolatitude 06 p0954 A71-18123

Cosmic ray mu meson intensity power spectrum frequency dependence, comparing to interplanetary field spectra 06 p0954 A71-18125

Cosmic ray intensity variations from magnetic fields of micrometeor streams in interplanetary plasma 06 p0954 A71-18126

Cosmic ray solar modulation anisotropy during 23 March 1966, 25 May 1967 and 26 January 1968 events in preForbush phase, evaluating multidirectional meson observations 06 p0956 A71-18138

Cosmic ray intensity Forbush decrease on 23 September 1966 coincidence with magnetic storm sudden commencement from satellite and ground based monitors data 07 p1184 A71-18750

Vertical planes at various points on lunar surface, calculating radiant energy fluxes 07 p1191 A71-18906

Planetary atmospheres radiant energy fluxes, developing validity of isolated line approximation in finite spectral intervals 07 p1191 A71-18908

Backscattered radiation energy during laser beam scanning of diffusely scattering surface 07 p1123 A71-19309

Atmospheric refractive index diurnal and seasonal variations determination by measuring He-Ne laser radiation intensity through turbulent inhomogeneous atmosphere 07 p1061 A71-19374

Electromagnetic and thermal energy fluxes during magnetic storms, using interplanetary spacecraft and D variation data 07 p1099 A71-19397

Cosmic ray intensity mean diurnal variation, taking into account angle between solar corotational velocity and earth equatorial plane 07 p1187 A71-19683

Near equilibrium shock layers nonequilibrium radiant emission calculation, noting application to Mars entry conditions [AIAA PAPER 70-773] 07 p1091 A71-19914

Laser beam evaporation of dense substances, examining luminous flux densities with gas dynamic equations 07 p1127 A71-20253

Radio telescope measurements of circular polarization and total flux of Jupiter at 13.1 cm wavelength 08 p1357 A71-20871

Long term fluctuations in pulsar radiation intensity due to interstellar scintillation 08 p1359 A71-20935

Low energy cosmic X ray observations, examining diffuse background and absolute flux values 08 p1349 A71-20936

Primary gamma radiation flux measurement, using spark chamber on satellite 08 p1350 A71-20954

Cosmic ray modulation processes, spectrum variation and intensity restoration delay, discussing solar activity indices and wind models 08 p1351 A71-20965

Interplanetary space cosmic ray density gradient from three dimensional anisotropic diffusion model 08 p1352 A71-20970

Galactic cosmic ray density space-time variations in interplanetary space with solar wind, using spherically symmetrical model with diffusion approximation 08 p1352 A71-20974

Galactic cosmic ray density modulation by solar wind, assuming heliolongitudinal asymmetry 08 p1353 A71-20975

Solar activity heliolongitudinal distribution effect on interplanetary space electromagnetic conditions governing galactic cosmic ray intensity 08 p1353 A71-20977

Cosmic ray intensity annual variations relationship to heliolongitudinal solar activity index HL, providing hysteresis curves for effective angular width parameter estimation 08 p1353 A71-20978

Atmospheric excess radiation flux azimuthal asymmetry in equatorial region, discussing angular intensity distribution data from Proton 2 Cerenkov counter 08 p1354 A71-21011

Solar X-ray flare region structure and emission flux density and spectral composition, using satellite-borne photometers and spectroheliographs 08 p1354 A71-21014

Aircraft altitude cosmic ray intensity measurements in lower atmosphere by neutron monitor, considering long term nucleonic intensity variations 08 p1355 A71-21629

Low energy cosmic ray intensity increase at propagating interplanetary shock wave front, discussing one dimensional model with particles undergoing convection and diffusion 08 p1356 A71-21630

Solar radiation flux standard instruments development for meteorological measurements, discussing calorimetric techniques and high precision radiometers 08 p1293 A71-21737

Radio source OZ-252 radiant flux density spectrographic observation, noting quasi-stellar object emission spectra 09 p1516 A71-22065

Radiant flux diffraction effectiveness of amplitude holograms with allowance for nonlinearity of photomaterial 09 p1442 A71-22400

Interplanetary magnetic field inhomogeneities structure from galactic cosmic rays intensity fluctuations observation 09 p1513 A71-22424

Primary cosmic gamma-quanta fluxes measured using telescope consisting of Cerenkov counters 09 p1513 A71-22556

Solar activity effects on midlatitude upper atmosphere corpuscular radiation intensity studied by rocket sounding 09 p1513 A71-22580

Cosmic ray and radiation belt data from vertical probes, determining radiation in instantaneous cross section of atmosphere 09 p1513 A71-22666

Optimum mounting angles for direct solar radiation flux on solar battery on circular orbit satellite 09 p1386 A71-22673

Predicted UV fluxes for main sequence stars, comparing stellar observations with models described by Kucz, Carbon and Gingerich 09 p1522 A71-22962

Giant elliptical galaxy Maffei I continuous radiation emission data at 1415 MHz, examining radio luminosity magnitude 09 p1523 A71-22982

Earth intrinsic radiation flux incident angular coefficient, examining effect on partially screened flat spacecraft elements 09 p1546 A71-23154

Solar surface radiation brightness and intensity for different disk regions and wavelengths 09 p1526 A71-23419

Soft X ray radiation correlations to radio emission flux at various frequencies in 20th solar activity cycle 09 p1515 A71-23529

Balloonborne radiometric instrumentation for solar and thermal radiations upward and downward flux measurements, discussing net radiation balance as function of solar elevation 09 p1515 A71-23558

Interplanetary shock waves sounding and geomagnetic storm forecasting based on cosmic ray intensity increases from ground observations 09 p1515 A71-23633

Twenty-seven day variation and cosmic ray intensity modulation relationship, examining 11 year variation from superposition of transient decreases 10 p1660 A71-23800

Flux density measurements of Ohio radio source survey at 1415 MHz compared with 1400 MHz measurements by Australian National Radio Astronomy Observatory telescope 10 p1668 A71-23881

Intensity variations of Cygnus X ray sources, analyzing high resolution results of Adelaide and Tasmania universities 10 p1661 A71-23882

Negative sudden phase anomalies, related signal strength enhancements and short wave fadeouts, considering maximum flux density of solar X-ray flares 10 p1575 A71-23883

Neutrino luminosity in strongly magnetized degenerate relativistic electron gas plasma from URCA energy loss rate calculations 10 p1671 A71-24303

Polar cap cosmic radiation intensity measurement for deducing electromagnetic conditions near earth and in interplanetary space 10 p1661 A71-24310

Spherical harmonics differential approximation generalized from one dimensional radiation specific intensity angular dependence Jacobi polynomial expansion 10 p1696 A71-24536

Extensive air showers and multiple muons frequencies, considering parent pions mean transverse momentum, multiplicity law form and primary cosmic ray intensity 10 p1664 A71-25046

Horizontal electric dipole gain dependence on height above plane lossy earth, deriving radiation intensity expression from Hertzian potential integral representation 11 p1730 A71-25249

Solar X-ray and radio fluxes at earth for high order temperatures by free-free transitions and Maxwell electron velocities in corona 12 p1947 A71-26770

Universe UV radiation intensity, estimating inverse Compton effect interaction of cosmic relativistic electrons with relict radiation 12 p1948 A71-27079

Earth surface formations and clouds angular brightness distribution based on reflected solar radiation intensity 12 p1901 A71-27102

Cosmic ray storm analysis, showing enhanced daily/shortlived variations, radiation intensity increase and solar flare observations 12 p1949 A71-27375

Cosmic radiation nucleonic component intensity diurnal variations relation to solar activity semiperiod 12 p1950 A71-27378

Soft solar X-ray bursts characteristics, discussing temporal and intensity differential distributions, flux measurements and decay time 12 p1953 A71-27654

Uniformly spaced linear arrays directivity as function of spacing, scan angle and current distribution, approximating element radiation intensity 13 p2028 A71-28000

Radiation intensity spatial dependence on laser polarization, giving three dimensional model for wave function phase calculation 13 p2077 A71-28046

- Transverse mode locking effect on radiation intensity of injection semiconductor laser as function of time and p-n junction refractivity 13 p2077 A71-28172
- Sky radiation background stellar component in far UV spectral region, determining intensity with Venera instruments 13 p2133 A71-28200
- Cosmic ray density distribution inside modulating spherical cone over long-lived solar wind regions, noting modulation depth quasi-periodic variation 13 p2129 A71-28550
- F 2 layer critical frequency variations relation to solar radio flux intensity, using mathematical approximations 13 p2062 A71-28557
- Long term pulsar intensity observations, noting periodic variations and power spectrum analysis 13 p2143 A71-29270
- Galactic cosmic ray intensity solar diurnal and semidiurnal variations outside magnetosphere 13 p2131 A71-29437
- Photometric IR observations of Nova Serpentis 1970, showing visual flux decrease 14 p2303 A71-29576
- Interstellar grain temperatures, considering radiant energy distribution and optical properties effects 14 p2305 A71-29679
- Magnetic cutoff variations during geomagnetic storm from counting rates of neutron monitors, noting cosmic ray intensity augmentation 14 p2298 A71-29748
- Flux estimates of gamma quanta with energies of 5 TeV from celestial objects due to bremsstrahlung and inverse Compton scattering of relativistic electrons 14 p2299 A71-29985
- Solar radio emission at 3.15 cm wavelength via 22-meter radio telescope, determining relation between source brightness and areas of sunspot groups 14 p2299 A71-29990
- Aries-Taurus region as soft X ray source, determining energy flux and source 14 p2301 A71-30426
- M87 nucleus radio flux density variations observation at 5 GHz 14 p2301 A71-30451
- Primary cosmic rays spectrum and intensity data in 4 to 10 BeV range, evaluating albedo particle effects 14 p2301 A71-30590
- High energy X ray flux from source in Centaurus Crux detected by balloon sounding 14 p2303 A71-30654
- Rapid fluctuations in high energy X ray flux from source in Centaurus Crux from balloon sounding 14 p2303 A71-30655
- Noise measurements on discrete radio sources spectra, studying Cas A and Cyg A flux density ratio 14 p2316 A71-30975
- Far zone field and radiated power equations for corner driven traveling wave loop antenna in warm plasma, comparing data for Ariel 3 satellite 14 p2283 A71-31040
- Positions and flux densities of radio sources from Fourth Cambridge catalog by pencil beam measurements at 408 MHz, using Molonglo telescope 15 p2485 A71-31697
- Cosmic ray mean intensity drop observation after Forbush decrease, noting rigidity dependence and daily variation from exponential recovery curve 15 p2474 A71-31777
- Cosmic ray intensities investigation by worldwide neutron- and supermonitors network, obtaining density and three dimensional current values 15 p2478 A71-31807
- Isotropic cosmic gamma ray flux, discussing extragalactic point sources detection by high resolution spectrometers 15 p2478 A71-31837
- VLF atmospherics integrated intensities changes probably due to ionization by meteors 15 p2371 A71-31839
- Cosmic ray intensity gradient measurement from Lost City meteorite Ar 37/Ar 39 ratio 15 p2479 A71-32361
- Axisymmetrical dense plasma, calculating radiation intensity radial distribution with approximate method 15 p2459 A71-32458
- Solar microwave bursts spectrum, calculating maximum radiation fluxes and frequencies from statistical data 15 p2480 A71-32749
- IR stars and galaxies measurements, determining 3.5 mm continuum radiation intensity 15 p2498 A71-32775
- Rayleigh scattering planetary atmosphere radiative transfer equation, calculating phase curves for flux and polarization 15 p2498 A71-32778
- Radiation flux calculation and divergence in regions with stepwise temperature and chemical composition distribution 16 p2661 A71-32798
- Cosmic ray annual intensity variations indicating gradient perpendicular to solar equatorial plane 16 p2625 A71-32801
- Equatorial airglow enhancement data, observing 6300 and 5577 A intensity variations 16 p2562 A71-32809
- W, Nb, Mo and Ta spectral emissive power at wavelengths from 0.66 to 5.12 μ m at various high temperatures 16 p2591 A71-33032
- Cygnus-X region radio photography, presenting radio brightness intensity modulated display supplementing contour map 16 p2630 A71-33124
- Pulsating gamma ray flux from pulsar NP 0532 in energy range from 250 keV to 2.3 MeV 16 p2626 A71-33389
- Gamma radiation flux distribution and spectral composition from Cosmos satellite observation, analyzing background effects 16 p2626 A71-33451
- Near space annihilation gamma radiation intensity and spectral energy composition by Cosmos satellite observation, considering possible antimatter nature of comets and meteor streams 16 p2626 A71-33452
- Upper atmosphere atomic hydrogen H sub alpha emission, correlating intensity and hydroxyl vibration temperature 16 p2564 A71-33665
- Ionospheric geocoronal L sub alpha emission intensity related to solar activity level from Cosmos 215 satellite data 16 p2564 A71-33667
- Background phonon X ray and gamma quanta intensities dependence on solar activity from Geiger counter recordings in outer space 16 p2626 A71-33675
- Optically dense plasma spectral characteristics, calculating reabsorbed line intensity distribution 16 p2619 A71-33707
- Altitude variation of forbidden line of 5577 A and 3914 A auroral emissions intensities ratio from rocket sounding 16 p2566 A71-33748
- Corpuscular flux intensities in upper atmosphere from meteorological rocket measurements in polar arctic region, discussing altitude-time dependence 16 p2627 A71-33777
- Solar modulation origin of sidereal diurnal variation in cosmic ray intensity anisotropies as function of interplanetary field direction, using underground muon telescopes 16 p2628 A71-33931
- Pulsating auroral patches with sudden intensity dependent spatial expansion, noting relation to triggering instabilities of precipitating electron beam 16 p2573 A71-33954
- Cyg X-1 X ray intensity and energy spectrum variation data, using balloon-borne telescope 16 p2629 A71-34076
- Pulsar emission data, presenting average phase shapes and pulse to pulse intensity fluctuations 17 p2797 A71-34372
- Large amplitude periodic X ray pulsations from Centaurus X-3, observing abrupt source intensity and pulse rate changes 17 p2798 A71-34375
- Convective flow at stagnation point relation to radiation flux decrease as result of absorption in cold boundary layer 17 p2671 A71-35259
- Critique of Vela 4 scattered Lyman alpha experiment, discussing maximum flux region and radiation intensity 17 p2805 A71-35380
- Extragalactic objects luminosity upper limits in hard gamma ray band, using Cosmos 208 scintillation Cerenkov telescope 17 p2796 A71-35736
- Gas flow energy transport, discussing thermal radiation, radiant flux density, planetary atmosphere entry, thermodynamic equilibrium and differential approximations 18 p2847 A71-36426
- Supermassive double galaxy spectrographic and photometric data for cluster Abell 1775, showing radial velocity difference, visual magnitude and mass estimates 18 p2969 A71-37041
- Optically identified B2 radio sources at 5 GHz, presenting flux density measurements, spectral index and visual identity 18 p2970 A71-37066
- Discrete galactic and extragalactic radio sources observations at 3.3 mm, detailing flux and variability measurements 18 p2970 A71-37067
- Light curve and apsidal motion of AR Cas from photoelectric photometry 18 p2971 A71-37069
- Universe UV radiation intensity, estimating inverse Compton effect interaction of cosmic relativistic electrons with relict radiation 19 p3126 A71-37429
- Electromagnetic and thermal energy fluxes during magnetic storms, using interplanetary spacecraft and D variation data 19 p3053 A71-37821
- Radiation energy density and radiation heat flux in small rectangular cavity, assuming modes excitation spectrum according to Planck distribution function [ASME PAPER 71-HT-16] 19 p3164 A71-37987
- NO, CO and Ar mixtures IR spectral emission radiant intensities behind shock tube generated reflected shock waves 19 p3012 A71-38087
- Earth radiation flux spectral intensity measurements, noting latitudinal distributions, day and night variations and oceanic and continental curves 19 p3056 A71-38355
- Power density prediction based on electromagnetic compatibility analysis of radar environments, comparing predicted propagation losses with measurements 19 p3021 A71-38455
- Peak optical flux density for catastrophic damage in close confined and double heterojunction injection Al-GaAs-GaAs lasers 19 p3075 A71-38507
- True central intensities of Fraunhofer lines, describing solar telescope and Czerny-Turner spectrometer 19 p3146 A71-38661
- Solar limb D3 He line intensity distribution measurements during eclipse of 22 September 1968 19 p3147 A71-38666
- Stray-light and sunspot intensity measurements of sunspot umbra and aureole during Mercury transit 19 p3147 A71-38668
- Sunspot intensity during 9 May 1970 Mercury transit with corrections for scattered light from solar limb observations 19 p3147 A71-38669
- Stray radiant flux effects on scanning IR radiometer for low temperature objects measurement 19 p3067 A71-38706
- Forbush decreases comparison with 11 year cosmic ray intensity variation, examining rigidity dependence and modulation functions 20 p3277 A71-38742
- Pulsar periods change rate and radio luminosity decay, discussing magnetic field braking 20 p3286 A71-38762
- Crab pulsar NP 0532 low energy gamma radiation emission data, observing flux ratios and pulsations 20 p3278 A71-39109
- Cygnus XR-1 X ray intensity fluctuations, discussing time scales and periodicities 20 p3278 A71-39111
- Daylight photometric flux derivation from filtered measurements of global sun and sky radiant energy, using natural illumination and short wave radiation relationship 20 p3234 A71-39175
- Automatic single beam recording spectroradiometer system for measurements of spectral irradiance, radiance, transmittance and reflectance 20 p3235 A71-39176
- Sunspot number relationship with solar radio flux, using cross spectral method for high and moderate activity periods 20 p3279 A71-39324
- Gamma ray production by pulsar-emitted particles interaction with surrounding nebula matter, investigating radiation intensity time variation 20 p3279 A71-39325
- Atmospheric excess radiation flux azimuthal asymmetry in equatorial region, discussing angular intensity distribution data from Proton 2 Cerenkov counter 20 p3279 A71-39591
- Solar X-ray flare region structure and emission flux density and spectral composition, using satellite-borne photometers and spectroheliographs 20 p3280 A71-39594
- Short wave radiation fluxes estimation for earth-atmosphere system from Cosmos satellite data, studying brightness field angle structure 20 p3260 A71-39681
- Mesospheric soft corpuscular radiation flux and temperature rocket observations, during solar flare activity 20 p3222 A71-39704
- Primary cosmic rays high energy gamma ray intensity spectrometric measurements onboard Cosmos 208 satellite, allowing for charged particles effects 20 p3283 A71-39753
- Trapped protons flux vs L profile measurement onboard sounding rocket near equator, comparing results with calculation from neutron albedo source and atmospheric losses 20 p3284 A71-39881
- Rhea and Titan UBV photoelectric observations, obtaining light curve magnitude variation 21 p3440 A71-40056
- Radio telescopic observations of Jupiter, Venus and radio source 3 C 273 at 2 and 8 mm wavelengths, determining brightness temperatures and radiation flux densities 21 p3445 A71-40258

Thin-shelled ensemble of noncolliding stars surrounding black hole, calculating spectral flux density and brightness

21 p3446 A71-40420

Seyfert galaxy micron photometry measurements, determining IR radiation flux changes with time

21 p3449 A71-40611

Cen X-3 source X ray flux periodic variations due to white dwarf star radial vibrations based on nonrotating model

21 p3449 A71-40613

Radiant monatomic gas flux boundary conditions derivation, considering all points in local thermodynamic equilibrium

21 p3475 A71-40660

Photometric determination of solar granulation rms intensity fluctuation, using ground telescope

22 p3596 A71-41453

Solar flares gamma ray flux, describing production by downward moving high energy particles

22 p3590 A71-41468

Diffuse 0.2-2 keV cosmic X ray flux, discussing energy spectrum and spatial distribution

22 p3591 A71-41914

Cosmic ray transport in random magnetic fields, deriving coupled integrodifferential equations for radiant intensity and flux

22 p3592 A71-41915

Astronomical polarimetry at 5 and 10 microns for intensity measurements of IR sources

22 p3545 A71-42147

Cosmic ray muons absolute intensity determination, using Durham vertical spectrograph

22 p3593 A71-42353

Variations in 10 micron flux from NGC 1068, noting strong nucleus emission modulation

22 p3605 A71-42397

Southern pulsars pulse energy flux average nightly values at 80 MHz

22 p3606 A71-42602

Astronomical radio sources from Parkes catalog, calculating daily and hourly variations in flux density

23 p3722 A71-42937

Two dimensional maps of circularly polarized solar emission at 7.8 GHz, noting flux density and polarization time dependence before flare

23 p3732 A71-43072

Scorpius X-1 X ray flux observations, noting high frequency oscillations responsible for radiation production

23 p3733 A71-43078

Linearly and circularly polarized electromagnetic field effective scattering surfaces relationships determination as value proportional to reflected and transmitted rms flux density ratio

23 p3644 A71-43285

Radiant flux from finite cylindrical volume to coaxial screen calculated under quasi-homogeneous medium and arbitrary optical thickness assumptions

23 p3782 A71-43920

Planetary nebulae microwave radiation emission survey by Algonquin Radio Observatory, determining flux densities

23 p3769 A71-43988

Mode changing in pulsar radiation, observing intensity profiles and polarization characteristics

23 p3769 A71-43995

Cygnus X1 short term X ray flux pulsation variability from Southern Hemisphere sounding rocket flight

24 p3865 A71-44445

Cloud and precipitation effects on radio echoes intensity measurement, discussing pulse dimensions influence on average signal magnitude

24 p3845 A71-44881

Radio echo average power measurement errors due to clouds

24 p3845 A71-44882

Pulsar CP 0950 radio emission intensity variation measurement, using dispersion removal technique for interstellar medium signal distortion

24 p3871 A71-44903

Ohio catalog radio source spectra and positions, presenting flux density and RMS errors

24 p3871 A71-44913

Laser radiation intensity modulation by time varying magnetic field

24 p3834 A71-45055

Radiation flux induced material dispersion of solid surface, taking into account radiation energy absorption by discontinuity introduction

24 p3835 A71-45225

RADIANT HEATING

F region electrons heating by RF energy at or near ionospheric plasma frequency, detecting temperature changes via optical nightglow intensity variations

01 p0040 A71-11533

Ionospheric modification by electrons radiant heating, discussing effects on 1.27 micron radiation

01 p0078 A71-11534

Ionosphere artificial Joule heating by RF energy, deriving expressions for deposition function frequency dependence

01 p0040 A71-11538

Laminar flow of liquid in duct with zero heat resistance of walls, calculating temperature distribution during radiative convective heating

03 p0519 A71-13745

Temperature field of radiation heated bodies, using analytic method based on backradiation law approximation by linear function with limit error in Stark range

03 p0519 A71-13746

Two dimensional incompressible laminar boundary layer flow along ablative blunt body in irradiant environment

04 p0679 A71-15467

Heat conduction three dimensional problem in radiation heated thin crystalline plates with temperature dependent thermophysical characteristics

05 p0831 A71-16184

Microwave radiation nonthermal biological damage, describing beetle pupae irradiation and radiant heating experiments

11 p1717 A71-25285

Calorimetric determination of reactor gamma source heating as function of specimens thickness and atomic number, discussing slab and cylindrical geometrical effects

11 p1797 A71-26078

Reentry heating simulation, noting UV radiation effects as shock layer thickness decreases

[AIAA PAPER 71-467]

11 p1859 A71-26248

Haze scattering effect on solar radiative heating rate due to water vapor absorption in near IR

17 p2736 A71-35561

Atmospheric radiant heat influx spectral distribution, evaluating vertical profiles of short wave radiation and aerosol effects

19 p3047 A71-37281

RADIANT INTENSITY

U RADIANT FLUX DENSITY

RADIATION ABSORPTION

NT ATMOSPHERIC ATTENUATION

NT AURORAL ABSORPTION

NT ELECTROMAGNETIC ABSORPTION

NT MOLECULAR ABSORPTION

NT PHOTOABSORPTION

NT POLAR CAP ABSORPTION

NT SELF ABSORPTION

NT ULTRAVIOLET ABSORPTION

NT X RAY ABSORPTION

Heat conduction effect on propagation of laser radiation absorption shock wave

01 p0092 A71-10068

Hot stellar atmospheres, calculating mean radiation absorption coefficients as function of temperature and electron pressure

01 p0158 A71-10805

Early phase model of F region heating and hydrodynamic expansion by deviative absorption of radio waves

01 p0040 A71-11530

Fat lean cellular and bone mineral mass determination in living bodies, using radiation absorption spectrometry

02 p0210 A71-12954

Ultrasonic absorption in hydrogen sulfide, measuring vibrational and rotational relaxation times as function of temperature

03 p0459 A71-13718

Cosmic rays intensity measurement in deep ocean with Cerenkov counter, determining Muon energy spectrum and absorption in water

03 p0477 A71-13862

Radiation absorbing detonation waves calculation by finite difference techniques based on pseudoviscosities

03 p0439 A71-14064

Visible radiation absorption by aerosol particles, noting gray absorption and imaginary portion of complex index of refraction

04 p0582 A71-15072

Thermal radiation absorbing and emitting medium in flow between parallel plates, examining heat transfer for simultaneous radiation and convection

04 p0685 A71-15517

Solar Lyman alpha radiation absorption by molecular oxygen, examining optical thickness with Intercomos-1 satellite

05 p0807 A71-16214

Nongray absorption and radiation cooling on smooth symmetric blunt bodies included in modified Maslen flow field method for radiation and large blowing

[AIAA PAPER 69-637]

05 p0694 A71-16566

Interaction between radiation from shock wave region and oncoming cold air flow in hypersonic flow past blunt body

07 p1014 A71-19730

Gas laser optical pumping based on photodissociation, calculating spatial temporal distributions of pump radiation absorption probability and main level population

07 p1125 A71-19806

Radiant heat transfer from heated cylindrical enclosure with black/gray walls to absorbing gas or gas having black particles, calculating absorption coefficients

07 p1224 A71-20018

Self focusing in media with resonance absorption, determining simulated Raman scattering threshold in bleachable absorbers as function of absorber concentration

07 p1161 A71-20381

Far IR cryogenic black paints absorptive throughout IR with surface stability at liquid He temperature and resistance to abrasion and flaking

08 p1335 A71-21383

Type 2 and 3 solar radio bursts, discussing models without reabsorption

08 p1356 A71-21755

Middle latitude night E region ionization, describing solar EM and corpuscular radiation absorption effects

08 p1286 A71-21853

Heat conduction effect on propagation of laser radiation absorption shock wave

09 p1464 A71-23263

Xe flash tube discharge saturable absorption effects, using YAG-Nd laser radiation for plasma attenuation measurements

09 p1465 A71-23484

Boundary layer equations for radiating and absorbing gas flow at large Reynolds numbers

10 p1593 A71-24367

Extinction parameters of submicron carbon, tungsten and Si particles in hydrogen measured at various temperatures, discussing scattering amplitude functions and Monte Carlo calculations

[AIAA PAPER 70-838]

11 p1854 A71-25507

HF electromagnetic waves absorption as function of discharge current intensity in ionized H, using gas pressure or uniform magnetic field as parameters

11 p1805 A71-25598

Observational test of Planck constant variation on cosmic scale in terms of radiation absorption by interstellar and intergalactic gases

11 p1832 A71-26183

Low resolution measurements of IR absorption of sulfur dioxide at room temperature

[ASME PAPER 70-WA/HT-4]

13 p2025 A71-28979

Rotational line overlap effect on laser IR radiation absorption in high pressure carbon dioxide, comparing calculated absorption coefficient with measurements

13 p2081 A71-29337

Cosmic radio noise absorption measurements at subauroral latitude for ionospheric absorption, discussing ionization regions spatial nonuniformity and horizontal extension

14 p2196 A71-30561

Black radiation absorption by isothermal gas in entire spectrum, discussing Hotel empirical formula

17 p2836 A71-34214

Atmospheric absorption of 10.6 micron laser beam radiation, noting effect on refractive index

18 p2910 A71-35843

Synchrotron radiation reabsorption in inhomogeneous sources, considering IR spectra of quasars and galactic nuclei

18 p2963 A71-36158

Gas dissociation in carbon dioxide laser by IR absorption method, investigating role in population inversion

18 p2932 A71-37008

Excited state absorption in sulfur hexafluoride traversed by carbon dioxide laser beam

18 p2933 A71-37014

Interstellar absorption at H alpha line wavelength in Orion nebula, obtaining contour map for comparison with radio intensity

19 p3131 A71-37230

Collisional broadening of IR absorption lines in vibration-rotation bands of carbon monoxide and hydrochloric acid

19 p3106 A71-37374

Argon plasma electron temperature by laser absorption and electron density measurements

19 p3110 A71-37406

Extragalactic background soft X ray diffuse flux consistent with absorption by Small Magellanic Cloud

20 p3278 A71-39108

Soviet book on optically dense plasma spectroscopy covering radiation reabsorption, transport equation, photon frequency, resonance energy, quantum mechanical calculations and spectral characteristics

20 p3274 A71-39145

Atmospheric optical stability control in ozone or other selectively absorbing gases measurements, filtering out spurious scattered light from aerosol particles

20 p3257 A71-39331

Young dust-filled planetary nebulae models with hot central stellar black body radiation, evaluating IR radiation absorption and reradiation in H region

21 p3446 A71-40417

Venus 3-4 micron region continuum absorption from high resolution spectra of Venus and sun

21 p3448 A71-40448

Traveling wave power resonances in ring laser with nonlinearly absorbing cell, noting role of absorbing component lamb saturation

21 p3394 A71-41257

Quantum theory of molecular or atomic spontaneous emission while simultaneously undergoing stimulated emissions or absorptions

21 p3421 A71-41401

- Interstellar Lyman alpha absorption equivalent widths in hot stars spectra, examining rocket and satellite observations
22 p3598 A71-41913
- UV and IR transmissivity and absorption coefficients of fused quartz between room temperature and 1500 C
22 p3565 A71-42559
- Cosmic rays intensity measurement in deep ocean with Cerenkov counter, determining muon energy spectrum and absorption in sea water
22 p3595 A71-42663
- UV absorber dyes in fluorescent tracers, discussing theory of dimensional sensitivity and use in liquid-film developers to quench background fluorescence
23 p3681 A71-43194
- Carbon dioxide photolysis at 1849 A and various pressures, suggesting gas dissociation at wavelengths with appreciable absorption
23 p3641 A71-43328
- Venusian atmosphere, observing dayside solar radiation absorption generated upward dayside and downward nightside vertical motions
23 p3735 A71-43333
- Jovian geometric albedo at 1800-1950 A decrease explained as absorption by gaseous and solid ammonia in cubic crystal form
23 p3736 A71-43345
- Monochromatic absorption coefficients determination for Ar heated in wall-stabilized arc at high temperatures and pressures
23 p3712 A71-43915
- Quasar and pulsar gamma ray absorption by critical energy collisions with low energy photons
24 p3866 A71-44917
- ## RADIATION BELTS
- NT INNER RADIATION BELT
NT OUTER RADIATION BELT
NT PROTON BELTS
- Jupiter decimetric emission circular polarization, observing equatorial magnetic field strength in radiation belt
02 p0317 A71-12868
- Intercoms 3 satellite for radiophysical and geophysical observations of radiation belts and ionosphere, discussing design, configuration and instrumentation
03 p0423 A71-13419
- C, N and O nuclei abundances in radiation belt near geometric equator, using data obtained by OGO-5 satellite in 1968
03 p0473 A71-13475
- Radiation intensity produced by inverse Compton effect between solar flux and Van Allen belt trapped high energy electrons
04 p0640 A71-14875
- Zone of unstable radiation in magnetosphere localizing auroral and quasi-captured particles
05 p0798 A71-16046
- Plasma containment in adiabatic magnetic traps, discussing particles, Coulomb collisions, instabilities, cyclotron resonance masers, Van Allen belts, etc
07 p1166 A71-19097
- Soviet book on active protection of space vehicles covering measures against penetrating radiation from Van Allen belts, solar flares and galactic cosmic rays
07 p1207 A71-19474
- Temporal intensity variations of geomagnetically trapped solar alpha particles from Injun 5 observations
08 p1356 A71-21644
- Electron loss by resonant interaction with whistlers in nonuniform magnetic field, taking Fokker-Planck equation as distribution function
09 p1513 A71-22423
- Cosmic ray and radiation belt data from vertical probes, determining radiation in instantaneous cross section of atmosphere
09 p1513 A71-22666
- Geomagnetically trapped particles radial diffusion across L shells, considering influence on steady state structure and dynamics of radiation belts
09 p1514 A71-23460
- Solar cycle time variations in trapped radiation belt proton flux, deriving proton transport equation from Boltzmann equation
10 p1663 A71-24785
- Earth radiation belts high energy electron flux intensity monotonic decrease during magnetically quiet periods from satellite data analysis
11 p1816 A71-25759
- Solar wind effects on space around earth, discussing dipole image of magnetic field, radiation belt feeding and atmospheric phenomena based on artificial satellite observations
11 p1817 A71-26337
- Soviet book on earth radiation belts and cosmic rays covering space-borne experiments, Van Allen belt, charged particle motion, origin hypotheses, etc
11 p1818 A71-26525
- Energetic charged particle motion in magnetosphere, considering radiation belt dynamics
12 p1949 A71-27372
- Magnetospheric electron echo probe experiment, using sounding rocket and injecting gun for controlled particle trapping investigation
12 p1953 A71-27674
- Charged particles magnetic scattering on cyclotron instability waves of radiation belt plasma, estimating proton relaxation time
13 p2129 A71-28552
- Trapped charged particle cyclotron, bounce and drift motion in distorted geomagnetic field
14 p2300 A71-30033
- Charged particles distribution in magnetosphere beyond radiation belts, proposing unstable radiation zone model containing auroral and semitrapped particles
16 p2626 A71-33450
- Electron lifetime in earth radiation belt due to resonant scattering with hiss VLF radiation
16 p2626 A71-33674
- Van Allen radiation belts and plasma sheet energy loss control, using cold plasma injection
16 p2629 A71-33976
- Radiation belt proton intensities and energy spectra measurements by Azur satellite solid state detector telescope with energy level discrimination electronics
19 p3125 A71-37417
- Energetic electrons, protons and alpha particle measurements by Azur satellite over polar cap and in radiation belt during March 1970 solar particle event
19 p3126 A71-37419
- Pioneer Jupiter probe missions as precursor to subsequent outer planets exploration, discussing primary objective of asteroid belt and Jupiter radiation belt hazards evaluation
19 p3152 A71-37911
- Jupiter radio observations, measuring nonthermal emission, magnetic field and trapped radiation belts
19 p3140 A71-37933
- Cosmic rays and solar energetic particles properties near earth and requirements on measurement during outer planets missions
19 p3127 A71-37940
- Cosmos satellite data on mainland China thermonuclear explosion of 27 December 1968, observing radiation effects on particles in natural radiation belts
20 p3278 A71-39128
- Magnetospheric electrons and protons acceleration and slot injection between radiation belts during magnetic storms, using flux measurements onboard Molniya 1 satellite
20 p3282 A71-39738
- High latitude auroral particle precipitation patterns and connections to plasma sheet, ring current, cusp and radiation belt sources, using rocket and satellite observations
21 p3439 A71-41179
- Radiation belt particles nonadiabatic changes, calculating rigidity as function of magnetic field lines
21 p3439 A71-41357
- Earth radiation belts high energy electron flux intensity monotonic decrease during magnetically quiet periods from satellite data analysis
22 p3591 A71-41527
- ## RADIATION CONTROL
- ### U RADIATION PROTECTION
- #### RADIATION COUNTERS
- NT CERENKOV COUNTERS
NT ELECTRON COUNTERS
NT GEIGER COUNTERS
NT NEUTRON COUNTERS
NT PARTICLE TELESCOPES
NT PROPORTIONAL COUNTERS
NT QUANTUM COUNTERS
NT SCINTILLATION COUNTERS
NT SPARK CHAMBERS
- Optical systems using photoelectron counter system for optical signal detection and demodulation
02 p0214 A71-12031
- Extensive air shower experiments, considering origin, particle interactions and detectors
03 p0475 A71-13838
- High energy cosmic ray particle charge and direction detector on Proton 3 satellite
04 p0596 A71-15122
- Energetic electron and proton precipitation measurements by sounding rocket-borne particle detectors in pulsating aurora
07 p1186 A71-19669
- Detectable information rate changes of photon counter with finite observation time and background noise
08 p1289 A71-21286
- Radiosonde with radiation sensor, minimizing temperature measurement errors in free atmosphere
08 p1293 A71-21745
- Micrometeoroid detector design for hypervelocity particle impacts, discussing solar radiation pressure effects on satellite measurements
11 p1761 A71-25544
- Alpha radiation machmeter with semiconductor pulse detectors, discussing supersonic regime effects on rate variations
12 p1908 A71-27607
- Critique on photomultiplier tube for photon counting, considering pulse height distribution, SNR and electron collection efficiency errors
16 p2578 A71-33146
- French monograph on system reliability of particle detection device covering methodology, functional
- models, Monte Carlo simulation, spectrometers and DC/DC converters
17 p2767 A71-35231
- Diamond radiation counters for C 14 containing carbon dioxide in extraterrestrial life detection, noting radioactivity curves as function of sample microflora
21 p3378 A71-40571
- Low cost two channel pulse counter (RUFAS) for astronomical photoelectric occultation observations, describing resolution, data output and computer interfacing
22 p3542 A71-41932
- Extensive air shower experiments, considering origin, particle interactions and detectors
22 p3594 A71-42639
- ## RADIATION DAMAGE
- Comparative radiation damage at different depth-dose tissue distributions in dogs
01 p0013 A71-11132
- Surface destruction of glass dielectric by pulsed laser beam, considering plasma clouds, shock waves, ablation and crack formation
02 p0258 A71-11640
- Vacuum UV degradation of thermal control coatings on ATS-1 satellite, comparing with laboratory simulation
04 p0618 A71-14896
- Impurity effects of annealing of radiation defects in p-type silicon, considering annealing temperature
04 p0636 A71-15037
- Si solar cells under low temperature electron irradiation, noting damage rate dependence on measurement temperature
05 p0701 A71-16076
- N-p Si solar cells, investigating mechanism of low energy proton irradiation damage to back contacts
05 p0702 A71-16084
- Defects and annealing in electron irradiated lithium diffused silicon solar cells
05 p0703 A71-16092
- Structural damage by laser radiation in polymethyl methacrylate, using polarized light microscopy
05 p0772 A71-16370
- Solar cells characteristics for space power systems, considering angle of incident sunlight, radiation damage, array design and mounting
05 p0705 A71-17151
- Radiation damage to HeLa cells at liquid nitrogen temperature and dry fern spores at room temperature
07 p1033 A71-18937
- Drug-radiation damage interaction relationship to radiosensitization in mammalian cells
07 p1034 A71-18946
- Embryo chemical sensitization to low radiation doses damage by radiosensitizer iodoacetamide
07 p1037 A71-18963
- Ionizing radiation induced surface damage dependence in matched oxide passivated silicon planar epitaxial transistors on junction fringing electric field strength during exposure
07 p1174 A71-19052
- Surface ionization effects on planar silicon bipolar transistors, considering damage reduction by device exposure to high ionizing radiation dose
07 p1174 A71-19057
- Neutron induced lifetime damage short term annealing dependence on minority carrier density in p-type silicon, considering majority carrier repulsion by positively charged centers
07 p1175 A71-19061
- Ion implantation lattice damage effects in crystalline silicon with allowance for optical reflectivity, considering annealing temperature and amorphous layer formation
07 p1175 A71-19062
- Statistical analysis of neutron induced gain degradation of silicon power transistors, determining failures distribution fit to Weibull function
07 p1070 A71-19063
- Nuclear radiation damage to ruby laser power output
07 p1121 A71-19067
- Neutron radiation damage on high efficiency microwave avalanche diode sources (TRAPATT oscillators)
07 p1071 A71-19068
- Neutron irradiation induced degradation in epitaxial Gunn diode performance
07 p1071 A71-19069
- Si surface barrier radiation detectors depletion region low energy proton irradiation damage determination from capacitance-voltage curves and capacitance recovery techniques
07 p1071 A71-19071
- Low energy proton irradiation damage to ATS and Intelsat satellites Si solar cells junction properties
07 p1022 A71-19072
- Electron radiation bulk damage effects on Si surface barrier detectors, determining reverse leakage current density and alpha particle response changes
08 p1345 A71-21842
- Metallic target in radiation damage from focused ruby laser beams as function of energy and luminous pulse duration
09 p1465 A71-23563

- Irreversible damage effects of visible light on retina in rats as function of irradiation, exposure time and vitamin A deficiency cell adaptation
10 p1563 A71-24327
- Cochlear/vestibular apparatus, ganglion cells, spinal roots and nerve trunk damage from ionizing radiation based on neural elements transirradiation in neoplasms
10 p1566 A71-25039
- Exposure time and power effects of CW Ar laser damage to rabbit iris, comparing with pulsed ruby laser effects
10 p1572 A71-25076
- Microwave radiation nonthermal biological damage, describing beetle pupae irradiation and radiant heating experiments
11 p1717 A71-25285
- Cataract production from microwave radiation exposure by lens nutrition alteration and surface shape changes
11 p1718 A71-25292
- Reflectance restoration of proton and UV degraded spacecraft thermal control coatings by low temperature oxygen plasma treatment applied to Surveyor 3 [AIAA PAPER 71-463]
11 p1800 A71-26244
- Chorioretinal temperature increases from naked solar eclipse observations for various observation angles and pupil diameters, considering solar irradiance and atmospheric transmittance spectra
11 p1726 A71-26484
- Spacecraft electric systems semiconductor devices radiation damage from high energy particles during space missions, noting radiation resistant devices development possibility
12 p1943 A71-26981
- Radiation resistance variations of n-type and p-type silicon photocells due to formation of one or two vacancy recombination centers
15 p2461 A71-31670
- Acoustical wave generation measurement during iris and retina photocoagulation and ruby laser burns, noting intraocular pressure surge simultaneous with ocular tissue explosion
15 p2365 A71-32346
- Histopathological and fluorescein angiographic studies of rhesus monkey chorioretinal lesions produced at threshold and suprathreshold power levels of Ar laser
15 p2365 A71-32347
- Thermomechanical damage by pulsed lasers in metals, discussing energy deposition and stress wave generation for optimal fracture conditions
15 p2422 A71-32555
- Silicon solar cells radiation damage from low energy protons, discussing current degradation as function of exposed area and particle energy
16 p2621 A71-33414
- IR absorption of oxygenated dislocationless phosphorus doped fast neutron irradiated n-type silicon, investigating dominant defects for different radiation dosages
17 p2790 A71-34199
- Focused laser beam interaction with liquid metal particles, discussing fluid phase light screening effect, droplet evaporation and mass expulsion characteristics
17 p2750 A71-34291
- Surface/volume damage induced by Nd-YAG laser irradiation to LiNbO₃ and KDP crystals in frequency doublers and Pockels cells, using scanning electron micrographs
17 p2790 A71-34376
- Curve power factors and radiation induced changes in silicon photovoltaic solar cells, considering junction depth, bulk resistivity, temperature and illuminating light intensity
17 p2677 A71-35049
- Carrier diffusion length change in damaged gamma irradiated silicon solar cells by numerical analysis, using experimentally obtained voltage or current
17 p2677 A71-35050
- Laser-induced retinal damage model based on energy interaction modes, including thermal and acoustic transients, vaporization and dielectric breakdown
18 p2863 A71-35955
- Radiation induced etch-pit dislocations and thermal decomposition kinetics in ammonium perchlorate crystals
18 p2955 A71-35967
- Retinal damage thresholds of rhesus monkeys to ocular radiation from yellow line 568.2 nm emitted by krypton CW gas laser
19 p3008 A71-38284
- Semiconductor neutron hardness assurance by irradiation of wafer, probe, die rejection and anneal screening technique
19 p3034 A71-38520
- Neutron irradiation effects on radiative, nonradiative and threshold currents in epitaxial GaAs laser diodes at room temperature
20 p3275 A71-38785
- Activation energy and temperature dependence of radiation induced free radical destruction in N-acetyl-DL-valine, using Arrhenius plots
21 p3345 A71-40203
- Beryllium reflector plate failure in NASA Plum Brook Reactor, discussing irradiation induced mechanical and physical property changes and internal/external stress effects
21 p3414 A71-40904
- Crystalline dislocations and impurity atmospheres role in kinetics of accumulation of radiation defects in Ge under fast electron bombardment
21 p3429 A71-41209
- CdS crystals faces damage caused by picosecond light pulses from free oscillating Nd-glass laser
21 p3432 A71-41305
- Low temperature proton irradiation damage and recovery in discontinuous Ta films sputtered in oxygen and nitrogen
22 p3585 A71-41804
- Prophylactic medication for radiation damage treatment, covering toxicity, pharmacological properties, metabolism, dosage and physiological action
22 p3505 A71-42711
- Rat organs pathomorphological changes under gamma neutron irradiation with head and abdomen shielding, noting intestines early damage
22 p3493 A71-42722
- Aminothiol class radiation protector influence on tissue damage of white rats under single and two-fold gamma radiation at various test conditions
22 p3494 A71-42729
- Thin film silicide resistors in monolithic IC for high sheet resistance or radiation hardness using sputtering deposition without protective overlayer
23 p3655 A71-43428
- Ultramicroscopic texture and radiation damage in Apollo 11 and 12 micron sized lunar dust grains compared with meteoritic rocks
23 p3758 A71-43756
- Proton irradiation damage on lunar surface, considering solar wind sputtering, reduction, chemical bond breakage and electron paramagnetic resonance
24 p3867 A71-44423
- Biological effects of ionizing radiation and non-radiative factors on radiation damage from satellite space flight tests on dogs and plants
24 p3798 A71-44891
- Electron transmission microscopy of Mo single crystals irradiated with fission neutrons and defect structures prior/after postirradiation anneal
24 p3839 A71-45192
- Irradiation defects and electrical quality of ion implanted silicon, using minority carrier lifetime measurements
24 p3863 A71-45357
- ### RADIATION DETECTORS
- #### NT DOSIMETERS
- #### NT GOLAY DETECTOR CELLS
- #### NT SILICON RADIATION DETECTORS
- #### NT THRESHOLD DETECTORS [DOSIMETERS]
- Solar radio bursts at 19 GHz, investigating single frequency proton warning technique
03 p0481 A71-14506
- IR astronomy, considering basic principles, instrumentation energy production and radiation, spectroscopy, detectors and atmospheric absorption and emission
04 p0649 A71-15254
- Soviet book on experimental methods in nuclear physics covering operation, structural features and application of radiation detectors
06 p0903 A71-18731
- Soviet book on thermal radiation sensing covering system functional circuits, radar conversion, military application and personnel training
07 p1060 A71-19100
- Optical astronomy instrumentation automation including telescopes, computer control, filters and detectors
07 p1114 A71-20051
- Gravitational radiation experimentation, discussing detector, directivity, equations of motion, etc
08 p1333 A71-21175
- Satellite-borne Ge radiation detectors, investigating design criteria and performance at elevated temperatures
08 p1267 A71-21847
- Heavy cosmic rays identification by charge spectrum analysis of balloon-borne combined plastic detectors and nuclear emulsions, noting astrophysical implications
09 p1514 A71-22804
- Cerenkov detectors and He filled spark chambers with large interelectrode spaces in high energy nuclear interaction studies, noting cosmic ray applications
10 p1612 A71-24667
- Large Cerenkov detectors in absorption spectrometers during high mountain cosmic ray measurements
10 p1612 A71-24668
- Gravitational shock waves from tachyons, considering capability for Weber gravitational radiation detection apparatus excitation across astronomical distances
11 p1798 A71-25591
- Solid propellant burning surface irradiance measurement, using optical lightpipe and radiation detector [AIAA PAPER 71-469]
11 p1859 A71-26250
- Cosmic ray neutrino results from deep underground detector near Johannesburg
12 p1952 A71-27399
- Cosmic ray muon flux at sea level, allowing for showers, multiple scattering, straggling, zigzag motion, detector efficiency and electronic equipment dead time
12 p1952 A71-27403
- Satellite-borne anisotropy and energy spectra measurement instruments for cosmic ray electrons and protons and solar and galactic X-rays
12 p1954 A71-27711
- Semiconductor radiation detectors, discussing minority charge carrier diffusion length measurements by nuclear method
13 p2065 A71-27957
- Planetary disks brightness temperature measurement using 22 m radio telescope with indium antimonide detector at 1.4 mm
13 p2141 A71-29102
- OSO-G satellite instrumentation for solar and celestial X ray detection, exploring spectral distribution, temporal intensity variations, sources and atmospheric albedo
13 p2070 A71-29135
- Sound radiation and pressure fields inside vibrating turbomachine blades, using miniaturized microphones and compact capacitive detectors
14 p2288 A71-30517
- Solar neutrino detection using capture reaction in perchloroethylene medium
15 p2478 A71-31803
- Proportional counters design for ionizing radiation detection, examining cosmic ray meson component
15 p2408 A71-31814
- He-Ne IR laser resonator as quadrature detector for modulated filtered laser radiation, noting strong LF noise
17 p2750 A71-34269
- Paraterphenyl coated photomultiplier as detector in far UV spectra, detailing efficiency range and sensitivity
17 p2745 A71-35589
- Specular reflecting passive radiators for synchronous satellite radiation detectors cooling [ASME PAPER 71-AV-30]
18 p2869 A71-36397
- Pulsed X ray emission from NP 0532 at 20-200 keV measured by balloon flown sun sensor controlled azimuth stabilized detectors
18 p2958 A71-36760
- End-on shock tube detection technique sensitivity for monitoring light emission behind reflected shock waves
20 p3209 A71-38830
- High resolution charged particle detector with wire cathode for synchrotron applications, discussing design and advantages
20 p3238 A71-39423
- High energy cosmic ray spectrometer onboard Proton 4, discussing ionization calorimeter, nuclear targets, particle charge and radiation detectors and primary measurements
20 p3283 A71-39755
- Semiconductor radiation detectors, discussing minority charge carrier diffusion length measurements by nuclear method
21 p3383 A71-41346
- P-type germanium photon drag detectors with carbon dioxide lasers, discussing response speed and sensitivity
22 p3543 A71-42129
- Auroral X rays passage through atmosphere, discussing integral spectral measurements with collimated and omnidirectional detectors
22 p3593 A71-42399
- Gravitational wave astronomy, discussing phenomenon relationship to Einstein relativity theory and detector configurations
23 p3733 A71-43120
- Electron emitter photomultipliers and photocathodes for low light level and scintillation counter applications, using negative electron affinity
23 p3651 A71-43432
- Wideband solid state converter circuit for quantization of signals from semiconductor nuclear radiation detectors, noting cost reduction
23 p3677 A71-43527
- He-Ne laser coherent radiation photodetection by variable diaphragm photomultiplier, analyzing photocurrent spectra as function of diaphragms aperture size and shape
23 p3687 A71-44175
- Millimeter and submillimeter wave radiation detection by paramagnetic materials, noting noise equivalent power dependence on various parameters
23 p3717 A71-44293
- Photon noise limited interferometer transducer for gravitational radiation antenna, using piezoelectric driver to generate subangstrom vibrations
24 p3835 A71-45209
- Microchannel plates detection efficiency for 2-150 keV electrons from C 14 pellet and electron gun
24 p3829 A71-45336
- ### RADIATION DISTRIBUTION
- #### NT ANTENNA RADIATION PATTERNS
- #### NT DIFFRACTION PATTERNS

**NT KOSSEL PATTERN
NT SIDELOBES**

Directional cosmic ray cut-off and loop-cone folding distribution at geomagnetic midlatitude sites
01 p0146 A71-11485

Statistical properties of multimode quantized optical fields, using density matrix in P-representation
02 p0259 A71-11932

Galactic radio corona existence, measuring northern galactic hemisphere sky brightness and cosmic ray distribution
03 p0483 A71-13204

GaAs heterojunction diode injection lasers, predicting high order transverse cavity modes and far field patterns from theoretical model
03 p0434 A71-13482

Room temperature spatial distribution of emission from injection lasers with single and triple heterojunctions in AlAs-GaAs system
03 p0439 A71-13980

Mathematical model of stellar atmospheres using radiation emission by elementary cylinder
04 p0647 A71-15236

Helicopter in-flight noise radiation pattern and spectra measurements for various operating parameters
04 p0531 A71-15406

Angular distribution and polarization of solar X-ray bremsstrahlung, taking into account magnetic field effects
05 p0000 A71-16032

Layer boundaries and critical concentrations of anomalous increase of radiation in earth and Venus atmospheres along tangential directions
05 p0738 A71-16044

Ruby laser with lens resonator, studying radiation patterns and angular divergence, lasing threshold and spectra width
05 p0763 A71-16831

Neodymium glass lasers, investigating pump-induced birefringence effect on polarization and radiation distribution
06 p0907 A71-17398

Soviet papers on satellite meteorology covering atmospheric radiation fields, wind determination, temperature distribution transformations and cloud forms identification
06 p0922 A71-17507

Meteorological satellite data interpretation, including atmospheric layers thermal balance and global absorbed and outgoing radiation distribution mapping
06 p0923 A71-17508

Radiation fields of various background and atmospheric cloud formations by reflected short wave radiation aircraft measurements
06 p0923 A71-17511

Radiation temperature fields and cloud distributions seasonal and latitude characteristics by meteorological earth satellite data
06 p0924 A71-17517

Global radiation temperature distribution inhomogeneities in underlying surfaces, atmosphere and radiation absorbing areas
06 p0924 A71-17518

Phenomenological one dimensional model of solar cosmic ray propagation for anisotropy and intensity as function of time during early phases of events
06 p0950 A71-18102

Isotropic galactic cosmic ray diffusion in interplanetary space from solar wind velocity and diffusion coefficient dependence on heliolatitude and heliolongitude
06 p0953 A71-18118

Cosmic rays transient north-south polar asymmetry, confirming time lag between Forbush decrease onsets
06 p0956 A71-18140

Tropospheric and lower stratospheric radiation balance components vertical profiles, using balloon sounding
07 p1151 A71-18913

Long wave radiation balance components vertical profiles, showing temperature stratification effect
07 p1151 A71-18914

Low profile optical system producing annular cone of radiation from point source for high speed aircraft beacon
07 p1107 A71-19203

Electron scattering effect on emission and absorption lines in stellar atmosphere, considering primary radiation sources uniform distribution and photosphere radiation transmission through electron atmosphere
07 p1192 A71-19291

Continuous optical conversion to IR and directional stellar radiation flow conversion to diffused radiation fields in circumstellar dust envelopes
07 p1187 A71-19821

Free nitrogen jets ejected from small orifices, measuring acoustic emission level and spectral pattern dependence on pressure
07 p1161 A71-20058

Compressible isotropic plasma slab effect on magnetic dipole radiation pattern, using reciprocity theorem
08 p1253 A71-21274

Electromagnetic wave scattering by perfectly conducting cylinder in anisotropic plasma with external

magnetic field, deriving radiation pattern from asymptotic expression
08 p1253 A71-21295

Statistical analysis of center-limb variations of intensity, spectrum and polarization of solar microwave impulsive bursts
08 p1364 A71-21419

Lunar surface electromagnetic sounding, presenting analysis of radiation fields and polarization characteristics for magnetic dipole situated on layered half space
10 p1576 A71-24054

Angular discretization effect on calculations of emerging radiation and integrated albedo from model cloudy atmosphere, using multiple scattering with terrestrial particle phase functions
10 p1643 A71-24972

Far field sound radiation pattern from vibrating circular piston set in nonrigid baffle for sonar detectors
11 p1798 A71-25186

Stimulated Compton effect in compact radio sources, giving formulas for energy flow between relativistic electron and radiation field
11 p1831 A71-26169

Power law dependence of lateral distribution function and core location of showers detected by Haverah Park array
13 p2122 A71-28068

Cerenkov light distribution calculation from gamma ray initiated air shower model obtained from Monte Carlo computer program
13 p2125 A71-28093

Book on laser physics covering radiation theory, atomic system interactions, Fresnel diffraction, Gaussian beam, Lamb theory and cavity engineering
13 p2078 A71-28429

Ultrasonic field distribution patterns from metallic and ceramic concave spherical reflectors under excitation by single or multiple piezoelectric elements
13 p2101 A71-29267

Radiation field description with spatial complex variables, considering application to scattering and waveguide problems
14 p2209 A71-29567

Galactic Lyman alpha emission, describing radiative transfer in radiation diffusion
14 p2306 A71-29683

Radiation patterns from piezoelectric transducers on Y face of lithium niobate, using Green function analysis
14 p2283 A71-29795

Radiation patterns and scattering cross sections of plane black disks excited by electromagnetic and acoustic waves
14 p2194 A71-30079

Acoustic tone radiation from subsonic rotor near potential field by interaction with nonuniform inlet flow based on Lighthill aerodynamic sound equation
14 p2225 A71-30210

Jet aircraft sound spectrum on ground and in air, comparing calculation with experiment
14 p2289 A71-30524

Solid state laser emission divergence, calculating far zone fields for arbitrary amplitude and phase distributions
15 p2418 A71-31243

Laser action internal differential quantum yield estimation using GaAs injection lasers near field emission patterns
15 p2422 A71-32461

Aperture field distribution for excitation of surface waves with high efficiency and gain
15 p2378 A71-32627

Optical detection of laser or scattered radiation transmitted through turbulent atmosphere, taking into account independent additive background radiation
16 p2608 A71-33145

Resonant energy exchanges between gaseous media and externally applied radiation fields from wavelength-tunable lasers
16 p2586 A71-33164

Plasma instabilities effectiveness for high energy cosmic rays confinement in galactic disk
16 p2625 A71-33238

Layer boundaries and critical concentrations of anomalous increase of radiation in earth and Venus atmospheres along tangential directions
16 p2635 A71-33448

Radiation attenuation volume coefficients for water clouds and fogs thermal sources and laser outputs
16 p2543 A71-33708

Atmospheric optics and geophysics problems modeling arrangement reproducing radiation field within light scattering medium
16 p2605 A71-34106

Temporal distribution of photons radiated by He-Ne laser operating in five modes
17 p2750 A71-34202

Pitch distribution of protons precipitated from auroral radiation region measured by scintillation detector aboard Cosmos 261 satellite in Northern Hemisphere
17 p2731 A71-34320

Laser longitudinal oscillation modes and maximum radiation envelope formation from noise at start of emission, using electric field strength recurrent relations
17 p2751 A71-34386

Scattering obstacle with surface currents and radiating fields, determining characteristic current distributions and values of elliptical loops, straight wires and circular arcs
17 p2700 A71-34753

Ray acoustic treatment, estimating diffusion of radiation patterns due to scattering by random inhomogeneities
17 p2783 A71-35036

Radiation field inhomogeneity effect on radiation gas jet flow, taking into account radiative energy transfer by differential approximation
17 p2728 A71-35117

Thermoluminescent dosimeter for skin basal layer dose measurement in mixed beta and gamma radiation fields
17 p2693 A71-35450

Incoherent radiation distribution analysis by image multiplex coding with SNR gain applied to IR region [ONERA-TP-972]
18 p2916 A71-36031

Coherent optical fields properties, discussing equivalence of quantum and classical descriptions
18 p2932 A71-36959

Azimuthal IR radiation distribution of atmospheric brightness cross sections at various zenith angles from balloon programmed-control radiometer data
19 p3054 A71-37969

Quasar red shifts distribution, indicating discretization in form of geometrical series
19 p3142 A71-38154

Wide angle paraboloid reflector electromagnetic field intensity distribution measurements in focal region
19 p3035 A71-38601

Diffraction loss equality in field distribution at con-focal laser resonator mirrors with circular coupling holes
20 p3242 A71-38850

Solar array technology for lunar surface applications including silicon cells, cadmium sulphide thin films, temperature effects, prototype module and radiation degradation
20 p3181 A71-38941

Elliptical cylinder pump cavity design for solid state laser with ideal beam geometry
20 p3246 A71-39493

Exact solutions to radiation-filled Brans-Dicke cosmologies, using Robertson-Walker metric
20 p3294 A71-39558

Earth-atmosphere system radiation budget, comparing meteorological satellites actinometric data with calculated climatological maps of planetary long wave radiation distribution
20 p3259 A71-39678

Earth atmosphere radiation fields analysis from Nimbus 3 five-channel scanning radiometer measurements, determining mean planetary albedo and temperature
20 p3259 A71-39679

Reflected radiation brightness field statistical structure in IR range from Cosmos 121 satellite measurements, calculating correlation functions and spectral densities
20 p3259 A71-39680

Stratosphere and mesosphere physics and dynamics, studying composition, radiation fields, temperature, winds, wave phenomena and relations to meteorological theory
20 p3230 A71-39872

Scorpius X-1 radio emission detection at 1415 MHz, discussing brightness distribution
21 p3441 A71-40068

Radiation energy contours of pulsed ruby laser beam in direct determination of thermal conductivity by flash technique, using heat flux transducer
21 p3391 A71-40180

Non-LTE picket fence model in radiative equilibrium solutions for thermal coupling and line strength parameter
21 p3438 A71-40243

Temperature control bracket energy equation as measure of temperature distribution in pure hydrogen stellar atmosphere, considering electron energy and radiation field
21 p3446 A71-40419

Diffuse radiation field inside homogeneous spherically symmetric dust nebula from radiative transfer equation solution as expansion after Legendre polynomials
21 p3451 A71-40716

GaAs luminescent p-n junction diode spontaneous emission measurement in magnetic field, noting redistribution in Lorentz force direction
21 p3432 A71-41303

Electromagnetic field distributions and far field radiation patterns of three layer waveguide GaAs heterostructure injection lasers, using Maxwell equations
22 p3555 A71-41688

- Electromagnetic wave propagation and radiation pattern of circular corrugated waveguide antenna feeds, considering unity azimuthally dependent modes 22 p3511 A71-42278
- Transfer equation formulation for radiation field determination in anisotropically scattering medium 22 p3621 A71-42598
- Long term vertical and horizontal variations of long wave radiation field in free atmosphere over U.S.S.R., using actinometric sounding data 22 p3570 A71-42848
- Radiation field profiles and applications of broadband ultrasonic transducers, including thickness and viscosity measurements 23 p3674 A71-42919
- Traveling wave laser with confocal, plane and semiconcentric resonators, calculating emission field spatial-temporal structure and inversion distribution 23 p3685 A71-43561
- Normal wave scattering on random permittivity inhomogeneities of stratified waveguide dielectric layer, calculating beam width and energy loss by perturbation procedure 23 p3645 A71-43567
- Ni-Fe film exposure to continuous IR laser light for laser radiation structure 23 p3686 A71-44056
- Mach bands appearance in red/green triangular wave intensity distributions generated on CRT, quantifying perceived brightness distribution by matching with variously positioned light slit 24 p3800 A71-44468
- Radiation diffusion in finite thickness medium with variable optical properties, giving equations for illumination levels and excited atom density in steady state medium 24 p3833 A71-44660
- Radiative transfer in linearly anisotropic-scattering conservative and nonconservative slabs with reflective boundaries, obtaining angular radiation distribution by normal mode expansion technique 24 p3888 A71-44966
- Airborne measurement of directional variation in reflected solar radiation over soil surface and vegetation, using scanning radiometer 24 p3826 A71-44984
- High energy charged particles angular distribution measurements in equatorial region cosmic radiation above atmosphere, using Proton 2 satellite data 24 p3866 A71-45027
- Lunar IR directional characteristics theory, noting agreement with observations at all observational and phase angles 24 p3874 A71-45188
- Liquid-state pulsed laser active element lens parameters effects on output radiation divergence 24 p3835 A71-45240
- RADIATION DOSAGE**
- Comparative radiation damage at different depth-dose tissue distributions in dogs 01 p0013 A71-11132
- Photogrammetry in precision three dimensional X ray stereoradiography, comparing doses with Kymography, Tomography and Seriescopy 02 p0203 A71-11951
- Absorbed dose equivalent from high energy neutrons and protons incident on tissue, using nucleon-meson cascade calculations 04 p0624 A71-14804
- Soviet papers on dosimetry of ionizing radiation intense fluxes covering electron collision, neutron spectra and gamma radiation 04 p0593 A71-14913
- Ionization chamber for high intensity isotopic gamma radiation dose measurement, discussing saturation current and Compton interaction process 04 p0594 A71-14917
- Computerized human body anatomical geometrical model with life size skeleton and organs scaling for radiation dosage analyses in space missions 04 p0546 A71-15282
- Radiation energy deposition profiles in transparent liquids, using holographic interferometer 05 p0748 A71-16263
- Radioprotectors and antibody formation in rats, determining ionizing radiation survival rate index for lethal dose and hematological indices 05 p0710 A71-16819
- Radial microdistribution of absorbed dose in heavy charged particle track, allowing for delta electron emission 06 p0963 A71-18365
- Relative biological effectiveness of multicharged C ions during single irradiation of *Chlorella*, noting dose dependent mutability 06 p0854 A71-18366
- Respiratory inhibitor KCN for killing increase from single radiation doses and reduction of dose fractionation sparing effect 07 p1036 A71-18962
- Embryo chemical sensitization to low radiation doses damage by radiosensitizer iodoacetamide 07 p1037 A71-18963
- Surface ionization effects on planar silicon bipolar transistors, considering damage reduction by device exposure to high ionizing radiation dose 07 p1174 A71-19057
- Failure criteria percentages for bipolar transistors, determining adequacy of Weibull distribution for low gamma ray dose survival probability 07 p1071 A71-19064
- Acceptable gamma radiation dosages for extended manned space flights based on prolonged irradiation of dogs 09 p1388 A71-22193
- Probable solar flare doses on interplanetary mission calculated by MCFLARE computer program using Monte Carlo methods 09 p1399 A71-22809
- Pyrolytic graphite microcalorimeter for X ray absorbed dose measurement, exploiting for calibration self heating 10 p1608 A71-23742
- Microwave/high frequencies safe exposure limits, discussing radiating aerial near field, radio hazards and human body absorption 10 p1573 A71-25080
- Microwave radiation nonthermal and cumulative biological effects, discussing dose/irradiation safety standards 11 p1717 A71-25283
- Microwave biological exposure systems implementation in limited space, describing focused prolate spheroid, absorber-lined horn and compact range illumination system 11 p1723 A71-25288
- Life prolongation during high intensity microwave exposures with ambient air temperature control for radiation bioeffects studies 11 p1717 A71-25291
- Cataract production from microwave radiation exposure by lens nutrition alteration and surface shape changes 11 p1718 A71-25292
- Spacecraft thermal control coatings for long-duration exposure to near-earth orbital conditions, determining optical properties degradation and solar absorptance [AIAA PAPER 71-454] 11 p1859 A71-26237
- Spacecraft systems radiation hardening design, discussing Tiroso satellite mission hazards and space exposure prediction for electronic parts, using flow chart rationale 11 p1839 A71-26333
- Soviet book on radiation dosimetry and spectrometry of ionizing radiations covering chemical, electrochemical, thermoluminescence, scintillation and diffuse reflection methods 11 p1797 A71-26450
- PAX intermediate spectrum reactor neutron and photon dose rates and fast and thermal neutron flux calculation, comparing results with experiment 13 p2099 A71-29258
- Human tissues neutron induced physical doses calculation 13 p2021 A71-29260
- Cosmic radiation doses measurement on Soyuz 3 spacecraft by nuclear emulsions, giving averaged doses absorbed by various cosmonaut tissues 15 p2362 A71-31314
- Hematopoietic injury and recovery from radiation exposure for dogs and monkeys, showing dose protraction effects 16 p2532 A71-33774
- Double standard for national levels of exposure and biological hazards of microwave radiation, comparing Soviet work to U.S. 19 p3008 A71-38442
- Irradiation dose effect on alpha particle irradiated Al foil electrical resistivity recovery, using Wheatstone bridge measurement 23 p3689 A71-42934
- Apollo 12 lunar core sample thermoluminescence dependence on radiation dose rates, detecting temperature gradients in regolith by differential thermal analysis 23 p3760 A71-43776
- Radiation exposure history from fossil tracks in Apollo 12 surface rocks and double core regolith samples, comparing with Saint Severin meteorite 23 p3764 A71-43802
- Radiation dose effects on polymer strain magnitude under critical cyclic loading 23 p3697 A71-44033
- Pion beam dosimetry with silicon detectors and plastic scintillators, presenting depth dose and isodose distributions and differential range curves 24 p3799 A71-44359
- Cosmic ray dosimetric monitoring in manned spacecraft, discussing ionization, thermoluminescent and nuclear photoemulsion methods of radiation measurement 24 p3826 A71-44888
- Manned spacecraft radiation protection against cosmic rays, considering proton attenuation in shielding materials and dose formation in body tissues 24 p3801 A71-44889
- Cosmic ray biological effects and admissible dose level normalization in space flight from prolonged tests on dogs 24 p3798 A71-44890
- RADIATION EFFECTS**
- NT RADIATION DAMAGE
- NT RADIATION INJURIES
- NT RADIOLYSIS
- Cryogenic fluids nucleate boiling dependence on solid surface characteristics, considering hysteresis, boiling site spreading and radiation effects 01 p0178 A71-10005
- Polymethyl methacrylate lifetime under simultaneous mechanical stresses and ionizing radiation 01 p0106 A71-10044
- C 14 incorporation from labeled glucose into cerebral glycogen of normal and X ray irradiated rats 01 p0011 A71-10850
- Bone marrow physiological regeneration after chronic gamma irradiation, noting effect on fission processes and chromosome apparatus of cells 01 p0014 A71-11146
- GaAs strongly doped p-n junctions, examining I-V characteristics changes under electron bombardment and mixed reactor field irradiation 01 p0140 A71-11458
- UV effect on airborne bacteria survival in simulated Martian dust clouds 01 p0019 A71-11557
- Free radicals role in photodynamic inactivation of Rhodotulra glutinis subjected to high intensity light irradiation 01 p0019 A71-11560
- Reactor gammas effects on thermionic diode output simulated in electron accelerator 02 p0238 A71-12228
- Kr 85 disposition following Mo-uranium oxide cermet fuels irradiation in test chamber 02 p0296 A71-12240
- Cylindrical thermionic converter irradiation tests under Incore Thermionic Reactor (ITR) Project, discussing postmortem examinations 02 p0195 A71-12243
- High temperature neutron irradiation properties of uranium oxides, carbides and nitrides coated with tungsten-rhenium 02 p0296 A71-12246
- Omega West Reactor isothermal irradiation experiments, determining long term fast neutron irradiation effects on Al 995, Lucalox and yttrium oxide insulator 02 p0280 A71-12251
- Microwave effects on living creatures, considering thermal and nonthermal effects on individual body organs and systems, permanent changes and protective measures 02 p0208 A71-12845
- Radiation effects on cylindrical magnetohydrodynamic shock propagation in plasma, deriving jump conditions in terms of Mach number and pressure ratios 02 p0294 A71-12847
- IR radiation effect on gas molecular dissociation, showing dissociation temperature decrease due to IR photon absorption 02 p0288 A71-12850
- Thermal radiation effects on M-2 double base solid propellant ignition, deflagration and burning rate 02 p0298 A71-12851
- Rare earth polycrystalline powders luminescence stimulation by ruby laser radiation, discussing two photon mechanism, luminous intensities relations and UV radiation 03 p0435 A71-13510
- X ray effects on dogs with and without UV preexposure, determining blood protein and chemical composition, hemoglobin content and thermostability 03 p0364 A71-13524
- Atmospheric air breakdown by mode-locked Q switched laser pulse train, investigating threshold electric field dependence on characteristic diffusion length 03 p0440 A71-14178
- Clear potting polymers, investigating temperature and ionizing particle irradiation effects on properties 04 p0618 A71-14898
- Ultrasonic viscosimeter for gamma irradiation effects on materials structure, determining fluid viscosity changes from rate of damping of plate vibrations 04 p0594 A71-14918
- Radiation effects on compression shock in hot gases, considering hypersonic flow around blunt body during planetary atmosphere entry [DFVLR-SONDDR-60] 04 p0526 A71-15101
- Amino acid content alteration in internal organs in rabbits under HF electromagnetic and ultrasound oscillations 04 p0547 A71-15573
- Nongray thermal radiation effect on laminar forced convection over heated horizontal flat plate, determining temperature profiles for optically thin and thick boundary layers 04 p0688 A71-15741
- Solar cells for Jupiter mission, discussing radiation and environmental tests concerning I-V characteristics 05 p0701 A71-16074

- Si solar cells electrical performance tests, considering 1 MeV electron irradiation effect on efficiency
05 p0702 A71-16082
- Electron, proton and UV irradiation effects on CdS solar cell protective plastic films with or without adhesive coatings, measuring transmission changes
05 p0771 A71-16087
- Surface roughness and thermal radiation effects on rural and urban boundary layer turbulence and diffusion by wind fluctuations observations
05 p0777 A71-16665
- Atmospheric ionization by vertical gamma and alpha radiation of natural radioactive products, comparing to vertical behavior of conductivity
05 p0799 A71-16843
- Ion-acoustic waves generation mechanism in outer space by strong electromagnetic radiation, considering quasars, supernovae shells, pulsars and solar super-corrna
05 p0800 A71-17196
- Geomagnetic field anomalous variations due to solar eclipse of 22 September 1968
05 p0746 A71-17211
- UV light starvation prevention, describing biological effects and illumination equipment for working areas
06 p0858 A71-17528
- Rectangular panel acoustic response by variational finite element method, including radiated sound field effects on structural vibration
06 p0984 A71-17622
- Apollo 11 igneous rocks potassium content vs irradiation exposure age, comparing lunar geology models
06 p0966 A71-17897
- Low and high linear energy transfer /LET/ cycloctron-accelerated alpha particles effects on *Drosophila melanogaster* longevity
06 p0853 A71-18028
- Radiation effects on thermal decomposition induction period in ammonium perchlorate and other pseudostable inorganic solids
06 p0944 A71-18301
- Gamma irradiation effects on physicochemical and organoleptic properties of food products
06 p0861 A71-18367
- X ray influence on protein and mineral content of blood serum in dogs
06 p0858 A71-18728
- Lethal radiation in *Escherichia coli* B/r, investigating post irradiation DNA breakdown inhibitors
07 p1033 A71-18940
- Methylhydrazine radiosensitization of Ehrlich ascites tumor cells, investigating X radiation enhanced cell killing effect via deoxyribonucleic acid strand breakage
07 p1035 A71-18955
- Ehrlich ascites tumor cell membrane potassium and electrophoretic mobility loss, investigating radiation effects under radiosensitizing and radioprotecting drugs
07 p1036 A71-18956
- Short and long term radiation effects reduction by chemical radioprotectors mixtures, noting improved survival and decrease in leukemia and cancer incidence in X ray irradiated mice
07 p1037 A71-18970
- Central nervous system role in radioprotective contribution of 5-hydroxytryptamine
07 p1038 A71-18972
- Nuclear and space radiation effects - NASA/IEEE Conference, University of California at San Diego, July 1970
07 p1070 A71-19051
- Permanent IR electron radiation effects on hardened MOS integrated inverter circuits, using units with plasma grown and vapor deposited aluminum oxide
07 p1174 A71-19053
- Long term IR X ray irradiation effects on complementary MOS logic networks with several p and n channels on single silicon, determining radiation induced failure modes
07 p1174 A71-19054
- X irradiation induced currents across aluminum oxide films sandwiched between thin metal electrodes as function of voltage and time
07 p1174 A71-19056
- Microcircuits component vulnerability, deriving time independent nonlinear terminal I-V characteristics, electrical switching response and ionizing radiation induced transient response
07 p1070 A71-19059
- Ionizing radiation effects on monolithic metal oxide semiconductor inverters, including testing and hardening techniques
07 p1070 A71-19060
- Radiation hardened semiconductor device technique by irradiating silicon wafers on lot to lot basis
07 p1071 A71-19065
- Electron-proton radiation effects on scintillating materials in space environment chamber, evaluating background light degradation of active source monitoring
07 p1175 A71-19066
- Light emitting diodes performance comparison under electron irradiation effect in space environment
07 p1071 A71-19070
- Luminescence excitation in chelates under pulsed ruby and neodymium laser radiation action, examining two photon absorption mechanism
07 p1122 A71-19130
- Negative resistance diodes characteristics under laser radiation, investigating switching properties, temperature effects and noise characteristics
07 p1076 A71-19373
- Laser ocular effects, discussing corneal /retinal/ lens lesion production, damage thresholds and application to clinical ophthalmological problems
07 p1049 A71-19792
- Scanning electron microscope for surface morphological investigations of materials after laser irradiation
07 p1113 A71-19793
- Soft galactic X rays role in interstellar grains alignment
07 p1188 A71-20056
- Heavy ion track registration in nonconductor minerals, discussing radiation damage and atomic species along trajectory
07 p1158 A71-20270
- Dinitrophenol inhibition of rejoining of X ray induced DNA breaks by L cells
07 p1045 A71-20447
- Al-Li alloy precipitation hardening after neutron irradiation, noting yield stress increase after aging at various temperatures
07 p1143 A71-20487
- Fast neutron irradiation effects on Mo recovery stages 1 to 3 in bcc metals using electrical resistivity measurements
07 p1143 A71-20491
- Neutron irradiation effects on Al-Mg alloys tensile properties, noting yield stress increase and appearance of Lueders strain
07 p1143 A71-20492
- Microwave irradiation effects on peripheral blood and bone marrow in dogs and rabbits
07 p1053 A71-20539
- Radiation-anneal hardening and radiation effects on yield stress temperature dependence in bcc metals
08 p1312 A71-21550
- Human gastrointestinal tract functional disturbances after prolonged work in UHF field
08 p1249 A71-21955
- Large gamma radiation doses effect on neodymium activated glass laser emission properties
09 p1460 A71-22256
- Transducer design selection for strain gage applications in high nuclear radiation environments based on system requirements
09 p1445 A71-22718
- Ionizing radiation inhibition of spinal cord neurons ribonucleic acid synthesis and enzyme activity in mice, using autoradiographic method
09 p1393 A71-22925
- Space travel genetic effects, discussing radiation, weightlessness, vibration and acceleration
09 p1394 A71-23149
- Radiative flux effect on magnetogasdynamical shock in self-gravitating gaseous stars
09 p1506 A71-23589
- Type I fluctuations experienced by extensive air showers generated by protons or heavy nuclei, discussing effect on primary cosmic ray energy determination
10 p1661 A71-23858
- Laser pulse induced rapid reversible crystallization of amorphous chalcogenide semiconductor films using photon flux model
10 p1655 A71-24044
- Soviet papers on radiation physics of nonmetallic crystals covering effects of neutron, proton, electron, gamma and X ray irradiation on physical properties
10 p1655 A71-24137
- Carrier concentration, radiation dose and temperature effects on radiation defect formation in Si and Ge during gamma irradiation
10 p1655 A71-24138
- Probability of quasi-chemical reactions between point defects in semiconductors due to ionizing radiation
10 p1655 A71-24139
- Radiation defects distribution in Si irradiated by protons, deuterons and alpha particles
10 p1655 A71-24140
- Gamma radiation effect on electrical properties of n-type GaAs single crystals with doping impurities, calculating defect introduction rate and forbidden zone energy levels
10 p1656 A71-24141
- Formation kinetics of radiation defects produced by gamma rays in Sb doped n-type Ge single crystals at 77 K
10 p1656 A71-24142
- Annealing and white light illumination effect on I-V characteristics of long Ge diodes irradiated by 5 MeV electrons at 77 K
10 p1583 A71-24144
- P-n junctions formation in p-silicon irradiated by alpha particles
10 p1656 A71-24145
- Ionizing radiation effect on piezoelectric properties of quartz plates, covering X rays, gamma rays, electrons, protons and alpha particles
10 p1656 A71-24146
- Lunar soil particle production, noting radiation erosion effects
10 p1673 A71-24414
- Radiation and gas-dust interactions, examining dispersion relation and instability for cosmological models
10 p1675 A71-24490
- Dry heat and Co 60 gamma radiation combined effects on spacecraft sterilization, discussing kinetic analysis of spore inactivation
10 p1565 A71-24613
- Coagulative and delayed cumulative cataract production by microwaves investigated by hypothermic technique
10 p1572 A71-25077
- Pathophysiological aspects of microwave irradiation, considering thermal response of human and animal organisms to electromagnetic radiation exposure
10 p1573 A71-25079
- Gravitational radiation damping of slowly moving systems, discussing treatment as singular perturbation problem with approximation solution by method of matched asymptotic expansions
11 p1797 A71-25139
- Fe meteorite Grant, measuring radial distribution of cosmogenic nuclides of K, Ca, Ti, V, Cr and Mn produced by cosmic rays
11 p1819 A71-25224
- Thermal and nonthermal effects of microwave and RF radiation in biological systems, discussing dielectric constant and conductivity for high water content tissues
11 p1716 A71-25281
- Low power density modulated RF energy illumination effects on mammalian biological functions, noting possible hazards to personnel
11 p1716 A71-25282
- Microwave radiation nonthermal and cumulative biological effects, discussing dose/irradiation safety standards
11 p1717 A71-25283
- Negative heart rate response during low level microwave irradiation of dorsal head in rabbits
11 p1717 A71-25284
- Life prolongation during high intensity microwave exposures with ambient air temperature control for radiation bioeffects studies
11 p1717 A71-25291
- Microwave irradiation of animals, noting analeptic effect and increased alertness
11 p1718 A71-25293
- Air- and vacuum-melted Hastelloy-N/Ni-based alloy/ creep-rupture properties dependence on irradiation temperature
11 p1781 A71-26077
- Spherical plasma ball thermokinetic expansion model, considering solid state laser irradiation
11 p1806 A71-26091
- Venus-Mercury flyby vehicle solar cells, cover glasses, adhesives and Kapton film, investigating space radiation effects on solar absorbance and transmittance
11 p1859 A71-26236
- Reentry heating simulation, noting UV radiation effects as shock layer thickness decreases
11 p1859 A71-26248
- Radiating laminar convective flow in vertical heated channel, noting radiation effects on temperature and velocity
11 p1860 A71-26446
- Lunar soil albedo, discussing radiation darkening, lunar rock particles size and mineral contents effects
11 p1835 A71-26460
- Thermal control coating materials, measuring separate and combined electron and UV radiation effects on reflectance and emittance in vacuum
11 p1800 A71-26519
- Intergalactic gas ionization and heating by UV radiation
12 p1955 A71-26579
- Solar energy absorbance changes in spacecraft thermal control surfaces exposed to particulate radiation at simulated synchronous altitude, using computerized model
12 p1928 A71-26761
- Space radiation environmental effects on reactively encapsulated zinc orthotitanates and paints
12 p1920 A71-26762
- MOS transistors on P substrates, investigating ionizing radiation effects on I-V characteristics
12 p1885 A71-26830

Photomagnetic effect in ferric borate, noting photoinduced change, radiation sensitivity and temperature effects

12 p1943 A71-26857

Book on electromagnetic fields and life environment covering biological effects of radio waves, protection, radiation sources, permissible intensities, working conditions

12 p1873 A71-26868

Gamma irradiation effect on conductivity of varistors made of p-type black SiC

12 p1886 A71-26897

Solar simulator with wide range irradiation strength variability for laboratory investigation of radiation effects on spacecraft components

12 p1894 A71-26982

Radiative emission effects on viscous flow in shock structure of low density hypersonic flow around blunt body

12 p1986 A71-27583

Radiation induced visual phosphores observed by dark adapted human subjects in fast neutron, X ray and positive pion beams at Berkeley comparative to primary cosmic ray effects

12 p1871 A71-27675

Thermal flutter of satellite storable tubular extensible members, determining static flexural and torsional vibrations due to solar radiation

12 p1984 A71-27736

Fast neutron irradiation effect on Ni-Cr alloy electrical resistivity as function of temperature and initial composition

13 p2083 A71-27964

Ion-acoustic waves generation in outer space by strong electromagnetic radiation, considering quasars, supernovae shells, pulsars and solar supercorona

13 p2128 A71-28251

Flash UV photolysis of ozone/water vapor mixtures, noting OH radical nonreaction with ozone

13 p2025 A71-28349

Soviet book on vestibular reactions covering functional relationship between stimulus parameters and labyrinth nonauditory part, adaptation to Coriolis forces and response to ionizing radiation

13 p2008 A71-28672

Mars physical conditions compared to earth, simulating Martian conditions and low temperature and UV effects on proteins

13 p2009 A71-28688

Atomic Ba excitation, ionization and oxidation during emission in sunlight at high altitudes

13 p2026 A71-29038

Microwave exposure effects on organisms and biological functions responses and thermal stresses as function of specific frequencies, power density and environmental temperature

13 p2021 A71-29325

Multiple starlike flashes and short streaks reported by subjects exposed to neutrons under 25 mev, discussing interaction with retinal rods by proton recoils

13 p2022 A71-29353

Preferential pairing detection in GaS at 4.2 K through electron radiation damage of donor-acceptor pair green edge emission, discussing resulting wavelength shift

14 p2284 A71-29818

Creep rupture strength and durability of Al, Ni and Cu irradiated by neutron flux

14 p2258 A71-30004

Electromagnetic field action on living organism simulated with infinite homogeneous cylinder in infinite cylindrical solenoid EM media

14 p2182 A71-30026

Melting body disintegration in hypersonic gas flow under radiation influence from shock layer, assuming optically thin boundary layer and intense vaporization

14 p2336 A71-30222

Neutron irradiation effects on diffusion-ion doped HF n-p-n silicon transistors of moderate power, showing radiation stability

14 p2213 A71-30625

Erythrocytes life span and bone marrow production in dogs subjected to gamma irradiation in doses simulating prolonged space flight conditions

15 p2356 A71-31307

Peripheral blood and bone marrow morphological composition in dogs subjected to chronic and repeated gamma irradiation

15 p2357 A71-31308

Amyotetrate and ATP effect on hemopoiesis of dogs subjected to chronic and repeated gamma irradiation

15 p2357 A71-31312

Neutron irradiation effect on lattice parameters and distortion energy of titanium and chromium carbides, using X ray analysis

15 p2430 A71-32152

Quartz, organic glass and plexiglass luminescence under giant pulse ruby laser radiation

15 p2422 A71-32462

Radiation effects on epoxy adhesive mechanical properties including compressive shear stress, modulus of elasticity and tensile strength

15 p2439 A71-32510

Radiation effects on bonding characteristics of epoxy-metal and epoxy-glass adhesive joints

15 p2439 A71-32511

Rat irradiated spinal cord, detailing orthodromic ventral root and monosynaptic reaction to rhythmic and increasing frequency stimulation

15 p2362 A71-32735

Soviet army medical appraisal of chronic microwave field induced affections, noting evaluation procedures inadequacy

16 p2534 A71-32827

Plasma generation by photon irradiation, radiolytic mechanism and high energy particle bombardment, discussing ionized media chemical reactions

16 p2540 A71-32971

Earth orbital radiation variations effect on climate, noting minor temperature, wind and hydrological changes

16 p2562 A71-33069

Plane and cylindrical waves three dimensional propagation, investigating finite electrical fluid conductivity and radiation effects in MGD

16 p2618 A71-33172

Plasma flow wave propagation, investigating compressibility, radiation and finite electrical conductivity effects with plane asymptotic solution combinations

16 p2618 A71-33173

Radiation defects isochronal annealing effects on absorption spectral distribution of gallium arsenide irradiated with fast neutron flux

16 p2620 A71-33184

GaAs single crystals defects formation during low temperature gamma photons and electron irradiation, considering electrical properties

16 p2620 A71-33185

Neutron and gamma radiation effects on electrophysical properties of high resistivity Si single crystals grown in hydrogen atmosphere

16 p2621 A71-33186

Gamma radiation induced changes in parameters of black silicon carbide nonlinear semiconductor resistors/varistors

16 p2546 A71-33464

Cosmic and telluric radiation biological effects on parameria, discussing relationship between dosage and growth rate

16 p2532 A71-33757

Tungsten single crystals under deuteron bombardment, noting structural defects formation as function of irradiation energy

16 p2595 A71-33883

Endurance limit of construction materials under fast and thermal neutron irradiation in reactor channel

16 p2598 A71-33986

Periodic orbits around Lagrange libration points of restricted three body problem disturbed by gravitational and radiative influences

17 p2809 A71-35599

Microwave radiation biological effects review and bibliography covering protein activity, genetic, central nervous system and cardiovascular effects

18 p2864 A71-35956

Apollo astronauts light flashes observation during lunar flight, discussing interpretation as scintillations in eye lens by multiply charged cosmic rays focusing on retina

19 p3001 A71-37299

Gas and surface temperature distributions for laminar flow in circular tube, considering conduction, convection and radiation effects

[ASME PAPER 71-HT-17]

19 p3164 A71-37988

Plasma radiation effects in gas tube electric arc heating, obtaining temperature and heat flux profiles and I-V characteristics from energy transport mathematical model

[ASME PAPER 71-HT-18]

19 p3164 A71-37989

Book on biological effects of radiation covering ionizing radiation properties and effects at molecular, cellular and tissue levels

19 p3002 A71-38048

Equivalent circuits for planar devices behavior under ionizing radiation, considering bipolar and MOS transistors

19 p3034 A71-38521

Cystine synthesis in simulated primitive conditions by UV irradiation of methane, ethane, ammonia, water vapor and hydrogen sulfide in spherical vessel

19 p3014 A71-38678

Cosmos satellite data on mainland China thermonuclear explosion of 27 December 1968, observing radiation effects on particles in natural radiation belts

20 p3278 A71-39128

Combined action of vibration and gamma irradiation on sporulation dynamics, survival rate and mutability of *Chlorella*

20 p3193 A71-39237

Gas heating by LF radiation due to Compton scattering near quasars, Seyfert galaxies nuclei and pulsars

20 p3289 A71-39293

Medical, zoological and biological effects of ELF signals in atmosphere, comparing with EEG alpha and gamma rhythm

20 p3193 A71-39478

Soyuz observation of tritium and He-3 nuclei in Al targets exposed to space radiation

20 p3280 A71-39601

Solar radiation effects on upper atmosphere soft electron flux and energy spectrum during day and night

20 p3281 A71-39724

Biosatellite 2 onboard experiments studying weightlessness effects on biological processes and interaction with radiation from Sr 85 gamma ray source

21 p3341 A71-40007

Radiation role in nonequilibrium boundary layer during atmospheric reentries at speeds exceeding escape velocity

21 p3368 A71-40694

Atmospheric wind, temperature, turbulence, hydrometeors, ozone, cosmic radiation and radio activity effects on commercial SST Concorde flight

21 p3325 A71-40829

Gangliosides and cerebroside content in rat brain under normal conditions, during hypoxia and under small X ray doses action

21 p3337 A71-41057

Semiconductor radiation-induced electrical conductivity changes correlation to forbidden band from theoretical model, considering radiation defects as conductivity compensators

21 p3431 A71-41230

Monte Carlo method computer simulation for displacement cascades energy and space structure in Ge, Si and PbS, interpreting semiconductor electrical properties under hard radiation

21 p3432 A71-41304

Auger recombination coefficient determination for nonequilibrium carriers in n-type InAs from photoconductivity and light absorption under laser excitation at high levels, noting electron mobility

21 p3433 A71-41310

Impurity photoconductivity spectra determination for n and p type Si crystals under 660 MeV proton irradiation

21 p3433 A71-41311

Gallium selenide excitation by ruby laser radiation, investigating impurity photoconductivity dependence on radiation intensity

21 p3395 A71-41352

Soviet book on animals morphophysiological changes in cardiovascular and nervous systems and various internal organs under RF wave exposure

21 p3344 A71-41369

Circumsolar radiation and atmospheric turbidity effects on readings of compensation type pyroheliometers with allowance for receiver sensitivity

21 p3384 A71-41382

Intense ionizing radiation and thermal treatment effects on electrical parameters of Si semiconductor devices

22 p3584 A71-41619

Kinetic theory of optically pumped gas, incorporating atomic line radiation effects on spatial and time evolution of velocity distribution

22 p3530 A71-41888

Electromagnetic radiation in stagnation flow region, determining temperature distribution absorption coefficient of carbon dioxide at rest between two parallel plates

22 p3621 A71-42024

Methane atmosphere polymerization by solar UV to form primordial oil slick, discussing importance to life development

22 p3535 A71-42074

Computer predictions of postirradiation reliability of electrical circuits, using Sceptre program and component tests

22 p3518 A71-42111

Neutron irradiation effects on Si p-n junction field effect transistors I-V characteristics, charge distribution in space charge region and transconductance

22 p3586 A71-42297

Radiation effects on components of science instruments used on outer planets Grand Tour mission

22 p3574 A71-42299

Book on high power laser radiation covering heating, melting, vaporization, particle emission, plasma production, gas and transparent material breakdown and biological effects

22 p3558 A71-42426

Optical second harmonic generation in excited tissues by Q switched ruby laser irradiation, observing narrow band emission line in collagenous tissues

22 p3559 A71-42567

Thermal radiation effect on laminar boundary layer of nonabsorbing fluid for plane heat emitting surface under natural and forced convection

22 p3622 A71-42680

Gamma emission effect on cystamine toxicity elimination in rats organism

22 p3492 A71-42715

Reactivity changes to pharmacological preparations under total proton and gamma ray irradiation of abdomen and head shielded rats

22 p3492 A71-42717

Glutamicoaspartic and glutamicoalanine aminotransferases activity in blood serum of dogs

- under gamma irradiation with shielded abdomen or head, observing hyperfermentemia
22 p3493 A71-42720
- Acceleration tolerance of gamma irradiated mice with and without radioprotectors
22 p3493 A71-42724
- Mice under combined gamma radiation and vibration and acceleration dynamic factors, studying radioresistance recovery rate
22 p3494 A71-42725
- Dogs peripheral blood reaction to complex action of transverse accelerations and gamma irradiation
22 p3494 A71-42727
- Radiation effects on rats peripheral blood state in low pressure environment with sea level value oxygen tension
22 p3494 A71-42732
- Composite tissue blocks method for comparative pathomorphological investigation of radiation pathology
22 p3505 A71-42734
- Radiation damage diagnosis in humans, investigating free amino acid excretion with urine by paper chromatography method
22 p3495 A71-42736
- Prolonged small radiation dosage effects on vestibular analyzer in normal and antiradiation drug protected dogs
22 p3495 A71-42798
- UV radiation effect on amino acids and peptides in different gas atmospheres in presence of salts and metal oxides
22 p3496 A71-42829
- Irradiation dose effect on alpha particle irradiated Al foil electrical resistivity recovery, using Wheatstone bridge measurement
23 p3689 A71-42934
- Ozone concentration measurements near sunrise by balloon-borne electrochemical ozonesonde, noting scattered radiation effect
23 p3667 A71-43074
- Mgd shock propagation in viscous heat conducting gas, investigating radiation escape effect
23 p3708 A71-43100
- Neutron bombardment effect on dislocation mobility in Ge single crystals investigated by bending and etching techniques
23 p3715 A71-43309
- Neutron irradiation effects on dissociative high temperature zinc diffusion in indium and gallium arsenides
23 p3716 A71-43480
- Microprobe measurements of rare gas composition for lunar rock 12013,10,31 mineral separates, noting cosmic ray bombardment role in K and Ar production
23 p3753 A71-43721
- Apollo 11 and 12 rocks luminescence under proton, electron, UV and X irradiation
23 p3760 A71-43774
- Apollo 12 returned Surveyor 3 component materials analysis for lunar exposure effects by nondestructive and destructive tests
23 p3765 A71-43811
- Nonsteady heat conduction of multilayer cylindrical and conical shells in periodic radiation flux, calculating temperature distribution
23 p3783 A71-44067
- Silicon carbide single crystal photoluminescence under pulsed ruby laser light irradiation at 77 K, discussing radiative recombination of excitons
24 p3833 A71-44666
- Cosmic ray biological effects and admissible dose level normalization in space flight from prolonged tests on dogs
24 p3798 A71-44890
- Monatomic gas flow in radiation field, noting effects on mass transfer
24 p3821 A71-45182
- Radiation flux induced material dispersion of solid surface, taking into account radiation energy absorption by discontinuity introduction
24 p3835 A71-45225
- Thermal dissociation reactions and radiation effects on flow variables in front of and behind strong normal shock, using gray gas approximation
24 p3822 A71-45368
- RADIATION EXPOSURE**
U RADIATION DOSEAGE
RADIATION FIELDS
U RADIATION DISTRIBUTION
RADIATION HAZARDS
Laser systems radiation hazards, considering operational requirements, personnel protective equipment, biological effects and exposure levels
01 p0021 A71-10008
- Cosmic ray heavy ion component biological effect, describing histological and radioautographic high altitude balloon experiment with black mice and rabbits
01 p0019 A71-11555
- Radiological risks of cosmic radiation during high altitude supersonic flights, considering galactic, solar and incident particles in aircraft atmosphere
03 p0473 A71-13099
- Control of biological laser radiation hazards
07 p1049 A71-19791
- Near field electromagnetic radiation probe for microwave measurements in proximity of hazard source
09 p1453 A71-23626
- Microwave/high frequencies safe exposure limits, discussing radiating aerial near field, radio hazards and human body absorption
10 p1573 A71-25080
- Source-subject coupling, reactive near field, multipath components and arbitrary polarization in hazardous EM fields quantification, discussing measuring techniques and instruments
11 p1717 A71-25286
- Radio frequency and microwave radiation hazards determination and elimination aboard naval ships
11 p1723 A71-25290
- Spacecraft systems radiation hardening design, discussing Tiroos satellite mission hazards and space exposure prediction for electronic parts, using flow chart rationale
11 p1839 A71-26333
- Biological tests of laser protective filters for eye as function of optical density and wavelength by sensitivity of in vivo ocular tissue response
13 p2020 A71-29035
- Aircraft personnel radiation hazards from radioactive luminous paint on instrument dials, signs and operational elements
13 p2021 A71-29145
- Environmental controls, health services and safety programs for outdoor range laser applications, considering USAF hazard regulations, public address system, etc
17 p2723 A71-34524
- Double standard for national levels of exposure and biological hazards of microwave radiation, comparing Soviet work to U.S.
19 p3008 A71-38442
- Environmental radiation exposure in air travel, comparing integral radiation dosages for conventional jet transport aircraft and SST
20 p3192 A71-38976
- High intensity light sources hazards analysis, discussing thermal detectors and vacuum and semiconductor photodiodes for pulsed laser outputs measurement
22 p3541 A71-41795
- Manned spacecraft hazard from charged particles radiation during solar flares and trapped particles by geomagnetic field, recommending protection methods
24 p3865 A71-44887
- RADIATION HEATING**
U RADIANT HEATING
RADIATION INDICATORS
U DOSIMETERS
U INDICATING INSTRUMENTS
RADIATION INJURIES
Book on eye injuries covering mechanical traumata, neuro-ophthalmology, chemical, thermal, radiation, electrical and sonic injuries, etc
05 p0711 A71-17010
- Respiratory inhibitor KCN for killing increase from single radiation doses and reduction of dose fractionation sparing effect
07 p1036 A71-18962
- Taurine restorative effect in patients with marked leucopenia induced by radiotherapy
07 p1040 A71-18991
- Chromosome radiation injury preservation in generations of X ray irradiated cells of human diploid strains
08 p1242 A71-21966
- Renal anatomical pathology in dogs long after high energy proton irradiation, noting similarity to natural aging
09 p1388 A71-22194
- Laser thermal/photochemical burns and electric shock prevention by preemployment/regular physical examinations and safety requirement education
09 p1402 A71-23412
- Hematopoietic injury and recovery from radiation exposure for dogs and monkeys, showing dose protraction effects
16 p2532 A71-33774
- RADIATION INTENSITY**
U RADIANT FLUX DENSITY
RADIATION LAWS
NT KIRCHHOFF LAW OF RADIATION
NT STEFAN-BOLTZMANN LAW
RADIATION MEASUREMENT
Radiometric temperature measurement via source radiated power/photon flux ratio, using Planck equation variation
01 p0178 A71-10140
- He-Ne laser LF radiation parameters calculations verified experimentally
01 p0092 A71-10334
- Global ozone distribution from inverted radiance measurements by IR interferometer spectrometer /IRIS/ on Nimbus 3 satellite
01 p0074 A71-11249
- Water vapor emission measurement, using shock tube for gas heating and black body calibrated optical system for radiation measurement
01 p0028 A71-11348
- Gain measurement on pulsed radiation from high voltage discharges in mixtures of carbon dioxide, nitrogen and helium
01 p0096 A71-11423
- Venera probes UV radiation measurement, discussing photometric equipment and spectra for hot stars and Milky Way in L alpha line
02 p0304 A71-11912
- Absolute measurements of solar flux density at 9500 MHz, comparing Nagoya and Heinrich-Hertz Institute radiometric observations
02 p0302 A71-12760
- Cosmic rays intensity measurement in deep ocean with Cerenkov counter, determining Muon energy spectrum and absorption in water
03 p0477 A71-13862
- Concave mirror interferometer for laser radiation spectra measurements, featuring piezoelectrically tuned optical system
03 p0439 A71-14000
- Zodiacal light interpretation based on ground-based, satellite and deep space probe Helios observations, considering particle flux measurements
03 p0491 A71-14012
- Night airglow spectral components by Cosmos 92 satellite measurements, considering UV region sources and intensity variations
03 p0417 A71-14050
- IR radiation measurement of chain branching rates in hydrogen-oxygen mixtures ignited by reflected shock waves
04 p0548 A71-14695
- Underground cosmic ray showers muon pairs lateral distribution measurement
04 p0640 A71-14815
- Simultaneous meteorological satellite IR radiation measurements and cloud photographs for superposition and mutual interpretation
05 p0752 A71-16676
- He I 584 A dayglow radiation measurement by retarding potential photoelectron analyzer on Javelin sounding rocket
06 p0887 A71-17267
- Monte Carlo calculations of intrinsic radiation and blackness degree of nonisothermal cavities with non-specific temperature profile
06 p0897 A71-17529
- Absolute intensities measurement method for spectrum of solar disk center at 2962-4087 A
06 p0967 A71-17902
- Statistical reliability tests for cosmic ray intensity records from ground stations, stressing time series aspect
06 p0951 A71-18108
- Morphology and dynamics of low intensity monochromatic midlatitude auroral arcs of 6300 A /O I/, comparing results with observation during IGY
07 p1103 A71-19766
- Ethylene diffusion flame radiation measurements, determining pressure effects and contributory ratio of carbon particles and gaseous radiation
08 p1346 A71-20859
- Solar radiation flux standard instruments development for meteorological measurements, discussing calorimetric techniques and high precision radiometers
08 p1293 A71-21737
- Longitudinal electron plasma waves generated by electron beam-plasma interactions, discussing simultaneous radiation and incoherent microwave scatter measurements in relation to theory
08 p1341 A71-21746
- Pyrolytic graphite hemispherical emissivity measurement on surface parallel and perpendicular to deposition surface at 1200-2300 K
08 p1323 A71-21921
- Be, V, Cu and Al foils low temperature integral radiant emission, describing calorimetric assembly
09 p1466 A71-22264
- SNAP 15A heat source gamma ray intensity measurements and identification of gamma ray producing isotopes, describing measurement apparatus
09 p1491 A71-22456
- Auroral X radiation at magnetoconjugate points Kerguelen/Archangel region, using balloon-borne spectrometers
09 p1438 A71-23146
- Balloonborne radiometric instrumentation for solar and thermal radiations upward and downward flux measurements, discussing net radiation balance as function of solar elevation
09 p1515 A71-23558
- Polar cap cosmic radiation intensity measurement for deducing electromagnetic conditions near earth and in interplanetary space
10 p1661 A71-24310
- IR astronomical background radiation measurements at very near IR and longer wavelengths for interplanetary, galactic and intergalactic sources
10 p1677 A71-24582
- Nuclear interactions superhigh energy measurements in cosmic particles on high mountain large sandwich assembly
10 p1662 A71-24666

Mean neutron monitor multiplicity time variations for solar cosmic ray events and Forbush decreases with modulation spectrum allowance

11 p1816 A71-25753

Quantum counting efficiency of commercial photomultiplier at 0328 Å by direct measurements, including signal and background dependence

11 p1766 A71-26300

Vertical geophysical sounding rocket research program and equipment for observing ionospheric parameters, solar UV and X rays, atmospheric absorption and meteorites

11 p1839 A71-26353

Thermal control coating materials, measuring separate and combined electron and UV radiation effects on reflectance and emittance in vacuum

11 p1800 A71-26519

Superfluid-helium-cooled rocket-borne far-IR radiometer for night sky radiation measurement, discussing cryogenic, optical detection and electronic systems design features and performance

12 p1903 A71-26791

Extensive air shower size measurements, relating energy spectra to primary energies up to 10 million TeV by calorimetric method

13 p2122 A71-28069

Radio particle correlation of extensive air showers at large zenith angles, using twofold coincident 44 MHz receiver trigger-scintillator system

13 p2127 A71-28108

Venera probes UV radiation measurement, discussing photometric equipment and spectra for hot stars and Milky Way in L alpha line

13 p2133 A71-28199

Primary component corrections for global cosmic ray variations from latitudinal expeditions, discussing method adaptation to computer

13 p2128 A71-28528

Zenith skylight spectral intensity distribution measurement during total solar eclipse of 7 March 1970, using optical scanning spectrometer

14 p2309 A71-30121

Extragalactic X ray sources from Explorer 42 flight, confirming explosive nature of Seyfert galaxies revealed by optical telescopes

14 p2313 A71-30401

Sidereal anisotropy in muon signal observed by cosmic ray telescope above sea level, indicating production by neutral particle and leakage relative to anticoincidence factor

15 p2477 A71-31797

Cosmic ray muon and neutrino measurements with deep underground scintillation detector array

15 p2477 A71-31800

Low energy gamma ray measurements by balloon flights, detecting peak energy due to electron-positron annihilation

15 p2479 A71-32077

Cosmic ray intensity gradient measurement from Lost City meteorite Ar 37/Ar 39 ratio

15 p2479 A71-32361

Cosmic ray produced radionuclides in Lost City meteorite, determining concentrations by nondestructive two-parameter gamma ray analysis

15 p2479 A71-32363

IR transducer with detector for space applications, measuring capacitance on electronic bridge circuit based on temperature and pressure effects [ONERA-TP-963]

16 p2576 A71-32845

Optical diagnosis and measurements for radiation from gases in nonequilibrium flow

16 p2578 A71-33153

Solar flare activity and sunspot distribution over central meridian from optical data by NASA solar particle alert network 1967-69

16 p2635 A71-33437

Primary cosmic ray nucleonic component observation by scintillator-Cerenkov telescope on OGO 3 satellite

16 p2628 A71-33932

Statistical measurements of solar protons, alpha particles and heavier nuclei by lunar orbiting Explorer 35

16 p2628 A71-33933

Solar protons penetration over polar cap during 25 February 1969 event from particle and magnetic field measurements inside and outside magnetosphere by satellites

16 p2628 A71-33934

Solar particle flux profile and low latitude cut-off observation by low altitude satellite during March 1969 to July 1970 events

16 p2628 A71-33936

German monograph on ozone determination from sky radiance, considering Rayleigh and Mie scattering

17 p2733 A71-34794

Pyrolytic graphite hemispherical emissivity measurement on surface parallel and perpendicular to deposition surface at 1200-2300 K

17 p2763 A71-35265

Flame temperature measurement by radiation and gas dynamic methods

17 p2745 A71-35440

Solar radiation field in polluted atmosphere, measuring intensity, polarization and flux due to aerosol scattering for comparison with Mie theory computation

17 p2736 A71-35563

Polarization measurement of cosmic ray muons at sea level as function of energy and zenith angle

19 p3124 A71-37284

Vertical 1 single stage geophysical rocket design and instrumentation for X rays, solar UV and meteoritic concentration measurements

19 p3154 A71-38530

Time resolved gain measurements of pulsed two level laser system, using computer for curve analysis

20 p3245 A71-39179

Radiometric measurement of total normal emittances of real surfaces at cryogenic temperatures

20 p3313 A71-39289

Vertical temperature profiles from Nimbus 3 satellite spectral radiance measurements, stressing importance for atmospheric circulation prediction

20 p3258 A71-39666

Relativistic primary cosmic rays chemical composition between Be and Fe from charge spectrum obtained with Cerenkov counters

20 p3284 A71-39756

Extensive air showers attenuation length measurement in Japan 1964-1968, using scintillator

20 p3284 A71-39863

Low energy solar particle observation by widely separated Mariner and Explorer spacecraft, noting flare-associated and nonflare intensity peak correlation with sun

20 p3284 A71-39876

Balloon Sonde I experiment, discussing telemetry from flying body and temperature effects on earth IR radiation measurement

22 p3535 A71-42053

Astronomical polarimetry at 5 and 10 microns for intensity measurements of IR sources

22 p3545 A71-42147

Cosmic rays intensity measurement in deep ocean with Cerenkov counter, determining muon energy spectrum and absorption in sea water

22 p3595 A71-42663

Isentropic nature of stratospheric air masses motion from balloon measurements of temperature and radiation

23 p3671 A71-43338

Lower stratosphere submillimeter wavelength radiation measurement using Fourier transform spectroscopy with phase modulation

24 p3822 A71-44448

Low energy primary cosmic gamma ray measurements for spectrum latitude dependence and time variations near earth by Cosmos satellite scintillation spectrometer

24 p3865 A71-44564

Airborne measurement of directional variation in reflected solar radiation over soil surface and vegetation, using scanning radiometer

24 p3826 A71-44984

RADIATION MEASURING INSTRUMENTS

NT ACTINOMETERS

NT BOLOMETERS

NT CERENKOV COUNTERS

NT DICKE RADIOMETERS

NT DOSIMETERS

NT ELECTRON COUNTERS

NT ELECTROPHOTOMETERS

NT ELECTROSTATIC PROBES

NT FABRY-PEROT SPECTROMETERS

NT GEIGER COUNTERS

NT GOLAY DETECTOR CELLS

NT HODOSCOPES

NT INFRARED DETECTORS

NT INFRARED INSTRUMENTS

NT INFRARED SCANNERS

NT MICROWAVE RADIOMETERS

NT RADIATION DETECTORS

NT RADIOMETERS

NT RIOMETERS

NT SILICON RADIATION DETECTORS

NT SOLAR SPECTROMETERS

NT SPECTORADIOMETERS

NT THRESHOLD DETECTORS [DOSIMETERS]

Long wave radiation earth-atmosphere balance measuring devices, discussing pyrogeometer, balometer and tests in Antarctica

01 p0080 A71-10541

Semiconductor photoelectric sensor for monitoring laser emission energy in conjunction with memory oscillograph or single pulse peak voltmeter

01 p0093 A71-10623

Radiation measuring instruments assembly for extensive air showers and cosmic ray particle nuclear interactions at high energies

01 p0084 A71-11367

Power meter for large or divergent CW or pulsed laser beams

03 p0427 A71-13919

Solar X-ray radiation measurements using real time telemetry from SOLRAD satellites

05 p0799 A71-17001

Optical system for spatially resolved measurement of extended bodies radiative emission and self absorption, describing design for measuring gas discharge plasma radiative properties

06 p0928 A71-18224

Magnetic Compton spectrometer for high intensity pulsed gamma ray environments and nuclear device spectral measurement

08 p1294 A71-21840

ATS-5 satellite-borne auroral electron and proton energy spectrum measuring instrument using cylindrical coordinate electrostatic analyzer

08 p1294 A71-21845

X ray astronomy, discussing measurement methods and equipment, radiation mechanism and cosmic sources, with particular reference to hot rarefied plasma and pulsar types

09 p1516 A71-22058

Near field electromagnetic radiation probe for microwave measurements in proximity of hazard source

09 p1453 A71-23626

Cosmic particle gradient perpendicular to solar equator plane and semiannual cosmic ray variations, using worldwide neutron monitor network

10 p1660 A71-23839

Total normal emittance under simulated reentry conditions, using emissometer with aluminum oxide reference cavity integral within sample

11 p1764 A71-26249

[AIAA PAPER 71-468] Barium titanate pyroelectric receivers for giant pulse laser emission measurements

12 p1915 A71-27756

Balloon-borne transistorized stratospheric cosmic ray probe, describing simultaneous gas discharge and dual coincidence telescope counters data transmission

14 p2247 A71-30596

Primary cosmic ray electron energy and intensity measuring equipment, using Cerenkov and scintillation counters, spark chamber, lead absorber and photorecorder

14 p2247 A71-30598

Cosmic ray measurements at various altitudes, describing magnet spectrograph for momentum spectra and particle identification

15 p2408 A71-31813

Integral wavelength solar radiation constant measurements by jet and rocket research aircraft, high level balloons and Mariner space probes

20 p3260 A71-39682

Atmospheric background radiation measurements with balloon-borne Michelson interferometer, noting data reduction and calibration methods

22 p3549 A71-42563

RADIATION MEDICINE

NT RADIOBIOLOGY

Unified approach to dosimetry in radiological protection, discussing practical application and instrument calibration to existent standards

06 p0859 A71-18030

Lethal radiation in *Escherichia coli* B/r, investigating post irradiation DNA breakdown inhibitors

07 p1033 A71-18940

Radiosensitizers indanetrione, menadione Synkavit and N-ethylmaleimide, noting effects on murine ascitic tumor

07 p1035 A71-18950

Anoxic fern spores X ray sensitization, observing diacetyl and isatin effects

07 p1036 A71-18961

6-azauridine effect on radiation induced inhibition of Yoshida sarcomas, Ehrlich carcinomas, benzopyrene-induced carcinomas and spontaneous mammary carcinomas growth and transplantability

07 p1039 A71-18978

Bromouridine as radiosensitizing agent improving effectiveness of radiation therapy of malignant brain tumor cells

07 p1040 A71-18990

Monograph on protection against ionizing radiation from external sources covering medical, veterinary and industrial uses

08 p1248 A71-21311

RADIATION METERS

U RADIATION MEASURING INSTRUMENTS

RADIATION NOISE

U ELECTROMAGNETIC NOISE

RADIATION PRESSURE

NT ELECTRON PRESSURE

NT ILLUMINANCE

NT LUMENS

NT LUMINANCE

NT LUMINOUS INTENSITY

NT SOUND PRESSURE

Gravity gradient satellite librational dynamics under solar radiation pressure, using analytical and numerical integration methods

01 p0163 A71-10755

Wolf-Rayet star atmospheres, discussing matter density distribution, light pressure effects on particle motion and H and He ionization levels

01 p0158 A71-10803

Optically thin medium convective instability, examining radiant pressure and magnetic field effects

01 p0158 A71-10804

Satellite orbit perturbations by solar radiation pressure, considering earth shadow in homogeneous field and long term effects

02 p0313 A71-12491

Magnetic and thermal pressures in solar wind from Explorer 34 data

05 p0797 A71-16016

Lunar satellite motion semianalytic solution, considering perturbative effects due to gravitational fields, solar radiation pressure and libration

05 p0809 A71-16541

Sunlight pressure forces and moments on complex shape artificial earth satellites, assuming uniform incident flux

09 p1492 A71-22374

Reflected radiative shock wave propagation velocity under transverse magnetic field, taking into account radiation pressure and energy

09 p1506 A71-23588

Solar radiation pressure acceleration effects on flat satellite in earth synchronous orbit, examining orbital shift and counteracting thrust velocity applications

10 p1671 A71-24333

Planetary nebulae mass ejection by radiation pressure, describing mathematical models for time independent outflowing envelopes

11 p1821 A71-25537

Spin dynamics and deformation measurements on PAGESOS balloon satellite by photoelectric photometry, noting solar radiation pressure torque

11 p1761 A71-25546

Short term interval satellite orbit perturbations, computing direct solar radiation pressure effects with computer program

13 p2137 A71-28477

Complex geometry surface light pressure momenta determination by body image projection onto photometric wedge and linear edge sliding screen procedure respectively, considering errors

13 p2071 A71-29154

Photoelectric, bolometric and photographic recording assembly for measurement of light pressure and aerodynamic forces on complex shape body in free molecular flow

13 p2071 A71-29155

Plane photogravitational restricted circular three body problem symmetrical periodic orbits closing on rotating plane after revolutions

15 p2483 A71-31340

PAGESOS spacecraft orbital acceleration prediction by radiation pressure perturbation theory accounting for nonisotropic scattering of solar spectra from rotating ellipsoidal body

16 p2641 A71-33772

German book on satellite geodesy covering two body problem, perturbation theory, earth gravitational field, gravitational effects of sun and moon, radiation pressure, etc

17 p2799 A71-34470

Light pressure measurement acting on Echo 1 satellite, considering integral reflection coefficient

20 p3306 A71-39132

Attitude control of gravity orientated satellite in arbitrary orbit by solar pressure, showing libration damping characteristics of radiation force

20 p3306 A71-39396

Mathematical model for studying solar radiation pressure effects on artificial satellite motion

21 p3438 A71-40104

Plasma confinement in bounded systems, considering externally induced field HF pressure effect on plasma density distribution

22 p3580 A71-41600

Jump conditions across three dimensional curved shock in radiation gas dynamics, considering radiation pressure number effect

22 p3530 A71-41695

Coupled librational dynamics of gravity oriented cylindrical satellite, calculating solar radiation pressure effects on attitude control behavior

22 p3611 A71-42042

Plane photogravitational restricted circular three body problem symmetrical periodic orbits closing on rotating plane after revolutions

22 p3606 A71-42615

Covariance analysis of Mars gravity harmonics, ephemeris and radiation pressure from Mariner 1971 range and Doppler radio tracking data [AAS PAPER 71-343]

23 p3727 A71-43016

Mathematical model of solar radiation pressure force and torque acting on spacecraft surface intercepting solar photon stream [AAS PAPER 71-352]

23 p3728 A71-43024

RADIATION PROTECTION

NT RADIATION SHIELDING

NT SOLAR RADIATION SHIELDING

Laser systems radiation hazards, considering operational requirements, personnel protective equipment, biological effects and exposure levels

01 p0021 A71-10008

Microwave effects on living creatures, considering thermal and nonthermal effects on individual body organs and systems, permanent changes and protective measures

02 p0208 A71-12845

Si solar cell radiation resistance improvement through Li doping, noting efficiencies in excess of state-of-art N/P cells after exposure to 1 MeV electrons

05 p0703 A71-16088

Radioprotectors and antibody formation in rats, determining ionizing radiation survival rate index for lethal dose and hematological indices

05 p0710 A71-16819

Prophylactic radiation protection through lipid toxicants reduction in white rats tissues by high efficiency chemical radioprotectors

06 p0849 A71-17391

Unified approach to dosimetry in radiological protection, discussing practical application and instrument calibration to existent standards

06 p0859 A71-18030

Biological radioprotectants in space flights including amino acids, bacterial polysaccharides, hormones and vitamins

06 p0861 A71-18358

Cosmic radiation protection of spacecrews by drugs, extrapolating animal data to humans

06 p0861 A71-18359

Radiation protection and sensitization - Conference, Rome, May 1969

07 p1031 A71-18926

Molecular mechanisms of bacterial cell radiosensitization and protection, discussing radiation produced free radicals interactions

07 p1031 A71-18927

Radiosensitizer and radioprotector action mode in altering X ray effects on DNA in biological systems of different complexity

07 p1032 A71-18928

Chemical protection against ionizing radiation by thiols and disulfides, discussing hydrogen transfer

07 p1032 A71-18930

Radioprotective action of amines and hypoxic agents by blocking oxygen transport to tissues

07 p1032 A71-18931

Radioprotective effect of cysteine on lysozyme in dilute aqueous solution, discussing scavenging water radicals

07 p1032 A71-18932

Chemical radioprotection by selenium containing compounds in biological and chemical systems tested in irradiated rats

07 p1032 A71-18933

Reactivity measurements of protective agent selenourea toward primary water radiolysis radicals

07 p1033 A71-18934

Structure-function studies of aminoethiol radioprotectants on *Escherichia coli* B/r, discussing radiation response at 274 and 77 K

07 p1033 A71-18936

Sulfur containing organic chelating compounds as radiation protective agents

07 p1034 A71-18941

Cysteamine protection of hydroxyurea sensitized Chinese hamster lung cells during X ray exposure

07 p1034 A71-18947

Thiol and disulphide compounds radiation protection capacity at cellular level in tissue culture, using reproductive integrity as protection criteria

07 p1034 A71-18948

Organic free radical radioprotective and radiosensitizing effect, reporting Chinese hamster cell line survival characteristics after treatment

07 p1035 A71-18949

Radioprotective drugs relationship to modification of glycolysis in Ehrlich ascites tumor cells

07 p1035 A71-18954

Para-aminopropiophenone and propylene glycol radiation protective effect on hematopoietic stem cells of mice

07 p1036 A71-18959

Hematoporphyrin chlorhydrate radioprotective effects on mice, removing, weighing and fixing spleens for hematopoietic colonies count

07 p1036 A71-18960

Chemical radioprotective effectiveness modification by open skin wounds, discussing results with whole body X ray irradiated mice

07 p1037 A71-18964

Toxicity reduction of aminoethylisothionium compounds through n-substitution with amino acids, noting slight decrease in radioprotective effectiveness

07 p1037 A71-18965

Hypoxia protection against ionizing irradiation by anaerobic glycolysis stimulation, lactic acid increase and blood glucose level elevation

07 p1037 A71-18966

Sodium fluoracetate as radiation protective agent, noting dependence on selective blockade of enzyme aconitase

07 p1037 A71-18967

Temperature effect in sodium fluoracetate protective action mechanism for mice irradiation

07 p1037 A71-18968

Cysteamine AET, serotonin and mexamine antiradiation drugs, investigating protective effect against fractionated lethal gamma irradiation

07 p1037 A71-18969

Short and long term radiation effects reduction by chemical radioprotectors mixtures, noting improved survival and decrease in leukemia and cancer incidence in X ray irradiated mice

07 p1037 A71-18970

Rat bone marrow chromosomes radiation protection, using 5-hydroxytryptamine

07 p1038 A71-18973

Irradiation protection in mice, dogs and sheep by bacterial endotoxin injection, discussing hematopoietic system stimulation and leukocyte counts

07 p1038 A71-18974

Mice protection against irradiation damage by adrenochrome monoguanilylhydrazine methan-sulphonate

07 p1038 A71-18977

Biochemical mechanism of radioprotective action of aminoethiols in mammals

07 p1039 A71-18979

Rats and mice blood redox potentials injected with cystamine, investigating increased radioprotection

07 p1039 A71-18980

Radioprotective mercaptoethylamine (MEA) effect on aerobic resynthesis of ATP in thymus nuclei and oxidative phosphorylation in rat liver mitochondria

07 p1039 A71-18984

Amino-ethyl-S-2-isothiuronium radio protective dose effects on enzyme activity, cardiovascular changes, blood transaminases concentration, bone marrow and peripheral circulation

07 p1040 A71-18986

Si solar cells transparent radiation protective coatings stability and degree of blackness, discussing UV irradiation and proton and electron bombardment

08 p1287 A71-21024

Monograph on protection against ionizing radiation from external sources covering medical, veterinary and industrial uses

08 p1248 A71-21311

Industry safe laser laboratory operating environments with reflection free walls, restrictive admittance and periodic personnel examinations

09 p1402 A71-23413

Book on electromagnetic fields and life environment covering biological effects of radio waves, protection, radiation sources, permissible intensities, working conditions

12 p1873 A71-26868

NASA space station design, describing operational procedures, structure, meteoroid, thermal and radiation insulation and living quarters

15 p2498 A71-31137

Magnetic shield design for protecting cylindrical space vehicle from space electron radiation, using simulator for engineering data

15 p2500 A71-32042

Antixposure suits physiological evaluation for subjective comfortableness, oral and skin temperatures and pulse rate, determining optimum environmental temperature

17 p2692 A71-35195

Si solar cells transparent radiation protective coatings stability and degree of blackness, discussing UV irradiation and proton and electron bombardment

20 p3240 A71-39604

Radiation protection drugs effects on albino rats hypoxia resistance, discussing hypoxic hypoxia response to intraperitoneally and perorally administered cysteamine and aminoethylisothiuronium

22 p3491 A71-42704

Radiation sickness prophylaxis chemical compounds, discussing protection mechanisms, radical activation and afflicted cell recovery

22 p3505 A71-42710

Prophylactic medication for radiation damage treatment, covering toxicity, pharmacological properties, metabolism, dosage and physiological action

22 p3505 A71-42711

Death rates, median life span and weight in mice exposed to gamma radiation after intra-abdominal injections of cysteamine

22 p3505 A71-42712

Chemical agents protective properties on albino mice under gamma-neutron radiation, noting dose and composition effects

22 p3492 A71-42713

Cystamine elimination rates in rats, extending radiation protective action by reinjection of eliminated portions

22 p3492 A71-42714

Cystamine hydrochloride or vitamin B complex with vitamin C for radiation sickness prevention and therapy

22 p3493 A71-42723

Mice acceleration before and after gamma irradiation, determining protective effect of cystamine in adrenaline and amphetamine mixture

22 p3494 A71-42726

Radioprotective effectiveness of cystamine and S beta-aminoethylisothiuronium in mice under combined gamma irradiation and transverse acceleration loads

22 p3494 A71-42730

- Radiation protection biological aspects - Conference, Kyoto, October 1969 23 p3638 A71-44325
- Radiation protection of Soyuz-9 crew, using solar activity forecasts 24 p3800 A71-44531
- Manned spacecraft hazard from charged particles radiation during solar flares and trapped particles by geomagnetic field, recommending protection methods 24 p3865 A71-44887
- Manned spacecraft radiation protection against cosmic rays, considering proton attenuation in shielding materials and dose formation in body tissues 24 p3801 A71-44889

RADIATION PYROMETERS

- Active cavity radiometric and international pyrheliometric scales comparison and solar constant from simultaneous solar irradiance measurements 16 p2581 A71-39399

RADIATION RESISTANCE

U RADIATION TOLERANCE

RADIATION SHIELDING

NT SOLAR RADIATION SHIELDING

- Hydrogen impregnated glass covers of solar cells preventing irradiation caused darkening and loss of power output under space environment conditions 05 p0700 A71-16066

- Self shielding effect of various substances under intense light 05 p0762 A71-16380

- Shielding effectiveness of different body portions during repeated proton irradiation on dogs 06 p0861 A71-18360

- Multilayer insulation systems for cryogenics protection aboard spacecraft, considering mechanical properties, radiation shielding, component evacuation rate and outgassing 08 p1375 A71-21748

- Nuclear radiation shielding design for space base SNAP 8 reactor, discussing geometry constraints for lithium hydride and U loop layers model 09 p1492 A71-22808

- Reactor shield weight optimization using FASTER-III Monte Carlo computer program for neutron and gamma ray transport 09 p1539 A71-22810

- Earth intrinsic radiation flux incident angular coefficient, examining effect on partially screened flat spacecraft elements 09 p1546 A71-23154

- Luneberg lens antenna theory and gain for communication satellite radio links, discussing shielding from hostile space environment 10 p1583 A71-24450

- X ray astronomy, including celestial sources emission, discrete cosmic sources, recording techniques, isotropic background and shielding 10 p1681 A71-25117

- In-core thermionic power system for manned space station application, discussing driver fuel elements, nuclear radiation shield, heat rejection and coolant outlet temperature 11 p1710 A71-25869

- Lunar dust deposition and brushing effects on spectral solar reflectance of thermal control materials in vacuum [AIAA PAPER 71-459] 11 p1799 A71-26241

- Spacecraft systems radiation hardening design, discussing Tiros satellite mission hazards and space exposure prediction for electronic parts, using flow chart rationale 11 p1839 A71-26333

- Self shielding effect of solid surfaces under intense light 12 p1915 A71-27457

- Biased angle selection in Monte Carlo shielding calculations, using importance function 13 p2099 A71-29253

- Reactor shielding design in U.S. based on Boltzmann transport equation solutions and Monte Carlo method 13 p2099 A71-29254

- Reactor shielding problems solutions involving removal-diffusion theory, two dimensional transport theory and Monte Carlo method 13 p2099 A71-29255

- Reactor-shield-containment system models under impact tests, noting cracks, leaks and deformations 16 p2606 A71-33250

- Fast neutron spectra in lead and water shielded reactor, comparing liquid scintillator measurements with discrete ordinates code calculations 16 p2606 A71-33253

- Multilayer insulation systems development and selection for cryogenics thermal protection on space vehicles, considering mechanical properties, radiation shielding, components, evacuation rate and outgassing 19 p3171 A71-38547

- Brayton cycle electric space power supply systems, describing shielded reactor and heat exchanger design 20 p3263 A71-38924

- Comparative abdomen and head shield effect during gamma irradiation of dogs on protein fractions in

- blood serum, noting increased globulins and glutamate aspartate transferases 20 p3188 A71-39222

- Radiation condenser computer program generalization to include effective radiative steady state node multiple enclosure simplification shield for thermal analysis optimization 20 p3314 A71-39357

- Nuclear characteristics of plutonium fuel for thermoelectric generators and required shield thicknesses for sensitive radiation experiment in outer planet spacecraft 22 p3592 A71-42300

- Partial body shielding effects on rats radiation sickness survival rates under gamma-neutron radiation, comparing head and belly shielding effectiveness at different intensities 22 p3492 A71-42716

- Reactivity changes to pharmacological preparations under total proton and gamma ray irradiation of abdomen and head shielded rats 22 p3492 A71-42717

- Head and abdomen shielding effects on radiation sickness evolution in dogs under lethal gamma irradiation 22 p3493 A71-42718

- Abdomen shielding effects on chromosome aberrations in bone marrow cells of guinea pigs and rats under gamma irradiation 22 p3493 A71-42719

- High energy proton irradiation of rats with partial shielding of abdominal region, observing pathomorphological changes in myocardium, nervous system and radiosensitive organs 22 p3493 A71-42721

- Rat organs pathomorphological changes under gamma neutron irradiation with head and abdomen shielding, noting intestines early damage 22 p3493 A71-42722

- Manned spacecraft radiation protection against cosmic rays, considering proton attenuation in shielding materials and dose formation in body tissues 24 p3801 A71-44889

RADIATION SICKNESS

- Muric preparation effect on DNA and RNA contents in hemopoietic organs during acute radiation sickness due to low power radiation 01 p0013 A71-11118

- Antihistamine treatment of hypotension and early transient incapacitation in monkeys under supralethal mixed gamma-neutron radiation 11 p1720 A71-26118

- Radiation sickness prophylaxis chemical compounds, discussing protection mechanisms, radical inactivation and afflicted cell recovery 22 p3505 A71-42710

- Partial body shielding effects on rats radiation sickness survival rates under gamma-neutron radiation, comparing head and belly shielding effectiveness at different intensities 22 p3492 A71-42716

- Head and abdomen shielding effects on radiation sickness evolution in dogs under lethal gamma irradiation 22 p3493 A71-42718

- White rats resistance to acute anoxic, anemic and histotoxic hypoxia during various phases of X radiation sickness, studying adrenal cortex histophysiological state 22 p3494 A71-42731

RADIATION SOURCES

NT MONOCHROMATORS

NT NEUTRON SOURCES

NT POINT SOURCES

- Coherent optical sources in form of lasers and parametric oscillators with usable power for communications 02 p0260 A71-12002

- Background noise in optical communication system, considering direct, reflected and scattered radiation sources in atmosphere 02 p0213 A71-12015

- Background emission characteristics, discussing cosmic electrons, X rays and radiation sources 02 p0300 A71-12092

- Very long baseline interferometry of galactic hydroxyl radical microwave emission sources 02 p0310 A71-12327

- Galactic and extragalactic sources of far IR radiation, discussing spectral distribution and luminosities 02 p0315 A71-12656

- Celestial sources far IR radiation detection using balloon-borne telescope 02 p0315 A71-12657

- Scorpius X-1 high energy X ray flux variations from balloon-borne scanner data 02 p0301 A71-12661

- Astronomical model for origins and time variations of compact strong sources radiation over all bands 02 p0315 A71-12663

- Low energy cosmic ray deuteron flux, examining energy spectral shapes of sources 02 p0303 A71-12871

- European X ray astronomy lunar occultation satellite, providing high resolution cosmic X ray source observation 02 p0303 A71-12952

- X ray sources location and grouping into supernova remnants and loose cluster categories, accounting for galactic background 03 p0483 A71-13187

- Stable tunable microwave source for spectroscopy using Gunn diode, giving microwave cavity spectrometer block diagram 03 p0428 A71-13924

- Carbon/oxygen and nitrogen/oxygen ratios in cosmic rays, considering energy dependence interstellar ionization loss and necessity for two component source model 03 p0480 A71-14051

- Three dimensional hologram reconstruction and recording, using extended source 03 p0428 A71-14057

- X ray sources at various flux levels, evaluating contribution to background radiation 03 p0481 A71-14269

- Intense X radiation source in Cetus region observation by Black Brant rocket 04 p0640 A71-15049

- Metagalactic background X rays origin, hypothesizing electron leakage from radio galaxy 04 p0657 A71-15748

- X ray background angular structure comparison with optical galaxies spatial distribution, ruling out universe models with sources following cosmological mass distribution 04 p0657 A71-15826

- H II regions compact radiation sources flux densities observation at centimeter wavelengths 05 p0812 A71-16690

- IR object IRC plus 10216 carbon monoxide emission at 2.6 mm, noting spectral line width, thermal emission and mass 05 p0812 A71-16695

- Transition radiation generation zones, determining physical cause 05 p0786 A71-17030

- X ray sources identification and position measurements near galactic center on basis of rocket experiments 05 p0814 A71-17234

- Spectral distribution reproduction of natural objects radiation by iodine lamp and glass filters 06 p0897 A71-17533

- Optimum line source approximation to desired radiation pattern, deriving least mean squared error expression 06 p0868 A71-17721

- Complex incident fields analysis by ray diffraction method, using set of simple sources with same amplitude and phase characteristics as actual incident field 06 p0868 A71-17728

- Uniqueness theorem for sources of electromagnetic fields expressible as magnitude integrable functions of time, considering implications for antenna aperture limitations on radar resolution 06 p0868 A71-17729

- Double star system with neutron star in pair with matter-losing star, discussing X ray sources variability causes 06 p0976 A71-18455

- Supersonic jet noise problem, discussing eddy-Mach wave radiation source mechanism from nonlinear streamwise development of inviscid instability waves in turbulent mixing layer [AIAA PAPER 71-150] 06 p0884 A71-18592

- Scorpius X-1 X ray emission temporal behavior on 3 March 1969 07 p1198 A71-19831

- Ammonia inversion radiation at 1.25 cm in direction of three galactic center sources, setting upper limits on densities in other areas 07 p1188 A71-19834

- X ray observations of NP0532 and other radio pulsars and galactic X ray sources 07 p1200 A71-20052

- Solar burst theories, considering type 3 radiation source model for determination of lower corona plasma waves energy densities 08 p1358 A71-20889

- Scorpius XR-1 simultaneous radio and optical measurements, discussing correlation of fluxes 08 p1360 A71-20985

- Background emission characteristics, discussing cosmic electrons, X rays and radiation sources 08 p1355 A71-21142

- Optimal time determination for using radioactive isotope as radiation source in nondestructive testing 08 p1332 A71-21898

- X ray astronomy, discussing measurement methods and equipment, radiation mechanism and cosmic sources, with particular reference to hot rarefied plasma and pulsar types 09 p1516 A71-22058

- X ray source in Perseus region, studying Aerobee rocket proportional counters measurements 09 p1512 A71-22348

- X ray spectrum measurement of Scorpius X-1 by Bragg spectrometer, explaining emission or absorption absence by source model with line weakened by electron scattering
09 p1518 A71-22349
- Cosmic X ray astronomy, discussing supernova, variable and extragalactic radiation sources, diffuse background radiation and Crab Nebula measurements
09 p1522 A71-22976
- Variable stars, quasars and X ray source ScoXr-1 UVB light photoelectric data, examining optical emissions and brightness variations
09 p1524 A71-23186
- Stellar X ray sources as close binary stars and old novae, calculating radiation by deceleration process
09 p1528 A71-23544
- OSO 3 satellite observations of diffuse X ray emission from galactic plane, eliminating straight line interpolation of spectrum between 3-10 keV X ray range and 100 MeV energy range
10 p1665 A71-23750
- Solar impulsive hard X-ray burst structure and location determination with balloon-borne modulation collimator, noting nonthermal electron origin
10 p1660 A71-23795
- Intensity variations of Cygnus X ray sources, analyzing high resolution results of Adelaide and Tasmania universities
10 p1661 A71-23882
- Boundary layer equations for radiating and absorbing gas flow at large Reynolds numbers
10 p1593 A71-24367
- Extraterrestrial hydrogen Lyman alpha emission source, investigating interstellar wind with OGO 5 satellite
10 p1601 A71-24438
- Lyman alpha sky background measurements by OGO 5 satellite, discussing absolute emission rate, spatial variations and origin
10 p1601 A71-24439
- IR astronomical background radiation measurements at very near IR and longer wavelengths for interplanetary, galactic and intergalactic sources
10 p1677 A71-24582
- Galactic X ray thermal emission model, discussing origin and location of sources
10 p1662 A71-24675
- Cosmic ray transport equation for solar sources, using Fisk numerical method by applying transformation of independent variable $U/r, T$
10 p1664 A71-24801
- Optimum frequency for detection of acoustic sources in upper atmosphere as function of altitude and turbulence
10 p1642 A71-24833
- X ray astronomy, including celestial sources emission, discrete cosmic sources, recording techniques, isotropic background and shielding
10 p1681 A71-25117
- Cygnus X-1 and X-2 X ray source location from Uhuru satellite measurements
11 p1814 A71-25213
- Seyfert galaxies NGC 1275 and NGC 4151 X ray flux detection, determining position and emission intensity
11 p1814 A71-25214
- M87, Cen A NGC 5128 and 3C 273 X ray emission observations in Virgo cluster, using Uhuru satellite
11 p1814 A71-25215
- Criticism of paper on synchrotron sources energy spectra formation, examining time dependent spectrum on boundary conditions
11 p1832 A71-26170
- Binary system of neutron star paired with matter-losing star, discussing X ray emission variability causes
12 p1956 A71-26605
- Milky Way Galaxy X ray sources, discussing bremsstrahlung, synchrotron radiation, Compton effect optical objects, supernova remnants and X ray astronomy
12 p1959 A71-26780
- Cosmic IR sources model based on assumption of cosmic ray particles emitting galactic sources surrounded by dust shells absorbing and reemitting energy
12 p1947 A71-26933
- Quasars and X ray sources, observing UVB magnitude variation with photoelectric data
12 p1963 A71-27077
- Cosmic ray diffusion from discrete sources in random galactic location, studying chemical constituents anisotropy and age with scattering model
12 p1948 A71-27367
- Atmospheric altitude of soft X ray source volume in solar flares from optical and radio observations
12 p1954 A71-27709
- Laser resonator properties with flat outlying mirrors, examining stimulated radiation generation and energy distribution
12 p1916 A71-27764
- Soft X ray background source, discussing north polar galactic spur as supernova outburst remnant
14 p2298 A71-29732
- German book on radiation climate of earth covering EM, corpuscular IR radiation sources, spectral composition, biological effects, etc
14 p2298 A71-29941
- Intense vacuum UV atomic line source excited in 2450 MHz microwave discharge cavity with clean spectrum, noting window deterioration and self absorption
14 p2240 A71-30127
- Aries-Taurus region as soft X ray source, determining energy flux and source
14 p2301 A71-30426
- High thrust density colloid emitting source development as basic microthruster for electrostatic propulsion systems
14 p2293 A71-30753
- [AIAA PAPER 71-694]
Laser radiation source time and spatial coherence effect on brightness distribution of image produced by hologram
15 p2402 A71-31254
- Fourier transform holography with partially coherent light from incoherent quasi-monochromatic source, considering bias problem
15 p2402 A71-31256
- Galactic discrete X ray sources identification with black nebulae, H II regions, close binary stars, Wolf-Rayet stars and planetary nebulae
15 p2482 A71-31330
- Neutron stars with pulsar characteristics in binary systems, discussing matter accretion relationship to X ray source evolution
15 p2483 A71-31342
- Thermal X ray sources associated with rotating collapsed stars with surrounding plasma shells, discussing plasma density profile and electron distribution in stellar magnetosphere
15 p2497 A71-32762
- Cygnus X-1 distance estimate based on low energy X ray spectrum obtained by sounding rocket
15 p2497 A71-32763
- Radiation from electrostatic waves in thin current sheet in geomagnetic tail into cold magnetized plasma, noting wave damping for wide frequency range
16 p2562 A71-32805
- Continuously tunable pulsed UV source using broadband dye laser emission input to rotatable KDP crystal
16 p2586 A71-33141
- Extragalactic cosmic X ray source, at high galactic latitude from sounding rocket experiments, correlating with galactic clusters
16 p2626 A71-33357
- Rotation measure and intrinsic angle of Crab pulsar emission, discussing optical and radio radiation origin
16 p2634 A71-33390
- Solar UV radiation data during 7 March 1970 eclipse from photometers sensitive to narrow bands, discussing sources, atmospheric absorption and D region ionosphere
16 p2627 A71-33773
- Solar flare X-ray emission source position during eclipse of 7 March 1970, using OSO-5 satellite data
16 p2627 A71-33813
- Cyg X-1 X ray intensity and energy spectrum variation data, using balloon-borne telescope
16 p2629 A71-34076
- Large amplitude periodic X ray pulsations from Centaurus X-3, observing abrupt source intensity and pulse rate changes
17 p2798 A71-34375
- Radiation source consisting of porous wall heated internally by hot gas, noting application as high altitude or space flare
17 p2728 A71-34888
- Critique of Vela 4 scattered Lyman alpha experiment, discussing maximum flux region and radiation intensity
17 p2805 A71-35380
- Coma cluster X ray source data from Uhuru satellite, observing size, luminosity, spectra, thermal bremsstrahlung mass and stability
17 p2796 A71-35413
- Vela X supernova remnant blast wave model and Gum Nebula formation, discussing kinetic and rotational energy transformation into radiation
17 p2807 A71-35414
- Lyman alpha resonant radiation in regions distant from cometary tails due to additional atomic hydrogen production from dust particles
17 p2809 A71-35595
- Extragalactic objects luminosity upper limits in hard gamma ray band, using Cosmos 208 scintillation Cerenkov telescope
17 p2796 A71-35736
- High intensity continuous gas discharge line source for extreme UV with low electromagnetic interference
18 p2914 A71-35845
- IR astronomy review covering semiconductor detectors and astronomical radiation sources including thermal and nonthermal sources
18 p2959 A71-35909
- IR radiation sources, discussing intermediate and early stars, galactic nucleus and extragalactic sources
18 p2958 A71-37029
- X ray source Cygnus X-1 position determination by Aerobee rocket-borne rotating modulation collimator
18 p2970 A71-37053
- Quasars and X ray sources, observing UVB magnitude variation with photoelectric data
19 p3133 A71-37427
- Nighttime D region behavior under ionization by X ray spectrum of Scorpius source
19 p3017 A71-37864
- Rotating magnetic white dwarf stars possibility as X ray sources with thermal spectrum, considering evidence based on Sco X-1 emission relationship to bremsstrahlung
19 p3127 A71-38010
- High peak power microwave oscillators, discussing pulsed limited space charge accumulation and TRAPATT diodes pulsed radiation sources performance
19 p3029 A71-38294
- Optimal radiant source power for photoelectric two axis autocollimation angle trackers, considering detector threshold sensitivity
19 p3067 A71-38659
- Finite thickness infinite slab with radiation from time dependent source, solving nonhomogeneous boundary value problem for linear transport equation
20 p3269 A71-39079
- Uniformly moving homogeneous isotropic non-dispersive conducting medium with arbitrarily distributed electromagnetic radiation sources, deriving solution in four dimensional covariant form
20 p3196 A71-39083
- Gamma radiation due to cosmic rays interaction with Mars surface/atmosphere and natural radioactive rocks elements decay, calculating intensity and spectral composition
20 p3280 A71-39630
- X ray rocket observations of Sco X-1 on 7-8 August 1969 compared to simultaneous optical observation, interpreting in terms of hot plasma model
20 p3283 A71-39751
- Vela pulsar interstellar scattering, studying pulse broadening, rotation measure and radiation origin near magnetic pole
20 p3303 A71-39937
- Jupiter and Saturn IR radiation sources, radio emission storms, magnetic fields, life existence, Grand Tour missions, etc
21 p3442 A71-40150
- Double radio emission sources during occultation period, noting structure, angular size components, positional errors and association to quasars
21 p3443 A71-40189
- Cosmic X and gamma radiation, discussing galactic and extragalactic sources, generation processes and spectrometric characteristics
21 p3438 A71-40522
- HF gravitational radiation due to quantum transitions, studying absorption, emission and sources
21 p3439 A71-40612
- Cen X-3 source X ray flux periodic variations due to white dwarf star radial vibrations based on nonrotating model
21 p3449 A71-40613
- Earth resources survey satellites, discussing natural sources/radiation, matter-energy interactions and perturbing media, remote sensors, space applications and reconnaissance
21 p3455 A71-40910
- High voltage source model for fast neutral particles, showing energy and yield as function of potential, pressure and magnetic field
21 p3421 A71-41295
- X ray variable source GX 1 plus 4 balloon observations in sky region near galactic center
22 p3592 A71-41927
- Circinus pulsating X ray source spectrum analysis, considering bremsstrahlung and black body models
22 p3592 A71-41928
- Variations in 10 micron flux from NGC 1068, noting strong nucleus emission modulation
22 p3605 A71-42397
- Galactic discrete X ray sources identification with black nebulae, H II regions, close binary stars, Wolf-Rayet stars and planetary nebulae
22 p3606 A71-42605
- Pulsar characteristics suppression in neutron stars of binary systems, discussing matter accretion relationship to X ray source evolution
22 p3606 A71-42617
- Highly compact X ray source spectrum fitted by black body model at 15 million K
23 p3732 A71-43076
- Scorpius X-1 optical and X ray flux transient short period oscillations correlation from Aerobee sounding rocket data
23 p3733 A71-43077
- Scorpius X-1 X ray flux observations, noting high frequency oscillations responsible for radiation production
23 p3733 A71-43078
- X ray astronomy, considering emissions and intensities of various classes of sources
23 p3736 A71-43449

Precision calibration system with adjustable temperature extended radiance source for long wavelength IR radiometer, discussing performance tests

23 p3676 A71-43512

Cosmic X ray astronomy, considering discrete sources and isotropic background X radiation

23 p3768 A71-43863

Cygnus X1 short term X ray flux pulsation variability from Southern Hemisphere sounding rocket flight

24 p3865 A71-44445

Vela X and Puppis A soft X ray observations using rocket-borne methane counter

24 p3866 A71-44907

X ray sources pulsation limits and locations determination by rocket-borne rotating modulation collimator

24 p3866 A71-44914

Galactic nucleus X ray source observations by Uhuru satellite, discussing emission and absorption spectra

24 p3866 A71-44915

RADIATION SPECTRA

NT ABSORPTION SPECTRA

NT BALMER SERIES

NT D LINES

NT ELECTROMAGNETIC SPECTRA

NT ELECTRONIC SPECTRA

NT EMISSION SPECTRA

NT FRAUNHOFER LINES

NT H ALPHA LINE

NT H BETA LINE

NT H GAMMA LINE

NT H LINES

NT HERZBERG BANDS

NT INFRARED SPECTRA

NT K LINES

NT LINE SPECTRA

NT LYMAN SPECTRA

NT MICROWAVE SPECTRA

NT RADIO SPECTRA

NT RAMAN SPECTRA

NT RYDBERG SERIES

NT SOLAR SPECTRA

NT STELLAR SPECTRA

NT TELLURIC LINES

NT ULTRAVIOLET SPECTRA

NT VIBRATIONAL SPECTRA

Radiation spectral and kinetic characteristics in neodymium glass laser in frequency scanning mode

01 p0095 A71-11029

Body radiative properties, examining degree of blackness dependence on surface roughness factor

02 p0331 A71-12188

Radio sources LF spectra distortions at critical value brightness temperature, noting induced Compton scattering effect on ambient gas thermal electrons

02 p0317 A71-12865

Venus spectra 10488 A carbon dioxide band from high dispersion spectroscopy

03 p0488 A71-13556

Extragalactic LF background radiation spectra, using model for free-free absorption in galactic disk

03 p0473 A71-13563

Concave mirror interferometer for laser radiation spectra measurements, featuring piezoelectrically tuned optical system

03 p0439 A71-14000

Radiation spectra kinetics of compound ruby lasers containing two crystals and Nicol prism

05 p0763 A71-16830

Absolute particle spectra above atmosphere and magnetosphere during solar flare of 23 February 1956

05 p0800 A71-17198

Solar modulation variation of secondary cosmic ray energy spectra, noting dependence on atmospheric depth and geomagnetic cut-off

06 p0955 A71-18135

Moon momentum spectra and charge ratio at 60 deg in east-west plane

06 p0961 A71-18176

Ce 138 excited states identification in beta decay spectra of Pr 138m and Pr 138 sources, using proton target bombardment

07 p1163 A71-19547

Ammonia inversion radiation at 1.25 cm in direction of three galactic center sources, setting upper limits on densities in other areas

07 p1188 A71-19834

Acoustic radiation spectra from turbulent jets, assuming approximate Gaussian statistics and second order velocity correlation space-time characteristics obtainable from frozen flow

07 p1016 A71-19959

Cosmic ray modulation spectrum function properties during Forbush decrease by spectrographic analysis

08 p1352 A71-20968

Statistics effect of quasi-monochromatic exciting radiation on generated radiation spectrum in nonlinear optics

09 p1461 A71-22396

High energy gamma rays in steady state universe assuming primary cosmic ray spectrum in extragalactic space by simple power law

10 p1664 A71-25045

Absolute spectra above atmosphere and magnetosphere and of particles accelerated in solar atmosphere during solar flare of 23 February 1956

13 p2128 A71-28253

Planetary nebula NGC 7009 narrow band filter photographs and spectra, detailing emission lines, intensity and velocity variations and model

14 p2313 A71-30430

Primary cosmic rays spectrum and intensity data in 4 to 10 BeV range, evaluating albedo particle effects

14 p2301 A71-30590

Body radiative properties, examining degree of blackness dependence on surface roughness factor

15 p2512 A71-31495

Cosmic ray rigidities spectra measurements above geomagnetic cutoff using balloon-borne emulsion plates in superconducting magnet field

15 p2407 A71-31805

Equatorial airglow enhancement data, observing 6300 and 5577 A intensity variations

16 p2562 A71-32809

Analytic approximations for ionization structure of nebula photoionized by flat spectrum

16 p2632 A71-33319

Low energy solar X-ray emission spectra observations, discussing nonthermal electron spectrum relation to acceleration by electric fields

16 p2626 A71-33725

Operational calibration of airborne IR spectrometer over hydrogeologically significant terrains, obtaining radiance spectra

18 p2920 A71-36363

Stellar rotation effects on radiation spectral characteristics, calculating He line profiles by LTE method

19 p3143 A71-38158

Electron distribution functions construction from spectrum of laser light Thomson scattering by rarefied plasma

19 p3074 A71-38215

Earth radiation flux spectral intensity measurements, noting latitudinal distributions, day and night variations and oceanic and continental curves

19 p3056 A71-38355

Galactic high energy electron differential spectrum, estimating spatial distribution and random magnetic field intensity

19 p3129 A71-38358

Cosmic ray spectrum at nonrelativistic energy region, noting ionization loss effects

19 p3129 A71-38359

Electromagnetic phenomena extraneous to established scientific and engineering disciplines, considering eclipotics, dowsing, hydronics, radionics, radiesthesia, orgone, backster phenomena, etc

19 p3031 A71-38441

Spectral measurements of nitrogen continuum radiation behind incident shocks at high speeds, suggesting free bound neutral atom-electron interactions origin

19 p3172 A71-38718

Spectrum and galactic isotropy of diffuse cosmic X rays by balloon-borne detector

21 p3438 A71-40605

Sea level high energy cosmic ray muon spectra calculation based on phenomenological model of nucleon-nucleus collisions

22 p3594 A71-42408

Magnetic modulation observation in plasma light scattering spectra experiments, noting dependence on angle between scattering and magnetic field vectors

23 p3713 A71-44150

Pulsar 0833-45 LF radiation spectrum decrease explained by pulse broadening due to interstellar scattering

24 p3868 A71-44565

Solar cosmic ray spectra at time of ejection from flare region and arrival near earth

24 p3866 A71-45040

RADIATION THERAPY

Mumie preparation effect on DNA and RNA contents in hemopoietic organs during acute radiation sickness due to low power radiation

01 p0013 A71-11118

L-erythro-alpha, beta-dihydroxybutyraldehyde radiosensitizing effect on adrenocarcinoma Ehrlich ascites tumor cells

07 p1035 A71-18952

Tumor DNA increase of halogenated pyrimidines incorporation compared to normal tissue DNA, discussing infraarterial infusion of radiosensitizing agents

07 p1040 A71-18989

Bromouridine as radiosensitizing agent improving effectiveness of radiation therapy of malignant brain tumor cells

07 p1040 A71-18990

Taurine restorative effect in patients with marked leucopenia induced by radiotherapy

07 p1040 A71-18991

Cystamine hydrochloride or vitamin B complex with vitamin C for radiation sickness prevention and therapy

22 p3493 A71-42723

RADIATION TOLERANCE

Optical bonding agent for calcite prism on Pioneer F/G mission, emphasizing optical and mechanical properties resistance to Jupiter high energy particles

01 p0081 A71-10835

Lithium concentration and defects in doped radiation resistant silicon solar cells during electron irradiation

05 p0703 A71-16089

Li doped Si solar cells recovery after irradiation, examining temperature dependence

05 p0704 A71-16105

Primary immune response chemical radioprotection in white mice during gamma irradiation, using serotonin as chemical protective and sheep red blood cells as immunizing agents

05 p0710 A71-16816

Ruby Q switched lasers with modular electro-optic shutters for low insertion loss and high optical radiation resistance

06 p0908 A71-18303

Radiation protection and sensitization - Conference, Rome, May 1969

07 p1031 A71-18926

Molecular mechanisms of bacterial cell radiosensitization and protection, discussing radiation produced free radicals interactions

07 p1031 A71-18927

Laboratory and clinical investigations of radiosensitization of cells and viruses by halogenated pyrimidine analogs

07 p1032 A71-18929

Sulfhydryl cysteamine and disulfide cystamine effect on bacteriophage survival rate at high anaerobic doses

07 p1033 A71-18938

DNA modification in Escherichia coli exposed to X rays and sensitized by triacetoneamine N-oxyl and oxygen

07 p1033 A71-18939

Cysteine incorporation in Escherichia coli B, noting X ray sensitivity and radioprotection

07 p1034 A71-18942

Radioreistant yeast strain Saccharomyces cerevisiae, discussing cycloheximide and gamma irradiation treatment influence on growth

07 p1034 A71-18943

Bacteria and mammalian cells radiosensitization, using phenylglyoxal and various carbonyl compounds

07 p1034 A71-18944

Age dependent changes in mammalian cells radiosensitivity, emphasizing endogenous nonprotein sulphhydryl effects

07 p1034 A71-18945

Drug-radiation damage interaction relationship to radiosensitization in mammalian cells

07 p1034 A71-18946

Organic free radical radioprotective and radiosensitizing effect, reporting Chinese hamster cell line survival characteristics after treatment

07 p1035 A71-18949

Radiosensitizers indanetrione, menadione Synkavit and N-ethylmaleimide, noting effects on murine ascitic tumor

07 p1035 A71-18950

Polycation effect on tumor cells, describing growth rate inhibitions, X ray sensitivity and DNA interference

07 p1035 A71-18951

L-erythro-alpha, beta-dihydroxybutyraldehyde radiosensitizing effect on adrenocarcinoma Ehrlich ascites tumor cells

07 p1035 A71-18952

Mouse Ehrlich ascites tumor cells, examining Co-60 gamma ray influence in presence of radiosensitizing 5,8-dihydroxypсорalen

07 p1035 A71-18953

Radiosensitizing effect of iodine compounds in dilute solution on Ehrlich ascites tumor cells and SH enzymes

07 p1036 A71-18957

Mitomycin C radiosensitizing effect on hematopoietic colony forming cells, using technique based on bone marrow cells spleen colonies forming ability

07 p1036 A71-18958

Anoxic fern spores X ray sensitization, observing diacetyl and isatin effects

07 p1036 A71-18961

Embryo chemical sensitization to low radiation doses damage by radiosensitizer iodoacetamide

07 p1037 A71-18963

Cytotoxic and radiosensitizing effect of thiol binding agents iodoacetamide (IAA), N-ethylmaleimide (NEM) and iodoacetic acid (IA) on crypt cells of mice duodenum

07 p1038 A71-18975

O-barenylacetic and methyl-O-benylcarboxylic acids effects on mice radiosensitivity to fast neutrons and gamma rays

07 p1038 A71-18976

Failure criteria percentages for bipolar transistors, determining adequacy of Weibull distribution for low gamma ray dose survival probability
07 p1071 A71-19064

Radiation resistance of center fed dipole antenna with transversely displaced feed points, using Schell-kunoff moment method
07 p1075 A71-19267

Radiation tolerant monolithic amplifier design, considering IF amplifier
07 p1080 A71-20411

Q switched and continuous laser collimated radiation exposure limits for eye cornea and skin, discussing environmental contamination
09 p1402 A71-23414

Seasonal effect on daily periodicity of mice radiosensitivity related to changes in bright/dark daytime proportion and feeding
10 p1565 A71-24654

Satellite square loop antennas radiation resistance in warm plasma, comparing calculated values with Ariel 3 satellite measurements
12 p1883 A71-27700

Radiation resistance of Alford loop antenna immersed in warm plasma, comparing theoretical values with measurements from Ariel 3 satellite experiment
13 p2034 A71-29290

Radiative capacity of materials with low thermal conductivity at high temperatures determination from reflectivity measurements for oblique light incidence
14 p2240 A71-30051

Antenna radiation resistance and efficiency in dissipative medium, using concept of modified power density
17 p2701 A71-34764

Nonplanar dipole antenna with transversely displaced feed points, considering effects on far field radiation patterns, radiation resistance, power gain, effective aperture and efficiency
18 p2887 A71-35970

Feed point axial displacement effects on radiation resistance and patterns of dipole antenna in weakly ionized plasma
18 p2875 A71-35971

Nonplanar dipole antenna with arbitrarily displaced feedpoints, considering far field radiation patterns, radiation resistance, power gain, effective aperture and efficiency
18 p2887 A71-35970

Radiation hardening of silicon solar cells, analyzing performance in low temperature environments
18 p2852 A71-36963

Equipment survival in natural and nuclear explosion electromagnetic and particle radiation environment
19 p3027 A71-37450

Semiconductor neutron hardness assurance by irradiation of wafer, probe, die rejection and anneal screening technique
19 p3034 A71-38520

Radiation resistance of small filamentary loop antenna in cold collisionless uniform multicomponent magnetoplasma, assuming uniform current distribution along loop
19 p3023 A71-38594

Surface cover materials thermal radiation characteristics and radiation resistance of plastics and solar cells, discussing friction in vacuum and spacecraft surface contamination by outgassing
20 p3210 A71-39453

Radioprotectants effect on mice against ionizing radiation and tolerance to back-to-chest accelerations in space flight
21 p3330 A71-40345

Radiation resistance, power gain, effective aperture and efficiency of modified log periodic dipole antenna
21 p3352 A71-40378

Living organisms life-sustaining possibility under simulated Martian temperature, humidity and atmospheric composition conditions, emphasizing unicellular organisms radiation resistance
21 p3334 A71-40572

High energy proton irradiation of rats with partial shielding of abdominal region, observing pathomorphological changes in myocardium, nervous system and radiosensitive organs
22 p3493 A71-42721

Mice under combined gamma radiation and vibration and acceleration dynamic factors, studying radioresistance recovery rate
22 p3494 A71-42725

Vibration influence on peripheral blood reaction to gamma radiation in dogs, using clinico-hematological indices
22 p3494 A71-42728

Unicellular organisms increased tolerance to UV radiation, discussing cells repairing ability in dark and pigments and protective compounds screening role
22 p3496 A71-42828

Polyethylene coating physicochemical properties under UV radiation, discussing density and modulus of elasticity, internal stresses, microcrack formation and preventive heat treatment
23 p3697 A71-44032

RADIATIVE HEAT TRANSFER

Nongray equilibrium radiative heat transfer in viscous radiating shock layer around blunt body entering high temperature nonisothermal carbon dioxide-nitrogen atmosphere
[AIAA PAPER 69-636] 01 p0180 A71-10938

Physiological effects of heat exchange between human organism and ambient medium by evaporation, radiation, conduction and convection
01 p0028 A71-11597

Long wave radiation fluxes calculation in troposphere based on principal radiant heat transfer components separation
02 p0277 A71-12117

Venus equatorial stratosphere structure, presenting approximate radiative dynamical calculation for zonal flow mechanism
03 p0488 A71-13552

Radiative and convective heat transfer from conducting fins on plane surface, describing interactions among heat conduction and radiant exchange
[ASME PAPER 70-HT-F] 03 p0519 A71-13701

High temperature gases radiative heat exchange, evaluating approximation methods
03 p0519 A71-13744

Radiative properties of construction properties and working media, noting importance to radiative heat transfer calculation
03 p0519 A71-13747

Radiation heat transfer from parallel plates with grooved surfaces for direction dependent radiation properties
03 p0521 A71-14293

Minimum core storage forms for radiant heat transfer doubly subscripted nonsymmetric equations, giving simple modifications for interchange between emitting and reflecting surfaces
03 p0522 A71-14454

Heat transfer - Conference, Versailles, August-September 1970, Volume 3, Forced convection and radiation
04 p0681 A71-15484

Total radiative interchange kernel measurements, describing remote excitation/detection
04 p0684 A71-15511

Radiative heat transfer between opaque interacting surfaces, investigating surface roughness effects
04 p0684 A71-15513

Radiative/convective heat transfer in moving media, reducing boundary problem to integral equations
04 p0685 A71-15514

Thermal radiation-conduction interaction in horizontal fluid layer, obtaining temperature profiles with Mach-Zehnder interferometer
04 p0685 A71-15515

Axisymmetrical, optically thick nonNewtonian, power law boundary layer with injection and suction, obtaining similarity transformations for simultaneous convection and radiation
04 p0685 A71-15516

Thermal radiation absorbing and emitting medium in flow between parallel plates, examining heat transfer for simultaneous radiation and convection
04 p0685 A71-15517

Blunt body nose protection from radiation-convective heat transfer, using porous injection of radiation absorbing substance
04 p0685 A71-15518

Atmospheric temperature, computing carbon dioxide concentration effect on radiative heating rates
05 p0742 A71-16677

Local radiative heat transfer and equilibrium temperature between identical uniform surface geometry planes, discussing directional dependent emittance and absorptance effects
[AIAA PAPER 71-76] 06 p1008 A71-18533

Heat transfer by radiation, convection and molecular thermal conductivity in gray absorbing medium flat layer bounded by parallel diffusively radiating planes
07 p1219 A71-18757

Radiative heat transfer during entry into shocked Venus model atmosphere
07 p1199 A71-19870

Radiant heat transfer from heated cylindrical enclosure with black/gray walls to absorbing gas or gas having black particles, calculating absorption coefficients
07 p1224 A71-20018

Combustion chamber radiant heat transfer measurements, describing radiometer
08 p1288 A71-21270

Combined radiative-convective heating test facility for atmospheric entry simulation
[AIAA PAPER 71-255] 08 p1273 A71-21984

Thermospheric heating by solar radiation in Schumann-Runge continuum, taking into account height and atmospheric components distribution
09 p1435 A71-22431

Steady one dimensional temperature field of cylindrical shell spacecraft, allowing for heat conduction and convective and radiative heat transfer within shell
09 p1546 A71-23148

Selective optical coatings efficiency and thermal properties under solar radiation and radiative heat exchange
09 p1510 A71-23418

Supernovae light curves theory based on numerical integration of gas dynamics and radiative heat conductivity equations
09 p1528 A71-23591

Turbulent mixing and radiative transfer relationship to micrometeorological temperature structure of atmospheric boundary layer
10 p1638 A71-23878

Mass entrainment products effect on radiative and convective heat transfer during decomposition of graphite blunt body in steady hypersonic flow of radiating air
10 p1696 A71-24364

Higher approximations of spherical harmonic method and moment method applied to propagation of periodic disturbances in radiating gas
10 p1696 A71-24545

Perturbation theory of supersonic flow with nonequilibrium radiative heat transfer, investigating pressure, density, temperature and velocity as function of relaxation time
10 p1697 A71-24943

IR radiative heat transfer in nongray nonisothermal gases, giving solutions for radiative equilibrium and combined conduction and radiation
10 p1698 A71-25094

Thermal louvers radiative heat transfer characteristics with solar irradiation effects, using Monte Carlo method
11 p1854 A71-25190

Satellite solar radiative heat input variations effect on optimal launch time, considering angular factor and thermal design
11 p1836 A71-25192

Radiatively interacting adjacent plates in presence of collimated solar flux, considering surface roughness effects on equilibrium temperature distribution
[AIAA PAPER 70-817] 11 p1854 A71-25511

Atmospheric modeling for earth and Venus heterosphere structure using multicomponent radiative hydrodynamic equations, determining atmospheric temperature and constituents height variation
11 p1828 A71-25764

Earth atmospheric zonal circulation model, using hydrothermodynamic equations with Newton law for radiative heat sources
11 p1795 A71-25919

Nongray surface property effects on radiant heat transfer between interacting opaque surfaces, analyzing spectral emittance wavelength and temperature dependence
[AIAA PAPER 71-464] 11 p1859 A71-26245

Spacecraft radiator thermal scale model, using forced convection, conduction and radiation heat transfer
11 p1860 A71-26517

Venusian atmosphere heat transfer processes, calculating radiant fluxes and convective motion model
12 p1958 A71-26640

Venus subcloud layer, investigating radiant heat transfer in convective lower atmosphere
12 p1958 A71-26646

Flowfields behind reflected shock waves, predicting end-wall pressure, radiative heat transfer and radiative gas dynamic coupling effects
[AIAA PAPER 70-774] 12 p1986 A71-27562

Soviet papers on upper atmosphere physics covering thermosphere, dynamic processes and radiative energy transport in stratosphere and mesosphere, and ionospheric parameters radio measurement
13 p2056 A71-28017

Upper atmosphere radiative energy transport equation derivation with allowance for deviations from Kirchhoff law, examining fluorescence mechanism and effect on radiative heating
13 p2057 A71-28025

Heat exchange during stabilized laminar flow of incompressible liquid in circular pipe with radiative cooling, deriving temperature profile and Nusselt number dependence
13 p2046 A71-28180

Radiant heat transfer measurements on sintered gauzes, considering mathematical model of porous wall with sweat cooling
13 p2161 A71-28750

Combined conductive and radiative heat transfer in absorbing and scattering materials, using two-flux model for transport and local energy balance equations solution
13 p2164 A71-28983

Honeycomb cell multilayer and reinforced structures, examining temperature field radiative heat transport and thermal conductivity and emissivity
13 p2165 A71-29180

Radiative and convective heat transfer for stagnation point flow of emitting carbon dioxide and nitrogen gas mixture, assuming thermodynamic equilibrium in shock layer
14 p2335 A71-30212

German monograph on network method application for conductive and radiative energy transfer coupling problems
14 p2336 A71-30231

Nuclear light bulb engine based on thermal radiation energy transfer from gaseous uranium fuel through internally cooled transparent wall to seeded hydrogen [AIAA PAPER 71-642] 14 p2274 A71-30719

Radiative heat transfer equilibrium in earth, Venus and Mars atmospheres, taking into account interaction with ground 15 p2395 A71-31448

Radiative heat transfer effects on small fires in zero gravity spacecraft and free falling chamber environments from diffusion flame models 15 p2514 A71-32084

Radiative heat transfer effects behind reflected and incident shock waves in high temperature air and xenon respectively 16 p2662 A71-32888

Temperature stabilization with self controlled water and radiation cooled heat pipes using argon in addition to K heat transfer medium 16 p2663 A71-34039

Optimal radiative capacity of star shaped radiator with mirror reflecting surfaces for vacuum cooling of elongated finned bodies 17 p2836 A71-34311

Cooling fin shape optimization for minimum volume, considering convective and radiative heat exchange for assumed temperature distribution 17 p2837 A71-34442

Radiative heat transfer in model water clouds by IR radiation, using method of discrete ordinates 17 p2735 A71-35560

Nonlinear radiative heat transfer in hydrogen plasma gas, obtaining temperature distributions 19 p3161 A71-37404

Radiative heat transfer in atomic lines through shock heated nonhomogeneous gases by analytical frequency integration, using separability approximation 19 p3162 A71-37407

Reflecting and ablating Teflon heat shields for radiative environment of outer planets atmosphere [AAS PAPER 71-147] 19 p3084 A71-37950

Radiation heat transfer volume interchange factors approximation for gases with nonuniform temperature, composition or pressure, comparing with exact numerical computations [ASME PAPER 71-HT-19] 19 p3164 A71-37990

Transient simultaneous conductive and radiative heat transfer in plane gray layer bounded by black walls, yielding nonlinear integrodifferential equation [ASME PAPER 71-HT-22] 19 p3165 A71-37993

Vertical motions, turbulent heat exchange and radiative heat input role in stratus clouds evolution, deriving humidity and heat transfer equations as functions of time 19 p3093 A71-38690

Earth atmospheric zonal circulation model, using hydrothermodynamic equations with Newton law for radiative heat sources 20 p3256 A71-39210

Heat transfer by radiation, conduction and convection, including various types of thermal insulation 20 p3311 A71-39244

Radiative-conductive heat transfer systems optimum thermal design, using nonlinear programming with mathematical model based on nodal analysis [ASME PAPER 71-VIBR-120] 21 p3474 A71-40339

Soviet book on long wavelength radiative heat exchange in atmosphere covering radiation relationship to circulation, cloud formation and weather prediction 21 p3411 A71-40873

Thermal stress distribution and temperature profiles in nearly opaque spherical shell under radiant and convective heating flux 21 p3476 A71-40942

Atmospheric rotation, anisotropic turbulence and long wave radiative heat transfer effects on cellular heat convection 21 p3412 A71-41387

Atmospheric modeling for earth and Venus heterosphere structure using multicomponent radiative hydrodynamic equations for atmospheric temperature and constituents height variation determination 22 p3598 A71-41532

Radiative and turbulent heat transfer in atmospheric surface layer, measuring radiative heat flux divergence and temperature fluctuations at different heights 22 p3534 A71-41860

Conductive and radiative axial heat transfer in packed/stagnant beds at 20-750 C, giving temperature profiles 22 p3620 A71-41877

Combined radiative and conductive heat transfer prediction in semitransparent solids by Taylor series expansion, defining radiative conductivity 22 p3620 A71-41883

Radiative heat transfer from lunar and Mercurian surfaces during eclipse 22 p3603 A71-42188

Laminar incompressible flow velocities and heat transfer by radiation and convection in inlet section of parallel plate duct 23 p3781 A71-43313

Nonstationary radiative heat transfer between cylindrical body and ambient medium, determining regular heating condition region 23 p3782 A71-43921

Radiant heat flux measurement during pulsed processes from surface in high temperature emitting gas, using thin film sensor with small time constant 23 p3782 A71-43922

Two dimensional radiative heat transfer in absorbing-emitting medium bounded by nonisothermal gray walls from Monte Carlo simulation, showing gas emissive power distribution 23 p3784 A71-44276

Nongray radiative heat transfer in finite slab with discrete absorption coefficient and specularly and diffusely reflecting boundary surfaces of uniform temperature 24 p3886 A71-44372

Solar coronal plasma radiative capacity and temperature structure from cooling function in thermal balance equation 24 p3869 A71-44806

Heat exchange during stabilized laminar flow of incompressible liquid in circular pipe with radiative cooling, deriving temperature profile and Nusselt number dependence 24 p3888 A71-44933

RADIATIVE LIFETIME

Fluorine ions excited levels mean lives from beam-foil line spectrum analysis 01 p0129 A71-10138

Ne, Ar, Kr and Xe ionized states transition and level lifetimes from photographically recorded beam foil spectra, discussing particle energies 04 p0629 A71-14805

Vibrationally excited ground state hydroxyl in fast flow system, considering mean radiative lifetime and reaction rate with ozone 08 p1250 A71-20662

Boron and carbon hydrides and carbon deuteride molecular ions radiative lifetime measurements, computing absolute oscillator strengths 08 p1250 A71-20671

Metastable radiative lifetimes of molecular states of nitrogen and CO, using time of flight and high resolution electron gun techniques 09 p1497 A71-22417

O I and II resonance transitions radiative lifetimes in vacuum UV, using beam foil method 10 p1676 A71-24501

Radiative lifetimes of UV multiplets in atomic C, N and O, using modified phase shift technique 10 p1645 A71-24547

Radiative mean lives and transition probabilities of electronic states in beam foil excited atomic and ionic carbon 11 p1803 A71-26061

Benzene, benzene-d sub 6 and sulfur dioxide radiative lifetime measurement comparison, investigating internal conversion behavior 14 p2190 A71-30570

Oxygen /super IS/ effective lifetime measurements in pulsating aurora, discussing mechanisms, quenching coefficients and heights 15 p2397 A71-31762

Ca, Mg, B and Al prominent resonance transitions radiative lifetimes and absolute oscillator strengths 15 p2452 A71-32596

Radiative mean life measurements by low energy beam foil excitation, considering branching ratio of transition probabilities equal to unity 16 p2576 A71-33051

Ion beam-foil produced oxygen spectra in wavelength range between 450 and 2200 A, determining mean radiative lives of O I - O VI excitation levels 16 p2529 A71-33183

Cosmic rays lifetime in Galaxy in presence of particle acceleration in interstellar space 16 p2626 A71-33463

Carbon monoxide in metastable state, considering quenching and radiative lifetime 16 p2615 A71-34089

Dynamic rate equation model of single wavelength flash lamp pumped rhodamine dye laser accounting for short molecular triplet state lifetimes 18 p2929 A71-35958

Deactivation and radiative lifetime of CO Cameron forbidden transition spectral bands produced by photon absorption 21 p3418 A71-40232

RADIATIVE RECOMBINATION

Stimulated recombination radiation from PbSe laser diodes at 77 K, showing stepwise curve of emission power vs pumping current 01 p0094 A71-10780

H-He partially ionized plasma bremsstrahlung, radiative and dielectronic recombination, discrete levels excitation and collisional ionization 05 p0787 A71-16489

Gallium phosphide current carriers radiative recombination, discussing electro- and photoluminescence phenomena 06 p0940 A71-17350

Nanosecond laser produced lithium hydride spherical plasma expansion model, taking into account three body and radiative recombinations 06 p0938 A71-18457

Recombination emission by atoms or radicals used with population for inversion thermal gas laser production 07 p1128 A71-20529

Metastable atom destruction, collision-radiative recombination and electron heating in low temperature decaying helium plasmas, using spectroscopic resonance line measurements 10 p1654 A71-24896

Li photoionization cross sections determined from spectral intensity measurements as function of threshold wavelength, discussing radiative electron-ion recombination into first excited state 10 p1646 A71-24992

Argon ionization and recombination in solar corona at electron temperatures of 2.0-4.5 times ten to sixth power K 11 p1832 A71-26180

Low temperature plasma collisional-radiative ionization and recombination coefficients, discussing nonequilibrium factors affecting electron density change rate 12 p1939 A71-27270

Collisional radiative volume recombination and ionization coefficients for quasi-stationary helium, considering singlet and triplet systems as two coupled individual systems 13 p2106 A71-28452

Metastable atom destruction, collision-radiative recombination and electron heating in low temperature decaying helium plasmas, using spectroscopic resonance line measurements 21 p3425 A71-41276

Jovian ionospheric electron and ion densities and temperatures, considering radiative association role 22 p3603 A71-42181

RADIATIVE TRANSFER

NT RADIATIVE HEAT TRANSFER

Galactic EM energy radiation, discussing flux upper limits in Low model 01 p1533 A71-10364

Radiative transfer equations averaging over quantum angles and energies, discussing use for nonsteady gas dynamic problems 01 p0179 A71-10666

Radiation transfer equation in extended hot stellar atmospheres, discussing scattering effects due to free electrons 01 p0158 A71-10802

Radiative transfer in plane layer of nongray absorbing and emitting medium bounded by black parallel plates, using rectangular model 01 p0180 A71-10945

Optical scatter channel transmission characteristics, using mathematical model consistent with radiative transfer theory and probability-computing receiver 02 p0249 A71-12012

Radiative transfer by shock profile spectral line in thermally inhomogeneous layers of radiating gas 02 p0240 A71-12184

Transformation properties of radiation field and electromagnetic energy fluxes of relativistic charged particles in magnetic field 02 p0312 A71-12362

Book on stellar atmospheres covering radiative transfer, opacity, equation of state, LTE, line spectra, atomic levels, etc 03 p0483 A71-13100

Solar chromosphere model, investigating radiative transfer effect on temperature structure of plane slab heated by thermal conduction 03 p0483 A71-13186

Cyclotron radiation emission and absorption in nonequilibrium plasma, deriving radiative transfer equation 03 p0465 A71-14268

German monograph on radiative transport in freely expanding gas clouds covering analytical and numerical calculations and experiments 03 p0418 A71-14369

Radiative transfer equation for atmospheres of rotating stars, deriving expression for flux distribution 03 p0495 A71-14381

Soviet book on optical properties of hot air covering spectral lines, radiative transfer, cross sections, pressure effects and absorptivity 03 p0460 A71-14397

Discrete values of inverse diffusion length occurring in solutions of anisotropic transfer equations 04 p0642 A71-14904

Soviet book on optics of scattering media covering visible radiation transfer in water, atmosphere, powders, tissues, dyes, inhomogeneous systems and photometry 04 p0626 A71-15224

Radiatively driven acoustic waves, studying radiative transfer-gas motion interaction under local molecular equilibrium for vibrational rate processes 05 p0836 A71-16532

One dimensional gas flow with radiative transfer, using time dependent difference scheme

05 p0735 A71-16714

Radiative transfer in nonuniform turbid medium with constant absorption coefficient

05 p0742 A71-16840

Unsteady heat conduction due to radiative energy transfer in dispersed powders, hydrosols and aerosols

06 p1009 A71-18729

Gas ionization relaxation phenomena behind strong shock waves, discussing ionization kinetics, radiation transfer effects, relaxation time and radiative heating

07 p1087 A71-19172

Radiation transport equations for stellar atmosphere model with variable depth magnetic field, considering absorption line formation and polarization characteristics

07 p1205 A71-20637

Low temperature plasma radiation transfer equation, discussing constraints to applicability in real radiation transfer problems

08 p1339 A71-21055

Atmospheric emission and absorption measurements at millimeter wavelengths, comparing with radiative transfer equation values

08 p1257 A71-21880

Radiative transfer theory extended to cosmological red shift and expansion effects on uniform isotropic X rays and gamma rays in homogeneous intergalactic medium

09 p1512 A71-22333

Optical-electrical analogy of thermal radiation impedance of thin dielectric films in low temperature insulation

09 p1494 A71-23003

Molecular flux distributions and capture by cryopanel in space simulation chamber using homogeneously emitting spherical gas source

09 p1428 A71-23006

Spherical harmonics differential approximation generalized from one dimensional radiation specific intensity angular dependence Jacobi polynomial expansion

10 p1696 A71-24536

Steady state photon transfer through homogeneous semiinfinite isothermal atmosphere with two level atoms, deriving linear integral equation for escape probability distribution

10 p1643 A71-24964

Vibrational nonequilibrium influence on IR radiative energy transfer in nongray nonisothermal gases

10 p1643 A71-24967

Analytic approximations in closed form for curves of growth of Doppler-Lorentz broadened lines, considering radiative transport in nonisotropic gases

10 p1646 A71-24991

Polarized radiation transfer in collective plasma, analyzing proper modes phase correlation effects by Liouville equation perturbation technique

10 p1654 A71-24996

Radiative transfer in nongray gas with local molecular and slightly disturbed radiative equilibrium, deriving linearized differential equation with application to radiatively driven acoustic waves

10 p1697 A71-25065

Spherically symmetric radiative transfer problems, constructing model with neutron transport theory [AIAA PAPER 71-466]

11 p1859 A71-26247

Visible and IR radiative transfer in water and ice clouds, calculating radiance and polarization from Mie theory

11 p1800 A71-26299

Quantitative UV radiative transfer and photolysis in model Jupiter atmosphere, considering coloration by ammonia and hydrogen sulfide gases in cloud region

11 p1834 A71-26455

Fredholm equation solution for radiative transfer between parallel plate configuration at midpoint

13 p2159 A71-27981

Electron scattering effects on spectral emission at optical and X ray wavelengths for homogeneous spherical ionized hydrogen plasma cloud, discussing radiation transfer

14 p2297 A71-29592

Galactic Lyman alpha emission, describing radiative transfer in radiation diffusion

14 p2306 A71-29683

Spherically symmetric systems radiative transfer problems using iteration on Eddington factor

14 p2307 A71-29864

Low temperature plasma radiation transfer equation, computing problems with absorption coefficient accounting for re-emission

14 p2280 A71-30168

Least squares method for inversion of radiative transfer equation, considering atmospheric temperature profiles determination from outgoing radiance

14 p2337 A71-30296

Atmospheric optics and radiative transfer, including earth albedo, sky brightness, heat balance, cloud/rain reflectance, molecular spectroscopy and multiple scattering

14 p2275 A71-30497

Radiative transfer equations averaging over quantum angles and energies, discussing use for nonsteady gas dynamic problems

14 p2339 A71-30999

Semiinfinite atmospheric multiple conservative Rayleigh scattering, describing polarized radiation transfer

15 p2449 A71-31333

Radiative transfer by shock profile spectral line in thermally inhomogeneous layers of radiating gas

15 p2511 A71-31492

Coupled radiative transfer-gas dynamic interactions in unsteady wave propagation, two dimensional steady flows and atmospheric motions

15 p2515 A71-32562

Bondi condition gravity waves, investigating radiation and energy transfer in given coordinate system

15 p2451 A71-32726

Radiative energy transfer equations solution in magnetic field, facilitating magnetograph calibration

15 p2496 A71-32740

Diffuse interstellar medium hydrogen radio recombination lines radiation transfer, investigating thermodynamic equilibrium effects

15 p2498 A71-32770

Rayleigh scattering planetary atmosphere radiative transfer equation, calculating phase curves for flux and polarization

15 p2498 A71-32778

Altitude and amplitude of winter stratospheric warmings from satellite measured radiance changes, considering radiative transfer equation and variable model of temperature structure

16 p2605 A71-33537

Radiation field inhomogeneity effect on radiation gas jet flow, taking into account radiative energy transfer by differential approximation

17 p2728 A71-35117

Non-LTE problems computation based on integral equation approach, using discrete operator for radiative transfer equation solution

17 p2808 A71-35552

Pulsating variable star spectral line formation from integral equation solution of radiative transfer and gas flow through shock front

17 p2808 A71-35553

Newton-Raphson method application to iterative solution of atomic excitations and radiative transfer in plasma

17 p2838 A71-35554

Radiative transfer in two-component stellar atmosphere, discussing lines corresponding to solar Ca K-line

17 p2839 A71-35555

Gray radiative transfer equations, bridging Planck and Rosseland mean absorption coefficients

17 p2839 A71-35557

Model cloudy atmosphere construction, reviewing computational techniques for radiative transfer analysis

17 p2735 A71-35559

Model radiative transfer across random air-sea interface, determining reflected sky radiance

17 p2736 A71-35562

Direct numerical integration for equation of radiative transfer in turbid atmosphere with allowance for scattering on molecules and aerosols

17 p2736 A71-35564

Radiative transfer in terrestrial clouds, inferring colloidal state from measurements of multiple scattering angular and wavelength dependence

17 p2736 A71-35566

Variational principle with reflectivity extremum for inhomogeneous planetary atmospheric line spectra profile calculation from radiative transfer equation

18 p2964 A71-36286

Physics and phenomenology of radiation field in spectral lines, considering radiation transfer with optical depth effects and kinetic energy transformation into radiation

18 p2968 A71-37035

Absorption intensities of R branch J manifolds of methane band, using half widths and pressure shifts

19 p3106 A71-37410

Sobolev function Q in radiative transfer, using invariant imbedding approach for integral equation transform

19 p3133 A71-37506

Surface relief effect on radiative properties of solid body with random surface roughness distribution

19 p3162 A71-37581

Radiation temperature profiles in low pressure oxygen-calcium wire diffusion flames from optical measurements based on radiative transfer equation

19 p3170 A71-38115

Radiative ignition of polymeric fuels /polystyrene and epoxy/ in oxygen/nitrogen mixtures

19 p3121 A71-38125

Nonlinear coupling between thermal conduction and radiative transfer in solar chromosphere by iterative method

19 p3143 A71-38159

Radiative transfer in inhomogeneous anisotropically scattering spherical shell atmospheres with radial symmetry, using invariant imbedding technique

20 p3287 A71-39082

Aircraft sounding of atmospheric microwave radiation transfer compared with IR method, measuring optical Mie characteristics, water vapor content, cloudiness, ice cover, etc

20 p3259 A71-39673

Ionization relaxation phenomena behind strong shock waves, discussing ionization kinetics, radiation transfer effects, relaxation time and radiative heating

21 p3365 A71-40087

Gas dynamic model for coupled vibrational and radiative nonequilibrium in carbon dioxide, obtaining macroscopic collisional and radiative transfer equations

21 p3418 A71-40233

Radiative transfer effects on hydromagnetic stellar atmospheres thermal-convective instability in presence of uniform rotation and uniform magnetic field

21 p3421 A71-40579

Diffuse radiation field inside homogeneous spherically symmetric dust nebula from radiative transfer equation solution as expansion after Legendre polynomials

21 p3451 A71-40716

UV and IR transmissivity and absorption coefficients of fused quartz between room temperature and 1500 C

22 p3565 A71-42559

Semiinfinite atmospheric multiple conservative Rayleigh scattering, describing polarized radiation transfer

22 p3576 A71-42608

Isotropic light scattering in unsteady plane layer of finite optical thickness, obtaining reflection and transmission coefficients for radiative transfer

22 p3607 A71-42869

Phase dependent spectra of Cepheids from multifrequency group calculations in radiative transfer model

23 p3723 A71-42946

Bondi condition gravitational waves, investigating radiation and energy transfer in given coordinate system

23 p3704 A71-43300

Iterative solution for radiant energy transport equation by Wiener Hopf operator equations, investigating convergence conditions

23 p3699 A71-43573

Spherical stellar atmosphere radiative transfer equation, using regional averaging method with opacity dependence on layer geometrical radius

23 p3766 A71-43828

Multiple scattering theory of Neumann transfer boundary value problems, showing Neumann intensity expansion coefficients relation to singular normal modes

24 p3848 A71-44788

Radiative thermal flux model of Venus atmosphere, using Venera data and greenhouse effect

24 p3870 A71-44822

Radiative transfer in linearly anisotropic scattering conservative and nonconservative slabs with reflective boundaries, obtaining angular radiation distribution by normal mode expansion technique

24 p3888 A71-44966

RADIATORS

Radiator systems field calculation based on waveguide and resonator excitation method, noting field amplitudes in two and three dimensional arrays

01 p0038 A71-11202

Plane curvilinear radiators synthesis for horizontal or vertical radiation patterns, obtaining current phase amplitude distributions by symmetrical striplines

01 p0056 A71-11205

Radiator system field calculation based on waveguide and resonator excitation method, noting field amplitudes in two and three dimensional arrays

17 p2697 A71-34254

Plane curvilinear radiators synthesis from horizontal or vertical radiation patterns, obtaining current phase amplitude distributions by symmetrical striplines

17 p2697 A71-34257

RADICALS

Dissociative electron attachment excess energy correlation with fragment ion translational energies, determining radical affinity

08 p1338 A71-21782

Excited radical and ion formation in unperturbed acetylene-air and superimposed HF discharge flames, determining activation energy

09 p1402 A71-22379

Propulsion system atom and radical concentrations measurements, using low pressure gas discharge flow system for combustion environment control

11 p1729 A71-26285

Flash photolysis produced methyl and methylene radical transitions maximum extinction coefficients and oscillator strength in vacuum UV

12 p1876 A71-26788

- Interstellar formyl radical and carbon 13 formyl ion search in galactic radio sources 13 p2142 A71-29103
- Radical and formaldehyde daytime concentrations predictions from steady state model of unpolluted surface atmosphere 16 p2575 A71-34048
- RADIO**
- Planet Mars polar and equatorial radii optical measurements comparison with radar and Mariner probes occultations results, determining optical ellipticity 03 p0493 A71-14200
- Gravity anomaly and lunar radar measurement at Apollo 12 landing site, using data telemetered to earth from surface module 16 p2636 A71-33507
- RADIO ALTIMETERS**
- Doppler radar velocity sensors and altimeters for lunar and planetary spacecraft instruments soft landing 04 p0597 A71-15324
- Radar altimeter use for ocean roughness determination 07 p1095 A71-18824
- Frequency modulated radio altimeters, discussing problems of altitude measurement independent of airplane motions in pitch and roll and immunity to fog effects 15 p2408 A71-31918
- Geodetic and oceanographic surface mapping by satellite radar altimeter system, discussing measurement technique, orbital parameters and data processing equipment [AIAA PAPER 71-845] 17 p2733 A71-34708
- GEOS-C geodetic satellite purpose and equipment, discussing earth gravitational field study, radar altimeter possibility and tracking systems usefulness 20 p3306 A71-39657
- Tidal analysis of sea surface elevations from satellite-borne altimeter as function of instrument errors and orbital determinations 22 p3536 A71-42549
- RADIO ANTENNAS**
- VHF/UHF telemetry antenna stellar calibration using radio stars 01 p0054 A71-10909
- Low loss cylinder loop as normalization antenna for meter waves 01 p0055 A71-11187
- Monograph on dual beam parabolic antennas in radio astronomy covering atmospheric effects, EM surface current density and scalar aperture field, etc 07 p1077 A71-19725
- Radio propagation and antennas transmission formulas, discussing fundamental circuit elements with inductors and capacitors 11 p1798 A71-25596
- Refractive errors in spaced antenna radio angle-of-elevation measurements based on comparison with use of single directional antenna 12 p1881 A71-27424
- Signal rejection characteristics of receiver preselector and antenna system, requiring receiver mixer efficiency and transmitter parameters 13 p2032 A71-28862
- Transhorizon radio propagation by atmospheric heterogeneities, discussing effect on attenuation, antenna gain reduction and transmission bandwidth 13 p2033 A71-29239
- Active antennas for frequency range 100 kHz to 250 MHz, discussing transistor circuitry optimization with respect to noise and linearity 14 p2210 A71-29822
- Airborne blade antenna tunable for 26-100 MHz by individual bands, using binary related inductors switched by miniature high vacuum relays 14 p2216 A71-31044
- Light aircraft notch antenna for efficient radiation at HF band lower end and minimal interference with aircraft structure 14 p2217 A71-31053
- Radio direction finding with discrete antenna scanning and multilevel beacon signal quantization, investigating accuracy 15 p2370 A71-31591
- Antenna tracking, RF and boresight alignment on ships and ground stations using Apollo lunar surface experiments package /ALSEP/ 18 p2876 A71-36473
- Minimum spacing between two base station antennas for mobile radio diversity reception 19 p3014 A71-37217
- Noise factor formula of multiple loop receiver input network with series connected stages for antenna matching and coupling parameters 19 p3022 A71-38498
- Linear antenna in anisotropic plasma, calculating reactance change with surrounding dielectric layer thickness with allowance for ion depletion 20 p3204 A71-39142
- Electronic broad banding of VLF/LF antennas for FSK radio communication through switched magnetically coupled reactor, determining antenna transient response 22 p3513 A71-42388

- RADIO ASTRONOMY**
- International joint optical and radio astronomical observations on Saturn rings and disk /1966/ 01 p0149 A71-10046
- Extra-atmospheric submillimeter astronomy, discussing emission observations between IR and RF region and astrophysical-cosmological applications 01 p0151 A71-10146
- Frequency allocations for radio astronomy 01 p0153 A71-10362
- Radio astronomy in millimeter and submillimeter ranges, surveying programs and equipment at various observatories 01 p0156 A71-10450
- L and S band paraboloidal dish antenna stellar calibration technique using absolute flux density from Cassiopeia A or Cygnus A 01 p0032 A71-10888
- Galactic radio emission sources high resolution observation by telescope, obtaining contour maps with positions and flux densities 02 p0303 A71-11820
- Galactic models from neutral H line profiles at 21 cm wavelength 02 p0307 A71-12084
- Orion Nebula /NGC 1976/ physical characteristics from H alpha line radio telescopic observation, discussing energy level population, electron density, collision mechanisms, etc 02 p0308 A71-12094
- Planetary and lunar thermal radio emission and brightness temperature measurements using sensitive receivers and large aperture radio telescopes 02 p0309 A71-12155
- Hydrogen maser time and frequency standards at Agassiz observatory for long baseline interferometry via radio telescope, discussing Loran C 02 p0261 A71-12334
- Radio sources position measurement with three-element interferometer by self calibrating technique 02 p0314 A71-12577
- Worldwide geophysical observatories network for observing solar optical, radio, particle X rays and geomagnetic and ionospheric effects [AIAA PAPER 70-1354] 02 p0239 A71-12692
- Long baseline radio interferometry, discussing phase difference measurement principles in terms of signal characteristics and wave forms, astronomy and geodesy applications 03 p0484 A71-13244
- Solar radio astronomy decimeter wave multichannel spectrograph for solar bursts fine structure spectrum analysis 03 p0488 A71-13530
- Mercury microwave and IR observations interpreted for thermophysical models for planetary subsurface, discussing rotation and heating 03 p0492 A71-14069
- Space radio astronomy of solar bursts at broad frequency range, using earth-remote probe experiment 04 p0642 A71-14901
- Solar eclipse of 22 September 1968 radio astronomical observations, examining sunspot groups during lunar occultation 04 p0650 A71-15558
- Type 3 solar radio bursts observed at low frequencies for half rotation, discussing occurrence, drift rates, propagation time and emission 05 p0804 A71-16031
- Ionospheric irregularity structure boundary variations shown by scintillation from satellite and radio star observations during quiet and disturbed magnetic conditions 06 p0887 A71-17269
- Atlas of 21 cm H I emission line profiles of outer part of Galaxy in Galactic anticenter region, plotting brightness temperature vs radial velocity 06 p0964 A71-17348
- Strip brightness distribution across Kepler supernova derived from occultation observation by radio telescope 06 p0971 A71-18241
- Precursor pulse disappearance of Crab Nebula pulsar NP 0532 at 606 MHz 07 p1190 A71-18864
- Lunar radioactive layer effective thickness by radio astronomical methods and from Apollo 11 flight 07 p1193 A71-19312
- Monograph on dual beam parabolic antennas in radio astronomy covering atmospheric effects, EM surface current density and scalar aperture field, etc 07 p1077 A71-19725
- Bubble of energetic charged particles embedded in interstellar or intergalactic magnetic field and in gas, discussing dynamic effects on radio astronomy observation 07 p1197 A71-19815
- Radio telescope measurements of circular polarization and total flux of Jupiter at 13.1 cm wavelength 08 p1357 A71-20871
- Galactic optical radial velocity measurements compared to 21 cm red shifts derived velocity 08 p1357 A71-20873
- Quasars radio structures observations in S band, using NRAO interferometer 08 p1358 A71-20934

- Formaldehyde line emission observed from trapezium H II region of Orion nebula, attributing to 140 GHz rotational transition 08 p1360 A71-20983
- Scorpius XR-1 simultaneous radio and optical measurements, discussing correlation of fluxes 08 p1360 A71-20985
- International joint optical and radio astronomical observations on Saturn rings and disk /1966/ 08 p1361 A71-21040
- Galactic models from neutral H line profiles at 21 cm wavelength 08 p1362 A71-21134
- Orion Nebula /NGC 1976/ physical characteristics from H alpha line radio telescopic observation, discussing energy level population, electron density, collision mechanisms, etc 08 p1362 A71-21144
- Modulation of long scale time variations of quasi-stellar radio sources and Seyfert galaxies due to intergalactic scintillations 08 p1364 A71-21414
- Solar corona structure on 22 September 1968 from radio astronomical and optical eclipse data 09 p1520 A71-22833
- Flux density measurements of Ohio radio source survey at 1415 MHz compared with 1400 MHz measurements by Australian National Radio Astronomy Observatory telescope 10 p1668 A71-23881
- Quasars or blue stars possibility of radio sources usually identified with galaxies 10 p1674 A71-24448
- Organic compounds astrochemistry, discussing hydroxyl absorption lines and molecular abundances in interstellar space 10 p1678 A71-24810
- Book on radio astronomy instruments and observations covering high sensitivity radiometers, masers, parametric amplifiers, radio telescope design, radio spectrometers, parabolic reflectors, etc 11 p1737 A71-25359
- OGO radio astronomy instrument for cosmic noise sky brightness distribution mapping by electrically short antenna ionospheric focusing 11 p1763 A71-26144
- Galactic radio source Sagittarius optically thick component evidence based on flux density measurement 12 p1956 A71-26612
- Radio astronomy in millimeter and submillimeter ranges, surveying programs and equipment at various observatories 12 p1967 A71-27421
- Radio mapping of Maffei 1 and 2 galaxies, confirming previously detected small diameter source 13 p2136 A71-28428
- Sizes, shapes and temporal characteristics of small scale inhomogeneities in F region, using vertical sounding, space diversity reception and radio astronomy 13 p2061 A71-28554
- Crab Nebula pulsar NP0532 radio observations, noting long term slowing down and irregular perturbations in periodicity 13 p2137 A71-28591
- Strong planetary nebulae measurement at short centimeter wavelengths, observing flux densities and thermal spectra 13 p2138 A71-28760
- Interstellar 21 cm and Na D lines comparison in directions of 30 stars at intermediate and high galactic latitudes 14 p2304 A71-29595
- Galaxy Maffei 2 observations in 21 cm neutral hydrogen line and in continuum at 1415 MHz with Nancy radio telescope 14 p2305 A71-29681
- H85 alpha recombination line in planetary nebula NGC 7027, considering IR physical parameters consistent with radio observations 14 p2313 A71-30432
- Radio pulses from Crab Nebula pulsar NP 0532, determining multipath scattering delay distribution function and distortion 14 p2314 A71-30641
- Galactic nebula YM 29 radiometric observations showing thermal source, mass and Balmer line fluxes comparable to planetary nebula 14 p2314 A71-30643
- Radioheliographic 80 MHz observations of harmonic type 2 solar burst near limb flare 15 p2472 A71-31688
- Culgoora 80 MHz radioheliographic observations of 13 October 1969 harmonic solar type 2 burst attributed to explosive flare behind west limb 15 p2472 A71-31689
- Harmonic type 3 solar bursts radioheliographic observations, discussing polarization characteristics 15 p2473 A71-31691
- Moving type 4 solar radio burst observation on 10 October 1969 with radioheliograph, noting circular polarization, movement direction, speed and structure 15 p2473 A71-31694

Lunar radioactive layer effective thickness by radio astronomical methods and from Apollo 11 flight
15 p2486 A71-31892

Mars radio spectrum discrepancy with elementary theory, assessing microwave observations
15 p2490 A71-32416

Data processing technique for radio mapping of sun, discussing unwanted harmonics elimination and noise reduction
15 p2491 A71-32447

Diffuse interstellar medium hydrogen radio recombination lines radiation transfer, investigating thermodynamic equilibrium effects
15 p2498 A71-32770

Dense interstellar cloud radio recombination lines in H I regions, calculating quadrupole effects on line splitting
15 p2498 A71-32771

Cygnus-X region radio photography, presenting radio brightness intensity modulated display supplementing contour map
16 p2630 A71-33124

Radio contour map of Crab nebula at 3.5 mm, giving brightness distribution and flux density
16 p2632 A71-33235

Fixed base two element interferometer for radio astronomy, obtaining beavertail radiation pattern by use of earth rotation
16 p2579 A71-33486

Radio astronomy signals reception and interpretation, detailing solar, galactic and extragalactic spectrum sources
17 p2797 A71-34242

Space radio astronomy, discussing frequency range in terrestrial atmosphere, RAE-1 satellite, cosmic and solar emissions and magnetopause generation, propagation and absorption processes
17 p2797 A71-34243

Decimeter wave multichannel spectrograph design for radio astronomy, stressing HF section
17 p2739 A71-34600

Lunar microwave thermal emission observation and theoretical predictions based on lunar surface models
17 p2804 A71-35177

Pulsar polarization characteristics and pulse profile observations in 250-450 MHz range
17 p2807 A71-35417

Filled aperture antennas for radio astronomy, considering mm wave observations, parabolic cylinder antennas and active/passive control of antenna surfaces
18 p2901 A71-37036

Radio astronomy, covering invisible stars discovery and instrumentation techniques comparison with UV and X ray astronomy
19 p3131 A71-37342

Cosmic radio astronomy, evaluating sensitivity and resolution limitation of ground based radio telescopes
19 p3138 A71-37762

Planetary LF radio emission experiments on Grand Tours, discussing models and spectrum, polarization, position and time variation measurements
19 p3141 A71-37965

Radio sources position data table based on high accuracy telescope observation including calibration uncertainties and measurement random errors
19 p3142 A71-38008

Electromagnetic compatibility in radio astronomy, discussing frequency spectrum pollution and national radio quiet zone
19 p3032 A71-38454

Joint American-Soviet astronomical radio interferometry, discussing resolution and quasar and galaxies structural difference
19 p3145 A71-38569

Monochromatic radio emission from decihertz years distant stars, discussing search experiment by low noise multichannel receivers
20 p3291 A71-39319

Microwave spectral line receivers for radio astronomy observation of molecular clouds in interstellar space
20 p3238 A71-39401

IAU Executive Committee, General Assembly and commissions reports on astronomy, including manuscripts preparation guidelines, handbook, etc
20 p3315 A71-39425

Heat release from elemental decay in radioactive layer from radio astronomical observations and lunar rock chemical analysis
20 p3295 A71-39620

Saturn planetary system optical and radio observations during 1966, discussing Janus satellite, D ring, rarefied envelope and brightness temperature distribution
20 p3297 A71-39632

Radio telescopic search for extraterrestrial oxygen 18 containing water microwave emission, suggesting water vapor maser pumping mechanism dependence on isotopic species
21 p3444 A71-40223

Cas A and Cyg A radio stars scintillation measurement by two element phase switched interferometers in ionospheric irregularities study
21 p3378 A71-40377

Radio observation for radial velocities in center region of Perseus cluster of galaxies
21 p3445 A71-40408

Tabular listing of frequency allocations for space services and radio astronomy made at Extraordinary Administrative Radio Conference
21 p3348 A71-40476

High resolution astronomical radio interferometry, discussing radio telescope system design
21 p3452 A71-41052

Australian National Radio Astronomy Observatory integrated time and frequency system with cesium beam frequency standard and digital computer for real time operation
22 p3547 A71-42498

Extragalactic radio sources catalog from Parkes Australian National Radio Astronomy Observatory 2700 MHz survey of plus/minus 4 deg zone and selected regions
22 p3607 A71-42769

Maffei 2 spiral galaxy hydrogen line and adjacent continuum observation by radio interferometry
23 p3733 A71-43080

Radio astronomic intercontinental base interferometry, discussing independent local oscillators requirements and atomic clock frequency standards
23 p3674 A71-43087

Planetary nebulae microwave radiation emission survey by Algonquin Radio Observatory, determining flux densities
23 p3769 A71-43988

RADIO ASTRONOMY EXPLORER SATELLITE
RAE satellite flexible boom vibration, obtaining antenna boom static deflection, natural frequencies and thermal bending effects
[ASME PAPER 71-DE-J]
12 p1977 A71-27319

RADIO ATTENUATION
Signal detection processes selection and components sizing for stand for echometric measurement of attenuation in long distance waveguide connection
01 p0029 A71-10309

Polar aurora pulsations of 4-12 sec intensity with associated cosmic radio noise absorption, using photometric measurements
02 p0242 A71-11761

Space-time structure of ionospheric regions of anomalous radio wave absorption during auroras, discussing ionization region
02 p0243 A71-11765

ELF and VLF radio attenuation for propagation below inhomogeneous isotropic ionosphere with realistic vertical variation models for electron density and collision frequency
02 p0212 A71-11964

Nondissipative focusing and ionospheric reflecting effects on MF radio wave absorption measurements for magnetically quiet and disturbed periods
03 p0409 A71-13391

Attenuation and phase velocities of ELF slow tail atmospherics for easterly and westerly nighttime propagation over Pacific Ocean
04 p0552 A71-15217

D region electron density profile relation to radio wave absorption frequency dependence
05 p0746 A71-17204

Time structure of auroral radio absorption from magnetically conjugate and closely spaced observations
06 p0892 A71-17977

Ionospheric radio wave absorption above polar aurora during solar activity minimum, discussing diurnal and annual behavior
09 p1435 A71-22429

Effect of asymmetrical inviscid flow from Trailblazer flight measurements, discussing windward leeward attenuation variation in transmitted VHF signal
09 p1406 A71-22916

Direct broadcast television service by satellite transmission, calculating trees and woods effects on attenuation and suggesting receiving system design modification
09 p1408 A71-23384

Venus atmosphere mm and cm radio wave propagation calculated from temperature, pressure and chemical composition data
11 p1823 A71-25695

Obliquely incident radio wave absorptions measurements from January-October 1968 vertical ionospheric soundings, correlating diurnal variations with solar zenith angular changes
11 p1732 A71-25787

Winter day absorption variability of HF radio waves reflected at oblique incidence from ionosphere, using ray tracing method
13 p2027 A71-27799

Nondeviative absorption of RF signal at 2.2 MHz in presence of cusp type sporadic E layer
13 p2055 A71-27926

D region electron density profile relation to radio wave absorption frequency dependence
13 p2059 A71-28259

Electron density profile determination in D region based on frequency dependence of radio waves absorption, discussing lower ionosphere anomalous ionization
13 p2061 A71-28539

Radio propagation attenuation calculation by tropodiffusion, using meteorological parameters from Brazilian weather stations
14 p2192 A71-29573

Venusian atmosphere RF refractive attenuation height dependence, field strength measurements comparison, inversion layer influence and surface echoes effects
14 p2309 A71-30098

Ionospheric absorption of 20 MHz radio waves as function of solar activity level, using electron density and temperature profiles
15 p2401 A71-32686

Ionospheric absorption measurements at 272 kHz, using surface wave attenuation factor as calibration technique
16 p2562 A71-33072

Percent-of-time distributions of attenuation by rain, clouds and atmospheric gases on earth-space paths at frequencies below 30 GHz
17 p2704 A71-35089

Radiometric measurements of frequency distribution of radio emission attenuation due to troposphere, noting sun-earth communication paths
17 p2707 A71-35124

Solar activity effects on equatorial ionospheric absorption of radio waves, deriving solar cycle constant
19 p3055 A71-38042

F region radio wave absorption dependence on electron-ion temperature difference from energy balance considerations, testing by radar backscatter measurements
19 p3055 A71-38045

D region ionization by electron fluxes as explanation for latitudinal radio wave absorption
19 p3057 A71-38370

Recalculated radio wave absorption during oblique transit through ionosphere from vertical measurements using rhombic antenna at 25 MHz
19 p3058 A71-38388

Broadband antenna twist reflector with wire grids, deriving design formulas and theoretical performance in terms of polarization attenuation
19 p3036 A71-38606

Rain attenuation measurements, noting limitations on microwave transmission at SHF
19 p3024 A71-38612

Cumulonimbus cloud hail danger, precipitation and water content measurements with scattering and attenuation of centimeter radar waves, including automated echo subtraction device
19 p3094 A71-38700

Sensitivity requirements for attenuation measurement radio receivers, considering minimum input SNR for absolute measurement error not to exceed preestablished value
20 p3197 A71-39550

Obliquely incident radio wave absorptions measurements from January-October 1968 vertical ionospheric soundings, correlating diurnal variations with solar zenith angular changes
22 p3509 A71-41555

Ionospheric geomagnetic field effect on ELF/VLF radio propagation
23 p3643 A71-42967

Phase integral correction for reflected radio wave absorption in ionosphere, comparing with ray theory
23 p3643 A71-42969

Stratospheric warmings effect on F 2 region parameters and ionospheric radio wave absorption, assessing time lag
23 p3673 A71-44049

Atmospheric vertical humidity profile from ground measurements of radio wave absorption at 1.35 cm water vapor line
24 p3822 A71-44820

Radio absorption in lower ionosphere, determining vertical distribution of electron density and production rates from solar protons energy spectrum
24 p3867 A71-45041

RADIO AURORAS
Magnetically conjugate range-time observations of E region radio aurora by pulsed VHF radar echoes
18 p2875 A71-35963

Radio and optical aurora correlation and control by polar electrojet, using VHF backscatter and geomagnetic recordings
20 p3229 A71-39853

Auroral ELF and VLF emission at high latitudes, discussing chorus and hiss generation regions and noise mechanism
20 p3229 A71-39854

RADIO BEACONS
Microwave local oscillator and beacon generator for Intelsat 3, discussing design, operation and performance
06 p0877 A71-18400

Sea trials with dummy payloads of sounding rocket recovery systems, using parachutes, flotation torus, radio beacons, fluorescent dyes and smoke generators
06 p0881 A71-18674

- French Geol spatial system utilization in polar zones, combining satellite with ground beacons, telemetry ground receiving station and computer 10 p1599 A71-23860
- Modeling of differences between actual and estimated flight times over radio beacon, obtaining cumulative frequency distributions 13 p2167 A71-28490
- Radio direction finding with discrete antenna scanning and multilevel beacon signal quantization, investigating accuracy 15 p2370 A71-31591
- Geodetic system with satellites and automatic radio beacons, establishing network on earth surface to track isolated points 18 p2913 A71-36529
- Single seater turbojet aircraft landing via automatic band switch for ARK-5 and ARK-10 radio compass 19 p3101 A71-38017
- Automatic pulsating locator beacons and receivers to determine emergency transmitters locations, using satellites with computer analysis 20 p3261 A71-38865
- Pulsars radio wave emission characteristics, intensity variation, duration, bandwidth, similarity to space radio beacons and evidence as neutron stars 21 p3442 A71-40144

RADIO BLACKOUT
U BLACKOUT [PROPAGATION]

RADIO BROADCASTING
U BROADCASTING

RADIO BURSTS

- NT SOLAR RADIO BURSTS
NT TYPE 2 BURSTS
NT TYPE 3 BURSTS
NT TYPE 4 BURSTS

Energy spectra of expanding relativistic particle clouds producing quasar and Seyfert galaxy nuclei outbursts 02 p0307 A71-12082

Energy spectra of expanding relativistic particle clouds producing quasar and Seyfert galaxy nuclei outbursts 08 p1362 A71-21132

Expanding source model verification for radio outbursts in quasars and Seyfert galaxy nuclei 08 p1365 A71-21424

Geomagnetic distributions of VLF hiss intensity and drifting frequency bursts near inner boundary of plasmopause on middle latitudes 09 p1411 A71-23634

Narrow band atmospheric radio noise burst average and rms field strength measurement 13 p2033 A71-28900

Solar wind velocity and Io phase relationship during decametric radio bursts from Jupiter, indicating plasmasphere existence 15 p2474 A71-31723

Pulse duration of atmospheric radio noise bursts at 3 MHz from lightning flashes, considering effect on data communication 23 p3643 A71-42970

RADIO COMMUNICATION

- NT PULSE FREQUENCY MODULATION
TELEMETRY
NT RADIO RELAY SYSTEMS
NT RADIO TELEGRAPHY
NT RADIO TELEMETRY
NT TELEPHONY

Optimum positioning and structure of light hogged antenna masts for radio communications and broadcasting networks 01 p0068 A71-11085

Cassegrain antenna electrical and structural design and control system for microwave propagation and communication research, using moon reflected signals as atmospheric probes 02 p0234 A71-12806

Extraterrestrial civilizations, discussing probability theory and radio communication 06 p0852 A71-17739

Radio amateur satellites contribution to space research and communications 07 p1057 A71-18814

Radio communication system hypersonic delay lines, investigating coupled resonators matching efficiency in parallel and series connection 07 p1074 A71-19142

Short wave communication channel quality estimate for discrete signal transmission based on signal level variations calculation with allowance for ionospheric parameters 08 p1252 A71-20773

Statistical properties of radio communication system polarization reception coefficient as function of receiving antenna and signal polarization characteristics 09 p1405 A71-22294

Optimal two stage signal search in frequency vs arrival time indeterminacy plane of communication system 10 p1579 A71-24714

Digital synthesizers design and operation for radio communications, discussing reception and transmiss-

sion noise performance, frequency stability and acquisition time 10 p1579 A71-24757

Airborne radio communication systems, stressing electronic equipment design reliability 12 p1878 A71-26880

Radio communication accuracy characteristics in calculation of maximum frequency, skip distance and emission angle by transmission curves for midlatitude ionosphere 13 p2030 A71-28544

Multichannel modular tropospheric scatter equipment as economic solution for medium range HF communication 13 p2034 A71-29317

ATS 1 and 3 satellite VHF transponders for ships and aircraft location, communication and remote sensing, discussing performance test results 14 p2198 A71-30898

Lunar roving vehicle telecommunication system requirements concerning vehicle functions, science experiments, crew operations and safety 14 p2200 A71-30915

Helicopter aerial design problems, considering antenna multiplicity use of nonmetallic structures and complexity of airborne radio systems 14 p2217 A71-31048

Communication blackout during missile and spacecraft high altitude flight, considering convective effects on gas breakdown by microwaves 14 p2206 A71-31071

Space radio communications, considering radio links reliability between multistage launcher rocket and ground stations 17 p2696 A71-34228

International radio regulations adopted by Geneva space conference with reference to frequency band allocations in 1-10 GHz range with equal rights to space and terrestrial services 17 p2697 A71-34246

International cooperation in space radio science, considering real time telemetry application via Solrad, Tiros and Alouette satellites 17 p2697 A71-34252

Radio communication system optimization from viewpoints of global synthesis including economics and partial synthesis based on noise stability, precision and reliability 17 p2698 A71-34392

Radio engineering of signal detection, filtration, information processing and recognition, discussing game theory methods for problems solution 17 p2698 A71-34393

Short wave frequency-diversity radio communication systems operating at extremal frequencies of group, estimating noise reduction effectiveness 17 p2698 A71-34395

Single sideband mechanical filters for voice multiplex transmission in radio and telephone systems, discussing material characteristics 17 p2714 A71-34608

Space radio communication - Conference, Paris, March 1971 17 p2699 A71-34676

Averaging method for nonlinear oscillations in celestial mechanics, radio engineering and electronics and for time lag, random forces and integrodifferential equations 17 p2779 A71-34904

Airborne communications with AN/ARC-154 transceiver in single radio, discussing extended frequency coverage, multimode operation, navigation and input/output provisions 17 p2775 A71-35758

Omnidirectional one slot aerial energized by dielectric waveguide for hypersonic vehicle-ground communication through ionized shock layer [ONERA-TP-949] 18 p2887 A71-36022

Earth-spacecraft radio communication requirements for future unmanned planetary missions, emphasizing imaging experiments and sensors 18 p2877 A71-36518

Performance characteristics and reuse intervals of high capacity mobile radio systems with dynamic channel assignment, using computer simulations 19 p3014 A71-37216

Radio wave propagation studies evolution, considering ionospheric signal reflection, equipment optimal characteristics and transversed medium composition and properties probing 19 p3016 A71-37341

Intercontinental point to point radio communication, discussing Hertzian beam /radio relay links/ and satellite communication comparison with underground and submarine cables 19 p3016 A71-37343

Marine navigation and data communications at L band via synchronous satellite, assessing capabilities by tests on ATS-5 satellite 19 p3102 A71-38070

RF communications spectrum pollution, discussing corrective and preventive electromagnetic compatibility measures 19 p3020 A71-38427

Soviet monograph on astronomical foundation of meteor communications, covering radio wave scattering by meteor trails and computer simulation of signal time-amplitude characteristics 21 p3349 A71-41373

Electronic broad banding of VLF/LF antennas for FSK radio communication through switched magnetically coupled reactor, determining antenna transient response 22 p3513 A71-42388

RADIO CONTROL

Telecontrolled Rotomobile flying crane with jet powered lifting rotor for carrying heavy loads over short distances 10 p1556 A71-24420

Radio controlled small aircraft as measurement platform for meteorological sensors, discussing development and performance from field tests 17 p2675 A71-35334

Soviet book on radio control of various flight vehicles covering closed loop synthesis, missile guidance, spacecraft trajectory correction and air traffic control 17 p2775 A71-35403

RADIO DIRECTION FINDERS

Frequency selective conical scanning for direction finding earth station antennas for communication satellite automatic tracking, using waveguide mode conversion 02 p0223 A71-12809

Satellite tracking by radio direction finder, noting periodic azimuth deviations related to ionospheric Faraday effect 03 p0377 A71-13169

Direction finding problems involving several waves of same frequency, discussing nonlinear computation methods with hybrid computers 06 p0927 A71-18205

Phase locked automatic direction finder /ADF/ flight test results, indicating signal to noise threshold reduction by coherent detection 07 p1057 A71-18815

Wideband microwave monopulse radar direction finding techniques, discussing concept, operation theory, characteristic equations and error analysis 07 p1059 A71-18846

Rawin system performance and technical features, describing radio direction finder design, operation, capabilities and carrier balloons 08 p1330 A71-21741

Radio direction finding of celestial bodies from moving platform, determining plane rotation effects on angle measurements 09 p1532 A71-22661

Phase sector direction finder for VHF range, using log periodic dipole arrays 11 p1738 A71-26338

Direction finder for point source signals from two simultaneous transmitters 14 p2210 A71-29810

Emitter location techniques for airborne passive ECM, discussing accuracies in terms of geometry, sample number, random and bias errors 15 p2375 A71-31205

Radio direction finding with discrete antenna scanning and multilevel beacon signal quantization, investigating accuracy 15 p2370 A71-31591

Polarization direction finder determining electromagnetic waves azimuth on basis of field intensity vectors 19 p3014 A71-37074

Atmosphere meteorological sounding, measuring geodetic quadrangle sides and diagonals by aircraft radio direction finder 19 p3065 A71-38175

Multicomponent signal arrival angles wave front analysis from antenna array phase and amplitude measurements for radio direction finding 24 p3803 A71-44647

RADIO ECHOES

Faint sporadic meteors mass distribution from forward and backscatter of radio echoes 01 p0151 A71-10254

Signal detection processes selection and components sizing for stand for echometric measurement of attenuation in long distance waveguide connection 01 p0029 A71-10309

D region electron density time variations, using partial radio reflection technique during solar eclipse of 20 May 1966 03 p0407 A71-13379

FM radio link fluctuating intermodulation distortions reduction by additive superpositioning of several compensating echoes with adaptive equalizer 03 p0380 A71-14334

Beam-plasma mechanism of very long delayed radio echoes from ionosphere 03 p0381 A71-14552

Electron concentration vertical profile in ionosphere as function of altitude of radio wave reflection and group refraction and velocity characteristics 06 p0895 A71-18278

- Group delay times criterion of multibeam propagation of ionospheric radio echoes for communications systems 06 p0869 A71-18281
- Topside sounders received frequencies of oblique echoes at plasma resonance, using WKB technique 07 p1168 A71-19676
- Trapped waveguide mode frequency of whispering gallery propagation in F region explaining round world echoes and long distance satellite observations 10 p1577 A71-24292
- Echo reflections and transition through critical coupling in D and E regions at low and medium frequencies, using nighttime electron density distributions 11 p1754 A71-25601
- Far ionospheric propagation of round-the-world echo signals from Moscow to Antarctic station Molodezhnaia and back to Moscow 11 p1731 A71-25773
- Small scale F layer inhomogeneities parameters and motion characteristics from radio echo observations 13 p2056 A71-27935
- Monograph on persistent radio meteor echoes fading relation to upper atmosphere wind structure 14 p2192 A71-29579
- Receiver triangle size effect on ionospheric drifts near 2 MHz, using partial and total reflections from lower ionosphere 14 p2230 A71-29710
- E layer phase height measurements with spaced receivers without ultra stable oscillators, calculating scale height 14 p2230 A71-29712
- Optimal noncoherent receiver for signal detection in mixture of noise and chaotic echoes in media with frequency dependent attenuation 15 p2369 A71-31231
- Ground based HF radio sounding of earth magnetosphere echoes due to propagation along electron density enhancement 15 p2398 A71-31769
- Magnetospheric whistler mode signal propagation paths and amplification, investigating echoes of ground to satellite transmission 19 p3016 A71-37400
- Polarization ellipse and depolarization coefficients for monochromatic radio waves reflected from F 2 ionosphere using Stokes parameters 19 p3056 A71-38362
- Electron concentration and collisions number fluctuations effect on D region profiles based on radio waves partial reflection data 19 p3057 A71-38365
- Meteor bodies mass distribution function for Geminid stream, determining parameter S from radio echoes 19 p3145 A71-38528
- Incident meteor flux density seasonal variations from radio reflections from trains and light scattering from micrometeoroids 20 p3298 A71-39642
- Sporadic and shower meteoroids mass distribution temporal variations as function of magnitude and solar longitude from visual and radio echo measurements 20 p3298 A71-39643
- Auroral radio reflections mechanism in terms of auroral plasma instability processes, identifying ion acoustic wave characteristics among other echo components 20 p3199 A71-39852
- Far ionospheric propagation of round-the-world echo signals from Moscow to Antarctic station Molodezhnaia and back to Moscow 22 p3509 A71-41541
- Rocket and radio wave wind profiles from 60 km to E region near 53N, presenting partial reflections and zonal winds time cross section 23 p3700 A71-43343
- Radio echoes from clouds and precipitation, determining detection threshold, station potential and statistical distribution numerical characteristics 24 p3844 A71-44879
- Cloud and precipitation effects on radio echoes intensity measurement, discussing pulse dimensions influence on average signal magnitude 24 p3845 A71-44881
- Radio echo average power measurement errors due to clouds 24 p3845 A71-44882
- Multiple mismatch reflection and mode conversion echo effect on error rate in guided millimeter wave phase shift keying systems 24 p3804 A71-44989
- Diurnal fluctuations in radio echo producing ionospheric region horizontal scale and height, discussing dependence on solar position 24 p3804 A71-45042
- RADIO ELECTRONICS**
- Soviet book on nonlinear and parametric radio circuits covering amplification, detection, modulation, oscillation generation and frequency division, multiplication and conversion 06 p0867 A71-17441
- Soviet papers on nonlinear and microwave radio engineering systems covering antenna arrays, tunnel diode multivibrators and binary logic elements, sub-harmonic oscillators, etc 11 p1739 A71-26535
- Culgoora radioheliograph electronic imaging system for diffraction pattern generation 24 p3828 A71-45205
- RADIO EMISSION**
- NT SOLAR RADIO BURSTS
- NT SOLAR RADIO EMISSION
- NT TYPE 2 BURSTS
- NT TYPE 3 BURSTS
- NT TYPE 4 BURSTS
- Explosion shock wave induced short wave radio emission, deriving time related gas ionization state of wave front 02 p0284 A71-11927
- Lunar radio emission measurements at 1.42 mm, using radio telescope and wideband superheterodyne radiometer 02 p0309 A71-12104
- Planetary and lunar thermal radio emission and brightness temperature measurements using sensitive receivers and large aperture radio telescopes 02 p0309 A71-12155
- Turbulent plasma radio emission theory of photon production and transport, considering application to quasars 02 p0292 A71-12587
- Small radio sources emission, examining correlation with optical photometric properties abnormalities 02 p0317 A71-12863
- Radio emission upper limits from galaxies in Markarian catalog 02 p0317 A71-12866
- Earth surface and atmosphere thermal radio emission measurement by radio telescope on Cosmos 243 satellite 03 p0409 A71-13420
- Electron-photon showers, discussing cascade theory equilibrium spectra, avalanches and radio emission 03 p0475 A71-13840
- Spatial distribution and polarization of radio emission from extensive air showers, using Geiger and scintillation counters, muon detectors and antennae 03 p0477 A71-13865
- Solar flare X ray and radio wave emission measurement byOGO 4 and Solrad 9 satellites 03 p0479 A71-14046
- Pulsar radio wave generation, discussing emission theory and frequency independence of beam width and polarization 03 p0493 A71-14208
- Radio source W58, investigating continuum emission structure and spectrum 04 p0641 A71-14736
- LF radio emission from Jupiter at 3-8 MHz 04 p0641 A71-14737
- Supernova remnant X ray and radio emission secular behavior, considering hot plasma and synchrotron models and continuous injection 04 p0640 A71-14874
- Coherent emission mechanisms for pulsar models, discussing plasma wave conversion into radio emission 04 p0650 A71-15582
- Phase modulation drift of radio emission from pulsar MF 0031-07 05 p0801 A71-15927
- Methyl alcohol detection in Sagittarius, examining radio line emission at 834 MHz 05 p0802 A71-15945
- Quasars radio spectra in 1-5 GHz frequency range, examining emission from expanding clouds due to synchrotron radiation with self absorption 05 p0805 A71-16112
- Radio emission from small galactic nebulosities, describing position, flux densities, identification and exciting stars 05 p0811 A71-16683
- Convective cyclotron instability in whistler mode, discussing magnetosphere as generation mechanism and taking into account magnetospheric plasma inhomogeneity 05 p0743 A71-17003
- Martian radio emission measurements at millimeter wavelength and surface thermal and electric parameters estimation 07 p1193 A71-19314
- Lunar radio emission measurements at 1.42 mm, using radio telescope and wideband superheterodyne radiometer 08 p1362 A71-21151
- Pulsars as rotating magnetic neutron stars, examining radio emission via maser amplification 08 p1363 A71-21174
- Optical quasi-stellar objects searched for radio emissions, disproving previously claimed detections 09 p1518 A71-22352
- Uranus radio emission model, considering presence of gaseous ammonia at saturation pressure in atmosphere 09 p1519 A71-22526
- Long wave cosmic radio background emission in circumlunar space by Luna 11 and 12 satellites, observing increase in earth magnetosphere tail 09 p1513 A71-22576
- Giant elliptical galaxy Maffei 1 continuous radiation emission data at 1415 MHz, examining radio luminosity magnitude 09 p1523 A71-22982
- Soft X ray radiation correlations to radio emission flux at various frequencies in 20th solar activity cycle 09 p1515 A71-23529
- Quasar radio emission fine structure measurements by very long baseline interferometry, using Goldstone Mars antenna and Haystack radio telescope 10 p1671 A71-24325
- Automatic frequency spectrum recorder related to monitor radio emissions in space service allocated bands 10 p1578 A71-24583
- Contour map of galactic radio emission in Cassiopeia and Cepheus region, noting discrete sources 11 p1831 A71-26132
- Jupiter magnetic field geometry related to Io modulated Jovian decametric radio emission 12 p1956 A71-26620
- Earth surface thermal radio emission measurements by UHF radiometry onboard Cosmos 243 satellite, showing brightness profiles of water, ice and land areas 12 p1899 A71-26639
- Galactic radio emission, considering continuum radiations, radio polarization, H I regions structure and physics, recombination and absorption lines 12 p1959 A71-26778
- Radio pulses at 2 MHz from cosmic ray air showers, using high speed digital techniques in statistical data analysis 12 p1948 A71-26936
- Uranus radio emission measurements at 8.22 mm wavelength, noting brightness temperature and atmospheric properties 12 p1965 A71-27226
- Antenna effective area and radiation pattern measurement using emission characteristics of extraterrestrial radio sources, sun and moon 12 p1967 A71-27422
- One- and two-component gas models for explaining interstellar gas kinematics and 21 cm line emission brightness temperature dependence on galactic longitude 12 p1970 A71-27747
- Hellswell VLF discrete emission theory application to determination of electron stream energy spectrum and structure 13 p2027 A71-27915
- Radio pulse production by extensive air shower charges geomagnetic separation 13 p2126 A71-28101
- Air showers emitted radio pulses polarization, noting inconsistency with geomagnetic origin 13 p2127 A71-28102
- Extensive air showers radio wave emission based on cascade theory, determining polarization characteristics 13 p2127 A71-28103
- Air shower radio emission properties, presenting electric field strength measurements at various frequencies 13 p2127 A71-28104
- Air shower radio pulse amplitude variations with zenith and azimuth angle, distance from shower axis and primary energy, examining frequency spectrum characteristics 13 p2127 A71-28105
- Radio emission measurement from extensive air showers by system of half wave dipoles in complex array of Moscow State University 13 p2127 A71-28106
- Extensive cosmic rays high and low frequency radio pulses investigation, using plastic scintillator triggered receivers 13 p2127 A71-28107
- Radio particle correlation of extensive air showers at large zenith angles, using twofold coincident 44 MHz receiver trigger-scintillator system 13 p2127 A71-28108
- Extensive air showers radio emission pulse shape, noting amplifying system response to input signal 13 p2128 A71-28109
- Average function for lateral distribution of radio emission in extensive air showers 13 p2128 A71-28170
- Galactic LF nonthermal radio emission origin, considering mechanisms of synchrotron radiation from cosmic ray electrons and enhanced bremsstrahlung 14 p2304 A71-29593
- LF whistler mode radio noise emissions observations in polar regions with Alouette 2, noting association with energetic particles influx into ionosphere 14 p2300 A71-30036
- Oscillations in second cavity of ammonia maser containing two resonators successively traversed by molecular beam, studying polarization and radioelectric emission 14 p2254 A71-30440

Cosmic radio emission coherent generation mechanism, involving derelativization and relativization of particles in small space

15 p2483 A71-31343

Light and radio emission from Orion nebula flare stars in meter waveband, discussing coherent mechanisms of plasma oscillations and gyro/synchrotron radiation amplification

15 p2485 A71-31696

Martian radio emission measurements at millimeter wavelength and surface thermal and electric parameters estimation

15 p2486 A71-31894

Astronomical 4C catalog radio sources statistical analysis, showing mean spectral indices dependence on radio emission fluxes and red shifts

15 p2487 A71-32037

Heat balance and 8.22 mm radio emission of Mars, evaluating surface thermal and electrical parameters including brightness temperature

15 p2490 A71-32411

Uranus radio emission measurement at 8.22 mm, obtaining brightness temperature

15 p2490 A71-32412

Mars and Jupiter radio emission at 2.3 mm and 8.15 mm, determining brightness temperature and electrical and thermal waves soil penetration depth ratio

15 p2490 A71-32413

Chromosphere and solar quiet regions transition zone model, investigating radio and UV emission and height dependence of temperature and density

15 p2497 A71-32745

Aperture synthesis observations of neutral hydrogen radio emission in spiral galaxy M 101, using twin-element interferometer

16 p2632 A71-33329

Rotation measure and intrinsic angle of Crab pulsar emission, discussing optical and radio radiation origin

16 p2634 A71-33390

Supernovae outburst remnant radio emission from Crab Nebula, discussing synchrotron mechanism and connection with pulsars

16 p2635 A71-33472

Saturn radio emission and brightness temperature measurements, determining rings optical thickness upper limit

16 p2639 A71-33692

Very long baseline interferometry of radio emissions from geostationary satellites, determining orbital elements and inertial position

16 p2544 A71-33845

Discrete VLF emissions triggered by naturally occurring whistler trains or man-made signals of constant frequency

16 p2544 A71-33950

Soft optical, radio and X ray emission during accretion of interstellar gas by neutron star with magnetic dipole moment

17 p2800 A71-34570

Field strength of radio emission from cosmic ray showers at 3.6 MHz, stressing data analysis procedure

17 p2732 A71-34623

Uranus radio emission model, indicating presence of gaseous ammonia at saturation pressure

17 p2807 A71-35501

Pulsar radiation generation by charged particles nonlinear Thomson scattering of strong LF electromagnetic wave and nonthermal radio emission

18 p2960 A71-35940

Radio emission from cosmic ray showers, discussing detection, particle populations and energy spectra

18 p2957 A71-36211

Uranus radio emission measurements at 8.22 mm wavelength, noting brightness temperature and atmospheric properties

19 p3132 A71-37378

Thermal radio emission of Jovian planets atmospheres, deriving brightness temperature [AAS PAPER 71-109]

19 p3139 A71-37909

Narrow band magnetospheric radio noise between electron plasma and upper hybrid resonance frequencies from satellite observations

20 p3285 A71-38728

Radio emission detection of para-formaldehyde and 2 mm formaldehyde distribution in Orion IR nebula

20 p3287 A71-39112

Monochromatic radio emission from decilight years distant stars, discussing search experiment by low noise multichannel receivers

20 p3291 A71-39319

Atmospheric moisture from Cosmos 243 satellite measurements of intrinsic atmospheric radiothermal emission

20 p3218 A71-39587

High latitude VLF radio emissions rate of occurrence at all magnetic times, noting diurnal variations

20 p3198 A71-39745

VLF emissions and low energy electrons relation to other auroral phenomena from satellite-borne data associating midnight maximum with particles from plasma sheet

20 p3229 A71-39855

ELF and VLF emissions during PCA, correlating data with particle and photometer recordings from ground based, satellite and rocket-borne observations

20 p3229 A71-39856

Continuous injection models for secular X ray and radio emission from supernova remnants in Crab Nebula, Cas A and Tycho

20 p3304 A71-39942

Pulsar radio emission via maser amplification, presenting model based on electrons behavior in intense magnetic field

20 p3285 A71-39949

Radio pulses from pulsars, noting relativistic energy of particles from volume emissivity and surface flux density

20 p3305 A71-39950

Radio pulses from pulsars based on model of coherent synchrotron radiation from magnetosphere trapped charged particles

20 p3285 A71-39951

Scorpius X-1 radio emission detection at 1415 MHz, discussing brightness distribution

21 p3441 A71-40068

Pulsars radio wave emission characteristics, intensity variation, duration, bandwidth, similarity to space radio beacons and evidence as neutron stars

21 p3442 A71-40144

Jupiter and Saturn IR radiation sources, radio emission storms, magnetic fields, life existence, Grand Tour missions, etc

21 p3442 A71-40150

Double radio emission sources during occultation period, noting structure, angular size components, positional errors and association to quasars

21 p3443 A71-40189

M supergiants hot corona base density determination from radio emissions observations, noting equivalence to solar type 4 microwave bursts

22 p3598 A71-41916

Pulsar radio emission from expanding charge sheets moving relativistically along dipolar magnetic field near neutron star polar caps, calculating energy distribution

22 p3604 A71-42336

Brightness and polarization distributions for supernova remnants IC443 and Puppis A, considering magnetic field orientation and thermal radio emission

22 p3606 A71-42601

Cosmic radio emission coherent generation mechanism involving derelativization and relativization of particles in small space

22 p3606 A71-42618

Electron-photon showers, discussing cascade theory, equilibrium spectra, avalanches and radio emission

22 p3594 A71-42641

Lateral distribution and polarization of radio emission from extensive air showers, using Geiger and scintillation counters, muon detectors and antennae

22 p3595 A71-42666

Red dwarf flare stars sporadic outbursts, considering light and radio emission curves, outburst energy and galactic emission

22 p3607 A71-42881

Atmospheric triggered VLF emissions theory, examining magnetospheric whistler Morse pulses

23 p3643 A71-43135

Planetary nebulae microwave radiation emission survey by Algonquin Radio Observatory, determining flux densities

23 p3769 A71-43988

Extensive air shower radio pulse emission by geomagnetic charge separation mechanism, using antenna and scintillation counters arrays

23 p3646 A71-44012

Pulsar CP 0950 radio emission intensity variation measurement, using dispersion removal technique for interstellar medium signal distortion

24 p3871 A71-44903

RADIO ENERGY

U RADIANT FLUX DENSITY

U RADIO WAVES

RADIO EQUIPMENT

NT IONOSPHERES

NT RADIO ANTENNAS

NT RADIO BEACONS

NT RADIO FILTERS

NT RADIO RECEIVERS

NT RADIO TELESCOPES

NT RADIO TRANSMITTERS

NT RADIOSONDES

NT RADIOTELEPHONES

NT RAWINSONDES

NT SPACECRAFT ANTENNAS

NT SUPERHETERODYNE RECEIVERS

NT TRANSMITTER RECEIVERS

NT TRANSPONDERS

NT VERY HIGH FREQUENCY RADIO EQUIPMENT

Nondestructive testing for reliability and lifetime of mass produced radio equipment under maximum load

02 p0257 A71-12530

Radio electronic equipment components reliability, using image recognition theory

03 p0384 A71-13422

Electronic synthesis using time structural properties of signals in radio systems

07 p1063 A71-20256

Soviet book on reliability and efficiency prediction of radio electronic devices covering a priori and posteriori random quality indices, mathematical and physical models and applications

10 p1582 A71-23900

Soviet book on aircraft ground support and onboard radio equipment operation and reliability increase by redundancy and rational methods, discussing preventive maintenance

10 p1583 A71-24670

Synchronous meteorological satellite data collection and transmission system error control, considering design tradeoffs for radio sets and coding techniques

14 p2198 A71-30899

Radio wave propagation studies evolution, considering ionospheric signal reflection, equipment optical characteristics and transversed medium composition and properties probing

19 p3016 A71-37341

Mobile LF air navigation AN/MRN-13 equipment, operation and maintenance

23 p3702 A71-43878

RADIO FILTERS

Radio sets integrated selection components, noting ceramic capacitors and filters and coil circuits

03 p0388 A71-14336

Finite memory radio filter synthesis for maximizing SNR with supplementary quadratic restrictions

04 p0550 A71-14617

Radio signals and receiving equipment structural synthesis, considering signal filtration under random additive noise

06 p0866 A71-17372

Computation of IF filter characteristics effect on angle modulation distortion

07 p1082 A71-20429

Radio engineering of signal detection, filtration, information processing and recognition, discussing game theory methods for problems solution

17 p2698 A71-34393

Space-time correlating antenna array forming matched filter for modulated signal reception with interference ejection

17 p2716 A71-34767

Capacitive memory storage for filtration of repetitive pulse radio signals mixed with additive noise

19 p3022 A71-38500

Finite memory linear radio filter synthesis for maximizing SNR under supplementary quadratic constraints

22 p3510 A71-42257

RADIO FREQUENCIES

NT C BAND

NT EXTREMELY HIGH FREQUENCIES

NT EXTREMELY LOW RADIO FREQUENCIES

NT HIGH FREQUENCIES

NT LOW FREQUENCIES

NT MICROWAVE FREQUENCIES

NT P BAND

NT SUPERHIGH FREQUENCIES

NT ULTRAHIGH FREQUENCIES

NT VERY HIGH FREQUENCIES

NT VERY LOW FREQUENCIES

Ionosphere artificial Joule heating by RF energy, deriving expressions for deposition function frequency dependence

01 p0040 A71-11538

Effective electron collision frequency and RF conductivity along geomagnetic lines in magnetosphere

03 p0377 A71-13272

NASA program concerning determination of RF spectrum sharing criteria and automatic data processing in aerospace systems

03 p0381 A71-14588

Absorption coefficient of plane wave scattering by thin spherical resistive shell for broadband RF radiation monitoring

04 p0558 A71-15149

Pulsar radiation intensity time variations at radio frequencies, noting observations of CP 1133

04 p0649 A71-15273

Measuring instruments for hyperabrupt varactor tuning diodes in RF, VHF and UHF ranges

05 p0728 A71-16396

Dynamic stabilization of drift dissipative instability by inhomogeneous RF electric field parallel to magnetic field

06 p0934 A71-17475

Drift wave instability suppression by homogeneous RF electric field in DC discharge diffused plasma

06 p0934 A71-17482

Low gain microwave amplifier cascade DC to RF conversion efficiency analysis

07 p1073 A71-19115

Second harmonic voltage effects on quenched domain mode Gunn effect oscillator for DC to RF conversion efficiency, discussing negative device conductance at multiharmonic frequencies

09 p1417 A71-22696

Lower ionosphere RF whistlers polarization and electromagnetic structure, determining earth-ionosphere waveguide resonance frequency

10 p1575 A71-23828

Thermal and nonthermal effects of microwave and RF radiation in biological systems, discussing dielectric constant and conductivity for high water content tissues
11 p1716 A71-25281

Low power density modulated RF energy illumination effects on mammalian biological functions, noting possible hazards to personnel
11 p1716 A71-25282

Radio frequency and microwave radiation hazards determination and elimination aboard naval ships
11 p1723 A71-25290

RF transparent ablator of silica filled elastomeric silicone, describing thermal, mechanical and electrical properties at various heating rates
11 p1790 A71-26046

IMPATT oscillators noise properties at large RF amplitudes, deriving expression for noise current as function of threshold current
11 p1733 A71-26369

Wide range nonimmersive RF coil with marginal oscillator for plasma electrical conductivity measurements tested for simulated reentry vehicle
12 p1908 A71-27285

Venusian atmosphere RF refractive attenuation height dependence, field strength measurements comparison, inversion layer influence and surface echoes effects
14 p2309 A71-30098

RF power absorption of uniform hot ion-electron plasma column, considering collision effects and EM radiation
14 p2281 A71-30556

Dynamic stabilization of plasma column drift dissipative instability by inhomogeneous RF electric field, using two fluid macroscopic equations
14 p2196 A71-30560

Primary and secondary standardization and precision measurement of thermal noise power at various radio frequencies and temperatures
14 p2204 A71-30977

Radio frequency measurements below 30 GHz, considering power, impedance, phase shift, voltage and current data
14 p2205 A71-30981

Radio frequency power meters comparison, reducing mismatch and directivity errors with directional coupler
14 p2205 A71-30984

Preferred frequencies for RF measurement and calibration based on Renard number series
14 p2205 A71-30986

Nonnose whistlers noise frequency and minimum group delay measurements
17 p2732 A71-34323

Magnetospheric conjugate ducts characteristics for HF radio propagation from Alouette 2 topside sounder ionograms analysis
19 p3016 A71-37369

Tabular listing of frequency allocations for space services and radio astronomy made at Extraordinary Administrative Radio Conference
21 p3348 A71-40476

RF power absorption by magnetized uniform hot electron-ion plasma column submitted to TE and TM waves
24 p3852 A71-44498

RADIO FREQUENCY DISCHARGE
Multiatomic molecules emission spectra excitation by superhigh frequency short duration pulsed gas discharges
02 p0286 A71-11889

Radio frequency electrostatic ion thruster using mercury ion source electrodeless self sustaining discharge
02 p0283 A71-12313

Steady state RF glow, abnormal glow and DC arc discharges in air at atmospheric pressure
12 p1881 A71-27274

RF discharge quasi-homogeneous plasma device for measuring antenna impedance and sheath effects
13 p2105 A71-27996

RF ion thruster /RIT-10/ optimization, investigating energy balance and plasma diagnostics [DGLR-71-041]
17 p2794 A71-35547

RF magnetic field radial distribution measurement in thermal argon induction plasma flame
20 p3273 A71-38841

RADIO FREQUENCY HEATING
Power transfer in plasma heating with combined RF and steady magnetic fields
01 p0137 A71-11481

Ionospheric modification of F region through high power HF transmitter heating
01 p0040 A71-11529

Plasma column ohmic and collisional heating by RF electromagnetic field, deriving energy transfer expressions
03 p0464 A71-13550

Electrical shock tube performance with RF induction heating of downstream gas
04 p0564 A71-14672

Stochastic model for electron-cyclotron plasma heating by high power microwaves in magnetic mirror
21 p3422 A71-40762

Off-resonance electron heating by microwaves in mirror contained high beta plasmas
24 p3852 A71-44486

Lower hybrid frequency heating and wave absorption efficiency in inhomogeneous HF cylindrical plasma
24 p3852 A71-44492

RADIO FREQUENCY IMPEDANCE PROBES
Series impedance elements in RF immittance measurements
07 p1112 A71-19772

Ionospheric electron density profiles at various altitudes determined by HF impedance probe method
09 p1436 A71-22575

High latitude F region electron density irregularity measurements, using rocket-borne impedance probe
11 p1755 A71-25617

Electric field angular distribution of short radio frequency probe in warm anisotropic plasma under magnetic field
13 p2104 A71-27852

Lower ionosphere charged particle concentrations and collision frequencies determination by LF impedance probe
13 p2058 A71-28028

Rocket-borne RF capacitance probe design for determining lower ionospheric electron densities
18 p2921 A71-36367

RADIO FREQUENCY INTERFERENCE
NT ATMOSPHERICS
NT BLACKOUT [PROPAGATION]
NT CHIRP SIGNALS
NT COSMIC NOISE
NT DAWN CHORUS
NT ELECTROMAGNETIC NOISE
NT HISS
NT IONOSPHERIC CROSS MODULATION
NT IONOSPHERIC NOISE
NT IONOSPHERICS
NT SHOT NOISE
NT SUDDEN ENHANCEMENT OF ATMOSPHERICS
NT THERMAL NOISE
NT WHISTLERS

Interference levels in UHF band measured from aircraft altitudes using LES-6 receiver adapted to KC-135 aircraft
01 p0037 A71-11166

Secondary currents on conducting cylinder near dipole antenna manifested as radio frequency interference, considering effect on radiation pattern
01 p0037 A71-11167

Papers on radio frequency interference and control
03 p0383 A71-13176

Radio frequency interference project control responsibilities and teamwork, noting communication transmitter design example
03 p0383 A71-13177

Statistical model for interference to terrestrial radio relay systems from geostationary satellites
07 p1060 A71-19214

Lightning and static electricity effects on helicopter design, considering rotor protection, cargo hook operation and passive dischargers for radio interference reduction
07 p1021 A71-19938

Optimal temporal and spatial temporal resolution for unknown parameter of interfering signal on white noise background
09 p1404 A71-22219

Radio interference suppression rules optimization, using mathematical model to characterize interference voltage, antenna sensitivity and radio transmitter field strength
11 p1733 A71-26339

Man-made HF noise interference with satellite broadcasting, giving special consideration to automotive ignition systems
12 p1878 A71-26994

Interference pattern of ground and sky waves at 16 kHz during summer near solar maximum
12 p1880 A71-27155

Interference threshold probabilities of pseudorandom frequency hopped signals in conventional spread spectrum communications relative to Gaussian receiver bandwidth
12 p1881 A71-27428

RF noise measurement instrumentation using statistical analysis for better interference characterization
13 p2035 A71-28865

Radar duct surface interference phenomena and focusing effects on radar beam energy propagation
14 p2201 A71-30936

Modal interference spacing in frequency range 13.6-22.3 kHz during sunrise transitions on middle latitude east-west propagation paths
15 p2369 A71-31432

Broadband radiated interference measurement of nonhyperbolic propellant rocket engine spark gap ignition for electromagnetic compatibility
15 p2471 A71-32372

Upper bound on error probability due to intersymbol interference for correlated and uncorrelated digital

signals, presenting examples for data communication systems
17 p2703 A71-35077

Computer simulation of error probability performances of binary coherent PSK system under thermal noise and intersymbol and interchannel radio interferences effects
17 p2707 A71-35476

Binary differentially coherent PSK modulated PCM radio link performance under noise and intersymbol and interchannel interferences effects, deriving error probability
17 p2707 A71-35477

Binary and quaternary PSK systems performance with intersymbol, interchannel and cochannel interferences and fading
17 p2707 A71-35478

HF radio communication receiver performance requirements and realization, considering gain, noise, interference, filtering, reciprocal mixing, intermodulation and frequency stability
18 p2895 A71-36998

RF communications spectrum pollution, discussing corrective and preventive electromagnetic compatibility measures
19 p3020 A71-38427

Linearization techniques for multiple signal interference reduction in broadband transistor power amplifiers in 225-400 MHz range
19 p3030 A71-38434

Time sharing technique application to RF interference with ATC resulting from transmitting and receiving antennas collocation
19 p3102 A71-38436

RF noise surveys in urban areas for effective space to earth communication link design at UHF
19 p3021 A71-38443

Radio frequency interference environment measurement in VHF range by subsynchronous Lincoln experimental satellites 5 and 6
19 p3021 A71-38452

Electromagnetic compatibility in radio astronomy, discussing frequency spectrum pollution and national radio quiet zone
19 p3032 A71-38454

Streamer discharges effects on integrated aircraft antenna and associated avionics, emphasizing RF interference and component damage
19 p3033 A71-38462

Parasitic radar echoes of meteorological, ground and sea origin
22 p3514 A71-42468

Demodulator interference noise in FM modulation radio relay system as function of ratio between interfered and interfering carrier powers and AM sensitivity
24 p3804 A71-44988

RADIO FREQUENCY NOISE
U ELECTROMAGNETIC NOISE
RADIO FREQUENCY RADIATION
U RADIO WAVES
RADIO FREQUENCY SHIELDING
Electronic equipment shielding against spurious signals, determining minimum metal thickness for desired effectiveness based on transmission line theory
03 p0383 A71-13178

Shielded enclosure resonance effects reduction on cavity impedance measurement by technique analogous to wave traps for notching out RF signal at selected frequencies
19 p3032 A71-38459

RADIO GALAXIES
Radio galaxies emission source, examining Patchy model for prestellar matter magnetic field strength
01 p0150 A71-10063

Energetic relativistic particles diffusion from radio galaxies
01 p0161 A71-11384

Transient annular structures in galaxies with nuclear explosion and fragmentation, examining radiogalaxy dynamics
04 p0655 A71-15724

Radio galaxies flux density measurements at 8000 MHz
08 p1357 A71-20869

Cosmological evolution in radio galaxies, discussing stellar populations, optical luminosity, model choice, red shift uncertainties, etc
09 p1522 A71-22974

Source count statistics of radio galaxy lifetimes and intergalactic heating, assuming multiple explosions
12 p1968 A71-27540

Exploding universe phenomena, considering supernovae, exploding galaxies, Crab Nebula, pulsars, quasars and radio galaxies
16 p2643 A71-34036

Photometric and spectroscopic study of NGC 3627 galaxy nucleus during optical observation of radio point galaxies
18 p2963 A71-36192

Critical evaluation of spectroscopic and photometric observations related to radio source 3C 386, sug-

- gesting foreground galactic star superposition on radio galaxy 21 p3447 A71-40443
- Book on cosmology covering stars, galaxies, radio galaxies, universe models, quasars, expansion, intergalactic matter and microwave radiation 22 p3607 A71-42773
- Radio galaxies cosmological evolution, discussing rate and spectrophotometric data 23 p3766 A71-43823
- Balloon flight detected gamma ray source Lib gamma-1, discussing possible identification with PKS 1514-24 radio galaxy 24 p3865 A71-44444

RADIO HORIZONS

- Propagation modes involved in HF or VHF reception at ground station of beyond-horizon satellite transmission 07 p1097 A71-19024

RADIO INTERFERENCE

U RADIO FREQUENCY INTERFERENCE

RADIO INTERFEROMETERS

- Ionospheric electron concentration measurement by bifrequency dispersion interferometer on Luna 14 orbiter 02 p0244 A71-11911
- Compact radio sources of high angular resolution observed via joint U.S.-U.S.S.R. radio interferometry 02 p0307 A71-12086
- Very long baseline interferometry (VLBI) of Jupiter decametric bursts at HF 02 p0310 A71-12326
- Very long baseline interferometry of galactic hydroxyl radical microwave emission sources 02 p0310 A71-12327
- Loran C transmissions for long baseline time and frequency synchronization 02 p0216 A71-12328
- Optimum frequency channels and delay estimates in very long baseline interferometry with large bandwidth for fringe and phase measurements 02 p0216 A71-12329
- Ionospheric and tropospheric effects on differential phase path in very long baseline interferometry, using ray tracing computer program 02 p0251 A71-12331
- Very long baseline interferometry (VLBI) one-bit instrumentation using videotape recorders in geodetic and geophysical measurements 02 p0251 A71-12332
- Frequency and phase analyses of cross correlated signals from very long baseline interferometry of decametric radiation from Jupiter 02 p0310 A71-12333
- Solar radio bursts multifrequency observation using simple image forming system with multielement interferometer 02 p0302 A71-12765
- Long baseline radio interferometry, discussing phase difference measurement principles in terms of signal characteristics and wave forms, astronomy and geodesy applications 03 p0484 A71-13244
- Servosystems errors of indicator-receiver for recording electromagnetic field pattern extremes in amplitude radio interferometers 04 p0557 A71-14635
- Long base line radio interferometry role in earth rotation rate measurement 06 p0891 A71-17892
- Long base line radio interferometry principles and geophysical applications 06 p0892 A71-17893
- Satellite radio interferometer multipath reflections effect on accuracy 07 p1106 A71-18839
- Quasars radio structures observations in S band, using NRAO interferometer 08 p1358 A71-20934
- Compact radio sources of high angular resolution observed via joint U.S.-U.S.S.R. radio interferometry 08 p1362 A71-21136
- Meteor trails azimuth angle measurement by radar interferometry, describing system advantages with respect to receiver noise, angular resolution and calibration 10 p1576 A71-24053
- Quasar radio emission fine structure measurements by very long baseline interferometry, using Goldstone Mars antenna and Haystack radio telescope 10 p1671 A71-24325
- Ionospheric electron concentration measurement by bifrequency dispersion interferometer on Luna 14 orbiter 13 p2058 A71-28198
- Radio interferometry techniques and instrumental advances, examining transionospheric waves coherence properties and ionospheric source distribution 13 p2031 A71-28783
- Optical synthetic aperture analogs of Covington-Drane and thin annular radio interferometers, discussing aperture resolution and spatial frequency response 14 p2238 A71-29802

- Solar image correction in high resolution radio interferometer by digital data processing technique maintaining required phase relations in antenna elements 15 p2373 A71-32446
- Minimum redundancy high resolution radio interferometer for observing H II, planetary nebulae, nonthermal supernova remnants, radio galaxies and solar features 15 p2385 A71-32463
- Long baseline radio interferometers, considering quasars, interstellar masers, geodesy and geology applications 15 p2412 A71-32705
- Water vapor emission map at 22 GHz from W 49, using three-station long baseline radio interferometer data 16 p2631 A71-33179
- Fixed base two element interferometer for radio astronomy, obtaining beavertail radiation pattern by use of earth rotation 16 p2579 A71-33486
- Quasar internal kinematics and fine structure rapid time variations from radio interferometry 17 p2799 A71-34502
- Joint American-Soviet astronomical radio interferometry, discussing resolution and quasar and galaxies structural difference 19 p3145 A71-38569
- Cas A and Cyg A radio stars scintillation measurement by two element phase switched interferometers in ionospheric irregularities study 21 p3378 A71-40377
- High resolution astronomical radio interferometry, discussing radio telescope system design 21 p3452 A71-41052
- Tracking servosystems errors of indicator-receiver of amplitude radio interferometers for recording electromagnetic field pattern extremes 22 p3521 A71-42275
- CH radical 10 cm line frequency determination by photographic Fabry-Perot interferometry 23 p3733 A71-43082

RADIO METEOROLOGY

- Passband circuits improving radio telemetry channel potential in atmospheric sounding system 01 p0080 A71-10543
- Atmospheric humidity and cloud moisture determination, considering meteorological satellites radio measurements errors relation to turbulent sea surface spectral radiant emittance ambiguity 04 p0621 A71-14638
- Radiometeorological measurements of atmospheric structure, using SHF troposcatter synchronously off-set beams on great circle propagation path 04 p0584 A71-15545
- Lower ionospheric irregularities drift from neutral air motion measurements compared to meteor radar system determination 12 p1900 A71-27057

RADIO METEORS

- Radio meteor orbit velocity and radiant measurements by pulse diffraction technique 09 p1520 A71-22829
- Atmospheric wind velocity radial components measurements for meteor drift as function of wind direction, using transmitter and receiver antennas synchronized orientation method 11 p1758 A71-25791
- Monograph on persistent radio meteor echoes fading relation to upper atmosphere wind structure 14 p2192 A71-29579
- Seasonal variations in semidiurnal tidal wind velocities in upper atmosphere for Northern Hemisphere radio meteor observations 14 p2231 A71-29720
- Atmospheric wind velocity radial components measurements for meteor drift as function of wind direction, using transmitter and receiver antennas synchronized orientation method 22 p3533 A71-41559

RADIO NAVIGATION

- NT HYPERBOLIC NAVIGATION
- NT LORAN
- NT LORAN C
- NT TACAN
- NT VHF OMNIRANGE NAVIGATION
- Aircraft radio compass navigation errors due to loop antenna inclinations during maneuvering 08 p1331 A71-20787
- Weather influence on long range radio navigation aids, considering supersonic aircraft operation and inertial navigation 10 p1640 A71-24963
- Area navigation system based on radio aids by airborne receivers and sensors for aircraft movement improvement, noting advantages of pilot displays (SAE PAPER 710457) 14 p2272 A71-30533
- Air navigation techniques history, considering radio, radar, loran Doppler and inertial navigation 14 p2272 A71-30712
- Radio and radar air navigation for civil aviation, discussing Doppler effect, inertia and satellite systems 19 p3100 A71-37344

- Unaided, integrated and differential OMEGA radio navigation configurations, comparing accuracy and suitability for airways system operations 22 p3571 A71-42082
- Agusta helicopter design and testing criteria, discussing four-blade rotor, fuselage and radio navigation equipment 22 p3482 A71-42224
- Aeronautical radio navigation aids photo-optical calibration, describing photogrammetric procedure and ground equipment for checking out airport ILS systems 23 p3702 A71-43587
- Long distance radio navigation and tracking systems, discussing Dioscures, Loran C and Omega 24 p3845 A71-44351

RADIO OBSERVATION

- Radio sources position errors, comparing optical and radio measurements 02 p0314 A71-12579
- Solar radio bursts multifrequency observation using simple image forming system with multielement interferometer 02 p0302 A71-12765
- Earth surface and atmosphere thermal radio emission measurement by radio telescope on Cosmos 243 satellite 03 p0409 A71-13420
- Soviet book on radio measurement methods and mathematical data processing in space trajectory measurements 04 p0555 A71-15375
- Sporadic E layer structure and disturbances from pulsed radio signal measurement, noting correlation to pressure oscillation at ground level 04 p0584 A71-15757
- Solar coronal magnetic field patterns from radio observations 05 p0802 A71-16014
- Interplanetary magnetic field sectors correlated to solar coronal active centers and condensations in metric wavelengths from radio observations 05 p0802 A71-16015
- Jupiter magnetospheric rotation period based on RF observations 06 p0971 A71-18240
- Geostationary radio beacon specifications and observational opportunities on ionospheric satellite ATS-F in 1972 07 p1096 A71-19016
- Ionospheric electron content observation by ATS-3 radio signals, noting gravity waves effect 07 p1098 A71-19034
- Atmospheric meteor zone turbulent motions under Archimedes forces based on radio observations 07 p1101 A71-19412
- Space vehicle landing trajectories calculation from visual and radio observations of orbital parameters 07 p1196 A71-19495
- Uranus physically self consistent atmosphere model based on spectroscopic, photometric and radio observational data 07 p1198 A71-19828
- Corotating solar wind electron number density from sun orbiting Pioneer spacecraft radio propagation measurements 07 p1189 A71-20320
- Radio emission observations at 8 mm wavelength from 3C 273 and 3C 279 07 p1204 A71-20626
- Orbital elements of small high velocity meteors determined by oblique radio sounding 09 p1520 A71-22840
- German space radio monitoring service, describing facilities for receiving and evaluating 20 MHz to 1 GHz transmissions 09 p1407 A71-23046
- Lunar rocks permissivity and density and surface roughness from radio wave scattering data 09 p1523 A71-23105
- F2 region ionospheric disturbances association with severe thunderstorms from radio observations 09 p1490 A71-23559
- Geminid meteoroids characteristics observation by radio, noting distributions of major semiaxes, plane inclination, elliptic eccentricities and day-by-day number variations 12 p1963 A71-26965
- Jovian atmosphere radio observations, discussing helium- and ammonium-hydrogen molecules ratio, brightness temperature spectra and RF wavelength absorbing agents 12 p1964 A71-27087
- Solar type 3 radio bursts polarization measurement by recording and subsequent digital processing 12 p1969 A71-27653
- Soviet papers on upper atmosphere physics covering thermosphere, dynamic processes and radiative energy transport in stratosphere and mesosphere, and ionospheric parameters radio measurement 13 p2056 A71-28017
- Pulsar CP 0834 pulse energy fluctuations spectra secondary periodicities fluctuations from radiohelio-graphic observation 13 p2141 A71-29099

- Satellite atmospheric temperature sounding by radiometric measurements, obtaining vertical temperature profile by mathematical inversion process
14 p2236 A71-30938
- Ionospheric drift rate measurements by closed space 2.2 MHz receiver method at vertical and oblique incidence, obtaining atmospheric circulation patterns
15 p2395 A71-31431
- Solar type 3 bursts with fundamental and second harmonic structure for corona reflected and direct rays at 80 MHz observed with Culgoora radioheliograph
15 p2473 A71-31690
- Polarized meandering type 4 burst of solar flare from 80 MHz radioheliographic observations, noting association with plasmoids containing synchrotron emitting relativistic electrons
15 p2473 A71-31695
- Ground based HF radio sounding of earth magnetosphere echoes due to propagation along electron density enhancement
15 p2398 A71-31769
- Daytime electron density profiles above 90 km from Doppler radio measurements by rockets launched from Southern Hemisphere site
16 p2567 A71-33779
- Jovian atmosphere radio observations, discussing helium- and ammonium-hydrogen molecules ratio, brightness temperature spectra and RF wavelength absorbing agents
19 p3133 A71-37437
- Lunar interior thermal radiation measurement in meter wavelength range during period of solar radio image behind limb, showing inverse temperature gradient with depth
19 p3138 A71-37756
- Atmospheric meteor zone turbulent motions under Archimedes forces based on radio observations
19 p3054 A71-37836
- Jupiter radio observations, measuring nonthermal emission, magnetic field and trapped radiation belts [AAS PAPER 71-108]
19 p3140 A71-37933
- Mars motion 1751-1969, comparing Clemence theory and Newcomb Tables of sun with meridian and radar ranging Mars observations
19 p3144 A71-38166
- Geminid meteoroids characteristics observation by radio, noting distributions of semiaxes, plane inclination elliptic eccentricities and day-by-day number variations
19 p3144 A71-38260
- Crab Nebula pulsar radio properties, observing energy release due to increase in period, multipath propagation effects, intensity and time dependence
20 p3302 A71-39923
- Radio observation for radial velocities in center region of Perseus cluster of galaxies
21 p3445 A71-40408
- Interplanetary scintillation radio observations interpretation by theory for atmospheric scintillations optical observations
21 p3447 A71-40426
- Radio-optical dispersometer for atmospheric water vapor density measurement with increased sensitivity
24 p3809 A71-44985
- Ionospheric integral electron concentration data from Elektron 1 and 3 satellites, using coherent radio wave measurements
24 p3866 A71-45028
- RADIO PHYSICS**
- Soviet papers on quantum radio physics covering injection lasers, high intensity beam and material interactions and laser dynamics
07 p1126 A71-20251
- Radio science - Conference, Ottawa, August 1969
14 p2203 A71-30966
- Solar gravitational deflection of radio waves measured by Cambridge one-mile telescope, observing radio source 3C 279 before/after 8 October 1970 occultation
23 p3769 A71-43990
- Radio-optics prospects in signal and information processing, image reconstruction, data transmission, computer storage, display and holographic movies and TV
23 p3681 A71-44344
- RADIO PROBING**
- Automatic aerological ground station with processing and transmission facilities for radio probe and radar data
01 p0029 A71-10360
- Ionospheric F layer modification by artificial heating, using radio echo detection of electron temperature changes
01 p0040 A71-11537
- Radio wave ionospheric heating effect on absorption of probing waves of different polarization
06 p0888 A71-17289
- Rocket-borne HF capacitance probe for measuring ionospheric electron density profile
07 p1116 A71-20498
- Ionospheric layers critical frequencies recording, using automatic interplanetary station type probe
09 p1436 A71-22450
- Radio wave propagation studies evolution, considering ionospheric signal reflection, equipment optimal characteristics and transverse medium composition and properties probing
19 p3016 A71-37341
- Lunar crust exploration by VLF surface waves, discussing frequency dependent depth penetration, conducting layers detection and communication or navigation use
20 p3291 A71-39313
- RADIO PROPAGATION**
- U RADIO TRANSMISSION**
- RADIO RANGE**
- LOLA /Location and Orientation of Lunar Astronauts/ system using RF ranging and solar sensor, discussing configuration, operation, accuracy and electronics
04 p0623 A71-15303
- Tropospheric height integral of refractivity for predicting atmospheric electromagnetic range at arbitrary elevation angle from surface weather data
08 p1257 A71-21881
- Long range tropospheric radio wave propagation, calculating signal impulse function and time lag between diffraction and reflection
09 p1404 A71-22217
- Short wave skip distance calculation as function of path inclination to ionospheric layer for linear and parabolic ionization distributions
13 p2030 A71-28556
- VHF and UHF ground reflection measurements for antenna site layout, showing feasible operations at short ranges
14 p2217 A71-31050
- Laboratory model for ionospheric perturbations effects on long range VLF paths
19 p3017 A71-37865
- RADIO RANGES**
- U RADIO BEACONS**
- RADIO RECEIVERS**
- NT SUPERHETERODYNE RECEIVERS**
- NT TRANSMITTER RECEIVERS**
- PCM telemetry receiving stations testing, comparing bit error probabilities of coherent and noncoherent methods of synchronizing pseudonoise sequences
01 p0033 A71-10890
- Microwave receiving and transmitting antennas proximity effects on permittivity measurements of dielectric layer
01 p0057 A71-11206
- Radio propagation at 84 MHz, investigating moving receiving terminal and aircraft reflection effects on signal distortions
02 p0216 A71-12344
- Skyнет ground stations operations and equipment, discussing receiving systems parametric amplifiers, local oscillators, demodulators, noise temperature, frequency flexibility and reliability
02 p0217 A71-12433
- Uncooled low noise microwave parametric amplifier for small receiving earth stations, describing three stage design, gain and bandwidth
02 p0234 A71-12814
- Radio sets integrated selection components, noting ceramic capacitors and filters and coil circuits
03 p0388 A71-14336
- Radio signals and receiving equipment structural synthesis, considering signal filtration under random additive noise
06 p0866 A71-17372
- Aircraft automatic landing improvement through use of space diversity ILS receiving system
07 p1153 A71-18830
- Radio signal receiving system design for group delay experiments with geostationary ATS-F for ionospheric and magnetospheric electron content
07 p1206 A71-19033
- Statistical dynamic response of FM receiver with frequency feedback
07 p1064 A71-20261
- Accurate single-sideband radio receiver tuning, observing reconstitution of harmonic tones in human speech strong vowel sounds
08 p1254 A71-21318
- Ground stations for communication satellites, discussing radio transmitter and receiver systems using low noise parametric amplifiers at low temperatures and extended demodulator threshold
10 p1590 A71-25101
- Communication satellite ground station radio receiver and transmitter systems including parametric amplifier and phase lock demodulators applications
10 p1590 A71-25102
- Satellite communication earth stations tracking receiver, describing operational principles with special attention to down-converter and demodulator circuits
12 p1887 A71-27001
- Solid state local oscillator for radio relay systems microwave receivers
13 p2039 A71-28899
- Field testing for radio telemetry receiving systems calibration, including tape recorder degradation effects during data processing
14 p2198 A71-30903
- Deep Space Communications System low noise microwave receiver, discussing operating noise temperature calibration, error analysis and programming
15 p2372 A71-32311
- Integrating discrete signal receiver with weighting proportional to signal, evaluating operational quality in presence of external stationary correlated noise
16 p2542 A71-33488
- UHF head for 225-400 MHz AM receiver, emphasizing choice of ring mixer and passband filter switching principle
16 p2548 A71-34124
- Microwave receiving and transmitting antennas proximity effects on permittivity measurements of dielectric layer
17 p2697 A71-34258
- Parametric up-converters for low noise broadband microwave receivers, discussing electronically tunable pump frequency accuracy and stability
17 p2714 A71-34606
- Low noise FET amplifiers for earth station radio receivers
17 p2715 A71-34687
- FM radio receiver SNR and noise spectra for arbitrary transmission band characteristics
17 p2701 A71-34778
- Sensitive mm wave receivers, using local oscillator and mixer functions in single Gunn diode for large dynamic signal input range and wide IF bandwidth capability
17 p2717 A71-35111
- Intelsat 3 satellite communication ground station radio receiving and transmitting equipment design
17 p2724 A71-35512
- Low noise parametric amplifiers for communication satellite ground station radio receivers, considering components characteristics
17 p2709 A71-35513
- Communication satellite ground station receiver-demodulator equipment using frequency double transposition and compression
17 p2717 A71-35514
- Parametric amplifiers for ground station low-noise receivers in communication satellite systems, considering frequency range extension effect on noise temperature and passband requirements
18 p2890 A71-36557
- HF radio communication receiver performance requirements and realization, considering gain, noise, interference, filtering, reciprocal mixing, intermodulation and frequency stability
18 p2895 A71-36998
- Electromagnetic compatibility characteristics in terms of receiver susceptibility to interference effects on selectivity and nonlinearity parameters
19 p3033 A71-38465
- Noise factor formula of multiple loop receiver input network with series connected stages for antenna matching and coupling parameters
19 p3022 A71-38498
- Hybrid microelectronics IC S band double conversion phase locked receiver, discussing fabrication, process requirements and component selection criteria
19 p3035 A71-38538
- Microwave spectral line receivers for radio astronomy observation of molecular clouds in interstellar space
20 p3238 A71-39401
- Sensitivity requirements for attenuation measurement radio receivers, considering minimum input SNR for absolute measurement error not to exceed preestablished value
20 p3197 A71-39550
- Microwave scanning beam guidance receiver design for aircraft landing aid, discussing time sharing and flight control
22 p3572 A71-42091
- Estimation-correlation principle application to harmonic signal receiver with unknown carrier frequency, using searching phase locked AFC circuit as estimation unit
22 p3512 A71-42313
- Incoherent receiver noise stability in multichannel system with channel frequency separation, deriving formula for receiver error probability
22 p3522 A71-42314
- Computer operated RF automatic test system for HF radio receiver spurious response measurements, giving test results
22 p3514 A71-42389
- Satellite-borne minimum bulk and weight K-band transmitter and receiver frequency converters design features and performance
22 p3524 A71-42522
- Three-receiver radio wave dispersion analysis application to ionospheric drift records to assess effects of velocity variation with time
22 p3515 A71-42599
- RADIO RECEPTION**
- Radio link diversity reception improvements by multiple baseband combinations in one or several stages
03 p0380 A71-14333

- Error probability during diversity reception under random radio noise 04 p0549 A71-14613
- Receiving equipment for navigation satellites of Naval Weapons Laboratory, considering 150 MHz channel 07 p1205 A71-19015
- Real noise stability of coherent FM receiver for case of spectrum limited signals due to passage through channel and selective networks 07 p1061 A71-19508
- Optimal reception of AM signal during nonlinear operation of radio system 07 p1064 A71-20258
- German space radio monitoring service, describing facilities for receiving and evaluating 20 MHz to 1 GHz transmissions 09 p1407 A71-23046
- Short wave radio reception and signal paths at magnetically conjugate point in Southern Hemisphere, using 40-110 msec delay times 13 p2030 A71-28536
- Minimum spacing between two base station antennas for mobile radio diversity reception 19 p3014 A71-37217
- Automatic pulsating locator beacons and receivers to determine emergency transmitters locations, using satellites with computer analysis 20 p3261 A71-38865
- Signal parameter estimation accuracy in nonoptimal reception on noise background with random uniformly distributed initial phase 20 p3199 A71-39817
- Adaptation algorithm for optimal synthesis of nonlinear radio reception system with additive noise 21 p3361 A71-41143
- Error probability during diversity reception under random radio noise 22 p3510 A71-42253

RADIO REFLECTION

U RADIO ECHOES

RADIO RELAY SYSTEMS

- Skyнет communication systems, describing long distance strategic communication links between ground and mobile air/helicopter stations via wide and narrow band pathways 02 p0218 A71-12439
- FM radio relay system modulation-demodulation equipment for multichannel FDM or TV signal transmission 05 p0728 A71-16146
- Statistical model for interference to terrestrial radio relay systems from geostationary satellites 07 p1060 A71-19214
- Intercontinental point to point radio communication, discussing Hertzian beam /radio relay links/ and satellite communication comparison with underground and submarine cables 19 p3016 A71-37343
- Relay data link and trajectory design integration for Viking orbiter 1975 mission [AAS PAPER 71-320] 23 p3726 A71-42994
- Jupiter atmospheric probe using relay-link communications geometry between probe and flyby spacecraft for 3.5 hr intervals [AAS PAPER 71-321] 23 p3726 A71-42995
- Demodulator interference noise in FM modulation radio relay system as function of ratio between interfered and interfering carrier powers and AM sensitivity 24 p3804 A71-44988

RADIO SCATTERING

- Faint sporadic meteors mass distribution from forward and backscatter of radio echoes 01 p0151 A71-10254
- Coherence matrix of elliptically polarized radio signal scattered by statistically rough conductive surface 04 p0550 A71-14619
- Radio wave propagation through extensive weakly scattering medium, presenting typical results for scintillation index, scintillation visibility and spatial autocorrelation function 07 p1196 A71-19576
- Lunar surface specific effective radio signal scattering area measured by Luna 9 and 13, describing signal fluctuations 09 p1523 A71-23145
- Synthetic aperture Doppler free coherent bistatic radar for high resolution maps of tropospheric radio scatterers 12 p1881 A71-27286
- Radio pulses from Crab Nebula pulsar NP 0532, determining multipath scattering delay distribution function and distortion 14 p2314 A71-30641
- Ionospheric propagation prediction accuracy problems, considering numerical mapping, horizontal gradients, absorption, scatter, maximum usable frequency and transequatorial propagation 14 p2202 A71-30949
- Bibliography on aurora covering observations, morphology, atomic and molecular processes, electric

fields, radio scattering, red arcs and particle precipitation 17 p2732 A71-34467

D region electron densities from HF radio waves ionospheric backscatter based on hypothesis of refractive index stochastic fluctuations 19 p3048 A71-37372

Multiple scattering of VHF and UHF radio waves from bundle conductor high voltage power transmission lines 19 p3021 A71-38446

Lunar surface layer density and dielectric permeability from radio wave scattering data from automatic spacecraft radar measurements 20 p3295 A71-39616

Soviet monograph on astronomical foundation of meteor communications, covering radio wave scattering by meteor trails and computer simulation of signal time-amplitude characteristics 21 p3349 A71-41373

Coherence matrix of elliptically polarized radio signal scattered by statistically rough conductive surface 22 p3510 A71-42259

Simultaneous ionosphere measurements by incoherent ground radio wave scattering and coherent signals from Intercosmos 2 and Cosmos 321 satellites 24 p3824 A71-45323

RADIO SIGNAL ABSORPTION

U ELECTROMAGNETIC ABSORPTION

U RADIO TRANSMISSION

RADIO SIGNAL PROPAGATION

U RADIO TRANSMISSION

RADIO SIGNALS

Radio signal reception error in cadence synchronization of binary data transmission systems with indeterminate signal arrival time 02 p0212 A71-11834

Pulsar radio signal characteristics, examining pulse profiles, nulls interstellar scintillation and optical and X ray bursts 02 p0318 A71-12914

Radio signals and receiving equipment structural synthesis, considering signal filtration under random additive noise 06 p0866 A71-17372

Stepped wideband radio signal power generator with manually controlled signal attenuator 06 p0876 A71-18078

Ships and aircraft position finding method based on satellite radio signals Doppler measurements, analyzing ionospheric influences 07 p1154 A71-19036

Small scale ionospheric irregularities from satellite radio signals fluctuations, using frequency scintillation measurements 07 p1060 A71-19037

Radio signal refractive index fluctuations in Venus atmosphere from Mariner 5 data 07 p1197 A71-19762

Cosmos 142 satellite measurements of VLF radio signals transmitted through ionosphere by ground based stations 09 p1408 A71-23143

Optimal reception of Markov radio signals with intrapulse FM, using nonlinear filtration theory 10 p1578 A71-24711

Coincident radio pulse effects on triggering antenna arrays, considering air shower mechanism 12 p1967 A71-27389

Geomagnetic effects on radio signals mechanism in extensive air showers, discussing scintillators array for east-west to north-south ratio polarization measurements 12 p1967 A71-27390

Random radio signals distributions properties with parameters subject to random variation 13 p2029 A71-28371

Sampled data delay-loop lock for tracking biphasic modulated pulsed-envelope RF signal arrival time 14 p2197 A71-30796

Radio power, insertion loss, frequency and dielectric measurements at mm wavelengths 14 p2205 A71-30982

VLF radio signals phase anomalies due to solar X-ray flares, monitoring by detectors onboard OSO-4 satellite 15 p2369 A71-31434

Radio signals fine structure examination by instantaneous pulsed voltage measurements, describing fast response digital voltmeter circuit with memory element 15 p2409 A71-32188

Cosmos satellites tracking and monitoring, decoding and interpreting radio signals 16 p2643 A71-34080

Radio astronomy signals reception and interpretation, detailing solar, galactic and extragalactic spectrum sources 17 p2797 A71-34242

Traffic capacity of systems for search and analysis of radio signals with random duration 19 p3015 A71-37258

Radio satellite scintillation producing small scale ionospheric irregularities, determining characteristic size variation with latitude by autocorrelation method 19 p3055 A71-38043

Radio signal group trajectory in ionosphere expressed as series expansion in terms of increasing power of beam reflection height 19 p3020 A71-38371

Holographic method of correlation and spectral analysis of radio signals applied to stable RF generator, random fields and stereophonic radio transmission measurements 19 p3067 A71-38492

Transient RF pulse dispersion along plasma loaded coaxial gas discharge, noting group delay 20 p3272 A71-38783

Bayesian estimates in nonlinear filtration of nonstationary non-Gaussian radio signals, deriving second central moments and parameter estimate errors 20 p3198 A71-39807

Signal parameter estimation accuracy in nonoptimal reception on noise background with random uniformly distributed initial phase 20 p3199 A71-39817

Ionospheric electron density measurements by differential Doppler and Faraday effects, using coherent radio signals of artificial earth satellites 22 p3508 A71-41526

Wave polarization and midpath ground reflection effects on power loss of two hop radio signal propagation through ionosphere 22 p3511 A71-42280

Lunik 14 spacecraft radio signal reflection from lunar surface, showing energy spectrum dependence on surface roughness 22 p3511 A71-42301

Radio pulse synchronous detection with wideband preamplifier, evaluating frequency mismatch effects on signal distortion by transient response analysis 23 p3644 A71-43287

Unmodulated and step-modulated HF pulse signal envelope calculation and diagram plotting 23 p3644 A71-43319

CW avalanche microwave oscillator frequency modulation /pulling/ by injected RF signal, discussing theory and experiment 23 p3646 A71-43903

Joint phase locked and delay tracking system dynamics for pseudorandom radio signal detection 23 p3646 A71-44267

RADIO SOURCES [ASTRONOMY]

- NT CASSIOPEIA A
- NT PULSARS
- NT QUASARS
- NT RADIO GALAXIES
- NT RADIO STARS
- Radio sources fine structure at 81.5 MHz, examining angular structure by interplanetary scintillation 01 p0158 A71-10769
- Radio sources, cosmic rays and X ray background origin, discussing synchrotron mechanism, Compton scattering and red shifts 01 p0144 A71-10770
- Galactic radio emission sources high resolution observation by telescope, obtaining contour maps with positions and flux densities 02 p0303 A71-11820
- Compact radio sources of high angular resolution observed via joint U.S.-U.S.S.R. radio interferometry 02 p3037 A71-12086
- Extragalactic radio source 3CR catalog, analyzing emission spectra 02 p3030 A71-12087
- Radio sources position measurement with three-element interferometer by self calibrating technique 02 p0314 A71-12577
- Radio sources optical position measurement on Schmidt plates 02 p0314 A71-12578
- Radio sources position errors, comparing optical and radio measurements 02 p0314 A71-12579
- Gain/temperature measurement test set for earth station receiving system by radio sources program tracking unit, noting antenna power ratios determination by attenuator 02 p0222 A71-12797
- Small radio sources emission, examining correlation with optical photometric properties abnormalities 02 p0317 A71-12863
- Radio sources LF spectra distortions at critical value brightness temperature, noting induced Compton scattering effect on ambient gas thermal electrons 02 p0317 A71-12865
- Physical processes in galactic and extragalactic sources of nonthermal radio emission, assuming pulsars as principal magnetic field and cosmic rays sources 03 p0483 A71-13201
- Coherent radiation mechanisms characterizing cosmic masers in molecular lines, sporadic solar radio emission and pulsar radiation 03 p0486 A71-13321

Discrete radio sources precise declinations and optical identifications, using prototype space frequency interferometer

04 p0641 A71-14735

Radio source W58, investigating continuum emission structure and spectrum

04 p0641 A71-14736

Precise radio sources positions by Schmidt telescope and AGK 3 reference frame, noting comparison with optical positions

04 p0644 A71-15048

Galactic sources 18 cm OH emission and/or absorption observation

04 p0657 A71-15759

Extragalactic radio sources relativistic electrons interaction with cosmic black body radiation, noting effect on sources lifetime and X ray background

04 p0641 A71-15838

Galaxies and universe evolution, discussing expansion, isotropic black body radiation, present matter distribution, radio source population density and galactic nuclei instability

04 p0661 A71-15895

Primeval intergalactic magnetic field existence, observing radio sources rotation distribution and red shift

05 p0805 A71-16108

Small elliptical galaxy associated with radio source 3C 386, noting luminosity, internal velocity dispersion and low metal abundance

05 p0805 A71-16109

Sagittarius A region observations with 80 MHz radioheliograph, noting radio sources flux density

05 p0805 A71-16116

Nonthermal extended radio source in pulsar CP 1919 area, proposing as supernova remnant

05 p0805 A71-16117

Extragalactic radio sources spectra, noting type C curvature and type S power law

05 p0805 A71-16120

Flat HF radio spectra from optically thin sources with low electron energy distribution indexes

05 p0808 A71-16399

H II regions compact radiation sources flux densities observation at centimeter wavelengths

05 p0812 A71-16690

Coma Berenices galaxy clusters, discussing radio sources detection

05 p0813 A71-17090

Pulsar 150 MHz radiation linear polarization measurements, correlating interstellar Faraday rotation with determinations from neighboring extragalactic radio sources

06 p0971 A71-18242

Radio wave propagation through extensive weakly scattering medium, presenting typical results for scintillation index, scintillation visibility and spatial autocorrelation function

07 p1196 A71-19576

Contour maps of antenna temperature in W31 region, discussing H I absorption features

07 p1198 A71-19816

Radio emission observations at 8 mm wavelength from 3C 273 and 3C 279

07 p1204 A71-20626

Small diameter radio sources, determining positions, flux densities and diameters

08 p1357 A71-20870

Compact radio sources of high angular resolution observed via joint U.S.-U.S.S.R. radio interferometry

08 p1362 A71-21136

Extragalactic radio source 3CR catalog, analyzing emission spectra

08 p1362 A71-21137

Radio source OZ-252 radiant flux density spectrographic observation, noting quasi-stellar object emission spectra

09 p1516 A71-22065

Compton scattering of relativistic electrons in cosmic plasma waves as source of HF radio emission from metagalactic objects

09 p1521 A71-22926

Extragalactic violent events energy from collapsing stars or pulsar bodies rotational energy, producing extended radio sources

09 p1522 A71-22977

Flux density measurements of Ohio radio source survey at 1415 MHz compared with 1400 MHz measurements by Australian National Radio Astronomy Observatory telescope

10 p1668 A71-23881

Cygnus A two component radio source scintillations power spectrum observation by dipole array

10 p1678 A71-24804

Supernova remnant HB 21 linear polarized radiation observed at 6 cm wavelength, correlating optical nebula shape with radio mapped contours

11 p1819 A71-25216

Extragalactic radio sources total and linearly polarized radiation one dimensional distributions, noting spectral variations, magnetic fields and rotation measurements

11 p1830 A71-26131

Stimulated Compton effect in compact radio sources, giving formulas for energy flow between relativistic electron and radiation field

11 p1831 A71-26169

Galactic radio source Sagittarius optically thick component evidence based on flux density measurement

12 p1956 A71-26612

Galactic radio emission, considering continuum radiations, radio polarization, H I regions structure and physics, recombination and absorption lines

12 p1959 A71-26778

Milky Way galaxy radio halo, investigating background brightness distribution and local spiral arm magnetic field structure

12 p1963 A71-27078

Jovian radio source angular diameter measurement by radio interferometry

12 p1967 A71-27310

Radio source 3C120 gamma quanta with energy above 100 MeV from Cosmos satellites scintillation and Cerenkov counter measurements

12 p1953 A71-27417

Extended galactic radio sources in anticenter quadrant, obtaining 408 MHz integrated flux densities and spectral indices

13 p2135 A71-28298

Radio source and associated elliptical galaxy major axes position angles correlation

13 p2135 A71-28299

Compton effect in variable radio sources, considering models of Seyfert galaxies 3C 84 and 3C 120 from baseline interferometry

13 p2141 A71-29100

Interstellar formyl radical and carbon 13 formyl ion search in galactic radio sources

13 p2142 A71-29103

Absorption, divergence and scattering attenuations and scintillation of microwaves from space sources, calculating frequency and distance dependence characteristics

13 p2034 A71-29390

Galactic H II regions 35 cm water source emission line profile observation, noting frequency and intensity variations

14 p2304 A71-29594

Matter density in universe, comparing delayed galactic growth with observed radio sources and quasars

14 p2305 A71-29675

Type 4 source movement out to 6 solar radii from solar center based on 80 MHz brightness temperature observations

14 p2306 A71-29694

Radio source 3C 273 observation at 8.2 mm wavelength, using traveling wave maser on radio telescope for tenfold sensitivity improvement

14 p2253 A71-29989

Solar radio emission at 3.15 cm wavelength via 22-meter radio telescope, determining relation between source brightness and areas of sunspot groups

14 p2299 A71-29990

BL Lac extragalactic source of radio, IR and visual radiation, estimating upper limit to distance based on spectrum model

14 p2313 A71-30452

Noise measurements on discrete radio sources spectra, studying Cas A and Cyg A flux density ratio

14 p2316 A71-30975

Absolute calibration of radio sources with variable flux density in microwave region

14 p2316 A71-30976

Astronomical radio sources angular structure, using lunar occultations in narrow frequency band at large SNR

15 p2482 A71-31329

Positions and flux densities of radio sources from Fourth Cambridge catalog by pencil beam measurements at 408 MHz, using Molonglo telescope

15 p2485 A71-31697

Submillimeter background radiation origin possibility from extragalactic discrete sources based on cosmological models

15 p2478 A71-31828

Radio sources 3C 48, 3C 144, 3C 161, 3C 273 and 3C 298 scintillations by interplanetary plasma at 60 MHz, determining electron density fluctuations

15 p2487 A71-32033

Astronomical 4C catalog radio sources statistical analysis, showing mean spectral indices dependence on radio emission fluxes and red shifts

15 p2487 A71-32037

Optical positions of 87 identified extragalactic radio sources between declinations plus 19 and minus 80 deg, using Palomar Sky Survey plates and prints

15 p2489 A71-32398

Radio sources interplanetary scintillations observation, discussing solar wind velocity and diffraction pattern scale

15 p2480 A71-32445

Water vapor emission map at 22 GHz from W 49, using three-station long baseline radio interferometer data

16 p2631 A71-33179

Extragalactic radio sources millimeter wavelength spectra measurements, investigating electron energy loss mechanism, magnetic field strengths and dynamics

16 p2631 A71-33234

Galactic H II regions radio sources observations by high resolution radio telescopes, comparing with optical appearance

16 p2632 A71-33326

IR line radiation from galactic center thermal radio sources, determining element abundances

16 p2633 A71-33336

Corotating solar plasma streams associated with variations of interplanetary scintillation from observed radio sources

16 p2634 A71-33386

Bright quasi-stellar radio sources B2 1215 plus 30 and ON231, discussing positions and spectrum

16 p2634 A71-33401

Irregular variable BL Lac photographic observations, equating object with radio source VRO 42.22.01

16 p2635 A71-33430

Galactic center isolated radio pulse search at 151.5 MHz, correlating with Weber gravitational events

17 p2805 A71-35378

Radio source PKS 1514-25 identification as E galaxy, investigating rapid optical variability and light curves

17 p2805 A71-35379

Time dependent multidimensional axisymmetric computations for extended extragalactic radio sources propagation into intergalactic media having different densities and temperatures

17 p2806 A71-35411

Interstellar silicon monoxide discovery from 130,246 MHz frequency line emission of galactic radio source Sag B2

17 p2807 A71-35416

Density and luminosity evolution of radio source population, considering counts per unit co-moving volume at cosmological epochs

18 p2961 A71-35966

Cyg X-1 X ray pulsar age determination and emission model speculations based on observation data for supernova remnant and radio counterpart absence explanation

18 p2962 A71-36151

Contour maps of radio source CTB 1 at UHF, suggesting supernova remnant superimposed on broad faint H II region

18 p2962 A71-36153

Double extragalactic radio sources luminosities and confinement observations, comparing with ram pressure prediction

18 p2963 A71-36156

Kinematic illusions in connection with retardation effects involving extragalactic sources with varying microwave output, noting occurrence in quasar 3C 279

18 p2925 A71-36924

Two dimensional structures of 76 extragalactic radio sources at 1425 MHz in tabular and graphical forms

18 p2970 A71-37064

Extragalactic centimeter radio sources flux density data and spectral distribution, presenting expression for error estimation

18 p2970 A71-37065

Optically identified B2 radio sources at 5 GHz, presenting flux density measurements, spectral index and visual identity

18 p2970 A71-37066

Discrete galactic and extragalactic radio sources observations at 3.3 mm, detailing flux and variability measurements

18 p2970 A71-37067

Milky Way galaxy radio halo, investigating background brightness distribution and local spiral arm magnetic field structure

19 p3133 A71-37428

Radio sources position data table based on high accuracy telescope observation including calibration uncertainties and measurement random errors

19 p3142 A71-38008

Negative search for radio pulsar near Cyg X-1 or associated variable radio source, using fast holding algorithm

20 p3292 A71-39408

Homogeneous large scale intergalactic magnetic field evidence in terms of Faraday rotation measurements of extragalactic radio sources

20 p3294 A71-39541

Identity relation of LF compact source to Crab pulsar NP 0532 with respect to interstellar scattering

20 p3302 A71-39924

Radio telescopic observations of Jupiter, Venus and radio source 3C 273 at 2 and 8 mm wavelengths, determining brightness temperatures and radiation flux densities

21 p3445 A71-40258

Critical evaluation of spectroscopic and photometric observations related to radio source 3C 386, suggesting foreground galactic star superposition on radio galaxy

21 p3447 A71-40443

RADIO SPECTRA

Bright star at radio source and X ray observations evaluation from optical identification of Cygnus X-1, taking into account spectrum and energy distribution characteristics

21 p3447 A71-40444

Compact radio sources in galactic nuclei, examining relation to IR emission

21 p3449 A71-40609

Extragalactic radio sources counts for proportional space volume determination, comparing various cosmological models

22 p3596 A71-41445

Small scale structure of extragalactic compact radio sources at 6 and 18 cm, obtaining magnetic field strengths and maximum brightness temperatures

22 p3598 A71-41912

Green Bank sky survey of radio sources at 1400 MHz, discussing 5C1 spectral analysis and overlaps

22 p3601 A71-42163

Extragalactic radio sources polarized radiation intensity statistical analysis, calculating magnetic field scale

22 p3602 A71-42175

Radio source counts interpretation by cosmological evolution models, suggesting luminosity role

22 p3606 A71-42600

Astronomical radio sources angular structure, using lunar occultations in narrow frequency band at large SNR

22 p3606 A71-42604

Extragalactic radio sources catalog from Parkes Australian National Radio Astronomy Observatory 2700 MHz survey of plus/minus 4 deg zone and selected regions

22 p3607 A71-42769

Astronomical radio sources from Parkes catalog, calculating daily and hourly variations in flux density

23 p3722 A71-42937

Solar gravitational deflection of radio waves measured by Cambridge one-mile telescope, observing radio source 3C 279 before/after 8 October 1970 occultation

23 p3769 A71-43990

Weak radio sources observations by lunar occultation method with large steerable radio telescope, discussing optical identification of sources

24 p3868 A71-44563

Spectral characteristics of continuous radio emission of extragalactic binary objects, discussing model of binary radio source formation from dipole nucleus

24 p3869 A71-44801

Ohio catalog radio source spectra and positions, presenting flux density and RMS errors

24 p3871 A71-44913

Photographic monitoring of radio sources with flat or peaked spectra, identifying as quasars or unstable galactic nuclei by optical variations

24 p3872 A71-44920

RADIO SPECTRA

NT MICROWAVE SPECTRA

Lunar upper crust structure and composition from radio wave reflection spectrum analysis

02 p0308 A71-12098

Atomic H excitation by electron impact, deriving cross sections for anomalous recombination lines in H II regions radio frequency spectrum

02 p0317 A71-12873

Small angular diameter radio source in central Crab Nebula association with pulsar NP 0532 based on spectra and pulse duration

03 p0483 A71-13203

Chromospheric flare north-south asymmetry aspects, calculating radio flux density correlation indices

03 p0417 A71-14193

Radio source W58, investigating continuum emission structure and spectrum

04 p0641 A71-14736

Planetary nebulae radio spectra observations by Jodrell Bank interferometer and total power instruments, using variable radius spherical shell model for flux density

04 p0658 A71-15836

Pulsars CP 0328, CP 0834, CP 1133 and CP 1919 radio spectra, examining interstellar scintillation model, transverse velocities and line widths

05 p0802 A71-15939

Quasars radio spectra in 1-5 GHz frequency range, examining emission from expanding clouds due to synchrotron radiation with self absorption

05 p0805 A71-16112

Extragalactic radio sources spectra, noting type C curvature and type S power law

05 p0805 A71-16120

Flat HF radio spectra from optically thin sources with low electron energy distribution indexes

05 p0808 A71-16399

Sunset and sunrise vertical displacement rate of lower ionosphere from spectral analysis of field intensities at 236, 557 and 1277 kHz

05 p0744 A71-17184

Thermal noise perturbed oscillator RF spectrum determination from frequency instability in time domain

[ONERA-TP-927]

07 p1075 A71-19265

Lunar upper crust structure and composition from radio wave reflection spectrum analysis

08 p1362 A71-21148

Radio spectrum use in space communications for satellite services, considering antenna design, modulation techniques and wave attenuation

09 p1406 A71-22871

Multicomponent whistler spectra due to discrete ionization inhomogeneities and complex structure nonuniformities forming diffuse whistlers in outer ionosphere

11 p1758 A71-25789

Optical variation and radio spectral index statistics of extragalactic sources, including quasars from photographic monitoring with 30 inch reflector

12 p1962 A71-26932

Sunset and sunrise vertical displacement rate of lower ionosphere from spectral analysis of field strength at 236, 557 and 1277 kHz

13 p2059 A71-28241

Quasar-like N-type and Seyfert galaxies optical characteristics, discussing optical variability and radio spectrum characteristics

14 p2307 A71-29866

Planetary nebulae observations in radio spectrum, determining interstellar extinction, electron temperature recombination theory and models

14 p2312 A71-30388

Noise measurements on discrete radio sources spectra, studying Cas A and Cyg A flux density ratio

14 p2316 A71-30975

Astronomical 4C catalog radio sources statistical analysis, showing mean spectral indices dependence on radio emission fluxes and red shifts

15 p2487 A71-32037

Mars radio spectrum discrepancy with elementary theory, assessing microwave observations

15 p2490 A71-32416

Bright quasi-stellar radio sources B2 1215 plus 30 and ON231, discussing positions and spectrum

16 p2634 A71-33401

Jupiter radio spectrum decametric component observations, emphasizing core and mantle rotation under coupled torsional oscillations

16 p2637 A71-33514

Sagittarius A model involving relativistic electron diffusion from point source due to Compton scattering for observed radio spectra explanation

18 p2957 A71-36155

Technological environment for international communications law, examining system design, radio spectrum resource management and communication satellites

18 p2986 A71-36164

Simple type centimeter solar radio bursts identification and relation to flare position, noting radio spectrum over sunspot

18 p2958 A71-36741

Extragalactic centimeter radio sources flux density data and spectral distribution, presenting expression for error estimation

18 p2970 A71-37065

Multicomponent whistler spectra due to discrete ionization inhomogeneities and complex structure nonuniformities forming diffuse whistlers in upper ionosphere

22 p3532 A71-41557

CH radical 10 cm line frequency determination by photographic Fabry-Perot interferometry

23 p3733 A71-43082

Ohio catalog radio source spectra and positions, presenting flux density and RMS errors

24 p3871 A71-44913

RADIO SPECTROSCOPY

High sensitivity radiospectrography, obtaining solar emission spectra on decametric waves by radio telescope, focal antenna and receivers

10 p1667 A71-23826

RADIO STARS

NT PULSARS

Antenna polar diagrams short range measurement, using far field approximation for incident plane waves source and radio star or satellite

02 p0223 A71-12801

Laboratory model for radio star scintillation and other diffraction phenomena by thin weak random phase changing screen including earth atmosphere or solar wind

10 p1678 A71-24797

Radio astronomy, covering invisible stars discovery and instrumentation techniques comparison with UV and X ray astronomy

19 p3131 A71-37342

Cas A and Cyg A radio stars scintillation measurement by two element phase switched interferometers in ionospheric irregularities study

21 p3378 A71-40377

Radio stars classes, discussing red dwarf flare, red supergiants, blue dwarf companion, novae, pulsars and X ray stars

21 p3448 A71-40582

RADIO TELEGRAPHY

Remotely controlled room temperature microwave parametric amplifier design for shipboard satellite telegraphy terminal

02 p0234 A71-12813

European telecommunication and TV distribution satellite system, including telephony, telegraphy, telex and wideband data transmission

17 p2696 A71-34232

RADIO TELEMETRY

NT PULSE FREQUENCY MODULATION TELEMETRY

Passband circuits improving radio telemetry channel potential in atmospheric sounding system

01 p0080 A71-10543

Computerized data management program for Minuteman radio telemetry instrumentation systems

01 p0050 A71-10884

Radio telemetry data transmission, investigating multipath propagation effects on signal to noise ratio and distortion

01 p0033 A71-10889

Harmonic and independent subcarrier DSB/FM telemetry systems implementation and utilization

01 p0033 A71-10898

Radio telemetry transmitter receiver systems notch noise testing for relationships between spectral power density, video and IF bandwidths and peak deviation

01 p0034 A71-10908

Universal UHF telemetry system for use on artillery projectiles and gun launched probes, describing components

01 p0034 A71-10911

Projectile P band FM/FM telemetry system for in-barrel data acquisition

01 p0034 A71-10912

Apollo lunar surface communications, discussing VHF system for voice and telemetry and TV hardware and techniques

01 p0035 A71-10914

Design criteria for implantable biotelemetry systems, discussing RF signal transmission through conductive body tissue

01 p0024 A71-10982

Nulls of radiation and input impedance of flush mounted rocket antennas for telemetry and transponder systems

02 p0228 A71-11674

Biotelemetry objectives, principles, implementation and applications, discussing wire and wireless systems, radio frequency selection, transmitting power and modulation methods

03 p0369 A71-13059

Telemetry systems prelaunch calibration tests, considering bit error rate, intermodulation distortion and antenna tracking

04 p0554 A71-15317

Real time missile radio telemetry data transmission to ground station, using instrumented aircraft

04 p0554 A71-15321

Solar cell and coverslide degradations measurement from telemetry data on satellites at near-synchronous altitudes

05 p0702 A71-16086

Multichannel EEG radio telemetry for remote recording of biological activity from subjects in motion and within human body

05 p0715 A71-17110

Rocket probe launched by aircraft for measuring pressure, temperature, magnetic field and wind velocity around tornado vortex through radio telemetry

05 p0778 A71-17140

Intelsat 3 satellite Communication, Telemetry, and Command system using transponders for multichannel voice and TV transmission

06 p0870 A71-18398

PAM/FM radio telemetry coder including electronic commutator for sampling and sequential time control, discussing design, operation, performance and reliability

06 p0870 A71-18399

Bioelectric activity of cerebral cortex in man under neuroemotional stress, using multichannel radioelectroencephalography

06 p0856 A71-18464

Suppressed RF carrier tracking for two channel interplex phase modulated telemetry

07 p1066 A71-20427

Wideband subcarrier frequencies demodulation technique for uncoded or coded PSK telemetry over large input SNR range for deep space interplanetary communication

08 p1254 A71-21316

Counting rate source encoding algorithm with orthogonal functions in space experiment data processing before telemetering to ground

08 p1259 A71-21592

Large capacity ferrite core buffer memory for spacecraft telemetry temporary data storage, using access circuitry with multichip and thin film circuits

09 p1421 A71-23735

Venus atmosphere determinations by Mariner 5 radio occultation measurements, deriving altitude profiles of refractivity, molecular number density, pressure, temperature and radio frequency absorption

10 p1669 A71-24176

Carrier suppression in angle modulated transponder telemetry by first order stationary stochastic processes

12 p1880 A71-27074

Field testing for radio telemetry receiving systems calibration, including tape recorder degradation effects during data processing

14 p2198 A71-30903

High efficiency autotrack strip-line-fed dipole antenna array for L and S band airborne telemetry

14 p2198 A71-30905

World Weather Watch global telemetry system including observing stations, and rockets, balloons and satellite-borne sensors, determining atmospheric states on ground and sea

14 p2199 A71-30913

Radio telemetry stimulator for conditioning large animals by applying high voltage short duration pulses to skin surface

16 p2534 A71-33050

International cooperation in space radio science, considering real time telemetry application via Solrad, Tiros and Alouette satellites

17 p2697 A71-34252

Soviet book on space radio telemetry systems characteristics, design, requirements and operation conditions covering noise stability, reliability and redundant codes

17 p2699 A71-34521

Tuned loop antenna for missile telemetric data transmission, discussing design, implementation and impedance and radiation measurements

17 p2718 A71-35749

Hadamard transform source encoding application to Apollo unified S-band telemetry links, considering possible system performance improvement

18 p2876 A71-36470

Telemetry systems with discrete compression-expansion function, calculating noise stability improvement as compared to linear and nonlinear signal conversion operations

22 p3515 A71-42859

Turnstile loop Yagi and hexafilar contrawound spiral antennas for microwave telemetry rocket data reception, describing design and radiation patterns

23 p3643 A71-43095

RADIO TELESCOPES

Steerable 100 m radio telescope design, surface accuracy, receiving installation and cryogenically cooled parametric amplifiers

01 p0068 A71-11342

Bonn 100 meter radio telescope, describing frequency range, antenna array, steering accuracy, construction and design

02 p0239 A71-12913

Soviet radio telescope tracking control system, describing feedback sensors, digital computer, servomotors, actuators and control panels

04 p0565 A71-14848

Performance tests for guidance accuracy and tracking smoothness of Crimean Astrophysical Observatory radio telescope, discussing pointing and tracking errors

04 p0565 A71-14849

Pulkovo radio telescope resolution improvement by range extension into millimeter wavelength region

07 p1109 A71-19341

Pulkovo radio telescope antenna surface precision and electrical characteristics at eight mm, using ground oscillators and solar, lunar and Venusian observations for radiation pattern

07 p1075 A71-19342

Pulkovo radio telescope effective frequency range extension beyond minimum 3 cm wavelength into millimeter range, installing high precision reflecting mirror surfaces

07 p1083 A71-19343

Pulkovo radio telescope reflector adjustment by phase comparator, using centimeter wave transmitting-receiving antenna for sun, moon and Venus observations

07 p1083 A71-19344

Radiotelescopic observations of period and declination of pulsar Mp 0450 in South India

07 p1201 A71-20499

Solar radio emission micropulsations observations at 10 cm, discussing primary and secondary bursts from different disk regions and radio telescope

07 p1189 A71-20639

Equatorially mounted parabolic reflector radio telescope, discussing structural design, mechanical drives and electronic control system

08 p1271 A71-21152

Parabolic radio telescope phase errors for field distribution, compensating for mirror system mass deformations

08 p1266 A71-21468

Highly directive radio telescope antenna parameters in near zone, using focusing at minimum distance

09 p1414 A71-22218

Receiver systems for 100 meter Effelsberg radio telescope using cryogenically cooled parametric amplifiers for receiver system noise minimization

10 p1578 A71-24510

Book on radio astronomy instruments and observations covering high sensitivity radiometers, masers, parametric amplifiers, radio telescope design, radio spectrometers, parabolic reflectors, etc

11 p1737 A71-25359

Venus maps from high resolution radio telescope observations, investigating surface pressure/temperature, planetary atmosphere and water vapor presence

11 p1830 A71-26109

Large steerable radio telescope with equatorially mounted parabolic cylinder for lunar occultation, pulsar and scintillation observations

12 p1894 A71-26930

Planetary disks brightness temperature measurement using 22 m radio telescope with indium antimonide detector at 1.4 mm

13 p2141 A71-29102

Radio source 3C 273 observation at 8.2 mm wavelength, using traveling wave maser on radio telescope for tenfold sensitivity improvement

14 p2253 A71-29989

Optical method for elastic deformations measurement of radio telescope reflector at various elevations

14 p2211 A71-29991

Max Planck Institute 100 m radio telescope at Bonn with all motions fully controllable, describing foundation constructional details, reflector structure and positioning gear

14 p2214 A71-30813

Filled aperture antennas for radio astronomy, considering mm wave observations, parabolic cylinder antennas and active/passive control of antenna surfaces

18 p2901 A71-37036

Cosmic radio astronomy, evaluating sensitivity and resolution limitation of ground based radio telescopes

19 p3138 A71-37762

Solar atmosphere oscillatory component observations at 3 mm wavelengths with two radio telescopes, obtaining power spectra

21 p3447 A71-40424

Hydrostatic bearings for large optical and radio telescopes, explaining lubricant flow control systems

23 p3661 A71-43862

Curved wire array to eliminate parasitic circular polarization of variable profile radio telescope antennas, applying to solar observations

23 p3655 A71-44326

Weak radio sources observations by lunar occultation method with large steerable radio telescope, discussing optical identification of sources

24 p3868 A71-44563

RADIO TRACKING

ATS 1 and 3 satellite VHF transponders for ships and aircraft location, communication and remote sensing, discussing performance test results

14 p2198 A71-30898

Interrogation, recording and location system satellite techniques for wildlife tracking and monitoring, describing collar antenna, battery pack and solar cells

14 p2200 A71-30923

Doppler effect satellite location of crystal controlled CW transmitters on earth surface for animal tracking

14 p2200 A71-30924

Lunar gravity measurements by Apollo 14 Doppler radio tracking during low altitude orbits, correlating variations with surface features

16 p2641 A71-33771

Correction method for satellite radio tracking errors due to VHF refraction in atmosphere

16 p2543 A71-33832

Satellite communication application to maritime mobile service and position determination, discussing VHF and UHF space and shipborne equipment and modulation systems

17 p2697 A71-34241

Radio tracking of aircraft by two geostationary satellites, discussing measurement, navigation and position errors

18 p2945 A71-36508

Navigation error sources and orbit determination accuracies for Jupiter planetary encounter, using earth based radio tracking data

[AAS PAPER 71-118]

19 p3101 A71-37937

Tracking servosystems errors of indicator-receiver of amplitude radio interferometers for recording electromagnetic field pattern extremes

22 p3521 A71-42275

Covariance analysis of Mars gravity harmonics, ephemeris and radiation pressure from Mariner 1971 range and Doppler radio tracking data

[AAS PAPER 71-343]

23 p3727 A71-43016

Earth based radio tracking data types involving simultaneous or near simultaneous spacecraft tracking from widely separated tracking

[AAS PAPER 71-399]

23 p3643 A71-43066

Lunar gravity estimate from low degree spherical harmonic coefficients in potential model and Lunar Orbiter 4 radio tracking data reduction

23 p3768 A71-43882

Long distance radio navigation and tracking systems, discussing Dioscures, Loran C and Omega

24 p3845 A71-44351

RADIO TRANSMISSION

NT DOUBLE SIDEBAND TRANSMISSION

NT IONOSPHERIC F-SCATTER PROPAGATION

NT IONOSPHERIC PROPAGATION

NT MICROWAVE TRANSMISSION

NT MULTIPATH TRANSMISSION

NT SHORT WAVE RADIO TRANSMISSION

NT SINGLE SIDEBAND TRANSMISSION

NT TRANSEQUATORIAL PROPAGATION

Proton Flare Project 1969 observation of VLF radio wave propagation, detecting sudden phase anomaly events due to solar activity

01 p0144 A71-10288

Adaptive retransmission for improving two-way communication between antenna arrays in randomly fading environment, calculating signal to noise ratio

01 p0052 A71-10468

Annular solar eclipse effects on VLF transmissions phase delay

02 p0212 A71-11969

Radio propagation at 84 MHz, investigating moving receiving terminal and aircraft reflection effects on signal distortions

02 p0216 A71-12344

VHF/UHF satellite transmission, predicting multiple ground reflection effects on signal fading and effective antenna gain by computerized method

06 p0868 A71-17732

Troposphere effects on radio wave propagation and satellite communication

07 p1059 A71-19010

Enhanced ionization density duct propagation of VLF radio waves in magnetosphere

07 p1062 A71-19578

Long range tropospheric radio wave propagation, calculating signal impulse function and time lag between diffraction and reflection

09 p1404 A71-22217

Book on applied diffraction theory covering scalar and vector wave theory, radio wave propagation, linear integral equations, microwave lens, Fabry-Perot interferometers, etc

09 p1494 A71-22959

Line-of-sight radio signal transmission, investigating sea surface reflections effects on phase of arrival and coherence

09 p1409 A71-23502

Meteor-reflected radio wave propagation directivity and diurnal and annual variations, comparing experimental and theoretical calculation results

10 p1576 A71-24033

Meteor-reflected radio wave propagation diurnal and annual variations prognosis, discussing indispensability of incident meteor particle velocity and density distributions

10 p1669 A71-24034

Solar particle effects on polar cap VLF radio propagation along polar and transpolar paths, considering short term phase effects

10 p1577 A71-24313

Diversified frequency radio data transmission and reception by linear modulation, considering error rate in white noise and selective/flat fading

10 p1580 A71-25109

Radio propagation and antennas transmission formulas, discussing fundamental circuit elements with inductors and capacitors

11 p1798 A71-25596

Coupled vacuum mode equations modified for cylindrical stratification for calculation of propagation characteristics of earth-ionosphere waveguide

11 p1731 A71-25664

Venus atmosphere mm and cm radio wave propagation calculated from temperature, pressure and chemical composition data

11 p1823 A71-25695

Ionospheric transverse inclinations from radio wave propagation characteristics obtained by circular oblique incidence sounding scans

11 p1758 A71-25788

Intelsat 4 transmission subsystems design, discussing alternative high power amplifier configurations, redundancy and emergency routing of transmitted RF carriers

12 p1894 A71-26992

Hamiltonian optics based model of ionospheric radio propagation, discussing earth magnetic field effects on radio wave angle-of-arrival changes

12 p1879 A71-27058

Polarization behavior of radio waves propagating through magnetoionic medium near and across transversal point of magnetic field

13 p2028 A71-27997

Smith method for radio wave propagation time lag calculation, assessing maximum error by comparing calculated with measured distance/frequency characteristics

13 p2030 A71-28561

Transhorizon radio propagation by atmospheric heterogeneities, discussing effect on attenuation, antenna gain reduction and transmission bandwidth

13 p2033 A71-29239

Conjugate and closely-spaced riometer observations of auroral radio absorption, considering explanation by alternation of particle precipitation between Northern and Southern Hemispheres

14 p2192 A71-29667

Optimal detection of rectangular radio signal pulse envelope distortions by multiplex fluctuations over white noise background

14 p2195 A71-30113

- Raisting ground radio station second antenna system, discussing design for all weather performance
14 p2214 A71-30812
- Radio wave propagation in ionosphere, measuring plasma frequency, cyclotron cut-off and noise level
15 p2373 A71-32443
- Orbiting satellites VHF radio signal transmissions enhancement, considering focusing effect of electron density contours resulting from gravity or acoustic wave in ionosphere
16 p2543 A71-33817
- Copyright protection of communication satellite transmitted radio and TV programs, discussing involvement of UN agencies and other international organizations
17 p2841 A71-34248
- Mode conversion and auroral effects observations on polar VLF propagation path, noting seasonal and solar cycle variations
17 p2731 A71-34319
- FM radio receiver SNR and noise spectra for arbitrary transmission band characteristics
17 p2701 A71-34778
- Long baseline atomic clock interferometry with meter wavelength cross polarized antenna arrays for spacecraft propagation experiments
17 p2744 A71-35098
- Book on communication satellites technology covering satellite transponders, spacecraft antennas and subsystems, high power transmission, launch vehicles, digital techniques, earth stations, etc
19 p3149 A71-37271
- Ionospheric transverse inclinations from radio wave propagation characteristics obtained by circular oblique backscatter sounding scans
22 p3532 A71-41556
- Radio regulation planning and frequency assignments for operational earth exploration satellite service
22 p3623 A71-41974
- Geometrical-optical approximation for residue series of obstacle /terminal/ gain in radio wave propagation over inhomogeneous earth
22 p3511 A71-42281
- Monochromatic radio wave propagation in interplanetary plasma, deriving frequency spectrum and phase and amplitude fluctuations
22 p3511 A71-42302
- Binary coding and phase displacement modulation of digital data in radio transmission
22 p3514 A71-42471
- Radio wave propagation characteristics in Venusian atmosphere and interplanetary plasma from Venera 7 probe data
24 p3805 A71-45312
- RADIO TRANSMITTERS**
NT IONOSPHERES
NT RADIO BEACONS
NT RADIOSONDES
NT RADIOTELEPHONES
NT RAWINSONDES
NT TRANSMITTER RECEIVERS
Constant bandwidth FM subcarrier oscillators signal preemphasis for FM and PM transmitters
01 p0033 A71-10897
- Microwave receiving and transmitting antennas proximity effects on permittivity measurements of dielectric layer
01 p0057 A71-11206
- Satellite communication system earth station transmitter with FDM-FM and SPADE carriers, noting intermodulation effect on channel capacity
02 p0223 A71-12810
- Transistorized transmitters constant phase low distortion AM system based on Chireix method, generating AM from two push-pull phase modulated signals
05 p0720 A71-16392
- High Q factor rotor systems applications in dielectrics electromagnetic viscosity measurement and radio transmitters with low oscillation phase drift
09 p1492 A71-22363
- ECG miniaturized single channel biotelemetry transmitter, discussing lightweight design and power supply
10 p1570 A71-24487
- Communication satellite ground station radio receiver and transmitter systems including parametric amplifier and phase lock demodulators applications
10 p1590 A71-25102
- Radio interference suppression rules optimization, using mathematical model to characterize interference voltage, antenna sensitivity and radio transmitter field strength
11 p1733 A71-26339
- Remote controlled automatically tuned 1-kw short wave transmitter with zero power tuning mode of power stage and drive unit frequency generation
12 p1887 A71-26989
- Signal rejection characteristics of receiver preselector and antenna system, requiring receiver mixer efficiency and transmitter parameters
13 p2032 A71-28862

- Microwave receiving and transmitting antennas proximity effects on permittivity measurements of dielectric layer
17 p2697 A71-34258
- Intelsat 3 satellite communication ground station radio receiving and transmitting equipment design
17 p2724 A71-35512
- Communication satellite ground station transmitting equipment, discussing carrier waves, FM, frequency converters and microwave amplifiers characteristics
17 p2717 A71-35515
- Emission transistor for Eole balloon transmitter power amplifier, discussing trouble-free emission, high output, wide temperature range, lightweight and reliability features
18 p2891 A71-36563
- Space communications period forecasting algorithm for limited power ground based transmitters and spacecraft in earth orbit
19 p3022 A71-38502
- Automatic pulsating locator beacons and receivers to determine emergency transmitters locations, using satellites with computer analysis
20 p3261 A71-38865
- Breadboard simulation model of laser space communications system consisting of carbon dioxide laser, transmitter telescope, GaAs phase modulator and attenuator
20 p3196 A71-39116
- Satellite-borne minimum bulk and weight K-band transmitter and receiver frequency converters design features and performance
22 p3524 A71-42522
- Phase discontinuity transmitter-receiver system for VLF/LF time signals
24 p3804 A71-44997

RADIO WAVE REFRACTION

- Tropospheric layers radio reflectivity as function of refractivity index and thickness/wavelength ratio
01 p0040 A71-11607
- Decimeter radio wave propagation in Venusian atmosphere, determining refraction and absorption coefficients height dependence based on Venera spacecraft data
05 p0718 A71-15993
- Venera satellites and Mariner 5 radio wave fluctuations and discontinuities of refractive index in Venusian atmosphere, considering atmospheric turbulence
05 p0719 A71-16042
- Irregularities heights in ionospheric refractivity responsible for radio-satellite scintillation from spaced receiver experiments at midlatitude and subauroral locations
06 p0868 A71-17985
- Ionospheric refraction during radio wave propagation using space diversity recordings of Faraday and Doppler effects for coherent signals from geophysical rockets
06 p0894 A71-18256
- Ionospheric columnar electron content using differential radio refraction measurements from satellite observation station
07 p1097 A71-19026
- Multipath distortion and wavenumber spectrum of refractive index in radio links
07 p1060 A71-19258
- Refractive errors in spaced antenna radio angle-of-elevation measurements based on comparison with use of single directional antenna
12 p1881 A71-27424
- Cosmic radio waves scattering in outer solar corona, considering refraction and gradients in electron density fluctuations
12 p1970 A71-27706
- Radio waves tropospheric refraction based on far field of vertical electrical dipole on impedance sphere
14 p2191 A71-29510
- Venera satellites and Mariner 5 radio wave fluctuations and discontinuities of refractive index in Venusian atmosphere, considering atmospheric turbulence
16 p2542 A71-33446
- Correction method for satellite radio tracking errors due to VHF refraction in atmosphere
16 p2543 A71-33832
- Tropospheric refraction effects and field strength dependence on height at frequencies below 10 MHz
19 p3017 A71-37862
- Atmospheric water vapor effects on microwave frequencies refraction index structure
19 p3024 A71-38611
- Venus atmosphere decimeter wave field intensity fluctuations and refraction coefficient variations
20 p3297 A71-39627
- Decimeter radio wave propagation in Venusian atmosphere, determining refraction and absorption coefficients height dependence based on Venera spacecraft data
22 p3515 A71-42742
- Microwave radio signals refraction angles and group delay times for biexponential model of ionospheric electron density profile
24 p3805 A71-45253

RADIO WAVES

- NT DECA-METRIC WAVES
NT DECIMETER WAVES

NT EXTRATERRESTRIAL RADIO WAVES

- NT GALACTIC RADIO WAVES
NT LONG WAVE RADIATION
NT MICROWAVES
NT MILLIMETER WAVES
NT RADIO EMISSION
NT SHORT WAVE RADIATION
NT SKY WAVES
NT SOLAR RADIO BURSTS
NT SOLAR RADIO EMISSION
NT SUBMILLIMETER WAVES
NT TYPE 2 BURSTS
NT TYPE 3 BURSTS
NT TYPE 4 BURSTS
- Atmospheric UHF attenuation observations by horn antenna
01 p0039 A71-11381
- HF radio wave Doppler shift by ionosphere effect in retransmitted and backscatter signals
01 p0040 A71-11524
- Early phase model of F region heating and hydrodynamic expansion by deviative absorption of radio waves
01 p0040 A71-11530
- F region reflected radio wave heating effect, considering electron temperature, collision frequency and heat conductivity
01 p0040 A71-11531
- Ionospheric absorption of radio waves reflected from sporadic E layer, noting attenuation frequency dependence
02 p0211 A71-11768
- Solar flare X ray and radio wave emission measurement byOGO 4 and Solrad 9 satellites
03 p0479 A71-14046
- Pulsar radio wave generation, discussing emission theory and frequency independence of beam width and polarization
03 p0493 A71-14208
- MF, LF and VLF ionospheric radio wave propagation theory using spherical wave functions for computer simulation
04 p0552 A71-15215
- Transient pulse plane wave reflection from ionospheric model with linear electron density profile
04 p0553 A71-15218
- Dipole antenna array coupling for circularly polarized radio waves amplitude fluctuations reflected from ionosphere at vertical incidence
05 p0738 A71-16216
- LF radio waves field strength monitoring for study of ionospheric effects due to celestial X rays
05 p0721 A71-16442
- Plasma instabilities role in ionospheric heating and radio wave attenuation
06 p0888 A71-17288
- Radio wave ionospheric heating effect on absorption of probing waves of different polarization
06 p0888 A71-17289
- Polarization fluctuations of radio waves reflected from ionosphere E and F layers, describing radio polarimeter and preliminary measurement results
07 p1061 A71-19384
- Radio wave absorption measurement at constant solar zenith angle of 65 deg, discussing seasonal variation
07 p1101 A71-19408
- Radio wave propagation at frequencies near proton gyrofrequency in horizontally stratified ionosphere, taking into account intermode coupling
07 p1102 A71-19666
- Pulsed radio wave interactions with various lower ionosphere models, estimating cross modulation by computer calculation for comparison with measurements
09 p1405 A71-22443
- Ionospheric radio waves scattering cross sections under time varying random irregularities, considering anisotropic behavior, dielectric tensor and geomagnetic field
09 p1411 A71-23587
- Anomalous winter ionospheric radio wave absorption related to amplitude increases of microbarometric oscillations at ground level
10 p1606 A71-24919
- HF and VHF radio propagation on earth surface, describing launchers used for generation and detection
10 p1579 A71-24950
- Radio propagation and antennas transmission formulas, discussing fundamental circuit elements with inductors and capacitors
11 p1798 A71-25596
- F region layers vertical drift from phase paths of radio waves reflected from constant electron density surfaces
11 p1756 A71-25646
- Sharp peaking of wave impedance characterizing propagation in earth-ionosphere waveguide from atmospheric radio noise measurements near 2 kHz
13 p2029 A71-28471
- Electron concentration profiles in D region from radio wave partial reflection coefficients
13 p2030 A71-28558

- Upper atmosphere aeronomy historical review, considering meteor trails, radio waves, auroral photography, terrestrial magnetic field and spectroscopy
14 p2229 A71-29704
- Vertically incident radio waves reflection from horizontally stratified ionosphere with random electron density irregularities
14 p2192 A71-29718
- Matrix solution for wave equation with mode coupling of VLF and ELF radio waves in horizontally stratified layer of anisotropic ionosphere plasma
15 p2373 A71-32444
- Polarization fluctuations of radio waves reflected from ionosphere E and F layers, describing radio polarimeter and preliminary measurement results
19 p3017 A71-37809
- Radio wave absorption measurement at constant solar zenith angle of 65 deg, discussing seasonal variation
19 p3053 A71-37832
- Radio wave scattering from ionosphere, considering plasma experiments in E and F region
19 p3018 A71-38247
- Pulsar periods change rate and radio luminosity decay, discussing magnetic field braking
20 p3286 A71-38762
- Mars ionosphere radio wave absorption integral coefficients, studying electron concentration and electron/gas molecular collisions frequency vertical profiles
20 p3297 A71-39629
- Mid- and high-latitude ionospheric radio wave transmission from spacecraft during solar cycle, considering latitudinal and longitudinal gradients and electron content change rate
20 p3197 A71-39715
- Limiting polarization of radio waves emerging obliquely from ionosphere into free space, describing numerical integration method and boundary conditions
21 p3348 A71-40525
- Soviet book on animals morphophysiological changes in cardiovascular and nervous systems and various internal organs under RF wave exposure
21 p3344 A71-41369
- Soviet monograph on radio wave propagation in fluctuating parameters media covering ionosphere /fluctuating electron concentration/ and troposphere /fluctuating inhomogeneities and refractive index values/
21 p3349 A71-41372
- Magnetoionic mode coupling of HF radio waves, considering Faraday rotation of satellite signals
23 p3642 A71-42963
- Electron periodic energization by magnetospheric RF wave propagation, examining cyclotron resonant interaction
23 p3644 A71-43321
- F layer perturbations by intense vertically upward radio waves for aeronomy and plasma control studies
23 p3671 A71-43543
- Radio brightness temperature relationship to sea surface state, noting ocean storm regions determination from radiometric satellite data
23 p3673 A71-44050
- Circularly polarized ultrashort radio wave reflection from lunar and planetary surfaces, determining angular scattering spectrum
24 p3805 A71-45313
- RADIOACTIVE AGE DETERMINATION**
Isotopic Rb/Sr age and initial chondritic ratio for silicate inclusions in Colomera iron meteorite
02 p0318 A71-12902
- Ar 40/Ar 39 age determination of Apollo 12 lunar rock 12013 fragments
03 p0494 A71-14220
- Trace element patterns of Apollo 12 lunar rock 12013 light and dark portions, discussing Rb-Sr age and Li, K, Rb, Sr, Ba and rare earth concentrations
03 p0494 A71-14222
- Apollo 12 lunar rock 12013 origin, determining age by U, Th and Pb isotopic study
03 p0494 A71-14223
- He, Ne, Ar and Xe from stepwise heating of Apollo 12 lunar rock 12013, discussing radiogenic and spallation components and He 3 and Ne 21 cosmic ray exposure ages
03 p0494 A71-14224
- Mn 53 age measurement of galactic cosmic rays
05 p0797 A71-15930
- Apollo 11 magnetic rocks and Apollo 12 rocks dating
06 p0966 A71-17742
- Atmospheric carbon 14 concentrations during past century, noting radioactive dating implications
07 p1102 A71-19580
- Decoupled nucleochronological isotopic equations for element age yielding solar system formation interval and supernova galactic distribution
08 p1251 A71-21694
- K-Ar age measurement by optimizing integrated neutron flux and sample size parameters, using graphical method
10 p1601 A71-24411
- Marine sediment age by fission track dating of volcanic glass shards, noting agreement with K-Ar, paleomagnetic and paleontologic ages
10 p1601 A71-24430
- Potassium-Argon dating analyses of neutron irradiated meteorites, discussing Chainpur chondrite chondrules gas retention ages
10 p1679 A71-24984
- Aubrite radiation age dating for stony meteorites lifetimes as function of collisional destruction, using Ne 21/Al 26 methods
10 p1680 A71-24989
- Cosmic ray spallation products and radiation age determination from spectral analysis of noble gas components in lunar rocks
11 p1829 A71-25837
- Lunar chronology and evolution from Rb and Sr internal isochrons on Apollo 11 and 12 crystalline rock samples
13 p2142 A71-29142
- U-Pb and Th-Pb age discrepancy in lunar dust, proposing Rn-222 emanation in decay chains
14 p2307 A71-29733
- Absolute production rates of He 3 and Ne 21 in average chondrites, determining radiation ages of stony meteorites aged less than two million years
15 p2486 A71-31991
- Radionuclides and noble gas isotopic abundances in recently fallen meteorites for cosmic ray exposure ages estimates
15 p2489 A71-32358
- Argon isotopes retention ages of crystalline lunar rocks 12002, 12051 and 12065 from lunar maria, using neutron activation and stepwise heating experiments
16 p2633 A71-33347
- K-Ar isotope ages of whole sample and feldspar concentrate from apollo 11 lunar rock 10003
16 p2633 A71-33349
- Bibliography and review of noble gases isotopic abundance in meteorites and lunar material, considering cosmic ray interactions, radiation ages and extinct radionuclides
17 p2798 A71-34451
- Bibliography and review of age determination of meteorites and lunar samples, considering chondrites, achondrites and iron meteorites
17 p2798 A71-34452
- Apollo 14 Fra Mauro rock fragment samples, determining Ar 40/Ar 39 ages
18 p2961 A71-35945
- Central Colorado basaltic lava flows tertiary paleomagnetic transition zone data, illustrating whole rock K-Ar dating difficulties
18 p2911 A71-35949
- K-Ar dating of shock metamorphosed rocks from Brent impact crater /Ontario, Canada/
19 p3050 A71-37658
- Uranium content correction for Ivory Coast microtektites, discussing effects on age values and correlation between tektite falls, geomagnetic reversals and faunal changes
20 p3292 A71-39405
- Apollo 14 flight Fra Mauro crystalline rocks age measurement, using Ar 40/39 ratio method
22 p3598 A71-41838
- Apollo 12 igneous rocks and fines from Ocean of Storms, presenting rubidium and strontium chronology and chemistry
23 p3752 A71-43709
- Rb-Sr isotopic composition in Apollo 12 regolith samples yielding 4.2-5.1 billion year ages
23 p3752 A71-43710
- Age determination of Apollo 12 rocks by U-Th-Pb method
23 p3752 A71-43713
- Cosmogenic radionuclide concentration and exposure ages of Apollo 12 rock from Ocean of Storms
23 p3754 A71-43730
- Lunar surface erosion and mixing from cosmogenic and primordial radionuclide measurement in Apollo 12 lunar rock and soil samples
23 p3755 A71-43731
- RADIOACTIVE DATING**
U RADIOACTIVE AGE DETERMINATION
RADIOACTIVE DECAY
NT NEUTRON EMISSION
Nd 147 decay gamma-gamma directional correlations, using coaxial Ge/LiJ and NaI/Tl detectors in conjunction with multichannel coincidence configuration
02 p0285 A71-11646
- Cosmic ray Be 7 equilibrium concentration, examining electron capture and radioactive decay
05 p0798 A71-16114
- Ce 138 excited states identification in beta decay spectra of Pr 138m and Pr 138 sources, using proton target bombardment
07 p1163 A71-19547
- Meteoritic Xe isotopes production mechanism covering spallation, neutron absorption, extinct I 129 and Pu 244 radiative decay and Xe component trapping
11 p1819 A71-25223
- Radioactive decay energy conversion of beta particle emitting cerium 144 into high voltage electricity in coaxial cylinder cell
15 p2447 A71-32211
- Heat release from elemental decay in radioactive layer from radio astronomical observations and lunar rock chemical analysis
20 p3295 A71-39620
- Gamma radiation due to cosmic rays interaction with Mars surface/atmosphere and natural radioactive rocks elements decay, calculating intensity and spectral composition
20 p3280 A71-39630
- Book on cosmic gamma rays covering secondary particle decay, electron-positron annihilation, proton-antiproton interactions, galactic radiation and cosmology
21 p3438 A71-40450
- Carbonaceous chondrite fission producing super-heavy element decay half life
22 p3605 A71-42398
- Apollo 11 and 12 rock samples examination, failing to observe radioactive halos
23 p3739 A71-43617
- RADIOACTIVE ELEMENTS**
U RADIOACTIVE ISOTOPES
RADIOACTIVE FALLOUT PARTICLES
U FALLOUT
RADIOACTIVE ISOTOPES
NT BERYLLIUM 7
NT BERYLLIUM 9
NT BERYLLIUM 10
NT CALIFORNIUM ISOTOPES
NT CARBON 14
NT CERIUM 144
NT COBALT 60
NT PLUTONIUM
NT PLUTONIUM 238
NT POLONIUM 210
NT TRANSURANIUM ELEMENTS
NT TRITIUM
NT XENON 133
- Pitts iron meteorite exposure history, noting consistency of rare gases isotopes contents in separated metal phase with prehistoric radiation flux increase
03 p0487 A71-13334
- Radioisotopes technical applications in industrial and aerospace sciences, discussing radioactive gas penetrants, radiation interaction and geometrical measurements
03 p0455 A71-13533
- Active cosmic ray modulation layer boundaries between sun and earth orbits, studying meteorite isotopes radioactivity
08 p1352 A71-20973
- Optimal time determination for using radioactive isotope as radiation source in nondestructive testing
08 p1332 A71-21898
- SNAP 15A heat source gamma ray intensity measurements and identification of gamma ray producing isotopes, describing measurement apparatus
09 p1491 A71-22456
- Radioisotope heat sources protection from reentry ablation and thermal stress with outer anisotropic pyrolytic graphite shield
13 p2099 A71-29259
- Lost City /Oklahoma/ and Uceru /Venezuela/ meteorites cosmogenic radionuclides data, using non-destructive analysis by gamma-gamma-coincidence counting system
15 p2489 A71-32357
- Radionuclides and noble gas isotopic abundances in recently fallen meteorites for cosmic ray exposure ages estimates
15 p2489 A71-32358
- Lost City meteorite secular and encounter perturbation effects on orbital evolution, interpreting short lived cosmic radiogenic isotopes formation
15 p2489 A71-32359
- Cosmic ray produced radionuclides in Lost City meteorite, determining concentrations by nondestructive two-parameter gamma ray analysis
15 p2479 A71-32363
- Human radioisotopic angiocardigraphy, emphasizing identification and physiological diagnosis of congenital and acquired cardiovascular defects
15 p2361 A71-32537
- Bibliography and review of noble gases isotopic abundance in meteorites and lunar material, considering cosmic ray interactions, radiation ages and extinct radionuclides
17 p2798 A71-34451
- Integrated waste collection and purification system using radioisotopes for thermal energy in 180-day space mission life support system
18 p2865 A71-36371
- [ASME PAPER 71-AV-4]
Long life radioisotope thermoelectric generators for space missions, discussing power degradation mechanisms and design trends
19 p3102 A71-37929
- Radionuclides depth distribution gradient in lunar samples, suggesting solar proton medium flux constancy over last million years
19 p3127 A71-38004

Radioisotopes as energy source for power conversion systems, discussing future availability of fission products and transuranium elements from commercial nuclear power reactors

20 p3265 A71-38948

Lung scanning, describing moving detectors, electronic apparatus adjustment and choice of radionuclide and labelled compound

20 p3192 A71-39072

Radioisotope testing methods for dissolution and mass transfer of alloying additives in Pb-Sb alloys during preparation in electromagnetic pumps

22 p3553 A71-41765

High energy proton spallation cross sections for several radionuclides from Ti targets, discussing application to lunar materials and meteorites analysis

23 p3706 A71-43199

Primordial radionuclides K, Th and U concentrations in Apollo 12 lunar rocks, breccias and fines, using gamma ray spectrometry

23 p3748 A71-43679

Apollo 11 and 12 fines cosmogenic He, Ne and Ar radionuclides composition determination, using electron microprobe analysis

23 p3754 A71-43727

Lunar cosmogenic radionuclides production time and spatial dependence calculations, comparing Apollo 11 and 12 measurements

23 p3754 A71-43729

Cosmogenic radionuclide concentration and exposure ages of Apollo 12 rock from Ocean of Storms

23 p3754 A71-43730

Lunar surface erosion and mixing from cosmogenic and primordial radionuclide measurement in Apollo 12 lunar rock and soil samples

23 p3755 A71-43731

Depth profiles of cosmogenic radionuclides in lunar rocks and soil samples from Apollo 11 and 12 flights, considering solar particle flux and spectra

23 p3755 A71-43732

Cosmogenic and primordial radionuclides in Apollo 12 surface rocks and fines from nondestructive gamma ray spectrometry

23 p3755 A71-43733

Tritium and argon radioactivities and depth variations in Apollo 12 rocks, discussing solar flare and cosmic ray exposure ages

23 p3755 A71-43737

RADIOACTIVE MATERIALS

Lunar radioactive layer effective thickness by radio astronomical methods and from Apollo 11 flight

07 p1193 A71-19312

Satellite studies of geocyclic particles and photoelectrons, including interactions with earth atmosphere

09 p1436 A71-22552

Alpha particle gas densitometric response to planet atmospheric density profiles in terms of radioactive source energy distribution, considering contoured baffle models

11 p1763 A71-26079

Aircraft personnel radiation hazards from radioactive luminous paint on instrument dials, signs and operational elements

13 p2021 A71-29145

Lunar radioactive layer effective thickness by radio astronomical methods and from Apollo 11 flight

15 p2486 A71-31892

Radioactive impurities transfer from lower stratosphere into upper troposphere based on vertical air transport data

15 p2400 A71-31970

Lost City meteorite Ar isotopes radioactivity measurements, considering cosmic ray flux radial gradient variations during meteoroid orbit

15 p2479 A71-32364

Lunar interior thermal history models for setting radioactive heat sources upper limits consistent with proposed temperature distribution

16 p2642 A71-33797

Radioactive rare gases and tritium in Apollo 12 lunar rocks and in sample return container, noting relationship to solar flare event

23 p3755 A71-43736

RADIOACTIVE NUCLIDES

U RADIOACTIVE ISOTOPES

RADIOBIOLOGY

Cosmic ray heavy ion component biological effect, describing histological and radioautographic high altitude balloon experiment with black mice and rabbits

01 p0019 A71-11555

Soviet papers on radiobiological aspects of reactivity of organisms in space flight covering radiation protection drugs, hypoxia, flight conditions, radiation pathology, etc

22 p3491 A71-42699

Composite tissue blocks method for comparative pathomorphological investigation of radiation pathology

22 p3505 A71-42734

Relative biological effectiveness of fast neutrons, allowing for gamma component contribution

22 p3494 A71-42735

Radiation protection biological aspects - Conference, Kyoto, October 1969

23 p3638 A71-44325

Physical and radiobiological studies on earth satellites covering radiation hazards and effects on animals, plants, unicellular organisms and biochemical systems

24 p3798 A71-44886

RADIOGRAPHY

Left ventricular volume determination by high speed cineangiocardiology, using optical scanning and automatic data processing

02 p0203 A71-11705

Photogrammetry in precision three dimensional X ray stereoradiography, comparing doses with Kymography, Tomography and Seriescopy

02 p0203 A71-11951

Electron photon cascades in multiplate substrate-free nuclear emulsion chamber with X ray films under lead plate

03 p0427 A71-13872

Submerged arc welding process, observing arc motion and metal transfer with X ray high speed photography

06 p0905 A71-18090

Portable Cf 252 neutron radiographic camera, noting reactor fuel and concrete polymer content measurements

07 p1119 A71-19950

Carbon fibers and composites nondestructive testing, discussing defect detection problems in ultrasonics, X ray diffraction and X radiography methods

[PLASTICS INST. PAPER 52]

08 p1296 A71-20918

Harmonic analysis of metals and alloys fine structure X ray photographs via digital computers

08 p1293 A71-21765

Spinal column radiographic examination after pilot ejection, discussing vertebral injuries detection

13 p2019 A71-28510

Neutron radiography facility using TRIGA reactor source, discussing design and performance

13 p2044 A71-28523

Al-Zn-Mg alloy plates welded with Al-Mg filler metals, observing ghost defects in radiographs

13 p2074 A71-28524

Ultrasonic/radiographic method for intraocular foreign body localization

13 p2013 A71-29031

Roentgenological analysis of paranasal sinuses in civil aviators, studying facial cavities infection

13 p2023 A71-29367

Multidirectional reinforced resin matrix composites inspection and nondestructive analysis by film/neutron radiography and X ray Vidicon

14 p2263 A71-29659

Neutron radiography and dosimetry as clinical diagnostic tool, calculating resolution through tissues for simulated human arm

17 p2693 A71-35449

Neutron radiography of Apollo ordnance, describing test facility and equipment

19 p3063 A71-37449

Electron photon cascades in multiplate substrate-free nuclear emulsion chamber with X ray films under lead plate

22 p3550 A71-42673

RADIOISOTOPE BATTERIES

NT SNAP 15

NT SNAP 19

NT SNAP 21

NT SNAP 23

NT SNAP 27

Operating experience with miniature thermionic radioisotope-fueled batteries, using thermal-thermionic models

02 p0196 A71-12273

Radionuclide batteries for energy supply in space, comparing with electrochemical sources

02 p0282 A71-12303

Technological development of thermoelectric radionuclide batteries for space applications using Ge-Si thermocouples

02 p0282 A71-12304

Space nuclear power developments, reviewing radioisotope heat sources, reactors and power conversion systems

04 p0624 A71-15284

Nimbus meteorological satellite program, discussing global cloud cover mapping and automatic picture taking, radioisotopic thermoelectric generator, sounder instrumentation and remote sensors

05 p0818 A71-17133

Radioisotope thermionic power supply for unmanned electric propulsion missions to outer planets, using 69 modules consisting of thermionic converter and emitter heat pipe

11 p1811 A71-25897

Impact resistant power packages for unmanned planetary probe landers, discussing radioisotope thermionic multiconverter array optimal configuration

11 p1713 A71-25898

Radioisotope thermoelectric generators integration for Pioneer 6/7 program, discussing design requirements

[AAS PAPER 71-150] 19 p3103 A71-37952

Pioneer Jupiter spacecraft, noting low weight, radioisotope thermoelectric generators and gyroscopic stabilization by spinning with antenna pointed at earth

[AAS PAPER 71-167] 19 p3141 A71-37964

Radioisotope thermoelectric generators in micro/milliwatt power range for biomedical applications

20 p3192 A71-38912

Isotope Brayton four module adaptable compact power system for space station, using plutonium 238 fuel and lithium hydride shielding for neutron attenuation

20 p3263 A71-38922

Long life performance predictions for lead telluride and silicon germanium radioisotope thermoelectric generators for deep space missions

20 p3263 A71-38925

Multihundred watt radioisotope thermoelectric generator for JPL outer planet missions, discussing vacuum/xenon filled performance and response to thermal/electrical transients

20 p3263 A71-38926

Multihundred watt radioisotope thermoelectric generator for spacecraft power supply, discussing system design, performance and safety requirements

20 p3263 A71-38927

Multihundred watt radioisotope thermoelectric generator heat source survivability in multiple skip reentry

20 p3264 A71-38931

Grand tour missions radioisotope thermoelectric generator power source, presenting optimization technique for hot thermocouple junction operation

20 p3264 A71-38932

Radioisotope thermoelectric generator safety and operations considerations for users of large nuclear space power systems

20 p3264 A71-38933

Radioisotopic power applications of beta and gamma emitting Co 60, noting powder ceramic fabrication of dense wafers for irradiation to convert natural Co 59

20 p3265 A71-38938

Long life radioisotope thermoelectric generator, discussing mathematical model to simulate expected performance profiles

20 p3266 A71-38958

RADIOLOGY

Aircrew radiological examination of spinal anatomical state, emphasizing traumatism due to vibration, acceleration, ejection and crashes

05 p0715 A71-16936

Chest and cardiovascular system optimal radiologic facilities, discussing X ray examination, catheterization-angiocardiac and nuclear radiology laboratories

07 p1053 A71-20354

Spine radiological examination for helicopter pilot fitness determination, discussing spinal weakness symptoms, special exercises, medical examinations and vibration reducing seat construction

22 p3500 A71-41578

RADIOLYSIS

Plasma generation by photon irradiation, radiolytic mechanism and high energy particle bombardment, discussing ionized media chemical reactions

16 p2540 A71-32971

Water radiolysis measurement in nuclear reactor tests, discussing experiment design as doubly telescoping sequences of blocks

21 p3345 A71-40202

RADIOMETERS

NT DICKE RADIOMETERS

NT INFRARED DETECTORS

NT INFRARED SCANNERS

NT MICROWAVE RADIOMETERS

NT SPECTRORADIOMETERS

ATS-5 satellite dual swept radiometer features, operation and specifications

01 p0082 A71-10985

Radiometric determination of diametrical distance between rotor and stator of turbomachines

03 p0421 A71-13003

Atmospheric temperature remote sounding from satellites using radiometer with selective chopper for carbon dioxide emission

03 p0422 A71-13355

Six channel selective chopper radiometer design and construction for carbon dioxide emission monitoring for remote atmospheric temperature sounding by Nimbus 4

03 p0423 A71-13356

Atmospheric temperature remote sounding via balloon-borne selective chopper radiometer

03 p0423 A71-13357

Differential radiometer with ultranarrow interference filter for daytime tracking of high altitude chemical vapor trails

03 p0424 A71-13636

Errors from multiple reflections between target environment viewed by IR thermometer or radiometer and background environment
05 p0752 A71-16672

Unicellular algae photosynthesis measurement by radiometric methods under optimum and equalized conditions of light, temperature and carbon dioxide supply
05 p0714 A71-16815

Ecological interpretation of daytime data from Nimbus 3 high resolution IR radiometer for hydrologic and plant distribution mapping
08 p1277 A71-20884

Combustion chamber radiant heat transfer measurements, describing radiometer
08 p1288 A71-21270

Device for rapid direct analysis of beryllium ores and concentrates in transport containers, using radiometric method
09 p1427 A71-22506

Balloonborne radiometric instrumentation for solar and thermal radiations upward and downward flux measurements, discussing net radiation balance as function of solar elevation
09 p1515 A71-23558

Infrared radiometer sea surface temperature measurements during oceanographic survey, examining inclination angle effect
09 p1440 A71-23590

Nimbus 4 satellite selective chopper radiometer data on IR radiation emitted by carbon dioxide, considering stratospheric warming
10 p1598 A71-23743

Temperature measurement techniques annual progress survey including contact and radiation thermometers, IR thermography, microwave radiometry, fluidic sensors, and liquid crystals
10 p1612 A71-24685

Cosmic background radiation ground based measurements at two high altitude sites, using radiometric technique
11 p1815 A71-25300

Book on radio astronomy instruments and observations covering high sensitivity radiometers, masers, parametric amplifiers, radio telescope design, radio spectrometers, parabolic reflectors, etc
11 p1737 A71-25359

Meteorological IR radiometer with thermosensitive element, chopper circuit and AC microvoltmeter, outlining calibration procedure
11 p1763 A71-26174

Water vapor dimer effects on atmospheric brightness temperature in cm and mm radiometric investigations from satellites above ocean areas
12 p1901 A71-27099

Double resonator ruby maser for observing transitions of interstellar hydroxyl, noting incorporation in modulation radiometer of astronomical telescope
13 p2077 A71-28373

Earth surface temperature measurement by airborne IR radiometers, discussing accuracy provided by narrow and wideband filters
14 p2240 A71-30126

Supplementary tables to SI nomenclature for radiometry and photometry including photon flux
14 p2242 A71-30157

Micrometeor mass data from radiometer measurements, detailing Cu and lanthanum hexaboride ionization probability
14 p2315 A71-30652

Hertzian radiometry experimental aspects covering background and medium temperature measurements, sky radiometry and absorbing gas total pressure measurements
14 p2204 A71-30969

Radiometric errors in cosmic background radiation measurement
14 p2204 A71-30970

Nimbus weather satellite with IR spectrometer, Michelson interferometer and selective chopping radiometer for atmospheric temperature remote sounding
15 p2445 A71-32295

Compact Q band magic tee with matched loads to check noise performance of two-input switched radiometer
16 p2579 A71-33385

Active cavity radiometric and international pyrheliometric scales comparison and solar constant from simultaneous solar irradiance measurements
16 p2581 A71-33939

Passive mapping of terrain with sidelooking radiometry by storing received signals from various elements over extended flight path
17 p2746 A71-35763

Meteorological objectives, radiometry and ground stations for Meteosat weather prediction system using geostationary satellite
18 p2878 A71-36527

Combined lidar and radiometric techniques for high layer cumulus and cirrus clouds IR emissivity determination
19 p3089 A71-37501

Atmospheric signal propagation study between satellite and earth, using solar radiometry
19 p3018 A71-38075

Stray radiant flux effects on scanning IR radiometer for low temperature objects measurement
19 p3067 A71-38706

Radiometric measurement of total normal emittances of real surfaces at cryogenic temperatures
20 p3313 A71-39289

Solar IR spectra referencing procedure based on filter reference radiometer, discussing technique theoretical foundation
20 p3237 A71-39327

Spacecraft-borne IR sequential filter radiometer design and performance for real time meteorological forecasting and atmospheric temperature measurements
22 p3544 A71-42143

IR atmospheric temperature profiles sounding by selective chopper radiometer launched into polar orbit on Nimbus 4 satellite
22 p3544 A71-42144

IR radiometer experiment for Mariner 1971 Mars orbiter mission, describing objectives and instrumentation
23 p3676 A71-43510

ITOS meteorological satellite scanning radiometer using point detector optical system for earth imaging
23 p3676 A71-43511

Night sky far IR background radiation measurements by rocket-borne superfluid HE cooled radiometer, determining average signal strength equivalency to black body temperature of 3.1 K
24 p3822 A71-44752

Airborne measurement of directional variation in reflected solar radiation over soil surface and vegetation, using scanning radiometer
24 p3826 A71-44984

RADIONUCLIDES
U RADIOACTIVE ISOTOPES
RADIOPATHOLOGY
Rat organs pathomorphological changes under gamma neutron irradiation with head and abdomen shielding, noting intestines early damage
22 p3493 A71-42722

RADIOPROTECTIVE AGENTS
U ANTIRADIATION DRUGS
RADIOSENSITIVITY
U RADIATION TOLERANCE
RADIOSONDES
NT IONOSONDES
NT RAWINSONDES
Reverse flow temperature probe design and calibration for vertical soundings from aircraft, comparing to radiosonde method
02 p0247 A71-11822

Mountainous region vertical air flow research, describing superspree balloon and precise pressure radiosonde system
02 p0189 A71-12420

High altitude rocket-borne radiosonde communication, examining transmission link characteristics, signal losses and antenna radiation patterns
04 p0551 A71-15012

Global computer processing scheme for aerological radiosonde observation, using coded telegrams as primary information data
06 p0922 A71-17502

Temperature measurement inaccuracies in 30 to 40 km region by balloonsonde sensors, involving IR cooling of thermistor
08 p1277 A71-20989

High altitude radiosonde thermometer and pressure sensor construction, discussing radiation error and wire lag
08 p1293 A71-21740

Radiosonde with radiation sensor, minimizing temperature measurement errors in free atmosphere
08 p1293 A71-21745

Solid state pulse modulated radiosonde for meteorological data transmission in digital form, using MOS integrated circuits
10 p1583 A71-24052

Stokes flow parachute extremely lightweight decelerator for increasing altitude and rocket-borne radiosondes atmospheric data sampling quality
11 p1707 A71-25277

VENTILATION rates and thermal factors of sensitive elements in radiosondes, using wind tunnel tests
11 p1761 A71-25382

Comparative accuracies of vertical atmospheric water vapor profiles by radiosonde and laser backscatter Raman component
11 p1794 A71-25383

Objective subsynoptic upper level analysis optimizing smaller scale radiosonde data over U.S.
16 p2604 A71-33533

Middle stratosphere monthly mean temperature maps based on radiosonde measurements, confirming anomalies with satellite IR spectrometer radiances
16 p2641 A71-33755

Hybrid thin film radiosonde transmitter design for atmospheric temperature and humidity data transmis-

sion from meteorological sounding balloon to ground station
19 p3035 A71-38539

Geostrophic wind measurements by radiosondes at various altitudes over British Isles, relating deviations from geostrophic equilibrium to vertical motions near tropospheric trough
20 p3258 A71-39551

Mathematical model of emission spectrum for PKZ radiosonde and radiosondes using superregenerative transceivers
21 p3383 A71-41243

Nimbus 3 satellite IR spectrometer atmospheric pressure height profiles, comparing with nearby radiosonde data
22 p3535 A71-42410

RADIOTELEPHONES
Aeronautical electronic equipment, discussing static transformer, radiotelephone sets, angle of approach meter, etc
03 p0383 A71-13018

RADIOTHERAPY
U RADIATION THERAPY
RADIUS
U RADII
RADOME MATERIALS
Book on radome engineering covering electromagnetic and thermal-mechanical design, organic and inorganic radomes, electrical evaluation and rain erosion
01 p0055 A71-11191

Reinforced plastics components in supersonic transport nose radome and missile radar antennas, discussing molding, sandwich materials and computer controlled spraying techniques
12 p1887 A71-27016

Materials and processing methods for rain erosion resistant ceramic coated plastic structures for supersonic aircraft, considering fiberglass reinforced polyimide radomes with alumina coating
14 p2262 A71-29645

RADOMES
Book on radome engineering covering electromagnetic and thermal-mechanical design, organic and inorganic radomes, electrical evaluation and rain erosion
01 p0055 A71-11191

Soviet book on antenna radomes of flight vehicles covering electromagnetic wave transmission through dielectric media, fabrication, construction materials, etc
01 p0057 A71-11322

Materials and processing methods for rain erosion resistant ceramic coated plastic structures for supersonic aircraft, considering fiberglass reinforced polyimide radomes with alumina coating
14 p2262 A71-29645

Microwave wideband and multiband radome design for strength, environmental and electrical requirements, achieving transmission efficiencies with dielectric and wall thickness selection
14 p2216 A71-31037

Antenna and radome constructions/shape effects on minimizing cross polarization produced by flat, cylindrical, conical and paraboloidal radomes in linear and circular beams
14 p2216 A71-31039

Radome design and production, considering construction, materials, shape, manufacturing techniques and technological problems
14 p2218 A71-31067

Radome lightning protection systems involving electrostatic shield, considering effect on electromagnetic characteristics and radiation patterns of nearby antennas
19 p3031 A71-38450

Antenna radome noise temperature under aerodynamic heating as function of losses in material, interface reflection and dielectric surfaces
23 p3647 A71-44324

RADON
NT RADON ISOTOPES
Apollo 11 lunar soil and rock samples under low level beta spectrometry, measuring radon daughter Pb 210
18 p2961 A71-35946

RADON ISOTOPES
U-Pb and Th-Pb age discrepancy in lunar dust, proposing Rn-222 emanation in decay chains
14 p2307 A71-29733

Radon 222 distribution in lunar atmosphere and top surface
21 p3449 A71-40607

RAE-1
U EXPLORER 38 SATELLITE
RAFTS
NT LIFE RAFTS
RAIL TRANSPORTATION
Rail track roughness and irregularities evaluation by railcar vibration measurements, using portable LF low amplitude acceleration measuring and recording system
11 p1845 A71-25349

[ALAA PAPER 71-384]
Integrated short-haul interurban transportation system, considering combination of conventional jet

RAILS

aircraft, STOL aircraft and high-speed ground transportation
[AIAA PAPER 71-508] 14 p2221 A71-29550
Asymptotic high velocity lift drag ratios for sheet and loop magnetic suspension train tracks
22 p3574 A71-41728

RAILS

Test rail system of Les Landes Testing Center, discussing optical and electromagnetic observation, measurement and test coordination and control facilities and equipment
04 p0567 A71-15817

Fiberglass reinforced plastic rocket launcher tubes with internal helical rails to impart spin to missiles, discussing design, fabrication and testing
11 p1786 A71-25419

RAIN

Mic extinction parameters tabulation for computed signal transmission through rain at microwave and visible frequencies
01 p0029 A71-10469

Reflectivity and attenuation observations of hail and radar bright band during storms, discussing rain effects
01 p0115 A71-10554

Storm reflectivity models using weather radar and surface rainfall data correlations
01 p0118 A71-10585

Rain and sand erosion materials tests, considering temperature and atmosphere pressure effects and relation between fatigue behavior and erosion/cavitation strength
03 p0444 A71-14289

Average radar cross section relative values for echoes from rain, considering horizontal, vertical and circular polarization in various sea states
04 p0551 A71-15008

Rain and drizzle millimeter wave attenuation and radar scattering cross section calculation
05 p0718 A71-15988

Submillimeter and millimeter waves attenuation in rain, comparing calculation results with measurement
05 p0718 A71-15990

Visible and IR radiation attenuation in rain and snow, comparing calculation based on Mie diffraction formulas with measurement
05 p0718 A71-15992

Atmospheric absorption by clouds, fog and rain on earth-space path at 90 GHz, using sun tracker
07 p1060 A71-19215

Freezing nucleus concentrations in hail and rain from different storms, showing dependence on precipitation type and intensity
08 p1326 A71-21451

Rain and fog modification concerning natural and artificial nuclei role, warm fog clearing and supercooled cloud experimentation
17 p2769 A71-34545

Percent-of-time distributions of attenuation by rain, clouds and atmospheric gases on earth-space paths at frequencies below 30 GHz
17 p2704 A71-35089

Rain attenuation measurements, noting limitations on microwave transmission at SHF
19 p3024 A71-38612

Atmospheric physics of cloud formation, rain, hail and snow precipitation, discussing intracloud temperature variations electric fields and air impurities on water condensation
21 p3410 A71-40146

Rain and drizzle submillimeter wave attenuation and radar scattering cross section calculation
22 p3515 A71-42737

Submillimeter waves attenuation in rain, comparing calculation with measurement
22 p3515 A71-42739

Visible and IR radiation attenuation in rain and snow, comparing calculation based on Mie diffraction formulas with measurement
22 p3515 A71-42741

Convective cloud dissipation after rainfall, calculating temporal behavior of temperature fields, water content, moisture and air motion rate
22 p3569 A71-42847

Vertically polarized millimeter and submillimeter wave attenuation measurement in rain
23 p3646 A71-43569

RAIN EROSION

U WATER EROSION

RAIN GAGES

Meteorological radar rainfall estimates comparison with dispersed tipping bucket gage measurements during storms
01 p0118 A71-10582

Italian book on microwave propagation covering electromagnetic wave attenuation, rainfall space-time structure and radioelectrical/meteorological data recording
11 p1731 A71-25650

Unified international scaling for annual and seasonal precipitations measured by national gages, comparing U.S.S.R. and U.S. reduction coefficients
21 p3383 A71-41377

Error factors of seasonal precipitation measurements by total precipitation gages
21 p3383 A71-41378

RAIN IMPACT DAMAGE

Book on radome engineering covering electromagnetic and thermal-mechanical design, organic and inorganic radomes, electrical evaluation and rain erosion
01 p0055 A71-11191

Plastic, elastomeric, ceramic glass, metallic and composite materials rain erosion resistance at supersonic speeds, examining rate-velocity dependence
03 p0444 A71-14288

Polyurethane coatings development for subsonic rain erosion protection for aircraft structures, using whirling arm apparatus with simulated rainfall
10 p1632 A71-24101

RAINDROPS

Radar precipitation measurement accuracy improvement, using various Z-R relationships for correlation of radar data and rainfall rates
01 p0117 A71-10581

Vertical air motions velocity in rainfall from Doppler spectrum total radar reflectivity and median velocity
07 p1150 A71-18798

Weather radar plan position indicator automatic film reading for digital mapping of rainfall intensity, discussing raindrop sizing
08 p1286 A71-20690

Fog droplet and rain effects on propagation of echo location signals from bats
10 p1638 A71-24423

Frequency response of rainfall attenuation for various dropsize distributions, plotting measured values at 890 and 110 GHz
15 p2374 A71-32696

Unified raindrop breakup theory, examining spherical liquid drop transient response under surface tension accelerated by uniform external gas flow
16 p2557 A71-32924

Automatic analyzer for rapid counting and sizing of raindrops, using collimated flashlamp source for illumination
18 p2918 A71-36076

Rainfall, aerosols and cloud water samples analyzed for chlorides and sulfates content and electrical properties
19 p3092 A71-38687

Ice formation and prevention on helicopters, taking into account presence of big drops of undercooled rain
20 p3178 A71-39374

Electrooptical measurement of high altitude rain cloud droplets size, shape and distribution
23 p3676 A71-43507

RAINSTORMS

NT THUNDERSTORMS

Meteorological radar rainfall estimates comparison with dispersed tipping bucket gage measurements during storms
01 p0118 A71-10582

Submillimeter wave attenuation measurement over 1 km path during summer rainstorms, comparing results with millimeter waves
05 p0718 A71-15989

Storm models for space-path attenuation calculations using digitized weather radar data for fine structure and surface rainfall data for extrapolation
17 p2704 A71-35090

Submillimeter wave attenuation measurement over 1 km path during summer rainstorms, comparing results with millimeter waves
22 p3515 A71-42738

RAMAN EFFECT

U RAMAN SPECTRA

RAMAN SCATTERING

U RAMAN SPECTRA

RAMAN SPECTRA

Q switched ruby laser-Raman radar for real time air pollution probe
02 p0213 A71-12014

Calcite and aragonite high pressure Raman line spectra comparisons, testing structural identification theory
07 p1054 A71-19369

Laser induced Raman scattering as diagnostic technique for measuring specie concentrations in gas mixtures
07 p1125 A71-19897

Lidar wavelength optimization for Raman scatter atmospheric studies, taking into account aerosol and weak signal statistical effects
08 p1254 A71-21458

Velocity components, species densities and temperature local measurements, using laser Doppler velocimeters, Raman scattering and tunable lasers
08 p1303 A71-22008

Frequency and spectral composition effect of incident radiation on stimulated Raman scattering of organic compounds, using ruby laser harmonic emission
09 p1461 A71-22395

High efficiency gas chamber for obtaining Raman spectra of corrosive gases at atmospheric pressure by He-Ne laser excitation
10 p1619 A71-23857

High power single mode CW tunable spin-flip Raman laser in InSb using CO pump
10 p1620 A71-24041

IR and Raman spectra vibrational analysis of crystalline and fluidic oxalyl bromide, explaining observations by two geometrical isomers existence
11 p1727 A71-25363

Comparative accuracies of vertical atmospheric water vapor profiles by radiosonde and laser backscatter Raman component
11 p1794 A71-25383

One magnon Raman scattering induced by light magnetic dipole coupling with YIG coherent spin waves
12 p1913 A71-26860

Measuring system for 180 degree Raman scattering in single crystals, powders, liquids and strongly absorbent solutions
12 p1915 A71-27673

Raman effect quantum theory, considering light scattering about atomic system
13 p2078 A71-28449

Monoclinic, stabilized and metastable tetragonal and cubic zirconias, noting IR and Raman spectra
13 p2093 A71-28991

High intensity tunable InSb spin flip stimulated Raman scattering from pulsed high pressure carbon dioxide laser radiation pumping
13 p2081 A71-29336

Parametric amplification of two laser waves with amplitude and phase modulation under exponential signal growth applied to Raman scattering in picosecond pulse field
15 p2418 A71-31188

Gaseous, liquid and polycrystalline biacetyl vibrational spectra and structure, noting mutual exclusion between IR and Raman radiation
16 p2538 A71-32874

Lasers as light sources, discussing Rayleigh, Tyndall, Raman and Thomson scatterings from various media
16 p2612 A71-33373

Ultrafast laser pulses, revealing fluorescence decay, stimulated Raman scattering and plasma formation transient details
16 p2588 A71-33873

Raman and IR reflection spectra of zinc tungstate single crystals
17 p2790 A71-34201

Photoelectric system for recording Raman spectra with He-Ne laser excitation source suitable for liquid, solution, crystal and powder and depolarization measurements
17 p2751 A71-34383

UV Raman remote gas sensors incorporating laser scattered radiation with high resolution monochromator
17 p2753 A71-35292

IR and Raman vibrational spectra and structure of tetrafluorocyclobutane
17 p2695 A71-35520

Solid glyoxal Raman spectrum data, showing operativity of mutual exclusion principle by IR comparison to Raman bands
18 p2873 A71-35830

Nonlinearities effects on inorganic liquid laser output, investigating Raman and Brillouin scatterings and self focusing
18 p2933 A71-37012

Ultrashort pulse formation in short pulse stimulated Raman oscillator, achieving partial group velocity matching
19 p3071 A71-37475

Gaseous and solid polycrystalline HNCS and DNCs IR and Raman spectra, studying LF of lattice vibrations
19 p3118 A71-37649

Mg compounds family of antifluorite structured small-gap semiconductors, investigating surface light scattering properties by Raman scattering techniques
19 p3119 A71-37870

Comparative IR and Raman spectra of gaseous, liquid and polycrystalline symmetrical dimethylhydrazine and deuterium analogs
19 p3013 A71-38345

Raman tensor, scattering efficiency and line widths in semiconductors due to optical phonons, discussing electro-optical coefficients
21 p3427 A71-40662

Molecular iodine vapor absorption filter for stray laser light in Brillouin and Raman scattering
21 p3393 A71-41042

Tunable spin-flip magneto-Raman IR laser, describing indium antimonide scattering, tuning range and applications
22 p3557 A71-42133

IR spectra of oxamide and diethoxamide, studying Raman spectrum in LF range
23 p3642 A71-43825

Raman microwave scattering on Langmuir oscillations, showing suprathreshold emission origin in theta pinch plasma
24 p3853 A71-44505

RAMAN SPECTROSCOPY

- Three mirror multiple beam interferometric rejection filter for laser Raman spectroscopy
08 p1289 A71-21379
- Multiphase gas flow, measuring gas concentration by laser Raman spectroscopy
[AIAA PAPER 71-286] 09 p1464 A71-23308
- Fluorochlorosilane preparation and identification by Raman laser spectroscopy, establishing line to vibration mode relation
14 p2189 A71-29746
- Gases high resolution Raman spectroscopy, using mirror system for exciting laser beam multiplication
15 p2423 A71-32600
- Optical cryostat suitable for Raman spectroscopy, using quartz tube optical cell and He evaporation by metal film resistor
20 p3268 A71-38833
- Spectral resolution of matrix Raman spectroscopy and depolarization measurements of isotope splitting, comparing with complementary IR data
20 p3194 A71-39404

RAMJET ENGINES

- NT SUPERSONIC COMBUSTION RAMJET ENGINES
- NT TURBORAMJET ENGINES
- Supersonic and subsonic combustion modes in constant area ramjet combustors, deriving dimensionless parameter for varying flow ratios as combustion stability criterion
[ASME PAPER 70-WA/AV-4] 03 p0521 A71-14148
- Supersonic combustion ramjet engine with liquid fuel injection, considering atomization process and ignition criteria
05 p0836 A71-16531
- German monograph on ignition and combustion processes in rapidly flowing gas mixtures covering supersonic flow, ramjet parameters, flow heating, etc
05 p0838 A71-16900
- Hypersonic ramjet reaction mechanisms for H combustion, discussing computational models, operation principles and atomic, radical and molecular collisions
06 p0865 A71-17410
- Shortest transfer time interstellar propulsion systems, considering nuclear pulse and electric rockets, fusion and photon rockets, and ramjets
15 p2469 A71-31748
- Book on aircraft propulsion covering design, dynamics, control, installation, gas turbine, ramjet, rocket and piston engines, compressors, combustion and energy cycles, etc
22 p3589 A71-42427

RAMS (PUMPS)

- Flexible ram air inflated keel and leading edge parawing design optimization for increased stability and reliability, introducing semirigid member concept
[AIAA PAPER 71-986] 24 p3791 A71-44582

RANDOM ACCESS MEMORY

- NT CORE STORAGE
- MOS LSI bipolar random access memory feasible at costs competitive with magnetics
02 p0228 A71-11653
- Large random access computer store based on redundancy in form of error correcting codes, discussing use for manufacturing yield improvements
24 p3806 A71-44655

RANDOM DISTRIBUTIONS

U STATISTICAL DISTRIBUTIONS

RANDOM ERRORS

- Single rotor gyrocompass with electromagnetic correction during random interactions involving intercardinal deviation, constructing correcting device to obtain optimal dynamic characteristics
03 p0430 A71-14353
- Optimal trajectory measurement program for orbit parameter determination, assuming random errors and nondegenerate weighting matrix of normal equations
09 p1519 A71-22542
- Error analysis of random and system degradation between calibrations for complex instrumentation by digital computer models
09 p1449 A71-22790
- Random failure definition based on stochastic processes mutual implication, producing unique characteristic events
11 p1771 A71-26160
- Aircraft onboard equipment tests in air navigation aid satellite project, estimating tracking random errors
18 p2877 A71-36509
- Dual stochastic relations of optimal control and minimal error observation under random noise, using programming method
21 p3361 A71-41136
- Gaussian errors effect in maximal ratio diversity combiner weighting factors on probability distribution of output SNR
22 p3513 A71-42384
- Random amplitude bounded measurement errors, describing nonlinear filtration method of noise smoothing
24 p3813 A71-44683
- Geometrical least squares model extension to maximum likelihood method for linear processes with additive Gaussian error
24 p3843 A71-44704

- Point motion in random error region applied to synchronous satellite trajectory control by single impulse correction
24 p3846 A71-45307

RANDOM LOADS

NT GUST LOADS

- Structural vibration response to nonhomogeneous random pressure fields based on homogeneous field theory
[ASME PAPER 70-WA/DE-11] 03 p0511 A71-14145
- Pinned steel lug joints fretting fatigue, examining cumulative damage under constant amplitude and narrow band random loading
03 p0513 A71-14244
- Linear elastic structure statistical response characteristics relation to natural environment random pressures, considering flexural vibrations of thin cylinder for modal density
05 p0826 A71-16732
- Equidistant multiple span rectangular plates vibration and acoustic radiation under random external forces
06 p0994 A71-17823
- On-off control system with crew motion caused random disturbing torques on spacecraft, determining waiting time, jet firing frequency and fuel consumption rate
07 p1208 A71-19885
- First passage time for snap-through of shallow cylindrical shell subject to stationary random loading, considering numerical solution by Pontryagin-Vitt equation
08 p1369 A71-20809
- Periodically supported beams response to random loading, using space-harmonic analysis
08 p1371 A71-21429
- Nonlinear panel flutter analysis and response under random excitation or nonlinear aerodynamic loading, using Rayleigh-Ritz approximation to Hamilton variational principle
09 p1534 A71-22080
- Linearly elastic cylindrical shells dynamic stability under combined axial and radial stochastic excitations, using Liapunov analysis
[AIAA PAPER 71-333] 11 p1842 A71-25312
- Internal structural design loads for aerospace vehicles subjected to random loads, considering shear, moment and torsion as random components of generalized internal load vector
11 p1838 A71-25516
- Forced vibrations of circular cylindrical shell under random normal load and internal pressure, noting stability of transversely pressurized flexible vs rigid structures
13 p2150 A71-28140
- Vibration absorbers optimization for multiple degree of freedom systems with random excitations, applying optimal control theory in frequency domain
13 p2158 A71-29427
- Column buckling under initially random bending and twisting, comparing numerical analysis accuracy with Bernoulli-Euler results
14 p2330 A71-30692
- Snap buckling instability of shallow shell type structures subject to random transverse load
15 p2502 A71-31417
- Reliability prediction of narrow band structures under random excitations, considering catastrophic and fatigue failure modes
15 p2506 A71-32094
- Elastic structures stability under randomly fluctuating external loads based on statistical methods
16 p2648 A71-32988
- Aircraft random heave-pitch response to taxiing on rough runways, analyzing dynamic loads and fatigue damage by power spectral techniques
18 p2850 A71-36675
- Nonlinear mechanical system stationary random forcing input and output response data, determining statistical linearization coefficients in Kazakov-Boon method
19 p3037 A71-37347
- Structures with random resistance, calculating upper and lower bounds for safety coefficients average value and variance
19 p3156 A71-37643
- S-N curve and structural failure probability due to combined random and primary loads based on mathematical model
19 p3157 A71-37847
- Aerodynamic control surfaces optimal location for flexible aircraft disturbed by random wind gusts, using matrix minimum principle and calculus of variations
19 p2998 A71-38713
- Structural vibrations excited by spatially and temporally random pressure loading, discussing power spectra and vibration measurement
21 p3467 A71-40912
- Complex structural systems response characteristics under steady state sinusoidal, transients and random loadings, developing hybrid elastodynamic equations
21 p3470 A71-41011

- Shallow two pinned sinusoidal arches stability under random symmetrically distributed lateral loads, observing deformation, buckling and critical value
22 p3612 A71-41429
- Random loading parameters adjustment in fatigue tests of welded aircraft structures
22 p3528 A71-41692

RANDOM NOISE

NT RANDOM SIGNALS

- Linear information feedback methods for white Gaussian noise channels
01 p0064 A71-10904
- Radio telemetry transmitter receiver systems notch noise testing for relationships between spectral power density, video and IF bandwidths and peak deviation
01 p0034 A71-10908
- Gaussian message optimal transmission through channel with white Gaussian noise in presence of total feedback
01 p0064 A71-11152
- Closed cylindrical shell response to random sound in contained fluid, investigating cylinder end acoustic boundary conditions with coupled oscillator theory
02 p0239 A71-11998
- Error probability during diversity reception under random radio noise
04 p0549 A71-14613
- Algorithms for optimal detection of weak determinate signal on background of Markov process approximated non-Gaussian noises
05 p0719 A71-16009
- FM discriminator with nonideal limiting, calculating signal to noise ratio under white Gaussian noise input
05 p0730 A71-17071
- Broad spectrum pseudorandom Gaussian noise generator, describing pseudorandom binary sequence filtering technique with desirable autocorrelation properties
06 p0877 A71-17327
- Radio signals and receiving equipment structural synthesis, considering signal filtration under random additive noise
06 p0866 A71-17372
- Random Gaussian noise driven damped nonlinear oscillator, discussing Duffing equation, consolidated expansions for response spectrum and common factors
06 p0926 A71-17499
- Binary signal parameters estimation mixed with Gaussian noise, using method of moments
07 p1065 A71-20420
- Woodward ambiguity function generalization for case of radar signal reflection from rapidly fluctuating target, mixed with white Gaussian noise
09 p1404 A71-22292
- Nonstationary colored noise linear shaping filter to transform white noise into nonstationary random process with specified covariance function
09 p1424 A71-23100
- Rate distortion over band limited feedback channels, considering capacity of additive Gaussian white noise channel
09 p1407 A71-23104
- Pulsed signal amplitude and delay time measurement in presence of interfering/reverberated/ signals and steady noise
09 p1407 A71-23111
- Spectrum analysis and probability distribution of burst noise pulses of silicon planar bipolar transistors consistent with Markov two state process
10 p1574 A71-23773
- Positive signal optimal detection system in unsteady non-Gaussian noise
10 p1577 A71-24282
- Random response of stationary linear system to pulse noise in time with independent amplitudes
10 p1588 A71-24901
- Structural system frequency response measurements under environmental noise conditions, discussing autocorrelation function for transient excitation damping
11 p1797 A71-25182
- Computer programs for random noise vibration test digital control, describing data base and logic programs
11 p1736 A71-26499
- Malfunction probabilities in presence of wideband noise for tunnel diode binary logic element /flip-flop/ pulse triggered into either of two output states
11 p1740 A71-26543
- Gram-Charlier error probabilities of digital satellite communication systems due to intersymbol interference and additive noise applied to Chebyshev, Gaussian and cutoff filters
12 p1879 A71-27069
- Amplitude-quantized random noise contaminated unknown signal sample, deriving conditional probability density function of combined output error and signal confidence interval
12 p1880 A71-27157
- Correlation function of modulation of radar sounding signals with nonwhite nonstationary Gaussian noise, obtaining target range and velocity maximum likelihood estimates
12 p1882 A71-27166

Output autocorrelation functions of zero memory nonlinear devices excited by signal plus Gaussian noise and interference

13 p2039 A71-28869

Coding for feedback communication system with additive white Gaussian noise, using mean-square estimation error

13 p2034 A71-29379

Heuristic signal design for digital communication over fast-fading Gaussian channels, stressing nonorthogonal signaling schemes

14 p2193 A71-30010

Optimal correlating detector of fluctuating two frequency radar signals in unknown random noise

14 p2195 A71-30112

Variances and covariances calculation for fluctuating numbers of semiconductor conduction electrons in terms of noise

14 p2211 A71-30292

Stochastic signal optimum linear estimation in multiplicative and measurement noises, deriving algorithms

14 p2197 A71-30794

Book on detection of signals in noise covering statistical theory principles and applications in digital communications, radar and sonar

15 p2369 A71-31507

Bayesian estimate of signal parameters in random noise background under mutually exclusive hypotheses about statistical properties

15 p2370 A71-31584

Weak signal detection in additive mixture of non-Gaussian random-correlated noise, deriving algorithms for discrete- and continuous-time and coherent detection problems

15 p2370 A71-31590

Book on detection, estimation and modulation theory, Part 3, Gaussian and radar-sonar signals in noise, covering point targets, random process and scatter channels

15 p2371 A71-31841

LF white Gaussian noise generator with continuously variable output, describing transistorized circuitry and output characteristics

15 p2371 A71-31851

Weak harmonic signal detection in narrow band Gaussian noise, using statistical algorithm

15 p2371 A71-32187

Plasma induced random noise and striation oscillations in carbon dioxide lasers as function of operational parameters

15 p2423 A71-32608

Optimal discrete time detection of radar signal parameters in nonGaussian correlated and noncorrelated noise, using Markov model

15 p2373 A71-32619

Signals detection of known form and unknown energy in Gaussian noise of unknown level, applying concept of invariance in hypothesis testing

16 p2541 A71-32820

Error probability and reception stability in synchronous detection of phase manipulated signals with additive Gaussian noise at multiplied carrier frequency

16 p2542 A71-33498

Multidimensional control system transmission matrix optimization in presence of random signals and noise

16 p2550 A71-33717

Bandlimiting effects on coherent detection of PSK, ASK and FSK signals in presence of white Gaussian noise, using SNR as performance criterion

17 p2704 A71-35085

German monograph on nonlinear distortion correction of binary bipolar signals in Gaussian noise covering receiver, decision theory and error probabilities

18 p2874 A71-35959

Random noise effects on oscillator short term frequency stability and velocity measurement by Doppler effect

18 p2879 A71-36531

Probability error calculation for digital signals contaminated by intersymbol interference and additive Gaussian noise

19 p3015 A71-37222

Output correlation functions of periodic signals limiting in random noise passing through zero memory devices, using Hermite polynomials method

20 p3195 A71-38857

Recursive algorithms for detection probabilities of fluctuating targets in Gaussian noise, including cell averaging constant false alarm rate (CFAR) extension

20 p3195 A71-38860

Noise variance maximum likelihood estimate based on order statistics for first order Reed-Muller code transmission over zero-mean white Gaussian noise channel

20 p3202 A71-38875

Gaussian and Poisson noise and SNR effects on subjective image quality rating, using transparency aerial scenes

20 p3235 A71-39190

Dual stochastic relations of optimal control and minimal error observation under random noise, using programming method

21 p3361 A71-41136

Statistical methods for calculating cross correlation function integrals of input and output coordinates of automatic control system in presence of random noise at input

22 p3525 A71-41437

Error probability during diversity reception under random radio noise

22 p3510 A71-42253

SNR of harmonic signal mixed with narrow band Gaussian noise, measuring correlation coefficients

22 p3510 A71-42255

Algorithms for optimal detection of weak determinate signal on background of Markov process approximated non-Gaussian noise

22 p3515 A71-42760

Algorithms for discrete message signal reception in background non-Gaussian additive noise with unknown statistical characteristics

23 p3647 A71-44321

Linear system under state dependent random noise, obtaining optimal steady control

24 p3814 A71-44684

RANDOM NUMBERS

Random numbers generation from natural random phenomena, discussing advantages, circuit and sampling rate

07 p1067 A71-18734

Time dependent dispersion simulation by random number generator, introducing horizontal and vertical shear, buoyancy and anisotropic turbulence

09 p1488 A71-23027

System design and optimization computer subroutines based on biological mutation and selection principles, using random number generator

11 p1734 A71-25639

Digital generation algorithm for random number sequences with specified autocorrelation and probability density function, illustrating computation accuracy and versatility

17 p2719 A71-34745

Aerial cameras performance prediction by computer simulation technique with random number generation

18 p2917 A71-36069

Stochastic linear systems stability with random processes coefficients, using differential equations

24 p3815 A71-44698

Summation theory of random number of independent random variables relation to queueing and reliability theories

24 p3843 A71-44873

RANDOM PROCESSES

NT RANDOM WALK

Limit theorems for spacewise inhomogeneous random walks on straight line with Markov chain transition probabilities

01 p0110 A71-10099

Nonlinear automatic control systems steady random processes approximate analysis by integral linearization of functions and operators

01 p0058 A71-10100

Computerized optimization of nonlinear dynamic control system subjected to random disturbances, using Monte Carlo method for quality functional

01 p0058 A71-10426

Quantum diffusion in scattering medium with absorption as sequence of random events

02 p0311 A71-12354

Soviet book on random functions theory in gravimetric observations over water covering ship dynamics, meter design, instrument damping, optimal linear filtering, etc

02 p0254 A71-12841

Controller characteristic adaptive control by disturbance of plant operation under random nonmanipulated action, considering cognitive system as Markovian automation-nature game

03 p0389 A71-13516

Narrow band random processes statistical characteristic relationship derived from upper and lower envelopes

03 p0452 A71-14390

Nonlinear control systems optimization methods formulation according to deterministic and random disturbances and initial conditions

03 p0391 A71-14402

Lunar seismic waves scattering as two dimensional random walk process, taking crust and rock compositions into account

04 p0650 A71-15544

Flexible bar as spatial filter for measuring wave number-frequency spectra of distributed random processes

05 p0822 A71-16405

Randomly used shared communication channels capacity, calculating probability function dependence on frequency assignment policy

05 p0721 A71-16467

Atmospheric turbulence steady random process correlation function, spectral density and probability distribution based on aircraft measurements

07 p1150 A71-18797

Random gain statistics of avalanche diode optical detectors, analyzing simple optical binary receivers

07 p1074 A71-19216

Multivariate and multidimensional random processes simulation with specified cross spectral density, applying to nonlinear structural vibration analysis

07 p1161 A71-19963

Soviet book on limit theorems for random walks covering random walk functionals, zero mean value, finite dispersion, sequences, normalized sums, Markov functionals, etc

07 p1148 A71-20300

Dominant diagrams of renormalization method in coherent random wave propagation

07 p1065 A71-20322

Multimass system oscillations due to viscous friction factor and kinematic random disturbances, considering dynamic behavior of wheeled vehicle on rough roadbed

07 p1162 A71-20469

Periodic nonstationary random process spectral representation derivation by applying Loeve harmonizability theorem

08 p1334 A71-21298

First order digital phase locked loops analysis for single channel command system, using random walk techniques

08 p1270 A71-21351

Random solution of stochastic integral equation of tagged point in continuous turbulent flow

08 p1276 A71-21357

Book on probability theory and applications covering stable distributions, renewal theory, large numbers laws, central limit theorem, Markov processes, random walks, etc

08 p1325 A71-21655

Nonlinear approximation for coherent Green function behavior in randomly fluctuating, unbounded and statistically homogeneous medium, emphasizing large scale fluctuations

08 p1325 A71-21883

Cylindrical shell dynamic response to random acoustic excitation within narrow frequency band of low modal density

09 p1534 A71-22082

Complex automatic systems with random switch-off, developing failure sequence models

09 p1422 A71-22119

Nonstationary colored noise linear shaping filter to transform white noise into nonstationary random process with specified covariance function

09 p1424 A71-23100

Electromagnetic wave propagation in anisotropic ionospheric plasma with time-varying random electron density irregularities

09 p1506 A71-23586

Soviet book on reliability and efficiency prediction of radio electronic devices covering a priori and posteriori random quality indices, mathematical and physical models and applications

10 p1582 A71-23900

Phi movement/pure motion/perception between successively presented, granular, moving objects, dichoptic and random dot Julesz patterns

10 p1567 A71-23987

Aircraft motion and traffic control at air corridors intersections for minimum flight schedule deviation under random disturbance due to weather, using statistical simulation

10 p1639 A71-24158

Continuous identification algorithm for system containing two delays for signal represented by stationary random process with autocorrelation function approximation

10 p1585 A71-24160

Peak structural response to nonstationary random excitations, approximating by Weibull distribution and Monte Carlo technique

11 p1843 A71-25326

Parameter optimization in linear control systems subject to random disturbances, using hybrid computer

11 p1735 A71-25840

Phase and log amplitude spectral and angular covariance of scintillation for propagation of two differing plane waves in randomly inhomogeneous medium

11 p1800 A71-26297

Computer aided statistical analysis of irregular quasi-optical transmission lines containing random inhomogeneities

11 p1733 A71-26347

Scattering matrix of stripline segment with random change in width of inner strip conductor

11 p1733 A71-26350

Convergence of identification scheme for scalar-input-scalar-output linear systems with random inputs, applying invariant set theorem for random systems

11 p1792 A71-26412

Signals as information carriers, comparing bounded spectrum carrier model, Gabor model, analytical signal model, steady random process model with bounded spectrum and Rice-Bunimovich model

11 p1734 A71-26463

Direct digital control system for random excitation environmental testing, discussing interfacing of TIME/DATA time series processor and minicomputer 11 p1736 A71-26500

Optimal stabilization system synthesis for multidimensional linear control plant in presence of random perturbation 12 p1892 A71-27176

E and F region irregularities random movements over Waltair, India, during IQSY, obtaining diurnal and seasonal variations 13 p2056 A71-27931

Verification, control and forecasting information characteristics for random process mixed with additive noise 13 p2041 A71-27942

Fiberglass reinforced plastics under constant strain rate, deriving failure models as random process for microscopic crack propagation 13 p2148 A71-28115

Statistical analysis of random oscillations excited in electron beam-plasma system based on signal recording data 13 p2106 A71-28364

Random radio signals distributions properties with parameters subject to random variation 13 p2029 A71-28371

Semiconductor random access memory components, discussing LSI circuits developments for RAM applications cost effectiveness in computer main-frame memories 13 p2035 A71-28772

Gaussian processes discrimination, considering correlation functions in integral control of nonlinear filter for image recognition 13 p2039 A71-28917

Oscillations in system of nonlinear cubic response with narrow-band random excitation, using statistical linearization 13 p2101 A71-29077

Stationary Gaussian Markovian form randomly fluctuating pressure gradient effects on steady incompressible channel flow velocity 14 p2223 A71-29924

Complex automatic systems with random switch-off, developing failure sequence models 14 p2220 A71-29997

Random ergodic process extremal behavior, determining mean time to reach original maximum or minimum 14 p2194 A71-30087

Velocity-aided Kalman filtering for one dimensional motion under random acceleration, obtaining steady state solution and transit time 14 p2197 A71-30793

Random time variation in sound radiation far field of point sources in subsonic circular rotational motion 15 p2450 A71-32129

PAM data transmission systems timing recovery, discussing maximum likelihood estimation method for timing parameter from random data 15 p2377 A71-32314

Structural dynamic responses as nonstationary narrow band random process, establishing peak values distribution functions with frequency interpretation 15 p2510 A71-32515

Random images transmission rates, comparing line-by-line and two dimensional encoding 16 p2541 A71-32819

Two-parameter statistical theory of material fatigue, considering random and ordered structural nonuniformities in space distributions 16 p2647 A71-32823

Numerical evaluation for individual samples of random processes obtained from nonstationary engineering experiments 16 p2602 A71-33341

Transition probabilities of random processes with rapid variability, using continuous Markov smoothing under Fokker-Planck equation 16 p2612 A71-33520

Kolmogoroff differential equations for probabilities of system states, showing validity for Markovian random processes and processes with aftereffects 16 p2603 A71-33891

HF amplifier statistical gain fluctuations effect on Dicke radiometer sensitivity, using Davenport-Root theory of random processes 16 p2548 A71-34132

Differentiable random processes, deriving approximate determination of correlation functions 17 p2777 A71-34348

Limits theorems of occupancy problem, concerning asymptotic behavior of random particle distribution to fixed cell with equal probabilities 17 p2764 A71-34574

Optimal structure and parameter adaptive estimation for continuous and discrete data Gaussian process models with linear dynamics 17 p2719 A71-34739

Linear unbiased estimates of mathematical expectation of random process optimal in sense of norm of symmetrical Banach space 17 p2765 A71-34861

Limited spectrum random processes interpolation, considering unequivocal recovery from values in infinite sequence of equidistant moments of time 17 p2765 A71-34862

Optimal extrapolation and filtration for class of random processes, considering functionals of solutions of stochastic differential equations 17 p2765 A71-34863

Fatigue life prediction for structure undergoing random steady Gaussian centered process, determining statistics of absolute maximums 17 p2832 A71-35471

Kinematic-dynamo theory with turbulent diffusivity effect, discussing resistivity as random function of position 18 p2969 A71-37045

Time optimal control for distributed systems with random properties, considering integral relations and flying wing vehicle torsional vibration problems 19 p2994 A71-37094

Recurrent procedure for probability characteristics analysis of stationary random process, using density functions and Euler equations 19 p3085 A71-37146

Jump phenomena of nonlinear control systems subjected to nonstationary Gaussian random inputs, using statistical linearization method 19 p3036 A71-37236

Economically optimal operation of circuits protecting object subject to stationary random process, determining object malfunction intensity 19 p3025 A71-37572

Binary systems formation probability during triple encounters, considering random initial conditions 20 p3290 A71-39301

Accuracy in maximum likelihood estimate for correlation function parameter of random process in signal reception on normal noise background 20 p3199 A71-39816

Self referencing holographic system for image compensation in fluctuating random medium, describing homodyning procedure 21 p3382 A71-40935

Stochastic optimal control of discrete processes with random disturbances 21 p3361 A71-41139

Random analogs of boundary value problems class for biharmonic functions, demonstrating unique solution existence 21 p3410 A71-41189

Book on dynamic programming application to optimal control covering discrete random processes, continuous deterministic and stochastic processes, etc 22 p3567 A71-42428

Digital computer simulation of random disturbances with uniform distribution, determining generated sequence correlation coefficient mean and variance 22 p3518 A71-42492

Random parietal environment representation by homogeneous distribution of independent sources, using boundary layer model [ONERA-TP-933] 22 p3576 A71-42500

Probabilistic system observation at random times, calculating Markov renewal processes optimal long run control 22 p3527 A71-42628

Smoothed randomized functionals and algorithms in adaptation and learning theory, accounting for constraints by generalized penalty function method 23 p3657 A71-44018

Reduced error spectral power density calculations for random processes with digital spectral analyzers 23 p3681 A71-44320

Statistical optimization of spherical gyroscope regarded as servocontrol system under random perturbation, using measured values of relative angles between sphere and inner gimbal 24 p3825 A71-44691

Linear systems with randomly varying parameters, deriving stability conditions from one dimensional distribution functions 24 p3815 A71-44699

Two rotor gyrocompass with random parameter excitation, calculating angular velocity random variation effects on drift 24 p3825 A71-44700

Random processes overshoots, determining probability distributions of overshoot duration and time of first attainment of given level for random sequences 24 p3815 A71-44703

Unsteady random processes structural analysis application to nonlinear dynamic systems, evaluating algorithms effectiveness and improvement by self adaptive operators with finite memory 24 p3815 A71-44705

Vibrational systems stability in presence of time dependent random parametric disturbances, using frequency analysis methods 24 p3848 A71-44851

RANDOM SAMPLING

On-off keying system digital detection using random sampling for achieving high bit rates 05 p0725 A71-17073

Random numbers generation from natural random phenomena, discussing advantages, circuit and sampling rate 07 p1067 A71-18734

Exact confidence intervals for probability and sampling quantiles of random quantity from beta distribution law 07 p2763 A71-34302

RANDOM SIGNALS

Optimal detection of narrow band signal with random phase and arrival time in radar or sonar, using nonlinear adaptive filter 02 p0211 A71-11720

Sampling and averaging techniques in fast random signal analysis using oscilloscope and memory unit 03 p0379 A71-13911

Optimal detector parameters for stochastic signals in noise, discussing analytic and simulation studies of adaptive techniques of pattern recognition 08 p1259 A71-21594

Adaptive control systems state variables and nonstationary parameters estimation in presence of random disturbance and measurement noise, using nonlinear filtering theory 09 p1423 A71-22612

Correlation estimates and optimal detector for incomplete a priori information signal reception on random and white noise background 10 p1579 A71-24878

Q factor of control systems as mathematical expectation of functional on input signal set with prescribed probabilistic measure and random initial conditions 10 p1588 A71-24904

Adaptive control systems probability characteristics in presence of random inputs, discussing improvements by coefficients and interpolation methods 12 p1891 A71-26727

Optimal receiver to detect multiple orthogonal signals on normal stationary noise background, assuming nonuniform a priori probability occurrence 12 p1883 A71-27618

Mathematical model for harmonic emission spectrum in FM and PM communication transmitters modulated by random signal 13 p2032 A71-28875

Continuous observation of resolvable signal random flows 13 p2033 A71-28916

Quality functional analysis for self adaptive filtration of random signal sequences 13 p2040 A71-28919

Nonlinear filtering synthesis of optimal receiver for pseudorandom phase shift keyed signal with arbitrary modulation angle and white noise background 14 p2195 A71-30107

Gaussian input signal nonlinear sampled data systems analysis using linear components and transfer function 14 p2220 A71-30800

Meteorologic bistatic radar equation for randomly distributed targets, applying to raindrops, refractivity perturbations, etc 14 p2197 A71-30830

Random turbulent signals from hot wires across pipe flow, studying form, skewness and flatness factors 15 p2391 A71-32108

Multidimensional control system transmission matrix optimization in presence of random signals and noise 16 p2550 A71-33717

Microfield double probe for plasma density and electron temperature determination, studying random signals crossed spectrum 17 p2789 A71-35350

Random access signaling system application to aircraft control, discussing signal redundancy requirement for access capability optimization based on radio environment model 17 p2747 A71-35783

Random aperiodic signals analysis, using two dimensional Fourier transforms 17 p2709 A71-35790

Distance measurement system with onboard transponder, discussing subcarrier and pseudorandom code signal techniques synthesis 18 p2879 A71-36532

Traffic capacity of systems for search and analysis of radio signals with random duration 19 p3015 A71-37258

Stochastic passband model of tropospheric communications channel, denoting random frequency duration above threshold level 19 p3022 A71-38501

Two phase flow speed transit time measurements by correlation methods with randomly fluctuating signals, noting use in small bore tubes and strip steel production 19 p3067 A71-38658

Probability functional formulas for quasi-determinate signal on unsteady normal noise background for use in false alarm and correct detection 20 p3199 A71-39815

RANDOM VARIABLES

Joint phase locked and delay tracking system dynamics for pseudorandom radio signal detection 23 p3646 A71-44267

Probabilistic analysis of random pulse signal gating on time selective zero lag converter with rectangular pulse input 23 p3647 A71-44322

Spatially distributed systems with random parameters, determining random output signals statistical moments 24 p3813 A71-44678

Optimal dynamic accuracy of control systems with random signals and parameter oscillations, using sensitivity theory 24 p3815 A71-44697

Ocean surface wave height /sea state/ measurement by high resolution random-signal radar based on model characterized by Poisson distributed scatterer density function 24 p3823 A71-45082

RANDOM VARIABLES

Straight line approximation of random two dimensional discrete set containing large measurement errors, comparing to least squares results 02 p0304 A71-11902

Linear ordinary differential equations system with random coefficients, proving mean stability theorem 03 p0450 A71-13119

Random parameter plant control, considering recursion formulas, optimal strategy and computerized simulation 03 p0391 A71-14379

Random graphs probabilistic characteristics, deriving algorithms for graph connectivity probability estimation 05 p0731 A71-16795

Photoelectron count of logarithmically fading optical signal, discussing noncentral chi square random variable approximation 05 p0726 A71-17085

Scalar Gaussian channel information optimal input capacity as function of random variable, assuming finite number of values for amplitude and variance constraints 11 p1730 A71-25374

Hybrid computer Monte Carlo technique for simulation and optimization of system with random parameters 11 p1735 A71-25843

Algorithm for nonparametric estimation of random parameters of general exponential family of unknown density distributions, investigating empirical estimates convergence to Bayes optimal estimates 12 p1892 A71-27022

Straight line approximation of random two dimensional discrete set containing large measurement errors, comparing to least squares results 13 p2133 A71-28189

Optimal control systems design with random parameters and initial state, considering open loop and feedback correction terms 13 p2042 A71-28708

Seasonal, irregular and long term earth rotation rate variations 14 p2310 A71-30198

German book on problems, mathematical foundations and investigation methods of technical reliability covering Boole model, random variables, distribution functions, failure rates, etc 16 p2583 A71-33524

Algorithm for nonparametric estimation of random parameters of general exponential family of unknown density distributions, investigating empirical estimates convergence to Bayes optimal estimates 19 p3038 A71-37691

Turbulent hydrodynamic line stretching problem, considering asymptotic rates as application of central limit theorem for dependent random variables sums 19 p3044 A71-37729

Frequency domain stability criteria for dynamical systems with random parameters, considering open loop stability, stochastic gain element rms value and linear element effective bandwidth 19 p3039 A71-38710

Canonical approximation of state correlation matrix and threshold crossings of variable systems with random turbulence type input vectors representing flight environment 21 p3408 A71-40614

Material random temperature and imperfection density effects on 3-bar truss nonlinear steady creep solutions for stress and velocity 22 p3615 A71-42211

Spatially distributed systems with random parameters, determining random output signals statistical moments 24 p3813 A71-44678

Parameters steady random variations effect on linear and nonlinear systems steady motion characteristics, using integral equation and averaging methods 24 p3815 A71-44696

Summation theory of random number of independent random variables relation to queueing and reliability theories 24 p3843 A71-44873

Pseudomoments estimation of convergence rate in central limit theorem for random variables series 24 p3843 A71-44874

RANDOM VIBRATION

Power gyrostabilizer optimal controlling section with random base frame oscillations, solving filtration problem as function of platform structure by Wiener method 01 p0079 A71-10427

Forced random oscillations of nonholonomic systems about equilibrium positions, deriving stability conditions in white noise disturbances 01 p0176 A71-11042

Book on mechanical vibration and shock measurements covering periodic and random vibrations characteristics, instrumentation, control, etc 02 p0251 A71-12175

Random vibrations nonlinear effects on gas bearing pendulous-integrating gyroscopic accelerometer response, using digital simulation 02 p0252 A71-12454

Covering plate steady state response to acoustic vibrations in viscoelastic half space, calculating interface displacement frequency spectra under zero shear stress assumption 03 p0459 A71-13719

Aircraft fuselage internal noise and structural frequency response due to random excitation, using transfer matrix analysis [ASME PAPER 70-WA/DE-9] 03 p0348 A71-14143

Fluid-loaded rectangular plates and membranes random vibration excitation by turbulent boundary layer flow [ASME PAPER 70-WA/DE-15] 03 p0511 A71-14147

First passage failure probabilities for single degree of freedom systems under random vibration [ASME PAPER 70-WA/APM-14] 03 p0512 A71-14155

Body position effect on dynamic characteristics of human operator under random vibration, considering pelvis-head amplitude-frequency characteristics 04 p0543 A71-14791

Mechanical oscillator mean square response to non-stationary random excitation 04 p0669 A71-15200

Null shift errors of compensated electromechanical pendulum accelerometers during random vibration of base 07 p1108 A71-19308

Stability, stationarity and amplitude damping of random parametric vibration system, using nonlinear differential equations 07 p1147 A71-19591

Coupling loss factor estimation, using wave transmission or natural frequency shift methods in statistical energy analysis 07 p1161 A71-19962

Rotor blade random vibrations in response to turbulence [AIAA PAPER 70-548] 09 p1381 A71-22081

Rumanian book on nonlinear and random vibrations covering dissipative and conservative nonlinear mechanical systems, deterministic excitation and applications of mathematics 09 p1543 A71-23619

Transverse spatial particle diffusion in plasma under random oscillations, examining interaction between collisionless plasma and longitudinal wave 10 p1649 A71-24318

Cylindrical panel vibration in supersonic flow under random effects, calculating stress-strain statistical properties as function of incident flow velocity 10 p1690 A71-24572

Random vibrations of statistically inhomogeneous elastic systems, using perturbation method 10 p1691 A71-24644

Buckled rectangular panels response to random excitation via single degree of freedom nonlinear vibration equation 11 p1841 A71-25196

Nonstationary random analysis of flight vehicle response to atmospheric turbulence, using Priestley evolutionary spectral method 11 p1836 A71-25320

Power spectral density analysis of aircraft structural response to taxiing produced random vibrations involving landing gear orifice damping and Coulomb friction 11 p1708 A71-26311

Two-shaker single input sinusoidal and random vibration tests, considering Hunter-Helmuth solution with constant cross coupling compensation in frequency band 11 p1745 A71-26491

Random vibration laboratory equalization by multiple taping of noise signals on recorder and manual processing 11 p1746 A71-26513

Automatic equalizer-analyzer system for random or shock vibration testing, including narrow-band

equalization, simplified display techniques and self-calibrating procedures 11 p1747 A71-26514

Asymptotic methods and Markov processes theory extension to unsteady vibration of nonlinear systems with slowly varying parameters and random perturbation 12 p1930 A71-27173

Deterministic and random nonlinear forced vibrations of one degree of freedom system with broken line elastic response 14 p2328 A71-30378

Pin-ended column stability and random behavior under white noise excitation, using analog simulation and application to vertical earthquake and aerospace vibration environments 14 p2330 A71-30683

Integrally stiffened five bay panel, calculating free vibration and random response to jet noise excitation [AIAA PAPER 71-585] 15 p2504 A71-31532

Probability theory of stresses during random vibrations of flat panel in acoustic field of jet engine exhaust 15 p2504 A71-31704

Automatic system for random vibration spectra control, consisting of spectrum shaper/analyzer and multidimensional controller 15 p2379 A71-31845

Mathematical model of multidimensional system stability for random vibration spectra control, including white noise generators, spectrum shaper/analyzer and summator 15 p2380 A71-31847

Man machine system dynamic properties and biomechanical model concepts, determining random vibration effects on sitting and working human body 15 p2366 A71-32728

Stationary narrow band Gaussian vibration excursion probability based on Markov point process [ASME PAPER 71-APM-19] 16 p2655 A71-33210

Cylindrical shells partially filled with liquid, calculating forced vibration under random loads and deterministic internal pressure 17 p2817 A71-34333

Two mirror Cassegrain antenna secondary reflector random fluctuations effects on drift in main lobe direction 17 p2713 A71-34397

Uniaxial gyroscopic stabilizer errors in presence of base random vibration, taking into account dry friction forces in bearings 17 p2738 A71-34560

Blower suction line random vibrations due to distributed random pressure, investigating various isolation arrangements for vibration reduction 20 p3308 A71-39085

Broadband random vibration simulation of force environment action on multimode structure [ASME PAPER 71-VIBR-2] 21 p3362 A71-40266

Random vibration testing digital computer control system and experiment design, considering discrete Fourier transform techniques application [ASME PAPER 71-VIBR-30] 21 p3360 A71-40285

Nonlinear Volterra integral equation system solution using almost periodic forced oscillations 21 p3409 A71-41081

Material fatigue failure under narrow band random vibration effects, deriving fatigue life prediction equation based on composite experimental design and statistical tests 22 p3615 A71-42002

Statistical approach to complex structural vibration under random excitation 23 p3775 A71-43214

Man machine system dynamic properties and biomechanical model concepts, determining random vibration effects on sitting and working human body 23 p3639 A71-43299

Point source average signal reflection from conductive plane in random oscillation 23 p3654 A71-44163

RANDOM WALK

Cosmic rays compound diffusion, considering combined effects of one dimensional diffusion along interstellar magnetic field lines and field lines three dimensional random walk 14 p2301 A71-30434

Random walk theory applied to electron motion in early stage of He breakdown in electric field, based on integral and differential cross section data 15 p2452 A71-31921

RANEY NICKEL

U CATALYSTS

U NICKEL

RANGE

Flight range and optimum angle of attack under wind conditions of constant velocity and direction, considering fuel consumption for given distance 06 p0847 A71-18325

RANGE (EXTREMES)

NT FREQUENCY RANGES

NT OCTAVES

NT PROPORTIONAL LIMIT

NT RADIO RANGE

NT ROCHE LIMIT

Nuclear reactor kinetic differential equations, ascertaining positive bounded solutions existence 01 p0126 A71-11290

Successive approximations of order K iterative methods for calculating inverse matrix, yielding lower and upper bounds 03 p0449 A71-13111

Narrow band random processes statistical characteristic relationship derived from upper and lower envelopes 03 p0452 A71-14390

Limiting bounds determination for existence of periodic orbits near known existing periodic orbit, presenting linear perturbation analysis 04 p0654 A71-15717

Stability loss of cylindrical shell at upper bound of buckling load under axial compression 06 p0983 A71-17365

Limiting analysis for upper estimate of carrying capacity of shell of revolution under load concentrated at center, evaluating stability loss 06 p0987 A71-17771

Swan band intensity upper limits in spectrum of 18 September 1966 sunspot 06 p0967 A71-17907

Natural frequency bounds for clamped beam with linearly varying compressive load and constant end load by Rayleigh-Ritz, Bazley-Fox second projection and Kato methods 08 p1368 A71-20806

Nonlinear control systems absolute stability range in parameter space 09 p1422 A71-22121

Extremal experiment planning for optimal search, defining intuitive acceptance of solutions during non-formal stages 12 p1988 A71-26710

Criterion on types of extrema of singular solutions of conditional equations in calculus of variations from Euler function behavior with respect to integration path 13 p2096 A71-29322

Nonlinear control systems absolute stability range in parameter space, using system of inequalities 14 p2220 A71-29999

Cosmological upper limit on gravitational constant time variation, extending Dicke theoretical bound to pressure filled cosmologies in flat space 17 p2801 A71-34651

German monograph on characteristics and upper and lower bound methods in plastic layer theory, deriving static and kinematic equations 17 p2748 A71-34798

Bounded integral manifolds existence for perturbed system of nonlinear differential equations near critical point, periodic orbit or periodic surface 17 p2769 A71-35795

Lower bound on distance between vertical asymptotes of second order differential equations solutions involving integral inequality 18 p2941 A71-36227

Error bounds and variational principles for nonlinear differential and integral equations, exemplifying by Liouville and Poisson-Boltzmann equations 20 p3255 A71-39496

Variational principle for obtaining upper and lower bounds on minimum drag on body of given volume in slow viscous flow 20 p3177 A71-39500

Pointwise bounds in Cauchy problem for fourth order quasi-linear equation using a priori inequality, applying Rayleigh-Ritz technique to elliptic partial differential equations 20 p3255 A71-39573

Gravitational and other forces involved in equilibrium of growing plants, showing gravity sensing ability lower limit existence 21 p3339 A71-39971

Limiting He 3 abundances in four H II regions 21 p3448 A71-40449

Photon mass terrestrial and extraterrestrial limit measurements, discussing speed of light frequency dependence, Coulomb law analog in magnetostatics energy conservation, etc 21 p3418 A71-40674

Eigenvalues lower bounds determination for arbitrary shape region, presenting domain constriction method 21 p3416 A71-41014

Constructive existence theorem for nonlinear elliptic equation with restricted bounded domain 21 p3409 A71-41078

Temperature and frequency dependence of electron phonon interaction maxima in rhenium, explaining transverse and longitudinal waves ultrasonic attenuation by two band theory 22 p3578 A71-42597

Boundedness theorem for Volterra equations, discussing applications 22 p3568 A71-42698

Optimal strategies in search of function global maximum 24 p3843 A71-44770

RANGE AND RANGE RATE TRACKING

Range and range rate measurement errors between ground station and artificial satellite, investigating atmospheric refraction effects 04 p0661 A71-15003

Correlation function of modulation of radar sounding signals with nonwhite nonstationary Gaussian noise, obtaining target range and velocity maximum likelihood estimates 12 p1882 A71-27616

Signals single set synthesis for simultaneous target information transmission and range and velocity measurement 12 p1883 A71-27617

Range and range rate measuring equipment for PCM-TDMA satellite communications system data feed and orbit observation 18 p2879 A71-36533

Apollo range instrumentation aircraft, describing C-135A modification with airborne lightweight optical tracking systems 19 p3022 A71-38546

Radar resolution performance for targets with range acceleration, determining matched filter or correlation radar effects 20 p3195 A71-38868

Estimation error covariance matrices of linearized Kalman tracker for ballistic reentering missiles, observing strong coupling of range and range rate with ballistic coefficient 23 p3646 A71-44083

RANGE CONTROL
U TRAJECTORY CONTROL

RANGE ERRORS

Rocket free flight ascent trajectory range error, approximating influence of stabilizers, nose cone and components misalignment along longitudinal axis 04 p0601 A71-14596

Coherent optical system for range and azimuth ambiguity simulation in radar systems 04 p0551 A71-15010

Tropospheric range error in EM signal arriving at earth zenith, measuring integral of refractivity through atmosphere from height, pressure, temperature and humidity 16 p2569 A71-33800

Analytic solution to range deviations along descending branch of free flight trajectory of ballistic vehicle in planetary atmosphere 24 p3872 A71-45015

RANGE FINDERS

NT LASER RANGE FINDERS

NT OPTICAL RANGE FINDERS

Noise effects on characteristics of automatic radar rangefinder with logarithmic receiver, showing discrimination curve deformation with increasing SNR 09 p1415 A71-22297

Model 6A geodimeter /photometric range finders/ laboratory and field tests 15 p2405 A71-31466

HEOS A-1 satellite telecommunication system, describing command, telemetry and ranging subsystems 18 p2875 A71-35984

Injection laser range finder with avalanche photodiode for Mars rover obstacle sensing, discussing range data processing methods 22 p3529 A71-42772

Range finder receiver based on Si avalanche detector coupled to tunnel diode circuit, with automatic gain control through tunnel diode bias control 23 p3677 A71-43518

RANGE INDICATORS
U INDICATING INSTRUMENTS

RANGE FINDERS

RANGE MEASUREMENT

U RANGEFINDING

RANGE SAFETY

Environmental controls, health services and safety programs for outdoor range laser applications, considering USAF hazard regulations, public address system, etc 17 p2723 A71-34524

Launch facility requirements for liquid fluorine upper stage, considering propellant storage and transfer, vapor disposal, leak detection, spills, aborts and range safety 18 p2898 A71-36457

RANGEFINDING

NT AIRBORNE RANGE AND ORBIT DETERMINATION

Geometric satellite geodesy, discussing simultaneous ranging from tracking station network 03 p0418 A71-14207

Lunar ephemeris for nanosecond resolution laser ranging systems by literal and numerical integration techniques 05 p0811 A71-16682

[JPL-TR-32-1517] Transionospheric ranging error correction by second difference of phase shift method 06 p0867 A71-17714

Navigation and communication experiment at L band on board S.S. Manhattan using ATS-5 satellite

with biphasic PSK modulation of three tones for ranging 07 p1057 A71-18816

X band radar system to compare electrical lengths in 100 m range with 10 to minus 6 accuracy, noting applications in geodetic and radio waves phase fluctuation measurements 07 p1075 A71-19345

Laser applications in physics research, discussing nonlinear optics and spectroscopy, time and distance measurements and Raman and Rayleigh light scattering 09 p1462 A71-22585

Satellite based position fixing data by ranging techniques, discussing application to navigation and ATC 18 p2945 A71-36493

RANGES (FACILITIES)
NT BALLISTIC RANGES
NT MISSILE RANGES
NT TEST RANGES

RANGING
U RANGEFINDING

RANKINE CYCLE

Reciprocating organic single cylinder Rankine cycle engine using thiophene working fluid 03 p0351 A71-13034

Natural gas organic Rankine cycle system for commercial on site electrical power generation and heating-cooling purposes 03 p0351 A71-13035

SNAP-8 mercury Rankine system performance data, investigating design change for reduced reactor operating temperatures 15 p2447 A71-32201

Helical induction boiler feed electromagnetic pump design, fabrication and testing for potassium Rankine cycle space power system 15 p2415 A71-32202

[GESP-455] Unalloyed tantalum as containment material in mercury Rankine cycle SNAP 8 system boiler for 5 year service life 15 p2448 A71-32221

Test facility and performance predictions for Rankine cycle power system components, including lithium heater, potassium boiler, condenser and preheater [GESP-451] 15 p2448 A71-32223

Rankine cycle turboelectric nuclear space power conversion system with liquid K as working fluid, discussing current technology status 16 p2526 A71-33525

Condensate removal devices for potassium vapor Rankine space power turbines to prevent blade erosion and efficiency degradation 20 p3262 A71-38918

Component performance of three loop Rankine cycle test rig using lithium, potassium and NaK-78 as working fluids 20 p3263 A71-38923

RANKINE TEMPERATURE SCALE
U TEMPERATURE SCALES

RANKINE-HUGONIOT RELATION

Alfven waves effect on MHD fast shock from numerical solution of extended Rankine-Hugoniot equations 10 p1667 A71-23798

Excess energy in fluid mechanics, breaking up equation into different orders by small perturbation approach and Rankine-Hugoniot shock relation 14 p2227 A71-30818

Low temperature shock waves in molecular hydrogen, discussing Rankine-Hugoniot equation behavior 16 p2555 A71-32895

Shock normal calculation by applying least squares technique to combined geomagnetic field and plasma data from single satellite, assuming Rankine-Hugoniot conservation relations 16 p2560 A71-33941

Boundary shock waves in electrically conducting gas under magnetic field, deriving Rankine-Hugoniot jump relations analogs and Prandtl relation 16 p2560 A71-34128

Shock wave data for Bame enstatite in 60-480 kb range, considering Hugoniot elastic limit and phase transition produced shock front 19 p3050 A71-37663

Two dimensional steady state detonation waves, obtaining generalized Rankine-Hugoniot equations 19 p3045 A71-38126

Collisionless shock waves downstream state, using Rankine-Hugoniot type relation model 19 p3117 A71-38650

RAPCON (CONTROL)
U RADAR APPROACH CONTROL

RAPID EYE MOVEMENT STATE

Rapid eye movements during nocturnal sleep of healthy human subjects, insomniacs and narcoleptics recorded on polygraphs 01 p0007 A71-10071

Heart rate variability in REM sleep, stage 4 sleep and wakeful state from ECG of normal males, calculating coefficient of temporal variability for each state 13 p2014 A71-29319

RAPID TRANSIT SYSTEMS

Human subjects REM sleep characteristics under 5-hydroxytryptophan influence, analyzing continuous polygraphic recordings of parietal EEG, horizontal eye movement and submental electromyographic activity

15 p2359 A71-13152
First and last rapid eye movement (REM) sleep differences in unrestrained chimpanzee

18 p2853 A71-35891
Oculomotor neural organization models, considering vestibular ocular reflex, saccadic eye movements and smooth pursuit systems

22 p3504 A71-42450

RAPID TRANSIT SYSTEMS

Sensing and communications technologies for short wayside headways, considering applicable equipment for personal rapid transit systems, modulation, coding and data transmission techniques

14 p2195 A71-30337

RARE EARTH ALLOYS

NT NEODYMIUM ALLOYS

Rare earth alloys spin disorder resistivity in crystal-line electric field absence and presence

04 p0637 A71-15797

Magnetic properties of sintered cobalt-rare earth alloy magnets using Sm, Pr, La or Ce misch metal for microwave device applications

14 p2284 A71-30703

Magnetic properties measurement of Co-rare earth permanent magnets, using Nb-Sn superconducting solenoid

14 p2284 A71-30704

Zinc and misch metal in Mg alloys, detailing rare earth metals distributions in various phases

16 p2594 A71-33714

Mechanical and crystallographic structure effect on cold brittleness temperature anisotropy and on ex-foliation of Cr alloyed with rare earth elements

17 p2755 A71-34416

RARE EARTH COMPOUNDS

NT CERIUM COMPOUNDS

NT EUROPIUM COMPOUNDS

NT SCANDIUM COMPOUNDS

NT SCANDIUM OXIDES

Rare earth polycrystalline powders luminescence stimulation by ruby laser radiation, discussing two photon mechanism, luminous intensities relations and UV radiation

03 p0435 A71-13510

IR lattice spectra of rare earth stannate and titanate pyrochlores

07 p1054 A71-19484

Rare earth metals di- and sesqui-carbides physical characteristics, establishing changing properties patterns during phase transitions

15 p2461 A71-32153

RARE EARTH ELEMENTS

NT CERIUM

NT CERIUM ISOTOPES

NT CERIUM 140

NT DYSPROSIUM

NT ERBIUM

NT EUROPIUM

NT GADOLINIUM

NT HOLMIUM

NT LANTHANUM

NT LUTETIUM

NT NEODYMIUM

NT NEODYMIUM ISOTOPES

NT PRASEODYMIUM

NT PROMETHIUM

NT SAMARIUM

NT SCANDIUM ISOTOPES

NT TERBIUM

NT YTTRIUM

Rare earth element concentrations in zircons and apatites separated from dacites and granites, explaining partition coefficients between phenocrysts and groundmass by crystal structure

03 p0407 A71-13338

Apollo 12 lunar rock 12013 rare earth, alkaline and alkali metal and Sr 87/Sr 86 data, discussing light and dark component composition

03 p0494 A71-14221

Rare earth abundance in Apollo 12 basalts and soils and achondritic meteorites, using partial melting model

06 p0966 A71-17899

Interlocking via photoexcitations and deexcitations due to lanthanide rare earths weak line solar spectra and ion atomic structure

06 p0969 A71-17970

Rare earth based liquid lasers, describing spectroscopic and performance properties of neodymium ions in aprotic solvents

07 p1124 A71-19788

Fluorapatite single crystals absorption spectra and luminescent characteristics under activation by rare earth ions, noting line widening dependence on crystal composition

09 p1507 A71-22390

Photochromic calcium fluoride preparation by rare earth additive coloration techniques

09 p1509 A71-23120

Physical properties, structure and sintering of refractory oxides of rare earth elements and actinides, including chromia

09 p1478 A71-23399

Compressive creep behavior of yttria rare earth stabilized zirconia storage heater refractories, determining stress time to failure

09 p1484 A71-23686

Rare earth and heavy elements determination in olivine hypersthene and enstatite chondrites by spark source mass spectroscopy, noting Fe meteorite silicate inclusions composition

11 p1819 A71-25225

Magnetization discontinuities in cobalt-rare earth particles at discrete imperfection levels as function of chemical, mechanical and heat treatment, noting Co-Y rectangular loop

12 p1943 A71-26861

Reagents for photometric determination of rare earth elements of yttrium subgroup in binary mixtures with La or Ce

15 p2367 A71-31646

Lost City /Oklahoma/ chondrites, determining alkali, alkaline earth and rare earth element concentrations and Rb-Sr model age

15 p2489 A71-32355

Refractory and rare metals single crystals - Conference, Moscow, December 1968

16 p2594 A71-33876

Refractory and rare metals absolute melting temperature dependence on atomic number, lattice constant, charge negativity and crystallographic, thermodynamic and mechanical parameters

16 p2594 A71-33878

Al-Cu-Li-Mn and magnesium/rare-earth-element alloys heat resistance and microhardness, determining strengthening by intermetallics

16 p2597 A71-33926

Quantum counter action in various media including trivalent and divalent rare earth ions, Fe group transition metal ions, semiconductors and gases

18 p2930 A71-36145

Longitudinal and transverse magnetostriction of polycrystalline iron garnets containing Gd, Tb, Dy and Ho in high magnetic fields

21 p3428 A71-41116

Rare earth, alkali and alkaline earth elements content of phenocrysts and acidic igneous magma

23 p3734 A71-43246

Rare earth trace elements abundance of Apollo 14 lunar soil samples from Fra Mauro, comparing with chondrites

23 p3735 A71-43248

Mineralogy, chemistry and origin of KREEP /potassium, rare earth element and phosphorus/ component in Apollo 12 soil and breccia samples from Ocean of Storms

23 p3741 A71-43632

Apollo 12 lunar soils, rocks and core samples, determining rare earth, alkali and alkaline earth elements concentrations

23 p3747 A71-43676

Apollo 12 lunar rock rare earth element abundances, comparing to Icelandic basalt flow

23 p3750 A71-43694

Rare earth elements and trace elements abundance in Apollo 12 igneous rocks, breccia and lunar soil

23 p3750 A71-43695

RARE GASES

NT ARGON

NT ARGON ISOTOPES

NT HELIUM

NT HELIUM ATOMS

NT HELIUM ISOTOPES

NT LIQUID HELIUM

NT NEON

NT NEON ISOTOPES

NT RADON

NT RADON ISOTOPES

NT XENON

NT XENON ISOTOPES

NT XENON 133

Saha equilibrium deviations in wall stabilized rare gas arc plasmas under normal pressure, describing numerical method for temperature and density distributions evaluation

01 p0133 A71-10746

Pressurized inert gas metal arc welding of Al, determining voltage, filler metal speed and chamber pressure effects by multiple regression analysis

02 p0255 A71-11709

Heat transfer to walls of quartz discharge tube in Ne, Ar and Xe, measuring integral energy flux

02 p0290 A71-12191

Upper stratosphere and mesosphere concentrations of Ne, Ar, and Kr from rocket-borne cryogenic air sampler

02 p0246 A71-12701

Primordial trapped planetary noble gases and solar isotopic ratios in separated meteoritic minerals from Orgueil carbonaceous chondrite

02 p0318 A71-12901

Pitts iron meteorite exposure history, noting consistency of rare gases isotopes contents in separated metal phase with prehistoric radiation flux increase

03 p0487 A71-13334

Transonic flow equations for chemically inert gases binary mixture, considering diffusion effect on dissipative process

03 p0401 A71-13906

He, Ne, Ar and Xe from stepwise heating of Apollo 12 lunar rock 12013, discussing radiogenic and spallation components and He 3 and Ne 21 cosmic ray exposure ages

03 p0494 A71-14224

Ne, Ar, Kr and Xe ionized states transition and level lifetimes from photographically recorded beam foil spectra, discussing particle energies

04 p0629 A71-14805

Human alveolar-arterial oxygen pressure differences, investigating inert gas effects

04 p0540 A71-15576

Charged particles-noble gases interactions with resultant vacuum UV radiation, considering conservation of energy principle and Jesse effect

04 p0630 A71-15652

High pressure rare gas UV emission spectra, examining wavelength cut-offs and flux ratios

04 p0549 A71-15691

Inert gas welding of Al with He as oxidation inhibitor, discussing penetration, welding rate and cost compared to Ar use

04 p0604 A71-15815

Rare gases interaction with focused multimode Q switched laser beam, measuring orders of nonlinearity and multiphoton ionization probabilities

05 p0761 A71-16335

Operational characteristics, spectroscopy and inversion mechanisms of noble gas ion lasers in light of plasma theories and atomic data [AIAA PAPER 70-82]

05 p0763 A71-16551

Spacecraft cabin rare gas-oxygen atmosphere decompression effects on animal metabolic rates

06 p0853 A71-17956

Molybdenum disulfide treated graphite brushes in electric contact with copper slip rings at high rates in dry pure inert gas atmospheres

07 p1120 A71-20275

Nitrogen molecule collision with metastable inert gas atoms and ions, investigating energy exchange mechanism

08 p1337 A71-20670

Superheavy elements formation due to fast neutron capture during supernova outbursts, discussing meteorites fission produced noble gases

08 p1337 A71-20959

Cosmic ray spallation products and radiation age determination from spectral analysis of noble gas components in lunar rocks

11 p1829 A71-25837

Solar wind noble gas composition on moon with aluminum foil exposure, confirming absence of lunar atmosphere and magnetic field

11 p1834 A71-26330

Formaldehyde vapor photodecomposition modes by end product analysis, utilizing mixed isotope, radical scavenger, inert gas pressurization and lamp intensity attenuation

12 p1877 A71-27758

Energy dependence of integral scattering cross sections of noble gas atoms in carbon dioxide

13 p2102 A71-27809

Linear nonequilibrium shock tunnel driven supersonic MHD generator operation under large scale power extraction and strong electromagnetic-rare gas interactions

14 p2287 A71-29879

Performance tests of electron bombardment ion thruster, using xenon, krypton argon, neon, nitrogen, helium and carbon dioxide

14 p2287 A71-29922

Neodymium glass laser free generation power with inert gas filled emission sources

14 p2254 A71-30274

Inert gases, hydrogen, deuterium and carbon dioxide flow in plane parallel glass slots over various Knudsen numbers, calculating slippage constants and volumetric discharge

14 p2227 A71-30673

Ti alloys inert gas shielded welding, determining relationship between welding current, electrode feed rate and electrode wire protruding length and diameter

15 p2413 A71-31219

Resonant charge transfer cross sections in inert rarefied gases from atomic screening parameters, considering positive charge conductivity of ionized dense gases

15 p2452 A71-31825

Three-phase plasmatrons with hot W electrodes for obtaining plasma of inert gases, nitrogen and hydrogen

15 p2457 A71-32267

Coaxial type MHD generator with steady magnetic field and plasma consisting of inert gases and ionizable alkali metal additives, obtaining electrical conductivity

15 p2355 A71-32268

- Lost City /Oklahoma/ and Suchy Dul /Czechoslovakia/ bronzite chondrites stable rare gas concentration determination 15 p2488 A71-32354
- Radionuclides and noble gas isotopic abundances in recently fallen meteorites for cosmic ray exposure ages estimates 15 p2489 A71-32358
- Water, carbon and rare gases in lunar crater breccias based on meteorites nature 15 p2494 A71-32490
- Rare gas ions molecular and dissociative charge transfer reactions with nitrogen, using statistical phase-space theory of chemical reactions 16 p2538 A71-32813
- Biological effects of inert gases in elevated pressure respiratory mixtures on human central nervous system 16 p2536 A71-33577
- Bibliography and review of noble gases isotopic abundance in meteorites and lunar material, considering cosmic ray interactions, radiation ages and extinct radionuclides 17 p2798 A71-34451
- High resolution differential cross section measurements for nonspherical potentials and molecular scattering of nitrogen and noble gases at thermal energies 18 p2949 A71-35898
- Added inert gases effect on gas phase H atoms recombination rate at room temperature, using electron spin resonance spectroscopy 19 p3011 A71-38080
- Ti alloys semiautomatic pulsed arc MIG welding, showing increased productivity and reduced distortion 19 p3070 A71-38423
- Windage data for inert gas in high speed generators rotor-stator gap, investigating turbulent velocity profiles 20 p3181 A71-38915
- Gas heating and energy balance of HF ring discharge in rare gases within cylindrical vessel, discussing electron energy distribution functions 20 p3273 A71-39044
- Heavy rare gases adsorption on terrigenous sediments, comparing earth atmospheric composition with meteoritic planetary primordial component 20 p3194 A71-39385
- Inert gases energy accommodation coefficients dependence on clean metal surface temperature based on lattice theory 21 p3415 A71-40538
- Field adsorption of inert gas atoms at metal surface from variational calculation 21 p3419 A71-40887
- Oscillations in He, Ne and Ar glow discharges, obtaining I-V characteristics 21 p3426 A71-41290
- Analytic approximation for radial integrals and electron excitation cross sections of inert gases, using atomic screening parameters 22 p3577 A71-41620
- Partial quenching of radiation from ionized inert gases during bases irradiation by IR produced with carbon dioxide lasers 22 p3581 A71-41808
- Iron meteorites total N abundances determination by inert carrier gas fusion extraction gas chromatography 23 p3734 A71-43243
- H transition excitation during atomic hydrogen collision with alkali elements and inert gases, discussing inner electron excitement 23 p3707 A71-43268
- German monograph on experimental determination of noble gas plasma conductivity under normal pressure in high temperature range, covering measurements under electric arc conditions 23 p3711 A71-43475
- Active and inert gases released by crushing Apollo 11 and 12 samples at room temperature and by low temperature heating 23 p3751 A71-43701
- Cosmic ray exposure ages and rare gas concentration profiles in Apollo 12 lunar rocks, discussing spallation products and neutron capture effects 23 p3753 A71-43719
- Rare gas concentrations and isotopic abundances in lunar rocks, fines and breccias from Apollo 11 and 12 flights, determining exposure and gas retention ages 23 p3753 A71-43720
- Microprobe measurements of rare gas composition for lunar rock 12013, 10, 31 mineral separates, noting cosmic ray bombardment role in K and Ar production 23 p3753 A71-43721
- Isotopic abundances and concentrations of spallogenic Ne, Kr and Xe in Apollo 12 rock 12002, constructing three stage model of irradiation history 23 p3753 A71-43722
- Apollo 12 lunar soil samples trapped rare gas analysis, observing solar wind He local variation from breccia 23 p3754 A71-43723
- Inert gases release from breccia 10065 by lunar rock vacuum crushing at room temperature, suggesting breccia formation from gas-rich parent materials 23 p3754 A71-43725
- Apollo 11 and 12 fines cosmogenic He, Ne and Ar radionuclides composition determination, using electron microprobe analysis 23 p3754 A71-43727
- Radioactive rare gases and tritium in Apollo 12 lunar rocks and in sample return container, noting relationship to solar flare event 23 p3755 A71-43736
- Velocity dependent HD beam scattering by inert gases, measuring total effective cross section in thermal energy range 23 p3707 A71-43879
- Stepwise ionization effects on ionic wave propagation and oscillation stability in inert gas DC discharges 24 p3857 A71-45230
- RAREFACTION**
Rarefaction and angle of attack effects on delta wing in hypersonic flow in wind tunnel 16 p2520 A71-33376
- RAREFACTION WAVES**
U ELASTIC WAVES
RAREFIED GAS DYNAMICS
Direct computerized simulation Monte Carlo method for numerical solution of Boltzmann equation in rarefied gas dynamics 01 p0113 A71-11472
- Kinetic equation for rarefied polyatomic gases derived from Liouville equation 02 p0286 A71-11883
- Rarefied gas linearized Poiseuille flow between parallel plates, using variational methods for Boltzmann equation 03 p0398 A71-13102
- Rarefied gas flow through long square tubes, solving continuum differential equation with nonequilibrium slip boundary conditions [ASME PAPER 70-WA/PID-1] 03 p0402 A71-14098
- Rarefied gas low speed slip flow over wedge, solving for velocity profiles and skin friction [ASME PAPER 70-WA/APM-26] 03 p0344 A71-14158
- Hypersonic rarefied nitrogen flow over wedge, investigating density field 04 p0570 A71-15033
- Binary gas mixture rarefied hypersonic flow structure near blunt body, investigating diffusive effects on recovery temperature dependence 04 p0528 A71-15488
- Monte Carlo simulation for studying rarefied hypersonic gas flow about slender cones and flat plates [AIAA PAPER 69-651] 05 p0694 A71-16562
- Rarefied gas Couette flow between concentric cylinders and heat transfer from wire to external cylinder, applying momentum method 05 p0736 A71-16723
- Thermal creep velocity in rarefied gas over infinite plane wall, using linearized Boltzmann-Krook equation 07 p1084 A71-18746
- Rarefied gas flow and heat transfer in plane Couette flow using Bhatnagar-Gross-Krook model with ellipsoidal distribution 07 p1224 A71-20024
- Finite element solution of plane Poiseuille rarefied gas flow between parallel infinite plates 07 p1093 A71-20284
- Linearized Boltzmann equation analytic solutions for rarefied gas dynamic problems, using ellipsoid model 07 p1093 A71-20285
- Rarefied gas steady and unsteady motions, proposing approximate method for various problems 09 p1382 A71-22372
- Rarefied gas flow density and velocity by total head and flow rate adapters, noting isentropic flow core region 09 p1382 A71-22728
- Rarefied gas thermal creep flow between parallel plates, using Boltzmann equation relaxation model for all Knudsen numbers 09 p1433 A71-23055
- Rarefied gas flow along boundary wall with temperature gradient, determining thermal creep and temperature slip effects 09 p1547 A71-23167
- Uniform magnetic field effect on rarefied gas slip flow over porous flat plate for skin friction response, using velocity and temperature fields equations 10 p1649 A71-24407
- Transport phenomena in rarefied gases, discussing sound dispersion in helium, weak shock waves, acoustic propagation in monatomic gases and kinetics in alternating fields 12 p1930 A71-27189
- Molecular collisional analysis of normal momentum transfer from flowing rarefied gas to monocrystalline surface 12 p1934 A71-27588
- Rarefied hypersonic flow in blunt body bow region, measuring density and rotational temperature fields by electron beam method 13 p1989 A71-27841
- Viscosity effect on initial highly underexpanded jets in Mach 1 to 5.7 nozzles for laminar, turbulent and rarefied air flows 13 p1989 A71-27889
- Dimensionless strength characteristics of convex bodies vs angles of attack in rarefied gas flows by linear regressive analysis using statistical model 13 p1991 A71-29147
- Weakly rarefied gas flow past bodies of various geometry, deriving equations of motion with approximate macroscopic integrodifferential equations 13 p1991 A71-29148
- Boundary conditions formulation for energy and mass transfer in weakly rarefied gas flows past bodies 13 p1991 A71-29149
- Closed system of macroequations for mass and energy conservation along symmetry axis of steady rarefied supersonic gas flow in front of blunt body 13 p1991 A71-29151
- Steady hypersonic nearly free molecular rarefied gas flow about convex body, applying kinetic operator 13 p1991 A71-29152
- Heat transfer on spheres and sharp cones in rarefied hypersonic gas flow at zero angles of attack in wind tunnel vacuum 13 p1992 A71-29176
- Compressible rarefied gas Couette flow over plane wall, calculating mean free path with Boltzmann equation relaxation model 13 p2051 A71-29357
- Boltzmann equation applicability to rarefied multatomic gases if distribution function is identical with integral of free molecular motion 14 p2276 A71-29561
- Method of characteristics application to steady rarefied gas flow from spherical source or sink 14 p2225 A71-30214
- Rarefied gas Poiseuille flow in parallel plates, cylindrical tube and annulus geometries, deriving subsonic flow velocity profiles by third order constitutive relations 14 p2227 A71-30574
- Hypersonic flow of dust containing gases at low density for distribution accuracy of cosmic dust collection by sounding rockets 15 p2387 A71-31171
- Conical converging nozzle flow of perfect monatomic gas in rarefied near continuum, transition and near free molecular regimes, using finite difference methods 15 p2390 A71-32045
- Colliding supersonic rarefied argon-helium jet flows diffusive separation in low density wind tunnel with electron beam diagnostics apparatus 16 p2554 A71-32800
- Nonlinear heat transfer in plane rarefied isothermal Couette gas flow, using BGK model 16 p2561 A71-34143
- Laminar convective heat transfer rates on hemisphere cylinder in rarefied hypersonic flow, comparing experimental results with Cheng, Davis and Lees theories 17 p2671 A71-34902
- Linearized Boltzmann equation solution for rarefied gas dynamics, discussing analytical, variational and numerical methods 17 p2784 A71-35572
- Rarefied gas dynamic models with velocity dependent collision frequencies, investigating linearized Boltzmann equations 17 p2729 A71-35573
- Inclined wedges in rarefied hypersonic flow conditions, investigating base and wake pattern geometrical and aerodynamic characteristics 18 p2849 A71-36756
- Rarefied gas flow characteristics through pipe orifice in intermediate range of rarefaction between free molecular flow and continuum flow 18 p2849 A71-37023
- Subliming nuclear microthruster design with Monte Carlo study of rarefied gas nozzle flow, noting application to spin stabilization 19 p3103 A71-38351
- Variable suction effects on two dimensional fluctuating slip flow of incompressible rarefied gas past infinite flat plate 20 p3211 A71-39466
- Viscosity effect on initial part of highly underexpanded jets in Mach 1 to 5.7 nozzles for laminar, turbulent and rarefied air flows 21 p3317 A71-40079
- Direct local density gradient measurement in rarefied free jet flow using electron beam deflection signal processed with lock-in amplifier 21 p3364 A71-40394
- Pitot tube interaction with subsonic rarefied gas flow, considering impact pressure 21 p3323 A71-40695
- Hydrodynamic equations for dense system fluctuations with stochastic terms in pressure tensor and heat flux vector evaluated for dilute gas 22 p3530 A71-41893
- Ion anemometer for measuring wind velocity magnitude and direction in rarefied Martian atmosphere 22 p3600 A71-41960
- Obstruction effects in rarefied gas flow through cylindrical ducts by numerical analysis, considering specular reflection, adsorption, absorption and finite molecular mean free path 22 p3531 A71-42343

RAREFIED GASES

- Distribution function integral representation application to steady motion of monocomponent rarefied gas containing amorphous particles, using successive approximation for kinetic equation solution 22 p3482 A71-42868
- Two dimensional and three dimensional wakes in supersonic and hypersonic rarefied gas wind tunnels, comparing cone and dihedral configurations 23 p3625 A71-43357
- Kinetic equations derivation for rarefied chemically reacting monatomic or stable molecular gases 23 p3707 A71-43924
- Flat face cylinders in rarefied supersonic gas flow, investigating perturbed region evolution 24 p3790 A71-45096

RAREFIED GASES

- NT COSMIC GASES
- NT INTERPLANETARY GAS
- NT INTERSTELLAR GAS
- Heat transfer between rarefied monatomic gas and porous wall, examining temperature jump with model kinetic equation for Knudsen layer 01 p0179 A71-10612

- Rotational temperature and density measurements in rarefied flow over sharp leading edge flat plate, obtaining shock layer static pressure 01 p0082 A71-10955

- Human gas metabolism under rarefied atmosphere via gas chromatography, discussing pulmonary ventilation determination and exhaled samples collection equipment 01 p0025 A71-11142

- Nonlinear heat transfer in rarefied gas between concentric cylinders, using modified discrete ordinate method based on BGK model equation 01 p0182 A71-11405

- Magnesium particle combustion in rarefied air at various pressures 01 p0182 A71-11444

- One dimensional steady heat transfer in rarefied gas between infinite parallel laws, using Boltzmann kinetic equation 03 p0462 A71-14570

- Be star rarefied gaseous envelopes emitting or absorbing region size determination, noting application to other rotating stellar systems 04 p0659 A71-15843

- Low density monatomic gases mixtures multicomponent thermal diffusion coefficients, demonstrating for heat conductivity and dissociated air equations 06 p0929 A71-18072

- Rarefied monatomic gas flow in axisymmetric jet exhaust into vacuum, noting expansion to low densities at thermodynamic nonequilibrium 07 p1090 A71-19894

- Density distribution, heat transfer and drag measurements in rarefied Ar cylindrical Couette flow, comparing results with Navier-Stokes and Burnett equations solutions 07 p1093 A71-20286

- Collision free ionizing wave propagation into cold low density unionized gas, showing wave oscillations damping due to ion velocities phase mixing 07 p1171 A71-20289

- Heat transfer in rarefied gases, discussing applicability of molecular-kinetic gas theory 09 p1544 A71-22287

- Rarefied gases heat transfer and density distribution between parallel plates at different temperatures 09 p1432 A71-22854

- Laboratory simulation of solid primordial condensation from low density partially excited gas for solar system origin 10 p1673 A71-24413

- Very weak magnetic field measurements by highly rarefied gases as sensors 10 p1642 A71-24697

- Large angle Rayleigh light scattering for density fluctuations determination in dilute gases with wavelength comparable to mean free path 10 p1642 A71-24835

- Amorphous particle rarefied gas in bounded volume, analyzing kinetic equation existence and uniqueness 13 p2103 A71-29146

- Heat flux between parallel plates in rarefied gas at various temperature ratios and Knudsen numbers, using Monte Carlo method 13 p2165 A71-29226

- German monograph on time dependent gas temperature in decaying plasmas, using frequencies of standing acoustic wave stimulated by pulsed discharges in rarefied gases 13 p2110 A71-29423

- Heat transfer in rarefied gases, considering gas at rest between flat plates, concentric spheres and cylinders and flowing through tubes, nozzles and between parallel plates 14 p2336 A71-30242

- Quantum-theoretical transport equation for dilute gases with internal degrees of freedom, generalizing for arbitrary spacing between internal energy levels 14 p2275 A71-30449

- Alkali metal, alkaline earth metal nitrates and sodium perchlorate mixed with powdered magnesium burned in rarefied air 14 p2338 A71-30616

- Heat transfer through stationary monatomic rarefied gas in annular space between coaxial cylinders, using two-flow Maxwellian function for approximate molecular velocity distribution 16 p2661 A71-32832

- Thermal equilibrium achievement by highly rarefied gas in closed container with space and time varying surface temperature, deriving gas particle distribution 17 p2784 A71-34195

- Temperature measurement by electron beam, using rarefied gas probing for determination of molecule distribution at various vibrational and rotational levels [ONERA-TP-960] 18 p2915 A71-36026

- Rarefied hypersonic flow density, velocity and temperature determination by electron beam technology, including ion production, calibration curves, collisions and spectroscopic analysis 18 p2949 A71-36419

- Moment and heat transfer coefficients for disks rotating in rarefied environment, noting transport characteristics decrease with increasing rarefaction 19 p3161 A71-37292

- Sealing coefficient and leakage performance model for multiple thread rarefied gas viscoelastic 20 p3241 A71-39801

- Transport properties of low density gas of rotating diatomic molecules, deriving quantum mechanical expression for relaxation time via restricted distorted wave approximation method 23 p3706 A71-42908

- Chaos propagation derivation from Boltzmann equation for dilute gas with intermolecular forces and collisions in pairs 23 p3705 A71-43873

- Heat conduction of rarefied air and argon in annuli between coaxial cylinders 23 p3783 A71-44068

- Current-optical effects of anisotropic absorption of polarized and unpolarized light in rarefied cosmic media 24 p3860 A71-45106

RAREFIED PLASMAS

- Nonlinear electrostatic vibrations in colliding antiparallel flows of rarefied plasma 02 p0289 A71-11928

- One dimensional unsteady barotropic fluid flow based on Euler equations, describing rarefied plasma nonlinear motions 03 p0462 A71-13289

- Microwave interferometer for low density electron laboratory plasmas 03 p0428 A71-13926

- Supersonic flow of rarefied plasma around plane bodies, allowing for electric field effect on ion motion 06 p0842 A71-18252

- Far wake asymptotic structure in rarefied plasma flow past charged bodies 07 p1165 A71-18878

- Rarefied plasma disturbances produced by large slowly moving charged spherical body, deriving electric field, ion and electron concentrations in body vicinity 07 p1195 A71-19380

- Low density plasma flow past bodies, measuring disturbed zone velocity, density and temperature distributions by Langmuir probes 07 p1173 A71-20528

- One dimensional unsteady barotropic fluid flow based on Euler equations, describing rarefied plasma nonlinear motions 09 p1504 A71-23265

- Flute oscillations stability in low density plasma within strong magnetic field of mirror geometry, calculating unstable oscillation spectrum by Galerkin method 10 p1650 A71-24526

- Numerical solution for planar ion sheath growth in low pressure plasma, calculating transient sheath thickness resulting from application of specific voltage waveforms 10 p1652 A71-24659

- Potential and nonpotential equation for Alfvén waves and ion cyclotron oscillations in low density nonisothermal plasma 12 p1936 A71-27035

- Bounded low pressure plasma oscillation frequency dependence on discharge chamber length, constant/variable potentials longitudinal profiles and density distribution 12 p1936 A71-27037

- Rarefied collisionless plasma, obtaining hydrodynamic equations for magnetic viscosity and thermal conductivity 13 p2106 A71-28564

- Metallic body motion in strongly rarefied plasma, determining compensating surface current distribution 13 p1991 A71-29158

- Electric field potential near sphere moving through rarefied collisionless plasma in condensation zone, determining ion and electron concentrations 13 p1991 A71-29159

- German monograph on drift waves in plasma with density gradient covering LF electrostatic disturbances in low density plasma 14 p2277 A71-29581

- Heterogeneous fluid flow-chemical processes interaction in low density plasma flow two phase boundary layer seeding, using physicochemical model 14 p2279 A71-29878

- Upper F region transpolar plasma distribution from Alouette 1 data, relating results to satellite measurements of magnetospheric low energy charged particles 14 p2234 A71-30041

- High beta diffuse plasma pinch configurations, deriving stability requirement hydromagnetic energy principle 14 p2281 A71-30540

- Ion-acoustic oscillations excitation in rarefied plasma layers confined by external high frequency TE wave electromagnetic field 14 p2281 A71-30555

- Ion cyclotron harmonic waves development in simulated low density and temperature space plasma, determining propagation upper and lower bounds 15 p2460 A71-32448

- Low density collisionally ionized plasma at equilibrium, calculating permitted, forbidden and semiforbidden radiative cooling coefficients 15 p2460 A71-32776

- Low density plasma in magnetic field, investigating existence possibilities of stationary isothermal jump and plane wave periodic solution 16 p2618 A71-33044

- Low density plasma diagnostics using Thomson scattering of laser light 16 p2618 A71-33161

- Rarefied plasma flow generation by Q-switched laser pulse focusing on solid target, measuring plasma properties with Langmuir probes and microwave interferometers 16 p2586 A71-33162

- Rarefied plasma disturbances produced by large slowly moving charged spherical body, deriving electric field, ion and electron concentrations in body vicinity 19 p3138 A71-37805

- Wavefront overturning in rarefied quasi-neutral plasma, investigating kinetic equations self similar solutions stability 19 p3114 A71-37859

- Electron distribution functions construction from spectrum of laser light Thomson scattering by rarefied plasma 19 p3074 A71-38215

- Electron beam for determining plasma potential and charge density as function of radius of inertially confined tenuous plasma cylinder 20 p3273 A71-39009

- Low density collisionless plasma stabilization in ion-accelerating external DC electric field 21 p3426 A71-41293

- Electron plasma waves and free streaming bursts response to fast rising voltage step in low density cylindrical plasma in strong magnetic field 22 p3582 A71-41899

- Wave phenomena in space chamber rarefied plasma, clarifying spontaneously excited noise wave properties by passive experiment 23 p3710 A71-43365

- Local thermodynamic equilibrium deviation theory and application in low density Ar plasma, noting difference in Langmuir probe and spectroscopic electron temperature measurements 23 p3714 A71-44154

- Rarefied theta pinch plasma collective interactions, examining kinetic instability, electron energy distribution, anisotropy, suprathermal microwave emission, cyclotron harmonics and oscillations 24 p3854 A71-44513

- Inhomogeneous rarefied plasma, investigating nonlocal, linear and nonlinear effects on electromagnetic wave reflection and transmission 24 p3857 A71-45117

RASERS

U MASERS

RATE METERS

U MEASURING INSTRUMENTS

RATE OF CLIMB INDICATORS

- Low resistance nozzles for complete power compensation in rate of climb indicators 01 p0079 A71-10350

RATES (PER TIME)

NT ACCELERATION (PHYSICS)

NT ACUSTIC VELOCITY

NT AIRSPEED

NT ANGULAR ACCELERATION

NT ANGULAR VELOCITY

NT ARRRHYTHMIA

NT BRADYCARDIA

NT BURNING RATE

NT COLLISION PARAMETERS

NT COLLISION RATES

NT CRITICAL VELOCITY

NT CURRENT DENSITY

NT DECAY RATES

NT DECELERATION

NT DRIFT RATE

NT ELECTRON DECAY RATE
 NT ELECTRON FLUX DENSITY
 NT ESCAPE VELOCITY
 NT EVAPORATION RATE
 NT EXHAUST VELOCITY
 NT FLOW VELOCITY
 NT FLUX [RATE]
 NT FLUX DENSITY
 NT GROUP VELOCITY
 NT HEART RATE
 NT HEAT FLUX
 NT HIGH ACCELERATION
 NT HIGH SPEED
 NT HYPERSONIC SPEED
 NT ILLUMINANCE
 NT IMPACT ACCELERATION
 NT ION PRODUCTION RATES
 NT IRRADIANCE
 NT LIGHT SPEED
 NT LOADING RATE
 NT LOW SPEED
 NT LUMENS
 NT LUMINANCE
 NT LUMINOUS INTENSITY
 NT MAGNETIC FLUX
 NT MASS FLOW RATE
 NT NEUTRON FLUX DENSITY
 NT ORBITAL VELOCITY
 NT PARTICLE ACCELERATION
 NT PARTICLE FLUX DENSITY
 NT PHASE VELOCITY
 NT PHOTON DENSITY
 NT PLASMA ACCELERATION
 NT PROPAGATION VELOCITY
 NT PROTON FLUX DENSITY
 NT PULSE RATE
 NT RADIAL VELOCITY
 NT RADIANCE
 NT RADIANT FLUX DENSITY
 NT RECOMBINATION COEFFICIENT
 NT RELATIVISTIC VELOCITY
 NT RESPIRATORY RATE
 NT ROTOR SPEED
 NT SIGNAL FADING RATE
 NT SOLAR CONSTANT
 NT SOLAR FLUX
 NT SOLAR FLUX DENSITY
 NT SOLAR VELOCITY
 NT SOUND INTENSITY
 NT SPIN REDUCTION
 NT STRAIN RATE
 NT SUBSONIC SPEED
 NT SUPERSONIC SPEEDS
 NT SYSTOLE
 NT TACHYCARDIA
 NT TERMINAL VELOCITY
 NT TIP SPEED
 NT TRANSONIC SPEED
 NT WIND VELOCITY

RATINGS
 Aircraft handling rating scales efficiency, noting difficulty in understanding and interpreting pilot opinion 12 p1875 A71-27253

RATIOMETERS
 Fuel cell system steam/hydrogen mixture mass ratio detector using fluidic delay line oscillator 17 p2745 A71-35294

RATIONAL FUNCTIONS
 Microwave circuits and components design using generalized rational function approximation in finite intervals with Zolotarev functions 08 p1252 A71-20757
 Algebraic criterion for positive realness of rational functions, using Routh algorithm 09 p1486 A71-23651
 Stationary covariance generation of matrix of rational functions of complex variable, solving factorization equation via algebraic Riccati equation 20 p3207 A71-38990
 Algorithm for rational function incomplete decomposition into partial fractions 20 p3255 A71-39490

RATIONS
 NT SPACE RATIONS

RATIOS
 NT ASPECT RATIO
 NT DIMENSIONLESS NUMBERS
 NT FROUDE NUMBER
 NT FUEL-AIR RATIO
 NT GRASHOF NUMBER
 NT HARTMANN NUMBER
 NT HIGH ASPECT RATIO
 NT INDEXES [RATIOS]
 NT LIFT DRAG RATIO
 NT LOW ASPECT RATIO
 NT MACH NUMBER
 NT MASS RATIOS
 NT NUSSELT NUMBER
 NT OPTICAL REFLECTION
 NT PAYLOAD MASS RATIO
 NT PECLET NUMBER
 NT PERVEANCE
 NT POISSON RATIO
 NT PRANDTL NUMBER
 NT RAYLEIGH NUMBER
 NT REYNOLDS NUMBER

NT RICHARDSON NUMBER
 NT SCALE [RATIO]
 NT SCHMIDT NUMBER
 NT SIGNAL TO NOISE RATIOS
 NT SIMILARITY NUMBERS
 NT STANDING WAVE RATIOS
 NT STANTON NUMBER
 NT STRESS RATIO
 NT STROUHAL NUMBER
 NT THICKNESS RATIO
 NT THRUST-WEIGHT RATIO
 NT VOID RATIO
 Modular ratios effect on structural composites, predicting property values from structural measurements 01 p0103 A71-11276

RATS
 Combined glucose-sodium chloride solution consumption by rats during normal and food deprivation conditions 02 p0201 A71-12874
 Emotionally induced osmotic pressure and thirst increase of rats during stress, noting eating behavior 02 p0201 A71-12875
 Microcathodes measurement of oxygen tension on arterioles external surface in hamster cheek pouch and hamster/rat cremaster muscle for blood flow regulation mechanism 03 p0363 A71-13487
 Reward magnitude effects on runway performance of rats with intertrial feeding 03 p0372 A71-13693
 Decaborane effects on amino acid metabolic patterns of various rat tissues, considering holoenzyme inactivation 05 p0706 A71-16294
 Prolonged water deprivation effects on hypothalamic self stimulation of rats with electrodes chronically implanted in posterior lateral hypothalamus 05 p0711 A71-17087
 Telemetric techniques for pharmacological effects of body temperature, motor activity and food and fluid intake on rat brain, describing recording and monitoring equipment 05 p0716 A71-17112
 Training effect on oxygen tension dynamics in rats brain cortex under progressive high altitude hypoxia conditions, noting adaptation influence on motor activity and survival rate 06 p0850 A71-17394
 Strain gage attachment to rat heart ventricle in situ with fine stainless steel pins 06 p0862 A71-18391
 Control and prolonged exercised rats adrenal and plasma catecholamine, corticosterone and epinephrine level comparisons using fluorometric analysis 07 p1044 A71-20330
 L-dopa multiinjection timed effects on rat brain norepinephrine metabolites concentrations, observing zero time control rated modifications 09 p1393 A71-22649
 Rats under various exercise programs, determining cardiac ventricle and gastrocnemius muscles calcium activated adenosine triphosphatase activities 09 p1400 A71-23361
 Thyroidectomized vitamin A deficient rats, noting visual sensitivity loss not correlated to thyroid 13 p2008 A71-28455
 Dark adapted albino rats behavioral assessment, measuring absolute visual thresholds to white and colored light 13 p2008 A71-28457
 Prolonged hypokinesia effect on rats serotonin [5-HT] metabolism, noting pronounced blood content deviation from normal during first to third and thirteenth to fifteenth day 20 p3187 A71-39218
 Myocardium reactions under 2G acceleration from histological, histochemical and electron microscopic observations on rats, noting dystrophic damage level relationship to duration 20 p3189 A71-39235

RAWINSONDES
 Rawinsonde reported extreme wind speed in arctic stratosphere at SST altitudes 05 p0777 A71-16700
 Rawin system performance and technical features, describing radio direction finder design, operation, capabilities and carrier balloons 08 p1330 A71-21741
 Nimbus 3 and 4 satellite observation data comparison with sounding rocket and rawinsondes based on temperature as function of pressure measurements 16 p2572 A71-33846

RAY TRACING
 Ray tracing in warm collisionless magnetoplasmas based on wave dispersion relation, discussing satellite communication 01 p0137 A71-11612
 Ionospheric and tropospheric effects on differential phase path in very long baseline interferometry, using ray tracing computer program 02 p0251 A71-12331
 Artificial satellite HF radio wave ionospheric guided propagation, considering ray tracing based on geometric-optics treatment 05 p0720 A71-16229

Complex rays for electromagnetic field construction, considering application to Gaussian laser beams 05 p0763 A71-16905
 Ray tracing near reflection level in ionosphere, considering magnetic field effect 06 p0927 A71-17687
 Radio ray tracing in complex space, describing plane stratified ionosphere 09 p1411 A71-23731
 Venus atmosphere critical refraction model, examining optical effects and ray paths 11 p1823 A71-25696
 Particle collisions effects on whistler ray paths, considering penetration through lower boundary of ionosphere 14 p2193 A71-29917
 Ray trace equations for conic surfaces, noting application in computer programs for unusual systems 17 p2768 A71-35592
 Book on electron optics covering image formation principles, field plotting and ray tracing analog and computational methods, electrostatic and magnetic lenses, etc 19 p3103 A71-37522
 Intensity and polarization for meteorological spherical and nonspherical particle size parameters, comparing exact Mie scattering and ray optics 23 p3704 A71-43337
 Human eye theoretical model with aspherical cornea front and lens back surfaces, computing astigmatism, coma, meridional and sagittal focal lengths by ray tracing method 24 p3798 A71-44978

RAYLEIGH DISTRIBUTION
 Area distributed incidental radio noise voltage envelope distribution functions conversion to Rayleigh distribution with range frequency relationships 01 p0037 A71-11165
 Symmetric operators family spectrum with generalized Rayleigh functional, showing analogy between linear and nonlinear theory at infinite spatial dimension 18 p2942 A71-36821
 Bayesian learning algorithm derivation for statistically optimum adaptive gain control in Rayleigh-distributed signal reception 20 p3206 A71-38874

RAYLEIGH EQUATIONS
 Rayleigh, baroclinic and Rossby waves instabilities effects on stellar structure during differential rotation 03 p0486 A71-13322
 Periodic solutions for strongly nonlinear differential system of n-coupled nonautonomous equations of Lienard and Rayleigh types 17 p2766 A71-34925

RAYLEIGH NUMBER
 Critical Rayleigh numbers for natural convection of water confined in square cells, noting heat transfer modes [ASME PAPER 70-WA/HT-7] 13 p2164 A71-28981
 Stability of governing parameters critical values /Taylor, Rayleigh or Reynolds numbers/ and periodic solutions in fluid mechanics 16 p2558 A71-33002

RAYLEIGH SCATTERING
 Light scattering geometry from infinite cylinder shown consistent with Rayleigh-Gans formalism 03 p0425 A71-13647
 Mars and Mercury polarization measurements, investigating Rayleigh scattering in atmospheres 05 p0806 A71-16204
 Relaxation theory of Rayleigh scattering of light by isotropic continuous medium, deriving spectral densities via fluctuation dissipation theorem 06 p0927 A71-17596
 Stimulated thermal Rayleigh scattering with picosecond pulses, discussing contributory processes 07 p1164 A71-19779
 Rayleigh-Brillouin light scattering in compressed hydrogen, hydrogen deuteride and deuterium, noting discrepancy between observed and theoretical spectra 08 p1301 A71-20743
 Daytime near horizon atmospheric luminescence measurement by Cosmos 224 satellite, discussing contributions of nitrogen and aerosol and Rayleigh scatterings 09 p1435 A71-22432
 Large angle Rayleigh light scattering for density fluctuations determination in dilute gases with wavelength comparable to mean free path 10 p1642 A71-24835
 Stimulated Mandelstam-Brillouin, Rayleigh line wing and thermal light scattering, discussing fine structure, glass fracture and components shift 10 p1621 A71-24837
 Tables of scattering functions and albedo for semiinfinite atmospheres according to nonconservative Rayleigh phase matrix for diffuse radiation computation 14 p2274 A71-30059
 Radar target detection in nonGaussian sea clutter, calculating trimmed-mean detector performance under Rayleigh fluctuation 14 p2197 A71-30805

RAYLEIGH WAVES

- Semiinfinite atmospheric multiple conservative Rayleigh scattering, describing polarized radiation transfer 15 p2449 A71-31333
- Rayleigh scattering planetary atmosphere radiative transfer equation, calculating phase curves for flux and polarization 15 p2498 A71-32778
- Polarized light multiple scattering in homogeneous plane parallel planetary atmospheres, considering Rayleigh scattering, test models and phase function obtained by neglecting polarization 16 p2632 A71-33320
- Lasers as light sources, discussing Rayleigh, Tyndall, Raman and Thomson scatterings from various media 16 p2612 A71-33373
- German monograph on ozone determination from sky radiance, considering Rayleigh and Mie scattering 17 p2733 A71-34794
- Light wave Rayleigh interferometer for concentration gradient measurements in liquid systems with mass transport 18 p2917 A71-36052
- Rayleigh scattering by obliquely oriented uniform thin cylindrical particles /needles/, using dielectric needle approximation 20 p3196 A71-39406
- Semiinfinite atmospheric multiple conservative Rayleigh scattering, describing polarized radiation transfer 22 p3576 A71-42608
- Resonance scattering laser radar for atmospheric pollution detection, discussing Rayleigh and Mie scattered light suppression 24 p3803 A71-44570
- RAYLEIGH WAVES**
- Rayleigh wave propagation in stochastically inhomogeneous elastic medium 01 p0169 A71-10637
- Interdigital Rayleigh wave transducer on piezoelectric ceramics with comb-to-comb polarization 01 p0055 A71-11174
- Mechanical characteristics of generalized Rayleigh waves in piezosemiconductors of cubic symmetry, deriving amplification and damping factors for zero diffusion coefficient 02 p0294 A71-11894
- Stimulated light scattering by capillary waves on incompressible fluid surface or by Rayleigh waves on surface of isotropic solid body with small opticoelastic moduli 02 p0285 A71-12505
- Surface tension effect on dispersion of Rayleigh waves in elastic body 04 p0673 A71-15882
- Rayleigh wave propagation in anisotropic substrates, using light diffraction by surface acoustic waves 05 p0783 A71-17078
- Rayleigh and phase change instability for olivine-spinel mantle convection 07 p1105 A71-20450
- Equivalent electrical circuits of interdigital transducers for piezoelectric generation and detection of ultrasonic Rayleigh waves 09 p1420 A71-23680
- Surface layer-bulk body interaction and Rayleigh wave propagation in elastic solid, using two dimensional continuum theory 10 p1691 A71-24645
- Rayleigh wave propagation along edge of thin plate, calculating velocity dependence on frequency 12 p1929 A71-26929
- Equivalent circuit for interdigital piezoelectric Rayleigh wave transducer 13 p2037 A71-28472
- Automatic classification of targets characterized by radar returns at discrete set of frequencies in Rayleigh region and first resonance range 17 p2747 A71-35773
- Thermoelastic plane harmonic and Rayleigh surface waves in elastic solids with thermal relaxation, using Maxwell heat conduction equation 20 p3310 A71-39779
- Rayleigh wave reflection from crack tip after propagation along open crack faces in elastic solid, determining surface wave energy loss 21 p3468 A71-41003
- Frequency dependence of Rayleigh wave propagation velocity along rough surfaces, based on smooth surface mass loading 23 p3703 A71-43203
- Acoustoelectrical current oscillations in GaAs films at low temperature under ultrasonic Rayleigh wave amplification 23 p3716 A71-43477
- RAYLEIGH-RITZ METHOD**
- Rectangular and circular thin orthotropic plates thermal buckling approximate solution using Rayleigh-Ritz energy method 05 p0819 A71-15978
- Clamped-free and clamped-ring-stiffened cylindrical shells free vibrations analysis for digital computer

programming, using Rayleigh-Ritz technique for approximate solution 08 p1371 A71-21427

Nonlinear panel flutter analysis and response under random excitation or nonlinear aerodynamic loading, using Rayleigh-Ritz approximation to Hamilton variational principle 09 p1534 A71-22080

Combined finite element method and Rayleigh-Ritz procedure for geometrically nonlinear problems solution of elastic plates with arbitrary shape, boundary and load distribution 16 p2653 A71-33088

Inelastic buckling process of axially compressed cylindrical shells with edge constraints, using variational principle and Rayleigh-Ritz method 19 p3158 A71-38182

Pointwise bounds in Cauchy problem for fourth order quasi-linear equation using a priori inequality, applying Rayleigh-Ritz technique to elliptic partial differential equations 20 p3255 A71-39573

RAYON

Graphite fibers mechanical properties based on rayon and polyacrylonitrile, considering tensile, flexural, compressive and shear strength 11 p1784 A71-25398

Polyacrylonitrile and rayon precursor graphite fibers diameter relation to Young modulus and tensile strength 15 p2438 A71-31817

RUE

U RELATIVE BIOLOGICAL EFFECTIVENESS [RBE]

RC CIRCUITS

Active filters of triple layer rectangular-shaped distributed RC elements, calculating components geometric variation effect on frequency response 01 p0058 A71-10312

Active RC filters synthesis, using expanded denominator of given transfer function 02 p0230 A71-11839

RC active filter with lumped-distributed components, discussing system stability at transition region between extreme electrical lengths 04 p0560 A71-14744

Periodically reverse switched capacitor network theory, deriving equivalent resonant transfer circuit and expression for voltage transfer ratio 04 p0561 A71-15699

Frequency generators using RC /RL/ designs with odd selective quadrupole element numbers as converters 07 p1078 A71-20062

Transfer function synthesis by RC fluidic circuits, presenting transfer function element circuits analysis and experimental verification 07 p1026 A71-20570

Analog information systems frequency modulators, describing network design consisting of phase shifting RC network, amplifier and inertialess resistor 09 p1415 A71-22296

Optimum synthesis and design of distributed RC filter for oscillator feedback circuit, using calculus of variations 09 p1425 A71-23652

Noise analysis of microelectronic active RC filters by cascade of passive and active networks, considering low pass filter 10 p1582 A71-23915

Active RC network realization of third order low-pass Butterworth characteristic with all capacitors having same value 14 p2210 A71-29798

RC analog fluidic circuits design for arbitrary transfer functions generation 15 p2351 A71-31682

Solid state RC network for single sideband frequency converter using phase difference carrier suppression 19 p3022 A71-38497

Dual input null networks application in RC feedback oscillators, examining frequency stability 20 p3206 A71-39915

Distributed RC network application as microelectronic delay line, discussing delay response improvement by compensating network 21 p3353 A71-40589

Distributed active RC filters design for low pass, bandpass and biquadratic network functions, including charts for element values determination 21 p3360 A71-40809

Tapered distributed RC low pass network configuration with voltage-controlled sources for sensitivity reduction low and high Q factors 21 p3361 A71-41409

Pulse trains of minimum spectral width generated from rectangular pulses by RC elements coupled without feedback 22 p3521 A71-42248

Regenerative nonlinear RC amplifier oscillations due to series opposed varicap diode capacitance 24 p3810 A71-45261

RC NETWORKS

U RC CIRCUITS

RCA SPECTRA 70 COMPUTER

Illiac 4 and Spectra 70 computers comparison in terms of logic circuit noise immunity and system noise sources 03 p0388 A71-13179

REACTANCE

Parasitic reactances in Gunn effect device packages from microwave equivalent circuit parameters 07 p1072 A71-19104

Movable metal iris with nearly frequency independent susceptance, relating characteristics to centered capacitive obstacle in waveguide 24 p3809 A71-45095

REACTION CONTROL

Proteins hydrolysis, investigating temperature effect on reaction, determining optimum conditions for maximum amino acids yields 11 p1728 A71-26066

Homogeneous fuel combustors with multistage reaction rate controlled system, determining linear relationships and heat release 21 p3437 A71-41049

REACTION JET ATTITUDE CONTROL

U ATTITUDE CONTROL

U JET THRUST

REACTION JETS

U JET FLOW

U JET THRUST

REACTION KINETICS

Photodissociation produced O/P3/ atoms detection and reaction rate measurements by resonance fluorescence scattering 01 p0130 A71-10369

Pyrolyzing vinyl polymers thermal degradation kinetics, deriving surface regression rates relationship to temperature 01 p0109 A71-10935

Book on fuel cells covering types, applications, thermodynamics, chemical reactions, direct electrical generation, etc 01 p0006 A71-11192

Oxygen uptake kinetics in human submaximal exercise during work load transitions and work-rest cycle 02 p0202 A71-11663

Mass transfer and Biot diffusion in MHD flows with mixed boundary reaction kinetics, considering Hartmann and plate problems 02 p0293 A71-12632

Spherical hydrogen-oxygen diffusion flame structure, discussing combustion processes chemical kinetics 02 p0210 A71-12856

Carbon kinetic isotope fractionation into carbon dioxide and organic compounds in meteorite-like Fischer-Tropsch reaction with nickel-iron or magnetic catalyst 03 p0483 A71-13013

Heterogeneous kinetics at elevated temperatures - Conference, Philadelphia, September 1969 03 p0374 A71-13121

Surface oxidation kinetics of iron by solid electrolyte techniques, comparing weight gain method 03 p0374 A71-13122

High melting point metal systems with nitrogen or oxygen, discussing engassing and degassing reactions kinetics and thermodynamic equilibrium 03 p0442 A71-13362

Atomic oxygen-nitrogen shock tube endothermic reaction under high translational and low vibrational energy, noting ozone loss 03 p0375 A71-13493

Hydrogen-oxygen induction period kinetics behind shock waves, monitoring OH concentration by UV line absorption method 03 p0376 A71-14276

Hydrogen-sensitized decomposition of hydrogen peroxide, taking oxygen inhibiting effect into account 03 p0376 A71-14277

Hydrogen peroxide decomposition acceleration by carbon monoxide, discussing reaction mechanisms and rate coefficients 03 p0376 A71-14280

Shock tube spectroscopic and reaction kinetic research, considering studies before LTE 04 p0547 A71-14692

IR radiation measurement of chain branching rates in hydrogen-oxygen mixtures ignited by reflected shock waves 04 p0548 A71-14695

Rate constant measurement for atomic hydrogen reaction with carbon dioxide yielding OH and CO, considering near IR emission spectroscopy applicability 04 p0548 A71-14697

Presulfidized Ni alloys and Cr oxidation rates 04 p0615 A71-15787

Stainless steel deoxidation by carbon in laboratory scale vacuum induction melting, explaining reaction kinetics 05 p0758 A71-16246

Detonation front at Chapman-Jouguet velocity demonstration by numerical transient flow calculations 05 p0834 A71-16510

Detonation wave with finite reaction velocity interaction with rarefaction wave from behind, noting oscillations development associated with attenuation 05 p0834 A71-16511

Hydrogen-oxygen reaction kinetics behind steady state shock waves under isothermal branched chain explosion limits 05 p0834 A71-16513

Gas dynamic processes effects on hydrogen-oxygen explosion chemical kinetics, calculating ignition delays under steady conditions behind plane reflected shock waves 05 p0716 A71-16514

Two-phase detonations, discussing importance of stripping mechanism and droplets deformation in reaction zone fuel consumption 05 p0834 A71-16515

Cr and Ti ionization rates, CO and NO reaction kinetics and decomposition products in shock tubes 05 p0716 A71-16521

Single pulse shock tube in high temperature chemical reaction kinetics, considering shock reflection theory 05 p0836 A71-16527

Chemiluminescent NO-O reaction spectral radiant intensity and absolute rate constant redetermination in premixed gaseous free jet and hydrogen flame atmosphere 05 p0837 A71-16568

High temperature diffusion controlled transient creep, considering unimolecular reaction kinetics stress and temperature dependence 05 p0830 A71-17239

Single layer graphite oxidation kinetics evaluated by electron microscopy, discussing removal rate 06 p0915 A71-17302

Hypersonic ramjet reaction mechanisms for H combustion, discussing computational models, operation principles and atomic, radical and molecular collisions 06 p0865 A71-17410

One dimensional kinetic calculations for hydrogen fluorine rocket nozzles compared to firing data, discussing Cl addition effect on performance [WSS/CI PAPER 70-21] 06 p0943 A71-17656

Acetylene pyrolysis kinetics, considering isothermal vs adiabatic conditions and surface catalyzed vs homogeneous gaseous [WSS/CI PAPER 70-18] 06 p0943 A71-17660

Indeterminacy interval reduction for ionospheric reaction rate constants by imposing supplementary condition on NO/oxygen molecular ion concentrations ratio 06 p0894 A71-18259

Cellulose, explosives and propellants thermal surface ignition, using heat transport and chemical kinetic equations 06 p0944 A71-18298

Chemical reaction kinetics optimal problem numerical solution based on Pontryagin maximum principle and gradient method 07 p1147 A71-19185

Interstitial solid solution hardening in pure Ni and Ni-C alloys, noting mechanism and C concentration effects 07 p1138 A71-19980

Co oxidation rate measurements over temperature range 475-1325 C at various oxygen pressures, determining oxide formation kinetic law and activation energy 07 p1139 A71-20225

Rate constant for oxygen uptake exponential increase during low intensity exercise by algebraic solution 07 p1052 A71-20336

Vibrationally excited ground state hydroxyl in fast flow system, considering mean radiative lifetime and reaction rate with ozone 08 p1250 A71-20662

Chemical reaction rate microscopic reversibility, observing rotational vibrational and/or translational states dependence of products reactants 08 p1250 A71-20666

MnO oxidation reduction kinetics measurement in carbon monoxide/dioxide atmospheres by gravimetry and electrical conductivity 08 p1318 A71-20698

Bismuth oxide and iron oxide equimolar mixtures solid state reactions, determining rates from integrated X ray diffraction and activation energies 08 p1318 A71-20699

Zinc electrode kinetics noting exchange reactions, anodic behavior in alkaline solutions and capacitance 08 p1233 A71-21080

Silver oxide electrodes electrochemical reaction kinetics, examining oxidation, anodic formation and cathodic reduction 08 p1234 A71-21086

Structural and kinetics investigation of oxides formation in silver-argentous oxide-argentous oxide system, using electron microscopy and electron diffraction methods 08 p1234 A71-21087

Al electrodes in molten salt electrolytes, investigating electrochemical kinetics by polarization measurements [ECS PAPER 200] 08 p1250 A71-21470

Papers on polymers thermal stability, Volume 1, covering molecular structure, reaction kinetics, scission, thermosetting resins, etc 08 p1323 A71-21474

Recombination frequency spectrum asymmetry in interaction between high and low frequency plasma oscillations, noting role of Doppler effect 08 p1340 A71-21495

Initial reaction rates of oxygen difluoride with diborane related to reactant concentration and temperature 09 p1510 A71-22071

Oxidation/vaporization kinetics of chromium oxide hot pressed and sintered pellets 09 p1480 A71-22113

Reaction dynamics for CO ion plus deuterium to yield COD ion plus D, noting polarization forces role 09 p1497 A71-22702

Molybdenite oxidation kinetics by thin layer technique with close temperature and gas composition control, measuring temperature, gas composition and particle size effects 09 p1472 A71-23128

Thoria containing Ni and Co base powders reduction in hydrogen atmosphere for precipitation hardened materials production, determining optimal thermodynamic and reaction kinetic factors 09 p1475 A71-23306

Equilibration rate of uncatalyzed carbon dioxide hydration reaction in open system at constant carbon dioxide partial pressure, examining buffering capacity effect 10 p1559 A71-23898

Ionization mechanisms for deviation of experimental altitude vs velocity curves of meteor trails, considering various electron and ion emissions and dissociation effects 10 p1669 A71-24032

Rate constant temperature dependence for ozone reaction with oxygen, considering airflow features due to singlet molecular oxygen 11 p1801 A71-25370

He-Zn ion laser, considering charge exchange and Penning collisions as primary excitation sources of Zn II levels 11 p1773 A71-25927

Nylon-phenolic composites pyrolysis, deriving kinetic coefficients from thermogravimetric analysis at various heating rates 11 p1728 A71-26043

Kinetic and ionization phenomena in Q switched laser produced plasmas, considering gas dynamic plasma parameters /velocity, density distribution, pressure and temperature/ 11 p1806 A71-26086

Kinetic processes in shock tubes, considering diagnostic techniques for monitoring time histories nonequilibrium distributions preparations 11 p1745 A71-26264

Reacting gases atom concentration quantitative measurements with electron spin resonance, discussing microwave power, saturation and modulation amplitude effects 11 p1765 A71-26284

Ionospheric ion formation and neutralization reaction rate coefficients determination by fitting rocket measured electron concentration profiles with computer generated profiles 13 p2062 A71-28560

Nitric oxide formation kinetics in shock induced combustion processes, considering hydrogen-oxygen-nitrogen reaction 13 p2113 A71-28616

Reaction rate controlling mechanisms in shock wave initiated oxidation of formaldehyde 13 p2113 A71-28617

Group properties of laminar boundary layer equations for incompressible binary fluid under various magnetic field distributions and reaction rates 13 p2048 A71-28735

Respiratory gas reaction mechanism on potassium superoxide in closed circuit breathing apparatus 13 p2021 A71-29113

Three body ion-neutral association reactions of NO ions with oxygen, nitrogen and carbon dioxide, noting temperature effect on rate constant 13 p2026 A71-29507

Bromine dissociation rates in presence of He, Ne, Ar, Kr and Xe, determining rate constant expressions from light absorption measurements behind incident shock waves 13 p2027 A71-29508

Carbon/graphite cloth reinforced aromatic/heterocyclic resins ablative composites pyrolysis kinetics by computer code analysis 14 p2262 A71-29649

Heterogeneous fluid flow-chemical processes interaction in low density plasma flow two phase boundary layer seeding, using physicochemical model 14 p2279 A71-29878

Chemical kinetic calculation of nitric oxide formation in spark ignition automobile engines and gas turbine combustors 14 p2190 A71-30454

Methane high temperature oxidation in steady flow system, predicting change rate of species concentrations and gas properties during reaction 14 p2285 A71-30457

Thermal emission analysis method for studying phase transformations and chemical conversion kinetics in multicomponent systems, applying to liquid evaporation rate measurement 14 p2338 A71-30618

Modular concept mathematical model for combustion and pollution formation processes in jet engine combustors, including turbulent mixing and reaction kinetics [AIAA PAPER 71-714] 14 p2294 A71-30766

Thermal decomposition rates and explosion of dinitroxydiethyl nitramine from heat release measurements at various pressures 15 p2462 A71-31376

Unmixed gases burning at finite reaction rate, analyzing steady laminar flames developing in mixing zone of fuel semiinfinite flow past static oxidizer 15 p2511 A71-31379

Oxidation kinetics of pure Al in dry oxygen as function of pressure and temperature, using manometric method 15 p2426 A71-31408

Calorimetrically measured energy feedback heat of reaction dependence from laminar diffusion flames above water cooler [WSS/CI PAPER 71-11] 15 p2463 A71-31621

CIF diluted solutions in Ne, investigating thermal decomposition mechanism behind shock waves by mass spectroscopy 15 p2367 A71-31874

Nitrogen and sulfur dioxide reactions in isolation, determining rate by concentration measurements using light absorption technique 15 p2465 A71-32082

Stoichiometric hydrogen-carbon monoxide-oxygen mixtures detonation wave propagation at critical Mach number, noting explosion limit chemical kinetics role 15 p2465 A71-32088

Zirconium dioxide reactions with chromium, molybdenum and tungsten carbides, studying reaction products, phase composition, sintering temperatures and chemical separation 15 p2432 A71-32166

Nickel sponge preparation by liquid nickel sulfide reaction with NiO under reduced pressure at various temperatures 15 p2433 A71-32178

Oxidation kinetics and scale morphology of chromium oxide forming thoriated and unthoriated Ni alloys, discussing rate controlling processes effects 16 p2590 A71-32871

Shock tube investigation of cyanogen and CN molecule dissociation at high temperatures, considering kinetics of CN decomposition 16 p2538 A71-32891

Elementary reactions in hydrocarbon combustion, using shock tube as chemical reactor to determine rate of reaction in 1600 to 2100 K range 16 p2539 A71-32892

Laminar boundary layers effect on chemical-kinetic measurements in shock tube, applying correction by computer program for subsonic diffuser 16 p2555 A71-32893

Reaction kinetic studies using hydrodynamic flow structure due to spherical shock wave from laser induced spark 16 p2616 A71-32903

Thermal decomposition kinetics of nitrous oxide in shock tube, measuring IR emission behind reflected wave 16 p2539 A71-32910

Nonequilibrium plasma chemical reaction kinetics problems, discussing time dependence, dissociation and recombination theories in pulsed EM field, equations and numerical calculations 16 p2539 A71-32965

Soviet book on gas phase chemical reactions rate constants determination covering elementary processes kinetics empirical methods 17 p2694 A71-34522

Rhodopsin kinetics mathematical analysis by cyclic five-component model, applying to flash and extended photolysis in rat retina 17 p2680 A71-34653

Time dependent corrections to one component monatomic systems equilibrium rate of reactions and temperature change, using moment method for integrating nonlinear Boltzmann equation 17 p2785 A71-34945

Thermobalance for studying high temperature silicon-carbon reaction kinetics, incorporating HF current, coaxial shielding of electrical connections and electromagnet balance 17 p2838 A71-35475

REACTION TIME

Electric field effects on town gas and hydrocarbon flame reaction rate, burning velocity and propagation speed due to free electrons in flame front
17 p2840 A71-35704

Singular perturbation theory for finite rate chemical kinetics effect on regression rate of seminfinit flat fuel plate in gas oxidizer stream
17 p2792 A71-35796

Reaction rate of vibrationally excited hydroxyl with ozone, obtaining hydroxyl emission spectra by Fourier transform spectroscopy
18 p2874 A71-35836

Mo, W and Mo-W alloys chlorination kinetics, investigating temperature and pressure effects on reaction rate from electron micrographs
18 p2938 A71-37002

Helium-cadmium laser discharge, discussing possible He trapping mechanisms and improved tube design to eliminate He cleanup
18 p2933 A71-37013

Detonation processes in gases, considering Zelovich-Doering-Neumann model and reaction kinetics
19 p3162 A71-37457

Diatomic gas molecules three body recombination and dissociation rate coefficients from modified phase-space theory of reaction rates
19 p3107 A71-38078

Hydrogen-oxygen reaction sensitized by ammonia, comparing with nitrogen dioxide and nitrosyl chloride activators
19 p3012 A71-38081

Reactions of H and O with hydrogen peroxide and water in discharge flow systems, measuring rate coefficients
19 p3012 A71-38083

Solid propellant combustion pressure oscillations amplification, developing mathematical model as function of reaction rate constant, chamber pressure, frequency and solid properties
19 p3123 A71-38096

Porous material slab pyrolysis, studying density and thermal conductivity changes and reaction kinetics
19 p3170 A71-38117

Oxygen uptake kinetics by hemoglobin layers, using Hill advancing front equation
19 p3010 A71-38567

Ionospheric effective recombination coefficient and reaction rate models for various solar activity periods and day and night conditions
20 p3224 A71-39714

Peptides formation from glycine in presence of trimetaphosphate, investigating mechanism
21 p3345 A71-40175

Phase-space theory of macroscopic fluctuations in nonlinear systems far from thermodynamic equilibrium, using chemical kinetics model
21 p3416 A71-40856

Chemical kinetics and fluid mechanics interaction effects in stagnation point boundary layer
21 p3475 A71-40860

Thermal dissociation rate of excited CsF, calculating ion-ion recombination rates
21 p3346 A71-40888

Nb nitriding kinetics and external effects observations, noting nitrogen diffusion through crystal lattices
21 p3404 A71-41163

Shock wave initiation of hydrogen-oxygen at 1200-1800 K, using UV absorption spectroscopy in shock tube studies
22 p3587 A71-42097

Urea hydrolysis reaction rates by urease at low water activity, noting use for Mars surface bioassay
22 p3487 A71-42226

Gas-metal reactions in refractory metals purification, discussing reaction kinetics, thermodynamic equilibria and dissolved gases induced mechanical properties changes
22 p3564 A71-42423

Apparatus for optical diagnostics of helioelectrochemical conversion reaction phototransformation kinetics including diffusion coefficient measurement in liquid phase
22 p3484 A71-42845

Corrosive oxide layer formation kinetics during interaction of oxygen with polycrystalline W at 500-1000 K, using desorption mass spectrometry
23 p3641 A71-42907

Delta-zirconium hydride hydrogen engassing experiment, investigating hydrogen absorption rate and diffusion constant temperature dependence
23 p3688 A71-42929

Carbon dioxide UV absorption and dissociation processes and reaction kinetics of dissociation products
23 p3642 A71-43329

Molecular oxygen partial pressure effect on nitrogen afterglow intensity, proposing three-body reaction kinetics
23 p3707 A71-43500

Shock-heated Mg/MgO particle dispersion, postulating kinetic mechanism consistent with spectrometric observations
24 p3863 A71-44940

Molecular oxygen dissociation rate constant determination during interaction with He atoms in cylindrical shock tube
24 p3850 A71-45056

REACTION TIME

Task difficulty involving simple and choice reaction time under stress of shock, threat of shock and noise
01 p0026 A71-11414

Reaction time diurnal variations to optical and acoustic stimuli, investigating disturbed natural sleep-waking rhythm effects
02 p0197 A71-11684

Nervous system activity changes relation to physical exercise type and extent, measuring visual response time
05 p0708 A71-16620

Changing rotational velocity recording device for vestibular apparatus tests, examining stimulus reaction speed
05 p0714 A71-16810

Pt electrode response time during unsteady oxygen partial pressures measurement
06 p0860 A71-18323

Motor learning error performance with discrimination reaction timer, discussing commitment to wrong response, group observations and specific error repetition
07 p1047 A71-19462

Gaseous nitromethane-oxygen mixtures detonation characteristics, determining reaction time by schlieren technique
08 p1346 A71-20862

Spatial and temporal patterned light flashes effects on dark adapted subjects, discussing cortical response changes in contrast depth
10 p1565 A71-24680

Lithium-like and sodium-like positive ions electron impact ionization, calculating cross sections and reaction rates with binary encounter model
11 p1801 A71-25211

Electroencephalographic and evoked cortical potential correlates of reaction time and visual discrimination in humans
13 p2022 A71-29345

Human performance after awakening at different times of night, considering reaction time and muscular coordination
15 p2362 A71-31201

Nonpremixed and premixed combustion theory in laminar flows, considering diffusion flame- reaction time ratio and activation energy effects
15 p2515 A71-32564

Visual latencies at photopic levels as function of binocular differences in retinal illuminance, using Limulus adaptation model and ERG correspondence
16 p2527 A71-32867

Light adaptation and visual latency, discussing temporal resolving properties of eye as function of binocular differences and target background contrast
16 p2527 A71-32868

Recognition response time experiments for word number effects in target set, discussing familiarity judgment and response decision
17 p2683 A71-35250

Reaction times distributions in visual or auditory mode single and multiple motor response units
17 p2686 A71-35433

Rhesus monkeys electrocortical events recorded during foreperiod of reaction time tasks
18 p2853 A71-35895

Human response to auditory stimuli start and cessation, noting time lag and perception duration
19 p3001 A71-37283

Surround luminance effect on relative perceptual latency of response, using test stimuli confined to rod free area of fovea
20 p3184 A71-38774

Hyperbaric normoxic breathing helium, nitrogen and neon gas mixture effects on EEG and reaction time in man
21 p3342 A71-40347

Prior muscle exertions effect on reaction time and duration of simple discrete movements, considering electromyogram frequency changes
22 p3503 A71-42194

Central panel luminance effect on peripheral visual detection time in search tasks
23 p3638 A71-42899

Proactive reaction time inhibition as indicator of immediate memory retention intensity in subjects receiving interpolated acoustic stimuli
23 p3634 A71-43865

Quantitative characterization of unit time response in visual system, mapping latency and synchronicity as functions of stimulus position
23 p3640 A71-43870

Light brightness and duration effect on central vision response time during dark adaptation
24 p3795 A71-44535

REACTION WHEELS

Three axis long life satellite attitude control, describing double gimbaled reaction wheel system
04 p0663 A71-15299

Spacecraft attitude control system with inertia wheels, determining stability by decomposition method
04 p0663 A71-15300

Reaction wheel satellite attitude control, describing nondimensional parameter for interaxis gyroscopic coupling effects in preliminary design estimates
17 p2722 A71-35185

Gravity gradient desaturation of momentum exchange attitude control system, considering control moment gyros and reaction wheels
19 p3098 A71-37185

Synchronous three-axes stabilized communication satellites attitude control system with double gimbaled reaction wheel control actuator, obtaining 0.1 degree pointing accuracy with pitch and roll sensors
19 p3098 A71-37190

Gimbaled reaction wheel for spacecraft accurate attitude stabilization and control
19 p3098 A71-37191

Twin wheel momentum bias/reaction jet spacecraft attitude control system, presenting mathematical model, stability analysis and design
19 p3099 A71-37192

Skewed and orthogonal redundant reaction wheels comparison for outer planet exploration spacecraft attitude control based on reliability analysis
19 p3101 A71-37926

Attitude stability of dual spin spacecraft with energy dissipation in flexible momentum wheel having two degrees of freedom
23 p3772 A71-43020

REACTIVITY

Perchloric acid reactivity with respect to hydrogen, methane, ethane and ethylene by flow method, using twin concentric jet reactor of Pyrex glass
17 p2792 A71-35709

Reactivity changes to pharmacocological preparations under total proton and gamma ray irradiation of abdomen and head shielded rats
22 p3492 A71-42717

REACTOR CORES

In-core thermionic reactor development for space applications
02 p0282 A71-12307

TV broadcast satellites with in-core thermionic reactor, discussing transmitting power, design and economy
02 p0283 A71-12308

Nuclear thermal rockets development, discussing reactor-engine tests, solid and gas cores and Saturn 5 application
02 p0283 A71-12314

Thermionic reactor core design for undersea conditions based on neutron data and calculation related with diode materials
11 p1711 A71-25882

Driver terrestrial in-core thermionic reactor dynamic behavior, discussing computerized simulation with respect to coolant loop
11 p1711 A71-25883

Thermionic reactor parametric criticality studies, evaluating fuel element and core design variations effects
11 p1712 A71-25885

Space base 100 kw thermionic reactor power plant featuring interchange core replacement package
11 p1713 A71-25895

Thermal and electrical characteristics of two nuclear type cylindrical converters with nonuniform emitter temperature
11 p1714 A71-25903

Critical mass calculation for open cycle gas core rocket reactors, considering cavity size, fuel radius, reflector thickness and hydrogen bypass flow
22 p3573 A71-41637

Volume fraction analysis of coaxial flow gas core nuclear rocket for mass flow ratios, fuel radius and density, using free jet computer code and eddy viscosity equations
22 p3573 A71-41638

REACTOR DESIGN

Low power thermionic reactors, comparing four types design, characteristics and performance estimates for power plants
02 p0281 A71-12263

Neutronic comparisons of design concepts for low power thermionic space power reactors based on uranium and uranium-based fuels
02 p0281 A71-12264

Thermionic performance influence on reactor design and operation, considering plant electrical ratings
02 p0281 A71-12266

Technology gap between thermionic converter physics and reactor engineering, emphasizing language problem
02 p0281 A71-12272

MHD system hydrodynamic stability using propellant and fuel filled reactor cavity to form three region two fluid vortex
06 p0882 A71-18318

Post burnout heat transfer to mist flow for nuclear reactor design, using two step model
07 p1221 A71-18789

Ground test reactor design based on colloid fueled reactor concept
[AIAA PAPER 70-688] 07 p1158 A71-19862

Nuclear radiation shielding design for space base SNAP 8 reactor, discussing geometry constraints for lithium hydride and U loop layers model
09 p1492 A71-22808

Liquid metal cooled, fast spectrum thermionic reactor experiment design based on Fast Reactor Core Test Facility use for dynamic and steady state characteristics determination
11 p1710 A71-25867

Thermionic reactor experiment design to evaluate U-235 fueled fast spectrum core dynamic and steady state characteristics, discussing system features
11 p1710 A71-25868

Thermionic reactor electric spacecraft propulsion system for unmanned outer planets missions, investigating voltage and radiator temperature effects on weight
11 p1811 A71-25872

Out-of-core thermionic converter system using heat pipes as electrical resistive elements, discussing design and performance
11 p1710 A71-25875

Design optimization of out-of-core cylindrical thermionic converter module with heat pipes and integral finned radiator
11 p1711 A71-25876

Thermionic reactor core design for undersea conditions based on neutron data and calculation related with diode materials
11 p1711 A71-25882

Design and operation of split fueled cores with axial heat pipes for 350 kwe out-of-core thermionic power converter system
11 p1712 A71-25884

Thermionic reactor parametric criticality studies, evaluating fuel element and core design variations effects
11 p1712 A71-25885

Space base 100 ekw thermionic reactor power plant featuring interchange core replacement package
11 p1713 A71-25895

Thermionic integrated Cs reservoir converter for in-pile applications, discussing design for various coolant temperatures
11 p1715 A71-25909

Reactor shielding design in U.S. based on Boltzmann transport equation solutions and Monte Carlo method
13 p2099 A71-29254

Reactor shielding problems solutions involving removal-diffusion theory, two dimensional transport theory and Monte Carlo method
13 p2099 A71-29255

SNAP-8 mercury Rankine system performance data, investigating design change for reduced reactor operating temperatures
15 p2447 A71-32201

Out-of-core nuclear thermionic converter system design feature concerning heat pipes, vapor-cooled radiators, modularity and reliability
15 p2448 A71-32224

Nuclear reactor design as heat source for electric power generation in space
16 p2606 A71-33249

Compact fast reactor design for space power with rotating fuel drums, Mo alloy reflectors and honeycomb support structure
16 p2606 A71-33252

REACTOR FUELS
U NUCLEAR FUELS
REACTOR MATERIALS

Test equipment for elasticity modulus measurement of neutron irradiated materials, noting u-c nuclear fuel and alloy samples
07 p1084 A71-20356

Endurance limit of construction materials under fast and thermal neutron irradiation in reactor channel
16 p2598 A71-33986

Water cooled reactor Zircaloy brazing filler metals, investigating corrosion resistance, joint strength and brazing capability
18 p2928 A71-36856

Mercury properties, chemistry, safety, handling and corrosion in nuclear coolant applications
19 p3102 A71-37071

German monograph on creep buckling tests of finned and unfinned thin walled pipes of heat resistant breeder reactor cladding materials
21 p3464 A71-40781

REACTOR PHYSICS

Thermionic reactor analytical model for systems analysis, considering complex interactions between reactor physics, thermionics and thermal/hydraulics
02 p0281 A71-12265

Plasma physics and fusion reactor development involving electric conduction, vibration and magnetic effects, stellarator containment, etc
07 p1168 A71-19602

Dynamic simulation of fission product heating in reactor using multigroup Way-Wigner method
07 p1158 A71-20350

REACTOR SAFETY

Nuclear powered long distance aircraft engines, discussing high burnup fuel, weight factors and safety problems
06 p0926 A71-17694

Nuclear power plants safety design and evaluation via probabilistic analysis
08 p1300 A71-21852

Nuclear surface effect vehicle and subsonic aircraft for transoceanic cargo shipping, discussing mobile reactor safety tests under high speed impact conditions
09 p1492 A71-22779

Reactor shield weight optimization using FASTER-III Monte Carlo computer program for neutron and gamma ray transport
09 p1539 A71-22810

Automatic control, safety and dynamics of thermionic reactor experiment under simulated spacecraft load requirements
11 p1712 A71-25888

Air breathing nuclear propulsion, considering reactor safety in air cushion vehicles and aircraft
14 p2273 A71-29930

Reactor-shield-containment system models under impact tests, noting cracks, leaks and deformations
16 p2606 A71-33250

Nuclear safety considerations for ground checkout, launch and in-orbit operations of reactors for earth-orbital manned space stations
20 p3262 A71-38920

Safe disposal for nuclear zirconium hydride reactors for manned space base mission
20 p3263 A71-38921

Radioisotope thermoelectric generator safety and operations considerations for users of large nuclear space power systems
20 p3264 A71-38933

REACTOR TECHNOLOGY

Fusion energy technology, discussing controlled reactor construction and operation
07 p1169 A71-20000

Out-of-core thermionic converter system using heat pipes as electrical resistive elements, discussing design and performance
11 p1710 A71-25875

Materials technology of Ta-W-Hf clad uranium mononitride fuel for lithium cooled compact fast space power reactor, including irradiation tests
16 p2606 A71-33254

READERS

Fluidic 8 track punched tape reader, discussing design simplicity, flexibility, accuracy, wear and long life operation
07 p1025 A71-20560

Flying spot scanner electron optical systems for reading data from photographic film for studies of recognition algorithms, image simulation and automatic particle track measurements
15 p2409 A71-32191

READING MACHINES

U READERS

READJUSTMENT

U ADJUSTING

READOUT

EEG analyzer voltage peaks recording on computer, using digital readout for simultaneous initial and terminal stage markings
08 p1248 A71-21446

Readout systems light emitting numerals legibility, determining threshold values from response categorization into correct responses, misreadings and missed signals
21 p3376 A71-40125

Coherent optical processing system coupled to electronic readout system incorporating image orthicon TV camera, small digital computer and cell generator
21 p3381 A71-40929

REAL GASES

German monograph on centered two dimensional nonequilibrium hypersonic expansion flow, considering real gas flow with chemical reactions
05 p0693 A71-16124

Shock wave propagation through converging nozzle, predicting real gas dissociation and vibrational excitation effects for comparison with shock tube measurement
05 p0735 A71-16528

Convective heat transfer in three dimensional stagnation point boundary layer flow characterized by real gas properties
10 p1698 A71-25098

Elliptical cones at large angle of attack, calculating three-component real gas properties effects on aerodynamic characteristics
13 p1993 A71-29191

Real gas mass flow rate computation through sonic nozzle
14 p2239 A71-29927

Methane and natural gas flow through critical flow nozzles, calculating real gas effects on mass flow rate
14 p2224 A71-29937

Boltzmann kinetic equation for imperfect gases in pair collision approximation, including terms propor-

tional to time and coordinate derivatives and van der Waal constants
15 p2387 A71-31193

High pressure pneumatic lines dynamics, considering equation of state for real gas with given compressibility function
16 p2527 A71-33618

Sound velocity in real gases as function of pressure and temperature, deriving by van Isterbeek result generalization for higher pressures
17 p2783 A71-35038

Shock tubes and shock tunnels, considering equilibrium expansion, relaxation phenomena and real gas effects
18 p2897 A71-36410

Dissipative fluid motion, discussing approaches to analysis of real fluids time dependent complex flow equations
19 p3089 A71-37499

Higher pressure ratios trend in aircraft gas turbines leading to higher exit temperatures from compressor, noting real gas effects
21 p3437 A71-40170

Blunt body heat transfer predictions for atmospheric reentry, discussing coupled effects of real gas behavior and slip/jump boundary conditions
21 p3474 A71-40256

REAL NUMBERS

NT INTEGERS

Algebraic criterion for positive realness of rational functions, using Routh algorithm
09 p1486 A71-23651

REAL TIME OPERATION

Operational memory share supervisor program with storage protection feature for real time multitask digital process control and teleprocessing of electrical power utility system
01 p0043 A71-10181

Real time systems design principles for processor organization, logic circuits, fault detection and diagnostic tests to facilitate high degree of reliability and maintainability
01 p0046 A71-10203

Real time graphic display monitoring of time sharing computer systems operational state
01 p0046 A71-10207

High speed real time interpretive language for biological calculations with PDP-8 computer
01 p0049 A71-10244

Manual tracking systems identification and real time display, developing software system
01 p0027 A71-11437

Real time six degree of freedom aircraft flight digital simulation using SL-1 continuous system simulation language
02 p0226 A71-11786

Hybrid real time computer simulation of external visual display cues for Apollo Command and Service Modules
02 p0237 A71-11791

Real time contourgram for monitoring ECG waveform data, describing cardiac measurement and data display
02 p0199 A71-12384

Real time oscilloscope observation of ultrafast photodiode response to mode locked laser pulses
03 p0438 A71-13886

Real time analysis and display of pulsed laser propagation data in rectangular X-Y field
03 p0427 A71-13920

Data system environment simulator /DASYS/ for real time test bed capability for software development and testing
04 p0556 A71-15294

MITOL problem-oriented compiler language for real time and postflight telemetry data processing
04 p0556 A71-15295

Real time missile radio telemetry data transmission to ground station, using instrumented aircraft
04 p0554 A71-15321

Real time processor design for sequential control of all-digital multiline data set
[IEEE PAPER 70-TP-375-COM]
05 p0725 A71-17067

USAF space missions information processing requirements relative to space transportation system, emphasizing real time image processing
05 p0727 A71-17229

Cathode ray tubes as real time display device in various types of professional equipment, describing functional performance and related tube design aspects
06 p0872 A71-17319

Real time solar flare image production for Skylab astronaut training, using films of H alpha, XUV and X ray solar images
06 p0902 A71-18530

Real time tracking filter candidates for implementation in systems tracking maneuvering vehicles compared in terms of accuracy and computer requirements for tactical applications
07 p1069 A71-18837

Development program for multiple access real time tactical information distribution system, designing and constructing tactical air control system test facility [AIAA PAPER 71-243] 07 p1156 A71-19718

Target detection performance in simulated real time airborne reconnaissance mission, taking into account search time and image type, contrast and rate of motion 08 p1248 A71-21227

ECG signals on-line and real time monitoring mathematical, statistical and bioengineering considerations 08 p1248 A71-21330

Adaptation algorithm for real time minimum mean square error array processing, using with multidimensional digital filter 08 p1256 A71-21605

Algorithms for continuous indirect sequential observations utilization with real time synoptic measurements in objective analysis 08 p1328 A71-21725

Real time low frequency narrow band spectrum analyzer using time compression technique for vibrating machinery diagnosis and prognosis 09 p1443 A71-22708

Real time and double exposure holographic interferometry measurements of strain on aluminum cylinder under internal pressure, noting discrepancy with strain gage values 09 p1444 A71-22711

Real time remote test site computation and display of complex engine inlet distortion parameters from dynamic pressure signal, using analog computer 09 p1446 A71-22726

Electronic imaging devices specifications, emphasizing real time reconnaissance systems performance requirements 10 p1609 A71-24059

Optimal models for time shared computer systems with real time multiprogramming 10 p1581 A71-24727

System identification, considering input signals classification, model structure, linear/nonlinear systems identifying and on-line/real time techniques 10 p1586 A71-24736

Digital simulation facility for airborne collision avoidance system effects on ATC terminal automation, discussing operation, hardware and software equipment 10 p1590 A71-24774

Real time spectrum analyzer, discussing data sampling rates, statistical uncertainties, waveform and bandwidth 10 p1612 A71-24832

Real time high resolution mass spectroscopy using digital computer techniques for data acquisition, processing and presentation 11 p1761 A71-25220

Computer controlled source data preparation Keycheck system, discussing real-time software support for documents audio/visual error detection 11 p1734 A71-25638

Complex real time hybrid computer simulator for captive two blade rotor platform dynamic problem solving 11 p1744 A71-25847

Flight test completed on onboard real time engine performance monitoring system, discussing thermodynamic analysis technique [ASME PAPER 71-GT-77] 11 p1813 A71-25991

Contamination degrading effects on optical surfaces, discussing application to real time monitors data analysis [AIAA PAPER 71-460] 11 p1800 A71-26242

Real time modal purity and data quality assessment techniques 11 p1853 A71-26501

MODAPS real time data processing system for modal vibration testing consisting of analog subsystems, digital interfaces and on-line minicomputer 11 p1746 A71-26502

Experiment planning, using digital computer in real time with programmed algorithm 12 p1883 A71-26713

Spatial filter synthesis for real time combined subtraction and correlation in coherent optical data processing system 12 p1905 A71-26808

MAC malfunction detection, analysis and recording system applications in commercial airlines, emphasizing real time response for maintenance function [SAE PAPER 710425] 13 p1995 A71-28311

Evoked brain potentials averaging in real time with computer linked by long distance communication lines 13 p2017 A71-28385

Real time holography using moving groundglass or fluorescent layer suitable for coherent matched filtering and seeing through fog 13 p2068 A71-28709

Real time computable partial recursive functions of n variables with expectancy estimate on Minsky machines 13 p2096 A71-28976

Adaptive controller consisting of real time identifier and minimum variance regulator approached through stochastic optimal control theory 14 p2219 A71-29696

Computer controlled acoustic data acquisition system with real time control of 16 high intensity acoustic generators 14 p2208 A71-30315

Real time radar instrumentation data processing and control system, discussing computer selection, software requirements and configuration, etc 14 p2196 A71-30338

Computer real time data monitoring and control software in satellite integration support and test operations, noting test oriented language 14 p2208 A71-30339

Real time systems programming techniques based on modular programs, integrated data stores, multiprocessor and special computer languages 14 p2208 A71-30381

Real time stroboscopic vibration analysis technique involving holographic interferometry 15 p2404 A71-31271

DC 10 flight test program improvement using data acquisition/processing with real time monitoring, instrument landing and laser tracking [AIAA PAPER 71-788] 16 p2553 A71-34018

On-line real time optimal control computations for aerial combat games between two aircraft, assessing airborne computer requirements [AIAA PAPER 71-797] 16 p2525 A71-34022

Apollo real time control center large software systems development management covering implementation, integration, testing, operation and maintenance 17 p2710 A71-34620

Mathematically oriented digital computer system implemented on IBM 360 with graphic remote consoles for engineering problems 17 p2710 A71-34622

Forty channel magnetography system including CRT display, digital controlled heliostat, real time computer and optical transducer 17 p2740 A71-34988

Real time system for solar spectrophotometry, noting application for scanning H alpha and other Balmer series lines profiles in solar flare regions 17 p2741 A71-34994

Videometer instrument for solar flares quantitative measurement, eliminating red sensitive vidicon for real time operation in H alpha region 17 p2742 A71-35003

French monograph on algorithms for parameters estimation for adaptive identification in real time of linear processes perturbed by related noise 17 p2767 A71-35232

Signal processing operation of real time optical correlator, using ultrasonic light modulators 17 p2708 A71-35484

Real time reconnaissance cockpit display system for airborne sensor systems, providing night combat imagery 17 p2747 A71-35772

BITSIM computer simulation technique for application to real time airborne photoreconnaissance imagery data transmission system design and performance analysis 18 p2917 A71-36070

Optimal models for time shared computer systems with real time multiprogramming 19 p3025 A71-37692

Real time holographic interferograms, achieving required beam intensities relationship by ordinary neutral light filters near collimator focus 19 p3065 A71-38196

Acoustic or microwave hologram reconstruction into visible three dimensional image in real time 19 p3066 A71-38412

Computer automated systems development for electromagnetic compatibility analysis, noting interactive processing in near real time mode 19 p3030 A71-38439

Real time lensless holographic recognition of spatially incoherent and self luminous patterns on diffusing backgrounds using optical matched multiple filters 20 p3235 A71-39184

Real time multitrack half tone recorder for displaying three dimensional information on instantaneous blood velocity measurement by Doppler effect 21 p3377 A71-40132

Real time mechanical strain measurement by optical correlation techniques, using coded matched-filter hologram and incoherent illumination 21 p3377 A71-40229

Hybrid electromechanical analog computer real time simulation technique for optimizing vibration response of two degree of freedom system with impact damper [ASME PAPER 71-VIBR-119] 21 p3350 A71-40338

Real time holographic interferometry of steady state mechanical vibrations of engineering structural components applicable to arbitrary small amplitude and large mode numbers 21 p3381 A71-40934

Real time coherent optical data processing, describing spatial filtering and reactive processor and image converter designs 22 p3540 A71-41750

Australian National Radio Astronomy Observatory integrated time and frequency system with cesium beam frequency standard and digital computer for real time operation 22 p3547 A71-42498

TV multiplexing and broadband multichannel real time telemetry data transmission without loss between Kennedy Space Center and ground station for computer operation 23 p3645 A71-43519

Error evaluation of digital real time simulation of nonlinear systems 24 p3813 A71-44571

REAL VARIABLES

NT ABEL FUNCTION

NT ASYMPTOTES

NT ASYMPTOTIC SERIES

NT BESSEL FUNCTIONS

NT BIHARMONIC EQUATIONS

NT BINARY INTEGRATION

NT BLASIU EQUATION

NT BOREL SETS

NT BURGER EQUATION

NT CALCULUS OF VARIATIONS

NT CAUCHY-RIEMANN EQUATIONS

NT COLLINEARITY

NT COPLANARITY

NT CUBIC EQUATIONS

NT CURL [VECTORS]

NT DELTA FUNCTION

NT DIFFERENTIAL EQUATIONS

NT DUFFING DIFFERENTIAL EQUATION

NT EINSTEIN EQUATIONS

NT ELLIPTIC DIFFERENTIAL EQUATIONS

NT EXISTENCE THEOREMS

NT EXTREMUM VALUES

NT FALKNER-SKAN EQUATION

NT FOKKER-PLANCK EQUATION

NT FOURIER SERIES

NT FUNCTIONAL INTEGRATION

NT GAUSS EQUATION

NT GREEN FUNCTION

NT HANKEL FUNCTIONS

NT HELMHOLTZ VORTICITY EQUATION

NT HYPERBOLIC FUNCTIONS

NT HYPERPLANES

NT INTEGRAL CALCULUS

NT JACOBI INTEGRAL

NT JACOBI MATRIX METHOD

NT KERNEL FUNCTIONS

NT LEBESGUE THEOREM

NT LIAPUNOV FUNCTIONS

NT LIMITS [MATHEMATICS]

NT LINEAR EQUATIONS

NT LIOUVILLE EQUATIONS

NT LIPSCHITZ CONDITION

NT MEASURE AND INTEGRATION

NT NEUMANN PROBLEM

NT NONLINEAR EQUATIONS

NT NUMERICAL INTEGRATION

NT PADE APPROXIMATION

NT PARABOLIC DIFFERENTIAL EQUATIONS

NT PARTIAL DIFFERENTIAL EQUATIONS

NT PERIODIC FUNCTIONS

NT POISSON EQUATION

NT POWER SERIES

NT QUADRATIC EQUATIONS

NT RUNGE-KUTTA METHOD

NT SERIES [MATHEMATICS]

NT SINE SERIES

NT STIELTJES INTEGRAL

NT STURM-LIOUVILLE THEORY

NT TAYLOR SERIES

NT TRIGONOMETRIC FUNCTIONS

NT VECTOR ANALYSIS

NT VLASOV EQUATIONS

NT VORTICITY

NT WIEIERSTRASS FUNCTIONS

NT WHITTAKER FUNCTIONS

N-body problem real singularities in celestial mechanics, considering present status and holomorphic motion 01 p0154 A71-10384

Average number of real roots of polynomials consisting of independent random quantities with identical distribution 23 p3699 A71-43571

REATTACHED FLOW

Turbulent separation and reattachment at turbomachine blade trailing edge at supersonic speeds, discussing various flow models 03 p0340 A71-13142

Leading edge bluntness and boundary layer displacement effects on attached and separated laminar boundary layers in high temperature hypersonic flow over compression corner [AIAA PAPER 68-68] 03 p0341 A71-13437

Flow separation and reattachment in confined jet mixing of air with secondary flow in duct [ASME PAPER 70-FE-B] 03 p0341 A71-13703

Three dimensional turbulent jet reattachment, investigating wall attachment distance with aspect and offset ratio and Reynolds number variations [ASME PAPER 70-WA/FLCS-5]

03 p0401 A71-14081
Simplified two dimensional jet reattachment model, using Goertler profile equation and constant spread parameter [ASME PAPER 70-WA/FLCS-8]

03 p0401 A71-14084
Leading edge bluntness and boundary layer displacement effects on attached and separated laminar boundary layers in high temperature hypersonic flow over compression corner [AIAA PAPER 68-68]

05 p0735 A71-16561
Interaction theory for supersonic separated and reattaching turbulent boundary layers, comparing to real flow past compression ramp [AIAA PAPER 71-128]

06 p0844 A71-18572
Fluidic diverting valve independent of turbulent reattachment, examining large scale model and digital element characteristics in closed loop system

07 p1024 A71-20553
Jet reattachment to adjacent flat plate, investigating back pressure effects

07 p1094 A71-20606
Fluidic OR-NOR element multiple regression analysis, investigating wall attachment, hysteresis switch pressure and percentage recovery

07 p1031 A71-20607
Wall attachment jet control volume model, examining flow momentum with restrictive force

07 p1031 A71-20609
Backward facing step in confined supersonic two dimensional flow, investigating turbulent shear layer reattachment

10 p1552 A71-24622
Interaction theory for supersonic separated and reattaching turbulent boundary layers, comparing to real flow past compression ramp [AIAA PAPER 71-128]

11 p1702 A71-25476
Streamwise vortices of distinct periodicity in laminar transitional turbulent reattaching flows over wide Mach number range

11 p1751 A71-25496
Heat transfer to airfoil in oscillating flow at large angles of attack, showing vortex shed reattachment and Nusselt numbers increase [ASME PAPER 71-GT-18]

11 p1703 A71-25963
Reattachment angle of supersonic laminar mixed boundary layer, using revolution model with Reynolds number allowance

11 p1704 A71-26194
Reattachment of single two dimensional turbulent air jet, investigating gas flow characteristics in combustion chambers

14 p2170 A71-30419
Separation controlled transonic drag-rise modification for V-shaped notches attributed to inviscid/viscid interaction controlling flow separation and reattachment [AIAA PAPER 71-568]

15 p2345 A71-31561
Attaching jet flow on inclined flat plate with small offset, obtaining centerline shape and velocity profile

15 p2391 A71-32056
Slow switching in wall attachment fluidic devices, determining flow characteristics

15 p2391 A71-32057
Ducted axisymmetric jet mixing flow, investigating flow separation and reattachment as function of diameter and velocity

15 p2392 A71-32252
Shock layer reattachment initiated by point explosion and driven continuously outward by inner contact surface

18 p2985 A71-36034
V shaped notches drag coefficients behavior in transonic regime, observing inviscid-viscid interaction controlling flow separation and reattachment

21 p3323 A71-40954

REBREATHING

Mixed venous oxygen tension oxide determination by nitrogen-carbon rebreathing method, considering pulmonary blood flow and oxygen carrying capacity

03 p0360 A71-13182
Chemosensitivity in normal, hypoxia and hypocapnia cases, using rebreathing techniques to construct isoxic carbon dioxide response curves and isocapnic oxygen response curves

07 p1052 A71-20329
Carbon dioxide tension in pulmonary arterial blood before/during prolonged rebreathing in oxygen mixtures at rest and exercise

10 p1558 A71-23895
Alveolar and arterial carbon dioxide partial pressure during rebreathing experiments at rest

13 p2007 A71-28435
Oxygen pulmonary diffusion capacity estimation by rebreathing procedure based on gas-blood partial-oxygen-pressure equilibration

17 p2678 A71-34173

RECEIVERS

NT LINEAR RECEIVERS

NT LOGARITHMIC RECEIVERS

NT RADIOTELEPHONES

NT SUPERHETERODYNE RECEIVERS

NT TELEVISION RECEIVERS

Coherent binary reception channels noiseproof qualities in presence of fluctuating noise and single concentrated bursts

01 p0030 A71-10473
Field tests for telemetry receiving systems solar calibration, describing antenna pointing

01 p0033 A71-10891
Quantum mechanical communication theory of optimal receivers, using statistical detection and estimation theory

02 p0213 A71-12016
Direct detection, heterodyne and optimum receivers for optical scattering channels in digital communication

02 p0214 A71-12020
Optical heterodyne receiver design, using nonlinear recursive techniques to estimate atmospheric fluctuation effects on IF signal characteristics

02 p0249 A71-12026
Solid state receiver for IR, using microwave biased Ge photoconductor

02 p0231 A71-12027
Optimal quantum receiver mathematical specification derivation for M-ary digital signal detection

02 p0215 A71-12036
Ground station integrated receiver cabinet formed by down-converter, demodulator and baseband equipment packaging

02 p0224 A71-12817
Earth station equipment for Intelsat 4, discussing thermal noise, transmitters, wideband receivers and demodulators

02 p0224 A71-12829
Servosystems errors of indicator-receiver for recording electromagnetic field pattern extremes in amplitude radio interferometers

04 p0557 A71-14635
Multiplexed PAM signal transmission over random time multichannel and diversity systems, discussing optimization for receiver frequency response by numerical solution [IEEE PAPER 70-TP-47-COM]

05 p0723 A71-17053
Adaptive/self synchronizing PSK receivers with common power and bandwidth, discussing analytical and numerical investigations of performance characteristics

05 p0723 A71-17054
All-digital multichannel narrow band FSK data receiver with time-shared arithmetic processor, discussing prototype design and performance [IEEE PAPER 70-TP-49-COM]

05 p0724 A71-17064
Receiving equipment for direct differential Doppler frequency measurement via beacon satellites observation

07 p1059 A71-19012
Intelsat 4 satellite transponder, examining receivers, transmitters, mechanical stability and heat transfer

10 p1578 A71-24509
Receiver systems for 100 meter Effelsberg radio telescope using cryogenically cooled parametric amplifiers for receiver system noise minimization

10 p1578 A71-24510
Monopulse receiver design system and image band noise factors tradeoffs, discussing preselector and integrated front end trends

11 p1737 A71-25676
Optimal receiver to detect multiple orthogonal signals on normal stationary noise background, assuming nonuniform a priori probability occurrence

12 p1883 A71-27618
Nonlinear filtering synthesis of optimal receiver for pseudorandom phase shift keyed signal with arbitrary modulation angle and white noise background

14 p2195 A71-30107
Electronically scanned circular array elements number in receiver design, discussing gain distribution

14 p2206 A71-31072
Optimal noncoherent receiver for signal detection in mixture of noise and chaotic echoes in media with frequency dependent attenuation

15 p2369 A71-31231
Noise stability and false response probabilities of receivers in circular remote control systems under harmonic interference for signal transmitted over power distribution grids

15 p2353 A71-32081
Probability density function of optimum phase locked loop synchronizer of sinusoidal signal with white Gaussian noise in partially coherent receiver

20 p3195 A71-38858

RECEIVING SYSTEMS

U RECEIVERS

RECEPTACLES [CONTAINERS]

U CONTAINERS

RECEPTORS [PHYSIOLOGY]

NT PROPRIOCEPTORS

African lungfish retina electron microscopy for Landolt club location, mitochondria, glycogen and microtubule content, considering relation to receptors and possible functions

01 p0009 A71-10272

Color matching discrepancies, considering rod blue qualities under photopic conditions, luminance level and trichromatic stimulus unsuitability for large field additive colorimetry

01 p0010 A71-10273
Alpha and beta receptor blocking drugs effects on oxygen consumption of methemoglobin-containing erythrocytes and hemolysates

03 p0363 A71-13483
Sensitivity, size and receptive fields position in cat retina ganglion cells

05 p0706 A71-16341
Simple nerve system receptor field organization in visual analyzer simulated by TV circuit with scanning beam controlled focusing

07 p1050 A71-20108
Human skin vibratory sensibility consideration as analyzer receptor for stimuli conversion into nervous processes

07 p1043 A71-20116
Vertebrate retina receptive field structure, suggesting interaction between receptor, horizontal and bipolar cells

07 p1046 A71-20623
Pattern recognition systems, considering receptor, preprocessing and decision making stages

10 p1568 A71-24225
Organisms olfactory extraction and interpretation of low intensity chemical signals from air, outlining receptor mechanism from fish physicochemistry

10 p1563 A71-24234
Human transversostriated muscle plate receptors morphogenesis

12 p1872 A71-27725
Accelerations effect on receptors in semicircular canals during human movements in rotating environment, using vector analysis

13 p2007 A71-28415
Cat single optic nerve fibers receptive field, observing functional organization and conduction velocity

13 p2008 A71-28458
Human odorant evoked response, considering stimulation of olfactory receptors and trigeminal afferences in nose

13 p2012 A71-28891
Visual sensation time theory validity investigation, discussing time elapsed between retinal receptor stimulation and perceptory sensation

14 p2189 A71-30406
Temperature, odor mixing and stimulation frequency effects on olfactory receptor potential of fly *Lucilia sericata*

14 p2186 A71-30568
Fly *Lucilia sericata* olfactory receptor and unit action potentials response to odor stimulation by homologous compounds

14 p2186 A71-30569
Snake IR receptor sense organs tested by IR stimulus from carbon dioxide laser, suggesting receptor operation on thermal principle

15 p2360 A71-32296
Reflex increase in ventilation induced by vibrations applied to cat triceps surae muscles, noting muscular and articular receptors role

17 p2678 A71-34175
Redundancy in receptive neuronal nets, examining structural and functional organization of generalized biological analyzer peripheral section

17 p2690 A71-34956
ACH retina application effects, showing second retinal neuron cholinergic receptors desensitization

17 p2686 A71-35490
Afferent nerve impulse traffic from atrial A-type receptor fibers in cats in relation to heart rate control

18 p2857 A71-36688
Canine ventricular myocardium as cardiac beta-adrenergic receptor, describing binding of norepinephrine to microsomal particles

19 p3002 A71-37900
Primary biological receptor element analogous electronic model for potential and afferent pulse train responses to stimuli

20 p3191 A71-38894
Visual projection, magnification and retina overlap on dorsal lateral geniculate nucleus in cats measured by random scatter in receptive field

21 p3335 A71-40668
Inhibitory binocular receptive fields in dorsal nucleus of lateral geniculate body for dominant and nondominant eye in cats, using moving slit and flash spot stimulation

21 p3335 A71-40669
Holography applications in ophthalmology to determine optical constants of living eye, including retinal receptors

22 p3540 A71-41753
Eye movement neurophysiology, discussing ocular proprioception, oculomotor muscle sensory receptor role, extraocular muscle afferent and efferent innervation and central nervous system control effect

22 p3488 A71-42433
Receptive fields of dark adapted cats striate cortex neurons as function of barbiturate anesthetic level

23 p3634 A71-43871

RECIPROCAL THEOREMS

- Quantitative variation in anesthetized cats striate cortex receptive fields as function of light and dark adaptation 23 p3634 A71-43872
- Human skin cold receptor diurnal activity rhythm 24 p3795 A71-44499

RECIPROCAL THEOREMS

- Compressible isotropic plasma slab effect on magnetic dipole radiation pattern, using reciprocity theorem 08 p1253 A71-21274
- Helmholtz reciprocity theorem extension to clear turbulent atmosphere, defining Green functions to characterize optical propagation in opposite directions between parallel planar apertures 10 p1641 A71-23949
- Reciprocity theorem for magnetoionic modes, considering arbitrary plane slab within magnetoplasma with parameter variation in direction normal to horizontal plane of stratification 10 p1577 A71-24293
- Linear elastokinetics tensorial field integral representation derivation from reciprocal dynamic theorem for equations of motion 10 p1687 A71-24350
- Cosserat-type bodies with linear elasticity, obtaining reciprocity theorem and stress solutions under concentrated load 18 p2984 A71-36949
- Monatomic gas beams scattering from gas surface interface with partially distributed energy states, confirming reciprocity or detailed balance principle 19 p3104 A71-38057

RECIPROCATING ENGINES

U PISTON ENGINES

RECIRCULATIVE FLUID FLOW

- Supersonic jet-bound subsonic wake interactions, determining recirculation zone boundaries 05 p0694 A71-16848
- Swirling effects on turbulent flow recirculation zone behavior in gas turbine main burners [AIAA PAPER 71-2] 06 p0946 A71-18477
- Heat transfer in cylindrical cavity with circulating flow as function of time and Peclet number 10 p1696 A71-24615
- Recirculation patterns in coaxial steady laminar mixing of homogeneous jets in confined tube, solving Navier-Stokes equations 11 p1748 A71-25151
- Recirculating cells and entrance conditions influence on confined heterogeneous jets laminar mixing, measuring velocity and concentration profiles [AIAA PAPER 71-601] 15 p2389 A71-31578
- Supersonic combustion flowfield transverse hydrogen jet injection into Mach 2.5 airstream, discussing recirculation region upstream [WSS/CI PAPER 71-15] 15 p2663 A71-31624
- Numerical analysis of laminar recirculating flow between shrouded rotating disks for interaction between vorticity and stream function and swirl-velocity field 18 p2905 A71-36309
- Two dimensional supersonic base flow with small Mach number recirculation zone, determining jet line by variational principle of Poisson equation 20 p3176 A71-39414
- Computer program for recirculating fluid flows applied to concentration curves obtained by gas injection on pipe center line with fully developed turbulent flow 24 p3820 A71-44956

RECLAMATION

- NT MATERIALS RECOVERY
- NT WATER RECLAMATION

RECOGNITION

- NT CHARACTER RECOGNITION
- NT PATTERN RECOGNITION
- NT SPEECH RECOGNITION
- NT TARGET RECOGNITION
- NT TIMBER IDENTIFICATION
- Computer programs parallel processable tasks recognition techniques survey, discussing algorithms 01 p0043 A71-10177
- Mathematical simulation of human recognition by black box approach as information conversion process 07 p1050 A71-20109

RECOIL ATOMS

- Scattering atom recoil effect in resonance line transfer with Doppler redistribution, discussing neglect from microscopic point of view 21 p3447 A71-40429

RECOIL PROTONS

- Proton recoil measurements of PuBe neutron source spectra, using pressurized hydrogen spherical proportional counter and liquid scintillator measurements 14 p2276 A71-29918

RECOMBINATION COEFFICIENT

- Atmospheric interaction layer large recombination coefficient existence possibility according to corpuscular model of radar head echo 01 p0159 A71-10871
- Molecular ion recombination coefficient of decaying plasma formed by UV irradiation of Cs vapor in inert gas, using microwave diagnostic method 04 p0634 A71-15115

- Air and oxygen electron-ion recombination coefficients, considering plasma deionization rate 05 p0756 A71-17208

- E layer electron concentrations, effective recombination coefficient and ionization sources during solar eclipse, noting soft X radiation intensity 06 p0894 A71-18260

- Ion-electron recombination coefficient measurement for ionized trails left by rocket exhausts in high atmosphere using radio observation 06 p0895 A71-18314

- MHD boundary layers with nonequilibrium ionization and recombination at finite rates 06 p0939 A71-18582 [AIAA PAPER 71-139]

- Three dimensional model of semiconductor diode current dependence on charge carrier diffusion length and surface recombination rate 09 p1414 A71-22189

- Two body N atoms recombination rate coefficient, using photometric analysis 09 p1498 A71-23400

- Pinch effect in nondegenerate intrinsic inhomogeneous semiconductors under nonuniform spatial volume recombination, resulting in nonlinear I-V characteristics 10 p1656 A71-24321

- Atmospheric molecular species, calculating electron impact ionization cross sections and recombination coefficients 10 p1645 A71-24970

- Dissociative recombination rates in partially ionized gases at elevated gas temperatures, using shock tube for limited ionization introduction 11 p1765 A71-26283

- Air and oxygen electron-ion recombination coefficients, considering plasma deionization rate 13 p2067 A71-28263

- Temperature dependence of current gain in p-n-p transistors due to increased surface recombination rate 14 p2213 A71-30623

- Metal additives catalytic effect on free radicals recombination rates in hydrogen-oxygen-nitrogen flames 15 p2515 A71-32552

- Oxygen dissociation and recombination rate constants at high temperatures from gas density interferometric measurement in relaxation zone of normal shock waves 15 p2367 A71-32570

- Physical model of Zn diffused GaAs electroluminescent diodes gradual degradation, establishing formation of new recombination centers through injected carrier lifetime measurement 15 p2377 A71-32607

- Hydrogen oxygen recombination rate constants from hydroxyl radical decay measurements in shock tube steady expansion 16 p2539 A71-32908

- Photoresonance cesium plasma development and decay, determining density spatial-temporal behavior and recombination and polar diffusion coefficients by probe measurements 17 p2787 A71-34287

- Electric fields effects on ionization and recombination rate in non-LTE Cs plasma 18 p2852 A71-36967

- Diatomic gas molecules three body recombination and dissociation rate coefficients from modified phase-space theory of reaction rates 19 p3107 A71-38078

- Added inert gases effect on gas phase H atoms recombination rate at room temperature, using electron spin resonance spectroscopy 19 p3011 A71-38080

- Metal additives catalytic effects on premixed hydrogen-oxygen-nitrogen flames free radical recombination rates, discussing heterogeneous and homogeneous schemes 19 p3012 A71-38082

- Partially ionized plasma expansion from spherical source into vacuum, obtaining equations of motion, collision integrals and recombination rate coefficient 19 p3115 A71-38213

- Ionospheric effective recombination coefficient and reaction rate models for various solar activity periods and day and night conditions 20 p3224 A71-39714

- Thermal dissociation rate of excited CsF, calculating ion-ion recombination rates 21 p3346 A71-40888

- Auger recombination coefficient determination for nonequilibrium carriers in n-type InAs from photoconductivity and light absorption under laser excitation at high levels, noting electron mobility 21 p3433 A71-41310

- Carbon ion and free electrons three body recombination rate coefficient measurement in carbon monoxide flows 24 p3802 A71-44607

- Identification of 417 Å line in solar EUV spectrum, calculating collision strengths and recombination rates for Fe XV 24 p3873 A71-45143

RECOMBINATION REACTIONS

- NT ATOMIC RECOMBINATION
- NT ELECTRON RECOMBINATION
- NT ELECTRON-ION RECOMBINATION
- NT HYDROGEN RECOMBINATIONS
- NT ION RECOMBINATION
- NT OXYGEN RECOMBINATION
- NT RADIATIVE RECOMBINATION

- Field effect photocurrent maximum in thin film semiconductors below Debye radius associating hole capture by recombination centers 01 p0139 A71-10781

- Atmospheric interaction layer large recombination coefficient existence possibility according to corpuscular model of radar head echo 01 p0159 A71-10871

- Electron density variations in ionospheric layers of different recombination types 01 p0074 A71-11080

- Electron density early time increase after artificial ionospheric heating, discussing F region recombination chemistry temperature dependence 01 p0040 A71-11532

- Three component two temperature plasma model of thermionic converter, including volume ionization-recombination processes 02 p0194 A71-12225

- Partially ionized bounded plasma LF natural oscillations due to ionization processes, ambipolar diffusion and charged particles recombination at walls 02 p0292 A71-12619

- Ionospheric Lyman alpha intensities and electron and positive ion densities during solar eclipse of 20 May 1966, discussing recombination model 03 p0407 A71-13380

- Diatomic molecules dissociation and recombination in presence of third body, considering quantum mechanical scattering theory 05 p0785 A71-16728

- Night D region ion kinetics data during thermonuclear detonation, discussing formation and conversion rates, electron concentration and recombination 08 p1278 A71-21009

- Recombination frequency spectrum asymmetry in interaction between high and low frequency plasma oscillations, noting role of Doppler effect 08 p1340 A71-21495

- I-V and capacitance characteristics of silicon diodes prepared by diffusive melting, considering recombination processes in p-n junctions 09 p1414 A71-22290

- Nonequilibrium recombination of dissociated combustion products of hydrogen in oxygen enriched heated air in supersonic nozzle 10 p1696 A71-24381

- Predawn enhancement structure of oxygen red line airglow at 6300 Å from time-latitude isophote diagrams, discussing F region photoelectrons recombination role 11 p1755 A71-25611

- Neutral wind effects on redistribution of E region ionization and recombination, comparing electron density profiles to vertical ion drift velocities 11 p1755 A71-25613

- Elementary particle recombination probabilities on solid body surface, using reactive gas model in form of quantum mechanics three body problem 12 p1934 A71-27546

- Photodissociative excitation of atomic oxygen dayglow emission, considering electron impact and dissociative recombination 13 p2056 A71-27933

- Interstellar H II regions high quantum number recombination line measurements, indicating Stark broadening 13 p2143 A71-29268

- Planetary nebulae observations in radio spectrum, determining interstellar extinction, electron temperature recombination theory and models 14 p2312 A71-30388

- Low temperature plasma reactions, discussing electron impact and collisions, ion formation, molecular excitation and thermal dissociation, vibrational relaxation, recombination, etc 16 p2539 A71-32964

- Selenium photocell photovoltaic effect, observing recombination and generation processes in space charge region 16 p2623 A71-34046

- Cometary dissociative recharging and recombination dissociation of water and hydrogen peroxide molecules in comets, giving empirical relation for effective cross sections 17 p2803 A71-34830

- Relaxation equations for dilute diatomic gas dissociation-recombination reactions, transforming kinetic equations to normal modes 19 p3107 A71-38079

- Night D region ion kinetics data during thermonuclear detonation, discussing formation and conversion rates, electron concentration and recombination 20 p3219 A71-39589

Hydrogen three-body recombination and dissociation rates in presence of molecular hydrogen, helium, argon and xenon collision partners 23 p3706 A71-42902

Interstellar medium recombination line emission origin from discrete distribution of cold and dense clouds 23 p3723 A71-42942

RECOMMENDATIONS

NT SUGGESTION

COMPRESSION

U COMPRESSING

RECONNAISSANCE

NT AERIAL RECONNAISSANCE

NT PHOTO RECONNAISSANCE

NT SPECTRAL RECONNAISSANCE

RECONNAISSANCE AIRCRAFT

NT EARTH RESOURCES SURVEY AIRCRAFT

NT MIRAGE 3 AIRCRAFT

NT TSR-2 AIRCRAFT

NT WEATHER RECONNAISSANCE AIRCRAFT

Navigator role in TACAN of reconnaissance and fighter aircraft, noting Weapon System Officer functions 01 p0123 A71-10503

Statistical diameter size distribution of random circles on plane or spheres in space from satellite and aircraft measurements for aerial and cloud photography 12 p1929 A71-27100

Tethered, ground supplied, rotor-borne, self stabilized surveillance platform (Kiebitz) system, discussing reconnaissance tasks, fire and communication control and data acquisition transmission and evaluation 15 p2347 A71-31212

Statistical diameter size distribution of random circles on plane or spheres in space from satellite and aircraft measurements for aerial and cloud photography 22 p3537 A71-41655

RECONNAISSANCE DRONE AIRCRAFT

U DRONE AIRCRAFT

U RECONNAISSANCE AIRCRAFT

RECONSTRUCTION

NT WAVE FRONT RECONSTRUCTION

Self reproduction of diffraction and reconstructed images of finite aperture in coherent radiation field by periodic transverse and longitudinal alternation 01 p0092 A71-10032

RECORDERS

Recorder circuit quick response enhancement in Grey code pulse counter, realizing parallel decoding in binary digits at high speeds 15 p2374 A71-31294

RECORDING

NT DATA RECORDING

NT DATA SMOOTHING

NT MAGNETIC RECORDING

NT PHOTOGRAPHIC RECORDING

RECORDING INSTRUMENTS

NT FLIGHT LOAD RECORDERS

NT FLIGHT RECORDERS

NT LUNAR SEISMOGRAPHS

NT OSCILLOGRAPHS

NT PLOTTERS

NT SEISMOGRAPHS

NT X-Y PLOTTERS

Thermal pattern visualizing and interpretation by imaging in far IR, noting equipment and uses of thermography in medicine, science and technology 01 p0078 A71-10135

Magnetic disk storage media for recording and reproducing wideband instrumentation data 01 p0082 A71-10893

Circumzenithal micrometric recording of almucantar passages of stars 03 p0422 A71-13011

Total solar eclipse of 7 March 1970, describing coronal spectrograph, TV, telescopic and photographic instruments 03 p0424 A71-13627

Upper atmosphere meteorological sounding facility for recording position and telemetry data from balloons, rocket payloads and meteor trails [AIAA PAPER 70-1392] 03 p0397 A71-13673

Circular Al rings under radial impulsive loading by curved magnetically driven Al flyer plates, recording strain-time histories on oscilloscopes [SESA PAPER 1644] 03 p0509 A71-13778

FM data recording system with transducers for converting varying parameters into frequency and tape recorder capable of playback for computer analysis 03 p0383 A71-14344

Solar magnetograph with potentiometers, recording magnetic fields, emission and absorption lines, radial velocity and brightness 04 p0589 A71-14836

Photoelectric device for recording stellar passages, discussing photocascade structure 04 p0592 A71-14858

Pulsed laser holography, discussing illumination source and holocameras for high contrast recording with Q switched ruby lasers 04 p0597 A71-15363

Stellar transit time recording by photoelectric instruments, discussing time constant and slit characteristics 04 p0598 A71-15377

Time lag between actual and measured stellar transit times by photoelectric recording instruments, noting atmospheric, spectral and instrumental factors 04 p0598 A71-15378

Magnetometers for space research, discussing instrumentation, spacecraft response, data, earth orbit, lunar, planetary and interplanetary measurements 05 p0748 A71-16228

Plasma echo and spin echo holophones for electrical signals temporal sequence recording and cued playback, noting human brain memory function analog 05 p0787 A71-16451

Changing rotational velocity recording device for vestibular apparatus tests, examining stimulus reaction speed 05 p0714 A71-16810

Impulse drive strip-chart recorder with low battery drain for high altitude balloon flights 05 p0755 A71-17143

Quartz magnetic variometer allowing simultaneous recording of magnetic field variations and suspension axis inclination changes 06 p0901 A71-18285

Magnetographic defectoscopy, discussing defect field magnetic recording techniques quality 07 p1106 A71-19143

Hologram recording material characterization concerning maximum diffraction, linearity and sensitivity 07 p1110 A71-19483

TV display eye movement monitor with automatic coordinate digital printout for permanent record 07 p1053 A71-20402

Electronic recording of cyclic strain diagrams of metals in wide loading frequency range using dynamic hysteresis method 07 p1218 A71-20485

Magnetic recording device for defect field recording by ferromagnetic tape polarization 08 p1273 A71-21900

Biotelemetric contactless recording of animal movements using centimeter band standing waves 09 p1397 A71-22216

Ionospheric layers critical frequencies recording, using automatic interplanetary station type probe 09 p1436 A71-22450

Power spectral density (PSD) analysis of multilevel binary coded signals for high density PCM recording 09 p1412 A71-22784

Pen actuators prototype models for fast response graphic recording instruments, using DC servomotors or galvanometers 09 p1452 A71-23386

Flight helmets speech intelligibility evaluation using in-flight manikin recording 10 p1572 A71-25069

Electromagnetic fields induction in biological tissues, recording energy absorption temperature distribution in phantom models with thermograph camera 11 p1717 A71-25289

Gas chromatography techniques, discussing carrier tank, flow control, injector, reactor, column, detector, recorder, flowmeter, etc 11 p1729 A71-26291

Thermal relaxation effects on thermal adjustment between gas and wall, comparing with thermograms from shock tube experiments 13 p2161 A71-28619

Compact head mounted six channel IC telemeter for artifact free EEG recording during laughter 13 p2020 A71-28889

Photoelectric, bolometric and photographic recording assembly for measurement of light pressure and aerodynamic forces on complex shape body in free molecular flow 13 p2071 A71-29155

Concorde SST flight test equipment installation with PCM recording and visual instruments 14 p2174 A71-30055

Cosmic ray nucleon-meson and barometric pressure data continuous recording equipment, comparing system to conventional instruments 14 p2248 A71-30602

Photoelectric system for recording Raman spectra with He-Ne laser excitation source suitable for liquid, solution, crystal and powder and depolarization measurements 17 p2751 A71-34383

Forty channel magnetography system including CRT display, digital controlled heliostat, real time computer and optical transducer 17 p2740 A71-34988

High spectral resolution image recording instrument with postrecording bandpass selection, discussing signature data base and sensor modes 18 p2917 A71-36066

Multichannel sound level meter capable of direct and continuous measurement and recording 18 p2897 A71-36221

Portable run-of-wind recorder featuring variable gear changes to facilitate range adjustments 18 p2925 A71-36960

Phonocardiograph design and calibration for accurate measuring and recording of cardiac vibration displacements, velocities and accelerations 19 p3005 A71-37231

Scanning densitometer for spectral transmission density continuous recording at low image contrast, discussing design and performance tests 19 p3063 A71-37248

Five component electromagnetic field station to record geomagnetic field magnetic and electric components variations 19 p3042 A71-38374

Automatic single beam recording spectroradiometer system for measurements of spectral irradiance, radiance, transmittance and reflectance 20 p2325 A71-39176

Real time multitrack half tone recorder for displaying three dimensional information on instantaneous blood velocity measurement by Doppler effect 21 p3377 A71-40132

Calibrated IR thermographic camera development and applications in medicine, X ray beam energy and reactor cooling rod measurements 22 p3545 A71-42148

Electron beam image recorder applications, discussing superior resolution, dynamic range width and high precision controllability advantages over laser or CRT techniques 22 p3548 A71-42516

Proton recording equipment onboard automatic interplanetary stations Zond 4 and 5 at 1.5-50 MeV using silicon drift counters 23 p3675 A71-43274

Photographic recording for graduated circle readings during stellar observation, discussing method, errors and system 23 p3680 A71-44264

Solar spectrum photoelectric recording instrument signal ratio accuracy, discussing divider circuit analysis 23 p3681 A71-44312

Transistorized AGC circuit for use with ultrasonic Doppler-cardiogram recording system to retain signal characteristics under strong fluctuations 24 p3801 A71-44543

RECOVERABLE SPACECRAFT

NT APOLLO SPACECRAFT

NT REUSABLE SPACECRAFT

NT SPACE SHUTTLES

NT VOSTOK 2 SPACECRAFT

RECOVERY

Recovery rate measurement during creep test by stress drop method 03 p0444 A71-14316

Cr plastic properties, investigating recovery and recrystallization effects from La and Y additions 09 p1476 A71-23316

Recovery factor for highly accelerated adiabatic compressible laminar boundary layer flow 15 p3391 A71-32114

RECOVERY PARACHUTES

Sea trials with dummy payloads of sounding rocket recovery systems, using parachutes, flotation torus, radio beacons, fluorescent dyes and smoke generators 06 p0881 A71-18674

Two stage parachute system RESY for water and land recovery of sounding rocket payloads 09 p1533 A71-23599

RECREATION

Recreational preferences among potential space crews from questionnaire analysis 08 p1248 A71-21231

RECRYSTALLIZATION

High quality quartz single crystal synthesis by hydrothermal recrystallization in autoclave 02 p0229 A71-11718

Alloying effects on room temperature mechanical properties of vacuum melted Mo-C-Ti, Mo-C-Zr and Mo-Ti-Zr under plastic deformation and recrystallization 02 p0265 A71-12520

Composition and annealing temperature effects on recrystallization of vacuum melted thin wire and rod Mo alloys 02 p0265 A71-12521

Mo single crystals polygonization and recrystallization, examining strain rate and deformation conditions effects 02 p0266 A71-12652

Doped W wire core porosity and anomalous recrystallization behavior microstructural observation by electron microscopy 02 p0268 A71-12890

Grain size refinement by alloy solute additions inhibition effect on growth and recrystallization, reducing boundary migration 03 p0446 A71-14489

Secondary recrystallization of Ti, Zr and Nb carbides within homogeneity ranges, determining activation energies as function of carbon deficiency in carbide lattice 04 p0609 A71-14749

Recrystallized annealed Ta, examining strain rate effect on mechanical properties

06 p0914 A71-18684

Optimal recrystallization of thin wire cast W-Re alloy subject to high size reduction

07 p1141 A71-20244

Recrystallized and overrecrystallized Al alloys, investigating factors controlling anisotropy of mechanical properties

08 p1305 A71-21033

Matrix stacking fault energy effects on steady state creep rate of recrystallized nickel-cobalt-aluminum oxide alloys, showing stress dependence

08 p1315 A71-21578

Cr plastic properties, investigating recovery and recrystallization effects from La and Y additions

09 p1476 A71-23316

Deformed Mo single crystals, noting polygonization processes relation to recrystallization during annealing

09 p1476 A71-23318

Polygonization and recrystallization processes in Fe-Cr alloy, using electron diffraction and microscopy

09 p1476 A71-23322

Primary, secondary and combinatory recrystallization kinetics and textures in tungsten wire of different compositions over 900-2300 C using X ray analysis and metallography

09 p1476 A71-23323

Recrystallization of V and V-Ti alloy, discussing hardness measurements, tensile tests, X ray diffraction, optical and electron microscopy

10 p1625 A71-24010

Al-Cu alloys recrystallization and age hardening irregularities, discussing inhomogeneous and anisotropic effects on ideal characteristics

10 p1628 A71-24823

Fiber textures formation in polycrystalline Zr from cold forging and cold drawing, observing fully developed recrystallization

10 p1629 A71-25028

Coarse grained recrystallized Mo ductile brittle transition temperature due to dislocation substructure and grain boundary state, noting low temperature annealing and critical straining

10 p1629 A71-25029

Cold rolled recrystallized Ni-Fe alloy, considering short range order structure effect on elastic limit

13 p2087 A71-29264

Structural disorientation dependent recrystallization of cold rolled and annealed Mo single crystals

14 p2258 A71-30006

Recrystallization nuclei linear growth rate activation energy relationship to Ni plastic deformation magnitude, temperature and purity

15 p2429 A71-31995

Cold worked pure Mo recrystallization kinetics, indicating dependence on deformation mode and techniques

15 p2433 A71-32177

Recrystallized and unrecrystallized deformed semipolished Al base alloy under cyclic and static loads, investigating macrofracture kinetics

16 p2594 A71-33713

Recrystallization of heat treated Fe-Ni alloys microstructures after hammer hardening

16 p2598 A71-34051

Low temperature tensile prestressing effect on recrystallization kinetics of polycrystalline large grain Ni by isothermal annealings method

17 p2755 A71-34194

Statistical microstructural analysis for nucleation and growth kinetics of recrystallization nuclei of metal single crystals

17 p2755 A71-34414

Diamonds in ureilites and carbonaceous chondrites, discussing formation due to recrystallization during asteroid collisions

17 p2810 A71-35723

Critical growth work hardening germination and recrystallization of oriented compression deformed Nb, Mo and W refractory cubic centered crystals

18 p2935 A71-36200

Microcrystal orientation in recrystallized tungsten structure by charged particles channelography

18 p2954 A71-36804

Lunar breccia, considering welded or sintered breccias, glassy breccias containing xenocrysts and xenoliths, instant rock breccias and recrystallized breccias

19 p3137 A71-37675

Vacuum-melted low-carbon low-manganese steel, investigating Ni and Cr additions effects on recrystallization textures

19 p3079 A71-37703

Recrystallization behavior of thorium dispersion hardened W-Re alloy compared to pure W by X ray diffraction, hardness tests, metallographic and electron microscopy methods

20 p3247 A71-38763

Dislocation structures of polycrystalline tungsten after deformation and recovery annealing, observing temperature dependence of critical strain for recrystallization

21 p3399 A71-40472

Soviet monograph on Canyon Diablo/Arizona/meteorite covering chemical composition, minerals, isotope composition, history, geology and impact recrystallization

21 p3452 A71-40874

High heat resistance of austenitic Cr-Ni-V-B steel by polygonization and recrystallization, using thermomechanical treatment

21 p3403 A71-41102

Copper wire laser welding to film on Cr substrate, exhibiting nonhomogeneous columnar structure and recrystallization

21 p3389 A71-41104

RECTANGLES

Harmonic mixed boundary value problem exact solution for rectangle with slit, outlining finite difference techniques convergence

15 p2441 A71-31356

Rectangular cylindrical shell finite element, deriving stiffness matrix with stress distribution

15 p2510 A71-32516

Alternating-direction Galerkin methods application to parabolic and hyperbolic differential equations for obtaining efficient iterative solution of heat equation on rectangle

19 p3087 A71-38305

RECTANGULAR BEAMS

Mixed plane elasticity theory of narrow rectangle imbedded in static walls under normal loads

08 p1373 A71-21943

Plastic strains, thermal residual stresses and buckling of rectangular cross section plates and beams subjected to asymmetric heating and cooling

08 p1375 A71-22056

Euler buckling of hinged slender prismatic bars of rectangular and elliptic cross sections with shear and transverse stress allowance

10 p1685 A71-23959

Shear deformation effect on optimal design of elastic beams, considering rectangular cross section circular ring by Timoshenko beam theory

11 p1849 A71-25677

Elastic deformation and plastic buckling of rectangular column with initial deflection under axial compression

13 p2157 A71-29287

Nonuniform cross section tapered, stepped rectangular and I section cantilever beams elastic lateral stability

14 p2330 A71-30689

Coupled natural frequencies in rectangular cross section pretwisted cantilever beams flexural vibrations

15 p2503 A71-31442

Rectangular composite prismatic bar with T shaped cross section, calculating torsion with summary representation method

17 p2824 A71-34847

Transverse waves propagation in vibrating orthotropic rectangular beams, noting inexact information regarding shear distribution

20 p3307 A71-39037

Effective shear modulus of multilayered rectangular elastic isotropic member in uniform torsion

22 p3618 A71-42587

Fiber reinforced viscoelastic rectangular beam, deriving asymptotic values of stress, curvature and position of neutral axis under constant moment

24 p3879 A71-44630

RECTANGULAR GUIDES

Electric potential and field distribution in dielectric plate insert of rectangular waveguide calculated by net point method using computer program

01 p0051 A71-10149

Wave dispersion and evanescent modes in rectangular waveguides filled with transversely inhomogeneous dielectric rod

01 p0056 A71-11196

Complex permittivity and impedance of dielectric samples in coaxial lines and rectangular waveguides by moving probe and resonant Q factor measurements

02 p0229 A71-11713

Integrated optical communication circuit technology adaptable to batch processing, considering encapsulated planar arrays of rectangular dielectric waveguides

02 p0231 A71-12008

Cylindrical post shunt impedance in rectangular waveguide, evaluating approximate theory for free space thin wire conductor

03 p0378 A71-13808

Rectangular waveguide with T junction, deriving characteristic impedance, maximum power and damping constant

05 p0719 A71-15997

Large aspect ratio rectangular duct with nonuniform surface texture, investigating turbulent flow, maximum velocity positions and zero shear stress

07 p1086 A71-18772

Flow field behind two dimensional roughness element in rectangular channel, discussing wall effects, reattachment point position, velocity distribution and turbulence intensity

07 p1086 A71-18775

Computer algorithms for scattering matrix of rectangular waveguide splitters in H plane

07 p1079 A71-20073

Radiation nulls suppression and broadband impedance matching of infinite rectangular waveguide phased arrays, giving numerical solutions

09 p1419 A71-23494

Y-shaped microwave power splitter, using dielectric wedge partially extending into rectangular metallic waveguide

11 p1733 A71-26349

Linear frequency beam scanning array antenna excited by individual phase shifter, studying rectangular waveguide in magnetic field plane

11 p1741 A71-26552

Rectangular cross section MHD channel spatial electrical field distribution, obtaining electrostatic potential, boundary conditions and efficiency

14 p2278 A71-29612

Microwave scattering by DC magnetized ferrimagnetic circular cylinder in rectangular waveguide

14 p2212 A71-30512

Scattering coefficients of thick inductive diaphragm in rectangular waveguide, using ray-optical method

15 p2376 A71-32023

TE modes propagation in rectangular guide partially filled with dielectric slab, considering two waveguides junction equivalent circuit

17 p2708 A71-35481

Transient thermal stresses in infinite cylinder of rectangular cross section with heat sources, using integral transforms

18 p2976 A71-36127

Wave diffraction at step junction of two rectangular waveguides and symmetrical diaphragm with dielectric fillers

19 p3019 A71-38332

Design algorithm for gyrotropic waveguide consisting of symmetrical rectangular coaxial with magnetized ferrite rods

19 p3019 A71-38333

Reflection and transmission coefficients of nonresonant slots in rectangular waveguide antenna with comb type slow wave structure

19 p3019 A71-38334

Rectangular waveguide with T shaped pedestal, deriving characteristic impedance, maximum power and damping constant

22 p3515 A71-42746

RECTANGULAR PANELS

Rectangular panel acoustic response by variational finite element method, including radiated sound field effects on structural vibration

06 p0984 A71-17622

Rectangular, square and circular cross section blanks dynamic metal cutting process by method of characteristics

08 p1295 A71-20794

Simply supported double layered rectangular mesh grids, solving finite difference equations under arbitrary loading

08 p1370 A71-21409

Dynamic behavior of circular and rectangular membrane panels with time and space dependent boundary conditions for aerospace structures

09 p1544 A71-23736

Acoustic damping of clamped and hinged rectangular panel at natural frequency, noting dependence on aspect ratio

21 p3416 A71-41200

RECTANGULAR PLANFORMS

NT RECTANGULAR PANELS

NT RECTANGULAR PLATES

NT RECTANGULAR WINGS

Elastoplastic unsteady thermally stressed state of square and rectangular planform bodies by calculated theory of small deformations, using strain compatibility equations with Airy stress function

02 p0323 A71-11743

Planar-rectangular shallow shells with double curvature geometry, analyzing natural oscillations by finite difference procedure

07 p1219 A71-20649

Lifting rectangular thin airfoil in symmetrical incompressible steady uniform orthogonal flow at small angle of attack, deriving Weissinger integral equation

23 p3625 A71-43487

Rectangular planform nonshallow spherical and elliptical shells, determining momentless stressed state

24 p3877 A71-44404

RECTANGULAR PLATES

Buckling analysis of rectangular waffle plates with multiple sizes of ribs in each stiffening direction, considering stability and design

01 p0178 A71-11583

Clamped rectangular metal plates dynamic plastic behavior under uniformly distributed impulsive velocities

02 p0321 A71-11678

Cracked rectangular plate bending under uniform transverse load, discussing crack geometry and propagation

02 p0321 A71-11681

Stress distribution in gelatin disk and rectangular plate compressed between horizontal slabs, using tangential difference method

02 p0328 A71-12512

Fluid-loaded rectangular plates and membranes random vibration excitation by turbulent boundary layer flow

[ASME PAPER 70-WA/DE-15] 03 p0511 A71-14147
Supported rectangular plates HF transverse vibrations by holographic interferometry

04 p0668 A71-15188

Nonlinear creep problems numerical time integration solution, applying to rectangular plate

04 p0672 A71-15755

Rectangular and circular thin orthotropic plates thermal buckling approximate solution using Rayleigh-Ritz energy method

05 p0819 A71-15978

Eccentrically stringer-reinforced rectangular plates buckling under linearly varying longitudinal compression, using Galerkin method

05 p0819 A71-15980

Rectangular thin elastic plate with circular holes under heat flow, solving thermoelastic problem by point matching

05 p0823 A71-16492

Rectangular plate with stiffener cross section for unit with constant mass, considering natural symmetric and antisymmetric mode frequencies

05 p0824 A71-16603

Singly curved rectangular plate free vibration characteristics obtained by partial differential equations of motion

05 p0825 A71-16605

Maximal deflection of square and rectangular thin plates with small initial concavities, using dynamic relaxation method for lateral and postbuckling in-plane edge loads

05 p0830 A71-17225

Rectangular plates and shallow shells large asymmetric deflection, using computerized finite difference technique

06 p0991 A71-17802

Elastic rectangular and thin plates design under dynamic loading, using Bubnov-Galerkin method for computer solutions

06 p0992 A71-17808

Equidistant multiple span rectangular plates vibration and acoustic radiation under random external forces

06 p0994 A71-17823

Rectangular plate bending with mixed boundary conditions, using paired trigonometric series

06 p1005 A71-18708

Dynamic elastic-plastic buckling of rectangular plates in sustained flow involving mass impact

07 p1211 A71-19251

Viscoelastic rectangular thin plate stability under buckling conditions, showing ratio of long term to instantaneous critical loads as function of hereditary properties

07 p1212 A71-19351

Stress concentration in planar rectangular shallow shells and plates with polygonal holes

07 p1218 A71-20470

Stress-strain state of rectangular transversely isotropic plate with clamped edge under uniformly distributed load, considering bending moments

07 p1218 A71-20473

Flat rectangular plate under plane stress, solving boundary condition problems with displacements and stresses from two neighboring edges

08 p1369 A71-20846

Free flexural vibrations of orthotropic rectangular plates subjected to large amplitude free or forced oscillations, using von Karman nonlinear equations

08 p1370 A71-21307

Transverse bending of hinged or clamped rectangular plates with different tensile and compressive resistance

08 p1373 A71-21945

Plastic strains, thermal residual stresses and buckling of rectangular cross section plates and beams subjected to asymmetric heating and cooling

08 p1375 A71-22056

Theory of plates under finite initial elastic deformation, applying to rectangular plate stability under compressions in two mutually perpendicular directions

09 p1537 A71-22521

Viscoelastic rectangular sandwich plate bending, stability, deflection and critical load calculation, assuming core stress-strain relation governed by Maxwell-Thompson differential equation

09 p1540 A71-22998

Flexural vibration analysis of rectangular isotropic and orthotropic polygonal elastic plates with constant or variable thickness, considering mass distribution and boundary conditions

10 p1625 A71-24019

Temperature induced bending of rectangular plate, obtaining stress-strain state

10 p1687 A71-24196

Rectangular plate and circular cylindrical shell segment under rotating moment and dynamic loads evaluated by Green function

10 p1691 A71-24812

Buckled rectangular panels response to random excitation via single degree of freedom nonlinear vibration equation

11 p1841 A71-25196

Finite element method for stiffness matrix free vibration analysis of thin rectangular plates under central planar loadings

[AIAA PAPER 71-334] 11 p1842 A71-25313

Harmonic vibrations of rib reinforced rectangular elastic plates with two freely supported parallel edges, deriving method for natural frequencies and forced vibration

11 p1848 A71-25580

Inextensible elastic Cosserat surfaces finite deformation mechanisms, applying theory to flexure of rectangular plate into closed circular cylinder and helical strip

11 p1849 A71-25681

Temperature and membrane thermal stress distribution in finite rectangular plate with insulated circular hole, considering steady state heat conduction equation

11 p1852 A71-26404

Plane stress distribution solution for rectangular elastic plastic plate under partial edge loading, using incremental theory

12 p1976 A71-27122

Spherical head projectiles collision with hemispherical shells and square plates with and without protective covering, calculating stress distribution

12 p1976 A71-27160

Natural frequencies and elastic stability of simply supported rectangular plate under linearly varying compressive loads

12 p1976 A71-27162

Stretching, twisting, pure bending and flexure of pretwisted elastic rectangular plates of rectangular cross section

13 p2147 A71-27783

Rectangular plate bending elements displacement functions representation by trigonometric expressions, using finite element method

13 p2147 A71-27790

Elastic stability and buckling behavior of transversely isotropic rectangular Mindlin plate under initial stress and displacement

14 p2324 A71-29871

Finite element midincrement stiffness matrices in postbuckling analysis of imperfect strut and rectangular plate

15 p2503 A71-31420

Rectangular plates with unidirectional stiffeners, calculating natural frequencies and mode shapes with approximate method

15 p2507 A71-32128

Optimal rectangular plates with adaptability, using convex programming

15 p2508 A71-32232

Monograph on rectangular shear elastic plates stability covering Cosserat plane, stress functions, buckling conditions, compressive forces and two dimensional equations

15 p2509 A71-32302

Rectangular plates under direct and shear in-plane forces, considering free lateral vibrations

15 p2509 A71-32512

Finite element method application to stress distribution analysis at crack tip of rectangular plate under tension, obtaining elastoplastic response to cyclic loading

16 p2653 A71-33086

Small deflection analysis within Cartesian coordinate system applicable to elastic-plastic rectangular plates bending under Tresca yield criterion

16 p2654 A71-33122

Stiffened rectangular plates parametric instability under in-plane sinusoidal dynamic forces, using mathematical model with stiffeners as discrete elements

[ASME PAPER 71-APM-26] 16 p2655 A71-33203

Isotropic sandwich plates with rigid cores due to shear boundary tractions, considering transverse strain and stress, displacement function and stability

16 p2660 A71-34035

Infinite length rectangular thin plate bent by uniform load, presenting exact solutions for stresses and displacements from couple-stresses plane strain elasticity theory

17 p2818 A71-34441

Rectangular plate with two adjacent sides clamped and two supported, solving bending problems with linear algebraic vector equations

17 p2824 A71-34846

Rectangular flexible plate displacement theory, solving boundary value problems with fractional step method

17 p2824 A71-34848

Thermal stressed state and bending theory of rectangular plate by initial function method, allowing for distributed transverse load

17 p2829 A71-35304

Equilibrium bifurcation for nonlinearly elastic incompressible body during finite subcritical homogeneous deformation, obtaining characteristic equations for cylindrical shell, circular and rectangular plates, etc

17 p2832 A71-35609

Free edge effect on critical loading of rectangular sandwich plate with asymmetrical structure and rigid filler

17 p2833 A71-35622

Clamped rectangular plate buckling under uniaxial and biaxial compression, obtaining critical loads for various aspect ratios

18 p2979 A71-36360

Fundamental frequency of large amplitude bending vibration of elastic and isotropic rectangular plates, considering effects of transverse shear and rotatory inertia

18 p2980 A71-36496

Rectangular cantilever plate free vibration under in-plane acceleration loads, calculating frequencies and mode shapes by Ritz method and computer technique

19 p3157 A71-37850

Isotropic viscoelastic plates of variable thickness subjected to mechanical and thermal stress, considering circular and rectangular plates vibration by external thermal shock

19 p3160 A71-38480

Compressible viscous gas supersonic flow, observing near wake region behind perpendicular trailing face of rectangular plate with motion, state, energy and continuity equations

21 p3318 A71-40081

Peak resonant response of thin rectangular plate with elastic edge restraint under concentrated load

[ASME PAPER 71-VIBR-6] 21 p3456 A71-40269

Five-layer rectangular sandwich plate containing two soft orthotropic cores and three plate stiff isotropic layers

[ASME PAPER 71-VIBR-48] 21 p3459 A71-40297

Flexural vibration of rectangular orthotropic plates under in-plane hydrostatic forces

21 p3464 A71-40768

Bending of semiinfinite rectangular plates clamped at long edges

21 p3464 A71-40770

Rectangular plate under lateral and inplane pressure pulses, examining transient response with Mathieu equation

21 p3471 A71-41023

Rectangular laminated orthotropic plates natural vibrations analysis, using extended Ritz technique

21 p3471 A71-41024

Stress intensity factors analysis of strip with longitudinal crack subject to tension and bending along edges and tension of rectangular plates with central crack

22 p3614 A71-41709

Plane wave propagation following thin elastic rectangular plate impact against smooth rigid obstacle, using difference scheme

22 p3531 A71-41910

Singly and nonsingly connected thin elastic rectangular plate stability analysis under arbitrary compression load on surface

23 p3777 A71-43423

Divergence behavior of flat rectangular panel at subsonic speeds, discussing boundary conditions, natural vibration modes and temperature effects

24 p3878 A71-44611

Geometrically nonlinear elastoplastic bending of rectangular flexible plates with various side ratios, using finite difference and strain theory

24 p3883 A71-44849

Small deflection theory for steady state creep bending of laminated anisotropic rectangular plate under uniform loads, using Galerkin method

24 p3841 A71-44957

RECTANGULAR WIND TUNNELS

Return circuit rectangular wind tunnel design, construction, instrumentation and calibration, discussing drive, jet inclination, velocity distribution, etc

08 p1272 A71-21305

Rectangular wind tunnel study of suction effect on velocity profiles and characteristics of turbulent boundary layer

20 p3213 A71-39788

RECTANGULAR WINGS

Thin rectangular wing load distribution in nonstationary incompressible flow, using downwash integral equation Fourier transform

09 p1383 A71-22946

Gust transfer functions relating lift and moments to upwash in single sinusoidal wave for large aspect ratio rectangular wings in turbulent incompressible flow

14 p1716 A71-30604

German monograph on incompressible potential flow field calculation about thick rectangular wings with control surfaces and ground effects

15 p2347 A71-32307

Space shuttle booster configuration design, comparing stowed, fixed straight and delta wing approaches, discussing air breathing engines, stage mating, fins, etc

18 p2972 A71-36444

Straight or moderately sweptback wings tip shape effect on vortex sheet roll, using detachment laws
20 p3176 A71-39418

Subsonic force effect calculations on rectangular wings, using downwash velocity potential method
24 p3789 A71-44613

RECTIFICATION

Specific contact resistance at zero bias as measure of ohmic or rectifying behavior of metal-semiconductor barrier under operating conditions
19 p3117 A71-37485

RECTIFIERS

NT AVALANCHE DIODES
NT CRYSTAL RECTIFIERS
NT GERMANIUM DIODES
NT THYRATRONS
NT THYRISTORS

Cyclotron wave rectifier for S band and X band microwave conversion to DC or LF AC power
07 p1080 A71-20451

Microwave receiving antenna with solid state power rectifier for converting energy from space solar cell array into DC power on earth
13 p2000 A71-28671

Monograph on strong signal behavior of control systems containing multiphase rectifier, covering stability of high power sources
19 p3039 A71-38550

RECTUM

Hemorrhagic rectocolitis in flying personnel in terms of etiologic, evolutive and therapeutic aspects
01 p0028 A71-11596

RECUPERATORS

U REGENERATORS
RECURSION FORMULAS
U RECURSIVE FUNCTIONS
RECURSIVE FUNCTIONS

Local invariants under axial rotation, deriving recurrence relations for time series expansions and perturbation methods
01 p0154 A71-10387

Recursive triangular algorithm for Lie transformation from introduction of small parameter into generating function and Hamiltonian
05 p0774 A71-16543

Perturbation method in nonlinear oscillations theory, using asymptotic recurrence formulas based on Lie transform
05 p0774 A71-16544

Thin isotropic plate nonstationary coupled thermoelasticity problem, obtaining recursion equation system for thermal stresses
06 p0983 A71-17367

Recursively defined infinite system convergence solutions for initial and boundary value inequalities, applying to differential game stability problems
06 p0920 A71-18237

Derivative approximation techniques for recursive signal detection, using computer program for solving optimum and suboptimum processes signal to noise ratio in effectiveness evaluation
08 p1255 A71-21596

Series inverse in powers of time and radius of convergence for universal form of Kepler equation, discussing recursion formulas for coefficients
09 p1516 A71-22174

Automatic computer program synthesis based on theorem proving approach for construction of recursive and iterative programs operating on natural numbers, lists and trees
10 p1581 A71-23968

Suboptimal estimation of remaining flight distance of aircraft at each radar range measurement by limited state recursive estimators
11 p1741 A71-25489

French monograph on nonlinear recurrences solutions and applications to sampled data systems
12 p1928 A71-26567

Recursion formulas for mapping entire earth ellipsoid on plane in single zone of Gauss-Kruger projection
12 p1900 A71-26970

Analog recursive computer with serial digital program for arithmetic unit and storage system control
12 p1884 A71-27150

Explicit recursive algorithms for construction of Lie and von Zeipel transformations
13 p2135 A71-28357

Real time computable partial recursive functions of n variables with expectancy estimate on Minsky machines
13 p2096 A71-28976

Electromagnetic wave multiple scattering by collinear spheres, computing radar cross sections with recursion relation for computer solution
17 p2701 A71-34757

Recursive algorithms for detection probabilities of fluctuating targets in Gaussian noise, including cell averaging constant false alarm rate (CFAR) extension
20 p3195 A71-38860

RED ARCS

Stable midlatitude red arc in night sky south of auroral zones, reviewing observed features, ionospheric behavior and formation theories
07 p1098 A71-19322

Subauroral red arcs phenomenon hypotheses based on associated ionospheric plasma properties measurements
07 p1102 A71-19663

Hydrogen ion concentration measurements by OGO 5 in plasmasphere during intense magnetic storms accompanied by stable auroral red arcs
10 p1605 A71-24787

Stable auroral red arcs on 29 September 1967, 31 October and 1 November 1968, comparing OGO 2 and OGO 4 VLF data on plasmapause crossings
15 p2397 A71-31757

Stable auroral red arcs generation at plasmapause from ion cyclotron wave turbulent dissipation of ring current proton energy
16 p2572 A71-33947

Stable auroral red arc excitation observations by HF radar scattering, scanning photometers and Alouette 1 satellite, noting local electron concentration increase
19 p3054 A71-38034

Plasmaspheric ambient hydrogen and helium atomic cations density measurement by OGO 5 ion mass spectrometer during magnetic storm, noting relationship to auroral red arcs
20 p3227 A71-39833

Stable auroral red and hydrogen arcs simultaneous spectrographic triangulation, noting correlation
20 p2322 A71-39895

RED BLOOD CELLS

U ERYTHROCYTES

RED SHIFT

Cosmological models with noninteracting matter and radiation, deriving red shift and luminosity-distance relationship
02 p0312 A71-12464

Mean cosmic density determinations, obtaining field galaxy luminosity function moments with red shift catalogs
02 p0313 A71-12499

Quasars spatial distribution and luminosity functions based on red shift observation
02 p0314 A71-12576

High red shift quasars linear polarization, examining absorption lines and depolarization due to Faraday rotation
04 p0649 A71-15272

Multiple absorption red shifts in quasars, discussing measured properties and negative clues
04 p0650 A71-15584

Primeval intergalactic magnetic field existence, observing radio sources rotation distribution and red shift
05 p0805 A71-16108

NGC 7320 as companion galaxy to NGC 7331 rather than member of Stephens quintet, considering red shift texture, lack of distortion and luminosity
05 p0805 A71-16110

Strong and weak emission red shifts of N galaxy 3C 390.3 in Balmer lines, indicating nonisothermal source and gas ejection
05 p0807 A71-16210

External galaxies radial velocity relationship to extragalactic nebulae spectral lines red shift
07 p1200 A71-20054

Quasars red shift and absorption lines observations, discussing distance measurement, brightness and intergalactic matter
07 p1200 A71-20211

Galactic optical radial velocity measurements compared to 21 cm red shifts derived velocity
08 p1357 A71-20873

Cosmic objects and phenomena research, considering matter and galaxy compacting and dispersing processes, red shift, quasars, etc
08 p1358 A71-20890

Field galaxy cosmological reddening from red shift data at faint magnitudes
09 p1516 A71-22063

Radiative transfer theory extended to cosmological red shift and expansion effects on uniform isotropic X rays and gamma rays in homogeneous intergalactic medium
09 p1512 A71-22333

Diffuse interstellar features in spectrum of reddened star in Cygnus OB2 stellar association, tabulating equivalent widths of H alpha and stellar He I line
10 p1665 A71-23749

Book on relativity and discretization in astronomy covering cosmic structures, galactic isopleths equilibrium theory, red shift discretizations, etc
10 p1670 A71-24210

Gravitational red shift in standard and isotropic forms of Schwarzschild metric
11 p1822 A71-25592

Quasar evolution, considering cosmological red shifts
12 p1958 A71-26695

Optical luminosity function and space density of quasars from 4C and Parker survey, assuming cosmological red shifts
12 p1966 A71-27233

Universe global structure and quasar frequency distribution based on red shifts and cosmological interpretations
12 p1968 A71-27642

Large and small red shift quasars relative probability correlation with cataloged galaxies clusters direction
14 p2315 A71-30656

White dwarf discovery method and properties, discussing color, spectra, parallaxes, luminosities, masses, red shifts, cluster and frequency distribution
14 p2316 A71-31005

Quasar mass lower limit estimation from emission and absorption red shift data
15 p2483 A71-31368

Astronomical 4C catalog radio sources statistical analysis, showing mean spectral indices dependence on radio emission fluxes and red shifts
15 p2487 A71-32037

Excess red shift of Fraunhofer lines at extreme limb explained by mechanism of radial currents in solar atmosphere
16 p2629 A71-32807

Scientific cosmology principles, considering distant galaxies red shift and galactic evolution
16 p2611 A71-33279

Statistical analysis of radio structure of quasars, considering red shift and anisotropy in angular size distribution
17 p2811 A71-35746

Upper limits to quasars masses with optical emission lines inside radio sources, using method independent of red shift composition
18 p2961 A71-35965

Quasar red shifts distribution, indicating discretization in form of geometrical series
19 p3142 A71-38154

Mass of virtual particle responsible for gravitation of vacuum and expansion of universe, considering correspondence to red shift in quasar spectra
19 p3146 A71-38644

Mass and discrepant red shifts theory, discussing time dependent gravitational constant, Friedmann cosmological model and Dirac equation
20 p3305 A71-39956

Closed formula for relation between luminosity and red shift in expanding Friedman universe for positive cosmological constant, positive space curvature and vanishing pressure
21 p3443 A71-40186

Quasars emission line red shifts distribution observations, evaluating selection effects
22 p3605 A71-42351

Sirius B white dwarf star effective temperature, radius and gravitational red shift determination from H-alpha and H-gamma line profile analysis
24 p3871 A71-44908

REDUCED GRAVITY

Mercury droplet dynamics in conducting liquid within electromagnetic field under reduced gravitation
02 p0293 A71-12631

Nonlinear free surface effects in low gravity tank draining, finding domains of validity for linearized and nonlinear analysis
03 p0399 A71-13439

Liquid oxygen nucleate boiling in simulated reduced gravity fields, obtaining heat transfer coefficients, departure frequency and bubble growth rate
04 p0687 A71-15536

Liquid sloshing in liquid propellant containing orbiting vehicle stabilized by active control system, examining expression for ring baffle slosh damping under reduced gravity
09 p1532 A71-22913

Biosatellite 3 reduced gravity environmental laboratory with subhuman primate on 30 day mission, discussing ground base tests, simulated and actual flight
09 p1400 A71-23238

Human performance in various locomotive tasks under simulated lunar reduced gravity conditions, classifying test stands and equipment
15 p2362 A71-31304

Low gravity field phenomena, discussing vertical jump on moon, ball trajectories launched from asteroid and voyage to neutron star
22 p3600 A71-41983

REDUCTION [CHEMISTRY]

NT DEOXYDIZING

NT HYDROGENATION

Double beam monochromatic differential cinespectrophotometer for recording oxidation/reduction reactions in intercellular pigments
01 p0021 A71-10243

Redox estimation from natural phase Eu ion concentrations in rocks
01 p0029 A71-11428

Niobium processing methods from economic standpoint, describing pyrochlore metallothermic reduction
02 p0271 A71-12938

Oxygen reduction on Teflon bonded Pt electrodes, eliminating concentrated overvoltage
02 p0210 A71-12955

Oxide bronzes as oxygen reduction catalysts in batteries and fuel cells, considering effects of varying compositions and crystal faces
03 p0374 A71-13054

- Zinc reduced di(4-pyridyl) ketone methiodides, examining electronic and electron spin resonance spectrum 03 p0377 A71-14301
- Rats and mice blood redox potentials injected with cystamine, investigating increased radioprotection 07 p1039 A71-18980
- Vitamin K3 effect on redox equilibria in red cell, discussing radiosensitizer mechanism 07 p1039 A71-18985
- MnO oxidation reduction kinetics measurement in carbon monoxide/dioxide atmospheres by gravimetry and electrical conductivity 08 p1318 A71-20698
- Silver oxides stability, considering solubility, reduction by hydrogen and thermal decomposition 08 p1234 A71-21085
- Thoria containing Ni and Co base powders reduction in hydrogen atmosphere for precipitation hardened materials production, determining optimal thermodynamic and reaction kinetic factors 09 p1475 A71-23306
- Thermal reduction methods for refractory metal powders of W, Mo, Zr, V, Hf, Nb, Ta and Ti 09 p1457 A71-23389
- High chromium low carbon steel, detailing oxygen content effects on high temperature reduction intercrystalline corrosion and grain growth 15 p2427 A71-31528
- Photoreduction regulation in Rhodospirillum rubrum by ammonium chloride, discussing nitrogen fixation and protein metabolism 16 p2527 A71-33058
- Gas exchange metabolic fluctuations of nitrogen fixation, hydrogen evolution and photoreduction in Rhodospirillum rubrum as function of culture conditions and age 16 p2528 A71-33059
- Proton irradiation damage on lunar surface, considering solar wind sputtering, reduction, chemical bond breakage and electron paramagnetic resonance 24 p3867 A71-44423
- REDUNDANCY**
- Data acquisition system using associative processor for redundancy removal algorithm 01 p0050 A71-10983
- Redundancy effects on human memorization working capacity, noting application to memory systems design 07 p1043 A71-20113
- Redundancy verification of parallel systems related to element MTBF and decision maker perspective involving acceptance risk of system failure 16 p2582 A71-33292
- Redundancy information effect on human performance in forced pace cognitive tasks under overload stimulus presentation rates 16 p2536 A71-33679
- Redundancy approach to information systems synthesis 17 p2720 A71-34952
- Statistical limits on reliability, informativeness, controllability and self organization of complex systems, determining minimum redundancy requirements for suppressing interfering factors 17 p2720 A71-34953
- Redundancy in receptive neuronal nets, examining structural and functional organization of generalized biological analyzer peripheral section 17 p2690 A71-34956
- Redundant information optimizer design, using nonlinear elements 17 p2720 A71-34957
- Redundancy utilization in automatic control systems synthesis, considering dynamic characteristics sensitivity 17 p2721 A71-34965
- Additional redundancy in information transmission systems with feedback to reduce error probability due to incorrect addressing 17 p2702 A71-34975
- Redundant strapdown Inertial Measurement Unit processor recovery requirements, investigating IMU information loss effects during recovery on spacecraft mission 17 p2772 A71-35058
- Reliability engineering, reviewing MTBF, redundancy, complexity effects on failure rate, reliability prediction, repair and replacement cost and test techniques 18 p2928 A71-36806
- Three degree of freedom perturbed two body problem, applying theory of redundant variables to Lagrangian equations of motion 19 p3143 A71-38163
- Error correction by tapped delay line coded equalizer and channel introduced redundancy, deriving upper bound for error probability 22 p3512 A71-42377
- REDUNDANCY ENCODING**
- Speech signals digital encoding with adaptive linear predictor for reducing redundancy, discussing digital simulation results and subjective comparison with log-PCM encoder 01 p0030 A71-10472
- PCM signal encoding redundancy reduction using discrete code transformation, considering telephony implementation 08 p1255 A71-21593
- Data transmission with redundancy, discussing optimum data compressing encoding of correlated source signals through linear transformation 12 p1883 A71-27009
- Soviet book on space radio telemetry systems characteristics, design, requirements and operation conditions covering noise stability, reliability and redundant codes 17 p2699 A71-34521
- Soviet papers on information systems redundancy using redundant algorithms and structures and redundant coding theory 17 p2720 A71-34951
- Redundant variables method as solution to problem of functional coding and algorithm synthesis, examining error control and correcting properties 17 p2701 A71-34963
- Analog error correcting redundancy codes, examining coding and decoding procedures 17 p2701 A71-34967
- Information effectiveness of redundant error detecting coding systems 17 p2702 A71-34968
- Redundancy encoding with error correcting codes for controlling results of rational operations series in residual classes system 17 p2710 A71-34976
- Random access signaling system application to aircraft control, discussing signal redundancy requirement for access capability optimization based on radio environment model 17 p2747 A71-35783
- Majority-logic decodable block codes construction by combining shorter length codes, obtaining correctable error bounds 20 p3201 A71-38873
- Large random access computer store based on redundancy in form of error correcting codes, discussing use for manufacturing yield improvements 24 p3806 A71-44655
- REDUNDANT COMPONENTS**
- Redundant structure dynamic analysis for forced and free vibrations, using finite element rank force method 05 p0829 A71-17120
- Two-unit redundant repairable system with standby, predicting periodic or random inspection effect on reliability through Laplace transforms 06 p0904 A71-18026
- Intelsat 3 satellite reliability program, discussing test procedures, redundancy, tradeoff against weight, etc 06 p0877 A71-18404
- Optimum orientation and accuracy of redundant sensor arrays in space navigation, guidance and attitude reference systems 06 p0925 A71-18518
- Spacecraft computer centered data systems with standby redundancy, automated flexibility and LSI devices for grand tour mission 08 p1260 A71-21846
- Reliability of redundant repairable systems with preventive maintenance, determining mean time between failures 11 p1769 A71-25660
- Parallel and standby redundancy systems with priority or noninstantaneous switchover, applying renewal theory integral equation 11 p1772 A71-26163
- Mission reliability calculations for systems with redundant units, considering design of airborne warning and control system and other radar control systems 12 p1885 A71-26675
- Intelsat 4 transmission subsystems design, discussing alternative high power amplifier configurations, redundancy and emergency routing of transmitted RF carriers 12 p1894 A71-26992
- Computerized minimum weight design of elastic redundant trusses under multiple static loads, using algorithms for generating upper and lower bounds for configuration [AIAA PAPER 71-362] 12 p1980 A71-27409
- Third Chance flight control system, discussing aircraft control capability with backup hydraulic system after loss of dual main hydraulic systems due to combat damage 13 p1998 A71-29382
- Aircraft ILS signal reception system, obtaining category III reliability performance by circuit redundancy and automatic incoming information surveillance 15 p2446 A71-31912
- Soviet papers on information systems redundancy using redundant algorithms and structures and redundant coding theory 17 p2720 A71-34951
- Redundant modules introduction in microelectronic systems for increased reliability 17 p2716 A71-34954
- Redundancy method for correct performance of flexible structure with faulty elements prepared from microelectronic information media 17 p2720 A71-34955
- Binary relation algebra application to diagnostics tests for system involving redundant subsystems 17 p2720 A71-34960
- Redundant algorithms and structures, analyzing anisotropic systems described by continuous differentiable functions 17 p2710 A71-34962
- Filtering methods for reducing systematic errors of measuring system with structural redundancy 17 p2740 A71-34964
- Reliability analysis of redundant information systems, deriving formulas for risk of failure and faultless operation probability 17 p2721 A71-34966
- Strapdown or gimbaled inertial measurement units for space shuttle program, considering reliability, redundancy and cost of ownership 17 p2772 A71-35059
- ST-224 redundant inertial measurement system, using conventional gimbaled platforms, each with three skewed single-degree-of-freedom control gyro and one caged gyro 17 p2773 A71-35060
- Optimum skew angle between redundant inertial systems, considering component weight, MTBF and duty cycle 17 p2773 A71-35062
- Redundant solid state sequencer programmable via core memory, using two identical channels to prevent wrong output 18 p2885 A71-36449
- Space shuttle avionics system redundancy, calculating costs for individual line replaceable units 18 p2889 A71-36479
- Space shuttle design concerning fault detection and isolation, redundancy and maintenance for cost and downtime minimization by application of airline methods 18 p2900 A71-36480
- Commercial aircraft reliability and maintainability design philosophy application to reusable space vehicles, considering optimum redundancy, dispatch with component inoperative and fault isolation 18 p2973 A71-36481
- Symphonic telecommunication satellite attitude control system, describing operational principle based on gyroscopic inertial reference and redundant IR sensors 18 p2974 A71-36525
- Computerized automatic redundancy management for space shuttle guidance, navigation and control, using fly by wire control technique for in-flight failure detection and correction [AIAA PAPER 71-946] 19 p3098 A71-37187
- Skewed and orthogonal redundant reaction wheels comparison for outer planet exploration spacecraft attitude control based on reliability analysis [AAS PAPER 71-157] 19 p3101 A71-37926
- Priority standby redundant system consisting of two repairable units, considering preemptive and non-preemptive repair for system failure 21 p3386 A71-40364
- Redundancy optimization of series-parallel k-out-of-n systems for maximum reliability subject to multiple cost constraints 21 p3388 A71-40878
- Memory cell fault tolerant sequential machine synthesis, considering masking feasibility and lower bounds on minimum redundancy 21 p3351 A71-41036
- Imaging with low redundancy arrays, noting holography role in image processing 22 p3538 A71-41736
- Soviet book on automatic control and computer components reliability, explaining redundancy principles and test and repair procedures 22 p3526 A71-41820
- Relcomp conversational time-sharing computer program for rapid calculation of reliability and MTBF of systems with serial and redundant units 22 p3517 A71-42103
- Computerized system redundancy optimization formulation as zero-one type variables integer programming problem, obtaining algorithmic solution for maximum reliability 22 p3517 A71-42106
- Optimal redundancy and availability allocation for MTBF and time to repair in multistage system, using dynamic programming 22 p3518 A71-42116
- Control system effectiveness improvement, using redundancy and self adaptive techniques 23 p3655 A71-43291
- REDUNDANT STRUCTURES**
- U REDUNDANT COMPONENTS**
- REENTRY**
- NT HYPERBOLIC REENTRY
- NT HYPERSONIC REENTRY
- NT SPACECRAFT REENTRY

REENTRY ANGLE

- Nonequilibrium electron temperature, concentration and reflection in reentry boundary layers, discussing heat transfer and ionization energy diffusion [AIAA PAPER 69-82] 07 p1015 A71-19879
- ## REENTRY ANGLE
- U ANGLES [GEOMETRY]
- ## REENTRY TRAJECTORIES
- ## REENTRY BODIES
- ## REENTRY VEHICLES
- ## REENTRY COMMUNICATION
- S band PCM telemetry system using frequency diversity for spin stabilized high velocity blunt nosed reentry vehicle signal reception 01 p0163 A71-10980
- ## REENTRY CONDITIONS
- ## REENTRY EFFECTS
- Reentry environment simulation at vehicle stations away from stagnation point, using arc heater with supersonic nozzle duct [AIAA PAPER 71-261] 08 p1274 A71-21988
- Entry vehicle carbon vapor thermochemistry uncertainties effects on nose tip ablation response concerning stagnation point surface recession and temperature levels [AIAA PAPER 71-414] 11 p1857 A71-26207
- Total normal emittance under simulated reentry conditions, using emissometer with aluminum oxide reference cavity integral within sample [AIAA PAPER 71-468] 11 p1764 A71-26249
- Rate constant measurements of hot plasma electron attachment from ion current collection plots for communication during atmospheric entry 12 p1939 A71-27272
- V groove cathode discharge produced He plasma parameters studied for reentry electron density and temperature simulation, correlating energy flux and microwave noise emission 12 p1895 A71-27273
- Wide range nonimmersive RF coil with marginal oscillator for plasma electrical conductivity measurements tested for simulated reentry vehicle 12 p1908 A71-27285
- Radiation pattern modification factors calculation for TE excited slot antenna in ground plane covered with inhomogeneous plasma reentry sheath 23 p3646 A71-44172
- ## REENTRY GLIDERS
- ## U LIFTING REENTRY VEHICLES
- ## REENTRY GUIDANCE
- Mathematical model for optimal control of spacecraft reentry into atmosphere 09 p1519 A71-22558
- Spacecraft banking control during reentry, deriving dynamic equations of angular motion 16 p2646 A71-33655
- Two step spacecraft reentry guidance involving skip trajectory at parabolic speeds, proposing algorithm for running coordinate and speed vector components values 24 p3846 A71-45301
- ## REENTRY PHYSICS
- Three dimensional ablation calculated for reentry sphere-cone taking into account shape changes and internal heat conduction [AIAA PAPER 70-199] 01 p0180 A71-10952
- Space aerodynamics, examining reentry, flow ranges, pressure field visualization and real gas and rarefaction effects 01 p0162 A71-11450
- Spacecraft reentry aerodynamics regarding hypersonic high altitude lifting bodies, shock wave and flow field, heat, mass and energy transfer, etc [ICAS PAPER 70-01] 02 p0185 A71-11686
- Mesosphere and stratosphere data from high level observations for supersonic transport and reentering space vehicle operations 08 p1328 A71-21724
- Water cooled channel flow test device for arc jet material ablation studies, simulating reentry environment of high energy turbulent boundary layer flow [AIAA PAPER 71-260] 08 p1273 A71-21987
- Reentry heating simulation, noting UV radiation effects as shock layer thickness decreases [AIAA PAPER 71-467] 11 p1859 A71-26248
- Hypersonic reentry flow over blunt nosed bodies, using water oxygen mixture to achieve simulation at lower stagnation temperatures 11 p1705 A71-26270
- Wire grid simulation of electron density, transmission and reflection of lossless and lossy reentry plasma sheath under microwave radiation at X and K bands 12 p1935 A71-26767
- Experimental proof of combustion phenomena in reinforced plastics ablation under simulated atmospheric reentry, using arc plasma jets 12 p1987 A71-27721
- Flow mechanics with emphasis on reentry problems - Conference, Goettingen, West Germany, March 1971, Volume I 18 p2845 A71-36407

- Reentry plasmas ionization and microwave and optical radiation properties, considering radar echo, electromagnetic scattering, thermal equilibrium and ablation products 18 p2952 A71-36422
- Radiation role in nonequilibrium boundary layer during atmospheric reentries at speeds exceeding escape velocity 21 p3368 A71-40694
- Spacecraft communication cut-off during atmospheric reentry due to thermal ionization of gas boundary layer, discussing sulfur hexafluoride injection alleviation and electrostatic probe 22 p3583 A71-41998
- Combustion and chemical reactions near wall, in forced convection, boundary layer transition, radiation and ablation of missile reentry 24 p3890 A71-45148
- Spacecraft motion control algorithm for reentry at escape velocity based on object motion model 24 p3846 A71-45305
- ## REENTRY SHIELDING
- Temperature profile similarity and thermal protective coating thickness for single reentered spacecraft [AIAA PAPER 71-37] 06 p0916 A71-18498
- Static aerodynamic characteristics of slender ablating reentry vehicle, discussing coupling between flow field and thermochemical analyses of heat shield materials response [AIAA PAPER 70-826] 11 p1854 A71-25512
- Protective coatings of Ta, Nb and TD alloys for high performance thermal protection systems, discussing space shuttle reentry heat shield 11 p1778 A71-25554
- Graphite materials for nosetip/reentry applications, discussing isostatically pressed short fiber-pitch composites and binderless graphites, ablation data and NDT procedures [AIAA PAPER 71-417] 11 p1790 A71-26341
- High hyperthermal ablation performance of reinforced carbon-carbon composites for reentry nosetip application [AIAA PAPER 71-416] 12 p1920 A71-26764
- Radioisotope heat sources protection from reentry ablation and thermal stress with outer anisotropic pyrolytic graphite shield 13 p2099 A71-29259
- Carbon-carbon spacecraft reentry heatshields evaluation and selection by nondestructive and destructive tests on flight cones 14 p2262 A71-29647
- Mechanical and thermal properties of chemical vapor deposited carbon composite felt material for reentry heat shielding 14 p2262 A71-29648
- Aerodynamic heating of reentry vehicle, suggesting shielding by radiative cooling 18 p2848 A71-36432
- ## REENTRY TRAJECTORIES
- Lifting oscillatory reentry trajectories, developing equation method to consider density and velocity distributions 02 p0320 A71-12403
- N interval trajectory estimation computer program minimum variance adjustment technique, discussing airborne astrogaphic camera system for reentry bodies position determination 04 p0556 A71-15330
- Atmospheric reentry trajectories optimization by differential dynamic programming 08 p1363 A71-21347
- Winged lifting body quasi-optimal reentry trajectory for minimum flight time, taking into account angle of attack control and angular motion inertia 08 p1367 A71-22038
- Lunar swingby trajectory analysis with atmospheric reentry, characteristics of geocentric portions of earth-moon and moon-earth transfers 09 p1519 A71-22546
- Graphite heat shield ablation during low velocity low altitude portion of satellite reentry trajectories [AIAA PAPER 71-415] 11 p1857 A71-26208
- Adaptive roll control of space vehicle on reentry trajectory, analyzing spacecraft angular motion dynamic equations for optimal conditions determination 12 p1926 A71-26719
- Computerized automatic control system for atmospheric reentry, combining computational prediction of motion parameters with closed loop feedback 12 p1926 A71-26720
- Spacecraft landing trajectory minimization for lower reentry maneuver space bound at orbital speeds and fixed point coordinates 13 p2145 A71-29177
- Spacecraft optimal atmospheric reentry trajectory for minimum flight distance, investigating angle of attack control with allowance for load constraints 13 p2143 A71-29229
- Spacecraft reentry trajectory angle of attack control by mechanically varying center of mass for axial loads 16 p2645 A71-33443

- Airborne astrogaphic camera system for simultaneous determination of multiple object reentry trajectories at Air Force test range 18 p2918 A71-36077
- Lifting entry trajectory control law based on uniform drag, affording heating rate and deceleration control [AIAA PAPER 71-915] 19 p3096 A71-37165
- Reentry glider approximate optimal atmospheric entry trajectories for maximizing function of terminal velocity, altitude, flight path and heading angle under terminal nonlinear constraints [AIAA PAPER 71-919] 19 p3096 A71-37168
- Three dimensional hypervelocity reentry trajectories, using aerodynamic lift and vehicle bank angle as optimal control parameter [AIAA PAPER 71-920] 19 p3096 A71-37169
- Reentry vehicles trajectory reconstruction by computer program and Kalman filter estimation theory, analyzing instrument errors [AIAA PAPER 71-933] 19 p3097 A71-37178
- Nonlinear filters performance comparison for reentry vehicle trajectory estimation from radar tracking, noting coordinate systems effect on extended Kalman filter accuracy 19 p3039 A71-38712
- Spacecraft trajectories for reentry at hypersonic velocity, examining aerodynamic control loads and characteristics in atmospheric skip 20 p3288 A71-39122
- ## REENTRY VEHICLES
- NT APOLLO SPACECRAFT
- NT BOOSTGLIDE VEHICLES
- NT LIFTING REENTRY VEHICLES
- NT REUSABLE SPACECRAFT
- NT VOSTOK 2 SPACECRAFT
- Ballistic reentry warheads atmospheric interception, investigating defensive nuclear bursts effects 01 p0163 A71-10268
- Shape and surface roughness effects on turbulent ablation of reentry body nose tip, noting recession rate [AIAA PAPER 69-717] 01 p0071 A71-10934
- S band PCM telemetry system using frequency diversity for spin stabilized high velocity blunt nosed reentry vehicle signal reception 01 p0163 A71-10980
- Antenna and telemetry system for spherical shell ICBM reentry vehicles data link to ground 01 p0036 A71-10986
- Soviet book on ballistics of flight vehicles during atmospheric reentry 02 p0319 A71-11844
- Reentry vehicle angle of attack control by mechanically varying center of mass for axial loads 05 p0779 A71-16039
- Roll resonance in reentry body motion under nonlinear pitch, damping and Magnus moments, using multiple scales method [AIAA PAPER 71-47] 06 p0979 A71-18508
- Dynamic damping coefficient extracted from flight test lateral rate data telemetering ablative reentry vehicle [AIAA PAPER 71-49] 06 p0980 A71-18510
- Atmospheric reentry dynamics of spinning body with trim angle of attack 07 p1205 A71-18892
- Ballistic reentry vehicle roll related to trim angles caused by inertia asymmetries [AIAA PAPER 70-204] 07 p1208 A71-19867
- Transpiration cooling of reentry vehicle nosetips, noting two dimensional aspects of porous wall coolant flow and matrix-coolant energy exchange [AIAA PAPER 69-96] 07 p1223 A71-19869
- Exact expression for minimum range sensitivity deribit from elliptical orbits for ballistic atmospheric entry vehicle, considering retrovelocity 07 p1199 A71-19873
- High turbulent flow simulation in hypervelocity wind tunnel for reentry vehicles operational testing, discussing nozzle gas dynamic and mechanical design [AIAA PAPER 71-253] 08 p1273 A71-21982
- Effect of asymmetrical inviscid flow from Trail-blazer flight measurements, discussing windward leeward attenuation variation in transmitted VHF signal 09 p1406 A71-22916
- Continuous flow arc air heater for reentry vehicle components ground testing, achieving combined high pressure and enthalpy [AIAA PAPER 71-259] 09 p1429 A71-23061
- Cylindrical spacecraft reentry body self-sustained pitching oscillations due to separation on downstream portion, examining stability derivatives 09 p1533 A71-23604
- European research on reentry vehicle configurations, noting French concentration on flow fields and German emphasis on overall shape and control surfaces 10 p1684 A71-24848
- Transient resonance response of slender entry vehicles in rolling trim at spin-pitch intersection for offset coplanar and orthogonal leading models 11 p1837 A71-25480

Reentry vehicles configuration lift and drag coefficients in hypersonic flow from pressure distribution and balance measurements, comparing with isolated cone data

11 p1702 A71-25487

Reentry vehicles fluidically controlled hydrazine rocket engine modules for roll rate control

[AIAA PAPER 70-650]

11 p1810 A71-25503

Static aerodynamic characteristics of slender ablating reentry vehicle, discussing coupling between flow field and thermochemical analyses of heat shield materials response

[AIAA PAPER 70-826]

11 p1854 A71-25512

Entry vehicle carbon vapor thermochemistry uncertainties effects on nose tip ablation response concerning stagnation point surface recession and temperature levels

[AIAA PAPER 71-414]

11 p1857 A71-26207

Prediction analysis of downstream effectiveness in high speed laminar boundary layer for reentry vehicular surfaces film cooling, using reference enthalpy method

[AIAA PAPER 71-425]

11 p1752 A71-26216

Roll rate variation and lift effect on reentry vehicle impact, comparing analytic treatment with six degree of freedom trajectory simulation

13 p2144 A71-27977

Vibration amplitudes and transverse acceleration of reentry vehicle during uncontrolled atmospheric descent trajectory

13 p2146 A71-29208

Lenticular reentry vehicle configuration, considering aerodynamics, trajectory heating and weight analysis and structural design

15 p2500 A71-31604

Analog analysis of shape history of ablating graphite nose tips of reentry vehicle, eliminating geometrical instabilities

18 p2984 A71-35953

Aerodynamic heating of reentry vehicle, suggesting shielding by radiative cooling

18 p2848 A71-36432

Static and dynamic stability characteristics of X-15 aircraft, lifting body and trapezoidal and delta wing reentry body

18 p2971 A71-36434

Nonlinear motion of asymmetric rolling reentry vehicle with variable roll rate, dynamic pressure and stability derivatives

[AIAA PAPER 71-932]

19 p3148 A71-37177

Aerodynamic heating tests of cone flap reentry vehicle using temperature sensitive paint

20 p3311 A71-39197

Liquid film cooling for slender body type hypersonic reentry vehicles, comparing active mass injection cooling systems to ablation type passive systems

22 p3621 A71-42006

Angular momentum vector orientation of reentry vehicle at end of spin-up, using helicoid precession concept to characterize rotational motion during constant thrust

22 p3611 A71-42029

Propulsive lift augmentation for horizontal landing of low and medium L/D reentry vehicles, determining optimum thrust program

22 p3612 A71-42046

REFERENCE ATMOSPHERES

International Reference Ionosphere (IRI), considering organization, electron density and temperature, ion composition and electron collision frequencies

05 p0742 A71-16971

Cargo airship standard atmosphere operation modes, discussing long range gas capacity and short range applications for large compact loads

11 p1708 A71-26309

Aircraft barometric altimeter errors caused by atmospheric temperature deviations from International Standard Atmosphere

14 p2244 A71-30323

COSPAR international reference atmosphere containing seasonal variations, solar flux and altitude models for density, temperature, pressure and wind

16 p2572 A71-33851

Harvard-Smithsonian reference atmosphere model of solar atmosphere, combining photosphere and quiet lower chromosphere

19 p3146 A71-38660

REFERENCE SYSTEMS

Equilateral tetrahedral and Frank systems compared for standard reference system applications in spatial vectorcardiography

01 p0022 A71-10400

Reference standards for nondestructive ultrasonic inspection for quality control

01 p0091 A71-11424

Neighboring optimum feedback guidance to motivate min-distance lookup parameter determined by minimizing metric function of perturbed state and reference trajectory

[AIAA PAPER 69-888]

03 p0454 A71-13446

Automatic solar and lunar reference guidance system with balanced photoelectric measuring equipment

04 p0591 A71-14846

International geomagnetic reference field 1965 geomagnetic potential rate of change and transformation to dipole coordinates

06 p0888 A71-17282

Lunar surface plan reference systems with no common points comparison with photomechanically obtained scale maps

06 p0976 A71-18448

Lunar reverse side, tabulating reference points on western libration zone and eastern sector

08 p1366 A71-21777

Earth international compartmentalization into equal area elements on reference sphere for spherical functions utilization

10 p1601 A71-24460

Stellar silicon brightness measurement for evaluating SNR and selecting reference star

10 p1679 A71-24951

Information support system for physiological studies of human performance, including indexing approach for references categorization, microfiche file and data bank

11 p1860 A71-25253

Lunar surface no common point systematic reference systems comparison with photomechanically obtained scale maps

12 p1955 A71-26598

Stability of first order gain model reference adaptive control system with sinusoidal input

12 p1973 A71-27580

Aerial and block triangulation error analysis accuracy dependence on reference point number, introducing camera internal orientation improvement

13 p2062 A71-28903

Relativistic formulation of thermodynamics and statistical mechanics in special theory of relativity, noting Ott presentation

13 p2102 A71-29324

Secular parallaxes of reference stars by photometric distances and relative proper motions of open clusters at low galactic latitude

15 p2483 A71-31341

Bibliographic references of articles on solar terrestrial research during IQSY, including geophysical phenomena, international projects and background material

15 p2397 A71-31617

Heading reference system feedback linear control circuits containing fluidic vortex rate sensor applied to turbine drive

15 p2353 A71-32070

Synthesis algorithms for model reference adaptive control systems using Liapunov second and Popov hyperstability methods

15 p2382 A71-32623

Special relativity distinguished from theories based on preferred frame of reference and physical Lorentz contraction by Michelson-Morley experiment in solid transparent medium

16 p2610 A71-33268

Atomic clocks on manned space stations, discussing stability in aerospace environment, techniques for earth based timer calibration, reference device, maintenance and corrections

17 p2743 A71-35056

Reduced state estimator for satellite orbital heading reference, describing decoupled single-skewed-gyro gyrocompass design for attitude control

19 p3148 A71-37206

[AIAA PAPER 71-965] Interference voltage prediction model of induced noise in reference ground of electronic systems

19 p3031 A71-38448

Single point grounding of electronic system providing personnel safety and voltage reference potential

19 p3032 A71-38451

Multivariate statistical analysis of parameters measuring reference stars effects on parallax and error estimates

21 p3444 A71-40195

Radar determination of reference change related to sudden acceleration, deducing Galilean-accelerated reference transition in two dimensional space-time

21 p3415 A71-40513

Self referencing holographic system for image compensation in fluctuating random medium, describing homodyning procedure

21 p3382 A71-40935

Dew point / frost point / reference hygrometer for humidity gage testing in thermohygrostat hygrochamber

21 p3384 A71-41379

Secular parallaxes of reference stars by photometric distances and relative proper motions of open clusters at low galactic latitude

22 p3606 A71-42616

Nitrous oxide dissociation as natural source of stratospheric nitric oxide, noting estimates use as yardstick for artificial source

23 p3642 A71-43347

Automatic resau detection and reference ground control points for computing and correcting geometric and radiometric image for earth resource data, noting correlation with reference system

[AIAA PAPER 71-978] 24 p3806 A71-44576

REFERENCES [STANDARDS] U STANDARDS

REFINING

NT ELECTROREFINING

NT ELECTROSLAG REFINING

Sintered or cast Re refining in vacuum electron beam furnace using water-cooled crystallizer, discussing metal losses during melting

06 p0904 A71-17948

Refining process of Fe-NiCu-Mn alloys, discussing aging kinetics, hardening mechanism and strength properties

11 p1781 A71-26159

Primary high purity Mg refining technique, composition, oxidation and structure

15 p2435 A71-32338

REFLECTANCE

Tropospheric layers radio reflectivity as function of refractivity index and thickness/wavelength ratio

01 p0400 A71-11607

Waveguide microwave load element with separate adjustment for reflection coefficient phase and magnitude

03 p0378 A71-13397

Semitransparent spherical dielectric shell under diffuse incident radiation, determining absorbance and reflectance by Monte Carlo method

03 p0518 A71-13648

Calorimetric method for measuring high signal reflection coefficients at microwave frequencies

04 p0586 A71-14656

Vacuum deposited Mo and Ru films optical properties, emphasizing reflectance measurements

04 p0627 A71-15693

Color sensations and retinex theory, discussing mathematics of lightness scheme and biologic correlate of reflectance

05 p0753 A71-16901

Two layer antireflection coatings on glass for He-Ne lasers, calculating optimal film thicknesses for various substrates and wavelengths

06 p0907 A71-18038

Integrating sphere coatings bidirectional reflectance characteristics, describing reflectometer data for smoked magnesium oxide and Au coated sandpaper samples

06 p0902 A71-18534

Fluoride overcoated Al reflectance measurements and polarization effects at various angles of incidence, noting utilization in vacuum UV instrumentation

08 p1335 A71-21381

Low energy proton irradiation induced thin polymer contaminant films effect on far UV reflecting mirrors reflectance and scattered light

08 p1290 A71-21382

Nonlinear theory of intrinsic semiconductors electromagnetic wave transmission under skin effect conditions, determining reflectance and carrier temperature

08 p1344 A71-21442

Ti dioxide-opacified porcelain enamel reflectance spectra analysis, deriving scattering cross sections and dispersed particle sizes and distribution

09 p1480 A71-22116

Multiple reflections method for complex reflection and transmission coefficients of microwave transmission line permitting use of digital computers

09 p1413 A71-22151

Mirror reflection coefficients effect on fringe characteristics of multibeam series interferometer, showing improvement by Fabry-Perot etalon system

09 p1451 A71-23174

Lossless radiating antenna element efficiency in circular cylindrical arrays of identical elements, relating to reflection coefficient

09 p1419 A71-23505

Pi-section waveguide with narrow slot in broad wall, calculating reflection and transmission coefficients as function of design parameters

10 p1584 A71-24719

Reflectance measurements of dielectric coating on metallic substrate, comparing with analytical model

[AIAA PAPER 71-448] 11 p1799 A71-26233

Reflectance restoration of proton and UV degraded spacecraft thermal control coatings by low temperature oxygen plasma treatment applied to Surveyor 3

[AIAA PAPER 71-463] 11 p1800 A71-26244

Bidirectional reflectance model for randomly rough surface, using distribution function for macroscopic probability of microscopic surface roughness elements with specific slopes

[AIAA PAPER 71-465] 11 p1800 A71-26246

Lunar radar reflectivity mapping at 7.5 m wavelength for maria and highlands echo powers, using interferometric techniques

11 p1834 A71-26451

Lower ionospheric irregularities drift from neutral air motion measurements compared to meteor radar system determination

12 p1900 A71-27057

Electron concentration profiles in D region from radio wave partial reflection coefficients

13 p2030 A71-28558

Variable target reflectivity effect on weather radar measurements, using extended echo fluctuation theory for average and maximum signals
13 p2031 A71-28723

Lead borosilicate glass with crystalline opacifiers, observing microstructure and reflectance
13 p2093 A71-28990

Normally incident electromagnetic wave propagation in inhomogeneous gyration medium, obtaining reflection and transmission coefficients and discussing resonance
13 p2108 A71-29088

Radiative capacity of materials with low thermal conductivity at high temperatures determination from reflectivity measurements for oblique light incidence
14 p2240 A71-30051

Microwave resonator Q factor measurement by reflection coefficient method, using swept signal generator to eliminate incidental FM problem
15 p2376 A71-32310

Microwave reflection factor analytical and graphical dependences on resistivity of variable thickness semiconductor layers
16 p2544 A71-34032

Spectral dependence of GaAs-CdSe alloys optical reflection coefficient
17 p2790 A71-34203

Magnetoplasma reflection coefficient for nonzero angle of incidence in Voigt configuration in superconducting coil, calculating effective intervening mass
17 p2789 A71-35348

Variational principle with reflectivity extremum for inhomogeneous planetary atmospheric line spectra profile calculation from radiative transfer equation
18 p2964 A71-36286

Reflection and transmission coefficients for electromagnetic propagation across magnetic field in parabolic plasma layer, determining EM-plasma wave conversion efficiency
19 p3014 A71-37079

Semiconductor instability effects on reflection and transmission coefficients of microwave control devices
19 p3026 A71-37252

Absorbance of anisotropically scattering medium compared with measured hemispherical reflectances and transmittances
19 p3165 A71-37991 [ASME PAPER 71-HT-20]

Electromagnetic wave scattering on single ellipsoidal inhomogeneity in cylindrical waveguide, obtaining relationship for electric and magnetic waves reflection coefficient
19 p3019 A71-38330

Reflection and transmission coefficients of nonresonant slots in rectangular waveguide antenna with comb type slow wave structure
19 p3019 A71-38334

Light pressure measurement acting on Echo 1 satellite, considering integral reflection coefficient
20 p3306 A71-39132

Lithium niobate hypersound attenuation and reflection coefficients frequency dependence determination by scattering laser light at hypersonic oscillations
20 p3244 A71-39162

Rhodochrosite /manganese carbonate/ complex refractivity determination for correlation between optical reflection, attenuation and scattering coefficients
20 p3269 A71-39185

Statistical processing of phase dependence of Martian integral brightness at 0.3-1.1 microns, noting abrupt reflectivity decrease
20 p3290 A71-39308

Reflection and transmission coefficients of long lossy single-wave waveguide line with random inhomogeneities
20 p3198 A71-39805

Photoelectric polarization curve, reflectivity and absolute diameter of Vesta, comparing with Lyot curve
22 p3602 A71-42177

Isotropic light scattering in unsteady plane layer of finite optical thickness, obtaining reflection and transmission coefficients for radiative transfer
22 p3607 A71-42869

Radio reflection and transmission coefficients for thin highly ionized layers under earth magnetic field, based on numerical integration of differential equations
23 p3665 A71-42962

Ionospheric propagation penetrating and nonpenetrating modes full wave reflection and transmission coefficients determination for height and frequency variation by thin film optical method
23 p3643 A71-42972

Infinite plane elastic wave reflection and refraction coefficients at fluid-solid interface, noting reflected beam lateral displacement at critical angles
23 p3703 A71-43202

Reflection coefficients measurement for scanning two-mirror interferometer with absorbing Ni film matched to external medium, discussing multilayered coatings
23 p3676 A71-43399

Double heterostructure GaAs injection laser mode reflectivity and waveguide properties, discussing

threshold current density and wavelength dependence on mirror reflectivity
24 p3832 A71-44433

Atmospheric attenuation effects on cloud and precipitation radar reflection coefficient
24 p3845 A71-44880

Reflection coefficient of multimode laser beam from dielectrics interface
24 p3833 A71-45044

REFLECTED RADIATION

U REFLECTED WAVES

REFLECTED RAYS

U REFLECTED WAVES

REFLECTED WAVES

Short wave reflected radiation fluxes in atmosphere with absorption allowance for water vapor, carbon dioxide and ozone
01 p0144 A71-10538

Complementary field component of radiation from Cassegrain subreflector
01 p0055 A71-11172

Reflected electromagnetic wave polarization parameters, obtaining correlation functions for radar echoes
04 p0557 A71-14632

Flow characteristics behind reflected shock wave flow and heat transfer at tube wall, noting unsteady and nonlinear effects
04 p0567 A71-14665

Spectroscopic studies of helium-hydrogen plasmas in first reflected shock region in electromagnetic T-tube
04 p0631 A71-14684

IR radiation measurement of chain branching rates in hydrogen-oxygen mixtures ignited by reflected shock waves
04 p0548 A71-14695

Air plasmas temperature measurements behind reflected shock wave, examining radiative cooling effects and total radiant energy
04 p0632 A71-14704

Magnetically reflecting nonducted whistler mode waves propagation noting dispersion, hybrid frequencies, ray curvature and field lines
06 p0868 A71-17983

Methyl radicals reactions produced by azomethane or ethane pyrolysis in reflected shock waves, describing chain reaction mechanism
08 p1250 A71-20668

One dimensional isentropic gas motion in acoustic wave reflection from cylindrical tube nonplane closed end under flow
08 p1276 A71-21478

Plane normal shock wave reflection in relaxing gas for shock tube endwall upstream and downstream dynamic pressures, using method of characteristics
09 p1546 A71-23166

Plane electromagnetic wave reflection from conducting convex cylinder in radially inhomogeneous absorbing medium, deriving equations for beam trajectory calculation
10 p1574 A71-23805

Ignition delay times behind reflected shock wave of alkanes methane through pentane in stoichiometric argon simulated air mixture
10 p1657 A71-24047

Amplitude curves of reflected wave vertical displacement component in horizontally stratified medium with simple layer velocity pattern
10 p1644 A71-25134

F region layers vertical drift from phase paths of radio waves reflected from constant electron density surfaces
11 p1756 A71-25646

Mach reflection of strong shock waves by sharp compressive corner in real gas in hypersonic tube, using laser Mach-Zehnder interferometer
11 p1752 A71-26190

Triple point trajectory of shock-shock Mach reflection off plane wall, comparing to Whitham theory
11 p1752 A71-26192

Autocorrelation functions of quasi-uniform solar radiation field reflected from earth with scattering allowance, using stationary random theory
12 p1901 A71-27097

Uniform asymptotic diffraction of plane wave from ideally reflecting cylinder, using parabolic equation method
13 p2027 A71-27900

Revolving cylindrical surface reflected energy from scanning fixed laser beam, noting signal frequency
13 p2077 A71-27948

Third harmonic component generation in reflected and transmitted waves from magnetoplasma slab, using Boltzmann transport equation and Maxwell equation
13 p2109 A71-29243

Receiver triangle size effect on ionospheric drifts near 2 MHz, using partial and total reflections from lower ionosphere
14 p2230 A71-29710

Acoustic waves reflection from nonplanar closed end of cylindrical tube with one dimensional isentropic gas flow from Riccati differential equation solution
14 p2227 A71-30665

Flat plate electrostatic probe for ionization rate measurements behind reflected shock waves, monitoring time evolution of electron production
14 p2248 A71-30884

Ethane-oxygen-argon mixtures ignition behind reflected shock wave, deriving composition temperature dependences correlation
15 p2463 A71-31625 [WSS/CI PAPER 71-16]

Pseudorandom binary codes for improved microwave antenna range measurements by suppressing unwanted reflections
15 p2373 A71-32370

Shock wave propagation in junction of straight duct with side branch for subsonic flow, analyzing reflected and transmitted waves
16 p2555 A71-32886

Radiative heat transfer effects behind reflected and incident shock waves in high temperature air and xenon respectively
16 p2662 A71-32888

Argon gas ionization behind reflected shock wave front investigation by double probe method with HF multistep pulse voltage
16 p2576 A71-32911

Calculational method for predicting angular distribution of sunlight upwelling flux scattered by atmosphere and reflected by ground, using Monte Carlo data
16 p2562 A71-33130

Signal waves amplifier in medium of high nonlinear electric polarization, considering reflected waves effect on amplification
16 p2544 A71-34131

Methane-oxygen-argon mixture ignition behind reflected shock waves in single pulse shock tube
17 p2792 A71-35707

Reflected shock wave interaction with shock tube contact surface
18 p2903 A71-36123

Carbon dioxide IR radiation measurements of duration of constant reflected shock temperature in over-tailored shock tunnel
19 p3041 A71-37893

NO, CO and Ar mixtures IR spectral emission radiant intensities behind shock tube generated reflected shock waves
19 p3012 A71-38087

End-on shock tube detection technique sensitivity for monitoring light emission behind reflected shock waves
20 p3209 A71-38830

Reflected radiation brightness field statistical structure in IR range from Cosmos 121 satellite measurements, calculating correlation functions and spectral densities
20 p3259 A71-39680

Solar and terrestrial IR reflected radiation from Cosmos satellites measurements, determining clouds upper boundary height
20 p3261 A71-39688

Autocorrelation functions of quasi-uniform solar radiation field reflected from earth, using stationary random theory and allowing for scattering
22 p3533 A71-41652

Reflected electromagnetic wave polarization parameters, obtaining correlation functions for radar echoes
22 p3510 A71-42272

Ne ionization relaxation time behind reflected shock waves from temperature and pressure measurements of combustion driven shock tube end wall
23 p3706 A71-42909

Reflected shock wave interaction with tangential discontinuity curve for supersonic incalculable jets, examining flow instability
23 p3665 A71-44337

Radio echoes from clouds and precipitation, determining detection threshold, station potential and statistical distribution numerical characteristics
24 p3844 A71-44879

REFLECTING TELESCOPES

Reflecting telescope with six meter mirror, describing optical and control systems and structure
02 p0254 A71-12712

Tunable filter reflecting telescope and accessory optics for H alpha monochromatic photography of electron corona during total eclipse
03 p0424 A71-13626

Optical design of image selector for Cassegrain telescope recording difference spectrum of targets in focal plane
03 p0425 A71-13646

Six meter reflector telescope construction, discussing design, components and control system
04 p0588 A71-14827

H II region high velocity observations by two etalon, propane scanned photoelectric Fabry-Perot spectrometer with reflecting telescope
04 p0581 A71-15044

Photoelectric reflector zenith telescope for determination of earth rotation and latitude variations, noting recording by photon counts
04 p0598 A71-15381

Three-mirror telescope third order dioptrics of astigmatism and coma suppression
06 p0901 A71-18313

Third order aberrations in Cassegrain type telescopes and coma correction in servo-stabilized images

07 p1107 A71-19202

Pulkovo radio telescope effective frequency range extension beyond minimum 3 cm wavelength into millimeter range, installing high precision reflecting mirror surfaces

07 p1083 A71-19343

Main mirror shape in three mirror telescopes permitting spherical aberration suppression

10 p1608 A71-23820

X ray astronomy orthogonal mirror telescopes, noting collecting efficiency, angular resolution and focusing

11 p1766 A71-26307

Four foci computer controlled Anglo-Australian reflecting telescope, considering design and applications

13 p2069 A71-28850

Four stage image intensifier testing for weak astronomical object photography in connection with 42 inch Cassegrain telescope

13 p2070 A71-29138

Trigonometric white dwarf star parallax measurements, using astrometric reflector to derive H-R diagram

14 p2316 A71-31007

Star EV Lac polarimetric observations during flare, using Cassegrainian reflector

15 p2487 A71-32031

High angular resolution optical telescopes, considering mirror materials, optical coatings and pointing systems

16 p2580 A71-33739

Astronomical reflecting telescope, discussing frictionless oil pressure bearing design, declination and hour axis drives operation and optical system

20 p3239 A71-39531

Reflecting telescope Schmidt camera photographic color system temperature dependency from cluster NGC 103 photographs

21 p3379 A71-40717

High resolution Mars photographs obtained with 61-in reflector telescope

24 p3872 A71-44998

REFLECTION

NT INFRARED REFLECTION

NT RETROREFLECTION

NT SIGNAL REFLECTION

NT SPECULAR REFLECTION

NT ULTRAVIOLET REFLECTION

NT WAVE REFLECTION

German monograph on beam shift at total reflection covering Goos-Hanchen optical effect, acoustics, quantum mechanics, plasma physics, Brewster law, holography, etc

05 p0780 A71-16122

Saturn satellites spectrophotometric observations at UV, visible and near IR, noting reflection spectra data

11 p1819 A71-25210

REFLECTION COEFFICIENT

U REFLECTANCE

REFLECTIVITY

U REFLECTANCE

REFLECTOMETRES

Integrating sphere coatings bidirectional reflectance characteristics, describing reflectometer data for smoked magnesium oxide and Au coated sandpaper samples

06 p0902 A71-18534

Total emittance measurements by portable IR reflectometer, tabulating nongray error effects

13 p2159 A71-27979

REFLECTOR SATELLITES

U PASSIVE SATELLITES

REFLECTORS

NT PARABOLIC REFLECTORS

NT PARABOLOID MIRRORS

NT RADAR CORNER REFLECTORS

NT RADAR REFLECTORS

NT SOLAR REFLECTORS

High efficiency spherical reflector antennas with scanning and multiple feed properties for communication satellite portable earth stations

02 p0233 A71-12792

Space communication reflector surface positioning and optical measuring techniques for best fit

02 p0234 A71-12805

Stray-source field on plane antenna reflector surface for arbitrary space direction

03 p0387 A71-14335

Reflector antenna under wideband noise radiation, determining directivity characteristics by solution for angle range homologous to region of irregular lobes

05 p0728 A71-16008

Pulkovo radio telescope reflector adjustment by phase comparator, using centimeter wave transmitting-receiving antenna for sun, moon and Venus observations

07 p1083 A71-19344

Solid state laser with different diffuse coatings on external reflector of pumping source, measuring energy output

07 p1125 A71-19812

Ideal reflector simulation of periodically supported infinite plane metallic wire gratings with rectangular mesh showing small sag

09 p1409 A71-23503

Far field diffraction pattern of corner reflector for normally incident monochromatic light, considering polarization characteristics

10 p1640 A71-23947

Space communications antennas main reflecting surface accuracy determination by statistical evaluation of efficiency degradation due to mechanical inaccuracies and structural flexibility

12 p1887 A71-27003

Ultrasonic field distribution patterns from metallic and ceramic concave spherical reflectors under excitation by single or multiple piezoelectric elements

13 p2101 A71-29267

Optical method for elastic deformations measurement of radio telescope reflector at various elevations

14 p2211 A71-29991

Minor planet Icarus earth approach observations with reflector and TV camera, determining spherical coordinates by comparison with reference stars

14 p2309 A71-29993

Reflectors group mean effective scattering cross section measurement by far field criterion

14 p2194 A71-30075

Corner reflector excitation by vertical or horizontal log-periodic dipole antenna for unidirectional wide-band radiation, deriving far field expression

18 p2895 A71-36994

Broadband antenna twist reflector with wire grids, deriving design formulas and theoretical performance in terms of polarization attenuation

19 p3036 A71-38606

Beryllium reflector plate failure in NASA Plum Brook Reactor, discussing irradiation induced mechanical and physical property changes and internal/external stress effects

21 p3414 A71-40904

Aircraft flash light designs, discussing tandem oscillating lights, fixed lamp rotating reflectors and lamps, xenon flashtube, quartz-iodine lamp and flash frequencies

22 p3483 A71-41494

Reflector antenna under wideband noise radiation, determining directivity characteristics by solution for angle range homologous to region of irregular sidelobes

22 p3524 A71-42757

REFLEXES

NT CAROTID SINUS REFLEX

NT RESPIRATORY REFLEXES

Conditioned reflexes in cats with mesencephalic reticular formation subject to food-signaling acoustic stimulation

01 p0007 A71-10034

Interhemispherical synthesis of conditioned reflex motor reactions at different running angles in mice

01 p0011 A71-11051

EEG dynamics and visual cortex neuron responses in cats to conditioned optical stimulus during defensive reflex formation

01 p0011 A71-11052

Temporary connection of neurons in visual and associative cortical regions of hemispheres in cats

01 p0012 A71-11053

Cortical vestibular projection zones in formation of conditioned reflexes and spatial orientation of cats

01 p0012 A71-11054

Orientation reflex in healthy and nervous human subjects from peripheral vessels blood pressure fluctuations in response to acoustic signals

01 p0012 A71-11055

Vasomotor reflexes latency in postganglionic cardiac and renal nerves in intact and spinalized cats, determining spinal mediation by electrophysiological methods

04 p0538 A71-15093

Reflex excitability of neuromuscular systems of Soyuz crewmembers during physical loads

06 p0855 A71-18372

Human operator psychophysiological analysis by memory-activity interdependence simulation, noting buffer memory, reflex system and habit acquisition

07 p1050 A71-20107

Muscle reflex action role in contralateral remote masking at high auditory signal sound pressure levels

08 p1246 A71-20803

Human spinal reflex effects during static work, suggesting cord segmental chiasmatic connections interaction with spinobulbar-spinal tract

08 p1249 A71-21973

Cerebrospinal knee and flexor reflex suppression observations in rabbits and cats during blood circulation disorders

09 p1391 A71-22480

Biophysical nature of human memory, investigating electrosensitivity phase modulators and variations by suprainensitive light stimulus to eye and adjustment reflex

09 p1391 A71-22484

Globus pallidus damage in cats, investigating effects on conditioned motor reflexes, learning and memory

10 p1564 A71-24466

Baroreflex regulation of pulse interval during bicycling exercise, using systolic pressure-pulse relation to express reflex sensitivity

13 p2012 A71-28951

Conditioned reflexes developed by prolonged training in two genetic strains of mice during adaptation to altitude hypoxia

15 p2356 A71-31248

Conditioned auditory reflex behavior in rats under influence of acceleration, noting ontogenetic effects

15 p2356 A71-31249

Sense organs conditioned reflex and physiology, investigating mechanisms and functional localization of discrimination function and differentiating inhibition

15 p2360 A71-32529

Arterial baroreceptor reflex action in rabbits, noting central noradrenergic neuron participation

16 p2528 A71-33075

Hypothermia effects on cat and dog vascular tone vasomotor reflex regulation, suggesting role of inhibition due to changed afference from cooled tissues

16 p2533 A71-34111

Soviet papers on higher nervous activity physiology, Part 1, Basic laws and mechanisms of conditioned reflex activity covering inhibition, and bioelectrical effects, with bibliography

17 p2684 A71-35357

Brain locking activity structural organization, discussing cerebral processes and control contact mechanisms activating conditioned reflexes

17 p2684 A71-35358

Orientation reflexes neuronal activity due to various stimuli, noting hippocampus reaction to sound and light

17 p2685 A71-35361

Bioelectrical aspects of conditioned reflex activity, discussing changes in cortex background, cortical and cerebral biopotentials and alpha-rhythm depression reactions

17 p2685 A71-35362

Reflexes dominant in organism throughout activity or temporarily dominating reflex system directing work of nervous centers

17 p2685 A71-35363

Physicochemical aspects of conditioned reflexes, including membrane mechanisms, effectiveness of synapses, mediation processes, ribonucleotides function and subcellular structures dynamics

17 p2685 A71-35364

Conditioned reflex activity, demonstrating development of individual signals systems interrelation

17 p2685 A71-35365

Sympathetic response in renal and splanchnic nerves to induced fall and rise of arterial blood pressure in anesthetized rabbits, investigating baroreceptor reflex effect

17 p2685 A71-35367

Bulbar and baroreceptor inhibition of spinal and supraspinal sympathetic reflex discharges recorded in cats from renal nerve

18 p2857 A71-36689

H reflex changes in spinal marrow of intact and labyrinthectomized rats under radial accelerations

20 p3188 A71-39221

Reflex mechanisms and programmed command in insect flight stabilization, discussing gravity proprioceptors, wind sensing and optomotor control

21 p3326 A71-39987

Flying personnel equilibrium tests with pendulum armchair, investigating labyrinth reflex by induced nystagmus

22 p3500 A71-41570

Vestibulo-colic reflex control of head movement in seated man under sinusoidal and stepwise rotational velocity stimulation, comparing with ocular stabilization

22 p3501 A71-41822

Neural control organization in vestibulo-ocular reflex arc, considering afferent and oculomotor neural signals

22 p3490 A71-42449

Oculomotor neural organization models, considering vestibular ocular reflex, saccadic eye movements and smooth pursuit systems

22 p3504 A71-42450

Sympathomimetic amines effects on central nervous system reflex activity of irradiated and desympathized animals

22 p3492 A71-42708

Human motor system control mechanism for stretch reflex loop gain with simplified central nervous system computation

23 p3639 A71-43354

Trace reflex formation in response to acoustic stimulus with verbal reinforcement, determining cross correlation connections between induced activity of auditory and motor areas

24 p3796 A71-44547

REFRACTED RADIATION
U REFRACTED WAVES

REFRACTED WAVES
U REFRACTED WAVES

REFRACTED WAVES
Alfven wave transformation into magnetoacoustic wave during passage across boundary between two

media in strong magnetic field, considering reflection and refraction laws

07 p1195 A71-19381

Short N wave refraction and diffraction by gas-filled soap bubble, discussing measurements to explain peaking and rounding in sonic boom pressure signature

10 p1642 A71-24811

Plane traveling electromagnetic wave existence, propagation and refraction in nonlinear dispersive nonmagnetic isotropic lossless medium

13 p2027 A71-27899

Acoustic refraction by two dimensional shear layer in duct, considering sound propagation and initial value problem solution

13 p2051 A71-29248

Reflection and refraction patterns of various wave number media vertical electromagnetic dipole fields at even and uneven interfaces

14 p2192 A71-29805

Venusian atmosphere RF refractive attenuation height dependence, field strength measurements comparison, inversion layer influence and surface echoes effects

14 p2309 A71-30098

Refraction and absorption length of coherent laser radiation propagating in high temperature cylindrical plasma column

15 p2458 A71-32390

Bounded sources gravitational waves generation and propagation, noting refraction phenomenon in matter presence

16 p2612 A71-33282

Refraction effects of moving inhomogeneous media in electromagnetic Doppler measurements, using Maxwell equations or relativistic ray tracing method for frequency variations

16 p2544 A71-33850

Alfven wave transformation into magnetoacoustic wave during passage across boundary between two media in strong magnetic field, considering reflection and refraction laws

19 p3138 A71-37806

Refractive imaging and scanning methods for thermal imaging systems, considering high performance IR lenses

22 p3544 A71-42137

Refraction of electromagnetic wave with electric field perpendicular to applied magnetic field in anisotropic plasma cylinder cross section

24 p3858 A71-45236

REFRACTING TELESCOPES

Mercury drawings from refractor observations /1964-1967/

09 p1520 A71-22834

REFRACTION

NT ATMOSPHERIC REFRACTION

NT BIREFRINGENCE

NT RADIO WAVE REFRACTION

Underwater objects plotted in double projectors, reconstructing water surface optical refraction

01 p0083 A71-11327

Neodymium glass laser with intracavity emission polarization, determining thermally induced double refraction effect on energy characteristics

03 p0435 A71-13505

Plane EM waves at two dimensional periodic media boundary, obtaining reflection and refraction for harmonics

05 p0723 A71-17029

Axisymmetric phase object holographic interferometry, showing light beam refraction effect on interference pattern

07 p1108 A71-19237

Linearized gravitation theory in macroscopic media, deriving refraction of gravitational waves based on classical electromagnetism

17 p2777 A71-34585

Refraction and image forming qualities of frog eye using measurement of intensity profile /point spread function/, confirming hyperopia

18 p2857 A71-36690

REFRACTIVE INDEX

U REFRACTIVITY

REFRACTIVITY

Threshold emission and self excitation of spatially inhomogeneous laser, considering active element gain and refractive index by electrodynamic model

01 p0094 A71-10687

Transparent solids unpolished samples refractive index and dispersion measurement using Abbe refractometer

01 p0128 A71-10837

Extended Spline Fit Technique for determining refractivity from interferograms of axisymmetric laminar diffusion flames

01 p0180 A71-10946

Structural properties of atmospheric refractive index, using single mode laser

01 p0120 A71-11102

Atmospheric refractive index average structural characteristics measurement over 25 km light propagation path, noting diurnal variation

02 p0245 A71-12011

Direction indicating color schlieren system displaying radial refractive index gradients, comparing with knife edge monochrome image resolution

03 p0423 A71-13459

Tropospheric diffraction fields computation in atmospheres with modified refractive index increasing monotonically with height, discussing IF and LF ground wave propagation

04 p0552 A71-15020

Visible radiation absorption by aerosol particles, noting gray absorption and imaginary portion of complex index of refraction

04 p0582 A71-15072

Australian tektites population polygons of bulk specific gravity and refractive index, indicating variations in chemical composition

04 p0582 A71-15133

Optical beam scintillation dependence on wavelength in strong refractive index turbulence

04 p0609 A71-15694

Refractive index equation for oblique wave propagation in inhomogeneous compressible electron plasmas

05 p0786 A71-16287

Magnetospheric whistlers, deriving group refractive index and velocity, propagation time and various L values

05 p0721 A71-16443

Carbon dioxide refractivity measurement, determining dielectric constant, Verdet constant and Rayleigh scattering cross section by dispersion formula

05 p0717 A71-16908

Small scale isotropic turbulence intensity and refractive index measurements by optical shadow devices

06 p0897 A71-17527

Pulsed carbon dioxide laser amplifier, examining spatial and temporal refractive index variations with interferometric measurements

06 p0910 A71-18667

Multipath distortion and wavenumber spectrum of refractive index in radio links

07 p1060 A71-19258

Small wavelength wave optics of media with inhomogeneous refractivity developed from geometric optics, representing probability amplitude of classical ray by wave function

07 p1110 A71-19476

Radio signal refractive index fluctuations in Venus atmosphere from Mariner 5 data

07 p1197 A71-19762

Plasma refractive index effects in pulsed HCN lasers, calculating stable cavity mirror curvatures construction as function of electron density by ray matrix approach

07 p1124 A71-19795

Interstellar extinction curve accounted for by graphite, iron and silicate grains, presenting refractive index values plotted as functions of wavelength

07 p1199 A71-20009

Threshold emission and self excitation of spatially inhomogeneous laser, considering active element gain and refractive index by electrodynamic model

07 p1125 A71-20148

Carbon dioxide laser IR pulses self focusing in liquid carbon disulfide, calculating nonlinear refractive index

07 p1128 A71-20396

Light rays bundle compression devices performance based on phase space treatment using Liouville theorem, comparing linear tapers and lenses performance to compressor with graded refractive index distribution

08 p1335 A71-21373

Far IR materials optical constants analysis by channeled spectra, using Fourier spectroscopy single signature in interferogram to yield real and imaginary parts of refractive index

08 p1335 A71-21384

Artificial dielectric refractive index with diffraction allowance as function of multilayer geometry, wave frequency, polarization and propagation direction

09 p1406 A71-22884

Aqueous HCl refractive indices measured for room temperature to Venus cloud temperature and various concentrations

09 p1522 A71-22937

Magnetoionic theory for drifting plasma whistler mode propagation, deriving magnetic field effects on imaginary and real parts of complex refractivity

09 p1505 A71-23385

Singularity free refractive index profiles, using hypergeometric function

10 p1642 A71-24590

Variable shear interferometer for infinite fringe operation and velocity measurement, discussing refractive index distributions in stationary and moving media

10 p1613 A71-24994

Aqueous HCl solutions refractive index calculation from concentration dependence for Venus clouds composition

10 p1680 A71-25012

Geomagnetic Pc1 pulsations propagation in F region, deriving hydromagnetic waves equations by ray tracing method and waves refractivity index in extraordinary mode

10 p1607 A71-25118

MHD waves incident at density step, calculating reflection, refraction and transmission coefficients and coupling modes

11 p1807 A71-26429

Nonstatic random isotropic medium geometrical optics, considering refractive index temporal fluctuation [ONERA-TP-970]

12 p1929 A71-26822

Venus polarimetric observational data comparison with polarization characteristics of radiation scattered at gamma-distribution particle sizes, determining refractivity and particle radius

12 p1964 A71-27088

Plasma refractive index and electron density measurements by He-Ne vernier interferometric laser

12 p1940 A71-27282

Refractive index and reflectivity of BiTeBr and BiTeI single crystals from interference measurements in transmission spectra

12 p1944 A71-27545

Ionospheric anisotropic plasma with mixture of different ions, deriving refractivity at whistler frequencies

13 p2058 A71-28027

Phase modulation in far IR interferometers applied to laser refraction measurements in solids and organic liquids

14 p2238 A71-29743

Complex refractive index equation of ionosphere for large values of vertical component of magnetic field, showing imaginary part independent of temperature effects

15 p2449 A71-31849

Gases refractive behavior, discussing constitutive properties, wave propagation, Lorentz electron theory of dispersion, spectral interferometry and hook method

16 p2608 A71-33156

Pulse laser holographic interferometry for refractivity measurement, considering wave front reconstruction principles

16 p2578 A71-33160

Atmospheric absorption of 10.6 micron laser beam radiation, noting effect on refractive index

18 p2910 A71-35843

Holographic fiber optics image-guiding structures preparation in sensitized polymethyl methacrylate cast sheet by refractive index gratings pair recording

18 p2946 A71-35852

Venus polarimetric observational data comparison with polarization characteristics of radiation scattered at gamma-distribution particle sizes, determining refractivity and particle radius

19 p3133 A71-37438

Refractive index changes by shock compression metamorphism of tektite, soda lime and silica glasses

19 p3084 A71-37661

Plasma optical refractivity, considering gas laser interferometry and holographic phase measurements

19 p3116 A71-38244

Ray statistics of electromagnetic wave scattering in homogeneous isotropic turbulent medium with ellipsoidal inhomogeneities of refractive index, using Fokker-Planck equation

19 p3020 A71-38364

Atmospheric water vapor effects on microwave frequencies refraction index structure

19 p3024 A71-38611

Ion beam deposition of insulating carbon thin films on room temperature substrates, considering transparency, index of refraction, insulating capacity, glass scratching ability, etc

20 p3241 A71-39011

Self induced thermal distribution due to laser beam, discussing effects on refractive index inhomogeneities and second harmonic generation

20 p3196 A71-39105

Rhodochrosite /manganese carbonate/ complex refractivity determination for correlation between optical reflection, attenuation and scattering coefficients

20 p3269 A71-39185

Venus atmosphere decimeter wave field intensity fluctuations and refraction coefficient variations

20 p3297 A71-39627

Transversally excited and atmospheric carbon dioxide laser, measuring time behavior of refraction index profile and lensing effects on resonator

21 p3392 A71-40547

Soviet monograph on radio wave propagation in fluctuating parameters media covering ionosphere /fluctuating electron concentration/ and troposphere /fluctuating inhomogeneities and refractive index values/

21 p3349 A71-41372

Infinite plane elastic wave reflection and refraction coefficients at fluid-solid interface, noting reflected beam lateral displacement at critical angles

23 p3703 A71-43202

Pressure histories from densification and relaxation measurements on lunar glass and synthetic samples, investigating refractive index changes after annealing 23 p3758 A71-43760

Lithium iodate hexagonal and tetragonal form crystal growth conditions from aqueous solution and recorded refractivity 23 p3717 A71-43935

REFRACTOMETERS

Onboard aircraft refractometer, design, operation principles and effectiveness 05 p0756 A71-17195

Onboard aircraft refractometer design, operation and effectiveness 13 p2067 A71-28250

REFRATORIES

Compressive creep behavior of yttria rare earth stabilized zirconia storage heater refractories, determining stress time to failure 09 p1484 A71-23686

REFRACTORY MATERIALS

NT CHROMIUM

NT MOLYBDENUM

NT MOLYBDENUM ALLOYS

NT NIOBIUM

NT NIOBIUM ALLOYS

NT OSMIUM ALLOYS

NT PORCELAIN

NT REFRATORIES

NT REFRACTORY METAL ALLOYS

NT REFRACTORY METALS

NT RHENIUM

NT RHENIUM ALLOYS

NT RHENIUM ISOTOPES

NT TANTALUM

NT TANTALUM ALLOYS

NT TUNGSTEN

NT TUNGSTEN ALLOYS

Gas flame heater for heat resistant samples under fatigue tests, simulating gas turbine engine operating conditions 01 p0067 A71-10041

Boride composites with high strength and thermal resistance suitable as nose cap and leading edge materials for reusable lifting reentry systems [AIAA PAPER 70-278] 01 p0109 A71-11282

High strength ceramics for high temperature applications, reviewing oxides, nitrides and carbides 01 p0109 A71-11601

Soviet book on Mg, Ca, Fe and Sn high temperature borates formation covering optimum synthesis conditions, properties, stability analysis, etc 02 p0208 A71-11800

K-beta and L-alpha X ray spectral emission bands of high melting vanadium compounds, considering chemical bonds 02 p0263 A71-11892

Hydraulic hot pressing equipment for producing large parts from high melting point metal powders and compounds by induction heating of dies 02 p0238 A71-12282

Reactive molecule and atom attack of refractory materials in dissociated gases at filament temperatures up to sublimation threshold 03 p0374 A71-13124

Soviet book on welding fillers based on high melting point compounds covering alloy selection, surfacing techniques, working machine maintenance, etc 03 p0432 A71-13689

High temperature specific heat of refractory molybdenum and uranium dioxide 04 p0612 A71-14959

Aircraft construction materials for 1990s, discussing need for high temperature resistant materials for supersonic and hypersonic airframe and engine structural components 05 p0839 A71-16141

Soviet monograph on refractory materials elasticity at high temperatures covering elastic and shear moduli, Poisson coefficient and resonance methods 05 p0766 A71-16400

Ni and Ti cutting, examining wear for various microcutting refractory materials 05 p0759 A71-16862

Refractory elements abundances in chondrites, basaltic achondrites and Apollo 11 fines, emphasizing Ca-Al relationship 06 p0966 A71-17894

Elastic and thermodynamic properties of transition metal carbides, comparing Debye temperatures obtained from elastic constant to those obtained from specific heat data 06 p0915 A71-18687

Grain growth inhibition in niobium diboride by TiN addition 07 p1144 A71-19390

Phase equilibria, microstructure and physical properties of high temperature vacuum sintered oxygen deficient zirconia and thorium 08 p1304 A71-20697

High melting compound tools wear resistance during Ti and Ni continuous microcutting 08 p1297 A71-21065

Conical metal core electrode erosion rates in pulsed plasma accelerators with refractory dielectric chamber 08 p1340 A71-21484

Columnar grain and single crystal high temperature gas turbine elements development through directional solidification 08 p1314 A71-21565

Refractory materials at normal and high temperatures, describing cyclic shear test methods 08 p1372 A71-21612

High temperature turbine parts protective coatings, discussing aluminum diffusion prevention and crack and oxidation resistance 09 p1456 A71-23290

Cermet antifriction and friction powder metallurgy sintered materials for working at high temperatures without lubricants, in vacuum and inert gases 09 p1483 A71-23392

Refractory oxygenless powder metallurgy products in high temperature technology, considering covalent bond formation 09 p1478 A71-23395

Physical properties, structure and sintering of refractory oxides of rare earth elements and actinides, including chromia 09 p1478 A71-23399

High temperature honeycomb woven fiberglass reinforced polyimide resin, asbestos reinforced composites and high modulus graphite materials, discussing specific strength and stiffness 10 p1618 A71-24771

Refractory composite inorganic materials technology, covering gas phase, single crystal and hydrothermal synthesis, physicochemical analysis and fabrication methods 13 p2090 A71-28006

Refractory materials production using chemical deposits from gaseous phase, discussing mechanical, physical and thermal properties of obtained coatings 13 p2074 A71-28526

Stainless steel wire fibers in refractory castables, noting flexural and compressive strength improvements 13 p2093 A71-28663

Microsphere formation by melting spinning refractory oxide rod tip in carbon dioxide laser focused emission 13 p2079 A71-28905

Conical metal core electrode erosion rates in pulsed plasma accelerators with refractory dielectric chamber 14 p2282 A71-30671

Galvanomagnetic properties of solid refractory zirconium and titanium compounds in two-band representation, measuring Hall effect and reluctance vs external magnetic field 15 p2426 A71-31512

Soviet papers on refractory carbides covering high purity and alloy products electrical, thermal, thermodynamic, mechanical, chemical, wear and abrasive properties 15 p2429 A71-32137

Porous refractory materials for thermochemical protection against high temperature plasma flow, discussing effectiveness in erosive wear reduction 15 p2432 A71-32164

Thermal stability test assembly for refractory materials cylindrical specimens, using argon plasma jet 15 p2385 A71-32238

Chromium carbides or borides high melting wear resistant surfacing material for machine components subjected to abrasive wear 15 p2418 A71-32669

Optimum sintering temperature, bulk composition and gas medium effects on structure and mechanical properties of silicon nitride and silicon carbide materials 15 p2437 A71-32670

Refractory tungsten boride with iron or nickel for powdery surfacing mixtures, showing hardness and wear resistance dependence on low melting component 15 p2438 A71-32675

Abrasive capability, shape and strength of refractory powders of fused titanium and niobium carbides and calcium boride compared with synthetic corundum 16 p2592 A71-33574

Materials stability testing in high temperature propane-butane combustion product flow, selecting compact silicon carbide for structural use in redox medium 17 p2761 A71-34310

Book on high temperature materials covering vacuum or inert gas properties for industrial and aerospace applications 17 p2760 A71-35623

Cyclic torsional shear testing of refractory materials at normal and high temperatures, describing test equipment 17 p2834 A71-35672

Refractory, superalloy and composite materials brazing process for space shuttle orbiter heat shield 18 p2928 A71-36854

High temperature four point bending vacuum furnace machine testing thin refractory sheets, noting strain rate, velocity jump and relaxation on tantalum carbide 19 p3063 A71-37554

Normal emission factors of dielectric materials at 1000-1500 C, using black bodies in study of thermal radiation of refractory materials 20 p3254 A71-39960

Refractory diborides in oxidizing environments, considering mechanical strength, thermal stability, oxidation resistance, heat conductivity, thermal expansion, specific heat and electrical resistance 21 p3405 A71-40138

Lime refractory fabrication and properties for high temperature applications, describing production of calcium oxide grain by sintering process from commercial calcium hydroxide 21 p3405 A71-40246

Heat resistant and refractory materials contact eutectic melting for surface coating production 21 p3390 A71-41175

High temperature structural application of refractory fiber reinforced ceramic composites 22 p3565 A71-42287

Refractory materials heat resistance criteria, taking into account hollow cylinder thermal stress distribution 23 p3698 A71-44212

Steel silicification in liquid media for high temperature oxidation resistance improvement 24 p3829 A71-44731

Temperature dependence of external friction coefficient between high-melting carbides in vacuum at constant normal load and slipping rate 24 p3830 A71-44863

REFRACTORY METAL ALLOYS

NT MOLYBDENUM ALLOYS

NT NIOBIUM ALLOYS

NT OSMIUM ALLOYS

NT RHENIUM ALLOYS

NT TANTALUM ALLOYS

NT TUNGSTEN ALLOYS

Nb based refractory metal alloys, discussing phase diagrams and electromagnetism separation method 02 p0270 A71-12934

Refractory metal alloys hot crack sensitivity testing by Vrestraint method, using ultrahigh purity inert atmosphere 06 p0912 A71-18042

Refractory alloys fatigue cracks kinetics based on endurance characteristics reflecting resistance to variable loads 07 p1129 A71-19153

Refractory alloys elastoplastic deformation under cyclic loading, deriving thermal fatigue equations 07 p1129 A71-19155

Refractory metals and alloys fabrication and mechanical and physical properties at high temperatures 07 p1134 A71-19581

Creep enhancement by additional microplastic deformation in refractory alloys during thermal cycling 08 p1317 A71-21618

Ti alloy powders and Ti-base refractory compounds production from Ti alloys wastes 08 p1317 A71-21856

Refractory metals and alloys thermal fatigue testing, describing test equipment allowing for variable test specimen constraints and arbitrarily programmed temperature control 09 p1425 A71-22317

Torsion pendulum for measuring internal friction and shear modulus of refractory metals and alloys 09 p1452 A71-23333

Hot deformation of superrefractory austenitic Ni alloy, considering elastic and plastic limits 09 p1479 A71-23625

Refractory metals and alloys products fabrication for aerospace applications, discussing hydrostatic bulge forming and aluminide coating in Nb alloy nozzle extension production 10 p1618 A71-24766

Book on computer calculation of phase diagrams covering quantitative computation of phase equilibrium and lattice stability parameters of refractory metal systems 11 p1777 A71-25197

Soviet monograph on physical metallurgy of refractory metals and alloys covering applicability, structure, phase diagrams, properties, chemistry, working, welding, etc 11 p1777 A71-25270

Refractory and structural steels and Al alloys, obtaining low cyclic plastic deformation and breaking stress curves 13 p2148 A71-28116

Refractory steels plastic deformation characteristics under isothermal creep 13 p2084 A71-28125

Hypersonic flight load bearing refractory alloy control surface protective coatings, emphasizing oxidation screening tests 14 p2262 A71-29646

REFRACTORY METALS

Ti alloy powders and Ti-based refractory compounds production from Ti alloy scrap, describing electrorefining, hydrogenation and carburization processing

14 p2260 A71-30835

Refractory alloys fatigue cracks formation kinetics based on endurance characteristics during symmetrical and asymmetrical load cycles

17 p2760 A71-35652

Refractory alloys elastoplastic deformation under cyclic loading, deriving thermal fatigue equations

17 p2760 A71-35653

Creep rate enhancement by additional microplastic deformation in refractory alloys during thermal cycling

17 p2761 A71-35678

Damping characteristics of Ni base refractory alloys at high temperatures, showing increase with cyclic strain amplitude

18 p2936 A71-36708

Chemical vapor deposited tungsten or other refractory metal alloys mechanical properties evaluation at high temperature, describing hoop stress measurement apparatus for induction heated specimens

[ECS PAPER 384-RPN] 20 p3252 A71-39553

TaC-WC, ZrC-WC and refractory compounds thermal expansion coefficient measurements

24 p3838 A71-44738

REFRACTORY METALS

NT CHROMIUM

NT MOLYBDENUM

NT NIOBIUM

NT RHENIUM

NT RHENIUM ISOTOPES

NT TANTALUM

NT TUNGSTEN

Electrical resistivity and structure of thin films of W, Mo and Cr evaporated in vacuum by neodymium laser

01 p0101 A71-10674

Materials for spacecraft design requirements, considering composite and refractory metals, Ti and heat resistant alloys

01 p0102 A71-10816

Refractory metal thermionic emitter-support systems, measuring surface interdiffusion at high temperatures

02 p0264 A71-12242

Vaporization chemistry in C, Si, Cr, Mo and Nb high temperature oxidation, using thermochemical diagrams

03 p0374 A71-13123

High melting point metal systems with nitrogen or oxygen, discussing engassing and degassing reactions kinetics and thermodynamic equilibrium

03 p0442 A71-13362

Refractory metal surfaces behavior in ultrahigh vacuum, using LEED and Auger electron spectroscopy

05 p0766 A71-16240

Refractory metal surface-gas reactions at high temperatures in vacuum, determining activation energies

05 p0766 A71-16241

Powdered W, Mo, Nb and Ta sulfides and compacts thermal vacuum behavior, examining phase compositions and transformations

05 p0769 A71-16861

Europium hexaboride-high melting point metals reaction for intermetallic compounds production, noting evaporation kinetics

06 p0913 A71-18087

Refractory metals and alloys fabrication and mechanical and physical properties at high temperatures

07 p1134 A71-19581

Refractory metals and carbides and borides, investigating laws governing electrodes erosion during electric spark breakdown

07 p1139 A71-20205

Optimal recrystallization of thin wire cast W-Re alloy subject to high size reduction

07 p1141 A71-20244

Refractory transition metals diborides thermoemissive properties for use in cathode materials

07 p1144 A71-20653

High temperature liquid propellant oxidative-erosion resistant ablative composites containing in situ reaction formed refractory metal carbides for rocket nozzles

08 p1318 A71-20696

Machining electrode materials, investigating high melting transition metals electroerosive stability and bending strength on basis of electronic theory

08 p1296 A71-20853

Refractory metals forming, coating, machining and joining operations, discussing parts manufacture

08 p1299 A71-21683

High temperature apparatus for enthalpy and specific heat measurements of refractory metals

08 p1273 A71-21936

Molten alumina and chromia reactions with refractory metals, calculating isobaric-isothermal potential variations

09 p1466 A71-22165

Refractory metals and alloys thermal fatigue testing, describing test equipment allowing for variable test specimen constraints and arbitrarily programmed temperature control

09 p1425 A71-22317

Hf, Ta, W and Re solubility in La and Ce hexaborides from lattice parameters, microhardness and X ray and metallographic analyses

09 p1509 A71-23066

Torsion pendulum for measuring internal friction and shear modulus of refractory metals and alloys

09 p1452 A71-23333

Thermal reduction methods for refractory metal powders of W, Mo, Zr, V, Hf, Nb, Ta and Ti

09 p1457 A71-23389

Sintering and pressing techniques for compact semifinished products of refractory metal powders including W, Mo, Ta, Nb, Zr and Ti

09 p1457 A71-23396

Refractory metals and alloys products fabrication for aerospace applications, discussing hydrostatic bulge forming and aluminate coating in Nb alloy nozzle extension production

10 p1618 A71-24766

Soviet monograph on physical metallurgy of refractory metals and alloys covering applicability, structure, phase diagrams, properties, chemistry, working, welding, etc

11 p1777 A71-25270

Refractory metals coating of various substrates by gaseous phase chemical deposition, discussing diffusion process theoretical analysis, experimental apparatus and coatings mechanical and physical properties

11 p1768 A71-25391

Bimetallic refractory metal joints electron beam welding and aging for applications to in-pile thermionic converters

11 p1769 A71-25857

W, Mo, Ta and W-Mo alloys hardness integrity, using high temperature microhardness tester

13 p2084 A71-28113

Temperature dependent diffusion coefficient of yttrium in refractory metal single crystals of Mo, W, Nb and Ta, using radiometric analysis

14 p2258 A71-30005

Refractory metals fatigue testing under nonstationary thermal loads, considering test data reliability improvement

14 p2259 A71-30268

Arc welding apparatus for chemically active high-melting metals in controlled superpure He atmosphere

14 p2253 A71-30486

Heat resistant metals long time creep prediction at low stresses or temperatures

15 p2428 A71-31859

Ti, Zr, Nb, Cr, Mo and W carbides compaction, investigating effects of compression, duration, pressing number, moisture and plasticizer contents and stress distribution

15 p2415 A71-32141

Nickel and cobalt pseudobinary eutectic alloys reinforced by refractory metal monocarbides whiskers, studying mechanical properties, solidification and phase equilibria

15 p2432 A71-32169

Refractory and rare metals single crystals - Conference, Moscow, December 1968

16 p2594 A71-33876

Refractory and rare metals absolute melting temperature dependence on atomic number, lattice constant, charge negativity and crystallographic, thermodynamic and mechanical parameters

16 p2594 A71-33878

High temperature apparatus for enthalpy and specific heat measurements of refractory metals

17 p2724 A71-35278

Critical growth work hardening germination and recrystallization of oriented compression deformed Nb, Mo and W refractory cubic centered crystals

18 p2935 A71-36200

Oxygen, hydrogen and nitrogen determination in high melting point metals

22 p3563 A71-42364

Gas-metal reactions in refractory metals purification, discussing reaction kinetics, thermodynamic equilibria and dissolved gases induced mechanical properties changes

22 p3564 A71-42423

REFRACTORY PERIOD

Short term central fatigue as causal factor of delayed psychological refractory period in multiple choice visual signal tasks

23 p3634 A71-43864

REFRASIL [TRADEMARK]

U FIBERS

U SILICON DIOXIDE

REFRIGERANTS

Film cooling effectiveness with He and refrigerant 12 injection into two dimensional turbulent boundary layer of supersonic airflow

03 p0517 A71-13453

Cryogenic fluids, considering refrigerants storage vessels, liquid surface detection devices, transfer lines, level gauges

20 p3270 A71-39241

REFRIGERATING

Cryogenic refrigeration requirements of low noise microwave amplifiers in satellite communications, discussing solid state masers and liquid helium parametric amplifiers

20 p3204 A71-39251

REFRIGERATING MACHINERY

NT REFRIGERATORS

Spacecraft cryogenic cooling systems, discussing passive, phase change and closed cycle coolers and refrigerators

04 p0535 A71-15343

Thermal separator type refrigerating machines design, discussing gas expansion under unsteady conditions

06 p0882 A71-18310

REFRIGERATORS

Ettingshausen refrigerator dynamic behavior mathematical models, using current density and potential gradient as controlling variables

04 p0678 A71-15465

Superconductors applications, noting low cost reliable closed cycle He refrigerators

06 p0941 A71-18017

One dimensional steady state performance characteristics of thermomagnetic generators and refrigerators in dimensionless form

09 p1387 A71-23647

Miniature high speed expansion turbines for helium liquefiers and refrigerators, discussing turbine flow passages and gas lubricated bearings

20 p3184 A71-39246

REFUELING

Quick connect/disconnect dry break couplings for aircraft fueling, describing design and operation

06 p0880 A71-18215

Static discharge hazards for aircraft, discussing causes for static charge build-up, dangers and precautionary methods during refueling operations

07 p1019 A71-19424

Automated fueling for Kennedy jet airport, using computer controlled underground bulk storage-satellite tank pipeline system

10 p1589 A71-24300

Flight and operation of IL-62 long distance jet aircraft, considering flight crew composition and training, passenger and cargo handling and refueling

11 p1706 A71-25260

Fuel tank gas cushion minimum volume during refueling, using method of successive approximations

16 p2623 A71-33610

REGENERATION

Time distribution of first passage through fixed level for nondecreasing whole number regeneration process with step trajectories

01 p0110 A71-10094

REGENERATION [ENGINEERING]

Astronaut space nutrition, discussing Apollo mission short range nonregenerative mode, long range closed loop regenerative cycles and waste recycling

01 p0027 A71-11572

Regenerative system reliability, examining oscillation mode selector

13 p2040 A71-28995

Ninety day manned test of regenerative life support system in space station simulator, presenting operational and maintenance data

[ASME PAPER 71-AV-3]

18 p2865 A71-36370

Waste management subsystem for 90-day space station simulator test of regenerative life support system

[ASME PAPER 71-AV-7]

18 p2865 A71-36374

Advanced regenerative portable life support system concept analysis for long duration and multiple extravehicular activity

[ASME PAPER 71-AV-10]

18 p2866 A71-36377

Zero-gravity circulating water electrolysis system prototype design for metabolic and leakage makeup oxygen supply in 12-man space station regenerative life support system

[ASME PAPER 71-AV-20]

18 p2867 A71-36387

Closed-loop solid electrolyte oxygen regeneration life support system, discussing 180-day life test

[ASME PAPER 71-AV-32]

18 p2869 A71-36399

Space station regenerative life support system 90-day manned test in simulator, discussing objectives, facilities and procedures

[ASME PAPER 71-AV-38]

18 p2870 A71-36405

Unidirectional regenerative ring carbon dioxide laser power amplifier tests for below and above threshold operations, noting saturation role in performance

20 p3242 A71-38843

Artificial ecological regenerative life support system design for space environments, discussing biotechnological properties

21 p3343 A71-40563

Extravehicular activity protection systems, discussing resource regeneration, technology, methodology and space station, lunar base and Martian missions schematic configurations

22 p3503 A71-41990

Oxidation of water in regeneration under spacecraft conditions, measuring organic impurities degree of oxidation in inhabited cabin atmospheric vapor condensates 22 p3506 A71-42814

REGENERATION [PHYSIOLOGY]
 Bone marrow physiological regeneration after chronic gamma irradiation, noting effect on fission processes and chromosome apparatus of cells 01 p0014 A71-11146
 Tritiated thymidine effects on splenic lymphocytes regeneration, discussing DNA synthesis, cycle completion and resident populations 11 p1719 A71-26055
 Mitotic response to various diets in normal and regenerating rat liver 14 p2182 A71-30069
 DNA replication in intercostal artery muscle cells during vascular wall physiological regeneration, noting cytophotometric study of polyploidization 16 p2531 A71-33467
 Erythrocyte disintegration products role in blood regeneration, showing erythropoiesis link to erythrodieresis for different forms of hypoxia 17 p2679 A71-34219
 Hydroponic plant cultivation with keramzit substrate, investigating replacement time effect and regenerative power of nutrient solution 22 p3506 A71-42816

REGENERATIVE COOLING
 Regeneratively cooled stainless steel thrust chamber failure related to internal carburization by fuel decomposition and propellant combustion 11 p1810 A71-25505
 Temperature field profiling along radius in front of gas turbine stage, applying to regeneratively cooled turbine engine 24 p3864 A71-45011

REGENERATIVE CYCLES
U REGENERATION [ENGINEERING]
REGENERATIVE FEEDBACK
U POSITIVE FEEDBACK
REGENERATIVE FUEL CELLS
 Alkaline fuel cells electrochemical regeneration for controlling carbonate concentration in electrolyte for performance improvement 03 p0353 A71-13057

REGENERATORS
NT THERMOSIPHONS
 Performance tests of two identical Brayton cycle heat exchanger units consisting of recuperator, heat sink exchanger and ducting in combination with turbine 15 p2355 A71-32213
 Pressure ratios and surface effects on regenerative heat exchanger in Brayton gas turbine cycles with intercooling or reheating 16 p2663 A71-34037

REGIONS
NT ANTARCTIC REGIONS
NT ARCTIC REGIONS
NT AURORAL ZONES
NT BRILLOUIN ZONES
NT D REGION
NT E REGION
NT F REGION
NT FRESNEL REGION
NT NULL ZONES
NT POLAR REGIONS
NT TEMPERATE REGIONS
NT TROPICAL REGIONS

REGISTERS [COMPUTERS]
NT SHIFT REGISTERS
 Transistorized multichannel registers for optical oscillograph records, discussing frame storage and digital processing circuitry 12 p1889 A71-27755

REGRESSION [STATISTICS]
U REGRESSION ANALYSIS
REGRESSION ANALYSIS
NT REGRESSION COEFFICIENTS
 Parameter estimation of mixed autoregressive moving-average (ARMA) time series using output data 06 p0878 A71-17332
 Fluidic OR-NOR element multiple regression analysis, investigating wall attachment, hysteresis switch pressure and percentage recovery 07 p1031 A71-20607
 Error analysis of adaptive estimators and gradient following algorithms for engineering regression equations, comparing stochastic approximation 08 p1269 A71-21332
 Iterative algorithms for regression function saddle point and applications in reliability and automatic control theories 10 p1585 A71-24156
 Second order experimental plans, obtaining regression analysis for matrix elements and regression coefficients variance 12 p1988 A71-26707
 Structural strength numerical evaluation, demonstrating effectiveness of regression equations in statistical data processing 16 p2651 A71-33063

Space flight sleep pattern data with EEG, using three descriptors and regression and linear discriminant analysis 16 p2528 A71-33108
 Maximum oxygen uptake prediction by stepwise regression technique from data collected during submaximum treadmill work 16 p2530 A71-33241
 Aircraft pilot physical examination for regression curves on near vision and eye accommodation, noting age effect 17 p2692 A71-35197
 Singular perturbation theory for finite rate chemical kinetics effect on regression rate of seminfinit flat fuel plate in gas oxidizer stream 17 p2792 A71-35796
 Mass, center of gravity and moment of inertia measurements curtailment by tolerance and regression analyses and Monte Carlo method [SAWE PAPER 883] 17 p2834 A71-35820
 Solar cycle effects on E region peak electron density, correlating sunspot number by regression analysis 21 p3372 A71-40036
 Linear regression optimal filtering application to aircraft target tracking 23 p3659 A71-44094
 Multivariable regression equations validity from dispersion analysis and limiting complexity with allowance for data sample volume 24 p3842 A71-44392
 Servosystems consisting of command and single executive elements error estimation based on mathematical planning of experiment for time loss reduction, deriving regression equation 24 p3808 A71-44395

REGRESSION COEFFICIENTS
 Polymer thermal degradation theory of pressure sensitive hybrid combustion, calculating linear regression rates 19 p3170 A71-38123

REGULARITY
 Grand Tour interplanetary trajectories regularization, removing singularities in equations of motion of space vehicles [AAS PAPER 71-315] 23 p3725 A71-42990

REGULATION
U CONTROL
REGULATIONS
 Radio interference suppression rules optimization, using mathematical model to characterize interference voltage, antenna sensitivity and radio transmitter field strength 11 p1733 A71-26339
 Book on air law and civil air policy covering international regulation, air traffic market, passenger and cargo services, etc 14 p2340 A71-29938
 SAE/DOT conference on aircraft and environments covering noise pollution, airport noise, sonic booms, regulatory/legal aspects and air pollution [AIAA PAPER 71-729] 14 p2295 A71-30776
 U.S. federal legislation and regulations for aircraft noise and sonic boom 15 p2516 A71-32245
 International radio regulations adopted by Geneva space conference with reference to frequency band allocations in 1-10 GHz range with equal rights to space and terrestrial services 17 p2697 A71-34246
 Aircraft industry license norms and standards, describing indexing procedures, storage techniques and data recovery operations with computer 18 p2886 A71-36810
 New IATA passenger and baggage international air transport conditions, discussing passenger/carrier legal relationships, with emphasis on differences between new and old regulations 18 p2989 A71-36918
 Finnish air traffic law based on international civil aviation convention, discussing regulations relative to aircraft, personnel and airports 18 p2989 A71-36919
 Warsaw air traffic convention agreements as amended at The Hague and Guatemala, presenting air transport regulations in present form 18 p2989 A71-36920
 Exchange regulation of standardized container loading units in air freight transportation 19 p3173 A71-38220
 Aircraft anticollision flashing lights, discussing current practices within national and international air traffic regulations regarding flash frequency, color and light sources 22 p3483 A71-41499
 Airport noise control regulations enforcement feasibility, noting financial burden 22 p3623 A71-41796
 Airlines procedures in conducting pilot training programs within ICAO recommendations and German regulations 23 p3639 A71-43230

REGULATORS
NT AUTOMATIC FREQUENCY CONTROL
NT CURRENT REGULATORS
NT FLOW REGULATORS

NT FREQUENCY CONTROL
NT FUEL FLOW REGULATORS
NT OXYGEN REGULATORS
NT PRESSURE REGULATORS
NT THERMOSTATS
NT VOLTAGE REGULATORS
 Approximate optimal control law formulation by harmonic linearization for nonlinear time invariant state regulator problem with high performance index 03 p0390 A71-14299
 Regulator logic synthesis using state variable feedback for stationary linear plants 03 p0393 A71-14467
 Nonlinear absolutely stable regulator design in parameter space, using computer simplex search 08 p1324 A71-21319
 Optimal output regulator for linear time invariant systems with reference vector and quadratic cost functional 12 p1893 A71-27430
 Ritz-Treffitz algorithm application to optimal state regulator problem computer processing to improve speed of solution and storage requirements 15 p2374 A71-31182
 Optimal zero-memory regulator for linear system with stochastic jump parameters, considering Bayes and minimax controllers 19 p0309 A71-38711
 Maximally achievable accuracy of linear optimal regulators and filters 23 p3659 A71-44099
 State estimation errors in quadratic optimal control feedback gain design of stochastic linear regulator 23 p3659 A71-44100
 Optimal stochastic control law derivation for linear regulator with quadratic performance criterion from limiting form of transfer function 24 p3816 A71-45134

REHEATING
U HEATING
REIGNITION
U IGNITION
REINFORCED MATERIALS
U COMPOSITE MATERIALS
REINFORCED PLASTICS
 Glass fiber-epoxy resin composites shear strength, considering fiber length and interfacial bond effects 01 p0106 A71-10277
 Fiberglass-reinforced plastics loading conditions effects on tensile strength, determining creep rupture strength from test data 01 p0107 A71-10413
 Viscoelastic behavior of boron fiber-epoxy resin composites at high temperature from torsion pendulum study, proposing linear model for damping peak effect 01 p0107 A71-10460
 Boundary value problem of elasticity theory for reinforced plastics with internal stresses due to shrinkage 01 p0107 A71-10495
 Reinforced polymers strength and deformation under tensile loads applied across fibers 01 p0107 A71-10496
 Contact problems of orthotropic fiberglass-reinforced plastic plate with low shear rigidity 01 p0169 A71-10498
 Heat conductivity equations for thermal stresses of thin cylindrically anisotropic plates made of reinforced laminar plastics 01 p0169 A71-10499
 Reinforced plastics - Conference, Freudenstadt, West Germany, October 1970 01 p0108 A71-10688
 Fiberglass reinforced plastics heavy duty structural parts quality control, discussing strength parameters, safety coefficients, testing methods, etc 01 p0088 A71-10689
 Lightweight structural elements fabrication from fiber reinforced plastic materials [prepregs], discussing manufacturing methods, structural design, production and testing of parts, etc 01 p0172 A71-10690
 Epoxy resin reinforcement by various fiberglass types, discussing effects of bond-enhancing agents, fatigue strength properties, etc 01 p0108 A71-10691
 Adhesive bonding and detachable joints in multilayered fiber reinforced plastic structures, discussing joint strength test methods, fiber and load force orientation effects, etc 01 p0108 A71-10692
 Fiber reinforced plastics fatigue strength investigation by cyclic tension-compression, bending and torsion tests, noting matrix-fiber interface shear stress capacity 01 p0108 A71-10693
 Thin wires mechanical properties compared for epoxy resin reinforcement applications, considering ductility, temperature and aging effects, cost, etc 01 p0108 A71-10694
 Glass fiber reinforced thermoplastics application possibilities and limitations, considering physical and mechanical properties 01 p0108 A71-10695

Glass fiber reinforced plastics strain properties under multiaxial loads, considering long and short time loading, temperature and environmental conditions
01 p0109 A71-10696

Glass fiber reinforced plastics stress and fracture analysis, using approximate and iterative methods for strength estimates and nonlinear stress-strain relationships
01 p0172 A71-10697

Buckling in fiber reinforced plastic thin walled shell structures, discussing structural stability problems and methods for prevention of buckling
01 p0172 A71-10698

Numerical stress-strain calculation for design of high pressure fiberglass-reinforced plastic balloons
01 p0176 A71-11048

Deformation and strength of pipes manufactured from oriented glass fiber reinforced plastics under axial tension
01 p0177 A71-11237

Automated machinery for reinforced plastic structural products manufacture by filament winding
[SME PAPER EM-70-135] 01 p0089 A71-11261

Polyimide/boron reinforced plastic structures fabrication, discussing use in leading edges
[SME PAPER EM-70-133] 01 p0090 A71-11263

Metal matrix and polymer matrix composite materials in aerospace industry, discussing selection factors for specific applications
01 p0104 A71-11283

Fiberglass reinforced plastic materials in steady temperature fields, determining creep and load carrying capacity
02 p0272 A71-11753

Fiberglass reinforced plastic cylindrical shells, investigating rheological effects during heating and concentrated radial loads
02 p0324 A71-11754

Corrosion resistant fiberglass reinforced plastic fluid storage vessels, noting structural characteristics, fabrication techniques, etc
02 p0256 A71-12348

Reinforced plastics - Conference, Brighton, October 1970
02 p0273 A71-12476

Carbon fiber reinforced epoxy composites, evaluating application as helicopter tail rotor blade material
02 p0273 A71-12477

Glass reinforced polyester laminates under static and repeated loading, investigating resin flexibility effects on fatigue strength
02 p0274 A71-12479

Fiber reinforced thermoplastics deformation characteristics, using uniaxial tensile test
02 p0274 A71-12480

Carbon fiber reinforced plastics, discussing mechanical and nondestructive testing for performance factors
02 p0274 A71-12482

Fire retardant glass reinforced polyester resins optimum formulation, examining burning properties, volatility, extinction time and flame propagation
02 p0274 A71-12483

Reinforced plastic laminates structural integrity, describing procedure for mechanical property evaluation
02 p0274 A71-12484

Carbon fiber surface treatment for reinforced plastic composites interlaminar strength increase, using wet oxidation process based on hypochlorous acid
02 p0274 A71-12485

Carbon fiber composites, examining epoxy resin matrix effects on mechanical performance and heat tolerance
02 p0274 A71-12486

High strength polyimide resin composites, discussing commercial and aerospace applications, chemistry, void content, volatiles and moisture absorption
02 p0274 A71-12487

Carbon fiber-epoxy resin composites in aircraft industry, examining fatigue life, cost, specific moduli and mechanical properties
02 p0275 A71-12488

Glass fiber reinforced plastics tensile strength under various continuous loading rates and elevated temperatures
02 p0275 A71-12667

Three phase particulate epoxy composite compressive yield strength, considering strain rate filler content, porosity and voids effect
03 p0442 A71-13538

Thermal cycle stresses at interface of composite glass tape-epoxy casting resin cylinder, using strain
03 p0508 A71-13763

Inextensible fiber-reinforced plastic-rigid solid, applying continuum theory to derive kinematic properties, yield condition and flow rule
03 p0514 A71-13439

Thermal expansion of unidirectional, angle-ply and complex laminated graphite-epoxy composites, con-

sidering fiber orientation, hysteresis and interlayer stress relaxation
03 p0449 A71-14459

Fiber reinforced plastics testing and mechanical parameters measurement, considering materials strength and fracture probability
04 p0618 A71-14887

Carbon fiber reinforced composite cryogenic fuel tanks development for post-Apollo programs, discussing fiber and resin physical properties
05 p0819 A71-15946

Aluminum reinforced epoxy model making, testing and stress analysis for aircraft structures, including creep, photoelastic coating and strain gage effects
05 p0821 A71-16346

Creep and long term strength of unidirectionally reinforced plastics under compression
05 p0771 A71-16361

Glass textolite materials strength during cooling under tensile, high rate tension and impact loads
05 p0771 A71-16362

Elastic and compression strength characteristics of fiberglass-reinforced plastics prepared by cold solidification
05 p0771 A71-16364

Orthotropic cylindrical shell stability under variable compression loads, considering glass fiber reinforced plastic tube
05 p0822 A71-16368

Low shear rigidity effect on stability of glass fiber reinforced plastic cylindrical shells under loads and elevated temperature
05 p0822 A71-16369

Elasticity and strength anisotropy changes of unidirectional fiberglass reinforced plastics during winding
05 p0759 A71-16372

Complex modulus of elasticity relation to viscoelastic cantilever beams stress or strain under forced vibration, considering fiber reinforced plastics
05 p0826 A71-16738

Glass fiber reinforced plastic plates static tensile and low cycle fatigue tests under pulsating tension
05 p0772 A71-16739

Unidirectional glass-epoxy filament wound composite material fracture strength based on three dimensional stress components of fiber-containing plane
05 p0826 A71-16740

Fracture strength of helical wound glass-epoxy composite cylinder under axial tension, determining tensile strength
05 p0826 A71-16741

Tensile test equipment for fiberglass reinforced plastics strength measurement under shear
05 p0772 A71-16888

Fiber reinforced plastics fatigue testing, discussing machines, specimen preparation and design, data analysis and environmental control
05 p0772 A71-16928

Injection molded thermoplastics with fiberglass reinforcement, examining mechanical properties and thermal and stress cracking resistance
05 p0773 A71-17123

Counterface nature effect on friction and wear processes of carbon fiber reinforced polymers, discussing formation of transfer film of wear debris
05 p0773 A71-17245

Combined deformation of reinforcing elements and polymer binder in monodirectional composite structure, determining stress distribution
06 p0915 A71-17380

Soviet book on fiber reinforced plastics design covering low strength rods, plates and thin walled rings, winding techniques, etc
06 p0983 A71-17435

High modulus boron-epoxy composite aircraft structures adhesive bonding, discussing mechanical properties, manufacturing techniques and quality control
[SAE PAPER 710110] 06 p0904 A71-17624

Fiberglass-reinforced plastics with and without water content, studying ablation performance
06 p0915 A71-17681

Carbon fibers for low weight aircraft plastic structural materials
06 p0915 A71-17743

Anisotropic fiberglass reinforced plastic shell stability under short term and prolonged loading, using geometrically nonlinear formulation and Galerkin method
06 p0994 A71-17825

High strength metal and ceramic reinforcement fibers, discussing properties and fabrication for plastic composites
06 p0916 A71-18088

High amplitude stress wave propagation in anisotropic quartz-phenolic composite, noting strong pulse amplitude attenuation
[AIAA PAPER 71-179] 06 p1004 A71-18618

Thermal stresses in annular plate of fiberglass reinforced epoxy resin
07 p1209 A71-18919

Glass fiber reinforced thermoplastics with increased room temperature mechanical properties, noting effect of heat, aging and chemical environment exposure
07 p1145 A71-19692

Lightning protective coatings for boron and graphite fiber reinforced plastics
07 p1021 A71-19944

High intensity electric current damage in boron and graphite filament reinforced epoxy resin composites
07 p1145 A71-19945

Stress rupture properties of S glass/epoxy single end strands at various load levels, considering distribution functions
07 p1145 A71-20126

Strain rate effect on fiber reinforced unidirectional epoxy composites tensile stress, noting steel, boron, beryllium and graphite/epoxy strands
07 p1139 A71-20137

Fiberglass reinforced plastic strength and deformability under tension as function of loading rate and test temperature
07 p1145 A71-20466

Organofunctional silane interfacial coupling for high strength glass reinforced thermoplastics
08 p1318 A71-20695

Charpy notched impact strength of carbon fiber reinforced epoxy resin composites over temperature range
[PLASTICS INST. PAPER 20] 08 p1318 A71-20891

Carbon fiber reinforced epoxy resin fatigue and crack propagation behavior in air, moisture and oil environments, using tensile, bending and torsion test methods
[PLASTICS INST. PAPER 49] 08 p1318 A71-20892

Carbon fiber reinforced plastics mechanical properties, discussing batch processing and specimen geometry variables effects on laminates
[PLASTICS INST. PAPER 24] 08 p1318 A71-20893

Carbon fiber reinforced carbon base composites manufacture by thermal decomposition of carbon fiber reinforced thermosetting resins, discussing polymer matrix shrinkage control
[PLASTICS INST. PAPER 36] 08 p1319 A71-20894

Carbon fiber reinforced polymers for self lubricating materials applications, discussing friction and wear characteristics under fresh and sea water, alcohols, mineral oils, etc
[PLASTICS INST. PAPER 31] 08 p1319 A71-20896

High strength flexible carbon fabrics from oxidized polyacrylonitrile yarns for reinforced plastic laminates
[PLASTICS INST. PAPER 39] 08 p1319 A71-20900

Filament wound carbon fiber reinforced plastics components fabrication and performance tests
[PLASTICS INST. PAPER 47] 08 p1296 A71-20902

Carbon fiber reinforced plastics applications for aero-engine components, considering mechanical and thermal properties and environmental conditions
[PLASTICS INST. PAPER 45] 08 p1347 A71-20905

Graphite fiber reinforced plastics adhesion and orientation effects on mechanical properties
[PLASTICS INST. PAPER 27] 08 p1320 A71-20906

Cross-ply carbon fiber reinforced epoxy resin laminates fatigue behavior under axial loading, discussing various failure mechanisms
08 p1321 A71-20912

Mechanical properties of plastic composites with boron, beryllium, silicon carbide and graphite fiber reinforcement
[PLASTICS INST. PAPER 29] 08 p1321 A71-20917

Heat resistant extended life carbon fiber/polyimide resin composites, noting aerospace applications
[PLASTICS INST. PAPER 34] 08 p1321 A71-20920

High speed ball impact tests and fracture energy of carbon fiber reinforced plastics
[PLASTICS INST. PAPER 25] 08 p1322 A71-20922

Tensile, flexural and compressive shear, impact and fatigue characteristics of carbon fiber-epoxy resin composites
[PLASTICS INST. PAPER 26] 08 p1322 A71-20923

Carbon fiber reinforced plastics potential aerospace structural applications, considering weight saving, mechanical properties, thermal expansion, stress concentration, impact resistance, corrosion and lightning problems
[PLASTICS INST. PAPER 43] 08 p1369 A71-20927

Failure analysis of unidirectionally reinforced fiberglass composites due to winding, using critical stress distribution function
08 p1323 A71-21011

Comparative tensile and creep tests of reinforced thermoplastics for performance/cost selection [PLASTICS INST. PAPER 4] 09 p1481 A71-22340

Reinforcement theory fiber filled thermoplastics, considering fiber strength and length [PLASTICS INST. PAPER 2] 09 p1481 A71-22341

Tribological characteristics of carbon fiber reinforced thermoplastics, noting improved sliding wear against metal surfaces [PLASTICS INST. PAPER 12] 09 p1481 A71-22344

Thermoplastics reinforcement with carbon, silicon nitride and silicon carbide fibers, noting fiber aspect ratio [PLASTICS INST. PAPER 5] 09 p1482 A71-22345

Interlayer shear modulus relation to thermal conductivity coefficient in oriented glass fiber reinforced plastics 09 p1482 A71-22814

Filament winding geodesic characteristics of shells of revolution made of glass fiber reinforced plastics 09 p1482 A71-22815

Numerical analysis of winding and heat treatment effects on residual stress distribution in cylindrical glass fiber reinforced plastic products 09 p1482 A71-22816

Steady multifiber winding process conditions in compact glass fiber packing for glass fiber reinforced plastic tubes 09 p1482 A71-22817

Stress concentration near hole in transversely isotropic cylindrical and spherical shells made of oriented glass fiber reinforced plastics 09 p1539 A71-22820

Stability characteristics of glass fiber reinforced plastic orthotropic cylindrical shell with elastic filler under torsion 09 p1539 A71-22821

Residual stresses in ring shaped specimens of wound glass fiber plastic products, using radial cutting technique 09 p1482 A71-22822

Optimal design parameters in minimization of reinforcement elements weight in cylindrical glass fiber reinforced orthotropic plastic shells under axial compression 09 p1539 A71-22826

Ultrasonic modulus vs strength of high modulus fiber reinforced epoxy matrix composites in non-destructive testing 09 p1484 A71-23687

Stress-strain curves for plastics with or without fiber reinforcements under impulsive compressive loading cycles, using split Hopkinson pressure bar apparatus 10 p1630 A71-23921

Surface treatment effects on high shear strength adhesive bonding of fiber reinforced plastics to metal substructures 10 p1630 A71-24069

Deformability and strength of soft fiber reinforced plastics under biaxial tension, determining low temperature critical tensile stresses and elongation ratios 10 p1634 A71-24194

High temperature testing assembly for reinforced plastics and binders in oxidizing and inert media under tension, compression, bending and cleavage loads 10 p1589 A71-24202

Performance-price relations of carbon, boron and glass fiber reinforced resin matrix composites in commercial and aerospace use 10 p1634 A71-24418

Filamentary composites for primary aircraft structural applications, emphasizing boron-epoxy material 10 p1618 A71-24770

Hardened and glass reinforced epoxy resin mechanical properties after 180 day hold in water, acid and alkaline solutions 10 p1635 A71-24827

Fiber reinforced plastics/epoxy resins/ electrical effects association with deformation and failure 10 p1635 A71-25013

Reinforced plastics - Conference, Washington, D.C., February 1971 11 p1784 A71-25392

Fiber length, diameter, bundle size, glass content and sizing effects on fiberglass reinforced plastic systems flexural, tensile and impact strength 11 p1784 A71-25395

SVAM glass reinforced plastics production and properties, discussing drawing, coating and forming oriented laminate on drum 11 p1784 A71-25396

Carbon fiber-epoxy resin composites Young modulus, thermal and electrical conductivities as function of fiber alignment and porosity 11 p1784 A71-25399

Nondestructive testing method obtaining relaxation modulus and accelerated degradation/stress corrosion of reinforced plastics 11 p1768 A71-25404

Carbon fiber reinforced plastics industrial engineering applications, noting cost effectiveness, strength and elasticity 11 p1861 A71-25407

Long term oxidative aging effects on interlaminar shear strength retention of low void graphite/ boron reinforced polyimide resin composites 11 p1785 A71-25410

Fiber reinforced thermoplastics fabrication by fluidized bed techniques, fusing powder matrix to fiber surface for continuous coating 11 p1768 A71-25415

Transverse impact resistive graphite fiber reinforced plastic (GFRP) lightweight sandwich panels and beam structures, using thin inner core facings 11 p1846 A71-25417

Winding equipment for continuous production of large diameter cylindrical filaments of reinforcing materials and polyester resins 11 p1768 A71-25418

Fiberglass reinforced plastic rocket launcher tubes with internal helical rails to impart spin to missiles, discussing design, fabrication and testing 11 p1786 A71-25419

Electrical properties, chemical resistance and reinforced plastics applications of telechelic ultrahigh vinyl polybutadiene resins 11 p1786 A71-25422

Plastics mold design improvements, discussing steel quality, guiding/heating systems, surface finish and chrome plating 11 p1768 A71-25432

Papers on glass fiber reinforced plastics covering end products and design criteria 11 p1788 A71-25651

Glass fiber reinforced plastics aerospace applications covering radomes, dielectric panels, aircraft ducting, secondary structures, furnishings, mouldings and tooling 11 p1788 A71-25652

Glass fiber reinforced plastics reinforcement techniques, emphasizing E glass filament manufacture, properties, advantages and products 11 p1788 A71-25653

Plastics reinforcement by combining high plastic deformation and fracture resistances with stiffness, discussing ceramics, whiskers, carbon and glass fibers 11 p1788 A71-25654

Glass fiber reinforced plastics mechanical properties, strain-stress characteristics and anisotropy, deriving orthotropic laminates tensile stiffness under deformation 11 p1849 A71-25656

Glass fiber reinforced plastics, discussing adhesion, wetting and adsorption effects on chemical reactions in glass-resin interfaces 11 p1788 A71-25657

Glass fiber reinforced plastics fatigue tests, discussing closed loop hydraulic servomechanism equipment, testing methods and materials and mean stress effects 11 p1789 A71-25658

Three dimensional reinforced composites for load bearing structural ablator 11 p1789 A71-26037

Elastic properties of bonded orthotropic layer plates, finding good agreement with fiberglass reinforced plastic laminates 11 p1851 A71-26199

Unidirectional glass fiber epoxy composite material nonlinear viscoelastic behavior, using isothermal uniaxial creep and recovery tests with thermodynamic constitutive equations 11 p1851 A71-26385

Fracture toughness and critical strain rate measurements in unidirectional glass reinforced plastics as function of resin, hardener, fiber and degree of cure 11 p1790 A71-26387

Maximum shear and hoop stress gradients in graphite-epoxy angle-ply laminated composite cylinders for axial and internal pressure loading 11 p1852 A71-26391

Boron and carbon fracture and debonding in epoxy matrix, using acoustic emission analysis 11 p1772 A71-26392

Filament winding techniques for glass fiber reinforced plastics, discussing processes, configurations and materials for achieving optimum strength 12 p1920 A71-27011

Stiffness factor in reinforced thermoplastics mechanical properties as function of glass fiber content, working temperature and duration of loading 12 p1920 A71-27012

Microcrack formation in carbon fiber-resin matrix composites under thermal stress 12 p1920 A71-27013

Izod impact testing of carbon fiber reinforced plastics, considering fiber volume loading, surface treatment and specimen and notch geometry 12 p1921 A71-27015

Reinforced plastics components in supersonic transport nose radome and missile radar antennas, discussing molding, sandwich materials and computer controlled spraying techniques 12 p1887 A71-27016

Coupled thermoelasticity, bending and stability of thin walled shells and plates of oriented fiberglass reinforced plastics with low shear rigidity, using Timoshenko theory 12 p1978 A71-27345

Fiberglass reinforced plastic structural elements heat induced deformation and carrying capacity due to material macroinhomogeneity and rigidities asymmetry 12 p1921 A71-27346

Perpendicularly woven fiberglass reinforced plastics stability, elasticity and viscoelasticity as function of temperature 12 p1921 A71-27347

Hand/machine sanded surfaces moderate environment exposure time effects on adhesive bonding of glass fiber reinforced plastic joints 12 p1921 A71-27411

Combined deformation of reinforcing elements and polymer binder in monodirectional composite structure, determining stress distribution 12 p1921 A71-27462

Experimental proof of combustion phenomena in reinforced plastics ablation under simulated atmospheric reentry, using arc plasma jets 12 p1987 A71-27721

Fiberglass reinforced plastics under constant strain rate, deriving failure models as random process for microscopic crack propagation 13 p2148 A71-28115

Tensile strength and fracture toughness of carbon fiber polyester composites, using mechanical testing and scanning electron microscopy 13 p2092 A71-28625

Probability characteristics of glass/epoxy plastics mechanical properties, considering tangential and axial tensile and bending strength, modulus of elasticity, buckling and compression strength 13 p2092 A71-28653

Stability loss, critical load and wave numbers for smooth conical and cylindrical shells of fiberglass reinforced plastics under uniform axial compression 13 p2157 A71-29181

Carbon and boron fiber reinforced plastics adhesive bonded and bolted joints, presenting results of hole deformation tests [DFVLR-SONDDR-96] 13 p2093 A71-29306

Hybrid boron-graphite filaments in epoxy matrix composite, describing increased tensile strength and modulus of elasticity 14 p2261 A71-29638

Materials and processing methods for rain erosion resistant ceramic coated plastic structures for supersonic aircraft, considering fiberglass reinforced polyimide radomes with alumina coating 14 p2262 A71-29645

Carbon/graphite cloth reinforced aromatic/heterocyclic resins ablative composites pyrolysis kinetics by computer code analysis 14 p2262 A71-29649

Advanced plastic composites fabrication and processing techniques, using resins, reinforcements and fillers 14 p2263 A71-29653

High modulus organic fiber for aerospace use, considering fiber-epoxy composite mechanical and physical properties 14 p2263 A71-29658

Multidirectional reinforced resin matrix composites inspection and nondestructive analysis by film/neutron radiography and X ray Vidicon 14 p2263 A71-29659

Stress-time superposition creep data for unfilled and coupled glass reinforced polypropylene at 23-80 C 14 p2264 A71-29835

Linear viscoelastic analysis of two dimensional plane stress model of polyphase composite material with rigid inclusions and voids and polymeric binder 14 p2263 A71-29836

Mechanical properties of fiberglass-epoxy cross-ply laminates, considering tensile strength, crack propagation and ultimate stress and strain 14 p2264 A71-29837

Soviet book on glass-reinforced plastic plates and shells covering engineering methods for anisotropic plates and shells stability and stress analysis 14 p2327 A71-30245

Geometrical parameters and load carrying capacity of fiberglass reinforced plastic composites with elastoplastic adhesive bonding, deriving relations for stress distribution 14 p2264 A71-30270

Fatigue strength of polyester laminates reinforced with glass cloth and mats 14 p2264 A71-30484

Dilatometric measurement for crazing rate in rubber-toughened plastics during tensile creep tests 15 p2438 A71-31369

Boron and graphite fiber reinforced plastics machining, discussing tools, operating parameters and process limitations [SME PAPER MR-71-820] 15 p2416 A71-32429

Epoxy and unsaturated polyester resin compounds for embedding glass fibers in fiberglass reinforced plastics 15 p2439 A71-32737

Ultrasonic pulse technique for plane transverse and longitudinal stress wave dispersion in boron fiber reinforced epoxy composite, determining group velocity dependence on frequency and elastic moduli [ASME PAPER 71-APM-27] 16 p2600 A71-33202

Prestressing of two layer fiberglass-reinforced plastic cylindrical shell under internal pressure 16 p2657 A71-33410

Stress-strain diagrams for oriented fiberglass-reinforced plastic under tension, taking into account temperature and anisotropy effects 16 p2601 A71-33411

Polymer binder setting degree effect on maximum strength of fiberglass cross reinforced plastic, analyzing compressive, bending, hardness, impact, thermal and porosity properties 16 p2601 A71-33682

Welded, bearing and interlocking joints and adhesive bonding in carbon fiber reinforced plastics, discussing anisotropy, thermal expansion and electrochemical corrosion problems 17 p2748 A71-34344

Monograph on fiber-resin composites covering glass, boron and carbon fibers and epoxy matrix materials tensile and thermoelastic properties 17 p2761 A71-34469

Dynamic compressive strength and failure of steel reinforced epoxy composites, discussing strain rate sensitivity 17 p2762 A71-34813

Vibration response NDT for fatigue crack damage in laminated filament-reinforced epoxy composites 17 p2824 A71-34815

Filament wound glass-reinforced plastic struts for cryogenic tank supports in long term planetary missions, testing thermal and mechanical properties 17 p2762 A71-35205

Gradient shape influence on connectivity in two phase graded structures, considering polyphase structure of filament reinforced composites 17 p2763 A71-35226

Oriented glass fiber-plastics plates and shells design, noting zero moment stress shells and filament overwrapped metallic pressure vessels 17 p2830 A71-35315

Metal-reinforced glass plastic composite conical shell with positive Gaussian curvature, estimating reliability and stability based on static tests 17 p2830 A71-35316

Thin multilayer pressurized glass fiber-plastic cylindrical shells, calculating stress redistribution due to crack initiation and prestressing effects 17 p2830 A71-35319

Fiber reinforced resins mechanical properties determination based on component materials characteristics 17 p2763 A71-35441

Optical transmission in unexposed phenolic resin base laminates with silica cloth reinforcements, studying stabilization treatments, pyrolysis and incident radiation spectral distribution 17 p2838 A71-35473

Optimal design of locally orthotropic elastic flat bodies of fiber reinforced plastics or metals 17 p2763 A71-35620

Boron-epoxy composite wing box beam design, describing preliminary weight estimation from layouts [SAWE PAPER 891] 17 p2834 A71-35815

Surface temperatures and ablation mechanism of combustion protective plastics reinforced by silica under intense heating measured by IR micropyrometer [ONERA-TP-962] 18 p2984 A71-36028

Carbon fiber reinforced plastics, reviewing properties, performance, development, applications and potential cost reduction 18 p2940 A71-36765

Uniaxially aligned glass and carbon fiber reinforced nylon composites prepared from caprolactam by anionic polymerization 19 p3083 A71-37339

Reinforced plastics for aerospace applications, giving special attention to heat shield and inflatable structures materials 19 p3085 A71-38069

Polyamides reinforced with finely chopped glass fiber, noting mechanical strength, Martens yield temperature and heat stability 19 p3085 A71-38476

Specimen support effects on three point bending tests of fiber-plastic composites, suggesting small diameter roller 21 p3405 A71-40596

Glass-fiber/glass-bead/resin beam stiffness and strength improvement with sandwiching between layers of unidirectional carbon fiber composite 21 p3405 A71-40597

Nondestructive testing of carbon fiber reinforced composites with resin matrices /CFRP/, suggesting ultrasonics for void detection 21 p3387 A71-40598

Carbon and boron fibers and whisker reinforced plastics fabrication, properties and costs, noting materials and optimum matrix combination 21 p3405 A71-40600

Hysteresis to strength relationship and particulate filler effect on reinforcement of rubbers and plastics 21 p3405 A71-40601

Friction, wear and adhesion of filler and matrix polymer composite bearing materials including glass,

carbon, lamellar solids, metal powders, carbons, nylons, PTFE, polyimides, etc 21 p3405 A71-40602

Carbon fiber reinforced plastics, considering aerospace and medical applications 21 p3406 A71-40702

Mechanical properties, applications and peculiarities of polymer composite materials reinforcement fibers 21 p3406 A71-40777

Nondestructive test for fiberglass reinforced plastic tank, using percussion method 21 p3466 A71-40838

Fatigue properties of satin woven fiberglass reinforced plastic cloth under various stress directions 21 p3406 A71-40839

Metal and polymer matrix materials research based on stringent requirements for thermal reactors, jet engines and space vehicles, discussing tests and analysis methods 21 p3401 A71-40901

Fiber reinforced elastic materials steady state plane wave propagation by modeling constituents as continua undergoing individual motions 21 p3469 A71-41004

Tensile fracture in grip section of fiber reinforced reduced cross section plastic composite specimens 22 p3564 A71-41591

Glass fiber reinforced flame retardant thermoplastic resins, tabulating flammability resistance and mechanical properties 22 p3565 A71-42076

Physical and mechanical properties of controlled flow vacuum cured glass reinforced polyimide prepreg laminates 22 p3565 A71-42595

Epoxy-alumina trihydrate composite system fracture energy data, noting interdependence of surface topography, phase dispersion volume fraction, particle size and spacing 23 p3696 A71-43102

Anisotropic glass fiber plastic material stress, strain and crack formation threshold measurements under long term static and cyclic axial loads 23 p3696 A71-43424

Carbon fiber reinforced plastics featuring high strength and Young modulus and low density for engineering applications 24 p3840 A71-44363

REINFORCED PLATES

Isotropic nonlinearly elastic plate weakened by doubly periodic reinforced curvilinear holes, calculating stress-strain state by Cauchy integrals 01 p0168 A71-10412

Composite beam of three thin plates reinforced by thin electric ribs, calculating stress strain state by Fourier transforms 01 p0176 A71-11044

Buckling analysis of rectangular waffle plates with multiple sizes of ribs in each stiffening direction, considering stability and design 01 p0178 A71-11583

Two dimensional stressed state of isotropic plate with elastically reinforced elliptical hole under biaxial tension 02 p0326 A71-12290

Stress concentration at free and reinforced curvilinear holes with random surface roughness applied to plane under hydrostatic tension 02 p0326 A71-12291

Thin reinforced viscoelastic isotropic multiconnected plate stress-strain state under bending due to concentrated loads and distributed normal forces 02 p0329 A71-12668

Flat sheet under uniform radial tension, varying thickness reinforcement around hole for high stress concentration avoidance 03 p0513 A71-14238

Thin circular cylindrical plate reinforced by longitudinal rigid stringers, deriving computer algorithm for calculating forced vibration 03 p0515 A71-14367

Eccentrically stringer-reinforced rectangular plates buckling under linearly varying longitudinal compression, using Galerkin method 05 p0819 A71-15980

Rectangular plate with stiffener cross section for unit with constant mass, considering natural symmetric and antisymmetric mode frequencies 05 p0824 A71-16603

Glass fiber reinforced plastic plates static tensile and low cycle fatigue tests under pulsating tension 05 p0772 A71-16739

Circular plates of anisotropic fiber-reinforced materials, calculating axisymmetric bending and buckling 06 p0995 A71-17829

Natural frequencies approximation for vibration modes of stiffened and singly curved panel structures 08 p1369 A71-20810

Free and forced vibrations of three layer freely suspended plate with allowance for energy dissipation 08 p1372 A71-21707

Buckling loads of square laminated anisotropic composite plates under compression, including bending-membrane coupling effects 11 p1847 A71-25462

Harmonic vibrations of rib reinforced rectangular elastic plates with two freely supported parallel edges, deriving method for natural frequencies and forced vibration 11 p1848 A71-25580

Reinforced plates flexural and torsional rigidity characteristics for stiffeners design, considering oblique angular coordinates system 12 p1982 A71-27509

Single fiber reinforced plate initial stress distribution due to linear expansion coefficients difference between matrix and fiber, using optical polarization 13 p2091 A71-28126

Longitudinal and transverse rib reinforced plates with parallel cracks extending to edge, obtaining flexural rigidity and stress-strain state 13 p2156 A71-29070

Elastic properties of orthotropic composite disks of fiber-reinforced materials, comparing actual stress in composite with permissible stress of fiber and matrix 14 p2329 A71-30472

Stress analysis of nonlinearly elastic plate with ring reinforced circular hole 14 p2332 A71-30854

Integrally stiffened five bay panel, calculating free vibration and random response to jet noise excitation [AIAA PAPER 71-585] 15 p2504 A71-31532

Stiffened rectangular plates parametric instability under in-plane sinusoidal dynamic forces, using mathematical model with stiffeners as discrete elements [ASME PAPER 71-APM-26] 16 p2655 A71-33203

Eccentrically stiffened thin cylindrical panels instability under uniform axial compression, uniform hoop compression and uniform shear 16 p2661 A71-34150

Fatigue crack propagation in Al alloy panels stiffened with bolted and integral stringers, determining stress intensity factor/crack growth rate relationship 17 p2827 A71-35156

Damage tolerant aircraft structures material toughness and residual strength, presenting fracture test results on precracked panels reinforced with crack stoppers 17 p2827 A71-35157

Stress and deflection analysis of plates reinforced with discrete stiffeners in form of simple beams and twisting elements, determining bending moments 18 p2983 A71-36845

Photoelastic analysis of maximum stress in wide plate with asymmetrically reinforced circular hole under tension, noting effects of rounded corner at hole edge 18 p2984 A71-37022

Stability of edge reinforced circular plate under uniform radial load, considering flexural and extensional stiffness of reinforcing beam 22 p3618 A71-42592

Fibers-matrix force interaction effects in metal composites, analyzing stress-strain state of reinforced plate 23 p3697 A71-44202

Dynamic response of thin walled structures natural frequency analyzed for formulating potential and kinetic energy for stiffness and mass matrices by minimization principle 24 p3878 A71-44555

Stress-strain state of nonlinearly elastic reinforced polymer plate with circular hole, deriving stress tensor components and first approximation solution for pure bending 24 p3882 A71-44838

REINFORCED SHELLS

Buckling of ring stiffened conical shells under axial compression, determining critical loads 01 p0168 A71-10342

Rib reinforced shells linear theory, deriving equilibrium equations with allowance for temperature terms 01 p0170 A71-10644

Discrete search method for stiffened cylindrical shell stability under combined uniform axial compression and lateral pressure loads 01 p0174 A71-10963

Reinforced cylindrical shells under external pressure, investigating longitudinal tensile stresses effect on stability 01 p0175 A71-11040

Homogeneous isotropic cylindrical shell stability, considering reinforcement by nonlinear dense symmetrical system of elastic threads under tension 01 p0176 A71-11124

Highly flexible nonlinearly elastic two layer cylinder reinforced by transversely isotropic shell, examining stressed state in axisymmetric temperature field 02 p0323 A71-11742

Corrosion resistant fiberglass reinforced plastic fluid storage vessels, noting structural characteristics, fabrication techniques, etc 02 p0256 A71-12348

Circular cylindrical shell with trapezoidal stringers reinforcement system along length, calculating strain during oscillation

03 p0514 A71-14359

Eccentrically stiffened thin spherical shell instability under uniform external pressure

04 p0669 A71-15199

Circular cylindrical shell reinforced by ring ribs, investigating dynamic characteristics under impulsive loading

04 p0672 A71-15756

Axial buckling tests on machined integrally ring stiffened cylindrical shells

05 p0823 A71-16559

Rib reinforced circular cylindrical shells, analyzing elementary and zero bending stress states

06 p0982 A71-17351

Cylindrical reinforced shells carrying capacity under dynamic external pressure

06 p0982 A71-17354

Weight-optimal cylindrical shells of revolution with uniform strength edge reinforcement, discussing pressure vessel design

06 p0982 A71-17356

Reinforced cylindrical minimum weight shells under combined axial compression and internal pressure, examining strength and buckling modes

06 p0982 A71-17357

Circular cylindrical orthotropic fiberglass-reinforced shell buckling under longitudinal impact, assuming initial surface imperfections

06 p0985 A71-17684

Elastic rib-reinforced flexible shallow shells theory, deriving variational equations for multicontact problem

06 p0985 A71-17752

Reinforced plate and shell theory, taking into account ribs arbitrary direction and contour profile

06 p0985 A71-17753

Stainless steel shells under uniform external pressure and constrained deformation, noting critical load increase

06 p0986 A71-17760

Local distributed load effects on bending of fiberglass reinforced plastic laminar orthotropic cylindrical shell

06 p0986 A71-17761

Cylindrical shell reinforced by transverse ribs under hydrostatic pressure, determining elastoplastic deformation

06 p0988 A71-17774

Side strain reactions of shells of revolution with meridional ribs, integrating equations by Green function

06 p0989 A71-17785

Eccentrically reinforced cylindrical shells stability equations under axisymmetric loading

06 p0993 A71-17813

Rib reinforced cylindrical shell stability under annular and axial stresses, determining eigenvalue of homogeneous integral equation

06 p0993 A71-17816

Eccentrically reinforced cylindrical shell stability, considering numerical analysis of structurally orthotropic shell parameters

06 p0993 A71-17817

Anisotropic fiberglass reinforced plastic shell stability under short term and prolonged loading, using geometrically nonlinear formulation and Galerkin method

06 p0994 A71-17825

Elastic and viscoelastic multilayer reinforced cylindrical shells stability, determining transverse shear stress role

06 p0996 A71-17841

Circular cylindrical shell stability with ribs of variable cross sections, using method based on semimomentless theory

06 p0997 A71-17850

Reinforced zero moment minimum weight shells strength analysis and optimal design algorithms, using discrete calculation scheme

06 p0998 A71-17854

Stability of rib stiffened and anisotropic shells, including composite and elastic filler structures

06 p1000 A71-17871

Contact theory of shells under local loads and reinforcing rib interactions

06 p1000 A71-17872

Axially compressed ring and stringer stiffened cylindrical shells minimum weight design, considering configuration instability

06 p1003 A71-18590

Cylindrical shells with arbitrary cross sectional contour, thickness and longitudinal stiffener spacing under tension or compression, presenting computer algorithm for determining stress-strain state

08 p1368 A71-20790

Reinforced shells of revolution carrying capacity upper limit subjected to internal adiabatic ideal gas flow

09 p1538 A71-22632

Filament winding geodesic characteristics of shells of revolution made of glass fiber reinforced plastics

09 p1482 A71-22815

Coaxial shells of revolution connected by meridional ribs, deriving elastic equilibrium conditions, stress-strain components and contact forces under thermal and mechanical loads

10 p1688 A71-24358

Shallow rib reinforced rectangular shells under normal load with infinite regularity estimates independent of rigidity, using double trigonometric series

10 p1689 A71-24564

Bidirectional stress-strain analysis of hinged cylindrical shells crosswise reinforced by rigid ribs using equilibrium equations

10 p1690 A71-24566

Orthotropic shells of revolution with concentrated masses and oscillator inclusions and reinforced by stringers and ribs, calculating free vibration by Ritz method

10 p1690 A71-24570

German monograph on circular cylindrical shells theory comparative studies covering energy and equilibrium methods, tensor representation, reinforced shells, etc

10 p1692 A71-24912

Thermal stability of cylindrical laminated fiberglass reinforced plastic shells, solving by linear shell stability theory

11 p1790 A71-26175

Zero moment stress state realization in thin macrohomogeneous shells by selecting adequate uniform multilayer structures for reinforcement

12 p1975 A71-26963

Soviet book on spherical bottoms weakened by openings covering shell stress/strain, elastic-plastic deformations, reinforcing elements and composite materials

12 p1977 A71-27293

Stress-strain state of closed circular cylindrical shells stiffened by longitudinal ribs, analyzing general solution of homogeneous equilibrium equations system

13 p2150 A71-28133

Soviet book on stability of thin walled reinforced and multilayer shells with various designs and boundary conditions

14 p2325 A71-29939

Reinforced toroidal shells stability under critical local loads, edge moment and heating, using finite difference method

14 p2332 A71-30847

Stability and stress analysis of elastic finned circular cylindrical shells reinforced by stringers

14 p2332 A71-30852

Stability of structurally orthotropic stringer reinforced cylindrical shell closed by spherical or plane bottoms under uniform external pressure

14 p2333 A71-30892

Stability loss of circular cylindrical shell with stepped wall thickness of central reinforcing sleeve under annular loading, determining critical load by thin shell theory

16 p2657 A71-33600

Critical loads and stability of longitudinally compressed circular cylindrical shells with eccentric ring and stringer reinforcement

16 p2657 A71-33603

Equivalent reinforcement of contact area between spherical shell and radial outlet cylindrical pipe under internal pressure and axial force

17 p2817 A71-34332

Bending of circular conical shell with discretely reinforced end cross section, deriving accurate closed form solution within limits of working model

17 p2828 A71-35302

Thin elastic spherical shells reinforced by stringers and frames and loaded by internal or external uniform pressure, calculating by energy method

17 p2829 A71-35311

Dynamic response of oddly stiffened circular cylindrical shells, using modified variational method

18 p2980 A71-36495

Photoelastic analysis of cylindrical shells of revolution with one hemispheric closed end and reinforcing flanges at opposite end rim, examining boundary conditions effects

18 p2981 A71-36718

Rib reinforced cylindrical shells deformation under local load, examining stress-strain distribution

18 p2981 A71-36719

Longitudinal edge stiffness and internal pressure effects on buckling and initial postbuckling behavior of axially compressed stringer reinforced cylindrical panels, discussing imperfection sensitivity

19 p3157 A71-37873

Hydrostatically loaded noncircular pressurized cylindrical shells with nonuniform rings, using asymptotic expansion procedure

19 p3157 A71-37875

Zero moment stress state realization in thin macrohomogeneous shells by selecting adequate uniform multilayer structures for reinforcement

19 p3159 A71-38266

In-plane boundary conditions effect on buckling loads of axially compressed simply supported ring stiffened cylindrical shells

19 p3159 A71-38270

Fiber reinforced tube under lateral compression between two flat dies, determining finite deformation from nonlinear elastic and elastoplastic shearing response analysis

20 p3311 A71-39966

Zero moment reinforced prismatic shells of rectangular cross section with arbitrary load distribution

21 p3472 A71-41146

Zero moment theory application to stability analysis of rib-reinforced cylindrical shell under external pressure

21 p3472 A71-41149

Natural vibrations of closed reinforced cylindrical shell clamped at end faces

21 p3473 A71-41153

Computer program for nonuniform thickness ring structure stress distribution under uniform radial line load based on reinforced circular cylindrical shell interaction under hydrostatic pressure

22 p3516 A71-41866

Stability formula for critical pressure in cylindrical shells orthotropically reinforced by closely spaced eccentric ribs

22 p3616 A71-42487

Stability and critical loads of reinforced geometrically nonlinear cylindrical shells, using strain energy method

24 p3882 A71-44842

Cyclic symmetrical deformation of thin elastic conical shells of revolution of variable thickness with meridional ribs under physical and thermal loads

24 p3882 A71-44843

Equivalent stiffening of circular hole in convex shell of revolution by short shell under symmetric and antisymmetric loads

24 p3882 A71-44845

Ring reinforced spherical shell and rib under concentrated normal forces, calculating force factors and displacement by simultaneous deformation analysis allowing moment stresses

24 p3883 A71-44896

REINFORCEMENT [PSYCHOLOGY]

Partial reinforcement effect in visual vigilance task, varying knowledge of results as incentive

16 p2537 A71-33680

Observing behavior in squirrel monkeys under multiple schedule of reinforcement availability

22 p3497 A71-42861

Trace reflex formation in response to acoustic stimulus with verbal reinforcement, determining cross correlation connections between induced activity of auditory and motor areas

24 p3796 A71-44547

REINFORCEMENT [STRUCTURES]

Glass fiber reinforced durometer and hard foam sandwich structures deformation characteristics under static loads, presenting theoretical and experimental results

01 p0172 A71-10700

Optimal cross sectional dimensions of thin walled longeron beams and ribs of skin reinforced delta wings minimizing weight

02 p0329 A71-12562

Inhomogeneously reinforced composite structures strengthening by internal stress matching

05 p0771 A71-16365

Thin metal sheet reinforcements effect on slow stable tear and catastrophic failure

06 p1003 A71-18563

Stiffened flat panel dynamic analysis, using finite element method

08 p1374 A71-22027

Airport runway surface strengthening, discussing overlaying additional rigid or flexible layers, replacing used sections and reinforcement problems

10 p1589 A71-24756

Composite morphology and mechanical properties relationship, considering reinforcing effect, filamentous systems, whisker growth ladder molecules synthesis and material production

10 p1635 A71-24768

Three dimensional composite reinforcement principles, discussing thermal strain reduction and mechanical properties

10 p1691 A71-24772

Material properties, impregnation, shaping, hardening and structural design in mass production of reinforced laminates for aircraft construction

12 p1920 A71-26954

Thin walled stiffened Duralumin box spars bending stress-strain states under unsteady creep

12 p1981 A71-27496

Spar box structure under pure bending noting flexural rigidity and stress and stability analysis with Kármán nonlinear equations

12 p1981 A71-27498

Compression strength theory for monodirectional reinforced homogeneous anisotropic and piecewise homogeneous materials, using microvolume stability loss failure mechanism

12 p1922 A71-27684

Honeycomb cell multilayer and reinforced structures, examining temperature field radiative heat transport and thermal conductivity and emissivity

13 p2165 A71-29180

Rectangular plates with unidirectional stiffeners, calculating natural frequencies and mode shapes with approximate method

15 p2507 A71-32128

Buckling for thin stress walled open sections on elastic foundation with constrained direction reinforcement

22 p3614 A71-41693

Fiber reinforced viscoelastic rectangular beam, deriving asymptotic values of stress, curvature and position of neutral axis under constant moment

24 p3879 A71-44630

REINFORCEMENT RINGS

Ring reinforced circular holes in cylindrical shells examining stress concentrations due to internal pressure

03 p0507 A71-13740

Stiff rings attached to elastic cylinders, analyzing stresses and deformations under concentrated loads and bending moments about radial and tangential axes [ASME PAPER 70-WA/PVP-1]

03 p0510 A71-14099

Circular cylindrical shell reinforced by ring ribs, investigating dynamic characteristics under impulsive loading

04 p0672 A71-15756

Axial buckling tests on machined integrally ring stiffened cylindrical shells

05 p0823 A71-16559

Eccentricity and clamping effects on stability and critical pressure of ring-reinforced cylindrical shells under internal pressure

08 p1369 A71-21122

Thermal buckling prediction for ring-stiffened cylinders, taking into account ring out-of-plane bending stiffness

17 p2825 A71-34896

Hydrostatically loaded noncircular pressurized cylindrical shells with nonuniform rings, using asymptotic expansion procedure

19 p3157 A71-37875

In-plane boundary conditions effect on buckling loads of axially compressed simply supported ring stiffened cylindrical shells

19 p3159 A71-38270

Cylindrical shell under opposing concentrated outwardly directed radial loads applied to reinforcing ring, presenting stress distributions and displacements

21 p3468 A71-40971

Photoelastic analysis of thermal stresses in polyurethane rubber ring reinforced polymers, cermets and rubber-metal composites

24 p3883 A71-44895

Ring reinforced spherical shell and rib under concentrated normal forces, calculating force factors and displacement by simultaneous deformation analysis allowing moment stresses

24 p3883 A71-44896

REINFORCING FIBERS

NT CARBON FIBERS

Glass fiber-epoxy resin composites shear strength, considering fiber length and interfacial bond effects

01 p0106 A71-10277

Fiber reinforced materials technology, reviewing basic principles, existing technologies and future trends, various composite materials characteristics, etc

01 p0107 A71-10315

Fiber reinforced materials industrial applications based on various matrix-fiber combinations, considering manufacturing processes, chemical and mechanical properties, etc

01 p0107 A71-10316

Fiberglass-reinforced plastics loading conditions effects on tensile strength, determining creep rupture strength from test data

01 p0107 A71-10413

Viscoelastic behavior of boron fiber-epoxy resin composites at high temperature from torsion pendulum study, proposing linear model for damping peak effect

01 p0107 A71-10460

Reinforced polymers strength and deformation under tensile loads applied across fibers

01 p0107 A71-10496

Epoxy resin reinforcement by various fiberglass types, discussing effects of bond-enhancing agents, fatigue strength properties, etc

01 p0108 A71-10691

Adhesive bonding and detachable joints in multilayered fiber reinforced plastic structures, discussing joint strength test methods, fiber and load force orientation effects, etc

01 p0108 A71-10692

Fiber reinforced plastics fatigue strength investigation by cyclic tension-compression, bending and torsion tests, noting matrix-fiber interface shear stress capacity

01 p0108 A71-10693

Thin wires mechanical properties compared for epoxy resin reinforcement applications, considering ductility, temperature and aging effects, cost, etc

01 p0108 A71-10694

Glass fiber reinforced thermoplastics application possibilities and limitations, considering physical and mechanical properties

01 p0108 A71-10695

Glass fiber reinforced plastics strain properties under multiaxial loads, considering long and short time loading, temperature and environmental conditions

01 p0109 A71-10696

Glass fiber reinforced plastics stress and fracture analysis, using approximate and iterative methods for strength estimates and nonlinear stress-strain relationships

01 p0172 A71-10697

High modulus graphite fiber composites, considering production, properties, utilization, availability and price/performance

[SME PAPER EM-70-114]

01 p0109 A71-11251

Fiber reinforced composites application in aerospace and aircraft, discussing boron and graphite and cost effectiveness

01 p0103 A71-11277

Boron vs graphite fiber reinforced composites, noting design application role

01 p0104 A71-11280

Ceramic fibers formation by particles mechanical deformation by extrusion in W matrix, describing grain structure of various extruded metal oxides

02 p0273 A71-12149

Composite materials with high strength short discontinuous fibers, considering manufacturing processes and mechanical properties

02 p0273 A71-12478

Fiber reinforced thermoplastics deformation characteristics, using uniaxial tensile test

02 p0274 A71-12480

Unidirectionally fiber reinforced composite materials, discussing compressive strength

02 p0274 A71-12481

Carbon fiber reinforced plastics, discussing mechanical and nondestructive testing for performance factors

02 p0274 A71-12482

Carbon fiber surface treatment for reinforced plastic composites interlaminar strength increase, using wet oxidation process based on hypochlorous acid

02 p0274 A71-12485

Carbon fiber composites, examining epoxy resin matrix effects on mechanical performance and heat tolerance

02 p0274 A71-12486

Carbon fiber-epoxy resin composites in aircraft industry, examining fatigue life, cost, specific moduli and mechanical properties

02 p0275 A71-12488

Carbon fiber reinforced plastics and metals structural components design, discussing properties, processing and applications

02 p0330 A71-12910

Load limit surfaces for composite plates with long elastic plastic fibers site bonded or imbedded in low strength matrix

03 p0504 A71-13429

Polymer binder effect photoviscoelastic stress analysis near discontinuous reinforcing fibers, comparing results with finite element method for time dependence

[SESA PAPER 1630]

03 p0507 A71-13755

Photoelastic study of stress wave propagation in composites under fiber matrix strip directed impulsive loading with exploding wire

[SESA PAPER 1708]

03 p0507 A71-13758

Cord reinforced elastic homogeneous isotropic cylindrical membrane axisymmetric deformation, using strain energy function

03 p0514 A71-13438

Inextensible fiber-reinforced plastic-rigid solid, applying continuum theory to derive kinematic properties, yield condition and flow rule

03 p0514 A71-14349

Carbon base multifiber yarns for metal matrix composites reinforcement, considering fiber strength degradation minimization methods

03 p0449 A71-14419

Thermal expansion of unidirectional, angle-ply and complex laminated graphite-epoxy composites, considering fiber orientation, hysteresis and interlayer stress relaxation

03 p0449 A71-14459

Fiber reinforced plastics testing and mechanical parameters measurement, considering materials strength and fracture probability

04 p0618 A71-14887

Whisker reinforced composites fabrication principles and methods, discussing constituents, mechanical, geometrical, physical and chemical requirements

04 p0603 A71-14949

Composite material of ductile matrix and straight reinforcing fibers, deriving yield condition

04 p0669 A71-15196

Plane wave propagation in layer direction in fiber reinforced viscoelastic materials

04 p0669 A71-15202

Composite materials of highly conductive metal fibers randomly distributed in low conductive matrices, investigating parameters affecting thermal conductivity from stochastic models

04 p0678 A71-15458

Fiber reinforced cryogenic pressure vessels design, manufacture and testing for space and terrestrial applications, comparing glass fibers to carbon fibers

04 p0618 A71-15650

Boron fiber-Al alloy composites linear thermal expansion as function of fiber volume fraction and orientation

04 p0615 A71-15788

Fiber reinforced Al and Al alloys, discussing physical properties and manufacturing methods

05 p0764 A71-15921

Carbon fiber reinforced composite cryogenic fuel tanks development for post-Apollo programs, discussing fiber and resin physical properties

05 p0819 A71-15946

Transverse elastic modulus and Poisson coefficient of composite materials as function of reinforcement, structure and fiber radius

05 p0771 A71-16360

Interlayer rigidity effects on strength of fiber reinforced composite materials under plane loads

05 p0771 A71-16366

Asbestos applications in aerospace technology, considering chemical and molecular structure, heat and radiation resistance, mechanical properties and reinforcement

05 p0772 A71-16465

Stress wave scattering in fiber reinforced composite material, using model of parallel elastic cylinders embedded in unbounded elastic medium

05 p0826 A71-16719

Bunched parallel reinforcing fibers of equal size and varying strength, deriving critical loads and stresses under gradual failure

05 p0772 A71-16751

Reinforced Ni-based composites, discussing barrier coating for tungsten fibers

05 p0769 A71-16860

Cu and Ni electroless deposition on carbon fibers for composites

05 p0759 A71-16927

Fiber reinforced plastics fatigue testing, discussing machines, specimen preparation and design, data analysis and environmental control

05 p0772 A71-16928

Fibrous composite materials stress and deformation analysis, using point matching numerical method and boundary point least squares method

05 p0829 A71-17119

Counterface nature effect on friction and wear processes of carbon fiber reinforced polymers, discussing formation of transfer film of wear debris

05 p0773 A71-17245

Combined deformation of reinforcing elements and polymer binder in monodirectional composite structure, determining stress distribution

06 p0915 A71-17380

Soviet book on fiber reinforced plastics design covering low strength rods, plates and thin walled rings, winding techniques, etc

06 p0983 A71-17435

Carbon fibers for low weight aircraft plastic structural materials

06 p0915 A71-17743

Circular plates of anisotropic fiber-reinforced materials, calculating axisymmetric bending and buckling

06 p0995 A71-17829

Mechanical property data for silicon nitride-silicon carbide fiber ceramic composites having high fracture values

06 p0916 A71-18035

High strength metal and ceramic reinforcement fibers, discussing properties and fabrication for plastic composites

06 p0916 A71-18088

Fiber composites reinforcement obtained in oriented solidification by structural precipitation hardening of matrix

[ONERA-TP-920]

06 p0913 A71-18094

Unidirectional discontinuous fiber composite longitudinal strength calculation based on perturbation effect and distortional energy criterion, using finite element method

06 p1001 A71-18100

Plane and spatial load transfer and diffusion in linear elastostatics, noting application to aircraft and civil engineering structures and fiber reinforced materials

06 p1001 A71-18222

Unidirectional fiber reinforced orthotropic composite materials elastic constants calculation as function of two isotropic components characteristics

06 p1001 A71-18309

Graphite fiber reinforced Al-Si alloy composite tensile strength and microstructure, observing tension failure modes

06 p0914 A71-18678

Continuous filament metal matrix composites fabrication from hot pressed composites by diffusion reaction process

06 p0915 A71-18688

Lightning protective coatings for boron and graphite fiber reinforced plastics

07 p1021 A71-19944

Laminate analogy predicting elastic and thermal expansion properties of short fiber reinforced composites, extending to two and three dimensional woven fabric composites

07 p1215 A71-20129

Unidirectional fiber reinforced composite longitudinal shear deformation, deriving analytical expression for stress distribution

07 p1216 A71-20132

Fiber reinforced materials machining, considering deformation and stress fields, forces required for continuous machining

07 p1120 A71-20133

Strain rate effect on fiber reinforced unidirectional epoxy composites tensile stress, noting steel, boron, beryllium and graphite/epoxy strands

07 p1139 A71-20137

W fiber reinforced Al strain distribution under tensile load, using moire grid method

07 p1144 A71-20495

Filament winding manufacturing methods using unidirectional glass reinforcements for design and fabrication of aircraft wing structure [SME PAPER EM-70-406]

07 p1120 A71-20546

Filament wound carbon fiber reinforced plastics components fabrication and performance tests [PLASTICS INST. PAPER 47]

08 p1296 A71-20902

Composite materials with metallic matrix and carbon fibers, discussing production techniques and mechanical properties [PLASTICS INST. PAPER 15]

08 p1320 A71-20907

Cross-ply carbon fiber reinforced epoxy resin laminates fatigue behavior under axial loading, discussing various failure mechanisms

08 p1321 A71-20912

High modulus graphite fiber reinforced composites tensile and compressive test methods and results [PLASTICS INST. PAPER 23]

08 p1321 A71-20913

Carbon fiber/carbon composites produced by moulded carbon technique, discussing mechanical properties and applications in rocket motors [PLASTICS INST. PAPER 38]

08 p1348 A71-20914

Mechanical properties of plastic composites with boron, beryllium, silicon carbide and graphite fiber reinforcement [PLASTICS INST. PAPER 29]

08 p1321 A71-20917

Carbon fiber evaluation of structural reinforcement potentialities for rocket motor cases and pressure vessels filament winding [PLASTICS INST. PAPER 48]

08 p1297 A71-20924

Cost aspects of carbon fiber reinforced composites in aircraft structures, suggesting increased aviation market for carbon fiber [PLASTICS INST. PAPER 46]

08 p1378 A71-20929

Carbon fiber reinforced Al composites fabrication and evaluation by metallographic examination, considering tensile strength [PLASTICS INST. PAPER 17]

08 p1322 A71-20930

Metals and alloys strengthening by in situ grown transition metal carbide fibers, noting whisker-like characteristics

08 p1315 A71-21586

W fibers reinforced Cu matrix work hardening rates as function of fiber diameter and volume fraction, using isolated tension pile-up model

09 p1535 A71-22279

Aligned fibers reinforced material hardening rate, taking into account elastic energy and external potential due to internal stress interaction with applied stress

09 p1467 A71-22286

Reinforcement theory fiber filled thermoplastics, considering fiber strength and length [PLASTICS INST. PAPER 2]

09 p1481 A71-22341

Filler and reinforcing agent effects on polypropylene rigidity, tensile strength and creep resistance at elevated temperatures [PLASTICS INST. PAPER 11]

09 p1481 A71-22342

Deformation and strength characteristics of fiber composite thermoplastic resins in terms of stiffness and reinforcement factors [PLASTICS INST. PAPER 3]

09 p1481 A71-22343

Thermoplastics reinforcement with carbon, silicon nitride and silicon carbide fibers, noting fiber aspect ratio [PLASTICS INST. PAPER 5]

09 p1482 A71-22345

Interlayer shear modulus relation to thermal conductivity coefficient in oriented glass fiber reinforced plastics

09 p1482 A71-22814

Filament winding geodesic characteristics of shells of revolution made of glass fiber reinforced plastics

09 p1482 A71-22815

Steady multifiber winding process conditions in compact glass fiber packing for glass fiber reinforced plastic tubes

09 p1482 A71-22817

Residual stresses in ring shaped specimens of wound glass fiber plastic products, using radial cutting technique

09 p1482 A71-22822

Mechanical strength and elastic properties under tension and bending of boron fibers, noting dependence on surface defects

09 p1482 A71-22823

Reinforced composite materials with curved fibers, considering one dimensional stress-strain relation and misalignment effect

09 p1539 A71-22917

Composite materials for compressor blades in aircraft engines, considering boron and carbon fiber reinforced materials

09 p1456 A71-23286

Heat resistant dispersion strengthened and fiber reinforced metal matrix superalloys for high temperature applications, considering superstrength alloys development

09 p1478 A71-23397

Co-Cr and Ni-Cr eutectic alloys with single crystal TaC fiber reinforcement, discussing unidirectional solidification

09 p1479 A71-23623

Stress-strain curves for plastics with or without fiber reinforcements under impulsive compressive loading cycles, using split Hopkinson pressure bar apparatus

10 p1630 A71-23921

Unidirectional fibrous composites brittle and ductile failures prediction under tension and torsion, comparing results with tests on glass-epoxy composites

10 p1686 A71-24017

Weather stress tests for determining optimum adhesive system for bonding reinforced fiberglass panels to Al extrusions held by steel beams

10 p1616 A71-24114

Deformability and strength of soft fiber reinforced plastics under biaxial tension, determining low temperature critical tensile stresses and elongation ratios

10 p1634 A71-24194

Composite morphology and mechanical properties relationship, considering reinforcing effect, filamentous systems, whisker growth ladder molecules synthesis and material production

10 p1635 A71-24768

Composites fabrication techniques, component materials and nature, emphasizing fiber orientation and matrix properties

10 p1618 A71-24769

Filamentary composites for primary aircraft structural applications, emphasizing boron-epoxy material

10 p1618 A71-24770

High temperature honeycomb woven fiberglass reinforced polyimide resin, asbestos reinforced composites and high modulus graphite materials, discussing specific strength and stiffness

10 p1618 A71-24771

Thornel graphite fibers modulus of elasticity, mechanical properties, applications and price

10 p1635 A71-24773

Short carbon and glass fiber reinforced composites, calculating modulus of elasticity from mathematical model

10 p1635 A71-24806

Fiber reinforced plastics/epoxy resins/electrical effects association with deformation and failure

10 p1635 A71-25013

Failure analysis of notched unidirectional composites under tensile load parallel to fiber, considering Griffith-Irwin-Orowan fracture theory applicability [AIAA PAPER 71-369]

11 p1784 A71-25343

Carbon fiber reinforced plastics industrial engineering applications, noting cost effectiveness, strength and elasticity

11 p1861 A71-25407

Carbon fiber reinforced high interlaminar shear strength composites, noting applications to advanced engineering structures

11 p1785 A71-25408

Long term oxidative aging effects on interlaminar shear strength retention of low void graphite/ boron reinforced polyimide resin composites

11 p1785 A71-25410

Epoxy resin in fiber reinforced composite prepreps, characterizing by thermomechanical analysis and gel permeation chromatography

11 p1786 A71-25411

Carbon fiber reinforcement in carbon fiber/glass fiber mat sandwich beams increasing tensile and compressive strength

11 p1846 A71-25412

Fiber reinforced thermoplastics fabrication by fluidized bed techniques, fusing powder matrix to fiber surface for continuous coating

11 p1768 A71-25415

Longitudinal and transverse residual stresses arising in lamination fabrication process of cross-ply fiber composites

11 p1786 A71-25421

Representative Thornel fiber aircraft fuselage component nondestructive testing and repair, and Thornel fiber, polysulfone and polyamide-imide composites fabrication and evaluation

11 p1787 A71-25427

Prototype graphite fiber/plastic fuselage component design, test and performance prediction, using structural analysis methods

11 p1787 A71-25428

Composite materials fiber-matrix interfacial behavior, determining polymer concentration on graphite fibers surface by Raman spectroscopy and composite shear strength increase

11 p1787 A71-25430

Thermally stable polyimide graphite fiber reinforced composites from solutions of monomeric reactions, comparing amide acid prepolymers

11 p1788 A71-25560

Glass fiber reinforced plastics aerospace applications covering radomes, dielectric panels, aircraft ducting, secondary structures, furnishings, mouldings and tooling

11 p1788 A71-25652

Plastics reinforcement by combining high plastic deformation and fracture resistances with stiffness, discussing ceramics, whiskers, carbon and glass fibers

11 p1788 A71-25654

Fiber reinforced composites, predicting mechanical properties, stress-strain behavior, interface failure, creep and fatigue by mathematical model

11 p1849 A71-25655

Mixed boundary value problem for fiber reinforced materials, analyzing shear response in multiply admissible kinematic deformations

11 p1850 A71-26105

Thermal stability of cylindrical laminated fiberglass reinforced plastic shells, solving by linear shell stability theory

11 p1790 A71-26175

Boron filaments and whiskers as reinforcements in high strength composite materials

11 p1790 A71-26336

Stress analysis near free surfaces in thin composite plates with unidirectionally oriented elastic isotropic fibers, applying boundary point least squares technique

11 p1851 A71-26382

Load-deformation characteristics in tension, compression and bending of two thin cement laminates reinforced with short random glass fibers, discussing stiffness and residual strain

11 p1790 A71-26384

Orientation dependent impact toughness and crack resistance of brittle fiber-ductile matrix composite of solidified carbide reinforced Co-Cr eutectic

11 p1782 A71-26386

Bounds for effective dielectric constant of fiber reinforced materials, using Miller geometry of matrix and inclusion

11 p1782 A71-26388

Interlaminar plane shear stress in fibrous composites under elastic deformation with edge effect, using membrane finite element analysis

11 p1852 A71-26394

Elastic stress-strain law and internal structure symmetry for three dimensional fibrous composites, including catrop reinforcement

11 p1852 A71-26396

Stiffness factor in reinforced thermoplastics mechanical properties as function of glass fiber content, working temperature and duration of loading

12 p1920 A71-27012

Izod impact testing of carbon fiber reinforced plastics, considering fiber volume loading, surface treatment and specimen and notch geometry

12 p1921 A71-27015

Combined deformation of reinforcing elements and polymer binder in monodirectional composite structure, determining stress distribution

12 p1921 A71-27462

Fiber composites monofilament and strand tests, considering fracture, fatigue, stress, corrosion and microstructure

12 p1921 A71-27635

Fiber reinforcements for structural composites, considering glass, polycrystals, vapor deposition, whiskers and metals

12 p1922 A71-27636

Ti, B and graphite fiber composites application to aircraft design, discussing mechanical properties and market competition

12 p1918 A71-27676

Fibrous composite materials experimental failure studies at high temperatures and cyclic loading

12 p1922 A71-27683

Large deformation of incompressible elastic body reinforced by unidirectional system of elastic fibers

12 p1922 A71-27695

Fiber reinforced composite materials plastic behavior shear stress theory, determining yield criteria and plastic strain rates associated with various failure modes

12 p1984 A71-27773

Fracture mechanics of metal matrix composite with ductile stainless steel reinforcing fibers

12 p1985 A71-27775

Single fiber reinforced plate initial stress distribution due to linear expansion coefficients difference between matrix and fiber, using optical polarization

13 p2091 A71-28126

Filament reinforced composite materials, considering spacecraft and missile applications mechanical and physical properties 13 p2144 A71-28166

Filamentary composite reinforced metal aircraft structures, considering boron/epoxy in combination with aluminum 13 p2151 A71-28168

Graphite epoxy composites fiber microstructure and surface condition, noting tensile fracture, crack propagation and brittleness 13 p2092 A71-28594

Tensile strength and fracture toughness of carbon fiber polyester composites, using mechanical testing and scanning electron microscopy 13 p2092 A71-28625

Al alloy matrix-graphite fiber reinforcement composites, discussing strength, temperature properties and processing techniques 13 p2092 A71-28660

Stainless steel wire fibers in refractory castables, noting flexural and compressive strength improvements 13 p2093 A71-28663

Carbon and boron fiber reinforced plastics adhesive bonded and bolted joints, presenting results of hole deformation tests [DFVLR-SONDDR-96] 13 p2093 A71-29306

Fiber strengthening of Cu-Fe-Cr wire by cold drawing and annealing, discussing age hardening process of chromium ferrite needles in ductile Cu matrix 13 p2088 A71-29402

Hybrid boron-graphite filaments in epoxy matrix composite, describing increased tensile strength and modulus of elasticity 14 p2261 A71-29638

Carbon/carbon composites, describing manufacturing techniques for fiber reinforced matrix structures 14 p2261 A71-29640

Three dimensional orthogonally woven reinforced felt-yarn composite for low density thermal insulation and chemical vapor deposition 14 p2262 A71-29651

Advanced plastic composites fabrication and processing techniques, using resins, reinforcements and fillers 14 p2263 A71-29653

High modulus organic fiber for aerospace use, considering fiber epoxy composite mechanical and physical properties 14 p2263 A71-29658

Impact strength of Cu, Cu-Ni alloy and superalloy matrices reinforced with W fibers, studying temperature, heat treatment and fiber content and toughness effects 14 p2258 A71-29919

Critical aspect ratio of W fibers in metal matrix composites for stress rupture applications 14 p2258 A71-29921

Elastic properties of orthotropic composite disks of fiber-reinforced materials, comparing actual stress in composite with permissible stress of fiber and matrix 14 p2329 A71-30472

Mechanical properties of composites consisting of Al matrix reinforced by boron fibers, considering high temperature creep, corrosion and thermal shock resistivity 14 p2259 A71-30473

Notched unidirectional composites failure mechanics under tensile load in fiber direction, considering debonding, plasticity and strength 15 p2428 A71-31971

Interfiber stress model for elastic matrix-fiber reinforced composites under inplane shear and transverse normal loading 15 p2507 A71-32096

Fiber reinforced materials with oriented armoring, calculating stress-strain state under transverse shear 15 p2439 A71-32235

Boron and graphite fiber reinforced plastics machining, discussing tools, operating parameters and process limitations [SME PAPER MR-71-820] 15 p2416 A71-32429

Ultrasonic pulse technique for plane transverse and longitudinal stress wave dispersion in boron fiber reinforced epoxy composite, determining group velocity dependence on frequency and elastic moduli [ASME PAPER 71-APM-27] 16 p2600 A71-33202

Specific strength of unidirectional fiber reinforced metal matrix composites, showing dependence on volume ratio and transmission coefficient 16 p2592 A71-33412

Composite materials reinforced by brittle sapphire and ductile copper whisker crystals, noting surface defects effect on mechanical properties 16 p2601 A71-33917

Fibrous composites with multiple and variable shear strength interfaces to improve longitudinal shear and transverse tensile strengths and toughness 17 p2817 A71-34342

Reinforcing fiber weaknesses, considering stress concentrators, cracks and steps due to handling damage and interaction with contaminants during heat treatment 17 p2817 A71-34343

Monograph on fiber-resin composites covering glass, boron and carbon fibers and epoxy matrix materials tensile and thermoelastic properties 17 p2761 A71-34469

Birefringent coating method for stress analysis of fiber-reinforced laminated composites, developing subsurface stress-surface strain relation [SESA PAPER 1837A] 17 p2761 A71-34528

Two phase fiber reinforced composites under polyaxial stresses, predicting plastic behavior by deformation theory 17 p2823 A71-34810

Gradient shape influence on connectivity in two phase graded structures, considering polyphase structure of filament reinforced composites 17 p2763 A71-35226

Fiber reinforced resins mechanical properties determination based on component materials characteristics 17 p2763 A71-35441

Bunched parallel reinforcing fibers of equal size and varying tensile strength, deriving critical loads and stresses under gradual failure 17 p2763 A71-35451

Optimal design of locally orthotropic elastic flat bodies of fiber reinforced plastics or metals 17 p2763 A71-35620

Boron, carbon, sapphire and glass fiber composite materials, considering brittleness, anisotropic properties, filament winding and plastic and metallic matrices 18 p2939 A71-35915

Incompressible fiber reinforced composite materials finite plane deformation continuum theory and stress analysis without restriction concerning elasticity, plasticity or viscoelasticity behavior [ASME PAPER 71-APM-V] 18 p2978 A71-36264

Fiber volume content, fiber-matrix bonding, heat treatment and age hardening effects on transverse modulus and tensile strength of unidirectional Al matrix fibrous composites 18 p2935 A71-36597

Carbon fiber reinforced plastics, reviewing properties, performance, development, applications and potential cost reduction 18 p2940 A71-36765

Carbon-fiber-reinforced carbon composites for high temperature applications, describing filament orientation, matrix composition and heat treatment effects on ablation performance 19 p3085 A71-38350

Polyamides reinforced with finely chopped glass fiber, noting mechanical strength, Martens yield temperature and heat stability 19 p3085 A71-38476

Exact solutions for cord reinforced materials with thermomechanical constraints of incompressibility and inextensibility and thermal constraint on temperature gradient 20 p3310 A71-39869

Fiber reinforced tube under lateral compression between two flat dies, determining finite deformation from nonlinear elastic and elastoplastic shearing response analysis 20 p3311 A71-39966

Carbon-carbon composites fabrication by electrostatic fiber deposition/flocking, using liquid impregnation-carbonization cycles with coal tar pitch 21 p3384 A71-40140

Specimen support effects on three point bending tests of fiber-plastic composites, suggesting small diameter roller 21 p3405 A71-40596

Carbon fiber reinforced plastics, considering aerospace and medical applications 21 p3406 A71-40702

Modulus of elasticity and Poisson ratio of composite material with anisotropic or isotropic fibers arranged in rectangular or square array 21 p3464 A71-40772

Mechanical properties, applications and peculiarities of polymer composite materials reinforcement fibers 21 p3406 A71-40777

Nondestructive test for fiberglass reinforced plastic tank, using percussion method 21 p3466 A71-40838

Fatigue properties of satin woven fiberglass reinforced plastic cloth under various stress directions 21 p3406 A71-40839

Fiber reinforced elastic materials steady state plane wave propagation by modeling constituents as continua undergoing individual motions 21 p3469 A71-41004

Dynamic photoelasticity for stress wave propagation in anisotropic fiber reinforced composites, using birefringent models and pulsed ruby laser beam 21 p3471 A71-41027

Tensile fracture in grip section of fiber reinforced reduced cross section plastic composite specimens 22 p3564 A71-41591

High temperature structural application of refractory fiber reinforced ceramic composites 22 p3565 A71-42287

Fiber reinforced metallic matrix composite under creep, discussing rigidity, stress distribution, rupture strength and failure time 23 p3697 A71-44201

Fibers-matrix force interaction effects in metal composites, analyzing stress-strain state of reinforced plate 23 p3697 A71-44202

Heat resistant Ni-base composite stiffened with W wires, investigating interaction between alloy and fibers from metallographic and X ray diffraction microscopy data 23 p3693 A71-44214

Porous fiber reinforced composite low density heat insulating materials thermal conductivity measurements, showing energy transport by heat transfer mechanisms 23 p3784 A71-44341

Carbon fiber reinforced plastics featuring high strength and Young modulus and low density for engineering applications 24 p3840 A71-44363

Fiber-reinforced composites mechanical properties based on analytical treatment as homogeneous orthotropic bodies 24 p3841 A71-44573

Fiber reinforced viscoelastic rectangular beam, deriving asymptotic values of stress, curvature and position of neutral axis under constant moment 24 p3879 A71-44630

Mechanical properties of fiber reinforced heat resistant alloys 24 p3837 A71-44726

Tungsten filaments as reinforcing agent of heat resistant composite chromium alloy, investigating long term high temperature effects 24 p3837 A71-44728

Heat resistant Nichrome composite alloy with tungsten filament reinforcement, discussing manufacture and mechanical properties at 1100 C 24 p3837 A71-44730

Stress-strain curve of unidirectional fiber reinforced composite Al and N-CI wire under axial compression loads, discussing buckling and shear instabilities 24 p3842 A71-45229

REISSNER THEORY

Stress distribution in infinite cracked elastic plate subjected to constant twisting on basis of Reissner thin plates theory 04 p0670 A71-15385

Thin walled prismatic shell constrained torsion problem, applying Reissner mixed variational method 06 p0992 A71-17806

Reissner shell theory equations for arbitrary internal and surface loads 06 p0996 A71-17836

Reissner variational theorem for boundary values in linear anisotropic and nonhomogeneous elasticity 10 p1691 A71-24809

Shear deformations effect on circular plates from Reissner theory, expressing bending moments and shear forces as functions of lateral deflection and stress function 15 p2507 A71-32112

Partitioning method for Reissner shell theory equations, constructing rod system 24 p3877 A71-44407

RELATIVE BIOLOGICAL EFFECTIVENESS [RBE]

Relative biological effectiveness of multicharged C ions during single irradiation of *Chlorella*, noting dose dependent mutability 06 p0854 A71-18366

Relative biological effectiveness of fast neutrons, allowing for gamma component contribution 22 p3494 A71-42735

RELATIVISTIC EFFECTS

Relativity and solar quadrupole moment effects in time delay measurements of signal traveling from earth to artificial satellites 05 p0808 A71-16446

Robertson metric beta and gamma coefficients and solar dynamic oblateness determination from probe motion under relativistic effects [ONERA-TP-893] 06 p0970 A71-18024

Magnetoplasma modulated waves nonlinear instability, taking into account relativistic effects 07 p1171 A71-20296

Boiling of relativistic heat conducting fluid in normal space-time manifold for nonstrict hyperbolic system, using Eckart scheme 10 p1694 A71-23831

Relativistic MHD waves based on ideal fluid compressibility and statistical mechanics for given space-time 10 p1650 A71-24586

Time unit definition by atomic clocks, taking into account relativistic effects 11 p1762 A71-25622

Carnot cycles generalization for thermodynamic systems with stationary gravitational fields, deriving temperature, thermodynamic equilibrium and entropy definitions for general relativistic systems 11 p1798 A71-25738

Relativistic fluid thermodynamics for compressible fluid reversible adiabatic flow, using variational principle to derive stress-energy tensor

11 p1798 A71-25739

Relativistic effects and optimization in Doppler geodetical measurements, using model computations for satellite azimuth-elevation relation

11 p1732 A71-25832

Stellar mass relativistic integral theorems and upper and lower bounds for gravitational potential theory

11 p1830 A71-26106

Relativity and neutronization effects on radial pulsations and density decrease of rotating cold white dwarfs near stability loss, using energetic method

12 p1966 A71-27236

Maximum toroidal magnetic fields of rotating neutron stars dependent on central density, using relativity corrections to plasma hydrodynamic and Maxwell equations

12 p1966 A71-27237

Radar reflection from Mercury and Venus, discussing observations of echo times predicted relativistic increase

12 p1967 A71-27419

Relativistic thermo-magnetoelastic wave propagation, considering elastic solid under magnetic and thermal fields

13 p2101 A71-29105

Strong gravitational wave bursts in galaxy, suggesting collapsed relativistic body cluster burning gravitational potential energy

13 p2142 A71-29137

Gravitational theory for black holes, presenting relativistic collapse in three dimensions identical to general relativity

14 p2303 A71-29583

Plane electromagnetic waves diffraction by moving periodic metal strip grating, taking into account relativistic effects

14 p0000 A71-30076

Gravitational potential tensor and equations of motion of relativistic mechanics for isolated system of masses

15 p2481 A71-31187

Nonlinear interaction between three resonant modified ordinary electromagnetic waves propagating perpendicular to static magnetic field in homogeneous electron plasma, studying relativistic effects

15 p2460 A71-32655

Rotating isothermic radially pulsating white dwarf evolution, considering neutronization and general relativistic effects

19 p3134 A71-37511

Entropy generation and survival of protogalaxies in expanding universe, deriving bulk/shear viscosity, heat transport and sound waves damping rate in relativistic fluid

20 p3287 A71-39051

Theorem proved for monotonic behavior of pressure within relativistic rotating star, assuming stationary axisymmetric gravitational field of Euclidean topology

20 p3293 A71-39447

General relativistic time delay and moon-earth masses and Mars mass-ephemeris ratios from S-band range and Doppler tracking

20 p3296 A71-39623

Icarus photographic observations, determining general relativity effects on orbital motion

21 p3443 A71-40187

Relativistic behavior of uniformly accelerated translational observer motion relative to inertial observer from space-time transformation

21 p3415 A71-40653

Relativistic equation derivation for dynamics of point with varying rest mass from Newtonian principle

21 p3415 A71-40659

Static magnetic fields configurations of magnetic and rotating neutron stars, considering general relativistic effects

21 p3450 A71-40714

Relativistic gravity in solar system, predicting Newtonian gravitational constant anisotropy measurements by Cavendish experiments

22 p3575 A71-41920

Interstellar space flight kinematics near light speed, discussing theoretical requirements for relativistic rocket engines

22 p3600 A71-42000

Particle collisions and relativistic effects on electromagnetic wave propagation within plasma in direction normal to external magnetic field near gyrofrequencies

23 p3645 A71-43559

RELATIVISTIC PARTICLES

Neutron star in accretion state, investigating generation of relativistic electrons, positrons and X ray and gamma emission

01 p0150 A71-10061

Energetic relativistic particles diffusion from radio galaxies

01 p0161 A71-11384

Galactic nuclei composition of dense core with small subunits generating relativistic particles

01 p0162 A71-11421

Relativistic self confined electron beam produced plasmas, measuring electron density profile by multiple pass Mach-Zehnder laser illuminated interferometer

02 p0289 A71-11546

Energy spectra of expanding relativistic particle clouds producing quasar and Seyfert galaxy nuclei outbursts

02 p0307 A71-12082

Nonrelativistic cosmic particles spectrum and chemical composition changes, examining ionization and heating energy loss effect

02 p0300 A71-12093

Transformation properties of radiation field and electromagnetic energy fluxes of relativistic charged particles in magnetic field

02 p0312 A71-12362

Relativistic electron spectra of cosmic rays accelerated by plasma turbulence, examining singularity in solution

03 p0483 A71-13202

Single pulse relativistic electron beam passage through plasma, calculating induced current density in axial direction

04 p0635 A71-15371

Extragalactic radio sources relativistic electrons interaction with cosmic black body radiation, noting effect on sources lifetime and X ray background

04 p0641 A71-15838

Solar flare delayed relativistic electron appearance, comparing radio, optical and X ray data for particle intensities

06 p0961 A71-18171

Energetic solar electron emission and cone propagation by IMP satellites, noting relation to proton and relativistic energy events

06 p0961 A71-18174

Relativistic velocity particles diffusion in cloud of scattering centers in centrifugal motion from Boltzmann equation solution by method of extensions

06 p0963 A71-18229

Supernovae expansion, investigating hydrodynamic model with interstellar magnetic fields and relativistic particles effects

06 p0973 A71-18335

Functional method application to ultrarelativistic particles in external fields quantum electrodynamics, discussing electromagnetic field superposition

07 p1162 A71-20549

Energy spectra of expanding relativistic particle clouds producing quasar and Seyfert galaxy nuclei outbursts

08 p1362 A71-21132

Nonrelativistic cosmic particles spectrum and chemical composition changes, examining ionization and heating energy loss effect

08 p1355 A71-21143

Relativistic electrons acceleration in solar proton flares, taking into account plasma density and magnetic field intensity

09 p1512 A71-22059

Relativistic electron beam instability and mean free path in dense plasma target, using Vlasov equation

09 p1500 A71-22238

Gravitational field effect on relativistic charge emission, noting gravitational waves detection

09 p1494 A71-22887

Compton scattering of relativistic electrons in cosmic plasma waves as source of HF radio emission from metagalactic objects

09 p1521 A71-22926

Strongly magnetized relativistic degenerate electron gas proton-proton reaction rates and electron capture over various temperatures, densities and magnetic field strengths

10 p1661 A71-24305

Quasi-linear relaxation of ultrarelativistic electron beam in homogeneous and inhomogeneous plasmas, noting initial divergence angle threshold

10 p1654 A71-24895

Model for relativistic electrons diffusion from IR sources, determining injected electron spectrum distortion due to inverse Compton losses and X ray spectrum

11 p1814 A71-25294

Relativistic quarks in cosmic rays at sea level and at mountain altitude, estimating production cross section vs absorption mean free path and mass

11 p1815 A71-25589

Small amplitude oscillations in system of relativistic electron beam penetrated plasma, calculating dispersion curves

12 p1936 A71-26919

Universe UV radiation intensity, estimating inverse Compton effect interaction of cosmic relativistic electrons with relic radiation

12 p1948 A71-27079

Long term storage of relativistic energetic electrons and protons in solar corona from IMP 4 and Pioneer 8 observations related to delayed emission from flares

12 p1969 A71-27657

Relativistic electrons associated with solar particle events, measuring occurrence frequency, electron propagation and diffusion anisotropy

13 p2129 A71-29057

Newton gravitation theory, showing extension by relativistic mass and vector gravitation potential addition

14 p2305 A71-29682

Flux estimates of gamma quanta with energies of 5 TeV from celestial objects due to bremsstrahlung and inverse Compton scattering of relativistic electrons

14 p2299 A71-29985

Cosmic radio emission coherent generation mechanism, involving derelativization and relativization of particles in small space

15 p2483 A71-31343

Moving type 4 solar radio burst, describing bipolar magnetic structure and origin in synchrotron radiation from relativistic electrons

15 p2473 A71-31692

Modulated relativistic electron beams interaction with plasma, investigating coherent energy loss

15 p2460 A71-32789

Relativistic electron precipitation during magnetic storms, showing cyclotron resonances with electromagnetic ion cyclotron waves

16 p2629 A71-33948

Collision rates in photon and relativistic particle gases, noting importance for cosmic radio and X ray sources processes calculations

18 p2949 A71-36100

Sagittarius A model involving relativistic electron diffusion from point source due to Compton scattering for observed radio spectra explanation

18 p2957 A71-36155

Solar flare X-ray origin model, discussing charged particle acceleration to relativistic energies, ambient gas heating and thermal and nonthermal X rays

18 p2958 A71-36740

Type 3 solar radio burst instantaneous emission frequency relationship to local plasma frequency in region with subrelativistic particles

18 p2958 A71-36742

Universe UV radiation intensity, estimating inverse Compton effect interaction of cosmic relativistic electrons with relic radiation

19 p3126 A71-37429

Pulsars electromagnetic radiation, considering bunch of relativistic charged particles

19 p3134 A71-37513

Heat and fictitious forces in variable rest mass relativistic particle dynamics for thermal energy conservation laws interpretation

19 p3162 A71-37641

Intense relativistic electron beam propagation in drift tube with neutral gas and plasma background, determining front velocity and energy transport

20 p3272 A71-38784

Foillless diode for production of high power relativistic electron beams, using multicathode system

20 p3202 A71-38831

Relativistic primary cosmic rays chemical composition between Be and Fe from charge spectrum obtained with Cerenkov counters

20 p3284 A71-39756

Radio pulses from pulsars, noting relativistic energy of particles from volume emissivity and surface flux density

20 p3305 A71-39950

Relativistic electron beam instability and mean free path in dense plasma target, using Vlasov equation

21 p3424 A71-41124

Quasi-linear relaxation of ultrarelativistic electron beam in homogeneous and inhomogeneous plasmas, noting initial divergence angle threshold

21 p3425 A71-41275

Relativistic neutralized cylindrical electron beam paraxial motion through uniform longitudinal magnetic field

21 p3426 A71-41289

Anisotropic solar ground level relativistic proton event of 18 November 1968, determining propagation mechanism characteristics from neutron monitor observations

22 p3591 A71-41470

Stochastic ion acceleration by relativistic electron beam in plasma traveling waves with different phase velocities

22 p3578 A71-42065

Cosmic radio emission coherent generation mechanism involving derelativization and relativization of particles in small space

22 p3606 A71-42618

Large area parallel-plate pulse ionization chamber for high altitude balloon measurements of relativistic cosmic ray heavy nuclei

22 p3550 A71-42887

Solar modulation of relativistic cosmic ray particles, noting step-like changes and rigidity dependence

23 p3719 A71-42948

Asymptotic expressions for electromagnetic field and currents induced in unbounded dense plasma by relativistic electron beam passage

23 p3711 A71-43410

Relativistic electron beam propagation entering vacuum or neutral gas filled region through grounded conducting wall, using one dimensional model

23 p3713 A71-44146

Electromagnetic waves excitation in coaxial resonator by relativistic electron beam, assuming presence of steady longitudinal magnetic field

24 p3833 A71-44663

Relativistic electron beam propagation in decelerating medium in crossed electric and magnetic fields, noting nonrelativistic instability condition

24 p3856 A71-44669

RELATIVISTIC PLASMAS

Cosmic objects relativistic plasma X ray and gamma ray background radiation increase, considering bremsstrahlung effect on radiation spectrum

04 p0657 A71-15747

Supraluminous waves modes in field free two component anisotropic plasma by linearized relativistic Vlasov equation

05 p0791 A71-16939

Collective longitudinal space charge waves in trapped relativistic one dimensional plasma, calculating inhibition/enhancement of cosmic ray Fermi acceleration

05 p0791 A71-16940

Neutrino luminosity in strongly magnetized degenerate relativistic electron gas plasma from URCA energy loss rate calculations

10 p1671 A71-24303

One dimensional plane adiabatic MHD free expansion of relativistic plasma

10 p1676 A71-24495

Fokker-Planck equation for Compton scattering in hot plasma, considering energy exchange rates for scattering in relativistic Maxwellian plasma

14 p2283 A71-30859

Temporal echo oscillations in collisionless relativistic electron plasma

17 p2786 A71-34198

Relativistic and/or degenerate electron gas equation of state formulae for density, temperature, entropy and internal energy

18 p2960 A71-35937

Dielectric permeability tensor of relativistic plasma stream, considering collisionless damping of surface waves in semiinfinite isotropic plasma

23 p3713 A71-44148

Zero temperature relativistic plasma ground state energy calculation using Fermi momentum and Green function

24 p3857 A71-45115

RELATIVISTIC THEORY

Chronometrically invariant formulation of relativistic thermodynamics second law distinguishing between three dimensional space and time

01 p0156 A71-10550

Quasi-classical equations of relativistic quantum mechanics, considering Klein-Gordon equation

01 p0129 A71-11293

Relativistic cosmology with singular point, using oscillatory model for Einstein equations general solution with time related physical singularity

02 p0285 A71-12527

Relativistic kinetic theory of particles with magnetic dipole moment in external EM field, deriving transport equations for distribution function

03 p0463 A71-13425

Lorentz invariants in relativistic fluid dynamics and thermodynamics in nonvacuo, suggesting determination through earth-moon space flight experiments

04 p0661 A71-14872

Classical and relativistic forces of inertia based on exact solution of Einstein nonlinear gravitational field equations, using general covariance principle

04 p0628 A71-15903

Relativistic electromagnetic field analysis, using fluid dynamic approach

04 p0628 A71-15917

Lagrangian methods yielding relativistically covariant formalism for wave packets in weakly inhomogeneous and time dependent plasma dynamics, obtaining motion equations from Euler-Lagrange equations

05 p0789 A71-16657

Equivalence principle in Einstein general relativity, discussing gravitation and inertial forces, cosmological postulate and metagalactic evolution

07 p1189 A71-18739

Relativistic gravitation theory and experimentation, surveying literature on gravity waves, EM propagation, gyroscopic precession, etc

07 p1158 A71-19096

Homogeneous isotropic relativistic cosmological model of universe, discussing construction

09 p1523 A71-23020

Static relativistic theory of isotropic spherically symmetric star equilibrium stability, assuming certain conditions with respect to mass-energy density and total baryon number

09 p1529 A71-23597

Linearized relativistic transport equation for mixture of isobaric Maxwellian molecules, solving in terms of eigenfunctions and eigenvalues of collision operators

10 p1645 A71-24609

Helmholtz and relativistic electrodynamics, discussing kinetic interaction potential using Lorentz invariance

10 p1644 A71-25110

General relativistic von Zeipel theorem providing necessary and sufficient condition for equidensity surfaces coincidence in stationary star axisymmetric rotating mass fluid

11 p1833 A71-26327

Relativistic formulation of thermodynamics and statistical mechanics in special theory of relativity, noting Ott presentation

13 p2102 A71-29324

Elastic properties relativistic theory, defining deformation tensor and constitutive laws

15 p2442 A71-31904

Relativistic stellar wind problem, discussing topological solutions

15 p2490 A71-32399

Relativistic kinetic theory of large amplitude transverse Alfven wave, discussing propagation in collisionless plasma

15 p2459 A71-32653

Chemical equilibria susceptibility to gravitational field effects, suggesting coincidence with conditions derived from relativistic thermodynamics

16 p2540 A71-33257

Uniformly rotating thin relativistic disks structure, stability and gravitational fields within general relativity framework

17 p2806 A71-35405

Post-Newtonian corrections for Maclaurin spheroids, presenting binding energy numbers

17 p2806 A71-35406

MHD detonation waves in relativistic perfect fluid of magnetic permeability μ immersed in electromagnetic field

18 p2951 A71-36189

Spectroscopic binary system with invisible major mass components, considering relativistic companion star

19 p3134 A71-37508

Tensors in relativistic asymmetrical field theory, generalizing Einstein gravitation and Maxwell electromagnetic equations for electrogravitational fields

19 p3105 A71-38580

Relativistic and Newtonian neutron star models with nuclear forces in equation of state, using unitary transformations for hard core and soft core potential

21 p3442 A71-40143

Lorentz invariant theory for relativistic gravity testing, deriving conservation laws and parameter constraints from parametrized post-Newtonian equations of motion

22 p3575 A71-41919

Relativistic gravitation theory, using Lorentz invariant scalar potential and gravitational metric

22 p3575 A71-42355

Cosmical constant role in relativistic cosmology, considering retention for additional freedom in linking relativity theory with other parts of physics theory

22 p3607 A71-42882

Least squares and sequential estimation techniques application to Mariner 6 and 7 tracking data analysis, verifying Einstein relativity theory on electromagnetic radiation propagation

23 p3731 A71-43054

RELATIVISTIC VELOCITY

High relativistic speed interstellar starship navigation, considering darkness cones, barrel, starbow, and near light speed problems

15 p2445 A71-31749

Stereoscopic effects and apparent shape or position of moving objects at relativistic speeds under binocular observation

16 p2535 A71-33166

Viscous relativistic fluid plane laminar flow, discussing incompressible thermally nonconducting case and stationary models

19 p3044 A71-37640

RELATIVITY

Light speed invariance in special theory of relativity concerning Galilean coordinates

01 p0127 A71-10601

Relativistic correction for planet perihelion rotation within Einstein gravitation theory, using proper magnitudes in terms of chronometric invariants

01 p0159 A71-10920

General relativistic formulation of massive magnetized rotating conductor, showing electrodynamical properties of surrounding empty space for explanation of stellar structure

01 p0160 A71-11273

Book on uncertainties of relativity and quantum theories covering potential energy, atomic clocks, coordinates and frames of reference, Doppler effect, gravity red shift, gravistatics, etc

02 p0284 A71-11843

Superfluid gyroscope for general relativity tests, using resonant phonon force field for drift reduction

02 p0248 A71-11943

Gyroscopic precession effects in earth polar orbital satellite experiments for Einstein general relativity tests

02 p0312 A71-12369

Pulsar pulse arrival times measurement for general relativity theory test, determining positions and period change rates

02 p0315 A71-12660

General relativity and gravitational collapse, discussing experimental tests, waves, use of Riemann geometry and Einstein field equations

03 p0482 A71-12972

Adiabatic temperature gradient requirement for neutral convection mode in general relativity of star in hydrostatic equilibrium

03 p0486 A71-13330

Centrifugal and Coriolis force in general relativity, discussing paradox associated with terms in mass shell test particles equations of motion

03 p0489 A71-13564

Energy relations in physical space of general relativity theory and inertia space of Newtonian classical mechanics

03 p0458 A71-13605

Einstein universe fictitious forces in noninertial frames, deriving equations from classical formulas by general covariance

03 p0490 A71-13942

Gravitational waves properties and detection, discussing relationship between electromagnetism and special relativity theory

03 p0459 A71-13950

Static charged dust distributions, investigating general relativity field equations with electromagnetic stress tensor

04 p0625 A71-14732

Gravitational waves collision analysis using coordinate system for general relativity

04 p0658 A71-15832

Chronometrically invariant formulation of Petrov gravitational fields algebraic classification at spacetime fixed point in general relativity

05 p0781 A71-16182

Static thin shells and disks gravitational fields in general relativity

05 p0781 A71-16447

Energy transfer in general relativity, discussing time sequences restriction of static deformable configurations in near field

05 p0781 A71-16729

Black hole model accounting for epsilon Aur eclipsing binary secondary component observations

06 p0970 A71-18031

General relativity theory tests, discussing Einstein effects existence and light velocity in gravitational field

06 p0971 A71-18246

Action at distance gravitation as alternative to general relativity, discussing gravitational frequency shift and light bending

07 p1189 A71-18747

Theoretical frameworks for testing relativistic gravity, using presence of metric and gravitational response equation from Dicke approach as postulates of parametrized post-Newtonian formalism

07 p1190 A71-18859

Parametrized post-Newtonian formalism for perfect fluids applied to Nordvedt effect in relativistic gravity

07 p1190 A71-18860

Time variable physical singularity in general relativistic cosmological solution of gravitation equations, constructing simplified models

07 p1191 A71-19173

Orbiting gyroscope de Sitter precession in different versions of Brans-Dicke theory, discussing term arising from anomalous scalar force in equations of motion

07 p1160 A71-19550

Physics laws and simplifications, discussing Newtonian mechanics, electrodynamics, relativity, atomic physics and quantum theory

07 p1163 A71-19603

Conformally flat universe class with short ranged scalar gravity, satisfying Einstein field equations

08 p1334 A71-21360

General relativity theory quantization, admitting kink states with fermion-like properties and spin

08 p1335 A71-21362

Hydrodynamic equations for behavior of thermally conducting viscous compressible fluid in first post-Newtonian approximation to general relativity, obtaining conservation laws

09 p1518 A71-22338

MHD equations for charged conducting fluid behavior in first post-Newtonian approximation to general relativity, obtaining conservation laws

09 p1518 A71-22339

Critique on Mach principle, discussing incompatibility between system inertia in universe and general relativity theory

09 p1522 A71-22980

Planetary rotational and translational motion interaction in Einstein gravitation theory, describing orbital elements secular disturbances in two body problem

09 p1526 A71-23339

General relativity theory applicability limits for strong gravitational fields and near singularities in cosmology

10 p1668 A71-24002

Book on relativity and discretization in astronomy covering cosmic structures, galactic isopleths equilibrium theory, red shift discretizations, etc

10 p1670 A71-24210

Viscous compressible fluid response to incident gravitational wave, deriving governing equations in linearized approximation to general relativity

10 p1676 A71-24496

Relativity - Conference, Cincinnati, June 1969

11 p1798 A71-25279

Rotating configurations in general relativity, considering infinitesimal quasi-static deformations

11 p1834 A71-26407

Gravitational field quantum fluctuations role in general theory of relativity and cosmological model

12 p1965 A71-27179

Hydrodynamic analogy for postulates in special relativity theory, analyzing steady and potential flow of inviscid compressible medium for Chaplygin gas with unreal time

12 p1932 A71-27547

General relativity gravitational field equations, giving composite sphere internal structure for core and shell

12 p1932 A71-27643

Closed universes quantization and gravitational field in general relativity, emphasizing superspace concept and finite-dimensional model quantum theories construction

13 p2100 A71-28395

Constant space curvature perturbations, considering density, rotational and propagation of gravitational waves with Lipschitz method

13 p2137 A71-28479

Gravitational theory for black holes, presenting relativistic collapse in three dimensions identical to general relativity

14 p2303 A71-29583

Relativistic gravitation theory quantitative study by space vehicle experiments, discussing earth orbit and deep space investigations

14 p2319 A71-29906

Gravitation theory with universe reference frame concept consistent with general relativity theory based on equivalence principle

14 p2315 A71-30860

Electromagnetic and gravitational waves scattering by static gravitational field, comparing classical general relativistic and quantum field theoretic results

14 p2275 A71-30861

Minkowski space-time concept, developing deviation function from geometric analysis

15 p2481 A71-31145

Physical meaning of fifth coordinate in five dimensional field theory, discussing relationship as parameter metric of de Sitter four dimensional space-time manifold

16 p2608 A71-33223

Relativity and gravitation - Conference, Technion City, Israel, July 1969

16 p2609 A71-33255

Particle motion in combined gravitational field of monopole and prolate quadrupole, deriving exact solution in Newtonian mechanics and general relativity

16 p2609 A71-33256

Energy-radiation problems in relativity theory, considering electromagnetic waves, Einstein equations, momentum tensors and moving charged particles

16 p2609 A71-33259

Spin weighted field functions for group SU(2) in gravitational radiation problems of general relativity, using Newman-Penrose formalism

16 p2609 A71-33260

Integral containing Heaviside and Dirac delta function in integrand with minus and plus infinity limits, computing value using thin spherical shells in general relativity

16 p2656 A71-33263

Natural symplectic structure for twistors on cotangent bundle over space-time manifold, considering Lagrange identity for Jacobi fields

16 p2609 A71-33264

Static electromagnetic fields in general relativity obtained for space-time metrics of group G automorphisms, considering Rainich unified field theory equations

16 p2610 A71-33265

Kinetic theory of gases in general relativity, including model of matter particle structure

16 p2610 A71-33267

Special relativity distinguished from theories based on preferred frame of reference and physical Lorentz contraction by Michelson-Morley experiment in solid transparent medium

16 p2610 A71-33268

Geometric object concept in third principle of relativity, obeying identity functional equations for infinitesimal general coordinate transformations

16 p2611 A71-33273

Relativistic cosmological models with nonzero pressure, considering matter as perfect gas-radiation mixture and isotropic/homogeneous three space

16 p2611 A71-33274

Landau-Lifshitz pseudotensor analogs of ten mechanical conservation laws in Einstein theory of gravitation

16 p2611 A71-33275

Scalar function expansion in relativistic invariant functions in pseudoeuclidian space, deriving direct and inverse formulas for spherical, hyperbolic and Lobachevskii coordinates

16 p2612 A71-33459

Book on relativistic astrophysics, Volume 1, Stars and relativity, covering stellar dynamics, astronomical models, cosmic objects evolution and star clusters

16 p2635 A71-33481

Sun as flattened ellipsoid of revolution, showing flatness effects on planet motion in relativity theory framework

16 p2612 A71-33567

General relativistic time delay of electromagnetic radiation propagation due to solar gravitational field measured from Mariner 6 and 7 range and Doppler data

16 p2640 A71-33737

Cauchy problem for nonlinear Boltzmann equation in general relativity, utilizing energy inequalities

16 p2612 A71-34059

Action-at-a-distance theory of gravitation generalized to tensor interactions of all orders, considering special relativity demands and perihelion advance of Mercury

17 p2797 A71-34368

Planetary dynamics bibliography and review, considering range determination and ephemerides, general relativity, tidal evolution and lunar orbit, solar system commensurabilities, etc

17 p2798 A71-34457

Quasi-closed Einstein universe model, showing orbits rotation similar to perihelions in Schwarzschild field

17 p2778 A71-34630

Gauge equations in general relativity theory for tetrad gravitational potential formulation, based on algebraic invariants method

17 p2778 A71-34636

Inertial effects induced by rotating thin walled shell of finite thickness, considering general relativity equations of motion for test particle

18 p2970 A71-37059

Relativistic hydrodynamic solution for gravitational interaction of vortex and potential motion of homogeneous medium

19 p3134 A71-37515

Covariant definition of radius vector in Riemann space, studying position operator in general relativity theory

19 p3105 A71-38582

Physical constraints on universe topology near collapsed-ordinary stars interaction in general relativity theory

19 p3105 A71-38583

Critique of cosmological theories based on spontaneous matter creation in strong gravitational fields, deriving particles discrete number constancy in general relativity

20 p3268 A71-38834

German monograph on static fields in general relativity theory covering covariant equilibrium conditions, two body problems, vacuum fields and Newtonian gravity principles

20 p3269 A71-39077

Equilibrium rotating superdense configurations in general relativity theory, determining integral parameters in low angular velocity approximation

20 p3289 A71-39297

Clock paradox problem resolution in relativity theory, considering space travel effects on time measurement and aging process

20 p3271 A71-39571

Time variable physical singularity in general relativistic cosmological solution of gravitation equations, constructing simplified models

21 p3441 A71-40088

Stationary signal space topology concept in special relativity, considering points neighborhoods as independent of signal sending time

21 p3346 A71-40091

Gravitational radiation interaction with uniform incompressible inviscid fluid in simple motion, considering response in linearized approximation to general relativity

21 p3446 A71-40421

Rapidly rotating polytropes in post-Newtonian approximation to general relativity

22 p3604 A71-42327

Schwarzschild constants evaluation from coupled gyroscopes spin axes observation, noting axes high angular velocities due to gravomagnetic effect in gravitational interaction

22 p3605 A71-42338

Generalized Einstein field equations in general relativity based on ennuple or tetrad variation, comparing with Schwarzschild solution

22 p3575 A71-42354

Trapped surface existence conditions and occurrence in strongly curved space-times

22 p3576 A71-42403

Gravitational field quantum fluctuations role in general theory of relativity and cosmological models

22 p3605 A71-42453

Gravitational wave astronomy, discussing phenomenon relationship to Einstein relativity theory and detector configurations

23 p3733 A71-43120

Spherically symmetric Gaussian coordinate systems completeness in spaces analogous to Lemaître and Kruskal spaces in general relativity

24 p3848 A71-44658

General theory of relativity for symmetric field, discussing De Donder incompressible fluid model and Tolman-Schwarzschild metrics

24 p3849 A71-45064

Newtonian analog construction, examining relativistic homogeneous anisotropic models

24 p3873 A71-45110

RELAXATION [MECHANICS]

NT STRESS RELAXATION

Thin glass fibers relaxation characteristics, discussing shear modulus, internal friction and temperature effects

03 p0448 A71-13298

Supersonic blunt body flow relaxation processes, calculating bow shock for various flow regimes and reaction rates

05 p0835 A71-16525

Relaxation theory of Rayleigh scattering of light by isotropic continuous medium, deriving spectral densities via fluctuation dissipation theorem

06 p0927 A71-17596

Thin glass fibers relaxation characteristics, discussing shear modulus, internal friction and temperature effects

09 p1483 A71-32371

Quasi-linear relaxation of ultrarelativistic electron beam in homogeneous and inhomogeneous plasmas, noting initial divergence angle threshold

10 p1654 A71-24895

Nondestructive testing method obtaining relaxation modulus and accelerated degradation/stress corrosion of reinforced plastics

11 p1768 A71-25404

Quantum electrodynamic analysis of relaxation processes in two level laser

11 p1774 A71-26005

Monoenergetic beam relaxation dynamics in plasma, describing oscillation excitation and diffusion allowing for instability

12 p1942 A71-27769

Nonlinear heredity theory related to Volterra-Freshet heredity theory under uniaxial tension, giving expression for polymers deformation relaxation processes

13 p2092 A71-28650

Unloading effects on elastoplastic stability of shells, using method based on successive approximations

13 p2156 A71-29073

Relaxation distance for sharp cone behavior from chemical nonequilibrium laminar boundary layer effects on simulated space shuttle configuration during reentry

13 p2146 A71-29504

Ion beam collisionless relaxation in hot electron plasma, observing oscillation spectra and velocity distributions

15 p2453 A71-31245

Plasma-electron beam system relaxation oscillations due to threshold excitation of transverse ionic oscillations by HF vibrations

15 p2460 A71-32706

Continuous light absorption, emission and ionization relaxation behind shock front in xenon

16 p2613 A71-32890

Fast argon plasma flow interaction with strong magnetic fields, describing ionization relaxation phenomena behind magnetically reflected shock fronts

16 p2615 A71-32898

Thin walled rod of strain hardenable material, developing constrained torsion approximation for creep and relaxation

16 p2651 A71-33060

Hypersonic magnetic spectrometer-relaxometer, comparing direct and indirect recording methods for hypersonic in metals at helium temperatures

16 p2580 A71-33928

Shock tubes and shock tunnels, considering equilibrium expansion, relaxation phenomena and real gas effects

18 p2897 A71-36410

Relaxation effects on velocity and temperature of solid particles in gas flows, emphasizing acoustic propagation, compression shock structure and nozzle flows

18 p2909 A71-36441

Radiation gas dynamics covering monatomic and molecular gases, chemical dissociation and vibrational relaxation

19 p3043 A71-37459

Magnetospheric high energy protons relaxation due to interaction with Alfvén waves, presenting Einstein-Kolmogoroff equation numerical solution for particle momentum distribution function

20 p3278 A71-39074

Small perturbations of stationary parallel flow with relaxation, considering boundary conditions around slender wings, partial differential equations and similarity law

20 p3213 A71-39569

Nitrogen alloying effects on relaxation resistance of Cr-Mn austenitic steel

21 p3402 A71-41092

Quasi-linear relaxation of ultrarelativistic electron beam in homogeneous and inhomogeneous plasmas, noting initial divergence angle threshold

21 p3425 A71-41275

Kinetic equations for electron density matrix of superconductors, describing two phase relaxation process

23 p3715 A71-43413

Review of papers at EUROMECH 23 colloquium on finite amplitude and diffusive effects in acoustics, covering acoustic damping by relaxation, dust and moisture, turbulence effects, etc

23 p3704 A71-43447

Pressure histories from densification and relaxation measurements on lunar glass and synthetic samples, investigating refractive index changes after annealing

23 p3758 A71-43760

MHD wave spectrum relaxation during wave-plasma interactions in weakly turbulent plasma, treating associated triplasma processes as elementary events

24 p3855 A71-44661

Electron beam and plasma nonlinear interactions, noting scattering zone, amplitude oscillation maximum, longitudinal velocity and relaxation patterns

24 p3856 A71-45097

RELAXATION [PHYSIOLOGY]

Diurnal rhythm of adrenaline secretion in subjects with different working habits, comparing catecholamine excretion under relaxation conditions

11 p1721 A71-26355

RELAXATION METHOD [MATHEMATICS]

Nonlinear relaxation iteration method for solving geometrically nonlinear problems in mechanics [ASME PAPER 70-WA/APM-43]

03 p0512 A71-14165

Dynamic relaxation method for solving simultaneous linear differential equations, comparing asymptotic rate of convergence with degenerate Chebyshev approximation

05 p0776 A71-17122

Theorems concerning relaxation in point total and single step iterative solution for Hammerstein type nonlinear equations

06 p0920 A71-18212

Asymmetric buckling of spherical caps with asymmetric imperfections, using nonlinear relaxation technique for treatment of finite difference representation of differential equations

09 p1541 A71-23090

Numerical search for optimum product space as extension of Gauss-Seidel relaxation method, noting applications to partial differential equations

10 p1637 A71-24841

Relaxation methods application to optimal control of systems described by equations with partial derivatives, studying minimizing sequences

13 p2043 A71-28817

Generalized relaxation methods application to transonic flow problems, combining with numerical integration theory for ordinary differential equations

18 p2906 A71-36324

Nonlinear structural frame analysis by dynamic relaxation for use with computers

24 p3879 A71-44632

RELAXATION OSCILLATORS

NT PHANTASTRONS

Pulsed semiconductor devices with S-shaped current-voltage curve, considering relaxation oscillator and voltage generator circuits

04 p0558 A71-15565

Fluidic relaxation oscillator experimental and theoretical analysis, investigating pressure and temperature effects on frequency stability

07 p1027 A71-20576

Statistical scatter of pulse duration in relaxation oscillator with common-emitter coupling concerning mass production

08 p1261 A71-20739

Temporary nonlinear feedback effect on stability of triggering potential and output pulse repetition rate of transistor self relaxing blocking oscillator

09 p1424 A71-23169

Physical process causing negative differential resistance segment on I-V curve of single junction transistor, describing thyristor-triggered relaxation oscillator

14 p2214 A71-30633

Cadmium doped silicon diodes I-V curve sinusoidal relaxation oscillations frequency and amplitude dependence on temperature

16 p2548 A71-34026

Relaxation processes in Michelson interferometer as integral part of carbon dioxide laser cavity in phase Q switching regime

19 p3071 A71-37389

Tunnel diode harmonic relaxation frequency divider, obtaining large division factors and wide synchronization bands with sinusoidal output signal

20 p3206 A71-39818

Precision relaxation oscillators design and error sources, discussing miniaturization by microelectronic approaches

21 p3355 A71-40736

RELAXATION TIME

Shock tube generated Xe plasma electron density measurements by spectroscopy and laser interferometry, deriving ionization relaxation time

01 p0134 A71-10995

Electron density fluctuations in nonstationary plasma under crossed electric and magnetic fields, relating times of instability development and background relaxation

02 p0289 A71-12179

Nitric oxide vibrational relaxation times in Ar from IR emission measurements at high temperature

02 p0287 A71-12495

Optimal relaxation time existence for Maxwell solid cylinder bonded to thin casing during forced vibration of rocket assembly, discussing Voigt solid

03 p0497 A71-13469

Ultrasonic absorption in hydrogen sulfide, measuring vibrational and rotational relaxation times as function of temperature

03 p0459 A71-13718

Molecular gas vibrational and rotational state equations, discussing relaxation times, sound propagation and transport processes

03 p0462 A71-14557

Time measurements of vibration relaxation in diatomic gases excited by shock waves

04 p0568 A71-14795

Hyperbolic heat conduction equation with small relaxation time parameter, studying convergence for Cauchy and boundary value problem

05 p0839 A71-17035

Transverse parity photomagnetic effect during intense illumination in isotropic semiconductor crystals with relaxation time independent of energy

05 p0794 A71-17041

Shock tube research instrumentation with fast response time for data on thermodynamic and transport properties, relaxation times and kinetics of high temperature gases

06 p0897 A71-17430

Relaxation time for nitrogen molecule vibration temperature in ionosphere due to thermal electron collisions

06 p0895 A71-18274

Gas ionization relaxation phenomena behind strong shock waves, discussing ionization kinetics, radiation transfer effects, relaxation time and radiative heating

07 p1087 A71-19172

Electron temperature in hydrocarbon air flame, discussing extra equilibrium excitation, energy relaxation rate and chemiluminescent emission

07 p1182 A71-19250

Ar-oxygen mixture in undiluted nitrogen, discussing relaxation time change during adiabatic excitation and molecule oscillations deactivation

07 p1163 A71-19276

Vibrational and rotational relaxation in sulfur dioxide, measuring relaxation time as function of temperature by ultrasonic absorption

07 p1054 A71-19370

Ion-molecule collision charge transfer and momentum transfer relaxation rates, using ion cyclotron resonance heterodyning method

07 p1054 A71-19371

Nonlinear Fokker-Planck equation solution by Mott-Smith bimodal distribution function method, investigating fully ionized nonequilibrium plasma relaxation time

07 p1171 A71-20295

Carbon dioxide laser molecular upper level vibrational relaxation time measurement

07 p1128 A71-20527

Rotating nonvibrating diatomic low density gas molecules rotational relaxation time and viscosity, based on quantum mechanics

08 p1336 A71-20659

Coulomb collisions in high density plasma beams, examining relaxation time

08 p1340 A71-21486

E layer near solar culmination relaxation, determining ion and electron concentration variations

08 p1286 A71-21855

Electron-ion plasma in HF electric and constant magnetic field, determining relaxation times and collision frequency for temperature compensation

09 p1502 A71-22539

Stress effects on electron relaxation time anisotropies in n-type Si, using high temperature piezoresistivity model for population transfer rates

09 p1508 A71-22692

Spatially uniform dense partially ionized plasmas asymptotic thermochemical relaxation processes due to heavy particle density, temperature or superimposed electric field changes

09 p1502 A71-22859

Plane normal shock wave reflection in relaxing gas for shock tube endwall upstream and downstream dynamic pressures, using method of characteristics

09 p1546 A71-23166

Bipolar photomagnetic effect relation to nonheating electric field in semiconductors with isotropic holes and multivalley electrons, obtaining surface intervalley relaxation rates

10 p1656 A71-24320

Electron beam relaxation in plasma, discussing experimental studies of oscillation amplitude and beam electrons energy distribution relationships during predominantly longitudinal plasma oscillation excitation

10 p1650 A71-24627

Perturbation theory of supersonic flow with nonequilibrium radiative heat transfer, investigating pressure, density, temperature and velocity as function of relaxation time

10 p1697 A71-24943

Pulsed ion laser electron density measurement by cavity method in S band, evaluating relaxation time

10 p1623 A71-25021

Hydrogen maser relaxation time measurement, using oscillator amplitude response

10 p1623 A71-25023

Electrostatic probe measurements of charged particles and thermal ionization relaxation in shock heated low density supersonic monatomic gas flows

11 p1766 A71-26286

Gas relaxation process equations of motion based on reversibility of time, considering application to particle systems with magnetic field moments

12 p1932 A71-27206

Charged particles magnetic scattering on cyclotron instability waves of radiation belt plasma, estimating proton relaxation time

13 p2129 A71-28552

Kinetic theory of nonspherical multiatomic molecules with electrons having rotational and oscillatory degrees of freedom, giving expressions for oscillatory relaxation times calculation

13 p2103 A71-29150

Solid state laser with slow relaxation bleachable filter, calculating modes self synchronization probability statistics relationship to relaxation time

14 p2253 A71-30109

Ar-oxygen mixture in undiluted nitrogen, discussing relaxation time change during adiabatic excitation and molecule oscillations deactivation

14 p2276 A71-30170

Coulomb collisions in high density plasma beams from numerical integration of Fokker-Planck equation for three initial distribution functions, studying relaxation time

14 p2283 A71-30674

Dielectric relaxation time in Debye binary liquid, comparing liquid filled coaxial transmission line step response measurements with Debye model

14 p2215 A71-30985

Electron density fluctuations in nonequilibrium plasma under crossed electric and magnetic fields, relating ionization instability development and background relaxation times

15 p2454 A71-31488

Nonequilibrium and equilibrium plasmas thermodynamic properties and molecular, atomic and ionic internal partition functions and relaxation times

16 p2617 A71-32955

EPR spectra and spin-lattice relaxation time in coal pitch and polyvinyl chloride during low temperature carbonization

17 p2763 A71-35245

Coherent electromagnetic excitation of optical transition levels by fluorescence measurement, obtaining dipole moment and relaxation times

18 p2929 A71-35903

Relaxation time model of solid state diodes based on equations for electrons of given energy, including p-n junction and tunnel diodes

19 p3027 A71-37495

Gas relaxation process equations of motion based on reversibility of time, considering application to particle systems with magnetic field moments

19 p3108 A71-38618

Ionization relaxation phenomena behind strong shock waves, discussing ionization kinetics, radiation transfer effects, relaxation time and radiative heating

21 p3365 A71-40087

Quantitative schlieren system for shock wave velocity, density ratio and relaxation time measurements, discussing electro-optical modification and calibration technique

21 p3364 A71-40404

Ne ionization relaxation time behind reflected shock waves from temperature and pressure measurements of combustion driven shock tube end wall
23 p3706 A71-42909

Electron velocity distribution relaxation in time dependent weakly ionized plasma within electric field, solving Boltzmann equation
23 p3708 A71-43151

Low frequency phase method application to fast electron processes and characteristic relaxation times in quick response Ge and Si junction diodes
23 p3650 A71-43307

Hydrogen fluoride vibrational relaxation times behind incident shock waves at various temperatures
24 p3802 A71-44922

Oxygen dissociation in He, Ar, Kr and Xe gas mixtures behind incident shock waves, calculating density gradients and vibrational relaxation time
24 p3802 A71-44924

RELAY

Lunar communications relay unit, discussing system design, capability and tradeoffs
01 p0035 A71-10919

Second order relay system with piecewise constant control, using phase plane analysis technique
03 p0451 A71-13964

Delay compensation in flip-flop element of optimal relay system with self oscillations, using optimal control algorithm constructed by phase space method
11 p1742 A71-26095

Relay advances - Conference, Oklahoma State University, April 1971
13 p2000 A71-28834

RELAY SATELLITES

Lunar far side communication, discussing libration point and lunar orbit relay system for high bit rate telemetry, TV and astronaut backpack communication
04 p0555 A71-15339

Tracking and data relay satellite system (TDRSS) impact on spacecraft mission support information management
07 p1197 A71-19704

Rendezvous equations near second lunar libration point, using Halo orbiting relay satellite for communication with spacecraft behind moon
09 p1521 A71-22912

Tacsat 1 telecommunications relay system, discussing UHF-SHF antenna radiation patterns, ground terminal equipment, nutation dampers and attitude and orbital correction procedures
12 p1882 A71-27611

Space station communications systems, discussing data relay satellites transmission paths to ground, multiple voice channels, two way color TV and onboard telephones
17 p2699 A71-34610

RELIABILITY

NT AIRCRAFT RELIABILITY

NT CIRCUIT RELIABILITY

NT COMPONENT RELIABILITY

NT SPACECRAFT RELIABILITY

NT STRUCTURAL RELIABILITY

Reliability prediction method effectiveness for control plant with efficiency represented by canonical forms
01 p0064 A71-10924

Stochastic processes applied to loaded redundancy systems reliability analysis
01 p0112 A71-11157

Complex systems potential effectiveness theory, establishing reliability, noise resistance and controllability limits
01 p0065 A71-11230

Satellite communications system earth station operation and reliability, discussing staffing, main and supporting communication equipment maintenance, utilities and redundancy
02 p0224 A71-12825

Terrain-following radar for TSR-2 aircraft, discussing reliability trials and improvement
07 p1062 A71-19557

Availability and failure frequency of systems of independent repairable units, using representation by network or reliability block diagram
15 p2415 A71-32341

Reliability and maintainability as concepts in life cycle costs applied to airline operations
16 p2552 A71-33287

Sequential analysis and Bayesian demonstration in hypothesis testing, considering weight ratios based on objective lower level program reliability test information
16 p2582 A71-33289

Human performance reliability data system using taxonomic structure for classifying behavioral studies and predicting man-machine performance
16 p2536 A71-33318

Space, radio communications, considering radio links reliability between multistage launcher rocket and ground stations
17 p2696 A71-34228

Low noise TWT amplifiers, performance, reliability and cost reduction
17 p2714 A71-34605

Gas lasers, discussing engineering developments for size and cost reduction, reliability, long life and high power
19 p3074 A71-38227

Direct measurements of cosmic dust particles in near earth environment and interplanetary space, noting reliability and calibration
20 p3300 A71-39655

Summation theory of random number of independent random variables relation to queueing and reliability theories
24 p3843 A71-44873

RELIABILITY ANALYSIS

Modular computer design for long term missions, discussing reliability estimation
01 p0046 A71-10205

Frame structures linear-mode failure probability estimation by reliability analysis
02 p0327 A71-12347

Gyroscope reliable performance life testing economic justification, noting cost lowering by deficient gyro rejection
05 p0749 A71-16304

[AGARDOGRAPH-128]

Statistical reliability tests for cosmic ray intensity records from ground stations, stressing time series aspect
06 p0951 A71-18108

Probabilistic weather forecasts reliability estimation
07 p1150 A71-18871

Ten-year old missile battery reliability programs based on two aspects of remotely activated one-shot battery
08 p1236 A71-21110

Mathematical model system analysis methods for reliability assurance, discussing worst case and Monte Carlo techniques
09 p1423 A71-23040

Timesaving reliability tests for Si transistors involving failure mechanism acceleration
09 p1418 A71-23042

Decoding computational work and time, discussing cost increases related to communication reliability
09 p1407 A71-23102

Nonrepairable elements reliability under external influences, discussing linear damage accumulation hypothesis
11 p1768 A71-25659

In-core thermionic reactor network reliability analysis, assuming component failures as equally probable stochastic events
11 p1713 A71-25893

Optimal reliability of system with nonlinear constraints, using mathematical model and sequential unconstrained minimization technique
11 p1771 A71-26161

Maximum entropy principle for prior distribution determination in Bayesian reliability estimation, comparing with statistical decision theory
11 p1772 A71-26164

Limited reliability mathematical model for radioisotopic thermoelectric generators semiconductor couples based on catastrophic failures
11 p1715 A71-26165

Hanle cascade effects on atomic lifetime reliability from collisional excitation experiments
11 p1803 A71-26370

Reliability analysis as essential input in trade studies for selecting system component designs, emphasizing NERVA program
12 p1928 A71-26664

Failure rate data in reliability analysis, considering material failure phenomena, and maintainability
12 p1909 A71-26665

Tabular system reliability analysis based on integration of fault tree, state variable and failure modes techniques
12 p1910 A71-26674

Mission reliability calculations for systems with redundant units, considering design of airborne warning and control system and other radar control systems
12 p1885 A71-26675

Reliability analysis method for systems cyclic operation, demonstrating application for satellite power subsystem
12 p1910 A71-26676

OA0 2 thermal test reliability analysis, using filtering process to eliminate component and subsystem level failures
12 p1971 A71-26681

Apollo program all-up spacecraft thermal vacuum tests, considering component and subsystem reliability analysis, thermal model verification and certification requirements
12 p1894 A71-26682

Cost effectiveness of reliability screening program from parts procurement through system test, using experience with attack radar for F-111 aircraft
12 p1885 A71-26683

Reliability analysis of solar thermoelectric generator module as function of individual photocells, circuit design and redundancy
15 p2351 A71-31672

Reliability prediction of narrow band structures under random excitations, considering catastrophic and fatigue failure modes
15 p2506 A71-32094

Gradual failure effects on operational reliability of centralized automatic control machine
15 p2374 A71-32192

Large nonrepairable systems reliability analysis by partitioning possible states into subsets
15 p2415 A71-32342

Dynamic stability and reliability analysis of pulse width modulated control systems by point-to-point mapping method
15 p2382 A71-32621

Information model for simulating systems reliability estimates uncertainty, noting state transition matrix, methodology and sensitivity analysis of effectiveness
16 p2583 A71-33304

Classification reliability of electromagnetic wave scattering fluctuating objects from statistical scattering matrices, obtaining incident wave polarization
17 p2698 A71-34260

Statistical limits on reliability, informativeness, controllability and self organization of complex systems, determining minimum redundancy requirements for suppressing interfering factors
17 p2720 A71-34953

Reliability analysis of universal computer system with identical elementary computers interconnected by communication channels
17 p2710 A71-34958

Reliability analysis of redundant information systems, deriving formulas for risk of failure and faultless operation probability
17 p2721 A71-34966

French monograph on system reliability of particle detection device covering methodology, functional models, Monte Carlo simulation, spectrometers and DC/DC converters
17 p2767 A71-35231

Probability density function for parameter of exponential measurement model based on structural inference theory, developing prediction densities as life test inferences
17 p2768 A71-35537

Reliability in key project decision making, including failure mode/effect analyses, design tradeoff, baseline meetings, hardware storage and data bases
18 p2926 A71-36491

Skewed and orthogonal redundant reaction wheels comparison for outer planet exploration spacecraft attitude control based on reliability analysis
19 p3101 A71-37926

[AAS PAPER 71-157]

Systems oriented components selection optimization technique by reliability/quality levels, considering repair and failure cost, storage time and mission duty cycle
19 p3034 A71-38518

Cathode ray tube, including electron beam peak power, resolution elements, luminescent materials, fabrication techniques, contrast preservation and reliability
20 p3234 A71-39062

Three phase code transformation task reliability and correlation, representing general factor analytic intellectual abilities and personality characteristics
20 p3192 A71-39073

Reliability controlled maintenance plan for avionics equipment based on mean time between failures
20 p3203 A71-39087

Discrete renewal processes applied to mathematical modeling of physical processes, using statistics of complicated events in reliability analysis
21 p3407 A71-40361

Generalized reliability function for systems of arbitrary configurations, using path enumeration approach based on probability theory
21 p3407 A71-40369

Semiconductor components reliability assurance under assumption of failure rate decrease with time for IC quality and performance improvement
21 p3356 A71-40746

Aircraft surveillance oceanic satellite systems design and reliability analysis, discussing position determination accuracy
22 p3572 A71-42094

Relcomp conversational time-sharing computer program for rapid calculation of reliability and MTBF of systems with serial and redundant units
22 p3517 A71-42103

Bias network analysis computer program for reliability analysis suited to failure mode, criticality, drift and catastrophic failures prediction
22 p3517 A71-42104

Computerized algorithm for redundant configuration system reliability function generation from Boolean algebra transmission function
22 p3517 A71-42107

Statistical fatigue life models, surveying failure probability distributions in reliability studies
22 p3566 A71-42117

Alcyon project PTA 1, considering balloon stabilization efficiency during night-day transition and system reliability
22 p3483 A71-42400

Multiple component logic circuit reliability analysis using Karnaugh diagram procedure for simplification 24 p3807 A71-45299

RELIABILITY CONTROL U QUALITY CONTROL U RELIABILITY ENGINEERING RELIABILITY ENGINEERING

Multiprogrammed and time shared multiaccess digital computers operating systems design, discussing dynamic memory protection structures 01 p0043 A71-10179

Real time systems design principles for processor organization, logic circuits, fault detection and diagnostic tests to facilitate high degree of reliability and maintainability 01 p0046 A71-10203

Modulo value influence on computer operation reliability, allowing for supplementary verification equipment reliability 01 p0049 A71-10531

Nonlinear control law for increased powered stabilization system accuracy in single-axis gyrostabilizer 01 p0079 A71-10533

Hybrid microcircuits reliability, discussing test data regarding receiving and sample inspection, environmental and performance testing, etc 01 p0053 A71-10733

Reliability test for fluidic digital comparison device 01 p0006 A71-10925

External actions effect on restorable products failure sequence, extending nonrestorable products reliability theory 01 p0088 A71-11231

Missile prototype reliability prediction, using reliability theory concepts in establishing computation and test programs without damage probability determination 02 p0298 A71-12366

Reliability prediction for machine parts subjected to cyclic stresses, using statistical analysis of fatigue data for failure rate calculation 02 p0327 A71-12367

Air transportation reliability through turbojet engine performance monitoring 02 p0298 A71-12368

Nondestructive testing for reliability and lifetime of mass produced radio equipment under maximum load 02 p0257 A71-12530

Single repairable unit system with spares deterioration in storage, calculating long-run availability and time to system failure 02 p0258 A71-12590

Apollo Applications Program command and service module test requirements to achieve reliable hardware for extended missions [ALAA PAPER 70-378] 03 p0500 A71-14436

NASA qualitative reliability technology applications to chemical industry 04 p0602 A71-14802

Product test duration and extent from reliability theory viewpoint 05 p0759 A71-16725

Two-unit redundant repairable system with standby, predicting periodic or random inspection effect on reliability through Laplace transforms 06 p0904 A71-18026

Navy avionics modular multiprocessing digital computer operating system reliability, comparing totally software and partly hardware approaches 07 p1067 A71-18833

Reliability in electronics - IEE Conference, London, December 1969 07 p1076 A71-19551

Satellite electronic equipment reliability engineering, considering circuit and system design, components screening, assembly and test procedures and quality assurance plans 07 p1207 A71-19563

Meteorological instrument design, emphasizing reliability and maintainability 08 p1293 A71-21734

MOSFET data systems evolution for IMP, discussing effects on system design and reliability approach 08 p1267 A71-21844

Book on reliability mathematics covering fundamental statistical concepts, logic diagrams, mathematical models, component reliability prediction, system prediction, reliability growth, assessment methods, etc 09 p1485 A71-22958

Iterative algorithms for regression function saddle point and applications in reliability and automatic control theories 10 p1585 A71-24156

Soviet book on aircraft ground support and onboard radio equipment operation and reliability increase by redundancy and rational methods, discussing preventive maintenance 10 p1583 A71-24670

Spacecraft structures weight optimization based on fracture mechanics and reliability cost constraints applied to pressure vessel design 11 p1847 A71-25464

Reliability test extent, duration, confidence limits and failure rate computed by nomograms 11 p1737 A71-25623

Random failure definition based on stochastic processes mutual implication, producing unique characteristic events 11 p1771 A71-26160

Reliability - IEEE Conference, Washington, D.C., January 1971 12 p1908 A71-26655

Statistical nature of time to complete MIL-STD-781 reliability sequential tests for military and space equipment, giving information about MTBF 12 p1908 A71-26656

Two-line all-equipment test and aeronautic systems division reliability testing, analyzing by Weibull Monte Carlo simulation 12 p1909 A71-26657

Computer aided reliability assurance system /CARAS/ for integrated circuits, correlating process and failure data 12 p1890 A71-26658

Particle impact noise detection of loose particles in electronic component cavities, discussing implementation, cost savings and reliability improvement 12 p1884 A71-26659

Total reliability requirement procedure for design, development and production of medium- and large-scale integrated circuits 12 p1884 A71-26660

Deferred state sampling plans using accept/reject decisions dependent on future lot disposition according to quality drift 12 p1909 A71-26661

Reliability experience acquired in collecting, processing and analyzing U.S. Army test and field data, stressing field data reduction work 12 p1909 A71-26662

Design analogies of aerospace and commercial systems, describing computerized simulation method for system design evaluation and reliability improvement 12 p1909 A71-26663

Equivalent circuit concepts in diagnostic metrology as converging logical-physical process, stressing electronic failure analysis 12 p1890 A71-26666

NASA reliability program provisions for aeronautical and space system contractors, reviewing evolution process 12 p1909 A71-26667

Reliability knowledge review, stressing learning curves for measuring and predicting reliability achievements and defect screens effectiveness measurement 12 p1909 A71-26668

Optimal reliability proposals for industry competitive posture improvement in difficult market environment, recommending military electronics reliability standards specification 12 p1909 A71-26669

Failure prevention, test discrepancy reporting and circuit analysis workshop techniques for program audits, integrating reliability managers, performers and customers 12 p1910 A71-26670

Pan American reliability program effect on airline maintenance, considering cost effectiveness, aircraft performance, data collection and analysis 12 p1910 A71-26671

Reliability assurance in product manufacturing, discussing specific tasks during design, preproduction and production phases 12 p1910 A71-26672

Risk assessment associated with reliability demonstration testing, considering fixed price procurement and cost effectiveness 12 p1910 A71-26677

Economic formulation in reliability engineering, expressing cost of failure and reliability improvement in comparable terms 12 p1987 A71-26678

Shillelagh missile reliability program development/deployment using part qualification levels and fly-before-buy procurement 12 p1885 A71-26684

Service life testing and reliability estimation, using ordinary and empirical Bayes approach in failure model with gamma probability distribution 12 p1910 A71-26685

Failure prediction from interval data for reliability and inventory problems, considering irregular inspection and manufacture for aging in calendar time 12 p1911 A71-26687

Statistical decision theory in reliability and project management, discussing Venus probe loss 12 p1911 A71-26690

Continuous loading method for accelerated reliability testing of circuit components 13 p2072 A71-27830

Small turbine type flowmeters for liquid hydrogen, discussing design, inspection, calibration and reliability 14 p2239 A71-29926

High temperature capacitance strain gage development for aircraft testing, discussing instrument configuration and data reliability 14 p2248 A71-30682

Soviet book on liquid rocket engines covering combustion chambers, fuel supply systems, static and dynamic characteristics, control and reliability 15 p2466 A71-31296

Book on durability and reliability in engineering design covering materials strength and service longevity concepts, failure modes, fabrication philosophies, etc 15 p2414 A71-31836

Performance category III all-weather capability ILS landing equipment standards, discussing high directivity antennas and transmission and control system redundancy techniques for reliability 15 p2445 A71-31909

Series and parallel complex systems reliability maximization by allocating optimum numbers of stocked spare parts 15 p2415 A71-32343

Reliability and maintainability - ASME/SAE/ALAA Conference, Anaheim, California, June 1971 16 p2582 A71-33284

Reliability implications of Boeing 747 program, considering problem detection and identification, parts fabrication and installation, airline operating variables, etc 16 p2522 A71-33285

Machine design strength criteria in development of formulas for lower bound estimates of mechanical components structural reliability 16 p2582 A71-33293

Unmanned spacecraft first day failures, discussing launch environment, duration tests in simulated space and performance improvement 16 p2645 A71-33296

Statistical procedure for maintainability allocation during early system design to meet specified overall goal 16 p2583 A71-33299

Cost distribution theory for various costs of failure, using probability distribution functions for modeling maintainability and reliability 16 p2583 A71-33305

System safety evaluation model with state-space network for representation of mission phase and hazard degradation 16 p2602 A71-33308

German book on problems, mathematical foundations and investigation methods of technical reliability covering Boole model, random variables, distribution functions, failure rates, etc 16 p2583 A71-33524

Large software systems development management, discussing pending disaster early identification, relationship to hardware, integrating contractor and programming tools 17 p2710 A71-34619

NASA space station electrical power systems discussing configurations, growth capacity, volume reliability and long term effects [ALAA PAPER 71-825] 17 p2677 A71-34720

Redundant modules introduction in microelectronic systems for increased reliability 17 p2716 A71-34954

Control reliability in automated system of discrete production management 17 p2721 A71-34961

Strapdown or gimbaled inertial measurement units for space shuttle program, considering reliability, redundancy and cost of ownership 17 p2772 A71-35059

Electronic two axis digitizer, discussing electromagnetic measuring concept, modular design, reliability and economics 17 p2711 A71-35291

Spacecraft system design with long life reliability for outer planet exploration missions [ALAA PAPER 71-831] 17 p2814 A71-35428

Reliability engineering, reviewing MTBF, redundancy, complexity effects on failure rate, reliability prediction, repair and replacement cost and test techniques 18 p2928 A71-36806

Nuclear power station design for optimal reliability levels, noting maintainability requirements 18 p2928 A71-36807

High reliability computers via multiprocessing for long duration space missions, discarding quad redundant and majority voter approaches [AAS PAPER 71-158] 19 p3152 A71-37927

Hardware reliability improvement techniques for long life unmanned space missions [AAS PAPER 71-156] 19 p3153 A71-37957

Simulation model for optimal cost time-independent component replacement of complex system subject to probabilistic deterioration 19 p3069 A71-38288

Reliability engineering techniques for design control of electromagnetic compatibility, employing statistical theory 19 p3030 A71-38437

Reliability physics - IEEE Conference, Las Vegas, April 1970 19 p3033 A71-38504

Reliable plastic encapsulated semiconductor devices design, production and evaluation, noting application to IC 19 p3033 A71-38509

Failure analysis of vacuum deposited Al film interconnections at contact windows, considering grain size effect and reliability improvement techniques 19 p3119 A71-38512

Discrete semiconductor devices test program assessing environmental screening for improved component reliability 19 p3034 A71-38517

Collector/base current ratio degradation in bipolar transistors, describing mechanisms characteristics and protective techniques 19 p3034 A71-38522

Emitter avalanche stress on gated silicon planar n-p-n transistors, investigating degradation phenomena 19 p3034 A71-38523

Probabilistic behavior of repairable two-state systems, assuming reliability measurability by operating time 21 p3407 A71-40362

Optimal design for system reliability and maintainability, using dynamic programming model 21 p3407 A71-40363

Conditional failure density evaluation from hazard rate, considering failure time distribution function, reliability function and conditional failure distribution 21 p3408 A71-40370

Fortran source listing for computer program approximating system reliability 21 p3351 A71-40371

Vibration tests of instruments, machines and apparatus, allowing for functional reliability 22 p3536 A71-41441

Reliability requirements in LSI technology, considering multilevel metallization and test vehicles for process control 22 p3519 A71-41633

Computerized reliability optimization system program for electronic equipment design and management methods to achieve high reliability and low cost 22 p3517 A71-42105

Computerized system redundancy optimization formulation as zero-one type variables integer programming problem, obtaining algorithmic solution for maximum reliability 22 p3517 A71-42106

Validity study of mathematical models representing failure rate variations of electronic components, considering thermal and electrical stresses 22 p3517 A71-42109

System quality analysis by reliability measures /mean time between failures/, using distribution free evaluation models 22 p3566 A71-42114

Static joint wear role in overall machine reliability and service life under working loads from mathematical prediction 22 p3619 A71-42852

In-flight monitoring of aircraft turbine engine reliability 23 p3718 A71-43233

Control system effectiveness improvement, using redundancy and self adaptive techniques 23 p3655 A71-43291

Nuclear test program management, considering reliability problems, delays and cost 23 p3786 A71-43462

NASA NHB reliability engineering provisions for aeronautical and space system contractors, considering criteria for program management, system engineering, manufacturing and facilities 23 p3682 A71-43497

RELIEF MAPS

Three dimensional lunar surface relief model from orbital photographs at different heights 08 p1360 A71-21023

Computer generated profile maps to fill military need for rapidly produced, easily interpreted terrain map 08 p1280 A71-21242

Martian surface relief details observation from earth distance, showing telescope resolution requirements above dense atmospheric layers 16 p2639 A71-33698

Passive mapping of terrain with sidelooking radiometry by storing received signals from various elements over extended flight path 17 p2746 A71-35763

Three dimensional lunar surface relief model from orbital photographs at different heights 20 p3294 A71-39603

RELUCTANCE

Hall effect and reluctance of TiN and ZrN specimens obtained by hot compression 15 p2427 A71-31515

Soviet book on synchronous reluctance motors covering operation principles, design features and starting characteristics 15 p2354 A71-32200

Four phase reluctance motor design for electromagnetic torque variation, examining function of commutation frequency and phase time constants 17 p2677 A71-35710

RELUCTIVITY

U RELUCTANCE

REMAGNETIZATION

U MAGNETIZATION

REMANENCE

Ancient geomagnetic intensity in Japan by comparing natural remanent magnetization with known thermoremanent magnetization induction, using stepwise heating method on antique pottery 04 p0582 A71-15127

Lunar magnetic field demagnetization effect hypothesis for explaining Apollo 11 lunar rock samples remanent magnetization 07 p1200 A71-20055

Carbonaceous chondrites natural remanent magnetization, revealing grey spinel oxide, Ni-Fe and iron sulfide as principal opaque minerals 10 p1674 A71-24429

Apollo 11 lunar rock and microbreccia examination for natural remanent magnetization, emphasizing viscous magnetization effect in terrestrial magnetic field 14 p2303 A71-29534

Ancient lunar magnetic field detection and origin from remanent magnetism in Apollo 11 breccia and basaltic rock samples 14 p2306 A71-29725

Lattice defect mechanism for high coercive force remanence production in meteorites and lunar samples by cosmic ray exposure 14 p2308 A71-29913

Apollo 11 and 12 crystalline rocks NRM natural remanent magnetization, discussing magnetizing fields origin 23 p3763 A71-43794

Lunar rocks 12002 and 12022 remanent magnetic moment as evidence for ancient lunar magnetic field 23 p3763 A71-43795

REMELTING

U MELTING

REMOTE CONSOLES

NASA Space Documentation Service on-line information retrieval system using direct access remote consoles 01 p0183 A71-10397

Digital computer operated from remote terminal for signal analysis including Fourier transform, complex multiplication and conjugation 05 p0727 A71-17144

Mathematically oriented digital computer system implemented on IBM 360 with graphic remote consoles for engineering problems 17 p2710 A71-34622

Interactive graphical computer system with remote on-line consoles for engineering problem modeling and analysis, giving illustrative examples 22 p3516 A71-41868

REMOTE CONTROL

NT RADIO CONTROL

Remote modules for spacecraft analog/digital telemetry distributing multiplexer input gates 01 p0036 A71-10988

Remotely controlled room temperature microwave parametric amplifier design for shipboard satellite telemetry terminal 02 p0234 A71-12813

Heat sterilizable remotely activated silver zinc battery for energy source of planetary lander capsule 03 p0352 A71-13043

Astronomical telescope automation and remote control, discussing advantages and problems 04 p0597 A71-15255

Single module unmanned Mars roving vehicle with flexible metal toroidal hoop-spoked wheels, discussing remote controlled scale model design for simulation on earth 04 p0566 A71-15333

Collisional drift instability remote feedback suppression in Q machine Cs plasma by microwave modulation at upper hybrid frequency 06 p0932 A71-17464

Unmanned lunar roving vehicle remote guidance, discussing onboard vs on-earth steering and velocity control, imaging system, obstacle detection and avoidance 08 p1331 A71-21325

Book on human factors application in teleoperator design and operation covering aerospace environments, transportation, remote control, sensors and actuator subsystems 09 p1399 A71-22613

Remote controlled automatically tuned l-kw short wave transmitter with zero power tuning mode of power stage and drive unit frequency generation 12 p1887 A71-26989

Direct digital control and data acquisition system for propulsion research testing, transmitting data over differential signal pairs to remote test cell 14 p2208 A71-30316

Nationwide man machine remote employment/personal services system including synchronous commu-

nication satellite, information and control network and remote terminals 14 p2199 A71-30914

Lunar roving vehicle telecommunication system requirements concerning vehicle functions, science experiments, crew operations and safety 14 p2200 A71-30915

Noise stability and false response probabilities of receivers in circular remote control systems under harmonic interference for signal transmitted over power distribution grids 15 p2353 A71-32081

Remote control and surveillance equipment for communication satellite ground station, discussing console and engineering service circuit designs 17 p2709 A71-35518

Remote power controller as static circuit protection device for aircraft and spacecraft automatically controlled electrical wiring system, discussing performance improvement 17 p2678 A71-35782

Remotely piloted vehicles development and limitations, considering air superiority, weapons delivery, sensors and survivability 18 p2849 A71-35899

REMOTE HANDLING

Frequency phase multistable elements, discussing automatic control, telemechanics and digital measurement applications 11 p1739 A71-26465

REMOTE SENSORS

Remote sea state information acquisition system using video attachment to radar for sea return spectrum recording and analysis 01 p0031 A71-10600

Atmospheric temperature profile in cloud presence, discussing remote sounding techniques with maximum probability method 01 p0120 A71-10854

Bibliography of bibliographies, manuals and books covering photointerpretation and remote sensing 01 p0084 A71-11379

Remote sensing systems for vegetation analysis, discussing machine-aided photointerpretation methods for data analysis 01 p0084 A71-11590

Atmospheric temperature remote sounding from satellites using radiometer with selective chopper for carbon dioxide emission 03 p0422 A71-13355

Six channel selective chopper radiometer design and construction for carbon dioxide emission monitoring for remote atmospheric temperature sounding by Nimbus 4 03 p0423 A71-13356

Atmospheric temperature remote sounding via balloon-borne selective chopper radiometer 03 p0423 A71-13357

Remote determination of temperature by operating and etalon thermistors resistances measurement with DC bridge 04 p0591 A71-14855

Microwave radiometric techniques for continuous all-weather remote sensing of sea conditions from satellites, discussing foam and surface ripple effects [AIAA PAPER 70-318] 05 p0743 A71-17101

Multichannel EEG radio telemetry for remote recording of biological activity from subjects in motion and within human body 05 p0715 A71-17110

Nimbus meteorological satellite program, discussing global cloud cover mapping and automatic picture taking, radioisotopic thermoelectric generator, sounder instrumentation and remote sensors 05 p0818 A71-17133

Satellites interrogation, recording and location system for data acquisition from deployed remote instrumented platforms 05 p0743 A71-17134

Drift type plasma instabilities, discussing feedback stabilization and remote sensing 06 p0932 A71-17465

Atmospheric path effects on spectral radiance intensity in remote airborne multispectral sensors 06 p0898 A71-17559

Airborne remote sensing application to agriculture and forestry for crop forecasting, soil mapping, insect infestation detection and range surveys 06 p0896 A71-18406

Agronomic research by remote sensing, discussing spatial, spectral and temporal measurements from electromagnetic multispectral response 06 p0896 A71-18407

Agricultural information and advisory service, utilizing remote sensing, computer sciences, research programs, educational involvement, satellites and aircraft 06 p1010 A71-18408

Worldwide remote sensing with satellites, high flying aircraft and computer data processing, discussing application in less developed countries 06 p0896 A71-18409

REMS

Earth resources coverage capabilities of manned orbital space station, comparing to remote measurement requirements
[AIAA PAPER 71-75] 06 p0980 A71-18532

Statistical methods for inventory boundary determination and data compression in automatic processing of multispectral scanner remote sensor earth observations from aircraft and spacecraft
[AIAA PAPER 71-234] 07 p1068 A71-19711

Earth resources survey remote sensor system with human for spatial and machine for spectral data processing
08 p1257 A71-20691

Meteorological satellites remote sensing advanced instruments and techniques, discussing retrograde polar and synchronous satellite orbits
08 p1366 A71-21744

Extensometer for evaluating remote reading strain gage performance at high and rapidly changing temperatures
09 p1445 A71-22720

Forested area landscape characteristics from remote sensed imagery, establishing base line information for vegetation mapping
09 p1438 A71-23210

Airborne multispectral remote sensing of forests, describing previsual detection of damage from insect infestations, disease organisms and oxidant air pollution
09 p1439 A71-23211

World crop areas, yield, production and land use data, using remote sensing devices
09 p1439 A71-23213

Urban housing environment data acquisition from remote sensor imagery, stressing rapid surveys and data timeless attribute
09 p1439 A71-23214

Geographic urban information and change detection systems with remote sensing inputs, discussing data storage and retrieval
09 p1439 A71-23214

Side-looking radar, thermal IR scanner and passive microwave radiometers for remote sensors for geologic mapping
09 p1452 A71-23215

Cartographic characteristics and applications of airborne radar sensors, stressing synthetic aperture radar and electronic techniques and equipment
09 p1452 A71-23219

Mean wind velocity and turbulence remote measurement with laser anemometry, using intensity modulation technique
10 p1623 A71-25091

Aerial and orbital remote sensing of water quality, considering waste materials effect on coastal marine environment
11 p1760 A71-26504

Mineral and water resources remote sensing, discussing sensor systems and data interpretation techniques with special reference to Colorado Bonanza project
11 p1760 A71-26531

Ground truth role in remote sensing surveys from space, considering field measurement techniques in calibrating sensor imagery and unknown terrestrial environment
11 p1760 A71-26532

Airborne remote sensing for oceanographic data acquisition in UV, visible, IR and microwave spectrum using reflected and emitted radiation instruments
12 p1902 A71-27260

Video tape recorder (VTR) for onboard storage of wideband analog and high rate digital sensor outputs of ERTS
14 p2249 A71-30901

Orbital Earth Resources Experiment Package sensor components, functions and crew tasks for operation
15 p2500 A71-31459

Earth Resources Remote Sensing Systems effectiveness, discussing sensor and satellite development, spectral and spatial recognition, data management and ecological and resource relationship
16 p2645 A71-33582

Canadian program of remote sensing for gathering information on earth resources and environment
16 p2566 A71-33749

Earth remote sensing in Brazil, discussing program organization and data acquisition related to NASA environmental resources technology satellites
16 p2570 A71-33826

Satellite remote sensing for crops and timber identification/detection, surface moisture measurements, soil mapping, marine hazard evaluation, etc
17 p2730 A71-34245

Electronic multimage processor for enhancement and interpretation of ERTS multiband remote sensor imagery data
17 p2737 A71-34273

Bibliography and review of solar system bodies surfaces, considering remote sensing at UV, optical, IR, microwave and radio wavelengths, in situ lunar measurement and surface exploration
17 p2798 A71-34458

UV Raman remote gas sensors incorporating laser scattered radiation with high resolution monochromator
17 p2753 A71-35292

Remote sensing imaging techniques for oil pollution survey, using airborne UV, IR, color and filtered panchromatic photography
17 p2735 A71-35386

ERTS remote sensor data processing, describing space and ground equipment and techniques
[AIAA PAPER 71-839] 17 p2814 A71-35429

Remote sounding of earth atmosphere temperature and composition
17 p2736 A71-35565

Remote sensing for geologic problems, using side-looking radar for fracture and fault detection and IR images for limestone, dolomite and granite discrimination
18 p2911 A71-35890

Remote subsurface oceanographic imagery from orbital altitudes in blue multispectral region, showing optimum filter passband
18 p2917 A71-36064

Raw remote sensor data acquisition relationship to economic activity and interpretation for earth resource/environmental information
18 p2912 A71-36067

Remote sensors for hydrogeologic prospecting in arid terrains, recommending vertical and horizontal polarized microwave radiometers
18 p2913 A71-36362

Thermal mapping performance of passive airborne IR scanners for remote environmental sensing, estimating SNR and noise equivalent irradiance
18 p2921 A71-36364

Lunar exploration system based on modified earth-orbit space station in polar lunar orbit as remote sensor platform and lander deployment base
18 p2972 A71-36443

Earth-spacecraft radio communication requirements for future unmanned planetary missions, emphasizing imaging experiments and sensors
18 p2877 A71-36518

Aircraft and satellite remote sensing techniques in geology, soil science, geography and hydrology
18 p2913 A71-36539

Aerial and satellite environmental water quality control surveillance, discussing remote sensing techniques and objectives
19 p3059 A71-38402

Environmental water pollution observation by remote sensing, discussing aerial photography
19 p3059 A71-38403

Digital pattern classification of oceanographic remote sensing multispectral airborne scanner data, considering sea surface color variations
19 p3060 A71-38405

Latent forest fire detection, describing airborne IR surveillance system
19 p3066 A71-38410

Multiple channel fringe counting interferometer for remote monitoring of large diameter microwave antenna under test in simulated solar thermal and vacuum environment
20 p3235 A71-39186

Remote image-forming sensors on satellites and aircraft, considering resolving power, contrast rendition, dynamic range, SNR, sensitivity, and reliability as performance measures
20 p3240 A71-39608

Atmospheric transmittance measurement errors in determining temperature, water vapor and ozone distributions from satellite remote sensing
20 p3258 A71-39671

Earth surface characteristics measurements with remote sensors, proposing overland albedo measurements for snows as to ground type /clouds, vegetation, sand and snow/
20 p3260 A71-39684

Remote sensing aerospace system for agriculture, considering soil mapping, forest fire reconnaissance, productivity evaluation and environmental and ecological conditions assessment
21 p3373 A71-40263

Earth resources survey satellites, discussing natural sources /radiation, matter-energy interactions and perturbing media/, remote sensors, space applications and reconnaissance
21 p3455 A71-40910

Laser remote sensing technique for tropospheric refractivity fluctuation profile measurement with tethered balloon-borne retroreflector tracking by ground based tracker
21 p3374 A71-40977

Aircraft heat viewer for underlying surfaces radiation properties, suggesting qualitative survey type thermal aerial photo combination with simultaneous radiometric measurements
21 p3383 A71-41300

Hot-wire anemometer remote operation, discussing coaxial cable length, terminal connection and bridge current
22 p3541 A71-41794

Global environmental monitoring and remote sensing from satellites, considering thermal, air and water pollution
22 p3534 A71-41961

ERTS remote sensing techniques, discussing objectives for southeastern U.S. in terms of agriculture, forestry, strip mine land reclamation and thermal pollution
22 p3534 A71-41967

Satellite observations for earth resources management, discussing operational ground-based remote sensor system and information extraction techniques
22 p3534 A71-41973

Remote sensing of chlorophyll and temperature in marine and fresh waters by spectroradiometer and differential and IR filter radiometers onboard airplane
22 p3534 A71-41986

Planning organization for global remote sensing information system operated and financed through international cooperation
22 p3623 A71-41987

Environmental quality indices from spaceborne or airborne remote sensing
22 p3534 A71-41995

Space technology applications to earth environment and resources management, discussing satellite-borne remote sensor systems and data processing techniques [SD-71-734] 22 p3535 A71-42047

Primary sensor transfer function selection to minimize rms error in information transmission over telemetry channel for subsequent digital processing
23 p3648 A71-43294

Unified procedure for detection of life on Mars by Viking program missions, using mass spectrometer for remote biologically oriented experiments
23 p3736 A71-43541

Earth resources technology satellites image processing system including electron beam recorder, image corrector, electro-optical systems and digital processors as design features
[AIAA PAPER 71-977] 24 p3825 A71-44575

ERTS remote sensing for ground system data management, emphasizing processing, correction, reproduction, storage, retrieval and distribution [AIAA PAPER 71-976] 24 p3817 A71-45294

Spacecraft orientation angle measurement by inertial sensors, analyzing equipment kinematic efficiency and limitations
24 p3829 A71-45318

REMS

U RAPID EYE MOVEMENT STATE

RENAL FUNCTION

Renin level in renal venous and peripheral blood in patients with renovascular hypertension
01 p0010 A71-10391

Flying personnel urinary lithiasis relationship with aeronautical activity, discussing etiopathological factors and augmented fluid intake
01 p0028 A71-11600

Renal function osmoregulation in Soyuz crew members
06 p0854 A71-18370

Human renal diluting capacity, examining prolonged absolute bed rest effects
09 p1401 A71-23365

Flight concomitant pathogenetic effects on urinary tract conditions, noting kidney descent, inflammatory episodes and calculus
10 p1566 A71-24977

Renal oxygenation in male Peruvian natives living permanently at high altitudes, determining reduced tubular function cause
12 p1873 A71-27127

Postflight metabolism and renal function of Soyuz 6, 7 and 8 crewmembers, associating weight loss during flight with water and salt discharges
13 p2006 A71-28409

Renal hemodynamic factors in whole kidney glomerulotubular balance in anesthetized dogs by manipulating filtration rate through constriction of aorta, thoracic vena cava, etc
16 p2529 A71-33194

Acute renal failure due to heat stress and physical exercise, noting discrepancy between physiological alterations and histopathological abnormalities
18 p2855 A71-36218

Circadian rhythms of human renal excretions in polar, temperate and equatorial regions
20 p3190 A71-39477

Water immersion effect on plasma renin activity, urinary aldosterone excretion and renal sodium and potassium handling in normal man
22 p3485 A71-41720

Antidiuretic action of chlorpropamide in mammalian kidney, considering intrarenal infusions effect on urinary concentration, free water clearance, glomerular filtration and sodium excretion
23 p3486 A71-41939

Hibernation effects on hedgehog electrolyte distributions and renal function, determining Na, K, Mg and Cl concentrations in muscles, liver, kidney, plasma red blood cells and bladder urine
22 p3488 A71-42416

RENDEZVOUS

NT EARTH ORBITAL RENDEZVOUS

SUBJECT INDEX

NT LUNAR ORBITAL RENDEZVOUS NT ORBITAL RENDEZVOUS NT SPACE RENDEZVOUS

Two controlled motions rendezvous problems treated as game between partners using quality criterion as payoff, deriving optimal strategies

03 p0392 A71-14405

RENDEZVOUS GUIDANCE

Minkey rendezvous computer program in Apollo 15 CSM aiding guidance, navigation and control system functions

17 p2772 A71-35055

Guidance and navigation requirements for rendezvous missions to two short period comets

[AAS PAPER 71-116] 19 p3101 A71-37913

RENDEZVOUS TRAJECTORIES

Soviet monograph on differential games of encounter of motions covering optimal control, rendezvous, pursuit, evasion, extremal guidance, etc.

06 p0926 A71-17438

Multiple impulsive spacecraft trajectory optimization technique application to comet rendezvous problem, using computer program

[ALAA PAPER 71-93] 06 p0977 A71-18548

Time series approximation of acceleration functions for analytical solution of low thrust interplanetary transfers, treating flyby and rendezvous mission modes

[ALAA PAPER 71-116] 06 p0977 A71-18566

Fuel optimal analytic multiburn transfer trajectories and shuttle rendezvous, assuming gravity vector linear dependence on position vector for burn arcs

[AAS PAPER 71-306] 23 p3724 A71-42982

REPAIRING

U MAINTENANCE

REPEATERS

Deception repeaters for erroneous information transmission to radar, considering echo signal level, burnthrough, target size, sensitivity, gain and bandwidth

04 p0555 A71-15359

Low distortion gain-controlled 140 MHz IF main amplifiers for 2700-channel microwave repeaters, discussing design and performance

05 p0730 A71-17069

Nonuniform feed effects on height of electrosark surface machining microasperities, investigating linear elliptical interpolator pulse sequence

08 p1296 A71-20851

Intelsat 4 satellite Spade communication system, using common reserve circuits and repeaters

15 p2373 A71-32640

Wideband fiber waveguide communication systems for optical frequencies, considering information carrying capacity limitation by components available for repeaters and terminal equipment

18 p2883 A71-36995

Linear digital interpolator in program controlled metal cutting tool circuit, determining transfer function with z transforms

22 p3525 A71-42876

REPETITION

High repetition rate TEA carbon dioxide laser up to 1000 pps with average power output up to 65 W

23 p3688 A71-44298

REPLACING

Simulation model for optimal cost time-independent component replacement of complex system subject to probabilistic deterioration

19 p3069 A71-38288

Replacement problem in stochastic point processes, obtaining cost over given time period and moments and correlations of replacement number

21 p3407 A71-40367

REPLICAS

Replica technique facilitating investigation of quenched solid propellant sandwich sample characteristics

08 p1271 A71-20868

REPORT GENERATORS

Computerized system evaluation and feedback data for assurance at hardware level, including reject and failure report documentation

12 p1890 A71-26673

REPRODUCTION

Bacteriophage Q beta ribonucleic acid variants, considering fluorescence determination of replication inhibition by ethidium bromide

04 p0548 A71-15267

REPRODUCTION (COPYING)

NT XEROGRAPHY

Self reproduction of diffraction and reconstructed images of finite aperture in coherent radiation field by periodic transverse and longitudinal alternation

01 p0092 A71-10032

Penta prism angle reduplication by interferometric measurements

14 p2241 A71-30139

REPRODUCTIVE SYSTEMS

NT UTERUS

Laser beam image reproducer systems, emphasizing pattern generators, automatic calibration subsystems, raster line merging apparatus, scanners and continuous film transport mechanism

22 p3559 A71-42515

REPTILES

NT SNAKES

NT TURTLES

REPULSION

U FORCE

RESCUE OPERATIONS

Space rescue operations, discussing notification, emergency location, terminal guidance systems and techniques application, international codes, etc.

01 p0164 A71-11438

Helicopter and V/STOL aircraft external noise and downwash measurements during simulated jungle rescue mission

04 p0531 A71-15409

Survival and rescue medical aspects, discussing water and food intake, dehydration, hygiene, sanitation, rest, injuries, heat and cold exposure, illnesses, rescue operations, etc.

08 p1245 A71-20718

Expandable structures for midair pilot rescue device with hot air filled BALLUTE, discussing BALLUTE material development

[ALAA PAPER 71-402] 11 p1707 A71-25278

German book on rescue systems for space emergencies covering mission failure, biological problems, escape vehicles, orbital operations safety and spacecraft transfer

12 p1972 A71-27185

Aircraft accident rescue system with helicopters, discussing cooperation between helicopter service and ground personnel

13 p2020 A71-28721

Night rescue terminal navigation, considering design, development and tests of Limited Night Recovery System for HH-53 helicopter

[AHS PREPRINT 534] 14 p2273 A71-31095

SK-5 air cushion vehicles evaluation including search/rescue, aids to navigation, law enforcement, safety logistics and oil pollution

[AHS PREPRINT 572] 14 p2180 A71-31113

Medical and technical aspects of air rescue and survival of astronauts in mountainous remote areas, noting dogs use for disaster victims location

22 p3482 A71-41982

Recovery, launch and landing operations of earth orbital shuttle vehicles, discussing space rescue capabilities

22 p3609 A71-41989

Docking with passive orbiting spinning or tumbling objects for space debris elimination and space rescue operations, describing remotely controlled despinning and retrieval methods

22 p3610 A71-42005

Space flight safety, discussing escape, rescue and survival design approaches for astronauts

22 p3611 A71-42037

Dynamic analysis of ATS 5 heat pipe fluid energy dissipation, confirming estimated stability of planned rescue approach configuration

22 p3611 A71-42038

IR radiation sensors application to fire protection and rescue operations

22 p3545 A71-42157

Extended launch windows for ground based rescue missions, using bi-elliptical rendezvous technique

[AAS PAPER 71-304] 23 p3638 A71-42980

Airport crash fire fighting equipment requirements and rescue operations

23 p3629 A71-43389

Helicopter, tilt wing and jet lift hovering aircraft outflow measurements to determine suitability as rescue vehicles

[ALAA PAPER 71-992] 24 p3791 A71-44586

RESEARCH

NT CRITICAL PATH METHOD

NT DYNAMIC PROGRAMMING

NT GAME THEORY

NT HIGH TEMPERATURE RESEARCH

NT LINEAR PROGRAMMING

NT MARKET RESEARCH

NT MINIMAX TECHNIQUE

NT NONLINEAR PROGRAMMING

NT NUCLEAR RESEARCH

NT OPERATIONS RESEARCH

NT SADDLE POINTS [GAME THEORY]

Turbulence research retrospective and new developments, reviewing contributions by Reynolds, Rayleigh, Prandtl, Taylor and Tollmien

11 p1751 A71-25578

Physics and astrophysics problem areas justifying intensified research

11 p1799 A71-25918

RESEARCH AIRCRAFT

NT B-70 AIRCRAFT

NT X-15 AIRCRAFT

NT X-24 AIRCRAFT

Q-Star experimental aircraft design and acoustical characteristics to study Quiet Aircraft Technology

08 p1231 A71-21441

RESEARCH AND DEVELOPMENT

Materials R and D economic considerations, emphasizing processing and assembly costs reduction and user benefits

01 p0183 A71-10279

RESEARCH AND DEVELOPMENT

Global Atmospheric Research Program /GARP/, discussing atmospheric motions, data acquisition, satellite networks, etc.

01 p0122 A71-11361

NACA/NASA rotating wing aircraft research history during 1955-1970 period, discussing wind tunnel research

01 p0005 A71-11377

Scientific research methods and tendencies, discussing theoretical and applied aspects, deductive and empirical procedures, technology interaction, practice criteria, etc.

02 p0335 A71-11853

Rational structure selection for scientific research organizations, using systems analysis

02 p0335 A71-11855

New information prediction in scientific research by data flow analysis

02 p0335 A71-11857

Satellite design developments by U.S. Navy

02 p0336 A71-11980

Technology assessment effects on science and engineering progress

02 p0336 A71-12121

Ossa R and D program noting budget allocations, satellite programs and international projects

04 p0690 A71-14934

Navy X ray research and utilization, discussing generation and interaction, radiography, radiation damage, dosimetry, spectroscopy, fluorescence analysis, etc.

04 p0625 A71-15095

Solar cell R and D in France, emphasizing thin film improvement

05 p0704 A71-16101

USAF weapons and support systems, discussing military R and D funding and resulting constraints

05 p0839 A71-16285

R and D money optimal reallocation due to total research budget decrement, based on computer program

05 p0840 A71-16743

R and D management decision making process structural model, discussing technological forecasting based on organized technical information, quantitized judgments, optimum resource allocation and hybrid technique

05 p0840 A71-16744

Earth resources satellite systems R and D planning, using case study approach in economic benefit analysis for parametric requirements determination

05 p0840 A71-17050

Combustion research for air breathing engines, discussing combustion stability in thrust augmentors, aircraft fire detection, MHD and external burning

06 p0946 A71-18476

Multinational corporate R and D laboratories, discussing problems with regard to language barriers, cultural differences and coordination

07 p1225 A71-19449

Information and technology transfer in multinational corporate R and D, discussing mechanisms of communication, use of common technical language and impediments due to attitude differences

07 p1225 A71-19450

Soviet book on research and design work optimization and automation based on mathematical methods and computer techniques

08 p1299 A71-21650

Laser technology R and D with respect to high average and/or peak power and chemical to coherent light energy conversion

09 p1462 A71-22584

High temperature steel and alloys metallurgical processes for stationary and aircraft gas turbine engine components, discussing production-quality control-research interrelationship

09 p1456 A71-23301

Research and development project funds allocation, developing mathematical dynamic modeling method for cost management

10 p1699 A71-24539

Motivations of scientists, engineers and technicians, considering changing nature of R and D projects

13 p2167 A71-28800

Organizational climate inventories in R and D establishments, comparing obstacles and incentives to creativity in government and industrial laboratories

14 p2339 A71-29852

Organization and funding criterion of unsuccessful R and D projects, considering project abandonment or failure

14 p2340 A71-29854

Mathematical programming models for resource allocation and project selection decision in R and D

14 p2340 A71-29855

Space research impact on general economy and ecology, noting royalty-free licensing to private industry by NASA

14 p2341 A71-30257

Weapons R and D flexible economical response to defense needs by emphasis on component and subsystem experimentation

14 p2341 A71-31130

- Commercial spinoff from government sponsored R and D, considering productivity and industry benefits 14 p2342 A71-31133
- Al alloys rods and sections extrusion process R and D, using lubricant without press residue 15 p2415 A71-32335
- West German parachute research, discussing stretching/filling shock, fabric material properties and static stability 15 p2350 A71-32373
- French aerospace research for aircraft, missiles, spacecraft and related power plant developments, discussing optimization methods, materials, reentry phenomena, etc 15 p2500 A71-32691
- Canadian R and D on fixed wing civil STOL aircraft, discussing augmentor wing concept using jet powered lift augmentor system 16 p2523 A71-33470
- Ion propulsion R and D at ONERA, discussing ionizer test control procedures, attitude control simulation and neutral fraction measurements [DGLR-71-027] 17 p2793 A71-35536
- Electrical propulsion systems research at Braunschweig installation covering plasma generation, ion sources, plasma accelerators, etc [DGLR-71-024] 17 p2794 A71-35544
- Parallel strategies effectiveness in R and D projects, discussing learning rate as critical parameter in project management decision making process 19 p3173 A71-37629
- Optimal investment model for R and D project evaluation and selection, using discrete cash flow and linear programming techniques 19 p3173 A71-37630
- Broadband point-to-point communication satellite systems for 1970s, discussing R and D effort, economics and international and domestic applications 20 p3197 A71-39606
- Low cost high performance rate gas bearing gyroscope development, emphasizing large scale production and overall instrument design optimization 22 p3551 A71-41664
- Economic analysis effect on R and D projects choice, assessing Space Shuttle system 22 p3624 A71-42526
- Industrial ownership in R and D markets, considering customer and supplier objectives compatibility in patent rights clauses 23 p3786 A71-43465
- Soviet aircraft industry R and D organizations and management 23 p3786 A71-44189
- Strategies and tactics for industrial R and D problems selection and solution for products innovation, noting element of chance 24 p3891 A71-44364
- Civil aviation research and development policy review covering aircraft noise, congestion, ATC, runway capacity and airport development problems [AIAA PAPER 71-1024] 24 p3892 A71-44602
- French R and D Directorate exhibits at 29th Le Bourget air show, discussing laser applications, telecommunication, navigation-guidance, energy conversion, test facilities and environmental studies 24 p3816 A71-44764
- Federal German Republic heat transfer research programs at universities, institutes, chemical industries and in nuclear process engineering 24 p3890 A71-45149
- RESEARCH FACILITIES**
- German book on Goettingen Aerodynamic Research Institute /1945-1969/ 01 p0068 A71-11406
- Industrial bioscience research laboratory information flow, product ideas, procedural innovations and scientific/technical literature reading 08 p1378 A71-20775
- Combustion research laboratory at Purdue University consisting of buildings, housing test cells, data acquisition system, propellant storage and instrument service area 09 p1427 A71-22727
- Noise research facility for fan and multistage compressor sound radiation, discussing anechoic chamber, power drive, test control, recording and real time analysis system 16 p2553 A71-33418
- European space research center, discussing satellite scientific and engineering data transmission and processing 16 p2553 A71-33422
- U.S. space program report to COSPAR covering organization, facilities, international activities, astronomy, lunar and planetary research, particles, fields, atmospheric, earth and life sciences 16 p2665 A71-33855
- Canadian report to COSPAR on space program and facilities covering scientific satellites, sounding rockets, etc 16 p2667 A71-33868
- Naval Air Rework Facility, discussing primary mission, technical disciplines and operational performance feedback [AIAA PAPER 71-765] 16 p2523 A71-34003

- Man-telescope-robot teams for space exploration facilities construction and operation, discussing lunar programs [AIAA PAPER 71-823] 17 p2723 A71-34722
- French monograph on medium term planning process for large basic research laboratory based on information system of functional activities presentations 19 p3174 A71-38548

RESEARCH MANAGEMENT

- Multinational corporate R and D laboratories, discussing problems with regard to language barriers, cultural differences and coordination 07 p1225 A71-19449
- Information and technology transfer in multinational corporate R and D, discussing mechanisms of communication, use of common technical language and impediments due to attitude differences 07 p1225 A71-19450
- Parallel strategies effectiveness in R and D projects, discussing learning rate as critical parameter in project management decision making process 19 p3173 A71-37629

RESEARCH PROJECTS

- Space research benefits from applications technology satellites and materials utilization, reviewing satellite communication networks, meteorology geodesy, navigation, geology and agriculture 03 p0524 A71-14245
- OART research projects covering space shuttle, vehicle configuration, heat transfer, thermal protection, lifting bodies, electronics, power studies, etc 04 p0661 A71-14931
- NACA/NASA rotary wing aircraft research, considering rotor loads and configurations, ground resonance, blade flutter and flapping, motion equations and VTOL 04 p0529 A71-15171
- NASA bilateral and multilateral international cooperation agreements in space research, discussing political objectives, program history, regulations and procedures 06 p1010 A71-17646
- Beam foil spectroscopy using van de Graaff accelerator, considering applications to atomic physics research and teaching 08 p1272 A71-21667
- Byurakan Astrophysical Observatory instrumentation and research program 09 p1429 A71-23352
- Organization and funding criterion of unsuccessful R and D projects, considering project abandonment or failure 14 p2340 A71-29854
- NASA Lewis Research Center Hg electron bombardment ion thrusters research programs 14 p2288 A71-29931
- Soviet research program relative to climatology, physical nature, morphology and dynamics of mesospheric clouds, discussing observational and experimental methods 14 p2233 A71-29968
- ONR human engineering research program concerning information input, display and processing concepts, decision making and motor output and control 16 p2536 A71-33529
- Rumanian space research, reviewing participation in socialist nations programs in physics, meteorology, communications and biology 16 p2665 A71-33854
- UK space research programs, discussing ground based, satellite and rocket-borne experiments 16 p2666 A71-33859
- Japanese space research report to COSPAR, discussing meteorology, atmospheric electricity, ionosphere, magnetosphere, galactic radiation, life sciences and planetology 16 p2666 A71-33860
- Italian report to COSPAR on 1970 space research, discussing 1971-72 programs for cosmic radiation, space plasma, meteorology, communications and international cooperation 16 p2666 A71-33862
- Indian report to COSPAR on space activities, discussing organization, facilities, experiments, applications, international collaboration and future plans 16 p2666 A71-33863
- Brazilian space research planning effort and activities covering rocket and satellite meteorology, satellite tracking, balloon experiments and ground based geophysical observations 16 p2667 A71-33869
- Space research system telecommunications, considering telemetry, tracking and telecommand systems 17 p2696 A71-34229
- General purpose manned space laboratory concept for multidisciplinary long term shuttle supported research investigations [AIAA PAPER 71-814] 17 p2812 A71-34727
- Long range near-earth orbit research and applications based on NASA goals, including laboratory/observatory definition [AIAA PAPER 71-812] 17 p2802 A71-34729

- Payload cost and response time reductions for shuttleborne space experiments, examining NASA Ames airborne research program management technique [AIAA PAPER 71-808] 17 p2813 A71-34731
- Shell structure computer analysis capability assessment covering U.S. industrial concerns, government agencies and universities research activities 22 p3516 A71-41864
- Physics and astrophysics problem areas justifying intensified research, discussing superconductivity, relativity, neutron stars, gravitational waves, etc 22 p3576 A71-42620
- Organization problems of research laboratory for space astronomy experiments, delineating roles of chief scientist, project manager and technical services 23 p3785 A71-43456

RESEARCH VEHICLES

- Sandwich metal construction with welded Norsial corrugated core for light weight and strength, discussing fabrication and application to hypersonic research vehicles 04 p0603 A71-15207

RESERVOIRS

- Thermionic converter integrated Cs reservoir module power efficiency and service life, considering diode technology 02 p0196 A71-12270
- Liquid Cs graphite integral reservoir effect on thermionic converter performance 02 p0196 A71-12271

RESIDUAL GAS

- ESRO 1 satellites space simulation chamber tests for residual gas effects, measuring spacecraft outgassing rate 09 p1533 A71-23732
- Computer program for interpretation of residual gas analyzer mass spectra, considering vacuum environmental testing of spacecraft 11 p1730 A71-26505
- Local shielding chambers for welding circumferential and longitudinal seams in Ti alloys with minimum residual oxygen concentrations 14 p2253 A71-30489
- Graphite properties in high and ultrahigh vacuum, suggesting use as electrode material in vacuum gages and residual gas analyzers 21 p3405 A71-40221
- Ultrahigh vacuum by condensate pump, defining vacuum level by mass spectrometric determination of residual gas content 23 p3661 A71-43271
- Langmuir electron oscillation excitation by ion beam at velocity exceeding average electron thermal velocity in plasma formed by residual gas ionization 24 p3858 A71-45234

RESIDUAL STRESS

- High compressive residual stress and high hardness for long life fatigue strength in nonrotating bending of notched machine parts 01 p0167 A71-10171
- Notched steel bars fatigue strength improvement via compressive self stresses /residual stresses/ 01 p0167 A71-10172
- Boundary value problem of elasticity theory for reinforced plastics with internal stresses due to shrinkage 01 p0107 A71-10495
- Diffusion bonding cycles for Al-B composite materials fabrication, relating strength enhancement to residual stress relief 01 p0104 A71-11284
- Simple variable loading and unloading in theory of small elastoplastic deformation under nonuniform heating for residual stress-strain determination 02 p0323 A71-11739
- Turbine disks cyclic nonisothermal deformation with allowance for Bauschinger effect, determining stress-strain state and residual microstresses 02 p0323 A71-11747
- German monograph on arbitrarily distributed internal stresses effect on elastic stability of plates, considering variational problem solution as matrix eigenvalue problem 02 p0327 A71-12375
- Superficial residual stresses measurement in plastic region by Hertzian hardness method, considering indentation by ball and proportionality to load variations 02 p0328 A71-12535
- Logarithmic damping of flexural oscillations produced by residual fretting stresses in circular plates 03 p0503 A71-13415
- Orthotropic photoelastic analysis of residual stresses in filament-wound composite ring structures, comparing with boring-out and cut-through methods 03 p0508 A71-13773
- Metal and glass composites with similar residual stress states under axial loading, examining yielding and fracture behavior 03 p0443 A71-14186
- Photoelasticity application for stress-strain state determination around bores made by electron beam, using epoxy models for internal stress distribution 03 p0429 A71-14272

Welded joints triaxial residual stress measurement by scanner 03 p0433 A71-14587

Two-member composite cylinders, predicting residual stress and axial loading behavior by elastoplastic analysis for comparison with experiment 04 p0666 A71-14893

Residual and mean stresses effects on fatigue strength of specimens with longitudinal nonload-carrying fillet welds 04 p0613 A71-15763

Inhomogeneously reinforced composite structures strengthening by internal stress matching 05 p0771 A71-16365

Embedded electrical resistance strain gages for three dimensional stress measurement, describing modifications for internal stresses reduction 05 p0830 A71-17242

Construction materials characteristic properties significance for design and structural reliability, discussing weldable Al alloys fatigue strength, internal stresses, inhomogeneity and corrosion behavior 06 p0981 A71-17341

Drag free spacecraft performance in deep space, examining inner residual disturbance forces for motion control systems [ONERA-TP-887] 06 p0900 A71-18022

Residual stress measurement in Hastelloy N gas tungsten arc welds by Sachs boring-out method, permitting stress distribution determination over short distance increments 06 p0912 A71-18043

Electron beam drilled workpieces, investigating residual stresses origin and character with photoelastic measurement 06 p0905 A71-18092

Elastic medium residual microstresses probability distribution, noting microdistortion tensor linear and transverse components and tangential and normal stresses relation 06 p1002 A71-18417

Residual stress effects on Al alloys stress corrosion crack growth rates as function of plane strain stress intensity, discussing residual stress elimination methods 07 p1137 A71-19974

Tubular compression members, examining residual stress profile effects on strength reduction 08 p1370 A71-21411

Loop patterns of secondary defect structures in quenched Al based alloys interpreted in terms of internal stress and stacking fault energy 08 p1310 A71-21531

Soviet papers on physics of metals and metallography covering residual stresses, energy dissipation after plastic deformation, heat treatment, etc 08 p1317 A71-21759

X ray analysis of oxide film structure, oxygen concentration and residual stresses at surface of oxidized Ti and Ti alloy 08 p1317 A71-21760

Plastic strains, thermal residual stresses and buckling of rectangular cross section plates and beams subjected to asymmetric heating and cooling 08 p1375 A71-22056

Heat resistant alloys low cycle fatigue tests at 20-800 C, establishing residual strain change patterns as function of stress and temperature 09 p1468 A71-22600

Numerical analysis of winding and heat treatment effects on residual stress distribution in cylindrical glass fiber reinforced plastic products 09 p1482 A71-22816

Residual stresses in ring shaped specimens of wound glass fiber plastic products, using radial cutting technique 09 p1482 A71-22822

Jetting collision effect on structural changes at interface between Ti and steel in explosive bonding, considering plastic deformation and residual stresses 10 p1629 A71-25030

Longitudinal and transverse residual stresses arising in lamination fabrication process of cross-ply fiber composites 11 p1786 A71-25421

Al and Al-Mg alloys average interdislocation internal stress measurement during steady state creep 12 p1916 A71-26895

Nondestructive magnetic method for measuring longitudinal residual stress in outer portions of ferromagnetic cylindrical bars 12 p1974 A71-26948

Residual stress at plate crack determined from elastic stress intensity factor measurements [ASME PAPER 71-MET-A] 12 p1977 A71-27311

Rigid plastic media dynamic model, showing yielding time delay effect on residual deflection as function of load duration 12 p1982 A71-27515

Residual stresses rapid X ray diffraction measurement, noting faster operation in go-no-go mode for nondestructive testing 12 p1912 A71-27533

Heat resistant alloys strengthened elements, studying high temperatures prolonged exposure effects on

surface layers strengthening and residual stresses relaxation 12 p1919 A71-27780

Strain gage method for residual stress determination in thin walled brass cylindrical shells produced by deep drawing 13 p2066 A71-28034

Helicopter component surface finish smoothness and residual stress requirements, using abrasive grinding belt machines with gear link mechanisms 13 p2075 A71-28943

Unidirectional fiber composites impact resistance, showing matrix modulus, fabrication process, fiber and void volume ratios and microresidual stress effects 14 p2264 A71-29920

Large circular plate residual stresses due to local spot heating and cooling, investigating effects of yield strain, heat input rate and peak temperature 14 p2329 A71-30462

Thin sheet Nb-Zr alloy welds, detailing residual stresses in butt joints 15 p2413 A71-31204

Finned solid cylinders surface layers, determining residual axial stresses distribution and amount with induction sensor 15 p2503 A71-31480

Residual stresses for fused contacts between metals and Si or gallium arsenide from polarization measurements in principal crystallographic planes 15 p2461 A71-31510

Hardened low alloy steel ultrasonic attenuation under magnetic field due to thermally introduced residual stresses 15 p2414 A71-31641

Elastic-plastic mechanics of steady crack growth under antiplane shear, discussing residual stress effect, plastic zones shape and strain distribution 15 p2428 A71-31974

Plastically deformed Ni powder specimens residual microstresses as function of applied hydrostatic pressure, using X ray diffraction measurements 15 p2429 A71-31996

Thermally induced residual stresses effect on yield behavior of unidirectionally solidified eutectic composites 15 p2432 A71-32171

Residual stress determination from stress intensity factor measurements, describing application to electron beam welded aluminum plate 15 p2508 A71-32259

Stress relaxation method using compliance measurement of bolted test assembly to determine initial and residual loads after exposure periods 15 p2436 A71-32507

Heat treatment effectiveness in reducing residual stress from stress relaxation data analysis 15 p2436 A71-32506

Stress relaxation as source of dimensional instability in precision devices, discussing thermal cycling role in residual stress relief 15 p2436 A71-32507

Optimum heat treatment for welds, investigating residual stress relief with higher harmonics method 15 p2417 A71-32664

Alternative approach to fracture mechanics, discussing thickness dependence of residual strength, crack initiation and crack propagation stability 15 p2510 A71-32725

Structural elements residual, principal and total stress determination, using photoelastic coating method 16 p2651 A71-33061

Stress-microstrain relationship for metal crystals prestrained in easy glide, obtaining mobile inelastic dislocation density and internal stress 16 p2654 A71-33102

Neuber elastoplastic analysis of residual notch stresses for improved cumulative damage predictions applied to aluminum alloy under overload [AIAA PAPER 71-776] 16 p2659 A71-34012

Circumferential notch effect on distribution of compressive self stresses produced by shallow skin layer expansion in round steel bars, using finite element method [SESA PAPER 1831] 17 p2819 A71-34529

Residual stress measurement in thin contoured Ti alloy sheets by X ray diffraction, using stress camera in normal incident beam mode 17 p2757 A71-34537

Logarithmic damping of bending oscillations produced by residual fretting stresses in circular plates 17 p2826 A71-35022

Stress annealing effects on Al 27 NMR lineshapes in pure Al powders filed and stored at room temperature, considering residual stress 17 p2759 A71-35225

Diffusion controlled order-disorder transformations kinetics, considering internal strain and gradient energy 21 p3397 A71-40431

Macroscopic residual stress and strain measurement and crack tip substructure, discussing crystal plastic deformation effect on fatigue crack propagation 21 p3466 A71-40831

Elastoplastic thermal stress analysis in axisymmetric bodies by finite element method, calculating residual stresses 21 p3466 A71-40841

Residual stress magnitude and distribution in metal strips rolled with ultrasonic vibrations 21 p3389 A71-41093

High temperatures prolonged exposure effects on surface layers hardening and residual stresses relaxation in heat resistant alloys 21 p3403 A71-41105

Open simply supported cylindrical shell internal stresses due to initial deformation based on thin elastic shell linear theory 22 p3613 A71-41563

Optically active material photoelastic properties utilization for residual stress distribution determination in machine elements after lathe working 22 p3617 A71-42575

Al-Zn solid solution mean effective and internal stresses and activation area during high temperature creep 23 p3691 A71-43900

Residual stress in closed spherical shell welded along equator, using stress-strain relations 23 p3778 A71-44035

Residual resistance measurements for studying recovery of high purity potassium wires deformed at/below 4.2 K, discussing anomalous difference with sodium 24 p3861 A71-45195

RESIDUES

Combustion residues particle size and distribution during rocket plume impingement on Al surface 01 p0183 A71-11594

RESIN BONDING

Axial compression of thin circular epoxy resin disks with three dimensional stress state produced by cementing to rigid platens, using triaxial analysis 01 p0109 A71-11008

Adhesive resin metal bond stability, examining surface finish and atmospheric moisture effects at various temperatures on exfoliation 06 p0904 A71-17944

Microencapsulation of bonded reactive resins in packaging, logistics and adhesive applications at room and elevated temperatures 10 p1634 A71-24120

Epoxy bond strength, cracking and failure of lapped joints as function of composition and mechanical properties 10 p1618 A71-24826

Stress distribution in plates and tubes bonded by stepped joints, assuming generalized plane stress 17 p2824 A71-34814

RESINS

NT ACRYLIC RESINS
NT EPOXY RESINS
NT ION EXCHANGE RESINS
NT NYLON [TRADEMARK]
NT PHENOLIC RESINS
NT POLYAMIDE RESINS
NT POLYESTER RESINS
NT POLYETHER RESINS
NT POLYIMIDE RESINS
NT POLYMETHYL METHACRYLATE
NT POLYURETHANE RESINS
NT SILICONE RESINS
NT SYNTHETIC RESINS
NT THERMOPLASTIC RESINS
NT THERMOSETTING RESINS
NT VINYL COPOLYMERS

High modulus carbon fiber wettability by matrix resin [PLASTICS INST. PAPER 21] 08 p1322 A71-20928

Performance-price relations of carbon, boron and glass fiber reinforced resin matrix composites in commercial and aerospace use 10 p1634 A71-24418

Resin systems for ablative composites, correlating hyperthermal performance characteristics via thermogravimetric, mechanical flexural and ablation tests 11 p1789 A71-26039

Multidirectional reinforced resin matrix composites inspection and nondestructive analysis by film/neutron radiography and X ray Vidicon 14 p2263 A71-29659

Elastic static and dynamic physicochemical characteristics of resin type amorphous materials under pulsed loads, using electromagnetic excitation of torsional vibrations 16 p2659 A71-33996

Glass-fiber/glass-bead/resin beam stiffness and strength improvement with sandwiching between layers of unidirectional carbon fiber composite 21 p3405 A71-40597

RESISTANCE COEFFICIENTS

U COEFFICIENTS

RESISTANCE HEATING

Resistively heated W-Re wire sublimation characteristics between 1550-1950 C in low pressure oxygen 02 p0264 A71-12255

Solar cell module joints welding technology development under ESRO sponsorship, emphasizing resistance welding and process optimization
05 p0704 A71-16095

Heating rate effect on parameters of resistance wire strain gages subjected to temperature gradients
09 p1443 A71-22634

Electric current heated thin resistance film thermoelectric transducer, measuring temperature rise with thermocouple
12 p1888 A71-27158

Ohmically heated collision plasma confinement in Uranan racetrack stellarator with large shear, describing magnetic field topography effects and plasma lifetime
17 p2785 A71-34196

Resistance NOR Ti BOND joining of Ti shapes, forming Ti-Cu eutectic at Cu plated Ti joint interface
21 p3387 A71-40620

Aluminum nitride crystals production by sublimation in resistance furnace with graphite heater
22 p3585 A71-41701

Transverse current conduction through MHD generator seeded hot plasma flow, showing Joule heating dominance in cathode boundary layer due to thermal instability
22 p3584 A71-42596

Joule heating effect on static negative differential resistance and switching of chalcogenide thin films
24 p3862 A71-45353

RESISTANCE THERMOMETERS

Rugged stable differential Pt resistance thermometer for Lunar Heat Flow Program, discussing construction, calibration and environmental test
03 p0427 A71-13917

Remote determination of temperature by operating and etalon thermistors resistances measurement with DC bridge
04 p0591 A71-14855

Resistance thermometer for temperature measurement in turbulent boundary layer near wall, giving expression for correction factor
07 p1106 A71-18786

Resistance thermometer using amorphous Pd-Si-Cr alloy for enhancing sensitivity at cryogenic temperatures
09 p1444 A71-22714

Resistance thermometry measurements near wall in turbulent flow, considering error causes
10 p1591 A71-23847

Substrate materials thermal characteristics determination for thin films resistance thermometers calibration, using pulse heating technique
12 p1908 A71-27593

Gas-solid interaction by shock tube method, determining thickness and thermal accommodation effects on thin metal film resistance thermometer response
16 p2576 A71-32922

Platinum resistance thermometers calibration normalized in resistance-difference ratios
18 p2916 A71-36047

Fluid phase discrimination temperature measurement system, using thin carbon film resistance thermometer with electrical power pulse sensing for liquid/gas phase discrimination
20 p3237 A71-39278

Resistance wire temperature sensor spatial resolution calculation, considering sensor length and isotropic turbulence effects on temperature spectrum and dissipation
22 p3542 A71-41904

Display system for scanning medium thermometer covering temperature range 28.0-37.4 C with 0.2 C accuracy, using liquid nitrogen cooled indium antimonide photoresistive detector
22 p3545 A71-42149

RESISTIVITY

U ELECTRICAL RESISTIVITY

RESISTOJET ENGINES

Spacecraft high performance resistojet engines, discussing design criteria for high temperature long term operation with minimum thermal losses
06 p0948 A71-18633

Resistojet design criteria for performance modeling of ammonia propellant thrusters and manned space stations using biowaste propellants
07 p1183 A71-18898

Concentric tube resistojet tested on hydrogen and ammonia propellants for use with biowaste propellants
09 p1387 A71-22908

Long term life test and vacuum tests of high temperature resistojets, using ammonia and hydrogen propellants
11 p1811 A71-25523

Biowaste resistojet propulsion system for NASA space station orbit-keeping, describing design and operation
14 p2293 A71-30748

High performance superheated subliming solid ammonium carbamate thruster using resistojet technology for specific impulse increase
15 p2469 A71-32048

Biowaste resistojet engine design and performance for various propellants and propellant mixtures
15 p2470 A71-32293

Resistojet power and specific impulse performance, investigating biowaste derived propellant chemical nonequilibrium effects
17 p2696 A71-35534

RESISTOJETS

U RESISTOJET ENGINES

RESISTORS

NT POTENTIOMETERS (RESISTORS)

NT PRINTED RESISTORS

NT THERMISTORS

FET as voltage controlled linear resistors, discussing use in attenuators, automatic gain control, volume compressors and RC networks frequency control elements
02 p0229 A71-11814

Carbon and metal film resistors stability, presenting service life characteristics prediction method for arbitrary electric loads and time
05 p0728 A71-16774

Resistor characteristics temperature dependence, considering platinum resistor and thermistor with negative temperature coefficient
06 p0900 A71-18186

Metal film resistors rapid evaluation method including thermal, load and shock tests devised by British electronic component manufacturers
07 p1076 A71-19553

Automatic test equipment for sorting large quantity resistors based on nonlinearity measurement
07 p1076 A71-19554

Planar-epitaxial IC resistors p-n junction parasitic effects on cut-off frequency, obtaining design formulas for capacitance and geometry
08 p1264 A71-21074

Defective resistors physical processes during thermal control method, appraising quality from surface temperature distribution
08 p1300 A71-21901

N-type single crystal silicon semiconductor resistors with high impurity concentrations and high accuracy
09 p1414 A71-22160

Hybrid integral microcircuits with thin film resistor heat sources, determining temperature fields on substrate and boundaries
09 p1416 A71-22495

Carbon dioxide production laser for automatic resistors trimming without current carrying capability reduction, noting accuracy, flexibility and speed
09 p1465 A71-23405

Noise temperature in microwave frequency mixers using nonlinear resistors, giving rectifier and diode loss formulas for rectangular and sinusoidal waves
19 p3027 A71-37494

Hybrid circuit methods for aligning resistors manufactured by different technologies, considering mechanical methods, electric erosion, electron and laser beam alignment, etc
20 p3208 A71-39434

Termination and interface aging resistance of thin film resistors under corrosion, noting Ti-Pd-Au materials
23 p3651 A71-43427

Thin film silicide resistors in monolithic IC for high sheet resistance or radiation hardness using sputtering deposition without protective overlayer
23 p3655 A71-43428

RESOLUTION

NT ANGULAR RESOLUTION

NT HIGH RESOLUTION

NT RADAR RESOLUTION

Linear continuous receiver and control systems resolution and statistical epsilon inventory
01 p0062 A71-10716

Microwave holography with artificial reference wave and receiver multiplier, improving linear resolution in image
02 p0248 A71-11876

Coherent optical data processing systems resolution testing, using multifrequency linear diffraction gratings
03 p0425 A71-13644

Microwave ultrasonic beam visualization techniques via Bragg diffraction of laser beam, investigating resolution capability
03 p0436 A71-13717

Two point resolution in Fourier holography with partially coherent recording and illuminating light
03 p0429 A71-14180

Pulkovo radio telescope resolution improvement by range extension into millimeter wavelength region
07 p1109 A71-19341

Astronomical telescope resolving power in focal plane emphasizing atmospheric turbulence
07 p1109 A71-19347

Statistical analysis of fiber optics imagery, considering resolution difference between static and dynamically scanned bundles
08 p1334 A71-21180

Aerial photography vs orbital acquired imagery resolution for land use data
09 p1439 A71-23212

Modulation-amplitude selective twofold increase of interferential spectrometer resolving power by asymmetric setup
10 p1613 A71-25020

Photographic materials in holography, examining resolving power dependence on size and angle between reference and signal light beams
12 p1903 A71-26756

Hologram size and film type limitations effects on resolution of reconstructed image in edge-line holography
14 p2241 A71-30131

Optical wave reconstruction from microwave holograms and application to interferometry, considering resolving power and visible images of microwave transparencies
15 p2405 A71-31281

Quadrupole mass spectrometer ultimate characteristics concerning resolution, range, recording speed, working pressure and sensitivity
17 p2737 A71-34288

Image amplifier camera resolution as function of light level based on photon statistics and cathode quantum efficiency
17 p2746 A71-35762

Photosystem resolution of coherent laser illuminated objects, discussing experimental investigation of image quality dependence on relative aperture
19 p3073 A71-38194

Hologram recording materials within and outside visible spectrum, considering sensitivity, reconstruction efficiency, resolution limitations, nonlinear and noise effects
21 p3380 A71-40920

Backward propagation method for ultrasonic image reconstruction, examining resolution in near field for high contrast objects
22 p3541 A71-41784

Resistance wire temperature sensor spatial resolution calculation, considering sensor length and isotropic turbulence effects on temperature spectrum and dissipation
22 p3542 A71-41904

Image detail reproduction quality and resolution, describing signal to noise and modulation transfer function effects
22 p3547 A71-42505

Holography capabilities of hypervelocity projectiles with front surface resolution, discussing fringes intensity and position from projectile spin
22 p3549 A71-42569

RESOLUTION CELL

Echoing area relation to radar range resolution cell size and aircraft dimensions, using mathematical model
02 p0210 A71-11643

RESOLUTS

U PROBLEM SOLVING

RESOLVING POWER

U RESOLUTION

RESONANCE

NT CYCLOTRON RESONANCE

NT ELECTRON PARAMAGNETIC

RESONANCE

NT FERROMAGNETIC RESONANCE

NT MAGNETIC RESONANCE

NT MAGNETOSONIC RESONANCE

NT MICROWAVE RESONANCE

NT NUCLEAR MAGNETIC RESONANCE

NT OPTICAL RESONANCE

NT PLASMA RESONANCE

NT PROTON MAGNETIC RESONANCE

NT PROTON RESONANCE

NT RESONANT VIBRATION

NT SPIN RESONANCE

Satellite topside sounders oblique echoes, investigating upper hybrid resonance with WKB technique
03 p0420 A71-14531

Neutron spectra measurement in epithermal energy range by activation of threshold and resonance foils, using expansion in orthonormal polynomials
04 p0594 A71-14915

Resonance in planar elliptic restricted three body problem, noting primaries eccentricity and long term effects
04 p0653 A71-15710

Stability and resonances in restricted three body problem, using method of surface-of-section
04 p0656 A71-15732

Deep resonance problem of conservative periodic Hamiltonian reduction to ideal form in celestial mechanics
04 p0657 A71-15736

Parametric resonance and first order instability region of Mathieu equation in nonlinear systems
04 p0620 A71-15737

Spinning symmetric satellite roll-yaw resonant attitude instabilities in circular orbit
06 p0980 A71-18544

Resonances stability and development in restricted three body problem with two degrees of freedom
07 p1202 A71-20514

Double resonance in natural satellite motion from long period perturbation prediction
07 p1202 A71-20517

Resonance line formation in multidimensional media, applying to non-LTE line transfer for two dimensional temperature variations 08 p1359 A71-20942

Finned configurations with nonlinear aerodynamic properties, obtaining solutions for angular motion at and near resonance [AIAA PAPER 70-535] 09 p1532 A71-22909

Ceres and Pallas orbital commensurability, considering resonance effects 09 p1527 A71-23537

Linear differential equations stability analysis by implicit equations applied to resonance phenomena, using Weierstrass theorem 10 p1640 A71-23803

Long time planetary atmosphere motions, investigating sideband resonance mechanism in Rossby wave packet interactions with weak shear zonal flow 12 p1925 A71-27195

Normally incident electromagnetic wave propagation in inhomogeneous gyration medium, obtaining reflection and transmission coefficients and discussing resonance 13 p2108 A71-29088

Superharmonic resonance in piecewise linear systems with unsymmetrical characteristics, investigating stability properties by Fourier series method 17 p2781 A71-34926

Hamiltonian systems equilibrium position stability conditions in presence of resonances, assuming neutrality in linear approximation 19 p3103 A71-37096

Variational methods application to high order dynamic systems resonance boundary value problem 20 p3309 A71-39487

Spiral wave dispersion, wave number and amplitude relationship in Galaxy near inner Lindblad resonance, noting correlation with ionized hydrogen density 21 p3451 A71-40855

Gas bearing ground clearance effects on pivoted pad resonance, pitching vibration mode, static journal displacement and friction 22 p3551 A71-41661

Absorption spectra of benzene, naphthalene and anthracene crystals, noting resonance coupling type effect on vibrational spectrum 24 p3851 A71-45171

Resonance charge exchange effect on gaseous ions mobility, noting cross sections structure due to resonance and wave interference 04 p0629 A71-14998

Ion-molecule collision charge transfer and momentum transfer relaxation rates, using ion cyclotron resonance heterodyning method 07 p1054 A71-19371

Multiphoton ionization cross section and charge number in neon near resonance under focused laser beam 13 p2081 A71-29338

Resonant charge transfer cross sections in inert rarefied gases from atomic screening parameters, considering positive gas conductivity of ionized dense gases 15 p2452 A71-31825

RESONANCE PROBES

Ionospheric low hybrid resonance measurements by rocket-borne quadrupole probe, deriving electron density and effective ion mass along trajectory 20 p3224 A71-39722

RESONANCE SCATTERING

Photodissociation produced O/P3/ atoms detection and reaction rate measurements by resonance fluorescence scattering 01 p0130 A71-10369

Self focusing in media with resonance absorption, determining stimulated Raman scattering threshold in bleachable absorbers as function of absorber concentration 07 p1161 A71-20381

Resonance line radiation polarization of potassium and cesium isotopes excited by electron impact 09 p1496 A71-22187

Superconducting alloys order parameter spatial variation and resonance scattering near nonmagnetic impurity at critical temperature, using Heinrich perturbation theory expansion solutions 12 p1942 A71-26744

Jupiter upper atmosphere extreme UV dayglow, involving resonant scattering and fluorescence of incident solar flux 12 p1961 A71-26888

Inhomogeneous planetary atmosphere resonantly scattered sunlight, calculating intensities with frequency redistribution functions 13 p2100 A71-28346

Electron lifetime in earth radiation belt due to resonant scattering with hiss VLF radiation 16 p2626 A71-33674

OH emission column density upper limit from rocket-borne UV spectrometer measurement of resonantly scattered sunlight intensity in electronic transition vibrational band 16 p2574 A71-33967

Energetic electrons pitch angle scattering during magnetic storms due to resonant interaction with proton generated Doppler shifted ion cyclotron waves 16 p2574 A71-33972

Excitation cross sections for resonance states by electron impact on atomic nitrogen and oxygen over aeronomical energy range 18 p2949 A71-36350

Airglow optical emission processes covering resonance scattering, fluorescence, chemical association, ionic reactions and excitation transfer 20 p3226 A71-39827

Scattering atom recoil effect in resonance line transfer with Doppler redistribution, discussing neglect from microscopic point of view 21 p3447 A71-40429

Atomic level interference and hyperfine splitting effects on angular and polarization distributions of resonantly scattered light in magnetic field 21 p3420 A71-41120

Photoelectron impact vs dissociative excitation cross sections of atomic oxygen resonance radiation in terrestrial airglow 23 p3669 A71-43171

Resonance scattering laser radar for atmospheric pollution detection, discussing Rayleigh and Mie scattered light suppression 24 p3803 A71-44570

RESONANCE TESTING

Elastic parameter dynamic measurements using resonance methods with electrostatic attraction 02 p0328 A71-12406

Fatigue limit of titanium alloy machine parts after finishing mechanical treatment under resonance testing 07 p1142 A71-20484

Oscillations generating mechanism in resonance tube fed by subsonic gas jet, determining oscillations amplitude and frequency at resonance 09 p1382 A71-22406

Single jet oscillations excitation of two resonant tubes, observing air motion with wool threads and stroboscopic lighting 10 p1591 A71-23823

Structural steady state vibration frequency response and resonance testing, investigating nonlinearity effects of large deflections 14 p2326 A71-30065

Nonstationary resonance analysis of forced flexural elastoplastic vibrations of beam of hardening/softening material under cyclic strain 18 p2981 A71-36709

French monograph on free and forced convection and external radiation from hot gas oscillating in resonance tube, considering heat balance and mass exchange 19 p3172 A71-38649

RESONANT CAVITIES

U CAVITY RESONATORS

RESONANT FREQUENCIES

Natural frequencies of cantilever turbine blade with asymmetric aerofoil under coupled bending-torsion vibrations, using Ritz-Galerkin method for equations of motion 01 p0143 A71-11014

Subsidiary resonance response time decay behavior in ionosphere, showing occurrence of principal resonances at higher orders 01 p0077 A71-11523

Fabry-Perot laser cavity resonant modes, noting host medium movement effects on diffraction loss and light beam intensity distribution 02 p0260 A71-12147

Partially ionized bounded plasma LF natural oscillations due to ionization processes, ambipolar diffusion and charged particles recombination at walls 02 p0292 A71-12619

Liquid sloshing frequencies in partially filled arbitrarily shaped vertical container 03 p0398 A71-13113

Turbomachine blades torsional-bending vibrations aerodynamic damping, noting natural frequency shift 03 p0340 A71-13141

Cantilever beam bending vibration, measuring driving point impedance and natural frequencies at low strain amplitudes for Mg alloy, Mn-Cu and coated Al beams 03 p0502 A71-13299

Clamped circular plates axisymmetric nonlinear resonant frequency response under uniform static pressure 04 p0668 A71-15187

Cantilever beam resonant frequencies measurement using electrodynamic vibration exciter 04 p0672 A71-15823

Arches and rings in-plane natural vibration frequencies determination based on Newmark numerical integration method for beams 05 p0820 A71-15985

Rectangular plate with stiffener cross section for unit with constant mass, considering natural symmetric and antisymmetric mode frequencies 05 p0824 A71-16603

Hafnium droplets burning in ultrapure oxygen at various pressures, considering combustion induced natural mode periodic oscillations [WSS/CI PAPER 70-14] 06 p0942 A71-17654

Material stiffness/weight ratio effects on helicopter blades uncoupled flapwise, chordwise and torsional natural frequencies by rapid estimation 06 p0985 A71-17691

Elastic composite liquid filled shell containers, calculating natural vibration with Ritz method 06 p0992 A71-17809

Dimensional resonances of standing helicon waves in two layer and multilayer semiconductor structures and crystals with growth inhomogeneities 07 p1176 A71-19273

Helicon wave resonance excitation and indication in intermediate magnetic fields in semiconductors 07 p1176 A71-19274

Cylindrical, conical and spherical shells natural frequencies and vibration modes determination using matrix series 07 p1212 A71-19365

Cylindrical shell panels with free supported curved edges and arbitrary boundary conditions, investigating natural frequencies and mode shapes 07 p1213 A71-19886

Thin cylindrical shell of revolution delaminations detection model, using free vibration natural frequency parameter under clamped-clamped conditions 07 p1216 A71-20135

Natural frequency bounds for clamped beam with linearly varying compressive load and constant end load by Rayleigh-Ritz, Bazley-Fox second projection and Kato methods 08 p1368 A71-20806

Box type structure free vibrations investigation by rectangular finite elements, comparing with natural frequencies and normal modes solution 08 p1369 A71-20807

Natural frequencies approximation for vibration modes of stiffened and singly curved panel structures 08 p1369 A71-20810

Electronic equipment for measuring resonant frequency drift during slow wave structure impedance measurements, considering mean square errors 08 p1264 A71-21073

Contained cross sectional deformation effects on turbine blades natural torsional vibration frequencies 08 p1372 A71-21617

Thin metallic disk radar cross sections for near resonance frequencies backscatter, comparing experimental and computer results 09 p1410 A71-23518

Vibrational characteristics of pretwisted cantilever beams with uniform rectangular cross section, investigating slenderness ratio effect on natural frequencies 09 p1543 A71-23661

Hinged sandwich beams loaded by concentrated masses, calculating natural vibration frequencies with and without allowance for rotatory mass inertia 10 p1690 A71-24571

Polygonal elastic plates natural frequencies investigation by conformal mapping and variational method, transforming holomorphic function into equivalent problem of circular boundary plate 10 p1691 A71-24813

Heterogeneous orthotropic cylindrical shells, calculating free natural vibration frequency spectra from refined equations of motion in Love and Donnell type theories 11 p1841 A71-25184

Elastic boundary conditions effect on natural frequencies and resonant displacement of thin isotropic circular cylindrical shell under concentrated load with harmonic time history 11 p1843 A71-25314

Rotating low aspect ratio turbomachinery blades natural frequencies and mode shapes, using finite element method for equilibrium equations eigenvalue problem [AIAA PAPER 71-374] 11 p1845 A71-25347

Computerized sloshing frequencies of tilting two dimensional tank of flat free surfaces with respect to effective gravity 11 p1752 A71-26198

Spherical shallow shell with hole, noting natural vibration frequency 12 p1975 A71-27108

Natural frequencies and elastic stability of simply supported rectangular plate under linearly varying compressive loads 12 p1976 A71-27162

Natural frequencies of finite circular cylinders in axially symmetric longitudinal vibration, using Rayleigh-Ritz method to derive differential equations for expansion functions coefficients 12 p1981 A71-27482

Frequencies and modes of natural vibrations of closed cylindrical shell with elastic filler 12 p1981 A71-27508

Vibration natural frequencies and mode shapes of cantilever plate mounted on rotating disk periphery, using finite element technique 13 p2147 A71-27788

Cylindrical microwave cavity partially containing cold nonuniform plasma enclosed by quartz tube, calculating resonant frequency by exact, multistrata and series methods

13 p2029 A71-28500

Adaptive automatic control systems, determining damping coefficient and natural oscillation frequencies with second order differential equations

13 p2041 A71-28639

Rotating ring resonator partially filled with dynamic isotropic medium, determining resonance properties

13 p2080 A71-29025

Transfer function optimization for linear tracking filter model with controlled resonant frequency, analyzing noise band performance

14 p2194 A71-30089

Extensional vibrations of thin cylindrical shell, discussing longitudinal and radial motions coupling and resonant frequency dependence on length/radius ratio

14 p2327 A71-30209

Spectral theory of linear differential operators for microwave oscillatory systems synthesis from inhomogeneous line segments, determining line characteristic impedances and local reflection function

15 p2369 A71-31233

Coupled natural frequencies in rectangular cross section pretwisted cantilever beams flexural vibrations

15 p2503 A71-31442

Rectangular plates with unidirectional stiffeners, calculating natural frequencies and mode shapes with approximate method

15 p2507 A71-32128

Arbitrary gravitational field effects on natural frequencies of rotating ring laser with traveling electromagnetic wave

15 p2421 A71-32408

Finite skin-stringer structures natural frequencies determination, using free flexural wave groups

15 p2510 A71-32518

Forced oscillations of system governed by one dimensional nonlinear wave equations, using perturbation procedure for solutions near linear resonant frequencies

16 p2606 A71-32857

Weakly nonlinear single degree of freedom cubic system under simultaneous time varying force and parametric excitation, presenting resonance frequencies classification

[ASME PAPER 71-APM-24] 16 p2655 A71-33205

Isoperimetric problem upper bounds for fundamental frequencies in free oscillations of incompressible fluid in container

16 p2559 A71-33483

Elastic spherical shell coupled to rigid body, calculating asymmetric free vibration natural frequencies and mode shapes from boundary conditions

17 p2817 A71-34339

Sloshing liquid natural frequencies change in cylindrical shell by movable devices, considering immersed thin elastic plate effect

17 p2726 A71-34579

Finite length thin circular cylindrical shells with clamped or simply supported edges, calculating flexural free vibration natural frequencies

17 p2822 A71-34643

Freely vibrating supported elastic isotropic oval cylindrical shells natural frequencies and mode shapes

17 p2825 A71-34873

Asymptotic methods for distributed system nonlinear time and space vibrations, discussing system dispersion effect on resonance conditions

17 p2780 A71-34914

Pretwisted cantilever airfoil cross section turbine and compressor blades vibration natural frequencies and mode shapes

17 p2828 A71-35282

Partially liquid filled cylindrical shells with elastically supported end rims, deriving algorithm for nonaxisymmetric natural vibration frequency calculations

17 p2833 A71-35614

Cross sectional warpage effects on turbine blades natural torsional vibration frequencies

17 p2834 A71-35677

Automatic classification of targets characterized by radar returns at discrete set of frequencies in Rayleigh region and first resonance range

17 p2747 A71-35773

Beam column with probabilistic material and geometric properties, axial loads and boundary conditions, obtaining free vibration and natural frequency stochastic equations

18 p2979 A71-36358

Fundamental frequency of large amplitude bending vibration of elastic and isotropic rectangular plates, considering effects of transverse shear and rotatory inertia

18 p2980 A71-36496

Parametric resonant circuit with low pumping frequency and transfer function variation according to arbitrary complex periodic law

18 p2896 A71-36623

Dynamic properties of turbine wheels under bending vibrations, classifying resonant frequencies on basis of vibration modes

18 p2981 A71-36722

Cylindrical shells under uniform external pressure loads, determining boundary conditions effects on natural frequencies and vibration mode shapes

19 p3155 A71-37529

Variable thickness and rigidity cylindrical shells, determining natural frequencies and vibration mode shapes with algorithm based on Ritz method

19 p3155 A71-37531

Edge clamped spherical shell natural vibration frequency determination using Vlasov shell theory equations

19 p3155 A71-37532

Linearly deformable beams with distributed parameters and lumped inclusions, determining natural transverse vibration frequencies and mode shapes

19 p3155 A71-37535

Minimum mass design of two dimensional plate-like structure with free vibration fundamental frequency or aeroelastic constraints, using optimal theory for extremum

19 p3158 A71-37877

Shielded enclosure resonance effects reduction on cavity impedance measurement by technique analogous to wave traps for notching out RF signal at selected frequencies

19 p3032 A71-38459

Dipole antenna with parallel parasitic element, investigating resonant length variation as function of spacing with matrix inversion method

19 p3035 A71-38599

Narrow band magnetospheric radio noise between electron plasma and upper hybrid resonance frequencies from satellite observations

20 p3285 A71-38728

Parametric resonance of single degree of freedom system with double bilinear hysteresis

20 p3267 A71-38793

Fundamental frequency of star shaped membrane with boundaries described by polar coordinates in Fourier series form

20 p3308 A71-39039

Free convective heat transfer in cryogenic liquid filled enclosure, studying effects of vibration near resonant frequency

20 p3314 A71-39292

Flat thin films in stripline cavity resonator with TEM mode, expressing bandwidth and resonance as frequency difference

20 p3239 A71-39426

Numerical analysis of natural frequency spectrum of elastic plate free vibrations in compressible inviscid fluid

20 p3310 A71-39784

Algorithm for linearly elastic structures vibration natural undamped frequency computation, assuming known dynamic stiffness matrix

20 p3311 A71-39964

Iterative method for linearly elastic structure undamped vibration natural frequency determination with fast convergence

20 p3311 A71-39965

High resolution spectroscopy of Na D resonance lines in saturated absorption with repetitively pulsed tunable dye laser

21 p3391 A71-40199

Peak resonant response of thin rectangular plate with elastic edge restraint under concentrated load

[ASME PAPER 71-VIBR-6] 21 p3456 A71-40269

Harmonic excitation response of masses on elastic half space, considering Poisson ratio effect, vibration amplitudes and resonant frequencies

[ASME PAPER 71-VIBR-59] 21 p3460 A71-40304

Torsional natural frequencies in coupled turbine and reciprocating engine system driving common propeller, using matrix techniques

[ASME PAPER 71-VIBR-83] 21 p3461 A71-40319

Transversely vibrating hollow cylindrical beam sound radiation and response to acoustic excitation, predicting resonant frequencies

[ASME PAPER 71-VIBR-84] 21 p3461 A71-40320

Five-span skin-stringer width and damping effects on vibrational response including resonant frequencies and mode shapes by transfer matrix analysis

[ASME PAPER 71-VIBR-101] 21 p3461 A71-40327

Free radial vibrations of curved beams by finite element method, using model to investigate variation with subtended angle of six lowest natural frequencies

21 p3462 A71-40529

Curved sandwich beams free flexural vibration by finite element method, noting parameters effects on natural frequencies

21 p3462 A71-40533

Bending resonance frequencies of beams for known external forces

21 p3463 A71-40550

Natural frequencies and vibration mode shapes of missile with idealized air friction force tangent to instantaneous neutral axis

21 p3455 A71-41012

Acoustic damping of clamped and hinged rectangular panel at natural frequency, noting dependence on aspect ratio

21 p3416 A71-41200

Extinguishing parametric vibrations, changing equivalent natural frequency from resonant state by supplementary load

21 p3473 A71-41368

Edge supported cylindrically curved panels flutter, investigating in-plane boundary conditions and geometry effects on natural frequency

22 p3616 A71-42216

Natural frequencies and vibration modes of perforated cylindrical, conical and spherical shells of revolution, using Ritz method

22 p3617 A71-42488

Elastic plates transverse vibrations fundamental frequency from constant deflection lines method

22 p3617 A71-42537

Closed phase lock loop FM demodulator design, determining resonant frequency parameters, attenuation factor and low pass filter elements

23 p3650 A71-43094

Dynamic response of thin walled structures natural frequency analyzed for formulating potential and kinetic energy for stiffness and mass matrices by minimization principle

24 p3878 A71-44555

Acoustic resonance excitation by vortex shedding from flat plate trailing edge in low speed wind tunnel

24 p3848 A71-44557

Flexural vibration of transversely isotropic composite material curved beams, deriving curvature effects on natural frequency

24 p3878 A71-44616

Traveling wave pair interaction with three energy level medium at resonance frequencies, deriving coupled differential equations for amplitude variations

24 p3833 A71-44662

SHF resonator small resonant frequency shift and Q factor changes measurement based on FM signal envelope shape analysis

24 p3858 A71-45237

RESONANT VIBRATION

Nonlinear single-degree of freedom mechanical system vibration under small random perturbations

01 p0127 A71-10548

Resonant excitation of plane dielectric waveguide by plane monochromatic wave

03 p0378 A71-13798

EM oscillations of open elliptic profile cylindrical mirrors resonator with dielectric elliptic cylinder

03 p0386 A71-13800

Power train systems gear induced noise analysis, using in-flight vibration and noise measurements for comparison with calculated noise spectra

[ASME PAPER 70-WA/DGP-1] 03 p0471 A71-14137

Heat transfer in flat plate, considering acoustic resonance vibration effect

04 p0684 A71-15505

Book on vibration measurements covering resonant and self excitation patterns, aerogenics, machine parts, transducers and engineering techniques

05 p0820 A71-16275

Isotropic circular plate natural vibrations for inhomogeneous boundary conditions, using net point method to derive finite difference equations

05 p0821 A71-16353

Thin cylindrical shell in ideal compressible fluid, calculating longitudinal resonance waves for acoustic excitation

06 p0985 A71-17755

Fourier resonance associated with electromagnetic wave diffraction from multilayer gratings

06 p0870 A71-18349

Spacecraft structures vibration testing nonlinear effects, extending asymptotic method for transition through resonance to nonresonant regions

[AIAA PAPER 71-211] 06 p1004 A71-18647

Satellite orbital elements, examining resonance due to earth potential

08 p1366 A71-21778

Oscillations generating mechanism in resonance tube fed by subsonic gas jet, determining oscillations amplitude and frequency at resonance

09 p1382 A71-22406

Sudden step changes in parameters of nonlinear resonance systems having several stable steady state solutions

09 p1543 A71-23612

Single jet oscillations excitation of two resonant tubes, observing air motion with wool threads and stroboscopic lighting

10 p1591 A71-23823

Small amplitude resonant thermal acoustic oscillations of inviscid polytropic gas contained in finite length tube

11 p1798 A71-25446

Natural vibration analysis method for circular cylindrical shell based on three dimensional theory of elasticity and energy principle, discussing boundary conditions effect

11 p1852 A71-26405

Hydromagnetic wave coupled solar wind-plasma sheet effects on resonant oscillations of geomagnetic tail, using two dimensional model

13 p2119 A71-27910

Passage through resonance of linear oscillator with slowly varying frequency, matching inner and outer asymptotic expansions

14 p2274 A71-29861

Particle displacements during resonance motion of shear and compression waves in linearly viscoelastic flat plate of finite thickness

14 p2332 A71-30851

Ionospheric electron resonance observation by sounders aboard rocket and satellites

14 p2202 A71-30947

Mechanical support system role in determination of aeroelastic stability of leeward cylinder immersed in wake using undamped flutter theory

14 p2334 A71-31021

Pressure gain resonant combustion chambers in gas turbines, discussing thermal efficiency and power output

15 p2467 A71-31445

Longitudinal wave absorbers attenuating resonance vibrations in rods and plates

15 p2504 A71-31707

End play influence on dynamic bending vibration stresses induced by aerodynamic forces in axial flow turbine rotor blades in case of resonant vibrations

15 p2508 A71-32298

External off-axis TEM wave transformation into natural oscillation modes in Fabry-Perot resonator under axially disturbance and impinging-excited wave mismatch

15 p2410 A71-32401

Nonlinear interaction between three resonant modified ordinary electromagnetic waves propagating perpendicular to static magnetic field in homogeneous electron plasma, studying relativistic effects

15 p2460 A71-32655

Satellite orbital elements perturbations, examining resonance due to earth geopotential

15 p2495 A71-32683

Imperfect circular cylindrical shell under external hydrostatic pressure loads, determining free and resonant vibration modes

16 p2651 A71-33062

Geomagnetic tail natural oscillations, applying model of plasma cylinder with free boundary immersed in interplanetary medium

16 p2564 A71-33673

Stationary small elastoplastic longitudinal forced vibrations of rods with internal resonance, obtaining asymptotic solution of nonlinear partial differential equations

16 p2659 A71-33980

Multiple mass rheonomic vibrational systems dynamic stability, presenting approximate solution and critical dissipation level for damping parametric resonances

17 p2777 A71-34346

Nonlinear resonance problems analysis by averaging schemes, considering Volosov and Morgunov stability conditions

17 p2781 A71-34929

Friction role in impact shock absorbers for elastic systems out of static equilibrium and resonance excitation in vibrations, noting harmful effects

17 p2834 A71-35679

Additive damping control of acoustic resonance fatigue of aerospace structures under severe environments, considering materials, tuned devices and layered techniques

18 p2979 A71-36494

Power balance and statistical analysis of energy flow and response in lightly damped resonant structures

20 p3268 A71-38960

Gas resonant oscillations in closed end tube, describing time-periodic motion by perturbation method with Mach number as flow parameter

20 p3211 A71-39078

Optimum geometry and vibration damping ability of laminated three layer elastic-viscoelastic-elastic beam at resonance

[ASME PAPER 71-VIBR-102] Rectangular laminated orthotropic plates natural vibrations analysis, using extended Ritz technique

21 p3461 A71-40328

Resonant oscillations effect on heat transfer across mixing length in cavities spanned by low speed turbulent shear layers

21 p3371 A71-41033

Circumferential flow direction nonuniformity effect in front of compressor wheel on intensity spread and resonant rotor blade vibrations

22 p3615 A71-41847

Resonance equation for rotating shaft natural vibration, using Timoshenko beam theory and gyroscopic moments

23 p3776 A71-43377

Dynamics of pipelines with nonstationary fluid flow, deriving equations for dynamic instability regions and for resonant vibration amplitudes

24 p3884 A71-45014

RESONATORS

NT CAVITY RESONATORS

NT MULTIMODE RESONATORS

Open barrel shaped resonators in plasma diagnostics, using waveguide concepts

01 p0133 A71-10683

Quartz crystal HF resonator unit for high g environments, discussing tradeoff between stiff support and stress-induced frequency instability

01 p0054 A71-10913

Resonance tube heat losses, discussing thermal exchange mechanism and wall temperature limits

01 p0180 A71-10993

Frequency division multiplexing of antenna feeder ducts without resonators using bridge circuits

01 p0054 A71-11084

Radiator systems field calculation based on waveguide and resonator excitation method, noting field amplitudes in two and three dimensional arrays

01 p0038 A71-11202

EM oscillations of open elliptic profile cylindrical mirrors resonator with dielectric elliptic cylinder

03 p0386 A71-13800

Resonators sequence delay system with external capacitance link, calculating dispersion characteristic and coupling resistance

03 p0386 A71-13802

Perturbation method in microwave electromagnetic field pattern determination and resonator design

04 p0586 A71-14657

Radio communication system hypersonic delay lines, investigating coupled resonators matching efficiency in parallel and series connection

07 p1074 A71-19142

Open barrel shaped resonators in plasma diagnostics, using waveguide concepts

07 p1170 A71-20145

Fluidic Helmholtz resonator for FM signal analysis, showing instantaneous phase difference between input and output pressures

07 p1026 A71-20568

Twin tube gas heating resonator using bistable air wall attaching supersonic power jet

07 p1028 A71-20582

Single gap klystron output resonator optimization, showing maximum electronic efficiency during bunched beam excitation

09 p1414 A71-22220

Microwave resonator Q factor and coupling and matching characteristics measurement using line probe with AM and FM signals

10 p1584 A71-24724

Ferrite resonator coupled to microwave transmission line, deriving instability effects threshold power level for comparison with measurement

10 p1584 A71-24725

Electric and magnetic surface current coefficients of antenna radiating elements in metallic waveguides and resonators by harmonics expansion applied to circular-cylindrical array

12 p1885 A71-26839

Parameters optimization for increasing tuning range of resonator with contactless piston based on numerical solution of transcendental equation

12 p1889 A71-27623

Laser resonator properties with flat outlying mirrors, examining stimulated radiation generation and energy distribution

12 p1916 A71-27764

Rotating ring resonator partially filled with dynamic isotropic medium, determining resonance properties

13 p2080 A71-29025

Planar Fabry-Perot optical resonator mirror rrs effect on modes and losses

14 p2254 A71-30138

Particle flux, energy storage and beam loading effects on superconducting traveling and standing wave resonators in linear accelerators

16 p2587 A71-33494

Microwave IC bandpass filters, utilizing dielectric resonators for high Q values

16 p2548 A71-33559

Radiator system field calculation based on waveguide and resonator excitation method, noting field amplitudes in two and three dimensional arrays

17 p2697 A71-34254

Frequency selection in He-Ne laser with Ne cell inside resonator effecting nonlinear frequency absorption

17 p2752 A71-34407

Fence guide waveguide on dielectric substrate for millimeter wave, applying to power dividers, directional couplers, hybrid rings and resonators

17 p2713 A71-34444

Vibrational combustion study of powder, using Helmholtz resonators with connected auxiliary combustion chamber

17 p2839 A71-35697

Longitudinal instability of bunch interacting with passive resonator, considering Landau damping influence by linear differential equations of motion solution

19 p3110 A71-37141

Green tensor function for waveguides, resonators and radiating devices with boundaries coinciding with orthogonal cylindrical coordinate systems surfaces

19 p3104 A71-38339

Asymmetrical single ring resonator with electric and magnetic waves, determining intrinsic fields

19 p3019 A71-38340

Contactless piston resonator ensuring one parallel resonance in tuning range, using quadrupole theory

19 p3030 A71-38341

Coupled resonator AT cut quartz crystal bandpass filter design in ladder configuration with low sensitivity and simple manufacturing methods

21 p3360 A71-40810

Hybrid lumped-distributed parameter resonant LC circuit design for nuclear magnetic resonance spectrometer

23 p3661 A71-44343

RESOURCE ALLOCATION

Computerized interactive scheduling system for modeling, optimization and priority requirements for NASA manned space flight network

10 p1581 A71-24297

Experimental computer-aided system evolution to integrate technology plans and evaluate potential resource allocations for mission-oriented technology programs

14 p2339 A71-29853

Mathematical programming models for resource allocation and project selection decision in R and D

14 p2340 A71-29855

RESOURCES

NT EARTH RESOURCES

RESPIRATION

NT HIGH ALTITUDE BREATHING

NT PRESSURE BREATHING

External respiration, gas exchange and energy expenditures during orthostatic tests involving immersion experiment

01 p0014 A71-11136

Russian book on perception of respiratory medium and gas preference in man and animals covering hypoxic or hypercapnic media, inhalation times, gas mixtures, etc

02 p0198 A71-11823

Low compensation point species capacity for carbon dioxide fixation, suggesting reduced photorespiration role

02 p0201 A71-12475

Biocontrol devices for artificial respiration and blood circulation, using information from organism

03 p0367 A71-12991

Chronic hypercapnia oxygen dissociation curves and red cell cation exchange in rats, considering compensated/uncompensated phases of respiratory acidosis

03 p0360 A71-13181

Cellular respiration and high altitude adaptation effect on cytochrome content and on oxidation and oxidative phosphorylation parameters of brain homogenates in rats

15 p2357 A71-31310

Optimal respiration mode based on controlled artificial feedback characteristics, making resistance to inhalation dependent on duration

17 p2680 A71-34644

Human olfactory perception of inspired air composition, noting sensory differentiation improvement with subsequent exposures in space flight training

22 p3505 A71-42800

Indole vapor inhalation and direct injection into mice, rats and rabbits, examining toxic qualities

22 p3506 A71-42812

Respiratory carbon dioxide and oxygen partial pressure effects on intraocular and blood pressure in rabbits under Somnifen narcosis

24 p3793 A71-44368

RESPIRATORY DISEASES

NT ASTHMA

NT PNEUMONIA

NT TUBERCULOSIS

Acute pulmonary embolism diagnoses, using vasculature angiography

07 p1042 A71-19838

High altitude pulmonary edema in unacclimatized humans, discussing symptoms, etiology incidence and prevention

14 p2183 A71-30277

High altitude pulmonary edema syndrome, investigating increased alveolar-arterial oxygen gradients of humans during treadmill exercise

14 p2184 A71-30279

RESPIRATORY IMPEDANCE

Respiratory inhibitor KCN for killing increase from single radiation doses and reduction of dose fractionation sparing effect

07 p1036 A71-18962

RESPIRATORY PHYSIOLOGY

Identification problems in mathematical model of respiratory function

02 p0206 A71-12108

Respiratory and circulatory responses in anesthetized cats to medullary ventral surface perfu-

sion with mock cerebrospinal fluid of varying K concentration or 2 percent procaine solutions
04 p0540 A71-15577

Hypoxia-hypercapnia interplay as respiratory chemoreceptors stimulants and depressants by investigating arterial oxygen and carbon dioxide tensions effects on phrenic nerve activity
06 p0854 A71-18061

Respiratory mechanics and ventilatory response to carbon dioxide during positive pressure breathing in conscious man
06 p0861 A71-18379

Hypoxic and hypercapnic ventilatory control and oxygen uptake in athletes, noting chemoreceptor function
06 p0862 A71-18384

Terminal bronchiole diameter changes with volume in isolated air filled lobes of cat lung
07 p1044 A71-20332

Electronic compensation of water vapor effects in respiratory mass spectrometry
07 p1052 A71-20335

Hypoxia from aerospace medicine viewpoint, discussing respiration physiology, oxygen transport, altitude effects, psychomotor functions, etc
08 p1238 A71-20705

German book on clinical pathophysiology of respiration covering respiratory physiology, pulmonary gas exchange, respiratory control, hypoxia, hyperoxia, pressure breathing, etc
09 p1394 A71-23069

Carbon dioxide tension in pulmonary arterial blood before/during prolonged rebreathing in oxygen mixtures at rest and exercise
10 p1558 A71-23895

Mean whole body intracellular pH and buffer capacity for arterial carbon dioxide tension in ventilated dogs
10 p1558 A71-23896

Equilibration rate of uncatalyzed carbon dioxide hydration reaction in open system at constant carbon dioxide partial pressure, examining buffering capacity effect
10 p1559 A71-23898

Respiratory diaphragmatic center, investigating motor-neuron system integral activity by recording and analyzing phrenic-nerve signals in rabbits
10 p1562 A71-24164

Respiration parameters digital recording system, describing analog signal recording and processing, analog to digital conversion and digital readout equipment and techniques
11 p1724 A71-25595

Tissue respiration and hemopoiesis in heterothermic and homothermic rodents under hypoxia
11 p1719 A71-25670

Afferent pulsed activity change in peripheral fibers of severed phrenic nerve during air inhalation and under asphyxia
11 p1719 A71-25671

Transient dynamics of ventilation and heart rate following positive and negative sustained step changes in work load initiated from different load levels
11 p1722 A71-26357

Temperature-respiration relations from isolated rat skeletal muscle mitochondria oxygen consumption measurements
11 p1723 A71-26408

Humans and animals vestibular stimuli effect on external respiration function and respiration center neuron activity
13 p2007 A71-28413

Respiratory responses and hyperventilation mechanism during static muscular work in maximal voluntary contraction, noting chemoreceptor and alarm-defense reaction
13 p2008 A71-28436

Respiratory gas reaction mechanism on potassium superoxide in closed circuit breathing apparatus
13 p2021 A71-29113

Respiratory air flow optimal regulation hypothesis, testing analytic prediction model results with experiment under stress and rest conditions
13 p2023 A71-29491

Factors affecting respiratory waves formation, modulating arterial blood pressure recordings and photoplethysmograms
14 p2185 A71-30411

Respiratory wave basic pattern during cat diaphragm artificial activation by electric rectangular stimulus to phrenic nerves
14 p2185 A71-30412

Human blood pH and gas composition regulation mechanism under response to carbon dioxide partial pressure changes in inhaled air
15 p2357 A71-31316

Alveolar-arterial oxygen pressure gradient derivation as sum of shunt, ventilation/perfusion inequalities and membrane and airway diffusions
15 p2363 A71-31444

Cortical neurodynamics during vestibular afferent activity and associated cardiovascular and respiratory reactions, noting EEG correlation to hemodynamics
16 p2527 A71-32828

Diaphragm mechanics, discussing thoracic pressure-lung volume and air flow relationships of respiratory system during electrophrenic stimulation in men and cats
16 p2530 A71-33239

Biological effects of inert gases in elevated pressure respiratory mixtures on human central nervous system
16 p2536 A71-33577

Spontaneous deep sighing breath physiological regulation in rats as lung inflation response due to vagally mediated mechanoreflex
17 p2679 A71-34176

Monograph on peripheral chemoreceptors and central chemosensitive area control of ventilation during chronic blood acid base changes and hypoxia in mammals
18 p2852 A71-35869

Respiratory aspects of hyperbaric thermal environments, considering heat exchange by convection
18 p2860 A71-36878

Human respiratory muscles electrical activity, discussing correlation analysis of interferential electromyograms from external intercostal muscles during breathing exercises
19 p3003 A71-38198

Maximum oxygen uptake measurement by two techniques, calculating heart rate
19 p3008 A71-38553

Variable tidal volume effects on lung test gas washout parameters
19 p3010 A71-38565

Respiratory chemoreceptors and acid-base alterations effects on adrenocortical activation during hypoxia in dogs
20 p3187 A71-38986

Heart rate and systolic pressure variability control through visual feedback of physiological information, obtaining respiratory measurements and ECG
21 p3344 A71-41037

Gangliosides inhibitory effects on active Ca ion transport in rat brain mitochondria, using succinate as respiratory substrate
21 p3338 A71-41075

Physiological relationship of young to old men, considering body composition, aerobic capacity and capillary-muscle fiber ratio
22 p3485 A71-41717

Water immersion or bed rest effects on basic metabolism and external respiration under simulated weightlessness
22 p3495 A71-42794

Dynamic characteristics of human respiratory and circulatory adaptation to muscular exercise, using systems analysis approach
23 p3634 A71-43905

External respiration, gas exchange and blood circulation during passive orthostatic tests
24 p3796 A71-44537

RESPIRATORY RATE

Pulmonary gas exchange relation to cyclical pattern of ventilatory flow, considering alveolar dead space and metabolic and respiratory rate effects
03 p0361 A71-13183

Central nervous system reactions to vasopressin and oxytocin presence in cerebrospinal fluid and blood, discussing respiratory frequency and antidiuretic tests
03 p0363 A71-13485

Shivering and heat polypnea threshold temperature shift in guinea pigs, considering thermal adaptation under cool environment exposure
03 p0364 A71-14250

Tidal volume and respiratory rate changes at start and end of exercise, considering ventilation control and neurogenic respiratory reflexes
04 p0545 A71-15161

High environmental carbon dioxide effects on cardiac depression and respiratory rate in rhesus monkeys and chimpanzees
06 p0851 A71-17612

Neural stimuli contribution to increasing respiration and hyperpnea during exercise
06 p0862 A71-18386

Respiratory rate and cardiac responses to exercise in man
07 p1052 A71-20326

Rats hypoxia tolerance, noting smoke effects on survival, respiratory rate, body temperature and glycolytic parameters
09 p1396 A71-23364

Jet pilots flight stresses assessment via biotelemetric transmission of pulse rate, respiratory rate, electrocardiographic data, flight altitude and velocity
10 p1567 A71-23880

Alveolar gas exchanges and cardiovascular functions during breath holding with air, determining resting oxygen consumption
12 p1870 A71-27135

Pulse wave velocity measurements in human veins by transcutaneous ultrasonic flow detectors, noting respiration and Valsalva effects
12 p1874 A71-27136

Sitting and supine position effect on exercise tolerance, heart rate, systolic pressure and respiration
12 p1874 A71-27136

rate in male subjects with coronary insufficiency, noting onset of angina pectoris
13 p2014 A71-29303

Equipment for prolonged measurement of oxygen consumption, respiratory quotient and insensitive perspiration in man, noting cost reduction and operation simplification
13 p2021 A71-29316

Respiratory air flow optimal regulation hypothesis, testing analytic prediction model results with experiment under stress and rest conditions
13 p2023 A71-29491

Metabolic, ventilator and cardiovascular response during free swimming and treadmill walking, relating oxygen consumption to work intensity
13 p2024 A71-29500

Regulation patterns of external respiration rate in man during physical exertion, showing load dependent pulmonary ventilation in accord with minimum energy expenditure principle
15 p2358 A71-31321

Optimal respiration mode based on controlled artificial feedback characteristics, making resistance to inhalation dependent on duration
17 p2680 A71-34644

Physiological tests for psychic stress effects on aircraft pilot tracking performance, respiration and heart rate
17 p2693 A71-35199

Hypothermia effect on brain nutritive processes and regulator activity, considering changes in brain blood supply, respiration and carbohydrate metabolism
22 p3486 A71-41940

Respiratory function and gas metabolism shift under high transverse accelerations in reclined confined subjects
22 p3495 A71-42795

Human nitrogen and water-salt metabolisms and respiratory activity during prolonged confinement in small volume chamber with cyclic varying hypoxic air
22 p3495 A71-42799

Physiological effects on mice of air pollution with gaseous toxic substances from urine and feces, noting increased respiration rate and choline esterase activity
22 p3486 A71-42807

Hypoxic respiratory reactions of highland natives and recently arrived residents to oxygen concentration change in inhaled mixtures
24 p3798 A71-45065

Respiratory sinus arrhythmia by spectral analysis and digital filtering, using linear model to approximate lung volume relationship to heart rate during normal breathing
24 p3802 A71-45067

RESPIRATORY REFLEXES

Tidal volume and respiratory rate changes at start and end of exercise, considering ventilation control and neurogenic respiratory reflexes
04 p0545 A71-15161

Dynamic respiratory and circulatory responses to hypoxia in anesthetized dogs, recording oxygen partial pressures, heart rate, blood pressure, blood flows, respiratory rate, etc
09 p1396 A71-23358

Human hypoxic ventilatory drive data for high altitude breathing, noting motivation reduction inversely related to time and altitude
14 p2185 A71-30288

Ventilatory control in acute hypoxia, detailing polycythemia effects on respiratory chemoreceptor sensitivity
14 p2185 A71-30289

Reflex increase in ventilation induced by vibrations applied to cat triceps surae muscles, noting muscular and articular receptors role
17 p2678 A71-34175

Spontaneous deep sighing breath physiological regulation in rats as lung inflation response due to vagally mediated mechanoreflex
17 p2679 A71-34176

Respiratory reflex mechanism of deep breath occurrence after period of airway occlusion in rabbits related to stimulation of vagal receptors
20 p3187 A71-39040

Transient heart rate response to square wave breathing in man under zero G parabolic flight
22 p3501 A71-41828

Chronic hypoxia exposure effects on human ventilatory response to carbon dioxide and oxygen deficiency
24 p3797 A71-44780

RESPIRATORY SYSTEM

NT BRONCHI

NT BRONCHIAL TUBE

NT DIAPHRAGM [ANATOMY]

NT LUNGS

NT NOSE [ANATOMY]

NT PHARYNX

Respiratory neuron structure in lateral zone of medulla oblongata in cats
01 p0013 A71-11097

Cardiovascular and ventilatory responses to room air and pure oxygen breathing under various exercise work load conditions
01 p0016 A71-11407

- Human respiratory parameters telemetry, discussing transducer development for ventilatory volume measurement 03 p0370 A71-13068
- Respiratory features for conscious or unconscious warning of impending exhaustion, noting work load-performance decrement relation 04 p0545 A71-15159
- Cardiovascular and respiratory systems afferent innervation in cats investigating pericardial, expiratory and pneumo-vascular mechanoreceptors 05 p0707 A71-16343
- Human physical exercise with stepwise increasing load noting working capacity, cardiovascular and respiratory system performance and blood composition interrelations 05 p0709 A71-16805
- Carbohydrate ingestion produced respiratory gas exchange ratio and alveolar ventilation effects on arterial oxygen tension in normal men 07 p1052 A71-20333
- Cardiopulmonary and circulatory mechanisms, adaptation limits and response to aerospace flight stress 08 p1238 A71-20720
- Central regulation mechanisms of acidic-alkaline equilibrium in ontogenesis, discussing midbrain intraterine and respiratory postnatal development 08 p1241 A71-21937
- Soyuz 9 spacecraft astronaut cardiovascular and respiratory systems responses to orthostatic effect after 18-day orbital flight from EKG measurements and sphygmography 09 p1389 A71-22208
- Book on clinical physiology techniques and anesthesiology measurements covering electronics, ECG analysis, blood pressure measurement, cardiac function, respiratory mechanics, etc 09 p1398 A71-22459
- Respiratory system self regulation and coordinated activity interference by bioccontrolled stimulator incorporation into natural nerve links 10 p1567 A71-24165
- Flow visualization and velocity measurements in repeatedly branching tube systems representative of human lung, estimating viscous dissipation and pressure drop 10 p1571 A71-24625
- High altitude aerobic working capacity limitations, examining oxygen transport system and circulator factors 14 p2183 A71-30276
- High altitude blood coagulation, determining hypercoagulability relationship to altered pulmonary hemodynamics 14 p2183 A71-30278
- Cardiovascular and respiratory systems, motor and muscular activity, metabolism and body energetics functional changes due to prolonged weightlessness 16 p2531 A71-33676
- Noisy environment effects on circulatory, respiratory and metabolic parameters during physical exercise, measuring heart rate, systolic blood pressure, oxygen intake and respiratory quotient 20 p3185 A71-38889
- Microbial contamination of human skin and upper respiratory tract during long term isolation in sealed environment 21 p3333 A71-40559
- RESPIROMETERS**
- Microbiological respirometer for oxidative metabolism for plants and small animals, considering manned space flight applications 14 p2189 A71-30344
- RESPONDERS**
- U TRANSDUCERS**
- RESPONSE BIAS**
- Voltage distribution in transistor base for forward and reverse biases, discussing nonuniform potential distribution 05 p0728 A71-16007
- Detection characteristics of transistor input circuit with automatic bias 11 p1740 A71-26545
- Voltage distribution in transistor base for forward and reverse biases, discussing nonuniform potential distribution 22 p3524 A71-42756
- RESPONSE TIME [COMPUTERS]**
- Rapid-response automatic control systems synthesis, using compensation signals based on external disturbances 01 p0063 A71-10722
- Holographic optical memory and computer output applications for rapid bulk data storage, considering various laser visualization systems 06 p0908 A71-18067
- Decision logic table application, utilizing valid response sets development maximum number and biparameter conditions 09 p1412 A71-23283
- RESPONSES**
- NT DYNAMIC RESPONSE**
- NT FREQUENCY RESPONSE**
- NT GALVANIC SKIN RESPONSE**
- NT HEMODYNAMIC RESPONSES**
- NT MODAL RESPONSE**
- NT PHYSIOLOGICAL RESPONSES**
- NT TIME RESPONSE**
- NT TRANSIENT RESPONSE**
- Composite material structural behavior prediction, emphasizing static, dynamic, buckling and post-buckling response of anisotropic plates laminated from unidirectional plies 11 p1846 A71-25429
- REST**
- NT BED REST**
- Position, exercise and lung volume effects on healthy males pulmonary diffusing capacity for CO at rest and during exercise 13 p2015 A71-29493
- Pulse frequency behavior during acquisition of perceptual and motor skills with particular attention to rest periods 15 p2362 A71-31195
- Resting and postexercise apexcardiogram correlation with maximal treadmill stress test, noting mean a-wave ratios 21 p3332 A71-40406
- Human response time for urgent signal after operational rest, showing effect of additional activation during waiting period 21 p3337 A71-41060
- RESTARTABLE ROCKET ENGINES**
- S-IVB liquid rocket engine and propellant feed systems restart shutdown in orbital operations [AIAA PAPER 70-672] 07 p1183 A71-19857
- Depressurization extinguishment of composite solid propellants for thrust termination, considering flame structure, surface characteristics and restart capability [DFVLR-SONDDR-129] 13 p2113 A71-28615
- RESTRAINTS**
- U CONSTRAINTS**
- RESTRICTIONS**
- U CONSTRUCTIONS**
- RESUSCITATION**
- Biocontrol devices for artificial respiration and blood circulation, using information from organism 03 p0367 A71-12991
- Artificial respiration in elevated gas pressure chamber to revive organism after clinical death by rapid decompression 12 p1876 A71-27745
- RETARDANTS**
- Book on chemistry and uses of fire retardants covering P, Sb, B, Cl, Br, cellulose, coatings and synthetic polymers 02 p0275 A71-12775
- RETENTION**
- Human nervous system stimulus trace retention in various age groups, using skin galvanic reaction 08 p1240 A71-21788
- RETENTION [PSYCHOLOGY]**
- Redundancy effects on human memorization working capacity, noting application to memory systems design 07 p1043 A71-20113
- Biological memory and perception processes electronic simulation by keyboard structure reenacting word reception, storage and delivery 07 p1051 A71-20118
- Learning sets development relation to transfer suppression, discussing previously learned discriminations retention 13 p2011 A71-28803
- Target value and exposure duration effects on recall in visual search tasks, discussing results in relation to previously reported inconsistencies 18 p2854 A71-36103
- Proactive reaction time inhibition as indicator of immediate memory retention intensity in subjects receiving interpolated acoustic stimuli 23 p3634 A71-43865
- RETICLES**
- Optimum AM reticle-detector models, discussing image resolution, electrical bandwidth and detection problems 07 p1115 A71-20368
- High accuracy angular precession measurements with autometric gyro for satellite relativity tests, using optical system with reticle coordinates 09 p1452 A71-23595
- RETICULOCYTES**
- Cellular damage to rat mitochondria and endoplasmic reticulum by injection of radioprotectors, discussing intracellular enzymes passage into plasma 07 p1039 A71-18981
- Spleen role as erythrocytic depot in reticulocytic reaction to acute hypoxia in splenectomized dogs inhaling air with reduced partial oxygen pressure 13 p2007 A71-28418
- RETINA**
- NT FOVEA**
- Visual cells outer segments structure and retinal photoreception characteristics, describing open thermodynamic system 01 p0009 A71-10231
- Cat retina ganglion cell /YCC-1/ threshold intensity, obeying reversed Weber law 01 p0009 A71-10234
- Rudd vision mechanism, considering daylength effect on spectral sensitivity and visual pigment retinal extract proportions 01 p0009 A71-10271
- African lungfish retina electron microscopy for Landolt club location, mitochondria, glycogen and microtubule content, considering relation to receptors and possible functions 01 p0009 A71-10272
- German monograph on frequency filter behavior of human retina regarding electric pulses, using ganglion model 03 p0373 A71-14372
- Binocular synchronization data, suggesting visual coordination dependent on continuous eye movement and retinal feedback timing 05 p0712 A71-16218
- Sensitivity, size and receptive fields position in cat retina ganglion cells 05 p0706 A71-16341
- Retinohypothalamic projection in rats by light microscope observations in unilateral retinal destruction 05 p0707 A71-16344
- Retinohypothalamic projection in rats by electron microscope observations of degenerating nerve fibers and boutons in arcuate nucleus after bilateral retinal destruction 05 p0707 A71-16345
- Human eye optical performance, noting retina anatomy and physiology, visual acuity, resolving power and reflectometry 05 p0713 A71-16482
- Retinal neurons receptive field center, examining excitation and direct inhibition interaction 05 p0707 A71-16596
- Retinal electronic model with about 700 photoreceptors and output cells and new interconnections technique 05 p0715 A71-17079
- Parafoveal sensitivity disruption /flash blindness/ due to retinal location and high intensity short duration adapting flash 06 p0851 A71-17605
- Unicocular oscillopsia with vertical retinal nystagmus and internuclear ophthalmoplegia due to multiple sclerosis 06 p0852 A71-17615
- Vertebrate retina receptive field structure, suggesting interaction between receptor, horizontal and bipolar cells 07 p1046 A71-20623
- Vestibular stimulation effects on bioelectrical activity in retina, optic tract, geniculum, visual cortex and ectosylvian gyrus in anesthetized cats 09 p1390 A71-22215
- Delayed e-wave like electrical response to light and inhibition in developing frog retina 09 p1393 A71-23011
- Stereoscopic vision dependent on vertical grating of different spatial frequency of retinal images 09 p1394 A71-23013
- Stiles-Crawford effect interpretation by geometrical scalar theory, calculating retinal cones mean diameters 10 p1560 A71-23991
- Peripheral visual resolution measurements, determining acuity thresholds at fovea and various points on temporal retina horizontal meridian over range of luminance values 10 p1564 A71-24608
- Model of retinal information in cats from physiological and anatomical evidence, considering processing of contrast and eye movement information 11 p1723 A71-25254
- Book on color and pattern vision physiology covering retinal induction, electrical excitation of eye, optical illusion, figural aftereffect, movement sensation, etc 12 p1870 A71-26769
- Distinctive visual evoked response potential field patterns resulting from human retina stimulation, using electrode array on occipital scalp 13 p2012 A71-28893
- Visual sensation time theory validity investigation, discussing time elapsed between retinal receptor stimulation and perceptory sensation 14 p2189 A71-30406
- Histopathological and fluorescein angiographic studies of rhesus monkey chorioretinal lesions produced at threshold and suprathreshold power levels of Ar laser 15 p2365 A71-32347
- Rhodopsin kinetics mathematical analysis by cyclic five-component model, applying to flash and extended photolysis in rat retina 17 p2680 A71-34653
- Photoc and electric release of afterdischarges in rats visual cortex, showing retina and Corpus geniculatum laterale role 17 p2686 A71-35489
- ACh retina application effects, showing second retinal neuron cholinergic receptors desensitization 17 p2686 A71-35490

- Laser-induced retinal damage model based on energy interaction modes, including thermal and acoustic transients, vaporization and dielectric breakdown
18 p2863 A71-35955
- Human cone visual pigments kinetic equation testing by comparing photolysis rate at equilibrium to regeneration rates
18 p2854 A71-36001
- Retina photosensitive cells properties and functions compared with films photosensitive chemicals, emphasizing retinal image transformation
18 p2864 A71-36068
- Signal propagation in model neuron network in terms of differential equations system, representing retina major cell types in planar model
19 p3003 A71-38276
- Retinal damage thresholds of rhesus monkeys to ocular radiation from yellow line 568.2 nm emitted by krypton CW gas laser
19 p3008 A71-38284
- Human retinal blood circulation changes and vision disturbance under transversely directed acceleration, using dark chamber teleophthalmoscopy
20 p3188 A71-39228
- Corned-retinal potential as generator of occipital alpha rhythm in human electroencephalogram modulated at 10 Hz by tremor in extraocular muscles
21 p3329 A71-40176
- Retinal directional effect measurements confirming mathematical model based on Gaussian distribution of retinal cones orientation, explaining brightness stimuli effectiveness and hue shift
21 p3335 A71-40670
- Circadian rhythm in isolated Aplysia eye due to retinal neurons population interaction
23 p3633 A71-43545
- Feline retinal neurons, noting span and density of branching amacrine cell protrusions and ganglion cells diversity
23 p3633 A71-43581
- Visual pigments in color blind subjects, using retinal densitometry
24 p3794 A71-44464
- Coriolis acceleration effect on human organism from optic functions and retinal hemodynamics study
24 p3795 A71-44534
- RETINAL ADAPTATION**
NT DARK ADAPTATION
NT LIGHT ADAPTATION
Visual threshold dependence on retinal location for various colors under conditions of scotopic, mesopic and photopic adaptation
01 p0009 A71-10233
- Sight of body and active locomotion effects on perceptual adaptation to tilted vision in male subjects
01 p0010 A71-10398
- Open and closed eyes electroretinogram, discussing lamellar electrode placed on lower eyelid
01 p0024 A71-11077
- Peak diameter differences of sensitization by annular surrounds in subjects, concerning scotopic increment threshold and retinal illuminance
03 p0365 A71-14376
- Rhodopsin dissociation and retina photochemical and bioelectrical processes after light flashes of various intensity
09 p1388 A71-22124
- Mean retinal threshold gradient along horizontal meridian for dark and light adapted eyes, considering dynamic neural mechanism
01 p1566 A71-24807
- Displaced and delayed retinal feedback adaptation theory for human factors problems in man machine systems
10 p1571 A71-24825
- Visual adaptation mathematical model, studying relation of brightness static transformation into luminance
17 p2692 A71-35174
- Retinal adaptation to prism-displaced hand image in terms of sensorimotor coordination central control change
19 p3006 A71-37543
- Proposed prism adaptation model suggesting visual motor control loop as linear system comprising independent subsystems
19 p3007 A71-37544
- Detectability measurement of foveal stimulus, suggesting nonuniformity of retinal illuminance in visual task
19 p3003 A71-38278
- Visual performance and retinal vascular changes under hypobaric elevation and hypoxia, noting stereopsis, binocular depth perception, critical flicker fusion, dark adaptation, etc
22 p3485 A71-41719
- Flicker adaptation effect on visual sensitivity to temporal fluctuations of light intensity
23 p3635 A71-43974
- HF signals adaptation dependence from human cornea potential measurements by presenting narrow band chromatic stimuli to subjects under photopic, mesopic and scotopic adaptation conditions
24 p3794 A71-44467
- Increment threshold for monoptic and dichoptic vision, showing spatial and luminance effects
24 p3801 A71-44979
- RETINAL IMAGES**
Soviet book on visual image formation on retina covering perception, stabilization, manipulative ability, etc
03 p0364 A71-13692
- Suprathreshold vision retinal image contrast loss measurement, suggesting role of balance between optical unsharpness and neural oversharpeness
04 p0540 A71-15833
- Color sensations and retinex theory, discussing mathematics of lightness scheme and biologic correlate of reflectance
05 p0753 A71-16901
- Optical perception constancy of object size, developing mathematical models of accommodation, convergence and retinal image size
07 p1051 A71-20120
- Retinal threshold along horizontal meridian for dark and light adapted eyes for stray light from small foveally fixated high luminance target
08 p1247 A71-21000
- Visual recognition process for simple achromatic image confined within simultaneous-perception viewing angles, deriving hypothetical model based on psychological factors
10 p1567 A71-24162
- Visual image propagation from retina to higher level formations in multichannel system of cat visual analyzer
10 p1561 A71-24163
- Retinal sine wave flicker transient response obtained with circular uniform field and counterphase grating targets
11 p1799 A71-26141
- Chorioretinal temperature increases from naked solar eclipse observations for various observation angles and pupil diameters, considering solar irradiance and atmospheric transmittance spectra
11 p1726 A71-26484
- Light flashes in eyes of dark adapted Apollo astronauts, considering Cerenkov radiation effects from primary cosmic ray single charged particles on retinal elements
12 p1933 A71-27383
- Visual perception theoretical models for liminal contrast prediction
13 p2023 A71-29442
- Human visual perception response to brightness under sinusoidal current, suggesting interaction with retinal neural structures
17 p2680 A71-34656
- Refraction and image forming qualities of frog eye using measurement of intensity profile /point spread function/, confirming hyperopia
18 p2857 A71-36690
- Apollo astronauts light flashes observation during lunar flight, discussing interpretation as scintillations in eye lens by multiply charged cosmic rays focusing on retina
19 p3001 A71-37299
- Retinal adaptation to prism-displaced hand image in terms of sensorimotor coordination central control change
19 p3006 A71-37543
- Stimulus patterns spatial intervals and line thickness effects on stabilized retinal images
19 p3004 A71-38280
- Visual evoked potential relationship to apparent size reduction of invariant retinal image
19 p3004 A71-38281
- Visual projection, magnification and retina overlap on dorsal lateral geniculate nucleus in cats measured by random scatter in receptive field
21 p3335 A71-40668
- Human cerebral EEG phenomena and evoked potential relationships to eye and retinal image movements
22 p3488 A71-42437
- Crossed retinal pathways in Siamese cats due to neuroanatomical defect impairing binocular vision and stereoscopic depth perception
23 p3633 A71-43546
- Afterimage induced smooth eye movements despite absence of moving visual stimulus, suggesting retinal image stabilization and saccadic behavior inhibiting processes
24 p3794 A71-44469
- Retinal image stabilization variables, noting whole fade characteristics sensitivity to stimulus pattern variations
24 p3795 A71-44470
- RETINENE**
Vitamin A initial uptake site and intracellular transport pathway in snails photoreceptors
01 p0009 A71-10230
- Vitamin A deficiency effect on rhodopsin loss dependent on illumination level in rat eye using electroretinography
10 p1563 A71-24326
- Irreversible damage effects of visible light on retina in rats as function of irradiation, exposure time and vitamin A deficiency cell adaptation
10 p1563 A71-24327
- Thyroidectomized vitamin A deficient rats, noting visual sensitivity loss not correlated to thyroid
13 p2008 A71-28455
- RETRACTABLE LANDING GEAR**
U LANDING GEAR
RETREIVAL
NT DATA RETRIEVAL
NT INFORMATION RETRIEVAL
RETROACTION
U RETROTHRUST
RETROFIRING
Impulsive retrofire deboost of rocket vehicles initially moving in elliptical orbits for maximum and minimum atmospheric entry angles
22 p3608 A71-41697
- RETROREFLECTION**
Q switched ruby laser ranging system of tracking station for use with retroreflecting satellites
03 p0379 A71-14007
- Laser radar system using retroreflector on lunar surface for measurement of distance between earth and moon
16 p2543 A71-33811
- Apollo optical retroreflector arrays characteristics and performance for laser range measurements from earth stations, describing multilensed receiver telescope
16 p2642 A71-33831
- Laser ranging of moon using retroreflector mounted on Lunokhod-1 lunar surface vehicle
17 p2707 A71-35402
- Laser ranging to retroreflector array placed on lunar surface during Apollo 11 mission
20 p3296 A71-39622
- RETROCKET ENGINES**
Stored gas rocketrocket total impulse expression, deriving from flow continuity equation in closed duct
08 p1366 A71-21308
- RETROSEQUENCING**
U RETROFIRING
U SEQUENTIAL CONTROL
RETROTHRUST
Exact expression for minimum range sensitivity deorbit from elliptical orbits for ballistic atmospheric entry vehicle, considering retrovelocity
07 p1199 A71-19873
- RETURN BEAM VIDICONS**
Return beam vidicon characteristics and applications for reconnaissance, optical storage and scan conversion, data and signal processing
22 p3548 A71-42509
- RETURN TO EARTH SPACE FLIGHT**
Thrust power optimization for spacecraft earth-planet round trip trajectories
12 p1957 A71-26633
- Trajectory analysis of geocentric phase and selenospherical motion of space vehicle leaving lunar surface and returning to earth atmosphere
13 p2143 A71-29209
- Earth-Jupiter-Saturn-earth trajectories, determining mission planning parameters
[AAS PAPER 71-361] 23 p3729 A71-43031
- REUSABLE LAUNCH VEHICLES**
NASA space transportation system economics, discussing cost analytic considerations in comparing reusable vs expendable launch systems
[AIAA PAPER 71-806] 17 p2841 A71-34733
- REUSABLE SPACECRAFT**
NT SPACE SHUTTLES
Boride composites with high strength and thermal resistance suitable as nose cap and leading edge materials for reusable lifting reentry systems
[AIAA PAPER 70-278] 01 p0109 A71-11282
- Abort and staging separation maneuvers of two equal size reusable lifting entry vehicles in wind tunnel tests
[AIAA PAPER 70-260] 01 p0165 A71-11579
- American-European space shuttle costs, comparing nonrecoverable Europa 3 with ballistic reusable devices
05 p0816 A71-16402
- Economical reusable space shuttle development for cargo and passenger transportation to and from orbit
07 p1206 A71-19090
- Space shuttle requirements from lifting body pilot viewpoint, noting booster and spacecraft reusability
07 p1206 A71-19091
- Two stage space shuttle, discussing NASA reusable spacecraft cost reduction and technological problems
07 p1209 A71-20226
- Space transportation system of two stage reusable space shuttle and orbit-to-orbit shuttle, supporting NASA and DOD missions
08 p1367 A71-21890
- Space based reusable manned/unmanned tug, discussing potential missions, system requirements and auxiliary hydrogen oxygen propulsion system
[AIAA PAPER 70-719] 09 p1511 A71-22902

Space shuttle phase B design, discussing British-American cooperation, fly-back orbital laboratory and Apollo 14 zero-gravity demonstration
11 p1839 A71-26320

Reusable Nuclear Shuttle using NERVA nuclear engine for low cost transportation to lunar and geosynchronous orbit, discussing design, operation, tests and problems
11 p1840 A71-26516

NASA evaluation of reports on space shuttles, discussing booster and orbiter design, mission requirements, payload capabilities, reusability, etc
14 p2320 A71-30421

Reusable nuclear shuttle design, considering various propellant tank configurations and expendable/reusable launch modes with respect to performance, development cost and cost effectiveness
[AIAA PAPER 71-640] 14 p2273 A71-30717

European Space Tug, discussing payload spectrum, multimode operation, reusable propulsion system and various missions application
15 p2499 A71-31215

Reusable nuclear shuttle concepts, performance and design requirements
17 p2813 A71-35072

Reusable nuclear shuttle guidance and control system requirements, using nuclear engine thrust pulse train for guidance
17 p2774 A71-35073

Navigation and guidance alternatives of reusable nuclear shuttle, stressing onboard sensors and processing systems for position and attitude determination
17 p2774 A71-35074

Reusable nuclear shuttle navigation systems evaluation by mission simulation, discussing reduced NERVA cooldown thrust pulses uncertainty effects
17 p2774 A71-35075

Reusable space shuttle optimization, discussing earth-to-orbit transportation, economic aspects, booster vehicles design, propellant cryogenic tanks and thermal protection
[AIAA PAPER 71-805] 17 p2814 A71-35430

Space shuttle with two stage booster and orbiter reusable vehicles, discussing performance, structural design and flight control system
[AIAA PAPER 71-804] 17 p2814 A71-35431

Commercial aircraft reliability and maintainability design philosophy application to reusable space vehicles, considering optimum redundancy, dispatch with component inoperative and fault isolation
18 p2973 A71-36481

Canard space shuttle reusable launch vehicle wing geometry variations effect on flyback systems weight, noting influence of aspect ratio and wing area
18 p2974 A71-36484

Space transportation system design concept based on reusable engines and partially external expendable tankage/REPEET, discussing economic factors
19 p3147 A71-37125

Mixed mode propulsion system for optimization of reusable space shuttle, discussing one-stage-to-orbit vehicle advantages and feasibility
19 p3121 A71-37126

European contribution to space shuttle and tug reusable space transportation systems, discussing post-Apollo programs cost analysis and hardware
19 p3150 A71-37310

Open cell lightweight cryogenic insulation for reusable liquid hydrogen fueled vehicles including space shuttle
20 p3312 A71-39271

Two stage reusable manned space shuttle computerized onboard data management system hardware and software
[IBM-712000405] 22 p3517 A71-41977

Two stage reusable space shuttle system for space transportation program, discussing budget, development and testing, international cooperation and information exchange
22 p3610 A71-42022

Computerized synthesis for fly-back system of first stage winged booster for earth-to-orbit reusable space transportation system
[FZA-456] 22 p3611 A71-42032

Reusable space tug payload injection missions, determining optimal round trip trajectories at earth escape energy levels
[AAS PAPER 71-370] 23 p3730 A71-43040

Reusable space transportation shuttle system, discussing design, operation, military uses, contract competition, economic analysis and political factors
23 p3784 A71-43353

NERVA reactor in-flight cooldown during engine shut-down phase of reusable earth-lunar transportation vehicle, discussing coolant management considerations
23 p3703 A71-44270

REUSEABLE SPACECRAFT
NT SPACE SHUTTLES
REVERBERATION
Surface energy absorption coefficient determination from decaying sound fields, deriving reverberation time and decay rate equations
23 p3703 A71-43201

REVERSE TIME
U REACTION TIME
REVERSED FLOW
Fredholm method for reversible transonic flow in computing aircraft wing and turbomachine or helicopter blade airfoils for compressibility law
01 p0003 A71-11022

Reversible transonic fluid flow through cylindrical blades cascade by hodographic singularities solution of potential and stream function
01 p0003 A71-11023

Reverse flow temperature probe design and calibration for vertical soundings from aircraft, comparing to radiosonde method
02 p0247 A71-11822

Channel flow and flow past bodies turbulent/laminar reverse transition for friction drag and heat transfer reduction
06 p0881 A71-17584

Cross flow profiles for compressible turbulent boundary layers with and without flow reversal via hodograph models family
08 p1229 A71-22033

Shielded hot-wire probe for mean and rms flow velocities in highly turbulent and rapidly reversing flows
24 p3828 A71-45075

REVERSING
Modified Landau-Lipschitz equation of thin ferromagnetic film for slowly reversing magnetic fields solved by interpolation, discussing magnetization curve subrelaxation segment
11 p1809 A71-26547

REWARD [PSYCHOLOGY]
Reward magnitude effects on runway performance of rats with intertrial feeding
03 p0372 A71-13693

Differentiation of hypothalamic drive and reward centers, applying electric stimulation via chronically implanted electrodes
17 p2681 A71-34944

REYNOLDS EQUATION
Positive pressure gradient turbulent boundary layer local characteristics in plane diffuser, using Reynolds stress change equations
07 p1086 A71-18770

Reynolds analogy of heat transfer applied to disk rotating near stator, including frictional dissipation and radial outflow in compressible or incompressible flow
13 p2048 A71-28599

Reynolds differential equations for three dimensional gas lubrication flows, noting linear velocity at rotating cylinder surface
17 p2749 A71-35639

Elastic boundary interaction with viscous sublayer of turbulent boundary layer for Reynolds stresses and drag reduction possibility
19 p3042 A71-37082

Book on statistical mechanics of turbulent fluid flows covering gas oscillations, correlation function, Reynolds equation, laminar flow, particle dispersion, etc
20 p3213 A71-39774

REYNOLDS LAW
U REYNOLDS EQUATION
REYNOLDS NUMBER
Temperature effects on heat transfer in turbulent boundary layer on cooled plate at various Reynolds numbers
01 p0179 A71-10609

Plane diffuser cascade losses at low main stream pressures, discussing Reynolds number role
01 p0003 A71-11062

Arc discharge plasma response to turbulent gas flow covering wide range of Reynolds numbers measured with Langmuir probes
01 p0136 A71-11479

Spherical particle motion investigation in plane Couette flow, predicting critical Reynolds number for transition to turbulent flow
03 p0398 A71-13112

Temperature sensitive paint and thermocouple techniques comparison for boundary layer transition data, considering aerodynamic heating and transition Reynolds numbers
03 p0518 A71-13468

Steady incompressible flow past oblate and prolate spheroids for Reynolds numbers up to 100, using spherical coordinates and finite difference method
03 p0400 A71-13729

Turbine blades with high aspect ratios, calculating behavior at small Reynolds number
[ASME PAPER 70-WA/GT-11] 03 p0343 A71-14119

Heated glass free jet characteristics at low Reynolds numbers, evaluating temperature distribution and two dimensional fluid dynamic effects
[ASME PAPER 70-WA/FE-3] 03 p0521 A71-14125

Compressible flow with closed streamlines at large Reynolds numbers, considering viscous and heat conduction cumulative secondary effects
04 p0569 A71-14987

Decay time of low Reynolds number weak turbulence generated by single and multistage grids, considering three dimensional energy spectrum
04 p0569 A71-15026

Pressure gradients and slot Reynolds number effects on impervious wall film cooling effectiveness in constant density flow
04 p0680 A71-15474

Local heat transfer to transverse circular cylinder at low Reynolds numbers, using iterative finite difference approach
04 p0683 A71-15493

Flat plate wake displacement sources in potential flow, considering high Reynolds numbers outside boundary layer
05 p0695 A71-16960

Viscous incompressible fluid flow with free boundary at large Reynolds numbers, deriving asymptotic expansion solution for wave motion
05 p0737 A71-16989

Steady two dimensional flow past flat plate in rectangular channel for low Reynolds number
05 p0738 A71-17249

Performance characteristics of horizontal and vertical stabilizers at medium Reynolds number from wind tunnel measurements, considering air foil and flap effects
06 p0842 A71-18249

Vortex streets behind circular cylinders at Reynolds numbers 50-160, discussing transition
06 p0842 A71-18322

Hypersonic cruise aircraft configuration reliable Reynolds numbers extrapolation from laminar boundary to turbulent layer
[AIAA PAPER 71-132] 06 p0883 A71-18576

Hypersonic flight test base pressure results at high Reynolds numbers for slender cone in turbulent flow, noting implications for ground test simulation
[AIAA PAPER 71-134] 06 p0883 A71-18578

Large diameter tube high Reynolds number air flow temperature profiles, using chromel-alumel thermocouple
07 p1220 A71-18762

Turbulent flame propagation at high Reynolds numbers, discussing nonthermal hydrodynamic mechanism, laminar front and fine structure
07 p1223 A71-19249

Small curvature radius/throat radius ratio supersonic nozzles mass flow rate coefficients at high Reynolds numbers, appraising isentropic flow prediction methods
07 p1015 A71-19877

Sphere and disk drag measurements for Reynolds numbers from 5 to 100,000, examining forces, moments, flow visualization, unsteady modes and constant acceleration
07 p1015 A71-19893

Computer calculation of high Reynolds number viscous and inviscid flow over arbitrary shaped two dimensional bodies and airfoils
07 p1017 A71-20313

Velocity distribution and Reynolds number relation to thickness in liquid films using turbulent viscosity
07 p1094 A71-20545

Low Reynolds number incompressible transient creep flow calculation by Marker-Cell numerical solution extension
07 p1094 A71-20613

Nonlinear subgrid scale eddy viscosity formulation for turbulence generated by mean shear or thermal instability at large Reynolds number
07 p1094 A71-20615

Boundary value problem of end effect in MHD channel with semiinfinite electrodes for arbitrary Reynolds numbers
09 p1499 A71-22130

Inviscid incompressible electrically conducting fluid flow past slender profile investigated by asymptotic power expansion of reciprocal magnetic Reynolds number
09 p1382 A71-22135

Steady boundary layer flow in viscous liquid thin down variable incline for large Reynolds and Froude numbers
09 p1432 A71-22451

Surface roughness ensuring turbulent reattachment at low Reynolds numbers on airfoil sections with separation near leading edge resulting in bubbles
[ONERA-TP-923] 10 p1549 A71-23762

Numerical calculation of Oseen hydrodynamic fields around sphere in unbounded fluid for various Reynolds numbers, obtaining flow velocity and drag
10 p1592 A71-23935

High Reynolds number transonic wind tunnel need in U.S., discussing wing maximum lift and pitching moment, shock induced flow separation, etc
10 p1589 A71-24174

Supersonic turbulent boundary layer density profile over flat plate at single Reynolds number, using Mach-Zender interferometer
10 p1593 A71-24270

Heat transfer at high Peclet number from sphere freely rotating in shear flow field at low Reynolds numbers
10 p1697 A71-24621

Laser heating induced turbulence in fluid medium, using dimensional analysis for effective Reynolds number
10 p1622 A71-24960

Constant property fluid laminar flow between rotating and stationary infinite disks for limiting Reynolds numbers based on gap width

11 p1748 A71-25154

Pipe flow hot wire measurements at turbulence onset Reynolds numbers, exhibiting axisymmetric laminar velocity profile distortion

11 p1748 A71-25155

Reynolds number effects on centrifugal compressor performance characteristics, discussing power losses in compressor, impeller and diffuser stages and compressor adiabatic efficiency

[ASME PAPER 71-GT-25] 11 p1703 A71-25967

Numerical analysis of steady symmetric incompressible flow past elliptical cylinders for Reynolds numbers up to 90

12 p1895 A71-26739

Bifurcation solutions of Navier-Stokes equations for time periodic motions of viscous incompressible fluid at critical Reynolds number

12 p1922 A71-26867

High Reynolds numbers asymptotic suction boundary layer linear stability analysis for viscous flow, using transformations to hypergeometric functions

12 p1896 A71-26923

Boundary layer suction optimization to achieve normal velocity component distribution for local Reynolds number equal to critical value at transition point

12 p1896 A71-26973

Vortex shedding characteristics of circular cylinders at low Reynolds numbers from experiment on tapered models wake structure

12 p1897 A71-27220

Plane parallel Couette flow stability with respect to small perturbations, considering positive wave numbers and Reynolds numbers

12 p1897 A71-27307

Transonic airfoil testing techniques in two dimensional flow, discussing wind tunnel conditions at various Reynolds numbers

12 p1864 A71-27467

Viscous convergent-divergent nozzle flow slender channel approximation, discussing nozzle geometry, Reynolds number and wall temperature effects

[AIAA PAPER 69-654] 12 p1865 A71-27556

Momentum thickness of boundary layer of circular cylinder in cross flow at high Reynolds numbers from static pressure and skin friction measurements

12 p1867 A71-27738

Unsteady acoustic wind in free sound field for random Reynolds numbers, using stream equation

13 p2101 A71-28847

Flow theory of steady separation zone near body at high Reynolds numbers, determining vortex parameters counterflow inviscid region

13 p2049 A71-29171

Asymptotic limiting viscous flow pattern and drag on flat plate with stationary separation zones at large Reynolds numbers

13 p2050 A71-29204

Friction factor for low Reynolds number turbulent flow in large aspect ratio rectangular ducts, comparing Blasius and Prandtl relations

[ASME PAPER 71-FE-A] 13 p2051 A71-29378

Supersonic mass flux probe description, discussing inlet geometry, angle of attack and Reynolds and Mach numbers effects on performance

14 p2239 A71-29925

Ekman boundary layer energy stability, determining effective Reynolds number critical value by Euler-Lagrange equations numerical integration

14 p2226 A71-30410

Flexible blades cascade at various pitch angles and Reynolds numbers

15 p2343 A71-31203

Low Reynolds number turbulent flow in large aspect ratio rectangular ducts, investigating Blasius and Prandtl circular tube friction factor relations

15 p2392 A71-32261

Stability of governing parameters critical values /Taylor, Rayleigh or Reynolds numbers/ and periodic solutions in fluid mechanics

16 p2558 A71-33002

Pipe Poiseuille flow instability with respect to finite amplitude disturbances, calculating Reynolds stress by linear wall mode

16 p2558 A71-33021

Damping disturbances structure in unbounded laminar flow stability at large Reynolds numbers, demonstrating damping modes eigensolutions in form of concentrated wave packets

16 p2559 A71-33022

Oscillating circular cylinder wake fluctuating velocity measurement at low Reynolds numbers, using hot-wire anemometer

[ASME PAPER 71-APM-33] 16 p2520 A71-33196

Free and enclosed disks rotation resistance at high Reynolds numbers, calculating fluid induced torque with logarithmic velocity profiles for turbulent boundary layer flow

[ASME PAPER 71-APM-25] 16 p2520 A71-33204

Helicopter rotor model testing in water tunnel, discussing advantages over wind tunnel testing due to

Reynolds number scaling and avoidance of wall interference effects

16 p2526 A71-34151

Two dimensional laminar separation bubbles in high Reynolds number flow fields, using finite difference solutions to Navier-Stokes equations

16 p2561 A71-34165

Wall roughness effects on laminar boundary layer velocity profile and Reynolds number, using Hankel functions and integrals

17 p2725 A71-34180

Incompressible turbulent boundary layers at low Reynolds numbers, using eddy viscosity and mixing length concepts for computation

17 p2728 A71-34884

Reynolds magnetic number effect on MHD channel conducting gas flow current distribution, taking into account Hall effect

17 p2790 A71-35642

Rotating liquid flow impulsive spin-up and spin-down in finite cylindrical containers, deriving simplified mathematical model at Reynolds number 1002

18 p2901 A71-35853

Transonic wind tunnel testing of air intake and afterbody of double flux engine nacelle at high subsonic Mach numbers and high Reynolds numbers

[ONERA-TP-943] 18 p2956 A71-36021

Liquid flow about oscillating flat plates, determining drag coefficient relationships to low Reynolds number and period parameter from graphical representation

18 p2902 A71-36033

Sting-free aerodynamic drag measurement on ellipsoidal cylinders in subsonic wind tunnel at transition Reynolds numbers

18 p2843 A71-36037

Pressure distribution over deflected flap as function of boundary layer separation, flap geometry, Reynolds number and Mach number

18 p2972 A71-36435

Inlet turbulent pressure data scaling hypothesis, investigating Reynolds number effect

[AIAA PAPER 71-669] 18 p2956 A71-36774

Asymptotic expansions for solution of wave motions of viscous incompressible fluid flow with free boundary at large Reynolds number

18 p2909 A71-36789

MHD channels end effects at finite magnetic Reynolds numbers, discussing wall conductivity and external magnetic field geometry effects

19 p3108 A71-37078

Discharge coefficient formula for supersonic nozzles at low throat Reynolds numbers, investigating boundary layer thickness for various nozzle geometries

19 p2993 A71-37896

Plane parallel Couette flow stability with respect to small perturbations, considering positive wave numbers and Reynolds numbers

19 p3046 A71-38263

Unstable thermal stratification and critical Reynolds number effects on dynamic instability of Ekman boundary layer vortex rolls

20 p3257 A71-39438

Viscous fluid stirring due to small amplitude rigid circular cylinder rotation, calculating steady flow velocity relationship to Reynolds number

20 p3177 A71-39481

Steady axisymmetric incompressible flow past sphere at low Reynolds numbers, reducing equations of motion to ordinary differential equations

20 p3212 A71-39506

Molecular chaos breakdown under shear flow, calculating thermodynamic fluctuation formula for unlimited Reynolds number increase

21 p3418 A71-40628

Magnetic field stabilizing effect on free shear layer of electrically conducting fluid at small Reynolds number

21 p3421 A71-40637

MHD flow stability under arbitrary three dimensional disturbances, considering energy estimate for interaction between magnetic field and velocity field at critical Reynolds number

21 p3422 A71-40676

Heat transfer from platinum wires in He and He-air mixtures, plotting Nusselt number variation with Reynolds number for various He concentrations

22 p3620 A71-41875

Turbulent flow of incompressible fluid in rough pipe, determining skin friction coefficient variation with Reynolds number

22 p3531 A71-42291

Boundary layer solution for initial flow around impulsively started sphere in viscous fluid at high Reynolds numbers

23 p3664 A71-44144

Laminar-turbulent boundary layer transition at Mach number 2-10, observing stabilizing effect of transition Reynolds number at increasing heat transfer intensity

24 p3818 A71-44745

RF-4 AIRCRAFT

U F-4 AIRCRAFT

RF-8 AIRCRAFT

U F-8 AIRCRAFT

RH-2 HELICOPTER

U UH-1 HELICOPTER

RHENIUM

NT RHENIUM ISOTOPES

Vacuum work function of thermionic converter using planar monocrystalline rhenium emitter over temperature range

02 p0192 A71-12206

Cesiated work functions of directed monocrystalline Re thermionic emitter from saturated electron emission currents over temperature range

02 p0295 A71-12207

Low temperature cylindrical thermionic converters with CVD Re electrodes, discussing design, fabrication and performance

02 p0193 A71-12219

Tungsten, molybdenum and rhenium single crystals hemispherical emissivity at high temperatures by electron beam heating, considering grain boundary contribution

04 p0613 A71-15581

Sintered or cast Re refining in vacuum electron beam furnace using water-cooled crystallizer, discussing metal losses during melting

06 p0904 A71-17948

Re hot rollability under low vacuum conditions as function of temperature, comparing with cold rolling

07 p1120 A71-20240

Rhenium effect on tungsten sensitivity to brittle fracture, measuring amplitude dependence of internal friction at temperatures from 77 to 1273 K

07 p1141 A71-20247

Electron beam welding of tungsten to tungsten/rhenium and tungsten/rhenium to niobium, discussing techniques for assembly of thermionic converter fuel elements

11 p1769 A71-25858

Adsorption states of Mo and Re surfaces during oxidation at low oxygen pressures and temperatures up to 2300 K, using noble gas molecular beams

14 p2190 A71-30402

Creep rupture behavior of electron beam melted polycrystalline sheet and powdered rhenium

21 p3397 A71-40454

Temperature and frequency dependence of electron phonon interaction maxima in rhenium, explaining transverse and longitudinal waves ultrasonic attenuation by two band theory

22 p3578 A71-42597

Re and Os abundance and meteoritic contamination levels in Apollo 11 and 12 rocks, fines and breccia

23 p3750 A71-43696

RHENIUM ALLOYS

Bare and cesiated work function of covapor deposited tungsten-rhenium electrodes from vacuum emission vehicle Schottky plots

02 p0295 A71-12205

W, W-Re and Re-Mo creep rupture properties investigation for selection of optimum materials for isotope containment for thermionic capsules

02 p0195 A71-12254

Rh alloys thermodynamic reactions with fluorinating agents including fluorine, bromine, pentafluoride and chlorine trifluoride

06 p0904 A71-17949

Phase transformations during tempering of rhenium steels using X ray, dilatometric and conductivity measurements

07 p1135 A71-19617

Rhenium in modern technology - Conference, Moscow, October 1968, Part 2

07 p1140 A71-20231

Equilibrium diagrams of Re with W, Mo, Co, Ni, discussing high strength system elastic components with torsional support applications

07 p1140 A71-20232

Groups IV-VIII transition metals reaction with Re and B, studying ternary compounds formation by X ray and metallographic analyses

07 p1140 A71-20233

Phase equilibria in Zr-Mo-Re and Zr-W-Re systems, studying isothermal section diagrams via X ray and metallographic techniques

07 p1140 A71-20234

W-Re-Ir ternary system phase diagrams, studying physicochemical properties via X ray and metallographic techniques

07 p1140 A71-20235

Mo-Re-Hf ternary alloys physical and mechanical properties, considering workability, electrical resistivity and expansion coefficient

07 p1140 A71-20237

Re based W alloys for electronic tube hot cathodes, discussing reduction and annealing effects on mechanical and plastic properties

07 p1140 A71-20238

W-Re alloy ingot nonmetallic inclusions complex phase structure, using electron probe, metallographic and electrolytic techniques

07 p1141 A71-20239

W-Re alloy microstructure creep, long term strength and plastic properties as function of temperature, using electron microscopy

07 p1141 A71-20241

- Mo-Re alloy wire structure and properties, observing heat treatment effect with metallographic techniques and X ray analysis 07 p1141 A71-20242
- W-Mo-Re high temperature alloys, discussing high strength, elastic properties, creep, thermal resistivity and expansion coefficient 07 p1141 A71-20243
- Optimal recrystallization of thin wire cast W-Re alloy subject to high size reduction 07 p1141 A71-20244
- Structure and mechanical properties of Mo alloy weld metal as function of Re concentration, using metallography, electron microscopy, X ray analysis and autoradiography 07 p1120 A71-20245
- Mo-Re alloys thermal and electrical properties from X ray analysis of two phase structure 07 p1141 A71-20246
- Elastic modulus as function of chemical composition and structure of binary alloys Mo-Re and Ni-Re 07 p1141 A71-20248
- Dynamic strength of elastic elements from wire and tapes of Mo-Re alloy 07 p1120 A71-20249
- Mechanical, heat resistant and thermoelectric properties of W-Re alloys for thermocouples 07 p1114 A71-20250
- Composition and annealing effects on mechanical and thermoelectric properties of sintered wire W-Re alloys 07 p1143 A71-20493
- Mo-Re alloy single crystals asymmetric mechanical properties, discussing shear tests of Mo and Mo-Re single crystals for hard and soft flow stress planes identification 11 p1777 A71-25372
- Chemical vapor deposition process for preparing W-Re alloys having uniform Re content and dense coherent grain structure 11 p1797 A71-25862
- Low temperature and composition effects on alloy softening in group 6A metals alloyed with Re 11 p1781 A71-26293
- Mo-Re alloy crystallographic features observation by transmission electron microscopy, noting equivalence of twin-slip and twin-twin interactions 11 p1783 A71-26477
- Comparative creep rupture properties of tungsten-rhenium consolidated by arc melting and powder metallurgy, considering rupture life and rupture ductility 15 p2427 A71-31818
- Creep rupture properties of W-Re arc melted and powder metallurgy materials at 1650 and 2200 C as function of time, void and grain size 15 p2428 A71-31819
- Nb-Re-C system, investigating polythermal NbC-Re cross section structure by metallographic chemical and X ray analyses and microhardness and melting point measurements 15 p2430 A71-32148
- Addition effects on polygonization of deformed single crystals of Mo and W with Re, using X ray analysis 16 p2596 A71-33887
- Arc melting consolidated W-Re-Hf-C alloy mechanical properties from tensile, creep and bend tests 20 p3247 A71-38766
- RHENIUM COMPOUNDS**
- Re intermetallic compounds structure and physical properties, examining chemical reactivity with transition metals as function of elements periodic table position 07 p1140 A71-20236
- Rhenium tellurides phase transformation during decomposition in Ar 16 p2621 A71-33566
- RHENIUM ISOTOPES**
- Re isotopic composition measurement in Apollo 12 rocks and regolith samples using neutron bombardment 23 p3750 A71-43697
- RHEOELECTRICAL SIMULATION**
- Sonic boom induced indoor acoustical waves, using electrical analog 14 p2274 A71-30200
- Heavy lift helicopter flight control system design, emphasizing fly by wire electrical analog [AHS PREPRINT 503] 14 p2178 A71-31079
- RHEOENCEPHALOGRAPHY**
- Rheoencephalography of cerebral hemodynamics during mental work, showing left hemisphere hyperemia 08 p1242 A71-21960
- RHEOGRAPHY**
- U RECORDING INSTRUMENTS**
- U RHEOMETERS**
- RHEOLOGY**
- Fiberglass reinforced plastic cylindrical shells, investigating rheological effects during heating and concentrated radial loads 02 p0324 A71-11754
- Soviet book on blood hydrodynamics covering circulatory system structure, rheology and mathematical models, pulsating flows, concentration effects and mass transfer 02 p0203 A71-11846
- Heat transfer - Conference, Versailles, August-September 1970, Volume 4, Natural convection and rheology 04 p0685 A71-15521
- Deformation stability of three dimensional body with rheological properties under compression 05 p0824 A71-16591
- Structural design optimization in rheology, classifying various objectives and constraints 09 p1540 A71-23086
- Brittle fracture mechanism models and connection with rheological properties of material, deriving relations for Griffith energy criterion 10 p1688 A71-24388
- Stress-strain state induced by concentrated forces in infinite medium with nonlocal rheological deformation law, obtaining particular solutions for quasi-static viscoelastic problems 13 p2149 A71-28128
- Yield pressure, starting torque, consistency and rheology of lubricating greases at low temperature in ball bearings [ASLE PREPRINT 71AM 1B-2] 13 p2076 A71-29489
- Rheological media viscoelastic relaxation theories generalization taking into account thermal stress and conduction 18 p2984 A71-37021
- Unsteady approach to nonisothermal flow theory for Couette flow, making general assumptions concerning rheological law and temperature dependence of fluidity 19 p3043 A71-37386
- Plastic strain hardening media stress-strain relations, discussing rheology, temperature effects, isotropy postulate and deformation processes 24 p3876 A71-44401
- Polymer systems molecular rheology based on statistical mechanics and simplified structural models 24 p3841 A71-44644
- RHEOMETERS**
- Female aircrews under moderate hypoxia, noting uterine rheography modification 06 p0860 A71-18194
- Weissenberg rheogoniometer modifications, providing upper cone motion elimination, unsteady/steady state measurements in constant stress field and amplitude/frequency variations 11 p1763 A71-26058
- RHODIUM**
- Evaporated Rh films preparation at various substrate temperatures in vacuum UV, determining reflectance and optical constants 08 p1343 A71-21183
- Dry reed sealer transfer contact design, operation and embodiment, noting Au diffused and Rh contacts with hydrogen gas 13 p2038 A71-28838
- Miniature dry reed switch for latching and speech path, using semihard magnetic material, sealing glass and electrodeplated rhodium contact 13 p2001 A71-28842
- RHODIUM ALLOYS**
- Rh and Ag-Pd alloys magnetic susceptibility, investigating hydrostatic pressure effects 21 p3432 A71-41269
- RHODIUM COMPOUNDS**
- Vacuum fusion sintered rhodium borides melting point, microhardness and conductivity and thermal emf temperature dependences determination by thermal metallographic and X ray analyses 23 p3717 A71-44024
- RHOMBIC ANTENNAS**
- Waves arrival directional fluctuations effect on power gain of horizontal rhombic antennas for high frequencies and various antenna and wave parameters 09 p1420 A71-23676
- Far field radiation patterns and optimum design of horizontal rhombic antenna in warm plasma, using linearized hydrodynamic theory 18 p2875 A71-35969
- RHOMBOHEDRONS**
- Beta rhombohedral boron whiskers production from hydrogen reduction of boron bromide and chloride by vapor-liquid-solid mechanism 22 p3564 A71-42533
- RHYTHM (BIOLOGY)**
- NT CIRCADIAN RHYTHMS**
- Heart rhythm coordinate curves for continuous EKG analysis using digital computer 01 p0025 A71-11153
- Biological rhythms and space nutrition - COSPAR Conference, Prague, May 1969, Life sciences and space research 01 p0017 A71-11551
- Human temporal performance of homogeneous discrete motor acts sequence, suggesting central nervous mechanism for movement rate generation 02 p0204 A71-12052
- Human discrete and continuous rhythmical movements rate control 02 p0204 A71-12054
- Acetylcholine endogenic formation in rabbit myocardium effect on ventricle rhythm guides automatic activity suppression by HF excitations 07 p1040 A71-19281
- Long term zero gravity effects on mammal physiologic rhythms characteristics, studying rats in biosatellite orbits 10 p1565 A71-24611
- Ectopic right atrial rhythms in ECG vectorial analysis 12 p1870 A71-27289
- DNA synthesis rhythm in aorta endothelial cells nuclei during direct division, noting effects of amitosis by autoradiography 12 p1872 A71-27752
- Endogenous short period rhythms in rotational movements of unifoliate leaves of Phaseolus angularis Wight grown under controlled environmental conditions 13 p2015 A71-29476
- Alpha rhythm activity, periodicity and mean frequency in cortex regions of healthy humans based on EEG frequency and correlation analyses 14 p2186 A71-30551
- First and last rapid eye movement (REM/ sleep differences in unrestrained chimpanzee 18 p2853 A71-35891
- Activity correlation of adjacent neurons of cat cerebral cortex somatosensory zone, considering distribution of same direction /cophase/ and different direction /counterphase/ of background rhythms 19 p3001 A71-37392
- Medical, zoological and biological effects of ELF signals in atmosphere, comparing with EEG alpha and gamma rhythm 20 p3193 A71-39478
- Summation dial vectorial representation of stationary and nonstationary time series data, relating rhythms in bed rest study 20 p3190 A71-39480
- Chronobiology purposes, techniques and applications, discussing rhythmic or cyclic variation calculation, biological rhythms spectra and classification and time structure alteration of organisms 21 p3329 A71-40149
- Corned-retinal potential as generator of occipital alpha rhythm in human electroencephalogram modulated at 10 Hz by tremor in extraocular muscles 21 p3329 A71-40176
- Electrical heart activity and ECG mathematical model with nonlinear oscillator system construction for normal and abnormal rhythms 21 p3336 A71-40986
- Vectorcardiographic analysis of patients with ECG diagnosed inferior atrial rhythm 22 p3490 A71-42519
- Frequency analysis of blood circulation rhythms and oxygen tension fluctuations in cerebra of rabbits, cats, monkeys and men 22 p3490 A71-42580
- Biorhythms and related physiological and psychic disturbances, stressing importance in aerospace medicine 23 p3637 A71-44245
- Respiratory sinus arrhythmia by spectral analysis and digital filtering, using linear model to approximate lung volume relationship to heart rate during normal breathing 24 p3802 A71-45067
- RIBBON PARACHUTES**
- Gliding guided ribbon parachute for transonic speed deployment, investigating turn capability, opening reliability, structural integrity and effective drag 10 p1557 A71-24868
- RIBBONS**
- Horizontal shear wave diffraction by finite crack and rigid ribbon in elastic medium 01 p0173 A71-10845
- RIBONUCLEIC ACIDS**
- Mumie preparation effect on DNA and RNA contents in hemopoietic organs during acute radiation sickness due to low power radiation 01 p0013 A71-11118
- In vitro lymphocyte antigen response measurements in cellular immunity evaluation under adverse logistical conditions, emphasizing RNA and DNA synthesis rates 02 p0199 A71-12390
- Biosynthesis of inosinic acid in transfer RNA in Escherichia coli by polynucleotide modification 03 p0375 A71-13173
- Structure and function of 50 S ribosomes of Escherichia coli based on determination of role of 5 S ribosomal RNA 04 p0548 A71-14733
- Bacteriophage Q beta ribonucleic acid variants, considering fluorescence determination of replication inhibition by ethidium bromide 04 p0548 A71-15267

RIBOSE

- Ionizing radiation inhibition of spinal cord neurons ribonucleic acid synthesis and enzyme activity in mice, using autoradiographic method
09 p1393 A71-22925
- High resolution X ray diffraction patterns of yeast phenylalanyl transfer RNA crystals, discussing double helical regional distribution characteristics
11 p1727 A71-25834
- Ultrasonic vibration effects on DNA and RNA content in skin and kidneys of albino rats
15 p2356 A71-31288
- Polysomal RNA disaggregation and attendant reduction in hepatic protein synthesis in rats as result of decreased feed ingestion during hypoxia
16 p2529 A71-33190
- Physicochemical aspects of conditioned reflexes, including membrane mechanisms, effectiveness of synapses, mediation processes, ribonucleotides function and subcellular structures dynamics
17 p2685 A71-35364
- Polyester formation by *Escherichia coli* ribosome catalyzed alpha-hydroxy acid incorporation into polymer chain
17 p2686 A71-35574
- Human body immune status normalization in prolonged space flight, investigating ribonucleic acid stimulated antibody formation
21 p3332 A71-40554
- Combined and individual effects of UV light, X ray irradiation and freezing-thawing cycles on ribonuclease
22 p3496 A71-42830

RIBOSE

- Abiogenic synthesis of nucleosides, heating adenine and ribose mixture at 170 C in atmosphere of oxygen, nitrogen and carbon dioxide
21 p3346 A71-40576

RIBS [SUPPORTS]

- Rib reinforced shells linear theory, deriving equilibrium equations with allowance for temperature terms
01 p0170 A71-10644
- Composite beam of three thin plates reinforced by thin electric ribs, calculating stress strain state by Fourier transforms
01 p0176 A71-11044
- Reinforced tube bundles thermal efficiency and convective heat transfer, discussing inter-rib cavity depth effects
01 p0181 A71-11229
- Buckling analysis of rectangular waffle plates with multiple sizes of ribs in each stiffening direction, considering stability and design
01 p0178 A71-11583
- Mechanical model for orthotropic elastoplastic plates with clamped torsion susceptible ribs
03 p0504 A71-13528
- Perturbed motion equations of body with liquid filled cylindrical cavity reinforced by elastically clamped ribs, solving boundary value problems
03 p0460 A71-14356
- Circular cylindrical shell reinforced by ring ribs, investigating dynamic characteristics under impulsive loading
04 p0672 A71-15756
- Reinforced plate and shell theory, taking into account ribs arbitrary direction and contour profile
06 p0985 A71-17753
- Side strain reactions of shells of revolution with meridional ribs, integrating equations by Green function
06 p0989 A71-17785
- Ribbed aluminum panels airborne sound transmission loss, evaluating structural damping effects
08 p1231 A71-21431
- Shallow rib reinforced rectangular shells under normal load with infinite regularity estimates independent of rigidity, using double trigonometric series
10 p1689 A71-24564
- Bidirectional stress-strain analysis of hinged cylindrical shells crosswise reinforced by rigid ribs using equilibrium equations
10 p1690 A71-24566
- Longitudinal and transverse rib reinforced plates with parallel cracks extending to edge, obtaining flexural rigidity and stress-strain state
13 p2156 A71-29070
- Rib reinforced cylindrical shells deformation under local load, examining stress-strain distribution
18 p2981 A71-36719
- Ribbed cylindrical shells modeling method for stress-strain state and stability
23 p3780 A71-44219
- Longitudinal rib reinforced cylindrical shell under axial compression loads, determining equilibrium stability with approximation of transcendental equations
23 p3780 A71-44222
- Ring reinforced spherical shell and rib under concentrated normal forces, calculating force factors and displacement by simultaneous deformation analysis allowing moment stresses
24 p3883 A71-44896

RICCATI EQUATION

- Optimal control discrete time matrix Riccati equation, establishing convergence, uniqueness and stability properties
02 p0275 A71-11673
- Unstable linear initial value problem numerical solution, using Riccati equations of invariant imbedding
02 p0277 A71-12727
- Correlated noise linear filtering problem analysis, introducing concept of invariant directions for Riccati equation
06 p0877 A71-17328
- Nonrecursive solution for discrete Riccati equation by finding eigenvalues and eigenvectors of canonical state-costate equations
06 p0878 A71-17335
- Structural properties of equilibrium solutions of quadratic matrix equation, using variational interpretation of associated Riccati equation, transform techniques and Parseval formula
13 p2095 A71-28815
- Linear systems with constant inputs optimal with respect to infinite terminal time quadratic performance, using Riccati equation
18 p2896 A71-36236
- Stationary covariance generation of matrix of rational functions of complex variable, solving factorization equation via algebraic Riccati equation
20 p3207 A71-38990
- Generalized Riccati equation reduction to integral equation, leading to asymptotic solution of second order linear differential equations
20 p3255 A71-39574
- Integrable linear differential equations application to Riccati equation and Bessel, Legendre and other functions relations in celestial mechanics
23 p3727 A71-43006
- Riccati equation reduction for optimal control of linear quadratic distributed parameter systems applied to temperature and heat flow regulation
23 p3653 A71-43969

RICHARDSON NUMBER

- Stratospheric turbulence induced aircraft buffeting dependence on vertical wind shear, Richardson number and thermal stability change from underlying to overlying layer
15 p2444 A71-31365
- Richardson number relationship to vertical heat diffusion coefficients in boundary layer
16 p2605 A71-34070
- Atmospheric structure near large amplitude Kelvin-Helmholtz billows in upper troposphere, deriving static stability, vertical wind shear and Richardson number
19 p3089 A71-37498
- Richardson criterion generalization for atmospheric turbulence onset, considering anisotropic turbulence conditions
24 p3844 A71-44447

RICHARDSON-DUSHMAN EQUATION

U TEMPERATURE EFFECTS

U THERMIONIC EMISSION

RIDGES

- Variable abyssal basalt populations, considering chemical analyses variations for ridges as function of ocean floor spreading rate
13 p2063 A71-29139

RIEMANN INTEGRAL

U MEASURE AND INTEGRATION

RIEMANN MANIFOLD

- General relativity and gravitational collapse, discussing experimental tests, waves, use of Riemann geometry and Einstein field equations
03 p0482 A71-12972
- Soviet monograph on meromorphic functions covering behavior variables, asymptotic properties and defects and Riemann surfaces application for values distribution analysis
05 p0773 A71-16249
- Riemann surfaces use in plane boundary value problems and singular integral equations, considering plane elasticity and filtration theories
07 p1148 A71-20079
- Maxwell equations analog for gravitational fields, considering Malybaeva equation as condition for gravitational waves existence in Riemann manifold
12 p1931 A71-27243
- Covariant definition of radius vector in Riemann space, studying position operator in general relativity theory
19 p3105 A71-38582
- Electromagnetic wave diffraction properties by ribbon metallic lattice in optically active media using Riemann-Hilbert method
24 p3804 A71-44716

RIEMANN PROBLEM

U CAUCHY PROBLEM

RIEMANN SPACE

U RIEMANN MANIFOLD

RIEMANN WAVES

- Nonself-similar wave type gas dynamic equations solutions, considering flow fields due to Riemann waves interaction in polytropic gas
05 p0693 A71-16376

- Nonself-similar wave type gas dynamic equations solutions, considering flow fields due to Riemann waves interaction in polytropic gas
12 p1898 A71-27453

- Arbitrary amplitude magnetoacoustic waves under gravitational field effects, obtaining exact Riemann wave solutions to MHD equations for compressible medium
19 p3112 A71-37741

- Ideal compressible fluid plane unsteady vortex-free self-similar flow, obtaining particular solutions families similar to Riemann waves and Prandtl-Meyer flows
22 p3532 A71-42866

RIGID BODIES

U RIGID STRUCTURES

RIGID ROTOR HELICOPTERS

NT CH-3 HELICOPTER

- Retreating blade stall experiments on model helicopter rotor, considering series of pressure distribution and boundary layer events
14 p2172 A71-31087
- Electromechanical control system synthesis for compound hingeless rotor helicopter, using root locus method with transfer functions from airframe motion linear model
14 p2179 A71-31096
- AH-56A compound helicopter rigid rotor stability and handling qualities, using flight, whirl tower and wind tunnel tests
14 p2180 A71-31115
- Coriolis coupled bending vibrations of hingeless helicopter rotor blades, noting out-of-plane component contribution to aerodynamic coupling
19 p3154 A71-37294
- Mil Mi-12 Soviet giant rigid rotor helicopter with 30,000 kg load or 250 passenger capacity
20 p3178 A71-39375

RIGID ROTORS

- Loads on compressor, ventilator and turbine rotor disks having large central holes, giving formulas for stress distributions
12 p1945 A71-26952
- Stiffened horizontal stoppable hingeless rotor conversion from helicopter to airplane flight speeds
14 p2178 A71-31078
- Forward flight performance of coaxial rigid rotor in NASA wind tunnel, comparing to aerodynamic stability with conventional rotors
14 p2178 A71-31090
- Hingeless rotor stability characteristics at high advance ratios, examining equations of motion and time variant aerodynamic coefficients
15 p2345 A71-31569
- Rigid rotor hub flapping stiffness tailoring for controllability, considering length and fatigue/structural strength
15 p2348 A71-31601
- Rigid rotor whirl dynamics in externally pressurized gas journal bearings, calculating frequencies in terms of stiffness and other parameters
22 p3552 A71-41670

RIGID STRUCTURES

NT RIGID ROTORS

NT RIGID WINGS

- Uniformly turbulized incompressible heavy fluid sloshing and free oscillations in rigid rotating vessel, using linear surface wave theory
01 p0069 A71-10411
- Impulsively loaded rigid plastic continua deformation lower bounds calculation, considering beams and plates
01 p0173 A71-10943
- Shallow shells of revolution of strain-hardening material, deriving stress strain state by rigid plastic body model
01 p0175 A71-11039
- Sound pressure radiation from infinite plate with rigid or pressure release baffles perpendicular to surface, using steepest descent method
02 p0325 A71-11997
- Convex functions theory of rigid perfectly plastic structures, formulating strain rate and stress fields relation in subgradients
02 p0326 A71-12339
- Rigid plane skeletal structures combinational properties, considering analytic geometry criteria and graphs from algorithm
02 p0327 A71-12395
- Rigid body free rotational stability, discussing initial conditions excursion
04 p0654 A71-15720
- Rigid heat conductors, using controllable states for heat flux-temperature gradient materials response function measurements
05 p0837 A71-16721
- Structural stability of incompressible elastic rod of variable rigidity flattened along axis, reducing boundary value problem to equation with continuous operator
05 p0828 A71-16987
- Rigid body stability studies with Hamiltonian as Liapunov function, noting application to flexible compact gravity gradient satellite planar motion
06 p0981 A71-18648

Rigid body motion implicit representation in curved finite elements

07 p1214 A71-19910

Homogeneous isotropic layers stack on rigid base with periodically varying elasticity parameters, calculating equilibrium under normal distributed load

07 p1217 A71-20460

Stiffened flat panel dynamic analysis, using finite element method

08 p1374 A71-20227

Linear coupling between orbital and attitude motions of rigid body, deriving 12th order six degrees of freedom linearized motion equation

09 p1516 A71-22173

Nontrivial expansion of rigid surface infinitesimal motions into analytical bendings, deriving differential equations system for n-order bendings of singly connected continuously differentiable surface

09 p1535 A71-22211

Elastic media damping effects on rigid bodies HF vertical and rotational vibrations, considering approximate solution for structural amplitude response

09 p1541 A71-23088

Shallow rib reinforced rectangular shells under normal load with infinite regularity estimates independent of rigidity, using double trigonometric series

10 p1689 A71-24564

Bidirectional stress-strain analysis of hinged cylindrical shells crosswise reinforced by rigid ribs using equilibrium equations

10 p1690 A71-24566

Limiting equilibrium of thin rigid plastic plate with piecewise smooth contour under skew symmetric load

10 p1690 A71-24568

Precessional equation of gyroscopic systems with rigid structural elements connected by single degree of freedom axial hinges

10 p1611 A71-24577

Plane rigid airfoil with fixed center of gravity, discussing motion in turbulent air and gust loads

10 p1557 A71-24947

Torsional-flexural stability of stiffened Ti panels for application to supersonic transport, using small deflection energy methods

[AIAA PAPER 71-338] 11 p1843 A71-25317

Nonlinear axisymmetric solution for cardiovascular system pulsatile flow, using long rigid tube and velocity profile representation

11 p1726 A71-26485

Iterative solution of semidefinite eigenvalue problems, identifying rigid body and deformation coordinates

12 p1974 A71-26873

Stability analysis of rigid frames and trusses, including effect of bending moments and shear forces before buckling

12 p1976 A71-27161

Reinforced plates flexural and torsional rigidity characteristics for stiffeners design, considering oblique angular coordinates system

12 p1982 A71-27509

Rigid plastic media dynamic model, showing yielding time delay effect on residual deflection as function of load duration

12 p1982 A71-27515

Shells of revolution plastic deformation problem, applying rigid viscoplastic strain hardenable material model

12 p1984 A71-27686

Approximate limiting loads with minimum yield stress for axisymmetric rigid-plastic body of arbitrary shape, using computerized static equilibrium method

13 p2150 A71-28137

Dynamically loaded rigid plastic bodies, solving limiting equilibrium problems by extremal principles

13 p2156 A71-29065

Differential rotational equations of motion for triaxial rigid body about center of mass under arbitrary torque

14 p2307 A71-29882

Stress-strain measurements in inelastic elements by photoelastic, laser, memory, load and plane deformation methods, considering plate with circular hole

14 p2333 A71-30894

Rigid framed dome structure stiffness analysis using multiglobal axes and joint equilibrium equations

15 p2507 A71-32105

Rigid-plastic solids with viscoplasticity extension, comparing stability with Hill condition

16 p2649 A71-33010

Elastic spherical shell coupled to rigid body, calculating asymmetric free vibration natural frequencies and mode shapes from boundary conditions

17 p2817 A71-34339

Rigid plastic framed structures minimum weight design and analysis formulation by network-topological approach based on yielding concept

17 p2831 A71-35356

Rigid sphere and concentric shells models approximation to turbulent motion in liquid-filled precessing spherical cavity

[ASME PAPER 71-APM-Y] 18 p2904 A71-36265

Structural stability of incompressible elastic rod of variable rigidity flattened along axis, reducing boundary value problem to equation with continuous operator

18 p2982 A71-36787

Space shuttle boost vehicle with various degrees of aerodynamic stability, discussing control laws effects on rigid body bending moment tradeoff

[AIAA PAPER 71-918] 19 p3147 A71-37167

Rigid body longitudinal impact against free end of variable cross sectioned viscoelastic cantilever beam, obtaining solution as rapidly converging Fourier series

19 p3160 A71-38485

Holographic interferometry application to two step static displacement measurement of diffusely reflecting surface of rigid body in motion

21 p3377 A71-40227

Dynamic influence of isotropic flat plates on spatial vibratory structures containing rigid bodies, considering compatibility and modal coupling

[ASME PAPER 71-VIBR-3] 21 p3456 A71-40267

Flexible rotating shafts high speed, rigid body and modal balancing machines

[ASME PAPER 71-VIBR-73] 21 p3460 A71-40311

Optimal trajectories and controls for dynamic systems modeled by coupled rigid bodies, applying to synthesis of robots and all-terrain vehicles

[ASME PAPER 71-VIBR-82] 21 p3414 A71-40318

Dual variational formulation for rigid plastic structure minimum cost design, applying to sandwich and fiber-reinforced plates

[ASME PAPER 71-VIBR-110] 21 p3462 A71-40333

Lower bound deformation theorem for rigid plastic continua and structures under impulsive loading, using kinematically admissible velocity field

22 p3614 A71-41608

GWU-FAP computer program for rigid frame elastic-inelastic analysis based on finite element method and plastic initial strain concept

22 p3516 A71-41867

Inertia-loaded elastic thin circular ring in rigid cavity with small initial clearance, calculating deformation by nonlinear bending theory

22 p3616 A71-42215

Near-normal plane shock wave reflection from rigid impermeable wall, obtaining nonstationary flow parameters in terms of Jacobi polynomials convergent series

22 p3531 A71-42865

Plane motion stability of rapidly rotating symmetric rigid body in atmosphere, deriving short-cut equations system by Bogoliubov-Zubarev method

24 p3847 A71-44416

Dynamic response of thin walled structures natural frequency analyzed for formulating potential and kinetic energy for stiffness and mass matrices by minimization principle

24 p3878 A71-44555

RIGID WINGS
Two dimensional rigid wings, investigating response characteristics to gust loads

09 p1383 A71-23440

RIGIDITY
Anisotropic rod elastic curve equilibrium shape for rigidity conditions, considering Goriachev solution to heavy solid body motion about fixed point

03 p0458 A71-13599

Interlayer rigidity effects on strength of fiber reinforced composite materials under plane loads

05 p0771 A71-16366

Aircraft systems assembly methods, discussing rigidity effects on error redistribution in external and internal force field application

08 p1295 A71-20792

Spar box structure under pure bending noting flexural rigidity and stress and stability analysis with Karman nonlinear equations

12 p1981 A71-27498

Center of rigidity position determination in cross section of thin walled beam under nonuniform temperature due to creep

13 p2154 A71-28642

Longitudinal and transverse rib reinforced plates with parallel cracks extending to edge, obtaining flexural rigidity and stress-strain state

13 p2156 A71-29070

Fiber reinforced metallic matrix composite under creep, discussing rigidity, stress distribution, rupture strength and failure time

23 p3697 A71-44201

MILLS
U VALLEYS
RING CURRENTS

Quiet day variations in earth surface magnetic field, examining magnetopause, neutral sheet and ring nonionospheric current models

03 p0421 A71-14535

Ring currents and polar magnetic substorms during intensive charged particle flux period in nighttime magnetosphere

07 p1101 A71-19414

Equatorial ring current asymmetry and change during magnetic storms studied by DR indices

08 p1279 A71-21212

Laminar geoelectromagnetic field excited by coaxial ring current, determining impedance and magnetic field ratios of spherical harmonics

09 p1435 A71-22434

Ring current indices by IGY data, attributing differences during great magnetic storms main phase to asymmetry of magnetospheric ring current

10 p1603 A71-24598

Atmospheric electric ring current in higher atmosphere with equatorial flow across magnetic lines, using dipole tensor conductivity model

10 p1603 A71-24701

Plasma sheet proton ring current, trapping boundary and plasmapause interrelations near magnetic equator and local midnight by satellite-borne analyzer array

10 p1605 A71-24781

Magnetospheric numerical model with two-monoenergy-component proton distribution function, examining ring current belt formation causing inflation

10 p1663 A71-24782

Extraterrestrial ring current under very quiet magnetic conditions from mean long term daily horizontal intensities

11 p1755 A71-25616

Compton electrons produced ring current effects on geomagnetic fields for gamma quantum source and air molecular interactions, considering exact analytical model

11 p1817 A71-25777

Magnetospheric location of SAR-arc field lines, discussing proximity to plasmapause, electron trough and ring current

13 p2055 A71-27918

Decreasing period micropulsations during elementary magnetospheric substorms, discussing relation to ring current asymmetry development

13 p2061 A71-28546

Ring current as source region for proton auroras, calculating energetic proton lifetimes for model magnetosphere

13 p2064 A71-29167

Geomagnetic disturbance vector distribution, computing three dimensional ring and ionospheric currents system models

14 p2229 A71-29672

Proton measurements in ring current by OGO-3 satellite compared with geomagnetic field data at low and high latitudes

16 p2626 A71-33663

OGO-2 rubidium vapor magnetometer measurements comparison with surface magnetic observatory data during geomagnetic storms, considering asymmetric ring current

16 p2572 A71-33946

Stable auroral red arcs generation at plasmapause from ion cyclotron wave turbulent dissipation of ring current proton energy

16 p2572 A71-33947

German monograph on self consistent ring current models of geomagnetic field interaction with charged particles

17 p2733 A71-34789

Ring currents and polar magnetic substorms during intensive charged particle flux period in nighttime magnetosphere

19 p3054 A71-37838

Ring current location in magnetosphere, noting electromagnetic ion cyclotron instability region as stable proton trapping boundaries

22 p3532 A71-41446

Compton electrons produced ring current effects on geomagnetic fields for gamma quantum source and air molecular interactions, considering exact analytical model

22 p3532 A71-41545

Worldwide geomagnetic disturbance during magnetic storm using DR-indices to express magnetospheric ring current induced perturbation

22 p3536 A71-42624

Large geomagnetic diurnal variations effects period determination by statistical method, considering partial ring currents in night magnetosphere

23 p3673 A71-43985

RING DISCHARGE
Ring laser two mode operation combination interaction and beat phasing, determining mode mismatch regions at synchronized frequencies

07 p1127 A71-20380

Gas heating and energy balance of HF ring discharge in rare gases within cylindrical vessel, discussing electron energy distribution functions

20 p3273 A71-39044

RING LASERS
Natural fluctuations sources intensity in annular lasers taking into account field strength dependence

02 p0261 A71-12507

Ring laser coupling phenomena, presenting angular measurements for laser-gyro with Langmuir-Fizeau and Faraday effect bias

04 p0607 A71-15022

Internally loss-modulated ring lasers unidirectional oscillation, analyzing two mode operation

06 p0906 A71-17300

RING STRUCTURES

- Annular gas laser beat frequency as function of Doppler shift emission, examining mirrors feedback, cavity Q and pumping variational effects
07 p1122 A71-19137
- Ring laser beat frequency response near parametric resonance
07 p1125 A71-19810
- Circularly polarized He-Ne ring laser operation, noting no traveling waves coupling via amplifying medium and locking due to cavity imperfections
07 p1127 A71-20388
- Single mode gas ring laser in longitudinal magnetic field, deriving lasing equations from semiclassical theory
07 p1129 A71-20532
- Beat and synchronization modes of opposed waves in rotating gas ring laser, examining frequency response asymptotic behavior
09 p1460 A71-22222
- Ring laser active medium polarization characteristics in strong field, taking into account spatial modulation of population
09 p1461 A71-22365
- He-Ne ring laser in locking range, studying opposing waves amplitude and phase differences dependence on cavity rotation and oscillation frequency tuning
09 p1461 A71-22382
- Gravitational field effect on phase difference of moving waves and polarization in rotating ring laser
09 p1462 A71-22398
- Mode multiplicity effect on ring laser independent beat and synchronized beat regimes
11 p1774 A71-26004
- Arbitrary gravitational field effects on natural frequencies of rotating ring laser with traveling electromagnetic wave
15 p2421 A71-32408
- Ring laser formed by single mode light guiding thin film, using nitrogen laser for pump source
19 p3071 A71-37478
- Unidirectional regenerative ring carbon dioxide laser power amplifier tests for below and above threshold operations, noting saturation role in performance
20 p3242 A71-38843
- Traveling wave power resonances in ring laser with nonlinearly absorbing cell, noting role of absorbing component lamb saturation
21 p3394 A71-41257
- IR ring laser rotation sensor, describing design principles for alignment and eliminating locking phenomenon
22 p3557 A71-42153
- Gas ring laser lock-in zone, showing dependence on resonator mirror curvature radius and mode competition between oppositely directed waves
23 p3683 A71-43393
- RING STRUCTURES**
NT REINFORCEMENT RINGS
NT RING WINGS
Nonlinearly elastic rings and arches under hydrostatic pressure, examining equilibrium with sixth order differential equations
02 p0325 A71-12125
- Annular structures on earth, moon and Mars, explaining cosmic origin on basis of lens-shaped subsurface breccia
02 p0310 A71-12298
- Orthotropic photoelastic analysis of residual stresses in filament-wound composite ring structures, comparing with boring-out and cut-through methods
03 p0508 A71-13773
- Circular Al rings under radial impulsive loading by curved magnetically driven Al flyer plates, recording strain-time histories on oscilloscopes
03 p0509 A71-13778
- Transient annular structures in galaxies with nuclear explosion and fragmentation, examining radiogalaxy dynamics
04 p0655 A71-15724
- Thin oval ring noncircularity effect on thermal instability based on small deflection analysis
05 p0820 A71-15983
- Doubly symmetric oval ring under lateral load, investigating creep behavior from equilibrium equations
05 p0820 A71-15984
- Arches and rings in-plane natural vibration frequencies determination based on Newmark numerical integration method for beams
05 p0820 A71-15985
- Axisymmetric problem solution method for ring shaped body of revolution in elasticity theory
06 p0983 A71-17366
- Critical parameters and vibration frequencies of homogeneous closed circular rings connected to thin shells determined for various boundary conditions
06 p0996 A71-17844
- Elliptic ring shaped disk with external and internal loading, determining stresses due to uniformly distributed loads
06 p1062 A71-18416
- Energy balance during ring blanks widening by electromagnetic pulses, establishing theoretical limit of mechanical efficiency
06 p0906 A71-18712

- Dynamic stress measurement of cantilever beams, frame structures and rings under impulsive loads
07 p1210 A71-19046
- Ring structure with nonlinear stress-strain law and linear strain-displacement relationship, deriving dynamic response to impulse
07 p1213 A71-19904
- Levitated superconducting ring in Princeton Spherator for plasma physics, describing Dewar, coil and feedback control systems
07 p1170 A71-20152
- Wet and dry lubricated slip ring systems long term application testing in ion pumped vacuum chambers
07 p1120 A71-20274
- Molybdenum disulfide treated graphite brushes in electric contact with copper slip rings at high rates in dry pure inert gas atmospheres
07 p1120 A71-20275
- Two dimensional concentric ring antenna arrays synthesis, describing radiation pattern formation
08 p1266 A71-21463
- Circular cylindrical shells on coaxial rings coupled by finite number of spokes as structural analytical models for engine casings, deriving formulas for arbitrary loads
08 p1374 A71-22040
- Residual stresses in ring shaped specimens of wound glass fiber plastic products, using radial cutting technique
09 p1482 A71-22822
- Liquid sloshing in liquid propellant containing orbiting vehicle stabilized by active control system, examining expression for ring baffle slosh damping under reduced gravity
09 p1532 A71-22913
- Rings elastic buckling problems under various loading conditions, using rate equations
11 p1840 A71-25138
- Shear deformation effect on optimal design of elastic beams, considering rectangular cross section circular ring by Timoshenko beam theory
11 p1849 A71-25677
- Long life vacuum tests of dry and wet lubricated slip ring systems for power and signal transfer, discussing wear, noise and contact resistance
11 p1771 A71-26050
- Thermal buckling and snapping of flat rings and of shallow conical rings under axisymmetric temperature distribution
12 p1977 A71-27317
- [ASME PAPER 71-DE-B] Characteristic equation of respiration vibrations of cylindrical ring in incompressible viscous fluid at rest, obtaining damping coefficient for large induced flow Reynolds numbers
13 p2047 A71-28397
- Rotating ring resonator partially filled with dynamic isotropic medium, determining resonance properties
13 p2080 A71-29025
- Approximate method for nonlinear ordinary differential equations with variable coefficients applied to cylinder oscillation and flexible ring deformation
14 p2324 A71-29881
- Twist-bending vibration of ring of rectangular cross section for entire range of length-to-diameter ratios, using Rayleigh shell theory
14 p2328 A71-30414
- Circular stresses and concentration coefficient variations in star shaped elastic surface projected onto ring under internal pressure
14 p2287 A71-30853
- Isotropic elastic thin oval rings nonlinear free and forced flexural vibrations calculation by Galerkin method
15 p2503 A71-31436
- Ring and cylindrical structures comparative stress relaxation at room temperature
15 p2508 A71-32229
- Stress relaxation in rings and rods, discussing errors in data correlation
15 p2508 A71-32230
- Circular rings coupled twist bending vibrations, considering rotatory inertia and shearing deformation effects
15 p2510 A71-32517
- Elastic rods and rings stability under compression beyond elasticity limit, determining equilibrium branching characteristics near bifurcation point
16 p2647 A71-32927
- Rotary inertia and shear deformation effects on three dimensional flexural vibrations of circular ring on elastic foundation
16 p2657 A71-33421
- Moment state stability of elastic hinged cylindrical shell and closed ring under pressure and concentrated load, using nonlinear equilibrium theory
16 p2660 A71-34114
- Cascade displacements and stresses in nozzle ring guide vanes with sectional diaphragm under axial and circumferential flow
18 p2980 A71-36706
- Tuff rings from Fort Rock-Christmas Lake Valley basin, investigating morphologic and volcanic features for surface water role in genesis
19 p3051 A71-37671

- Computer program for nonuniform thickness ring structure stress distribution under uniform radial line load based on reinforced circular cylindrical shell interaction under hydrostatic pressure
22 p3516 A71-41866
- Inertia-loaded elastic thin circular ring in rigid cavity with small initial clearance, calculating deformation by nonlinear bending theory
22 p3616 A71-42215
- Function construction procedure for ring-shaped structure conformal mapping onto doubly connected regions with simple contours, applying to prismatic rod torsion problem
23 p3776 A71-43419
- Thermal and mechanical stresses concentration near peripheral notches on ring-shaped graphite, noting notch sensitivity relationship to tip curvature and graphite grain size
23 p3698 A71-44230
- RING WINGS**
Lift characteristics of semicircular channel wing with pusher propeller at trailing edge, comparing theoretical, wind tunnel and flight test results
10 p1553 A71-24857
- RINGS**
Nonlinear elastoplastic ring buckling under compression
09 p1534 A71-22145
- Chinese remainder theorem for noncommutative rings with divisors of zero and without two-sided unity element in number theory
18 p2976 A71-36096
- Interference rings formation mechanism near main beam emitted by ruby laser with plane and reflecting terminal faces
21 p3392 A71-40515
- RINGS [MATHEMATICS]**
Mixed boundary value problem solution for ring in class of functions with given singularities, using Keldysh-Sedov formulas
09 p1485 A71-22525
- Relationships among topologies definable on commutative algebraic ring
24 p3843 A71-44798
- RIOMETERS**
Riometers accuracy and stability, considering measurement error of ionospheric radio wave absorption
02 p0247 A71-11774
- Ionospheric absorption at solar maximum and minimum, comparing riometer measurements with ray tracing calculations and electron density, collision frequency or temperature profiles
02 p0245 A71-11962
- Hourly changes in auroral conjugate location from ionospheric absorption and riometer magnetograms, noting electrojet triangulation
08 p1279 A71-21210
- Equatorial and precipitating solar proton fluxes in interrelationship in magnetosphere from riometer absorption in auroral and polar cap regions
19 p3125 A71-37360
- Riometer measurement of ionospheric absorption, comparing with IQSY method
24 p3822 A71-44525
- RIOMETRY**
U MEASUREMENT
U RIOMETERS
- RIPPLES**
Low speed angular contact bearings surface geometry effects on friction perturbation torque ripple frequency
18 p2928 A71-36764
- RISK**
Average risk minimization based on empirical data, showing relationship of problem to uniform convergence of averages toward expectation value
12 p1892 A71-27020
- Producer risk determination and tables for Method 4 maintainability demonstration plan of MIL-STD-471
16 p2583 A71-33303
- Risk additivity in portfolios from experiments on accommodation role in binocular rivalry control
17 p2684 A71-35254
- Average risk minimization based on empirical data, showing relationship of problem to uniform convergence of averages toward expectation value
19 p3037 A71-37689
- RITZ AVERAGING METHOD**
Elastic composite liquid filled shell containers, calculating natural vibration with Ritz method
06 p0992 A71-17809
- Ritz-Galerkin method for solving nonlinear operator equations in Hilbert space, discussing convergence and error estimate
06 p0919 A71-18204
- Difference equations derivation for flat plates plane stress extension as localized Ritz process, providing common classification of finite difference and finite element methods
13 p2147 A71-27784
- Ridged waveguide complete eigenvalue solution by integral equation formulation and Ritz-Galerkin method
14 p2212 A71-30516

Ritz-Treffitz algorithm application to optimal state regulator problem computer processing to improve speed of solution and storage requirements
15 p2374 A71-31182

Global-local finite element combined Ritz methods for beam and plate vibration analysis
24 p3880 A71-44638

RL CIRCUITS
NT LC CIRCUITS
NT RLC CIRCUITS
Frequency generators using RC /RL/ designs with odd selective quadrupole element numbers as converters
07 p1078 A71-20062

RLC CIRCUITS
Rectangular diagrams for solving linear RLC networks by digital computer graphics
03 p0390 A71-14308
Stability of RLC networks with negative resistances, applying Liapunov functions
12 p1891 A71-26998

RLC NETWORKS
U RLC CIRCUITS

RNA
U RIBONUCLEIC ACIDS

ROBOTS
Man-telemotor-robot teams for space exploration facilities construction and operation, discussing lunar programs
[AIAA PAPER 71-823] 17 p2723 A71-34722
Robots structural description and computer modeling based on various algorithms
17 p2691 A71-35167
Self adaptive controlled robot velocipedist, discussing speed control and equations of motion
19 p3039 A71-38540
Optimal trajectories and controls for dynamic systems modeled by coupled rigid bodies, applying to synthesis of robots and all-terrain vehicles
[ASME PAPER 71-VIBR-82] 21 p3414 A71-40318

ROCHE LIMIT
Semidetached eclipsing binary stars mass exchange, examining stellar evolution, luminosity, mass loss and exchange and Roche limit
02 p0313 A71-12497

ROCKET BOOSTERS
U BOOSTER ROCKET ENGINES

ROCKET CHAMBERS
U COMBUSTION CHAMBERS
U THRUST CHAMBERS

ROCKET COMBUSTORS
U COMBUSTION CHAMBERS
U THRUST CHAMBERS

ROCKET ENGINE CASES
Sounding rockets motors with integrally molded plastic case and nozzle, discussing cost effectiveness and demonstration tests
[AIAA PAPER 70-1386] 03 p0470 A71-13669
Carbon fiber evaluation of structural reinforcement potentialities for rocket motor cases and pressure vessels filament winding
[PLASTICS INST. PAPER 48] 08 p1297 A71-20924
Composite rocket engine casing thermal flux approximation from multilayer plate heat conductivity
17 p2837 A71-34568
Strength, ductility and notch toughness research on base materials and welds of nickel maraging steel rocket motor cases
21 p3389 A71-40913

ROCKET ENGINE CONTROL
Switching analysis for high order vehicle systems with magnitude and direction constraints in attitude control for Saturn rocket with sloshing motion
08 p1269 A71-21331
Soviet book on design of self guidance systems for aerodynamically controlled rockets
10 p1640 A71-24731
Reentry vehicles fluidically controlled hydrazine rocket engine modules for roll rate control
[AIAA PAPER 70-650] 11 p1810 A71-25503
Soviet book on aircraft and rocket engines control automation, discussing nuclear power plant/fuel systems design and control simulation methods
11 p1814 A71-26403
Solid impulse control using solid quench system and wafer demand gas generator for solid propellants
[AIAA PAPER 71-751] 14 p2297 A71-30844
Acoustic damping of small amplitude waves by non-burning particles in T burners and rocket motors, noting propellant seeding with zirconium oxide
[AIAA PAPER 71-633] 15 p2471 A71-32574
Relative motion interaction dynamics in rocket biaxial control with azimuth and elevation servos, using Mathieu equation and stability criterion
22 p3526 A71-41971

ROCKET ENGINE DESIGN
FOILAC solid propellant rocket motors for high thrust short action time propulsion, reviewing development status and performance
[AIAA PAPER 70-1385] 03 p0470 A71-13668
Astrobee D low cost high performance sounding rocket with long duration radial burning propulsion system for D region and meteorological research
[AIAA PAPER 70-1387] 03 p0498 A71-13670

Motor design parameters effects on solid propellant extinguishment predicted from mathematical combustion model
[AIAA PAPER 70-664] 03 p0469 A71-14442
Cs ion microrocket engine development, discussing Cs fueling device, ionizer heating, fabrication and control methods
[ONERA-TP-847] 04 p0639 A71-15351
Europa 3B launcher first stage, discussing design concept with emphasis on reliability and low cost
05 p0816 A71-16401
Spacecraft high performance resistor engines, discussing design criteria for high temperature long term operation with minimum thermal losses
[AIAA PAPER 71-193] 06 p0948 A71-18633
Low, medium and high specific impulse microthrusters development in France, using cold gases, subliming solids, hydrazine, ammonia and cesium ions
[AIAA PAPER 70-617] 07 p1184 A71-19865
Plastics and metals as construction materials in aircraft, missile and rocket design
07 p1215 A71-20044
Sounding rocket design parameters optimization, investigating apogee-payload relations, thrust as function of time, total weight, maximum altitude and acceleration
09 p1531 A71-22127
Soviet book on space electric rocket engines design and stress analysis covering nuclear reactors, radioactive isotope energy sources and energy converters
13 p2118 A71-29421
NASA Lewis Research Center Hg electron bombardment ion thrusters research programs
14 p2288 A71-29931
Ion thruster technology and subsystem development program status, describing design and performance characteristics
[AIAA PAPER 71-690] 14 p2293 A71-30750
Throtttable bipropellant rocket engine, discussing cryogenic and space storable propellants and injection system optimization based on combustion mechanism photographic observation
[AIAA PAPER 71-740] 14 p2296 A71-30783
Solid propellant rocket engine design, discussing combustion instability technology applications in damping and driving mechanisms influence determination
[AIAA PAPER 71-754] 14 p2296 A71-30788
Soviet book on liquid rocket engines covering combustion chambers, fuel supply systems, static and dynamic characteristics, control and reliability
15 p2466 A71-31296
Space shuttle engine design based on reusable XLR129 rocket engine, presenting performance data
15 p2467 A71-31469
High pressure gaseous hydrogen oxygen auxiliary propulsion systems /APS/ thruster design and cold flow and hot fire testing for space shuttle requirements
[AIAA PAPER 71-737] 15 p2470 A71-32291
Biowaste resistor engine design and performance for various propellants and propellant mixtures
[AIAA PAPER 71-687] 15 p2470 A71-32293
AJ-550 liquid hydrogen/oxygen staged combustion cycle space shuttle engine, describing preburner and main injector, turbopump and combustion chamber construction
[AIAA PAPER 71-660] 15 p2471 A71-32575
Rocket engine burning oxygen and hydrogen propellants at 3000 psia combustion chamber pressure for space shuttle booster and orbiter stages
[AIAA PAPER 71-659] 16 p2624 A71-33106
Time constant dependence of hybrid rocket combustion chamber on engine parameters and structure
16 p2625 A71-33619
Jupiter orbiter spacecraft propulsion system design, noting advantages of fluorine/hydrazine propellant combination
[AAS PAPER 71-154] 19 p3122 A71-37925
Vertical 1 single stage geophysical rocket design and instrumentation for X rays, solar UV and meteoritic concentration measurements
19 p3154 A71-38530
Frozen bipropellants as self supporting structural member for booster weight reduction, considering mechanical and thermal properties and melting rate requirement
20 p3276 A71-39609
Interstellar space flight kinematics near light speed, discussing theoretical requirements for relativistic rocket engines
22 p3600 A71-42000

ROCKET ENGINE NOISE
Transient mean square response of simple structural systems to forcing function representing rocket engine noise, comparing with stationary mean square response for each launch stage
[AIAA PAPER 71-348] 11 p1837 A71-25327

ROCKET ENGINES
NT BOOSTER ROCKET ENGINES
NT ELECTRIC ROCKET ENGINES
NT ELECTROSTATIC ENGINES
NT HYBRID PROPELLANT ROCKET ENGINES
NT HYDRAZINE ENGINES
NT HYDROGEN OXYGEN ENGINES

NT J-2 ENGINE
NT LIQUID PROPELLANT ROCKET ENGINES
NT MICROROCKET ENGINES
NT NUCLEAR ENGINE FOR ROCKET VEHICLES
NT NUCLEAR ROCKET ENGINES
NT RESTARTABLE ROCKET ENGINES
NT RETROCKET ENGINES
NT SOLID PROPELLANT ROCKET ENGINES
Energy sources for rockets and satellites, comparing chemical, solar and nuclear supplies
02 p0282 A71-12302
Astronautics and rocket technology history - Conference, Belgrade, September 1967, covering rocket engines, fuels and materials, ramjet engines, control systems, etc
05 p0816 A71-16500
Rocket engines with nitrogen tetroxide/hydrazine injectors destructive instability due to pressure disturbances, establishing origin, propagation velocity and pops extent by streak photography
[WSS/CI PAPER 70-25] 06 p0942 A71-17653
Nitrogen tetroxide/hydrazine pulse mode rocket engines structural failure due to chemically reactive gaseous hot spots causing high pressure spiking and detonation initiation
[WSS/CI PAPER 70-24] 06 p0944 A71-17663
Parameters influence on mercury hollow cathode neutralizers for Kaufman ion thruster
[AIAA PAPER 70-1090] 07 p1184 A71-19863
Metal powders hypergolic ignition in gaseous chlorine trifluoride, examining use in air augmented rockets primary combustors
07 p1183 A71-19875
Soviet book on space flight mechanics covering vehicle motion, engine systems, gravitational fields and trajectories
08 p1361 A71-21050
Rocket engine thermodynamic characteristics and parameters determination, using extrapolation formulas with initial fuel composition
08 p1346 A71-21264
Control jets interaction with airstream surrounding typical tactical missile configuration, considering rear mounted bistable fluidic thrusters and circular sonic jets
11 p1837 A71-25506
Analytical method for optimal rocket motors cluster arrangement in multistage spacecraft, considering horizontal trajectories rated terminal velocity performance
11 p1839 A71-26335
Rocket propulsion systems local heat transfer investigation, comparing experimental data to Bartz formula estimates over wide combustion chamber pressure range
12 p1945 A71-26983
Thrust measurement of aircraft and rocket propulsion systems, comparing cost and characteristics of mechanical, electrical and hydraulic systems
12 p1894 A71-26991
Electrostatic spray generated charged colloids adaptation to thruster with metal capillary needles under AC voltage, evolving low thrust propellants
13 p2118 A71-29503
Steady state thermonuclear fusion rockets, considering specific impulse, space propulsion and research priorities
14 p2288 A71-29929
Beam vector control from ion bombardment thrusters with dual grid electrostatic, movable screen electrode and discharge chamber extraction systems
[AIAA PAPER 71-691] 14 p2293 A71-30751
Frequency analysis of open loop transfer function, determining combustion instability for catalytic monopropellant thrusters
[AIAA PAPER 71-701] 14 p2286 A71-30759
Combustion efficiencies of staged rocket motor consisting of gas generator, secondary combustor and converging-diverging nozzle
[AIAA PAPER 71-739] 14 p2296 A71-30782
Minuteman 2 third stage rocket engine instrumentation performance evaluation for oscillatory combustion characteristics analysis
[AIAA PAPER 71-755] 14 p2248 A71-30789
Low pressure gaseous hydrogen/gaseous oxygen APS rocket engines operating with propellant stored as liquids and fed to thruster without pressure augmentation
[AIAA PAPER 71-738] 15 p2467 A71-31326
Space shuttle main engine based on high pressure, staged combustion, reusable, minimum risk and low cost concepts
[AIAA PAPER 71-658] 15 p2470 A71-32290
Broadband radiated interference measurement of nonhyperbolic propellant rocket engine spark gap ignition for electromagnetic compatibility
15 p2471 A71-32372
Turbulent combustion stability in rocket engine with allowance for walls reflecting acoustic waves excited by flame
16 p2663 A71-33605
Skylab pointing and control system using control moment gyros and cold gas reaction thruster system to provide attitude control
17 p2813 A71-35064

ROCKET EXHAUST

Electron bombardment mercury ion rocket engine, considering mass flow rate and magnetic field strength effect on performance 17 p2794 A71-35540

Cold gas rocket propulsion systems design parameters, determining performance and weight formulae 21 p3437 A71-41050

Book on aircraft propulsion covering design, dynamics, control, installation, gas turbine, ramjet, rocket and piston engines, compressors, combustion and energy cycles, etc 22 p3589 A71-42427

ROCKET EXHAUST

Combustion residues particle size and distribution during rocket plume impingement on Al surface 01 p0183 A71-11594

Spacecraft propellant condensation on low temperature surfaces near cesium ion thruster exhaust, considering neutral atoms impingement and charge exchange 03 p0522 A71-14455

Ion-electron recombination coefficient measurement for ionized trails left by rocket exhausts in high atmosphere using radio observation 06 p0895 A71-18314

Liquid rocket propellant engine exhaust plume flow field, discussing mathematical models for combustion chamber, throat region and nozzle [AIAA PAPER 70-844] 07 p1183 A71-19861

Surface heating and pressure distribution on Lunar Module from rocket exhaust plume impingement tests in vacuum [AIAA PAPER 71-256] 08 p1377 A71-21985

Rocket engine exhaust jet simulation in wind tunnel tests, discussing principles derived from aerodynamic geometrical and physical similarity laws 12 p1945 A71-27466

Slender cone at Mach 10 with underexpanded exhaust plume, determining flow field interactions separation pattern and aerodynamic coefficients [AIAA PAPER 71-562] 15 p2347 A71-32280

Multistep rocket mass ratios optimization, including exhaust gas velocities, structure and efficiency 16 p2644 A71-32843

Ionospheric disturbances due to supersonic shock from missile exhaust plume, noting F region compressions and undulations 16 p2563 A71-33358

Spectral scanning method for determining temperature profile of jet- or rocket-engine exhaust stream by gas radiation and transmittance measurements, discussing radiometric effects 18 p2916 A71-36048

Base pressure of cluster rocket exhaust with several jets simultaneously ejecting from nozzles 18 p2903 A71-36116

Base flow characteristics in four-nozzle rocket exhaust as functions of nozzle axis interspaces, nozzle exit section-base surface distance and Mach number 18 p2903 A71-36117

Chemical composition and size distribution of particulate matter in solid propellant combustor of boron loaded rocket motor 21 p3436 A71-40944

Microwave scattering noise spectrum from turbulent rocket-exhaust jet illuminated by plane wave 22 p3510 A71-42208

Scattering from turbulent rocket-exhaust jet illuminated by focused microwave beam, calculating noise spectrum by approximate theory 22 p3510 A71-42209

Flow field calculation in intermediate altitude rocket exhaust plumes by modified Lagrangian finite difference technique 22 p3590 A71-42774

ROCKET FIRING

NT RETROFIRING

Self regulating steady state cryopump system for simulated altitude testing during rocket engine firings 20 p3184 A71-39198

ROCKET FLIGHT

Soviet book on rocket flight dynamics covering center of mass motion characteristics, guided missiles, external ballistics, multistage design and flight optimization 02 p0320 A71-12724

Sounding rocket dispersion analysis, discussing roll rate errors, earth rotation and wind effects and improved computational techniques [AIAA PAPER 70-1379] 03 p0498 A71-13662

Unguided, attitude stabilized and velocity controlled sounding rockets impact dispersion, discussing system selection and servomechanism [AIAA PAPER 70-1381] 03 p0498 A71-13664

Rocket free flight ascent trajectory range error, approximating influence of stabilizers, nose cone and components misalignment along longitudinal axis 04 p0601 A71-14596

Rocket optimum control synthesis for powered flight phase, determining angle of attack for transfer to maximum velocity by Cauchy problem 05 p0779 A71-16038

Optimal vacuum rocket trajectories over spherical earth, deriving nonlinear differential equations for position and velocity [AIAA PAPER 71-20] 06 p0976 A71-18487

Two stage rocket trajectory optimization for prescribed flight range, maximizing hit probability for given number of launches 08 p1367 A71-22036

Impact dispersion reduction of uncontrolled sounding rocket ZENIT with CUCKOO booster by canard control, noting flight path angle error by tracking radar 09 p1533 A71-23598

Optimal thrust programming for rocket near spherical planet, transfer between circular orbits and lunar landing at predicted point 10 p1683 A71-24847

Two stage rocket flight optimization for minimum propellant consumption, using calculus of variations 13 p2145 A71-28734

Kalman filter in preflight postflight analysis of velocity increment by spin rocket plume impingement at preentry altitudes [AIAA PAPER 71-934] 19 p3148 A71-37179

ROCKET FUEL TANKS

U PROPELLANT TANKS

ROCKET LAUNCHERS

Churchill research range auroral sounding rocket launcher facility, describing design, construction and performance [AIAA PAPER 70-1391] 03 p0397 A71-14275

Fiberglass reinforced plastic rocket launcher tubes with internal helical rails to impart spin to missiles, discussing design, fabrication and testing 11 p1786 A71-25419

ROCKET LAUNCHING

NT LUNAR LAUNCH

NT ORBITAL LAUNCHING

Sounding rocket-moving target spatial relationship trajectory modeling by digital simulation, applying to vehicle launching during solar eclipse of March 1970 [AIAA PAPER 70-1374] 03 p0497 A71-13657

Thrust vector control system of reduced impact dispersion of Skylark sounding rocket [AIAA PAPER 70-1375] 03 p0497 A71-13658

Wind compensation method for launching sounding rockets susceptible to nonlinear wind effects, using data generated by six degree of freedom trajectory digital simulation program [AIAA PAPER 70-1390] 03 p0498 A71-13672

Vacuum tube launchers and boosters for launching small to medium size meteorological probe rocket into lower atmosphere [AIAA PAPER 70-1393] 03 p0498 A71-13674

Rocket/launcher aerodynamic interference effects investigation by wind tunnel simulation, determining interference coefficients for rockets ballistic dispersion calculations [AIAA PAPER 71-269] 08 p1274 A71-21995

German monograph on determination of instantaneous position of polar electrojet for rocket launching parameters computation 18 p2911 A71-35920

Rockets and launch operations protection from atmospheric electricity at Kennedy Space Center, discussing current and future lightning suppression 18 p2913 A71-36451

Seasonal stratospheric wind effects on infrasound propagation to U.S. northeast coast from rockets launched at Cape Kennedy 20 p3306 A71-39762

Frequency shift in air-coupled surface waves during Saturn 5 launches, computing apparent phase velocity experienced by ground 23 p3672 A71-43883

ROCKET LININGS

Graphite fiber reinforced ablative composites fabricated into rocket propulsion test units for oxidative liquid high temperature and pressure environments 09 p1459 A71-23685

Elastomeric rocket motor thermal insulants ablation, considering composite properties, heat transfer, compounding and tests 21 p3406 A71-40603

ROCKET MOTOR CASES

U ROCKET ENGINE CASES

ROCKET NOSE CONES

Meteorological rocket nose portion thermal regime, determining housing, insulation coating and compartments temperature 19 p3172 A71-38632

Meteorological rocket nose thermal shield, discussing design and effectiveness 19 p3172 A71-38636

ROCKET NOZZLES

U-tube rocket nozzle and fuel element fabrication methods for NERVA space engine, emphasizing coating process 01 p0126 A71-10006

Sounding rockets motors with integrally molded plastic case and nozzle, discussing cost effectiveness and demonstration tests [AIAA PAPER 70-1386] 03 p0470 A71-13669

Secondary gas injection at right angles into supersonic rocket nozzle, investigating side force characteristics 03 p0470 A71-13736

Nuclear rocket nozzle cooling passages, discussing heat transfer and friction correlations for single-phase hydrogen turbulent flow [AIAA PAPER 70-661] 03 p0456 A71-14444

One dimensional kinetic calculations for hydrogen fluorine rocket nozzles compared to firing data, discussing Cl addition effect on performance [WSS/CI PAPER 70-21] 06 p0943 A71-17656

Axial Mach number distribution of supersonic flow in rocket nozzle with Rao optimum contour 07 p1093 A71-20366

High temperature liquid propellant oxidative-erosion resistant ablative composites containing in situ reaction formed refractory metal carbides for rocket nozzles 08 p1318 A71-20696

SIRIO spacecraft cavity backed antenna around apogee motor nozzle operating at 40 and 360 MHz 14 p2218 A71-31069

Inviscid compressible transonic flow field equations for perfect gas in conical rocket nozzles, measuring wall and center line pressures 15 p2390 A71-32040

Laser holographic inspection for disbands in metal/phenolic rocket nozzles of two divergent geometries, corroborating by ultrasonics and dye penetrants 24 p3829 A71-45278

ROCKET OXIDIZERS

German monograph on high energy propellant-oxidizer systems changes of state under high temperature conditions with chemical relaxation taken into account 05 p0795 A71-17106

Solid propellant oxidizers hydroxylammonium perchlorate and hydrazine nitroform self deflagration, determining combustion temperatures and burning rate pressure relationships 06 p0944 A71-18299

Erosive burning of composite propellants based on ammonium perchlorate, studying oxidizer grain size effect 10 p1658 A71-25122

Compositional and oxidizer particle size effects on combustion instability of plastic propellant based on ammonium perchlorate and polyisobutene [AIAA PAPER 69-478] 11 p1809 A71-25454

Red fuming nitric acid-sulfur dioxide as oxidizer for auxiliary ignition in liquid rocket motors 15 p2465 A71-32110

Hybrid rocket /Barbarella I/ design, tests, engine, feed system oxidizer tank, fairings fins, propellants and launch facilities 22 p3589 A71-42049

ROCKET PLANES

NT X-15 AIRCRAFT

ROCKET PROPELLANT TANKS

U PROPELLANT TANKS

ROCKET PROPELLANTS

NT CRYOGENIC ROCKET PROPELLANTS

NT GASEOUS ROCKET PROPELLANTS

NT HYPERGOLIC ROCKET PROPELLANTS

NT LIQUID ROCKET PROPELLANTS

NT METAL PROPELLANTS

NT MONOPROPELLANTS

NT SLURRY PROPELLANTS

NT SOLID ROCKET PROPELLANTS

Thermodynamic calculation of chemical equilibrium of rocket propellants and gun powders using computer program in Fortran IV 01 p0141 A71-10343

Spacecraft propellant condensation on low temperature surfaces near cesium ion thruster exhaust, considering neutral atoms impingement and charge exchange 03 p0522 A71-14455

Rocket propellants and gun powders performance calculation, using FORTRAN IV program 04 p0637 A71-15678

One dimensional kinetic calculations for hydrogen fluorine rocket nozzles compared to firing data, discussing Cl addition effect on performance [WSS/CI PAPER 70-21] 06 p0943 A71-17656

Initial reaction rates of oxygen difluoride with diborane related to reactant concentration and temperature 09 p1510 A71-22071

Rocket propellant performance improvement with boron, giving boiling temperature vs pressure and calculation methods for combustion products composition 11 p1809 A71-25573

Liquid hydrogen rocket propellant tanks insulation problems in space shuttle and orbiter 15 p2499 A71-31216

Biowaste resistojet engine design and performance for various propellants and propellant mixtures [AIAA PAPER 71-687] 15 p2470 A71-32293

Pulsed plasma rail mercury propellant thruster for satellite attitude control, measuring thrust and exhaust velocity with balance and Langmuir probe respectively 18 p2956 A71-36243

Pulsed plasma thrusters, propellants, trigger and feed systems developments for long life secondary spacecraft propulsion

22 p3588 A71-41975

Small hybrid rocket engine using aromatic amines mixture as fuel and nitric acid as oxidizer, discussing regression rate relations and internal ballistics design

22 p3589 A71-42019

ROCKET PROPELLED SLEDS

Test rail system of Les Landes Testing Center, discussing optical and electromagnetic observation, measurement and test coordination and control facilities and equipment

04 p0567 A71-15817

Laser velocity measuring system for tracking high speed rocket sleds on Holloman test track

18 p2932 A71-36616

Automatic argon ion laser tracking system for high speed rocket sleds, describing apparatus configuration and error correcting devices

18 p2883 A71-36908

ROCKET SONDES

U SOUNDING ROCKETS

ROCKET SOUNDING

Position finding for auroral electrojet using magnetometer measurements onboard Black Brant 3 rockets

01 p0075 A71-11331

Rocket-borne mass spectrometer observation of NO in auroral arc

01 p0077 A71-11522

Noctilucent cloud particle size composition and origin from sounding rocket flight and control collecting surfaces

02 p0246 A71-12702

Cosmic dust in mesosphere and upper atmosphere during weak noctilucent cloud from rocket collecting flight

02 p0246 A71-12703

Particle size collected on electron microscope grids attached to Luster rocket sampling surfaces during noctilucent cloud display

02 p0246 A71-12705

Photographic observation of noctilucent cloud occurrence over geographical location during sounding rocket flight

02 p0246 A71-12706

Parallel and perpendicular electric fields in auroral arcs from rocket-borne experiment

03 p0406 A71-13303

Sodium dayglow rocket measurements, comparing emission intensities with ground based measurements

03 p0407 A71-13312

Sounding rocket attitude monitoring and control, using digital output roll stabilized gyro platform

[AIAA PAPER 70-1407] 03 p0455 A71-13686

Cosmic dust size distribution measurement by electron microscopic examination of in-flight shadowed substrates during particle collection on ESRO rocket

03 p0491 A71-14015

Thermospheric neutral particle molecular nitrogen density and temperature measurements by rockets, noting correlations with diurnal, solar cycle and other variations

03 p0414 A71-14020

Rocket observations of far IR radiation from upper atmosphere

03 p0415 A71-14026

Rocket-borne Na-K vapor release for upper atmosphere winds profiles and diffusion measurements by ballistic camera photography

03 p0415 A71-14027

Rocket experiments during 1964 solar eclipse, obtaining D region parameters from parachute-borne blunt probe measurements of atmospheric positive and negative conductivities

03 p0416 A71-14033

Ionospheric plasma drift from spinning rocket shadow effect, using retarding potential analyzer

03 p0416 A71-14034

Black Brant rocket measurement of PCA event at Churchill, Canada on 19 November 1968, discussing electron density and alpha particle and proton flux

03 p0417 A71-14038

Daytime ionosphere rocket observations at Antarctica, examining electron density profiles

05 p0743 A71-17006

Rocket probe launched by aircraft for measuring pressure, temperature, magnetic field and wind velocity around tornado vortex through radio telemetry

05 p0778 A71-17140

X ray sources identification and position measurements near galactic center on basis of rocket experiments

05 p0814 A71-17234

He I 584 A dayglow radiation measurement by retarding potential photoelectron analyzer on Javelin sounding rocket

06 p0887 A71-17267

Upper atmosphere nitric oxide density measurement by scanning UV spectrometers on Nike-Apache rockets, noting ionization consequences for D region

06 p0888 A71-17273

Magnus effects on Apache sounding rocket at supersonic speeds, discussing spinning model and static tests

[AIAA PAPER 70-207] 07 p1205 A71-18893

Particle diffusion modulation by simultaneous VLF and ULF electromagnetic waves during rocket experiment

07 p1062 A71-19680

Differential secondary electron flux measurement in aurora with Aerobee rocket spectrometer

08 p1282 A71-21635

Polar ionosphere ion composition measurement by meteorological rocket-borne RF mass spectrometer

09 p1435 A71-22444

Satellite, rocket and Thomson scatter data application to communications - IEE Conference, London, January 1971

10 p1575 A71-23864

Flux and shape variability of X ray emission from M87 using proportional counters onboard Aerobee-Hi rocket

10 p1661 A71-24421

Brightness ratio near solar horizon from Ly alpha predawn and postdawn rocket observations consistent with radiation multiple scattering coronal model

10 p1605 A71-24794

Auroral pulsation analysis from rocket soundings, investigating oxygen green linear excitation sources

11 p1753 A71-25549

High altitude probe design and optimization, discussing hybrid propellant propulsion system peak altitude payloads and combustion temperatures

11 p1811 A71-25575

High latitude F region electron density irregularity measurements, using rocket-borne impedance probe

11 p1755 A71-25617

Stratospheric seasonal wind reversals morphological classification for comparing atmospheric processes over different rocket sounding stations

12 p1900 A71-27065

Stratospheric and mesospheric wind measurements over Leba sounding rocket station

12 p1900 A71-27066

Stratospheric wind seasonal reversals over Polish coast of Baltic Sea in 1967-1969 from rocket sounding and upper air synoptic analysis

12 p1900 A71-27067

Rocket-borne wind measurements at 40-70 km by glass fiber and Cu chaff clouds

12 p1901 A71-27068

D region atomic oxygen measurement via Nike Cajun sounding rocket flight

13 p2056 A71-27932

Ionospheric ion formation and neutralization reaction rate coefficients determination by fitting rocket measured electron concentration profiles with computer generated profiles

13 p2062 A71-28560

Multiple periodicity of Cygnus X-1 X ray emission from rocket sounding

14 p2302 A71-30653

Ionospheric electron resonance observation by sounders aboard rocket and satellites

14 p2202 A71-30947

Hypersonic flow of dust containing gases at low density for distribution accuracy of cosmic dust collection by sounding rockets

15 p2387 A71-31171

Rocket chemical release clouds into atmosphere during IQSY, discussing wind profiles, diffusion coefficients, turbulence, temperatures and atomic O distribution

15 p2396 A71-31615

Rocket observation for spatial distribution of far UV nightglow at Lyman alpha and shorter wavelengths

15 p2398 A71-31764

Diffuse low energy cosmic X rays rocket measurements, noting excess over extrapolated power law valid for higher energies

15 p2480 A71-32761

Atmospheric density measurements at 70 to 115 km altitude range from rocket soundings with accelerometer instrumented inflatable spheres

16 p2562 A71-33066

Corpuscular and solar electromagnetic ionizing radiation simultaneous measurement by sounding rockets, evaluating contribution to lower ionosphere formation

16 p2627 A71-33776

Daytime electron density profiles above 90 km from Doppler radio measurements by rockets launched from Southern Hemisphere site

16 p2567 A71-33779

Nike Apache solar X-ray observations during 7 March 1970 eclipse, determining residual fluxes and atmospheric absorption profiles for ion production rates

16 p2627 A71-33790

Electron temperature profiles in ionosphere from rocket probes, noting correlation with geomagnetic activity indexes

16 p2569 A71-33798

Normal angle determination by rocket observations for whistler mode waves propagation through magnetosphere and ionosphere from conjugate VLF ground station signals

16 p2569 A71-33805

Rocket-borne electron spectrometer measurements of low energy electrons during auroral events, noting influx sudden enhancement

16 p2570 A71-33820

Conjugate photoelectrons existence from rocket measurements during total solar eclipse of 7 March 1970

16 p2570 A71-33823

Pakistani space research including satellite geodesy, ionospheric sounding, rocket experiments, VLF studies and time keeping

16 p2666 A71-33857

UK space research programs, discussing ground based, satellite and rocket-borne experiments

16 p2666 A71-33859

Brazilian space research planning effort and activities covering rocket and satellite meteorology, satellite tracking, balloon experiments and ground based geophysical observations

16 p2667 A71-33869

Australian space research 1970 report to COSPAR covering rocket sounding, X ray and gamma ray astronomy, tracking stations and international cooperation

16 p2667 A71-33871

Molecular oxygen densities at 80-160 km by rocket sounding with absorption of solar Lyman alpha line and C IV doublet at 1550 A

16 p2574 A71-33966

Ionospheric electron concentration and proton flux rocket-borne measurements during nighttime PCA event, discussing atomic oxygen role in recombination processes

16 p2575 A71-33974

D region winter anomaly causes from coordinated rocket measurements, discussing electron density profiles and electron-ion recombination

17 p2731 A71-34315

German monograph on rocket measurements in auroral zone with proton magnetometer covering magnetosphere, spin-lattice and spin-spin relaxation time and data processing

18 p2910 A71-35885

German monograph on three component magnetometer for position determination of polar electrojet by sounding rocket

18 p2915 A71-35921

German monograph on calibrating induction coil and proton precession magnetometers for polar electrojet rocket experiments

18 p2915 A71-35922

Cosmic X ray astronomy by rocket and balloon soundings and discrete emission source measurements, considering energy spectra

18 p2957 A71-36212

German monograph on geomagnetic reference field for rocket measurements covering mathematical model for northern Scandinavia

18 p2913 A71-36682

Auroral zone proton measurements during slowly varying cosmic noise absorption, obtaining energy spectrum by rocket soundings

19 p3125 A71-37418

Nighttime E region ion composition and concentration profiles, using rocket sounding

19 p3061 A71-38628

Electrojet currents association with visible aurorae, using sounding rockets with rubidium vapor magnetometers

20 p3215 A71-38733

Equatorial electrojet region ionospheric currents during magnetically quiet day and nighttime from rocket measurements

20 p3218 A71-39524

Combined micrometeoroid collection and detection rocket experiment using foil penetration and plasma emission at impact for flux, masses and particle velocity determination

20 p3299 A71-39645

Sounding rockets sampling of cosmic dust in upper atmosphere during and after Zeta Perseid and Arietid meteor showers

20 p3299 A71-39651

Midlatitude ionospheric electron density and electron temperature measurements by rocket experiments, noting diurnal and seasonal variations

20 p3224 A71-39718

Day and night E and F region ion composition under solar maximum winter conditions from rocket measurements with RF mass spectrometers

20 p3280 A71-39719

Cosmic soft X ray detection by proportional counters with thin polypropylene windows onboard sounding rocket, considering galactic emission possibility

20 p3283 A71-39750

X ray rocket observations of Sco X-1 on 7-8 August 1969 compared to simultaneous optical observation, interpreting in terms of hot plasma model

20 p3283 A71-39751

Earth UV dayglow observation by Aerobee rocket-borne scanning spectrometer, noting features due to atomic oxygen and nitrogen and nitrogen oxide gamma band
20 p3226 A71-39830

Low energy hydrogen and helium ions composition of primary aurora precipitation from rocket-borne spectrometer experiment, suggesting direct solar wind origin of primaries
20 p3301 A71-39850

Trapped protons flux vs L profile measurement on-board sounding rocket near equator, comparing results with calculation from neutron albedo source and atmospheric losses
20 p3284 A71-39881

Polar cap electric field and relationship to magnetic disturbances from measurements on Ba ion clouds released by rockets
20 p3230 A71-39883

Night and daytime auroral zone ionospheric electric field measurement by rocket-borne Langmuir probe, noting components parallel and perpendicular to magnetic field
20 p3231 A71-39891

Atmospheric neutral and singly ionized He extreme UV emission altitude distribution measurement by sounding rocket-borne thin film photon counters
20 p3199 A71-39894

Rocket-borne explosive charge initiated detonation wave effects on decimeter wavelength radio waves in lower E layer
20 p3199 A71-39894

Cosmic soft X rays in energy range 0.14-7 keV from rocket soundings with thin polypropylene window proportional counters, covering field of view in Cygnus-Cassiopeia region
22 p3593 A71-42330

Rocket measured exospheric temperatures correlation with global model values based on incoherent scatter measurements
23 p3670 A71-43187

Cygnus X1 short term X ray flux pulsation variability from Southern Hemisphere sounding rocket flight
24 p3865 A71-44445

Venus upper atmospheric UV spectra from rocket-borne telescope spectrophotometer, considering O I and H I emission features
24 p3872 A71-44919

Ionospheric and neutral atmospheric temperature profile, composition and electron density and energy measurements by MR-12 rocket
24 p3824 A71-45310

ROCKET TEST FACILITIES

Meteor meteorological rocket flight testing, describing performance, instrumentation and technical and organizational problems
05 p0817 A71-16639

Modal characteristic pick-up system for vibration tests of rockets or aircraft on ground, using small size accelerometers with individual electronic circuit
12 p1895 A71-27719

Self regulating steady state cryopump system for simulated altitude testing during rocket engine firings
20 p3184 A71-39198

Hybrid rocket /Barbarella I/ design, tests, engine, feed system oxidizer tank, fairings fins, propellants and launch facilities
22 p3589 A71-42049

ROCKET THRUST

NT RETROTHRUST
Continuous thrust spacecraft optimal trajectory regularization, obtaining differential equations for three dimensional motion
01 p0154 A71-10381

Swirling flow through multiple nozzles of simulated solid propellant rocket motors, determining thrust and mass flow effects on passage
01 p0072 A71-11592

Thrust equation, control volume and propulsive efficiency for rockets and air breathing jets from energy conservation principle
02 p0299 A71-12681

Postflight analysis including six degree of freedom trajectory digital simulation of Aerobee 350 sounding rocket behavior under large thrust misalignment
03 p0498 A71-13663

FOILAC solid propellant rocket motors for high thrust short action time propulsion, reviewing development status and performance
03 p0470 A71-13668

Stored gas retrorocket total impulse expression, deriving from flow continuity equation in closed duct
06 p1366 A71-21308

Sounding rocket design parameters optimization, investigating apogee-payload relations, thrust as function of time, total weight, maximum altitude and acceleration
09 p1531 A71-22127

Thrust power optimization for spacecraft earth-planet round trip trajectories
12 p1957 A71-26633

German monograph on linear theory of optimization problems for low thrust rockets covering orbital calculations, flight characteristics and Coast Arc problem
14 p2319 A71-30233

Cooling effectiveness of liquid film barrier injected into rocket thrust chamber with vortex motion, considering heat transfer and performance
14 p2291 A71-30740

Optimal trajectory analysis for constant thrust optimal-coast minimum propellant control of rocket powered space vehicle
15 p2488 A71-32091

Component assembly effect on dynamic stability of liquid propellant rocket engine spacecraft during thrust sections of trajectory
16 p2646 A71-33657

Optimal fuel trajectories involving intermediate thrust arcs, considering strong thrust variations, mid-course guidance and numerical results
22 p3600 A71-41959

Angular momentum vector orientation of reentry vehicle at end of spin-up, using helicoid precession concept to characterize rotational motion during constant thrust
22 p3611 A71-42029

Iterative solution of least squares programming problem for finite thrust rocket trajectory optimization
23 p3724 A71-42984

Optimal singular control conditions for intermediate rocket thrust arc nonoptimality in Newtonian gravitational field for minimum fuel fixed time trajectory
23 p3718 A71-43378

ROCKET VEHICLES

NT AEROBEE ROCKET VEHICLE
NT AGENA ROCKET VEHICLES
NT APACHE ROCKET VEHICLE
NT ASTROBEE ROCKET VEHICLES
NT BLACK BRANT SOUNDING ROCKETS
NT BLACK BRANT 3 SOUNDING ROCKET
NT BLACK BRANT 4 SOUNDING ROCKET
NT CENTAUR LAUNCH VEHICLE
NT DIAMANT LAUNCH VEHICLE
NT ELDO LAUNCH VEHICLE
NT KAPPA 9 ROCKET VEHICLE
NT LAMBDA ROCKET VEHICLES
NT MULTISTAGE ROCKET VEHICLES
NT NIKE-APACHE ROCKET VEHICLE
NT NIKE-TOMAHAWK ROCKET VEHICLE
NT RUBIS ROCKET VEHICLE
NT SATURN LAUNCH VEHICLES
NT SATURN S-1C STAGE
NT SATURN S-2 STAGE
NT SATURN S-4B STAGE
NT SATURN 5 LAUNCH VEHICLES
NT SINGLE STAGE ROCKET VEHICLES
NT SKYLARK ROCKET VEHICLE
NT SOUNDING ROCKETS
NT THOR DELTA LAUNCH VEHICLE
NT THOR LAUNCH VEHICLES
NT VIKING ROCKET VEHICLE

Spinning rocket vehicle with aerodynamic asymmetry, deriving equations of motion and steady aerolelastic behavior
03 p0499 A71-13678

Sounding rocket vehicle static stability reduction due to aerolelastic bending, using flight characteristics and wind tunnel test data for computerized analysis
03 p0499 A71-13681

Horizontally coherent supersonic velocity LF sound signals from Apollo rocket vehicles at high elevations
07 p1208 A71-20149

Soviet book on long range rocket ballistics covering control system, dynamics, firing distance, motion equations, stage separation and nominal trajectories
13 p2146 A71-29438

Infinite-time linear dynamic system suboptimal control derivation from lower dimension models, exemplifying by flexible-bodied rocket vehicle pitch plane dynamics
17 p2720 A71-34871

Rocket propulsion system equipped space shuttle dynamics, discussing aerodynamic forces and moments measurement in supersonic wind tunnels
19 p3151 A71-37318

Impulsive retrofire boost of rocket vehicles initially moving in elliptical orbits for maximum and minimum atmospheric entry angles
22 p3608 A71-41697

ROCKET-BORNE INSTRUMENTS

Aerobee 150 sounding rocket cryogenic air sampler, discussing design, operation and air constituents reaction to cooling
01 p0084 A71-11442

Nulls of radiation and input impedance of flush mounted rocket antennas for telemetry and transponder systems
02 p0228 A71-11674

Upper stratosphere and mesosphere concentrations of Ne, Ar, and Kr from rocket-borne cryogenic air sampler
02 p0246 A71-12701

Langmuir probe DC detector for rocket quasi-static and AC electric field measurements in auroral zone ionosphere
03 p0406 A71-13302

Stellar Tracking Rocket Attitude Positioning System /STRAP/ for sounding rocket payloads three-axis orientation control with accuracy
03 p0455 A71-13683

Sounding rocket Solar Eclipse Sensor for 7 March 1970 event, discussing mission, capabilities, data acquisition and design
03 p0455 A71-13685

Zodiacal light IR spectroscopy by rocket-borne detector, providing information on interplanetary dust properties
03 p0491 A71-14013

Cosmic dust detection equipment onboard Centaur and Nike-Apache rockets, using recoverable metallic collector and telemetered tungsten target plasma emission detector
03 p0491 A71-14016

Cosmic dust fluxes determination by rocket-borne micrometeorite experiments, using piezoelectric acoustic type impact detectors
03 p0492 A71-14017

Ionospheric measurements by rocket-borne HF capacitance probe during solar flare of 26 February 1969, determining electron density vertical stratification
03 p0416 A71-14032

Low energy particle variable flux measurement in midlatitude ionosphere, using rocket-borne thin window proportional counters
03 p0421 A71-14539

High altitude rocket-borne radiosonde communication, examining transmission link characteristics, signal losses and antenna radiation patterns
04 p0551 A71-15012

Rocket UV astronomy, discussing atmospheric and interstellar absorption, equipment design and OAO experiments
04 p0649 A71-15253

Rocket-borne beta ray atmospheric densitometer errors due to cosmic rays
05 p0752 A71-16673

Rocket probe launched by aircraft for measuring pressure, temperature, magnetic field and wind velocity around tornado vortex through radio telemetry
05 p0778 A71-17140

IR radiation measuring circuit with pneumatic detector usable on rockets and satellites
06 p0900 A71-18023

Rocket-borne solid state spectrometer with liquid nitrogen-cooled Li drifted silicon detector and optical feedback preamplifier for solar X-ray measurements
06 p0901 A71-18223

UV solar spectrum rocket-borne high resolution spectroscopy by Fabry-Perot interferometer and echelle grating, discussing design parameters and recorded data
06 p0903 A71-18718

Energetic electron and proton precipitation measurements by sounding rocket-borne particle detectors in pulsating aurora
07 p1186 A71-19669

Nitrogen Vegard-Kaplan and second positive band systems emission, using rocket-borne spectrometer in UV aurora
07 p1102 A71-19670

Parachute ejectable rocket-borne instrument package with telemetry system for lower ionosphere measurements, describing electrical and mechanical design and operation
07 p1208 A71-19803

Rocket-borne HF capacitance probe for measuring ionospheric electron density profile
07 p1116 A71-20498

X ray source in Perseus region, studying Aerobee rocket proportional counters measurements
09 p1512 A71-22348

Mesosphere charged particles concentration and mobility measurements, using rocket-borne aspiration probes
10 p1604 A71-24705

Daytime lower ionosphere electron density profiles over equator, using rocket-borne Langmuir and plasma noise probes
10 p1606 A71-24913

Stokes flow parachute extremely lightweight decelerator for increasing altitude and rocket-borne radiosondes atmospheric data sampling quality
11 p1707 A71-25277

Superfluid-helium-cooled rocket-borne far-IR radiometer for night sky radiation measurement, discussing cryogenic, optical detection and electronic systems design features and performance
12 p1903 A71-26791

Rocket sonde prototype for wind and temperature measurements, discussing electrical circuits, mechanical design and operation
12 p1972 A71-27064

Cosmic X ray background observations, using rocket-borne proportional counter
13 p2131 A71-29269

Rocket-borne Cassegrain telescope system design for stellar spectra in UV region of EM spectrum between 900 and 3300 A
14 p2238 A71-29727

Rocket-borne twin-channel photoelectric stellar photometer for use in 1400-3000 A region, describing nondispersive wavelength isolation methods
14 p2240 A71-30124

Short low noise transistorized receiving antennas for rockets with nonconducting hoods and conducting surface 14 p2218 A71-31063

Sounding rockets, outlining experimental missions, design and payload varieties, auxiliary systems and electronic equipment 15 p2499 A71-31213

Rocket-borne coronagraph photometry of solar corona during solar eclipse of 7 March 1970 16 p2640 A71-33733

OH emission column density upper limit from rocket-borne UV spectrometer measurement of resonantly scattered intensity in electronic transition vibrational band 16 p2574 A71-33967

Rocket-borne RF capacitance probe design for determining lower ionospheric electron densities 18 p2921 A71-36367

X ray source Cygnus X-1 position determination by Aerobee rocket-borne rotating modulation collimator 18 p2970 A71-37053

High resolution solar UV spectrum observation between 200 and 220 nm by sun-pointed Skylark rocket-borne echelle spectrograph 19 p3135 A71-37611

Solar Mg II H and K line profiles from rocket-borne echelle interferometer spectrograph and densitometer data 19 p3135 A71-37612

Vertical 1 single stage geophysical rocket design and instrumentation for X rays, solar UV and meteoritic concentration measurements 19 p3154 A71-38530

Ionospheric electron concentration and temperature measurements, describing rocket-borne asymmetrical Langmuir probe 19 p3067 A71-38631

Meteorological research rockets instrument composition and systematization, discussing functional schemes, arrangement and onboard location 19 p3067 A71-38637

Ionospheric low hybrid resonance measurements by rocket-borne quadrupole probe, deriving electron density and effective ion mass along trajectory 20 p3224 A71-39722

Ground based optical observation of raylike artificial auroras produced by rocket-borne accelerator generated electron beams, using image orthicon TV system 20 p3231 A71-39886

Taurus X-1 X ray emission polarization from rocket-borne polarimeter measurements, utilizing incoherent scattering 20 p3302 A71-39921

Auroral far UV spectrum and intensity measurements, discussing atmospheric absorption effects on rocket-borne spectrometer sensitivity 21 p3372 A71-40039

Night sky far IR background radiation measurements by rocket-borne superfluid HE cooled radiometer, determining average signal strength equivalency to black body temperature of 3.1 K 24 p3822 A71-44752

Vela X and Puppis A soft X ray observations using rocket-borne methane counter 24 p3866 A71-44907

ROCKET-BORNE PHOTOGRAPHY

Oxygen red-green line emission intensity in quiet auroral arc, using rocket-borne photometers 11 p1754 A71-25551

Solar disk photographs taken by Skylark rocket in EUV and soft X ray region 20 p3293 A71-39534

ROCKETRY

U ROCKETS

ROCKETS

Dissipative mechanical filter for rocket self excited vibrations to eliminate oscillatory instability, describing transfer function and modal characteristics 01 p0164 A71-11021

Rocket body longitudinal autooscillation modes, taking into account pipeline fluid discontinuous cavitation oscillations 16 p2644 A71-32834

ROCKS

NT ANDESITE

NT ANORTHOSITE

NT BASALT

NT BRECCIA

NT CARBONACEOUS ROCKS

NT COAL

NT ENSTATITE

NT GNEISS

NT GRANITE

NT IGNEOUS ROCKS

NT LAVA

NT LIMESTONE

NT LUNAR ROCKS

NT MAGMA

NT OLIVINE

NT PYROXENES

NT QUARTZ

NT SANDSTONES

NT SERPENTINE

Reduced pressure effects on thermal expansion and fragmentation of rocks 03 p0418 A71-14460

Exposed rock bodies thickness determination using normalized peak gravity effect diagrams 04 p0583 A71-15271

North American feldspathoidal and silica unsaturated rocks progression in space and time 04 p0584 A71-15775

Photographic and IR multiband spectral discrimination for rock and soil mapping from orbiting ERTS satellites 06 p0898 A71-17562

[ALAA PAPER 70-303] Extraterrestrial microorganisms penetration into rocks and meteorites under various climate conditions, noting effects of humidity 13 p2010 A71-28693

High moisture content rock samples electrical conductivity and permittivity by VLF electrospectroscopic investigations based on signal phase shift 14 p2238 A71-29514

Ultrahigh energy muons intensity distribution as function of zenith angle at fixed slant depth of rock 15 p2476 A71-31793

Thermally stabilized volcanic rock magnetic properties and coupling hysteresis effect changes due to reheating in weak magnetic field 18 p2912 A71-36197

Coesite-stishovite content in Ries crater nonporous crystalline rocks of variable composition and degree of shock metamorphism 19 p3050 A71-37660

Mercury determination in terrestrial and nonterrestrial rock samples by atomic absorption spectroscopy, noting high temperature release patterns 21 p3346 A71-40863

RODENTS

NT GUINEA PIGS

NT HAMSTERS

NT MICE

NT RABBITS

NT RATS

Frequency spectra and cosinor for circadian rhythms in rodents and in man during Gemini and Vostok flights, considering future biosatellites 01 p0020 A71-11569

Adrenocortical function in garden dormouse during autumnal preparation for hibernation, considering environmental temperature factors 13 p2014 A71-29315

RODS

German monograph on nonlinear flexural-torsional stress analysis of thin walled rods with open profiles covering fork supported and cantilever beam systems 01 p0166 A71-10112

Color matching discrepancies, considering rod blue qualities under photopic conditions, luminance level and trichromatic stimulus unsuitability for large field additive colorimetry 01 p0010 A71-10273

Polish book on limiting load capacity of structural elements covering notched rods and plates with hole under elastoplastic stress 02 p0330 A71-12750

Console rod free and forced transverse vibrations amplitude dependent damping, considering longitudinal tensile force effect and hysteresis 03 p0502 A71-13405

Static tension effect on damping capacity of drawn rods under flexural vibrations, considering materials with strong magneto-mechanical hysteresis 03 p0503 A71-13413

Anisotropic thin rods deformation, extending Nikolai constraints condition on Kirchhoff analogy for isotropic rods 03 p0506 A71-13598

Anisotropic rod elastic curve equilibrium shape for rigidity conditions, considering Goriachev solution to heavy solid body motion about fixed point 03 p0458 A71-13599

Thin rod deformation by gyrostat motion analysis, deriving anisotropic curved rods equilibrium shapes 03 p0458 A71-13600

Infinite elastic beam normal impact by semiinfinite elastic rod, using Timoshenko beam and one dimensional bar theory to describe elastic waves [ASME PAPER 70-WA/APM-54] 03 p0513 A71-14171

Polish book on impact in discrete mechanical systems covering beams, curved rods, plates, nonlinear damping, numerical analysis, subjected to shock loading 03 p0513 A71-14297

Radiation patterns of dielectric rod antennas with axial emission in near field 04 p0557 A71-14630

Staticogeometrical relations of thin torus shaped shell and closed curvilinear rods 05 p0824 A71-16594

Boundary layer development on slender rod in axial shear flow for different profiles 05 p0694 A71-16711

Structural stability of incompressible elastic rod of variable rigidity flattened along axis, reducing boundary value problem to equation with continuous operator 05 p0828 A71-16987

Homogeneous rod heat transfer inverse problem, considering temperature distribution determination 06 p1005 A71-17325

Structural behavior of rods and cylindrical shells under dynamic impact loads 06 p0989 A71-17783

Thermal diffusivity in disks and rods irradiated by sinusoidally modulated thermal radiation beam, measuring temperature phase difference across front and back faces 07 p1223 A71-19622

Wave dispersion in transversely isotropic rods, discussing phase velocities, spectral lines and cut-off frequencies 07 p1214 A71-19957

Infinitely long dielectric rod waveguide HE sub 11 surface wave mode launching efficiency, using Fourier integral 08 p1262 A71-20754

Energy dissipation during independent flexural-torsional vibrations of rods, noting alternating shear stress superposition effect on damping 09 p1538 A71-22629

Statically indeterminate rod system design, using linear strengthened materials strain diagrams and Castigliano principle 09 p1538 A71-22650

Welding rods chemical composition and welding procedures for heat resistant austenitic and martensitic steels for gas turbines, considering maraging steels heat treatment influence 09 p1456 A71-23291

Nonhomogeneous variable diameter rods plastic torsion, deriving stress function and distribution 11 p1848 A71-25620

Optimal elastic beam structural design for given deflection in presence of body forces, considering rod under centrifugal loads 11 p1849 A71-25680

Free vibrations of three dimensional system of rods subjected to transverse vibrations in two planes of symmetry 12 p1930 A71-27172

Physically nonlinear bent rod, deriving strain method equations for plasticity with hardening according to broken line law 12 p1978 A71-27336

Asymptotic solutions of improved equations for elastic and elastoplastic waves in rods, considering longitudinal waves propagation 12 p1980 A71-27449

Load bearing capacity of thin walled box shaped rod of strain hardening material during bending beyond elastic limit 13 p2153 A71-28294

Approximate critical stresses during longitudinal compression of nonmetallic rods of medium flexibility, using stability loss curve tangent to Euler hyperbola 13 p2091 A71-28295

Free elastically joined composite rod under tracking forces, calculating stability and oscillations by numerical method 13 p2154 A71-28644

Torsion of circular composite rods of sectors with different shear moduli and radial cracks 14 p2326 A71-30193

Force method equations for linear viscoelastic system of incompressible rods obeying small deformations theory 14 p2328 A71-30376

Stress-strain state of finite length elastic rod free of bending moments and coupled to semiinfinite plate 14 p2332 A71-30868

Equilibrium stability of rods, shells and plates during creep due to applied load 14 p2333 A71-30893

Low temperature and tensile loading rates effects on static and dynamic strength of steel rods with ground and rolled threads 15 p2505 A71-31862

Stress relaxation in rings and rods, discussing errors in data correlation 15 p2508 A71-32230

Rods stability under nonconservative loads, applying Liapunov functions to boundary value problems 16 p2607 A71-32977

Rods instability with cross sectional stress concentration dependent properties, presenting buckling and bending problems 16 p2648 A71-32990

Thin walled rod of strain hardenable material, developing constrained torsion approximation for creep and relaxation 16 p2651 A71-33060

Logarithmic decrement of flexural, longitudinal and torsional vibration damping of various size rods, taking into account surface layer energy loss 16 p2659 A71-33979

Stationary small elastoplastic longitudinal forced vibrations of rods with internal resonance, obtaining asymptotic solution of nonlinear partial differential equations 16 p2659 A71-33980

ROGALLO WINGS

- Time dependent bending of circular cross sectioned rod under constant load compression and creep
17 p2821 A71-34564
- Static tension effect on damping capacity of stretched rods under flexural vibrations, considering materials with strong magneto-mechanical hysteresis
17 p2826 A71-35020
- Stress-strain state of thin walled curvilinear frame-type rods of variable cross section with variable elastic moduli along length and contour
17 p2829 A71-35309
- Green functions difference interpretation for finite and semiinfinite heat receiving rods, using dimensionless unsteady heat transfer parameter
18 p2985 A71-36124
- R and C parameters determination for electric circuit simulating heat transfer in rod by amplitude-frequency characteristics
18 p2985 A71-36125
- Structural stability of incompressible elastic rod of variable rigidity flattened along axis, reducing boundary value problem to equation with continuous operator
18 p2982 A71-36787
- Torsion of hollow beam consisting of two homogeneous isotropic rods with different elastic properties and simply connected cross sections, solving by conformal mapping
19 p3155 A71-37387
- Nonlinear behavior of compressed elastic and elastoplastic rods in presence of large deformations, determining bearing capacity by step method
20 p3269 A71-39164
- Plastic wave propagation along rods and through slabs, describing finite deformation elastic-plastic theory
21 p3464 A71-40785
- Semiinfinite rods in maximal plastic deformation, observing impulse and energy constraint distinction
21 p3467 A71-40961
- Radiation patterns of dielectric rod antennas with axial emission in near field
22 p3521 A71-42270
- Flexural wave propagation in thin curved rod oscillating in plane, calculating frequency and velocity from boundary conditions according to Saint Venant
22 p3617 A71-42574
- Rod buckling under creep conditions, evaluating stability with Shenley model
24 p3877 A71-44405
- Partitioning method for Reissner shell theory equations, constructing rod system
24 p3877 A71-44407
- Closed profile thin walled curvilinear rods, deriving static and strain integrals with Hookes law
24 p3877 A71-44410
- Thermally loaded rod structures optimization, presenting method for estimating canonical equations influence parameters
24 p3842 A71-44642
- Stress wave propagation in rod consisting of viscoelastic finite and semiinfinite elastic parts during pulsed sinusoidal load at end
24 p3885 A71-45223

ROGALLO WINGS

U FLEXIBLE WINGS
U FOLDING STRUCTURES

ROLL

- Launch vehicle under influence of random fin misalignments, predicting roll rate by statistical analysis
[AIAA PAPER 70-1382] 03 p0498 A71-13665
- Sounding rocket attitude monitoring and control, using digital output roll stabilized gyro platform
[AIAA PAPER 70-1407] 03 p0455 A71-13686
- Ballistic reentry vehicle roll related to trim angles caused by inertia asymmetries
[AIAA PAPER 70-204] 07 p1208 A71-19867
- Cone roll dynamics-ablation patterns coupling in hypersonic wind tunnels
[AIAA PAPER 70-562] 07 p1208 A71-19868
- Roll rate variation and lift effect on reentry vehicle impact, comparing analytic treatment with six degree of freedom trajectory simulation
13 p2144 A71-27977
- Aircraft flight characteristics dependence on angle of attack, roll and pitch
13 p1997 A71-29043
- Roll moment of inertia to static margin ratio effect on yaw of repose angle magnitude in ballistic match of projectiles
14 p2325 A71-29890
- ROLL CONTROL
U LATERAL CONTROL
ROLL FORMING
- Plastic flow of metal during rolling in T groove, determining particle velocity and strain energy distributions
02 p0257 A71-12565
- Thick strips widening by rolling, deriving formula for maximum widening from plastic deformation process description by displacement-rate fields
04 p0602 A71-14608
- Sheet blanks shaping into conical products by rolling, discussing stress-strain state in blank and time dependent rolling process
06 p0906 A71-18711

Corrugated blank cross section distortion under bending on three roller mill
08 p1295 A71-20795

- Rolled metals crystallographic texture and pole figure determination using X ray diffractometer
09 p1467 A71-22307
- Residual stress magnitude and distribution in metal strips rolled with ultrasonic vibrations
21 p3389 A71-41093

ROLLER BEARINGS

- Radially loaded bearings rolling on flat track, determining slip-stick areas and creep conditions
01 p0086 A71-10298
- Thermally induced preload changes in roller bearings due to temperature gradients measured, using strain gage bridges and thermocouples
01 p0088 A71-11006
- Heat resistant roller bearings for vacuum applications at high temperature, discussing cage design and self lubricating materials
02 p0258 A71-12599
- High traction fluid effect on high speed roller bearing cage skidding, comparing with military specification oil
[ASME PAPER 70-LUB-E] 03 p0432 A71-13707
- Rolling contact body displacement effect on bearings rigidity with allowance for inner ring transverse vibration
08 p1295 A71-20689
- Cylinder roller bearing for heavy axial and radial loads, determining carrying capacity by sliding surfaces
10 p1617 A71-24683
- EHD lubricant film thickness and friction forces effects on ball and roller bearings selection and design
[ASME PAPER 71-DE-3] 12 p1911 A71-27322
- High speed roller bearing design with long fatigue life and weight reduction for high temperature operation in inert environment
[ASME PAPER 71-DE-50] 12 p1912 A71-27328
- Static load and stress distribution in rolling element bearings, using elastic contact area analysis method
[ASLE PREPRINT 71AM 1D-1] 13 p2076 A71-29487
- Spalling fatigue life prediction in rolling contact, studying ductility, compressive stresses, inclusions, surface imperfections and bearing ring deflections effects with mathematical model
14 p2251 A71-29830
- Tapered roller bearing lubrication, considering application to CH-47 Boeing helicopter transmission
17 p2749 A71-35300

ROLLING

- Sintered W rolling in vacuum over reduction and temperature ranges
02 p0256 A71-12514
- Oxidation potential criterion for metal sticking to rolls during rolling in vacuum, considering Ta, Zr, Mo, W, Ni, Cu, Nb and V
02 p0256 A71-12515
- Longitudinal and cross rolling effects on anisotropy of mechanical properties and deep drawability of sintered thin sheet Mo
02 p0257 A71-12518
- Mechanical properties of Ti alloys subjected to rolling and heat treatment
02 p0265 A71-12522
- High purity Mg deformation by remelting and rolling, investigating grain growth based on size measurement
03 p0445 A71-14341
- Abnormal microstructure in hot rolled plates and sheets of alpha plus beta Ti alloys
05 p0766 A71-16349
- Re hot rollability under low vacuum conditions as function of temperature, comparing with cold rolling
07 p1120 A71-20240
- Tall thin strip rolling in ribbed grooves, determining critical area reductions causing plastic stability loss
08 p1295 A71-20841
- Apparatus for rolling and stretching metals at cryogenic temperatures, describing structural features
08 p1300 A71-21810
- Cr specimens containing Y, investigating microscopic breakdown at high temperatures as function of deformation during vacuum rolling
09 p1474 A71-23235
- Pure W single crystals grown by electron beam zone melting technique, noting rolling workability
12 p1919 A71-27761
- Rolling contact spalling fatigue failure incidence in subsurface defects, using engineering model based on crack growth rate
14 p2251 A71-29828
- Contacting surface rolling spalling fatigue failure incidence prediction using engineering model with preexistent discontinuities and microgeometrical asperities
14 p2251 A71-29829
- Hot rolled powder metallurgy Mo, noting texture during annealing and cold rolling
15 p2425 A71-31396
- Müky Way galaxy interstellar neutral hydrogen rolling motion phenomenon confirmed by 21 cm line survey data
16 p2630 A71-33053

AMG6M alloy hot rolling butt joints, showing ductility and strength of welds
19 p3070 A71-38424

ROLLING CONTACT BEARINGS

U ANTIFRICTION BEARINGS

ROLLING CONTACT LOADS

- Elastohydrodynamic oil film measurements for rolling point contact of ball bearing under starvation using optical interferometry
01 p0087 A71-10481
- Rolling ball fatigue and lubrication with fluorinated polyethers at cryogenic temperatures compared to superfinned mineral oil
01 p0107 A71-10484
- Test time and contact stresses effect on jet fuels antiwear properties under rolling friction
02 p0298 A71-12570
- Device for jet fuels antiwear properties measurement under rolling friction
07 p1111 A71-19493
- Two dimensional effects of cylinders rolling on elastic half space, investigating inflated tire shear stress and slip region
11 p1850 A71-26101
- Photoelastic analysis of oil film effects on rolling/sliding contact stresses of plastic and glass cylinders on steel ring, showing discrepancy with Hertzian distribution
15 p2414 A71-31946
- Local slip theory in elastic contact region with dry friction, assuming Amontons-Coulomb law for displacement, rolling and sticking
17 p2747 A71-34327
- Rheological factors and error sources in X ray measurements of lubricant film thickness in rolling contact
24 p3830 A71-44947
- Multiple rig rolling fatigue life tester, evaluating aviation gas turbine lubricants
[ASLE PREPRINT 71LC-15] 24 p3832 A71-45292
- Non-Newtonian film thickness, load capacity and maximum viscoelastic stress effect in point contact with second order fluid lubricant for slide/roll ratio
[ASLE PREPRINT 71LC-16] 24 p3832 A71-45293
- ROLLING MOMENTS
- Roll resonance in reentry body motion under nonlinear pitch, damping and Magnus moments, using multiple scales method
[AIAA PAPER 71-47] 06 p0979 A71-18508
- Nonlinear resonant roll motion of passive magnetic attitude control satellites, using Hill and Mitropolskii methods
11 p1837 A71-25458
- Transient resonance response of slender entry vehicles in rolling trim at spin-pitch intersection for offset coplanar and orthogonal leading modes
11 p1837 A71-25480
- Projectiles yawing and rolling over long flight paths, describing onboard solar aspect sensor and telemetry link to ground stations
[AIAA PAPER 70-538] 11 p1761 A71-25513
- ROOM TEMPERATURE
- Aqueous HCl refractive indices measured for room temperature to Venus cloud temperature and various concentrations
09 p1522 A71-22937
- Friction coefficient and wear of steel in vacuum and air at low and room temperatures
13 p2072 A71-27870
- Low resolution measurements of IR absorption of sulfur dioxide at room temperature
[ASME PAPER 70-WA/HT-4] 13 p2025 A71-28979
- Plastic deformation of aluminum oxide by indentation and abrasion at room temperature, using transmission electron microscopy
13 p2093 A71-28989
- Ring and cylindrical structures comparative stress relaxation at room temperature
15 p2508 A71-32229
- Room temperature ultrasonic frequency fatigue behavior of Al-base superalloy single crystals
17 p2756 A71-34493
- Stress annealing effects on Al 27 NMR lineshapes in pure Al powders filed and stored at room temperature, considering residual stress
17 p2759 A71-35225
- Experimental comparison between double drift and single drift region mm wave IMPATT diodes on room temperature metal heat sinks
18 p2895 A71-36984
- Semiconductor lasers, noting AlGaAs-GaAs p-n heterojunction structure contribution to room temperature efficiency of diode lasers
19 p3074 A71-38230
- Room temperature ionic instability on p channel silicon gate MOS devices due to processing method, noting threshold voltage change
19 p3033 A71-38506
- Ni-Mo-V, Ni-Cr-Mo-V and Cr-Mo-V high strength rotor forging steels fatigue crack growth characteristics tests at room temperature
20 p3247 A71-38768
- Fatigue crack propagation in high yield strength steels at room temperature in air environments, considering primary influence of applied stress intensity range
20 p3248 A71-38769

Evaporated pure Ni coatings effects on carbon fiber fracture strength and microstructure at room temperature 20 p3248 A71-38815

High efficiency room temperature laser operation assisted by energy transfer in holmium doped yttrium lithium fluoride 20 p3247 A71-39761

ROOT-MEAN-SQUARE ERRORS

Star image vibration trail amplitude, determining rms deviation with automatic system 04 p0590 A71-14843

Adaptation algorithm for real time minimum mean square error array processing, using with multidimensional digital filter 08 p1256 A71-21605

Meteor trails distance determination by radar pulses reflection observation, estimating reflected signal delay dispersion and plotting mean square errors 10 p1576 A71-24037

Exact formulas and graphs for RMS error in object position and velocity prediction for long time intervals based on least squares polynomial smoothing 12 p1881 A71-27425

Radio noise amplitude probability distribution, considering RMS voltage, average voltage and average logarithm of voltage 13 p2031 A71-28861

Coding for feedback communication system with additive white Gaussian noise, using mean-square estimation error 13 p2034 A71-29379

Nonlinear free oscillations, discussing linearization for nonlinear functions by weighted mean square method 14 p2325 A71-30060

Rapidly converging first order training algorithm for adaptive equalizer design in PAM signal reception, using variable step sizes for mean-square error minimization 16 p2545 A71-32821

Root-mean-square and uniform approximations of signals by Fourier and Haar series 16 p2550 A71-33720

Mean-square-error determination for binary code data transmission in symmetrical channels with slowly changing parameters, noting dependence on fading level 17 p2702 A71-34974

Least squares prediction of gravity anomalies, tabulating interpolation coefficients and mean square errors 17 p2734 A71-35189

Optimality in classification of stochastic processes in recognition system, using predicting filter rms error as discriminating function 19 p3038 A71-37779

Statistical analysis of digital automatic control system with unreliable communication channel, determining system mean square error 22 p3525 A71-41439

Solar constant calculations, discussing rms error and effective temperature 22 p3596 A71-41451

Nonlinear filtering for noise reduction of image data by mean-squared error minimization, discussing zero memory technique 22 p3547 A71-42507

Primary sensor transfer function selection to minimize rms error in information transmission over telemetry channel for subsequent digital processing 23 p3648 A71-43294

Astronomical telescopes stellar image motion dependence on zenith distance, determining RMS value of jitter 23 p3771 A71-44259

Ohio catalog radio source spectra and positions, presenting flux density and RMS errors 24 p3871 A71-44913

ROOTS

Square root function approximation in interval, using Heron iteration and Chebyshev method 06 p0919 A71-18206

ROOTS OF EQUATIONS

Perturbed motion stabilization in nonlinear control system with applicable equation containing zero root and imaginary roots 01 p0128 A71-11158

Control systems root contours boundary lines, dividing a plane into realizability regions for system characteristic equation complex conjugate roots 06 p0878 A71-17337

Time vector method extension to equations of motion with real roots, noting applications to aircraft flight control problems 06 p0925 A71-18049

Complex zeros of complex polynomials, matrix inequalities and nonlinear programming, constructing areas intersection in complex plane defined by inequality bounds on eigenvalues of companion matrix 09 p1485 A71-22970

Two-differential equations system in critical case of double zero root, deriving motion stability criteria with aid of Liapunov functions 09 p1495 A71-23430

Differential equations of root loci motions for stationary linear automatic control design by hodograph and Evan method 10 p1637 A71-24906

Existence proof of periodic solutions to second order partial differential equations with imaginary roots 12 p1923 A71-27240

Approximate determination of first characteristic root of equation for plate, hollow sphere and hollow cylinder, using variational method for heat conduction problem 13 p2159 A71-28184

Low pass equiripple insertion loss functions roots for commensurate microwave filters with stubs and unit elements 13 p2038 A71-28610

Variable structure automatic control system synthesis, giving roots distribution of characteristic equation for fluttering mode 13 p2041 A71-28636

Closed loop circuit stability determination based on predetermined area requirement for characteristic equation roots 13 p2043 A71-28793

Variable structure control system synthesis with roots of equation of perturbed motion of characteristic point in dead zone 13 p2096 A71-28934

Orders of convergence for iterative procedures for finding zero of nonlinear function, considering secant and Steffenson method 17 p2768 A71-35685

Sound attenuation in lined duct, using Newton-Raphson method for complex roots of equations 18 p2947 A71-36499

Motion stability for critical case of characteristic equation with purely imaginary roots, deriving solution by nonlinear mechanics asymptotic method 19 p3104 A71-38013

Rotating shaft critical speed determination as root of polynomial from frequency equation /characteristic determinant/ without iterative search [ASME PAPER 71-VIBR-53] 21 p3385 A71-40300

Branch points of root locus curves for rational transfer functions and transfer functions with recovery time [DFVLR-SONDDR-110] 22 p3566 A71-41854

Polynomial equation roots determination, analyzing floating point arithmetic errors 23 p3698 A71-43097

Average number of real roots of polynomials consisting of independent random quantities with identical distribution 23 p3699 A71-43571

ROSETTE SHAPES

Strain analysis by moire-rosette method, using fringe patterns from pair of crossed gratings through optical spatial filtering 03 p0423 A71-13549

ROSSBY REGIMES

Nonlinear interaction between long planetary waves and zonal circulation in atmospheric model with negative viscosity 01 p0113 A71-10537

Planetary scale Rossby waves, examining vertical structure for zonal flow blocking and polar stratosphere warming 01 p0120 A71-10860

Rayleigh, baroclinic and Rossby waves instabilities effects on stellar structure during differential rotation 03 p0486 A71-13322

Mean zonal flow effects on Rossby waves in barotropic atmosphere, deriving formulas for energy of spectral components 07 p1151 A71-19146

Long time planetary atmosphere motions, investigating sideband resonance mechanism in Rossby wave packet interactions with weak shear zonal flow 12 p1925 A71-27195

Horizontal flat plate moving transversely in rotating stratified fluid, calculating boundary layer blocking conditions for entire Rossby and Russell numbers range 12 p1897 A71-27222

Axisymmetric small Rossby number flow driven by axially distributed heat sources, examining core multiboundary layer structure 20 p3212 A71-39507

Rotating fluid axisymmetric flow into point sink, investigating Rossby number 24 p3817 A71-44419

ROTARY DRIVES

U MECHANICAL DRIVES

ROTARY GYROSCOPES

NT FLUID ROTOR GYROSCOPES

Two-rotor gyrocompass accelerated reduction to meridian 01 p0080 A71-10630

Hodograph of asymmetrical gyrostator with self excitation, determining angular velocity dependence on flywheel momentum 01 p0163 A71-10656

Soviet book on rotary and oscillatory vibrational gyroscopes covering equations of motion, stability, error correction, applications, etc 02 p0247 A71-11824

Stability problems of free rotor and driven rotor gyrostats, considering spin stabilized spacecraft 04 p0662 A71-15192

Euler problem on permanent axes of rotation with extension to spinning gyrostator 04 p0662 A71-15195

Stability of steady motions of satellite gyroscope in Newtonian central force field, allowing for rotor bearing elasticity 05 p0751 A71-16585

Liapunov stability of unperturbed motion of single rotor correctable gyrocompasses with liquid-torsion suspension 05 p0751 A71-16586

Gyroscope in gimbal system with elastic rotor bearings, determining dynamic stability in Newtonian central force field 06 p0899 A71-17929

Damping effects in three frame rotor gyroscope due to force originated by static joint housing design 09 p1449 A71-22794

Forced rotation influence of gimbal suspension on astatic gyroscope motion with respect to inertial coordinates, demonstrating pseudoregular precession 09 p1451 A71-23172

Turn rate gyro installation angle and airspeed effects on instrument reliability, presenting in-flight investigation results relative to turn rate information usefulness under various flight conditions [SAE PAPER 710380] 10 p1610 A71-24245

Deterministic steady state error model for floated inertial gyroscope, considering lateral or rotational float displacement and temperature distribution variations 11 p1761 A71-25517

Liapunov stability of gyroscopic stabilizers as electromechanical systems, assuming nonrigidity of rotor, gimbal and platform suspension 13 p2069 A71-28726

Routh-Liapunov stability of lasting rotation of dynamically symmetrical gyrostator in force field of two stationary centers 13 p2145 A71-28729

Variable mass body rotational motion stability in central Newtonian field with gyroscope on symmetry axis 14 p2275 A71-30880

Hodograph of asymmetrical gyrostator with self excitation, determining angular velocity dependence on flywheel momentum 14 p2275 A71-30990

High speed spin effect on amplified or damped nutations in low friction rotary gyroscope mounted on gimbals 15 p2401 A71-31178

Gyroscope errors with gimbal suspension mounted on slowly moving base, discussing base steady rotation 17 p2746 A71-35605

Rotor asymmetry effect on errors of two degrees of freedom gyro mounted on dynamic platform 17 p2746 A71-35608

Free spinning gyrostats classical problems equivalence, discussing interaction torque between body and rotor on axis of rotation 21 p3415 A71-40771

Schwarzschild constants evaluation from coupled gyroscopes spin axes observation, noting axes high angular velocities due to gravomagnetic effect in gravitational interaction 22 p3605 A71-42338

ROTARY STABILITY

NT GYROSCOPIC STABILITY

Ellipsoidal plasmod equilibrium in external HF field, calculating rotation rate and potential energy 01 p0132 A71-10151

Motion stability of satellite with rigid connection to symmetric rotors rotation axes 01 p0164 A71-11156

Rayleigh, baroclinic and Rossby waves instabilities effects on stellar structure during differential rotation 03 p0486 A71-13322

Rigid body free rotational stability, discussing initial conditions excursion 04 p0654 A71-15720

Dry friction autocompensation in inertial navigation accelerometers by forced rotation of platform 05 p0751 A71-16589

Stability of slowly rotating stars with phase transition in center, determining critical density jump for stability loss 07 p1193 A71-19296

Fluid rotational stability between coaxial cylinders rotating at same angular velocity in presence of radial temperature gradient 10 p1696 A71-24374

Stress redistribution and static inertioclastic instability of rotating beams and disks of low modulus high yield strength materials 11 p1848 A71-25495

ROTARY WING AIRCRAFT

Semielastic body rotational stability, investigating elastic coupling effects on controllability of rotating space stations in earth orbit 12 p1973 A71-27590

Variable mass body rotational motion stability in central Newtonian field with gyroscopic on symmetry axis 14 p2275 A71-30880

Helicopter rotor system vibratory and mechanical stability characteristics, investigating anisotropically mounted flexible swash plate and blade out of track effects [AHS PREPRINT 511] 14 p2178 A71-31082

AH-56A compound helicopter rigid rotor stability and handling qualities, using flight, whirl tower and wind tunnel tests [AHS PREPRINT 574] 14 p2180 A71-31115

Rotational stability of spin stabilized satellite with liquid filled propellant tanks, investigating viscous effects on motion coupling between rigid body and liquid 15 p2499 A71-31175

Hingeless rotor stability characteristics at high advance ratios, examining equations of motion and time variant aerodynamic coefficients [AIAA PAPER 71-580] 15 p2345 A71-31569

Externally pressurized gas journal bearing whirl instability stabilization system, predicting whirl onset threshold speed 22 p3551 A71-41662

Rigid rotor whirl dynamics in externally pressurized gas journal bearings, calculating frequencies in terms of stiffness and other parameters 22 p3552 A71-41670

ROTARY WING AIRCRAFT

NT ALOUETTE HELICOPTERS

NT AUTOGYROS

NT BO-105 HELICOPTER

NT CH-3 HELICOPTER

NT CH-46 HELICOPTER

NT CH-47 HELICOPTER

NT CH-54 HELICOPTER

NT COMPOUND HELICOPTERS

NT H-53 HELICOPTER

NT H-56 HELICOPTER

NT HELICOPTERS

NT MILITARY HELICOPTERS

NT OH-6 HELICOPTER

NT RIGID ROTOR HELICOPTERS

NT UH-1 HELICOPTER

NACA/NASA rotating wing aircraft research history during 1955-1970 period, discussing wind tunnel research 01 p0005 A71-11377

NACA/NASA rotary wing aircraft research, considering rotor loads and configurations, ground resonance, blade flutter and flapping, motion equations and VTOL 04 p0529 A71-15171

Army rotorcraft hot day standard design hover criterion, developing analytical models for hovering aircraft, cost, climatology and environmental features 04 p0533 A71-15431

Rotary wing and VTOL aircraft controllability requirements definition through in-flight simulation of visual and kinetic impressions and environmental conditions by BO-105 helicopter 05 p0696 A71-16135

Book on fixed and rotary winged aircraft air cooled piston engine design, performance and maintenance in business and military operators manual terminology 05 p0796 A71-17125

Army rotorcraft performance data, discussing hovering and forward flight performance out of ground and level flight power requirements and drag and compressibility effects [AHS PREPRINT 500] 14 p2177 A71-31076

Rotorcraft sound characteristics, discussing rotor noise spectrum, directivity, measurement and instrumentation 16 p2523 A71-33417

Rotorcraft and VTOL aircraft noise characteristics, noting implications of reduction to acceptable levels 16 p2523 A71-33419

Convertible rotor transport aircraft, considering ATC, mass transportation systems, safety, noise and socio-economics 20 p3178 A71-39387

Rotor performance and design for hover and cruise VTOL flights 22 p3482 A71-42238

ROTARY WINGS

NT LIFTING ROTORS

NT RIGID ROTORS

NT TILTING ROTORS

NT TIP DRIVEN ROTORS

Carbon fiber reinforced epoxy composites, evaluating application as helicopter tail rotor blade material 02 p0273 A71-12477

Analog periodometer with short response time for helicopter blade vibration studies 05 p0752 A71-16736

Material stiffness/weight ratio effects on helicopter blades uncoupled flapwise, chordwise and torsional natural frequencies by rapid estimation 06 p0985 A71-16791

Lightning and static electricity effects on helicopter design, considering rotor protection, cargo hook operation and passive dischargers for radio interference reduction 07 p1021 A71-19938

Lightning protection for nonmetallic helicopter rotor blades 07 p1021 A71-19939

Boundary layer discontinuity on helicopter rotor blade in hovering using flow visualization [AIAA PAPER 69-197] 07 p1017 A71-20307

Helicopter rotor inertial system kinetic energy, examining takeoff advantages 09 p1385 A71-23670

Contoured silicone internal pressure bag mandrels for helicopter rotor blades fabrication 10 p1615 A71-24096

Sound radiation from time varying point force in accelerative motion, applying to fan or helicopter rotor noise at subsonic tip speeds 12 p1867 A71-26702

Helicopter blades inherent vibration damping, comparing theoretical and semiempirical predictions to experimental results 12 p1976 A71-27123

Unsteady flow measurement around wing sections during rapid angle of attack variations, emphasizing helicopter rotor blades 12 p1864 A71-27468

Marginal vortex effects on aerodynamics of helicopter lifting surfaces, considering blade form and noise spectrum tested in hydrodynamic tunnel 12 p1864 A71-27473

Airfoils unsteady stall by testing two dimensional model in harmonic pitching oscillation for helicopter rotor blades characteristics [ONERA-TP-936] 12 p1866 A71-27609

Structure and shape of vortex wake associated with oblique flow past multiblade hinged rotor, using cavitation method 13 p1993 A71-29217

Helicopter rotor vortex system and induced velocity field for various angles of attack, flight conditions and unit loads, using smoke visualization technique 13 p1994 A71-29235

Noise production during aerodynamic tests on helicopter rotor in wind tunnel 14 p2176 A71-30519

Stiffened horizontal stoppable hingeless rotor conversion from helicopter to airplane flight speeds [AHS PREPRINT 502] 14 p2178 A71-31078

Helicopter rotor blade airload by applying lifting surface solution [AHS PREPRINT 510] 14 p2171 A71-31081

Helicopter rotor system vibratory and mechanical stability characteristics, investigating anisotropically mounted flexible swash plate and blade out of track effects [AHS PREPRINT 511] 14 p2178 A71-31082

Helicopter fuselage vertical and in-plane main rotor head vibratory forces isolation with hydropneumatic servocentered system at transmission/airframe interface [AHS PREPRINT 514] 14 p2253 A71-31085

Helicopter rotor stall characteristics, investigating blade flexibility, unsteady aerodynamics and variable inflow effects [AHS PREPRINT 520] 14 p2171 A71-31086

Flow field velocity distribution at rotating wing devices tip vortices [AHS PREPRINT 522] 14 p2172 A71-31088

Wake model and computer program to compute geometries, flows and velocity influence coefficients for helicopter blade load calculations [AHS PREPRINT 523] 14 p2172 A71-31089

Rotor stability derivatives determination from instrumented OH-6A prototype helicopter wind tunnel tests, comparing data with analytical results obtained by digital computing technique [AHS PREPRINT 543] 14 p2179 A71-31100

Fail-safe helicopter rotor control design, discussing damage tolerant components, redundant system, failure warning and maintenance [AHS PREPRINT 550] 14 p2179 A71-31102

Size effects on large rotor systems design, considering weight, blade loading, tip speed, etc [AHS PREPRINT 552] 14 p2180 A71-31104

Optimal turbofan engine and reaction drive rotor combinations for helicopter design [AHS PREPRINT 561] 14 p2297 A71-31108

High performance UH-1 compound helicopter high speed flight research, considering rotor loads, stability, control and flying qualities [AHS PREPRINT 570] 14 p2180 A71-31111

Helicopter stability, using Lockheed rotor system with gyro coupled to cantilevered blades 15 p2348 A71-31599

Unmanned flight vehicles recovery system, describing built-in rotor design for navigation and high precision landing [DGLR-71-020] 15 p2351 A71-32787

Helicopter rotor model testing in water tunnel, discussing advantages over wind tunnel testing due to Reynolds number scaling and avoidance of wall interference effects 16 p2526 A71-34151

Helicopter rotor blades fail-safe design, presenting criteria for fatigue loaded structures residual strength and life based on crack propagation rate methods 17 p2828 A71-35163

Dirichlet problem in hodograph plane of compressible fluid flow from aircraft, helicopter blades or turbine blade airfoils 17 p2672 A71-35470

Analytical weight determination of articulated shaft driven helicopter main rotor blades, presenting computer program [SAWE PAPER 893] 17 p2835 A71-35826

Helicopter rotor noise due to blade-vortex interaction, using linear gust model 18 p2849 A71-36934

Review of September 1970 aerodynamic noise symposium covering jet and helicopter rotor noise, nonlinear acoustics and diffraction theory 19 p2994 A71-38205

Optimum rotor/jet thrust ratio determination procedure for tip jet driven rotors, considering performance upper bound 19 p2998 A71-38653

Vortex flow over helicopter rotor square tips, using visualization technique with ammonia vapor boundary layer flow over diazonium salt solution 21 p3318 A71-40169

Jet flaps application to autogyro rotor, using pressure jump for air centrifugation 21 p3324 A71-41399

Photogrammetric recording of helicopter rotor induced aerodynamic effects using wind tunnel test smoke visualization technique 23 p3678 A71-43588

Technology developments in rotor, drive, flight controls and cargo handling systems of heavy lift helicopter system, noting military and commercial applications [AIAA PAPER 71-994] 24 p3792 A71-45296

ROTATING

U ROTATION

ROTATING BODIES

NT COMPRESSOR ROTORS

NT FLYWHEELS

NT IMPELLERS

NT LIFTING ROTORS

NT PUMP IMPELLERS

NT RIGID ROTORS

NT ROTARY WINGS

NT ROTATING CYLINDERS

NT ROTATING DISKS

NT ROTATING SPHERES

NT ROTORS

NT TILTING ROTORS

NT TIP DRIVEN ROTORS

NT TURBINE WHEELS

Uniformly turbulized incompressible heavy fluid sloshing and free oscillations in rigid rotating vessel, using linear surface wave theory 01 p0069 A71-10411

Inertial navigation system error reduction by gyroplatform rapid rotation 01 p0122 A71-10421

Regular optimal motion problem for nonlinear controls reduced to degenerate problem for solving optimal control of solid rotating body angular velocity 01 p0065 A71-11234

General relativistic formulation of massive magnetized rotating conductor, showing electrodynamic properties of surrounding empty space for explanation of stellar structure 01 p0160 A71-11273

Euler-Poisson equations for heavy solid body motion about fixed point, deriving particular solution 03 p0457 A71-13581

Kinematic interpretation of body motion about fixed point for case of traveling angular velocity hodograph integrable in closed form 03 p0457 A71-13589

Hess solution for heavy body rotating about fixed point, considering cavities filled with ideal incompressible fluid in turbulent and irrotational motion and linear invariant relation 03 p0458 A71-13591

Heavy solid body rotation about fixed point, using fixed and traveling hodograph 03 p0458 A71-13592

Anisotropic rod elastic curve equilibrium shape for rigidity conditions, considering Goriachev solution to heavy solid body motion about fixed point 03 p0458 A71-13599

Mathematical models for heat transfer by laminar free convection to rotating central plate passing through synchronously rotating surroundings, considering Coriolis effect 03 p0518 A71-13617

Laminar boundary layer on spinning bodies of revolution in oncoming stream, using implicit finite difference technique [AIAA PAPER 70-1377] 03 p0341 A71-13660

Spinning rocket vehicle with aerodynamic asymmetry, deriving equations of motion and steady aeroelastic behavior [AIAA PAPER 70-1397] 03 p0499 A71-13678

Variable inertia rotating rigid body stabilization by nonlinear optimal control problem, using Hamilton-Jacobi and Riccati equations 03 p0391 A71-14314

Gyrostatic system with center of mass in uniform circular motion, deriving rotary motion equations invariant 03 p0460 A71-14386

Population I Cepheids studies applied to galactic rotation and solar motion parameters estimation, discussing stellar distances inaccuracy effects 04 p0643 A71-14908

Rigid body free rotational stability, discussing initial conditions excursion 04 p0654 A71-15720

Lense-Thirring effect in test masses approaching in same orbit around rotating body, noting correction dependence on central body geometry and angular velocity 05 p0806 A71-16183

Incompressible turbulent boundary layer flow over steadily rotating flat plate blade, discussing centrifugal pumping and shear stress 05 p0694 A71-16581

Action-angle variables for Euler-Poinsot problem of solid body free rotation about stationary point 05 p0783 A71-16996

Equations of motion solution of heavy solid body about stationary point applied to Hess gyroscope 05 p0754 A71-16998

Angle of attack amplification due to body trim plane rotation, obtaining pertinent relations by method of stationary phase [AIAA PAPER 71-48] 06 p0980 A71-18509

Hypersonic boundary layer of spinning circular cone at angle of attack, using finite difference method [AIAA PAPER 71-57] 06 p0843 A71-18516

Axisymmetric body rapid rotation under center of gravity velocity vector conditions, solving for plane gliding motion stability in air 07 p1159 A71-19354

Active control moments construction of solid body rotating about stationary point 07 p1161 A71-20268

Rotating cantilever beams flexural vibrations, developing tables for frequency equation determination 08 p1370 A71-21306

Translation-rotation motion of elongated body in Vinti potential field 10 p1667 A71-23814

Cylindrical shock wave in solid body rotating gas for angular variation effects on shock velocity, using similarity method 10 p1593 A71-24405

Blowing and suction effects on laminar boundary layer flow of quiet fluid over permeable rotating cone, discussing skin friction and heat transfer 10 p1594 A71-24406

Solid body finite rotation theory involving formal operations on quaternions 10 p1642 A71-24576

Axisymmetric incompressible boundary layer flow, temperature distribution and heat exchange near critical point of rotating body with varying surface temperature 11 p1854 A71-25239

Cascade and single stage rotating rig data comparison with aerodynamic predictions based on intrablade analysis, including wall boundary layer model [ASME PAPER 71-GT-13] 11 p1703 A71-25959

General relativistic von Zeipel theorem providing necessary and sufficient condition for equidensity surfaces coincidence in stationary star axisymmetric rotating mass fluid 11 p1833 A71-26327

Hercules galaxies cluster rotation, determining radial velocities, axis position angle and center position 12 p1962 A71-26911

Rotating spacecraft attitude control system, using sun-earth albedo sensor for attitude determination [DFVLR-SONDDR-113] 12 p1972 A71-26986

Unsteady vibrations of rotating free solid body entering atmosphere at hypersonic velocity, taking into account nonlinearity of aerodynamic moments 12 p1972 A71-27171

Lifting force of wing with rotating flap, deriving lift increase due to circulation redistribution at surface 12 p1865 A71-27491

Laminar boundary layer equations for rotating plate with surface of arbitrary curvilinear shape, determining external flow pressure gradient leading to separation 12 p1865 A71-27502

Semielastic body rotational stability, investigating elastic coupling effects on controllability of rotating space stations in earth orbit 12 p1973 A71-27590

Metal temperatures in rotating cooled gas turbine blades, discussing coolant flow aerodynamics 13 p2117 A71-28748

Monograph on heat transfer from rotating heated surface with induced turbulent boundary layers covering disk, cone and sphere geometries 13 p2162 A71-28882

Rotating ring resonator partially filled with dynamic isotropic medium, determining resonance properties 13 p2080 A71-29025

Computer algorithm for liquid sloshing in rotating cavities, using finite difference scheme 13 p2050 A71-29211

Endogenous short period rhythms in rotational movements of unifoliate leaves of *Phaseolus angularis* Wight grown under controlled environmental conditions 13 p2015 A71-29476

Differential rotational equations of motion for triaxial rigid body about center of mass under arbitrary torque 14 p2307 A71-29882

Angular momentum influence on linear axisymmetric motions of centrally condensed bodies, considering finite amplitude pulsations of rapidly rotating columns 15 p2481 A71-31202

Random time variation in sound radiation far field of point sources in subsonic circular rotational motion 15 p2450 A71-31219

Square cross section rectangular rotating grains dynamic behavior in magnetic fields, obtaining orientation data with Monte Carlo method 15 p2498 A71-32772

Schuster hypothesis on celestial object relation between angular momentum and magnetic fields 16 p2637 A71-33513

Nonlinear theory for rotating shallow shells of revolution, deriving edge zone boundary layer solutions for differential equations 16 p2660 A71-34071

Autonomous location determination for rotating dynamic plant with inertial platform by constructing finite rotation vector 17 p2775 A71-35601

Counterrotating antenna without mechanical contact, using magnetic bearings for spin stabilized geostationary telecommunications satellites 18 p2892 A71-36574

Coriolis forces influence on rotating spacecraft design, estimating relationships between coriolis force, artificial g, rotational radius and speed and velocity of motion 18 p2871 A71-36638

Dynamic seal development for space base rotating hubs, describing simulated environmental tests for elastomer inflatable seals and lubricants evaluation [AIAA PAPER 71-863] 18 p2927 A71-36651

Action-angle variables for Euler-Poinsot problem of solid body free rotation about stationary point 18 p2948 A71-36796

Equations of motion solution of heavy solid body about stationary point applied to Hess gyroscope 18 p2925 A71-36798

Inertial effects induced by rotating thin walled shell of finite thickness, considering general relativity equations of motion for test particle 18 p2970 A71-37059

Equilibrium rotating superdense configurations in general relativity theory, determining integral parameters in low angular velocity approximation 20 p3289 A71-39297

Time dependent analysis of swirling flow boundary layers in rotating container using modified Oseen method 21 p3367 A71-40639

Cat and human eye movement control system measurements, studying isolated oculomotor muscles and globe restraining tissues dynamics 22 p3489 A71-42441

Gravitational and aerodynamic perturbation moment effects on nonsymmetric solid body rotary motion near mass center, using precession model 22 p3612 A71-42870

Three-legged slewing about nonorthogonal axes, solving single-axis reorientations by two successive rotations about arbitrary fixed lines [AAS PAPER 71-389] 23 p3773 A71-43057

Lagrange equations for variable mass systems with rotational transport and relative motions 23 p3773 A71-43093

Ellipticity of weakly rotating configurations, determining $5m/4$ delta ratio for white dwarfs 23 p3770 A71-44063

Plane motion stability of rapidly rotating symmetric rigid body in atmosphere, deriving short-cut equations system by Bogolubov-Zubarev method 24 p3847 A71-44416

Thermally driven motion of water with free surface in rotating annulus, investigating steady wave flow by three dimensional nonlinear Navier-Stokes equations numerical integration 24 p3844 A71-44417

Couple-stress theory application to body model with constrained rotations, discussing elasticity theory modifications in relation to real physical phenomena 24 p3848 A71-44643

Rotating solid body nutations damping by pendulums system oscillating in plane normal to rotation axis, deriving optimal conditions 24 p3848 A71-44855

ROTATING CONES U CONICAL BODIES U ROTATING BODIES

ROTATING CYLINDERS

Blowing air conditions and flow parameters effects on film cooling efficiency for rotating cylinder 01 p0178 A71-10416

Thick walled slowly rotating viscoelastic cylinder deformation under varying gravitational loads, using theory of elasticity 01 p0169 A71-10500

Couette flow stability between coaxial rotating cylinders, calculating eigenvector in first approximation small perturbation equations 03 p0404 A71-14231

Buoyancy effects on transient free convection heat transfer in revolving tube for zero to 100 g centrifugal acceleration [ASME PAPER 70-HT-10] 03 p0521 A71-14292

Plane monochromatic electromagnetic wave scattering by moving and rotating cylinder 04 p0549 A71-14612

Couette flow between rotating cylinders and Taylor vortex formation by Liapunov-Schmidt method and spectrum perturbation theory, discussing secondary flow determination accuracy 04 p0575 A71-15603

Rotating fluid cylinder in magnetic field parallel to rotation axis, discussing hydromagnetic precession rate, resonance phenomena and magnetic Reynolds number flows 06 p0882 A71-18319

Viscous incompressible fluid partly filling rotating cylindrical cavity, considering motion under centrifugal forces in adjoining unperturbed free surface region 07 p1093 A71-20467

Flutter analysis of rotating thin cylindrical shell with outer surface exposed to inviscid helical air flowfield 09 p1533 A71-22078

Finite length rotating cylinder, calculating axisymmetric creep under thermal effects in power series from theory of small elastoplastic deformation 09 p1537 A71-22516

Periodic rotation reversal effect on hollow cylinder surface temperature distribution in space simulation testing of spin stabilized orbiting satellites 09 p1430 A71-23733

Fluid rotational stability between coaxial cylinders rotating at same angular velocity in presence of radial temperature gradient 10 p1696 A71-24374

Flutter analysis of long thin cylindrical shells rotating in circular helical air flow field [AIAA PAPER 71-373] 11 p1845 A71-25346

Tangential velocity profile in steady incompressible electrically conducting viscous axial flow between concentric rotating cylinders with radial magnetic field, solving Navier-Stokes equations 11 p1752 A71-26048

Rotation effects on vibration traveling waves in rotating cylindrical shells, considering Coriolis, centrifugal and torque loads [ASME PAPER 71-DE-A] 12 p1977 A71-27316

Flow transition to laminar drag law for thin cylinder freely suspended in Hg in rotating vertical cylindrical MHD channel 14 p2279 A71-29615

Incompressible homogeneous isotropic fluid Couette flow between stationary inner and rotating concentric outer cylinders, examining Weissenberg effect 14 p2226 A71-30445

Nonuniform rotation of nonhomogeneous isotropic elastic cylindrical shell, obtaining steady state axisymmetric vibrations 14 p2331 A71-30842

Stokes second problem solution, obtaining transient and steady state fluid flow pattern near cylinder executing harmonic rotational oscillations around axis 15 p2393 A71-32263

Viscous incompressible fluid flow stability between concentric rotating cylinders, developing nonlinear model of two disturbance interaction 16 p2558 A71-32985

Momentum transfer secondary flow between rotating cylinders in terms of effective/molecular viscosity ratio as function of Taylor number [ASME PAPER 71-APM-30] 16 p2559 A71-33199

Viscous incompressible fluid flow between two rotating nonconcentric cylinders, presenting transverse velocity profiles 17 p2725 A71-34177

Rotating cylindrical shell symmetrical deformation under external load, obtaining three dimensional axisymmetric problem solution in elastic theory 17 p2816 A71-34330

Smallest Taylor number corresponding to Couette flow stability between two rotating cylinders subjected to rotationally symmetrical perturbation 18 p2902 A71-36093

Finite radius rotating cylinder stability analysis, using equilibrium functions of distribution with trajectory integration method 19 p3134 A71-37512

Lense-Thirring spin-spin gravitational forces measurement between disks and cylinders, using weak field low velocity relativity approximation 20 p3292 A71-39409

ROTATING DISKS

- Viscous fluid stirring due to small amplitude rigid circular cylinder rotation, calculating steady flow velocity relationship to Reynolds number
20 p3177 A71-39481
- Oscillatory modes of perturbation in onset of flow instability for Newtonian liquid between concentric rotating cylinders with transverse pressure gradient
20 p3212 A71-39484
- Gortler-Taylor vortices visualization in liquids between rotating concentric cylinders using pulverized aluminum
20 p3213 A71-39781
- Hydrodynamic stability of incompressible conducting fluid flow between two moving linearly and rotating coaxial cylinders in longitudinal magnetic field
21 p3367 A71-40688
- Stress-strain state of rotating viscoelastic hollow cylinder with mobile inner boundary under internal pressure and temperature effects
21 p3472 A71-41145
- Centrifugally driven thermal convection in rotating cylinder of fluid heated from above, calculating heat flux through wall and effect on Nusselt number
22 p3620 A71-41879
- Plane monochromatic electromagnetic wave scattering by moving and rotating cylinder
22 p3510 A71-42252
- Taylor vortex flow stability between rotating concentric cylinders, using fifth order amplitude expansions in matrix form
24 p3817 A71-44420

ROTATING DISKS

- Incompressible fluid laminar flow between stationary and rotating porous disks with equal suction and injection
02 p0240 A71-12337
- Turbulent flow mean velocity beyond rotating disk edge, using momentum integral method
[ASME PAPER 70-FE-C] 03 p0400 A71-13702
- Unsteady MHD forced flow of viscous incompressible electrically conducting fluid against rotating disk
03 p0459 A71-13902
- Three dimensional nonboundary layer laminar radially inward incompressible Newtonian fluid flow between corotating disks, using integral method
[ASME PAPER 70-WA/FE-4] 03 p0402 A71-14126
- Optimal design of rotating disks of nonuniform thickness with integral shafts, using two and three dimensional numerical analysis for stress distribution
[ASME PAPER 70-WA/DE-6] 03 p0511 A71-14141
- Rotor and rotor-disk system response to constant and pulsating torque, experimentally examining critical whirl speed and lateral vibration
[ASME PAPER 70-WA/DE-14] 03 p0511 A71-14146
- Axisymmetric free transverse vibration frequencies of centrally clamped spinning membrane disks
04 p0668 A71-15186
- Single disk rotating in still air, calculating temperature profiles and local heat transfer coefficients
04 p0683 A71-15494
- Horizontal clinostat rotation rate for optimal and acceptable weightlessness simulation in plants, comparing with wheat seedlings growth in Biosatellite 2
05 p0712 A71-16150
- Heat transfer from rotating disk to parallel nonrotating disk, investigating turbulence effect from air flow pattern observation
06 p1007 A71-18315
- Unsteady viscous incompressible flow over impulsively started rotating disk by acceleration averaging method
07 p1088 A71-19356
- Rotating axisymmetric disk algorithm using method of local variations in strength and rigidity
07 p1212 A71-19357
- Skewed turbulent boundary layer and incompressible laminar flow on rotating disk, considering effective viscosity relations and applications domain
07 p1090 A71-19889
- Fluidic rotational speed sensor, using boundary layers attached to rotating disk surfaces to deflect fluid jets
07 p1031 A71-20604
- Integral transform methods for analytic solutions to current and potential distribution on disk in infinite plane for four limiting cases
08 p1237 A71-21471
- Thirring effect experimental measurements in gravitation theory, magnetic suspension system or torsion balance with two rotating disks generating angular momentum
10 p1642 A71-24467
- Constant property fluid laminar flow between rotating and stationary infinite disks for limiting Reynolds numbers based on gap width
11 p1748 A71-25154
- Stress redistribution and static inertioclastic instability of rotating beams and disks of low modulus high yield strength materials
11 p1848 A71-25495
- Rotationally symmetric flow above rotating disk by nonexistence proof and uniqueness theorem
12 p1896 A71-26924

- Laminar source flow between rotating parallel porous disks with equal suction/injection rates solved for infinite radius series, discussing radial velocity and shear stress distributions
12 p1896 A71-27052
- Vibration natural frequencies and mode shapes of cantilever plate mounted on rotating disk periphery, using finite element technique
13 p2147 A71-27788
- Reynolds analogy of heat transfer applied to disk rotating near stator, including frictional dissipation and radial outflow in compressible or incompressible flow
13 p2048 A71-28599
- Disk rotating in gimbal system, describing gyroscopic moments and precession
13 p2068 A71-28632
- Monograph on boundary layer theory covering unsteady heat transfer from rotating disk, thermal free convection in corners, etc
14 p2223 A71-29934
- Low cycle fatigue strength of high speed rotating aluminum and brass disks, comparing with uniaxial push-pull fatigue test
14 p2328 A71-30418
- Axisymmetrical three component flow equations for incompressible viscous fluid in cylinder with rotating disk
14 p2227 A71-30855
- Incompressible laminar flow between rotating and stationary disks with small gap width and radial mass flow, using Navier-Stokes and continuity equations
15 p2387 A71-31168
- Turbulent flow field mean velocity components measurements near thin rotating disk
15 p2392 A71-32253
- Free and enclosed disks rotation resistance at high Reynolds numbers, calculating fluid induced torque with logarithmic velocity profiles for turbulent boundary layer flow
[ASME PAPER 71-APM-25] 16 p2520 A71-33204
- Laminar flow in incompressible fluid between rotating disk and fixed wall at small distances with radial mass stream, using finite difference method for Navier-Stokes equations
17 p2726 A71-34581
- Rupturing rotations estimates for turbine disks, considering failure modes and load bearing capacity
17 p2829 A71-35305
- Uniformly rotating thin relativistic disks structure, stability and gravitational fields within general relativity framework
17 p2806 A71-35405
- Thin circular disk rotating at constant angular velocity, solving three dimensional elasticity problem with formal power series of thickness-diameter ratio
[ASME PAPER 71-APM-Q] 18 p2978 A71-36260
- Numerical analysis of laminar recirculating flow between shrouded rotating disks for interaction between vorticity and stream function and swirl-velocity field
18 p2905 A71-36309
- Accelerating rotating disks with variable thickness, presenting shear stress distribution
18 p2982 A71-36771
- Moment and heat transfer coefficients for disks rotating in rarefied environment, noting transport characteristics decrease with increasing rarefaction
19 p3161 A71-37292
- Rotating disk flow system for Fe vaporizing into cold Ar atmosphere, investigating effect of condensation in boundary layer on mass transfer
19 p3162 A71-37727
- Sound radiation from subsonically rotating annular disk source, calculating far field pressure and efficiency
19 p2997 A71-37845
- Elastic field and stress distribution in composite circular rotating disk under constant normal pressure
19 p3159 A71-38187
- Anisotropic material circular rotating disks of various thickness, calculating stress and deformation
19 p3160 A71-38473
- Stress analysis of rotating orthotropic disks mounted on elastic shafts, obtaining closed form solution for governing differential equations
20 p3308 A71-39088
- Lense-Thirring spin-spin gravitational forces measurement between disks and cylinders, using weak field low velocity relativity approximation
20 p3292 A71-39409
- Laminar and turbulent incompressible viscous flow with spiral vortices between two parallel rotating disks
20 p3213 A71-39778
- Spalding-Patankar numerical integration for heat transfer from air cooled disk rotating near stator, considering frictional heating, disk temperature distribution and nonunity Prandtl numbers
22 p3620 A71-41878
- Axially symmetric flow in half space above rotating disk, proving boundary value problem solution existence by fixed point technique
22 p3531 A71-42402

- Buckling thermal gradients for rotating orthotropic annular plates under edge pull load
22 p3619 A71-42842
- Laminar convective heat transfer from rotating isothermal disk in uniform forced stream, using pressure distribution measurements
23 p3781 A71-43314
- Rotating disks optimal design allowing for creep from additional coupling imposition and contour displacement
23 p3780 A71-44220
- Rotating disk creep analysis by Van Fo Fi-Ozerov nonlinear equation, obtaining numerical solution for total creep equation and time to failure for two angular velocities
24 p3882 A71-44839
- ## ROTATING ELECTRICAL MACHINES
- Electric potential and current density in rotor of thin disk unipolar engine with zonal removal, formulating Neumann problem
13 p2002 A71-28930
- ## ROTATING ENVIRONMENTS
- Mathematical models for heat transfer by laminar free convection to rotating central plate passing through synchronously rotating surroundings, considering Coriolis effect
03 p0518 A71-13617
- Vestibular problems in long manned space flight, discussing weightlessness and rotating environment for artificial gravity
04 p0541 A71-14753
- Human rotation perception, discussing man-carrying rotation device, angular acceleration threshold, etc
04 p0541 A71-14756
- Gravity effects on human caloric and rabbits rotational nystagmus, noting semicircular canals role
04 p0542 A71-14757
- Resonant proton drift in axisymmetric rotating magnetosphere, discussing flow from boundary or tail to auroral region
05 p0800 A71-17178
- Turbulent diffusion flame laminarization by superimposed rotating flow field, discussing boundary layer stabilizing effect of external centrifugal force field
10 p1695 A71-24048
- Resonant proton drift in asymmetric rotating magnetosphere, discussing flow from boundary or tail to auroral zone
13 p2128 A71-28235
- Accelerations effect on receptors in semicircular canals during human movements in rotating environment, using vector analysis
13 p2007 A71-28415
- Medical physiological requirements of angular velocity and g level for artificial gravity creation by rotating space vehicle, considering human tolerances and vehicle design
[AIAA PAPER 71-871] 18 p2870 A71-36627
- Human performance in rotating environment, discussing Stromberg Dexterity, pursuit rotor, mental arithmetic, verbal learning and NAMI Ataxia tests
[AIAA PAPER 71-888] 18 p2871 A71-36637
- Human physiological responses to rotating environment, evaluating heart rates, blood pressure, pulmonary functions, visual observations and vital capacities
[AIAA PAPER 71-890] 18 p2856 A71-36639
- Modeling human disorientation and motion sickness in rotating spacecraft, stressing sensors dynamic response
[AIAA PAPER 71-870] 18 p2872 A71-36654
- Human psychomotor performance measurements in rotating environments, using Langley complex coordinator and decision response time devices
[AIAA PAPER 71-887] 19 p3006 A71-37275
- Artificial gravity field produced by rotating spacecraft in earth orbit, examining astronaut physical responses and centrifugal force effects on work tasks
21 p3342 A71-40255
- Earth-like ecology for habitation in space, considering hollow sunlit rotating space chamber for life cycles in controlled weather environment
21 p3343 A71-40360
- ## ROTATING FLUIDS
- ### NT ROTATING LIQUIDS
- Dynamic behavior of liquids in partially filled mobile tanks under almost centrifugal force fields
01 p0069 A71-10396
- Magnetosonic wave instability in differentially rotating gas
01 p0160 A71-11119
- Rotating inviscid incompressible fluids in tubes, investigating axisymmetric nonlinear waves motion in relation to vortex breakdown
01 p0072 A71-11224
- Global atmospheric circulation theory relation to flow pattern of free thermal convection in rotating fluid subjected to horizontal temperature gradient
01 p0122 A71-11359
- Astrophysical bodies dynamo equations describing large scale magnetic fields generation by small scale cyclonic turbulence in rotating fluid body
02 p0314 A71-12588

Nonstationary rotating MHD viscoplastic medium between coaxial cylinders in crossed electric and magnetic fields, determining zone interface position and stress distribution

03 p0464 A71-13601

Thermal instabilities in rapidly rotating fluids by buoyancy force and depth gradient, noting geophysical analogy of self gravitating sphere

03 p0409 A71-13727

Turbulent hydrodynamics and heat transfer in rotating flows of incompressible fluid

04 p0578 A71-15631

Setting spherical particle into rotation in fluid characterized by uniform rotational motion far from particle

05 p0735 A71-16159

Nonuniformly rotating Hg fluid, noting hydromagnetic stability and velocity control by imposed radial current distribution between coaxial ring shaped electrodes

05 p0788 A71-16608

Purely azimuthal magnetic toroidal-meridional component poloidal field conversion by slow precessional motion superimposition on rotating fluid under uniform current distribution

06 p0894 A71-18016

Rotating fluid cylinder in magnetic field parallel to rotation axis, discussing hydromagnetic precession rate, resonance phenomena and magnetic Reynolds number flows

06 p0882 A71-18319

Neutral hydrogen subsystem rotation in inner Galaxy from equal angular velocity surfaces

09 p1518 A71-22375

Rotating self gravitating axisymmetric fluid mass structure steady state equations, examining Clairaut theory asymptotic nature

09 p1527 A71-23532

Rapidly rotating fluid flows, calculating inertia waves by geometrical optics method

10 p1591 A71-23854

Inhomogeneous rotating self-gravitating system kinetic theory, linearizing collisionless Boltzmann equation to two dimensional linear integral equation for obtaining small oscillation modes

10 p1641 A71-24278

Flow instability and secondary circulation in pressure-driven rotating rectangular channel

10 p1595 A71-24617

Asymptotic stability of rapidly rotating horizontally bounded fluid heated from below, considering conductive state and Ekman layers

10 p1595 A71-24618

Waves generated by obstacle steady motion along axis of uniformly rotating electrically conducting homogeneous fluid, using Lighthill technique

10 p1595 A71-24624

Local instability of curved flow, considering stability of fluid flow between rotating cylinders for instability onset criterion establishment

10 p1597 A71-24941

Constant property fluid laminar flow between rotating and stationary infinite disks for limiting Reynolds numbers based on gap width

11 p1748 A71-25154

Hydromagnetic flow of conducting viscous incompressible fluid in rotating straight annular pipe under constant pressure gradient

11 p1804 A71-25433

Stabilization effect of rotation on Rayleigh-Taylor instability of stratified compressible inviscid fluid of variable density for noncritical wave numbers

11 p1749 A71-25434

Rotating plane layer viscous incompressible conducting fluid flow between two parallel walls with temperature gradient subject to perpendicular gravitational and magnetic fields

11 p1757 A71-25767

Horizontal flat plate moving transversely in rotating stratified fluid, calculating boundary layer blocking conditions for entire Rossby and Russell numbers range

12 p1897 A71-27222

Nonlinear limit rotation velocity and circulation induced by wheel in axial flow turbomachine for incompressible ideal fluid, using iterative numerical algorithm

12 p1866 A71-27715

Steady flow of electrically conducting incompressible viscous fluid in rotating parallel-plane channel under constant transverse magnetic field

13 p2110 A71-29296

Spinning sphere impulsively starting rotation from rest in compressible viscous fluid, calculating boundary layer growth by matched asymptotic expansions method

14 p2225 A71-30295

Gravitational instability of heat conducting compressible fluid relative to class of axisymmetric perturbations, considering viscosity, magnetic field and uniform rotation

14 p2226 A71-30397

Book on fluid mechanics covering rotating fluids, flow between concentric cylinders, emulsions, standing waves on water, etc

14 p2226 A71-30554

Vertical magnetic field and Coriolis forces effect on equilibrium of heavy viscous incompressible infinitely conducting rotating fluid

15 p2453 A71-31183

Torsionally oscillating disk in steadily rotating incompressible second order fluid, calculating transverse and radial shear stress

15 p2387 A71-31185

Free jets in rotating homogeneous fluids, investigating inertial and friction effects for various jet-rotational velocity ratios

15 p2390 A71-31926

Steady nonlinear regime of Benard convection in uniformly rotating fluid, using two-dimensional primitive equation numerical model with rigid boundaries

15 p2393 A71-32638

Perfect incompressible fluid steady rotational linearized three dimensional flows, calculating complex waves system

16 p2560 A71-34056

Density perturbation effect on transient spin down of incompressible dissipative rotating stratified fluid in cylindrical container

16 p2561 A71-34164

Fixed sphere on axis of unbounded rotating fluid /R greater than unity/, suggesting flow of Taylor column type

17 p2726 A71-34576

Ideally incompressible fluid with free surface, analyzing interfacial tension forces effects on rotational-translational motion stability

17 p2730 A71-35648

Rotating liquid flow impulsive spin-up and spin-down in finite cylindrical containers, deriving simplified mathematical model at Reynolds number 1002

18 p2901 A71-35853

Impulsively started time-dependent rotational Couette flow stability analysis by initial value problem and quasi-steady approaches

18 p2902 A71-36038

Time dependent rotating laminar flow of viscous incompressible fluid in closed cylindrical container, presenting numerical solutions to Navier-Stokes equations

18 p2908 A71-36343

Three dimensional rotational gas flows, using Berker compatibility equations

19 p3045 A71-37795

Rotating viscous fluid flow between concentric circular cylinders, predicting velocity field dependence on position and time during inner cylinder sudden stop

21 p3366 A71-40543

Unsteady boundary layer of viscous incompressible rotating fluid flow due to infinite flat plate accelerated motion, calculating velocity and skin friction

21 p3367 A71-40657

Rotating plane layer viscous incompressible conducting fluid flow between two parallel walls with temperature gradient subject to perpendicular gravitational and magnetic fields

22 p3532 A71-41535

Backflow region and shock interaction in rotating and swirling gas streams and jets in supersonic nozzle with separation and thrust effects

22 p3480 A71-42682

Plane steady rotational flow of inviscid gas with arbitrary state equation for straight or circular streamlines

23 p3662 A71-43236

Fluid flow friction and combined free and forced convective heat transfer characteristics in rotating curved circular tube, using finite difference scheme and iterative solution

23 p3783 A71-44192

Rotating fluid axisymmetric flow into point sink, investigating Rossby number

24 p3817 A71-44419

Isothermal gas rotation in circular cylinder, calculating symmetric normal frequency modes

24 p3818 A71-44590

ROTATING GENERATORS

NT AC GENERATORS

NT DYNAMOMETERS

NT TURBOGENERATORS

Energy converters for satellite nuclear power plants, discussing rotating, MHD, thermionic and thermoelectric systems

02 p0282 A71-12306

Galaxy gaseous disk as low mode dynamo, calculating turbulent diffusion coefficient for passive magnetic fields

05 p0811 A71-16688

Hot performance tests of three identical Brayton rotating units on gas bearings

15 p2355 A71-32226

Parasitic speed controller for alternator rotational speed and frequency regulation in dynamic space power systems, investigating phase controlled loading improvement

20 p3262 A71-38916

ROTATING LIQUIDS

Incompressible nonviscous rotating fluid in toroidal shell, obtaining flow patterns steady state solutions for turbomachinery design

10 p1552 A71-24520

Large gas bubble migration in rotating liquid without gravity, noting velocity dependence on stagnation point distance and radius of curvature

15 p2392 A71-32119

Gas bubble in liquid under surface tension, weightlessness and rotation, determining angular velocity for fluid system disintegration

16 p2560 A71-34142

Hydraulic resistance and heat transfer in annular channel with rotating flow, comparing to axial flow

24 p3888 A71-44747

ROTATING MATTER

Rotating configurations in general relativity, considering infinitesimal quasi-static deformations

11 p1834 A71-26407

Angular momentum of rotating Einstein-Rosen bridge, comparing neutron star models

16 p2609 A71-33262

Rapidly rotating polytropes in post-Newtonian approximation to general relativity

22 p3604 A71-42327

Kinetic theory of collisionless system in closed anisotropic cosmologies including rotation effects

23 p3705 A71-44123

Einstein equations for universes with expansion, rotation, shear and Bianchi type IX spaces, obtaining diagrammatic solutions

23 p3770 A71-44124

ROTATING MIRRORS

Carbon dioxide laser with simultaneous active rotating mirror Q switch and passive absorbing gas cell

05 p0760 A71-16256

Air bearings design for laser scanner high speed rotating mirror in vacuum, describing static and dynamic tests for rotor inversion point

07 p1117 A71-19506

Doppler effect mechanism for laser Q switching with rotating mirror, noting pulse width dependence on wavelength

08 p1302 A71-21434

Slave sweep plane-parallel mirror systems design for maximum picture taking rates in high speed cameras

11 p1767 A71-26467

Rotating mirror wavelength shifter of laser light source for use in electronic spectroscopy, noting measurements with high speed Doppler wheel in vacuum

13 p2067 A71-28445

ROTATING PLASMAS

Electron gas column rotating about axis parallel to uniform external magnetic field, considering equilibria within Vlasov-Maxwell model

01 p0136 A71-11478

Plasma rotation effects on toroidal systems diffusion, considering pressure gradient, rotational velocity, transverse electric field and path lengths

03 p0464 A71-13931

Partially ionized rotating plasma centrifuge for isotope and element separation, controlling velocity distribution of conducting magnetic fluid by isorotation law

05 p0788 A71-16607

Rotating streaming plasma stability, including ion Larmor finite radius effects in presence of coriolis forces

05 p0788 A71-16628

High pressure electrodeless HF gas discharge plasmas, investigating effects of external magnetic field, gas and pressure on discharge rotation frequency

08 p1342 A71-21915

Plasma jet drift stabilization in toroidal magnetic field with diverter producing 180 degree field line rotation

12 p1941 A71-27548

Rotating spole in unstable pulsed MPD arc, noting rotation frequency and resemblance to plasma rotation

12 p1941 A71-27568

Massive rotating plasma cloud contraction with magnetic field perpendicular to rotation axis, causing magneto-rotational explosions

14 p2312 A71-30386

Magnetogravitational instability model with allowance for finite Larmor radius effect, considering plasma rotation parallel to magnetic field

15 p2459 A71-32654

Rotating arc plasma jet exhaust flow pattern visualization, using bifocal lens system and photographic flash technique in particle track photography

16 p2579 A71-33339

Corotating solar plasma streams associated with variations of interplanetary scintillation from observed radio sources

16 p2634 A71-33386

Interelectrode gap position control of discharge in coaxial gas heater with arc rotated by magnetic field

17 p2676 A71-34309

High pressure electrodeless HF gas discharge plasmas, investigating effects of external magnetic

ROTATING SHAFTS

- field, gas and pressure on discharge rotation frequency 17 p2789 A71-35260
- Weakly ionized gas plasma confined by cylindrical electrodes and dielectric fronts, calculating rotational movement behavior in transverse electric and longitudinal magnetic fields 18 p2952 A71-36943
- Equilibrium diffusion of rotating plasma in toroidal systems, deriving two fluid hydrodynamic equations with allowance for ion temperature perturbation 19 p3109 A71-37140
- Rotating magnetic field plasma pinch, discussing streak and framing photography, electron line density profiles, magnetic probes and ion and electron temperature measurements 19 p3111 A71-37632
- Resistive instability in uniformly rotating magnetoplasmas with finite Larmor radius, using guiding center equations 19 p3115 A71-38208
- Element and isotope separation effects under centrifugal acceleration in rotating plasma, using mass spectrometric diagnostics 22 p3580 A71-41584
- Plasma flow around disk in single ended Q machine with magnetic field parallel to flow velocity, measuring density profile for wake structure 22 p3580 A71-41587
- Earth corotating plasma tail evidence in plasmopause variations from high resolution proton distribution data obtained by Ogo 4 satellite during magnetic storm 23 p3668 A71-43166
- Rotating plasma theory and devices, noting applications to fusion, cosmic physics and technical systems 24 p3852 A71-44494
- ## ROTATING SHAFTS
- ### NT SHAFTS [MACHINE ELEMENTS]
- ### NT TURBOSHAFTS
- Plain bearing oil whirl onset speed, using matrix manipulation for unbalanced shaft self induced vibration amplitudes prediction 03 p0431 A71-13072
- Rotating shafts stability under torsion with two unequal flexural rigidities 04 p0672 A71-15773
- Optoelectronic signal transfer from rotating shafts to stationary equipment without rubbing contacts 05 p0723 A71-16973
- Elastoplastic tubular rods rotation under constant bending moments, solving for large rotational angles 07 p1212 A71-19352
- Stationary motion stability of shaft in cylindrical MHD finite length bearing, assuming incompressible lubrication and small lubrication clearance 09 p1453 A71-22139
- Accelerometer for direct measurements of angular acceleration of rotating shafts, using semiconductor transducers 09 p1443 A71-22706
- Stress threshold for crack growth in rotating shaft bending fatigue 10 p1693 A71-25058
- Rotational effects on laminar subsonic compressible viscous flow across shaft face seals, noting leakage rates and pressure profiles 14 p2251 A71-29936
- Optimal cross section of minimum volume rotating shaft with complex fatigue strength, accounting for tension and shear effects 17 p2822 A71-34595
- Vertical statically unbalanced rotating shaft with two degrees of freedom, investigating internal damping, flexural vibrations and equation of motion 19 p3154 A71-37348
- Rotating shaft critical speed determination as root of polynomial from frequency equation /characteristic determinant/ without iterative search [ASME PAPER 71-VIBR-53] 21 p3385 A71-40300
- Stability of rotating unsymmetrically mass distributed cantilever shaft with unsymmetrical rotor, determining unstable region boundaries by theoretical analysis and experiment [ASME PAPER 71-VIBR-58] 21 p3385 A71-40303
- Flexible rotating shafts high speed, rigid body and modal balancing machines [ASME PAPER 71-VIBR-73] 21 p3460 A71-40311
- Heavy load transportation Mi 12 helicopter design and performance, noting gas turbine rigid shaft connection 23 p3627 A71-42926
- Resonance equation for rotating shaft natural vibration, using Timoshenko beam theory and gyroscopic moments 23 p3776 A71-43377
- ## ROTATING SPHERES
- Setting spherical particle into rotation in fluid characterized by uniform rotational motion far from particle 05 p0735 A71-16159
- Heat transfer at high Peclet number from sphere freely rotating in shear flow field at low Reynolds numbers 10 p1697 A71-24621

- Temperature distribution inside solid sphere rotating in viscous incompressible liquid with constant strength heat source at center, discussing flow field around sphere 11 p1853 A71-25146
- Spherical celestial bodies with linear equatorial velocities, deriving anomalous rotation law 11 p1833 A71-26260
- Gravitational constant determination, using rotating mounted W sphere and gas tight chamber with cylinder suspended from quartz fiber 12 p1931 A71-27245
- Spinning sphere impulsively starting rotation from rest in compressible viscous fluid, calculating boundary layer growth by matched asymptotic expansions method 14 p2225 A71-30295
- Two spheroid rigid bodies rotational and translational motion, using linear and Hill type differential equations for angular variables and coordinates 14 p2312 A71-30384
- Magnus or Robins effect on rotating spheres, obtaining lift coefficients from conical pendulum periodic time measurements 15 p2346 A71-31927
- Convective motions in differentially rotating thin spherical shells, explaining solar differential rotation 16 p2630 A71-33055
- Energy dissipation measurement in liquid filled spinning precessing spherical cavity by gimbaled mechanism [ASME PAPER 71-APM-4] 16 p2644 A71-33219
- Spinning centrally clamped thin shallow spherical shell free vibration numerical analysis by considering perturbation about equilibrium configuration [ASME PAPER 71-APM-G] 18 p2977 A71-36254
- Large scale convection solar magnetic field patterns calculations based on rotating thin spherical shells, noting solar cycle activity 19 p3147 A71-38667
- Elastico-viscous liquid steady secondary flow induced by oblate or prolate spheroid rotating about axis of symmetry from linear partial differential equations solution 20 p3214 A71-39967
- Viscous incompressible flow between concentric rotating spheres, investigating hydrodynamic stability 23 p3663 A71-43443
- ## ROTATING STALLS
- Rotating stall in axial flow compressor high pressure stages, taking into account boundary layer separation 01 p0003 A71-11063
- Rotating stall analysis, using small perturbation method 04 p0569 A71-14984
- ## ROTATING VEHICLES
- ### U ROTATING BODIES
- ## ROTATION
- ### NT AUTOROTATION
- ### NT EARTH ROTATION
- ### NT MOLECULAR ROTATION
- ### NT PLANETARY ROTATION
- ### NT SATELLITE ROTATION
- ### NT SOLAR ROTATION
- ### NT STELLAR ROTATION
- Figural noise and rotation effects on visual form perception, using random and redundancy figures in figure cancellation task 01 p0026 A71-11417
- Rotation direction perception by three cue system for polar projection of dotted line, considering differential retinal velocity relative to axis of rotation 05 p0713 A71-16550
- Jupiter magnetospheric rotation period based on RF observations 06 p0971 A71-18240
- Hind limb antagonistic muscles bioelectric activity dependence on animal rotation direction and head fixation 09 p1388 A71-22196
- Moon shape, translational and rotational motion determination by optical tracking, discussing possible refinements as function of distance measurement accuracy 09 p1525 A71-23337
- Interstellar medium dispersion and rotation measurements, calculating electron concentration fluctuation effects 16 p2608 A71-33227
- Mathematical feature selection transformations by multidimensional rotations, considering character recognition experiment 19 p3026 A71-38490
- IR ring laser rotation sensor, describing design principles for alignment and eliminating locking phenomenon 22 p3557 A71-42153
- Translational and rotational vibrational motion correlation of solid body mass center in Newtonian force field 24 p3872 A71-45047

ROTOR AERODYNAMICS

- Rotor loss coefficients for prediction of radial gas turbine performance using one dimensional analysis 01 p0143 A71-11016
- Turbulence level effects on aerodynamic losses of axial flow turbomachines, discussing boundary layer of blades 03 p0340 A71-13143
- Sound generation by rotor-stator interaction in subsonic axial flow compressors, using acceleration potential and wake technique 03 p0469 A71-13277
- Turbulent and laminar jet propagation and mixing in rotor downwash field [DGLR-70-050] 05 p0795 A71-15961
- Aerodynamic synthesis of helicopter rotor under hover and vertical ascent conditions, using nonlinear vortex approach 07 p1014 A71-19740
- Probabilistic estimate of aerodynamic imbalance of aircraft gas turbine rotors due to production errors in compressor blade angle 08 p1349 A71-22045
- Comparative vertical turbulence and loss restrictive stochastic models for threshold crossing rotor blade flapping vibrations at low lift high advance ratio [AIAA PAPER 71-389] 11 p1846 A71-25351
- Aerodynamic design of VTOL propellers, demonstrating possibility of cyclic control of XC-142 experimental propeller [DGLR-71-017] 15 p2347 A71-32784
- Perturbation study of subharmonic rotor instability due to elastic symmetry, obtaining equations of motion [ASME PAPER 71-VIBR-57] 21 p3385 A71-40302
- Transient and steady state flexible rotor dynamics analysis [ASME PAPER 71-VIBR-92] 21 p3461 A71-40325
- Helicopter wake and boundary layer effects on rotor aerodynamic performance in hovering, low and high speed forward flight [AIAA PAPER 71-581] 22 p3479 A71-41500
- Photogrammetric recording of helicopter rotor induced aerodynamic effects using wind tunnel test smoke visualization technique 23 p3678 A71-43588
- Lifting rotors aerodynamic damping in forward flight, describing methods for blade response variance matrix computation 24 p3789 A71-44559
- Rotor elements eccentricity effect on rotor dynamic deflection, discussing rotor unbalance determination 24 p3884 A71-45010
- ## ROTOR BLADES
- Tip vortex effects on rotor blade flutter in hovering flight, discussing compressibility and oscillation frequency 05 p0694 A71-16564
- Rotating blade noise technology, discussing vehicles and components, noise nature, generation, reduction and prediction 05 p0695 A71-17158
- Sound radiation by rotor from interaction with nonuniform flow, considering multiple blades 05 p0697 A71-17159
- Far field sound radiated from steady loading of isolated subsonic rotor, noting dependence on spatial uniformity of flow entering rotor 05 p0697 A71-17160
- Inlet turbulence interaction with rotor potential flow as noise source in axial flow fans, developing expression for sound power radiated 05 p0738 A71-17163
- Short rotor blade span supersonic fan for pressure wave forward propagation elimination, obtaining acoustic and aerodynamic characteristics [AIAA PAPER 71-182] 06 p0885 A71-18621
- Transonic compressor rotors blade camberline shape optimization by various tip diffusion factor-ratio combinations 07 p1184 A71-20200
- Boundary layer discontinuity on helicopter rotor blade in hovering using flow visualization [AIAA PAPER 69-197] 07 p1017 A71-20307
- Rotor blade random vibrations in response to turbulence [AIAA PAPER 70-548] 09 p1381 A71-22081
- Cyclic creep test for simulating helicopter rotor blades start-stop cycles effect on adhesive bonded joints, using fixed load-unload cycle 10 p1631 A71-24076
- Stability analysis and design optimization with dynamics and aeroelastics constraints for helicopter rotor blade minimum weight with bending torsion flutter and favorable frequency placements [AIAA PAPER 71-388] 11 p1846 A71-25352
- Complex real time hybrid computer simulator for captive two blade rotor platform dynamic problem solving 11 p1744 A71-25847
- Discrete frequency rotor interaction noise from lifting fans, using rotor harmonics acting on blades [ASME PAPER 71-GT-12] 11 p1812 A71-25958

- Helicopter blades inherent vibration damping, comparing theoretical and semiempirical predictions to experimental results 12 p1976 A71-27123
- Incompressible fluid motion in laminar boundary layer on blade rotating uniformly about axis perpendicular to wing span 14 p2170 A71-30218
- Advancing Blade Concept helicopter lifting rotor development, discussing full scale analysis, design, fabrication and wind tunnel tests [AHS PREPRINT 504] 14 p2178 A71-31080
- Rotor blade stall induced helicopter control loads, combining unsteady aerodynamics with aeroelastic rotor analysis [AHS PREPRINT 513] 14 p2178 A71-31084
- Retreating blade stall experiments on model helicopter rotor, considering series of pressure distribution and boundary layer events [AHS PREPRINT 521] 14 p2172 A71-31087
- Integral spar inspection system for making CFI-46 rotor blade fail-safe [AHS PREPRINT 551] 14 p2180 A71-31103
- Size effects on large rotor systems design, considering weight, blade loading, tip speed, etc [AHS PREPRINT 552] 14 p2180 A71-31104
- Dynamic stress on rotor blades of aircraft engine axial compressor stages with low hub/diameter ratio 16 p2624 A71-33345
- Noise generation due to inlet free stream turbulence incident on isolated stators and rotors, using flat plate cascade blade row model 18 p2956 A71-36498
- Coriolis coupled bending vibrations of hingeless helicopter rotor blades, noting out-of-plane component contribution to aerodynamic coupling 19 p3154 A71-37294
- Discrete frequency sound radiation from rotating periodic sources covering rotor blade noise in near field and from disk loading asymmetries 19 p2997 A71-38466
- Acoustic measurement of rotor tones in duct of four blade ventilation fan 19 p3000 A71-38655
- ROTOR BLADES (TURBOMACHINERY)**
- Normal stress analysis at tooth of turbine rotor blade root, taking into account friction force 01 p0143 A71-11247
- Flow research on blading - Conference, Baden, Switzerland, March 1969 03 p0339 A71-13139
- Two stage compressors with subsonic and supersonic air velocity and high camber rotor blades, discussing strength against centrifugal force 05 p0796 A71-16647
- Heat transfer coefficients of various jet systems impinging on gas turbine blade inner surfaces, discussing cooling flow rates and solid particles injection into air flow [ASME PAPER 71-GT-9] 11 p1811 A71-25955
- Flow variation effect on velocity and flow angle distribution at exit of shrouded radial flow impeller with backward swept blades, using streamline curvature method [ASME PAPER 71-GT-15] 11 p1703 A71-25961
- Optimum weight protective system against uncontained rotor failure with radial fragment passage through turbine engine casing [ASME PAPER 71-GT-70] 11 p1813 A71-25985
- Glass fiber rotor blades design with longitudinal pressure tapings for cascade wind tunnel and turbomachinery flow research applications 11 p1772 A71-26316
- Loads on compressor, ventilator and turbine rotor disks having large central holes, giving formulas for stress distributions 12 p1945 A71-26952
- Air cooling methods for aircraft engine turbine rotor blades, considering heat distribution in rotor disk 15 p2467 A71-31461
- Single phase and evaporative systems for liquid cooling high temperature gas turbine rotor blades, reviewing heat transfer performance evaluation 15 p2469 A71-31734
- Jet engine high pressure turbine high temperature alloy blades and vanes grinding operation, discussing testing, operating conditions and coolant application [SME PAPER MR-71-802] 15 p2416 A71-32432
- Thermal stresses in gas turbine rotor blade with two dimensional temperature field, using closed/Saint Venant/plate solutions 16 p2657 A71-33543
- Rotor blade stability, calculating unsteady local lift and effects of blade profile camber and steady angle of attack 17 p2672 A71-35468
- Axial flow turbines, calculating effects of axial clearance between stator and rotor bladings on rotor impulse blades bending vibration strength 18 p2979 A71-36299
- Sweep and dihedral geometry effects on blade to blade and meridional flows in turbomachinery blade rows, using actuator disk theory 19 p2994 A71-38274
- Normal shock existence in blade spacings of rotor and guide vanes of axial flow supersonic compressor as function of pressure nonuniformity 22 p3479 A71-41843
- Vibration amplitudes and phases /excitation modes/ during flutter for weakly inhomogeneous annular cascade flow with blade interaction and random inhomogeneity 22 p3615 A71-41846
- Circumferential flow direction nonuniformity effect in front of compressor wheel on intensity spread and resonant rotor blade vibrations 22 p3615 A71-41847
- Centrifugal pump pressure characteristics calculation by pressure quality coefficient dependence on relative flow rate, assuming arbitrary number of blades 22 p3554 A71-41848
- Flow rate and heating analysis of centrifugal pumps with variable cross section impeller blade ring inlet 22 p3554 A71-41850
- High temperature gas turbine engines rotor blades cooling, deriving generalized dimensionless relations for heat transfer data extension from static tests to operational conditions 23 p3718 A71-44066
- Flow models for turbomachinery, averaging equations for flow through blade cascades across pitch 23 p3627 A71-44348
- Liquid particles motion over variable profile turbine rotor blade edge, concave and fanning surfaces as function of Coriolis and centrifugal force 24 p3819 A71-44932
- ROTOR DISCS**
- U TURBINE WHEELS**
- ROTOR HUBS**
- U HUBS**
- U ROTORS**
- ROTOR LIFT**
- ViSTOL civil aircraft, considering rotor lift and variable sweep wings 10 p1556 A71-24850
- Large crane heavy lift helicopter stability and controllability, considering effects of slung loads, performance improvement, automatic flight control and physical size 19 p2998 A71-38651
- Optimum rotor/jet thrust ratio determination procedure for tip jet driven rotors, considering performance upper bound 19 p2998 A71-38653
- ROTOR SPEED**
- Free three degrees of freedom gyroscope motion with exponential attenuation of rotor kinetic moment 01 p0079 A71-10532
- Thin gas turbine disk strength under axisymmetric flexural vibrations, noting agreement of calculated and experimental rotor rpm danger zone 04 p0671 A71-15639
- Acoustic tone radiation from subsonic rotor near potential field by interaction with nonuniform inlet flow based on Lighthill aerodynamic sound equation 14 p2225 A71-30210
- High speed gas lubricated foil supported nonmetallic rotor for nuclear magnetic resonance research 22 p3553 A71-41678
- High rpm effect on centrifugal pump efficiency, considering hydraulic, volume and mechanical losses 22 p3554 A71-41849
- Optimal control of self excited vibration of high speed rotor with thrust magnetic bearing, using analog simulation 23 p3681 A71-43311
- Radial thrust bearing balls ovality effect on axial vibration of rapidly rotating turbine engine rotor 24 p3864 A71-45006
- ROTORCRAFT**
- U ROTARY WING AIRCRAFT**
- ROTORCRAFT AIRCRAFT**
- Rotorcraft ideal height-velocity boundary and critical decision point height prediction, discussing pilots optimal control under emergency conditions 04 p0527 A71-15414
- Low disk-loading prop rotor application to propeller and fanjet STOL and fanjet VTOL short haul aircraft [AIAA PAPER 71-781] 17 p2674 A71-34481
- ROTORS**
- NT COMPRESSOR ROTORS**
- NT FLYWHEELS**
- NT IMPELLERS**
- NT LIFTING ROTORS**
- NT PUMP IMPELLERS**
- NT RIGID ROTORS**
- NT ROTARY WINGS**
- NT TILTING ROTORS**
- NT TIP DRIVEN ROTORS**
- NT TURBINE WHEELS**
- Motion stability of satellite with rigid connection to symmetric rotors rotation axes 01 p0164 A71-11156
- Rotor and rotor-disk system response to constant and pulsating torque, experimentally examining critical whirling speed and lateral vibration [ASME PAPER 70-WA/DE-14] 03 p0511 A71-14146
- Jet engine rotor strain and temperature data transmission, examining special purpose telemeters design 07 p1062 A71-19628
- High Q factor rotor systems applications in dielectrics electromagnetic viscosity measurement and radio transmitters with low oscillation phase drift 09 p1492 A71-22363
- Surface geometry effect of polycentric gas bearing on rotor stability in dynamic equilibrium without radial load 09 p1454 A71-22799
- Rotating blade /rotors/ and stationary /stators/ rows in axial flow molecular pump, deriving overall and individual transmission probabilities 09 p1455 A71-23058
- Electric potential and current density in rotor of thin disk unipolar engine with zonal removal, formulating Neumann problem 13 p2002 A71-28930
- Natural vibrations of two coaxial rotors with unbalanced disk and different angular velocities, solving equations of motion by energy balance method 19 p3156 A71-37536
- Windage data for inert gas in high speed generators rotor-stator gap, investigating turbulent velocity profiles 20 p3181 A71-38915
- Stability of rotating unsymmetrically mass distributed cantilever shaft with unsymmetric rotor, determining unstable region boundaries by theoretical analysis and experiment [ASME PAPER 71-VIBR-58] 21 p3385 A71-40303
- Single mass flexible rotor in elastic bearings mounted on damped flexible supports, analyzing dynamic unbalance response and transient motions [ASME PAPER 71-VIBR-72] 21 p3460 A71-40310
- Flexible rotor multiplane field balancing analysis, investigating test validity and accuracy and sensing instruments effects [ASME PAPER 71-VIBR-74] 21 p3460 A71-40312
- Flexible rotor balancing by exact point speed influence coefficient method [ASME PAPER 71-VIBR-91] 21 p3386 A71-40324
- Air pressurized bearing mounted rotor with vertical shaft, discussing elastically suspended foundation mass and damping effect on self excited vibration 22 p3550 A71-41659
- Cayley-Klein parameters application to quasisynchronous motion of satellite with multiple rotors, using perturbation method 24 p3848 A71-44830
- ROUGHNESS**
- NT SEA ROUGHNESS**
- NT SURFACE ROUGHNESS**
- ROUND TRIP TRAJECTORIES**
- NT CIRCUMLUNAR TRAJECTORIES**
- Circumunar trajectories with return to earth atmosphere, comparing various methods 09 p1519 A71-22662
- Thrust power optimization for spacecraft earth-planet round trip trajectories 12 p1957 A71-26633
- Space tug optimal round trip trajectories for payload earth escape injection missions, obtaining boundary value problem solution by Newton-Raphson iteration technique 21 p3452 A71-40908
- Orbit-to-orbit shuttles as earth capture systems for round trip planetary missions, using hyperbolic rendezvous technique with returning interplanetary spacecraft 22 p3600 A71-41954
- Impulsive trajectory optimization for asteroid Eros round trip sample return mission using chemical propulsion [AAS PAPER 71-369] 23 p3730 A71-43039
- Reusable space tug payload injection missions, determining optimal round trip trajectories at earth escape energy levels [AAS PAPER 71-370] 23 p3730 A71-43040
- ROUNDED LEADING EDGES**
- U LEADING EDGES**
- ROVER PROJECT**
- Manned mars exploration, discussing excursion module, surface rover and base construction 13 p2143 A71-29251
- ROVING VEHICLES**
- NT LUNAR ROVING VEHICLES**
- RUBBER**
- NT ELASTOMERS**
- NT SILICONE RUBBER**
- Photoelastic compensator of urethane rubber, describing construction and applications 01 p0082 A71-11009
- Stillman rubber elastomers tests by cyclic exposure to hydrazine and air, water vapor or carbon dioxide, considering suitability as valve seat 05 p0772 A71-16466
- Rubber seals performance testing, discussing measuring methods 06 p0905 A71-18216
- Inflation of initially spherical balloon of elastic rubber-like material, discussing tensile instability 11 p1707 A71-25445

RUBIDIUM

Electron paramagnetic resonance atomic scale stress analysis of high polymer fibers and rubber, measuring chain scission and bond rupture for different loading histories

13 p2091 A71-28440

Heating by thermoelastic damping through sudden removal of stresses on homogeneously strained elastic body, comparing elastic deformation of rubber and steels

17 p2821 A71-34584

Molecular bond rupture and strain energy release rates correlation during ozone cracking of rubber from electron paramagnetic resonance and stress elongation measurements

18 p2939 A71-36244

RUBIDIUM

NT RUBIDIUM ISOTOPES

Optically pumped rubidium maser short term frequency instability caused by thermal noise and resonator temperature and pumping power fluctuation

01 p0095 A71-11211

Miniaturized Rb atomic frequency source having 1 in 10 to 8th power stability in year and 5 minute warm-up time

02 p0252 A71-12422

Optical hyperfine splitting of Rb resonance lines of atomic beam light source, using Fabry-Perot interferometer

07 p1111 A71-19488

Light-microwave signal relation in optical pumping and detection in Rb atomic oscillator

08 p1289 A71-21273

Rubidium viscosity near solidification point from thin immersed plate forced vibrations amplitude

09 p1508 A71-22540

OGO-2 rubidium vapor magnetometer measurements comparison with surface magnetic observatory data during geomagnetic storms, considering asymmetric ring current

16 p2572 A71-33946

Optically pumped rubidium maser short term frequency instability caused by thermal noise and resonator temperature and pumping power fluctuations

17 p2750 A71-34262

Apollo 12 igneous rocks and fines from Ocean of Storms, presenting rubidium and strontium chronology and chemistry

23 p3752 A71-43709

Atomic time standards, discussing Cs 133, hydrogen maser, ammonia maser and rubidium gas cell equipment

24 p3827 A71-44994

RUBIDIUM ISOTOPES

Optically pumped Rb laser theory, taking into account superfine and Zeeman structure of atoms

05 p0763 A71-16872

Rb-Sr isotopic composition in Apollo 12 regolith samples yielding 4.2-5.1 billion year ages

23 p3752 A71-43710

RUBIS ROCKET VEHICLE

Barium ion cloud experiments for ionospheric vapor release determination from Rubis Rocket trajectory visible markings

11 p1755 A71-25643

RUBY

Laser rubies optical properties, considering orientation, homogeneity and inner stresses, emission in spiking and Q switched operation

05 p0761 A71-16329

EPR line width in ruby under charged dislocations and electric fields of lattice defects, using statistical method

06 p0942 A71-18348

Electron-nuclear interactions in ruby by magnetoacoustic double resonance, comparing experimental and theoretical data

07 p1181 A71-20526

Spectral and relaxation characteristics in antiStokes two photon luminescence of polycrystalline ruby exposed to filtered light pulses

09 p1508 A71-22392

Optimal location of nonreciprocal disk shaped YIG element of traveling wave quantum ruby paramagnetic amplifier for weak magnetic field levels

10 p1585 A71-24883

Ruby watch jewels as pinhole diaphragms in laser beam broadening systems, determining optimal size

16 p2588 A71-34102

Solid state lasers, considering ruby and YAG-Nd ion materials pumped at room temperature

19 p3074 A71-38229

RUBY LASERS

Pulse transmission control equipment for Q switched ruby laser output

01 p0095 A71-11171

Q switched monomode ruby laser coherence length measurements, using holography at various beam intensities

01 p0096 A71-11374

Free generation regime of ruby laser studied by electro-optical method of smoothing spatial inversion inhomogeneities

02 p0261 A71-12502

Potassium vapor emission spectrum fine structure in high power ruby laser field, noting dependence on vapor pressure

02 p0262 A71-12612

Polarization characteristics of dual rod ruby laser emission, determining phase coincidence and energy output

03 p0434 A71-13503

Rare earth polycrystalline powders luminescence stimulation by ruby laser radiation, discussing two photon mechanism, luminous intensities relations and UV radiation

03 p0435 A71-13510

Emission kinetics for linearly polarized waves from composite ruby laser, describing pumping power effects

03 p0435 A71-13513

Q switched ruby laser ranging system of tracking station for use with retroreflecting satellites

03 p0379 A71-14007

Spectroscopic hole burning in coupled saturable dye-ruby lasers with frequency locking

04 p0607 A71-14725

Photodetector triggered single pulse selection from mode locked ruby laser

04 p0608 A71-15595

Atmospheric aerosol vertical distribution by lidar system, describing ruby Q switched giant pulse laser design and operation

05 p0720 A71-16221

Phase objects holography using pulsed ruby laser with plane-parallel and hemispherical cavity

05 p0752 A71-16748

Radiation spectra kinetics of compound ruby lasers containing two crystals and Nicol prism

05 p0763 A71-16830

Ruby laser with lens resonator, studying radiation patterns and angular divergence, lasing threshold and spectra width

05 p0763 A71-16831

Contact electro-optic KDP crystal shutters for Q switching ruby laser

06 p0907 A71-17530

Ruby Q switched lasers with modular electro-optic shutters for low insertion loss and high optical radiation resistance

06 p0908 A71-18303

Nuclear radiation damage to ruby laser power output

07 p1121 A71-19067

Ruby laser passive Q switching by phototropic thin film shutter, outlining advantages over bleachable dyes

07 p1122 A71-19140

Focused ruby laser beam degradation of various gaseous aliphatic and alicyclic hydrocarbons

07 p1124 A71-19789

Electro-optical shutter with low control voltage /3 kV/ for ruby laser consisting of Pockels cell and Porro prism

07 p1125 A71-19808

Emission of ruby laser with resonator containing passive Q switch solution and lenses, investigating regular self oscillation region

07 p1125 A71-19811

Optically pumped pulsed ruby laser welding unit, noting joining and hole drilling problems

07 p1119 A71-19968

Ruby laser driven luminous waves during breakdown and heating within freely expanding gas jet observed with streak photography

07 p1126 A71-20168

Pulsed ruby laser radiation energy characteristics relation to crystal temperature distribution, thermal deformation and compensating lens focal length

07 p1126 A71-20188

Optical pumping efficiency in ruby laser for different rod cross sections

08 p1301 A71-21220

Near Gaussian intensity distributions from multimode high power pulsed ruby lasers, using rotating diffuser

08 p1302 A71-21407

Metallic target in radiation damage from focused ruby laser beams as function of energy and luminous pulse duration

09 p1465 A71-23563

Dynamics of focusing electric discharges generated by coaxial plasma gun illuminated by ruby laser beam, using schlieren photography

10 p1653 A71-24758

Microwave frequency sound generation in solids with Q switched ruby laser

10 p1621 A71-24838

Q switched ruby laser time dependent spectrum analysis by high speed camera with Fabry-Perot interferometer, noting holographic interferometry application

10 p1622 A71-24962

Q switched ruby laser emission effect on long wave pigment system of photosynthesizing organisms

11 p1774 A71-26006

Plane and three dimensional dynamic holograms recording in bleachable dyes, using ruby laser with gal-

lium chloride phthalocyanin in chlorobenzene as Q switch

11 p1767 A71-26565

Deuterium gas breakdown by ruby laser, using quantum kinetic equation for electron interactions with molecules and photon field

12 p1915 A71-27284

P-type gallium selenide crystals impurity photoconductivity measurements by Q switched ruby laser

13 p2077 A71-27959

Subnanosecond interferograms with high spatial resolution of plasma filaments in ruby laser produced spark

13 p2077 A71-28047

Fine crystalline substances forced combination scattering at liquid nitrogen temperature, using ultrashort ruby laser pulses for excitation spectra

13 p2080 A71-29022

Holographic stroboscope using ruby laser with passive shutter for HF vibration measurement

14 p2254 A71-30584

Cloud energy dissipation coefficient determination by ruby laser device, applying to water content and liquid particle concentration, vapor cloud and aerosol concentration

15 p2445 A71-31449

Motion and collision of plasma blobs generated by giant pulse ruby laser irradiation on lithium plate

15 p2455 A71-31643

Ultrasonic effects on synchronization of ruby laser radiation, investigating emission pulse structure and peak sequence

15 p2419 A71-31712

Hexamethylindotricarbocyanine iodide ethanol dye solution stimulated fluorescence during excitation by ruby laser radiation in spike generation quasi-continuous monopulse modes

15 p2421 A71-32406

Quartz, organic glass and plexiglass luminescence under giant pulse ruby laser radiation

15 p2422 A71-32462

Ruby laser pumped tunable organic dye laser to excite atomic flame fluorescence of 5535.5 A barium resonance line, obtaining intensity vs concentration

15 p2422 A71-32582

Giant pulse ruby laser, using potassium dihydrophosphate crystals linear electro-optical effect for Q modulation

15 p2424 A71-32758

Single mode ruby laser emission on transparent dielectrics, observing surface luminescence, free electrons production and adsorbed gases heating

16 p2585 A71-32797

Three dimensional hologram recording, showing He-Ne laser reconstruction of Q switched ruby laser hologram image of mosquito flight

16 p2579 A71-33528

Self focusing effect of Q switched single mode ruby laser emission in CdS crystal, noting 60 kW minimum threshold power

16 p2588 A71-33645

Ruby laser ranging of moon, describing Pic du Midi Observatory laser telemetry station and Luna 17 retroreflectors

16 p2640 A71-33752

Plane mirror ruby laser pseudosteady regime, discussing fundamental TEM mode case

16 p2588 A71-34062

Luminescence quenching in Hg tube activated ZnS-Cu phosphors under action of ruby laser red light

17 p2752 A71-34404

Upper atmosphere density observation by Q switched ruby laser radar

17 p2753 A71-34748

Magnetic field effects on ruby laser radiation kinetics and spectral composition, studying crystal heating and light emission

17 p2753 A71-35242

Plane and three dimensional dynamic holograms recording in bleachable dyes, using ruby laser with gallium chloride phthalocyanin in chlorobenzene as Q switch

17 p2745 A71-35507

Holography with single transverse longitudinal mode pulsed ruby laser, emphasizing carrier frequency shift as limiting factor on depth of field

17 p2745 A71-35587

Ruby laser sources of short duration and high energy emission in holography, considering oscillator amplifier illuminator, contour spacings, transmission holocameras, etc

18 p2930 A71-36057

Q switched ruby laser holography, using controlled multimode emission for contour recordings of reflected light scenes

18 p2920 A71-36102

Pulsed ruby laser high speed photography for accurate measurements of models contours in hypervelocity flight within aeroballistic range

18 p2923 A71-36612

Fluorescence spectra of anthracene ethyl alcohol solution and powdery crystalline anthracene by single and two photon ruby laser excitation

19 p3071 A71-37263

Ruby laser Q switching by hydrogen and copper phthalocyanin vapors, obtaining nanosecond single pulses with high power density

19 p3072 A71-37768

Oscillatory variation of optical length of pulsed laser resonators during lasing, testing with ruby laser in free emission mode

19 p3073 A71-37791

Ruby laser microwelding machine for simultaneous welding of several points with one discharge suitable for micromechanics, computer manufacturing, watchmaking, etc

19 p3069 A71-38232

Pulsed ruby laser holographic instrumentation for materials tests, detailing reflected wave front complex amplitude characterization

20 p3245 A71-39347

Nanosecond ruby laser pulse generation using electro-optic shutter switching circuit external to Q-spoiled cavity

21 p3391 A71-40179

Radial energy contours of pulsed ruby laser beam in direct determination of thermal conductivity by flash technique, using heat flux transducer

21 p3391 A71-40180

Interference rings formation mechanism near main beam emitted by ruby laser with plane and reflecting terminal faces

21 p3392 A71-40515

Self induced transparency in ruby attenuator, detailing phase relaxation effects at various temperatures

21 p3427 A71-40546

Pulsed ruby laser holography improvement by coherence length increase with temperature controlled multitelons and beam uniformity through ruby crystals improvement

21 p3393 A71-40925

High resolution portable hologram recording camera with pulsed ruby laser light source and rechargeable storage batteries as self contained power supply

21 p3380 A71-40926

Two photon absorption coefficients of ZnSe and zinc cadmium selenide crystals for ruby laser radiation, showing energy gap reduction effect

21 p3395 A71-41340

Gallium selenide excitation by ruby laser radiation, investigating impurity photoconductivity dependence on radiation intensity

21 p3395 A71-41352

Optical spacecraft tracking, using pulsed ruby lasers at Baker-Nunn camera stations of Smithsonian Astrophysical Observatory for retroreflector-equipped satellites ranges

21 p3349 A71-41404

Q-switched ruby laser holographic interferometry for hypersonic flame combustion recording

22 p3559 A71-41742

Pulsed ruby laser transmission and reflection holography in single transverse and axial electromagnetic mode, stressing safety aspects

22 p3556 A71-41743

Single mode ruby laser spatiotemporal coherence characteristics with emission moment controlled by Q switch operating on modulated ultrasonic traveling waves

23 p3683 A71-43394

Interferometric fringes from study of gas plasma produced by ruby laser pulses, using Nd glass laser for heating

23 p3710 A71-43409

Steady power pulsation measurement and operation mode theory of ruby laser with bleachable dye filters

23 p3684 A71-43416

Holographic evaluation of low power ruby laser emitted wave spatial coherence factor via fringe visibility measurements

23 p3679 A71-43894

Absorption spectrum of atmospheric gases from laser spectrometer based on tunable ruby laser, measuring water vapor absorption coefficients in multipass cell

24 p3834 A71-45207

Nanosecond solid dielectric discharger fired by Q switched ruby laser for commutation of coaxial line forming high amplitude voltage pulses

24 p3835 A71-45238

Ruby laser radiation modulation by ultrasonic mirror oscillations, discussing mechanism

24 p3836 A71-45269

RUDDERS

NT AERIAL RUDDERS

Solar rudder for spacecraft steering in form of right circular cone with ideally reflecting surface

20 p3306 A71-39136

RULES

NT FLIGHT RULES

NT INSTRUMENT FLIGHT RULES

NT PALMGREN-MINER RULE

NT PHASE RULE

NT SUM RULES

NT WHITHAM RULE

RUMBLE INSTABILITY

U ACOUSTIC INSTABILITY

RUN TIME (COMPUTERS)

Probabilistic cyclic queue model of overhead time and channel utilization in multiprogrammed computer systems under demand memory paging

13 p2035 A71-28973

Accelerated procedures for Markov chain model optimal control problems solution with computation time advantage over usual dynamic programming

17 p2719 A71-34737

Discrete Kalman filter computational efficiency improvement by iterative processing technique for covariance matrix updating

17 p2722 A71-35182

Hardware executive control with associative memory for avionic digital computer system, comparing computation speed, cost and reliability with software method

17 p2712 A71-35778

Nonlinear time varying systems digital integration simulation techniques by variational equations approach, discussing accuracy, execution time and limitations

18 p2884 A71-36141

Transonic flow numerical analysis, discussing initial conditions and imbedded shocks choice for computation efficiency

18 p2905 A71-36307

Picture processing using general purpose digital computer simulation for reduction of processing time and special purpose hardware investments

21 p3376 A71-40111

Branched space trajectory optimization by steepest descent method with coasting arcs, obviating numerical integration for accuracy increase and computing time reduction

[AAS PAPER 71-309]

23 p3725 A71-42985

Computer generation of sensitivity functions for nonlinear sampled data control systems, discussing simulator components and computational time economy problems

23 p3648 A71-43859

RUNGE-KUTTA METHOD

Keplerian orbit numerical integration, considering Runge-Kutta method and transformations

01 p0154 A71-10377

Initial value problems differential equations discontinuities, describing step-size adjustment for fourth order Runge-Kutta methods

02 p0277 A71-12728

Algebraic equations system solution by eighth order Runge-Kutta process with eleven function evaluations per step

04 p0619 A71-14812

Spiral plate heat exchanger temperature-length profile calculation by Runge-Kutta technique

04 p0678 A71-15464

Numerical integration of Poisson kinematic equations for direction cosines, using Runge principle for accuracy values proportional to third power of integration step

05 p0780 A71-16051

Initial value problems involving linear ordinary differential equations, deriving theorems for Runge-Kutta and Adams methods effectiveness

06 p0917 A71-17566

Matrix eigenvalue problem solution by reducing to nonlinear algebraic equations for iterative solution or integration by Runge-Kutta method

06 p0921 A71-18342

Runge-Kutta type difference methods for calculating unsteady gas flow with shock waves

07 p1087 A71-19184

Boundary value problems solution, using Runge-Kutta method with computer for eigenfunctions of ordinary differential equations

09 p1484 A71-22177

Semiimplicit Runge-Kutta schemes absolute stability, using schematization of algorithm

10 p1636 A71-23841

Classic fourth and lower order Runge-Kutta formulas with stepsize control, applying to heat transfer problems

10 p1636 A71-23924

Numerical integration of Poisson kinematic equations for direction cosines, using Runge principle for accuracy values proportional to third power of integration step

16 p2605 A71-33455

Supersonic flow field computation for wing-body combinations by shock-capturing finite difference techniques, discussing improvement based on Runge-Kutta method

18 p2844 A71-36303

Stefan problem reduction to order n differential flow equation solution using Runge-Kutta method

18 p2905 A71-36314

Local error estimators comparison for Runge-Kutta method in production code design for ordinary differential equations numerical solution

18 p2941 A71-36353

Computerized solutions of gas turbine engines motion equations, considering Euler, fourth order and fifth order Runge-Kutta, Adams, Bashforth and implicit methods

18 p2957 A71-36809

RUNNING

Tarahumara Indian runners cardiovascular system physical conditioning for endurance extremes

08 p1240 A71-21887

Trained college and recreational swimmers cardiac output and maximum oxygen consumption during tethered swimming and treadmill running

13 p2024 A71-29496

World champion marathon runner metabolic responses during submaximal and maximal treadmill running, recording oxygen consumption, heart rate and lactic acid

20 p3185 A71-38890

RUNUP

U ENGINE TESTS

RUNWAY CONDITIONS

Airport runway mechanical fog dispersal, using trailer mounted rotating wire mesh sieves

04 p0566 A71-14983

Runway visual range automatic assessment, discussing data handling, digital display and error sources

04 p0623 A71-15023

Runway deicing methods, discussing spreading of chemicals by ground vehicles and aircraft

07 p1083 A71-19425

Fog removal by high power carbon dioxide lasers, evaluating possibility of clearing airport runways [AIAA PAPER 69-670]

07 p1153 A71-20308

Noise abatement power cutback takeoff procedures, maximum altitude approaches and preferential runway systems for noise relief

08 p1232 A71-21813

Aircraft aquaplaning skidding prevention by runway resurfacing and water depth sensor warning indicators

10 p1609 A71-23946

Crosswind components measurement for different runways of important German civil airports

10 p1639 A71-25041

Flexible runway surfaces classification by LCN method, calculating for Ilyushin aircraft

11 p1745 A71-26201

Mutual aerodynamic effects of SM-1 helicopters during simultaneous takeoff and landing, determining minimum distances between helicopters

12 p1867 A71-26953

Fog clearance from airport runways, discussing available techniques, economic aspects and importance for military operations

12 p1925 A71-27247

Airport pavement design principles, considering imposed stresses at flight operation areas, runways, taxiways, apron and waiting position overrun areas, shoulders and strips

13 p2045 A71-29311

Uneven runway taxiing vibration effects on supersonic transport aircraft, comparing calculation with measurement

14 p2175 A71-30305

Civil aircraft arresting on runway overshoots, describing safe deceleration method by use of soft ground arresters

17 p2674 A71-35210

Systems approach to airfield pavement for future aircraft, integrating design, construction, operation and maintenance

18 p2897 A71-36346

Aircraft random heave-pitch response to taxiing on rough runways, analyzing dynamic loads and fatigue damage by power spectral techniques

18 p2850 A71-36675

Airport congestion as constraint on air travel, considering runway capacity and adjusted demand

19 p3042 A71-38028

Braking performance of runway surfaces and skidding resistance of aircraft tires, considering load and inflation pressure, tread materials and weather conditions effects

22 p3529 A71-42234

Aircraft skidding accidents investigation, comparing airplane stopping distance computations and observations

23 p3628 A71-43228

Laser technique for runway and slant visibility range, lower cloud boundary and atmospheric damping coefficient

23 p3701 A71-43889

RUNWAY LIGHTS

Psychophysical evaluation of glide slope detection accuracy by diamond vs square shape in runway centerline stripping as aircraft landing aid

12 p1875 A71-27252

Horizontal visibility range determination of lights on landing strip

15 p2443 A71-31360

Flashing civil aviation lights history, progress and photometric characteristics, discussing navigation and landing aids

22 p3499 A71-41489

RUNWAYS

Aircraft pavement design - Conference, London, November 1970

02 p0237 A71-12162

Transport aircraft tire pressure and multiwheeled landing gear limitations regarding pavement design

02 p0189 A71-12163

- Aircraft multiwheel undercarriage effect on rigid and flexible pavements, examining failure modes 02 p0189 A71-12164
- Municipal airport rigid pavements design considering supporting effects of soil subgrade, asphaltic concrete subbase and pavement strength 02 p0237 A71-12165
- Flexible pavements design for giant transports considering load repetitions, total systems, environmental effects, etc 02 p0238 A71-12166
- Rigid and flexible pavement design and construction in Europe, discussing unreinforced and crack reinforced slabs and CBR method 02 p0238 A71-12167
- Aircraft pavements in UK, discussing reinforced and unreinforced concrete, tar-bound bases and surface coatings 02 p0238 A71-12168
- Runways, aprons and taxiways strengthening to accommodate higher tire pressures and landing speeds, heavier aircraft and surface riding requirements 02 p0238 A71-12169
- Aircraft pavements design and construction problems regarding adverse soil conditions 02 p0238 A71-12170
- Maximum throughput-rate capacity for runway and final approach path airspace involving multiple IFR landings 02 p0279 A71-12893
- Floating airport structural design, using hollow concrete blocks filled with polystyrene foam as runway basic unit 09 p1428 A71-22949
- Airport runway surface strengthening, discussing overlaying additional rigid or flexible layers, replacing used sections and reinforcement problems 10 p1589 A71-24756
- Roissey-en-France airport, describing construction, passenger handling, terminal facilities, traffic volume and runway system 13 p2045 A71-29309
- Melbourne/Tullamarine airport, describing facilities, capacity, road system, cargo and passenger handling areas and runway layout 13 p2045 A71-29310
- Binational Basle-Mulhouse airport, discussing traffic structure, buildings and runway development 18 p2897 A71-35996
- Narita site Tokyo international airport, discussing transportation, runways, ground handling, navigation aids, lighting, etc 18 p2897 A71-35997
- Asphalt pavement design for heavy multiwheel aircraft, using BISTRO computer program 18 p2897 A71-36000
- Operating costs and runway lengths for V/STOL in city and suburban short haul air transportation 18 p2897 A71-36347
- Atlanta airport instant runway construction using concrete pavement, compacted subbase and longitudinal/herringbone underdrain 18 p2897 A71-36349
- Super CTOL airport planning, discussing location of runway pairs, aircraft operations, noise reduction, community relations and efficiency 19 p3041 A71-38023
- International airport planning, considering runways, hangars, second level loading, cargo handling and safety 20 p3209 A71-39388
- Airport operation costs affected by runway utilization, parking bays alignment, baggage handling and aircraft noise 20 p3209 A71-39390
- STOL aircraft system, discussing ground installations, runways, three dimensional area navigational aids, noise reduction, air traffic and short haul productivity [ALAA PAPER 71-983] 24 p3791 A71-44579
- RUPTURING**
- Bond rupture and fracture in semicrystalline polymers, noting agreement with random length molecular tie chain scission model 04 p0670 A71-15388
- Strengthening curve determination by tensile tests for plastic yield limit, strength and elongation at rupture 04 p0673 A71-15898
- Pure polycrystalline Al under uniaxial tension, noting vacancy rupture mechanism 06 p1000 A71-17940
- Unidirectionally aligned fiber phase solidified eutectic composites model, discussing high temperature rupture and creep properties 08 p1323 A71-21585
- Low carbon steel welds, investigating low cycle deformation and rupture resistance as function of weld zones 08 p1316 A71-21609
- Short term creep and rupture model, considering strain hardening effect 08 p1371 A71-21610

- Carbon and oxygen inclusions effects on polycrystalline molybdenum rupture due to precipitation and chemisorption 11 p1781 A71-26323
- Rupturing rotations estimates for turbine disks, considering failure modes and load bearing capacity 17 p2829 A71-35305
- Composite failure model tested for short term creep and rupture in Mo alloy at constant loads and 785-1400 C, considering strain hardening 17 p2834 A71-35670
- Linear-elastic fracture mechanics limits concerning toughness based on elastic-plastic rupture model for yielding materials 19 p3161 A71-38726
- RUTHENIUM**
- Vacuum deposited Mo and Ru films optical properties, emphasizing reflectance measurements 04 p0627 A71-15693
- RUTHENIUM ALLOYS**
- Near equiatomic Ta-Ru alloys phase transformations by resistance and susceptibility changes and X ray powder patterns of cooled structure 04 p0614 A71-15777
- RUTILE**
- Two center bound polaron in rutile single crystal, studying dielectric behavior in applied magnetic field 08 p1345 A71-21690
- Variable Nb composition of meteoritic rutile grains from quantitative electron microprobe analysis 20 p3292 A71-39384
- RYAN AIRCRAFT**
- NT XC-142 AIRCRAFT**
- RYDBERG SERIES**
- Time of flight energy spectra of high lying and Rydberg metastable atoms by electron impact dissociation of molecular oxygen, noting atmospheric applications 16 p2614 A71-34043

S

- S BAND**
- U SUPERHIGH FREQUENCIES**
- U ULTRAHIGH FREQUENCIES**
- S CURVES**
- Langmuir S curves for W /110/-Cs and Mo /100/-Sr adsorption determined by thermionic electron emission microscope, noting minimum work function 02 p0295 A71-12203
- S GLASS**
- Stress rupture properties of S glass/epoxy single end strands at various load levels, considering distribution functions 07 p1145 A71-20126
- Stress rupture behavior of S glass/epoxy multifilament strands, developing tensile and creep test apparatus installed in controlled environment building 11 p1784 A71-25397
- S MATRIX THEORY**
- Circulation adjustment of m-port waveguide single junction circulator by scattering matrix eigenvalues 01 p0056 A71-11197
- Classification of electromagnetic wave scattering fluctuating objects from statistical scattering matrices, obtaining incident wave polarization 01 p0038 A71-11208
- Radar target backscattering characteristics description using scattering matrix invariants 04 p0619 A71-15329
- Charged scalar static model, using dispersion theory to include two-meson effects in two nucleons binding energy at zero separation 05 p0785 A71-16449
- Computer algorithms for scattering matrix of rectangular waveguide splitters in H plane 07 p1079 A71-20073
- Multicomponent microwave equipment, discussing design automation by matrix notation with computer calculations 09 p1416 A71-22468
- Electromagnetic scattering matrix formulation, considering volume and surface type scattering for objects of arbitrary shape, comparing numerical results with experimental measurements 09 p1493 A71-22806
- Scattering matrix of stripline segment with random change in width of inner strip conductor 11 p1733 A71-26350
- S matrices application to nonlinear electric circuits and media with nonlinear permittivity coefficients, biological neurons and optical frequency integrators 14 p2220 A71-30025
- Classification reliability of electromagnetic wave scattering fluctuating objects from statistical scattering matrices, obtaining incident wave polarization 17 p2698 A71-34260
- Electromagnetic scattering by imperfectly conducting circular and square cylinders, using matrix technique based on conformal transformation from polygonal to circular cross section 22 p3512 A71-42361

- Two sided error estimates for electrodynamic impedance, admittance and scattering matrices in diffraction theory 24 p3805 A71-45256
- S WAVES**
- Electrical resistance spot weld penetration measurement via ultrasonic method using shear waves 01 p0086 A71-10305
- Horizontal shear wave diffraction by finite crack and rigid ribbon in elastic medium 01 p0173 A71-10845
- Shear wave propagation into heat conducting viscoelastic fluids, considering steady one dimensional flow stability 01 p0181 A71-11188
- Transient axisymmetric rotary shear wave propagation in nonhomogeneous viscoelastic media with cylindrical hole 04 p0671 A71-15752
- Shearing gravity waves /Kelvin-Helmholtz/ instability in isothermal layer model discontinuous interface application to CAT 05 p0777 A71-16667
- Thin single layer orthotropic circular cylindrical shell shear coupled traveling wave reflections, determining stresses in terms of particle velocities 07 p1216 A71-20134
- Lower earth mantle shear velocity models derivation and core radius estimation based on S travel times observation 11 p1760 A71-26060
- S wave scattering from H and He positron systems at low energies, applying Kohn and Harris variational methods 11 p1803 A71-26373
- Cylindrical cavities in infinite series, examining shear wave diffraction 12 p1975 A71-27109
- Elastic plane shear wave diffraction on elliptical cylinders in half space, using elliptical wave function series and linear algebraic equations 12 p1978 A71-27332
- Particle displacements during resonance motion of shear and compression waves in linearly viscoelastic flat plate of finite thickness 14 p2332 A71-30851
- Face shear and thickness twist waves in bcc crystal plates, presenting numerical computation results for Fe and W 15 p2426 A71-31418
- S shock wave and magnetic field interaction at supersonic speed, using shock tube and MHD channel with sectioned electrodes 17 p2790 A71-35643
- Secondary floating shock generation in supersonic ideal gas flow about blunt bodies, investigating body configuration and flight regime effects 18 p2845 A71-36331
- S-wave elastic positron-hydrogen scattering in ionization region, estimating error in extrapolated t matrix from complex energy 19 p3106 A71-37375
- Shear layers acoustic excitation, considering coupling between sound waves and rotational excited shear waves in flow detachment line 21 p3317 A71-40014
- S-N DIAGRAMS**
- Metallic materials semimicroscopic damage in fatigue of S/N gage under constant strain 01 p0104 A71-11396
- Low-cycle fatigue curve determination for plane elastoplastic bending with flexible loading, deriving rated fatigue life 09 p1536 A71-22502
- Notched age hardening Al alloys sheets, obtaining fatigue damage test data and S-N curves 14 p2326 A71-30067
- Fatigue S-N curves discontinuities associated with plastic yield and crack path tested on mild steel notched specimens 16 p2591 A71-33346
- Stiffened panel acoustically induced stress estimation using experimentally determined random S-N curves with various structural parameters 17 p2826 A71-35033
- Statistical methods for S-N curve and fatigue limit tests, including iterative method, probit analysis, etc 18 p2936 A71-36695
- Nickel base alloy under axisymmetric tension compression tests, obtaining breaking load diagrams and fatigue and creep curves 18 p2937 A71-36716
- S-N curve and structural failure probability due to combined random and primary loads based on mathematical model 19 p3157 A71-37847
- S-3 SATELLITE**
- U EXPLORER 12 SATELLITE**
- S-18 SATELLITE**
- U OAO**
- S-27 SATELLITE**
- U ALOUETTE 1 SATELLITE**
- S-50 SATELLITE**
- U OGO-C**

S-51 SATELLITE

U ARIEL 1 SATELLITE

S-52 SATELLITE

U ARIEL 2 SATELLITE

S-64 HELICOPTER

U CH-54 HELICOPTER

SAAB AIRCRAFT

NT SAAB 37 AIRCRAFT

SAAB 37 AIRCRAFT

Technical aspects of tactical all-weather instrument landing system of Swedish STOL aircraft Saab 37 Viggen

11 p1796 A71-25233

SABATIER REACTION

Photometry of head and tail regions of comets Kosik, Akhamarov-Iurllov-Hassel, Arend-Roland and Mrkos by equidensity method, using Sabatier effect

15 p2484 A71-31668

Spacecraft closed loop oxygen recovery system using electrochemical carbon dioxide concentrator, Sabatier reactor and water electrolysis subsystem

22 p3503 A71-42017

SABOT PROJECTILES

Small caliber smoothbore powder sabot guns generating planar shock wave in solids, using streak camera monitoring of impact and recoil velocities

14 p2223 A71-30885

SACCHARIDES

U CARBOHYDRATES

SADDLE POINTS [GAME THEORY]

Iterative algorithms for regression function saddle point and applications in reliability and automatic control theories

10 p1585 A71-24156

Saddle point type differential game problem structure, determining optimal player strategies for fixed point termination

12 p1931 A71-27521

Search for saddle points of function, presenting sub-gradient and penalty methods for solving differential, finite and infinite games

13 p2095 A71-28813

Stationary saddle points phase method for wave diffraction problems in inhomogeneous medium, deriving asymptotic expansion for surface integrals

14 p2194 A71-30078

SAFETY

NT AIRCRAFT SAFETY

NT FLIGHT SAFETY

NT INDUSTRIAL SAFETY

NT RANGE SAFETY

NT REACTOR SAFETY

SAFETY DEVICES

NT ARRESTING GEAR

NT EJECTION SEATS

NT ESCAPE CAPSULES

NT ESCAPE ROCKETS

NT HELMETS

NT SEAT BELTS

NT SPACE SUITS

Cylindrical transparent plastic antismoke hood with metallized dome, noting respiratory volume and air supply

01 p0028 A71-11599

Helicopter turbine engine protection device design guidelines

04 p0533 A71-15434

Aircraft midair collision avoidance, discussing Elimination Range Zero system operation procedures and cost

07 p1154 A71-19079

Cargo aircraft crew safety and survival, describing restraint, escape, flight deck interior doors, fire and smoke hazards and personnel environmental protection

07 p1019 A71-19643

Fluidics application to weapon systems safety and arming devices, investigating reliability and immunity to environmental conditions

07 p1025 A71-20561

Crashworthy personnel restraint systems for general aviation including upper torso restraint [SAE PAPER 710396]

10 p1569 A71-24260

German book on rescue systems for space emergencies covering mission failure, biological problems, escape vehicles, orbital operations safety and spacecraft transfer

12 p1972 A71-27185

Concorde power plant fire protection system, describing prototype engine bay overheat detection system and additional UV optical fire detection system

14 p2288 A71-30300

High precision safety couplings performance, discussing flexible clutches enhancing effects

15 p2413 A71-31481

Air transportation safety review covering weather knowledge, aircraft structures, instrumentation, radio aids and power plants

18 p2849 A71-36175

Performance monitor for aircraft automatic landing systems safety control [AIAA PAPER 71-958]

19 p3099 A71-37199

Extravehicular activity protection systems, discussing resource regeneration, technology, methodology and space station, lunar base and Martian missions schematic configurations

22 p3503 A71-41990

Aircraft ditching and flying personnel survival, stressing passenger briefing and crew jacket equipment with VHF transceiver for rescue operations coordination

23 p3628 A71-43229

SAFETY FACTORS

Aircraft galley design safety criteria, considering injuries from routine use, normal, crash or ditching conditions component dislodgment, equipment malfunctions and defects

01 p0004 A71-10029

Social quantitative benefit vs risk assessment of new technologies, considering atomic power safety

02 p0336 A71-12120

Ellipsoidal pressure vessel heads failure mode analysis, considering buckling under internal pressure and design formula with safety factors

[ASME PAPER 70-PVP-26] 04 p0665 A71-14769

Laser thermal/photochemical burns and electric shock prevention by preemployment/regular physical examinations and safety requirement education

09 p1402 A71-23412

VTOL propulsion systems safety requirements, considering single and double breakdowns

10 p1659 A71-24752

Radio frequency and microwave radiation hazards determination and elimination aboard naval ships

11 p1723 A71-25290

Fatigue failure probabilistic model under variable amplitude loading, considering relation between safety factor and fatigue failure probability

11 p1848 A71-25492

Fracture-safe design, discussing strength transition, ratio analysis diagram, R-curve resistance, weldability and computer techniques

11 p1778 A71-25747

Plug-in relay hazards and minimization for aircraft flight safety applications

13 p2001 A71-28841

Lunar roving vehicle telecommunication system requirements concerning vehicle functions, science experiments, crew operations and safety

14 p2200 A71-30915

Emergency surface decompression and treatment procedures for project Tektite aquanauts, determining safe interval and schedules for return to habitat on ocean floor

16 p2535 A71-33110

System safety evaluation model with state-space network for representation of mission phase and hazard degradation

16 p2602 A71-33308

Aircraft structures fatigue properties, discussing stresses, life estimates, safety factors and descriptive curves

16 p2656 A71-33343

Space shuttle operation phases hazards, emphasizing propellant loading, fire suppression systems, survival equipment and self contained life support devices

17 p2813 A71-34784

Single sortie or clustered mode orbital space stations systems safety, noting effects on operations, configurations and design

[AIAA PAPER 71-826] 17 p2814 A71-35425

Electrical medical apparatus with electrodes and intracardiac catheters, considering electric current danger threshold, electrocution hazards and safety precautions

17 p2693 A71-35486

Structures with random resistance, calculating upper and lower bounds for safety coefficients average value and variance

19 p3156 A71-37643

Single point grounding of electronic system providing personnel safety and voltage reference potential

19 p3032 A71-38451

Multihundred watt radioisotope thermoelectric generator for spacecraft power supply, discussing system design, performance and safety requirements

20 p3263 A71-38927

Radioisotope thermoelectric generator safety and operations considerations for users of large nuclear space power systems

20 p3264 A71-38933

Convertible rotor transport aircraft, considering ATC, mass transportation systems, safety, noise and socio-economics

20 p3178 A71-39387

Jet engine advent impact on aviation fuels safety, discussing gasoline hazards in prejet aircraft

23 p3718 A71-43231

NASA program fire safety goals, discussing development of nonflammable materials covering fibrous asbestos, glass, polyimides, Teflon, metallics and halogenated materials

[AIAA PAPER 71-1011] 24 p3841 A71-44595

SAFETY HAZARDS

U HAZARDS

SAFETY MANAGEMENT

Space systems safety programs, discussing failure mode and single point failure analysis techniques, escape mechanisms and redundancy design

14 p2320 A71-30258

Safety engineers integration into overall system through basic development programs, involving management, manufacturing, testing and integrated logistic support

16 p2664 A71-33309

Airport certification and safety inspection program mandated by Airport and Airway Development Act of 1971

23 p3661 A71-43235

SAGITTARIUS CONSTELLATION

Methyl alcohol detection in Sagittarius, examining radio line emission at 834 MHz

05 p0802 A71-15945

Sagittarius A region observations with 80 MHz radioheliograph, noting radio sources flux density

05 p0805 A71-16116

Galactic radio source Sagittarius optically thick component evidence based on flux density measurement

12 p1956 A71-26612

Interstellar silicon monoxide discovery from 130,246 MHz frequency line emission of galactic radio source Sag B2

17 p2807 A71-35416

Sagittarius A model involving relativistic electron diffusion from point source due to Compton scattering for observed radio spectra explanation

18 p2957 A71-36155

Three color photometry of star field in Sagittarius cloud, determining interstellar absorption, density and luminosity for main sequence stars

19 p3144 A71-38169

Interstellar formamide detection in Sgr direction by microwave emission, showing hyperfine components and rest frequencies

22 p3599 A71-41930

SAHA EQUATIONS

Saha equilibrium deviations in wall stabilized rare gas arc plasmas under normal pressure, describing numerical method for temperature and density distributions evaluation

01 p0133 A71-10746

SAILPLANES

U GLIDERS

SAILS

NT SAILWINGS

NT SOLAR SAILS

SAILWINGS

Statics and aerodynamics of lifting decelerators /parawings and sailwings/ at supersonic and hypersonic speeds

[AIAA PAPER 68-945] 01 p0002 A71-10927

Sailing aerodynamic characteristics, obtaining aerodynamic loading by two dimensional flexible airfoil and Prandtl lifting line theories

07 p1017 A71-20303

SAINT VENANT FLEXURE PROBLEM

U SAINT VENANT PRINCIPLE

SAINT VENANT PRINCIPLE

Torsion computation for bar with rectangular cross section by analogy with electrical networks, comparing with Saint Venant results

01 p0167 A71-10340

Nonhomogeneous orthotropic beam Saint Venant bending, using finite element method

09 p1534 A71-22104

Infinitely slender cylinder elastic equilibrium, deriving Saint Venant problem solution in power series form

10 p1692 A71-25202

Saint Venant principle generalization for transient creep and stress relaxation analysis in rectilinear thin walled multiply connected beam under torsion

17 p2833 A71-35612

Flexural wave propagation in thin curved rod oscillating in plane, calculating frequency and velocity from boundary conditions according to Saint Venant

22 p3617 A71-42574

SALINITY

Airborne surveillance for environmental management, discussing earth resources program, aerial sensors for thermal water pollution, crop disease, salinity and geological structure

07 p1018 A71-19080

SALT BATHS

CdS single crystals treatment in salt melts to obtain given conductivity and photosensitivity, discussing LiCl, Ag, Cu, Na, Cd and In concentration effects

05 p0793 A71-16822

Hydrogen embrittlement in hot salt stress corrosion of Ti alloy

07 p1142 A71-20372

Al electrodes in molten salt electrolytes, investigating electrochemical kinetics by polarization measurements

08 p1250 A71-21470

Salt bath application to steels and Al alloys heat treatment, discussing carburizing, neutral hardening, austempering, martempering, annealing and brazing

18 p2927 A71-36665

SALT SPRAY TESTS

- Stress corrosion testing of Al alloy in NaCl bath under tensile stress, using Weibull distributions
22 p3560 A71-41627
- SALT SPRAY TESTS**
Adhesive/metal interface corrosion resistance tests, discussing salt fog chamber for shear, compression buckling and cleavage stresses
05 p0770 A71-17248
- SALTS**
Ti hot salt stress corrosion, considering effects of oxygen, air velocity, moisture, thermal cycling, fatigue and type of salt
11 p1781 A71-26261
- Airport jet fuel delivery system salt driers for reducing water content below saturation, lengthening filter life and improving downstream system components performance
[SAE PAPER 710440]
13 p2113 A71-28322
- Gaseous chromium carbonyl or aqueous chromium salt spray additives behavior photometric investigations in premixed hydrogen-oxygen-nitrogen flames
16 p2540 A71-33374
- Oxygen consumption by nitrogen starved nonsynchronous *Chlorella* culture during different assimilation of nitrogen salts in darkness and light
16 p2531 A71-33461
- Bivalent metal salts effect on blood serum albumin crystallization by isolating pure protein
16 p2531 A71-33468
- Halophilic bacteria electron transport chain, studying protein, phospholipids, flavoproteins and cytochromes sedimentation properties by electron microscopy and light scattering technique
21 p3334 A71-40593
- Beta-aminoethylthiophosphoric acid monosodium salt effect on mice stability to lateral accelerations
22 p3491 A71-42701
- UV radiation effect on amino acids and peptides in different gas atmospheres in presence of salts and metal oxides
22 p3496 A71-42829
- SAMARITAN AIRCRAFT**
U C-131 AIRCRAFT
- SAMARIUM**
Sm double plus ion sites distribution in KCl by spectroscopy
09 p1506 A71-22147
- Hysteresis loop measurements and functional measurements correlation on periodic permanent magnet stacks of TWT ring magnets of Sm-Co alloy
14 p2285 A71-30705
- SAMPLED DATA**
U DATA SAMPLING
SAMPLED DATA SYSTEMS
U DATA SAMPLING
- SAMPLERS**
Molecular mass gage with chambers interconnected by porous membranes for injected small gas samples
02 p0250 A71-12137
- Astrometric instruments optimal spatial sampling with parallel slits grill in focal plane, studying error minimization
10 p1608 A71-23825
- Biological instrumentation and soil sampler aboard Viking lander for 1975 mission to Mars
16 p2537 A71-33808
- Apollo 12 returned Surveyor 3 surface sampler examination for micrometeorite pits and soil, glassy spheres and other granular materials adhesion to paint
23 p3766 A71-43817
- SAMPLES**
Monolayer submicron self supporting particle film samples preparation for sintering by transmission electron microscopy
11 p1763 A71-26150
- SAMPLING**
NT AIR SAMPLING
NT CORE SAMPLING
NT DATA SAMPLING
NT RANDOM SAMPLING
- Dynamic cross-field photomultiplier sampling function characteristics measurement using self-mode-locked He-Ne pulsed laser
02 p0248 A71-12006
- Fourier transform formalism of sampling theorem in frequency domain used in coherent optical processor, obtaining multiple reproduction of space limited functions
04 p0627 A71-15686
- MIL-STD-414 sampling procedures and tables for inspection by variables for percent defective
06 p0905 A71-18059
- Reacting gases analysis by mass spectroscopy, discussing stable products microprobe and molecular beams effective samplings for free radicals and active atoms
11 p1765 A71-26278
- Deferred state sampling plans using accept/reject decisions dependent on future lot disposition according to quality drift
12 p1909 A71-26661
- Conditional distribution density formation for signal-noise mixture based on learning sampling with dependent values
15 p2370 A71-31586

- End wall sampling of high pressure shock tube, using abrupt pressure rise to drive test gas flow through duct to sample bottle
15 p2383 A71-31627
- [WSS/CI PAPER 71-18]
Truncated sequential test for production models based on preproduction testing with allowance for unequal sample sizes
15 p2416 A71-32344
- ASTM Committee F-7-C status report on contamination methods including sampling, processing samples and particulate analysis
19 p3000 A71-38324
- SAMPLING DEVICES**
U SAMPLERS
- SAN MARCO SATELLITE**
San Marco satellite attitude determination from on-board aerodynamic drag measurements, using least squares method for three components calculation
01 p0122 A71-10390
- Upper atmosphere exploration by San Marco 2 satellite, studying diurnal density variations and effects of large geomagnetic storms
14 p2236 A71-30817
- Equatorial ionospheric density measurements on quiet and perturbed days, using San Marco 2 satellite balance
21 p3373 A71-40047
- SAN MARCO SATELLITES**
NT SAN MARCO 2 SATELLITE
- SAN MARCO 2 SATELLITE**
Space shuttle reentry in quiet and geomagnetic storm perturbed atmosphere with reference to density variations, using San Marco 2 satellite
[ICAS PAPER 70-04]
03 p0497 A71-13149
- Diurnal minimum and geomagnetic storms effect on equatorial air density from San Marco 2 satellite drag experiment
03 p0415 A71-14024
- SANDS**
Rain and sand erosion materials tests, considering temperature and atmosphere pressure effects and relation between fatigue behavior and erosion/cavitation strength
03 p0444 A71-14289
- Sand and dust effects on military helicopter flight controls and equipment service life, discussing relief program
04 p0533 A71-15430
- SANDSTONES**
Shock metamorphism of Coconino sandstone at Meteor Crater, Arizona, examining porosity role in rock compression and in high pressure phases formation
19 p3050 A71-37659
- SANDWICH CONSTRUCTION**
U SANDWICH STRUCTURES
- SANDWICH PLATES**
U PLATES [STRUCTURAL MEMBERS]
U SANDWICH STRUCTURES
- SANDWICH STRUCTURES**
Sandwich structure cores of foamglass granulate filled unsaturated polyester paste, discussing development of highly thixotropic paste mixtures
01 p0172 A71-10699
- Glass fiber reinforced durometer and hard foam sandwich structures deformation characteristics under static loads, presenting theoretical and experimental results
01 p0172 A71-10700
- Three-layer spherical shell, determining filler effects on stress-strain state at circular hole
01 p0176 A71-11047
- Metallurgical and structural production of diffusion bonded titanium honeycomb sandwich panels for aerospace hardware weight saving
01 p0090 A71-11270
- Sandwich structures applications in aircraft and space vehicles, discussing component characteristics, manufacturing processes and mechanical testing procedures
02 p0324 A71-11959
- Axisymmetric and unsymmetric free vibrations of orthotropic sandwich cylindrical or conical shells under various boundary conditions
02 p0325 A71-11999
- Nb alloys in hypersonic glider fabrication, discussing mechanical properties, oxidation resistance and sandwich panel design
02 p0270 A71-12935
- Equations of motion for free vibrations of three layer plate, considering energy dissipation in soft low modulus of elasticity middle layer
03 p0502 A71-13404
- Stress concentration in buckling proof clamped sandwich rod with multicut rectangular cross section under torsional bending
03 p0504 A71-13527
- Mathematical stress wave model for sandwich plates under high velocity impact, considering structural multiple reflections and various material combinations
[SESA PAPER 1633]
03 p0508 A71-13774
- Sandwich metal construction with welded Norsial corrugated core for light weight and strength,

- discussing fabrication and application to hypersonic research vehicles
04 p0603 A71-15207
- Orthotropic sandwich and homogeneous single layer circular cylindrical shells optimal design
05 p0822 A71-16419
- Sandwich structures fabrication of foam core and solid polymer skin by automated injection molding
05 p0759 A71-16931
- Stress-strain state in elasticity theory of three layer symmetrical plate
05 p0828 A71-16986
- Sandwich panels with conical shell or elongated honeycomb fillers, calculating stability and elastic properties
06 p0986 A71-17757
- Applicability limits of equations of theory of three-layer plates and shells of asymmetric structure
06 p0987 A71-17766
- Stress-strain state of isotropic three-layer plates and shells with rigid and light weight fillers, noting weakening by curvilinear holes
06 p0987 A71-17769
- Circular cylindrical sandwich shell natural vibrations reduced to shell and filler contact problem, using two and three dimensional models
06 p0990 A71-17792
- Cylindrical sandwich shells with multiple isotropic load carrying and transversely compressible filler layers, deriving local stability equations
06 p0990 A71-17793
- Forced vibrations of three layer plates and shells made from physically nonlinear materials, deriving nonlinear equations with allowance for rigid filler tangential displacement
06 p0991 A71-17797
- Three layer plate with metallic carrier surfaces and plastic foam filler, calculating stress state near applied concentrated moment
06 p0995 A71-17831
- Boundary layer construction near free edge of laminar plates by asymptotic integration of three dimensional equations of elasticity theory
06 p0997 A71-17849
- Axisymmetric deformed state of three layer circular conical shell with rigidly clamped edges, obtaining equilibrium equations by Bubnov-Galerkin method
06 p0997 A71-17851
- Stress-strain state of three-layer polymer plate having different thicknesses, Poisson coefficients and creep functions
06 p1005 A71-18707
- Soviet book on computer calculation of three-layer elastic plates and shells covering programs, initial equations, input number language, numerical solution, etc
07 p1210 A71-19047
- X irradiation induced currents across aluminum oxide films sandwiched between thin metal electrodes as function of voltage and time
07 p1174 A71-19056
- Free vibration of spherical sandwich shell under axisymmetric static and dynamic loading
07 p1212 A71-19590
- Spherical sandwich shells free vibration motion equations, taking into account transverse shear deformation and rotary inertia effects
07 p1215 A71-20095
- Bending stiffness matrix for sandwich folded plate, reproducing core shearing deformations
08 p1367 A71-20748
- Replica technique facilitating investigation of quenched solid propellant sandwich sample characteristics
08 p1271 A71-20868
- Complex Al brazing alloy for honeycomb core joining to Ti alloy face sheets, discussing fillet formation and strength optimization
08 p1299 A71-21686
- Symmetric three-layer girder with contact deformations and transverse compression of filler, calculating vibration under elastic impact by numerical analysis
09 p1538 A71-22522
- Multilayer plate vibrations calculated with allowance for energy dissipation in material, deriving equations of motion
09 p1538 A71-22602
- Honeycomb sandwich core elastic modulus measurement under transverse compression
09 p1470 A71-22994
- Viscoelastic rectangular sandwich plate bending, stability, deflection and critical load calculation, assuming core stress-strain relation governed by Maxwell-Thompson differential equation
09 p1540 A71-22998
- Continuous seam diffusion bonding of Ti alloy thin gage and sandwich structures in air, considering joint types
[ASM PAPER W71-23.4]
09 p1455 A71-23094
- Plane sandwich plates in supersonic gas flow, investigating aeroelastic stability, transverse shear flexibility and axial loads
09 p1543 A71-23609

Multilayer sandwich plates with transverse shear resistant inner layers and bending and twisting moment resistant outer layers, calculating critical buckling loads by finite elements

10 p1686 A71-24020

Single ply sandwich composite prepregs for use with honeycomb reinforcement, noting one step curing for light weight structural panels

10 p1630 A71-24065

Degradation rate tests on adhesive bonded sandwich panels of temperature resistant composite structural materials at varying atmospheric pressures

10 p1614 A71-24073

Corrosion resistant adhesive bonding tested by exposing sandwich structure to outdoor weathering and salt spray environments

10 p1616 A71-24111

Hinged sandwich beams loaded by concentrated masses, calculating natural vibration frequencies with and without allowance for rotatory mass inertia

10 p1690 A71-24571

Weight minimization of semiinfinite flat sandwich panel at constant dynamic pressure in supersonic flow subject to flutter constraint, using finite element model

11 p1842 A71-25310

Carbon fiber reinforcement in carbon fiber/glass fiber mat sandwich beams increasing tensile and compressive strength

11 p1846 A71-25412

Transverse impact resistive graphite fiber reinforced plastic (GFRP)/ lightweight sandwich panels and beam structures, using thin inner core facings

11 p1846 A71-25417

Reinforced plastics components in supersonic transport nose radome and missile radar antennas, discussing molding, sandwich materials and computer controlled spraying techniques

12 p1887 A71-27016

Vibration damping of simply supported sandwich beam with viscoelastic core, using energy method

12 p1977 A71-27318

Asymmetric structure elastic transversely isotropic sandwich panels bending equations, taking into account transverse shear strain and stability

12 p1981 A71-27497

Minimum volume design of sandwich axisymmetric plates obeying Mises criterion, using calculus of variations

13 p2146 A71-27782

Eigenvalue problems in theory of sandwich plates with rigid cores, obtaining solutions by Galerkin method

14 p2322 A71-29734

Closed circular cylindrical shell nonlinear problem solvability extended to anisotropic sandwich shell, using mean deflection theory

14 p2332 A71-30866

Curved sandwich plate strain and kinetic energy expression derivation for use with finite element displacement method

15 p2508 A71-32136

Shear modulus, flexure and buckling of web stiffened sandwich structures, using core layer model based on continuum theory

16 p2656 A71-33217

Stability and critical load of constant thickness cylindrical sandwich hinge supported shell under annular loading, using variational method

16 p2657 A71-33601

Isotropic sandwich plates with rigid cores due to shear boundary tractions, considering transverse strain and stress, displacement function and stability

16 p2660 A71-34035

Nonlinear creep analysis of clamped pressurized circular cylindrical sandwich shells representing stress, membrane force and bending moment as displacement based on Mises criterion

17 p2816 A71-34297

Equations of motion for free vibrations of three layer plate, considering energy dissipation in soft low modulus of elasticity middle layer

17 p2825 A71-35014

Clamped-clamped sandwich beam with thin face sheets and soft viscoelastic core, investigating forced, damped, nonlinear and LF flexural vibrations

17 p2826 A71-35032

High modulus graphite-boron composites design and application to lightweight structures, illustrating sandwich construction for race boat main boom stiffness and compressive strength

17 p2762 A71-35203

Free edge effect on critical loading of rectangular sandwich plate with asymmetrical structure and rigid filler

17 p2833 A71-35622

Stress-strain state in elasticity theory of three layer symmetrical plate

18 p2982 A71-36786

Wave propagation in three layered plates, giving frequency spectrum

19 p3158 A71-37884

Buckling and initial postbuckling behavior of clamped thin shallow spherical sandwich shells under axisymmetrical loads

19 p3159 A71-38185

Four layer sandwich damping with viscoelastic material, noting frequency dependent effectiveness

[ASME PAPER 71-VIBR-20] 21 p3458 A71-40278

Five-layer rectangular sandwich plate containing two soft orthotropic cores and three plate stiff isotropic layers

[ASME PAPER 71-VIBR-48] 21 p3459 A71-40297

Curved sandwich beams free flexural vibration by finite element method, noting parameters effects on natural frequencies

21 p3462 A71-40533

Static characteristics and free vibration of doubly curved honeycomb sandwich plates, using finite element method

21 p3462 A71-40534

Glass-fiber/glass-bead/resin beam stiffness and strength improvement with sandwiching between layers of unidirectional carbon fiber composite

21 p3405 A71-40597

Elastic buckling and initial postbuckling behavior of clamped shallow spherical sandwich shells under axisymmetrical load

21 p3469 A71-41007

Stress concentration in layers of sandwich beams with holes under bending and tension

21 p3473 A71-41156

Nonlinear finite element analysis of sandwich arches elastic buckling, using straight beam-column type model

22 p3618 A71-42586

Critical compression loads and stability equations for clamped and hinged circular three layer plates with light filler, using Bessel functions

23 p3778 A71-44043

Multicore circular sandwich plates under various symmetrical loading and boundary conditions, deriving bending equations

24 p3879 A71-44619

SANITATION

Sanitary, chemical and toxic properties of polymeric materials in isolation chamber with contaminated outgassing atmosphere at moderate temperature

01 p0024 A71-11128

Jet aircraft and hygiene, considering communicable diseases spread control measures and sanitation methods by airlines

09 p1400 A71-23071

Urine conservation in spacecraft cabin sanitation facilities by phenol-containing preparations, emphasizing PNF method for long period operation

22 p3507 A71-42822

SAPPHIRE

High temperature annealing effect on sapphire single whiskers structure, using electron microscopy

01 p0106 A71-10276

Pure shear mode propagation in sapphire, determining acoustic axes velocity

02 p0294 A71-11947

Sapphire whiskers production by melt growth technique, describing process and whiskers mechanical properties

04 p0636 A71-14944

Boron, carbon, sapphire and glass fiber composite materials, considering brittleness, anisotropic properties, filament winding and plastic and metallic matrices

18 p2939 A71-35915

Single crystal silicon films deposited on sapphire substrates, determining disorientation angles, block dimensions, dislocation density, orientation and structure

22 p3586 A71-42061

Silicon thin film on sapphire for bipolar and MOSFET transistors for microwave IC and subnanosecond switching circuits

23 p3715 A71-43434

Structural and electrical properties of sublimation deposited GaAs films on sapphire and semiinsulating substrate in vacuum

24 p3863 A71-45358

SARCOMA

U CANCER

SAS

U SMALL ASTRONOMY SATELLITES

SAS-A

X ray astronomy with SAS-A satellite, discussing proportional counters, detectors and short period pulsation discovery

18 p2965 A71-36598

SATAN [SENSOR]

U TERRAIN ANALYSIS

SATELLITE ANTENNAS

Electrical stability of double sphere dipole antennas for FR-1 satellite ionospheric plasma electric fields measurements

02 p0229 A71-11714

VLF Poynting flux measurement technique on Injun 5 satellite using one electric and one magnetic antenna, discussing magnetic orientation errors effects

07 p1062 A71-19668

Satellite altitude dipole source effectiveness in lower ionosphere, comparing to ground based source with same dipole moment

07 p1064 A71-20319

Satellite-borne long wave transmitting antenna excitation, calculating electromagnetic field near earth surface by earth-ionosphere waveguide model

08 p1252 A71-20744

Luneberg lens antenna theory and gain for communication satellite radio links, discussing shielding from hostile space environment

10 p1583 A71-24450

Satellite antenna power density contours on earth, using pattern operator for coordinate transformation

12 p1881 A71-27423

Error introduced into coherent two-way Doppler tracking measurements on spinning satellite, using turnstile antenna

12 p1882 A71-27431

Satellite square loop antennas radiation resistance in warm plasma, comparing calculated values with Ariel 3 satellite measurements

12 p1883 A71-27700

Earth-ionosphere waveguide excitation by satellite-borne horizontal dipole antenna, deriving fields at earth surface based on idealized model

14 p2196 A71-30562

Four arm conical spiral microwave antenna with circularly polarized hemispherical radiation pattern for satellite and rocket applications

14 p2216 A71-31042

Computer program for processing of UHF radiation patterns of ESRO 4 scientific satellite omnidirectional antenna systems

14 p2217 A71-31051

Multifunctional communications satellite for TV distribution and trunk line, domestic, aeronautical, maritime, small user and space vehicle services

17 p2699 A71-34613

European regional satellite communication system, discussing TV coverage, spot beam antennas, frequency reuse, speech interpolation and circuits allocation

17 p2700 A71-34679

Composite ATS 6 and 7 satellite antenna feed capable of illuminating large space-deployable parabolic antenna

17 p2716 A71-35096

Short helical antenna performance and characteristics, discussing radiation patterns, efficiency, bandwidth and space vehicle use

18 p2888 A71-36023

European regional satellite communication system, discussing TV coverage, spot beam antennas, frequency reuse, speech interpolation and circuits allocation

18 p2877 A71-36516

Counterrotating antenna without mechanical contact, using magnetic bearings for spin stabilized geostationary telecommunications satellites

18 p2892 A71-36574

Isotropic and quasi-isotropic satellite antennas, considering circumferential arrays fed in phase or with progressing phase and systems with orthogonally polarized radiators

18 p2893 A71-36577

Satellite systems contributions to transmission technology, considering economic factors, satellite antennas and receiver noise figures

19 p3017 A71-37519

Tracking meteorological satellite receiving antenna orientation data computer calculation, obtaining methods for geographic picture gridding

21 p3410 A71-40824

SATELLITE ATTITUDE CONTROL

Two-gyro attitude control system with conical suspension, analyzing vehicle motion asymptotic stability in circular orbit

01 p0081 A71-10634

Gimballed reaction boom attitude control systems for gravity gradient stabilization of earth-pointing satellites, investigating performance by dynamic model simulation

01 p0165 A71-11585

Nonlinear precision attitude control system stability analysis algorithm based on quadratic Liapunov function

02 p0278 A71-11648

Skyнет satellite attitude determination and adjustment by IR and solar sensors, electronics processing equipment, nutation damping and pulsed axial thrusters

02 p0320 A71-12430

Limit cycle oscillations in satellite attitude control system, producing control moment by pulse modulated controller

03 p0499 A71-14074

Satellite time optimal attitude control, using gravity gradient technique with active libration damping

03 p0500 A71-14434

Three axis long life satellite attitude control, describing double gimbaled reaction wheel system

04 p0663 A71-15299

ITOS-1 meteorological satellite launch and operational sequences in orbit, discussing thermal and at-

Attitude control, power and communications and sensor equipment

04 p0663 A71-15314

SkyLab earth-orbiting manned space station attitude and pointing control systems design

04 p0623 A71-15323

Sirio synchronous orbit satellite configuration, emphasizing attitude control system, telemetry encoders and electric power supply

05 p0816 A71-16404

Optimal momentum exchange desaturation in attitude control systems for orbiting spacecraft, concerning gravity gradient and disturbance torques

05 p0817 A71-16552

Two-horizon-sensors system for low orbit satellite with three-axis attitude stabilization

06 p0899 A71-17966

Digital attitude reference systems for three axis stabilized earth oriented satellites using sun sensor measurements

06 p0926 A71-18520

Gravity gradient torque and near earth environment effects on rotationally damped dual spin satellite attitude motion

06 p0980 A71-18546

Synchronous satellites orbit and attitude control systems for correcting orbital errors due to launch inaccuracies, solar and lunar effects and terrestrial potential anisotropy

07 p1207 A71-19532

Optimal orientation control of axisymmetric rotating space vehicle, using cyclic sliding mode theory

09 p1532 A71-22659

Hybrid coordinate formulation for flexible space vehicle attitude control system design

09 p1532 A71-22907

SIRIO satellite project, discussing orbital dynamics, propulsion system, attitude control, onboard and ground electronic equipment

10 p1682 A71-24272

Nonlinear satellite system attitude control for minimum fuel consumption, deriving linear programming algorithm based on optimal control theory

10 p1683 A71-24522

Satellite solar radiative heat input variations effect on optimal launch time, considering angular factor and thermal design

11 p1836 A71-25192

Nonlinear resonant roll motion of passive magnetic attitude control satellites, using Hill and Mitropolskii methods

11 p1837 A71-25458

Inertia effects on coupled librations and stability bounds of axisymmetric gravity oriented satellites in circular orbits, using integral manifold

11 p1838 A71-26195

Attitude control of spin stabilized satellite with autonomous maneuverability, discussing correction maneuver method with one quasi-constant inertial reference direction

12 p1971 A71-26985

Rotating spacecraft attitude control system, using sun-earth albedo sensor for attitude determination [DUNFLR-SONDDR-113]

12 p1972 A71-26986

Flexible spacecraft attitude control and classification systems based on mathematical models

12 p1973 A71-27604

Tacsat 1 telecommunications relay system, discussing UHF-SHF antenna radiation patterns, ground terminal equipment, nutation dampers and attitude and orbital correction procedures

12 p1882 A71-27611

SIMCON simulation of physical systems using IBM 360/91 computer illustrated by satellite attitude control application

14 p2207 A71-30022

Gyrostat satellite steady motion and relative position optimal stabilization by additional forces application

14 p2275 A71-30871

Asymptotic stability of equilibrium position of vibrating linear mechanical systems with semidefinite damping matrix applicable to satellite attitude stabilization

15 p2502 A71-31174

Aeros satellite active magnetic attitude control system design, operation and testing

15 p2499 A71-31210

European electric propulsion systems for flight trajectories within low gravity fields and orbital parameter attitude control and correction

15 p2469 A71-31730

Azur satellite mission report, discussing major anomalies, energy supply, position control, temperature behavior and orbit

15 p2501 A71-32779

In-flight operation of Azur satellite magnetic attitude control system during period between booster separation and steady orbital motion

15 p2501 A71-32782

Axisymmetric satellite optimal reorientation into prescribed rotary motion by gas operated control jets, considering space navigation problems

16 p2645 A71-33440

Control moment gyro for attitude pointing control system of Skylab space station

17 p2743 A71-35063

Reaction wheel satellite attitude control, describing nondimensional parameter for interaxis gyroscopic coupling effects in preliminary design estimates

17 p2722 A71-35185

X 4 satellite of British National Space Program, discussing design features, orbit, configuration, power subsystem, data handling and attitude control

17 p2814 A71-35330

French monograph on satellite stabilization by ion propulsion and attitude control logic element design covering geostationary and geocentric satellites, mass and power balances

17 p2814 A71-35500

Artificial g space station configurations, developing movable control mass attitude stabilization system

18 p2971 A71-36277

Magnetic torquer for satellite attitude control consisting of solenoid with hard magnetic material core

18 p2973 A71-36463

Symphonic telecommunication satellite attitude control system, describing operational principle based on gyroscopic inertial reference and redundant IR sensors

18 p2974 A71-36525

Satellite attitude control principles for studies requiring satellite orientation relative to orbital coordinate system

19 p3062 A71-37149

Electromagnetic actuator for momentum desaturation of control moment gyros used for attitude stabilization and control of space stations

[AIAA PAPER 71-939]

19 p3098 A71-37184

Synchronous three-axes stabilized communication satellites attitude control system with double gimbaled reaction wheel control actuator, obtaining 0.1 degree pointing accuracy with pitch and roll sensors

[AIAA PAPER 71-949]

19 p3098 A71-37190

Attitude dynamics and control of apogee motor assembly with paired satellites, discussing energy dissipation and spin axis reorientation time

[AIAA PAPER 71-953]

19 p3099 A71-37194

Reduced state estimator for satellite orbital heading reference, describing decoupled single-skewed-gyro gyrocompass design for attitude control

[AIAA PAPER 71-965]

19 p3148 A71-37206

Right ascension and declination accuracy for Sirio satellite attitude determination in transfer orbit, describing computer program

19 p3150 A71-37312

Attitude control of gravity orientated satellite in arbitrary orbit by solar pressure, showing libration damping characteristics of radiation force

20 p3306 A71-39396

Three axis and dual-spin attitude control subsystems for communications satellites, considering flywheel stabilization advantage

21 p3454 A71-40478

German monograph on locking process in earth satellites with passive magnetic attitude control covering satellite rotational motion mathematical model, stability analysis, etc

21 p3455 A71-40773

Time optimal semiautomatic attitude control for circular orbiting satellite pitch motion, using gravitational and aerodynamic torques

22 p3570 A71-42001

Coupled librational dynamics of gravity oriented cylindrical satellite, calculating solar radiation pressure effects on attitude control behavior

22 p3611 A71-42042

Orbital spacecraft trajectory and attitude dynamics, using computerized state model for mission planning, orbit determination, satellite geodesy and reentry analysis

[AAS PAPER 71-344]

23 p3727 A71-43017

Nonlinear controlled plant dynamic behavior sensitivity in parameter perturbation derived from mathematical model, applying to satellite attitude control

[ASME PAPER 70-WA/AUT-5]

24 p3816 A71-45136

Apparatus for dynamically equivalent ground tests of satellite instrumentation and attitude control system

24 p3817 A71-45273

SATELLITE ATTITUDE DISTURBANCE

U ATTITUDE STABILITY

U SPACECRAFT STABILITY

SATELLITE COMMUNICATIONS

U SPACECRAFT COMMUNICATION

SATELLITE COMMUNICATIONS SHIPS

SkyNet system shipborne earth station design and specifications, discussing size and weight restrictions, radar proximity, gun shocks, antenna stabilization and power budgets

02 p0217 A71-12435

SkyNet system small communications terminal specifications and equipment for ship to shore telegraphic traffic, considering small dish antenna for shipboard installation

02 p0217 A71-12436

Shipborne satellite communications terminal, describing antenna, control and monitoring systems and performance characteristics

02 p0221 A71-12785

Remotely controlled room temperature microwave parametric amplifier design for shipboard satellite telegraphy terminal

02 p0234 A71-12813

Navigation and communication experiment at L band on board S.S. Manhattan using ATS-5 satellite with biphasic PSK modulation of three tones for ranging

07 p1057 A71-18816

Civil aviation and merchant marine satellites, considering aircraft and surface vessel antenna characteristics and modulation techniques for optimum communication channel frequencies

17 p2775 A71-35582

SATELLITE CONFIGURATIONS

Sirio synchronous orbit satellite configuration, emphasizing attitude control system, telemetry encoders and electric power supply

05 p0816 A71-16404

Advanced communications satellites system engineering, including configuration based on active body stabilization, rechargeable hydrogen oxygen fuel cells and ion engines

[AIAA PAPER 71-843]

17 p2812 A71-34710

X 4 satellite of British National Space Program, discussing design features, orbit, configuration, power subsystem, data handling and attitude control

17 p2814 A71-35330

SATELLITE CONTROL

NT SATELLITE ATTITUDE CONTROL

SkyNet satellite mission profile, onboard equipment and control system, discussing communications, command/telemetry processing equipment, electrical power sources, and secondary propulsion

02 p0320 A71-12429

Auxiliary propulsion devices for satellite stabilization, discussing monopropellant, bipropellant, post-combustion, hydrazine plenum, electrical, plasma jet, ion and colloid systems

02 p0299 A71-12749

Flight testing of automatic orbital operations system for satellites and space probes

[DGLR-70-080]

05 p0779 A71-15958

Stability of steady motions of satellite gyroscopes in Newtonian central force field, allowing for rotor bearing elasticity

05 p0751 A71-16585

Defense Satellite Communications System Phase II design and implementation, considering earth, space and control subsystems

07 p1057 A71-18818

Central station of German ground system for satellite data acquisition, tracking and telecommand

07 p1082 A71-19021

Computer controlled ground based command and data acquisition software system for OAO-A2 spacecraft remote control stations, discussing interface with monitor and interrupt capabilities

08 p1259 A71-21658

Angular motion of deformable earth satellite as solid-elastic system with distributed masses, applying automatic control transfer function

09 p1491 A71-22548

Satellite rendezvous programmed control with allowance for thrust limitation by free trajectories method, determining impulse duration, magnitude and time

09 p1531 A71-22571

Mission objectives and orbit parameters of Azur satellite, considering satellite control and data transmission as function of ground support system

10 p1589 A71-23927

Krylov-Bogoliubov averaging method in optimal satellite motion programming of transfer orbit and low thrust correction

10 p1587 A71-24843

Satellite pitching oscillations optimal stabilization, obtaining approximate solution for finite time

12 p1972 A71-27026

Ion microthruster for satellite orbit and position corrections, describing optimum performance characteristics and test facility

[DGLR-71-032]

17 p2795 A71-35548

Satellite pitching oscillations optimal stabilization, obtaining approximate solution for finite time

19 p3152 A71-37695

Dual-spin vs three-axis stabilization and control systems for synchronous communication satellite design

21 p3454 A71-40477

Rotating space station simulator for translational and rotational motion determination under gravity gradient torque action and control under input state conditions

[IBM-712000406]

22 p3529 A71-41970

SATELLITE DESIGN

Satellite system design digital simulation model in GPSS language for performance interrelationships between subsystems and reliability gain in orbit from redundancy

02 p0318 A71-11782

Satellite design developments by U.S. Navy

02 p0336 A71-11980

Heat pipes structural material and heat carrier for various temperature ranges in satellite technology

02 p0331 A71-12069

Auxiliary propulsion devices for satellite stabilization, discussing monopropellant, bipropellant, post-combustion, hydrazine plenum, electrical, plasma jet, ion and colloid systems

02 p0299 A71-12749

Satellite and earth station parameters effects on SPADE communication systems link budget, considering carrier power statistics, amplitude and phase nonlinearities

02 p0221 A71-12779

Intercosmos 3 satellite for radiophysical and geophysical observations of radiation belts and ionosphere, discussing design, configuration and instrumentation

03 p0423 A71-13419

German monograph on research satellite design based on information gain criterion

03 p0380 A71-14371

Large multipurpose synchronous communication satellite, discussing design versatility, applications and operating characteristics

04 p0663 A71-15311

OAQ 2 design and performance features concerning pointing accuracy and stability, command capability, data handling, thermal environment, orbit constraints, ultraviolet spectroscopy, etc

05 p0818 A71-17128

Defense Satellite Communications System Phase II design and implementation, considering earth, space and control subsystems

07 p1057 A71-18818

Satellite electronic equipment reliability engineering, considering circuit and system design, components screening, assembly and test procedures and quality assurance plans

07 p1207 A71-19563

ERTS A and B projects, describing satellite communications, data handling, telemetry, tracking and command, thermal control, orbit-adjut, image processing and ground equipment

10 p1682 A71-24172

Satellite solar radiative heat input variations effect on optimal launch time, considering angular factor and thermal design

11 p1836 A71-25192

Drag-free satellite design and propulsion requirements, noting orbit perturbation mechanisms [AIAA PAPER 70-1145]

11 p1838 A71-25522

European scientific experiments satellite, describing design features and mission capabilities

15 p2501 A71-32693

Azur satellite structure and mechanism requirements, design and tests, noting damping characteristics and Yo-Yo system [DGLR 71-014]

15 p2501 A71-32783

NASA earth resources technology satellites system, discussing ERTS A and B development, payloads and ground support systems and international aspects

16 p2630 A71-32854

Symphonic communication satellite subsystem, discussing geostationary positions, launchers, frequency ranges and transmission zones

16 p2543 A71-33583

First generation domestic communications satellite system, discussing various proposals for FCC authorization [AIAA PAPER 71-842]

17 p2700 A71-34711

Space shuttle economic and design impact on satellite payloads, noting variations in flight frequency and cost, hardware and performance [AIAA PAPER 71-807]

17 p2813 A71-34732

Reaction wheel satellite attitude control, describing nondimensional parameter for interaxis gyroscopic coupling effects in preliminary design estimates

17 p2722 A71-35185

X 4 satellite of British National Space Program, discussing design features, orbit, configuration, power subsystem, data handling and attitude control

17 p2814 A71-35330

Small satellite role in meteorological, earth observation, communications and navigation missions, discussing orbit, weight, electrical power, attitude control, data handling and modular design concepts

17 p2805 A71-35331

Itos 1 and Noaa 1 meteorological satellite systems design and operation, outlining attitude and thermal control, sensors, power supply and orbital performance [AIAA PAPER 71-836]

17 p2814 A71-35432

Italian SIRIO experimental SHF telecommunications satellite, noting trapped radiation and high energy electron experiments

18 p2974 A71-36521

Franco-German Symphonic communication satellite, discussing missions and subsystems design features

18 p2974 A71-36522

Technical parameters and performance tradeoffs of ESRO preoperational aeronautical satellite program

19 p3153 A71-38067

NASA 12-man 10-year space station program, discussing design, information management, environmental control and life support system

19 p3153 A71-38147

Salyut space station design, operation and mission, describing docking and undocking procedures for Soyuz 11 supply craft

19 p3153 A71-38148

NASA modular space station program, describing design and equipment

19 p3153 A71-38149

NASA space station program, discussing design, guidance, navigation, electrical power and environmental control

19 p3154 A71-38150

Critical solar cell battery power system design parameters and performance characteristics affecting post 1977 satellites and manned vehicles design

20 p3179 A71-38902

Reliable and low cost electrical solar array/silver zinc battery power system for Agena satellite, discussing design features and flight tests results

20 p3182 A71-38943

Dual-spin vs three-axis stabilization and control systems for synchronous communication satellite design

21 p3454 A71-40477

Three-axis and dual-spin stabilization systems for future synchronous communication satellites, considering reliability, mission flexibility and growth potential

21 p3455 A71-40479

Attitude stiffness and pointing accuracy of three-axis and dual-spin stabilization system for future synchronous communication satellites

21 p3455 A71-40481

Scientific objectives and satellite design of ESRO sponsored geostationary space mission, describing Europa II launcher design and operation

22 p3608 A71-41952

Aircraft surveillance oceanic satellite systems design and reliability analysis, discussing position determination accuracy

22 p3572 A71-42094

SATELLITE DRAG

High drag satellite 1968-59A orbits from optical and radar observations, obtaining rotational speed of upper atmosphere

03 p0407 A71-13305

Satellite dynamics applications in determination of atmospheric drag, earth and moon gravitational fields and Mars and Venus mass from trajectory construction

03 p0491 A71-14003

Upper atmosphere densities from satellite drag data, noting semiannual variations

03 p0414 A71-14021

Diurnal minimum and geomagnetic storms effect on equatorial air density from San Marco 2 satellite drag experiment

03 p0415 A71-14024

Atmospheric density and rotation measurements below 195 km from high resolution drag analysis of satellite OV1-15 using least squares fitting

06 p0887 A71-17272

Earth oblateness and air drag effects on satellite trajectories by asymptotic method of nonlinear mechanics, obtaining closed form solutions for first order approximation

10 p1678 A71-24928

Drag-free satellite design and propulsion requirements, noting orbit perturbation mechanisms [AIAA PAPER 70-1145]

11 p1838 A71-25522

Spacecraft intermediate orbit osculating elements first order secular disturbances due to atmospheric resistance

13 p2132 A71-27936

Upper atmosphere density fluctuations associated with solar activity and local time values, using Cosmos 14 satellite drag data

16 p2564 A71-33666

Semiannual density variation in heterosphere as function of height based on satellite drag and atmospheric models

16 p2564 A71-33723

Diurnal variation of atmospheric parameters in thermosphere deduced from incoherent scatter and satellite drag, discussing atmospheric model correspondence to observed data

16 p2566 A71-33742

Ionospheric density diurnal variations and atmospheric rotation data from OV1-15 satellite drag measurements, noting geomagnetic activity effects

16 p2566 A71-33746

Thermospheric composition determination from satellite drag derived densities, comparing with data computed from mass spectroscopic observations

16 p2566 A71-33750

Global model of atmospheric temperature, chemical composition and density for altitudes from 25 to 1000 km, using satellite drag determined density values

16 p2567 A71-33782

Seasonal density variations in thermosphere and exosphere, obtaining model from Explorers 19 and 39 drag measurements for comparison withOGO-6 mass spectroscopy

16 p2569 A71-33802

Upper atmosphere density determination from Cosmos satellite deceleration data, allowing for diurnal and semiannual variations and solar radio emission intensity effects

16 p2571 A71-33837

Semiannual ionospheric density variations from Cosmos artificial satellites drag, noting agreement with solar corpuscular radiation geoefficiency

16 p2571 A71-33841

Exospheric density semiannual variations from June 1968 to December 1970 at altitudes of 900 and 1070 km, using satellite drag determination by orbital period rate of change measurement

16 p2643 A71-33848

Orbital elements determination for Osumi Japanese satellite, describing trajectory correction for atmospheric effect

17 p2802 A71-34746

Energy considerations of satellite orbit paradox, discussing speed increase under drag, librational motion and secular month length

18 p2962 A71-36099

Analog mass center estimator for spinning drag-free orbiting satellite, using free-falling proof mass shielded from external forces inside satellite cavity as reference [AIAA PAPER 71-947]

19 p3148 A71-37188

Satellites interaction with ionosphere, concerning applications to particle density, electric field, flux and drag measurements

19 p2992 A71-37560

Atmospheric density variations calculation, using aerodynamic drag coefficient data from gas flow-satellite surface interactions

20 p3223 A71-39706

Diurnal and semiannual variations in upper atmosphere density from Cosmos satellite drag observations, noting calculation systematic errors

20 p3223 A71-39707

Upper atmosphere density variations and time lag with respect to geomagnetic disturbances, using satellite drag measurements

20 p3223 A71-39709

Semiannual upper atmosphere density variations near solar maximum from satellite drag data, relating height amplitude profile with exospheric temperatures

20 p3223 A71-39710

Long term orbit calculation by superposition of gravity and drag perturbations, taking into account solar and geomagnetic induced density variations [AAS PAPER 71-376]

23 p3730 A71-43046

SATELLITE GROUND SUPPORT

Earth station technology - IEE Conference, London, October 1970

02 p0219 A71-12776

Mission objectives and orbit parameters of Azur satellite, considering satellite control and data transmission as function of ground support system

10 p1589 A71-23927

Computer real time data monitoring and control software in satellite integration support and test operations, noting test oriented language

14 p2208 A71-30339

Satellite geodesy in Netherlands, discussing measurement and instrumentation techniques and ground station equipment and operation

16 p2563 A71-33368

German space operations center for performing ground operations for Azur research satellite

16 p2563 A71-33747

Intelsat system, describing organization, satellites, space segment support elements and ground stations

17 p2811 A71-34230

Satellite telecommunication systems, considering standard and small transportable ground stations and Intelsat system

17 p2696 A71-34233

Communications capability of Canadian domestic satellite system, outlining performance parameters of satellite and earth stations

17 p2703 A71-35080

Reduced cost ground stations for satellite communications system and applicability to small nations, using single channel per carrier FM and compandors

17 p2704 A71-35087

Earth stations operating in Intelsat System, discussing mandatory performance requirements and design approaches

17 p2705 A71-35100

SATELLITE GROUND TRACKS

Circular sun synchronous earth satellites, investigating swathing patterns control by orbit selection and modification [AAS PAPER 71-353]

23 p3728 A71-43025

SATELLITE GUIDANCE

Satellite optimal guidance, discussing gyroscopic application for stabilization and orientation control

03 p0500 A71-14227

NASA space station program, discussing design, guidance, navigation, electrical power and environmental control

19 p3154 A71-38150

SATELLITE INSTRUMENTS

NT LASER ALTIMETERS

SATELLITE INTERCEPTORS

Satellite with onboard equipment for astronomical IR spectroscopy, considering stabilization accuracy and measurement duration effects on spectral resolution

01 p0163 A71-10395

ATS-5 satellite dual swept radiometer features, operation and specifications

01 p0082 A71-10985

Azur research satellite scientific instruments and objectives and design parameters

01 p0164 A71-11334

Satellite static inverter for voltage wave form synthesis by time optimal response closed loop technique, providing input insensitive AC output

02 p0190 A71-11675

Intercoms 3 satellite for radiophysical and geophysical observations of radiation belts and ionosphere, discussing design, configuration and instrumentation

03 p0423 A71-13419

Proton 4 satellite high and superhigh energy cosmic ray spectrometer, discussing principles of operation and parameters

03 p0426 A71-13833

High energy cosmic ray particle charge and direction detector on Proton 3 satellite

04 p0596 A71-15122

NASA satellites meteorological IR instruments, considering purpose, design, operation and performance

04 p0598 A71-15365

Earth satellites ferrite core buffer storage replacement by magnetic tape unit noting design, performance, volume and operation [DGLR-70-082]

05 p0726 A71-15952

Precession equations of gyroscope onboard near earth satellite, comparing Schiff and Brans-Dicke theories

05 p0781 A71-16488

Satellite ion energy analyzer with onboard data reduction for ionospheric ion temperature and concentration measurement with high temporal resolution

05 p0755 A71-17139

Two-horizon-sensors system for low orbit satellite with three-axis attitude stabilization

06 p0899 A71-17966

IR radiation measuring circuit with pneumatic detector usable on rockets and satellites [ONERA-TP-874]

06 p0900 A71-18023

Satellite cosmic ray monitors data, examining correlation with sun to obtain interplanetary magnetic field spatial structure

06 p0951 A71-18106

Satellite radio interferometer multipath reflections effect on accuracy

07 p1106 A71-18839

ESRO 1 small scientific satellite attitude measurement system, discussing design and flight test results

07 p1154 A71-18840

ATS-5 satellite-borne auroral electron and proton energy spectrum measuring instrument using cylindrical coordinate electrostatic analyzer

08 p1294 A71-21845

Satellite-borne Ge radiation detectors, investigating design criteria and performance at elevated temperatures

08 p1267 A71-21847

Elektron 2 and 4 satellites orientation based on onboard solar and magnetic sensors

09 p1531 A71-22570

Optimum mounting angles for direct solar radiation flux on solar battery on circular orbit satellite

09 p1386 A71-22673

Satellite-borne sensor for ionospheric ions velocity measurement, describing design and operation principles

09 p1438 A71-23141

Ionospheric ions drift velocity horizontal and vertical components distribution, using satellite-borne sensor

09 p1438 A71-23142

High accuracy angular precession measurements with autometric gyro for satellite relativity tests, using optical system with reticle coordinates

09 p1452 A71-23595

Satellite instruments to measure intensity and energy spectrum of high energy electrons and protons

10 p1683 A71-24464

Mariner 6 and 7 UV spectrometers, describing technical details, operating characteristics and calibration of planetary coronagraph and Ebert-Fastie monochromator used for Martian atmosphere analysis

11 p1766 A71-26301

Satellite-borne anisotropy and energy spectra measurement instruments for cosmic ray electrons and protons and solar and galactic X-rays

12 p1954 A71-27711

Ocean height measurement by orbit determination from satellite altimetry, considering least squares solutions and instrument errors

13 p2066 A71-27983

OSO-G satellite instrumentation for solar and celestial X ray detection, exploring spectral distribu-

tion, temporal intensity variations, sources and atmospheric albedo

13 p2070 A71-29135

Binary data compression for satellite-borne instrumentation for space physics measurements, discussing redundancy reduction technique

13 p2033 A71-29274

Michelson interferometer onboard Nimbus 4 satellite for recording earth IR emission spectrum

14 p2241 A71-30140

X ray telescopes and neutron cameras telephoto lenses for satellites and space stations, discussing optical design and correction methods

14 p2246 A71-30391

Instrumentation and orbital parameters of meteorological satellites observing winds, tropical circulations, heat budget, hydrology and ocean surfaces

14 p2270 A71-30498

IR scanning vertical temperature profile radiometer for Ilos meteorological satellites, describing electronic signal processing

14 p2200 A71-30916

Simultaneous two magnetometer measurements of weak magnetic fields in interplanetary space, near moon and planets by satellites in presence of spacecraft field

15 p2406 A71-31753

Satellite skin potential and errors in electron density and temperature determinations by Langmuir probe measurements, using model ionosphere

15 p2398 A71-31768

Satellite-borne semiconductor telescope for relativistic heavy primary cosmic rays identification, increasing resolving power by minimum pulse selection method

15 p2407 A71-31806

Nimbus weather satellite with IR spectrometer, Michelson interferometer and selective chopping radiometer for atmospheric temperature remote sounding

15 p2445 A71-32295

Spatially periodic static field mass spectrometers for upper atmosphere composition measurements on board satellite and sounding rocket

15 p2400 A71-32350

Meteoroid velocity measurement by satellite-borne meteoroid detectors, giving Geminid meteor shower measurements results

16 p2639 A71-33724

Skylab earth resources experimental equipment, describing sensing and recording instrumentation for electromagnetic spectral pattern recognition studies [ALAA PAPER 71-841]

17 p2739 A71-34712

High reliability integrated complementary MOS circuit fabrication chain in Concerto satellite program, discussing technological process with account of physicochemical data

18 p2890 A71-36536

Ferrite core memories for information storage of digital computer onboard Eole satellite, discussing design and reliability measures

18 p2891 A71-36560

X ray astronomy with SAS-A satellite, discussing proportional counters, detectors and short period pulsation discovery

18 p2965 A71-36598

Transient performance of phase locked loop on-board tumbling satellite, noting relation to time, SNR and fade modulation

20 p3196 A71-38871

Remote image-forming sensors on satellites and aircraft, considering resolving power, contrast rendition, dynamic range, SNR, sensitivity, and reliability as performance measures

20 p3240 A71-39608

Satellite data techniques and instrumentation in earth geometry and kinetics, reviewing geopotential models, pole positions, tides, ocean physics and international cooperation

20 p3219 A71-39656

Atmospheric transmittance measurement errors in determining temperature, water vapor and ozone distributions from satellite remote sensing

20 p3258 A71-39671

HEOS-A2 eccentric orbit satellite for interplanetary space and high latitude magnetosphere data, discussing onboard experiments, major subsystems and design philosophy

22 p3607 A71-41505

Global three dimensional atmospheric temperature mapping by selective chopper radiometer on Nimbus 4 satellite, measuring carbon dioxide IR emission

22 p3533 A71-41629

Space technology applications to earth environment and resources management, discussing satellite-borne remote sensor systems and data processing techniques [SD-71-734]

22 p3535 A71-42047

IR atmospheric temperature profiles sounding by selective chopper radiometer launched into polar orbit on Nimbus 4 satellite

22 p3544 A71-42144

Satellite-borne minimum bulk and weight K-band transmitter and receiver frequency converters design features and performance

22 p3524 A71-42522

Proton 4 satellite high and superhigh energy cosmic ray spectrometer, discussing operational principles and parameters

22 p3594 A71-42634

IR radiometer experiment for Mariner 1971 Mars orbiter mission, describing objectives and instrumentation

23 p3676 A71-43510

ITOS meteorological satellite scanning radiometer using point detector optical system for earth imaging

23 p3676 A71-43511

Apparatus for dynamically equivalent ground tests of satellite instrumentation and attitude control system

24 p3817 A71-45273

Single channel electron multiplier applications to sounding rockets, orbital satellites and deep space probes, discussing fatigue effects, ultrahigh vacuum environments and UV and X ray studies

24 p3811 A71-45333

SATELLITE INTERCEPTORS

Nuclear, hydrogen/oxygen and solid propellant satellite interceptors effectiveness measurement, considering warhead kill radius, propellant weight and specific impulse

13 p2144 A71-27982

SATELLITE LAUNCHING

U SPACECRAFT LAUNCHING

SATELLITE LIFETIME

North Atlantic communications, navigation and ATC systems requirements for geostationary satellite operation, considering lifetime rated data and voice channels transmissions volume

11 p1839 A71-26332

Artificial planetary satellites lifetime estimation from atmospheric drag, discussing critical height-atmospheric density relationship, satellite design and initial orbit height

16 p2638 A71-33671

Reliability and maintenance of satellites, launchers and other space systems

18 p2975 A71-36534

Lunar orbit space station lifetime, using averaged variational equations numerical integration for terrestrial, solar and lunar gravitational field effects [AAS PAPER 71-377]

23 p3730 A71-43047

SATELLITE MANEUVERS

U SPACECRAFT MANEUVERS

SATELLITE NAVIGATION SYSTEMS

Air traffic control by satellite, discussing CNES-SGAC and ESRO experiments within Dioscures project test program

01 p0125 A71-10748

U.S. Navy Satellite Navigation System error study, considering dead reckoning accuracy, random instrument errors, mathematical error model and statistical analysis procedure

08 p1331 A71-21168

North Atlantic communications, navigation and ATC systems requirements for geostationary satellite operation, considering lifetime rated data and voice channels transmissions volume

11 p1839 A71-26332

ESRO preoperational aeronautical satellite system for Atlantic and Pacific coverage, noting position determination for reduced aircraft separation, frequency selection and performance trade-offs

16 p2644 A71-32850

Satellite communication application to maritime mobile service and position determination, discussing VHF and UHF space and shipborne equipment and modulation systems

17 p2697 A71-34241

Onboard orbit navigation scheme free from sensor uncertainty cause constraints, using satellite ejected from spacecraft into near orbit

17 p2772 A71-35053

Skylab strapdown attitude navigation system using components designed for predecessor projects ATM and Saturn I Workshop

17 p2773 A71-35065

Doppler satellite/airborne inertial navigation system integration with delayed state Kalman filter

17 p2776 A71-35766

Radio and radar air navigation for civil aviation, discussing Doppler effect, inertia and satellite systems

19 p3100 A71-37344

Satellite navigation system for aviation and marine use, examining operational requirements, economic viability and technical solutions

22 p3570 A71-41509

Aircraft surveillance oceanic satellite systems design and reliability analysis, discussing position determination accuracy

22 p3572 A71-42094

SATELLITE NETWORKS

Geostationary communication satellites system with timed orbital motions for avoiding serial sun transit outages and eclipses

01 p0030 A71-10471

Ultrawide bandwidth optical data relay link between earth satellites, discussing system design concept

02 p0214 A71-12024

Skylink satellite communications system configuration and specifications, discussing geostationary satel-

lite multiple access, SSMA transmission system, power budgets, reliability and repeater specifications
02 p0217 A71-12428

Skyнет types 3 and 4 ground stations performance, discussing antenna gain, FM carrier to noise ratio, channel capacity, error rates and system reliability
02 p0217 A71-12438

Skyнет communication systems, describing long distance strategic communication links between ground and mobile air/helicopter stations via wide and narrow band pathways
02 p0218 A71-12439

Satellite regional broadcasting and telephony/data services cost model
02 p0221 A71-12781

Regional European communications satellite system operation, discussing coverage area, performance requirements, meteorological aspects of propagation, etc
02 p0221 A71-12782

Cost optimal direct broadcast and redistribution satellite systems
02 p0221 A71-12783

Atmosphere effects on antenna noise temperature variations in G/T value for earth station performance in satellite communication system
02 p0222 A71-12799

Ground station central control and monitoring of satellite communications systems
02 p0224 A71-12822

Satellite communications system earth station operation and reliability, discussing staffing, main and supporting communication equipment maintenance, utilities and redundancy
02 p0224 A71-12825

Ground based data derivation and transmission system for multicontrol satellite communication system
02 p0225 A71-12834

Nondegenerate parametric amplifiers above X band for satellite communication systems, discussing circuitry, varactors, diode packaging and solid state pump sources improvements
02 p0235 A71-12906

Intelsat system earth station on-site planning considerations for integration with existing wideband communication system and traffic growth demand
03 p0380 A71-14343

Satellite meteorology, discussing system, observational data, weather prediction, communications sensors, TV imaging and global atmospheric research program
04 p0621 A71-15308

Synchronous orbit satellite links in tandem for government and military telephone communications, discussing subjective evaluation for acceptability
05 p0725 A71-17070

Intelsat global network demand assignment multiple access system, discussing traffic density and earth station functional requirements
06 p0869 A71-18234

Intelsat 3 global satellite communication system design and performance
06 p0870 A71-18393

Satellite communication system parameters optimization based on economical and technical constraints, applying to Intelsat 3
07 p1063 A71-20040

Disclosures project commercial satellite system for telecommunications, air traffic control and navigation, describing simulation method used in cost effectiveness study
09 p1547 A71-22276

Satellite communications systems international planning, discussing Intelsat system limitations
09 p1548 A71-23354

Australian satellite domestic telecommunications network design, discussing population distribution, existing systems and Intelsat 3 F-4
11 p1730 A71-25264

Aircraft phased arrays for L-band ATC satellite system application, alleviating problems of power budget and vulnerability to multipath and interference
14 p2217 A71-31054

Circular orbit patterns for continuous whole earth surface coverage with five satellites
16 p2630 A71-32840

Meteorological satellite system for weather forecasting in Mediterranean area, including visible and IR ranges survey and automatic stations and buoys interoperation
16 p2604 A71-32846

Communication satellite systems vs conventional terrestrial methods, emphasizing economic comparison
17 p2697 A71-34236

Satellite communication system selection vs underground cable or hybrid systems, based on power requirements and economics
17 p2700 A71-34678

First generation domestic communications satellite system, discussing various proposals for FCC authorization
[AIAA PAPER 71-842] 17 p2700 A71-34711

Communications capability of Canadian domestic satellite system, outlining performance parameters of satellite and earth stations
17 p2703 A71-35080

Transmission performance of thin route satellite communication system for northern Canada, comparing FM, PCM and delta modulation techniques
17 p2703 A71-35081

Earth stations operating in Intelsat System, discussing mandatory performance requirements and design approaches
17 p2705 A71-35100

Intelsat communications satellite system network operation, describing reliability outages, maintenance and economy
17 p2705 A71-35101

Queueing theory approach to communication satellite network design, applying to ocean air traffic control and worldwide military broadcast systems
17 p2721 A71-35106

Itos 1 and Noaa 1 meteorological satellite systems design and operation, outlining attitude and thermal control, sensors, power supply and orbital performance
[AIAA PAPER 71-836] 17 p2814 A71-35432

Satellite communication ground station center in conjunction with Intelsat 3 satellites system for transcontinental telephone links
17 p2708 A71-35508

Geodetic system with satellites and automatic radio beacons, establishing network on earth surface to track isolated points
18 p2913 A71-36529

Aeronautical satellite systems program planning for improved aircraft communications, ATC and other air traffic services in airspace over oceanic areas
22 p3573 A71-42096

Intelsat 1, 2, 3 and 4 satellite network development for world telecommunication coverage, discussing expected future replacement and modulation and multiple access technologies
23 p3643 A71-43250

Experimental ATS-1 satellite medical network for geographically and climatically isolated areas, noting impact on emergency treatment and anxiety level reduction
[AIAA PAPER 71-1003] 24 p3801 A71-44592

SATELLITE OBSERVATION

Proton Flare Project 1969 observation of solar radio bursts by Alouette 2 satellite
01 p0144 A71-10287

Satellite with onboard equipment for astronomical IR spectroscopy, considering stabilization accuracy and measurement duration effects on spectral resolution
01 p0163 A71-10395

Synoptic and moisture content charts from Kosmos-243 satellite measurements of escaping thermal RF flux
01 p0073 A71-10540

Higher geodesy problems, determining earth dimensions and figure, gravitational field and absolute and relative point positions with artificial earth satellites
01 p0159 A71-10809

Global ozone distribution from inverted radiance measurements by IR interferometer spectrometer /IRIS/ on Nimbus 3 satellite
01 p0074 A71-11249

Directed proton fluxes measurements in bow shock, magnetosheath and solar wind by OGO 5 satellite ion spectrometer
01 p0147 A71-11491

Low energy particle environment at synchronous altitude during magnetically quiet times from ATS 5 auroral particles experiment
01 p0147 A71-11497

Whistler ducts as enhanced ionization from OGO 3 satellite observations near magnetic equator, noting magnetospheric ionization hydrostatic model and predicted cut-off
01 p0076 A71-11499

Magnetospheric VLF electric field emissions above electron cyclotron frequency from OGO 5 observation at magnetic equator
01 p0076 A71-11500

Lyman alpha and O I 1304 A airglow depressions over poles from OGO 4 satellite observations
01 p0076 A71-11503

Satellite sounding of atmospheric pollution by spectral analysis of outgoing thermal radiation
02 p0241 A71-11689

Electron concentration and temperature data from Langmuir probe on Explorer 22, discussing magnetic storms effects
02 p0244 A71-11910

Ionospheric electron concentration measurement by bifrequency dispersion interferometer on Luna 14 orbiter
02 p0244 A71-11911

Monograph on visibility of satellite in elliptic orbit covering probabilistic aspects, communication, navigation, weather, reconnaissance and scientific satellites
02 p0319 A71-11970

Earth-moon mass ratio correction, observing artificial satellite motion near triangular libration point
02 p0308 A71-12100

Brightness field spatial structure of solar radiation reflected from earth by Cosmos 149 satellite, discussing homogeneity and isotropy
02 p0246 A71-12114

Earth radiation measurement at 10-12 microns by Cosmos 243 satellite-borne radiometer, comparing temperatures for boundary air layers in cloudless conditions
02 p0246 A71-12115

Soft solar X-ray flares six minute periodicity from satellite observation
02 p0300 A71-12472

Diffuse cosmic X ray spectrum obtained from telescope aboard OSO 3 satellite
02 p0300 A71-12580

Diffuse cosmic X rays observation by telescope aboard OSO 3 satellite, determining isotropy
02 p0301 A71-12581

Scorpius X-1 X ray and optical variations observation by Vela 5 satellites
02 p0315 A71-12662

Satellites applications in French space programs, discussing telecommunication, meteorology, air navigation aids, space geodesy and earth resources
02 p0337 A71-12918

European X ray astronomy lunar occultation satellite, providing high resolution cosmic X ray source observation
02 p0303 A71-12952

Solar eclipse of 7 March 1970 ionospheric ionization observations via satellites, correlating data with Wallops Island vertical ionograms
03 p0406 A71-13174

ESRO 1 satellite hydrogen and ionized nitrogen auroral emissions photometric measurements, discussing electron/proton phenomena relation to geomagnetic activity
03 p0406 A71-13248

Comparative simultaneous ionospheric temperature and plasma concentration by Explorer 31 probes and ground based radar measurements
03 p0407 A71-13311

Atmospheric temperature remote sounding from satellites using radiometer with selective chopper for carbon dioxide emission
03 p0422 A71-13355

Six channel selective chopper radiometer design and construction for carbon dioxide emission monitoring for remote atmospheric temperature sounding by Nimbus 4
03 p0423 A71-13356

Upper ionosphere electron concentration enhancement in polar cap from satellite probe measurements
03 p0408 A71-13385

Orbital space stations for earth studies, considering atmospheric, hydrological and meteorological observations, astronomy, medico-biological and technological experiments and interplanetary spacecraft bases construction
03 p0497 A71-13418

Intercoms 3 satellite for radiophysical and geophysical observations of radiation belts and ionosphere, discussing design, configuration and instrumentation
03 p0423 A71-13419

Earth surface and atmosphere thermal radio emission measurement by radio telescope on Cosmos 243 satellite
03 p0409 A71-13420

C, N and O nuclei abundances in radiation belt near geomeric equator, using data obtained by OGO-5 satellite in 1968
03 p0473 A71-13475

European ground stations geodetic surveys by laser range measurements and photographic observations of satellites with reflectors
03 p0413 A71-14008

Atmospheric reflection latitude and angular dependence on wavelengths from satellite UV measurements, noting ozone content seasonal variation of ozonosphere
03 p0413 A71-14010

Zodiacal light interpretation based on ground-based, satellite and deep space probe Helios observations, considering particle flux measurements
03 p0491 A71-14012

Picogram dust particle flux measurements in selenocentric cislunar and interplanetary space by Mariner 4, OGO 3 and Explorer 35
03 p0491 A71-14014

Atmospheric density curves by satellite observation, obtaining schematic models for fine structure of semiannual variation
03 p0414 A71-14023

Theoretical vs observed atmospheric densities between 350 and 1500 km, using models and satellite observations
03 p0415 A71-14025

Lyman alpha radiation scattering observation by satellites, obtaining geocoronal atomic hydrogen distribution in thermosphere and exosphere
03 p0415 A71-14028

SATELLITE OBSERVATION

Ionospheric electron temperature global pattern from satellite observations

03 p0415 A71-14029

Solar energetic protons measurements by ESRO 1 satellite following flare of 18 November 1968, noting cut-off latitude over northern polar cap

03 p0478 A71-14039

Electron and proton energy measurements by near-polar orbit ESRO 1 satellite, noting anisotropy and isotropy near and in proton zones

03 p0479 A71-14040

Polar orbiting satellite observed transient plasma density enhancements relation to geomagnetic activity

03 p0417 A71-14042

Solrad 8 satellite monitoring of Lyman alpha and UV radiation, discussing flux variation at 1080-1350 A

03 p0479 A71-14043

Solar radiation spectral distribution at 0-16 A by photometers on Solrad 9, computing theoretical ratios with gray body assumption

03 p0479 A71-14044

Atmospheric absorption models of solar X-rays at occultation times, using Solrad satellites

03 p0480 A71-14048

Night airglow spectral components by Cosmos 92 satellite measurements, considering UV region sources and intensity variations

03 p0417 A71-14050

Three dimensional traverse in geocentric Cartesian coordinates for connection of two adjacent satellite observation stations

03 p0418 A71-14324

Solar UV radiation measurements by OSO-3, obtaining flux variation over solar rotation period

03 p0481 A71-14508

Magnetospheric electron density trough measurements by Explorer 22 Langmuir probe during rising solar cycle

03 p0420 A71-14529

Whistler-mode waves circular polarization measurement by OGO 6 satellite, noting application to hiss, chorus and ion density studies

03 p0421 A71-14538

Ionospheric electron content persistent longitudinal anomalies observed by low orbiting satellites

03 p0421 A71-14541

Magnetotail energetic electron event simultaneous observations by Vela 3A and Imp 3 satellites, evaluating plasma sheet boundary motion hypotheses

03 p0421 A71-14545

Lower limit of neutral line in geomagnetic tail merging, noting inconclusiveness of direct spacecraft observations

03 p0421 A71-14551

Escaping-earth radiation actinometric measurement by meteorological satellites, discussing seasonal thermal radiation variations in Southern Hemisphere polar regions

04 p0579 A71-14637

Satellite monitoring impacts on global ecological and natural resource public policy issues

04 p0689 A71-14820

Small satellites for radiation and solar cell damage measurements, surface friction and cold welding experiments and Apollo communications testing

04 p0662 A71-15018

Earth ellipsoid physical constants using satellite measurements of geocentric gravitational constant, earth-moon mass ratio and geopotential harmonic coefficients

04 p0581 A71-15066

Solar proton recording during flare by Proton 3 satellite

04 p0641 A71-15124

Nimbus meteorological sensor and photographic data application to geology and hydrology for repeat global and synoptic observations, terrestrial mapping and event classification

04 p0583 A71-15290

Geodetic survey adjustment and accuracy improvement using satellite radar range and ballistic camera data

04 p0583 A71-15302

Geodetic position rapid determination accuracy by Doppler satellite observation

04 p0583 A71-15304

Earth gravitational environment critical parameters at synchronous altitudes by satellite drift observation, discussing geopotential field determination

04 p0583 A71-15306

Satellite meteorology, discussing system, observational data, weather prediction, communications sensors, TV imaging and global atmospheric research program

04 p0621 A71-15308

Nimbus AVCS imagery applied to studies of bedrock geology, geomorphology and climate

04 p0597 A71-15309

DIAL satellite project, discussing geocoronal hydrogen concentration, upper atmosphere electron density, magnetic field measurement, etc

04 p0664 A71-15649

Galactic Lyman alpha observation by Vela 7, discussing error possibility of data interpretation based on interstellar hydrogen shock wave

04 p0658 A71-15831

Photospheric and interplanetary magnetic field polarity and magnitude comparison, using Explorer observations

05 p0802 A71-16012

Magnetic and thermal pressures in solar wind from Explorer 34 data

05 p0797 A71-16016

Large scale ionospheric irregularities from Faraday fading records by satellite observations, studying height, fluctuations, electron contents, horizontal size and orientations

05 p0741 A71-16439

Solar wind upstream waves ahead of earth bow shock by dual satellite observations

05 p0741 A71-16629

Earth bow shock configuration model from dual satellite observation

05 p0742 A71-16632

Hurricane Gladys structure and dynamics observations by Apollo 7 spacecraft, satellites and radar, noting large cloud feature

05 p0777 A71-16662

Simultaneous meteorological satellite IR radiation measurements and cloud photographs for superposition and mutual interpretation

05 p0752 A71-16676

Scientific applications of satellite photometric observations, considering geomagnetic effects on spacecraft rotation, satellite size and reflection properties, etc

05 p0723 A71-16970

Solar X-ray radiation measurements using real time telemetry from SOLRAD satellites

05 p0799 A71-17001

Microwave radiometric techniques for continuous all-weather remote sensing of sea conditions from satellites, discussing foam and surface ripple effects [ALAA PAPER 70-318]

05 p0743 A71-17101

Nimbus meteorological satellite program, discussing global cloud cover mapping and automatic picture taking, radioisotopic thermoelectric generator, sounder instrumentation and remote sensors

05 p0818 A71-17133

Vertical NO profile at 100-220 km from 1968 Cosmos 224 measurement of atmospheric glow near horizon

05 p0744 A71-17186

Short duration proton energy increases observation by Explorer 34, considering interpretation as acceleration associated interplanetary shocks

06 p0949 A71-17254

Solar electrons access to closed field lines in geomagnetosphere quasi-trapping region from satellite observation

06 p0949 A71-17257

Magnetopause crossing observation of ATS 5 satellite during magnetic storm

06 p0887 A71-17258

Geomagnetic storm disturbance fields measurement by ATS 1 satellite compared with simultaneous low altitude observation, noting cavity sudden commencement compression effect

06 p0887 A71-17259

Inner radiation zone electrons loss and replenishment observation by Pegasus satellite during magnetically quiet and active periods

06 p0949 A71-17264

Ionospheric irregularity structure boundary variations shown by scintillation from satellite and radio star observations during quiet and disturbed magnetic conditions

06 p0887 A71-17269

Meteorological satellites scan zones latitudinal overlap for circular or elliptical orbits

06 p0898 A71-17649

Magnetospheric sudden impulses amplitude and rise time distributions observation by OGO 3 and 5 satellites

06 p0889 A71-17686

Alpha particle abundance in solar wind positive ions observed by ESRO satellite HEOS-1

06 p0950 A71-17919

Early type stars radiant flux observation from OGO 6 satellite

06 p0969 A71-17975

Quiet time fluxes and differential energy spectra of protons and alpha particles at 2-20 MeV measured by cosmic ray detectors on OGO-3

06 p0954 A71-18127

Solar and galactic cosmic rays interactions with interplanetary magnetic field 28 January-25 February 1967 based on Explorer 33 and 28 satellite observations

06 p0957 A71-18145

Solar flare induced cosmic ray intensity increases registered by high latitude neutron monitors and Explorer 35 satellite, presenting intensity time profiles analyses

06 p0957 A71-18146

HEOS A-1 satellite solar proton flux measurements from 25 and 27 February 1969 solar flares, noting strong backscattering of 360 MeV particles

06 p0957 A71-18149

Low energy solar and galactic cosmic ray propagation in interplanetary medium from Zond 3 and Venus 2-4 space probes measurements

06 p0958 A71-18152

Solar proton event on 9 June 1968 observed at polar caps by ESRO 2 satellite, noting flux profile structure

06 p0958 A71-18154

Astronautical TV camera and photogrammetric systems use on manned and unmanned lunar probes, discussing applications to earth surface surveys

06 p0901 A71-18287

Agricultural information and advisory service, utilizing remote sensing, computer sciences, research programs, educational involvement, satellites and aircraft

06 p1010 A71-18408

Worldwide remote sensing with satellites, high flying aircraft and computer data processing, discussing application in less developed countries

06 p0896 A71-18409

Columnar electron content measurements by geostationary satellites, discussing research in developing countries for cost reduction

07 p1096 A71-19007

Receiving equipment for direct differential Doppler frequency measurement via beacon satellites observation

07 p1059 A71-19012

Ionospheric columnar electron content using differential radio refraction measurements from satellite observation station

07 p1097 A71-19026

Ionospheric electron content from Faraday rotation measurements of earth satellite and deep space probe

07 p1098 A71-19029

Ionospheric electron mean content by polar satellites, using combination of Doppler differential and Faraday rotation hybrid methods

07 p1206 A71-19032

Ionospheric electron content observation by ATS-3 radio signals, noting gravity waves effect

07 p1098 A71-19034

Solar vicinity particle storage implication from flare proton energy spectrum observation by Injun 5 satellite

07 p1186 A71-19653

Upstream discrete wave packets propagation interplanetary medium from Ogo 5 observation

07 p1197 A71-19656

Energetic electrons distribution in magnetotail plasma sheet from Explorer 35 satellite observation data

07 p1186 A71-19657

Energetic electrons in magnetospheric tail plasma sheet, investigating flux time profiles and correlation with local magnetic fields from Imp 3 satellite observation data

07 p1186 A71-19658

Low energy electron and proton fluxes observation by Isis 1 satellite, concluding solar wind penetration to low altitudes through magnetopause cusp

07 p1186 A71-19659

VLF Poynting flux measurement technique on Injun 5 satellite using one electric and one magnetic antenna, discussing magnetic orientation errors effects

07 p1062 A71-19668

Comparison of experimental and gas dynamic fluid parameter jumps across earth bow shock, suggesting reappraisal of gas dynamic analog from satellite observation

07 p1103 A71-19678

Solar optical flares association with type 3 bursts from OGO-3 observations, suggesting temporary creation or enhancement of electron stream propagation by filament or sunspot structure change

07 p1187 A71-19724

Energy transfer at colliding streams in solar wind from Explorer 34 and Vela 4B measurements of proton, alpha particle, electron and magnetic field parameters

07 p1188 A71-19824

Solar constant and spectral energy distribution standard values by high altitude aircraft, balloon and spacecraft measurements

07 p1199 A71-20005

Space vehicle apparent distance magnitude estimation judgments, investigating stimulus range effects on response range and Stevens type power function exponent

07 p1051 A71-20217

Lunar bulk modulus, viscosity, inertia moments and density calculation from gravity potential values obtained by Luna 10 and Lunar Orbiter satellites

07 p1203 A71-20520

Equatorial proton belt radial profile analysis by satellite electron distribution data

08 p1351 A71-20962

Polarimetric measurements of solar X-ray flares by Intercoms 1 satellite

08 p1354 A71-21013

Galactic cosmic rays interaction with interplanetary magnetic field from Venera 4 measurements June-October 1967

08 p1354 A71-21015

Earth-moon mass ratio correction, observing artificial satellite motion near triangular libration point
08 p1362 A71-21150

VLF hiss directions from Injun 5 Poynting flux observations, proposing propagation across plasmapause boundary
08 p1282 A71-21633

Temporal intensity variations of geomagnetically trapped solar alpha particles from Injun 5 observations
08 p1356 A71-21644

World Weather Watch plan, discussing upper air, surface and satellite observations, telecommunication and data processing
08 p1328 A71-21719

Satellite role in future observing systems for global atmospheric research program, describing satellite instrumentation
08 p1328 A71-21721

Sounding system constant level superpressure balloons for atmospheric circulation global description at all levels and latitudes in conjunction with satellite observations
08 p1231 A71-21742

Planet rotation vector determination, using satellite stellar observations and planetary surface reference points
08 p1365 A71-21776

Earth twilight aureole and cloud spectra from satellite photometry
08 p1285 A71-21792

Earth gravity field in physical geodesy, considering satellite geodesy, gravitation-inertia interrelation, etc
08 p1285 A71-21799

Satellite geodesy, discussing reference orbits calculation, gravity field spherical harmonics, station positions, etc
08 p1285 A71-21800

Satellite geodesy for determining tracking station coordinates and gravity field
08 p1285 A71-21801

Satellite geodetic data interpretation of geoid undulations and gravity anomalies
08 p1285 A71-21803

Weather satellite data for numerical analysis and forecasts, reconstructing geopotential field
09 p1486 A71-22300

Quasi-captured and escaped electron flux angular dependence and latitudinal variations observations at low altitudes by Cosmos 228 satellite
09 p1512 A71-22362

Daytime near horizon atmospheric luminescence measurement by Cosmos 224 satellite, discussing contributions of nitrogen and aerosol and Rayleigh scatterings
09 p1435 A71-22432

Venusian atmospheric models of troposphere, stratosphere and thermosphere based on satellites observation data
09 p1519 A71-22527

Satellite studies of geoeactive particles and photoelectrons, including interactions with earth atmosphere
09 p1436 A71-22552

Satellite-borne spectrometer for low energy electrons measurement, describing virgin photoelectrons equilibrium energy spectrum for different latitudes and pitch angles
09 p1436 A71-22553

Satellite-borne spectrometer for low energy ion measurement
09 p1436 A71-22554

Satellite-borne scintillation spectrometers for medium and high energy electron and proton measurements
09 p1513 A71-22555

Plasmasphere ion concentration measurements on-board Elektron 2 and 4 satellites, observing dependence on geomagnetic activity
09 p1513 A71-22574

Long wave cosmic radio background emission in circumplanar space by Luna 11 and 12 satellites, observing increase in earth magnetosphere tail
09 p1513 A71-22576

High energy electrons in near space excess radiation from high altitude balloon and satellite data
09 p1513 A71-22667

Earth optical radiation environment observation from satellites, reviewing solar spectra, near IR cloud spectra and vacuum UV radiometer scans
09 p1437 A71-22739

Cosmos 142 satellite measurements of VLF radio signals transmitted through ionosphere by ground based stations
09 p1408 A71-23143

Artificial earth satellite circular orbit determination from topocentric directions measurement by optical and electronic observations
09 p1408 A71-23176

Plasma intrusion into simulated magnetosphere compared with satellite observations, discussing spatial distribution and interplanetary magnetic field effects
09 p1529 A71-23707

Comets gaseous atmospheres related to 1970 OAO discovery of vast hydrogen atmosphere, indicating

molecular hydrogen abundance and gas production rate
10 p1665 A71-23745

OSO 3 satellite observations of diffuse X ray emission from galactic plane, eliminating straight line interpolation of spectrum between 3-10 keV X ray range and 100 MeV energy range
10 p1665 A71-23750

Soft X ray bursts involving solar flares from satellite observations, discussing thermal nature and total activity related H-alpha emission rates
10 p1660 A71-23794

Satellite, rocket and Thomson scatter data application to communications - IEE Conference, London, January 1971
10 p1575 A71-23864

Satellite data for ionospheric radio communication forecasting involving maximum usable radio frequencies, discussing F 2 region large scale disturbances
10 p1575 A71-23868

Trapped waveguide mode frequency of whispering gallery propagation in F region explaining round world echoes and long distance satellite observations
10 p1577 A71-24292

Longitude precessional constant determined by long baseline interferometry through dynamical behavior observation of earth orbiting or interplanetary artificial spacecraft
10 p1674 A71-24437

Solar geomagnetic seasonal ionization control of upper ionosphere longitudinal composition variations from polar satellite observations
10 p1602 A71-24555

Solar wind-magnetosphere interaction modes from Explorer 33 and 35 interplanetary plasma and magnetic field data
10 p1663 A71-24780

Plasma sheet proton ring current, trapping boundary and plasmapause interrelations near magnetic equator and local midnight by satellite-borne analyzer array
10 p1605 A71-24781

Low latitude DS ionospheric current component and auroral electrojet intensity for intense geomagnetic storms, considering particle observations by ATS 5 synchronous satellite
10 p1605 A71-24790

Upper atmosphere statistical structure based on analysis of deviations of satellite-determined air densities from theoretical Jacchia model, noting latitudinal, seasonal and diurnal variations
10 p1607 A71-25024

Galactic plane X ray scan by NASA small astronomy satellite Uhuru, discussing satellite instrumentation, detector and sensor sensitivity and preliminary measurements
11 p1814 A71-25212

Cygnus X-1 and X-2 X ray source location from Uhuru satellite measurements
11 p1814 A71-25213

M87, Cen A NGC 5128 and 3C 273 X ray emission observations in Virgo cluster, using Uhuru satellite
11 p1814 A71-25215

Tornado producing thunderstorms upper level outflow synoptic and dynamic processes from ATS 3 pictures, discussing convective warming effects
11 p1794 A71-25381

Micrometeoroid detector design for hypervelocity particle impacts, discussing solar radiation pressure effects on satellite measurements
11 p1761 A71-25544

VLF propagation in low latitude ionosphere from FR-1 satellite observations, obtaining electron density model of equatorial anomaly
11 p1755 A71-25642

Earth radiation belts high energy electron flux intensity monotonic decrease during magnetically quiet periods from satellite data analysis
11 p1816 A71-25759

Planetary distribution of primary cosmic rays and residual charged particles over atmosphere from Cosmos 208 and 228 satellite data
11 p1816 A71-25761

International coordinated measurements of solar activity geophysical effects in upper atmosphere, discussing synchronized observations of Cosmos 261 satellite and ground based ionospheric station network
11 p1816 A71-25762

International coordinated solar chromospheric flare effects on D region lower boundary and ionospheric propagation by Cosmos 261 satellite and ground based observatories
11 p1816 A71-25763

Galactic cosmic rays solar modulation and intensity gradient in interplanetary space from satellite observation data
11 p1817 A71-25766

Solar flux from 7 July 1966 flare observation via Proton 3 satellite, obtaining cosmic rays integral spectra
11 p1817 A71-25781

Interplanetary magnetic field parameters for various heliocentric distances from 1959-1967 satellite observations, discussing cavity position and solar activity phase correlations
11 p1829 A71-25782

Midlatitude topside ionospheric electron density mean diurnal and seasonal variations from Alouette 1 satellite observation
11 p1757 A71-25784

N/z profiles of upper ionosphere from Alouette 1 vertical sounding data, proposing model for ionosphere shape
11 p1758 A71-25786

Polish papers on artificial earth satellite observation covering celestial mechanics and orbit determination, geodetic applications, upper atmosphere and instruments
11 p1758 A71-25806

Geodetic geographic coordinate transformations and ellipsoid heights, azimuth and length determination from synchronous photographic observations and distance measurements of artificial satellites
11 p1759 A71-25813

Tetrahedrometric leveling of spatial networks with independent bases between satellite points confirmed for Baja-Cairo direction
11 p1759 A71-25814

Variation coefficient and corrections to dependent observations for space triangulation leveling by least squares method, comparing closing directions
11 p1759 A71-25815

Satellite geodetic global networks employing triangulation, trilateration and height measurements, deriving dominant point observation stations /Hazay-Tarczy method/
11 p1759 A71-25816

Eccentric satellite observation, considering geodesic determination of coordinate difference between observation station and reference point
11 p1732 A71-25818

Satellite geodesy progress over 12 years since artificial earth satellites, considering gravitational field and station position measurement accuracies
11 p1759 A71-25820

Solar activity effects on atmospheric density variations from satellite observations, using random process isocorrelation charts
11 p1759 A71-25821

Atmospheric density semiannual variations from satellite observation, comparing with atmospheric models
11 p1760 A71-25824

Satellite orbit period variation data for PERLO program visual observations, calculating topocentric celestial equator transits
11 p1732 A71-25826

Artificial earth satellite observation by Soviet universal and semiautomatic cameras with quartz clocks and four component mirror lens optical system
11 p1762 A71-25829

Computer program algorithm for satellite photographic observation data processing based on measurement at one station
11 p1733 A71-25833

Cloud shape data, comparing meteorological satellite measurements and ground based visual observations
11 p1795 A71-26559

Earth surface thermal radio emission measurements by UHF radiometry onboard Cosmos 243 satellite, showing brightness profiles of water, ice and land areas
12 p1899 A71-26639

German low altitude polar orbiting research satellite AZUR orbital characteristics and bearing on auroral zone substorm phenomena
12 p1899 A71-26833

Direction of chord in space from synchronous photographic satellite observations, considering optimum satellite altitude
12 p1900 A71-26969

Latitudinal distribution of integral water content of clouds in droplet form above Pacific, Atlantic and Indian oceans from Cosmos 243 measurements
12 p1924 A71-27098

Radio source 3C120 gamma quanta with energy above 100 MeV from Cosmos satellites scintillation and Cerenkov counter measurements
12 p1953 A71-27417

Pioneer F spacecraft investigation of Jupiter regions and outer interplanetary space, discussing design, communication system and possible future missions
12 p1973 A71-27603

Hot coronal components of solar active regions observations with satellite-borne grazing incidence X ray telescope, discussing emission dependency on photospheric magnetic field
12 p1954 A71-27707

Translation of geodetic geographical coordinates and ellipsoidal altitudes by synchronous photographic satellite observations and satellite-distance measurements from two ground stations
12 p1903 A71-27753

Interplanetary magnetic field north-south component from Mariner 2, 4 and 5 measurements
13 p1311 A71-27907

Band limited micropulsations observed in space during magnetospheric substorm by fluxgate magnetometer onOGO 5
13 p2119 A71-27913

Color frequency-time spectrograms of VLF electric and magnetic field Poynting flux data from Injun 5 satellite

13 p2054 A71-27914

Venus atmospheric turbulence from Venera 4, 5, 6 and Mariner 5 observations, discussing scaling laws and normalized signal-amplitude standard deviation

13 p2132 A71-27928

Differential energy spectrum of cosmic ray deuterium flux of galactic origin from IMP 5 satellite measurements

13 p2120 A71-27974

Ocean height measurement by orbit determination from satellite altimetry, considering least squares solutions and instrument errors

13 p2066 A71-27983

X ray pulsations from Cygnus X-1 observed from Uhuru satellite, suggesting exstar discovery

13 p2120 A71-28004

Quark flux and generation cross sections above atmosphere from Proton 3 satellite elementary particle spectrometer data

13 p2121 A71-28053

Inelastic proton-proton and proton-carbon interaction cross sections, measuring proton energy with ionization calorimeter on Proton 1, 2 and 3 satellites

13 p2121 A71-28060

Ionospheric electron concentration and temperature data from Langmuir probe on Explorer 22, discussing magnetic storms effects

13 p2058 A71-28197

Ionospheric electron concentration measurement by bifrequency dispersion interferometer on Luna 14 orbiter

13 p2058 A71-28198

Vertical NO profile at 100-220 km from 1968 Cosmos 224 measurement of atmospheric glow near horizon

13 p2059 A71-28243

Earth surface nighttime, twilight and daytime horizons visual observations by Soyuz 9 spacecraft

13 p2060 A71-28426

Longitudinal variations of inner radiation belt particle flux density at low altitudes from Proton 2 satellite data

13 p2128 A71-28548

OGO 4 satellite micrometeoroid flux detection, emphasizing noise control procedures for data correlation

13 p2145 A71-28700

Solar wind heavy ion data, using Heos-1 satellite observations of 31 March 1970 interplanetary shock

13 p2130 A71-29059

Solar wind speed data, investigating variations in satellite observations

13 p2130 A71-29062

Orbital space stations for earth studies, considering atmospheric, hydrological and meteorological observations, astronomy, medico-biological and technological experiments and interplanetary spacecraft bases construction

14 p2319 A71-29695

Geomagnetic field models validity from satellite data

14 p2231 A71-29903

Relativistic gravitation theory quantitative study by space vehicle experiments, discussing earth orbit and deep space investigations

14 p2319 A71-29906

Space vehicle observation effect on Mars and Venus conceptions, considering origins of life, runaway greenhouse effect on earth and atmospheric circulation

14 p2308 A71-29909

Noctilucent cloud observation from space, discussing instruments, radiation spectrum, global scale formation, time dependent structures and satellite orbit requirements

14 p2232 A71-29963

High latitude measurements of low energy electron precipitation by Auroral 1 satellite, explaining anomalous high level F region ionization near dark pole

14 p2299 A71-30031

LF whistler mode radio noise emissions observations in polar regions with Alouette 2, noting association with energetic particles influx into ionosphere

14 p2300 A71-30036

Upper F region transpolar plasma distribution from Alouette 1 data, relating results to satellite measurements of magnetospheric low energy charged particles

14 p2234 A71-30041

High latitude upper ionospheric structures and plasma flow in magnetosphere from Alouette/ISIS topside sounders, noting solar UV and particle ionization sources

14 p2234 A71-30042

Spread F ionospheric electron density irregularities and satellite scintillation over polar cap

14 p2300 A71-30043

Double star measurements precision obtainable in space with stable and perfect instrument, comparing to ground observations

14 p2246 A71-30364

Instrumentation and orbital parameters of meteorological satellites observing winds, tropical circulations, heat budget, hydrology and ocean surfaces

14 p2270 A71-30498

Random multiple access technique for satellite data collection, taking advantage of frequency instability associated with oscillator circuits

14 p2199 A71-30908

Nimbus 4 Interrogation Recording and Location System meteorological information for tropical region upper atmosphere experiment

14 p2200 A71-30917

Interrogation, recording and location system satellite techniques for wildlife tracking and monitoring, describing collar antenna, battery pack and solar cells

14 p2200 A71-30923

Doppler effect satellite location of crystal controlled CW transmitters on earth surface for animal tracking

14 p2200 A71-30924

Satellite atmospheric temperature sounding by radiometric measurements, obtaining vertical temperature profile by mathematical inversion process

14 p2236 A71-30938

Ionospheric electron resonance observation by sounders aboard rocket and satellites

14 p2202 A71-30947

Satellite measurements of cold plasma density and plasmopause in magnetosphere, comparing Whistler, Langmuir probe and ion trap data

14 p2237 A71-30951

Atmospheric VLF electromagnetic emissions and electron instabilities data from satellite observation, detailing source regions, large amplitude electrostatic waves and wave-particle correlation

14 p2202 A71-30952

Hydromagnetic approximation of ELF propagation modes and emission in magnetosphere, using satellite and ground based observations

14 p2202 A71-30953

Automatic camera for international synchronous observations of geodetic satellites

14 p2250 A71-31117

Photographic observations of Paoeos satellite during 1968 with PO-2 camera

14 p2250 A71-31118

Trace length analysis of Paoeos and Echo 2 satellites by camera observations

14 p2318 A71-31119

Coordinate measurement accuracy for star and satellite photographic observation using Zeiss Ascorecord

14 p2250 A71-31121

Brightness variations of satellite during passage in circular orbit as function of distance, phase and atmospheric extinction

14 p2318 A71-31122

Photographic and laser observations during passage of satellite for determination of distance between observer and earth rotational axis

14 p2250 A71-31123

Simultaneous ionospheric electron density measurements from Isis satellite topside and incoherent scatter soundings

15 p2394 A71-31428

Magnetospheric plasma clouds equatorial observation by ATS 5 satellite, revealing plasma injection during substorms and dispersion by earth magnetic and electric fields

15 p2397 A71-31755

High energy primary cosmic ray program of Goddard Space Flight Center involving charge composition and energy spectra studies in balloon and satellite experiments

15 p2478 A71-31804

Satellite IR photography, discussing camera systems, photointerpretation, applications in glaciology, hydrology, oceanography, geology, volcanology and environmental protection

15 p2408 A71-31835

Lunar subsurface water detection from satellite in polar orbit around moon by electromagnetic measurement

15 p2492 A71-32476

Planetary exploration from space, recommending flights to moons of outer planets due to possible presence of atmospheres and water ice

15 p2494 A71-32495

Planet intrinsic rotation vector determination, using satellite stellar observations and planetary surface reference points

15 p2495 A71-32681

Mesospheric noctilucent cloud formations observations from space by cosmonaut on 9 June 1970 over Arabian peninsula

15 p2496 A71-32727

Pc 2-4 pulsations relationship to interplanetary magnetic field strength and orientation, using IMP 3 and 4 satellite data

15 p2401 A71-32732

Monsoonal response of Somali Current in Indian Ocean, using spacecraft IR observations of sea surface horizontal temperature gradients

16 p2562 A71-33068

Satellite geodesy in Netherlands, discussing measurement and instrumentation techniques and ground station equipment and operation

16 p2563 A71-33368

Spatial and angular distribution of upper atmospheric IR emission layers from Cosmos 65 observation

16 p2563 A71-33449

Altitude and amplitude of winter stratospheric warmings from satellite measured radiance changes, considering radiative transfer equation and variable model of temperature structure

16 p2605 A71-33537

Satellite view of earth surface, deriving expressions for cone-sphere intersections in terms of geographic coordinates

16 p2638 A71-33539

Earth Resources Remote Sensing Systems effectiveness, discussing sensor and satellite development, spectral and spatial recognition, data management and ecological and resource relationship

16 p2645 A71-33582

Fast charged particles measurement in inner radiation belt by Cerenkov counter mounted on Cosmos 137 satellite indicating presence of high energy electrons

16 p2626 A71-33664

Upper atmosphere heating at high latitudes, analyzing air density variations from Molniya 1K satellite observations over 2 year period

16 p2565 A71-33740

Upper atmospheric composition and density variations with latitude and local time, using OV3-6 satellite measurements

16 p2566 A71-33756

Upper atmosphere parameters determination by simultaneous positional and photometric satellite observations

16 p2568 A71-33793

Air density observation near 150 km heights from Cosmos 316 orbit, noting geomagnetic disturbance effects and semiannual variation

16 p2569 A71-33806

Orbiting satellites VHF radio signal transmissions enhancement, considering focusing effect of electron density contours resulting from gravity or acoustic wave in ionosphere

16 p2543 A71-33817

Semiannual atmospheric density variation measurements by OV3-6 satellite

16 p2570 A71-33821

Soft X ray emission line behavior during solar flares based on OSO-6 satellite-borne Bragg crystal spectrometer data

16 p2627 A71-33835

Nimbus 3 and 4 satellite observation data comparison with sounding rocket and rawinsondes based on temperature as function of pressure measurements

16 p2572 A71-33846

Pakistani space research including satellite geodesy, ionospheric sounding, rocket experiments, VLF studies and time keeping

16 p2666 A71-33857

UK space research programs, discussing ground based, satellite and rocket-borne experiments

16 p2666 A71-33859

Brazilian space research planning effort and activities covering rocket and satellite meteorology, satellite tracking, balloon experiments and ground based geophysical observations

16 p2667 A71-33869

Primary cosmic ray nucleonic component observation by scintillator-Cerenkov telescope on OGO 3 satellite

16 p2628 A71-33932

Statistical measurements of solar protons, alpha particles and heavier nuclei by lunar orbiting Explorer 35

16 p2628 A71-33933

Solar protons penetration over polar cap during 25 February 1969 event from particle and magnetic field measurements inside and outside magnetosphere by satellites

16 p2628 A71-33934

Energetic solar protons asymmetric access to north south polar caps by satellite observation during 24 January 1969 event

16 p2628 A71-33935

Solar particle flux profile and low latitude cut-off observation by low altitude satellite during March 1969 to July 1970 events

16 p2628 A71-33936

Shock normal calculation by applying least squares technique to combined geomagnetic field and plasma data from single satellite, assuming Rankine-Hugoniot conservation relations

16 p2560 A71-33941

Earth bow shock internal structure based on correlated observations of magnetic field, ELF magnetic fluctuations and suprathermal electrons by OGO 5 satellite

16 p2628 A71-33943

Time variations of magnetotail plasma sheet from electron energy spectral measurements on Vela satellites

16 p2629 A71-33945

- Geomagnetic equatorial ionospheric ion temperature, comparing incoherent scatter radar and OGO-D retarding potential analyzer values 16 p2573 A71-33956
- Magnetospheric observations by Imp 3 satellite of energetic electron and magnetotail field variations near neutral sheet as function of substorm time 16 p2574 A71-33971
- Atmospheric electron density irregularities observations, using Alouette 2 satellite electrostatic probe 16 p2574 A71-33973
- Space radio astronomy, discussing frequency range in terrestrial atmosphere, RA-E-1 satellite, cosmic and solar emissions and magnetopause generation, propagation and absorption processes 17 p2797 A71-34243
- Meteorological satellites characteristics, reviewing Tiros, Itos, Nimbus, ATS, SMS and IGAR programs and vehicles 17 p2812 A71-34244
- Satellite remote sensing for crops and timber identification/detection, surface moisture measurements, soil mapping, marine hazard evaluation, etc 17 p2730 A71-34245
- Pitch distribution of protons precipitated from auroral radiation region measured by scintillation detector aboard Cosmos 261 satellite in Northern Hemisphere 17 p2731 A71-34320
- Micrometeoroids bibliography and review, considering ground based photometry and scattering theory, satellite flux measurements, particle collection and craters 17 p2798 A71-34456
- German book on satellite geodesy covering two body problem, perturbation theory, earth gravitational field, gravitational effects of sun and moon, radiation pressure, etc 17 p2799 A71-34470
- ERTS system, considering multispectral data acquisition, relay devices and spacecraft and ground information processing 17 p2812 A71-34611
- Synchronous meteorological satellite programs, noting earth imaging, data transmission, collection and relay and space environment monitoring 17 p2812 A71-34612
- Geodetic and oceanographic surface mapping by satellite radar altimeter system, discussing measurement technique, orbital parameters and data processing equipment [AIAA PAPER 71-845] 17 p2733 A71-34708
- Jupiter atmospheric entry probe mission, discussing descent depths, atmospheric pressure and temperature effects, data return techniques and Grand Tour Missions [AIAA PAPER 71-832] 17 p2802 A71-34715
- Satellite and gravimetric data combination procedure for determining geocentric station coordinates and earth gravitational field 17 p2734 A71-35031
- Sea surface slope distribution and wind velocity determination by sun glitter photography from synchronous satellite 17 p2734 A71-35215
- Critique of Vela 4 scattered Lyman alpha experiment, discussing maximum flux region and radiation intensity 17 p2805 A71-35380
- Coma cluster X ray source data from Uhuru satellite, observing size, luminosity, spectra, thermal bremsstrahlung mass and stability 17 p2796 A71-35413
- Manned orbital research modules design for atmospheric physics, weather and earth resources observations and stellar astronomy [AIAA PAPER 71-815] 17 p2814 A71-35426
- OSO satellites observations, studying X ray flare phases, temperatures and spectra 17 p2808 A71-35521
- Twilight glow spectrophotometry and visual observations from Soyuz 5 spacecraft, determining atmospheric optics and vertical aerosol profile 18 p2911 A71-36006
- Twilight aureole visual observation and objective colorimetry from Soyuz spacecraft, noting importance for atmospheric composition determination 18 p2911 A71-36007
- Earth IR radiance at 5-20 microns from interferometric spectrometer /IRIS/ aboard NIMBUS 3 satellite 18 p2912 A71-36101
- Venus atmospheric model based on Mariner 5 and Venera satellites observation, comparing with optical observation from earth 18 p2965 A71-36293
- Global atmospheric research with balloons, buoys and orbiting satellites for meteorological and oceanographic data recovery 18 p2913 A71-36486
- Geodetic satellite data utilization for test range specific point positioning, control densification, earth gravitational model determination and tracking station locations 18 p2913 A71-36492
- Satellite based position fixing data by ranging techniques, discussing application to navigation and ATC 18 p2945 A71-36493
- X ray astronomy with SAS-A satellite, discussing proportional counters, detectors and short period pulsation discovery 18 p2965 A71-36598
- Soyuz 9 cosmonaut meteorological experiments, observations and atmospheric formations photographs 18 p2944 A71-36686
- OSO-6 measurements of gegenschein, comparing relative sky brightness data with ground based observations 18 p2966 A71-36766
- Satellite applications to cartographic and geodetic surveys, discussing photographic difficulties 19 p3047 A71-37302
- Solar wind plasma density and flow speed semiannual variations from Vela 3 and 4 satellite observations, noting dependence on heliographic latitude 19 p3124 A71-37351
- Plasma in dayside polar magnetosphere, analyzing Imp 5 and other earth satellites measurements data 19 p3047 A71-37357
- Diurnal distribution, latitudinal occurrence and intensity patterns of ELF, VLF and LF whistler-mode noise emissions from Alouette 2 satellite observation 19 p3016 A71-37364
- Solar studies with emphasis on space observations - Conference, London, April 1970 19 p3135 A71-37608
- Far UV solar spectra observations, using OSO-2, 4, 5 and 6 spectroheliograms 19 p3136 A71-37614
- Lunar near-side tectonic patterns, including mare ridges, rills, highland ridges and crater walls features within maria from Lunar Orbiter photographs 19 p3052 A71-37676
- Outer planet satellite missions for optimal imaging conditions in terms of proximity and lighting [AAS PAPER 71-138] 19 p3140 A71-37942
- Brightness profiles of earth daytime horizon from Soyuz spacecraft photographic photometry, deriving atmospheric scattering coefficient relation to optical thickness vertical distribution 19 p3054 A71-37967
- Cloud cover areal distribution estimation model using multichannel IR radiometer data from Nimbus 2 satellite 19 p3056 A71-38267
- Primary cosmic ray proton energy spectrum in 50 GeV to 300 TeV range, using Proton 1, 2 and 3 satellite-borne counters 19 p3128 A71-38352
- Electron flux and energy spectra measurements at 200-600 km altitude by Cerenkov counters onboard Proton 1 and 2 19 p3129 A71-38375
- Aerial and satellite environmental water quality control surveillance, discussing remote sensing techniques and objectives 19 p3059 A71-38402
- Radio frequency interference environment measurement in VHF range by subsynchronous Lincoln experimental satellites 5 and 6 19 p3021 A71-38452
- Meteosat satellite for taking earth photographs and relating between weather stations 19 p3154 A71-38474
- Auroral luminosity patterns over northern Scandinavia based on ESRO all-sky camera recordings, noting relationship to electron and proton precipitation 19 p3060 A71-38573
- Auroral electrons and protons precipitation patterns from ESRO 1A northern polar cap observations, identifying electron energy zones 19 p3060 A71-38574
- Magnetic activity effect on pitch angle distribution of low energy auroral electrons from ESRO 1A measurements 19 p3060 A71-38575
- ESRO-1A /Aurora/ observations of variations in low energy electron spectrum, noting relationship to magnetic activity 19 p3060 A71-38576
- Lightning observation by OSO-E satellite, suggesting maximum thunderstorm incidence over North Atlantic Ocean 19 p3061 A71-38675
- Artificial satellites optical characteristics from amateur observers, discussing brightness and absolute magnitude 20 p3305 A71-38731
- Automatic pulsating locator beacons and receivers to determine emergency transmitters locations, using satellites with computer analysis 20 p3261 A71-38865
- Cosmos satellite data on mainland China thermonuclear explosion of 27 December 1968, observing radiation effects on particles in natural radiation belts 20 p3278 A71-39128
- Fast charged particle flux measurement in inner radiation belt by Cosmos 137 satellite in January-February 1967 20 p3278 A71-39140
- Satellite data on solar wind velocity, ion composition, temperature and magnetic field characteristics near earth orbit 20 p3279 A71-39445
- Cloud cover charts for North Atlantic-European-North African region, comparing satellite and ground station visual observations 20 p3258 A71-39552
- Continuous solar UV and X rays monitoring by SOLRAD 10 satellite, investigating solar activity and flares effect on shortwave communications and manned space travel 20 p3294 A71-39580
- Polarimetric measurements of solar X-ray flares by Intercoms 1 satellite 20 p3280 A71-39593
- Galactic cosmic rays interaction with interplanetary magnetic field from Venera 4 measurements of June-October 1967 20 p3280 A71-39595
- Soyuz observation of tritium and He-3 nuclei in Al targets exposed to space radiation 20 p3280 A71-39601
- Dust particle measurements in selenocentric and cislunar space /1967-1969/ by Lunar Explorer 35 and OGO 3 20 p3298 A71-39640
- Geopotential temporal variations from earth Baker-Nunn satellite observations 20 p3219 A71-39658
- Geodetic parameters describing earth gravity field and satellite tracking stations positions in geocentric reference frame, using satellite observation and deep space probes 20 p3220 A71-39659
- Base triangle determination by geometric geodesy, using laser telemetry and satellite optical observations with cataphotic reflecting prisms 20 p3220 A71-39661
- Geodetic satellite observational data condensation by substitution for all measurements of pass above station with pseudomeasurement expressed by vector with atmost six components 20 p3220 A71-39663
- Atmospheric temperature and water vapor profile calculation from Nimbus satellite IR spectrometer data, noting Southern Hemisphere tropospheric and stratospheric pressure analyses 20 p3258 A71-39667
- Atmospheric temperature profile from satellite soundings of outgoing radiation in IR carbon dioxide band, using regularization and Chahine methods 20 p3258 A71-39669
- Microwave sounding of ocean and earth surface thermal emission and atmospheric water vapor content by Cosmos 243 satellite-borne radiometers 20 p3259 A71-39672
- Atmospheric radiative energy budget based on structure and cloudiness distribution data from satellites and in situ observations 20 p3259 A71-39677
- Earth-atmosphere system radiation budget, comparing meteorological satellites actinometric data with calculated climatological maps of planetary long wave radiation distribution 20 p3259 A71-39678
- Reflected radiation brightness field statistical structure in IR range from Cosmos 121 satellite measurements, calculating correlation functions and spectral densities 20 p3259 A71-39680
- Short wave radiation fluxes estimation for earth-atmosphere system from Cosmos satellite data, studying brightness field angle structure 20 p3260 A71-39681
- Earth surface effective temperature map from meteorological satellites IR imagery interpretation 20 p3260 A71-39686
- Solar and terrestrial IR reflected radiation from Cosmos satellites measurements, determining clouds upper boundary height 20 p3261 A71-39688
- Meteorological satellite IR imagery for calculating spectral values of cloudiness radiation contrasts against underlying surface background 20 p3261 A71-39689
- Long term upper atmosphere density variations correlated with solar flux, using satellite observations 20 p3223 A71-39708
- Solar proton enhancement over auroral zone observed aboard near earth polar orbiting ESRO 2 satellite 20 p3282 A71-39735
- Interplanetary H scattered solar Lyman alpha background observations by Vela 7 and OGO 3 satellites, showing 72 day correlation with intensity curve 20 p3300 A71-39736
- Plasmasphere evening ionization anomalies observations from spherical electrostatic analyzers onboard

OV3-1 polar orbiting satellite, noting thermal plasma depletion during orbit night sector

20 p3225 A71-39741

Cosmos 142 and 259 experiments on ionospheric VLF propagation, discussing diurnal variations of daytime electron density

20 p3197 A71-39743

Drifting whistler frequency cutoff phenomena /striations/ observation in low latitude by POGO satellites, discussing interpretation based on propagation effect

20 p3198 A71-39746

Nonflare solar X-ray emission from Cosmos 230 observation, noting presence of sunspot groups with complicated magnetic fields during enhanced short wave emission

20 p3283 A71-39749

Plasmaspheric ambient hydrogen and helium atomic cations density measurement by OGO 5 ion mass spectrometer, during magnetic storm, noting relationship to auroral red arcs

20 p3227 A71-39833

Low energy auroral particle measurements from polar satellites, obtaining electron and proton precipitations location, and angular and energy distributions

20 p3228 A71-39847

VLF emissions and low energy electrons relation to other auroral phenomena from satellite-borne data associating midnight maximum with particles from plasma sheet

20 p3229 A71-39855

Magnetospheric plasma convection electric field double-probe measurement at high latitude by Injun-5 satellite, noting east-west velocity reversals or discontinuities at auroral zone

20 p3230 A71-39882

Proton precipitation satellite observation, comparing with simultaneous ground based measurement of auroral radar echoes

20 p3285 A71-39887

Polar ionospheric ion density enhancement correlation to low energy electron precipitation from observations by polar satellite

20 p3231 A71-39888

Thermospheric atomic hydrogen concentration temporal variations in situ measurement by Explorer 32 satellite

20 p3232 A71-39898

Magnetospheric plasma observation by Sirio 1 satellite, measuring protons, electrons and magnetic field with sensors

20 p3307 A71-39959

Equatorial ionospheric density measurements on quiet and perturbed days, using San Marco 2 satellite balance

21 p3373 A71-40047

Nimbus 2 satellite observed 6.7 micron water vapor radiation, compared to calculated radiances

21 p3373 A71-40224

Upper atmospheric density numerical calculation from draconite period by Perlo program using satellite observation near celestial equator

21 p3374 A71-40655

Solar proton flare prediction with microwave radio burst data, using satellite measurements

22 p3590 A71-41464

Solar low energy cosmic ray population anisotropy from satellite observations during flare event, describing rise time, decay, field alignment and time constant

22 p3591 A71-41469

Earth radiation belts high energy electron flux intensity monotonic decrease during magnetically quiet periods from satellite data analysis

22 p3591 A71-41527

Planetary distribution of primary cosmic rays and residual charged particles over atmosphere from Cosmos 208 and 228 satellite data

22 p3591 A71-41529

International coordinated measurements of solar activity geophysical effects in upper atmosphere, discussing synchronized observations of Cosmos 261 satellite and ground based ionospheric station network

22 p3591 A71-41530

International coordinated measurements of solar chromospheric flare effects on D region lower boundary and ionospheric propagation by Cosmos 261 satellite and ground based observatories

22 p3591 A71-41531

Galactic cosmic rays solar modulation and particle intensity gradient in interplanetary space from satellite observation data

22 p3591 A71-41534

Solar proton flux from 7 July 1966 flare observation via Proton 3 satellite, obtaining cosmic rays integral spectra

22 p3591 A71-41549

Interplanetary magnetic field parameters for various heliocentric distances from 1959-1967 satellite observations, discussing cavity position and solar activity phase correlations

22 p3598 A71-41550

Midlatitude topside ionospheric electron density mean diurnal and seasonal variations from Alouette 1 satellite observation

22 p3532 A71-41552

Ionization profiles of upper ionosphere from Alouette 1 vertical sounding data, proposing model for ionosphere shape

22 p3532 A71-41554

Latitudinal distribution of integral water drop content of clouds above Pacific, Atlantic and Indian oceans from Cosmos 243 measurements

22 p3568 A71-41653

Water vapor dimer effects on atmospheric brightness temperature in cm and mm radiometric investigations from satellites above oceans

22 p3533 A71-41654

Global environmental monitoring and remote sensing from satellites, considering thermal, air and water pollution

22 p3534 A71-41961

Atmospheric trace and pollutant molecules global survey, using airborne/spaceborne high resolution Fourier interference IR spectrometer

22 p3542 A71-41963

Satellite observations for earth resources management, discussing operational ground-based remote sensor system and information extraction techniques

22 p3534 A71-41973

Geothermic processes determination and registration in volcanic activity range by satellite IR measurements

22 p3534 A71-42004

Differential correction for redetermination of satellite observation stations geodetic coordinates as related to earth center of gravity and terrestrial potential coefficients

22 p3534 A71-42023

Direct observation of cosmic ray kinetic energy losses in interplanetary region by measurements at separated spacecraft

22 p3593 A71-42331

Tidal analysis of sea surface elevations from satellite-borne altimeter as function of instrument errors and orbital determinations

22 p3536 A71-42549

Gulf Stream and Middle Atlantic Bight complex synoptic sea surface temperature distribution from ITOS 1 satellite high resolution IR imagery

22 p3536 A71-42885

Geodetic locations of Doppler satellite observing stations consistent with CIO pole and astronomical determinations

[AAS PAPER 71-341]

23 p3666 A71-43014

Grand Tour mission satellite planetary imaging analyses and science scan platform pointing requirements, utilizing computer graphic techniques

[AAS PAPER 71-379]

23 p3731 A71-43049

Interplanetary plasma and magnetic field observations by Vela 3 and Imp 3 satellites

23 p3708 A71-43154

Magnetopause and bow shock location from IMP measurements, discussing solar wind momentum flux induced orbit-to-orbit changes in boundary positions

23 p3667 A71-43159

Equatorial proton and electron pitch angle distributions in loss cone and at large angles from geostationary ATS 5 satellite observation

23 p3720 A71-43165

Earth corotating plasma tail evidence in plasmopause variations from high resolution proton distribution data obtained by Ogo 4 satellite during magnetic storm

23 p3668 A71-43166

Vela 4A and 4B satellite observation of impulsive energetic electron fluxes in distant magnetotail associated with magnetospheric polar substorms

23 p3670 A71-43184

Premidnight asymmetry in directional 40 keV ionospheric electron flux profiles in magnetic local time observed on Azur satellite

23 p3721 A71-43185

Helmholtz vorticity equation application for indirect determination of inaccessible area geopotential field from satellite data

23 p3700 A71-43305

OSO satellite observed soft solar X-ray data correlation to solar activity

23 p3721 A71-43840

High energy particle environment model at synchronous altitudes during quiet geomagnetic periods from satellite observation, establishing outer radiation belt distribution function

23 p3722 A71-43978

Equatorial convective cloud mesosystems formation from Apollo 6 data, investigating Hadley circulation energy generation

23 p3701 A71-44011

Vertical atmospheric humidity profile variations relationship to clouds water vapor content from thermal radio emission measurements onboard Cosmos 243 satellite

23 p3673 A71-44048

Radio brightness temperature relationship to sea surface state, noting ocean storm regions determination from radiometric satellite data

23 p3673 A71-44050

Atmospheric vertical humidity profile determination by measuring microwave radiation from satellite

24 p3822 A71-44350

Low energy primary cosmic gamma ray measurements for spectrum latitude dependence and time variations near earth by Cosmos satellite scintillation spectrometer

24 p3865 A71-44564

Ionospheric integral electron concentration data from Elektron 1 and 3 satellites, using coherent radio wave measurements

24 p3866 A71-45028

SATELLITE ORBIT CALCULATION

U ORBIT CALCULATION

SATELLITE ORBITS

NT PARKING ORBITS

NT POLAR ORBITS

NT STATIONARY ORBITS

Highly eccentric satellite orbit, determining analytical solution for HEOS 1 launch window

01 p0154 A71-10386

Satellites initial circular orbit determination from incomplete observations

01 p0155 A71-10444

Geostationary communication satellites system with timed orbital motions for avoiding serial sun transit outages and eclipses

01 p0030 A71-10471

Kalman optimal linear filter application to near earth satellite orbit calculation based on earth radar observations

01 p0156 A71-10518

Canonical transformations for method of variations applied to differential equations describing satellite orbit perturbations

01 p0156 A71-10544

Liapunov method applied to nonlinear differential equations for distant satellite orbit secular perturbations

01 p0156 A71-10546

Cable-connected spinning and orbiting satellite spring-mass system, deriving in-plane motion equations by Hamilton principle for numerical analysis

01 p0165 A71-11587

Optimal two impulse correction with minimum energy for planetary approach trajectory and subsequent satellite orbit transfer

02 p0304 A71-11901

Geopotential coefficient recovery, using resonant satellite orbits long arc elements

02 p0245 A71-11995

Semiannual variation in upper atmosphere air density from satellite orbit data

03 p0407 A71-13304

High drag satellite 1968-59A orbits from optical and radar observations, obtaining rotational speed of upper atmosphere

03 p0407 A71-13305

Satellite dynamics applications in determination of atmospheric drag, earth and moon gravitational fields and Mars and Venus mass from trajectory construction

03 p0491 A71-14003

Oblate planet artificial satellite motion, obtaining secular and periodic perturbations to third and second order

04 p0642 A71-14739

Venus low retrograde spin rate explained as result of capture of moonlike object from retrograde orbit, transforming planet rotational energy into heat

04 p0642 A71-14823

Orbital solutions based on critical optical tracking and Doppler observations, comparing with GEOS 1 and 2 satellite orbits

04 p0553 A71-15305

Orbiting satellite targets assignment and scheduling to ground stations, presenting mathematical formulation and numerical example

04 p0555 A71-15332

Generalized von Zeipel treatment of lunar and artificial satellite theories, generating single canonical transformation by variable separation technique

04 p0654 A71-15719

Two dynamic systems on borderline of wildness, assuming one moving in oblate planet field

04 p0655 A71-15721

Satellite motion in orbits with semilatus rectum of 1/6 equatorial radius of oblate planet, discussing errors outside planetary radius

04 p0656 A71-15735

Elektron 2 and 4 satellites rotary motion with orbital variance of precession parameters and kinetic moment vector, considering gravitational and magnetic forces

05 p0815 A71-16034

Satellite motion stability in axisymmetric field of oblique rotating planet

05 p0815 A71-16050

Illumination charts for operational satellite, discussing orbit geometry and times, evolution trajectories and launch parameters

06 p0966 A71-17702

Synchronous satellites orbit and attitude control systems for correcting orbital errors due to launch inaccuracies, solar and lunar effects and terrestrial potential anisotropy

07 p1207 A71-19532

High power pulsed laser applications, considering satellite orbit determination, distant satellite ranging and precise triggering of high voltage spark gaps

07 p1124 A71-19780

Satellite orbital motion, discussing idealized perturbations limiting problem from point mass

08 p1360 A71-21004

Satellite orbital elements, examining resonance due to earth potential

08 p1366 A71-21778

Aerodynamic moment on satellite with asymmetrically positioned solar cell platforms, analyzing motion around center of mass for diffuse scattering flow

09 p1531 A71-22568

Intermediate elliptical orbits for planetary satellites with small inclination to equatorial plane

09 p1520 A71-22671

Computer algorithm for optimal linear impulse corrections to satellite orbit under inequality type constraints

09 p1424 A71-23135

Monkey physiological responses from lift-off to orbital insertion, showing EEG and EMG arousal reactions, motion sickness development, cardiovascular and respiratory changes

09 p1394 A71-23239

Orbiting Biosatellite 3 monkey environmental and physiological parameters circadian rhythms, investigating desynchronization or arrhythmia

09 p1395 A71-23241

Satellite orbital period variation under earth gravitational potential tesseral and sectorial harmonics

09 p1526 A71-23341

Computer controlled electromechanical system for luminous projection on world map of satellite orbits, using Ne-He laser beam

09 p1430 A71-23627

Artificial satellite orbital velocity tangential component time variation from variational calculus direction law

10 p1674 A71-24441

Long term zero gravity effects on mammal physiologic rhythms characteristics, studying rats in biosatellite orbits

10 p1565 A71-24611

Earth oblateness and air drag effects on satellite trajectories by asymptotic method of nonlinear mechanics, obtaining closed form solutions for first order approximation

10 p1678 A71-24928

Algorithms for close earth satellite orbit calculation developed by numerical integration methods, discussing solution efficiency [AIAA PAPER 69-948]

11 p1820 A71-25463

Jupiter, Saturn and Uranus satellite systems orbital radius and mass correlation, suggesting satellite orbital tidal evolution and energy dissipation at planetary atmospheric boundary layer

11 p1827 A71-25729

NonKeplerian intermediate orbit of artificial earth satellite motion with account of zonal harmonics, using fixed centers

11 p1829 A71-25807

Topocentric satellite trajectory approximation along circular orbit by n-degree equation, using coordinate-time relation

11 p1829 A71-25809

Satellite orbit elements over short time intervals from basic and asynchronous observations, using rectangular geocentric coordinates

11 p1829 A71-25810

Quasi-draconic and draconic orbital periods of earth satellites, showing ascending and descending passage variations

11 p1829 A71-25811

Optimal synchronous plane accuracy for space triangulation as function of geometrical position of artificial satellite relative to earth sphericity

11 p1758 A71-25812

PERLO program for analysis of satellite orbital period changes to determine celestial equator crossings from sequence of positions

11 p1829 A71-25825

Satellite orbit period variation data for PERLO program visual observations, calculating topocentric celestial equator transits

11 p1732 A71-25826

Lozinskii method orbit periods, comparing with quasi-draconic orbit periods from subsatellite point method

11 p1732 A71-25827

Photographic quasi-draconic period measurements from satellite transit across topocentric celestial equator tested on Echo 2 and Pagesos A

11 p1732 A71-25828

Four axis Zeiss camera unit for satellite small circle arc orbit observations, determining axial parameters equalization by least squares method and rotation rates

11 p1762 A71-25830

Relativistic effects and optimization in Doppler geodetical measurements, using model computations for satellite azimuth-elevation relation

11 p1732 A71-25832

Lunar gravitational field application for placing spacecraft into static earth satellite orbit with standing position with respect to rotating earth

12 p1957 A71-26627

Solar activity and geomagnetic disturbance effects on upper atmosphere density from ATS 2 satellite orbit observations

12 p1899 A71-26886

Planetary satellites intermediate orbits, obtaining angular orbital elements secular perturbations

12 p1964 A71-27091

Optimal two impulse correction with minimum energy for planetary approach trajectory and subsequent satellite orbit transfer

13 p2133 A71-28188

Hill-Brown differential equations for satellite coordinates transformed for integration with analytical programming language

13 p2135 A71-28352

Artificial satellites eccentric orbits commensurable with earth rotation, noting resonance effects of geopotential

13 p2135 A71-28354

Short term interval satellite orbit perturbations, computing direct solar radiation pressure effects with computer program

13 p2137 A71-28477

Approximate analytical method for nonlinear coupled equations of axisymmetric satellite librations in circular orbit, using constant Hamiltonian

14 p2319 A71-29892

Gravity field determination from satellite orbit analysis, using surface gravity and astrogodetic data

14 p2313 A71-30488

Forced vibration damping of satellites in elliptical orbits by variable cantilevers and rotor

15 p2499 A71-31177

Radar ranging experiment onboard Jupiter orbiter, concerning perturbations, gravitational harmonics and short arc orbit determination

15 p2487 A71-32041

Plane librational motion of axially symmetric satellite in elliptic orbit, developing periodic solution

15 p2488 A71-32092

Satellite orbital elements perturbations, examining resonance due to earth geopotential

15 p2495 A71-32683

Elliptic restricted three body problem, calculating fictitious retrograde Jovian satellites orbits in rotating-pulsating axes for sun-Jupiter case

16 p2633 A71-33337

Elektron 2 and 4 satellites rotary motion with orbital variance of precession parameters and kinetic angular momentum vector, considering gravitational and magnetic effects

16 p2645 A71-33438

Satellite motion stability in axisymmetric field of oblique rotating planet

16 p2645 A71-33454

Artificial planetary satellites lifetime estimation from atmospheric drag, discussing critical height-atmospheric density relationship, satellite design and initial orbit height

16 p2638 A71-33671

Upper atmosphere rotational speed variations from measurements of orbital inclination of satellites

16 p2569 A71-33807

X 4 satellite of British National Space Program, discussing design features, orbit, configuration, power subsystem, data handling and attitude control

17 p2814 A71-35330

Energy considerations of satellite orbit paradox, discussing speed increase under drag, librational motion and secular month length

18 p2962 A71-36099

Martian satellites motion along arbitrary elliptical orbits, expressing planet gravitational potential

18 p2962 A71-36108

Reduced state estimator for satellite orbital heading reference, describing decoupled single-skewed-gyro gyrocompass design for attitude control

19 p148 A71-37206

Artificial earth satellite orbital decay rate measurement for upper atmosphere density data, using combined directional observations and orbit data

19 p3048 A71-37394

Planetary satellites intermediate orbits, obtaining angular orbital elements secular perturbations

19 p1333 A71-37441

Satellite capture by Jupiter, calculating satellite orbits based on aphelion and perihelion conditions derived from planetary elliptical orbit three body problem

20 p3287 A71-38978

Satellite circular orbit trajectory plane time optimal relocation, examining turn angle angular position and modulus of maximum lateral acceleration

20 p3288 A71-39121

Attitude control of gravity orientated satellite in arbitrary orbit by solar pressure, showing libration damping characteristics of radiation force

20 p3306 A71-39396

Satellite orbital motion, discussing idealized perturbations limiting problem from point mass

20 p3294 A71-39584

Space triangulation and orbital methods of geodetic surveying of earth with satellites, using simultaneous observations from two and three stations

21 p3374 A71-40584

Automatic methods for equations of motion solution for artificial satellites orbits

22 p3600 A71-41951

Diamant launch vehicle multistage development for placing satellites in low perigee and high eccentricity and high and low circular orbits

22 p3610 A71-42020

Earth gravitational field effect on dual spin satellite motion in circular orbit, using Vigneron averaging method for linearized equations of motion

22 p3612 A71-42782

Trajectory aiming plane in optimum satellite orbit selection for planetary flyby and orbiter missions [AAS PAPER 71-305]

23 p3724 A71-42981

Circular sun synchronous earth satellites, investigating swathing patterns control by orbit selection and modification [AAS PAPER 71-353]

23 p3728 A71-43025

Automatic multi-satellite ephemeris maintenance by mathematical procedures, describing computer automated scheduling system program [AAS PAPER 71-355]

23 p3728 A71-43026

Upper atmosphere rotation rate decrease at altitudes above 350 km, determining zonal wind variations by satellite orbits analysis from Hewitt camera observations

23 p3667 A71-43140

Artificial lunar satellite motion in gravitational fields of nonspherical moon, earth and sun, deriving orbit perturbations

24 p3874 A71-45174

Mars orbiters and Kepler laws, discussing planetary motion, satellite orbits and orbital characteristics

24 p3875 A71-45268

SATELLITE ORIENTATION

San Marco satellite attitude determination from onboard aerodynamic drag measurements, using least squares method for three components calculation

01 p0122 A71-10390

Variance estimates and error expectations for satellite coordinates and velocity vectors from star altitude measurements

02 p0278 A71-11903

Earth radiation latitude nonuniformity effect on error in onboard satellite local vertical determinations, using Cosmos satellite data

02 p0304 A71-11915

Satellite orientation determination from single vector measurements, discussing coordinate systems transition

02 p0319 A71-11917

Oscillating satellite orientation from geomagnetic field strength vector, using least squares method

02 p0319 A71-11918

Satellite optimal guidance, discussing gyroscope application for stabilization and orientation control

03 p0500 A71-14227

Space vehicle local orientation by method of least squares determination of matrix for conditions of orthogonality, assuming random measurement errors

05 p0815 A71-16035

Axisymmetric satellite optimal reorientation into prescribed rotary motion by gas operated control jets, considering space navigation problems

05 p0815 A71-16036

Satellite onboard local vertical detection, emphasizing IR horizon sensors role

06 p0892 A71-17964

Manometric equipment arrangement in nose cone of oriented satellite with aerodynamic system stabilization

08 p1287 A71-21022

Artificial earth satellites orientation determined by onboard telemetric measurements, constructing model for rotational motion around center of mass

09 p1531 A71-22569

Elektron 2 and 4 satellites orientation based on onboard solar and magnetic sensors

09 p1531 A71-22570

Optimal orientation control of axisymmetric rotating space vehicle, using cyclic sliding mode theory

09 p1532 A71-22659

Space vehicles dimensions effects on working fluid mass and power required for orientation

09 p1532 A71-23133

Artificial earth satellite orbit perigee motion, calculating perturbation effect due to gravitational and magnetic fields on orientation and rotation

09 p1523 A71-23150

Sensitivity algorithms and application to attitude estimation of rigid body satellite in circular earth orbit

10 p1587 A71-24747

Equilibrium orientations of gravity gradient stabilized gyrostabilized satellites with rotor axis in principal plane, using Hamiltonian as Liapunov testing function

10 p1684 A71-24929

Attitude control of spin stabilized satellite with autonomous maneuverability, discussing correction

- maneuver method with one quasi-constant inertial reference direction
12 p1971 A71-26985
- Variance estimates and error expectations for satellite coordinates and velocity vectors from star altitude measurements
13 p2098 A71-28190
- Earth radiation latitude nonuniformity effect on error in onboard satellite local vertical determinations, using Cosmos satellite data
13 p2133 A71-28202
- Artificial earth satellite orientation determination from single vector measurements, discussing coordinate systems transition
13 p2145 A71-28204
- Oscillating artificial earth satellite orientation determination from geomagnetic field strength vector, using least squares method
13 p2145 A71-28205
- Spacecraft local attitude determination from measurements with random errors by least squares method
16 p2645 A71-33439
- Axissymmetric satellite optimal reorientation into prescribed rotary motion by gas operated control jets, considering space navigation problems
16 p2645 A71-33440
- Pulsed relay control system for stabilizing spacecraft orientation in flight, allowing for changes in characteristics of guidance sensor systems and slave mechanisms
16 p2646 A71-33660
- Angular position of sun nonoriented artificial earth satellites with angular velocities not exceeding 0.5 deg/sec, using harmonic analysis of magnetometric data
16 p2543 A71-33662
- Rotating dumbbell shaped satellites orientation optimization by system of jets, calculating energy losses
16 p2646 A71-33672
- Navigation and guidance alternatives of reusable nuclear shuttle, stressing onboard sensors and processing systems for position and attitude determination
17 p2774 A71-35074
- Satellite attitude control principles for studies requiring satellite orientation relative to orbital coordinate system
19 p3062 A71-37149
- Manometric equipment arrangement in nose cone of oriented satellite with aerodynamic system stabilization
20 p3240 A71-39602
- SATELLITE PERTURBATION**
- Planetary satellites intermediate orbits calculation in three dimensional Hill problem, allowing for solar disturbances
01 p0156 A71-10447
- Satellite orbit perturbations by solar radiation pressure, considering earth shadow in homogeneous field and long term effects
02 p0313 A71-12491
- Oblate planet artificial satellite motion, obtaining secular and periodic perturbations to third and second order
04 p0642 A71-14739
- Stationary satellite stationkeeping, considering triaxiality and graphical technique for corrections for luni-solar perturbations and solar pressure
04 p0649 A71-15326
- Three body stellar problem libration calculation using nonlinear mechanics methods, and application to lunar satellite perturbation by earth and lunar gravitational effects
04 p0655 A71-15728
- Satellite orbital elements perturbation due to tesseral and sectorial harmonics of earth gravitational potential
06 p0976 A71-18451
- Gravity oriented satellites librational dynamics in elliptic orbits, emphasizing atmospheric adverse effects [AIAA PAPER 71-89]
06 p0980 A71-18545
- Stochastic Liapunov stability of satellite motion influenced by aerodynamic and gravity gradient torques, considering atmospheric density uncertainty [AIAA PAPER 70-37]
07 p1208 A71-19883
- Jovian and solar perturbation of hypothetical artificial Callisto satellites, using Delaunay method
09 p1518 A71-22373
- Aerodynamic moment on satellite with asymmetrically positioned solar cell platforms, analyzing motion around center of mass for diffuse scattering flow
09 p1531 A71-22568
- Artificial earth satellite orbit perigee motion, calculating perturbation effect due to gravitational and magnetic fields on orientation and rotation
09 p1523 A71-23150
- Satellite orbital period variation under earth gravitational potential tesseral and sectorial harmonics
09 p1526 A71-23341
- Spin dynamics and deformation measurements on PAGEOS balloon satellite by photoelectric photometry, noting solar radiation pressure torque
11 p1761 A71-25546
- Spherical harmonics of secular perturbations in artificial satellites motion due to atmospheric gravitation
11 p1829 A71-25808
- Quasi-draconic and draconic orbital periods of earth satellites, showing ascending and descending passage variations
11 p1829 A71-25811
- Satellite orbital elements perturbation due to tesseral and sectorial harmonics of earth gravitational potential
12 p1955 A71-26601
- Tumbling triaxial satellite in elliptical orbit about spherical planet, determining resonant and nonresonant gravity gradient perturbations
13 p2145 A71-28356
- Equilibrium position stability of nonlinear two body satellite system in circular orbits in gravitational central force field, using linearized equations of motion
15 p2499 A71-31176
- Maximum nutation-precession angles of spin stabilized satellites during extension of long flexible booms
15 p2500 A71-32046
- Lumped fifteenth order spherical harmonics in geopotential from Ariel 3 satellite orbital inclination corrected for lunar-solar oscillatory perturbations
16 p2563 A71-33387
- Pageos spacecraft orbital acceleration prediction by radiation pressure perturbation theory accounting for nonisotropic scattering of solar spectra from rotating ellipsoidal body
16 p2641 A71-33772
- Weightlessness simulation for aerospace mechanisms, using tower release and gyrometric system for testing stage separation, satellite perturbation, yo-yos, probes and mast development [ONERA-TP-940]
18 p2971 A71-36018
- Error independence and elasticity allowance for moon librations and satellite perturbations
20 p3286 A71-38759
- Earth gravitational field fine structure via circular orbit satellite perturbations
20 p3220 A71-39660
- Mathematical model for studying solar radiation pressure effects on artificial satellite motion
21 p3438 A71-40104
- Earth-orbiting space vehicle attitude motion under constantly acting disturbances based on mathematical total stability of equilibrium
22 p3608 A71-41968
- Altitude dynamics and motion stability analysis of gravity oriented synchronous satellite under perturbation effects of environmental forces due to sun, earth, albedo and cosmic rays
22 p3612 A71-42050
- Long term orbit calculation by superposition of gravity and drag perturbations, taking into account solar and geomagnetic induced density variations [AAS PAPER 71-376]
23 p3730 A71-43046
- Cayley-Klein parameters application to quasi-precessional motion of satellite with multiple rotors, using perturbation method
24 p3848 A71-44830
- SATELLITE RENDEZVOUS**
- U ORBITAL RENDEZVOUS**
- SATELLITE ROTATION**
- Motion stability of satellite with rigid connection to symmetric rotors rotation axes
01 p0164 A71-11156
- Cable-connected spinning and orbiting satellite spring-mass system, deriving in-plane motion equations by Hamilton principle for numerical analysis
01 p0165 A71-11587
- Satellite oscillations about center of mass, allowing for energy dissipation due to magnetic hysteresis
02 p0319 A71-11907
- Damping in gravity graded satellite passive stabilization systems under eddy currents and dry friction induced by magnet motion
02 p0319 A71-11908
- Uniaxial satellite rotational motion, examining magnetic and gravitational torque effects on gyro dynamic properties
02 p0320 A71-11975
- Pageos 1 balloon satellite rotation observation over two years, determining period as time function
03 p0379 A71-14005
- Elektron 2 and 4 satellites rotary motion with orbital variance of precession parameters and kinetic moment vector, considering gravitational and magnetic forces
05 p0815 A71-16034
- Axissymmetric satellite optimal reorientation into prescribed rotary motion by gas operated control jets, considering space navigation problems
05 p0815 A71-16036
- Dynamically symmetrical satellite optimal transfer into steady axial rotation state with simultaneous alignment of symmetry axis, considering control jets moments
05 p0779 A71-16037
- Two-body satellite of axissymmetric rigid bodies interconnected by lossy universal joint, calculating transient oscillation damping of forced precession under external torque
07 p1205 A71-18895
- Aerodynamic moment on satellite with asymmetrically positioned solar cell platforms, analyzing motion around center of mass for diffuse scattering flow
09 p1531 A71-22568
- Artificial earth satellites orientation determined by onboard telemetric measurements, constructing model for rotational motion around center of mass
09 p1531 A71-22569
- Magnetic damper motions in rapidly spinning satellite
09 p1533 A71-23140
- Artificial earth satellite orbit perigee motion, calculating perturbation effect due to gravitational and magnetic fields on orientation and rotation
09 p1523 A71-23150
- Periodic rotation reversal effect on hollow cylinder surface temperature distribution in space simulation testing of spin stabilized orbiting satellites
09 p1430 A71-23733
- Passive nutation damping of spin stabilized orbital satellites with mechanical and pendulum dampers involving nonlinear interaction of vibrational and rotational motions
10 p1683 A71-24562
- Error introduced into coherent two-way Doppler tracking measurements on spinning satellite, using turnstile antenna
12 p1882 A71-27431
- Satellite rotation about center of mass, allowing for energy dissipation due to magnetic hysteresis
13 p2144 A71-28194
- Damping in gravity gradient satellite passive stabilization systems under eddy currents and dry friction induced by magnet motion
13 p2144 A71-28195
- Iapetus photometric observations, obtaining light curve by plotting rotational phase angle against magnitude
13 p2136 A71-28390
- Gravity stabilized satellite in elliptic orbit, examining rotational motion equations stability
15 p2499 A71-31159
- Elektron 2 and 4 satellites rotary motion with orbital variance of precession parameters and kinetic angular momentum vector, considering gravitational and magnetic effects
16 p2645 A71-33438
- Axissymmetric satellite optimal reorientation into prescribed rotary motion by gas operated control jets, considering space navigation problems
16 p2645 A71-33440
- Dynamically symmetrical satellite optimal transfer into steady axial rotation state with simultaneous alignment of symmetry axis, considering control jets moments
16 p2605 A71-33441
- Rotating dumbbell shaped satellites orientation optimization by system of jets, calculating energy losses
16 p2646 A71-33672
- Compound pendulum in artificial satellite for establishing attitude reference or detecting rotation rate variations
17 p2813 A71-34870
- Optimal maneuvers of axissymmetrical rotating satellite, minimizing orbital transfer
17 p2815 A71-35603
- Analog mass center estimator for spinning drag-free orbiting satellite, using free-falling proof mass shielded from external forces inside satellite cavity as reference [AIAA PAPER 71-947]
19 p3148 A71-37188
- Artificial gravity field produced by rotating spacecraft in earth orbit, examining astronaut physical responses and centrifugal force effects on work tasks
21 p3342 A71-40255
- German monograph on locking process in earth satellites with passive magnetic attitude control covering satellite rotational motion mathematical model, stability analysis, etc
21 p3455 A71-40773
- Rotating space station simulator for translational and rotational motion determination under gravity gradient torque action and control under input state conditions [IBM-712000406]
22 p3529 A71-41970
- Earth gravitational field effect on dual spin satellite motion in circular orbit, using Vigneron averaging method for linearized equations of motion
22 p3612 A71-42782
- Motion stability analysis for force-free spinning satellites with flexible appendages by Liapunov direct method [AAS PAPER 71-345]
23 p3772 A71-43018
- Canonical transformations application to spinning satellite with nutation damper [AAS PAPER 71-346]
23 p3728 A71-43019
- SATELLITE TELEVISION**
- TV broadcast satellites with in-core thermionic reactor, discussing transmitting power, design and economy
02 p0283 A71-12308
- Large earth station control for satellite communications system, including traffic capacity, TV transmission path breaks and logic equipment
02 p0224 A71-12824

Television satellites orbital transfer from low to geostationary orbit using ion propulsion

03 p0378 A71-13742

Satellite educational TV for developing nations, using cost benefit approach for system selection

04 p0691 A71-15277

TV systems for earth resources survey satellites, discussing high resolution return beam vidicon tubes, laser beam image reproducer and electron beam recorder systems

05 p0816 A71-16143

Mars Mariner 6 and 7 flyby missions, discussing surface and atmospheric information and data processing techniques

06 p0965 A71-17626

Mars surface TV pictures from Mariner 6 and 7, including cratered and uncratered terrains, light and dark markings and south polar cap

06 p0965 A71-17628

Circularly polarized parabolic reflector UHF antenna with helical feed for direct TV reception from satellite, discussing design and performance

09 p1417 A71-23034

Direct broadcast television service by satellite transmission, calculating trees and woods effects on attenuation and suggesting receiving system design modification

09 p1408 A71-23384

Communication satellites telephone, telex and high speed data transmission systems engineering, discussing intercontinental TV, synchronous orbit injection and solar panel deployment

12 p1973 A71-27610

Sirio B European communication satellite, discussing electronic equipment for simultaneous multichannel telephony and color TV transmission

14 p2319 A71-29820

Education satellite technology, discussing transmission levels, low cost high sensitivity receiver design and TV broadcasting

16 p2638 A71-33581

Satellite systems for educational TV program distribution, discussing orbit utilization, ground stations and ATS program

16 p2645 A71-33588

European telecommunication and TV distribution satellite system, including telephony, telegraphy, telex and wideband data transmission

17 p2696 A71-34232

Communication satellite TV and sound broadcasting system design without unreasonable cost

17 p2697 A71-34237

Satellite broadcasting defined by UN, discussing community and home direct reception modes and educational TV potentialities and problems

17 p2697 A71-34238

Satellite TV educational applications, outlining joint Indian Atomic Energy Department and NASA project

17 p2841 A71-34239

Copyright protection of communication satellite transmitted radio and TV programs, discussing involvement of UN agencies and other international organizations

17 p2841 A71-34248

Multifunctional communications satellite for TV distribution and trunk line, domestic, aeronautical, maritime, small user and space vehicle services

17 p2699 A71-34613

European regional satellite communication system, discussing TV coverage, spot beam antennas, frequency reuse, speech interpolation and circuits allocation

17 p2700 A71-34679

Satellite instructional TV experiment for direct community broadcasting to Indian villages

17 p2700 A71-34709

Juridical and institutional aspects of problems raised by TV programs content transmitted by communication satellites, noting applicability of international law

18 p2986 A71-36166

Joint India-U.S. satellite instructional television experiment for national development using ATS-F spacecraft

18 p2988 A71-36502

Satellite broadcasting of TV programs, assessing cost for European community

18 p2876 A71-36503

Satellite TV broadcasting development in European community, giving cost estimation procedure and program reception methods

18 p2876 A71-36504

Mixed satellite TV broadcasting system for France, estimating cost

18 p2988 A71-36505

TV broadcasting by satellite to isolated users via cable transmission, estimating cost and satellite optimal radiating power

18 p2877 A71-36507

European regional satellite communication system, discussing TV coverage, spot beam antennas, frequency reuse, speech interpolation and circuits allocation

18 p2877 A71-36516

Direct broadcast satellite TV communications, discussing international regulations and legal aspects

18 p2989 A71-36578

Low cost TV ground receiving systems for signals transmitted from synchronous satellites, describing reception techniques, manufacturing and performance characteristics

23 p3646 A71-43594

Explorer SAS-D astronomical satellites for UV spectra recording by TV cameras

24 p3876 A71-45275

SATELLITE TEMPERATURE

Cylindrical shell spacecraft thermal control coating system optimization, using truncated series representation

[ASME PAPER 70-WA/AUT-13]

03 p0499 A71-14151

ITOS-1 meteorological satellite launch and operational sequences in orbit, discussing thermal and attitude control, power and communications and sensor equipment

04 p0663 A71-15314

Thermal control surfaces experiment onboard Black Arrow X3 satellite

06 p0981 A71-18675

Outer planet large satellite steady state thermal models, indicating interiors at temperatures above ice-ammonia eutectic

14 p2318 A71-31125

Azur satellite mission report, discussing major anomalies, energy supply, position control, temperature behavior and orbit

[DGLR-71-008]

15 p2501 A71-32779

Azur satellite flight data evaluation, discussing heat balance and temperature monitoring

[DGLR-71-013]

15 p2501 A71-32780

ATS F and G thermal control, discussing heat pipe, louver and model tests

[ASME PAPER 71-AV-28]

18 p2868 A71-36395

SATELLITE TRACKING

Equatorial ionosphere correlation distance regarding VHF telemetry disturbances and satellite tracking, determining antenna ground spacing

01 p0074 A71-11307

Skynet ground stations design, equipment and operations, discussing antennas movement control, Cassegrain reflectors, receiving system amplifier noise temperature and tracking demodulator

02 p0233 A71-12432

Communication satellite autotracking by step track technique for exclusion of tracking feeds and multiple receiver channels in earth stations

02 p0222 A71-12789

Communication satellite ground station steerable antenna autotracking, evaluating on-line optimal search techniques by digital simulation

02 p0222 A71-12791

Multiple beam antenna with fixed spherical reflector and movable dual subreflector feedhorns, comparing with conventional Cassegrain antenna for satellite tracking

02 p0233 A71-12794

Antenna primary feed design and sample and store technique tracking system with conical scan control for Intelsat 3 satellite ground station

02 p0223 A71-12802

High efficiency feeds for large satellite autotracking earth station antennas, using focal plane distribution

02 p0223 A71-12808

Frequency selective conical scanning for direction finding earth station antennas for communication satellite automatic tracking, using waveguide mode conversion

02 p0223 A71-12809

Satellite ground station autotracking receivers, discussing antenna position control systems

02 p0239 A71-12816

Radar station-satellite contact times using horizon crossing, lunar occultation and keyhole constraints

02 p0280 A71-12898

Satellite tracking by radio direction finder, noting periodic azimuth deviations related to ionospheric Faraday effect

03 p0377 A71-13169

Transportable photoelectric satellite tracking system with 4-axis support for Schmidt-Cassegrain telescope, discussing field testing results

03 p0397 A71-14004

Q switched ruby laser ranging system of tracking station for use with retroreflecting satellites

03 p0379 A71-14007

Satellite triangulation network adjustment based on simultaneous errors observations, using filtering equations for matrix manipulations reduction

03 p0413 A71-14009

Artificial satellite photographic tracking, discussing Baker-Nunn cameras, international projects and future research

03 p0455 A71-14070

Geometric satellite geodesy, discussing simultaneous ranging from tracking station network

03 p0418 A71-14207

Range and range rate measurement errors between ground station and artificial satellite, investigating atmospheric refraction effects

04 p0661 A71-15003

Orbit determination accuracy using synchronous satellite system for tracking near earth spacecraft

04 p0553 A71-15312

Orbiting satellite targets assignment and scheduling to ground stations, presenting mathematical formulation and numerical example

04 p0555 A71-15332

Satellites interrogation, recording and location system for data acquisition from deployed remote instrumented platforms

05 p0743 A71-17134

Intelsat 3 Ground Control System functions, design and operation of tracking, telemetry and command stations subsystems

06 p0870 A71-18394

Central station of German ground system for satellite data acquisition, tracking and telecommand

07 p1082 A71-19021

Atmospheric propagation errors of satellite tracking system in VHF region

07 p1059 A71-19028

Tracking and data relay satellite system (TDRSS) impact on spacecraft mission support information management

07 p1197 A71-19704

Passive airborne computer augmented aircraft antenna pointing control system for communication satellites tracking

07 p1077 A71-19710

Satellite carrier tracking and phase lock carrier loops, evaluating lock and reacquisition performance loss by linear model and Monte Carlo digital simulation

08 p1270 A71-21352

Satellite laser tracking for geodetic data acquisition

08 p1285 A71-21802

NASA pulsed laser ranging systems for scientific satellite tracking, determining accuracy by trajectory and long arc orbital comparison

10 p1576 A71-24051

Camera vibration, and refraction anomaly effects on error of designated position for star or satellite

14 p2250 A71-31120

Ionospheric refraction errors in satellite tracking, computing elevation, range and range rate corrections

16 p2640 A71-33734

Correction method for satellite radio tracking errors due to VHF refraction in atmosphere

16 p2543 A71-33832

Polish space research covering satellite tracking, solar physics interplanetary gas dynamics, meteorological rockets and aerospace medicine

16 p2666 A71-33856

Cosmos satellites tracking and monitoring, decoding and interpreting radio signals

16 p2643 A71-34080

Earth gravity field and satellite tracking stations positions geodetic parameters in geocentric reference frame

17 p2733 A71-35027

NASA ERTS program, discussing system concept automatic data processing capability, compatibility with tracking ground stations and international cooperation

17 p2805 A71-35329

Satellite distance measurement by laser, describing energy calculation, equipment parameters, ground tests, cloud echo and Geos B satellite experiments

17 p2709 A71-35598

Range and range rate measuring equipment for PCM-TDMA satellite communications system data feed and orbit observation

18 p2879 A71-36533

Communication satellites automatic tracking system, noting low cost

18 p2881 A71-36555

Five-gate automatic acquisition star and satellite TV tracker with video signal from vidicon or image orthicon, using line-to-line correlation for SNR improvement

18 p2882 A71-36904

Three-channel monopulse tracking receiver for automatic steering of satellite tracking antennas, noting gain controlled IF amplifier module

18 p2884 A71-36996

Orbit computation and tracking system for Iris satellite using differential correction program

19 p3142 A71-38066

Ballistic measurement system for photographing satellites, illustrating minimum brightness relation to satellite distance

20 p3240 A71-39536

Geodetic parameters describing earth gravity field and satellite tracking stations positions in geocentric reference frame, using satellite observation and deep space probes

20 p3220 A71-39659

Condition equations for zonal harmonics using low inclination DIAL satellite interferometric measurements over perigee revolution

20 p3300 A71-39664

Pageos satellite optical tracking experiment, discussing camera, point image quality and quartz clocks rms error

21 p3347 A71-40260

Narrow beam acquisition and angle tracking for spaceborne laser communication links between low earth orbiting and synchronous satellite 21 p3348 A71-40805

Tracking meteorological satellite receiving antenna orientation data computer calculation, obtaining methods for geographic picture gridding 21 p3410 A71-40824

Nikolajev-Helwan space direction determination between satellite tracking stations at long distances, using simultaneous circle method 21 p3374 A71-41051

Satellite tracking ground antenna servocontrol, discussing system requirements and automatic and programmed operating modes [DFVLR-SONDDR-125] 22 p3483 A71-41520

SATELLITE TRACKING AND DATA ACQ NETWORK

U STADAN [SATELLITE TRACKING NETWORK]

SATELLITE TRANSMISSION

Small Astronomy Satellite PCM/PM telemetry transmitting split phase encoded data at 136 MHz 01 p0036 A71-10987

Widely separated microwave oscillators phase synchronization via satellite transponder 02 p0216 A71-12330

Precision measurement of satellite microwave flux and polarization at ground, involving Skynet tests 02 p0218 A71-12444

Artificial satellite HF radio wave ionospheric guided propagation, considering ray tracing based on geometric-optics treatment 05 p0720 A71-16229

Ionospheric electron content measurement from Faraday fading of Explorer 22 satellite transmissions during low and high solar activity 05 p0741 A71-16444

Ionospheric total electron content determination by Faraday fading of 40 MHz radio transmissions from Explorer 22 satellite, considering seasonal variations 05 p0741 A71-16445

Meteorological satellite systems, discussing earth image transmission by TV cameras IR photography, data processing and cloud pictures 05 p0817 A71-16641

Irregularities heights in ionospheric refractivity responsible for radio-satellite scintillation from spaced receiver experiments at midlatitude and subauroral locations 06 p0868 A71-17985

Wideband mixer for Intelsat 3 satellite, describing design, operation and performance 06 p0877 A71-18401

Microwave transmitting and receiving duplexers for Intelsat 3 satellite, discussing design, operation and performance 06 p0877 A71-18402

Error free SATCOM computer to computer data communication via satellite link 07 p1058 A71-18822

Geodetic satellite transmissions for ionospheric research, discussing orbital elements and frequency data 07 p1095 A71-19004

Troposphere effects on radio wave propagation and satellite communication 07 p1059 A71-19010

Satellites for time dissemination, discussing clock synchronization and signal propagation 07 p1154 A71-19011

Low angle signal strength enhancements from ionospheric beacon satellite BE-B transmissions 07 p1096 A71-19018

Low elevation polarimetric recordings of 136.44 MHz transmission from Early Bird geostationary satellite 07 p1206 A71-19022

Ionospheric error correction in distance measurements involving satellites, noting simultaneous differential Doppler and Faraday signal measurements 07 p1097 A71-19023

Propagation modes involved in HF or VHF reception at ground station of beyond-horizon satellite transmission 07 p1097 A71-19024

Small scale ionospheric irregularities from satellite radio signals fluctuations, using frequency scintillation measurements 07 p1060 A71-19037

UHF sharing between space and terrestrial services, discussing relationships between frequency choice, satellite relay performance, RF power requirements and system costs 07 p1065 A71-20419

Multiuser satellite communications system transmission capacity, comparing time division with Walsh multiplexing 08 p1269 A71-21334

Radio spectrum use in space communications for satellite services, considering antenna design, modulation techniques and wave attenuation 09 p1406 A71-22871

International telephone transmission, comparing technical and economic characteristics between submarine cable and satellite systems 10 p1577 A71-24267

Scintillation effects on synchronous satellite signal fading observed through polar ionosphere 10 p1577 A71-24315

Diurnal and seasonal variations of scintillations in short wave radio signals transmitted from earth satellites and spacecraft, noting relationship to ionospheric inhomogeneities 12 p1898 A71-26635

Man-made HF noise interference with satellite broadcasting, giving special consideration to automotive ignition systems 12 p1878 A71-26994

Gram-Charlier error probabilities of digital satellite communication systems due to intersymbol interference and additive noise applied to Chebyshev, Gaussian and cutoff filters 12 p1879 A71-27069

Microwave power transmission from satellite solar energy station to earth, discussing atmospheric attenuation mechanisms and wavelength and power density optimization 13 p2000 A71-28670

Faraday rotation of satellite signals, deriving relations for second order effects 13 p2031 A71-28784

Receiving system for phase measurement on coherent signals from satellites, discussing frequency conversion through phase locked filter 13 p2033 A71-29275

Faraday rotation of Transit 4A satellite signals recorded at three stations within Southeast Asian equatorial zone, showing latitudinal variation of ionospheric electron content at sunspot minimum 14 p2235 A71-30249

ATS 1 and 3 satellite VHF transponders for ships and aircraft location, communication and remote sensing, discussing performance test results 14 p2198 A71-30898

Performance and cost design tradeoff between HF and synchronous meteorological satellite data collection systems, considering platform transmitting power and SNR 14 p2198 A71-30900

Satellite telemetry systems for data transmission to developing nations ground stations decoding equipment 14 p2199 A71-30910

ERTS telecommunication system for space tracking and high resolution multispectral image data acquisition and commanding 14 p2199 A71-30912

Faraday rotation of satellite signals across transverse region, considering sudden jumps at transverse point in lower and topside ionosphere 16 p2544 A71-33959

Satellite broadcasting defined by UN, discussing community and home direct reception modes and educational TV potentialities and problems 17 p2697 A71-34238

Ionospheric electron content measurements from satellite signals Faraday rotation, criticizing graphical procedure for ambiguity reduction 17 p2732 A71-34322

Space station communications systems, discussing data relay satellites transmission paths to ground, multiple voice channels, two way color TV and onboard telephones 17 p2699 A71-34610

Low elevation angle tropospheric fading relationship to satellite communications and broadcasting at frequencies between 1 and 20 GHz 17 p2703 A71-35083

German TDMA system based on satellite repeater, discussing network configuration, transmission parameters, control, frame/burst format and field trial 18 p2875 A71-36050

ERTS satellite-based laser communication system, calculating cloud cover effect on clear line-of-sight light transmission probability through atmosphere to ground station 18 p2876 A71-36472

Pilot system of satellite transmitted educational TV involving lines reduction on TV screen 18 p2988 A71-36506

Aircraft onboard equipment tests in air navigation aid satellite project, estimating tracking random errors 18 p2877 A71-36509

ESRO part of joint ATC communication experiment for L band satellite use, giving voice and data transmission and distance measurement techniques tests results 18 p2945 A71-36510

Satellite to aircraft radio link simulation, evaluating electronic scanning antenna operation, intelligibility, data transmission rate and distance measurement accuracy 18 p2945 A71-36511

Meter wave aircraft slot antenna for Concorde air to ground communication via satellite, presenting synthetic radiation patterns 18 p2889 A71-36514

Rectilinear correction of geometric errors of images transmitted from earth resources satellites, using digital computer 18 p2886 A71-36540

Intelsat 3 and 4 RF demodulator design with tracking filters, using varactor for frequency control and discriminator for frequency drift compensation 18 p2890 A71-36558

Ground-aircraft link via synchronous communication satellite, discussing transmission frequency selection, ionospheric effect on propagation and satellite antenna 19 p3016 A71-37314

Magnetospheric whistler mode signal propagation paths and amplification, investigating echoes of ground to satellite transmission 19 p3016 A71-37400

Satellite systems contributions to transmission technology, considering economic factors, satellite antennas and receiver noise figures 19 p3017 A71-37519

Synchronous satellite transmission Faraday rotation conversion into total electron content, removing n pi ambiguity 19 p3128 A71-38032

Atmospheric signal propagation study between satellite and earth, using solar radiometry 19 p3018 A71-38075

Mid- and high-latitude ionospheric radio wave transmission from spacecraft during solar cycle, considering latitudinal and longitudinal gradients and electron content change rate 20 p3197 A71-39715

Ionospheric electron density measurements by differential Doppler and Faraday effects, using coherent radio signals of artificial earth satellites 22 p3508 A71-41526

Magnetoionic mode coupling of HF radio waves, considering Faraday rotation of satellite signals 23 p3642 A71-42963

Ionospheric HF wave ordinary (O) and extraordinary (E) modes coupling effect on satellite signal Faraday rotation 23 p3642 A71-42964

SATELLITE-BORNE PHOTOGRAPHY

In- and outflow fields in hurricane Debbie, using airborne radar echoes and ATS 3 satellite pictures 01 p0118 A71-10589

Wind speed field estimations from wind direction, using satellite cloud photographs 01 p0119 A71-10851

Tropics role in global circulation from satellite photography, discussing convection, cloud clusters, momentum fluxes, etc 01 p0121 A71-11356

Nimbus meteorological sensor and photographic data application to geology and hydrology for repeat global and synoptic observations, terrestrial mapping and event classification 04 p0583 A71-15290

Sea morphology from satellite photographs corresponding to sun reflex zone 05 p0739 A71-16274

Atmospheric high pressure axis determination from satellite photographed sea surface sunglint reflection patterns, using model calculations 05 p0778 A71-17045

Multispectral and multitemporal digital imagery spectral registration using fast Fourier transform techniques, applying to earth resources satellite imagery preprocessing 05 p0756 A71-17147

Environmental satellite data on-line processing and extraction procedures, including visible and IR imagery mapping and cloud pictures analysis 07 p1067 A71-18806

Computer pattern recognition technique for determining cloud motions in real time from ATS satellite photographs 08 p1326 A71-21453

Photographic image acquisition from planet orbiters, examining systems performance and lens selection 09 p1447 A71-22749

Aerial photography vs orbital acquired imagery resolution for land use data 09 p1439 A71-23212

Biosatellite 3 onboard camera time lapse photography of monkey sleep/wake activity patterns during weightlessness 09 p1394 A71-23240

Latent heat convective transport from lower to tropical upper troposphere, noting periodic energy fluctuations from time lapse synchronous satellite cloud photographs 09 p1489 A71-23553

Geodetic azimuth between two remote points on earth surface based on synchronous satellites positions and photographs 11 p1759 A71-25817

Four axis Zeiss camera unit for satellite small circle arc orbit observations, determining axial parameters equalization by least squares method and rotation rates 11 p1762 A71-25830

Computer program algorithm for satellite photographic observation data processing based on measurement at one station
11 p1733 A71-25833

Statistical diameter size distribution of random circles on plane or spheres in space from satellite and aircraft measurements for aerial and cloud photography
12 p1929 A71-27100

Satellite paralactical mounted camera installation for adjusting axis parallel to earth rotation axis
13 p2070 A71-29120

Satellite scale imagery potential for land-use mapping, using photomosaic simulation at 1/400000 scale
13 p2064 A71-29395

Land use classification schemes selection with orbital imagery for U.S. thematic mapping
13 p2064 A71-29397

Photogrammetric coordinate relation of points on lunar surface and stereopanoramas of scanning photographs by Luna 9 and 13 orbiters
15 p2406 A71-31618

Satellite IR photography, discussing camera systems, photointerpretation, applications in glaciology, hydrology, oceanography, geology, volcanology and environmental protection
15 p2408 A71-31835

Optical center position on negative and lens distortion of satellite camera verified on zenith area photos of stellar coordinate measurements
16 p2575 A71-32835

Polynomial fitting for information compression of Wild BC-4 satellite photographs, comparing short arc with geometric compensation methods
16 p2581 A71-34041

Sea surface slope distribution and wind velocity determination by sun glitter photography from synchronous satellite
17 p2734 A71-35215

Monograph on satellite-borne orbital photographic imaging techniques application to natural resources survey, discussing remote areas geomorphological and geological reconnaissance maps preparation
18 p2915 A71-35905

Aircraft and satellite remote sensing techniques in geology, soil science, geography and hydrology
18 p2913 A71-36539

Rectilinear correction of geometric errors of images transmitted from earth resources satellites, using digital computer
18 p2886 A71-36540

Satellite applications to cartographic and geodetic surveys, discussing photographic difficulties
19 p3047 A71-37302

Cloud amount and cloud cover interpretation from satellite data compared with ground, noting radiometric limitations
20 p3258 A71-39549

Global, regional and local earth IR imagery for earth sciences from space TV, photography and spectrophotometry
20 p3220 A71-39665

Earth surface characteristics relationship to meteorological elements based on interpretation of color space photographs from automated Zond 7 station
20 p3260 A71-39687

Statistical diameter size distribution of random circles on plane or spheres in space from satellite and aircraft measurements for aerial and cloud photography
22 p3537 A71-41655

Cumulus clouds photographs above Northern Hemisphere by meteorological satellite during active periods of earth atmospheric circulation
23 p3701 A71-44047

Crop surveys from multiband and multibase satellite photography during Apollo 9 mission, using statistical multispectral pattern recognition digital techniques
24 p3827 A71-44987

SATELLITE-BORNE RADAR
K band satellite transmit/receive frequency converters, describing design features and performance tests under simulated environmental conditions
19 p3028 A71-37697

SATELLITES
NT AEROS SATELLITE
NT ALOUETTE SATELLITES
NT ALOUETTE 1 SATELLITE
NT ALOUETTE 2 SATELLITE
NT APPLICATIONS TECHNOLOGY SATELLITES
NT ARIEL 1 SATELLITE
NT ARIEL 2 SATELLITE
NT ARIEL 3 SATELLITE
NT ARTIFICIAL SATELLITES
NT ATS 1
NT ATS 5
NT ATS 6
NT ATS 7
NT AZUR SATELLITE
NT BEACON SATELLITES
NT BIOSATELLITE 2
NT BIOSATELLITE 3
NT BIOSATELLITES
NT COMMUNICATION SATELLITES

NT COSMOS SATELLITES
NT DEIMOS
NT DIAL SATELLITE
NT EARLY BIRD SATELLITES
NT EARTH RESOURCES TECHNOLOGY SATELLITES
NT EARTH SATELLITES
NT ECHO 1 SATELLITE
NT ECHO 2 SATELLITE
NT ELEKTRON SATELLITES
NT ELEKTRON 2 SATELLITE
NT ELEKTRON 4 SATELLITE
NT ENVIRONMENTAL RESEARCH SATELLITES
NT EOSS
NT ESRO 1 SATELLITE
NT ESRO 2 SATELLITE
NT EXPLORER SATELLITES
NT EXPLORER 12 SATELLITE
NT EXPLORER 22 SATELLITE
NT EXPLORER 26 SATELLITE
NT EXPLORER 28 SATELLITE
NT EXPLORER 31 SATELLITE
NT EXPLORER 33 SATELLITE
NT EXPLORER 35 SATELLITE
NT EXPLORER 37 SATELLITE
NT EXPLORER 38 SATELLITE
NT EXPLORER 40 SATELLITE
NT FR-1 SATELLITE
NT GEODETIC SATELLITES
NT GEOPHYSICAL SATELLITES
NT GEOS 1 SATELLITE
NT GEOS 2 SATELLITE
NT GEOS-C SATELLITE
NT GRAVITY GRADIENT SATELLITES
NT HEOS A SATELLITE
NT HEOS SATELLITES
NT IAPETUS
NT IMP
NT INJUN SATELLITES
NT INTELSAT SATELLITES
NT IRIS SATELLITES
NT ISIS SATELLITES
NT ITO 1
NT LINCOLN EXPERIMENTAL SATELLITES
NT LUNAR ORBITER
NT LUNAR SATELLITES
NT METEOROLOGICAL SATELLITES
NT MOLNIYA SATELLITES
NT MOON
NT NATURAL SATELLITES
NT NAVIGATION SATELLITES
NT NIMBUS SATELLITES
NT NIMBUS 2 SATELLITE
NT NIMBUS 3 SATELLITE
NT NIMBUS 4 SATELLITE
NT OAO
NT OGO
NT OGO-B
NT OGO-C
NT OGO-D
NT OGO-E
NT ORBITAL WORKSHOPS
NT OSO
NT OSO-E
NT OSO-F
NT OSO-G
NT OSO-3
NT OUTER PLANETS EXPLORERS
NT OV-1 SATELLITES
NT OV-3 SATELLITES
NT PAGEOS SATELLITE
NT PASSIVE SATELLITES
NT PHOBOS
NT PROTON 1 SATELLITE
NT PROTON 2 SATELLITE
NT PROTON 4 SATELLITE
NT RADIO ASTRONOMY EXPLORER SATELLITE
NT RELAY SATELLITES
NT SAN MARCO SATELLITE
NT SAN MARCO 2 SATELLITE
NT SAS-A
NT SCIENTIFIC SATELLITES
NT SKYNET SATELLITES
NT SMALL ASTRONOMY SATELLITES
NT SMALL SCIENTIFIC SATELLITES
NT SPUTNIK SATELLITES
NT SYNCHRONOUS METEOROLOGICAL SATELLITE
NT SYNCHRONOUS SATELLITES
NT SYNCOM SATELLITES
NT TELSTAR SATELLITES
NT TIROS SATELLITES
NT VELA SATELLITES
NT VENERA SATELLITES
NT VENERA 4 SATELLITE
NT VENERA 6 SATELLITE

Satellite solar power station for microwave generation, transmission and energy conversion to electrical power on earth
13 p1999 A71-28665

Book on sources and availability of IQSY data, Volume 7, covering stations, sounding rockets, satellites, space probes and World Data Centers catalog
15 p2395 A71-31518

SATURATED HYDROCARBONS
U ALKANES

SATURATION
Stellar scintillation saturation at large zenith angles, examining atmospheric dispersion and multiple scattering roles
01 p0127 A71-10141

CW carbon dioxide laser beam IR absorption by sulfur hexafluoride, investigating saturation parameter relationship to pressure, temperature and relaxation time
03 p0437 A71-13879

Ni aluminoboronizing process by circulation method, discussing thermodynamic analysis for saturation possibility and parameters experimental determination
03 p0432 A71-13961

Viscosity measurements for saturated liquid state of Ne, Ar, H, N, O, CO and methane
06 p0929 A71-17315

He-Cd laser output description by rate equations, investigating saturation effects, discharge processes and optimization
06 p0910 A71-18666

Analog to digital converter noise power generation due to quantization and saturation effects under Gaussian input
07 p1059 A71-18852

Modified Ebers-Moll equivalent circuit model for saturation characteristics of high voltage transistors
07 p1174 A71-19058

Steels in stressed state, determining hydrogen saturation and occlusion
09 p1467 A71-22309

Model of curved channel multipliers saturation gain at high applied voltages
09 p1446 A71-22736

MOS transistor saturation range transconductance, internal resistance and gain factor calculation, allowing for field effect on space charge near drain
12 p1889 A71-27626

Microhardness dependent saturation of glass powders by iron, nickel and titanium during sintering of cermet metal matrix materials in vacuum
16 p2601 A71-33573

Saturation effects and mode selection for monofrequency He-Ne lasers with nonlinear absorption
17 p2752 A71-34406

Critical point anomaly in saturation curves of reduced temperature-compressibility planes of pure substances, using metric differential geometry and thermodynamics
18 p2985 A71-36452

Saturated Hg vapor pressure at 650-900 K by boiling point method
19 p3162 A71-37591

He-Ne lasers, investigating possible saturation effect usage in strong field to obtain single-mode operation
19 p3072 A71-37769

Nonlinear equations for traveling wave amplifiers using transverse wave interaction modes /cyclotron and synchronous electron beam waves/, calculating saturation characteristics
20 p3203 A71-39003

Ion cyclotron resonance power absorption, deriving expression for average ion kinetic energy at saturation in steady state limit
21 p3418 A71-40231

Mathematical description by Gaussian error function for metals diffusive saturation and diffusion constants determination
21 p3403 A71-41160

Numerical modeling and analysis of homocentric light beams propagation in cubic and nonlinearity saturation medium, using parabolic equation approximation
21 p3417 A71-41259

Pressure dependent absorption of carbon dioxide laser by boron chloride, considering saturation and line overlapping effects
22 p3556 A71-41805

Current and charge saturation effects on channel electron multipliers in continuous and pulse operation
24 p3811 A71-45330

SATURN [PLANET]
NT SATURN RINGS
Saturn millimeter wave spectrum and brightness temperature measurements, showing ammonia absorption characteristics in atmosphere
04 p0659 A71-15851

Saturn satellite Iapetus periodic light variation curve explanation in terms of meteoroids impact erosion
04 p0660 A71-15861

Jupiter and Saturn magnetosphere calculations, considering solar wind characteristics and planetary magnetic fields
06 p0977 A71-18494

[AIAA PAPER 71-30]
Saturn natural satellites commensurabilities evolution from analysis of libration amplitude change with time for interaction under tidal friction with planet
07 p1202 A71-20519

- Jupiter and Saturn gravitational moments calculation procedure based on planetary density angular distribution 08 p1361 A71-21054
- Titan visual photometric observations, describing measurement procedures and error sources 09 p1528 A71-23549
- Saturn satellites spectrophotometric observations at UV, visible and near IR, noting reflection spectra data 11 p1819 A71-25210
- Saturn cloud layer molecular absorption from spectral /photographic and photoelectric/ observations 11 p1827 A71-25730
- H and He concentrations upper limit for Titan atmosphere from molecular diffusion time constant 11 p1828 A71-25732
- Saturn, Titan and ring IR photometric observations, examining brightness temperature albedos, optical thickness and individual particles 13 p2134 A71-28283
- Saturncentric latitude measurements tabulation for use with standard drawings 13 p2136 A71-28388
- Jupiter and Saturn magnetic field differences, considering metallic interior models 14 p2304 A71-29599
- Jupiter and Saturn gravitational moments calculation procedure based on planetary density angular distribution 14 p2310 A71-30167
- Saturn atmospheric structure and optical properties, investigating methane absorption bands 15 p2483 A71-31337
- Saturn and Jupiter mass determination from Schwassmann-Wachmann 1 comet motion observations, using perturbation program based on Schubart-Stumpf n-body integration program 18 p2970 A71-37062
- Launch opportunities for Grand Tour outer planets missions using Saturn-Jupiter instead of Jupiter-Saturn flyby sequence [AAS PAPER 71-139] 19 p3140 A71-37943
- Mimas-Tethys resonance motions under short period gravitational perturbations and tidal dissipation functions 20 p3286 A71-38760
- Saturn planetary system optical and radio observations during 1966, discussing Janus satellite, D ring, rarefied envelope and brightness temperature distribution 20 p3297 A71-39632
- Rhea and Titan UVB photoelectric observations, obtaining light curve magnitude variation 21 p3440 A71-40056
- Jupiter and Saturn IR radiation sources, radio emission storms, magnetic fields, life existence, Grand Tour missions, etc 21 p3442 A71-40150
- Saturn internal constitution, discussing Ramsey theory of planetary interior composition of hydrogen-helium mixture 22 p3596 A71-41450
- Saturn disk monochromatic albedos observation by multicolor photoelectric photometry, comparing with Jupiter 22 p3602 A71-42178
- Saturn atmospheric structure and optical properties, investigating methane absorption bands 22 p3606 A71-42612
- Earth-Jupiter-Saturn-earth trajectories, determining mission planning parameters [AAS PAPER 71-361] 23 p3729 A71-43031
- Hydrogen and helium thermal dissociation and ionization at Jupiter and Saturn adiabatic atmospheric models conditions 24 p3850 A71-44809
- Computer processed photographic observations of Pluto, 10 Hygiea, 433 Eros and Saturn satellites VII, VIII and IX 24 p3874 A71-45178
- SATURN LAUNCH VEHICLES**
- NT SATURN 5 LAUNCH VEHICLES**
- Saturn launch vehicle gust penetration loads, presenting separated flow and associated time lag effects [AIAA PAPER 71-178] 06 p1004 A71-18617
- Saturn launch vehicle navigation, guidance and control system, discussing optimal system design for flight path optimization 07 p1155 A71-19527
- Interactive Saturn flight program simulator for real time graphics operations of navigation, guidance, engine control, event sequencing and communications 08 p1272 A71-21237
- Switching analysis for high order vehicle systems with magnitude and direction constraints in attitude control for Saturn rocket with sloshing motion 08 p1269 A71-21331
- Prelaunch automatic azimuth alignment theodolites for Saturn 1B and Saturn 5 space vehicles inertial guidance system, discussing return images separation and error signal generation 08 p1289 A71-21375
- Separated flow and time lag effects on sinusoidal gust penetration loads and elastic launch vehicle response of Apollo-Saturn class [AIAA PAPER 71-344] 11 p1836 A71-25323
- High vacuum mass spectrometric hazardous gas detection system used during cryogenic loading of Saturn vehicles, discussing application to environmental pollution detection 22 p3542 A71-41988
- SATURN PROJECT**
- Information management system to schedule, control and status work on Apollo/Saturn Program at Kennedy Space Center [AIAA PAPER 71-239] 07 p1207 A71-19715
- SATURN RINGS**
- International joint optical and radio astronomical observations on Saturn rings and disk 1/1966/ 01 p0149 A71-10046
- Saturn rings physical properties concerning optical thickness, particle features, albedo and mass 02 p0310 A71-12158
- Soviet book on Saturn rings covering observations, brightness change with phase angle and dynamics 03 p0483 A71-13125
- Saturn rings spectral reflectivity measurement and compositional implications concerning water frosts and silicates 04 p0659 A71-15857
- Saturn rings radial structure model featuring purely gravitational forces association with primary and perturbers, using planar restricted three body problem formalism 07 p1202 A71-20518
- International joint optical and radio astronomical observations on Saturn rings and disk 1/1966/ 08 p1361 A71-21040
- Mimas /Saturn satellite/ perturbations effect on Cassini division in Saturn rings 10 p1673 A71-24425
- Saturn polarimetric observation, noting rings polarization Stokes parameters, methane absorption bands and continuous spectrum 15 p2482 A71-31336
- Saturn radio emission and brightness temperature measurements, determining rings optical thickness upper limit 16 p2639 A71-33692
- Dynamic model for Saturn rings radial structure, considering outside composition material, Titan perturbation effect and particle space density 22 p3603 A71-42186
- Saturn polarimetric observation, noting rings polarization, Stokes parameters, methane absorption bands and continuous spectrum 22 p3606 A71-42611
- Saturn ring motion stability factors for atomized material resistance to gravitational field, discussing ring thickness, density and other parameters 24 p3869 A71-44810
- SATURN S-1C STAGE**
- Space shuttle development and certification test program comparison with large aircraft and spacecraft programs, considering Boeing 747 aircraft and Apollo Saturn S-1C stage [AIAA PAPER 71-306] 09 p1531 A71-22619
- SATURN S-2 STAGE**
- Saturn S-2 stage propellant feedlines and V-2 engines simulating structural longitudinal oscillation by analog computer [AIAA PAPER 70-626] 03 p0472 A71-14430
- Spray foam insulation for Saturn S-2 stage, consisting of phenolic honeycomb core composite purged with helium 20 p3312 A71-39270
- SATURN S-4B STAGE**
- S-IVB liquid rocket engine and propellant feed systems restart chidown in orbital operations [AIAA PAPER 70-672] 07 p1183 A71-19857
- Saturn S-4B continuous vent system for propellant tanks during parking orbit to prevent excessive pressure, requiring liquid settling with auxiliary ullaging rockets 18 p2973 A71-36453
- SATURN STAGES**
- NT SATURN S-1C STAGE**
- NT SATURN S-2 STAGE**
- NT SATURN S-4B STAGE**
- SATURN 5 LAUNCH VEHICLES**
- Saturn V second stage longitudinal oscillation from structure and propulsion system interaction examined by transfer function simulator subroutine /TRANSIM/ computer program 02 p0318 A71-11788
- Nuclear thermal rockets development, discussing reactor-engine tests, solid and gas cores and Saturn 5 application 02 p0283 A71-12314
- Skylab program, describing equipment based on Saturn 5 workshop experiments and objectives 07 p1206 A71-19088
- Missile vibrations during acceleration calculated in matrix form for Saturn 5/Apollo booster configuration 20 p3306 A71-39412
- Apollo/Saturn 5 propulsion system design, development, testing and integration 22 p3589 A71-42026
- Mobile concept and automated checkout applications in Apollo/Saturn 5 Launch Complex 39, discussing performance 22 p3611 A71-42044
- Frequency shift in air-coupled surface waves during Saturn 5 launches, computing apparent phase velocity experienced by ground 23 p3672 A71-43883
- SAWTOOTH WAVEFORMS**
- Pulse rise, fall times and peak current values in sawtooth-voltage generator relaxation circuits with avalanche transistors 03 p0387 A71-13998
- Quadratic sawtooth voltage and sweep frequency generators design based on periodic parabolic pulse phase modulation of quartz oscillators HF output 04 p0559 A71-15568
- Sawtooth structure of convective plasma column in sulfur hexafluoride at cross flow Mach numbers, using thermionic rail accelerator 09 p1498 A71-22096
- Linear sawtooth generator, using MOS unijunction transistors to switch and maintain constant discharge current from timing capacitor 11 p1740 A71-26549
- Linear sawtooth voltage phantastron type generator, presenting operation time diagrams and circuit advantages 12 p1906 A71-26900
- Avalanche transistors circuits, generating rectangular and sawtooth pulses for use in time delay devices 14 p2213 A71-30582
- High speed rotating optical attenuator for sub-second sawtooth radiance pulse generation for detection, cooling or heating experiments 19 p3063 A71-37249
- SCALARS**
- Scalar theory for nonstatic gravitational fields, using tensor and linearized equations 10 p1641 A71-23975
- Scalar function expansion in relativistic invariant functions in pseudoeuclidian space, deriving direct and inverse formulas for spherical, hyperbolic and Lobachevskii coordinates 16 p2612 A71-33459
- Scalar material transport in incompressible inhomogeneous turbulent fluid based on one point correlations equations 17 p2835 A71-34211
- Scalar-tensor field self consistent interaction theory eliminating Einstein gravitational model paradox 17 p2801 A71-34629
- Neutral functional equation including scalar differential-difference equation, determining sufficient conditions for zero solution 20 p3254 A71-38899
- Linear time-varying system state space representation determination based on scalar differential equation, considering advantages 22 p3566 A71-41853
- Relativistic gravitation theory, using Lorentz invariant scalar potential and gravitational metric 22 p3575 A71-42355
- Semiinfinite atmospheric multiple conservative Rayleigh scattering, describing polarized radiation transfer 22 p3576 A71-42608
- SCALE [CORROSION]**
- Fe-Ni alloy oxidations parabolic kinetics and activation energies, noting scale development as function of oxidation amount and temperature 05 p0770 A71-17098
- Comparative isothermal oxidation of Fe-Cr-Al, Ni-Cr-Al and Co-Cr-Al alloys with protective scales 10 p1624 A71-23971
- Manganese and silicon effects on oxidation and scale mechanisms of Co-Cr alloys, using thermogravimetric, metallographic and microprobe techniques 10 p1625 A71-23973
- Oxidation kinetics and scale morphology of chromium oxide forming thoriated and unthoriated Ni alloys, discussing rate controlling processes effects 16 p2590 A71-32871
- Oxidation resistance and scale fracture healing by Al additions to Co-Cr alloys at high temperatures, using electron probe and scanning electron microscope analyses 21 p3405 A71-41420
- Boron addition effects on scaling resistance of Ni-Cr steel at high temperatures 23 p3690 A71-43278
- X ray analysis of scale formation in precipitation hardened nickel, investigating thermal resistance and oxidation rates 23 p3691 A71-43520
- SCALE [RATIO]**
- Level ampoule inner surface curvature nonuniformity, noting correction determination in level scale division 04 p0592 A71-14857

Design and fabrication of frequency multipliers from 10 to 30 GHz on silica substrates by scaling and integrated circuit processing

- 19 p3026 A71-37219
- Lunar maps classification, nomenclature and scales sequence
- 21 p3448 A71-40549
- Time scale and time interval characteristics for scientific use, tabulating associated units
- 24 p3827 A71-44995

SCALE EFFECT

- Scale effect in cavitation flow, discussing flow parameters and model size effects on similar flows
- 04 p0570 A71-15063
- Gyroscopes motor couple scale factor measurement [AGARDOGRAPH-128]
- 05 p0750 A71-16311
- Viscous similitude reduction to Mach number independent Birkhoff binary scaling for hypersonic flow over slender bodies
- [AIAA PAPER 71-252]
- 08 p1377 A71-21981
- High Reynolds number transonic wind tunnel need in U.S., discussing wing maximum lift and pitching moment, shock induced flow separation, etc
- 10 p1589 A71-24174

Thermal scale modeling limitations for radiation-conduction system of unmanned spacecraft, discussing material thermal properties, model dimensions, instrumentation effects and environment simulation

- 13 p2159 A71-27988
- Size effects on large rotor systems design, considering weight, blade loading, tip speed, etc
- [AHS PREPRINT 552]
- 14 p2180 A71-31104
- Scale factor effect on brittle fracture strength for Ti and Al alloys and high strength steels
- 16 p2657 A71-33409

Helicopter rotor model testing in water tunnel, discussing advantages over wind tunnel testing due to Reynolds number scaling and avoidance of wall interference effects

- 16 p2526 A71-34151
- Brittle fracture under stress concentrations, calculating scale factor based on technical cohesive strength statistical theory
- 17 p2833 A71-35619

Dimensionless products associated with scale factor effects of parachute critical opening /squidding/ velocity

- 19 p2996 A71-37293
- Multivalley semiconductors scale effect due to nonuniform electron heating by electric field, determining effective conductivity as function of plate thickness and surface characteristics
- 22 p3585 A71-42058

Scale effect in semiconductor magnetoresistance due to carrier separation across plate thickness under perpendicular magnetic field

- 23 p3715 A71-43476
- Uniform model universes with matter and black body radiation, obtaining radiation temperature dependence on scale factor
- 23 p3769 A71-43994

Solid powder metallurgy tungsten alloys, determining scale factor effect on bending strength and fatigue limit

- 23 p3693 A71-44226

SCALE HEIGHT

High atmosphere X ray absorption grazing scale height variations from satellite measurement of solar X-ray flux during sunrise and sunset

- 03 p0480 A71-14049
- E layer phase height measurements with spaced receivers without ultra stable oscillators, calculating scale height
- 14 p2230 A71-29712

Upper ionosphere electron density scale height data, noting conjugate point sunrise heating effects from Alouette I data

- 17 p2731 A71-34313
- Atmospheric temperature and density scale height seasonal variations near mesopause, using meteor theory mass and luminosity equations
- 17 p2737 A71-35740

High altitude aerosol layer effects on atmospheric UV albedo, correcting ozone scale height spaceborne measurements

- 20 p3221 A71-39695

SCALE MODELS

Computerized human body anatomical geometrical model with life size skeleton and organs scaling for radiation dosage analyses in space missions

- 04 p0546 A71-15282
- Single module unmanned Mars roving vehicle with flexible metal toroidal hoop-spoked wheels, discussing remote controlled scale model design for simulation on earth
- 04 p0566 A71-15333

Airfoil profile drag measurements, correlating full scale flight tests and scale model tests in transonic and high Reynolds number wind tunnels

- [AIAA PAPER 71-289]
- 08 p1229 A71-22012
- Structurally similar models, investigating space vehicles dynamic characteristics
- 09 p1532 A71-22658

Large space structures zero backlash deployment mechanism, discussing dynamically scaled model for mechanical and structural design and dynamic analysis [AIAA PAPER 71-400]

- 11 p1836 A71-25276
- Aircraft tires mechanical data from small models, discussing mechanical properties, tire stresses and tire temperatures
- [AIAA PAPER 71-346]
- 11 p1707 A71-25325

Numerical and scale modeling interaction for spacecraft thermal design verification

- [AIAA PAPER 71-439]
- 11 p1838 A71-26227
- Free flight ranges application to high temperature gas dynamics, using mathematical model to relate sub and full scale observations
- 11 p1705 A71-26269

Spacecraft radiator thermal scale model, using forced convection, conduction and radiation heat transfer

- 11 p1860 A71-26517
- Lunar ground effect machine, discussing operation principles, design, construction, terrain advantage and scale model testing
- 11 p1747 A71-26528

Thermal scale modeling limitations for radiation-conduction system of unmanned spacecraft, discussing material thermal properties, model dimensions, instrumentation effects and environment simulation

- 13 p2159 A71-27988
- Surface roughness causes and effects in planar fluidic elements, using large scale models
- 15 p2351 A71-32059

Reactor-shield-containment system models under impact tests, noting cracks, leaks and deformations

- 16 p2606 A71-33250
- Electromagnetic coupling measurement between two antennas in cluttered communications system, emphasizing scale model prediction technique
- 17 p2703 A71-35078

Fixed multiple beam toroidal reflector antenna operating above 12 GHz, analyzing 10 by 15 ft scaled model parabolic torus

- 17 p2704 A71-35091
- Long time failure modeling of real structure behavior in short times by scale and mathematical models, noting nonaccountability of crack propagation time
- 17 p2834 A71-35669

Near field noise measurement on quarter-scale model to estimate fuselage pressure in VTOL aircraft for conventional, short and vertical takeoff configurations

- 19 p2997 A71-37844
- Aerothermodynamics and scale modeling techniques for prediction of plastic burning rates, using Spalding mass transfer theory and dimensional analysis
- 19 p3171 A71-38250

Two dimensional seismic mathematical and scale techniques appropriate to inertial navigation devices test pads noise isolation examination

- [AIAA PAPER 71-912]
- 19 p3056 A71-38326
- Subscale modeling of aircraft trailing vortices in controllable laboratory environment
- 21 p3318 A71-40488

SCALERS

Multichannel scaler as interface between edge scan unit and calculator to generate optical transfer functions

- 13 p2066 A71-28159

SCALING LAWS

Faraday rotation near ferromagnetic critical temperature of chromium bromide, discussing scaling laws validity and experimental confirmation

- 04 p0637 A71-15796
- Electric propulsion spacecraft mission performance scaling laws for invariant trajectory, obtaining optimum gross payload over wide range of system input parameters
- [AIAA PAPER 71-160]
- 06 p0981 A71-18602

Rational scale selection for theoretical and experimental graphs, investigating slopes and angles between line segments for various parameters

- 09 p1439 A71-23347
- Temperature gradients effect on density distribution in material near critical point, using classical and scaling-law theories and Ising model
- 12 p1929 A71-27031

Venus atmospheric turbulence from Venera 4, 5, 6 and Mariner 5 observations, discussing scaling laws and normalized signal-amplitude standard deviation

- 13 p1322 A71-27928
- Differential equation systems optimal scaling for analog computer, proposing amplitude and time scaling factors and disposition parameters with linear programming
- 15 p2440 A71-31155

Intermittence and scale similarity in turbulent flow structure, analyzing eddies distribution inhomogeneity

- 16 p2557 A71-32932
- Inlet turbulent pressure data scaling hypothesis, investigating Reynolds number effect
- [AIAA PAPER 71-669]
- 18 p2956 A71-36774

Electron production cross sections in inelastic atomic collisions, evaluating classical scaling law and quantum mechanical statistical methods against experimental results [AIAA PAPER 71-995]

- 24 p3850 A71-44587

SCANDIUM

NT SCANDIUM ISOTOPES

SCANDIUM COMPOUNDS

NT SCANDIUM OXIDES

Mass spectrometric determination of vapor phase dissociation energies of scandium dicarbide and scandium tetracarbide

- 08 p1250 A71-20673

SCANDIUM ISOTOPES

Inelastic alpha particle scattering experiment for studying energy spectrum and angular distribution of Sc-45 excited states

- 03 p0462 A71-14417

SCANDIUM OXIDES

Transparent scandium oxide powder development by hot pressing, plotting IR transmission vs wavelength

- 20 p3253 A71-38819

SCANDIUM 46

U SCANDIUM ISOTOPES

SCANNERS

NT FLYING SPOT SCANNERS

NT HORIZON SCANNERS

NT INFRARED SCANNERS

NT OPTICAL SCANNERS

Current profile monitor for scanning electron beam irradiations from accelerator, using storage oscilloscope or X-Y recorder for display

- 02 p0249 A71-12127
- Scanning electron microscopy for microstructures of various eutectic Ni alloys, discussing rod-plate transition
- 06 p0914 A71-18681

Follow-up scanning systems and reading volume reduction in biological image descriptions facilitating computer aided microstructure analysis

- 06 p0871 A71-18697
- Follow-up scanning system input of microobject data with maximum contraction for biological computer analysis, noting karyotype or blood formula applications
- 06 p0864 A71-18698

Multielectrode ultrasonic transducer with multiplexing circuits for electronic readout scanning, discussing application in rapid inspection of plate or strip isotope heat sources

- 08 p1287 A71-20950
- V/STOL microwave scanning beam approach and landing system, describing ground and airborne station equipment and operation
- 08 p1332 A71-21680

Telescope plate scanner automated computerized operation, evaluating faint stars identification and color classification for annual motion surveys

- 09 p1443 A71-22646
- Search scanning system synthesis based on forces optimal distribution over investigated field, using Pontryagin maximum principle
- 10 p1586 A71-24167

Direct analysis of IC by laser beams, considering homogeneity test scanning of Ge semiconductor crystals through photovoltaic injector microscopy

- 12 p1914 A71-27041
- Scanning system with hydropneumatic drive for Fabry-Perot spectrometers in IR region, describing He-Ne laser tests
- 14 p2247 A71-30587

Statistical detection theory applied to images against background of laser produced speckle, using flying-spot type scanning machine

- 17 p2754 A71-35324
- Scanning electron microscope for poor metallization detection in manufacturing cycle of semiconductor devices
- 19 p3034 A71-38519

Grand Tour mission satellite planetary imaging analyses and science scan platform pointing requirements, utilizing computer graphic techniques [AAS PAPER 71-379]

- 23 p3731 A71-43049
- Eye and orbit A and B ultrasonography scanning technique, showing minimal echogram distortions in meridional arc scans
- 24 p3799 A71-44367

SCANNING

NT CONICAL SCANNING

NT FREQUENCY SCANNING

NT PANORAMIC SCANNING

NT RADAR SCANNING

Weather radar signals decorrelation times due to vertical wind shear and azimuth scanning

- 01 p0030 A71-10598
- Horizontal aperture equalization for desired waveform response, describing scanning methods and quantitative effect on noise
- 02 p0211 A71-11645

Meteorological satellites scan zones latitudinal overlap for circular or elliptical orbits

- 06 p0898 A71-17649

Precise Brorfelde transit circle reading by photoelectric scanning, determining diameter and group corrections 06 p0899 A71-17967

Data handling system with digital computer and multichannel scanning, processing and recording for simultaneously conducting two environmental tests of satellites 07 p1069 A71-20403

Ionospheric transverse inclinations from radio wave propagation characteristics obtained by circular oblique incidence sounding scans 11 p1758 A71-25788

Thermal imaging devices scanning systems for producing television-like images, noting alternate line scanning 15 p2412 A71-32759

Ionospheric transverse inclinations from radio wave propagation characteristics obtained by circular oblique backscatter sounding scans 22 p3532 A71-41556

Refractive imaging and scanning methods for thermal imaging systems, considering high performance IR lenses 22 p3544 A71-42137

SCANNING DEVICES

U SCANNERS

SCAT

U SUPERSONIC COMMERCIAL AIR TRANSPORT

SCATTER PROPAGATION

NT IONOSPHERIC F-SCATTER PROPAGATION

Long range troposcatter, evaluating antenna directivity effects on signal fading rate and fluctuation 01 p0037 A71-11087

SCATTERERS

U SCATTERING

SCATTERING

NT ACOUSTIC SCATTERING

NT ATMOSPHERIC SCATTERING

NT BACKSCATTERING

NT COHERENT SCATTERING

NT COMPTON EFFECT

NT ELASTIC SCATTERING

NT ELECTROMAGNETIC SCATTERING

NT ELECTRON SCATTERING

NT FORWARD SCATTERING

NT INCOHERENT SCATTERING

NT ION SCATTERING

NT IONOSPHERIC F-SCATTER PROPAGATION

NT LIGHT SCATTERING

NT MICROWAVE SCATTERING

NT MIE SCATTERING

NT NEUTRON SCATTERING

NT NUCLEON-NUCLEON SCATTERING

NT PROTON SCATTERING

NT RADAR SCATTERING

NT RAMAN SPECTRA

NT RAYLEIGH SCATTERING

NT RESONANCE SCATTERING

NT REVERBERATION

NT THOMSON SCATTERING

NT TROPOSPHERIC SCATTERING

NT WAVE SCATTERING

NT X RAY SCATTERING

He-Ne laser atomic scattering theory 06 p0907 A71-17997

Monatomic gas beams scattering from gas surface interface with randomly distributed energy states, confirming reciprocity or detailed balance principle 19 p3104 A71-38057

SCATTERING AMPLITUDE

Atmospheric aerosols role in Martian opposition effect, applying Mie theory to integrated scattering intensities calculation for submicron particles 03 p0489 A71-13558

Scatter effects of transistor parameters on maximum undistorted output-voltage amplitude of single stage amplifier 07 p1080 A71-20263

Electromagnetic field amplitude and phase scattering diagrams analysis for shape information capacity 13 p2029 A71-28369

Three particle elastic scattering amplitudes calculation using local Yukawa potentials 14 p2277 A71-30862

Glauber scattering amplitudes for atomic hydrogen excitation by electrons or protons, presenting closed form expressions requiring no numerical integration 21 p3420 A71-41195

SCATTERING COEFFICIENTS

Light scattering and attenuation coefficients calculation by small particle approximation, determining applicability limits from comparison with use of exact Mie formulas 07 p1160 A71-19809

Cross couplings in wideband antenna arrays, determining scattering coefficients, self/mutual impedances and admittances of two radiating elements 11 p1738 A71-26344

Scattering coefficients of thick inductive diaphragm in rectangular waveguide, using ray-optical method 15 p2376 A71-32023

Standard visibility and scattering coefficient changes due to humidity variation from maritime aerosol particles equilibrium radii calculations 16 p2605 A71-34084

Atmospheric short wave radiation angular and vertical distribution relation to aerosol scattering parameters, using transport equation 16 p2605 A71-34104

Upper atmosphere dust scattering indicatrix from twilight sky brightness at solar vertical, determining total directed scattering coefficient 19 p3132 A71-37390

Aerosol scattering coefficient in atmosphere, determining statistical characteristics of vertical and spectral structure 19 p3090 A71-37970

Atmospheric directional scattering coefficients from vertical measurements of IR spectral sky brightness near solar almucantar and direct radiation 19 p3090 A71-37976

Altitude variation of atmospheric air scattering coefficient from Soyuz 3 spacecraft measurements, considering aerosol stratification 20 p3259 A71-39676

Antennas scattering coefficients measurement by ground and atmospheric radiation, permitting antenna noise temperature components determination 20 p3205 A71-39803

SCATTERING CROSS SECTIONS

Atomic ion-ion recombination total inelastic cross sections calculation by Landau-Zener method, noting agreement with experiment 01 p0129 A71-10366

Microwave attenuation cross section of wet ice spheres, tabulating as function of wavelength, sphere diameter and water thickness 01 p0030 A71-10555

Negative pion elastic scattering differential cross section measurements from 1.71 to 5.53 GeV/c, using zero gradient synchrotron beam on liquid hydrogen target 02 p0286 A71-11647

Surveyor lunar probes alpha scattering chemical analysis technique tested on rocks of known composition 02 p0305 A71-11984

Multicomponent plasma electrical and thermal conductivities from quantum mechanical scattering cross sections 02 p0289 A71-12176

Cs doped Mg vapor arc discharge, determining electron mobility and diffusion cross section 02 p0286 A71-12180

Fast electron elastic and inelastic scattering Ar plasma at large Rutherford cross section, obtaining charged particle density 02 p0291 A71-12317

He excitation by He, Ne, Ar and Kr collisions, calculating first Born wave cross section 03 p0460 A71-13498

Na-Cs unpolarized and spin exchange differential scattering cross sections calculation by phenomenological and difference potential methods 04 p0630 A71-15654

Rain and drizzle millimeter wave attenuation and radar scattering cross section calculation 05 p0718 A71-15988

Perturbation theory diagrammatic version for describing lattice vibrations effect on scattering cross sections of low energy electrons from single crystal solid surfaces 05 p0792 A71-16316

DWBA optical model coupled channels comparison in 2s-1d shell for predicting proton scattering elastic cross sections 06 p0929 A71-17579

Hydrogen-slow electron collision cross sections, calculating Jovian upper atmosphere Lyman alpha and Balmer H alpha emission 06 p0929 A71-17679

Proton irradiation on Fe and Ni targets, measuring spallation cross sections 07 p1158 A71-19074

Radio wave propagation through extensive weakly scattering medium, presenting typical results for scintillation index, scintillation visibility and spatial autocorrelation function 07 p1196 A71-19576

Tropospheric temperature and aerosol to molecule ratio measurements by optical radar to determine relative concentrations and scattering cross section contributions 07 p1153 A71-20007

Single Born scattering theory applicability to critical electron density fluctuations 07 p1171 A71-20293

Nonadiabatic H-H collisions cross sections in two state time dependent impact parameter approximation, including electron exchange 08 p1337 A71-21193

Electron loss and capture by hydrogen atoms, protons and negative ions during collisions between atoms and molecules in gases, interpreting cross section data 08 p1338 A71-21491

Ti dioxide-opacified porcelain enamel reflectance spectra analysis, deriving scattering cross sections and dispersed particle sizes and distribution 09 p1480 A71-22116

Quantum mechanical theory of nonrelativistic fast electron backscattering from continuous media, considering scattering cross sections 09 p1496 A71-22236

Average radar backscattering cross section calculation for conducting obstacles for arbitrary transmitter and receiver antenna polarizations, obtaining results for straight wires, circular loops and helices 09 p1410 A71-23516

Ionospheric radio waves scattering cross sections under time varying random irregularities, considering anisotropic behavior, dielectric tensor and geomagnetic field 09 p1411 A71-23587

Observation range determination numerically for cyclotron resonances of effective scattering cross section of light wave by collisionless plasma in magnetic field 10 p1646 A71-23848

Nitrogen excitation by fast protons and electrons impact, obtaining primary collision cross sections by measurements extrapolation to zero pressure 10 p1664 A71-24793

Al and Pb atoms nuclei inelastic interaction cross section with nuclear active particles, using ionization calorimeter and wide gap spark chambers 11 p1760 A71-25165

CO Fourth Positive band system excitation cross sections by electron impact on carbon monoxide and carbon dioxide 11 p1727 A71-25366

Radiation from long lived ionic excited states, studying emission spectra, electron impact cross sections and positive nitric oxide ions band system 11 p1727 A71-25368

Inelastic scattering cross sections, using measured neutron leakage spectra from thick spherical shells of Ta, W, Mo and Be 11 p1802 A71-25556

Cross section for electron and muon neutrino-antineutrino pair production by photons, using intermediate boson theory 11 p1802 A71-25588

Fe ion photodetachment cross section polarization dependence on a sites in YIG-Si to explain photoinduced uniaxial anisotropy, using crystal field theory 12 p1943 A71-26858

Proton form factors and radius determination from experimental data analysis of cross sections of electron scattering by protons over wide transferred-momentum range 12 p1901 A71-27180

Energy dependence of integral scattering cross sections of noble gas atoms in carbon dioxide 13 p2102 A71-27809

Electromagnetic backscatter cross section for HF irradiated turbulent dielectric media by rigorous and heuristic derivations 13 p2028 A71-27998

Inelastic proton-proton and proton-carbon interaction cross sections, measuring proton energy with ionization calorimeter on Proton 1, 2 and 3 satellites 13 p1211 A71-28060

Reflectors group mean effective scattering cross section measurement by far field criterion 14 p2194 A71-30075

Radiation patterns and scattering cross sections of plane black disks excited by electromagnetic and acoustic waves 14 p2194 A71-30079

Electron production by proton impact on nitrogen, oxygen, neon and argon, measuring cross sections angular and energy distribution by electrostatic analysis and electron counting 14 p2277 A71-30660

Multicomponent plasma electrical and thermal conductivities from Debye potential quantum mechanical scattering cross sections 15 p2454 A71-31485

Chemically interacting gases transfer properties at various temperatures, determining collision parameters and interaction cross sections and energies 15 p2451 A71-31494

Resonant charge transfer cross sections in inert rarefied gases from atomic screening parameters, considering positive charge conductivity of ionized dense gases 15 p2452 A71-31825

Energy dependence of collisional time delay functions computed for H/IS/ atoms interacting with hydrogen potential, determining scattering cross sections 16 p2613 A71-32811

Electron loss and capture by hydrogen atoms, protons and negative ions during collisions between atoms and molecules in gases, interpreting cross section data 16 p2614 A71-33042

Inelastic electron scattering cross sections and energy spectra from Al and Au targets, using magnetic analyzer with high resolution detector
16 p2614 A71-34042

Production cross section of Lee-Wick hypothetical massive electromagnetic bosons by muons at high energy, giving Feynman diagrams
17 p2785 A71-34750

Electronic to vibrational energy transfer in mercury vapor reaction with hydrogen fluoride, studying IR emission and scattering cross section
18 p2874 A71-35834

High resolution differential cross section measurements for nonspherical potentials and molecular scattering of nitrogen and noble gases at thermal energies
18 p2949 A71-35898

Excitation cross sections for resonance states by electron impact on atomic nitrogen and oxygen over aeronautical energy range
18 p2949 A71-36350

Absorptance of anisotropically scattering medium compared with measured hemispherical reflectances and transmittances
[ASME PAPER 71-HT-20]
19 p3165 A71-37991

Electromagnetic wave arbitrary incidence on conducting circular disk for polarization parallel and perpendicular to incidence plane, calculating backscattering cross section for comparison with measurement
20 p3194 A71-38840

Glauber and Vainshtein approximations for cross sections of 1s-2p excitation during inelastic electron-atomic hydrogen scattering
20 p3272 A71-39470

Close coupling calculation for low energy hydrogen atom-molecule collision, discussing cross section, transition probabilities and elastic scattering
20 p3272 A71-39579

Reversible electron transitions selection rule in diatomic molecules excitation by electron impact, obtaining differential cross sections
21 p3417 A71-40198

Fast charged particles inelastic collisions with atoms and molecules, investigating Bethe differential cross section theory
21 p3418 A71-40675

Slow negative atomic oxygen ion production in collisions of fast protons and hydrogen atoms with oxygen molecules, measuring scattering cross sections
21 p3419 A71-41109

Quantum mechanical theory of nonrelativistic fast electron backscattering from continuous media, considering scattering cross sections
21 p3419 A71-41118

Kinematic theory of resonant gamma rays diffraction by single crystals, calculating differential cross sections of Bragg scattering for total degeneracy and Zeeman splitting
21 p3420 A71-41123

Analytic approximation for radial integrals and electron excitation cross sections of inert gases, using atomic screening parameters
22 p3577 A71-41620

Criticism of paper on spallation cross section for Be 10 production from oxygen high energy fragmentation in meteorites
22 p3508 A71-42350

Atomic model potentials for spectroscopic and scattering data, using perturbation theory
22 p3578 A71-42420

Proton form factors and radius determination from experimental data analysis of cross sections of electron scattering by protons over wide momentum transfer range
22 p3578 A71-42454

Ocean surface condition correlation to radar backscattering cross sections and wind velocity from scatterometer data
22 p3569 A71-42545

Rain and drizzle submillimeter wave attenuation and radar scattering cross section calculation
22 p3515 A71-42737

Electron impact excited carbon monoxide and dioxide 1260-5000 A spectral emission, discussing cross sections of Cameron and fourth positive bands
23 p3706 A71-42904

Carbon dioxide spectral emission at 1260-4500 A from electron impact excitation, discussing cross sections and Mars atmosphere application
23 p3706 A71-42905

High energy proton spallation cross sections for several radionuclides from Ti targets, discussing application to lunar materials and meteorites analysis
23 p3706 A71-43199

High energy proton spallation cross sections for several radionuclides from Fe targets, discussing application to beam monitoring and meteoritic studies
23 p3706 A71-43200

Boundary value problem for plane wave scattering by spherical cap, obtaining scattering cross section for Helmholtz resonator and hemispherical shell
23 p3703 A71-43208

Linearly and circularly polarized electromagnetic field effective scattering surfaces relationships deter-

mination as value proportional to reflected and transmitted rms flux density ratio
23 p3644 A71-43285

Large scale electron-neutral and neutral-neutral correlation effects on turbulent weakly ionized plasma electromagnetic scattering cross section
23 p3711 A71-43524

Velocity dependent HD beam scattering by inert gases, measuring total effective cross section in thermal energy range
23 p3707 A71-43879

He, HD and deuterium scattering by various gas molecules, measuring total effective cross sections for comparison with calculation
23 p3707 A71-43880

Total and momentum transfer cross sections for low energy electron scattering by atomic and diatomic molecules
23 p3707 A71-43898

Experimental techniques for differential, total and momentum transfer electron-molecule scattering cross sections at low electron energies, discussing rotational excitation
23 p3707 A71-43899

Coulomb interactions within dense Boltzmann plasma in transition from ideal to nonideal state, proposing effective Coulomb pair cross section concept
23 p3712 A71-43913

Effective excitation cross sections of molecular CO ion bands in comet tails due to He ions collisions with CO molecules, considering deviation from adiabatic hypothesis
23 p3708 A71-44314

Suprathermal proton bremsstrahlung cross section calculation, using Weizsacker-Williams method
24 p3865 A71-44905

Wave interference phenomena associated with elastic scattering of atoms, considering differential inelastic scattering cross sections anomalies
24 p3851 A71-45166

SCATTERING FUNCTIONS

Reflecting and scattering models of line formation in planetary atmospheres allowing for inhomogeneously distributed gas and particles and for anisotropic scattering phase function
03 p0486 A71-13320

Unsteady scattering patterns analysis, determining atmospheric extinction coefficient by reflected light oscillograms, formulas or signal amplitude time recording
09 p1487 A71-22385

Plasma electron temperature measurement from scattering indicatrix of laser radiation
09 p1501 A71-22394

Stochastic scattering process charged particle flux by Lagrange expansion based on Fokker-Planck equation
09 p1529 A71-23594

N body system variables evolution, discussing complete scattering based on mean quadratic and harmonic distances
10 p1642 A71-24432

Electromagnetic wave diffraction on arbitrary spheres, including scattering and attenuation by four water droplets
10 p1579 A71-24877

Autocorrelation functions of quasi-uniform solar radiation field reflected from earth with scattering allowance, using stationary random theory
12 p1901 A71-27097

Tables of scattering functions and albedo for semiinfinite atmospheres according to nonconservative Rayleigh phase matrix for diffuse radiation computation
14 p2274 A71-30059

Electromagnetic inverse scattering model of electrical radius of conducting spherical radar target employing expansion of scattered field in vector wave functions
14 p2196 A71-30564

Satellite-to-aircraft links propagation characteristics, considering specular reflected signals, diffuse scattering and scattering function
17 p2705 A71-35097

Configuration space theory of nonrelativistic three body scattering covering transition amplitudes of three-three chemical reaction rates
22 p3577 A71-41651

Autocorrelation functions of quasi-uniform solar radiation field reflected from earth, using stationary random theory and allowing for scattering
22 p3533 A71-41652

Ocean surface wave height /sea state/ measurement by high resolution random-signal radar based on model characterized by Poisson distributed scatterer density function
24 p3823 A71-45082

SCATTERING MATRIX

U S MATRIX THEORY

SCF

U SELF CONSISTENT FIELDS

SCHAUDER FIXPOINT THEOREM

Functional analysis application to nonlinear integral equations, stressing Schauder fixpoint theorem
18 p2943 A71-36952

SCHEDULING

NT PREDICTION ANALYSIS TECHNIQUES
Orbiting satellite targets assignment and scheduling to ground stations, presenting mathematical formulation and numerical example
04 p0555 A71-15332

Aircraft motion and traffic control at air corridors intersections for minimum flight schedule deviation under random disturbance due to weather, using statistical simulation
10 p1639 A71-24158

Computerized interactive scheduling system for modeling, optimizational and priority requirements for NASA manned space flight network
10 p1581 A71-24297

Premature scheduled maintenance, providing model for duplication between repair and overhaul/replacement cost
16 p2552 A71-33313

Stochastic optimal control theory application to airplane rescheduling model, obtaining dynamic programming algorithm for optimal landing and takeoff rules
23 p3702 A71-44104

SCHLICKUNOFF PRINCIPLE

Radiation resistance of center fed dipole antenna with transversely displaced feed points, using Schlickunoff moment method
07 p1075 A71-19267

SCHEMATICS

U CIRCUIT DIAGRAMS

SCHIZOPHRENIA

Auditory averaged evoked potential as measure correlating with degree of psychopathology in schizophrenia
01 p0011 A71-10765

Step-wise discriminant analysis in auditory evoked potential variability in schizophrenia
01 p0011 A71-10766

SCHLIEREN PHOTOGRAPHY

Laser schlieren crossed beam measurements in shear layer of shock free Mach 2.46 jet
01 p0094 A71-10953

Direction indicating color schlieren system displaying radial refractive index gradients, comparing with knife edge monochrome image resolution
03 p0423 A71-13459

Modified Ashby-Jephcott laser interferometer schlieren system for HF gas density measurements
03 p0427 A71-13922

Three dimensional opacity function for phase objects measurements using interferometry, holography or schlieren methods
04 p0596 A71-14969

Laser produced schlieren interferometry diffraction pattern determination, using Doppler frequency shift law
04 p0596 A71-15222

Color schlieren system with wedge type interference filter between high quality lenses pair for obtaining undistorted real image
04 p0598 A71-15364

Two dimensional hypersonic flow field density gradient distribution measurement by space-time resolved laser schlieren system
04 p0600 A71-15592

Schlieren device for visualization of thermal gradients in boundary layer of any orientation, replacing natural astigmatism with arbitrarily adjustable one
05 p0749 A71-16266

Ultrasound propagation visualization in solids, describing sensitive schlieren apparatus
06 p0903 A71-17323

Multiple source schlieren system for flow visualization in Canadian trisonic wind tunnel, using integrated logic circuitry for control
07 p1083 A71-19924

Pulsed laser schlieren system for ultrasonic wave front imaging in nondestructive testing techniques
08 p1286 A71-20949

Schlieren system conversion to holographic visualization in operational wind tunnels and test facilities
09 p1449 A71-22788

Density gradient visualization with schlieren optical system, discussing propeller aerodynamics
10 p1616 A71-24103

Nondestructive evaluation of ultrasonic wave propagation in adhesively bonded test specimens, using schlieren method
10 p1616 A71-24104

Wind tunnel hypersonic flow visualization by schlieren and phase contrast methods at low volumetric mass
11 p1764 A71-26273

Subsonic turbulent jet flow optical measurement by quantitative schlieren technique to overcome hot-body anemometry difficulties due to temperature and velocity fluctuations
12 p1896 A71-27215

Schlieren visualization for supersonic annular fixed cascade and freon compressor wind tunnels, using vane holding cylinder devices [ONERA-TP-948] 12 p1867 A71-27717

Interaction between viscous mixing shear layer induced by tangential injection and external supersonic flow field, obtaining spark schlieren photographs and wall pressure distributions [ASME PAPER 71-FE-24] 13 p2053 A71-29461

Shock wave attenuation in perforated duct, using pressure transducers and schlieren photography 16 p2554 A71-32884

Optical interferometry and schlieren photography involving high power pulsed lasers, discussing applications to plasma diagnostics and holography 16 p2586 A71-33159

Turbulent multispecies gas mixing measurements using dark field laser schlieren system 18 p2930 A71-36059

Wave reconstruction from gaseous flow hologram analysis with differential interferometry in polarized light and schlieren techniques with phase filter defocusing 20 p3239 A71-39461

Laser dye cell optical quality dependence on light pumping and liquid dye flow velocity, using schlieren method 20 p3246 A71-39489

Quantitative schlieren system for shock wave velocity, density ratio and relaxation time measurements, discussing electro-optical modification and calibration technique 21 p3364 A71-40404

Light intensity distribution inhomogeneity in transmission by GaAs single crystals, using schlieren method 21 p3428 A71-41201

SCHMIDT CAMERAS

Precise radio sources positions by Schmidt telescope and AGK 3 reference frame, noting comparison with optical positions 04 p0644 A71-15048

Photometric field error of Abastumani Schmidt camera determined from Hyad cluster photographs attributed to distance errors from vignetting of optics 07 p1115 A71-20442

Folded all-reflecting Schmidt camera UV image converter system for space astronomy applications, discussing pressure sensitivity effects on UV direct recording emulsion 09 p1447 A71-22751

Schmidt telescope as astrometric instrument, comparing mean error with catalog positions 16 p2578 A71-33322

GALAXY measuring engine for automatic measurement of glass photographic plates taken from Schmidt telescopes, discussing performance 17 p2741 A71-34997

Reflecting telescope Schmidt camera photographic color system temperature dependency from cluster NGC 103 photographs 21 p3379 A71-40717

SCHMIDT NUMBER

Heterogeneous chemical reaction for visualization of wall streamlines on moving obstacle, discussing boundary layer structure at large Prandtl and Schmidt numbers 10 p1591 A71-23835

Mass transfer in turbulent flow region downstream of circular pipe sudden enlargement for high Schmidt numbers, using diffusion controlled electrolysis technique 17 p2837 A71-34692

High Prandtl /Schmidt/ number fluids turbulent flow temperature profile derivation by turbulent transport mathematical model 23 p3664 A71-44199

SCHOTTKY EFFECT

U WORK FUNCTIONS

SCHROEDINGER EQUATION

Limiting absorption principle and Schroedinger nonelliptic spectral theory for steady state wave propagation in inhomogeneous anisotropic media 12 p1929 A71-26866

WKB wave functions for one dimensional non-relativistic problems by simple transformation derivation, solving by application of Liouville substitution to Schroedinger equation 12 p1923 A71-27666

Moliere high energy solution of Schroedinger scattering equation for optical propagation in turbulent atmosphere, noting inconsistency of Born-Rytov approximation 13 p2102 A71-29441

Canonical quantization, discussing Schroedinger equation, Hamilton-Jacobi theory, Feynman integrals and sandwich conjecture 16 p2609 A71-33258

Feinman integral definition and relation to Schroedinger equation for square summable potentials with lower bound 17 p2765 A71-34866

Numerical integration of Schroedinger equation for spontaneous ionization of hydrogen atom in electric field 19 p3107 A71-38056

German monograph on comparison between quantum mechanical approximate methods through quantization of approximated eigenfunctions covering Schroedinger equation, wave functions, Born-Oppenheimer approximation, etc 20 p3271 A71-39042

Rapidly converging iterative solution to radial Schroedinger equation in oscillatory region 21 p3408 A71-40845

SCHUMANN-RUNGE BANDS

Thermospheric heating by solar radiation in Schumann-Runge continuum, taking into account height and atmospheric components distribution 09 p1435 A71-22431

Oxygen molecular excitation behind incident shock waves in pure oxygen and oxygen-argon and oxygen-neon mixtures, examining Schumann-Runge band system [AVERL-RR-352] 15 p2451 A71-31674

Oxygen Schumann-Runge bands system from photographic and photoelectric spectra recording for arc jet heated air and oxygen-noble gas mixtures [AVERL-RR-354] 24 p3850 A71-45088

SCHWARTZ METHOD

Schwarz differential invariant in Kepler problem, describing point motion under Newtonian force effect 05 p0811 A71-16640

SCHWARZ-CHRISTOFFEL TRANSFORMATION

Schwarz-Christoffel conformal transformation inversion for electrostatic field integral equation formulation, applying to stepped-guide junction 14 p2212 A71-30515

SCHWARZSCHILD METRIC

Gravitational stresses derived from Friedmann-Lobachevskii and Schwarzschild spaces 03 p0456 A71-13297

Spectral line intensities, discussing equivalent width, broadening, transition probability, Schuster-Schwarzschild model, solar abundances, etc 04 p0630 A71-15237

White dwarfs, neutron stars and black holes origin and characteristics, discussing density, mass radius, gravitation and structure 07 p1199 A71-19999

Gravitational stresses derived from Friedmann-Lobachevskii and Schwarzschild spaces 09 p1495 A71-23270

Gravitational red shift in standard and isotropic forms of Schwarzschild metric 11 p1822 A71-25592

Zerilli equation solutions for even-parity gravitational perturbations on Schwarzschild geometry, considering gravitational collapse and black hole effects 13 p2133 A71-27972

Kerr-Newman black hole as generic final state of gravitational collapse developed from Schwarzschild geometry and mass, angular momentum and charge parameters 16 p2631 A71-33177

Quasi-closed Einstein universe model, showing orbits rotation similar to perihelions in Schwarzschild field 17 p2778 A71-34630

Weyl and Schwarzschild field metric equivalence, showing nonreducibility from one to other by coordinate transformation 17 p2778 A71-34637

Space-time model of torsion tensor effect on geodesic lines under Schwarzschild metric, evaluating orbital perihelion motion of planets and light ray bending 18 p2967 A71-36826

Schwarzschild constants evaluation from coupled gyroscopes spin axes observation, noting axes high angular velocities due to gravomagnetic effect in gravitational interaction 22 p3605 A71-42338

Generalized Einstein field equations in general relativity based on ennuple or tetrad variation, comparing with Schwarzschild solution 22 p3575 A71-42354

Arbitrary multipole structure spherical wave propagation in Schwarzschild metric, using Bondi coordinate system and negative powers of r 23 p3704 A71-43826

General theory of relativity for symmetric field, discussing De Donder incompressible fluid model and Tolman-Schwarzschild metrics 24 p3849 A71-45064

SCHWASSMANN-WACHMANN COMET

Saturn and Jupiter mass determination from Schwassmann-Wachmann I comet motion observations, using perturbation program based on Schubart-Stumpf n-body integration program 18 p2970 A71-37062

SCIATIC REGION

Rana temporaria isolated sciatic nerve excitation process, investigating continuous ultrasound effect 09 p1391 A71-22486

Differential lipid and phospholipid composition of white matter in brain, cervical, thoracic and lumbosacral sections of spinal cord and sciatic nerve in dogs 21 p3338 A71-41074

SCIENCE

Science studies, prediction and information procurement - Conference, Kiev, December 1967 02 p0334 A71-11851

Science and technology trend forecasting for planning, organization and program selection 02 p0335 A71-11852

Scientific research methods and tendencies, discussing theoretical and applied aspects, deductive and empirical procedures, technology interaction, practice criteria, etc 02 p0335 A71-11853

New information prediction in scientific research by data flow analysis 02 p0335 A71-11857

Soviet book on science of science covering information concept, control, organization and economics of scientific labor and advances prognostication 10 p1699 A71-24730

SCIENTIFIC SATELLITES

NT APPLICATIONS TECHNOLOGY SATELLITES

NT ATS 1

NT ATS 5

NT ATS 6

NT ATS 7

NT AZUR SATELLITE

NT DIAL SATELLITE

NT ENVIRONMENTAL RESEARCH SATELLITES

NT OV-1 SATELLITES

NT OV-3 SATELLITES

NT SMALL SCIENTIFIC SATELLITES

Azur research satellite scientific instruments and objectives and design parameters 01 p0164 A71-11334

Small scientific spacecraft onboard computers, discussing integration into satellite telemetry system and relationship with ground based data processing facilities 03 p0382 A71-13246

German monograph on research satellite design based on information gain criterion 03 p0380 A71-14371

ESRO 1 small scientific satellite attitude measurement system, discussing design and flight test results 07 p1154 A71-18840

SIRIO project mission analysis, discussing space communication and magnetospheric investigations by scientific satellite in geostationary orbit 10 p1670 A71-24268

Galactic plane X ray scan by NASA small astronomy satellite Uhuru, discussing satellite instrumentation, detector and sensor sensitivity and preliminary measurements 11 p1814 A71-25212

German low altitude polar orbiting research satellite AZUR orbital characteristics and bearing on auroral zone substorm phenomena 12 p1899 A71-26833

European scientific experiments satellite, describing design features and mission capabilities 15 p2501 A71-32693

Scientific goals and mission behavior of Dial aeronomy satellite for spatial distribution determination of atmospheric hydrogen concentration [DGLR-71-004] 15 p2501 A71-32781

European space research center, discussing satellite scientific and engineering data transmission and processing 16 p2553 A71-33422

Canadian report to COSPAR on space program and facilities covering scientific satellites, sounding rockets, etc 16 p2667 A71-33668

Italian SIRIO experimental SHF telecommunications satellite, noting trapped radiation and high energy electron experiments 18 p2974 A71-36521

HEOS-A2 eccentric orbit satellite for interplanetary space and high latitude magnetosphere data, discussing onboard experiments, major subsystems and design philosophy 22 p3607 A71-41505

German Aeros satellite for upper atmosphere aeronomy research, describing objectives regarding atmospheric composition and density 22 p3610 A71-42008

SCIENTISTS

Branching model of scientific information propagation and influence networks, exemplifying problem of hypersonic flow around blunt bodies 02 p0335 A71-11854

Social factors of labor organization and control in scientific teams for industry 02 p0335 A71-11856

Mathematical model for optimizing observational data sampling and working time losses by scientific research personnel 02 p0336 A71-11859

Scientist-astronauts work in manned space flight program support/backup crews and Skylab missions scientific/medical experiments

07 p1046 A71-19089

Motivations of scientists, engineers and technicians, considering changing nature of R and D projects

13 p2167 A71-28800

SCINTILLATION

Stellar scintillation saturation at large zenith angles, examining atmospheric dispersion and multiple scattering roles

01 p0127 A71-10141

Radio sources fine structure at 81.5 MHz, examining angular structure by interplanetary scintillation

01 p0158 A71-10769

Pulsar radio signal characteristics, examining pulse profiles, nulls interstellar scintillation and optical and X ray bursts

02 p0318 A71-12914

Pulsar radiation intensity time variations at radio frequencies, noting observations of CP 1133

04 p0649 A71-15273

Optical beam scintillation dependence on wavelength in strong refractive index turbulence

04 p0609 A71-15694

Ionospheric irregularity structure boundary variations shown by scintillation from satellite and radio star observations during quiet and disturbed magnetic conditions

06 p0887 A71-17269

Irregularities heights in ionospheric refractivity responsible for radio-satellite scintillation from spaced receiver experiments at midlatitude and subauroral locations

06 p0868 A71-17985

Plasma density irregularities in solar wind, showing wavelength dependence of interplanetary scintillation inconsistent with magnetic variations

07 p1184 A71-18862

Midlatitude scintillation diurnal and seasonal variations, using satellite communications data

07 p1095 A71-19003

Ionospheric electron density irregularity effects on communication satellite scintillation in auroral zone, using Doppler and Faraday measurements

07 p1098 A71-19035

Electron-proton radiation effects on scintillating materials in space environment chamber, evaluating background light degradation of active source monitoring

07 p1175 A71-19066

Statistical optical measurements of solar scintillation due to atmospheric conditions

07 p1111 A71-19489

Photoelectron counting distribution for random medium passage scintillated stochastic light, considering low level amplitude stabilized and chaotic radiation transmission through turbulent atmosphere

07 p1159 A71-19513

Radio wave propagation through extensive weakly scattering medium, presenting typical results for scintillation index, scintillation visibility and spatial autocorrelation function

07 p1196 A71-19576

Long term fluctuations in pulsar radiation intensity due to interstellar scintillation

08 p1359 A71-20935

Atmospheric scintillation, refractive and diffusive attenuation of microwaves from outer space at low elevation angles

08 p1364 A71-21421

Organic scintillators as active laser materials, discussing absorption, oscillation and emission spectra and luminescence quantum yield

09 p1461 A71-22386

Multiwavelength laser beam scintillations and atmospheric turbulence spectra, investigating saturation phenomena, transverse amplitude correlation lengths and signal fluctuations receiver aperture smoothing

09 p1464 A71-22780

Ionospheric scintillation effects on fading of oppositely circularly polarized VHF signals in space communications

09 p1410 A71-23522

Scintillation effects on synchronous satellite signal fading observed through polar ionosphere

10 p1577 A71-24315

Interplanetary medium small scale plasma irregularities by scintillation techniques, considering electron density deviations

10 p1674 A71-24434

Laboratory model for radio star scintillation and other diffraction phenomena by thin weak random phase changing screen including earth atmosphere or solar wind

10 p1678 A71-24797

Cygnus A two component radio source scintillations power spectrum observation by dipole array

10 p1678 A71-24804

Phase and log amplitude spectral and angular covariance of scintillation for propagation of two differing plane waves in randomly inhomogeneous medium

11 p1800 A71-26297

Diurnal and seasonal variations of scintillations in short wave radio signals transmitted from earth satellites

lites and spacecraft, noting relationship to ionospheric inhomogeneities

12 p1898 A71-26635

Atmospheric scintillation light detection from air shower, determining interaction mean free path of .1-10 million TeV primary particles

13 p2122 A71-28070

Absorption, divergence and scattering attenuations and scintillation of microwaves from space sources, calculating frequency and distance dependence characteristics

13 p2034 A71-29390

Spread F ionospheric electron density irregularities and satellite scintillation over polar cap

14 p2300 A71-30043

Laser beam scintillation covariance beyond turbulent atmospheric layer in Fresnel and Fraunhofer zones

14 p2254 A71-30423

Radio sources 3C 48, 3C 144, 3C 161, 3C 273 and 3C 298 scintillations by interplanetary plasma at 60 MHz, determining electron density fluctuations

15 p2487 A71-32033

Quasar 3C 48 observations at 408 MHz, noting scintillations due to interplanetary plasma inhomogeneities

15 p2487 A71-32035

Radio sources interplanetary scintillations observation, discussing solar wind velocity and diffraction pattern scale

15 p2480 A71-32445

Corotating solar plasma streams associated with variations of interplanetary scintillation from observed radio sources

16 p2634 A71-33386

Scintillation fading of signals in SHF band due to electron density irregularities in F region

17 p2699 A71-34624

Communications systems using carbon dioxide laser wave propagation, considering wave extinction by absorption and scattering, scintillations due to atmospheric turbulence, etc

17 p2700 A71-34749

Apollo astronauts light flashes observation during lunar flight, discussing interpretation as scintillations in eye lens by multiply charged cosmic rays focusing on retina

19 p3001 A71-37299

Ionospheric electron density irregularities measurement, comparing scintillation, spread F and electrostatic probe methods

19 p3128 A71-38035

Radio satellite scintillation producing small scale ionospheric irregularities, determining characteristic size variation with latitude by autocorrelation method

19 p3055 A71-38043

Astronomical telescopes image motion, distortion and scintillation, examining atmospheric refractive index and density/temperature variation effects

19 p3010 A71-38571

Cas A and Cyg A radio stars scintillation measurement by two element phase switched interferometers in ionospheric irregularities study

21 p3378 A71-40377

Interplanetary scintillation radio observations interpretation by theory for atmospheric scintillations optical observations

21 p3447 A71-40426

Effective flashes by scintillating Xe arc flash tube, considering perception by human eye

22 p3499 A71-41492

Pulsar JP 1933 distance lower limit from 21 cm absorption and galactic rotation model, noting scintillation parameters consistency with observations in thin screen model

24 p3873 A71-45141

SCINTILLATION COUNTERS

Hard solar X-ray spectra measurements, reinterpreting OSO 3 scintillation counter response due to pulse pile-up

02 p0302 A71-12766

Interstellar scintillation index and fading time of pulsar signals at 2388 MHz

05 p0807 A71-16208

Cosmic rays solar diurnal variation, using underground recordings in Bolivia and New Mexico from multiple two fold coincidence scintillator telescopes

06 p0952 A71-18114

Sensitive fast response scintillation electron detector for use with signal energy analyzer

07 p1115 A71-20358

Satellite-borne scintillation spectrometers for medium and high energy electron and proton measurements

09 p1513 A71-22555

Solar wind motion irregularities near sun from interplanetary scintillation observations, using receivers at Goldstone deep space tracking station

10 p1674 A71-24435

Fast neutrons scintillation counters effectiveness, presenting calculation procedure with corrections for double carbon-hydrogen scattering and nuclear reaction effects

11 p1761 A71-25577

TeV hadrons lateral energy distributions in air shower cores from Ne hodoscope measurements for

fluctuations between primary energy and shower size, discussing French alpine scintillators array

12 p1951 A71-27386

Geomagnetic effects on radio signals mechanism in extensive air showers, discussing scintillators array for east-west to north-south ratio polarization measurements

12 p1967 A71-27390

Quarks search in cosmic rays at sea level and mountain altitude, using telescope with plastic scintillation counters and wire spark chambers

13 p2121 A71-28055

Extensive air showers hadronic component observation by nuclear emulsion chambers combined with scintillation detectors

13 p2124 A71-28080

Extensive air showers cores structure observed with plastic scintillators and multiplate cloud chamber at 2770 m

13 p2124 A71-28082

Radio particle correlation of extensive air showers at large zenith angles, using twofold coincident 44 MHz receiver trigger-scintillator system

13 p2127 A71-28108

Versatile pulse amplifier for use with scintillation counters, surface barrier detectors, proportional counters or channel electron multipliers

13 p2067 A71-28163

Plastic scintillators anomalous pulse spectra in sea level transition region attributed to EM cascades single particles /muons/ production

14 p2301 A71-30425

Time coordinate compensator for time variable spectrometers operating on long plastic scintillators with two terminal photomultipliers

14 p2247 A71-30579

Cosmic ray telescopes with scintillation and Cerenkov counters for 2 to 8 BeV energy range, describing structural details and operational specifications

14 p2247 A71-30597

Cosmic ray secondary background of balloon-borne X ray scintillation astronomical telescopes for equatorial latitudes with reference to shutter technique and NaI/Tl crystal

15 p2406 A71-31751

Cosmic ray muon and neutrino measurements with deep underground scintillation detector array

15 p2477 A71-31800

Neutrino emission from collapsing stars, discussing possibility of detection by large mass organic scintillator

15 p2478 A71-31802

Balloon X ray astronomy techniques and observations, noting collimated scintillation counter instrumentation and PCM telemetry

16 p2641 A71-33754

Scintillation spectrometers sensitivity evaluation for low energy electrons in various regions of magnetosphere

20 p3234 A71-39127

Electron emitter photomultipliers and photocathodes for low light level and scintillation counter applications, using negative electron affinity

23 p3651 A71-43432

Circuits for scintillation counters signals identification, describing protective measures against electrical interference and background radiation

23 p3677 A71-43526

Extensive air shower radio pulse emission by geomagnetic charge separation mechanism, using antenna and scintillation counters arrays

23 p3646 A71-44012

Pion beam dosimetry with silicon detectors and plastic scintillators, presenting depth dose and isodose distributions and differential range curves

24 p3799 A71-44359

SCINTILLATION SPECTROMETERS

U SCINTILLATION COUNTERS

U SPECTROMETERS

SCINTILLATORS

U SCINTILLATION COUNTERS

SCINTILLOMETERS

U SCINTILLATION COUNTERS

SCISSION

U CLEAVAGE

SCORPIO CONSTELLATION

U SCORPIUS CONSTELLATION

SCORPIUS CONSTELLATION

Scorpius X-1 high energy X ray flux variations from balloon-borne scanner data

02 p0301 A71-12661

Scorpius X-1 X ray and optical variations observation by Vela 5 satellites

02 p0315 A71-12662

Sco X-1 optical spectroscopic and photometric observations, noting H alpha and H ion emission lines pattern-continuum brightness relationship

05 p0812 A71-16698

H I and H beta emission, Sco-Cen association stellar members near Sco X-1, discussing X ray heating and ionization

07 p1187 A71-19818

Scorpius X-1 X ray emission temporal behavior on 3 March 1969 07 p1198 A71-19831

Scorpius XR-1 simultaneous radio and optical measurements, discussing correlation of fluxes 08 p1360 A71-20985

X ray spectrum measurement of Scorpius X-1 by Bragg spectrometer, explaining emission or absorption absence by source model with line weakened by electron scattering 09 p1518 A71-22349

Interstellar absorption and color excesses in Sco OB-1 from spectral observation and photometry for star cluster and association background 11 p1831 A71-26133

Scorpio-Centaurus association and Gould belt proper motion, discussing convergent point in FK4 catalog with maximum likelihood method 15 p2483 A71-31470

Scorpius X-1 cocoon pulsar thermal X ray emission model, describing hot gaseous region around rotating neutron star 18 p2969 A71-37043

Nighttime D region behavior under ionization by X ray spectrum of Scorpius source 19 p3017 A71-37864

X ray rocket observations of Sco X-1 on 7-8 August 1969 compared to simultaneous optical observation, interpreting in terms of hot plasma model 20 p3283 A71-39751

Scorpius X-1 radio emission detection at 1415 MHz, discussing brightness distribution 21 p3441 A71-40068

Scorpius X-1 optical and X ray flux transient short period oscillations correlation from Aerobee sounding rocket data 23 p3733 A71-43077

Scorpius X-1 X ray flux observations, noting high frequency oscillations responsible for radiation production 23 p3733 A71-43078

SCRAMBLING [COMMUNICATION]

Uniform signal energy distribution in wideband synchronous data transmission channels using linear sequential filters with scramblers 23 p3647 A71-44345

SCRAMJET ENGINES

U SUPERSONIC COMBUSTION RAMJET ENGINES

SCRAMJETS

U SUPERSONIC COMBUSTION RAMJET ENGINES

SCREEN EFFECT

Monopole radiation on ground screens, deriving modified elevation angle to transform quasi-far zone measurements 06 p0868 A71-17716

Term splitting of Li I, B I, Na I and other sequences with one electron spectra, using screening parameters obtained from Hartree-Fock calculations 08 p1337 A71-21182

Electrical screening layers around charged clouds, giving numerical model for space charge accumulation, electric field distribution and forces acting on cloud droplets 12 p1925 A71-27290

Reflection, diffraction and transmission of plane microwave incident on conducting screen perforated periodically with circular holes, using transmission line analysis and dipole moments method 14 p2192 A71-29568

Sound passage through rigid screen of arbitrary wave thickness with apertures, using linear algebraic equations 15 p2449 A71-31709

Aerodynamic characteristics of arbitrary planform wing moving near screen, ground or water surface, using vortex model 16 p2521 A71-33596

Focused laser beam interaction with liquid metal particles, discussing fluid phase light screening effect, droplet evaporation and mass expulsion characteristics 17 p2750 A71-34291

Free space diffraction of E-polarized plane electromagnetic wave by slit in thick conducting screen, deriving approximate solution from Wiener Hopf equation by matrix techniques 19 p3023 A71-38592

Radiant flux from finite cylindrical volume to coaxial screen calculated under quasi-homogeneous medium and arbitrary optical thickness assumptions 23 p3782 A71-43920

Conical monopole antenna imaging above hemispherical ground of variable radius, plotting finite screen effectiveness from analytical and numerical solutions 23 p3655 A71-44168

Plane electromagnetic wave diffraction on dense periodic array at conducting screen, showing far field asymptotic behavior for E and H polarization 23 p3647 A71-44331

SCREENING

Hydrogen molecule-atom short range interaction energy, calculating multicenter integrals for screening constants 02 p0286 A71-11954

Ozone screening heights from sunrise effects on D region VLF wave reflection 02 p0212 A71-11968

Integrated circuit life testing, comparing functional and pin-to-pin screening data 19 p3034 A71-38516

SCREENS

Turbulent heat and mass exchange intensity at gas screen, investigating nonisothermality and wall penetrability effects 04 p0683 A71-15497

Diffraction by perfectly conducting plane screens solved by Hilbert space formulation of EM diffraction 19 p3018 A71-38192

Acoustical field from streamlined body of revolution moving in homogeneous gaseous medium past semiinfinite rigid screen, using Wiener-Hopf method for diffraction radiation 20 p3175 A71-38809

X ray monitoring process optimization with pmb-6 betatron, discussing intensifying screens thickness and composition effects on defects detectability 22 p3553 A71-41762

Computerized screen construction for surfaces with net characterized by singularity-free and curve-edges properties 22 p3518 A71-42395

Low temperature thermal insulation using diffraction effects of multilayer perforated reflecting screens 22 p3622 A71-42678

SCREW DISLOCATIONS

Bcc metals single and multilayer stacking faults, twin boundaries and screw dislocations observations, using central force atomic model 08 p1310 A71-21537

Stress-strain curve and single crystal dislocation structure of Al alloys with coherent precipitates, noting screw dislocations predominance 10 p1629 A71-25033

Linear isotropic and centro-symmetric second-grade elastic material and special case with coupling stress, calculating stress field of long straight screw and edge dislocations 14 p2327 A71-30290

Surface effects of transverse slip screw dislocations in metal fatigue crack nucleation, relating stacking fault energy and number of cycles to failure 16 p2593 A71-33681

Elastic cracks and screw dislocation pile-ups crossing bimaterial interface, deriving dual singular integral equations 22 p3615 A71-41710

SCREWS

Machine screws and metal joints stress distribution, using electric simulation with adaptability to digital computation 03 p0432 A71-13957

Micrometer screw revolution value determined by method of scale pairs for Bamberg zenith telescope, noting dependence on temperature and declination differences of star pairs 08 p1292 A71-21675

Ocular micrometer screw revolution value of instruments of astronomical universal type from scale pair outside of meridian 08 p1292 A71-21676

SCRUBBERS

Agema rocket engine pollutants, considering pollution control by scrubbers, engine system modification and micrometeorological data gathering [AIAA PAPER 71-716] 14 p2294 A71-30768

SCRUBBING

U WASHING

SDF [COMPUTERS]

U SITE DATA PROCESSORS

SE-210 AIRCRAFT

Caravelle aircraft all-weather Sud Lear automatic landing system operation and performance 15 p2446 A71-31913

European automatic flight control systems for landing in category IIIA conditions, discussing triplex system in Trident and simplex in Caravelle 24 p3846 A71-44456

SEA KNIGHT HELICOPTER

U CH-46 HELICOPTER

SEA ROUGHNESS

Radar altimeter use for ocean roughness determination 07 p1095 A71-18824

Model aspects of sea echoes and clutter unsteadiness on radar 22 p3514 A71-42470

SEA STATES

Remote sea state information acquisition system using video attachment to radar for sea return spectrum recording and analysis 01 p0031 A71-10600

Average radar cross section relative values for echoes from rain, considering horizontal, vertical and circular polarization in various sea states 04 p0551 A71-15008

Radar detection ranges on nonfading targets as function of sea state in marine environment 05 p0723 A71-16972

Soviet book on physics of interaction between atmosphere and ocean covering heat transfer, wave formation, vertical mixing in upper sea layer, etc 10 p1639 A71-24671

Earth and ocean surface state and cloud height determination using airborne laser radar observations 16 p2568 A71-33786

Sea surface slope distribution and wind velocity determination by sun glitter photography from synchronous satellite 17 p2734 A71-35215

Wideband spectrum utilization above 10 GHz for high rate digital communications and ecology monitoring of sea state, earth surface contour and atmospheric pollutants 19 p3020 A71-38407

Ocean layer mixing from aerial photographs using dye injections and floating cards under various wind, sea state and thermal profile conditions 22 p3569 A71-42547

Tidal analysis of sea surface elevations from satellite-borne altimeter as function of instrument errors and orbital determinations 22 p3536 A71-42549

Radio brightness temperature relationship to sea surface state, noting ocean storm regions determination from radiometric satellite data 23 p3673 A71-44050

Upwind/downwind differential Doppler spectra of radar sea echo for P, L and C bands 23 p3646 A71-44173

Ocean surface wave height/sea state measurement by high resolution random-signal radar based on model characterized by Poisson distributed scatterer density function 24 p3823 A71-45082

Airborne radar sea return averaged pulse shape measurements over various water surfaces, noting clear distinction between specular and scattered reflection components 24 p3824 A71-45083

SEA WATER

Cosmic rays intensity measurement in deep ocean with Cerenkov counter, determining Muon energy spectrum and absorption in water 03 p0477 A71-13862

Turbulent pressure pulsations at surface of floating body of revolution moving unsteadily in sea water during boundary layer development 04 p0576 A71-15613

Microwave radiometric techniques for continuous all-weather remote sensing of sea conditions from satellites, discussing foam and surface ripple effects [AIAA PAPER 70-318] 05 p0743 A71-17101

Aerial and orbital remote sensing of water quality, considering waste materials effect on coastal marine environment 11 p1760 A71-26504

Ti-Al binary alloy embrittlement in sea water by notched cantilever beam stress corrosion test, investigating alpha 2 particle precipitation effect on cracking susceptibility 14 p2256 A71-29522

Cosmic rays intensity measurement in deep ocean with Cerenkov counter, determining muon energy spectrum and absorption in sea water 22 p3595 A71-42663

SEALANTS

U SEALERS

SEALERS

Heat and corrosion resistant vacuum tight ceramic to metal brazed seals 07 p1119 A71-19972

Supersonic transport fuel tank environments and sealant requirements, describing Boeing laboratory environment approach 09 p1385 A71-23424

Elastomers for aerospace vehicles extreme environments, discussing fuel tank integral high temperature sealants 10 p1631 A71-24078

Long term exposure effects on high temperature resistant supersonic aircraft fuel tank sealants 10 p1631 A71-24081

Accelerated testing of jet fuel containment sealant, using reduced pressure and hybrid fluorocarbon silicone 10 p1632 A71-24083

Outdoor five year aging tests on polysulfide and silicone adhesive sealants under semiarid, marine and high humidity environments 10 p1634 A71-24119

Aircraft power plants sealing materials, emphasizing porous cermet seals heat resistance under thermal cyclic loads 12 p1895 A71-27688

- Sealing porous metal castings and powdered parts, discussing impregnation by vacuum-pressure and internal circulatory methods and sealant types
18 p2928 A71-36838
- SEALING**
- NT SELF SEALING**
- Sequential environmental testing effects on large hybrid microcircuit packages, reviewing solder sealing processes and repair methods
01 p0053 A71-10732
- High pressure and temperature seals and sealing in aircraft and spacecraft, including O rings and elastomers use
06 p0905 A71-18056
- Fluorosilicone sealants for aircraft fuel containment, discussing resistance to heat, jet fuel, moisture and heat aging
10 p1631 A71-24080
- Electron beam welding of metal-metal and metal-ceramic joints and sapphire sealing under vacuum
11 p1745 A71-26399
- Dry reed sealer transfer contact design, operation and embodiment, noting Au diffused and Rh contacts with hydrogen gas
13 p2038 A71-28838
- Fluid sealing capabilities of silicone, fluorosilicone and fluoroacarbon elastomers above 250 F [ASLE PREPRINT 71AM 3B-1]
13 p2093 A71-29488
- Sealing materials adhesion to fiberglass and metals based on rupturing force in loading tests
15 p2414 A71-31655
- SEALS [STOPPERS]**
- NT GLANDS [SEALS]**
- NT HERMETIC SEALS**
- NT O RING SEALS**
- NT PACKINGS [SEALS]**
- NT PLUGS**
- Computerized analysis of seal temperature, elastic displacements and seal force balance in iterative design method for gas turbine mainshaft seals
01 p0142 A71-10479
- Aircraft high temperature polyimide hydraulic actuator rod seals, discussing design and performance tests [SAE PAPER 700790]
01 p0091 A71-11543
- Static seals - IME Conference, London, December 1970
06 p0905 A71-18214
- Rubber seals performance testing, discussing measuring methods
06 p0905 A71-18216
- Static seals design and applications, taking into account operating temperature and pressure
06 p0905 A71-18217
- Piston expulsion seals for storable fueled and ready liquid rockets
06 p0905 A71-18218
- Hydrogen peroxide immersion effects on dimethyl silicone seal rubber tensile properties and tear strength
10 p1631 A71-24082
- Low compression set and volume swell of vulcanizates of fluoroelastomer at elevated temperatures for sealing applications
10 p1632 A71-24099
- High performance precision shaft and face seal design and applications
10 p1617 A71-24417
- Atmospheric seal leakage control tests for long orbital lifetime space station designs, discussing vacuum chamber monitored pressure shell penetrations [AIAA PAPER 71-337]
11 p1836 A71-25316
- Liquid fluorine feed system valves, seals and seats, discussing design criteria for flight weight components [AIAA PAPER 70-705]
11 p1709 A71-25519
- Resilient metal seals for extreme temperatures or minimum leakage and weight
12 p1911 A71-27060
- Long life labyrinth seal designs based on actual service experience and component or factory engine tests [SAE PAPER 710435]
13 p2073 A71-28319
- Sealing coefficient and leakage performance model for multiple thread rarefied gas viscoseals
20 p3241 A71-39801
- Compressible flow across shaft face seals and narrow slots, examining fluid inertia, viscous friction and entrance losses
23 p3663 A71-43592
- SEAMS [JOINTS]**
- Portable xerographic unit construction and electric circuitry, discussing application for welded seams X ray imagery
09 p1450 A71-22895
- SEAPLANES**
- Seaplane step /flat plate/ ricochet off ideal incompressible fluid surface, determining free surface shape by accounting for trailing vortices effects
07 p1088 A71-19355
- SEARCH PROFILES**
- Optimal unconditional sequential search for defects, using rejection function
08 p1300 A71-22020
- Search scanning system synthesis based on forces optimal distribution over investigated field, using Pontryagin maximum principle
10 p1586 A71-24167
- SEARCH RADAR**
- Acquisition and processing of aircraft search radar data obtained by track-while-scan technique, using off-line digital computer
01 p0040 A71-11392
- Stochastic model for analysis of track-while-scan technique for aircraft search radar, based on Kalman filter theory
01 p0065 A71-11393
- Radar energy loss estimate over space targets, considering various energy distributions in given search volume, target acquisition probability, signal to noise ratio, etc
02 p0212 A71-11879
- Double curved reflectors assembly methods for rotating search radar antennas, considering parabolic and elliptic strip shapes for sidelobe suppression modification
09 p1409 A71-23495
- Circular aperture illuminations for high beam efficiency and low sidelobes in search radar antenna applications, using Fredholm integral equation
24 p3809 A71-44990
- SEARCHING**
- NT SEARCH PROFILES**
- Linear programming functional control solution by generalized searching gradient algorithm at admissible region boundary
03 p0389 A71-13517
- Practice effects on visual vigilance task performance with and without search
04 p0540 A71-15845
- Time optimal hierarchical failure-search systems by varying structure for four different search algorithms
10 p1585 A71-24161
- Search methods for nonlinear identification problems solution, evaluating and comparing nonlinear programming methods of conjugate gradients and of Davidson
12 p1892 A71-27023
- Search methods for nonlinear identification problems solution, evaluating and comparing nonlinear programming methods of conjugate gradients and of Davidson
19 p3038 A71-37693
- SEARCHLIGHTS**
- Searchlight problem with isotropic scattering for semiinfinite and finite geometries, computing transmission functions for Fourier intensity components by kernel approximation method
17 p2839 A71-35571
- SEAS**
- NT MEDITERRANEAN SEA**
- NT NORTH SEA**
- SEASONAL VARIATIONS**
- U ANNUAL VARIATIONS**
- SEASONS**
- NT SUMMER**
- NT WINTER**
- SEAT BELTS**
- General aviation aircraft accidents involving seat belt and shoulder harness restrained occupants, discussing vertical force effects on survivability and injuries in severe crashes [SAE PAPER 710399]
10 p1555 A71-24261
- SEATS**
- NT EJECTION SEATS**
- SECANTS**
- U TRIGONOMETRIC FUNCTIONS**
- SECONDARY AIR**
- U AIR**
- SECONDARY COSMIC RAYS**
- Negative pi-N NN interactions in emulsion at high energies, plotting angular distributions of secondary particles in cosmic ray showers
03 p0476 A71-13847
- Ultrahigh energy electrons and gamma quanta in ground produced by cosmic rays, plotting mean free path vs energy
03 p0478 A71-13868
- Cosmic ray secondaries mean transverse momentum from muons lateral distribution measurement
04 p0640 A71-14816
- Solar modulation variation of secondary cosmic ray energy spectra, noting dependence on atmospheric depth and geomagnetic cut-off
06 p0955 A71-18135
- Secondary cosmic ray spectrum latitude knee based on nucleon, proton and muon energy spectra
06 p0960 A71-18167
- Nuclear emulsion produced cosmic ray jets secondaries angular distribution, primary energy and anisotropy
13 p2121 A71-28056
- Nucleon-nucleon and meson-nucleon collisions, determining secondary cosmic ray multiplicity dependence on primary particles energy spectra
13 p2121 A71-28057
- Fireball transverse momentum effect on angular distribution of secondary particles, considering high energy nuclear interactions
13 p2058 A71-28063
- Upper atmospheric primary cosmic ray layer ionization, considering secondary particles, X rays, neutrons, tritons and mesons as ionizing agents
22 p3591 A71-41647
- Primary and secondary cosmic ray muon variations in vertical and zenith angles, determining coupling coefficients
22 p3593 A71-42357
- Negative pi minus N and NN interactions in emulsion at high energies, plotting angular distributions of secondary particles in cosmic ray showers
22 p3594 A71-42648
- Ultrahigh energy electrons and gamma quanta in ground produced by primary cosmic rays, plotting mean free path vs energy
22 p3595 A71-42669
- SECONDARY EMISSION**
- Secondary electron emission during RbBr, Se and CdTe film bombardment by sodium ions and atoms
01 p0139 A71-11099
- Space TV systems using SEC /secondary electron conduction/ camera tube
04 p0597 A71-15289
- Mass spectrometer application to study of secondary ion emission during metal surface bombardment by argon ion beam
07 p1112 A71-19621
- Solar radio emission micropulsations observations at 10 cm, discussing primary and secondary bursts from different disk regions and radio telescope
07 p1189 A71-20639
- Differential secondary electron flux measurement in aurora with Aerobee rocket spectrometer
08 p1282 A71-21635
- Secondary ion component on tungsten target surface during sputtering by alkali metal ions
09 p1494 A71-22878
- Excited atom density determination for two-photon light absorption in one-dimensional medium, obtaining energy balance equation asymptotic solution and secondary radiation intensity
12 p1914 A71-27028
- Fireballs existence, discussing maxima in angular distribution due to secondary particles transversal momenta limitation
13 p2058 A71-28062
- Electromagnetic showers triggered in lead by 6 GeV primary cosmic ray electrons, calculating spatial distribution with Monte Carlo method
14 p2302 A71-30594
- Cosmic ray secondary background of balloon-borne X ray scintillation astronomical telescopes for equatorial latitudes with reference to shutter technique and NaI/Tl crystal
15 p2406 A71-31751
- Cosmic ray high energy pion and nucleon nuclear interaction observations, determining statistical fluctuations in secondary particles angular distribution
15 p2479 A71-32076
- Secondary electrons and photons energy spectra and depth dependence in upper atmosphere from numerical solution of one dimensional transport equations
16 p2628 A71-33937
- Secondary emission analog for improved Auger spectroscopy to eliminate objectionable feature of electron spectra taken with retarding potential analyzer
18 p2922 A71-36579
- Atomic and molecular gases electron impact ionization, measuring secondary particle energy distribution and angular dependence
24 p3850 A71-44925
- Channel electron multiplier principles and characteristics, discussing secondary electron production probability during electron irradiation of surface in vacuum
24 p3811 A71-45326
- SECONDARY FLOW**
- Secondary jet action on circular horizontal plate located above parallel screen, using Poisson equation
02 p0186 A71-12552
- Flow separation and reattachment in confined jet mixing of air with secondary flow in duct [ASME PAPER 70-FE-B]
03 p0341 A71-13703
- Laminar corner boundary layer secondary flow, taking into account velocity and skin friction distributions
03 p0404 A71-14239
- Couette flow between rotating cylinders and Taylor vortex formation by Liapunov-Schmidt method and spectrum perturbation theory, discussing secondary flow determination accuracy
04 p0575 A71-15603
- Streamwise vorticity formation by wall turbulence nonuniformities, deducing secondary currents direction
05 p0736 A71-16963

Tangential velocity and total temperature distribution axial and radial gradients from secondary flow functions and turbulent energy equations
06 p0883 A71-18321

Centerline velocity and concentration decay predictions of free and confined jet models without secondary flows, considering turbulent mixing
[AIAA PAPER 71-3] 06 p0883 A71-18478

Weakly ionized gas discharge three dimensional unsteady motion of viscous incompressible gas discharge plasma in homopolar device curvilinear channel, emphasizing secondary overflow during acceleration
07 p1167 A71-19235

Mathematical model for secondary flow in turbulent boundary layer in corners and salients, confirming existence of transversal pressure gradient variation
10 p1592 A71-23979

Flow instability and secondary circulation in pressure-driven rotating rectangular channel
10 p1595 A71-24617

Primary/secondary flow density ratio effect on rotary jet flow induction, describing experimental results with 1/7-1/1 density ratios
10 p1553 A71-24853

Head end secondary flows in solid propellant rocket motor combustion chamber due to transverse acoustic waves in quiescent fluid
14 p2335 A71-29877

Time independent three dimensional streaming secondary motion due to vibrating flexible plate
14 p2325 A71-30061

Vortex induced shear and secondary flow through row of spheres, curved channel, turbine blades, rotating impeller, suction pipe and upstream boundary layers
14 p2224 A71-30176

German monograph on accelerating grids in wind tunnel and axial flow turbine, covering plane/secondary flows past cascades and stator/rotor blading
15 p2347 A71-32303

Momentum transfer secondary flow between rotating cylinders in terms of effective/molecular viscosity ratio as function of Taylor number
[ASME PAPER 71-APM-30] 16 p2559 A71-33199

Jet induced secondary flow interaction with circular plate, showing ring vortex effects on pressure distribution
17 p2669 A71-34334

Adversely heated fluid flow layers between rigid boundaries, studying thermal instability due to formation of stationary secondary rolls
[ASME PAPER 71-APM-00] 18 p2985 A71-36269

Elastico-viscous liquid steady secondary flow induced by oblate or prolate spheroid rotating about axis of symmetry from linear partial differential equations solution
20 p3214 A71-39967

Noise sources in axial flow fans, considering radiation from turbulent boundary layers, scattering of incident turbulence and secondary flow influence
21 p3323 A71-40710

Two phase flow in asymmetrically roughened ducts, investigating secondary flow effects on heat transfer characteristics
21 p3477 A71-40995

Heat transfer and temperature field calculation in turbulent flows through channels of noncircular cross sections, allowing for secondary flow
22 p3619 A71-41871

SECONDARY HARMONIC GENERATION
U HARMONIC GENERATIONS

SECONDARY INJECTION
Secondary gas injection at right angles into supersonic rocket nozzle, investigating side force characteristics
03 p0470 A71-17376

Jet deviation by secondary gas injection, predicting lateral thrust performance
04 p0525 A71-14793

Liquid properties effect on secondary injection from spray nozzle, determining jet penetration in supersonic stream by scattered light and schlieren photographs
09 p1381 A71-22089

Aerodynamic flame stabilization by secondary air jets obliquely directed toward combustion chamber main flow, comparing with mechanical devices characteristics
[DFVLR-SONDDR-120] 15 p2472 A71-32719

Heat and mass exchange coefficients and critical separation for turbulent boundary layer with secondary fluid injection under nonisothermal conditions
20 p3210 A71-38897

SECONDARY RADAR
Secondary surveillance radar in ATC systems, discussing advantages and implications for controllers
09 p1406 A71-22955

SECONDARY WAVES
U S WAVES

SECRETIONS
NT ENDOCRINE SECRETIONS
NT HORMONES
NT INSULIN
NT SWEAT

Stomach secretory function and histomorphological changes in dogs under stress
09 p1390 A71-22263

Secretory function intensity of salivary glands, liver and stomach of animals and humans with different water-salt metabolism conditions
11 p1719 A71-25669

SECULAR PERTURBATION
U LONG TERM EFFECTS

SECURITY
ADEPT-50 resource sharing system for classified data processing, describing time sharing security control model
01 p0044 A71-10188

Confidential information management, discussing designer and data system user role as foundation for basic privacy control system
01 p0044 A71-10189

SEDIMENTARY ROCKS
NT CARBONACEOUS ROCKS
NT COAL
NT LIMESTONE
NT SANDSTONES

SEDIMENTS
Marine sediment age by fission track dating of volcanic glass shards, noting agreement with K-Ar, paleomagnetic and paleontologic ages
10 p1601 A71-24430

Sterols isolation and identification from Pleistocene sediment by gas-liquid chromatography and combined gas chromatography-mass spectrometry
15 p2366 A71-31367

Bound sugar content in marine sediments by capillary gas chromatographic-mass spectrometric analysis of trimethylsilyl derivatives
19 p3055 A71-38146

Heavy rare gases adsorption on terrigenous sediments, comparing earth atmospheric composition with meteoritic planetary primordial component
20 p3194 A71-39385

Biogenicity and significance of oldest stromatolites from optical microscopic and carbon isotopic studies
22 p3533 A71-41616

SEEBECK COEFFICIENT
U SEEBECK EFFECT

SEEBECK EFFECT
Liquid sodium and potassium thermoelectric potentials, calculating Seebeck coefficients to 600 C
01 p0141 A71-11602

Electrical conductivity measurement for thorium oxide at 1000-1600 C and at low oxygen partial pressures, discussing Seebeck coefficient behavior
07 p1177 A71-19569

Measuring instrument for amorphous and polycrystalline materials resistivity and Seebeck coefficient as function of temperature and pressure
09 p1446 A71-22737

SEEDING (INOCULATION)
U INOCULATION

SEEDS
Spaceflight effects on dry crepis capillaris seeds in five day orbit, showing chromosome rearrangements and increased mutagenic sensitivity
09 p1392 A71-22563

Orbital space flight effects on dry barley seeds, noting increased intracellular rearrangements
09 p1392 A71-22564

Hawaiian silversword seed germination and inhibition showing extraordinary heat sensitivity
16 p2527 A71-33049

Lettuce seedlings growth reduction and geotopic and phototropic behavior modification by 3-prime chlorophenyl 3-methoxy phthalide, noting gravity response elimination through action on statoliths
23 p3639 A71-43143

SEEKERS
U HOMING DEVICES

SEGREGATION
U SEPARATION

SEISMIC ENERGY
Lunar seismic energy diffusion, calculating transmitted and reflected acoustic wave intensities as time function after explosion
16 p2637 A71-33511

Pulsar speedup due to neutron starquakes, deriving self gravitating elastic incompressible sphere model for time prediction
23 p3722 A71-42894

SEISMIC WAVES
NT RAYLEIGH WAVES
Long seismic reverberations from man-made impacts on moon, using Apollo 12 lunar surface station recordings
01 p0159 A71-10824

Seismograph recording of Apollo 12 lunar module impact as result of secondary ejecta spray around seismometer or translunar seismic wave propagation
04 p0644 A71-15128

Lunar seismic waves scattering as two dimensional random walk process, taking crust and rock compositions into account
04 p0650 A71-15544

Seismic waves scattering mechanism in heterogeneous medium from lunar seismograms
04 p0650 A71-15546

Chandler wobble seismic excitation by dislocations: elasticity theory, discussing pole path changes: earthquake correlation
06 p0891 A71-178864

Soviet book on nonstationary waves covering gravity waves development, moving periodic pressure systems, seismic disturbances and nonhomogeneous ideal liquids
10 p1595 A71-246501

Lunar seismic energy diffusion, calculating transmitted and reflected acoustic wave intensities as time function after explosion
16 p2637 A71-335111

Elastic seismic waves attenuation in polycrystalline ceramics and rocks by grain boundary relaxation, noting strong frequency dependence of earth mantle internal friction
17 p2735 A71-353901

Seismic wave velocity measurements in pahoehoe basal flows in lava beds, comparing with laboratory dilatational velocities
19 p3052 A71-376855

Lunar near surface seismic velocity distribution for cold accretion and meteorite impact models, comparing travel times
21 p3450 A71-406455

P times least squares analysis complications by systematic earthquake location errors and azimuthal station anomalies variation
23 p3672 A71-438844

SEISMOCARDIOGRAPHY
Optimal contactless kinetocardiography recording of LF patient chest vibrations, comparing short wave method
06 p0863 A71-184683

Space research utilization in medicine, discussing remote blood pressure measurements, seismocardiography visual analysis, sterilization procedures and equipment for physically handicapped
10 p1571 A71-247541

SEISMOGRAPHS
NT LUNAR SEISMOGRAPHS
Acoustical holography principles properties and applications, discussing liquid surface levitation, Bragg diffraction and undersea and seismic utilization
21 p3381 A71-409311

SEISMOLOGY
Theoretical equations of state in geophysics, considering systematics approach to laboratory data, seismic velocity profiles, finite strain and atomistic approach
12 p1931 A71-27415

Two dimensional seismic mathematical and scale techniques appropriate to inertial navigation devices test pads noise isolation examination
[AIAA PAPER 71-912] 19 p3056 A71-38326

Deep lunar interior elastic properties, seismic speeds and Debye temperature determination from equations of equilibrium and state and measured moment of inertia
20 p3286 A71-38738

P times least squares analysis complications by systematic earthquake location errors and azimuthal station anomalies variation
23 p3672 A71-438844

SEISMOMETERS
U SEISMOGRAPHS

SEIZURES
Acoustic priming of audiogenic seizures in mice, noting high susceptibility to convulsions under intense sound
03 p0360 A71-13160

Genetics and temporal audiogenic seizures in mice, noting age and exposure effects on susceptibility
03 p0360 A71-13161

Audioconditioned convulsive response (ACCR) characterization, investigating age, auditory conditioning and environmental noise effects on sound-induced seizures in mice
03 p0360 A71-13162

Neurochemical factors in auditory stimulation and susceptibility to audiogenic seizures, noting gamma-aminobutyric acid (GABA) inhibitor
03 p0360 A71-13164

Cortical and subcortical electrical activity during electrically and drug induced convulsive seizures in cats, correlating with spinal monosynaptic reflex variations
15 p2359 A71-31957

Cerebral gamma-aminobutyric acid metabolism and hyperbaric oxygen induced seizures in chicks during brain development, noting increased membrane permeability
20 p3186 A71-38970

SELECTION
NT PERSONNEL SELECTION
NT PILOT SELECTION

Selection index estimation from partial multivariate normal data for precision improvement, discussing procedure and Monte Carlo simulation results
07 p1147 A71-19599

SELECTIVE FADING
Fading microwave radio channel baseband gain and noise stability, assuming nonuniform frequency selective fading effects
07 p1066 A71-20426

Telegraphy binary data transmission through channels with frequency-selective fading, investigating noise stability improvement by programmed carrier frequency variation and receiver passband shifting
17 p2698 A71-34394

Quasars emission line red shifts distribution observations, evaluating selection effects
22 p3605 A71-42351

SELECTIVITY
Radio sets integrated selection components, noting ceramic capacitors and filters and coil circuits
03 p0388 A71-14336

Electromagnetic compatibility characteristics in terms of receiver susceptibility to interference effects on selectivity and nonlinearity parameters
19 p3033 A71-38465

SELECTORS
Simple pressure selector switch for measurement up to 40 input pressures
06 p0900 A71-18055

Signal rejection characteristics of receiver preslector and antenna system, requiring receiver mixer efficiency and transmitter parameters
13 p2032 A71-28862

SELENIDES
NT CADMIUM SELENIDES
NT COPPER SELENIDES
NT GALLIUM SELENIDES
NT LEAD SELENIDES
NT ZINC SELENIDES

Anisotropic transport coefficients valence band model of TlSe, measuring electric conductivity, Hall effect and thermo-emf as function of temperature
21 p3434 A71-41328

SELENIUM
Amorphous Se p-type conductivity, discussing temperature and crystalline phase dependence
05 p0792 A71-16379

CW laser transitions in Se II, investigating current saturation behavior and output power and structure
15 p2422 A71-32581

Selenium photocell photovoltaic effect, observing recombination and generation processes in space charge region
16 p2623 A71-34046

SELENIUM ALLOYS
PbTe-GeTe-PbSe solid solution alloyed by lead chloride, investigating structure, composition and distribution of basic elements
15 p2460 A71-31283

Thermoelectric properties of quaternary Sb-Bi-Te-Se solid solutions, noting low thermal conductivity
22 p3584 A71-41618

SELENIUM COMPOUNDS
NT CADMIUM SELENIDES
NT COPPER SELENIDES
NT GALLIUM SELENIDES
NT LEAD SELENIDES
NT SELENIDES
NT ZINC SELENIDES

Chemical radioprotection by selenium containing compounds in biological and chemical systems tested in irradiated rats
07 p1032 A71-18933

Reactivity measurements of protective agent selenourea toward primary water radiolysis radicals
07 p1033 A71-18934

Stimulated and spontaneous emission from InSe single crystal under focused fast electron beam bombardment
21 p3434 A71-41326

SELENOGRAPHY
Selenographic position determination method based on stellar observations
09 p1530 A71-23714

Physical selenography, discussing lunar mantle structure, lunar topology, lunar evolution, etc
10 p1670 A71-24209

Lunar geometrical and dynamical properties, deriving force function from density distribution and surface equation
11 p1822 A71-25687

Lunar center figure position determination by harmonic analysis, comparing with Mills III catalog
15 p2483 A71-31344

Selenography and selenodesy with Apollo whole-disk lunar photograph, providing positions catalog in tabular form
18 p2965 A71-36294

Morphological features of crater Copernicus as lunar caldera, observing agreement with volcanic origin
19 p3137 A71-37681

Lunar center figure position determination by harmonic analysis, comparing with Mills III catalog
22 p3607 A71-42619

Lunar physical libration effect on lunar satellite orbital elements, considering reorientation of selenographic axes fixed in true moon
23 p3727 A71-43004

Equatorial lunar radius determinations from image motion compensation sensor onboard Lunar Orbiter 1 spacecraft
23 p3727 A71-43010

Optimal method selection for astronomical measurements on lunar surface, discussing instrumental and technical difficulties with selenographic longitudes and latitudes determination
24 p3870 A71-44812

Determination method for selenographic coordinates of points on lunar surface, discussing astronomical observations from moon
24 p3870 A71-44813

Selenodetic catalog centers mutual positions determination from lunar near side hypsometric charts
24 p3875 A71-45316

SELENOLOGY
NT LUNAR CORE

Moon surface basic points catalogs differences, estimating position dispersion by residuals of transformations
03 p0484 A71-13216

Selenodesy and planetary geodesy of moon, inner and outer planets, including sun-planet mass ratios
08 p1366 A71-21798

Papers on lunar astronomy and physics covering motions in space, librations, earth-moon system dynamics, geometrical and optical properties and origin
11 p1822 A71-25683

Lunik spacecraft soil sampler landing site geological-morphological analysis from television images, indicating formation patterns similar to equatorial zone seas microrelief
12 p1966 A71-27302

Lunar dynamics and structure data from two lunar seismic stations installed during Apollo 11 and 12 missions as part of ALSEP
12 p1967 A71-27416

Lunik spacecraft soil sampler landing site geological-morphological analysis from TV images, indicating formation patterns similar to equatorial zone seas microrelief
19 p3145 A71-38261

Deep lunar interior elastic properties, seismic speeds and Debye temperature determination from equations of equilibrium and state and measured moment of inertia
20 p3286 A71-38738

Dust particle measurements in selenocentric and cislunar space /1967-1969/ by Lunar Explorer 35 and OGO 3
20 p3298 A71-39640

Apollo 11 and 12 regolith and breccia samples, discussing shock effects detection and interpretation, chemical composition, grain size distribution and impact origin
23 p3745 A71-43660

Lunar surface history model, discussing mascons, chemical composition, isochron ages and seismic and electrical properties of samples
23 p3746 A71-43670

Apollo 12 magnetic measurements of lunar interior electroconductivity simultaneously on lunar surface and in circumlunar orbit
23 p3762 A71-43789

SELF ABSORPTION
Quasars circular polarization measurements at 21 cm, noting synchrotron self absorption
14 p2307 A71-29867

Intense vacuum UV atomic line source excited in 2450 MHz microwave discharge cavity with clean spectrum, noting window deterioration and self absorption
14 p2240 A71-30127

Synchrotron radiation reabsorption in inhomogeneous sources, considering IR spectra of quasars and galactic nuclei
18 p2963 A71-36158

SELF ADAPTIVE CONTROL SYSTEMS
Automatic control with twofold invariance properties, describing use as nonsearch self adaptive system
01 p0061 A71-10707

Complex control systems using self adjustment compensation of error signals according to input derivative
01 p0063 A71-10723

Dynamic programming and Bayes algorithm for self organizing and self adjusting Markovian systems
03 p0389 A71-13515

Soviet book on self adjusting control systems with reference models covering harmonic linearization method, phase plane technique, deterministic signals, etc
04 p0560 A71-14641

Adaptive/self synchronizing PSK receivers with common power and bandwidth, discussing analytical and numerical investigations of performance characteristics
05 p0723 A71-17054

Onboard self adaptive multichannel data reduction for redundancy by oversampling
07 p1063 A71-19709

Self adaptive systems with dynamic characteristics stabilization, obtaining algorithm for adaptive loop optimization
09 p1422 A71-22120

Nonlinear self adjusting and variable structure automatic control systems for piloted and pilotless flight vehicles, considering oscillations due to electric servosystems nonlinear characteristics
12 p1926 A71-26716

Adaptive control systems components stability and accuracy requirements, demonstrating functional multipliers and quorum elements operation by functional diagrams, transient equations and signal waveforms
12 p1890 A71-26717

Aeroelastic aircraft self adjusting automatic control systems, discussing elimination of elastic oscillations caused noise from angular velocity sensing circuits
12 p1926 A71-26718

Standard transfer function choice method for self adjusting automatic control system design, establishing relations between transient properties and poles and zeros distribution
12 p1891 A71-26725

Marks searchless self adjusting control system calculation, using method of total motion separation into characteristic components
12 p1891 A71-26726

Flight vehicles nonsearching self adjusting control systems synthesis, using gradient method with simplified sensitivity models
12 p1926 A71-26729

Criterion for fixed adjustment adaptive control systems comparison with self adjusting systems, using frequency range of plant information required for synthesis of correcting devices
12 p1891 A71-26730

Synthesis of high speed digital computer non-searching adaptive control program to ensure closed system required dynamic characteristics for complex linear unsteady control plant
12 p1926 A71-26731

Self adjusting autopilot synthesis with capability for control plant changing parameters and structural vibrations effects compensation
12 p1927 A71-26732

Self adaptive control system for selective assembly process, ensuring matching of size distribution curves within identical batches
12 p1912 A71-27341

Self adaptive systems with dynamic characteristics stabilization, obtaining algorithm for adaptive loop optimization
14 p2220 A71-29998

Mathematical modeling and convergence analysis of nonscanning self adaptive control systems for linear objects, using Liapunov second method
15 p2379 A71-31519

Russian papers on complex control systems covering hierarchical structures, automatic, optimal, self adaptive, multidimensional and nonlinear systems analysis and synthesis
15 p2379 A71-31842

Optimal stabilization of self adjusting control system for nonstationary plant in limited time by linear model using Lagrange multipliers
15 p2382 A71-32622

Central nervous system self regulating properties analysis by automatic control theory, using parametric functional model of brain electrical activity
16 p2538 A71-34107

Soviet book on self adjusting systems dynamics with frequency stabilization characteristics, covering linearized motion equations, narrow band processes, etc
17 p2722 A71-35175

Grand Tour missions centralized data handling, describing computer aided telemetry system and self testing and repairing control computer
19 p3025 A71-37954

Self adaptive controlled robot velocipedist, discussing speed control and equations of motion
19 p3039 A71-38540

Envelope process transfer function calculation for self adaptive systems parametric control dynamic characteristics
21 p3361 A71-41138

Mathematical modeling and convergence analysis of nonscanning self adaptive control systems for linear objects, using Liapunov second method
22 p3528 A71-42884

Control system effectiveness improvement, using redundancy and self adaptive techniques
23 p3655 A71-43291

SELF ALIGNMENT
Air lubricated bearing elements lifting force, restoring moment and translational rigidity, considering dependence on minimum clearance, sliding rate, pressing force and geometric parameters
05 p0758 A71-16351

Direct in-orbit alignment of integrated optical strap-down inertial guidance system for space application, considering self contained prelaunch alignment and calibration
17 p2774 A71-35071

Time optimal self alignment methods for inertial platforms, using mathematical model based on torque iteration and bang bang misalignment angles control
21 p3413 A71-40544

SELF BIAS

SELF BIAS

U BIAS

SELF CONSISTENT FIELDS

Charged particle motion in self consistent continuous wave spectrum from Vlasov and Poisson equations solution 02 p0289 A71-11955

Classical many component plasma dynamics with collective particle interactions in self consistent longitudinal electric field, deriving complex wave equations 06 p0937 A71-18062

Self consistent Darwin model for slow wave electromagnetic plasma simulation 07 p1172 A71-20297

Self consistent field (SCF) calculations of dipyrindine glyoxal and bianthrone photoproduct molecules with triplet ground state, using unrestricted Hartree-Fock theory 11 p1727 A71-25576

Nitrogen dioxide ground and excited state self consistent fields energy calculations, discussing electron transitions probable assignments in spectrum 12 p1934 A71-27759

Nonlinear Fokker-Planck equation numerical tests for collision effects on self consistent field first order component and plasma electron distribution function perturbation 15 p2453 A71-31146

Oxygen molecules lower states diffuse orbitals, using self consistent fields configuration-interaction calculation method 17 p2785 A71-34948

SELF DEPLOYING SPACE STATIONS

U SELF ERECTING DEVICES

U SPACE STATIONS

SELF DIFFUSION

U DIFFUSION

SELF ERECTING ANTENNAS

U ANTENNAS

U SELF ERECTING DEVICES

SELF ERECTING DEVICES

Large space structures zero backlash deployment mechanism, discussing dynamically scaled model for mechanical and structural design and dynamic analysis [AIAA PAPER 71-400] 11 p1836 A71-25276

Stowable extendible structures for spacecraft and space experiments, discussing inflatable, rigidized cloth and mechanically deployable apparatus 22 p3609 A71-41981

Planar librational motion prediction for gravity gradient satellite with extendible booms during deployment 22 p3610 A71-42014

SELF EXCITATION

Hodograph of asymmetrical gyrostat with self excitation, determining angular velocity dependence on flywheel momentum 01 p0163 A71-10656

Threshold emission and self excitation of spatially inhomogeneous laser, considering active element gain and refractive index by electrodynamic model 01 p0094 A71-10687

Dissipative mechanical filter for rocket self excited vibrations to eliminate oscillatory instability, describing transfer function and modal characteristics 01 p0164 A71-11021

Nonautonomous vibrations of self excited catclaver beam with tangential force 01 p0177 A71-11295

Self excited cavity oscillators with tunnel and parametric diodes and nonequilibrium medium, noting single and multimodes, energy capabilities and frequency interactions 02 p0231 A71-11874

Book on vibration measurements covering resonant and self excitation patterns, aerodynamics, machine parts, transducers and engineering techniques 05 p0820 A71-16275

Threshold emission and self excitation of spatially inhomogeneous laser, considering active element gain and refractive index by electrodynamic model 07 p1125 A71-20148

Noise thermometry by Josephson effect, demonstrating self excitation random frequency modulation with thermal noise and thermometer having microkelvin noise temperature measurement capability 07 p1114 A71-20157

Harmonic oscillations frequency dividers with small asynchronous component of nonlinear element conductance, showing self excitation and wide synchronization bandwidth 09 p1413 A71-22152

Cylinder vibration due to wake force in wind tunnel, discussing self exciting force induction 09 p1540 A71-23057

Power amplifier klystron self excitation in linear electron accelerators, describing tunable driver circuit with quartz reference oscillator 12 p1889 A71-27754

Hodograph of asymmetrical gyrostat with self excitation, determining angular velocity dependence on flywheel momentum 14 p2275 A71-30990

Self excited and transient oscillations parameters determination in nonlinear control systems, using control area concept 15 p2383 A71-32697

Self excitation and amplitude limitation of powder vibratory combustion, considering pressure and sample length effects 17 p2840 A71-35701

Asynchronous generators classification based on primary distinction by independent or self operated excitation and stabilized or controlled frequency 19 p3000 A71-38639

Self induction function and stability for vortex with finite core at aircraft wing, confirming Crow theory 21 p3320 A71-40502

Modulation instability of dispersion type NMR stabilizer of resonance conditions, determining critical frequency of self excitation and maximum amplification 22 p3519 A71-41444

Optimal control of self excited vibration of high speed rotor with thrust magnetic bearing, using analog simulation 23 p3681 A71-43311

Microwave power distributed self excited oscillator synchronization using elements insensitive to external disturbances 23 p3655 A71-44318

SELF FOCUSING

Weakly divergent electromagnetic wave beam propagation in optically nonlinear laminarily inhomogeneous medium, considering absorption coefficient and self focusing 01 p0037 A71-11201

Neodymium laser emission in mode locked operation, examining self focusing and modulation effect in active element 02 p0261 A71-12323

Galactic cosmic rays nonlinear interactions with solar wind, taking into account autofocusing effect 06 p0951 A71-18103

Self focusing in media with resonance absorption, determining stimulated Raman scattering threshold in bleachable absorbers as function of absorber concentration 07 p1161 A71-20381

Carbon dioxide laser IR pulses self focusing in liquid carbon disulfide, calculating nonlinear refractive index 07 p1128 A71-20396

Self focusing effect of Q switched single mode ruby laser emission in CdS crystal, noting 60 kW minimum threshold power 16 p2588 A71-33645

Weakly divergent electromagnetic wave beam propagation in optically nonlinear laminarily inhomogeneous medium, considering absorption coefficient and self focusing 17 p2697 A71-34253

Thermal self focusing of pulsed millimeter waves transmitted through cylindrical plasma, observing power dependence and beam asymmetry 18 p2951 A71-35986

Nonlinearities effects on inorganic liquid laser output, investigating Raman and Brillouin scatterings and self focusing 18 p2933 A71-37012

Hydrodynamic effects on laser beam propagation through gases by finite difference solution, applying to trapping, acoustic and light amplifications and banana self focusing 20 p3242 A71-38838

Nonlinear losses in ultrashort light pulse generators and amplifiers, attributing to self focusing of laser radiation in active and optical media 22 p3558 A71-42457

Differential equation solution for plane self focusing and one dimensional self modulation of waves interacting in nonlinear media 23 p3704 A71-43408

Self focusing in gas breakdown produced by nanosecond laser pulses, using schlieren photography and laser light forward transmission measurements 24 p3832 A71-44358

SELF INDUCED VIBRATION

NT PANEL FLUTTER

NT SUPERSONIC FLUTTER

NT TRANSONIC FLUTTER

Plain bearing oil whirl onset speed, using matrix manipulation for unbalanced shaft self induced vibration amplitudes prediction 03 p0431 A71-13072

Polymer neck autooscillatory expansion under drawing as result of interaction between elastic deformation and heat release during orientational transformation 03 p0448 A71-14362

Laser beam self induced thermal distortion in near field absorbing moving medium by theoretical model based on geometrical optics 07 p1128 A71-20389

Limit cycle bounds in phase plane for self sustained vibrations of autonomous systems, using Poincare-Bendixson theorem 11 p1841 A71-25179

SELF LUBRICATING MATERIALS

Heat resistant roller bearings for vacuum applications at high temperature, discussing cage design and self lubricating materials 02 p0258 A71-12599

Carbon fiber reinforced polymers for self lubricating materials applications, discussing friction and wear characteristics under fresh and sea water, alcohols, mineral oils, etc [PLASTICS INST. PAPER 31] 08 p1319 A71-20896

Cermet antifriction and friction powder metallurgy sintered materials for working at high temperatures without lubricants, in vacuum and inert gases 09 p1483 A71-23392

SELF LUBRICATION

Friction-wear characteristics of self lubricating composites under sliding conditions in air and vacuum [ASLE PREPRINT 70LC-17] 08 p1298 A71-21160

SELF ORGANIZING SYSTEMS

Cerebellum substrate for memory list processing in brain assuming Perceptron mechanism 01 p0015 A71-11313

Dynamic programming and Bayes algorithm for self organizing and self adjusting Markovian systems 03 p0389 A71-13515

Series connected three level perceptron type learning system with sensory, association and response units, establishing performance selection and prediction parameters 07 p1068 A71-20102

Perceptron learning systems with cross connections in single functional elements class, discussing visual patterns training schemes 07 p1068 A71-20103

Adaptive flight control systems, emphasizing bionics approach to self organizing systems 10 p1682 A71-24227

Adaptive self-organizing and -learning control systems with long and short term memory retention, using logic random searches to find parameter values [ASME PAPER 71-DE-22] 12 p1892 A71-27324

Minerva digital computing system with learning cells and electronic microcircuit elements capable of self organizing similar to human intelligence 19 p3025 A71-37420

Hybrid computer control of engine start-up using adaptive logic, adaptive programming and self organizing storage 20 p3208 A71-38998

Adaptive random search optimization of optical tracking self organizing feedback control system under inherent coupling signals 23 p3657 A71-43942

SELF OSCILLATION

Biological clocks self oscillating mechanism as temperature dependent component of circadian clocks in multicellular organisms, assuming small enzyme concentrations 01 p0020 A71-11566

Stellar variability emphasizing pulsations, noting role of He II critical ionization zone in maintaining self oscillations 03 p0485 A71-13259

Computerized statistical simulation of steady state, ergodic, self oscillatory processes in plane magnetron 03 p0386 A71-13811

Pendulum clock with contactless drive for isochronal autooscillation period, outlining pulse amplitude and duration stabilization 04 p0592 A71-14863

Two stream electron plasma with Coulomb particle collisions, considering autooscillations and nonlinear friction characteristic 04 p0633 A71-15109

Multicircuit vacuum tube oscillator with delay, calculating self oscillation line width reduction by two external resonators with high Q factor 04 p0558 A71-15121

Spontaneous oscillations in semiconductors with deep traps, deriving conditions for soft or hard excitation 07 p1176 A71-19226

Self pumped parametric amplification and oscillation of Gunn effect diodes 07 p1075 A71-19262

Emission of ruby laser with resonator containing passive Q switch solution and lenses, investigating regular self oscillation region 07 p1125 A71-19811

Transistorized ultrasonic oscillator active conductances and other circuit parameters effects on self oscillation frequency stability 07 p1078 A71-20060

Self oscillatory system behavior under sinusoidal external force, using nonlinear differential equations transformation 08 p1334 A71-21292

Closed loop systems with odd-symmetrical nonlinear components and distributed delay, calculating self oscillations 09 p1422 A71-22367

Optical parametric oscillator, observing simultaneous oscillation and second harmonic and difference frequency generation 09 p1493 A71-22760

Cylindrical spacecraft reentry body self-sustained pitching oscillations due to separation on downstream portion, examining stability derivatives
09 p1533 A71-23604

Avalanche diode microwave oscillator stabilized by two external resonant circuits, investigating self oscillation characteristics
10 p1582 A71-23808

Delay compensation in flip-flop element of optimal relay system with self oscillations, using optimal control algorithm constructed by phase space method
11 p1742 A71-26095

Equivalent-to-adaptive parametrically invariant automatic control, discussing compensation, variable structure, autooscillatory, HF nonlinear, ultrasonic and nonsearching self adjusting systems
12 p1890 A71-26723

Gyroscopic integrating accelerometer dynamics on high frequency angular vibrating base, determining self oscillations and drift motions
13 p2065 A71-27946

Time optimal systems with control lag, showing elimination of self oscillations
13 p2042 A71-28640

Magnetospheric model calculation for self oscillation period and amplitude dependence on longitude and plasma density estimation from observed geomagnetic pulsation period
14 p2228 A71-29531

Optical and microwave multifrequency autooscillatory drift and reflex klystrons, TWT and electronic oscillators, comparing to He-Ne lasers
14 p2211 A71-30091

Noise rejection in step type extremal self oscillating system with variable control period, estimating process precision
15 p2381 A71-31981

Self induced second order mode locking optical pulsing of double heterostructure stripe geometry junction lasers operating continuously at room temperature
15 p2421 A71-32388

Rocket body longitudinal autooscillation modes, taking into account pipeline fluid discontinuous cavitation oscillations
16 p2644 A71-32834

Open microwave resonators self oscillations damping, using Sommerfeld radiation conditions
16 p2546 A71-33479

Controlled motion dynamics of spacecraft performing maneuvers, applying point transformation to third-order nonlinear system moving about center of mass in lateral motion
16 p2646 A71-33658

Second order and degenerate third order nonlinear automatic control systems analysis by point mapping method, considering global stability and self oscillation mode
17 p2783 A71-35128

Nonlinear feedback control system with two nonlinear memoryless energyless elements separated by linear device, discussing grapho-analytical method for self sustained oscillation determination
17 p2722 A71-35183

Exhaust pipe or diffusion kinetic flame type relaxational autooscillatory fuel combustion system, calculating vibration frequency, amplitude and mode
17 p2839 A71-35695

Vibrating systems behavior under combined parametric excitation and self oscillation mechanism, investigating damping and generation control
19 p3155 A71-37526

On-off temperature control system with distributed parameters under boundary conditions, investigating symmetric self oscillation
19 p3163 A71-37780

Nonlinear autonomous oscillation systems stability conditions derivation by Kamenkov method for quasi-linear systems
20 p3269 A71-39201

Air pressurized bearing mounted rotor with vertical shaft, discussing elastically suspended foundation mass and damping effect on self excited vibration
22 p3550 A71-41659

Automatic control theory application to pneumatic self vibration /hammer/ occurrence criteria derivation for externally-pressurized gas-lubricated thrust collar bearings
22 p3551 A71-41660

Small autooscillations of high order differential equations system, investigating bifurcation occurrence relationship to zero equilibrium position stability change
23 p3699 A71-43572

Dynamic characteristics of self oscillating systems from response to sinusoidal test signals, using Abel integral equations
24 p3881 A71-44835

Pneumatic hammer /self oscillation/ occurrence in gas lubricated externally pressurized annular thrust bearing, comparing experimental and theoretical stability data
24 p3830 A71-44948

Vertical shaft stability on elastic sliding bearings, considering passage through autooscillations zone
24 p3831 A71-45051

Liquid transition through critical value, considering self oscillation mode frequency
24 p3821 A71-45340

SELF REGULATING
U AUTOMATIC CONTROL
SELF REPAIRING DEVICES
Grand Tour missions centralized data handling, describing computer aided telemetry system and self testing and repairing control computer
[AAS PAPER 71-152] 19 p3025 A71-37954

Failure analysis of memory organization in self repair memory system, using various coding and modularization techniques on subsystems
21 p3350 A71-40365

SELF SEALING
High speed low power loss spiral groove bearings self sealing grease lubricants with high shear stability and good boundary lubrication
[ASLE PREPRINT 70LC-6] 08 p1322 A71-21157

Aircraft self sealing fuel tank and fuel cell systems damage control, considering chemical, precompressed foam and swellable elastomer seal concepts
10 p1554 A71-24079

SELF STIMULATION
Oxygen respiration effect on self stimulation and emotional reactions in rabbits during hypothalamus electrical stimulation
06 p0855 A71-18376

SELSYNS (TRADEMARK)
U SERVOMOTORS
SEMICIRCULAR CANALS
Biocybernetic model of vestibular control system for spatial orientation, considering semicircular canals fluid motion angular velocity sensors and linear displacement perception
03 p0367 A71-12982

Elasmobranch fish labyrinth electrophysiology, analyzing semicircular canals linear acceleration response
04 p0536 A71-14755

Gravity effects on human caloric and rabbits rotational nystagmus, noting semicircular canals role
04 p0542 A71-14757

Semicircular canal ducts dynamic response characteristics, using suspended liquid filled inner tube for endolymph simulation
04 p0542 A71-14789

Vestibular system semicircular canals mathematical model determination of galvanic stimulation and directional preponderance, considering visual, postural and vehicle orientation feedback loops
04 p0543 A71-14790

Semicircular canal ducts dynamic behavior, using mathematical model for wave transmission of elastic fluid-filled toroidal shell in rigid channel
04 p0547 A71-15772

Centrifugal force effect on pigeon head nystagmus, acting on semicircular canal via otoliths or cupula
09 p1388 A71-22123

Semicircular canal influence on otolith reactions in pigeons, noting caudal and rostral shifts evoking levator and depressor coccygei contractions during horizontal acceleration
09 p1390 A71-22214

Coriolis effects on endolymph shift direction in semicircular canals of man under rotation with head movements in sagittal plane, involving nystagmus and illusory sensations
09 p1392 A71-22640

Neural transmission to vestibular nuclei of semicircular canal response to rotational stimulation, discussing test methods and results with decerebrated or anesthetized cats
10 p1566 A71-25047

Accelerations effect on receptors in semicircular canals during human movements in rotating environment, using vector analysis
13 p2007 A71-28415

Lateral and anterior semicircular canal neural reactions to caloric stimulation in frogs, indicating hydrodynamic interactions
16 p2532 A71-33912

Semicircular canal and otolithic organ function in free swimming fish angular orientation behavior
21 p3328 A71-39996

Coordination structure of human hand arbitrary movements during stimulation of horizontal semicircular canals in vestibular apparatus by negative angular acceleration
24 p3796 A71-44545

SEMICONDUCTING FILMS
Field effect photocurrent maximum in thin film semiconductors below Debye radius associating hole capture by recombination centers
01 p0139 A71-10781

Secondary electron emission during RbBr, Se and CdTe film bombardment by sodium ions and atoms
01 p0139 A71-11099

Solid state traveling wave amplifier using thin n-type epitaxial GaAs layer
03 p0384 A71-13316

Transport mechanism for holes in polycrystalline Ge films based on Matthiessen rule, considering surface scattering and dislocation
03 p0468 A71-14464

Optical and photoelectrical properties of thin amorphous thallium arsenic sulfide, thallium antimony sulfide and thallium bismuth sulfide films obtained by vacuum deposition
05 p0794 A71-16835

Microwave measurements of semiconductors and semiconductor films including resistivity, permittivity and carrier mobility
06 p0873 A71-17538

Organic thin film layer semiconductors photoconductivity, developing semiempirical theory of pulse formation
06 p0941 A71-17735

Conductivity of films with surface roughness dimensions large in proportion to screening radius and carrier free path length, presenting refined analysis
07 p1175 A71-19223

Intermetallic III-V compound semiconductor films and layers charge carrier transport phenomena and optical properties
07 p1178 A71-19850

Amorphous semiconducting thin films quenching fabrication techniques and electrical properties
07 p1181 A71-20410

Laser pulse induced rapid reversible crystallization of amorphous chalcogenide semiconductor films using photon flux model
10 p1655 A71-24044

Current oscillations and switching effect in amorphous chalcogenide compound films sputtered thermally on unheated glass and pyroceram substrates
13 p2111 A71-28173

I-V and capacitance characteristics of chalcogenide-glass based matrix-film diode sandwich and film-face switching structures with/without memory
13 p2112 A71-28922

Antimony trisulfide semiconductor films, noting chemical composition effects on photosensitive properties
15 p2461 A71-31286

Al distribution in gallium aluminum arsenide films obtained by epitaxial growth from liquid phase, showing temperature variation dependence during deposition
18 p2954 A71-36161

Hall coefficient and resistivity in undoped heteroepitaxial GaAs on aluminum oxide films grown by trimethylgallium arsine process
20 p3276 A71-38881

Multilayer microwave semiconducting film piezoelectric acoustic transducer loss and frequency response derivation from electromechanical power conversion theory
20 p3240 A71-39764

Transition layer structure formation of epitaxial semiconducting films, discussing model for dislocations origin
21 p3427 A71-40727

Thermal switching and negative resistance model and measurements of amorphous semiconductor thin films of Ge, Si and chalcogenide glasses
21 p3428 A71-40741

Deep level impurity compensation of high resistivity epitaxial films of GaAs by chromium, complex lattice defects and copper acceptors, using cathodoluminescence spectra
21 p3430 A71-41220

I-V and capacitance characteristics of chalcogenide-glass based matrix-film diode sandwich and film-face switching structures with/without memory
21 p3433 A71-41317

Evaporated tellurium thin films electrical properties, discussing fabrication techniques, temperature dependence, field effect and Hall mobilities, threshold voltage and stability
23 p3715 A71-43435

Acoustoelectrical current oscillations in GaAs films at low temperature under ultrasonic Rayleigh wave amplification
23 p3716 A71-43477

Large photomagnetic effect in semiconductor films using multilayered Cd-Te p-n microjunctions
23 p3716 A71-43484

Electron energy spectrum in periodic semiconductor structures of super thin p-n junction layers
23 p3716 A71-43485

Phase composition and defect structure of thin film CdTe islet compensates on NaCl and KBr cleavage faces
23 p3718 A71-44316

Current amplification in CdS and CdSe single crystals and thin films by fast electron bombardment
24 p3859 A71-44386

Cd doped thin polycrystalline CdTe films rectification mechanism and DC conductivity, discussing light, electric field and temperature effects
24 p3861 A71-45248

Structural and electrical properties of sublimation deposited GaAs films on sapphire and seminsulating substrate in vacuum
24 p3863 A71-45358

SEMICONDUCTOR DEVICES
NT AVALANCHE DIODES
NT FIELD EFFECT TRANSISTORS
NT GALLIUM ARSENIDE LASERS

NT GERMANIUM DIODES
 NT JUNCTION DIODES
 NT JUNCTION TRANSISTORS
 NT METAL OXIDE SEMICONDUCTORS
 NT MIS [SEMICONDUCTORS]
 NT NEURISTORS
 NT PARAMETRIC DIODES
 NT PHOTODIODES
 NT PHOTOVOLTAIC CELLS
 NT SEMICONDUCTOR LASERS
 NT SILICON TRANSISTORS
 NT THERMISTORS
 NT THYRISTORS
 NT TRANSISTOR AMPLIFIERS
 NT TRANSISTORS
 NT VARACTOR DIODES
 NT VARISTORS
 Semiconductor photoelectric sensor for monitoring laser emission energy in conjunction with memory oscillograph or single pulse peak voltmeter
 01 p0093 A71-10623
 Semiconductor quantum amplifier dynamic range in steady operation mode, analyzing monochromatic signal gain
 01 p0096 A71-11219
 Aircraft electric systems control by solid state switching, discussing reliability, service life, versatility and compatibility
 01 p0007 A71-11627
 Time-pulse converter for semiconductor triodes DC amplification factor measurement
 02 p0230 A71-11832
 High energy batteries electronic discharge mechanisms, examining use of semiconductor cathodes
 03 p0352 A71-13042
 Semiconductor devices for continuous blood pressure telemetry
 03 p0370 A71-13069
 Photoemitter technology based on GaAs/Cs photocathodes
 03 p0468 A71-14466
 Pulsed semiconductor devices with S-shaped current-voltage curve, considering relaxation oscillator and voltage generator circuits
 04 p0558 A71-15565
 Masking techniques for printed and thin film circuits and semiconductor devices fabrication
 05 p0759 A71-16775
 Microwave semiconductor limiter diode for decimeter operation using spark gap analog
 06 p0873 A71-17540
 Semiconductor devices for frequency multiplication including variable capacitance, charge storage effect and composite varactor diodes
 06 p0873 A71-17541
 Operating mode of semiconductor AFC mixer of radar receiver under large signal
 06 p0874 A71-17546
 Surface illuminated semiconductor excess current carriers nonstationary distribution and space charge, solving equation system by operational technique
 06 p0942 A71-18185
 Radiation hardened semiconductor device technique by irradiating silicon wafers on lot to lot basis
 07 p1071 A71-19065
 Transferred electron devices (TED), reviewing physics of transferred electron effect, theory and design of amplifiers and oscillators
 07 p1072 A71-19102
 Monolithic optically written and electrically read semiconductor-ferroelectric memory device employing single crystal barium titanate
 07 p1067 A71-19261
 Measuring transformer for AC input signal with pulse width modulated semiconductor multiplier feedback
 08 p1261 A71-20737
 Bulk effect microwave oscillators energy source design, reviewing operation mode and circuit tuning control parameters
 08 p1266 A71-21623
 Limited space charge accumulation layer diodes operating characteristics, using GaAs devices with uniform doping for microwave peak power
 08 p1266 A71-21624
 High purity Ge crystals growth, studying Hall effect and resistivity for semiconductor detector fabrication
 08 p1345 A71-21841
 Nondegenerate and degenerate semiconductor current flow equilibrium at low temperatures based on Boltzmann transport equation
 09 p1414 A71-22251
 Semiconductor integrated circuit fabrication optimization, considering defect density, component number, crystal size and cost analysis
 09 p1416 A71-22490
 Integrated circuits semiconductor components, determining effects of heat energy production/withdrawal and strong field on electric current carriers mobility and concentration
 09 p1416 A71-22496
 Electron transfer bulk oscillators negative conductivity as function of geometry, field and doping nonu-

niformities, using computerized simulation for device frequency-voltage characteristics
 09 p1417 A71-22689

Accelerometer for direct measurements of angular acceleration of rotating shafts, using semiconductor transducers
 09 p1443 A71-22706

Semiconductor element design flexibility, providing greater reliability and reduced size/weight for space vehicles and missiles
 09 p1445 A71-22722

Analog type semiconductor switches for aircraft and spacecraft automatic checkout systems, discussing component transistor types, optoelectronic devices and materials
 09 p1418 A71-23041

Inhomogeneous semiconductor model leading to anomalously high apparent mobility
 09 p1510 A71-23486

Electroluminescent semiconductor diodes based on GaP and GaAlAs, discussing design, properties, uses and production
 11 p1737 A71-25569

Limited reliability mathematical model for radioisotopic thermoelectric generators semiconductor couples based on catastrophic failures
 11 p1715 A71-26165

Semiconductor wafers examination with He-Ne IR laser scan microscope, producing oscilloscope shadowgraph displays of IR transmission variations in wafers
 11 p1763 A71-26186

Tunable Gunn oscillator obtained by semiconductor surface loading, discussing oscillation frequency as function of anode to edge distance
 11 p1738 A71-26365

Signal stability in distributed active lines of HF semiconductor devices with negative leakage resistance
 12 p1878 A71-26843

Spacecraft electric systems semiconductor devices radiation damage from high energy particles during space missions, noting radiation resistant devices development possibility
 12 p1943 A71-26981

Output power stabilization of He-Ne laser, using vacuum photodiodes or semiconductor diodes for discharge current regulation
 12 p1915 A71-27733

Batch fabricated three dimensional planar coaxial microelectronic interconnection and packaging technique for semiconductor chips
 12 p1890 A71-27771

Semiconductor radiation detectors, discussing minority charge carrier diffusion length measurements by nuclear method
 13 p2065 A71-27957

Book on integrated circuits and semiconductor devices covering MOSFET, optoelectronic devices, silicon controlled rectifiers and thyristors
 13 p2036 A71-28042

Unmodulated microwave oscillations power stabilizer with semiconductor attenuator
 13 p2036 A71-28367

Voltage regulating diodes, discussing development and principal characteristics of Epi-Z family of Zener diodes
 13 p2037 A71-28575

Semiconductor random access memory components, discussing LSI circuits developments for RAM applications cost effectiveness in computer main-frame memories
 13 p2035 A71-28772

Multilayered semiconductor structures with p-n junctions, discussing I-V characteristics, noninjection component effects, carrier transport and negative resistance
 13 p2111 A71-28920

Dispersion and boundary equation concerning space-charge wave propagation under diffusion effect in Gunn semiconductors with anisotropic conductivity and finite thickness
 14 p2283 A71-29793

Semiconductor thermoelectric battery p-n cell elements joining with mercury amalgam for commutating
 14 p2181 A71-29953

Millimeter wave semiconductor isolator using circular waveguide with coaxial n-type InSb in longitudinal magnetic field
 14 p2212 A71-30510

Transient response and design formulas for microwave power stabilizer with nonlinear inertial feedback containing semiconductor attenuator
 15 p2378 A71-31230

Book on hot electron microwave generators covering semiconductor physics, collision theory, Gunn effect, domain dynamics, avalanche breakdown, etc
 15 p2375 A71-31509

Satellite-borne semiconductor telescope for relativistic heavy primary cosmic rays identification, increasing resolving power by minimum pulse selection method
 15 p2407 A71-31806

Metal-semiconductor-metal low noise microwave oscillator, using single crystal n-type Si wafers sandwiched between two PtSi Schottky barrier contacts
 15 p2377 A71-32315

Impedance variations vs electrophysical properties of epitaxial and diffusive semiconductor structures for electronic equipment, applying microwave fields for parameter control
 18 p2954 A71-35874

Bulk semiconductor microwave control components, considering dielectric and conductive properties of plasma state
 18 p2894 A71-36980

Semiconductor device with stable negative conductance over wide range of microwave frequencies and power levels, using transferred electron effect in epitaxial GaAs
 18 p2895 A71-36985

Semiconductor instability effects on reflection and transmission coefficients of microwave control devices
 19 p3026 A71-37252

Microwave reflection from semiconductor wafers with dielectric film, presenting electromagnetic field parameters as function of electrophysical properties
 19 p3117 A71-37264

Reliable plastic encapsulated semiconductor devices design, production and evaluation, noting application to IC
 19 p3033 A71-38509

Discrete semiconductor devices test program assessing environmental screening for improved component reliability
 19 p3034 A71-38517

Scanning electron microscope for poor metallization detection in manufacturing cycle of semiconductor devices
 19 p3034 A71-38519

Maximum efficiency of 10-20 W output semiconductor amplifier at 2.3 GHz, discussing possible replacement of vacuum tubes
 20 p3205 A71-39456

Microwave waveguide semiconductor modulator with p-n-n diode as control element, taking into account semiconductor control element conductivity change along waveguide wall
 20 p3206 A71-39813

Holographic methods for etching masks of IC and other semiconductor components
 21 p3354 A71-40731

Cholesterol liquid crystals technique for thermal analysis of microcircuits, multilayer circuit boards, semiconductor devices and other electronic components
 21 p3355 A71-40738

Semiconductor components reliability assurance under assumption of failure rate decrease with time for IC quality and performance improvement
 21 p3356 A71-40746

Metals and systems for semiconductor devices metallization, evaluating conductivity, adhesion, contact resistance, deposition ease, electrochemical corrosion, reliability and stability
 21 p3356 A71-40802

Ion implanted depletion mode MOS/LSI devices in conjunction with conventional P channel processing
 21 p3358 A71-40821

Ceramic semiconductor atmospheric humidity detector with hydrophilic properties, using complex capillary porous body composed of crystals and amorphous substance
 21 p3383 A71-41237

Multilayered semiconductor structure with p-n junctions, discussing I-V characteristics, noninjection current component effects, carrier transport and negative resistance
 21 p3433 A71-41306

Semiconductor radiation detectors, discussing minority charge carrier diffusion length measurements by nuclear method
 21 p3383 A71-41346

Intense ionizing radiation and thermal treatment effects on electrical parameters of Si semiconductor devices
 22 p3584 A71-41619

Semiconductor diode image tube system as digital multichannel photometer, noting cost, weight and size advantages over photomultiplier tube array with pulse counting electronics
 22 p3541 A71-41793

High intensity light sources hazards analysis, discussing thermal detectors and vacuum and semiconductor photodiodes for pulsed laser outputs measurement
 22 p3541 A71-41795

Electronic techniques in optronics /optoelectronics/, discussing CRT, image tubes, semiconductor devices and lasers
 22 p3559 A71-42467

Thick film technology and tests for hybrid microcircuits and semiconductor packaging
 23 p3651 A71-43430

- Semiconductor package designs for high performance miniature IR sensors, including flat packs, TO, custom metal and glass dewar configurations
23 p3676 A71-43509
- High power semiconductor devices in pulsed operation mode for transient thermal resistance and p-n junction temperature estimation
23 p3652 A71-43584
- Design and performance of semiconductor devices with heterojunctions, covering injection laser without cooling, emission frequency converter and negative resistance triode
24 p3808 A71-44383
- Phase shift and attenuation measurements in high power microwave ferrite tetrodes circuits, using semiconductor transducers/digadectors/
24 p3809 A71-44871
- Phase sensitive magnetic semiconductor pulse width modulator with diode bridge consisting of single saturable-core choke input and transistor circuit output arms
24 p3810 A71-45155
- ## SEMICONDUCTOR JUNCTIONS
- NT JOSEPHSON JUNCTIONS
NT N-P-N JUNCTIONS
NT P-I-N JUNCTIONS
NT P-N JUNCTIONS
NT P-N-P JUNCTIONS
NT P-N-P-N JUNCTIONS
NT SILICON JUNCTIONS
- Junction-casing and junction-ambient medium thermal resistance determined in power transistors and diodes
01 p0055 A71-11125
- Emission threshold current in semiconductor heterojunction p-p-n laser
03 p0439 A71-13977
- Room temperature spatial distribution of emission from injection lasers with single and triple heterojunctions in AlAs-GaAs system
03 p0439 A71-13980
- AlAs-GaAs heterojunction laser threshold currents and CW operation at room temperature as function of p- and n-type emitter regions
03 p0439 A71-13987
- Tunneling in boron doped p-type silicon metal-semiconductor and MIS tunnel junctions
04 p0636 A71-14973
- Copper sulfide-cadmium disulfide heterojunctions photocapacitance effects, discussing current generating mechanism and modulation by trapped charge with heat treatment effects taken into account
05 p0699 A71-16054
- CaAs Schottky tunnel junctions properties and bias independent structure evaluation by excess noise generation
06 p0940 A71-17312
- Semiconductor thermocell junction polishing effects on bilateral layers tensile strength and electrical contact resistance
07 p1023 A71-19145
- Josephson maximum DC current plot for linear overlap junctions, discussing junction area geometry to current perimetric proportionality
09 p1423 A71-22693
- Thermoelectric microwave radiation sensors with small area n-n junctions, investigating carrier heating effects on I-V characteristics
10 p1584 A71-24723
- Gunn diodes and heterojunction laser applications in optical pulse communication systems synthesis
11 p1772 A71-25235
- Distribution laws of statistical Q characteristics and of junction capacitance of varicaps
11 p1740 A71-26542
- Nonlinear analog function generators using semiconductor junctions and combined diode-resistor network
13 p2039 A71-28914
- Time dependence of peak emission energy shift due to junction temperature rise in GaAs junction lasers operated with flat topped current pulse
15 p2420 A71-32027
- Continuous automatic recording of semiconductor diodes integral conductivity components, using circuit with controlled steady voltage bias
17 p2713 A71-34569
- Tunnelling conductance anomaly in metal-insulator-metal junctions containing paramagnetic impurities, analyzing I-V characteristics during switching effect
18 p2954 A71-36802
- Superconducting microjunctions I-V characteristic at critical temperature, investigating voltage fluctuations effects in external circuit
19 p3119 A71-37860
- Electrons interaction with impurities and longitudinal optical phonon in metal-insulator-semiconductor tunnel junctions
19 p3119 A71-37869
- Copper sulfide-cadmium sulfide photovoltaic solar cell electronic processes observation at heterojunction, noting electron trapping and hole injection roles in long term stability
19 p3119 A71-38140
- GaAs laser diode junction temperature measurement methods for verification of stimulated emission quenching due to heating
19 p3074 A71-38231
- Peak optical flux density for catastrophic damage in close confined and double heterojunction injection Al-GaAs-GaAs lasers
19 p3075 A71-38507
- Monolithic alphanumeric array of planar light-emitting GaAsP diode matrix on common chip for programmed function keyboard use in display devices
21 p3349 A71-40108
- Junction structures and electrical properties of silicon n-p-n transistors fabricated by various combinations of diffusion and ion implantation
21 p3354 A71-40728
- Beam-lead nitride-passivated IC seal junction chip reliability evaluation by life tests for optimum packaging into functional modules
21 p3357 A71-40813
- Beam-lead devices, discussing comparison to conventional transistor chip, reliability, applications and assembly techniques
21 p3357 A71-40815
- Optical investigation of metal-semiconductor interface blocking layer and photo-Hall effect in high resistivity crystals
21 p3433 A71-41316
- Multijunction functional devices for operation as decade digital counter, step voltage generator, analog/digital converter, binary counter, neuristor line, etc
22 p3520 A71-41706
- Characteristic energies of exponential band tails in GaAs junction lasers from wavelength shift with cavity Q and spontaneous emission line width
22 p3558 A71-42360
- Photoeffect efficiency of solar energy converters based on semiconductor cadmium sulfide-copper sulfide heterojunctions
22 p3483 A71-42536
- Numerical analysis of large signal output characteristics for directly modulated GaAs junction injection lasers, investigating resonance phenomenon
23 p3683 A71-43351
- Negative resistance in high resistance compensated semiconductor diodes with double injection associated with diffusion growth
23 p3652 A71-43482
- Design and performance of semiconductor devices with heterojunctions, covering injection laser without cooling, emission frequency converter and negative resistance triode
24 p3808 A71-44383
- Heterostructure/multisemiconductor junctions/injection laser with reduced current density requirement for continuous operation at room temperature
24 p3833 A71-44974
- Thermal resistance, junction temperature and maximum power meter for semiconductor transistors and diodes with/without heat sinks
24 p3810 A71-45203
- ## SEMICONDUCTOR LASERS
- NT GALLIUM ARSENIDE LASERS
- Semiconductor lasers direct amplitude, pulse and frequency modulation methods, comparing advantages and limitations
02 p0260 A71-12004
- Nd glass laser radiation time and spectral structure
03 p0437 A71-13885
- Emission threshold current in semiconductor heterojunction p-p-n laser
03 p0439 A71-13977
- Room temperature spatial distribution of emission from injection lasers with single and triple heterojunctions in AlAs-GaAs system
03 p0439 A71-13980
- IR lasers, discussing carbon dioxide CW and Q-switched operation and semiconductor lasers
04 p0606 A71-14712
- Optical signal amplifiers operational principles, discussing parametric, semiconductor laser, and solid state amplifiers and amplifiers using gas in Fabry-Perot resonator
04 p0608 A71-15079
- Semiconductor laser diodes structural and operational characteristics, discussing applications in aircraft and construction machines guidance systems
05 p0761 A71-16328
- Semiconductor laser threshold current temperature dependence, considering maximum power gain and compensation techniques
06 p0908 A71-18424
- Semiconductor injection lasers, discussing energy characteristics of state density distribution, coherent emission, etc
07 p1126 A71-20252
- Electron beam pumped CdS laser, investigating output pulse time duration based on laser oscillation quenching model
08 p1302 A71-21433
- Semiconductor lasers properties, operational characteristics, power outputs and efficiency
09 p1462 A71-22586
- Spectral mode and CW operation of stripe geometry double heterostructure GaAs junction lasers above room temperature
09 p1463 A71-22763
- High power single mode CW tunable spin-flip Raman laser in InSb using CO pump
10 p1620 A71-24041
- Accuracy requirements on crystal orientation for p-n junction laser with tilted mirrors and various resonator lengths concerning output vs current characteristics
12 p1914 A71-27095
- Transverse mode locking effect on radiation intensity of injection semiconductor laser as function of time and p-n junction refractivity
13 p2077 A71-28172
- Accelerator with electron pregrouping for exciting semiconductor lasers based on amplifying klystrons
13 p2079 A71-28858
- Nd-YAG laser operation with simultaneous intracavity frequency doubling and mode locking, observing mode-locked pulse lengthening and circulating power decrease
13 p2081 A71-29335
- High intensity tunable InSb spin flip stimulated Raman scattering from pulsed high pressure carbon dioxide laser radiation pumping
13 p2081 A71-29336
- Continuous visible operation of semiconductor laser at room temperature, discussing lasing thresholds
13 p2081 A71-29340
- Semiconductor injection laser output transient response, analyzing stepshaped impressed current by differential rate equations
13 p2081 A71-29391
- Cadmium sulfide pulsed laser spectrum analysis, discussing output stabilization by mode selection and electron beam scanning
14 p2253 A71-30092
- Semiconductor lasers with fast electron pencil beam excitation for high capacity computer storage application
14 p2207 A71-30110
- Pulsed semiconductor laser as high resolution optical range spectroscopy, noting application to Cs hyperfine absorption
15 p2421 A71-32403
- Semiconductor heterostructure junction diode lasers for operation at room temperature, discussing energy band structure and mass communications application
16 p2587 A71-33471
- Semiconductor laser continuous emission conditions at room temperature, assuming output power drop with increasing current due to p-n junction heating
16 p2587 A71-33492
- Dynamic amplification ranges of monochromatic signal by semiconductor, solid state and gas lasers in steady operation mode
17 p2750 A71-34270
- Short pulse Nd-YAG direct detection laser system for space communications, noting RF links complementation, high data rates, practical size, weight and power requirements
17 p2705 A71-35093
- Double heterojunction structure improvements in injection laser diodes and arrays
18 p2931 A71-36603
- Stimulated emission in double heterojunction Al-GaAsP quaternary lasers, considering solution grown crystals advantages
19 p3071 A71-37476
- IR pumped stimulated light emission in semiconductor, noting upconversion due to energy transfer between impurity ions
19 p3071 A71-37479
- Semiconductor lasers, noting AlGaAs-GaAs p-n heterojunction structure contribution to room temperature efficiency of diode lasers
19 p3074 A71-38230
- Papers on semiconductor, carbon dioxide and dye lasers
20 p3243 A71-39065
- Semiconductor lasers, discussing laser action concepts, optical waveguiding, power conversion efficiency, thermal properties, reliability, crystal imperfections, GaAs laser properties, transient phenomena, etc
20 p3243 A71-39066
- Plasmaron coupling and laser emission in optically excited Ag-doped cadmium tin diphosphide
21 p3391 A71-40200
- Emitted signal delay time effect on operational precision of semiconductor laser radar for measuring lower cloud boundary heights
21 p3394 A71-41239
- Prebunching electron accelerator for exciting semiconductor lasers based on amplifying klystrons
21 p3394 A71-41296
- Circuit generating short rectangular current pulses for pumping semiconductor lasers
23 p3685 A71-43528

Indium gallium phosphide p-n junction laser operation at 4.2 and 77 K, considering threshold currents magnitude

23 p3687 A71-44138

Heterostructure /multisemiconductor junctions/ injection laser with reduced current density requirement for continuous operation at room temperature

24 p3833 A71-44974

SEMICONDUCTORS [MATERIALS]

NT ACCEPTOR MATERIALS

NT DONOR MATERIALS

NT METAL OXIDE SEMICONDUCTORS

NT MIS (SEMICONDUCTORS)

NT N-TYPE SEMICONDUCTORS

NT ORGANIC SEMICONDUCTORS

NT P-TYPE SEMICONDUCTORS

NT PHOTOCONDUCTORS

Semiconductors optical properties, measuring Franz-Keldysh effect in specimen under strong sinusoid electric field perpendicular to light beam direction

01 p0137 A71-10089

Polycrystalline semiconductors Hall effect by grain structure model for low and high resistivity boundaries, giving vapor deposited cadmium selenide film data

01 p0137 A71-10283

LF spiral monochromatic wave pulse propagation from vacuum into semiinfinite semiconductor, considering bandwidth relation to electron heating

01 p0138 A71-10431

Electromagnetic wave nonlinear propagation in semiconductors, considering field amplitude and electron temperature for strong electron phonon interaction and degenerate semimetals

01 p0138 A71-10434

Sasaki effect in doped semiconductors at low temperatures concerning conduction anisotropy and intervalley impurity electron scattering

01 p0139 A71-10777

Thermodynamic distribution of amphoteric Ge impurities in sublatitudes of GaAs semiconductor for compensation by acceptor vacancies

01 p0139 A71-10778

Wave propagation in plane neutral electron beam near interface with semiconductor

01 p0139 A71-10782

Minority current carrier mobility in anisotropic semiconductors, using Dember and photomagnetic effects

01 p0139 A71-11035

Semiconductor with charged impurities in strong electromagnetic field, investigating scattering effects on electron energy spectrum

01 p0140 A71-11463

Mechanical characteristics of generalized Rayleigh waves in piezosemiconductors of cubic symmetry, deriving amplification and damping factors for zero diffusion coefficient

02 p0294 A71-11894

High resistance semiconductors minority carriers mean diffusion length based on induced charge dependence on applied voltage during illumination by absorbable light

02 p0294 A71-11898

Strain free insulated mounting technique for semiconductors onto cold finger at liquid He 3 temperatures

02 p0294 A71-12142

Electron states in highly doped semiconductors, describing energies in conduction and forbidden bands

02 p0297 A71-12616

LF EM wave absorption in disordered semiconductors, calculating frequency dependence of conductivity due to electron transitions between discrete local levels

02 p0297 A71-12618

Space charge hypersurface layer conductance in semiconductors, allowing for three dimensional surface impurity fields

03 p0467 A71-13976

Magnetic field effect on mean electron impact ionization probability in valent semiconductors with ellipsoidal equienergetic surfaces

03 p0467 A71-13978

Nonequilibrium injected carrier distribution effect on bipolar drift mobility in compensated semiconductors

03 p0467 A71-13983

Semiconductor cadmium sulfide crystal structure changes during high power electron beam and optical pumping, using stimulated emission spectra measurements

03 p0439 A71-13984

Homogeneous and inhomogeneous photoelectric semiconductors, examining photomagnetolectric, photomechanic, photovoltaic and Dember effects

03 p0468 A71-14303

Monograph on helicon and Alfvén wave propagation in nonmagnetic semiconductors and semimetals covering active and passive waves

04 p0635 A71-14088

Arsenic doped Si single crystal impurity segregation striae and central faceted area observations by scanned laser IR microscope

04 p0608 A71-15039

Electron mobility and thermal emf in nondegenerate ferromagnetic semiconductors, considering entrainment of electrons by magnons at temperatures below Curie point

04 p0636 A71-15102

Transducer with single crystal Ge for high heat flux measurement, noting calibration by direct conduction

04 p0599 A71-15589

Aging process effects on thermoelectric semiconductors physical stability for cryogenic applications

05 p0793 A71-16799

Acoustic and surface plasma waves in superconducting semiconductor metal films and laminates

05 p0793 A71-16826

One conduction band semiconductor surface drift waves in presence of current carrier drift

05 p0794 A71-16836

Low electrical conductivity semiconductor melts thermal conductivity, discussing energy quasi-gap existence

05 p0794 A71-16881

Radioelectric /Hall/ effect due to electromagnetic wave propagation in semiconductors, noting longitudinal electric field generation by thermoelectric forces

05 p0794 A71-16882

Transverse parity photomagnetic effect during intense illumination in isotropic semiconductor crystals with relaxation time independent of energy

05 p0794 A71-17041

Soviet book on kinetic effects in semiconductors covering galvanoresistive and thermomagnetic effects, energy bands, quantum theory, oscillation theory, etc

06 p0941 A71-17431

Porphyrins optical and semiconductor properties concerning absorption, electrical conductivity and photoconductivity spectra

06 p0941 A71-17526

Microwave measurements of semiconductors and semiconductor films including resistivity, permittivity and carrier mobility

06 p0873 A71-17538

Polycrystalline semiconductors grain boundaries effect on conductivity, Hall mobility and current carriers concentration

06 p0942 A71-18187

Lamb wave interaction with current carriers in cubic symmetry piezosemiconductors, obtaining amplification factor

06 p0942 A71-18352

Carrier mobility in noncompensated highly doped semiconductors, presenting derivation from Rogachev expression for scattering Coulomb center screening charge density

07 p1175 A71-19218

Semiconductors isoelectronic impurity states, using semiempirical delta-potential method to calculate bonding energy for GaP containing nitrogen as impurity

07 p1175 A71-19220

Nonhomogeneous arbitrarily formed semiconductor layers, using Van der Pauw method for measuring conductivity and Hall mobility

07 p1175 A71-19221

Schottky barrier diode shot noise, examining dependence on potential barrier gap thickness, height and permittivity, impurity distribution, Schottky layer thickness and semiconductor dielectric constant

07 p1075 A71-19225

Spontaneous oscillations in semiconductors with deep traps, deriving conditions for soft or hard excitation

07 p1176 A71-19226

Dimensional resonances of standing helicon waves in two layer and multilayer semiconductor structures and crystals with growth inhomogeneities

07 p1176 A71-19273

Helicon wave resonance excitation and indication in intermediate magnetic fields in semiconductors

07 p1176 A71-19274

Quadrupole interaction in crystals of diamond-like semiconductors gallium telluride and indium telluride

07 p1177 A71-19275

SHF electric fields effects on free carrier redistribution in semiconductors and surface effect influence on sample conductivity

07 p1177 A71-19496

Amorphous semiconductors theories and models, considering structural, optical and electrical characteristics

07 p1178 A71-19847

Soviet papers on solid state electronics problems covering semiconductors photoelectric, magnetic, surface properties, autoemission, photoemission, etc

07 p1178 A71-19917

Heterojunctions with II-VI compound semiconductors, evaluating electro-optical performance

07 p1181 A71-20409

Noncrystalline amorphous solids electro-optical effects, studying semiconductor energy band models

07 p1181 A71-20422

Multiple valued Sasaki effect concerning electron transitions in multivalley Ge semiconductors

07 p1181 A71-20537

Nonlinear theory of intrinsic semiconductors electromagnetic wave transmission under skin effect conditions, determining reflectance and carrier temperature

08 p1344 A71-21442

Hydrogen-like centers in semiconductors, investigating secondary optical absorption

09 p1506 A71-22144

Semiconductor thermoelectric materials in intercrystalline boundaries porosity effects on electrical and thermal conductivity

09 p1506 A71-22162

Electron entrainment by photons during intraband light absorption by free carriers in Ge semiconductors

09 p1507 A71-22232

Macroscopic model of impurity electron centers for strong exchange interactions in ferromagnetic and paramagnetic semiconductors

09 p1508 A71-22880

Amorphous semiconductors for memory and logic devices, using reversible structural transformations between disordered and ordered states

09 p1509 A71-23114

Probability of quasi-chemical reactions between point defects in semiconductors due to ionizing radiation

10 p1655 A71-24139

Bipolar photomagnetic effect relation to nonheating electric field in semiconductors with isotropic holes and multivalley electrons, obtaining surface intervalley relaxation rates

10 p1656 A71-24320

Pinch effect in nondegenerate intrinsic inhomogeneous semiconductors under nonuniform spatial volume recombination, resulting in nonlinear I-V characteristics

10 p1656 A71-24321

Hall effect mechanical vibration transducer with indium arsenide semiconductors and elastically suspended magnets

10 p1612 A71-24639

Photoelectret effects in semiconductor materials containing deep lying impurity centers, discussing inhomogeneity regions and noise and reverse current levels

11 p1808 A71-25915

Automatic control application to liquid metal and semiconductor materials, plasma flows, charged particle beams and similar media interacting with magnetic fields

12 p1936 A71-26972

Direct analysis of IC by laser beams, considering homogeneity test scanning of Ge semiconductor crystals through photovoltaic injector microscopy

12 p1914 A71-27041

Alkali and rare earth metal hexaborides energetic structure, discussing semiconductor, semimetallic and metallic compounds on basis of energy bands and effective valence

12 p1944 A71-27094

Semiconductor or gas-discharge two-component plasmas, calculating permittivity variation due to carrier heating and diffusion during strong plane monochromatic, electromagnetic wave propagation

12 p1937 A71-27184

Amorphous semiconductors, including electrical conductivity, temperature dependence, germanium/silicon structural model and mobility energy

12 p1944 A71-27244

Ovonic systems involving electrothermal switching effects on semiconductor glasses, discussing threshold voltage characteristics as function of temperature distribution and glass thickness

12 p1944 A71-27638

Semiconductors high carrier densities at low temperatures, showing possible soft plasma branch and electron sound

12 p1944 A71-27770

Semiconductor zinc selenide and zinc cadmium selenide crystals two photon absorption coefficients, noting forbidden bandwidth relation

13 p2077 A71-27954

Semiconductor materials technologies, discussing optoelectronic and microwave components, photodiode arrays, HF diodes and transistors and IC Doppler radar units

13 p2111 A71-28908

Electron-hole scattering effect on carrier heating and I-V characteristics in semiconductors, using relaxation time and self consistent analysis

13 p2111 A71-28921

Electron energy spectra of amorphous semiconductors by cell method, replacing conditions for splicing wave functions by extremum integral

13 p2112 A71-28925

Carrier mobility, conductivity and optical absorption in strong electric fields of chalcogenide glasses for switching and memory effect amorphous semiconductors

13 p2112 A71-28926

Variances and covariances calculation for fluctuating numbers of semiconductor conduction electrons in terms of noise
14 p2211 A71-30292

Surface state energy positions determination in high-energy gap semiconductors by photovoltage spectral distribution
14 p2284 A71-30404

Electron hole plasma in plate shaped semiconductor under rapidly increasing external magnetic field, examining density
15 p2453 A71-31247

Test equipment for radiometric analysis of impurities concentration distribution in semiconductors, using thin plane-parallel layers continuous removal method
15 p2383 A71-31657

Nonlinear optical effects associated with free holes and electrons in semiconductors, including higher harmonics generation and frequency mixing
16 p2621 A71-33375

Crystal defects and electrical and optical properties changes due to electron bombardment of semiconductors
16 p2622 A71-33622

Thermoelectric and thermomagnetic phenomena in semiconductors with impurity ions, solving electric conductivity and diffusion and Poisson equations for weak magnetic fields
16 p2622 A71-34027

I-V characteristics of compensated semiconductors during nonequilibrium carrier injection from contacts
16 p2622 A71-34028

Electromagnetic absorption cross sections from wave function of free carriers in semiconductors with point defects
16 p2623 A71-34031

Microwave reflection factor analytical and graphical dependences on resistivity of variable thickness semiconductor layers
16 p2544 A71-34032

Anisotropic carrier redistribution near semiconductor charged surface with energy band bending, discussing relaxation rate
17 p2790 A71-34197

Composite piezoelectric transducer subjected to current flow in semiconducting boundary layer under polarization gradient, determining mechanical response by Laplace transform
17 p2739 A71-34669

Semiconductor defects, including stoichiometric vacancies in sphalerite lattices, epitaxial interfaces and dislocations in Ge
18 p2953 A71-35870

Impure GaAs and InP semiconductors compensation by introducing diffusible temperature dependent impurities
18 p2953 A71-35871

Laminar semiconductor and metallic structures electromagnetic impedance dependence on layers thickness, resistances and permittivities
18 p2953 A71-35873

Quantum counter action in various media including trivalent and divalent rare earth ions, Fe group transition metal ions, semiconductors and gases
18 p2930 A71-36145

Concentration broadening of impurity levels in compensated semiconductors, proposing averaging procedure
19 p3117 A71-37262

Specific contact resistance at zero bias as measure of ohmic or rectifying behavior of metal-semiconductor barrier under operating conditions
19 p3117 A71-37485

Temperature dependence of ionization rates in aluminum gallium arsenides for samples with varying Al contents
19 p3117 A71-37486

Thin film Au-CdS-Al type metal-semiconductor barriers, determining barrier height from temperature dependence measurements of I-V characteristics
19 p3118 A71-37488

Charge neutrality in semiconductors with implanted dopant ions profiles, considering junction field penetration into Gaussian profile
19 p3118 A71-37489

Mg compounds family of antiferroelectric structured small-gap semiconductors, investigating surface light scattering properties by Raman scattering techniques
19 p3119 A71-37870

Failure prediction for metal film semiconductor contacts on silicon substrate by electromigration, considering current density and temperature gradients
19 p3119 A71-38510

Semiconductor neutron hardness assurance by irradiation of wafer, probe, die rejection and anneal screening technique
19 p3034 A71-38520

Cascaded thermoelectric generator using Si-Ge and Pb-Te elements with heat pipe interstage coupling
20 p3264 A71-38929

Nonlinear Faraday effect in nonparabolic semiconductors subjected to strong electromagnetic field and

steady magnetic field, deriving distribution function of charge carriers
20 p3276 A71-39010

Crystal growth of III-V compound semiconductors from vapor phase, studying deposition processes chemistry by mass spectrometry
21 p3427 A71-40216

Silicon semiconductor surface passivation with thermally grown silicon dioxide films
21 p3427 A71-40218

Raman tensor, scattering efficiency and line widths in semiconductors due to optical phonons, discussing electro-optical coefficients
21 p3427 A71-40662

Optical mixing and higher harmonics generation by free carriers in semiconductors, using carbon dioxide laser
21 p3393 A71-40663

Amorphous semiconductors electrical switching effects and applications covering computer memory, visual display control and printing
21 p3355 A71-40740

Microwave MESFET HF circuits, discussing noise factor advantage over bipolar transistors in low noise preamplifiers
21 p3355 A71-40743

Hybrid circuit heat sensitive semiconductor chips mounting methods for preventing thermal degradation
21 p3356 A71-40744

Optical phonons and temperature dependent phase transitions in paraelectric antimony and ferroelectric sulfoxide semiconductors, using polarized IR and Raman spectra measurements
21 p3428 A71-40775

Light intensity distribution inhomogeneity in transmission by GaAs single crystals, using schlieren method
21 p3428 A71-41201

Photoelectret effects in semiconductor materials containing deep lying impurity centers, discussing inhomogeneity regions and noise and reverse current levels
21 p3429 A71-41205

Switching effects in diode structure formed by two tungsten point contacts on glassy cadmium germanium arsenide surface
21 p3358 A71-41207

Semiconductor surface state effects on p-n junction photodiode frequency characteristics under short and open circuit conditions, noting nonequilibrium capacitance during illumination
21 p3358 A71-41215

Sound waves interaction in piezoelectric semiconductors under pumping, deriving basic equations for parametric amplification investigation
21 p3430 A71-41216

Ge and Si point contact semiconductor diodes anisotropic deformation, investigating pressure effects on current and negative resistance in forward branch of I-V characteristics
21 p3430 A71-41222

Semiconductor radiation-induced electrical conductivity changes correlation to forbidden band from theoretical model, considering radiation defects as conductivity compensators
21 p3431 A71-41230

Semiconductor materials compensated trapping levels analysis, applying thermally simulated capacitor discharge technique
21 p3431 A71-41231

Nonlinear absorption in transparent semiconductors of picosecond light pulses from Nd laser with locked modes
21 p3431 A71-41256

Exchange interaction in excitons for arbitrary band structure of semiconductors in effective mass approximation allowing correction
21 p3431 A71-41262

Semiconductor surface layer noise generation physical model with allowance for relaxation effects due to traps in space charge region
21 p3432 A71-41301

Monte Carlo method computer simulation for displacement cascades energy and space structure in Ge, Si and PbS, interpreting semiconductor electrical properties under hard radiation
21 p3432 A71-41304

Electron-hole scattering effect on carrier heating and I-V characteristics in semiconductors, using relaxation time and self consistent analysis
21 p3433 A71-41308

Optical investigation of metal-semiconductor interface blocking layer and photo-Hall effect in high resistivity crystals
21 p3433 A71-41316

Electron energy spectra of amorphous semiconductors by cell method, replacing wave functions condition extremum integral
21 p3434 A71-41321

Semiconductor surface relaxation behavior with allowance for inhomogeneity and charge exchange between slow states and space charge
21 p3434 A71-41322

Solid and liquid Ge thermal conductivity measurement at high temperatures by coaxial cylinder and flat layer methods
21 p3435 A71-41334

Photoelectric properties of gold doped germanium semiconductor structures, investigating long wavelength background illumination effect on nonequilibrium conductivity
21 p3435 A71-41336

GeTe alloyed with Zn, Cd or Hg, measuring electrical conductivity and thermoelectric power temperature dependence
21 p3435 A71-41345

Negative differential conductance in semiconductors containing attractive centers with Maxwellian distribution function and temperature dependence on carrier energy
21 p3436 A71-41351

Gallium selenide excitation by ruby laser radiation, investigating impurity photoconductivity dependence on radiation intensity
21 p3395 A71-41352

Piezosemiconductors nonequilibrium electron plasma current oscillations under strong electric and magnetic field interactions
22 p3584 A71-41644

Transverse surface wave amplification in piezosemiconductor, considering cases of total or drift current in thin near-surface semiconducting layer
22 p3585 A71-41707

Multivalley semiconductors scale effect due to nonuniform electron heating by electric field, determining effective conductivity as function of plate thickness and surface characteristics
22 p3585 A71-42058

Antiferromagnetic semiconductors and metals in magnetic field, obtaining Fourier components of electromagnetic fluctuation correlators for dielectric permittivity and magnetic permeability tensors
22 p3586 A71-42062

Semiconductors submillimeter and far IR reflection spectra and cyclotron resonance measurements
22 p3586 A71-42140

Microwave antenna near field apparent image and phase-amplitude distribution measurement with photocontrolled semiconductor panel
22 p3523 A71-42318

Semiconductor or gas-discharge two-component plasmas, calculating permittivity variation due to carrier heating and diffusion during strong plane monochromatic electromagnetic wave propagation
22 p3584 A71-42461

Polycrystalline thin film CdSe-CdS and CdSe-CdTe solid solution semiconductor alloys Hall mobility and carrier concentration dependence on substrate temperature
23 p3715 A71-43433

Coulomb interaction effect between charged traps in amorphous semiconductor, noting state density reduction at Fermi energy
23 p3715 A71-43472

Scale effect in semiconductor magnetoresistance due to carrier separation across plate thickness under perpendicular magnetic field
23 p3715 A71-43476

Dynamic carrier density instabilities for semiconductor-metal electric phase transition by Frenkel-Poole effect in semiconductor with donors
23 p3716 A71-43478

Urbach absorption-photon energy law for excitons in AII-BVI semiconductors
23 p3716 A71-43481

Waveguide system for measuring semiconductors electrical and photoelectric properties at SHF, observing temperature effects
23 p3652 A71-43531

Soviet book on microwelding by pressure covering semiconductor-metal bonding, ultrasonic soldering and thermal processes
23 p3682 A71-44125

Symbiotic shifts of conductivity compensation effect in glassy chalcogenide semiconductors unaffected by heat treatment of blanks or impurities
23 p3717 A71-44315

Nondiffusion theory for I-V characteristics of monopolar and quasi-monopolar photosensitive semiconductors with various carrier injection levels
24 p3859 A71-44385

Semiconductor applications of alpha SiC single crystals, showing mechanical separation of polytypes from druses
24 p3841 A71-44742

Dielectric and semiconductor crystals surface defects, considering electric polarization structures
24 p3860 A71-45098

Transition from metallic to activation conductivity in doped semiconductors, noting activation energy dependence on compensation degree
24 p3860 A71-45121

Hot electrons in semiconductors within crossed and parallel electric and quantizing magnetic fields, examining collision frequencies and energy relaxation
24 p3861 A71-45165

High purity Sb, In and Ag by vacuum distillation, zone melting and electrolytic refining for semiconductor electronics 24 p3861 A71-45201

Surface potential barrier models for thermionic and photoelectric emissions from semiconductors in Schottky deviation region 24 p3862 A71-45350

Experimental verification for electrostatic field gradient effects on charge carrier concentration in diffused regions of semiconductors 24 p3863 A71-45359

Luminescence time decay in optically excited thin direct gap semiconductor with surface losses, establishing phase shift method for carrier lifetime and semiconductor surface properties 24 p3863 A71-45360

SEMIEMPIRICAL EQUATIONS

Incompressible fluid turbulent boundary layer equations, examining approximate semiempirical calculations 04 p0573 A71-15555

Organic thin film layer semiconductors photoconductivity, developing semiempirical theory of pulse formation 06 p0941 A71-17735

Equations systems for free turbulent boundary layer in incompressible fluid, deriving semiempirical formulas for turbulent viscosity coefficient 07 p1089 A71-17935

SEMIEMPIRICAL EQUATIONS

U METALLOIDS

SENDERS

U TRANSMITTERS

SENSATIONS

U PERCEPTION

SENSE ORGANS

NT BARORECEPTORS
NT CHEMORECEPTORS
NT CHOROID MEMBRANES
NT COCHLEA
NT CORNEA
NT CORTI ORGAN
NT EAR
NT EYE [ANATOMY]
NT FOVEA
NT GRAVIRECEPTORS
NT LABYRINTH
NT MASTOIDS
NT MECHANORECEPTORS
NT MIDDLE EAR
NT OCULOMOTOR NERVES
NT OTOLITH ORGANS
NT PHOTORECEPTORS
NT PROPRIOCEPTORS
NT PUPILS
NT RETINA
NT SEMICIRCULAR CANALS
NT THERMORECEPTORS
NT VESTIBULES

Vibrotactile information transmission, discussing skin mechano-receptive systems and similarities or differences between auditory and tactile characteristics 10 p1563 A71-24231

Intraocular pressure self regulating nervous system components, discussing fluctuation sensors, cortical centers to eye impulse conveyors and glaucoma diagnostic applications 11 p1716 A71-25199

Skin temperature sensitivity factors, discussing neural correlates of thermal sensation and skin receptors causing thermal stimulation sensitivity 14 p2183 A71-30253

Snake IR receptor sense organs tested by IR stimulus from carbon dioxide laser, suggesting receptor operation on thermal principle 15 p2360 A71-32296

Sense organs conditioned reflex and physiology, investigating mechanisms and functional localization of discrimination function and differentiating inhibition 15 p2360 A71-32529

SENSES

U SENSORY PERCEPTION

SENSIBILITY

U SENSITIVITY

SENSING

U DETECTION

SENSITIVITY

NT IMPACT RESISTANCE
NT LIGHT ADAPTATION
NT NOTCH SENSITIVITY
NT PAIN SENSITIVITY
NT PHOTSENSITIVITY
NT PHOTOTROPISM
NT RADIATION TOLERANCE

Low pass active filters with various characteristics, comparing amplitude-frequency responses 01 p0051 A71-10259

Computer methods for calculating sensitivity of amplitude and phase frequency response functions in automatic control systems to system parameter changes 01 p0059 A71-10529

Shadow and interference methods sensitivity for low density gas flows improved via monochromatic light source 02 p0248 A71-11937

Translational vs deformation displacement motion in sensitivity of double exposure holographic interferometry 03 p0429 A71-14181

High speed automated network design method for optimum value determination of system parameters, using sensitivity analysis and hybrid computer optimization techniques 03 p0390 A71-14305

Linear optimal control systems with penalty on state and control vector sensitivities, avoiding mathematical difficulties 03 p0391 A71-14313

Peak diameter differences of sensitization by annular surrounds in subjects, concerning scotopic increment threshold and retinal illuminance 03 p0365 A71-14376

Stellar spectrometers design features and performance with photomultipliers, emphasizing sensitivity 04 p0589 A71-14834

Spectral analysis increased sensitivity for dispersion systems, using optimum filtering of spatial frequencies 04 p0590 A71-14838

Dicke type radiometer sensitivity and spectrum, recommending antenna gain improvement, intrinsic receiver noise reduction and large averaging times 04 p0596 A71-15065

Multiparameter sensitivity functions in network theory, discussing auxiliary, adjoint and direct methods 04 p0560 A71-15148

Flight simulators simulation width and parameter sensitivity analysis by state vector feedback method, using multiparameter control root-locus technique 05 p0733 A71-15970

Sensitivity threshold measurement of photoelectric shadow instrument with test adapter simulating periodic input signal 06 p0898 A71-17536

Etchant type, concentration and temperature effect on various plastics track etching ratio and sensitivity 07 p1145 A71-20272

Linear ordinary differential equation systems first order output sensitivity coefficients generation and application to second order cross sensitivities 07 p1148 A71-20416

Minimum-sensitivity network synthesis using continuously equivalent transformations and weighted sum of sensitivities square magnitudes as criterion 08 p1268 A71-21272

Sensitivity algorithms and application to attitude estimation of rigid body satellite in circular earth orbit 10 p1587 A71-24747

Holographic multiple pass two-beam optical interferometer with greater sensitivity than single pass instrument (Mach-Zehnder) 15 p2402 A71-31259

Sensitivity functions of phase canonical form for single input linear time invariant controllable systems, using frequency domain techniques 15 p2382 A71-32442

Automatic control systems sensitivity, including literature survey 16 p2550 A71-33703

HF amplifier statistical gain fluctuations effect on Dicke radiometer sensitivity, using Davenport-Root theory of random processes 16 p2548 A71-34132

Ideal laser gyro sensitivity against background of natural emission fluctuations 17 p2737 A71-34411

Angular accelerometer with paddle torsion damper, comparing sensitivity with ordinary inertial instrument 17 p2739 A71-34562

Optimal control systems synthesis with reduced sensitivity to parameter variations by trajectory sensitivity feedback with cost minimization 17 p2719 A71-34744

Redundancy utilization in automatic control systems synthesis, considering dynamic characteristics sensitivity 17 p2721 A71-34965

Nonlinear automatic control systems sensitivity to changes in prescribed operating conditions and component parameters 17 p2784 A71-35136

Weber antenna sensitivity for short pulses of gravitational radiation, giving limit for connection coefficient of piezotransducer with detector 18 p2946 A71-35979

Sensitivity formula and graphical interpretation for IR scanner, assuming object and ambient medium as Lambertian radiators 19 p3068 A71-38707

Constant coefficient linear systems sensitivity functions computational procedure using nth order differential equations linear transformations 19 p3039 A71-38714

Scintillation spectrometers sensitivity evaluation for low energy electrons in various regions of magnetosphere 20 p3234 A71-39127

Actinometer thermobatteries surface sensitivity distribution effect on solar radiation flux measurement accuracy 20 p3237 A71-39330

Tridrant star sensor, noting superior photometric and geometrical sensitivities 20 p3239 A71-39535

Sensitivity requirements for attenuation measurement radio receivers, considering minimum input SNR for absolute measurement error not to exceed preestablished value 20 p3197 A71-39550

Hologram recording materials within and outside visible spectrum, considering sensitivity, reconstruction efficiency, resolution limitations, nonlinear and noise effects 21 p3380 A71-40920

Tapered distributed RC low pass network configuration with voltage-controlled sources for sensitivity reduction low and high Q factors 21 p3361 A71-41409

Pyroelectric IR detectors performance, investigating strontium barium nitrate, lithium sulphate and triglycine sulfate materials effects on frequency range and sensitivity 22 p3542 A71-42122

Computer generation of sensitivity functions for nonlinear sampled data control systems, discussing simulator components and computational time economy problems 23 p3648 A71-43859

Human eyes macular pigment optical density curves through spectral sensitivity measurements, noting differences due to race, environment, age, skin, eye and hair color 24 p3794 A71-44466

Weakly damped nonstationary linear systems analysis by modified sensitivity function method, evaluating solution error 24 p3816 A71-45001

SENSITIZING

Hydrogen-oxygen reaction sensitized by ammonia, comparing with nitrogen dioxide and nitrosyl chloride activators 19 p3012 A71-38081

SENSOR-AIRBORNE TERRAIN ANALYSIS

U SENSORS

U TERRAIN ANALYSIS

SENSOMOTOR PERFORMANCE

NT PSYCHOMOTOR PERFORMANCE
NT PSYCHOSOMATICS

Motor and sensory nerve conduction impairment in upper extremities in vibration disease 01 p0010 A71-10394

Sensorimotor performance of flight and nonflight personnel, investigating motions speed and accuracy 01 p0024 A71-11110

Aural and visual limitations effects on athletes rowing rhythms, examining afferent systems interactions 02 p0205 A71-12059

Human motor skills acquisition during manual control problem solving, modeling operator as single channel data processing system 03 p0368 A71-12998

Motor cortex sensory input in animals and man, using evoked responses recording 05 p0706 A71-16319

Knowledge of results and rest pauses effect on sensorimotor skills at different training conditions 05 p0714 A71-16618

Visual-tactile dominance relationship as function of tactual judgment accuracy 07 p1045 A71-20385

Signals temporal uncertainty and sensory modality influence on watchkeeping performance, discussing signal density effect on pulses duration increments detection 10 p1568 A71-24183

Muscular fibers analysis for motoneuron split potentials, using needle electrode 10 p1564 A71-24484

Central nervous system responsiveness changes after exhausting physical exercise, giving electroencephalogram and sensorimotor reaction records 11 p1719 A71-25668

Psychobiological stress of prolonged weightlessness /bed rest/ in man in terms of adaptive homeostatic state and decreased sensory-motor-muscular input 11 p1725 A71-26120

Sensomotor activity tests of operator perceiving high speed stimuli in broad visual field for psychological selection of aircraft and spacecraft pilots 13 p2018 A71-28416

Cerebral ischemia effects on sensorimotor cortex function in cats, recording spontaneous EEG and pyramidal response to cortical electrical stimulation 15 p2359 A71-31956

Speed and accuracy relation of hand movement aimed at target, showing error as function of length of uncontrolled terminal phase 16 p2536 A71-33372

- Human motor control behavior sampling hypothesis of open loop system at voluntary effort initiation, discussing validity based on ankle rotation physiological test
17 p2690 A71-34741
- Retinal adaptation to prism-displaced hand image in terms of sensorimotor coordination central control change
19 p3006 A71-37543
- Proposed prism adaptation model suggesting visual motor control loop as linear system comprising independent subsystems
19 p3007 A71-37544
- Human observer performance in imaging systems, detailing contrast, ambient illumination, resolution, exposure time, display size, field of view and image blur and enhancement
22 p3547 A71-42503
- ## SENSORS
- Design principles for sensitive elements of capacitive sensors for distance measurement via electrostatic induction effects
01 p0079 A71-10527
- Calibration of condenser microphone micrometeoroid sensor, using bead drop and hypervelocity impact tests
03 p0422 A71-13284
- Sounding rocket Solar Eclipse Sensor for 7 March 1970 event, discussing mission, capabilities, data acquisition and design
[AIAA PAPER 70-1406] 03 p0455 A71-13685
- Fluoric oscillators as sensors for carbon dioxide concentration detection in exhaled breathing gases, noting frequency dependence on gas properties
[ASME PAPER 70-WA/FLCS-10] 03 p0372 A71-14086
- Fluidic inertial instruments for space sensing, guidance and control including gyroscopes, accelerometers and rate sensors
04 p0535 A71-15322
- Inertial quantity sensors testing, discussing environmental control, calibration, inspection, etc
[AGARDOGRAPH-128] 05 p0749 A71-16302
- Ultrasonic position sensor for automatic control, using short pulses for azimuth and range resolution
06 p0896 A71-17321
- Monolith thermal flux sensors inertia characteristics on various surfaces
06 p0899 A71-18005
- Annihilation quanta detector and positron source for gas density measurement, noting sensitivity, counting interval and Be covering thickness
07 p1164 A71-20178
- Fluidics, discussing wave operated sensors, control systems, future developments and applications
07 p1024 A71-20208
- Manned aircraft crew long range navigation, discussing sensor, information processing and display systems for future commercial and military missions
07 p1157 A71-20343
- Fluidic noncontact position sensor, investigating flapper insertion effect on laminar jet flow
07 p1030 A71-20599
- Fluidic coincidence position sensors, using wall attachment amplifiers and nozzle displacement
07 p1030 A71-20601
- Target detection improvement in reconnaissance by black and white TV system, using narrow band filters for conversion to multispectral sensor system
08 p1287 A71-21240
- Global meteorological systems, discussing variables information content, measurements frequency and accuracy, horizontal/vertical resolution, sensor bearing platform and cost
08 p1327 A71-21715
- Inertial sensors, considering electromechanical devices, single and two degrees of freedom floated gyros and electromagnetic rebalance pendulous accelerometers
09 p1443 A71-22594
- Fluidic inertial instruments, describing sensor or transducer components, flight control systems, rate damper systems and attitude control systems
09 p1387 A71-22785
- Photoelectron noise limited low light level imaging sensors, investigating resolving power, signal degradation and camera tube performance
10 p1610 A71-24061
- High accuracy deflector and diffraction sensors for optical tracking systems, noting dependence on ultrasonic frequency
10 p1610 A71-24169
- Lateral separation focus sensors for high angular resolution optical systems, reviewing autocollimating optics and operational patterns
10 p1644 A71-25090
- Automatic gust alleviation system employing inertial sensors and feedback devices with wing flaps and elevators, considering linkage control, noninteracting control and split control
11 p1706 A71-25195
- Miniature aerodynamic turbulence gage using axisymmetric lifting body sensor
13 p2066 A71-28158
- Time dependence of signal emf induced in toroidal proton precession magnetometer sensor with elliptical cross section
14 p2246 A71-30481
- Jet edge tone sensor and internal feedback fluidic oscillator for temperature measurement, using dependence of sound speed in gas
15 p2352 A71-32065
- Fluidic ammeter for measuring electric current in uninsulated wire, using fluoric oscillator sensor
16 p2576 A71-32974
- Integrated vehicular information management systems consisting of computers, multiprocessors, multiplexers, dedicated subsystem processors, sensors and effectors
17 p2743 A71-35057
- Angular acceleration measuring device based on closed loop wide bandwidth sensor, discussing theory of operation, performance and applications
[AIAA PAPER 71-909] 19 p2995 A71-37160
- Tridant star sensor, noting superior photometric and geometrical sensitivities
20 p3239 A71-39535
- Brewer bubbler as continuous surface ozone sensor, measuring ozone vertical distribution in atmosphere
21 p3377 A71-40181
- Light sources selection and design for visibility range sensors employing backscattering
21 p3382 A71-41236
- Temperature field of thermochemical sensor in automatic control systems, developing thermal energy transport models for circular disk with energy source at center
22 p3537 A71-41443
- Two-axis pneumatic rate gyroscope with externally pressurized gas bearing for airborne vehicle fluidic autostabilizer sensor
22 p3551 A71-41666
- IR ring laser rotation sensor, describing design principles for alignment and eliminating locking phenomenon
22 p3557 A71-42153
- Equatorial lunar radius determinations from image motion compensation sensor onboard Lunar Orbiter 1 spacecraft
[AAS PAPER 71-337] 23 p3727 A71-43010
- Pulmonary circulation pressure and flow telemetry of free ranging intact animals, describing instrumentation and technique for transduction and transmission
23 p3640 A71-44243
- Differential magnetic circuit sensor with movable screen, analyzing neutral point lag for calculation of emf distributed output winding and neutral point displacement
24 p3810 A71-45153
- ## SENSORY DEPRIVATION
- Motor and sensory nerve conduction impairment in upper extremities in vibration disease
01 p0010 A71-10394
- Aural and visual limitations effects on athletes rowing rhythms, examining afferent systems interactions
02 p0205 A71-12059
- Somatic concentration and brief sensory deprivation effects on rod and frame and embedded figures test performance
07 p1045 A71-20382
- Prolonged perceptual deprivation effects on behavioral, physiological and chemical reactions, discussing EEG mean frequency changes
11 p1724 A71-25362
- Luminance and luminous flux discrimination in light and dark reared rats after early visual deprivation
13 p2011 A71-28810
- Visual perceptual masking under binocular and dichoptic conditions separating peripheral and central interference effects
21 p3342 A71-40225
- Normal females electrophysiological changes during sensory isolation of water tank variety from EEG, EMG, EOG, EKG and electrodermal measurements, considering cortical activities reduction
21 p3330 A71-40346
- ## SENSORY DISCRIMINATION
- NT BRIGHTNESS DISCRIMINATION
NT TACTILE DISCRIMINATION
NT VISUAL DISCRIMINATION
- Perceived and responded to discriminative stimuli identification in probability learning, using parameter free model of event pattern association strength
07 p1049 A71-19775
- Brief light flash duration discrimination, discussing luminance and time between flashes
10 p1570 A71-24607
- Sense organs conditioned reflex and physiology, investigating mechanisms and functional localization of discrimination function and differentiating inhibition
15 p2360 A71-32529
- Human olfactory perception of inspired air composition, noting sensory differentiation improvement with subsequent exposures in space flight training
22 p3505 A71-42800
- ## SENSORY FEEDBACK
- Human tracking of external targets and body point projections, examining visual feedback role
02 p0205 A71-12057
- Average minimum time for incorrect movement amendment, based on performer ability to process visual feedback
07 p1045 A71-20386
- Displaced and delayed retinal feedback adaptation theory for human factors problems in man machine systems
10 p1571 A71-24825
- Mathematical fatigue models based on permeability variations in synaptic membranes and feedback regulation due to working organ metabolic changes
17 p2687 A71-34354
- Proposed prism adaptation model suggesting visual motor control loop as linear system comprising independent subsystems
19 p3007 A71-37544
- Visual target pursuit tracking test confirming error amending by central mechanism without sensory feedback
19 p3007 A71-37545
- ## SENSORY PERCEPTION
- NT AUDITORY PERCEPTION
NT AUTOKINESIS
NT CONSCIOUSNESS
NT CRITICAL FLICKER FUSION
NT OLFACTORY PERCEPTION
NT PAIN SENSITIVITY
NT PROPRICEPTION
NT SPACE PERCEPTION
NT TACTILE DISCRIMINATION
NT TASTE
NT VERTICAL PERCEPTION
NT VIBRATION PERCEPTION
NT VISUAL DISCRIMINATION
NT VISUAL PERCEPTION
- Rapid identification of steels and other metals by chemical, instrumental and organoleptic methods
01 p0183 A71-10256
- Russian book on perception of respiratory medium and gas preference in man and animals covering hypoxic or hypercapnic media, inhalation times, gas mixtures, etc
02 p0198 A71-11823
- Human response to and perception of angular acceleration, discussing implications for motion capability in flight simulator
[AIAA PAPER 70-350] 10 p1571 A71-24860
- Somatosensory cortical and cuneate evoked responses and EEG amplitude/frequency changes due to hypovolemic shock
13 p2003 A71-27836
- Rotation perception in dark and oculogyril illusion, using power law to describe subjective vestibular sensation relation to angular acceleration stimulus pulses
13 p2022 A71-29327
- Papers on anatomy and mechanisms of mammalian sensory systems including vision, audition and touch
14 p2183 A71-30251
- Pulse frequency behavior during acquisition of perceptual and motor skills with particular attention to rest periods
15 p2362 A71-31195
- Speed overestimation in intermittent illumination of moving bars and textures as function of frequency, using Piaget and brightness enhancement phenomena
15 p2366 A71-32713
- Anatomical load sensing method, determining torso pain thresholds by sensitivity tests
[SESA PAPER 1823A] 17 p2689 A71-34539
- Spinal cord ascending neurons temperature sensitivity, comparing data from cats experiments with hydrothalamic temperature sensors sensitivity
18 p2861 A71-36894
- Visual signal detection from noise, investigating mental images effects in six sense modalities
18 p2862 A71-37016
- Human response to auditory stimuli start and cessation, noting time lag and perception duration
19 p3001 A71-37283
- Activity correlation of adjacent neurons of cat cerebral cortex somatosensory zone, considering distribution of same direction /cophase/ and different direction /counterphase/ of background rhythms
19 p3001 A71-37392
- Plants and animals reactions to environment gravitational component, showing organisms perception of accelerating force
21 p3326 A71-39970
- Gravitational and other forces involved in equilibrium of growing plants, showing gravity sensing ability lower limit existence
21 p3339 A71-39971
- Gravity susception by higher plants, proving starch statolith hypothesis
21 p3339 A71-39977
- Gravity susception by higher plants, analyzing geotonic data for georeception theories
21 p3340 A71-39978
- Arguments against statolith theory of gravitational perception in plants
21 p3340 A71-39979
- Physiological systems connected with sensory perception of equilibrium and orientation on ground and in air, discussing pilot training and selection
23 p3632 A71-43148

SENSORY STIMULATION

Human thermoregulatory response to ambient temperature variations, considering deep body and skin temperature interrelations 02 p0202 A71-11667

Cardiovascular and biochemical effects of chronic intermittent neurogenic stimulation, noting alaphamethyltyrosine antihypertension agent 03 p0359 A71-13157

Motor cortex sensory input in animals and man, using evoked responses recording 05 p0706 A71-16319

Somatosensory and viscerosensory stimulation effects on cortex neuron amygdala complex and convergent interrelations 06 p0849 A71-17384

Physiological interaction between conscious and unconscious trace processes during time count by pairing acoustic, tactile, proprioceptive and photic stimuli 06 p0850 A71-17599

Gestalt psychology perceptual organization, analyzing contextual background and residual stimuli, interaction concepts, configurational principles and organismic factors 07 p1042 A71-19696

Ambient temperature effects on flicker fusion threshold, using constant stimuli and forced choice methods for determination of test subjects sensory sensitivity to heat and cold exposure 10 p1568 A71-24184

Signal transformation laws of central nervous system motor command patterns construction from sensory impulse streams 10 p1569 A71-24236

Cat type I and II optic nerve fibers response to flicker stimulation, noting receptive field organization, conduction velocity and temporal and spatial information processing 13 p2008 A71-28459

Evoked cortical responses to taste solutions of acid and salt applied to human tongue surface, using averaging technique 13 p2012 A71-28887

Habituation and dishabituation of human vertex response, using auditory or somatosensory stimuli 13 p2012 A71-28890

Human odorant evoked response, considering stimulation of olfactory receptors and trigeminal afferences in nose 13 p2012 A71-28891

Repetitive stimulation effects on auditory evoked potentials in cochlear nucleus, inferior colliculus and medial geniculate body of unanesthetized cats 13 p2012 A71-28892

Spatial and temporal discrimination functions in vision, audition and touch, establishing and controlling stimuli by vibrators 14 p2188 A71-30252

Temperature, odor mixing and stimulation frequency effects on olfactory receptor potential of fly *Lucilia sericata* 14 p2186 A71-30568

Fly *Lucilia sericata* olfactory receptor and unit action potentials response to odor stimulation by homologous compounds 14 p2186 A71-30569

Performance differences between tactile and visual localization and temporal ordering ability, using sequential presentation of high rate point stimuli 15 p2363 A71-31948

Radio telemetry stimulator for conditioning large animals by applying high voltage short duration pulses to skin surface 16 p2534 A71-33050

Visual and auditory evoked potentials enhancement in cats using cryogenic blockage of nonspecific thalamo-cortical system in inferior thalamic peduncle region 17 p2682 A71-35112

Visual evoked potentials and cortical recovery cycle data for normal and psychiatric subjects of various ages 17 p2682 A71-35113

Variables affecting processing mode/serial or parallel/ of complex stimuli information 17 p2684 A71-35255

Accommodometer for automatic measurement of eye response to accommodation stimulus 18 p2863 A71-35849

Gross locomotion and cargo handling in simulated artificial gravity environments, studying effects of Coriolis forces, angular accelerations, oculo-vestibular stimuli and traction variations [ALAA PAPER 71-886] 18 p2871 A71-36636

Positive and negative deflections in human electroretinogram off response to stimuli 19 p3007 A71-38058

Signals convergence of various sensory modalities as function of impulse reactions of individual brain neurons in mammals 19 p3003 A71-38197

Hue shifts by intermittent stimulation, suggesting interaction between stimulus intermittency and temporal color coding in visual system 19 p3004 A71-38283

Primary biological receptor element analogous electronic model for potential and afferent pulse train responses to stimuli 20 p3191 A71-38894

Cortical responses of awake cat to narrow-band FM noise stimuli, proposing neuronal model 20 p3190 A71-39767

Central nervous tissue sensitivity, considering direct sensing of gravitational stimuli of vibratory character 21 p3328 A71-39997

Taste modalities identification by factor analysis technique based on correlation matrix between independent stimuli 21 p3341 A71-40073

Psychophysiological reactions to understimulation and overstimulation, noting catecholamine output, heart rate and performance efficiency in humans 21 p3329 A71-40177

Functional lability of human tactual analyzer by measuring minimum interval between two discrete controlled stimuli 21 p3344 A71-41064

Posterolateral thalamus nucleus neurons response to visual, acoustic and somatic stimuli in cats with microelectrodes 22 p3490 A71-42578

SENTENCES
NT SYLLABLES
NT WORDS [LANGUAGE]
SEPARATED FLOW
NT BOUNDARY LAYER SEPARATION

Thin delta wing with leading edge separation, obtaining drag lift and rolling moment coefficients and pressure distribution 02 p0185 A71-12408

Turbulent separation and reattachment at turbomachine blade trailing edge at supersonic speeds, discussing various flow models 03 p0340 A71-13142

Flow separation and reattachment in confined jet mixing of air with secondary flow in duct [ASME PAPER 70-FE-B] 03 p0341 A71-13703

Supersonic flow past notch in lateral body surface or in two closely lying coaxial bodies, applying turbulent jet theory to separation zone 04 p0528 A71-15626

Dynamic model of flow separation of plane fluid past body in channel with eddy wake formation 04 p0578 A71-15630

Interaction theory for supersonic separated and reattaching turbulent boundary layers, comparing to real flow past compression ramp [ALAA PAPER 71-128] 06 p0844 A71-18572

Saturn launch vehicle gust penetration loads, presenting separated flow and associated time lag effects [ALAA PAPER 71-178] 06 p1004 A71-18617

Separated turbulent eddy viscosity models incompressible similar reverse flow velocity profiles from Falkner-Skan equations [ALAA PAPER 71-203] 06 p0886 A71-18641

Vortex flow theory, developing computer program for various separation flows 07 p1086 A71-18776

Blunt cylinder with small thrust in anomalous seeded flow in hypersonic wind tunnels, observing separated shock wave distortion 07 p1013 A71-18924

Two link approximation of Chaplygin function by coupling to integral equations, applying to ideal gas jet separation flow past symmetrical arc 07 p1016 A71-20084

Similarity criterion for volute centrifugal pumps via supersonic model, considering cavitation parameters influence throughout angular velocities range at flow separation 08 p1347 A71-20784

Twin vortex development in unsteady separated flow past thin flat plate, using flow visualization 09 p1432 A71-22582

Supersonic flow separation around cross shaped horizontal tail plane with subsonic leading edge, obtaining pressure distribution and aerodynamic characteristics 09 p1384 A71-23608

Separated flow and time lag effects on sinusoidal gust penetration loads and elastic launch vehicle response of Apollo-Saturn class [ALAA PAPER 71-344] 11 p1836 A71-25323

Capillary pressure and contact angle drop of two fluid flow separated by parallel plate interface 11 p1750 A71-25443

Interaction theory for supersonic separated and reattaching turbulent boundary layers, comparing to real flow past compression ramp [ALAA PAPER 71-128] 11 p1702 A71-25476

Hele-Shaw flow viscous tails from airfoil, observing high Reynolds number trailing edge flow for separation and initiation of Kutta condition 11 p1705 A71-26447

Three dimensional steady separated liquid and gas flows past low aspect ratio bodies, deriving similarity laws for reduction to two dimensional problem 13 p2049 A71-29169

Flow theory of steady separation zone near body at high Reynolds numbers, determining vortex parameters counterflow inviscid region 13 p2049 A71-29171

Air inlet for simulation of shock wave separated flow in supersonic diffusers, deriving pressure variation profile along free boundary 13 p1992 A71-29175

Blowing and wall curvature effects on gas flow separation and critical pressure gradient in Couette flow examples 13 p1993 A71-29193

Asymptotic limiting viscous flow pattern and drag on flat plate with stationary separation zones at large Reynolds numbers 13 p2050 A71-29204

Separation control of two dimensional air flow with turbulent boundary layer along circular cylindrical wall by jets or suction 13 p2051 A71-29433

Surface curvature effects in nonsimilar second order boundary layer solutions for subsonic plane flow over cylinder with separation 14 p2170 A71-30442

Shock and pressure gradient induced turbulent transonic flow separation, using two dimensional circular arc model for flow field investigation [ALAA PAPER 71-565] 15 p2344 A71-31559

Separation controlled transonic drag-rise modification for V-shaped notches attributed to inviscid/viscid interaction controlling flow separation and reattachment [ALAA PAPER 71-568] 15 p2345 A71-31561

Turbulent wall jet with initial boundary layer, calculating growth and separation in arbitrary pressure gradient by integral method 15 p2389 A71-31581

Helmholtz, half and full mode standing pressure waves for separated flow induced acoustic resonance in open cavities 15 p2391 A71-32106

Ducted axisymmetric jet mixing flow, investigating flow separation and reattachment as function of diameter and velocity 15 p2392 A71-32252

Slender cone at Mach 10 with underexpanded exhaust plume, determining flow field interactions separation pattern and aerodynamic coefficients [ALAA PAPER 71-562] 15 p2347 A71-32280

Colliding supersonic rarefied argon-helium jet flows diffusive separation in low density wind tunnel with electron beam diagnostics apparatus 16 p2554 A71-32800

Pressure histories due to weak shock wave propagation through dividing flow junction, describing wave decay in side branch duct 16 p2555 A71-32887

Approximate calculation of pressure distribution, separation points and drag on circular cylinder in viscous liquid flow, using ideal fluid jet model 16 p2560 A71-33597

Aperture angle effect on flow separation in inlet section of diffuser with cylindrical to conical channel transition 16 p2521 A71-33611

Two vortex model for downwash variations in supersonic flow past thin delta wing with separation at leading edges 17 p2669 A71-34190

Negative pressure gradient effect on separation of supersonic flow over notches, comparing theory with wind tunnel determination 17 p2671 A71-34898

Wall pressure spectra and rms wall pressure levels measurements in subsonic separated flows, postulating model for pressure fluctuation estimation 17 p2728 A71-35037

Pressures, velocities and aerodynamic characteristics of supersonic flow around slender delta wings with forced asymmetry and separation at leading edges 18 p2843 A71-36134

Experimental materials for axial flow vane pumps operating under cavitation conditions, considering separated flow around impeller blades 20 p3241 A71-39169

V shaped notches drag coefficients behavior in transonic regime, observing inviscid-viscid interaction controlling flow separation and reattachment 21 p3323 A71-40954

Hypersonic flow over rearward facing step by rotational characteristics method, describing inviscid and viscous dominated regions 21 p3324 A71-40969

Dimensionless parameters effect on divided blood flow characteristics in large arterial bifurcation 24 p3801 A71-44622

Establishment time measurement for laminar separated flow, using shock tunnel driver section to give long test time at low incident Mach number 24 p3818 A71-44628

- SEPARATION**
 Simultaneous identification and control by separation method of two separate problems solution, one being set of unknown parameters estimation
 03 p0394 A71-14485
 Blue edge anodize technique for revealing segregation in Ti alloys without affecting mechanical properties
 18 p2938 A71-37058
 Ti-Fe and Ti-Cr binary alloys microsegregation genetic trend measurement by electron probe microanalysis, observing critical cooling rate from beta phase
 22 p3562 A71-41945
 Free surface equilibrium segregation in solid solutions of Cu-Al alloys single crystals by Auger electron spectroscopy and low energy electron diffraction
 24 p3839 A71-45123
- SEPARATORS**
 NT AIR FILTERS
 NT CLASSIFIERS
 NT DIVIDERS
 NT DUST COLLECTORS
 NT EVAPORATORS
 NT FLUID FILTERS
 NT SPIRALS [CONCENTRATORS]
 Inlet particle separators for engine erosion prevention, discussing tests of various models for separation efficiency, clogging resistance, pressure loss and flow distortion
 04 p0639 A71-15435
 Polymeric materials for silver zinc battery separators, discussing porous and solvent-type pore free membranes
 08 p1234 A71-21091
 Cellulose application as zinc silver oxide battery separator, considering chemical stability, cellophane properties, polymerization and crystallinity
 08 p1234 A71-21093
 Aluminosilicate separators for silver zinc cells, using compaction and sintering techniques
 08 p1235 A71-21096
- SEPTUM**
 Ventricular septal defect, discussing incidence, human physiological responses, morbidity and mortality in various age groups
 13 p2004 A71-27862
- SEQUENCING**
 Stacking sequence effect on laminate strength, considering specific layer orientations for optimal protection against delamination under uniaxial static and fatigue loadings
 07 p1216 A71-20130
 Binary sequences with relaxed Barker criterion, examining correlation coefficients
 07 p1149 A71-20418
 Monkeys trained to observe and report two-member serial position sequences with delayed matching-to-sample procedure
 14 p2187 A71-29519
 Boundary value problem for Laplace equations, noting conditions for convergence of solutions sequence
 17 p2765 A71-34867
 Serial edge absolute coded and parallel alphanumeric timing on engineering sequential films, discussing frame selection, marking, offset, pull down and exposure correction
 18 p2919 A71-36085
 Redundant solid state sequencer programmable via core memory, using two identical channels to prevent wrong output
 18 p2885 A71-36449
 Generalized computing machines deductive systems, introducing sequence of partial functions
 18 p2886 A71-36823
- SEQUENTIAL ANALYSIS**
 Sequential environmental testing effects on large hybrid microcircuit packages, reviewing solder sealing processes and repair methods
 01 p0053 A71-10732
 Thevenin and Norton equivalent circuits determination using sequential method of network analysis
 02 p0236 A71-12041
 Ascending aorta blood flow sequential velocity measurement using conical hot-film probe with linearized constant temperature anemometer circuit
 [ASME PAPER 70-WA/BHF-13]
 03 p0373 A71-14111
 Eight channel physiological data scanning and timing control, sequential conversion, printing and punching
 05 p0714 A71-16923
 Asynchronous sequence detectors and similar circuits design, discussing method for flow table reduction and merging
 06 p0896 A71-17320
 Space-time interactions and associated input-output mismatches from overprinting, sequential blanking and displacement visual perceptual information processing
 07 p1049 A71-19695
 Soviet book on limit theorems for random walks covering random walk functionals, zero mean value, finite dispersion, sequences, normalized sums, Markov functionals, etc
 07 p1148 A71-20300
 Error correction coding/decoding techniques integration, discussing convolutional and block coding and Viterbi, Sequential and Threshold decoding algorithms
 07 p1066 A71-20425
 Algorithms for continuous indirect sequential observations utilization with real time synoptic measurements in objective analysis
 08 p1328 A71-21725
 Optimal unconditional sequential search for defects, using rejection function
 08 p1300 A71-22020
 Pattern recognition feature subset selection based on sequential decision model for on-line processes
 09 p1411 A71-22624
 Optimal reliability of system with nonlinear constraints, using mathematical model and sequential unconstrained minimization technique
 11 p1771 A71-26161
 Motion sequential analysis of airways utilization, using mathematical-statistical methods
 12 p1927 A71-27143
 Heuristic algorithm for computation of failures detection tests in asynchronous sequential logic circuits
 14 p2218 A71-29520
 Truncated sequential test for production models based on preproduction testing with allowance for unequal sample sizes
 15 p2416 A71-32344
 Sequential analysis and Bayesian demonstration in hypothesis testing, considering weight ratios based on objective lower level program reliability test information
 16 p2582 A71-33289
 Modular component computational algorithm for sequential least squares estimation /filtering/ with process noise for straightforward computer code conversion
 20 p3201 A71-38757
 Digital sequential detector based on range sampling technique, comparing performance to digital sequential probability test /SPRT/ detector
 20 p3206 A71-39906
 Water radiolysis measurement in nuclear reactor tests, discussing experiment design as doubly telescoping sequences of blocks
 21 p3345 A71-40202
 Spacecraft-borne IR sequential filter radiometer design and performance for real time meteorological forecasting and atmospheric temperature measurements
 22 p3544 A71-42143
 Sequential dual wavelength IR gas analyzers for anesthetics research and chemical plant process streams analysis
 22 p3545 A71-42156
 Fano and stack algorithms comparison by computer simulation of two sequential decoding algorithms
 22 p3512 A71-42379
 Reed-Solomon erasure-correcting sequential decoder implementation for hybrid coding scheme, using digital circuitry
 22 p3513 A71-42387
 Least squares and sequential estimation techniques application to Mariner 6 and 7 tracking data analysis, verifying Einstein relativity theory on electromagnetic radiation propagation
 [AAS PAPER 71-384]
 23 p3731 A71-43054
 Sequential processor performance prediction error with linear method from Monte Carlo cycle analysis of Apollo 14 early rendezvous profile
 [AAS PAPER 71-386]
 23 p3731 A71-43056
 Automatic resseau detection and reference ground control points for computing and correcting geometric and radiometric image for earth resource data, noting correlation with reference system
 [AIAA PAPER 71-978]
 24 p3806 A71-44576
- SEQUENTIAL COMPUTERS**
 Angular function computation in Mie theory of light scattering, considering sequential computer programming economics
 14 p2207 A71-30150
 Memory cell fault tolerant sequential machine synthesis, considering masking feasibility and lower bounds on minimum redundancy
 21 p3351 A71-41036
- SEQUENTIAL CONTROL**
 Human motor reactions sequential systems control characteristics, considering effects of external stimulus and repetition time interval
 03 p0357 A71-12988
 Computer aided design for fluidic-pneumatic sequential control circuits synthesis, discussing algorithms and computer programs
 [ASME PAPER 70-WA/FLCS-17]
 03 p0354 A71-14090
 Huffman /impulse-equivalent/ pulse sequence design, examining energy distribution form control of signal in time-frequency plane
 04 p0551 A71-15005
- Real time processor design for sequential control of all-digital multiline data set
 [IEEE PAPER 70-TP-375-COM]
 05 p0725 A71-17067
 Linear sequential circuits feedforward inverse transfer function matrix existence condition and construction procedure
 07 p1081 A71-18735
 Iterative method for good aperiodic binary sequences in radar range resolution
 07 p1148 A71-19769
 Sequence solution to multidimensional time varying Fokker-Planck equation for phase locked nonlinear systems
 08 p1324 A71-21342
 Distribution functions of initial and established intervals of stochastic and Poisson sequences in automatic control, reliability and communications theories
 10 p1588 A71-24902
 Switch series data checking and sequence identification in program controlled computer systems, exemplifying tape reading procedure
 11 p1734 A71-25637
 Performance differences between tactile and visual localization and temporal ordering ability, using sequential presentation of high rate point stimuli
 15 p2363 A71-31948
 Distributed Fetch sequencing computer technique, discussing system speeds, throughput rates, bus requirement and arithmetic processor demand reduction and task performing capability
 17 p2712 A71-35779
 Sequential control with fluid logic programmers, considering decimal and binary counters, shift registers, gray code generator and integrated devices
 24 p3793 A71-45087
- SEQUENTIAL DETECTION**
 U SEQUENTIAL ANALYSIS
 SERIES [MATHEMATICS]
 NT ASYMPTOTIC SERIES
 NT FOURIER SERIES
 NT PADE APPROXIMATION
 NT POWER SERIES
 NT SINE SERIES
 NT TAYLOR SERIES
 Diffraction on smooth convex body, constructing convergent series for homogeneous wave equation solution
 01 p0038 A71-11203
 Fluid lines transient response obtained in infinite series form
 [ASME PAPER 70-WA/FE-22]
 03 p0403 A71-14132
 Finite maximum and minimum angular zero densities of integral functions, noting relationship to angular additive measure
 04 p0618 A71-14647
 Stokes multipliers first approximations for outer expansions of Orr-Sommerfeld flow equation solutions
 04 p0570 A71-15096
 Periodic orbits representation in trigonometric series with numerical coefficients and truncation for applications
 04 p0654 A71-15716
 FORTRAN-based list processor subroutines for computing Poisson series used in celestial mechanics
 04 p0660 A71-15890
 Antenna aperture random radiation field representation in expansion in eigenfunctions, comparing results with linear antenna statistical theory
 05 p0727 A71-15994
 German monograph on vibration fields representation by superposition of planar waves with complex wave vectors, considering convergent series of Hankel and Bessel functions
 05 p0782 A71-16898
 F 2 region critical frequency diurnal variation forecasting, using series expansion of natural orthogonal components
 06 p0895 A71-18276
 Rectangular plate bending with mixed boundary conditions, using paired trigonometric series
 06 p1005 A71-18708
 Uniqueness theorem for Dirichlet series bounded on real axis
 07 p1146 A71-19040
 Analytic function steady approximation with aid of polynomials in given region, considering Dirichlet series
 07 p1146 A71-19042
 Jacobi series coefficient relation to convergent series sum singularities in lemniscate bounded domain
 07 p1149 A71-20643
 Point matching techniques, discussing effects of metal boundary on divergence of series and error from numerical examples of rectangular waveguide and scattering
 08 p1252 A71-20755
 Optimum one term series solution for multidimensional heat conduction problem with initial profiles
 10 p1698 A71-25086
 Series solution for unbounded mixing of two incompressible homogeneous coaxial fluids with constant properties, using successive approximations method
 11 p1748 A71-25159

Lagerstrom mathematical model for two dimensional viscous flow at low Reynolds number, discussing asymptotic solutions for limit process expansions analysis 11 p1752 A71-26010

Nonlinear systems response to arbitrary multiple frequency inputs, deriving series expansion for nonlinear modulation products 11 p1793 A71-26424

Laminar boundary layer growth along moving flat plate wall, obtaining series solution relating shear stress to velocity ratio 15 p2390 A71-32018

Scalar function expansion in relativistic invariant functions in pseudoeuclidian space, deriving direct and inverse formulas for spherical, hyperbolic and Lobachevskii coordinates 16 p2612 A71-33459

Linear heat transfer boundary value problem series solution in Cartesian and cylindrical coordinate systems 16 p2663 A71-33904

Self adjoint expansion of Laplace operator with point spectrum, establishing uniform convergence and Riesz summability conditions of spectral decomposition 16 p2603 A71-33999

Diffraction on smooth convex body, constructing convergent series for homogeneous wave equation solution 17 p2697 A71-34255

Asymptotic expansion of spectral functions expressed by Cauchy integral over smooth open segment 17 p2763 A71-34419

Elastodynamics three dimensional mixed initial and boundary value problems, presenting infinite series solution 18 p2979 A71-36359

Radio signal group trajectory in ionosphere expressed as series expansion in terms of increasing power of beam reflection height 19 p3020 A71-38371

Automated algebraic manipulation in celestial mechanics, discussing use of Poisson series in perturbation theory problem 19 p3088 A71-38400

Computer implementation for Hansen theory of general perturbations, constructing program based on automatic Poisson series processor 21 p3445 A71-40257

Three dimensional solution for statics and dynamics of homogeneous plates, laminates and orthotropic materials in series form, noting Mindlin analysis 21 p3456 A71-40262

Continuous analog iterative methods and solution of nonlinear two point boundary value problems, producing convergent series of iterates 21 p3408 A71-40585

Buoyancy and surface-tension induced fluid instabilities in open and closed vertical circular cylindrical containers from series solution by Jeffreys-Goldstein method 21 p3367 A71-40667

Diffuse radiation field inside homogeneous spherically symmetric dust nebula from radiative transfer equation solution as expansion after Legendre polynomials 21 p3451 A71-40716

Orthonormal series expansion for features generation with predetermined properties, applying to handwritten numerals recognition 22 p3515 A71-41512

Antenna aperture random radiation field representation in expansion in eigenfunctions, comparing results with linear antenna statistical theory 22 p3524 A71-42743

Equations of motion averaging method, constructing series representation of function [AAS PAPER 71-334] 23 p3727 A71-43007

Asymptotic expansion method for hyperbolic and parabolic differential equations fundamental solutions featuring validity near surface and in interior of characteristic conoid 23 p3698 A71-43096

Validity theorems derived for complex parameter elasticity theory equations by vector functions expansion 23 p3777 A71-43583

Pseudomoments estimation of convergence rate in central limit theorem for random variables series 24 p3845 A71-44874

Extragalactic astronomical approximate dependences in cosmology of homogeneous isotropic universe from series expansion, considering Einstein field theory and Hoyle matter creation tensor 24 p3874 A71-45175

SERIES EXPANSION

U SERIES [MATHEMATICS]

SERPENTINE

Montmorillonite and serpentine as major crystalline constituents of Orgueil meteorite 10 p1679 A71-24983

SERT [ROCKET TESTS]

U SPACE ELECTRIC ROCKET TESTS

SERT 2 SPACECRAFT

Electric propulsion systems integration into SERT 2 spacecraft, discussing launch imposed environment, thrust vector control, thruster breakdown, power conditioning, etc 09 p1511 A71-22898

SERT 2 spacecraft ion thruster ground tests and flight operation, tabulating performance data [AIAA PAPER 70-1125] 09 p1511 A71-22899

SERT 2 power conditioning, describing operating requirements, components construction, overload protection, system performance, etc 09 p1511 A71-22900

SERT 2 solar array power system in sun synchronous orbit, considering power conditioning and deployment technique [AIAA PAPER 70-1159] 09 p1387 A71-22901

SERUMS

Myocardial infarction noting serum prealbumins changes 06 p0849 A71-17293

Bicycle ergometer workout effects on serum proteins, noting intravascular redistribution, tissue damage and membrane permeability 07 p1052 A71-20328

Quantitative determination of phenylalanine in serum by gas-liquid chromatographic analysis method 13 p2026 A71-29477

Bivalent metal salts effect on blood serum albumin crystallization by isolating pure protein 16 p2531 A71-33468

Cholesterol and esterified cholesterol distribution in human skin from analysis on fat, epidermis, corium, subcutaneous tissue and serum by chromatographic/colorimetric methods 20 p3185 A71-38892

SERVICE LIFE

Modular computer design for long term missions, discussing reliability estimation 01 p0046 A71-10205

Ball bearing cage life, examining angular misalignment effect 01 p0086 A71-10297

Sirene 311 cylindrical thermionic converter in-pile life testing in Triton swimming pool nuclear reactor 02 p0193 A71-12220

Cylindrical thermionic converter for Incore Thermionic Reactor, discussing diodes engineering problems and performance test for lifetime 02 p0194 A71-12221

Flame-fired thermionic diode service life, output power and voltage efficiency and weight reduction 02 p0196 A71-12269

Thermionic converter integrated Cs reservoir module power efficiency and service life, considering diode technology 02 p0196 A71-12270

Service life and manufacturing yield of Apollo 25-IRIG /inertial reference integrating gyroscope/ ball bearing 02 p0252 A71-12458

Nondestructive testing for reliability and lifetime of mass produced radio equipment under maximum load 02 p0257 A71-12530

Oscillatory motion effects on bonded solid film lubricants wear life, discussing oscillation arc and frequency, surface finish and load 02 p0258 A71-12593

Organic dye laser output and service life enhancement, using filters for absorption of UV pumping radiation photodecomposition of rhodamine 6G alcohol solution 03 p0435 A71-13509

Titanium alloy turbine disks creep rupture strength and service life, considering pressing and forming manufacturing technology 04 p0664 A71-14604

Service life of pin jointed connections with elastoplastic strains in bore walls 04 p0602 A71-14606

Biosatellite hydrogen oxygen fuel cell/silver zinc battery combination power system for long aerospace missions, discussing optimal design tradeoff 04 p0535 A71-15286

Gyroscope reliable performance life testing economic justification, noting cost lowering by deficient gyro rejection [AGARDGRAPH-128] 05 p0749 A71-16304

Dry reed switches service life relation to crossing or switching current, considering contact degradation and operational conditions 05 p0728 A71-16747

Gas turbine engines materials and components equivalent service life estimation 05 p0796 A71-16753

Gas turbine engine nozzle guide vanes under pulsed thermal operation, discussing service life evaluation and increase 05 p0827 A71-16756

Aircraft gas turbine engine components equivalent testing by shortening testing time required to increase service life 05 p0796 A71-16761

Carbon and metal film resistors stability, presenting service life characteristics prediction method for arbitrary electric loads and time 05 p0728 A71-16774

Aircraft generator service life improvement and weight minimization by close coupling with drive and heat producing components cooling with oil spray and mist 06 p0849 A71-18463

Geometries and technical specifications deviation effects on service life and fatigue characteristics of thin walled structural components under cyclic loads 06 p1005 A71-18710

Colloid microthruster system life test, discussing design and steady state performance [AIAA PAPER 70-1110] 07 p1184 A71-19864

Aircraft gear pumps bearing elements design for increasing service life 08 p1295 A71-20793

Thermal fatigue testing apparatus for material longevity, simulating tensile stresses due to centrifugal forces on gas turbine engine blade during thermal loading 08 p1271 A71-20837

Semipermeable polyethylene grafted membranes /separators/ for extended cycle life in silver zinc cells 08 p1235 A71-21094

Zinc-silver oxide batteries underwater and aerial applications, designing medium high rate long life cells 08 p1236 A71-21103

Military aircraft zinc silver oxide battery service requirements and performance 08 p1236 A71-21103

Service performance and tests of zinc silver oxide batteries on Explorers 17 and 32 08 p1236 A71-21105

Complex airframe design for economic and safe operation and long life using fatigue and fracture mechanics [AIAA PAPER 70-512] 08 p1374 A71-22025

Expansion bellows fatigue strength based on load and displacement measurements performed during low cycle model tests 09 p1538 A71-22604

Turboprop aircraft engine service life extension, correcting deficiencies via accelerated tests based on relation between failure rate and usage 09 p1511 A71-22633

Service life of solid molybdenum sulfide based plastic coatings with different binders under high vacuum friction investigated by mass spectroscopy 09 p1454 A71-22819

Potting compounds service life estimation based on accelerated hydrolytic reversion data at high temperatures and humidities 10 p1633 A71-24117

Steel sheet specimens under temperature and stress cycles, studying creep, plastic deformation and service life 10 p1686 A71-24189

Thermal fatigue and service life of thin walled tubular pearlite steel notched specimens in various oxidizing media 10 p1626 A71-24191

Elementary component constant failure rate for systems with prolonged operation without maintenance, determining mathematical model for confidence levels and dependability figures 10 p1617 A71-24266

Long term life test and vacuum tests of high temperature resistojets, using ammonia and hydrogen propellants [AIAA PAPER 70-1136] 11 p1811 A71-25523

Thermionic converter 9000 hour endurance test, performing metallographic, spectrographic and chemical analysis on emitter, collector, metal ceramic seal, brazing and alumina spacers 11 p1715 A71-25913

Long life vacuum tests of dry and wet lubricated slip ring systems for power and signal transfer, discussing wear, noise and contact resistance 11 p1771 A71-26050

Life tests and properties of organic working fluids heat pipes for electronic component cooling [AIAA PAPER 71-408] 11 p1856 A71-26203

Millimeter backward wave oscillators, discussing cooling, operating characteristics, frequency pulling and pushing, life and reliability 11 p1739 A71-26436

Helicopter auxiliary power unit [APU] life cycle cost computation 12 p1988 A71-26679

Service life testing and reliability estimation, using ordinary and empirical Bayes approach in failure model with gamma probability distribution 12 p1910 A71-26685

Bleached hologram lifetime extension, decreasing light induced decay rate by gelatin hardening 12 p1905 A71-26815

Structure service life and storage failure probability calculation with current load measurements and laboratory fatigue testing 13 p2076 A71-29231

Long-life self-contained solid lubricated ball bearing systems operating under combined high-temperature, high-speed, high-load conditions 14 p2252 A71-30192

Cutting angle effect on service life of broaching tools for Ti alloys annealed forgings, using high-speed P18 tool steel 14 p2259 A71-30271

Iridium-based long life hydrazine catalyst with multiple cold start capability, describing development program for substrate evaluation and physical properties and process optimization [AIAA PAPER 71-704] 14 p2286 A71-30761

Book on durability and reliability in engineering design covering materials strength and service longevity concepts, failure modes, fabrication philosophies, etc 15 p2414 A71-31836

SNAP 8 turbine-alternator as nuclear-electric space power converter, discussing rotating machinery components design and 10,000 hr endurance testing results 15 p2447 A71-32208

Unalloyed tantalum as containment material in mercury Rankine cycle SNAP 8 system boiler for 5 year service life 15 p2448 A71-32221

Materials evaluation of SNAP 8 power conversion system breadboard assembly after 8700 hour test, extrapolating service life for space flight application 15 p2448 A71-32222

Temperature effects on service life of cermet bronze-graphite bearings using different lubricants 15 p2418 A71-32674

Reliability and maintainability as concepts in life cycle costs applied to airline operations 16 p2552 A71-33287

Life cycle cost optimization of STOL aircraft and tracked air cushion vehicles for operating transportation system 16 p2522 A71-33306

Service life/stress testing, failure analysis and corrective action from technical and cost positions 16 p2583 A71-33315

Plastic deformation, creep rupture strength, endurance limit and service life of prestressed strain hardenable material 16 p2659 A71-33985

Service failure prediction by photoelastic methods, discussing failure sources and analysis techniques 17 p2820 A71-34554

Jovian turbopause probe mission, discussing atmospheric composition measurements and nonsurvivable system concept [AIAA PAPER 71-833] 17 p2802 A71-34714

Gas turbine engines materials and components equivalent service life estimation 17 p2793 A71-35452

Gas turbine engine nozzle guide vanes under pulsed thermal operation, discussing service life evaluation and increase 17 p2832 A71-35455

Aircraft gas turbine engine components equivalent testing by shortening testing time required to increase service life 17 p2793 A71-35460

Probability density function for parameter of exponential measurement model based on structural inference theory, developing prediction densities as life test inferences 17 p2768 A71-35537

Integrated drive generator for aircraft electrical power systems, improving weight, life and reliability 17 p2678 A71-35781

Fluid contamination and protective filter in hydraulic power components for design service life 18 p2851 A71-36204

Life support water management subsystem 4-man 90-day test in space station simulator with closed water and oxygen loops and no resupply [ASME PAPER 71-AV-6] 18 p2865 A71-36373

Closed-loop solid electrolyte oxygen regeneration life support system, discussing 180-day life test [ASME PAPER 71-AV-32] 18 p2869 A71-36399

Viking Mars spacecraft pressure vessel design, incorporating linear elastic fracture mechanics for long life 18 p2979 A71-36487

Transistors life testing for temperature and voltage dependence of failure rates 18 p2893 A71-36805

Polymer materials strength and lifetime prediction under natural conditions from mathematical model based on laboratory accelerated test data 19 p3084 A71-37781

TOPS spacecraft parts and technology development, reliability and contribution to long life system design [AAS PAPER 71-159] 19 p3152 A71-37928

Long life radioisotope thermoelectric generators for space missions, discussing power degradation mechanisms and design trends [AAS PAPER 71-160] 19 p3102 A71-37929

Hardware reliability improvement techniques for long life unmanned space missions [AAS PAPER 71-156] 19 p3153 A71-37957

Gas lasers, discussing engineering developments for size and cost reduction, reliability, long life and high power 19 p3074 A71-38227

Mass transport at high current densities in Al and Mo thin film conducting stripes, noting effect on IC life 19 p3119 A71-38511

Integrated circuit life testing, comparing functional and pin-to-pin screening data 19 p3034 A71-38516

Cost effectiveness screening program for integrated circuits, considering four stages of life cycle 20 p3202 A71-38753

Automated endurance testing of 2-15 kW Brayton power conversion system, using rotating unit, heat exchanger, electronic voltage regulator, parasitic speed control 20 p3180 A71-38907

Long life performance predictions for lead telluride and silicon germanium radioisotope thermoelectric generators for deep space missions 20 p3263 A71-38925

Nickel-zinc batteries for use in hybrid heat engine/electric systems of low pollutant passenger cars, increasing service life by aerospace technology 20 p3181 A71-38936

Life tested thermoelements postoperative diagnostic analysis, using thermoelectric techniques 20 p3182 A71-38952

SNAP 19 TAGS thermoelectric generator life tests at high temperature in Ar, predicting long term performance including thermoelectric material and isotope fuel decay effects 20 p3266 A71-38963

Fracture mechanics application to proof testing for components life determination, exemplifying concept by flawed pressure vessel 20 p3308 A71-39459

Beam-lead nitride-passivated IC seal junction chip reliability evaluation by life tests for optimum packaging into functional modules 21 p3357 A71-40813

Gas turbine engine turbine blades service life increase by Cr and Al vacuum diffusion metallization, presenting full scale endurance test results 21 p3390 A71-41173

Spacecraft tape recorder design for five years minimum continuous unattended reliable operation, describing quality control and environmental/life testing procedures 22 p3608 A71-41507

Pulsed plasma thrusters, propellants, trigger and feed systems developments for long life secondary spacecraft propulsion 22 p3588 A71-41975

Static joint wear role in overall machine reliability and service life under working loads from mathematical prediction 22 p3619 A71-42852

SERVICE MODULES

Apollo 13 in flight emergencies and countermeasures, discussing fire in Service Module oxygen tank causes and effects on spacecraft systems and solutions 07 p1206 A71-19087

Adhesives in Apollo command, service and lunar modules primary load carrying structures, electrical potting and sealing medium 10 p1630 A71-24067

Space shuttle applications and utilization, discussing payloads, performance modes, Mission Support Module, ancillary equipment, system interfaces and related profiles [AIAA PAPER 71-816] 17 p2812 A71-34726

SERVICES

Large capacity aircraft reception and servicing problems consideration for facilitating traffic 06 p1010 A71-17588

SERVO LOOPS

U FEEDBACK CONTROL

U SERVOCONTROL

SERVOACTUATORS

U ACTUATORS

U SERVOMOTORS

SERVOAMPLIFIERS

Servoamplifier dynamic response effects on dynamic characteristics of fluid-filled pendulous accelerometers 02 p0252 A71-12455

Beam deflection fluidic circuit design by linear static matching method, considering servoamplifier feedback control system 07 p1026 A71-20569

Wind tunnel model trajectory simulation system with closed loop control by digital computer, describing instrumentation, system servoamplifiers and testing procedures 14 p2208 A71-30334

Fluidic servo amplifier operation by PWM mode with PD computation and ripple removal circuit 15 p2352 A71-32069

SERVOCONTROL

Dissipative gyroscopic system with servo link, obtaining steady motion stability 02 p0252 A71-12402

Dynamic automatic control and servo systems with distributed parameters, discussing synthesis and precision 03 p0389 A71-13373

Stellar photoelectric servo guide with photon counting in mismatch sensor for telescope positioning 04 p0590 A71-14845

Third order aberrations in Cassegrain type telescopes and coma correction in servo-stabilized images 07 p1107 A71-19202

Papers on modern practice in servo design covering digital techniques, applications of analog and hybrid computers and thyristors, reliability engineering, etc 08 p1268 A71-21195

Sinusoidal vibration tests using narrowband tracking filters, considering automatic servocontrols and feedback loop optimum matching 14 p2175 A71-30310

Telescope automation using servocontrolled drive with spur gearing and dual opposed motors for data acquisition separation and minimum program interaction 17 p2740 A71-34982

Electronic and hydraulic devices for communication satellite ground station steerable antenna servocontrol, driving and pointing, discussing tracking error signals 17 p2724 A71-35511

Structural synthesis of on-off servo feedback control system with combined dynamic and counterconnection braking of actuating motor within relay dead zone limits 19 p3038 A71-37776

Photogrammetric instruments digital servo, using printed disk DC motor drive, incremental measurement, nonlinear feedback and digital integrated circuit logic 20 p3233 A71-38829

Satellite tracking ground antenna servocontrol, discussing system requirements and automatic and programmed operating modes [DFVLR-SONDDR-125] 22 p3483 A71-41520

Relative motion interaction dynamics in rocket biaxial control with azimuth and elevation servos, using Mathieu equation and stability criterion 22 p3526 A71-41971

Digital servo system with signal quantization by level and time, evaluating oscillating motion in steady state mode 23 p3655 A71-43292

Statistical optimization of spherical gyroscope regarded as servocontrol system under random perturbation, using measured values of relative angles between sphere and inner gimbal 24 p3825 A71-44691

SERVOMECHANISMS

NT SERVOAMPLIFIERS

NT SERVOMOTORS

Complex servo systems with feedback loop and anticipating path, demonstrating equivalence to systems based on error measurements 01 p0062 A71-10719

Discrete servo position gage accuracy in presence of high uncorrelated noise level, using Markov chain 01 p0038 A71-11233

Hydraulic servomechanism with piston-type control valve, examining oil compressibility and sustained oscillations effects on system stability 01 p0007 A71-11378

Book on fluid power circuits and systems covering switching theory, closed loop systems, pneumatic circuits, servo systems and pressure control 02 p0190 A71-11871

Unguided, attitude stabilized and velocity controlled sounding rockets impact dispersion, discussing system selection and servomechanism [AIAA PAPER 70-1381] 03 p0498 A71-13664

Servosystems errors of indicator-receiver for recording electromagnetic field pattern extremes in amplitude radio interferometers 04 p0557 A71-14635

Electro-hydraulic servomechanisms dynamic performance variation probabilistic model, presenting sixth order system variable parameters for Monte Carlo simulation 06 p0848 A71-17318

Pneumatic and hydraulic fluidic power control systems, discussing moving part position servos and cold gas reaction systems 07 p1028 A71-20585

Papers on modern practice in servo design covering digital techniques, applications of analog and hybrid computers and thyristors, reliability engineering, etc 08 p1268 A71-21195

Photoelectric servosystem for three dimensional positioning of slit image, discussing system applications and accuracy 08 p1291 A71-21395

Spring coupled inertially damped instrument servomechanisms design, applying phase margin maximization criterion 11 p1716 A71-26417

Wind gust effect on autotracking antenna servosystem tracking error, evaluating torque disturbance admittance

12 p1868 A71-27002

Simple sensitive multichannel servo system thermobarometer for volume changes corrections, noting adaptation to five channel closed circuit respiratory apparatus

12 p1874 A71-27138

Flight vehicle equations of motion for computer simulation, calculating optimal servosystem parameters and optimal range control by hybrid computer scheme

14 p2319 A71-30001

Helicopter fuselage vertical and in-plane main rotor head vibratory forces isolation with hydropneumatic servovercentered system at transmission/airframe interface

[AHS PREPRINT 514] 14 p2253 A71-31085

Pulsed relay control system for stabilizing spacecraft orientation in flight, allowing for changes in characteristics of guidance sensor systems and slave mechanisms

16 p2646 A71-33660

N-dimensional phase spaces of nonlinear nth order automatic control systems at parameter space sections /hyperplanes/, considering nonlinearities effects in servomechanisms

17 p2783 A71-35129

Hydraulic servo equipment filtration systems design, discussing contamination effects and servo components physical characteristics effects on tolerance level

19 p2999 A71-38320

Instrument servomechanisms with spring-coupled inertial dampers, evaluating dimensional design parameters from analytical root locus

21 p3326 A71-40616

Soviet book on digital servomechanisms dynamics covering logarithmic frequency characteristics and pulsed and hybrid control systems

22 p3526 A71-41800

Tracking servosystems errors of indicator-receiver of amplitude radio interferometers for recording electromagnetic field pattern extremes

22 p3521 A71-42275

Variable structure digital control servomechanism flutter mode analysis, using nonlinear differential equation

22 p3528 A71-42878

Optimal gyroscopic servosystems feasibility analysis, using approximation technique for finite memory optimal filter transfer function

23 p3675 A71-43296

Servosystems consisting of command and single executive elements error estimation based on mathematical planning of experiment for time loss reduction, deriving regression equation

24 p3808 A71-44395

SERVOMOTORS

Pen actuators prototype models for fast response graphic recording instruments, using DC servomotors or galvanometers

09 p1452 A71-23386

Piecewise-linear approximation of nonlinear friction effect on interferometric servosystem stability, deriving formulas for harmonic linearization coefficient of linearity

13 p2041 A71-28375

Basket wound and printed circuit moving coil electric and servomotors design characteristics

13 p2000 A71-28794

Structural synthesis of on-off servo feedback control system with combined dynamic and countercontrol braking of actuating motor within relay dead zone limits

19 p3038 A71-37776

SERVOS

U SERVOMOTORS

SERVOSTABILITY CONTROL

U SERVOCONTROL

SET THEORY

NT BOREL SETS

NT EQUIVALENCE

NT THRESHOLD LOGIC

Straight line approximation of random two dimensional discrete set containing large measurement errors, comparing to least squares results

02 p0304 A71-11902

Dynamic polysystems stability and optimization, discussing minimality and recurrence in state space set

03 p0450 A71-13120

Flows on 3-manifolds near isolated invariant sets

04 p0620 A71-15727

Noninferior set for static optimization of systems with vector valued objective function using dual linear inequality

06 p0878 A71-17333

Closed invariant sets of smooth flow on compact manifold involving homoclinic or heteroclinic point theory of Poincare

06 p0918 A71-17640

Control sets bound structure, discussing invariance theorems

09 p1422 A71-22377

Straight line approximation of random two dimensional discrete set containing large measurement errors, comparing to least squares results

13 p2133 A71-28189

Solid nontrivial trajectory existence conditions near connected set of strong bilateral attraction, examining dynamic system in connected noncompact space

13 p2094 A71-28497

Systems concept formalization, including structural relations on basis of set theory, topological considerations and flow theory

17 p2777 A71-34599

Linear dynamic system recursive state estimation for set-membership description of uncertainty under unknown input disturbances and observation errors

17 p2718 A71-34734

Unique linear product approximations of continuous functions of several variables extended to general convex sets

17 p2768 A71-35682

Sufficient conditions for differential game encounter, considering conflict controlled motion guidance onto given set

18 p2947 A71-36776

Dielectric potential operator as arbitrary bounded Lebesgue measurable set, obtaining eigenvalues and eigenfunctions spectrum

18 p2942 A71-36820

Continuous machines basic properties, introducing tau computation and tau computable sets union, intersection, difference and parallel product

18 p2886 A71-36824

Continuous machine arithmetical properties, introducing tau generable set

18 p2886 A71-36825

Differential games with deviation from encounter, considering strategies for continuous, programmed and discontinuous control classes to bring motion to given set

19 p3103 A71-37093

Set covering algorithm based on single branch search coupled with linear programming and suboptimization techniques

19 p3025 A71-37546

Extremal problems approximation conditions in optimal value and elements set senses, applying to study of convergence in presence of constraints

19 p3088 A71-38413

Holomorphic matrix valued function on connected open subset of complex plane, obtaining conditions for satisfying homogeneous linear differential equation

21 p3410 A71-41185

SEX

Sexual behavior of male cats after parachlorophenylalanine injections, noting unchanged or diminished performance and serotonin lowering in brain

02 p0199 A71-12365

Sex differences in rat body weight regulation due to lateral hypothalamic lesions

11 p1720 A71-26074

SFERICS

U ATMOSPHERICS

SHADOWGRAPH PHOTOGRAPHY

NT SCHLIEREN PHOTOGRAPHY

Shadow photography applied to Mach reflections in argon, carbon dioxide and Freon 12 in shock tube, using Huygens principle for pressure mechanism

02 p0239 A71-11635

Sensitivity threshold measurement of photoelectric shadow instrument with test adapter simulating periodic input signal

06 p0898 A71-17536

Finite amplitude waves from supersonic jet, discussing pressure fluctuations measurement for explaining wave patterns visible on spark shadowgraphs [AIAA PAPER 71-151]

06 p0845 A71-18593

Shock induced combustion by firing spheres or cone cylinders into air- or oxygen-hydrogen mixtures, taking shadow photographs of resulting disturbances

11 p1860 A71-26268

Shock wave interaction with duct cross section changes, discussing experimental apparatus and shadowgraph results

15 p2393 A71-32265

Theoretical and photographic study of underexpanded air jets ejected simultaneously from several mutually interacting nozzles near origin

18 p2903 A71-36115

Collisionless momentum transfer between interstreaming ions in laser produced plasma, using fast photography, shadowgraphy and electric potential probes

19 p3114 A71-38177

Holographic investigation of acoustical fields, describing shadowgraph recording apparatus for sound pressure amplitude distribution

20 p3232 A71-38811

Three dimensional imaging of objects from white light or X ray shadowgraphs by holographic phase implantation

24 p3824 A71-44356

Two dimensional reflection supersonic nozzle shock wave initiated unsteady starting process, presenting shadowgraphs from shock tube investigation

24 p3821 A71-45367

SHADOWGRAPHS

U SHADOWGRAPH PHOTOGRAPHY

SHADOWS

NT LUNAR SHADOW

NT PENUMBRAS

Umbral rotational temperatures determined from equivalent widths of molecular lines

06 p0967 A71-17908

Shadow projector creating visual illusion of space surrounding flying aircraft for aviation training, relating perceived distortions to system parameters

06 p0864 A71-18716

Light source displacement distortions in shadow visualization for flight trainers involving terrain scale and landing simulation

08 p1271 A71-20796

Sunspot umbra empirical model, deriving temperature and optical depth relationship from IR continuous limb darkening

10 p1666 A71-23787

Vibrational and rotational temperatures diurnal variations of upper atmospheric OH emissions from IR spectroscopic measurements, discussing earth shadow effects on mean intensity

11 p1753 A71-25541

Optical effects observation by air traveler during takeoff, including haze or cloud droplet scattering, halos, shock wave shadows, shallow watercolors and twilight wedge

13 p2022 A71-29350

Shadow band observations during 7 March 1970 solar eclipse, determining spectral energy distribution from magnetic tape recordings of collimated photocells output

16 p2566 A71-33761

SHAFTS [MACHINE ELEMENTS]

NT TURBOSHAFTS

Computerized analysis of seal temperature, elastic displacements and seal force balance in iterative design method for gas turbine mainshaft seals

01 p0142 A71-10479

Optimal design of rotating disks of nonuniform thickness with integral shafts, using two and three dimensional numerical analysis for stress distribution [ASME PAPER 70-WA/DE-6]

03 p0511 A71-14141

High performance precision shaft and face seal design and applications

10 p1617 A71-24417

Solid circular Ti shaft torsion boundary value problem solution, using elastic-viscoplastic materials thermodynamics and constitutive relations

11 p1849 A71-25801

Resolved stress formula for shafts under simultaneous tangential bending and torsion acting at dangerous points of cross section

18 p2981 A71-36721

Stress analysis of rotating orthotropic disks mounted on elastic shafts, obtaining closed form solution for governing differential equations

20 p3308 A71-39088

Axisymmetric stress and strain states calculation for linear elastic field in cylindrical tight fits between hub and shaft

21 p3463 A71-40656

Air pressurized bearing mounted rotor with vertical shaft, discussing elastically suspended foundation mass and damping effect on self excited vibration

22 p3550 A71-41659

Regular and singular perturbation solutions for beam bending under axial forces and shaft warping in torsion

22 p3616 A71-42214

Compressible flow across shaft face seals and narrow slots, examining fluid inertia, viscous friction and entrance losses

23 p3663 A71-43592

Curvilinear elasticity solutions to stress concentrations at fine necks in cylindrical shaft under torsion, considering semicircle, semiellipse, rectangle, triangle and arc shapes

24 p3882 A71-44846

Vertical shaft stability on elastic sliding bearings, considering passage through autooscillations zone

24 p3831 A71-45051

SHAKERS

Two-shaker single input sinusoidal and random vibration tests, considering Hunter-Helmuth solution with constant cross coupling compensation in frequency band

11 p1745 A71-26491

SHALLOW SHELL EQUATIONS

Comparative shallow shell finite element analyses using different stiffness matrices

01 p0175 A71-11012

Shallow shells of revolution of strain-hardening material, deriving stress strain state by rigid plastic body model

01 p0175 A71-11039

Nonlinear stability of shallow spherical shells under concentrated loads, showing critical loads dependence on shallowness

01 p0177 A71-11239

Stress-strain state variability associated with optimal local heating of shallow shells of revolution

02 p0322 A71-11727

Shallow spherical shell thermally stressed state produced by temperature gradients

02 p0322 A71-11728

Bending of thin elastic orthotropic shallow shells, taking into account large deflections, temperature distribution and material nonuniformities

02 p0325 A71-12288

Perforated thick shallow spherical shell, solving boundary value problem for external loads

02 p0329 A71-12671

Doubly curved thin shallow shells nonlinear stability, using piecewise linearization for postbuckling load-displacement curves

03 p0501 A71-13073

Clamped shallow spherical and conical shells axisymmetric dynamic buckling under step loads of infinite duration, showing similarity with static buckling

03 p0504 A71-13455

Shallow shell theory boundary value problems, calculating stress concentration for domes and shells with holes

03 p0513 A71-14230

Successive approximation algorithm for stress concentrations at holes in nonlinear shallow shells, applying to cylindrical and spherical shells with circular and elliptical holes

04 p0664 A71-14602

Constant/variable thickness isotropic elastoplastic shallow shells stress analysis and limiting load determination, using numerical method based on successive approximation technique

04 p0664 A71-14603

Shallow spherical shells with periodically spaced holes, discussing stress analysis by least squares method for curved perforated plates [ASME PAPER 70-PVP-11]

04 p0665 A71-14771

Thin shallow shell theory boundary value problem, discussing reduction to Fredholm integral equations system

05 p0828 A71-16893

Thin orthotropic shallow elastic shells with initial defects, analyzing critical pressure states

06 p0982 A71-17355

Elastic rib-reinforced flexible shallow shells theory, deriving variational equations for multicontact problem

06 p0985 A71-17752

Axisymmetric vibration frequencies, form shapes and apparent masses for vertical fluid filled coaxial cylindrical shells resting on shallow spherical shell

06 p0986 A71-17763

Shallow spherical shells stability under constant external pressure

06 p0987 A71-17768

Thin shallow shell theory, describing asymptotic method for nonlinear equations integration

06 p0988 A71-17776

Orthotropic shallow shells nonlinear theory, examining inverse bending problems

06 p0988 A71-17778

Flexible plates and shallow shells supercritical deformation in high temperature field, taking into account modulus of elasticity and thermal expansion coefficient temperature dependence

06 p0990 A71-17796

Rectangular plates and shallow shells large asymmetric deflection, using computerized finite difference technique

06 p0991 A71-17802

Stress-strain state of shallow shells under concentrated heat load, obtaining asymptotic expressions for various parameters

06 p0997 A71-17845

Critical dynamic snap-through of shallow clamped arches under concentrated loads, using finite difference method [AIAA PAPER 71-176]

06 p1004 A71-18615

Thin shallow elastic shells boundary value problem, deriving existence and multiplicity of equilibrium state critical points for bending and buckling

07 p1213 A71-19639

Shallow orthotropic cylindrical shells with weak anisotropy, deriving equations for stress concentration at circular hole

07 p1217 A71-20457

Stress concentration in planar rectangular shallow shells and plates with polygonal holes

07 p1218 A71-20470

Planar-rectangular shallow shells with double curvature geometry, analyzing natural oscillations by finite difference procedure

07 p1219 A71-20649

Thin shallow shells under surface loads with allowance for electric field induced body forces and moments, deriving four equations system

08 p1368 A71-20788

First passage time for snap-through of shallow cylindrical shell subject to stationary random loading, considering numerical solution by Pontryagin-Vitt equation

08 p1369 A71-20809

Shallow shell triangular finite element method application to cylindrical shell theory

09 p1534 A71-22106

Flexible elastoplastic shallow shell theory, using mixed variational principle for flexure velocity and stress function

09 p1535 A71-22179

Positive curvature type shallow shells computation for optimum efficiency and minimum material expenditure by dimensionless modeling method

09 p1537 A71-22517

Shallow conical shells local heat treatment, determining optimal temperature fields

09 p1546 A71-23084

Clamped shallow spherical caps under uniform pressure, computing axisymmetric buckling

09 p1541 A71-23091

Edge loading effects on shallow hyperbolic parabolic shell elastic damping, discussing flat plate theory analog solution

10 p1686 A71-23995

Axisymmetric snap-through of shallow clamped spherical caps under uniform pressure, revealing existence of higher modes as isolated closed loops from approximate solution

10 p1689 A71-24518

Shallow rib reinforced rectangular shells under normal load with infinite regularity estimates independent of rigidity, using double trigonometric series

10 p1689 A71-24564

Shallow spherical shell thermal stability, investigating factors affecting Galerkin method validity

10 p1690 A71-24574

German monograph on nonnumerical transformation of tensor equations by computers, applying to shallow shell theory

10 p1692 A71-25038

Nonlinear dynamic analysis of shells of revolution under symmetric and asymmetric loads, obtaining solutions for shallow cap buckling

11 p1847 A71-25465

Shallow laminated shells nonlinear bending equations, using variational principle with allowance for transverse shear strain of layers

12 p1975 A71-27104

Spherical shallow shell with hole, noting natural vibration frequency

12 p1975 A71-27108

Numerical solution of equations describing stress-strain state of shallow nonuniformly heated shell

12 p1979 A71-27355

Thin walled elastic isotropic shallow shell with thermal boundary conditions, obtaining thermoelastic solution in series form

12 p1984 A71-27687

Dynamic snapthrough of shallow circular cylindrical shell undergoing plane motion in response to nearly symmetric impulsive pressure

13 p2146 A71-27781

Elastoplastic plates and shallow shells with rigid orthotropic filler, bending and buckling beyond elastic limit

13 p2156 A71-29066

Critical load of shallow shell of revolution as function of geometric and material parameters

14 p2321 A71-29624

Axisymmetrical snap buckling of clamped shallow spherical shell with initial deformation under external pressure, using energy method

14 p2322 A71-29689

Nonlinear stability of saddle-like deformed circular and square flat plates and shallow shells under transverse loadings

14 p2322 A71-29692

Curvature effects on shallow shell free vibration frequencies, solving linear eigenvalue problem

14 p2325 A71-30062

Clamped shallow spherical cap buckling and initial postbuckling behavior under axisymmetric band type loads, using numerical analysis

14 p2330 A71-30690

Symmetric and asymmetric dynamic buckling of shallow elastic arches under uniform loads, using nonlinear finite difference method

14 p2331 A71-30695

Stresses and deformations of shallow spherical shells with specified edge displacements

15 p2502 A71-31186

Snap buckling instability of shallow shell type structures subject to random transverse load

15 p2502 A71-31417

Thin plates and shallow shells stability, investigating weak solutions of wall displacement differential equations

16 p2649 A71-32993

Mathematical techniques of equilibrium states and periodic vibrations in nonlinear elastic systems illustrated by thin plate and shallow cap buckling under uniform pressure

16 p2649 A71-32998

Linearized shell theory, proposing improvement of Marguerre-Vlasov shallow shell equations in terms of invariant displacement and stress functions

16 p2649 A71-33000

Mixed finite element formulation for shallow shells, discussing element matrix generation phase and governing variational principle

16 p2652 A71-33080

Clamped shallow spherical shells buckling and postbuckling behavior under axisymmetric ring loads, examining effect of load location and shell geometry variations

[ASME PAPER 71-APM-9] 16 p2656 A71-33216

Initial interaction phase between thin shallow conical shell vibrating axisymmetrically and ideal incompressible fluid, determining hydrodynamic pressure effects

16 p2560 A71-33901

Nonlinear theory for rotating shallow shells of revolution, deriving edge zone boundary layer solutions for differential equations

16 p2660 A71-34071

Transverse shear deformation and normal stresses effect on shallow shell with normal concentrated loads

17 p2822 A71-34594

Multilayer asymmetrical shallow shells with transverse shear strains, deriving finite deflection nonlinear equations

17 p2833 A71-35613

Channel type closed shallow shells stress states calculation, applying asymptotic integration technique to load decomposition

18 p2976 A71-36178

Spinning centrally clamped thin shallow spherical shell free vibration numerical analysis by considering perturbation about equilibrium configuration [ASME PAPER 71-APM-G]

18 p2977 A71-36254

Shallow spherical shell under uniform external pressure loads, obtaining boundary conditions effects on stress-strain state

19 p3155 A71-37530

Shallow lattice shell equations approximated by generalization of asymptotic theories for lattice-type disks and plates

19 p3158 A71-38151

Buckling and initial postbuckling behavior of clamped thin shallow spherical sandwich shells under axisymmetrical loads

19 p3159 A71-38185

Thin shallow spherical shell weakened by circular hole, calculating stressed state from boundary value problem solution

20 p3308 A71-39165

Forced and free vibrations of shallow cylindrical shell in rectangular duct filled with ideal fluid

20 p3310 A71-39785

Elastic buckling and initial postbuckling behavior of clamped shallow spherical sandwich shells under axisymmetrical load

21 p3469 A71-41007

Variational stress-strain equation for flexible shallow orthotropic multilayer shells with large deflections under normal pressure and contour loading

23 p3778 A71-44040

Cylindrical shell with elliptical hole, calculating elastic stress concentration due to axial tension based on shallow shell theory

24 p3879 A71-44625

Discrete element finite deflection analysis of shallow arches using numerical method of potential energy minimization

24 p3879 A71-44636

Asymptotic design formulas for thermoelastic supercritical strains in thin elastic shallow spherical shells under external pressure

24 p3881 A71-44827

Natural and forced joint vibrations of liquid and shallow spherical shells

24 p3881 A71-44829

SHANKS

U JOINTS (JUNCTIONS)

SHANNON INFORMATION THEORY

U INFORMATION THEORY

SHAPES

NT ELLIPTICITY

NT LINE SHAPE

NT ROSETTE SHAPES

NT T SHAPE

Shape and surface roughness effects on turbulent ablation of reentry body nose tip, noting recession rate

[AIAA PAPER 69-717] 01 p0071 A71-10934

Minimum suction rate preventing laminar boundary layer separation from curvilinear porous surface in jet flow

02 p0186 A71-12553

Shell shape without bending stresses due to external load

05 p0828 A71-16891

Figural change perception in apparent motion, considering resolving capabilities and visual stimuli for plastic deformation and shape rotation

07 p1048 A71-19516

Electromagnetic field amplitude and phase scattering diagrams analysis for shape information capacity

13 p2029 A71-28369

SHARING

Interstellar grain temperatures, determining shape effects on emissivities 14 p2305 A71-29680

Coordinate transformations of shape and position of cometary tails on orbit plane suitable for digital computer 15 p2485 A71-31669

SHARING

U COORDINATION

SHARKS

Small spotted dogfish shark epiphysis cerebri, determining light sensitivity and properties 13 p2008 A71-28456

SHARP LEADING EDGES

Rotational temperature and density measurements in rarefied flow over sharp leading edge flat plate, obtaining shock layer static pressure 01 p0082 A71-10955

Circular stagnation line position on axisymmetrical blunt bodies with circular sharp edge 09 p1384 A71-23672

Leading edge suction analogy for predicting low speed lift and drag-due-to-lift characteristics of sharp edge delta and related wing planforms [AIAA PAPER 69-1133] 10 p1553 A71-24851

SHATTERING

U FRAGMENTATION

SHEAR CREEP

Al alloy biaxial shear creep under abrupt temperature and stress changes, noting surface size, shape and location [ASME PAPER 70-WA/APM-41] 03 p0443 A71-14164

Novozhilov complex transformation method extended to Timoshenko theory of elastic shells constructed with allowance for transverse shear deformation 05 p0820 A71-16187

SHEAR DISTURBANCES

U S WAVES

SHEAR FATIGUE

U SHEAR STRESS

SHEAR FLOW

Spatial and temporal structure in turbulent breakdown of shear flows in stably stratified atmosphere from radar images of vertical cross sections 01 p0116 A71-10569

Transverse wave instability of unmagnetized collisionless plasma subjected to shear flow 01 p0136 A71-1477

Shear flow turbulent friction in boundary layer, deriving Navier-Stokes equation integrodifferential formulation 02 p0241 A71-12411

Turbulent flow near porous wall with pressure gradient, calculating velocity and shear distribution by modified Van Driest theory 03 p0399 A71-13432

Plane Couette flow turbulence, discussing wall region shear and core homogeneity 03 p0400 A71-13546

Axially loaded finite stringer bonded to infinite elastic sheet, considering adhesive shear flow 03 p0514 A71-14350

Boundary layer development on slender rod in axial shear flow for different profiles 05 p0694 A71-16711

Grid turbulence interaction with uniform mean shear flow, examining initial disturbance length scale effects 05 p0695 A71-16965

Three dimensional transonic shear flow structure in turbomachine cascade, using time dependent numerical solution [AIAA PAPER 71-83] 06 p0843 A71-18540

Airfoils in two dimensional nonuniformly sheared slipstreams, predicting pressure distribution from mathematical model for comparison with measurement [AIAA PAPER 71-94] 06 p0843 A71-18549

Turbulent shear flows transport properties, computing atmospheric and vortex motions by invariant modeling of Reynolds stress term in boundary layer momentum equation [AIAA PAPER 71-217] 06 p0886 A71-18653

Two dimensional thermal convection through shallow layer with vertical shear using numerical model 07 p1152 A71-19752

Nondissipative heterogeneous shear flow stability in presence of uniform magnetic field in streaming direction 07 p1169 A71-20023

Nonlinear subgrid scale eddy viscosity formulation for turbulence generated by mean shear or thermal instability at large Reynolds number 07 p1094 A71-20615

Atmospheric Kelvin waves interaction with mean zonal flow in westerly shear zone, noting momentum flux divergence distribution correlation with observed zonal accelerations 09 p1489 A71-23552

Heat transfer at high Peclet number from sphere freely rotating in shear flow field at low Reynolds numbers 10 p1697 A71-24621

Stratified shear flow stability, investigating diffuse interface between two miscible fluids 10 p1595 A71-24623

Turbulent shear flows, examining zero and negative entrainment in boundary layers 10 p1595 A71-24626

Nonuniform transonic shear compressible flow past symmetric airfoil, using linearized small disturbance theory 10 p1552 A71-24761

Static pressure recovery and core region velocity profile in rectangular wall diffusers with uniform shear flow [ASME PAPER 71-GT-5] 11 p1751 A71-25951

Three dimensional turbine end wall boundary layer with shear term, using momentum integral analysis and cross flow velocity profiles [ASME PAPER 71-GT-6] 11 p1751 A71-25952

Maximum velocity position in turbulent shear flow for differential pressure effect between double pitot tubes, using inductance type transducer 11 p1767 A71-26313

Thermally stratified turbulent shear flow, calculating turbulent energy balance and temperature inhomogeneity spectral equations 12 p1895 A71-26899

Destabilizing buoyancy forces effect on weak homogeneous shear flow turbulence in gases, discussing turbulence decay with time and turbulence energy growth 12 p1896 A71-26940

Boussinesq stratified fluid zonal flow with vertical and horizontal shear, studying stability to hydrostatic neutral wave perturbations 12 p1925 A71-27194

Computer program for aerodynamic forces on flexible plate undergoing transient motion in shear flow, applying to panel flutter 12 p1866 A71-27559

Boundary layer equations based on eddy viscosity model for turbulent free shear flow, solving numerically in Crocco coordinate plane [ASME PAPER 71-FE-17] 13 p2052 A71-29456

Vortex induced shear and secondary flow through row of spheres, curved channel, turbine blades, rotating impeller, suction pipe and upstream boundary layers 14 p2224 A71-30176

Boundary layer effect on sound transmission in acoustically treated circular duct with shear flow, reducing governing equations to two-point boundary value problem 14 p2224 A71-30199

Nonlinear dynamical evolution of two dimensional unstable shear flows, using numerical integration of time dependent incompressible Navier-Stokes equations 14 p2226 A71-30409

Velocity profile of steady two dimensional incompressible laminar boundary layer flow with suction or injection, noting wall shear function 15 p2388 A71-31441

Shearing flows in steady vortex around airfoil in perturbed velocity, considering aerodynamic forces torque 15 p2346 A71-31903

Stationary nonparallel plane flow stability with horizontal shear to three dimensional nondivergent disturbances in Boussinesq fluid, using Arnold method 15 p2393 A71-32637

Unsteady waves in parallel shear flows, noting viscous and nonlinear effects 16 p2558 A71-33011

Stream function and velocity of shear flow vortex in infinitely thin profile from linearized Euler equations for boundary value problem 16 p2561 A71-34161

Uniform shear flow past semiinfinite flat plate, studying diffuse and heat transfer near leading edge 16 p2561 A71-34162

Extension of Heisenberg model for spectral transfer to second order fluids in turbulent shear flow, noting accompanying weakening of anisotropic influences 17 p2725 A71-34181

Incompressible turbulent shear boundary layer equations of motion, developing integrodifferential formulation of Navier-Stokes theory 18 p2904 A71-36184

Dense fluids linearized general transport equations solution, obtaining explicit expressions for shear viscosity 18 p2950 A71-37061

Perturbed problem of rotational steady compressible flow in three dimensional channel at upstream infinity/shear flow, using linearization by current functions 20 p3211 A71-39419

Stability problem in hydrodynamics of perturbed heterogeneous shear flow, solving initial value problem for Couette flow 20 p3213 A71-39783

Stepwise change in wall roughness effects on turbulent shear flow through two dimensional channel, measuring mean velocity, turbulent intensity and shear stress 21 p3365 A71-40015

Straight line vortices in uniform two dimensional straining field, detailing irrotational strain and simple shear 21 p3320 A71-40501

Sound propagation in sheared fluid in duct, determining energy flux from linearized gas dynamic equations 21 p3366 A71-40536

Molecular chaos breakdown under shear flow, calculating thermodynamic fluctuation formula for unlimited Reynolds number increase 21 p3418 A71-40628

Thermal convection induced perturbations in unstably stratified horizontal shear Couette flow of Boussinesq fluid in rectangular channel heated from below 21 p3475 A71-40641

Inhomogeneous plasma shear flow instability with ion-ion collision, using BGK model 22 p3579 A71-41581

Shear flow effects on sound propagation in rigid rectangular ducts, taking into account boundary layer thickness 23 p3704 A71-43212

Minimum drag and lifting line characteristics of large aspect ratio wing in uniform shear flow with velocity variations along span 23 p3625 A71-43312

Fluid elements streamwise dispersion in two dimensional turbulent shear open channel flow, using Markovian model for numerical simulation 24 p3817 A71-44421

Stability of dissipative shear flow of inviscid incompressible electrically conductive fluid in presence of magnetic field, deriving instability modes phase velocity limiting conditions from MHD equations 24 p3855 A71-44645

SHEAR LAYERS

Temperature distribution and heat transfer across transitional separated shear layer under subsonic air flow, using interferometric measurements 04 p0679 A71-15470

Optical crossed-beam measurements of turbulence intensities in cold subsonic air jet shear layer [AIAA PAPER 71-137] 06 p0902 A71-18580

Prediction method for turbulent boundary layer development using shear work integral for range from wall jet to adverse pressure gradient flow 07 p1085 A71-18764

Transverse velocity shear effects on low-beta resistive plasma LF stability in uniform magnetic field 07 p1166 A71-18882

Approximate bridging relations for heat transfer, surface shear and drag in transitional regime between free molecule and continuous flows 07 p1087 A71-18894

Clear air turbulence role in general atmosphere circulation, considering energy dissipation, momentum transfer and shear layer producing mesoscale processes 07 p1153 A71-20221

Static pressure port errors in hypersonic turbulent flow, using approximate shear layer momentum balance for pressure increase derivation [AIAA PAPER 71-270] 08 p1228 A71-21996

Laminar mixing region stratified free shear layer stability between two uniform streams from numerical solution of linear sixth order equation for disturbance amplitude function 09 p1432 A71-22851

Backward facing step in confined supersonic two dimensional flow, investigating turbulent shear layer reattachment 10 p1552 A71-24622

Transonic aircraft jet exhaust wave structure, examining reflection geometry at shear layer and shock diamond train 10 p1553 A71-24867

Directional acoustic radiation from supersonic jet, discussing generation mechanism theory based on shear layer instability close to nozzle 12 p1945 A71-27221

Acoustic refraction by two dimensional shear layer in duct, considering sound propagation and initial value problem solution 13 p2051 A71-29248

Interaction between viscous mixing shear layer induced by tangential injection and external supersonic flow field, obtaining spark schlieren photographs and wall pressure distributions [ASME PAPER 71-FE-24] 13 p2053 A71-29461

Atmospheric turbulent shear layer model, giving velocity, stable, unstable and neutral profiles 14 p2267 A71-29759

Nonlinear stability theory, considering velocity and vorticity perturbations in circular Couette plane Poiseuille and shear layer flows 15 p2393 A71-32568

Variable density effect on inviscid free shear layer instability at small Mach numbers, deriving difference equation for inviscid disturbance [DFVLR-SONDDR-114] 19 p3043 A71-37300

Thin layers shear strength and friction under high pressure, describing rotating-anvil shear press with

high sensitivity strain gage equipped load and torque cells
20 p3241 A71-38878

Shear layers acoustic excitation, considering coupling between sound waves and rotational excited shear waves in flow detachment line
21 p3317 A71-40014

Magnetic field stabilizing effect on free shear layer of electrically conducting fluid at small Reynolds number
21 p3421 A71-40637

Two dimensional supersonic turbulent free shear layer recompression process from flow model numerical calculation
21 p3371 A71-40998

Free shear layer similarity flow profiles correlation for turbulent isobaric jet mixing by spread rate parameters, using viscosity models
21 p3371 A71-41032

Resonant oscillations effect on heat transfer across mixing length in cavities spanned by low speed turbulent shear layers
21 p3371 A71-41033

Electric current shear at auroral arcs due to electron precipitation into lower ionosphere
22 p3536 A71-42623

Hypersonic axisymmetric slender body near wake shear layer determination by shock expansion method for numerical computation accuracy and efficiency
23 p3626 A71-44194

SHEAR PROPERTIES

NT SHEAR STRENGTH

Ta alloys single crystals elastic compliance constants over temperature range, deriving bulk and shear moduli and anisotropy factor
01 p0100 A71-10373

Pure shear mode propagation in sapphire, determining acoustic axes velocity
02 p0294 A71-11947

Thin glass fibers relaxation characteristics, discussing shear modulus, internal friction and temperature effects
03 p0448 A71-13298

Shear deformation and rotary inertia in heterogeneous laminated plates of bonded anisotropic layers, discussing bending-extensional coupling
04 p0668 A71-15185

Turbulent flow of nonlinear Stokes fluids with transverse shear, determining nonlinear properties effects
04 p0575 A71-15605

Soviet monograph on refractory materials elasticity at high temperatures covering elastic and shear moduli, Poisson coefficient and resonance methods
05 p0766 A71-16400

Rail shear test theoretical and experimental analysis, comparing high modulus reinforced composites test data with predicted values from lamination theory
07 p1215 A71-20128

Refractory materials at normal and high temperatures, describing cyclic shear test methods
08 p1372 A71-21612

Nonshallow spherical shells of small shear modulus materials, examining boundary conditions and axisymmetric deformation
09 p1535 A71-22184

Interlayer shear modulus relation to thermal conductivity coefficient in oriented glass fiber reinforced plastics
09 p1482 A71-22814

Thin glass fibers relaxation characteristics, discussing shear modulus, internal friction and temperature effects
09 p1483 A71-23271

Torsion pendulum for measuring internal friction and shear modulus of refractory metals and alloys
09 p1452 A71-23333

Mo-Re alloy single crystals asymmetric mechanical properties, discussing shear tests of Mo and Mo-Re single crystals for hard and soft flow stress planes identification
11 p1777 A71-25372

Axial compression buckling of elastic core filled circular cylindrical shells with transverse shear flexibility, noting solid propellant rocket cases design application
13 p2148 A71-27984

Bending and torsional oscillations in rectangular specimens of femur and tibia, calculating elastic and shear moduli of compact bone tissues
13 p2019 A71-28658

Disperse systems dynamic behavior, considering density ratio, discontinuity diameter, viscosity and shear modulus
14 p2256 A71-29518

Torsion of circular composite rods of sectors with different shear moduli and radial cracks
14 p2326 A71-30193

Monograph on rectangular shear elastic plates stability covering Cosserat plane, stress functions, buckling conditions, compressive forces and two dimensional equations
15 p2509 A71-32302

Circular rings coupled twist bending vibrations, considering rotatory inertia and shearing deformation effects
15 p2510 A71-32517

Shear modulus, flexure and buckling of web stiffened sandwich structures, using core layer model based on continuum theory
[ASME PAPER 71-APM-8] 16 p2656 A71-33217

Cyclic torsional shear testing of refractory materials at normal and high temperatures, describing test equipment
17 p2834 A71-35672

Fundamental frequency of large amplitude bending vibration of elastic and isotropic rectangular plates, considering effects of transverse shear and rotatory inertia
18 p2980 A71-36496

Microscopically homogeneous and isotropic two-phase composite material shear modulus formula derivation
19 p3155 A71-37481

Transverse waves propagation in vibrating orthotropic rectangular beams, noting inexact information regarding shear distribution
20 p3307 A71-39037

Effective shear modulus of multilayered rectangular elastic isotropic member in uniform torsion
22 p3618 A71-42587

Magnetic field effects on complex Young and shear moduli for nonferromagnetic metals, describing experimental technique and frequency resolution criterion
23 p3689 A71-43206

Thin isotropic shells with terminal shear rigidity, deriving complex version of classical theory of thermoelasticity for plastic shells with low shear resistance
24 p3878 A71-44482

Solid lubricant-epoxy compounds shear modulus measurement by cantilever beam specimens dynamic testing, calculating wear life coefficients for molybdenum disulfide in epoxy resin
[ASLE PREPRINT 71LC-1] 24 p3842 A71-45284

Shear modulus and stress-strain relations for different plastic strain rates
24 p3886 A71-45362

SHEAR STRAIN

Multilayer asymmetric plates deflection, stability and vibrations, deriving nonlinear bending equations with allowance for transverse shear strains
06 p0995 A71-17833

Unidirectional fiber reinforced composite longitudinal shear deformation, deriving analytical expression for stress distribution
07 p1216 A71-20132

Anisotropic material failure under combined loading, predicting strength from uniaxial and shear tests
[AIAA PAPER 71-368] 11 p1845 A71-25342

Shear deformation effect on optimal design of elastic beams, considering rectangular cross section circular ring by Timoshenko beam theory
11 p1849 A71-25677

Shallow laminated shells nonlinear bending equations, using variational principle with allowance for transverse shear strain of layers
12 p1975 A71-27104

Spherical shell stressed state weakened by holes, investigating shear deformation effect
12 p1975 A71-27107

Stability analysis of rigid frames and trusses, including effect of bending moments and shear forces before buckling
12 p1976 A71-27161

Asymmetric structure elastic transversely isotropic sandwich panels bending equations, taking into account transverse shear strain and stability
12 p1981 A71-27497

Stress concentration due to holes and other stress raisers in plates and shells, taking into account transverse shear strains effects
13 p2149 A71-28127

Cartesian shear and rigid rotation moire patterns by spatial filtering of superposed diffraction gratings
14 p2329 A71-30464

Rotary inertia and shear deformation effects on three dimensional flexural vibrations of circular ring on elastic foundation
16 p2657 A71-33421

Isotropic sandwich plates with rigid cores due to shear boundary tractions, considering transverse strain and stress, displacement function and stability
16 p2660 A71-34035

Orthotropic thin walled bars with rigidly connected rectangular elements, applying displacement under torsion with allowance for shear to H beam
17 p2823 A71-34782

Multilayer asymmetrical shallow shells with transverse shear strains, deriving finite deflection nonlinear equations
17 p2833 A71-35613

Two parallel noncoplanar cracks extension in elastically isotropic solid by applied shear stress with deformation in antiplane strain mode
19 p3157 A71-37797

Finite strain theory for elastic-plastic deformation, considering isothermal shear of neo-Hookean material before yielding and during elastic unloading
20 p3267 A71-38794

Shear deformation and rotary inertia effects on flexural vibration frequencies of pretwisted, nonpretwisted and tapered cantilever beams
[ASME PAPER 71-VIBR-79] 21 p3461 A71-40316

Thin truncated conical shells axisymmetric free vibrations, considering shear deformation and rotary inertia effects
21 p3462 A71-40528

Shear deformation theory of axisymmetric cylindrical shells in contact with smooth rigid surfaces
21 p3470 A71-41017

Strength and deformation characteristics of glass plastic under torsional and compressive shear loads, investigating temperature effects on elastic modulus
23 p3697 A71-44204

SHEAR STRENGTH

Glass fiber-epoxy resin composites shear strength, considering fiber length and interfacial bond effects
01 p0106 A71-10277

Shell theory of anisotropic shells and plates with low shear rigidity, using Timoshenko-type model
01 p0169 A71-10497

Contact problems of orthotropic fiberglass-reinforced plastic plate with low shear rigidity
01 p0169 A71-10498

Tungsten plasma coatings on steel, examining shear strength dependence on vaporization distance, microstructure and residual stresses
01 p0088 A71-10788

Thin web shear test device demonstrated on aluminum foil and glass fiber composites
03 p0508 A71-13765

Pressure and strain rate effects on polycrystalline Be shear strength, determining activation energy for dislocation motion
03 p0445 A71-14463

Shearing strength of and lubrication effect on metal-plastic adhesion bond, using solid rotating indenter technique
05 p0759 A71-16363

Low shear rigidity effect on stability of glass fiber reinforced plastic cylindrical shells under loads and elevated temperature
05 p0822 A71-16369

Moment loads and stress functions of orthotropic laminar shells with low shear rigidity
05 p0822 A71-16371

Carbon fibers, light metal alloys and composites, studying moduli of elasticity and shear thermal variations
[PLASTICS INST. PAPER 16] 08 p1320 A71-20904

High speed low power loss spiral groove bearings self sealing grease lubricants with high shear stability and good boundary lubrication
[ASLE PREPRINT 70LC-6] 08 p1322 A71-21157

Measuring instrument for determining shear strength of adhesive bond
09 p1443 A71-22503

Ultrasonic waves propagation in hydraulic and lubricating oils, testing shear resistance
09 p1484 A71-23673

Polyurethane structural adhesives with excellent tensile shear and T-peel strengths at cryogenic temperatures, long pot lives and good processing characteristics
10 p1630 A71-24068

Surface treatment effects on high shear strength adhesive bonding of fiber reinforced plastics to metal substructures
10 p1630 A71-24069

Low temperature curing long open time epoxy adhesives evaluation for 3500 psi shear strength
10 p1631 A71-24072

Carboxyl terminated butadiene-acrylonitrile/epoxy carbon fiber composites fracture energy, noting fracture strength, short beam shear strength and tensile strength at cryogenic temperatures
11 p1785 A71-25403

Carbon fiber reinforced high interlaminar shear strength composites, noting applications to advanced engineering structures
11 p1785 A71-25408

Long term oxidative aging effects on interlaminar shear strength retention of low void graphite/ boron reinforced polyimide resin composites
11 p1785 A71-25410

Impact composite materials with reactive resins as binders for polyester fabric, determining peel resistance, tensile shear strength and high temperature aging effect
11 p1786 A71-25416

Composite materials fiber-matrix interfacial behavior, determining polymer concentration on graphite fibers surface by Raman spectroscopy and composite shear strength increase
11 p1787 A71-25430

Coupled thermoelasticity, bending and stability of thin walled shells and plates of oriented fiberglass

reinforced plastics with low shear rigidity, using Timoshenko theory 12 p1978 A71-27345

Shear strength effect on axisymmetrical stress-strain state of orthotropic cylindrical shell subjected to nonuniform surface heating 13 p2148 A71-27825

Be, U and W shear strength measurements, detailing strain, strain rate and pressure effects [ASME PAPER 70-WA/PT-2] 15 p2434 A71-32260
Fibrous composites with multiple and variable shear strength interfaces to improve longitudinal shear and transverse tensile strengths and toughness 17 p2817 A71-34342

Optimal cross section of minimum volume rotating shaft with complex fatigue strength, accounting for tension and shear effects 17 p2822 A71-34595

Thin layers shear strength and friction under high pressure, describing rotating-anvil shear press with high sensitivity strain gage equipped load and torque cells 20 p3241 A71-38878

Polycrystalline body macrohomogeneous plastic deformation, deriving basic postulates for slippage and plane relationships to tangential stress and shear strength dependence on elastic deformation 23 p3777 A71-43576

Cone penetration resistance tests on granular lunar soil simulants for in-place shear strength and packing characteristics under various gravity conditions 23 p3757 A71-43751

Strength and deformation characteristics of glass plastic under torsional and compressive shear loads, investigating temperature effects on elastic modulus 23 p3697 A71-44204

SHEAR STRESS

NT TORSIONAL STRESS

Laminar boundary layer free convection at vertical plate with exponentially decreasing surface temperature, determining thermal flux and shear stress 01 p0179 A71-10610

Cu addition effects in solid solution on grain boundary sliding in Al at constant shear stress, considering accompanying crystal dislocations 01 p0102 A71-10739

I-beam plastic moment under shear force, using empirical curve for interaction between bending moment and shear force 01 p0174 A71-11000

Strain rate effect on critical shear and cross slip stresses of Al and Al-Mg single crystals, obtaining stacking fault energy 03 p0442 A71-13364

Steady incompressible laminar pipe flow within porous wall cylinder, determining velocity, pressure distribution and shear stress [ASME PAPER 70-WA/FLCS-3] 03 p0401 A71-14079

Axisymmetric mixed boundary problem for elastic infinite cone, obtaining solution by assuming zero shearing stresses 03 p0513 A71-14234

Direct pointwise stress determination in twisted cracked elastic bars under torsion and longitudinal shear by numerical methods 04 p0667 A71-15180

Thermomechanical coupling in axially symmetric viscoelasticity of cylindrical cavity under shear stress, determining stress concentration from temperature distribution 04 p0669 A71-15203

Frictional resistance reduction in hydrodynamics, considering critical shear stress in ducted flow 04 p0571 A71-15209

Crack extension by incident elastic wave diffraction for specific shear stress character at wave front 05 p0825 A71-16709

Small surface elements local skin friction sensor measurements near wall during laminar and turbulent flow, making direct shear force measurements 05 p0752 A71-16734

Tensile test equipment for fiberglass reinforced plastics strength measurement under shear 05 p0772 A71-16888

Turbulent boundary layer theories and classification according to prediction ability relative to heat transfer rates, shear stress distribution and fields of concentration 07 p1085 A71-18752

Turbulent boundary layer laminarization prediction in moderate accelerations, using Pathankar-Spalding finite difference formulation and experimental results for shear stress model selection 07 p1085 A71-18752

Two dimensional turbulent channel flow, determining local mean wall shear stress from velocity gradient 07 p1087 A71-18784

Hot-wire anemometer calibration, measuring shear stress and turbulence distributions in circular channel 07 p1106 A71-18785

Technical equations of shells of slowly varying curvature with transverse shear deformation and normal stress 07 p1211 A71-19252

Compressibility effect on turbulent pipe flow shear stress distribution, presenting high subsonic Mach number theoretical results from Kjellstroem-Hedberg momentum equation integration 07 p1088 A71-19423

Multilayered composite mathematical model, studying interfacial delamination under antiplane shear load 07 p1215 A71-20127

Fastener group behavior under combination of direct shear and moment, obtaining load deformation response of individual connections 08 p1370 A71-21410

Bolted joint assemblies under sustained loading, examining joint and fastener coating, bolt design and strength level and shear and tension stress effects 08 p1371 A71-21412

Bcc Ti-V single crystals deformation modes and resolved shear stresses as function of temperature and composition 08 p1307 A71-21510

Titanium single crystal prism slip dislocation dynamics, examining temperature and strain rate effects on shear stress 08 p1309 A71-21521

Gallium oxide particles effects on Ag-Ga matrix single crystals critical resolved shear stress 08 p1311 A71-21543

Grain boundary sliding and shear deformation in bicrystal Al and Al-Co solid solutions 08 p1345 A71-21576

Energy dissipation during independent flexural-torsional vibrations of rods, noting alternating shear stress superposition effect on damping 09 p1538 A71-22629

Book on elastic plate theory covering bending and transverse shear effects, boundary problems, rectangular isotropic, structurally orthotropic, circular and annular plates under various loads 09 p1544 A71-23701

Fracture models of stress field produced by accelerating crack under shear loading, using pulse diffraction method 10 p1684 A71-23932

Euler buckling of hinged slender prismatic bars of rectangular and elliptic cross sections with shear and transverse stress allowance 10 p1685 A71-23959

Failure/yield points, stiffness and failure energy from adhesive shear stress elongation curves, using computer assisted thick adherend tests 10 p1631 A71-24071

Homogeneous wave turbulence-MHD tangential discontinuity structures interaction, resulting in shear stress across discontinuity surface 10 p1652 A71-24663

Simultaneous determination of first and second mode photoelastic maximum shear stress intensity patterns of epoxy model, using computer plotted ellipses 10 p1694 A71-25060

High precision finite element for static analysis of loaded thin elastic shells of revolution including shear deformations 11 p1844 A71-25339

Shear stress and eddy viscosity distribution in Mach 20 compressible turbulent boundary layer, using mixing length flow theory 11 p1751 A71-25499

Mixed boundary value problem for fiber reinforced materials, analyzing shear response in multiply admissible kinematic deformations 11 p1850 A71-26105

Time dependent shear stress, temperature and boundary layer pressure in laminar flow over stepwise accelerated flat plate at hypersonic speed 11 p1856 A71-26193

Vapor flow passage wall shear stress effect on sonic velocity limit in Na heat pipes [ALAA PAPER 71-407] 11 p1856 A71-26202

S-shape lines of axial displacement field and interlaminar shear edge effect in laminated composites verified by moire technique 11 p1852 A71-26390

Maximum shear and hoop stress gradients in graphite-epoxy angle-ply laminated composite cylinders for axial and internal pressure loading 11 p1852 A71-26391

Interlaminar plane shear stress in fibrous composites under elastic deformation with edge effect, using membrane finite element analysis 11 p1852 A71-26394

Three dimensional turbulent boundary layer calculations, using two dimensional method based on turbulent energy equation empirical conversion into shear stress transport equation 11 p1753 A71-26443

Laminated plates transverse shear effects on deformation and stress distribution, using finite element analysis 12 p1982 A71-27571

Fiber reinforced composite materials plastic behavior shear stress theory, determining yield criteria and plastic strain rates associated with various failure modes 12 p1984 A71-27773

Eigenvalue, shooting and parallel shooting methods for solving Falkner-Skan boundary layer equation with positive or negative wall shear 13 p2047 A71-28230

Vertical variations of Reynolds stress and heat flux in atmospheric surface layer attributed to sub-mesoscale circulations, using sonic, thermometer and drag measurements 13 p2097 A71-28724

Incompressible planar fluid flow magnitude, direction and turbulent shear stress measurement by hot-wire anemometer 14 p2239 A71-29928

Shear stress distribution and local heat flux at surface of axisymmetric bodies for laminar and turbulent boundary layer flow 14 p2170 A71-30219

Shear stress, eddy viscosity and mixing length distributions in compressible turbulent boundary layers with air and carbon dioxide injection 14 p2228 A71-31025

Torsionally oscillating disk in steadily rotating incompressible second order fluid, calculating transverse and radial shear stress 15 p2387 A71-31185

Elastic-plastic mechanics of steady crack growth under antiplane shear, discussing residual stress effect, plastic zones shape and strain distribution 15 p2428 A71-31974

Shear deformations effect on circular plates from Reissner theory, expressing bending moments and shear forces as functions of lateral deflection and stress function 15 p2507 A71-32112

Energy dissipation in material under complex vibrations, noting role of summary shear stress 15 p2508 A71-32234

Fiber reinforced materials with oriented armoring, calculating stress-strain state under transverse shear 15 p2439 A71-32235

German monograph on thermally stressed shear soft shells with finite deformation covering tensor analysis, thermoelasticity, temperature fields and two dimensional bodies 15 p2509 A71-32305

Radiation effects on epoxy adhesive mechanical properties including compressive shear stress, modulus of elasticity and tensile strength 15 p2439 A71-32510

Rectangular plates under direct and shear in-plane forces, considering free lateral vibrations 15 p2509 A71-32512

Wall shear stress, momentum and displacement thickness of shock induced boundary layer interaction in tube and over flat plate, using integral method [ASME PAPER 71-APM-21] 16 p2559 A71-33208

Eccentrically stiffened thin cylindrical panels instability under uniform axial compression, uniform hoop compression and uniform shear 16 p2661 A71-34150

Transverse shear deformation and normal stresses effect on shallow shell with normal concentrated loads 17 p2822 A71-34594

Laminar boundary layer flow theory for arbitrary curved surfaces, predicting shear stress, thickness and velocity and pressure distributions 18 p2844 A71-36319

Laminar hypersonic boundary layer equations, calculating heat transfer and shear stress in stagnation point 18 p2847 A71-36428

Strain rate dependence of shear stress, plastic cross-slip and stacking fault energy of Al single crystals at 77 K 18 p2937 A71-36749

Accelerating rotating disks with variable thickness, presenting shear stress distribution 18 p2982 A71-36771

Thin walled beam structures under external torsional loading, calculating distribution of longitudinal and shear stresses 18 p2982 A71-36808

Two parallel noncoplanar cracks extension in elastically isotropic solid by applied shear stress with deformation in antiplane strain mode 19 p3157 A71-37797

Forced axisymmetric motion of circular viscoelastic plate, including effects of rotatory inertia, transverse shear and time dependent boundary conditions 19 p3157 A71-37848

Shear envelope of thin walled beam with semicircular cross section under creep 19 p3159 A71-38186

Incompressible turbulent boundary layer with pressure gradients, calculating Clauser equilibrium model and flow with constant wall shear stress 20 p3210 A71-39030

Stress distribution in adhesive lapped joints with emphasis on shear stress 21 p3384 A71-40139

Laminar viscous flow past semfinite flat plate to second Oseen type approximation, obtaining shear stress on plate 21 p3368 A71-40707

Hypersonic flat plate under impulsive loads, calculating time dependent transient wall shear stress and boundary layer induced pressure
21 p3369 A71-40964

Interlaminar shear stress and midsurface displacement of thin orthotropic laminated cylindrical shells, using linear deformation theory
21 p3470 A71-41018

Thin liquid films under simultaneous shear and gravity forces, noting data incorporation into transport equations for heat and mass transfer
22 p3620 A71-41884

Longitudinal shear induced stress field around rigid circular cylindrical inclusion and parallel crack, using Jacobi elliptic function in conformal mapping procedure
23 p3777 A71-43495

Flow field generation by coaxial turbulent jets, determining velocity distribution, turbulence intensities and shear stresses by hot-wire anemometers
23 p3627 A71-44198

Ni-Cr single crystals plastic deformation, presenting work hardening characteristics and critical resolved shear stress
23 p3694 A71-44278

Strongly curved wall jets development in thick boundary layer upstream of blowing slot, discussing calculation method, correction for shear stresses and comparison with experimental results
24 p3819 A71-44952

Stress-strain curve of unidirectional fiber reinforced composite Al and N-CI wire under axial compression loads, discussing buckling and shear instabilities
24 p3842 A71-45229

SHEAR WAVES
U S WAVES
SHEARING STRESS
U SHEAR STRESS
SHEATHS
NT ION SHEATHS
NT PLASMA SHEATHS
Breakdown voltage and high power tests for pressure bonded collector sheath tubes with cracked alumina insulators and flowing liquid metal coolant
11 p1709 A71-25859

SHEET METAL
U METAL SHEETS
SHEETS
Stress intensity factors for infinite sheet rectangular cut-out with symmetrical edge internal cracks under axial tension
04 p0670 A71-15387

Large plastic strains in fiber in sheet bending for wide angle range, using Hill theory
17 p2816 A71-34298

Optimal bar design for tangential load transmission into sheet, determining stress distribution
17 p2821 A71-34591

SHELL STABILITY
Nonlinear viscoelastic material with stress dependent properties, solving for thick walled shells deformation under internal pressure
01 p0168 A71-10423

Stability of longitudinally hinged isotropic cylindrical shells under external pressure, using finite difference method
01 p0170 A71-10645

Cylindrical shell stability under combined axial compression and heating, using finite difference method
01 p0170 A71-10646

Buckling in fiber reinforced plastic thin walled shell structures, discussing structural stability problems and methods for prevention of buckling
01 p0172 A71-10698

Discrete search method for stiffened cylindrical shell stability under combined uniform axial compression and lateral pressure loads
01 p0174 A71-10963

Load deflection relations for rigid plastic cylindrical shells beyond incipient collapse load
01 p0175 A71-11011

Reinforced cylindrical shells under external pressure, investigating longitudinal tensile stresses effect on stability
01 p0175 A71-11040

Elastic shell filled with ideal fluid, analyzing dynamic stability under periodic impulses
01 p0176 A71-11049

Homogeneous isotropic cylindrical shell stability, considering reinforcement by nonlinear dense symmetrical system of elastic threads under tension
01 p0176 A71-11124

Nonlinear stability of shallow spherical shells under concentrated loads, showing critical loads dependence on shallowness
01 p0177 A71-11239

Simply supported cylindrical shell buckling under linearly varying lateral pressure
01 p0178 A71-11399

Thin shells of revolution local stability during nonuniform stressed state development under heating
02 p0324 A71-11755

Spherical shell plastic deformations under internal pressure, discussing stress instability condition
02 p0325 A71-12123

Temperature fields without induced stress, considering relation between thermal and dislocation stresses in shells of revolution
02 p0325 A71-12283

Stability loss of cylindrical and spherical shells under heating and external force, determining critical temperature and loads
02 p0325 A71-12286

Stability loss of circular cylindrical shells under bending beyond elastic limit
02 p0325 A71-12287

Cylindrical shell deflection under concentrated radial force expressed in terms of algebraic polynomials
02 p0326 A71-12295

Prebuckling deformations influence on circular cylindrical shell buckling under external pressure, applying Galerkin method to Donnell equations
02 p0329 A71-12602

Continuous elastic filler effects on axisymmetric stability loss in cylindrical shell under subcritical compression loads, using three dimensional linearized equations
02 p0329 A71-12665

Skin friction effect on cylindrical shell critical loads at various supersonic gas flow velocities, noting application to flutter analysis
02 p0329 A71-12666

Doubly curved thin shallow shells nonlinear stability, using piecewise linearization for postbuckling load-displacement curves
03 p0501 A71-13073

Spherical shells deformation subjected at elevated temperature to high velocity impact on planar rigid target
03 p0503 A71-13427

Marguerre equations for deflection and buckling of partially and fully loaded spherical caps, noting inaccuracy of finite difference approximation
03 p0503 A71-13428

Postbuckling behavior of open cylindrical shells under uniform axial compression loads, solving finite difference equations by Newton-Raphson method
03 p0505 A71-13539

Axisymmetrically loaded shells of revolution made of work hardening materials, determining inelastic finite deformations and buckling loads by incremental variational method
03 p0505 A71-13543

Open cylindrical shells with end eccentricity or initial deflection imperfections, investigating buckling under axial compression by Newton-Raphson method
03 p0505 A71-13544

Thin walled circular cylindrical shells creep buckling under radial pressure and thermal gradients
03 p0512 A71-14152

Thin walled cylindrical shells with filler, determining stability under axial compression by computer calculation
03 p0514 A71-14360

Cylindrical shells axisymmetric nonlinear strain discontinuities propagation, using Timoshenko equations
03 p0515 A71-14380

Thin spherical shell with circular cutout under HF axisymmetric excitation by concentrated radial force
04 p0667 A71-15181

Cylindrical cantilever shells/silos/ under wind loads by semimembrane analysis, discussing cross section distortion and stress prediction
04 p0667 A71-15182

Eccentrically stiffened thin spherical shell instability under uniform external pressure
04 p0669 A71-15199

Free transverse oscillations of closed prismatic shell of flexible rectangular panels filled with compressible inviscid liquid
04 p0573 A71-15564

Thin circular cylindrical shell stability subjected to axisymmetric thermal pulse, describing buckling process by mathematical model
05 p0820 A71-16186

Orthotropic cylindrical shell stability under variable compression loads, considering glass fiber reinforced plastic tube
05 p0822 A71-16368

Low shear rigidity effect on stability of glass fiber reinforced plastic cylindrical shells under loads and elevated temperature
05 p0822 A71-16369

Computerized nonlinear collapse analysis of elliptical cylinders and cones under axial compression
05 p0823 A71-16555

Local axisymmetric dimple imperfection effects on buckling load of circular cylindrical shell under axial compression
05 p0823 A71-16557

Local buckling tests on machined integrally ring stiffened cylindrical shells
05 p0823 A71-16559

Axisymmetric stability of fluid filled cylindrical shells under rapid axial compression
05 p0824 A71-16592

Isotropic elastic spherical shells stability under combined axial compression and local loads
05 p0824 A71-16593

Staticogeometrical relations of thin torus shaped shell and closed curvilinear rods
05 p0824 A71-16594

End face frame stiffness effects on cylindrical shell critical pressure
06 p0982 A71-17352

Cylindrical shells with large arbitrary defects, deriving stability equations from shell theory
06 p0982 A71-17353

Stability loss of cylindrical shell at upper bound of buckling load under axial compression
06 p0983 A71-17365

Shells with arbitrary moment initial stressed state, calculating stability by energy method
06 p0986 A71-17758

Stainless steel shells under uniform external pressure and constrained deformation, noting critical load increase
06 p0986 A71-17760

Local distributed load effects on bending of fiberglass reinforced plastic laminar orthotropic cylindrical shell
06 p0986 A71-17761

Equilibrium stability of orthotropic cylindrical shell under longitudinal compression, discussing critical stresses
06 p0986 A71-17762

Axisymmetric vibration frequencies, form shapes and apparent masses for vertical fluid filled coaxial cylindrical shells resting on shallow spherical shell
06 p0986 A71-17763

Shallow spherical shells stability under constant external pressure
06 p0987 A71-17768

Axisymmetric stability loss of thin long cylindrical shell with elastic filler under uniformly distributed compressive forces over shell ends
06 p0987 A71-17770

Limiting analysis for upper estimate of carrying capacity of shell of revolution under load concentrated at center, evaluating stability loss
06 p0987 A71-17771

Closed cylindrical shells behavior under static loads, determining stability
06 p0988 A71-17775

Cylindrical shells buckling under subcritical loads, considering internal and external hydrostatic pressure and axial compression
06 p0988 A71-17779

Plates and shells stability under plastic deformations at subcritical strains, using three dimensional linearized equations
06 p0989 A71-17787

Elastic cylindrical shells stability under dynamic load consisting of conservative forces and normal compression
06 p0990 A71-17789

Acceleration inequalities of dynamically loaded elastoplastic shells, using permissible stress and displacement velocity fields
06 p0990 A71-17790

Cylindrical shell stability under nonuniform loading, solving infinite homogeneous algebraic equations system by Bunnov-Galerkin method
06 p0990 A71-17791

Cylindrical sandwich shells with multiple isotropic load carrying and transversely compressible filler layers, deriving local stability equations
06 p0990 A71-17793

Circular cylindrical shell stability under uniform tension, taking into account support flexibility and temperature difference
06 p0990 A71-17794

Cylindrical structure longitudinal stress wave propagation characteristics, analyzing wave induced structural instability and destruction process
06 p0991 A71-17801

Local imperfection and stress effects on cylindrical shell stability under various single and combined loads
06 p0991 A71-17803

Cylindrical shell compression stability in presence of creep, determining initial surface dent effects
06 p0992 A71-17805

Eccentrically reinforced cylindrical shells stability equations under axisymmetric loading
06 p0993 A71-17813

Thin imperfect cylindrical shell stability, considering statistical analysis of initial irregularities
06 p0993 A71-17815

Rib reinforced cylindrical shell stability under annular and axial stresses, determining eigenvalue of homogeneous integral equation
06 p0993 A71-17816

Eccentrically reinforced cylindrical shell stability, considering numerical analysis of structurally orthotropic shell parameters
06 p0993 A71-17817

Smooth cylindrical shell stability, considering internal pressure effect on critical axial stresses
06 p0993 A71-17819

Closed circular cylindrical shell stability and buckling during axial compression, using energy method in geometrically nonlinear formulation

06 p0994 A71-17824

Anisotropic fiberglass reinforced plastic shell stability under short term and prolonged loading, using geometrically nonlinear formulation and Galerkin method

06 p0994 A71-17825

Rigid plastic shells carrying capacity by kinematic method based on linear programming

06 p0996 A71-17839

Elastic and viscoelastic multilayer reinforced circular cylindrical shells stability, determining transverse shear stress role

06 p0996 A71-17841

Elastoplastic conical shells strain under longitudinal impact by large rigid body, analyzing plastic bending

06 p0996 A71-17842

Cylindrical shell stability under critical dynamic radial pressure, discussing geometrical and mechanical parameters and loading law

06 p0997 A71-17847

Cylindrical shell stability under arbitrary external pressure, discussing forces and displacements of precritical stressed state

06 p0997 A71-17848

Circular cylindrical shell stability with ribs of variable cross sections, using method based on semimomentless theory

06 p0997 A71-17850

Axisymmetric deformed state of three layer circular conical shell with rigidly clamped edges, obtaining equilibrium equations by Bubnov-Galerkin method

06 p0997 A71-17851

Reinforced zero moment minimum weight shells strength analysis and optimal design algorithms, using discrete calculation scheme

06 p0998 A71-17854

Multilayer plates and shells, considering bending, stability, boundary layer stress state, rigid filters theory and local strength

06 p0998 A71-17857

Complex shells strength analysis using limiting equilibrium theory and mathematical programming

06 p0998 A71-17859

Thin walled flexible shell theory and equilibrium under large deformation

06 p0999 A71-17862

Numerical algorithms of elastic stability solutions for thin walled axisymmetrically loaded shells of revolution with finite difference schemes

06 p0999 A71-17864

Deformation theory of dynamic bending, buckling and stability of plates and shells beyond elastic limit

06 p0999 A71-17865

Stress nonuniformity and initial imperfection influence on cylindrical shell stability

06 p0999 A71-17868

Stability of rib stiffened and anisotropic shells, including composite and elastic filler structures

06 p1000 A71-17871

Axially compressed ring and stringer stiffened cylindrical shells minimum weight design, considering configuration instability

[AIAA PAPER 71-147]

06 p1003 A71-18590

Plastic deformation of circular plates and shells from material with different yield and strengthening moduli in tension and compression

07 p1211 A71-19164

Thin spherical roller supported domes stability and axisymmetric deformation under apex point loads, investigating plastic buckling and inelastic strain effects

07 p1216 A71-20222

Conical shell stability under dynamic longitudinal compression

07 p1218 A71-20472

First passage time for snap-through of shallow cylindrical shell subject to stationary random loading, considering numerical solution by Pontryagin-Vitt equation

08 p1369 A71-20809

Eccentricity and clamping effects on stability and critical pressure of ring-reinforced cylindrical shells under internal pressure

08 p1369 A71-21122

Energy dissipation in free oscillations of multilayer shells consisting of alternating rigid elastic layers and soft fillers, deriving equations of motion

08 p1369 A71-21123

Stability analysis of cylindrical shells hinged over ends under critical destabilizing axisymmetric radial displacements

08 p1373 A71-21946

Shells of revolution under combined thermal and mechanical loading, presenting analytical basis of BOSOR 3 digital stress analysis program

09 p1533 A71-22079

Circular cylindrical shell initial geometrical imperfections effect on stability under nonuniform composite loading

09 p1537 A71-22518

Reinforced shells of revolution carrying capacity upper limit subjected to internal adiabatic ideal gas flow

09 p1538 A71-22632

Stability characteristics of glass fiber reinforced plastic orthotropic cylindrical shell with elastic filler under torsion

09 p1539 A71-22821

Thin cylindrical shell deformation under concentrated transverse loads applied through rigid boss, determining displacement variations as function of applied loads and edge constraints

09 p1543 A71-23659

Thin spherical shell under uniform normal pressure using dynamic stability criterion and energy method for asymptotic nonlinear shell equations

10 p1685 A71-23937

Elastic cylindrical shells oscillations and stability in inviscid incompressible liquid flow, reducing problem to integro-differential equation by Fourier integral transformation

10 p1688 A71-24357

Dynamic deformation of cylindrical shells by elastic body impact, using sequence boundary value solutions in plate theory

10 p1689 A71-24561

Critical load and elastic base one-sided contact effects on cylindrical shell stability under uniform external pressure, using nonlinear programming

10 p1689 A71-24563

Boundary value problem concerning stability and oscillations of shells of revolution through reduction to Cauchy problem based on direct integration of equilibrium equations

10 p1690 A71-24569

Shallow spherical shell thermal stability, investigating factors affecting Galerkin method validity

10 p1690 A71-24574

In-plane boundary conditions influence on clamped conical shells buckling under external pressure, using displacement method based on Donnell stability equations

11 p1841 A71-25158

Linearly elastic cylindrical shells dynamic stability under combined axial and radial stochastic excitations, using Liapunov analysis

[AIAA PAPER 71-333]

11 p1842 A71-25312

High precision finite element for static analysis of loaded thin elastic shells of revolution including shear deformations

[AIAA PAPER 71-360]

11 p1844 A71-25339

Digital computerization for cylindrical shells post-buckling stability analysis, discussing FORMAC and REDUCE formula manipulation systems

[AIAA PAPER 71-363]

11 p1845 A71-25341

Dynamic response of rotationally symmetric open-ended thin shells of revolution under transient impulsive and thermal loadings, using FORTRAN 4 finite difference program

11 p1847 A71-25466

Optimum buckling load of cylindrical shells under lateral pressure using Rayleigh-Ritz method

11 p1848 A71-25484

Prestress vibration hardening of shells of revolution for circumferential 0 and 1 wave number, using VALORS and BALORS programs

11 p1848 A71-25486

Orthotropic conical shell subjected to torsion, using Ritz approximate energy method for linear stability problem solution

11 p1848 A71-25618

Buckling load scatter reduction in axially compressed thin walled circular shells as function of manufacturing accuracy

[DFVLR-SONDDR-92]

12 p1974 A71-26869

Frequency equation of flexural vibration of fluid filled circular cylindrical shells, using linear elasticity

12 p1974 A71-26928

Soviet book on spherical bottoms weakened by openings covering shell stress/strain, elastic-plastic deformations, reinforcing elements and composite materials

12 p1977 A71-27293

Coupled thermoelasticity, bending and stability of thin walled shells and plates of oriented fiberglass reinforced plastics with low shear rigidity, using Timoshenko theory

12 p1978 A71-27345

Thermal stress analysis of hinged thin circular cylindrical shells of variable thickness by computerized discrete orthogonalization method

12 p1979 A71-27357

Long circular cylindrical shell stability under action of bending moments at end face, deriving neutral equilibrium equations

12 p1981 A71-27495

Forced vibrations of circular cylindrical shell under random normal load and internal pressure, noting stability of transversely pressurized flexible vs rigid structures

13 p2150 A71-28140

Static problems of shells of revolution under local loads, solving by stable numerical process

13 p2152 A71-28276

Friction forces between expansion die sectors and blank, describing effect on closed contour shell stress-strain state and shaping process

13 p2074 A71-28939

Unloading effects on elastoplastic stability of shells, using method based on successive approximations

13 p2156 A71-29073

Biaxial plastic extension stability of anisotropic sheets and cylindrical shells, using Hill plasticity theory of orthotropic materials

13 p2156 A71-29074

Stability loss, critical load and wave numbers for smooth conical and cylindrical shells of fiberglass reinforced plastics under uniform axial compression

13 p2157 A71-29181

Critical stress and stability analysis of cylindrical shell with initial indentation of length comparable to radius under axial compression

14 p2321 A71-29536

Axisymmetrical snap buckling of clamped shallow spherical shell with initial deformation under external pressure, using energy method

14 p2322 A71-29689

Nonlinear stability of saddle-like deformed circular and square flat plates and shallow shells under transverse loadings

14 p2322 A71-29692

Clamped and hinged spherical and paraboloidal shell caps elastic stability tests under external pressure loading, determining critical pressure

14 p2323 A71-29846

Heavy hinged nonshallow circular arches stability during buckling sideways with bifurcations in critical load deflection curves

14 p2324 A71-29885

Radial free vibration frequency of pressurized orthotropic shells with bending terms

14 p2325 A71-29886

Soviet book on stability of thin walled reinforced and multilayer shells with various designs and boundary conditions

14 p2325 A71-29939

Critical loads and stability loss equations near edge of thin convex clamped elliptical shell of revolution under uniform external compression loads

14 p2325 A71-30024

Soviet book on glass-reinforced plastic plates and shells covering engineering methods for anisotropic plates and shells stability and stress analysis

14 p2327 A71-30245

Parametric differentiation technique for axisymmetric stability of spherical shells, using Reissner nonlinear differential equations

14 p2329 A71-30506

Simply supported nearly circular cylindrical shell, calculating nonlinear damped dynamic response due to exponentially decaying radial pressure

14 p2330 A71-30688

Reinforced toroidal shells stability under critical local loads, edge moment and heating, using finite difference method

14 p2332 A71-30847

Load carrying capacity of edge clamped spherical shells of revolution with Tresca yield condition under uniform internal pressure

14 p2332 A71-30848

Strength analysis of shells of revolution and plates under axisymmetric loads for rigidly plastic material with Tresca yield condition

14 p2332 A71-30849

Stability and stress analysis of elastic finned circular cylindrical shells reinforced by stringers

14 p2332 A71-30852

Soviet papers on three dimensional structures covering strength and stability of compound curvature shells, bodies of revolution and multilayer plates

14 p2332 A71-30888

Momentless axisymmetric stress state and stability loss in thin convex shells of revolution in linear approximation

14 p2333 A71-30891

Stability of structurally orthotropic stringer reinforced cylindrical shell closed by spherical or plane bottoms under uniform external pressure

14 p2333 A71-30892

Equilibrium stability of rods, shells and plates during creep due to applied load

14 p2333 A71-30893

Linear stability equations derivation from vector equilibrium conditions in engineering shell theory

15 p2502 A71-31160

Snap buckling instability of shallow shell type structures subject to random transverse load

15 p2502 A71-31417

German monograph on iterative procedure for sectional parameters of shells of revolution with meridian form under peripheral loads described by harmonic functions

15 p2509 A71-32374

Asymptotic eigenvalue density estimates for edge-hinged thin elastic rectangular shell, determining shell stability linear equation solution conditions

16 p2647 A71-32937

Aeroelastic stability of flat plates and shells, considering panel flutter

16 p2648 A71-32987

Thin plates and shallow shells stability, investigating weak solutions of wall displacement differential equations

16 p2649 A71-32993

Buckling and postbuckling loads of initially imperfect orthotropic cylindrical shells under axial compression and internal pressure, using potential energy principle

16 p2651 A71-33025

Elements movement and stability loss of circular cylindrical shells during snap, using Gauss least constraint principle

16 p2651 A71-33027

Clamped shallow spherical shells buckling and postbuckling behavior under axisymmetric ring loads, examining effect of load location and shell geometry variations

[ASME PAPER 71-APM-9] 16 p2656 A71-33216

Stability loss of circular cylindrical shell with stepped wall thickness of central reinforcing sleeve under annular loading, determining critical load by thin shell theory

16 p2657 A71-33600

Stability and critical load of constant thickness cylindrical sandwich hinge supported shell under annular loading, using variational method

16 p2657 A71-33601

Critical loads and stability of longitudinally compressed circular cylindrical shells with eccentric ring and stringer reinforcement

16 p2657 A71-33603

Closed circular cylindrical shell stability under dynamic axial compressive loading with static internal pressure

16 p2658 A71-33719

Moment state stability of elastic hinged cylindrical shell and closed ring under pressure and concentrated load, using nonlinear equilibrium theory

16 p2660 A71-34114

Strain energy and stability of nonlinear plate and shell bending under Love-Kirchhoff hypothesis, using three dimensional elasticity theory

17 p2815 A71-34296

Rotating cylindrical shell symmetrical deformation under external load, obtaining three dimensional axisymmetric problem solution in elastic theory

17 p2816 A71-34330

Circular cylindrical shell stability under combined axial tensile (compressive) loads and torque, verifying theory by experiments on stainless steel shell

17 p2817 A71-34336

Finite oval cylindrical shells with clamped boundaries, investigating stability and elastic buckling under axial compression for comparison with circular cylindrical shells

[SESA PAPER 1832] 17 p2819 A71-34536

Metal-reinforced glass plastic composite conical shell with positive Gaussian curvature, estimating reliability and stability based on static tests

17 p2830 A71-35316

Cylindrical shell with continuous filler, calculating stability and axisymmetric buckling in axial compression

17 p2830 A71-35321

Isotropic circular cylindrical shell stability with longitudinal hinges under uniform external pressure, determining critical load

17 p2831 A71-35322

Toroidal shell stability analysis for asymmetric buckling based on small deflection theory linearized relations, deriving upper critical pressure by Bubnov-Galerkin method

17 p2831 A71-35323

Cantilevered elastic cylindrical shell stability during bending by transverse load uniformly distributed over entire surface or applied at end

17 p2833 A71-35615

Plastic deformation of circular plates and shells of material with different yield and hardening moduli in tension and compression from creep theory relationships

17 p2834 A71-35660

Circular cylindrical shells creep buckling in pure bending, deriving formula for critical time

18 p2980 A71-36674

Rib reinforced cylindrical shells deformation under local load, examining stress-strain distribution

18 p2981 A71-36719

Elastic buckling load of cylindrical shells with dimple imperfections under external pressure, applying perturbation expansion to Karman-Donnell equations

18 p2982 A71-36839

Elastic stability and buckling modes of cylindrical shell under critical gravity load, using double Fourier series and linear theory

18 p2983 A71-36847

Cylindrical shell stability under radial pressure or axial compression from load-distributing filler model solution

20 p3308 A71-39166

Buckling load reduction for axially compression loaded geometrically perfect cylindrical shells by wall temperature gradients induced partial yielding

21 p3469 A71-41006

Zero moment theory application to stability analysis of rib-reinforced cylindrical shell under external pressure

21 p3472 A71-41149

Frequency and buckling stability eigenvalue evaluation for anisotropic circular cylindrical shells under nonuniform lateral prestress

22 p3615 A71-42210

Stability formula for critical pressure in cylindrical shells orthotropically reinforced by closely spaced eccentric ribs

22 p3616 A71-42487

Oval cross sectioned cylindrical shells, deriving free oscillation solution

23 p3775 A71-43310

Plastic buckling stability of hinged arches for perfect and imperfect structures with linear work hardening stress-strain behavior

23 p3776 A71-43372

Soviet book on elastoplastic deformations of plates and cylindrical shells made of low strain hardening materials, covering strength and stability calculations

23 p3779 A71-44186

Ribbed cylindrical shells modeling method for stress-strain state and stability

23 p3780 A71-44219

Longitudinal rib reinforced cylindrical shell under axial compression loads, determining equilibrium stability with approximation of transcendental equations

23 p3780 A71-44222

Power series analysis of circular cylindrical shells stability under biaxial compression, expressing critical loadings

24 p3878 A71-44612

Stability and critical loads of reinforced geometrically nonlinear cylindrical shells, using strain energy method

24 p3882 A71-44842

Buckling stability and critical loads of thin elastic cylindrical shells with hollow core in axial compression

24 p3882 A71-44844

Stability under uniform external pressure of closed spherical shell with axisymmetric initial imperfection in equatorial region, using finite difference technique

24 p3883 A71-44853

Circular cylindrical shell critical stress level leading to stability loss during high speed clogging process based on kinetic energy method

24 p3884 A71-44897

SHELL THEORY

Shells with positive Gaussian curvature, deriving p analytic functions for zero bending stress state and infinitesimal deflections of middle surface

01 p0168 A71-10415

Shell theory of anisotropic shells and plates with low shear rigidity, using Timoshenko-type model

01 p0169 A71-10497

Rib reinforced shells linear theory, deriving equilibrium equations with allowance for temperature terms

01 p0170 A71-10644

Finite length elastic cylindrical shell deformation approximate solution by Legendre polynomials

01 p0173 A71-10942

Kirchoff triangular shell element design via linear shell theory

01 p0174 A71-10967

Comparative shallow shell finite element analyses using different stiffness matrices

01 p0175 A71-11012

Transversely isotropic spherical shell of small shear modulus material, deriving stress concentration at circular holes

01 p0175 A71-11038

Elastic thin walled shells of variable thickness with zero Gaussian curvature, deriving stress strain state with allowance for elastoplasticity

01 p0176 A71-11041

Numerical method for stress distribution around openings in shells, using orthogonal coordinate system

02 p0321 A71-11649

Stress-strain state variability associated with optimal local heating of shallow shells of revolution

02 p0322 A71-11727

Thin circular cylindrical perforated shell, analyzing stress distribution around circular hole by coordinate transformation and partial differential equations

02 p0326 A71-12346

German monograph on displacement elimination method in viscoelastic shell theory covering shearing loads derivation from stress functions

02 p0327 A71-12398

Zero bending moment shells of revolution under concentrated load, using boundary value problem for p analytic functions

02 p0328 A71-12539

Perforated thick shallow spherical shell, solving boundary value problem for external loads

02 p0329 A71-12671

General nonlinear finite deformation shell and strain membrane theories in terms of reference state quantities by direct physical derivation

03 p0502 A71-13353

Laminated cylindrical shells of orthotropic layers, deriving linear theory and equations of motion

03 p0504 A71-13430

Shell of revolution bending deformation, assessing Trefftz approximation error

03 p0506 A71-13597

Variational methods applied to shells transition into plastic state during cylindrical bending, giving critical load formulas

03 p0509 A71-13873

Shells and plate disk structures elastoplasticity analysis problems, considering limit loads, large deflections, boundary state theory, optical design, etc

03 p0510 A71-13944

Spherical shell segments stresses and displacement due to arbitrary axisymmetric surface tractions and edge boundary conditions, using axisymmetric elasticity solutions

[ASME PAPER 70-WA/APM-27]

03 p0512 A71-14159

Laminated circular cylindrical shells under axisymmetric mechanical and thermal loads, including transverse isotropy and shear deformation effects in stress analysis theory

[ASME PAPER 70-WA/APM-53]

03 p0513 A71-14170

Geometrically nonlinear shell dynamics, basing equations of motion and compatibility on variational principles

03 p0514 A71-14346

Computer program TENSOR for numerical solutions of shell theory

03 p0515 A71-14396

Thin shells of revolution formed of closed box sections, using numerical integration and stiffness matrix for solution

[ASME PAPER 70-PVP-12] 04 p0665 A71-14770

Soviet book on perforated plates and shells covering strength, rigidity, lattice tension and bending, stress and strain states, boundary value problems, etc

04 p0671 A71-15398

Novozhilov complex transformation method extended to Timoshenko theory of elastic shells constructed with allowance for transverse shear deformation

05 p0820 A71-16187

Anisotropic shell theory with allowance for transverse stresses, using triorthogonal curvilinear coordinates

05 p0821 A71-16367

Semiinfinite simply supported cylindrical shell transient response due to axisymmetrically engulfing step pressure wave, investigating moving load critical velocity

[AIAA PAPER 70-18]

05 p0823 A71-16556

Shell shape without bending stresses due to external load

05 p0828 A71-16891

Thin shallow shell theory boundary value problem, discussing reduction to Fredholm integral equations system

05 p0828 A71-16893

Cylindrical shells with large arbitrary defects, deriving stability equations from shell theory

06 p0982 A71-17353

Thickness variation law for plates and shells with minimal elastic strain energy

06 p0982 A71-17358

Boundary conditions of line of symmetry and antisymmetry types for stress-strain state of halved shells

06 p0984 A71-17666

Shell and plate theory - Conference, Dnepropetrovsk, U.S.S.R., September 1969

06 p0985 A71-17751

Elastic rib-reinforced flexible shallow shells theory, deriving variational equations for multicontact problem

06 p0985 A71-17752

Reinforced plate and shell theory, taking into account ribs arbitrary direction and contour profile

06 p0985 A71-17753

Elastic shell dynamics under initial and boundary conditions, developing variational principle algorithm

06 p0986 A71-17756

Anisotropic shells theory, discussing displacement components

06 p0986 A71-17759

Applicability limits of equations of theory of three-layer plates and shells of axisymmetric structure

06 p0987 A71-17766

Stress-strain state of isotropic three-layer plates and shells with rigid and light weight fillers, noting weakening by curvilinear holes

06 p0987 A71-17769

Plates and shells under concentrated loads, determining stress-strain state

06 p0988 A71-17773

Thin shallow shell theory, describing asymptotic method for nonlinear equations integration

06 p0988 A71-17776

Iteration method application to shell design nonlinear differential equations solution 06 p0988 A71-17777

Geometrically nonlinear thin nonshallow shells of revolution, deriving axisymmetrical elastic deformation equations 06 p0988 A71-17780

Equilibrium equations for flexible plates and shells with nonlinear terms in one dimensional case 06 p0989 A71-17782

Static and kinematic adaptability of plates and shells under progressive structural failure 06 p0989 A71-17784

Side strain reactions of shells of revolution with meridional ribs, integrating equations by Green function 06 p0989 A71-17785

Cost-optimal zero moment shell geometry, developing digital computer algorithm with dynamic programming 06 p0992 A71-17804

Relation uniaxial stressed state relationship to internal geometry of flexible shell 06 p0993 A71-17814

Variable thickness truncated hollow cone elastic equilibrium, considering asymptotic analysis of axisymmetric problem 06 p0994 A71-17820

Heavy liquid shells of revolution, determining equilibrium form in gravitational and surface tension forces from condition of minimal functional of total free energy 06 p0994 A71-17827

Elastic spherical shell three dimensional stress-strain state asymptotic behavior near concentrated force as function of parameter characterizing relative thickness and curvature 06 p0995 A71-17830

Shells of revolution of different forms, discussing numerical solution of inverse problem 06 p0995 A71-17832

Axisymmetric isotropic shells of revolution, using matrix-operator notation for differential equations systems solution 06 p0995 A71-17835

Reissner shell theory equations for arbitrary internal and surface loads 06 p0996 A71-17836

Solution behavior of zero-curvature shells under concentrated loads with increasing distance from application point 06 p0996 A71-17843

Thin walled two layer bimetallic shells of revolution under large deformation, analyzing equilibrium by zero moment theory 06 p0998 A71-17856

Multilayer plates and shells, considering bending, stability, boundary layer stress state, rigid filters theory and local strength 06 p0998 A71-17857

Complex shells strength analysis using limiting equilibrium theory and mathematical programming 06 p0998 A71-17859

General linear shell theory, considering elastic processes in structural design 06 p0998 A71-17860

Thin walled flexible shell theory and equilibrium under large deformation 06 p0999 A71-17862

Thermoelasticity, mechanical and thermal processes in deformation of elastic plates and shells 06 p0999 A71-17866

Static computations of thin walled shells and honeycombs, examining variational, matrix, finite element, initial function, small parameter and plate bending methods 06 p0999 A71-17867

Vibration and wave analysis in dynamic deformation of elastic shells and plates with environmental allowance 06 p1000 A71-17870

Contact theory of shells under local loads and reinforcing rib interactions 06 p1000 A71-17872

Prismatic shells vibration, buckling and stress analysis, applying computer solutions to complex bodies of revolution [ALAA PAPER 71-112] 06 p1003 A71-18562

Flat triangular elements for shell analysis, describing membrane and bending displacements by identical quadratic polynomials [ALAA PAPER 71-114] 06 p1003 A71-18564

Soviet book on computer calculation of three-layer elastic plates and shells covering programs, initial equations, input number language, numerical solution, etc 07 p1210 A71-19047

Technical equations of shells of slowly varying curvature with transverse shear deformation and normal stress 07 p1211 A71-19252

Resistive network computation in plate and shell dynamics, exemplifying skew plate under central concentrated load 08 p1370 A71-21303

Momentless theory of anisotropic shells, using three dimensional elasticity theory 08 p1373 A71-21867

Tensor elasticity relations in linear theory of thin elastic shells in Kirchhoff-Love range 08 p1373 A71-21868

Shallow shell triangular finite element method application to cylindrical shell theory 09 p1534 A71-22106

Flexible elastoplastic shallow shell theory, using mixed variational principle for flexure velocity and stress function 09 p1535 A71-22179

Positive curvature type shallow shells computation for optimum efficiency and minimum material expenditure by dimensionless modeling method 09 p1537 A71-22517

Physically nonlinear theory of isotropic elastic shells and plates eliminating Love-Kirchhoff hypothesis 09 p1543 A71-23613

Thin spherical shell under uniform normal pressure using dynamic stability criterion and energy method for asymptotic nonlinear shell equations 10 p1685 A71-23937

Circular cylindrical shells stress-strain state in elastic medium, obtaining criteria for boundary conditions limiting values for linear theory applicability 10 p1688 A71-24356

Axisymmetric snap-through of shallow clamped spherical caps under uniform pressure, revealing existence of higher modes as isolated closed loops from approximate solution 10 p1689 A71-24518

German monograph on circular cylindrical shells theory comparative studies covering energy and equilibrium methods, tensor representation, reinforced shells, etc 10 p1692 A71-24912

German monograph on basic equations for isotropic elastic homogeneous thin shell subjected to infinitesimal displacements, determining work of form change 10 p1692 A71-25037

German monograph on nonnumerical transformation of tensor equations by computers, applying to shallow shell theory 10 p1692 A71-25038

Duality in doubly curved shells analysis by finite element method, applying Kirchhoff-Love shells boundary conditions and energy variational principle 10 p1693 A71-25049

Heterogeneous orthotropic cylindrical shells, calculating free natural vibration frequency spectra from refined equations of motion in Love and Donnell type theories 11 p1841 A71-25184

Natural vibration analysis method for circular cylindrical shell based on three dimensional theory of elasticity and energy principle, discussing boundary conditions effect 11 p1852 A71-26405

Error estimate for solution of approximately linear elastic boundary value problems of shells with no strain energy functional, discussing stress-strain relations 12 p1974 A71-26943

Transversally isotropic spherical shell with constant thickness, calculating equation system for equilibrium 12 p1975 A71-27105

Large elastic deformations of incompressible materials shells with inclusion of transverse normal strain, considering thickness change at boundaries 12 p1976 A71-27159

Oscillation theorem for natural vibrations of thin shells of revolution, considering boundary value problem eigenvalues 12 p1977 A71-27304

Static and dynamic stress analysis and limiting loads of plastic shells and plates with temperature field in structural element, using deformation theory 12 p1979 A71-27350

Shells of revolution plastic deformation problem, applying rigid viscoplastic strain hardenable material model 12 p1984 A71-27686

Reduced order numerical integration technique for plate and shell problems solution 13 p2147 A71-27791

Forced axisymmetric vibrations of composite cylindrical shell with spherical bottom, obtaining influence coefficients and inhomogeneous boundary conditions 13 p2150 A71-28141

Curvature effects on shallow shell free vibration frequencies, solving linear eigenvalue problem 14 p2325 A71-30062

Incompressible plastic shells behavior, discussing deformation, energy dissipation rate, equilibrium equations and boundary conditions 14 p2328 A71-30380

Closed membrane shell of revolution finite creep due to uniform pressure, applying large deformation incremental theory 14 p2328 A71-30396

Thermoelastic shells and plates approximate linear theory, detailing uniqueness theorem for initial mixed boundary value problem 14 p2329 A71-30446

Generalized elastic thin shell nonlinear theory, deriving equilibrium equations and boundary conditions from shape dependent energy considerations 14 p2329 A71-30448

Closed circular cylindrical shell nonlinear problem solvability extended to anisotropic sandwich shell, using mean deflection theory 14 p2332 A71-30866

Linear stability equations derivation from vector equilibrium conditions in engineering shell theory 15 p2502 A71-31160

Thin conical shell under longitudinal impact, deriving theory for transverse and rotary inertias and transverse shear deformation effects 15 p2506 A71-32017

German monograph on thermally stressed shear soft shells with finite deformation covering tensor analysis, thermoelasticity, temperature fields and two dimensional bodies 15 p2509 A71-32305

Linearized shell theory, proposing improvement of Marguerre-Vlasov shallow shell equations in terms of invariant displacement and stress functions 16 p2649 A71-33000

Cosserat surface static stability, considering construction of direct theories of thin shells 16 p2649 A71-33001

Thin elastic shells Koiter-Sanders mathematical model finite element analysis using Ritz method [ASME PAPER 71-APM-32] 16 p2655 A71-33197

Elastoplasticity shell theory, demonstrating analogy between stresses and strains in three dimensional medium 16 p2660 A71-34067

Nonlinear theory for rotating shallow shells of revolution, deriving edge zone boundary layer solutions for differential equations 16 p2660 A71-34071

Yield surface approximations for thin shell made of material obeying von Mises yield criterion, considering transverse shear effect 16 p2661 A71-34118

Error estimates in thin elastic shell linear theory, modifying three dimensional displacement field 17 p2815 A71-34224

Vlasov theory application to nonshallow shells, suggesting discretization procedure with quadrilateral finite elements for calculation by finite differences 17 p2816 A71-34325

Stress-strain state of circular cylindrical shell hinged at edges under local radial loads 17 p2817 A71-34340

Numerical method for limit analysis of axisymmetric shells of revolution, considering truncated conical shells and pressure vessels with rigid circular plates 17 p2818 A71-34400

Book on asymptotic approximation in three dimensional thin and thick elastic shell theory including interior and Kirchhoff edge zone equations 17 p2822 A71-34770

Anisotropic laminated cylinders under combined axial load, torsion and internal pressure, calculating stresses with Vlasov-Ambartsumyan shell theory 17 p2823 A71-34811

Shell analysis in curvilinear coordinates, obtaining edge effect equation with canonical kinematic unknowns in plane sections law 17 p2830 A71-35314

Small strain theory of shells derived from three dimensional equations of equilibrium and compatibility by asymptotic approach 18 p2982 A71-36840

Natural axisymmetric vibration of thin elastic shell of revolution, deriving eigenvalues convergence to spectrum lower bound by asymptotic method 19 p3154 A71-37097

Edge clamped spherical shell natural vibration frequency determination using Vlasov shell theory equations 19 p3155 A71-37532

Shallow lattice shell equations approximated by generalization of asymptotic theories for lattice-type disks and plates 19 p3158 A71-38151

Edge effect in elastic lattice shells generalized from lattice plates and disks 19 p3158 A71-38152

Inelastic buckling process of axially compressed cylindrical shells with edge constraints, using variational principle and Rayleigh-Ritz method 19 p3158 A71-38182

Transient response of Euler-Bernoulli and Timoshenko beams and cylindrical shells with moving loads 19 p3158 A71-38183

Oscillation theorem for natural vibrations of thin shells of revolution, considering boundary value problem eigenvalues 19 p3159 A71-38264

Partially nonlinear theory of anisotropic shells of uniform thickness, obtaining variational integrals of stress equations of motion 20 p3307 A71-38796

Membrane theory of anisotropic shells, using three dimensional elasticity theory 20 p3308 A71-39366

Tensor elasticity relations in linear theory of thin elastic shells in Kirchhoff-Love range 20 p3308 A71-39367

Asymptotic geometric optics methods application to thin shell theory, reducing transport equation to ordinary differential equation 20 p3310 A71-39865

Axial vibration transmission characteristics of shells of revolution, stressing shell mass and thickness, internal damping and edge restraint effects [ASME PAPER 71-VIBR-7] 21 p3457 A71-40270

Transfer matrix and finite element combination technique for plates and shells vibration analysis [ASME PAPER 71-VIBR-85] 21 p3461 A71-40321

Circular cylindrical shells analysis by Koiter strain energy method for small finite deflections, considering simplifying modifications of energy functionals 21 p3468 A71-40976

Shear deformation theory of axisymmetric cylindrical shells in contact with smooth rigid surfaces 21 p3470 A71-41017

Circular cylindrical shell under longitudinal parametric load, obtaining nonstationary responses with deformation theory 21 p3471 A71-41029

Paraboloidal shells of revolution inextensional vibrations comparison to Sanders theory, using finite element method 21 p3471 A71-41030

Zero moment reinforced prismatic shells of rectangular cross section with arbitrary load distribution 21 p3472 A71-41146

Nonlinear periodically oscillating motions in shell theory, examining buckling characteristics of thin walled structures under dynamic and shock loads action 21 p3473 A71-41152

Natural vibrations of closed reinforced cylindrical shell clamped at end faces 21 p3473 A71-41153

Open simply supported cylindrical shell internal stresses due to initial deformation based on thin elastic shell linear theory 22 p3613 A71-41563

Sound transmission through finite closed shells, considering statistical energy analysis, modal coupling and noise reduction 23 p3704 A71-43213

Plastic shells under finite bending, deriving large deflection theory from nonlinear continuum mechanics by yield criterion Lagrangian formulation 23 p3775 A71-43317

Elastic and inelastic thin shell nonlinear theory derivation by integrating material continuity equations of motion over shell thickness 23 p3775 A71-43318

Axisymmetrical elastic deformation of thin helicoidal shell with rectilinear profile, deriving equilibrium equations and stress-strain relationships 23 p3778 A71-44038

Thin closed circular cylindrical shell under arbitrary loading 23 p3778 A71-44039

Soviet book on computerized finite difference solutions for physically nonlinear plates and shells covering material anisotropy, creep, thermal, radiative and cyclic load effects 23 p3779 A71-44184

Complex configuration shell theory, considering successive approximation method 24 p3876 A71-44403

Rectangular platform nonshallow spherical and elliptical shells, determining momentless stressed state 24 p3877 A71-44404

Partitioning method for Reissner shell theory equations, constructing rod system 24 p3877 A71-44407

Rigidly plastic shell theory Lagrangian formulation for moderately large deflections, defining kinematic and dynamic tensors for field equations 24 p3880 A71-44640

Circular conical shell initial deformation under impulsive load, using Timoshenko theory 24 p3883 A71-44852

Shell of revolution natural vibration spectrum, investigating moment and momentless type systems of differential equations 24 p3886 A71-45342

SHELLS [STRUCTURAL FORMS]

NT ANISOTROPIC SHELLS

NT CIRCULAR SHELLS

NT CONICAL SHELLS

NT CYLINDRICAL SHELLS

NT DOMES [STRUCTURAL FORMS]

NT ELASTIC SHELLS

NT HEMISPHERICAL SHELLS

NT LIQUID FILLED SHELLS

NT METAL SHELLS

NT ORTHOTROPIC SHELLS

NT PERFORATED SHELLS

NT RADOMES

NT REINFORCED SHELLS

NT SPHERICAL CAPS

NT SPHERICAL SHELLS

NT THIN WALLED SHELLS

NT TOROIDAL SHELLS

Elastic waves excitation by pressure wave in shells of revolution, investigating acoustic medium effects on frontal discontinuities intensity 01 p0176 A71-11148

Papers on structural mechanics covering plates and shells buckling and vibration behavior 05 p0819 A71-15977

Fe powder filled tubular shell compression by magnetic fields and pulse sequences 05 p0759 A71-17168

Forced vibrations of three layer plates and shells made from physically nonlinear materials, deriving nonlinear equations with allowance for rigid filler tangential displacement 06 p0991 A71-17797

Nonstationary temperature fields and thermal stresses in plates and shells for discontinuous boundary conditions 06 p0991 A71-17799

Rectangular plates and shallow shells large asymmetric deflection, using computerized finite difference technique 06 p0991 A71-17802

Plate and shell designs, considering thin walled structures optimization for minimum weight, volume and cost vs maximum stresses 06 p0998 A71-17858

Influence coefficients closed forms for one and two sheet hyperboloids and ellipsoidal and paraboloidal shells under axisymmetrical edge loads 06 p1002 A71-18413

Stress concentration analysis at arbitrarily oriented cracks in shell, noting curvature influence by single integral equations with Cauchy kernel 07 p1217 A71-20458

Elastic collapse analysis of shell structures with variable rectangular grid spacing based on modified finite difference computer program 11 p1844 A71-25338

[AIAA PAPER 71-359]

Stress concentration due to holes and other stress raisers in plates and shells, taking into account transverse shear strains effects 13 p2149 A71-28127

Oriented glass fiber-plastics plates and shells design, noting zero moment stress shells and filament overwrapped metallic pressure vessels 17 p2830 A71-35315

Filament wound shell of revolution optimum configuration, deriving equations for orthotropic filament axes coincidence with principal stress trajectories 17 p2830 A71-35317

Real weight formula for shell fuselages based on theoretical similarity considerations 20 p3178 A71-39411

High precision displacement functions for finite element models of rotational shell and plate bending problems 21 p3470 A71-41019

Shell structure computer analysis capability assessment covering U.S. industrial concerns, government agencies and universities research activities 22 p3516 A71-41864

Approximate periodic Green matrix solution to equilibrium equations in displacements for shell of revolution under linear loads 24 p3881 A71-44826

SHIELDS

NT LUNAR SHELTERS

Bare base shelter/hangar expandable structures for rapid worldwide Tactical Fighter Organization deployment, noting foam and honeycomb fabrication [AIAA PAPER 71-398] 11 p1744 A71-25274

SHIELDING

NT ELECTROMAGNETIC SHIELDING

NT ELECTROSTATIC SHIELDING

NT HEAT SHIELDING

NT MAGNETIC SHIELDING

NT RADIATION SHIELDING

NT RADIO FREQUENCY SHIELDING

NT REENTRY SHIELDING

NT SOLAR RADIATION SHIELDING

NT SPACECRAFT SHIELDING

Ground space facilities protection from lightning and electromagnetic interference 07 p1084 A71-19947

SHIFT

German monograph on beam shift at total reflection covering Goos-Hanchen optical effect, acoustics, quantum mechanics, plasma physics, Brewster law, holography, etc 05 p0780 A71-16122

Fiberglass shift moduli based on twist tests, using ratio of deformations on adjacent faces 15 p2438 A71-31654

SHIFT REGISTERS

Shift register based on coplanar Gunn diodes for pulse processing, considering diodes application to

logic circuits of digital instrumentation and communication systems 01 p0052 A71-10323

Linear feedback function for r-stage feedback shift register resulting in equal length branchless cycles [JPL-TR-32-1511] 03 p0388 A71-13282

Uniform frequency distribution pseudorandom digital sequences, using shift register generator 04 p0560 A71-14745

Computer shift registers synthesis technique based on block buildup, estimating logic elements amount 06 p0871 A71-17521

M-ary linear feedback shift register cycle structure determination, relating behavior to p-ary LFSR 08 p1269 A71-21345

Binary sequences generated by conventional pseudorandom shift register sequences for communication and system identification 18 p2881 A71-36568

Sequential control with fluid logic programmers, considering decimal and binary counters, shift registers, gray code generator and integrated devices 24 p3793 A71-45087

SHILLELAGH MISSILES

Shillelagh missile reliability program development/deployment using part qualification levels and fly-before-buy procurement 12 p1885 A71-26684

SHIMS

U COMPENSATORS

SHIP PROPULSION

U MARINE PROPULSION

SHIPS

NT AIRCRAFT CARRIERS

NT CARGO SHIPS

NT NUCLEAR POWERED SHIPS

NT SATELLITE COMMUNICATIONS SHIPS

Marine traffic control via satellite telemetry, describing merchant and powered fishing fleet distribution and navigation requirements 01 p0125 A71-10978

Radio frequency and microwave radiation hazards determination and elimination aboard naval ships 11 p1723 A71-25290

SHIVERING

Shivering and heat polypnea threshold temperature shift in guinea pigs, considering thermal adaptation under cool environment exposure 03 p0364 A71-14250

Young guinea pigs thermal adaptation tests at different temperatures and environmental conditions, observing threshold temperature shifting for shivering and heat polypnea 18 p2858 A71-36863

Skeletal muscles shivering thermogenesis during cold adaptation, investigating thermoregulation effects on organ and system heat production 18 p2862 A71-36895

Guinea pig thermoregulation of shivering and nonshivering thermogenesis, showing intrahypothalamic noradrenaline injection effects on threshold temperature elevation 18 p2862 A71-36901

SHOCK

Clinical and hemodynamic profile of cardiogenic shock after acute myocardial infarction 04 p0541 A71-15914

SHOCK ABSORBERS

Shock absorber selection for reducing one dimensional oscillations of elastic linearly damped body on supporting base 01 p0127 A71-10633

Steady state motion equations of multiple unit impact damper attached to periodically excited primary system, developing solution for mathematical model 03 p0505 A71-13547

Friction role in impact dampers for elastic systems out of static equilibrium 08 p1372 A71-21619

Parachute decelerator towline energy absorber shock attenuation characteristics, discussing drop test results [AIAA PAPER 70-1202] 11 p1708 A71-25527

Nonlinear elastic suspension springs with symmetrically hardened behavior for shock and vibration isolation of aerospace instruments and controls 17 p2825 A71-34890

Friction role in impact shock absorbers for elastic systems out of static equilibrium and resonance excitation in vibrations, noting harmful effects 17 p2834 A71-35679

Linear multidegree of freedom shock isolation system optimum design, masses, spring and damping coefficients, using mathematical programming [ASME PAPER 71-VIBR-81] 21 p3461 A71-40317

SHOCK DIFFUSERS

U DIFFUSERS

U SHOCK WAVE ATTENUATION

SHOCK DISCONTINUITY

Shock structure in crystalline solids, including dissipative processes, discontinuities, continuum mechanics and lattice dynamics 04 p0664 A71-14662

SHOCK FRONTS

- Photographic study of early vortex formation in flow started by shock diffracting over edge 04 p0586 A71-14702
- Unsteady analogy for hypersonic flows past blunt bodies with shock deformation 08 p1227 A71-21863
- Numerical solution of nonuniform enthalpy mixed axisymmetric gas flow in curvilinear regions with upper boundary and discontinuity using build-up method 10 p1551 A71-24376
- High entropy layer in hypersonic flow with arbitrary large freestream Mach number behind shock 14 p2334 A71-29559
- Slow MHD shock wave profile discontinuity corresponding to conventional gas dynamics isothermal jump 16 p2615 A71-32793
- Collisionless plasma shock front microstructure, examining isomagnetic discontinuity with high spatial resolution probes 19 p3045 A71-37853
- Unsteady analogy for hypersonic flows past blunt bodies with shock deformation 20 p3176 A71-39362
- Normal shock wave propagation in nonuniform gases with arbitrary property gradients based on modified method of infinitesimal contact discontinuities 20 p3212 A71-39482
- Physical model for electric current carrying shock discontinuity driven through nonconducting gas by Lorentz force, investigating uniqueness and stability 22 p3581 A71-41889
- Reflected shock wave interaction with tangential discontinuity curve for supersonic incalculable jets, examining flow instability 23 p3665 A71-44337

SHOCK FRONTS

- Boundary layer thickness measurement behind shock wave front using oscillogram of electrostatic probe current 01 p0078 A71-10160
- Magnetic probes effectiveness study of electron heating behind shock wave front in plasma, measuring electron temperature 02 p0288 A71-11636
- Shock wave front propagation instability in decreasing density medium, applying to stellar structure 02 p0241 A71-12510
- Boundary motion between media during transport phenomena under Stefan conditions, establishing shock front coordinates by Hadamard algorithm 03 p0520 A71-13951
- Solar wind and magnetopause shock front location at 1969 maximum, examining proton parameters from Heos 1 observations 03 p0482 A71-14513
- Laminar and turbulent boundary layer effects on flow velocity and Mach number behind shock front 04 p0567 A71-14664
- Detonation waves Mach configuration, noting frontal structure similarity, lead shock velocity and non-reactive blast wave model 05 p0833 A71-16507
- Multiple wave intersections at marginal detonation front, determining dynamic behavior by soot technique 05 p0833 A71-16508
- Detonation front at Chapman-Jouguet velocity demonstration by numerical transient flow calculations 05 p0834 A71-16510
- Shock structure at Venus and Mars dependence on interplanetary magnetic field orientation from Mariners 4 and 5 data, indicating magnetosheaths existence 05 p0810 A71-16636
- Electron temperature and concentration profiles behind shock front from IR emission and absorption simultaneous measurement, applying method to xenon ionization and recombination processes 06 p0936 A71-17594
- Heliosphere boundary interactions with interstellar medium, considering galactic plasma shock front and boundary radius as function of solar activity level [AIAA PAPER 71-33] 06 p0977 A71-18495
- Gas ionization relaxation phenomena behind strong shock waves, discussing ionization kinetics, radiation transfer effects, relaxation time and radiative heating 07 p1087 A71-19172
- Charged particles interactions with shock fronts or MHD discontinuities, indicating contributory effects to cosmic rays acceleration 07 p1184 A71-19376
- Shock wave interaction with wedge moving at supersonic speed, calculating geometry of regions formed intersecting wavefronts 07 p1014 A71-19741
- Arbitrary strength and shape shock front propagation past ocean surface, calculating diffraction at interface 07 p1094 A71-20614

- Time estimation for plasma front propagation in quartz glass circular pipes without imposition of axial magnetic field 08 p1338 A71-20829
- Low energy cosmic ray intensity increase at propagating interplanetary shock wave front, discussing one dimensional model with particles undergoing convection and diffusion 08 p1356 A71-21630
- Detonation wave of gas in circular cylinder with nonsimultaneous axisymmetric initiation at plane boundary, obtaining solution for small perturbation flow behind detonation front 11 p1853 A71-25152
- Double structured perpendicular magnetoplasma shock waves possessing precursor foot due to ion reflection from resistive shock front 12 p1936 A71-26918
- Shock front detection by Fraunhofer diffraction of narrow parallel Gaussian laser beam 13 p2067 A71-28162
- Three dimensional spatial unsteady hypersonic gas flow about bodies behind strong shock wave front 14 p2169 A71-30182
- Differential equation describing nonstationary reflection of symmetrical shock front from spherical and cylindrical blunt bodies 14 p2170 A71-30216
- Shock front electron number density profile due to ground state precursor atoms photoionization, assuming LTE in heated gas 15 p2392 A71-32120
- Continuous light absorption, emission and ionization relaxation behind shock front in xenon 16 p2613 A71-32890
- Fast argon plasma flow interaction with strong magnetic fields, describing ionization relaxation phenomena behind magnetically reflected shock fronts 16 p2615 A71-32898
- Plane shock front collapse through logarithmic spiral contraction, obtaining pressure and temperature conditions downstream of front 16 p2556 A71-32919
- Ionization and excitation kinetics of Hg in relaxation flow zone behind shock wave front, considering electron impact role in ground state atoms ionization 18 p2951 A71-35980
- Shock wave data for Bamle enstatite in 60-480 kb range, considering Hugoniot elastic limit and phase transition produced shock front 19 p3050 A71-37663
- Charged particles interactions with shock fronts or MHD discontinuities, indicating contributory effects to cosmic rays acceleration 19 p3127 A71-37801
- Collisionless plasma shock front microstructure, examining isomagnetic discontinuity with high spatial resolution probes 19 p3045 A71-37853
- Shock fronts diffraction and reflection with vortices generation at discontinuities, predicting wave shape and strength distribution in two dimensional or axisymmetric situations 21 p3365 A71-40016
- Ionization relaxation phenomena behind strong shock waves, discussing ionization kinetics, radiation transfer effects, relaxation time and radiative heating 21 p3365 A71-40087
- Jump conditions across three dimensional curved shock in radiation gas dynamics, considering radiation pressure number effect 22 p3530 A71-41695
- Interplanetary magnetic shock front location and geometry determination, using interstellar hydrogen density measurements 23 p3720 A71-43133
- Hypersonic shock wave front motion into air at one atmosphere, measuring reflectivity and curvature for comparison with theory 23 p3626 A71-43929
- Spherical projectile hypervelocity impact on compressible fluid, showing viscous effects on velocity and stress distribution behind shock front 24 p3877 A71-44426
- Piezoelectric probe for pressure measurement in plasma behind shock front, discussing design and measuring circuit 24 p3825 A71-44750
- Pressure and flow direction defects behind Mach reflected shock near three shock intersection, considering steady flow theoretical model 24 p3820 A71-44953
- Pressure and mass velocity profiles behind two dimensional shock wave generation on Al flat plates explosive surface 24 p3839 A71-45228

SHOCK HEATING

- Magnetic probes effectiveness study of electron heating behind shock wave front in plasma, measuring electron temperature 02 p0288 A71-11636

- Population inversions in shock induced dissociation of alkali halides in 2000 to 7000 K range, considering rate constants and molecular relaxation 04 p0629 A71-14694
- Radiation effects on compression shock in hot gases, considering hypersonic flow around blunt body during planetary atmosphere entry [DFVLR-SONDDR-60] 04 p0526 A71-15101
- Shock heating effects due to compression and plastic dissipation on basis of finite one dimensional waves in strain rate sensitive elastic viscoplastic solids 05 p0830 A71-17238
- Convective plus radiative shock tube model stagnation point heating rate measurements for planetary entry heating rate in air and Venus gas [AIAA PAPER 69-635] 09 p1382 A71-22092
- Dissociation and particle velocity in shock heated molecular beams of oxygen or hydrogen and argon mixtures, using mass spectroscopic measurements 11 p1765 A71-26282
- Electrostatic probe measurements of charged particles and thermal ionization relaxation in shock heated low density supersonic monatomic gas flows 11 p1766 A71-26286
- Shock heated Ar thermal conductivity measurements by following temperature boundary layer with time resolved interferograms with HF laser stroboscope light source 12 p1986 A71-27578
- Shock wave heated atmospheric model computation for solar chromosphere and corona 14 p2306 A71-29684
- Temperature measurements in shock heated carbon monoxide by IR emission-absorption technique 15 p2411 A71-32554
- Monatomic mercury gas excitation and ionization mechanisms ahead of and behind shock front, establishing electron gas heating kinetics in relaxation zone 16 p2616 A71-32902
- Ionization profiles of shock heated argon with impurities, using microwave and pulsed Langmuir probe measurements 16 p2616 A71-32912
- Spectroscopic measurement of vacuum UV radiation from shock heated krypton plasma, noting self reversed resonance lines indicating cold boundary layer 17 p2787 A71-34589
- Vibrational population inversions due to molecular energy exchanges from rapid heating behind normal shock wave in carbon dioxide-nitrogen-helium mixtures 17 p2728 A71-34883
- Radiative heat transfer in atomic lines through shock heated nonhomogeneous gases by analytical frequency integration, using separability approximation 19 p3162 A71-37407
- Hypervelocity impact melts, considering meteorite crater igneous rocks or glasses associated with shock deformation 19 p3051 A71-37666
- Carbon dioxide IR radiation measurements of duration of constant reflected shock temperature in over-tailored shock tunnel 19 p3041 A71-37893
- Spectral measurements of nitrogen continuum radiation behind incident shocks at high speeds, suggesting free bound neutral atom-electron interactions origin 19 p3172 A71-38718
- Critical atomic carbon to oxygen ratio measurement for incipient soot formation in shock heated acetylene, ethylene and ethane/oxygen/argon mixtures 21 p3436 A71-40859
- Shock wave initiation of hydrogen-oxygen at 1200-1800 K, using UV absorption spectroscopy in shock tube studies 22 p3587 A71-42097
- Shock-heated Mg/MgO particle dispersion, postulating kinetic mechanism consistent with spectrometric observations 24 p3863 A71-44940

SHOCK LAYERS

- Nongray equilibrium radiative heat transfer in viscous radiating shock layer around blunt body entering high temperature nonisothermal carbon dioxide-nitrogen atmosphere [AIAA PAPER 69-636] 01 p0180 A71-10938
- Shock-reflection interferometry of electron and mass density profiles of ionized argon end wall thermal layer 04 p0674 A71-14701
- Chemical nonequilibrium effects on hypersonic, blunt body shock layers flow in reacting planetary carbon dioxide-nitrogen atmospheres [AIAA PAPER 71-35] 06 p0866 A71-18496
- Radiative heat transfer during entry into shocked Venus model atmosphere 07 p1199 A71-19870
- Nonequilibrium multicomponent ionization calculations for stagnation merged shock layer of hypersonic blunt body by successive accelerated replacement [AIAA PAPER 69-655] 07 p1015 A71-19890

Inviscid air nonequilibrium shock layer properties correlation based on plenum entropy, predicting composition of downstream converging-diverging nozzle expanding air flow
[AIAA PAPER 70-866] 07 p1090 A71-19905

Near equilibrium shock layers nonequilibrium radiant emission calculation, noting application to Mars entry conditions
[AIAA PAPER 70-773] 07 p1091 A71-19914

Reentry heating simulation, noting UV radiation effects as shock layer thickness decreases
[AIAA PAPER 71-467] 11 p1859 A71-26248

High temperature aerodynamics with electromagnetic radiation, considering thermally radiating shock layers, electric arc driven wind tunnels and gas dynamic lasers
12 p1940 A71-27277

Radiative emission effects on viscous flow in shock structure of low density hypersonic flow around blunt body
12 p1986 A71-27583

Small spherical solid or liquid particles deceleration, melting and shattering due to spherical and conical bodies in compressible hypersonic shock layer flow field
[AIAA PAPER 69-712] 14 p2334 A71-29873

Melting body disintegration in hypersonic gas flow under radiation influence from shock layer, assuming optically thin boundary layer and intense vaporization
14 p2336 A71-30222

Asymmetries in magnetospheric shock layer due to upstream interplanetary magnetic field, considering forward stagnation region of solar wind-magnetosphere interaction
[AIAA PAPER 71-610] 15 p2395 A71-31546

Nonequilibrium dissociating gas flow past blunt body using time dependent shock layer analysis
15 p2346 A71-32049

Shock standoff distance and Mach disk diameter measurements in underexpanded sonic jets, using nitrogen dioxide-tetroxide working fluid
17 p2670 A71-34895

Detonation wave with dual front structure, calculating attenuation in Chapman-Jouquet regime by boundary shock layer method
17 p2839 A71-35635

Viscous relaxing gas hypersonic flow around sphere in presence of nonequilibrium chemical reactions in shock layer
17 p2673 A71-35637

Shock layer reattachment initiated by point explosion and driven continuously outward by inner contact surface
18 p2985 A71-36034

Shock layer parameters of supersonic viscous gas flow past blunt bodies of heat insulated and cooled surfaces, using Navier-Stokes equations
19 p2991 A71-37089

Shock layer pressure distribution for axisymmetric bodies moving at supersonic velocity in gas at rest, deriving nonstationary analog of Newton-Busemann formula
22 p3481 A71-42864

SHOCK LOADS
NT BLAST LOADS

Quasi-plastic impact in shock interaction between free body and moving plane, using nonlinear finite difference equation
01 p0127 A71-10636

Substructures and properties of Ni, Chromel A, Inconel 600 and TD-NiCr following explosive shock load deformation, using electron microscope
02 p0268 A71-12889

Polish book on impact in discrete mechanical systems covering beams, curved rods, plates, nonlinear damping, numerical analysis, subjected to shock loading
03 p0513 A71-14297

Thermal recovery in stainless steel after explosive shock loading and forming
04 p0614 A71-15781

Bent structure failure under pulse floor acceleration shocks, concerning aircraft seat damage during crash landing
08 p1367 A71-20747

Supersonic compressor performance, discussing shock and dump losses and wave structure model errors
10 p1553 A71-24869

Lunar surface properties, noting shock effects from impact induced pressures and temperatures
11 p1834 A71-26453

Explosive shock loading effect on materials properties, describing test equipment
12 p1895 A71-27689

Plate excitation by supersonic turbulent and shock boundary layers, measuring wall pressure fluctuation and panel displacement
15 p2507 A71-32132

West German parachute research, discussing stretching/filling shock, fabric material properties and static stability
15 p2350 A71-32373

Shock produced stress relaxation in thin walled Al tubes, comparing strain-time profiles with thin shell theory
16 p2647 A71-32923

Coesite-stishovite content in Ries crater nonporous crystalline rocks of variable composition and degree of shock metamorphism
19 p3050 A71-37660

Refractive index changes by shock compression metamorphism of tektite, soda lime and silica glasses
19 p3084 A71-37661

Diaplectic glass formation by experimental shock loading of orthoclase in porous mixtures
19 p3084 A71-37662

Flight test measurements of shock cell noise loading of aircraft tail planes, noting alleviation by nozzle and mirror structural modifications
19 p2998 A71-38467

Explosively shock strengthened austenitic stainless steel, investigating mechanical properties at elevated temperatures
21 p3398 A71-40462

Porous Cu and W shock loading properties, discussing principal Hugoniot data for P alpha dynamic response model
21 p3466 A71-40796

Nonlinear periodically oscillating motions in shell theory, examining buckling characteristics of thin walled structures under dynamic and shock loads action
21 p3473 A71-41152

Apollo 11 and 12 unshocked and shocked microbreccias petrology, noting shock compression and shock welding
23 p3745 A71-43658

Alloying elements effects on high-carbon steels phase transformation under shock loading to form martensite-austenitic structure
24 p3840 A71-45376

SHOCK MEASURING INSTRUMENTS

Machine for measuring inertial and structural responses to shock in single degree of freedom and more complex systems having dominant resonant frequency
01 p0068 A71-11548

Ionization measurement in detonation and shock waves in reactive gas mixtures by microwave cavity techniques
15 p2411 A71-32556

SHOCK RESISTANCE
NT IMPACT RESISTANCE

Quartz crystal HF resonator unit for high g environments, discussing tradeoff between stiff support and stress-induced frequency instability
01 p0054 A71-10913

Air to air and air to ground missile zinc silver oxide batteries capabilities, including energy density, long storage life and shock and temperature resistance
08 p1236 A71-21104

Elastic plastic wave cancellation in energy absorbing materials, considering polymer group efficiency for shock mitigation from weight and volume standpoint
11 p1843 A71-25329

Shock wave caused chemical reactions between solids and cryogenic liquids, discussing shock sensitivity tester for liquid propellant- structural material systems
14 p2222 A71-30546

Hot pressed TiC cylinder thermal shock resistance from tests to failure after heat cycling at 1000-1200 C
17 p2760 A71-35664

Quenching effects on glazed and unglazed alumina rods in various media, noting improved flexural and tensile strength, thermal shock resistance and impact resistance
22 p3565 A71-42342

Aerospace materials and structures shock sensitivity from derivation of dynamic fracture propagation relationship to stress wave
24 p3886 A71-45370

SHOCK SENSITIVITY
U SHOCK RESISTANCE
SHOCK SIMULATORS

Gases, condensed phases and blast simulation for high explosive driven shock tubes
04 p0565 A71-14677

Finite difference simulation of high energy Mach 120 to 40 air shock experiment
04 p0565 A71-14678

Large scale explosive driven conical shock tube nuclear air blast simulator
04 p0624 A71-14681

SHOCK SPECTRA

Frequency analysis and Fourier transform evaluation of mechanical shocks and single impulses, outlining theory for filter response to pulses
11 p1853 A71-26521

Free piston double diaphragm shock tube for hypersonic speeds without attenuation in argon, discussing time resolved channeled spectra measurements of electron density
16 p2551 A71-32916

SHOCK TESTS

Machine for measuring inertial and structural responses to shock in single degree of freedom and more complex systems having dominant resonant frequency
01 p0068 A71-11548

Book on mechanical vibration and shock measurements covering periodic and random vibrations characteristics, instrumentation, control, etc
02 p0251 A71-12175

Incident shock test time and reflected pressure for turbulent boundary layer at high Mach numbers in air and nitrogen
04 p0563 A71-14663

Shock pulse measurements for detecting damage to ball and roller bearings due to fatigue
04 p0604 A71-15673

Metal film resistors rapid evaluation method including thermal, load and shock tests devised by British electronic component manufacturers
07 p1076 A71-19553

Anomalous resistivity due to weak electrostatic turbulence in plasma, discussing applications to perpendicular collisionless shock experiments
12 p1940 A71-27418

Environmental rationale behind thermal shock testing, discussing approaches for temperature cycle provision
23 p3682 A71-43902

SHOCK TUBES
NT SHOCK TUNNELS

Shock formation in cylindrical and two dimensional tubes investigated numerically by FLIC method for compressible fluid flow
01 p0069 A71-10130

Spherical and cylindrical electrostatic probes for point ion density measurements in continuum flowing plasmas in hypersonic wake, discussing shock tube program for calibration
03 p0423 A71-13441

Atomic oxygen-nitrogen shock tube endothermic reaction under high translational and low vibrational energy, noting ozone loss
03 p0375 A71-13493

Shock wave dynamic behavior in shock tube under variable diaphragm opening time for high pressure gas flow into lower pressure section
03 p0472 A71-14261

Hydrogen-oxygen induction period kinetics behind shock waves, monitoring OH concentration by UV line absorption method
03 p0376 A71-14276

Shock tubes - Conference, University of Toronto, June 1969
04 p0562 A71-14661

Flow characteristics behind reflected shock wave flow and heat transfer at tube wall, noting unsteady and nonlinear effects
04 p0567 A71-14665

Boundary layer growth effects on two dimensional flow field in low pressure test gas of circular and rectangular shock tubes
04 p0568 A71-14667

Shock tube run time in acceleration region at turbulent regime for air, using pitot pressure measurements
04 p0563 A71-14668

High performance shock tube driving techniques, determining effectiveness and flow properties predictability
04 p0564 A71-14669

Shock wave attenuation delay in air heated shock tube by use of He-Ar mixture as driver gas
04 p0673 A71-14670

Imploding wire trigger technique for high shock velocity electric arc drivers in shock tubes
04 p0674 A71-14671

Electrical shock tube performance with RF induction heating of downstream gas
04 p0564 A71-14672

High temperature bypass piston shock tube for helium and nitrogen
04 p0564 A71-14673

Free piston shock drivers concerning plateau pressure reduction
04 p0564 A71-14674

Double diaphragm shock tube with detonable buffer hydrogen-oxygen mixture
04 p0564 A71-14676

Gases, condensed phases and blast simulation for high explosive driven shock tubes
04 p0565 A71-14677

Implosion driven shock tube using hydrogen-oxygen mixtures detonated by short exploding wire
04 p0673 A71-14679

Shock tubes with linear explosive driver for helium and air, determining performance by high speed camera measurements
04 p0565 A71-14680

Large scale explosive driven conical shock tube nuclear air blast simulator
04 p0624 A71-14681

Ionizing shock waves and high speed gas flow generation in tubes using high explosives
04 p0674 A71-14683

Shock tube flow interaction with EM field, using two step Lax-Wendroff finite difference method for partial differential equations 04 p0631 A71-14686

Electron temperature measurement in electromagnetic shock tube by spectroscopy and ruby laser light scattering in plasma, examining validity of local thermal equilibrium assumption 04 p0632 A71-14688

Shock tube current sheet speed variations, describing discharge voltage, pressure and test gas effects 04 p0632 A71-14689

Compressible magnetofluid dynamics studies in cesium shock tube 04 p0632 A71-14690

Shock tube spectroscopic and reaction kinetic research, considering studies before LTE 04 p0547 A71-14692

Shock tube measurements of vibrational energy transfer in molecular carbon dioxide-nitrogen-water system 04 p0629 A71-14693

Free radical effect on exchange reaction between ammonia and deuterium in high diluted argon shock tube 04 p0548 A71-14698

Shock tube diagnostics, instrumentation and rapid photography in nonequilibrium gas dynamics 04 p0565 A71-14699

Flow and radiative properties of air in high explosive shock tube 04 p0586 A71-14700

Reflected shock wave interaction with boundary layer and contact surface in shock tube, examining flow uniformity 04 p0568 A71-14703

Hypersonic shock wave production into air at one atmosphere in tube with electrical discharge gas heating 04 p0566 A71-14970

Air/Ar with ionizable lithium oxide plasma stream electric properties determination by shock tube wall electrode pair, using ambipolar diffusion theory 04 p0634 A71-15113

Shock induced exothermic reactions on boundary layer transition in shock tube, investigating free stream thermal energy release effects 04 p0572 A71-15503

Pulsed supersonic nozzle source molecular beam for shock tube target, detecting viscous effects from transient flux observation 04 p0600 A71-15596

Cr and Ti ionization rates, CO and NO reaction kinetics and decomposition products in shock tubes 05 p0716 A71-16521

Gas dynamic coupling effect on vibrational deactivation of carbon monoxide at 1400 to 2200 K range in shock tube 05 p0835 A71-16523

Single pulse shock tube in high temperature chemical reaction kinetics, considering shock reflection theory 05 p0836 A71-16527

Perturbations effect on tube flow and density variations due to noninstantaneous shock wave formation 05 p0836 A71-16529

Dwell or dark pause measurements of shock tube driver high pressure arc discharge for various gases 05 p0788 A71-16578

Shock tube diaphragm bursting by passing heavy current through overlapping heated wire under pressure 05 p0734 A71-16583

Bursting diaphragm shock tube as research tool for high temperature phenomena in energy transfer processes, reaction kinetics, hypersonic flow and astrophysics 05 p0734 A71-17240

Shock tube research instrumentation with fast response time for data on thermodynamic and transport properties, relaxation times and kinetics of high temperature gases 06 p0897 A71-17430

Hypersonic shock tube for aerodynamic measurements at high Reynolds numbers [DFVLR-SONDDR-95] 06 p0880 A71-18046

N and CO thermal conductivity shock tube measurements, discussing pressure distribution and high temperature effects 06 p1007 A71-18075

Solid particle impurity effects on hypersonic shock tube flow, determining error in blunt body measurements 07 p1013 A71-18916

Shock tube testing of acoustic materials at high sound amplitudes 07 p1083 A71-19586

Binary gas mixtures shock tube flow kinetic theory, indicating shock wave formation, contact layer diffusion and expansion wave dispersion 07 p1093 A71-20287

Plane normal shock wave reflection in relaxing gas for shock tube endwall upstream and downstream dynamic pressures, using method of characteristics 09 p1546 A71-23166

Hypervelocity projectile material impact on ultimate reflectance of bombarded polished metals from shock tube tests 11 p1799 A71-25835

Kinetic processes in shock tubes, considering diagnostic techniques for monitoring time histories nonequilibrium distributions preparations 11 p1745 A71-26264

Spectral studies on radiation from molecules, atoms and electrons, demonstrating shock tube applications in opacity measurements 11 p1764 A71-26265

Shock tube facility with two-phase system of solid particles and gases as primary driven fluid, applying to hypervelocity impact phenomena observation 11 p1745 A71-26266

Dissociative recombination rates in partially ionized gases at elevated gas temperatures, using shock tube for limited ionization introduction 11 p1765 A71-26283

High temperature plasmas optical properties measurement by plasma spectroscopy, using gas driven shock tube as light source 12 p1940 A71-27276

Diaphragm opening time influence on gas flow in shock tubes 12 p1897 A71-27451

Thermal relaxation effects on thermal adjustment between gas and wall, comparing with thermograms from shock tube experiments 13 p2161 A71-28619

Low pressure gas heating in shock tube, considering stagnation temperature increase 13 p2049 A71-29198

Soviet book on experimental aerodynamics covering wind tunnels, shock tubes, liquid and gas physical properties, flow parameter measurement equipment, etc 14 p2221 A71-29524

Shock tube high temperature air viscosity from laminar boundary layer heat exchange data 14 p2224 A71-30047

Slender body interaction with interface forming after bursting of membrane separating low and high pressure gas supersonic flow in shock wave tube 15 p2386 A71-31162

Thermal dissociation rate of undiluted nitrogen in shock tube over 5700 to 12,000 K range, using pressure measurements [ALAA PAPER 71-620] 15 p2451 A71-31549

End wall sampling of high pressure shock tube, using abrupt pressure rise to drive test gas flow through duct to sample bottle [WSS/CIPAPER 71-18] 15 p2383 A71-31627

Boron particles ignition theory and shock tube experiments, measuring ignition delay as function of temperature, pressure, gas composition and particle size [WSS/CIPAPER 71-20] 15 p2464 A71-31629

Unsteady one dimensional MHD shock wave evolution and separation in shock tube, using single fluid continuum equations with numerical dissipation 15 p2457 A71-32389

Shock tubes - Conference, London, July 1971 16 p2554 A71-32876

Shock wave propagation in ducts and cavities of different shapes and cross sections, compensating errors in recorded signals for shock tube pressure measuring equipment development 16 p2555 A71-32885

Shock tube investigation of cyanogen and CN molecule dissociation at high temperatures, considering kinetics of CN decomposition 16 p2538 A71-32891

Elementary reactions in hydrocarbon combustion, using shock tube as chemical reactor to determine rate of reaction in 1600 to 2100 K range 16 p2539 A71-32892

Laminar boundary layers effect on chemical-kinetic measurements in shock tube, applying correction by computer program for subsonic diffuser 16 p2555 A71-32893

Shock tube production of vibrationally excited molecules for mass spectra studies in hot gases 16 p2613 A71-32894

Shock tube measurements of vibration-vibration energy exchange probability in nitrogen-carbon monoxide-argon mixtures 16 p2613 A71-32896

Vibrational relaxation of CO by Fe atoms in Ar shock tube following iron pentacarbonyl decomposition 16 p2539 A71-32897

Nonequilibrium corner expansion flow of ionized argon induced by normal shock waves in hypervelocity shock tube 16 p2555 A71-32905

Thermal decomposition kinetics of nitrous oxide in shock tube, measuring IR emission behind reflected wave 16 p2539 A71-32910

High sensitivity helium neon laser interferometer for transient phase objects designed for shock tube and tunnel experiments 16 p2576 A71-32913

Low pressure shock tubes performance, investigating wave and contact surface trajectories and ideal velocity deviations 16 p2556 A71-32915

Free piston double diaphragm shock tube for hypersonic speeds without attenuation in argon, discussing time resolved channelled spectra measurements of electron density 16 p2551 A71-32916

Closed path recycling shock tubes, presenting numerical simulation of circular path continuous shock wave driven by successive electrical discharges in presence of perpendicular magnetic field 16 p2551 A71-32917

Temporal and spatial flow velocity profiles produced by shock tube generated pressure wave propagation in open-end pipe 16 p2556 A71-32921

Gas-solid interaction by shock tube method, determining thickness and thermal accommodation effects on thin metal film resistance thermometer response 16 p2576 A71-32922

Shock wave generated plasmas elementary reactions, discussing shock tubes and noble and diatomic gases chemionization 16 p2540 A71-32970

Shock tube spectroscopy as tool for atomic and molecular research, describing applications in chemical physics, astrophysics, gas dynamics, etc 16 p2578 A71-33152

Wall shear stress, momentum and displacement thickness of shock induced boundary layer interaction in tube and over flat plate, using integral method [ASME PAPER 71-APM-21] 16 p2559 A71-33208

French shock tube test facility for reproducing and investigating effects of sonic booms on vision and physiological processes 16 p2552 A71-33350

Turbulent boundary layer transition in shock tube with thickness inhomogeneity regions, using schlieren photographs 16 p2559 A71-33404

German monograph on pressure changes as boundary layer effect in tube wind tunnels covering test equipment and experimental design, Becker theory, pipe flow, etc 17 p2670 A71-34792

Free piston shock tube with air driver producing strong waves at speeds corresponding to gas effects 17 p2724 A71-34892

Double-diaphragm shock tube optimal parameters with allowance for boundary layer effect behind shock wave propagating in central chamber 17 p2730 A71-35634

S shock wave and magnetic field interaction at supersonic speed, using shock tube and MHD channel with sectioned electrodes 17 p2790 A71-35643

Reflected shock wave interaction with shock tube contact surface 18 p2903 A71-36123

Shock tubes and shock tunnels, considering equilibrium expansion, relaxation phenomena and real gas effects 18 p2897 A71-36410

Shock tube isomerization of cyclopropane to propylene as model system for small ring compounds, noting rate constants 19 p3010 A71-37272

Vibrational relaxation behind incident shock waves in CO based on shock tube pressure measurements at 2400-6000 K 19 p3106 A71-37880

Water vapor effect on vibrational relaxation of CO in shock tubes, measuring IR emissions 19 p3012 A71-38084

High temperature oxidation of ammonia, carbon monoxide and methane by nitrous oxide in shock tubes, using optical interferometry and UV/IR emission 19 p3012 A71-38086

Ignition delays of propane-oxygen-argon mixtures in shock tubes from pressure and heat flux measurements in reflected region 19 p3169 A71-38109

Shock tube investigation of solid polymeric hydrocarbon fuel ignition in hot oxidizing gas stream 19 p3121 A71-38124

Pressure, time and attenuation measurements of high explosive driven air shock in steel pipe, comparing with numerical simulation 20 p3208 A71-38787

End-on shock tube detection technique sensitivity for monitoring light emission behind reflected shock waves 20 p3209 A71-38830

Room temperature and heated driver gas low attenuation electric shock tube, investigating diaphragm opening process and effect on shock wave motion 20 p3209 A71-38837

Electromagnetically driven shock tube with precursor effect due to ionization of impurities by UV radiation from discharge, using gages to tag gas flow 20 p3239 A71-39431

Flow velocity measurement in electromagnetically driven unsteady shock tube from charged particles extraction, using ionization gages 20 p3329 A71-39432

High performance electric arc driven shock tube for shock velocities to 45 km/sec and test times over 4 microseconds, using 80/20 helium-hydrogen mixture 21 p3365 A71-40975

Thermal conductivity determination of Ar at extremely high temperatures, using temporal development of thermal boundary layer at shock tube wall 22 p3619 A71-41523

Shock wave attenuation in two diaphragm tube, obtaining velocity profiles with microwave phase detector system 23 p3674 A71-43086

Neon red lines Stark widths and shifts in function of electron and neutral Ne densities in shock tube 23 p3707 A71-43585

Two dimensional reflection supersonic nozzle shock wave initiated unsteady starting process, presenting shadowgraphs from shock tube investigation 24 p3821 A71-45367

SHOCK TUNNELS

Nonreflected shock tunnels hypersonic air flow, determining beginning and end times for optimum testing periods 04 p0563 A71-14666

Shock tunnel extremely high enthalpy and pressure for scramjet engine combustion research 11 p1860 A71-26267

Monograph on hypersonic shock tunnel supersonic combustion research techniques covering test facilities, optical and electromagnetic flow measurement methods, etc 14 p2334 A71-29578

Linear nonequilibrium shock tunnel driven supersonic MHD generator operation under large scale power extraction and strong electromagnetic-rare gas interactions 14 p2287 A71-29879

Flap induced flow deflection effects in hypersonic shock tunnel, obtaining turbulent heating, skin friction and pressure data [AIAA PAPER 71-598] 15 p2343 A71-31540

Turbulent boundary layer growth over flat plate and compression corner model in hypersonic gun tunnels, measuring pressure and heat transfer rate distributions 16 p2554 A71-32880

Shock tunnel investigation of two dimensional supersonic turbulent mixing with and without combustion, using Mach-Zehnder interferometer and piezoelectric transducers 16 p2554 A71-32881

Film cooling studies in subsonic and supersonic flows, using shock tunnel for gas turbine conditions simulation 16 p2551 A71-32882

Heat transfer, density and pressure measurements of hypersonic two dimensional centered nonequilibrium corner expansion oxygen flow with frozen boundary in shock tunnel 16 p2555 A71-32906

High sensitivity helium neon laser interferometer for transient phase objects designed for shock tube and tunnel experiments 16 p2576 A71-32913

Electron density and temperature distribution in boundary layer flow of reflected shock tunnel conical nozzle 17 p2727 A71-34877

Shock tubes and shock tunnels, considering equilibrium expansion, relaxation phenomena and real gas effects 18 p2897 A71-36410

Gas flow through hypersonic conical nozzle in shock-gun tunnel, measuring pressure ratio and Mach number distributions at test section 18 p2849 A71-37024

Carbon dioxide IR radiation measurements of duration of constant reflected shock temperature in over-tailored shock tunnel 19 p3041 A71-37893

Shock tunnel drag measurements on sharp slender cones in near free molecule hypersonic flow in air and He 19 p2993 A71-37897

Establishment time measurement for laminar separated flow, using shock tunnel driver section to give long test time at low incident Mach number 24 p3818 A71-44628

SHOCK WAVE ATTENUATION

Shock wave attenuation delay in arc heated shock tube by use of He-Ar mixture as driver gas 04 p0673 A71-14670

Detonation wave with finite reaction velocity interaction with rarefaction wave from behind, noting oscillations development associated with attenuation 05 p0834 A71-16511

Interaction between perfect gas ionizing shock wave and transverse magnetic field in coaxial channel, indicating incident wave attenuation and reflected shock wave formation 09 p1498 A71-22128

Elastic plastic wave cancellation in energy absorbing materials, considering polymer group efficiency for shock mitigation from weight and volume standpoint [AIAA PAPER 71-350] 11 p1843 A71-25329

Supersonic flight path curvature effects on local shock wave production, considering no boom zone and ground rules 11 p1708 A71-26310

Solar atmospheric model, calculating shock wave dissipation in chromosphere for photosphere central iron line intensity correlation with magnetic field intensity 15 p2497 A71-32746

Shock wave attenuation along uniform perforated tube, considering rarefaction and compression waves in resulting unsteady flow 16 p2554 A71-32883

Shock wave attenuation in perforated duct, using pressure transducers and schlieren photography 16 p2554 A71-32884

Pressure, time and attenuation measurements of high explosive driven air shock in steel pipe, comparing with numerical simulation 20 p3208 A71-38787

Room temperature and heated driver gas low attenuation electric shock tube, investigating diaphragm opening process and effect on shock wave motion 20 p3209 A71-38837

Shock wave attenuation in two diaphragm tube, obtaining velocity profiles with microwave phase detector system 23 p3674 A71-43086

Supersonic aircraft shape for shock waves minimization based on channel configuration with converging inlet and diverging outlet section 24 p3791 A71-44572

SHOCK WAVE CONTROL

Numerical analysis of plane transonic flows past shock free airfoils without boundary layer separation using inverse method of complex characteristics 19 p2994 A71-38307

SHOCK WAVE GENERATORS

NT SHOCK TUBES

NT SHOCK TUNNELS

Shock formation in cylindrical and two dimensional tubes investigated numerically by FLIC method for compressible fluid flow 01 p0069 A71-10130

Cylindrical shock waves generation from instantaneous energy release along line in quiescent atmosphere studied by numerical integration of flow equations 01 p0072 A71-11471

Strong shock wave generation by detonation with simultaneous working gas heating and compression 05 p0735 A71-16381

Ultrafast Q switched laser induced shock waves in solids, discussing model for picosecond impulse 06 p0907 A71-17311

Plane compression waves propagation into constant state nonviscous fluid, considering shock formation of pressure pulses and overpressure as function of time 07 p1091 A71-19961

Weak discontinuities propagation and growth in MGD with finite electrical and thermal conductivity, calculating shock wave generation critical time 07 p1170 A71-20094

Collisionless shock waves generation in theta pinches, plasma formation, experimental devices, diagnostic methods and magnetic probes 07 p1172 A71-20507

Spherical magnetogasdynamic shock production in conducting gas by explosion into homogeneous self gravitating system, assuming density dependence on inverse power of distance 09 p1505 A71-23585

Plane shock wave formation in dense Ar, using molecular dynamics numerical technique 10 p1694 A71-23953

Pulsed magnetic piston produced shock waves propagation along field in collisionless hydrogen plasma 10 p1654 A71-24894

Fast shock waves electromagnetic production in light gases, discussing interferometric measurements at optical and microwave frequencies in H 11 p1764 A71-26272

Strong shock wave generation by detonation with simultaneous working gas heating and compression 12 p1898 A71-27460

Small caliber smoothbore powder sabot guns generating planar shock wave in solids, using streak camera monitoring of impact and recoil velocities 14 p2223 A71-30885

Secondary floating shock generation in supersonic ideal gas flow about blunt bodies, investigating body configuration and flight regime effects 18 p2845 A71-36331

Multiple tone generation by axial flow transonic compressors, considering shock waves production and propagation associated with supersonic elements of blading 18 p2848 A71-36497

Infrasonic shock wave generation in troposphere by powerful earthquakes, causing upper atmosphere density rise due to heating 20 p3219 A71-39599

SST sonic boom generation, discussing aircraft design and atmospheric conditions effects and property damage 21 p3325 A71-40705

Pulsed magnetic piston produced shock waves propagation along field in collisionless plasma 21 p3425 A71-41274

SHOCK WAVE INTERACTION

Plane shock wave diffraction at wedge, analyzing role of gas specific heats ratio 01 p0070 A71-10664

Monograph on plane shock wave interactions covering supersonically moving two dimensional thin airfoils, slender bodies of revolution and thin wings 01 p0003 A71-11227

Fluid mechanics of interaction of shock wave and turbulent boundary layer at transonic-supersonic speeds 03 p0399 A71-13138

Flow characteristics in turbomachine blade cascades with transonic regime, emphasizing shock-boundary layer interaction phenomena 03 p0340 A71-13140

Ionizing shock wave interaction with transverse magnetic field, examining magnetic field distribution behind shock front, interface discontinuity and wave reflection 03 p0462 A71-13234

Laminar shock induced boundary layers, examining velocity, pressure gradients and enthalpy 03 p0400 A71-13739

Plane transonic flow with curved compression shock wave between subsonic and supersonic regions 03 p0345 A71-14560

Shock tube flow interaction with EM field, using two step Lax-Wendroff finite difference method for partial differential equations 04 p0631 A71-14686

Incident shock tube flow interaction with one dimensional MHD channel flow 04 p0632 A71-14687

Reflected shock wave interaction with boundary layer and contact surface in shock tube, examining flow uniformity 04 p0568 A71-14703

Time measurements of vibration relaxation in diatomic gases excited by shock waves 04 p0568 A71-14795

Strong blast wave interaction and transient pressure on conical slender supersonic bodies 04 p0525 A71-14979

Ionizing shock wave interaction incident on transverse magnetic field 05 p0786 A71-15975

Far and near field solutions of plane steady transonic flow past thin airfoil including imbedded shock waves, using small disturbance theory [AIAA PAPER 70-188] 05 p0694 A71-16565

Incident shock wave interaction with liquid hydrocarbon fuel drops in oxidizing and inert atmospheres, considering combustion characteristics and ignition mechanism [AIAA PAPER 71-206] 06 p0886 A71-18642

Interaction between radiation from shock wave region and oncoming cold air flow in hypersonic flow past blunt body 07 p1014 A71-19730

Shock wave interaction with wedge moving at supersonic speed, calculating geometry of regions formed intersecting wavefronts 07 p1014 A71-19741

Plasma ring vortices in crossed electrical discharges attributed to shock wave induced plasma flow across lines of force of azimuthal magnetic field 08 p1338 A71-20785

Low energy cosmic ray intensity increase at propagating interplanetary shock wave front, discussing one dimensional model with particles undergoing convection and diffusion 08 p1356 A71-21630

Hypersonic strong interaction flow over inclined surface, using asymptotic expansion in powers of hypersonic interaction parameter for boundary layer equations reduction 09 p1382 A71-22109

Interaction between perfect gas ionizing shock wave and transverse magnetic field in coaxial channel, indicating incident wave attenuation and reflected shock wave formation 09 p1498 A71-22128

Weak magnetic field disturbance by strong spherical shock wave propagation in finite conductivity gas 09 p1430 A71-22140

Shock wave interaction with evaporating aerosol for diffusive and ablative models taking into account thermal conductivity 09 p1433 A71-22856

Magnetosonic waves generation by interaction of bow shock with frozen tangential discontinuities in solar wind 09 p1521 A71-22866

Laminar boundary layer interaction with shock wave in viscous supersonic flow near concave compression corner

09 p1384 A71-23618

Normal shock wave interaction with deformable solid walls, determining explosion or sonic booms effects on elastic structures and protection devices

10 p1556 A71-24483

Traveling shock waves interaction with orifice inside ducts, noting anomalous phenomena probably due to unsteady boundary layer growth or time lag

10 p1596 A71-24923

Normal shock wave acceleration of water droplets by external pressure, observing distortion and breakup through shadowgraph techniques

[ALAA PAPER 71-325] 11 p1749 A71-25305

Water drops deformation and fragmentation due to shock wave impact in high velocity air stream

[ALAA PAPER 71-392] 11 p1749 A71-25354

Compressible turbulent boundary layer interaction with wedge or corner induced oblique shock waves, using transformation methods

11 p1750 A71-25481

Triple point trajectory of shock-shock Mach reflection off plane wall, comparing to Whitman theory

11 p1752 A71-26192

Soviet papers on wave propagation in viscoelastic and elastoplastic media covering shock wave interaction, magnetoelectric waves, etc

12 p1980 A71-27444

Shock wave incidence on wedge moving at supersonic speed, considering uniform flow region on upper wedge surface for specific values of Mach number and vertex angle

12 p1897 A71-27445

Hypersonic cruise vehicles viscous interactions areas, examining compression corners, shock interactions, laminar and turbulent flow, boundary layer separation, etc

[ALAA PAPER 70-781] 12 p1865 A71-27551

Shock wave ignition of liquid fuel drop in oxidizing atmosphere, discussing combustion process

[ALAA PAPER 70-9] 12 p1986 A71-27566

Shock interaction effects on flapped delta wing at hypersonic speed, presenting method for estimating reflected expansion wave impingement boundaries and resulting aerodynamic coefficients

12 p1868 A71-27598

Flow and heat transfer measurements in dihedrons simulating patterns about supersonic conical edge and shock wave interaction line, using thermindicator-coating technique

13 p1992 A71-29174

Plane shock wave diffraction at wedge, analyzing role of gas specific heats ratio

14 p2228 A71-30997

Combustion acceleration of molar oxygen-methane mixtures in cylindrical chamber during flame-shock wave interaction, using motion picture techniques

15 p2511 A71-31381

Sonic boom pressure signature laboratory scale measurement after modification by traveling through air jet turbulence, comparing with statistical prediction

[ALAA PAPER 71-618] 15 p2388 A71-31547

Sonic boom wave interaction with topographic models, measuring surface pressure time history

[ALAA PAPER 71-619] 15 p2389 A71-31548

Shock wave interaction with duct cross section changes, discussing experimental apparatus and shadowgraph results

15 p2393 A71-32265

Drag coefficients of bodies of revolution from wind tunnel shock induced steady flow data, considering blast loading experiments in shock tube

16 p2519 A71-32878

Shock wave reflection process model in magnetic fields, describing time development of interaction process

16 p2616 A71-32901

Wall shear stress, momentum and displacement thickness of shock induced boundary layer interaction in tube and over flat plate, using integral method

[ASME PAPER 71-APM-21] 16 p2559 A71-33208

Liquid hydrocarbon fuel drop interaction with incident shock wave in oxidizing and inert atmospheres, investigating aerodynamic shattering and combustion

17 p2836 A71-34435

S shock wave and magnetic field interaction at supersonic speed, using shock tube and MHD channel with sectioned electrodes

17 p2790 A71-35643

Shock layer reattachment initiated by point explosion and driven continuously outward by inner contact surface

18 p2985 A71-36034

Reflected shock wave interaction with shock tube contact surface

18 p2903 A71-36123

Shock wave interaction with laminar boundary layer on flat plate using modified Lax-Wendroff difference technique

18 p2906 A71-36320

V shaped conical wing in supersonic and hypersonic flow with shock attached to leading edge, investigating

complex wave system with time dependent and analytical methods

18 p2845 A71-36339

One dimensional nonsteady combustion processes accompanying self sustained detonation waves initiated by merger of two weak shock waves, using Lax finite difference method

19 p3170 A71-38127

Transverse hydromagnetic shock structure in partially ionized gas, calculating ions, electrons and atoms temperatures, velocities and momentum

21 p3444 A71-40239

Neutral gas acceleration to high velocity at low ionization level by electromagnetic plasma gun formed unionized shock wave

21 p3423 A71-40766

Viscous slipstream flow downstream of triple shock wave intersection in supersonic diffuser air flow, using Pitot and static pressure probe measurements

21 p3324 A71-40981

Coherence theory of strong shock induced explosive gas ignition limit

22 p3621 A71-42099

Backflow region and shock interaction in rotating and swirling gas streams and jets in supersonic nozzle with separation and thrust effects

22 p3480 A71-42682

Reflected shock wave interaction with tangential discontinuity curve for supersonic incalculable jets, examining flow instability

23 p3665 A71-44337

Flare induced laminar boundary layer/shock wave interactions on axisymmetric bodies at zero incidence in supersonic flow under adiabatic conditions

24 p3789 A71-44604

Hydrogen fluoride vibrational relaxation times behind incident shock waves at various temperatures

24 p3802 A71-44922

Oxygen dissociation in He, Ar, Kr and Xe gas mixtures behind incident shock waves, calculating density gradients and vibrational relaxation time

24 p3802 A71-44924

Pressure and flow direction defects behind Mach reflected shock near three shock intersection, considering steady flow theoretical model

24 p3820 A71-44953

SHOCK WAVE PROFILES

Collisionless shock waves in magnetized plasma as function of Alfvén-Mach number, measuring electron temperature jump on wave front spectroscopically

01 p0132 A71-10153

Shock wave dynamics of brightness curve reflecting supernova outbursts

02 p0307 A71-12088

Radiative transfer by shock profile spectral line in thermally inhomogeneous layers of radiating gas

02 p0240 A71-12184

Plane straight shock wave stability in inviscid compressible medium, discussing gas dynamic equation discontinuous solution

03 p0401 A71-13967

MHD shock waves structure capable of ionizing gases, using law of conductivity variation with temperature

03 p0465 A71-14063

Liquid/gas repeated injection into ideal gas plane supersonic flow, determining resultant shock wave radius relation to Mach number and temperature

03 p0404 A71-14254

Shock structure in crystalline solids, including dissipative processes, discontinuities, continuum mechanics and lattice dynamics

04 p0664 A71-14662

Plasma accelerator self ionizing current free stable radiative shock wave structure in hydrogen, using time resolved spectroscopic measurements

04 p0548 A71-14696

Collisionless electrostatic shock formation and structure, using one dimensional two species numerical simulation code

04 p0634 A71-15174

Multidimensional detonation wave structure, presenting spacing prediction by transverse wave strength

05 p0834 A71-16509

Earth bow shock configuration model from dual satellite observation

05 p0742 A71-16632

Finite electrical conductivity effects on solar flare-induced interplanetary shock waves, discussing solar wind time dependent bulk flow characteristics

05 p0810 A71-16634

Shock waves with high equilibrium temperature, calculating structure during multiple ionization of atoms

07 p1087 A71-19186

Caret wing serial tests in Mach 8 to 15 hypersonic flow, including three component force, spanwise direction pressure distribution and shock wave angular measurements by flow visualization

07 p1016 A71-20015

Plane steady state MHD shock wave structure in infinitely conducting fluid under magnetic field perpen-

dicular to shock velocity, introducing quadratic artificial viscosity factor

07 p1174 A71-20616

Shock wave dynamics of brightness curve reflecting supernova outbursts

08 p1362 A71-21138

Shock wave shape attached to cone moving in ideal gas studied by Pade-Shanks approximation method, considering angle of attack

09 p1431 A71-22405

Steady plane plasma shock wave structure in partially ionized and radiating gas, using Navier-Stokes equations in three fluid continuum approach

09 p1504 A71-23202

Boltzmann equation for shock wave structure, comparing errors of variational principles and moment methods of approximation

10 p1593 A71-24279

Plane stationary shock wave propagation through one component vapor-liquid mixture, calculating profile and mixture parameters under evaporation and condensation

10 p1593 A71-24348

Three dimensional convergence for spherical shock wave by linear pinch wall shaping based on Whitman ray-shock theory

11 p1752 A71-26191

Monograph on shock wave structure in nonequilibrium partially ionized gas flow covering plasma diagnostics, electron temperature, ion density, induced potential gradient, etc

13 p2048 A71-28738

Strong shock wave structure parameters variations calculation, considering various applications

13 p2049 A71-29200

Convergence and accuracy of modified Gauss-Seidel finite difference scheme, calculating one dimensional Navier-Stokes shock structure

13 p2051 A71-29429

Monograph on shock and detonation waves ionization and structure covering diagnostic techniques, heat transfer, particle flow, pressure measurements, etc

14 p2335 A71-29933

Collisionless magnetic slow shocks laminar wave train structure, using two-fluid hydromagnetics with ion cyclotron radius dispersion

14 p2282 A71-30558

Entropy layer in hypersonic flows, determining body configuration from shock wave shape described by coordinates power function

14 p2171 A71-30875

Shock wave splitting in KBr, determining shock profiles and velocities by electromagnetic method

15 p2463 A71-31385

Radiative transfer by shock profile spectral line in thermally inhomogeneous layers of radiating gas

15 p2511 A71-31492

Slow MHD shock wave profile discontinuity corresponding to conventional gas dynamics isothermal jump

16 p2615 A71-32793

Shock wave diffraction patterns on plane walled convex corners in air, nitrogen and carbon dioxide at various Mach numbers

16 p2556 A71-32918

Transverse shock waves fine structure and saturation of ion-acoustic turbulence in collisionless plasma, using magnetic field probe and MHD equations

16 p2619 A71-33649

Supersonic underexpanded submerged gas jet at various Mach and Knudsen numbers and pressure ratios, observing trailing shock wave geometry

17 p2669 A71-34218

Design shock wave correspondence to strong oblique shock, discussing off design behavior of caret wing

17 p2671 A71-35280

Shock wave profile nonlinear one dimensional problems in gas dynamics, using monotonic difference scheme

18 p2907 A71-36333

Shock wave structure prediction by nonlinear kinetic models with Monte Carlo solutions of full Boltzmann equation

18 p2907 A71-36334

Relaxation effects on velocity and temperature of solid particles in gas flows, emphasizing acoustic propagation, compression shock structure and nozzle flows

18 p2909 A71-36441

Collisionless shock waves downstream state, using Rankine-Hugoniot type relation model

19 p3117 A71-38650

Shock fronts diffraction and reflection with vortices generation at discontinuities, predicting wave shape and strength distribution in two dimensional or axisymmetric situations

21 p3365 A71-40016

Convergence of progressive shock wave solutions for higher order equations of conservation laws with dissipation and dispersion terms, proving shock curves existence

21 p3414 A71-40141

- Delta wing shock envelope visualization at hypersonic speed, obtaining flow field photographs by vapor screen technique 21 p3324 A71-40973
- Shock wave structure in liquid-gas bubble mixture with varying volumetric gas content, bubble size, shock strength and liquid viscosity 24 p3820 A71-45128
- ## SHOCK WAVE PROPAGATION
- Heat conduction effect on propagation of laser radiation absorption shock wave 01 p0092 A71-10068
- Shock wave propagation in channel with MHD interaction between compressed gas and nonuniform magnetic field 01 p0132 A71-10662
- Similar solution of strong shock wave propagation with nonequal heat coefficients, approximating energy of dissociation ionization and free molecular oscillation 01 p0070 A71-10663
- Proton fluxes at 300 keV associated with propagating interplanetary shock waves, noting alpha particle enhancement 01 p0146 A71-11487
- Shock wave front propagation instability in decreasing density medium, applying to stellar structure 02 p0241 A71-12510
- Radiation effects on cylindrical magnetohydrodynamic shock propagation in plasma, deriving jump conditions in terms of Mach number and pressure ratios 02 p0294 A71-12847
- Shock wave propagation in bent and branched ducts, discussing schlieren method flow visualization, diffraction measurement with differential interferometer and interaction between shock and vortex 03 p0400 A71-13696
- Shock wave dynamic behavior in shock tube under variable diaphragm opening time for high pressure gas flow into lower pressure section 03 p0472 A71-14261
- High beta plasma, calculating turbulence for fast shock propagating perpendicular to magnetic field 03 p0496 A71-14514
- Plane shock wave propagation in polytropic gas of variable density, using successive approximation technique 03 p0345 A71-14558
- One dimensional ionized gas flow behind shock wave propagating in MGD duct 03 p0466 A71-14569
- Imploding wire trigger technique for high shock velocity electric arc drivers in shock tubes 04 p0564 A71-14671
- Ionizing shock wave propagation through MHD channel flow, determining induction emf current and electron density and concentration 04 p0632 A71-14691
- Shock wave stability with respect to infinitesimal disturbances, using Burger and Korteweg-de Vries equations via Liapunov method application 04 p0570 A71-15080
- Hydrodynamic model describing intermediate stages of propagation of plasma shock wave created by laser light focusing 05 p0787 A71-16333
- Shock wave propagation through converging nozzle, predicting real gas dissociation and vibrational excitation effects for comparison with shock tube measurement 05 p0735 A71-16528
- Perturbations effect on tube flow and density variations due to noninstantaneous shock wave formation 05 p0836 A71-16529
- Finite electrical conductivity role in interplanetary piston driven shock waves propagation in solar wind 05 p0810 A71-16635
- Collisionless plasma shock longitudinal wave propagation perpendicular to magnetic field, demonstrating ion acoustic/electron Bernstein modes instability 05 p0789 A71-16655
- Shock wave propagation in three dimensional elastic media, calculating finite strains effect on behavior 05 p0828 A71-16988
- Nonlinear acoustics propagation theoretical solutions by weak shock theory and Burger equation, noting differences in exactness and complexity of methods 05 p0784 A71-17156
- Shock formation and chemical activation in solid secondary explosives detonation, considering propagation acceleration by pressure rise in terms of reaction products thermodynamic properties 07 p1223 A71-19246
- Self similar shock wave propagation in exponentially varying density at constant pressure, solving by method of successive approximation 07 p1089 A71-19731
- Cylindrical shock wave propagation in inhomogeneous exponential atmosphere from extension of method for spherical wave 07 p1089 A71-19742
- Pressure shocks propagation through electrically and thermally conducting viscous gas in presence of uniform magnetic field 07 p1169 A71-20025
- Arbitrary strength and shape shock front propagation past ocean surface, calculating diffraction at interface 07 p1094 A71-20614
- Short shock wave equations for two dimensional steady motions of ideal gas 08 p1276 A71-21871
- Hanging shock wave in small supersonic flow past profile with broken generatrix in plane ideal gas 08 p1228 A71-21872
- Weak magnetic field disturbance by strong spherical shock wave propagation in finite conductivity gas 09 p1430 A71-22140
- Fluctuations effect on MHD shock wave propagating in plasma perpendicular to external magnetic field, obtaining field amplitude distribution function 09 p1500 A71-22242
- Blast wave propagation following explosions at center of generalized Roche model, discussing core radius and envelope thickness 09 p1431 A71-22371
- Curved shock reflection from straight rigid boundary, calculating relationship between incident and reflected wave curvatures 09 p1433 A71-22855
- Sonic boom and explosion shock wave propagation over long distances through turbulence modeled by sound speed fluctuation, including acoustic scattering effect 09 p1433 A71-22858
- Gas dynamic solutions of plane shock wave propagation in moving medium, considering conservation laws 09 p1525 A71-23198
- Heat conduction effect on propagation of laser radiation absorption shock wave 09 p1464 A71-23263
- Reflected radiative shock wave propagation velocity under transverse magnetic field, taking into account radiation pressure and energy 09 p1506 A71-23588
- Alfvén waves effect on MHD fast shock from numerical solution of extended Rankine-Hugoniot equations 10 p1667 A71-23798
- Stationary shock wave propagation perpendicular to magnetic field in Vlasov collisionless plasmas 10 p1647 A71-23892
- Plane stationary shock wave propagation through one component vapor-liquid mixture, calculating profile and mixture parameters under evaporation and condensation 10 p1593 A71-24348
- Shock wave propagation in electronically excited hot plasma in electromagnetic field, assuming negligible electron-ion collisions 10 p1653 A71-24828
- Pulsed magnetic piston produced shock waves propagation along field in collisionless hydrogen plasma 10 p1654 A71-24894
- Heterogeneous detonation propagation in mixture of liquid fuel droplets suspended in gaseous oxidizer, discussing droplets disintegration time and shock wave parameters 10 p1698 A71-25124
- Transonic compressor shock wave noise generation and decay rates at multiple tones, using sonic boom analysis [ASME PAPER 71-GT-7] 11 p1703 A71-25953
- Mach reflection of strong shock waves by sharp compressive corner in real gas in hypersonic tube, using laser Mach-Zehnder interferometer 11 p1752 A71-26190
- Algorithm for numerical analysis of cylindrical shock wave propagation in stationary ideal gas 13 p2046 A71-27903
- Shock wave propagation in channel with MHD interaction between compressed gas and nonuniform magnetic field 14 p2283 A71-30995
- Similar solution of strong shock wave propagation with nonequal heat coefficients, approximating dissociation, ionization and excitation energy of molecules vibrational degrees of freedom 14 p2228 A71-30996
- Similarity solutions describing flow characteristics behind plane hydromagnetic shock propagating into uniform ideal gas at rest in presence of transverse magnetic field 15 p2391 A71-32074
- Unsteady one dimensional MHD shock wave evolution and separation in shock tube, using single fluid continuum equations with numerical dissipation 15 p2457 A71-32389
- Sonic boom phenomena, discussing supersonic flow near aircraft, atmospheric propagation, distortion, focusing, caustics, turbulence effects and reduction 15 p2350 A71-32566
- Gas dynamics of explosions, considering electromagnetic fields and chemical reactions effects on blast wave propagation in unbounded media 15 p2515 A71-32567
- Shock wave propagation in ducts and cavities of different shapes and cross sections, compensating errors in recorded signals for shock tube pressure measuring equipment development 16 p2555 A71-32885
- Shock wave propagation in junction of straight duct with side branch for subsonic flow, analyzing reflected and transmitted waves 16 p2555 A71-32886
- Pressure histories due to weak shock wave propagation through dividing flow junction, describing wave decay in side branch duct 16 p2555 A71-32887
- Radiative heat transfer effects behind reflected and incident shock waves in high temperature air and xenon respectively 16 p2662 A71-32888
- Approximation analysis for laminar two dimensional boundary layer behind plane shock wave moving over infinite flat plate 16 p2556 A71-32914
- Low pressure shock tubes performance, investigating wave and contact surface trajectories and ideal velocity deviations 16 p2556 A71-32915
- Closed path recycling shock tubes, presenting numerical simulation of circular path continuous shock wave driven by successive electrical discharges in presence of perpendicular magnetic field 16 p2551 A71-32917
- Blast wave propagation in explosive gaseous mixtures, presenting analysis based on detonation decay to Chapman-Jouget state 16 p2556 A71-32920
- Critical induced acceleration for shock propagation as function of strain in polymethyl methacrylate [ASME PAPER 71-APM-14] 16 p2600 A71-33213
- Free piston shock tube with air driver producing strong waves at speeds corresponding to gas effects 17 p2724 A71-34892
- Weak shock propagation in three dimensional unsteady flow, obtaining shock construction rule 17 p2729 A71-35423
- Double-diaphragm shock tube optimal parameters with allowance for boundary layer effect behind shock wave propagating in central chamber 17 p2730 A71-35634
- Bernstein mode wave instability growth rate in collisionless shocks propagating perpendicular to magnetic field, including pressure gradient effects 18 p2950 A71-35928
- Nonuniform self propagation of cylindrical imploding shock waves in electrically conducting gas 18 p2951 A71-36005
- Type 2 radio burst disturbances in coronal magnetic field, considering shock wave travel parallel to magnetic field lines 18 p2957 A71-36159
- Shock wave diffraction propagation through nonuniform fluid, noting application to two dimensional unsteady flows 18 p2907 A71-36332
- Finite difference technique for convective flow equations involving shock wave propagation, discussing heuristic analysis for truncation error 18 p2907 A71-36338
- Multiple tone generation by axial flow transonic compressors, considering shock waves production and propagation associated with supersonic elements of blading 18 p2848 A71-36497
- Finiteness of deformations and convective terms effect on medium velocity in terms of displacements on shock wave propagation in three dimensional elastic medium 18 p2982 A71-36788
- Nonlinear diffraction of weak shock waves near rigid wall with sharp bend, obtaining approximate solution by matched asymptotic expansion method 19 p3043 A71-37100
- Flow parameters behind shock waves propagating in carbon dioxide-nitrogen mixtures at Mach numbers from 5 to 10 19 p3044 A71-37583
- Decane and hexadecane fog detonation propagation in gaseous oxygen 19 p3170 A71-38128
- Short shock wave equations solutions for two dimensional steady flow of ideal gas 20 p3211 A71-39370
- Hanging compression shock wave in plane supersonic ideal gas flow past body with broken generatrix 20 p3176 A71-39371
- Normal shock wave propagation in nonuniform gases with arbitrary property gradients based on modified method of infinitesimal contact discontinuities 20 p3212 A71-39482

SHOCK WAVES

Earth bow shock multiple crossings identification by magnetic field experiment onboard Pioneer 8 at geocentric distances 20 p3230 A71-39878

Convergence of progressive shock wave solutions for higher order equations of conservation laws with dissipation and dispersion terms, proving shock curves existence 21 p3414 A71-40141

Quantitative schlieren system for shock wave velocity, density ratio and relaxation time measurements, discussing electro-optical modification and calibration technique 21 p3364 A71-40404

Strain rate dependent constitutive relation for shock propagation in porous materials, discussing relaxation time 21 p3465 A71-40794

High performance electric arc driven shock tube for shock velocities to 45 km/sec and test times over 4 microseconds, using 80/20 helium-hydrogen mixture 21 p3365 A71-40975

Fluctuations effect on MHD shock wave propagating in plasma perpendicular to external magnetic field, obtaining field amplitude distribution function 21 p3424 A71-41131

Pulsed magnetic piston produced shock waves propagation along field in collisionless plasma 21 p3425 A71-41274

Plasma shock wave propagation along weak magnetic field, considering energy dissipation 21 p3425 A71-41279

Laminar collisionless shock propagation perpendicular to magnetic field into hot plasma, calculating temperature effects on leading edge growth rate 22 p3579 A71-41580

Mgd shock propagation in viscous heat conducting gas, investigating radiation escape effect 23 p3708 A71-43100

Solar high energy particles directional and temporal properties, investigating single encounter model with propagating interplanetary shock waves 23 p3720 A71-43153

Hypersonic shock wave front motion into air at one atmosphere, measuring reflectivity and curvature for comparison with theory 23 p3626 A71-43929

Self similar solutions for ideal gas flow driven by piston ahead of shock propagating in medium at rest with power law density distribution 23 p3719 A71-44143

Hypersonic axisymmetric slender body near wake shear layer determination by shock expansion method for numerical computation accuracy and efficiency 23 p3626 A71-44194

SHOCK WAVES

NT DETONATION WAVES

NT MACH CONES

NT NORMAL SHOCK WAVES

NT OBLIQUE SHOCK WAVES

NT RIEMANN WAVES

NT SONIC BOOMS

Shock wave diffraction at sharp edges, discussing physical principles, angle and pressure ratio effects 01 p0001 A71-10109

Compression shock wave development in compressible media, deriving wave amplitude/time relationship via velocity distribution approximation by discontinuous Mach wave series 01 p0069 A71-10122

Gas temperature measurement behind strong shocks in diaphragmless electric shock tube by spectral line inversion method, noting application to gas dynamics 01 p0078 A71-10156

Solar flare proton propagation, examining interplanetary shock wave effects on cosmic ray scattering 01 p0146 A71-13386

Stationary waves produced by earth bow shock, calculating cyclotron radiation amplitude and polarization characteristics by thin current sheet model 01 p0075 A71-1490

Directed proton fluxes measurements in bow shock, magnetosheath and solar wind by OGO 5 satellite ion spectrometer 01 p0147 A71-1491

Magnetic field fluctuations in magnetosheath from Pioneer observations, noting bow shock correlation 01 p0075 A71-1492

Sunward magnetosheath magnetic field fluctuations, noting power levels spatial variations, transverse shock aligned fields and longitudinal waves 01 p0075 A71-1493

Slow mode shocks in interplanetary space detected by Mariner 5 spacecraft 3.5 and 27 million km from earth 01 p0148 A71-11527

Shadow photography applied to Mach reflections in argon, carbon dioxide and Freon 12 in shock tube, using Huygens principle for transfer mechanism 02 p0239 A71-11635

Weak nonlinear ion-acoustic shock waves in cold ion-warm electrons plasma, using nonlinear perturbation method 02 p0288 A71-11868

Pseudoshock mechanism model, explaining supersonic diffuser main flow static pressure increase and decrease alternately and wall increase monotonously 02 p0239 A71-11870

Explosion shock wave induced short wave radio emission, deriving time related gas ionization state of wave front 02 p0284 A71-11927

Shock waves behavior and effects in Sc galaxies spiral arms, attributing dark lanes at inward edges to shock waves in gas flow 02 p0307 A71-12083

Quasi-spherical divergent shock waves produced by Pt wire explosion in air 02 p0332 A71-12336

Nonlinear instabilities in shock wave numerical calculations, using Shuman short wave filtering operator 02 p0240 A71-12396

Hydrocarbon fuels high temperature oxidation behind shock waves, investigating reaction process by combustion products IR emissions and density gradient 02 p0298 A71-12860

Amino acid synthesis in simulated primitive environments, discussing possible effects of meteoric kinetic energy and lightning-associated shock waves 03 p0358 A71-13015

Free wave reflection measurements of normal acoustic impedance of ground surfaces in relation to shock waves from large supersonic commercial aircraft 03 p0347 A71-13278

Anisotropic plasma discontinuities in solar wind, noting shock misidentification 03 p0463 A71-13307

Two dimensional free gas jet expansion into quiescent medium, predicting terminal shock position 03 p0400 A71-13466

Vibrational relaxation behind incident shock waves in pure nitrogen, using end wall pressure measurements 03 p0375 A71-13496

Sodium atom excitation by high energy particle collisions behind shock waves, measuring electron and vibrational temperatures 03 p0376 A71-13992

Acoustic shock wave scattering by cylindrical cavities in inviscid fluid medium, noting shielding effect, peak excitation and inverse logarithmic decay [ASME PAPER 70-WA/APM-57] 03 p0459 A71-14173

Hypersonic conical flow with attached shock waves over delta wings 03 p0344 A71-14243

Hydrogen-oxygen induction period kinetics behind shock waves, monitoring OH concentration by UV line absorption method 03 p0376 A71-14276

Blunt body problem with detached shock, considering methods of lines and integral relations agreement for wide range of Mach numbers 03 p0344 A71-14449

Flow characteristics behind reflected shock wave flow and heat transfer at tube wall, noting unsteady and nonlinear effects 04 p0567 A71-14665

Hemispherical imploding shock wave reflection, noting cold wall presence and gas density effects 04 p0568 A71-14682

Spectroscopic studies of helium-hydrogen plasmas in first reflected shock region in electromagnetic T-tube 04 p0631 A71-14684

High Mach number collisionless shock waves in low density argon plasma, measuring electron heating and shock thickness 04 p0631 A71-14685

IR radiation measurement of chain branching rates in hydrogen-oxygen mixtures ignited by reflected shock waves 04 p0548 A71-14695

Air plasmas temperature measurements behind reflected shock wave, examining radiative cooling effects and total radiant energy 04 p0632 A71-14704

Electron density measurement behind shock waves in air/argon mixture by free molecular Langmuir probes 04 p0629 A71-14705

Flat plate ion density probe with convection and ion production in electric sheath, comparing to shock waves in air 04 p0632 A71-14706

Inviscid nonheat conducting gas flow parameters behind shock wave reflection from solid wall at obtuse angle using linear approximation from variable separation method 04 p0572 A71-15554

Linearized shock waves and periodic disturbances propagation by discrete ordinates method in planar radiative gas dynamics 04 p0689 A71-15742

Hydrodynamic equations for discontinuity problems of origin and disruption of vortices, 04 p0689 A71-15742

transonic gas flow and shock wave formation, using Lagrange equations 04 p0579 A71-15813

Galactic Lyman alpha observation by Vela 7, discussing error possibility of data interpretation based on interstellar hydrogen shock wave 04 p0658 A71-15831

Shock waves and chemical reactions due to plane, cylindrical and spherical point explosions in combustible gaseous mixtures 05 p0833 A71-16503

Cylindrical blast waves analytical solutions by combined parameter, coordinate and matched asymptotic expansions 05 p0833 A71-16504

Hydrogen-oxygen reaction kinetics behind steady state shock waves under isothermal branched chain explosion limits 05 p0834 A71-16513

Shock waves in nitrogen, carbon dioxide and mixtures, measuring Mach number for deviation evaluation from vibrational and dissociation equilibria 05 p0835 A71-16522

Initial ionization, relaxation kinetics and nonequilibrium radiation behind strong shock waves in monatomic gases and air 05 p0835 A71-16524

Supersonic blunt body flow relaxation processes, calculating bow shock for various flow regimes and reaction rates 05 p0835 A71-16525

Strong shock wave Mach reflection, determining pressure and temperature at wedge surface by shock tube experiment 05 p0835 A71-16526

Single pulse shock tube in high temperature chemical reaction kinetics, considering shock reflection theory 05 p0836 A71-16527

Energy deposition, vacuum expansion and vaporization of barium in two phase jets, using combustion and solid state shock waves 05 p0836 A71-16538

Solar wind upstream waves ahead of earth bow shock by dual satellite observations 05 p0741 A71-16629

Earth bow shock configuration model from dual satellite observation 05 p0742 A71-16632

German monograph on shock wave diffraction wedge angular changes in ideal gas region, comparing experimental with perturbation theoretical results 05 p0737 A71-17107

Short duration proton energy increases observation by Explorer 34, considering interpretation as acceleration associated interplanetary shocks 06 p0949 A71-17254

Diamagnetic moment of strong shock waves from high temperature light spark explosion in gases 06 p0930 A71-17399

Shock wave bisector rule improvement, applying to asymptotic behavior of bow shock attached to airfoil in two dimensional supersonic flow 06 p0841 A71-17420

Shell-fluid interaction problems, considering liquid filled shells oscillations, acoustic shock waves action, body impact against water, etc 06 p0998 A71-17861

Interstellar medium characteristics, examining H I and II regions thermal properties and shock waves 06 p0972 A71-18329

Extended stellar atmospheres production mechanism involving outward acceleration of material in rarefaction wave following shock wave arrival at atmosphere edge 06 p0976 A71-18472

Inviscid mixed subsonic-supersonic gas flows with shocks, developing time dependent numerical method [AIAA PAPER 71-45] 06 p0883 A71-18506

Hypersonic flow over cones with attached and detached shock waves, using Lax differencing technique and time dependent formulation for reentry flow fields 06 p0846 A71-18655

Blunt cylinder with small throat in anomalous seeded flow in hypersonic wind tunnels, observing separated shock wave distortion 07 p1013 A71-18924

Runge-Kutta type difference methods for calculating unsteady gas flow with shock waves 07 p1087 A71-19184

Nitromethane detonation initiation by long duration low amplitude shock waves 07 p1182 A71-19242

Shock wave diffraction by two dimensional weak disturbances, using aerodynamics blast method 07 p1223 A71-19255

Solar wind fast shock wave and simultaneous ground geomagnetic disturbance related to magnetospheric deformation 07 p1185 A71-19396

Comparison of experimental and gas dynamic fluid parameter jumps across earth bow shock, suggesting 07 p1185 A71-19396

- reappraisal of gas dynamic analog from satellite observation
07 p1103 A71-19678
- Two dimensional flow MHD in plasmas with anisotropic pressure, considering weak shock waves parameter changes in linear approximation
07 p1168 A71-19726
- Static pressure measurements near oblique shock waves using short probe, evaluating readings accuracy
07 p1090 A71-19911
- Hot plasma production by strong shock wave heating, using EM shock tubes under laboratory controlled conditions
07 p1172 A71-20506
- Nonideal plasma thermodynamically complete equation of state based on shock wave experiments
07 p1173 A71-20533
- Methyl radicals reactions produced by azomethane or ethane pyrolysis in reflected shock waves, describing chain reaction mechanism
08 p1250 A71-20668
- Chromosphere-flare and galactic cosmic ray hypotheses of Forbush decrease and strong shock waves in interplanetary medium
08 p1352 A71-20967
- Artificial solar wind experiments, describing interaction between hydrogen plasma shock wave and simulated geomagnetic field
08 p1354 A71-21010
- Shock waves behavior and effects in Sc galaxies spiral arms, attributing dark lanes at inward edges to shock waves in gas flow
08 p1362 A71-21133
- Electric breakdown in supersonic Ar or air flow behind shock wave, determining threshold discharge currents
08 p1276 A71-21485
- Two phase Hg tunnel for shock wave visualization by RF discharge between test model body and external ring, comparing measurements with supersonic flow theory
08 p1272 A71-21751
- Closing shock position in supersonic underexpanded single and two phase jets, determining liquid phase concentration effects on Mach number and nozzle pressure in wind tunnel
08 p1228 A71-21925
- Shock wave free surface velocity measurement using moiré method for photographic recording with image converter streak camera
09 p1444 A71-22715
- High beta collisionless shock wave turbulence, discussing frequency and wavenumber spectra and turbulence level measurements by light scattering technique
09 p1504 A71-23255
- Radiative flux effect on magnetogasdynamic shock in self-gravitating gaseous stars
09 p1506 A71-23589
- Interplanetary shock waves sounding and geomagnetic storm forecasting based on cosmic ray intensity increases from ground observations
09 p1515 A71-23633
- Combustion reactions development with velocity gradient downstream steady shock wave, considering aerodynamic field in supersonic wind tunnel
10 p1694 A71-23813
- Dissipative fluid sonic flow and shock conditions downstream of symmetrical plane barrier
10 p1549 A71-23824
- Ignition delay times behind reflected shock wave of alkanes methane through pentane in stoichiometric argon simulated air mixture
10 p1657 A71-24047
- Pseudo-stationary shock wave in plane MHD flow of conducting gases, deriving existence theorem for linear relations between vorticity and current density
10 p1648 A71-24281
- Aerodynamic characteristics and flow pattern in wake behind star-shaped body at supersonic speed, determining drag and shock waves location
10 p1551 A71-24371
- Cylindrical shock wave in solid body rotating gas for angular variation effects on shock velocity, using similarity method
10 p1593 A71-24405
- Relativistic MHD waves based on ideal fluid compressibility and statistical mechanics for given spacetime
10 p1650 A71-24586
- Shock and turbulent ray interactions of plasma streams with neutral gas cloud, noting comet tail similarity
10 p1652 A71-24653
- Hydromagnetic shock wave structure, treating plasma in two fluid approximation with collisional transport coefficients in changing density and temperature
10 p1596 A71-24657
- Acoustic and shock waves propagation in quasi-steady supersonic flow in duct with varying cross section
10 p1598 A71-25083
- Generation mechanism of magnetohydrodynamic shock waves associated with sudden commencements of 27-day recurrent geomagnetic disturbances
10 p1608 A71-25120
- Gravitational shock waves from tachyons, considering capability for Weber gravitational radiation detection apparatus excitation across astronomical distances
11 p1798 A71-25591
- Linear longitudinal ion wave instabilities in electrostatic shock in plasma by double humped /bump in tail/ velocity distribution
12 p1935 A71-26916
- Double structured perpendicular magnetoplasma shock waves possessing precursor foot due to ion reflection from resistive shock front
12 p1936 A71-26918
- Transport phenomena in rarefied gases, discussing sound dispersion in helium, weak shock waves, acoustic propagation in monatomic gases and kinetics in alternating fields
12 p1930 A71-27189
- Flowfields behind reflected shock waves, predicting end-wall pressure, radiative heat transfer and radiative gas dynamic coupling effects
[AIAA PAPER 70-774] 12 p1986 A71-27562
- Collisionless plasma with thermal ions in magnetic field absence, investigating stationary ion shock wave propagation
12 p1941 A71-27767
- Thermalization processes in earth bow shock with emphasis on ion heating, using electromagnetic dispersion relation for ion-ion streaming instability
13 p2054 A71-27908
- Solar wind-Mercury interaction, discussing planet physical properties, magnetized wind parameters and bow shock wave existence
13 p2120 A71-27924
- Isomagnetic potential discontinuity of electrostatic character in collisionless plasma shock waves, studying Mach number effect
13 p2105 A71-28169
- MHD discontinuities effect on earth magnetosphere, computing bow shock wave and magnetopause positions from satellite observation data
13 p2059 A71-28252
- Collisionless plasma thermal shock wave, showing heat in electron component transportable along magnetic field at lower rates than thermal velocity
13 p2106 A71-28425
- Earth magnetosphere boundary position, head shock wave, transition region width and current magnetic field changes during magnetopause in geomagnetic storm periods
13 p2061 A71-28549
- Reaction rate controlling mechanisms in shock wave initiated oxidation of formaldehyde
13 p2113 A71-28617
- Electron and laser pulse plumes, using thermomechanical shock wave theory
13 p2079 A71-28768
- German monograph on bimolecular reactions of H and O atoms in shock waves with hydrogen peroxide and dioxide and nitrous oxide
13 p2102 A71-28881
- Book on shock waves in collisionless plasmas covering basic equations and classification of shock structures, magnetosonic waves, shocks and solitons, electrostatic shocks and solitons, etc
13 p2108 A71-28896
- Electron thermal anisotropy effect on oblique whistlers preceding strong collisionless shock waves, using linear Vlasov theory
13 p2064 A71-29168
- Air inlet for simulation of shock wave separated flow in supersonic diffusers, deriving pressure variation profile along free boundary
13 p1992 A71-29175
- Shock wave strength for laminar boundary layer separation at transonic speeds with external flow freestream Mach number near one
14 p2324 A71-29883
- Electron and ion concentrations, electron temperature and electrical conductivity of ionized air before shock wave, using shock tube with He driver gas
14 p2225 A71-30225
- German monograph on shock waves in anisotropic plasma covering parameters derivation based on kinetic plasma theory and experimental verification possibilities
14 p2280 A71-30235
- Incident sonic boom shock wave reflection factors off smooth surface, discussing pressure rise and flight near threshold Mach number
14 p2177 A71-30610
- Electrical breakdown of supersonic Ar and air stream behind shock wave, determining threshold discharge currents
14 p2227 A71-30672
- Hypersonic flow pattern past windward side of delta wing with supersonic leading edges, joining potential and vortex regions behind shock wave
14 p2171 A71-30874
- Flat plate electrostatic probe for ionization rate measurements behind reflected shock waves, monitoring time evolution of electron production
14 p2248 A71-30884
- Shock compressed tetranitromethane mixtures with various benzene ethyl iodide proportions, investigating lateral discharge wave effects on detonation process structure
15 p2511 A71-31382
- Nonequilibrium effects in Ar free jet plasma, using cooled Langmuir probe for electron temperature and ion density measurements through shock wave in front of blunt body
[AIAA PAPER 71-591] 15 p2454 A71-31536
- Shock and pressure gradient induced turbulent transonic flow separation, using two dimensional circular arc model for flow field investigation
[AIAA PAPER 71-565] 15 p2344 A71-31559
- Temperature and shock structure effects on choked jet noise characteristics, using axisymmetric convergent and convergent-divergent nozzles for radiated noise fields investigation
[AIAA PAPER 71-582] 15 p2468 A71-31570
- Ethane-oxygen-argon mixtures ignition behind reflected shock wave, deriving composition temperature dependences correlation
[WSS/CI PAPER 71-16] 15 p2463 A71-31625
- Hydrogen fluoride vibrational excitation behind incident shock waves at 1400-4100 K, describing experimental procedure and results
[WSS/CI PAPER 71-17] 15 p2463 A71-31626
- Oxygen molecular excitation behind incident shock waves in pure oxygen and oxygen-argon and oxygen-neon mixtures, examining Schumann-Runge band system
[AVERL-RR-352] 15 p2451 A71-31674
- Coronal emission from turbulent plasma excited by shock wave, discussing relation to type 2 radio bursts
15 p2473 A71-31719
- Solar wind ion thermalization in earth bow shock by counterstreaming instability related to interplanetary magnetic field
15 p2399 A71-31774
- CIF diluted solutions in Ne, investigating thermal decomposition mechanism behind shock waves by mass spectroscopy
15 p2367 A71-31874
- Viscous boundary layer induced shock decay from analysis of disturbances generated by power law bodies in otherwise uniform two dimensional flow
15 p2392 A71-32115
- Finite ion temperature effect on large amplitude magnetosonic disturbances and collisionless shock waves formation in plasmas, using one dimensional macroparticle code
15 p2458 A71-32394
- Collisionless small amplitude shocks in plasmas, considering wave dispersion and critical Mach number effects
15 p2459 A71-32561
- Book on hodograph equations covering plane transonic flow, Tricomi boundary value problems, weak shocks and pressure density relations
15 p2394 A71-32766
- Low temperature shock waves in molecular hydrogen, discussing Rankine-Hugoniot equation behavior
16 p2555 A71-32895
- Reaction kinetic studies using hydrodynamic flow structure due to spherical shock wave from laser induced spark
16 p2616 A71-32903
- Ionizing shocks in argon produced by pressure driven shock tube, measuring velocity and ionization within and behind nozzle
16 p2616 A71-32904
- Pure carbon monoxide dissociation rate behind incident shock wave in high temperature environment, using two wavelength IR emission data
16 p2539 A71-32909
- Argon gas ionization behind reflected shock wave front investigation by double probe method with HF multistep pulse voltage
16 p2576 A71-32911
- Transient response of water drops to shock wave induced accelerations at near critical Weber numbers
16 p2557 A71-32925
- Flame, laser and shock wave plasma generation, considering afterglows, ionized gas flows and high temperature effects
16 p2617 A71-32958
- Ionospheric disturbances due to supersonic shock from missile exhaust plume, noting F region compressions and undulations
16 p2563 A71-33358
- Shock normal calculation by applying least squares technique to combined geomagnetic field and plasma data from single satellite, assuming Rankine-Hugoniot conservation relations
16 p2560 A71-33941
- Earth bow shock internal structure based on correlated observations of magnetic field, ELF magnetic fluctuations and suprathermal electrons by OGO 5 satellite
16 p2628 A71-33943

Boundary shock waves in electrically conducting gas under magnetic field, deriving Rankine-Hugoniot jump relations analogs and Prandtl relation 16 p2560 A71-34128

Nonlinear analysis of arterial flow pulses and shock waves, simulating aortic insufficiency under pathological conditions by mathematical model 16 p2538 A71-34145

Transonic flow fields in slender symmetric profiles, incorporating shock relations at trailing edge 16 p2522 A71-34163

Bibliography and review of interplanetary magnetic fields and plasmas, considering solar wind properties, magnetosheath, bow shock and magnetospheric tail 17 p2799 A71-34460

Hypersonic small perturbation flow past two dimensional or axisymmetric slender bodies supporting logarithmic shock waves 17 p2670 A71-34658

Thermal radiation effect on normal shock wave structure in gas-particle flows, deriving approximate closed form solution for gray absorbing particle cloud 17 p2727 A71-34879

Closing shock position in supersonic under-expanded single and two phase jets, determining liquid phase concentration effects on Mach number and nozzle pressure in wind tunnel 17 p2671 A71-35269

Tubular models sealed at one end with cavity facing oncoming steady gas flow, measuring increased stagnation temperature associated with shock wave formation 17 p2672 A71-35628

Shock wave formation in stationary flow adjacent to supersonic flow region, using Friedrich simple wave theory 17 p2673 A71-35645

Methane-oxygen-argon mixture ignition behind reflected shock waves in single pulse shock tube 17 p2792 A71-35707

Water vapor effects on shock compressed air in thermodynamic equilibrium by computer program, noting temperature and electron concentration reduction 18 p2984 A71-35857

Transonic flow numerical analysis, discussing initial conditions and imbedded shocks choice for computation efficiency 18 p2905 A71-36307

One-dimensional numerical model of nonisothermal plasma, showing soliton separation from leading front by ion-acoustic shock waves after reversal stage 19 p3042 A71-37076

Photographic observations of plasma eruptions from metal and opaque dielectric targets subjected to neodymium laser pulses, discussing successive shock wave formation 19 p3070 A71-37085

Spectroscopic analysis of continuous light emission from molecular oxygen-nitrogen mixtures in Mach 9 shock waves, stressing radiative reaction role 19 p3106 A71-37462

Shock wave data for Bamlé enstatite in 60-480 kb range, considering Hugoniot elastic limit and phase transition produced shock front 19 p3050 A71-37663

Spectroscopic study of imploding shock waves in hemispherical chamber filled with oxygen-hydrogen-helium mixture at high pressure 19 p3163 A71-37735

Solar wind fast shock wave and simultaneous ground geomagnetic disturbance related to magnetospheric deformation 19 p3127 A71-37820

Vibrational relaxation behind incident shock waves in CO based on shock tube pressure measurements at 2400-6000 K 19 p3106 A71-37880

Dissociation reaction in presence of halogen atoms produced in shock wave by thermal decomposition of hydrogen fluoride 19 p3012 A71-38085

NO, CO and Ar mixtures IR spectral emission radiant intensities behind shock tube generated reflected shock waves 19 p3012 A71-38087

Shock induced ignition in explosive homogeneous hydrogen-oxygen gaseous mixtures 19 p3171 A71-38130

Astronomical models of solar wind interaction with interstellar medium, determining magnetic field effects on shock wave 20 p3278 A71-39139

Soviet book on unsteady motions of continuous media covering gas dynamics, thermodynamics, shock and plane detonation waves, three dimensional gas motions, etc 20 p3211 A71-39144

Complex three dimensional shock waves about space shuttle configuration, visualizing hypersonic nitrogen flow with electron beams 20 p3211 A71-39356

Photometric and spectroscopic observations of pulsating stars, noting shock waves in atmospheres of W Virginis and RR Lyrae 20 p3292 A71-39446

Artificial solar wind experiments, describing interaction between hydrogen plasma shock wave and simulated geomagnetic field 20 p3279 A71-39590

Collisionless plasma thermal shock wave, showing heat in electron component transportable along magnetic field at lower rates than thermal velocity 21 p3421 A71-40083

Shock wave diffraction at symmetric lenticular wing profile with free stream critical Mach number of 0.87, using Godunov difference scheme 21 p3322 A71-40679

Noise sources in axial flow fans, considering radiation from turbulent boundary layers, scattering of incident turbulence and secondary flow influence 21 p3323 A71-40710

Shock waves and mechanical properties of solids - Conference, Raquette Lake, New York, September 1970 21 p3464 A71-40784

Shock stress waves dispersion in laminated composite materials 21 p3465 A71-40790

Computationally convenient equation of state describing porous materials shock response 21 p3466 A71-40795

Radially symmetric shocked flows computation method, using momentum equation in conservation form in original Cartesian coordinates 21 p3368 A71-40848

Soviet monograph on unsteady motion of compressible fluids covering acoustic and shock wave reflection from solid boundaries, impact penetration and pressure propagation 21 p3369 A71-40869

Molecular beam extraction from equilibrium gas flows, describing shock beam formation model with associated escape probability 21 p3419 A71-40956

Sonic boom minimization including front and rear shocks, exemplifying by SST aircraft 21 p3324 A71-40972

Stationary collisional shock observation in continuous supersonic plasma wind tunnel involving Q device modified into magnetic de Laval nozzle 21 p3426 A71-41403

Prior stressing and thermal treatments effect on shock induced substructures in polycrystalline Mo, using transmission electron microscopy 21 p3404 A71-41416

Two dimensional supersonic flow pattern, velocity and loss in shock waves in front of blade cascade 22 p3479 A71-41842

Hybrid computer simulation of nonlinear ion-acoustic shocks in diaphragms 22 p3577 A71-41896

Turbulent low Mach number electrostatic ion shocks evolution, correlating turbulence spatial growth with reflected ions distribution 23 p3708 A71-42892

High Mach number turbulent magnetosonic shocks generation by driving reflecting piston into plasma, simulating by electromagnetic particle code 23 p3708 A71-42893

Ne ionization relaxation time behind reflected shock waves from temperature and pressure measurements of combustion driven shock tube end wall 23 p3706 A71-42909

Sonic line position measurement in supersonic flow behind detached shock wave preceding axisymmetric or plane blunt bodies 23 p3625 A71-43092

Translational and rotational temperature and density variations through shock waves in oxygen and nitrogen, using Monte Carlo scheme 23 p3781 A71-43444

Plane supersonic ionizing shock wave in magnetic field under small wave plane perturbation from equilibrium position, calculating stability from linearized equations 23 p3663 A71-43575

Gravitational shock waves study by tensor distribution technique including Einstein equations solution 23 p3770 A71-44006

Approximate solution for position and strength of shock waves about cones in steady supersonic flow 24 p3790 A71-44624

Shock initiation problem collisionless solution for transport properties of gas flow, considering departure from Navier-Stokes solution 24 p3819 A71-44791

Working gas parameter determination for valve supply main system during feed opening, explaining heating effect for second valve by shock wave theory 24 p3793 A71-45021

Solar radio burst generation model based on effects of strong shock waves during chromospheric flares for geomagnetic storm prediction 24 p3867 A71-45081

Nonlinear equations of compressible medium motion near point of contact between shock and diffraction waves 24 p3821 A71-45365

Two dimensional reflection supersonic nozzle shock wave initiated unsteady starting process, presenting shadowgraphs from shock tube investigation 24 p3821 A71-45367

SHOOTING STAR AIRCRAFT

U T-33 AIRCRAFT

SHORT CIRCUITS

Temperature effects on Si solar cell short circuit currents, considering solar spectrum, photon absorption coefficient and diffusion length 05 p0700 A71-16067

Static fluid logic elements, discussing short circuit during switchover, snap action, pressure loss and circuit examples 07 p1027 A71-20573

LF transistor power amplifier protection from power overloads in case of short circuit at output 12 p1889 A71-27625

Lumped model for two dimensional current flow in grown junction transistor base, predicting small signal common emitter short circuit input impedance 22 p3523 A71-42359

SHORT HAUL AIRCRAFT

Economic contributions of U.S. domestic airline industry in 1970s regarding air transportation constraints and impact on short haul 01 p0004 A71-10486

Short haul air transportation in U.S., interagency cooperation and federal involvement 01 p0184 A71-10875

Short haul air transportation technological factors for VTOL, STOL, CTOL and light aircraft, considering operating costs, passenger service and environment impact 02 p0188 A71-11700

V/STOL short haul transport systems, discussing interurban applications, all-weather operation, operating costs, noise and atmospheric pollution 03 p0523 A71-13565

Intercity V/STOL air transportation system, discussing traffic movements, cost and terminals 03 p0454 A71-13566

Intercity V/STOL aircraft transport system, solving congestion problems through all weather superiority, low noise level and separate ATC 03 p0347 A71-13571

VTOL systems for commercial short haul air transportation, discussing large helicopters and compound aircraft applications for system capacity profitability and efficiency increases 03 p0347 A71-13575

Short haul STOL aircraft transport system, discussing neighborhood stoptop ownership, technical feasibility and economic, emotional, ecological and sociological viability 03 p0523 A71-13618

Compound and VTOL aircraft and prototype compact downtown V-ports for short haul air transportation improvement and expansion 03 p0348 A71-13619

Short haul STOL concepts including stoptop potentials, onboard avionics, vehicle characteristics, tradeoffs and current nonproductive flying due to traffic congestion 03 p0348 A71-13620

Area navigation in commuter/air taxi operations concerning airborne equipment, airport utilization and CTOL, STOL and VTOL aircraft 04 p0622 A71-14650

Optimum flight paths for V/STOL aircraft operating in short haul transportation near city centers 04 p0624 A71-15443

V/STOL component of unified transportation system, discussing transportation modes, airport locations, noise reduction, cost factors, etc 10 p1556 A71-24274

Turbofan VTOL or STOL intercity aircraft, examining high bypass lift engine design 10 p1557 A71-24861

European airbus, considering flight trials of first A.300B high capacity transport aircraft 12 p1867 A71-26921

Prop-fan propulsion system for V/STOL short haul transport aircraft, discussing performance, noise and weight characteristics [SAE PAPER 710470] 13 p2115 A71-28338

Dassault Mercure short range twin jet aircraft capable of using powerful engine 13 p1997 A71-29276

Aircraft capabilities in intraurban transportation for Detroit metropolitan area, considering vehicle design, fleet size, cost and terminal location [AIAA PAPER 71-504] 14 p2172 A71-29548

Integrated short-haul interurban transportation system, considering combination of conventional jet aircraft, STOL aircraft and high-speed ground transportation [AIAA PAPER 71-508] 14 p2221 A71-29550

French contribution to air transportation, discussing international cooperation on supersonic Concorde, medium range airbus and short range Mercure 15 p2350 A71-32688

Low disk-loading propfan application to propeller and fanjet STOL and fanjet VTOL short haul aircraft [AIAA PAPER 71-781] 17 p2674 A71-34481

- Operating costs and runway lengths for V/STOL in city and suburban short haul air transportation 18 p2987 A71-36347
- Future air transportation concepts, discussing short haul travel market, economic, environmental, safety, convenience and reliability aspects 18 p2989 A71-36671
- European air traffic employed in transportation of tourists, considering European Airbus A-300B super twin 19 p3172 A71-37273
- Mercury short range passenger aircraft design conception, analyzing cost 19 p2997 A71-38242
- Short haul air transportation, discussing performance requirements, community acceptance and navigation and landing aids 22 p3482 A71-42073
- STOL aircraft system, discussing ground installations, runways, three dimensional area navigational aids, noise reduction, air traffic and short haul productivity [AIAA PAPER 71-983] 24 p3791 A71-44579
- ## SHORT RANGE BALLISTIC MISSILES
- Short range air to ground attack missile system, discussing nuclear warhead, propulsion system, performance characteristics and program cost analysis 10 p1682 A71-24286
- Linear closed loop optimal intercept guidance law compensating for short range tactical missile time lag, guidance command saturation and target acceleration 15 p2446 A71-32113
- Image recording system low light /IR/SILL/ camera design for long range attitude and events /LORAE/ telescopes in short missile instrumentation 18 p2919 A71-36086
- ## SHORT TAKEOFF AIRCRAFT
- ### NT DHC 4 AIRCRAFT
- Aladin 2 interurban Stoll transport design with blown wings and jet deflection by wing flaps, emphasizing engine noise reduction 01 p0005 A71-10749
- High lift systems for four-engine Mach 0.8 turbofan STOL aircraft, discussing propulsion, aerodynamics and design trends [SAE PAPER 700811] 01 p0003 A71-11545
- STOL navigation equipment and microwave landing instruments test programs, noting data recording and flight operations 03 p0454 A71-13286
- STOL future performance and safety level, considering current jet aircraft fatal accident record and proportional perpetuation, airworthiness and operational considerations 03 p0347 A71-13568
- Short haul STOL aircraft transport system, discussing neighborhood stolport ownership, technical feasibility and economic, emotional, ecological and sociological viability 03 p0523 A71-13618
- Short haul STOL concepts including stolport potentials, onboard avionics, vehicle characteristics, tradeoffs and current nonproductive flying due to traffic congestion 03 p0348 A71-13620
- STOL and boundary layer control aircraft takeoff and landing distance, considering jet suction action influence on lift and drag coefficients 04 p0529 A71-14595
- STOL aircraft for tactical support, discussing USAF intertheater requirements 04 p0529 A71-15024
- IFR design requirements for STOL navigation equipment from flight tests 04 p0623 A71-15424
- Three axis flight director for precise helicopter control, deflected slipstream STOL or VTOL attitude and power under low ceiling and visibility landing 04 p0624 A71-15428
- VTOL and STOL port federal design criteria, outlining planning and construction 04 p0567 A71-15441
- Public-use ground level and rooftop helicopter and STOL aircraft landing facilities for city and suburban traffic 04 p0567 A71-15442
- Light amphibian passenger STOL P-300 Equator aircraft, using single turbosupercharged engine driving two blade propeller at tail assembly 05 p0696 A71-16132
- Universal mini carrier UMC-120 light turboprop STOL transport 05 p0696 A71-16133
- ARAVA STOL aircraft, describing payloads, configuration, design flight testing, stability and landing characteristics 07 p1018 A71-19082
- Ground boundary layer effects of fixed ground plane for powered STOL wind tunnel model, discussing flow breakdown criteria, contraction lag, strut fairing interference, etc [AIAA PAPER 71-266] 08 p1232 A71-21992
- Power augmented lift STOL aircraft operating costs reduction by channel wing concept, discussing aerodynamic theory and structural applications to high lift flaps aircraft 09 p1385 A71-22592
- Fluid mechanics of atmospheric environment and flow on swept wings in short and medium range aircraft design, concerning STOL capability in India 09 p1383 A71-23199
- NASA aerodynamic research applicable to business aircraft concerning wind tunnel and flight tests, STOL performance and high speed cruise technology [SAE PAPER 710378] 10 p1554 A71-24244
- Aladin 2 French STOL project, consisting of suitably flapped wings with multiple propulsion units with fishtail exhaust nozzles inside rectangular ejectors 10 p1556 A71-24283
- Turbofan VTOL or STOL intercity aircraft, examining high bypass lift engine design 10 p1557 A71-24861
- Wing flap slipstream deflection correction method for evaluation of propeller power effect on lift and drag coefficients of Arava twin engine STOL aircraft 11 p1706 A71-25164
- Technical aspects of tactical all-weather instrument landing system of Swedish STOL aircraft Saab 37 Viggen 11 p1796 A71-25233
- Wing design criteria imposed by high speed requirement for short takeoff aircraft, considering thin swept-back wing with small aspect ratio for lateral control 12 p1867 A71-27471
- Turbofan STOL transport application to air transportation congestion, discussing conditioning landing field length, navigational/control problems and jet flap concepts 12 p1868 A71-27602
- Vortex wakes behind STOL operations high lift wings, discussing height above ground and various wind tunnel dimensions effects 13 p1990 A71-28033
- STOL aircraft electric power variable frequency generation and high voltage DC distribution with secondary square wave AC distribution [SAE PAPER 710444] 13 p1998 A71-28325
- Military/commercial STOL transport design, discussing performance, payload and equipment requirements with emphasis on production cost benefits [SAE PAPER 710468] 13 p1996 A71-28336
- STOL aircraft/engine integrated systems for medium distance air transportation, discussing tradeoff factors involving performance, noise, weight and cost [SAE PAPER 710469] 13 p2115 A71-28337
- Integrated short-haul interurban transportation system, considering combination of conventional jet aircraft, STOL aircraft and high-speed ground transportation [AIAA PAPER 71-508] 14 p2221 A71-29550
- Two dimensional flow research on high lift airfoils for STOL aircraft, using vorticity distribution and wind tunnel wall blowing techniques 14 p2169 A71-29910
- Civil aviation customer /operator, passenger and community/ needs, describing STOL and V/STOL aircrafts 14 p2340 A71-30162
- VTOL and STOL aircraft comparative study covering site area, cost and noise and toxic gas production 14 p2175 A71-30163
- Air transport development trends, considering increased speed and capacity, STOL aircraft, urban service, and European cooperation for manufacturing 14 p2341 A71-30302
- STOL vehicle and systems air transportation expansion by reducing trip time, congestion, noise exposures and pollution for DOT, DOD and NASA roles [SAE PAPER 710464] 14 p2176 A71-30535
- Commercial vs military design criteria for STOL transport aircraft, noting landing and takeoff distances and noise levels [SAE PAPER 710465] 14 p2176 A71-30536
- STOL aerodynamics of leading edge high lift devices on thick profiles, externally blown flaps, boundary layer control and jet flap effect 15 p2343 A71-31214
- STOL commercial aircraft propulsion systems, considering two stream augmentor wing engine and high bypass ratio three stream engine [AIAA PAPER 71-746] 15 p2467 A71-31325
- Aladin II four-jet engined STOL intercity transport aircraft, noting low noise characteristics and passenger capacity 15 p2347 A71-31412
- Three dimensional jet flap and lifting line/ surface theories application to STOL aerodynamic systems with externally blown flaps and augmentor wing [AIAA PAPER 71-578] 15 p2345 A71-31568
- Quiet turbofan STOL feasibility, discussing structural, propulsive and technical aspects, economy, passenger comfort and performance estimates 15 p2348 A71-31605
- STOL jet aircraft noise reduction by using engines with moderate dilution rate 15 p2349 A71-31882
- STOL aircraft flight characteristics in proximity to ground, comparing analytical results with wind tunnel test data [AIAA PAPER 71-579] 15 p2349 A71-32281
- Life cycle cost optimization of STOL aircraft and tracked air cushion vehicles for operating transportation system 16 p2522 A71-33306
- Canadian R and D on fixed wing civil STOL aircraft, discussing augmentor wing concept using jet powered lift augmentor system 16 p2523 A71-33470
- Twin turboprop STOL aircraft lateral directional oscillation traced to rudder vibration due to aerodynamic hinge moments interaction with friction [AIAA PAPER 71-792] 16 p2525 A71-34019
- Low disk-loading propeller application to propeller and fanjet STOL and fanjet VTOL short haul aircraft [AIAA PAPER 71-781] 17 p2674 A71-34481
- STOL aircraft guidance capability with onboard digital computer, maintaining time of arrival envelope at way points along complex flight paths [AIAA PAPER 71-770] 17 p2775 A71-35528
- Passenger travel demand model for STOL transportation in underdeveloped areas 18 p2987 A71-36348
- Aircraft control design by implicit model-following technique with optimal feedback sampled data and continuous control algorithm, exemplifying STOL aircraft landing approach control [AIAA PAPER 71-956] 19 p2995 A71-37197
- Airport system utilization, discussing aircraft noise, ATC, STOL development and passenger handling capacity problems [CASI PAPER 72/3] 19 p3041 A71-37594
- Costs/benefits strategy for investment in STOL fleets reducing delay and airport congestion, using heuristic computer model 19 p3173 A71-38029
- VTOL and fan lift STOL aircraft, discussing simulation and head-up displays for roll demand, vertical speed and ILS beam 21 p3413 A71-40134
- Modular step scan microwave aircraft landing system /TALAR/ design and operation, noting short takeoff and landing 22 p3572 A71-42088
- Takeoff and landing performance evaluation for commercial STOL aircraft, noting high bypass ratio turbofans and high lift systems use 22 p3483 A71-42286
- Canadian STOL program, discussing Quebec-Windsor corridor passenger traffic [AIAA PAPER 71-982] 24 p3791 A71-44578
- STOL aircraft system, discussing ground installations, runways, three dimensional area navigational aids, noise reduction, air traffic and short haul productivity [AIAA PAPER 71-983] 24 p3791 A71-44579
- Performance prediction and evaluation of propulsion-augmented high lift systems for STOL aircraft, considering weight, thrust and wing loading [AIAA PAPER 71-990] 24 p3791 A71-44585
- AIAA members comments on STOL, VTOL and V/STOL aircraft merits and developments [AIAA PAPER 71-1015] 24 p3791 A71-44596
- STOL aircraft flight control problems, discussing Mach trim, artificial feel, stability, feedback system responses and lateral/directional laws [AIAA PAPER 71-993] 24 p3792 A71-45297
- ## SHORT WAVE RADIATION
- ### NT DECIMETER WAVES
- ### NT MICROWAVES
- ### NT MILLIMETER WAVES
- ### NT SUBMILLIMETER WAVES
- Short wave reflected radiation fluxes in atmosphere with absorption allowance for water vapor, carbon dioxide and ozone 01 p0144 A71-10538
- Explosion shock wave induced short wave radio emission, deriving time related gas ionization state of wave front 02 p0284 A71-11927
- Short radio wave propagation over single jump lines in F 2 critical frequency gradient presence, examining maximum usable frequency increase 09 p1405 A71-22439
- Atmospheric short wave radiation angular and vertical distribution relation to aerosol scattering parameters, using transport equation 16 p2605 A71-34104
- Short wave radiation fluxes estimation for earth-atmosphere system from Cosmos satellite data, studying brightness field angle structure 20 p3260 A71-39681
- Angular distribution of outgoing short wave radiation field intensity as function of sun height on basis of actinometric data from Cosmos 184 satellite 21 p3374 A71-41299
- Neutral helium short wave solar radiation in quiescent and loop prominences 23 p3768 A71-43844

SHORT WAVE RADIO TRANSMISSION

Short wave broadcasting and ionospheric reflection during solar eclipse of 7 March 1970, relating to nighttime free electron distributions
01 p0151 A71-10119

Short wave signal polarization fading minimization by dispersed reception of circularly polarized components, discussing power gain relation to antenna configuration
02 p0219 A71-12543

Short wave double log periodic antenna for 8-26 MHz transmission over long path lengths
07 p1080 A71-20265

Ionospheric absorption relation to solar X-ray flux enhancement during short wave fade-outs from OGO-4 and Solrad 9 satellites
07 p1064 A71-20318

Short wave communication channel quality estimate for discrete signal transmission based on signal level variations calculation with allowance for ionospheric parameters
08 p1252 A71-20773

Diurnal and seasonal variations of scintillations in short wave radio signals transmitted from earth satellites and spacecraft, noting relationship to ionospheric inhomogeneities
12 p1898 A71-26635

Remote controlled automatically tuned 1-kw short wave transmitter with zero power tuning mode of power stage and drive unit frequency generation
12 p1887 A71-26989

Short wave radio reception and signal paths at magnetically conjugate point in Southern Hemisphere, using 40-110 msec delay times
13 p2030 A71-28536

Short wave skip distance calculation as function of path inclination to ionospheric layer for linear and parabolic ionization distributions
13 p2030 A71-28556

Reflected short wave signal frequency shift due to reflecting ionospheric layer movement and electron concentration changes, considering oblique incidence on isotropic and anisotropic layers
16 p2542 A71-33484

Quasi-specular and Lambert reflection of short radio waves from lunar surface dependent on central portion of near side
16 p2543 A71-33668

Short wave frequency-diversity radio communication systems operating at extremal frequencies of group, estimating noise reduction effectiveness
17 p2698 A71-34395

Short wave radio signal analyzer for joint distribution of phase and amplitude probabilities and PSK communications noise stability in ionosphere
19 p3028 A71-37784

Continuous solar UV and X rays monitoring by SOLRAD 10 satellite, investigating solar activity and flares effect on shortwave communications and manned space travel
20 p3294 A71-39580

SHOT NOISE

Phase fluctuations in nonautonomous reflex klystron oscillators due to shot noise in electron beams
04 p0557 A71-14624

Schottky barrier diode shot noise, examining dependence on potential barrier gap thickness, height and permittivity, impurity distribution, Schottky layer thickness and semiconductor dielectric constant
07 p1075 A71-19225

Shot noise effect on ambient plasma magnetosphere electric field measurements with Langmuir and double probes for electron density and temperature
11 p1756 A71-25644

Distributed tunnel diode traveling wave amplifier load noise thermal and shot components, noting impedance boundaries
20 p3206 A71-39814

Fluctuation in synchronized reflex klystron oscillators due to shot noise in electron beams
22 p3521 A71-42264

Electron bombardment effects on shot noise of silicon junction transistors, noting generation-recombination current increase in emitter junction
22 p3586 A71-42298

SHOWERS

Zero gravity whole body shower system for space station, describing air drag and vacuum methods for water collection
[ASME PAPER 71-AV-2] 18 p2865 A71-36369

High power radar identification of preferred areas of shower development, analyzing thermal convective areas distribution
19 p3089 A71-37503

SHRINKAGE

Boundary value problem of elasticity theory for reinforced plastics with internal stresses due to shrinkage
01 p0107 A71-10495

Two semiinfinite strips joined to form one infinite strip, determining stresses by joint shrinkage
03 p0509 A71-13898

Stability loss in microvolume of laminated composites with small filler concentrations during shrinkage, using three dimensional linearized equations
12 p1978 A71-27344

SHROUDED BODIES

U SHROUDS

SHROUDED NOZZLES

Convolute nozzle extension in engine with low pressure exit seal released and blown off by venting internal pressure
[AIAA PAPER 71-677] 14 p2292 A71-30741

SHROUDED PROPELLERS

Lift characteristics of semicircular channel wing with pusher propeller at trailing edge, comparing theoretical, wind tunnel and flight test results
10 p1553 A71-24857

SHROUDED TURBINES

Shrouded aircraft engine turbine blades vibration stresses found minimum by setting up paired blades with fixed tension along shroud
09 p1538 A71-22595

SHROUDS

Space environment simulation chamber shrouds, developing mathematical expressions for temperature distributions in flat plates and trapezoidal fins
05 p0733 A71-16137

Flow induced vibration suppression by perforated concentric shroud around circular cylinder, investigating porosity and shroud/cylinder diameter ratio effects [ASME PAPER 71-VIBR-28] 21 p3458 A71-40283

SHUNTS

U BYPASSES

U CIRCUITS

SHUTTERS

Contact electro-optic KDP crystal shutters for Q switching ruby laser
06 p0907 A71-17530

Holographic stroboscope using ruby laser with passive shutter for HF vibration measurement
14 p2254 A71-30584

SIBERIA

Noctilucent cloud observations at Tomsk, Novosibirsk and other Siberian locations from 1965 to 1968
14 p2233 A71-29970

SIC [COEFFICIENT]

U STRUCTURAL INFLUENCE COEFFICIENTS

SICKNESSES

NT ALTITUDE SICKNESS

NT DECOMPRESSION SICKNESS

SID [IONOSPHERIC DISTURBANCES]

U SUDDEN IONOSPHERIC DISTURBANCES

SIDE INLETS

Secondary gas injection at right angles into supersonic rocket nozzle, investigating side force characteristics
03 p0470 A71-13736

SIDE-LOOKING RADAR

NT RADAR IMAGERY

Side-looking airborne radar /SLAR/ imagery and site selection for soil pattern topography
02 p0244 A71-11952

Side-looking airborne radars ground and slant range imagery mosaic preparation and geoscience interpretation, analyzing terrain geometry, radar shadow and layover
06 p0898 A71-17561

Mapping by position data extraction from airborne high resolution side-looking radar
06 p0869 A71-18295

Side-looking airborne radar and IR line scan systems, discussing instrumental correction of image distortion
09 p1450 A71-22967

Side-looking radar, thermal IR scanner and passive microwave radiometers for remote sensors for geologic mapping
09 p1452 A71-23215

Side-looking airborne radar /SLAR/ for sea ice identification, mapping and ship routing in Northwest Passage
09 p1439 A71-23448

Target movement effects on airborne coherent side-looking synthetic aperture imaging radar during scan rate and compression ratio increases
14 p2197 A71-30798

Structural design, mechanical stability and aircraft compatibility for airborne side-looking radar antennas, using end fed slotted waveguide arrays
14 p2205 A71-31041

Pulse compression and optical data correlation in side-looking radar, considering Doppler effect
15 p2374 A71-32650

Remote sensing for geologic purposes, using side-looking radar for fracture and fault detection and IR images for limestone, dolomite and granite discrimination
18 p2911 A71-35890

Vegetation penetration with K-band side-looking airborne imaging radars, noting multifrequency multipolarization system application for terrain reconnaissance
18 p2875 A71-36365

Side-looking airborne radars and image recording scanners design for geoscience applications, discussing gray scale improvement, multispectral sensing, target discrimination, etc
18 p2875 A71-36366

SIDEBANDS

Long time planetary atmosphere motions, investigating sideband resonance mechanism in Rossby wave packet interactions with weak shear zonal flow
12 p1925 A71-27195

Optimal design for minimum noise maximum gain bandwidth of lower sideband parametric up-converters
23 p3630 A71-42917

SIDELobe REDUCTION

Reception and transmission of reduced sideband pseudorandom FM signals using quaternary S-sequence synthesis
01 p0037 A71-11082

Optimal synthesis of antenna array radiation patterns with minimum square deviation from zero in sidelobe
04 p0557 A71-14629

Phased arrays sidelobe reduction by digital phase shifters, considering scan angle and phase quantization step size
06 p0875 A71-17711

Wideband radar array antenna system with suppressed grating lobes
06 p0867 A71-17712

Phased arrays sidelobe reduction through reflection lobe dispersion
06 p0875 A71-17718

Fluctuating radar target detection in clutter by sidelobe blanking system, discussing false alarm adaptive threshold procedure
07 p1154 A71-18842

Longitudinal direction positioning error effects on grating lobe field deviation and reduction in uniform linear arrays
08 p1257 A71-21885

Linear and circular apertures sum and difference radiation patterns for minimum sidelobes power
09 p1407 A71-23108

Double curved reflectors assembly methods for rotating search radar antennas, considering parabolic and elliptic strip shapes for sidelobe suppression modification
09 p1409 A71-23495

Linear antenna arrays synthesis with Z transforms permitting sidelobe reduction and nulls in antenna radiation patterns
09 p1419 A71-23498

Sparse antenna arrays with small sidelobe level, estimating error due to radiation pattern substitution by statistical method
11 p1741 A71-26556

Long conical multimode horn with corrugated surface throat to suppress sidelobes and equalize E and H plane beamwidths
17 p2716 A71-35095

Far field minimum radiation over angular sector for directional broadside array with optimum interelement spacing, considering sidelobe reduction
18 p2875 A71-35972

Constrained optimization of array antennas performance for obtaining radiation pattern with desired sidelobe levels
19 p3023 A71-38591

Optimal synthesis of antenna array radiation patterns with minimum square deviation from zero in sidelobe
22 p3510 A71-42269

Circular aperture illuminations for high beam efficiency and low sidelobes in search radar antenna applications, using Fredholm integral equation
24 p3809 A71-44990

SIDELOBES

Chebyshev antenna arrays minimum length for given sidelobe levels
04 p0557 A71-14631

Chebyshev array directivity for various element spacings and sidelobe ratios, presenting formulas for computer calculations
06 p0875 A71-17725

Polar diagrams computation for large Cassegrain antennas, obtaining sidelobe peaks envelope at wider angles of radiation by near field measurements
15 p2368 A71-31139

Line source excitation for maximum aperture efficiency with given sidelobe level
19 p3035 A71-38596

Chebyshev antenna arrays minimum length for given sidelobe levels
22 p3521 A71-42271

Reflector antenna under wideband noise radiation, determining directivity characteristics by solution for angle range homologous to region of irregular sidelobes
22 p3524 A71-42757

SIDERITE METEORITES

U IRON METEORITES

SIDESLIP

NT EARTH ORBITAL RENDEZVOUS

NT LUNAR ORBITAL RENDEZVOUS

NT ORBITAL RENDEZVOUS
NT SPACECRAFT DOCKING
Systems analysis application to stability of aerodynamic cross coupling in flight vehicle motions with steady sideslip, using feedback and root locus techniques
02 p0190 A71-12687
Automatic control system for fighter aircraft sideslip correction, using rudder position sensor, transverse accelerometer and high pass filter for anticipatory sideslip reduction
10 p1556 A71-24288
Side forces on ogive cylinder bodies at large incidence as function of Mach number, nose fineness and bluntness ratios for laminar and turbulent boundary layers
[AIAA PAPER 71-570] 15 p2345 A71-31563
Digital simulation for predicting static directional aerodynamic forces and moments characteristics of air cushion vehicle configuration through 180 degrees of sideslip
[AIAA PAPER 71-907] 19 p2995 A71-37158
SIDEWASH
U BACKWASH
SIGHT
U VISUAL PERCEPTION
SIGNAL ANALYSIS
Radar tracking systems stretcher detector circuit output signal amplitude and spectral distribution analysis
01 p0029 A71-10308
Weather radar signals decorrelation times due to vertical wind shear and azimuth scanning
01 p0030 A71-10598
Chi-square distributions fitted to observed telecommunication variables distributions
01 p0041 A71-11609
Straight and curved edges produced vidiosignal amplitude spectra discrimination in TV image scanning of nuclear particle path photographs, using filtering device
02 p0248 A71-11827
Rectilinear edge aperture filtration, examining mismatch angle effects on videosignal amplitude
02 p0248 A71-11828
Monochromatic signal spectrum determination from circulating realization spectrum analysis
02 p0248 A71-11833
Ionization gage detector signal interpretation as function of reflected molecule velocity distribution, noting shutter speed errors
02 p0286 A71-12128
Frequency and phase analyses of cross correlated signals from very long baseline interferometry of decametric radiation from Jupiter
02 p0310 A71-12333
Spacecraft signal amplitude and phase modulation and fault diagnosis by VLF analysis
02 p0218 A71-12447
Radar signal probability ratio over finite interval
02 p0219 A71-12620
Correlator circuit for low level signal extraction from noise and for analysis of frequency spectrum of complex AC signals
03 p0377 A71-13241
Long baseline radio interferometry, discussing phase difference measurement principles in terms of signal characteristics and wave forms, astronomy and geodesy applications
03 p0484 A71-13244
Noiselike signals frequency modulation via pseudorandom sequence, deriving relationships for spectra and combined /frequency-lag/ correlation functions
03 p0378 A71-13393
Sampling and averaging techniques in fast random signal analysis using oscilloscope and memory unit
03 p0379 A71-13911
Preshwhitening technique for acoustic turbulent flow data recording and analysis
04 p0600 A71-15598
Field of determinate signal with normal noise, considering representation as superposition of two circularly polarized components of directly opposite rotation
05 p0719 A71-16010
EEG topography continuous recording for signal analysis based on regression theory
05 p0713 A71-16321
Digital computer operated from remote terminal for signal analysis including Fourier transform, complex multiplication and conjugation
05 p0727 A71-17144
Frequency domain and time domain methods analysis of signal from laser velocimeter
06 p0900 A71-18053
GaAs lasers self-induced pulses signal structure, measuring pulse width, repetition rate and amplitude fluctuations
06 p0910 A71-18671
Large signal oscillation mode model for GaAs devices operational prediction, including space charge and intervalley transfer time effects
07 p1070 A71-18867

Large signal microwave equivalent circuits analysis of IMPATT diodes, allowing carrier multiplication by impact ionization at every point in diode
07 p1072 A71-19108
Electronic synthesis using time structural properties of signals in radio systems
07 p1063 A71-20256
Temporal registration efficiency of rectangular pulse by position of front at ideal band filter output
07 p1064 A71-20259
Statistical dynamic response of FM receiver with frequency feedback
07 p1064 A71-20261
Sequence spectrum of phase modulated discrete signal for frequency division multiplex filters
07 p1064 A71-20264
Binary signal parameters estimation mixed with Gaussian noise, using method of moments
07 p1065 A71-20420
Multisignal characteristics of high power noise modulated microwave traveling wave tube amplifiers
07 p1064 A71-20452
Fluidic Helmholtz resonator for FM signal analysis, showing instantaneous phase difference between input and output pressures
07 p1026 A71-20568
Analog surveillance radar signal analysis by digital storage and evaluation methods
08 p1252 A71-20745
Spatial resolution improvement by utilizing temporal degree of freedom of transmitted signal, discussing hologram plate recording during exposition intervals
08 p1287 A71-21191
Neuroelectric signal analysis using real time nerve spike recognition and separation based on nuclear instrumentation techniques
08 p1249 A71-21839
Signaling sensitivity leveling by introduction of automatic defect indicator into defectoscope
08 p1273 A71-21904
Signals statistical parameters and phase space properties, deriving functional relationships for signal processing correlation techniques
09 p1405 A71-22298
Spectral analysis of laser Doppler flowmeter signals, considering time independent systems
09 p1463 A71-22691
Constant, programmed and random amplitude spectral analysis and signal averaging correlation with failure statistics, noting laboratory simulation
09 p1444 A71-22709
Time series analysis techniques concerning correlation, auto and cross power spectral density, amplitude and period histograms, real time pattern recognition and filtering
09 p1405 A71-22783
Power spectral density /PSD/ analysis of multilevel binary coded signals for high density PCM recording
09 p1412 A71-22784
Solar radio burst types occurrences at various frequencies in relation to radio emission slowly varying component
09 p1514 A71-22793
Applied transducer signals from surface and internal fractures of various lengths, depths and positions
09 p1450 A71-22896
Orthogonal signal analysis and synthesis with Walsh functions, giving practical implementations of required operations
09 p1406 A71-23030
Signal mean and noise variance as direct functions of phase angle between signal component passed by bandpass limiter and coherent reference
10 p1582 A71-23765
Correlation, transfer and coherence functions in measurements, using digital signal analysis
11 p1731 A71-25597
Signals as information carriers, comparing bounded spectrum carrier model, Gabor model, analytical signal model, steady random process model with bounded spectrum and Rice-Bunimovich model
11 p1734 A71-26463
Small signal characteristics mathematical models of carotid sinus baroreceptors of rabbits
12 p1870 A71-27133
Signals single set synthesis for simultaneous target information transmission and range and velocity measurement
12 p1883 A71-27617
Continuous observation of resolvable signal random flows
13 p2033 A71-28916
Small-signal gain radial variation in cylindrical electrically excited carbon dioxide laser amplifier, characterizing discharge properties by modified Schottky analysis
13 p2080 A71-29330
Class structure of system identification problems with input and output signals and transform H, applying to stochastic operators
14 p2219 A71-29697

Strong level crossing signals in stepwise fluorescence, investigating fine and hyperfine structure of atomic Li
14 p2277 A71-30508
Bayesian estimate of signal parameters in random noise background under mutually exclusive hypotheses about statistical properties
15 p2370 A71-31584
Optimal Bayesian system for simultaneous discrimination and parameter estimation of several signals in noise background
15 p2370 A71-31585
Conditional distribution density formation for signal-noise mixture based on learning sampling with dependent values
15 p2370 A71-31586
Weak signal detection in additive mixture on non-Gaussian random-correlated noise, deriving algorithms for discrete- and continuous-time and coherent detection problems
15 p2370 A71-31590
Synchronous data transmission system digital signal harmonic analysis based on stochastic process theory, applying to amplitude and phase modulation
15 p2372 A71-32321
Arbitrary shape pulsed AM systems prediction technique improvement, using time-domain signal
15 p2373 A71-32371
Root-mean-square and uniform approximations of signals by Fourier and Haar series
16 p2550 A71-33720
Steady and linear systems discretization by Laguerre transformation and isomorphism between continuous and discrete signals
16 p2550 A71-34058
Cosmos satellites tracking and monitoring, decoding and interpreting radio signals
16 p2643 A71-34080
Radio astronomy signals reception and interpretation, detailing solar, galactic and extragalactic spectrum sources
17 p2797 A71-34242
Random aperiodic signals analysis, using two dimensional Fourier transforms
17 p2709 A71-35790
Self consistent one dimensional large signal analysis of Read type IMPATT diode oscillator, taking into account device-circuit interaction
18 p2888 A71-36130
Binary sequences generated by conventional pseudorandom shift register sequences for communication and system identification
18 p2881 A71-36568
Traffic capacity of systems for search and analysis of radio signals with random duration
19 p3015 A71-37258
Second approximation estimates of spatial-temporal signals parameters
19 p3015 A71-37260
Holographic method of correlation and spectral analysis of radio signals applied to stable RF generator, random fields and stereophonic radio transmission measurements
19 p3067 A71-38492
Beam direction weight center of signal spectrum and effective antenna centers of airborne Doppler velocimeter in horizontal flight
19 p3033 A71-38496
Monograph on strong signal behavior of control systems containing multiphase rectifier, covering stability of high power sources
19 p3039 A71-38550
Analog computer analysis of EEG wave asymmetry for organism functional state detection illustrated on human reaction response to threshold acoustic stimuli
21 p3344 A71-41068
Polarimeter for simultaneous determination of Stokes parameters, analyzing electric signal in frequency and phase
22 p3537 A71-41474
Signal design and error rate of impulse noise channel, analyzing error probability of smear-desmear and standard data channels through Rice integral evaluation
22 p3513 A71-42381
Deterministic signal with normal noise, considering field representation as superposition of two circularly polarized components of directly opposite rotation
22 p3515 A71-42758
Continuous signal representations in time and frequency domains by Fourier series
23 p3644 A71-43284
Unmodulated and step-modulated HF pulse signal envelope calculation and diagram plotting
23 p3644 A71-43319
Optical anemometers for local nondestructive flow velocity measurements, discussing signal analysis possibilities
23 p3679 A71-43952
Solar spectrum photoelectric recording instrument signal ratio accuracy, discussing divider circuit analysis
23 p3681 A71-44312

Muscular bioelectric potential input processing into digital computer, describing amplitude, frequency and time domain analysis of electromyogram signals
24 p3801 A71-44542

SIGNAL ANALYZERS

Matrix switch amplitude analyzer for EEG signals providing feedback stimuli to subject
01 p0021 A71-10246

Sensitive fast response scintillation electron detector for use with signal energy analyzer
07 p1115 A71-20358

EEG analyzer voltage peaks recording on computer, using digital readout for simultaneous initial and terminal stage markings
08 p1248 A71-21446

Real time low frequency narrow band spectrum analyzer using time compression technique for vibrating machinery diagnosis and prognosis
09 p1443 A71-22708

Amplitude discriminating Goto circuit with four tunnel diodes operating on negative and positive half periods as amplitude distribution analyzer at 40 MHz
10 p1582 A71-23954

Visual image propagation from retina to higher level formations in multichannel system of cat visual analyzer
10 p1561 A71-24163

Real time spectrum analyzer, discussing data sampling rates, statistical uncertainties, waveform and bandwidth
10 p1612 A71-24832

Automatic equalizer-analyzer system for random or shock vibration testing, including narrow-band equalization, simplified display techniques and self-calibrating procedures
11 p1747 A71-26514

Microwave spectrum analyzer, discussing capabilities and applications in ECM, surveillance, communications, circuit design and analysis and electromagnetic compatibility
15 p2368 A71-31208

Short wave radio signal analyzer for joint distribution of phase and amplitude probabilities and PSK communications noise stability in ionosphere
19 p3028 A71-37784

Ternary delta modulation evolution from binary system by addition of encoder-analyzer, calculating SNR
20 p3202 A71-39468

Analog statistical analyzer for measuring one dimensional EEG amplitude distribution functions, illustrating reaction response to threshold acoustic stimuli
21 p3344 A71-41067

SIGNAL DETECTION

NT CORRELATION DETECTION

Signal detection processes selection and components sizing for stand for echometric measurement of attenuation in long distance waveguide connection
01 p0029 A71-10309

Differential PSK signal detection, using decoding circuit with uncontrolled oscillator
01 p0031 A71-10822

Adaptive optimal electromagnetic and acoustic detection antenna synthesis, considering signal direction and spatial noise structure
02 p0229 A71-11716

Optimal detection of narrow band signal with random phase and arrival time in radar or sonar, using nonlinear adaptive filter
02 p0211 A71-11720

Quantum mechanical communication theory of optimal receivers, using statistical detection and estimation theory
02 p0213 A71-12016

Optical systems using photoelectron counter system for optical signal detection and demodulation
02 p0214 A71-12031

Optimal quantum receiver mathematical specification derivation for M-ary digital signal detection
02 p0215 A71-12036

Paraboloidal mirror array of spherical segments for direct detection optical receiver, discussing minimum time dispersion and blur circle
03 p0425 A71-13650

Capacitive and floating Langmuir probes paired comparison measurements of electrostatic potential fluctuations spectrum in steady state turbulent magnetically confined plasma
03 p0430 A71-14416

Invariant detection law for signals with single phase differential keying, considering application to signal fading
04 p0550 A71-14616

Maximum likelihood estimation algorithm for arrival direction of narrowband signal under correlated noise
04 p0550 A71-14618

Algorithms for optimal detection of weak determinate signal on background of Markov process approximated non-Gaussian noises
05 p0719 A71-16009

Optimal quasi-regular signal detection on amplitude and frequency modulated noise background
05 p0723 A71-17020

Phase-coherent communication systems with phase locked loops for data detector synchronization, calculating noisy timing effects on detection efficiency
05 p0724 A71-17059

On-off keying system digital detection using random sampling for achieving high bit rates
05 p0725 A71-17073

Coherent light photoelectric detection probability in background light passing through narrow band filter of rectangular or Lorentz frequency characteristics
07 p1059 A71-18848

Band limiting effects on PCM/split phase signal detection, considering signal to noise ratio degradation
07 p1061 A71-19263

FM discriminator detection, calculating false click probability and effect on output signal to noise ratio
07 p1061 A71-19535

PCM bit synchronization and signal detection by nonlinear filter theory, giving optimum sequential estimator
07 p1061 A71-19536

Signal detection payoff in symmetrical auditory task, studying effect on rates and error analysis
07 p1045 A71-20384

Bandlimiting effects on PCM/split phase signal detection
07 p1066 A71-20431

Derivative approximation techniques for recursive signal detection, using computer program for solving optimum and suboptimum processes signal to noise ratio in effectiveness evaluation
08 p1255 A71-21596

Two-sample nonparametric adaptive detection using computer test statistics selection
08 p1259 A71-21600

Adaptive array processor analysis and optimum design for passive detection of sonar type directional stochastic signals
08 p1256 A71-21602

Algorithmic threshold directivity pattern for adaptive array processors in quasi-stationary signal and noise fields
08 p1256 A71-21603

Frequency signal structure selection to ensure maximum information capacity for given SNR at receiver output in discrete information transmission
08 p1257 A71-21980

Algorithmic analysis of detection characteristics of periodic compensation systems used in moving targets signal detection
09 p1404 A71-22153

Geographic urban information and change detection systems with remote sensing inputs, discussing data storage and retrieval
09 p1439 A71-23214

Geometry optimization of error-free distributed nondirectional aperture array receivers, using signal detectability technique
09 p1408 A71-23491

Signals temporal uncertainty and sensory modality influence on watchkeeping performance, discussing signal density effect on pulses duration increments detection
10 p1568 A71-24183

Organisms olfactory extraction and interpretation of low intensity chemical signals from air, outlining receptor mechanism from air physicochemistry
10 p1563 A71-24234

Positive signal optimal detection system in unsteady non-Gaussian noise
10 p1577 A71-24282

Optimal two stage signal search in frequency vs arrival time indeterminacy plane of communication system
10 p1579 A71-24714

Optimum frequency for detection of acoustic sources in upper atmosphere as function of altitude and turbulence
10 p1642 A71-24833

HF and VHF radio propagation on earth surface, describing launchers used for generation and detection
10 p1579 A71-24950

Binary on-off laser communication channels, calculating atmospheric turbulence effect on Poisson detection error probability
11 p1730 A71-25198

Forced choice visual signal detection tasks scanning strategies and differential sensitivity to various target locations
11 p1724 A71-26075

Detection characteristics of transistor input circuit with automatic bias
11 p1740 A71-26545

Paired comparison tests of relative signal detected by capacitive and floating Langmuir probes in steady state turbulent plasma confined in magnetic mirror geometry
13 p2066 A71-28155

Amplitude modulated optical band signal detection, comparing optimal direct photodetection and superheterodyne receivers sensitivities
13 p2029 A71-28365

Algol 60 object time error messages detection with test run in-core load-and-go compiler
13 p2035 A71-29014

Asymptotically optimal detection/discrimination algorithms for weak signals on correlated noise background
14 p2195 A71-30105

Optimal detection of rectangular radio signal pulse envelope distortions by multiplex fluctuations over white noise background
14 p2195 A71-30113

Optimal noncoherent receiver for signal detection in mixture of noise and chaotic echoes in media with frequency dependent attenuation
15 p2369 A71-31231

Book on detection of signals in noise covering statistical theory principles and applications in digital communications, radar and sonar
15 p2369 A71-31507

Asymptotically optimal rank algorithms for signal resolution at phase and amplitude detectors outputs
15 p2370 A71-31587

Signal detection in noise, investigating quantiles position optimization in nonparametric test statistics
15 p2370 A71-31588

Signal detection in stationary, Markov and other noise background, discussing functional method of statistical and probabilistic representation
15 p2370 A71-31589

Weak signal detection in additive mixture on non-Gaussian random-correlated noise, deriving algorithms for discrete- and continuous-time and coherent detection problems
15 p2370 A71-31590

Output probability distributions and covariance functions of nonlinear transformations of Gaussian stochastic processes occurring in signal detection and control theory
15 p2379 A71-31822

Book on detection, estimation and modulation theory, Part 3, Gaussian and radar-sonar signals in noise, covering point targets, random process and scatter channels
15 p2371 A71-31841

Weak harmonic signal detection in narrow band Gaussian noise, using statistical algorithm
15 p2371 A71-32187

Atmospheric laser link with automatic sensitivity control during reception, measuring detector output signal fluctuation reduction characteristics
15 p2372 A71-32319

Signals detection of known form and unknown energy in Gaussian noise of unknown level, applying concept of invariance in hypothesis testing
16 p2541 A71-32820

Human auditory signal detection related to averaged evoked potential in scalp by electrophysiological measurements
16 p2534 A71-32951

Three color photoelectric photometer improvements by introducing synchronous signal detection and electronic gates by field effect transistors
16 p2579 A71-33434

Error probability and reception stability in synchronous detection of phase manipulated signals with additive Gaussian noise at multiplied carrier frequency
16 p2542 A71-33498

Radio engineering of signal detection, filtration, information processing and recognition, discussing game theory methods for problems solution
17 p2698 A71-34393

Bandlimiting effects on coherent detection of PSK, ASK and FSK signals in presence of white Gaussian noise, using SNR as performance criterion
17 p2704 A71-35085

Book on synchronous communications theory covering statistical detection, decision and estimation and source and channel encoding
17 p2707 A71-35218

Optical homodyne detection of light signal wave front scattered by moving surface with normally distributed roughness, calculating conditions for optimum SNR
18 p2930 A71-36058

Radio emission from cosmic ray showers, discussing detection, particle populations and energy spectra
18 p2957 A71-36211

Visual signal detection from noise, investigating mental images effects in six sense modalities
18 p2862 A71-37016

Signal detection on Gaussian noise background, deriving error probabilities and optimal processing algorithms
19 p3015 A71-37224

Asymptotic optimal rank criterion for noncoherent detection of fluctuating radar signal in noise of unknown intensity
19 p3015 A71-37253

Fourier transform holograms as complex matched filter for pattern recognition and signal detection in coherent optical systems
19 p3066 A71-38239

Single-shot joint detection-estimation for discrete and continuous data and generalization to Bayesian

system identification, considering optimal nonlinear estimator realization
20 p3201 A71-38847

Recursive algorithms for detection probabilities of fluctuating targets in Gaussian noise, including cell averaging constant false alarm rate (CFAR)/extension
20 p3195 A71-38860

Comments on optimum bandwidth of low pass RC filter for pulse signal detection in nonstationary noise
20 p3203 A71-38867

Critique of paper on additional signal power for optimum performance of PCM binary signal detection under channel band limiting effect in white noise
20 p3196 A71-38870

Adaptive reception of weak repetitive signals on background of intense fluctuating noise, synthesizing adaptive detection system for multipath propagation and small SNR
20 p3199 A71-39809

Probability functional formulas for quasi-determinate signal on unsteady normal noise background for use in false alarm and correct detection
20 p3199 A71-39815

HF electric signal detection, using acoustoelectric surface wave field in piezo semiconducting crystal
21 p3436 A71-41363

Optical holographic detection and measurement of ultrasonic waves, providing practical method of investigating LF sound waves
22 p3541 A71-41785

Invariant detection law for signals with singular phase difference modulation, considering application to signal fading
22 p3510 A71-42256

Maximum likelihood estimation algorithm for arrival direction of narrowband signal under correlated noise
22 p3510 A71-42258

Decoding of correlative level coding or partial response signaling systems with ambiguity zone detection, discussing error correction algorithm
22 p3513 A71-42382

Algorithms for optimal detection of weak determinate signal on background of Markov process approximated non-Gaussian noise
22 p3515 A71-42760

Radio pulse synchronous detection with wideband preamplifier, evaluating frequency mismatch effects on signal distortion by transient response analysis
23 p3644 A71-43287

Circuits for scintillation counters signals identification, describing protective measures against electrical interference and background radiation
23 p3677 A71-43526

Joint phase locked and delay tracking system dynamics for pseudorandom radio signal detection
23 p3646 A71-44267

Radio echoes from clouds and precipitation, determining detection threshold, station potential and statistical distribution numerical characteristics
24 p3844 A71-44879

SIGNAL DETECTORS

Radar tracking systems stretcher detector circuit output signal amplitude and spectral distribution analysis
01 p0029 A71-10308

Modified integrate and dump detector using FM click mechanism for improving bit decision and reducing error rates in FSK system
01 p0032 A71-10879

Optical heterodyne mixing efficiency invariance to thin detector position for small frequency difference between signal and local oscillator
02 p0249 A71-12033

Fluidic acoustic signal detector for output determination of HF fluid oscillators, discussing performance, constant loading effect and signal amplitude
[ASME PAPER 70-WA/FLCS-7]

03 p0428 A71-14083

FM optical signals detection using Fabry-Perot interferometer with air gap between mirrors
05 p0753 A71-16875

Asynchronous tunnel diode microwave detector, considering frequency properties and sensitivity
06 p0874 A71-17547

Optimum AM reticle-detector models, discussing image resolution, electrical bandwidth and detection problems
07 p1115 A71-20368

Optimal detector parameters for stochastic signals in noise, discussing analytic and simulation studies of adaptive techniques of pattern recognition
08 p1259 A71-21594

Single and dual channel weak signal adaptive detectors theoretical performance under statistically undefined noise background
08 p1256 A71-21601

Metal-oxide-metal tunnel diode properties, discussing parametric effects on small and large signals detector operation
09 p1416 A71-22684

Cophase ad hoc statistic for data processing of detectors array sensing signal propagating in uncorrelated noise
09 p1408 A71-23452

Correlation estimates and optimal detector for incomplete a priori information signal reception on random and white noise background
10 p1579 A71-24878

Detectors for deterministic signals in noise with rational spectral density, considering analog filter for continuous input sampling and discrete filter for point sampling
14 p2195 A71-30108

Optimal correlating detector of fluctuating two frequency radar signals in unknown random noise
14 p2195 A71-30112

Radar target detection in nonGaussian sea clutter, calculating trimmed-mean detector performance under Rayleigh fluctuation
14 p2197 A71-30805

Pulse detection equipment by peak voltage and current value sampling, using avalanche transistors
15 p2377 A71-32324

Two stage noncoherent rank detector of fluctuating radar signals in noise with unknown distribution
15 p2373 A71-32630

Computer algorithm for diode detector static and dynamic I-V characteristics calculation by trial and error process with piecewise linear approximation
16 p2546 A71-33399

Schottky barrier, point contact and Ge back diodes for microwave mixers and detectors, noting burnout characteristics
18 p2894 A71-36979

Comparative detection performance of Siebert and Dicke-fix constant false alarm rate (CFAR)/ radar detectors for signals in Gaussian noise
20 p3195 A71-38866

Digital sequential detector based on range sampling technique, comparing performance to digital sequential probability test (SPRT)/ detector
20 p3206 A71-39906

Trigonometric synthesizers with nonuniformly sectioned tapped delay line and summation circuit for signal distortion correction in telephone channel
23 p3650 A71-43288

SIGNAL DISCRIMINATORS U SIGNAL DETECTORS SIGNAL DISTORTION

Invariant automatic control system performance improvement by signal predistortion for reproducibility increase
01 p0062 A71-10717

Radio telemetry data transmission, investigating multipath propagation effects on signal to noise ratio and distortion
01 p0033 A71-10889

Magnetic tape recording system FM distortion derivation from head-to-tape spacing transfer function
01 p0033 A71-10892

Information feedback distortion and countertraining effects on learning and performance in lever displacement-target test
01 p0026 A71-11415

EM pulse distortion in resonant and nonresonant gases, discussing applications to homogeneous tropospheric propagation
01 p0040 A71-11608

Noise stability in single-channel FM transmission system via maximum SNR obtained with optimal predistortion
02 p0212 A71-11836

Radio propagation at 84 MHz, investigating moving receiving terminal and aircraft reflection effects on signal distortions
02 p0216 A71-12344

Double balanced cross coupled transistor mixer, predicting conversion gain and inter and cross modulation distortion performances
02 p0233 A71-12345

ECG signal analog to digital conversion at sampling rate and quantizing accuracy for minimal losses and/or distortion
02 p0208 A71-12949

FM radio link fluctuating intermodulation distortions reduction by additive superpositioning of several compensating echoes with adaptive equalizer
03 p0380 A71-14334

Transient waveform distortion of arbitrarily modulated signal propagating through ideal waveguide
04 p0553 A71-15219

Optical channel capacity and laser signal distortion through turbulent atmosphere
05 p0720 A71-16288

Signals measurement distortions in FM recording-reproducing channel due to recorder magnetic tape speed fluctuations, discussing compensation methods
05 p0752 A71-16724

Path intermodulation data distortion derivation from noise power ratio measurements over five tropospheric scatter paths during system acceptance tests
05 p0723 A71-17055

Optimal discrete signal filters with finite duration transient process, describing approximation procedure to restore noise distorted signals
06 p0876 A71-17928

Unresolved radar targets or multipath distortion determination by measurement of complex indicated angle on two pulses separated by short interval
07 p1058 A71-18843

Ionospheric electron density irregularity effects on communication satellite scintillation in auroral zone, using Doppler and Faraday measurements
07 p1098 A71-19035

Multipath distortion and wavenumber spectrum of refractive index in radio links
07 p1060 A71-19258

Computation of IF filter characteristics effect on angle modulation distortion
07 p1082 A71-20429

Telephone channel phase-frequency distortions effects on discrete signal transmission quality from phase-delay-time frequency characteristics criterion
08 p1253 A71-20774

Magnetic tape recording systems nonlinear amplitude distortion in terms of transfer function characteristics applied to analog instrumentation
09 p1449 A71-22786

Rate distortion over band limited feedback channels, considering capacity of additive Gaussian white noise channel
09 p1407 A71-23104

Distortion effects in switching diode modulators due to local oscillator interference
09 p1420 A71-23681

Polarization distortion of partially polarized wave emission and reception by two channel horn antennas, noting radio astronomy, radar and optics applications
10 p1584 A71-24876

Millimeter wave waveguide time delay distortion characteristics equalization using directional filter cascades
14 p2210 A71-29572

Two theorems on minimax transversal filter equalization at receiver for digital communication systems distortion reduction
14 p2193 A71-30012

Optimal detection of rectangular radio signal pulse envelope distortions by multiplex fluctuations over white noise background
14 p2195 A71-30113

Radio pulses from Crab Nebula pulsar NP 0532, determining multipath scattering delay distribution function and distortion
14 p2314 A71-30641

Linear passive network steady state FM distortion numerical calculation, applying to Chebyshev-response bandpass filter
14 p2197 A71-30806

Steady state analysis of phase controlled parasitic current, discussing reduction of alternator apparent power requirements and harmonic distortion
15 p2355 A71-32218

Quasi-stationary method applicability for determining distortion of FM signal passing through linear circuit
15 p2373 A71-32631

Restrictions on signals effective bandwidth, determining uniform upper bounds for use in design of systems with minimum distortion
16 p2542 A71-33458

Intelsat 4 communication system simulation by transponder engineering model to test performance objective concerning baseband distortion and intermodulation
17 p2705 A71-35102

Automatic control system output signal changes due to finite variations, noting expansion into Taylor series
17 p2723 A71-35344

German monograph on nonlinear distortion correction of binary bipolar signals in Gaussian noise covering receiver, decision theory and error probabilities
18 p2874 A71-35959

Amplifier effects on phase distortion of pulse signals passing through power amplifier stages of coherent pulse communication systems
19 p3015 A71-37257

Physical factors affecting electromagnetic signal propagation in earth-ionosphere waveguide
19 p3017 A71-37811

Message distortions analysis in PCM communications systems due to phase fluctuations of synchronization signal
19 p3022 A71-38494

Intermodulation distortion in abrupt junction current pumped varactor frequency converter
20 p3202 A71-38848

Transfer function for transmission through maser medium, cancelling signal distortions due to propagation
20 p3242 A71-38877

Bandpass filter harmonic signal phase shift distortion effect on transient response in PSK of multichannel transmission
23 p3644 A71-43286

SIGNAL ENCODING

Radio pulse synchronous detection with wideband preamplifier, evaluating frequency mismatch effects on signal distortion by transient response analysis
23 p3644 A71-43287

Trigonometric synthesizers with nonuniformly sectioned tapped delay line and summation circuit for signal distortion correction in telephone channel
23 p3650 A71-43288

SIGNAL ENCODING

Speech signals digital encoding with adaptive linear predictor for reducing redundancy, discussing digital simulation results and subjective comparison with log-PCM encoder
01 p0030 A71-10472

PCM telemetry signal encoding, investigating aliasing and pulse width errors dependence on frequency band occupied by bandpass signal
01 p0032 A71-10881

Reception and transmission of reduced sidelobe pseudorandom FM signals using quaternary S-sequence synthesis
01 p0037 A71-11082

Convolutional code words minimum distance-arbitrary length relationship for path memory performance measurement
08 p1258 A71-21313

Counting rate source encoding algorithm with orthogonal functions in space experiment data processing before telemetering to ground
08 p1259 A71-21592

PCM signal encoding redundancy reduction using discrete code transformation, considering telephony implementation
08 p1255 A71-21593

Image data coding by linear transformation and block quantization, considering Fourier, Hadamard and Karhunen-Loeve methods
10 p1580 A71-23766

Information processing by living systems, considering nervous system and brain operation with emphasis on neuron structure, message coding, programming and information storage
10 p1562 A71-24223

Sensing and communications technologies for short wayside headways, considering applicable equipment for personal rapid transit systems, modulation, coding and data transmission techniques
14 p2195 A71-30337

Book on synchronous communications theory covering statistical detection, decision and estimation and source and channel encoding
17 p2707 A71-35218

Noise stability and rejection probability of code sequence in real multifrequency communications systems with multipositional frequency shift keying
19 p3022 A71-38495

Pulse compression circuit techniques combined with radar system philosophy for signal encoding application to pulse radar
20 p3201 A71-39911

Signal to quantizing noise ratios for differential PCM systems used to encode analog signals from Markov processes into digital form
22 p3514 A71-42391

SIGNAL FADEOUT

U SIGNAL FADING

SIGNAL FADING

NT SELECTIVE FADING

Adaptive retransmission for improving two-way communication between antenna arrays in randomly fading environment, calculating signal to noise ratio
01 p0052 A71-10468

Short wave signal polarization fading minimization by dispersed reception of circularly polarized components, discussing power gain relation to antenna configuration
02 p0219 A71-12543

Traffic capacity of Gaussian communications channel with Rayleigh fading, examining code transmission coefficient under discrete control mode
03 p0378 A71-13394

TWT microwave amplifier parameters effect on power threshold for electron beam signal control loss
03 p0385 A71-13790

Invariant detection law for signals with single phase differential keying, considering application to signal fading
04 p0550 A71-14616

High altitude rocket-borne radiosonde communication, examining transmission link characteristics, signal losses and antenna radiation patterns
04 p0551 A71-15012

Interstellar scintillation index and fading time of pulsar signals at 2388 MHz
05 p0807 A71-16208

Ionospheric drift measurements during solar cycle based on fading of radio waves reflected from E and F regions
05 p0741 A71-16437

Ionospheric electron content measurement from Faraday fading of Explorer 22 satellite transmissions during low and high solar activity
05 p0741 A71-16444

Ionospheric total electron content determination by Faraday fadings of 40 MHz radio transmissions from Explorer 22 satellite, considering seasonal variations
05 p0741 A71-16445

Photoelectron count of lognormally fading optical signal, discussing noncentral chi square random variable approximation
05 p0726 A71-17085

VHF/UHF satellite transmission, predicting multiple ground reflection effects on signal fading and effective antenna gain by computerized method
06 p0868 A71-17732

Ionospheric scintillation effects on fading of oppositely circularly polarized VHF signals in space communications
09 p1410 A71-23522

Complex and envelope covariance for Rician fading communication channel, deriving equation for unsymmetric power spectrum
10 p1574 A71-23767

Negative sudden phase anomalies, related signal strength enhancements and short wave fadeouts, considering maximum flux density of solar X-ray flares
10 p1575 A71-23883

Scintillation effects on synchronous satellite signal fading observed through polar ionosphere
10 p1577 A71-24315

Diversified frequency radio data transmission and reception by linear modulation, considering error rate in white noise and selective/flat fading
10 p1580 A71-25109

Array spacing dependence of ionospheric irregularities horizontal drift and anisotropy, using statistical properties of ground diffraction patterns
11 p1731 A71-25614

Computer simulation of fading records in spaced antenna ionospheric drift experiment, detecting mean direction and diffraction pattern velocity with correlation analysis
13 p2054 A71-27800

Monograph on persistent radio meteor echoes fading relation to upper atmosphere wind structure
14 p2192 A71-29579

Heuristic signal design for digital communication over fast-fading Gaussian channels, stressing nonorthogonal signaling schemes
14 p2193 A71-30010

Mathematical model for predicting microwave signal fading characteristics due to reflections from ocean surface
15 p2368 A71-31140

Scintillation fading of signals in SHF band due to electron density irregularities in F region
17 p2699 A71-34624

Mean-square-error determination for binary code data transmission in symmetrical channels with slowly changing parameters, noting dependence on fading level
17 p2702 A71-34974

Low elevation angle tropospheric fading relationship to satellite communications and broadcasting at frequencies between 1 and 20 GHz
17 p2703 A71-35083

Binary and quaternary PSK systems performance with intersymbol, interchannel and cochannel interferences and fadings
17 p2707 A71-35478

Theoretical signal strength reduction on USAF Eastern Test Range based on missile antenna radiation pattern characteristics
18 p2876 A71-36471

Phase and amplitude variations of multipath fading of microwave signals relating atmospheric irregularities
19 p3015 A71-37221

Noise stability during noncoherent reception of frequency shift keyed signal by receiver with finite Q predetector integrators in presence of fading
20 p3196 A71-39258

GBR wavefield above winter nighttime ionosphere, noting latitudinal profile due to D region spatial variations and signal fading with F region structure
20 p3197 A71-39744

Transmission characteristics of communication systems with incoherent carriers through fading and nonfading media, showing advantage of PFM-AM with clipped noise carrier
20 p3201 A71-39913

Italian Sirio synchronous satellite for SHF propagation and communication experiments on fading statistics, frequency dependence, path diversity and TV transmission
21 p3347 A71-40474

Line-of-sight microwave multipath fading, predicting attenuation distribution as function of pathlength by piecewise linear approximation of atmospheric refraction index
21 p3349 A71-41196

Invariant detection law for signals with singular phase difference modulation, considering application to signal fading
22 p3510 A71-42256

SIGNAL FADING RATE

Long range troposcatter, evaluating antenna directivity effects on signal fading rate and fluctuation
01 p0037 A71-11087

Field amplitude distribution parameter in long distance tropospheric communications based on fading depth
05 p0722 A71-16866

SIGNAL FLOW GRAPHS

Topological unistor graph solutions to linear equations of electronic circuits by structural conjugate numbers on digital computer
11 p1792 A71-26376

Laser cavity analysis for etalon effects on mode, using signal flow graphs
14 p2254 A71-30143

SIGNAL GENERATORS

NT FREQUENCY SYNTHESIZERS

NT FUNCTION GENERATORS

Alphanumeric character generation from resistive storage of time derivatives for CRT displays
01 p0047 A71-10216

Logarithmic signal converter with parallel circuits arrangement for large dynamic range operation
02 p0231 A71-12040

Variable microwave thermal noise temperature standard generator with output ranging from below 40 to above 370 K
02 p0250 A71-12139

Stepped wideband radio signal power generator with manually controlled signal attenuator
06 p0876 A71-18078

Microwave local oscillator and beacon generator for Intelsat 3, discussing design, operation and performance
06 p0877 A71-18400

Random numbers generation from natural random phenomena, discussing advantages, circuit and sampling rate
07 p1067 A71-18734

Transient signal generation by propagation of large amplitude pulses, discussing angular dependence in water
07 p1063 A71-19960

Frequency generators using RC (RL) designs with odd selective quadrupole element numbers as converters
07 p1078 A71-20062

C and higher band pulse modulated signal generation with nanosecond duration, using TEM-mode pulse-forming network
10 p1577 A71-24211

Random vibration laboratory equalization by multiple taping of noise signals on recorder and manual processing
11 p1746 A71-26513

EMC susceptibility test equipment consisting of portable buzzing relay noise generator
13 p2045 A71-28874

Quartz-tube LF measuring generator with low linear instability, using frequency divider and narrow band RC filter
13 p2040 A71-28936

Kalman-Bucy filter construction as true time varying Wiener filter with covariances independent of signal generation, applying to data smoothing problem
14 p2220 A71-30460

Atmospheric and man-made noise measurement techniques, using signal generator as reference standard for absolute amplitudes
14 p2204 A71-30978

LF white Gaussian noise generator with continuously variable output, describing transistorized circuitry and output characteristics
15 p2371 A71-31851

Speech envelope masking noise generation with constant S/N ratio for intelligibility studies
15 p2372 A71-32297

Frequency stability definition for signal generator, proposing spectral density measure
21 p3414 A71-40222

German monograph on Gunn oscillators frequency stabilization by synchronization with external oscillator emitting HF signals
23 p3649 A71-43045

SIGNAL MEASUREMENT

Signal detection processes selection and components sizing for stand for echometric measurement of attenuation in long distance waveguide connection
01 p0029 A71-10309

Low level optical signal transient response measuring instrument with nsec resolution and automatic photomultiplier current gain control
02 p0249 A71-12131

Optimum frequency channels and delay estimates in very long baseline interferometry with large bandwidth for fringe and phase measurements
02 p0216 A71-12329

Precision measurement of satellite microwave flux and polarization at ground, involving Skyline tests
02 p0218 A71-12444

Nondissipative focusing and ionospheric reflecting effects on MF radio wave absorption measurements for magnetically quiet and disturbed periods
03 p0409 A71-13391

High impedance source with shunt capacitance, discussing periodic output measurement using operational amplifier

03 p0427 A71-13923

Minority carrier bulk lifetime from large signal response time of MOS capacitor in deep inversion

03 p0388 A71-14474

Photoelectric recording devices for star passages, describing automatic compensation for signal delay instability

04 p0592 A71-14864

Relativity and solar quadrupole moment effects in time delay measurements of signal traveling from earth to artificial satellites

05 p0808 A71-16446

Signals measurement distortions in FM recording-reproducing channel due to recorder magnetic tape speed fluctuations, discussing compensation methods

05 p0752 A71-16724

AC signal amplitude measurements, describing circuit design with DC voltage generation proportional to input AC voltage

06 p0899 A71-17926

Ionospheric refraction during radio wave propagation using space diversity recordings of Faraday and Doppler effects for coherent signals from geophysical rocks

06 p0894 A71-18256

Low angle signal strength enhancements from ionospheric beacon satellite BE-B transmissions

07 p1096 A71-19018

Ionospheric error correction in distance measurements involving satellites, noting simultaneous differential Doppler and Faraday signal measurements

07 p1097 A71-19023

Mode locked picosecond laser pulse duration measurement by beat frequency detection

07 p1123 A71-19211

Measuring transformer for AC input signal with pulse width modulated semiconductor multiplier feedback

08 p1261 A71-20737

FM type system for measurement of wear narrow band noise power based on phase components processing

08 p1253 A71-21289

Lidar wavelength optimization for Raman scatter atmospheric studies, taking into account aerosol and weak signal statistical effects

08 p1254 A71-21458

Unsteady scattering patterns analysis, determining atmospheric extinction coefficient by reflected light oscillograms, formulas or signal amplitude time recording

09 p1487 A71-22385

Error reduction in reconstructions of time concentrated band limited signals from given set of linear measurements

09 p1407 A71-23101

Pulsed signal amplitude and delay time measurement in presence of interfering /reverberated/ signals and steady noise

09 p1407 A71-23111

Lunar surface specific effective radio signal scattering area measured by Luna 9 and 13, describing signal fluctuations

09 p1523 A71-23145

Periodic signal input effects on stationary linear system, using closed form Laplace transformation

10 p1643 A71-24909

Measurement system for communication satellite ground station equipment including parametric amplifier, wideband receiver, power oscillators, and radio transmitters and receivers

10 p1590 A71-25103

Intelsat system ground station equipment testing including antenna radiometric gain, noise temperature, energy dissipation, telephone and TV performance measurements

10 p1580 A71-25104

Phase measurement at millimeter wavelengths in free space, using reference signal and interference pattern of slowly varying electric field

13 p2030 A71-28609

Variable target reflectivity effect on weather radar measurements, using extended echo fluctuation theory for average and maximum signals

13 p2031 A71-28723

Isolation technique for recording low level ECG and deep body temperature signals in animals exposed to large amplitude RF fields

13 p2020 A71-28864

Receiving system for phase measurement on coherent signals from satellites, discussing frequency conversion through phase locked filter

13 p2033 A71-29275

Threshold SNR for signal frequency meter based on zero number count method, determining reliability

14 p2194 A71-30088

Frequency measurements of square wave signal with unknown amplitude by two mismatched channels, comparing rms error with effective estimate variance

14 p2195 A71-30106

Transmission loss measurements at HF over 960 km temperate latitude path for wave polarization calculations and ionospheric absorption estimation

14 p2196 A71-30468

Microwave oscillations small phase difference variation measurement, using polarization effects

14 p2196 A71-30636

Small signal impedance of avalanche region in microwave IMPATT diode

14 p2215 A71-30833

Truncated pulse signal height distributions of atmospheric sources

14 p2203 A71-30960

Radio power, insertion loss, frequency and dielectric measurements at mm wavelengths

14 p2205 A71-30982

Preferred frequencies for RF measurement and calibration based on Renard number series

14 p2205 A71-30986

Radio signals fine structure examination by instantaneous pulsed voltage measurements, describing fast response digital voltmeter circuit with memory element

15 p2409 A71-32188

Microwave resonator Q factor measurement by reflection coefficient method, using swept signal generator to eliminate incidental FM problem

15 p2376 A71-32310

Mode locked laser pulse signal recovery from time integrated correlation functions of arbitrary order, including field amplitude fluctuations

16 p2588 A71-34075

CO lasing processes using small signal single pass gain measurements on flowing CO-air-He laser

17 p2751 A71-34378

Recalculated radio wave absorption during oblique transit through ionosphere from vertical measurements using rhombic antenna at 25 MHz

19 p3058 A71-38388

Small signal gain and saturation intensity measurement of carbon dioxide laser as function of gas flow velocity

20 p3244 A71-39099

Doppler carrier frequency shift measurement accuracy

20 p3198 A71-39808

Digital servo system with signal quantization by level and time, evaluating oscillating motion in steady state mode

23 p3655 A71-43292

Wideband solid state converter circuit for quantization of signals from semiconductor nuclear radiation detectors, noting cost reduction

23 p3677 A71-43527

E layer vertical velocity fluctuations from scattered signal phase and amplitude correlation measurements, using perturbation technique

23 p3647 A71-44334

Multicomponent signal arrival angles wave front analysis from antenna array phase and amplitude measurements for radio direction finding

24 p3803 A71-44647

Cloud and precipitation effects on radio echoes intensity measurement, discussing pulse dimensions influence on average signal magnitude

24 p3845 A71-44881

SHF resonator small resonant frequency shift and Q factor changes measurement based on FM signal envelope shape analysis

24 p3858 A71-45237

Simultaneous ionosphere measurements by incoherent ground radio wave scattering and coherent signals from Intercosmos 2 and Cosmos 321 satellites

24 p3824 A71-45323

SIGNAL MIXING

Optical heterodyne mixing efficiency invariance to thin detector position for small frequency difference between signal and local oscillator

02 p0249 A71-12033

Laser light frequency mixing and doubling in isotropic bodies in crossed magnetic and electric fields, examining magneto-electro-optical processes

02 p0261 A71-12171

Stellar spectroscopy by optical heterodyning of laser and star light mixing, using He-Ne laser, high speed photocell and RF power measurement equipment

03 p0487 A71-13331

SNR of harmonic signal mixed with narrow band noise, measuring correlation coefficients

04 p0550 A71-14615

Signal-white noise mixture filtration, determining maximum SNR position and magnitude and filter bandwidth

09 p1416 A71-22466

High order harmonic mixing of klystron microwave and far IR laser radiation using Josephson junction

09 p1464 A71-22766

Production rates for beat and sum frequencies mixing from interaction of two parallel laser beams with free electrons, using nonrelativistic radiation theory

09 p1465 A71-23546

Single and double balanced diode mixers characteristics comparisons for spurious response suppression, considering RF third order intercept technique

11 p1737 A71-25674

Superheterodyne radiometers for millimeter and submillimeter waves, using Mach-Zehnder interferometer frequency mixer for parasitic signal suppression

12 p1886 A71-26847

Laser light enhanced scattering by optical mixing of beams in plasma

13 p2079 A71-28797

Signal rejection characteristics of receiver preselector and antenna system, requiring receiver mixer efficiency and transmitter parameters

13 p2032 A71-28862

Nonlinear optical effects associated with free holes and electrons in semiconductors, including higher harmonics generation and frequency mixing

16 p2621 A71-33375

Sensitive mm wave receivers, using local oscillator and mixer functions in single Gunn diode for large dynamic signal input range and wide IF bandwidth capability

17 p2717 A71-35111

HF radio communication receiver performance requirements and realization, considering gain, noise, interference, filtering, reciprocal mixing, intermodulation and frequency stability

18 p2895 A71-36998

Laser beam frequency mixing, discussing optical harmonics generation, light reflection/transmission and picosecond pulse measurements

21 p3392 A71-40661

Optical mixing and higher harmonics generation by free carriers in semiconductors, using carbon dioxide laser

21 p3393 A71-40663

Millimeter wave klystrons phase locking to HCN far IR laser line via harmonic mixing in Si and metal-oxide-metal Josephson point contacts

22 p3555 A71-41599

SNR of harmonic signal mixed with narrow band Gaussian noise, measuring correlation coefficients

22 p3510 A71-42255

SIGNAL NOISE

U SIGNAL TO NOISE RATIOS

SIGNAL PROCESSING

Contour-mapped and digital data field processing and analysis for National Severe Storms Laboratory /NSSL/ radar signal processing and decoding system

01 p0118 A71-10590

Solid state digital integrator for weather radar signals, using recursive integration scheme

01 p0050 A71-10593

Invariant automatic control system performance improvement by signal predistortion for reproducibility increase

01 p0062 A71-10717

Instrumentation magnetic tape recorder reproduce systems equalization using active circuits and signal processing to develop required transfer function

01 p0082 A71-10894

Constant bandwidth FM subcarrier oscillators signal preemphasis for FM and PM transmitters

01 p0033 A71-10897

Digital FM discriminator for demodulating FM signals with high deviation percentage

01 p0033 A71-10899

NRZ PCM signal conditioning, bit and group synchronization and decommutation techniques

01 p0034 A71-10901

PCM telemetry bit synchronizer/signal conditioner, discussing bit acquisition, error and slippage rates

01 p0053 A71-10907

Transient processes in transistor with strong input signal, using substitution parameter for nonlinear differential equation

01 p0055 A71-11155

Continuous signal discretization for communication channels maximum information compression rates

02 p0211 A71-11826

Logarithmic signal converter with parallel circuits arrangement for large dynamic range operation

02 p0231 A71-12040

Tan-lock type compared to other phase demodulators in communication signal processing system, describing basic lock configuration

03 p0377 A71-13242

Filter output voltage in pseudorandom signals correlation processing, using Duhamel integral

03 p0378 A71-13392

Radar information digital extractors for processing signals from airborne transponder

03 p0382 A71-13570

Signal optimization for binary data transmission system with noiseless feedback channel, considering receiver signal energy and structure

04 p0560 A71-14743

Huffman /impulse-equivalent/ pulse sequence design, examining energy distribution form control of signal in time-frequency plane

04 p0551 A71-15005

Optical fields holographic subtraction for SNR enhancement 05 p0748 A71-16262

Arbitrary patterns recognition by parallel processing, deriving mathematical instructions for signal processing based on statistical communication theory 05 p0726 A71-16391

Decision-directed digital adaptive signal equalizer for high speed data transmission, discussing design and advantages 05 p0725 A71-17065

Multichannel on-line data terminals using minicomputer for communication control, error detection and data buffering [IEEE PAPER 68-TP-448-COM] 05 p0727 A71-17068

Soviet book on radar signal processing optimization covering detection and measurement, electronic analog and discrete digital filters design, etc 06 p0867 A71-17445

Transistorized four-quadrant control signals voltage multiplier, analyzing operation and circuit diagrams 06 p0879 A71-17493

Temporal stability of operating points on curves of signals from time interval sensors in angle code converters 06 p0873 A71-17522

Signal cross correlation processing in unstable and turbulent plasmas, comparing correlational and spectral analyses of plasma dispersion and transfer function measurements 06 p0938 A71-18456

Digital adaptive spectral filtering canceling undesired power spectra based on measured mean square values ratio and stochastic approximation methods 07 p1082 A71-20408

Fluidic pneumatic control system compensator for digital signal processing 07 p1026 A71-20567

Deep space probes telemetry system a priori data compression ratio evaluation using channel activities under unknown output signals cross correlation [AIAA PAPER 71-231] 08 p1258 A71-20799

Kalman filter application as observer of observable signals derivatives, using gain matrix to minimize variance estimate for instrument landing systems 08 p1269 A71-21343

Phase quantization theoretical derivation, applying mathematical technique used in signal processing nonlinear problems 08 p1291 A71-21403

Adaptive array processor analysis and optimum design for passive detection of sonar type directional stochastic signals 08 p1256 A71-21602

Optimum antenna array processing design for target detection in nonuniform clutter background, using decision-theoretic processor with digital computer 08 p1256 A71-21604

Areal precipitation quantitative radar measurements, describing signal processing and digital system for contour mapped displays and numerical summaries 08 p1257 A71-21738

Optimal phase regulated AFC system for FM signal filtration in presence of internal noise 09 p1404 A71-22155

Optimal temporal and spatial temporal resolution for unknown parameter of interfering signal on white noise background 09 p1404 A71-22219

Signals statistical parameters and phase space properties, deriving functional relationships for signal processing correlation techniques 09 p1405 A71-22298

Phase locked loop as versatile building block for integrated circuit design, discussing basic principles and applications in analog and digital signal processing 09 p1415 A71-22354

Wideband photographic signal recording by modulated laser beams, discussing performance characteristics in terms of signal to noise ratio and laser power 09 p1460 A71-22355

Real time low frequency narrow band spectrum analyzer using time compression technique for vibrating machinery diagnosis and prognosis 09 p1443 A71-22708

Real time remote test site computation and display of complex engine inlet distortion parameters from dynamic pressure signal, using analog computer 09 p1446 A71-22726

Variable capacitance signal transducers characteristics, circuitry and pulse width modulation 09 p1448 A71-22771

Add transfer characteristics, demonstrating summation method for signal to noise ratio improvement 09 p1407 A71-23049

Spectrum economy by passing signal through symmetrical bandpass filter using FSK keyer 10 p1574 A71-23769

Materials microstrain determination using automatic capacitance bridge gage and analog or hybrid computer for measurement signal processing 10 p1609 A71-23916

Neurophysiological auditory information processing, considering mechanical transformation of two dimensional pressure-time signal and three dimensions for presentation to nervous system 10 p1562 A71-24228

Organisms olfactory extraction and interpretation of low intensity chemical signals from air, outlining receptor mechanism from air physicochemistry 10 p1563 A71-24234

Signal transformation laws of central nervous system motor command patterns construction from sensory impulse streams 10 p1569 A71-24236

Rapid scan astronomical spectrophotometer with 1024 channel for signal averaging on slow change in sky transparency for improving accuracy 12 p1904 A71-26803

Amplitude-quantized random noise contaminated unknown signal sample, deriving conditional probability density function of combined output error and signal confidence interval 12 p1880 A71-27157

Stretch technique for pulse time transformation including signal slowdown, speedup or time reversal performed within window with duration determined by time-bandwidth product 12 p1881 A71-27427

Signal processing using arrays, solving for monochromatic plane wave by transforming gain equation 12 p1882 A71-27532

Signal rejection characteristics of receiver preselector and antenna system, requiring receiver mixer efficiency and transmitter parameters 13 p2032 A71-28862

Power line and signal line transients in digital systems 13 p2032 A71-28863

Thick film flat spiral inductor filter design for television signals, using linear analysis computer program 13 p2039 A71-28913

Discretization interval in discrete analog filters for optimal processing of complex radar signals, estimating systematic errors 14 p2194 A71-30081

Optico-acoustic autocorrelator for linear FM signals spatial compression, discussing design and performance 14 p2194 A71-30085

Combined heterodyning, beam forming and cross correlation of broadband multichannel signal from multidimensional phased array, using coherent optical system 14 p2241 A71-30142

Stochastic signal optimum linear estimation in multiplicative and measurement noises, deriving algorithms 14 p2197 A71-30794

Gaussian input signal nonlinear sampled data systems analysis using linear components and transfer function 14 p2220 A71-30800

Image classification by optical and electro-optic processing methods for spatial signal perception and treatment in natural form 14 p2248 A71-30816

CW 28 micron signal resonant regenerative amplification in pulsed wave vapor laser, showing pulse to pulse frequency coherence 14 p2255 A71-30832

Walsh orthogonal functions application in signal processing and as carrier waves in telemetry data transfer systems 14 p2199 A71-30909

IR scanning vertical temperature profile radiometer forITOS meteorological satellites, describing electronic signal processing 14 p2200 A71-30916

Quasi-harmonic signal suppression in theta-power amplifier as function of nonlinearity at various noise levels 15 p2375 A71-31229

Radio direction finding with discrete antenna scanning and multilevel beacon signal quantization, investigating accuracy 15 p2370 A71-31591

Solar system interstellar communication with Galaxy, discussing information transmission, coding decoding, recording, display, pulse use and economics 15 p2371 A71-31747

Electro-pneumatic transducer for conversion of electrical into fluidic signals, using temperature dependence of laminar gas jet deflection angle in flow along heated curved wall 15 p2353 A71-32072

Coincidence adders with digit by digit alteration of direct and inverse signals, discussing synthesis and reliability 15 p2376 A71-32183

Low voltage signal conversion to digital code, emphasizing SNR improvement 15 p2382 A71-32452

Optimal sensing recording and signal processing in multispectral photography for aerial reconnaissance capability 15 p2410 A71-32470

Large signal saturation effects in cyclotron resonance oscillators, using helical electron beam-cavity interaction model 16 p2545 A71-33394

Clutter signals simulation with predetermined auto- and cross correlation, describing mathematical method for filter weighting function 16 p2541 A71-33424

Frequency multiplier or divider output signal spectral line form and width conversion from monochromatic input signal 16 p2542 A71-33490

Optimal inertialess transformation of output signals from several devices, noting method application to analog data processing systems 16 p2550 A71-33892

Satellite communications use of geostationary orbit, considering ground station antennas radiation patterns, signal processing, stationkeeping, etc 17 p2696 A71-34234

Communication satellite systems integration into general telecommunication network, considering telephone circuit data transmission characteristics, routing and signal processing 17 p2696 A71-34235

Radio engineering of signal detection, filtration, information processing and recognition, discussing game theory methods for problems solution 17 p2698 A71-34393

Signal processing operation of real time optical correlator, using ultrasonic light modulators 17 p2708 A71-35484

Silicon microwave transistors frequency response theory, considering application as small-signal and power amplifiers 18 p2894 A71-36978

Wideband communications theory applied to continuous/analog signals using frequency and amplitude modulation 19 p3015 A71-37254

Cumulonimbus cloud hail danger, precipitation and water content measurements with scattering and attenuation of centimeter radar waves, including automated echo subtraction device 19 p3094 A71-38700

Output correlation functions of periodic signals limiting in random noise passing through zero memory devices, using Hermite polynomials method 20 p3195 A71-38857

Harmonic analysis of signal processing radar antennas spatial filtering process, noting application to physical optics theory 20 p3200 A71-39903

Signal processing techniques for clutter suppression in moving target indicator radar 20 p3200 A71-39908

Optical correlation for surveillance and pulse Doppler radar receivers signal processing 20 p3200 A71-39910

Pulse compression dispersive filters for signal processing 20 p3206 A71-39912

Direct local density gradient measurement in rarefied free jet flow using electron beam deflection signal processed with lock-in amplifier 21 p3364 A71-40394

Digital techniques for tactical radar signal processing functions, discussing low cost integrated circuitry, moving target indicators, and analog to digital converters 21 p3348 A71-40588

Signal processing circuits for 1000 MS/S optical communication link using multiplier/signal switch, bit synchronizer and data regenerator 21 p3357 A71-40807

Surface wave digital and analog signal processing filters for time delayed, frequency or phase coded transmission and reception applications 21 p3357 A71-40811

Signal quantization induced low amplitude oscillations in digital control systems, discussing relationship to digital controller programming form 21 p3361 A71-40980

Signal process models choice in Kalman-Bucy filtering, proving smallest error covariance matrix existence 21 p3349 A71-41190

Signal AM-PM conversion by locking oscillator with single external injection 22 p3523 A71-42480

Optimal nonlinear discrete filters with finite memory for polynomial signals, discussing synthesis with aid of minimax method 22 p3527 A71-42856

Telemetry systems with discrete compression-expansion function, calculating noise stability improve-

ment as compared to linear and nonlinear signal conversion operations

22 p3515 A71-42859

Signal filtration algorithms and parameter estimation in additive non-Gaussian noise background by conditional Markov process theory

23 p3644 A71-43290

Uniform signal energy distribution in wideband synchronous data transmission channels using linear sequential filters with scramblers

23 p3647 A71-44345

Data transmitting and receiving instruments and systems development problems covering signal shaping and converters and information channel and data reception theories

24 p3806 A71-44375

Kalman filter literature covering structure, applications, fundamental properties, shortcomings, filter synthesis and degradation factors

24 p3808 A71-44398

Optimum signal processing for distance measurement with lasers, considering propagation, detection and measure process statistical properties, optical radar and sine wave modulation

24 p3834 A71-45206

SIGNAL RECEPTION

NT SYLLABLES

NT SYMBOLS

NT TELEVISION RECEPTION

S band PCM telemetry system using frequency diversity for spin stabilized high velocity blunt nosed reentry vehicle signal reception

01 p0163 A71-10980

He-Ne IR laser resonator as quadratic receiver for modulated filtered laser emission, noting strong LF noise

01 p0096 A71-11218

Two-directional digital data transmission system, determining probability of not obtaining message for arbitrary interrogation signals number

01 p0039 A71-11319

Antenna gain, transmission efficiency and receiving cross sections in dissipative isotropic medium

01 p0041 A71-11614

Radio signal reception error in cadence synchronization of binary data transmission systems with indeterminate signal arrival time

02 p0212 A71-11834

Radio propagation at 84 MHz, investigating moving receiving terminal and aircraft reflection effects on signal distortions

02 p0216 A71-12344

Electronic equipment shielding against spurious signals, determining minimum metal thickness for desired effectiveness based on transmission line theory

03 p0383 A71-13178

Optimal and nonoptimal signal reception under conditions of incomplete a priori information based on approximation by Markov processes in white noise

05 p0730 A71-16000

Nonhomogeneous signal fields reception in presence of homogeneous noise using two-element subtractive antenna array, noting S/N improvement

05 p0721 A71-16469

Radar echo signal amplitude probability distribution during fully polarizational reception

05 p0723 A71-16873

Radar receiver dynamic range centering for log-normal target statistics for minimum probability of signal exclusion

05 p0725 A71-17084

Noise stability during complex signals reception and lag measurement on fluctuating noise background

06 p0866 A71-17371

Propagation modes involved in HF or VHF reception at ground station of beyond-horizon satellite transmission

07 p1097 A71-19024

Radio signal receiving system design for group delay experiments with geostationary ATS-F for ionospheric and magnetospheric electron content

07 p1206 A71-19033

Communication satellite station at Fucino (Italy), testing receiving and transmitting equipment transmission quality

07 p1063 A71-20041

Noise rejection of two channel asynchronous storage circuit with internal detection for weak signal reception

08 p1252 A71-20734

FM demodulator system with parametric tracking filters for threshold improvement, discussing reception performance

08 p1265 A71-21279

Maximum likelihood estimates for deterministic signal parameter during optimal reception on stationary normal noise background

09 p1405 A71-22465

Multiwavelength laser beam scintillations and atmospheric turbulence spectra, investigating saturation phenomena, transverse amplitude correlation lengths and signal fluctuations receiver aperture smoothing

09 p1464 A71-22780

Optical signal heterodyne reception, discussing reduced atmospheric distortion effects

10 p1575 A71-23812

Signal fluctuation effect on directional properties of multipole receiving antenna, calculating radiation pattern

10 p1583 A71-24708

Optimal reception of Markov radio signals with intrapulse FM, using nonlinear filtration theory

10 p1578 A71-24711

Noise stability during noncoherent reception of frequency shift keyed signal by receiver with finite Q predetector integrators in presence of fading

11 p1733 A71-25938

Receiving system for phase measurement on coherent signals from satellites, discussing frequency conversion through phase locked filter

13 p2033 A71-29275

Nonlinear filtering synthesis of optimal receiver for pseudorandom phase shift keyed signal with arbitrary modulation angle and white noise background

14 p2195 A71-30107

Aircraft ILS signal reception system, obtaining category III reliability performance by circuit redundancy and automatic incoming information surveillance

15 p2446 A71-31912

Rapidly converging first order training algorithm for adaptive equalizer design in FPM signal reception, using variable step sizes for mean-square error minimization

16 p2545 A71-32821

Integrating discrete signal receiver with weighting proportional to signal, evaluating operational quality in presence of external stationary correlated noise

16 p2542 A71-33488

Error probability and reception stability in synchronous detection of phase manipulated signals with additive Gaussian noise at multiplied carrier frequency

16 p2542 A71-33498

Radio astronomy signals reception and interpretation, detailing solar, galactic and extragalactic spectrum sources

17 p2797 A71-34242

He-Ne IR laser resonator as quadratic detector for modulated filtered laser radiation, noting strong LF noise

17 p2750 A71-34269

Space-time correlating antenna array forming matched filter for modulated signal reception with interference ejection

17 p2716 A71-34767

Optimum pulse transmission through thin exponentially inhomogeneous plasma region for maximum amplitude signal reception, using matched filter theory

17 p2788 A71-34768

Decoding of linear codes combinations for non-identical domains of correct reception, noting dependence on signal structure

17 p2702 A71-34973

Passive mapping of terrain with sidelooking radiometry by storing received signals from various elements over extended flight path

17 p2746 A71-35763

German monograph on nonlinear distortion correction of binary bipolar signals in Gaussian noise covering receiver, decision theory and error probabilities

18 p2874 A71-35959

Gyrator circuit design with two antiparallel transistor amplifier stages for minimal DC current reception

18 p2888 A71-36223

Bayesian learning algorithm derivation for statistically optimum adaptive gain control in Rayleigh-distributed signal reception

20 p3206 A71-38874

Noise stability during noncoherent reception of frequency shift keyed signal by receiver with finite Q predetector integrators in presence of fading

20 p3196 A71-39258

Submillimeter plane monochromatic waves propagation in ground layer of turbulent atmosphere, deriving received signals levels fluctuations

20 p3198 A71-39804

Adaptive reception of weak repetitive signals on background of intense fluctuating noise, synthesizing adaptive detection system for multipath propagation and small SNR

20 p3199 A71-39809

Accuracy in maximum likelihood estimate for correlation function parameter of random process in signal reception on normal noise background

20 p3199 A71-39816

Signal reception noise stability by superregenerative transceiver in meteorological system

21 p3383 A71-41242

Optimal and nonoptimal signal reception under conditions of incomplete a priori information based on approximation by Markov processes in white noise

22 p3527 A71-42749

Algorithms for directional antenna boresight orientation estimation errors relative to spacecraft attitude

sensor, based on measurement of received signal strength

22 p3525 A71-42775

Weak modulated signal sensitivity of photodetectors with strong background as function of bias voltage and illumination power

23 p3678 A71-43533

Algorithms for discrete message signal reception in background non-Gaussian additive noise with unknown statistical characteristics

23 p3647 A71-44321

Wideband transistorized active dipole antenna for reception at 100-1000 MHz, calculating impedance and effective height by linear theory

24 p3807 A71-44360

Data transmitting and receiving instruments and systems development problems covering signal shaping and converters and information channel and data reception theories

24 p3806 A71-44375

SIGNAL REFLECTION

Calorimetric method for measuring high signal reflection coefficients at microwave frequencies

04 p0586 A71-14656

Delay time between beams reflected from different parts of meteor trail, using phase invariant and frequency scanning methods

06 p0869 A71-18263

Satellite radio interferometer multipath reflections effect on accuracy

07 p1106 A71-18839

Signal reflection from sporadic E layer, investigating multiplicity relationship to earth surface, ionization level, D region and nighttime absorption

07 p1100 A71-19403

Piezoelectric transducer echo signals spectral analysis, taking into account electrical load and electromechanical coupling degree

08 p1294 A71-21896

Long range tropospheric radio wave propagation, calculating signal impulse function and time lag between diffraction and reflection

09 p1404 A71-22217

External SHF signal effects on multifrequency spectrum of reflex klystron coupled with long waveguide

09 p1414 A71-22221

Woodward ambiguity function generalization for case of radar signal reflection from rapidly fluctuating target, mixed with white Gaussian noise

09 p1404 A71-22292

E region electron concentration profiles, using ground sounding equipment allowing accurate signal reflection altitude measurements

09 p1435 A71-22441

Line-of-sight radio signal transmission, investigating sea surface reflections effects on phase of arrival and coherence

09 p1409 A71-23502

Ideal reflector simulation of periodically supported infinite plane metallic wire gratings with rectangular mesh showing small sag

09 p1409 A71-23503

Meteor-reflected radio wave propagation directivity and diurnal and annual variations, comparing experimental and theoretical calculation results

10 p1576 A71-24033

Meteor-reflected radio wave propagation diurnal and annual variations prognosis, discussing indispensability of incident meteor particle velocity and density distributions

10 p1669 A71-24034

Meteor trails distance determination by radar pulses reflection observation, estimating reflected signal delay dispersion and plotting mean square errors

10 p1576 A71-24037

Fog droplet and rain effects on propagation of echo location signals from bats

10 p1638 A71-24423

Covariance matrix of coordinate fluctuations of instantaneous radar center of reflection from set of scatterers

10 p1578 A71-24709

Low density plasma-double gridded antenna system for ion and electron signal propagation studies, observing multiple reflections of acoustic and ballistic pulses and bulk phenomenon

12 p1935 A71-26913

Radar reflection from Mercury and Venus, discussing observations of echo times predicted relativistic increase

12 p1967 A71-27419

Lumped inhomogeneities reflections effect on characteristics of AM signal along transmission line

12 p1883 A71-27624

Instantaneous frequency statistical characteristics of passive noise spectra and fluctuating signals reflected from nonpoint moving radar targets

14 p2195 A71-30111

Mathematical model for predicting microwave signal fading characteristics due to reflections from ocean surface

15 p2368 A71-31140

Airborne ECM receiver, determining conditions for detecting victim radar signal before signal reflection from aircraft 15 p2368 A71-31207

Reflected short wave signal frequency shift due to reflecting ionospheric layer movement and electron concentration changes, considering oblique incidence on isotropic and anisotropic layers 16 p2542 A71-33484

Radar observation of lunar distance, motion and surface statistical nature, noting enhanced reflectivity associated with craters 17 p2804 A71-35178

Airborne Doppler velocity sensors, considering hydrometers effects on HF signal attenuation and reflection 17 p2747 A71-35768

Radio wave propagation studies evolution, considering ionospheric signal reflection, equipment optimal characteristics and transversed medium composition and properties probing 19 p3016 A71-37341

Signal reflection from sporadic E layer, investigating multiplicity relationship to earth surface, ionization level, D region and nighttime absorption 19 p3053 A71-37827

Harmonically modulated reflected light signals phase shift and demodulation, assuming single scattering 19 p3018 A71-37975

Automatic interplanetary station adapter to obtain reflected signals amplitude-altitude-frequency characteristics during ionospheric probes 19 p3058 A71-38392

Computer programming for on-line correction of microwave measurements of loss and reflection effects between network analyzer and device/circuit under test 20 p3205 A71-39377

Wave polarization and midpath ground reflection effects on power loss of two hop radio signal propagation through ionosphere 22 p3511 A71-42280

Lunik 14 spacecraft radio signal reflection from lunar surface, showing energy spectrum dependence on surface roughness 22 p3511 A71-42301

Point source average signal reflection from conductive plane in random oscillation 23 p3654 A71-44163

Anomalous ultrasonic attenuation in pure superconducting Nb from pulse echo amplitude measurements 24 p3860 A71-44751

SIGNAL STABILIZATION

Analog transducers and tape recorders measurement sensitivity and conversion factor stabilization using push-pull signals 05 p0747 A71-16144

Oscillator signal frequency instability relationship with spectral purity based on thermal noise effects [ONERA-TP-912] 05 p0722 A71-16706

Temporal stability of operating points on curves of signals from time interval sensors in angle code converters 06 p0873 A71-17522

Transient stabilization analysis for electronic circuits containing diverse components with variable parameters, considering active low pass filter example 07 p1078 A71-20061

Optimal reception of AM signal during nonlinear operation of radio system 07 p1064 A71-20258

Frequency stabilized lasers as absolute wavelength standards, discussing perturbation causes for optical resonant cavities and atomic transitions 10 p1621 A71-24581

Microwave discriminators with IF error signal ensuring high stabilization of master oscillator frequency without complex tuning operations 11 p1737 A71-25939

Signal stability in distributed active lines of HF semiconductor devices with negative leakage resistance 12 p1878 A71-26843

Stabilizing system for retransmission beam of direct TV broadcast satellite, considering rebroadcast antenna, electronic sensor and antenna pointing subsystem 18 p2892 A71-36576

Gain and stability of MOS transistor small signal amplifier as function of frequency, using lumped element equivalent circuit 19 p3028 A71-37563

Noise stability and rejection probability of code sequences in real multifrequency communications systems with multipositional frequency shift keying 19 p3022 A71-38495

Microwave discriminators with IF error signal ensuring high stabilization of master oscillator frequency without complex tuning operations 20 p3205 A71-39259

Supercritical transfer electron amplifier using GaAs CW Gunn diode with cathode doping notch and profiles sloping upward for stabilization 22 p3521 A71-42204

SIGNAL TO NOISE RATIOS

Holography theory, analyzing coherent, incoherent and modulated incoherent forms in SNR terms 01 p0078 A71-10142

Adaptive retransmission for improving two-way communication between antenna arrays in randomly fading environment, calculating signal to noise ratio 01 p0052 A71-10468

Coherent binary reception channels noiseproof qualities in presence of fluctuating noise and single concentrated bursts 01 p0030 A71-10473

Radio telemetry data transmission, investigating multipath propagation effects on signal to noise ratio and distortion 01 p0033 A71-10889

He-Ne IR laser resonator as quadratic receiver for modulated filtered laser emission, noting strong LF noise 01 p0096 A71-11218

Noise stability in single-channel FM transmission system via maximum SNR obtained with optimal predistortion 02 p0212 A71-11836

Free space optical channel analog and digital communication theory, considering SNR, M-ary signaling, error probabilities and information rates, etc 02 p0213 A71-12018

ECG signal analog to digital conversion at sampling rate and quantizing accuracy for minimal losses and/or distortion 02 p0208 A71-12949

Parametric amplifier with nonlinear capacitance varying as quadratic function of voltage, deriving power gain, bandwidth and noise figure from equivalent circuit 03 p0383 A71-13270

Chopper amplifier modulator and demodulator circuits analysis, discussing SNR performance 03 p0387 A71-13821

Boxcar integrator attachment for oscilloscopes, improving S/N ratio of repetitive signal 03 p0427 A71-13918

Locking characteristics of automatic phase control circuits in noisy environment 03 p0391 A71-14311

Signal parameter estimation during pulse sequence reception on background of nonstationary additive noise 04 p0549 A71-14614

SNR of harmonic signal mixed with narrow band noise, measuring correlation coefficients 04 p0550 A71-14615

Finite memory radio filter synthesis for maximizing SNR with supplementary quadratic restrictions 04 p0550 A71-14617

Maximum likelihood estimation algorithm for arrival direction of narrowband signal under correlated noise 04 p0550 A71-14618

Hologram Fresnel zone with monochromatic signal and background noise, determining precision of object image coordinates 04 p0584 A71-14633

Interference reduction in logic circuits using combined signal amplitude-pulse duration discrimination 04 p0562 A71-15893

Field of determinate signal with normal noise, considering representation as superposition of two circular polarized components of directly opposite rotation 05 p0719 A71-16010

Optical fields holographic subtraction for SNR enhancement 05 p0748 A71-16262

Nonhomogeneous signal fields reception in presence of homogeneous noise using two-element subtractive antenna array, noting S/N improvement 05 p0721 A71-16469

Doppler pulse radar signal reception, calculating noise signal optimal relationship for comparison with adapted filtration technique 05 p0722 A71-16707

Optimal quasi-regular signal detection on amplitude and frequency modulated noise background 05 p0723 A71-17020

Path intermodulation data distortion derivation from noise power ratio measurements over five tropospheric scatter paths during system acceptance tests 05 p0723 A71-17055

Absolute value type early-late gate bit synchronizer steady state phase noise performance evaluation by Fokker-Planck method 05 p0730 A71-17060

FM discriminator with nonideal limiting, calculating signal to noise ratio under white Gaussian noise input 05 p0730 A71-17071

PSK pseudonoise/spread spectrum communication systems with SNR reduction, examining phase nonlinearities effect 05 p0725 A71-17074

Photodetector-transistor amplifier coupling for maximum SNR in optical communication systems 06 p0866 A71-17370

Phase locked automatic direction finder /ADF/ flight test results, indicating signal to noise threshold reduction by coherent detection 07 p1057 A71-18811

Radar performance with multipath using complex angle /CA/ method for resolving low angle targets comparing S/N ratio with monopulse system without CA 07 p1058 A71-18844

Optimum low pass filter bandwidth for pulse detection in exponential noise, using two dimensional spectrum 07 p1059 A71-18845

Linear delay input effects on analog cross correlation mean performance, plotting output SNR vs integration time 07 p1059 A71-18855

Broadband pulling cavity stabilized X band Gunn oscillator, using measured circuit and diode admittance 07 p1073 A71-19111

Band limiting effects on PCM/split phase signal detection, considering signal to noise ratio degradation 07 p1061 A71-19265

FM discriminator detection, calculating false click probability and effect on output signal to noise ratio 07 p1061 A71-19533

Quasi-single sideband frequency modulation system response to noise above threshold for Gaussian signal [IEEE PAPER 70-TP-70-COM] 07 p1062 A71-19533

Incomplete separation influence of composite signal components on noise stability of coherent communication systems 07 p1064 A71-20253

Binary signal parameters estimation mixed with Gaussian noise, using method of moments 07 p1065 A71-20420

Baseband recorder flutter, pilot and AGC noise effects on quadrature double sideband /QDSB/ FM systems 07 p1066 A71-20430

Nd-glass laser amplified mode locked pulse measurements, noting signal to noise ratio above 10,000 07 p1129 A71-20611

Noise rejection of two channel asynchronous storage circuit with internal detection for weak signals reception 08 p1252 A71-20734

Optical data storage photodetector output signal to noise and signal to background ratios, using Fourier transform amplitude and phase holograms 08 p1287 A71-21180

Holographic recording intermodulation noise suppression by image wave field distortion and retrieval considering signal to noise ratio 08 p1287 A71-21187

Photographic emulsion model for signal to average noise irradiance ratio analysis in hologram reconstruction 08 p1287 A71-21188

Correlation detection systems, calculating DC component effects on output signal to noise ratio 08 p1253 A71-21280

Information transmission rate and error probability in analog feedback systems, showing normalized maximum transmission speed dependence on signal to noise ratio 08 p1268 A71-21283

Hadamard-transform spectrometer experimental verification for multiplex advantage in signal to noise ratio 08 p1289 A71-21370

Optimal detector parameters for stochastic signals in noise, discussing analytic and simulation studies on adaptive techniques of pattern recognition 08 p1259 A71-21594

Derivative approximation techniques for recursive signal detection, using computer program for solving optimum and suboptimum processes signal to noise ratio in effectiveness evaluation 08 p1255 A71-21596

Observational data statistical evaluation, considering meteorological instrument bias, corresponding instrument fluctuations and noise/signal separation by linear algebraic filter 08 p1329 A71-21726

Signal fluctuation noise reduction with input screen inertia by lagging component introduction to introscopic system 08 p1294 A71-21903

Frequency signal structure selection to ensure maximum information capacity for given SNR at receiver output in discrete information transmission 08 p1257 A71-21980

Optimal recognition system for optical spatial and background inhomogeneous Gaussian signals in noise 08 p1257 A71-22022

Optimal phase regulated AFC system for PM signal filtration in presence of internal noise 09 p1404 A71-22155

Wideband photographic signal recording by modulated laser beams, discussing performance characteristics 09 p1404 A71-22155

teristics in terms of signal to noise ratio and laser power

09 p1460 A71-22355
Maximum likelihood estimates for deterministic signal parameter during optimal reception on stationary normal noise background

09 p1405 A71-22465
Signal-white noise mixture filtration, determining maximum SNR position and magnitude and filter bandwidth

09 p1416 A71-22466
External and transistor noise temperature effects on SNR of transistorized microwave receiving antennas

09 p1417 A71-23038
Adder transfer characteristics, demonstrating summation method for signal to noise ratio improvement

09 p1407 A71-23049
Cophase ad hoc statistic for data processing of detectors array signal propagating in uncorrelated noise

09 p1408 A71-23452
Threshold carrier to noise ratio for phase lock demodulators, using computerized prediction model

10 p1574 A71-23764
Signal mean and noise variance as direct functions of phase angle between signal component passed by bandpass limiter and coherent reference

10 p1582 A71-23765
Wave structure and mutual coherence functions of optical wave propagating in turbulent atmosphere, considering signal to noise ratio

10 p1641 A71-23948
Detection characteristics of optimal interperiod processing radar pulse systems for arbitrary correlation of signal and noise fluctuations

10 p1578 A71-24710
Stellar silicon brightness measurement for evaluating SNR and selecting reference star

10 p1679 A71-24951
Ne absorption tube in alternating magnetic field for He-Ne laser frequency stabilization reference, discussing laser output SNR effects

12 p1913 A71-26926
Slip vs static error offset for first and passive second order phase locked loop as function of signal to noise ratio via computer simulation

12 p1892 A71-27073
Adaptive array antennas with control loop, deriving noise expression for maximizing signal to noise ratio

12 p1881 A71-27426
Interference threshold probabilities of pseudorandom frequency hopped signals in conventional spread spectrum communications relative to Gaussian receiver bandwidth

12 p1881 A71-27428
Interaural phase angle control, using equal masker/signal narrow noise bands and phase shifting network between channels

12 p1871 A71-27534
Signal to noise ratio measurement in hologram reconstructions by vibration interferograms

13 p2068 A71-28447
Phase hologram nonlinearities effects, determining signal to noise power ratio in terms of Chebyshev series coefficients

13 p2069 A71-28714
Threshold SNR for signal frequency meter based on zero number count method, determining reliability

14 p2194 A71-30088
Optimal antennas statistical synthesis for minimum noise power for given signal gain

14 p2195 A71-30108
Detectors for deterministic signals in noise with rational spectral density, considering analog filter for continuous input sampling and discrete filter for point sampling

14 p2195 A71-30108
Noise stability at reduced peak signal power of PTM-AM communications using wideband linearly frequency modulated carrier pulses

15 p2368 A71-31228
Quasi-harmonic signal suppression in theta-power amplifier as function of nonlinearity at various noise levels

15 p2375 A71-31229
Optimal noncoherent receiver for signal detection in mixture of noise and chaotic echoes in media with frequency dependent attenuation

15 p2369 A71-31231
Conditional distribution density formation for signal-noise mixture based on learning sampling with dependent values

15 p2370 A71-31586
Input signal preservation in nonlinear dynamic system described by finite difference equation in presence of noise, deriving algorithms for discrete time computers

15 p2381 A71-31982
Facility for signal noise measurement in proportional fluidic amplifiers, discussing stored sweep spectra interpretation

15 p2351 A71-32053
Noise stability and false response probabilities of receivers in circular remote control systems under har-

monic interference for signal transmitted over power distribution grids

15 p2353 A71-32081
Speech envelope masking noise generation with constant S/N ratio for intelligibility studies

15 p2372 A71-32297
Low voltage signal conversion to digital code, emphasizing SNR improvement

15 p2382 A71-32452
Laser output speckle removal with slowly moving and motionless diffusers system, reducing integration time for obtaining SNR

15 p2451 A71-32590
Optimal discrete time detection of radar signal parameters in nonGaussian correlated and noncorrelated noise, using Markov model

15 p2373 A71-32619
Spectroscopic plate emulsion with excellent signal to noise characteristics, investigating baking time response in controlled nitrogen atmosphere

16 p2577 A71-33137
Signal to noise ratios for coaxial laser radar system heterodyning signal backscattered from atmospheric aerosol

16 p2541 A71-33138
He-Ne IR laser resonator as quadratic detector for modulated filtered laser radiation, noting strong LF noise

17 p2750 A71-34269
Low noise operation of CW devices with GaAs vapor grown p-n junctions, observing optimum AM SNR of minus 140 dB

17 p2713 A71-34445
FM radio receiver SNR and noise spectra for arbitrary transmission band characteristics

17 p2701 A71-34778
Stellar spectrograms digital filtering for SNR improvement for photographic plate with line widths larger than granulation noise mean period

17 p2743 A71-35008
Bandlimiting effects on coherent detection of PSK, ASK and FSK signals in presence of white Gaussian noise, using SNR as performance criterion

17 p2704 A71-35085
Flow velocity measurement by laser differential Doppler heterodyning, obtaining SNR from frequency difference between shifted beams

18 p2914 A71-35848
Image intensifier tube coupled to smoothing dissector to improve SNR in electronic scanning spectrometer

18 p2914 A71-35850
Incoherent radiation distribution analysis by image multiplex coding with SNR gain applied to IR region [ONERA-TP-972]

18 p2916 A71-36031
Noise equivalent irradiance equation for airborne IR scanner at peak response detector wavelength, involving target scene radiance and hot iridome emittance

18 p2917 A71-36053
Pattern recognition multiplex arrangement with optical relay tube and point hologram for image distribution onto spatially separated channels to obtain SNR improvement

18 p2917 A71-36054
Optical homodyne detection of light signal wave front scattered by moving surface with normally distributed roughness, calculating conditions for optimum SNR

18 p2930 A71-36058
IMPATT diode amplifiers and oscillators AM and FM noise spectra and SNR prediction for comparison with experiment

18 p2888 A71-36271
Thermal mapping performance of passive airborne IR scanners for remote environmental sensing, estimating SNR and noise equivalent irradiance

18 p2921 A71-36364
Five-gate automatic acquisition star and satellite TV tracker with video signal from vidicon or image orthicon, using line-to-line correlation for SNR improvement

18 p2882 A71-36904
Image dissectors in optical tracking applications, discussing design, operation, SNR performance, tracking modes, relative merits and disadvantages

18 p2883 A71-36915
Probability error calculation for digital signals contaminated by intersymbol interference and additive Gaussian noise

19 p3015 A71-37222
Asymptotic optimal rank criterion for noncoherent detection of fluctuating radar signal in noise of unknown intensity

19 p3015 A71-37253
Phase locked loop models with off-tuned binary PSK interfering signal and angle modulated signal and noise at input, noting performance degradation

19 p3020 A71-38429
Interference voltage prediction model of induced noise in reference ground of electronic systems

19 p3031 A71-38448
Noise factor formula of multiple loop receiver input network with series connected stages for antenna matching and coupling parameters

19 p3022 A71-38498

Capacitive memory storage for filtration of repetitive pulse radio signals mixed with additive noise

19 p3022 A71-38500
Signal shape matched suboptimum self bit synchronizer for high SNR and timing error variance, reducing jitter

20 p3203 A71-38862
Envelope limiting in control loops of adaptive array antennas, reducing varying noise interference

20 p3195 A71-38863
Gaussian and Poisson noise and SNR effects on subjective image quality rating, using transparency aerial scenes

20 p3235 A71-39190
Ternary delta modulation evolution from binary system by addition of encoder-analyzer, calculating SNR

20 p3202 A71-39468
Sensitivity requirements for attenuation measurement radio receivers, considering minimum input SNR for absolute measurement error not to exceed preestablished value

20 p3197 A71-39550
Information producing capabilities of various combinations of SNR, bandwidth and contrast in simulated digital encoding TV systems

21 p3347 A71-40130
Incoherent carrier communications system, obtaining message SNR of 60-70 dB for analog signals with compound pulse modulation and carrier clipping

21 p3347 A71-40375
Photographically recorded image enhancement, discussing filtering, SNR and film grain noise

21 p3382 A71-40936
Signal reception noise stability by superregenerative transceiver in meteorological system

21 p3383 A71-41242
Digital programmable matched filter for LSI technology, considering signal/noise discrimination

22 p3519 A71-41511
Ultrasonic defectoscopy of steel samples, considering grain size effects on SNR

22 p3528 A71-41757
Brillouin scattering effect on noise of Bragg imaging in ultrasonic band at room temperature, using convergent illuminating light beam

22 p3541 A71-41779
Signal parameter estimation during pulse sequence reception on background of nonstationary additive noise

22 p3510 A71-42254
SNR of harmonic signal mixed with narrow band Gaussian noise, measuring correlation coefficients

22 p3510 A71-42255
Finite memory linear radio filter synthesis for maximizing SNR under supplementary quadratic constraints

22 p3510 A71-42257
Maximum likelihood estimation algorithm for arrival direction of narrowband signal under correlated noise

22 p3510 A71-42258
Hologram Fresnel zone with monochromatic signal and background noise, determining precision of object image coordinates

22 p3546 A71-42273
Mixed base modulation technique performance, considering SNR in transmission problem

22 p3512 A71-42380
Bit synchronization in high SNR digital communication system, using Kalman filtering algorithm

22 p3513 A71-42383
Gaussian errors effect in maximal ratio diversity combiner weighting factors on probability distribution of output SNR

22 p3513 A71-42384
Signal to quantizing noise ratios for differential PCM systems used to encode analog signals from Markov processes into digital form

22 p3514 A71-42391
Nonlinear and syllabic companded digital delta modulation systems, discussing SNR measurement and computer simulation for optimum design

22 p3514 A71-42392
Combined injection locking with indirect synchronization for FM signals in noisy environment with allowance for bias oscillator LF time constant effect

22 p3514 A71-42393
Image detail reproduction quality and resolution, describing signal to noise and modulation transfer function effects

22 p3547 A71-42505
Noise-free linear wave front reconstruction from nonlinearly recorded holograms, noting importance of amplitude transfer function

22 p3550 A71-42571
Deterministic signal with normal noise, considering field representation as superposition of two circularly polarized components of directly opposite rotation

22 p3515 A71-42758
Millimeter and submillimeter wave radiation detection by paramagnetic materials, noting noise equivalent power dependence on various parameters

23 p3717 A71-44293

- Demodulator interference noise in FM modulation radio relay system as function of ratio between interfering and interfering carrier powers and AM sensitivity 24 p3804 A71-44988
- Optimal number of parallel connections of transistors in amplifier for improving SNR 24 p3810 A71-45260
- Two component I/f noise measurements in p-channel MOS transistors 24 p3812 A71-45352
- Substrate effect on MOSFET noise and y-parameters using wave equation 24 p3862 A71-45354

SIGNAL TRANSMISSION

- NT AUTOMATIC PICTURE TRANSMISSION
- NT BIOTELEMETRY
- NT DATA TRANSMISSION
- NT DOUBLE SIDEBAND TRANSMISSION
- NT IONOSPHERIC F-SCATTER PROPAGATION
- NT IONOSPHERIC PROPAGATION
- NT MICROWAVE TRANSMISSION
- NT MULTIPATH TRANSMISSION
- NT PCM TELEMETRY
- NT PULSE FREQUENCY MODULATION TELEMETRY
- NT RADAR TRANSMISSION
- NT RADIO TELEMETRY
- NT RADIO TRANSMISSION
- NT SATELLITE TRANSMISSION
- NT SHORT WAVE RADIO TRANSMISSION
- NT SINGLE SIDEBAND TRANSMISSION
- NT TELEMETRY
- NT TELEVISION TRANSMISSION
- NT TRANSEQUATORIAL PROPAGATION
- Quantization in data transmission and extraction, considering analog signals transmission in digital form and radar echoes recognition by digital integration systems 01 p0029 A71-10307
- Mie extinction parameters tabulation for computed signal transmission through rain at microwave and visible frequencies 01 p0029 A71-10469
- HF radio wave Doppler shift by ionosphere effect in retransmitted and backscatter signals 01 p0040 A71-11524
- Signal sources output impedance matching effect on phase difference measurement accuracy 02 p0212 A71-11842
- Ultrawide bandwidth laboratory laser communication link for high fidelity signal transmission, discussing system configuration, components and preliminary test results 02 p0214 A71-12025
- Heat rotation induced eye movements in cats by neuron level determination, considering vestibular apparatus of signal transmission loop for mathematical model 03 p0356 A71-12983
- Real time analysis and display of pulsed laser propagation data in rectangular X-Y field 03 p0427 A71-13920
- Fluid limits transient response to frequency modulated signal inputs, considering Newtonian fluids or perfect gases [ASME PAPER 70-WA/FLCS-1] 03 p0354 A71-14078
- Coherence matrix of elliptically polarized radio signal scattered by statistically rough conductive surface 04 p0550 A71-14619
- Wideband signal processing via multiple narrow band channels, discussing performance limitations due to amplitude and phase distortion and spurious outputs 04 p0555 A71-15341
- Time interval maximum transmittable energy under spectral limitation, deriving time limited pulse functions for minimum energy loss 05 p0720 A71-16393
- Optoelectronic signal transfer from rotating shafts to stationary equipment without rubbing contacts 05 p0723 A71-16973
- Nonlinear planar propagation of sinusoidal and band-limited noise signals in air, extending to spherical waves 05 p0784 A71-17157
- Communication satellite systems for long distance telephone connections, comparing transmission possibilities between links and terrestrial extensions 06 p0869 A71-18013
- Satellites for time dissemination, discussing clock synchronization and signal propagation 07 p1154 A71-19011
- Linearly polarized CW signal transmission through near solar corona, measuring Faraday rotation 07 p1191 A71-19030
- Communication satellite station at Fucino (Italy), testing receiving and transmitting equipment transmission quality 07 p1063 A71-20041
- Short wave communication channel quality estimate for discrete signal transmission based on signal level

- variations calculation with allowance for ionospheric parameters 08 p1252 A71-20773
- Cosmos 142 satellite measurements of VLF radio signals transmitted through ionosphere by ground based stations 09 p1408 A71-23143
- Electromagnetic transient signal nonlinear dispersion in homogeneous isotropic partially ionized plasma medium 09 p1505 A71-23520
- Visual image propagation from retina to higher level formations in multichannel system of cat visual analyzer 10 p1561 A71-24163
- Microwave signal attenuation in LF oscillation beam plasma discharge, comparing to braking cyclotron absorption effect 10 p1653 A71-24880
- Long life vacuum tests of dry and wet lubricated slipping systems for power and signal transfer, discussing wear, noise and contact resistance 11 p1771 A71-26050
- Minimum error pre- and post-filtered sampled signals for pulse modulation and data compression optimization 12 p1879 A71-27070
- Lumped inhomogeneities reflections effect on characteristics of AM signal along transmission line 12 p1883 A71-27624
- Direction finder for point source signals from two simultaneous transmitters 14 p2210 A71-29810
- Noise effect on signal parameter control in linear measurement devices 14 p2194 A71-30082
- Mammalian neurons, neuroendocrine transducer /pinealocytes and adrenomedullary chromaffin/ and endocrine cells communication properties, noting signal transmission 14 p2182 A71-30180
- VLF signal propagation during low and high solar activity, discussing equipment precision, diurnal and seasonal phase variations and phase anomalies correlation 14 p2204 A71-30973
- Microsecond time synchronization potential through cycle identification of VLF multiple frequency transmissions 14 p2204 A71-30974
- Telemetry polarization diversity combiners for data dropout elimination, considering input signal characteristics and propagation 15 p2370 A71-31642
- Solar system interstellar communication with Galaxy, discussing information transmission, coding decoding, recording, display, pulse use and economics 15 p2371 A71-31747
- Performance category III all-weather capability ILS landing equipment standards, discussing high directivity antennas and transmission and control system redundancy techniques for reliability 15 p2445 A71-31909
- C band SYDAC system compatible with conventional ILS, considering transmission sensitivity to ground reflection and lateral obstacles 15 p2445 A71-31910
- Restrictions on signals effective bandwidth, determining uniform upper bounds for use in design of systems with minimum distortion 16 p2542 A71-33458
- Error estimates in transmission of pulse code telemetering signals by nonredundant binary code through asymmetric channel 16 p2543 A71-33706
- Multidimensional control system transmission matrix optimization in presence of random signals and noise 16 p2550 A71-33717
- Discrete VLF emissions triggered by naturally occurring whistler trains or man-made signals of constant frequency 16 p2544 A71-33950
- Signal waves amplifier in medium of high nonlinear electric polarization, considering reflected waves effect on amplification 16 p2544 A71-34131
- Long distance FM signal pulse propagation and maximum compression synthesis in dispersive media, using asymptotic theory for mathematical treatment 17 p2701 A71-34761
- Laser Doppler anemometer, defining signal transmission region and spectrum bandwidth/amplitude from photocurrent and single moving scattering particle emission 17 p2745 A71-35328
- Random access signaling system application to aircraft control, discussing signal redundancy requirement for access capability optimization based on radio environment model 17 p2747 A71-35783
- Distance measurement system with onboard transponder, discussing subcarrier and pseudorandom code signal techniques synthesis 18 p2879 A71-36532

- Commutation and combined transmission free access system, discussing error probability 18 p2880 A71-36552
- Semiconductor instability effects on reflection and transmission coefficients of microwave control devices 19 p3026 A71-37252
- Magnetospheric whistler mode signal propagation paths and amplification, investigating echoes of ground to satellite transmission 19 p3016 A71-37400
- Atmospheric signal propagation study between satellite and earth, using solar radiometry 19 p3018 A71-38075
- Signal propagation in model neuron network in terms of differential equations system, representing retina major cell types in planar model 19 p3003 A71-38276
- Cadence synchronization of multichannel communications systems using orthogonal signals with overlapping transmission spectra 19 p3022 A71-38493
- Conversion losses as function of signal power and circuit impedance in narrow band triode frequency converter 19 p3022 A71-38499
- Optical parametric oscillator signal wave amplitude fluctuations during nonresonant pumping, calculating damping term governing temporal behavior of deviation from stationary value 20 p3268 A71-38835
- Noise variance maximum likelihood estimate based on order statistics for first order Reed-Muller code transmission over zero-mean white Gaussian noise channel 20 p3202 A71-38875
- Ear inherent channel capacity estimation by applying Shannon equations for binary signal transmission 20 p3191 A71-39765
- Stationary signal space topology concept in special relativity, considering points neighborhoods as independent of signal sending time 21 p3346 A71-40090
- Incoherent carrier communications system, obtaining message SNR of 60-70 dB for analog signals with compound pulse modulation and carrier clipping 21 p3347 A71-40376
- Standard frequency and UTC time signal transmission coherent with SI/atomic/second 22 p3509 A71-42087
- Coherence matrix of elliptically polarized radio signal scattered by statistically rough conductive surface 22 p3510 A71-42259
- Mixed base modulation technique performance considering SNR in transmission problem 22 p3512 A71-42380
- Common channel signaling system for demand assigned multiple access satellite communication, discussing design features and applications to PCMTDMA 22 p3514 A71-42520
- PAM signal transmission through statistically rough waveguide, calculating wall roughness effects on transient response by multiple scattering theory 23 p3645 A71-43566
- Low cost TV ground receiving systems for signals transmitted from synchronous satellites, describing reception techniques, manufacturing and performance characteristics 23 p3646 A71-43594
- SIGNALS
- Microwave negative resistance diode avalanche region, deriving four element incremental signal model 01 p0055 A71-11168
- SIGNATURE ANALYSIS
- Carbon dioxide lasers signature, considering 10.4 micron band P/20/ and P/16/ lines dominant modes for wide gain curve and operating conditions 05 p0760 A71-16259
- Sonic boom problem, investigating pressure signature of large models in supersonic wind tunnels [AIAA PAPER 71-184] 06 p0886 A71-18623
- Small scaled low power carbon dioxide lasers, noting signature variations as function of mirror distance variations 06 p0910 A71-18669
- Far IR materials optical constants analysis by channeled spectra, using Fourier spectroscopy single signature in interferogram to yield real and imaginary parts of refractive index 08 p1335 A71-21384
- Boron and carbon fracture and debonding in epoxy matrix, using acoustic emission analysis 11 p1772 A71-26392
- Pulsar signature on diffuse X ray background, converting fraction of luminosity into k series photons 14 p2297 A71-29584
- Polynomial Hamiltonian for type VIII and IX vacuum cosmologies, suggesting quantized versions involving fluctuations of 3-space signature and topology 18 p2946 A71-35983

Carbon dioxide laser signatures prediction from multiple application of optical resonant equation by computer program, studying line competition effects 20 p3247 A71-39771

SIGNATURES
 NT MAGNETIC SIGNATURES
 NT RADAR SIGNATURES
 NT SPECTRAL SIGNATURES

SIGNS [SYMBOLS]
 U SYMBOLS

SIGNS AND SYMPTOMS
 NT ASPHYXIA
 NT BRADYCARDIA
 NT LEUKOPENIA
 NT VERTIGO
 Thermal state symptoms characterizing limit of human tolerance to heat loads at rest and during physical exercise 01 p0014 A71-11135
 Psychopathology identification by manifest phenotypic behavior, discussing syndrome identification, misperceptions and distorted impressions 07 p1042 A71-19697
 Early and prognostic signs of arteriosclerosis in aircraft pilots from medical examination records 07 p1045 A71-20541
 Subjective fatigue feeling correlation to symptoms based on bank clerks and broadcasting workers work load assessment ratings 17 p2688 A71-34367
 Decompression sickness, investigating surface excursion diving and selection of limb bends vs CNS symptoms by tests on goats 21 p3330 A71-40344
 Human ocular control system supranuclear disorder syndromes and signs in terms of physiological concepts 22 p3488 A71-42438

SIKORSKY AIRCRAFT
 NT CH-3 HELICOPTER
 NT CH-54 HELICOPTER
 NT H-53 HELICOPTER
 NT H-56 HELICOPTER

SIKORSKY S-64 HELICOPTER
 U CH-54 HELICOPTER

SIKORSKY S-65 HELICOPTER
 U H-53 HELICOPTER

SILANES
 NT CHLOROSILANES
 Silane for polycrystalline films deposition on oxidized silicon wafers, noting substrate temperature effects on preferred orientation of deposits 02 p0297 A71-12958
 Organofunctional silane interfacial coupling for high strength glass reinforced thermoplastics 08 p1318 A71-20695
 Silyl peroxides as promotion agents for polymeric materials adhesion to solid substrates and for cross-linking polyethylene to other polymers 10 p1633 A71-24109
 Shelf stable two component urethane adhesives with prepolymer reactive silane coupling agents for high peel strength retention in humid environment 14 p2261 A71-29637

SILENCERS
 One dimensional flow models of internal combustion engine exhaust silencers in noisy systems 11 p1810 A71-25180
 Gas turbine exhaust silencer performance prediction by transmission line theory, considering LF requirements effect on size and cost [ASME PAPER 71-GT-8] 11 p1811 A71-25954
 French disengageable silencer for jet engine noise attenuation during aircraft takeoff 15 p2471 A71-32695

SILICA
 U SILICON DIOXIDE

SILICA GLASS
 MOS large scale IC phosphosilicate glass substrate vapor deposits effects, including hardness, pinhole density and electromigration 07 p1070 A71-18868
 Microcrater morphology in soda-lime-silica glass by polystyrene spheres, detailing shape, density, velocity and incidence angle effects 18 p2961 A71-35948
 Refractive index changes by shock compression metamorphism of tektite, soda lime and silica glasses 19 p3084 A71-37661
 Hypervelocity impact melts, considering meteorite crater igneous rocks or glasses associated with shock deformation 19 p3051 A71-37666

SILICATES
 NT ALUMINUM SILICATES
 NT ANDESITE
 NT ARAGONITE
 NT ENSTATITE
 NT FELDSPARS
 NT FLUOROSILICATES
 NT GARNETS
 NT KAOLINITE
 NT MONTMORILLONITE
 NT PYROPHYLLITE
 NT PYROXENES

TALC
 NT YTTRIUM-ALUMINUM GARNET
 NT YTTRIUM-IRON GARNET
 Soviet book on oxide and silicate materials chemistry and technology covering corrosion, thermophysical properties shear stress, drying, etc 02 p0272 A71-11825
 Particulate silicates IR emission spectra under simulated lunar conditions, noting existence of nearly optimum conditions on moon surface 02 p0305 A71-11987
 Liquid silicate systems density calculation from partial molar volumes of oxide components 05 p0716 A71-16407
 Nuclear tracks high density in Apollo core small silicate crystals, discussing extralunar dust and photo-spheric iron-hydrogen ratio 07 p1189 A71-18740
 Interstellar silicate extinction related to 2200 Å band from determination of enstatite optical constants 07 p1200 A71-20053
 Heavy ion tracks in silicate minerals, using thermal annealing to identify origins 07 p1158 A71-20273
 UVB colors and polarization models for reflection nebulae based on Mie scattering functions for exponential size distribution of silicate particles 09 p1517 A71-22332
 Mafic silicates condensation in primordial solar nebula, explaining meteoritic abundance patterns by two component elemental volatility model and trace element distribution 09 p1521 A71-22932
 Lunar and terrestrial ilmenite basalt, considering hornfels from Keweenaw Duluth complex in Minnesota and Apollo 11 samples 09 p1529 A71-23657
 Pluto iron richness from analysis of similarities between Pluto spectra and Fe bearing terrestrial silicate crystals 10 p1673 A71-24426
 Optical fluorescence of lunar transients in UV to IR range for rock forming silicates, using electron microprobe with cathode luminescence capability 15 p2492 A71-32472
 Crystallization temperatures of lunar gabbroid rocks from Tranquillity base, comparing with dry silicate melts 15 p2401 A71-32498
 Sikhote-Aline shower region soil samples and meteorite and micrometeorite fragment morphology, emphasizing silicate spherules 17 p2810 A71-35718
 Lithium magnesium zinc silicates crystallization phase equilibria, noting temperature effects, structure, melting and solubility 20 p3253 A71-38818
 Interstellar silicate absorption search using VI Cyg No 12 spectrum observations 22 p3605 A71-42349
 Tranquillity silicate mineral in crystalline basaltic rocks from Apollo 11 and 12 samples 23 p3737 A71-43605
 IR vibrational spectroscopic analysis of Apollo 11 and 12 rocks and dust isolated silicate minerals, using LF absorption bands 23 p3759 A71-43766

SILICIDES
 NT DISILICIDES
 L-alpha X ray spectral band and K absorption edges in vanadium silicides and high temperature superconductors, obtaining energy bands electron distribution 02 p0294 A71-11893
 Nb oxidation protection by Ti or Cr modified silicide coating, noting results with various Cr-Si mixtures 02 p0272 A71-12944
 Structure and durability of self healing silicide based coatings for niobium oxidation protection at high temperatures 02 p0272 A71-12947
 Superalloy dispersion strengthened and fused slurry silicide coatings for aircraft gas turbine engines and space shuttle heat shields 11 p1778 A71-25555
 Silicide coated Nb alloys for gas turbine engine components operating at temperatures above 2000 F [SAE PAPER 710460] 13 p2115 A71-28334
 Boridosilicide and boridoaluminide diffusion coatings on iron and steel, investigating formation kinetics structure and properties 21 p3390 A71-41171
 Thin film silicide resistors in monolithic IC for high sheet resistance or radiation hardness using sputtering deposition without protective overlayer 23 p3655 A71-43428
 Steel silicification in liquid media for high temperature oxidation resistance improvement 24 p3829 A71-44731
 Boron silicide coatings wear resistance in vacuum and air, determining slipping rate and working medium influence on friction process in active surface layers 24 p3830 A71-44859

SILICON
 NT SILICON ISOTOPES

Mg, Al and Si ions spectral analysis, discussing energy levels and transition lines 01 p0129 A71-10136
 Acoustic surface wave amplification using accumulation layer on Si in MOS structures 02 p0249 A71-12039
 Gaseous impurities diffusion into silicon via open tube microelectronic method 02 p0297 A71-12922
 Optical fibers scattering loss measurement, describing Si solar cell integrating cube scattering detector 03 p0424 A71-13638
 Crystal growth mechanism involving vapor, liquid and solid phases, discussing Si whiskers and impurities effects 04 p0636 A71-14943
 Silicon and gallium arsenide photovoltaic solar cells, examining performance at high illumination intensities 04 p0535 A71-15006
 Lithium concentration and defects in doped radiation resistant silicon solar cells during electron irradiation 05 p0703 A71-16089
 Production and annealing of defects in lithium diffused bulk silicon after irradiation with 30 MeV electrons and fission neutrons at 300 K 05 p0703 A71-16091
 Power loss processes in Si solar cells, noting improvement in collection, voltage and curve factors 05 p0704 A71-16104
 Silicon single crystal dislocation free growth by Czochralski and Dash methods 05 p0792 A71-16292
 Neutron induced lifetime damage short term annealing dependence on minority carrier density in p-type silicon, considering majority carrier repulsion by positively charged centers 07 p1175 A71-19061
 Ion implantation lattice damage effects in crystalline silicon with allowance for optical reflectivity, considering annealing temperature and amorphous layer formation 07 p1175 A71-19062
 Metal ceramic microstrip L band oscillator circuit with high efficiency silicon avalanche diodes in capacitively loaded TEM coupled lines 07 p1074 A71-19122
 N-type Si surface barriers and finishing effects on photoconductivity and photoelectric effect 07 p1179 A71-19921
 N-type single crystal silicon semiconductor resistors with high impurity concentrations and high accuracy 09 p1414 A71-22160
 Epitaxial deposition of discrete separated p- and n-type silicon on single sapphire substrate, considering technique for MOS devices fabrication 09 p1509 A71-23116
 Pyrolytic aluminum oxide thin films on Si substrate by thermodecomposition, measuring vapor deposition parameters and Si surface preparation effects on dielectric and interface properties 09 p1509 A71-23117
 Carrier concentration, radiation dose and temperature effects on radiation defect formation in Si and Ge during gamma irradiation 10 p1655 A71-24138
 Radiation defects distribution in Si irradiated by protons, deuterons and alpha particles 10 p1655 A71-24140
 P-n junctions formation in p-silicon irradiated by alpha particles 10 p1656 A71-24145
 Stellar silicon brightness measurement for evaluating SNR and selecting reference star 10 p1679 A71-24951
 Boron or phosphorus doping of silicon, noting microhardness increase and friction coefficient reduction 12 p1911 A71-26820
 Photocurrent frequency dependence in thin-base silicon photodiodes for carrier optical generation behind p-n junction and depleted region 12 p1886 A71-26848
 Fe ion photodetachment cross section polarization dependence on a sites in YIG-Si to explain photoinduced uniaxial anisotropy, using crystal field theory 12 p1943 A71-26858
 Residual stresses for fused contacts between metals and Si or gallium arsenide from polarization measurements in principal crystallographic planes 15 p2461 A71-31510
 Neutron and gamma radiation effects on electrophysical properties of high resistivity Si single crystals grown in hydrogen atmosphere 16 p2621 A71-33186
 IR absorption of oxygenated dislocationless phosphorus doped fast neutron irradiated n-type silicon, investigating dominant defects for different radiation dosages 17 p2790 A71-34199
 Radiation hardening of silicon solar cells, analyzing performance in low temperature environments 18 p2852 A71-36963

- Intermetallic formation in Au-Al systems via diffusion couples, determining activation energy, silicon effect and tensile strength 19 p3119 A71-38513
- Silicon reactions with aluminum surfaces, using low energy electron diffraction technique 20 p3194 A71-38882
- Fluorinated ethylene propylene covers for silicon solar cells, describing processing parameters effects on optical and electrical characteristics 20 p3182 A71-38944
- GaAs solar batteries for spacecraft power supplies, comparing effectiveness with Si cells for optimum utilization 20 p3183 A71-39133
- Papers on astronomy covering eclipsing binaries, eclipse functions computations, silicon in sun, Magellanic clouds and stellar kinematics 20 p3300 A71-39819
- Solar silicon line spectra of photosphere, chromosphere and corona, including ionic spectra over wide ionization potentials range 20 p3301 A71-39822
- External and internal absorption spectra of silicon crystal doubly doped with boron and indium acceptors, interpreting line broadening and cross section decrease 21 p3426 A71-40071
- Silicon semiconductor surface passivation with thermally grown silicon dioxide films 21 p3427 A71-40218
- Silicon gate process effect on MOS circuits application, noting bipolar compatibility, circuit layout compactness and reliability 21 p3354 A71-40729
- Si addition effect on Ni-Cr alloy calorized layer depth, microhardness, phase structure, chemical composition and scaling resistance 21 p3390 A71-41168
- Ge and Si point contact semiconductor diodes anisotropic deformation, investigating pressure effects on current and negative resistance in forward branch of I-V characteristics 21 p3430 A71-41222
- Monte Carlo method computer simulation for displacement cascades energy and space structure in Ge, Si and PbS, interpreting semiconductor electrical properties under hard radiation 21 p3432 A71-41304
- Cyclotron resonance measurement for holes in uniaxially compressed Si, determining pressure and temperature effects on relative half width of hole line by relaxation time 21 p3433 A71-41309
- Impurity photoconductivity spectra determination for n and p type Si crystals under 660 MeV proton irradiation 21 p3433 A71-41311
- Plasma anodization of Si in positive column of DC oxygen glow discharge, considering silicon dioxide growth rate in negative glow, Faraday dark space and anode fall 22 p3581 A71-41809
- Interconnection Ta thin films and silicon encapsulation for solid state components in hybrid IC under high humidity 23 p3656 A71-43431
- Electron microscopic investigation of Au thin film deposits on Si single crystals in ultrahigh vacuum, noting semiconductor-like resistance/temperature behavior at liquid He temperatures 24 p3862 A71-45347
- ### SILICON ALLOYS
- Boride coatings for Fe-Si alloy, testing corrosion and wear resistances in aqueous salt, acid and alkali solutions 01 p0097 A71-10039
- Al-Si alloys corrosion resistance in humid atmosphere and acid medium, investigating effects of refining process and hydrogen content 01 p0097 A71-10040
- Cr-Si steels cold shortness tests, identifying low temperature failure mechanisms 01 p0098 A71-10082
- Self ignition temperature of aerosols of Al-Si powders as function of dispersion and alloy composition 01 p0182 A71-11449
- Cr and Mo thin film coatings on Si-Fe, examining effect on plastic deformation and mechanical properties 02 p0266 A71-12655
- Si-Fe fatigue crack growth in vacuum at various temperatures, discussing stress intensity, cleavage and ductility effects 02 p0267 A71-12882
- Protective oxide formation on single phased Cu-Al-Si alloys during high temperature oxidation 05 p0770 A71-17099
- Maraging steels precipitation hardening due to alloying with Si, obtaining improved strength with satisfactory plasticity 08 p1305 A71-21026
- Fe-Si alloy with pronounced texture and large grain size, determining lattice period from X ray diffractogram obtained by reverse response method 09 p1467 A71-22308
- Ti-TiSS13 eutectic oriented solidification structures, showing unidirectional growth faceted silicide fibers and disorientation 10 p1626 A71-24402
- Al-Mg-Si alloy development with low quenching sensitivity and high tensile strength 14 p2259 A71-30471
- Si-B-C alloy phase diagram near SiC-B cross section, noting B solubility limit, microhardness and electrical resistivity 16 p2592 A71-33565
- Cold hardened Cr-Si steels strength/plasticity thermal dependence and brittleness from short torsion and compression tests, identifying low temperature failure mechanisms 16 p2593 A71-33638
- Al-Mg-Si alloy vibration creep endurance under single step loading, emphasizing strain and defect accumulation 17 p2757 A71-34593
- Physicomechanical properties of cermet sintered thermoelectric materials, considering n- and p-type samples of Si-Ge alloys 19 p3075 A71-37111
- Performance tests of high temperature silicon-germanium alloy thermoelectric generator for outer planet mission spacecraft 20 p3264 A71-38928
- Protective xenon atmospheres in sealed silicon-germanium alloy thermoelectric generators, discussing leakage and pressure levels 20 p3265 A71-38934
- Orientational magneto-optic effect in nickel and ferrosilicon monocrystals, discussing anisotropy influence on frequency dependence 21 p3431 A71-41263
- ### SILICON CARBIDES
- I-V characteristics of low and high resistance p(SiC)/n(CdS) junctions prepared by different methods 01 p0139 A71-11116
- Mechanical property data for silicon nitride-silicon carbide fiber ceramic composites having high fracture values 06 p0916 A71-18035
- Transfer function voltage controlled transistorized amplifier using silicon carbide nonlinear resistance element 07 p1075 A71-19301
- Thin oxide films on solution grown single crystals of cubic beta-silicon carbide, discussing physical and electronic properties measurements 07 p1177 A71-19571
- Epitaxial boron phosphides single crystals growth, using thermal decomposition and reduction for deposition on hexagonal silicon carbide substrates basal plane 07 p1180 A71-20174
- Thermoplastics reinforcement with carbon, silicon nitride and silicon carbide fibers, noting fiber aspect ratio 09 p1482 A71-22345
- Gamma irradiation effect on conductivity of varistors made of p-type black SiC 12 p1886 A71-26897
- Black SiC varistors IV characteristics and conductivity, investigating fast neutron irradiation and isochronal annealing effects 12 p1886 A71-26898
- Nonporous polycrystalline silicon carbide production by reaction sintering, applying to high temperature technology 15 p2430 A71-32142
- Silicon-boron melts, investigating B and C concentration effects on carbide layer thickness on graphite/melt interface 15 p2439 A71-32144
- Truncated-cone hot-pressed silicon carbide samples, measuring enthalpy and heat capacity as temperature function at high temperatures 15 p2431 A71-32160
- Tensile strength of boron, silicon carbide coated boron, silicon carbide, stainless steel and tungsten fibers after exposure to air, argon and aluminum at high temperatures 15 p2435 A71-32440
- Optimum sintering temperature, bulk composition and gas medium effects on structure and mechanical properties of silicon nitride and silicon carbide materials 15 p2437 A71-32670
- Gamma radiation induced changes in parameters of black silicon carbide nonlinear semiconductor resistors/varistors/ 16 p2546 A71-33464
- Si-B-C alloy phase diagram near SiC-B cross section, noting B solubility limit, microhardness and electrical resistivity 16 p2592 A71-33565
- Materials stability testing in high temperature propane-butane combustion product flow, selecting compact silicon carbide for structural use in redox medium 17 p2761 A71-34310
- Electrical conductivity and thermoelectric power measurements for polycrystalline beta-SiC heavily doped with nitrogen, estimating electron effective mass and carrier mobility at high temperatures 21 p3433 A71-41307
- Oxygen effects on SiC electrical properties by comparison of photoluminescence spectra of alpha-SiC crystals grown by sublimation in Ar atmosphere 21 p3436 A71-41348
- Alumina, boron carbide and silicon carbide notched and unnotched impact strength tests, using drop weight technique 22 p3565 A71-42542
- Sintered construction material with high SiC content, investigating thermal stability in nitrogen, air, carbon dioxide and water vapor above 2000 K 23 p3696 A71-44020
- Silicon carbide single crystal photoluminescence under pulsed ruby laser light irradiation at 77 K, discussing radiative recombination of excitons 24 p3833 A71-44666
- Semiconductor applications of alpha SiC single crystals, showing mechanical separation of polytypes from druses 24 p3841 A71-44742
- ### SILICON COMPOUNDS
- NT ALUMINUM SILICATES
- NT ANDESITE
- NT ARAGONITE
- NT CHLOROSILANES
- NT COESITE
- NT DISILICIDES
- NT ENSTATITE
- NT FELDSPARS
- NT FLUOROSILICATES
- NT GARNETS
- NT KAOLINITE
- NT MONTMORILLONITE
- NT MUSCOVITE
- NT ORGANIC SILICON COMPOUNDS
- NT PYROPHYLLITE
- NT PYROXENES
- NT QUARTZ
- NT SILANES
- NT SILICATES
- NT SILICIDES
- NT SILICON CARBIDES
- NT SILICON DIOXIDE
- NT SILICON NITRIDES
- NT SILICON OXIDES
- NT SILICON TETRACHLORIDE
- NT TALC
- NT YTTRIUM-ALUMINUM GARNET
- NT YTTRIUM-IRON GARNET
- Nb strips siliconization by silicon hydride decomposition and silicide or silicon oxidation, noting Si surface enrichment and bulk diffusion processes 02 p0272 A71-12943
- Silicon difluoride reactions and properties, describing production from commercial silicon tetrafluoride and versatility of reactions with organic and inorganic compounds 19 p3011 A71-37647
- SiH molecular ion identification in solar atmosphere by solar absorption spectra 20 p3294 A71-39547
- Coherent stimulated recombination radiation emission by p-type cadmium silicon arsenide single crystals in liquid nitrogen cryostat under various pumping levels 21 p3431 A71-41229
- ### SILICON DIOXIDE
- NT COESITE
- NT QUARTZ
- Silane for polycrystalline films deposition on oxidized silicon wafers, noting substrate temperature effects on preferred orientation of deposits 02 p0297 A71-12958
- Damkohler analysis of nitrogen-silica gel absorption isotherm in multimolecular range, noting vapor phase transport and absorbed phase diffusivities 03 p0517 A71-13175
- North American feldspathoidal and silica unsaturated rocks progression in space and time 04 p0584 A71-15775
- Fused silica and single crystal NaCl nonlinear parameters from ultrasonic beams mixing studies 05 p0793 A71-16410
- Oxidation resistance of silica gel lubricants, noting optimum diphenyl amine inhibitor 06 p0916 A71-18470
- Silicon dioxide space charge distribution dependence on photoinjected currents in MOS structures, showing charge effects on I-V characteristics 07 p1174 A71-19055
- Gate voltage drift in enhanced p-channel MIS transistors having either pure silicon dioxide insulation or silicon dioxide with silicon nitride 09 p1413 A71-22156
- Silica minerals in interstellar dust as source of 2200 A interstellar absorption band from comparisons to 2250 A band in Fe or Al bearing quartz spectra 09 p1522 A71-22936

Capacitance voltage measurements on interface of pyrolytically deposited n-type silicon dioxide- InAs MOS diodes as function of admittance at room and 77 K temperatures 10 p1582 A71-23774

Thermodynamic equilibrium constants of Fe-MgO-SiO₂-O₂ system reactions at one atmosphere and 900-1300 C 14 p2190 A71-29875

Crystallization behavior and chemical compositions of Apollo 11 lunar basalts including olivine and silica normative varieties 16 p2637 A71-33512

Optical transmission in unexposed phenolic resin base laminates with silica cloth reinforcements, studying stabilization treatments, pyrolysis and incident radiation spectral distribution 17 p2838 A71-35473

Amino silica gels absorption properties with respect to carbon dioxide, hydrogen sulfide and water vapor, comparing affinity 20 p3193 A71-39233

Thin dielectric films on germanium substrates, using oxygen diffusion through silicon dioxide 20 p3205 A71-39435

Silicon semiconductor surface passivation with thermally grown silicon dioxide films 21 p3427 A71-40218

Plasma anodization of Si in positive column of DC oxygen glow discharge, considering silicon dioxide growth rate in negative glow, Faraday dark space and anode fall 22 p3581 A71-41809

Tridymite structure in lunar pigeonite porphyry 12021 by single crystal X ray diffraction, comparing with meteorite and silica brick 23 p3738 A71-43613

Hydrogen dissolution in fused silica, investigating temperature effects during impregnation on reactive defect sites number 24 p3841 A71-44869

SILICON FILMS

Silane for polycrystalline films deposition on oxidized silicon wafers, noting substrate temperature effects on preferred orientation of deposits 02 p0297 A71-12958

Radiation resistance variations of n-type and p-type silicon photocells due to formation of one or two vacancy recombination centers 15 p2461 A71-31670

Molybdenum hemicarbid layer as diffusion barrier between metal and disilicide, investigating system thermal stability 21 p3399 A71-40526

Single crystal silicon films deposited on sapphire substrates, determining disorientation angles, block dimensions, dislocation density, orientation and structure 22 p3586 A71-42061

Silicon thin film on sapphire for bipolar and MOSFET transistors for microwave IC and subnanosecond switching circuits 23 p3715 A71-43434

Impurity redistribution errors in C-V characteristics of MOS capacitors due to Si thermal oxidation 24 p3809 A71-44993

Excess minority carrier diffusion length measurement in thin silicon wafers, using light-spot and dark-spot methods 24 p3861 A71-45202

Irradiation defects and electrical quality of ion implanted silicon, using minority carrier lifetime measurements 24 p3863 A71-45357

SILICON ISOTOPES

Apollo 12 lunar rock 12013 oxygen 18 and silicon 30 ratios, comparing to terrestrial basalts and gabbros, Apollo 11 rocks and oceanic rhyolite obsidians 03 p0495 A71-14225

Apollo 11 and 12 lunar samples O 18/O 16, Si 30/Si 28, D/H and C 13/C 12 ratio determination, examining whole rocks, breccias, soils, plagioclases and fines 23 p3751 A71-43705

SILICON JUNCTIONS

Silicon avalanche photodiode detectors for near IR laser pulse receivers, discussing quantum efficiencies, internal gains and room temperature responsivities 01 p0092 A71-10011

Si diffusion p-n junctions at high injection levels in strong electric fields, discussing I-V characteristics, minority carrier lifetime, barrier capacitance, etc 03 p0384 A71-13374

N-p Si solar cells controlled lifetime doping effects on electrical performance 05 p0700 A71-16063

Ti-Ag contact N-P and P-N single crystal Si solar cells electrical and mechanical performance characteristics 05 p0700 A71-16069

Si solar cells with and without cover slides performance in severe thermal and light environment /near sun missions/ 05 p0701 A71-16070

N-p Si solar cells, investigating mechanism of low energy proton irradiation damage to back contacts 05 p0702 A71-16084

Defects and annealing in electron irradiated lithium diffused silicon solar cells 05 p0703 A71-16092

Silicon junction avalanche diodes as S band oscillators and amplifiers, presenting peak power efficiency and gain data 05 p0729 A71-16921

Avalanche diodes as solid state noise sources, observing planar silicon junctions breakdown voltages 06 p0940 A71-17324

Ionizing radiation induced surface damage dependence in matched oxide passivated silicon planar epitaxial transistors on junction fringing electric field strength during exposure 07 p1174 A71-19052

Low energy proton irradiation damage to ATS and Intelsat satellites Si solar cells junction properties 07 p1022 A71-19072

Power amplification with anomalous mode Si p-n-n mesa structure avalanche diodes under input driving power at system resonance frequency 07 p1073 A71-19116

Si step-junction avalanche diodes conduction current pulse waveforms during large signal operation, using numerical calculation 08 p1265 A71-21290

Light emission of microplasmas and mesoplasmas in silicon p-n junctions, determining spectral distribution 09 p1507 A71-22190

I-V and capacitance characteristics of silicon diodes prepared by diffusive melting, considering recombination processes in p-n junctions 09 p1414 A71-22290

Si Read diode computer simulated large-signal operation, determining temperature effect on microwave oscillating efficiency 09 p1417 A71-22966

Si p-n-n junction avalanche diode, investigating experimental evidence of microwave generation at subharmonics of transit time excitation and trapped-plasma mode 12 p1887 A71-27047

Thermal oxidation and metal evaporation effects on electrical properties of silicon-silicon dioxide wafer interface in MOS structures 12 p1944 A71-27096

Diffusive p-type Si valve photocells, investigating barrier capacitance 17 p2713 A71-34565

Si p-n junctions microplasmas I-V characteristics, discussing avalanche breakdown, temperature dependence and light emission 18 p2953 A71-35872

Integrated complementary MOS circuit technology, discussing low power consumption, high speed, n and p regions realization on Si plates and design parameters relations 18 p2891 A71-36562

One- and two-sided abrupt junction IMPATT diodes, investigating Si junction type effects on avalanche region and diode design 18 p2895 A71-36987

Hall effect measurements utilization for simultaneous determination of donors and acceptors concentration in semiconductors, applying to n-type silicon 19 p3118 A71-37487

Vacuum deposition of silica and alumina thin films on silicon substrate MOS diodes, using CW carbon dioxide laser 19 p3074 A71-38233

GaAs and silicon IMPATT diodes applications and performance, discussing power levels, amplifier applications, injection locked oscillators and microwave signal source 21 p3357 A71-40818

Avalanche Si photodiode current pulse formation frequency governing mechanism, considering roles of free carriers and electron tunneling 21 p3358 A71-41344

Si Pt-n-p transit time microwave diode source noise measurement, noting low noise characteristics and suitability for local oscillator applications 21 p3359 A71-41413

Spherical avalanche diodes in silicon and silicon-germanium mixed crystals, describing IR detection properties 22 p3543 A71-42125

Neutron irradiation effects on Si p-n junction field effect transistors I-V characteristics, charge distribution in space charge region and transconductance 22 p3586 A71-42297

Electron bombardment effects on shot noise of silicon junction transistors, noting generation-recombination current increase in emitter junction 22 p3586 A71-42298

Flatband voltage stabilization of metal-glass-oxide-silicon systems for phosphosilicate glass 22 p3587 A71-42532

Silicon resistance strain gages sensitivity as function of variable signed load cycles 22 p3550 A71-42880

Low frequency phase method application to fast electron processes and characteristic relaxation times in quick response Ge and Si junction diodes 23 p3650 A71-43307

Silicon Schottky tunnel MOS diodes, discussing effect of thin interfacial film between metal and semiconductor on I-V characteristics 23 p3652 A71-43936

Silicon avalanche diodes for microwave TRAP-PATT amplifiers and self excited oscillators with IMPATT triggering 23 p3653 A71-43964

SILICON NITRIDES

Physical, chemical and electrical properties of silicon nitride thin films deposited pyrolytically on Si substrates, analyzing deposition process effects 03 p0468 A71-14001

Mechanical property data for silicon nitride-silicon carbide fiber ceramic composites having high fracture values 06 p0916 A71-18035

Gate voltage drift in enhanced p-channel MIS transistors having either pure silicon dioxide insulation or silicon dioxide with silicon nitride 09 p1413 A71-22156

Thermoplastics reinforcement with carbon, silicon nitride and silicon carbide fibers, noting fiber aspect ratio [PLASTICS INST. PAPER 5] 09 p1482 A71-22345

Optimum sintering temperature, bulk composition and gas medium effects on structure and mechanical properties of silicon nitride and silicon carbide materials 15 p2437 A71-32670

Current-voltage hysteresis and memory properties of silicon-silicon nitride capacitors as function of oxide layer and stacking fault traps 22 p3516 A71-41684

Polycrystalline beta silicon nitride foils containing glide dislocations from room temperature fracture, determining Burgers vectors and slip planes 24 p3842 A71-45194

SILICON OXIDES

NT COESITE

NT MUSCOVITE

NT QUARTZ

NT SILICON DIOXIDE

Elemental analysis for lunar rocks and regolith, comparing silicon oxide and titanium oxide composition in Apollo 12 and Apollo 11 samples 10 p1672 A71-24389

SiO₂ antireflection coatings for GaAs injection lasers, discussing single layer quarter-wave coatings for loss minimization and bandwidth maximization 16 p2585 A71-33136

Interstellar silicon monoxide discovery from 130,246 MHz frequency line emission of galactic radio source Sag B2 17 p2807 A71-35416

Charge injection in metal-aluminum oxide-silicon dioxide-silicon systems using capacitance voltage technique 22 p3587 A71-42531

Microstrip line on silicon-silicon oxide system, investigating propagation modes and fringing effect by parallel-plate waveguide model 24 p3809 A71-45091

SILICON POLYMERS

NT SILICONE RESINS

NT SILICONES

Fluid sealing capabilities of silicone, fluorosilicone and fluorocarbon elastomers above 250 F [ASLE PREPRINT 71AM 3B-1] 13 p2093 A71-29488

SILICON RADIATION DETECTORS

Rocket-borne solid state spectrometer with liquid nitrogen cooled Li drifted silicon detector and optical feedback preamplifier for solar X-ray measurements 06 p0901 A71-18223

Si surface barrier radiation detectors depletion region low energy proton irradiation damage determination from capacitance-voltage curves and capacitance recovery techniques 07 p1071 A71-19071

Silicon detector measurements of energy deposition in aluminum by monoenergetic electrons 07 p1106 A71-19073

Electron radiation bulk damage effects on Si surface barrier detectors, determining reverse leakage current density and alpha particle response changes 08 p1345 A71-21842

Uncooled Si nuclear particle detector charge sensitive and pulse shaping amplifier design, discussing spacecraft instrumentation and fabrication requirements 08 p1267 A71-21848

Star sensor telescope, employing digitally coded silicon photocell detector for precise optical image location 18 p2925 A71-36910

Onboard silicon detector TV guidance sensor for establishing outer planet mission spacecraft orientation with precise targeting, based on patched conic trajectory simulation [AAS PAPER 71-120] 19 p3101 A71-37915

Proton recording equipment onboard automatic interplanetary stations Zond 4 and 5 at 1.5-50 MeV using silicon drift counters

23 p3675 A71-43274

Range finder receiver based on Si avalanche detector coupled to tunnel diode circuit, with automatic gain control through tunnel diode bias control

23 p3677 A71-43518

Pion beam dosimetry with silicon detectors and plastic scintillators, presenting depth dose and isodose distributions and differential range curves

24 p3799 A71-44359

Operational principles and circuit diagram of transistorized preamplifier for Si p-n gamma quanta radiant flux detector, noting noise properties and possible improvements

24 p3810 A71-45151

SILICON RECTIFIERS

U CRYSTAL RECTIFIERS

SILICON SOLAR CELLS

U SOLAR CELLS

SILICON: TETRACHLORIDE

Titanium and silicon tetrachlorides oxygen-containing impurities determination without hydrolysis, describing measuring device design

15 p2383 A71-31659

SILICON TRANSISTORS

Impurity effects of annealing of radiation defects in p-type silicon, considering annealing temperature

04 p0636 A71-15037

Ionizing radiation induced surface damage dependence in matched oxide passivated silicon planar epitaxial transistors on junction fringing electric field strength during exposure

07 p1174 A71-19052

Surface ionization effects on planar silicon bipolar transistors, considering damage reduction by device exposure to high ionizing radiation dose

07 p1174 A71-19057

Statistical analysis of neutron induced gain degradation of silicon power transistors, determining failures distribution fit to Weibull function

07 p1070 A71-19063

Electron trapping in MIS transistor, discussing thermal annealing process activation energy and trap production by radiation

07 p1076 A71-19499

Bipolar silicon microwave transistors process technology improvements related to extensions of frequency, power handling or low noise performance

08 p1263 A71-20991

Timesaving reliability tests for Si transistors involving failure mechanism acceleration

09 p1418 A71-23042

Spectrum analysis and probability distribution of burst noise pulses of silicon planar bipolar transistors consistent with Markov two state process

10 p1574 A71-23773

Current controlled unstable pulse oscillator, discussing depletion layer transistors and upper frequency limit as function of thermal loads and switching times

12 p1887 A71-27043

P channel enhanced MOS transistors, logic elements and digital integrated circuits in silicon films on sapphire substrates

13 p2038 A71-28716

Silicon planar transistors at low injection levels, showing current transfer function temperature dependence

14 p2213 A71-30624

Neutron irradiation effects on diffusion-ion doped HF n-p-n silicon transistors of moderate power, showing radiation stability

14 p2213 A71-30625

Silicon microwave transistors frequency response theory, considering application as small-signal and power amplifiers

18 p2894 A71-36978

MOS transistors thin monocrystalline silicon layers formation by epitaxial growth and substrate selective electrochemical etching

19 p3028 A71-37565

Emitter avalanche stress on gated silicon planar n-p-n transistors, investigating degradation phenomena

19 p3034 A71-38523

Microwave Si MESFET for 15 GHz oscillation with reduced gate metallization resistance and pad parasitics, improving gain and noise figure

22 p3520 A71-41683

Gold doping effect on minority carrier lifetime and other electrical properties of epitaxial Si transistors

22 p3520 A71-41702

Electron bombardment effects on shot noise of silicon junction transistors, noting generation-recombination current increase in emitter junction

22 p3586 A71-42298

Thermal feedback modification of Si JFETs AC and DC characteristics at low operating temperatures

23 p3649 A71-43070

SILICONE RESINS

Outdoor five year aging tests on polysulfide and silicone adhesive sealants under semiarid, marine and high humidity environments

10 p1634 A71-24119

SILICONE RUBBER

Hydrogen peroxide immersion effects on dimethyl silicone seal rubber tensile properties and tear strength

10 p1631 A71-24082

Contoured silicone internal pressure bag mandrels for helicopter rotor blades fabrication

10 p1615 A71-24096

Flame retardant silicone elastomers for use as aircraft construction materials, describing fabrication techniques, mechanical, aging and weathering properties

12 p1921 A71-27412

SILICONES

Natural convection heat transfer between two isothermal concentric spheres, using water and silicone oils as convective fluids

07 p1222 A71-18995

Accelerated testing of jet fuel containment sealant, using reduced pressure and hybrid fluorocarbon silicone

10 p1632 A71-24083

Ablation residue, including silicone elastomer foam heat shield material ablative degradation

11 p1855 A71-26040

RF transparent ablator of silica filled elastomeric silicone, describing thermal, mechanical and electrical properties at various heating rates

11 p1790 A71-26046

Performance testing of fluorosilicone hydraulic fluid in high temperature supersonic aircraft piston pumps

12 p1921 A71-27040

High density nitric acid oxidizer and unsymmetrical dimethyl hydrazine with silicone fluid additive application to Agena rocket engine for higher performance [AIAA PAPER 71-736]

14 p2287 A71-30781

SILICONIZING

Nb strips siliconization by silicon hydride decomposition and silicide or silicon oxidation, noting Si surface enrichment and bulk diffusion processes

02 p0272 A71-12943

Thermodynamic calculation of silicon chloride gas for high temperature two stage molybdenum silicification in glowing discharge under vacuum conditions

11 p1770 A71-25944

Cermet iron chromosilicization and sinter compactness effects on depth and structure, noting wear, corrosion and thermal resistance

19 p3075 A71-37110

Thermodynamic equilibrium calculation and demonstration of Mo siliciding by circulation method in hydrogen-free gaseous medium containing silicon chlorides

21 p3390 A71-41169

SILOS [MISSILE STORAGE]

U MISSILE SILOS

SILVER

Silver-silver oxide electrode chemistry in alkaline solutions, describing oxide structure, solubility and stability

08 p1234 A71-21083

Sealed secondary Ag cells, controlling H and O recombination by auxiliary electrode

08 p1236 A71-21106

Platinum, palladium and gold detection in silver assay buttons by atomic absorption spectrophotometry

15 p2367 A71-31649

Epitaxial Ag thin film with controlled surface roughness on mica, measuring electrical resistivity as function of temperature, thickness and surface specularly

15 p2461 A71-32376

Electric field effect of epitaxial thin silver films on mica in vacuum as function of temperature, thickness and surface specularly

15 p2461 A71-32377

Ga spreading over Ag and Au thin films surfaces from electronographic and optical experiments, noting volume heterodiffusion

20 p3276 A71-39153

Electrical properties and electroluminescence measurements for p-n junctions in Au- and Ag-doped GaP, noting negative resistance in I-V characteristics

21 p3433 A71-41312

High purity Sb, In and Ag by vacuum distillation, zone melting and electrolytic refining for semiconductor electronics

24 p3861 A71-45201

SILVER ALLOYS

Gallium oxide particles effects on Ag-Ga matrix single crystals critical resolved shear stress

08 p1311 A71-21543

Rh and Ag-Pd alloys magnetic susceptibility, investigating hydrostatic pressure effects

21 p3432 A71-41269

SILVER COMPOUNDS

NT SILVER HALIDES

NT SILVER IODIDES

NT SILVER OXIDES

SILVER HALIDES

NT SILVER IODIDES

Anomalous temperature dependent silver halide photoemission related to lattice vibrationally dependent hybridization of valence states

01 p0137 A71-10144

TV and silver halide emulsion application to planetary photography from space orbit, providing film system immediate information storage and high resolution

09 p1447 A71-22744

Reversal processing technique for producing high diffraction efficiency, low noise and good light stability phase holograms on silver halide emulsions

13 p2068 A71-28711

SILVER IODIDES

Electric properties of solid modified AgI electrolyte batteries

03 p0351 A71-13010

SILVER OXIDE ZINC BATTERIES

U SILVER ZINC BATTERIES

SILVER OXIDES

Silver-silver oxide electrode chemistry in alkaline solutions, describing oxide structure, solubility and stability

08 p1234 A71-21083

Silver oxides crystal structures and physical and electrochemical properties

08 p1234 A71-21083

Silver oxides stability, considering solubility, reduction by hydrogen and thermal decomposition

08 p1234 A71-21083

Silver oxide electrodes electrochemical reaction kinetics, examining oxidation, anodic formation and cathodic reduction

08 p1234 A71-21083

Structural and kinetics investigation of oxides formation in silver-silver oxide-silver-silver oxide system, using electron microscopy and electron diffraction methods

08 p1234 A71-21083

Chemically prepared silver oxide for silver zinc batteries bivalent electrode fabrication

08 p1298 A71-21090

SILVER ZINC BATTERIES

Design, testing and flight performance of sealed AgO-Zn cells of Mariner Mars 1969 spacecraft

03 p0350 A71-13027

Heat sterilizable remotely activated silver zinc battery for energy source of planetary lander capsule

03 p0352 A71-13044

Temperature controlled zinc-silver oxide reserve battery, describing design for high power/energy density, broad operating temperature range and high altitude environmental capability

03 p0352 A71-13044

Biosatellite hydrogen oxygen fuel cell/silver zinc battery combination power system for long aerospace missions, discussing optimal design tradeoff

04 p0535 A71-15288

Zinc-silver oxide batteries - Conference, Montreal, October 1968

08 p1233 A71-21070

Zinc-silver oxide batteries thermodynamic characteristics obtained from silver-silver oxide and zinc-zinc hydroxide electrodes data

08 p1233 A71-21070

Zinc electrodes manufacturing processes, describing materials used in electrodeposition and pressure powder methods, quality control procedures and Zn-Ag batteries electrical characteristics

08 p1297 A71-21088

Manufacture and mechanical properties of sintered silver electrodes involving oxide, powder and resin bonding methods

08 p1297 A71-21088

Chemically prepared silver oxide for silver zinc batteries bivalent electrode fabrication

08 p1298 A71-21090

Polymeric materials for silver zinc battery separators, discussing porous and solvent-type pore free membranes

08 p1234 A71-21093

Cellulose application as zinc silver oxide battery separator, considering chemical stability, cellophane properties, polymerization and crystallinity

08 p1234 A71-21093

Semipermeable polyethylene grafted membranes/separators/ for extended cycle life in silver zinc cells

08 p1235 A71-21094

Heat sterilizable separator material for development of heat sterilizable Ag-Zn batteries meeting contamination requirements in interplanetary exploration

08 p1235 A71-21094

Aluminosilicate separators for silver zinc cells using compaction and sintering techniques

08 p1235 A71-21094

Silver zinc batteries and cells case cover materials and sealing techniques for space missions

08 p1235 A71-21094

Primary and secondary silver oxide-zinc cells performance capability

08 p1235 A71-21094

Zn-Ag oxide cell discharge, determining heat generation rate and voltage production model

08 p1235 A71-21094

Unactivated dry charged zinc-silver oxide cells storage life, determining chemical composition changes at various temperatures and time lengths
08 p1235 A71-21100

Activated storage effect on life of secondary Zn-Ag oxide cells, discussing degradation rate of charge retention
08 p1235 A71-21101

Zinc-silver oxide batteries underwater and aerial applications, designing medium high rate long life cells
08 p1236 A71-21102

Military aircraft zinc silver oxide battery service requirements and performance
08 p1236 A71-21103

Air to air and air to ground missile zinc silver oxide batteries capabilities, including energy density, long storage life and shock and temperature resistance
08 p1236 A71-21104

Service performance and tests of zinc silver oxide batteries on Explorers 17 and 32
08 p1236 A71-21105

Quality control for Minuteman zinc silver oxide battery production
08 p1298 A71-21109

Reliable and low cost electrical solar array/silver zinc battery power system for Agena satellite, discussing design features and flight tests results
20 p3182 A71-38943

SIMICOR [IMAGE CORRELATOR]
U IMAGE CORRELATORS

SIMILARITIES
U ANALOGIES

SIMILARITY NUMBERS
Compressible flow similarity parameters, establishing dimensionless relations for radial turbomachines design
03 p0343 A71-13830

Supersonic jet expansion in variable geometry channels, obtaining pressure dependence on injection rate and similarity parameters
17 p2669 A71-34216

SIMILARITY THEOREM
NT LAGRANGE SIMILARITY HYPOTHESIS
Similar solution of strong shock wave propagation with nonequal heat coefficients, approximating energy of dissociation ionization and free molecular oscillation
01 p0070 A71-10663

Nonaffine similarity laws and transformations subject to limitations of Newtonian impact theory for two dimensional bodies, obtaining aerodynamic coefficients
01 p0002 A71-10948

Thermodynamic similarity laws for rocket fuel tanks with cryogenic propellants, using dimensional analysis for unsteady temperature distributions
02 p0332 A71-12526

Solid fuels and propellants heterogeneous ignition mechanism, using local similarity and related methods
02 p0333 A71-12853

Multilayer structures dynamic phenomena during switching, examining similarity theory with simple p-n junctions
03 p0388 A71-14387

Similarity methods, partial differential numerical analysis, dispersive wave and perturbation theory applications to mechanics
06 p0920 A71-18220

Electromagnetic pulse propagation over flat impedance surface, determining similarity parameters
07 p1060 A71-19187

Unsteady incompressible laminar boundary layer equations, obtaining similarity solutions from momentum integral equation
07 p1093 A71-20365

Similarity criterion for volute centrifugal pumps via supersonic model, considering cavitation parameters influence throughout angular velocities range at flow separation
08 p1347 A71-20784

Discrete fluidic element dynamic tests, using magnified models with similarity criteria
09 p1386 A71-22653

Prandtl equations derivation, initial value problem and similarity theory models for steady plane incompressible laminar flow
11 p1749 A71-25302

Similarity comparisons of isotropic and anisotropic scattering patterns in cloudy atmospheres for haze effects on Mars image contrast, using asymptotic method
11 p1825 A71-25710

Dynamics of planetary atmospheres large scale motions, using similarity theory and dimensional analysis methods for atmospheric circulation characteristics calculation
11 p1826 A71-25720

Expanding laser generated plasma self similarity model from hydrodynamic equations, describing thermokinetic properties
11 p1806 A71-26092

Similarity solution of boundary layer equations for nonuniform external flow
14 p2225 A71-30217

German monograph on similarity transformations application to MGD channel flows covering mechanical, electromagnetic and thermodynamic equations
14 p2283 A71-30863

Similar solution of strong shock wave propagation with nonequal heat coefficients, approximating dissociation, ionization and excitation energy of molecules vibrational degrees of freedom
14 p2228 A71-30996

Laminar boundary layer of free vortex and source flow, obtaining similarity transform of Navier-Stokes equation
14 p2228 A71-31027

Similarity solutions describing flow characteristics behind plane hydrodynamic shock propagating into uniform ideal gas at rest in presence of transverse magnetic field
15 p2391 A71-32074

German monograph on similarity principle as design method in electromechanics covering similarity laws in mechanics, thermodynamics and electricity
17 p2748 A71-34791

Compressible boundary layer equations similarity solutions uniqueness proof, using asymptotic behavior
18 p2909 A71-36814

French monograph on similar solutions of laminar boundary layer problem in supersonic flow covering finite difference methods and convective heat flux
19 p2994 A71-38648

Small perturbations of stationary parallel flow with relaxation, considering boundary conditions around slender wings, partial differential equations and similarity law
20 p3213 A71-39569

Nonself-similar problem of developing plane turbulent jet in unbounded space, obtaining second and third terms of asymptotic series of stream function
21 p3368 A71-40692

Existence and uniqueness of boundary layer equations similarity solution for viscous incompressible fluid flow past paraboloid
22 p3531 A71-42197

Nonlinear automatic control system statistical optimization using similarity theory
24 p3813 A71-44681

SIMILITUDE LAW
Viscous similitude reduction to Mach number independent Birkhoff binary scaling for hypersonic flow over slender bodies
08 p1377 A71-21981

Anisotropy tensor and figurative vector components relation with eigenvector correspondence to eigenstate and eigenmodulus in similitude ratio
10 p1688 A71-24451

Similarity laws for gas discharges in carbon dioxide lasers verified by longitudinal electric field measurements
12 p1914 A71-27209

Electron avalanche processes in gas discharges, deriving electron energy distribution function and similarity laws
13 p2103 A71-29079

Viscous gas jets in uniform oncoming flow, deriving similarity laws by dimensionality theory
13 p1994 A71-29223

Approximate similitude relation for vibrating thin shells with scaled surface geometry, using Love equations of motion
14 p2327 A71-30204

German monograph on similarity principle as design method in electromechanics covering similarity laws in mechanics, thermodynamics and electricity
17 p2748 A71-34791

Interior region of incompressible turbulent boundary layer with pressure gradient on permeable wall, discussing local similitude hypothesis
17 p2729 A71-35346

Similarity laws for gas discharges in carbon dioxide lasers verified by longitudinal electric field measurements
19 p3075 A71-38621

SIMULATION
NT ACOUSTIC SIMULATION
NT ALTITUDE SIMULATION
NT ANALOG SIMULATION
NT ATMOSPHERIC ENTRY SIMULATION
NT COMPUTERIZED SIMULATION
NT CONTROL SIMULATION
NT DIGITAL SIMULATION
NT ENVIRONMENT SIMULATION
NT EXHAUST FLOW SIMULATION
NT FLIGHT SIMULATION
NT LANDING SIMULATION
NT RHEOELECTRICAL SIMULATION
NT SOLAR SIMULATION
NT SPACE ENVIRONMENT SIMULATION
NT THERMAL SIMULATION
NT WEIGHTLESSNESS SIMULATION
Data reduction accuracy estimation via simulation technique, using method of least squares
01 p0073 A71-10357

Traveling wave tubes electric simulation, giving block diagram for circuit model
03 p0386 A71-13806

Computer systems performance simulation, discussing data collection and preparation and language selection
05 p0727 A71-17048

Rocket/launcher aerodynamic interference effects investigation by wind tunnel simulation, determining interference coefficients for rockets ballistic dispersion calculations
08 p1274 A71-21995

[AIAA PAPER 71-269]
Satellite scale imagery potential for land-use mapping, using photomosaic simulation at 1/400000 scale
13 p2064 A71-29395

Absorbent materials test methods and acoustic data reduction with simulation principle
14 p2275 A71-30525

SIMULATOR TRAINING
U TRAINING SIMULATORS

SIMULATORS
NT COCKPIT SIMULATORS
NT CONTROL SIMULATION
NT ENVIRONMENT SIMULATORS
NT FLIGHT SIMULATORS
NT LUNAR ORBIT AND LANDING SIMULATORS
NT SHOCK SIMULATORS
NT SOLAR SIMULATORS
NT SPACE SIMULATORS
NT SPACECRAFT CABIN SIMULATORS
NT TARGET SIMULATORS
NT TRAINING SIMULATORS
NT VIBRATION SIMULATORS
General information system model, producing human performance simulator for various equipment, personnel and procedure mixes
07 p1046 A71-19456

Electromagnetic waves propagation in inhomogeneous medium, using simulation chamber with NaCl and ethyl alcohol diffused agar-agar
17 p2724 A71-34755

Moire equivalence device for simulating fringe patterns in hologram interferometry, using loci of constant pathlength
20 p3235 A71-39188

Ultrasonic radar simulator to produce data for radar system performance evaluation, describing automated short range and manual long range systems
20 p3196 A71-39376

SIMULTANEOUS EQUATIONS
Differential equations systems construction from given integral manifold, deriving steady state functional and stability conditions
01 p0111 A71-10487

Parametric differentiation method for reducing structural optimization and nonlinear programming problems to solution of simultaneous nonlinear algebraic equations
01 p0174 A71-10951

Algebraic equations system solution by eighth order Runge-Kutta process with eleven function evaluations per step
04 p0619 A71-14812

Differential equations system continuability theorem for specific initial conditions
05 p0775 A71-16885

Dynamic relaxation method for solving simultaneous linear differential equations, comparing asymptotic rate of convergence with degenerate Chebyshev approximation
05 p0776 A71-17122

Axisymmetric isotropic shells of revolution, using matrix-operator notation for differential equations systems solution
06 p0995 A71-17835

Simultaneous dual integral equations coupled pairs with constant coefficients involving Bessel functions of orders zero and unity
13 p2094 A71-28484

Convergence of Brodyan single-rank iterative solution for nonlinear equations systems involving approximation to Jacobian matrix
18 p2941 A71-36357

Geodetic grid points coordinates accuracy estimate based on normal equations system cracovian matrix, determining arbitrary elements by numerical process without error equations linearization
24 p3822 A71-44768

SIMULTANEOUS IMAGE CORRELATOR
U IMAGE CORRELATORS

SINE
U TRIGONOMETRIC FUNCTIONS

SINE SERIES
Altitude and azimuth angle values computation using logarithmic and natural haversines table
02 p0280 A71-12899

SINE WAVES
Monograph on nonlinear theory of one dimensional homogeneous collisionless plasma resonance covering charged particle motion in sinusoidal and standing potential waves
01 p0131 A71-10101

Low cost multichannel peak/average sine vibration control system with acceleration selector and averager
01 p0067 A71-10864

Gyroscopic drift tests, using sinusoidal linear VLF acceleration [AGARDOGRAPH-128] 05 p0750 A71-16312
CW Nd-YAG laser response to sinusoidal cavity perturbation, observing resonance modes 05 p0761 A71-16332
Nonlinear planar propagation of sinusoidal and band-limited noise signals in air, extending to spherical waves 05 p0784 A71-17157
Short elastic sine waves propagation in cylindrical shells, applying nonclassical equations 06 p0982 A71-17359
Digital control systems for electrodynamic vibration exciters, discussing computer ranged instrumentation amplifier, digitally controlled sine wave oscillator and FFT processor 11 p1746 A71-26503
Sinusoidal vibration tests using narrowband tracking filters, considering automatic servocontrols and feedback loop optimum matching 14 p2175 A71-30310
Collector current delay and rise times in transistor common emitter configuration for linear, sine and exponential input signals 14 p2213 A71-30630
Charged particle acceleration by nonstationary sinusoidal electric fields in earth magnetosphere based on mathematical model 19 p3129 A71-38377
Universal dispersion curve for steady state sinusoidal flexural wave propagation in plates and bars, using Poisson ratio as single parameter 21 p3463 A71-40535

SINGLE CRYSTALS
NT WHISKERS [SINGLE CRYSTALS]
Te-doped In Sb single crystal growth in transverse magnetic fields, using Czochralski crystal puller 01 p0100 A71-10281
Ta alloys single crystals elastic compliance constants over temperature range, deriving bulk and shear moduli and anisotropy factor 01 p0100 A71-10373
Gd-As direct synthesis from components elements and single crystal growth using chemical transport reactions 01 p0138 A71-10404
Microwave permittivity dispersion in segnetoelectrics as function of single crystal domains size, considering barium titanate dielectric spectrum resonance 01 p0138 A71-10433
Edge dislocations in deformed single crystals of Nb-Mo and Nb-Re alloys at various temperatures 01 p0101 A71-10738
Intermetallic Ni-Al volume fraction dependent deformation of single crystals of binary Ni-Al system, using X ray and transmission electron microscopy 01 p0102 A71-10740
Thermoemissive and adsorptive properties of Nb single crystals in Cs atomic beam at various temperatures 01 p0139 A71-11100
Electroacoustic properties of GaAs diffusion layer transducers as function of resistivity and charge carrier concentration in single crystals 01 p0140 A71-11122
Iron single crystal wavy slip pattern of plastic deformation under tension at room temperature, noting relation between yield point and crystal orientation 01 p0105 A71-11621
High quality quartz single crystal synthesis by hydrothermal recrystallization in autoclave 02 p0229 A71-11718
High purity Nb and Nb-O solid solution single crystals, investigating temperature dependence of yield stress 02 p0263 A71-11866
Vacuum work function of thermionic converter using planar monocrystalline rhenium emitter over temperature range 02 p0192 A71-12206
Cesium work functions of directed monocrystalline Re thermionic emitter from saturated electron emission currents over temperature range 02 p0295 A71-12207
Single crystal facet angles and surface energy planes by light reflection for W emitter in vacuum, Cs and iodine 02 p0251 A71-12208
Thermionic converter with single crystal 110 W emitter surfaces and Nb collector, measuring I-V performance 02 p0193 A71-12212
Mo single crystals polygonization and recrystallization effects, examining strain rate and deformation conditions 02 p0266 A71-12652
Nb single crystals, examining structure in initial deformed and annealed states at various low temperatures 02 p0266 A71-12654
Ni base superalloy single crystal fatigue crack propagation 02 p0268 A71-12886

Zn deposition on Zn single crystals in KOH solution, examining time and potential effects on deposit morphology 02 p0210 A71-12956
Nb-Mo alloys single crystals deformed in compression, considering work hardening and slip relation to temperature, Mo content and stress level 03 p0441 A71-13313
Strain rate effect on critical shear and cross slip stresses of Al and Al-Mg single crystals, obtaining stacking fault energy 03 p0442 A71-13364
Single crystal indium gallium phosphide solid solution synthesis, discussing crystallophysical and electrophysical properties 03 p0467 A71-13424
Single crystal creep strain rate measurement under cryogenic temperatures by hybrid photoelectric servo system with optical extensometer avoiding physical contact with specimen [SESA PAPER 1699] 03 p0426 A71-13759
CdS single crystals green edge emission and optical flash spectra, discussing wavelength, UV excitation intensity and temperature effects 03 p0468 A71-14384
CdS single crystals with Cu and Cl additives, observing optical flash and thermoluminescence in IR band 03 p0468 A71-14385
Arsenic doped Si single crystal impurity segregation striae and central faceted area observations by scanned laser IR microscope 04 p0608 A71-15039
Diffusion and solubility of thermally induced acceptors in indium antimonide single crystals 04 p0636 A71-15085
Barium titanate single crystals domain structure and electrical properties at room temperature under uniaxial tensile stresses, measuring dielectric hysteresis loops 04 p0637 A71-15104
Tungsten, molybdenum and rhenium single crystals hemispherical emissivity at high temperatures by electron beam heating, considering grain boundary contribution 04 p0613 A71-15581
Ta single crystals solution hardening, discussing interstitial impurities effects on bcc metals flow stress temperature dependence 05 p0765 A71-16162
Silicon single crystal dislocation free growth by Czochralski and Dash methods 05 p0792 A71-16292
Perturbation theory diagrammatic version for describing lattice vibrations effect on scattering cross sections of low energy electrons from single crystal solid surfaces 05 p0792 A71-16316
Cracks nucleation by spark discharge in Mo single crystals, using optical and transmission electron microscopy 05 p0766 A71-16323
Fused silica and single crystal NaCl nonlinear parameters from ultrasonic beams mixing studies 05 p0793 A71-16410
CdS single crystals treatment in salt melts to obtain given conductivity and photosensitivity, discussing LiCl, Ag, Cu, Na, Cd and In concentration effects 05 p0793 A71-16822
Photoelectrical and thermoelectrical properties of CdS, CdS-CdSe and CdSe single crystals epitaxial films 05 p0793 A71-16823
Ti microcrystals on single crystal tungsten substrate, discussing phase transformations 05 p0768 A71-16854
Al single crystals creep deformation, noting thermally activated mechanism at cryogenic temperatures 05 p0769 A71-16879
Yttrium-iron garnet single crystals angle between variable and constant fields influence on spin wave thresholds 05 p0794 A71-16883
Te doped InAs single crystals structural characteristics investigation by X ray diffraction, noting laminar growth with alloying impurity varying concentrations 06 p0940 A71-17388
Contact electro-optic KDP crystal shutters for Q switching ruby laser 06 p0907 A71-17530
Potassium niobate single crystals domain structures by interferometry, discussing surface deformations, dipole couplings and temperature dependent angles 06 p0941 A71-18039
Microwave Gunn diodes made from GaAs single crystals, describing fabrication by diffusion process 06 p0876 A71-18082
Li concentration effect on CdS single crystals brittle fracture anisotropy by metallographic techniques 06 p0941 A71-18083
Structure changes of Al single and polycrystals with initial cube orientation under cold rolling 06 p0913 A71-18420

Nb-W single crystal deformation, discussing athermal solid solution strengthening 06 p0914 A71-18683
Mg-Cd single crystals deformation by prismatic slip as function of testing temperature and state of order 07 p1132 A71-19437
Mechanical properties of supersaturated Ni-Al alloys aged at 700 F, discussing composition effects on single crystals deformation and polycrystal strength variation 07 p1133 A71-19442
High temperature creep behavior of nickel base alloys with L12 and B2 type lattices, discussing single crystals of beta-NiAl 07 p1133 A71-19446
Undoped and Nd doped synthetic fluorapatite single crystals heat capacity, thermal expansion and thermal conductivity measurements, yielding Debye temperature 07 p1180 A71-20164
Epitaxial boron phosphides single crystals growth, using thermal decomposition and reduction for deposition on hexagonal silicon carbide substrates basal plane 07 p1180 A71-20174
Electron paramagnetic resonance and optical absorption spectra of transition metal ions in zoisite crystal 08 p1343 A71-20658
Nickel ion diffusion coefficients in high purity magnesium oxide single crystals in high temperature argon atmosphere 08 p1343 A71-20664
W and Mo single crystals metallographic microanalysis for temperature cycles effects on microstructure 08 p1305 A71-21056
GaAs-InAs type single crystals, polycrystals and epitaxial films solid solutions, studying optical, electrical and luminescent properties 08 p1344 A71-21443
Ta single crystals with interstitial carbon, nitrogen and oxygen, examining Peierls and interstitial hardening stresses additivity 08 p1307 A71-21503
Interstitial nitrogen effects on thermally activated flow in Nb single crystals, determining yield and flow stresses and strain-rate sensitivity dependences on temperature 08 p1307 A71-21504
Ta and W single crystals yield stress temperature dependence, confirming asymmetric Peierls barrier 08 p1307 A71-21507
Nb single crystals dislocation substructure correlation with strength properties 08 p1307 A71-21508
Mo single crystals dislocation velocity, discussing slip systems and stress and temperature effects 08 p1307 A71-21509
Bcc Ti-V single crystals deformation modes and resolved shear stresses as function of temperature and composition 08 p1307 A71-21510
Stoichiometric NiAl single crystals plastic deformation study by transmission electron microscopy, determining dislocations by image matching technique 08 p1308 A71-21511
Nb single crystals heterogeneous deformation at very low temperatures, observing jerky flow due to adiabatic temperature rise during plastic deformation 08 p1308 A71-21512
Titanium single crystal prism slip dislocation dynamics, examining temperature and strain rate effects on shear stress 08 p1309 A71-21521
Li and temperature effects on mechanical properties of Mg base single crystals in basal and prismatic slip 08 p1309 A71-21525
Magnesium indium alloys single crystal plastic deformation, investigating basal and prismatic slip at various temperatures 08 p1309 A71-21528
Dilute Al alloys single crystals amplitude dependent internal frictions measurement, obtaining binding energies between substitutional alloying atoms and dislocations 08 p1310 A71-21535
Electrochemical polarization effects on Ni single crystals mechanical behavior under tensile deformation 08 p1310 A71-21539
Gallium oxide particles effects on Ag-Ga matrix single crystals critical resolved shear stress 08 p1311 A71-21543
Columnar grain and single crystal high temperature gas turbine elements development through directional solidification 08 p1314 A71-21565
Tilt boundary intersections during creep in Mo single crystals 08 p1315 A71-21577
Gamma prime precipitate effects on flow stresses of Ni alloys single crystals at various strain rates and elevated temperatures 08 p1315 A71-21580

Single crystal TiC-VC alloys mechanical properties, considering room temperature hardness, high temperature deformation and brittle to ductile transition temperature

08 p1316 A71-21589

Two center bound polaron in rutile single crystal, studying dielectric behavior in applied magnetic field

08 p1345 A71-21690

Single crystal W thermal conductivity measurement at 1200-2500 K, discussing apparatus and error sources

08 p1318 A71-21920

N-type single crystal silicon semiconductor resistors with high impurity concentrations and high accuracy

09 p1414 A71-22160

Artificially grown corundum homogeneous single crystals structure relationship to thermodynamic and kinetic growth conditions

09 p1481 A71-22164

Fluorapatite single crystals absorption spectra and luminescent characteristics under activation by rare earth ions, noting line widening dependence on crystal composition

09 p1507 A71-22390

Single crystal indium gallium phosphide p-n junction preparation by epitaxial vapor phase growth technique, determining energy gap dependence on alloy composition

09 p1510 A71-23121

Deformed Mo single crystals, noting polygonization processes relation to recrystallization during annealing

09 p1476 A71-23318

Subgrain growth kinetics for tungsten deformed by rolling and polygonizing annealing, using metallography, X ray microradiography and crystal spectrometry

09 p1476 A71-23324

Ultrasonic irradiation effect on single tungsten crystals deformation characteristics and structure

09 p1477 A71-23327

Strain effect on ultrasound damping in single W crystals, considering microhardness

09 p1477 A71-23328

Debye-Waller factors for Nb and Sn atoms in intermetallic niobium stannide by X ray intensity measurements on single crystal

10 p1655 A71-23770

Gamma radiation effect on electrical properties of n-type GaAs single crystals with doping impurities, calculating defect introduction rate and forbidden zone energy levels

10 p1656 A71-24141

Formation kinetics of radiation defects produced by gamma rays in Sb doped n-type Ge single crystals at 77 K

10 p1656 A71-24142

Gamma radiation influence on photomechanical effect in GaP and GaAs single crystals, using microhardness tester

10 p1656 A71-24143

GaAs single crystals conductivity and surface capacitance under transverse electric field at low temperatures

10 p1657 A71-24322

Stress-strain curve and single crystal dislocation structure of Al alloys with coherent precipitates, noting screw dislocations predominance

10 p1629 A71-25033

Mo-Re alloy single crystals asymmetric mechanical properties, discussing shear tests of Mo and Mo-Re single crystals for hard and soft flow stress planes identification

11 p1777 A71-25372

High strain rate effects on Al single crystals deformation, presenting overall and local strain and lattice rotation measurements in impact tested specimens

11 p1779 A71-26014

Niobium alloys single crystals deformations, studying microyielding to macroflow transitions by dynamic microstrain technique

11 p1780 A71-26019

MgO single crystals dominant coloration in solar spectral region by electron hole pair diffusion, trapping and recombination

[AIAA PAPER 71-450]

11 p1808 A71-26234

Vanadium oxide thin vapor transport films on single crystal aluminum oxide, using RF sputtering of powdered targets

11 p1809 A71-26397

LiF single crystals temperature, strain rate and positive Mg ionic impurity effects on work hardening characteristics

11 p1809 A71-26478

Solid solution hardening in Nb alloys single crystals, explaining in terms of elastic interaction of dislocations with substitutional atoms

12 p1916 A71-26927

Activation energy anisotropy for Mo and Nb single crystals dislocation relaxation, noting temperature dependence

12 p1917 A71-27300

Molecular collisional analysis of normal momentum transfer from flowing rarefied gas to monocrystalline surface

12 p1934 A71-27588

Ferromagnetic and antiferromagnetic single crystals thermal conductivity at 193-673 K, analyzing anomalies on basis of magnetic and structural characteristics

12 p1944 A71-27661

Measuring system for 180 degree Raman scattering in single crystals, powders, liquids and strongly absorbent solutions

12 p1915 A71-27673

Pure W single crystals grown by electron beam zone melting technique, noting rolling workability

12 p1919 A71-27761

Nb single crystals structure and properties after cold rolling and annealing, determining crystallographic parameters of plastic deformation

13 p2086 A71-28579

Monoclinic, stabilized and metastable tetragonal and cubic zirconias, noting IR and Raman spectra

13 p2093 A71-28991

Cylindrical lithium niobate single crystal acoustic propagation, determining speed, damping and sound reflection with He-Ne laser light scattering at hyper-sonic oscillations

13 p2080 A71-29024

Elastically and plastically anisotropic single crystals randomly oriented in polycrystalline aggregate, noting initial yield surface in fcc lattice

13 p2155 A71-29063

Antiperthitic intergrowths from single crystal X ray studies of lunar rock plagioclase

13 p2142 A71-29140

Solution hardening and softening of single crystals, considering deformation in Nb-Mo and Nb-Re alloys

13 p2088 A71-29344

Stage 1 fatigue fracture mechanism in Ni-based superalloy single crystals, observing air and vacuum effects

13 p2088 A71-29405

Mo and W single crystals mechanical properties, considering C and iron group additions influence

14 p2255 A71-29516

Kinetics of Ti single crystals tensile deformation by prismatic gliding, studying moving dislocations interactions with metal impurities

14 p2257 A71-29844

Structural disorientation dependent recrystallization of cold rolled and annealed Mo single crystals

14 p2258 A71-30006

Nb single and polycrystalline thermal conductivity /diffusivity, specific heat, electrical resistivity and monochromatic/ integrated degree of blackness at high temperatures

14 p2258 A71-30052

W and Mo single crystals metallographic microanalysis for thermal cycling effects on microstructure

14 p2259 A71-30172

GaAs single crystals real surface electrical characteristics, using pulsed field effect techniques

14 p2284 A71-30403

Combination light scattering in liquids, single crystal and crystal powders, employing long lived argon laser with internal mirrors and large diameter capillaries

14 p2255 A71-30585

Surface conductivity and current carrier mobility vs surface potential in CdSe single crystal films deposited on mica base by vacuum vaporization

15 p2461 A71-31511

Combustion characteristics of single boron carbide particles, studying minimum gas temperatures for self-ignition and burning times

15 p2464 A71-31630

Single crystal and polycrystalline alumina specimens strengthening by annealing with various metal oxide powders

15 p2438 A71-31975

Aluminum single crystals tensile deformation and annealing to produce polygonized substructure

15 p2432 A71-32172

Laser radiation second harmonic generation susceptibility in molecular crystals due to charge transfer accompanied lowest energy electronic transitions

15 p2421 A71-32402

Compressive creep of aluminum oxide single crystals deformed by dislocation glide and rhombohedral twinning, investigating activation energy and rate controlling mechanism

15 p2439 A71-32439

Oxygen adsorption kinetics at Nb single crystal surface at high temperatures and low pressures

15 p2436 A71-32547

Thermionic emission and adsorption characteristics of Ta single crystal faces in cesium atom streams, using thermoelectronic and surface ionization methods

15 p2453 A71-32643

Thermal characteristics of emission and work functions of spherical Ta single crystal faces by Martin microscope measurements

15 p2453 A71-32644

GaAs single crystals defects formation during low temperature gamma photons and electron irradiation, considering electrical properties

16 p2620 A71-33185

Neutron and gamma radiation effects on electrophysical properties of high resistivity Si single crystals grown in hydrogen atmosphere

16 p2621 A71-33186

Single crystal Ni-base superalloy anisotropic hollow cylinder creep under biaxial loading, studying rate dependence on crystallographic axis orientation and stresses ratio

[ASME PAPER 71-APM-1]

16 p2591 A71-33222

Iron single crystals plastic deformation under tension, studying ductile/brittle fractures mechanisms and transition temperature

16 p2591 A71-33369

Refractory and rare metals single crystals - Conference, Moscow, December 1968

16 p2594 A71-33876

Polyhedral Nb single crystals production from niobium pentachloride and hydrogen reaction, determining growth rate

16 p2594 A71-33877

Oriented Mo single crystals substructure during growth, showing crystallographic orientation

16 p2595 A71-33879

Mo single crystal growth by vacuum melting without oil vapors, noting reduced carbon content and increased ductility

16 p2595 A71-33880

Molybdenum-niobium alloys single crystals electron work function in vacuum from emission patterns and anisotropy

16 p2595 A71-33881

Molybdenum single crystals isotropic thermal conductivity, electrical resistivity and total hemispheric degree of blackness at high temperatures

16 p2595 A71-33882

Tungsten single crystals under deuteron bombardment, noting structural defects formation as function of irradiation energy

16 p2595 A71-33883

Deformation conditions and annealing temperature effects on fine structure of Mo single crystals, noting polygonization

16 p2595 A71-33884

Cyclic heat treatment effect on fine structure and properties of Mo single crystals in He atmosphere

16 p2595 A71-33885

Neutron irradiated Mo single crystals polygonization after cold rolling, using X ray topology methods

16 p2596 A71-33886

Addition effects on polygonization of deformed single crystals of Mo and W with Re, using X ray analysis

16 p2596 A71-33887

Mo single crystals physicomechanical and microstructural anisotropy under tension at different temperatures, noting strength and plasticity dependence on crystallographic orientation

16 p2596 A71-33888

Alloying elements effect on structural stability and properties of W and Mo alloys single crystals, studying thermal cycling response

16 p2596 A71-33908

Fractographic investigation of fatigue crack propagation in pure monocrystalline and polycrystalline Al

16 p2599 A71-34095

Raman and IR reflection spectra of zinc tungstate single crystals

17 p2790 A71-34201

Room temperature ultrasonic frequency fatigue behavior of Ni-base superalloy single crystals

17 p2756 A71-34493

Consistency examination of thermal activation analysis in Nb, determining strain rate sensitivity of pure Nb and Nb-Mo single crystals subjected to compression at 178 and 273 K

17 p2759 A71-35223

Thermal and athermal yield stresses of Nb and Nb-Mo single crystals, considering strain rate sensitivity and thermal stress increase with increasing plastic strain

17 p2759 A71-35224

Single crystal W thermal conductivity measurement at 1200-2500 K, discussing apparatus and error sources

17 p2759 A71-35264

German monograph on high temperature measurement of thermal and electrical conductivity of W and Mo single crystals

18 p2915 A71-35960

Strain rate dependence of shear stress, plastic cross-slip and stacking fault energy of Al single crystals at 77 K

18 p2937 A71-36749

Electron concentration and mobility of heavily doped n-type InSb single crystals at high temperatures, investigating temperature dependence of Hall coefficient

18 p2954 A71-36803

Single crystal Ni-Al solid solutions deformations, examining temperature and concentration dependence of critical cleavage stresses

19 p3076 A71-37120

Ni-Mo single crystals under isothermal aging, observing long range order parameter, domain size and microstrains

19 p3077 A71-37411

Surface properties and environmental effects on fatigue striations development and crack initiation in Cu single crystals 19 p3077 A71-37412

Copper single crystals fatigue as statistical work hardening phenomenon 19 p3081 A71-38072

Slip line deformation of ordered and disordered Cu-Au intermetallic single crystals from microstrain and electron micrographic studies 20 p3249 A71-38967

Nucleate boiling of liquid helium I on gallium single crystal surfaces 20 p3312 A71-39282

Transient photoconductivity measurements of room temperature electron mobility in deuterated anthracene single crystals, discussing isotope effect 20 p3194 A71-39348

Ta-W polycrystals and single crystals oxidation at 850-1100 C, noting anisotropic scale-fracture morphologies 20 p3252 A71-39373

Single crystal vanadium carbide magnetic susceptibility decrease with increasing carbon content attributed to orbital paramagnetism 21 p3395 A71-40025

Thin single crystalline film deposition by molecular beam epitaxy of GaAs, describing surface structure observation with high energy electron diffraction 21 p3427 A71-40217

Stress-strain curves of dual slip orientation in Ge single crystals deformed in compression, using interference, optical and electron microscopy 21 p3397 A71-40457

Nitrogen adsorption on single crystal W planes by flash desorption experiment, noting work function change dependence on planes 21 p3345 A71-40539

Elastic-plastic stress wave attenuation, applying theory of wave propagation in single crystals to flow field numerical solution 21 p3465 A71-40786

Kinematic theory of resonant gamma rays diffraction by single crystals, calculating differential cross sections of Bragg scattering for total degeneracy and Zeeman splitting 21 p3420 A71-41123

Light intensity distribution inhomogeneity in transmission by GaAs single crystals, using schlieren method 21 p3428 A71-41201

Microwave photoconductivity of boron single crystals under pulsed illumination, determining temperature effects on carrier mobility, recombination coefficients and relaxation times 21 p3428 A71-41202

Temperature dependence of impurity photoluminescence of Cr-doped GaAs single crystals, measuring activation energy 21 p3430 A71-41214

Negative differential conductance of anthracene single crystals in electrolytes, observing N-shaped I-V characteristics 21 p3430 A71-41221

Tellurium concentrations and photocurrent spectra in Te-doped InSb single crystal samples, determining Te diffusion after annealing 21 p3430 A71-41225

Cyclotron absorption and resonance spectra of hot electrons in p-type InSb samples cut from single crystals containing different amounts of impurities 21 p3430 A71-41226

Orientational magneto-optic effect in nickel and ferrosilicon monocrystals, discussing anisotropy influence on frequency dependence 21 p3431 A71-41263

Bismuth telluride single crystals thermal conductivity and thermoelectric power temperature dependence 2.3-100 K, discussing magnetic field effects 21 p3433 A71-41314

Quasi-binary InAs-GaP single crystals absorption and diffuse reflection spectra, determining forbidden bandwidth as function of compound composition 21 p3434 A71-41332

GaAs-InAs solid solutions single crystal ingots, investigating optical absorption and reflection spectra, energy gap width and carrier mobility temperature dependence 21 p3435 A71-41335

Germanium single crystal surface conductivity, observing carbon monoxide adsorption effects at various pressures 21 p3435 A71-41341

CdS single crystal acoustoelectric domain determination, using light diffraction method 21 p3436 A71-41364

Edge dislocations mobility in zone refined alpha Ti single crystals in bending, using etch pit techniques at 77, 200 and 300 K 21 p3404 A71-41415

Single crystal silicon films deposited on sapphire substrates, determining disorientation angles, block dimensions, dislocation density, orientation and structure 22 p3586 A71-42061

Pulse shape of mode locked frequency doubled Nd-YAG laser, using single crystal for second harmonic generation and phase modulation 22 p3558 A71-42348

Monocrystalline and polycrystalline Ta-Hf oxidation at 750-1050 C, noting orientation 22 p3563 A71-42363

Nonlinear optical properties of phase matchable crystal cadmium germanium arsenide for carbon dioxide laser second harmonic generation and parametric interactions 23 p3714 A71-42960

Neutron bombardment effect on dislocation mobility in Ge single crystals investigated by bending and etching techniques 23 p3715 A71-43309

Single crystal structure of shocked terrestrial and lunar ilmenite from X ray precession and Laue analyses 23 p3740 A71-43623

Photorecombination model explaining kinetics of negative photoconductivity effect during illumination of impurity region in high resistivity p-type ZnTe-CdTe single crystals at room temperatures 23 p3717 A71-43948

Laser use in computer technology, reporting lithium and barium sodium niobate single crystals capacity for data storage 23 p3686 A71-43959

Vacuum annealing and residual gas effects on Mo single crystal dislocation structure and microhardness 23 p3692 A71-44060

Ni-Cr single crystals plastic deformation, presenting work hardening characteristics and critical resolved shear stress 23 p3694 A71-44278

Current amplification in CdS and CdSe single crystals and thin films by fast electron bombardment 24 p3859 A71-44386

Adhesion, recombination and electron-band curvature nomograms for space charge region in photosensitive CdS single crystals 24 p3859 A71-44388

LiF and MgO high purity single crystals plastic deformation geometric characteristics, discussing nucleation probability on different slip planes 24 p3859 A71-44450

Silicon carbide single crystal photoluminescence under pulsed ruby laser light irradiation at 77 K, discussing radiative recombination of excitons 24 p3833 A71-44666

Barium titanate single crystal solid solution electro-optic characteristics at 6328 A and temperatures above Curie point, determining temperature dependences 24 p3860 A71-44667

High purity Be single crystal transverse bending tests, plotting yield stress and bending angle vs temperature 24 p3836 A71-44673

Semiconductor applications of alpha SiC single crystals, showing mechanical separation of polytypes from druses 24 p3841 A71-44742

W and Mo single and polycrystals structural changes by ion bombardment in Li vapor atmosphere at 1500 C, using mass spectrometer 24 p3838 A71-44862

Free surface equilibrium segregation in solid solutions of Cu-Al alloys single crystals by Auger electron spectroscopy and low energy electron diffraction 24 p3839 A71-45123

Stress and magnetic field induced spin density wave polarization vectors rotation in Cr single crystals, accounting for Young modulus temperature and magnetic field dependence 24 p3861 A71-45131

Electron transmission microscopy of Mo single crystals irradiated with fission neutrons and defect structures prior/after postirradiation anneal 24 p3839 A71-45192

Surface segregation, adhesion and friction of monocrystalline Cu-Al, Cu-Sn and Fe-Al alloys from Auger emission spectroscopy and low energy electron diffraction experiments [ASLE PREPRINT 71LC-5] 24 p3839 A71-45287

Surface oxide, organic and lead film effects on friction and plastic deformation of Zn single crystal during sliding [ASLE PREPRINT 71LC-6] 24 p3839 A71-45288

Electron microscopic investigation of Au thin film deposits on Si single crystals in ultrahigh vacuum, noting semiconductor-like resistance/temperature behavior at liquid He temperatures 24 p3862 A71-45347

SINGLE SIDEBAND DEMODULATION

U SINGLE SIDEBAND TRANSMISSION

SINGLE SIDEBAND MODULATION

U SINGLE SIDEBAND TRANSMISSION

SINGLE SIDEBAND RECEIVERS

U SINGLE SIDEBAND TRANSMISSION

SINGLE SIDEBAND TRANSMISSION

Single sideband phase modulation compared with conventional PM or FM effect on spectrum conservation 01 p0037 A71-11164

Quasi-single sideband frequency modulation system response to noise above threshold for Gaussian signal [IEEE PAPER 70-TP-70-COM] 07 p1062 A71-19537

Accurate single-sideband radio receiver tuning, observing reconstitution of harmonic tones in human speech strong vowel sounds 08 p1254 A71-21318

Single sideband mechanical filters for voice multiplex transmission in radio and telephone systems, discussing material characteristics 17 p2714 A71-34608

Automatic equalizer with fast startup time for digital communication systems including partial response and single sideband Nyquist systems 19 p3026 A71-37220

Solid state RC network for single sideband frequency converter using phase difference carrier suppression 19 p3022 A71-38497

Independent sideband transmitter checkout and maintenance for maximum communication circuit performance 21 p3353 A71-40519

Q band relative phase measurement using single sideband suppressed carrier ferrite modulator in serrodyne phase bridge 24 p3803 A71-44649

SINGLE STAGE ROCKET VEHICLES

NT AGENA ROCKET VEHICLES

NT BLACK BRANT SOUNDING ROCKETS

NT BLACK BRANT 3 SOUNDING ROCKET

NT BLACK BRANT 4 SOUNDING ROCKET

NT VIKING ROCKET VEHICLE

Vertical 1 single stage geophysical rocket design and instrumentation for X rays, solar UV and meteoritic concentration measurements 19 p3154 A71-38530

SINGLE-PHASE FLOW

Heat transfer intensification under forced one and two phase flow in channels 04 p0675 A71-14782

Closing shock position in supersonic under-expanded single and two phase jets, determining liquid phase concentration effects on Mach number and nozzle pressure in wind tunnel 08 p1228 A71-21925

Closing shock position in supersonic under-expanded single and two phase jets, determining liquid phase concentration effects on Mach number and nozzle pressure in wind tunnel 17 p2671 A71-35269

SINGULAR INTEGRAL EQUATIONS

Three dimensional wings harmonic oscillation with arbitrary frequency in subsonic flow, presenting approximation method for singular integral equation 01 p0173 A71-10844

Soviet monograph on singular integral equations and boundary value problems involving Cauchy kernels 04 p0619 A71-15400

Nonlinear singular integropartial differential equation numerical integration extension 06 p0917 A71-17553

Boundary value problems of analytic functions and singular integral equations, considering hydromechanics and elasticity theory applications 07 p1148 A71-20077

Riemann surfaces use in plane boundary value problems and singular integral equations, considering plane elasticity and filtration theories 07 p1148 A71-20079

Contact heat conduction boundary value problems, applying parabolic potentials method to Volterra singular integral equation systems 09 p1545 A71-22876

Dirichlet problem for elliptic differential equations with lowest derivatives coefficients and leading term in Bitsadze operator, discussing reduction to singular integral equation 12 p1923 A71-27511

Numerical stress analysis of elastic three-dimensional fracture specimen with edge crack, using singular integral equations analogous to Green boundary formula in potential theory 16 p2655 A71-33181

Singular integral equation theory application to design of cylindrical antennas with small length-to-radius ratio 19 p3035 A71-38597

Supercavitating bounded flow of weightless fluid past slender bodies, deriving singular integral equations in terms of pressure gradient and cavern thickness derivative 20 p3213 A71-39787

SINGULARITY (MATHEMATICS)

Charged particle motion in magnetic dipole field, investigating singularity and topological flow nature 01 p0127 A71-10382

N-body problem real singularities in celestial mechanics, considering present status and holomorphic motion 01 p0154 A71-10384

Solution singularity of laminar boundary layer structure near separation point 02 p0240 A71-12379

Relativistic cosmology with singular point, using oscillatory model for Einstein equations general solution with time related physical singularity 02 p0285 A71-12527

Couple stress effects on thermoelastic problem for half space with heat doublet on bounding plane, discussing singularity behavior and order 03 p0510 A71-13910

Singularity carrier auxiliary curves in airfoil cascade design, formulating and proving existence theorem 05 p0693 A71-16397

Low energy magnetoacoustic wave with finite conductivity, determining gas parameters near singular points 06 p0936 A71-17652

Time variable physical singularity in general relativistic cosmological solution of gravitation equations, constructing simplified models 07 p1191 A71-19173

Jacobi series coefficient relation to convergent series sum singularities in lenslike bounded domain 07 p1149 A71-20643

Potential flow past cylinder with sources and sinks singularities, deriving formulas for aerodynamic characteristics of infinite span wings with boundary layer control 08 p1227 A71-20777

Mixed boundary value problem solution for ring in class of functions with given singularities, using Keldysh-Sedov formulas 09 p1485 A71-22525

General relativity theory applicability limits for strong gravitational fields and near singularities in cosmology 10 p1668 A71-24002

Singularity free refractive index profiles, using hypergeometric function 10 p1642 A71-24590

Hyperon stars thermodynamics, deriving hot neutron stars equation of state with particular reference to center singularities 11 p1828 A71-25737

Criterion on types of extrema of singular solutions of conditional equations in calculus of variations from Euler function behavior with respect to integration path 13 p2096 A71-29322

Singularities in linear elliptic partial differential equations, considering Cartesian and cylindrical polar coordinate problems 15 p2440 A71-31348

Linear elastic body stress field singularities, investigating local geometry and boundary condition effects 16 p2654 A71-33175

Incompressible laminar boundary layer on parabolic profile at angle of attack, noting singularity in all vanishing shear stress/separation points [ASME PAPER 71-APM-31] 16 p2520 A71-33198

German monograph on corner singularities in oblique plates calculation with aid of displacement and stress functions, covering bending theory 17 p2823 A71-34796

Smooth solutions of functional and differential-difference equations in neighborhood of singular points with deviation of argument tending to zero 17 p2767 A71-34938

Continuity and smoothness properties of piecewise optimal control at junction between singular and nonsingular subarcs, developing necessary conditions 17 p2723 A71-35296

Cosmological singularity, considering homogeneous Newtonian universes expanding or contracting with shear and rotation 17 p2806 A71-35382

Loaded crack ending at bimaterial composite interface, analyzing crack tip stress field singularity order dependence on material elastic constants [ASME PAPER 71-APM-O] 18 p2978 A71-36258

Singularities of Euler equations in turbulent flow problems, studying design of difference schemes 18 p2907 A71-36335

Weakly singular integrals numerical compound quadrature error bound and convergence rate estimate by applying Peano theorem with modification for avoiding singularity 18 p2941 A71-36355

Convergence theorem for singular integrands numerical quadratures, assuming domination near singularity by monotone integrable function 18 p2941 A71-36356

Projection iterative method for solving singular linear equations, noting use for matrix conversion 18 p2942 A71-36699

Stress field singularities at interface corners in bonded dissimilar isotropic elastic materials under plane force field applied to wedge subregion 18 p2983 A71-36843

Regular boundary value problems singularities for linear second order analytic elliptic equations solutions in two independent variables 18 p2942 A71-36925

Autonomous two dimensional system with given trajectory and singular points, describing differential equations construction 19 p3085 A71-37350

Transverse curvature effect on singularity at separation for laminar boundary layer from analogy with flat-plate compressible boundary layer 19 p3044 A71-37726

Bianchi type IX universe homogeneous cosmological model, noting oscillatory evolution near singularity and rotating axes of alternating Kaser epochs 19 p3138 A71-37851

Externally pressurized thin walled elastic spherical shells influence coefficients singularity 19 p3158 A71-37886

Critical time calculation for singularity in solutions of homogeneous nonlinear hyperbolic differential equations with smooth initial data, discussing application examples 20 p3254 A71-38790

Excising neighborhood of singularity from manifold with vector field definition, making possible regularization of two and three body problems 20 p3254 A71-38900

Flight mechanics of point with limited power propulsion system and energy storage unit, investigating variational maximum payload problem with singular control optimization 20 p3288 A71-39125

Arutunian method application to crack problems in power law elastic materials and contact problems in nonlinear creep, noting error for crack tip singularity 20 p3310 A71-39868

Time variable physical singularity in general relativistic cosmological solution of gravitation equations, constructing simplified models 21 p3441 A71-40088

Singularities of Green matrix in steady state wave propagation in homogeneous anisotropic media 21 p3416 A71-41245

Double forces surface distributions, investigating displacement and stress fields singularities of static Lamé equations 22 p3614 A71-41603

First kind Fredholm integral equation approximation by numerical quadrature formulas plus collocation, using singular value decomposition for solution 22 p3567 A71-42296

Computerized screen construction for surfaces with net characterized by singularity-free and curve-edges properties 22 p3518 A71-42395

Irregularly shaped thin elastic plates under uniform transverse or point loads with singularities resulting from loading or corner conditions 22 p3618 A71-42591

Lifting configurations unsteady air loads prediction, investigating loading singularities in linearized potential theory 22 p3481 A71-42832

Discrete system high order optimality sufficient conditions and methods for singular and nonsingular controls study 22 p3527 A71-42854

Grand Tour interplanetary trajectories regularization, removing singularities in equations of motion of space vehicles [AAS PAPER 71-315] 23 p3725 A71-42990

Gas dynamics nonstationary linearized equation solutions based on nonstationary source- and vortex-like singularities 23 p3663 A71-43491

Stress concentrations and singularities at interface corners, presenting procedure for standardized mathematical formulation of conditions for different physical problems 23 p3777 A71-43494

Singular optimal control theory generalization using appropriate transformations, considering stability results for bang-bang solutions 23 p3657 A71-43941

Indirect numerical method for solving optimal control problems with singular arcs 23 p3658 A71-44086

Initial singularity removal in model big bang universe compatible with 3K black body radiation in terms of renormalized gravitational theory 23 p3770 A71-44182

Multiple scattering theory of radiative transfer boundary value problems, showing Neumann intensity expansion coefficients relation to singular normal modes 24 p3848 A71-44788

SINKS

NT HEAT SINKS

Entrainment induced potential flow near free jets, using equivalent sink distribution derived from known boundary layer solutions 10 p1596 A71-24937

Rotating fluid axisymmetric flow into point sink, investigating Rossby number 24 p3817 A71-44419

SINTERING

Transition metals powders and carbides sintering by high temperature hot pressing in homogeneity region, determining optimum conditions and activation energy 02 p0256 A71-12276

Sintered W rolling in vacuum over reduction and temperature ranges 02 p0256 A71-12514

One chamber vacuum furnace for dewax, presinter and sinter of cemented carbides, referring to Cox chart for system design 05 p0758 A71-16248

Metal powders sintering computer simulated dynamic volume diffusion model based on Laplace equation, comparing calculated growth rates with electron microscope data 06 p0903 A71-17344

Sintered Al-Ni-Co alloys, investigating magnetic properties and density after heat treatment 06 p0913 A71-18099

Tungsten boride sintering bonds with molten Ni as function of wettability low dihedral angle, discussing cermet porosity range 07 p1130 A71-19297

Microporosity morphology relationship to grain size and boundaries in alloys solidification and pores removal kinetics from castings by sintering 07 p1119 A71-19977

Forged superhigh density sintered steels strength and fracture mechanism 08 p1304 A71-20995

Dispersed alumina inclusions strengthening effect during nichrome alloy sintering 08 p1305 A71-21060

Manufacture and mechanical properties of sintered silver electrodes involving oxide, powder and resin bonding methods 08 p1297 A71-21089

Niobium carbides sintering by hot pressing at various temperatures, discussing kinetics, relative compactness and activation energy 09 p1466 A71-22163

Sponge iron sintered powder compacts deformation behavior from uniaxial compression tests, proposing plasticity prediction criteria 09 p1466 A71-22169

WC-Co system binder phase composition and properties, studying W content as function of initial carbide grain size, Co content, sintering and quenching time 09 p1466 A71-22170

Ultrasonic vibration effects on TiC sintering during isothermal heating with and without pressure 09 p1470 A71-23063

High temperature Ni and Co alloys powder metallurgy, discussing production, preparation, pressing and sintering 09 p1456 A71-23300

Soviet papers on powder metallurgy covering metal powder fabrication, forming and sintering techniques and materials for friction, antifriction, and heat resistant applications 09 p1478 A71-23388

Solid state sintering of metal ceramics, discussing diffusion-viscous, pure diffusion and activation mechanisms 09 p1457 A71-23390

Liquid-solid interface phenomena during sintering and porous materials impregnation by liquid metals, using spherical and nonspherical particle models 09 p1457 A71-23391

Cermet antifriction and friction powder metallurgy sintered materials for working at high temperatures without lubricants, in vacuum and inert gases 09 p1483 A71-23392

Sintering and pressing techniques for compact semifinished products of refractory metal powders including W, Mo, Ta, Nb, Zr and Ti 09 p1457 A71-23396

Physical properties, structure and sintering of refractory oxides of rare earth elements and actinides, including chromia 09 p1478 A71-23399

Shape and size variations of dispersed particles of Tn, Zr, La and Y in tungsten during sintering 10 p1624 A71-23904

Air sintered oxides stabilized hafnia body compositions and phases from X ray diffraction and electron microprobe correlation, noting monoclinic and cubic grains 10 p1630 A71-23976

Low temperature sintering of Ni-P alloy coated tungsten, discussing diffusion phenomena 10 p1625 A71-23999

Spark sintering powder metallurgy using alternating and direct current plus pressure, discussing use in Be components production for aerospace applications 10 p1618 A71-24765

Alumina trichite reinforcement of nickel base matrix using magnetic alignment and sintering under low pressure below melting point [ONERA-TP-911] 11 p1777 A71-25238

Monolayer submicron self supporting particle film samples preparation for sintering by transmission electron microscopy

11 p1763 A71-26150

Titanium nitride sintering in vacuum, noting strain by grain sliding to pore center under surface tension force effects

12 p1918 A71-27527

Forgeability and tensile properties of spark sintered unstrained Ti-Al-V preforms from prealloyed powders in uncontrolled atmosphere

13 p2084 A71-28147

Sintering time effect on initial permeability of Ni-Fe-Cu-Mo alloy made by powder metallurgy

13 p2086 A71-28626

Magnesia rich magnesium aluminum oxide spinel ceramics, discussing sintering, grain growth inhibition and strength increase

13 p2092 A71-28662

Lead zirconate-titanate point defects crystal chemistry, interpreting sintering and grain growth behavior

13 p2093 A71-28992

Nonporous polycrystalline silicon carbide production by reaction sintering, applying to high temperature technology

15 p2430 A71-32142

Pressed or sintered steel powder joining to wrought mild steel parts, evaluating welded joints with torsion test

15 p2417 A71-32615

Optimum sintering temperature, bulk composition and gas medium effects on structure and mechanical properties of silicon nitride and silicon carbide materials

15 p2437 A71-32670

Microhardness dependent saturation of glass powders by iron, nickel and titanium during sintering of cermet metal matrix materials in vacuum

16 p2601 A71-33573

Prealloyed Al powder liquid phase sintering without precompacting, discussing oxidation and density control

18 p2928 A71-36667

Ni-Cr-Mo cermet alloys sinterability, physicochemical properties and microstructure

19 p3075 A71-37109

Cermet iron chromosilicidization and sinter compact effects on depth and structure, noting wear, corrosion and thermal resistance

19 p3075 A71-37110

Physicochemical properties of cermet sintered thermoelectric materials, considering n- and p-type samples of Si-Ge alloys

19 p3075 A71-37111

Lunar breccia, considering welded or sintered breccias, glassy breccias containing xenocrysts and xenoliths, instant rock breccias and recrystallized breccias

19 p3137 A71-37675

Calcium difluoride powder under sintering, examining optical transparency and morphological features

19 p3069 A71-38049

Transition metals addition effect on W sintering behavior in 1000-2000 C range, explaining by electron exchange between alloy components

21 p3396 A71-40031

Lime refractory fabrication and properties for high temperature applications, describing production of calcium oxide grain by sintering process from commercial calcium hydroxide

21 p3405 A71-40246

Mechanical and frictional properties of sintered copper matrix glass compacts, considering lubricating or seizure preventing effects of glass presence

21 p3406 A71-40759

Sintered metals and powder metallurgy technology, discussing methods and materials available to widen applications

22 p3562 A71-42225

WC and TiC-Co solid solution phase after sintering inhomogeneous structure, investigating grain growth and phase decomposition behavior at various temperatures

23 p3689 A71-43103

Glass particles crystallization in sintered metal matrix glass materials, examining microcracks and temperature and cyclic heating effects

23 p3696 A71-43251

High temperature sintering kinetics of tungsten, observing heating rate effects

23 p3690 A71-43257

Sintering of Ni based heat resistant alloy, determining phase composition, lattice constant and microhardness of compressed specimens

23 p3691 A71-43521

Precipitation hardenable Cr-Cu liquid phase sintered powder composite, showing matrix properties variations

23 p3695 A71-44291

Platinoid boride production, determining reaction sintering temperature with thermal metallographic and X ray analysis

24 p3838 A71-44735

Total-to-open porosity ratio for carbide-iron type materials sintering, noting relative density and chemical composition effects

24 p3838 A71-44736

SINUSES

NT PARANASAL SINUSES

Aortic and sinus nerves afferent electric impulsion under adrenalin and nicotine, considering age peculiarities

03 p0363 A71-13522

SINUSOIDS

U SINE WAVES

SITE DATA PROCESSORS

Integrated vehicular information management systems consisting of computers, multiprocessors, multiplexers, dedicated subsystem processors, sensors and effectors

17 p2743 A71-35057

SITES

NT LAUNCHING PADS

NT LUNAR LANDING SITES

Site selection and area planning for major airport, illustrating Montreal and Toronto systems [CASI PAPER 72/2]

19 p3040 A71-37593

SITTING POSITION

Lower vertebral column forces and moments in seated human under seat-to-head acceleration

04 p0542 A71-14788

Body position effect on dynamic characteristics of human operator under random vibration, considering pelvis-head amplitude-frequency characteristics

04 p0543 A71-14791

Regional pulmonary vasomotor activity in sitting man, determining pulmonary flow distribution with Xe 133 technique

10 p1561 A71-24126

Sitting and supine position effect on exercise tolerance, heart rate, systolic pressure and respiration rate in male subjects with coronary insufficiency, noting onset of angina pectoris

13 p2014 A71-29303

Xe 133 elimination from anterior tibial muscles in dry and water immersed sitting subjects, discussing effects of air and oxygen breathing

13 p2022 A71-29358

Vertical translational acceleration perception threshold of aircraft pilot seated in upright position

14 p2188 A71-29780

Upright tilt stress effects on cardiac cycle phases in healthy subjects, using noninvasive techniques

15 p2358 A71-31453

SIZE [DIMENSIONS]

Carbon steel specimens size effect on energy dissipation and damping characteristics under transverse flexural vibrations

03 p0503 A71-13412

Electrode size effects on voltage loss and boundary layer conductivity of combustion driven MHD generator

14 p2287 A71-29880

Dwarf elliptical and irregular galaxies of small intrinsic size, small absolute luminosity and low surface brightness

18 p2967 A71-37028

Size classification of limonite Mars simulation samples, noting surface roughness of 0.02-10 microns

21 p3449 A71-40642

SIZE DETERMINATION

NT PRECIPITATION PARTICLE MEASUREMENT

Metal flaw size measurement, discussing ultrasonic echo amplitude and defect scanning methods

01 p0086 A71-10304

Meteor particle speed and size estimation using accelerated glass microsphere bombardment in plasmoid

02 p0304 A71-11914

Planets and satellites diameter determination, reviewing double image technique

02 p0309 A71-12153

High purity Mg deformation by remelting and rolling, investigating grain growth based on size measurement

03 p0445 A71-14341

Steels prior austenite and martensite grain size control by thermal cycling

03 p0446 A71-14492

Exposed rock bodies thickness determination using normalized peak gravity effect diagrams

04 p0583 A71-15271

Be star rarefied gaseous envelopes emitting or absorbing region size determination, noting application to other rotating stellar systems

04 p0659 A71-15843

Optical perception constancy of object size, developing mathematical models of accommodation, convergence and retinal image size

07 p1051 A71-20120

Antimatter body size determination, using primary high energy cosmic ray flux

09 p1515 A71-23535

Heart size estimated from chest X rays related to corrected orthogonal ECG findings in patients with congestive heart failure symptoms

12 p1875 A71-27288

Meteor particle speed and size estimation using accelerated glass microsphere bombardment in plasmoid

13 p2133 A71-28201

Seyfert galaxy NGC 1068 IR observations, noting angular extent and size

14 p2303 A71-29585

Bright comets particles albedo, absorptivity and size observation by combined IR and optical photometry

14 p2314 A71-30649

Neptune diameter and flattening, using photographic and photoelectric observations

17 p2799 A71-34477

Gum Nebula size, density and electron temperature data from RAE-1 and OGO-5 satellites and ground based telescopes observations, correlating with Vela X supernova outburst

17 p2806 A71-35409

Crystal laser elliptic cavity size determination for maximum emission efficiency, using photochemical method for energy transfer measurement

17 p2754 A71-35748

Spot size and spatial intensity distribution determination of low-power laser, using optical laboratory components

18 p2931 A71-36585

Small lunar and terrestrial craters, determining impact or volcanic origin by depth-diameter ratio

19 p3137 A71-37677

ASTM Committee F-7-C status report on contamination methods including sampling, processing samples and particulate analysis

19 p3000 A71-38324

Planetary and lunar meteorite craters classification according to radius logarithm to base ten, covering diameter size from 2 microns to 2000 km

21 p3444 A71-40206

Relative size cue for facilitating stereoscopic depth perception in ambiguous disparity stereograms

23 p3638 A71-43110

SIZE PERCEPTION

U SPACE PERCEPTION

SIZE SEPARATION

Gel permeation chromatography for polymer molecules size /hydrodynamic volume/ separation

04 p0548 A71-15265

SIZING

Turbulence amplifier optimal dimensioning for maximum fan-out factor and minimal signal transport time

07 p1024 A71-20554

SIZING [SEPARATION]

U SIZE SEPARATION

SIZING [SHAPING]

Shape effect of compressed solid fuel on thermal ignition delay time in heated gas flow for pyroxyline

03 p0520 A71-13993

SKELETON

U MUSCULOSKELETAL SYSTEM

SKID LANDINGS

Aircraft skidding accidents investigation, comparing airplane stopping distance computations and observations

23 p3628 A71-43228

SKIDDING

Braking performance of runway surfaces and skidding resistance of aircraft tires, considering load and inflation pressure, tread materials and weather conditions effects

22 p3529 A71-42234

SKIN [ANATOMY]

NT EPIDERMIS

NT EPITHELIUM

Human skin blood flow and venous tone in middle finger and forearm during leg muscle exercise to exhaustion

01 p0016 A71-11410

Human skin biomechanical properties, observing extensibility, resiliency and elasticity

05 p0710 A71-16807

Human skin analyzer excitability test, discussing threshold response

05 p0710 A71-16809

Asphyxia induced changes in regional cutaneous and visceral sympathetic activity in anesthetized rabbits, noting relationship with ear blood flow increase

06 p0854 A71-18324

Oxygen tension in skin and kidneys using chronoamperometric measurements

06 p0857 A71-18724

Human skin vibratory sensibility consideration as analyzer receptor for stimuli conversion into nervous processes

07 p1043 A71-20116

Decompression urticaria response in subjects after inert gas breathing at constant ambient pressure, noting osmosis mechanism

08 p1246 A71-20813

Skin tissues automicroflora composition and natural immunity indices changes after 18 day orbital flight from microbiological and immunological examinations

09 p1389 A71-22204

Q switched and continuous laser collimated radiation exposure limits for eye cornea and skin, discussing environmental contamination

09 p1402 A71-23414

Carbon dioxide elimination across human skin, investigating perspiration effects 14 p2186 A71-30567

Ultrasonic vibration effects on DNA and RNA content in skin and kidneys of albino rats 15 p2356 A71-31288

Radio telemetry stimulator for conditioning large animals by applying high voltage short duration pulses to skin surface 16 p2534 A71-33050

Tannic acid and water washing effects on prevention of monomethylhydrazine absorption through skin in dogs 16 p2535 A71-33119

Skin surface burns effect on neurosecretory processes in hypothalamus supraoptic and paraventricular nuclei and neurosecretory admission into hypophysis 17 p2680 A71-34647

Thermoluminescent dosimeter for skin basal layer dose measurement in mixed beta and gamma radiation fields 17 p2693 A71-35450

Human sweat gland duct filling and skin epidermal hydration behavior by analysis of time delays between sweat emergence and steady state, using electrical stimulation 18 p2858 A71-36865

Cholesterol and esterified cholesterol distribution in human skin from analysis on fat, epidermis, corium, subcutaneous tissue and serum by chromatographic/colorimetric methods 20 p3185 A71-38892

Microbial contamination of human skin and upper respiratory tract during long term isolation in sealed environment 21 p3333 A71-40559

Local and central body temperature effects on human cutaneous venomotor reflexes, monitoring venous wall tension by measuring hand dorsal veins pressure during temporary arrest of hand circulation 24 p3797 A71-44777

SKIN [STRUCTURAL MEMBER]

Pulse response of unsheathed coaxial umbilical cable connector mounted flush with missile skin 10 p1585 A71-25072

Boron-epoxy structural skins design for F-14 honeycomb horizontal stabilizer, using computer program 11 p1786 A71-25420

Graphite-epoxy composite skins for commercial aircraft flight spoiler, discussing multiangle ply design and fabrication 12 p1921 A71-27413

Artificial corrosion pits effect on fatigue durability of smooth samples and aircraft duraluminum skin elements 13 p1995 A71-27819

Finite skin-stringer structures natural frequencies determination, using free flexural wave groups 15 p2510 A71-32518

Three layer trapezoidally corrugated panels with skin under longitudinal compression, determining local stability and stress-strain diagrams 17 p2830 A71-35320

Five-span skin-stringer width and damping effects on vibrational response including resonant frequencies and mode shapes by transfer matrix analysis [ASME PAPER 71-VIBR-101] 21 p3461 A71-40327

SKIN FRICTION

NT AERODYNAMIC DRAG

NT FRICTION DRAG

NT VISCOUS DRAG

Near separation flow in laminar compressible boundary layer on cold wall near zero skin friction, suggesting added terms for previous expansion 02 p0332 A71-12378

Skin friction effect on cylindrical shell critical loads at various supersonic gas flow velocities, noting application to flutter analysis 02 p0329 A71-12666

Compressible turbulent boundary layer skin friction measurements on adiabatic flat plate, discussing drag balance calibration [ASME PAPER 70-WA/FE-26] 03 p0403 A71-14134

Rarefied gas low speed slip flow over wedge, solving for velocity profiles and skin friction [ASME PAPER 70-WA/APM-26] 03 p0344 A71-14158

Laminar corner boundary layer secondary flow, taking into account velocity and skin friction distributions 03 p0404 A71-14239

Skin friction, Stanton numbers, velocity and temperature profiles in accelerating turbulent boundary layer flows, using Prandtl mixing length 04 p0680 A71-15478

Small surface elements local skin friction sensor measurements near wall during laminar and turbulent flow, making direct shear force measurements 05 p0752 A71-16734

Nozzle wall hypersonic boundary layers in helium tunnel, presenting skin friction measurements and heat transfer rates [AIAA PAPER 71-161] 06 p0884 A71-18603

Turbulent skin friction and boundary layer velocity measurements on nonadiabatic flat plates at hypersonic Mach numbers [AIAA PAPER 71-167] 06 p0885 A71-18609

Flow between parallel planes of dissimilar surface texture, obtaining mixing length models velocity profiles, skin friction coefficients and zero shear stress position 07 p1086 A71-18773

Unsteady boundary layers on sphere or cone moving along axis, determining skin friction angular response 07 p1016 A71-20098

Turbulent boundary layer skin friction measurement by dual pitot tube, taking into account mean velocity profile 08 p1275 A71-21309

Compressible boundary layer separation near zero skin friction by Kaplan perturbation technique, studying nonlinear integral equation with Abel kernel 09 p1432 A71-22455

Uniform magnetic field effect on rarefied gas slip flow over porous flat plate for skin friction response, using velocity and temperature fields equations 10 p1649 A71-24407

Compressible flow in two dimensional boundary layers in arbitrary pressure gradient, using turbulent energy equation for skin frictions and free stream Mach numbers 10 p1598 A71-25082

Pulsating incompressible two dimensional laminar boundary layer flow past insulated plate at zero incidence, calculating skin friction and surface temperature 10 p1697 A71-25084

Heat transfer in laminar free-convection boundary layers adjacent to plane and axisymmetric walls at constant temperature, deriving skin friction and mass flow rate 12 p1985 A71-26941

Instrument for skin friction measurements in adiabatic turbulent compressible boundary layers [ASME PAPER 71-FF-27] 13 p2072 A71-29463

Skin friction drag and velocity profile measurements on flat plate in two phase circular pipe flow in subsonic wind tunnel for gas-solid media, using photographic technique [ASME PAPER 71-FF-32] 13 p2053 A71-29467

Turbulent skin friction and heat transfer prediction on flat plates and wind tunnel walls at supersonic and hypersonic Mach numbers, using Van Driest theory 14 p2334 A71-29868

Flap induced flow deflection effects in hypersonic shock tunnel, obtaining turbulent heating, skin friction and pressure data [AIAA PAPER 71-598] 15 p2343 A71-31540

Flat plate surface film cooling by two dimensional tangent slot injection in hypersonic turbulent flow, measuring equilibrium temperatures and skin friction [AIAA PAPER 71-599] 15 p2343 A71-31541

Incompressible laminar skin friction calculation on porous plate by Karman-Pohlhausen method, considering surface blowing 15 p2392 A71-32118

Integral analysis of incompressible turbulent boundary layer with mass transfer and pressure gradient, including Stevenson velocity profiles and skin friction law [ASME PAPER 71-APM-2] 16 p2559 A71-33221

Skin friction, trailing edge boundary profiles and tuft flow patterns on model F-4D aircraft in transonic flow [AIAA PAPER 71-762] 16 p2521 A71-34001

Laminar constant pressure boundary layer hypersonic limits, estimating skin friction and heat transfer 17 p2728 A71-34885

Preston skin friction measuring tube calibration, presenting Patel analytic method simplification 17 p2729 A71-35284

Boundary layer approximation for isothermal turbulent plane semibounded jet expanding over porous surface, deriving friction stresses and flow velocity in skin and stream regions 20 p3214 A71-39795

Unsteady boundary layer of viscous incompressible rotating fluid flow due to infinite flat plate accelerated motion, calculating velocity and skin friction 21 p3367 A71-40657

Viscous fluid layer surface waves nonlinear theory, analyzing surface friction and gravity force angle effects on wave characteristics 21 p3367 A71-40682

Turbulent flow of incompressible fluid in rough pipe, determining skin friction coefficient variation with Reynolds number 22 p3531 A71-42291

SKIN FRICTION DRAG

U FRICTION DRAG

SKIN RESISTANCE

Nonlinear theory of intrinsic semiconductors electromagnetic wave transmission under skin effect conditions, determining reflectance and carrier temperature 08 p1344 A71-21442

Electrocardiography from unprepared skin without paste, using integrated stainless steel electrode-buffer amplifiers 13 p2023 A71-29399

Plasma losses in high current plasma configuration due to inverse skin effect by observation for discharge regimes in theta pinch, zeta and Tokamak systems 21 p3422 A71-40763

Auditory stimulus conditioning of human skin resistance responses on escape-avoidance schedule 22 p3497 A71-42862

SKIN TEMPERATURE [BIOLOGY]

Digital simulation mathematical model describing simultaneous energy and mass transfer process in clothing-air-space-skin system 02 p0203 A71-11806

Skin temperature and metabolism changes magnitude, duration and variability in unacclimatized male subjects during cold stress 02 p0208 A71-12836

Thermal shock physiological effects, determining skin-air convective heat exchange coefficient 06 p0860 A71-18190

Venomotor responses of forearm and hand veins to rapid changes in skin temperature in exercising man 06 p0861 A71-18382

Venomotor responses of forearm veins to local and remote thermal stimuli to skin in exercising man 06 p0862 A71-18383

Skin cooling effect on awake exercising dog ventilation, noting carbon dioxide response curve, arterial partial pressure and hyperpnea 09 p1396 A71-23366

Organic thermoregulator control signal generation as function of body peripheral to central temperature ratios, using skin temperature rise measurements 10 p1564 A71-24485

Thermal environment effect on human skin temperature and final temperature and tolerance time prediction from early exposure 11 p1725 A71-26117

Local cutaneous heat regulation in man, using thermocutane method in analyzing response to constant temperature thermode application to small skin surface 13 p2014 A71-29314

Skin temperature sensitivity factors, discussing neural correlates of thermal sensation and skin receptors causing thermal stimulation sensitivity 14 p2183 A71-30253

Antiexposure suits physiological evaluation for subjective comfortableness, oral and skin temperatures and pulse rate, determining optimum environmental temperature 17 p2692 A71-35195

Human body weight and skin sweat gland water loss rates effects on thermoregulation 18 p2858 A71-36864

Local skin thermoregulation mechanism in man controlled by cooperative bradykinin biosynthesis, using IR thermometry recording of thermal stimulus 18 p2859 A71-36868

Skin temperature and perspiration role in metabolic heat elimination, considering evaporation coefficient relationship to convection coefficient 18 p2859 A71-36873

Human temperature tolerance during exposure to hot and cold environments, using skin temperature as indicator 18 p2859 A71-36875

Chill level index for skin temperature effects on rate of evaporative heat loss and thermal information to central controller during heavy work 18 p2860 A71-36876

Impulse skin temperature encoding in primate cutaneous thermoreceptors in dynamic thermal conditions 18 p2860 A71-36877

Temperature regulation during exercise by proportional control, investigating skin temperature effect on set point temperature, sweat rate and skin thermal conductance 18 p2860 A71-36879

Cats preoptic and skin temperature change effects on posterior hypothalamic neurons 18 p2861 A71-36888

Cutaneous circulation control by venous thermoregulatory reactions to temperature variations, using dog saphenous veins perfused with autologous blood or Krebs-Ringer solution 18 p2862 A71-36898

Heart rate variation during and after muscular exercise, discussing correlated measurements of rectal and mean skin temperatures, blood lactate, pyruvate and glucose 20 p3185 A71-38891

Cold climate clothed human windchill tables, considering various heat transfer modes and skin temperature 20 p3192 A71-39205

Mean body temperature computation in neutral and hot environments from rectal and skin temperatures 22 p3485 A71-41723

Human skin cold receptor diurnal activity rhythm 24 p3795 A71-44499

SKIRTS

Air cushion vehicle technology, considering economics, propulsion, structures, controllability, flexible skirt systems and R and D [SAE PAPER 710183] 08 p1231 A71-21713

SKULL

NT CRANIUM

Localized focused ultrasonic beam action on brain portions without skull trepanation in animals and man, visualizing sonic field by Tepler effect 15 p2356 A71-31291

SKY

NT NIGHT SKY

SKY BRIGHTNESS

Sky brightness scattering indicatrix in effective atmospheric layer free from underlying surface multiple scattering and reflection distortions 02 p0246 A71-12119

Galactic radio corona existence, measuring northern galactic hemisphere sky brightness and cosmic ray distribution 03 p0483 A71-13204

Cloudless day sky brightness expressions, discussing singular points 05 p0778 A71-16842

Brightness ratio near solar horizon from Ly alpha predawn and postdawn rocket observations consistent with radiation multiple scattering geocoronal model 10 p1605 A71-24794

OGO radio astronomy instrument for cosmic noise sky brightness distribution mapping by electrically short antenna ionospheric focusing 11 p1763 A71-26144

Meteoritic aerosols optical manifestation from photometric measurements on stratospheric balloons, demonstrating Orionids effects on twilight sky brightness 12 p1960 A71-26832

Circumterrestrial meteoroid dust cloud properties based on night sky brightness photometric observation 12 p1964 A71-27090

Earth surface formations and clouds angular brightness distribution based on reflected solar radiation intensity 12 p1901 A71-27102

Photometric analysis of manned spacecraft twilight brightness photographs for spherical atmosphere in single scattering approximation 12 p1901 A71-27103

Sky brightness measurements during total solar eclipses, discussing solar elevation, cloud cover and albedo effects 14 p2309 A71-30117

Zenith sky brightness and color change during total solar eclipse of 12 November 1966 at Santa Ines, Peru, using interference filter photometers 14 p2309 A71-30118

Zenith sky intensity and spectral distribution changes during solar eclipse of 12 November 1966, discussing dependence on height and terrain 14 p2309 A71-30119

Day sky brightness and polarization observation during total solar eclipse of 7 March 1970 14 p2309 A71-30120

Atmospheric optics and radiative transfer, including earth albedo, sky brightness, heat balance, cloud/terrain reflectance, molecular spectroscopy and multiple scattering 14 p2275 A71-30497

Sky brightness broadband measurements by Skylark sounding rocket, noting relationship to zodiacal light 16 p2575 A71-32842

Model radiative transfer across random air-sea interface, determining reflected sky radiance 17 p2736 A71-35562

OSO-6 measurements of gegenschein, comparing relative sky brightness data with ground based observations 18 p2966 A71-36766

Upper atmosphere dust scattering indicatrix from twilight sky brightness at solar vertical, determining total directed scattering coefficient 19 p3132 A71-37390

Circumterrestrial meteoroid properties based on night sky brightness photometric observation 19 p3133 A71-37440

Brightness profiles of earth daytime horizon from Soyuz spacecraft photographic photometry, deriving atmospheric scattering coefficient relation to optical thickness vertical distribution 19 p3054 A71-37967

Azimuthal IR radiation distribution of atmospheric brightness cross sections at various zenith angles from balloon programmed-control radiometer data 19 p3054 A71-37969

Atmospheric directional scattering coefficients from vertical measurements of IR spectral sky brightness near solar almucantar and direct radiation 19 p3090 A71-37976

Water and ice clouds spectral brightness coefficients in IR region of spectra from aircraft measurements 19 p3090 A71-37977

Circumterrestrial dust cloud characteristics from night sky brightness photometric measurements, noting seasonal changes 20 p3219 A71-39646

SKY RADIATION

NT AIRGLOW

NT DAYGLOW

NT GEOCORONAL EMISSIONS

NT NIGHTGLOW

NT TWILIGHT GLOW

Sky radiation background in far UV spectral region, calculating stellar component 02 p0304 A71-11913

Radio sky background temperature measurement with telescope, using moon as screen 03 p0487 A71-13472

Polarization and sky radiance data before, during and after 7 March 1970 solar eclipse 03 p0425 A71-13688

Lyman alpha sky background measurements by OGO 5 satellite, discussing absolute emission rate, spatial variations and origin 10 p1601 A71-24439

Sky noise temperature measurements for ATS-5 millimeter wave radiometers, taking into account variations due to atmospheric temperature and humidity conditions 12 p1877 A71-26608

Sky radiation background stellar component in far UV spectral region, determining intensity with Venera instruments 13 p2133 A71-28200

Skylight polarization dispersion in relation to multiple scattering in molecular atmosphere 13 p2063 A71-29110

Zenith skylight spectral intensity distribution measurement during total solar eclipse of 7 March 1970, using optical scanning spectrometer 14 p2309 A71-30121

Altitude size distribution of atmospheric aerosol from sky radiance measurements in sun aureole region, calculating sunlight forward single scattering 14 p2310 A71-30125

Hertzian radiometry experimental aspects covering background and medium temperature measurements, sky radiometry and absorbing gas total pressure measurements 14 p2204 A71-30969

German monograph on ozone determination from sky radiance, considering Rayleigh and Mie scattering 17 p2733 A71-34794

Planetary, stellar, galactic, sky and extragalactic UV radiation from OAO-2 spectrophotometric observations, noting interstellar extinction curves 20 p3300 A71-39747

SKY WAVES

Average electron density profiles for forecasting MF sky waves field strengths, using nocturnal ionospheric measurements 10 p1575 A71-23866

Interference pattern of ground and sky waves at 16 kHz during summer near solar maximum 12 p1880 A71-27155

SKYCRANE HELICOPTER

U CH-54 HELICOPTER

SKYLAB PROGRAM

Manned space flight network telemetry system modification for Skylab, ERTS and Apollo J missions, giving data flow diagrams and equipment electrical characteristics 01 p0035 A71-10917

AAP electrical power system simulation for Skylab earth orbit missions, taking environmental effects into account 02 p0190 A71-11795

Skylab design and mission objectives, describing attitude control, MDA, quarters, Apollo telescope mount and proposed experiments 02 p0321 A71-12738

Post Apollo manned space operation, emphasizing Skylab program, space shuttles and long term space station 04 p0689 A71-14927

Skylab, space station and shuttle programs covering economics, international participation and ground and flight tests 04 p0661 A71-14928

Skylab earth-orbiting manned space station attitude and pointing control systems design 04 p0623 A71-15323

Real time solar flare image production for Skylab astronaut training, using films of H alpha, XUV and X [AIAA PAPER 71-73] 06 p0902 A71-18530

Orbital environment contamination and effect on optical instruments and astronomical experiments in Skylab Program [AIAA PAPER 71-74] 06 p0902 A71-18531

Skylab program, describing equipment based on Saturn 5 workshop experiments and objectives 07 p1206 A71-19088

Scientist-astronauts work in manned space flight program support/backup crews and Skylab missions scientific/medical experiments 07 p1046 A71-19089

Charge sensitive low power amplifier and fast coincidence system for solid state detectors and random counting rates in Skylab application 08 p1267 A71-21849

Skylab workshop as orbital manned platform for scientific investigation, discussing system design details and technical evaluation 10 p1682 A71-24276

Apollo lunar and Skylab photographic systems: discussing topographic, panoramic, metric, stellar and multispectral cameras and instrumentation 12 p1907 A71-27257

Skylab habitability facilities for astronaut work effectiveness and physical well being 15 p2363 A71-31455

Skylab program organization and management system design, operations and equipment 15 p2499 A71-31457

Skylab as orbital factory, worksite and observatory for experiments in science, technology, materials science and manufacturing 15 p2500 A71-31460

Skylab earth resources experimental equipment, describing sensing and recording instrumentation for electromagnetic spectral pattern recognition studies [AIAA PAPER 71-841] 17 p2739 A71-34712

Control moment gyro for attitude pointing control system of Skylab space station 17 p2743 A71-35063

Skylab pointing and control system using control moment gyros and cold gas reaction thruster system to provide attitude control 17 p2813 A71-35064

Skylab strapdown attitude navigation system using components designed for predecessor projects ATM and Saturn I Workshop 17 p2773 A71-35065

Skylab life support systems design and performance prediction covering thermal and humidity control, atmospheric supply, carbon dioxide removal, water and waste management [ASME PAPER 71-AV-14] 18 p2866 A71-36381

Consumable usage as function of mission time computed with computer program simulating NASA Skylab mission 18 p2885 A71-36461

Skylab checkout and launch facilities and operations, describing modifications required for Apollo lunar missions facilities utilization at Cape Kennedy 18 p2899 A71-36476

Skylab habitability considerations in Orbital Workshop design, discussing waste management, food management and sleeping compartments [AIAA PAPER 71-872] 18 p2870 A71-36628

Skylab and space station crew garments, discussing personal preference and style integration with function and overall system impact [AIAA PAPER 71-875] 18 p2870 A71-36630

Skylab manned earth orbital artificial gravity experiment, describing mission objectives and requirements [AIAA PAPER 71-861] 18 p2975 A71-36649

Artificial gravity Skylab wobble damping, using ATM control moment gyros [AIAA PAPER 71-862] 18 p2975 A71-36650

Optimized momentum and attitude control system /MACS/ for Skylab class space stations employing control moment gyro and reaction jet elements [AIAA PAPER 71-938] 19 p3098 A71-37183

Skylab electrical power system located on Orbital Workshop and Airlock Module and on ATM, discussing capabilities, characteristics and limitations 20 p3179 A71-38903

Skylab manned scientific space laboratory for medical, solar astronomy, earth resources, technology and engineering experiments 22 p3608 A71-41950

Skylab life support, habitability and thermal comfort system, discussing ventilation, humidity, carbon dioxide and odor control and water, food and waste management 22 p3609 A71-41976

Skylab program data management systems, discussing onboard data collection, transmission and ground facilities 22 p3610 A71-42007

Optical orientation determination and star pattern recognition for Skylab in solar inertial attitude by digital and hybrid simulations [AAS PAPER 71-397] 23 p3732 A71-43065

SKYLARK
U SKYLARK ROCKET VEHICLE

Skylark rocket vehicle, describing mission objectives and effect on optical instruments and astronomical experiments in Skylab Program [AIAA PAPER 71-74] 06 p0902 A71-18531

Skylark sounding rocket attitude control by three axis star pointing system, using strapdown gyro and plus 5 magnitude stellar sensor [AIAA PAPER 70-1401] 03 p0455 A71-13682

Intensity calibrated grazing incidence spectrographs on Skylark sounding rockets, recording solar soft X-ray and XUV spectra 06 p0967 A71-17903

Sky brightness broadband measurements by Skylark sounding rocket, noting relationship to zodiacal light 16 p2575 A71-32842

High resolution solar UV spectrum observation between 200 and 220 nm by sun-pointed Skylark rocket-borne echelle spectrograph 19 p3135 A71-37611

Solar disk photographs taken by Skylark rocket in EUV and soft X ray region 20 p3293 A71-39534

Equatorial modulation in pulsating aurora, discussing electron measurements with channel multipliers and electrostatic analyzers aboard ERSO Skylark S29/2 20 p3228 A71-39841

SKYNET SATELLITES

SkyNet - IEE Conference, London, April 1970 02 p0216 A71-12426

SkyNet project UK and U.S. cooperation, discussing system scope, coordination, contract placing and PERT critical path analysis in management planning 02 p0337 A71-12427

SkyNet satellite communications system configuration and specifications, discussing geostationary satellite multiple access, SSMA transmission system, power budgets, reliability and repeater specifications 02 p0217 A71-12428

SkyNet satellite mission profile, onboard equipment and control system, discussing communications, command/telemetry processing equipment, electrical power sources, and secondary propulsion 02 p0320 A71-12429

SkyNet satellite attitude determination and adjustment by IR and solar sensors, electronics processing equipment, nutation damping and pulsed axial thrusters 02 p0320 A71-12430

SkyNet telemetry and command stations configuration and equipment functions, discussing antenna subsystem parabolic reflector and positioning, PCM demodulation and computer systems 02 p0217 A71-12431

SkyNet ground stations design, equipment and operations, discussing antennas movement control, Cassegrain reflectors, receiving system amplifier noise temperature and tracking demodulator 02 p0233 A71-12432

SkyNet ground stations operations and equipment, discussing receiving systems parametric amplifiers, local oscillators, demodulators, noise temperature, frequency flexibility and reliability 02 p0217 A71-12433

SkyNet and SCAT ground stations system noise temperature, considering receiver, antenna and sky sources, measurement techniques and error analysis 02 p0217 A71-12434

SkyNet system shipborne earth station design and specifications, discussing size and weight restrictions, radar proximity, gun shocks, antenna stabilization and power budgets 02 p0217 A71-12435

SkyNet system small communications terminal specifications and equipment for ship to shore telegraphic traffic, considering small dish antenna for shipboard installation 02 p0217 A71-12436

SkyNet type 3 and 4 transportable ground stations, describing antenna, radio cabin with IF and control equipment and channeling cabin with baseband equipment 02 p0217 A71-12437

SkyNet types 3 and 4 ground stations performance, discussing antenna gain, FM carrier to noise ratio, channel capacity, error rates and system reliability 02 p0217 A71-12438

SkyNet communication systems, describing long distance strategic communication links between ground and mobile air/helicopter stations via wide and narrow band pathways 02 p0218 A71-12439

SkyNet satellites in orbit communications, repeaters testing, describing test facilities, spacecraft communication subsystems operation, terminals calibration and atmospheric losses 02 p0218 A71-12440

Test terminal for SkyNet satellite communications, describing parabolic antenna, computer, receiver system, calibration program, etc 02 p0218 A71-12441

Transmitter system for SkyNet spacecraft performance tests using calibrated automatic level control and microwave calorimeters 02 p0218 A71-12442

Test laboratory for SkyNet spacecraft communications subsystems at microwave frequencies 02 p0238 A71-12443

Precision measurement of satellite microwave flux and polarization at ground, involving SkyNet tests 02 p0218 A71-12444

SkyNet project earth station effective radiated power and gain by dual satellite access measurements 02 p0218 A71-12445

SkyNet types III and IV ground stations design, discussing signal flow, antenna system, SNR, tracking and transmitter channels and test facilities 02 p0221 A71-12784

SkyNet satellites earth stations design, structure, transportation and erection ease, considering operational and stowed position survivability in high velocity winds 02 p0223 A71-12804

SLABS

Elastic and perfectly plastic plane stress problems yield point load lower bounds by finite element method, considering weakened slabs 03 p0505 A71-13541

Finite thickness infinite slab with radiation from time dependent source, solving nonhomogeneous boundary value problem for linear transport equation 20 p3269 A71-39079

Plastic wave propagation along rods and through slabs, describing finite deformation elastic-plastic theory 21 p3464 A71-40785

Nongray radiative heat transfer in finite slab with discrete absorption coefficient and specularly and diffusely reflecting boundary surfaces of uniform temperature 24 p3886 A71-44372

Radiative transfer in linearly anisotropic-scattering conservative and nonconservative slabs with reflective boundaries, obtaining angular radiation distribution by normal mode expansion technique 24 p3888 A71-44966

SLAGS

Sulfur effervescing molten slag/gas systems causing planetary vulcanism, examining patterns on earth, moon and Mars 15 p2496 A71-32708

Nitrogen equilibrium solubility dependence on slag basicity and gas phase nitrogen/carbon monoxide contents in aluminosilical melts 21 p3399 A71-40470

SLANT

U SLOPES

SLANT PERCEPTION

U SPACE PERCEPTION

SLATS

U LEADING EDGE SLATS

SLEDS

NT ROCKET PROPELLED SLEDS

SLEEP

NT HYPNOSIS

NT INSOMNIA

Rapid eye movements during nocturnal sleep of healthy human subjects, insomniacs and narcoleptics recorded on polygraphs 01 p0007 A71-10071

Digital delta filter for quantifying sleep EEG slow wave activity 01 p0011 A71-10767

Neuron pairs discharge sequence temporal correlation in cats association cortex during natural sleep and wakefulness 01 p0011 A71-10849

Simulated sonic booms effects on sleeping humans, considering intensity levels, age factors, sleep stage, adaptability and housing 03 p0371 A71-13165

Hippocampal, neocortical and somatic effects of HF electrical stimulation of mesencephalic reticular formation during different stages of sleep in cats 05 p0707 A71-16424

Electroencephalographic and motor effects of electrically stimulated reinforcing and negative subcortical structures in sleeping cats 06 p0852 A71-17669

Sleep period time displacement effect on sleep using EEG recordings 08 p1239 A71-20816

Biosatellite 3 monkey sleep and wake states based on visual and computer analysis of telemetered EEG data from earth orbital flight 09 p1395 A71-23242

Human heart beat phase frequency changes after acoustic stimulation during natural sleep from EEG, EKG, EMG of musculus hypoglossus and eye motions 11 p1721 A71-26292

Subsonic jet aircraft noise and simulated sonic booms awakening effects on human sleep 11 p1726 A71-26510

Brain subcortical structure neuronal assemblies impulse activity during sleeping and dreaming in patients treated with implanted electrodes 13 p2005 A71-28378

Behavioral arousal and EEG thresholds changes during sleep due to electrical and audio stimulation 13 p2005 A71-28379

Natural sleep and wakefulness stages neurophysiology based on bioelectric activity spectral and correlation analyses 13 p2005 A71-28380

Heart rate variability in REM sleep, stage 4 sleep and wakefull state from ECG of normal males, calculating coefficient of temporal variability for each state 13 p2014 A71-29319

Subcortical-cortical EEG recording of unrestrained chimpanzees sleep cycles, using computer analysis and biotelemetry techniques 15 p2359 A71-31951

Human subjects REM sleep characteristics under 5-hydroxytryptophan influence, analyzing continuous polygraphic recordings of parietal EEG, horizontal eye movement and submental electromyographic activity 15 p2363 A71-31958

Polygraphic sleep recordings automatic analysis, presenting numerical results for rapid and slow eye movements, muscle tone, heart and respiratory rates 15 p2359 A71-31952

Simulated sonic booms and subsonic jet aircraft noise effects on human subjects of various ages during different sleep stages 15 p2364 A71-32250

Space flight sleep pattern data with EEG, using three descriptors and regression and linear discriminant analysis 16 p2528 A71-33108

Sounds effects on natural nocturnal sleep of healthy humans with normal hearing 17 p2679 A71-34479

Cat thalamus ventrolateral nucleus neuronal discharges during waking and slow and fast wave sleeps 17 p2680 A71-34689

First and last rapid eye movement (REM) sleep differences in unrestrained chimpanzee 18 p2853 A71-35891

Human blood pressure in brachial artery during spontaneous night sleep, recording EEG, EKG and horizontal eye movements 21 p3329 A71-40185

Transport aircrew sleep patterns effects on fatigue and sleep disturbances, discussing physiologic debt and stresses 21 p3342 A71-40341

Young adult males split-period sleep regimes dependence on intervening wakefulness time interval, periods length and onset sidereal time 21 p3330 A71-40348

Pilot EEG, behavioral and subjective correlates of natural and drug induced sleep at atypical hours, using calculation and vigilance tests 22 p3502 A71-41835

Prolonged bed rest effects on EEG sleep patterns in young healthy subjects with and without exercise 23 p3631 A71-43109

SLEEP DEPRIVATION

Time zone change effects on worldwide schedule flight crews sleep patterns, considering biological functions Circadian rhythm changes 04 p0544 A71-15057

Human sleep deprivation research, discussing task performance, man machine interaction and work-rest cycles 04 p0540 A71-15848

Surface negative slow EEG potential (CNV) in human brain after total sleep loss 06 p0850 A71-17428

Clinical value of electroencephalogram following sleep deprivation in detecting abnormalities in neurological patients 09 p1395 A71-23248

Community aircraft noise intensity indexes from annoyance and physiological reaction standpoint, discussing sleep interruption, hearing loss, communication interference, etc 15 p2364 A71-32242

Human fatigue with emphasis on chronic conditions unrelieved by rest or sleep, recommending elimination of conditions resulting in excessive stress, anxiety or boredom 17 p2687 A71-34353

Protein content in cytoplasm of neurons and glial satellite cells in supraoptical and red nuclei of white rat brains during natural and paradoxical phase deprived sleep 19 p3005 A71-38545

Sleep related fatigue in pilot performance and flight safety, considering sleep lack and disruption and irregular duty patterns 21 p3343 A71-40590

SLENDER BODIES

NT SLENDER CONES

Whitman supersonic flow theory application to mid-or near-field sonic boom of slender bodies in wind tunnel research 01 p0005 A71-10956

Monograph on plane shock wave interactions covering supersonically moving two dimensional thin airfoils, slender bodies of revolution and thin wings 01 p0003 A71-11227

Lift of slender aircraft with rectangular cross section fuselage and high wing 03 p0342 A71-13737

Boundary layer higher order effects on zero-lift drag of short slender bodies, emphasizing shock generated vorticity 04 p0569 A71-15029

Tail assembly load distribution in steady uniform flow for nonzero angles of attack, using slender body theory

04 p0527 A71-15367

Boundary layer development on slender rod in axial shear flow for different profiles

05 p0694 A71-16711

Slender beams transverse vibration, including nonlinear bending inertia in motion equation

05 p0825 A71-16716

Plane steady incompressible MHD flow past slender nonconducting profile, determining magnetic field components boundary conditions

05 p0695 A71-16892

Slender bodies of revolution with cylindrical afterbodies in subsonic wind tunnel, examining vortex systems and aerodynamic forces

06 p0842 A71-18048

Boundary layer turbulence decay in slender body supersonic near wake expansion region, using linear theory for assessment of change in fluctuation level and turbulent scale size

06 p0845 A71-18638

Aerodynamic characteristics of conical and pyramidal configurations with various planforms by slender body theory, replacing three dimensional flow by two dimensional flow

08 p1227 A71-20776

Viscous similitude reduction to Mach number independent Birkhoff binary scaling for hypersonic flow over slender bodies

08 p1377 A71-21981

Vortex breakdown on slender sharp edged and modified delta wings with varying sweep angles investigated in wind tunnel using schlieren system for flow visualization

08 p1229 A71-22028

Boundary layer model of laminar viscous flow around high speed slender bodies with surface mass transfer

09 p1381 A71-22084

Inviscid incompressible electrically conducting fluid flow past slender profile investigated by asymptotic power expansion of reciprocal magnetic Reynolds number

09 p1382 A71-22135

Heat transfer to slender bodies in hypersonic flow, comparing wind tunnel measurements with modified reference enthalpy method predictions for laminar and turbulent flow

09 p1545 A71-22941

Reactive equilibrium hypersonic gas flow over slender pointed body, neglecting rate chemistry

09 p1383 A71-23054

Aerodynamic characteristics of slender body of revolution traveling in long tube with circular cross section, deriving static and dynamic stability derivatives formulas

11 p1702 A71-25477

Static aerodynamic characteristics of slender ablating reentry vehicle, discussing coupling between flow field and thermochemical analyses of heat shield materials response

11 p1854 A71-25512

Three dimensional incompressible flow about slender foil in perfect fluid, stressing vortex field effect

12 p1865 A71-27477

Flow field model for steady asymmetric vortex system shed from slender body of revolution in coning motion

12 p1865 A71-27552

Hypersonic wakes of two dimensional slender wedges and flat plate, testing stability in transition region in wind tunnel

12 p1866 A71-27561

Error in determining pressure and loading distribution on surface of slender bodies of revolution

13 p1994 A71-29323

Pressure distribution and drag prediction over slender axisymmetric fuselages and afterbodies and exhaust nozzles at transonic Mach numbers

14 p1270 A71-30771

Slender body interaction with interface forming after bursting of membrane separating low and high pressure gas supersonic flow in shock wave tube

15 p2386 A71-31162

Supersonic potential flow at large distance from slender body of revolution at angle of attack, deriving nonlinear partial differential equations system

15 p2343 A71-31170

Near field flow pattern of inclined slender body of revolution, using Whitman far field theory of supersonic flow

15 p2344 A71-31554

Small disturbance equations for steady transonic flows past thin lifting airfoils and slender bodies

15 p2344 A71-31560

Two dimensional viscous hypersonic flow past thin, needle shaped and highly blunted bodies with strong boundary layer interaction on outer stream

15 p2347 A71-32569

Hypersonic small perturbation flow past two dimensional or axisymmetric slender bodies supporting logarithmic shock waves

17 p2670 A71-34658

Viscous compressible flow around slender body in hypersonic slip flow regime, using finite difference method

18 p2908 A71-36344

Flow field and model wall on slender bodies in low density hypersonic flows ranging from free molecular flow to continuum flow

18 p2846 A71-36418

Nonspherical nose bluntness effects on slender vehicle dynamics, considering conical geometry as approximate nose shape after ablation due to turbulent heating

[AIAA PAPER 71-931] 19 p3148 A71-37176

Hypersonic flow theory evolution, considering friction and high temperature effects and flows about slender, blunt and bluff bodies

19 p2992 A71-37455

Laminar compressible wakes instability behind planar and axisymmetric slender bodies, solving integral conservation equations for fluctuation amplitude variations

19 p2993 A71-37879

Water tunnel walls effect on supercavitating flows past slender bodies

20 p3213 A71-39786

Supercavitating bounded flow of weightless fluid past slender bodies, deriving singular integral equations in terms of pressure gradient and cavern thickness derivative

20 p3213 A71-39787

Viscous incompressible flow past semiinfinite slender body with upper and lower surface forced vibrations, solving ideal fluid and boundary layer equations by Shkadov method

21 p3367 A71-40683

Slender body of revolution in supersonic and subsonic air flow, calculating boundary conditions with Lagrange formulation

21 p3323 A71-40963

Axially loaded slender beam mass and deformation effect on constrained bending motion system stability and dynamic response

21 p3469 A71-41010

Liquid film cooling for slender body type hypersonic reentry vehicles, comparing active mass injection cooling systems to ablation type passive systems

22 p3621 A71-42006

Motion equations derived for slender beam transverse vibrations on continuous viscoelastic foundation, considering nonlinearities from external couplings, longitudinal displacements and curvature

22 p3617 A71-42539

Hypersonic axisymmetric slender body near wake shear layer determination by shock expansion method for numerical computation accuracy and efficiency

23 p3626 A71-44194

SLENDER CONES

Three dimensional attached compressible laminar boundary layer on slender cones in hypersonic flight at high angles of attack derived by numerical integration

01 p0070 A71-10926

Strong blast wave interaction and transient pressure on conical slender supersonic bodies

04 p0525 A71-14979

Monte Carlo simulation for studying rarefied hypersonic gas flow about slender cones and flat plates

05 p0694 A71-16562

Slender cone hypersonic laminar three dimensional boundary layer separation at angle of attack, proposing helical vortex model

[AIAA PAPER 71-129] 06 p0845 A71-18573

Hypersonic flight test base pressure results at high Reynolds numbers for slender cone in turbulent flow, noting implications for ground test simulation

[AIAA PAPER 71-134] 06 p0883 A71-18578

Nose bluntness, angle of attack and oscillation amplitude effect on hypersonic unsteady aerodynamics of slender cones

[AIAA PAPER 70-216] 07 p1016 A71-19895

Aerodynamic effects of bluntness on slender cones in free flight tests at Mach 17

[AIAA PAPER 70-554] 09 p1381 A71-22090

Slender cone boundary layer transition under angle of attack at Mach 21 with promoted leeward and fixed windward ray

14 p2335 A71-29887

Flow field measurement about sharp and slightly blunted slender cone at hypersonic speed and zero angle of attack

[AIAA PAPER 71-625] 15 p2344 A71-31553

Slender cone at Mach 10 with underexpanded exhaust plume, determining flow field interactions separation pattern and aerodynamic coefficients

[AIAA PAPER 71-562] 15 p2347 A71-32280

Near wake streamline configuration in symmetry plane of slender cone in hypersonic flow at free stream Mach number 7

18 p2848 A71-36754

Shock tunnel drag measurements on sharp slender cones in near free molecule hypersonic flow in air and He

19 p2993 A71-37893

Turbulent hypersonic wake density and temperature measurement for slender cone model in shock tunnel using dual electron beam excitation technique

21 p3364 A71-40399

SLENDER WINGS

NT INFINITE SPAN WINGS

Lift of slender aircraft with rectangular cross section fuselage and high wing

03 p0342 A71-13778

Slender deformable airfoil in bounded fluid flow, determining lift coefficient by one dimensional integrodifferential equation for elastic large aspect ratio wing

04 p0567 A71-14590

Ground effects on pressure distribution on slender wing bodies with low aspect ratio and thick cross sections

06 p0842 A71-18047

Hypersonic minimum drag slender wing leading edge shape for given airfoil section, using Newtonian theory

08 p1229 A71-22039

Loads induced on infinite aspect ratio wing by straight infinite free vortex in subsonic compressible freestream, using planar lifting surface theory

11 p1702 A71-25474

Unsteady flow downwash behind finite span slender wing during supersonic motion at finite Strouhal numbers

12 p1866 A71-27697

Pressures, velocities and aerodynamic characteristics of supersonic flow around slender delta wings with forced asymmetry and separation at leading edges

18 p2843 A71-36134

Slender wing lift in supersonic flow, analyzing suction force on leading edge and viscosity and nonlinear effects

[DFVLR-SONDDR-138] 18 p2848 A71-36677

Vortex-induced heating alleviation to lee side of slender wings in hypersonic flow by contouring leading edge planform

19 p2993 A71-37892

Small perturbations of stationary parallel flow with relaxation, considering boundary conditions around slender wings, partial differential equations and similarity law

20 p3213 A71-39569

Free vortices from slender wings, controlling strength, position, core stability and thickness on basis of one dimensional flow model

21 p3319 A71-40492

Minimum drag and lifting line characteristics of large aspect ratio wing in uniform shear flow with velocity variations along span

23 p3625 A71-43312

Slender two dimensional wedge wings aerodynamic characteristics in hypersonic strong interaction flow, determining wall shear stress and lift drag ratio effects

24 p3789 A71-44621

SLEWING

Three-legged slewing about nonorthogonal axes, solving single-axis reorientations by two successive rotations about arbitrary fixed lines

[AAS PAPER 71-389] 23 p3773 A71-43057

SLICING

Electrolytic saw for slicing strain-free metal crystals without damage, noting improved surface flatness

02 p0255 A71-12141

SLIDING

High traction fluid effect on high speed roller bearing cage skidding, comparing with military specification oil

[ASME PAPER 70-LUB-E] 03 p0432 A71-13707

Grain boundary sliding on Mg-Al alloy polycrystalline specimens measured at successive strains during creep under 2800 psi stress

03 p0443 A71-14184

SLIDING CONTACT

Stress concentration and free surface shape at sliding contact for elastic semiinfinite cylinder, discussing mixed boundary value problem

01 p0171 A71-10658

Thermal contact resistance measurements between sliding contacts after load application under various temperatures, using transient pulse technique

[AIAA PAPER 71-438] 11 p1858 A71-26226

Stress concentration and free surface shape at sliding contact for elastic semiinfinite cylinder, discussing mixed boundary value problem

14 p2333 A71-30992

Photoelastic analysis of oil film effects on rolling/sliding contact stresses of plastic and glass cylinders on steel ring, showing discrepancy with Hertzian distribution

15 p2414 A71-31946

Sliding contact between closed annulus and elastic cylinder, deriving integral expressions

21 p3472 A71-41147

SLIDING FRICTION

Isotactic polypropylene and high pressure polyethylene in contact with steel, examining temperature effect on friction and adhesion 01 p0106 A71-10299

Sliding friction and wear of metal pairs under vacuum, using gravimetric and electron optical methods 03 p0432 A71-13366

Magnetic suspension apparatus for temperature measurement near interface of sliding bodies in vacuum 03 p0397 A71-13914

Static metallic adhesion model for sliding friction, using contact resistance measurements 05 p0758 A71-16239

Penetration model of thin solid film lubricant friction on sliding surfaces of finite roughness [ASLE PREPRINT 70LC-15] 08 p1298 A71-21159

Friction-wear characteristics of self lubricating composites under sliding conditions in air and vacuum [ASLE PREPRINT 70LC-17] 08 p1298 A71-21160

Sliding load history effects on friction of thin burnished films of molybdenum disulfide in vacuum [ASLE PREPRINT 70LC-18] 08 p1298 A71-21161

Machine tool friction slides dynamics simulation for phase diagrams analysis, using Szoke model 10 p1614 A71-23994

Arbitrary direction harmonic vibration effects on kinetic friction coefficient between sliding bodies 11 p1767 A71-25267

Gold sliding electric contacts friction behavior, studying adsorbed gas lubrication in ultrahigh purity environments 12 p1912 A71-27637

Redistribution of carbon, copper, nickel and chromium on friction surfaces of powder metallurgy antifriction cermet slide bearings by spectral analysis 15 p2418 A71-32673

Stress, slip and damping of clamped elastic plate with finite friction under alternating axial load, using finite element method 16 p2581 A71-33174

Cobalt and lanthanum with face and body centered lattices, studying plastic deformation during allotropic transformations under sliding friction and gripping 16 p2584 A71-33895

Structural design of gyroscope ball bearings, considering additional sliding friction force moment 17 p2739 A71-34561

Low speed angular contact bearings surface geometry effects on friction perturbation torque ripple frequency 18 p2928 A71-36764

Polyethylene, polypropylene and copolymers sliding friction viscoelastic nature, obtaining relationship between sliding force, adhesion bond shear strength and contact area 19 p3068 A71-37425

Microfriction anisotropy of graphite at small loads for sliding on basal and edge planes, using scanning electron microscope 20 p3253 A71-39410

Aircraft parts lubrication friction and wear problems, discussing failure modes, solid and liquid lubricants, component damage and lubrication systems 21 p3389 A71-40902

Humidity effects on molybdenum disulfide bonded solid film lubricant friction properties at low load and slow speed, noting mechanical escapement timers accuracy [ASLE PREPRINT 71LC-2] 24 p3831 A71-45285

Surface oxide, organic and lead film effects on friction and plastic deformation of Zn single crystal during sliding [ASLE PREPRINT 71LC-6] 24 p3839 A71-45288

Non-Newtonian film thickness, load capacity and maximum viscoelastic stress effect in point contact with second order fluid lubricant for slide/roll ratio [ASLE PREPRINT 71LC-16] 24 p3832 A71-45293

SLIP

Interstitial role in bcc metals slip anisotropy at low temperatures, examining stress differential effect in Nb-oxygen solid solutions 08 p1307 A71-21505

Fcc binary alloys cross slip difficulty due to solute atoms and small short range order regions 08 p1309 A71-21527

Deformation modes with associated structural defects for slip, viscous slip and climb processes in gamma prime precipitation hardened nickel based alloys 08 p1315 A71-21583

Two dimensional effects of cylinders rolling on elastic half space, investigating inflated tire shear stress and slip region 11 p1850 A71-26101

Elastoplastic buckling of structures, considering strain hardening materials, slip and Bauschinger effect 16 p2650 A71-33024

Local slip theory in elastic contact region with dry friction, assuming Amontons-Coulomb law for displacement, rolling and sticking 17 p2747 A71-34327

Slip line deformation of ordered and disordered Cu-Au intermetallic single crystals from microstrain and electron micrographic studies 20 p3249 A71-38967

Second order theory of plane plastic flow, investigating characteristic slip lines of perturbed velocity field and stress equations 23 p3774 A71-43144

SLIP BANDS

U EDGE DISLOCATIONS

SLIP FLOW

Rarefied gas flow through long square tubes, solving continuum differential equation with noncontinuum slip boundary conditions [ASME PAPER 70-WA/PID-1] 03 p0402 A71-14098

Rarefied gas low speed slip flow over wedge, solving for velocity profiles and skin friction [ASME PAPER 70-WA/APM-26] 03 p0344 A71-14158

Kinetic theory approximate method application to model equation with velocity dependent collision frequency, obtaining solution for Kramers problem and expression for slip coefficient 06 p0931 A71-17450

Uniform magnetic field effect on rarefied gas slip flow over porous flat plate for skin friction response, using velocity and temperature fields equations 10 p1649 A71-24407

Slip flow development in parallel plate channel entrance, discussing center line velocity and excess pressure distributions 15 p2393 A71-32262

Simple gas thermal creep/velocity slip and temperature jump coefficients by applying variational technique to linearized Boltzmann equation with boundary conditions 17 p2785 A71-35446

Viscous compressible flow around slender body in hypersonic slip flow regime, using finite difference method 18 p2908 A71-36344

Thermal creep slip velocity expression in power series for arbitrary fraction of molecules diffusely reflected from surface by Bhatnagar-Gross-Krook model solution 19 p3163 A71-37734

Variable suction effects on two dimensional fluctuating slip flow of incompressible rarefied gas past infinite flat plate 20 p3211 A71-39466

Blunt body heat transfer predictions for atmospheric reentry, discussing coupled effects of real gas behavior and slip/jump boundary conditions 21 p3474 A71-40256

Diffusing gas mixtures slipping rate along wall at arbitrary accommodation coefficients, deriving expression based on molecule distribution functions from linearized Boltzmann equations solution 21 p3418 A71-40678

Continuum dislocation theory, discussing initial stress couple problem, slip motion and dislocation rate tensor 21 p3468 A71-41000

Slip, surface permeability and temperature gradient effects on surface friction and heat transfer in boundary layer near cylinder critical point 24 p3887 A71-44743

SLIPSTREAMS

NT PROPELLER SLIPSTREAMS

Dispersion model of turbulent mixing of isothermal and nonisothermal slipstreams of air-gasoline combustion products in nozzles 04 p0577 A71-15622

Airfoils in two dimensional nonuniformly sheared slipstreams, predicting pressure distribution from mathematical model for comparison with measurement [AIAA PAPER 71-94] 06 p0843 A71-18549

Intensified molecular diffusion during turbulent mixing of supersonic slipstreams in cylindrical mixing chamber, using optical Prudnikov method 07 p1089 A71-19733

Plane and circular turbulent jet boundary layer expansion in slipstream, comparing analytical with experimental results 12 p1898 A71-27505

Turbulence level effects on mixing of three plane parallel slipstreams with equal velocities and temperature from smoke visualization 13 p2163 A71-28962

Incompressible conducting fluid plane jet expansion in homogeneous slipstream, deriving partial differential equations for nonconduction approximation 14 p2278 A71-29610

Slipstream due to supersonic source in hypersonic stream, determining shape of limiting surface 15 p2346 A71-32116

Viscous slipstream flow downstream of triple shock wave intersection in supersonic diffuser air flow, using Pitot and static pressure probe measurements 21 p3324 A71-40981

SLITS

Mixed boundary value problem in elasticity theory for piecewise homogeneous isotropic plate with slits, reducing to integral equations 06 p0983 A71-17361

Photomaterial nonlinear effects on contour distortion in holographic recording of Fourier image slit for graphic memory use 10 p1612 A71-24716

Harmonic mixed boundary value problem exact solution for rectangle with slit, outlining finite difference techniques convergence 15 p2441 A71-31356

Free space diffraction of E-polarized plane electromagnetic wave by slit in thick conducting screen, deriving approximate solution from Wiener Hopf equation by matrix techniques 19 p3023 A71-38592

SLOPES

NT GLIDE PATHS

Visual slant averaging mechanism evidence from binocular disparator tests, considering gradient slant perception theory and neurophysiological averaging mechanism 04 p0546 A71-15170

Rational scale selection for theoretical and experimental graphs, investigating slopes and angles between line segments for various parameters 09 p1439 A71-23347

Edge waves on sloping beach in exponentially stratified fluid, finding lowest mode/Stoke edge wave/insensitivity to density field 11 p1749 A71-25358

SLOSHING

U LIQUID SLOSHING

SLOT ANTENNAS

Shadow current method for asymptotic solution to two dimensional problem of electromagnetic wave far diffraction field on ideally conducting plane with infinite rectilinear slot 02 p0210 A71-11629

Radiation patterns of diametrically opposed slot antenna arrays on infinitely long cylinders 04 p0559 A71-15878

Doubly shunt loaded short slot antenna, determining optimum capacitive loadings for enhanced radiation or improved directivity 06 p0876 A71-17740

Aperture antennas gain loss due to aperture phase errors 07 p1075 A71-19268

Conducting disk with slot dipole at center, determining asymptotic expressions for radiation field far zone 08 p1266 A71-21465

Self and mutual admittance, isolation and radiation pattern of slots on infinite cylinder covered by inhomogeneous lossy plasma 08 p1341 A71-21886

Cylindrical slot antennas radiation patterns in plane perpendicular to axis, discussing field emission and angular position of each slot for phase multiplier 09 p1415 A71-22458

Axial slits circular array pattern in large conducting cylinders fed by waveguides 09 p1419 A71-23497

Asymptotic expression for mutual admittance between axial rectangular slots on large conducting cylinder 09 p1419 A71-23507

Admittance of aperture antenna radiating into lossy warm overdense plasma half space, considering electron energy 09 p1505 A71-23521

Flush mounted annular slot missile antenna theory application to near zone field strength instrumentation calibration and plane wave electromagnetic field pulse response determination 10 p1580 A71-25071

Synthesis of slot antenna on metallic wedge for amplitude radiation pattern, determining RMS approximation and fixed phase diagram 14 p2195 A71-30103

Structural design, mechanical stability and aircraft compatibility for airborne side-looking radar antennas, using end fed slotted waveguide arrays 14 p2205 A71-31041

Slotted waveguide arrays in precision Doppler radar antennas, correlating predicted and actual performance 14 p2206 A71-31073

Aerospace antenna design, calculating one-wavelength circular slot aperture radiation from circular cylindrical surface 14 p2206 A71-31075

Linear aperture antenna radiation pattern interpolation based on complex-valued function satisfying integral equations system 16 p2546 A71-33497

Electronically scanned cruciform slot-array aircraft antenna for satellite controlled navigation aid, discussing circularly polarized wave radiation 16 p2548 A71-34123

Slot antennas electromagnetic radiation patterns in conducting ground plane coated with moving isotropic cold plasma sheath 17 p2701 A71-34758

Worst case criterion for finite circular antenna aperture illuminations effectiveness comparison and optimization in synthesizing ideal radiation pattern 17 p2715 A71-34763

- Omnidirectional one slot aerial energized by dielectric waveguide for hypersonic vehicle-ground communication through ionized shock layer
[ONERA-TP-949] 18 p2887 A71-36022
- Meter wave aircraft slot antenna for Concorde air to ground communication via satellite, presenting synthetic radiation patterns 18 p2889 A71-36514
- Numerical method for near field antenna coupling over conducting surface of aerospace vehicles applied to L band slot antennas on F-4 Phantom aircraft 19 p3031 A71-38445
- Line source excitation for maximum aperture efficiency with given sidelobe level 19 p3035 A71-38596
- Parabolic reflector aperture antennas with Gaussian distributed random phase deviations, obtaining asymptotic expansion for radiation pattern 19 p3036 A71-38605
- Wave diffraction by air gap multilayered dielectric coated sphere with azimuthal slot for low loss transmission, obtaining radiation pattern 22 p3522 A71-42283
- Narrow strongly radiating slot voltage distribution, investigating cavity coupling with integral equation 22 p3522 A71-42305
- Dual integral equations solutions to electromagnetic wave diffraction at plane conducting slotted screen 23 p3644 A71-43258
- Radiation pattern modification factors calculation for TE excited slot antenna in ground plane covered with inhomogeneous plasma reentry sheath 23 p3646 A71-44172
- SLOTS**
- NT WING SLOTS**
- Polarization control of emission from cross-shaped slots on square and circular waveguide walls via phase and amplitude adjustment 03 p0386 A71-13809
- Pi-section waveguide with narrow slot in broad wall, calculating reflection and transmission coefficients as function of design parameters 10 p1584 A71-24719
- Two layer thermal and velocity model of gaseous film cooling with constant turbulent step slot flow [ASME PAPER 71-GT-3] 11 p1855 A71-25949
- Three dimensional slot lip geometry effects on tangential and splash film cooling of gas turbines [ASME PAPER 71-GT-11] 11 p1855 A71-25957
- Self- and mutual admittances for axial rectangular slots in inhomogeneous cylindrical plasma layer, giving coupled radial transmission line model for propagation 13 p2105 A71-28002
- Two dimensional prediction of adiabatic wall temperature and heat transfer coefficient downstream of film cooling slots, using Prandtl mixing length forms 13 p2160 A71-28598
- Waveguide systems coupled through slots in lattice partition approximated by anisotropic dielectric layer 19 p3019 A71-38338
- Plane electromagnetic wave diffraction by circular cylinder with longitudinal slot, determining scattered field by Riemann-Hilbert method 19 p3020 A71-38417
- Slide valve slot fluid flow oscillation frequency range estimate for quasi-stationarity 20 p3183 A71-39168
- Hemispherical and spherical pressurized gas bearing design with narrow circumferential feed slot as laminar flow restrictors, predicting static load performance 22 p3551 A71-41667
- Modular slot fed fluid bearing using jacking gas effects for pumping power conservation under high speed steady state, discussing design and application 22 p3552 A71-41669
- Thick Al alloy sheet with central slot under cyclic loads, examining striation spacings and fatigue crack propagation rates with electron fractography 22 p3561 A71-41708
- Compressible flow across shaft face seals and narrow slots, examining fluid inertia, viscous friction and entrance losses 23 p3663 A71-43592
- Discrete slot pressurized fluid journal bearing design for low L/D ratios and small size configuration 24 p3830 A71-44942
- Quasi-stationary electric field in toroidal metallic ionization chamber with meridional and equatorial slots, deriving formulas for components as function of coordinates 24 p3857 A71-45231
- SLOTTED ANTENNAS**
- U SLOTT ANTENNAS**
- SLOTTED WIND TUNNELS**
- Lift correction in perforated two dimensional transonic wind tunnels, considering incidence angle and streamline curvature effects on airfoil models 10 p1590 A71-24953
- SLOW NEUTRONS**
- U THERMAL NEUTRONS**

SLURRY PROPELLANTS

- Mg slurry fuel mixing, ignition and combustion characteristics for injection into high speed air flow [AIAA PAPER 71-6] 06 p1007 A71-18480
- Ignition and combustion tests of storable boron/magnesium/hexane slurry injected directly in high speed air stream 14 p2286 A71-30773
- SLUSH**
- Microwave systems for cryogenic liquid and slush density and flow velocity measurements 04 p0586 A71-14659
- Hydrogen slush storage and transfer density and flow measuring instrumentation, emphasizing capacitance measurement 08 p1292 A71-21695
- Microwave methods for nitrogen or hydrogen densities and flow rate measurement in single phase liquid and slush state 08 p1292 A71-21696
- Capacitance measurement technique for density and mass flow measurements for hydrogen slush storage and transfer 20 p3237 A71-39276

SLV (SOFT LANDING VEHICLES)

- U SOFT LANDING SPACECRAFT**
- SMALL ASTRONOMY SATELLITES**
- Small Astronomy Satellite PCM/PM telemetry transmitting split phase encoded data at 136 MHz 01 p0036 A71-10987
- Galactic plane X ray scan by NASA small astronomy satellite Uhuru, discussing satellite instrumentation, detector and sensor sensitivity and preliminary measurements 11 p1814 A71-25212

SMALL PERTURBATION FLOW

- Small perturbation subsonic flows aerodynamic noise, using matched asymptotic expansions method 02 p0240 A71-12377
- Rotating stall analysis, using small perturbation method 04 p0569 A71-14984
- Turbulent flow main characteristics calculation based on maximum stability hypothesis with respect to most dangerous perturbation, presenting numerical solutions by digital computer 07 p1085 A71-18755
- Hydrodynamic stability of viscous conducting fluid plane Couette-Poiseuille flow in transverse magnetic field by linear theory, considering complete spectrum of small disturbances 07 p1169 A71-19727
- Airborne hot wire measurements of small scale structure of atmospheric turbulence 07 p1153 A71-20276
- Stability of two concentrically flowing fluids in straight circular tube, investigating axisymmetric and asymmetric disturbances by small perturbation method 07 p1093 A71-20282
- Oscillating airfoil wake interaction with fixed cascade, considering two dimensional incompressible inviscid small perturbation flow theory 09 p1511 A71-22943
- Detonation wave of gas in circular cylinder with nonsimultaneous axisymmetric initiation at plane boundary, obtaining solution for small perturbation flow behind detonation front 11 p1853 A71-25152
- Mesoscale gravity waves and jet stream stability in temperature-stratified atmosphere with small wave perturbations, estimating wave phase velocities and amplitude functions 12 p1924 A71-26736
- Plane parallel Couette flow stability with respect to small perturbations, considering positive wave numbers and Reynolds numbers 12 p1897 A71-27307
- Cavity cross sections deformation in heavy ideal liquid, deriving nonlinear system of equations for time dependence within framework of small perturbation theory 13 p2047 A71-28279
- Stability of steady states of physical system with respect to finite perturbations 13 p2100 A71-28451
- Excess energy in fluid mechanics, breaking up equation into different orders by small perturbation approach and Rankine-Hugoniot shock relation 14 p2227 A71-30818
- Small disturbance equations for steady transonic flows past thin lifting airfoils and slender bodies [AIAA PAPER 71-566] 15 p2344 A71-31560
- Hypersonic small perturbation flow past two dimensional or axisymmetric slender bodies supporting logarithmic shock waves 17 p2670 A71-34658
- Oswatitsch expansion method of characteristics for weak perturbations in nonlinear propagation processes 19 p2992 A71-37452
- Plane parallel Couette flow stability with respect to small perturbations, considering positive wave numbers and Reynolds numbers 19 p3046 A71-38263

Turbulent flow stability with respect to small disturbances, applying maximum stability principle to stable averaged flow 20 p3210 A71-38895

Small perturbations of stationary parallel flow with relaxation, considering boundary conditions around slender wings, partial differential equations and similarity law 20 p3213 A71-39569

Heat transfer of short hot wire normal to ambient incompressible air flow, using small perturbation energy equation 21 p3379 A71-40664

Linear stability equations for two dimensional compressible supersonic boundary layer with three dimensional disturbances including thickness growth term 21 p3370 A71-40995

Upstream influence and interfacial waves in open channel two fluid small perturbation flow 23 p3663 A71-43446

Small perturbation development of plane potential motion of ideal incompressible fluid in elliptical region, confirming instability 24 p3821 A71-45219

SMALL SCIENTIFIC SATELLITES

Small satellites for radiation and solar cell damage measurements, surface friction and cold welding experiments and Apollo communications testing 04 p0662 A71-15018

SMEAD

Astronomical data correction for smearing effects applying Fast Fourier Transform algorithm 18 p2960 A71-35933

SMELL

U OLFACTORY PERCEPTION

SMOKE

- Cylindrical transparent plastic antismoke hood with metallized dome, noting respiratory volume and air supply 01 p0028 A71-11599
- Flame retardant effects on smoke density and oxygen index of polystyrene, acrylonitrile-butadiene-styrene (ABS) and polyester systems 07 p1144 A71-19572
- Combustor design for minimum exhaust smoke emission from aircraft gas turbine jet engines, considering air pollution 08 p1347 A71-20867
- Aircraft engine smoke emission control, discussing Ringelmann chart assessment for various commercial jet aircraft and airport gaseous pollutants 08 p1380 A71-21832
- Aircraft smoke emission control, outlining legal action by New Jersey State Department of Health 08 p1380 A71-21833
- Rats hypoxia tolerance, noting smoke effects on survival, respiratory rate, body temperature and glycolytic parameters 09 p1396 A71-23364
- Standard equipment and procedures for aircraft gas turbine engine exhaust smoke measurement [ASME PAPER 71-GT-88] 11 p1813 A71-25995
- SMOKE TRAILS**
- Visible exhaust smoke trails from aircraft jet engines, measuring optical density by photographic photometry 13 p2114 A71-28314
- Kerosene type fuels for aircraft gas turbine engines, discussing combustion problems, smoke emission reduction and bacterial or fungal contamination 13 p2113 A71-28754
- Dispersal of jet aircraft exhaust emissions near airports and of smoke trails in upper atmosphere, assessing pollutant levels near large urban airports 15 p2349 A71-32244

SMOOTHING

NT DATA SMOOTHING

- Rough metal surface smoothing through annealing in vacuum, deriving governing equations from Mullins theory of thermal grooving and solid surface capillary morphology 22 p3554 A71-42424
- Astronomical observations weighted estimation based on smoothing Pearson curves empirical distribution 23 p3771 A71-44257
- Random amplitude bounded measurement errors, describing nonlinear filtration method of noise smoothing 24 p3813 A71-44683

SMS

U SYNCHRONOUS SATELLITE

METEOROLOGICAL

SNAILS

Vitamin A initial uptake site and intracellular transport pathway in snails photoreceptors 01 p0009 A71-10230

SNAKES

Snake IR receptor sense organs tested by IR stimulus from carbon dioxide laser, suggesting receptor operation on thermal principle 15 p2360 A71-32296

SNAKING

U LATERAL OSCILLATION

SNAP
 NT SNAP 8
 NT SNAP 15
 NT SNAP 19
 NT SNAP 21
 NT SNAP 23
 NT SNAP 27
 NT SPACE POWER UNIT REACTORS
SNAP 8
 Nuclear radiation shielding design for space base SNAP 8 reactor, discussing geometry constraints for lithium hydride and U loop layers model
 09 p1492 A71-22808
SNAP-8 mercury Rankine system performance
 data, investigating design change for reduced reactor operating temperatures
 15 p2447 A71-32201
SNAP 8 turbine-alternator as nuclear-electric space power converter, discussing rotating machinery components design and 10,000 hr endurance testing results
 15 p2447 A71-32208
Startup testing of SNAP 8 power conversion system coupled with nuclear reactor simulator
 15 p2447 A71-32217
Tantalum/stainless steel mercury boilers for SNAP 8, evaluating performance
 15 p2448 A71-32219
Unalloyed tantalum as containment material in mercury Rankine cycle SNAP 8 system boiler for 5 year service life
 15 p2448 A71-32221
Materials evaluation of SNAP 8 power conversion system breadboard assembly after 8700 hour test, extrapolating service life for space flight application
 15 p2448 A71-32222
SNAP 15
SNAP 15A heat source gamma ray intensity measurements and identification of gamma ray producing isotopes, describing measurement apparatus
 09 p1491 A71-22456
SNAP 19
Nimbus 3/SNAP 19 radioisotopic thermoelectric generator design and performance
 05 p0780 A71-17136
Orbital performance of SNAP 19 radioisotopic thermoelectric generator for nuclear power supply on Nimbus 3 observatory
 20 p3266 A71-38962
SNAP 19 TAGS thermoelectric generator life tests at high temperature in Ar, predicting long term performance including thermoelectric material and isotope fuel decay effects
 20 p3266 A71-38963
Thermal protection and electrical and mechanical evaluation of SNAP 19 radioisotope thermoelectric generator for integration with Viking Mars lander
 20 p3267 A71-38964
SNAP 19 Radioisotope Thermoelectric Generator (RTG) for advanced space missions, using lead telluride and silver antimony germanium telluride as conversion materials
 20 p3267 A71-38965
SNAP 21
Long term performance of lead telluride thermoelectric generators tested under SNAP 21, 23A and 27 programs
 20 p3266 A71-38955
SNAP 23
Long term performance of lead telluride thermoelectric generators tested under SNAP 21, 23A and 27 programs
 20 p3266 A71-38955
SNAP 27
Long term performance of lead telluride thermoelectric generators tested under SNAP 21, 23A and 27 programs
 20 p3266 A71-38955
SNATCHING
U SPACECRAFT RECOVERY
SNOW
Snowflakes melting region radar observation, discussing fall speed, reflectivity profile, particle size distribution, Doppler characteristics, etc
 01 p0117 A71-10575
Snow storms wind field and turbulent region detection, using Doppler VAD pattern and mapping
 01 p0117 A71-10576
Doppler radar techniques for turbulent kinetic energy budget in boundary layer, discussing wind profile and turbulence in snow conditions
 01 p0117 A71-10577
VTOL operation under snow and ice conditions, discussing adhesion, radiation absorption and electrical properties of ice
 04 p0533 A71-15437
Submillimeter wave attenuation in snow, comparing results of calculation based on Mie theory with measurement
 05 p0718 A71-15991
Visible and IR radiation attenuation in rain and snow, comparing calculation based on Mie diffraction formulas with measurement
 05 p0718 A71-15992

Neutron monitor counting rate at Sanae, Antarctica, observing snow and atmospheric pressure and temperature effects
 06 p0960 A71-18168
Elemental abundance ratio patterns in microscopic spherules collected from atmosphere and polar snows, comparing to terrestrial and lunar rocks
 20 p3298 A71-39638
Earth surface characteristics measurements with remote sensors, proposing overlaid albedo measurements for clues as to ground type /clouds, vegetation, sand and snow/
 20 p3260 A71-39684
Atmospheric physics of cloud formation, rain, hail and snow precipitation, discussing intracloud temperature variations electric fields and air impurities on water condensation
 21 p3410 A71-40146
Submillimeter wave attenuation in snow, comparing results of calculation based on Mie theory with measurement
 22 p3515 A71-42740
Visible and IR radiation attenuation in rain and snow, comparing calculation based on Mie diffraction formulas with measurement
 22 p3515 A71-42741
SNOWPLOW EFFECT
U PLASMA DYNAMICS
SOAPS
Li quantitative determination in soaps and lubricants by gamma spectroscopy of nuclear reactions with alpha particles from radioactive source
 01 p0106 A71-10093
Metallic soaps polarity and micellar bond energy effects on pliable lubricants structure and properties
 07 p1144 A71-19491
SOCIAL FACTORS
Social factors of labor organization and control in scientific teams for industry
 02 p0335 A71-11856
Social quantitative benefit vs risk assessment of new technologies, considering atomic power safety
 02 p0336 A71-12120
Technology assessment effects on science and engineering progress
 02 p0336 A71-12121
Superior jet pilots social, military and flying case histories, noting predominance of firstborn children with close father-son relationships
 03 p0371 A71-13325
Short haul STOL aircraft transport system, discussing neighborhood stolport ownership, technical feasibility and economic, emotional, ecological and sociological viability
 03 p0523 A71-13618
German monograph on socioeconomic evaluation of air transportation systems for developing nations, using cost-benefit analysis
 04 p0691 A71-15125
Human circadian rhythms in continuous darkness, noting social cues entrainment sufficiency
 06 p0849 A71-17303
Meteorological observing program execution legal and legislative aspects, noting social adjustment to weather effects
 08 p1329 A71-21731
Noise disturbance near large airports, considering aircraft noise, public annoyance and socio-psychological conditions
 12 p1875 A71-27478
Human position in socialist productive system, examining pedagogical aspects of leadership
 13 p2019 A71-28491
Processes involved in obtaining materials required for socialist organization operation, discussing operations, cost reduction by work mechanization and optimum data processing
 13 p2167 A71-28492
Aerospace business future, discussing political, military and social factors effect
 17 p2841 A71-34575
Shower habitability requirements for adequate cleansing of body and hair to satisfy physiological, psychological and social needs of crew members on long space missions
 18 p2870 A71-36629
Book on space technology for developing countries covering economic, social and educational reform, solar system exploration and extraterrestrial civilizations
 22 p3623 A71-42066
SOCIAL ISOLATION
Circadian work-rest cycles in isolated humans
 01 p0017 A71-11411
Fighting between male mice isolated at early age or reared in small groups, considering ontogenetic and experiential determinants
 13 p2011 A71-28805
Color and music distraction for operator in isolated environment and counteract psychophysiological activity impairment
 20 p3193 A71-39225

Human microflora variation in long term confinement, examining anaerobic and aerobic microorganisms responses
 21 p3333 A71-40557
Microbial contamination of human skin and upper respiratory tract during long term isolation in sealed environment
 21 p3333 A71-40559
Bacterial contamination in confined sealed space during long term human occupation, observing hemolytic microflora spreading dynamics on bodies, clothes, wall and air
 21 p3343 A71-40560
Prolonged manned space flight infectious disease hazards, discussing confinement, zero gravity, high oxygen content, personal hygiene, waste disposal and preflight immune status
 21 p3333 A71-40561
Time sense modifications among human groups isolated in underground environment and deprived of timekeeping means, evaluating average individual behavior
 22 p3500 A71-41577
Pharyngeal streptococcal flora of men confined in sealed chamber, observing microbial transfer
 24 p3800 A71-44530
Experimental ATS-1 satellite medical network for geographically and climatically isolated areas, noting impact on emergency treatment and anxiety level reduction
 24 p3801 A71-44592
SOCIOLOGY
NT SOCIAL FACTORS
Socioeconomic changes in aeronautics, discussing faster long range aircraft, airport access problems, technological advances, short haul transportation and industry/government relations
 12 p1868 A71-27601
SODIUM
NT LIQUID SODIUM
NT SODIUM VAPOR
Secondary electron emission during RbBr, Se and CdTe film bombardment by sodium ions and atoms
 01 p0139 A71-11099
Sodium counterflow from serosal to mucosal surface of short-circuited acid-killed turtle bladder
 01 p0015 A71-11182
Sodium dayglow rocket measurements, comparing emission intensities with ground based measurements
 03 p0407 A71-13312
Sodium atom excitation by high energy particle collisions behind shock waves, measuring electron and vibrational temperatures
 03 p0376 A71-13992
Accelerated cavitation damage in Na, examining pressure and temperature effects
 03 p0443 A71-14286
Na-Cs unpolarized and spin exchange differential scattering cross sections calculation by phenomenological and difference potential methods
 04 p0630 A71-15654
Dispersion medium effects on thermal hardening of lubricating oils with Na or Li additives
 05 p0772 A71-16385
Solar Na I Fraunhofer lines empirical constants and abundance, discussing van der Waal attraction, Stark broadening and radiative damping
 06 p0969 A71-17974
Gas agent temperature measurement by sodium spectral line reversal method using MHD generators experimental research
 09 p1512 A71-23671
Na I absorption spectrum interpretation between 150 and 900 A in vacuum UV, noting various discrete features
 10 p1676 A71-24500
Vapor flow passage wall shear stress effect on sonic velocity limit in Na heat pipes
 11 p1856 A71-26202
Heat acclimatization effects on sweat Na concentration over wide sweat rates range, discussing possible mechanisms
 13 p2024 A71-29498
High average power flash lamp pumped pulsed dye laser development and application in atmospheric sodium probing
 16 p2586 A71-33148
Na and K transition oscillator strengths, noting core polarization effects on mathematical model
 16 p2615 A71-34088
Glass fibers and rods from thallium-sodium ion exchanging, investigating flexibility, focusing and light conduction without distortion
 16 p2588 A71-34120
Sodium and cations elimination by kidneys during water-salt metabolism changes due to high temperature and hypodynamia
 20 p3189 A71-39232
F, Na and Al origin in galactic cosmic radiation, investigating production as spallation fragments and generation in source
 23 p3719 A71-42943

SODIUM ALLOYS

NaK lubricated segmented hydrodynamic fluid film tilting pad type journal bearings and Kingsbury type self aligning thrust bearings

15 p2447 A71-32210

SODIUM CARBONATES

Sodium bicarbonate intravenous effects on cat and rabbit otolithic reactions to accelerations and motion

06 p0861 A71-18375

Commercial sodium bicarbonate powder for methane air diffusion flames extinction, noting particle surface areas

07 p1182 A71-19248

Thermal conductivity of Li and Na carbonates alone and combined in mixture with magnesia at various temperatures

08 p1377 A71-21933

SODIUM CHLORIDES

Combined glucose-sodium chloride solution consumption by rats during normal and food deprivation conditions

02 p0201 A71-12874

Fused silica and single crystal NaCl nonlinear parameters from ultrasonic beams mixing studies

05 p0793 A71-16410

Voluntary body water and salt deficits decreasing human heat tolerance

05 p0708 A71-16597

Warm fog modification by condensation nucleus seeding, discussing droplet concentrations, cloud height and aerosol content effects on salt seeding material optimal size and dosage

09 p1488 A71-23253

Long term immersion effects on human water-salt metabolism, noting increased erythrocyte water contents and hematocrit index

13 p2006 A71-28403

Electromagnetic waves propagation in inhomogeneous medium, using simulation chamber with NaCl and ethyl alcohol diffused agar-agar

17 p2724 A71-34755

Dehydration effects on blood parameters in Somali donkeys and zebu steers, observing increases in plasma osmolality, sodium chloride, hemoglobin, packed cell volume, etc

17 p2681 A71-34940

Nickel maraging steel in NaCl solution, investigating susceptibility to stress corrosion cracking

18 p2935 A71-36595

Corrosion fatigue crack propagation in Ni-Cr-Mo maraging steel in room temperature NaCl solution at various stress intensity ranges

20 p3248 A71-38778

Trapped hydrogen atoms detection in proton irradiated KCl and NaCl single crystals at 77 K, using electron paramagnetic resonance spectroscopy

24 p3802 A71-44425

SODIUM COMPOUNDS

NT CRYOLITE

NT SODIUM CARBONATES

NT SODIUM CHLORIDES

NT SODIUM FLUORIDES

NT SODIUM HYDRIDES

NT SODIUM IODIDES

NT SODIUM PEROXIDES

NT TALC

Hemoglobin-sodium nitrite reaction in absence of oxygen, discussing methemoglobin formation by autocatalysis

03 p0363 A71-13486

Catalytic decomposition of sodium chlorate using cobalt oxide catalysts

04 p0549 A71-15750

Sodium fluoroacetate as radiation protective agent, noting dependence on selective blockade of enzyme acetylase

07 p1037 A71-18967

Temperature effect in sodium fluoroacetate protective action mechanism for mice irradiation

07 p1037 A71-18968

Sodium oxide-titanium dioxide-water ternary system, determining sodium titanates formation regions in equilibria in 300 C isotherm

15 p2367 A71-31902

Orthorhombic-tetragonal phase transition in barium sodium niobate, investigating expansion curve discontinuities due to crystallographic changes from dilatometric studies

20 p3275 A71-38816

SODIUM D-LINE

U D LINES

SODIUM FLUORIDES

Light transmitting vacuum deposited NaF polycrystal for IR measurements

08 p1343 A71-21288

SODIUM HYDRIDES

Na D lines broadening by atomic H, discussing interatomic forces between Na and H atoms in terms of NaH molecular potentials

16 p2614 A71-33101

SODIUM IODIDES

NaI-glycerol solution resistivity values, determining measurement frequency, temperature, outgas procedures, purity and doping level effects

24 p3802 A71-44614

SODIUM PEROXIDES

Sodium superoxide isothermal decomposition, detailing metallic oxide effects with differential thermal analysis, thermogravimetry and differential thermogravimetry

17 p2694 A71-34672

SODIUM SILICATES

NT TALC

SODIUM VAPOR

Rocket-borne Na-K vapor release for upper atmosphere winds profiles and diffusion measurements by ballistic camera photography

03 p0415 A71-14027

Single plate interferometer tested by Na vapor anomalous dispersion near D lines, considering application to hook interferometry

16 p2578 A71-33158

Winds and diffusion measurements in lower atmosphere using sodium vapor cloud release from Centaur IIB rocket

20 p3221 A71-39692

SOFT LANDING

Space capsule reentry into Martian atmosphere for soft landing, using onboard nonlinear filter and stochastic control for random wind gusts

03 p0500 A71-14479

Doppler radar velocity sensors and altimeters for lunar and planetary spacecraft instruments soft landing

04 p0597 A71-15324

Venus atmospheric temperature and pressure measurements during and after Venera 7 soft landing

09 p1528 A71-23560

Venera 7 satellite data during descent through Venus atmosphere and activity after soft landing on 15 December 1970, noting temperature and pressure measurements

20 p3289 A71-39130

Apollo command module land landing capability in case of abort after liftoff, describing Monte Carlo simulation procedure

22 p3573 A71-42776

SOFT LANDING SPACECRAFT

NT APOLLO SPACECRAFT

NT LANDING MODULES

NT LUNAR LANDING MODULES

NT LUNAR MODULE

NT MARS EXCURSION MODULE

NT SURVEYOR LUNAR PROBES

NT SURVEYOR 1 LUNAR PROBE

NT SURVEYOR 3 LUNAR PROBE

NT SURVEYOR 5 LUNAR PROBE

NT VOSTOK 2 SPACECRAFT

Single stage to orbit space shuttle system /SERV/ concept with VTOL capability, discussing configurational and operational characteristics with emphasis on flexibility and versatility

04 p0664 A71-15336

Soft lunar landing powered descent optimal control for cost functional minimization, considering linear analytic approach with fuel consumption reduction

10 p1682 A71-24330

SOFT RECOVERY

U SOFT LANDING

SOFTENING

Low strain cyclic hardening and softening in Al-Mg alloy, comparing measurements by monitoring and tensile testing methods

03 p0444 A71-14315

Medium alloy structural steels tempering, investigating Mn, Ni, Cr and Mo effect on activation energy of softening

03 p0445 A71-14338

Pure Fe and Fe-Ni alloys thermal stress component temperature dependence measurement, investigating Ni addition effect on alloy softening

05 p0765 A71-16188

Bcc metals low temperature strength, examining solution softening in Fe-Mo alloys

08 p1307 A71-21506

Solution hardening and softening of single crystals, considering deformation in Nb-Mo and Nb-Re alloys

13 p2088 A71-29344

SOFTWARE [COMPUTERS]

U COMPUTER PROGRAMS

U COMPUTER SYSTEMS PROGRAMS

SOIL MAPPING

Side-looking airborne radar /SLAR/ imagery and site selection for soil pattern topography

02 p0244 A71-11952

Photographic and IR multiband spectral discrimination for rock and soil mapping from orbiting ERTS satellites

[AIAA PAPER 70-303]

06 p0898 A71-17562

Crop species and soil condition computerized identification from film optical density differences, using multibase and multimulsion photography

08 p1282 A71-21436

Satellite remote sensing for crops and timber identification/detection, surface moisture measurements, soil mapping, marine hazard evaluation, etc

17 p2730 A71-34245

Remote sensing aerospace system for agriculture, considering soil mapping, forest fire reconnaissance,

productivity evaluation and environmental and ecological conditions assessment

21 p3373 A71-40263

SOIL MECHANICS

Aircraft pavements design and construction problems regarding adverse soil conditions

02 p0238 A71-12176

Apollo 12 lunar rock examination, discussing soil mechanics, mineralogical and petrological aspects and surface features and fines

05 p0806 A71-16148

Gas exchange between air or gas mixture flows and terrestrial soil in extraterrestrial microorganisms detection, using continuous sampling and gas chromatography

21 p3346 A71-40575

SOIL SCIENCE

Soil microorganisms multiplication under simulated Martian conditions in limonite and garden soil mixture

01 p0019 A71-11558

Earth and planetary surface soil dielectric constants and conductivity determination based on p-wave velocity data correlation

05 p0743 A71-17142

Airborne remote sensing application to agriculture and forestry for crop forecasting, soil mapping, insect infestation detection and range surveys

06 p0896 A71-18406

Soil and ground rock amino acids preparation and analysis by desalting method

08 p1251 A71-21891

Lunar soil particle production, noting radiation erosion effects

10 p1673 A71-24414

Lunar soil albedo, discussing radiation darkening, lunar rock particles size and mineral contents effects

11 p1835 A71-26460

Optimal mineral-organic nutrient medium and soil selection for microorganism detection on Mars

13 p2009 A71-28681

Color and color IR films for soil identification, performing optical density measurements on film transparencies with densitometer

13 p2071 A71-29394

Meteoritic material magnetic fraction determination by chemical analysis for spherules in soil surrounding meteorite craters at Henbury, Australia

15 p2488 A71-32351

Sikhote-Alin 1967 meteoritic expedition, discussing collected fragments and soil samples, crater and hole structures and mapped sites

17 p2809 A71-35715

Sikhote-Aline shower region soil samples and meteorite and micrometeorite fragment morphology, emphasizing silicate spherules

17 p2810 A71-35718

Aircraft and satellite remote sensing techniques in geology, soil science, geography and hydrology

18 p2913 A71-36539

Italian soil particles of cosmic origin, noting space research activities relation to micrometeorites and dust studies

20 p3298 A71-39644

Lunar soil samples 12001.1, 12037, 12042.25 and 12070.100 exterior morphology and chemistry, noting environmental temperature decrease, crater formation and meteorite impact

23 p3745 A71-43662

Martian surface materials determination by comparing albedo and brightness with spectral and photometric characteristics of crushed reddish volcanic rock and silicate sand mixed with limonite

23 p3770 A71-44052

Lunar topsoil density variations from Lunik and Surveyor radio wave, alpha and gamma scattering data, discussing Lunik 13 and Surveyor 7 landing sites

24 p3875 A71-45314

SOILS

NT CLAYS

NT LUNAR DUST

NT LUNAR SOIL

NT SANDS

Gravitational fields and atmospheric pressure effects on soils subjected to static and dynamic loading, using aircraft parabolic gravity simulation

[AIAA PAPER 69-1009]

01 p0068 A71-11581

Xerophyte soil microorganisms reproductive stability in artificial Mars environment chamber at maximum hygroscopic moisture

13 p2019 A71-28690

Biological instrumentation and soil sampler aboard Viking lander for 1975 mission to Mars

16 p2537 A71-33808

SOLAR ACTIVITY

NT FACULAE

NT SOLAR FLARES

NT SOLAR PROMINENCES

NT SOLAR STORMS

NT SPICULES

NT SUNSPOTS

Solar active regions lambda 10 830 line from photometric observations, determining optical thickness, Doppler width and radiation source activity

02 p0306 A71-12080

Solar activity long term variations in 11 year cycle maxima, noting preferred locations on disk [AIAA PAPER 70-1368] 02 p0315 A71-12695

Solar active regions, examining development and occurrence of solar flares 02 p0301 A71-12758

Wolf numbers monthly fluctuations, giving histogram of fluctuation amplitude distribution 03 p0484 A71-13211

E layer atmospheric densities from decaying satellites observation, discussing solar activity and geomagnetic correlations 03 p0414 A71-14022

North-south asymmetry in solar disk microwave bursts sources distribution 03 p0496 A71-14536

Solar protons energy spectrum upper cut-off based on worldwide neutron monitors recordings of 28 January 1967 solar event 06 p0950 A71-17998

Solar proton entry into geomagnetic field during 9 June 1968 event 06 p0958 A71-18153

Radial velocity distribution-magnetic fields connection in solar atmosphere active and quiet regions 06 p0975 A71-18437

F 2 layer nighttime ionization seasonal fluctuations, considering dependence on geographical longitude and latitude and solar activity levels 07 p1098 A71-19382

Fokker-Planck equation for convection dominated transport of solar cosmic rays solved for exponential decay phase of solar particle events 07 p1185 A71-19651

Solar disk active region gas development radial velocities on two levels /4 July 1966/, using double magnetograph 07 p1205 A71-20636

Primary cosmic ray variations energy spectra on rising and declining solar activity arm, analyzing stratospheric particle intensities 08 p1353 A71-20980

Solar active regions lambda 10 830 line from photometric observations, determining optical thickness, Doppler width and radiation source activity 08 p1361 A71-21130

Coronal magnetic field geometry maps, using high altitude photospheric field measurements for correlations with active sun 08 p1363 A71-21154

Quiet time galactic component of geomagnetic field variations excluding solar-terrestrial disturbances 08 p1363 A71-21199

Solar activity cycle model, considering dynamo equations with only radial rotation differentiability 08 p1365 A71-21774

Geomagnetic solar quiet day horizontal current and electrostatic potential field model in ionosphere, using dynamo equations 09 p1442 A71-23708

Discrete solar proton event three digit classification system, covering proton intensity, riometer absorption and neutron monitor increase 10 p1660 A71-23799

Generation mechanism of 27-day recurrent geomagnetic disturbances sudden commencements, analyzing interrelationship between recurrent disturbances, solar data and solar plasma physical parameter 10 p1607 A71-25119

Interplanetary magnetic field parameters for various heliocentric distances from 1959-1967 satellite observations, discussing cavity position and solar activity phase correlations 11 p1829 A71-25782

Yearly cosmic rays intensity variations in meridional plane from 1955-1969 ionization temperature coefficient recordings as function of solar activity levels 11 p1817 A71-25783

Radial velocity fields-magnetic fields relationship in solar atmosphere active and quiet regions 12 p1955 A71-26587

Eleven year solar activity cycles interrelationship, giving empirical expression for Wolf numbers in consecutive events 12 p1961 A71-26903

Cosmic radiation nucleonic component intensity diurnal variations relation to solar activity semiperiod 12 p1950 A71-27378

Velocity and magnetic field measurements in solar active regions, using fine scan simultaneous Doppler and magnetogram observations 12 p1968 A71-27646

Hot coronal components of solar active regions observations with satellite-borne grazing incidence X ray telescope, discussing emission dependency on photospheric magnetic field 12 p1954 A71-27707

Solar and geophysical morphology of radio burst of active sun, treating bremsstrahlung, gyro, synchrotron and Cerenkov radiation and plasma waves 13 p2137 A71-28514

Radio model of brightness temperature and electron density in transition layer of solar active regions, using

Laplace transformation and hydrostatic equilibrium equation 13 p2141 A71-29050

Solar sunspot activity cycles, correlating intensities with duration 13 p2142 A71-29119

Solar chromospheric activity of 8 February 1971, obtaining brightness temperature maps at 400, 800 and 1200 microns 13 p2143 A71-29271

Solar active regions velocity field at different levels, discussing transition region from photosphere to chromosphere 14 p2308 A71-29973

Solar active region photospheric radial velocity field time variations, using magnetograph in Fe I line 14 p2308 A71-29977

Solar atmospheric active regions, comparing longitudinal and transverse magnetic field strengths at various levels 14 p2308 A71-29981

Magnetometer network operation during IQSY, establishing Sq variations in polar regions on quiet days and nature of geomagnetic disturbances 15 p2396 A71-31607

Bibliographic references of articles on solar terrestrial research during IQSY, including geophysical phenomena, international projects and background material 15 p2397 A71-31617

Moving type 4 solar radio burst observation on 10 October 1969 with radioheliograph, noting circular polarization, movement direction, speed and structure 15 p2473 A71-31694

Scattering effects on decimeter wavelength quiet sun emissions flux densities, frequencies and brightness temperatures 15 p2485 A71-31716

Solar activity cycle model, considering magnetic dynamo equations with radial rotation differentiability 15 p2495 A71-32679

Chromosphere and solar quiet regions transition zone model, investigating radio and UV emission and height dependence of temperature and density 15 p2497 A71-32745

Solar wind outflow from active regions by numerical integration of hydrodynamics equations, using corona temperature distribution 15 p2480 A71-32753

Honda 1968 comet activity from photographic and visual brightness observations, establishing relation between brightness fluctuations and solar activity 17 p2803 A71-34831

Homologous solar microwave bursts from different active centers recorded with 7 GHz polarimeter 18 p2957 A71-35964

Geomagnetic diurnal variations near Sq current vortex focus, indicating existence of ionospheric diverging or converging currents 18 p2912 A71-36298

Doppler velocity field recording method over two dimensional solar active region image, using narrow band filter with video photographic subtraction technique 18 p2924 A71-36730

Solar activity and intensity ratios of O VII X-ray coronal emission lines, giving upper bound on electron density 18 p2965 A71-36734

Nonspherical axisymmetric model of minimum type solar corona, investigating light scattering electrons density distribution relation to brightness and polarizations 19 p3131 A71-37240

Coherent periodic compressional micropulsations of geomagnetic field intensity and energetic electron fluxes at synchronous altitude during quiet day 19 p3016 A71-37361

Quiet sun, active regions and flares far UV space observations interpretation based on models 19 p3136 A71-37615

Helium-like ion forbidden line emission and transition probabilities, deriving solar densities in active regions 19 p3136 A71-37621

F 2 layer nighttime ionization seasonal fluctuations, considering dependence on geographical longitude and latitude and solar activity levels 19 p3052 A71-37807

Quiet sun diurnal variations of intertropical F 2 ionization in true heights over Tamanrasset meridian 19 p3054 A71-37863

Atmospheric composition and temperature effects on F 1 region ion concentration structure from 140 to 220 km for low solar activity conditions 19 p3058 A71-38382

Forbush decreases comparison with 11 year cosmic ray intensity variation, examining rigidity dependence and modulation functions 20 p3277 A71-38742

Time variation of average values of magnetic field strength and size in solar polar regions, noting field element decrease before solar activity maximum 20 p3291 A71-39322

Harmonic residuum of solar quiet, considering mean deviation and correlation coefficients 20 p3217 A71-39514

Extrasolar influence on solar activity, considering north-south asymmetry of sunspots distribution and annual June/December sunspots incidence extremes 20 p3294 A71-39540

Semiannual upper atmosphere density variations near solar maximum from satellite drag data, relating height amplitude profile with exospheric temperatures 20 p3223 A71-39710

Solar activity tabulation and review covering International Geophysical Year and International Quiet Sun Year 21 p3442 A71-40151

Solar radioelectric activity in 1966, tabulating mean daily density and variability of solar flux 21 p3442 A71-40152

Absorption variation with solar activity and seasons, reexamining vertical incidence absorption measurements at 3.65 MHz /1958 and 1959/ at Walair 21 p3373 A71-40374

Related solar active regions during 14 January-1 June 1969, associating largest flares with inverted polarity 22 p3597 A71-41460

Interplanetary magnetic field parameters for various heliocentric distances from 1959-1967 satellite observations, discussing cavity position and solar activity phase correlations 22 p3598 A71-41550

OSO satellite observed soft solar X-ray data correlation to solar activity 23 p3721 A71-43840

Longitudinal dependence of solar quiet geomagnetic field horizontal component at equator, discussing discrepancy between theory and observation 23 p3673 A71-43986

Radiation protection of Soyuz-9 crew, using solar activity forecasts 24 p3800 A71-44531

SOLAR ACTIVITY EFFECTS

Solar activity cycles correlation with planets positions over ecliptic 01 p0149 A71-10053

Proton Flare Project 1969 observation of VLF radio wave propagation, detecting sudden phase anomaly events due to solar activity 01 p0144 A71-10288

Proton Flare Project 1969 observation of flares and subsequent ionospheric disturbances during retrospective interval 01 p0144 A71-10290

Power spectra and cross spectra of surface pressure variations in polar regions compared to solar emission, noting Antarctic-Arctic relationship 01 p0119 A71-10741

Cosmic ray nuclear component during solar activity minimum, using Cerenkov counters onboard Elektron satellites 01 p0146 A71-11371

Interplanetary magnetic sector structure near sunspot maximum 01 p0163 A71-11521

SD geomagnetic variations and electron jet spread over polar cap stream during solar cycle 02 p0243 A71-11763

Polar region semitransparent sporadic ionospheric layers nighttime temporal and cyclic ionization variations, determining solar activity effects and corpuscular stream densities by ionogram 02 p0243 A71-11767

Ionospheric electron content at mid to high latitudes from satellite and station data, discussing possible solar control 02 p0244 A71-11960

Ionospheric absorption at solar maximum and minimum, comparing riometer measurements with ray tracing calculations and electron density, collision frequency or temperature profiles 02 p0245 A71-11962

Annular solar eclipse effects on VLF transmissions phase delay 02 p0212 A71-11969

Ionospheric electron concentration enhancement at different heights during solar flare, using incoherent scatter radar technique 02 p0300 A71-12471

Worldwide geophysical observatories network for observing solar optical, radio, particle X rays and geomagnetic and ionospheric effects [AIAA PAPER 70-1354] 02 p0239 A71-12692

Comet brightness fluctuation phenomenon, discussing solar wind interaction with Platt particles in cometary atmosphere 02 p0303 A71-12867

Neutral upper atmosphere response to solar activity variations, discussing temperature, density and helium/oxygen composition 03 p0409 A71-13577

Solar flare particles effects on magnetospheric energetic particle population, discussing magnetic activity effects on trapped particles [AIAA PAPER 70-1357] 03 p0473 A71-13578

Solar radiation spectral distribution at 0-16 Å by photometers on Solrad 9, computing theoretical ratios with gray body assumption

03 p0479 A71-14044

Solar cosmic ray phenomena, noting ionospheric effects and physical processes near sun

03 p0480 A71-14067

Night airglow, discussing spectrum, latitudinal dependency, diurnal variation, time and space correlations and sunspot cycle and solar activity effects

03 p0417 A71-14071

Solar activity effects on day airglow atomic oxygen red line, calculating production rates for photodissociation, dissociative recombination and electron impact excitation

03 p0418 A71-14265

Solar radio centers and interplanetary sector structures in connection with recurrent geomagnetic storms

03 p0496 A71-14512

Lower ionosphere electron density changes with solar zenith angle during active sun year

04 p0583 A71-15213

Sunspot region birth and growth, noting arch filament systems with H alpha time lapse movies

05 p0801 A71-15935

Interplanetary magnetic field sectors correlated to solar coronal active centers and condensations in metric wavelengths from radio observations

05 p0802 A71-16015

SCL nomenclature denoting solar flare effect on long wave field intensity

05 p0804 A71-16033

Ionospheric electron content measurement from Faraday fading of Explorer 22 satellite transmissions during low and high solar activity

05 p0741 A71-16444

Solar prominence interaction, observing coronal rain and mound

05 p0809 A71-16474

D region exponential model application to high solar activity conditions, using absorption measurement data

05 p0742 A71-16813

Geomagnetic field anomalous variations due to solar eclipse of 22 September 1968

05 p0746 A71-17211

Solar stimulated X ray fluorescence by photoelectric ionization in upper atmosphere, discussing effects on X ray astronomy experiments

06 p0949 A71-17268

Galactic cosmic ray solar modulation in interplanetary medium, discussing spherically symmetric model

06 p0949 A71-17275

Models for solar wind modulation of galactic cosmic rays by anisotropic diffusion approximation

06 p0951 A71-18104

Force field model for galactic cosmic rays modulation by solar cycles, noting agreement with Fokker-Planck equation analytic and numerical solutions

06 p0952 A71-18110

Galactic cosmic ray proton and He spectrum measurements in 1968 compared to electron spectra, explaining solar modulation features by models incorporating energy loss effects

06 p0952 A71-18112

Primary cosmic ray solar modulation calculations using Trilling formula for response functions and upper limiting rigidity to diurnal variation

06 p0953 A71-18119

Solar activity correlation with cosmic ray intensity and solar wind properties, analyzing hysteresis diagrams for wind modulation characteristics dependence on heliolatitude

06 p0954 A71-18123

Quiet time fluxes and differential energy spectra of protons and alpha particles at 2-20 MeV measured by cosmic ray detectors on OGO-3

06 p0954 A71-18127

Low energy cosmic rays modulation and heliocentric gradient during solar minimum, comparing OGO 1 and 2 ion chamber measurements with other space and ground observations

06 p0954 A71-18128

Heavy cosmic ray nuclei intensity and energy spectra, investigating solar modulation effects

06 p0954 A71-18129

Galactic cosmic ray solar modulation with 20 year periodicity, suggesting nearby galactic magnetic field direction

06 p0955 A71-18130

Residual modulation from 1954-1964 solar cycle, considering 19th cycle hysteresis loop from cosmic ray balloon data

06 p0955 A71-18131

Sunspot heliographic latitude role in 11 year galactic cosmic ray modulation

06 p0955 A71-18133

Galactic cosmic ray modulation region dimensions calculated during various solar activity cycles

06 p0955 A71-18134

Solar modulation variation of secondary cosmic ray energy spectra, noting dependence on atmospheric depth and geomagnetic cut-off

06 p0955 A71-18135

Forbush decrease rigidity dependence relation to cosmic ray solar modulation, using neutron monitors counting rate variations at different vertical cut-off rigidities

06 p0956 A71-18136

Cosmic ray solar modulation anisotropy during 23 March 1966, 25 May 1967 and 26 January 1968 events in preForbush phase, evaluating multidirectional meson observations

06 p0956 A71-18138

High latitude neutron monitors during 15 November 1960 solar cosmic ray event, calculating asymptotic directions for protons with magnetospheric model

06 p0959 A71-18161

Cosmic ray equator position dependence on solar activity level, discussing shipborne neutron monitor observations during IGY and IQSY

06 p0959 A71-18162

Solar flare delayed relativistic electron appearance, comparing radio, optical and X ray data for particle intensities

06 p0961 A71-18171

Galactic cosmic rays solar modulation effects on fast neutron flux in atmosphere

06 p0962 A71-18182

Atmospheric fast neutron flux, discussing solar proton events and Forbush decreases effects

06 p0963 A71-18183

Solar activity sudden perturbations effect on earth pressure field and atmospheric circulation

06 p0924 A71-18265

Ionization rate experimental profiles during maximum solar activity compared with calculations, showing additional source of ionization in E region

06 p0895 A71-18272

Vertical electron density profile variations during ionospheric perturbations in years of solar activity maximum and minimum

06 p0895 A71-18277

Heliosphere boundary interactions with interstellar medium, considering galactic plasma shock front and boundary radius as function of solar activity level

[AIAA PAPER 71-33]

06 p0977 A71-18495

Ionospheric electron mean content 1964-1969 from density, ionization, slab thickness and solar flux diurnal and equinoctial peaks

07 p1097 A71-19025

Electron and ion temperature in ionosphere, discussing measurements, solar heating, F and E region, variability over solar cycle, etc

07 p1098 A71-19320

Galactic and solar cosmic rays diffusion as function of solar activity and interstellar medium properties, considering particle velocity and proton scattering transport

07 p1185 A71-19379

Twilight helium emission diurnal and seasonal variations relationship to geomagnetic activity and solar depression, using Abastumani observations

07 p1099 A71-19389

Nighttime ionospheric absorption frequency dependence during solar activity cycle

07 p1100 A71-19400

Equatorial zone daytime F 2 maximum height diurnal variation latitude change with decreasing solar activity from vertical sounding

07 p1100 A71-19401

Ionospheric characteristics recording concerning critical frequencies and minimum heights above Sverdrlovsk during solar eclipse of 22 September 1968

07 p1101 A71-19407

Seasonal variations in F 2 region, using critical frequencies during descending solar activity phase

07 p1102 A71-19672

Geomagnetic field quiet solar diurnal variations, examining dynamo theory in lower ionosphere at middle latitudes

07 p1104 A71-20045

Geomagnetic solar quiet field and terrestrial currents diurnal variations, discussing interrelations and vector polarization

07 p1104 A71-20047

Terrestrial electrical current distribution diagram based on solar quiet variation hodographs

07 p1104 A71-20048

Morning and evening H alpha hydrogen line in twilight glow, establishing connection with solar activity level

07 p1105 A71-20439

Cosmic ray modulation processes, spectrum variation and intensity restoration delay, discussing solar activity indices and wind models

08 p1351 A71-20965

Eleven year galactic cosmic ray amplitude variation, determining modulation by sunspot groups and latitude

08 p1352 A71-20972

Galactic cosmic ray density modulation by solar wind, assuming heliolongitudinal asymmetry

08 p1353 A71-20975

Irregularity levels changes in interplanetary magnetic field during solar activity cycle from cosmic ray neutron component measurement data obtained on azimuthal muon telescopes

08 p1353 A71-20976

Solar activity heliolatitudinal distribution effect on interplanetary space electromagnetic conditions governing galactic cosmic ray intensity

08 p1353 A71-20977

Cosmic ray intensity annual variations relationship to heliolatitudinal solar activity index HL, providing hysteresis curves for effective angular width parameter estimation

08 p1353 A71-20978

Solar activity cycles correlation with planets positions over eclipses

08 p1361 A71-21047

Galactic cosmic ray proton and He nuclei spectra measurements aboard Pioneer 8 spacecraft over large energy range, considering solar modulation parameters

08 p1355 A71-21628

Nighttime E layer behavior during geomagnetic storms in quiet sun years, investigating corpuscular flux effects

08 p1356 A71-21854

E layer near solar culmination relaxation, determining ion and electron concentration variations

08 p1286 A71-21855

Ionospheric radio wave absorption above polar aurorae during solar activity minimum, discussing diurnal and annual behavior

09 p1435 A71-22429

E region additional ionization source during solar activity maximum, analyzing ion production function and electron concentration

09 p1435 A71-22440

Interplanetary magnetic field intensity and geomagnetic activity level correlation with 27-day solar activity cycle based on Venera 4 and Mariner 5 data comparison

09 p1519 A71-22577

Low latitude atmospheric vertical density variations, comparing solar and geomagnetic activities effects

09 p1436 A71-22578

Solar activity effects on midlatitude upper atmosphere corpuscular radiation intensity studied by rocket sounding

09 p1513 A71-22580

Torsional pendulum behavior variations during solar eclipse of 7 March 1970

09 p1493 A71-22805

Midlatitude spread F, sunspot activity and geomagnetic activity variations related, discussing fast solar particles

09 p1437 A71-22938

Pc and Pi micropulsations, correlating magnetospheric cavity eigenmodes with sunspot activity

09 p1440 A71-23637

Twenty-seven day variation and cosmic ray intensity modulation relationship, examining 11 year variation from superposition of transient decreases

10 p1660 A71-23800

Cosmic particle gradient perpendicular to solar equator plane and semiannual cosmic ray variations, using worldwide neutron monitor network

10 p1660 A71-23839

Atmospheric Pb 210 / radium D / aerosols concentration relationship to solar activity from measurement with blue filter

10 p1599 A71-23859

Ionospheric propagation forecasting as function of solar and magnetic activity conditions for maximum usable communications frequencies, using F2 layer peak electron density

10 p1575 A71-23865

Negative sudden phase anomalies, related signal strength enhancements and short wave fadeouts, considering maximum flux density of solar X-ray flares

10 p1575 A71-23883

Solar cycle effects on diurnal variations of F 2 region critical frequency and maximum ionization height

10 p1600 A71-23884

Phase and frequency instabilities in electromagnetic wave propagation - NATO/AGARD Conference, Ankara, Turkey, October 1967

10 p1576 A71-24185

Ionospheric computer model, describing electron and ion densities in middle latitudes as function of latitude, longitude, altitude, season, time and solar activity

10 p1577 A71-24290

Solar particle effects on polar cap VLF radio propagation along polar and transpolar paths, considering short term phase effects

10 p1577 A71-24313

Eleven year cycle cosmic ray modulation mechanism, considering solar wind and interplanetary magnetic field parameters

10 p1662 A71-24472

Solar geomagnetic seasonal ionization control of upper ionosphere longitudinal composition variations from polar satellite observations

10 p1602 A71-24555

Solar and lunar modulation of geophysical parameters, atmospheric electricity and thunderstorms in complex space-meteorology scope

10 p1604 A71-24706

- Earth outer radiation belt electrons intensity, differential energy spectra and radial diffusion during maximum solar activity
10 p1663 A71-24783
- Solar cycle time variations in trapped radiation belt proton flux, deriving proton transport equation from Boltzmann equation
10 p1663 A71-24785
- Midlatitude D region considering electron concentration height distribution, ionization process and solar activity effects
10 p1606 A71-24916
- Midlatitude whistlers propagation paths during minimum solar activity for estimating magnetospheric electron density profile
10 p1580 A71-25135
- Solar wind distribution with respect to interplanetary magnetic field structure, interaction with planets and effect on earth magnetosphere
11 p1814 A71-25262
- Cosmic ray intensity diurnal data recorded during maximum and minimum solar activity periods, relating to 27 day and shorter variations
11 p1815 A71-25590
- Midlatitude ionosphere electron production rates during quiet solar activity, deriving seasonally varying electron density profiles
11 p1755 A71-25609
- International coordinated measurements of solar activity geophysical effects in upper atmosphere, discussing synchronized observations of Cosmos 261 satellite and ground based ionospheric station network
11 p1816 A71-25762
- International coordinated solar chromospheric flare effects on D region lower boundary and ionospheric propagation by Cosmos 261 satellite and ground based observatories
11 p1816 A71-25763
- Galactic cosmic rays solar modulation and intensity gradient in interplanetary space from satellite observation data
11 p1817 A71-25766
- Solar activity effects on atmospheric density variations from satellite observations, using random process isocorrelation charts
11 p1759 A71-25821
- Diurnal temperature variations in middle ionosphere by rocket probes, noting solar activity changes influence
11 p1759 A71-25823
- Solar wind effects on space around earth, discussing dipole image of magnetic field, radiation belt feeding and atmospheric phenomena based on artificial satellite observations
11 p1817 A71-26337
- Neutral H concentration in upper atmosphere during solar minimum, using ion thermal energies from rocket and satellite mass spectrometric, radio and proton whistler measurements
12 p1898 A71-26637
- Solar activity and geomagnetic disturbance effects on upper atmosphere density from ATS 2 satellite orbit observations
12 p1899 A71-26886
- Interference pattern of ground and sky waves at 16 kHz during summer near solar maximum
12 p1880 A71-27155
- Diurnal solar variation of cosmic radiation observed by two Argentine meson telescopes
12 p1950 A71-27379
- Type 3 radio bursts at hectometric wavelengths from 13 to 25 August 1968, noting effect of large active sunspot groups
12 p1969 A71-27652
- Sunrise behavior of midlatitude topside ionosphere from low sunspot numbers from Alouette 1 electron density and plasma scale height profiles
13 p2055 A71-27920
- Two dimensional atmospheric model including oxygen and nitrogen photodissociation, recombination and photoionization, investigating solar activity and ionizing radiation effects on temperature stratification
13 p2057 A71-28018
- Geomagnetic field anomalous variations due to solar eclipse of 22 September 1968
13 p2060 A71-28266
- Cosmic ray density distribution inside modulating spherical cone over long-lived solar wind regions, noting modulation depth quasi-periodic variation
13 p2129 A71-28550
- Cosmic ray energetic spectrum variation from observed latitudinal effects during 1954-1962 solar activity cycle
13 p2129 A71-28551
- F 2 layer critical frequency variations relation to solar radio flux intensity, using mathematical approximations
13 p2062 A71-28557
- Daily Ap activity response of magnetosphere to sunspots, using 38 year geomagnetic storminess levels
13 p2062 A71-28785
- Cosmic rays galactic component intensity observed on earth correlated with solar phenomena
13 p2130 A71-29061
- Solar flares effect on potential gradient and air-earth current characteristics, suggesting solar triggered increase in thunderstorm frequency
13 p2130 A71-29107
- Galactic cosmic ray intensity solar diurnal and semidiurnal variations outside magnetosphere
13 p2131 A71-29437
- Midlatitude daytime ionospheric electron density profile during low solar activity based on rocket sounding data
14 p2228 A71-29535
- Noctilucent cloud incidences relation to solar activity variations, determining frequency spectrum and four year occurrence cycles
14 p2233 A71-29967
- Faraday rotation of Transit 4A satellite signals recorded at three stations within Southeast Asian equatorial zone, showing latitudinal variation of ionospheric electron content at sunspot minimum
14 p2235 A71-30249
- Nitrogen molecular excitation by photoelectron impacts in dayglow, investigating 1 PG band emission intensity variation with solar activity
14 p2235 A71-30349
- Atmospheric neutron data at various altitudes, relating densities, fluxes and spectra to solar activity
14 p2301 A71-30589
- Cosmic ray modulation by solar wind, developing model with time variations based on magnetic bending power
14 p2302 A71-30647
- VLF signal propagation during low and high solar activity, discussing equipment precision, diurnal and seasonal phase variations and phase anomalies correlation
14 p2204 A71-30973
- F 2 layer peak electron density diurnal and seasonal variations, noting geomagnetic latitude and solar activity effects
15 p2394 A71-31427
- VLF radio signals phase anomalies due to solar X-ray flares, monitoring by detectors onboard OSO-4 satellite
15 p2369 A71-31434
- Long thin spacecraft antennas and gravity gradient booms, explaining solar induced oscillations with lumped parameter and Lagrangian equation models
15 p2504 A71-31598
- Ionospheric absorption of 20 MHz radio waves as function of solar activity level, using electron density and temperature profiles
15 p2401 A71-32686
- Cosmic ray modulation by angle dependent solar wind, detailing adiabatic deceleration and radial anisotropy effects
15 p2481 A71-32777
- Upper atmosphere density fluctuations associated with solar activity and local time values, using Cosmos 14 satellite drag data
16 p2564 A71-33666
- Ionospheric geocoronal L sub alpha emission intensity related to solar activity level from Cosmos 215 satellite data
16 p2564 A71-33667
- Background phonon X ray and gamma quanta intensities dependence on solar activity from Geiger counter recordings in outer space
16 p2626 A71-33675
- F 2 and E layers peak electron densities semiannual variations, suggesting association with solar activity and charged particles penetration
16 p2568 A71-33785
- Midlatitude E region electron density profile data for various solar activity levels, investigating formation theory and atmospheric models
16 p2570 A71-33822
- Upper atmospheric neutral composition diurnal variations as function of altitude, local time and solar activity
16 p2570 A71-33829
- Lower thermosphere atomic nitrogen concentration during maximum solar activity, using rocket-borne radio frequency and time of flight mass spectrometers
16 p2572 A71-33843
- COSPAR international reference atmosphere containing seasonal variations, solar flux and altitude models for density, temperature, pressure and wind
16 p2572 A71-33851
- Solar modulation origin of sidereal diurnal variation in cosmic ray intensity anisotropies as function of interplanetary field direction, using underground muon telescopes
16 p2628 A71-33931
- Energetic solar protons asymmetric access to north south polar caps by satellite observation during 24 January 1969 event
16 p2628 A71-33935
- Solar particle flux profile and low latitude cut-off observation by low altitude satellite during March 1969 to July 1970 events
16 p2628 A71-33936
- Solar Lyman alpha emission line monitoring by OSO 5 satellite during 1969, noting solar activity effects
16 p2643 A71-33938
- Lunar surface anomalous brightness during 26 March 1970 photometric and polarimetric observations, discussing possible correlation to solar activity
17 p2797 A71-34183
- Harmonic analysis of F 2 region critical frequency in antarctic region, emphasizing solar activity effects
17 p2731 A71-34317
- Solar wind modulation effects on galactic protons and cosmic rays, using radial magnetic field mathematical model and Monte Carlo method
17 p2795 A71-34373
- Bibliography and review of solar activity relevant to sun-planet relationships, considering magnetic fields, transient events, corona and solar wind
17 p2799 A71-34459
- Sq day to day variability relation to interplanetary plasma parameters including magnetic field and solar wind velocity and kinetic energy
17 p2801 A71-34625
- Geomagnetic micropulsation data, emphasizing behavior during 11 year solar cycle
17 p2732 A71-34671
- HF radio absorption in antarctic night ionosphere, discussing solar activity effects
17 p2733 A71-34776
- Statistical analysis of polar auroras visual observation, discussing solar activity effects
17 p2733 A71-34836
- Solar corona formation relation to geomagnetic storm generation
17 p2734 A71-35191
- Stratospheric pressure surfaces height over polar, middle and tropical latitudes as function of long term solar activity
18 p2944 A71-36220
- Statistical determination of solar radio emission S-component average flux spectrum during solar cycle peak phase
18 p2966 A71-36739
- Galactic and solar cosmic rays diffusion coefficient as function of solar activity and interstellar medium properties, considering particle velocity and proton scattering transport
19 p3127 A71-37804
- Twilight helium emission diurnal and seasonal variations relationship to geomagnetic activity and solar depression, using Abastumani observations
19 p3053 A71-37814
- Nighttime ionospheric absorption frequency dependence during solar activity cycle
19 p3053 A71-37824
- Equatorial zone daytime F 2 maximum height diurnal variation latitude change with decreasing solar activity from vertical sounding
19 p3053 A71-37825
- Ionospheric characteristics recording concerning critical frequencies and minimum heights above Sverdlensk during solar eclipse of 22 September 1968
19 p3053 A71-37831
- Nighttime sporadic E layer behavior near magnetic equator, discussing occurrence frequency, seasonal variation and solar activity effects
19 p3055 A71-38037
- Solar activity effects on equatorial ionospheric absorption of radio waves, deriving solar cycle constant
19 p3055 A71-38042
- Solar effects contradictory relationships with earth atmosphere, discussing geomagnetic disturbance, annual variations, stratospheric transport and high energy particles
19 p3128 A71-38354
- Ionospheric neutral composition variations as function of height, local time and solar activity
19 p3056 A71-38356
- Latitudinal distribution of electron temperature in F 2 layer during summer daytime period of low solar activity from electron density profile geometrical parameters
19 p3057 A71-38369
- Arctic polar region geomagnetic perturbations during IQSY, noting diurnal variations
19 p3059 A71-38399
- Chromospheric flares effect on sporadic E layer under low solar activity conditions
19 p3130 A71-38527
- Geomagnetic storms association with atmospheric pressure trough development during sporadic solar activity
20 p3214 A71-38729
- Martian lower ionospheric models during solar proton event, determining electron density profiles
20 p3286 A71-38741
- Midlatitude solar quiet geomagnetic field dynamics morphology, emphasizing regular diurnal and annual changes and irregular fluctuations
20 p3217 A71-39510
- Emf dynamo nonuniformities effect on magnetospheric field aligned electric currents associated with solar quiet geomagnetic variations, calculating ionospheric electrostatic fields
20 p3217 A71-39516
- Continuous solar UV and X rays monitoring by SOLRAD 10 satellite, investigating solar activity and flares effect on shortwave communications and manned space travel
20 p3294 A71-39580

Neutral upper atmosphere observations, discussing lower thermospheric density and composition diurnal, seasonal and latitudinal variations and solar activity effects

20 p3220 A71-39690

Neutral-ionized parts interactions in upper atmosphere, discussing ionospheric plasma modulation, solar control and seasonal anomalies in lower ionosphere and ionic reactions

20 p3223 A71-39712

Ionospheric effective recombination coefficient and reaction rate models for various solar activity periods and day and night conditions

20 p3224 A71-39714

Mid- and high-latitude ionospheric radio wave transmission from spacecraft during solar cycle, considering latitudinal and longitudinal gradients and electron content change rate

20 p3197 A71-39715

Day and night E and F region ion composition under solar maximum winter conditions from rocket measurements with RF mass spectrometers

20 p3280 A71-39719

Low energy solar particle observation by widely separated Mariner and Explorer spacecraft, noting flare-associated and nonflare intensity peak corotation with sun

20 p3284 A71-39876

Solar cycle effects on E region peak electron density, correlating sunspot number by regression analysis

21 p3372 A71-40036

Planetary luminosity correlated with solar activity, discussing far UV and solar wind particle interactions with atmosphere

22 p3591 A71-41472

International coordinated measurements of solar activity geophysical effects in upper atmosphere, discussing synchronized observations of Cosmos 261 satellite and ground based ionospheric station network

22 p3591 A71-41530

International coordinated measurements of solar chromospheric flare effects on D region lower boundary and ionospheric propagation by Cosmos 261 satellite and ground based observatories

22 p3591 A71-41531

Galactic cosmic rays solar modulation and particle intensity gradient in interplanetary space from satellite observation data

22 p3591 A71-41534

Yearly cosmic rays intensity variations in meridional plane from 1955-1969 ionization temperature coefficient recordings as function of solar activity levels

22 p3591 A71-41551

Sporadic E layer initial height seasonal variations at mean geographic latitudes, considering solar zenith angle and activity effects

22 p3533 A71-41646

Solar cycle variation effects on interstellar hydrogen within solar system, discussing thermal motion, density, far UV ionization and charge transfer reactions

22 p3601 A71-42169

Periodic variations in amount of dark material present in Jupiter atmospheric belts, noting uncorrelation with solar activity

22 p3603 A71-42182

Ionospheric responses to solar flares, correlating sudden frequency deviations with sudden total electron content enhancement

22 p3592 A71-42222

Solar modulation of relativistic cosmic ray particles, noting step-like changes and rigidity dependence

23 p3719 A71-42948

Subequatorial ionospheric upward moving irregularities during high sunspot activity, explaining phenomenon at F2 region level by Hall drift from daytime west-east electric field

23 p3665 A71-42971

Cosmic ray solar diurnal variation anomaly at 1954 minimum, discussing diffusion and scattering in interplanetary medium

23 p3720 A71-43136

Solar flare induced E and F regions electron density enhancement observation by Thomson scatter, noting relationship to EUV ionizing radiation

23 p3721 A71-43173

Nuclear track densities in lunar core and fine samples, relating erosion history, solar activity and surface stirring

23 p3764 A71-43799

Planetary tidal forces correlation with solar activity distribution, observing Ca flocculi spectrum

23 p3768 A71-43851

Spread F observing irregularities at Nairobi, investigating nocturnal and seasonal variations and magnetic and solar activity effects

23 p3672 A71-43971

Atmospheric wind velocity time variations at 80-100 km altitudes from ionospheric drift data, finding planetary oscillation periodicities relationship to solar activity cycle

24 p3822 A71-44349

Solar unipolar magnetic regions relation to geomagnetic disturbances variability, discussing 11 year cycle

24 p3823 A71-45036

Hysteresis effect at solar cycle maximum for midlatitude E layer electron density response to solar activity

24 p3824 A71-45125

Solar activity effects on biosphere, examining solar-geomagnetic and medico-biological indexes relationships and clinico-statistical evidence of human organism effects

24 p3799 A71-45197

SOLAR ATMOSPHERE

Solar photospheric spectrum, investigating deuterium abundance relative to hydrogen

01 p0157 A71-10762

Solar granules velocity profiles, establishing horizontal outflow and vertical upflow from filtergrams at 6569.2 Å absorption

02 p0316 A71-12754

Solar line blanketing effect data derivation and analysis for model atmosphere computer programs, considering application to spectrally similar stars

02 p0316 A71-12755

Spicule horizontal component motion from H alpha spectra movies with slit tangential to solar limb

02 p0316 A71-12756

Solar chromosphere model, investigating radiative transfer effect on temperature structure of plane slab heated by thermal conduction

03 p0483 A71-13186

Sunspots initial appearance east-west asymmetry interpretation by conical atmospheric model, including foreshortening and absorption effects

03 p0483 A71-13188

Eclipse photon counting for solar atmosphere height determination, describing spectrograph-photomultiplier apparatus

03 p0424 A71-13632

Solar atmosphere semiempirical models taking into account non-LTE conditions

04 p0651 A71-15667

Solar chromosphere structure and Lyman continuum, examining brightness and kinetic temperatures, limb variations, radiative transfer and models

05 p0803 A71-16023

Solar chromosphere mass motion, studying macroturbulence influences on visible spectrum lines high resolution profiles from rocket spectrograms

06 p0967 A71-17904

Solar photosphere oscillations, suggesting convection zone acting as resonant cavity

06 p0971 A71-18243

Radial velocity distribution-magnetic fields connection in solar atmosphere active and quiet regions

06 p0975 A71-18437

Solar photosphere macroturbulence effects on Fraunhofer lines and central intensities of various absorption lines

06 p0975 A71-18443

Heliosphere boundary interactions with interstellar medium, considering galactic plasma shock front and boundary radius as function of solar activity level [AIAA PAPER 71-33]

06 p0977 A71-18495

Atmospheric noise effect on solar granulation photographic observation based on cross correlation between identical measurements

07 p1200 A71-20037

Solar photosphere faculae, applying Schuster-Schwarzschild model for molecular lines and bedding level of carbon hydride

08 p1365 A71-21772

Solar photosphere turbulent velocity, taking into account instrumental profile effects

09 p1524 A71-23193

Solar granular or convective motion velocities vs photospheric oscillations for Doppler shifts in line spectra

10 p1665 A71-23776

Empirical solar photosphere continuum models, calculating temperature distribution for absolute intensities at center and limb darkening ratios

10 p1666 A71-23779

Solar lower chromosphere two dimensional models, using relative RMS line center intensity variations and mean limb darkening curves

10 p1666 A71-23781

Solar chromospheric emission line identification at 4097.3 Å, discussing N III transition

10 p1666 A71-23783

Sunspot group magnetic field distribution and radial velocities, investigated at H alpha and 6302.499 Å atmospheric levels

10 p1666 A71-23788

Radial velocity fields-magnetic fields relationship in solar atmosphere active and quiet regions

12 p1955 A71-26587

Solar photosphere macroturbulence effects on Fraunhofer lines and central intensities of various absorption lines

12 p1955 A71-26593

Active unperturbed solar photosphere, determining variations in spectral line profiles

12 p1963 A71-27082

Solar plasma emission capacity, using atmospheric ionization theory

12 p1964 A71-27084

Downward moving large scale surface velocity fields of solar atmosphere from magnetograph data

12 p1968 A71-27645

Hydrodynamic wave modes calculation for solar atmospheric model with ionization effects, noting trapped resonant gravity waves calculation agreement with observed oscillations

12 p1969 A71-27647

Photospheric layers supergranular motion and oscillations as function of solar atmosphere height and sun position, investigating velocity fields two dimensional structure

12 p1970 A71-27701

Atmospheric altitude of soft X ray source volume in solar flares from optical and radio observations

12 p1954 A71-27709

Solar chromosphere model, explaining spicule origin and relation to small scale nonuniformities

13 p2136 A71-28430

Solar atmosphere center limb observations, describing line intensity fluctuations in Na D and Na 5888 doublets and Mg 4571 line

13 p2140 A71-29044

Shock wave heated atmospheric model computation for solar chromosphere and corona

14 p2306 A71-29684

Solar atmosphere line broadening by neutral hydrogen, noting discrepancy in van der Waals interaction

14 p2306 A71-29686

Solar atmospheric active regions, comparing longitudinal and transverse magnetic field strengths at various levels

14 p2308 A71-29981

Solar photosphere and faculae temperature, gas/electron pressures, density and turbulence velocity from Schuster-Schwarzschild model

15 p2495 A71-32677

Solar atmosphere vertical temperature and density distribution measurements, using spatially averaged H and K resonance line profiles central reversals

15 p2496 A71-32742

Solar atmosphere structure inhomogeneities, describing Ca II H and K line spectra profiles

15 p2497 A71-32743

Solar atmospheric model, calculating shock wave dissipation in chromosphere for photosphere central iron line intensity correlation with magnetic field intensity

15 p2497 A71-32746

Excess red shift of Fraunhofer lines at extreme limb explained by mechanism of radial currents in solar atmosphere

16 p2629 A71-32807

Solar atmosphere mean radial velocity relation to low excitation potential based on Fraunhofer lines blue shifts observations

17 p2808 A71-35576

Solar photospheric velocity field measurements, using balloon-borne sodium resonance cell with diffraction limited telescope

18 p2965 A71-36729

UV studies of solar atmosphere in quiet and active regions, considering low and high chromosphere, transition zone, quiet corona and inhomogeneity

18 p2968 A71-37034

Active unperturbed solar photosphere, determining variations in spectral line profiles

19 p1313 A71-37432

Solar plasma emission capacity, using atmospheric ionization theory

19 p1313 A71-37434

Solar photosphere and low chromosphere models temperature-height profile

19 p1315 A71-37609

Solar photosphere iron abundance data from Fraunhofer spectrum and EUV line measurements

19 p1315 A71-37610

Nonlinear coupling between thermal conduction and radiative transfer in solar chromosphere by iterative method

19 p1343 A71-38159

Harvard-Smithsonian reference atmosphere model of solar atmosphere, combining photosphere and quiet lower chromosphere

19 p1346 A71-38660

Bright-dark asymmetry testing in solar granulation photography by objective method

19 p1346 A71-38663

Short periodical pulsations in solar atmosphere related to magnetosound propagation in area of temperature minimum with directed perpendicular magnetic field

20 p3290 A71-39305

SiH molecular ion identification in solar atmosphere by solar absorption spectra

20 p3294 A71-39547

Solar silicon line spectra of photosphere, chromosphere and corona, including ionic spectra over wide ionization potentials range

20 p3301 A71-39822

Solar atmosphere oscillatory component observations at 3 mm wavelengths with two radio telescopes, obtaining power spectra

21 p3447 A71-40424

Solar atmosphere closed magnetic loop system model, determining surface differential rotation rate and angular velocity distribution 22 p3596 A71-41452

Photometric determination of solar granulation rms intensity fluctuation, using ground telescope 22 p3596 A71-41453

Morphological relationships in solar chromospheric H alpha fine structure involving bushes, fibrils, threads and filaments 22 p3597 A71-41457

Solar transition layer and inner corona empirical minimum equator model, using radio, UV, white and monochromatic radiation data 22 p3601 A71-42161

Acoustic wave propagation and heating in solar atmosphere, using Harvard Smithsonian reference atmosphere and Stein frequency spectra 22 p3601 A71-42170

Power spectrum analysis of solar granular intensity fluctuations and velocities, noting asymmetry behavior of Ba II line in individual convection cells 23 p3767 A71-43834

Mg isotopes in solar atmosphere, analyzing absorption bands in sunspot spectrum 23 p3767 A71-43837

Solar atmosphere electron densities from ion emission line intensities in Be isoelectronic sequence 23 p3721 A71-43839

Radiation attenuation effect on solar photosphere turbulence determination by Goldberg-Unno method 23 p3772 A71-44311

Electric conductivity correlation between solar faculae and Bilderberg model of photosphere and chromosphere 24 p3868 A71-44458

Scattered light effect on measured facula-to-photosphere contrast, leading to hotter average facula model 24 p3868 A71-44460

Search for CH molecular ion lines in solar photospheric spectrum, discussing profiles and equivalent widths 24 p3873 A71-45144

SOLAR AUXILIARY POWER UNITS

Electric power system for satellites, considering energy conversion, storage and processing from chemical, solar and nuclear sources 17 p2676 A71-34227

SOLAR AZIMUTH

U AZIMUTH

SOLAR POSITION

SOLAR CELLS

Solar cell array for high radiation intensity application in Helios solar probe 02 p0191 A71-12068

Optical fibers scattering loss measurement, describing Si solar cell integrating cube scattering detector 03 p0424 A71-13638

Silicon and gallium arsenide photovoltaic solar cells, examining performance at high illumination intensities 04 p0535 A71-15006

Solar cells - IEEE Conference, Seattle, August 1970 05 p0697 A71-16053

CdS solar cells thermal stability and performance, discussing satellite applications 05 p0699 A71-16056

Copper sulfide-cadmium disulfide thin film solar cells degradation under simulated orbital conditions, determining electrochemically induced copper filament growth as electric shorts causes 05 p0699 A71-16057

Integrated high voltage CdS solar batteries with interconnected cells in series without grid 05 p0699 A71-16058

CdTe thin film solar cell characterization, showing low carrier concentration of base layer and improved stability at elevated temperatures 05 p0699 A71-16059

Ti-Ag and Ti-Pd-Ag solar cell contacts structure and degradation dependence on high temperature and humidity environmental exposure 05 p0699 A71-16060

Solderless Ag-Ti solar cell contacts humidity degradation mechanism 05 p0699 A71-16061

Electroformed Al contact solar cells without soldering, investigating process parameters effects on performance 05 p0699 A71-16062

N-p Si solar cells controlled lifetime doping effects on electrical performance 05 p0700 A71-16063

Si solar cells with titanium oxide antireflection coatings, discussing environmental test results 05 p0700 A71-16064

Si solar cells with antireflection titanium dioxide layer, comparing performance with conventional adhesive cover system 05 p0700 A71-16065

Hydrogen impregnated glass covers of solar cells preventing irradiation caused darkening and loss of power output under space environment conditions 05 p0700 A71-16066

Temperature effects on Si solar cell short circuit currents, considering solar spectrum, photon absorption coefficient and diffusion length 05 p0700 A71-16067

Solar cells lumped series resistance determination, comparing dark forward characteristics method and two light level approach 05 p0000 A71-16068

Ti-Ag contact N-P and P-N single crystal Si solar cells electrical and mechanical performance characteristics 05 p0700 A71-16069

Si solar cells with and without cover slides performance in severe thermal and light environment /near sun missions/ 05 p0701 A71-16070

Si solar cells low temperature and solar intensity performance optimization by identifying and eliminating low output problems 05 p0701 A71-16071

Si solar cells spectral responses at low temperatures 05 p0701 A71-16072

Si solar cell low temperature low solar illumination intensity I-V performance deficiencies, considering corrective design modifications 05 p0701 A71-16073

Solar cells for Jupiter mission, discussing radiation and environmental tests concerning I-V characteristics 05 p0701 A71-16074

Si solar cells I-V characteristics measurement at low temperature 05 p0701 A71-16075

Si solar cells under low temperature electron irradiation, noting damage rate dependence on measurement temperature 05 p0701 A71-16076

Si solar cell performance improvement from use of achromatic antireflective coatings 05 p0701 A71-16077

Low stress integral coverslips deposition by high vacuum ion beam sputtering for solar cell manufacturing cost reduction 05 p0702 A71-16078

Si solar cell cover glass assembly and packaging improvements using Teflon 05 p0702 A71-16079

Helios solar probe satellite solar array techniques for high temperature and illumination intensity 05 p0702 A71-16080

CdS solar cells performance under simulated synchronous orbit conditions, describing test equipment 05 p0702 A71-16081

Si solar cells electrical performance tests, considering 1 MeV electron irradiation effect on efficiency 05 p0702 A71-16082

Si solar cells electron spectrum irradiation, simulating space environment synchronous altitude trapped electrons omnidirectional and flux/energy characteristics 05 p0702 A71-16083

N-p Si solar cells, investigating mechanism of low energy proton irradiation damage to back contacts 05 p0702 A71-16084

LES 6 synchronous orbit solar cells experiments, determining various type cells degradation due to low energy proton damage 05 p0702 A71-16085

Solar cell and coverslide degradations measurement from telemetry data on satellites at near-synchronous altitudes 05 p0702 A71-16086

Si solar cell radiation resistance improvement through Li doping, noting efficiencies in excess of state-of-art N/P cells after exposure to 1 MeV electrons 05 p0703 A71-16088

Lithium concentration and defects in doped radiation resistant silicon solar cells during electron irradiation 05 p0703 A71-16089

Lithium-containing p-n solar cells photovoltaic performance and stability tests at room temperature 05 p0703 A71-16090

Defects and annealing in electron irradiated lithium diffused silicon solar cells 05 p0703 A71-16092

Silicon solar cell lightweight integrated array for large arrays, discussing deployment and orientation mechanisms, ribbon coverglass technique and cost estimates 05 p0703 A71-16093

High voltage solar cell array operation for satellite in ionosphere, discussing plasma leakage current minimization by electrical insulation 05 p0703 A71-16094

Solar cell module joints welding technology development under ESRO sponsorship, emphasizing resistance welding and process optimization 05 p0704 A71-16095

Solar cell array for probe mission, using optimized high temperature low resistance modules combined with mirrors of high thermal emissivity 05 p0704 A71-16096

Solar cell array fabrication for operation at 173-383 K, discussing honeycomb sandwich substrate using epoxy-novolac-fiberglass facings and Al core 05 p0756 A71-16097

Pulsed xenon solar simulator system for testing single and group cells and panels for flight spacecraft programs 05 p0733 A71-16098

Si solar cells lightweight economical deployable arrays, discussing temperature performance, assembly, coverslips, interconnection, stowage and telescopic mast and ends 05 p0704 A71-16099

Electrical power generation from sunlight without pollution, using solar cell elevated rug technology 05 p0704 A71-16100

Solar cell R and D in France, emphasizing thin film improvement 05 p0704 A71-16101

Si solar cells with high electrical output in space sunlight, discussing device limitations 05 p0704 A71-16102

Si solar cell technology, discussing contacts, low temperature performance and conversion efficiency 05 p0757 A71-16103

Power loss processes in Si solar cells, noting improvement in collection, voltage and curve factors 05 p0704 A71-16104

Li doped Si solar cells recovery after irradiation, examining temperature dependence 05 p0704 A71-16105

Si solar cell test for electrical discharge effect on series resistance, curve power factor, conversion efficiency and spectral response 05 p0705 A71-16169

Solar cells characteristics for space power systems, considering angle of incident sunlight, radiation damage, array design and mounting 05 p0705 A71-17151

Low energy proton irradiation damage to ATS and Intelsat satellites Si solar cells junction properties 07 p1022 A71-19072

Si solar cells transparent radiation protective coatings stability and degree of blackness, discussing UV irradiation and proton and electron bombardment 08 p1287 A71-21024

Optimum mounting angles for direct solar radiation flux on solar battery on circular orbit satellite 09 p1386 A71-22673

Balloon flight instrumentation for solar cell I-V measurements, using semiconductor selection circuits and RF telemetry 09 p1446 A71-22734

SERT 2 solar array power system in sun synchronous orbit, considering power conditioning and deployment technique 09 p1387 A71-22901

Satellite power supply systems, discussing solar cell generators with emphasis on reliability 10 p1683 A71-24641

I-V characteristics and electrical properties of n-p silicon solar cells at low temperature and low illumination intensities 12 p1869 A71-27434

Solar arrays for satellite electrical power supply, discussing mathematical model for reliability calculation 13 p2002 A71-29273

Energy conversion efficiency improvement of silicon solar cells, noting power loss effects 14 p2181 A71-29702

GaAs solar cells photoelectric energy characteristics as function of light flux, comparing with Si cells 14 p2181 A71-29952

Low cost solar array unfolded by centrifugal spinning force, considering application to spin and 3-axis stabilized spacecraft 16 p2526 A71-32852

Silicon solar cells radiation damage from low energy protons, discussing current degradation as function of exposed area and particle energy 16 p2621 A71-33414

Curve power factors and radiation induced changes in silicon photovoltaic solar cells, considering junction depth, bulk resistivity, temperature and illuminating light intensity 17 p2677 A71-35049

Carrier diffusion length change in damaged gamma irradiated silicon solar cells by numerical analysis, using experimentally obtained voltage or current 17 p2677 A71-35050

Telecommunication satellites photoelectric power systems, discussing solar generators with silicon cells 18 p2851 A71-36572

Thickness monitoring technique for thin films, using silicon solar cell mounted adjacent to substrate with iron deposition 18 p2922 A71-36591

Radiation hardening of silicon solar cells, analyzing performance in low temperature environments 18 p2852 A71-36963

Copper sulfide-cadmium sulfide photovoltaic solar cell electronic processes observation at heterojunctions 18 p2852 A71-36963

- tion, noting electron trapping and hole injection roles in long term stability
19 p3119 A71-38140
- Oxygen contamination effect on GaP solar cell electroluminescence and photoluminescence characteristics from electrical and mass spectroscopic analysis data
19 p2998 A71-38143
- European research, development and production of solar cells, discussing Intelsat 4 program applications
20 p3179 A71-38851
- Lightweight solar cell structural failure modes under automatic thermal cycling for prolonged period in wide temperature range and by immersion in liquid nitrogen
20 p3179 A71-38852
- Critical solar cell battery power system design parameters and performance characteristics affecting post 1977 satellites and manned vehicles design
20 p3179 A71-38902
- Solar array technology for lunar surface applications including silicon cells, cadmium sulphide thin films, temperature effects, prototype module and radiation degradation
20 p3181 A71-38941
- Power conditioning electronics for integrally regulated and controlled high voltage solar array spacecraft power system, increasing reliability and reducing weight
20 p3181 A71-38942
- Reliable and low cost electrical solar array/silver zinc battery power system for Agena satellite, discussing design features and flight test results
20 p3182 A71-38943
- Fluorinated ethylene propylene covers for silicon solar cells, describing processing parameters effects on optical and electrical characteristics
20 p3182 A71-38944
- Hot spots and voltage breakdowns due to open or shadowed solar cells, studying effect in orbital workshop array
20 p3182 A71-38945
- Copper sulfide-cadmium sulfide thin film solar cells under simulated orbital conditions, including thermal cycling, constant illumination and temperature effects
20 p3182 A71-38946
- Recoverable usable energy maximization from solar oriented spacecraft electrical power system, using silicon cell array and nickel cadmium batteries
20 p3182 A71-38956
- GaAs solar batteries for spacecraft power supplies, comparing effectiveness with Si cells for optimum utilization
20 p3183 A71-39133
- Surface cover materials thermal radiation characteristics and radiation resistance of plastics and solar cells, discussing friction in vacuum and spacecraft surface contamination by outgassing
20 p3210 A71-39453
- Si solar cells transparent radiation protective coatings stability and degree of blackness, discussing UV irradiation and proton and electron bombardment
20 p3240 A71-39604
- Solar to electric energy conversion efficiency and electrical properties of photoconverters using compressed sintered CdS
24 p3808 A71-44390
- SOLAR CHROMOSPHERE**
U CHROMOSPHERE
U SOLAR ATMOSPHERE
SOLAR COLLECTORS
NT SOLAR REFLECTORS
SOLAR COMPASSES
Lunar surface vehicle navigation system, describing dead reckoning and sun aspect compass for initial gyro alignment
01 p0124 A71-10514
- SOLAR CONSTANT**
Solar constant and zero air mass spectrum, discussing new standard values
01 p0159 A71-10861
- Solar constant and spectral energy distribution standard values by high altitude aircraft, balloon and spacecraft measurements
07 p1199 A71-20005
- Solar constant value and spectral distribution of solar radiation outside atmosphere
13 p2056 A71-28013
- Active cavity radiometric and international pyrheliometric scales comparison and solar constant from simultaneous solar irradiance measurements
16 p2581 A71-33939
- U.S.S.R. and U.S. balloon measurements of direct solar radiation integral fluxes, deriving solar constant values
20 p3260 A71-39683
- Solar constant calculations, discussing rms error and effective temperature
22 p3596 A71-41451
- SOLAR CONVERTERS**
U SOLAR GENERATORS
SOLAR CORONA
Solar corona radioliograph observations, discussing burst types, prominences, shock waves, etc
01 p0152 A71-10329

- Solar corona radio emission enhancement, comparing thermal and nonthermal streamer models
01 p0152 A71-10332
- Solar corona evolution in contraction phase, calculating models based on dissipation theory
01 p0157 A71-10760
- Type IV solar radio emission broadband intensity fluctuations explained by MHD pulsations in flux tubes in corona
01 p0162 A71-11387
- Quiet corona temperature from solar equator soft X ray flux measurement by satellite-borne heliograph
02 p0300 A71-12077
- Solar coronal plasma electromagnetic wave amplification, discussing maser action effect on radar echoes
02 p0306 A71-12078
- Solar coronal structure and interplanetary magnetic fields prediction based on magnetic models, testing accuracy at solar eclipses
02 p0315 A71-12694
- [AIAA PAPER 70-1363] Solar X-ray flare activity statistical prediction based on correlation to coronal electron temperature and emission measure
02 p0301 A71-12698
- [AIAA PAPER 70-1371] Solar flare trigger mechanism, proposing inner corona thermal runaway of radiative power function
02 p0302 A71-12761
- Quasi-stationary coronal magnetic field and electron density from Faraday rotation experiment, using theoretical model
02 p0302 A71-12769
- Solar corona and wind composition, accounting for He flux and heavy elements from diffusion equations solution
02 p0303 A71-12770
- Tunable filter reflecting telescope and accessory optics for H alpha monochromatic photography of electron corona during total eclipse
03 p0424 A71-13626
- Total solar eclipse of 7 March 1970, describing coronal spectrograph, TV, telescopic and photographic instruments
03 p0424 A71-13627
- K corona radially and tangentially polarized components color differences from 7 March 1970 eclipse photographs analysis
03 p0489 A71-13628
- Fabry-Perot spectrometer systems for solar corona emission spectra and temperature measurements during eclipses
03 p0489 A71-13629
- Solar corona lines during 7 March 1970 eclipse, using Lallemand electrostatic cameras
03 p0489 A71-13630
- Computer controlled eclipse telescope for coronal thermal emission IR spectrum observation
03 p0424 A71-13633
- Solar proton flares, coronal radio diameter and cosmic radiation intensity relationship
03 p0473 A71-13788
- Heavy ion diffusion in solar corona, emphasizing flow velocity and density
03 p0495 A71-14503
- Electron excitation coefficient rate of green coronal line by quantum defect method, discussing energy levels of Fe ions
04 p0643 A71-14906
- Solar corona isophotes ellipticity and equal polarization curves during 7 March 1970 eclipse, using isodensitometric and polarimetric techniques
04 p0651 A71-15666
- Solar corona magnetic fields and structure during 12 November 1966 eclipse, determining electron densities and temperatures
05 p0802 A71-16013
- Solar coronal magnetic field patterns from radio observations
05 p0802 A71-16014
- Interplanetary magnetic field sectors correlated to solar coronal active centers and condensations in metric wavelengths from radio observations
05 p0802 A71-16015
- Monochromatic coronal structure in prominences, explaining light diminution by density reduction
05 p0804 A71-16027
- Coronal condensations emission changes after microwave solar bursts, discussing circular polarization and flare mechanism based on collisionless dissipation of magnetic energy
05 p0804 A71-16029
- Coronal magnetic structure mechanical diagnosis, using flare associated hydromagnetic disturbances
05 p0799 A71-16471
- Solar prominence interaction, observing coronal rain and mound
05 p0809 A71-16474
- Solar coronal plasma X ray emission, using simplified thermal continuum function
05 p0800 A71-17095
- Cooperative international program of monochromatic coronal photography with interference filters for 1973-1976
06 p0968 A71-17911

- Cooling models for flare produced plasmas in solar corona, considering collisional, radiative and conductive mechanisms
06 p0968 A71-17913
- Coronal magnetic fields before/after solar proton flares
06 p0950 A71-17917
- Solar corona emissions, discussing very high temperatures origin, eclipses and electromagnetic radiation spectrum
06 p0970 A71-18058
- Solar corona active regions thermal model, taking into account X ray emission and temperature distribution
06 p0963 A71-18439
- Inner solar corona polarization during 22 September 1968 total eclipse based on isolines from polarimetric photographs
06 p0975 A71-18440
- Thomson scattering role in solar corona electron cooling
06 p0976 A71-18454
- Linearly polarized CW signal transmission through near solar corona, measuring Faraday rotation
07 p1191 A71-19030
- Coronal line observation of autoionizing states by dielectronic recombination in solar spectrum
07 p1198 A71-19827
- Solar chromosphere and corona wave motions, presenting solar radio emission fluctuations correlation functions
07 p1199 A71-20010
- Meridional solar magnetic field shape determination, discussing latitude drift of spot forming zones, coronal penetrations and 80 year sunspot periodicity
08 p1358 A71-20887
- Solar burst theories, considering type 3 radiation source model for determination of lower corona plasma waves energy densities
08 p1358 A71-20889
- Quiet corona temperature from solar equator soft X ray flux measurement by satellite-borne heliograph
08 p1361 A71-21127
- Solar coronal plasma electromagnetic wave amplification, discussing maser action effect on radar echoes
08 p1361 A71-21128
- Coronal magnetic field geometry maps, using high altitude photospheric field measurements for correlations with active sun
08 p1363 A71-21154
- Coronal and prominence IR photography during 7 March 1970 solar eclipse
09 p1442 A71-22066
- Solar corona structure on 22 September 1968 from radio astronomical and optical eclipse data
09 p1520 A71-22833
- Solar eclipse measurements at 1.18 cm on 11 September 1969, describing limb brightening and center and coronal emission
10 p1666 A71-23790
- Solar limb darkening measurement with high temporal resolution and inner corona photometry by white and polarized light during 7 March 1970 eclipse
10 p1678 A71-24829
- Protosun and primordial solar nebula evolution based on dust particles behavior
11 p1819 A71-25221
- Argon ionization and recombination in solar corona at electron temperatures of 2.0-4.5 times ten to sixth power K
11 p1832 A71-26180
- Green corona corrections of position-angle errors, east-west asymmetry, photometric scale instability and threshold measurements
11 p1832 A71-26181
- Solar corona active regions thermal model, considering X ray emission and temperature distribution
12 p1946 A71-26589
- Inner solar corona polarization during 22 September 1968 total eclipse based on isolines from polarimetric photographs
12 p1955 A71-26590
- Solar corona electrons cooling by Thomson scattering, calculating electron energy loss
12 p1955 A71-26604
- Solar coronal heating homopolar generator model, proposing neutrons as energy source
12 p1961 A71-26877
- Solar corona plasma turbulence spectra, evaluating radar echo structure
12 p1963 A71-27080
- Solar corona photometry during 22 September 1968 eclipse, determining brightness variations and decrease from limb
12 p1966 A71-27231
- Solar inner corona forbidden emission lines and continuum enhancement during 30 May 1965 eclipse as function of heliocentric position angle
12 p1969 A71-27650
- Green line intensity and electron/ion density contours as function of height over solar limb for March 1970 coronal enhancement
12 p1969 A71-27651

Long term storage of relativistic energetic electrons and protons in solar corona from IMP 4 and Pioneer 8 observations related to delayed emission from flares
12 p1969 A71-27657

Solar corona high radial and tangential polarization during 7 March 1970 eclipse from photographs with neutral density filter and rotating linear polaroid sectors
12 p1970 A71-27705

Cosmic radio waves scattering in outer solar corona, considering refraction and gradients in electron density fluctuations
12 p1970 A71-27706

Hot coronal components of solar active regions observations with satellite-borne grazing incidence X ray telescope, discussing emission dependency on photospheric magnetic field
12 p1954 A71-27707

Solar corona soft X ray emission, investigating temperature and flare activity effects
13 p2129 A71-29051

Solar corona XUV resonance line spectrum interpretation, using thermal emission from inhomogeneous regions
14 p2297 A71-29678

Shock wave heated atmospheric model computation for solar chromosphere and corona
14 p2306 A71-29684

Supersonic to subsonic solar corona transition, using supersonic solution for solar wind inviscid equations
14 p2302 A71-30648

Solar corona visible lines, indentifying V VI to Fe IX electron transitions with variable inductance three electrode spark source
14 p2314 A71-30650

Solar prominences formation, discussing coronal thermal instability, chromospheric heat balance, magnetic field and gas heating
15 p2482 A71-31334

Coronal flare onset, examining dynamic processes of plasma compression with longitudinal magnetic field
15 p2482 A71-31335

Solar type 3 bursts with fundamental and second harmonic structure for corona reflected and direct rays at 80 MHz observed with Culgoora radioheliograph
15 p2473 A71-31690

Coronal emission from turbulent plasma excited by shock wave, discussing relation to type 2 radio bursts
15 p2473 A71-31719

Cosmic ray gradient perpendicular to solar equator plane related to coronal intensity
15 p2479 A71-31906

Green corona activity longitudinal distribution from solar cycle observations, noting underphotospheric rigid body rotation
15 p2497 A71-32748

Solar wind outflow from active regions by numerical integration of hydrodynamics equations, using corona temperature distribution
15 p2480 A71-32753

Large coronal streamer with active region enhancement during total eclipse on 22 September 1968, giving model of enhancement
16 p2625 A71-33328

IR Fe XIII lines in solar corona during total eclipse of 12 November 1966
16 p2640 A71-33729

Rocket-borne coronagraph photometry of solar corona during solar eclipse of 7 March 1970
16 p2640 A71-33733

Solar corona green line observations with Lallemand electrostatic camera during 7 March 1970 eclipse, showing equivalent width, electron density and temperature vs height above limb
16 p2640 A71-33745

Coronal IR emission lines during solar eclipse of 7 March 1970, using high altitude aircraft-borne Fourier transform spectrometer
16 p2640 A71-33751

Coronal and interplanetary magnetic fields during 7 March 1970 solar eclipse, comparing calculated field line maps with coronal structure photographs
16 p2641 A71-33775

Coronal line measurements on slit spectrogram during solar eclipse of 7 March 1970, showing fine structure in inner corona
16 p2642 A71-33784

Spectrographic observation of coronal lines in chromosphere during solar eclipse of 7 March 1970
16 p2642 A71-33787

Outer corona polarization determination from airborne photographic observations in March solar eclipse, presenting preliminary results of photometric data reduction
16 p2642 A71-33803

Solar corona photometric intensity and polarization measurements during 1970 solar eclipse
16 p2580 A71-33819

Bibliography and review of solar activity relevant to sun-planet relationships, considering magnetic fields, transient events, corona and solar wind
17 p2799 A71-34459

Carbonaceous chondrites chemical and mineralogical composition densities and structure due to condensation at various temperatures within early solar nebula
17 p2799 A71-34512

Solar corona studies at Kiev University during 1952, 1954, 1961, 1965 and 1968 solar eclipses, showing coronal fine structure relation to chromosphere
17 p2802 A71-34827

Hydrostatic, dynamic, hydrodynamic and two-component corona models and solar corpuscular radiation, considering heat conductivity and viscosity effects on solar wind dynamic characteristics
17 p2795 A71-34828

Solar corona formation relation to geomagnetic storm generation
17 p2734 A71-35191

Solar coronal line photometry eliminating inherent systematic measurement errors of previous methods
17 p2809 A71-35597

Type 2 radio burst disturbances in coronal magnetic field, considering shock wave travel parallel to magnetic field lines
18 p2957 A71-36159

Wavelength prediction for coronal transitions at various atomic configurations, deriving semiempirical expressions from observed data for energy level intervals determination
18 p2965 A71-36733

Solar activity and intensity ratios of O VII X-ray coronal emission lines, giving upper bound on electron density
18 p2965 A71-36734

Solar Fe XIV 5303 coronal line isolation, using solid Fabry-Perot interferometer as monochromator
18 p2966 A71-36736

Solar corona model for structure and dynamic properties, investigating gas-magnetic field interactions
18 p2966 A71-36737

Solar chromospheric plane area related to peak K coronal brightness at limb
18 p2966 A71-36738

UV studies of solar atmosphere in quiet and active regions, considering low and high chromosphere, transition zone, quiet corona and inhomogeneity
18 p2968 A71-37034

Nonspherical axisymmetric model of minimum type solar corona, investigating light scattering electrons density distribution relation to brightness and polarization
19 p3131 A71-37240

Brightness and polarization of solar corona at total eclipse on 12 November 1966 from polarigraphic observations
19 p3131 A71-37243

Solar corona photometry during 22 September 1968 eclipse, determining brightness variations and decrease from limb
19 p3132 A71-37383

Solar corona plasma turbulence spectra, evaluating radar echo structure
19 p3133 A71-37430

Solar chromosphere and corona manifold structure data, using high resolution filter photography
19 p3136 A71-37616

Solar limb and disk intensity spectra in chromosphere-corona transition region, calculating models, element abundances structure, electron pressure and hydrostatic equilibrium equations
19 p3136 A71-37617

Solar flare X ray spectrum analysis for lower corona physical conditions, discussing continuum and line emission
19 p3126 A71-37623

Proposed model with with neutrons as energy source for solar corona, discussing validity based on capture gamma ray flux expectation
19 p3127 A71-38009

Solar wind acceleration due to Alfvén wave pressure gradient, taking into account coronal parameters of temperature, magnetic field and energy density
19 p3128 A71-38162

Two dimensional isophotes of extreme solar corona from integrated vidicon pictures taken from moon surface by Surveyors 6 and 7
19 p3147 A71-38670

Emission characteristics above solar limb in four EUV lines, comparing with K-coronameter measurements to estimate element abundances
19 p3130 A71-38671

Solar coronal X ray spectrum calculation of high-temperature low-density plasma, considering line emission from electron collisional excitation and radiation
20 p3278 A71-39058

Solar wind origin in active regions by radar exploration, noting signal backscattering from coronal plasma turbulent pulsations
20 p3281 A71-39732

Time variable dispersion of Crab Nebula pulsar, showing coincidence with occultation by solar corona
20 p3302 A71-39927

Solar wind theory, discussing thermal conduction and MHD wave energy supply mechanisms of large scale solar corona expansion
21 p3439 A71-41183

Solar corona current sheet magnetic model, computing polar plume orientations and radial and nonradial streamers
21 p3453 A71-41359

Solar transition layer and inner corona empirical minimum equator model, using radio, UV, white and monochromatic radiation data
22 p3601 A71-42161

Solar corona O VII and Ne IX helium line triplets observations, examining electron density limits
22 p3605 A71-42352

Solar prominences formation, discussing coronal thermal instability, chromospheric heat balance, magnetic field and gas heating
22 p3606 A71-42609

Coronal flare onset, examining dynamic processes of plasma compression with longitudinal magnetic field
22 p3606 A71-42610

Calcium abundance in solar corona, using measured values for total intensity of continuum and integrated intensities ratio
23 p3768 A71-43845

Monochromatic observations of coronal loop, using isophotal map from coronagraph through Fabry-Perot interferometer
23 p3768 A71-43846

Solar coronal heating neutron theory based on solar gamma ray flux considerations
23 p3770 A71-44014

Solar coronal plasma radiative capacity and temperature structure from cooling function in thermal balance equation
24 p3869 A71-44806

Photographic far UV solar spectra during eclipse of 7 March 1970, discussing coronal lines, prominences and quiet atmosphere structure
24 p3871 A71-44911

SOLAR CORPUSCULAR RADIATION

NT SOLAR PROTONS
High energy albedo neutrons energy and angular distributions, determining solar neutron flux upper limit
01 p0147 A71-11517

Energetic solar neutrons near maximum, calculating continuous flux and proton emission from balloon measurements
02 p0302 A71-12768

Absolute particle spectra above atmosphere and magnetosphere during solar flare of 23 February 1956
05 p0800 A71-17198

Solar electrons access to closed field lines in geomagnetosphere quasi-trapping region from satellite observation
06 p0949 A71-17257

Nitrogen dioxide and molecular oxygen ions densities in lower ionosphere as function of solar corpuscular radiation
06 p0895 A71-18275

Temporal intensity variations of geomagnetically trapped solar alpha particles from Injun 5 observations
08 p3356 A71-21644

Nighttime E layer behavior during geomagnetic storms in quiet sun years, investigating corpuscular flux effects
08 p3156 A71-21854

Solar particle effects on polar cap VLF radio propagation along polar and transpolar paths, considering short term phase effects
10 p1577 A71-24313

Partial mixing effects on solar neutrino flux and stellar evolution
10 p1662 A71-24497

Solar corpuscular radiation differential and integral spectrum, assessing energetic electron flux in D region at sunrise
11 p1815 A71-25587

Solar neutron flux measurements compared to previous spark chamber scintillation experiment flown at Hyderabad, India
13 p2120 A71-27927

Absolute spectra above atmosphere and magnetosphere and of particles accelerated in solar atmosphere during solar flare of 23 February 1956
13 p2128 A71-28253

Relativistic electrons associated with solar particle events, measuring occurrence frequency, electron propagation and diffusion anisotropy
13 p2129 A71-29057

Solar neutrons and compact luminous objects, discussing unsolved problems and theoretical-observational discrepancies
14 p2309 A71-30015

Point sources of solar neutrino radiation, explaining negative experimental results without drastic change of main assumptions concerning stellar evolution
15 p2478 A71-31801

Solar neutrino detection using capture reaction in perchloroethylene medium
15 p2478 A71-31803

Semiannual ionospheric density variations from Cosmos artificial satellites drag, noting agreement with solar corpuscular radiation geoeffectivity
16 p2571 A71-33841

- Solar particle flux profile and low latitude cut-off observation by low latitude satellite during March 1969 to July 1970 events 16 p2628 A71-33936
- Hydrostatic, dynamic, hydrodynamic and two-component corona models and solar corpuscular radiation, considering heat conductivity and viscosity effects on solar wind dynamic characteristics 17 p2795 A71-34828
- Energetic electrons, protons and alpha particle measurements by Azur satellite over polar cap and in radiation belt during March 1970 solar particle event 19 p3126 A71-37419
- Cosmic rays and solar energetic particles properties near earth and requirements on measurement during outer planets missions [AAS PAPER 71-126] 19 p3127 A71-37940
- D region ionization by solar corpuscular streams, considering formation of charged particle concentration profiles 20 p3216 A71-39141
- Low energy solar particle observation by widely separated Mariner and Explorer spacecraft, noting flare-associated and nonflare intensity peak corotation with sun 20 p3284 A71-39876
- Solar high energy particles directional and temporal properties, investigating single encounter model with propagating interplanetary shock waves 23 p3720 A71-43153
- Comet brightness variations correlation with geomagnetic field and solar corpuscular flux variations in interplanetary space 24 p3870 A71-44814
- ### SOLAR COSMIC RAYS
- Solar cosmic ray phenomena, noting ionospheric effects and physical processes near sun 03 p0480 A71-14067
- PCA ionization, using range-energy ratio of solar cosmic rays penetrating spirally into polar atmosphere for electron production rate determination 05 p0742 A71-16812
- Phenomenological one dimensional model of solar cosmic ray propagation for anisotropy and intensity as function of time during early phases of events 06 p0950 A71-18102
- Solar cosmic ray diurnal variations latitude effect explained by two way anisotropy model 06 p0952 A71-18109
- Solar cosmic ray intensity yearly variation by pressure corrected neutron monitor, discussing atmospheric temperature effects, coronal emission heliolatitude distribution and annual wave amplitude 06 p0953 A71-18117
- Solar cosmic ray proton event of 18 November 1968 studied with neutron monitor data from worldwide network, considering associated flare 06 p0957 A71-18147
- Low energy solar and galactic cosmic ray propagation in interplanetary medium from Zond 3 and Venus 2-4 space probes measurements 06 p0958 A71-18152
- Stratospheric soft photon anomalous fluxes associated with May 1967 solar cosmic ray bursts 06 p0959 A71-18157
- Solar cosmic ray activity near sunspot maximum, discussing events of 18 November 1968 and 11 April 1969 06 p0959 A71-18158
- High latitude neutron monitors during 15 November 1960 solar cosmic ray event, calculating asymptotic directions for protons with magnetospheric model 06 p0959 A71-18161
- Galactic and solar cosmic rays diffusion as function of solar activity and interstellar medium properties, considering particle velocity and proton scattering transport 07 p1185 A71-19379
- Fokker-Planck equation for convection dominated transport of solar cosmic rays solved for exponential decay phase of solar particle events 07 p1185 A71-19651
- Recurrent solar cosmic ray events and M region magnetic storms 07 p1186 A71-19654
- Cosmic ray intensity mean diurnal variation, taking into account angle between solar corotational velocity and earth equatorial plane 07 p1187 A71-19683
- Solar cosmic ray interaction with oblique shock wave MHD discontinuity, noting energy particle buildup and acceleration 08 p1351 A71-20964
- Ionization measurements of high latitude and altitude cosmic rays covering four solar maxima 08 p1355 A71-21628
- Proton energy change effects on charged particles propagating in interplanetary space, using low energy solar flare proton fluxes observations 09 p1514 A71-22801
- Energy spectrum of iron group solar cosmic ray particles determined from glass removed from Surveyor 3 spacecraft, considering lunar erosion implications 09 p1515 A71-23656

- Cosmic ray transport equation for solar sources, using Fisk numerical method by applying transformation of independent variable U/r 10 p1664 A71-24801
- Time dependence of atmospheric ionization at polar cap absorption event, obtaining relativistic and non-relativistic solar cosmic rays ionization equations 11 p1754 A71-25586
- Mean neutron monitor multiplicity time variations for solar cosmic ray events and Forbush decreases with modulation spectrum allowance 11 p1816 A71-25753
- Solar flux from 7 July 1966 flare observation via Proton 3 satellite, obtaining cosmic rays integral spectra 11 p1817 A71-25781
- Anisotropy of solar cosmic ray electrons, considering parallel diffusion coefficients for ions and electrons 12 p1954 A71-27712
- Solar cosmic ray acceleration and propagation from time variation and heliocentric distance dependence of relative abundance of protons to helium nuclei 13 p2129 A71-29058
- Solar flare cosmic ray propagation, investigating bounded interplanetary diffusion medium effects 13 p2130 A71-29060
- Solar cosmic ray flare catalog, using polar region absorption radio burst and proton event data 14 p2299 A71-29986
- Astronomical photography of solar eclipse of 7 March 1970 from two locations indicating negative evidence of bulk particle movements above 20 km/sec related to cosmic rays 16 p2642 A71-33810
- Solar cosmic ray data, discussing multicharged nuclei relative abundances in photosphere and propagation models 19 p3126 A71-37625
- Galactic and solar cosmic rays diffusion coefficient as function of solar activity and interstellar medium properties, considering particle velocity and proton scattering transport 19 p3127 A71-37804
- Anomalous distribution in heliocentric longitude of solar injected cosmic radiation, suggesting interplanetary magnetic field lines of force stochastic wandering 19 p3130 A71-38674
- Solar high energy cosmic ray proton burst observations, examining maximum flux delay time with Venus 6 satellite 20 p3281 A71-39734
- Solar low energy cosmic ray population anisotropy from satellite observations during flare event, describing rise time, decay, field alignment and time constant 22 p3591 A71-41469
- Solar and galactic iron group cosmic ray track distributions in Apollo 12 lunar rocks, investigating surface residence times 23 p3764 A71-43800
- Galactic and solar cosmic ray effects on Apollo 11 lunar soil and rock samples, analyzing Xe isotopic anomalies 23 p3722 A71-44016
- Solar cosmic ray spectra at time of ejection from flare region and arrival near earth 24 p3866 A71-45040
- ### SOLAR CYCLES
- #### NT SUNSPOT CYCLE
- Nonrecurrent sunspot clusters latitudinal motion speed correlation with solar activity cycle phase 01 p0149 A71-10052
- Solar activity cycles correlation with planets positions over ecliptic 01 p0149 A71-10053
- Proton Flare Project 1969 observations concerning retrospective interval activity during maximum phase of solar cycle 01 p0144 A71-10286
- Geomagnetic field perturbation as function of 11-year solar activity cycle, using magnetic observatory 01 p0073 A71-10921
- Regularities of polar auroras and ionospheric disturbances during solar cycle with decreased low energy corpuscular flux 02 p0242 A71-11760
- SD geomagnetic variations and electron jet spread over polar cap stream during solar cycle 02 p0243 A71-11763
- Solar activity cycles mechanism, deriving nonlinear equations from quasisymmetric magnetic dynamo models 02 p0307 A71-12081
- Solar activity long term variations in 11 year cycle maxima, noting preferred locations on disk [AIAA PAPER 70-1368] 02 p0315 A71-12695
- Thermospheric neutral particle molecular nitrogen density and temperature measurements by rockets, noting correlations with diurnal, solar cycle and other variations 03 p0414 A71-14020
- Magnetospheric electron density trough measurements by Explorer 22 Langmuir probe during rising solar cycle 03 p0420 A71-14529

- Sunspots visual observations in 1969, giving Wolf numbers and rotational means by Carrington elements 04 p0644 A71-15070
- Polarity pattern of interplanetary magnetic field near solar maximum, using poloidal model 05 p0803 A71-16017
- Ionospheric absorption measurements noting diurnal, seasonal and solar cycle variations 05 p0740 A71-16429
- Ionospheric drift measurements during solar cycles based on fading of radio waves reflected from E and F regions 05 p0741 A71-16437
- Residual modulation from 1954-1964 solar cycle, considering 19th cycle hysteresis loop from cosmic ray balloon data 06 p0955 A71-18131
- Galactic cosmic ray modulation region dimensions calculated during various solar activity cycles 06 p0955 A71-18134
- Solar cosmic ray activity near sunspot maximum, discussing events of 18 November 1968 and 11 April 1969 06 p0959 A71-18158
- Solar half cycle total ionospheric electron content and slab thickness diurnal and seasonal variations from Syncom 3 beacon signal 07 p1097 A71-19020
- Solar radio emission constant and slowly varying components, investigating sunspots, activity cycle and flux rate 07 p1195 A71-19340
- Theoretical and observed Balmer alpha distributions over solar cycle by Lyman beta scattering on hydrogen in upper atmosphere 07 p1187 A71-19671
- Nonrecurrent sunspot clusters latitudinal motion speed correlation with solar activity cycle phase 08 p1361 A71-21046
- Solar activity cycles correlation with planets positions over ecliptic 08 p1361 A71-21047
- Solar activity cycles mechanism, deriving nonlinear equations from quasi-symmetric magnetic dynamo models 08 p1362 A71-21131
- Solar wind speed distributions /1962-1970/ as function of solar cycle 08 p1356 A71-21641
- Solar activity cycle model, considering dynamo equations with only radial rotation differentiability 08 p1365 A71-21777
- Sunspot activity and 107 mm solar flux 27 day variations during 11 year solar cycle 09 p1513 A71-22792
- Solar cycle effects on diurnal variations of F 2 region critical frequency and maximum ionization height 10 p1600 A71-23884
- Solar cycle large sunspot groups as function of heliographic longitude, noting structure/distribution stability responsible for phenomena 10 p1674 A71-24459
- Eleven year cycle cosmic ray modulation mechanism, considering solar wind and interplanetary magnetic field parameters 10 p1662 A71-24472
- Solar cycle time variations in trapped radiation belt proton flux, deriving proton transport equation from Boltzmann equation 10 p1663 A71-24785
- Pulsar mechanism relation to solar cycle mechanism, discussing magnetic flux correlation to period 10 p1681 A71-25071
- Eleven year solar activity cycles interrelationship, giving empirical expression for Wolf numbers in consecutive events 12 p1961 A71-26903
- Twenty-two year solar cycles, relating Wolf numbers with minima and maxima in secular cycle 12 p1961 A71-26904
- Oscillatory hydromagnetic dynamo model of large scale solar magnetic field of variable sign, using Bénard convective cell with Coriolis velocity disturbance 13 p2137 A71-28529
- Sunspot groups frequency as function of mean area, comparing distributions in Northern and Southern Hemispheres for 11 year cycles 13 p2143 A71-29329
- Solar activity cycle model, considering magnetic dynamo equations with radial rotation differentiability 15 p2495 A71-32679
- Green corona activity longitudinal distribution from solar cycle observations, noting underphotospheric rigid body rotation 15 p2497 A71-32748
- Total electron content throughout solar cycle maximum, discussing annual variations 16 p2571 A71-33833
- Daytime occurrence of maximum wave reflection frequency and blanketing frequency for period of two solar cycles at Rarotonga and Christchurch stations 16 p2574 A71-33970

- Mode conversion and auroral effects observations on polar VLF propagation path, noting seasonal and solar cycle variations 17 p2731 A71-34319
- Geomagnetic micropulsation data, emphasizing behavior during 11 year solar cycle 17 p2732 A71-34671
- Statistical determination of solar radio emission S-component average flux spectrum during solar cycle peak phase 18 p2966 A71-36739
- Solar cycle variation of planetary exospheric temperature from heat balance equation solution 19 p3131 A71-37334
- Solar activity effects on equatorial ionospheric absorption of radio waves, deriving solar cycle constant 19 p3055 A71-38042
- Large scale convection solar magnetic field patterns calculations based on rotating thin spherical shells, noting solar cycle activity 19 p3147 A71-38667
- Viscous torsional vibrations inadequacy for interpreting solar activity cycles relative to magnetic field 20 p3290 A71-39303
- Solar magnetic field generation by gyrotropic turbulence, noting inadequacy of Steenbeck explanation for quantitative estimates of solar cycle parameters 20 p3291 A71-39317
- Solar cycle effects on E region peak electron density, correlating sunspot number by regression analysis 21 p3372 A71-40036
- Solar cycle variation effects on interstellar hydrogen within solar system, discussing thermal motion, density, far UV ionization and charge transfer reactions 22 p3601 A71-42169
- Ionospheric propagation hysteresis relationship to secular variation in F region response to sunspot number, noting differences in succeeding solar cycles 22 p3536 A71-42419
- Atmospheric wind velocity time variations at 80-100 km altitudes from ionospheric drift data, finding planetary oscillation periodicities relationship to solar activity cycle 24 p3822 A71-44349
- Solar unipolar magnetic regions relation to geomagnetic disturbances variability, discussing 11 year cycle 24 p3823 A71-45036
- SOLAR DISK**
- U SUN**
- SOLAR ECLIPSES**
- Meteorological, optical and coronographical observations of total solar eclipse of 7 March 1970 01 p0151 A71-10116
- Solar eclipse observations of 7 March 1970, discussing site selection, shadows, corona, prominences, temperature measurements and photographs 01 p0151 A71-10117
- Meteorological observations during solar eclipse of 7 March 1970 concerning temperature, wind, humidity, pressure, air circulation and optical phenomena 01 p0151 A71-10118
- Short wave broadcasting and ionospheric reflection during solar eclipse of 7 March 1970, relating to nighttime free electron distributions 01 p0151 A71-10119
- Solar emission line spectra second observation outside total eclipse, noting big coronal condensation above eastern limb 01 p0159 A71-10869
- Annular solar eclipse effects on VLF transmissions phase delay 02 p0212 A71-11969
- Solar coronal structure and interplanetary magnetic fields prediction based on magnetic models, testing accuracy at solar eclipses [AIAA PAPER 70-1363] 02 p0315 A71-12694
- Solar eclipse of 7 March 1970 ionospheric ionization observations via satellites, correlating data with Wallops Island vertical ionograms 03 p0406 A71-13174
- Hydrogen Lyman alpha radiation intensity and atmospheric absorption before and during solar eclipse of 20 May 1966, considering D region ion production 03 p0407 A71-13376
- Solar X-rays role in D region ionization from ion probe sounding during eclipse of 20 May 1966 03 p0407 A71-13377
- Ionospheric electron collision frequency and concentration height distribution during annular solar eclipse of 20 May 1966 03 p0407 A71-13378
- D region electron density time variations, using partial radio reflection technique during solar eclipse of 20 May 1966 03 p0407 A71-13379
- Ionospheric Lyman alpha intensities and electron and positive ion densities during solar eclipse of 20 May 1966, discussing recombination model 03 p0407 A71-13380
- Total solar eclipse of 7 March 1970, describing coronal spectrograph, TV, telescopic and photographic instruments 03 p0424 A71-13627
- K corona radially and tangentially polarized components color differences from 7 March 1970 eclipse photographs analysis 03 p0489 A71-13628
- Fabry-Perot spectrometer systems for solar corona emission spectra and temperature measurements during eclipses 03 p0489 A71-13629
- Solar corona lines during 7 March 1970 eclipse, using Lallemand electrostatic cameras 03 p0489 A71-13630
- Eclipse photon counting for solar atmosphere height determination, describing spectrograph-photomultiplier apparatus 03 p0424 A71-13632
- Computer controlled eclipse telescope for coronal thermal emission IR spectrum observation 03 p0424 A71-13633
- Photoelectric photometer with mechanical chopper for extreme limb darkening measurement at total eclipse 03 p0424 A71-13635
- Solar eclipse sounding rocket study of totality path over Wallops Station for 7 March 1970 event, discussing payload launch, ground support equipment, planning, etc [AIAA PAPER 70-1395] 03 p0397 A71-13676
- Sounding rocket Solar Eclipse Sensor for 7 March 1970 event, discussing mission, capabilities, data acquisition and design [AIAA PAPER 70-1406] 03 p0455 A71-13685
- Polarization and sky radiance data before, during and after 7 March 1970 solar eclipse 03 p0425 A71-13688
- Rocket experiments during 1964 solar eclipse, obtaining D region parameters from parachute-borne blunt probe measurements of atmospheric positive and negative conductivities 03 p0416 A71-14033
- Solar soft X ray and extreme UV relative contribution to E layer ion production rates during solar eclipse of 12 November 1966 03 p0481 A71-14511
- Solar eclipse of 22 September 1968 radio astronomical observations, examining sunspot groups during lunar occultation 04 p0650 A71-15558
- Solar corona isophotes ellipticity and equal polarization curves during 7 March 1970 eclipse, using isodensitometric and polarimetric techniques 04 p0651 A71-15666
- Solar corona magnetic fields and structure during 12 November 1966 eclipse, determining electron densities and temperatures 05 p0802 A71-16013
- Geomagnetic field anomalous variations due to solar eclipse of 22 September 1968 05 p0746 A71-17211
- Eclipse observations interpretation for transition region between extreme limb and low chromosphere 06 p0967 A71-17905
- Mauna Loa coronagraph observations before, during and after 7 March 1970 solar eclipse 06 p0968 A71-17912
- E layer electron concentrations, effective recombination coefficient and ionization sources during solar eclipse, noting soft X radiation intensity 06 p0894 A71-18260
- Inner solar corona polarization during 22 September 1968 total eclipse based on isolines from polarimetric photographs 06 p0975 A71-18440
- Ionospheric characteristics recording concerning critical frequencies and minimum heights above Sverdlovsk during solar eclipse of 22 September 1968 07 p1101 A71-19407
- Solar chromosphere and prominences observations during total eclipse of 12 November 1966 by slitless spectrograph, using grazing incidence method 08 p1365 A71-21423
- Coronal and prominence IR photography during 7 March 1970 solar eclipse 09 p1442 A71-22066
- Torsional pendulum behavior variations during solar eclipse of 7 March 1970 09 p1493 A71-22805
- Solar corona structure on 22 September 1968 from radio astronomical and optical eclipse data 09 p1520 A71-22833
- Ozone distribution measurements in mesosphere and stratosphere by rocket during seasonal ionospheric disturbance and solar eclipse 09 p1490 A71-23562
- Solar eclipse measurements at 1.18 cm on 11 September 1969, describing limb brightening and center and coronal emission 10 p1666 A71-23790
- Lunar shadow effects on bow wave mechanism during 7 March 1971 solar eclipse, considering traveling ionospheric disturbance measurements from satellite 10 p1600 A71-23885
- Solar limb darkening measurement with high temporal resolution and inner corona photometry by white and polarized light during 7 March 1970 eclipse 10 p1678 A71-24829
- Chorioretinal temperature increases from naked solar eclipse observations for various observation angles and pupil diameters, considering solar irradiance and atmospheric transmittance spectra 11 p1726 A71-26484
- Inner solar corona polarization during 22 September 1968 total eclipse based on isolines from polarimetric photographs 12 p1955 A71-26590
- Solar corona photometry during 22 September 1968 eclipse, determining brightness variations and decrease from limb 12 p1966 A71-27231
- Solar inner corona forbidden emission lines and continuum enhancement during 30 May 1965 eclipse as function of heliocentric position angle 12 p1969 A71-27650
- Spectral analysis of solar prominences observed during Peruvian eclipse of 12 November 1966, obtaining two dimensional distribution of kinetic temperature, density and turbulent velocity 12 p1970 A71-27702
- Solar corona high radial and tangential polarization during 7 March 1970 eclipse from photographs with neutral density filter and rotating linear polaroid sectors 12 p1970 A71-27705
- Ionospheric continuity in F2 region during partial solar eclipses, using EUV radiation and additional corpuscular source of ionization 13 p2053 A71-27792
- Geomagnetic field anomalous variations due to solar eclipse of 22 September 1968 13 p2060 A71-28266
- Sky brightness measurements during total solar eclipses, discussing solar elevation, cloud cover and albedo effects 14 p2309 A71-30117
- Zenith sky brightness and color change during total solar eclipse of 12 November 1966 at Santa Ines, Peru, using interference filter photometers 14 p2309 A71-30118
- Zenith sky intensity and spectral distribution changes during solar eclipse of 12 November 1966, discussing dependence on height and terrain 14 p2309 A71-30119
- Day sky brightness and polarization observation during total solar eclipse of 7 March 1970 14 p2309 A71-30120
- Zenith skylight spectral intensity distribution measurement during total solar eclipse of 7 March 1970, using optical scanning spectrometer 14 p2309 A71-30121
- Solar eclipse on 7 March 1970, determining midlatitude geomagnetic pulsations with dynamic power spectral analysis 15 p2397 A71-31761
- Canadian observational sites for solar eclipse of 10 July 1972, describing expected weather conditions, totality time/duration and location accessibility 16 p2630 A71-33125
- Large coronal streamer with active region enhancement during total eclipse on 22 September 1968, giving model of enhancement 16 p2625 A71-33328
- IR Fe XIII lines in solar corona during total eclipse of 12 November 1966 16 p2640 A71-33729
- Solar extreme UV flash spectrum from spectroheliographs aboard Aerobee 170 rocket launched during March 1970 eclipse, comparing with homogeneous and inhomogeneous temperature models 16 p2640 A71-33730
- Thermospheric electron heating rate and ion chemistry above Wallops Island during 7 March 1970 solar eclipse, measuring ion composition and concentration 16 p2565 A71-33732
- Rocket-borne coronagraph photometry of solar corona during solar eclipse of 7 March 1970 16 p2640 A71-33733
- Wavelike ionospheric undulations of total columnar electron content and of true height of bottomside plasma frequencies before and during solar eclipse of 7 March 1970 16 p2565 A71-33738
- Solar corona green line observations with Lallemand electrostatic camera during 7 March 1970 eclipse, showing equivalent width, electron density and temperature vs height above limb 16 p2640 A71-33745
- Coronal IR emission lines during solar eclipse of 7 March 1970, using high altitude aircraft-borne Fourier transform spectrometer 16 p2640 A71-33751
- Shadow band observations during 7 March 1970 solar eclipse, determining spectral energy distribution from magnetic tape recordings of collimated photocells output 16 p2566 A71-33761

Solar eclipse effects on atmospheric structure, circulation and meridional flow, using rocket measured temperature and wind data for pressure and density variations near stratopause

16 p2567 A71-33764

Solar UV radiation data during 7 March 1970 eclipse from photometers sensitive to narrow bands, discussing sources, atmospheric absorption and D region ionosphere

16 p2627 A71-33773

Coronal and interplanetary magnetic fields during 7 March 1970 solar eclipse, comparing calculated field line maps with coronal structure photographs

16 p2641 A71-33775

Coronal line measurements on slit spectrogram during solar eclipse of 7 March 1970, showing fine structure in inner corona

16 p2642 A71-33784

Spectrographic observation of coronal lines in chromosphere during solar eclipse of 7 March 1970

16 p2642 A71-33787

Nike Apache solar X-ray observations during 7 March 1970 eclipse, determining residual fluxes and atmospheric absorption profiles for ion production rates

16 p2627 A71-33790

Outer corona polarization determination from airborne photographic observations in March solar eclipse, presenting preliminary results of photometric data reduction

16 p2642 A71-33803

Astronomical photography of solar eclipse of 7 March 1970 from two locations indicating negative evidence of bulk particle movements above 20 km/sec related to cosmic rays

16 p2642 A71-33810

Solar flare X-ray emission source position during eclipse of 7 March 1970, using OSO-5 satellite data

16 p2627 A71-33813

Solar corona photometric intensity and polarization measurements during 1970 solar eclipse

16 p2580 A71-33819

Conjugate photoelectrons existence from rocket measurements during total solar eclipse of 7 March 1970

16 p2570 A71-33823

Intra-Mercurial planets and comets discovered during solar eclipses, discussing size, orbital eccentricity, albedo and equilibrium temperature

16 p2642 A71-33830

Meteorological planning study for 1973 African solar eclipse observation site selection

16 p2572 A71-33844

Traveling ionospheric disturbances due to gravity wave interactions during solar eclipse of 7 March 1970, confirming electron content variations from ATS 3 polarization data

16 p2575 A71-33975

Atmospheric potential gradient measurements during solar eclipse of 7 March 1970, using airborne and ground observations

17 p2731 A71-34321

Metallic lines in high-dispersion spectrograms in 1966 Peruvian eclipse for lower chromosphere excitation temperature

17 p2799 A71-34476

Brightness and polarization of solar corona at total eclipse on 12 November 1966 from polarographic observations

19 p3131 A71-37243

Solar corona photometry during 22 September 1968 eclipse, determining brightness variations and decrease from limb

19 p3132 A71-37383

Ionospheric characteristics recording concerning critical frequencies and minimum heights above Sverlovsk during solar eclipse of 22 September 1968

19 p3053 A71-37831

Iso-line charts showing F 2 layer critical frequency deviations and negative disturbance zones during solar eclipse of 22 September 1968

19 p3058 A71-38385

Solar limb D3 He line intensity distribution measurements during eclipse of 22 September 1968

19 p3147 A71-38666

Midlatitude ionospheric irregularities, electron density vertical distribution and electron and ion temperature variation measurements, during solar eclipse of 22 September 1968

20 p3224 A71-39716

Electron content spatial and temporal variation during ionospheric storm of 8 March 1970 after total solar eclipse

20 p3232 A71-39899

Radiative heat transfer from lunar and Mercurian surfaces during eclipse

22 p3603 A71-42188

Solar eclipse induced atmospheric gravity waves interference, considering resulting bow wave discrepancy with wavelike ionospheric disturbance

23 p3670 A71-43190

Solar chromospheric data for 1952, 1958, 1962 and 1966 eclipses, showing helium abundance in prominences

23 p3767 A71-43842

Photographic far UV solar spectra during eclipse of 7 March 1970, discussing coronal lines, prominences and quiet atmosphere structure

24 p3871 A71-44911

SOLAR ENERGY

Solar energy thermionic converter life test program and equipment, noting failure due to loss of intraelectrode Cs

02 p0194 A71-12223

Energy sources for rockets and satellites, comparing chemical, solar and nuclear supplies

02 p0282 A71-12302

Solar core to surface energy transfer mechanism, discussing chromosphere spectrographic, photoelectric and telescopic observations

02 p0312 A71-12373

Static solar H II region ionization balance, energy, UV radiation transfer, gravitational equilibrium and interstellar gas temperature

06 p0975 A71-18442

Satellite solar power station for microwave generation, transmission and energy conversion to electrical power on earth

13 p1999 A71-28665

Microwave power transmission from orbiting solar power station to earth, discussing design optimization problems

13 p1999 A71-28666

Microwave power transmission from satellite solar energy station to earth, discussing atmospheric attenuation mechanisms and wavelength and power density optimization

13 p2000 A71-28670

Microwave receiving antenna with solid state power rectifier for converting energy from space solar cell array into DC power on earth

13 p2000 A71-28671

Solar energy degradation heat trapping-dissipating walls for inhabited living space on lunar surface

22 p3529 A71-42844

SOLAR ENERGY ABSORBERS

Solar energy absorptance changes in spacecraft thermal control surfaces exposed to particulate radiation at simulated synchronous altitude, using computerized model

12 p1928 A71-26761

SOLAR FACULAE

U FACULAE

SOLAR FLARES

Proton Flare Project 1969 observations concerning retrospective interval activity during maximum phase of solar cycle

01 p0144 A71-10286

Proton Flare Project 1969 observation of solar radio bursts by Alouette 2 satellite

01 p0144 A71-10287

Proton Flare Project 1969 observation of VLF radio wave propagation, detecting sudden phase anomaly events due to solar activity

01 p0144 A71-10288

Proton Flare Project 1969 observation of polar cap ionospheric disturbance due to proton event by VLF propagation phase measurement

01 p0073 A71-10289

Proton Flare Project 1969 observation of flares and subsequent ionospheric disturbances during retrospective interval

01 p0144 A71-10290

Limb flares relationships to solar soft X ray bursts intensity growth phase

01 p0144 A71-10868

Solar chromospheric flares observations tabulation /1969/ and H alpha line width curves graph

01 p0144 A71-10870

Solar flare proton propagation, examining interplanetary shock wave effects on cosmic ray scattering

01 p0146 A71-11386

Solar flare particles entrance into geomagnetic tail, modifying diffusion model

01 p0147 A71-11494

Ionospheric electron concentration enhancement at different heights during solar flare, using incoherent scatter radar technique

02 p0300 A71-12471

Soft solar X-ray flares six minute periodicity from satellite observation

02 p0300 A71-12472

Solar magnetic field polarity mapping from H-alpha filtergrams, using magnetic configurations in flare location and time forecasting

02 p0316 A71-12696

Solar flare classification based on X ray intensity, offering geophysical significance advantage

02 p0301 A71-12697

Solar X-ray flare activity statistical prediction based on correlation to coronal electron temperature and emission measure

02 p0301 A71-12698

Solar flare forecasting based on statistical correlation to magnetic fields inferred from H alpha filtergrams

02 p0301 A71-12699

Real time solar flare locations and region activity levels prediction based on hydrogen alpha inferred magnetic configuration

02 p0301 A71-12700

Solar active regions, examining development and occurrence of solar flares

02 p0301 A71-12758

Solar flare trigger mechanism, proposing inner corona thermal runaway of radiative power function

02 p0302 A71-12761

Solar microwave bursts and associated optical flares homologous characteristics, discussing radio emission mechanism

02 p0302 A71-12763

Solar flare of 30 March 1969, determining differential rigidity spectral index and small anisotropy

02 p0302 A71-12767

Solar flare particles effects on magnetospheric energetic particle population, discussing magnetic activity effects on trapped particles

[AIAA PAPER 70-1357]

03 p0473 A71-13578

Solar proton flares, coronal radio diameter and cosmic radiation intensity relationship

03 p0473 A71-13788

Sunspot areas and chromospheric flares relationship to distance from central meridian, noting Earth negative influence on solar activity and geometrical observational conditions

03 p0490 A71-13936

Oppositely polarized maximal magnetic field strengths in sunspot regions during proton flares

03 p0478 A71-13937

Ionospheric measurements by rocket-borne HF capacitance probe during solar flare of 26 February 1969, determining electron density vertical stratification

03 p0416 A71-14032

Solar proton and electron events from viewpoint of particle acceleration and magnetic field configuration in active region

03 p0478 A71-14036

Solar proton flares associated with 1968 and 1969 strong particle events, noting correlation with hard X ray and microwave bursts

03 p0478 A71-14037

Solar energetic protons measurements by ESR0 1 satellite following flare of 18 November 1968, noting cut-off latitude over northern polar cap

03 p0478 A71-14039

Solar X-ray emissions dynamic spectra at flare times by E-T tracing

03 p0479 A71-14045

Solar flare X ray and radio wave emission measurement byOGO 4 and Solrad 9 satellites

03 p0479 A71-14046

Solar X-rays emission anisotropy, questioning correlation with optical flares

03 p0480 A71-14047

Chromospheric flare north-south asymmetry aspects, calculating radio flux density correlation indices

03 p0417 A71-14193

Solar proton recording during flare by Proton 3 satellite

04 p0641 A71-15124

Impulsive solar flare X rays spectral characteristics, examining electron energy, bremsstrahlung, microwave bursts and particle escape, collisions and injection

05 p0797 A71-15937

Solar flare relative abundance and energy spectra of He 3 and He 4, using charged particle telescope on IMP 4

05 p0797 A71-15943

White light flares due to photosphere heating by flux of energetic ions and electrons impinging from above

05 p0797 A71-16028

Coronal condensations emission changes after microwave solar bursts, discussing circular polarization and flare mechanism based on collisionless dissipation of magnetic energy

05 p0804 A71-16029

SCL nomenclature denoting solar flare effect on long wave field intensity

05 p0804 A71-16033

Coronal magnetic structure mechanical diagnosis, using flare associated hydromagnetic disturbances

05 p0799 A71-16471

D region aeronomy characteristics and ionizing radiation energy spectra during solar flare of 22 October 1969

05 p0799 A71-16818

Absolute particle spectra above atmosphere and magnetosphere during solar flare of 23 February 1956

05 p0800 A71-17198

Cooling models for flare produced plasmas in solar corona, considering collisional, radiative and conductive mechanisms

06 p0968 A71-17913

Coronal magnetic fields before/after solar proton flares

06 p0950 A71-17917

Emission structure of large electron active region McMath plage 8905 mapped by 40 keV solar flare electrons

06 p0950 A71-17918

Diurnal cosmic ray neutron variations after proton flares, comparing calculated radial and azimuthal gradients to experimental data

06 p0951 A71-18105

Solar flare event of 28 January 1967, observing parent flare location, particle fluxes and diffusion and spectral exponent

06 p0957 A71-18143

Protons and alpha particles energy spectra during 25 February 1969 solar event from Centaur rocket observations as part of ESRO PCA campaign

06 p0957 A71-18144

Solar flare induced cosmic ray intensity increases registered by high latitude neutron monitors and Explorer 35 satellite, presenting intensity time profiles analyses

06 p0957 A71-18146

Solar cosmic ray proton event of 18 November 1968 studied with neutron monitor data from worldwide network, considering associated flare

06 p0957 A71-18147

Solar flare associated increases in cosmic ray intensity during November 1968-April 1969, correcting anisotropic peak and decay rates to standard barometric coefficients

06 p0957 A71-18148

HEOS A-1 satellite solar proton flux measurements from 25 and 27 February 1969 solar flares, noting strong backscattering of 360 MeV particles

06 p0957 A71-18149

Solar flares of 25-27 February 1969 effects on polar cap and interplanetary space flux rates, confirming magnetospheric modulation of proton density peaks

06 p0958 A71-18151

Solar flare on 9 June 1968, observing proton energy spectra and flux variation with time profiles

06 p0958 A71-18155

Particle flux energy spectra and time dependence of 25 February 1969 solar proton event

06 p0959 A71-18156

Solar flare electrons at 10-200 MeV region, discussing energy spectra and time history

06 p0961 A71-18170

Solar flare delayed relativistic electron appearance, comparing radio, optical and X ray data for particle intensities

06 p0961 A71-18171

Solar flare high energy electrons, examining rise time and decay

06 p0961 A71-18173

Neutron and gamma ray production by nuclear interactions in solar flares

06 p0961 A71-18175

Real time solar flare image production for Skylab astronaut training, using films of H alpha, XUV and X ray solar images

06 p0902 A71-18530

Quasi-exponential model of electron vertical profile in D region for aeronomic and ionizing radiation characteristics during solar flare of 30 October 1969

07 p1195 A71-19393

Soviet book on active protection of space vehicles covering measures against penetrating radiation from Van Allen belts, solar flares and galactic cosmic rays

07 p1207 A71-19474

Computational model for post acceleration propagation of solar flare charged particles

07 p1185 A71-19652

Solar vicinity particle storage implication from flare proton energy spectrum observation by Injun 5 satellite

07 p1186 A71-19653

Solar optical flares association with type 3 bursts fromOGO-3 observations, suggesting temporary creation or enhancement of electron stream propagation by filament or sunspot structure change

07 p1187 A71-19724

Impulsive hard X ray and far UV emission during solar flares

07 p1188 A71-19825

X ray line emission from heliumlike calcium during solar flare of 2 November 1969

07 p1188 A71-19826

Powerful solar flare H lines spectrophotometric observation, noting hydrogen atom upper energy levels overexcitation

07 p1188 A71-20033

Hydrogen atoms upper energy levels overexcitation in solar flare, suggesting role of stimulated photorecombinations

07 p1188 A71-20034

Spectrophotometric observation of solar weak chromospheric flare of 15 June 1964, determining flare origin

07 p1188 A71-20039

Time and spectral distribution of hard X ray radiation during solar flare, using nonrelativistic electron bremsstrahlung model

07 p1189 A71-20638

Interplanetary magnetic field in plane perpendicular to ecliptic, investigating force lines configuration by solar proton events

07 p1189 A71-20640

Critique on existence of one hundred million degree K solar flare plasma

08 p1350 A71-20944

Solar flare model, computing thermal X ray emission

08 p1350 A71-20945

Chromosphere-flare and galactic cosmic ray hypotheses of Forbush decrease and strong shock waves in interplanetary medium

08 p1352 A71-20967

Polarimetric measurements of solar X-ray flares by Intercoms 1 satellite

08 p1354 A71-21013

Solar X-ray flare region structure and emission flux density and spectral composition, using satellite-borne photometers and spectroheliographs

08 p1354 A71-21014

Solar flare electron spectra in interplanetary space and within earth magnetosphere, investigating simultaneous observations by satellite-borne magnetic electron spectrometers

08 p1354 A71-21037

Solar flare EUV radiation and ionospheric currents dynamo region ground based detection by geomagnetic crochets time structure analysis

08 p1355 A71-21198

Ionospheric electron density and reflection height during sudden phase anomaly in solar X-ray flare

08 p1355 A71-21222

Relativistic electrons acceleration in solar proton flares, taking into account plasma density and magnetic field intensity

09 p1512 A71-22059

Proton energy change effects on charged particles propagating in interplanetary space, using low energy solar flare proton fluxes observations

09 p1514 A71-22801

Probable solar flare doses on interplanetary mission calculated by MCFLEARE computer program using Monte Carlo methods

09 p1399 A71-22809

Unusual sunspot rotation from 30 September to 8 October 1969 in plage region No. 10344, noting flare activity and rotational motion

10 p1666 A71-23786

Sodium D line flare emission on solar surface vs comet scattering, using photoelectric observation in undisturbed center disk region

10 p1660 A71-23791

Solar flares explosive phase in photometric terms for flash onset correlations with 10.7 cm radio and hard X ray bursts, using H alpha film records

10 p1660 A71-23793

Soft X ray bursts involving solar flares from satellite observations, discussing thermal nature and total activity related H-alpha emission rates

10 p1660 A71-23794

Solar flare produced hard X-ray bursts, examining thermal processes and nonthermal electron distribution

10 p1660 A71-23796

Solar flare spectral line features at 1.9 A, considering iron ion origin

10 p1660 A71-23797

Negative sudden phase anomalies, related signal strength enhancements and short wave fadeouts, considering maximum flux density of solar X-ray flares

10 p1575 A71-23883

Polar caps energetic particle environment involving solar flare proton and electron fluxes

10 p1600 A71-24309

Solar wind blast wave dependence on initial disturbance energy and angular extent by time dependent two dimensional hydrodynamic flow simulation

10 p1663 A71-24779

Iron nuclei emission during 1967-1969 solar flares from spacecraft window and lunar camera lens etched tracks, discussing Fe/He ratio and lunar soil densities

11 p1815 A71-25299

International coordinated solar chromospheric flare effects on D region lower boundary and ionospheric propagation by Cosmos 261 satellite and ground based observatories

11 p1816 A71-25763

Solar flux from 7 July 1966 flare observation via Proton 3 satellite, obtaining cosmic rays integral spectra

11 p1817 A71-25781

Turbulent photosphere and chromosphere, investigating finite resistivity effects on solar flare phenomena

11 p1832 A71-26173

Type 3 solar radio bursts in absence of H alpha flares, noting soft X-ray emission

12 p1946 A71-26619

Solar flare two stage particle acceleration from X-ray burst observations, discussing induced electric field and Fermi mechanism

12 p1946 A71-26624

Geomagnetic crochet associated solar optical flares and microwave bursts during four year period, showing north-south asymmetry over disk

12 p1947 A71-26768

Cosmic ray storm analysis, showing enhanced daily/shortlived variations, radiation intensity increase and solar flare observations

12 p1949 A71-27375

Energetic solar X-rays, microwaves and EUV ionizing radiation during periodic bursts of solar flare

12 p1953 A71-27655

Energetic electrons generating solar flares position relation with active regions associated with type 1 radio noise storms

12 p1953 A71-27656

Long term storage of relativistic energetic electrons and protons in solar corona from IMP 4 and Pioneer 8 observations related to delayed emission from flares

12 p1969 A71-27657

Atmospheric altitude of soft X ray source volume in solar flares from optical and radio observations

12 p1954 A71-27709

Absolute spectra above atmosphere and magnetosphere and of particles accelerated in solar atmosphere during solar flare of 23 February 1956

13 p2128 A71-28253

Solar chromospheric flares in 1969, constructing tables of observation data commencement and end time and H alpha line maximum width

13 p2128 A71-28480

Solar corona soft X ray emission, investigating temperature and flare activity effects

13 p2129 A71-29051

Continuous emission in solar flare spectra from spectroheliographic data, suggesting photospheric origin

13 p2129 A71-29052

Plasmoid ejection during flare and condensation by radiative instability, interpreting Simple 3 solar radio bursts in terms of thermal emission

13 p2129 A71-29054

Solar radio burst of 27 September 1969, associating flare with dynamic spectrum

13 p2129 A71-29055

Nonthermal X rays and 10-100 KeV electron acceleration and emission from solar flares, using spacecraft observations

13 p2129 A71-29056

Relativistic electrons associated with solar particle events, measuring occurrence frequency, electron propagation and diffusion anisotropy

13 p2129 A71-29057

Solar flare cosmic ray propagation, investigating bounded interplanetary diffusion medium effects

13 p2130 A71-29060

Solar flares effect on potential gradient and air-earth current characteristics, suggesting solar triggered increase in thunderstorm frequency

13 p2130 A71-29107

Astronaut protection from solar flare high energy protons, discussing spacesuit, spacecraft orientation and solid, electrostatic, magnetic and plasma shielding

13 p2021 A71-29252

Motions in chromospheric limb and disk flares based on H alpha photography

14 p2298 A71-29974

Solar limb flare evolution on 11 July 1966, observing filament structure, vertical velocity and branching

14 p2298 A71-29975

Chromospheric flare on 11 July 1966, comparing solar radio emissions at 10 cm and 1.5 m wavelengths

14 p2298 A71-29976

Sunspots with proton flares of 7 July and 2 September 1969, examining longitudinal and transverse magnetic field components and total field vector

14 p2298 A71-29980

Solar cosmic ray flare catalog, using polar region absorption radio burst and proton event data

14 p2299 A71-29986

Coronal flare onset, examining dynamic processes of plasma compression with longitudinal magnetic field

15 p2482 A71-31335

VLF radio signals phase anomalies due to solar X-ray flares, monitoring by detectors onboard OSO-4 satellite

15 p2369 A71-31434

IQSY solar magnetic field, radio emission and corona observations, including flare data reevaluation

15 p2483 A71-31613

Radioheliographic 80 MHz observations of harmonic type 2 solar burst near limb flare

15 p2472 A71-31688

Culgoora 80 MHz radioheliographic observations of 13 October 1969 harmonic solar type 2 burst attributed to explosive flare behind west limb

15 p2472 A71-31689

Polarized meandering type 4 burst of solar flare from 80 MHz radioheliographic observations, noting association with plasmoids containing synchrotron emitting relativistic electrons

15 p2473 A71-31695

Statistical tests of solar flares based on maximum likelihood method, discussing longitude distribution, rigid rotation, planetary effects, etc.

15 p2480 A71-32751

Solar flare radiation data from Pioneer spacecraft, detailing anisotropy, heliocentric longitude gradients, decay time constants and energy spectra

15 p2480 A71-32752

Solar flare activity and sunspot distribution over central meridian from optical data by NASA solar particle alert network 1967-69

16 p2635 A71-33437

Geomagnetic field daily variation amplitude increase under equatorial electrojet during 7 July 1966 solar proton flare

16 p2567 A71-33768

Solar flare X-ray emission source position during eclipse of 7 March 1970, using OSO-5 satellite data

16 p2627 A71-33813

Soft X-ray emission line behavior during solar flares based on OSO-6 satellite-borne Bragg crystal spectrometer data

16 p2627 A71-33835

Solar flares forecasting based on group total sunspot area, largest spot area and spots number observations

16 p2627 A71-33903

Periodic solar flare X-ray emission, presenting time separation from Vela 5 and 6 scintillation detectors

16 p2629 A71-34078

Real time system for solar spectrophotometry, noting application for scanning H alpha and other Balmer series lines profiles in solar flare regions

17 p2741 A71-34994

Videometer instrument for solar flares quantitative measurement, eliminating red sensitive vidicon for real time operation in H alpha region

17 p2742 A71-35003

Sudden phase anomalies relation to solar flares, radio bursts and X radiation from severe worldwide ionospheric storm observation

17 p2796 A71-35349

Solar X-ray flares recorded by SOLRAD-9 on Explorer 37 satellite occurring in optical flares-microwave bursts-X ray flares sequence

17 p2796 A71-35391

OSO satellites observations, studying X ray flare phases, temperatures and spectra

17 p2808 A71-35521

Solar flare X-ray origin model, discussing charged particle acceleration to relativistic energies, ambient gas heating and thermal and nonthermal X rays

18 p2958 A71-36740

Simple type centimeter solar radio bursts identification and relation to flare position, noting radio spectrum over sunspot

18 p2958 A71-36741

Proton flares in McMath Region 8461 /August-September 1966/, describing solar wind plasma ejection and helium enriched interplanetary medium

18 p2958 A71-36743

Solar flare observations /14-19 November 1969/, obtaining H alpha line profile

19 p3124 A71-37229

Particle acceleration in solar flares, examining current layer generation in magnetic field above bipolar spot group

19 p3126 A71-37520

Quiet sun, active regions and flares far UV space observations interpretation based on models

19 p3136 A71-37615

Solar flare X and gamma rays, radio and far UV emission, discussing model for chromospheric cool plasma heating by flow through magnetic instability

19 p3126 A71-37620

Solar flare X ray spectrum analysis for lower corona physical conditions, discussing continuum and line emission

19 p3126 A71-37623

Solar prompt and delayed discrete particle events, discussing proton and electron sources, distribution and flare association

19 p3126 A71-37624

Quasi-exponential model of electron vertical profile in D region for aeronomic and ionizing radiation characteristics during solar flare of 30 October 1969

19 p3127 A71-37817

Ionization rates induced by solar flares charged particles in planetary atmospheres

19 p3142 A71-38047

Chromospheric flares effect on sporadic E layer under low solar activity conditions

19 p3130 A71-38527

Solar X-ray line emission, using crystal spectrometers during large chromospheric flare

19 p3130 A71-38672

Dynamic energy spectra of nonthermal electrons in solar flares from balloon-borne high resolution hard X ray observations

19 p3130 A71-38673

High frequency plasma turbulence in solar flares due to nonlinear conversion of ion-acoustic plasmons to Langmuir plasmons

20 p3279 A71-39304

Continuous solar UV and X rays monitoring by SOLRAD 10 satellite, investigating solar activity and flares effect on shortwave communications and manned space travel

20 p3294 A71-39580

Polarimetric measurements of solar X-ray flares by Intercoms 1 satellite

20 p3280 A71-39593

Solar X-ray flare region structure and emission flux density and spectral composition, using satellite-borne photometers and spectroheliographs

20 p3280 A71-39594

Mesospheric soft corpuscular radiation flux and temperature rocket observations, during solar flare activity

20 p3222 A71-39704

Low energy solar particle observation by widely separated Mariner and Explorer spacecraft, noting flare-associated and nonflare intensity peak correlation with sun

20 p3284 A71-39876

Solar boundary conditions effect on interplanetary propagation of solar flare particles for anisotropic diffusion model

20 p3285 A71-39896

Thermal effects in loop prominences formation after solar flares from model computer simulation

22 p3597 A71-41459

Related solar active regions during 14 January-1 June 1969, associating largest flares with inverted polarity

22 p3597 A71-41460

Solar proton flare prediction with microwave radio burst data, using satellite measurements

22 p3590 A71-41464

Electron acceleration and solar flare triggering due to quasi-static electric field caused by gas motion near photosphere

22 p3590 A71-41466

Neutron flux estimate from protons number needed for white light solar flare caused by energetic particle penetration into photosphere

22 p3590 A71-41467

Solar flares gamma ray flux, describing production by downward moving high energy particles

22 p3590 A71-41468

Solar low energy cosmic ray population anisotropy from satellite observations during flare event, describing rise time, decay, field alignment and time constant

22 p3591 A71-41469

International coordinated measurements of solar chromospheric flare effects on D region lower boundary and ionospheric propagation by Cosmos 261 satellite and ground based observatories

22 p3591 A71-41531

Ionospheric responses to solar flares, correlating sudden frequency deviations with sudden total electron content enhancement

22 p3592 A71-42222

Coronal flare onset, examining dynamic processes of plasma compression with longitudinal magnetic field

22 p3606 A71-42610

Mathematical model for solar flares formation based on magnetic/kinetic energy conversion, investigating plasma instability

23 p3719 A71-42950

Solar flare induced E and F regions electron density enhancement observation by Thomson scatter, noting relationship to EUV ionizing radiation

23 p3721 A71-43173

Interplanetary energy spectrum of solar flare Fe nuclei from tracks in Surveyor 3 glass filter and rock 12022

23 p3765 A71-43813

Material distribution as function of temperature in postflare loop system after east limb proton flare of 12 August 1970

23 p3768 A71-43847

High velocity H alpha ejections in association with important solar flare on 12 March 1969, suggesting mass motions control by gravitational field

23 p3721 A71-43848

Magnetic fields, bremsstrahlung and synchrotron emission in impulsive flare of 24 October 1969

23 p3721 A71-43849

Heliographic longitude effect on delay time between solar proton observation and flare occurrence from HEOS A1 data, noting magnetic field influence

23 p3768 A71-43852

Plasma current driven sheet at neutral point of cusp and quadrupole magnetic field for space physical simulation of solar flare and geomagnetic tail

23 p3714 A71-44277

He excitation and ionization in chromospheric flares, performing calculations for 10,000-50,000 K electron temperatures and 0.5-9.0 times 10 to 13th power per cc electron densities

23 p3722 A71-44310

Solar cosmic ray spectra at time of ejection from flare region and arrival near earth

24 p3866 A71-45040

Solar radio burst generation model based on effects of strong shock waves during chromospheric flares for geomagnetic storm prediction

24 p3867 A71-45081

SOLAR FLUX

Fesenkov photometer for aureole flux observations eliminating solar diffraction

01 p0080 A71-10542

Solar UV radiation measurements by OSO-3, obtaining flux variation over solar rotation period

03 p0481 A71-14508

Radiation intensity produced by inverse Compton effect between solar flux and Van Allen belt trapped high energy electrons

04 p0640 A71-14875

HEOS A-1 satellite solar proton flux measurements from 25 and 27 February 1969 solar flares, noting strong backscattering of 360 MeV particles

06 p0957 A71-18149

Ionospheric electron mean content 1964-1969 from density, ionization, slab thickness and solar flux diurnal and equinoctial peaks

07 p1097 A71-19025

Interplanetary space solar wind flux variations-earth electromagnetic field pulsations comparison by spacecraft and geophysical station observations

07 p1187 A71-19677

Sunspot activity and 107 mm solar flux 27 day variations during 11 year solar cycle

09 p1513 A71-22792

Radiatively interacting adjacent plates in presence of collimated solar flux, considering surface roughness effects on equilibrium temperature distribution [AIAA PAPER 70-817]

11 p1854 A71-25511

Solar proton anisotropy measurements, discussing flux directional distribution

14 p2297 A71-29670

Spectral analysis of solar microwave bursts, examining flux and energy variation with frequency

19 p3146 A71-38577

Long term upper atmosphere density variations correlated with solar flux, using satellite observations

20 p3223 A71-39708

Balloon measurement of solar flux and brightness temperature in 12-24 micron range

24 p3873 A71-45142

SOLAR FLUX DENSITY

NT SOLAR CONSTANT

Absolute measurements of solar flux density at 9500 MHz, comparing Nagoya and Heinrich-Hertz Institute radiometric observations

02 p0302 A71-12760

Solar radiation fluxes at earth surface in presence of cumulus clouds, relating fluxes to cloud magnitude and sunshine duration by regression relations

06 p0889 A71-17648

Solar flux from 7 July 1966 flare observation via Proton 3 satellite, obtaining cosmic rays integral spectra

11 p1817 A71-25781

Solar limb flocculus on 15 June 1967, noting electron temperature and concentration, effective length, emission and luminescence

12 p1964 A71-27083

Solar neutron flux measurements compared to previous spark chamber scintillation experiment flown at Hyderabad, India

13 p2120 A71-27927

Solar limb flocculus on 15 June 1967, noting electron temperature and concentration, effective length, emission and luminescence

19 p3133 A71-37433

Solar radioelectric activity in 1966, tabulating mean daily density and variability of solar flux

21 p3442 A71-40152

Solar flux density measurements at 2980 MHz, noting integration with spectral curve

22 p3590 A71-41463

Solar proton flux from 7 July 1966 flare observation via Proton 3 satellite, obtaining cosmic rays integral spectra

22 p3591 A71-41549

SOLAR GENERATORS

NT SOLAR AUXILIARY POWER UNITS

NT SOLAR CELLS

CdS-CuS n-p junction solar converters, noting long-wave sensitivity dependence on light extrinsic absorption

02 p0190 A71-11896

Reliable brushless direct-drive system design for controlling position and rate of solar power arrays on orbiting spacecraft

12 p1869 A71-27432

Satellite solar power station for microwave generation, transmission and energy conversion to electrical power on earth

13 p1999 A71-28665

Microwave power transmission from orbiting solar power station to earth, discussing design optimization problems

13 p1999 A71-28666

High efficiency and power long life cross field amplifier generator for solar energy conversion in space into microwave, discussing magnetron and amplifier

13 p2000 A71-28668

Cost optimization for solar generator thermobatteries by selecting temperature, contact resistance, material parameters and fabrication technology

15 p2351 A71-31671

Reliability analysis of solar thermoelectric generator module as function of individual photocells, circuit design and redundancy

15 p2351 A71-31672

Solar-array space station environmental control and life support system design for 12-man 10-year mission capability with 180-day resupply

18 p2866 A71-36379

Orbital electric power system performance simulation for analysis of solar array/battery lock-up, comparing graphical and computer techniques

20 p3183 A71-38957

Photoeffect efficiency of solar energy converters based on semiconductor cadmium sulfide-copper sulfide heterojunctions

22 p3483 A71-42536

CNES hypotheses and methods determining current delivered by solar generator of FR 1 satellite, discussing electrical performance due to electron and proton irradiation

24 p3793 A71-44760

SOLAR GRAVITATION

Two dimensional motion stability near sun-perturbed earth-moon triangular libration points, using computerized high order treatment

04 p0653 A71-15708

Robertson metric beta and gamma coefficients and solar dynamic oblateness determination from probe motion under relativistic effects

[ONERA-TP-893]

06 p0970 A71-18024

Lunar motion theory, discussing radial perturbation, variation, parallactic and annual inequalities, secular acceleration and evection

11 p1822 A71-25684

Static solar H II region ionization balance and energy, UV radiation transfer, gravitational equilibrium and interstellar gas temperature

12 p1955 A71-26592

Venus upper atmosphere retrograde circulation correlation with solar couple effect on thermal semidiurnal atmospheric tide

13 p2134 A71-28286

General relativistic time delay of electromagnetic radiation propagation due to solar gravitational field measured from Mariner 6 and 7 range and Doppler data

16 p2640 A71-33737

Gyroscope apparent precession due to reference star light deflection by solar gravitational field

20 p3270 A71-39559

Lunar and solar gravitation effects on leveling from formulas and nomogram, noting seasonal maximum effect in southern latitudes and Northern Hemisphere

23 p3670 A71-43302

Solar gravitational deflection of radio waves measured by Cambridge one-mile telescope, observing radio source 3C 279 before/after 8 October 1970 occultation

23 p3769 A71-43990

Cometary nucleus outbursts and splitting moments spatial distribution, indicating solar radiation and tidal action effects

24 p3868 A71-44457

SOLAR HEAT FLOW

U HEAT FLUX

U SOLAR FLUX

SOLAR HEATING

Flexible Storable Tubular Extendible Member (STEM) in-plane bending vibrations under solar heating

01 p0173 A71-10941

Venus atmosphere rotational model, considering nonlinear instability due to wind shear from solar heat induced convection

03 p0489 A71-13607

Thermospheric heating by solar radiation in Schumann-Runge continuum, taking into account height and atmospheric components distribution

09 p1435 A71-22431

Liquid water natural occurrence on Martian surface, considering possibility of ice melting by sunlight or other heat sources

11 p1826 A71-25718

Glazing lunar craterlet interiors in Apollo 11 observations, comparing solar flash heating and volcanic bomb impact formation

15 p2493 A71-32484

Haze scattering effect on solar radiative heating rate due to water vapor absorption in near IR

17 p2736 A71-35561

Acoustic wave propagation and heating in solar atmosphere, using Harvard Smithsonian reference atmosphere and Stein frequency spectra

22 p3601 A71-42170

Mars and Venus carbon dioxide atmospheres, covering solar EUV heating efficiency, upper atmosphere temperature and chemical recombinations

23 p3735 A71-43334

Governing equations numerical integration for Venusian atmosphere circulation, calculating solar heating distribution in spherical polar coordinates

23 p3735 A71-43340

Solar coronal heating neutron theory based on solar gamma ray flux considerations

23 p3770 A71-44014

SOLAR INSTRUMENTS

NT SPECTROHELIOGRAPHS

Horizontal AT&U solar telescope and ASP-20 and DFS-3 diffraction spectroscopes, discussing performance, time relay and resolution

04 p0589 A71-14830

TV techniques for solar optical image, describing equipment for recording and conversion

04 p0589 A71-14835

Solar telescope coelostat and auxiliary mirror hydropneumatic unloading mechanism

04 p0566 A71-14870

OAO continuous observation capability, Project STAR telescopes, solar and X ray instruments and resupply missions based on space shuttle concept

05 p0818 A71-17132

Solar polar magnetic field simultaneous measurements at Crimea and Mount Wilson from magnetographs

06 p0967 A71-17901

High resolution UV solar photographs by stratospheric balloon-borne Cassegrain telescope

10 p1680 A71-25018

Green corona corrections of position-angle errors, east-west asymmetry, photometric scale instability and threshold measurements

11 p1832 A71-26181

Vertical geophysical sounding rocket research program and equipment for observing ionospheric parameters, solar UV and X rays, atmospheric absorption and meteorites

11 p1839 A71-26353

Space vehicles solar orientation sensors, discussing construction, configuration and direction finding characteristics

12 p1972 A71-27485

Apollo Telescope Mount for high resolution solar observation and manned instruments evaluation in space environment, discussing attitude and pointing control systems

15 p2500 A71-31458

Polarization characteristics of solar coude telescope and Littrow spectrograph at Okayama Astrophysical Laboratory

19 p3062 A71-37241

Statistical analysis of microphotometer scan of solar granulation photographs blurring during partial eclipse of 20 May 1966, correcting image for atmospheric and instrument effects

21 p3439 A71-40053

SOLAR LIMB

Spicule horizontal component motion from H alpha spectra movies with slit tangential to solar limb

02 p0316 A71-12756

Quiescent and sunspot prominences line of sight velocity measurements on limb, investigating statistical properties of velocity field

02 p0316 A71-12759

Center limb linearized impulsiveness calculations for type 2 solar bursts recorded with circular polarization features

02 p0302 A71-12762

Photoelectric photometer with mechanical chopper for extreme limb darkening measurement at total eclipse

03 p0424 A71-13635

Portable photoelectric recorder for solar limb vibration frequency spectrum and amplitude measurements

04 p0590 A71-14844

Solar chromosphere structure and Lyman continuum, examining brightness and kinetic temperatures, limb variations, radiative transfer and models

05 p0803 A71-16023

Eclipse observations interpretation for transition region between extreme limb and low chromosphere

06 p0967 A71-17905

Solar center-limb Fraunhofer line profile variations observed with double diffraction monochromator

09 p1524 A71-23192

Fraunhofer lines at solar disk center and near limb, investigating profiles for asymmetry

09 p1524 A71-23194

Solar simplified geometrical model, observing emission peak center to limb variation of Mg II, H and K lines and optical thickness

10 p1666 A71-23782

Solar eclipse measurements at 1.18 cm on 11 September 1969, describing limb brightening and center and coronal emission

10 p1666 A71-23790

Solar limb darkening measurement with high temporal resolution and inner corona photometry by white and polarized light during 7 March 1970 eclipse

10 p1678 A71-24829

Solar limb flocculus on 15 June 1967, noting electron temperature and concentration, effective length, emission and luminescence

12 p1964 A71-27083

Solar corona photometry during 22 September 1968 eclipse, determining brightness variations and decrease from limb

12 p1966 A71-27231

Green line intensity and electron/ion density contours as function of height over solar limb for March 1970 coronal enhancement

12 p1969 A71-27651

Solar Na D lines Doppler width, describing limb darkening data, assuming source function frequency dependent

12 p1970 A71-27748

Solar atmosphere center limb observations, describing line intensity fluctuations in Na D and Na 5688 doublets and Mg 4571 line

13 p2140 A71-29044

Motions in chromospheric limb and disk flares based on H alpha photography

14 p2298 A71-29974

Radioheliographic 80 MHz observations of harmonic type 2 solar burst near limb flare

15 p2472 A71-31688

Culgoora 80 MHz radioheliographic observations of 13 October 1969 harmonic solar type 2 burst attributed to explosive flare behind west limb

15 p2472 A71-31689

Excess red shift of Fraunhofer lines at extreme limb explained by mechanism of radial currents in solar atmosphere

16 p2629 A71-32807

Solar Fraunhofer line wavelengths shifts at disk center and at limb, evaluating Stark broadening contribution

18 p2962 A71-36106

Center to limb solar brightness distribution at 1.4 mm, discussing chromospheric models and antenna beam pattern effects

18 p2965 A71-36735

Solar chromospheric plage area related to peak K coronal brightness at limb

18 p2966 A71-36738

Solar corona photometry during 22 September 1968 eclipse, determining brightness variations and decrease from limb

19 p3132 A71-37383

Solar limb flocculus on 15 June 1967, noting electron temperature and concentration, effective length, emission and luminescence

19 p3133 A71-37433

Solar limb and disk intensity spectra in chromosphere-corona transition region, calculating models, element abundances structure, electron pressure and hydrostatic equilibrium equations

19 p3136 A71-37617

Solar limb H alpha spicules spectrograms, noting oscillations and time intervals

19 p3147 A71-38665

Solar limb D3 He line intensity distribution measurements during eclipse of 22 September 1968

19 p3147 A71-38666

Sunspot intensity during 9 May 1970 Mercury transit with corrections for scattered light from solar limb observations

19 p3147 A71-38669

Emission characteristics above solar limb in four EUV lines, comparing with K-coronameter measurements to estimate element abundances

19 p3130 A71-38671

Solar limb high resolution photography at different H-alpha wavelengths, using tunable 1-8A and 1A Halle filters in tandem for parasitic light elimination

22 p3596 A71-41455

Oscillations of visible chromosphere boundary and regularity in position of spicule groups along limb, studying H alpha filtergrams

22 p3597 A71-41456

Material distribution as function of temperature in postflare loop system after east limb proton flare of 12 August 1970

23 p3768 A71-43847

SOLAR LONGITUDE

Green corona activity longitudinal distribution from solar cycle observations, noting underphotospheric rigid body rotation

15 p2497 A71-32748

Sporadic and shower meteoroids mass distribution temporal variations as function of magnitude and solar longitude from visual and radio echo measurements

20 p3298 A71-39643

Heliographic longitude effect on delay time between solar proton observation and flare occurrence from HEOS A1 data, noting magnetic field influence

23 p3768 A71-43852

SOLAR MAGNETIC FIELD

Solar magnetic field regions, bright line structures and faculae from Fraunhofer lines analysis, discussing magnetic downward velocities

01 p0152 A71-10328

Solar magnetic fields configuration and evolution, discussing sunspots and white light faculae

01 p0152 A71-10330

Turbulent diffusion role in magnetic fields origin in sun, planets and galactic gaseous disk

01 p0162 A71-11419

Spectraspectroheliograph observations, noting correlations between contour maps of solar continuum intensity and magnetic fields

[AIAA PAPER 70-1360]

02 p0315 A71-12693

Solar magnetic field polarity mapping from H-alpha filtergrams, using magnetic configurations in flare location and time forecasting

[AIAA PAPER 70-1369]

02 p0316 A71-12696

Solar flare forecasting based on statistical correlation to magnetic fields inferred from H alpha filtergrams

[AIAA PAPER 70-1372]

02 p0301 A71-12699

Real time solar flare locations and region activity levels prediction based on hydrogen alpha inferred magnetic configuration

[AIAA PAPER 70-1373]

02 p0301 A71-12700

Photospheric magnetic field direction autocorrelation showing differential and rigid rotation properties at various heliographic latitudes

02 p0316 A71-12751

Solar general magnetic field determination by measuring visually small displacements on photographic plate 02 p0316 A71-12752

Solar magnetic fine structure production by gas motion in supergranular convection 02 p0316 A71-12753

Solar faculae semiempirical models, cospatial with strong photospheric magnetic fields constructed from continuum observations 02 p0316 A71-12757

Quasi-stationary coronal magnetic field and electron density from Faraday rotation experiment, using theoretical model 02 p0302 A71-12769

Sunspot spectrograms analysis, observing wavelength shift in Zeeman triplet circular components and magnetic splitting inequality under different circular polarizations 03 p0484 A71-13210

Oppositely polarized maximal magnetic field strengths in sunspot regions during proton flares 03 p0478 A71-13937

Solar proton and electron events from viewpoint of particle acceleration and magnetic field configuration in active region 03 p0478 A71-14036

Solar magnetograph with potentiometers, recording magnetic fields, emission and absorption lines, radial velocity and brightness 04 p0589 A71-14836

Lunar and solar periodic magnetic variations, using time series analysis based on discrete Fourier transforms for frequency spectrum lines 04 p0582 A71-15097

Solar magnetic field variation observation, revealing sun as quadrupole magnetic rotator 04 p0657 A71-15828

Photospheric and interplanetary magnetic field polarity and magnitude comparison, using Explorer observations 05 p0802 A71-16012

Solar corona magnetic fields and structure during 12 November 1966 eclipse, determining electron densities and temperatures 05 p0802 A71-16013

Solar coronal magnetic field patterns from radio observations 05 p0802 A71-16014

Line formation calculations for different spot models and arbitrary depth dependence of magnetic field vector, interpreting pi component anomalous splitting 05 p0803 A71-16021

Circular polarization measurement in various lines, finding magnetic field strength influenced by line absorption coefficient variations from photosphere to spot and faculae 05 p0803 A71-16025

Longitudinal magnetic field component measurement quiescent prominences, relating to angle between prominence and north-south direction on sun 05 p0804 A71-16026

Coronal magnetic structure mechanical diagnosis, using flare associated hydromagnetic disturbances 05 p0799 A71-16471

Solar polar magnetic field simultaneous measurements at Crimea and Mount Wilson from magnetographs 06 p0967 A71-17901

Longitudinal magnetic field in quiescent prominences from magnetograph recording of Zeeman effect on hydrogen, helium and metal lines 06 p0967 A71-17909

Coronal magnetic fields before/after solar proton flares 06 p0950 A71-17917

Sun daily mean-interplanetary polarized magnetic fields correlation, using source surface model 06 p0968 A71-17920

Sun as variable star, discussing brightness, rotation and magnetic characteristics 06 p0971 A71-18245

Radial velocity distribution-magnetic fields connection in solar atmosphere active and quiet regions 06 p0975 A71-18437

Sunspot observations on 3 July and 14 September 1967, examining transverse magnetic field distribution and radial gas velocities and motion with magnetograph 07 p1195 A71-19338

Meridional solar magnetic field shape determination, discussing latitude drift of spot forming zones, coronal penetrations and 80 year sunspot periodicity 08 p1358 A71-20887

Coronal magnetic field geometry maps, using high altitude photospheric field measurements for correlations with active sun 08 p1363 A71-21154

Earth and sun magnetic field production models as function of dynamo states, discussing solar field effects on terrestrial space environment 09 p1517 A71-22334

Neutrino magnetic moment spin precession effects on solar magnetic fields, discussing electromagnetic field-charged particles interaction 09 p1528 A71-23593

Sunspot group magnetic field distribution and radial velocities, investigated at H alpha and 6302.499 A atmospheric levels 10 p1666 A71-23788

Magnetostatic sunspot model with twisted field showing radial dependence of azimuthal component 10 p1666 A71-23789

Quiet solar wind two component model, including viscosity, magnetic field and reduced heat conduction 10 p1662 A71-24498

Radial velocity fields-magnetic fields relationship in solar atmosphere active and quiet regions 12 p1955 A71-26587

Terrestrial, solar and galactic magnetic fields, discussing generation by combined nonuniform rotation and cyclonic turbulence based on dynamo equation 12 p1961 A71-26859

Velocity and magnetic field measurements in solar active regions, using fine scan simultaneous Doppler and magnetogram observations 12 p1968 A71-27646

Oscillatory hydromagnetic dynamo model of large scale solar magnetic field of variable sign, using Bernard convective cell with Coriolis velocity disturbance 13 p2137 A71-28529

Magnetic field strength measurements from Zeeman splittings of sunspots molecular lines, considering saturation effects 13 p2140 A71-29047

Unipolar sunspot magnetic field and electric currents, comparing chromosphere and photosphere total field vector 14 p2298 A71-29978

Sunspot umbra, calculating vertical magnetic field strength distribution from Fraunhofer lines 14 p2308 A71-29979

Sunspots with proton flares of 7 July and 2 September 1969, examining longitudinal and transverse magnetic field components and total field vector 14 p2298 A71-29980

Solar atmospheric active regions, comparing longitudinal and transverse magnetic field strengths at various levels 14 p2308 A71-29981

Coronal flare onset, examining dynamic processes of plasma compression with longitudinal magnetic field 15 p2482 A71-31335

ISQY solar magnetic field, radio emission and corona observations, including flare data reevaluation 15 p2483 A71-31613

Moving type 4 solar radio burst, describing bipolar magnetic structure and origin in synchrotron radiation from relativistic electrons 15 p2473 A71-31692

Circular polarization and fadeout of moving solar type 4 burst related to magnetic arch and synchrotron emitting electrons deceleration 15 p2473 A71-31693

Solar atmospheric model, calculating shock wave dissipation in chromosphere for photosphere central iron line intensity correlation with magnetic field intensity 15 p2497 A71-32746

MHD planetary waves existence on sun, estimating mean toroidal solar magnetic field and rotation rate 15 p2497 A71-32756

Seasonal and annual longitudinal variations in ionospheric ion distribution, stressing solar geomagnetic control importance 16 p2567 A71-33762

Coronal and interplanetary magnetic fields during 7 March 1970 solar eclipse, comparing calculated field line maps with coronal structure photographs 16 p2641 A71-33775

Sunspot convective heat transfer in terms of magnetic field convection theory, considering motion in photosphere 17 p2802 A71-34826

High resolution quiescent and active solar prominences and magnetic field observations, discussing Zeeman effect and line spectrum polarization 17 p2806 A71-35393

Solar alpha effect dynamo effect model, determining nonaxisymmetric magnetic field generation 18 p2960 A71-35936

Type 2 radio burst disturbances in coronal magnetic field, considering shock wave travel parallel to magnetic field lines 18 p2957 A71-36159

Profile changes of magnetically non-split lines in faculae, explaining observations by outer layers temperature increase 18 p2965 A71-36731

Telescopic phase retardation effect on polarization in Zeeman split Fraunhofer line, discussing consequence for solar magnetic field determination 18 p2965 A71-36732

Solar corona model for structure and dynamic properties, investigating gas-magnetic field interactions 18 p2966 A71-36737

Polarized solar millimeter emission associated with sunspot magnetic field compatible with multiple sources from chromosphere 18 p2966 A71-36762

MHD systems equilibrium and stability involved in quiescent prominences, considering temperature dependence of heat conductivity, magnetic field and initial gas compression 18 p2967 A71-36927

Particle acceleration in solar flares, examining current layer generation in magnetic field above bipolar spot group 19 p3126 A71-37520

Optical space observations need in solar physics, stressing 0.2 sec angular resolution for extreme UV and magnetic field measurement 19 p3136 A71-37619

Large scale alternating solar magnetic field generation by outer shell convective flow, constructing oscillator hydromagnetic dynamo model 19 p3145 A71-38353

Solar prominences magnetic fields, determining strength and orientation with Zeeman effect 19 p3146 A71-38572

Large scale convection solar magnetic field patterns calculations based on rotating thin spherical shells, noting solar cycle activity 19 p3147 A71-38667

Viscous torsional vibrations inadequacy for interpreting solar activity cycles relative to magnetic field 20 p3290 A71-39303

Short periodical pulsations in solar atmosphere related to magnetosound propagation in area of temperature minimum with directed perpendicular magnetic field 20 p3290 A71-39305

Solar magnetic field generation by gyrotropic turbulence, noting inadequacy of Steenbeck explanation for quantitative estimates of solar cycle parameters 20 p3291 A71-39317

Time variation of average values of magnetic field strength and size in solar polar regions, noting field element decrease before solar activity maximum 20 p3291 A71-39322

MHD models of photospheric layers of sunspots emphasizing magnetic forces distribution 20 p3292 A71-39444

Astronomical models relating sunspots to solar magnetic field existence 20 p3293 A71-39530

Nonflare solar X-ray emission from Cosmos 230 observation, noting presence of sunspot groups with complicated magnetic fields during enhanced short wave emission 20 p3283 A71-39749

Solar corona current sheet magnetic model, computing polar plume orientations and radial and nonradial streamers 21 p3453 A71-41359

Solar atmosphere closed magnetic loop system model, determining surface differential rotation rate and angular velocity distribution 22 p3596 A71-41452

Spiral topology of chromospheric fibrils and filaments in H alpha near sunspots, noting similarity with axisymmetric force free magnetic field configuration 22 p3597 A71-41458

Coronal flare onset, examining dynamic processes of plasma compression with longitudinal magnetic field 22 p3606 A71-42610

Polarized solar radio emission at millimeter wavelength in active regions associated with sunspot magnetic fields 23 p3733 A71-43125

Dynamo theory of solar and lunar magnetic fields diurnal variations, determining ionospheric wind velocities and pressure changes 23 p3669 A71-43174

Magnetic fields, bremsstrahlung and synchrotron emission in impulsive flare of 24 October 1969 23 p3721 A71-43849

Molecular gas dissociation equilibrium and carbon monoxide overtone line widths dependences on magnetic field strength in sunspots 24 p3868 A71-44459

Transverse magnetic field measurement over sunspot in chromosphere, noting fan-shaped field line divergence 24 p3870 A71-44817

Solar unipolar magnetic regions relation to geomagnetic disturbances variability, discussing 11 year cycle 24 p3823 A71-45036

SOLAR NEBULA

U SOLAR CORONA

SOLAR NOISE

U SOLAR RADIO EMISSION

SOLAR OBSERVATORIES

NT OSO

NT OSO-E

NT OSO-3

Worldwide geophysical observatories network for observing solar optical, radio, particle X rays and geomagnetic and ionospheric effects [AIAA PAPER 70-1354] 02 p0239 A71-12692

Mauna Loa coronagraph observations before, during and after 7 March 1970 solar eclipse 06 p0968 A71-17912

Balloon heliophysics, discussing equipment and working program of first Soviet stratospheric solar station 07 p1195 A71-19336

ATM for manned solar observation, discussing thermal design, thermal vacuum test philosophy, mathematical models and analytical and test data correlation [AIAA PAPER 71-433] 11 p1838 A71-26222

Canadian observational sites for solar eclipse of 10 July 1972, describing expected weather conditions, totality time/duration and location accessibility 16 p2630 A71-33125

Meteorological planning study for 1973 African solar eclipse observation site selection 16 p2572 A71-33844

Sunspot relative number observation accuracy test by least squares method for solar observatories 19 p3130 A71-37226

SOLAR ORBITS

NT PERIHELIONS

Hilda minor planet group and Thule motion, examining real orbit relation to Schwarzschild type periodic orbits 01 p0155 A71-10441

Comet distributions near Jupiter orbit 03 p0487 A71-13375

Hyperbolic, elliptical and parabolic heliocentric motion, determining location of body in orbit with unitary method 03 p0493 A71-14194

Sunspot cycle period relationship to planetary orbital periods 03 p0493 A71-14210

Pluto-Neptune system implications for solar system evolution theories, discussing deterministic and statistical models and a body problem approaches 04 p0655 A71-15726

Hill lunar solution of a planet problem in rectangular heliocentric coordinates 04 p0656 A71-15733

Neptune orbital motion prediction, determining effect of variations in time and mean distance on accuracy 05 p0810 A71-16542

Nearly parabolic comets orbital orientation relation to sun peculiar motion direction, noting repulsive particles capture mechanism 06 p0976 A71-18449

Minor planets mean motions commensurability with Jupiter in restricted three body problem 07 p1202 A71-20515

Active cosmic ray modulation layer boundaries between sun and earth orbits, studying meteorite isotopes radioactivity 08 p1352 A71-20973

Small natural vibrations effect of solar sail-propelled system on heliocentric orbit motion 09 p1531 A71-22559

SERT 2 solar array power system in sun synchronous orbit, considering power conditioning and deployment technique [AIAA PAPER 70-1159] 09 p1387 A71-22901

Planetary motion mutual perturbation, presenting method for expansion of disturbing function 09 p1525 A71-23334

Observations distribution influence on accuracy of almost circular planetary orbits determining elements, considering geocentric distances and ecliptic longitudes and latitudes 09 p1526 A71-23345

Mercury and Venus transit periodicity before solar disk, examining celestial mechanics and solar system distances determination 10 p1680 A71-25003

Asteroid ring origin, discussing osculating and corresponding secular orbital elements of mother planet 11 p1820 A71-25245

Meteoroids orbital elements statistically compared to asteroids 11 p1820 A71-25246

Planetary formation, obtaining retrograde orbit probability and distances and masses expectation by stochastic model 11 p1830 A71-26110

Nearly parabolic comets orbital orientation relation to sun peculiar motion direction, noting repulsive particles capture mechanism 12 p1955 A71-26599

Pales /49/ orbit motion analysis for Jupiter mass, noting discrepancies between old and new observations 15 p2488 A71-32198

Earth velocity vector right ascension, declination and magnitude determination from cosmic 3 K background radiation anisotropy 16 p2563 A71-33402

Sun as flattened ellipsoid of revolution, showing flatness effects on planet motion in relativity theory framework 16 p2612 A71-33567

Mars, Uranus and Jupiter observations with Sao Paulo Observatory Danjon astrolabe, presenting east and west transits right ascension and declination tables 18 p2961 A71-35943

Space-time model of torsion tensor effect on geodetic lines under Schwarzschild metric, evaluating orbital perihelion motion of planets and light ray bending 18 p2967 A71-36826

Sun-earth distance and earth orbital eccentricity effect on E region peak electron density, discussing Chapman-Like model 21 p3372 A71-40035

Icarus photographic observations, determining general relativity effects on orbital motion 21 p3443 A71-40187

Outer planets masses determination from orbit perturbations analysis and optical observations [AAS PAPER 71-312] 23 p3725 A71-42988

Mars orbiters and Kepler laws, discussing planetary motion, satellite orbits and orbital characteristics 24 p3875 A71-45268

SOLAR PARALLAX

Stellar intrinsic motions with respect to galaxies, including solar apex coordinates, secular parallax and Oort constants 07 p1194 A71-19331

SOLAR PHYSICS

Solar diatomic molecules vibrational degree of freedom model, applying Boltzmann distribution 08 p1365 A71-21773

Granular features of solar surface, describing television equipment used aboard balloon for image in 1.2-2 microns region 10 p1680 A71-25004

Protosun and primordial solar nebula evolution based on dust particles behavior 11 p1819 A71-25221

Krause-Steenbeck solar dynamo eigenvalue evaluation assuming step function differential rotation and delta function alpha-effect for approximation 12 p1971 A71-27749

Solar X-ray line spectra observation, noting K alpha transition indicative of suprathermal events 14 p2297 A71-29598

Supersonic to subsonic solar corona transition, using supersonic solution for solar wind inviscid equations 14 p2302 A71-30648

Sun and interplanetary medium, considering pure atomic physics, radio emission, IR excess, solar wind, sunspots and solar radio astronomy 15 p2486 A71-31924

Solar diatomic molecules vibrational degree of freedom model, applying Boltzmann distribution 15 p2495 A71-32678

Swedish space research activity covering upper atmospheric physics, ionosphere, magnetosphere and solar phenomena 16 p2665 A71-33853

Polish space research covering satellite tracking, solar physics interplanetary gas dynamics, meteorological rockets and aerospace medicine 16 p2666 A71-33856

German Democratic Republic space research, reviewing meteorological, ionospheric, geomagnetic and solar physics studies 16 p2666 A71-33864

Solar corona studies at Kiev University during 1952, 1954, 1961, 1965 and 1968 solar eclipses, showing coronal fine structure relation to chromosphere 17 p2802 A71-34827

Solar oblateness and Li abundance interpretation by model of thermally driven turbulence terminated at rotating core surface containing partial mass 17 p2806 A71-35385

ESRO sounding rocket program covering atmospheric and ionospheric physics and solar and auroral phenomena 18 p2896 A71-35926

Solar studies with emphasis on space observations - Conference, London, April 1970 19 p3135 A71-37608

Optical space observations need in solar physics, stressing 0.2 sec angular resolution for extreme UV and magnetic field measurement 19 p3136 A71-37619

Stellar chromosphere detection through H, K and metastable He lines observation, noting importance for solar physics 19 p3136 A71-37627

Proposed model with neutrons as energy source for solar corona, discussing validity based on capture gamma ray flux expectation 19 p3127 A71-38009

Electron acceleration and solar flare triggering due to quasi-static electric field caused by gas motion near photosphere 22 p3590 A71-41466

Neutron flux estimate from protons number needed for white light solar flare caused by energetic particle penetration into photosphere 22 p3590 A71-41467

Solar spaceborne astronomy, examining progress in temperature and density profiles determination 22 p3605 A71-42524

SOLAR PLASMA [RADIATION]

U SOLAR WIND

SOLAR POSITION

Lower ionosphere electron density changes with solar zenith angle during active sun year 04 p0583 A71-15213

Atmospheric ion concentration at 100-200 km related to solar zenith angle, describing diurnal and vertical behavior by photochemical theory 05 p0744 A71-17182

F I layer occurrence frequency probability vs solar elevation 07 p1100 A71-19399

Radio wave absorption measurement at constant solar zenith angle of 65 deg, discussing seasonal variation 07 p1101 A71-19408

Balloonborne radiometric instrumentation for solar and thermal radiations upward and downward flux measurements, discussing net radiation balance as function of solar elevation 09 p1515 A71-23558

Obliquely incident radio wave absorptions measurements from January-October 1968 vertical ionospheric soundings, correlating diurnal variations with solar zenith angular changes 11 p1732 A71-25787

Atmospheric zero light polarization points, examining solar vertical and various aluminanters, horizontal and vertical nonuniformities and albedo variations 11 p1795 A71-25925

Green corona corrections of position-angle errors, east-west asymmetry, photometric scale instability and threshold measurements 11 p1832 A71-26181

Directional thermal emission from rough lunar surface as function of crater frequency, aspect ratio and solar deviation angle, comparing to Lambertian behavior [AIAA PAPER 71-480] 11 p1833 A71-26256

Atmospheric ion concentration at 100-200 km related to solar zenith angle, describing vertical and diurnal density pattern by photochemical theory 13 p2059 A71-28239

Time between noon and evening maxima in F2 layer critical frequency compared with evening maximum period, showing dependence on nighttime solar zenith angle 13 p2062 A71-28559

Cosmic ray annual intensity variations indicating gradient perpendicular to solar equatorial plane 16 p2625 A71-32801

F I layer occurrence frequency probability vs solar elevation 19 p3053 A71-37823

Radio wave absorption measurement at constant solar zenith angle of 65 deg, discussing seasonal variation 19 p3053 A71-37832

Atmospheric zero light polarization points, examining solar vertical and various aluminanters, horizontal and vertical nonuniformities and albedo variations 20 p3257 A71-39216

Day airglow columnar emission rates for Lyman-Birge-Hopfield system of molecular nitrogen as function of solar zenith angle, using OGO 4 observations 20 p3231 A71-39892

Obliquely incident radio wave absorptions measurements from January-October 1968 vertical ionospheric soundings, correlating diurnal variations with solar zenith angular changes 22 p3509 A71-41555

SOLAR POWER GENERATION

U SOLAR GENERATORS

SOLAR POWER SOURCES

U SOLAR GENERATORS

SOLAR PROBES

Solar cell array for high radiation intensity application in Helios solar probe 02 p0191 A71-12068

Si solar cells with and without cover slides performance in severe thermal and light environment /near sun missions/ 05 p0701 A71-16070

Helios solar probe satellite solar array techniques for high temperature and illumination intensity 05 p0702 A71-16080

Robertson metric beta and gamma coefficients and solar dynamic oblateness determination from probe motion under relativistic effects [ONERA-TP-893] 06 p0970 A71-18024

Helios solar probe antenna system for S-band radio communication, discussing electrical and mechanical design 09 p1533 A71-23734

Quasi-isotropic directional, omnidirectional and auxiliary antennas of Helios Solar Probe S band

system, discussing design, radiation patterns, adaptability and X band measurements

14 p2217 A71-31052

Helios 6 interplanetary solar probe, investigating particle propagation, energy spectra, direction distributions and spatial gradients

15 p2499 A71-31211

SOLAR PROMINENCES

Solar eclipse observations of 7 March 1970, discussing site selection, shadows, corona, prominences, temperature measurements and photographs

01 p0151 A71-10117

Quiescent and sunspot prominences line of sight velocity measurements on limb, investigating statistical properties of velocity field

02 p0316 A71-12759

Solar H alpha prominences on 29, 30, 31 July and 1 August 1967, using filtergrams and spectroheliograms

04 p0641 A71-15661

Longitudinal magnetic field component measurement quiescent prominences, relating to angle between prominence and north-south direction on sun

05 p0804 A71-16026

Monochromatic coronal structure in prominences, explaining light diminution by density reduction

05 p0804 A71-16027

Solar prominence interaction, observing coronal rain and mound

05 p0809 A71-16474

Longitudinal magnetic field in quiescent prominences from magnetograph recording of Zeeman effect on hydrogen, helium and metal lines

06 p0967 A71-17909

Quiescent metallic and ordinary prominences continuum spectra measurements, showing hydrogen ionization dependence on microstructure

06 p0975 A71-18438

Solar chromosphere and prominences observations during total eclipse of 12 November 1966 by slitless spectrograph, using grazing incidence method

08 p1365 A71-21423

Coronal and prominence IR photography during 7 March 1970 solar eclipse

09 p1442 A71-22066

Solar prominence spectra, presenting equivalent line widths, central line intensities and Doppler half widths

09 p1524 A71-23190

Bright quiescent solar prominences metastable He excitation, studying electron temperatures and densities in interfilament areas

09 p1525 A71-23197

Quiescent metallic and ordinary prominences continuum spectra measurements, showing hydrogen ionization dependence on fine structure

12 p1955 A71-26588

Spectral analysis of solar prominences observed during Peruvian eclipse of 12 November 1966, obtaining two dimensional distribution of kinetic temperature, density and turbulent velocity

12 p1970 A71-27702

Soft X ray emission from solar loop prominences, noting data compatibility with fast protons injection model

12 p1954 A71-27703

Solar limb flare evolution on 11 July 1966, observing filament structure, vertical velocity and branching

14 p2298 A71-29975

Solar prominences formation, discussing coronal thermal instability, chromospheric heat balance, magnetic field and gas heating

15 p2482 A71-31334

High resolution quiescent and active solar prominences and magnetic field observations, discussing Zeeman effect and line spectrum polarization

17 p2806 A71-35393

Thermal, turbulent and macroscopic motions in solar loop prominence of 4 May 1960, using spectral line composition by Gaussian profiles

17 p2809 A71-35596

High performance solar prominence telescope, showing objective diameter effect on image contrast

18 p2915 A71-35977

MHD systems equilibrium and stability involved in quiescent prominences, considering temperature dependence of heat conductivity, magnetic field and initial gas compression

18 p2967 A71-36927

Solar prominences magnetic fields, determining strength and orientation with Zeeman effect

19 p3146 A71-38572

High performance solar prominence telescope components design, considering lenses and diaphragms with special attention to image degrading influences

21 p3378 A71-40523

Solar corona current sheet magnetic model, computing polar plume orientations and radial and nonradial streamers

21 p3453 A71-41359

Thermal effects in loop prominences formation after solar flares from model computer simulation

22 p3597 A71-41459

Solar thermal radio component observations at 169 MHz with east-west radioheliograph related to helmet and active coronal streamers

22 p3597 A71-41461

Solar prominences formation, discussing coronal thermal instability, chromospheric heat balance, magnetic field and gas heating

22 p3606 A71-42609

Solar rotation evidence from H alpha and K line spectra of quiescent prominences for westward wind

23 p3767 A71-43841

Solar chromospheric data for 1952, 1958, 1962 and 1966 eclipses, showing helium abundance in prominences

23 p3767 A71-43842

Energy balance in cool quiescent solar prominences, using 6000 km 6000 K isothermal slab model

23 p3767 A71-43843

Neutral helium short wave solar radiation in quiescent and loop prominences

23 p3768 A71-43844

He ionization and excitation in optically thick solar prominences, considering recombination excitation for observed triplet-level populations at 5000-10,000 K electron temperature

24 p3869 A71-44805

SOLAR PROPULSION

Electric rocket propulsion systems using nuclear or solar energy and electrothermal, electromagnetic or electrostatic principle

02 p0283 A71-12309

Solar electric propulsion (SEP) for automated planetary missions, discussing system characteristics, capabilities and costs

[AIAA PAPER 69-1103]

03 p0500 A71-14426

Small natural vibrations effect of solar sail-propelled system on heliocentric orbit motion

09 p1531 A71-22559

Hollow cathode ion thruster and lightweight power conditioner of solar-electric propulsion system for unmanned deep space probes

09 p1511 A71-22904

Solar electric propulsion and transfer system for higher payloads of SECOM communication satellites, using Europa 2 launcher

16 p2644 A71-32855

Solar electric propulsion system design for interplanetary spacecraft, describing Hg bombardment ion engine

17 p2794 A71-35546

Solar electric multimission spacecraft design, discussing off-optimum propulsion parameters effects on low thrust performance by characteristic surface representation

[AAS PAPER 71-324]

23 p3772 A71-42998

Solar electric propulsion application to Halley Comet flythrough and rendezvous missions, describing trajectory characteristics and payload capabilities

[AAS PAPER 71-363]

23 p3729 A71-43033

SOLAR PROTONS

Proton Flare Project 1969 observations concerning retrospective interval activity during maximum phase of solar cycle

01 p0144 A71-10286

Proton Flare Project 1969 observation of solar radio bursts by Alouette 2 satellite

01 p0144 A71-10287

Proton Flare Project 1969 observation of VLF radio wave propagation, detecting sudden phase anomaly events due to solar activity

01 p0144 A71-10288

Proton Flare Project 1969 observation of polar cap ionospheric disturbance due to proton event by VLF propagation phase measurement

01 p0073 A71-10289

Proton Flare Project 1969 observation of flares and subsequent ionospheric disturbances during retrospective interval

01 p0144 A71-10290

Solar flare proton propagation, examining interplanetary shock wave effects on cosmic ray scattering

01 p0146 A71-11386

Oppositely polarized maximal magnetic field strengths in sunspot regions during proton flares

03 p0478 A71-13937

Solar proton flares associated with 1968 and 1969 strong particle events, noting correlation with hard X ray and microwave bursts

03 p0478 A71-14037

Solar energetic protons measurements by ESRO 1 satellite following flare of 18 November 1968, noting cut-off latitude over northern polar cap

03 p0478 A71-14039

Solar radio bursts at 19 GHz, investigating single frequency proton warning technique

03 p0481 A71-14506

Solar wind and magnetopause shock front location at 1969 maximum, examining proton parameters from Heos 1 observations

03 p0482 A71-14513

Large amplitude upstream wave solar wind event of 10 March 1968 with suprathermal protons, correlating magnetometer plasma probe and Lepedea proton data

03 p0482 A71-14550

Solar proton recording during flare by Proton 3 satellite

04 p0641 A71-15124

Lunar atomic hydrogen atmosphere from solar wind proton bombardment, considering detection by scattered Lyman alpha radiation measurements

04 p0659 A71-15854

Type 3 solar radio bursts, examining proton and electron stream exciters

05 p0804 A71-16030

Solar microwave bursts correlation to solar proton emissions

05 p0798 A71-16115

Solar protons and electrons latitude profiles, discussing dependence on magnetic rigidity

06 p0964 A71-17272

Coronal magnetic fields before/after solar proton flares

06 p0950 A71-17917

Solar protons energy spectrum upper cut-off based on worldwide neutron monitors recordings of 28 January 1967 solar event

06 p0950 A71-17998

Diurnal cosmic ray neutron variations after proton flares, comparing calculated radial and azimuthal gradients to experimental data

06 p0951 A71-18105

Protons and alpha particles energy spectra during 25 February 1969 solar event from Centaur rocket observations as part of ESRO PCA campaign

06 p0957 A71-18144

Solar cosmic ray proton event of 18 November 1968 studied with neutron monitor data from worldwide network, considering associated flare

06 p0957 A71-18147

HEOS A-1 satellite solar proton flux measurements from 25 and 27 February 1969 solar flares, noting strong backscattering of 360 MeV particles

06 p0957 A71-18149

Solar particles propagation to earth during solar proton event of 25 February 1969, discussing local interplanetary field

06 p0958 A71-18150

Solar proton entry into geomagnetic field during 9 June 1968 event

06 p0958 A71-18153

Solar proton event on 9 June 1968 observed at polar caps by ESRO 2 satellite, noting flux profile structure

06 p0958 A71-18154

Solar flare on 9 June 1968, observing proton energy spectra and flux variation with time profiles

06 p0958 A71-18155

Particle flux energy spectra and time dependence of 25 February 1969 solar proton event

06 p0959 A71-18156

High latitude neutron monitors during 15 November 1960 solar cosmic ray event, calculating asymptotic directions for protons with magnetospheric model

06 p0959 A71-18161

Solar proton event energy spectra based on multiplicity measurements of cosmic ray neutron intensity increases

06 p0960 A71-18164

Energetic solar electron emission and cone propagation by IMP satellites, noting relation to proton and relativistic energy events

06 p0961 A71-18174

Atmospheric fast neutron flux, discussing solar proton events and Forbush decreases effects

06 p0963 A71-18183

Solar vicinity particle storage implication from flare proton energy spectrum observation by Injun 5 satellite

07 p1186 A71-19653

Interplanetary magnetic field in plane perpendicular to ecliptic, investigating force lines configuration by solar proton events

07 p1189 A71-20640

Relativistic electrons acceleration in solar proton flares, taking into account plasma density and magnetic field intensity

09 p1512 A71-22059

Solar radio bursts power spectra associated with proton events, noting extension to millimeter waves

09 p1514 A71-22933

Discrete solar proton event three digit classification system, covering proton intensity, riometer absorption and neutron monitor intensity

10 p1660 A71-23799

Polar caps energetic particle environment involving solar flare proton and electron fluxes

10 p1600 A71-24309

Interplanetary magnetic field irregularities and solar proton diffusion mean free path during 25 February 1969 event

10 p1677 A71-24556

Solar wind composition of protons, He isotopes and heavy rare gas ions from Apollo lunar samples

11 p1814 A71-25263

Long term storage of relativistic energetic electrons and protons in solar corona from IMP 4 and Pioneer 8 observations related to delayed emission from flares

12 p1969 A71-27657

Solar cosmic ray acceleration and propagation from time variation and heliocentric distance dependence of relative abundance of protons to helium nuclei
13 p2129 A71-29058

Solar proton anisotropy measurements, discussing flux directional distribution
14 p2297 A71-29670

Sunspots with proton flares of 7 July and 2 September 1969, examining longitudinal and transverse magnetic field components and total field vector
14 p2298 A71-29980

Solar cosmic ray flare catalog, using polar region absorption radio burst and proton event data
14 p2299 A71-29986

Diurnal variations of electron number density against height in lower ionosphere over Resolute Bay, relating to solar proton events
14 p2300 A71-30044

Statistical measurements of solar protons, alpha particles and heavier nuclei by lunar orbiting Explorer 35
16 p2628 A71-33933

Solar protons penetration over polar cap during 25 February 1969 event from particle and magnetic field measurements inside and outside magnetosphere by satellites
16 p2628 A71-33934

Energetic solar protons asymmetric access to north south polar caps by satellite observation during 24 January 1969 event
16 p2628 A71-33935

Proton flares in McMath Region 8461 (August-September 1966), describing solar wind plasma ejection and helium enriched interplanetary medium
18 p2958 A71-36743

Balloon observations of solar protons on 29-30 September 1968 over Iceland with GM telescopes and scintillation detectors, considering energy spectrum and time behavior
18 p2958 A71-36744

Diurnal variations in equatorial and precipitating low energy solar proton-produced gamma rays in magnetosphere
19 p3125 A71-37359

Equatorial and precipitating solar proton fluxes interrelationship in magnetosphere from riometer absorption in auroral and polar cap regions
19 p3125 A71-37360

Solar prompt and delayed discrete particle events, discussing proton and electron sources, distribution and flare association
19 p3126 A71-37624

Radionuclides depth distribution gradient in lunar samples, suggesting solar proton medium flux constancy over last million years
19 p3127 A71-38004

Polar cap absorption event, investigating solar high energy protons precipitation effects
19 p3129 A71-38360

Solar wind proton penetration through earth magnetosphere, taking into account drift, force lines curvature and nonstationary plasma boundary
19 p3129 A71-38376

Martian lower ionospheric models during solar proton event, determining electron density profiles
20 p3286 A71-38741

Solar proton trajectories calculations in Williams-Mead geomagnetic field model, showing longitude difference in tail region
20 p3216 A71-38747

PCA due to solar proton event, measuring electron/ion densities and temperatures, proton/electron energy flux spectrum, Lyman alpha radiation and X rays
20 p3281 A71-39730

Solar high energy cosmic ray proton burst observations, examining maximum flux delay time with Venus 6 satellite
20 p3281 A71-39734

Solar proton enhancement over auroral zone observed aboard near earth polar orbiting ESRO 2 satellite
20 p3282 A71-39735

Solar proton flare prediction with microwave radio burst data, using satellite measurements
22 p3590 A71-41464

Solar proton events intensity forecasts using time parameters of microwave bursts
22 p3590 A71-41465

Neutron flux estimate from protons number needed for white light solar flare caused by energetic particle penetration into photosphere
22 p3590 A71-41467

Anisotropic solar ground level relativistic proton event of 18 November 1968, determining propagation mechanism characteristics from neutron monitor observations
22 p3591 A71-41470

Solar proton flux from 7 July 1966 flare observation via Proton 3 satellite, obtaining cosmic rays integral spectra
22 p3591 A71-41549

Solar protons contribution to spallogenic Mn 53 production in Apollo 12 lunar rock and soil from neutron activation analysis
23 p3755 A71-43734

Heliographic longitude effect on delay time between solar proton observation and flare occurrence from HEOS A1 data, noting magnetic field influence
23 p3768 A71-43852

SOLAR RADIATION

NT SOLAR CORPUSCULAR RADIATION

NT SOLAR COSMIC RAYS

NT SOLAR PROTONS

NT SOLAR RADIO BURSTS

NT SOLAR RADIO EMISSION

NT SOLAR WIND

NT SOLAR X-RAYS

NT SUNLIGHT

NT TYPE 2 BURSTS

NT TYPE 3 BURSTS

NT TYPE 4 BURSTS

Semiautomatic electrophotometer with interference light filters for atmospheric ozone, aerosol and solar radiation recording
01 p0080 A71-10602

Gravity gradient satellite librational dynamics under solar radiation pressure, using analytical and numerical integration methods
01 p0163 A71-10755

Satellite orbit perturbations by solar radiation pressure, considering earth shadow in homogeneous field and long term effects
02 p0313 A71-12491

Solrad 8 satellite monitoring of Lyman alpha and UV radiation, discussing flux variation at 1080-1350 Å
03 p0479 A71-14043

Solar UV radiation measurements by OSO-3, obtaining flux variation over solar rotation period
03 p0481 A71-14508

Earth hydrogen geocorona models comparison with solar Lyman alpha spectrographic data from Aerobee rocket flight measurements
03 p0496 A71-14509

Actinometric network for monthly sums of overall solar radiation and earth surface radiative balance, estimating random errors mean square values
04 p0621 A71-14640

Aerosol-induced solar radiation attenuation correlation to humidity in atmospheric boundary layer
04 p0641 A71-15119

Solar H alpha prominences on 29, 30, 31 July and 1 August 1967, using filtergrams and spectroheliograms
04 p0641 A71-15661

Corrections derived for Labs-Neckel 1968 solar radiation tables transformation into 1968 International Practical Temperature Scale
05 p0797 A71-16018

Solar disk computed continuum and estimated line polarizations compared to BCA photosphere values, discussing metal abundances
05 p0803 A71-16019

Si solar cells with and without cover slides performance in severe thermal and light environment /near sun missions/

05 p0701 A71-16070

Solar Lyman alpha radiation absorption by molecular oxygen, examining optical thickness with Intercomsol-1 satellite
05 p0807 A71-16214

Electron temperature anisotropy in lower ionosphere, discussing effects of solar UV radiation propagating along geomagnetic field during daytime
05 p0744 A71-17183

Static solar H II region ionization balance, energy, UV radiation transfer, gravitational equilibrium and interstellar gas temperature
06 p0975 A71-18442

Statistical optical measurements of solar scintillation due to atmospheric conditions
07 p1111 A71-19489

Solar flare EUV radiation and ionospheric currents dynamo region ground based detection by geomagnetic crochets time structure analysis
08 p1355 A71-21198

Solar radiation flux standard instruments development for meteorological measurements, discussing calorimetric techniques and high precision radiometers
08 p1293 A71-21737

Middle latitude night E region ionization, describing solar EM and corpuscular radiation absorption effects
08 p1286 A71-21853

Solar color index calibration from Mg b triplet photoelectrical measurement from dwarfs and Jupiter satellites
09 p1516 A71-22064

Solar radiation energy distribution simulated by vacuum monochromator, discussing Ar-Kr-Xe-methane mixture
09 p1513 A71-22557

Selective optical coatings efficiency and thermal properties under solar radiation and radiative heat exchange
09 p1510 A71-23418

Solar surface radiation brightness and intensity for different disk regions and wavelengths
09 p1526 A71-23419

Balloonborne radiometric instrumentation for solar and thermal radiations upward and downward flux measurements, discussing net radiation balance as function of solar elevation
09 p1515 A71-23558

Solar particle tracks in clear filter glass from Surveyor 3 spacecraft, comparing with lunar rocks track results
09 p1529 A71-23655

Brightness temperature from solar UV continuum in 1680 to 600 Å in photosphere-chromosphere transition model
10 p1666 A71-23780

Solar radiation pressure acceleration effects on flat satellite in earth synchronous orbit, examining orbital shift and counteracting thrust velocity applications
10 p1671 A71-24333

Brightness ratio near solar horizon from Ly alpha predawn and postdawn rocket observations consistent with radiation multiple scattering geocoronal model
10 p1605 A71-24794

Spectroscopic observation of comet Bennett near perihelion, noting solar continuum intensity dependence on wavelengths
10 p1681 A71-25062

Thermal louvers radiative heat transfer characteristics with solar irradiation effects, using Monte Carlo method
11 p1854 A71-25190

Thermal louver models in space simulation chambers, determining heat dissipation, optical efficiencies, blade geometry and solar radiation effects
11 p1854 A71-25191

Micrometeoroid detector design for hypervelocity particle impacts, discussing solar radiation pressure effects on satellite measurements
11 p1761 A71-25544

Spin dynamics and deformation measurements on PAGEOS balloon satellite by photoelectric photometry, noting solar radiation pressure torque
11 p1761 A71-25546

Lunar dust deposition and brushing effects on spectral solar reflectance of thermal control materials in vacuum
[AIAA PAPER 71-459]
11 p1799 A71-26241

Solar absorptance sensitivity to thermal surface particulate contamination as function of particle composition, quantity, size and linearity with obscured area [AIAA PAPER 71-473]
11 p1800 A71-26253

Chorioretinal temperature increases from naked solar eclipse observations for various observation angles and pupil diameters, considering solar irradiance and atmospheric transmittance spectra
11 p1726 A71-26484

Static solar H II region ionization balance and energy, UV radiation transfer, gravitational equilibrium and interstellar gas temperature
12 p1955 A71-26592

Solar simulator with wide range irradiation strength variability for laboratory investigation of radiation effects on spacecraft components
12 p1894 A71-26982

Autocorrelation functions of quasi-uniform solar radiation field reflected from earth with scattering allowance, using stationary random theory
12 p1901 A71-27097

Earth surface formations and clouds angular brightness distribution based on reflected solar radiation intensity
12 p1901 A71-27102

Intense solar microwave burst indication of high energy electron production, discussing synchrotron radiation, interplanetary medium particle propagation and cosmic ray modulation
12 p1950 A71-27381

Thermal flutter of satellite storable tubular extensible members, determining static flexural and torsional vibrations due to solar radiation
12 p1984 A71-27736

Electron temperature anisotropy in lower ionosphere, discussing effects of solar UV radiation propagating along geomagnetic field during daytime at middle latitudes
13 p2059 A71-28240

Short term interval satellite orbit perturbations, computing direct solar radiation pressure effects with computer program
13 p2137 A71-28477

Submillimeter wave region solar radiation atmospheric absorption by Fourier spectrometry and double output Michelson interferometer with Golay cell detectors
14 p2307 A71-29740

Thermal emissivity and solar absorptivity of Al coated with surface layers of aluminum oxide and silicon oxide, describing fabrication techniques and performance measurements
14 p2335 A71-30128

Chronic and acute gamma irradiation facilities used in animal experiments simulating steady cosmic radiation

tion and powerful solar flare radiation expected in prolonged space flight

15 p2357 A71-31313

Solar UV radiation atmospheric absorption during IQSY by ion chamber measurements, considering upper atmosphere oxygen concentration

15 p2396 A71-31616

Scattered light effects on sunspot intensities observations during Mercury occultation and near solar limb

15 p2496 A71-32739

Solar flare radiation data from Pioneer spacecraft, detailing anisotropy, heliocentric longitude gradients, decay time constants and energy spectra

15 p2480 A71-32752

Solar flare activity and sunspot distribution over central meridian from optical data by NASA solar particle alert network 1967-69

16 p2635 A71-33437

Pagcos spacecraft orbital acceleration prediction by radiation pressure perturbation theory accounting for nonisotropic scattering of solar spectra from rotating ellipsoidal body

16 p2641 A71-33772

Solar UV radiation data during 7 March 1970 eclipse from photometers sensitive to narrow bands, discussing sources, atmospheric absorption and D region ionosphere

16 p2627 A71-33773

Corpuscular and solar electromagnetic ionizing radiation simultaneous measurement by sounding rockets, evaluating contribution to lower ionosphere formation

16 p2627 A71-33776

Thermospheric dynamics, including global compositional structure, winds and temperature response to solar radiation and vertical mass diffusion

16 p2571 A71-33838

West German space research activities during 1970 on meteorology, ionospheric physics, solar radiation, cosmic rays and life sciences

16 p2666 A71-33866

Sea surface slope distribution and wind velocity determination by sun glitter photography from synchronous satellite

17 p2734 A71-35215

Solar radiation field in polluted atmosphere, measuring intensity, polarization and flux due to aerosol scattering for comparison with Mie theory computation

17 p2736 A71-35563

Venus surface temperature dependence on incident solar flux based on runaway greenhouse nongray calculation, considering water vapor as IR opacity source in models

18 p2964 A71-36285

Atmospheric directional scattering coefficients from vertical measurements of IR spectral sky brightness near solar almucantar and direct radiation

19 p3090 A71-37976

Atmospheric signal propagation study between satellite and earth, using solar radiometry

19 p3018 A71-38075

Hydrogen ionization and excitation equilibrium, using slab model atmospheres irradiated from both sides by photospheric, chromospheric and coronal radiation

19 p3146 A71-38664

Thermospheric atomic oxygen and molecular nitrogen number densities, discussing earth atmospheric absorption of solar UV lines

20 p3214 A71-38727

Earth thermosphere models, discussing shortwave solar radiation as major energy source during quiet conditions, diurnal variations of structure, neutral-charged components interconnection, etc

20 p3216 A71-39117

Daylight photometric flux derivation from filtered measurements of global sun and sky radiant energy, using natural illumination and short wave radiation relationship

20 p3234 A71-39175

Circumsolar scattered radiation effects on ozonometer reading accuracy, taking into account effect of sun angular altitude under cloudless conditions

20 p3237 A71-39329

Actinometer thermobatteries surface sensitivity distribution effect on solar radiation flux measurement accuracy

20 p3237 A71-39330

Attitude control of gravity orientated satellite in arbitrary orbit by solar pressure, showing libration damping characteristics of radiation force

20 p3306 A71-39396

Integral wavelength solar radiation constant measurements by jet and rocket research aircraft, high level balloons and Mariner space probes

20 p3260 A71-39682

U.S.S.R. and U.S. balloon measurements of direct solar radiation integral fluxes, deriving solar constant values

20 p3260 A71-39683

Solar and terrestrial IR reflected radiation from Cosmos satellites measurements, determining clouds upper boundary height

20 p3261 A71-39688

Solar radiation effects on upper atmosphere soft electron flux and energy spectrum during day and night

20 p3281 A71-39724

Interplanetary H scattered solar Lyman alpha background observations by Vela 7 and OGO 3 satellites, showing 27 day correlation with intensity curve

20 p3300 A71-39736

Mathematical model for studying solar radiation pressure effects on artificial satellite motion

21 p3438 A71-40104

Circumsolar radiation and atmospheric turbidity effects on readings of compensation type pyroheliometers with allowance for receiver sensitivity

21 p3384 A71-41382

Solar flares gamma ray flux, describing production by downward moving high energy particles

22 p3590 A71-41468

Autocorrelation functions of quasi-uniform solar radiation field reflected from earth, using stationary random theory and allowing for scattering

22 p3533 A71-41652

Alouette and Isis satellites flight data comparison with attitude and spin dynamics theory, considering solar radiation pressure and gravitation and magnetic field effects

22 p3609 A71-41997

Coupled librational dynamics of gravity oriented cylindrical satellite, calculating solar radiation pressure effects on attitude control behavior

22 p3611 A71-42042

Mathematical model of solar radiation pressure force and torque acting on spacecraft surface intercepting solar photon stream

[AAS PAPER 71-352]

23 p3728 A71-43024

Venusian thermosphere, observing dayside solar radiation absorption generated upward dayside and downward nightside vertical motions

23 p3735 A71-43333

Neutral helium short wave solar radiation in quiescent and loop prominences

23 p3768 A71-43844

Planetary atmospheric motions, discussing solar radiation, internal heat sources, planetary rotation and magnetic field effects

23 p3672 A71-43891

Cometary nucleus outbursts and splitting moments spatial distribution, indicating solar radiation and tidal action effects

24 p3868 A71-44457

Airborne measurement of directional variation in reflected solar radiation over soil surface and vegetation, using scanning radiometer

24 p3826 A71-44984

SOLAR RADIATION OBSERVATION

U SOLAR RADIATION

SOLAR RADIATION SHIELDING

Expandable rigidizable solar shields operational, structural and thermal performance tests conducted with spherical models for cryogenically fueled space vehicles

03 p0500 A71-14432

Astronaut protection from solar flare high energy protons, discussing spacesuit, spacecraft orientation and solid, electrostatic, magnetic and plasma shielding

13 p2021 A71-29252

SOLAR RADIO BURSTS

NT TYPE 2 BURSTS

NT TYPE 3 BURSTS

NT TYPE 4 BURSTS

Proton Flare Project 1969 observation of solar radio bursts by Alouette 2 satellite

01 p0144 A71-10287

Solar corona radioheliograph observations, discussing burst types, prominences, shock waves, etc

01 p0152 A71-10329

Solar microwave bursts and associated optical flares homologous characteristics, discussing radio emission mechanism

02 p0302 A71-12763

Solar bursts position and motion measurements at decimeter wavelengths, using sweep frequency grating interferometer

02 p0302 A71-12764

Solar radio bursts multifrequency observation using simple image forming system with multielement interferometer

02 p0302 A71-12765

Solar mm bursts impulsive component correlation with associated soft X ray burst

03 p0473 A71-13184

Solar radio astronomy decimeter wave multichannel spectrograph for solar bursts fine structure spectrum analysis

03 p0488 A71-13530

Solar proton flares associated with 1968 and 1969 strong particle events, noting correlation with hard X ray and microwave bursts

03 p0478 A71-14037

Solar radio bursts at 19 GHz, investigating single frequency proton warning technique

03 p0481 A71-14508

Solar radio centers and interplanetary sector structures in connection with recurrent geomagnetic storm

03 p0496 A71-14508

North-south asymmetry in solar disk microwave bursts sources distribution

03 p0496 A71-14508

Space radio astronomy of solar bursts at broad frequency range, using earth-remote probe experiments

04 p0642 A71-14508

Coronal condensations emission changes at microwave solar bursts, discussing circular polarization and flare mechanism based on collisionless dissipation of magnetic energy

05 p0804 A71-16000

Solar microwave bursts correlation to solar proton emissions

05 p0798 A71-16100

Solar radio bursts monitoring at 71 GHz /July 1968/ December 1969/

06 p0968 A71-17911

Solar 3.3 mm bursts observation, showing temporal correlation with soft X ray bursts

06 p0968 A71-17911

Solar radio short term and fast drifting bursts observations with high spectral resolution, describing duration, frequencies bandwidth and polarization

06 p0963 A71-18444

Solar radio emission micropulsations observations at 10 cm, discussing primary and secondary bursts from different disk regions and radio telescope

07 p1189 A71-20630

Statistical analysis of center-limb variations of intensity, spectrum and polarization of solar microwave impulsive bursts

08 p1364 A71-21411

Solar radio burst types occurrences at various frequencies in relation to radio emission slowly varying component

09 p1514 A71-22790

Solar radio bursts power spectra associated with proton events, noting extension to millimeter waves

09 p1514 A71-22930

Solar impulsive microwave bursts, showing association with types D, E and F sunspots

10 p1667 A71-23790

Solar flares explosive phase in photometric terms for flash onset correlations with 10.7 cm radio and hard X ray bursts, using H alpha film records

10 p1660 A71-23790

Redundancy reduction method based on least squares approximation for recording solar radio bursts emissions

10 p1661 A71-23920

Supernova explosion or solar outburst theory of climatic effects on mass extinction of organisms at Cretaceous-Tertiary boundary

10 p1673 A71-24420

Solar radio short and fast-drifting bursts observations with high spectral resolution, describing duration, frequencies bandwidth and polarization

12 p1946 A71-26590

Geomagnetic crochet associated solar optical flares and microwave bursts during four year period, showing north-south asymmetry over disk

12 p1947 A71-26760

Solar X-ray and radio fluxes at earth for high order temperatures by free-free transitions and Maxwellian electron velocities in corona

12 p1947 A71-26770

Energetic solar X-rays, microwaves and EUV ionizing radiation during periodic bursts of solar flare

12 p1953 A71-27650

Solar and geophysical morphology of radio burst of active sun, treating bremsstrahlung, gyro, synchrotron and Cerenkov radiation and plasma waves

13 p2137 A71-28510

Plasmoid ejection during flare and condensation by radiative instability, interpreting Simple 3 solar radio bursts in terms of thermal emission

13 p2129 A71-29050

Solar radio burst of 27 September 1969, associating flare with dynamic spectrum

13 p2129 A71-29050

Solar cosmic ray flare catalog, using polar region absorption radio burst and proton event data

14 p2299 A71-29980

Decimeter solar radio bursts time splitting data, presenting high time and frequency resolution on decimeter bursts

15 p2473 A71-31720

Solar microwave burst frequency occurrence statistical analysis

15 p2495 A71-32680

Solar microwave bursts spectrum, calculating maximum radiation fluxes and frequencies from statistical data

15 p2480 A71-32740

Sudden phase anomalies relation to solar flares, radio bursts and X radiation from severe worldwide ionospheric storm observation

17 p2796 A71-35340

Solar X-ray flares recorded by SOLRAD-9 on Explorer 37 satellite occurring in optical flares-microwave bursts-X ray flares sequence
17 p2796 A71-35391

Homologous solar microwave bursts from different active centers recorded with 7 GHz polarimeter
18 p2957 A71-35964

Simple type centimeter solar radio bursts identification and relation to flare position, noting radio spectrum over sunspot
18 p2958 A71-36741

Solar radio bursts circular polarization data, presenting single and multiple inversion analysis at microwave frequencies
19 p3128 A71-38170

Spectral analysis of solar microwave bursts, examining flux and energy variation with frequency
19 p3146 A71-38577

Solar low energy X-ray spectra observation during impulsive bursts, discussing thermal and nonthermal emission properties
21 p3438 A71-40425

Solar radio bursts and noise storms frequency band spectra, investigating warm plasma wave propagation and mode coupling theories
22 p3579 A71-41462

Solar proton flare prediction with microwave radio burst data, using satellite measurements
22 p3590 A71-41464

Solar proton events intensity forecasts using time parameters of microwave bursts
22 p3590 A71-41465

M supergiant hot corona base density determination from radio emissions observations, noting equivalence to solar type 4 microwave bursts
22 p3590 A71-41916

Tables for aurora correlation with solar radio bursts at 185 MHz
23 p3769 A71-43908

Solar radio burst generation model based on effects of strong shock waves during chromospheric flares for geomagnetic storm prediction
24 p3867 A71-45081

SOLAR RADIO EMISSION

NT SOLAR RADIO BURSTS
NT TYPE 2 BURSTS
NT TYPE 3 BURSTS
NT TYPE 4 BURSTS

Solar corona radio emission enhancement, comparing thermal and nonthermal streamer models
01 p0152 A71-10332

Solar local SHF emission sources circular polarization, discussing sunspot clusters effects
02 p0306 A71-12076

Absolute measurements of solar flux density at 9500 MHz, comparing Nagoya and Heinrich-Hertz Institute radiometric observations
02 p0302 A71-12760

Solar proton flares, coronal radio diameter and cosmic radiation intensity relationship
03 p0473 A71-13788

Solar radio waves varying component local sources relationship with sunspots development, describing characteristics based on thermal bremsstrahlung and cyclotron/synchrotron fast electrons radiation
07 p1195 A71-19339

Solar radio emission constant and slowly varying components, investigating sunspots, activity cycle and flux rate
07 p1195 A71-19340

Solar chromosphere and corona wave motions, presenting solar radio emission fluctuations correlation functions
07 p1199 A71-20010

Solar radio emission micropulsations observations at 10 cm, discussing primary and secondary bursts from different disk regions and radio telescope
07 p1189 A71-20639

Solar local SHF emission sources circular polarization, discussing sunspot clusters effects
08 p1361 A71-21126

Superthermal electrons continuous stream release into interplanetary medium during hectometric solar noise storm activities
09 p1518 A71-22353

Solar radio burst types occurrences at various frequencies in relation to radio emission slowly varying component
09 p1514 A71-22793

High sensitivity radiospectrography, obtaining solar emission spectra on decametric waves by radio telescope, focal antenna and receivers
10 p1667 A71-23826

Chromospheric millimetric emission through 250 GHz atmospheric passband on isophoto maps, showing higher brightness temperatures compared with solar disk
12 p1969 A71-27649

F 2 layer critical frequency variations relation to solar radio flux intensity, using mathematical approximations
13 p2062 A71-28557

Measuring instrument for solar radio emission at 8 mm, using GaAs Schottky barrier diode mixer for system noise temperature reduction
14 p2239 A71-29916

Mesospheric cloud statistics compared with 200 MHz solar radio emission during summers of 1958-1966
14 p2232 A71-29961

Chromospheric flare on 11 July 1966, comparing solar radio emissions at 10 cm and 1.5 m wavelengths
14 p2298 A71-29976

Solar radio emission at 3.15 cm wavelength via 22-meter radio telescope, determining relation between source brightness and areas of sunspot groups
14 p2299 A71-29990

IQSY solar magnetic field, radio emission and corona observations, including flare data reevaluation
15 p2483 A71-31613

Forward/reverse drift pair bursts relation to decameter type 3 solar radio emission, postulating existence of electron acceleration sources in upper corona
15 p2485 A71-31714

Data processing technique for radio mapping of sun, discussing unwanted harmonics elimination and noise reduction
15 p2491 A71-32447

Statistical analysis of radiometer measurement data of solar emission atmospheric attenuation at 19 GHz
15 p2496 A71-32710

Type 3 solar emission bursts, investigating time profiles and quasi-oscillatory decay
15 p2480 A71-32750

Radio astronomy signals reception and interpretation, detailing solar, galactic and extragalactic spectrum sources
17 p2797 A71-34242

Radiometric measurements of frequency distribution of solar emission attenuation due to troposphere, noting sun-earth communication paths
17 p2707 A71-35124

Statistical determination of solar radio emission S-component average flux spectrum during solar cycle peak phase
18 p2966 A71-36739

Polarized solar millimeter emission associated with sunspot magnetic field compatible with multiple sources from chromosphere
18 p2966 A71-36762

Solar flare X and gamma rays, radio and far UV emission, discussing model for chromospheric cool plasma heating by flow through magnetic instability
19 p3126 A71-37620

Sunspot number relationship with solar radio flux, using cross spectral method for high and moderate activity periods
20 p3279 A71-39324

Solar radioelectric activity in 1966, tabulating mean daily density and variability of solar flux
21 p3442 A71-40152

Solar thermal radio component observations at 169 MHz with east-west radioheliograph related to helmet and active coronal streamers
22 p3597 A71-41461

Metric frequency solar radio noise active regions relationship to interplanetary magnetic field polarity distribution
22 p3597 A71-41471

Two dimensional maps of circularly polarized solar emission at 7.8 GHz, noting flux density and polarization time dependence before flare
23 p3732 A71-43072

Polarized solar radio emission at millimeter wavelength in active regions associated with sunspot magnetic fields
23 p3733 A71-43125

Curved wire array to eliminate parasitic circular polarization of variable profile radio telescope antennas, applying to solar observations
23 p3655 A71-44326

SOLAR RADIO WAVES
U SOLAR RADIO EMISSION
SOLAR REFLECTORS

Apollo spacecraft and lunar landing module thermal control surfaces, considering inorganic silicate bonded paint
09 p1533 A71-23426

Solar rudder for spacecraft steering in form of right circular cone with ideally reflecting surface
20 p3306 A71-39136

SOLAR ROTATION

German monograph on differential solar rotation resulting from anisotropic turbulent viscosity in hydrogen convection zone
02 p0317 A71-12846

Solar UV radiation measurements by OSO-3, obtaining flux variation over solar rotation period
03 p0481 A71-14508

Solar magnetic field variation observation, revealing sun as quadrupole magnetic rotator
04 p0657 A71-15828

Type 3 solar radio bursts observed at low frequencies for half rotation, discussing occurrence, drift rates, propagation time and emission
05 p0804 A71-16031

Sun as variable star, discussing brightness, rotation and magnetic characteristics
06 p0971 A71-18245

Cosmic ray intensity mean diurnal variation, taking into account angle between solar corotational velocity and earth equatorial plane
07 p1187 A71-19683

Preferred orientations of rotational and tangential discontinuities in solar wind from Mariner 5 data
08 p1356 A71-21642

Differential rotation in sun, giant planets and upper atmospheres of earth and Venus, attributing solar rotation to tides caused by planets
09 p1522 A71-22961

Unusual sunspot rotation from 30 September to 8 October 1969 in plage region No. 10344, noting flare activity and rotational motion
10 p1666 A71-23786

Sunspot group magnetic field distribution and radial velocities, investigated at H alpha and 6302.499 A atmospheric levels
10 p1666 A71-23788

Rotation-convection model of solar equatorial acceleration and temperature, assuming inhomogeneous isotropic latitude dependent turbulent energy transport
12 p1968 A71-27644

Krause-Steenbeck solar dynamo eigenvalue evaluation assuming step function differential rotation and delta function alpha-effect for approximation
12 p1971 A71-27749

Pioneer 9 interplanetary observations, presenting deep space data for solar rotations and radial gradient in VLF electric field behavior
13 p2064 A71-29163

Nucleus brightness of comet Ikeya-Seki from plates in photographic and photovisual spectral regions, indicating relation to solar rotation
15 p2484 A71-31667

Solar activity cycle model, considering magnetic dynamo equations with radial rotation differentiability
15 p2495 A71-32679

Sunspot butterfly diagram interpretation based on heliographic latitude drift relation to gradient of solar rotational velocity
15 p2495 A71-32707

MHD planetary waves existence on sun, estimating mean toroidal solar magnetic field and rotation rate
15 p2497 A71-32756

Convective motions in differentially rotating thin spherical shells, explaining solar differential rotation
16 p2630 A71-33055

Solar oblateness and Li abundance interpretation by model of thermally driven turbulence terminated at rotating core surface containing partial mass
17 p2806 A71-35385

Doppler velocity field recording method over two dimensional solar active region image, using narrow band filter with video photographic subtraction technique
18 p2924 A71-36730

Low energy solar particle observation by widely separated Mariner and Explorer spacecraft, noting flare-associated and nonflare intensity peak correlation with sun
20 p3284 A71-39876

Solar atmosphere closed magnetic loop system model, determining surface differential rotation rate and angular velocity distribution
22 p3596 A71-41452

Streamline pattern deduction for sun large scale flow from Doppler line of sight velocities
22 p3596 A71-41454

Solar wind angular momentum calculation from short term directional, density and velocity fluctuations, using Vela 3 satellite data
22 p3592 A71-42162

Solar rotation evidence from H alpha and K line spectra of quiescent prominences for westward wind
23 p3767 A71-43841

SOLAR SAILS

Small natural vibrations effect of solar sail-propelled system on heliocentric orbit motion
09 p1531 A71-22559

SOLAR SENSORS

SkyNet satellite attitude determination and adjustment by IR and solar sensors, electronics processing equipment, nutation damping and pulsed axial thrusters
02 p0320 A71-12430

Automatic solar and lunar reference guidance system with balanced photoelectric measuring equipment
04 p0591 A71-14846

LOLA /Location and Orientation of Lunar Astronauts/ system using RF ranging and solar sensor, discussing configuration, operation, accuracy and electronics
04 p0623 A71-15303

Digital attitude reference systems for three axis stabilized earth oriented satellites using sun sensor measurements
06 p0926 A71-18520

Solar aspect sensors as navigation components for rolling vehicle heading angle determination
07 p1157 A71-20415

- Magnetometer for indicating position of constant level meteorological balloons provided with solar sensors 10 p1612 A71-24759
- Projectiles yawing and rolling over long flight paths, describing onboard solar aspect sensor and telemetry link to ground stations [AIAA PAPER 70-538] 11 p1761 A71-25513
- Sun sensor design accuracy and stability parameters for spacecraft ultrafine guidance, comparing bias error with solar simulator measurements 11 p1767 A71-26334
- Rotating spacecraft attitude control system, using sun-earth albedo sensor for attitude determination [DFVLR-SONDDR-113] 12 p1972 A71-26986
- Reliable brushless direct-drive system design for controlling position and rate of solar power arrays on orbiting spacecraft 12 p1869 A71-27432
- ### SOLAR SIMULATION
- UK 3 spacecraft support sting for solar simulation and thermal vacuum testing in 2.5 meter test chamber, describing design and construction 06 p0881 A71-18720
- Solar radiation energy distribution simulated by vacuum monochromator, discussing Ar-Kr-Xe-methane mixture 09 p1513 A71-22557
- High intensity vacuum UV solar simulator, using high pressure jet pinched xenon arc lamp with magnesium fluoride envelope 11 p1747 A71-26515
- Solar simulator with wide range irradiation strength variability for laboratory investigation of radiation effects on spacecraft components 12 p1894 A71-26982
- Copper sulfide-cadmium sulfide thin film solar cells under simulated orbital conditions, including thermal cycling, constant illumination and temperature effects 20 p3182 A71-38946
- Multiple channel fringe counting interferometer for remote monitoring of large diameter microwave antenna under test in simulated solar thermal and vacuum environment 20 p3235 A71-39186
- ### SOLAR SIMULATORS
- Toulouse space environment simulator artificial sun assembly consisting of xenon lamp and projection optics for cylindrical light beam production 02 p0239 A71-12748
- Electro-optical solar simulator, describing system design, performance and applications for spacecraft testing 04 p0567 A71-15366
- Pulsed xenon solar simulator system for testing single and group cells and panels for flight spacecraft programs 05 p0733 A71-16098
- Sun sensor design accuracy and stability parameters for spacecraft ultrafine guidance, comparing bias error with solar simulator measurements 11 p1767 A71-26334
- ### SOLAR SPECTRA
- Solar line spectra formation and analysis, discussing transfer equation, atomic levels, line shape, etc 01 p0152 A71-10327
- Solar photospheric spectrum, investigating deuterium abundance relative to hydrogen 01 p0157 A71-10762
- Solar constant and zero air mass spectrum, discussing new standard values 01 p0159 A71-10861
- Solar emission line spectra second observation outside total eclipse, noting big coronal condensation above eastern limb 01 p0159 A71-10869
- Solar Li abundance determined from selected sunspot spectra observations 01 p0161 A71-11382
- Solar Hg abundance low value by photosphere spectrum absence of Hg I lines, comparing higher content in carbonaceous chondrites 02 p0306 A71-12048
- Photosphere and facula turbulent velocities and damping constants from Ni and Fe IR lines analysis 02 p0306 A71-12079
- Solar active regions lambda 10 830 line from photometric observations, determining optical thickness, Doppler width and radiation source activity 02 p0306 A71-12080
- Spectroscopoheliograph observations, noting correlations between contour maps of solar continuum intensity and magnetic fields [AIAA PAPER 70-1360] 02 p0315 A71-12693
- Solar line blanketing effect data derivation and analysis for model atmosphere computer programs, considering application to spectrally similar stars 02 p0316 A71-12755
- Solar radiation spectral distribution at 0.16 A by photometers on Solrad 9, computing theoretical ratios with gray body assumption 03 p0479 A71-14044
- Solar He II Lyman alpha line, measuring long term absolute intensity variations 03 p0496 A71-14507

- Solar Lyman alpha emission line absorption by geocoronal atomic hydrogen, comparing observational data with prediction from models 03 p0496 A71-14510
- Solar spectrum line digital recording, discussing design and operation principles 04 p0590 A71-14842
- Linearly polarized light measurements of solar spectral lines Zeeman effects, describing calibration method based on Fraunhofer lines broadening due to magnetic fields 04 p0642 A71-14903
- Spectral line intensities, discussing equivalent width, broadening, transition probability, Schuster-Schwarzschild model, solar abundances, etc 04 p0630 A71-15237
- Impulsive solar flare X rays spectral characteristics, examining electron energy, bremsstrahlung, microwave bursts and particle escape, collisions and injection 05 p0797 A71-15937
- Solar line spectra wavelength improvement in 7780 to 7925 A range, using carbon dioxide bands 05 p0803 A71-16020
- Line formation calculations for different spot models and arbitrary depth dependence of magnetic field vector, interpreting pi component anomalous splitting 05 p0803 A71-16021
- Circular polarization measurement in various lines, finding magnetic field strength influenced by line absorption coefficient variations from photosphere to spot and faculae 05 p0803 A71-16025
- OSO 4 satellite small grazing incidence monochromator as monitor for flux variations in solar He II Lyman alpha line ionizing radiation source 05 p0748 A71-16251
- Absolute intensities measurement method for spectrum of solar disk center at 2962-4087 A 06 p0967 A71-17902
- Intensity calibrated grazing incidence spectrographs on Skylark sounding rockets, recording solar soft X-ray and XUV spectra 06 p0967 A71-17903
- Swan band intensity upper limits in spectrum of 18 September 1966 sunspot 06 p0967 A71-17907
- Solar X-ray resonance, intercombination and forbidden lines variations of O VII emission 06 p0968 A71-17910
- Interlocking via photoexcitations and deexcitations due to lanthanide rare earths weak line solar spectra and ion atomic structure 06 p0969 A71-17970
- CuH lines in sunspot spectra and solar isotopic ratio of Cu obtained from Cu I lines 06 p0969 A71-17971
- Fraunhofer line resonance polarization from solar spectral bands statistical analysis, noting collisional depolarization 06 p0969 A71-17973
- Solar Na I Fraunhofer lines empirical constants and abundance, discussing van der Waal attraction, Stark broadening and radiative damping 06 p0969 A71-17974
- UV solar spectrum rocket-borne high resolution spectroscopy by Fabry-Perot interferometer and echelle grating, discussing design parameters and recorded data 06 p0903 A71-18718
- Pulkovo observatory six channel two slit single photomultiplier rotating photographic plate magnetograph, for solar spectra polarization and radial velocities observation 07 p1109 A71-19337
- Coronal line observation of autoionizing states by dielectronic recombination in solar spectrum 07 p1198 A71-19827
- Weak and average intensity Fraunhofer lines contours variation over solar disk 07 p1200 A71-20038
- Sunspot boundary displacement toward limb in Fe I, Ti I and H alpha lines in passing from continuum to absorption line observations, discussing Wilson effect 07 p1205 A71-20635
- Night sky H beta photometry, showing solar type spectrum at high galactic latitudes and net emission at low latitudes 08 p1350 A71-20946
- Wilson-Bappu effect and asymmetric K line emission in sun 08 p1359 A71-20947
- Solar flare electron spectra in interplanetary space and within earth magnetosphere, investigating simultaneous observations by satellite-borne magnetic electron spectrometers 08 p1354 A71-21037
- Photosphere and facula turbulent velocities and damping constants from Ni and Fe IR lines analysis 08 p1361 A71-21129
- Solar active regions lambda 10 830 line from photometric observations, determining optical thickness, Doppler width and radiation source activity 08 p1361 A71-21130

- Secondary umkehr effect in solar UV region at twilight, proposing origin mechanism by ozone layer optical properties 08 p1357 A71-21875
- Earth optical radiation environment observation from satellites, reviewing solar spectra, near IR cloud spectra and vacuum UV radiometer scans 09 p1437 A71-22739
- CH molecule line formation mechanism for 4300 A transition in solar photosphere, studying collisions with hydrogen atoms 09 p1520 A71-22842
- Solar prominence spectra, presenting equivalent line widths, central line intensities and Doppler half widths 09 p1524 A71-23194
- Fraunhofer line profiles, determining optical depth at various points in photosphere 09 p1524 A71-23191
- Solar center-limb Fraunhofer line profile variations observed with double diffraction monochromator 09 p1524 A71-23192
- Fraunhofer lines at solar disk center and near limb, investigating profiles for asymmetry 09 p1524 A71-23194
- Telluric lines from 6327.5 to 6330.0 A in solar spectrum from photoelectric observations 09 p1525 A71-23196
- Solar spectra of far IR absorption of atmosphere above 4.2 km, using interferometer and cryogenic bolometer measurements 09 p1490 A71-23557
- Solar particle tracks in clear filter glass from Surveyor 3 spacecraft, comparing with lunar rocks track results 09 p1529 A71-23655
- Solar granular or convective motion velocities via photospheric oscillations for Doppler shifts in line spectra 10 p1665 A71-23776
- Solar Doppler widths from spectral line profiles by Goldberg profile intercomparison method, determining solar microturbulence depth dependence 10 p1665 A71-23777
- Solar lower chromosphere two dimensional models, using relative RMS line center intensity variations and mean limb darkening curves 10 p1666 A71-23781
- Solar simplified geometrical model, observing emission peak center to limb variation of Mg II, H and K lines and optical thickness 10 p1666 A71-23782
- Solar chromospheric emission line identification at 4097.3 A, discussing N III transition 10 p1666 A71-23783
- Sunspot molecular lines and rotational temperatures of MgH, CaH and TiO using model umbral atmospheres and photographic spectrograms 10 p1666 A71-23784
- Sunspots umbrae spectrum analysis in 4000-8000 A region, identifying molecular absorption lines photoelectrically 10 p1666 A71-23785
- Sodium D line flare emission on solar surface vs comet scattering, using photoelectric observation in undisturbed center disk region 10 p1660 A71-23791
- Solar flare spectral line features at 1.9 A, considering iron ion origin 10 p1660 A71-23797
- Solar spectrum observations in water band at 1.87 micron by stratospheric balloon sounding 10 p1667 A71-23863
- Solar corpuscular radiation differential and integral spectrum, assessing energetic electron flux in D region at sunrise 11 p1815 A71-25587
- Sunspots forbidden Fe I lines, calculating magnetic dipole and electric quadrupole transition probabilities 11 p1830 A71-26112
- MgO single crystals dominant coloration in solar spectral region by electron hole pair diffusion, trapping and recombination [AIAA PAPER 71-450] 11 p1808 A71-26234
- Quiet sun extreme UV spectrum measurements by OSO-4 Harvard scanning spectrometer, discussing instrument design and experimental results 12 p1956 A71-26618
- Solar corona plasma turbulence spectra, evaluating radar echo structure 12 p1963 A71-27080
- Solar photosphere vibrational temperature determination, using Franck-Condon factor with equivalent line widths for five CN vibrational bands 12 p1963 A71-27081
- Active unperturbed solar photosphere, determining variations in spectral line profiles 12 p1963 A71-27082
- Solar inner corona forbidden emission lines and continuum enhancement during 30 May 1965 eclipse as function of heliocentric position angle 12 p1969 A71-27650
- Green line intensity and electron/ion density contours as function of height over solar limb for March 1970 coronal enhancement 12 p1969 A71-27651

Fe XIV intensities in solar EUV spectrum, calculating equilibrium population of energy levels in coronal conditions 12 p1970 A71-27704

Solar Na D lines Doppler width, describing limb darkening data, assuming source function frequency dependent 12 p1970 A71-27748

Solar constant value and spectral distribution of solar radiation outside atmosphere 13 p2056 A71-28013

Photoelectric umbral scans at 6200-6700 Å identifying NiH lines, showing equal solar and terrestrial abundance isotopic ratios 13 p2135 A71-28301

Solar atmosphere center limb observations, describing line intensity fluctuations in Na D and Na 5688 doublets and Mg 4571 line 13 p2140 A71-29044

Solar Ca II K line core formation, discussing models for high spatial resolution spectra 13 p2140 A71-29045

Solar quiet region chromosphere K emission line behavior, identifying surface characteristics for width absolute magnitude relation 13 p2140 A71-29046

Magnetic field strength measurements from Zeeman splittings of sunspots molecular lines, considering saturation effects 13 p2140 A71-29047

Solar vacuum UV spectrum analysis, using echelle grating spectrograph onboard Skylark sounding rockets 13 p2070 A71-29048

Solar spicules H alpha and beta, D3 and K line profiles, considering radial and turbulent velocities, optical thickness, atomic density and He emission 13 p2140 A71-29049

Continuous emission in solar flare spectra from spectroheliographic data, suggesting photospheric origin 13 p2129 A71-29052

Solar X-ray line spectra observation, noting K alpha transition indicative of suprathermal events 14 p2297 A71-29598

Solar atmosphere line broadening by neutral hydrogen, noting discrepancy in van der Waals interaction 14 p2306 A71-29686

Gas pressure gradient and transmittance of sunspots, obtaining contours of D2 Na I and 5173 Å Mg I lines 14 p2309 A71-29983

Solar corona visible lines, identifying V VI to Fe IX electron transitions with variable inductance three electrode spark source 14 p2314 A71-30650

Solar image correction in high resolution radio interferometer by digital data processing technique maintaining required phase relations in antenna elements 15 p2373 A71-32446

Solar atmosphere structure inhomogeneities, describing Ca II H and K line spectra profiles 15 p2497 A71-32743

Low energy solar X-ray emission spectra observations, discussing nonthermal electron spectrum relation to acceleration by electric fields 16 p2626 A71-33725

Solar wind turbulence spectrum from Mariner 6 and 7 space probe radar measurements, using differenced range vs integrated Doppler technique 16 p2627 A71-33728

Solar extreme UV flash spectrum from spectroheliographs aboard Aerobee 170 rocket launched during March 1970 eclipse, comparing with homogeneous and inhomogeneous temperature models 16 p2640 A71-33730

Solar corona green line observations with Lallemand electrostatic camera during 7 March 1970 eclipse, showing equivalent width, electron density and temperature vs height above limb 16 p2640 A71-33745

Coronal IR emission lines during solar eclipse of 7 March 1970, using high altitude aircraft-borne Fourier transform spectrometer 16 p2640 A71-33751

Coronal line measurements on slit spectrogram during solar eclipse of 7 March 1970, showing fine structure in inner corona 16 p2642 A71-33784

Spectrographic observation of coronal lines in chromosphere during solar eclipse of 7 March 1970 16 p2642 A71-33787

Solar Lyman alpha emission line monitoring by OSO 5 satellite during 1969, noting solar activity effects 16 p2643 A71-33938

Real time system for solar spectrophotometry, noting application for scanning H alpha and other Balmer series lines profiles in solar flare regions 17 p2741 A71-34994

Thermal, turbulent and macroscopic motions in solar loop prominence of 4 May 1960, using spectral line composition by Gaussian profiles 17 p2809 A71-35596

Solar Fraunhofer line wavelengths shifts at disk center and at limb, evaluating Stark broadening contribution 18 p2962 A71-36106

Center to limb solar brightness distribution at 1.4 mm, discussing chromospheric models and antenna beam pattern effects 18 p2965 A71-36735

Solar Fe XIV 5303 coronal line isolation, using solid Fabry-Perot interferometer as monochromator 18 p2966 A71-36736

Solar flare observations /14-19 November 1969/, obtaining H alpha line profile 19 p3124 A71-37229

Solar corona plasma turbulence spectra, evaluating radar echo structure 19 p3133 A71-37430

Solar photosphere vibrational temperature determination, using Franck-Condon factor with equivalent line widths for five CN vibrational bands 19 p3133 A71-37431

Active unperturbed solar photosphere, determining variations in spectral line profiles 19 p3133 A71-37432

Solar photosphere iron abundance data from Fraunhofer spectrum and EUV line measurements 19 p3135 A71-37610

High resolution solar UV spectrum observation between 200 and 220 nm by sun-pointed Skylark rocket-borne echelle spectrograph 19 p3135 A71-37611

Solar Mg II H and K line profiles from rocket-borne echelle interferometer spectrograph and densitometer data 19 p3135 A71-37612

Far UV solar spectra observations, using OSO-2, 4, 5 and 6 spectroheliograms 19 p3136 A71-37614

Quiet sun, active regions and flares far UV space observations interpretation based on models 19 p3136 A71-37615

Solar limb and disk intensity spectra in chromosphere-corona transition region, calculating models, element abundances structure, electron pressure and hydrostatic equilibrium equations 19 p3136 A71-37617

Solar flare X ray spectrum analysis for lower corona physical conditions, discussing continuum and line emission 19 p3126 A71-37623

Solar limb H alpha spicules spectrograms, noting oscillations and time intervals 19 p3147 A71-38665

Solar limb D3 He line intensity distribution measurements during eclipse of 22 September 1968 19 p3147 A71-38666

Solar X-ray line emission, using crystal spectrometers during large chromospheric flare 19 p3130 A71-38672

Solar coronal X ray spectrum calculation of high-temperature low-density plasma, considering line emission from electron collisional excitation and radiation 20 p3278 A71-39058

Sunspot number relationship with solar radio flux, using cross spectral method for high and moderate activity periods 20 p3279 A71-39324

Solar IR spectra referencing procedure based on filter reference radiometer, discussing technique theoretical foundation 20 p3237 A71-39327

SiH molecular ion identification in solar atmosphere by solar absorption spectra 20 p3294 A71-39547

Solar silicon line spectra of photosphere, chromosphere and corona, including ionic spectra over wide ionization potentials range 20 p3301 A71-39822

Solar atmosphere oscillatory component observations at 3 mm wavelengths with two radio telescopes, obtaining power spectra 21 p3447 A71-40424

Solar low energy X-ray spectra observation during impulsive bursts, discussing thermal and nonthermal emission properties 21 p3438 A71-40425

Solar radio bursts and noise storms frequency band spectra, investigating warm plasma wave propagation and mode coupling theories 22 p3379 A71-41462

Solar flux density measurements at 2980 MHz, noting integration with spectral curve 22 p3390 A71-41463

Sunspot umbrae molecular line spectra, observing equivalent widths, isotopic abundances and band intensities 22 p3602 A71-42174

Solar X-ray spectra satellite lines observed by Bragg crystal spectrometers on Skylark rocket launched from Sardinia in December 1970 22 p3592 A71-42219

Solar chromosphere spectrum analysis, measuring H alpha line relative shifts variation with altitude 22 p3607 A71-42872

Solar far UV Fe and Ni ion lines 23 p3723 A71-42951

Interferometric measurements of 142 solar absorption lines in light from solar disk center 23 p3767 A71-43835

Solar K-line profile absolute intensity calibration from elements of fine structure on surface, determining brightness temperature 23 p3767 A71-43836

Mg isotopes in solar atmosphere, analyzing absorption bands in sunspot spectrum 23 p3767 A71-43837

Solar spectrum photoelectric recording instrument signal ratio accuracy, discussing divider circuit analysis 23 p3681 A71-44312

Photographic far UV solar spectra during eclipse of 7 March 1970, discussing coronal lines, prominences and quiet atmosphere structure 24 p3871 A71-44911

Identification of 417 Å line in solar EUV spectrum, calculating collision strengths and recombination rates for Fe XV 24 p3873 A71-45143

Search for CH molecular ion lines in solar photospheric spectrum, discussing profiles and equivalent widths 24 p3873 A71-45144

SOLAR SPECTROMETERS

Multiplex spectrometer for eclipse spectra photoelectric observation, using pseudorandom binary sequences as encoding pattern 03 p0424 A71-13634

Solar spectrograph data transmission to digital computer, discussing intermediate magnetic tape storage 04 p0590 A71-14841

Plage intensity variations on basis of photometrically analyzed Lyot filtergrams and ionosonde records 05 p0740 A71-16435

Intensity calibrated grazing incidence spectrographs on Skylark sounding rockets, recording solar soft X-ray and XUV spectra 06 p0967 A71-17903

Rocket-borne solid state spectrometer with liquid nitrogen cooled Li drifted silicon detector and optical feedback preamplifier for solar X-ray measurements 06 p0901 A71-18223

Quiet sun extreme UV spectrum measurements by OSO-4 Harvard scanning spectrometer, discussing instrument design and experimental results 12 p1956 A71-26618

Crimean astrophysical observatory horizontal solar telescope, describing spectrograph spectral bandwidth and dispersion characteristics 14 p2240 A71-29984

Polarization characteristics of solar coude telescope and Littrow spectrograph at Okayama Astrophysical Laboratory 19 p3062 A71-37241

SOLAR STORMS

Type 3 solar radio burst storms at low frequencies, suggesting electron packet exciters propagating with little deceleration 06 p0968 A71-17916

Recurrent solar cosmic ray events and M region magnetic storms 07 p1186 A71-19654

Suprathermal electrons continuous stream release into interplanetary medium during hectometric solar noise storm activities 09 p1518 A71-22353

Type 3 solar LF radio burst storms, considering streamer density, inhomogeneities and solar wind speed 13 p2141 A71-29053

Auroral X ray radiation measurements in midnight sector during solar storm of 8 March 1970 24 p3823 A71-45034

SOLAR STREAMS

U SOLAR CORPUSCULAR RADIATION

SOLAR SYSTEM

Solar activity cycles correlation with planets positions over ecliptic 01 p0149 A71-10053

Solar system exploration, discussing planets characteristics, trajectory utilization, grand tours, etc 01 p0151 A71-10269

Deuterium formation in early solar system by examining autogenetic spallogenic model 01 p0157 A71-10763

Three body gravitational capture of interstellar dust in solar system, examining zodiacal cloud 01 p0158 A71-10771

Solar system origin, structure and evolution, discussing planet and satellite orbital motion, resonance effects, tides and postaccretional changes 01 p0161 A71-11335

Accretion theory of planet and satellite formation in solar system, including earth-moon model 03 p0495 A71-14262

URCA neutrino emission processes explaining anomalous isotopic heavy element abundance in solar system

04 p0651 A71-15660

Pluto-Neptune system implications for solar system evolution theories, discussing deterministic and statistical models and a body problem approaches

04 p0655 A71-15726

Mg 26 isotopic abundance in meteoritic, lunar and terrestrial feldspar by mass spectrometry, suggesting limits on Al 26 in early solar system

06 p0966 A71-17896

Solar system evolutionary problems - Conferences, University of Rome, November 1968 and February 1969

07 p1202 A71-20512

Angular velocity and momentum vector evolution of isolated bodies in solar system, considering models to trace rotational motion evolution

07 p1203 A71-20525

Solar activity cycles correlation with planets positions over ecliptic

08 p1361 A71-21047

Newton inverse square law of gravitation in solar system, considering closed orbit trajectories

08 p1363 A71-21320

Decoupled nucleochronological isotopic equations for element age yielding solar system formation interval and supernova galactic distribution

08 p1251 A71-21694

Nomogram construction for graphical solution of two body problem using radius-vector and velocity components applied to solar system

09 p1520 A71-22844

Mafic silicates condensation in primordial solar nebula, explaining meteoritic abundance patterns by two component elemental volatility model and trace element distribution

09 p1521 A71-22932

Agglomeration process of dust particles growth in primordial solar nebula, considering early evolutionary phase of nearly free contraction and later phase with nebula flattening into gaseous disk rotating about protosun

09 p1523 A71-23045

Extraterrestrial Lyman alpha radiation source attributed to solar Lyman alpha scattering on cold interplanetary hydrogen penetrating to inner solar system

09 p1526 A71-23462

Media resistance effects on three body problem three dimensional periodic orbits, discussing implications to solar system formation from surrounding nebula

09 p1527 A71-23534

Chemical elements abundance in ordinary chondrites, terrestrial magma and lunar rocks, considering Alven theory of solar system origin

10 p1665 A71-23741

Collinear libration centers of spacecraft motion in sun perturbed three dimensional earth-moon system

10 p1671 A71-24329

Laboratory simulation of solid primordial condensation from low density partially excited gas for solar system origin

10 p1673 A71-24413

Supernovae detonation model, examining nucleosynthesis for solar system abundances

10 p1675 A71-24492

Planetary mass system as pulsar timing error sources, noting change in barycenter of solar system

10 p1675 A71-24493

Dust grain condensation and primordial elements transport into interplanetary space during early stage solar evolution

11 p1819 A71-25222

Planetary condensation under conditions of Woolfson solar system origin capture theory

11 p1820 A71-25296

Solar system space physics review covering earth atmospheric temperature, density and models, solar wind, auroras, and moon, Venus and Mars data from space missions

13 p2131 A71-27877

Hydrodynamic model of coalescing meteors substantiating cosmogonic Laplace-Schmidt hypotheses of solar system planetary formation from cosmic dust

13 p2131 A71-27892

Exobiological survey of solar system beyond Mars, considering asteroids, Jovian planets and moons, Pluto and comets

13 p2133 A71-28040

CI chondrites approximating primordial solar system matter condensable fractions based on isotopic/elemental abundance continuity, fractionation patterns and chondrules absence

14 p2306 A71-29708

Gravity decrease effects on planetary orbits, considering two bodies in circular and elliptical orbits and many bodies solar system with interaction between planets

16 p2631 A71-33167

Planetary dynamics bibliography and review, considering range determination and ephemerides, general

relativity, tidal evolution and lunar orbit, solar system commensurabilities, etc

17 p2798 A71-34457

Bibliography and review of solar system bodies surfaces, considering remote sensing at UV, optical, IR, microwave and radio wavelengths, in situ lunar measurement and surface exploration

17 p2798 A71-34458

Apollo 11 and 12 lunar rocks composition, suggesting depletion of K, Rb and Pb in solar nebula prior to final accretion of moon

18 p2963 A71-36228

Small bodies collisions in solar system, using Newtonian mechanics to indicate formation of meteor and asteroid streams

18 p2967 A71-36923

Chondrite classification, primordial matter composition and early solar system chemical processes, discussing cosmic gas condensation and refractory element fractionation

18 p2967 A71-37027

Magnetic field measurements on Outer Planets Grand Tour to yield solar system origin and evolution and interstellar medium data

[AAS PAPER 71-123]

19 p3139 A71-37918

Balanced terrestrial and outer planets NASA solar system exploration strategy for 1970s, outlining earth based observations and flight missions program

[AAS PAPER 71-100]

19 p3140 A71-37930

Time arrival measurements of optical pulses from Crab Nebula pulsar correlated to solar system barycenter

20 p3303 A71-39931

Five outer planets orbital perturbations by four inner planets, comparing second differentials with disturbing force numerical values

21 p3441 A71-40096

Relativistic gravity in solar system, predicting Newtonian gravitational constant anisotropy measurements by Cavendish experiments

22 p3575 A71-41920

Skylab manned scientific space laboratory for medical, solar astronomy, earth resources, technology and engineering experiments

22 p3608 A71-41950

Book on space technology for developing countries covering economic, social and educational reform, solar system exploration and extraterrestrial civilizations

22 p3623 A71-42066

Supernova shell fragmentation as basis for solar system formation model, considering meteoritic materials heavy elements formation by nucleosynthesis followed by r-process event

22 p3604 A71-42192

Planetary formation from sun ejected charged bodies captured in orbit due to electromagnetic effects, considering Sarvajna model

22 p3604 A71-42334

Solar system organic compounds detection and evolution, considering element, isotope and pigment composition, optical activity and polymerization

22 p3496 A71-42824

Early solar system organic matter origin, discussing amino acid synthesis from CO, H and ammonia reaction with N, alumina or clay catalysts

23 p3633 A71-43244

Prebiotic organic matter in solar system, investigating contamination free amino acid catalytic synthesis from deuterated reactants

23 p3633 A71-43245

Space plasma physics, considering solar system origin

24 p3874 A71-45169

SOLAR TEMPERATURE

Quiet corona temperature from solar equator soft X ray flux measurement by satellite-borne heliograph

02 p0300 A71-12077

Solar photosphere temperature constancy in thin CO layer from equivalent spectral line width determination

03 p0484 A71-13208

UV scanning polychromator spectroheliometer on Apollo Telescope Mount, examining temperature distribution on sun

03 p0430 A71-14435

Subphotospheric trapped standing acoustic wave mechanism of 5 minute oscillations on solar surface

05 p0801 A71-15936

Critique on existence of one hundred million degree K solar flare plasma

08 p1350 A71-20944

Solar flare model, computing thermal X ray emission

08 p1350 A71-20945

Quiet corona temperature from solar equator soft X ray flux measurement by satellite-borne heliograph

08 p1361 A71-21127

Empirical solar photosphere continuum models, calculating temperature distribution for absolute intensities at center and limb darkening ratios

10 p1666 A71-23779

Sunspot molecular lines and rotational temperatures of MgH, CaH and TiO using model umbral atmospheres and photographic spectrograms

10 p1666 A71-23784

Sunspot umbra empirical model, deriving temperature and optical depth relationship from IR continuous limb darkening

10 p1666 A71-23787

Solar temperature after formation, using isotopic composition differences in terrestrial and extraterrestrial xenon

10 p1668 A71-23871

Solar coronal heating homopolar generator model, proposing neutrons as energy source

12 p1961 A71-26877

Solar photosphere vibrational temperature determination, using Franck-Condon factor with equivalent line widths for five CN vibrational bands

12 p1963 A71-27081

Rotation-convection model of solar equatorial acceleration and temperature, assuming inhomogeneous isotropic latitude dependent turbulent energy transport

12 p1968 A71-27644

Solar neutrino astronomy, investigating interior central temperature, energy generation mechanism and model

13 p2142 A71-29116

Solar corona XUV resonance line spectrum interpretation, using thermal emission from inhomogeneous regions

14 p2297 A71-29678

Solar atmosphere vertical temperature and density distribution measurements, using spatially averaged H and K resonance line profiles central reversals

15 p2496 A71-32742

Solar extreme UV flash spectrum from spectroheliographs aboard Aerobee 170 rocket launched during March 1970 eclipse, comparing with homogeneous and inhomogeneous temperature models

16 p2640 A71-33730

Profile changes of magnetically non-split lines in faculae, explaining observations by outer layers temperature increase

18 p2965 A71-36731

Solar photosphere vibrational temperature determination, using Franck-Condon factor with equivalent line widths for five CN vibrational bands

19 p3133 A71-37431

Solar brightness temperature measurements using balloon-borne Michelson interferometer

19 p3135 A71-37613

Electron temperatures for lithium-like ions O VI, Ne VIII and Mg X formation in solar chromosphere and corona, using rocket spectrometric measurements

19 p3136 A71-37618

Short periodical pulsations in solar atmosphere related to magnetosound propagation in area of temperature minimum with directed perpendicular magnetic field

20 p3290 A71-39305

Solar constant calculations, discussing rms error and effective temperature

22 p3596 A71-41451

Solar spaceborne astronomy, examining progress in temperature and density profiles determination

22 p3605 A71-42524

SOLAR VELOCITY

Downward moving large scale surface velocity fields of solar atmosphere from magnetograph data

12 p1968 A71-27645

Sunspot butterfly diagram interpretation based on heliographic latitude drift relation to gradient of solar rotational velocity

15 p2495 A71-32707

Spectroheliogram Doppler movies of solar velocity fields showing oscillatory and slowly varying components

18 p2965 A71-36728

Solar velocity field decomposition into oscillatory and slowly varying components by spectroheliograms with high spatial resolution

19 p3146 A71-38662

Streamline pattern deduction for sun large scale flow from Doppler line of sight velocities

22 p3596 A71-41454

SOLAR WIND

Mathematical model for interaction between solar wind and interstellar gas

01 p0144 A71-10066

Artificial solar wind production by plasma electrodynamic acceleration, investigating simulated earth-wind interaction

01 p0160 A71-11067

Solar wind injection into magnetosphere, noting effects of magnetopause outward velocity and electric field strength

01 p0146 A71-11452

Solar wind elemental and isotopic He and Ne compositions from mass spectrometry of ions collected in metal foils deployed during Apollo 11 and 12 landings

01 p0146 A71-11486

Lunar Mach cone in flow of magnetized warm collisionless solar plasma from Explorer 35 observations

01 p0162 A71-11489

- Directed proton fluxes measurements in bow shock, magnetosheath and solar wind byOGO 5 satellite ion spectrometer 01 p0147 A71-11491
- Polytrope solar wind equations, expressing distance and flow velocity as functions of mass density 01 p0147 A71-11510
- Two parameter asymptotic solutions for viscous model of solar wind flow 01 p0147 A71-11511
- Solar wind ion abundances from satellite observation, discussing energy spectra, particle distributions, etc 01 p0147 A71-11518
- Solar wind ion energy per charge spectra, comparing to Vela 3A observations for composition 01 p0148 A71-11519
- Near earth solar wind Fe, Si and O ions, using electrostatic analyzer on Vela 5A satellite 01 p0148 A71-11520
- Plasma motion in magnetosphere under undisturbed geomagnetic conditions, taking solar wind into account 02 p0244 A71-11919
- Solar wind plasma composition and dynamics, discussing element and ion abundances, solar activity effects, plasma stability, etc 02 p0300 A71-12374
- Solar corona and wind composition, accounting for He flux and heavy elements from diffusion equations solution 02 p0303 A71-12770
- Symmetrical solar wind model solutions with thermal conductivity, showing constant mass and total energy flux conditions relationship to critical line 02 p0303 A71-12771
- Solar wind interaction with moon, using two dimensional guiding center model 02 p0303 A71-12772
- Comet brightness fluctuation phenomenon, discussing solar wind interaction with Platt particles in cometary atmosphere 02 p0303 A71-12867
- Boundary position and thickness between geomagnetic field and solar wind plasma, simulating interaction with magnetosphere 03 p0473 A71-13107
- Anisotropic plasma discontinuities in solar wind, noting shock misidentification 03 p0463 A71-13307
- Solar wind lunar impingement induction of magnetic fields used for global sounding of moon structure 03 p0486 A71-13323
- Solar wind microscopic structure, examining interplanetary wave-particle interactions 03 p0480 A71-14068
- Supersonic solar wind flow termination, examining interstellar neutral hydrogen effect 03 p0481 A71-14502
- Simple two fluid solar wind speed and proton temperature model, discussing nonthermal energy dissipation 03 p0481 A71-14504
- Solar wind and magnetopause shock front location at 1969 maximum, examining proton parameters from Heos 1 observations 03 p0482 A71-14513
- Large amplitude upstream wave solar wind event of 10 March 1968 with suprathermal protons, correlating magnetometer plasma probe and Lepedea proton data 03 p0482 A71-14530
- Geomagnetic microfluctuations noting magnetospheric dimensions, solar wind velocity, magnetic activity indicators and latitude effects on rapid variations 04 p0584 A71-15369
- Solar wind plasma power spectra noting frequency dependence, particle density and speed and interplanetary magnetic fields 05 p0802 A71-15942
- Magnetic and thermal pressures in solar wind from Explorer 34 data 05 p0797 A71-16016
- Solar wind velocity and ion temperature measurement by modulation-type ion trap onboard interplanetary Venera 3 satellite 05 p0798 A71-16052
- Solar wind upstream waves ahead of earth bow shock by dual satellite observations 05 p0741 A71-16629
- Finite electrical conductivity effects on solar flare-induced interplanetary shock waves, discussing solar wind time dependent bulk flow characteristics 05 p0810 A71-16634
- Finite electrical conductivity role in interplanetary piston driven shock waves propagation in solar wind 05 p0810 A71-16635
- Two fluid model solar wind, predicting electron temperature and heat flow 05 p0799 A71-16692
- Solar wind parameters-terrestrial electromagnetic field micropulsations relation based on interplanetary probes and time correlated ground observations 05 p0800 A71-17170
- Solar wind torque on earth magnetic dipole based on magnetosphere model analytic solution in rotating reference frame 06 p0891 A71-17885
- Alpha particle abundance in solar wind positive ions observed by ESRO satellite HEOS-1 06 p0950 A71-17919
- Solar wind velocity relationship with F 2 layer electron density 06 p0950 A71-17991
- Galactic cosmic rays nonlinear interactions with solar wind, taking into account autofocusing effect 06 p0951 A71-18103
- Models for solar wind modulation of galactic cosmic rays by anisotropic diffusion approximation 06 p0951 A71-18104
- Solar wind asymmetric component on basis of 27-day cosmic ray variations 06 p0953 A71-18121
- Solar activity correlation with cosmic ray intensity and solar wind properties, analyzing hysteresis diagrams for wind modulation characteristics dependence on heliolatitude 06 p0954 A71-18123
- Energetic solar wind particles, discussing interplanetary magnetic field curvature and gradient effects 06 p0956 A71-18142
- Solar and galactic cosmic rays interactions with interplanetary magnetic field 28 January-25 February 1967 based on Explorer 33 and 28 satellite observations 06 p0957 A71-18145
- Geomagnetic activity relation to large scale variations in interplanetary magnetic field and solar wind deformation velocity, using satellite and space probe observations 06 p0963 A71-18254
- Solar wind observations, accounting for cosmic plasma and stellar wind properties 06 p0973 A71-18336
- Jupiter and Saturn magnetosphere calculations, considering solar wind characteristics and planetary magnetic fields [AJAA PAPER 71-30] 06 p0977 A71-18494
- Plasma density irregularities in solar wind, showing wavelength dependence of interplanetary scintillation inconsistent with magnetic variations 07 p1184 A71-18862
- Solar wind fast shock wave and simultaneous ground geomagnetic disturbance related to magnetospheric deformation 07 p1185 A71-19396
- Low energy electron and proton fluxes observation by Isis 1 satellite, concluding solar wind penetration to low altitudes through magnetopause cusp 07 p1186 A71-19659
- Quiet day geomagnetic field measurements at synchronous orbit ATS 1, calculating equatorial component of interaction force between solar wind and earth 07 p1102 A71-19664
- Interplanetary space solar wind flux variations-earth electromagnetic field pulsations comparison by spacecraft and geophysical station observations 07 p1187 A71-19677
- Energy transfer at colliding streams in solar wind from Explorer 34 and Vela 4B measurements of proton, alpha particle, electron and magnetic field parameters 07 p1188 A71-19824
- Corotating solar wind electron number density from sun orbiting Pioneer spacecraft radio propagation measurements 07 p1189 A71-20320
- Spin-orbit coupling and angular momentum transfer between planets and sun by interaction with solar wind 07 p1203 A71-20522
- Proton flux range between solar wind and cosmic radiation protons energy by spacecraft observation 08 p1350 A71-20952
- Cosmic ray modulation processes, spectrum variation and intensity restoration delay, discussing solar activity indices and wind models 08 p1351 A71-20965
- Diurnal cosmic ray anisotropy, investigating solar wind velocity and interplanetary magnetic field effects 08 p1352 A71-20971
- Galactic cosmic ray density space-time variations in interplanetary space with solar wind, using spherically symmetrical model with diffusion approximation 08 p1352 A71-20974
- Galactic cosmic ray density modulation by solar wind, assuming heliolongitudinal asymmetry 08 p1353 A71-20975
- Artificial solar wind experiments, describing interaction between hydrogen plasma shock wave and simulated geomagnetic field 08 p1354 A71-21010
- Geomagnetic cavity heuristic model with solar wind driven unipolar induction current in ionosphere 08 p1280 A71-21218
- Magnetohydrodynamical effects of spirally twisted interplanetary field on solar wind velocity and density 08 p1355 A71-21420
- Solar wind speed distributions /1962-1970/ as function of solar cycle 08 p1356 A71-21641
- Preferred orientations of rotational and tangential discontinuities in solar wind from Mariner 5 data 08 p1356 A71-21642
- Solar wind flux correlation with earth EM field pulsations, noting flare-generated shock front effects on magnetosphere 09 p1513 A71-22422
- Solar wind electric field relation to ground magnetic disturbances during magnetic storm from Explorer 28 and ground data 09 p1435 A71-22433
- Magnetic disturbances caused by magnetospheric-solar wind filamentary inhomogeneity interaction observed by Pioneer 6 09 p1513 A71-22560
- Interplanetary plasma disturbances in Venus proximity from Venera measurements 09 p1520 A71-22669
- Deceleration of low energy cosmic rays in solar wind involving Fermi acceleration by MHD waves and adiabatic energy change 09 p1514 A71-22802
- Magnetosonic waves generation by interaction of bow shock with frozen tangential discontinuities in solar wind 09 p1521 A71-22866
- Solar wind static and dynamic pressures on earth magnetosphere, using geomagnetic parameters 09 p1514 A71-23152
- Mathematical model for interaction between solar wind and interstellar gas 09 p1514 A71-23259
- Solar wind simulation for interaction with lunar magnetic field, discussing particle shadowing effects generation of electric fields 09 p1514 A71-23310
- Cosmic rays propagation in solar wind, presenting statistical theory of interplanetary magnetic field effect on charged particles transport 09 p1515 A71-23461
- Quasi-radial hypervelocity approximation of rotating azimuthally dependent solar wind under magnetic field 09 p1515 A71-23709
- Solar wind interaction with field free planetary ionospheres, giving three dissimilar models 10 p1661 A71-24005
- Trapped solar wind He and Ne in Surveyor 3 unpainted Al tube, comparing with Apollo 11 and 12 solar wind composition 10 p1672 A71-24390
- Solar wind motion irregularities near sun from interplanetary scintillation observations, using receivers at Goldstone deep space tracking station 10 p1674 A71-24435
- Quiet solar wind two component model, including viscosity, magnetic field and reduced heat conduction 10 p1662 A71-24498
- Lunar rock analysis, discussing heavy ion impact traces and amorphous skin relation to solar wind 10 p1677 A71-24696
- Interplanetary space low energy cosmic ray protons steady state anisotropy based on radial gradient model of outward convection at solar wind speeds 10 p1663 A71-24777
- Solar wind heat conduction evaluation by electron energy equation dimensional analysis 10 p1663 A71-24778
- Solar wind blast wave dependence on initial disturbance energy and angular extent by time dependent two dimensional hydrodynamic flow simulation 10 p1663 A71-24779
- Solar wind-magnetosphere interaction modes from Explorer 33 and 35 interplanetary plasma and magnetic field data 10 p1663 A71-24780
- Solar wind origin of auroral ions from low energy hydrogen and helium ion spectral measurements 10 p1664 A71-24791
- Laboratory model for radio star scintillation and other diffraction phenomena by thin weak random phase changing screen including earth atmosphere or solar wind 10 p1678 A71-24797
- Solar wind distribution with respect to interplanetary magnetic field structure, interaction with planets and effect on earth magnetosphere 11 p1814 A71-25262
- Solar wind composition of protons, He isotopes and heavy rare gas ions from Apollo lunar samples 11 p1814 A71-25263
- Anomalous dispersion and instability in solar wind plasma with thermal anisotropy and high beta ratio, applying magnetosonic wave-particle interactions 11 p1816 A71-25754
- Hydrogen plasma simulation of solar wind-planetary body interaction, showing electric fields behind moon and Venus 11 p1816 A71-25755
- Dust particle angular momentum orientation in comet tails through bombardment by solar wind protons, noting role in scattered light polarization 11 p1832 A71-26182

Solar wind noble gas composition on moon with aluminum foil exposure, confirming absence of lunar atmosphere and magnetic field

11 p1834 A71-26330

Solar wind effects on space around earth, discussing dipole image of magnetic field, radiation belt feeding and atmospheric phenomena based on artificial satellite observations

11 p1817 A71-26337

Collisionless motion of solar wind ions in helical magnetic field, giving transfer function of charged particles

12 p1947 A71-26636

Interplanetary magnetic field measurements from lunar surface and lunar orbit, discussing solar wind effects on bulk electrical conductivity of lunar crust

12 p1947 A71-26691

Solar plasma emission capacity, using atmospheric ionization theory

12 p1964 A71-27084

Lunar samples mineralogy, petrology and geochemistry, considering lunar surface processes, cosmic ray flux and solar wind

12 p1967 A71-27414

Solar system space physics review covering earth atmospheric temperature, density and models, solar wind, auroras, and moon, Venus and Mars data from space missions

13 p2131 A71-27877

Lunar diamagnetic cavity signatures from Ames magnetometer experiment on Explorer 35 orbiter, indicating solar wind interaction

13 p2132 A71-27909

Hydromagnetic wave coupled solar wind-plasma sheet effects on resonant oscillations of geomagnetic tail, using two dimensional model

13 p2119 A71-27910

Solar wind-Mercury interaction, discussing planet physical properties, magnetized wind parameters and bow shock wave existence

13 p2120 A71-27924

Plasma motion in magnetosphere under undisturbed geomagnetic conditions, taking into account solar wind

13 p2058 A71-28206

Interplanetary magnetic field angular gradient and sectorial effects on solar wind, discussing wind velocity

13 p2128 A71-28527

Cosmic ray density distribution inside modulating spherical cone over long-lived solar wind regions, noting modulation depth quasi-periodic variation

13 p2129 A71-28550

Solar wind deflection due to permanent lunar surface magnetism

13 p2129 A71-28780

Type 3 solar LF radio burst storms, considering streamer density, inhomogeneities and solar wind speed

13 p2141 A71-29053

Solar wind heavy ion data, using Heos-1 satellite observations of 31 March 1970 interplanetary shock

13 p2130 A71-29059

Solar wind speed data, investigating variations in satellite observations

13 p2130 A71-29062

Rotating solar wind nonradial oscillations and energy transport, showing internal solar gravity waves effects

13 p2130 A71-29118

Distant geomagnetic tail longitudinal magnetic field gradient model based on pressure balance between internal field and solar wind, discussing tail flux content

13 p2064 A71-29162

Solar wind-magnetosphere interaction based on electric fields and currents, discussing energy transfer and magnetic field reversal at magnetopause

13 p2064 A71-29165

Ionic and thermal structure model of daytime Venus ionosphere with solar wind heating based on Mariner 5 flyby mission

14 p2305 A71-29661

Initial phase duration of geomagnetic storms inverse dependence on sudden commencement amplitude in accord with solar wind-magnetosphere interaction

14 p2231 A71-29724

Polar magnetic disturbances, discussing correlation with interplanetary magnetic field and interaction effects between solar wind and magnetosphere

14 p2231 A71-29907

Solar wind interaction with planetary atmospheres, discussing various models relationship to observational data

14 p2298 A71-29908

Atmospheric and cosmic origin of noctilucent clouds, discussing solar wind effects on H, O and water vapor molecules in mesosphere and thermosphere

14 p2232 A71-29956

MHD processes of upper atmosphere in mesospheric cloud formation, discussing solar wind-magnetic field interactions and equilibrium for Pikelner bomb

14 p2232 A71-29960

Solar equatorial plane interplanetary plasma and magnetic field features from cosmic ray variation anomaly observation

14 p2299 A71-29988

Solar wind compressed magnetic field in sunward magnetosphere and extended geomagnetic tail observation by Pioneer 7 spacecraft

14 p2234 A71-30028

Cosmic ray modulation by solar wind, developing model with time variations based on magnetic bending power

14 p2302 A71-30647

Supersonic to subsonic solar corona transition, using supersonic solution for solar wind inviscid equations

14 p2302 A71-30648

Asymmetries in magnetospheric shock layer due to upstream interplanetary magnetic field, considering forward stagnation region of solar wind-magnetosphere interaction

15 p2395 A71-31546

Solar wind velocity and Io phase relationship during decametric radio bursts from Jupiter, indicating plasmasphere existence

15 p2474 A71-31723

Solar wind torque on geomagnetic cavity by rotational unipolar induction currents, including Joule heating of ionospheric plasma and directional magnetic fields

15 p2474 A71-31773

Solar wind ion thermalization in earth bow shock by counterstreaming instability related to interplanetary magnetic field

15 p2399 A71-31774

Quasar 3C 48 observations at 408 MHz, noting scintillations due to interplanetary plasma inhomogeneities

15 p2487 A71-32035

Radio sources interplanetary scintillations observation, discussing solar wind velocity and diffraction pattern scale

15 p2480 A71-32445

Solar wind outflow from active regions by numerical integration of hydrodynamics equations, using corona temperature distribution

15 p2480 A71-32753

Thermal properties of solar wind plasma, determining electron and proton temperature distributions, proton heating rate, electron thermal conductivity and energy exchange rates

15 p2480 A71-32754

Cosmic ray modulation by angle dependent solar wind, detailing adiabatic deceleration and radial anisotropy effects

15 p2481 A71-32777

Corotating solar plasma streams associated with variations of interplanetary scintillation from observed radio sources

16 p2634 A71-33386

Solar wind velocity and ion temperature measurement by modulation-type ion trap onboard interplanetary Venera 3 satellite

16 p2626 A71-33456

Solar wind turbulence spectrum from Mariner 6 and 7 space probe radar measurements, using differenced range vs integrated Doppler technique

16 p2627 A71-33728

Lunar, meteoroid and asteroid surface erosion, investigating hypervelocity impact, solar wind flux and ion sputtering effect

16 p2642 A71-33818

Swiss space research, surveying international cooperative scientific activity relative to upper atmosphere satellite geodesy, solar wind, lunar samples analysis, IR and UV astronomy and celestial mechanics

16 p2665 A71-33852

Interplanetary hydrogen and helium from cosmic dust deionizing effect on solar wind, calculating gas density and flux

16 p2628 A71-33940

Solar wind rotational to tangential discontinuities ratio determination and hypothesis concerning origin in interplanetary magnetic field

16 p2628 A71-33942

Magnetotail changes relationship to solar wind magnetic field and magnetospheric substorms from ground and satellite data

16 p2629 A71-33944

Low energy auroral thermal electrons flux after geomagnetic substorm, entering magnetosphere from solar wind

16 p2629 A71-33953

Solar wind modulation effects on galactic protons and cosmic rays, using radial magnetic field mathematical model and Monte Carlo method

17 p2795 A71-34373

Bibliography and review of solar activity relevant to sun-planet relationships, considering magnetic fields, transient events, corona and solar wind

17 p2799 A71-34459

Bibliography and review of interplanetary magnetic fields and plasmas, considering solar wind properties, magnetosheath, bow shock and magnetospheric tail

17 p2799 A71-34460

Sq day to day variability relation to interplanetary plasma parameters including magnetic field and solar wind velocity and kinetic energy

17 p2801 A71-34625

Hydrostatic, dynamic, hydrodynamic and two-component corona models and solar corpuscular radiation, considering heat conductivity and viscosity effects on solar wind dynamic characteristics

17 p2795 A71-34828

He, Ne and Ar isotopic distribution and origin in Apollo 12 lunar samples, considering solar wind implantation

17 p2695 A71-35036

Apollo 11 and 12 lunar landings, discussing retrieved lunar material, seismographs, solar wind and light reflector for measuring earth-moon distance

18 p2959 A71-35906

Jovian magnetospheric plasma densities, discussing roles of centrifugal ejection, solar wind plasma injection and photoelectron diffusion

18 p2964 A71-36291

Asteroid magnetospheres effects on magnetic moments and whistler mode noise propagation in solar wind

18 p2964 A71-36292

Proton flares in McMath Region 8461 (August-September 1966), describing solar wind plasma ejection and helium enriched interplanetary medium

18 p2958 A71-36743

Comet Tago-Sato-Kosaka isophotometry, obtaining surface brightness distribution and solar wind velocity estimate

19 p3130 A71-37228

Solar wind plasma density and flow speed semiannual variations from Vela 3 and 4 satellite observations, noting dependence on heliographic latitude

19 p3124 A71-37351

Second order MHD equations for density fluctuations driven by Alfvén waves with relation to solar wind

19 p3110 A71-37352

Nonthermal electrons interaction with electron plasma oscillations and HF transverse waves in upstream solar wind

19 p3125 A71-37353

Substorm signature in interplanetary medium relating southward component with solar wind energy transformation

19 p3132 A71-37356

Solar plasma emission capacity, using atmospheric ionization theory

19 p3133 A71-37434

Solar wind MHD interaction with magnetosphere, taking into account photospheric origin, velocity in interplanetary space and Parker theory

19 p3126 A71-37460

Solar wind fast shock wave and simultaneous ground geomagnetic disturbance related to magnetospheric deformation

19 p3127 A71-37820

Solar wind formation of heliosphere, discussing solar wind-interstellar medium interaction region probes by Pioneers F and G

19 p3141 A71-37962

Solar wind acceleration due to Alfvén wave pressure gradient, taking into account coronal parameters of temperature, magnetic field and energy density

19 p3128 A71-38162

Interplanetary plasma and magnetic field interaction with earth magnetosphere using spacecraft measurements during storms

19 p3145 A71-38272

Solar wind proton penetration through earth magnetosphere, taking into account drift, force lines curvature and nonstationary plasma boundary

19 p3129 A71-38376

Astronomical models of solar wind interaction with interstellar medium, determining magnetic field effects on shock wave

20 p3278 A71-39139

Jupiter decametric radio emission relation to solar wind, geomagnetic activity and shock waves causing Forbush decreases

20 p3291 A71-39312

Satellite data on solar wind velocity, ion composition, temperature and magnetic field characteristics near earth orbit

20 p3279 A71-39445

Artificial solar wind experiments, describing interaction between hydrogen plasma shock wave and simulated geomagnetic field

20 p3279 A71-39590

Lunar dust potential as function of solar wind flux and particle photoefficiency

20 p3298 A71-39639

Solar wind origin in active regions by radar exploration, noting signal backscattering from coronal plasma turbulent pulsations

20 p3281 A71-39732

Low energy hydrogen and helium ions composition of primary aurora precipitation from rocket-borne spectrometer experiment, suggesting direct solar wind origin of primaries

20 p3301 A71-39850

VLF ion wave instabilities in polar wind based on plasma kinetic theory, comparing with electrostatic wave observation by OV3-3 satellite

20 p3231 A71-39890

Outwardly propagating coronal Alfvén waves pressure exertion on solar wind, using one fluid polytrope model

21 p3438 A71-40423

Solar wind angular momentum flux transport from nonradial velocity components measurements by Mariner 5, noting agreement with comet tail observations

21 p3438 A71-40428

Shock free transonic deceleration of solar wind due to interacting interactions, discussing plasma flow

21 p3438 A71-40604

Large scale spiral variations of interplanetary magnetic field related to structures in solar wind, including polar field and out of eclipses models

21 p3453 A71-41181

Solar wind theory, discussing thermal conduction and MHD wave energy supply mechanisms of large scale solar corona expansion

21 p3439 A71-41183

Radial electric field and electrostatic potential in solar wind from two fluid model

22 p3592 A71-41921

Solar wind angular momentum calculation from short term directional, density and velocity fluctuations, using Vela 3 satellite data

22 p3592 A71-42162

Steady state transition layer between cold solar plasma flow and geomagnetic field in one dimensional model

22 p3536 A71-42622

Solar wind velocity increase by magnetic field energy conversion to kinetic energy, constructing steady state MHD one fluid model

23 p3719 A71-42949

Interplanetary plasma and magnetic field observations by Vela 3 and Imp 3 satellites

23 p3708 A71-43154

Suprathermal electron beam induced HF wave instability in solar wind upstream from earth bow shock, interpreting OGO 5 observations

23 p3720 A71-43158

Magnetopause and bow shock location from IMP measurements, discussing solar wind momentum flux induced orbit-to-orbit changes in boundary positions

23 p3667 A71-43159

Model prediction for magnetospheric electric field dependence on solar wind velocity, comparing results with plasmaspheric measurements for different Kps

23 p3721 A71-43177

Interstellar He photoionization effect on solar wind abundance

23 p3721 A71-43182

Magnetospheric substorms relationship to interplanetary magnetic field and solar wind plasma parameters, noting dominant effect of interplanetary southward component

23 p3734 A71-43183

Li, B, Mg and Ti isotopic abundances and search for trapped solar wind Li in Apollo 11 and 12 rocks

23 p3752 A71-43708

Apollo 11 and 12 lunar samples history of irradiation exposure to galactic cosmic rays and solar wind, using rare gas and Gd isotope measurements

23 p3754 A71-43724

Solar rotation evidence from H alpha and K line spectra of quiescent prominences for westward wind

23 p3767 A71-43841

Proton irradiation damage on lunar surface, considering solar wind sputtering, reduction, chemical bond breakage and electron paramagnetic resonance

24 p3867 A71-44423

Outer radiation belt parameters dependence on interplanetary magnetic field sectorial structure and solar wind velocity

24 p3866 A71-45039

Artificial magnetosphere interaction with 8 keV electrons in hydrogen plasma beam simulating solar wind, noting penetration caused by boundary instability

24 p3823 A71-45043

SOLAR X-RAYS

Limb flares relationships to solar soft X ray bursts intensity growth phase

01 p0144 A71-10868

Solar hard X ray absorption in D region, calculating integral flux radiation

01 p0145 A71-11076

Quiet corona temperature from solar equator soft X ray flux measurement by satellite-borne heliograph

02 p0300 A71-12077

Soft solar X-ray flares six minute periodicity from satellite observation

02 p0300 A71-12472

Solar flare classification based on X ray intensity, offering geophysical significance advantage

02 p0301 A71-12697

Solar X-ray flare activity statistical prediction based on correlation to coronal electron temperature and emission measure

02 p0301 A71-12698

Hard solar X-ray spectra measurements, reinterpreting OSO 3 scintillation counter response due to pulse pile-up

02 p0302 A71-12766

Solar mm bursts impulsive component correlation with associated soft X ray burst

03 p0473 A71-13184

Solar X-rays role in D region ionization from ion probe sounding during eclipse of 20 May 1966

03 p0407 A71-13377

Solar proton flares associated with 1968 and 1969 strong particle events, noting correlation with hard X ray and microwave bursts

03 p0478 A71-14037

Solar X-ray emissions dynamic spectra at flare times by E-T tracing

03 p0479 A71-14045

Solar flare X ray and radio wave emission measurement by OGO 4 and Solrad 9 satellites

03 p0479 A71-14046

Solar X-rays emission anisotropy, questioning correlation with optical flares

03 p0480 A71-14047

Atmospheric absorption models of solar X-rays at occultation times, using Solrad satellites

03 p0480 A71-14048

High atmosphere X ray absorption grazing scale height variations from satellite measurement of solar X-ray flux during sunrise and sunset

03 p0480 A71-14049

Solar soft X ray and extreme UV relative contribution to E layer ion production rates during solar eclipse of 12 November 1966

03 p0481 A71-14511

Impulsive solar flare X rays spectral characteristics, examining electron energy, bremsstrahlung, microwave bursts and particle escape, collisions and injection

05 p0797 A71-15937

Angular distribution and polarization of solar X-ray bremsstrahlung, taking into account magnetic field effects

05 p0000 A71-16032

Solar X-ray radiation measurements using real time telemetry from SOLRAD satellites

05 p0799 A71-17001

Solar coronal plasma X ray emission, using simplified thermal continuum function

05 p0800 A71-17095

Intensity calibrated grazing incidence spectrographs on Skylark sounding rockets, recording solar soft X-ray and XUV spectra

06 p0967 A71-17903

Solar X-ray resonance, intercombination and forbidden lines variations of O VII emission

06 p0968 A71-17910

Solar 3.3 mm bursts observation, showing temporal correlation with soft X ray bursts

06 p0968 A71-17915

Solar X-ray control of lower ionospheric radio wave absorption determined from Solrad 9 and Panska Ves Observatory data

06 p0892 A71-17921

Solar flare delayed relativistic electron appearance, comparing radio, optical and X ray data for particle intensities

06 p0961 A71-18171

Rocket-borne solid state spectrometer with liquid nitrogen cooled Li drifted silicon detector and optical feedback preamplifier for solar X-ray measurements

06 p0901 A71-18223

Impulsive hard X ray and far UV emission during solar flares

07 p1188 A71-19825

X ray line emission from heliumlike calcium during solar flare of 2 November 1969

07 p1188 A71-19826

Ionospheric absorption relation to solar X-ray flux enhancement during short wave fade-outs from OGO-4 and Solrad 9 satellites

07 p1064 A71-20318

Time and spectral distribution of hard X ray radiation during solar flare, using nonrelativistic electron bremsstrahlung model

07 p1189 A71-20638

Solar flare model, computing thermal X ray emission

08 p1350 A71-20945

Polarimetric measurements of solar X-ray flares by Intercoms 1 satellite

08 p1354 A71-21013

Solar X-ray flare region structure and emission flux density and spectral composition, using satellite-borne photometers and spectroheliographs

08 p1354 A71-21014

Quiet corona temperature from solar equator soft X ray flux measurement by satellite-borne heliograph

08 p1361 A71-21127

Ionospheric electron density and reflection height during sudden phase anomaly in solar X-ray flare

08 p1355 A71-21222

Solar flares explosive phase in photometric terms for flash onset correlations with 10.7 cm radio and hard X ray bursts, using H alpha film records

10 p1660 A71-23793

Soft X ray bursts involving solar flares from satellite observations, discussing thermal nature and total activity related H-alpha emission rates

10 p1660 A71-23794

Solar impulsive hard X-ray burst structure and location determination with balloon-borne modulation collimator, noting nonthermal electron origin

10 p1660 A71-23795

Solar flare produced hard X-ray bursts, examining thermal processes and nonthermal electron distribution

10 p1660 A71-23796

Negative sudden phase anomalies, related signal strength enhancements and short wave fadeouts, considering maximum flux density of solar X-ray flares

10 p1575 A71-23883

Sudden geomagnetic storm effects on low ionosphere state, discussing solar X-ray and particle radiation

11 p1815 A71-25581

Thermal fluctuations in earth upper atmosphere, related to satellite deceleration and X ray solar radiation changes by autocorrelation and cross correlation analyses

11 p1817 A71-25822

Solar corona active regions thermal model, considering X ray emission and temperature distribution

12 p1946 A71-26589

Type 3 solar radio bursts in absence of H alpha flares, noting soft X-ray emission

12 p1946 A71-26619

Solar flare two stage particle acceleration from X-ray burst observations, discussing induced electric field and Fermi mechanism

12 p1946 A71-26624

Solar X-ray and radio fluxes at earth for high order temperatures by free-free transitions and Maxwell electron velocities in corona

12 p1947 A71-26770

Soft solar X-ray bursts characteristics, discussing temporal and intensity differential distributions, flux measurements and decay time

12 p1953 A71-27654

Energetic solar X-rays, microwaves and EUV ionizing radiation during periodic bursts of solar flare

12 p1953 A71-27655

Soft X ray emission from solar loop prominences, noting data compatibility with fast protons injection model

12 p1954 A71-27703

Solar X ray flux and spectral energy distribution calculation in 0-20 A band, using 9.1 cm spectroheliograms

12 p1954 A71-27708

Atmospheric altitude of soft X ray source volume in solar flares from optical and radio observations

12 p1954 A71-27709

Satellite-borne anisotropy and energy spectra measurement instruments for cosmic ray electrons and protons and solar and galactic X-rays

12 p1954 A71-27711

Solar corona soft X ray emission, investigating temperature and flare activity effects

13 p2129 A71-29051

Nonthermal X rays and 10-100 KeV electron acceleration and emission from solar flares, using spacecraft observations

13 p2129 A71-29056

OSO-G satellite instrumentation for solar and celestial X ray detection, exploring spectral distribution, temporal intensity variations, sources and atmospheric albedo

13 p2070 A71-29135

Solar X-ray line spectra observation, noting K alpha transition indicative of suprathermal events

14 p2297 A71-29598

VLF radio signals phase anomalies due to solar X-ray flares, monitoring by detectors onboard OSO-4 satellite

15 p2369 A71-31434

Low energy solar X-ray emission spectra observations, discussing nonthermal electron spectrum relation to acceleration by electric fields

16 p2626 A71-33725

Nike Apache solar X-ray observations during 7 March 1970 eclipse, determining residual fluxes and atmospheric absorption profiles for ion production rates

16 p2627 A71-33790

Solar flare X-ray emission source position during eclipse of 7 March 1970, using OSO-5 satellite data

16 p2627 A71-33813

Soft X ray emission line behavior during solar flares based on OSO-6 satellite-borne Bragg crystal spectrometer data

16 p2627 A71-33835

Periodic solar flare X-ray emission, presenting time separation from Vela 5 and 6 scintillation detectors

16 p2629 A71-34078

Sudden phase anomalies relation to solar flares, radio bursts and X radiation from severe worldwide ionospheric storm observation

17 p2796 A71-35349

Solar X-ray flares recorded by SOLRAD-9 on Explorer 37 satellite occurring in optical flares-microwave bursts X ray flares sequence

17 p2796 A71-35391

OSO satellites observations, studying X ray flare phases, temperatures and spectra

17 p2808 A71-35521

Solar activity and intensity ratios of O VII X-ray coronal emission lines, giving upper bound on electron density

18 p2965 A71-36734

Solar flare X-ray origin model, discussing charged particle acceleration to relativistic energies, ambient gas heating and thermal and nonthermal X rays

18 p2958 A71-36740

Solar flare X and gamma rays, radio and far UV emission, discussing model for chromospheric cool plasma heating by flow through magnetic instability

19 p3126 A71-37620

Solar flare X ray spectrum analysis for lower corona physical conditions, discussing continuum and line emission

19 p3126 A71-37623

Solar X-ray line emission, using crystal spectrometers during large chromospheric flare

19 p3130 A71-38672

Dynamic energy spectra of nonthermal electrons in solar flares from balloon-borne high resolution hard X ray observations

19 p3130 A71-38673

Solar coronal X ray spectrum calculation of high-temperature low-density plasma, considering line emission from electron collisional excitation and radiation

20 p3278 A71-39058

Solar disk photographs taken by Skylark rocket in EUV and soft X ray region

20 p3293 A71-39534

Continuous solar UV and X rays monitoring by SOLRAD 10 satellite, investigating solar activity and flares effect on shortwave communications and manned space travel

20 p3294 A71-39580

Polarimetric measurements of solar X-ray flares by Intercoms 1 satellite

20 p3280 A71-39593

Solar X-ray flare region structure and emission flux density and spectral composition, using satellite-borne photometers and spectroheliographs

20 p3280 A71-39594

Upper atmospheric temperature and soft solar X-ray time scale fluctuation data, using satellite drag observations and statistical analysis

20 p3280 A71-39705

Nonflare solar X-ray emission from Cosmos 230 observation, noting presence of sunspot groups with complicated magnetic fields during enhanced short wave emission

20 p3283 A71-39749

Solar low energy X-ray spectra observation during impulsive bursts, discussing thermal and nonthermal emission properties

21 p3438 A71-40425

Solar X-ray spectra satellite lines observed by Bragg crystal spectrometers on Skylark rocket launched from Sardinia in December 1970

22 p3592 A71-42219

Solar soft X-rays scattering in upper atmosphere, providing background against cosmic X rays

23 p3721 A71-43363

OSO satellite observed soft solar X-ray data correlation to solar activity

23 p3721 A71-43840

SOLDERING

NT ULTRASONIC SOLDERING

Sequential environmental testing effects on large hybrid microcircuit packages, reviewing solder sealing processes and repair methods

01 p0053 A71-10732

Metal coatings and thin films wetting by soldering materials, emphasizing oxide removal

06 p0903 A71-17426

Optimum temperature for Zr and Mo soldering of graphite materials with formation of carbide interlayer for ensuring maximum heat resistance

15 p2439 A71-32145

SOLDERS

Accelerated creep rupture tests on metals and solder alloys, comparing constant stretch rate and load methods

[SESA PAPER 1672] 03 p0508 A71-13762

SOLENOID VALVES

Differential circuit for bilateral stopping control of double action piston cylinders, discussing solenoids valves operation

11 p1716 A71-26324

SOLENOIDS

Cu clad Nb-Ti wire wound superconducting solenoids with large fields at 1.6-5.2 K

24 p3809 A71-45105

SOLID ARGON

U SOLIDIFIED GASES

SOLID LUBRICANTS

Solid molybdenum disulfide lubricants antifriction properties and performance under atmospheric and high vacuum conditions, noting humidity effects and composition of friction-evolved gases

01 p0106 A71-10036

Solid metal lubricant films bonding by ion plating using diode method, noting interface type and structure examination by electron microscopy

01 p0087 A71-10483

Oscillatory motion effects on bonded solid film lubricants wear life, discussing oscillation arc and frequency, surface finish and load

02 p0258 A71-12593

Atmospheric and high vacuum performance tests of solid lubricant coatings based on molybdenum disulfide

05 p0757 A71-16174

Polybenzothiazole as solid film formulations binder for friction wear improvements, noting thermal and oxidative stability, toughness, adhesive properties and handling ease

05 p0772 A71-16375

Film thickness effect on solid powdered graphite, molybdenum disulfide and calcium fluoride lubricants friction coefficients

07 p1116 A71-18998

Metallic soaps polarity and micellar bond energy effects on pliable lubricants structure and properties

07 p1144 A71-19491

Penetration model of thin solid film lubricant friction on sliding surfaces of finite roughness

[ASLE PREPRINT 70LC-15] 08 p1298 A71-21159

Graphite lubricants superconducting properties under high pressures and low temperatures, suggesting new superconductors developments and metal free electron model modification

10 p1656 A71-24299

Molybdenum disulfide bonded solid film lubricants performance characteristics, considering load, speed and temperature effects

[ASLE PREPRINT 71AM 2D-1] 13 p2076 A71-29486

Long-life self-contained solid lubricated ball bearing systems operating under combined high-temperature, high-speed, high-load conditions

14 p2252 A71-30192

Extruding complex structural shapes of Ti alloys, considering use of glass as lubricant

[SME PAPER MF-71-139] 18 p2927 A71-36662

Solid lubricant molybdenum disulfide physicochemical interaction with Ag, Ni, Fe and Co at high temperatures, using X ray structural and spectrometric analyses

23 p3697 A71-44029

Solid lubricant-epoxy compounds shear modulus measurement by cantilever beam specimens dynamic testing, calculating wear life coefficients for molybdenum disulfide in epoxy resin

[ASLE PREPRINT 71LC-1] 24 p3842 A71-45284

Humidity effects on molybdenum disulfide bonded solid film lubricant friction properties at low load and slow speed, noting mechanical escapement timers accuracy

[ASLE PREPRINT 71LC-2] 24 p3831 A71-45285

Nimbus B-2 satellite-borne IR spectrometer lubrication using solid film technique, discussing real time and accelerated vacuum environmental tests

[ASLE PREPRINT 71LC-3] 24 p3831 A71-45286

SOLID PHASES

Phase relationships in magnesium ferrate-magnesium chromate systems subjected to annealing in air and hydrogen atmospheres

01 p0107 A71-10403

Apollo 11 flight glass basal, determining crystallization sequence and phase assemblage of high Ti specimens as oxygen fugacity function

06 p0970 A71-18235

Cadmium arsenide alpha and beta phases Hall constant temperature dependence, studying photoelectric and optical properties

07 p1177 A71-19279

Lithium tetrafluoroaluminate equilibrium vapor pressure over solid aluminum fluoride plus solid lithium cryolite examined by weight-loss effusion method

07 p1055 A71-19624

Metastable beta phase Ti-Mo and Ti-V alloys ternary additions effect on decomposition

07 p1138 A71-19982

Boron nitride and aluminum nitride particles behavior in Mo matrix, considering solid metallic phase formation

09 p1470 A71-23067

Ice, solid carbon dioxide and alcohols oxygen K spectra from long wave X ray spectroscopy

09 p1498 A71-23479

Ti-Al-Cr-Fe alloys microstructure, investigating alpha and beta phases with X ray diffraction

10 p1627 A71-24531

Liquid and solid phase relations in Be-Al-Ti system by chemical, thermal, microscopic and X ray investigation, discussing solubility range of ternary phase and intermetallic compounds

10 p1629 A71-25034

Nb-Pd system concentration profiles and thermal diffusion coefficients, investigating phase formations by electron probe microanalysis

10 p1629 A71-25035

Thin gallium films metastable gamma and delta phase ring diagrams using electron diffraction techniques

12 p1942 A71-26821

Ti alloys aging, noting hardness increase and fine structure alpha phase coherent with beta solid solution matrix

12 p1917 A71-27296

Long term aged heat resistant Ni base alloys, investigating gamma prime phase chemical composition

12 p1917 A71-27298

Mo-Zr-Cr alloy samples cast annealed and quenched at 1500 C, calculating phase equilibrium diagram

12 p1918 A71-27528

Plastic deformation and alloying effect of small additions of interstitial elements on decomposition of metastable beta phase

13 p2086 A71-28580

Fe/Ti pair diffusion coefficients at various temperatures, showing thin central and two single phase zone formation

13 p2087 A71-29263

Gamma phase composition estimation in Ni base superalloys by phase rule principles and analytic geometry

13 p2089 A71-29407

Vacuum melted Ni base superalloys, determining Mo and hardener effects on gamma prime solvus temperature and solutioning rate

13 p2090 A71-29418

Horse Creek, Mount Egerton and Norton County enstatite meteorites metal phases and pyrrhotite inclusions from electron microprobe data

13 p2144 A71-29474

Cast Nb-W-Mo-Zr-C alloys heat treatment effect on microstructure and phase composition, noting ductility improvement

15 p2426 A71-31406

Sigma phase intergranular precipitation in low carbon Ni-Co-Cr-Mo alloys, noting temperature effect on morphology

15 p2436 A71-32546

Complex alloyed steel under electroslag welding, investigating heat treatment effect on heat affected zone phase composition

15 p2437 A71-32661

Zinc and misch metal in Mg alloys, detailing rare earth metals distributions in various phases

16 p2594 A71-33714

Yttrium effect on phase composition of V-Ga alloys from microstructural, X ray structural and microdiffraction analysis

16 p2622 A71-33909

Ti alloys metastable omega phase precipitation effect on mechanical properties, using thin film microscopy

17 p2756 A71-34492

Cylindrical powder samples combustion stability, noting gaseous and condensed phase interaction effects on sound emission

17 p2840 A71-35699

Solid glyoxal Raman spectrum data, showing operativity of mutual exclusion principle by IR comparison to Raman bands

18 p2873 A71-35830

Omega phase embrittlement in aged Ti-Mo alloy, giving tensile properties and load-elongation diagrams

19 p3082 A71-38176

Eutectoid decomposition of tantalum carbide, noting X ray phase identification during carburization of tantalum ribbons

20 p3252 A71-39961

Diffusion layer structure and phase composition during quenched and annealed steel saturation by Cr at high heating rates

21 p3404 A71-41170

Heat resistant Ni alloys hot strength level and temperature dependence as function of gamma-prime-phase particle size, discussing aging effect on creep rate

22 p3561 A71-41841

Ti-Fe and Ti-Cr binary alloys microsegregation genetic trend measurement by electron probe microanalysis, observing critical cooling rate from beta phase

22 p3562 A71-41945

Beta eutectoid and solid solution Ti binary alloys omega phase morphology observation by transmission electron microscopy, noting elliptical and cubic types hexagonal crystal structure

22 p3562 A71-41946

Metastable beta type Ti binary alloys isothermal transformation microstructure observation by microscopic and X ray diffraction methods

22 p3562 A71-41947

Co-Mn binary alloy phase diagram redetermination, noting sigma phase formation after heavy deformation

23 p3689 A71-42933

Fine structure dislocation and phase composition of Cr-Mo steel at elevated temperature in steam pipe applications, noting recrystallization stability
23 p3690 A71-43277

Microalloying effects on phase composition, surface phenomena, fine crystalline structure and microstructure of E1417L steel
24 p3836 A71-44374

Aluminized layer phase and chemical composition of heat resistant iron and nickel alloys
24 p3837 A71-44732

Speed of sound measurement in solid and liquid phase suspensions, considering dense phase inertia forces and particles thermal retardation effects
24 p3827 A71-45019

SOLID PROPELLANT IGNITION

Thermal radiation effects on M-2 double base solid propellant ignition, deflagration and burning rate
02 p0298 A71-12851

Solid fuels and propellants heterogeneous ignition mechanism, using local similarity and related methods
02 p0333 A71-12853

Shape effect of compressed solid fuel on thermal ignition delay time in heated gas flow for pyroxyline
03 p0520 A71-13993

Adsorption role in empirical ignition laws of various solid nitric acid based hypergolic propellant systems, discussing ignition delay relation to acid concentration
04 p0548 A71-14825

Engine pressure spiking restart preignition products, determining hydrazine nitrate and dinitrate presence by spectrum analysis
06 p0945 A71-18296

Gas phase ignition of solid propellants involving gas phase variable density for constant density based equations by Howarth transformation
10 p1695 A71-24332

Solid propellant combustion stability theory for two dimensional disturbances, considering process as elastic body transformation into gaseous combustion products
13 p2159 A71-28138

Boron particles ignition theory and shock tube experiments, measuring ignition delay as function of temperature, pressure, gas composition and particle size
[WSS/CI PAPER 71-20] 15 p2464 A71-31629

Catalytic role in ammonium perchlorate solid rocket propellants ignition and combustion
17 p2792 A71-34434

Shock tube investigation of solid polymeric hydrocarbon fuel ignition in hot oxidizing gas stream
19 p3121 A71-38124

Radiative ignition of polymeric fuels/polystyrene and epoxy in oxygen/nitrogen mixtures
19 p3121 A71-38125

Thermal energy requirement for homogeneous solid propellant ignition, measuring flame formation time and temperature
24 p3863 A71-44762

SOLID PROPELLANT ROCKET ENGINES

Swirling flow through multiple nozzles of simulated solid propellant rocket motors, determining thrust and mass flow effects on passage
01 p0072 A71-11592

FOILAC solid propellant rocket motors for high thrust short action time propulsion, reviewing development status and performance
[AIAA PAPER 70-1385] 03 p0470 A71-13668

Burning rate manual determination for solid propellant rocket motors with sliverless grains
03 p0522 A71-14451

Solid propellant rocket chamber unstable motion, discussing pressure and velocity coupling
06 p0946 A71-18297

Solid propellant engine structural analysis, examining transient thermal loading and internal pressure effects
[AIAA PAPER 71-115] 06 p1003 A71-18565

Solid propellant rocket motor combustion control by fluidic vortex valve, considering thrust variation
[AIAA PAPER 70-643] 07 p1183 A71-18904

Transverse acoustic wave amplification in solid propellant rocket motor, using discrete mass injection as excitation source
12 p1946 A71-27565

Monograph on solid propellant rockets combustion instability covering pressure oscillations at acoustic frequencies, swirling nozzle flow, chamber pressure, etc
14 p2287 A71-29577

Head end secondary flows in solid propellant rocket motor combustion chamber due to transverse acoustic waves in quiescent fluid
14 p2335 A71-29877

In-flight base heating and thermal environment measurements from Thor Delta launch vehicle using six strap-on solid propellant motors
[AIAA PAPER 71-644] 14 p2320 A71-30721

Low modulus solid propellants family for low thrust-to-mass ratio fully case bonded end-burning motors, using polymer network theory for binder formulation
[AIAA PAPER 71-654] 14 p2285 A71-30729

Design provisions for captive fired testing of solid rocket motors, describing equipment and procedures for monitoring motor phenomena during testing
[AIAA PAPER 71-678] 14 p2292 A71-30742

Combustion instability with wave motion coupling in solid propellant rocket motors due to energy gain and loss mechanisms within chamber
[AIAA PAPER 71-753] 14 p2296 A71-30787

Solid propellant rocket engine design, discussing combustion instability technology applications in damping and driving mechanisms influence determination
[AIAA PAPER 71-754] 14 p2296 A71-30788

Missile component vibration environments generation by Minuteman 2 and 3 third stage motors solid propellant oscillatory burning
[AIAA PAPER 71-756] 14 p2296 A71-30790

Solid propellant rocket engines combustion instability, reexamining Culick analysis of longitudinal oscillations with pressure and velocity coupling
15 p2467 A71-31473

High performance superheated subliming solid ammonium carbamate thruster using resistojel technology for specific impulse increase
[WSS/CI PAPER 70-210] 15 p2469 A71-32048

Solid propellant missiles underground silo self eject mode launching simulation, obtaining heat transfer, pressure and acoustic measurements
[AIAA PAPER 71-707] 15 p2385 A71-32576

Elastic adhesive interlayer effect on bond fracture strength, considering propellant-liner-steel combination in solid rocket motors
18 p2977 A71-36245

Critique of paper on explosive hazards of large solid rocket motors, suggesting extrapolation of fractional TNT equivalent
18 p2955 A71-36284

Momentum transfer between gas and condensed phase in metalized solid propellant rocket motors, measuring noncontinuum and turbulence effects on sphere drag
21 p3437 A71-40861

Solid propellant rocket motor stable operation region, describing propellant response function to pressure and velocity fluctuations
[ONERA-TP-1016] 22 p3588 A71-41956

Low thrust long burning solid rocket propellant motor for orbit insertion maneuvers, discussing design, static tests, nozzle composition, igniter and performance
22 p3589 A71-42016

Transverse acoustic wave amplification due to mass injection around submerged nozzle in solid propellant rocket engines, noting annular flow role
22 p3589 A71-42034

Internal ballistics equations of powder solid fuel rocket motor treated as homogeneous chemical reactor
24 p3890 A71-45107

SOLID PROPELLANTS

NT CASE BONDED PROPELLANTS

NT COMPOSITE PROPELLANTS

NT METAL PROPELLANTS

NT PLASTIC PROPELLANTS

NT SOLID ROCKET PROPELLANTS

Erosive burning resulting from nonplanar surface structure of solid propellant
02 p0334 A71-12858

Solid propellants stress measurement using piezoresistive transducer
03 p0501 A71-13172

AP composite solid propellant combustion model based on multiple flame structure surrounding individual oxidizer crystals
03 p0469 A71-13440

Nonlinear elastic effect on stress concentration of incased tubular solid propellant grain
03 p0504 A71-13462

Motor design parameters effects on solid propellant extinguishment predicted from mathematical combustion model
[AIAA PAPER 70-664] 03 p0469 A71-14442

Stress concentration at interface between bonding agent and fuel element in solid propellant grain
05 p0000 A71-15981

Transient response of solid propellant combustion to pressure variations and sudden depressurization
05 p0795 A71-16540

Combustion instability data with same solid propellants by T-burner and L super asterisk burner, discussing theoretical models of transient combustion
05 p0837 A71-16570

Solid propellant oxidizers hydroxylammonium perchlorate and hydrazine nitroform self deflagration, determining combustion temperatures and burning rate pressure relationships
06 p0944 A71-18299

Solid propellant combustion instability, considering burning propellant mass flux response to periodic thermal radiation
[AIAA PAPER 71-209] 06 p0948 A71-18645

Replica technique facilitating investigation of quenched solid propellant sandwich sample characteristics
08 p1271 A71-20868

Burning rate temperature sensitivity of composite solid propellants, using granular diffusion flame model
09 p1510 A71-22911

Composite solid propellant binders thermal decomposition investigation by differential scanning calorimetry method, discussing kinetic data relevance to solid propellant combustion
10 p1657 A71-24046

Solid propellant burning surface irradiance measurement, using optical lightpipe and radiation detector
[AIAA PAPER 71-469] 11 p1859 A71-26250

Phenol furfuraldehyde-ammonium perchlorate solid propellant combustion, investigating burning rate
12 p1944 A71-26742

Fast burning rates in thin film solid composite propellants composed of McCormick-Selph 510, 164 monopropellant, oxidizer and polyvinyl chloride binder
[AIAA PAPER 71-655] 14 p2285 A71-30730

Solid propellants based on low cost hydroxyl terminated polybutadiene binders meeting burning rate, mechanical properties and processing requirements for large booster motors
[AIAA PAPER 71-708] 14 p2286 A71-30764

Solid propellants extinguishment by depressurization, using transient flame model
[AIAA PAPER 71-631] 15 p2466 A71-32283

High energy solid propellants use in Europa 2 launch vehicle perigee-apogee motor, considering synchronous satellite payload increase
16 p2645 A71-33365

Stresses and deformation in solid propellants charges under gravitational load, assuming homogeneous isotropic and linearly viscoelastic charge material
17 p2829 A71-35307

Ammonium perchlorate based solid propellants combustion, assuming pyrolysis of solid binder
17 p2792 A71-35549

Solid fuel vibrational combustion devices and operational analysis, considering various chamber configurations
17 p2840 A71-35702

Solid propellant combustion pressure oscillations amplification, developing mathematical model as function of reaction rate constant, chamber pressure, frequency and solid properties
19 p3123 A71-38096

Al and Mg powder dispersed in solid ammonium perchlorate oxidizer, investigating various combustion mechanics
19 p3120 A71-38120

Photographic study of acceleration and pressure effects on Al agglomerates and combustion processes on solid propellant surface, describing pit growth by combustion model
19 p3120 A71-38121

Chemical composition and size distribution of particulate matter in solid propellant combustor of boron loaded rocket motor
21 p3436 A71-40944

Holographic inspection of bond between inert solid propellant grain and polymer liner, using double exposure to record surface deformation of fiberglass case
22 p3549 A71-42570

Solid propellant combustion simplified laminar flame theory, calculating pressure effect on burning rate, surface energy loss and temperature effects
24 p3888 A71-44938

Solid fuel combustion in presence of unsteady heat propagation in heated layer, solving fuel heat conduction equation for sudden combustion rate change
24 p3891 A71-45218

SOLID ROCKET PROPELLANTS

NT METAL PROPELLANTS

Pressure-temperature equivalences in elasticity problems, considering applications to case bonded solid propellant rocket grains
04 p0638 A71-15197

Europa 2 booster payload increase by using beryllium-containing solid fuels in perigee and apogee stages
05 p0815 A71-15969

Stability criteria for longitudinal combustion instability tested for generality using data from various solid propellant formulations
[AIAA PAPER 69-480] 05 p0837 A71-16569

Electric field effects on burning rates of composite metalized solid propellant containing ammonium perchlorate
[AIAA PAPER 71-174] 06 p0947 A71-18613

Solid propellant instantaneous burning rates prediction methods based on flame structure model and steady state burning data as functions of pressure and initial temperature
[AIAA PAPER 70-667] 09 p1510 A71-22905

Strain energy calculation of V notched crack in elastic continuum from finite element computer programs applied to fractures in solid propellant rocket motor cartridges or grains
10 p1693 A71-25056

Nuclear, hydrogen/oxygen and solid propellant satellite interceptors effectiveness measurement, considering warhead kill radius, propellant weight and specific impulse
13 p2144 A71-27982

- Solid composite propellant mixing influence on viscosity, pot life and motor reject rates based on bench scale production [AICHE PAPER 32D] 13 p2113 A71-28894
- Continuous burning rate measurement for metalized composite solid propellants, using optical sensor for servo tracking propellant surface 14 p2244 A71-30328
- Low modulus solid propellants family for low thrust-to-mass ratio fully case bonded end-burning motors, using polymer network theory for binder formulation [AIAA PAPER 71-654] 14 p2285 A71-30729
- Ammonium perchlorate propellants sterilizability, using medium resolution mass spectrometer and regression analysis of results in thermal stability studies [AIAA PAPER 71-718] 14 p2286 A71-30769
- Solid impulse control using solid quench system and wafer demand gas generator for solid propellants [AIAA PAPER 71-751] 14 p2297 A71-30844
- Catalytic role in ammonium perchlorate solid rocket propellants ignition and combustion 17 p2792 A71-34434

SOLID ROTATION

U ROTATING BODIES

SOLID SOLUTIONS

- Crystalline structural changes during decomposition of supersaturated solid solution of Ta in Co 01 p0101 A71-10608
- Decomposition structure of supersaturated solid solution in Co-Nb alloy, showing beta phase transformation inhibition 01 p0101 A71-10671
- Cu adding effects in solid solution on grain boundary sliding in Al at constant shear stress, considering accompanying crystal dislocations 01 p0102 A71-10739
- Electron mobility in gallium arsenide phosphide solid solutions, discussing temperature effects 01 p0141 A71-11465
- High purity Nb and Nb-O solid solution single crystals, investigating temperature dependence of yield stress 02 p0263 A71-11866
- Decomposition of unstable beta solid solution of Ti-V alloy, using X ray and microscopic analyses 02 p0263 A71-11929
- Nb-impurity binary solid solutions, calculating interdiffusion and heterodiffusion coefficients 02 p0270 A71-12930
- Nb binary solid solutions with various Ti, Mo and Zr percentages, examining structure and mechanical properties 02 p0270 A71-12931
- Nitrogen austenite solute-solute binding energy derivation from experimental data for comparison with carbon austenite 03 p0441 A71-13314
- Solute core redistribution and dendritic refinement in highly undercooled Fe-Ni alloy, using metallographic and electron microprobe analyses 03 p0442 A71-13365
- Single crystal indium gallium phosphide solid solution synthesis, discussing crystallophysical and electrophysical properties 03 p0467 A71-13424
- Fine coherent precipitate morphologies by spinodal mechanism, reviewing clustering in binary solid solutions 03 p0446 A71-14491
- Alpha titanium-oxygen solid solutions surface structure, using low energy electron diffraction for determination of order-disorder transition and superlattice reflections 04 p0610 A71-14895
- Ti alloys beta phase solid solution decomposition during cooling and plastic deformation at low temperatures 05 p0767 A71-16770
- Nb-W single crystal deformation, discussing athermal solid solution strengthening 06 p0914 A71-18683
- Ni-W eutectic alloy unidirectional solidification to obtain composite structure in Ni-W solid solution 06 p0915 A71-18689
- Nb-V-Mo alloys lattice structure, examining continuous solid solutions with X ray and metallographic analysis 07 p1129 A71-19144
- Al alloy rapidly crystallized film structure, studying atomic diffusion mobility effects on formation of supersaturated solid solutions 07 p1130 A71-19299
- Zr solid state solubility in Mo as function of quenching temperature, using optical microscopy and microhardness testing techniques 07 p1130 A71-19300
- Mechanical properties of supersaturated Ni-Al alloys aged at 700 F, discussing composition effects on single crystals deformation and polycrystal strength variation 07 p1133 A71-19442

- Spinodal decay of supersaturated solid solutions with nonenergetic phase nucleus formation 07 p1135 A71-19616
- Metastable Al-rich Al-Fe solid solutions decomposition during isothermal and isochronal annealing, from X ray diffraction patterns 07 p1137 A71-19979
- Interstitial solid solution hardening in pure Ni and Ni-C alloys, noting mechanism and C concentration effects 07 p1138 A71-19980
- Solid solution reactions analysis for Ti/C powder formation 08 p1304 A71-20993
- Cemented carbides based on TiC-molybdenum carbide-Ni, studying properties as function of molybdenum carbide and C contents in primary solid solution 08 p1304 A71-20994
- Al-Be-Mg alloys under solution treatment, noting aging and prolonged heating effects on mechanical properties from solid solution decomposition diagram 08 p1305 A71-21034
- C solubility in Mo-W solid solution at various temperatures 08 p1306 A71-21063
- GaAs-InAs type single crystals, polycrystals and epitaxial films solid solutions, studying optical, electrical and luminescent properties 08 p1344 A71-21443
- Bcc metals low temperature strength, examining solution softening in Fe-Mo alloys 08 p1307 A71-21506
- Solid solution hardening theories, discussing point obstacles random distribution effect on strength and superposition of multiple hardening mechanisms 08 p1309 A71-21522
- Solid solution hardening of Ta base alloys as function of elastic interaction between dislocations and solute atoms 08 p1309 A71-21523
- Internal friction solid solution weakening of bcc group V-B alloys 08 p1309 A71-21524
- Fcc binary alloys cross slip difficulty due to solute atoms and small short range order regions 08 p1309 A71-21527
- Guinier-Preston zone formation by mixed substitutional-interstitial solute-atom clustering in bcc metals, considering steel strengthening 08 p1311 A71-21541
- Grain boundary sliding and shear deformation in bicrystal Al and Al-Co solid solutions 08 p1345 A71-21576
- Barium titanate-fluorine substitutional solid solutions production and X ray analysis, examining Curie point behavior 09 p1506 A71-22166
- Anomalous electrical resistivity during decomposition of supersaturated solid solution of Fe-Co-Mo alloy 09 p1468 A71-22359
- Multilayer liquid phase epitaxy heterostructures growth with crystalline solid solutions of aluminum gallium arsenide for injection lasers 09 p1464 A71-23122
- Hf alloys containing transition metals, discussing phase transformations and solid solutions 09 p1473 A71-23225
- Materials with prescribed magnetic properties and expansion coefficients developed using relationships between solid solutions structure and physical properties 10 p1623 A71-23901
- Superconductivity transition of Nb-Ti solid solutions with varying Ti content, using specific heat measurements between 2.5 and 20 K 10 p1628 A71-24890
- Rapid melt quenching in Al alloys metastably extended supersaturated solid solutions, discussing strengthening mechanisms, high temperature decomposition and powder metallurgy utilization 10 p1628 A71-25027
- Thermodynamic properties of interstitial solid solutions with fcc metals from atomically discrete model by computer simulation 11 p1778 A71-25531
- Crystallographic relationships between Ni- and Cr-rich solid solutions, noting preferred interphase interfaces in Ni-Cr eutectic alloy 11 p1778 A71-25532
- Atomic bond strength of solid solution hardening as function of composition for calcium/strontium difluorides, using vibrational IR and laser Raman spectra 12 p1877 A71-26804
- Al-Ni alloys rapidly quenched from melt, determining solid solutions mechanical and microstructural properties 12 p1916 A71-26893
- Solid solution hardening in Nb alloys single crystals, explaining in terms of elastic interaction of dislocations with substitutional atoms 12 p1916 A71-26927

- Nb-N and Ta-N alloys, calculating electrical resistivity and solid solutions lattice constants at various temperatures 12 p1917 A71-27292
- Ti alloys aging, noting hardness increase and fine structure alpha phase coherent with beta solid solution matrix 12 p1917 A71-27292
- Boron solubility in Mo-W solid solution, discussing microstructure, electrical and mechanical properties for range of alloying ratios 12 p1918 A71-27660
- Cadmium mercury telluride solid solutions electron energy spectrum at low temperatures, calculating electron mobility in crystals with zero forbidden band 13 p2110 A71-27952
- Curie point of solid solutions in ternary system of zirconate-titanate and lead metaniobate, using maxima on temperature dependence curve of permittivity 13 p2111 A71-28152
- Binary interstitial solid solutions thermodynamic properties calculation with Kirkwood expansion, allowing crystal first order partition function measurement without degeneracy error 13 p2087 A71-29133
- Matthiessen rule validity proof by Renucci method, applying to Nb-base solid solutions 13 p2087 A71-29328
- Equilibria of molybdenum-nitrogen solid solutions at various temperatures 14 p2260 A71-30474
- PbTe-GeTe-PbSe solid solution alloyed by lead chloride, investigating structure, composition and distribution of basic elements 15 p2460 A71-31283
- Al-Zn-Mg-Li solid solutions isothermal phase diagrams, obtaining Al-rich alloys phase compositions for quenching and aging temperatures 15 p2426 A71-31405
- Solidus-liquidus surfaces and isothermal phase diagrams of quaternary system of Cr with Ti, Zr, Nb and Ta, showing Laves phase interactions and continuous solid solutions 15 p2426 A71-31407
- High temperature creep in Al-Zn solid solution, using isothermal tests 15 p2429 A71-31997
- Thermal coefficient of resistivity of carbides and solid solutions of Ti, Zr, Hf, V and Nb, noting inverse dependence of covalent bond in Me-Me band 15 p2430 A71-32154
- Strength, plastic properties, electrical conductivity and fine structure associated with decomposition kinetics of Al alloy supersaturated solid solution 15 p2435 A71-32333
- Low temperature heat capacities from 1.5 to 15 K for transition metal borides and solid solutions 15 p2437 A71-32649
- Anomalous electrical resistivity variation during decomposition of supersaturated solid solution of Fe-Co-Mo alloy 16 p2593 A71-33632
- Heat transfer in interstitial solid solutions, interpreting thermal diffusion measurements in transition metals mixed crystals 16 p2599 A71-34093
- Triple Knudsen cell method to determine thermodynamic activity of Cu in bcc solid solution of Ti-Cu alloys 17 p2756 A71-34488
- Gallium antimonide-germanium system solid solution lattice constant determination, using X ray and microstructural analysis and microhardness measurements 17 p2791 A71-34566
- Beta Ti-Pu solid solution, constructing diffusion phase diagrams from electron beam microprobe analysis and autoradiography 18 p2935 A71-36174
- Ionic conduction in perovskite-type oxide solid solution, discussing application to high temperature hydrogen oxygen fuel cells 18 p2852 A71-36966
- Electrolytic behavior of yttria-hafnia solid solutions from X ray analysis and electroconductivity measurements 18 p2874 A71-37001
- Single crystal Ni-Al solid solutions deformations, examining temperature and concentration dependence of critical cleavage stresses 19 p3076 A71-37120
- Iron precipitation rate from supersaturated Al alloy solid solution in structures with low and high dislocation densities 19 p3079 A71-37702
- Interstitial solute thermomigration of C in Ti, V, Fe, Co, Ni and Pd, using radioactive tracer technique 19 p3079 A71-37710
- Carbon activity, free energy entropy and enthalpy in fcc solid solution of Fe-Ni-C alloy 19 p3080 A71-37714
- Partial configurational thermodynamic functions of interstitial species in ternary solid solutions containing substitutional and interstitial solute atoms 20 p3194 A71-38804

Ternary solid solutions with substitutional and interstitial solute atoms, developing statistical mechanical interaction model

20 p3194 A71-38805

Polycrystalline barium titanates solid solutions with fluorine displacement of oxygen atoms, observing IR absorption spectra

20 p3276 A71-39151

Solid solution hardening in Ta alloy single crystals, investigating temperature effects on interstitial impurities scavenging and lattice mechanism

21 p3395 A71-40027

Thermodynamic ion current ratios of solid solution V-Ti alloys, using Knudsen effusion and time of flight mass spectrometric methods

21 p3398 A71-40463

Solid Ni-Co and Ni-Cu alloys, investigating hydrogen solubility

21 p3398 A71-40466

Mn-Ge solid solutions coercive force and magnetization, investigating temperature dependence and heat treatment effects

21 p3432 A71-41264

Superconductivity transition of Nb-Ti solid solutions with varying Ti content, using specific heat measurements at 2.5-20 K

21 p3432 A71-41266

GaAs-InAs solid solutions single crystal ingots, investigating optical absorption and reflection spectra, energy gap width and carrier mobility temperature dependence

21 p3435 A71-41335

Solid solution electron energy spectrum at low temperatures, considering electron mobility in cadmium-mercury telluride crystals with zero forbidden band

21 p3435 A71-41342

Thermoelectric properties of quaternary Sb-Bi-Te solid solutions, noting low thermal conductivity

22 p3584 A71-41618

Beta eutectoid and solid solution Ti binary alloys omega phase morphology observation by transmission electron microscopy, noting elliptical and cubic types hexagonal crystal structure

22 p3562 A71-41946

WC and TiC-Co solid solution phase after sintering inhomogeneous structure, investigating grain growth and phase decomposition behavior at various temperatures

23 p3689 A71-43103

Polycrystalline thin film CdSe-CdS and CdSe-CdTe solid solution semiconductor alloys Hall mobility and carrier concentration dependence on substrate temperature

23 p3715 A71-43433

Al-Zn solid solution mean effective and internal stresses and activation area during high temperature creep

23 p3691 A71-43900

Copper-indium-tellurides homogeneity region components solubility in different cross sections of concentration triangle at room temperature

23 p3717 A71-44023

Permittivity increase in fluor-substituted barium titanate solid solutions for ceramic capacitor microminiaturization

24 p3859 A71-44387

Barium titanate single crystal solid solution electro-optic characteristics at 6328 A and temperatures above Curie point, determining temperature dependences

24 p3860 A71-44667

Free surface equilibrium segregation in solid solutions of Cu-Al alloys single crystals by Auger electron spectroscopy and low energy electron diffraction

24 p3839 A71-45123

SOLID STATE

Lunar solid state thermal convection throughout interior, noting pressure release production of basaltic magmas consistent with Apollo 11 rocks composition

02 p0305 A71-11988

Nonpairwise van der Waal interactions effects on vacancy formation energies in monatomic solids, using Lorentz oscillator and two body models for comparison

08 p1344 A71-21367

Solid state solubility of B in Nb, determining binary Nb-B alloys phase diagram by microscopic, X ray and thermal analyses

13 p2085 A71-28224

Soviet monograph on EM waves in solid state plasma covering propagation, amplification, generation and penetration

13 p2112 A71-29078

Molten Co-Cr alloy structural transitions at increasing temperatures, relating to change in solid state with increasing Cr content

15 p2425 A71-31393

SOLID STATE DEVICES

NT AVALANCHE DIODES
NT CRYOTRONS
NT CRYSTAL RECTIFIERS
NT FIELD EFFECT TRANSISTORS
NT GALLIUM ARSENIDE LASERS
NT GERMANIUM DIODES
NT JUNCTION DIODES
NT JUNCTION TRANSISTORS
NT METAL OXIDE SEMICONDUCTORS

NT MIS [SEMICONDUCTORS]

NT NEURISTORS

NT PARAMETRIC DIODES

NT PHOTODIODES

NT PHOTOVOLTAIC CELLS

NT RUBY LASERS

NT SEMICONDUCTOR DEVICES

NT SEMICONDUCTOR LASERS

NT SILICON TRANSISTORS

NT SOLID STATE LASERS

NT THERMISTORS

NT THYRISTORS

NT TRANSISTOR AMPLIFIERS

NT TRANSISTORS

NT VARACTOR DIODES

NT VARISTORS

Automatic temperature monitor and proportional solid state DC controller for electrophysiological use

01 p0022 A71-10247

Electron beam welding system, discussing solid state controls, programmed operation and type and thickness of welded materials

01 p0087 A71-10451

Solid state digital integrator for weather radar signals, using recursive integration scheme

01 p0050 A71-10593

Solid state receiver for IR, using microwave biased Ge photoconductor

02 p0231 A71-12027

Solid state electrochemical energy storage device using rubidium silver iodide electrolyte

03 p0350 A71-13031

High energy density solid state electrolyte cell with lithium anode

03 p0351 A71-13033

Heat pipe improvement of capacitor energy storage and I-V, analyzing in terms of heat loss vs conducted heat

03 p0352 A71-13045

Onboard monitoring sensor trends for airborne computer automatic data systems, noting digital transducers, LSI logic and solid state devices

03 p0395 A71-13081

Solid state traveling wave amplifier using thin n-type epitaxial GaAs layer

03 p0384 A71-13316

Papers on solid state maser development covering theory, materials and applications

03 p0435 A71-13531

Biological heuristic programming in cybernetics, discussing solid state logic elements limiting factors in modeling

03 p0383 A71-14394

Solid state transferred electron broadband amplifiers in electronic countermeasure memory systems for radar pulse replica retransmission, comparing with low noise traveling wave tubes

04 p0558 A71-15361

Apparatus for thin film solid state devices fabrication under ultrahigh vacuum

05 p0733 A71-16233

Solid state circuit digital frequency discriminator with low pass filter in ESRO stations telemetry receivers AFC and antiseband system

05 p0720 A71-16326

Solid state single injection diodes with shallow traps, calculating trapping noise

06 p0872 A71-17313

Low energy protons radial gradient in interplanetary space measured with intercalibrated solid state detectors on Venus bound Mariner 5 and earth orbiting Explorer 33

06 p0952 A71-18113

Rocket-borne solid state spectrometer with liquid nitrogen cooled Li drifted silicon detector and optical feedback preamplifier for solar X-ray measurements

06 p0901 A71-18223

Spacecraft phased arrays design, considering solid state amplifiers effect on total array performance and transistors and varactors output power efficiency

07 p1069 A71-18813

Strapdown solid state compass based on magnetometer principle, describing gyro feedback correction system and circuitry

08 p1287 A71-21171

Charge sensitive low power amplifier and fast coincidence system for solid state detectors and random counting rates in Skylab application

08 p1267 A71-21849

Programmable solid state pulse generator for charge-sensitive amplifier excitation at high pulse repetition rates, discussing circuit elements and applications

08 p1267 A71-21850

High temperature ultraminiature pressure transducers, reviewing p-n junctions thermal limitations and thermal properties of dielectric oxides used with solid state epitaxially grown sensors

09 p1448 A71-22772

Microwave and modular solid state ILS designs, discussing accelerated progress, international standard and present system life expectancy

10 p1639 A71-23943

Piezotron accelerometer for vibration measurement, combining quartz sensing element with sub-miniature solid state electrostatic amplifier

11 p1767 A71-26442

Annular solid state microwave diodes temperature distribution at diode/heat sink interface, presenting closed form solution for calculation of absolute temperature rise

12 p1889 A71-27699

Microwave receiving antenna with solid state power rectifier for converting energy from space solar cell array into DC power on earth

13 p2000 A71-28671

Solid state vs electrical-mechanical relay switching and isolation technology

13 p2001 A71-28845

Solid state local oscillator for radio relay systems microwave receivers

13 p2039 A71-28899

Low power vertical-incidence solid state pulse compression FM ionosonde

14 p2246 A71-30480

Thermal noise in space charge limited solid state diodes with field dependent mobility and hot carriers

14 p2284 A71-30502

Book on solid state power supplies covering transistorized DC/DC converters and DC/AC inverters, oscillators, power amplifiers, transformers, inductors, magnetic amplifiers, voltage regulators, etc.

14 p2182 A71-30857

Small scale solid state digital computer for experimental medical data statistical processing

15 p2365 A71-32534

Solid state light emitting diodes in aerial camera data recording system for enhanced spectral matching, increased photo conversion efficiency and lower power drive

18 p2920 A71-36089

Redundant solid state sequencer programmable via core memory, using two identical channels to prevent wrong output

18 p2885 A71-36449

Design considerations for bulk solid state acoustic devices in light diffraction and modulation applications

19 p3066 A71-38411

Spurious emissions from CW and pulsed GaAs solid state oscillators as function of material active layer thickness and contacting procedure

19 p3032 A71-38460

Solid state RC network for single sideband frequency converter using phase difference carrier suppression

19 p3022 A71-38497

Solid state linear array piezoelectric hydroacoustic image transducer for underwater viewing in turbid oceanic environments

20 p3233 A71-38828

High voltage solid state electrolytic cell battery with Li anodes, testing storage and discharge characteristics

20 p3181 A71-38935

AN/ARC-144 solid state ultrareliable UHF multimode aircraft transceiver, discussing tuning, frequency synthesis and broadband power amplifier

20 p3196 A71-39209

Performance levels prediction for airborne solid state phased array radar transmission sources, considering TRAPPAT devices

22 p3509 A71-41630

Solid state charge controlled electroluminescent display panel with image memory capability, describing negative oxygen ions and photoconductive charge control methods

22 p3548 A71-42514

Laser pumped solid state masers operational characteristics, describing spontaneous emission noise

23 p3683 A71-43084

Wideband solid state converter circuit for quantization of signals from semiconductor nuclear radiation detectors, noting cost reduction

23 p3677 A71-43527

Solid state airborne weather radar for civil aviation, discussing design, weight and power requirement reduction

23 p3647 A71-44273

SOLID STATE LASERS

NT RUBY LASERS

Er laser efficiency dependence on dopants in Li-Ca-silicate glass host, determining energy transfer rates for optimum concentration

01 p0092 A71-10010

Continuous Nd-YAG laser welding, considering power, penetration depth and applications

01 p0087 A71-10453

Laser microspectral investigations of meteorites microrregions and nonhomogeneities relevant to astrophysics and nucleosynthesis

01 p0158 A71-10764

Stimulated recombination radiation from PbSe laser diodes at 77 K, showing stepwise curve of emission power vs pumping current

01 p0094 A71-10780

Radiation spectral and kinetic characteristics in neodymium glass laser in frequency scanning mode
01 p0095 A71-11029

Spectral properties of solid state laser with cavity lengthened by optical delay line
01 p0095 A71-11096

Lithium niobate crystal electro-optical shutter to Q switch calcium difluoride-Dy laser emitting giant pulses at high repetition rate
01 p0095 A71-11210

Solid state laser transverse modes maximum dependence on resonator geometrical parameters usable for producing stable kinetic emission model with narrow spectral line
02 p0259 A71-11878

Nd-glass pulsed solid state laser amplifier gain characteristics, deriving flux density and population inversion equations
02 p0261 A71-12173

Neodymium laser emission in mode locked operation, examining self focusing and modulation effect in active element
02 p0261 A71-12323

Transverse mode selection techniques for solid state laser brightness increase
02 p0262 A71-12717

Mode locked continuously pumped Nd-YAG laser pulse shape, using optical correlation technique
02 p0262 A71-12730

Neodymium glass laser with intracavity emission polarization, determining thermally induced double refraction effect on energy characteristics
03 p0435 A71-13505

Nd-YAG laser with intracavity lithium niobate phase modulator, investigating frequency sweeping/modulation/ mode operation
03 p0437 A71-13878

Nd-YAG pulsed laser, comparing Kr and Xe flash lamps for pumping performance
03 p0437 A71-13880

Nd-YAG pulsed laser mode locking with internal FM modulation
03 p0437 A71-13883

Single mode locked Nd-glass laser pulse time synchronization with Q switched ruby laser
03 p0438 A71-13891

AlAs-GaAs heterojunction laser threshold currents and CW operation at room temperature as function of p- and n-type emitter regions
03 p0439 A71-13987

Ruby and Nd-YAG laser basic mechanisms, properties and performance characteristics, discussing material problems and frequency width considerations
04 p0605 A71-14708

Glass laser types, properties and applications, noting welding and cutting, plasma generation, controlled thermonuclear reactions, neutron generation, intense short duration X ray fields, etc
04 p0605 A71-14709

Self giant pulsed operation of ruby and Nd-YAG lasers obtained by mirror misalignment
04 p0606 A71-14714

Input-output properties of Nd-YAG rods in W pumped continuous lasers
04 p0606 A71-14715

Optical signal amplifiers operational principles, discussing parametric, semiconductor laser, and solid state amplifiers and amplifiers using gas in Fabry-Perot resonator
04 p0608 A71-15079

High power continuously pumped Nd-YAG laser operating characteristics and design parameters
04 p0608 A71-15586

Calorimeter for ruby or neodymium laser output energy measurement
05 p0748 A71-16254

Glass lasers characteristics and applications, discussing material compositions, ion imbeddings and manufacturing techniques
05 p0761 A71-16327

CW Nd-YAG laser response to sinusoidal cavity perturbation, observing resonance modes
05 p0761 A71-16332

Pulse transmission mode Q switched neodymium laser, discussing pulse duration
05 p0762 A71-16374

Pulse repetition rate of Q switched YAG-Nd oscillator-amplifier laser systems
05 p0762 A71-16479

CdS laser wavelength and relative threshold excitation levels as function of temperature based on band edge absorption effects
05 p0763 A71-16498

Nd-YAG laser branching ratios measurement for all transitions during oscillations at room temperature
05 p0764 A71-16912

High repetition rate Q switched Nd-YAG lasers, graphing theoretical Q switching from rate equations of ideal four-level laser
05 p0764 A71-17076

Multimode power obtainable in TEM in solid laser, using convex mirror and in cavity polarization rotator
06 p0906 A71-17304

Traveling medium solid state lasers spike generation due to spatiotemporal fluctuations of losses and pumping
06 p0907 A71-17379

Neodymium glass lasers, investigating pump-induced birefringence effect on polarization and radiation distribution
06 p0907 A71-17398

Neodymium glass solid state laser transverse mode locking and capture due to active medium nonlinear properties
06 p0907 A71-17400

Traveling medium solid state lasers radiation intensity modulation by active element motion
06 p0907 A71-17593

ND and Yb ions stimulated emission from spirally wound glass fibers, comparing activator pumping energy peaks
07 p1122 A71-19135

Nd glass traveling wave laser single frequency emission luminescence stability as function of pumping power, using dispersive ring resonator
07 p1122 A71-19136

Q switched Nd laser pulse duration control as function of KDP crystal orientation and pumping power
07 p1122 A71-19138

Solid state laser with different diffuse coatings on external reflector of pumping source, measuring energy output
07 p1125 A71-19812

Erbium ions stimulated emission, spectroscopic properties, pulsed laser action and absorption spectra in yttrium orthoaluminate
07 p1126 A71-20165

Single mode ruby and Nd glass lasers axial mode selection by dye filters, noting radiation spectra and spatial coherence
07 p1126 A71-20190

Nd-glass laser amplified mode locked pulse measurements, noting signal to noise ratio above 10,000
07 p1129 A71-20617

YAG-Nd laser rods CW pumping by cooled and room temperature GaAsP diodes, determining threshold temperature dependence
07 p1129 A71-20621

Mode locked Nd-glass laser, describing dispersion and Kerr effects on pulse frequency modulation
08 p1301 A71-21125

Solid state laser oscillation transient features analysis by dynamic rate equations, taking into account electric field phase variations in mode locking
08 p1301 A71-21277

Dy-ion-doped calcium fluoride laser with monochromatic pumping, examining mode selection and coupling
08 p1303 A71-21791

Spectral properties of solid state laser with cavity lengthened by optical delay line
08 p1303 A71-21954

Nonlinear effects of IR beam passage from continuous neodymium-yttrium garnet laser trough defocusing media
09 p1460 A71-22231

Large gamma radiation doses effect on neodymium activated glass laser emission properties
09 p1460 A71-22256

Controllable pulse length Q switched Nd-YAG laser using lithium iodate doubling crystal
09 p1463 A71-22757

Temperature dependent wavelength tuning of Pb-Sn-Te diode lasers, noting air pollution detection use
09 p1463 A71-22764

Spectral mode, band to band carrier decay, pulsed and CW operation of laser quality In-Ga-P
09 p1463 A71-22765

Nd-YAG laser mode locking via variable loss element introduction into cavity
09 p1464 A71-23157

Continuously pumped Q switched neodymium doped YAG laser micromachining tool for resistor trimming, resonator/filter frequency tuning and diode/transistor vaporizing
09 p1457 A71-23402

Long pulse glass laser welder-driller, determining mean energy densities and spot sizes
09 p1464 A71-23404

Xe flash tube discharge saturable absorption effects, using YAG-Nd laser radiation for plasma attenuation measurements
09 p1465 A71-23484

Strongly coherent Nd doped glass laser development by decreasing cavity Fresnel number, discussing maximized radiance and infrared output
09 p1465 A71-23564

Parasitic noise reduction in CW Nd-YAG laser output
10 p1620 A71-24154

Book on glass lasers covering absorption and fluorescence of glasses, glass structure, energy transfer, nonradiative transitions, quenching, etc
11 p1772 A71-25450

Nd-YAG laser cavity dumping for continuously pumped efficient pulsing at various repetition rates
11 p1773 A71-25797

Electron and ion plasma heating by subnanosecond neodymium laser pulses, using computer calculations of hydrodynamic equations
11 p1806 A71-26085

Spherical plasma ball thermokinetic expansion model, considering solid state laser irradiation
11 p1806 A71-26091

Traveling medium solid state lasers spike generation due to spatiotemporal fluctuations of losses and pumping
12 p1915 A71-27451

Optical losses and quantum efficiencies of electron-beam pumped CdS lasers, determining extinction coefficient from dependence of threshold current on resonator length
12 p1915 A71-27601

Laser parameters of Nd-doped hydrate-phosphorus oxychloride-stannic chloride liquid system compared with YAG and Nd-doped glass, studying optical evolution and losses
13 p2078 A71-28400

Subpicosecond structure and frequency sweep observation results of single pulse of Nd-glass laser, considering explanation by mode locking theory
13 p2079 A71-28712

Solid state laser with slow relaxation bleachable filter, calculating modes self synchronization probability statistics relationship to relaxation time
14 p2253 A71-30109

Spectral filter effects on Nd-YAG laser performance stability and output
14 p2254 A71-30155

Neodymium glass laser free generation power with inert gas filled emission sources
14 p2254 A71-30274

Axial mode locking and equidistant frequency generation in solid state lasers due to active medium saturation, using self consistent equations with broadened amplification line
15 p2418 A71-31189

Synchronization time of nine solid state lasers as function of frequency alignment
15 p2375 A71-31226

Solid state laser emission angular divergence, considering active medium optical inhomogeneity and cavity parameters effects
15 p2418 A71-31236

Solid state laser emission divergence, calculating far zone fields for arbitrary amplitude and phase distributions
15 p2418 A71-31243

Frequency composition in glass laser with Fabry-Perot resonator producing polarized radiation components, discussing transverse modes selection
15 p2420 A71-32000

High gain parametric generation of coherent light in ammonium dihydrogen phosphate crystal continuously tunable across visible spectrum with UV harmonic of Nd-YAG laser
15 p2420 A71-32383

Self induced second order mode locking optical pulsing of double heterostructure stripe geometry junction lasers operating continuously at room temperature
15 p2421 A71-32388

Optimal pulsed power output of continuously pumped Q switched Nd-YAG laser as function of mode parameters
15 p2423 A71-32603

Nd-YAG laser spatial hole burning effects, considering number of oscillating modes, transverse mode degeneracy and sinusoidal phase perturbation influence
15 p2423 A71-32604

Frequency doubling of 2.06 micron holmium doped oxyapatite laser output by proustite single crystal
15 p2423 A71-32610

Cavity loss dependent erbium glass laser line oscillations in lower threshold region under Q switch and long pulse conditions
15 p2424 A71-32611

High voltage power supply for optically pumped solid state lasers, including water cooling of ruby and discharge tube jacket
16 p2585 A71-33070

Krypton arc lamps of high conversion efficiency for optical pumping of neodymium lasers, setting lamp and Nd-YAG rod in prolate ellipsoidal cavity
16 p2585 A71-33144

Stimulated emission of ZnO laser by electron beam excitation at 82-250 K near A-L-O line, considering exciton interactions
16 p2589 A71-34121

Dynamic amplification ranges of monochromatic signal by semiconductor, solid state and gas lasers in steady operation mode
17 p2750 A71-34271

Surface/volume damage induced by Nd-YAG laser irradiation to LiNbO₃ and KDP crystals in frequency doublers and Pockels cells, using scanning electron micrographs
17 p2790 A71-34371

Neodymium-yttrium-aluminate laser for high average power operation and second harmonic and parametric generation

17 p2753 A71-34802

High coherence Q switched spatially filtered Nd-glass laser operating in fundamental mode for high power

17 p2754 A71-35747

Crystal laser elliptic cavity size determination for maximum emission efficiency, using photochemical method for energy transfer measurement

17 p2754 A71-35748

Emission characteristics of neodymium glass laser with polymethylene dye-passive shutters of finite relaxation time, investigating ultrashort pulse separation

18 p2929 A71-35985

Papers on quantum electronics, Volume 1, covering carbon dioxide and YAG lasers, quantum counter action and interference holography

18 p2930 A71-36144

Solid state laser with Nd ions in YAG, discussing crystal growth and structure, optical pumping continuous and Q switched operation and mode locking

18 p2930 A71-36146

Reflection, material and resonator losses correlation in solid state lasers, investigating pulse power in Q switched operation

18 p2932 A71-36801

Transportable high radiance lunar ranging laser system, describing optical equipment in ruby and Nd-glass laser experiments

18 p2883 A71-36917

Nd-YAG laser optimum single frequency output operation, discussing two-component-mode filters methods using intracavity tilted Fabry-Perot and metallic film reflector etalons

18 p2932 A71-37005

Thermal effects of continuously tungsten iodine lamp pumped Nd-YAG laser, measuring rod temperature distribution by microprobe beam

18 p2932 A71-37009

Photographic observations of plasma eruptions from metal and opaque dielectric targets subjected to neodymium laser pulses, discussing successive shock wave formation

19 p3070 A71-37085

Neodymium-glass lasers active elements thermal-stress-induced birefringence effects on energetic and polarization characteristics

19 p3072 A71-37767

Crystal laser pyrotechnic illumination lamps with noncompacted explosive mixture, noting Nd ion doped calcium tungstate and YAG laser tests

19 p3073 A71-37788

Solid state lasers, considering ruby and YAG-Nd ion materials pumped at room temperature

19 p3074 A71-38229

Elliptical cylinder pump cavity design for solid state laser with ideal beam geometry

20 p3246 A71-39493

IR spectroscopy of CO using tunable PbSe diode laser, measuring Doppler linewidth and room temperature absorption coefficient at line center

20 p3246 A71-39757

Short-pulse high-rate space digital laser communication components technology, discussing mode locked and frequency doubled Nd-YAG laser source

21 p3348 A71-40806

Holographic detection of transient phase objects in Nd oxide doped laser glass

21 p3382 A71-40938

Nonlinear effects in high power Nd-YAG CW IR laser beam transmission through defocusing media

21 p3394 A71-41110

Nonlinear absorption in transparent semiconductors of picosecond light pulses from Nd laser with locked modes

21 p3431 A71-41256

CdS crystals faces damage caused by picosecond light pulses from free oscillating Nd-glass laser

21 p3432 A71-41305

High capacity holographic storage system including frequency doubled Nd-YAG laser, Si integrated photodetector array and digital light deflector

22 p3540 A71-41754

Mode locked Nd-glass laser transient effects, examining pulse width limitations by side band generation

22 p3556 A71-41801

Room temperature visible surface laser action in praseodymium chloride and bromide, obtaining optical pumping into upper laser level by wavelength tunable dye laser

22 p3556 A71-41802

Pulse shape of mode locked frequency doubled Nd-YAG laser, using single crystal for second harmonic generation and phase modulation

22 p3558 A71-42348

Second harmonic mode locked frequency doubled pulsed neodymium-yttrium-aluminum oxide garnet laser using single intracavity barium sodium niobate

23 p3683 A71-42957

Neodymium glass laser emission kinetics control with positive and negative feedback by introducing

nonlinear media into plane-parallel resonator with two positive lenses

23 p3684 A71-43418

Nd positive ion cross section for stimulated emission with glass composition determined by laser and fluorescence measurements

23 p3685 A71-43938

Solid state lasers, discussing ruby lasers application for welding and drilling, mode coupling of glass lasers and extremely short pulses generation

23 p3685 A71-43953

Nd glass laser system with Pockels cell Q switched oscillator for producing highly ionized plasmas

23 p3686 A71-43954

Gallium arsenide phosphide electroluminescent junction diode pumped Nd-YAG laser room temperature CW and pulsed outputs

23 p3687 A71-44139

SOLID STATE PHYSICS

Solid state physicists and metallurgy, discussing high strength materials, composites, radiation tolerance, fatigue, oxidation, superconductors, etc

05 p0794 A71-16957

Soviet book on multicomponent systems of oxides covering solid state structure, mathematical techniques, metal-metal and metal-oxide binary systems, etc

06 p0865 A71-17436

Solid state phenomena investigation by hypersonic methods, discussing frequency and temperature dependence of hypersonic phonons damping in crystals, elastic wave interactions in semiconductors, etc

06 p0942 A71-18199

Soviet papers on solid state electronics problems covering semiconductors photoelectric, magnetic, surface properties, autoemission, photoemission, etc

07 p1178 A71-19917

Bismuth oxide and iron oxide equimolar mixtures solid state reactions, determining rates from integrated X ray diffraction and activation energies

08 p1318 A71-20699

Electron spectrophotometry in molecular and solid state physics, comparing to X ray analysis

10 p1645 A71-24695

Current induced flow of superconducting domains in superconductor intermediate state, presenting theoretical analysis of motion of domains of arbitrary topology

12 p1942 A71-26745

Solid state reaction of titanium carbide with Ti, Zr and V in vacuum at high temperatures

13 p2082 A71-27821

Book on hot electron microwave generators covering semiconductor physics, collision theory, Gunn effect, domain dynamics, avalanche breakdown, etc

15 p2375 A71-31509

Relaxation time model of solid state diodes based on equations for electrons of given energy, including p-n junction and tunnel diodes

19 p3027 A71-37495

SOLID SURFACES

NT CRYSTAL SURFACES

Liquid droplet diameter effect on solid surface erosive wear

01 p0072 A71-11242

Isotropic incompressible viscoelastic solid deformation field under uniaxial and equal biaxial relaxation, determining constitutive equation

09 p1534 A71-22142

Multiple echo of impurity atom during collisions with solid body surface, contributing to vaporization from layer

12 p1932 A71-27034

Self shielding effect of solid surfaces under intense light

12 p1915 A71-27457

Elementary particle recombination probabilities on solid body surface, using reactive gas model in form of quantum mechanics three body problem

12 p1934 A71-27546

Longitudinal solid surface curvature effects on heat transfer, calculating velocity and temperature fields by similarity analysis via boundary layer equations

12 p1987 A71-27737

Atom interaction potential with solid body surface, discussing experiments and results

13 p2103 A71-29160

Gas atoms collisions with linear harmonic oscillator and solid surface simulated by semiinfinite elastically coupled atomic lattice, using combined asymptotic expansions method

13 p2103 A71-29227

Classical and quantum mechanical theories of gas atom-solid surface scattering with applications to different physical regimes

14 p2276 A71-30405

Boiling at solid heated surfaces, discussing nucleation, bubble formation, pool boiling factors, heat transfer correlation and forced convection

15 p2515 A71-32565

Molecular beam scattering at solid surfaces, outlining scattered particles angular and velocity distribution measurement

18 p2848 A71-36439

Wave motions in viscous fluid layer in presence of surfactant elastic substances adjoining solid surface or gas, using Navier-Stokes equations

19 p3042 A71-37084

Ion beam milling techniques for device fabrication involving atomic interactions on solid surfaces

21 p3384 A71-40219

Low loss images from smooth solid specimens in surface scanning electron microscope by collecting backscattered electrons

23 p3674 A71-42959

Radiation flux induced material dispersion of solid surface, taking into account radiation energy absorption by discontinuity introduction

24 p3835 A71-45225

SOLID SUSPENSIONS

Particle energy spectrum function effect on fluid energy spectrum in turbulent gas-solid suspension flow

[ASME PAPER 71-FE-15] 13 p2052 A71-29454

Relaxation effects on velocity and temperature of solid particles in gas flows, emphasizing acoustic propagation, compression shock structure and nozzle flows

18 p2909 A71-36441

Laser illuminated Mach-Zehnder interferometer system including high speed cameras for studying flame propagation among polythene particles suspended in air

19 p3064 A71-38063

Solid particle or droplet admixture effect on turbulent gas jet structure

22 p3530 A71-41872

SOLID-SOLID INTERFACES

Irreversible processes during formation of contact between indium telluride thin film and metal in vacuum at high temperature

01 p0137 A71-10150

Cu compatibility with refractory Ta-W alloy interface at high temperature, noting eutectic formation

01 p0100 A71-10374

Elastic body-vibrating surface interaction, examining friction coefficient under various modes

01 p0088 A71-10626

Electron tunneling through interfaces of MIS structures, calculating conductance and current characteristics

01 p0140 A71-11413

Sliding friction and wear of metal pairs under vacuum, using gravimetric and electron optical methods

03 p0432 A71-13366

Electron beam welding penetration depth, using constant melt temperature boundary interface

[ASME PAPER 70-WA/HT-2] 03 p0432 A71-14094

Interfacial wetting, bonding and chemical and mechanical stabilities in whisker composites, discussing system stability

04 p0611 A71-14948

Crack perpendicular to planar interface between isotropic half spaces, noting elastic constants effect on stress components distribution and relative magnitudes

04 p0670 A71-15384

Thermal conductance of contacts between dissimilar solids with interstitial fluids, calculating heat flow direction effect by double constriction model

04 p0678 A71-15459

Stress concentration at interface between bonding agent and fuel element in solid propellant grain

05 p0000 A71-15981

Counterface nature effect on friction and wear processes of carbon fiber reinforced polymers, discussing formation of transfer film of wear debris

05 p0773 A71-17245

Compressive contact interaction problem for elastic circular cylindrical shell lying in circular cylindrical cavity of elastic body

06 p0987 A71-17764

Thermal resistance to heat transfer at interface between hard smooth flat surface and softer turned surface

[AIAA PAPER 71-80] 06 p1008 A71-18537

Explosive metal welding bond interface, investigating heat treatment effect on microstructure

06 p0914 A71-18680

Surface temperature radiation interaction between two solid half spaces using Green function reduction method

07 p1223 A71-19254

Titanium diboride contact interaction with Ti, Zr and V in vacuum at various temperatures

09 p1471 A71-23083

Pyrolytic aluminum oxide thin films on Si substrate by thermodecomposition, measuring vapor deposition parameters and Si surface preparation effects on dielectric and interface properties

09 p1509 A71-23117

Capacitance voltage measurements on interface of pyrolytically deposited n-type silicon dioxide-InAs MOS diodes as function of admittance at room and 77 K temperatures

10 p1582 A71-23774

Surface layer-bulk body interaction and Rayleigh wave propagation in elastic solid, using two dimensional continuum theory

10 p1691 A71-24645

Temperature distribution in composite media sections involving solid interfacial sources, using Vodicica orthogonality equations

10 p1697 A71-24694

Jetting collision effect on structural changes at interface between Ti and steel in explosive bonding, considering plastic deformation and residual stresses

10 p1629 A71-25030

Mathematical model for heat transfer coefficients between two identical metal surfaces in contact

11 p1853 A71-25157

Interfacial bonding effect on fracture toughness of glass sphere filled epoxy and polyester resins, using tapered cleavage specimen

11 p1846 A71-25413

Strength transfer at glass-epoxy laminates interface in reference to critical surface tension of coupling agent on fabrics

11 p1786 A71-25414

Thermal oxidation and metal evaporation effects on electrical properties of silicon-silicon dioxide wafer interface in MOS structures

12 p1944 A71-27096

Tantalum disilicide kinetic interaction with Ta, investigating formation rate at various temperatures

13 p2089 A71-29415

Dissimilar elastic half spaces joined over circular region, calculating interfacial traction stresses induced by arbitrary loading from coupled integral equations

14 p2328 A71-30293

Internal frictionless contact stress determination for two telescoped cylinders with different diameters, using integrodifferential equation

14 p2331 A71-30845

Displacements produced by impulsive torsional body force situated within elastic half space bonded to half space of different material properties

16 p2647 A71-32859

Local slip theory in elastic contact region with dry friction, assuming Amontons-Coulomb law for displacement, rolling and sticking

17 p2747 A71-34327

Metal joint explosive bonding, investigating wavy interface formation mechanism by aerohydrodynamic analogy

17 p2748 A71-34494

Stress distribution in isotropic and anisotropic half spaces with crack in interface bonding, reducing boundary value problem to Hilbert problem

17 p2819 A71-34509

Thermal distortion effect on heat flow between two contacting semiinfinite solids of different materials

17 p2837 A71-34691

Circular contact area in theory of elasticity with allowance for surface structure of bodies in contact, solving Hertz axisymmetrical problem of elastic bodies

17 p2833 A71-35610

Contact problem for elasticity theory taking hereditarity in deformation into account, proving existence and uniqueness theorems

19 p3156 A71-37538

Bulk and surface diffusion roles in clean and contaminated Cu-Ni surfaces adhesion

19 p3080 A71-37713

Molybdenum hemicarbidic layer as diffusion barrier between metal and disilicide, investigating system thermal stability

21 p3399 A71-40526

Shear deformation theory of axisymmetric cylindrical shells in contact with smooth rigid surfaces

21 p3470 A71-41017

Solid body contact interaction devices at high temperatures in vacuum, gas and air for evaluation of surface coatings, adhesion, diffusion, mechanical properties, etc

21 p3382 A71-41174

Bonding conditions effect on wave mode formation at explosive bonded interface in bullet experiments on thin metal targets

22 p3617 A71-42495

Thermal conductivity of elastic, elastoplastic and plastic contact area between two compressed rough surfaces

22 p3622 A71-42686

Two-component composite cylindrical body thermomechanical stresses near junction-surface edge under plane deformation conditions

23 p3776 A71-43420

Silicon Schottky tunnel MOS diodes, discussing effect of thin interfacial film between metal and semiconductor on I-V characteristics

23 p3652 A71-43936

Solid lubricant molybdenum disulfide physicochemical interaction with Ag, Ni, Fe and Co at high temperatures, using X ray structural and spectrometric analyses

23 p3697 A71-44029

Nonlinear vibrations of circular plate with variable boundary contact on rigid base

24 p3881 A71-44831

Seizing of flat and flat/spherical steel samples pairs in vacuum as function of temperature, pressure and time of contact, using compression-tension machine

24 p3838 A71-44857

Adhesion effects on interactions between abrasive and metal surfaces in grinding operations as function of grinding speed and contact surfaces properties

24 p3830 A71-44860

Previous plastic loading deformation effect on contact area, print number, size distribution and thermal conductivity for flat surfaces

24 p3830 A71-44943

SOLIDIFICATION

Ultrafine grain metallic structures by solidification, describing various techniques

03 p0446 A71-14488

Nonlinear two dimensional free boundary problem of axisymmetric fluid flow in tubes with surface solidification, obtaining numerical solution based on finite difference equations

04 p0677 A71-15454

Al ingot level pouring casting, considering solidification effect on subsurface segregation and cyclic pattern of macrostructure

04 p0614 A71-15783

Apollo lunar rock sample solidification and impact rates, deriving cratering time behavior

04 p0660 A71-15863

Temperature gradients and cooling rates of Ti alloy sheet moving arc weld pools, discussing instantaneous solidification

05 p0757 A71-16212

Heat flow in unidirectional solidification of vacuum cast alloy turbine blades, using analog thermal model

05 p0758 A71-16244

Phase change solidification phenomena in n-hexadecane for spacecraft thermal control systems, considering two or three dimensional models

07 p1223 A71-19876

Microporosity morphology relationship to grain size and boundaries in alloys solidification and pores removal kinetics from castings by sintering

07 p1119 A71-19977

Wrought high strength Al alloy nonequilibrium second phase particles formation effect on mechanical behavior during solidification

07 p1137 A71-19978

Solidification process for unidirectionally cast airfoil shaped turbine components from Ni superalloys, discussing mold withdrawal

08 p1299 A71-21682

Ti-Ti5S13 eutectic oriented solidification structures, showing unidirectional growth faceted silicide fibers and disorientation

10 p1626 A71-24402

Al alloys microstructure and mechanical properties after rapid solidification, considering rapid quenching techniques and resulting metastable variations

10 p1627 A71-24596

Point matching technique applied to two dimensional solidification of viscous flow over semiinfinite flat plate, transforming moving free boundary problem to stationary domain

[ASME PAPER 70-APM-R] 10 p1596 A71-24733

Phase changes (droplet solidification/ effect on two phase nozzle flow, considering perturbation treatment

[ASME PAPER 71-FE-11] 13 p2052 A71-29452

Quantitative description of solidification structures of Al-Cu, Al-Cu-Ti, Al-Si, Al-Mg and Al-Si-Cu, discussing dendritization index, cooling rate and tensile strength

14 p2257 A71-29842

Solidification pressure of nuclear and neutron star matter, suggesting modifications to equation of state

15 p2452 A71-32548

Al-Cu-Mg monovariant alloys directional solidification, considering criterion for plane front growth breakdown based on constitutional supercooling

19 p3078 A71-37701

Binary alloy solidification in electroslag remelting process, determining temperature distribution and solidus, mushy and liquidus zones by heat transfer analysis

19 p3079 A71-37706

Sn-Pb alloy solidification point analysis around liquid-solid front with interface visualization by electron microprobe

20 p3238 A71-39416

Zirconium oxide-lanthanum oxide systems near melting point, plotting solidification and phase diagrams

20 p3254 A71-39962

Ni-Cu alloy castings solidification experiments on catalytically clean metals to avoid heterogeneous nucleation

21 p3387 A71-40460

Al-Co and Al-Ni alloy rods unidirectionally solidified, discussing compositional range in eutectic structures at high solidification rates

23 p3689 A71-43101

Mechanical properties of Al-aluminum intermetallic eutectic alloys after rapid solidification in semicontinuous casting technique, noting flow stress and tensile strength increase

23 p3695 A71-44286

SOLIDIFIED GASES

Liquefied and solidified gas IR measurements describing versatile optical cell

02 p0250 A71-12133

Ozone in Mars solid carbon dioxide polar cap, using UV reflection-absorption spectra

04 p0661 A71-15897

Thermal conductivity measurement of cryopumped solid gas deposits in thin walled stainless steel cylinder with temperature gradients

09 p1546 A71-23007

Hydrogen condensation and evaporation on liquid helium cooled surfaces in cryopump with reduced thermal radiation loading

09 p1546 A71-23008

Hydrogen-helium gas mixtures high pressure phase behavior, considering solidified gas core under Jupiter and Jovian planets atmospheres

11 p1827 A71-25728

Solid Ne isotopes specific heat at constant pressure and volume, entropy, enthalpy and Gruneisen parameters

13 p2102 A71-29481

Two component solid gas vortex flows with end wall injection eliminating boundary layer losses for colloid core nuclear rocket engine concept

[AIAA PAPER 71-637] 14 p2273 A71-30715

Hydrogen condensation in interstellar gas clouds onto solid dust grains from vapor pressure measurements of solid hydrogen at low temperatures

16 p2634 A71-33392

Martian polar caps heat balance, noting albedo differences due to irregularities in solid carbon dioxide cover

22 p3603 A71-42190

Solid helium and molecular metallic hydrogen thermodynamic properties and phase diagrams as functions of pressures corresponding to Jupiter and Saturn interiors

22 p3606 A71-42613

Iron meteorites total N abundances determination by inert carrier gas fusion extraction gas chromatography

23 p3734 A71-43243

Jovian geometric albedo at 1800-1950 A decrease explained as absorption by gaseous and solid ammonia in cubic crystal form

23 p3736 A71-43345

SOLIDS

NT SOLIDIFIED GASES

Weibull density functions applied to fracture location distribution in brittle solids

01 p0167 A71-10294

Transparent solids unpolished samples refractive index and dispersion measurement using Abbe refractometer

01 p0128 A71-10837

Transient heat conduction of solids obeying Fourier law, deriving numerical solution for boundary value problem by Laplace transformation

01 p0180 A71-10937

High temperature calorimetry of solids for heat capacity and thermal processes thermodynamic and thermokinetic characteristics, considering calorimeter design engineering

01 p0083 A71-11226

Corrosion processes in and on solids, noting techniques and instrumentation for control

03 p0441 A71-13254

Euler-Poisson equations for heavy solid body motion about fixed point, deriving particular solution

03 p0457 A71-13581

Hess solution for motion of heavy solid body with fixed point, surveying various methods

03 p0458 A71-13599

Heavy solid body rotation about fixed point, using fixed and traveling hodograph

03 p0458 A71-13592

Solid body motion kinematics about fixed point for Euler-Poisson equations

03 p0458 A71-13594

Characteristic energy absorption spectra of dielectric solids from direct IR measurements for single crystal and thin film specimens

03 p0385 A71-13645

Solid electrolyte batteries development, considering design, performance, advantages and applications

03 p0355 A71-14322

Inextensible fiber-reinforced plastic-rigid solid, applying continuum theory to derive kinematic properties, yield condition and flow rule

03 p0514 A71-14349

Soviet book on fracture physics /crack growth in solid bodies/ covering glass, polymers, single crystals and polycrystalline metals, etc

03 p0515 A71-14398

Shock structure in crystalline solids, including dissipative processes, discontinuities, continuum mechanics and lattice dynamics

04 p0664 A71-14662

Thermophysical properties of solids at high temperatures - Conference, Salford, England, July-September 1970, Part I

04 p0594 A71-14953

Thermal diffusivity and total emissivity measurements of solids between 1500 K and melting point, using arc image furnace

04 p0595 A71-14966

Elastic solids mechanical characterization using finite element formulation of minimum potential energy theorem

04 p0671 A71-15751

Solid deformable body combined brittle and plastic elements model for strain analysis

05 p0827 A71-16758

Solid metal plates breakdown mechanism at high temperatures and supersonic plasma jet action

05 p0768 A71-16778

Dilatometric thermal expansion method for determining cylindrical solid body thermal conductivity coefficient

05 p0838 A71-16790

Action-angle variables for Euler-Poinsot problem of solid body free rotation about stationary point

05 p0783 A71-16996

Complex configuration solid bodies boundary value problems numerical solution algorithm using R functions

05 p0775 A71-17013

High energy electron penetration and scattering in solids, obtaining beam density profiles by polymethyl methacrylate resist exposure

06 p0940 A71-17305

Ultrasound propagation visualization in solids, describing sensitive schlieren apparatus

06 p0903 A71-17323

Nonlinear interaction between waves with random phases in magnetoactive plasma of solid body, discussing weak turbulence theory

06 p0930 A71-17404

Stress distribution at cracks in solid bodies, discussing crack models, plasticity and elasticity theories and continuum mechanical basis of fracture theory

06 p0911 A71-17413

Semiinfinite solid elastic cylinder under self equilibrium end loading, obtaining elastostatic solution

06 p1000 A71-18027

One dimensional nonstationary temperature field in solid body with linearly related heat conductivity and capacity

07 p1221 A71-18921

Elastic solids fourth order anharmonic equation of state from finite strain theory, resolving ambiguities by Mie-Grüneisen equation

07 p1178 A71-19800

Noncrystalline amorphous solids electro-optical effects, studying semiconductor energy band models

07 p1181 A71-20422

Crystalline solids strain rate effects due to simultaneous operation of plastic deformation mechanisms including diffusion controlled creep and dislocation-drag processes

08 p1371 A71-21560

Cryostat design and operation for investigating solids mechanical properties and structure at liquid He temperature

09 p1426 A71-22321

Models for nonferromagnetic solid body mechanics allowing for relationships among mechanical, thermal and electromagnetic processes

09 p1509 A71-23076

Thermophysical properties of solids at high temperatures - Conference, University of Salford, England, April 1970

10 p1624 A71-23906

Time optimal control for massive solids heating or cooling from initial into prescribed finite state with constraints

10 p1695 A71-24159

Solid body finite rotation theory involving formal operations on quaternions

10 p1642 A71-24576

Microwave frequency sound generation in solids with Q switched ruby laser

10 p1621 A71-24838

Self consistent hydrodynamic heating of solid substance by laser pulse for nonequilibrium ionization

10 p1653 A71-24887

Solids evaporation into vacuum, considering interconnected problems of heat conduction and evaporation front boundary conditions

10 p1697 A71-25063

Negative differential conductance of homogeneous nonequilibrium electronic solid-body plasma in electromagnetic field upon Cherenkov interaction

11 p1807 A71-25584

Equilibrium thermodynamics of ideal elastic solids under stress, using Cauchy stress tensor

11 p1799 A71-25740

Free solid body carrying heavy pendulum, calculating oscillations as function of geometrical and inertial characteristics during motion under tangential force

12 p1929 A71-27117

Solid bodies crack development theory, emphasizing crack tip fine and hyperfine structures concepts and time dependent effects

13 p2149 A71-28121

Solids continuum mechanics and fracture criteria, emphasizing intermixed elastic, plastic or viscoelastic types materials behavior idealization

13 p2151 A71-28214

Stabilization of solid body orientation with twin gyros under slave engine drive, producing control moments to gimbal axis

13 p2145 A71-28935

Temperature dependent thermophysical properties effect on temperature distribution in step-heated semiinfinite solid, deriving time limited perturbation solution

13 p2164 A71-28988

Three dimensional elastic plastic solid, calculating stress and deformation with finite difference procedure

14 p2322 A71-29737

Statically determinate plane strains in plastic solids, establishing geometrical relations between constant normal-shear stresses and principal directions curves

14 p2323 A71-29816

Solid additives, graphite and molybdenum disulfide concentration effects on liquid lubricants and greases antiwear performance

14 p2251 A71-29827

Conjugate functions theory variational application to solid mechanics, generalizing concept of potential for nonlinear behavior laws in viscosity and plasticity

14 p2329 A71-30447

Reactive solids ignition by constant energy flux from asymptotic analysis of activation energy limit

14 p2337 A71-30458

Monograph on crack problems in mathematical theory of thermoelasticity covering crack effects on stress distribution in circular cylinders, thick plates and infinite solid bodies

14 p2329 A71-30501

Crack propagation model in linearly viscoelastic solid strip based on thermodynamics first law

15 p2506 A71-32011

Crack propagation in brittle solids under constant deformation or thermal shock, verifying behavior by results with polycrystalline aluminum oxides

16 p2590 A71-32941

Thermoelastic stability of finitely deformed solids under nonconservative surface tractions without body force

16 p2649 A71-33009

Rigid-plastic solids with viscoplasticity extension, comparing stability with Hill condition

16 p2649 A71-33010

Solid metal plates erosion mechanism at high temperatures under supersonic plasma jet action, noting dependence on specific heat and latent heat of fusion

16 p2591 A71-33030

Creep tests of admissible stress states in viscoelastic isotropic compressible or incompressible linear and nonlinear solids

16 p2591 A71-33206

Finite elasticity theory for isotropic incompressible solids, formulating Ericksen problem for requirements of statically possible radially symmetric deformations in equilibrium

16 p2661 A71-34147

Soviet monograph on plasticity and strength of solid bodies at low temperatures covering solidifying gases, static tests, dynamic properties and creep

17 p2724 A71-35186

Axisymmetric dynamic deformation of elastic solid, obtaining characteristic properties and solutions of mixed initial and boundary value problems

17 p2831 A71-35353

Combined brittle and plastic elements model for strain analysis of nonelastic deformed solid

17 p2832 A71-35457

Structural stability regions construction for solid body with liquid filled cavities

17 p2730 A71-35607

Action-angle variables for Euler-Poinsot problem of solid body free rotation about stationary point

18 p2948 A71-36796

Oblique shock wave incident on plane boundary of nonlinear homogeneous elastic solid, proving wave reflection pattern uniqueness

18 p2982 A71-36813

Surface relief effect on radiative properties of solid body with random surface roughness distribution

19 p3162 A71-37581

Test facility for thermal diffusivity measurements in solids by method of plane temperature waves using periodic optical heating at 1500 K

19 p3063 A71-37589

Solid cylindrical particles interaction under entrainment in pipe by viscous incompressible fluid, obtaining numerical solution by reduction to flow past moving body

19 p3046 A71-38418

Deformation and stress distribution three dimensional state around flat parabolic cracks in elastic solids

20 p3307 A71-38772

Dual beam pulsed gas laser magnetic resonance spectrometer for magneto-optic studies of solids in far IR frequencies

20 p3244 A71-39177

Thermal stresses and couples in micropolar elastic solid cavity and rigid inclusion during uniform heat flow

20 p3309 A71-39560

Thermoelastic plane harmonic and Rayleigh surface waves in elastic solids with thermal relaxation, using Maxwell heat conduction equation

20 p3310 A71-39779

Shock waves and mechanical properties of solids - Conference, Raquette Lake, New York, September 1970

21 p3464 A71-40784

Rayleigh wave reflection from crack tip after propagation along open crack faces in elastic solid, determining surface wave energy loss

21 p3468 A71-41003

Generalized radiation cooling of convex solid, demonstrating existence of unique stable positive solution to boundary value problem related to temperature distribution

21 p3477 A71-41184

Self consistent hydrodynamic heating of solid substance by laser pulse for nonequilibrium ionization

21 p3424 A71-41253

Discrete approximations for continuous fields in solid body nonlinear theory with differential and nonlinear equations replaced by algebraic and linear equations respectively

22 p3616 A71-42218

Rotating solid body nutations damping by pendulums system oscillating in plane normal to rotation axis, deriving optimal conditions

24 p3848 A71-44855

Translational and rotational vibrational motion correlation of solid body mass center in Newtonian force field

24 p3872 A71-45047

Plastic deformation of solid body in terms of slip dislocations displacement rate

24 p3885 A71-45052

SOLIDUS

InAs-AIAs pseudobinary system solidus boundary determination from pellet phase diagram

08 p1344 A71-21472

Coarse grained lunar basalt from Oceanus Procellarum, examining ground mass and subsolidus cooling history

14 p2313 A71-30427

Mo-Ni-C ternary alloy X ray analysis, determining solidus temperature from phase diagrams

15 p2424 A71-31237

Ta-V-C ternary system solidus surface and equilibrium diagram determination by metallographic techniques and X ray and thermal analyses

15 p2430 A71-32147

Binary alloy solidification in electroslag remelting process, determining temperature distribution and solidus, mushy and liquidus zones by heat transfer analysis

19 p3079 A71-37706

Equilibrium phase relations in lunar rocks and synthesized analogs, determining liquidus and solidus temperatures

23 p3742 A71-43640

SOLSTICES

Spatial-temporal harmonics of noctilucent cloud occurrences during IQSY with maximum displays after summer solstice in both hemispheres

14 p2233 A71-29965

SOLUBILITY

Diffusion and solubility of thermally induced acceptors in indium antimonide single crystals

04 p0636 A71-15085

Nitrogen diffusion and solubility in W, deriving expression for permeation constant

04 p0614 A71-15784

Oxygen solubility and activity in Fe-Al and Fe-Ti melts, using neutron activation analysis

04 p0614 A71-15785

Manometric apparatus determining solubility of inert gases in water, blood and other liquids, establishing partition coefficients of ethyl ether

06 p0862 A71-18390

Zr solid state solubility in Mo as function of quenching temperature, using optical microscopy and microhardness testing techniques

07 p1130 A71-19300

Hydrogen solubility in alpha Ti, using electrical resistivity measurement at liquid nitrogen temperature

07 p1139 A71-19991

Ce, Pr and Nd solubility in Cr, investigating temperature dependence, microhardness, deoxidation and alpha phase by X ray, metallographic and durometric analyses

07 p1144 A71-20652

C solubility in Mo-W solid solution at various temperatures

08 p1306 A71-21063

Silver oxides stability, considering solubility, reduction by hydrogen and thermal decomposition

08 p1234 A71-21085

Hf, Ta, W and Re solubility in La and Ce hexaborides from lattice parameters, microhardness and X ray and metallographic analyses

09 p1509 A71-23066

- Fe-Ni alloys, determining hydrogen permeability, diffusion coefficient and solubility as function of composition by electrochemical method 09 p1472 A71-23127
- Phase diagram of Ti-Ta-Mo alloy system, obtaining solubility and electrical conductivity for various cross sections 09 p1480 A71-23706
- Mo-Ti-C ternary alloy, examining solid state solubility, equilibrium conditions and microhardness 10 p1628 A71-24647
- Mo-Fe-C ternary system, investigating various concentrations, microhardness measurements, solid state solubility and ductility 10 p1628 A71-24648
- Solid state solubility of B in Nb, determining binary Nb-B alloys phase diagram by microscopic, X ray and thermal analyses 13 p2085 A71-28224
- Nitrogen solubility in W at high temperature, using metal high vacuum apparatus and mass filter partial pressure measuring instrument 14 p2260 A71-30475
- Nitrogen solubility in Ni-Mo and Ni-W melts, detailing Ti and pressure effects 15 p2424 A71-31392
- Boron solubility in molybdenum, showing grain size decrease, plastic deformation change and elongation 15 p2425 A71-31399
- Graphite solubility in Co and Ni, discussing solution energies and entropies 19 p3081 A71-37723
- Solid Ni-Co and Ni-Cu alloys, investigating hydrogen solubility 21 p3398 A71-40466
- Nitrogen equilibrium solubility dependence on slag basicity and gas phase nitrogen/carbon monoxide contents in aluminosilicate melts 21 p3399 A71-40470
- Copper-indium-tellurides homogeneity region components solubility in different cross sections of concentration triangle at room temperature 23 p3717 A71-44023
- Hydrogen solubility in alpha phase Ti-Al alloys, using resistometric technique and electron microscopy 23 p3694 A71-44282
- Hydrogen solubility in liquid Cr, Ni and Co alloys containing Si for various concentrations and temperatures 24 p3840 A71-45371

SOLUTES

- Binding energies between solute atoms and vacancies in dilute Al alloys measured by quantitative transmission electron microscopy 08 p1310 A71-21530
- Solute diffusion coefficients dependence on proteins concentrations in human plasma from experiment, presenting equation for prediction 23 p3637 A71-44253
- Interstitial solute carbon distribution in martensite, using generalized perfect lattice gas statistical mechanics 23 p3694 A71-44281

SOLUTION

- Nonlinear global strong cellular branching solutions stability of Navier-Stokes equations 16 p2558 A71-32997

SOLUTIONS

- NT AQUEOUS SOLUTIONS
- NT DETONABLE GAS MIXTURES
- NT GAS MIXTURES
- NT NUCLEAR EMULSIONS
- NT PHOTOGRAPHIC EMULSIONS
- NT SOLID SOLUTIONS
- Solution concentration, solid content, specific gravity and bulk modulus measurements by sound velocity measurement 15 p2409 A71-32197

SONAR

- Optimal detection of narrow band signal with random phase and arrival time in radar or sonar, using nonlinear adaptive filter 02 p0211 A71-11720
- Book on detection, estimation and modulation theory, Part 3, Gaussian and radar-sonar signals in noise, covering point targets, random process and scatter channels 15 p2371 A71-31841

SONDES

- NT IONOSONDES
- NT RADIOSONDES
- NT RAWINSONDES
- Umkehr technique vs Mast-Brewer sondes for ozone vertical distributions 01 p0073 A71-10857
- Vacuum tube launchers and boosters for launching small to medium size meteorological probe rocket into lower atmosphere [AIAA PAPER 70-1393] 03 p0498 A71-13674
- Rocket sonde prototype for wind and temperature measurements, discussing electrical circuits, mechanical design and operation 12 p1972 A71-27064

SONIC ANEMOMETERS

- Wind speed measurement by cup and sonic anemometers, considering errors due to tower structure effect 05 p0752 A71-16663

SONIC BOOMS

- Whitham supersonic flow theory application to mid-or near-field sonic boom of slender bodies in wind tunnel research 01 p0005 A71-10956
- High intensity sonic boom effects on heart rate of dogs, noting conditioning benefit 03 p0358 A71-13097
- Simulated sonic booms effects on sleeping humans, considering intensity levels, age factors, sleep stage, adaptability and housing 03 p0371 A71-13165
- Sound and sonic booms effects on farm animals physiology and behavior, considering milk production, reproduction, food intake and growth rate 03 p0360 A71-13166
- Physiological and psychological human responses to sonic booms in France, UK and U.S. considered as acceptability criteria 03 p0371 A71-13167
- Sonic boom wave pressure history prediction on arbitrarily oriented plane walls by explicit fixed mesh time dependent numerical method [ASME PAPER 70-WA/APM-9] 03 p0349 A71-14153
- Pointed body of revolution in gravitationally stratified atmosphere, discussing supersonic boom and minimum drag [DFVLR-SONDDR-97] 05 p0694 A71-16712
- Supersonic jet transport legal aspects in land overflight, discussing ground noise and sonic boom effects on persons and property 06 p0846 A71-17644
- Sonic boom problem, investigating pressure signature of large models in supersonic wind tunnels [AIAA PAPER 71-184] 06 p0886 A71-18623
- Sonic boom near field behavior, discussing N wave focusing [AIAA PAPER 71-185] 06 p0886 A71-18624
- Far field sonic boom pressure profiles simulation by methane-oxygen mixture detonation in balloons [AIAA PAPER 71-186] 06 p0886 A71-18625
- Sonic boom effects on human physiology and behavior and structures, based on theoretical studies and simulators 08 p1232 A71-21812
- Legal aspects of military sonic booms, discussing administrative remedies, liability and various cases 08 p1379 A71-21830
- Sonic boom wind tunnel testing techniques at high Mach numbers, giving sample pressure signatures [AIAA PAPER 71-280] 08 p1229 A71-22006
- Sonic boom and explosion shock wave propagation over long distances through turbulence modeled by sound speed fluctuation, including acoustic scattering effect 09 p1433 A71-22858
- Cut-off Mach number of sonic bang propagation on ground for flight track in relation to atmospheric parameters 09 p1383 A71-23577
- Normal shock wave interaction with deformable solid walls, determining explosion or sonic booms effects on elastic structures and protection devices 10 p1556 A71-24483
- Short N wave refraction and diffraction by gas-filled soap bubble, discussing measurements to explain peaking and rounding in sonic boom pressure signature 10 p1642 A71-24811
- Atmospheric turbulence effects on sonic boom rise times by statistical theory 10 p1556 A71-24817
- Structures dynamic loading and damage by sonic booms, discussing structural response prediction by boom pressure wave model 10 p1693 A71-25052
- Transonic compressor shock wave noise generation and decay rates at multiple tones, using sonic boom analysis [ASME PAPER 71-GT-7] 11 p1703 A71-25953
- Supersonic flight path curvature effects on local shock wave production, considering no boom zone and ground rules 11 p1708 A71-26310
- Subsonic jet aircraft noise and simulated sonic booms awakening effects on human sleep 11 p1726 A71-26510
- Plate and acoustic finite elements simulation of window-room system coupled transient response to sonic booms, discussing equations of motion and cavity depth effect 12 p1981 A71-27481
- Sonic boom induced indoor acoustical waves, using electrical analog 14 p2274 A71-30200
- Incident sonic boom shock wave reflection factors off smooth surface, discussing pressure rise and flight near threshold Mach number 14 p2177 A71-30610

SST sonic boom minimization, discussing cross-country flight 14 p2177 A71-30820

- Sonic boom pressure signature laboratory scale measurement after modification by traveling through air jet turbulence, comparing with statistical prediction [AIAA PAPER 71-618] 15 p2388 A71-31544
- Sonic boom wave interaction with topographic models, measuring surface pressure time history [AIAA PAPER 71-619] 15 p2389 A71-31548
- U.S. federal legislation and regulations for aircraft noise and sonic boom 15 p2516 A71-32244
- Simulated sonic booms and subsonic jet aircraft noise effects on human subjects of various ages during different sleep stages 15 p2364 A71-32250
- Room with windows and open doors under sonic boom, determining cavity resonance model for impulsive loading conditions 15 p2450 A71-32514
- Sonic boom phenomena, discussing supersonic flow near aircraft, atmospheric propagation, distortion, focusing, caustics, turbulence effects and reduction 15 p2350 A71-32566
- French shock tube test facility for reproducing and investigating effects of sonic booms on vision and physiological processes 16 p2552 A71-33350
- SST sonic booms, investigating intensity and transonic aircraft supersonic flight feasibility 16 p2525 A71-34100
- Sonic boom implications and decision on acceptability with alternative policies of complete banning, controlled corridors and overflight limitations [CASI PAPER 72/4] 19 p2996 A71-37595
- Meteorological problems of operation of commercial supersonic aircraft, including sonic boom intensity and extent [CASI PAPER 72/7] 19 p2996 A71-37597
- Sonic boomless transonic transports design, performance, economics and airline routes at Mach 1.2 and 0.98 [CASI PAPER 72/8] 19 p2996 A71-37598
- Sonic booms loudness as function of peak overpressures and rise times, using semiempirical formulae 21 p3325 A71-40536
- SST sonic boom generation, discussing aircraft design and atmospheric conditions effects and property damage 21 p3325 A71-40705
- Sonic boom minimization including front and rear shocks, exemplifying by SST aircraft 21 p3324 A71-40972

SONIC FLOW

U TRANSONIC FLOW

SONIC NOZZLES

- Sonic nozzle design for precise mass flow measurement, determining nozzle profile for axial velocity distribution in conformity with laminar boundary layer equations solution 10 p1597 A71-24944
- Real gas mass flow rate computation through sonic nozzle 14 p2239 A71-29927
- Steady state partially ionized monatomic gas expansion from sonic orifice, investigating electron-ion recombination effects on flow properties 15 p2457 A71-32101
- Discharge coefficient correction factor for curvature effect on mass flow rate measurement by sonic throat for axisymmetric nozzles [ONERA-TP-956] 18 p2915 A71-36024

SONIC SOLDERING

U ULTRASONIC SOLDERING

SONIC SPEED

U ACOUSTIC VELOCITY

SONIC WAVEGUIDES

U ACOUSTIC DELAY LINES

SONOGRAMS

- Eye and orbit A and B ultrasonography scanning technique, showing minimal echogram distortions in meridional arc scans 24 p3799 A71-44367

SOOT

- Back mixing effects on hydrocarbons combustion comparing well-stirred reactor with flat flame soot yields 07 p1181 A71-19246
- Air polluting nitric oxide and soot production by jet aircraft, discussing mixing process and atmospheric dispersion [AIAA PAPER 70-115] 12 p1946 A71-27566
- Aircraft piston and turbine engine soot extracts can cerogenic activity in hybrid mice 12 p1872 A71-27724
- Critical atomic carbon to oxygen ratio measurements for incipient soot formation in shock heated acetylene ethylene and ethane/oxygen/argon mixtures 21 p3436 A71-40855
- Soot emission suppression from propane diffusion flame by metallic additives 22 p3588 A71-42101

SORBENTS

NT ABSORBENTS
NT ADSORBENTS

Decontaminating methods for water regenerated from urine under space flight conditions by filtering water condensate through sorbents

22 p3506 A71-42815

SORPTION

NT ADSORPTION
NT CHEMISORPTION

Thermogravimetric analysis of goethite-rich sample of Mars type limonite, considering sorption process relation to Mars environment and polar caps

04 p0644 A71-15131

Stress corrosion cracking, discussing stress effect, environmental and metallurgical factors and electrochemical and sorption theories

13 p2085 A71-28221

Molecular hydrogen sorption pumping by cold carbon dioxide cryodeposits, showing absorbed molecules surface diffusion into disordered frost structure

17 p2695 A71-35138

Oxygen sorption rate by Ti at low pressure from measurement in stainless steel ultrahigh vacuum chamber

17 p2695 A71-35139

Hydrogen sorption capacity by sulfur dioxide frost from cryodeposit formation on stainless steel sphere in vacuum chamber and equilibrium isotherms measurement

17 p2695 A71-35142

Vacuum covered gage measurements in sorption and cryogenic systems with activated pumping surfaces, concerning molecular gas flux leaving specimen

21 p3417 A71-41298

Maximum bubble pressure automatic capillary electrometer for salt solutions and organic compounds electroosorption, comparing with Lippmann instrument and capacitance bridge

22 p3548 A71-42529

SORTING

U CLASSIFYING

SOUND

U ACOUSTICS

SOUND ABSORPTION

U SOUND TRANSDUCERS

SOUND AMPLIFICATION

Microwave emission from InSb due to sound amplification by piezoelectric electron-phonon coupling at low magnetic fields

01 p0052 A71-10321

Acoustic surface wave amplification using accumulation layer on Si in MOS structures

02 p0249 A71-12039

Transverse acoustic wave amplification in solid propellant rocket motor, using discrete mass injection as excitation source

12 p1946 A71-27565

Interdigital broadband hybrid junction transducer terminated in negative resistances for acoustic surface waves amplification

13 p2037 A71-28476

Hydrodynamic effects on laser beam propagation through gases by finite difference solution, applying to trapping, acoustic and light amplifications and banana self focusing

20 p3242 A71-38838

Transverse acoustic wave amplification due to mass injection around submerged nozzle in solid propellant rocket engines, noting annular flow role

22 p3589 A71-42034

Ultrasonic subharmonic waves amplified in standing waves through utilization of propagation medium nonlinearity and cavity reflector induced dispersion

23 p3704 A71-43362

SOUND BARRIER

U ACOUSTIC VELOCITY

SOUND DETECTORS

U SOUND TRANSDUCERS

SOUND FIELDS

Superfluid gyroscope for general relativity tests, using resonant phonon force field for drift reduction

02 p0248 A71-11943

Point source acoustic radiation field in presence of absorbing plane, presenting solutions and approximations based on plane wave reflection and modified image method

03 p0456 A71-13276

Sound and vibration disorder measure for choosing statistical or deterministic models for system/response situation

[ASME PAPER 70-WA/DE-1] 03 p0459 A71-14138

Sound field in multiple source enclosures, discussing noise and vibration control, acoustic modes excitation and environment simulation

[ASME PAPER 70-WA/DE-8] 03 p0511 A71-14142

Inlet turbulence interaction with rotor potential flow as noise source in axial flow fans, developing expression for sound power radiated

05 p0738 A71-17163

Near and far noise fields from coaxial interacting supersonic jet flows

[AIAA PAPER 71-152] 06 p0884 A71-18594

Sound field due to point source inside absorbent lined enclosure for anechoic chamber performance prediction

07 p1160 A71-19587

Beam pattern near vibrating piston near sound field, discussing boundary between far field

07 p1113 A71-19953

Sound field interaction with sinusoidally corrugated surface, considering aircraft noise measurement implications

08 p1333 A71-21162

Large space vehicle acoustic environment test facility, investigating combined direct and/or reverberant sound field effects

08 p1272 A71-21430

Aeroacoustic phenomena in free turbulent gas jets, discussing structure, noise-turbulence correlations and acoustic field generation at subsonic/critical velocities

09 p1384 A71-23607

Noise reduction by antisound, using directly opposing field with identical wave geometry and reversed phase

10 p1643 A71-24948

Far field sound radiation pattern from vibrating circular piston set in nonrigid baffle for sonar detectors

11 p1798 A71-25186

Axial flow fan noise, investigating louvers effects on sound field

12 p1945 A71-26704

Unsteady acoustic wind in free sound field for random Reynolds numbers, using stream equation

13 p2101 A71-28847

Quasi-unsteady approximation of mutual hydrodynamic drift velocity of aerosol particles in high power sound field

13 p2101 A71-28849

Cost efficient sound limit expenditures per parameter unit in commercial transport aircraft design

13 p2167 A71-28945

Point and large sources acoustic free field measurement, predicting reflecting ground surface effects on accuracy

14 p2274 A71-30066

Circular air jet velocity, turbulence intensity and energy spectra distributions, investigating longitudinal acoustic field influence

14 p2225 A71-30226

Sound fields of flying aircraft from noise measurements, discussing engine operating conditions, speed and attitude

14 p2176 A71-30521

Jet aircraft sound spectrum on ground and in air, comparing calculation with experiment

14 p2289 A71-30524

Localized focused ultrasonic beam action on brain portions without skull trepanation in animals and man, visualizing sonic field by Tepler effect

15 p2356 A71-31291

Jet noise reduction by foam injection, developing mathematical model for foam behavior in sound field

[AIAA PAPER 71-734] 15 p2388 A71-31327

Fan induced low speed jet noise from turbofan engines, discussing results of far field sound measurements for simulated nacelle configurations with and without acoustic liners

[AIAA PAPER 71-586] 15 p2467 A71-31533

Computational technique for acoustic field of jet aerodynamic noise, using Lighthill theory for spectral calculations

[AIAA PAPER 71-583] 15 p2468 A71-31571

Probability theory of stresses during random vibrations of flat panel in acoustic field of jet engine exhaust

15 p2504 A71-31704

Pressure fluctuations in acoustic field of boundary layer under slot suction, considering vortex formation and separation on edges

15 p2389 A71-31713

Sound field of point acoustic stresses in arbitrary motion, investigating uniform straight line and circular motion and pure rotation effects

15 p2450 A71-32130

Sound reflection by dense doubly periodic lattice parallel to rigid screen, describing asymptotic characteristics by double lattice virtual mass including mirror image

20 p3268 A71-38807

Acoustical field from streamlined body of revolution moving in homogeneous gaseous medium past semiminfinite rigid screen, using Wiener-Hopf method for diffraction radiation

20 p3175 A71-38809

Acoustic field HF asymptotic characteristics after sound passage through elastic shell, expressing sound fields inside and outside by integro-differential equations system

20 p3268 A71-38810

Holographic investigation of acoustical fields, describing shadowgraph recording apparatus for sound pressure amplitude distribution

20 p3232 A71-38811

Sound field excitation by wedge shaped transducer in liquid filled wedge extension region, determining

sound field distribution as function of frequency and wedge angle

20 p3268 A71-38812

Acoustic holography imaging technology, discussing sound field visualization and applications in nondestructive testing, medical diagnostics, ultrasonic microscopy, seismology and underwater viewing

22 p3546 A71-42478

Surface energy absorption coefficient determination from decaying sound fields, deriving reverberation time and decay rate equations

23 p3703 A71-43201

Sound field measurement in circular and rectangular air duct with sound-absorbing walls /mufflers/, deriving empirical formula for attenuation frequency characteristics

24 p3849 A71-45271

SOUND GENERATORS

Mechanical transducers for generating and detecting second sound in He isotopes at millidegree temperatures, discussing construction and performance

02 p0250 A71-12135

Sound generation by rotor-stator interaction in subsonic axial flow compressors, using acceleration potential and wake technique

03 p0469 A71-13277

Sound field in multiple source enclosures, discussing noise and vibration control, acoustic modes excitation and environment simulation

[ASME PAPER 70-WA/DE-8] 03 p0511 A71-14142

Aerodynamic sound generation dependence on convective derivative of hydrodynamic pressure within turbulence source region

05 p0784 A71-17154

Sound radiation by rotor from interaction with nonuniform flow, considering multiple blades

05 p0697 A71-17159

Far field sound radiated from steady loading of isolated subsonic rotor, noting dependence on spatial uniformity of flow entering rotor

05 p0697 A71-17160

Axial and swirling mean flow effects on sound transmission and generation in hard walled ducts

06 p0945 A71-17620

Sound generation by frontal collision of double pair vortices, showing pressure proportional to Mach number

10 p1641 A71-24346

Microwave frequency sound generation in solids with Q switched ruby laser

10 p1621 A71-24838

Directional acoustic radiation from supersonic jet, discussing generation mechanism theory based on shear layer instability close to nozzle

12 p1945 A71-27221

Computer controlled acoustic data acquisition system with real time control of 16 high intensity acoustic generators

14 p2208 A71-30315

Combination tone noise generation from turbofans with supersonic fan blade tip speed, determining sound power distribution among engine rotation frequency harmonics

[AIAA PAPER 71-730] 14 p2295 A71-30777

Combustion generated aerodynamic noise, considering sound radiation from open turbulent flames, spectral content, power output and origin

[AIAA PAPER 71-735] 14 p2338 A71-30780

Airfoils broadband noise generation mechanism in turbulent flow in anechoic chamber

[AIAA PAPER 71-587] 15 p2468 A71-31573

Turbomachinery rotor and stator row aerodynamic interaction, describing discrete tone noise generation from far field measurements

15 p2450 A71-32134

Jet aircraft noise generation, transmission and reduction, emphasizing turbofan engine acoustics, operational characteristics and exhaust sound

15 p2349 A71-32241

Ultrasonic surface wave generation by infinite interdigital electrode array on piezoelectric material, predicting behavior from equivalent circuit by variational principle

17 p2717 A71-35491

Multiple tone generation by axial flow transonic compressors, considering shock waves production and propagation associated with supersonic elements of blading

18 p2848 A71-36497

Fluid mechanics of human whistling as function of resonant cavity and orifice jet velocities, comparing Rayleigh bird call and Pfeifentone

18 p2910 A71-36935

SOUND INTENSITY

Synthesized glottal consonant imitation by human voice, analyzing stimulus and response intensity levels relationship

02 p0206 A71-12062

Acoustic priming of audiogenic seizures in mice, noting high susceptibility to convulsions under intense sound

03 p0360 A71-13160

Control valves aerodynamically generated sound pressure level prediction, using empirical method

[ASME PAPER 70-WA/FE-28] 03 p0403 A71-14136

SOUND LOCALIZATION

- Acoustic intensity and exposure time duration for threshold lesion in cat brain 05 p0712 A71-16283
- Shock tube testing of acoustic materials at high sound amplitudes 07 p1083 A71-19586
- Noise exposure index from mean sound intensity measurement, considering harmful effects on humans 13 p2021 A71-29284
- Niese procedure for sound intensity determination, considering measurement practice 13 p2101 A71-29285
- Turbulent flow and high sound level effects on acoustic attenuation in narrow rectangular duct 14 p2224 A71-30207
- Combination tone noise generation from turbofans with supersonic fan blade tip speed, determining sound power distribution among engine rotation frequency harmonics [AIAA PAPER 71-730] 14 p2295 A71-30777
- Sounds effects on natural nocturnal sleep of healthy humans with normal hearing 17 p2679 A71-34479
- Frequency distribution of heart sounds in precordium, studying slope of attenuation and relative peaking 20 p3185 A71-38803
- Broadcast sound loudness level monitor as measuring and indicating instrument, discussing technological and psychoacoustical evolution 20 p3271 A71-39763
- Lined ducts design for flow with intense sound, discussing analysis methods, testing procedures, liner materials development and acoustic attenuation 21 p3361 A71-40212
- Comparative residual and reversed microinterval masking signals and human auditory perception capacity measurements using sound level estimates 22 p3490 A71-42579
- ## SOUND LOCALIZATION
- Vascular effector structure in orientation reaction of peripheral vessels to sound, using plethysmogram and rheoencephalogram indications 08 p1242 A71-21962
- Echo location systems theorem concerning ambiguity density relationship to signal bandwidth 14 p2194 A71-30063
- ## SOUND MEASUREMENT
- ### U ACOUSTIC MEASUREMENTS
- ### SOUND PERCEPTION
- ### U AUDITORY PERCEPTION
- ### SOUND PRESSURE
- Sound pressure radiation from infinite plate with rigid or pressure release baffles perpendicular to surface, using steepest descent method 02 p0325 A71-11997
- Noise generation increase with unchanged mass flow rate by cone angle diffusers in jet nozzles, considering far field sound pressure level [ASME PAPER 70-WA/GT-5] 03 p0402 A71-14117
- Control valves aerodynamically generated sound pressure level prediction, using empirical method [ASME PAPER 70-WA/FE-28] 03 p0403 A71-14136
- Auditory meatus sound pressure levels measurements in subjects with fabricated human earmolds with canal modifications, considering frequency responses and resonance 05 p0712 A71-16279
- Muscle reflex action role in contralateral remote masking at high auditory signal sound pressure levels 08 p1246 A71-20803
- Fan noise random propagation and sound power in cylindrical air ducts from modal spectra and pressure measurements 10 p1596 A71-24834
- Subsonic turbulent boundary layer noise generation and acoustic pressure on aircraft surface, using Lighthill theory 10 p1553 A71-24952
- Structures dynamic loading and damage by sonic booms, discussing structural response prediction by boom pressure wave model 10 p1693 A71-25052
- Condenser microphones aerodynamically induced noise, investigating acoustic pressure lower limit dependence on air flow velocity and turbulence 12 p1888 A71-27063
- Jet fighter-bomber aircraft noise survey, discussing sound pressure levels and frequency analysis during ground running, speech interference levels and ear protectors requirements 12 p1875 A71-27629
- Noise emission and acoustic efficiency in pulsating combustors, considering sound pressure level 13 p2113 A71-28618
- Fan-produced sound pressure fluctuation in very low speed subsonic wind tunnel test stream, noting resulting anemometer calibration errors 14 p2275 A71-30526
- Probability theory of stresses during random vibrations of flat panel in acoustic field of jet engine exhaust 15 p2504 A71-31704

- Error analysis of Corcos hypothesis concerning cross spectra of pseudoacoustic LF turbulent pressure pulsations on flat plate 15 p2389 A71-31708
- Structural panel under acoustic loading by supersonic convected turbulence, deriving responses with finite Fourier transforms 15 p2507 A71-32131
- Frequency and level dependent discrepancy between free field and pressure thresholds at low frequencies due to physiological noise produced under earcap 17 p2681 A71-34699
- Near field noise measurement on quarter-scale model to estimate fuselage pressure in VTOL aircraft for conventional, short and vertical takeoff configurations 19 p2997 A71-37844
- Sound radiation from subsonically rotating annular disk source, calculating far field pressure and efficiency 19 p2997 A71-37845
- Simple source theory of aerodynamic noise, approximating relationship between radiated sound power and jet pressure spectra 19 p3124 A71-38531
- Holographic investigation of acoustical fields, describing shadowgraph recording apparatus for sound pressure amplitude distribution 20 p2332 A71-38811
- Prediction methods for human aircraft noise perception, assessing weighted sound pressure level or complex loudness-noisiness computation scales 21 p3325 A71-40866
- ## SOUND PROPAGATION
- ### NT VOICE
- Sound radiation from finite span airfoil in three dimensional turbulent flow, considering lift function effect 03 p0399 A71-13280
- Molecular gas vibrational and rotational state equations, discussing relaxation times, sound propagation and transport processes 03 p0462 A71-14557
- Sound waves propagation and scattering in moving media, deriving wave equation for acoustical pressure by iterative process 11 p1747 A71-25147
- Transport phenomena in rarefied gases, discussing sound dispersion in helium, weak shock waves, acoustic propagation in monatomic gases and kinetics in alternating fields 12 p1930 A71-27189
- Sound dispersion in monatomic gases from viewpoint of linearized hydrodynamic, Boltzmann and model equations 12 p1930 A71-27190
- Acoustic refraction by two dimensional shear layer in duct, considering sound propagation and initial value problem solution 13 p2051 A71-29248
- Nonlinearity effects on slow variation of small amplitude constant profile periodic sound waves propagating in radiating gas, deriving nonlinear model wave equations 16 p2607 A71-32858
- Noise research facility for fan and multistage compressor sound radiation, discussing anechoic chamber, power drive, test control, recording and real time analysis system 16 p2553 A71-33418
- Sound velocity in real gases as function of pressure and temperature, deriving by van Isterbeek result generalization for higher pressures 17 p2783 A71-35038
- Experimental research at Building Research Station on outdoor sound propagation for building design in relation to aircraft and road traffic noise 17 p2674 A71-35237
- Ultrasound propagation velocity dependence on high pressure and temperature in carbon dioxide, considering Rao rule applicability to highly compressed gases 17 p2784 A71-35506
- Open singing flame from propane-butane and oxygen jet mixture, constructing oscillogram model of sound emission 17 p2839 A71-35696
- Cylindrical powder samples combustion stability, noting gaseous and condensed phase interaction effects on sound emission 17 p2840 A71-35699
- Sound propagation in sheared fluid in duct, determining energy flux from linearized gas dynamic equations 21 p3366 A71-40536
- Frequency, density, thickness and structural factors/stiffness/ influence on sound insulation of uncoated and foil coated absorbers 22 p3575 A71-42401
- Ultrasonic subharmonic waves amplified in standing waves through utilization of propagation medium nonlinearity and cavity reflector induced dispersion 23 p3704 A71-43362

- Spinning acoustic modes transmission and backscatter in nonuniform long cylindrical ducts with throat 24 p3848 A71-44556
- ## SOUND TRANSDUCERS
- ### NT ELECTROACOUSTIC TRANSDUCERS
- ### NT MICROPHONES
- Mechanical transducers for generating and detecting second sound in He isotopes at millidegree temperatures, discussing construction and performance 02 p0250 A71-12135
- Sound field excitation by wedge shaped transducer in liquid filled wedge extension region, determining sound field distribution as function of frequency and wedge angle 20 p3268 A71-38812
- Papers on ultrasonic transducer materials covering magnetostrictive metals and alloys and piezoelectric crystals and ceramics 20 p3236 A71-39253
- Magnetostrictive metals and piezomagnetic ceramics as transducer materials for ultrasonic wave generation, detection and filtration 20 p3236 A71-39254
- Piezoelectric crystals and ceramics for acoustics power detectors and radiators, considering crystal symmetry and coupling factor effect on piezoelectricity 20 p3253 A71-39255
- Multilayer microwave semiconducting film piezoelectric acoustic transducer loss and frequency response derivation from electromechanical power conversion theory 20 p3240 A71-39764
- ## SOUND TRANSMISSION
- Normal incidence sound absorption coefficient by propagating narrow bandwidth sinusoidal pulse and measuring amplitude before and after reflection 05 p0781 A71-16276
- Axial and swirling mean flow effects on sound transmission and generation in hard walled ducts 06 p0945 A71-17620
- Ribbed aluminum panels airborne sound transmission loss, evaluating structural damping effects 08 p1231 A71-21431
- Partition walls sound insulation by porous absorbers, discussing differential equations and acoustic properties 12 p1929 A71-27062
- Beef liver cell nuclei acoustic absorption at various frequencies, determining relation to protein content 12 p1928 A71-27535
- Boundary layer effect on sound transmission in acoustically treated circular duct with shear flow, reducing governing equations to two-point boundary value problem 14 p2224 A71-30199
- Sound passage through rigid screen of arbitrary wave thickness with apertures, using linear algebraic equations 15 p2449 A71-31709
- Soundproofing of air inlets and fan exhausts with reference to absorbent systems with resonant cavities, technologies, environmental conditions and material fatigue 15 p2469 A71-31880
- Acoustic vibrations generation and transmission in nonadiabatic gas containing heat sources, taking into account conductive and radiative heat transfer and momentum loss 16 p2662 A71-33029
- Communication satellite TV and sound broadcasting system design without unreasonable cost 17 p2697 A71-34237
- First heart sound changes, discussing sound vibration and transmission and cardiac function 19 p3000 A71-37232
- Telecommunication developments covering coaxial cables, waveguides, error elimination, information theory, sound transmission and radars 19 p3016 A71-37340
- Kinematic analysis and simulation of transmission modes of sound energy through middle ear 19 p3002 A71-38062
- Acoustic field HF asymptotic characteristics after sound passage through elastic shell, expressing sound fields inside and outside by integro-differential equations system 20 p3268 A71-38810
- Ultrasound absorption in liver tissue due to macromolecular relaxation processes 20 p3191 A71-39770
- Plane sound waves transmission and reflection through finite plates single cascade by Wiener Hopf technique 21 p3437 A71-40537
- Plane acoustic wave transmission problem through finite chord plate array in subsonic gas flow, using factorization method in diffraction theory 21 p3322 A71-40686
- ## SOUND VELOCITY
- ### U ACOUSTIC VELOCITY
- ### SOUND WAVES
- ### NT AERODYNAMIC NOISE
- ### NT AIRCRAFT NOISE

NT ELECTROACOUSTIC WAVES
 NT ENGINE NOISE
 NT JET AIRCRAFT NOISE
 NT LAMB WAVES
 NT NOISE [SOUND]
 NT ROCKET ENGINE NOISE
 NT SONIC BOOMS
 NT THERMAL NOISE
 Artery wall elasticity relation to Korotkoff sound wave frequency by upper arm blood pressure model, using cylindrical rubber tubes and canine specimens 01 p0009 A71-10240
 Nonlinear resonance excitation of ion acoustic plasma waves by weak external electric field, using partial differential equations 01 p0134 A71-11027
 Plane acoustic wave diffraction by dense periodic grating, using crimped surface scattering with Neumann and mixed boundary conditions 01 p0128 A71-11120
 Plane acoustic wave diffraction and acting force on sphere in low viscosity medium, obtaining asymptotic formulas for pressure, velocity and intensity 01 p0128 A71-11123
 Turbulent jet noise estimation taking into account retarded time effect on acoustic radiation 01 p0072 A71-11468
 Weak nonlinear ion-acoustic shock waves in cold ion-warm electrons plasma, using nonlinear perturbation method 02 p0288 A71-11868
 Sound pressure radiation from infinite plate with rigid or pressure release baffles perpendicular to surface, using steepest descent method 02 p0325 A71-11997
 Closed cylindrical shell response to random sound in contained fluid, investigating cylinder end acoustic boundary conditions with coupled oscillator theory 02 p0239 A71-11998
 Warm continuously stratified electron plasma fields behavior in coupling region excited by incident electron-acoustic wave 02 p0293 A71-12742
 Finite amplitude sound interaction with Helmholtz resonator, attributing losses to viscous damping and orifice jet flow kinetic energy dissipation 03 p0456 A71-13279
 Dispersion relation for LF quasi-static ion acoustic waves in finite geometry plasma 03 p0464 A71-13933
 Plane acoustic wave diffraction at thin semiinfinite elastic plate, reducing to Riemann boundary problems for Helmholtz equation in half space 03 p0459 A71-14061
 Linear theory of acoustoelectric oscillator with sandwiched piezoelectric plate accounting for mode enhancement and quenching 04 p0558 A71-15146
 Acoustic plane waves transient interaction with cylindrical elastic shell, using Volterra integral equations 04 p0668 A71-15189
 Ion acoustic waves in streaming ion plasma, discussing wave modes and energy exchange 04 p0634 A71-15258
 Heat transfer in flat plate, considering acoustic resonance vibration effect 04 p0684 A71-15505
 Quantitative acoustic vibration effects on cooldown rate of bodies from room temperature to liquid nitrogen or helium temperature 04 p0686 A71-15525
 Bragg diffracted light intensity increase from standing resonating acoustic wave, considering applicability for laser communication multiplexing and demultiplexing 05 p0720 A71-16269
 Radiatively driven acoustic waves, studying radiative transfer-gas motion interaction under local molecular equilibrium for vibrational rate processes 05 p0836 A71-16532
 Sound wave damping by chemical relaxation, showing dependence on dimensionless reaction heat, equilibrium constant and Damkohler number 05 p0717 A71-16533
 Internal combustion engine exhaust system sound radiation, discussing pressure wave effects, energy flux and boundary conditions 05 p0796 A71-16604
 Nonadiabatic gas acoustic oscillation instability, examining heat release fluctuations 05 p0838 A71-16777
 Acoustic and surface plasma waves in superconducting semiconductor metal films and laminates 05 p0793 A71-16826
 Thermoanemometer frequency characteristic determination, simulating turbulent oscillations by plane acoustic waves 05 p0753 A71-16845
 Rayleigh wave propagation in anisotropic substrates, using light diffraction by surface acoustic waves 05 p0783 A71-17078
 Ion-acoustic waves generation mechanism in outer space by strong electromagnetic radiation, considering

quasars, supernovae shells, pulsars and solar supercorona 05 p0800 A71-17196

Equidistant multiple span rectangular plates vibration and acoustic radiation under random external forces 06 p0994 A71-17823

Shell-fluid interaction problems, considering liquid filled shells oscillations, acoustic shock waves action, body impact against water, etc 06 p0998 A71-17861

Electromagnetic wave trapping by nonlinear resonant interactions involving ion sound wave and two electromagnetic waves in isotropic plasma 06 p0869 A71-17988

Supersonic jet noise problem, discussing eddy-Mach wave radiation source mechanism from nonlinear streamwise development of inviscid instability waves in turbulent mixing layer [AIAA PAPER 71-150] 06 p0884 A71-18592

Plane sound waves incident on flat plate airfoils lattice, obtaining transmitted and reflected pressure amplitudes [AIAA PAPER 71-181] 06 p0885 A71-18620

Whistler indicator generation, relating VLF emissions to iono-acoustic oscillations in magnetosphere 07 p0199 A71-19387

Acoustic radiation spectra from turbulent jets, assuming approximate Gaussian statistics and second order velocity correlation space-time characteristics obtainable from frozen flow 07 p0106 A71-19959

Free nitrogen jets ejected from small orifices, measuring acoustic emission level and spectral pattern dependence on pressure 07 p1161 A71-20058

One dimensional isentropic gas motion in acoustic wave reflection from cylindrical tube nonplane closed end under flow 08 p1276 A71-21478

Magnetic field generation in acoustically turbulent medium, deriving spectral function equation 08 p1341 A71-21795

Nonisothermal plasma ion acoustic oscillations spectral energy density in electromagnetic wave field, calculating HF conductivity and absorption coefficient 09 p1500 A71-22243

Ultrasound propagation velocity dependence on high pressure and temperature in carbon dioxide, considering Rao rule applicability to highly compressed gases 09 p1492 A71-22529

FET transistors on epitaxial GaAs as input and output transducers for acoustic surface waves 09 p1417 A71-22755

Ion acoustic waves propagation and structure measurements with metal electrode technique and continuous channel electron multiplier in plasma wind tunnel 10 p1611 A71-24517

Lift/cruise engine design and thrust vector control influence on VTOL transport aircraft transition characteristics and ground acoustic field [DGLR-70-040] 10 p1556 A71-24749

Thin flexible panel acoustic power radiation due to turbulent boundary layer wall pressure fluctuations excitation 10 p1596 A71-24814

Airfoils accelerating near sound velocity, calculating acoustic radiation by linear theory 10 p1553 A71-24816

Cosmological enhancement of density perturbations and amplitude variation of acoustic and gravitational waves in anisotropic homogeneous universe 10 p1678 A71-24886

Noise reduction by antisound, using directly opposing field with identical wave geometry and reversed phase 10 p1643 A71-24948

Radiative transfer in nongray gas with local molecular and slightly disturbed radiative equilibrium, deriving linearized differential equation with application to radiatively driven acoustic waves 10 p1697 A71-25065

Acoustic and shock waves propagation in quasi-steady supersonic flow in duct with varying cross section 10 p1598 A71-25083

Two dimensional sound wave equation solution in terms of time retarded arguments, deriving analytical expressions for aircraft noise intensity and power 11 p1797 A71-25144

Small amplitude resonant thermal acoustic oscillations of inviscid polytropic gas contained in finite length tube 11 p1798 A71-25446

Sound radiation and wake turbulence spectra from axial compressor single airfoils, including double circular arc profiles [ASME PAPER 71-GT-4] 11 p1703 A71-25950

Aerodynamic noise scattering near Lighthill multiples, considering intense near-field energy conversion into sound waves 11 p1705 A71-26448

Sound radiation from time varying point force in accelerative motion, applying to fan or helicopter rotor noise at subsonic tip speeds 12 p1867 A71-26702

Nonlinear theory of ion-sound plasma turbulence for strong wave-particle interaction near resonance 12 p1935 A71-26915

Nonlinear waves in weakly dispersing media, discussing packet self-focusing and -compression, electromagnetic radiation with acoustic oscillations, geometric optics and HF-LF interactions 12 p1929 A71-27166

Directional acoustic radiation from supersonic jet, discussing generation mechanism theory based on shear layer instability close to nozzle 12 p1945 A71-27221

Topside ionospheric instabilities of electrostatic ion acoustic and ion cyclotron waves to field aligned currents in single and multion plasmas 13 p2054 A71-27917

Ion-acoustic waves generation in outer space by strong electromagnetic radiation, considering quasars, supernovae shells, pulsars and solar supercorona 13 p2128 A71-28251

MHD wave coupling in homogeneous plasma in field dependent on single coordinate, obtaining modified Alfven and acoustic waves stability conditions 13 p2106 A71-28498

MHD waves nonlinear interaction in magnetosphere, calculating transverse Alfven and magnetosonic and longitudinal acoustic wave decay instabilities 13 p2106 A71-28562

Collisionless heat propagation along plasma magnetic field, showing relation to ion sound velocity 13 p2107 A71-28568

Combustion chambers unstable acoustic oscillations, calculating equations for nonlinear growth and decay rate and limiting amplitude 13 p2160 A71-28613

Harmonic pressure generator design based on plane sound waves principle 13 p2071 A71-29293

Acoustic holography for simultaneous three-dimensional image and internal structure insight, discussing applications to submarine exploration and medical diagnostics 13 p2071 A71-29299

German monograph on time dependent gas temperature in decaying plasmas, using frequencies of standing acoustic wave stimulated by pulsed discharges in rarefied gases 13 p2110 A71-29423

High coupling low diffraction loss cut for acoustic surface wave propagation on lithium niobate 14 p2283 A71-29796

Head end secondary flows in solid propellant rocket motor combustion chamber due to transverse acoustic waves in quiescent fluid 14 p2335 A71-29877

Acoustooptic deflector modulation transfer function calculated from autocorrelation theorem 14 p2241 A71-30141

Sonic boom induced indoor acoustical waves, using electrical analog 14 p2274 A71-30200

Acoustic tone radiation from subsonic rotor near potential field by interaction with nonuniform inlet flow based on Lighthill aerodynamic sound equation 14 p2225 A71-30210

Sound radiation and pressure fields inside vibrating turbomachine blades, using miniaturized microphones and compact capacitive detectors 14 p2288 A71-30517

Hot jet aerodynamic parameters from emissions of electromagnetic and acoustic energies by crossed beam IR probing 14 p2288 A71-30520

Ion-acoustic oscillations excitation in rarefied plasma layers confined by external high frequency TE wave electromagnetic field 14 p2281 A71-30555

Acoustic waves reflection from nonplanar closed end of cylindrical tube with one dimensional isentropic gas flow from Riccati differential equation solution 14 p2227 A71-30665

Acoustic wave after passage through turbulent wake, measuring phase fluctuations 15 p2387 A71-31169

One dimensional acoustic tunnel effect for incident wave normal to barrier analogous to macroscopic spin waves and quantum mechanics 15 p2449 A71-31703

Green function or Huygens principle for radiation and diffraction of electromagnetic or acoustic waves in anisotropic media 15 p2449 A71-31869

Pressure and velocity distributions in gas filled cavity undergoing resonant acoustic oscillations due to heat addition 15 p2392 A71-32126

Random time variation in sound radiation far field of point sources in subsonic circular rotational motion 15 p2450 A71-32129

Numerical analysis of far field gain pattern of shielded acoustic antenna by Kirchhoff integral, assuming circular symmetry and perfectly absorbing walls

15 p2372 A71-32193

Acoustical wave generation measurement during iris and retina photocoagulation and ruby laser burns, noting intracocular pressure surge simultaneous with ocular tissue explosion

15 p2365 A71-32346

Airfoils with turbulent boundary layers, calculating acoustic radiation from surface distribution of pressure fluctuations

15 p2347 A71-32520

Acoustic vibrations generation and transmission in nonadiabatic gas containing heat sources, taking into account conductive and radiative heat transfer and momentum loss

16 p2662 A71-33029

Atmospheric space charge and distribution measurement through oscillating electric field modulation by sound waves

16 p2562 A71-33067

Magnetic field generation in acoustically turbulent MHD medium, deriving spectral function equation and eigenvectors

16 p2619 A71-33545

Orbiting satellites VHF radio signal transmissions enhancement, considering focusing effect of electron density contours resulting from gravity or acoustic wave in ionosphere

16 p2543 A71-33817

Ray acoustic treatment, estimating diffusion of radiation patterns due to scattering by random inhomogeneities

17 p2783 A71-35036

Time decrease of acoustically irradiated aerosol concentration involving coagulation processes

17 p2784 A71-35347

Decay instability at ion-sound frequency induced by large amplitude Bernstein mode wave in plasma

18 p2951 A71-35929

Space time structure of acoustic waves propagating in cylindrical duct with weakly absorbing walls and axial inviscid time dependent fluid flow [ONERA-TP-965]

18 p2946 A71-36030

Acoustic radiation of supersonic jet toward nozzle exit section, plotting pressure pulsations vs active/passive pressure ratio

18 p2903 A71-36122

One-dimensional numerical model of nonisothermal plasma, showing soliton separation from leading front by ion-acoustic shock waves after reversal stage

19 p3042 A71-37076

First heart sound changes, discussing sound vibration and transmission and cardiac function

19 p3000 A71-37232

Plasmapause Alfvén, ion-acoustic, electron and ion drift wave modes coupling, calculating instability condition and growth rate

19 p3110 A71-37371

Electromagnetic wave propagation through magnetoplasma disturbed by acoustic wave, calculating transmitted and reflected waves amplitude modulation

19 p3110 A71-37480

Whistler indicator generation, relating VLF emissions to iono-acoustic oscillations in magnetosphere

19 p3052 A71-37812

Sound radiation from subsonically rotating annular disk source, calculating far field pressure and efficiency

19 p2997 A71-37845

Baffled piston source sound radiation impedance from numerical solution of Fredholm integral equation for vibrating disk in finite rigid concentric baffle

19 p3104 A71-37849

Ion acoustic instability in ionosphere in presence of fast particles inhomogeneity, estimating ions and electrons drift velocities

19 p3129 A71-38366

Design considerations for bulk solid state acousto-optic devices in light diffraction and modulation applications

19 p3066 A71-38411

Acoustic or microwave hologram reconstruction into visible three dimensional image in real time

19 p3066 A71-38412

Discrete frequency sound radiation from rotating periodic sources covering rotor blade noise in near field and from disk loading asymmetries

19 p2997 A71-38466

Finite amplitude entropic waves with propagated acoustic radiation-fluid particle motion energy coupling, using thermodynamic J function methods

20 p3315 A71-39772

Shear layers acoustic excitation, considering coupling between sound waves and rotational excited shear waves in flow detachment line

21 p3317 A71-40014

Transversely vibrating hollow cylindrical beam sound radiation and response to acoustic excitation, predicting resonant frequencies [ASME PAPER 71-VIBR-84]

21 p3461 A71-40320

Jet and turbulence mechanism of vascular murmurs associated with stenosis for minimum flow Reynolds numbers, using aorta orifice plates in dogs

21 p3336 A71-40864

Soviet monograph on unsteady motion of compressible fluids covering acoustic and shock wave reflection from solid boundaries, impact penetration and pressure propagation

21 p3369 A71-40869

Nonisothermal turbulent plasma ion acoustic oscillations spectral energy density in electromagnetic wave field, calculating HF conductivity and absorption coefficient

21 p3424 A71-41132

Surface acoustic waves in layered substructure of piezoelectric epitaxial film of cadmium sulfide on germanium substrate

21 p3429 A71-41208

Sound waves interaction in piezoelectric semiconductors under pumping, deriving basic equations for parametric amplification investigation

21 p3430 A71-41216

Cosmological enhancement of density perturbations and amplitude variation of acoustic and gravitational waves in anisotropic homogeneous universe

21 p3453 A71-41251

Sound wave dispersion in metals in inclined magnetic field, noting sound velocity deviation

21 p3417 A71-41265

Sound waves excitation and amplification in weakly ionized plasma within alternating electric field

21 p3425 A71-41282

Acoustic wave detection in K-seeded methane-oxygen flame plasma, using I-V characteristic modulation of fixed electrostatic probe

22 p3580 A71-41622

Phase aberrations in Bragg imaging for sound components projecting out of plane normal to light beam

22 p3540 A71-41778

Optical holographic detection and measurement of ultrasonic waves, providing practical method of investigating LF sound waves

22 p3541 A71-41785

Resonant coupling of two electron plasma waves with ion sound wave at large electron Larmor radii under weak magnetic field

22 p3583 A71-42418

Finite plates coincidence effect occurrence with sound waves, examining backing cavity and incidence angle influence

22 p3576 A71-42538

Nonlinear waves in weakly dispersing media, discussing packet self-focusing and -compression, electromagnetic radiation with acoustic oscillations, geometric optics and HF-LF interactions

22 p3576 A71-42621

Ion acoustic waves dispersion relation, presenting attenuation and phase velocity tables

23 p3667 A71-43138

Three dimensional transient interaction of spherical acoustic waves with cylindrical elastic shell, using integral transform techniques

23 p3775 A71-43207

Acoustic waves transmitted through solid elastic cylinders, calculating wavefront loci and waves amplitudes

23 p3704 A71-43210

Wave phenomena in space chamber rarefied plasma, clarifying spontaneously excited noise wave properties by passive experiment

23 p3710 A71-43365

Sound waves propagation in fully ionized gas, considering electron plasma frequency

23 p3705 A71-44001

SOUNDERS

U SOUNDING

SOUNDING

NT BALLOON SOUNDING

NT IONOSPHERIC SOUNDING

NT ROCKET SOUNDING

Satellite topside sounders oblique echoes, investigating upper hybrid resonance with WKB technique

03 p0420 A71-14531

Soviet monograph on thermal sounding of atmosphere by satellite covering moisture content, cloud surfaces and stratosphere temperatures and thermal radiation distribution

05 p0738 A71-16197

Earth atmosphere thermal sounding problems, considering indirect temperature profile determination, various degrees of cloudiness and Planck function dependence on pressure

07 p1151 A71-18909

Lower atmosphere meteorological parameters remote determination by acoustic sounding, discussing range and resolution characteristics

08 p1330 A71-21743

Lidar soundings of troposphere, investigating multilayer echo structure of haze layers, clouds and rainstorms

17 p2770 A71-34706

SOUNDING ROCKETS

NT AEROBEE ROCKET VEHICLE

NT APACHE ROCKET VEHICLE

NT ASTROBEE ROCKET VEHICLES

NT BLACK BRANT SOUNDING ROCKETS

NT BLACK BRANT 3 SOUNDING ROCKET

NT BLACK BRANT 4 SOUNDING ROCKET

NT KAPPA 9 ROCKET VEHICLE

NT LAMBDA ROCKET VEHICLES

NT SKYLARK ROCKET VEHICLE

Upper atmosphere micrometeorite research with sounding rockets, considering interplanetary particle flux

03 p0485 A71-13250

Sounding rocket-moving target spatial relationship, trajectory modeling by digital simulation, applying to vehicle launching during solar eclipse of March 1970

[AIAA PAPER 70-1374] 03 p0497 A71-13657

Cassiopee attitude control device for sounding rocket impulse trajectory correction, discussing spinning nose cones, corrective algorithm and final impact accuracy

[AIAA PAPER 70-1378] 03 p0498 A71-13661

Sounding rocket dispersion analysis, discussing roll rate errors, earth rotation and wind effects and improved computational techniques

[AIAA PAPER 70-1379] 03 p0498 A71-13662

Unguided, attitude stabilized and velocity controlled sounding rockets impact dispersion, discussing system selection and servomechanism

[AIAA PAPER 70-1381] 03 p0498 A71-13664

Sounding rockets nonlinear aerodynamic characteristics from full scale and supersonic wind tunnel free flight data, using wobble analysis

[AIAA PAPER 70-1383] 03 p0498 A71-13666

Sounding rockets motors with integrally molded plastic case and nozzle, discussing cost effectiveness and demonstration tests

[AIAA PAPER 70-1386] 03 p0470 A71-13669

Wind compensation method for launching sounding rockets susceptible to nonlinear wind effects, using data generated by six degree of freedom trajectory digital simulation program

[AIAA PAPER 70-1390] 03 p0498 A71-13672

Sounding rocket dispersion reduction using optimum wind filter for impact prediction based wind statistics and measurement

[AIAA PAPER 70-1394] 03 p0499 A71-13675

Solar eclipse sounding rocket study of totality path over Wallops Station for 7 March 1970 event, discussing payload launch, ground support equipment, planning, etc

[AIAA PAPER 70-1395] 03 p0397 A71-13676

Sandhawk research sounding rocket performance, aerodynamic and flight characteristics for heavy payload transport to high altitude

[AIAA PAPER 70-1398] 03 p0499 A71-13679

Sounding rockets aerodynamic heating effects approximate prediction methods using computer programs

[AIAA PAPER 70-1399] 03 p0518 A71-13680

Sounding rocket vehicle static stability reduction due to aeroelastic bending, using flight characteristics and wind tunnel test data for computerized analysis

[AIAA PAPER 70-1400] 03 p0499 A71-13681

Stellar Tracking Rocket Attitude Positioning System (STRAP) for sounding rocket payloads three-axis orientation control with accuracy

[AIAA PAPER 70-1402] 03 p0455 A71-13683

Gyro-inertial three axis attitude control systems for sounding rockets, using two degrees of freedom gyro as orientation reference

[AIAA PAPER 70-1405] 03 p0455 A71-13684

Sounding rocket Solar Eclipse Sensor for 7 March 1970 event, discussing mission, capabilities, data acquisition and design

[AIAA PAPER 70-1406] 03 p0455 A71-13685

Churchill research range auroral sounding rocket launcher facility, describing design, construction and performance

[AIAA PAPER 70-1391] 03 p0397 A71-14275

UK space program, discussing international cooperation, sounding rocket development and performance and military communication satellites

05 p0806 A71-16148

Cassiopee attitude control system for sounding rockets using stellar and inertial sensors for orientation and pointing

[AIAA PAPER 70-1404] 05 p0780 A71-16416

Bora-Sond rocket for upper atmosphere low cost sounding, describing propulsion system design and chemistry

[AIAA PAPER 70-1388] 05 p0816 A71-16417

Meteor meteorological rocket flight testing, describing performance, instrumentation and technical and organizational problems

05 p0817 A71-16639

Sea trials with dummy payloads of sounding rocket recovery systems, using parachutes, flotation torus, radio beacons, fluorescent dyes and smoke generators

06 p0881 A71-18674

Sounding rockets and experimental results - Conference, Cardiff, Wales, April 1970

06 p0903 A71-18717

Sounding rocket design parameters optimization, investigating apogee-payload relations, thrust as function of time, total weight, maximum altitude and acceleration

09 p1531 A71-22127

Impact dispersion reduction of uncontrolled sounding rocket ZENIT with CUCKOO booster by canard control, noting flight path angle error by tracking radar 09 p1533 A71-23598

Two stage parachute system RESY for water and land recovery of sounding rocket payloads 09 p1533 A71-23599

Sounding rocket flight accurate trajectory data, determining cost effective radar tracking system 10 p1610 A71-24149

Rocketsonde instrumentation noise separation from stratospheric variability, discussing paired soundings based large scale discrepancies in temperature and wind observations 11 p1794 A71-25386

Vertical geophysical sounding rocket research program and equipment for observing ionospheric parameters, solar UV and X rays, atmospheric absorption and meteorites 11 p1839 A71-26353

Dynamic Test Chamber for sounding rocket or spacecraft functional testing in simulated flight environment 11 p1746 A71-26508

Sounding rockets aerodynamic characteristics, comparing wind tunnel and flight test data 12 p1864 A71-27474

Optimal omnidirectional antenna array located on cylindrical head section of sounding rocket for L band telemetry 14 p2216 A71-31035

Sounding rockets, outlining experimental missions, design and payload varieties, auxiliary systems and electronic equipment 15 p2499 A71-31213

Book on sources and availability of IQSY data, Volume 7, covering stations, sounding rockets, satellites, space probes and World Data Centers catalog 15 p2395 A71-31518

Stratospheric circulation synoptic and detailed structure from meteorological rocket network sensors 15 p2396 A71-31614

Corpuscular flux intensities in upper atmosphere from meteorological rocket measurements in polar arctic region, discussing altitude-time dependence 16 p2627 A71-33777

Life support systems test under weightlessness environment in Nike Tomahawk sounding rockets launched from Wallops Island 16 p2537 A71-33816

Nimbus 3 and 4 satellite observation data comparison with sounding rocket and rawinsondes based on temperature as function of pressure measurements 16 p2572 A71-33846

Polish space research covering satellite tracking, solar physics interplanetary gas dynamics, meteorological rockets and aerospace medicine 16 p2666 A71-33856

ESRO report to COSPAR on sounding rockets and geostationary satellites development, orbits and decay during extraterrestrial gamma radiation 16 p2667 A71-33867

Canadian report to COSPAR on space program and facilities covering scientific satellites, sounding rockets, etc 16 p2667 A71-33868

ESRO sounding rocket program covering atmospheric and ionospheric physics and solar and auroral phenomena 18 p2896 A71-35926

Meteorological rocket nose portion thermal regime, determining housing, insulation coating and compartments temperature 19 p3172 A71-38632

Meteorological rocket nose thermal shield, discussing design and effectiveness 19 p3172 A71-38636

Meteorological research rockets instrument composition and systematization, discussing functional schemes, arrangement and onboard location 19 p3067 A71-38637

Meteorological rocketsonde film mounted thermistor bead temperature sensor, developing mathematical model for thermometric correction formulas in automatic data processing 20 p3236 A71-39208

Woomera /Australia/ meteorological rocket firings, using temperature and wind profiles to assess sensors and parachutes performance 20 p3221 A71-39691

Valentine technique difficulty in testing stationary solution for control optimality, discussing overcoming method for problem of sounding rocket thrust control in vacuo 23 p3773 A71-43856

Ram current effect in sounding rockets for plasma ion density measurement 24 p3822 A71-44793

Single channel electron multiplier applications to sounding rockets, orbital satellites and deep space probes, discussing fatigue effects, ultrahigh vacuum environments and UV and X ray studies 24 p3811 A71-45333

SOURCE PROGRAMS

Computer source code generation for symbolic partial differentiation program for continuous system digital simulation 02 p0226 A71-11778

Computer controlled source data preparation Keycheck system, discussing real-time software support for documents audio/visual error detection 11 p1734 A71-25638

SOUTH AMERICA

Atmospheric turbulence over South America from Lufthansa data, noting occurrence, location, strength and dimensions 14 p2268 A71-29766

SOUTHERN HEMISPHERE

NT ANTARCTIC REGIONS

Geomagnetic activity winter-summer difference in Northern and Southern Hemisphere middle latitudes 08 p1283 A71-21645

Southern Hemisphere general atmospheric circulation data, using constant volume balloons dispersion 11 p1755 A71-25641

Geomagnetic and interplanetary magnetic fields, considering inverse direction of electric currents in Northern and Southern Hemispheres 11 p1757 A71-25776

Sensible heat meridional transport frequency spectra wavenumber in Southern Hemisphere midtroposphere 13 p2063 A71-29108

Angular momentum meridional transport flux wave number-frequency spectral characteristics in mid-troposphere of Southern Hemisphere 13 p2063 A71-29109

Conjugate and closely-spaced riometer observations of auroral radio absorption, considering explanation by alternation of particle precipitation between Northern and Southern Hemispheres 14 p2192 A71-29667

Mesospheric height-temperature measurements in noctilucent cloud zone of Southern Hemisphere 14 p2232 A71-29958

Southern Hemisphere stratosphere and mesosphere meteorological parameters seasonal variation, comparing rocket sounding data with standard models 15 p2400 A71-31968

Neutral lower thermosphere density variations at high and middle latitude in Southern Hemisphere from OVI-15 /SPADES/ satellite accelerometer measurements 16 p2570 A71-33824

Galactic weak X ray sources observation in Southern Hemisphere for flux and energy spectrum 17 p2796 A71-35408

Southern Hemisphere extended operational meteorological prediction using six level primitive equation model 20 p3256 A71-39202

Atmospheric temperature and water vapor profile calculation from Nimbus satellite IR spectrometer data, noting Southern Hemisphere tropospheric and stratospheric pressure analyses 20 p3258 A71-39667

Four-color and H beta photometric data tabulation for bright B type stars in Southern Hemisphere 21 p3443 A71-40192

Geomagnetic and interplanetary magnetic fields, considering inverse direction of electric currents in Northern and Southern Hemispheres 22 p3532 A71-41544

SOVEREIGNTY

Air and cosmic space common law, discussing boundaries, sovereignty over state territories and jurisprudence related to travel development 11 p1861 A71-26325

SOYBEANS

Chlorella ration effect on internal organs of protein-deficient mice compared with casein and soybean rations 01 p0025 A71-11145

In vivo green soybean and corn leaves bidirectional IR reflection and transmission distribution functions 05 p0739 A71-16253

SOYUZ SPACECRAFT

Soyuz 4 and 5 self contained cosmonaut life support system for extravehicular activity, discussing principal components block diagram 01 p0025 A71-11141

Biomedical experiments and man machine relationship on Soyuz 9 record endurance flight 01 p0164 A71-11457

Soyuz spacecraft command cabin equipment, describing control panel, command signal systems and routine operations 03 p0497 A71-13196

Soyuz 9 scientific and technical experiments during prolonged orbital flight, discussing day and night horizon 03 p0495 A71-14391

Soyuz 9 prolonged space flight biomedical effects on human organism, emphasizing weightlessness 03 p0365 A71-14392

Soyuz 9 flight manned biomedical mission, evaluating 18 day exposure effect on human physiology and work capacity 08 p1246 A71-20820

Soyuz 9 spacecraft crew medical support and post-flight examination, discussing earth environment readaptation 09 p1397 A71-22197

Soyuz 9 cosmonauts physiological monitoring instrumentation and procedures, describing bioinstrumentation harness for data telemetry 09 p1397 A71-22198

Soyuz 9 cosmonauts medical monitoring, discussing physiological changes, vagotonic reactions and work capacity 09 p1389 A71-22199

Soyuz 9 cosmonauts postflight clinical examination, noting muscle pain, eyelid edema, leg muscle atrophy, etc 09 p1389 A71-22200

Soyuz 9 spacecraft crew food diet description including products and packaging 09 p1397 A71-22205

Soyuz 9 spacecraft astronauts space flight effect on digestive system enzyme secretion function based on pre- and post-flight examinations 09 p1389 A71-22206

Soyuz 9 spacecraft astronauts otorhinolaryngological organs response to 18-day orbital flight, observing pathological changes from clinical post flight examination 09 p1389 A71-22207

Soyuz 9 spacecraft astronauts cardiovascular and respiratory systems responses to orthostatic effect after 18-day orbital flight from EKG measurements and sphygmography 09 p1389 A71-22208

Soyuz 9 spacecraft simulator prolonged confinement effect on human cardiovascular system functional state 09 p1390 A71-22209

Postflight metabolism and renal function of Soyuz 6, 7 and 8 crewmembers, associating weight loss during flight with water and salt discharges 13 p2006 A71-28409

Cosmic radiation doses measurement on Soyuz 3 spacecraft by nuclear emulsions, giving averaged doses absorbed by various cosmonaut tissues 15 p2362 A71-31314

Soviet report to COSPAR on upper atmosphere and cosmic space including Soyuz spacecraft, lunar soil sample recovery and surface vehicle delivery 16 p2666 A71-33865

Saliut 1/Soyuz 10 mission, discussing configuration, size orbits and docking procedure 18 p2975 A71-36685

Soyuz 9 cosmonaut meteorological experiments, observations and atmospheric formations photographs 18 p2944 A71-36686

Salyut space station design, operation and mission, describing docking and undocking procedures for Soyuz 11 supply craft 19 p3153 A71-38148

Altitude variation of atmospheric air scattering coefficient from Soyuz 3 spacecraft measurements, considering aerosol stratification 20 p3259 A71-39676

Astronaut work capacity and adaptation during long term flight of space vehicle Soyuz 9 21 p3342 A71-40259

Radiation protection of Soyuz-9 crew, using solar activity forecasts 24 p3800 A71-44531

SPACE BASES

Space base biomedical center based on Integrated Medical and Behavioral Laboratory Measurement System /IMBLMS/ concept 04 p0546 A71-15280

Nuclear radiation shielding design for space base SNAP 8 reactor, discussing geometry constraints for lithium hydride and U loop layers model 09 p1492 A71-22808

In-core thermionic reactor flight system for space base applications, providing electric power and thermal shielding 11 p1710 A71-25870

Conceptual design of nuclear thermionic power plant for Space Base application, discussing plant efficiency, radiator area requirements, launch weight and shielding 11 p1710 A71-25871

Space base 100 kw thermionic reactor power plant featuring interchange core replacement package 11 p1713 A71-25895

Dynamic seal development for space base rotating hubs, describing simulated environmental tests for elastomer inflatable seals and lubricants evaluation [ALAA PAPER 71-863] 18 p2927 A71-36651

Safe disposal for nuclear zirconium hydride reactors for manned space base mission 20 p3263 A71-38921

SPACE BIOLOGY

U EXOBIOLOGY

SPACE CAPSULES

NT ESCAPE CAPSULES

Space capsule reentry into Martian atmosphere for soft landing, using onboard nonlinear filter and stochastic control for random wind gusts
03 p0500 A71-14479

SPACE CHARGE

Computer analysis of microwave circuit parameters effects on limited space charge accumulation oscillation in CW transferred electron devices
01 p0055 A71-11169

Tungsten cathode current partitioning in dense Ar plasma, noting electron emitter work function reduction due to ion space charge field
02 p0289 A71-11940

Space charge problem for thermionic converter emitter sheath for electrons and ions with half-Maxwellian distribution
02 p0291 A71-12234

Atmospheric electrical properties derivation from continuity equation, considering ion concentration, conductivity, space charge density and electric field
03 p0409 A71-13610

Space charge hypersurface layer conductance in semiconductors, allowing for three dimensional surface impurity fields
03 p0467 A71-13976

Field aligned currents and high potential drop space charge regions above aurora associated with electron acceleration
03 p0419 A71-14525

Flow patterns modification through space charges, demonstrating laminarization of turbulent flow and boundary layer separation prevention
04 p0569 A71-14985

Rotating electron beam cyclotron and space charge waves interaction with fast electromagnetic waves
05 p0719 A71-16002

Field effect transistors with nonuniform doping profiles along channel, calculating carrier accumulation and space charge limited current flow by two dimensional model analysis
05 p0791 A71-16166

Collective longitudinal space charge waves in trapped relativistic one dimensional plasma, calculating inhibition/enhancement of cosmic ray Fermi acceleration
05 p0791 A71-16940

Space charge effects on fog precipitation, taking droplet size into account
05 p0779 A71-17141

Surface illuminated semiconductor excess current carriers nonstationary distribution and space charge, solving equation system by operational technique
06 p0942 A71-18185

Large signal oscillation mode model for GaAs devices operational prediction, including space charge and intervalley transfer time effects
07 p1070 A71-18867

Silicon dioxide space charge distribution dependence on photoinjected currents in MOS structures, showing charge effects on I-V characteristics
07 p1174 A71-19055

Ion source emitter plasma column generated by electron beam injection through gas filled chamber, compensating ion space charge with fast discharge electrons
07 p1170 A71-20180

Limited space charge accumulation layer devices operating characteristics, using GaAs devices with uniform doping for microwave peak power
08 p1266 A71-21624

Transferred electron bulk negative differential conductivity devices, analyzing combined doping and geometry effects on space charge and domain dynamics
09 p1507 A71-22250

Space charge sign distribution sounding in atmosphere by electrode potential difference measurement
09 p1437 A71-22677

Atmospheric electrical effects due to aurora, discussing negative space charge, bremsstrahlung flux and electrojet plasma instability
10 p1604 A71-24703

Microwave devices with transmission lines excited by curvilinear electron beams, deriving dispersion equations for TWT with allowance for space charge effect
10 p1584 A71-24717

Quasi-linear theory of inhomogeneities generation in equatorial jet, considering space charge waves excitation by electric current perpendicular to geomagnetic field
11 p1757 A71-25772

Linear and nonlinear laser induced ion emission from solid targets with and without magnetic field, considering electron space charge accelerator
11 p1775 A71-26085

Electrical screening layers around charged clouds, giving numerical model for space charge accumulation, electric field distribution and forces acting on cloud droplets
12 p1925 A71-27290

Electron electrostatic or space charge oscillations in nonneutral plasma columns with cylindrical symmetry around axial magnetic field
13 p2104 A71-27848

Low temperature space charge mechanism of threshold switching, using pulse measurements on thin layer multicomponent chalcogenide glasses
13 p2110 A71-28044

Dispersion and boundary equation concerning space-charge wave propagation under diffusion effect in Gunn semiconductors with anisotropic conductivity and finite thickness
14 p2283 A71-29793

Space charge delay angle, RF induced current and mode instability interrelated for actual high power heavy duty magnetrons, using electron bunch model
14 p2211 A71-29831

Thermal noise in space charge limited solid state diodes with field dependent mobility and hot carriers
14 p2284 A71-30502

Epitaxial film thickness and resistivity effect on transistor cut-off frequency, discussing collector junction space charge region boundary location
14 p2213 A71-30626

Atmospheric space charge and distribution measurement through oscillating electric field modulation by sound waves
16 p2562 A71-33067

Poisson equation for space charge layer of reverse-biased p-n junction in p-n-p-n structure with allowance for two types of moving current carriers
16 p2546 A71-33495

Plane diode electrode gap differential capacitance for operation with anode negative voltage, current saturation and space charge limitation
16 p2548 A71-33709

Selenium photocell photo voltaic effect, observing recombination and generation processes in space charge region
16 p2623 A71-34046

He ion beam space charge neutralization by thermal electrons injection
17 p2784 A71-34200

Moving plasma beam capture by transverse magnetic field due to polarization space charges electrostatic separation
17 p2786 A71-34280

German monograph on electron production effect on channel breakdown in nitrogen, showing positive space charge accumulation near anode in gas discharge
17 p2788 A71-34775

Noise, admittance and I-V characteristics of hot holes in space charge limited Ge diodes at high voltage and frequencies to 22 MHz
19 p3029 A71-38141

High peak power microwave oscillators, discussing pulsed limited space charge accumulation and TRAPATT diodes pulsed radiation sources performance
19 p3029 A71-38294

Soviet book on cloud electricity covering space charge and electrical characteristics
19 p3091 A71-38533

Thermal motion effects on space charge waves propagation along plasma columns in weak magnetic field, comparing measured wavelength/frequency relationship with theoretical prediction
20 p3273 A71-38879

Semiconductor surface layer noise generation physical model with allowance for relaxation effects due to traps in space charge region
21 p3432 A71-41301

Photocurrent for two stage transition in space charge layer in p-n junctions of germanium with radiation defects
21 p3435 A71-41333

Quasi-linear theory of inhomogeneities generation in equatorial jet, considering space charge waves excitation by electric current perpendicular to geomagnetic field
22 p3532 A71-41540

Rotating electron beam cyclotron and space charge waves interaction with fast electromagnetic waves
22 p3515 A71-42751

GaAs LSA mode V band oscillator CW and pulsed operations power and efficiency limitations
23 p3649 A71-42915

Space charge density and carrier mobility in disordered regions of p-n microjunctions
23 p3717 A71-43486

Adhesion, recombination and electron-band curvature nomograms for space charge region in photosensitive CdS single crystals
24 p3859 A71-44388

SPACE COMMUNICATION

NT INTERPLANETARY COMMUNICATION

NT LUNAR COMMUNICATION

NT REENTRY COMMUNICATION

NT SPACECRAFT COMMUNICATION

Optical communications for terrestrial and space applications, assessing state of art of optics devices, systems and theory
02 p0212 A71-12001

Optical components and technology for acquisition, tracking, transmit-beam offset and background noise discrimination functions in optical space communications
02 p0213 A71-12007

Free space optical channel analog and digital communication theory, considering SNR, M-ary signaling, error probabilities and information rates, etc
02 p0213 A71-12018

Antenna gain of Space Communications and Tracking terminal from feedhorn radiation pattern and reflector geometry
02 p0219 A71-12448

INTELSAT IV earth stations communications standards, discussing receiver gain-noise temperature ratio, feed polarization, radiation power and control transmission modes, etc
02 p0221 A71-12777

Satellite operating conditions effects on INTELSAT IV earth station design, emphasizing communications aspects
02 p0221 A71-12777

Space communication reflector surface positioning and optical measuring techniques for best fit
02 p0234 A71-12809

Carbon dioxide lasers for wideband data transmission in space
04 p0556 A71-15648

Flexible telemetry systems for space flight applications, considering component exchangeability and electric connections variability by mechanical and electronic means
05 p0718 A71-15959

Radio spectrum use in space communications for satellite services, considering antenna design, modulation techniques and wave attenuation
09 p1406 A71-22871

German space radio monitoring service, describing facilities for receiving and evaluating 20 MHz to 1 GHz transmissions
09 p1407 A71-23046

Computerized finite element techniques for stress and structural analysis for space communication and radar applications
10 p1684 A71-23756

SIRIO project mission analysis, discussing space communication and magnetospheric investigations by scientific satellite in geostationary orbit
10 p1670 A71-24268

French space telecommunication policy report, noting European, autonomous and educational options
11 p1861 A71-26522

Space communications antennas main reflecting surface accuracy determination by statistical evaluation of efficiency degradation due to mechanical inaccuracies and structural flexibility
12 p1887 A71-27003

Binary, uncoded and M-ary FSK with convolutional codes for low powered planetary entry probes communicating to earth
14 p2200 A71-30921

Marconi 90 ft space communication antennas and waveguide components, using feed horn radiation patterns to compute gain
15 p2374 A71-31141

Deep Space Communications System low noise microwave receiver, discussing operating noise temperature calibration, error analysis and programming
15 p2372 A71-32311

International space telecommunication systems, emphasizing legal aspects of operation
16 p2665 A71-33585

Launch vehicles for space telecommunications applications, considering payload capacity for missions involving earth resources, radio and visual astronomy and meteorology
17 p2811 A71-34226

Space radio communications, considering radio links reliability between multistage launcher rocket and ground stations
17 p2696 A71-34228

Space research system telecommunications, considering telemetry, tracking and telecommand systems
17 p2696 A71-34229

Satellite communication application to maritime mobile service and position determination, discussing VHF and UHF space and shipborne equipment and modulation systems
17 p2697 A71-34241

International radio regulations adopted by Geneva space conference with reference to frequency band allocations in 1-10 GHz range with equal rights to space and terrestrial services
17 p2697 A71-34246

Legal problems in space telecommunications, discussing UN and international nongovernmental organizations solutions for interference protection, pirate space stations and spacecraft distress or emergency
17 p2841 A71-34247

UN leadership in space communications international cooperation, emphasizing communication satellite systems application to educational TV
17 p2841 A71-34249

Global broadcasting from space, suggesting international cooperation and UN role
17 p2841 A71-34250

International cooperation in space radio science, considering real time telemetry application via Solrad, Tiros and Alouette satellites
17 p2697 A71-34252

Soviet book on space radio telemetry systems characteristics, design, requirements and operation conditions covering noise stability, reliability and redundant codes
17 p2699 A71-34521

Space radio communication - Conference, Paris, March 1971
17 p2699 A71-34676

Wideband Cassegrain microwave antenna for space communication, discussing reflecting horn for maximum radiation gain
17 p2715 A71-34686

Electrical performance of Cassegrain antenna reflector for space communication via ATS and deep space research
17 p2700 A71-34747

Nonlinear gain and AM/PM conversion in FDMA communication through satellite repeater, using traveling wave tubes plus postzonal filter
17 p2703 A71-35082

Short pulse Nd-YAG direct detection laser system for space communications, noting RF links complementation, high data rates, practical size, weight and power requirements
17 p2705 A71-35093

Aerospace data bus for multiplexed transmission within vehicles, considering control and sequencing methods terminal concepts, capability noise reduction and reliability
17 p2712 A71-35785

East-West cooperation in space telecommunications, outlining Intelsat and Intersputnik organizational structure
18 p2987 A71-36167

Space communication - Conference, Paris, March-April 1971, Volumes 1 and 2
18 p2876 A71-36501

Gridistor microwave FET for space communication equipment, combining advantages of FET and bipolar transistors
18 p2892 A71-36565

IR CdTe-HgTe detectors for laser space communications at 10.6 microns, using directivity of light waves in vacuo for wideband transmission
18 p2892 A71-36566

Error occurrence due to perturbations in space communication channels for digital data transmission, describing binary channels models based on Markov chains
18 p2881 A71-36567

Spacecraft conical antenna design for planetary communications, investigating impact on other subsystems
[AAS PAPER 71-151] 19 p3018 A71-37953

Beam pointing and tracking requirements for optical space communication system, from energy transfer considerations
19 p3018 A71-38235

RF noise surveys in urban areas for effective space to earth communication link design at UHF
19 p3021 A71-38443

Space communications period forecasting algorithm for limited power ground based transmitters and spacecraft in earth orbit
19 p3022 A71-38502

Breadboard simulation model of laser space communications system consisting of carbon dioxide laser, transmitter telescope, GaAs phase modulator and attenuator
20 p3196 A71-39116

Tabular listing of frequency allocations for space services and radio astronomy made at Extraordinary Administrative Radio Conference
21 p3348 A71-40476

Short-pulse high-rate space digital laser communication components technology, discussing mode locked and frequency doubled Nd-YAG laser source
21 p3348 A71-40806

SPACE DEBRIS

Dynamics and thermodynamics of water and oxygen particles ejected into space by Apollo during translunar flight, using ground based photographic observations
[AIAA PAPER 71-474] 11 p1833 A71-26254

Docking with passive orbiting spinning or tumbling objects for space debris elimination and space rescue operations, describing remotely controlled despinning and retrieval methods
22 p3610 A71-42005

Satellites explosion debris distribution and orbital characteristics as data base for earth force field and geopotential resonance phenomena analysis
[AAS PAPER 71-351] 23 p3728 A71-43023

SPACE DENSITY

Expanding universe adiabatic density fluctuation evolution, describing photon distribution function collision equation for plasma recombination
05 p0801 A71-15929

Spiral arms formation on galactic scale in terms of density waves produced by gravitational perturbations
11 p1832 A71-26184

Statistical analysis of gravitational instability for isotropic cosmological models, examining density perturbations as random functions of coordinates and comparing with galactic mass statistics
12 p1965 A71-27178

Optical luminosity function and space density of quasars from 4C and Parker survey, assuming cosmological red shifts
12 p1966 A71-27233

Statistical space density and velocity perturbations of galaxies relative to origin of rotation in range of Friedman cosmological model
12 p1966 A71-27235

Galactic spirals density wave theory based on three models rotation curve patterns observation
14 p2314 A71-30639

Interstellar clouds internal structure investigation by photographic photometry, determining maximum density
21 p3451 A71-40718

Spiral wave dispersion, wave number and amplitude relationship in Galaxy near inner Lindblad resonance, noting correlation with ionized hydrogen density
21 p3451 A71-40855

Intergalactic dust density limits using absorption magnitude and red shift of distant galaxies
22 p3599 A71-41924

Mean ratio of mass to three-halves power of luminosity for elliptical and lenticular galaxies based on catalog mass data emphasizing uncertainties
22 p3599 A71-41935

Three body problem involving large mass ratio by backward numerical integration in constant density resisting medium
22 p3601 A71-42164

Dynamic model for Saturn rings radial structure, considering outside composition material, Titan perturbation effect and particle space density
22 p3603 A71-42186

Statistical analysis of gravitational instability for isotropic cosmological models, examining density perturbations as random functions of coordinates and comparing with galactic mass statistics
22 p3605 A71-42452

Stellar density function outside symmetry plane of galactic phase-space model
24 p3868 A71-44461

SPACE DETECTION AND TRACKING SYSTEM

ERTS telecommunication system for space tracking and high resolution multispectral image data acquisition and commanding
14 p2199 A71-30912

Space research system telecommunications, considering telemetry, tracking and telecommand systems
17 p2696 A71-34229

SPACE ELECTRIC ROCKET TESTS

SERT II electron bombardment thruster operation with Ar and Hg propellants
[AIAA PAPER 71-157] 06 p0947 A71-18599

SPACE ENVIRONMENT

U AEROSPACE ENVIRONMENTS

SPACE ENVIRONMENT SIMULATION

NT WEIGHTLESSNESS SIMULATION

Particulate silicates IR emission spectra under simulated lunar conditions, noting existence of nearly optimum conditions on moon surface
02 p0305 A71-11987

Electro-optical solar simulator, describing system design, performance and applications for spacecraft testing
04 p0567 A71-15366

CdS solar cells performance under simulated synchronous orbit conditions, describing test equipment
05 p0702 A71-16081

Si solar cells electron spectrum irradiation, simulating space environment synchronous altitude trapped electrons omnidirectional and flux/energy characteristics
05 p0702 A71-16083

Space environment simulation chamber shrouds, developing mathematical expressions for temperature distributions in flat plates and trapezoidal fins
05 p0733 A71-16137

OAQ simulation system including prototype spacecraft and digital computer for verifying ground system performance
05 p0734 A71-17131

Electron-proton radiation effects on scintillating materials in space environment chamber, evaluating background light degradation of active source monitoring
07 p1175 A71-19066

Soyuz 9 spacecraft simulator prolonged confinement effect on human cardiovascular system functional state
09 p1390 A71-22209

Free molecular flow on cryosurface in cylindrical space simulation chamber with spherical test object
09 p1433 A71-23005

Molecular flux distributions and capture by cryopanel in space simulation chamber using homogeneously emitting spherical gas source
09 p1428 A71-23006

Solar wind simulation for interaction with lunar magnetic field, discussing particle shadowing effects generation of electric fields
09 p1514 A71-23310

ESRO 1 satellites space simulation chamber tests for residual gas effects, measuring spacecraft outgassing rate
09 p1533 A71-23732

Periodic rotation reversal effect on hollow cylinder surface temperature distribution in space simulation testing of spin stabilized orbiting satellites
09 p1430 A71-23733

Thermal louver models in space simulation chambers, determining heat dissipation, optical efficiencies, blade geometry and solar radiation effects
11 p1854 A71-25191

Hydrogen plasma simulation of solar wind-planetary body interaction, showing electric fields behind moon and Venus
11 p1816 A71-25755

Apollo command module guidance computer and environment hybrid simulation for flight software and crew procedures verification
11 p1744 A71-25845

Dynamic Test Chamber for sounding rocket or spacecraft functional testing in simulated flight environment
11 p1746 A71-26508

Thermal/vacuum space simulation assembly level testing for prelaunch confidence of Mariner spacecraft
12 p1893 A71-26680

Solar simulator with wide range irradiation strength variability for laboratory investigation of radiation effects on spacecraft components
12 p1894 A71-26982

Multiple circumferential heat pipes construction and tests for spacecraft thermal control, using simulated space environment
12 p1972 A71-27408

Space simulation - Conference, Gaithersburg, Maryland, September 1970
13 p2044 A71-28302

Spacecraft propane boiler system, obtaining heat transfer behavior under simulated aerospace conditions
14 p2319 A71-29726

In-flight UV spectrometric measurements of simulated Jupiter atmosphere, using sunlit gas mixture released from Mariner spacecraft in interplanetary space
14 p2308 A71-29914

Man and equipment instrumentation in simulated space environment, considering training and interface of man and life support systems
14 p2188 A71-30312

Human performance in various locomotive tasks under simulated lunar reduced gravity conditions, classifying test stands and equipment
15 p2362 A71-31304

Erythrocytes life span and bone marrow production in dogs subjected to gamma irradiation in doses simulating prolonged space flight conditions
15 p2356 A71-31307

Chronic and acute gamma irradiation facilities used in animal experiments simulating steady cosmic radiation and powerful solar flare radiation expected in prolonged space flight
15 p2357 A71-31313

Ion cyclotron harmonic waves development in simulated low density and temperature space plasma, determining propagation upper and lower bounds
15 p2491 A71-32448

Laboratory simulation of satellite motion in ionospheric plasma, specifying maximum current density, electron velocity distribution and temperature range
[AIAA PAPER 71-608] 15 p2385 A71-32545

Molecular incidence rate and emission over surface of cold wall and spherical test object in cylindrical space simulation chamber
15 p2393 A71-32703

Ninety day manned test of regenerative life support system in space station simulator, presenting operational and maintenance data
[ASME PAPER 71-AV-3] 18 p2865 A71-36370

Waste management subsystem for 90-day space station simulator test of regenerative life support system
[ASME PAPER 71-AV-7] 18 p2865 A71-36374

High enthalpy plasma jet wind tunnels, considering arc heaters and simulation range extension to higher adiabatic static pressures to avoid nonequilibrium expansion in nozzle
18 p2898 A71-36413

Orbital cargo transfer simulation techniques involving zero-g aircraft and water immersion
18 p2899 A71-36469

Gross locomotion and cargo handling in simulated artificial gravity environments, studying effects of Coriolis forces, angular accelerations, oculo-vestibular stimuli and traction variations
[AIAA PAPER 71-886] 18 p2871 A71-36636

Impact and explosive craters production in same target material under controlled laboratory conditions, determining depth of burst simulating impingement
19 p3156 A71-37682

Multiple channel fringe counting interferometer for remote monitoring of large diameter microwave antenna under test in simulated solar thermal and vacuum environment 20 p3235 A71-39186

Living organisms life-sustaining possibility under simulated Martian temperature, humidity and atmospheric composition conditions, emphasizing unicellular organisms radiation resistance 21 p3334 A71-40572

Space environment simulation for ultrahigh vacuum effects on crystalline enzymes activity, measuring by chemiluminescence techniques 21 p3334 A71-40573

Wave phenomena in space chamber rarefied plasma, clarifying spontaneously excited noise wave properties by passive experiment 23 p3710 A71-43365

Plasma current driven sheet at neutral point of cusp and quadrupole magnetic field for space physical simulation of solar flare and geomagnetic tail 23 p3714 A71-44277

SPACE ENVIRONMENTAL LUBRICATION

U SPACECRAFT LUBRICATION

SPACE ERECTABLE STRUCTURES

NT BEACON SATELLITES

NT EXPLORER 22 SATELLITE

Silicon solar cell lightweight integrated array for large arrays, discussing deployment and orientation mechanisms, ribbon coverglass technique and cost estimates 05 p0703 A71-16093

Full scale models, nonflammable materials and tests for manned space expandable structures including airlocks, transfer tunnels, station modules, lunar shelters and flexible windows [AIAA PAPER 71-399] 11 p1744 A71-25275

Large space structures zero backlash deployment mechanism, discussing dynamically scaled model for mechanical and structural design and dynamic analysis [AIAA PAPER 71-400] 11 p1836 A71-25276

Stowable extendible structures for spacecraft and space experiments, discussing inflatable, rigidized cloth and mechanically deployable apparatus 22 p3609 A71-41981

SPACE EXPLORATION

NT VIKING MARS PROGRAM

European governmental and industrial roles in space programs, discussing cost efficiency requirements 01 p0183 A71-10265

Solar system exploration, discussing planets characteristics, trajectory utilization, grand tours, etc 01 p0151 A71-10269

Dry heat spacecraft sterilization-compatibility tests of reagents and growth media for planetary biological exploration 01 p0027 A71-11563

Solar electric propulsion (SEP) for automated planetary missions, discussing system characteristics, capabilities and costs [AIAA PAPER 69-1103] 03 p0500 A71-14426

Planetary and interplanetary exploration missions, discussing U.S. planetary space program budgets and costs 04 p0657 A71-15818

Optimal space experiments selection for satellites and space probes, discussing criteria and techniques for guidance in program management decision making 05 p0816 A71-16138

Book on geochemical exploration of moon and planets covering orbital, compositional and surface studies, Apollo missions, Lunar Receiving Laboratories and data processing 05 p0813 A71-16950

Heat sterilizable separator material for development of heat sterilizable Ag-Zn batteries meeting contamination requirements in interplanetary exploration 08 p1235 A71-21095

Composite rocket cum hypersonic airbreathing propulsion reducing space exploration program cost 08 p1348 A71-21301

N-channel PSK/PM digital telemetry system modulation scheme for space exploration 08 p1254 A71-21315

Mass spectroscopy applications to neutral and ionized terrestrial upper atmosphere, lunar atmosphere and space research 11 p1726 A71-25218

Spectroscopic search for water on Mars during 1963-1970, summarizing conclusions concerning quantity and variations with location, season and from year to year 11 p1826 A71-25715

Soviet book on earth radiation belts and cosmic rays covering space-borne experiments, Van Allen belt, charged particle motion, origin hypotheses, etc 11 p1818 A71-26525

Solar system space physics review covering earth atmospheric temperature, density and models, solar wind, auroras, and moon, Venus and Mars data from space missions 13 p2131 A71-27877

Space flight, discussing stellar trips, propulsion systems and planetary exploration 13 p2145 A71-29130

Planetary exploration from space, recommending flights to moons of outer planets due to possible presence of atmospheres and water ice 15 p2494 A71-32495

German book on models and constructions for interplanetary space flights covering Helios project, grand tour, Mars landing, planetary exploration, etc 16 p2645 A71-33523

Outer space legal survey and prospects, emphasizing UN resolutions for international law and space exploration problems 16 p2665 A71-33586

International space exploration management and organization, emphasizing NASA cooperative programs 16 p2665 A71-33587

Man-teleoperator-robot teams for space exploration facilities construction and operation, discussing lunar programs [AIAA PAPER 71-823] 17 p2723 A71-34722

Exploration, science and applications goals of U.S. space effort 19 p3131 A71-37326

Nuclear rocket propulsion for human post-Apollo space programs, including Mars exploration 19 p3131 A71-37328

Balanced terrestrial and outer planets NASA solar system exploration strategy for 1970s, outlining earth based observations and flight missions program [AAS PAPER 71-100] 19 p3140 A71-37930

Scientific unmanned exploration of near stellar systems, discussing target star selection, extraterrestrial life, propulsion systems and kinematic and energy requirements 19 p3141 A71-37963

Space research - COSPAR Conference, Leningrad, May 1970 20 p3219 A71-39612

NASA program for lunar and planetary exploration, listing missions, instrumentation, experiments and future aims 23 p3736 A71-43498

SPACE FLIGHT

NT APOLLO FLIGHTS

NT APOLLO 7 FLIGHT

NT APOLLO 8 FLIGHT

NT APOLLO 9 FLIGHT

NT APOLLO 11 FLIGHT

NT APOLLO 12 FLIGHT

NT APOLLO 13 FLIGHT

NT APOLLO 14 FLIGHT

NT APOLLO 15 FLIGHT

NT GEMINI 4 FLIGHT

NT GEMINI 10 FLIGHT

NT HYPERBOLIC REENTRY

NT HYPERSONIC REENTRY

NT INTERPLANETARY FLIGHT

NT INTERSTELLAR TRAVEL

NT LUNAR FLIGHT

NT MANNED SPACE FLIGHT

NT RETURN TO EARTH SPACE FLIGHT

NT SPACECRAFT REENTRY

NT VIKING MARS PROGRAM

Space aerodynamics, examining reentry, flow ranges, pressure field visualization and real gas and rarefaction effects 01 p0162 A71-11450

Space flight biological effects on parasitic wasp *Habrobracon*, investigating genetic, mutational, biochemical, behavioral and physiological parameters 01 p0019 A71-11553

Space flight effects on survival, mutation and cell development of *Chlorella* cells suspensions onboard Zond 5 spacecraft 01 p0019 A71-11554

Soviet book on radio measurement methods and mathematical data processing in space trajectory measurements 04 p0555 A71-15375

German yearbook on air and space flight covering mechanics, control, aerodynamics and test facilities 06 p0847 A71-18044

Biological radioprotectants in space flights including amino acids, bacterial polysaccharides, hormones and vitamins 06 p0861 A71-18358

Soviet book on space flight mechanics covering vehicle motion, engine systems, gravitational fields and trajectories 08 p1361 A71-21050

Space flight biological effects on lysogenic bacteria and human cells in culture 12 p1872 A71-26641

Astronautics progress review from earliest space flights to present, discussing stabilization, recovery, ballistic reentry and latitude determination 16 p2634 A71-33396

Space flight aerodynamic problems and wind tunnel simulation, considering satellites, maneuverability for landing and synergetic orbit rotation, hypersonic problems of reentry, etc 18 p2846 A71-36408

ALOFT computer language for checkout and operation of complex space oriented equipment such as space shuttle 18 p2885 A71-36446

TOTAL checkout computer language for future space vehicles, considering objectives, characteristics and merits 18 p2885 A71-36447

Clock paradox problem resolution in relativity theory, considering space travel effects on time measurement and aging process 20 p3271 A71-39571

Biomedical effects of Apollo 14 space flight, considering weightlessness adaptation 22 p3487 A71-41981

Space flight safety, discussing escape, rescue and survival design approaches for astronauts 22 p3611 A71-42031

Unfavorable high intensity noise effects on auditory and motor analyzers during space flight 22 p3495 A71-42799

Cosmic ray biological effects and admissible dose level normalization in space flight from prolonged tests on dogs 24 p3798 A71-44890

Biological effects of ionizing radiation and non-radiative factors on radiation damage from satellite space flight tests on dogs and plants 24 p3798 A71-44891

SPACE FLIGHT FEEDING

Regenerated nutrients as foods for long duration space missions, discussing physicochemical methods for metabolic waste products conversion into safe synthetic nutrient compounds 01 p0026 A71-11250

Biological rhythms and space nutrition - COSPAR Conference, Prague, May 1969, Life sciences and space research 01 p0017 A71-11551

Astronaut space nutrition, discussing Apollo mission short range nonregenerative mode, long range closed loop regenerative cycles and waste recycling 01 p0027 A71-11572

Space diets for maximum energy consisting of fats and proteins from biological systems and carbohydrates from chemical systems 01 p0027 A71-11573

Space shuttle life support, protective and crew system interfaces, discussing food and waste management and accident procedures 07 p1052 A71-20230

Potential foods synthesis for long duration space missions by physicochemical methods, discussing regeneration of carbohydrates from metabolic waste carbon dioxide and electrolytic byproduct hydrogen 07 p1056 A71-20375

Feeding systems, potable water and waste disposal in space cabins 08 p1245 A71-20730

Soyuz 9 spacecraft crew food diet description including products and packaging 09 p1397 A71-22205

Yeasts growth on synthetic carbohydrates with crude formose sugars, discussing application as regenerating food in long term closed life support system 19 p3011 A71-37576

Manned spacecraft life support system dehydrated food ration effects on human organisms health, metabolism and immunoreactivity during long space flight 22 p3507 A71-42823

SPACE FLIGHT STRESS

Medical support of extended manned space missions, considering functional disturbances, diseases, drug reactivity and timing of in-flight aid 01 p0024 A71-11131

Space motion sickness causes and prevention, discussing syndromes, psychophysiological factors, vestibular mechanics and adaptation 04 p0539 A71-15283

Renal function osmoregulation in Soyuz crew members 06 p0854 A71-18370

Automated vision tester for evaluating space environment effects and multiphasic health screening 07 p1046 A71-18805

Cardiopulmonary and circulatory mechanisms, adaptation limits and response to aerospace flight stress 08 p1238 A71-20720

Medical flight information on astronaut response to space flight environment in confined and unconfined state and during intra- and extravehicular activities 08 p1246 A71-20731

Soyuz 9 flight manned biomedical mission, evaluating 18 day exposure effect on human physiology and work capacity 08 p1246 A71-20820

Biosatellite postflight experiment evaluating effects of forced electrolyte imbalance in Macaca nemestrina 08 p1239 A71-20821

Circumlunar space flight effects on spiderwort, dry seeds and onion bulbs germinating capacity, growth stimulation and chromosome rearrangements 08 p1247 A71-21025

- Bone tissue optical density and blood serum and urine calcium content of Soyuz 9 crew members during and after flight 09 p1389 A71-22201
- Weightlessness effects on muscular reflexes, tonus and contractibility in Soyuz 9 astronauts 09 p1389 A71-22202
- Soyuz 9 spacecraft astronauts space flight effect on digestive system enzyme secretion function based on pre- and post-flight examinations 09 p1389 A71-22206
- Soyuz 9 spacecraft astronauts otorhinolaryngological organs response to 18-day orbital flight, observing pathological changes from clinical post flight examination 09 p1389 A71-22207
- Soyuz 9 spacecraft astronauts cardiovascular and respiratory systems responses to orthostatic effect after 18-day orbital flight from EKG measurements and sphygmography 09 p1389 A71-22208
- Soyuz 9 spacecraft simulator prolonged confinement effect on human cardiovascular system functional state 09 p1390 A71-22209
- Spaceflight effects on dry crepis capillaris seeds in five day orbit, showing chromosome rearrangements and increased mutagenic sensitivity 09 p1392 A71-22563
- Orbital space flight effects on dry barley seeds, noting increased intracellular rearrangements 09 p1392 A71-22564
- Biosatellite 3 monkey sleep and wake states based on visual and computer analysis of telemetered EEG data from earth orbital flight 09 p1395 A71-23242
- In-flight monkey cardiovascular observations, discussing central venous pressure, urine volume, electrolyte imbalances and heart rate 09 p1395 A71-23244
- German book on space medicine covering stresses on human organism during ascent into space, weightlessness and radiation effects, spacecraft environment, nutritional problems, etc 10 p1558 A71-23753
- Space flight factors effects on human physiology and psychology, discussing spacecraft gaseous medium control, food supply, closed ecological systems and weightlessness effects 13 p2016 A71-27876
- Postflight metabolism and renal function of Soyuz 6, 7 and 8 crewmembers, associating weight loss during flight with water and salt discharges 13 p2006 A71-28409
- Calcium, potassium and iron loss by astronauts during Apollo space missions, using instrumental neutron activation analysis 16 p2528 A71-33111
- Pyridoxine and serotonin metabolism changes and vestibular disorders observation in space flight 16 p2532 A71-33677
- Turtles organs and tissues responses during Zond 5 and 7 lunar probes circumlunar flight 16 p2532 A71-33678
- Afferent mechanisms of orthostasis in space flight, discussing plasma fluid volume reduction and cardiovascular adjustments on passive tilting [AIAA PAPER 71-883] 18 p2856 A71-36634
- Astronaut chromosome aberrations, presenting peripheral blood leukocytes cytogenetic tests for pre and post space flight 20 p3188 A71-39227
- Circumlunar space flight effects on spiderwort, dry seeds and onion bulbs germinating capacity, growth stimulation and chromosome rearrangements 20 p3193 A71-39605
- Astronaut work capacity and adaptation during long term flight of space vehicle Soyuz 9 21 p3342 A71-40259
- Radioprotectants effect on mice against ionizing radiation and tolerance to back-to-chest accelerations in space flight 21 p3330 A71-40345
- Weightlessness effect on vestibular apparatus from bullfrogs vestibular nerve single fibers spike train data during orbital flight 22 p3598 A71-41689
- Space station legal regime covering prolonged flight psychological and behavioral factors, misconduct jurisprudence and earthbound law liability 22 p3623 A71-42021
- Soviet papers on radiobiological aspects of reactivity of organisms in space flight covering radiation protection drugs, hypoxia, flight conditions, radiation pathology, etc 22 p3491 A71-42699
- Human orthostatic and vestibular stability responses to weightlessness during extended space flights noting acceleration tolerance, physical efficiency, infection resistance and medication sensitivity 22 p3495 A71-42790
- SPACE FLIGHT TRAINING**
 - Soviet book on psychology and outer space covering astronauts experiences and emotions during training and flights, daily routine, equipment, food, habits and personal characteristics 21 p3336 A71-40876
 - Human olfactory perception of inspired air composition, noting sensory differentiation improvement with subsequent exposures in space flight training 22 p3505 A71-42800
- SPACE GLIDERS**
 - U LIFTING REENTRY VEHICLES
- SPACE LABORATORIES**
 - NT MANNED ORBITAL LABORATORIES
 - NT MANNED ORBITAL RESEARCH LABORATORIES
 - Materials science and manufacturing in space, discussing potential technologies and laboratory techniques using vacuum, weightlessness, temperature and radiation environment 02 p2555 A71-11973
 - Book on space observatories covering atmospheric structure, space astronomy applications, atmospheric attenuation, balloon IR sounding, satellite observation, etc 14 p2316 A71-30895
 - Long range near-earth orbit research and applications based on NASA goals, including laboratory/observatory definition 17 p2802 A71-34729
 - Satellite stabilization techniques, noting application to space laboratories and shuttles 19 p3150 A71-37317
 - Space and orbital laboratories construction and operation legitimacy problem covering satellites, stations and space transport concepts and international management 19 p3151 A71-37323
 - Experimental determination of gravitational constant in orbiting space laboratory by gravitational centrifugal balance of test objects [AAS PAPER 71-350] 23 p3728 A71-43022
- SPACE LAW**
 - International law for states jurisdiction in aerospace, emphasizing airspace lateral to national territories and high seas, vertical to earth surface and outer space 06 p1010 A71-17645
 - Jurisdiction of air traffic and space law, noting applicability to start and landing phases of spacecraft 09 p1548 A71-23000
 - Air and cosmic space common law, discussing boundaries, sovereignty over state territories and jurisprudence related to travel development 11 p1861 A71-26325
 - International Telecommunications Satellite Consortium, reviewing legal order, organization structural framework, objectives and financial aspects 16 p2664 A71-33584
 - International space telecommunication systems, emphasizing legal aspects of operation 16 p2665 A71-33585
 - Outer space legal survey and prospects, emphasizing UN resolutions for international law and space exploration problems 16 p2665 A71-33586
 - Legal problems in space telecommunications, discussing UN and international nongovernmental organizations solutions for interference protection, pirate space stations and spacecraft distress or emergency 17 p2841 A71-34247
 - Direct broadcast satellite TV communications, discussing international regulations and legal aspects 18 p2989 A71-36578
 - U.S. and U.S.S.R. space stations with European participation, discussing design, international cooperation and legal and political problems 19 p3149 A71-37305
 - Space and orbital laboratories construction and operation legitimacy problem covering satellites, stations and space transport concepts and international management 19 p3151 A71-37323
 - Space station legal regime covering prolonged flight psychological and behavioral factors, misconduct jurisprudence and earthbound law liability 22 p3623 A71-42021
- SPACE LOGISTICS**
 - Space shuttle cargo handling systems, considering space logistics, space missions, vehicle traffic, satellite maintenance, rescue modules, etc [AIAA PAPER 71-319] 09 p1427 A71-22615
 - Logistics system for synchronous orbit space stations supply, discussing parking to synchronous orbit transfer of reusable and disposable logistics vehicles 11 p1838 A71-25530
 - Consumable usage as function of mission time computed with computer program simulating NASA Skylab mission 18 p2885 A71-36461
 - Spacecraft housekeeping relation to logistics elements of maintenance and up and down cargo supply 18 p2899 A71-36467
 - ELDO space tug development, discussing uses for earth orbital space stations and applications satellites logistics and interplanetary injection 22 p3609 A71-41978
- SPACE MAINTENANCE**
 - Economic evaluation of automatic support systems for maintainability of low quantity high technology space programs 03 p0396 A71-13091
 - Space shuttle cargo handling systems, considering space logistics, space missions, vehicle traffic, satellite maintenance, rescue modules, etc [AIAA PAPER 71-319] 09 p1427 A71-22615
 - Space shuttle flight test instrumentation for launcher, spacecraft and airplane triple operational and maintenance system requirements, discussing digital data bus monitoring concept [AIAA PAPER 71-313] 10 p1609 A71-23974
 - Manned spacecraft maintenance simulation model, applying complex systems operational availability assessments 12 p1894 A71-26689
 - Space station prototype environmental thermal control and life support systems, considering maintainability, reliability, weight penalties and fault detection and isolation [ASME PAPER 71-AV-22] 18 p2867 A71-36389
 - Orbital maintenance in pressurized environment, incorporating limited habitability, electronic/pneumatic bench access, critical spares storage racks, extravehicular activity manipulators and repair area 18 p2899 A71-36468
 - Space shuttle design concerning fault detection and isolation, redundancy and maintenance for cost and downtime minimization by application of airline methods 18 p2900 A71-36480
 - Space shuttle tests and flight operation, discussing launching, maintenance, booster/orbiter mating, payload installation and orbital mechanics 18 p2974 A71-36490
 - Reliability and maintenance of satellites, launchers and other space systems 18 p2975 A71-36534
 - Manned orbital operations economy for space station utilization, discussing laboratory equipment, on-orbit supervision, maintenance and remote communications limitations [MDAC-WD-1746] 22 p3611 A71-42030
 - Computerized simulation of reliability and in-flight subsystem maintenance for increased space mission success probability, using priority and waiting queue method 22 p3518 A71-42112
- SPACE MECHANICS**
 - NT ASTRODYNAMICS
 - NT CELESTIAL MECHANICS
 - NT KEPLER LAWS
 - NT ORBITAL MECHANICS
- SPACE MISSIONS**
 - Pioneer spacecraft flight missions, discussing interplanetary, solar-earth and deep space observations 01 p0160 A71-10990
 - Space mission reflex vestibular disturbance and motion sickness prevention, examining artificial gravity and drugs 02 p0198 A71-11979
 - Power sources for future NASA programs, discussing requirements in relation to various types of space missions 03 p0351 A71-13037
 - Earth-moon mission fuel cells, discussing development of direct, indirect and redox cells 04 p0535 A71-15082
 - Planetary and interplanetary exploration missions, discussing U.S. planetary space program budgets and costs 04 p0657 A71-15818
 - Silver zinc batteries and cells case cover materials and sealing techniques for space missions 08 p1235 A71-21097
 - Biosatellite 3 reduced gravity environmental laboratory with subhuman primate on 30 day mission, discussing ground base tests, simulated and actual flight 09 p1400 A71-23238
 - German book on rescue systems for space emergencies covering mission failure, biological problems, escape vehicles, orbital operations safety and spacecraft transfer 12 p1972 A71-27185
 - European Space Tug, discussing payload spectrum, multimode operation, reusable propulsion system and various missions application 15 p2499 A71-31215
 - Electrostatic ion propulsion systems for interplanetary missions, using experimental engine characteristics as basis for flight studies [DFVLR-SONDDR-121] 15 p2496 A71-32722
 - Launch vehicles for space telecommunications applications, considering payload capacity for missions involving earth resources, radio and visual astronomy and meteorology 17 p2811 A71-34226
 - High reliability low energy camera tubes for video communication in space missions, considering vidicons with photoconducting layer with large time constant 17 p2739 A71-34683

Phobos and Deimos missions, examining lander and lander/orbiter configurations and Titan-Centaur and space shuttle-Centaur launch systems
[AIAA PAPER 71-830] 17 p2802 A71-34716

Integrated waste collection and purification system using radioisotopes for thermal energy in 180-day space mission life support system
[ASME PAPER 71-AV-4] 18 p2865 A71-36371

Wide heat load range space radiator design for space mission environmental control/life support system, using stagnation control
[ASME PAPER 71-AV-5] 18 p2865 A71-36372

Roving vehicle design for 1979 Mars mission
18 p2898 A71-36445

Shower habitability requirements for adequate cleansing of body and hair to satisfy physiological, psychological and social needs of crew members on long space missions
[AIAA PAPER 71-873] 18 p2870 A71-36629

Heuristic approaches for generating perturbations to automatically evaluate partial derivatives for interplanetary space missions
19 p3135 A71-37561

Requirements and opportunities for comet and asteroid missions including flyby, rendezvous, docking and sample return
[AAS PAPER 71-104] 19 p3139 A71-37906

Planetary quarantine constraint effect on multiple outer planet missions, considering navigation error sources and midcourse maneuvers
[AAS PAPER 71-122] 19 p3002 A71-37917

Long life radioisotope thermoelectric generators for space missions, discussing power degradation mechanisms and design trends
[AAS PAPER 71-160] 19 p3102 A71-37929

Plasma ion and electron distribution functions measurement on outer planet missions
[AAS PAPER 71-124] 19 p3114 A71-37938

Plasma wave instrument for measuring AC electrical and magnetic field levels in outer planet missions
[AAS PAPER 71-125] 19 p3064 A71-37939

Outer planet satellite missions for optimal imaging conditions in terms of proximity and lighting
[AAS PAPER 71-138] 19 p3140 A71-37942

Jovian probe and spacecraft mission feasibility, discussing launch opportunities, targeting, objectives and data transmission
[AAS PAPER 71-141] 19 p3141 A71-37944

Spacecraft electronic equipment design for reliability in long duration space missions
[AAS PAPER 71-155] 19 p3153 A71-37956

Hardware reliability improvement techniques for long life unmanned space missions
[AAS PAPER 71-156] 19 p3153 A71-37957

Missions beyond solar system for studying origin and evolution of life, planets and stars
[AAS PAPER 71-163] 19 p3141 A71-37960

Ultraplannetary probes for exploration beyond solar system, discussing heliosphere, cometary, interstellar and stellar mission categories propulsion system selection
[AAS PAPER 71-164] 19 p3141 A71-37961

Salyut space station design, operation and mission, describing docking and undocking procedures for Soyuz 11 supply craft
19 p3153 A71-38148

Viking Lander power system design, discussing functional requirements by mission and science objectives and reliability features
20 p3181 A71-38940

SNAP 19 Radioisotope Thermoelectric Generator (RTG) for advanced space missions, using lead telluride and silver antimony germanium telluride as conversion materials
20 p3267 A71-38965

Europa 3 launch vehicle, considering background history, mission requirements and performance profile
21 p3454 A71-40157

Mission tasks and design problems of European space tug, considering geostationary transfer missions and cargo bay geometry
21 p3454 A71-40158

Stereophotogrammetric measurement of body and limb volume changes after prolonged space mission
22 p3502 A71-41861

Scientific objectives and satellite design of ESRO sponsored geostationary space mission, describing Europa II launcher design and operation
22 p3608 A71-41952

Outer planet explorers design for Grand Tour mission, discussing launch parameters, flight paths, environmental hazards, communications, ground control, navigation and power generation
22 p3601 A71-42028

Astronaut teleoperators use for space operations cost reduction and future experiments productivity increase
22 p3503 A71-42033

Astronomical and earth resources observations accommodation by space shuttle orbital sortie missions, obtaining sensor use rate estimate from worldwide cloud cover statistical distribution
[AAS PAPER 71-303] 23 p3724 A71-42979

Grand Tour missions set optimization for 1976 to 1982, defining flight opportunity launch/arrival date space for various mission types
[AAS PAPER 71-358] 23 p3728 A71-43028

Lunar impact targeting technique improvement for Apollo 14 mission preflight analyses and flight support operations
[AAS PAPER 71-392] 23 p3732 A71-43060

SPACE NAVIGATION

NT INTERPLANETARY NAVIGATION

Space navigation variation problem, examining perturbation differential equation for semimajor axis and eccentricity and momentum and eccentric anomaly relationship
01 p0122 A71-10389

Space navigator operations, procedures and computer interface and manually aided onboard Apollo cislunar navigation system possible improvement
01 p0124 A71-10510

Space vehicle onboard navigation and guidance systems capability, considering Apollo transition from direct task interaction and supervision to functional man machine communication
01 p0124 A71-10511

Spacecraft navigation, guidance and control for manual rendezvous with orbiting target, examining error sources perturbing effects
01 p0022 A71-10513

Mariner Mars 1969 navigation, guidance and control systems design, mechanization and flight testing
03 p0455 A71-14073

Proportional navigation vs optimally evasive constant speed target in two dimensions, considering lateral acceleration and time constraints in pursuer control
03 p0455 A71-14438

Axisymmetric satellite optimal reorientation into prescribed rotary motion by gas operated control jets, considering space navigation problems
05 p0815 A71-16036

Optimum orientation and accuracy of redundant sensor arrays in space navigation, guidance and attitude reference systems
[AIAA PAPER 71-59] 06 p0925 A71-18518

Grand Tour mission design, discussing navigation, trajectory parameters, launch vehicles and satellite flybys
[AIAA PAPER 71-187] 06 p0978 A71-18626

Computer requirements of self contained guidance, navigation and control system onboard manned orbital space station
[AIAA PAPER 71-221] 07 p1155 A71-19702

Nonlinear proportional navigation guided homing missile and minimum time to turn, developing quadratic equation with close larger positive root approximation
07 p1156 A71-19878

Apollo cislunar navigation capability and procedures, describing onboard data acquisition and digital processing equipment
13 p2098 A71-29386

High relativistic speed interstellar starship navigation, considering darkness cones, barrel, starbow, and near light speed problems
15 p2445 A71-31749

Precision landing guidance system using microwave scanning beam technique, stressing application to aerospace transportation
15 p2446 A71-32723

Axisymmetric satellite optimal reorientation into prescribed rotary motion by gas operated control jets, considering space navigation problems
16 p2645 A71-33440

Space shuttle, space station and nuclear shuttle navigation - Conference, Huntsville, Alabama, February 1971
17 p2772 A71-35051

Onboard orbit navigation scheme free from sensor uncertainty cause constraints, using satellite ejected from spacecraft into near orbit
17 p2772 A71-35053

NASA space station navigation system, considering landmark and ground tracking, ground beacons and satellite concepts, long term effects, operational requirements and design goals
17 p2772 A71-35054

Autonomous unknown landmark tracking space shuttle navigation system performance assessment by digital computer program providing error analysis and Monte Carlo simulation
17 p2773 A71-35067

Low cost navigation equipment selection for space shuttle system updating during orbital coast, rendezvous and atmospheric flight
17 p2774 A71-35069

Navigation and guidance alternatives of reusable nuclear shuttle, stressing onboard sensors and processing systems for position and attitude determination
17 p2774 A71-35074

Reusable nuclear shuttle navigation systems evaluation by mission simulation, discussing reduced NERVA cool-down thrust pulses uncertainty effects
17 p2774 A71-35075

NASA space station program, discussing design, guidance, navigation, electrical power and environmental control
19 p3154 A71-38150

Luna 18 mission accomplishments in lunar orbital automatic navigation techniques and arrival point coordinate accuracy
22 p3597 A71-41500

Actual navigation dispersions, estimation uncertainties and resultant Mars orbit insertion statistical deviation requirements for six Mars approach angles in 1971 Mars window
[AAS PAPER 71-323] 23 p3726 A71-42949

N-body integrated reference trajectories and navigation requirements for extended Venus/Mercury 1973 mission midcourse correction
[AAS PAPER 71-362] 23 p3729 A71-43000

Onboard optical tracking effectiveness for Grand Tour deep space navigation, considering star-planet angles, plane diameter angles and natural satellite observations
[AAS PAPER 71-394] 23 p3732 A71-43006

Book on electronic aids for navigation systems for marine and aerospace transport operation covering measuring and display instruments, radio wave properties, etc
23 p3702 A71-43222

SPACE ORIENTATION

Cortical vestibular projection zones in formation of conditioned reflexes and spatial orientation of cats
01 p0012 A71-11054

Proprioceptive gravity perception in Hymenoptera noting joint located hair plates and constant angle space orientation in dark
21 p3327 A71-39988

Gravity receptors and locomotion orientation in Crustacea, discussing statocyst, stimulation, input and compensatory eye movements with respect to gravitational field
21 p3327 A71-39990

Functional anatomy of vertebrate gravity receptor system in spatial orientation, discussing otolith organs, sensory cells and hair cell topography in elasmobranch labyrinth
21 p3327 A71-39990

Epidemiology statistics of USAF spatial disorientation aircraft accidents, noting pilot training, flight environment and indoctrination remedy programs
21 p3342 A71-40359

SPACE PERCEPTION

NT AUTOKINESIS

Contour effects on brightness paradox, investigating contrast and perception of luminance gradients in space by constant sum estimation method
03 p0365 A71-14377

Visual slant averaging mechanism evidence from binocular disparator tests, considering gradient slant perception theory and neurophysiological averaging mechanism
04 p0546 A71-15174

Input-output transformations for judgments of area of circles and paired weights, using nonmetric scaling
05 p0713 A71-16544

Rotation direction perception by three cue systems for polar projection of dotted line, considering differential retinal velocity relative to axis of rotation
05 p0713 A71-16554

Orienting response and apparent motion toward away from observer, using galvanic skin response and finger pulse volume studies
07 p1048 A71-19511

Figural change perception in apparent motion, considering resolving capabilities and visual stimuli for plastic deformation and shape rotation
07 p1048 A71-19511

Optical perception constancy of object size, developing mathematical models of accommodation, convergence and retinal image size
07 p1051 A71-20120

Mathematical simulation of visual distance perception capacity of man from ground reference landmark observation during vertical flight
07 p1051 A71-20120

Space vehicle apparent distance magnitude estimation judgments, investigating stimulus range effects on response range and Stevens type power function exponent
07 p1051 A71-20211

Intrareversal times for figures eliciting and not eliciting apparent depth in flat drawings
07 p1045 A71-20388

Stereoscopic depth perception mechanisms, studying stereocanomaly in binocular vision for crossed near-zero and uncrossed disparity ranges
08 p1247 A71-21188

Stereoscopic vision dependent on vertical grating or different spatial frequency of retinal images
09 p1394 A71-23011

Phi movement /pure motion/ perception between successively presented, granular, moving objects dichoptic and random dot Julesz patterns
10 p1567 A71-23988

- Saccadic and smooth pursuit eye movements modification to visual targets instantaneous velocity changes at varying intervals 10 p1560 A71-23988
- Vestibular system functions physical analog model, predicting responses to motion inputs and possible problems for flight situations 10 p1569 A71-24237
- Human visual system response to moving spatially periodic stimuli, developing mathematical model for motion perception 10 p1572 A71-24999
- Human vision spatial and temporal resolution relationship, examining image contrast sensitivity and target size, viewing distance and luminance reduction effects 10 p1572 A71-25000
- Astronomical methods for determination of distances to planets, stars and galaxies, considering human distance perception 12 p1962 A71-26955
- Human visual geometrical illusions and figural aftereffects, determining mechanism locations for spatial patterns physical and phenomenal properties 13 p2018 A71-28464
- Behavioral effects of electrically induced EEG abnormalities in inferotemporal and occipital cortex in monkeys on visual pattern discrimination and successive spatial reversals 13 p2011 A71-28806
- Spatial and temporal discrimination functions in vision, audition and touch, establishing and controlling stimuli by vibrators 14 p2188 A71-30252
- Speed overestimation in intermittent illumination of moving bars and textures as function of frequency, using Piaget and brightness enhancement phenomena 15 p2366 A71-32713
- Pilots illusory attitude perception causes, suggesting psychological and medical remedies 16 p2534 A71-32830
- Horizontal-vertical velocity illusions relationship, noting independent determinants 17 p2691 A71-35109
- Mathematical models of distance perception under flight conditions according to visible brightness of luminous surface 17 p2691 A71-35166
- Human visual depth impression by gradient patterns, discussing experimental verification for hypothesis concerning perceptual economy principle 17 p2684 A71-35252
- Stereoscopic vision and depth discrimination tests in cats, using conditioned suppression and rod-like shadow disparity stimuli 20 p3191 A71-39958
- Perceived distance effect on induced movement from stereoscopic cues 21 p3344 A71-41199
- Depth perception variability under central and peripheral illumination conditions, using Duncan multiple range test for data analysis 22 p3498 A71-41481
- Projection type 3-D display lenticular lens sheet optimum design and depth resolution 22 p3549 A71-42560
- Relative size cue for facilitating stereoscopic depth perception in ambiguous disparity stereograms 23 p3638 A71-43110
- Crossed retinal pathways in Siamese cats due to neuroanatomical defect impairing binocular vision and stereoscopic depth perception 23 p3633 A71-43546
- Apparent movement due to closely spaced sequentially flashed dots in human peripheral field of vision, considering eye movement role 23 p3634 A71-43970
- Stereoacuity role in pilot ability to land aircraft at minima, questioning adequacy of Verhoeff depth perception test administration conditions 23 p3637 A71-44244
- ## SPACE PHOTOGRAPHY
- ### U SPACEBORNE PHOTOGRAPHY
- ### SPACE POWER UNIT REACTORS
- #### NT SNAP 8
- Space nuclear power developments, reviewing radioisotope heat sources, reactors and power conversion systems 04 p0624 A71-15284
- Parametric performance of quasi-vacuum mode thermionic multicell space power generator, discussing surface parameters, fuel form, emitter geometry, helium management and generator reliability 11 p1714 A71-25900
- Nuclear reactor design as heat source for electric power generation in space 16 p2606 A71-33249
- Compact fast reactor design for space power with rotating fuel drums, Mo alloy reflectors and honeycomb support structure 16 p2606 A71-33252
- Nuclear safety considerations for ground checkout, launch and in-orbit operations of reactors for earth-orbital manned space stations 20 p3262 A71-38920
- Safe disposal for nuclear zirconium hydride reactors for manned space base mission 20 p3263 A71-38921
- ## SPACE PROBES
- ### NT JUPITER PROBES
- ### NT LUNAR PROBES
- ### NT LUNIK 14 LUNAR PROBE
- ### NT MARINER SPACE PROBES
- ### NT MARINER SPACECRAFT
- ### NT MARINER VENUS-MERCURY 1973
- ### NT MARINER 5 SPACE PROBE
- ### NT MARINER-MERCURY 1973
- ### NT MARS PROBES
- ### NT PIONEER SPACE PROBES
- ### NT PIONEER 6 SPACE PROBE
- ### NT PIONEER 7 SPACE PROBE
- ### NT PIONEER 8 SPACE PROBE
- ### NT PIONEER 9 SPACE PROBE
- ### NT SOLAR PROBES
- ### NT SURVEYOR LUNAR PROBES
- ### NT SURVEYOR 1 LUNAR PROBE
- ### NT SURVEYOR 3 LUNAR PROBE
- ### NT SURVEYOR 5 LUNAR PROBE
- ### NT VENERA SATELLITES
- ### NT VENERA 3 SATELLITE
- ### NT VENERA 4 SATELLITE
- ### NT VENERA 6 SATELLITE
- ### NT VENUS PROBES
- ### NT VIKING MARS PROGRAM
- ### NT ZOND 3 SPACE PROBE
- ### NT ZOND 5 SPACE PROBE
- Lagrange points role in three body problem, discussing applications to space probe positioning 02 p0316 A71-12739
- Rocket probe with constant tangential acceleration in planetary gravitational field, investigating flight direction 03 p0495 A71-14388
- Flight testing of automatic orbital operations system for satellites and space probes [DGLR-70-080] 05 p0779 A71-15958
- Solar cell array for probe mission, using optimized high temperature low resistance modules combined with mirrors of high thermal emissivity 05 p0704 A71-16096
- Solar wind parameters-terrestrial electromagnetic field micropulsations relation based on interplanetary probes and time correlated ground observations 05 p0800 A71-17170
- Ionospheric electron content from Faraday rotation measurements of earth satellite and deep space probe 07 p1098 A71-19029
- Deep space probes telemetry system a priori data compression ratio evaluation using channel activities under unknown output signals cross correlation [AIAA PAPER 71-231] 08 p1258 A71-20799
- Hollow cathode ion thruster and lightweight power conditioner of solar-electric propulsion system for unmanned deep space probes [AIAA PAPER 70-648] 09 p1511 A71-22904
- Integral electron flux and current in retarding-potential plasma probes, considering application to nonconcave geometry and spacecraft probes 11 p1805 A71-25615
- Impact resistant power packages for unmanned planetary probe landers, discussing radioisotope thermionic multiconverter array optimal configuration 11 p1713 A71-25898
- Distant artificial cosmic objects coordinate determination by image converter/closed TV system screen photography and TV observations of space probes 14 p2309 A71-29992
- Book on sources and availability of IQSY data, Volume 7, covering stations, sounding rockets, satellites, space probes and World Data Centers catalog 15 p2395 A71-31518
- Jovian turbopause probe mission, discussing atmospheric composition measurements and nonsurvivable system concept [AIAA PAPER 71-833] 17 p2802 A71-34714
- Jupiter atmospheric entry probe mission, discussing descent depths, atmospheric pressure and temperature effects, data return techniques and Grand Tour Missions [AIAA PAPER 71-832] 17 p2802 A71-34715
- Graphitic ablative heat shield fractions and forebody configurations for probe entry into atmospheres of Saturn, Uranus and Neptune [AAS PAPER 71-145] 19 p3141 A71-37948
- Ultraplanetary probes for exploration beyond solar system, discussing heliosphere, cometary, interstellar and stellar mission categories propulsion system selection [AAS PAPER 71-164] 19 p3141 A71-37961
- Deep space plasma measurement techniques by instruments on earth satellites 19 p3116 A71-38245
- Two-parametric models of interplanetary dust distribution predictions involving zodiacal light scattering
- measurements from space probes for in- and out-of-ecliptic missions 20 p3219 A71-39637
- Geodetic parameters describing earth gravity field and satellite tracking stations positions in geocentric reference frame, using satellite observation and deep space probes 20 p3220 A71-39659
- Exospheric ion composition determination by vertical-cathode probe mass spectrometer measurements, obtaining H, He, N, O and NO ion concentration vertical profiles 20 p3280 A71-39720
- Probe for circular polar Mercury orbit, obtaining missions values 22 p3600 A71-42010
- Single channel electron multiplier applications to sounding rockets, orbital satellites and deep space probes, discussing fatigue effects, ultrahigh vacuum environments and UV and X ray studies 24 p3811 A71-45333
- ## SPACE PROGRAMS
- ### NT APOLLO PROJECT
- ### NT EUROPEAN SPACE PROGRAMS
- ### NT FRENCH SPACE PROGRAMS
- ### NT LUNAR PROGRAMS
- ### NT TEKTTITE PROJECT
- ### NT U.S.S.R. SPACE PROGRAM
- Space flight in Japan, discussing satellites applications, test facilities, research agencies, high altitude rockets, etc 03 p0524 A71-13723
- Defense and space programs management systems, discussing structured activities planning for efficient resources use [ASME PAPER 70-WA/MGT-5] 03 p0524 A71-14097
- NASC future active role, discussing advisory capacity to Executive Branch, problems handled and space programs 04 p0689 A71-14926
- Space shuttle program plans, economics, operational characteristics, contracting and management planning 04 p0689 A71-14929
- Cooperative international space ventures, discussing mission programs, global needs, successes and deficiencies 04 p0690 A71-14935
- Space applications international programs in 1970s, discussing political, legal, economic and management aspects of earth resources survey [ERS/ satellite program] 04 p0691 A71-15348
- Cooperative international scientific space programs, discussing NASA, ESRO and other foreign space activities 04 p0692 A71-15350
- Space activities in Japan, discussing satellite program, launch bases, tracking stations and communications ground stations 05 p0839 A71-16130
- Optimal space experiments selection for satellites and space probes, discussing criteria and techniques for guidance in program management decision making 05 p0816 A71-16138
- Space research goals emphasizing solar system formation, and plasma physics and chemistry 14 p2310 A71-30197
- Manned space projects U.S./European cooperation, discussing economic and population factors involved in international space cooperation programs 14 p2341 A71-30261
- Post-Apollo program European participation, discussing need for multilateral international agreements on space shuttle, space tug and space station projects 14 p2341 A71-30262
- Astronautics progress review from earliest space flights to present, discussing stabilization, recovery, ballistic reentry and latitude determination 16 p2634 A71-33396
- Organizing space activities for world needs - Conference, New York, October 1968 16 p2664 A71-33580
- Space program economics, discussing applications benefits, spending and byproduct effects cost planning, funding and organization 16 p2665 A71-33590
- Pakistani space research including satellite geodesy, ionospheric sounding, rocket experiments, VLF studies and time keeping 16 p2666 A71-33857
- Japanese space research report to COSPAR, discussing meteorology, atmospheric electricity, ionosphere, magnetosphere, galactic radiation, life sciences and planetology 16 p2666 A71-33860
- Indian report to COSPAR on space activities, discussing organization, facilities, experiments, applications, international collaboration and future plans 16 p2666 A71-33863
- Canadian report to COSPAR on space program and facilities covering scientific satellites, sounding rockets, etc 16 p2667 A71-33868

Brazilian space research planning effort and activities covering rocket and satellite meteorology, satellite tracking, balloon experiments and ground based geophysical observations
16 p2667 A71-33869

Australian space research 1970 report to COSPAR covering rocket sounding, X ray and gamma ray astronomy, tracking stations and international cooperation
16 p2667 A71-33871

Meteorological satellites characteristics, reviewing Tiros, Itos, Nimbus, ATS, SMS and IGAR programs and vehicles
17 p2812 A71-34244

Long range near-earth orbit research and applications based on NASA goals, including laboratory/observatory definition
[AIAA PAPER 71-812] 17 p2802 A71-34729

Small satellite role in meteorological, earth observation, communications and navigation missions, discussing orbit, weight, electrical power, attitude control, data handling and modular design concepts
17 p2805 A71-35331

International communications law development, discussing capital investment, information dissemination, 1967 space treaty and Intelsat program
18 p2986 A71-36163

International Telecommunication Union report on telecommunication and peaceful uses of outer space, covering space programs, communication satellites, UN role, etc
19 p3172 A71-37517

Space program management - Conference, Paris and Neuilly-sur-Seine, February 1970
23 p3784 A71-43451

Industrial project management executive work team for space programs, emphasizing responsibilities of prime contractor
23 p3786 A71-43461

Quality control for space programs hardware suppliers, discussing contractual aspects
23 p3786 A71-43468

Balanced space programs for 1970s and beyond, discussing unmanned planetary missions, manned Apollo, Skylab and space shuttle projects, private, foreign and international programs
[AIAA PAPER 71-1020] 24 p3892 A71-44598

Earth observation system design decision making, considering data needs, technology readiness, man role in earth resources programs and space program schedule
24 p3892 A71-44867

SPACE RADIATION

U EXTRATERRESTRIAL RADIATION

SPACE RADIATORS

U SPACECRAFT RADIATORS

SPACE RATIONS

Manned spacecraft life support system dehydrated food ration effects on human organisms health, metabolism and immunoreactivity during long space flight
22 p3507 A71-42823

SPACE RENDEZVOUS

NT EARTH ORBITAL RENDEZVOUS

NT LUNAR ORBITAL RENDEZVOUS

NT ORBITAL RENDEZVOUS

Deep space shuttles operating modes and vehicle types, considering chemical vs nuclear propulsion, direct vs near-orbit rendezvous, refueling, etc
01 p0165 A71-11593

Requirements and opportunities for comet and asteroid missions including flyby, rendezvous, docking and sample return
[AAS PAPER 71-104] 19 p3139 A71-37906

Shuttle/Centaur injection stage, considering application to comet rendezvous mission via Jovian powered swingby
[AAS PAPER 71-113] 19 p3139 A71-37912

Guidance and navigation requirements for rendezvous missions to two short period comets
[AAS PAPER 71-116] 19 p3101 A71-37913

Extended launch windows for ground based rescue missions, using bi-elliptic rendezvous technique
[AAS PAPER 71-304] 23 p3638 A71-42980

Solar electric propulsion application to Halley Comet flythrough and rendezvous missions, describing trajectory characteristics and payload capabilities
[AAS PAPER 71-363] 23 p3729 A71-43033

Sequential processor performance prediction error with linear method from Monte Carlo cycle analysis of Apollo 14 early rendezvous profile
[AAS PAPER 71-386] 23 p3731 A71-43056

SPACE RENDEZVOUS MANEUVERS

U SPACE RENDEZVOUS

U SPACECRAFT MANEUVERS

SPACE SCIENCES

U AEROSPACE SCIENCES

SPACE SHUTTLES

Deep space shuttles operating modes and vehicle types, considering chemical vs nuclear propulsion, direct vs near-orbit rendezvous, refueling, etc
01 p0165 A71-11593

Space shuttle integrated electronic onboard and ground reusable systems design, considering data flow

management, checkout, computer decentralization, electronic switching and redundancy
02 p0231 A71-11978

Hypersonic aerodynamic characteristics of flat delta and caret wing models at high incidence angles for space shuttles
03 p0344 A71-14445

Lifting body flight test program applications in manned space shuttle
04 p0661 A71-14819

Post Apollo manned space operation, emphasizing Skylab program, space shuttles and long term space station
04 p0689 A71-14927

Skylab, space station and shuttle programs covering economics, international participation and ground and flight tests
04 p0661 A71-14928

Space shuttle program plans, economics, operational characteristics, contracting and management planning
04 p0689 A71-14929

OART research projects covering space shuttle, vehicle configuration, heat transfer, thermal protection, lifting bodies, electronics, power studies, etc
04 p0661 A71-14931

Space shuttle systems structural joints thermal control, discussing contact conductance with and without interstitial fillers
04 p0676 A71-15334

Single stage to orbit space shuttle system (SERV) concept with VTOL capability, discussing configurational and operational characteristics with emphasis on flexibility and versatility
04 p0664 A71-15336

Manned space vehicle unsteady aerodynamics, considering flow separation, vortex interference, shock and stall flutter problems in space shuttle design
04 p0526 A71-15337

Post-Apollo space programs European collaboration, discussing space shuttle and space tug projects [DGLR-70-067] 05 p0839 A71-15957

American-European space shuttle costs, comparing nonrecoverable Europa 3 with ballistic reusable devices
05 p0816 A71-16402

Delta shuttle orbiter for space transportation system, discussing structural design and economic aspects with reference to future space programs
05 p0819 A71-17227

Maximum stagnation temperature on swept wing leading edge for equilibrium glide entry of space shuttle
07 p1013 A71-18902

Economical reusable space shuttle development for cargo and passenger transportation to and from orbit
07 p1206 A71-19090

Space shuttle requirements from lifting body pilot viewpoint, noting booster and spacecraft reusability
07 p1206 A71-19091

Manned flight from Montgolfier Balloon to Apollo 13, discussing future space programs including lunar base and space shuttle
07 p1195 A71-19417

Space shuttle integrated information management system, emphasizing software element requirements and data processor hardware
[AIAA PAPER 71-222] 07 p1155 A71-19703

Elastic, inertial and aerodynamic forces aeroelastic triangle, examining lift changes due to aircraft structure deformation, dynamic flight stability and space shuttle development problems
07 p1215 A71-20063

Two stage space shuttle, discussing NASA reusable spacecraft cost reduction and technological problems
07 p1209 A71-20226

Space shuttle technology, discussing wind tunnel studies, aerothermal and operational flight mechanics, model characteristics, orbiter configurations and booster-orbiter separation
07 p1209 A71-20227

Space shuttle structures and materials, considering booster arrangements thermal protection, high temperature metals and composite materials
07 p1216 A71-20228

Space shuttle vibrational characteristics, investigating dynamic models, aeroelasticity, reentry, wing stall flutter and buffet boundaries
07 p1209 A71-20229

Space shuttle life support, protective and crew system interfaces, discussing food and waste management and accident procedures
07 p1052 A71-20230

Space transportation system of two stage reusable space shuttle and orbit-to-orbit shuttle, supporting NASA and DOD missions
08 p1367 A71-21890

Space shuttle as post-Apollo key project for technology advancement, discussing predesign studies and technical problem areas in propulsion, materials, structures and avionics
09 p1531 A71-22273

Space shuttle ground operations analysis emphasizing cost effectiveness, discussing breakdown into ground support activities, facilities and equipment
[AIAA PAPER 71-317] 09 p1427 A71-22614

Space shuttle cargo handling systems, considering space logistics, space missions, vehicle traffic, satellite maintenance, rescue modules, etc
[AIAA PAPER 71-319] 09 p1427 A71-22615

Space shuttle safety, discussing rocket engine durability, turbine life, flaw detection, radiation hazards, etc
[AIAA PAPER 71-302] 09 p1511 A71-22616

Space shuttle design, emphasizing reliability and safety
[AIAA PAPER 71-303] 09 p1531 A71-22617

Space shuttle development and certification test program comparison with large aircraft and spacecraft programs, considering Boeing 747 aircraft and Apollo Saturn S-IC stage
[AIAA PAPER 71-306] 09 p1531 A71-22618

Space shuttles thermal-structural cost effective ground testing
[AIAA PAPER 71-307] 09 p1531 A71-22620

Optimum test logic and constraint network for space shuttle program
[AIAA PAPER 71-309] 09 p1531 A71-22621

Space shuttle onboard vs ground checkout systems, considering vehicle autonomy and cost reduction
[AIAA PAPER 71-311] 09 p1427 A71-22623

Space shuttle development test program, discussing low cost dynamic structural and flight testing
[AIAA PAPER 71-308] 09 p1532 A71-23017

Space shuttle flight test instrumentation for launcher, spacecraft and airplane triple operational and maintenance system requirements, discussing digital data bus monitoring concept
[AIAA PAPER 71-313] 10 p1609 A71-23974

Space shuttle main, auxiliary and air breathing propulsion systems, describing various design concepts
10 p1682 A71-24284

Hypersonic air transportation future prospects, discussing technical problems and feasibility in view of space shuttle development
10 p1699 A71-24285

Space shuttle application to periodic interplanetary orbit making flyby without stopping, discussing trajectory requirements and relative orientation of earth, Venus and Mars
10 p1676 A71-24515

Space shuttle launch and turnaround operational sequences, vehicle processing facilities and alternate methods for vehicle erection, mating and transport to pad
[AIAA PAPER 71-320] 10 p1683 A71-24830

Space shuttle vehicles and assembly flow manufacturing, development and operations requirements, including ground rules, verification test facilities, cost reduction and interrelationships
[AIAA PAPER 71-316] 10 p1590 A71-24831

Radiative and high temperature insulative space shuttle thermal protection systems with actively cooled, passively cooled and uncooled substructures
[AIAA PAPER 71-443] 11 p1838 A71-26228

Space shuttle thermal protection system optimal weight by numerical parameterization, discussing temperature constraints and material rearrangement effects
[AIAA PAPER 71-444] 11 p1839 A71-26229

Performance prediction of fixed wing leading edges radiative, ablative and active cooling thermal protection systems and system weights comparison for space shuttle entry mission
[AIAA PAPER 71-445] 11 p1839 A71-26230

Lightweight oxidation resistant carbon-carbon composites for space shuttle leading edge components thermal protection
[AIAA PAPER 71-446] 11 p1790 A71-26231

Space shuttle phase B design, discussing British-American cooperation, fly-back orbital laboratory and Apollo 14 zero-gravity demonstration
11 p1839 A71-26230

Reusable Nuclear Shuttle using NERVA nuclear engine for low cost transportation to lunar and geosynchronous orbit, discussing design, operation, tests and problems
11 p1840 A71-26516

Earth-to-orbit space shuttle booster and orbiter unit design considerations including low development cost, risk and time, weight and payloads
11 p1840 A71-26529

Space shuttle program sustaining engineering and hardware logistics support
[AIAA PAPER 71-318] 12 p1894 A71-26698

Ceramic fiber external insulation thermal protection systems for space shuttles, considering use with Al and Ti
[AIAA PAPER 71-442] 12 p1985 A71-26763

Space shuttle thermal protection systems, discussing design requirements and constraints, materials selection, tradeoff and cost effectiveness studies
12 p1971 A71-26984

- Space shuttle comparison with transport aircraft, discussing high thermal resistant and cryogenic insulator material concepts, with application to Concorde structural computations 12 p1973 A71-27605
- Space shuttle propulsion systems, describing main engine prototype designs, booster attitude and docking control systems 12 p1946 A71-27606
- Composite materials application to space shuttles, considering resulting weight reduction 13 p2144 A71-28167
- Relaxation distance for sharp cone behavior from chemical nonequilibrium laminar boundary layer effects on simulated space shuttle configuration during reentry 13 p2146 A71-29504
- International space transport systems, discussing shuttle system optimal sizing considerations 14 p2320 A71-30260
- NASA evaluation of reports on space shuttles, discussing booster and orbiter design, mission requirements, payload capabilities, reusability, etc 14 p2320 A71-30421
- Reusable nuclear shuttle design, considering various propellant tank configurations and expendable/reusable launch modes with respect to performance, development cost and cost effectiveness [AIAA PAPER 71-640] 14 p2273 A71-30717
- Space shuttle airbreathing propulsion systems requirements and design studies, considering cruise, landing, go-around and ferry capabilities [AIAA PAPER 71-662] 14 p2290 A71-30731
- Gaseous oxygen/gaseous hydrogen auxiliary propulsion engines, considering cold flow experiments with nonreactive simulant gases 14 p2291 A71-30737
- Simulated altitude test facilities selection for Space Shuttle Orbiter Engine [AIAA PAPER 71-679] 14 p2292 A71-30743
- Liquid hydrogen rocket propellant tanks insulation problems in space shuttle and orbiter 15 p2499 A71-31216
- Space shuttle engine design based on reusable XLR129 rocket engine, presenting performance data 15 p2467 A71-31469
- Space shuttle vehicle models, calculating surface flow patterns and pressure and aerodynamic heating distributions for comparison with test data [AIAA PAPER 71-594] 15 p2343 A71-31539
- Space shuttle main engine based on high pressure, staged combustion, reusable, minimum risk and low cost concepts [AIAA PAPER 71-658] 15 p2470 A71-32290
- High pressure gaseous hydrogen oxygen auxiliary propulsion systems /APS/ thruster design and cold flow and hot fire testing for space shuttle requirements [AIAA PAPER 71-737] 15 p2470 A71-32291
- High performance low cost space shuttle propulsion systems airbreathing engines, attitude control thruster and orbital maneuvering [AIAA PAPER 71-656] 15 p2470 A71-32292
- AJ-550 liquid hydrogen/oxygen staged combustion cycle space shuttle engine, describing preburner and main injector, turbopump and combustion chamber construction [AIAA PAPER 71-660] 15 p2471 A71-32575
- Propulsion system design and performance requirements for space shuttle booster and orbiter vehicle, considering low cost, long life, reliability, safety and minimum maintenance [AIAA PAPER 71-657] 15 p2471 A71-32577
- European satellite telecommunications network design, discussing shuttle-tug launcher use and economy 16 p2644 A71-32848
- Rocket engine burning oxygen and hydrogen propellants at 3000 psia combustion chamber pressure for space shuttle booster and orbiter stages [AIAA PAPER 71-659] 16 p2624 A71-33106
- Niobium alloy use for space shuttle thermal protection, examining oxidation and mechanical properties 17 p2757 A71-34495
- Earth orbital space stations modular design, discussing space shuttle use, crew training and program management [AIAA PAPER 71-824] 17 p2812 A71-34721
- Space shuttle applications and utilization, discussing payloads, performance modes, Mission Support Module, ancillary equipment, system interfaces and related profiles [AIAA PAPER 71-816] 17 p2812 A71-34726
- Space shuttle cost effectiveness and utilization analyzed for system-level requirements to maximize economic benefits [AIAA PAPER 71-810] 17 p2813 A71-34730
- Payload cost and response time reductions for shuttleborne space experiments, examining NASA Ames airborne research program management technique [AIAA PAPER 71-808] 17 p2813 A71-34731
- Space shuttle economic and design impact on satellite payloads, noting variations in flight frequency and cost, hardware and performance 17 p2813 A71-34732
- Space shuttle operation phases hazards, emphasizing propellant loading, fire suppression systems, survival equipment and self contained life support devices 17 p2813 A71-34784
- Space shuttle, space station and nuclear shuttle navigation - Conference, Huntsville, Alabama, February 1971 17 p2772 A71-35051
- Geolunar interorbital transportation based on shuttle trajectories, interorbital rendezvous, elliptic orbits and terminal transfer 17 p2804 A71-35052
- Strapdown or gimbaled inertial measurement units for space shuttle program, considering reliability, redundancy and cost of ownership 17 p2772 A71-35059
- Space shuttle guidance, evaluating performance of strapdown and gimbaled systems by nominal and abort trajectories 17 p2773 A71-35061
- Autonomous unknown landmark tracking space shuttle navigation system performance assessment by digital computer program providing error analysis and Monte Carlo simulation 17 p2773 A71-35067
- Space shuttle scanning beam landing guidance system, discussing accuracy in penetration, alignment, flare out and touchdown maneuvers and trajectories 17 p2773 A71-35068
- Low cost navigation equipment selection for space shuttle system updating during orbital coast, rendezvous and atmospheric flight 17 p2774 A71-35069
- Reusable nuclear shuttle concepts, performance and design requirements 17 p2813 A71-35072
- Reusable nuclear shuttle guidance and control system requirements, using nuclear engine thrust pulse train for guidance 17 p2774 A71-35073
- Navigation and guidance alternatives of reusable nuclear shuttle, stressing onboard sensors and processing systems for position and attitude determination 17 p2774 A71-35074
- Reusable nuclear shuttle navigation systems evaluation by mission simulation, discussing reduced NERVA cooldown thrust pulses uncertainty effects 17 p2774 A71-35075
- On-orbit payload handling for space shuttles, including manipulator arms for drawing docking vehicles together, closed circuit TV and airolocking [AIAA PAPER 71-811] 17 p2814 A71-35427
- Reusable space shuttle optimization, discussing earth-to-orbit transportation, economic aspects, booster vehicles design, propellant cryogenic tanks and thermal protection [AIAA PAPER 71-805] 17 p2814 A71-35430
- Space shuttle with two stage booster and orbiter reusable vehicles, discussing performance, structural design and flight control system [AIAA PAPER 71-804] 17 p2814 A71-35431
- Space shuttle auxiliary propulsion subsystems for attitude control, orbit maneuvering and power supply, discussing design requirements with emphasis on fail-operational and fail-safe criteria [AIAA PAPER 71-661] 17 p2795 A71-35624
- Space Shuttle Orbiter Environmental Control and Life Support Systems, discussing maintenance [ASME PAPER 71-AV-15] 18 p2866 A71-36382
- Space shuttle environmental control and life support system design covering atmospheric pressure, composition, humidity, temperature, water and waste management [ASME PAPER 71-AV-16] 18 p2867 A71-36383
- Space shuttle aerothermodynamics, discussing heat transfer measurements, phase change patterns, electron beam flow visualization and boundary layer transition 18 p2847 A71-36430
- Hypersonic aircraft design usable as transport or space shuttle, determining aerodynamic behavior in viscous flow 18 p2847 A71-36431
- Aerodynamic characteristics of space shuttle configurations over entire flight velocity range, stressing coupling effects of control surfaces at large angles of attack 18 p2972 A71-36437
- Space shuttle booster configuration design, comparing stowed, fixed straight and delta wing approaches, discussing air breathing engines, stage mating, fins, etc 18 p2972 A71-36444
- ALOFT computer language for checkout and operation of complex space oriented equipment such as space shuttle 18 p2885 A71-36446
- Zero-g propellant tank quantity gaging methods, suggesting large cryogenic propellant tanks for space shuttle orbiter stage 18 p2922 A71-36455
- Space shuttle attitude control propulsion and orbit maneuver, considering high and low chamber pressure gaseous systems 18 p2973 A71-36456
- Computer programs for functional analysis, planning and control of space stations and shuttles operation 18 p2885 A71-36459
- Titanium and superalloy radiative heat shield design for space shuttle booster, recommending postsupported honeycomb configuration 18 p2973 A71-36462
- Premium mechanical properties for materials in space shuttle orbiter project, emphasizing cost and weight reductions 18 p2979 A71-36465
- System engineering techniques application to end-to-end space shuttle cargo handling system 18 p2899 A71-36466
- Airline operations approach to Cape Kennedy launch processing system for reduced hardware and operational costs of shuttle support 18 p2899 A71-36475
- Centaur/shuttle integration and operations, considering ground tanking modes and in-flight propellant transfer 18 p2973 A71-36477
- Space shuttle facilities planning, discussing vehicles, overall assembly flow, manufacturing, tests and operations 18 p2926 A71-36478
- Space shuttle avionics system redundancy, calculating costs for individual line replaceable units 18 p2889 A71-36479
- Space shuttle design concerning fault detection and isolation, redundancy and maintenance for cost and downtime minimization by application of airline methods 18 p2900 A71-36480
- Canard space shuttle reusable launch vehicle wing geometry variations effect on flyback systems weight, noting influence of aspect ratio and wing area 18 p2974 A71-36484
- Space shuttle vehicles landing with emergency arrestment aids, describing tailhook/cable, net and landing gear/cable engagement methods 18 p2900 A71-36488
- European space tug orbit to orbit autonomous shuttle system, discussing participation in post-Apollo programs 18 p2988 A71-36489
- Space shuttle tests and flight operation, discussing launching, maintenance, booster/orbiter mating, payload installation and orbital mechanics 18 p2974 A71-36490
- Housekeeping systems for manned modular space station and shuttle, discussing steward duties and waste control [AIAA PAPER 71-880] 18 p2871 A71-36633
- Diffusion bonding in production of shuttle type vehicles, considering fluxless brazing of refractory superalloys for heat shielding [SME PAPER AD-71-246] 18 p2927 A71-36660
- Refractory, superalloy and composite materials brazing process for space shuttle orbiter heat shield 18 p2928 A71-36854
- Mixed mode propulsion system for optimization of reusable space shuttle, discussing one-stage-to-orbit vehicle advantages and feasibility 19 p3121 A71-37126
- Optimal lateral guidance switching thresholds for low L/D shuttle vehicle entry, using optimal stochastic control theory for problem formulation in conjunction with dynamic programming [AIAA PAPER 71-914] 19 p3096 A71-37164
- Space shuttle boost vehicle with various degrees of aerodynamic stability, discussing control laws effects on rigid body bending moment tradeoff [AIAA PAPER 71-918] 19 p3147 A71-37167
- Control strategies for space shuttle transition at 45,000-150,000 ft, emphasizing terminal conditions and stability and control boundaries [AIAA PAPER 71-921] 19 p3147 A71-37170
- Computerized automatic redundancy management for space shuttle guidance, navigation and control, using fly by wire control technique for in-flight failure detection and correction [AIAA PAPER 71-946] 19 p3098 A71-37187
- Space shuttle orbital centrifuge systems configuration, comparing artificial gravity experiment performance options [AIAA PAPER 71-860] 19 p3006 A71-37274
- Orbiting stations and space shuttles - Conference, Rome, April 1971 19 p3149 A71-37301
- Space station, shuttle and tug as post-Apollo space program, discussing objective, designs and systems analysis 19 p3149 A71-37303
- European contribution to space shuttle and tug reusable space transportation systems, discussing post-Apollo programs cost analysis and hardware 19 p3150 A71-37310

Space shuttle structural heat problems, discussing shield design configurations and cooling systems
19 p3150 A71-37311

Temperature distribution in space shuttle during short radius reentry
19 p3161 A71-37316

Satellite stabilization techniques, noting application to space laboratories and shuttles
19 p3150 A71-37317

Rocket propulsion system equipped space shuttle dynamics, discussing aerodynamic forces and moments measurement in supersonic wind tunnels
19 p3151 A71-37318

Lift and drag coefficients for arbitrary body form in hypersonic flow calculated for cylindrical surface with reference to space shuttle reentry
19 p2992 A71-37320

Longitudinal dynamic stability of space shuttle during atmospheric entry, noting magnetic storms effects
19 p3151 A71-37322

Technical prospects of European aerospace industries participation in post-Apollo program, noting space shuttle development role
19 p3151 A71-37324

European launcher programs and participation in post-Apollo shuttles and orbital stations development in partnership with U.S.
19 p3151 A71-37330

Open cell lightweight cryogenic insulation for reusable liquid hydrogen fueled vehicles including space shuttle
20 p3312 A71-39271

Complex three dimensional shock waves about space shuttle configuration, visualizing hypersonic nitrogen flow with electron beams
20 p3211 A71-39356

Attitude control propulsion system for booster and orbiter of space shuttle in European participation package
21 p3454 A71-40159

Orbit-to-orbit shuttles as earth capture systems for round trip planetary missions, using hyperbolic rendezvous technique with returning interplanetary spacecraft
22 p3600 A71-41954

Space shuttle optimal lifting trajectory analysis, examining boost launch system performance increase
22 p3608 A71-41955

Two stage reusable manned space shuttle computerized onboard data management system hardware and software
[IBM-712000405] 22 p3517 A71-41977

Recovery, launch and landing operations of earth orbital shuttle vehicles, discussing space rescue capabilities
22 p3609 A71-41989

Space shuttle impact on cost reduction in NASA space operations, considering operations costs of payloads
22 p3609 A71-41994

Spacecraft and payload design under influence of space shuttle availability, discussing program cost savings
22 p3610 A71-42003

Space shuttle trajectory design optimization by nonlinear programming, proposing mathematical model to handle equality and inequality constraints
22 p3600 A71-42013

Two stage reusable space shuttle system for space transportation program, discussing budget, development and testing, international cooperation and information exchange
22 p3610 A71-42022

Scientific research methods and applications experiments from orbiting Space Shuttle, noting environmental control and life support provision
22 p3611 A71-42039

Economic analysis effect on R and D projects choice, assessing Space Shuttle system
22 p3624 A71-42526

Space shuttle operations analysis for cislunar space, including transfer trajectory inclination and long term effects
[AAS PAPER 71-300] 23 p3724 A71-42976

Mission analysis aspects of space shuttle operations between earth orbit station and lunar orbit station
[AAS PAPER 71-301] 23 p3724 A71-42977

Earth orbit shuttle payload increase, discussing refueling and auxiliary hydrogen tank concept
[AAS PAPER 71-302] 23 p3772 A71-42978

Astronomical and earth resources observations accommodation by space shuttle orbital sortie missions, obtaining sensor use rate estimate from worldwide cloud cover statistical distribution
[AAS PAPER 71-303] 23 p3724 A71-42979

Fuel optimal analytic multiburn transfer trajectories and shuttle rendezvous, assuming gravity vector linear dependence on position vector for burn arcs
[AAS PAPER 71-306] 23 p3724 A71-42982

Branched trajectory optimization algorithm using steepest descent method applied to space shuttle vehicle mission design
[AAS PAPER 71-326] 23 p3726 A71-43000

Optimal ascent trajectories for delta wing space shuttle flight, using accelerated gradient methods
[AAS PAPER 71-328] 23 p3726 A71-43001

Space shuttle optimal design problem, applying accelerated gradient parameter optimization technique
[AAS PAPER 71-329] 23 p3727 A71-43002

Reusable space transportation shuttle system, discussing design, operation, military uses, contract competition, economic analysis and political factors
23 p3784 A71-43353

Design parameter optimization for two-stage space shuttle atmospheric flight from spherical nonrotating earth by sequential straight line approximation
23 p3774 A71-44115

SPACE SIMULATORS

Oil diffusion pumped space simulation vacuum chamber performance improvement methods including water vapor and carbon dioxide desorption, Ti sublimation pumping and 20 K cryopumping
06 p0881 A71-18462

Design, calibration and computer control of orbital heating simulator, using heat flux sensor feedback for ATM thermal vacuum tests
[AIAA PAPER 71-432] 11 p1745 A71-26221

Space simulation - Conference, Gaithersburg, Maryland, September 1970
13 p2044 A71-28302

Space station regenerative life support system 90-day manned test in simulator, discussing objectives, facilities and procedures
[ASME PAPER 71-AV-38] 18 p2870 A71-36405

Long duration orbital simulator for technical planning activities, discussing capabilities, options, accuracy and central processing unit usage
18 p2885 A71-36460

Operating principles of spaceflight simulators, considering star coordinates errors in collimator simulator of stellar sky
19 p3062 A71-37150

Rotating space station simulator for translational and rotational motion determination under gravity gradient torque action and control under input state conditions
[IBM-712000406] 22 p3529 A71-41970

Cylindrical space simulation chamber with spherical test subject, deriving molecular incidence rate from integral equations with probability matrix for finite partial surfaces
24 p3816 A71-45138

SPACE STATIONS

NT ORBITAL SPACE STATIONS

NT ORBITAL WORKSHOPS

Spinning space stations with mass geometry changes, discussing attitude and angular velocity optimal control
01 p0164 A71-11435

Space station crew operations, discussing vehicle and research duties, habitability, etc
02 p0203 A71-11976

Post Apollo manned space operation, emphasizing Skylab program, space shuttles and long term space station
04 p0689 A71-14927

Skylab, space station and shuttle programs covering economics, international participation and ground and flight tests
04 p0661 A71-14928

Space station program characteristics, discussing technology, sciences, exploration, public services, foreign relations and national defense
04 p0689 A71-14930

OART space station development, discussing long term effects, artificial gravity, environmental problems, electric power, life support, protection systems and human factors
04 p0643 A71-14932

Space station information management, examining data processing and distribution to space and ground users
04 p0661 A71-15001

Space station and interplanetary flight research programs, discussing design, grand tour and Jupiter flyby
05 p0817 A71-16642

Space station experiments fine pointing and stability, discussing attached or coorbiting free flying mode with zero G conditions
[AIAA PAPER 71-62] 06 p0980 A71-18521

Common module series for NASA candidate experiment program for manned space stations in 1975-1985 era, discussing configuration and subsystem design
[AIAA PAPER 71-70] 06 p0980 A71-18528

Space station plasma physics experiments, investigating electron and ion wakes, resonance, VLF electromagnetic energy propagation and magnetospheric phenomena
[AIAA PAPER 71-71] 06 p0938 A71-18529

Ammonia design criteria for performance modeling of ammonia propellant thrusters and manned space stations using biowaste propellants
[AIAA PAPER 70-211] 07 p1183 A71-18898

Earth-moon libration point space station optimal control, considering restricted four body problem
08 p1363 A71-21323

Full scale models, nonflammable materials and tests for manned space expandable structures including airlocks, transfer tunnels, station modules, lunar shelters and flexible windows
[AIAA PAPER 71-399] 11 p1744 A71-25275

In-core thermionic power system for manned space station application, discussing driver fuel elements, nuclear radiation shield, heat rejection and coolant outlet temperature
11 p1710 A71-25869

Statistical analysis of equipment selection for multipurpose scientific laboratory onboard space stations under economic and time constraints
13 p2094 A71-28187

Microwave power transmission from orbiting solar power station to earth, discussing design optimization problems
13 p1999 A71-28666

Microwave power transmission for supplying electric power to space station complex for performing scientific experiments over long periods in earth orbits
13 p2000 A71-28667

High power linear beam tube devices for space power generation station, considering use of klystron with heat pipes for low weight and high efficiency
13 p2000 A71-28669

Chemical evolution and extraterrestrial life detection, noting cell proliferation methods, automatic biological stations and Mars microorganisms
13 p2009 A71-28680

Space stations - AAS Conference, Anaheim, California, June 1970
14 p2320 A71-30256

NASA space station program, discussing relationship between space stations, Skylab and space shuttle, electric power generation, habitability, safety and communications networks
14 p2320 A71-30259

NASA space station design, describing operational procedures, structure, meteoroid, thermal and radiation insulation and living quarters
15 p2498 A71-31137

Space station communications systems, discussing data relay satellites transmission paths to ground, multiple voice channels, two way color TV and onboard telephones
17 p2699 A71-34610

Earth orbital space stations modular design, discussing space shuttle use, crew training and program management
[AIAA PAPER 71-824] 17 p2812 A71-34721

General purpose manned space laboratory concept for multidisciplinary long term shuttle supported research investigations
[AIAA PAPER 71-814] 17 p2812 A71-34727

Space station common module concept, discussing NASA functional program elements accommodating multidisciplinary scientific applications and technology experiment modes
[AIAA PAPER 71-813] 17 p2813 A71-34728

Space shuttle, space station and nuclear shuttle navigation - Conference, Huntsville, Alabama, February 1971
17 p2772 A71-35051

Control moment gyro for attitude pointing control system of Skylab space station
17 p2743 A71-35063

Artificial g space station configurations, developing movable control mass attitude stabilization system
18 p2971 A71-36277

Zero gravity whole body shower system for space station, describing air drag and vacuum methods for water collection
[ASME PAPER 71-AV-2] 18 p2865 A71-36369

Ninety day manned test of regenerative life support system in space station simulator, presenting operational and maintenance data
[ASME PAPER 71-AV-3] 18 p2865 A71-36370

Life support water management subsystem 4-man 90-day test in space station simulator with closed water and oxygen loops and no resupply
[ASME PAPER 71-AV-6] 18 p2865 A71-36373

Waste management subsystem for 90-day space station simulator test of regenerative life support system
[ASME PAPER 71-AV-7] 18 p2865 A71-36374

Solar-array space station environmental control and life support system design for 12-man 10-year mission capability with 180-day resupply
[ASME PAPER 71-AV-12] 18 p2866 A71-36379

Environmental control and life support subsystems selection and definition for 12-man space station
[ASME PAPER 71-AV-13] 18 p2866 A71-36380

Composition and daily fluctuations of trace contaminants during 90-day space station simulator test
[ASME PAPER 71-AV-17] 18 p2867 A71-36384

Oxygen generation system for 90-day space station simulator, considering carbon dioxide removal and reduction and water electrolysis
[ASME PAPER 71-AV-18] 18 p2867 A71-36385

Zero-gravity circulating water electrolysis system prototype design for metabolic and leakage makeup oxygen supply in 12-man space station regenerative life support system
[ASME PAPER 71-AV-20] 18 p2867 A71-36387

Space station prototype environmental thermal control and life support systems, considering maintainability, reliability, weight penalties and fault detection and isolation
[ASME PAPER 71-AV-22] 18 p2867 A71-36389

Space station life support prototype vapor diffusion water reclamation system for pure and sterile water distillation from urine process stream
[ASME PAPER 71-AV-31] 18 p2869 A71-36398

Prototype space station environmental thermal control and life support system digital simulation for transient design and performance prediction
[ASME PAPER 71-AV-34] 18 p2869 A71-36401

Space station thermal control systems design, discussing pumped loop, air cooled semipassive and heat pipe systems
[ASME PAPER 71-AV-36] 18 p2869 A71-36403

Hydrogen depolarized fuel cell for space station prototype carbon dioxide concentrator, describing modular design concept and operation
[ASME PAPER 71-AV-37] 18 p2870 A71-36404

Space station regenerative life support system 90-day manned test in simulator, discussing objectives, facilities and procedures
[ASME PAPER 71-AV-38] 18 p2870 A71-36405

Lunar exploration system based on modified earth-orbit space station in polar lunar orbit as remote sensor platform and lander deployment base
18 p2972 A71-36443

Computer programs for functional analysis, planning and control of space stations and shuttles operation
18 p2885 A71-36459

Space station facilities and launch and prelaunch operations at Kennedy Space Center, discussing statistical analysis for activity optimization and integrated mission management concept
18 p2899 A71-36474

Space station assembly in earth orbit, providing low transportation costs, modular elements return and incremental growth
18 p2974 A71-36485

Skylab and space station crew garments, discussing personal preference and style integration with function and overall system impact
[AIAA PAPER 71-875] 18 p2870 A71-36630

Housekeeping systems for manned modular space station and shuttle, discussing steward duties and waste control
[AIAA PAPER 71-880] 18 p2871 A71-36633

Breadboard attitude control system for scale model space station using control moment gyros
[AIAA PAPER 71-935] 19 p3097 A71-37180

Optimized momentum and attitude control system /MACS/ for Skylab class space stations employing control moment gyro and reaction jet elements
[AIAA PAPER 71-938] 19 p3098 A71-37183

Electromagnetic actuator for momentum desaturation of control moment gyros used for attitude stabilization and control of space stations
[AIAA PAPER 71-939] 19 p3098 A71-37184

Space station, shuttle and tug as post-Apollo space program, discussing objective, designs and systems analysis
19 p3149 A71-37303

U.S. and U.S.S.R. space stations with European participation, discussing design, international cooperation and legal and political problems
19 p3149 A71-37305

NASA 12-man 10-year space station program, discussing design, information management, environmental control and life support system
19 p3153 A71-38147

Salyut space station design, operation and mission, describing docking and undocking procedures for Soyuz 11 supply craft
19 p3153 A71-38148

NASA modular space station program, describing design and equipment
19 p3153 A71-38149

NASA space station program, discussing design, guidance, navigation, electrical power and environmental control
19 p3154 A71-38150

Isotope Brayton four module adaptable compact power system for space station, using plutonium 238 fuel and lithium hydride shielding for neutron attenuation
20 p3263 A71-38922

Space station legal regime covering prolonged flight psychological and behavioral factors, misconduct jurisprudence and earthbound law liability
22 p3623 A71-42021

Dynamic unbalances effects for axially symmetrical dual spin space station with rigid or low coupling interconnections, considering control moment gyros use
22 p3612 A71-42770

Fuel optimal transfer from circular orbit space station to rendezvous with vehicles in different circular orbits
[AAS PAPER 71-365] 23 p3729 A71-43035

SPACE STORAGE

Superinsulation for long term storage of cryogenic propellants in space tanks using double aluminized Mylar with Dacron needles
09 p1546 A71-23009

Mixed ullage heating, convection and conduction models of thermal stratification of cryogenic propellants stored in low gravity environment
11 p1810 A71-26507

Jet mixing control of thermodynamic state of space stored cryogenic fluids, minimizing mass penalties resulting from equilibrium departures
[AIAA PAPER 71-646] 14 p2285 A71-30723

Orbital maintenance in pressurized environment, incorporating limited habitability, electronic/pneumatic bench access, critical spares storage racks, extravehicular activity manipulators and repair area
18 p2899 A71-36468

Stowable extendible structures for spacecraft and space experiments, discussing inflatable, rigidized cloth and mechanically deployable apparatus
22 p3609 A71-41981

SPACE SUITS

Thermal environment loads in lunar ambulation, discussing Apollo EVA suit system and internally produced heat
02 p0207 A71-12386

Liquid cooled space suit fluidic temperature control, using pressure differential variations across garment for cooling level modulation
[ASME PAPER 70-WA/FLCS-19] 03 p0355 A71-14092

Astronaut electrode-amplifier helmet harness for cable and radiotelemetry acquisition of EEG, EGO, EMG and blood pressure data on noninterference basis
10 p1570 A71-24475

Book on space suit evolution covering balloon flight, tropopause, stratosphere, astromonks, astronauts, etc
16 p2537 A71-33872

Antixposure suits physiological evaluation for subjective comfortableness, oral and skin temperatures and pulse rate, determining optimum environmental temperature
17 p2692 A71-35195

Advanced regenerative portable life support system concept analysis for long duration and multiple extravehicular activity
[ASME PAPER 71-AV-10] 18 p2866 A71-36377

Heat removal from space suit, discussing anatomic and physiological features suitable for cooling
20 p3188 A71-39224

SPACE SURVEILLANCE

Radar target optimal detection algorithms in cloud of passive reflectors, noting space surveillance regularities
05 p0722 A71-16870

Time and frequency synchronization for EROS airborne collision avoidance system, considering impact on aeronautical communication, navigation and surveillance
[CASI PAPER 72/17] 19 p3100 A71-37604

SPACE SURVEILLANCE (GROUND BASED)

Multiradar tracking system with monoradar units interconnected by central digital computers for wide air-space surveillance
08 p1255 A71-21598

Navigation and surveillance interdependence in ATC
22 p3571 A71-42085

SPACE SURVEILLANCE (SPACEBORNE)

Satellite remote sensing for crops and timber identification/detection, surface moisture measurements, soil mapping, marine hazard evaluation, etc
17 p2730 A71-34245

Aircraft surveillance oceanic satellite systems design and reliability analysis, discussing position determination accuracy
22 p3572 A71-42094

Geostationary satellite oceanic automated ATC center design, estimating cost
22 p3572 A71-42095

SPACE SYSTEMS ENGINEERING

U AEROSPACE ENGINEERING

SPACE TRANSPORTATION

Stapleblock fabrication method for low mass, high strength ferrite core memory storage blocks in space travel applications
02 p0232 A71-12071

Space transportation system performance risks due to design parameter uncertainties, presenting analysis method for tradeoff studies based on figure of merit calculation
04 p0663 A71-15335

Space transportation system profitability conditions, discussing optimal cost reduction and launcher/booster characteristics
04 p0692 A71-15821

Delta shuttle orbiter for space transportation system, discussing structural design and economic aspects with reference to future space programs
05 p0819 A71-17227

USAF space missions information processing requirements relative to space transportation system, emphasizing real time image processing
05 p0727 A71-17229

Economical reusable space shuttle development for cargo and passenger transportation to and from orbit
07 p2106 A71-19090

Circadian rhythms from aerospace medicine viewpoint, discussing cycle stability and flexibility, air and space travel, etc
08 p2138 A71-20704

Space transportation vehicles thermal protection systems, discussing reusable ceramic and oxidation resistant carbon-carbon composite materials properties and weight saving potential
[SAE PAPER 700771] 08 p1375 A71-21370

Space transportation system of two stage reusable space shuttle and orbit-to-orbit shuttle, supporting NASA and DOD missions
08 p1367 A71-21890

Space travel genetic effects, discussing radiation, weightlessness, vibration and acceleration
09 p1394 A71-23149

Manned planetary precursor missions size, cost and operational characteristics, discussing effects of transportation system for projection
14 p2319 A71-30247

International space transport systems, discussing shuttle system optimal sizing considerations
14 p2320 A71-30260

NASA space transportation system economics, discussing cost analytic considerations in comparing reusable vs expendable launch systems
[AIAA PAPER 71-806] 17 p2841 A71-34733

Geolunar interorbital transportation based on shuttle trajectories, interorbital rendezvous, elliptic orbits and terminal transfer
17 p2804 A71-35052

Space transportation system design concept based on reusable engines and partially external expendable tankage/REPEAT, discussing economic factors
19 p3147 A71-37125

Space transport systems, discussing spaceship earth survival problem from cosmospic criteria
19 p3149 A71-37304

Space transport rendezvous and docking techniques, emphasizing guidance, propulsion system configuration and sensors
19 p3149 A71-37306

Aerodynamic testing for space transport vehicle design, discussing experimental gas dynamics role in high stagnation enthalpy systems
19 p3161 A71-37315

Space and orbital laboratories construction and operation legitimacy problem covering satellites, stations and space transport concepts and international management
19 p3151 A71-37323

Space transportation orbiter design covering thermal protection, aerodynamics and cross range problems during earth reentry
22 p3609 A71-41979

Two stage reusable space shuttle system for space transportation program, discussing budget, development and testing, international cooperation and information exchange
22 p3610 A71-42022

Computerized synthesis for fly-back system of first stage winged booster for earth-to-orbit reusable space transportation system
[FZA-456] 22 p3611 A71-42032

Reusable space transportation shuttle system, discussing design, operation, military uses, contract competition, economic analysis and political factors
23 p3784 A71-43353

Civil aeromedical standards for aerospace transportation vehicles including occupant selection, vehicle design and operational guidelines
23 p3641 A71-44251

NERVA reactor in-flight cooldown during engine shut-down phase of reusable earth-lunar transportation vehicle, discussing coolant management considerations
23 p3703 A71-44270

SPACE TUGS

Post-Apollo space programs European collaboration, discussing space shuttle and space tug projects
[DGLR-70-067] 05 p0839 A71-15957

Space based reusable manned/unmanned tug, discussing potential missions, system requirements and auxiliary hydrogen oxygen propulsion system
[AIAA PAPER 70-719] 09 p1511 A71-22902

Post Apollo program European participation in space tug design and orbiter model flight tests, considering mini shuttle support applications
11 p1839 A71-26331

European Space Tug, discussing payload spectrum, multimode operation, reusable propulsion system and various missions application
15 p2499 A71-31215

European satellite telecommunications network design, discussing shuttle-tug launcher use and economy
16 p2644 A71-32848

European space tug orbit to orbit autonomous shuttle system, discussing participation in post-Apollo programs

18 p2988 A71-36489

Space station, shuttle and tug as post-Apollo space program, discussing objective, designs and systems analysis

19 p3149 A71-37303

European unmanned interorbital tug, investigating configurations, structure, hookup system, docking and propellant supply

19 p3150 A71-37309

European contribution to space shuttle and tug reusable space transportation systems, discussing post-Apollo programs cost analysis and hardware

19 p3150 A71-37310

ELDO studies of interorbital space tug for transfer of satellites in geosynchronous orbits

19 p3151 A71-37327

Mission tasks and design problems of European space tug, considering geostationary transfer missions and ca_{20} bay geometry

21 p3454 A71-40158

Space tug optimal round trip trajectories for payload earth escape injection missions, obtaining boundary value problem solution by Newton-Raphson iteration technique

21 p3452 A71-40908

ELDO space tug development, discussing uses for earth orbital space stations and applications satellites logistics and interplanetary injection

22 p3609 A71-41978

Space tug assist to escape branched trajectories optimization

[AAS PAPER 71-330]

23 p3727 A71-43003

Reusable space tug payload injection missions, determining optimal round trip trajectories at earth escape energy levels

[AAS PAPER 71-370]

23 p3730 A71-43040

SPACE VEHICLE CHECKOUT PROGRAM

Europa I/II third stage integration and systems testing, discussing checkout hardware and software

[DGLR-70-058]

05 p0815 A71-15971

Europa 2 booster rocket third stage attitude control system, describing measuring, controlling and actuating functions dynamic integration and checkout

05 p0815 A71-16134

Space shuttle development and certification test program comparison with large aircraft and spacecraft programs, considering Boeing 747 aircraft and Apollo Saturn S-IC stage

[AIAA PAPER 71-306]

09 p1531 A71-22619

Optimum test logic and constraint network for space shuttle program

[AIAA PAPER 71-309]

09 p1531 A71-22621

Space shuttle onboard vs ground checkout systems, considering vehicle autonomy and cost reduction

[AIAA PAPER 71-311]

09 p1427 A71-22623

Programming language SCOPE for Europa 2 booster vehicle operational checkout system, describing simple coding procedure for test program

11 p1734 A71-25250

Skylab checkout and launch facilities and operations, describing modifications required for Apollo lunar missions facilities utilization at Cape Kennedy

18 p2899 A71-36476

SPACE VEHICLE CONTROL

U SPACECRAFT CONTROL

SPACE VEHICLES

U SPACECRAFT

SPACE-TIME CONTINUUM

U RELATIVITY

SPACE-TIME FUNCTIONS

Chronometrically invariant formulation of relativistic thermodynamics second law distinguishing between three dimensional space and time

01 p0156 A71-10550

Static solutions to equations of gravity, showing nonequilibrium universe with negatively determinate time-similar Ricci curvature

01 p0160 A71-11117

Space-time structure of ionospheric regions of anomalous radio wave absorption during auroras, discussing ionization region

02 p0243 A71-11765

Cosmic ray anisotropy fluctuation and propagation function dimensionality relationship, demonstrating essentially one dimensional propagation

02 p0300 A71-12370

Physical and geometrical properties of dust filled universes, using left invariant metrics compatible with Einstein equations

05 p0773 A71-15925

Chronometrically invariant formulation of Petrov gravitational fields algebraic classification at spacetime fixed point in general relativity

05 p0781 A71-16182

Space-time and time correlation functions for classical many body system, proving Chapman-Enskog equivalence to correlation function methods

05 p0786 A71-16864

Robertson metric beta and gamma coefficients and solar dynamic oblateness determination from probe motion under relativistic effects

[ONERA-TP-893]

06 p0970 A71-18024

Theoretical frameworks for testing relativistic gravity, using presence of metric and gravitational response equation from Dicke approach as postulates of parameterized postNewtonian formalism

07 p1190 A71-18859

Space metric as similarity criterion for meteorological element field synoptic setup, discussing probability for forecasting by analogy

07 p1150 A71-18872

Homogeneous cosmological models evolution theory, considering Einstein equations analytic solution for lengthy era

07 p1204 A71-20536

Curved space-time mathematical structure /quasi-groups/, investigating 10-parametric classes of coordinate systems and Poincare groups

08 p1334 A71-21358

Boiling of relativistic heat conducting fluid in normal space-time manifold for nonstrict hyperbolic system, using Eckart scheme

10 p1694 A71-23831

Thermodynamic, electrodynamic and cosmological time asymmetry, discussing arrow-of-time concept as fundamental to physical space/time relationships

11 p1828 A71-25735

Four dimensional space-time meteorological observation data assimilation schemes and problems

13 p2096 A71-28014

Test particle uniform acceleration motion in curved space-time, requiring torsion free and constant curvature particle world line

14 p2274 A71-29575

Minkowski space-time concept, developing deviation function from geometric analysis

15 p2481 A71-31145

Physical meaning of fifth coordinate in five dimensional field theory, discussing relationship as parameter metric of de Sitter four dimensional space-time manifold

16 p2608 A71-33223

Wave fronts in Einstein-Maxwell theory, showing perturbation propagation along background space-time metric field

16 p2609 A71-33261

Natural symplectic structure for twistors on cotangent bundle over space-time manifold, considering Lagrange identity for Jacobi fields

16 p2609 A71-33264

Static electromagnetic fields in general relativity obtained for space-time metrics of group G automorphisms, considering Rainich unified field theory equations

16 p2610 A71-33265

Classification of curvature tensor of relativistic Riemann space-time gravitational metric field

16 p2611 A71-33276

Elementary particle geometrical-group model assuming negative curvature de Sitter space inside and flat space outside

17 p2778 A71-34627

Simultaneous solution of Einstein and elementary particle motion equations for space-time curvature within particle resulting from self gravitation

17 p2778 A71-34628

Quasi-closed Einstein universe model, showing orbits rotation similar to perihelions in Schwarzschild field

17 p2778 A71-34630

Gravitational equations in Maxwellianized form, investigating Bianchi qualities

17 p2778 A71-34631

Weyl and Schwarzschild field metric equivalence, showing nonreducibility from one to other by coordinate transformation

17 p2778 A71-34637

Deformation field of continuous medium in Minkowski space-time, defining tensor in Euclidean space of initial configuration

18 p2947 A71-36191

Space-time model of torsion tensor effect on geodesic lines under Schwarzschild metric, evaluating orbital perihelion motion of planets and light ray bending

18 p2967 A71-36826

Brans-Dicke cosmologies in arbitrary units, deriving power law solutions in flat Friedmann space

20 p3294 A71-39557

Radar determination of reference change related to sudden acceleration, deducing Galilean-accelerated reference transition in two dimensional space-time

21 p3415 A71-40513

Relativistic behavior of uniformly accelerated translational observer motion relative to inertial observer from space-time transformation

21 p3415 A71-40653

Relativistic gravitation theory, using Lorentz invariant scalar potential and gravitational metric

22 p3575 A71-42355

Trapped surface existence conditions and occurrence in strongly curved space-times

22 p3576 A71-42403

Arbitrary multipole structure spherical wave propagation in Schwarzschild metric, using Bondi coordinate system and negative powers of r

23 p3704 A71-43826

Spherically symmetric Gaussian coordinate systems completeness in spaces analogous to Lemaitre and Kruskal spaces in general relativity

24 p3848 A71-44659

SPACE-TIME METRIC

U SPACE-TIME FUNCTIONS

SPACEBORNE ASTRONOMY

Solar spaceborne astronomy, examining progress in temperature and density profiles determination

22 p3605 A71-42524

SPACEBORNE PHOTOGRAPHY

NT SATELLITE-BORNE PHOTOGRAPHY

Celestial body gravitational field from satellite photogrammetry

01 p0083 A71-11326

Information retrieval system at Extra-terrestrial Photographic Information Center /EPIC/ for identification of extraterrestrial photographs from satellites and manned space explorations

[NSSDC PAPER 69-09]

01 p0184 A71-11425

Mars surface areodetic control net from Mariner 6 and 7 TV pictures, determining initial coordinate points and far and near encounter frames

06 p0965 A71-17630

Digital computer techniques for Mars surface imagery systematic video data distortions quantification and correction onboard Mariner 6 and 7

06 p0871 A71-17631

EROS program mapping cameras, discussing wide angle, narrow angle and telescopic imaging

08 p1288 A71-21243

Image specifications and data interpretation techniques for regional resource survey using small scale aerial and space photography

08 p1288 A71-21245

Space Optics - ESSA-USAF Conference, Santa Barbara, September 1969

09 p1446 A71-22738

Full photographic spectral range spaceborne cameras photometric calibration, involving determination of absolute magnitude and illuminance spatial variation in image plane

09 p1447 A71-22744

TV and silver halide emulsion application to planetary photography from space orbit, providing film system immediate information storage and high resolution

09 p1447 A71-22746

Mercator chart of Mars surface between 70 deg north and 70 deg south latitude from Mariner 6 and 7 photography

09 p1452 A71-23220

Space photography for earth resource assessment, discussing multi-band, -date and -stage techniques advantages, image analysis and conference systems

11 p1767 A71-26530

Direction of chord in space from synchronous photographic satellite observations, considering optimum satellite altitude

12 p1900 A71-26969

Photometric analysis of manned spacecraft twilight-brightness photographs for spherical atmosphere in single scattering approximation

12 p1901 A71-27103

Apollo 9 So65 multispectral color space photography for basic land use pattern determinations

12 p1907 A71-27259

Translation of geodetic geographical coordinates and ellipsoidal altitudes by synchronous photographic satellite observations and satellite-distance measurements from two ground stations

12 p1903 A71-27753

Space photos for land use and forestry, considering IR color photographs from Apollo 9 flight

13 p2064 A71-29398

X ray telescopes and neutron cameras telephoto lenses for satellites and space stations, discussing optical design and correction methods

14 p2246 A71-30391

Hadley, Prinz and Schroter lunar sinuous rills morphology from Orbiter photography, discussing rills origin

15 p2493 A71-32489

Remote subsurface oceanographic imagery from orbital altitudes in blue multispectral region, showing optimum filter passband

18 p2917 A71-36064

Aerospace vehicles high resolution photography, introducing phase rate image tracking sensors for forward motion compensation

18 p2883 A71-36909

Lunar Apennine-Hadley region geological implications from high resolution earth-based radar map and Lunar Orbiter photography

20 p3287 A71-38977

Global lunar map coordinate grid from spaceborne photography and rectification on spherical screen noting rays and maria

20 p3296 A71-39621

Spectrophotometry and photography of earth twilight aureole, clouds and underlying surface from manned Soyuz 5 and 7 spacecraft

20 p3240 A71-39675

Earth orbital photography for geologic applications, discussing advantages over aerial photography 22 p3534 A71-41962

Limited interval definitions of photometric functions of lunar crater walls by photography from orbiting Apollo 11 22 p3603 A71-42187

Atmospheric wind speed estimation, using ATS geostationary satellite cloud photographs 22 p3535 A71-42411

Apollo 12 multispectral lunar photography experiment using four camera configuration, verifying by ground photoelectric photometry 23 p3761 A71-43780

SPACEBORNE TELESCOPES

Large aperture telescope in-orbit maintainability packaging, examining optical systems replacement tolerances and astronauts EVA mode accessibility 09 p1446 A71-22742

Large spaceborne telescope primary mirrors materials under microstructural loads, considering low expansion ceramics and metallics applications 09 p1446 A71-22743

Hot coronal components of solar active regions observations with satellite-borne grazing incidence X ray telescope, discussing emission dependency on photospheric magnetic field 12 p1954 A71-27707

Spaceborne astronomical telescope image stabilization system, utilizing field splitting technique 18 p2925 A71-36903

SPACECRAFT

Large space vehicle acoustic environment test facility, investigating combined direct and/or reverberant sound field effects 08 p1272 A71-21430

Space shuttle vehicles and assembly flow manufacturing, development and operations requirements, including ground rules, verification test facilities, cost reduction and interrelationships [AIAA PAPER 71-316] 10 p1590 A71-24831

Space shuttle facilities planning, discussing vehicles, overall assembly flow, manufacturing, tests and operations 18 p2926 A71-36478

SPACECRAFT ANTENNAS

Antenna and telemetry system for spherical shell ICBM reentry vehicles data link to ground 01 p0036 A71-10986

Unfurlable spacecraft antenna design with conical main and parabolic subreflector 02 p0232 A71-12324

Spacecraft phased arrays design, considering solid state amplifiers effect on total array performance and transistors and varactors output power efficiency 07 p1069 A71-18813

Optimum transmitted data volume, orientation accuracy and size of narrow beam parabolic spacecraft antennas, defining optimum parabola for approximate radiation pattern 07 p1078 A71-19871

Helios solar probe antenna system for S-band radio communication, discussing electrical and mechanical design 09 p1533 A71-23734

RAE satellite flexible boom vibration, obtaining antenna boom static deflection, natural frequencies and thermal bending effects [ASME PAPER 71-DE-J] 12 p1977 A71-27319

Omnidirectional broadband telemetry antenna array for spacecraft providing near isotropic circular polarized radiation with open line microstrip feed 14 p2199 A71-30907

Quasi-isotropic directional, omnidirectional and auxiliary antennas of Helios Solar Probe S band system, discussing design, radiation patterns, adaptability and X band measurements 14 p2217 A71-31052

Tape helix radiators for spacecraft phased antenna arrays, analyzing performance for proposed L band system 14 p2217 A71-31057

Near-isotropic six radiator antenna array for large aerospace vehicles, calculating three dimensional radiation distribution 14 p2218 A71-31066

Numerical prediction of radiation patterns for antennas mounted on spacecraft, noting booms and solar cell panels effects 14 p2218 A71-31068

SIRIO spacecraft cavity backed antenna around apogee motor nozzle operating at 40 and 360 MHz 14 p2218 A71-31069

Aerospace antenna design, calculating one-wavelength circular slot aperture radiation from circular cylindrical surface 14 p2206 A71-31075

Long thin spacecraft antennas and gravity gradient booms, explaining solar induced oscillations with lumped parameter and Lagrangian equation models 15 p2504 A71-31598

Short helical antenna performance and characteristics, discussing radiation patterns, efficiency, bandwidth and space vehicle use [ONERA-TP-950] 18 p2888 A71-36023

Spacecraft conical antenna design for planetary communications, investigating impact on other subsystems [AAS PAPER 71-151] 19 p3018 A71-37953

Oil for lubricating ball bearings in spacecraft antenna despin system, investigating weight loss, sorption, surface migration and contamination danger 20 p3184 A71-39352

SPACECRAFT CABIN ATMOSPHERES

Spacecraft cabin rare gas-oxygen atmosphere decompression effects on animal metabolic rates 06 p0853 A71-17956

Spacecraft cabin atmospheres, discussing controlled atmosphere composition, barometric pressure, physiological effects, trace constituents, fire hazards, etc 08 p1245 A71-20729

Ion exchange resin carbon dioxide removal and concentration system for space cabin environments, describing monitoring and control instrumentation 14 p2189 A71-30313

Materials selection for manned spacecraft, discussing environmental interactions between man, materials and atmosphere 16 p2601 A71-33874

Self contained one man module cell design and tests of electrochemical carbon dioxide concentrating system for space applications [ASME PAPER 71-AV-21] 18 p2867 A71-36388

Hydrogen depolarized fuel cell for space station prototype carbon dioxide concentrator, describing modular design concept and operation [ASME PAPER 71-AV-37] 18 p2870 A71-36404

Spacecraft cabin artificial atmospheric composition and variation effects on human immunocompetence, examining lymphoid cell immunity reactions after lymphocytes blast transformations 21 p3332 A71-40556

Oxidation of water in regeneration under spacecraft conditions, measuring organic impurities degree of oxidation in inhabited cabin atmospheric vapor condensates 22 p3506 A71-42814

SPACECRAFT CABIN SIMULATORS

Life support water management subsystem 4-man 90-day test in space station simulator with closed water and oxygen loops and no resupply [ASME PAPER 71-AV-6] 18 p2865 A71-36373

Composition and daily fluctuations of trace contaminants during 90-day space station simulator test [ASME PAPER 71-AV-17] 18 p2867 A71-36384

Oxygen generation system for 90-day space station simulator, considering carbon dioxide removal and reduction and water electrolysis [ASME PAPER 71-AV-18] 18 p2867 A71-36385

Manned 90 day test of closed chamber regenerative life support system simulator, describing subsystems, crew nutrition, hygiene, maintenance and leisure activities 22 p3503 A71-42043

SPACECRAFT CABINS

Feeding systems, potable water and waste disposal in space cabins 08 p1245 A71-20730

Crew performance as information input factor based on USAF two man space cabin research 09 p1400 A71-23245

Urine conservation in spacecraft cabin sanitation facilities by phenol-containing preparations, emphasizing PNF method for long period operation 22 p3507 A71-42822

SPACECRAFT COMMUNICATION

NT REENTRY COMMUNICATION

Carbon dioxide laser intersatellite communication systems as economical alternative to microwave and millimeter systems, noting use onboard ATS satellites 01 p0091 A71-10009

Scientific data transmission systems signal design considerations for Apollo lunar exploration missions 01 p0035 A71-10915

Unified S band communication system for manned space flight network ground stations 01 p0035 A71-10916

Telemetry and communications roles in Apollo flight operations, describing data system management 01 p0035 A71-10918

Marine traffic control via satellite telemetry, describing merchant and powered fishing fleet distribution and navigation requirements 01 p0125 A71-10978

Information collection from ocean data stations networks by satellite and HF digital data communications, noting feasibility of VHF telemetry communications 01 p0037 A71-10991

Ray tracing in warm collisionless magnetoplasmas based on wave dispersion relation, discussing satellite communication 01 p0137 A71-11612

Ultrawide bandwidth optical data relay link between earth satellites, discussing system design concept 02 p0214 A71-12024

Skyнет satellites in orbit communications, repeaters testing, describing test facilities, spacecraft communication subsystems operation, terminals calibration and atmospheric losses 02 p0218 A71-12440

Test terminal for Skyнет satellite communications, describing parabolic antenna, computer, receiver system, calibration program, etc 02 p0218 A71-12441

Test laboratory for Skyнет spacecraft communications subsystems at microwave frequencies 02 p0238 A71-12443

Spacecraft signal amplitude and phase modulation and fault diagnosis by VLF analysis 02 p0218 A71-12447

Satellite and earth station parameters effects on SPADE communication systems link budget, considering carrier power statistics, amplitude and phase nonlinearities 02 p0221 A71-12779

INTELSAT earth station operations via SPADE demand-assignment system, discussing interference requirements, frequency stability, gain flatness, etc 02 p0221 A71-12780

Shipborne satellite communications terminal, describing antenna, control and monitoring systems and performance characteristics 02 p0221 A71-12785

Earth station modifications for INTELSAT IV operation, discussing transmission parameters, distortion control, amplifier design, etc 02 p0221 A71-12786

Two stage parametric SHF amplifier for Skyнет V Naval receiver system 02 p0234 A71-12812

Linear low noise wideband frequency modulator for Intelsat 4 satellite telephony communication, considering channel capacity 02 p0234 A71-12819

Narrow band FM modems with high carrier frequency stability for satellite communication terminals with small dish antennas 02 p0234 A71-12820

Microstrip double down-converter receiver for satellite earth stations, describing thin film integrated circuits and carrier selection 02 p0235 A71-12835

S band transponder for vehicle-space-ground link subsystem /VSGLS/ of USAF integrated telemetry, tracking and command system 05 p0719 A71-16151

Artificial satellite HF radio wave ionospheric guided propagation, considering ray tracing based on geometric-optics treatment 05 p0720 A71-16229

Relativity and solar quadrupole moment effects in time delay measurements of signal traveling from earth to artificial satellites 05 p0808 A71-16446

Satellites interrogation, recording and location system for data acquisition from deployed remote instrumented platforms 05 p0743 A71-17134

Book on earth satellite telecommunications systems and international law covering historical, scientific, economic, legal and political background 06 p1010 A71-18020

Low noise temperature high gain satellite communication antenna feeds optimal design using stepped aperture 06 p0877 A71-18395

Ionospheric total electron content specification for satellite transponders time delay error reduction 07 p1095 A71-19002

Midlatitude scintillation diurnal and seasonal variations, using satellite communications data 07 p1095 A71-19003

Troposphere effects on radio wave propagation and satellite communication 07 p1059 A71-19010

Ships and aircraft position finding method based on satellite radio signals Doppler measurements, analyzing ionospheric influences 07 p1154 A71-19036

Onboard self adaptive multichannel data reduction for redundancy by oversampling [AIAA PAPER 71-232] 07 p1063 A71-19709

Data handling system with digital computer and multichannel scanning, processing and recording for simultaneously conducting two environmental tests of satellites 07 p1069 A71-20403

Optimal algorithmic coordination of spaceborne computer-transmitter coupling, using SIMSCRIPT language simulation 08 p1259 A71-21599

Noise stability of synchronous phase demodulator in satellite and tropospheric communications, considering threshold characteristics 09 p1413 A71-22146

Rendezvous equations near second lunar libration point, using Halo orbiting relay satellite for communication with spacecraft behind moon

09 p1521 A71-22912

Helios solar probe antenna system for S-band radio communication, discussing electrical and mechanical design

09 p1533 A71-23734

Large capacity ferrite core buffer memory for spacecraft telemetry temporary data storage, using access circuitry with multichip and thin film circuits

09 p1421 A71-23735

Australian satellite domestic telecommunications network design, discussing population distribution, existing systems and Intelsat 3 F-4

11 p1730 A71-25264

North Atlantic communications, navigation and ATC systems requirements for geostationary satellite operation, considering lifetime rated data and voice channels transmissions volume

11 p1839 A71-26332

Diurnal and seasonal variations of scintillations in short wave radio signals transmitted from earth satellites and spacecraft, noting relationship to ionospheric inhomogeneities

12 p1898 A71-26635

Satellite communication earth stations time division multiple access systems, discussing operational principles and configurations

12 p1895 A71-27000

Satellite communication earth stations tracking receiver, describing operational principles with special attention to down-converter and demodulator circuits

12 p1887 A71-27001

Analytic optimization of Cassegrain antennas of revolution used in satellite telecommunications

13 p2033 A71-29241

Transmitter clock phase lock loop for PCM-TDMA satellite communication system, applying to control system design having time lag

13 p2034 A71-29392

Acquisition system consisting of positioning of local station burst signal in time slot for PCM-TDMA satellite communication system, discussing design and performance tests

13 p2034 A71-29393

Combined data compression and error control by digital sequential decoding for space to earth data links using digital computers

14 p2193 A71-30023

Lunar roving vehicle telecommunication system requirements concerning vehicle functions, science experiments, crew operations and safety

14 p2200 A71-30915

Microstrip p-i-n diode controlled L band digital phase shifter for aircraft-satellite communication

14 p2217 A71-31055

Blade antenna linear array design for aircraft-satellite communication, determining mutual influences by array measurements in simulated electrical environment

14 p2206 A71-31062

Communication blackout during missile and spacecraft high altitude flight, considering convective effects on gas breakdown by microwaves

14 p2206 A71-31071

European satellite telecommunications network design, discussing shuttle-tug launcher use and economy

16 p2644 A71-32848

Apollo 14 communications support by USAF, discussing voice and data relay between spacecraft and control center, global weather support, cartographic and geodetic services, etc

16 p2541 A71-33178

Space station communications systems, discussing data relay satellites transmission paths to ground, multiple voice channels, two way color TV and onboard telephones

17 p2699 A71-34610

Multifunctional communications satellite for TV distribution and trunk line, domestic, aeronautical, maritime, small user and space vehicle services

17 p2699 A71-34613

FDMA single channel per carrier satellite communication system voice processing and modulation techniques, discussing analog frequency modulation and phase shift keying

17 p2704 A71-35086

Comparison of demand assignment multiple access/modulation techniques for satellite communication using high quality telephone channels

17 p2706 A71-35103

Satellite voice communications system for small terminals in remote areas, discussing feasibility, design, cost and frequency allocation

17 p2706 A71-35123

Intelsat satellite-earth station communications technology, considering microwave line of sight techniques

17 p2707 A71-35333

HEOS A-1 satellite telecommunication system, describing command, telemetry and ranging subsystems

18 p2875 A71-35984

Unilateralism in U.S. satellite communications policy, suggesting international cooperation for frequency spectrum management

18 p2986 A71-36165

Satellite communication role in disseminating information and promoting technology in underdeveloped countries

18 p2987 A71-36168

Satellite broadcasting to West African countries, discussing communications policies, NASA tracking stations in Africa and U.S.-Nigeria agreement for Comsat and Intelsat programs

18 p2987 A71-36169

South American contributions to satellite communication juridical problems solution, suggesting adherence to international law

18 p2987 A71-36170

International satellite broadcasting practices and laws, discussing effect on free information dissemination

18 p2987 A71-36171

Frequency memories application to earth-satellite-aircraft UHF communications, repeater apparatus and multiple access transmission of half tone images in worldwide satellite communication

18 p2881 A71-36553

Cassegrain antennas with reflector horn feed for satellite communication, noting gain and noise temperature

18 p2890 A71-36554

Digital filtering in PCM communication systems with active repeater satellites and space vehicle telemetry

18 p2881 A71-36569

Book on communication satellites technology covering satellite transponders, spacecraft antennas and subsystems, high power transmission, launch vehicles, digital techniques, earth stations, etc

19 p3149 A71-37271

Jupiter probe design and communication for deep penetration into atmosphere, concerning mission phases through entry and descent to sample altitudes

19 p3153 A71-37946

Space communications period forecasting algorithm for limited power ground based transmitters and spacecraft in earth orbit

19 p3022 A71-38502

Narrow beam acquisition and angle tracking for spaceborne laser communication links between low earth orbiting and synchronous satellite

21 p3348 A71-40805

Spacecraft communication cut-off during atmospheric reentry due to thermal ionization of gas boundary layer, discussing sulfur hexafluoride injection alleviation and electrostatic probe

22 p3583 A71-41998

SkyLab program data management systems, discussing onboard data collection, transmission and ground facilities

22 p3610 A71-42007

Jupiter atmospheric probe using relay-link communications geometry between probe and flyby spacecraft for 3.5 hr intervals

23 p3726 A71-42995

Simultaneous ionosphere measurements by incoherent ground radio wave scattering and coherent signals from Intercosmos 2 and Cosmos 321 satellites

24 p3824 A71-45323

SPACECRAFT COMPONENTS

NT COMMAND MODULES

NT LANDING MODULES

NT LUNAR LANDING MODULES

NT LUNAR MODULE

NT MARS EXCURSION MODULE

NT SERVICE MODULES

NT SPACECRAFT CABINS

NT SPACECRAFT MODULES

ESRO/ELDO space documentation service involving NASA file remote processing and data bank for space component selection

07 p1225 A71-20001

Lightweight oxidation resistant carbon-carbon composites for space shuttle leading edge components thermal protection

11 p1790 A71-26231

Solar simulator with wide range irradiation strength variability for laboratory investigation of radiation effects on spacecraft components

12 p1894 A71-26982

Component assembly effect on dynamic stability of liquid propellant rocket engine spacecraft during thrust sections of trajectory

16 p2646 A71-33657

Orbital nonpropulsive vent system to remove excess or residual propellant vapors and waste gases with minimum impulse imbalances imparted to vehicle

18 p2973 A71-36454

Communication satellite components reliability assurance method, discussing production and qualification tests

18 p2890 A71-36538

SPACECRAFT CONFIGURATIONS

NT APOLLO TELESCOPE MOUNT

NT SATELLITE CONFIGURATIONS

OART research projects covering space shuttle, vehicle configuration, heat transfer, thermal protection, lifting bodies, electronics, power studies, etc

04 p0661 A71-14931

Space shuttle technology, discussing wind tunnel studies, aerothermal and operational flight mechanics, model characteristics, orbiter configurations and booster-orbiter separation

07 p1209 A71-20227

Space shuttle structures and materials, considering booster arrangements thermal protection, high temperature metals and composite materials

07 p1216 A71-20228

Structurally similar models, investigating space vehicles dynamic characteristics

09 p1532 A71-22658

Space vehicles dimensions effects on working fluid mass and power required for orientation

09 p1532 A71-23133

European research on reentry vehicle configurations, noting French concentration on flow fields and German emphasis on overall shape and control surfaces

10 p1684 A71-24848

Space shuttle phase B design, discussing British-American cooperation, fly-back orbital laboratory and Apollo 14 zero-gravity demonstration

11 p1839 A71-26320

Permanent orbital space station design proposal for launch in latter 1970s, discussing systems concepts and configurations

14 p2320 A71-30422

Lenticular reentry vehicle configuration, considering aerodynamics, trajectory heating and weight analysis and structural design

15 p2500 A71-31604

Phobos and Deimos missions, examining lander and lander/orbiter configurations and Titan-Centaur and space shuttle-Centaur launch systems

17 p2802 A71-34716

Venus planetology missions, discussing objectives, experimental packages, payloads, costs and entry/lander configurations

17 p2802 A71-34717

Single sortie or clustered mode orbital space stations systems safety, noting effects on operations, configurations and design

17 p2814 A71-35425

Artificial g space station configurations, developing movable control mass attitude stabilization system

18 p2971 A71-36277

Aerodynamic characteristics of space shuttle configurations over entire flight velocity range, stressing coupling effects of control surfaces at large angles of attack

18 p2972 A71-36437

Grand Tour spacecraft configuration design involving system requirements, communications, power, guidance, etc

19 p3152 A71-37924

Mariner 9 spacecraft mission, discussing configuration, data handling and TV surface mapping of Mars

24 p3876 A71-45267

SPACECRAFT CONSTRUCTION MATERIALS

Fiber reinforced composites application in aerospace and aircraft, discussing boron and graphite and cost effectiveness

01 p0103 A71-11277

Boride composites with high strength and thermal resistance suitable as nose cap and leading edge materials for reusable lifting reentry systems

01 p0109 A71-11282

Be mechanical and physical properties, corrosion behavior, toxicity, fabrication and application as aircraft and spacecraft structural material

01 p0104 A71-11539

Multilayer insulation systems for cryogenics protection aboard spacecraft, considering mechanical properties, radiation shielding, component evacuation rate and outgassing

08 p1375 A71-21748

Full scale models, nonflammable materials and tests for manned space expandable structures including airlocks, transfer tunnels, station modules, lunar shelters and flexible windows

11 p1744 A71-25275

Spacecraft thermal control coatings for long-duration exposure to near-earth orbital conditions, determining optical properties degradation and solar absorptance

11 p1859 A71-26237

Space shuttle comparison with transport aircraft, discussing high thermal resistant and cryogenic insulator material concepts, with application to Concorde structural computations

12 p1973 A71-27605

Materials selection for manned spacecraft, discussing environmental interactions between man, materials and atmosphere

16 p2601 A71-33874

Premium mechanical properties for materials in space shuttle orbiter project, emphasizing cost and weight reductions

18 p2979 A71-36465

Reinforced plastics for aerospace applications, giving special attention to heat shield and inflatable structures materials

19 p3085 A71-38069

Polymer materials for aerospace construction, considering behavior in cryogenic and high temperature environments

22 p3564 A71-41510

Metal embrittlement by gaseous hydrogen, discussing countermeasures against hydrogen metal interaction and cracking

22 p3562 A71-41999

SPACECRAFT CONTAMINATION

Lunar Module Ag coated stranded Cu wire, analyzing fluorine contamination with proton microprobe

02 p0209 A71-12592

Orbital environment contamination and effect on optical instruments and astronomical experiments in Skylab Program

[AIAA PAPER 71-74] 06 p0902 A71-18531

Quadrupole mass spectroscopy of spacecraft critical surfaces vapor contamination, using lubricating oil covered titanium dioxide colorimetric sample

10 p1609 A71-23930

Optical ground contamination monitoring devices for Apollo Telescope Mount collecting time-line and integrated data

[AIAA PAPER 71-458] 11 p1764 A71-26240

Spacecraft windows optical degradation from contamination with condensed particles, presenting light scatter measurement results

[AIAA PAPER 71-472] 11 p1833 A71-26252

Solar absorptance sensitivity to thermal surface particulate contamination as function of particle composition, quantity, size and linearity with obscured area

[AIAA PAPER 71-473] 11 p1800 A71-26253

Spacecraft surface contamination, noting effects on thermal control and optical equipment

[AIAA PAPER 71-457] 11 p1840 A71-26421

Planetary quarantine including background, program evolution, sterilization technology and contamination sources

16 p2537 A71-33744

Planetary quarantine analysis for unmanned Mars orbiter, considering accidental spacecraft impact, loose particles and gases used for attitude control and pressurization

16 p2537 A71-33799

Long mission duration manned spacecraft contaminant control system design, discussing catalytic, oxidation, chemisorption and charcoal adsorption removal techniques and computerized performance prediction

[ASME PAPER 71-AV-19] 18 p2867 A71-36386

Oil for lubricating ball bearings in spacecraft antenna despun system, investigating weight loss, sorption, surface migration and contamination danger

20 p3184 A71-39352

Surface cover materials thermal radiation characteristics and radiation resistance of plastics and solar cells, discussing friction in vacuum and spacecraft surface contamination by outgassing

20 p3210 A71-39453

Biosphere contamination, discussing sterilization and quarantine experiments at Lunar Receiving Laboratory, flight crew testing and microbiological studies

21 p3448 A71-40569

Surveyor 3 surfaces discoloration and lunar dust contamination, noting Apollo 12 lunar module caused disturbances by on-site observation

23 p3766 A71-43816

SPACECRAFT CONTROL

NT SATELLITE ATTITUDE CONTROL

NT SATELLITE CONTROL

Spacecraft navigation, guidance and control for manual rendezvous with orbiting target, examining error sources perturbing effects

01 p0022 A71-10513

Mission requirements in decision processes for guidance and control system design of aerospace vehicles

[AIAA PAPER 70-1231] 01 p0126 A71-11301

Axisymmetric spacecraft fuel optimal reorientation control by reaction jets determined using Pontryagin maximum principle

01 p0165 A71-11586

N-body real time trajectory simulation of Apollo Command and Service module G and C systems and mission

02 p0237 A71-11793

Control programs realizability for optimal escape trajectories of low thrust vehicles with motion about mass of center and with or without artificial gravity

02 p0319 A71-11905

Skylark sounding rocket attitude control by three axis star pointing system, using strapdown gyro and plus 5 magnitude stellar sensor

[AIAA PAPER 70-1401] 03 p0455 A71-13682

Spacecraft attitude suboptimal control by orthogonal set of amplitude limited PWM reaction control jets, presenting spacecraft controlled motion computer simulation

[AIAA PAPER 70-997] 03 p0499 A71-13722

Mariner Mars 1969 navigation, guidance and control systems design, mechanization and flight testing

03 p0455 A71-14073

Spacecraft and aircraft automatic control man machine interface, bionics and traffic control systems

03 p0455 A71-14393

Spin stabilized spacecraft fuel optimal direction cosine attitude control, considering relation to inertial system

03 p0500 A71-14448

Space capsule reentry into Martian atmosphere for soft landing, using onboard nonlinear filter and stochastic control for random wind gusts

03 p0500 A71-14479

Spacecraft attitude control system with inertia wheels, determining stability by decomposition method

04 p0663 A71-15300

Pulsed plasma thruster system as secondary propulsion unit for spacecraft attitude, station and trajectory control

04 p0638 A71-15325

Space vehicle local orientation by method of least squares determination of matrix for conditions of orthogonality, assuming random measurement errors

05 p0815 A71-16035

Reentry vehicle angle of attack control by mechanically varying center of mass for axial loads

05 p0779 A71-16039

Algorithm for spacecraft rotational maneuver control based on single turn around specific axis, using onboard computer

05 p0816 A71-16176

Delta booster second stage packaged attitude control three-axis system, discussing electronic implementation for gyroscopic action control

05 p0818 A71-17138

Drag free spacecraft performance in deep space, examining inner residual disturbance forces for motion control systems

[ONERA-TP-887] 06 p0900 A71-18022

Lunar module digital autopilot design, considering attitude state estimator, reaction control system and thrust vector control

[AIAA PAPER 70-991] 07 p1154 A71-18897

Apollo 12 Lunar Module high landing accuracy, discussing control actions, trajectory error sources and power descent

07 p1206 A71-19086

Automatic control in space - Conference, Toulouse, March 1970

07 p1154 A71-19526

Computer requirements of self contained guidance, navigation and control system onboard manned orbital space station

[AIAA PAPER 71-221] 07 p1155 A71-19702

Spacecraft attitude control microthrusters utilizing catalytically reactive gas mixtures during pulse mode and steady state operation

[AIAA PAPER 70-614] 07 p1183 A71-19859

Phase change solidification phenomena in n-hexadecane for spacecraft thermal control systems, considering two or three dimensional models

07 p1223 A71-19876

Lunar Module physical characteristics and control system function, emphasizing automated vs manual flight degree and astronaut overriding capability

07 p1208 A71-19915

Interactive Saturn flight program simulator for real time graphics operations of navigation, guidance, engine control, event sequencing and communications

08 p1272 A71-21237

Earth-moon libration point space station optimal control, considering restricted four body problem

08 p1363 A71-21323

Coupled control of space vehicle orientation with reference to three celestial bodies, reducing plane vibrations to dynamic third order system

09 p1491 A71-22547

Spacecraft autonomous control algorithm to ensure geographically specified landing accuracy, noting atmospheric density

09 p1491 A71-22565

Multistage rockets terminal control synthesis based on linear functionals

09 p1532 A71-22660

Liquid sloshing in liquid propellant containing orbiting vehicle stabilized by active control system, examining expression for ring baffle slosh damping under reduced gravity

09 p1532 A71-22913

Heat pipe applications for space vehicle thermal control, discussing spacecraft radiators, thermal exchangers and structure isothermalization

11 p1856 A71-26205

Adaptive roll control of space vehicle on reentry trajectory, analyzing spacecraft angular motion dynamic equations for optimal conditions determination

12 p1926 A71-26719

Computerized automatic control system for atmospheric reentry, combining computational prediction of motion parameters with closed loop feedback

12 p1926 A71-26720

Spacecraft attitude measurement using spatial coherence of laser or star light beam, discussing feasibility and detection equipment

12 p1927 A71-27429

Space vehicles solar orientation sensors, discussing construction, configuration and direction finding characteristics

12 p1972 A71-27485

Control programs reliability for optimal escape trajectories of low thrust vehicles with motion about mass of center and with or without artificial gravity

13 p2144 A71-28192

Spacecraft optimal atmospheric reentry trajectory for minimum flight distance, investigating angle of attack control with allowance for load constraints

13 p2143 A71-29229

Apollo cislunar navigation capability and procedures, describing onboard data acquisition and digital processing equipment

13 p2098 A71-29386

Control, navigation and guidance review, considering application of earth reference coordinates for aircraft, missiles and spacecraft

14 p2272 A71-30710

Spacecraft local attitude determination from measurements with random errors by least squares method

16 p2645 A71-33439

Spacecraft reentry trajectory angle of attack control by mechanically varying center of mass for axial loads

16 p2645 A71-33443

Spacecraft banking control during reentry, deriving dynamic equations of angular motion

16 p2646 A71-33655

Dynamic stability of controlled spacecraft with liquid propellant rocket engines, considering acceleration and braking sections of trajectory

16 p2646 A71-33656

Controlled motion dynamics of spacecraft performing maneuvers, applying point transformation to third-order nonlinear system moving about center of mass in lateral motion

16 p2646 A71-33658

Pulsed relay control system for stabilizing spacecraft orientation in flight, allowing for changes in characteristics of guidance sensor systems and slave mechanisms

16 p2646 A71-33660

Optimal control algorithm for spacecraft descent in atmosphere at speed near escape velocity, using game theory

16 p2646 A71-33702

Apollo real time control center large software systems development management covering implementation, integration, testing, operation and maintenance

17 p2710 A71-34620

Quaternon representation of successive rotations in space vehicle control, locating final position of coordinate frame with respect to original position

17 p2773 A71-35066

Lunik 16 and 17 automatic lunar landing stations and Lunokhod-1 lunar surface vehicle, describing propulsion systems, control elements and scientific equipment

17 p2724 A71-35401

Fluidic gyroscope technology, reviewing current development and problems associated with severe environmental conditions affecting inertial guidance and spacecraft control

18 p2922 A71-36482

Lifting entry trajectory control law based on uniform drag, affording heating rate and deceleration control

[AIAA PAPER 71-915] 19 p3096 A71-37165

Space shuttle boost vehicle with various degrees of aerodynamic stability, discussing control laws effects on rigid body bending moment tradeoff

[AIAA PAPER 71-918] 19 p3147 A71-37167

Breadboard attitude control system for scale model space station using control moment gyros

[AIAA PAPER 71-935] 19 p3097 A71-37180

Gravity gradient desaturation of momentum exchange attitude control system, considering control moment gyros and reaction wheels

[AIAA PAPER 71-940] 19 p3098 A71-37185

Gimballed reaction wheel for spacecraft accurate attitude stabilization and control

[AIAA PAPER 71-950] 19 p3098 A71-37191

Twin wheel momentum bias/reaction jet spacecraft attitude control system, presenting mathematical model, stability analysis and design

[AIAA PAPER 71-951] 19 p3099 A71-37192

Active precession control devices for spin stabilized spacecraft, noting energy dissipation effect

[AIAA PAPER 71-952] 19 p3148 A71-37193

Integrated system for precision attitude determination and pointing control of spacecraft gimballed payloads

[AIAA PAPER 71-962] 19 p3099 A71-37203

Full mission engineering simulator/flight controls integration laboratory utilization in Apollo program, describing equipment for control systems testing, monitoring and troubleshooting

[AIAA PAPER 71-970] 19 p3040 A71-37211

- Solar rudder for spacecraft steering in form of right circular cone with ideally reflecting surface
20 p3306 A71-39136
- Spacecraft manual control investigation, using human operator models described by linear transfer function with variable coefficients
20 p3193 A71-39226
- Thrusting lifting orbital vehicle nonlinear longitudinal dynamics in near-circular orbit, deriving orbital elements variation behavior and angle of attack mode period and damping
21 p3454 A71-40094
- Europa 3 electrical system as integrated vehicle control system using central processor and data bus
22 p3608 A71-41957
- Spacecraft pointing control system with momentum exchange controllers, considering near optimal control policy for control moment gyro system
22 p3608 A71-41966
- Spinning and dual spin spacecraft angular momentum and axis control, investigating optimal fuel and small angle reorientation techniques
22 p3611 A71-42045
- Analysis and stability of multiloop attitude control systems for flexible spacecraft
23 p3773 A71-44091
- Space vehicle low thrust minimum terminal variance guidance problem reduced to stochastic bang-bang optimal control system
23 p3702 A71-44101
- Jump type behavioral uncertainties in stochastic optimal control problems, considering control of spinning spacecraft
23 p3659 A71-44112
- Parabolic velocity atmospheric reentry navigation algorithm for spacecraft control, demonstrating guidance accuracy to landing point
24 p3846 A71-45304
- Spacecraft motion control algorithm for reentry at escape velocity based on object motion model
24 p3846 A71-45305
- ### SPACECRAFT DESIGN
- #### NT SATELLITE DESIGN
- Compact aerodynamic reentry vehicle development problems and costs, discussing lifting body vehicle for wind tunnel, ground and flight tests and reentry trajectories
02 p0320 A71-12066
- SkyLab design and mission objectives, describing attitude control, MDA, quarters, Apollo telescope mount and proposed experiments
02 p0321 A71-12738
- Black Brant 3B sounding rocket design and development, discussing payload capability, static and dynamic stability, flight and ground handling loads
[AIAA PAPER 70-1396] 03 p0499 A71-13677
- Spacecraft structural design and thermal control, discussing requirements and responsibilities of designer
03 p0499 A71-13741
- Apollo Applications Program command and service module test requirements to achieve reliable hardware for extended missions
[AIAA PAPER 70-378] 03 p0500 A71-14436
- Single stage to orbit space shuttle system/SERV/concept with VTOL capability, discussing configurational and operational characteristics with emphasis on flexibility and versatility
04 p0664 A71-15336
- Manned space vehicle unsteady aerodynamics, considering flow separation, vortex interference, shock and stall flutter problems in space shuttle design
04 p0526 A71-15337
- Unmanned scientific missions to outer planets in late 1970s, discussing instruments requirements, flight paths, spacecraft designs and payloads
04 p0649 A71-15347
- Optimization of multistage rockets with given payload, propellants and explosive separation of stages
05 p0817 A71-16613
- Delta shuttle orbiter for space transportation system, discussing structural design and economic aspects with reference to future space programs
05 p0819 A71-17227
- Soviet book on manned space flight covering spacecraft design, life support systems, mission characteristics, medical considerations, etc
06 p0864 A71-18700
- Economical reusable space shuttle development for cargo and passenger transportation to and from orbit
07 p1206 A71-19090
- Toxicology in aerospace vehicles design and operation, discussing occupational exposures, propellant operations, medical aspects, hazards, etc
08 p1244 A71-20712
- Space shuttle as post-Apollo key project for technology advancement, discussing predesign studies and technical problem areas in propulsion, materials, structures and avionics
09 p1531 A71-22273
- Space shuttle design, emphasizing reliability and safety
[AIAA PAPER 71-303] 09 p1531 A71-22617
- Hybrid coordinate formulation for flexible space vehicle attitude control system design
[AIAA PAPER 70-20] 09 p1532 A71-22907
- SkyLab workshop as orbital manned platform for scientific investigation, discussing system design details and technical evaluation
10 p1682 A71-24276
- Atmospheric seal leakage control tests for long orbital lifetime space station designs, discussing vacuum chamber monitored pressure shell penetrations
[AIAA PAPER 71-337] 11 p1836 A71-25316
- Papers on heat transfer and spacecraft thermal control covering solid-vacuum interfaces thermal and visible radiation properties, multilayer insulation, thermal control devices, etc
11 p1854 A71-25360
- Unmanned lunar logistics vehicle for extended manned lunar exploration station, discussing general design, propulsion and control systems
[AIAA PAPER 70-613] 11 p1838 A71-25529
- Numerical and scale modeling interaction for spacecraft thermal design verification
[AIAA PAPER 71-439] 11 p1838 A71-26227
- System and component models for spacecraft thermal control design, considering materials, environmental degradation, measurement errors, manufacturing and quality assurance
[AIAA PAPER 71-456] 11 p1859 A71-26239
- Space shuttle phase B design, discussing British-American cooperation, fly-back orbital laboratory and Apollo 14 zero-gravity demonstration
11 p1839 A71-26320
- Post Apollo program European participation in space tug design and orbiter model flight tests, considering mini shuttle support applications
11 p1839 A71-26331
- Spacecraft systems radiation hardening design, discussing Tiros satellite mission hazards and space exposure prediction for electronic parts, using flow chart rationale
11 p1839 A71-26333
- Analytical method for optimal rocket motors cluster arrangement in multistage spacecraft, considering horizontal trajectories rated terminal velocity performance
11 p1839 A71-26335
- Reusable Nuclear Shuttle using NERVA nuclear engine for low cost transportation to lunar and geosynchronous orbit, discussing design, operation, tests and problems
11 p1840 A71-26516
- Earth-to-orbit space shuttle booster and orbiter unit design considerations including low development cost, risk and time, weight and payloads
11 p1840 A71-26529
- Space shuttle thermal protection systems, discussing design requirements and constraints, materials selection, tradeoff and cost effectiveness studies
12 p1971 A71-26984
- NASA evaluation of reports on space shuttles, discussing booster and orbiter design, mission requirements, payload capabilities, reusability, etc
14 p2320 A71-30421
- Permanent orbital space station design proposal for launch in latter 1970s, discussing systems concepts and configurations
14 p2320 A71-30422
- Reusable nuclear shuttle design, considering various propellant tank configurations and expendable/reusable launch modes with respect to performance, development cost and cost effectiveness
[AIAA PAPER 71-640] 14 p2273 A71-30717
- NASA space station design, describing operational procedures, structure, meteoroid, thermal and radiation insulation and living quarters
15 p2498 A71-31137
- SkyLab program organization and management, system design, operations and equipment
15 p2499 A71-31457
- Apollo Lunar Module design evolution, considering mission requirements, reliability objectives, environmental factors, manned operation, weight and configuration
15 p2500 A71-31603
- Magnetic shield design for protecting cylindrical space vehicle from space electron radiation, using simulator for engineering data
15 p2500 A71-32042
- Apollo 15-17 CSM design modifications, discussing increased mission duration capability, lunar orbital science instruments operation and weight increase
[AIAA PAPER 71-821] 17 p2812 A71-34723
- Space shuttle economic and design impact on satellite payloads, noting variations in flight frequency and cost, hardware and performance
[AIAA PAPER 71-807] 17 p2813 A71-34732
- Reusable nuclear shuttle concepts, performance and design requirements
17 p2813 A71-35072
- Reusable nuclear shuttle guidance and control system requirements, using nuclear engine thrust pulse train for guidance
17 p2774 A71-35073
- Single sortie or clustered mode orbital space stations systems safety, noting effects on operations, configurations and design
[AIAA PAPER 71-826] 17 p2814 A71-35425
- Space shuttle auxiliary propulsion subsystems for attitude control, orbit maneuvering and power supply, discussing design requirements with emphasis on fail-operational and fail-safe criteria
[AIAA PAPER 71-661] 17 p2795 A71-35624
- Wide heat load range space radiator design for space mission environmental control/life support system, using stagnation control
[ASME PAPER 71-AV-5] 18 p2865 A71-36372
- Solar-array space station environmental control and life support system design for 12-man 10-year mission capability with 180-day resupply
[ASME PAPER 71-AV-12] 18 p2866 A71-36379
- SkyLab life support systems design and performance prediction covering thermal and humidity control, atmospheric supply, carbon dioxide removal, water and waste management
[ASME PAPER 71-AV-14] 18 p2866 A71-36381
- Space shuttle environmental control and life support system design covering atmospheric pressure, composition, humidity, temperature, water and waste management
[ASME PAPER 71-AV-16] 18 p2867 A71-36383
- Long mission duration manned spacecraft contaminant control system design, discussing catalytic, oxidation, chemisorption and charcoal adsorption removal techniques and computerized performance prediction
[ASME PAPER 71-AV-19] 18 p2867 A71-36386
- Thermal design, analysis, testing and flight performance of ITOS-1 spacecraft, noting fail-safe temperature regulation
[ASME PAPER 71-AV-23] 18 p2868 A71-36390
- Design and performance testing of arterial wick circular heat pipes for OAO-C spacecraft
[ASME PAPER 71-AV-26] 18 p2868 A71-36393
- Prototype space station environmental thermal control and life support system digital simulation for transient design and performance prediction
[ASME PAPER 71-AV-34] 18 p2869 A71-36401
- Space shuttle booster configuration design, comparing stowed, fixed straight and delta wing approaches, discussing air breathing engines, stage mating, fins, etc
18 p2972 A71-36444
- Roving vehicle design for 1979 Mars mission
18 p2988 A71-36445
- Computer simulation model for experimental data in post-SkyLab space station design
18 p2973 A71-36458
- Space shuttle design concerning fault detection and isolation, redundancy and maintenance for cost and downtime minimization by application of airline methods
18 p2900 A71-36480
- Commercial aircraft reliability and maintainability design philosophy application to reusable space vehicles, considering optimum redundancy, dispatch with component inoperative and fault isolation
18 p2973 A71-36481
- Medical physiological requirements of angular velocity and g level for artificial gravity creation by rotating space vehicle, considering human tolerances and vehicle design
[AIAA PAPER 71-871] 18 p2870 A71-36627
- Architectural and environmental design tools for space system habitability, discussing work and living areas, hygienic facilities, etc
[AIAA PAPER 71-879] 18 p2871 A71-36632
- Coriolis forces influence on rotating spacecraft design, estimating relationships between coriolis force, artificial g, rotational radius and speed and velocity of motion
[AIAA PAPER 71-889] 18 p2871 A71-36638
- Space transportation system design concept based on reusable engines and partially external expendable tankage/REPEAT, discussing economic factors
19 p3147 A71-37125
- U.S. and U.S.S.R. space stations with European participation, discussing design, international cooperation and legal and political problems
19 p3149 A71-37305
- Jupiter orbiters and probes noting objectives, spacecraft design and mission description
[AAS PAPER 71-103] 19 p3152 A71-37905
- Grand Tour spacecraft configuration design involving system requirements, communications, power, guidance, etc
[AAS PAPER 71-149] 19 p3152 A71-37924
- TOPS spacecraft parts and technology development, reliability and contribution to long life system design
[AAS PAPER 71-159] 19 p3152 A71-37928
- Multipoint gravity assist grand tours in outer solar system, discussing launch opportunities and mission effects on spacecraft design
[AAS PAPER 71-102] 19 p3140 A71-37932
- Outer planet exploration spacecraft subsystems reliability and ten year flight requirements for planet orbiting and flyby missions
[AAS PAPER 71-112] 19 p3140 A71-37934

Jupiter probe design and communication for deep penetration into atmosphere, concerning mission phases through entry and descent to sample altitudes [AAS PAPER 71-143] 19 p3153 A71-37946

Jupiter entry probe integration on TOPS and Pioneer outer planet spacecraft for flyby missions, discussing design feasibility and spacecraft modification requirements [AAS PAPER 71-153] 19 p3153 A71-37955

Spacecraft electronic equipment design for reliability in long duration space missions [AAS PAPER 71-155] 19 p3153 A71-37956

Parts qualification and acceptance for outer planet mission spacecraft, minimizing random and wear-out failures to meet weight and other constraints [AAS PAPER 71-161] 19 p3153 A71-37958

Multilayer insulation systems development and selection for cryogenics thermal protection on space vehicles, considering mechanical properties, radiation shielding, components, evacuation rate and outgassing [AAS PAPER 71-171] 19 p3171 A71-38547

Critical solar cell battery power system design parameters and performance characteristics affecting post 1977 satellites and manned vehicles design [AAS PAPER 71-179] 20 p3179 A71-38902

Viking Lander power system design, discussing functional requirements by mission and science objectives and reliability features [AAS PAPER 71-181] 20 p3181 A71-38940

Polyvinyl chloride foam insulation system for liquid hydrogen-liquid oxygen space vehicles tested under groundhold and simulated flight conditions [AAS PAPER 71-183] 20 p3253 A71-39269

Mission tasks and design problems of European space tug, considering geostationary transfer missions and cargo bay geometry [AAS PAPER 71-185] 21 p3454 A71-40158

Attitude control propulsion system for booster and orbiter of space shuttle in European participation package [AAS PAPER 71-187] 21 p3454 A71-40159

Spacecraft-borne high voltage system breakdown prevention by avoiding high electric field and critical gas pressure [AAS PAPER 71-189] 21 p3358 A71-41192

Space transportation orbiter design covering thermal protection, aerodynamics and cross range problems during earth reentry [AAS PAPER 71-191] 22 p3609 A71-41979

Spacecraft and payload design under influence of space shuttle availability, discussing program cost savings [AAS PAPER 71-193] 22 p3610 A71-42003

Outer planet explorers design for Grand Tour mission, discussing launch parameters, flight paths, environmental hazards, communications, ground control, navigation and power generation [AAS PAPER 71-195] 22 p3601 A71-42028

Solar electric multimission spacecraft design, discussing off-optimum propulsion parameters effects on low thrust performance by characteristic surface representation [AAS PAPER 71-197] 23 p3772 A71-42998

Space shuttle optimal design problem, applying accelerated gradient parameter optimization technique [AAS PAPER 71-199] 23 p3727 A71-43002

Reusable space transportation shuttle system, discussing design, operation, military uses, contract competition, economic analysis and political factors [AAS PAPER 71-201] 23 p3784 A71-43353

Design parameter optimization for two-stage space shuttle atmospheric flight from spherical nonrotating earth by sequential straight line approximation [AAS PAPER 71-203] 23 p3774 A71-44115

Space vehicle radiative cooling system rib temperature field calculation, taking into account material heat conductivity temperature dependence [AAS PAPER 71-205] 24 p3889 A71-45023

SPACECRAFT DOCKING

Apollo simulator navigation and docking training techniques, discussing manned LM and CSM key role performance [AAS PAPER 71-207] 07 p1156 A71-20342

Space shuttle propulsion systems, describing main engine prototype designs, booster attitude and docking control systems [AAS PAPER 71-209] 12 p1946 A71-27606

On-orbit payload handling for space shuttles, including manipulator arms for drawing docking vehicles together, closed circuit TV and airlocking [AIAA PAPER 71-811] 17 p2814 A71-35427

Salut 1/Soyuz 10 mission, discussing configuration, size orbits and docking procedure [AAS PAPER 71-211] 18 p2975 A71-36685

Space transport rendezvous and docking techniques, emphasizing guidance, propulsion system configuration and sensors [AAS PAPER 71-213] 19 p3149 A71-37306

Satellite docking systems, discussing laser radar feasibility and device design [AAS PAPER 71-215] 19 p3149 A71-37307

European unmanned interorbital tug, investigating configurations, structure, hookup system, docking and propellant supply [AAS PAPER 71-217] 19 p3150 A71-37309

Requirements and opportunities for comet and asteroid missions including flyby, rendezvous, docking and sample return [AAS PAPER 71-104] 19 p3139 A71-37906

Salut space station design, operation and mission, describing docking and undocking procedures for Soyuz 11 supply craft [AAS PAPER 71-106] 19 p3153 A71-38148

Docking with passive orbiting spinning or tumbling objects for space debris elimination and space rescue operations, describing remotely controlled despinning and retrieval methods [AAS PAPER 71-108] 22 p3610 A71-42005

SPACECRAFT ELECTRONIC EQUIPMENT

NT AIRBORNE/SPACEBORNE COMPUTERS

Remote modules for spacecraft analog/digital telemetry distributing multiplexer input gates [AAS PAPER 71-110] 01 p0036 A71-10988

Space shuttle integrated electronic onboard and ground reusable systems design, considering data flow management, checkout, computer decentralization, electronic switching and redundancy [AAS PAPER 71-112] 02 p0231 A71-11978

Soyuz spacecraft command cabin equipment, describing control panel, command signal systems and routine operations [AAS PAPER 71-114] 03 p0497 A71-13196

Intelsat 3 satellite mechanical and electronic components fabrication, emphasizing quality and reliability assurance procedures and assembly techniques [AAS PAPER 71-116] 06 p0905 A71-18403

Variable conductance inert gas type heat pipe for spacecraft electronic equipment fine temperature control, noting design to eliminate start-up problems [AIAA PAPER 71-422] 11 p1857 A71-26213

Spacecraft electric systems semiconductor devices radiation damage from high energy particles during space missions, noting radiation resistant devices development possibility [AAS PAPER 71-424] 12 p1943 A71-26981

Sirio B European communication satellite, discussing electronic equipment for simultaneous multichannel telephony and color TV transmission [AAS PAPER 71-426] 14 p2319 A71-29820

Spacecraft electronic equipment design for reliability in long duration space missions [AAS PAPER 71-155] 19 p3153 A71-37956

Earth resources experiments package electromagnetic compatibility with Apollo Applications Program [AAS PAPER 71-157] 19 p3032 A71-38453

Interplanetary navigation TV camera in-flight calibration, discussing instrument error sources elimination [AAS PAPER 71-159] 22 p3573 A71-42771

Thick film hybrid microcircuits for spacecraft electronic systems component reliability [AAS PAPER 71-161] 23 p3650 A71-43123

SPACECRAFT ENVIRONMENTS

Cosmonaut water supply and regeneration in spacecraft using self contained biological cycle [AAS PAPER 71-163] 01 p0025 A71-11150

Lethal recessive point mutation in *Drosophila melanogaster* eggs on Zond 5 spacecraft [AAS PAPER 71-165] 01 p0018 A71-11552

Spacecraft structural design and thermal control, discussing requirements and responsibilities of designer [AAS PAPER 71-167] 03 p0499 A71-13741

Cylindrical shell spacecraft thermal control coating system optimization, using truncated series representation [AAS PAPER 71-169] 03 p0499 A71-14151

Permanent magnets for footwear restraint and mobility in zero gravity spacecraft, testing neutral buoyancy and six degree of freedom simulation effects [AAS PAPER 71-171] 07 p1048 A71-19607

Spacecraft cabin atmospheres, discussing controlled atmosphere composition, barometric pressure, physiological effects, trace constituents, fire hazards, etc [AAS PAPER 71-173] 08 p1245 A71-20729

Steady one dimensional temperature field of cylindrical shell spacecraft, allowing for heat conduction and convective and radiative heat transfer within shell [AAS PAPER 71-175] 09 p1546 A71-23148

Orbiting Biosatellite 3 monkey environmental and physiological parameters circadian rhythms, investigating desynchronization or arrhythmia [AAS PAPER 71-177] 09 p1395 A71-23241

Temperature uncertainties determination in spacecraft thermal analysis, using influence coefficients obtained from steady state heat balance equation [AAS PAPER 71-179] 11 p1858 A71-26219

Manned space station optimal thermal control design, investigating heat pipe and semipassive/air cooled concepts [AAS PAPER 71-181] 11 p1838 A71-26220

Space station thermal control system design, verifying radiator adequacy by parametric computer analysis with allowance for thermal coating degradation, vehicle attitude and other variables [AAS PAPER 71-183] 11 p1858 A71-26223

Computer program for interpretation of residual gas analyzer mass spectra, considering vacuum environmental testing of spacecraft [AAS PAPER 71-185] 11 p1730 A71-26505

Spacecraft radiator thermal scale model, using forced convection, conduction and radiation heat transfer [AAS PAPER 71-187] 11 p1860 A71-26517

Human nervous reactions to monochromatic red, yellow green and blue light for optimal color climate in spacecraft cabins [AAS PAPER 71-189] 13 p2018 A71-28411

Radiative heat transfer effects on small fires in zero gravity spacecraft and free falling chamber environments from diffusion flame models [AAS PAPER 71-191] 15 p2514 A71-32084

Human energy requirements in weightless environments, correlating metabolic data from Gemini and Apollo missions with food consumption and energy balance measurements [AAS PAPER 71-193] 16 p2532 A71-33778

Environmental thermal control/life support system for manned space station, discussing maintenance, weight, power and volume [AIAA PAPER 71-827] 17 p2690 A71-34719

Visual detection of stars in spacecraft environment, considering window cleanliness and antireflection coating effect on light scattering [AAS PAPER 71-829] 18 p2864 A71-36278

Space Shuttle Orbiter Environmental Control and Life Support Systems, discussing maintenance [AAS PAPER 71-831] 18 p2866 A71-36382

Space station thermal control systems design, discussing pumped loop, air cooled semipassive and heat pipe systems [AAS PAPER 71-833] 18 p2869 A71-36403

Spacecraft housekeeping relation to logistics elements of maintenance and up and down cargo supply [AAS PAPER 71-835] 18 p2899 A71-36467

Liquid He containment in space zero-g environment, proposing use of high thermal conductivity porous plug operating in superfluid regime [AAS PAPER 71-837] 20 p3184 A71-39280

Microorganisms under closed environmental ecological conditions with reference to astronauts infectious diseases, discussing bacteria growth in Biosatellite 2 and earth based closed chamber experiments [AAS PAPER 71-839] 21 p3343 A71-40562

Space conditions exposure of lysogenic strains of *Escherichia coli* and monolayer cultures of human cells aboard Zond 5 and 7 flights [AAS PAPER 71-841] 21 p3333 A71-40565

Chlorella viability and mutability aboard Soyuz and Zond spacecraft, noting trend toward growth of anomalies in autosporeulation [AAS PAPER 71-843] 21 p3343 A71-40566

SkyLab life support, habitability and thermal comfort system, discussing ventilation, humidity, carbon dioxide and odor control and water, food and waste management [AAS PAPER 71-845] 22 p3609 A71-41976

Spacecraft closed loop oxygen recovery system using electrochemical carbon dioxide concentrator, Sabatier reactor and water electrolysis subsystem [AAS PAPER 71-847] 22 p3503 A71-42017

Oxidation of water in regeneration under spacecraft conditions, measuring organic impurities degree of oxidation in inhabited cabin atmospheric vapor condensates [AAS PAPER 71-849] 22 p3506 A71-42814

SPACECRAFT GUIDANCE

NT SATELLITE GUIDANCE

Space vehicle onboard navigation and guidance systems capability, considering Apollo transition from direct task interaction and supervision to functional man machine communication [AAS PAPER 71-851] 01 p0124 A71-10511

Spacecraft navigation, guidance and control for manual rendezvous with orbiting target, examining error sources perturbing effects [AAS PAPER 71-853] 01 p0022 A71-10513

Star charts as orientation and navigation aids in manned space flight [AAS PAPER 71-855] 01 p0125 A71-10517

Mission requirements in decision processes for guidance and control system design of aerospace vehicles [AIAA PAPER 70-1231] 01 p0126 A71-11301

Space rescue operations, discussing notification, emergency location, terminal guidance systems and techniques application, international codes, etc [AAS PAPER 71-857] 01 p0164 A71-11438

N-body real time trajectory simulation of Apollo Command and Service module G and C systems and mission [AAS PAPER 71-859] 02 p0237 A71-11793

Neighboring optimum feedback guidance to motivate min-distance lookout parameter determined by minimizing metric function of perturbed state and reference trajectory [AIAA PAPER 69-888] 03 p0454 A71-13446

Mariner Mars 1969 navigation, guidance and control systems design, mechanization and flight testing [AAS PAPER 71-861] 03 p0455 A71-14073

Space launchers flight control and guidance systems technology, emphasizing use of onboard digital computers

05 p0817 A71-16678

Spacecraft midcourse guidance technique for lunar and interplanetary trajectories based on matched asymptotic expansions

[AIAA PAPER 71-117] 06 p0978 A71-18567

Minimum propellant deterministic guidance law for bounded-thrust constant jet exhaust velocity spacecraft, using neighboring extremal theory

[AIAA PAPER 71-118] 06 p0978 A71-18568

Linear and nonlinear filtering, discussing theory and application in space guidance systems

07 p1081 A71-19533

Computer requirements of self contained guidance, navigation and control system onboard manned orbital space station

[AIAA PAPER 71-221] 07 p1155 A71-19702

Strapdown inertial navigator alignment by digital filtering techniques, discussing application to aircraft and spacecraft

08 p1331 A71-21170

Prelaunch automatic azimuth alignment theodolites for Saturn 1B and Saturn 5 space vehicles inertial guidance system, discussing return images separation and error signal generation

08 p1289 A71-21375

Soviet book on design of self guidance systems for aerodynamically controlled rockets

10 p1640 A71-24731

Precision landing guidance system using microwave scanning beam technique, stressing application to aerospace transportation

15 p2446 A71-32723

NASA space station navigation system, considering landmark and ground tracking, ground beacons and satellite concepts, long term effects, operational requirements and design goals

17 p2772 A71-35054

Redundant strapdown Inertial Measurement Unit processor recovery requirements, investigating IMU information loss effects during recovery on spacecraft mission

17 p2772 A71-35058

Space shuttle guidance, evaluating performance of strapdown and gimbaled systems by nominal and abort trajectories

17 p2773 A71-35061

Space shuttle scanning beam landing guidance system, discussing accuracy in penetration, alignment, flare out and touchdown maneuvers and trajectories

17 p2773 A71-35068

Direct in-orbit alignment of integrated optical strapdown inertial guidance system for space application, considering self contained prelaunch alignment and calibration

17 p2774 A71-35071

Reusable nuclear shuttle guidance and control system requirements, using nuclear engine thrust pulse train for guidance

17 p2774 A71-35073

Navigation and guidance alternatives of reusable nuclear shuttle, stressing onboard sensors and processing systems for position and attitude determination

17 p2774 A71-35074

Optimal lateral guidance switching thresholds for low L/D shuttle vehicle entry, using optimal stochastic control theory for problem formulation in conjunction with dynamic programming

[AIAA PAPER 71-914] 19 p3096 A71-37164

Outer planets Grand Tour spacecraft onboard optical guidance instruments, discussing vidicon and image dissector systems designs

[AIAA PAPER 71-945] 19 p3098 A71-37186

Computerized automatic redundancy management for space shuttle guidance, navigation and control, using fly by wire control technique for in-flight failure detection and correction

[AIAA PAPER 71-946] 19 p3098 A71-37187

Space transport rendezvous and docking techniques, emphasizing guidance, propulsion system configuration and sensors

19 p3149 A71-37306

Space and missile guidance performance analysis based on error sources, using Monte Carlo simulation

19 p3101 A71-37754

Guidance and navigation requirements for rendezvous missions to two short period comets

[AAS PAPER 71-116] 19 p3101 A71-37913

Onboard approach guidance instrument for Grand Tour to outer planets missions reducing fuel for corrective maneuvers by estimating trajectories

[AAS PAPER 71-119] 19 p3101 A71-37914

Terminal guidance sensing from spinning spacecraft in swagby mission to outer planets

[AAS PAPER 71-121] 19 p3101 A71-37916

Spacecraft interplanetary guidance trajectory correction, deriving algorithm for optimal accuracy and minimum fuel expenditure

20 p3288 A71-39124

Solid state modulation for spacecraft horizon sensing via IR carbon dioxide atmospheric radiation,

proposing Fabry-Perot structure with controlled plate separation

22 p3537 A71-41475

Aerospace guidance technology evolution at MIT with emphasis on inertial systems

22 p3570 A71-41993

Minimum propellant guidance laws comparison for impulsive and bounded thrust spacecraft, considering jump and controllability conditions for one burn trajectories

22 p3611 A71-42025

Guidance system figure of merit determining relative effectiveness of launch vehicle in delivering spacecraft onto interplanetary trajectory

22 p3573 A71-42788

Minimum propellant deterministic guidance law for bounded thrust constant jet exhaust velocity rocket guidance law, comparing to minimum propellant impulsive thrust guidance law

[AAS PAPER 71-310] 23 p3725 A71-42986

Monte Carlo simulation of navigation and guidance for Grand Tour Jupiter-Saturn-Uranus 1977 mission, using graphics computer program /STEP VII/

[AAS PAPER 71-374] 23 p3701 A71-43044

Midcourse and planetary approach guidance by onboard optical measurements, noting application to earth-Mars trajectories and Grand Tour missions

[AAS PAPER 71-393] 23 p3702 A71-43061

Vehicle attitude determination and guidance sensor orientation by vector space matrix method, minimizing errors by weighted least squares affine transformation technique

[AAS PAPER 71-396] 23 p3773 A71-43064

Optimal timing for interplanetary midcourse guidance maneuvers for realistic cost function, indicating first and last maneuver sensitivity

23 p3702 A71-43939

Space vehicle low thrust minimum terminal variance guidance problem reduced to stochastic bang-bang optimal control system

23 p3702 A71-44101

SPACECRAFT INSTRUMENTS

NT LASER ALTIMETERS

NT SATELLITE INSTRUMENTS

NT SPACECRAFT POSITION INDICATORS

Venera-borne gas analyzers for parachute descent probing of Venus atmosphere, describing design and operation

02 p0248 A71-11916

Low brightness spacecraft photometer calibration using moonlit earth radiance as reference

02 p0249 A71-12075

Soviet book on flight vehicle instruments and sensors static and dynamic characteristics, instrument errors and reliability

02 p0254 A71-12720

Soyuz spacecraft command cabin equipment, describing control panel, command signal systems and routine operations

03 p0497 A71-13196

Trapped protons east-west asymmetry observations during Gemini 4 flight, using on-board high sensitivity plastic-scintillation spectrometer

03 p0479 A71-14041

Atmospheric pollution long term effects measurement and control using spacecraft-mounted instruments

04 p0581 A71-14821

Fluidic inertial instruments for space sensing, guidance and control including gyroscopes, accelerometers and rate sensors

04 p0535 A71-15322

Doppler radar velocity sensors and altimeters for lunar and planetary spacecraft instruments soft landing

04 p0597 A71-15324

Unmanned scientific missions to outer planets in late 1970s, discussing instruments requirements, flight paths, spacecraft designs and payloads

04 p0649 A71-15347

Magnetometers for space research, discussing instrumentation, spacecraft response, data, earth orbit, lunar, planetary and interplanetary measurements

05 p0748 A71-16228

OAO experiments instrument packages for UV observations from orbit, discussing telescopes pointing accuracy and stability, mission objectives, etc

05 p0755 A71-17129

Long life spacecraft tape recorders, considering digital and analog equipment and life and reliability testing of components and complete units

07 p1106 A71-18812

Manometric equipment arrangement in nose cone of oriented satellite with aerodynamic system stabilization

08 p1287 A71-21022

Uncooled Si nuclear particle detector charge sensitive and pulse shaping amplifier design, discussing spacecraft instrumentation and fabrication requirements

08 p1267 A71-21848

Semiconductor element design flexibility, providing greater reliability and reduced size/weight for space vehicles and missiles

09 p1445 A71-22722

Viking Mars 1975 surface meteorological transducers, discussing measurements, environment and mission constraints

09 p1448 A71-22777

Liquid wastes venting into space environment, producing ice particle clouds interference with spacecraft optical instruments

11 p1753 A71-26506

Spaceborne optical sensors cleanliness requirements, considering particle size distribution, shape, population densities, chemical composition and origin

[AIAA PAPER 71-471] 12 p1873 A71-26758

Venera-borne gas analyzers for parachute descent probing of Venus atmospheric composition, describing design and operation

13 p2067 A71-28201

Instrumentation in aerospace industry - Conference Las Vegas, May 1971

14 p2243 A71-30309

Man and equipment instrumentation in simulated space environment, considering training and interface of man and life support systems

14 p2188 A71-30312

Holographic techniques, optical data processing and laser properties for aerospace instrumentation

14 p2244 A71-30329

High reliability low energy camera tubes for video communication in space missions, considering vidicons with photoconducting layer with large time constant

17 p2739 A71-34683

Outer planets Grand Tour spacecraft onboard optical guidance instruments, discussing vidicon and image dissector systems designs

[AIAA PAPER 71-945] 19 p3098 A71-37186

Lightweight precision gimbal design for spaceborne star tracker with arc-second accuracy for stellar updated inertial system independent of spacecraft stabilization

[AIAA PAPER 71-963] 19 p3062 A71-37204

Onboard silicon detector TV guidance sensor for establishing outer planet mission spacecraft orientation with precise targeting, based on patched conic trajectory simulation

[AAS PAPER 71-120] 19 p3101 A71-37915

Physical, chemical and biochemical instrumentation and measurements for probe entering Jupiter atmosphere

[AAS PAPER 71-148] 19 p3153 A71-37951

Impedance determination for symmetrical spherical probes and spacecraft housing with flat screen separation, using partial capacitance formula

19 p3066 A71-38388

Manometric equipment arrangement in nose cone of oriented satellite with aerodynamic system stabilization

20 p3240 A71-39602

Space vehicle measurements of sporadic meteor particle flux near earth, using detectors insensitive to acoustic and vibrational noise

20 p3299 A71-39648

Spacecraft tape recorder design for five years minimum continuous unattended reliable operation, describing quality control and environmental/life testing procedures

22 p3608 A71-41507

IR modulator in space equipment, considering Fabry-Perot cavity with variable plate separation

22 p3544 A71-42138

Spacecraft-borne IR sequential filter radiometer design and performance for real time meteorological forecasting and atmospheric temperature measurements

22 p3544 A71-42143

Radiation effects on components of science instruments used on outer planets Grand Tour mission

22 p3574 A71-42299

Nuclear characteristics of plutonium fuel for thermoelectric generators and required shield thicknesses for sensitive radiation experiment in outer planet spacecraft

22 p3592 A71-42300

Equatorial lunar radius determinations from image motion compensation sensor onboard Lunar Orbiter 1 spacecraft

[AAS PAPER 71-337] 23 p3727 A71-43010

Onboard optical tracking effectiveness for Grand Tour deep space navigation, considering star-planet angles, plane diameter angles and natural satellite observations

[AAS PAPER 71-394] 23 p3732 A71-43062

Proton recording equipment onboard automatic interplanetary stations Zond 4 and 5 at 1.5-50 MeV using silicon drift counters

23 p3675 A71-43274

Cosmic ray dosimetric monitoring in manned spacecraft, discussing ionization, thermoluminescent and nuclear photoemulsion methods of radiation measurement

24 p3826 A71-44888

Spacecraft orientation angle measurement by inertial sensors, analyzing equipment kinematic efficiency and limitations

24 p3829 A71-45318

SPACECRAFT LANDING

NT HORIZONTAL SPACECRAFT LANDING

- NT LUNAR LANDING
NT MARS LANDING
NT PLANETARY LANDING
Doppler radar velocity sensors and altimeters for lunar and planetary spacecraft instruments soft landing
04 p0597 A71-15324
Space vehicle landing trajectories calculation from visual and radio observations of orbital parameters
07 p1196 A71-19495
Spacecraft autonomous control algorithm to ensure geographically specified landing accuracy, noting atmospheric density
09 p1491 A71-22565
Venus atmospheric temperature and pressure measurements during and after Venera 7 soft landing
09 p1528 A71-23560
Spacecraft landing trajectory minimization for lower reentry maneuver space bound at orbital speeds and fixed point coordinates
13 p2145 A71-29177
Unmanned flight vehicles recovery system, describing built-in rotor design for navigation and high precision landing
[DGLR 71-020] 15 p2351 A71-32787
Space shuttle vehicles landing with emergency arrestment aids, describing tailhook/cable, net and landing gear/cable engagement methods
18 p2900 A71-36488
Spacecraft entry into planetary atmosphere, considering heating, deceleration and landing
20 p3305 A71-38814
Spacecraft reentry into random medium atmosphere, determining optimal control procedure for prescribed arrival region and time with simulation equation
20 p3269 A71-39123
Artificial illumination for Venus surface pictures from landed space vehicle
22 p3608 A71-41953
Climatological studies and weather forecast support for Apollo 14 mission prelaunch, launch, emergency landing and terminal areas
24 p3845 A71-44981
Landing control algorithm using onboard digital computer for spacecraft hyperbolic velocity reentry, discussing simulation test results
24 p3846 A71-45303
- SPACECRAFT LAUNCHING**
Minuteman missile technology application as boosters for near earth spacecraft launching, emphasizing tradeoff between reliability and cost
04 p0663 A71-15313
Diamant B French satellite booster development program, discussing general aims, specific objectives, program implementation, organization and industrial facilities
04 p0664 A71-15820
Spacecraft launch trajectory optimization, combining thrust vector, inclination constraints and final adjustment parameters
07 p1207 A71-19529
Monkey physiological responses from lift-off to orbital insertion, showing EEG and EMG arousal reactions, motion sickness development, cardiovascular and respiratory changes
09 p1394 A71-23239
Space shuttle launch and turnaround operational sequences, vehicle processing facilities and alternate methods for vehicle erection, mating and transport to pad
[AIAA PAPER 71-320] 10 p1683 A71-24830
Satellite launcher flight plan maximizing mass in orbit or apogee for rocket trajectories optimal control
13 p2139 A71-28827
German monograph on spacecraft systems launch readiness prediction covering reliability requirements, configuration analysis, tradeoffs, failure analysis, mathematical techniques, etc
13 p2146 A71-29482
Space station facilities and launch and prelaunch operations at Kennedy Space Center, discussing statistical analysis for activity optimization and integrated mission management concept
18 p2899 A71-36474
Airline operations approach to Cape Kennedy launch processing system for reduced hardware and operational costs of shuttle support
18 p2899 A71-36475
Skylab checkout and launch facilities and operations, describing modifications required for Apollo lunar missions facilities utilization at Cape Kennedy
18 p2899 A71-36476
Space shuttle tests and flight operation, discussing launching, maintenance, booster/orbiter mating, payload installation and orbital mechanics
18 p2974 A71-36490
Large synchronous communication satellite launching by propulsion stages assembling in orbit through automatic rendezvous maneuvers
18 p2975 A71-36526
ELDO studies of interorbital space tug for transfer of satellites in geosynchronous orbits
19 p3151 A71-37327
- Outer planets combined orbiter/flyby missions, investigating single launch feasibility with INT-20/Centaur launch vehicle
[AAS PAPER 71-114] 19 p3140 A71-37935
Jovian probe and spacecraft mission feasibility, discussing launch opportunities, targeting, objectives and data transmission
[AAS PAPER 71-141] 19 p3141 A71-37944
Space shuttle optimal lifting trajectory analysis, examining boost launch system performance increase
22 p3608 A71-41955
International cooperation in astronautics, reviewing European satellites launching and world distribution of lunar rock and soil samples
22 p3623 A71-42012
Diamant launch vehicle multistage development for placing satellites in low perigee and high eccentricity and high and low circular orbits
22 p3610 A71-42020
Climatological studies and weather forecast support for Apollo 14 mission prelaunch, launch, emergency landing and terminal areas
24 p3845 A71-44981
- SPACECRAFT LUBRICATION**
Fluoro-alkyl s-triazines as high temperature lubricants and energy transfer fluids for aerospace systems
[ASLE PREPRINT 70LC-5] 08 p1322 A71-21155
- SPACECRAFT MANEUVERS**
Abort and staging separation maneuvers of two equal size reusable lifting entry vehicles in wind tunnel tests
[AIAA PAPER 70-260] 01 p0165 A71-11579
Optimal two impulse correction with minimum energy for planetary approach trajectory and subsequent satellite orbit transfer
02 p0304 A71-11901
Soviet book on maneuvering of spacecraft covering trajectory calculation, thrust control, translunar and interplanetary flights, atmospheric reentry, orbital rendezvous, optimal control, etc
02 p0321 A71-12725
Orbiting vehicle state variables at ballistic transfer termination for known injection errors, calculating fuel consumption for final adjustments
03 p0485 A71-13249
Algorithm for spacecraft rotational maneuver control based on single turn around specific axis, using onboard computer
05 p0816 A71-16176
Launch vehicle attitude control system for lateral drift minimization and prevention of structural load limit exceeding maneuvers, presenting stability analysis
06 p0979 A71-17338
Optimal low thrust power plant for spacecraft payload-maneuver tradeoff
09 p1512 A71-23139
Attitude control of spin stabilized satellite with autonomous maneuverability, discussing correction maneuver method with one quasi-constant inertial reference direction
12 p1971 A71-26985
Spacecraft capture by ballistic aerobraking during passage through planet atmosphere, proposing analytic models
13 p2133 A71-27987
Optimal two impulse correction with minimum energy for planetary approach trajectory and subsequent satellite orbit transfer
13 p2133 A71-28188
Communication satellites electric propulsion economic tradeoff studies, considering propellant requirements for north-south stationkeeping, and near-synchronous orbit maneuvers
[AIAA PAPER 71-683] 14 p2292 A71-30746
Controlled motion dynamics of spacecraft performing maneuvers, applying point transformation to third-order nonlinear system moving about center of mass in lateral motion
16 p2646 A71-33658
Ion microthruster for satellite orbit and position corrections, describing optimum performance characteristics and test facility
17 p2795 A71-35548
[DGLR 71-032] 17 p2795 A71-35548
Optimal maneuvers of axisymmetrical rotating satellite, minimizing orbital transfer
17 p2815 A71-35603
Large synchronous communication satellite launching by propulsion stages assembling in orbit through automatic rendezvous maneuvers
18 p2975 A71-36526
Low thrust long burning solid rocket propellant motor for orbit insertion maneuvers, discussing design, static tests, nozzle composition, igniter and performance
22 p3589 A71-42016
Spin stabilized spacecraft inversion by mass translation with momentum vector fixed in inertial space, calculating control mass dynamics
22 p3612 A71-42777
Mariner 9 Mars 71 mission orbit determination, trajectory and maneuver strategy for near earth, cruise, planetary approach and satellite phases, using in-flight tracking data
[AAS PAPER 71-391] 23 p3732 A71-43059
- Optimal timing for interplanetary midcourse guidance maneuvers for realistic cost function, indicating first and last maneuver sensitivity
23 p3702 A71-43939
- SPACECRAFT MODELS**
Space shuttle technology, discussing wind tunnel studies, aerothermal and operational flight mechanics, model characteristics, orbiter configurations and booster-orbiter separation
07 p1209 A71-20227
Space shuttle vibrational characteristics, investigating dynamic models, aeroelasticity, reentry, wing stall flutter and buffet boundaries
07 p1209 A71-20229
Numerical and scale modeling interaction for spacecraft thermal design verification
[AIAA PAPER 71-439] 11 p1838 A71-26227
Post Apollo program European participation in space tug design and orbiter model flight tests, considering mini shuttle support applications
11 p1839 A71-26331
Apollo program all-up spacecraft thermal vacuum tests, considering component and subsystem reliability analysis, thermal model verification and certification requirements
12 p1894 A71-26682
Space shuttle vehicle models, calculating surface flow patterns and pressure and aerodynamic heating distributions for comparison with test data
[AIAA PAPER 71-594] 15 p2343 A71-31539
- SPACECRAFT MODULES**
NT LANDING MODULES
NT LUNAR LANDING MODULES
NT LUNAR MODULE
NT MARS EXCURSION MODULE
Apollo Command and Service Module simulation of flight phases in lunar landing missions
02 p0237 A71-11792
Common module series for NASA candidate experiment program for manned space stations in 1975-1985 era, discussing configuration and subsystem design
[AIAA PAPER 71-70] 06 p0980 A71-18528
High energy three stage booster system for geostationary orbiter, discussing interstage propellant transfer, apogee impulse system and mission rated payload modular configurations
11 p1838 A71-25574
Earth orbital space stations modular design, discussing space shuttle use, crew training and program management
[AIAA PAPER 71-824] 17 p2812 A71-34721
Manned orbital research modules design for atmospheric physics, weather and earth resources observations and stellar astronomy
[AIAA PAPER 71-815] 17 p2814 A71-35426
Space station assembly in earth orbit, providing low transportation costs, modular elements return and incremental growth
18 p2974 A71-36485
NASA modular space station program, describing design and equipment
19 p3153 A71-38149
- SPACECRAFT MOTION**
Satellite translational motion in circular problem of three bodies, discussing existence of equations integral
03 p0484 A71-13223
Satellite motion stability in axisymmetric field of oblique rotating planet
05 p0815 A71-16050
Geometrical solutions to central motion and space vehicle dynamics, including Chaplygin problem, position and velocity transfer and comet tail separation
05 p0810 A71-16584
Optimal viscous damping effect of cylindrical filled fuel tanks on satellite nutations
06 p0979 A71-17417
Space vehicle motion on planetary flyby trajectories, using Chebyshev polynomial series and Picard successive approximations method to solve two point boundary value problem
[AIAA PAPER 71-192] 06 p0978 A71-18630
On-off control system with crew motion caused random disturbing torques on spacecraft, determining waiting time, jet firing frequency and fuel consumption rate
07 p1208 A71-19885
Soviet book on spacecraft motion parameters measurements accuracy covering electronic systems error sources and reduction in design and data processing
08 p1251 A71-20675
Motion perturbation equations for guided space vehicles, allowing for sloshing liquid propellant viscosity effects
09 p1532 A71-22657
Intermediate orbit calculation, allowing for spacecraft large gravitational perturbation during motion near planetary sphere of influence
09 p1519 A71-22663
Elastic deformable satellite motion stability in central Newtonian force field
09 p1532 A71-23134
Collinear libration centers of spacecraft motion in sun perturbed three dimensional earth-moon system
10 p1671 A71-24329

Spacecraft motion during flight toward planet, including trajectory correction energy loss, autonomous angular measurements and attractive forces

13 p2146 A71-29237

Plane librational motion of axially symmetric satellite in elliptic orbit, developing periodic solution

15 p2488 A71-32092

Laboratory simulation of satellite motion in ionospheric plasma, specifying maximum current density, electron velocity distribution and temperature range

[AIAA PAPER 71-608] 15 p2385 A71-32545

Satellite motion stability in axisymmetric field of oblique rotating planet

16 p2645 A71-33454

Earth satellite plane periodic oscillations damping with respect to center of mass in orbital plane during motion on elliptical Kepler orbit

16 p2646 A71-33659

Graviplane flight theory, spacecraft center of mass motion in central gravitational field with continuous mass geometry variation

16 p2646 A71-33661

Modeling human disorientation and motion sickness in rotating spacecraft, stressing sensors dynamic response

[AIAA PAPER 71-870] 18 p2872 A71-36654

Cayley-Klein parameters application to quasi-precessional motion of satellite with multiple rotors, using perturbation method

24 p3848 A71-44830

Spacecraft motion stabilization about mass center and optimal angular velocity control using minimax technique

24 p3846 A71-45308

SPACECRAFT ORBITAL ASSEMBLY

U ORBITAL ASSEMBLY

SPACECRAFT ORBITS

NT INTERPLANETARY TRANSFER ORBITS

NT PARKING ORBITS

NT POLAR ORBITS

NT SATELLITE ORBITS

NT STATIONARY ORBITS

NT TRANSFER ORBITS

NT TROJAN ORBITS

Linear algorithms for determining spacecraft relative orbital state using angle data with digital computer

01 p0163 A71-11588

Mathematical model for determining thrust interplanetary spacecraft orbit, considering time history of position, velocity and thrust acceleration

[AIAA PAPER 69-901] 03 p0487 A71-13451

Spacecraft single parameter orbital correction, considering correction impulse error effects and error minimization

07 p1155 A71-19530

Orbiting spacecraft local attitude determination, analyzing second order gyrocompass filter, third order steady state filter and fourth order time varying gyrocompass filter

07 p1207 A71-19531

Spacecraft orbital elements determination, using statistical analysis in processing observed motion data

08 p1360 A71-21005

Microthrust powered spacecraft earth escape, using lunar attraction by orbiting spacecraft with vector opposite to moon

12 p1968 A71-27579

Spacecraft intermediate orbit osculating elements first order secular disturbances due to atmospheric resistance

13 p2132 A71-27936

Lunar gravitational field application in interplanetary travel, investigating spacecraft orbits by data processing machine

17 p2797 A71-34186

Space shuttle attitude control propulsion and orbit maneuver, considering high and low chamber pressure gaseous systems

18 p2973 A71-36456

Salut 1/Soyuz 10 mission, discussing configuration, size orbits and docking procedure

18 p2975 A71-36685

Spacecraft orbital elements determination, using statistical analysis in processing observed motion data

20 p3294 A71-39585

Scientific research methods and applications experiments from orbiting Space Shuttle, noting environmental control and life support provision

22 p3611 A71-42039

Actual navigation dispersions, estimation uncertainties and resultant Mars orbit insertion statistical delta V requirements for six Mars approach angles in 1977 Mars window

[AAS PAPER 71-323] 23 p3726 A71-42997

Batch and sequential consider filters data processing methods for Mars orbiting spacecraft state estimation, investigating error sources

[AAS PAPER 71-385] 23 p3731 A71-43055

Near circular orbit elements determination as functions of spacecraft initial speed and coordinates deviation by mathematical expectation procedure

24 p3876 A71-45317

SPACECRAFT PERFORMANCE

Satellite system design digital simulation model in GPSS language for performance interrelationships between subsystems and reliability gain in orbit from redundancy

02 p0318 A71-11782

Black Brant 3B sounding rocket design and development, discussing payload capability, static and dynamic stability, flight and ground handling loads

[AIAA PAPER 70-1396] 03 p0499 A71-13677

Drag free spacecraft performance in deep space, examining inner residual disturbance forces for motion control systems

[ONERA-TP-887] 06 p0900 A71-18022

Electric propulsion spacecraft mission performance scaling laws for invariant trajectory, obtaining optimum gross payload over wide range of system input parameters

[AIAA PAPER 71-160] 06 p0981 A71-18602

Space shuttle applications and utilization, discussing payloads, performance modes, Mission Support Module, ancillary equipment, system interfaces and related profiles

[AIAA PAPER 71-816] 17 p2812 A71-34726

Reusable nuclear shuttle concepts, performance and design requirements

17 p2813 A71-35072

Space shuttle with two stage booster and orbiter reusable vehicles, discussing performance, structural design and flight control system

[AIAA PAPER 71-804] 17 p2814 A71-35431

Cost-performance tradeoffs of aerospace launch vehicle expandable structural components, investigating program factors, materials and construction technologies

[SAWE PAPER 884] 17 p2750 A71-35828

Space shuttle tests and flight operation, discussing launching, maintenance, booster/orbiter mating, payload installation and orbital mechanics

18 p2974 A71-36490

Europa 3 launch vehicle, considering background history, mission requirements and performance profile

21 p3454 A71-40157

Earth orbit shuttle payload increase, discussing refueling and auxiliary hydrogen tank concept

[AAS PAPER 71-302] 23 p3772 A71-42978

SPACECRAFT POSITION INDICATORS

Coupled control of space vehicle orientation with reference to three celestial bodies, reducing plane vibrations to dynamic third order system

09 p1491 A71-22547

Navigation and guidance alternatives of reusable nuclear shuttle, stressing onboard sensors and processing systems for position and attitude determination

17 p2774 A71-35074

Satellite based position fixing data by ranging techniques, discussing application to navigation and ATC

18 p2945 A71-36493

SPACECRAFT POWER SUPPLIES

Spacecraft onboard power supply problem, discussing relative merits of electric and nuclear thermal propulsion systems

01 p0143 A71-11434

Nuclear electric space power plant rejecting waste heat by heat pipes

01 p0126 A71-11576

AAP electrical power system simulation for Skylab earth orbit missions, taking environmental effects into account

02 p0190 A71-11795

Neutronic comparisons of design concepts for low power thermionic space power reactors based on uranium and uranium-based fuels

02 p0281 A71-12264

Energy sources for rockets and satellites, comparing chemical, solar and nuclear supplies

02 p0282 A71-12302

Radionuclide batteries for energy supply in space, comparing with electrochemical sources

02 p0282 A71-12303

Technological development of thermoelectric radionuclide batteries for space applications using Ge-Si thermocouples

02 p0282 A71-12304

Nuclear reactors for space power supply with turboelectric, thermoelectric and thermionic converters

02 p0282 A71-12305

Energy converters for satellite nuclear power plants, discussing rotating, MHD, thermionic and thermoelectric systems

02 p0282 A71-12306

TV broadcast satellites with in-core thermionic reactor, discussing transmitting power, design and economy

02 p0283 A71-12308

Ni-Cd batteries for OAO 2 spacecraft, considering manufacturing, materials, components and tests

03 p0350 A71-13027

Design, testing and flight performance of sealed AgO-Zn cells of Mariner Mars 1969 spacecraft

03 p0350 A71-13029

Electric power source requirements of USAF aircraft, missile and spacecraft electrical systems

03 p0351 A71-13036

Power sources for future NASA programs, discussing requirements in relation to various types of space missions

03 p0351 A71-13037

Heat sterilizable remotely activated silver zinc battery for energy source of planetary lander capsule

03 p0352 A71-13043

Spacecraft electric power transformation and control techniques enhancement, using DC to DC converter, voltage converter/regulator and solar array reorientation system

03 p0352 A71-13049

High voltage power supply for NASA orbital gravity substitute electrostatic workbench, including abnormal load and oxygen environment tests

03 p0394 A71-13050

Nonlinear vector potential analysis of aerospace homopolar inductor alternators, considering fully armature currents

03 p0353 A71-13053

OART space station development, discussing long term effects, artificial gravity, environmental problems, electric power, life support, protection systems and human factors

04 p0643 A71-14932

Biosatellite hydrogen oxygen fuel cell/silver zinc battery combination power system for long aerospace missions, discussing optimal design tradeoff

04 p0353 A71-15286

CdS solar cells thermal stability and performance, discussing satellite applications

05 p0699 A71-16056

High voltage solar cell array operation for satellite in ionosphere, discussing plasma leakage current minimization by electrical insulation

05 p0703 A71-16094

Si solar cells lightweight economical deployable arrays, discussing temperature performance, assembly, coverslips, interconnection, stowage and telescopic mast and ends

05 p0704 A71-16099

Fuel cell technology in astronautics, reviewing design and operational characteristics, functional and economic merits as spacecraft power supply sources

05 p0705 A71-16140

Sirio synchronous orbit satellite configuration, emphasizing attitude control system, telemetry encoders and electric power supply

05 p0816 A71-16404

Solar cells characteristics for space power systems, considering angle of incident sunlight, radiation damage, array design and mounting

05 p0705 A71-17151

Low energy proton irradiation damage to ATS and Intelsat satellites Si solar cells junction properties

07 p1022 A71-19072

Spacecraft power system batteries performance, specifications, development, reliability and manufacture

08 p1236 A71-21108

SERT 2 solar array power system in sun synchronous orbit, considering power conditioning and deployment technique

[AIAA PAPER 70-1159] 09 p1387 A71-22901

Satellite power supply systems, discussing solar cell generators with emphasis on reliability

10 p1683 A71-24641

Symphonic communication satellite power supply system voltage control, discussing controlled system properties based on closed circuit frequency characteristics

10 p1683 A71-24642

Reliability analysis method for systems cyclic operation, demonstrating application for satellite power subsystem

12 p1910 A71-26676

Microthrust powered spacecraft earth escape, using lunar attraction by orbiting spacecraft with vector opposite to moon

12 p1968 A71-27579

Heat rejection radiator influence on space nuclear power system as function of mass/area for Brayton, Rankine, thermoelectric and thermionic conversion schemes

13 p1999 A71-28597

Microwave power transmission for supplying electric power to space station complex for performing scientific experiments over long periods in earth orbits

13 p2000 A71-28667

Solar arrays for satellite electrical power supply, discussing mathematical model for reliability calculation

13 p2002 A71-29273

Turbo-MHD cycle technology of nuclear electric power systems with high temperature reactor for space and terrestrial applications

[AIAA PAPER 71-638] 14 p2273 A71-30716

Thick film microcircuit DC-TO-DC converter electronics design for TOPS spacecraft power subsystem

14 p2214 A71-30801

- Helical induction boiler feed electromagnetic pump design, fabrication and testing for potassium Rankine cycle space power system
[GESP-455] 15 p2415 A71-32202
- Brayton space power system for NASA manned space missions, discussing control system requirements, design and performance 15 p2354 A71-32203
- Brayton power system electrical subsystem and component performance tests, discussing engine control package, DC supply, inverters and instrumentation 15 p2354 A71-32204
- Mercury column electrochemical coulometer as amper-hour type of state-of-charge indicator for secondary batteries in space power applications 15 p2354 A71-32206
- SNAP 8 turbine-alternator as nuclear-electric space power converter, discussing rotating machinery components design and 10,000 hr endurance testing results 15 p2447 A71-32208
- Three stage potassium vapor turbine for space systems electric power generation, discussing erosion and endurance tests 15 p2415 A71-32214
- Steady state and transient interactions due to thermal integration of isotope Brayton space power and life support systems 15 p2364 A71-32220
- Materials evaluation of SNAP 8 power conversion system breadboard assembly after 8700 hour test, extrapolating service life for space flight application 15 p2448 A71-32222
- Pulse charging methods for improved storage batteries performance in space power supply systems, noting solar array voltage variations use in spinning satellites 16 p2526 A71-32847
- Low cost solar array unfolded by centrifugal spinning force, considering application to spin and 3-axis stabilized spacecraft 16 p2526 A71-32852
- Incore thermionic reactor as low cost power supply for direct-to-home TV satellite, converting thermal power to electrical without moving masses 16 p2526 A71-32853
- Materials technology of Ta-W-Hf clad uranium mononitride fuel for lithium cooled compact fast space power reactor, including irradiation tests 16 p2606 A71-33254
- Rankine cycle turboelectric nuclear space power conversion system with liquid K as working fluid, discussing current technology status 16 p2526 A71-33525
- Electric power system for satellites, considering energy conversion, storage and processing from chemical, solar and nuclear sources 17 p2676 A71-34227
- NASA space station electrical power systems discussing configurations, growth capacity, volume reliability and long term effects [AIAA PAPER 71-825] 17 p2677 A71-34720
- Telecommunication satellites photoelectric power systems, discussing solar generators with silicon cells 18 p2851 A71-36572
- High power nickel cadmium battery for geostationary communications satellites for replacement in Intelsat 4 series 18 p2852 A71-36573
- Electrical power systems for spacecraft, reviewing solar cells, batteries, fuel cells and radioisotope thermoelectric generators 19 p3121 A71-37122
- Future space flight energy requirements for onboard power supplies and propulsion, considering high temperature reactors with nuclear fuel in plasma state 19 p3122 A71-37319
- Long life radioisotope thermoelectric generators for space missions, discussing power degradation mechanisms and design trends [AAS PAPER 71-160] 19 p3102 A71-37929
- Critical solar cell battery power system design parameters and performance characteristics affecting post 1977 satellites and manned vehicles design 20 p3179 A71-38902
- Skylab electrical power system located on Orbital Workshop and Airlock Module and on ATM, discussing capabilities, characteristics and limitations 20 p3179 A71-38903
- Brayton cycle 2-15 kW power system for space application and potential gains from component improvements, discussing current status 20 p3180 A71-38906
- Post test inspection of Brayton Rotating Unit for closed Brayton cycle electric power conversion system for long space missions 20 p3180 A71-38909
- Nuclear reactor Brayton cycle space power system design point characteristics, discussing cycle parameters, working fluid, turbine inlet temperature, operating pressure level, etc 20 p3262 A71-38913
- Parasitic speed controller for alternator rotational speed and frequency regulation in dynamic space power systems, investigating phase controlled loading improvement 20 p3262 A71-38916
- Condensate removal devices for potassium vapor Rankine space power turbines to prevent blade erosion and efficiency degradation 20 p3262 A71-38918
- Reactor power systems for earth orbital space station, considering thermoelectric and Brayton cycle power conversion modules 20 p3262 A71-38919
- Isotope Brayton four module adaptable compact power system for space station, using plutonium 238 fuel and lithium hydride shielding for neutron attenuation 20 p3263 A71-38922
- Brayton cycle electric space power supply systems, describing shielded reactor and heat exchanger design 20 p3263 A71-38924
- Multihundred watt radioisotope thermoelectric generator for JPL outer planet missions, discussing vacuum/xenon filled performance and response to thermal/electrical transients 20 p3263 A71-38926
- Multihundred watt radioisotope thermoelectric generator for spacecraft power supply, discussing system design, performance and safety requirements 20 p3263 A71-38927
- Performance tests of high temperature silicon-germanium alloy thermoelectric generator for outer planet mission spacecraft 20 p3264 A71-38928
- Performance potential of MHD generators utilizing nonequilibrium ionization in nuclear space power systems 20 p3264 A71-38930
- Grand tour missions radioisotope thermoelectric generator power source, presenting optimization technique for hot thermocouple junction operation 20 p3264 A71-38932
- Radioisotope thermoelectric generator safety and operations considerations for users of large nuclear space power systems 20 p3264 A71-38933
- Viking Lander power system design, discussing functional requirements by mission and science objectives and reliability features 20 p3181 A71-38940
- Power conditioning electronics for integrally regulated and controlled high voltage solar array spacecraft power system, increasing reliability and reducing weight 20 p3181 A71-38942
- Reliable and low cost electrical solar array/silver zinc battery power system for Agena satellite, discussing design features and flight tests results 20 p3182 A71-38943
- PbTe thermoelectric converter for ZrH reactor space power supply, discussing operational performance, design and materials technology 20 p3265 A71-38951
- Tubular compact air cooled thermoelectric module endurance and performance tests and computer simulation for space reactor power system 20 p3266 A71-38954
- Recoverable usable energy maximization from solar oriented spacecraft electrical power system, using silicon cell array and nickel cadmium batteries 20 p3182 A71-38956
- Orbital electric power system performance simulation for analysis of solar array/battery lock-up, comparing graphical and computer techniques 20 p3183 A71-38957
- Orbital performance of SNAP 19 radioisotopic thermoelectric generator for nuclear power supply on Nimbus 3 observatory 20 p3266 A71-38962
- GaAs solar batteries for spacecraft power supplies, comparing effectiveness with Si cells for optimum utilization 20 p3183 A71-39133
- Synchronous communication satellites stabilization for implementation in 1970-1975 time frame, considering antenna size, power system capacity and vehicle pointing 21 p3348 A71-40480
- Brushless DC motor as power source for meteorological, communications and geological satellites, describing electromechanical design features and operating characteristics 21 p3326 A71-40724
- Dead ended compartments concentration and current distributions calculation in space hydrogen-oxygen fuel cells, using mathematical model with convective diffusion equation 21 p3326 A71-41249
- ATS power supply concepts, considering growth capability, control, reliability, thermal dissipation and weight minimization 22 p3588 A71-41958
- Liquid metal MHD cycles for spacecraft power supply systems, proposing counterflow condensation at nozzle outlet 22 p3574 A71-42431
- SPACECRAFT PRELAUNCH TESTS
- U SPACE VEHICLE CHECKOUT PROGRAM
- SPACECRAFT PROPULSION
- NT ELECTROMAGNETIC PROPULSION
- NT ELECTROSTATIC PROPULSION
- NT ION PROPULSION
- NT PHOTONIC PROPULSION
- NT PLASMA PROPULSION
- NT SOLAR PROPULSION
- Spacecraft onboard power supply problem, discussing relative merits of electric and nuclear thermal propulsion systems 01 p0143 A71-11434
- Deep space shuttles operating modes and vehicle types, considering chemical vs nuclear propulsion, direct vs near-orbit rendezvous, refueling, etc 01 p0165 A71-11593
- Papers on nuclear engineering for satellites and rockets covering radioisotope batteries and reactor energy sources, nuclear-electric and nuclear-thermal propulsions 02 p0281 A71-12301
- Nuclear thermal rockets development, discussing reactor-engine tests, solid and gas cores and Saturn 5 application 02 p0283 A71-12314
- Auxiliary propulsion devices for satellite stabilization, discussing monopropellant, bipropellant, post-combustion, hydrazine plenum, electrical, plasma jet, ion and colloid systems 02 p0299 A71-12749
- Solar electric propulsion (SEP) for automated planetary missions, discussing system characteristics, capabilities and costs [AIAA PAPER 69-1103] 03 p0500 A71-14426
- Pulsed plasma thruster system as secondary propulsion unit for spacecraft attitude, station and trajectory control 04 p0638 A71-15325
- Thermonuclear microbombs for manned spacecraft propulsion to solar system boundary, describing system design and performance 04 p0625 A71-15647
- Nuclear electric space propulsion size and cost factors, discussing scaling laws use for size-performance relationships 06 p0947 A71-18631
- Spacecraft high performance resistojel engines, discussing design criteria for high temperature long term operation with minimum thermal losses [AIAA PAPER 71-195] 06 p0948 A71-18633
- Soviet book on interplanetary electric spacecraft covering chemical and nuclear jet engines and rockets, electrothermal engines, plasma thrusters, etc 06 p0981 A71-18732
- Spacecraft propellant expulsion systems, comparing capillary with conventional techniques [AIAA PAPER 70-685] 07 p1183 A71-19856
- Electric propulsion systems integration into SERT 2 spacecraft, discussing launch imposed environment, thrust vector control, thruster breakdown, power conditioning, etc [AIAA PAPER 70-1123] 09 p1511 A71-22898
- Concentric tube resistojel tested on hydrogen and ammonia propellants for use with biowaste propellants [AIAA PAPER 70-1133] 09 p1387 A71-22908
- Thermionic reactor electric propulsion for unmanned outer planets exploration, discussing spacecraft design, launch vehicle, weight factors, etc [AIAA PAPER 70-1122] 09 p1492 A71-22914
- Optimal control of composite spacecraft propulsion system incorporating high thrust-weight ratio chemical engine and low thrust ion engine 09 p1512 A71-23138
- Soviet monograph on electric space propulsion systems theory covering ion and plasma engines, gas turbine engines, nuclear energy sources, solar cells, etc 10 p1658 A71-24011
- Space shuttle main, auxiliary and air breathing propulsion systems, describing various design concepts 10 p1682 A71-24284
- Kaufman ion thruster providing electric propulsion for satellite spiraling from parking to synchronous orbit [AIAA PAPER 70-1101] 11 p1810 A71-25501
- Drag-free satellite design and propulsion requirements, noting orbit perturbation mechanisms [AIAA PAPER 70-1145] 11 p1838 A71-25522
- Thermionic reactor electric spacecraft propulsion system for unmanned outer planets missions, investigating voltage and radiator temperature effects on weight 11 p1811 A71-25872
- Automatic control, safety and dynamics of thermionic reactor experiment under simulated spacecraft load requirements 11 p1712 A71-25888
- Space flight, discussing stellar trips, propulsion systems and planetary exploration 13 p2145 A71-29130

Steady state thermonuclear fusion rockets, considering specific impulse, space propulsion and research priorities

14 p2288 A71-29929

Nuclear fusion powered pulsed space propulsion systems with laser initiation, discussing energy conversion to momentum, limitations, vehicle configuration and mission performance

[AIAA PAPER 71-636] 14 p2288 A71-30095

Total and vapor pressure sensing and hybrid analog/digital electronic controller for multiburn cryogenic spacecraft propulsion pressurization

[AIAA PAPER 71-647] 14 p2290 A71-30724

Space shuttle airbreathing propulsion systems requirements and design studies, considering cruise, landing, go-around and ferry capabilities

[AIAA PAPER 71-662] 14 p2290 A71-30731

Satellite auxiliary electric propulsion systems survey for program managers and systems engineers, considering cost and component reliability

[AIAA PAPER 71-685] 14 p2292 A71-30747

Blowdown resistojet propulsion system for NASA space station orbit-keeping, describing design and operation

[AIAA PAPER 71-686] 14 p2293 A71-30748

Nuclear space power systems computer simulation for preliminary system and mission analysis, considering Brayton, Rankine and thermionic systems

[AIAA PAPER 71-689] 14 p2208 A71-30749

Space shuttle engine design based on reusable XLR129 rocket engine, presenting performance data

15 p2467 A71-31469

NERVA nuclear rocket engine for space propulsion and long duration auxiliary power generation

[AIAA PAPER 71-639] 15 p2448 A71-32285

Propulsion system design and performance requirements for space shuttle booster and orbiter vehicle, considering low cost, long life, reliability, safety and minimum maintenance

[AIAA PAPER 71-657] 15 p2471 A71-32577

Lunik 16 and 17 automatic lunar landing stations and Lunokhod-1 lunar surface vehicle, describing propulsion systems, control elements and scientific equipment

17 p2724 A71-35401

ESRO activity in low thrust electric propulsion systems development for attitude stabilization and stationkeeping, using colloid and field emission thruster concepts

[DGLR-71-035] 17 p2794 A71-35541

Propulsion systems evaluation for Mars and Jupiter missions, using bundled ESKA 28 electrostatic ion thrusters and incore thermionic reactors

[DGLR-71-046] 17 p2794 A71-35545

Solar electric propulsion system design for interplanetary spacecraft, describing Hg bombardment ion engine

17 p2794 A71-35546

Space shuttle auxiliary propulsion subsystems for attitude control, orbit maneuvering and power supply, discussing design requirements with emphasis on fail-operational and fail-safe criteria

[AIAA PAPER 71-661] 17 p2795 A71-35624

Energy requirements for antihydrogen production in interstellar photonic drives, discussing feasibility

18 p2956 A71-36683

Mixed mode propulsion system for optimization of reusable space shuttle, discussing one-stage-to-orbit vehicle advantages and feasibility

19 p3121 A71-37126

Future space flight energy requirements for onboard power supplies and propulsion, considering high temperature reactors with nuclear fuel in plasma state

19 p3122 A71-37319

Traveling wave plasma accelerator, discussing use for spacecraft propulsion

19 p3122 A71-37321

Nuclear rocket propulsion for human post-Apollo space programs, including Mars exploration

19 p3131 A71-37328

Space propulsion by plasma deflagration gun, measuring specific impulse by piezoelectric probe and pendulum methods

19 p3122 A71-37871

Jupiter orbiter spacecraft propulsion system design, noting advantages of fluorine/hydrazine propellant combination

[AAS PAPER 71-154] 19 p3122 A71-37925

Ultraterrestrial probes for exploration beyond solar system, discussing heliosphere, cometary, interstellar and stellar mission categories propulsion system selection

[AAS PAPER 71-164] 19 p3141 A71-37961

Cryogenic rocket propulsion technology covering propellant selection, pumping, cavitation, starting, tank stratification, instrumentation, hydrogen uses, nuclear propulsion, cost, availability, toxicity and storability

20 p3306 A71-39250

Pulsed plasma thrusters, propellants, trigger and feed systems developments for long life secondary spacecraft propulsion

22 p3588 A71-41975

SPACECRAFT RADIATORS

Spacecraft cryogenic cooling systems, discussing passive, phase change and closed cycle coolers and refrigerators

04 p0535 A71-15343

Heat pipe applications for space vehicle thermal control, discussing spacecraft radiators, thermal exchangers and structure isothermalization

[AIAA PAPER 71-410] 11 p1856 A71-26205

Variable conductance heat pipes feedback mechanisms for spacecraft electrical temperature control system design, using steady state analysis based performance model

[AIAA PAPER 71-421] 11 p1857 A71-26212

Airlock thermal capacitor for radiator performance augmentation by absorbing heat on orbit hot side and rejecting on cold, providing coolant temperature level damping

[AIAA PAPER 71-429] 11 p1858 A71-26218

Multiple circumferential heat pipes construction and tests for spacecraft thermal control, using simulated space environment

[AIAA PAPER 71-412] 12 p1972 A71-27408

Heat rejection radiator influence on space nuclear power system as function of mass/area for Brayton, Rankine, thermoelectric and thermionic conversion schemes

13 p1999 A71-28597

Wide heat load range space radiator design for space mission environmental control/life support system, using stagnation control

[ASME PAPER 71-AV-5] 18 p2865 A71-36372

Spectral reflecting passive radiators for synchronous satellite radiation detectors cooling

[ASME PAPER 71-AV-30] 18 p2869 A71-36397

Low temperature space radiator to reject thermal power from isotope Brayton cycle power system for future space missions

20 p3181 A71-38917

SPACECRAFT RECOVERY

Sea trials with dummy payloads of sounding rocket recovery systems, using parachutes, flotation torus, radio beacons, fluorescent dyes and smoke generators

06 p0881 A71-18674

Unmanned flight vehicles recovery system, describing built-in rotor design for navigation and high precision landing

[DGLR-71-020] 15 p2351 A71-32787

Astronautics progress review from earliest space flights to present, discussing stabilization, recovery, ballistic reentry and latitude determination

16 p2634 A71-33396

Recovery, launch and landing operations of earth orbital shuttle vehicles, discussing space rescue capabilities

22 p3609 A71-41989

Docking with passive orbiting spinning or tumbling objects for space debris elimination and space rescue operations, describing remotely controlled despinning and retrieval methods

22 p3610 A71-42005

SPACECRAFT REENTRY

Spacecraft reentry aerodynamics regarding hypersonic high altitude lifting bodies, shock wave and flow field, heat, mass and energy transfer, etc

[ICAS PAPER 70-01] 02 p0185 A71-11686

Space shuttle reentry in quiet and geomagnetic storm perturbed atmosphere with reference to density variations, using San Marco 2 satellite

[ICAS PAPER 70-04] 03 p0497 A71-13149

Mesosphere and stratosphere data from high level observations for supersonic transport and reentering space vehicle operations

08 p1328 A71-21724

Mathematical model for optimal control of spacecraft reentry into atmosphere

09 p1519 A71-22558

Spacecraft optimal impulsive braking by onboard engine to ensure maximum angle of atmospheric reentry

09 p1519 A71-22567

Cylindrical spacecraft reentry body self-sustained pitching oscillations due to separation on downstream portion, examining stability derivatives

09 p1533 A71-23604

Skipping entry trajectories up to fifth extremal points in planetary atmosphere, using matched asymptotic solution

11 p1837 A71-25483

Graphite heat shield ablation during low velocity low altitude portion of satellite reentry trajectories

[AIAA PAPER 71-415] 11 p1857 A71-26208

Soviet book on dynamics of spacecraft descent to earth covering reentry vehicles trajectory optimization, with allowance for atmospheric perturbation effects

11 p1840 A71-26375

Game theory application to spacecraft reentry problem, obtaining optimal control algorithms

12 p1972 A71-27017

Spacecraft optimal atmospheric reentry trajectory for minimum flight distance, investigating angle of attack control with allowance for load constraints

13 p2143 A71-29229

Spacecraft reentry trajectory angle of attack control by mechanically varying center of mass for axial loads

16 p2645 A71-33443

Continuous hypersonic wind tunnels with low gas density simulating flow states during reentry phase of space vehicles

18 p2898 A71-36417

Temperature distribution in space shuttle during short radius reentry

19 p3161 A71-37314

Game theory application to spacecraft reentry problem, obtaining optimal control algorithms

19 p3152 A71-37687

Spacecraft reentry into random medium at atmosphere, determining optimal control procedure for prescribed arrival region and time with simulation equation

20 p3269 A71-39123

Estimation error covariance matrices of linearized Kalman tracker for ballistic reentering missiles, observing strong coupling of range and range rate with ballistic coefficient

23 p3646 A71-44083

Two step spacecraft reentry guidance involving skip trajectory at parabolic speeds, proposing algorithm for running coordinate and speed vector components values

24 p3846 A71-45301

Spacecraft roll stabilization during parabolic earth atmosphere reentry, developing single parameter multistep algorithm

24 p3846 A71-45302

Landing control algorithm using onboard digital computer for spacecraft hyperbolic velocity reentry discussing simulation test results

24 p3846 A71-45303

Parabolic velocity atmospheric reentry navigation algorithm for spacecraft control, demonstrating guidance accuracy to landing point

24 p3846 A71-45304

Spacecraft motion control algorithm for reentry at escape velocity based on object motion model

24 p3846 A71-45305

SPACECRAFT RELIABILITY

Satellite system design digital simulation model in GPSS language for performance interrelationships between subsystems and reliability gain in orbit from redundancy

02 p0318 A71-11787

Missile prototype reliability prediction, using reliability theory concepts in establishing computation and test programs without damage probability determination

02 p0298 A71-12366

Economic evaluation of automatic support systems for maintainability of low quantity high technology space programs

03 p0396 A71-13097

Minuteman missile technology application at boosters for near earth spacecraft launching emphasizing tradeoff between reliability and cost

04 p0663 A71-15313

Europa 3B launcher first stage, discussing design concept with emphasis on reliability and low cost

05 p0816 A71-16401

Intelsat 3 satellite reliability program, discussing test procedures, redundancy, tradeoff against weight etc

06 p0877 A71-18400

ESRO 2 satellite program reliability prediction and procedures in design and manufacture, defects during development and tests and performance in orbit

07 p1207 A71-19555

Space shuttle safety, discussing rocket engine durability, turbine life, flaw detection, radiation hazards etc

[AIAA PAPER 71-302] 09 p1511 A71-22611

Space shuttle design, emphasizing reliability and safety

[AIAA PAPER 71-303] 09 p1531 A71-22611

Thermal/vacuum space simulation assembly level testing for prelaunch confidence of Mariner spacecraft

12 p1893 A71-26688

QAO 2 thermal test reliability analysis, using filtering process to eliminate component and subsystem level failures

12 p1971 A71-26688

Manned spacecraft maintenance simulation model applying complex systems operational availability assessments

12 p1894 A71-26688

Reliable brushless direct-drive system design for controlling position and rate of solar power arrays on orbiting spacecraft

12 p1869 A71-27433

German monograph on spacecraft systems launch readiness prediction covering reliability requirements configuration analysis, tradeoffs, failure analysis mathematical techniques, etc

13 p2146 A71-29488

Voltage breakdown in scientific spacecraft system during test and flight, discussing factors affecting gas discharges

14 p2181 A71-29866

- Unmanned spacecraft first day failures, discussing launch environment, duration tests in simulated space and performance improvement 16 p2645 A71-33296
- Space shuttle operation phases hazards, emphasizing propellant loading, fire suppression systems, survival equipment and self contained life support devices 17 p2813 A71-34784
- Intelsat communications satellite system network operation, describing reliability outages, maintenance and economy 17 p2705 A71-35101
- Spacecraft system design with long life reliability for outer planet exploration missions [AIAA PAPER 71-831] 17 p2814 A71-35428
- Solar-array space station environmental control and life support system design for 12-man 10-year mission capability with 180-day resupply [ASME PAPER 71-AV-12] 18 p2866 A71-36379
- Space station prototype environmental thermal control and life support systems, considering maintainability, reliability, weight penalties and fault detection and isolation [ASME PAPER 71-AV-22] 18 p2867 A71-36389
- Space shuttle design concerning fault detection and isolation, redundancy and maintenance for cost and downtime minimization by application of airline methods 18 p2900 A71-36480
- Commercial aircraft reliability and maintainability design philosophy application to reusable space vehicles, considering optimum redundancy, dispatch with component inoperative and fault isolation 18 p2973 A71-36481
- Franco-German Symphonie communication satellite reliability measures, describing component selection methods 18 p2889 A71-36524
- Reliability and maintenance of satellites, launchers and other space systems 18 p2975 A71-36534
- Communication satellite components reliability assurance method, discussing production and qualification tests 18 p2890 A71-36538
- Skewed and orthogonal redundant reaction wheels comparison for outer planet exploration spacecraft attitude control based on reliability analysis [AAS PAPER 71-157] 19 p3101 A71-37926
- TOPS spacecraft parts and technology development, reliability and contribution to long life system design [AAS PAPER 71-159] 19 p3152 A71-37928
- Outer planet exploration spacecraft subsystems reliability and ten year flight requirements for planet orbiting and flyby missions [AAS PAPER 71-112] 19 p3140 A71-37934
- Spacecraft electronic equipment design for reliability in long duration space missions [AAS PAPER 71-155] 19 p3153 A71-37956
- Hardware reliability improvement techniques for long life unmanned space missions [AAS PAPER 71-156] 19 p3153 A71-37957
- Viking Lander power system design, discussing functional requirements by mission and science objectives and reliability features 20 p3181 A71-38940
- Three-axis and dual-spin stabilization systems for future synchronous communication satellites, considering reliability, mission flexibility and growth potential 21 p3455 A71-40479
- Spacecraft-borne high voltage system breakdown prevention by avoiding high electric field and critical gas pressure 21 p3358 A71-41192
- Computerized simulation of reliability and in-flight subsystem maintenance for increased space mission success probability, using priority and waiting queue method 22 p3518 A71-42112
- SPACECRAFT RENDEZVOUS**
U SPACE RENDEZVOUS
SPACECRAFT SENSORS
U SPACECRAFT INSTRUMENTS
SPACECRAFT SHIELDING
- Expandable rigidizable solar shields operational, structural and thermal performance tests conducted with spherical models for cryogenically fueled space vehicles 03 p0500 A71-14432
- Vacuum UV degradation of thermal control coatings on ATS-1 satellite, comparing with laboratory simulation 04 p0618 A71-14896
- Temperature profile similarity and thermal protective coating thickness for single reentered spacecraft [AIAA PAPER 71-37] 06 p0916 A71-18498
- Soviet book on active protection of space vehicles covering measures against penetrating radiation from Van Allen belts, solar flares and galactic cosmic rays 07 p1207 A71-19474
- Electron trapping in dielectrics, providing effective light and inexpensive spacecraft bremsstrahlung shield and lower average radiation energy at synchronous altitudes 07 p1164 A71-20625
- Reactor shield weight optimization using FASTER-III Monte Carlo computer program for neutron and gamma ray transport 09 p1539 A71-22810
- Arc heated duct facilities providing high temperature supersonic turbulent boundary layer flows over large samples for orbital logistic vehicle thermal protection tests [AIAA PAPER 71-262] 09 p1429 A71-23060
- Earth intrinsic radiation flux incident angular coefficient, examining effect on partially screened flat spacecraft elements 09 p1546 A71-23154
- Construction and hypervelocity impact tests of penetration resistive dual bumper wall for spacecraft meteoroid protection [AIAA PAPER 71-339] 11 p1843 A71-25318
- Superalloy dispersion strengthened and fused slurry silicide coatings for aircraft gas turbine engines and space shuttle heat shields 11 p1778 A71-25555
- Test streams and chemical composition effects on ablative composites for hypervelocity heat protection of manned atmospheric entry vehicles 11 p1855 A71-26031
- System and component models for spacecraft thermal control design, considering materials, environmental degradation, measurement errors, manufacturing and quality assurance [AIAA PAPER 71-456] 11 p1859 A71-26239
- Reflectance restoration of proton and UV degraded spacecraft thermal control coatings by low temperature oxygen plasma treatment applied to Surveyor 3 [AIAA PAPER 71-463] 11 p1800 A71-26244
- Magnetic shield design for protecting cylindrical space vehicle from space electron radiation, using simulator for engineering data 15 p2500 A71-32042
- Mechanical design of frictionless bimetal actuated louver system for spacecraft thermal control [ASME PAPER 71-AV-39] 18 p2870 A71-36406
- Heat shields for space applications, reviewing heat sinks, double wall cooling techniques and radiative, transpiration and ablation cooling systems 18 p2848 A71-36433
- Space shuttle structural heat problems, discussing shield design configurations and cooling systems 19 p3150 A71-37311
- Reflecting and ablating Teflon heat shields for radiative environment of outer planets atmosphere [AAS PAPER 71-147] 19 p3084 A71-37950
- SPACECRAFT STABILITY**
Motion stability of satellite with rigid connection to symmetric rotors rotation axes 01 p0164 A71-11156
- Auxiliary propulsion devices for satellite stabilization, discussing monopropellant, bipropellant, post-combustion, hydrazine plenum, electrical, plasma jet, ion and colloid systems 02 p0299 A71-12749
- Computerized simulation of disturbance torques of spin stabilized spacecraft in near earth orbit 03 p0500 A71-14433
- Dual spin spacecraft high performance nutation damper, using wheel of uniform mass distribution 04 p0661 A71-15002
- Stability problems of free rotor and driven rotor gyrostats, considering spin stabilized spacecraft 04 p0662 A71-15192
- Space vehicle attitude stabilization system, using sensor with hysteresis relay characteristic for vibration damping 05 p0780 A71-16049
- Free flight space vehicle nonlinear bending vibrations due to harmonic and pulse excitation 05 p0825 A71-16679
- Solid propellant rocket chamber unstable motion, discussing pressure and velocity coupling 06 p0946 A71-18297
- Space station experiments fine pointing and stability, discussing attached or coorbiting free flying mode with zero G conditions [AIAA PAPER 71-62] 06 p0980 A71-18521
- Spinning symmetric satellite roll-yaw resonant attitude instabilities in circular orbit [AIAA PAPER 71-88] 06 p0980 A71-18544
- Representative data of actual forces and moments applicable to large spacecraft attitude control system for typical crew activities obtained through simulation programs [AIAA PAPER 69-1006] 07 p1208 A71-19866
- Algorithm for simultaneous estimate of spacecraft state and covariance matrix with observation error vector 07 p1148 A71-19882
- Stochastic Liapunov stability of satellite motion influenced by aerodynamic and gravity gradient torques, considering atmospheric density uncertainty [AIAA PAPER 70-37] 07 p1208 A71-19883
- Linearized equations of motion for stability of dual spin satellite composed of platform, rotor, platform mounted damper and rotor mounted damper 11 p1837 A71-25514
- Spacecraft nonlinear stabilization system phase space structure, transient processes and system stability domain, using point-to-point transformation method 12 p1972 A71-27018
- Dual spin spacecraft bearing assembly flexibility effects on attitude stability, discussing time constant [AIAA PAPER 70-1043] 12 p1973 A71-27569
- Gravity stabilized satellite in elliptic orbit, examining rotational motion equations stability 15 p2499 A71-31159
- Rotational stability of spin stabilized satellite with liquid filled propellant tanks, investigating viscous effects on motion coupling between rigid body and liquid 15 p2499 A71-31175
- European geostationary telecommunication satellite stabilization using ion thrusters 16 p2623 A71-32851
- Space vehicle attitude stabilization system, using sensor with hysteresis relay characteristic for vibration damping 16 p2605 A71-33453
- Stroboscopic and analytical studies of oscillations and stability regions of gravity gradient satellite in eccentric orbit 18 p2963 A71-36282
- Electromagnetic actuator for momentum desaturation of control moment gyros used for attitude stabilization and control of space stations [AIAA PAPER 71-939] 19 p3098 A71-37184
- Gimbaled reaction wheel for spacecraft accurate attitude stabilization and control [AIAA PAPER 71-950] 19 p3098 A71-37191
- Active precession control devices for spin stabilized spacecraft, noting energy dissipation effect [AIAA PAPER 71-952] 19 p3148 A71-37193
- Fuel slosh energy dissipation and dynamic stability of Intelsat 4, discussing spacecraft and tank selection [AIAA PAPER 71-954] 19 p3148 A71-37195
- Satellite stabilization techniques, noting application to space laboratories and shuttles 19 p3150 A71-37317
- Longitudinal dynamic stability of space shuttle during atmospheric entry, noting magnetic storms effects 19 p3151 A71-37322
- Stability of uncontrolled space vehicles with on-board masses vibrating at small amplitude 19 p3152 A71-37537
- Spacecraft nonlinear stabilization system phase space structure, transient processes and system stability domain, using point-to-point transformation method 19 p3152 A71-37688
- Parameter optimization of linear time invariant nutation damper by second Liapunov method 20 p3306 A71-38853
- Earth-orbiting space vehicle attitude motion under constantly acting disturbances based on mathematical total stability of equilibrium 22 p3608 A71-41968
- Dynamic stability analysis, ground testing and corrective accumulator devices for POGO oscillations in space booster structure 22 p3609 A71-41992
- Dynamic analysis of ATS 5 heat pipe fluid energy dissipation, confirming estimated stability of planned rescue approach configuration 22 p3611 A71-42038
- Altitude dynamics and motion stability analysis of gravity oriented synchronous satellite under perturbation effects of environmental forces due to sun, earth, albedo and cosmic rays 22 p3612 A71-42050
- Earth pointing satellites gravity gradient stabilization by thin inextensible fibers with end tip masses 22 p3590 A71-42779
- Motion stability analysis for force-free spinning satellites with flexible appendages by Liapunov direct method [AAS PAPER 71-345] 23 p3772 A71-43018
- Mathematical model of solar radiation pressure force and torque acting on spacecraft surface intercepting solar photon stream [AAS PAPER 71-352] 23 p3728 A71-43024
- Trap states existence in OSO type satellites, considering damping mechanism and computer results 23 p3773 A71-44092
- Spacecraft roll stabilization during parabolic earth atmosphere reentry, developing single parameter multistep algorithm 24 p3846 A71-45302
- Spacecraft motion stabilization about mass center and optimal angular velocity control using minimax technique 24 p3846 A71-45308
- SPACECRAFT STERILIZATION**
Dry heat spacecraft sterilization-compatibility tests of reagents and growth media for planetary biological exploration 01 p0027 A71-11563

Dry heat destruction rates for microorganisms encapsulated in and on spacecraft hardware, concluding temperature and water conditions in spore as major factors

01 p0027 A71-11564

Ethylene oxide and methyl bromide sporidial activity compared for spacecraft sterilization of *B. subtilis* var niger spores

01 p0027 A71-11565

Heat sterilizable remotely activated silver zinc battery for energy source of planetary lander capsule

03 p0352 A71-13043

Spacecraft sterilization by microbial inactivation, comparing thermoradiation and dry heat methods

06 p0853 A71-17959

Heat sterilizable separator material for development of heat sterilizable Ag-Zn batteries meeting contamination requirements in interplanetary exploration

08 p1235 A71-21095

Dry heat and Co 60 gamma radiation combined effects on spacecraft sterilization, discussing kinetic analysis of spore inactivation

10 p1565 A71-24613

Soviet papers on extraterrestrial life and detection methods covering biological conditions, extremal environmental factors and spacecraft sterilization

13 p2009 A71-28677

Space objects sterilization techniques in Soviet Union and United States, covering hot air, ionizing radiation, UV light, ethylene oxide with or without Freon, etc

13 p2019 A71-28694

Spacecraft sterilization, discussing space environment effects on microorganisms, interplanetary unmanned lander sterilization, crew quarantine, etc

13 p2019 A71-28696

Low temperature condensed phase ammonium perchlorate decomposition effects on ballistic and postheat sterilization properties of CTPB propellant [AIAA PAPER 71-717]

15 p2465 A71-32282

Planetary quarantine including background, program evolution, sterilization technology and contamination sources

16 p2537 A71-33744

Combined dry heat and ionizing radiation for spacecraft sterilization process, detailing synergistic effect on microbes

16 p2537 A71-33770

Bacterial spore distribution and dry heat resistance on Mariner-Mars 1969 spacecraft, using randomly selected aerobic mesophilic isolates

19 p3002 A71-37646

Biosphere contamination, discussing sterilization and quarantine experiments at Lunar Receiving Laboratory, flight crew testing and microbiological studies

21 p3448 A71-40569

SPACECRAFT STRUCTURES

Metallurgical and structural production of diffusion bonded titanium honeycomb sandwich panels for aerospace hardware weight saving

01 p0090 A71-11270

Plastic low emittance Au coating for spacecraft, controlling thickness via electron bombardment method

01 p0109 A71-11271

Sandwich structures applications in aircraft and space vehicles, discussing component characteristics, manufacturing processes and mechanical testing procedures

02 p0324 A71-11959

Graphite/epoxy composite structural spacecraft panels, discussing design analysis and fabrication procedure

04 p0618 A71-15344

Spacecraft structures vibration testing nonlinear effects, extending asymptotic method for transition through resonance to nonresonant regions [AIAA PAPER 71-211]

06 p1004 A71-18647

Space shuttle structures and materials, considering booster arrangements thermal protection, high temperature metals and composite materials

07 p1216 A71-20228

Dynamic behavior of circular and rectangular membrane panels with time and space dependent boundary conditions for aerospace structures

09 p1544 A71-23736

Climbing drum peel adhesion test anomaly in spacecraft adhesive bonded honeycomb structure under lap shear and flatwise tension

10 p1614 A71-24075

Spacecraft deployable booms, discussing structural design, self loading, weight, stowage volume and thermal stability requirements [AIAA PAPER 71-396]

11 p1841 A71-25272

Spacecraft structures weight optimization based on fracture mechanics and reliability cost constraints applied to pressure vessel design

11 p1847 A71-25464

Glass fiber reinforced plastics aerospace applications covering radomes, dielectric panels, aircraft ducting, secondary structures, furnishings, mouldings and tooling

11 p1788 A71-25652

Grooved Al heat pipes experimental performance in moderate temperature for space vehicle applications [AIAA PAPER 71-409]

11 p1856 A71-26204

Transient pressures in spacecraft and volume compartments with outgassing for ambient pressure decrease and low pressures unattainable with large chambers

11 p1840 A71-26398

Filament reinforced composite materials, considering spacecraft and missile applications mechanical and physical properties

13 p2144 A71-28166

Spacecraft propane boiler system, obtaining heat transfer behavior under simulated aerospace conditions

14 p2319 A71-29726

Multistep rocket mass ratios optimization, including exhaust gas velocities, structure and efficiency

16 p2644 A71-32843

Cost-performance tradeoffs of aerospace launch vehicle expandable structural components, investigating program factors, materials and construction technologies

[SAWE PAPER 884]

17 p2750 A71-35828

Composite structures development, discussing wing, fuselage, aeropropulsion and missile development, weight savings of hardware and fighter empenage applications

[AIAA PAPER 71-367]

18 p2979 A71-36275

Viking Mars spacecraft pressure vessel design, incorporating linear elastic fracture mechanics for long life

18 p2979 A71-36487

Space shuttle structural heat problems, discussing shield design configurations and cooling systems

19 p3150 A71-37311

Stowable extendible structures for spacecraft and space experiments, discussing inflatable, rigidized cloth and mechanically deployable apparatus

22 p3609 A71-41981

Quality control organization in British spacecraft projects, discussing material selection system and subsystem tests, process engineering and inspector training

23 p3681 A71-43470

SPACECRAFT TELEVISION

NT SATELLITE TELEVISION

Apollo lunar surface communications, discussing VHF system for voice and telemetry and TV hardware and techniques

01 p0035 A71-10914

Space TV systems using SEC /secondary electron conduction/ camera tube

04 p0597 A71-15289

Mars Mercator projection photomap, using Mariner 6 and 7 spacecraft TV images

06 p0965 A71-17630

Mars surface areodetic control net from Mariner 6 and 7 TV pictures, determining initial coordinate points and far and near encounter frames

06 p0965 A71-17630

Mariner Mars 1969 TV cameras instrument design and calibration techniques

06 p0898 A71-17632

Astronautical TV camera and photogrammetric systems use on manned and unmanned lunar probes, discussing applications to earth surface surveys

06 p0901 A71-18287

Surveyor 3 spacecraft TV camera surface discoloration patterns caused by lunar soil blown by Apollo 12 exhaust

08 p1363 A71-21219

Mars surface maps from visual and photographic observations for TV picture interpretation of Mariner orbital flights

11 p1834 A71-26432

Lunar dust reflectance degradation of thermal control paint on Surveyor 3 TV camera, separating solar radiation effects by analytical model

[AIAA PAPER 71-478]

12 p1920 A71-26760

Apollo lunar surface S band communications and TV systems and equipment, including ground commanded TV assembly

18 p2878 A71-36519

Global, regional and local earth IR imagery for earth sciences from space TV, photography and spectrophotometry

20 p3220 A71-39665

Mars orbiting spacecraft trajectory from spacecraft based TV pictures of Phobos and Deimos [AAS PAPER 71-372]

23 p3730 A71-43042

Mars surface cartography and orbit determination using TV data from Mars orbiting spacecraft [AAS PAPER 71-373]

23 p3730 A71-43043

Alpha radioactivity in Surveyor 3 camera visor, calculating upper limit of Po 210 at equilibrium of Oceanus Procellarum

23 p3765 A71-43812

Mars surface mapping, discussing computer reconstruction process for Mariner 6 and 7 TV picture quality improvement

24 p3875 A71-45266

Mariner 9 spacecraft mission, discussing configuration, data handling and TV surface mapping of Mars

24 p3876 A71-45267

SPACECRAFT TRACKING

NT SATELLITE TRACKING

Earth based orbit determination for Mars orbiting spacecraft, comparing batch and sequential tracking filter data processing methods

[AIAA PAPER 71-119]

06 p0978 A71-18657

Guiana Space Center facilities and equipment describing computerized and automated real time telemetering and data processing systems for spacecraft tracking

09 p1425 A71-22274

Optical spacecraft tracking, using pulsed ruby lasers at Baker-Nunn camera stations of Smithsonian Astrophysical Observatory for retroreflector-equipped satellites ranges

21 p3349 A71-41401

Low thrust interplanetary spacecraft tracking, using spectral factorization for Kalman filtering equations steady state solution

[AAS PAPER 71-395]

23 p3732 A71-43067

Earth based radio tracking data types involving simultaneous or near simultaneous spacecraft tracking from widely separated tracking

[AAS PAPER 71-399]

23 p3643 A71-43066

SPACECRAFT TRAJECTORIES

NT CIRCUMLUNAR TRAJECTORIES

NT EARTH-MARS TRAJECTORIES

NT EARTH-MOON TRAJECTORIES

NT INTERPLANETARY TRAJECTORIES

NT LUNAR TRAJECTORIES

NT MOON-EARTH TRAJECTORIES

Continuous thrust spacecraft optimal trajectory regularization, obtaining differential equations for three dimensional motion

01 p0154 A71-10381

Space vehicle trajectories, discussing programming method to control motion for prescribed boundary conditions

03 p0495 A71-14236

Soviet book on radio measurement methods and mathematical data processing in space trajectory measurements

04 p0555 A71-15375

Satellite flight trajectories construction, proposing algorithms for computer and automatic curve plotter

05 p0779 A71-16040

Optimal vacuum rocket trajectories over spherical earth, deriving nonlinear differential equations for position and velocity

[AIAA PAPER 71-20]

06 p0976 A71-18487

Multiple impulsive spacecraft trajectory optimization technique application to comet rendezvous problem, using computer program

[AIAA PAPER 71-93]

06 p0977 A71-18548

Jupiter atmospheric probe approach trajectory uncertainties and navigation requirements during 1978 mission

[AIAA PAPER 71-120]

06 p0926 A71-18569

Electric propulsion spacecraft mission performance scaling laws for invariant trajectory, obtaining optimum gross payload over wide range of system input parameters

[AIAA PAPER 71-160]

06 p0981 A71-18602

Numerical integration for continuously thrusting spacecraft optimal trajectory, considering rectangular Cartesian and polar cylindrical coordinates characteristics

[AIAA PAPER 69-903]

07 p1191 A71-18891

Spacecraft minimum impulse /or fuel/ ellipse-clipse transfer, discussing computer survey results of 650 trajectories

07 p1199 A71-19899

Spacecraft motion parameters maximum probability estimates, using approximate weight-matrix inversion techniques

08 p1360 A71-21003

Spacecraft orbital elements determination, using statistical analysis in processing observed motion data

08 p1360 A71-21005

Soviet book on space flight mechanics covering vehicle motion, engine systems, gravitational fields and trajectories

08 p1361 A71-21050

Selection of uncorrelated measurement composition ensuring optimal accuracy of space vehicle trajectory

09 p1519 A71-22541

Satellite rendezvous programmed control with allowance for thrust limitation by free trajectories method, determining impulse duration, magnitude and time

09 p1531 A71-22571

Manual onboard orbit determination assuming electronic equipment failure, discussing geometric in-plane orbital parameters and safe orbit check [AIAA PAPER 70-159]

09 p1521 A71-22910

Space vehicle trajectories power-optimal single parameter nonlinear correction, assuming ideal impulse performance

09 p1523 A71-23136

Midlatitude stratosphere and lower ionosphere density model, discussing vertical, diurnal and seasonal variations effects on spacecraft trajectories

09 p1438 A71-23137

Trans-Mars launch window problem, discussing minimum delta-V three-impulse noncoplanar transfer

from circular parking orbit onto asymptotic velocity vector

10 p1671 A71-24331

Soviet book on dynamics of spacecraft descent to earth covering reentry vehicles trajectory optimization, with allowance for atmospheric perturbation effects

11 p1840 A71-26375

Spacecraft flight trajectory parameters estimation from unknown second moment matrix of navigation measurement errors

12 p1957 A71-26628

Maximum likelihood method for accuracy of spacecraft trajectory determination by complex expressions in multidimensional geometric representation

12 p1957 A71-26629

Optimal measurement programs for instrument controlled spacecraft trajectory sections, using maximum likelihood method

12 p1957 A71-26630

Thrust power optimization for spacecraft earth-planet round trip trajectories

12 p1957 A71-26633

Satellite launcher flight plan maximizing mass in orbit or apogee for rocket trajectories optimal control

13 p2139 A71-28827

Spacecraft landing trajectory minimization for lower reentry maneuver space bound at orbital speeds and fixed point coordinates

13 p2145 A71-29177

Spacecraft trajectory optimization during atmospheric reentry with allowance for total-load restriction, using Pontryagin maximum principle

13 p2143 A71-29195

Trajectory analysis of geocentric phase and selenospherical motion of space vehicle leaving lunar surface and returning to earth atmosphere

13 p2143 A71-29209

European electric propulsion systems for flight trajectories within low gravity fields and orbital parameter attitude control and correction

15 p2469 A71-31730

Optimal trajectory analysis for constant thrust optimal-coast minimum propellant control of rocket powered space vehicle

15 p2488 A71-32091

Satellite flight trajectories construction, proposing algorithms for computer and automatic curve plotter

16 p2605 A71-33444

Dynamic stability of controlled spacecraft with liquid propellant rocket engines, considering acceleration and braking sections of trajectory

16 p2646 A71-33656

Component assembly effect on dynamic stability of liquid propellant rocket engine spacecraft during thrust sections of trajectory

16 p2646 A71-33657

Space trajectory radars for measurements on military firing ranges and civil space centers, using microelectronics for data processing

16 p2544 A71-34098

Geolunar interorbital transportation based on shuttle trajectories, interorbital rendezvous, elliptic orbits and terminal transfer

17 p2804 A71-35052

Soviet book on radio control of various flight vehicles covering closed loop synthesis, missile guidance, spacecraft trajectory correction and air traffic control

17 p2775 A71-35403

Pioneer F and G spacecraft Jupiter flyby postencounter mission options ranging from solar system escape to high-inclination low-perihelion trajectories

19 p3139 A71-37921

Two body orbits problem concerning satellite flightpath transfer possibility to orbit touching cyclic or elliptical trajectories

20 p3287 A71-38849

Interplanetary single impulse flight trajectories optimization and computation, determining geometrical and kinematic characteristics

20 p3288 A71-39120

Spacecraft trajectories for reentry at hyperbolic velocity, examining aerodynamic control loads and characteristics in atmospheric skip

20 p3288 A71-39122

Spacecraft motion parameters maximum probability estimates, using approximate weight-matrix inversion techniques

20 p3294 A71-39583

Optimal fuel trajectories involving intermediate thrust arcs, considering strong thrust variations, mid-course guidance and numerical results

22 p3600 A71-41959

Space shuttle operations analysis for cislunar space, including transfer trajectory inclination and long term effects

23 p3724 A71-42976

Branched space trajectory optimization by steepest descent method with coasting arcs, obviating numerical integration for accuracy increase and computing time reduction

23 p3725 A71-42985

Herrick-Gibbs preliminary orbit determination method in matrix form for spacecraft extended to process greater than three inertial position vectors

[AAS PAPER 71-317] 23 p3725 A71-42991

Relay data link and trajectory design integration for Viking orbiter 1975 mission

[AAS PAPER 71-320] 23 p3726 A71-42994

Orbital spacecraft trajectory and attitude dynamics, using computerized state model for mission planning, orbit determination, satellite geodesy and reentry analysis

[AAS PAPER 71-344] 23 p3727 A71-43017

Asteroids flyby approaches during Jupiter missions and Grand Tours, obtaining gravitational deflection of spacecraft trajectories and mass cost estimates

[AAS PAPER 71-360] 23 p3729 A71-43030

Reusable space tug payload injection missions, determining optimal round trip trajectories at earth escape energy levels

[AAS PAPER 71-370] 23 p3730 A71-43040

Mars orbiting spacecraft trajectory from spacecraft based TV pictures of Phobos and Deimos

[AAS PAPER 71-372] 23 p3730 A71-43042

Fast spacecraft trajectory computation in n-body inverse square force field, developing closed form recurrence formula for onboard computers

[AAS PAPER 71-382] 23 p3731 A71-43052

Solar system escape trajectory analysis for Jupiter-Saturn-Pluto and Jupiter-Uranus-Neptune Grand Tour missions, presenting flyby characteristics and heliocentric postencounter directions

[AAS PAPER 71-383] 23 p3731 A71-43053

Second variation for general space trajectories in terms of pseudo-Hamiltonian of Pontryagin, applying to singular arc optimality in space vehicle escape maneuver

23 p3768 A71-43857

SPACECREWS

Space station crew operations, discussing vehicle and research duties, habitability, etc

02 p0203 A71-11976

Cosmic radiation protection of spacecrews by drugs, extrapolating animal data to humans

06 p0861 A71-18359

Renal function osmoregulation in Soyuz crew members

06 p0854 A71-18370

Scientist-astronauts work in manned space flight program support/backup crews and Skylab missions scientific/medical experiments

07 p1046 A71-19089

Representative data of actual forces and moments applicable to large spacecraft attitude control system for typical crew activities obtained through simulation programs

[AIAA PAPER 69-1006] 07 p1208 A71-19866

Crew performance as information input factor based on USAF two man space cabin research

09 p1400 A71-23245

Postflight metabolism and renal function of Soyuz 6, 7 and 8 crewmembers, associating weight loss during flight with water and salt discharges

13 p2006 A71-28409

Space crew members muscle tone, determining weightlessness effect by rigidity and bioelectric activity

15 p2357 A71-31317

Radiation protection of Soyuz-9 crew, using solar activity forecasts

24 p3800 A71-44531

SPACERS

Lateral heat transfer along parallel conducting and radiating plates spaced by absorbing and isotropically scattering dielectric

[AIAA PAPER 70-849] 11 p1788 A71-25524

SPACING

NT AIRCRAFT APPROACH SPACING

Ignited mode theory applied to wide-spaced thermionic diodes, verifying LTE plasma column development

02 p0291 A71-12233

Minimum spacing between two base station antennas for mobile radio diversity reception

19 p3014 A71-37217

SPADATS [TRACKING SYSTEM]

U SPACE DETECTION AND TRACKING SYSTEM

SPALLATION

Deuterium formation in early solar system by examining autogenetic spallogenic model

01 p0157 A71-10763

Proton irradiation on Fe and Ni targets, measuring spallation cross sections

07 p1158 A71-19074

Meteoritic Xe isotopes production mechanism covering spallation, neutron absorption, extinct I 129 and Pu 244 radiative decay and Xe component trapping

11 p1819 A71-25223

Cosmic ray spallation products and radiation age determination from spectral analysis of noble gas components in lunar rocks

11 p1829 A71-25837

Crack extension criterion for time dependent spallation, correlating simple mechanistic model with Al alloys data

12 p1919 A71-27774

Surface melting, spallation and stress response prediction for metals under pulsed electron beam heating, using one dimensional finite difference computer program

15 p2390 A71-32005

Pulsed electron beam heating of metals, determining surface melting, spallation and induced stresses with one dimensional computer programs

15 p2429 A71-32006

Mass spectrometric studies of origin of light elements Li, Be and B in universe, considering spallation of stellar and galactic gases by high energy particles

18 p2959 A71-35914

Tensile strain response for spallation fracture in metals by impact and electron beam heating of Al, Cu and Ti alloys

21 p3466 A71-40798

Criticism of paper on spallation cross section for Be 10 production from oxygen high energy fragmentation in meteorites

22 p3508 A71-42350

F, Na and Al origin in galactic cosmic radiation, investigating production as spallation fragments and generation in source

23 p3719 A71-42943

High energy proton spallation cross sections for several radionuclides from Ti targets, discussing application to lunar materials and meteorites analysis

23 p3706 A71-43199

High energy proton spallation cross sections for several radionuclides from Fe targets, discussing application to beam monitoring and meteoritic studies

23 p3706 A71-43200

Isotopic abundances and concentrations of spallogenic Ne, Kr and Xe in Apollo 12 rock 12002, constructing three stage model of irradiation history

23 p3753 A71-43722

Primary cosmic ray and spallation track density distribution in Apollo 12 deep core soil samples

23 p3764 A71-43801

SPALLING

Rolling contact spalling fatigue failure incidence in subsurface defects, using engineering model based on crack growth rate

14 p2251 A71-29828

Contacting surface rolling spalling fatigue failure incidence prediction using engineering model with preexistent discontinuities and microgeometrical asperities

14 p2251 A71-29829

Spalling fatigue life prediction in rolling contact, studying ductility, compressive stresses, inclusions, surface imperfections and bearing ring deflections effects with mathematical model

14 p2251 A71-29830

SPARE PARTS

Single repairable unit system with spares deterioration in storage, calculating long-run availability and time to system failure

02 p0258 A71-12590

Service support for hardware engineering models from breadboard to preproduction stages, determining spare parts location, quantity and cost requirements

09 p1430 A71-23477

Series and parallel complex systems reliability maximization by allocating optimum numbers of stocked spare parts

15 p2415 A71-32343

Logistics support planning technique for determining number of spares with prechosen probability level, using asymptotic approximation method

16 p2552 A71-33302

SPARK CHAMBERS

Primary gamma radiation flux measurement, using spark chamber on satellite

08 p1350 A71-20954

Cerenkov detectors and He filled spark chambers with large interelectrode spaces in high energy nuclear interaction studies, noting cosmic ray applications

10 p1612 A71-24667

Quarks search in cosmic rays at sea level and mountain altitude, using telescope with plastic scintillation counters and wire spark chambers

13 p2121 A71-28055

SPARK DISCHARGES

U ELECTRIC SPARKS

SPARK GAPS

High power pulsed laser applications, considering satellite orbit determination, distant satellite ranging and precise triggering of high voltage spark gaps

07 p1124 A71-19780

Electrodischarge machining operational principles, discussing spark energy, gap, discharge time, liquid dielectric, spark generator and electrode

09 p1455 A71-23251

Laser triggered switching, discussing ability to trigger high voltage spark gaps with nsec delay and subnsec jitter

11 p1775 A71-26083

- Laser triggered switching, considering theory of laser induced voltage breakdown of gas filled spark gap 12 p1915 A71-27283
- Broadband radiated interference measurement of nonhyperbolic propellant rocket engine spark gap ignition for electromagnetic compatibility 15 p2471 A71-32372
- Controllable overhead arc spark gap discharger system design and characteristics for high power research, communication or industrial electrical installations 19 p3000 A71-38642
- Carbon dioxide laser triggered pressurized spark gap producing high voltage fast risetime pulses for use in IR radiation control by electro-optic shutters 20 p3244 A71-39106
- SPARK IGNITION**
- Spark discharge ignition in air by Q switched ruby laser 01 p0093 A71-10684
- Spark ignited hydrogen-oxygen detonations in supersonic wind tunnel, using schlieren photographs 05 p0835 A71-16520
- Two phase mixture spark ignition dynamics, investigating probabilistic character and ignition energy 07 p1224 A71-20068
- Spark discharge ignition in air by Q switched ruby laser 07 p1125 A71-20146
- High pressure laser spark ignition in argon by extraneous plasma source 09 p1460 A71-22235
- Spark ignition of polystyrene suspensions during free fall in air, investigating ignition mechanism by high speed photography 12 p1986 A71-26967
- High pressure laser spark ignition in argon by external plasma source 21 p3394 A71-41115
- SPARK MACHINING**
- Nonuniform feed effects on height of electrosark surface machining microasperities, investigating linear elliptical interpolator pulse sequence 08 p1296 A71-20851
- Electroerosion and electrochemical combined effects on machining surface removal, discussing optimal anodic removal rates and electrolyte concentrations 08 p1296 A71-20852
- Machining electrode materials, investigating high melting transition metals electroerosive stability and bending strength on basis of electronic theory 08 p1296 A71-20853
- Junction diode effects on spark erosion machining, noting reduction in tool wear 08 p1297 A71-20998
- Electrodischarge machining operational principles, discussing spark energy, gap, discharge time, liquid dielectric, spark generator and electrode 09 p1455 A71-23251
- Electric discharge machining process for hard and brittle materials, based on metal erosion by interrupted electric spark 13 p2075 A71-28946
- Metal removal rate optimization in electro-discharge machining process, considering governing parameters of relaxation circuit 13 p2075 A71-28947
- Aircraft jet engine application of electric discharge machining for repetitive continuous production, considering automated closed cycle equipment [SME PAPER MR-71-143] 18 p2927 A71-36658
- SPARK SHADOWGRAPH PHOTOGRAPHY**
- U SHADOWGRAPH PHOTOGRAPHY**
- SPARKS**
- NT ELECTRIC SPARKS**
- Energy distribution of laser spark spectrum in air, He and Ar, determining transmission coefficients of spark plasmas by self absorption method 02 p0258 A71-11638
- SPATIAL DEPENDENCIES**
- Free generation regime of ruby laser studied by electro-optical method of smoothing spatial inversion inhomogeneities 02 p0261 A71-12502
- Agronomic research by remote sensing, discussing spatial, spectral and temporal measurements from electromagnetic multispectral response 06 p0896 A71-18407
- Radiation intensity spatial dependence on laser polarization, giving three dimensional model for wave function phase calculation 13 p2077 A71-28046
- Temporal and spatial relations between impulsive Pi bursts near midnight at polar substorms onset and IPDP micropulsation events in afternoon-evening hours 16 p2573 A71-33952
- Space time structure of acoustic waves propagating in cylindrical duct with weakly absorbing walls and axial inviscid time dependent fluid flow [ONERA-TP-965] 18 p2946 A71-36030

- Space-time correlation measurements in grid-generated isotropic turbulence, determining full- and narrow-band velocity signals Eulerian time correlation 18 p2902 A71-36035
- Spatial relaxation of electron energy distribution with inelastic and Coulomb collisions, integrating Boltzmann equation 18 p2949 A71-36969
- Second approximation estimates of spatial-temporal signals parameters 19 p3015 A71-37260
- Plasma sheath formation near absorbing wall, calculating electric potential and current variations in space and time 19 p3117 A71-38723
- Geomagnetic activity daily variability index statistical dependence on geomagnetic latitude, noting maximum below equatorial electrojet 20 p3217 A71-39513
- GBR wavefield above winter nighttime ionosphere, noting latitudinal profile due to D region spatial variations and signal fading with F region structure 20 p3197 A71-39744
- Time-space description of steady and homogeneous turbulence in incompressible fluid flow 21 p3367 A71-40690
- Lunar cosmogenic radionuclides production time and spatial dependence calculations, comparing Apollo 11 and 12 measurements 23 p3754 A71-43729
- Longitudinal dependence of solar quiet geomagnetic field horizontal component at equator, discussing discrepancy between theory and observation 23 p3673 A71-43986
- Increment threshold for monoptic and dichoptic vision, showing spatial and luminance effects 24 p3801 A71-44979

SPATIAL DISTRIBUTION**NT STAR DISTRIBUTION**

- Solar activity cycles correlation with planets positions over eclipse 01 p0149 A71-10053
- Minor planet distribution in asteroid belt central area, noting inclination angle, eccentricity, ascending node and perihelion longitude 01 p0155 A71-10442
- Pulsars periods distribution at different galactic latitudes 01 p0161 A71-11339
- Spatial-temporal distribution of laser spark plasma electron density and temperature based on holographic interferometry 02 p0258 A71-11639
- Brightness field spatial structure of solar radiation reflected from earth by Cosmos 149 satellite, discussing homogeneity and isotropy 02 p0246 A71-12114
- Quasars spatial distribution and luminosity functions based on red shift observation 02 p0314 A71-12576
- RV Tau type stars general and spectral classification, covering color indices, line-of-sight velocities, kinematics and spatial distribution 03 p0485 A71-13262
- Semiregular and irregular variable stars spatial densities and distributions, amplitudes and periods 03 p0486 A71-13268
- Charged particles momenta and spatial arrangement during cosmic ray particles nuclear interactions, describing recording equipment 03 p0476 A71-13845
- Muons spatial distribution function in mountain level extensive air showers 03 p0476 A71-13855
- Muon spatial distribution fluctuations at mountain level, using approximate methods 03 p0477 A71-13858
- High energy muons in extensive air showers, studying spatial distribution, spectrum and electron showers by photon spark chamber telescope underground 03 p0477 A71-13860
- Spatial distribution and polarization of radio emission from extensive air showers, using Geiger and scintillation counters, muon detectors and antennae 03 p0477 A71-13865
- Cosmic ray shower particles spatial and angular distribution structure near electron-photon cascade core 03 p0478 A71-13867
- Room temperature spatial distribution of emission from injection lasers with single and triple heterojunctions in AlAs-GaAs system 03 p0439 A71-13980
- He-Ne laser light beam double slit experiments, investigating multimode operation effect on spatial coherence 03 p0440 A71-14177
- Spatial vector calculations using laser distance measurement and optical observations 03 p0380 A71-14191
- Lower limit of neutral line in geomagnetic tail merging, noting inconclusiveness of direct spacecraft observations 03 p0421 A71-14551

Noctilucent cloud observations and research covering geographic distribution, annual and diurnal variations, kinematics, volcanic connections, cosmic dust eruptions, etc

04 p0584 A71-15677

X ray background angular structure comparison with optical galaxies spatial distribution, ruling out universe models with sources following cosmological mass distribution

04 p0657 A71-15826

Galaxies and universe evolution, discussing expansion, isotropic black body radiation, present matter distribution, radio source population density and galactic nuclei instability

04 p0661 A71-15895

Blue and red supergiants ratio as function of radial distance from Galactic center, noting distribution in M33

05 p0805 A71-16119

German monograph on hot-wire anemometry in fluids, taking into account partial differential equation solution for temporal and spatial temperature distribution along wire

05 p0753 A71-16899

Polar auroral arc orientations spatial and diurnal distribution and morphological characteristics for grouping into four types, discussing aurora borealis

05 p0744 A71-17188

Geomagnetic activity diurnal variation dependence on latitude and longitude during IGY

05 p0746 A71-17210

Earth variable electromagnetic field spatial harmonics asymptotic properties

05 p0746 A71-17212

Solar protons and electrons latitude profiles, discussing dependence on magnetic rigidity

06 p0964 A71-17276

Plasma confinement in specified bounded spatial domain by feedback control localized to outer shell

06 p0931 A71-17453

Magnetospheric sudden impulses amplitude and rise time distributions observation by OGO 3 and 5 satellites

06 p0889 A71-17686

Small scale spatially periodic auroral arc distortion observations, using low light level TV reception

06 p0893 A71-17981

Satellite cosmic ray monitors data, examining corotation with sun to obtain interplanetary magnetic field spatial structure

06 p0951 A71-18106

Plane and spatial load transfer and diffusion in linear elastostatics, noting application to aircraft and civil engineering structures and fiber reinforced materials

06 p1001 A71-18222

Optical system for spatially resolved measurement of extended bodies radiative emission and self absorption, describing design for measuring gas discharge plasma radiative properties

06 p0928 A71-18224

Optimal control for distributed parameter system described by linear hyperbolic partial differential equation, deriving existence theorem and cost function

07 p1147 A71-19471

Spatial potential measurements in magnetized non-Maxwellian hydrogen plasma, using Zaitsev-Mnev method

07 p1171 A71-20192

Target field luminance, interstimulus interval and target-mask spatial separation effects on visual backward masking, estimating inhibitory region radius

07 p1051 A71-20218

Solar activity cycles correlation with planets positions over eclipse 08 p1361 A71-21047

Pulsed optical parametric oscillators, investigating effects of spatially nonuniform pumping with beams having Gaussian intensity profiles

08 p1302 A71-21432

Horizontal He distribution in upper atmosphere from OGO 6 mass spectrometric data normalization for altitude by Jacchia model atmosphere

08 p1283 A71-21647

Optimal temporal and spatial temporal resolution for unknown parameter of interfering signal on white noise background

09 p1404 A71-22219

Quasi-captured and escaped electron flux angular dependence and latitudinal variations observations at low altitudes by Cosmos 228 satellite

09 p1512 A71-22362

Closed loop systems with odd-symmetrical nonlinear components and distributed delay, calculating self oscillations

09 p1422 A71-22367

Soft electron fluxes spatial distribution and temporal variations in magnetosphere based on Elektron 2 charged particle trap data

09 p1513 A71-22573

Image restoration from random fluctuations, developing analog procedure from time dependent functions of spatial frequencies and approximation

09 p1407 A71-23048

- Stellar spatial densities in cluster NGC 6913 area, based on two color photometry and spectral classifications 09 p1524 A71-23185
- Optimum synthesis and design of distributed RC filter for oscillator feedback circuit, using calculus of variations 09 p1425 A71-23652
- Plasma intrusion into simulated magnetosphere compared with satellite observations, discussing spatial distribution and interplanetary magnetic field effects 09 p1529 A71-23707
- Pulsar dispersion measures for spatial distributions above galactic plane, determining mean interstellar electron density of local spiral arm 10 p1671 A71-24304
- Lyman alpha sky background measurements byOGO 5 satellite, discussing absolute emission rate, spatial variations and origin 10 p1601 A71-24439
- Spatial distribution of aurorae in O and molecular nitrogen ion emissions 10 p1602 A71-24553
- Human visual system response to moving spatially periodic stimuli, developing mathematical model for motion perception 10 p1572 A71-24999
- Newtonian gravitational system n body problem infinite time approach, obtaining spatial distribution of star clusters 11 p1819 A71-25208
- Planetary distribution of primary cosmic rays and residual charged particles over atmosphere from Cosmos 208 and 228 satellite data 11 p1816 A71-25761
- Energy transfer during charged particles passage through material media as function of spatial distribution, discussing electron production rates 11 p1802 A71-25769
- Galactic clusters statistical analysis for relative sky areas at various distances, discussing inverse apparent diameters and interstellar obscuration effects 11 p1833 A71-26329
- Preferential orientation of physical galactic pairs, obtaining equatorial plane inclinations and major axes positional angles distribution 12 p1955 A71-26582
- Superconducting alloys order parameter spatial variation and resonance scattering near nonmagnetic impurity at critical temperature, using Heinrich perturbation theory expansion solutions 12 p1942 A71-26744
- Early type stars, open clusters, associations and stellar rings space distribution and state of motion 12 p1959 A71-26776
- Lenslike media with parabolic index profiles, deriving equivalent transformation theorem for distributed optical systems design 12 p1928 A71-26810
- Spherically symmetric galactic and star clusters at Hubble expansion, deriving spatial density 12 p1962 A71-26909
- Plasma plate under vacuum conditions, examining transient radiation and spatial dispersion 12 p1937 A71-27118
- Optical luminosity function and space density of quasars from 4C and Parker survey, assuming cosmological red shifts 12 p1966 A71-27233
- Sidereal distribution of arrival directions of extensive air showers containing high energy hadrons 13 p1213 A71-28074
- TeV hadronic component in air shower cores, comparing energy spectra and lateral distributions to Monte Carlo simulations 13 p1213 A71-28078
- Average function for lateral distribution of radio emission in extensive air showers 13 p1218 A71-28170
- Auroral arc orientation spatial and diurnal distribution, location and morphological characteristics, grouping into four types 13 p2059 A71-28245
- Geomagnetic activity diurnal variation dependence on latitude and longitude during IGY 13 p2060 A71-28265
- Earth variable electromagnetic field spatial harmonics asymptotic properties 13 p2060 A71-28267
- Spatio-temporal patterns in visual contrast sensitivity, noting exaggerated eye movements effects 13 p2018 A71-28462
- Sporadic E layer occurrence frequency distribution during 1958-1960, investigating characteristics over equatorial, temperate and auroral zones 13 p2061 A71-28540
- Large scale clustering of galaxies and galactic clusters, comparing observed and Poisson distributions 13 p2138 A71-28759
- Solar Ca II K line core formation, discussing models for high spatial resolution spectra 13 p2140 A71-29045
- Magnetospheric model calculation for self oscillation period and amplitude dependence on longitude and plasma density estimation from observed geomagnetic pulsation period 14 p2228 A71-29531
- Spatial variations in cosmic He abundance attributed to primordial temperature fluctuations at early epochs in Friedmann universe 14 p2303 A71-29587
- Spiral galaxy NGC 2403 neutral hydrogen distribution model fitting of observed velocity profiles 14 p2303 A71-29589
- Spatial MHD flow in diffuser bounded by two diverging and two parallel walls, showing solutions with axial symmetry in cylindrical and spherical coordinate systems 14 p2278 A71-29605
- Rectangular cross section MHD channel spatial electrical field distribution, obtaining electrostatic potential, boundary conditions and efficiency 14 p2267 A71-29612
- Atmospheric turbulence space-time relationships measurements, discussing computerized time series, spatial and phase spectral analysis for sensors data 14 p2267 A71-29754
- Spatial-temporal harmonics of noctilucent cloud occurrences during IQSY with maximum displays after summer solstice in both hemispheres 14 p2233 A71-29965
- Electron beam instability in cylindrical magnetically confined plasma column, calculating quasi-static oscillations spatial growth increments 14 p2279 A71-30090
- Extraterrestrial slow neutron flux and decay density, calculating spatial distribution by power function 14 p2302 A71-30592
- Electromagnetic showers triggered in lead by 6 GeV primary cosmic ray electrons, calculating spatial distribution with Monte Carlo method 14 p2302 A71-30594
- Electromagnetic showers in lead, using 20 GeV primary cosmic ray electrons to calculate spatial evolution 14 p2302 A71-30603
- External galaxies neutral hydrogen distribution from interferometric observations, discussing interpretation consistent with optically derived rotation curves 14 p2314 A71-30638
- Daniel comet minimum distance distributions between asteroids, determining minor planet masses 15 p2482 A71-31302
- Rocket observation for spatial distribution of far UV nightglow at Lyman alpha and shorter wavelengths 15 p2398 A71-31764
- Water distribution in space, natural satellites and terrestrial planets, discussing Clarke abundance values and hydrochlorosphere concept 15 p2494 A71-32493
- Multiple laser cavities in single lasing medium, describing spatial separation of single giant pulses 15 p2422 A71-32584
- Two-parameter statistical theory of material fatigue, considering random and ordered structural nonuniformities in space distributions 16 p2647 A71-32823
- Young open star cluster NGC 6823 membership based on relative proper motions data and color-magnitude diagram 16 p2631 A71-33180
- M 13 spherical star cluster, determining spatial distribution, center coordinates, radius and dynamic behavior 16 p2634 A71-33428
- Spatial and angular distribution of upper atmospheric IR emission layers from Cosmos 65 observation 16 p2563 A71-33449
- Upper atmosphere neutral species latitudinal and seasonal distributions, using turbulent transport coefficients and photochemical reaction rate constants in finite difference solution 16 p2569 A71-33804
- Plasma potentials spatial distribution measurement, describing switching circuit and probe design 16 p2620 A71-33905
- Earth upper mantle electrical conductivity as function of depth based on geomagnetic variation field spatial distribution data 16 p2572 A71-33907
- Pulsating auroral patches with sudden intensity dependent spatial expansion, noting relation to triggering instabilities of precipitating electron beam 16 p2573 A71-33954
- Cometary dust polydispersion, showing particle distribution near nuclei similar to meteor streams 17 p2803 A71-34829
- Distribution functions of observed and true sphericities/axis ratios/of Sculptor-type dwarf galaxies 17 p2804 A71-34842
- Heat exchange between atmosphere and earth surface, calculating nonadiabatic term size and spatial distribution 17 p2734 A71-35193
- Symmetrically distributed nebulae around Wolf-Rayet stars, detailing Ngc 7635 and associated star BD plus 60 deg 2522 17 p2806 A71-35410
- Double galaxies relative number determination, taking into account differences of components absolute magnitudes 17 p2808 A71-35578
- Spot size and spatial intensity distribution determination of low-power laser, using optical laboratory components 18 p2931 A71-36585
- Symmetric operators family spectrum with generalized Rayleigh functional, showing analogy between linear and nonlinear theory at infinite spatial dimension 18 p2942 A71-36821
- Time optimal control for distributed systems with random properties, considering n integral relations and flying wing vehicle torsional vibration problems 19 p2994 A71-37094
- Precipitating protons measurement in 2.5-200 KeV energy range by OVI-15 satellite, comparing spatial distribution with plasmopause profile 19 p3125 A71-37358
- Diurnal distribution, latitudinal occurrence and intensity patterns of ELF, VLF and LF whistler-mode noise emissions from Alouette 2 satellite observation 19 p3016 A71-37364
- Spatial distribution, ion density and space potential measurements in plasma boundary layer at conducting sphere 19 p3112 A71-37738
- Cloud cover areal distribution estimation model using multichannel IR radiometer data from Nimbus 2 satellite 19 p3056 A71-38267
- Galactic high energy electron differential spectrum, estimating spatial distribution and random magnetic field intensity 19 p3129 A71-38358
- F 2 region electron density spatial and temporal distribution, investigating plasma vertical drift effects 19 p3058 A71-38384
- Auroral electrons temporal and spatial structure from ground based optical observations and rocket-borne electron detector measurements 20 p3228 A71-39849
- Pulsars luminosity, z-distance and period distribution in Galaxy, comparing supernova remnants 20 p3303 A71-39933
- Origin and evolution of multiring basins on lunar surface, giving crater diameter distribution 21 p3448 A71-40548
- Radon 222 distribution in lunar atmosphere and top surface 21 p3449 A71-40607
- Geographic distribution pattern of Australasian tektites, considering origin and crater theory of tektite events 21 p3450 A71-40646
- Martian surface clouds distribution in graph, noting statistical correlation with surface radar altitude 21 p3450 A71-40712
- Internal structure investigation of interstellar clouds in Cassiopeia, discussing color equation, photographic plate characteristics and accuracy 21 p3451 A71-40719
- Extragalactic radio sources counts for proportional space volume determination, comparing various cosmological models 22 p3596 A71-41445
- Planetary distribution of primary cosmic rays and residual charged particles over atmosphere from Cosmos 208 and 228 satellite data 22 p3591 A71-41529
- Energy transfer during charged particles passage through material media as function of spatial distribution, discussing electron production rates 22 p3577 A71-41537
- Three dimensional imaginary object reconstruction by holographic stereogram method 22 p3538 A71-41734
- Diffuse 0.2-2 keV cosmic X ray flux, discussing energy spectrum and spatial distribution 22 p3591 A71-41914
- UK 5 spacecraft experiments in X ray astronomy, investigating spatial distribution and energy spectra of emissions in space, polarization and pulsar periodicities 22 p3610 A71-42015
- Spatial dispersion effect on circular polarized cyclotron radiation spontaneous emission coefficient in nonequilibrium plasma 22 p3583 A71-42326
- Charged particles momenta and spatial arrangement during cosmic ray particles nuclear interactions, describing recording equipment 22 p3594 A71-42646
- Muons lateral distribution function in mountain level extensive air showers 22 p3595 A71-42656
- Muon lateral distribution fluctuations at mountain level, using approximate methods 22 p3595 A71-42659

SPATIAL FILTERING

High energy muons in extensive air showers, studying spatial distribution, spectrum and electron photon showers by underground photon spark chamber telescope

22 p3595 A71-42661

Lateral distribution and polarization of radio emission from extensive air showers, using Geiger and scintillation counters, muon detectors and antennae

22 p3595 A71-42666

Cosmic ray shower particles lateral and angular distribution structure near electron-photon cascade core

22 p3595 A71-42668

Spiral galaxy M33 observations at 21 cm, deriving hydrogen atoms distribution and kinematic properties

23 p3722 A71-42938

Satellites explosion debris distribution and orbital characteristics as data base for earth force field and geopotential resonance phenomena analysis [AAS PAPER 71-351]

23 p3728 A71-43023

Distributed parameter system optimal feedback control with quadratic performance indices dependence on discrete point states, applying to uniform bar temperature control

23 p3656 A71-43853

Cometary nucleus outbursts and splitting moments spatial distribution, indicating solar radiation and tidal action effects

24 p3868 A71-44457

Spatially distributed systems with random parameters, determining random output signals statistical moments

24 p3813 A71-44678

Meteorological formation classification problems from radar data, discussing optimal solution with discrete selection space

24 p3844 A71-44877

Upper atmosphere minor component distribution rearrangement, investigating transition time to diffusion equilibrium

24 p3823 A71-45031

SPATIAL FILTERING

Spatial filtering equipment for unwanted images and diffraction in holography, interferometry, etc

01 p0092 A71-10336

Parallel matched spatial filtering by optically superposed Fourier holograms, detecting simultaneously different image details

01 p0081 A71-10686

Spectral analysis increased sensitivity for dispersion systems, using optimum filtering of spatial frequencies

04 p0590 A71-14838

Spatial filtering for digitally deconvolving noisy degraded image by exploiting fundamental identity between vector convolution and polynomial multiplication

04 p0627 A71-15685

Flexible bar as spatial filter for measuring wave number-frequency spectra of distributed random processes

05 p0822 A71-16405

Matched spatial filters for holographic image recognition in biological studies

06 p0903 A71-18695

IR system with moving space filter, calculating detector output and noise due to background radiation

07 p1058 A71-18828

Nonredundant array filtering and postdetection processing for aberration compensation in incoherent imaging

07 p1110 A71-19480

Optical data processing by incoherent matched filtering with Fourier holograms

08 p1291 A71-21401

Holographic generation of high efficiency, extended range spatial filters, applying to defocused images restoration

10 p1612 A71-24585

Spatial filter synthesis for real time combined subtraction and correlation in coherent optical data processing system

12 p1905 A71-26808

Optical synthetic aperture analogs of Covington-Drane and thin annular radio interferometers, discussing aperture resolution and spatial frequency response

14 p2238 A71-29802

Cartesian shear and rigid rotation moire patterns by spatial filtering of superposed diffraction gratings

14 p2329 A71-30464

Phase-only complex valued spatial filter for holographic wave front construction involving amplitude and phase modulations, investigating performance

17 p2745 A71-35590

High coherence Q switched spatially filtered Nd-glass laser operating in fundamental mode for high power

17 p2754 A71-35747

Pattern recognition techniques application to metallurgical data analysis, discussing spatial filtering and classification process

17 p2749 A71-35791

Human visual system biological model for pattern recognition based on spatial filtering covering Fourier transform modification for application to discrete case

17 p2694 A71-35793

Partially spatially coherent illumination influence on measurement of correlation function of two dimensional patterns, obtaining formula for optical filtering

18 p2929 A71-35973

Sinusoidal image distributions generation by changing frequency response of optical system by exit pupil function/incoherent spatial filtering/modification

18 p2918 A71-36073

Harmonic analysis of signal processing radar antennas spatial filtering process, noting application to physical optics theory

20 p3200 A71-39903

Digital picture processing and holography, considering spatial filtering computer simulation and image synthesis

22 p3539 A71-41745

Computer synthesis of holograms and spatial filters for coherent optical data processing systems, noting large computational volume required for three dimensional objects

22 p3539 A71-41746

Real time coherent optical data processing, describing spatial filtering and reactive processor and image converter designs

22 p3540 A71-41750

Rotated pattern detection by optical spatial filtering with superposed holograms, obtaining optimal rotation angle for triangle with digital computer

22 p3546 A71-42475

Digital computer holography, discussing generation, reconstruction, applications in optical spatial filtering and surface testing and sampling and quantization effects

22 p3546 A71-42479

Flat modulation transfer functions obtained by spatial filtering of high aspect ratio annular apertures images in coherent optical processor

22 p3549 A71-42552

SPATIAL ISOTROPY

U ISOTROPY

SPATIAL ORIENTATION

U ATTITUDE [INCLINATION]

SPECIES DIFFUSION

Diffusion boride protective coatings on Nb, Ta, Mo and W against carbon diffusion from carburizing agents

01 p0100 A71-10401

Inclusions diffusive motion effects on heterogeneous systems creep properties, determining creep rate as function of stress and temperature

13 p2148 A71-27960

Ternary systems chemical composition of contacting and equilibrium states due to directional flow in multicomponent diffusion layer, noting relationship to phase diagrams

16 p2541 A71-33929

Concentration profiles around burning droplet, assuming constant binary diffusion coefficients for all species

17 p2840 A71-35705

Chromium casting steel, investigating annealing effects on alloying elements diffusion

18 p2934 A71-36150

Lattice and grain boundary diffusion of Ce and Nd in Ni using radioactive tracer sectioning technique

21 p3398 A71-40468

Co-Ni alloy interdiffusion coefficient determination as function of concentration by magnetic transformation effect

21 p3399 A71-40700

Elements distribution in ternary alloy system during simultaneous saturation and burning-out of two components and successive diffusion into third

21 p3403 A71-41161

Cr diffusion into Ni-Cr alloys in presence of colorized layer, noting increased diffusive mobility

21 p3390 A71-41167

Tellurium concentrations and photocurrent spectra in Te-doped InSb single crystal samples, determining Te diffusion after annealing

21 p3430 A71-41225

Radiation flux induced material dispersion of solid surface, taking into account radiation energy absorption by discontinuity introduction

24 p3835 A71-45225

SPECIFIC HEAT

NT HEAT OF DISSOCIATION

NT HEAT OF SOLUTION

Plane shock wave diffraction at wedge, analyzing role of gas specific heats ratio

01 p0070 A71-10664

Apollo 11 lunar rocks excess heat capacity and thermal conductivity at liquid He temperatures due to peaks in vibrational frequency distribution

02 p0306 A71-11989

Tantalum and niobium disilicides enthalpy and heat capacity temperature dependences

02 p0263 A71-12198

Computer solutions of one dimensional flow of constant composition and specific heat ratio fluids, using influence coefficients

03 p0405 A71-14440

Heat capacity and thermodynamic properties of alpha beryllium nitride from 20 to 315 K, using precision calorimeter

04 p0674 A71-14722

Beta-Li hexafluoroaluminate heat capacity and thermodynamic properties from 15 to 380 K

04 p0674 A71-14722

Compressed liquid and gaseous fluorine constant volume specific heat measurements, tabulating results

04 p0674 A71-14722

High temperature specific heat of refractory molybdenum and uranium dioxide

04 p0612 A71-14939

W-Mo alloy enthalpy and specific heat measurements at high temperatures by drop calorimetry

04 p0613 A71-14939

Elastic and thermodynamic properties of transition metal carbides, comparing Debye temperatures obtained from elastic constant to those obtained from specific heat data

06 p0915 A71-18688

One dimensional nonstationary temperature field in solid body with linearly related heat conductivity and capacity

07 p1221 A71-18922

High temperature apparatus for enthalpy and specific heat measurements of refractory metals

08 p1273 A71-21939

Thermal conductivity, electrical resistivity and specific heat of hot pressed beryllium

10 p1624 A71-23900

Lunar crust regolith thermophysical properties concerning particle size and mass, specific heat and thermal conductivity from Luna 16 automatic station sampler

12 p1963 A71-26966

Solid Ne isotopes specific heat at constant pressure and volume, entropy, enthalpy and Gruneisen parameters

13 p2102 A71-29488

Plane shock wave diffraction at wedge, analyzing role of gas specific heats ratio

14 p2228 A71-30999

Tantalum and niobium disilicides enthalpy and specific heat temperature dependences in 1200-2100 K range

15 p2426 A71-31500

Thermochemistry data changes influence in form of heat of formation, partition functions, specific free energy or specific heat on high temperature gas mixtures composition

15 p2514 A71-32099

Niobium and zirconium carbides enthalpy and specific heat dependence on temperature and composition

15 p2431 A71-32159

Truncated-cone hot-pressed silicon carbide samples, measuring enthalpy and heat capacity as temperature function at high temperatures

15 p2431 A71-32166

Low temperature heat capacities from 1.5 to 15 K for transition metal borides and solid solutions

15 p2437 A71-32646

Wide range specific heat measurements of dense simple fluids /helium, neon, argon, krypton, parahydrogen, oxygen and fluorine/

15 p2515 A71-32700

Solid metal plates erosion mechanism at high temperatures under supersonic plasma jet action, noting dependence on specific heat and latent heat of fusion

16 p2591 A71-33035

Specific heat measurement in magnetic field for graphite under neutron irradiation at low temperatures, noting Schottky anomaly

16 p2600 A71-33377

Anisotropic carbon-graphite materials and metal temperature dependence of thermal expansion coefficients, noting approximation by Debye heat capacity function

16 p2601 A71-33378

High temperature apparatus for enthalpy and specific heat measurements of refractory metals

17 p2724 A71-35272

Ammonium chloride specific heat measurements near order-disorder transition, comparing results using model behavior

17 p2791 A71-35754

Pressure change accompanying mixing of two ideal gases, assuming constant specific heats

18 p2904 A71-36269

Electroconductivity, thermal conductivity and diffusivity, specific heat and emissivities of Ti at 1000-1700 K

19 p3078 A71-37558

Test facility for studying temperature dependence of thermal diffusivity and true heat capacity of metals between minus 150 and plus 400 C

19 p3063 A71-37558

Lunar crust regolith thermophysical properties concerning particle size and mass, specific heat and thermal conductivity from Luna 16 automatic station sampler

19 p3144 A71-38222

Deep lunar interior elastic properties, seismic speeds and Debye temperature determination from equations of equilibrium and state and measured moment of inertia

20 p3286 A71-38738

Materials behavior at low temperatures, investigating lattice vibrational spectra relation to specific heat, conducting electron energies, thermal expansion, etc

20 p3270 A71-39242

Glass transition temperature and specific heat of Apiezon N and T greases used as thermal bonding agent at cryogenic temperatures

20 p3253 A71-39267

Inviscid gas flow from supersonic nozzle into submerged region, considering specific heat ratio effect on dimensionless parameters, jet boundaries and suspended shock profiles

21 p3322 A71-40693

Crystal lattice vibration and molecular libration effects on solid carbon tetrachloride heat capacity at 0-20 and 200-230 K

22 p3585 A71-42059

Apollo 11 and 12 rocks specific heat and thermal conductivity at 2-5 K, comparing elastic properties

23 p3761 A71-43785

Specific heat of Apollo 11 breccia and Apollo 12 olivine dolerite at 95-340 K

23 p3762 A71-43786

Thermal conductivity, diffusivity and specific heat of lunar soil and basalt analogs, using Luna 16 samples

24 p3873 A71-45103

SPECIFIC IMPULSE

NERVA XE-Prime test series, discussing computer simulation full power and high specific impulse operation and startup under varying initial conditions [AIAA PAPER 70-709]

03 p0456 A71-14428

Low, medium and high specific impulse microthrusters development in France, using cold gases, subliming solids, hydrazine, ammonia and cesium ions

07 p1184 A71-19865

Nuclear, hydrogen/oxygen and solid propellant satellite interceptors effectiveness measurement, considering warhead kill radius, propellant weight and specific impulse

13 p2144 A71-27982

Steady state thermonuclear fusion rockets, considering specific impulse, space propulsion and research priorities

14 p2288 A71-29929

High performance superheated subliming solid ammonium carbamate thruster using resistojet technology for specific impulse increase [WSS/CI PAPER 70-210]

15 p2469 A71-32048

Resistojet power and specific impulse performance, investigating biowaste derived propellant chemical nonequilibrium effects

17 p2696 A71-35534

Space propulsion by plasma deflagration gun, measuring specific impulse by piezoelectric probe and pendulum methods

19 p3122 A71-37871

SPECIFICATIONS

NT AIRCRAFT SPECIFICATIONS

NT EQUIPMENT SPECIFICATIONS

Criteria for converting aeronautical project operational targets into actual requirements and technical specifications, emphasizing cost effectiveness

14 p2177 A71-30824

Heat treatment specifications selection for Ni alloy by mathematical method based on cylindrical specimens elongation under tensile loads

23 p3691 A71-43523

SPECIMENS

Creep test results scatter, considering non-homogeneity of specimen properties and deviation from test conditions

20 p3250 A71-39021

SPECTRA

NT ABSORPTION SPECTRA

NT ATOMIC SPECTRA

NT BALMER SERIES

NT D LINES

NT ELECTROMAGNETIC SPECTRA

NT ELECTRONIC SPECTRA

NT EMISSION SPECTRA

NT ENERGY SPECTRA

NT FRAUNHOFER LINES

NT H ALPHA LINE

NT H BETA LINE

NT H GAMMA LINE

NT H LINES

NT HERZBERG BANDS

NT INFRARED SPECTRA

NT K LINES

NT LINE SPECTRA

NT LYMAN SPECTRA

NT MASS SPECTRA

NT MICROWAVE SPECTRA

NT MOLECULAR SPECTRA

NT NEUTRON SPECTRA

NT NOISE SPECTRA

NT OXYGEN SPECTRA

NT PLASMA SPECTRA

NT POWER SPECTRA

NT RADIATION SPECTRA

NT RADIO SPECTRA

NT RAMAN SPECTRA

NT RYDBERG SERIES

NT SCHUMANN-RUNGE BANDS

NT SHOCK SPECTRA

NT SOLAR SPECTRA

NT SPECTRAL BANDS

NT STELLAR SPECTRA

NT SWAN BANDS

NT TELLURIC LINES

NT UV SPECTRA

NT ULTRAVIOLET SPECTRA

NT VEGARD-KAPLAN BANDS

NT VIBRATIONAL SPECTRA

SPECTRAL ABSORPTION

U ABSORPTION SPECTRA

SPECTRAL ANALYSIS

U SPECTRUM ANALYSIS

SPECTRAL BANDS

NT ABSORPTION SPECTRA

NT FRAUNHOFER LINES

NT HERZBERG BANDS

NT SCHUMANN-RUNGE BANDS

NT SWAN BANDS

NT TELLURIC LINES

NT VEGARD-KAPLAN BANDS

Carbon dioxide band radiances measured by Nimbus 3 satellite IR spectrometer, noting seasonal temperature changes in stratosphere due to meridional circulation

01 p0119 A71-10743

K-beta and L-alpha X ray spectral emission bands of high melting vanadium compounds, considering chemical bonds

02 p0263 A71-11892

L-alpha X ray spectral band and K absorption edges in vanadium silicides and high temperature superconductors, obtaining energy bands electron distribution

02 p0294 A71-11893

Interstellar dust, examining diffuse line and band origin, absorption spectra and silicate grains

02 p0312 A71-12466

Sunspot observation of 22 June 1959, discussing two MgO bands spectrographic analysis

02 p0313 A71-12536

Astronomical model for origins and time variations of compact strong sources radiation over all bands

02 p0315 A71-12663

Venus spectra 10488 A carbon dioxide band from high dispersion spectroscopy

03 p0488 A71-13556

High dispersion spectroscopic observations of Venus carbon dioxide bands for deriving rotational temperature

03 p0488 A71-13557

Narrow band random processes statistical characteristic relationship derived from upper and lower envelopes

03 p0452 A71-14390

Venus high dispersion spectra used for line positions and constants of carbon dioxide 7820 and 7883 A bands

04 p0629 A71-14806

Nocturnal intensity and excitation temperature variation of hydroxyl vibrational rotational band in air-glow

04 p0581 A71-15050

Carbon monoxide fundamental band spectral absorptivity distributions at various high temperatures and optical densities

04 p0549 A71-15512

Venus high resolution spectra interpretation for sub II band of carbon dioxide isotope

04 p0659 A71-15859

Solar line spectra wavelength improvement in 7780 to 7925 A range, using carbon dioxide bands

05 p0803 A71-16020

Equivalent line widths of 5520 A ammonia band in Jupiter spectrum

07 p1198 A71-19829

Hydrogen and deuterium oscillator strengths and transition probabilities for Lyman and Werner system individual bands by electronic dipole moment functions

07 p1164 A71-20019

Carbon dioxide 7883 and 7820 A band strengths compared in Venus atmosphere

08 p1338 A71-21396

Bands and gray levels number selection for Mars surface multispectral imaging

09 p1447 A71-22750

High altitude low latitude aurora, observing intense spectral bands and lines and excitation due to optical resonance, atom- and molecule- electron collisions

09 p1441 A71-23643

Twilight airglow measurements of hydroxyl and molecular oxygen bands by balloon-borne instruments including IR grating spectrometer and filter photometers

10 p1601 A71-24400

Diffuse interstellar bands polarization and extinction based on silicate and graphite grain composition and sizes

10 p1675 A71-24469

Methane spectral band analysis, examining J manifolds self broadening coefficients of R branch

10 p1573 A71-24546

CO half-width calculations for carbon dioxide broadened fundamental and first overtone bands from Anderson-Tsao-Curnutte theory

10 p1645 A71-24969

Granular features of solar surface, describing television equipment used aboard balloon for image in 1.2-2 microns region

10 p1680 A71-25004

Radiation from long lived ionic excited states, studying emission spectra, electron impact cross sections and positive nitric oxide ions band system

11 p1727 A71-25368

Auroral pulsation analysis from rocket soundings, investigating oxygen green linear excitation sources

11 p1753 A71-25549

Isotope effects in Lyman and Werner systems of molecular hydrogen, HD and molecular deuterium, calculating band strengths, oscillator strengths and Franck-Condon factors

11 p1803 A71-26072

Solar X ray flux and spectral energy distribution calculation in 0-20 A band, using 9.1 cm spectroheliograms

12 p1954 A71-27708

Experimental solar blind photomultipliers for stellar photometry above earth atmosphere at 1450-2800 A, giving spectral response and quantum efficiency

14 p2240 A71-30122

Nitrogen molecular excitation by photoelectron impacts in dayglow, investigating I PG band emission intensity variation with solar activity

14 p2235 A71-30349

Reflecting layer model for methane band absorption spectrum in Jovian atmosphere

17 p2807 A71-35412

Hot water vapor total emissivity charts at various temperatures, using band model parameters with spectroscopic data

18 p2985 A71-36592

Integral wavelength solar radiation constant measurements by jet and rocket research aircraft, high level balloons and Mariner space probes

20 p3260 A71-39682

Dayglow neutral and ionized diatomic nitrogen band system emission excitation mechanism from vibrational and rotational intensity distributions observations

20 p3226 A71-39829

Narrow band and UVB photoelectric photometry of Uranus geometric albedo and magnitude at unit distance as functions of wavelength

21 p3443 A71-40191

Deactivation and radiative lifetime of CO Cameron forbidden transition spectral bands produced by photon absorption

21 p3418 A71-40232

Effective cross section and excitation functions measurements for molecular nitrogen ion first negative system spectral bands by fast electrons

21 p3419 A71-41108

Semiempirical model for molecular band mean transmission, applying to ammonia 10 and 16 micron lines

22 p3602 A71-42179

Photometric study of short term variations of Jupiter atmospheric activity in UV, blue, green, red and near IR spectral ranges

22 p3603 A71-42185

K and M class stars B and V magnitudes in UVB system based on atomic lines and molecular bands spectral absorption

23 p3771 A71-44306

Martian height gradients from 1.6 micron carbon dioxide band intensity, using telescopes with prismatic quartz spectrometer

24 p3869 A71-44807

Werner band system and Lyman alpha radiation emission from molecular hydrogen excitation by electron impact

24 p3850 A71-44923

High dispersion spectroscopic observations of Venus, finding carbon dioxide band rotational temperature

24 p3873 A71-45079

SPECTRAL CORRELATION

Ionized Xe laser lines in spontaneous emission, establishing correlation with unidentified lines

03 p0438 A71-13887

SPECTRAL EMISSION

Quark regions in massive stars internal structure, discussing plasma superconductivity and spectral line emission

01 p0160 A71-11112

Water vapor emission measurement, using shock tube for gas heating and black body calibrated optical system for radiation measurement

01 p0028 A71-11348

Astronomical model for origins and time variations of compact strong sources radiation over all bands

02 p0315 A71-12663

Six channel selective chopper radiometer design and construction for carbon dioxide emission monitoring for remote atmospheric temperature sounding by Nimbus 4

03 p0423 A71-13356

Ta spectral emissivity in red and green and relationship to surface structure change induced by heat treatment

03 p0460 A71-14465

Spectral emittance of Ti at high temperatures in visible region under vacuum

04 p0611 A71-14956

Transition metal diborides X ray emission K alpha band, establishing asymmetry index, bandwidth and maximum power shift deviations from B

05 p0770 A71-17169

Spectral and relaxation characteristics in antiStokes two photon luminescence of polycrystalline ruby exposed to filtered light pulses

09 p1508 A71-22392

Carbon dioxide laser design and characteristics, discussing lasing action, spectral properties of continuous and Q switching output power

10 p1623 A71-25089

Dye emission frequency variation during quasi-stationary emission process

11 p1774 A71-26002

Collision effects on atomic spectral line profiles, using quantum mechanical description of atomic center-of-mass motion with particular application to lasers

11 p1803 A71-26147

Nongray surface property effects on radiant heat transfer between interacting opaque surfaces, analyzing spectral emittance wavelength and temperature dependence

[AIAA PAPER 71-464]

11 p1859 A71-26245

Spectral emission and level populations of diffusion and principal series lines of cesium vapor in 5 mm discharge plasma diode with hot cathode

12 p1941 A71-27549

Electron scattering effects on spectral emission at optical and X ray wavelengths for homogeneous spherical ionized hydrogen plasma cloud, discussing radiation transfer

14 p2297 A71-29592

Solar corona XUV resonance line spectrum interpretation, using thermal emission from inhomogeneous regions

14 p2297 A71-29678

Spectral luminance and transmittance of noctiluent clouds for spaceborne photometric observation, using American-Swedish rocket particle experiment

14 p2232 A71-29962

W, Nb, Mo and Ta spectral emissive power at wavelengths from 0.66 to 5.12 μ at various high temperatures

16 p2591 A71-33032

Spectral line emission from nitrogen ions, identifying charge by Doppler shift technique application to beam foil light source

16 p2615 A71-34129

Non-LTE physics of He atoms in hot stellar atmospheres, presenting numerical results for He I and II line spectra variations explanation

17 p2808 A71-35558

Thermal, turbulent and macroscopic motions in solar loop prominence of 4 May 1960, using spectral line composition by Gaussian profiles

17 p2809 A71-35596

Spectral emittance ranges of Apollo 12 lunar fines dependent on density for 2.5-14 micron wavelengths [ASME PAPER 71-HT-21]

19 p3142 A71-37992

Atomic oxygen concentration from 5577 A green line emission of airglow and chemiluminescence of nitric oxide

20 p3215 A71-38739

Vertical temperature profiles from Nimbus 3 satellite spectral radiance measurements, stressing importance for atmospheric circulation prediction

20 p3258 A71-39666

Electron impact excited carbon monoxide and dioxide 1260-5000 A spectral emission, discussing cross sections of Cameron and fourth positive bands

23 p3706 A71-42904

Carbon dioxide spectral emission at 1260-4500 A from electron impact excitation, discussing cross sections and Mars atmosphere application

23 p3706 A71-42905

Spectral properties and tunability of far IR from ZnTe and lithium niobate crystals from difference-frequency mixing of mode-locked Nd glass laser pulses

23 p3686 A71-43997

SPECTRAL ENERGY DISTRIBUTION

Quantum theory for spontaneous parametric light scattering, determining photon spectral distribution

02 p0285 A71-12506

RR Lyr type stars kinematic behavior, line of sight velocities, spectral energy distribution and temperature

03 p0485 A71-13263

Physical chemistry of arc plasma, considering radial distribution, spectral density and energy relations for spectrochemical applications

03 p0465 A71-13973

Spectroscopic hole burning in coupled saturable dye-ruby lasers with frequency locking

04 p0607 A71-14725

Gamma radiation flux distribution and spectral composition by satellite observation, analyzing background effects

05 p0798 A71-16047

Near space annihilation gamma radiation intensity and spectral energy composition by satellite observation, considering possible antimatter nature of comets and meteor streams

05 p0798 A71-16048

Si solar cells spectral responses at low temperatures

05 p0701 A71-16072

Spectral distribution reproduction of natural objects radiation by iodine lamp and glass filters

06 p0897 A71-17533

CW electric discharge mixing chemical lasers, identifying molecular transitions responsible for radiations from output spectral distribution measurements

[AIAA PAPER 71-216]

06 p0909 A71-18652

Solar constant and spectral energy distribution standard values by high altitude aircraft, balloon and spacecraft measurements

07 p1199 A71-20005

Time and spectral distribution of hard X ray radiation during solar flare, using nonrelativistic electron bremsstrahlung model

07 p1189 A71-20638

Wilson-Bappu effect and asymmetric K line emission in sun

08 p1359 A71-20947

Light emission of microplasmas and mesoplasmas in silicon p-n junctions, determining spectral distribution

09 p1507 A71-22190

Nonisothermal plasma ion acoustic oscillations spectral energy density in electromagnetic wave field, calculating HF conductivity and absorption coefficient

09 p1500 A71-22243

Approximate photocount statistics for superposition of coherent and chaotic radiation of Gaussian, triangular, square and Lorentzian shaped spectra

09 p1462 A71-22686

Energy distribution in dark and light details on Venus spectrograms, considering relation to clouds in upper atmosphere

09 p1520 A71-22838

Spectral distributions of absorption cross sections of IR radiation by quasi-local oscillations

09 p1494 A71-22885

Ray transformation after passing through optical resonator with Brewster prism, calculating spectral energy losses dependence by geometrical optics method

09 p1464 A71-23072

ELF atmospheric pulse trains recordings at widely separated stations for spectral amplitude ratio differentials, using lightning and ionospheric heating mechanisms

09 p1489 A71-23445

Spectral bandwidth of Q switched giant pulse laser as function of single pass gain, optical switch and resonator loss

10 p1619 A71-23955

Frequency domain spectral energy equations for large scale atmospheric motions, discussing earth rotation effects on kinetic energy spectrum

10 p1638 A71-23963

Collision induced spectral cross relaxation radiative saturation and Lamb dip formation in carbon dioxide molecular lasers, using rate equations

10 p1620 A71-24151

Organic lasers with xanthene dyes solutions, investigating triplet states molecular population effect on output energy characteristics in pumping

10 p1620 A71-24344

Li photoionization cross sections determined from spectral intensity measurements as function of threshold wavelength, discussing radiative electron-ion recombination into first excited state

10 p1646 A71-24992

Intermediate band photometric system for three dimensional star classification based on published stellar spectral energy distribution data

10 p1681 A71-25129

Early stars Vilnius intermediate band and UVB systems comparison for color excess ratios and magnitudes, obtaining reddening line slopes by spectral energy distributions

10 p1682 A71-25131

Cepheids broadband photometric study of temperature and blanketing variations as function of turbulent velocity and gravity, using atmospheric models

11 p1818 A71-25206

Angular, spectral and temporal properties of Cerenkov radiation in cosmic ray extensive air showers

11 p1815 A71-25594

Solar flux from 7 July 1966 flare observation via Proton 3 satellite, obtaining cosmic rays integral spectra

11 p1817 A71-25781

Optimal estimate of spectral density of vibration process over finite time interval, using spectral analyzer

12 p1930 A71-27175

Solar X ray flux and spectral energy distribution calculation in 0-20 A band, using 9.1 cm spectroheliograms

12 p1954 A71-27708

Cosmic ray energetic spectrum variation from observed latitudinal effects during 1954-1962 solar activity cycle

13 p2129 A71-28555

Extreme turbulence measurement during low level flights of Mirage A3-76 fighter aircraft, determining true gust velocities and power spectral energy distributions

14 p2267 A71-29756

Zenith sky intensity and spectral distribution changes during solar eclipse of 12 November 1966, discussing dependence on height and terrain

14 p2309 A71-30119

Zenith skylight spectral intensity distribution measurement during total solar eclipse of 7 March 1970, using optical scanning spectrometer

14 p2309 A71-30121

Surface state energy positions determination in high-energy gap semiconductors by photovoltage spectral distribution

14 p2284 A71-30404

White dwarf stars effective temperature measurements, matching absolute spectral energy distributions with fluxes from model atmospheres

14 p2317 A71-31013

UV spectral energy distribution of Jupiter from rocket-borne Cassegrain telescope observation, computing planet geometric reflectivity in 2100-3600 A range

15 p2491 A71-32422

IR stellar object HD 45677, discussing IR spectral energy distribution in terms of black body temperature range

15 p2497 A71-32765

Gamma radiation flux distribution and spectral composition from Cosmos satellite observation, analyzing background effects

16 p2626 A71-33451

Near space annihilation gamma radiation intensity and spectral energy composition by Cosmos satellite observation, considering possible antimatter nature of comets and meteor streams

16 p2626 A71-33452

Shadow band observations during 7 March 1970 solar eclipse, determining spectral energy distribution from magnetic tape recordings of collimated photocells output

16 p2566 A71-33761

Atmospheric radiant heat influx spectral distribution, evaluating vertical profiles of short wave radiation and aerosol effects

19 p3047 A71-37281

Vibrational energy distribution and emission lines of fluorine atoms plus chloroform reactions in chemical laser, using equal gain measurements

19 p3071 A71-37331

Dumb-bell Nebula forbidden O III line profiles observation with two-etalon scanning Fabry-Perot

19 p3144 A71-38171

Spectral analysis of solar microwave bursts, examining flux and energy variation with frequency

19 p3146 A71-38577

Broadband electrostatic VLF wave observation in polar magnetosphere by OV3-3 satellite, noting emission power spectra density relationship to frequency

20 p3199 A71-39889

Frequency stability definition for signal generator, proposing spectral density measure

21 p3414 A71-40222

Nonisothermal turbulent plasma ion acoustic oscillations spectral energy density in electromagnetic wave field, calculating HF conductivity and absorption coefficient

21 p3424 A71-41132

Cr-doped n-type seminsulating GaAs single crystal photoconductivity measurement, noting spectral peaks dependence on temperature

21 p3434 A71-41324

Solar proton flux from 7 July 1966 flare observation via Proton 3 satellite, obtaining cosmic rays integral spectra

22 p3591 A71-41549

Quasars emission line red shifts distribution observations, evaluating selection effects

22 p3605 A71-42351

Power spectral density of N-ary orthogonal continuous phase FSK waveforms for ELF/VLF communications

22 p3513 A71-42385

Absolute spectral energy distribution and K-corrections for giant elliptical galaxies in Virgo cluster

23 p3722 A71-42935

- Absolute spectral energy distribution and K-corrections for giant elliptical galaxies from scanner observations 23 p3722 A71-42936
- Solar K-line profile absolute intensity calibration from elements of fine structure on surface, determining brightness temperature 23 p3767 A71-43836
- Reduced error spectral power density calculations for random processes with digital spectral analyzers 23 p3681 A71-44320
- SPECTRAL LINE WIDTH**
- Solar chromospheric flares observations tabulation /1969/ and H alpha line width curves graph 01 p0144 A71-10870
- Plasma electric field effects on atomic spectral line shape by plasma kinetic theory 01 p0130 A71-11349
- Solid state laser transverse modes maximum dependence on resonator geometrical parameters usable for producing stable kinetic emission model with narrow spectral line 02 p0259 A71-11878
- Solar photosphere temperature constancy in thin CO layer from equivalent spectral line width determination 03 p0484 A71-13208
- Ionized gas flow temperature distribution effects on half width of H beta line 04 p0633 A71-15064
- Multicircuit vacuum tube oscillator with delay, calculating self oscillation line width reduction by two external resonators with high Q factor 04 p0558 A71-15121
- Lithium line strength indicator of stellar age, discussing T Tauri, A, carbon, S and Ba II stars 04 p0646 A71-15232
- Spectral line intensities, discussing equivalent width, broadening, transition probability, Schuster-Schwarzschild model, solar abundances, etc 04 p0630 A71-15237
- Neutral Ar and Ne resonance lines Stark broadening constant from Stark width-oscillator strength product 04 p0630 A71-15651
- Pulsars CP 0328, CP 0834, CP 1133 and CP 1919 radio spectra, examining interstellar scintillation model, transverse velocities and line widths 05 p0802 A71-15939
- IR object IRC plus 10216 carbon monoxide emission at 2.6 mm, noting spectral line width, thermal emission and mass 05 p0812 A71-16695
- Ruby laser with lens resonator, studying radiation patterns and angular divergence, lasing threshold and spectra width 05 p0763 A71-16831
- Stark broadening of hydrogen lines in plasma, noting role of amplitude modulation and nonadiabaticity 06 p0930 A71-17406
- Umbral rotational temperatures determined from equivalent widths of molecular lines 06 p0967 A71-17906
- EPR line width in ruby under charged dislocations and electric fields of lattice defects, using statistical method 06 p0942 A71-18348
- Equivalent line widths of 5520 A ammonia band in Jupiter spectrum 07 p1198 A71-19829
- Laser dynamic theory with uniformly broadened and Doppler spectral lines based on nonlinear interactions between harmonic oscillations 07 p1127 A71-20255
- Sr-Cr-Eu class Ap magnetic stars mean surface field estimates, using broadened absorption line measurements 08 p1359 A71-20939
- Equivalent widths of CO lines in interstellar absorption spectrum of zeta Ophiuchi 08 p1360 A71-20982
- Temperature induced spectral line widening of trivalent positive Pr ions in lanthanum niobate crystals 09 p1507 A71-22391
- Class M supergiants alpha Sco, delta Sge, R Lyr and alpha Her spectra between 7000 and 6000 A wavelengths, tabulating equivalent bandwidths 09 p1524 A71-23189
- Solar prominence spectra, presenting equivalent line widths, central line intensities and Doppler half widths 09 p1524 A71-23190
- Fraunhofer line profiles, determining optical depth at various points in photosphere 09 p1524 A71-23191
- Solar center-limb Fraunhofer line profile variations observed with double diffraction monochromator 09 p1524 A71-23192
- Fraunhofer lines at solar disk center and near limb, investigating profiles for asymmetry 09 p1524 A71-23194
- Emission line profile and source function in finite optical thickness plane layer, using matrix equation 09 p1525 A71-23195
- Micropulsations power spectrum from magnetospheric model based on transient current sheets, approximating background frequency dependence and daytime/nighttime spectral line widths 09 p1441 A71-23638
- Solar Doppler widths from spectral line profiles by Goldberg profile intercomparison method, determining solar microturbulence depth dependence 10 p1665 A71-23777
- NGC 2655 galaxy nucleus emissive gas/absorption line widths and stellar population, using network spectrographs 10 p1667 A71-23827
- He-Ne laser 0.63 micron line collisional broadening dependence on gas temperature 10 p1620 A71-24342
- Methane spectral band analysis, examining J manifolds self broadening coefficients of R branch 10 p1573 A71-24546
- Internal asynchronous modulation of He-Ne laser with Doppler broadened line of working transition in multifrequency mode 10 p1621 A71-24881
- High resolution measurement of carbon dioxide broadened half widths for water vapor lines in fundamental band 10 p1645 A71-24965
- Half widths calculation for carbon dioxide broadened water vapor absorption lines in nu sub 2 fundamental, considering dipole-quadrupole interactions 10 p1645 A71-24966
- CO absorption spectrum in carbon dioxide atmosphere, comparing self- and nitrogen- broadened half widths 10 p1645 A71-24968
- CO half-width calculations for carbon dioxide broadened fundamental and first overtone bands from Anderson-Tsao-Curnutte theory 10 p1645 A71-24969
- Analytic approximations in closed form for curves of growth of Doppler-Lorentz broadened lines, considering radiative transport in nonisotropic gases 10 p1646 A71-24991
- Broadened energy distributions in electron beams, discussing energy spread delta E and C prime values relationship for studying weak Coulomb interactions 11 p1802 A71-25631
- Laser pulse intensity and spectral width effect on measured cross section of stimulated emission 11 p1774 A71-26007
- Quiescent metallic and ordinary prominences continuous spectra measurements, showing hydrogen ionization dependence on fine structure 12 p1955 A71-26588
- Constant Doppler wide-angle laser beam scanning, presenting expressions for Doppler shift, spread in spectral width of scanned laser beam and scan angle 12 p1913 A71-26814
- Time and space variable echo waves in electron plasma by wave packets interaction, considering spectral line width finiteness influence 12 p1937 A71-27038
- Solar photosphere vibrational temperature determination, using Franck-Condon factor with equivalent line widths for five CN vibrational bands 12 p1963 A71-27081
- Active unperturbed solar photosphere, determining variations in spectral line profiles 12 p1963 A71-27082
- Single loop quartz vacuum tube oscillators, calculating oscillation spectral line width due to thermal and shot noise and circuit parameters fluctuations 12 p1889 A71-27622
- Monomode laser frequency fluctuations, considering line width separation 12 p1915 A71-27640
- Solar Na D lines Doppler width, describing limb darkening data, assuming source function frequency dependent 12 p1970 A71-27748
- Prototype two stage maser extended passband broadening and stability increase at high cooling temperature 13 p2078 A71-28374
- Solar chromospheric flares in 1969, constructing tables of observation data commencement and end time and H alpha line maximum width 13 p2128 A71-28480
- Solar Ca II K line core formation, discussing models for high spatial resolution spectra 13 p2140 A71-29045
- Solar quiet region chromosphere K emission line behavior, identifying surface characteristics for width absolute magnitude relation 13 p2140 A71-29046
- Solar spicules H alpha and beta, D3 and K line profiles, considering radial and turbulent velocities, optical thickness, atomic density and He emission 13 p2140 A71-29049
- Interstellar H II regions high quantum number recombination line measurements, indicating Stark broadening 13 p2143 A71-29268
- Upper atmosphere temperature measurements using red emission Doppler contour width data of atomic oxygen at 6300 A 14 p2229 A71-29673
- Solar atmosphere line broadening by neutral hydrogen, noting discrepancy in van der Waals interaction 14 p2306 A71-29686
- X ray interference lines widening in Al-Mo alloy foil obtained from melt by rapid cooling attributed to stress relieving 14 p2258 A71-30008
- Temperature dependent absorption line width and secondary moments of nuclear magnetic resonance spectra of Ti-Zr-H system 14 p2258 A71-30009
- Pulsed nitrogen-pumped dye laser output spectral narrowing by injection of argon laser monochromatic radiation into cavity 15 p2420 A71-32382
- Spectral lines Doppler broadening reduction in spectroscopy using foil and gas excited accelerator beams as light sources 15 p2412 A71-32579
- Solar atmosphere structure inhomogeneities, describing Ca II H and K line spectra profiles 15 p2497 A71-32743
- Ba atoms excitation and optical transitions line broadening by collisions with Ar atoms behind shock waves, using atomic absorption spectroscopy 16 p2613 A71-32889
- Na D lines broadening by atomic H, discussing interatomic forces between Na and H atoms in terms of NaH molecular potentials 16 p2614 A71-33101
- Peak contour positions of rotation lines of hydrogen chloride as function of spectral slitwidth for wavenumber calibration of far IR spectrometers 16 p2577 A71-33134
- Equivalent width of metallic lines for pole-on main sequence stars, examining effect of rotational axis inclination with respect to line of sight on washout of lines 16 p2633 A71-33334
- Frequency multiplier or divider output signal spectral line form and width conversion from monochromatic input signal 16 p2542 A71-33490
- Collisionless turbulent plasmas nonequilibrium electric fields determination from hydrogen spectral lines Stark broadening 16 p2619 A71-33549
- Stark widening in hydrogen Lyman alpha line, considering atomic state operator of evolution thermal mean effects 16 p2614 A71-34061
- Ne 20 transition line width behavior vs pressure in He-Ne laser at 3.19 microns wavelength 17 p2752 A71-34402
- Radiative width of laser transition in Ne 20 atom and line frequency shift vs pressure in dual He-Ne laser assembly effectuating atom collisions 17 p2752 A71-34403
- X ray diffraction lines diffusion of deformed Ni and Nb, attributing absence to small block dispersion 17 p2755 A71-34415
- Metallic lines in high-dispersion spectrograms in 1966 Peruvian eclipse for lower chromosphere excitation temperature 17 p2799 A71-34476
- Solar Fraunhofer line wavelengths shifts at disk center and at limb, evaluating Stark broadening contribution 18 p2962 A71-36106
- Ar ion laser plasma spectral lines widths and shifts at various pressures and current densities, noting role of ion-neutral charge exchange collisions 18 p2932 A71-37007
- Collisional broadening of IR absorption lines in vibration-rotation bands of carbon monoxide and hydrochloric acid 19 p3106 A71-37374
- Stark contours of hydrogen spectral lines in turbulent plasma with high noise level due to HF Langmuir oscillations 19 p3110 A71-37388
- Nonadiabatic effects in van der Waal line broadening, taking into account mixing between degenerate magnetic sublevels in atomic collisions 19 p3106 A71-37409
- Absorption intensities of R branch J manifolds of methane band, using half widths and pressure shifts 19 p3106 A71-37410
- Solar photosphere vibrational temperature determination, using Franck-Condon factor with equivalent line widths for five CN vibrational bands 19 p3133 A71-37431
- Active unperturbed solar photosphere, determining variations in spectral line profiles 19 p3133 A71-37432
- Resonance broadening measurements of alkali metals, giving relation between optically thick and thin full widths for Lorentzian and Gaussian line shapes 19 p3105 A71-38721

He II alpha lines scanned by electromagnetically driven T tube, comparing with Stark broadening theory

20 p3272 A71-39576

IR spectroscopy of CO using tunable PbS₂ diode laser, measuring Doppler linewidth and room temperature absorption coefficient at line center

20 p3246 A71-39757

External and internal absorption spectra of silicon crystal doubly doped with boron and indium acceptors, interpreting line broadening and cross section decrease

21 p3426 A71-40071

Raman tensor, scattering efficiency and line widths in semiconductors due to optical phonons, discussing electro-optical coefficients

21 p3427 A71-40662

Cyclotron resonance measurement for holes in uniaxially compressed Si, determining pressure and temperature effects on relative half width of hole line by relaxation time

21 p3433 A71-41309

Interstellar Lyman alpha absorption equivalent widths in hot stars spectra, examining rocket and satellite observations

22 p3598 A71-41913

Pulse trains of minimum spectral width generated from rectangular pulses by RC elements coupled without feedback

22 p3521 A71-42248

Optical second harmonic generation in excised tissues by Q switched ruby laser irradiation, observing narrow band emission line in collagenous tissues

22 p3559 A71-42567

H II regions kinematic properties in Large Magellanic Cloud, presenting emission line profiles and radial velocities

23 p3723 A71-42939

Formaldehyde transitions in ground and excited states at 6 cm, attaining line widths and hyperfine structure at 1-3 kHz

23 p3723 A71-42953

Spectral line broadening due to radiating atom-electron gas interaction in nonequilibrium partially ionized plasma

23 p3710 A71-43392

Coalescence /collapse/ of overlapping spectral lines due to nonadiabatic broadening for Stark structure of hydrogen and helium lines in discharge plasma

23 p3707 A71-43407

Traveling wave laser emission phase and amplitude fluctuations and spectral line width determination from single-mode distributed parameter model

23 p3685 A71-43563

Neon red lines Stark widths and shifts in function of electron and neutral Ne densities in shock tube

23 p3707 A71-43585

Automated analysis of high resolution IR astronomical spectra by computer program, presenting procedures for spectral line width, depth and frequency determination

24 p3867 A71-44438

Molecular gas dissociation equilibrium and carbon monoxide overtone line widths dependences on magnetic field strength in sunspots

24 p3868 A71-44459

Laser light emission from system of four-level centers with variably widened asymmetric luminescence line

24 p3833 A71-44659

Seyfert galaxy NGC 5548 H alpha profile spectroscopic observations, discussing broad emission lines

24 p3870 A71-44901

Search for CH molecular ion lines in solar photospheric spectrum, discussing profiles and equivalent widths

24 p3873 A71-45144

SPECTRAL LINES

U LINE SPECTRA

SPECTRAL NOISE

U WHITE NOISE

SPECTRAL RECONNAISSANCE

Black and white television scanning ability of color differentiation and gray tone identification by signal fluctuations in aerial imagery

12 p1907 A71-27261

SPECTRAL REFLECTANCE

Planetary surfaces photometry, discussing parameters, phase laws, albedos, spectral reflectivities, phase function theory and light scattering

02 p0309 A71-12156

Galilean satellites spectral reflectivity from photometric observations during Jupiter apparitions

03 p0488 A71-13554

Spectral reflectance measurement, comparing oxidized meteoritic material and Martian surface

03 p0489 A71-13559

Radar interferometric mapping of Venus surface reflectivity in polarized mode at 70 cm wavelength

03 p0490 A71-13782

Saturn rings spectral reflectivity measurement and compositional implications concerning water frosts and silicates

04 p0659 A71-15857

Aerial photographic measurements of terrain spectral reflectance and analysis of water resource color and quality by scene color standard technique

09 p1439 A71-23218

Hypervelocity projectile material impact on ultimate reflectance of bombarded polished metals from shock tube tests

11 p1799 A71-25835

Spectral reflectance of water cryodeposits on liquid nitrogen cooled surfaces in vacuum IR integrating sphere

[AIAA PAPER 71-447] 11 p1858 A71-26232

Lunar dust deposition and brushing effects on spectral solar reflectance of thermal control materials in vacuum

[AIAA PAPER 71-459] 11 p1799 A71-26241

Reflecting Au films deposition on glass substrates by evaporation in vacuo, discussing optical devices, reproduction and bonding improvements

11 p1809 A71-26431

Space stable thermal control coatings, noting reflectance optical spectroscopy of zinc oxide based paints and zinc orthotitanate

11 p1747 A71-26520

Surveyor 3 thermal control surfaces analysis from Apollo 12 samples collection, discussing spectral reflectance and lunar dust effects on surface finishes optical properties

[AIAA PAPER 71-479] 12 p1920 A71-26759

Lunar dust reflectance degradation of thermal control point on Surveyor 3 TV camera, separating solar radiation effects by analytical model

[AIAA PAPER 71-478] 12 p1920 A71-26760

Martian continents, seas and polar caps spectrum analysis, noting spectral reflectivity and brightness distributions

12 p1965 A71-27225

Refractive index and reflectivity of BiTeBr and BiTeI single crystals from interference measurements in transmission spectra

12 p1944 A71-27545

Jupiter Galilean satellites narrowband photometric data, observing albedos, spectral reflectivity, rotational phase, and brightness variations

13 p2135 A71-28292

Carbon dioxide frosts spectral absolute reflectance measurements at 0.5-12 microns, applying results to problems associated with cryogenically cooled surfaces

15 p2514 A71-32098

Mars surface narrow-band spectrophotometric observation, obtaining spectral reflectivities for geometric albedos calculation

18 p2970 A71-37048

Martian continents, seas and polar caps spectrum analysis, noting spectral reflectivity and brightness distributions

19 p3132 A71-37377

Water and ice clouds spectral brightness coefficients in IR region of spectra from aircraft measurements

19 p3090 A71-37977

Automatic single beam recording spectroradiometer system for measurements of spectral irradiance, radiance, transmittance and reflectance

20 p2325 A71-39176

Ashen light over Venus nocturnal hemisphere due to reflected earthlight and starlight

23 p3733 A71-43128

Visible and near IR spectral reflectivity measurements of basalt separates, glass and anorthositic fragments from Apollo 12 mare samples

23 p3760 A71-43770

Spectral directional reflectance of Apollo 11 and 12 fines as function of bulk density

23 p3760 A71-43771

Luminescence, thermoluminescence and spectral reflectance of lunar samples from Oceanus Procellarum and Mare Tranquillitatis

23 p3760 A71-43775

X ray probe, scanning electron microscopy and spectral reflectance analysis of lunar environment effects on Apollo 12 returned Surveyor 3 materials surface cratering

23 p3766 A71-43818

Martian surface materials determination by comparing albedo and brightness with spectral and photometric characteristics of crushed reddish volcanic rock and silicate sand mixed with limonite

23 p3770 A71-44052

SPECTRAL RESOLUTION

Satellite with onboard equipment for astronomical IR spectroscopy, considering stabilization accuracy and measurement duration effects on spectral resolution

01 p0163 A71-10395

Xenon resonance lamp with high spectral purity, discussing construction, life and refilling ease

04 p0600 A71-15599

Lunar ephemeris for nanosecond resolution laser ranging systems by literal and numerical integration techniques

[JPL-TR-32-1517] 05 p0811 A71-16682

Solar radio short term and fast drifting bursts observations with high spectral resolution, describing duration, frequencies bandwidth and polarization

06 p0963 A71-18441

Photographic materials in holography, examining resolving power dependence on size and on angle between reference and signal light beams

07 p1108 A71-19238

Mossbauer spectrometer with constant speed mechanical drive, describing special design features to avoid vibration induced lowering of spectral resolution

09 p1442 A71-22319

Laser fluid flow velocimeter pulse output resolution approximation, using spectrum analyzer or discriminator measurements

09 p1453 A71-23726

Photoelectric imaging devices resolution performance, considering modulation transfer function and measurement methods

10 p1610 A71-24066

Phase and log amplitude spectral and angular covariance of scintillation for propagation of two differing plane waves in randomly inhomogeneous medium

11 p1800 A71-26297

Solar radio short and fast-drifting bursts observations with high spectral resolution, describing duration, frequencies bandwidth and polarization

12 p1946 A71-26591

High resolution Fabry-Perot spectrometer with stepwise automatic scanning, discussing reproducibility, flexibility and stability

12 p1908 A71-27672

Error analysis of Corcos hypothesis concerning cross spectra of pseudoacoustic LF turbulent pressure pulsations on flat plate

15 p2389 A71-31708

High spectral resolution image recording instrument with postrecording bandpass selection, discussing signature data base and sensor modes

18 p2917 A71-36066

Spectral resolution of matrix Raman spectroscopy and depolarization measurements of isotope splitting, comparing with complementary IR data

20 p3194 A71-39404

SPECTRAL SIGNATURES

Agronomic research by remote sensing, discussing spatial, spectral and temporal measurements from electromagnetic multispectral response

06 p0896 A71-18407

Partly time invariant and periodically time varying gain equations based on Banach algebras spectral mapping theorem and higher order circle criteria

11 p1742 A71-26411

SPECTRAL THEORY

Solar line spectra formation and analysis, discussing transfer equation, atomic levels, line shape, etc

01 p0152 A71-10327

Acoustic turbulence spectrum in compressible fluid with potential motion, using complex traveling wave amplitudes in hydrodynamic equations

02 p0239 A71-11924

Crab Nebula pulsar PSR 0531 plus 21 at 410-1664 MHz, noting mean pulse profiles and spectral indices

05 p0812 A71-16697

Magnetospheric cold plasma dispersive and amplifying combined effects on pearl elements spectral shape, considering wave packet propagation applications

11 p1730 A71-25543

Limiting absorption principle and Schroedinger nonelliptic spectral theory for steady state wave propagation in inhomogeneous anisotropic media

12 p1929 A71-26866

Spectral theory of linear differential operators for microwave oscillatory systems synthesis from inhomogeneous line segments, determining line characteristic impedances and local reflection function

15 p2369 A71-31233

SPECTROGRAMS

High dispersion spectrograms of manganese Ap stars alpha And and pi Boo A, estimating electron concentration

07 p1204 A71-20632

Color frequency-time spectrograms of VLF electric and magnetic field Poynting flux data from Injun 5 satellite

13 p2054 A71-27914

Metallic lines in high-dispersion spectrograms in 1966 Peruvian eclipse for lower chromosphere excitation temperature

17 p2799 A71-34476

Computerized microphotometry of stellar spectrograms for converting input density data to intensity scales, coding tube sensometer plates, wedge/strip spectrograms and step wedges

17 p2742 A71-35006

Stellar spectrograms digital filtering for SNR improvement for photographic plate with line widths larger than granulation noise mean period

17 p2743 A71-35008

SPECTROGRAPHS

U SPECTROMETERS

SPECTROHELIOGRAPHS

- Solar corona radioheliograph observations, discussing burst types, prominences, shock waves, etc
01 p0152 A71-10329
- Spectraspectroheliograph observations, noting correlations between contour maps of solar continuum intensity and magnetic fields
[AIAA PAPER 70-1360] 02 p0315 A71-12693
- UV scanning polychromator spectroheliometer on Apollo Telescope Mount, examining temperature distribution on sun
03 p0430 A71-14435
- Sagittarius A region observations with 80 MHz radioheliograph, noting radio sources flux density
05 p0805 A71-16116
- Solar cycle large sunspot groups as function of heliographic longitude, noting structure/distribution stability responsible for phenomena
10 p1674 A71-24459
- Pulsar CP 0834 pulse energy fluctuations spectra secondary periodicities fluctuations from radioheliographic observation
13 p2141 A71-29099
- Spectroheliogram Doppler movies of solar velocity fields showing oscillatory and slowly varying components
18 p2965 A71-36728
- Far UV solar spectra observations, using OSO-2, 4, 5 and 6 spectroheliograms
19 p3136 A71-37614
- Solar velocity field decomposition into oscillatory and slowly varying components by spectroheliograms with high spatial resolution
19 p3146 A71-38662
- Two dimensional velocity field observations in and around sunspots from Doppler spectroheliograms
23 p3767 A71-43838

SPECTROHELIOSCOPES

U SPECTROHELIOGRAPHS

SPECTROMETERS

- NT FABRY-PEROT SPECTROMETERS
- NT INFRARED SPECTROMETERS
- NT MASS SPECTROMETERS
- NT SOLAR SPECTROMETERS
- NT SPECTROHELIOGRAPHS
- NT TIME OF FLIGHT SPECTROMETERS
- NT ULTRAVIOLET SPECTROMETERS
- Portable direct reading spectrometer for monitoring oxygen-hydrogen containing contaminants in gas tungsten arc welding process
02 p0247 A71-11712
- Spectrograph design for simultaneous measurement of velocity spectra and charge-to-mass ratios of ions, using magnetic and electric fields deflection effects
02 p0249 A71-12126
- Echelle grating and transmission optics spectrographs using image intensifier tubes for increased sensitivity
02 p0250 A71-12138
- Soviet spectral instrumentation for industry and research
02 p0254 A71-12710
- Fat lean cellular and bone mineral mass determination in living bodies, using radiation absorption spectrometry
02 p0210 A71-12954
- Organic compounds carbon K emission spectra, using light element X ray spectrometer for aliphatic, aromatic and partly ionic substances spectral analysis
03 p0375 A71-13200
- Solar radio astronomy decimeter wave multichannel spectrograph for solar bursts fine structure spectrum analysis
03 p0488 A71-13530
- Eclipse photon counting for solar atmosphere height determination, describing spectrograph-photomultiplier apparatus
03 p0424 A71-13632
- Proton 4 satellite high and superhigh energy cosmic ray spectrometer, discussing principles of operation and parameters
03 p0426 A71-13833
- Stable tunable microwave source for spectroscopy using Gunn diode, giving microwave cavity spectrometer block diagram
03 p0428 A71-13924
- ESCA /Electron Spectroscopy for Chemical Analysis/ spectrometer using small digital computer as process regulator
03 p0428 A71-13925
- Spectrographic method for simultaneous determination of constituents in hard metals by rotating disk solution technique
03 p0375 A71-13972
- Trapped protons east-west asymmetry observations during Gemini 4 flight, using on-board high sensitivity plastic-scintillation spectrometer
03 p0479 A71-14041
- Stellar spectrograph with image converter, obtaining optimal ratio between telescope and collimator diameters
04 p0589 A71-14833

- Astronomical spectrometers covering prism, grating, dye filter, plane Fabry-Perot, monochromator, Michelson and coherent detection laser spectrometers
04 p0593 A71-14871
- Stellar spectra and spectral types, discussing spectrographs, identification of lines, intensity measurements, absorption lines, Harvard system, etc
04 p0646 A71-15229
- Electron accelerator with broad stable beam for calibration of spectrometers and channel electron multipliers
04 p0599 A71-15587
- Minimum image size in parallel plate electrostatic spectrograph under focusing with small angular aberrations
04 p0600 A71-15593
- Clean cryogenic vacuum high speed gas pumping system for calibrating spectrometers for use on Apollo telescope mount
07 p1160 A71-19854
- Hadamard-transform spectrometer experimental verification for multiplex advantage in signal to noise ratio
08 p1289 A71-21376
- Magnetic Compton spectrometer for high intensity pulsed gamma ray environments and nuclear device spectral measurement
08 p1294 A71-21840
- Gamma ray spectrometers made from high purity p-type Ge crystal, observing performance
08 p1345 A71-21843
- Mossbauer spectrometer with constant speed mechanical drive, describing special design features to avoid vibration induced lowering of spectral resolution
09 p1442 A71-22319
- Satellite-borne spectrometer for low energy electrons measurement, describing virgin photoelectrons equilibrium energy spectrum for different latitudes and pitch angles
09 p1436 A71-22553
- Satellite-borne spectrometer for low energy ion measurement
09 p1436 A71-22554
- Satellite-borne scintillation spectrometers for medium and high energy electron and proton measurements
09 p1513 A71-22555
- Large Cerenkov detectors in absorption spectrometers during high mountain cosmic ray measurements
10 p1612 A71-24668
- Modulation-amplitude selective twofold increase of interferential spectrometer resolving power by asymmetric setup
10 p1613 A71-25020
- Negative ions photodetachment by continuously tunable laser and ion cyclotron resonance spectrometer
11 p1772 A71-25371
- Water vapor latitude variation on Mars from Coude spectrograph of 107 inch telescope
11 p1826 A71-25716
- Parallel plate electrostatic analyzer design, discussing second order focusing, angular aberrations and magnification
12 p1903 A71-26570
- Fiber optics for spectroscopic illumination, discussing absolute and angular transmission measurements and optical angular transfer function calculation
12 p1905 A71-26806
- Interferential spectrometer with selection by amplitude modulation with double passage mirrors arrangement for obtaining double resolution
12 p1905 A71-26811
- Interference spectrography and spectrometry techniques, describing transverse achromatic light source beam splitting and frequency analysis of photographed fringes
14 p2238 A71-29804
- Spectrometric imager device providing information on spatial and spectral distribution of light from extended objects, discussing signal encoding and decoding devices and techniques
14 p2242 A71-30145
- Mossbauer gamma spectrometer for operation at constant and adjustable velocities, incorporating springless vibrator and automatic zero stabilization
14 p2247 A71-30577
- Proton flux measuring spectrometer with automatic tracking of distribution maxima over energy range from 0.15 to 4 keV
14 p2247 A71-30578
- Time coordinate compensator for time variable spectrometers operating on long plastic scintillators with two terminal photomultipliers
14 p2247 A71-30579
- Large volume Cerenkov detector design for cosmic ray energy total absorption spectrometer measurements
14 p2247 A71-30599
- High energy cosmic muons momentum spectrum and charge ratio measurements at large zenith angles, describing magnetic spectrometer
14 p2247 A71-30601

- Balloon-borne ionization spectrometer for high energy cosmic ray measurement, discussing calibration and accuracy
15 p2407 A71-31811
- Cosmic ray measurements at various altitudes, describing magnet spectrograph for momentum spectra and particle identification
15 p2408 A71-31813
- Nuclear magnetic resonance spectrometer for moisture content measurement of lunar and terrestrial soils and rocks
15 p2411 A71-32474
- Steady plasma flow velocity measurements, describing two channel high resolution spectrometer
17 p2787 A71-34390
- Decimeter wave multichannel spectrograph design for radio astronomy, stressing HF section
17 p2739 A71-34600
- Flame atomic fluorescence-atomic emission DC spectrometer for trace wear metals analysis in jet engine oils, covering spectral wavelengths below and above 3500 A
17 p2695 A71-35150
- French monograph on system reliability of particle detection device covering methodology, functional models, Monte Carlo simulation, spectrometers and DC/DC converters
17 p2767 A71-35231
- Airglow surveys using extended field large aperture interferometer-spectrometer with optical wedge compensators and digital recording
18 p2914 A71-35842
- Apollo 11 lunar soil and rock samples under low level beta spectrometry, measuring radon daughter Pb 210
18 p2961 A71-35946
- Double electron-nuclear resonance spectrometer using HF modulation of magnetic field for observation of electron paramagnetic resonance signal
18 p2924 A71-36626
- Dispersive photoelectron spectrometers, considering entrance area and solid angle product /etendue/
19 p3063 A71-37553
- True central intensities of Fraunhofer lines, describing solar telescope and Czerny-Turner spectrometer
19 p3146 A71-38661
- Performance measurement of electrostatic spectrometers as monochromators by calculation of electron energy distribution
20 p3233 A71-38821
- Scintillation spectrometers sensitivity evaluation for low energy electrons in various regions of magnetosphere
20 p3234 A71-39127
- High energy cosmic ray spectrometer onboard Proton 4, discussing ionization calorimeter, nuclear targets, particle charge and radiation detectors and primary measurements
20 p3283 A71-39755
- Echelle gratings in single pass spectrometers, discussing properties, instrument profiles quality and accuracy
22 p3537 A71-41473
- Cosmic ray muons absolute intensity determination, using Durham vertical spectrograph
22 p3593 A71-42353
- Proton 4 satellite high and superhigh energy cosmic ray spectrometer, discussing operational principles and parameters
22 p3594 A71-42634
- Hybrid lumped-distributed parameter resonant LC circuit design for nuclear magnetic resonance spectrometer
23 p3661 A71-44343
- Shock-heated Mg/MgO particle dispersion, postulating kinetic mechanism consistent with spectrometric observations
24 p3863 A71-44940
- Absorption spectrum of atmospheric gases from laser spectrometer based on tunable ruby laser, measuring water vapor absorption coefficients in multipass cell
24 p3834 A71-45207

SPECTROMETRY

U SPECTROMETERS

SPECTROPHOTOMETERS

NT INFRARED SPECTROPHOTOMETERS

- Double beam monochromatic differential cinespectrophotometer for recording oxidation/reduction reactions in intercellular pigments
01 p0021 A71-10243
- Double beam spectrophotometer for small transmission changes, discussing measurement range and uncertainty
02 p0247 A71-11721
- Spectrophotometric instrumentation in physics and chemistry, discussing developments in automation, accuracy and measurement time
03 p0429 A71-14326
- TV spectrophotometer with photographic and photoelectric measurement techniques advantages for measuring astronomical telescope spectral passbands
07 p1109 A71-19349

Rapid scan astronomical spectrophotometer with 1024 channel for signal averaging on slow change in sky transparency for improving accuracy

12 p1904 A71-26803

Spectrophotometers photometric accuracy measurement technique, using Bouguer law and optical fields superposition

14 p2240 A71-30123

Rapid scanning dual wavelength spectrophotometer for recording oxidation-reduction and membrane bound reactions in turbid suspensions of biological materials

18 p2922 A71-36580

SPECTROPHOTOMETRY

NT STELLAR SPECTROPHOTOMETRY

Rapid internal standard identification method for metals by atomic absorption spectrophotometry, using diluted acid solution of specimen

01 p0028 A71-10257

Upper atmospheric gas components vertical distribution by airborne photometric absorption and attenuation measurements in UV spectrum

02 p0246 A71-12118

Quasars spectrophotometry data, obtaining physical conditions, abundances and electron temperature

05 p0811 A71-16685

Soviet lunar surface rocks physical properties ground observation including colorimetry, spectrophotometry and polarimetry

07 p1193 A71-19311

Electron spectrophotometry in molecular and solid state physics, comparing to X ray analysis

10 p1645 A71-24695

NGC 3351 galaxy core spectrophotometry of optical spectrum covering emission and absorption lines

12 p1960 A71-26831

Platinum, palladium and gold detection in silver assay buttons by atomic absorption spectrophotometry

15 p2367 A71-31649

Soviet lunar surface rocks physical properties ground observation including colorimetry, spectrophotometry and polarimetry

15 p2485 A71-31891

Rapid photoelectric spectrum scanning techniques using multichannel analyzer and triggering mechanism

17 p2741 A71-34991

Real time system for solar spectrophotometry, noting application for scanning H alpha and other Balmer series lines profiles in solar flare regions

17 p2741 A71-34994

Twilight glow spectrophotometry and visual observations from Soyuz 5 spacecraft, determining atmospheric optics and vertical aerosol profile

18 p2911 A71-36006

Mars surface narrow-band spectrophotometric observation, obtaining spectral reflectivities for geometric albedos calculation

18 p2970 A71-37048

Global, regional and local earth IR imagery for earth sciences from space TV, photography and spectrophotometry

20 p3220 A71-39665

Spectrophotometry and photography of earth twilight aureole, clouds and underlying surface from manned Soyuz 5 and 7 spacecraft

20 p3240 A71-39675

Photoelectric and photographic spectrophotometric observations of relatively bright moderate excitation planetary nebula NGC 6826, obtaining electron density and ion concentration

21 p3446 A71-40415

Radio galaxies cosmological evolution, discussing rate and spectrophotometric data

23 p3766 A71-43823

SPECTRORADIOMETERS

Soviet book on radiation dosimetry and spectrometry of ionizing radiations covering chemical, electrochemical, thermoluminescence, scintillation and diffuse reflection methods

11 p1797 A71-26450

Automatic single beam recording spectroradiometer system for measurements of spectral irradiance, radiance, transmittance and reflectance

20 p3235 A71-39176

Remote sensing of chlorophyll and temperature in marine and fresh waters by spectroradiometer and differential and IR filter radiometers onboard airplane

22 p3534 A71-41986

SPECTROSCOPES

U SPECTROMETERS

SPECTROSCOPIC ANALYSIS

Thermionic converter Cs plasmas electron temperature and density gradients spectroscopic measurements compared with prediction from energy transport analysis and ionization coefficients

02 p0194 A71-12226

Thermionic converter spectroscopic measurements in several regions of I-V characteristics, noting plasma radiation intensity periodic waveform

02 p0195 A71-12238

Sulfur hexafluoride absorption lines observation by inverted Lamb dip high resolution spectroscopy, using heterodyne methods

02 p0209 A71-12731

Material testing - Conference, Budapest, October 1970, Section 3, Spectrochemical analysis

03 p0375 A71-13968

Plasma generators for spectrochemical analysis, discussing properties and design

03 p0465 A71-13969

Analytical sensitivity and reproducibility in plasma jet excitation for spectrochemical applications

03 p0465 A71-13970

Aerosol powder suspensions for spectrochemical objectives in plasma jets

03 p0465 A71-13971

Spectrographic method for simultaneous determination of constituents in hard metals by rotating disk solution technique

03 p0375 A71-13972

Physical chemistry of arc plasma, considering radial distribution, spectral density and energy relations for spectrochemical applications

03 p0465 A71-13973

Spectrochemical analysis of alloy steels using microspark method

03 p0375 A71-13974

Quantitative spectrographic microanalysis using laser pulse vaporization and spark discharge

03 p0438 A71-13975

Ar-Ag arc, microwave discharge and plasma torch techniques in emission spectroscopy of trace elements in biological materials

03 p0377 A71-14421

Electron temperature measurement in electromagnetic shock tube by spectroscopy and ruby laser light scattering in plasma, examining validity of local thermal equilibrium assumption

04 p0632 A71-14688

Shock tube spectroscopic and reaction kinetic research, considering studies before LTE

04 p0547 A71-14692

Plasma accelerator self ionizing current free stable radiative shock wave structure in hydrogen, using time resolved spectroscopic measurements

04 p0548 A71-14696

Muscovite mica substrate surface composition as function of preparation and processing, using Auger electron spectroscopy

06 p0941 A71-17408

Halogens atomic transition probabilities spectroscopic measurements in visible and near IR spectra, using gas driven shock tube

07 p1163 A71-19685

Rare earth based liquid lasers, describing spectroscopic and performance properties of neodymium ions in aprotic solvents

07 p1124 A71-19788

Uranus physically self consistent atmosphere model based on spectroscopic, photometric and radio observational data

07 p1198 A71-19828

Erbium ions stimulated emission, spectroscopic properties, pulsed laser action and absorption spectra in yttrium orthoaluminate

07 p1126 A71-20165

Relative elevation differences on Mars surface revealed by near IR carbon dioxide bands spectroscopic observations

11 p1825 A71-25713

Mars surface pressure and elevation differences determined by spectroscopic observation of carbon dioxide band

11 p1825 A71-25714

Spectrometer slit-width cancellation by Doppler shift of light emission by fast ion beams, resulting in spectral lines increased intensities

13 p2071 A71-29331

Plasma local thermodynamic equilibrium relation to continuum, molecular band, atomic lines intensity and absorption line reversal/equivalent widths measurements

16 p2617 A71-32959

Apollo 11 and 12 lunar soil and rock samples abundance comparison based on Mossbauer spectroscopy

16 p2637 A71-33509

Flame atomic fluorescence-atomic emission DC spectrometer for trace wear metals analysis in jet engine oils, covering spectral wavelengths below and above 3500 A

17 p2695 A71-35150

Spectroscopic analysis of continuous light emission from molecular oxygen-nitrogen mixtures in Mach 9 shock waves, stressing radiative reaction role

19 p3106 A71-37462

Mercury determination in terrestrial and nonterrestrial rock samples by atomic absorption spectroscopy, noting high temperature release patterns

21 p3346 A71-40863

Cosmogenic and primordial radionuclides in Apollo 12 surface rocks and fines from nondestructive gamma ray spectrometry

23 p3755 A71-43733

Spectroscopic analysis of pulsed gas discharge in crossed electric and magnetic fields of gas magnetron diode in 3100-4660 A wavelength range

23 p3712 A71-43933

SPECTROSCOPIC TELESCOPES

Horizontal ATsU solar telescope and ASP-20 and DFS-3 diffraction spectroscopes, discussing performance, time delay and resolution

04 p0589 A71-14831

Water vapor latitude variation on Mars from Couder spectrograph of 107 inch telescope

11 p1826 A71-25711

Criean astrophysical observatory horizontal solar telescope, describing spectrograph spectral bandwidth and dispersion characteristics

14 p2240 A71-29984

Climatological European southern observatory in Chile, describing spectroscopic and photometric telescopes, grand prism objective and double astrophotograph

20 p3210 A71-39521

SPECTROSCOPY

NT ABSORPTION SPECTROSCOPY

NT ASTRONOMICAL SPECTROSCOPY

NT AURORAL SPECTROSCOPY

NT GAS SPECTROSCOPY

NT INFRARED SPECTROSCOPY

NT MAGNETIC SPECTROSCOPY

NT MASS SPECTROSCOPY

NT MOLECULAR SPECTROSCOPY

NT NUCLEAR RADIATION SPECTROSCOPY

NT OPTICAL EMISSION SPECTROSCOPY

NT RADIO SPECTROSCOPY

NT RAMAN SPECTROSCOPY

NT SPECTROPHOTOMETRY

NT SPECTROSCOPIC ANALYSIS

NT STELLAR SPECTROPHOTOMETRY

NT ULTRAVIOLET SPECTROSCOPY

NT VACUUM SPECTROSCOPY

NT X RAY SPECTROSCOPY

Hadamard transform spectroscopy, discussing spectral intensity calculation for cyclic measurement matrices

04 p0549 A71-15690

Papers on optics, Volume 8, covering synthetic apertures, light beating spectroscopy, multilayer antireflection coatings, interference microscopy, photoelectron counting, human eye performance, laser light, etc

05 p0713 A71-16481

Laser microprobe emission spectroscopy of biological matrix elements, investigating bovine albumin effect on spectrum analysis

07 p1113 A71-19785

Beam foil spectroscopy using van de Graaff accelerator, considering applications to atomic physics research and teaching

08 p1272 A71-21667

Laser applications in physics research, discussing nonlinear optics and spectroscopy, time and distance measurements and Raman and Rayleigh light scattering

09 p1462 A71-22585

Terrestrial spectroscopy by cryogenic gravity meter with hollow superconducting niobium sphere in cylindrically symmetric magnetic field, detecting earth spheroidal oscillations

10 p1598 A71-23737

Spectroscopic measurement of high temperatures for ionized gases/plasmas in local thermodynamic equilibrium

11 p1761 A71-25571

High resolution holographic Fourier transform spectroscopy, discussing interferometer localized interference fringes direct recording method and heterodyning technique

12 p1905 A71-26805

Spectroscopy and collisional transfer in methyl chloride by microwave laser double resonance, measuring population changes in various rotation vibration levels

12 p1877 A71-27004

Xe plasma flash tubes with very low discharge current magnetic field for spectroscopic and laser applications in presence of Zeeman effect

14 p2243 A71-30272

Shock tube spectroscopy as tool for atomic and molecular research, describing applications in chemical physics, astrophysics, gas dynamics, etc

16 p2578 A71-33152

Secondary emission analog for improved Auger spectroscopy to eliminate objectionable feature of electron spectra taken with retarding potential analyzer

18 p2922 A71-36579

Hot water vapor total emissivity charts at various temperatures, using band model parameters with spectroscopic data

18 p2985 A71-36592

SPECTRUM ANALYSIS

Mg, Al and Si ions spectral analysis, discussing energy levels and transition lines

01 p0129 A71-10136

Solar line spectra formation and analysis, discussing transfer equation, atomic levels, line shape, etc

01 p0152 A71-10327

Remote sea state information acquisition system using video attachment to radar for sea return spectrum recording and analysis

01 p0031 A71-10600

Aircraft response to atmospheric gust, discussing spectral analysis procedures and calculation results on T-tail aircraft design

01 p0005 A71-10752

Atmospheric surface layer turbulence spectra and cospectra observations in July-August 1969 at Edithvale, Australia

01 p0120 A71-10858

Instrumentation tape recorder time base error effects on signal carrier amplitude and spectral purity

01 p0033 A71-10896

Spectra of faint optical meteors for chemical abundance, discussing radiative processes during atmospheric entry, Leonid meteors and data acquisition

01 p0161 A71-11275

Energy distribution of laser spark spectrum in air, He and Ar, determining transmission coefficients of spark plasmas by self absorption method

02 p0258 A71-11638

Satellite sounding of atmospheric pollution by spectral analysis of outgoing thermal radiation

02 p0241 A71-11689

Straight and curved edges produced vidiosignal amplitude spectra discrimination in TV image scanning of nuclear particle path photographs, using filtering device

02 p0248 A71-11827

Monochromatic signal spectrum determination from circulating realization spectrum analysis

02 p0248 A71-11833

Frequency-wavenumber power spectrum estimators probability distribution, using Gaussian distribution probability density function

02 p0215 A71-12046

Extragalactic radio source 3CR catalog, analyzing emission spectra

02 p0300 A71-12087

Nonrelativistic cosmic particles spectrum and chemical composition changes, examining ionization and heating energy loss effect

02 p0300 A71-12093

Nitrogen inductive low pressure discharge, determining vibrational and rotational temperatures, ionization degree, electron temperature and energy balance by spectroscopic technique

02 p0286 A71-12178

Ionized intergalactic and pregalactic matter 3K microwave background, examining spectrum and degree of anisotropy

02 p0312 A71-12467

Sunspot observation of 22 June 1959, discussing two MgO bands spectrographic analysis

02 p0313 A71-12536

Computer controlled mass spectrometer system, processing spectral information data for on-line graphic system output

02 p0253 A71-12550

Diffuse cosmic X ray spectrum obtained from telescope aboard OSO 3 satellite

02 p0300 A71-12580

Solar flare of 30 March 1969, determining differential rigidity spectral index and small anisotropy

02 p0302 A71-12767

Relativistic electron spectra of cosmic rays accelerated by plasma turbulence, examining singularity in solution

03 p0483 A71-13202

Active nitrogen afterglow complex spectrum analysis from vacuum UV to IR, proposing energy transfer mechanism

03 p0460 A71-13352

Commercially produced metallic wire gratings reflection spectra measurement, determining use as high performance filters and light polarizers in far IR region

03 p0457 A71-13507

Solar radio astronomy decimeter wave multichannel spectrograph for solar bursts fine structure spectrum analysis

03 p0488 A71-13530

Laser action on six lines of ionized Xe spectrum, discussing discharge tube, optical resonator and spectrograph characteristics

03 p0438 A71-13895

Solar X-ray emissions dynamic spectra at flare times by E-T tracing

03 p0479 A71-14045

Night airglow spectral components by Cosmos 92 satellite measurements, considering UV region sources and intensity variations

03 p0417 A71-14050

Night airglow, discussing spectrum, latitudinal dependency, diurnal variation, time and space correlations and sunspot cycle and solar activity effects

03 p0417 A71-14071

Martian dayglow spectrum, examining excitation processes for carbon monoxide Cameron bands

03 p0497 A71-14544

Ne, Ar, Kr and Xe ionized states transition and level lifetimes from photographically recorded beam foil spectra, discussing particle energies

04 p0629 A71-14805

Spectral analysis increased sensitivity for dispersion systems, using optimum filtering of spatial frequencies

04 p0590 A71-14838

Hadamard transform spectroscopy, discussing spectral intensity calculation for cyclic measurement matrices

04 p0549 A71-15690

Saturn millimeter wave spectrum and brightness temperature measurements, showing ammonia absorption characteristics in atmosphere

04 p0659 A71-15851

Shading reflector transverse motion effect on radar signal spectrum based on geometric optics approximation

05 p0719 A71-15999

Circular polarization measurement in various lines, finding magnetic field strength influenced by line absorption coefficient variations from photosphere to spot and faculae

05 p0803 A71-16025

Fast transformations algorithm for generalized spectral analysis

05 p0774 A71-16415

Radiation spectra kinetics of compound ruby lasers containing two crystals and Nicol prism

05 p0763 A71-16830

Ruby laser with lens resonator, studying radiation patterns and angular divergence, lasing threshold and spectra width

05 p0763 A71-16831

Vertical behavior of stratospheric optical thickness and dispersion coefficient in red region of spectrum from photometric analysis of Soyuz 3 photographs of daytime horizon

05 p0742 A71-16839

Book on optical data processing covering light characteristics, Fourier transforms, spectrum analysis, photographic film, filtering, holography, etc

05 p0754 A71-17124

Sunset and sunrise vertical displacement rate of lower ionosphere from spectral analysis of field intensities at 236, 557 and 1277 kHz

05 p0744 A71-17184

Absolute particle spectra above atmosphere and magnetosphere during solar flare of 23 February 1956

05 p0800 A71-17198

Western frequency drift effects on spectrum time evolution azimuthal asymmetry in diminishing period geomagnetic pulsation intervals

05 p0747 A71-17214

Atmospheric path effects on spectral radiance intensity in remote airborne multispectral sensors

06 p0898 A71-17559

Differential operator determination in spectral analysis of inverse problem stability

06 p0865 A71-17582

Intensity calibrated grazing incidence spectrographs on Skylark sounding rockets, recording solar soft X-ray and XUV spectra

06 p0967 A71-17903

Vertical structure of solar faculae from spectroscopic method for three dimensional information derivation

06 p0967 A71-17908

Statistical equilibrium equations solved for atom/ion with complex energy level structure and weak spectral lines, discussing deviations from LTE

06 p0969 A71-17969

Forbush decreases and long term cosmic ray particle intensity changes, investigating spectral variations

06 p0956 A71-18137

Solar flare event of 28 January 1967, observing parent flare location, particle fluxes and diffusion and spectral exponent

06 p0957 A71-18143

Secondary cosmic ray spectrum latitude knee based on nucleon, proton and muon energy spectra

06 p0960 A71-18167

Engine pressure spiking restart preignition products, determining hydrazine nitrate and dinitrate presence by spectrum analysis

06 p0945 A71-18296

Wave number/phase velocity spectrum of wall pressure measurements beneath two dimensional turbulent boundary layer

06 p0882 A71-18317

Quiescent metallic and ordinary prominences continuum spectra measurements, showing hydrogen ionization dependence on microstructure

06 p0975 A71-18438

Spectral analysis of five-day pulsations in earth rotational velocity, estimating amplitudes of suspected velocity fluctuations

06 p0896 A71-18452

Signal cross correlation processing in unstable and turbulent plasmas, comparing correlational and spectral analyses of plasma dispersion and transfer function measurements

06 p0938 A71-18456

Atmospheric boundary layer IR transmittance spectra compared to spectrum calculated from transmittance functions

07 p1152 A71-19149

Volume spectra during heat treatment in metallic systems, using automatic dilatometry

07 p1112 A71-19613

Coherent optical data processing techniques, discussing diffraction phenomena, spectral analysis and holography

07 p1067 A71-19629

Laser microprobe emission spectroscopy of biological matrix elements, investigating bovine albumine effect on spectrum analysis

07 p1113 A71-19785

Relative spectral sensitivity /amplitude frequency characteristics/ applicability to describing nonlinear systems

07 p1043 A71-20111

Self similar laser produced plasma examination, using irradiated multilayer targets and spectrum analysis

07 p1170 A71-20169

Electrophotometric and spectral observations of continuous airglow spectrum

07 p1105 A71-20438

Correlation and spectrum analysis of simultaneous EEG data in mono and dizygotic twins using computer and FFT algorithm

08 p1246 A71-20746

Planetary nucleus BD plus 30.3639 degrees and Wolf-Rayet star HD 164270, comparing spectrum and ionization potential

08 p1359 A71-20937

Cosmic ray modulation spectrum function properties during Forbush decrease by spectrographic analysis

08 p1352 A71-20968

Second spherical harmonic generation mechanisms in axisymmetric diurnal and semidiurnal cosmic ray spectrum variations

08 p1352 A71-20969

Fe powder concentration in Ni powder by spectral analysis, examining particle size and HF generator spark condensation effects

08 p1306 A71-21066

Zinc-hydroxy system spectrum analysis, using laser source Raman spectrometer and modified IR reflectance accessory

08 p1233 A71-21079

Extragalactic radio source 3CR catalog, analyzing emission spectra

08 p1362 A71-21137

Nonrelativistic cosmic particles spectrum and chemical composition changes, examining ionization and heating energy loss effect

08 p1355 A71-21143

Term splitting of Li I, B I, Na I and other sequences with one electron spectra, using screening parameters obtained from Hartree-Fock calculations

08 p1337 A71-21182

Periodic nonstationary random process spectral representation derivation by applying Loeve harmonizability theorem

08 p1334 A71-21298

Matrix multiplication algorithm based on degrees of freedom analysis for various transformations and spectral analysis

08 p1260 A71-21662

Turbulent plasmas nonequilibrium electric fields determination from hydrogen spectral lines Stark broadening

08 p1341 A71-21790

Piezoelectric transducer echo signals spectral analysis, taking into account electrical load and electromechanical coupling degree

08 p1294 A71-21896

Ti dioxide-opacified porcelain enamel reflectance spectra analysis, deriving scattering cross sections and dispersed particle sizes and distribution

09 p1480 A71-22116

Holographic spectrum analyzer for plasma diagnostics in microwave band, deriving formulas for emission spectrum based on interference patterns intensities in waveguide

09 p1499 A71-22150

Comet 1969g spectrum at 3800-8500 A, noting upper H alpha surface brightness limit consistency with chromospheric resonance fluorescence model

09 p1517 A71-22335

Spectral analysis of laser Doppler flowmeter signals, considering time independent systems

09 p1463 A71-22691

Real time low frequency narrow band spectrum analyzer using time compression technique for vibrating machinery diagnosis and prognosis

09 p1443 A71-22708

Constant, programmed and random amplitude spectral analysis and signal averaging correlation with failure statistics, noting laboratory simulation

09 p1444 A71-22709

Ray transformation after passing through optical resonator with Brewster prism, calculating spectral

energy losses dependence by geometrical optics method 09 p1464 A71-23072

Airborne multispectral remote sensing of forests, describing previal detection of damage from insect infestations, disease organisms and oxidant air pollution 09 p1438 A71-23210

Sunspots umbrae spectrum analysis in 4000-8000 Å region, identifying molecular absorption lines photoelectrically 10 p1666 A71-23785

Solar spectrum observations in water band at 1.87 micron by stratospheric balloon sounding 10 p1667 A71-23863

Isotopic emission features at 11.7/cm, discussing high resolution ground based spectrum measurement 10 p1599 A71-23869

Spectral sensitivity by stimulus control and presentation in barred pattern alternatives and photopic system monitoring by visual evoked responses 10 p1560 A71-23986

Pluto iron richness from analysis of similarities between Pluto spectra and Fe bearing terrestrial silicate crystals 10 p1673 A71-24426

Jovian band color variation spectral observations using narrow band photometry 10 p1676 A71-24499

Na I absorption spectrum interpretation between 150 and 900 Å in vacuum UV, noting various discrete features 10 p1676 A71-24500

Methane spectral band analysis, examining J manifolds self broadening coefficients of R branch 10 p1573 A71-24546

Magnetospheric VLF banded emissions spectral analysis, investigatingOGO-5 data by high time resolution spectral techniques 10 p1579 A71-24788

Solar wind origin of auroral ions from low energy hydrogen and helium ion spectral measurements 10 p1664 A71-24791

Real time spectrum analyzer, discussing data sampling rates, statistical uncertainties, waveform and bandwidth 10 p1612 A71-24832

Q switched ruby laser time dependent spectrum analysis by high speed camera with Fabry-Perot interferometer, noting holographic interferometry application 10 p1622 A71-24962

Mars atmospheric CO abundances and rotational temperature from Voigt line profiles 10 p1646 A71-24993

Binary star 112 Herculis elemental abundances by atmospheric model analysis of spectra 10 p1680 A71-25001

Saturn satellites spectrophotometric observations at UV, visible and near IR, noting reflection spectra data 11 p1819 A71-25210

Jupiter far IR emission spectra models, examining atmospheric composition, temperature and structure 11 p1821 A71-25538

Neutral pion decay and galactic gamma radiation from demodulated cosmic ray spectrum, discussing neutral pion meson production 11 p1815 A71-25593

Venus atmosphere composition and structure from microwave spectrum, noting surface pressure and temperature and water vapor 11 p1823 A71-25694

Water vapor latitude variation on Mars from Coude spectrograph of 107 inch telescope 11 p1826 A71-25716

Spectral studies on radiation from molecules, atoms and electrons, demonstrating shock tube applications in opacity measurements 11 p1764 A71-26265

Nb-Ti alloys internal friction spectra due to oxygen content, applying graphical decomposition method 11 p1781 A71-26322

Waking and sleeping EEG signals bispectrum analysis, correlating component waves interactions with alpha activity, lead placement and state of consciousness 11 p1722 A71-26378

Mars 1969 opposition effects, describing Syrtis Major, Arabia and disk brightness, color and spectrum 11 p1835 A71-26456

Quiescent metallic and ordinary prominences continuous spectra measurements, showing hydrogen ionization dependence on fine structure 12 p1955 A71-26588

Spectral analysis of five day pulsations in earth rotational velocity, estimating periods and amplitudes of suspected velocity fluctuations 12 p1898 A71-26602

Electron paramagnetic resonance spectral investigation of dynamic Jahn-Teller effect in La doped strontium chloride, discussing structural variations as function of temperature 12 p1942 A71-26743

Astronomical photometry and photometric systems, discussing spectral classification, U, V, B, Y, beta system, energy distributions and seven color photography 12 p1903 A71-26774

Turbulent boundary layer thermal flux fluctuation spectral distribution determination by applying fluctuation diagram method to filtered signals 12 p1985 A71-26828

Thermally stratified turbulent shear flow, calculating turbulent energy balance and temperature inhomogeneity spectral equations 12 p1895 A71-26899

Cepheids UVB spectrum analysis, examining brightness shapes and color index curves 12 p1962 A71-26907

Spectral analysis methods for detection of water on celestial bodies, considering possible abundance on planets and stars 12 p1962 A71-26956

Quasars and X ray sources, observing UVB magnitude variation with photoelectric data 12 p1963 A71-27077

Waveform and spectral analysis program for electronic system designs, discussing fast Fourier transform modular staging and noise control applications 12 p1884 A71-27148

Optimal estimate of spectral density of vibration process over finite time interval, using spectral analyzer 12 p1930 A71-27175

Martian continents, seas and polar caps spectrum analysis, noting spectral reflectivity and brightness distributions 12 p1965 A71-27225

Bolide spectrum on 6 June 1969, determining stellar magnitude and periodic pulsations and asynchronous flares characteristics along trajectory 12 p1965 A71-27229

Apollo 9 So65 multispectral color space photography for basic land use pattern determinations 12 p1907 A71-27259

Cortico- and subcorticograms rhythm dynamics in sleeping and awake cats by spectral analysis and EEG integration 12 p1871 A71-27486

Isotropic turbulence three dimensional velocity spectrum function, using absolute mean strain rate constant and variable Reynolds number 12 p1898 A71-27581

Spectral line broadening theory applications to qualitative interpretation and quantitative determination of spectrograms from hydrogen line profiles of stellar atmospheric parameters 12 p1969 A71-27667

Spectral analysis of solar prominences observed during Peruvian eclipse of 12 November 1966, obtaining two dimensional distribution of kinetic temperature, density and turbulent velocity 12 p1970 A71-27702

Solar X ray flux and spectral energy distribution calculation in 0-20 Å band, using 9.1 cm spectroheliograms 12 p1954 A71-27708

Frequency vs time spectral shapes of magnetospheric VLF discrete emissions for field line and electron stream parameters 13 p2027 A71-27916

Line emission in X ray background in galactic plane and at galactic pole based on rocket flight data 13 p2120 A71-28005

Density spectrum of cosmic ray showers, discussing altitude effects, structure function and transition 13 p2125 A71-28087

Sunset and sunrise vertical displacement rate of lower ionosphere from spectral analysis of field strength at 236, 557 and 1277 kHz 13 p2059 A71-28241

Absolute spectra above atmosphere and magnetosphere and of particles accelerated in solar atmosphere during solar flare of 23 February 1956 13 p2128 A71-28253

Western frequency drift effects on spectrum time evolution azimuthal asymmetry in decreasing period geomagnetic pulsation intervals 13 p2060 A71-28269

Venus carbon dioxide spectrum, observing spatial and temporal variation in abundance 13 p2134 A71-28287

Extended galactic radio sources in anticenter quadrant, obtaining 408 MHz integrated flux densities and spectral indices 13 p2135 A71-28298

Photoelectric umbral scans at 6200-6700 Å identifying NiH lines, showing equal solar and terrestrial abundance isotopic ratios 13 p2135 A71-28301

Strong planetary nebulae measurement at short centimeter wavelengths, observing flux densities and thermal spectra 13 p2138 A71-28760

Precision Stark spectroscopy of methane by nonlinear laser absorption, observing Lamb-dip spectra by tuning stable single mode laser 13 p2079 A71-28950

Faint meteor spectra recording, using high sensitive image orthicon 13 p2070 A71-29017

Solar Ca II K line core formation, discussing models for high spatial resolution spectra 13 p2140 A71-29045

Solar vacuum UV spectrum analysis, using echelle grating spectrograph onboard Skylark sounding rockets 13 p2070 A71-29048

Long term pulsar intensity observations, noting periodic variations and power spectrum analysis 13 p2143 A71-29270

Atmospheric turbulence space-time relationships measurements, discussing computerized time series, spatial and phase spectral analysis for sensors data 14 p2267 A71-29755

Electromagnetic interference measurements, considering direct reading with RI-FI receiver, impulse generators and spectrum analysis 14 p2193 A71-29915

Cadmium sulfide pulsed laser spectrum analysis, discussing output stabilization by mode selection and electron beam scanning 14 p2253 A71-30092

Early type close binary systems AO Cas, HD 47129, HD 190918 and HD 193793 spectral observations 14 p2311 A71-30369

Errors in spectral estimates by single-mode filters using analog computer for geoscientific data processing 14 p2246 A71-30482

Auto- and cross-spectral estimation from irregularly sampled data by extending complex demodulation 14 p2246 A71-30483

Monograph on planetary nebulae covering structure, luminosity, spectra, origin, chemical composition, temperature, magnetic fields, etc 15 p2481 A71-31148

Microwave spectrum analyzer, discussing capabilities and applications in ECM, surveillance, communications, circuit design and analysis and electromagnetic compatibility 15 p2368 A71-31208

Pc micropulsations spectra fine structure and diurnal variations, analyzing rubidium magnetometer recordings by power spectral density method 15 p2394 A71-31425

Computational technique for acoustic field of jet aerodynamic noise, using Lighthill theory for spectral calculations [AIAA PAPER 71-583] 15 p2468 A71-31571

Noise and spectral analysis for measuring fluid flow with random temperature fluctuations by transit times 15 p2406 A71-31596

Titanium alloys analysis by dissolution in sulfuric acid and aerosol injection into spark discharge, discussing standard solution preparation 15 p2367 A71-31650

Solar eclipse on 7 March 1970, determining midlatitude geomagnetic pulsations with dynamic power spectral analysis 15 p2397 A71-31761

Cosmic ray rigidities spectra measurements above geomagnetic cutoff using balloon-borne emulsion plates in superconducting magnet field 15 p2407 A71-31805

Mu, VV, ST and RW Cephei cold supergiants polarization data, noting spectral dependence 15 p2487 A71-32030

Mars IR spectral geometric albedo of bright and dark regions for surface composition model 15 p2491 A71-32419

Optical fluorescence spectra of rock forming minerals for quantitative analysis of lunar surface 15 p2411 A71-32471

Nitrogen beam foil spectrum analysis, calculating transitions and decay times 15 p2452 A71-32598

Beam foil excited Ar spectrum between 500 and 1000 Å, tabulating lines with ionization stages based on line intensity variation with beam energy 15 p2368 A71-32601

Polyatomic molecule photoelectron spectroscopy, emphasizing spectra interpretation by quantum mechanical procedures 16 p2541 A71-33398

Meteor spectrum analysis presenting tables for Soviet observations 16 p2639 A71-33694

Uniqueness theorem for second order differential equation associated with inverse problem of spectral analysis, developing operator transformation procedure 16 p2603 A71-33890

Laser spectral-isotopic determination of oxygen content in metals, noting analysis variant dependence on metal purity 17 p2751 A71-34384

Rapid photoelectric spectrum scanning techniques using multichannel analyzer and triggering mechanism 17 p2741 A71-34991

Direct spectra analysis system using refrigerated image isocan TV camera as detector for astronomical spectrograph 17 p2741 A71-34993

X-Y programmed microdensitometer for stellar spectra analysis, imaging adjustable slit on spectrogram by interchangeable microscope objectives, using Kohler illumination 17 p2742 A71-35000

Automated stellar spectrophotometry, defining possible measurements on crowded spectra 17 p2742 A71-35005

Finite length heterogeneous thin layered cylindrical shell axisymmetric free vibration frequency spectrum analysis 17 p2826 A71-35035

Magnetic field effects on ruby laser radiation kinetics and spectral composition, studying crystal heating and light emission 17 p2753 A71-35242

Thermal, turbulent and macroscopic motions in solar loop prominence of 4 May 1960, using spectral line composition by Gaussian profiles 17 p2809 A71-35596

Solid glyoxal Raman spectrum data, showing operativity of mutual exclusion principle by IR comparison to Raman bands 18 p2873 A71-35830

Bispectral analysis of EEG frequency bands interrelations 18 p2863 A71-35896

Cross power spectral analysis of atmospheric electric potential gradient relation to meteorological parameters, noting diurnal variations 18 p2944 A71-36010

Infrared Michelson interferometer system digital data processing by computer, developing spectral density plots 18 p2920 A71-36092

Spectral distribution moments of light scattering due to polarizability changes in colliding molecule pair 18 p2947 A71-36196

Statistical determination of solar radio emission S-component average flux spectrum during solar cycle peak phase 18 p2966 A71-36739

Computer interpretation of Mossbauer effect spectra with iterative, integration and comparison procedure 18 p2887 A71-36858

N stars Y CVn, RY Dra and 19 Psc IR synthetic cyanide radical spectrum analysis, determining C 12/C 13 ratio 18 p2969 A71-37044

Virgo XR-1 X rays observation with rocket-borne proportional counters, noting photo index or bremsstrahlung temperature consistency with spectrum 18 p2959 A71-37050

Magellanic clouds X rays observation, interpreting spectrum analysis data as due to few strong sources 18 p2959 A71-37051

GX 17 X ray observation, noting exponential spectrum characteristic of thermal bremsstrahlung and resemblance with Sco X-1 radiation 18 p2959 A71-37054

Frequencies, rotational constants, molecular structure and moments of inertia of five isotopic species of vinylene carbonate from microwave spectrum analysis 19 p3011 A71-37373

Martian continents, seas and polar caps spectrum analysis, noting spectral reflectivity and brightness distributions 19 p3132 A71-37377

Bolide spectrum on 6 June 1969, determining stellar magnitude and periodic pulsations and asynchronous flares characteristics along trajectory 19 p3132 A71-37381

CN radical red system molecular constants, considering degenerate perturbation effects in shifts between electronic states 19 p3106 A71-37405

Quasars and X ray sources, observing UBV magnitude variation with photoelectric data 19 p3133 A71-37427

Aircraft observed stratospheric gravity waves spectral analysis, noting differentiation between atmospheric turbulence and waves 19 p3089 A71-37500

Spectral composition of emitted radiation, emissivity and absorptivity of Venus atmosphere at high temperatures 19 p3135 A71-37580

Quiet sun, active regions and flares far UV space observations interpretation based on models 19 p3136 A71-37615

Solar flare X ray spectrum analysis for lower corona physical conditions, discussing continuum and line emission 19 p3126 A71-37623

Spectroscopic study of imploding shock waves in hemispherical chamber filled with oxygen-hydrogen-helium mixture at high pressure 19 p3163 A71-37735

Far IR collision induced spectrum in carbon dioxide, observing temperature and pressure dependence in gas phase and absorption in liquid 19 p3106 A71-38051

Flash photolysis produced gaseous carbon difluoride IR spectrum analysis by rapid scan IR spectroscopy 19 p3011 A71-38053

Holographic method of correlation and spectral analysis of radio signals applied to stable RF generator, random fields and stereophonic radio transmission measurements 19 p3067 A71-38492

Beam direction weight center of signal spectrum and effective antenna centers of airborne Doppler velocimeter in horizontal flight 19 p3033 A71-38496

Spectral analysis of solar microwave bursts, examining flux and energy variation with frequency 19 p3146 A71-38577

Spectral measurements of nitrogen continuum radiation behind incident shocks at high speeds, suggesting free bound neutral atom-electron interactions origin 19 p3172 A71-38718

Solar coronal X ray spectrum calculation of high-temperature low-density plasma, considering line emission from electron collisional excitation and radiation 20 p3278 A71-39058

Lunar surface microstructure inhomogeneities bimodal distribution from IR and UV spectral analysis 20 p3295 A71-39617

Power spectral analyses of auroral light and X ray pulsations, discussing damping due to velocity dispersions of electrons with various energies 21 p3373 A71-40069

Spectral analysis of Markarian galaxies, observing emission and absorption lines and hydrogen reversal 21 p3441 A71-40105

Neutral atoms and ions collision damping constants estimation for spectrum synthesis, using approximate formula based on Stark broadening effect 21 p3442 A71-40160

Ion pairing study in unresolved metal hyperfine splitting spectral region, using electron spin resonance line shape analysis 21 p3345 A71-40372

Venus 3-4 micron region continuum absorption from high resolution spectra of Venus and sun 21 p3448 A71-40448

Atmospheric and wake turbulence effects on aircraft from discrete gust and spectral interpretations, discussing load production and uncontrollable rolling moments 21 p3321 A71-40507

Electronic transitions in oxygen molecule due to ion impact from kinetic energy loss spectrum 21 p3418 A71-40886

Gain and spectral characteristics of transverse flow CW chemical laser with hydrogen and deuterium fluorides active medium 21 p3393 A71-41041

Spectral dependence of photon capture cross section of negative Zn center in Zn-doped n-type silicon during electron excitation to conduction band 21 p3429 A71-41206

Mathematical model of emission spectrum for PKZ radiosonde and radiosondes using superregenerative transceivers 21 p3383 A71-41243

Impurity photoconductivity spectra determination for n and p type Si crystals under 660 MeV proton irradiation 21 p3433 A71-41311

Spectra and correlation functions for ion sound turbulence, calculating anomalous resistivity for plasma in external electric field 22 p3579 A71-41582

Holographic spectral analysis to determine modes oscillating in multilongitudinal and multitransverse mode laser 22 p3541 A71-41791

Cascade mountains volcanic ash deposits elemental abundances correlation by computerized gamma ray spectra analysis of TRIGA reactor activated glass separates 22 p3533 A71-41855

Circinus pulsating X ray source spectrum analysis, considering bremsstrahlung and black body models 22 p3592 A71-41928

Green Bank sky survey of radio sources at 1400 MHz, discussing SC1 spectral analysis and overlaps 22 p3601 A71-42163

Low dispersion luminosity criteria in A and F stars, computing synthetic spectra for atmospheric temperature surface gravity microturbulence and abundance 22 p3601 A71-42166

Solar X-ray spectra satellite lines observed by Bragg crystal spectrometers on Skylark rocket launched from Sardinia in December 1970 22 p3592 A71-42219

Shading reflector transverse motion effect on radar signal spectrum based on geometric optics approximation 22 p3515 A71-42748

Highly compact X ray source spectrum fitted by black body model at 15 million K 23 p3732 A71-43076

Far IR spectrum analysis using Michelson interferometer with beam splitter 23 p3676 A71-43400

Power spectrum analysis of solar granular intensity fluctuations and velocities, noting asymmetry behavior of Ba II line in individual convection cells 23 p3767 A71-43834

Computer programs based on least squares numerical analysis for complex internal friction spectra due to Snoek and grain boundary relaxation 23 p3648 A71-43927

SbSI crystal reflection spectra anisotropy and band structure at 90,273 and 300 K, comparing experimental data with group analysis 23 p3717 A71-43947

Magnetic modulation observation in plasma light scattering spectra experiments, noting dependence on angle between scattering and magnetic field vectors 23 p3713 A71-44150

Classification method for unwidened low dispersion stellar spectra, giving table for weak stars in region around NGC 6913 cluster 23 p3772 A71-44308

Reduced error spectral power density calculations for random processes with digital spectral analyzers 23 p3681 A71-44320

Harmonic analysis applicability to amplitude-frequency characteristics of plasma current fluctuations, governing spectral characteristics determination accuracy by passband filter delineation precision 24 p3851 A71-44394

Automated analysis of high resolution IR astronomical spectra by computer program, presenting procedures for spectral line width, depth and frequency determination 24 p3867 A71-44438

Spectral characteristics of continuous radio emission of extragalactic binary objects, discussing model of binary radio source formation from dipole nucleus 24 p3869 A71-44801

Respiratory sinus arrhythmia by spectral analysis and digital filtering, using linear model to approximate lung volume relationship to heart rate during normal breathing 24 p3802 A71-45067

Search for CH molecular ion lines in solar photospheric spectrum, discussing profiles and equivalent widths 24 p3873 A71-45144

Turbulence spectral function asymptotic behavior with infinitely increasing wave number, using graphic technique 24 p3821 A71-45220

Color photography of magnetic particle and penetrant indications, discussing light sources, camera types, filter and film selection, exposure and spectral characteristics of indications 24 p3829 A71-45283

SPECULAR REFLECTION

Diffraction of cylindrical wave on thin infinite weakly reflecting cylindrical shell 01 p0128 A71-11121

Visual accommodation measurement based on apparent motion of laser specular reflection pattern 04 p0609 A71-15697

Handedness formula for elliptical polarization after specular metallic reflection of linearly polarized light 07 p1111 A71-19485

Angular dependence of specularly parameter /probability of specular scattering of electron incident upon surface/ via magnetic field dependence of magnetomorphonic harmonic oscillations 10 p1655 A71-23771

Solar absorptance sensitivity to thermal surface particulate contamination as function of particle composition, quantity, size and linearity with obscured area [AIAA PAPER 71-473] 11 p1800 A71-26253

Transverse electromagnetic wave penetration in semibounded plasma with specular electron reflection 12 p1878 A71-26958

Longitudinal plasma layer waves kinetic theory, considering particles specular reflection from layer boundaries 12 p1937 A71-27203

Quasi-specular and Lambert reflection of short radio waves from lunar surface dependent on central portion of near side 16 p2543 A71-33668

Satellite-to-aircraft links propagation characteristics, considering specular reflected signals, diffuse scattering and scattering function 17 p2705 A71-35097

Laser beam reflection from arbitrary geometric surface, considering reverse problem of response of flat or curved mirror to incident collimated light 18 p2929 A71-36055

Spectral reflecting passive radiators for synchronous satellite radiation detectors cooling [ASME PAPER 71-AV-30] 18 p2869 A71-36397

Thermal creep slip velocity expression in power series for arbitrary fraction of molecules diffusely reflected from surface by Bhatnagar-Gross-Krook model solution 19 p3163 A71-37734

- Longitudinal plasma sheath waves kinetic theory, considering particles specular reflection from sheath boundaries 19 p3116 A71-38615
- Polarized plane electromagnetic waves oblique specular reflection from discretely layered lunar models based on Apollo 11 and 12 data, determining near-surface layers electrical properties 21 p3450 A71-40644
- Telescopic observations of Apollo 8-14 spacecraft, suggesting addition of specular reflecting surfaces or transmitters radiating at optical frequencies 21 p3449 A71-41406
- Hologram interference fringes formation and location using grating model of diffusely reflecting surface 22 p3539 A71-41739
- Nongray radiative heat transfer in finite slab with discrete absorption coefficient and specularly and diffusely reflecting boundary surfaces of uniform temperature 24 p3886 A71-44372

SPEECH

- NT ARTICULATION
- NT PHONEMES
- NT PHONETICS
- NT SYLLABLES
- NT WORDS [LANGUAGE]
- Transducer for measuring mandibular dynamic movements during speech 01 p0079 A71-10346
- Aerospace environments noise effects on human physiology and speech communication 08 p1244 A71-20710
- Accurate single-sideband radio receiver tuning, observing reconstitution of harmonic tones in human speech strong vowel sounds 08 p1254 A71-21318
- Cerebral speech mechanisms division into cortical centers and basal ganglia centers 10 p1563 A71-24229
- Healthy subject speech speed effect on phonation phase length, noting relation to normal articulator phase 16 p2531 A71-33462
- Speech intelligibility prediction in time varying aircraft noise based on test score relationship to articulation index for steady state noise 20 p3271 A71-39766
- Book on noise effects on man covering audiometry, aural reflex, hearing damage risk, physiological responses, motor performance and speech communication 20 p3193 A71-39874

SPEECH DEFECTS

- Pure tone, air/bone conducting and speech audiometry, considering hearing tests, artificial mastoids, environmental requirements and physical principles 06 p0859 A71-18029
- Transverse accelerations effect on human speech features 24 p3795 A71-44471

SPEECH DISCRIMINATION

U SPEECH RECOGNITION

SPEECH RECOGNITION

- Computer for speaking and answering verbal questions, using continuous frequency spectrum analysis and phonemes spectra in memory storage 06 p0871 A71-18057
- Auditory illusions, investigating phonemic restorations, verbal transformations and perceptual organization 07 p1051 A71-20212
- Electronic apparatus isolating temporal segments from spoken syllable for speech analysis 09 p1408 A71-23383
- Speech processing and recognition, considering progressive data reduction by ear and physiological limitations imposed information rate time variation 10 p1568 A71-24230
- Computer simulation of automatic voice communication link intelligibility measurement, using speech recognition techniques 13 p2032 A71-28872
- Gundefender earplug evaluation tests, using temporary threshold shift reduction and modified rhyme techniques for speech intelligibility measurement in noise 15 p2364 A71-32196
- Speech envelope masking noise generation with constant S/N ratio for intelligibility studies 15 p2372 A71-32297
- Pattern recognition machine construction for written alphanumeric symbols and human voice identification, providing bibliography 15 p2372 A71-32316
- Time varying aircraft noise effect on speech intelligibility, discussing test for relation to articulation index 21 p3343 A71-40709
- Damped exponential cosine probability distribution function for clipped waveforms of voiced speech signal 23 p3645 A71-43439

SPEED

U VELOCITY

SPEED BRAKES

U BRAKES [FOR ARRESTING MOTION]

SPEED CONTROL

- Unguided, attitude stabilized and velocity controlled sounding rockets impact dispersion, discussing system selection and servomechanism [AIAA PAPER 70-1381] 03 p0498 A71-13664
- Attitude and velocity control for VTOL aircraft takeoff and landing operations in hovering flight, discussing simulation devices and testing operations [DGLR-70-073] 05 p0779 A71-15948
- Concorde automatic flight control, noting reduced weight and speed accuracy limit at Mach 2 05 p0751 A71-16325
- Aircraft with automatic thrust controller, calculating transfer functions characterizing speed and attitude control modes 10 p1640 A71-24910
- Pulse width modulation controlled DC motors, deriving formulas for speed and torque characteristics 13 p1999 A71-28630
- En route turbojet aircraft flight speed control, assessing impact on ATC procedures 13 p2098 A71-28884
- Self adaptive controlled robot velocipedist, discussing speed control and equations of motion 19 p3039 A71-38540
- Parasitic speed controller for alternator rotational speed and frequency regulation in dynamic space power systems, investigating phase controlled loading improvement 20 p3262 A71-38916
- Adjustable speed drive with brushless DC synchronous motor using rotor position sensor and three phase bridge inverter 23 p3630 A71-43499

SPEED INDICATORS

NT ANEMOMETERS

NT HOT-FILM ANEMOMETERS

NT HOT-WIRE ANEMOMETERS

NT SONIC ANEMOMETERS

Balloon and glider vertical speed indicators, considering barometric devices and electric variometer 06 p0901 A71-18248

Fluidic rotational speed sensor, using boundary layers attached to rotating disk surfaces to deflect fluid jets 07 p1031 A71-20604

Laser Doppler velocimeter, determining basic operational parameters including required particle density, number, type, size, output signal to noise ratio, etc [AIAA PAPER 71-288] 08 p1304 A71-22011

Alpha radiation machometer with semiconductor pulse detectors, discussing supersonic regime effects on rate variations 12 p1908 A71-27607

Backscattering laser Doppler velocimeter for water flow and moving opaque object measurements, discussing velocity resolution and optical geometry 19 p3072 A71-37552

Beam direction weight center of signal spectrum and effective antenna centers of airborne Doppler velocimeter in horizontal flight 19 p3033 A71-38496

Atmospheric self-aligning dual-scatter laser Doppler velocimeter, calculating backscattered power, range, wavelength and scatter centers number relationships 22 p3559 A71-42564

Aircraft pitot static systems design with removable drain plug, noting line installation problems 23 p3675 A71-43387

SPEED REGULATION

U SPEED CONTROL

SPEEDOMETERS

U SPEED INDICATORS

SPHALERITE

U ZINC BLEND

SPHERES

NT CELESTIAL SPHERE

NT FALLING SPHERES

NT POINCARÉ SPHERES

NT ROTATING SPHERES

Spheres drag coefficient at hypersonic Mach numbers for near free molecular flow 01 p0002 A71-10969

Plane acoustic wave diffraction and acting force on sphere in low viscosity medium, obtaining asymptotic formulas for pressure, velocity and intensity 01 p0128 A71-11123

Spheres Oseen drag, extending Goldstein expansion for Navier-Stokes equation in powers of Reynolds number 02 p0185 A71-12380

Radially deforming sphere dynamic behavior during translational motion in infinite incompressible static medium 02 p0241 A71-12669

Ballistic data reduction for drag coefficient of spherical projectiles, using time distance relation for constant coefficient 03 p0341 A71-13467

Parallel nonuniform supersonic flow of two coaxial gas jets past sphere 03 p0345 A71-14562

Free convection temperature field about isothermal spheres in air, using interferometer for axisymmetric field 04 p0686 A71-15522

Poisson-Boltzmann equation solution for potential of charged sphere with radius not larger than Debye radius 05 p0781 A71-16380

Axisymmetric body stationary motions around sphere, investigating secular and ordinary stability 05 p0809 A71-16470

Plasma coated spherical antenna radiation, discussing hot and cold plasmas frequency and electroacoustic wave effects 06 p0875 A71-17730

Unsteady heat conduction in thermally coupled spherical regions, discussing duration, penetration depth and temperature histories 06 p1006 A71-18071

Axisymmetric stress in sphere and space with spherical cavity, using p-analytic functions 06 p1001 A71-18343

Sphere and disk drag measurements for Reynolds numbers from 5 to 100,000, examining forces, moments, flow visualization, unsteady modes and constant acceleration 07 p1015 A71-19893

Unsteady boundary layers on sphere or cone moving along axis, determining skin friction angular response 07 p1016 A71-20098

Field intensity of plane electromagnetic wave diffracted at conducting sphere 08 p1252 A71-20735

Electromagnetic wave scattering by perfectly conducting sphere, using integral equation formulation 08 p1253 A71-21294

Free fall of sphere in viscous fluid, expressing fluctuations frequency as function of interfacial tension, sphere density and diameter 08 p1276 A71-21878

Convective heat transfer coefficient for supersonic flow past sphere, considering kinetic heating by flow 08 p1378 A71-22047

Numerical calculation of Oseen hydrodynamic fields around sphere in unbounded fluid for various Reynolds numbers, obtaining flow velocity and drag 10 p1592 A71-23935

Multilayered spherical model induced fields and static heating patterns, approximating primate cranial structure EM plane wave irradiation 11 p1717 A71-25287

Spherically symmetric radiative transfer problems, constructing model with neutron transport theory [AIAA PAPER 71-466] 11 p1859 A71-26247

Transversally isotropic sphere and orthotropic cylinder in symmetrical temperature field, calculating thermal stress equations 12 p1975 A71-27112

Flow in vicinity of stagnation point of sphere and cylinder during pulsating motion in nonuniform stream 12 p1897 A71-27448

Monograph on heat transfer from rotating heated surface with induced turbulent boundary layers covering disk, cone and sphere geometries 13 p2162 A71-28882

Electric field potential near sphere moving through rarefied collisionless plasma in condensation zone, determining ion and electron concentrations 13 p1991 A71-29159

Surface impedance of sphere based on received electromagnetic field amplitude-frequency characteristics 14 p2191 A71-29511

Spherically symmetric systems radiative transfer problems using iteration on Eddington factor 14 p2307 A71-29864

Elastic sphere equilibrium with penny shaped crack under inner surface pressure, observing stress distribution 14 p2326 A71-30096

Flow measurements in axisymmetric turbulent wake of sphere in low speed wind tunnel 15 p2346 A71-32123

Sphere drag in hypersonic jet transition flow near free molecule limit, using magnetic suspension method 15 p2347 A71-32124

Radiative cooling system for nearly spherical or polyhedral bodies using radially attached diverging conical elements 17 p2836 A71-34307

Fixed sphere on axis of unbounded rotating fluid R greater than unity, suggesting flow of Taylor column type 17 p2726 A71-34576

Multiple EM scattering by two spheres, using multipole expansion and ray optics 17 p2701 A71-34756

Electromagnetic wave multiple scattering by collinear spheres, computing radar cross sections with recursion relation for computer solution 17 p2701 A71-34757

- Finite difference method application to three dimensional boundary layer calculation on sphere-segment surfaces in supersonic flow 17 p2672 A71-35632
- Viscous relaxing gas hypersonic flow around sphere in presence of nonequilibrium chemical reactions in shock layer 17 p2673 A71-35637
- Kinematic-dynamo equations for stationary unsheared conducting nonrotating sphere dynamo action in isotropic velocity turbulence 18 p2969 A71-37046
- Unsteady flow of incompressible micropolar fluid due to sphere oscillations, calculating velocity, drag and stress components 19 p3045 A71-37799
- Curvature effect on heat and mass transfer from isothermal sphere in potential flow [ASME PAPER 71-HT-7] 19 p3164 A71-37984
- Free stream turbulence effects on local heat transfer from sphere situated in forced convection air flow [ASME PAPER 71-HT-8] 19 p3164 A71-37985
- Steady axisymmetric incompressible flow past sphere at low Reynolds numbers, reducing equations of motion to ordinary differential equations 20 p3212 A71-39506
- Momentum transfer between gas and condensed phase in metallized solid propellant rocket motors, measuring noncontinuum and turbulence effects on sphere drag 21 p3437 A71-40861
- Free falling spheres rocking/lateral motions, deriving nonlinear damped pendulum equation with motion coupling expressed as Reynolds number dependent phase shift effect 21 p3416 A71-40953
- Fluctuating lift and drag forces on accelerating free falling sphere, discussing relation to asymmetrical wake vortex shedding 21 p3324 A71-40970
- Steady slow free molecule flow past sphere, obtaining distribution function and surface boundary conditions 21 p3370 A71-40987
- Stress and contact time calculation for impact of spheres on finite thickness elastic plate overlying rigid foundation 21 p3472 A71-41031
- Glass spheres formation on moon, suggesting mineral melt atomization in high speed gas stream 21 p3454 A71-41421
- Temperature stresses relaxation in transversely isotropic viscoelastic sphere calculated numerically for 500 and 100 hour periods 22 p3616 A71-42486
- Rough spheres, cylinders and annuli in contact, determining surface roughness and waviness effects on surface geometry under elastic and plastic deformations 23 p3682 A71-43928
- Boundary layer solution for initial flow around impulsively started sphere in viscous fluid at high Reynolds numbers 23 p3664 A71-44144
- Spherical projectile hypervelocity impact on compressible fluid, showing viscous effects on velocity and stress distribution behind shock front 24 p3877 A71-44426
- Sword shaped tip on plastic sphere front portion, detailing hydrodynamic drag reduction at various Reynolds numbers 24 p3818 A71-44711
- SPHERICAL ANTENNAS**
- Transverse feed design for spherical reflector antennas, noting efficiency and field distribution 17 p2700 A71-34751
- Wave diffraction by air gap multilayered dielectric coated sphere with azimuthal slot for low loss transmission, obtaining radiation pattern 22 p3522 A71-42283
- SPHERICAL CAPS**
- Marguerre equations for deflection and buckling of partially and fully loaded spherical caps, noting inaccuracy of finite difference approximation 03 p0503 A71-13428
- Thin elastic shallow spherical dome nonlinear motion under uniformly distributed external pressure 06 p0982 A71-17360
- Asymmetric buckling of spherical caps with asymmetrical imperfections, using nonlinear relaxation technique for treatment of finite difference representation of differential equations 09 p1541 A71-23090
- Clamped shallow spherical caps under uniform pressure, computing axisymmetric buckling 09 p1541 A71-23091
- Axisymmetric snap-through of shallow clamped spherical caps under uniform pressure, revealing existence of higher modes as isolated closed loops from approximate solution 10 p1689 A71-24518
- Clamped shallow spherical cap buckling and initial postbuckling behavior under axisymmetric band type loads, using numerical analysis 14 p2330 A71-30690
- Spherical caps under step pressure loading, noting elastic damping effects on dynamic stability 15 p2506 A71-32093
- Spherical cap bubbles in water and mineral oil at various dynamic viscosities, measuring laminar and turbulent wakes character, rise speed and shape 21 p3365 A71-40017
- Shallow spherical cap and deep thin spherical shell buckling, solving integral equations by iterative procedure 21 p3463 A71-40542
- Boundary value problem for plane wave scattering by spherical cap, obtaining scattering cross section for Helmholtz resonator and hemispherical shell 23 p3703 A71-43208
- SPHERICAL HARMONICS**
- Earth spherical and ellipsoidal gravity potential coefficients association using Lamé orthogonal function properties 01 p0155 A71-10388
- Long term evolution of close low eccentricity lunar satellite orbits, describing lunar gravity effects by spherical harmonic expansion 04 p0655 A71-15723
- Spherical harmonic analysis of worldwide cosmic ray variations during geomagnetic storms, using ground station and satellite data 06 p0949 A71-17253
- Spherical harmonic analysis of geomagnetic field strength for global magnetic anomaly charts 06 p0894 A71-18267
- Hypersonic radiating gas inviscid flow past blunt bodies, using spherical harmonics approximation 07 p1013 A71-19183
- Cyclic variations in geomagnetic field from 1550 through 1960 using spherical harmonic analysis of magnetic declination 07 p1099 A71-19395
- Second spherical harmonic generation mechanisms in axisymmetric diurnal and semidiurnal cosmic ray spectrum variations 08 p1352 A71-20969
- Satellite geodesy, discussing reference orbits calculation, gravity field spherical harmonics, station positions, etc 08 p1285 A71-21800
- Spherical harmonics differential approximation generalized from one dimensional radiation specific intensity angular dependence Jacobi polynomial expansion 10 p1696 A71-24536
- Higher approximations of spherical harmonic method and moment method applied to propagation of periodic disturbances in radiating gas 10 p1696 A71-24545
- Spherical harmonics of secular perturbations in artificial satellites motion due to atmospheric gravitation 11 p1829 A71-25808
- Spherical harmonic expansion for volumes of tubes of unit flux in geomagnetic field for use in magnetospheric dynamics 14 p2229 A71-29668
- Lumped fifteenth order spherical harmonics in geopotential from Ariel 3 satellite orbital inclination corrected for lunar-solar oscillatory perturbations 16 p2563 A71-33387
- Spherical and ellipsoidal functions relationship for terrestrial gravitational field anomalies 16 p2564 A71-33571
- Spherical harmonic expansion of nonhomogeneous oblate spheroid mass distribution potential, giving convergence criterion 17 p2733 A71-35029
- Cyclic variations in geomagnetic field from 1550 through 1960, using spherical harmonic analysis of magnetic declinations 19 p3053 A71-37819
- Orbital equations of motion and associated variational equations numerical integration, calculating geopotential in terms of spherical harmonics [AAS PAPER 71-390] 23 p3666 A71-43058
- Lunar gravity estimate from low degree spherical harmonic coefficients in potential model and Lunar Orbiter 4 radio tracking data reduction 23 p3768 A71-43882
- SPHERICAL SHELLS**
- NT SPHERICAL CAPS**
- Antenna and telemetry system for spherical shell ICBM reentry vehicles data link to ground 01 p0036 A71-10986
- Transversely isotropic spherical shell of small shear modulus material, deriving stress concentration at circular holes 01 p0175 A71-11038
- Spherical elastic shell axisymmetric vibrations in compressible fluid with free surface 01 p0071 A71-11046
- Three-layer spherical shell, determining filler effects on stress-strain state at circular hole 01 p0176 A71-11047
- Stress-strain state of anisotropic inhomogeneous viscoelastic solid fuel charge sphere with annihilating internal boundary 01 p0177 A71-11238
- Nonlinear stability of shallow spherical shells under concentrated loads, showing critical loads dependence on shallowness 01 p0177 A71-11239
- Shallow spherical shell thermally stressed state produced by temperature gradients 02 p0322 A71-11728
- Spherical shell plastic deformations under internal pressure, discussing stress instability condition 02 p0325 A71-12123
- Stability loss of cylindrical and spherical shells under heating and external force, determining critical temperature and loads 02 p0325 A71-12286
- Nonlinear quadratic elasticity theory of isotropic tube and hollow sphere under small linear deformations, obtaining stress-strain relation 02 p0326 A71-12294
- Perforated thick shallow spherical shell, solving boundary value problem for external loads 02 p0329 A71-12671
- Spherical shells deformation subjected at elevated temperature to high velocity impact on planar rigid target 03 p0503 A71-13427
- Clamped shallow spherical and conical shells axisymmetric dynamic buckling under step loads of infinite duration, showing similarity with static buckling 03 p0504 A71-13455
- Semitransparent spherical dielectric shell under diffuse incident radiation, determining absorbance and reflectance by Monte Carlo method 03 p0518 A71-13648
- Spherical shell segments stresses and displacement due to arbitrary axisymmetric surface tractions and edge boundary conditions, using axisymmetric elasticity solutions [ASME PAPER 70-WA/APM-27] 03 p0512 A71-14159
- Multicavity thin walled containers of spheres and intersecting plane partitions, comparing structural properties with single sphere of equal overall volume 03 p0515 A71-14366
- Shallow spherical shells with periodically spaced holes, discussing stress analysis by least squares method for curved perforated plates [ASME PAPER 70-PVP-11] 04 p0665 A71-14771
- Absorption coefficient of plane wave scattering by thin spherical resistive shell for broadband RF radiation monitoring 04 p0558 A71-15149
- Thin spherical shell with circular cutout under HF axisymmetric excitation by concentrated radial force 04 p0667 A71-15181
- Eccentrically stiffened thin spherical shell instability under uniform external pressure 04 p0669 A71-15199
- Spherical or conical shells of revolution axisymmetric oscillations, analyzing zero moment equations system spectrum 05 p0822 A71-16377
- Internal pressure load carrying capacity of intersecting spherical and cylindrical shells based on limit or plastic design concept 05 p0823 A71-16493
- Isotropic elastic spherical shells stability under combined axial compression and local loads 05 p0824 A71-16593
- Axisymmetric vibration frequencies, form shapes and apparent masses for vertical fluid filled coaxial cylindrical shells resting on shallow spherical shell 06 p0986 A71-17763
- Shallow spherical shells stability under constant external pressure 06 p0987 A71-17768
- Multilayer conical and spherical shells of revolution axisymmetric elastic deformation, deriving stress-strain state equations with allowance for transverse shear 06 p0990 A71-17795
- Natural vibrations of partially liquid filled closed spherical shell for arbitrary boundary conditions, using approximate method 06 p0991 A71-17798
- Vertical circular cylindrical tank with shallow spherical shell bottom filled partially by ideal incompressible liquid, calculating joint oscillations 06 p0994 A71-17826
- Elastic momentless conical tank with spherical bottom partially filled by liquid, calculating axisymmetric oscillation 06 p0995 A71-17828
- Elastic spherical shell three dimensional stress-strain state asymptotic behavior near concentrated force as function of parameter characterizing relative thickness and curvature 06 p0995 A71-17830
- Nonlinear statics of thin walled cylindrical and spherical shells, including buckling under various end conditions 06 p0999 A71-17869
- Axisymmetrical potential theory for two spherical circular disks system, using X-analytic functions for reducing to Fredholm equation 06 p0928 A71-18345

Natural convection heat transfer between two isothermal concentric spheres, using water and silicone oils as convective fluids

07 p1222 A71-18995

Cylindrical, conical and spherical shells natural frequencies and vibration modes determination using matrix series

07 p1212 A71-19365

Free vibration of spherical sandwich shell under axisymmetric static and dynamic loading

07 p1212 A71-19590

Thin shallow spherical shell vertical impact against ideal incompressible liquid surface, calculating axisymmetric deformation and hydrodynamic load distribution

07 p1089 A71-19738

Spherical sandwich shells free vibration motion equations, taking into account transverse shear deformation and rotary inertia effects

07 p1215 A71-20095

Stress waves in elastic spherical shell due to external pressure pulse, approximating near field by saddle point technique

07 p1215 A71-20097

Thin spherical roller supported domes stability and axisymmetric deformation under apex point loads, investigating plastic buckling and inelastic strain effects

07 p1216 A71-20222

Free vibrations of closed spherical shell immersed in ideal incompressible fluid at arbitrary depth

09 p1535 A71-22182

Nonshallow spherical shells of small shear modulus materials, examining boundary conditions and axisymmetric deformation

09 p1535 A71-22184

Closed spherical shell, calculating optimal internal temperature fields for keeping thermal stresses at low level under local axisymmetric heating

09 p1537 A71-22520

Metallic spherical shell shielding of electromagnetic waves, deriving approximation for first n terms for EM fields inside due to impinging plane monochromatic wave

09 p1405 A71-22683

Stress concentration near hole in transversely isotropic cylindrical and spherical shells made of oriented glass fiber reinforced plastics

09 p1539 A71-22820

Liquid shell about solid spherical core, analyzing vibrations and sphere gravitational effects on material particle motion

09 p1495 A71-23342

Thin spherical shell under uniform normal pressure using dynamic stability criterion and energy method for asymptotic nonlinear shell equations

10 p1685 A71-23937

Spherical and paraboloid shells of revolution internal and external forces correlation, considering boundary value problem differential solution

10 p1686 A71-23996

Shallow spherical shell thermal stability, investigating factors affecting Galerkin method validity

10 p1690 A71-24574

Spherical shell containing through crack, calculating in-plane and Kirchhoff bending stresses under periodic transverse vibrations

10 p1693 A71-25054

Inelastic scattering cross sections, using measured neutron leakage spectra from thick spherical shells of Ta, W, Mo and Be

11 p1802 A71-25556

Plastic spherical shell containing cylindrical section under Tresca yield conditions, obtaining upper critical load limits

11 p1850 A71-25943

Transversally isotropic spherical shell with constant thickness, calculating equation system for equilibrium

12 p1975 A71-27105

Spherical shell stressed state weakened by holes, investigating shear deformation effect

12 p1975 A71-27107

Spherical shallow shell with hole, noting natural vibration frequency

12 p1975 A71-27108

Soviet book on spherical bottoms weakened by openings covering shell stress/strain, elastic-plastic deformations, reinforcing elements and composite materials

12 p1977 A71-27293

Spherical or conical shells of revolution axisymmetric oscillations, analyzing zero moment equations system spectrum

12 p1981 A71-27463

Local plastic deformation analysis of spherical and cylindrical shells subjected to yield point loads through rigid boss, using nonlinear programming

13 p1247 A71-27787

Approximate determination of first characteristic root of equation for plate, hollow sphere and hollow cylinder, using variational method for heat conduction problem

13 p1259 A71-28184

Hollow carbon microspheres from pitch material, emphasizing applications in porous composites

14 p2263 A71-29657

Axisymmetrical snap buckling of clamped shallow spherical shell with initial deformation under external pressure, using energy method

14 p2322 A71-29689

Clamped and hinged spherical and paraboloidal shell caps elastic stability tests under external pressure loading, determining critical pressure

14 p2323 A71-29846

Gas-filled spherical cavity in infinite compressible liquid, deriving radial oscillations by numerical solution

14 p2225 A71-30229

Parametric differentiation technique for axisymmetric stability of spherical shells, using Reissner nonlinear differential equations

14 p2329 A71-30506

Flexible spherical domes elastic-plastic deformation, using variational equation and iterative algorithm

14 p2331 A71-30840

Load carrying capacity of edge clamped spherical shells of revolution with Tresca yield condition under uniform internal pressure

14 p2332 A71-30848

Stresses and deformations of shallow spherical shells with specified edge displacements

15 p2502 A71-31186

Coupled elastic buckling in continuous systems, determining postbuckling paths for strut, spherical shell and flat plate

16 p2650 A71-33017

Convective motions in differentially rotating thin spherical shells, explaining solar differential rotation

16 p2630 A71-33055

Clamped shallow spherical shells buckling and postbuckling behavior under axisymmetric ring loads, examining effect of load location and shell geometry variations

[ASME PAPER 71-APM-9]

16 p2656 A71-33216

Energy dissipation measurement in liquid filled spinning precessing spherical cavity by gimbaled mechanism

[ASME PAPER 71-APM-4]

16 p2644 A71-33219

Equivalent reinforcement of contact area between spherical shell and radial outlet cylindrical pipe under internal pressure and axial force

17 p2817 A71-34332

Elastic spherical shell coupled to rigid body, calculating axisymmetric free vibration natural frequencies and mode shapes from boundary conditions

17 p2817 A71-34339

Thin elastic spherical shells reinforced by stringers and frames and loaded by internal or external uniform pressure, calculating by energy method

17 p2829 A71-35311

Optimal design of axisymmetrical annular plate and cylindrical and spherical shells by maximum principle

17 p2833 A71-35621

Spinning centrally clamped thin shallow spherical shell free vibration numerical analysis by considering perturbation about equilibrium configuration

[ASME PAPER 71-APM-G]

18 p2977 A71-36254

Rigid sphere and concentric shells models approximation to turbulent motion in liquid-filled precessing spherical cavity

[ASME PAPER 71-APM-Y]

18 p2904 A71-36265

Axisymmetric plastic deformation of imperfection sensitive spherical shell after elastic buckling, considering load carrying capacity

[ASME PAPER 71-APM-FF]

18 p2978 A71-36266

Shallow spherical shell under uniform external pressure loads, obtaining boundary conditions effects on stress-strain state

19 p3155 A71-37530

Edge clamped spherical shell natural vibration frequency determination using Vlasov shell theory equations

19 p3155 A71-37532

Variable thickness thin orthotropic spherical shell with hole, calculating stressed state with successive approximation technique

19 p3155 A71-37533

Stress concentration formulas for elliptical hole in spherical shell with or without cap

19 p3156 A71-37540

Externally pressurized thin walled elastic spherical shells influence coefficients singularity

19 p3158 A71-37886

Buckling and initial postbuckling behavior of clamped thin shallow spherical sandwich shells under axisymmetrical loads

19 p3159 A71-38185

Large scale convection solar magnetic field patterns calculations based on rotating thin spherical shells, noting solar cycle activity

19 p3147 A71-38667

Radiative transfer in inhomogeneous anisotropically scattering spherical shell atmospheres with radial symmetry, using invariant imbedding technique

20 p3287 A71-39082

Thin shallow spherical shell weakened by circular hole, calculating stressed state from boundary value problem solution

20 p3308 A71-39165

Shallow spherical cap and deep thin spherical shell buckling, solving integral equations by iterative procedure

21 p3463 A71-40547

Small deformation dynamic response of vibrating isotropic linearly elastic spherical shell to radial and time dependent body force field

21 p3464 A71-40766

Thermal stress distribution and temperature profiles in nearly opaque spherical shell under radiant and convective heating flux

21 p3476 A71-40944

Elastic buckling and initial postbuckling behavior of clamped shallow spherical sandwich shells under axisymmetrical load

21 p3469 A71-41066

Natural frequencies and vibration modes of perforated cylindrical, conical and spherical shells of revolution, using Ritz method

22 p3617 A71-42486

Residual stress in closed spherical shell welded along equator, using stress-strain relations

23 p3778 A71-44035

Rectangular planform nonshallow spherical and elliptical shells, determining momentless stressed state

24 p3877 A71-44404

Two layer anisotropic spherical shell of elastoheterodyne material under uniform pressure, investigating stress-strain state

24 p3880 A71-44710

Asymptotic design formulas for thermoelastic supercritical strains in thin elastic shallow spherical shells under external pressure

24 p3881 A71-44827

Natural and forced joint vibrations of liquid and shallow spherical shells

24 p3881 A71-44829

Stability under uniform external pressure of closed spherical shell with axisymmetric initial imperfection in equatorial region, using finite difference technique

24 p3883 A71-44853

Ring reinforced spherical shell and rib under concentrated normal forces, calculating force factors and displacement by simultaneous deformation analysis allowing moment stresses

24 p3883 A71-44896

Linearly polarized plane electromagnetic wave scattering by radially inhomogeneous spherical shell, presenting boundary value problems solutions and approximations

24 p3805 A71-45184

SPHERICAL TANKS

LP axisymmetric vibrations of spherical completely filled tank with free liquid surface in upper tank and pipeline

16 p2657 A71-33602

SPHERICAL WAVES

Frequency correlation between amplitude and phase fluctuations of different-frequency spherical waves propagating in turbulent medium

01 p0073 A71-10545

Polarization structure of paraboloid mirror antennas circular emission by geometrical diffraction theory of spherical edge waves

01 p0056 A71-11204

Electromagnetic wave Poynting vector trajectories in absorbing inhomogeneous media, discussing reversibility and energy propagation of spherical and plane structures

02 p0210 A71-11631

Quasi-spherical divergent shock waves produced by Pt wire explosion in air

02 p0332 A71-12336

MF, LF and VLF ionospheric radio wave propagation theory using spherical wave functions for computer simulation

04 p0552 A71-15215

Nonlinear planar propagation of sinusoidal and band-limited noise signals in air, extending to spherical waves

05 p0784 A71-17157

Laser resonator mode representation with oblate spheroidal vector wave function through boundary value problem formulation

08 p1301 A71-21293

Spherical wave scattering on thin conducting truncated bodies of revolution, deriving equations system for field pattern

08 p1254 A71-21460

Weak magnetic field disturbance by strong spherical shock wave propagation in finite conductivity gas

09 p1430 A71-22140

Spherical magnetogasdynamic shock production in conducting gas by explosion into homogeneous self-gravitating system, assuming density dependence on inverse power of distance

09 p1505 A71-23585

Electromagnetic wave diffraction on arbitrary spheres, including scattering and attenuation by four water droplets

10 p1579 A71-24877

Strong cylindrical and spherical electromagnetic wave propagation in plasmas, calculating amplitude and electron temperature

11 p1805 A71-25768

Three dimensional convergence for spherical shock wave by linear pinch wall shaping based on Whitham ray-shock theory

11 p1752 A71-26191

Charge particle motion and radiation in strong plane and spherical electromagnetic waves with nonthermal astrophysical applications

12 p1877 A71-26616

Diffraction of spherical wave on triangular prism, using reduction by group theory of point sources

12 p1878 A71-26838

Spherical wave expansion theory application to near field and far field patterns, using analytical, experimental and numerical data

13 p2028 A71-27993

Reaction kinetic studies using hydrodynamic flow structure due to spherical shock wave from laser induced spark

16 p2616 A71-32903

Plasma energy cumulation by concentric spherical and cylindrical waves, calculating stability limit by integral solution

16 p2619 A71-33355

Polarization structure of parabolic reflector antennas circular radiation by geometrical diffraction theory of spherical edge waves

17 p2697 A71-34256

Strong cylindrical and spherical electromagnetic wave propagation in plasmas, calculating amplitude and electron temperature

22 p3579 A71-41536

Temporal frequency spectra for spherical wave propagating through atmospheric turbulence, using covariance functions and Taylor hypothesis

22 p3575 A71-41788

Spherical wave technique adaptation to antenna radiation determination by equivalent current sheets

22 p3509 A71-42200

Plastic work hardening produced by pressure application to spherical cavity surface in infinite elastoplastic medium, considering spherical elastic wave attenuation

23 p3775 A71-43147

Three dimensional transient interaction of spherical acoustic waves with cylindrical elastic shell, using integral transform techniques

23 p3775 A71-43207

Arbitrary multipole structure spherical wave propagation in Schwarzschild metric, using Bondi coordinate system and negative powers of r

23 p3704 A71-43826

SPHEROIDS

NT OBLATE SPHEROIDS

NT PROLATE SPHEROIDS

Spheroidal solutions near center for free oscillations of self gravitating rheological spherical mass

01 p0127 A71-10462

Spheroidal cavity effects on elastic medium under axisymmetric stress field, using Legendre potential functions

07 p1212 A71-19253

Paraboloidal, hyperboloidal and flattened spheroidal telescope mirrors testing with optical compensation lenses by Foucault shadow and Ronchi methods

07 p1116 A71-20641

Post-Newtonian corrections for Maclaurin spheroids, presenting binding energy numbers

17 p2806 A71-35406

Spheroid with two dielectric separated halves and mixed boundary conditions, determining spreading currents L_f electromagnetic field

22 p3484 A71-42879

Glass spherical particles formation mechanisms for lunar surface, discussing size limitation factors

23 p3757 A71-43753

SPHERULES

NT SPHERULITES

Spherules and finely dispersed meteorite materials on earth, discussing detection, collection, morphology phase and chemical composition, incidence and formation mechanisms

12 p1965 A71-27224

Microsphere formation by melting spinning refractory oxide rod tip in carbon dioxide laser focused emission

13 p2079 A71-28905

Meteorite material magnetic fraction determination by chemical analysis for spherules in soil surrounding meteorite craters at Henbury, Australia

15 p2488 A71-32351

Sikhote-Aline shower region soil samples and meteorite and micrometeorite fragment morphology, emphasizing silicate spherules

17 p2810 A71-35718

Spherules and finely dispersed meteorite materials on earth, discussing detection, collection, morphology phase and chemical composition, incidence and formation mechanisms

19 p3132 A71-37376

Elemental abundance ratio patterns in microscopic spherules collected from atmosphere and polar snows, comparing to terrestrial and lunar rocks

20 p3298 A71-39638

Size distribution and concentration of magnetic spherules in troposphere from electron and optical microscopy

23 p3665 A71-42965

Apollo 12 lunar glass spherules chemical composition, homogeneity, densities and thermal histories, using electron probe analysis

23 p3758 A71-43758

SPHERULITES

Spherulitic linear polyethylene rod cold drawing, observing fibrous structure formation by light and electron microscopy and X ray scattering

19 p3084 A71-37650

Cooling history of magma containing spherulite growth forms on basis of morphological variations in glassy and crystalline rocks

19 p3051 A71-37673

SPHYGMOGRAPHY

Circulation parameters in vascular network by bloodless zonal ultrasonic sphygmography based on acoustic bioecholocation

17 p2689 A71-34648

SPICULES

Spicule horizontal component motion from H alpha spectra movies with slit tangential to solar limb

02 p0316 A71-12756

Solar chromosphere model, explaining spicules origin and relation to small scale nonuniformities

13 p1236 A71-28430

Solar spicules H alpha and beta, D3 and K line profiles, considering radial and turbulent velocities, optical thickness, atomic density and He emission

13 p2140 A71-29049

Solar limb H alpha spicules spectrograms, noting oscillations and time intervals

19 p3147 A71-38665

Oscillations of visible chromosphere boundary and regularity in position of spicule groups along limb, studying H alpha filtergrams

22 p3597 A71-41456

SPIKE ANTENNAS

U MONOPOLE ANTENNAS

SPIKE POTENTIALS

Neuroelectric signal analysis using real time nerve spike recognition and separation based on nuclear instrumentation techniques

08 p1249 A71-21839

Superposition model of spontaneous activity of cerebellar Purkinje cells for spike triggering

13 p2014 A71-29289

Neural spikes and LF components separation from background noise, describing feedback amplifiers circuit

15 p2356 A71-31251

Functional relation of primary responses and unit spike activity at subcortical visual centers in cats

19 p3001 A71-37443

Weightlessness effect on vestibular apparatus from bullfrogs vestibular nerve single fibers spike train data during orbital flight

22 p3598 A71-41689

SPIKING

Traveling medium solid state lasers spike generation due to spatiotemporal fluctuations of losses and pumping

06 p0907 A71-17379

Nitrogen tetroxide/hydrazine pulse mode rocket engines structural failure due to chemically reactive gaseous hot spots causing high pressure spiking and detonation initiation

06 p0944 A71-17663

Traveling medium solid state lasers spike generation due to spatiotemporal fluctuations of losses and pumping

12 p1915 A71-27459

SPIN

NT ELECTRON CAPTURE

NT ELECTRON SPIN

NT METAL SPINNING

NT NUCLEAR SPIN

NT PARTICLE SPIN

NT SPIN-ORBIT INTERACTIONS

NT SPIN-SPIN COUPLING

SPIN DYNAMICS

Motion components about center of mass of body using flywheel attitude control by small parameter method

02 p0279 A71-11906

Alouette 2 satellite spin dynamics measurement based on telemetered optical data

03 p0379 A71-14006

Pulsar free rotational dynamics accounting for amplitude and time variations in signals, considering non-rigidity and viscosity effects

03 p0493 A71-14211

Na-Cs unpolarized and spin exchange differential scattering cross sections calculation by phenomenological and difference potential methods

04 p0630 A71-15654

Atmospheric reentry dynamics of spinning body with trim angle of attack

07 p1205 A71-18892

A-7 low altitude tactical fighter spin evaluation program, discussing maneuvering capability, external stores and departure mode

07 p1018 A71-19094

USAF F-4E Stall/Near Stall Investigation, discussing testing requirements, fighter aircraft improvement, spin avoidance and high angle of attack limitations

07 p1019 A71-19095

Control of time varying mechanical torque normal to ball bearing pair common spin axis by cross torque control through misalignment coupling

08 p1298 A71-21156

Low latitude air density correlation to magnetic disturbance deduced from Ariel 2 satellite spin rate changes

10 p1602 A71-24552

Transient resonance response of slender entry vehicles in rolling trim at spin-pitch intersection for offset coplanar and orthogonal leading modes

11 p1837 A71-25480

Spin dynamics and deformation measurements on PAGEOS balloon satellite by photoelectric photometry, noting solar radiation pressure torque

11 p1761 A71-25546

Atomic and molecular spin in cosmic medium, discussing static/dynamic orientation, resonance mechanism, hyperfine structure and magnetic sublevels

12 p1933 A71-27420

Motion components about center of mass of body using flywheel attitude control by small parameter method

13 p2098 A71-28193

High speed spin effect on amplified or damped nutations in low friction rotary gyroscope mounted on gimbals

15 p2401 A71-31178

Rotating liquid flow impulsive spin-up and spin-down in finite cylindrical containers, deriving simplified mathematical model at Reynolds number 1002

18 p2901 A71-35853

Lumped parameter simulation model for flexible turbine rotor dynamics in nonspinning coordinate system, discussing bearing constraints modeling methods and eigenanalysis applicability

21 p3385 A71-40309

Free spinning gyrostats classical problems equivalence, discussing interaction torque between body and rotor on axis of rotation

21 p3415 A71-40771

Alouette and Isis satellites flight data comparison with attitude and spin dynamics theory, considering solar radiation pressure and gravitation and magnetic field effects

22 p3609 A71-41997

ISIS-I ionospheric sounding satellite spin rate behavior

22 p3612 A71-42786

SPIN FORGING

U METAL SPINNING

SPIN REDUCTION

Venus low retrograde spin rate explained as result of capture of moonlike object from retrograde orbit, transforming planet rotational energy into heat

04 p0642 A71-14823

Density perturbation effect on transient spin down of incompressible dissipative rotating stratified fluid in cylindrical container

16 p2561 A71-34164

Oil for lubricating ball bearings in spacecraft antenna despun system, investigating weight loss, sorption, surface migration and contamination danger

20 p3184 A71-39352

SPIN RESONANCE

Gravitational and tidal torque effects on Mercury spin rate as model of passage through resonance

04 p0657 A71-15738

Asymmetric missile angular response to spin varying through resonance

06 p0979 A71-18507

[AIAA PAPER 71-46] Mercury spin orbit resonance probability computation, making a priori assumptions for long term orbital variations, tidal torque and equatorial asymmetry

07 p1203 A71-20521

Ferromagnetic and antiferromagnetic characteristics relation to electromagnetic and spin waves coupling in nonresonant and resonant regions

10 p1656 A71-24317

Tumbling triaxial satellite in elliptical orbit about spherical planet, determining resonant and nonresonant gravity gradient perturbations

13 p2145 A71-28356

Nucleation, growth and spinodal decomposition during aging in Fe-Cr alloys, using Mossbauer spectroscopy

13 p2089 A71-29414

Coupling effects between two Permalloy films for different interface treatments, using standing spin wave resonances

18 p2955 A71-36941

Mimas-Tethys resonance motions under short period gravitational perturbations and tidal dissipation functions

20 p3286 A71-38760

- Optical absorption and electron spin resonance in KCl with and without KOH, noting F band existence 21 p3414 A71-40070
- Ferromagnetic electron spin resonance spectra of Apollo 11 lunar samples, using model for polycrystalline spectra simulation 23 p3734 A71-43242
- ### SPIN STABILIZATION
- S band PCM telemetry system using frequency diversity for spin stabilized high velocity blunt nosed reentry vehicle signal reception 01 p0163 A71-10980
- Spinning space stations with mass geometry changes, discussing attitude and angular velocity optimal control 01 p0164 A71-11435
- Satellite oscillations about center of mass, allowing for energy dissipation due to magnetic hysteresis 02 p0319 A71-11907
- Computerized simulation of disturbance torques of spin stabilized spacecraft in near earth orbit 03 p0500 A71-14448
- Spin stabilized spacecraft fuel optimal direction cosine attitude control, considering relation to inertial system 03 p0500 A71-14448
- Dual spin spacecraft high performance nutation damper, using wheel of uniform mass distribution 04 p0661 A71-15002
- Spinning aerospace vehicle optimal attitude control system by minimizing reaction fuel, noting application of Pontryagin maximum principle 04 p0623 A71-15143
- Stability problems of free rotor and driven rotor gyrostats, considering spin stabilized spacecraft 04 p0662 A71-15192
- Trajectories prediction for subsonic spin stabilized projectiles via water tunnel tests, considering blunt nose and tail and rounded nose right circular cylinders [AIAA PAPER 71-296] 08 p1275 A71-22016
- Periodic rotation reversal effect on hollow cylinder surface temperature distribution in space simulation testing of spin stabilized orbiting satellites 09 p1430 A71-23733
- Passive nutation damping of spin stabilized orbital satellites with mechanical and pendulum dampers involving nonlinear interaction of vibrational and rotational motions 10 p1683 A71-24562
- Dual spin spacecraft bearing assembly flexibility effects on attitude stability, discussing time constant [AIAA PAPER 70-1043] 12 p1973 A71-27569
- Rotational stability of spin stabilized satellite with liquid filled propellant tanks, investigating viscous effects on motion coupling between rigid body and liquid 15 p2499 A71-31175
- Maximum nutation-precession angles of spin stabilized satellites during extension of long flexible booms 15 p2500 A71-32046
- Low cost solar array unfolded by centrifugal spinning force, considering application to spin and 3-axis stabilized spacecraft 16 p2526 A71-32852
- Digital systems synthesis for stabilization of triaxial gyrostabilizer consisting of three uniaxial gyrostabilizers with cross couplings 17 p2738 A71-34559
- Kalman filter in preflight postflight analysis of velocity increment by spin rocket plume impingement at preentry altitudes 19 p3148 A71-37179
- Active precession control devices for spin stabilized spacecraft, noting energy dissipation effect [AIAA PAPER 71-952] 19 p3148 A71-37193
- Terminal guidance sensing from spinning spacecraft in swingly mission to outer planets [AAS PAPER 71-121] 19 p3101 A71-37916
- Subliming nuclear microthruster design with Monte Carlo study of rarefied gas nozzle flow, noting application to spin stabilization 19 p3103 A71-38351
- Dual-spin vs three-axis stabilization and control systems for synchronous communication satellite design 21 p3454 A71-40477
- Three-axis and dual-spin stabilization systems for future synchronous communication satellites, considering reliability, mission flexibility and growth potential 21 p3455 A71-40479
- Attitude stiffness and pointing accuracy of three-axis and dual-spin stabilization system for future synchronous communication satellites 21 p3455 A71-40481
- Rotating space station simulator for translational and rotational motion determination under gravity gradient torque action and control under input state conditions [IBM-712000406] 22 p3529 A71-41970
- Spinning and dual spin spacecraft angular momentum and axis control, investigating optimal fuel and small angle reorientation techniques 22 p3611 A71-42045

- Spin stabilized spacecraft inversion by mass translation with momentum vector fixed in inertial space, calculating control mass dynamics 22 p3612 A71-42777
- Spin stabilized lunar satellite attitude determination, using Kalman filter for processing telemetered sun aspect angle measurements from satellite sensor 22 p3573 A71-42780
- Earth gravitational field effect on dual spin satellite motion in circular orbit, using Vigneron averaging method for linearized equations of motion 22 p3612 A71-42782
- Motion stability analysis for force-free spinning satellites with flexible appendages by Liapunov direct method [AAS PAPER 71-345] 23 p3772 A71-43018
- ### SPIN TESTS
- Wind tunnel apparatus for reproducing coning and spinning motions of bodies of revolution, using six-component strain gage balance for aerodynamic forces 01 p0002 A71-10930
- Aircraft spin tests preparation and evaluation, describing pilot errors 15 p2348 A71-31462
- ### SPIN WAVES
- #### U MAGNONS
- ### SPIN-LATTICE RELAXATION
- Fe 57 nuclei longitudinal and transverse relaxation in yttrium iron oxide sublattices at various temperatures and magnetic field strengths 05 p0794 A71-16878
- Critical temperature short to long range ordering mechanism theories, discussing lattice type, transition continuity and spinodal decomposition factors 07 p1131 A71-19432
- EPR spectra and spin-lattice relaxation time in coal pitch and polyvinyl chloride during low temperature carbonization 17 p2763 A71-35245
- German monograph on rocket measurements in auroral zone with proton magnetometer covering magnetosphere, spin-lattice and spin-spin relaxation time and data processing 18 p2910 A71-35885

SPIN-ORBIT INTERACTIONS

NT ELECTRON CAPTURE

- Spin-orbit coupling and angular momentum transfer between planets and sun by interaction with solar wind 07 p1203 A71-20522
- Hartree-Fock energy levels, transition probabilities and wave functions for highly ionized atoms in B I isoelectronic sequences, including spin-orbit interactions 15 p2452 A71-32597
- Atomic structure constants numerical calculation, obtaining H matrix of complex including spin-orbit interaction and configuration mixing 19 p3142 A71-38155
- Trigonal crystal field and spin-orbit interaction matrices for ion energy levels in vanadium corundum in strong g scheme, using symmetry group tensor operators 21 p3427 A71-40075
- Potassium photoionization cross section, including spin-orbit interaction, orientation of photoejected electrons and dipole transition moment correction due to core polarization 21 p3417 A71-40197
- ### SPIN-SPIN COUPLING
- Lense-Thirring spin-spin gravitational forces measurement between disks and cylinders, using weak field low velocity relativity approximation 20 p3292 A71-39409

SPINAL CORD

NT SPINE

- Soviet book on spinal cord conducting paths electrophysiology covering anatomical and clinical data and neuron theory 03 p0364 A71-13691
- Ascending neuron vestibulo-ocular reflex arc, emphasizing medial longitudinal fasciculus 04 p0537 A71-14763
- Ascending pathways from spinal thermosensitive region to hypothalamic temperature control center, considering spinohalamic tract impulse frequency temperature response and bilateral RF coagulations 04 p0539 A71-15094
- Cyclic muscular voluntary movements, noting spinal segmental apparatus function 05 p0709 A71-16804
- Antagonistic descending characteristics of medial and lateral hypothalamic nuclei on excitation of spinal cord motoneurons 06 p0856 A71-18465
- Human spinal reflex effects during static work, suggesting cord segmental chiasmatic connections interaction with spinobulbar-spinal tract 08 p1249 A71-21973
- Ionizing radiation inhibition of spinal cord neurons ribonucleic acid synthesis and enzyme activity in mice, using autoradiographic method 09 p1393 A71-22925
- Ventral spinocerebellar tract cellular level control transmission to motoneurons, considering monitoring 16 p2609 A71-33260

- of inhibitory interneurons output against excitatory input 12 p1869 A71-26705
- Rat irradiated spinal cord, detailing orthodromic ventral root and monosynaptic reaction to rhythmic and increasing frequency stimulation 15 p2362 A71-32735
- Cardiovascular responses to hypothalamic, spinal cord and stellate ganglion stimulation as function of intensity, pulse duration and frequency in cats 16 p2531 A71-33367
- Bulbar and baroreceptor inhibition of spinal and supraspinal sympathetic reflex discharges recorded in cats from renal nerve 18 p2857 A71-36689
- Temperature effects on spinal excitation and inhibition in cats, investigating spinal motoneurons discharge frequency 18 p2861 A71-36890
- Spinal cord ascending neurons temperature sensitivity, comparing data from cats experiments with hydrothalamic temperature sensors sensitivity 18 p2861 A71-36894
- H reflex changes in spinal marrow of intact and labyrinthectomized rats under radial accelerations 20 p1888 A71-39221
- Sensory transmission of spinal heat and cold sensitivity in ascending spinal neurons of anesthetized cats 21 p3334 A71-40630
- Differential lipid and phospholipid composition of white matter in brain, cervical, thoracic and lumbosacral sections of spinal cord and sciatic nerve in dogs 21 p3338 A71-41074
- Healthy males immersion in water containing NaCl, determining modified gravitational field effect on motor functions 22 p3505 A71-42792
- ### SPINDLES
- Neuromuscular spindles sensory information processing, determining fibers selective data transmission functions by frequency meter and model for electrical and mechanical properties 03 p0366 A71-12977
- Human neuromuscular activity description by model for muscle spindles functions, considering systems parameters oscillations relation to mean muscle stress 03 p0366 A71-12978
- Externally pressurized air lubricated bearing boring spindle performance tests, considering circular accuracy, maintenance, tool life and cost effectiveness 22 p3552 A71-41675
- ### SPINE
- Vasomotor reflexes latency in postganglionic cardiac and renal nerves in intact and spinalized cats, determining spinal mediation by electrophysiological methods 04 p0538 A71-15093
- Aircrew radiological examination of spinal anatomical state, emphasizing traumas due to vibration, acceleration, ejection and crashes 05 p0715 A71-16936
- Spinal column radiographic examination after pilot ejection, discussing vertebral injuries detection 13 p2019 A71-28510
- Inertial properties of segmented cadaver trunk for mathematical model of spinal response to impact in seat ejection acceleration injuries in high speed aircraft 16 p2528 A71-33117
- Spine radiological examination for helicopter pilot fitness determination, discussing spinal weakness symptoms, special exercises, medical examinations and vibration reducing seat construction 22 p3500 A71-41578
- ### SPINEL
- Opaque minerals in Apollo 12 rocks, emphasizing spinel compositions 01 p0162 A71-11426
- Phonon-magnon absorption bands temperature dependences in Ni, Co and Li ferrimagnetic spinels, giving graphical data for Curie points 04 p0637 A71-15106
- Lunar 12 spinel compositional variation and textures as petrogenetic indicators, showing magma differentiation by crystal settling after lunar surface extrusion 10 p1672 A71-24394
- Magnesia rich magnesium aluminum oxide spinel ceramics, discussing sintering, grain growth inhibition and strength increase 13 p2092 A71-28662
- Opaque mineral compositions in Apollo 12 lunar rocks, noting ilmenite, spinels, native iron and troilite 23 p3739 A71-43620
- ### SPINNING [METALLURGY]
- #### U METAL SPINNING
- ### SPINOR GROUPS
- Spin weighted field functions for group SU (2) in gravitational radiation problems of general relativity, using Newman-Penrose formalism 16 p2609 A71-33260

- Electromagnetic field theory formulation, using Maxwell equations for spinors 23 p3705 A71-43827
- SPIRAL ANTENNAS**
- NT LOG SPIRAL ANTENNAS
- Multimode slow wave planar spiral antenna design and radiation field characteristics 09 p1420 A71-23510
- Conical equiangular spiral antenna active region boundary calculation, considering radiation vector 10 p1584 A71-24718
- Single- and two-tyr cylindrical spiral antenna, calculating end reflection, current damping and in-phase excitation component effects of radiation characteristics distortion 11 p1741 A71-26553
- Four arm conical spiral microwave antenna with circularly polarized hemispherical radiation pattern for satellite and rocket applications 14 p2216 A71-31042
- Turnstile loop Yagi and hexafilar contrawound spiral antennas for microwave telemetry rocket data reception, describing design and radiation patterns 23 p3643 A71-43095
- SPIRAL GALAXIES**
- NT MILKY WAY GALAXY
- Spiral galaxy NGC 6946 photometric observations, examining stellar magnitudes, color indices, associations distribution and distance 01 p0149 A71-10055
- Shock waves behavior and effects in Sc galaxies spiral arms, attributing dark lanes at inward edges to shock waves in gas flow 02 p0307 A71-12083
- Spiral galaxies mass-luminosity relationship from optical and radio astronomy data 02 p0308 A71-12102
- Galactic spiral structure model, examining nonlinear stellar density waves in plasma cylinder 03 p0484 A71-13205
- Resonance phenomena in spiral galaxies, determining stellar orbits, potential and distribution functions 04 p0655 A71-15725
- Spiral waves in galaxies, using crossed stream inclined wave model 04 p0658 A71-15842
- NGC 7320 as companion galaxy to NGC 7331 rather than member of Stephens quintet, considering red shift texture, lack of distortion and luminosity 05 p0805 A71-16110
- Spiral structure of galaxies identified with growing wave propagation in finite thickness axisymmetric disk hydrodynamic theory 05 p0813 A71-17036
- Interstellar grain formation relation with stellar evolution in terms of density wave theory of spiral structure origin 06 p0973 A71-18339
- Shock waves behavior and effects in Sc galaxies spiral arms, attributing dark lanes at inward edges to shock waves in gas flow 08 p1362 A71-21133
- Galactic spiral structure production mechanism observation by method based on photometry of individual stars 09 p1517 A71-22331
- Spiral galaxies orientation anisotropy explanation by hypothetical model of cosmological magnetic field 11 p1831 A71-26166
- Spiral arms formation on galactic scale in terms of density waves produced by gravitational perturbations 11 p1832 A71-26184
- Measuring methods for internal velocities of stars and gas within spiral galaxy, considering emission lines and Fabry-Perot interferometer 12 p1960 A71-26786
- Spiral galaxy structure formation and stability explanation in terms of wave theory of stellar subsystems interaction 12 p1967 A71-27309
- Spiral galaxy NGC 4569 member of Virgo cluster, using measurements of central velocity field, rotation and density estimates 13 p2132 A71-27965
- Spiral galaxy NGC 2403 neutral hydrogen distribution model fitting of observed velocity profiles 14 p2303 A71-29589
- Elliptical and spiral galaxies in coma cluster central zone, presenting observed radius vs magnitude diagrams 14 p2313 A71-30429
- Galactic spirals density wave theory based on three models rotation curve patterns observation 14 p2314 A71-30639
- Spiral density wave structure in computer simulations of evolution of galaxies, showing azimuthal dependence on gravitational and radial forces 15 p2497 A71-32769
- Aperture synthesis observations of neutral hydrogen radio emission in spiral galaxy M 101, using twin-element interferometer 16 p2632 A71-33329
- Spiral structure of Galaxy, using perturbation method for analysis of steady state interstellar gas with differential rotation due to coupling with stellar gas 16 p2643 A71-34069
- Galaxies spiral structure interpretation in terms of gravitation theory of pressure and density waves 20 p3293 A71-39528
- Statistical space velocity distributions, gravitation field strength and vertex deviation for nearby young stars, using density wave theory of galactic spirals 21 p3444 A71-40196
- Spiral galaxies N/O abundance gradients across disks from H II regions spectra 21 p3445 A71-40409
- Spiral structure OB associations in outer regions of Andromeda nebula, investigating blue objects in U and B plates of Schmidt telescope 21 p3451 A71-40723
- Spiral galaxy M33 observations at 21 cm, deriving hydrogen atoms distribution and kinematic properties 23 p3722 A71-42938
- Maffei 2 spiral galaxy hydrogen line and adjacent continuum observation by radio interferometry 23 p3733 A71-43080
- SPIRALS**
- Symmetrical wave excitation by electric dipole of conical surface ideally conducting along hyperbolic spirals, obtaining solution by integral transformation 05 p0727 A71-15996
- Symmetrical wave excitation by electric dipole of conical surface ideally conducting along hyperbolic spirals, obtaining solution by integral transformation 22 p3524 A71-42745
- SPIRALS (CONCENTRATORS)**
- Plane shock front collapse through logarithmic spiral contraction, obtaining pressure and temperature conditions downstream of front 16 p2556 A71-32919
- Large scale spiral variations of interplanetary magnetic field related to structures in solar wind, including polar field and out of ecliptic models 21 p3453 A71-41181
- SPLASH POINTS**
- U WATER LANDING
- Oxygen balance of intact and denervated dog spleen during asphyxia, distinguishing splenic contraction and metabolic rate-storage capacity ratio 04 p0538 A71-15087
- Hematoporphyrin chlorhydrate radioprotective effects on mice, removing, weighing and fixing spleens for hematopoietic colonies count 07 p1036 A71-18960
- Tritiated thymidine effects on splenic lymphocytes regeneration, discussing DNA synthesis, cycle completion and resident populations 11 p1719 A71-26055
- Human heart, kidneys, liver and spleen tissues antigen composition analysis by isolation of pure antibodies 12 p1872 A71-27723
- Spleen role as erythrocytic depot in reticulocytic reaction to acute hypoxia in splenectomized dogs inhaling air with reduced partial oxygen pressure 13 p2007 A71-28418
- SPLINE FUNCTIONS**
- Nonlinear boundary value problems numerical solutions using spline and Hermitian functions in Ritz-Galerkin setting 06 p0917 A71-17565
- Tchebycheffian spline functions, solving Hermite-Birkhoff interpolation as stochastic prediction and filtering 07 p1147 A71-19325
- German monograph on spline functions interpolation for solving integral equations and stress calculation in curvilinear edged disks 13 p2157 A71-29420
- SPLITTING**
- Sunspot spectrograms analysis, observing wavelength shift in Zeeman triplet circular components and magnetic splitting inequality under different circular polarizations 03 p0484 A71-13210
- SPOILERS**
- Light aircraft spoilers to minimize landing risk, discussing spoiler/dive brake area effects on glide path angular control [SAE PAPER 710387] 10 p1555 A71-24251
- Graphite-epoxy composite skins for commercial aircraft flight spoiler, discussing multiangle ply design and fabrication 12 p1921 A71-27413
- SPONTANEOUS COMBUSTION**
- Self ignition temperature of aerogels of Al-Mg alloys during heating of powders 01 p0182 A71-11448
- Self ignition temperature of aerosols of Al-Si powders as function of dispersion and alloy composition 01 p0182 A71-11449
- Supersonic hydrogen diffusion flames ignition aids at near-thermal self ignition point, discussing catalytically induced prereactions [DFVLR-SONDDR-118] 15 p2466 A71-32718
- Ignitability limits of hydrogen/air and hydrocarbon/oxygen mixtures at high temperatures near self ignition range 23 p3782 A71-44007
- SPONTANEOUS EMISSION**
- Ionized Xe laser lines in spontaneous emission, establishing correlation with unidentified lines 03 p0438 A71-13887
- Electron plasma waves one dimensional quasi-linear instability with allowance for spontaneous emission 03 p0464 A71-13929
- Polarization of spontaneous emission in Zn-doped GaAs p-n junctions as function of electric field strength 03 p0467 A71-13985
- GaAs lasers p-n junction active region thickness from minority carrier mobility and spontaneous emission measurements in threshold current determination 09 p1460 A71-22305
- Spontaneous emission decreases at CdS and GaAs lasing onset observed visually in internal reflection cavity under electron beam pumping 20 p3243 A71-39007
- GaAs luminescent p-n junction diode spontaneous emission measurement in magnetic field, noting redistribution in Lorentz force direction 21 p3432 A71-41303
- Stimulated and spontaneous emission from InSe single crystal under focused fast electron beam bombardment 21 p3434 A71-41326
- Quantum theory of molecular or atomic spontaneous emission while simultaneously undergoing stimulated emissions or absorptions 21 p3421 A71-41401
- Spatial dispersion effect on circular polarized cyclotron radiation spontaneous emission coefficient in nonequilibrium plasma 22 p3583 A71-42326
- Characteristic energies of exponential band tails in GaAs junction lasers from wavelength shift with cavity Q and spontaneous emission line width 22 p3558 A71-42360
- Laser pumped solid state masers operational characteristics, describing spontaneous emission noise 23 p3683 A71-43084
- SPONTANEOUS IGNITION TEMPERATURE**
- U IGNITION TEMPERATURE
- U SPONTANEOUS COMBUSTION
- SPORADIC E LAYER**
- Polar region semitransparent sporadic ionospheric layers nighttime temporal and cyclic ionization variations, determining solar activity effects and corpuscular stream densities by ionogram 02 p0243 A71-11767
- Ionospheric absorption of radio waves reflected from sporadic E layer, noting attenuation frequency dependence 02 p0211 A71-11768
- F 2 layer anomalies association with equatorial electrojet from F 2 and sporadic E critical frequencies analysis 02 p0245 A71-11963
- Sporadic E layer structure and disturbances from pulsed radio signal measurement, noting correlation to pressure oscillation at ground level 04 p0584 A71-15757
- Sporadic E and FEs regions multiples enhancement during squall thunderstorms, noting effects on lower ionospheric ionization 05 p0740 A71-16436
- Auroral sporadic E layer events relationship to pi 1 type irregular magnetic pulsations generation in Arkhangelsk region 05 p0744 A71-17187
- Sporadic E layer effect on F 2 region critical frequencies 05 p0745 A71-17201
- Sporadic E layer formation based on wind shift theory with drift data 05 p0746 A71-17202
- Sporadic E layers magnetic field variations, examining charged particle redistribution with air turbulence model 05 p0746 A71-17203
- Sporadic ionization occurrences nighttime observation in auroral E region, describing vertical electron concentration profile 06 p0895 A71-18280
- Sporadic E layer and critical frequency relationship to traveling ionospheric disturbances, suggesting role of atmospheric internal gravity waves 07 p1100 A71-19402
- Signal reflection from sporadic E layer, investigating multiplicity relationship to earth surface, ionization level, D region and nighttime absorption 07 p1100 A71-19403
- Lunar tides in sporadic E layer critical frequency, considering wind shears and electrostatic fields associated with lunar current system 08 p1363 A71-21202
- E layer critical frequencies interrelationship, assuming equal electron production rates 10 p1599 A71-23876

Microbarometric oscillations enhancement due to atmospheric pressure waves generation and cold fronts passage, considering relationship to sporadic E critical frequency

10 p1606 A71-24918

Sporadic E wind shear theory, discussing time variation in metallic ion content

13 p2055 A71-27923

Nondeviative absorption of RF signal at 2.2 MHz in presence of cusp type sporadic E layer

13 p2055 A71-27926

Auroral sporadic E layer events relationship to Pi 1 type irregular magnetic pulsations generation in Arkhangelsk region

13 p2059 A71-28244

Sporadic E layer effect on F 2 region critical frequencies

13 p2059 A71-28256

Sporadic E layer formation, using wind shear theory and drift data

13 p2059 A71-28257

Sporadic E layers magnetic field variations, examining charged particle redistribution with air turbulence model

13 p2059 A71-28258

Sporadic E layer occurrence frequency distribution during 1958-1960, investigating characteristics over equatorial, temperate and auroral zones

13 p2061 A71-28540

Ionospheric propagation, considering traveling disturbances, sporadic E phenomena, plasma frequency distributions and D region parameters

14 p2202 A71-30950

Ionized magnesium dayglow measurement in sporadic E layer by rocket-borne UV spectrometer, determining ion to atom ratio

15 p2398 A71-31765

Sporadic E layer enhancement by zonal transport within layer, considering gravity waves interaction effect on ion density horizontal redistribution

16 p2573 A71-33960

Daytime occurrence of maximum wave reflection frequency and blanketing frequency for period of two solar cycles at Rarotonga and Christchurch stations

16 p2574 A71-33970

Sporadic E layer and critical frequency relationship to traveling ionospheric disturbances, suggesting role of atmospheric internal gravity waves

19 p3053 A71-37826

Signal reflection from sporadic E layer, investigating multiplicity relationship to earth surface, ionization level, D region and nighttime absorption

19 p3053 A71-37827

Nighttime sporadic E layer behavior near magnetic equator, discussing occurrence frequency, seasonal variation and solar activity effects

19 p3055 A71-38037

Daytime ionogram corrections for underlying ionization in absence of x-trace of sporadic E layer

19 p3058 A71-38386

Chromospheric flares effect on sporadic E layer under low solar activity conditions

19 p3130 A71-38527

Midlatitude sporadic E layer formation mechanism, considering wind shear theory

19 p3061 A71-38630

Sporadic E layer initial height seasonal variations at mean geographic latitudes, considering solar zenith angle and activity effects

22 p3533 A71-41646

Sporadic E layer thickness measurement by Phase Ionosonde, measuring phase advance on F region echoes

23 p3666 A71-42975

Blanketing sporadic E layer diurnal and seasonal variations from equatorial stations ionosonde data obtained during IGY, discussing wind shear mechanism

23 p3667 A71-43134

Midlatitude sporadic E layer changes during increased geomagnetic activity, considering skin effect and current shear

23 p3670 A71-43189

Sporadic E layer ionization relation to thunderstorm surface pressure disturbance, considering gravity wave propagation

23 p3670 A71-43322

Sporadic E layer observation by reference electrode of electron temperature probe on sounding rocket, determining electron density below 85 km in D region

23 p3671 A71-43367

SPORADIC METEORIODS

Faint sporadic meteoroids mass distribution from forward and backscatter of radio echoes

01 p0151 A71-10254

Sporadic meteoroids geocentric velocity distribution over celestial sphere by photographic observation and oblique radio sounding, noting annual variations

10 p1668 A71-24029

High order conditional algebraic equations in determination from azimuthal radar observation sporadic meteor density distribution over celestial sphere, discussing solution procedure and convergence

10 p1576 A71-24030

Sporadic and shower meteoroids mass distribution temporal variations as function of magnitude and solar longitude from visual and radio echo measurements

20 p3298 A71-39643

Space vehicle measurements of sporadic meteor particle flux near earth, using detectors insensitive to acoustic and vibrational noise

20 p3299 A71-39648

Sporadic and cometary meteor particles concentration along earth orbit, using optical and radiant measurements

20 p3299 A71-39650

SPORES

Ethylene oxide and methyl bromide sporicidal activity compared for spacecraft sterilization of *B. subtilis* var niger spores

01 p0027 A71-11565

Radiation damage to HeLa cells at liquid nitrogen temperature and dry fern spores at room temperature

07 p1033 A71-18937

Anoxic fern spores X ray sensitization, observing diacetyl and isatin effects

07 p1036 A71-18961

Dry heat and Co 60 gamma radiation combined effects on spacecraft sterilization, discussing kinetic analysis of spore inactivation

10 p1565 A71-24613

Stearothermophilus spore germination stimulation, investigating effects of preheating and amino acid and carbohydrate concentration

13 p2010 A71-28695

Spores released from solids interiors by aeolian erosion on planetary surface, noting application to microbes in planetary quarantine

16 p2537 A71-33796

Bacterial spore distribution and dry heat resistance on Mariner-Mars 1969 spacecraft, using randomly selected aerobic mesophilic isolates

19 p3002 A71-37646

Combined action of vibration and gamma irradiation on sporulation dynamics, survival rate and mutability of *Chlorella*

20 p3193 A71-39237

Bacterial spores survival under simulated lunar surface conditions, comparing results with vegetable cells experiments

21 p3334 A71-40567

SPOT WELDS

Electrical resistance spot weld penetration measurement via ultrasonic method using shear waves

01 p0086 A71-10305

Aluminum spot welding specification consistency, examining surface conditions, cleaning procedures, weld schedules and bond design effects

04 p0603 A71-14923

Al alloy spot welding, investigating defects effects on welded joint fatigue strength under dynamic tests by metallographic and X ray examinations

15 p2436 A71-32467

Fatigue lifetime of overlapping joint spot welds of Al alloys, investigating shrinkage crack initiation and propagation

24 p3830 A71-44786

Statistical analysis of spot welded and adhesive joints of high strength Al alloy sheet in aircraft structures

24 p3831 A71-45012

SPRAY CHARACTERISTICS

V/STOL spray generation tests concerning pilot visibility impairment in low altitude overwater hover

04 p0534 A71-15444

Rocket engine propellant injectors with noncircular orifice geometry, presenting experimental spray patterns and predicted performance for noncircular and circular orifice configurations

11 p1810 A71-25520

Single and multibeam holography application to size, trajectory, distribution, population density and velocity measurements of water and electric arc welding sprays droplets

14 p2243 A71-30299

Liquid spray steady evaporation and mixing in gaseous swirl, using continuum mechanics

17 p2727 A71-34693

SPRAY NOZZLES

Liquid properties effect on secondary injection from spray nozzle, determining jet penetration in supersonic stream by scattered light and schlieren photographs

09 p1381 A71-22089

SPRAYED COATINGS

Ground deicing system for transport aircraft, discussing antifreeze liquid spray application after mechanical snow removal

09 p1428 A71-22948

Apollo spacecraft and lunar landing module thermal control surfaces, considering inorganic silicate bonded paint

09 p1533 A71-23426

SPRAYED PROTECTIVE COATINGS

U PROTECTIVE COATINGS

U SPRAYED COATINGS

SPRAYERS

Atomization drop size distributions in sprays from convergent pneumatic nozzles for molten wax and polyethylene mixtures

13 p2049 A71-29010

SPRAYING

NT FLAME SPRAYING

NT PLASMA SPRAYING

Hollow cone water spray from pressure jet swaging atomizer into uniform air stream, observing droplet velocities and trajectories by high speed photography

13 p2049 A71-28717

SPRAYING APPARATUS

U SPRAYERS

U SPRAYERS

SPREAD F

Ionospheric heating self amplification and spread F triggering by disturbances, calculating ray path through model ionospheric irregularities

01 p0078 A71-11536

VHF radar measurements of scattering by field-aligned irregularities associated with equatorial spread F

03 p0420 A71-14535

Midlatitude spread F, sunspot activity and geomagnetic activity variations related, discussing fast solar wind particles

09 p1437 A71-22930

Conjugate duct irregularities in magnetosphere involving interchange of plasma tubes by spatially varying electric fields, applying to spread F formation

14 p2230 A71-29712

Spread F ionospheric electron density irregularities and satellite scintillation over polar cap

14 p2300 A71-30043

Ionospheric electron density irregularities measurement, comparing scintillation, spread F and electron static probe methods

19 p3128 A71-38037

Spread F configuration irregularities at Nairobi, investigating nocturnal and seasonal variations and magnetic and solar activity effects

23 p3672 A71-43977

SPREAD REFLECTION

U DIFFUSE RADIATION

U REFLECTION

SPRINGS [ELASTIC]

Light aircraft steel landing gear springs structural design at Cessna, considering certification requirements

10 p1555 A71-24266

[SAE PAPER 710400] Spring coupled inertially damped instrument servomechanisms design, applying phase margin maximization criterion

11 p1716 A71-26417

Spring loaded intermittent contact devices vibrating system parameters for computer programmed transfer matrix solution, noting gravity loaded variant

12 p1931 A71-27480

Complex media and plasticity theory deformation models based on central friction mechanisms, discussing elastic spring analog

14 p2332 A71-30877

Nonlinear elastic suspension springs with symmetrically hardened behavior for shock and vibration isolation of aerospace instruments and controls

17 p2825 A71-34890

Linear multidegree of freedom shock isolation system optimum design, masses, spring and damping coefficients, using mathematical programming [ASME PAPER 71-VIBR-81]

21 p3461 A71-40317

Instrument servomechanisms with spring-coupled inertial dampers, evaluating dimensional design parameters from analytical root locus

21 p3326 A71-40616

SPUR [REACTORS]

U SPACE POWER UNIT REACTORS

SPUTNIK SATELLITES

East-West cooperation in space telecommunications, outlining Intelsat and Intersputnik organizational structure

18 p2987 A71-36167

Stainless steel sputter deposits equilibrium phases, determining deposition temperature ranges for austenite and ferrite formation

02 p0267 A71-12884

Fuel cell electrodes preparation by sputtering thin Ta and Pt layers on porous Vycor

03 p0353 A71-13056

Micrometeorite sputtering in ionosphere producing influx of meteorite atoms and ions in atmosphere, considering temperature dependence of stone meteorite sputtering coefficient

03 p0486 A71-13305

Low stress integral coverslips deposition by high vacuum ion beam sputtering for solar cell manufacturing cost reduction

05 p0702 A71-16078

Facility backspattered material effect on performance of glass-coated accelerator grids for Kaufman electron bombardment thrusters [AIAA PAPER 71-156]

06 p0947 A71-18596

High transition temperature superconducting materials thin films composition control by sputtering from hot pressed powder mixture ingots targets
07 p1178 A71-19849

Secondary ion component on tungsten target surface during sputtering by alkali metal ions
09 p1494 A71-22878

Sputtered tantalum films oxygen content determination by anodization current efficiency measurements
16 p2621 A71-33187

QUALLS

Sporadic E and FEs regions multiples enhancement during squall thunderstorms, noting effects on lower ionospheric ionization
05 p0740 A71-16436

SQUARE WAVES

Frequency measurements of square wave signal with unknown amplitude by two mismatched channels, comparing rms error with effective estimate variance
14 p2195 A71-30106

Ninety degree phase shifter and frequency multiplier for square waves
15 p2376 A71-32025

Stability conditions for square wave sustaining voltage, including complex rectangular waveforms with pulsed discharges in plasma display
20 p3233 A71-39060

QUEEZING

U COMPRESSING

U VENANT FLEXURE PROBLEM

U SAINT VENANT PRINCIPLE

STABILITY

NT ACOUSTIC INSTABILITY

NT AERODYNAMIC STABILITY

NT AIRCRAFT STABILITY

NT ATTITUDE STABILITY

NT BOUNDARY LAYER STABILITY

NT COMBUSTION STABILITY

NT CONTROL STABILITY

NT DIMENSIONAL STABILITY

NT DIRECTIONAL STABILITY

NT DYNAMIC STABILITY

NT FLAME STABILITY

NT FLOW STABILITY

NT FREQUENCY STABILITY

NT GYROSCOPIC STABILITY

NT HOVERING STABILITY

NT LATERAL STABILITY

NT LONGITUDINAL STABILITY

NT LOW SPEED STABILITY

NT MAGNETOHYDRODYNAMIC STABILITY

NT MAGNETOSPHERIC INSTABILITY

NT MOTION STABILITY

NT ROTARY STABILITY

NT SHELL STABILITY

NT SPACECRAFT STABILITY

NT STATIC STABILITY

NT STORAGE STABILITY

NT STRUCTURAL STABILITY

NT SURFACE STABILITY

NT SYSTEMS STABILITY

NT THERMAL STABILITY

Liapunov stability of neutral first order nonlinear differential equations solutions with time lag
01 p0112 A71-10655

Triangular libration points stability in elliptic restricted three body problem, determining parametric resonance region
03 p0495 A71-14226

Normal shock wave stability in perfect gas with viscosity and heat conduction under arbitrary small one dimensional disturbances, formulating eigenvalue problem
07 p1224 A71-20288

Three body problem stability investigation, using Liapunov perturbation function
08 p1361 A71-21052

Book on matrix methods in stability theory covering matrix algebra, Liapunov theory and functions, stability matrices properties and optimal control theory applications
09 p1539 A71-22872

Stability of trapped particle equilibrium, considering contribution to plasma wave dispersion
13 p2104 A71-27847

Three body problem stability investigation, using Liapunov perturbation function
14 p2310 A71-30169

Liapunov stability of neutral first order nonlinear differential equations solutions with time lag
14 p2266 A71-30989

Stars with central He burning and loop occurrence in H-R diagram, suggesting secular instabilities with high stellar mass
16 p2633 A71-33332

Finite beta microinstabilities inherent in magnetic mirror confined plasmas, considering wave propagation across magnetic field at multiples of ion cyclotron frequency
18 p2950 A71-35861

STABILITY AUGMENTATION

U FEEDBACK CONTROL

U STABILIZATION

STABILITY DERIVATIVES

NT PITCHING MOMENTS

NT ROLLING MOMENTS

NT YAWING MOMENTS

Spanwise distribution of induced drag in subsonic flow by vortex lattice method, noting applicability to rotary derivatives in stability analysis
02 p0187 A71-12691

Time vector method for aircraft flight test data evaluation, discussing control deflections effects on phugoid motion, lateral stability derivatives and error estimation
03 p0347 A71-13341

Nonlinear aerodynamic moments for arbitrary motions of bodies of revolution in free flight
[AIAA PAPER 70-205] 03 p0341 A71-13435

Nonlinear aerodynamic moment system for nonaxisymmetric bodies free flight motion analysis, taking into account interactions excluded in classical treatment
[AIAA PAPER 71-275] 08 p1228 A71-22000

Aerodynamic moment on satellite with asymmetrically positioned solar cell platforms, analyzing motion around center of mass for diffuse scattering flow
09 p1531 A71-22568

Cylindrical spacecraft reentry body self-sustained pitching oscillations due to separation on downstream portion, examining stability derivatives
09 p1533 A71-23604

Pitching stability derivatives of sharp oscillating wedges at zero incidence in viscous hypersonic flow from perturbation method, including thickness and wave reflection effects
14 p2171 A71-31023

Rotor stability derivatives determination from instrumented OH-6A prototype helicopter wind tunnel tests, comparing data with analytical results obtained by digital computing technique
[AHS PREPRINT 543] 14 p2179 A71-31100

Twin turboprop STOL aircraft lateral directional oscillation traced to rudder vibration due to aerodynamic hinge moments interaction with friction
[AIAA PAPER 71-792] 16 p2525 A71-34019

Digital simulation for predicting static directional aerodynamic forces and moments characteristics of air cushion vehicle configuration through 180 degrees of sideslip
[AIAA PAPER 71-907] 19 p2995 A71-37158

Nonlinear motion of asymmetric rolling reentry vehicle with variable roll rate, dynamic pressure and stability derivatives
[AIAA PAPER 71-932] 19 p3148 A71-37177

Rocket propulsion system equipped space shuttle dynamics, discussing aerodynamic forces and moments measurement in supersonic wind tunnels
19 p3151 A71-37318

Soviet book on practical aerodynamics of aircraft with turboprop engines covering piloting, forces and moments, stability, controllability, takeoff, landing, etc
19 p2994 A71-38534

Maximum vector values for stability and rigidity of elastic systems under modulo limited disturbances, applying to beam deflection and second derivative
21 p3473 A71-41154

Medium compressibility effect on gas dynamic characteristics and aerodynamic forces and moments in centrifugal compressor end stage bladed diffuser
23 p3626 A71-43552

STABILITY TESTS

NT FLIGHT STABILITY TESTS

NT WIND TUNNEL STABILITY TESTS

Thermionic stability life tests of cylindrical diodes with W emitters at constant current and optimal Cs and collector temperatures
02 p0194 A71-12222

Trilayer niobium-alumina-niobium sheath insulator thermal stability test under electrical load
02 p0232 A71-12253

Lithium-containing p-n solar cells photovoltaic performance and stability tests at room temperature
05 p0703 A71-16090

Liapunov function time derivative for autonomous system asymptotic stability tests by exact differential method
05 p0774 A71-16579

Perpendicularly woven fiberglass reinforced plastics stability, elasticity and viscoelasticity as function of temperature
12 p1921 A71-27347

Clamped and hinged spherical and paraboloidal shell caps elastic stability tests under external pressure loading, determining critical pressure
14 p2323 A71-29846

Stability test for Routh-Hurwitz problem using step by step method based on algorithm
19 p3086 A71-37898

Copper sulfide-cadmium sulfide photovoltaic solar cell electronic processes observation at heterojunction, noting electron trapping and hole injection roles in long term stability
19 p3119 A71-38140

STABILIZATION

NT SIGNAL STABILIZATION

NT SPIN STABILIZATION

Inertially stabilized tactical missile control system performance analysis using hybrid computer simulation methods
02 p0226 A71-11785

Giant pulse laser emission stabilization, describing technique for eliminating short time oscillations in subnanosecond range
02 p0261 A71-12321

C-5 military transport stability augmentation for pitch and yaw inertia at low speed, using pilot evaluation on cockpit simulator
02 p0190 A71-12684

Satellite optimal guidance, discussing gyroscope application for stabilization and orientation control
03 p0500 A71-14227

Variable inertia rotating rigid body stabilization by nonlinear optimal control problem, using Hamilton-Jacobi and Riccati equations
03 p0391 A71-14314

Plate critical surface temperature in case of stabilization by supersonic boundary layer cooling
05 p0695 A71-16852

HF stabilization of plasma instabilities, noting electrostatic instability suppression by ordinary and helicon type waves
06 p0934 A71-17476

Ion source for double focusing magnetic mass spectrometer for use with gas chromatograph on Mars mission, requiring electron beam stabilization in space
07 p1113 A71-19851

Optimal stabilization system synthesis for multidimensional linear control plant in presence of random perturbation
12 p1892 A71-27176

Stabilization of solid body orientation with twin gyros under slave engine drive, producing control moments to gimbal axis
13 p2145 A71-28935

Afterglow plasma drift-dissipative instability stabilization by RF magnetic and electric fields
14 p2800 A71-30504

Spurious effects on stabilizing circuits with loaded Zener diodes for reference voltage source
18 p2893 A71-36800

Marginal stabilization of MHD instabilities of linear pinch by force free magnetic fields, comparing with energy method
20 p3275 A71-39462

Shearless magnetic fields discontinuities in marginal stabilization of MHD instabilities for constant pinch force free fields, including toroidal effects
20 p3275 A71-39463

Alcyon project PTA 1, considering balloon stabilization efficiency during night-day transition and system reliability
22 p3483 A71-42400

Retinal image stabilization variables, noting whole fade characteristics sensitivity to stimulus pattern variations
24 p3795 A71-44470

Unstable systems dynamic stabilization, deriving conditions from second order linear differential equations with variable coefficients
24 p3849 A71-45048

STABILIZED PLATFORMS

Power gyrostabilizer optimal controlling section with random base frame oscillations, solving filtration problem as function of platform structure by Wiener method
01 p0079 A71-10427

Sounding rocket attitude monitoring and control, using digital output roll stabilized gyro platform
[AIAA PAPER 70-1407] 03 p0455 A71-13686

Liapunov stability of gyroscopic stabilizers as electromechanical systems, assuming nonrigidity of rotor, gimbal and platform suspension
13 p2069 A71-28726

Nutation damping and vibration isolation in dual spin spacecraft, using flexible dissipative coupling between platform and rotor
18 p2971 A71-36276

Errors equations for space stable inertial navigation systems, considering rotating platforms and velocity and altitude damping
20 p3261 A71-38854

STABILIZERS

Transient response and design formulas for microwave power stabilizer with nonlinear inertial feedback containing semiconductor attenuator
15 p2378 A71-31230

Wideband stabilizer design for high acuity aerial reconnaissance camera to obtain high degree of attenuation to roll and pitch rotational motion inputs
18 p2919 A71-36087

Modulation instability of dispersion type NMR stabilizer of resonance conditions, determining critical frequency of self excitation and maximum amplification
22 p3519 A71-41444

Two-axis pneumatic rate gyroscope with externally pressurized gas bearing for airborne vehicle fluidic autostabilizer sensor
22 p3551 A71-41666

Gyroscopic systems dynamic drift reduction by inertial damping, using astatic and static stabilizers
23 p3675 A71-43295

- Transistor compensation stabilizers design and fabrication with enhanced voltages 24 p3807 A71-44382
- STABILIZERS [AGENTS]**
- Beta stabilizers effects on Ti strength, plasticity and stress concentration sensitivity at low temperatures 05 p0767 A71-16766
- Soviet book on automotive and jet aircraft engine fuel chemical stabilizers under storage, transit and operational conditions, examining additives in relation to stability ratings 06 p0942 A71-17433
- Beta stabilizers effect on mechanical properties of alpha structure Ti-Al-V alloys subjected to different heat treatments 13 p2083 A71-27874
- Beta stabilizers effects on Ti base binary alloys strength, plasticity and stress concentration sensitivity at low temperatures 17 p2760 A71-35465
- Allosteric adenosine monophosphate nucleosidase stabilization by inorganic salts, substrate and essential activator, investigating enzyme inactivation mechanism in low ionic strength environments 23 p3642 A71-44268
- STABILIZERS [FLUID DYNAMICS]**
- NT HORIZONTAL TAIL SURFACES**
- Performance characteristics of horizontal and vertical stabilizers at medium Reynolds number from wind tunnel measurements, considering air foil and flap effects 06 p0842 A71-18249
- Stabilizer structure effect on flame stability of atomized liquid fuel, studying excess air ratio relation to air flow velocity 13 p2163 A71-28963
- STABLE OSCILLATIONS**
- Object constant speed motion in terrestrial orthodromy, examining Shuler vertical small oscillations stability 01 p0125 A71-10628
- Soviet book on mechanical oscillator threshold sensitivity to small moment of forces, covering light friction and radiometric oscillatory instability effects and estimates 02 p0285 A71-12839
- Magnetron oscillators frequency and oscillation stability, examining phase mismatch angle, filament current and cathode thermal balance 03 p0386 A71-13805
- Incompressible viscous liquid forced oscillations stability, developing linearization procedure for nonlinear operator equation of perturbations 08 p1275 A71-21051
- Satellite pitching oscillations optimal stabilization, obtaining approximate solution for finite time 12 p1972 A71-27026
- Two dimensional periodic and doubly periodic boundary value problems solution in theory for stable oscillations of elastic and viscoelastic bodies perturbed by circular holes 12 p1980 A71-27447
- Unmodulated microwave oscillations power stabilizer with semiconductor attenuator 13 p2036 A71-28367
- Stable oscillation development time in phantastion oscillator, using linearization of nonlinear term 14 p2211 A71-30114
- Stability analysis of nonradial oscillations of cold nonrotating relativistic neutron stars by linearized Einstein equations with coupled gravitational waves 16 p2635 A71-33482
- Steady oscillation frequencies in systems described by nonlinear differential equations, including external perturbations 17 p2782 A71-34931
- Stroboscopic and analytical studies of oscillations and stability regions of gravity gradient satellite in eccentric orbit 18 p2963 A71-36282
- Satellite pitching oscillations optimal stabilization, obtaining approximate solution for finite time 19 p3152 A71-37695
- STACKING FAULT ENERGY**
- Plastic deformation and phase transformation in textured austenitic stainless steel, considering stacking fault energy contribution 01 p0101 A71-10737
- Polycrystalline Ni single and overlapping stacking faults production by tensile deformation in premacroyield region, noting stress concentration effects 02 p0268 A71-12888
- Strain rate effect on critical shear and cross slip stresses of Al and Al-Mg single crystals, obtaining stacking fault energy 03 p0442 A71-13364
- Intrinsic stacking fault energy temperature dependence in austenitic Fe-Cr-Ni alloys determination from dislocation mode measurements by high temperature transmission electron microscopy 07 p1138 A71-19984
- Loop patterns of secondary defect structures in quenched Al based alloys interpreted in terms of internal stress and stacking fault energy 08 p1310 A71-21531

- Matrix stacking fault energy effects on steady state creep rate of recrystallized nickel-cobalt-aluminum oxide alloys, showing stress dependence 08 p1315 A71-21578
- Stacking faults and fcc precipitation of Ti beta alloys after high temperature heating 09 p1469 A71-22850
- Surface effects of transverse slip screw dislocations in metal fatigue crack nucleation, relating stacking fault energy and number of cycles to failure 16 p2593 A71-33681
- Strain rate dependence of shear stress, plastic cross-slip and stacking fault energy of Al single crystals at 77 K 18 p2937 A71-36749
- Ni-Co alloy fine structure under plastic deformations, determining stacking fault energy effects with X ray diffraction lines 19 p3076 A71-37119
- Matrix stacking fault energy effect on tensile creep deformation modes in gamma prime precipitation hardened nickel-base alloys 19 p3080 A71-37721
- STACKING FAULTS**
- U CRYSTAL DEFECTS**
- STADAN [SATELLITE TRACKING NETWORK]**
- NASA Stadan and Speopt optical and laser tracking sites dynamic position estimations from GEOS 1 and 2 observations, analyzing model error effects 20 p3220 A71-39662
- STAGE SEPARATION**
- Abort and staging separation maneuvers of two equal size reusable lifting entry vehicles in wind tunnel tests [AIAA PAPER 70-260] 01 p0165 A71-11579
- Optimization of multistage rockets with given payload, propellants and explosive separation of stages 05 p0817 A71-16613
- Soviet book on long range rocket ballistics covering control system, dynamics, firing distance, motion equations, stage separation and nominal trajectories 13 p2146 A71-29438
- Weightlessness simulation for aerospace mechanisms, using tower release and gyrometric system for testing stage separation, satellite perturbation, yo-yos, probes and mast development [ONERA-TP-940] 18 p2971 A71-36018
- STAGING [ROCKETS]**
- U STAGE SEPARATION**
- STAGNATION**
- U STAGNATION POINT**
- STAGNATION FLOW**
- Vorticity amplification in stagnation flow by stretching, discussing effects on average boundary layer profile 03 p0398 A71-13104
- Uniform flow stability near two dimensional stagnation region formed by blunt body immersion in cross flow 03 p0400 A71-13728
- Stagnation point flow flame sheet model, showing density-viscosity product variation for injection rate effect on velocity profile 08 p1375 A71-20865
- Radiative and convective heat transfer for stagnation point flow of emitting carbon dioxide and nitrogen gas mixture, assuming thermodynamic equilibrium in shock layer 14 p2335 A71-30212
- Binary laminar boundary layer in hypersonic axisymmetric stagnation point flow with temperature dependent material properties, presenting exact and approximate calculation methods 17 p2671 A71-35422
- Conductive and radiative axial heat transfer in packed/stagnant beds at 20-750 C, giving temperature profiles 22 p3620 A71-41877
- Electromagnetic radiation in stagnation flow region, determining temperature distribution absorption coefficient of carbon dioxide at rest between two parallel plates 22 p3621 A71-42024
- STAGNATION POINT**
- Numerical analysis of complex boundary layer at axisymmetric stagnation point with massive blowing 01 p0071 A71-10964
- Hydrogen fuel injection into hot oncoming air flow, investigating boundary layer chemical behavior at stagnation point of diffusion flame 02 p0334 A71-12857
- Boundary layer theory extended to cross vorticity transport in outer flow approaching two dimensional stagnation point 03 p0398 A71-13103
- Plane ideal incompressible fluid jet impact on curvilinear surface, considering flow characteristics near stagnation point 04 p0567 A71-14592
- Free stream turbulence enhanced stagnation line heat and mass transfer on two dimensional blunt body 04 p0681 A71-15481

- Blunt body stagnation point heat transfer in hypersonic flow, describing gas dynamic equations, field viscosity and conductivity 04 p0528 A71-11578
- Unsteady viscous rotational stagnation point flow, solving vorticity transport equation 05 p0736 A71-16766
- Quasi-stagnation levels in ion motion induced by external atmospheric gravity waves at ionospheric height 06 p0888 A71-17433
- Plasma torch stagnation point heat transfer measurements, using heat pipe calorimetry [AIAA PAPER 71-81] 06 p0902 A71-11578
- Viscous incompressible axisymmetrical flow, examining vortices near stagnation point of infinitesimal obstacle 07 p1089 A71-16766
- Nonequilibrium multicomponent ionization calculations for stagnation merged shock layer of hypersonic blunt body by successive accelerated replacement [AIAA PAPER 69-655] 07 p1015 A71-11578
- Reentry environment simulation at vehicle stagnation away from stagnation point, using arc heater with periscope nozzle duct [AIAA PAPER 71-261] 08 p1274 A71-28963
- Convective plus radiative shock tube model stagnation point heating rate measurements for planetary entry heating rate in air and Venus gas [AIAA PAPER 69-635] 09 p1382 A71-28963
- Circular stagnation line position on axisymmetric blunt bodies with circular sharp edge 09 p1384 A71-28963
- Heat fluxes from premixed methane-oxygen and propane-oxygen flames measurement by transpiration calorimetric method, comparing forward stagnation point results with calculated values 10 p1695 A71-28963
- Villat problem of ideal incompressible two dimensional fluid flow around plate, determining stagnation point location 10 p1594 A71-28963
- Convective heat transfer in three dimensional stagnation point boundary layer flow characterized by gas properties 10 p1698 A71-28963
- Two dimensional laminar boundary layer equation local drag coefficient from one and two term Merkle expansion in regions upstream of stagnation point 12 p1896 A71-27026
- Flow in vicinity of stagnation point of sphere and cylinder during pulsating motion in nonuniform stream 12 p1897 A71-27026
- Equilibrium air boundary layer flows at two dimensional stagnation points, discussing flow characteristics and real gas heat transfer parameters [AIAA PAPER 70-809] 12 p1866 A71-27026
- Mass injection effect on heat transfer reduction three dimensional stagnation points as function of shape, enthalpy and gas properties 14 p2335 A71-28963
- Multicomponent gas nonequilibrium viscous flow near blunt body stagnation point, presenting stagnation layer parameter variations effects on heat exchange 14 p2336 A71-30212
- Asymmetries in magnetospheric shock layer due to upstream interplanetary magnetic field, considering forward stagnation region of solar wind-magnetosphere interaction [AIAA PAPER 71-610] 15 p2395 A71-30212
- Large gas bubble migration in rotating liquid with gravity, noting velocity dependence on stagnation point distance and radius of curvature 15 p2392 A71-30212
- Laminar boundary layer flow at stagnation point with intensive injection of different absorbing medium, calculating temperature profiles and thermal fluxes 17 p2725 A71-34931
- Cold combustible gas mixture ignition temperature at flat plate forward stagnation point, investigating inert gas concentration, activation energy and Dankohler number effects 17 p2837 A71-34931
- Convective flow at stagnation point relation to radiation flux decrease as result of absorption in boundary layer 17 p2671 A71-35422
- Low density hypersonic flow around blunt body considering total pressure and flow velocity on stagnation point line 18 p2846 A71-36282
- Laminar hypersonic boundary layer equations, calculating heat transfer and shear stress in stagnation point 18 p2847 A71-36282
- Combustion dynamics, including fire spread in fuels, ignition, turbulent/laminar fields and boundary layer, stagnation point and opposed jet burning 19 p3166 A71-37695
- Counterflow methane diffusion flames structure forward stagnation region of porous cylinder, measuring velocity, temperature, concentration, reaction and heat release rate profiles 19 p3168 A71-37695

Flow instability in stagnation point region of circular under in turbulent channel flow, using hydrogen bubble method for flow visualization

20 p3211 A71-39454

Second order viscoelastic fluid two dimensional stagnation point flow, solving boundary layer equations

20 p3213 A71-39564

Chemical kinetics and fluid mechanics interaction effects in stagnation point boundary layer

21 p3475 A71-40860

Transonic nozzle flow with variable stagnation speed of sound across flow, deriving governing equations with stream function as independent variable

21 p3324 A71-40978

STAGNATION PRESSURE

Liquid-vapor interactions in constant area steam-jet condensing ejector mixing section, measuring initial static and stagnation pressure profiles [ASME PAPER 71-FE-21]

13 p2052 A71-29459

Stagnation pressure changes in unsteady flow downstream of turbomachine blades with fluctuating circulation related to vortex sheets

17 p2671 A71-35279

STAGNATION REGION

STAGNATION POINT

Heat transfer boundary conditions determination in studying heat protective coatings effectiveness, discussing measurement methods for stagnation temperatures and heat fluxes from exhaust gases

04 p0600 A71-15643

Maximum stagnation temperature on swept wing leading edge for equilibrium glide entry of space shuttle

07 p1013 A71-18902

Shielded fine wire probe for total temperature rapid measurement in high speed flows, discussing construction and theoretical considerations

11 p1761 A71-25528

Hypersonic reentry flow over blunt nosed bodies, using water oxygen mixture to achieve simulation at lower stagnation temperatures

11 p1705 A71-26270

High enthalpy flow temperature probe, determining stagnation temperature of combustion gases by chromel-alumel thermocouple

11 p1765 A71-26277

Chemically nonequilibrium laminar boundary layer profiles in axisymmetric hypersonic conical nozzle at high air stagnation temperature, calculating wall friction, displacement and momentum loss thickness

13 p1889 A71-27904

Low pressure gas heating in shock tube, considering stagnation temperature increase

13 p2049 A71-29198

Geometrical parameters effect on operation of high pressure two-stage nozzle ejector with conical mixing chamber, measuring gas flow rates, total pressures and stagnation temperatures

16 p2521 A71-33612

Tubular models sealed at one end with cavity facing incoming steady gas flow, measuring increased stagnation temperature associated with shock wave formation

17 p2672 A71-35628

Hypersonic wind tunnel air condensation detection by light scattering instrumentation, discussing stagnation temperature condensation

21 p3364 A71-40405

STAINLESS STEELS

NT AUSTENITIC STAINLESS STEELS

NT MARTENSITIC STAINLESS STEELS

Ferritic steel with 17 percent Cr, examining dynamic behavior under high speed tension test regarding heterogeneity of plastic deformation, stress peak, etc

01 p0105 A71-11616

Stainless steel sputter deposits equilibrium phases, determining deposition temperature ranges for austenite and ferrite formation

02 p0267 A71-12884

Titanium, Inconel and stainless steel alloys deep drawing press loads under various lubrication and temperature conditions, considering work hardening, friction and anisotropic coefficients [ASME PAPER 70-WA/PROD-26]

03 p0433 A71-14114

Water impact erosion on stainless steel, Ni and Al and Ti alloys, observing impact velocity relationship with number

03 p0444 A71-14287

Stainless steel-Al joining techniques, describing gas tungsten arc process

04 p0603 A71-14920

Thermal recovery in stainless steel after explosive shock loading and forming

04 p0614 A71-15781

Stainless steel deoxidation by carbon in laboratory scale vacuum induction melting, explaining reaction kinetics

05 p0758 A71-16246

Stainless steel physicochemical properties stability, discussing equipment for industrial materials test-

ing under various environmental and loading conditions

05 p0769 A71-16897

Cr-Ni stainless steel tensile and compressive stresses effect on hydrogen permeability at elevated temperatures

06 p0912 A71-17946

He embrittled stainless steel stress-rupture behavior under vacuum and elevated temperature conditions, discussing microstructural characteristics

06 p0914 A71-18685

Stainless steel coatings vacuum deposition on Ti alloy plates, considering product cryogenic and mechanical properties

07 p1118 A71-19853

Stainless steel fatigue crack growth characteristics at liquid metal fast breeder type nuclear reactors elevated temperatures

07 p1138 A71-19983

Granulometric composition effects on stainless steel powders bulk weight, friability and compactability, taking into account particle shape

09 p1470 A71-23062

Relaxation analysis of strain range, hold time and cycle number in low cycle fatigue testing of annealed stainless steel at 1200 F [ASM PAPER W71-24.1]

09 p1471 A71-23093

High strength stainless steel dislocation structure and mechanical properties, discussing tempering, tensile strength, precipitation hardening and temperature effects

11 p1776 A71-25167

Liquid Na heat exchanger fabrication, using electron beam welding technique for stainless steel components assembly

11 p1768 A71-25390

Regeneratively cooled stainless steel thrust chamber failure related to internal carburation by fuel decomposition and propellant combustion

11 p1810 A71-25505

Spreading, wettability, diffusion and aggressive properties of nickel base brazing filler metals on stainless steels

11 p1769 A71-25750

Fracture mechanics of metal matrix composite with ductile stainless steel reinforcing fibers

12 p1985 A71-27775

Deformation substructures, strain rates and terminal properties of explosively-formed thin walled stainless steel cylinders, using transmission electron microscopy

13 p2153 A71-28501

Stainless steel wire fibers in refractory castables, noting flexural and compressive strength improvements

13 p2093 A71-28663

Al matrix-stainless steel composites under tensile loading parallel to reinforcement direction, noting creep behavior at ambient temperature

13 p2089 A71-29413

Surface roughness of 304 stainless steel by Brunauer-Emmett-Teller measurements, using ethylene as adsorbate

14 p2284 A71-30073

Co-Mo and Co-Mo-Ti stainless maraging steels tensile strength after quenching, establishing Mo and Co alloying limits

15 p2427 A71-31526

Tensile strength of boron, silicon carbide coated boron, silicon carbide, stainless steel and tungsten fibers after exposure to air, argon and aluminum at high temperatures

15 p2435 A71-32440

Annealed stainless steel and Ti alloy in solution heat treated aged condition, detailing elevated temperature and high strain rate effects on fatigue life and tensile properties

15 p2438 A71-32791

Notch effect on stainless steel and alpha brass rods and plates ductility and fracture strength

16 p2591 A71-32947

High strength structural stainless steels with good toughness and little crack sensitivity, noting brittleness due to oxidation, precipitation and carbide network

16 p2597 A71-33916

Aluminum effect on nickel diffusion in iron from stainless and aluminum steels study

16 p2599 A71-34053

Circular cylindrical shell stability under combined axial tensile/compressive loads and torque, verifying theory by experiments on stainless steel shell

17 p2817 A71-34336

Minimum output power required for CW carbon dioxide laser drilling of thin stainless steel sheets in vacuum and air, using cylindrical source model

17 p2750 A71-34369

Tensile properties, plane strain fracture toughness and stress corrosion threshold of high strength precipitation hardening stainless steels

17 p2755 A71-34438

Strength and toughness optimization in high strength stainless steels by austenitizing and removing delta ferrite by isothermal transformation

17 p2756 A71-34491

Mechanical properties of explosively clad plates, considering stainless steel/mild steel and brass/mild steel composites

17 p2757 A71-34663

Chromium stainless steels fine structure, noting quenching and tempering temperatures effects

19 p3076 A71-37118

Stainless steel and Al alloy creep rupture life apparent reduction by frequent beam leveling

19 p3082 A71-38135

Electron microprobe analysis of cavity surface and lip of cosmic dust impact craters in stainless steel plates exposed at 400 km altitude in Gemini S-D10 experiment

20 p3299 A71-39652

Electron beam hearth refined ferritic stainless steel, presenting weldability with gas tungsten arc process

21 p3388 A71-40623

High strength stainless steel dislocation structure and mechanical properties, discussing tempering, tensile strength, precipitation hardening and temperature effects

21 p3402 A71-41088

Stainless steels nitriding in presence of halogen compounds with heat treatment, observing thermodynamic potential shift

21 p3389 A71-41099

Carbon and stainless steels chemical composition effects on diffusion layer structure and fatigue strength after diffusive boriding

21 p3403 A71-41162

Vacuum contactless metallization of carbon steels, stainless steels and nickel alloys, considering Si, Cr and Al coatings

21 p3390 A71-41172

Low temperature aging behavior of maraging stainless steels from electrical resistivity measurements

22 p3562 A71-41948

Reduced oxygen effect on structure and mechanical, technological and corrosive properties of stainless steel melted in open and vacuum furnaces

23 p3690 A71-43279

STALL

U BOUNDARY LAYER SEPARATION

STAMPING

Axisymmetric mixed boundary value problem of thermoelasticity for hot stamp penetration into transversely isotropic half space, deriving contact stresses

01 p0175 A71-11036

Wall thickness change to prescribed value by controlling stress-strain state in sheet stamping operations

24 p3831 A71-45013

STANDARD ATMOSPHERES

U REFERENCE ATMOSPHERES

STANDARD DEVIATION

Standard deviation of atmospheric turbulence velocity components over flat arid terrain

02 p0278 A71-12707

Mean and standard deviation of fraction of total primary cosmic ray energy losses not measurable by ionization spectrometers

15 p2407 A71-31809

STANDARDIZATION

LSI device standardized set for implementing digital computer systems of varying functional complexities

01 p0044 A71-10183

Aerospace systems instrumentation magnetic tape standardization and testing

04 p0597 A71-15298

Standard printing color identification system for DOD mapping, charting and geodesy services standardization

08 p1281 A71-21259

Destructive and nondestructive material testing techniques, discussing equipment design and procedures standardization

13 p2074 A71-28493

Primary and secondary standardization and precision measurement of thermal noise power at various radio frequencies and temperatures

14 p2204 A71-30977

Basic parameters of echo and mirror shadow methods for ultrasonic defectoscopy of welded joints, considering standardization principles

24 p3829 A71-44784

STANDARDS

NT FREQUENCY STANDARDS

NT REFERENCE ATMOSPHERES

Aircraft emergency evacuation illumination standards, considering independent power source, crash survivable installation, operation initiation and exit visibility

01 p0004 A71-10030

Aerospace engine starting systems military and industry specifications and standards, considering cartridge pneumatic, electric, gas turbine, hydraulic and mechanical types

01 p0067 A71-10103

Reference standards for nondestructive ultrasonic inspection for quality control

01 p0091 A71-11424

Variable microwave thermal noise temperature standard generator with output ranging from below 40 to above 370 K

02 p0250 A71-12139

Maintenance free cryogenic noise temperature standard for continuous microwave antenna operation independent of elevation angle

04 p0550 A71-14658

Army rotorcraft hot day standard design hover criterion, developing analytical models for hovering aircraft, cost, climatology and environmental features

04 p0533 A71-15431

Thorium wavelength measurements by interferometry, noting weighted averages as secondary standards of length

04 p0627 A71-15692

MIL-STD-414 sampling procedures and tables for inspection by variables for percent defective

06 p0905 A71-18059

Continuous flow oxygen regulators construction, performance and testing SAE standard, covering automatic, adjustable and preset types

07 p1049 A71-19648

Four-ring stable capacitor for reference standard and application to precision angle measurement

07 p1080 A71-20315

NBS traceable nonferrous conductivity standards for eddy current testing, discussing error analysis, long term drift, grain direction and stratification effects

09 p1469 A71-22710

Dynamic pressure primary standard in terms of mass, time, length and temperature, describing phenomenon selection, error analysis and physical and mathematical models

09 p1448 A71-22769

Standard equipment and procedures for aircraft gas turbine engine exhaust smoke measurement

[ASME PAPER 71-GT-88] 11 p1813 A71-25995

Airport certification and safety inspection procedures and minimum safety standards

[SAE PAPER 710413] 13 p2167 A71-28305

Field strength standards and calibrations for frequencies from audio to 1 GHz range, discussing uncertainties

14 p2205 A71-30980

Performance category III all-weather capability ILS landing equipment standards, discussing high directivity antennas and transmission and control system redundancy techniques for reliability

15 p2445 A71-31909

Producer risk determination and tables for Method 4 maintainability demonstration plan of MIL-STD-471

16 p2583 A71-33303

In situ metal-gas secondary standard assembly for ultrahigh vacuum gage calibration, using repeatable pressure generation from binary erbium-hydrogen system

17 p2744 A71-35140

Center of gravity and moment of inertia measurement system based on standards of comparison principle

[SAE PAPER 880] 17 p2835 A71-35822

British civil aircraft airworthiness requirements, discussing aircraft industry management philosophy ensuring quality standards in design, development, production, inspection and product support

18 p2989 A71-36673

V/STOL airworthiness certification, considering standards developed by FAA in cooperation with industry

[CASI PAPER 72/21] 19 p2997 A71-37607

Bulk and surface hydrogen concentration comparison in NBS hydrogen-in-titanium standards

19 p3080 A71-37718

Double standard for national levels of exposure and biological hazards of microwave radiation, comparing Soviet work to U.S.

19 p3008 A71-38442

Liquid nitrogen cooled microwave low temperature noise standard in WR-51 waveguide

20 p3202 A71-38832

Mica selection quality criteria for capacitors, outlining electrical, physical and optical properties standards

22 p3520 A71-41712

Civil aeromedical standards for aerospace transportation vehicles including occupant selection, vehicle design and operational guidelines

23 p3641 A71-44251

Atomic time standards, discussing Cs 133, hydrogen maser, ammonia maser and rubidium gas cell equipment

24 p3827 A71-44994

STANDING WAVE RATIOS

Impedance measurement and standing wave ratios at microwave frequencies, using directional couplers

03 p0377 A71-13269

X band Schottky barrier diodes RF impedance mismatch and noise factor, calculating dependence on microwave oscillator voltage-standing wave ratio

09 p1421 A71-23723

Electromagnetic compatibility, measuring microwave antennas characteristics, including frequency range, gain, beamwidth, voltage standing wave ratio, impedance and radiation patterns

13 p2039 A71-28877

Nonreflecting dielectric support washers design in coaxial-stripline junctions, calculating VSWR as function of dimensions and frequency

19 p3019 A71-38335

STANDING WAVES

Monograph on nonlinear theory of one dimensional homogeneous collisionless plasma resonance covering charged particle motion in sinusoidal and standing potential waves

01 p0131 A71-10101

Kinetic energy and available potential energy balance in atmospheric stationary disturbances (standing waves), using atmospheric flow statistics

01 p0119 A71-10853

Strain-optical constants determination by ultrasonic technique, using Raman-Nath theory for optical diffraction produced by standing ultrasonic wave

03 p0425 A71-13716

Pontryagin maximum principle applied to optimal control of standing TE wave electric field strength in microwave gyrotron

03 p0386 A71-13813

Bragg diffracted light intensity increase from standing resonating acoustic wave, considering applicability for laser communication multiplexing and demultiplexing

05 p0720 A71-16269

Laser cavity standing wave field electro-optic modulation for uniform population inversion, producing spontaneous single frequency output

05 p0764 A71-17232

Dimensional resonances of standing helicon waves in two layer and multilayer semiconductor structures and crystals with growth inhomogeneities

07 p1176 A71-19273

Biotelemetric contactless recording of animal movements using centimeter band standing waves

09 p1397 A71-22216

German monograph on time dependent gas temperature in decaying plasmas, using frequencies of standing acoustic wave stimulated by pulsed discharges in rarefied gases

13 p2110 A71-29423

Helmholtz, half and full mode standing pressure waves for separated flow induced acoustic resonance in open cavities

15 p2391 A71-32106

Wideband four probe waveguide impedance meters design for standing wave structure measurement

15 p2378 A71-32634

Magnetospheric resonator properties bounded by ionosphere/earth system lines of force, examining nonuniform plane wave generation and standing wave pulsation period

15 p2401 A71-32731

Longitudinal modes in standing wave gas laser with Brewster windows in presence of active level emission capture

17 p2753 A71-34412

Coupling effects between two Permalloy films for different interface treatments, using standing spin wave resonances

18 p2955 A71-36941

Spatially periodic inhibition of gold vapor condensation by intense optical standing wave using Q switched laser radiation

20 p3245 A71-39403

Electron oscillation induced longitudinal standing wave excitation and suppression in beam-plasma system by passing electron beam through axially bounded plasma

20 p3275 A71-39864

Ultrasonic subharmonic waves amplified in standing waves through utilization of propagation medium nonlinearity and cavity reflector induced dispersion

23 p3704 A71-43362

STANDS

U SUPPORTS

STANNIDES

NT NIOBIUM STANNIDES

STANTON NUMBER

Skin friction, Stanton numbers, velocity and temperature profiles in accelerating turbulent boundary layer flows, using Prandtl mixing length

04 p0680 A71-15478

Heat exchange at large Prandtl numbers near porous flat wall with liquid injection, calculating Stanton number

13 p2046 A71-28181

Heat transfer to transpired turbulent boundary layer, reviewing theoretical models and experimental results for friction coefficient and Stanton number

[ASME PAPER 71-HT-44] 19 p3166 A71-38003

STAPHYLOCOCCUS

Pulmonary antibacterial defenses with pure oxygen breathing mice, noting inhibition of early intrapulmonary clearance of *Staphylococcus aureus* and enhanced clearance of *Klebsiella pneumoniae*

22 p3487 A71-42241

STAR CLUSTERS

NT VIRGO STAR CLUSTER

Planetary nebulae and scattered stellar cluster visible coincident distribution near galactic center

02 p0308 A71-12103

Open cluster NGC 7789 blue stragglers data acquisition from image tube spectrograms and four color and H beta photometry, obtaining location along main sequence

02 p0314 A71-12586

Peculiar velocities nonisotropic distribution in stationary differentially rotating stellar system based on Boltzmann equation solution

03 p0484 A71-13222

Spectral classification parameters, discussing spectral-type indicators, luminosity indicators, spectra of clusters and galaxies, abundance, population and low mass objects

04 p0646 A71-15231

White dwarfs, investigating spectral classification clusters, motions and location on H-R diagram

04 p0647 A71-15241

UBV photometry of RR Lyrae variables in metal rich globular cluster NGC 6171

04 p0649 A71-15372

Variable stars GR 181-202 in galactic cluster IC 1848 field examined by Schmidt telescope

04 p0651 A71-15663

NonMarkoffian kinetic theory for hierarchical structure of clusters in expanding universe

06 p0964 A71-17314

Stellar velocities distribution in nonrotating clusters, examining mass dispersion role in evolution

06 p0974 A71-18430

Evolutionary cooling sequences and lifetimes for low mass white dwarfs in Hyades cluster, considering near surface convection in models with hydrogen envelopes

07 p1190 A71-18856

Superassociations in late morphological type galaxies, discussing photometric and colorimetric observations

07 p1192 A71-19284

O-B stars velocity distribution in synthetic association, proposing method for space velocities mean value determination

07 p1192 A71-19289

Large Magellanic Cloud stellar associations system physical properties from object characteristics and spatial distribution

07 p1197 A71-19723

H I and H beta emission, Sco-Cen association stellar members near Sco X-1, discussing X ray heating and ionization

07 p1187 A71-19818

Globular cluster star velocities distribution, examining dynamic evolution models and gravitational effects

08 p1362 A71-21155

Random gravitational encounter effects of passing stars on dynamical evolution of spherically symmetric stellar system, using modified Monte Carlo method

09 p1517 A71-22330

Star group formation theory, proposing hypothesis on toroidal stages in stellar evolution

09 p1524 A71-23183

Milky Way northern portion absorption values obtained from star cluster data

09 p1524 A71-23184

Stellar spatial densities in cluster NGC 6913 area, based on two color photometry and spectral classifications

09 p1524 A71-23185

Diffuse interstellar features in spectrum of reddened star in Cygnus OB2 stellar association, tabulating equivalent widths of H alpha and stellar He I line

10 p1665 A71-23749

Individual M-type red supergiants luminosity, masses and periodicities based on cluster membership and pulsational Q value

10 p1674 A71-24433

Scattered stellar clusters region stars and interstellar matter from photographic magnitudes diagrams and color indices, determining absorption fluctuations by color excess technique

10 p1681 A71-25127

Newtonian gravitational system n body problem infinite time approach, obtaining spatial distribution of star clusters

11 p1819 A71-25208

Interstellar absorption and color excesses in Sco OB-1 from spectral observation and photometry for star cluster and association background

11 p1831 A71-26133

Open star cluster NGC 6819 photoelectric and photographic data, indicating age, color magnitude diagram and main sequence turnoff

11 p1831 A71-26134

Stellar velocity distribution in nonrotating clusters, examining mass dispersion role in evolution

12 p1955 A71-26580

Young cluster NGC 2264 main sequence A and F stars four color and H beta observation, suggesting evidence of circumstellar gas shells

12 p1956 A71-26615

Galactic structure historical approach, discussing stellar astronomy foundations, Milky Way, cluster and spiral position, etc

12 p1958 A71-26772

Early type stars, open clusters, associations and stellar rings space distribution and state of motion 12 p1959 A71-26776

Stellar cluster evolution equations in terms of free particle physics based on Boltzmann equation, describing computerized integrations 12 p1960 A71-26785

Spherically symmetric galactic and star clusters at Hubble expansion, deriving spatial density 12 p1962 A71-26909

K giants, subgiants, M67 and NGC 188 abundances, noting high metallicities 13 p2136 A71-28431

German monograph on membership in open star clusters, covering M67, pseudocluster M39 and stellar brightness and motions 13 p2139 A71-28879

Star and galaxy clusters total kinetic energy content, using line of sight velocity data and astronomical models 14 p2312 A71-30390

Spherical stellar system dynamical evolution model, applying constant point mass technique 14 p2314 A71-30640

Globular star clusters and spherical galaxies stability, proposing rotating gravitating masses spherically symmetrical system model 15 p2482 A71-31331

Secular parallaxes of reference stars by photometric distances and relative proper motions of open clusters at low galactic latitude 15 p2483 A71-31341

Pleiades flare stars photographic magnitude and brightness data, establishing relation between amplitude and duration 15 p2486 A71-32029

Self gravitating time independent disk-like stellar system model, investigating mass and velocity distributions 16 p2630 A71-33054

Young open star cluster NGC 6823 membership based on relative proper motions data and color-magnitude diagram 16 p2631 A71-33180

Photometry and structure of young open cluster NGC 7380, obtaining magnitudes in UVB and positions on Hamburg-Schmidt plates 16 p2632 A71-33321

Ap and Am stars distribution and ages, considering high proportion in Hyades, Sirius, Praesepe and Coma Berenice clusters 16 p2633 A71-33333

M 13 spherical star cluster, determining spatial distribution, center coordinates, radius and dynamic behavior 16 p2634 A71-33428

Book on relativistic astrophysics, Volume 1, Stars and relativity, covering stellar dynamics, astronomical models, cosmic objects evolution and star clusters 16 p2635 A71-33481

Galactic star cluster K 4 and Ba 10 observations with RGU photographic photometry, noting distances and types 18 p2960 A71-35938

Cosmic ray injection by clusters of dense magnetic neutron stars, giving particle number for Galaxy 18 p2957 A71-35962

Stellar evolution, discussing semiconvective regions, mass loss, red giants and supergiants, He flash structures and globular clusters 18 p2967 A71-36999

Planetary nebulae central stars, considering elementary stellar evolution theory, globular cluster stars and ejection mechanism 18 p2968 A71-37031

Globular cluster NGC 6541 UVB photometric investigation, determining distance from sun and galactic plane 19 p3143 A71-38164

Stellar systems existence with positive total energy, using numerical integration of equations of motion for components of Trapezium in Orion 20 p3290 A71-39300

Globular clusters with inhomogeneous composition, deriving partial densities of masses 20 p3291 A71-39318

Supermassive stars observational data and origin likelihood at center of galaxy or star cluster 20 p3292 A71-39421

Spectrophotometric observations of asymptotic giant and red giant branch stars in metal weak globular clusters 21 p3440 A71-40063

Open stellar clusters Tr 14, 15, 16 and eta Carinae Nebula distance determination, using photoelectric and photographic photometry 21 p3441 A71-40064

RR Lyrae variables period-frequency distribution in Oosterhoff types I and II globular clusters, interpreting in terms of pulsation theory 21 p3445 A71-40413

Photographic photometry of M67 to 200-inch telescope limit for main sequence star evolution track 21 p3446 A71-40414

Open star clusters characteristic parameter derivation for boundary potential, radius, stellar mean distance, masses and mean angular velocities based on strip counts 21 p3450 A71-40711

Stellar evolution on horizontal branch and parameters of state of RR Lyrae stars in globular clusters of various ages 21 p3451 A71-40720

Open clusters membership probabilities and frequency distribution function parameters calculation by fitting relative proper motions to model with maximum likelihood procedure 22 p3601 A71-42165

Globular star clusters and spherical galaxies stability, modeling as rotating gravitating masses in spherically symmetrical system 22 p3606 A71-42606

Secular parallaxes of reference stars by photometric distances and relative proper motions of open clusters at low galactic latitude 22 p3606 A71-42616

Globular cluster RR Lyrae horizontal branch stellar models, investigating masses luminosities and compositions 23 p3723 A71-42944

Classification method for unviewed low dispersion stellar spectra, giving table for weak stars in region around NGC 6913 cluster 23 p3772 A71-44308

Stars origin theories, discussing stellar associations, young stars, galaxies instability and cosmology and cosmogony 24 p3875 A71-45198

STAR DISTRIBUTION

Spiral galaxy NGC 6946 photometric observations, examining stellar magnitudes, color indices, associations distribution and distance 01 p0149 A71-10055

Star charts as orientation and navigation aids in manned space flight 01 p0125 A71-10517

Program and auxiliary tables for stellar azimuth determination by observations near elongation 01 p0159 A71-10810

Star origin position in Galaxy, computing meridional galactic orbits for nearby late B types 01 p0161 A71-11385

Automatic instrument for star detection and azimuth derivation, scanning nighttime zenith star field [AIAA PAPER 69-861] 01 p0126 A71-11584

Planetary nebulae and scattered stellar cluster visible coincident distribution near galactic center 02 p0308 A71-12103

Galactic spiral structure model, examining nonlinear stellar density waves in plasma cylinder 03 p0484 A71-13205

Clock corrections determinations by stars pairs situated symmetrically around zenith, obtaining formulas by various methods 03 p0484 A71-13219

Proper motions of stars for distance scale of universe using position, relative and fixed reference methods 04 p0646 A71-15228

Morgan two dimensional stellar spectral system with luminosity classes, comparing to Harvard scheme 04 p0646 A71-15230

Resonance phenomena in spiral galaxies, determining stellar orbits, potential and distribution functions 04 p0655 A71-15725

Pulsar number-period distribution, using oblique rotator model under electromagnetic and gravitational torque effects 05 p0804 A71-16106

Visible brightness of Milky Way for various galactic structure models, discussing star and dust distribution effects 06 p0975 A71-18444

O-B stars velocity distribution in synthetic association, proposing method for space velocities mean value determination 07 p1192 A71-19289

Pulkovo astronomical expedition in Chile, concerning faint star coordinates and equipment for telescopic, electrophotometric and spectral observations 07 p1083 A71-19326

Latitude observation program at Pulkovo from 1968 through 1987 with zenith telescope, noting faint star declination and motion errors in General Catalog 07 p1194 A71-19328

Large Magellanic Cloud stellar associations system physical properties from object characteristics and spatial distribution 07 p1197 A71-19723

Stellar spatial densities in cluster NGC 6913 area, based on two color photometry and spectral classifications 09 p1524 A71-23185

Lunar Mapping Camera ground support operations, describing pre and post mission assistance, stellar field calibration and data reduction 09 p1429 A71-23221

Star orbit computation in galactic potential fields, using Hamming modified predictor corrector scheme for numerical integration 10 p1678 A71-24927

Newtonian gravitational system n body problem in infinite time approach, obtaining spatial distribution of star clusters 11 p1819 A71-25208

RR Lyrae type variable star statistical population indices evaluation based on space and radial velocities and position 11 p1820 A71-25247

Galaxy M33 density wave velocity and detection, discussing star distribution, H II regions red and blue supergiant and hot stars 11 p1821 A71-25540

Visible brightness of Milky Way for various galactic structure models, discussing star and dust distribution effects 12 p1955 A71-26594

Galactic structure historical approach, discussing stellar astronomy foundations, Milky Way, cluster and spiral position, etc 12 p1958 A71-26772

Early type stars, open clusters, associations and stellar rings space distribution and state of motion 12 p1959 A71-26776

C, gM and S spectral type stars, considering distribution, absolute magnitudes and intrinsic colors 12 p1959 A71-26777

Stellar orbits for nearby stars, examining short arc statistics and galactic field models 12 p1959 A71-26781

White dwarf discovery method and properties, discussing color, spectra, parallaxes, luminosities, masses, red shifts, cluster and frequency distribution 14 p2316 A71-31005

White dwarfs from Catalog of Nearby Stars, indicating radial and tangential velocities, proper motions, positions luminosity and UVB spectra 14 p2317 A71-31009

Scorpio-Centaurus association and Gould belt proper motion, discussing convergent point in FK4 catalog with maximum likelihood method 15 p2483 A71-31470

Central Galactic region star distribution, considering RR Lyrae and metal-rich stars 15 p2495 A71-32704

Subdwarf star data, reviewing spectra, kinematics, nucleosynthesis, interiors, atmospheres, angular momentum, formation, abundances and distribution 16 p2631 A71-33126

Stellar ring in Aquila, reducing proper motions of stars in all catalogs to General Catalog system and to Brosche FK 4 system 16 p2632 A71-33327

Ap and Am stars distribution and ages, considering high proportion in Hyades, Sirius, Praesepe and Coma Berenice clusters 16 p2633 A71-33333

M 13 spherical star cluster, determining spatial distribution, center coordinates, radius and dynamic behavior 16 p2634 A71-33428

Lunar libration detection by photographing double exposure of stellar field and moon 16 p2636 A71-33503

Automatic precise centering on photographic plate star image by movement across scanning slits for orthogonal coordinates and processing in on-line computer 17 p2742 A71-34999

Star counting device, showing stellar fields contribution to total brightness 17 p2742 A71-35004

Automatic data reduction system for TV images of star fields acquired from OAO 17 p2743 A71-35009

Symmetrically distributed nebulae around Wolf-Rayet stars, detailing Ngc 7635 and associated star BD plus 60 deg 2522 17 p2806 A71-35410

Stellar calibration of lunar mapping camera for precision metric photography and time correlated postflight attitude determination 18 p2925 A71-36916

Stellar composition analysis of Small and Large Magellanic clouds using Hertzprung-Russell, color magnitude and two color diagrams 20 p3301 A71-39823

Pulsars luminosity, z-distance and period distribution in Galaxy, comparing supernova remnants 20 p3303 A71-39933

Thin-shelled ensemble of noncolliding stars surrounding black hole, calculating spectral flux density and brightness 21 p3446 A71-40420

Space distribution of OB stars from revised Victoria H gamma spectrophotometric magnitudes by MK spectral classification 21 p3448 A71-40594

Stellar population data, discussing star distribution and galactic evolution 22 p3599 A71-41931

STAR FIELDS

Optical orientation determination and star pattern recognition for Skylab in solar inertial attitude by digital and hybrid simulations
[AAS PAPER 71-397] 23 p3732 A71-43065

STAR FIELDS
U STAR DISTRIBUTION
STAR TRACKERS
Automatic instrument for star detection and azimuth derivation, scanning nighttime zenith star field
[AIAA PAPER 69-861] 01 p0126 A71-11584
Variance estimates and error expectations for satellite coordinates and velocity vectors from star altitude measurements
02 p0278 A71-11903
Skylark sounding rocket attitude control by three axis star pointing system, using strapdown gyro and plus 5 magnitude stellar sensor
[AIAA PAPER 70-1401] 03 p0455 A71-13682
Stellar Tracking Rocket Attitude Positioning System /STRAP/ for sounding rocket payloads three-axis orientation control with accuracy
[AIAA PAPER 70-1402] 03 p0455 A71-13683
Camera focal distance, optical center position and distortion determination of Zeiss Astrographic objective by moving star pairs method
03 p0428 A71-13941
Stellar photoelectric servo guide with photon counting in mismatch sensor for telescope positioning
04 p0590 A71-14845
Automatic telescope instrumentation, considering polychromator, photometer and photoelectric star finders
04 p0597 A71-15256
Automated radar calibration system using star tracker and computerized control
04 p0554 A71-15318
Cassiopee attitude control system for sounding rockets using stellar and inertial sensors for orientation and pointing
[AIAA PAPER 70-1404] 05 p0780 A71-16416
Variance estimates and error expectations for satellite coordinates and velocity vectors from star altitude measurements
13 p2098 A71-28190
Coordinate measurement accuracy for star and satellite photographic observation using Zeiss Ascorecord
14 p2250 A71-31121
Optical telescopes automatic electronic control by positioning mechanical axis to specified coordinates and tracking guide star
17 p2740 A71-34983
Automatic star follower for camera by optically splitting stellar image and measuring radial displacement by comparing signals
17 p2740 A71-34987
Five-gate automatic acquisition star and satellite TV tracker with video signal from vidicon or image orthicon, using line-to-line correlation for SNR improvement
18 p2882 A71-36904
Star sensor telescope, employing digitally coded silicon photocell detector for precise optical image location
18 p2925 A71-36910
Lightweight precision gimbal design for spaceborne star tracker with arc-second accuracy for stellar updated inertial system independent of spacecraft stabilization
[AIAA PAPER 71-963] 19 p3062 A71-37204
Gyro and star tracker precision attitude determination system, assessing computational and other error effects on system performance
[AIAA PAPER 71-964] 19 p2996 A71-37205
Electro-optic direction sensor, discussing single axis star tracking application
[AIAA PAPER 71-966] 19 p3100 A71-37207
Star comparator automatic azimuth system using long evacuated tunnel transfer to underground inertial guidance laboratory
[AIAA PAPER 71-925] 19 p3102 A71-38328
Tridant star sensor, noting superior photometric and geometrical sensitivities
20 p3239 A71-39535
Multivariate statistical analysis of parameters measuring reference stars effects on parallax and error estimates
21 p3444 A71-40195

STAR TRACKING
U STAR TRACKERS
STARFIGHTER AIRCRAFT
U F-104 AIRCRAFT
STAR EFFECT
Electrostatic vibrations from turbulent plasma heating on basis of Stark broadening of hydrogen spectral lines, obtaining electric field strength
01 p0131 A71-10069
Neutral Ar and Ne resonance lines Stark broadening constant from Stark width-oscillator strength product
04 p0630 A71-15651
Stark induced quantum beats in H Ly alpha emission, using beam foil excited hydrogen
05 p0785 A71-16701

Stark broadening of hydrogen lines in plasma, noting role of amplitude modulation and nonadiabaticity
06 p0930 A71-17406

H lines Stark broadening in turbulent plasma, considering Langmuir vibrations nonadiabatic action and energy density
07 p1168 A71-19277

Turbulent plasmas nonequilibrium electric fields determination from hydrogen spectral lines Stark broadening
08 p1341 A71-21790

H beta, H gamma and H delta Stark broadened profiles, investigating perturbing electron-radiating atom inelastic collisions, Gaunt factors and half widths
09 p1496 A71-22413

Electrostatic vibrations from turbulent plasma heating on basis of Stark broadening of hydrogen spectral lines, obtaining electric field strength
09 p1504 A71-23264

Precision Stark spectroscopy of methane by nonlinear laser absorption, observing Lamb-dip spectra by tuning stable single mode laser
13 p2079 A71-28950

Interstellar H II regions high quantum number recombination line measurements, indicating Stark broadening
13 p2143 A71-29268

H lines Stark broadening in turbulent plasma, considering Langmuir vibrations nonadiabatic action and energy density
14 p2280 A71-30171

Stark effect saturable absorber modulation of passively Q switched carbon dioxide laser, using difluoroethane, difluoroethylene, methyl fluoroform, trichloroethylene and vinyl chloride
16 p2586 A71-33147

Collisionless turbulent plasmas nonequilibrium electric fields determination from hydrogen spectral lines Stark broadening
16 p2619 A71-33549

Stark widening in hydrogen Lyman alpha line, considering atomic state operator of evolution thermal mean effects
16 p2614 A71-34061

Solar Fraunhofer line wavelength shifts at disk center and at limb, evaluating Stark broadening contribution
18 p2962 A71-36106

Carbon dioxide laser high efficiency driven Q switching, using Stark effect in molecular gases
18 p2933 A71-37015

Stark contours of hydrogen spectral lines in turbulent plasma with high noise level due to HF Langmuir oscillations
19 p3110 A71-37388

Resonance broadening measurements of alkali metals, giving relation between optically thick and thin full widths for Lorentzian and Gaussian line shapes
19 p3105 A71-38721

He II alpha lines scanned by electromagnetically driven T tube, comparing with Stark broadening theory
20 p3272 A71-39576

Neutral atoms and ions collision damping constants estimation for spectrum synthesis, using approximate formula based on Stark broadening effect
21 p3442 A71-40160

Coalescence /collapse/ of overlapping spectral lines due to nonadiabatic broadening of Stark structure of hydrogen and helium lines in discharge plasma
23 p3707 A71-43407

Neon red lines Stark widths and shifts in function of electron and neutral Ne densities in shock tube
23 p3707 A71-43585

Charged particles effect on plasma negative ions, examining Stark effect in energy level
24 p3857 A71-45114

STARS
NT A STARS
NT B STARS
NT BINARY STARS
NT CEPHEID VARIABLES
NT COMPANION STARS
NT DWARF STARS
NT EARLY STARS
NT ECLIPSING BINARY STARS
NT EXTARs
NT GIANT STARS
NT HOT STARS
NT INFRARED STARS
NT MAGNETIC STARS
NT MAIN SEQUENCE STARS
NT NEUTRON STARS
NT NOVAE
NT O STARS
NT PROTOSTARS
NT PULSARS
NT RADIO STARS
NT SUN
NT SUPERGIANT STARS
NT SUPERNOVAE
NT T TAURI STARS
NT VARIABLE STARS
NT WHITE DWARF STARS

NT ZETA AURIGAE STAR

Metal poor stars eccentric galactic orbits, considering interstellar medium accretion effect
02 p0312 A71-12468

Star image vibration trail amplitude, determining rms deviation with automatic system
04 p0590 A71-14843

Soviet book on stellar physics covering evolution, internal structure, mass, luminosity, radius, density, temperature, bolometric magnitude, energy transfer, etc
04 p0645 A71-15225

Papers on stellar astronomy, Volume 1, covering observation techniques, spectral classification, stellar atmospheres and line formation and stellar rotation
04 p0645 A71-15226

Papers on stellar astronomy, Volume 2, covering angular momentum, binaries, white dwarfs, magnetic stars, UV and IR astronomy and theoretical models
04 p0647 A71-15239

Soviet papers on sun and stars covering atmospheric structure and physics, nonstationary stars, evolution and galaxies
09 p1524 A71-23182

Soviet book on stars, galaxies and metagalaxy covering stellar luminosities, spectra, novae and supernovae
10 p1668 A71-24015

M stars mass loss, determining dust shells radii and densities with IR observations of circumstellar emission
11 p1818 A71-25204

C, gM and S spectral type stars, considering distribution, absolute magnitudes and intrinsic colors
12 p1959 A71-26777

Astronomical methods for determination of distances to planets, stars and galaxies, considering human distance perception
12 p1962 A71-26955

Spectral analysis methods for detection of water on celestial bodies, considering possible abundance on planets and stars
12 p1962 A71-26956

Visual detection of stars in spacecraft environment, considering window cleanliness and antireflection coating effect on light scattering
18 p2864 A71-36278

Physical constraints on universe topology near collapsed-ordinary stars interaction in general relativity theory
19 p3105 A71-38583

Astronomical telescopes stellar image motion dependence on zenith distance, determining RMS value of jitter
23 p3771 A71-44259

STARTERS
NT ENGINE STARTERS
Determinate phases formation mechanisms in unbalanced parametric oscillators, considering periodic shunting and bias modulation methods for oscillator starting
05 p0727 A71-16004

Unsteady processes in starting period of supersonic Ludwig tube, initiating flow by quick opening diaphragm downstream of nozzle
05 p0734 A71-16563

Determinate phases formation mechanisms in unbalanced parametric oscillators, considering periodic shunting and bias modulation methods for oscillator starting
22 p3524 A71-42753

Operational characteristics of starting igniters for gas turbine engine combustion chambers
24 p3864 A71-45003

STARTING
Liquid bipropellant rocket engine ignition and start transient calculation for hypergolic and externally ignited starts at sea level and high altitude pressures
[WSS/CI PAPER 70-23] 06 p0943 A71-17655

Startup testing of SNAP 8 power conversion system coupled with nuclear reactor simulator
15 p2447 A71-32217

STATE EQUATIONS
U EQUATIONS OF STATE
STATE ESTIMATION
U ORBITAL POSITION ESTIMATION
STATE VECTORS
Control system problems with state space constraints, deriving sufficient conditions for optimality
04 p0561 A71-15868

Noninferior set for static optimization of systems with vector valued objective function using dual linear inequality
06 p0878 A71-17333

Model theory identification application to aeronautical systems, discussing transfer function representation, state variable and direct methods
10 p1587 A71-24748

Dynamic optimization with constrained state and control vectors, solving problems by hybrid method with partial derivatives
11 p1735 A71-25842

Equivalence relationship between state space defined parameter and difference order of time-variable scalar differential equation
[DFVLR-SONDDR-79] 12 p1922 A71-27006

Optimal output regulator for linear time invariant systems with reference vector and quadratic cost functional 12 p1893 A71-27430

V/STOL aircraft flight path and attitude controls in turbulence, discussing design based on state variable methods of control theory 14 p2173 A71-29776

Optimal stabilization of self adjusting control system for nonstationary plant in limited time by linear model using Lagrange multipliers 15 p2382 A71-32622

Multivariable control system state variable feedback decoupling theory generalization to include output subset, using matrices 17 p2718 A71-34736

Linear dynamic systems state estimation, using empirical Bayes decision theory to develop filter set 17 p2825 A71-34897

Interceptor aircraft optimal nonlinear command guidance scheme for reduction of airborne computation load with forward prediction of interceptor and target state vectors AIAA PAPER 71-916 19 p3096 A71-37166

Minimum order state vector reconstruction linear filters for constant plants optimal control, applying to aircraft flight multiple control-point problem 23 p3657 A71-44077

Flight test measurements for improved estimates of aircraft states and aerodynamic parameters, using relinearized Kalman filter 23 p3629 A71-44089

Generalized matrix inverses application to estimation of state vector in dynamic control system, determining covariance matrix of estimator 23 p3700 A71-44117

Modified perturbation method for solving optimal control boundary value problems with state variable inequality constraints, noting application to reentry trajectories 24 p3876 A71-44608

STATIC AERODYNAMIC CHARACTERISTICS

Static aerodynamic data correlation for high subsonic speed transport aircraft model in transonic wind tunnels, including relative buoyancy and turbulence effects AIAA PAPER 71-2911 09 p1429 A71-23423

STATIC DEFORMATION

Static computations of thin walled shells and honeycombs, examining variational, matrix, finite element, initial function, small parameter and plate bending methods 06 p0999 A71-17867

Nonlinear statics of thin walled cylindrical and spherical shells, including buckling under various end conditions 06 p0999 A71-17869

Strain continuity equations in statics using equivalent integrodifferential form 07 p1218 A71-20465

Rotating configurations in general relativity, considering infinitesimal quasi-static deformations 11 p1834 A71-26407

Statistical scatter approximation of creep characteristics using relation to accumulated static damage and time to failure 12 p1979 A71-27352

Thermal flutter of satellite storable tubular extendible members, determining static flexural and torsional vibrations due to solar radiation 12 p1984 A71-27736

Static ductile deformation in quartz, olivine, pyroxenes and plagioclase, noting plastic deformation and recovery 19 p3050 A71-37664

STATIC DISCHARGERS

Lightning current transfer tests of p-static discharger for aircraft installations 07 p1020 A71-19935

STATIC ELECTRICITY

Lightning and static electricity - Conference, San Diego, December 1970 07 p1019 A71-19926

Statistical information on lightning and static hazards relative to airworthiness 07 p1020 A71-19929

Lightning and static electricity effects on helicopter design, considering rotor protection, cargo hook operation and passive dischargers for radio interference reduction 07 p1021 A71-19938

Lightning and static electricity hazards at Kennedy Space Center, discussing meteorological aspects 07 p1084 A71-19948

Weakly turbulent plasmas static electric conductivity derivation from kinetic equation for linear response to one-particle distribution function 09 p1503 A71-22861

STATIC FRICTION

Static friction influence on readings of gyrotachometer with pulse width modulated torque sensor current 07 p1108 A71-19306

Static friction in steel-polymer couples under vacuum, considering temperature, contact time, normal load and physicochemical properties effects 09 p1454 A71-22818

Force equations for static and dynamic friction under external forced vibration, determining mean values from mechanical model 19 p3068 A71-37346

Gas bearing ground clearance effects on pivoted pad resonance, pitching vibration mode, static journal displacement and friction 22 p3551 A71-41661

Contactless oscillography of static and kinetic moments of friction in ball bearings in aggressive gas media, discussing experimental assembly design 22 p3529 A71-42489

STATIC INVERTERS

Satellite static inverter for voltage wave form synthesis by time optimal response closed loop technique, providing input insensitive AC output 02 p0190 A71-11675

Inner FET and FET static and dynamic inverters in digital IC, discussing switching characteristics, gates, memory cells, etc 02 p0228 A71-11812

Aircraft variable frequency electrical generating systems, discussing weight and size reduction in motors and static inverters by gate controlled switches 02 p0197 A71-12908

Single phase static inverter module with voltage waveform synthesis by time optimal response /bang-bang/ closed loop technique 04 p0535 A71-15287

STATIC LOADS

Welded joints ductile and brittle static tensile strength at low temperatures, allowing for mechanical inhomogeneities 01 p0085 A71-10085

Static tension effect on damping capacity of drawn rods under flexural vibrations, considering materials with strong magneto-mechanical hysteresis 03 p0503 A71-13413

Metallic components strain localization and concentration factors under high pressures or temperatures involving plastic strain, noting static and cyclic load effects 04 p0666 A71-14882

Circular arches static equilibrium path and dynamic response due to concentrated static and step loading using energy approach 04 p0668 A71-15184

Closed cylindrical shells behavior under static loads, determining stability 06 p0988 A71-17775

Thermal contact resistance as function of time during static load 07 p1116 A71-18917

Free vibration of spherical sandwich shell under axisymmetric static and dynamic loading 07 p1212 A71-19590

First passage time for snap-through of shallow cylindrical shell subject to stationary random loading, considering numerical solution by Pontryagin-Vitt equation 08 p1369 A71-20809

Isotropic material structures under static external loads, considering stress rupture strength models 08 p1371 A71-21608

Thermal fatigue testing of materials under static load with allowance for creep 09 p1426 A71-22497

Static wind loading on large radar antenna structures from wind tunnel tests, considering forces and moments reduction by perforated reflectors and shallow curved cover 10 p1591 A71-23757

Metal-metal adhesive bonds temperature effects, long term static loads, dynamic strength and aging behavior 10 p1618 A71-24684

Axisymmetric deformation of thin elastic shell of revolution under combined effect of static surface load and nonuniform heating 12 p1979 A71-27359

Computerized minimum weight design of elastic redundant trusses under multiple static loads, using algorithms for generating upper and lower bounds for configuration AIAA PAPER 71-3621 12 p1980 A71-27409

Gas turbine blades thermal fatigue test and analysis, investigating static tensile loading effects on heat resistance under thermal cycling 13 p2149 A71-28124

Machine for corrosion testing materials under various static and dynamic axial tension, torsion and bending loads 13 p2045 A71-29374

Plates analysis under static and dynamic loads based on finite difference, lattice analogs, mathematically consistent lumped parameters and finite element models 15 p2503 A71-31438

Welded joints ductile and brittle static tensile strength at low temperatures, allowing for mechanical inhomogeneities 16 p2584 A71-33641

Automatic testing machine for materials corrosive strength under varying and combined complex static or dynamic stresses 16 p2580 A71-33687

Recrystallized and unrecrystallized deformed semicrystalline Al base alloy under cyclic and static loads, investigating macrofracture kinetics 16 p2594 A71-33713

Static tension effect on damping capacity of stretched rods under flexural vibrations, considering materials with strong magneto-mechanical hysteresis 17 p2826 A71-35020

Aircraft structural panels under cyclic static loads, examining fatigue life with probability theory, statistics and regression analysis 17 p2829 A71-35312

Finite element analysis codes for complex two layered linear elastic shells of revolution under static and dynamic loads 17 p2831 A71-35351

Aircraft weighing in place during maintenance operations, describing load cell equipped jacks design for time saving weight determination [SAWE PAPER 898] 17 p2724 A71-35814

Al-Zn-Mg alloy welded joints under repeated static loads, determining shape, filler wire composition and aging effects on fatigue strength 19 p3083 A71-38425

Cylindrical shell under opposing concentrated outwardly directed radial loads applied to reinforcing ring, presenting stress distributions and displacements 21 p3468 A71-40971

Complex structural systems response characteristics under steady state sinusoidal, transients and random loadings, developing hybrid elastodynamic equations 21 p3470 A71-41011

Hemispherical and spherical pressurized gas bearing design with narrow circumferential feed slot as laminar flow restrictors, predicting static load performance 22 p3551 A71-41667

Bar forces in statically determinate planar truss due to arbitrary loads at joints, describing computer program for sequential solution 22 p3517 A71-41869

Equations of elastic wave propagation in isotropic materials in presence of static surface stresses and body forces 23 p3775 A71-43205

Fatigue test equipment for 293-233 K and 50-100 ton static or 25-50 ton cyclic loads, using Freon 22 as coolant 23 p3661 A71-44234

Closed profile thin walled curvilinear rods, deriving static and strain integrals with Hookes law 24 p3877 A71-44410

STATIC PRESSURE

NT HYDROSTATIC PRESSURE

Pseudoshock mechanism model, explaining supersonic diffuser main flow static pressure increase and decrease alternately and wall increase monotonously 02 p0239 A71-11870

Noncircular cross section static pressure probes theoretically insensitive to pitch, yaw and Mach number, testing performance 03 p0341 A71-13730

Clamped circular plates axisymmetric nonlinear resonant frequency response under uniform static pressure 04 p0668 A71-15187

Started supersonic axisymmetric parallel diffuser, examining wall static pressure and heat transfer 04 p0528 A71-15489

Supersonic air flow pattern over rectangular indentations on plane and axisymmetric surfaces, examining static pressure and adiabatic temperature distributions 07 p1014 A71-19744

Static pressure measurements near oblique shock waves using short probe, evaluating readings accuracy 07 p1090 A71-19911

Large model fluid proportional amplifier, investigating optimum static and dynamic pressure gain by methodological and transmission line approach 07 p1025 A71-20558

Gas turbine rotor axial load determination, using static pressure distribution 08 p1348 A71-21268

Static pressure port errors in hypersonic turbulent flow, using approximate shear layer momentum balance for pressure increase derivation [AIAA PAPER 71-270] 08 p1228 A71-21996

Static pressure measuring instruments operating principles and characteristics 09 p1448 A71-22768

Solar wind static and dynamic pressures on earth magnetosphere, using geomagnetic parameters 09 p1514 A71-23152

STATIC STABILITY

Turbulent incompressible air flow in-stream static pressure fluctuations measurement, describing bleed type pressure transducer theory, design and operational characteristics

10 p1611 A71-24516

Static pressure recovery and core region velocity profile in rectangular wall diffusers with uniform shear flow

[ASME PAPER 71-GT-5] 11 p1751 A71-25951
Flutter of buckled plate exposed to static pressure differential and streamwise applied in-plane load, comparing experimental results with stability boundary calculations

12 p1983 A71-27584

Liquid-vapor interactions in constant area steam-water condensing ejector mixing section, measuring axial static and stagnation pressure profiles

[ASME PAPER 71-FB-21] 13 p2052 A71-29459
Oxygen metabolic rate in isolated canine lungs at various static inflation levels and cyclic ventilation, examining mechanical deformation effects

17 p2683 A71-35145

Photographic study of colliding underexpanded and normally expanded supersonic jets in two-wind-tunnel assembly with atmospheric static working pressure

18 p2903 A71-36118

High enthalpy plasma jet wind tunnels, considering arc heaters and simulation range extension to higher adiabatic static pressures to avoid nonequilibrium expansion in nozzle

18 p2898 A71-36413

Pitot and static pressure measurement in low density hypersonic flows, considering thermal transpiration, gas nonequilibrium near measurement cavity and nature of inlet geometry

18 p2921 A71-36415

Static and transient pressure measurement in turbulent boundary layers, using transducer with piezoelectric sensing element

20 p3233 A71-38822

STATIC STABILITY

NT DIMENSIONAL STABILITY

NT SHELL STABILITY

NT STRUCTURAL STABILITY

Ball bearings with irregular surfaces, analyzing static equilibrium conditions

01 p0088 A71-10635

Critical static strength of Duralumin under cyclic impact loads, analyzing statistically load distribution function applicability

01 p1013 A71-11240

Soviet book on flight vehicle instruments and sensors static and dynamic characteristics, instrument errors and reliability

02 p0254 A71-12720

Sounding rocket vehicle static stability reduction due to aeroelastic bending, using flight characteristics and wind tunnel test data for computerized analysis

03 p0499 A71-13681

[AIAA PAPER 70-1400] Circular arches static equilibrium path and dynamic response due to concentrated static and step loading using energy approach

04 p0668 A71-15184

Magnetohydrostatic stellar interior instability, noting magnetic buoyancy

05 p0802 A71-15938

Jet interference effects on aircraft static stability with ejector afterbody, noting wind tunnel methods of drag minimization and measurement

05 p0696 A71-15953

[DGLR-70-048] Long time static strength, durability and thermal stability relations determined for heat resistant alloys at operational temperatures

08 p1306 A71-21112

Aerodynamic characteristics of slender body of revolution traveling in long tube with circular cross section, deriving static and dynamic stability derivatives formulas

11 p1702 A71-25477

Monograph on turbine blade fir tree roots, calculating stress-strain state of long term static strength under elastic and elastoplastic deformation and unsteady creep

11 p1852 A71-26400

Metallic materials static to dynamic transition in creep noting temperature and purity effects

13 p2084 A71-28110

Static problems of shells of revolution under local loads, solving by stable numerical process

13 p2152 A71-28276

Gravitohydrodynamic instability of static and constraining composite systems composed of infinitely conducting fluids, using normal mode analysis

13 p2108 A71-29164

Free flight static and dynamic stability tests on lightweight cone shaped models in longshot tunnel at hypersonic speeds, using spark recording

16 p2519 A71-32879

Static stability criterion dynamic extension for nonlinear continua under conservative loads, using Liapunov functions

16 p2607 A71-32980

Cosserat surface static stability, considering construction of direct theories of thin shells

16 p2649 A71-33001

Probabilistic approach to prolonged lifetime design and static strength of structures of monocoque and multi spar wings, using fatigue characteristics of individual elements

16 p2657 A71-33604

Control configured vehicle design longitudinal requirements due to application of relaxed static stability and maneuver load control

[AIAA PAPER 71-786] 16 p2525 A71-34016

Thin elastic shallow cylindrical panel in steady conducting supersonic gas flow, detailing magnetic field effects on static and dynamic stability and flutter

17 p2816 A71-34326

Nonlinear elastic incompressible bodies with small deformations, obtaining three dimensional static and dynamic stability variational equation

17 p2816 A71-34328

Static and dynamic stability characteristics of X-15 aircraft, lifting body and trapezoidal and delta wing reentry body

18 p2971 A71-36434

Atmospheric structure near large amplitude Kelvin-Helmholtz billows in upper troposphere, deriving static stability, vertical wind shear and Richardson number

19 p3089 A71-37498

STATIC TESTS

Apollo integrated shell static and dynamic testing, describing data acquisition system techniques

01 p0067 A71-10863

Static and dynamic testing of fluidic elements as function of geometrical and operating parameters

03 p0355 A71-14296

Whisker composites mechanical properties analysis, discussing stiffness and strength under static loads, elastic moduli, stress analysis, statistical tensile failure model, etc

04 p0667 A71-14947

Acoustic emission monitoring system for real time detection of crack initiation and propagation in complex structure during static and fatigue tests

06 p0906 A71-18461

Plane discrete fluidic switching element external static characteristics tests in relay and trigger modes

07 p1023 A71-19362

Digital active fluid amplifiers static and dynamic behavior, defining complex parameters for system engineering

07 p1026 A71-20564

F-111 airframe static test instrumentation, describing computerized processing of simultaneous inputs from 400 channels of tape recorded strain, load and deflection data

09 p1444 A71-22717

Engine inlet noise prediction from static test and flyover data as function of time at various observer locations, examining suppression effects on total spectra

[SAE PAPER 710386] 10 p1659 A71-24250

Yak 40 aircraft flight test program, discussing airworthiness requirements, static structural, vibration and wind tunnel tests

14 p2174 A71-29911

Dual Flex nozzle concept, discussing design equations derivation, cold flow testing, fabrication and static tests

14 p2296 A71-30843

Diffusely reflecting in-plane surface displacement measurement by holographic interferometry, comparing static and dynamic methods for accuracy

15 p2403 A71-31265

Cast ZrC hot hardness measurement by static tests at high temperatures, comparing with hot-pressed samples

15 p2431 A71-32161

Elastic static and dynamic physicochemical characteristics of resin type amorphous materials under pulsed loads, using electromagnetic excitation of torsional vibrations

16 p2659 A71-33996

Soviet monograph on plasticity and strength of solid bodies at low temperatures covering solidifying gases, static tests, dynamic properties and creep

17 p2724 A71-35186

Metal-reinforced glass plastic composite conical shell with positive Gaussian curvature, estimating reliability and stability based on static tests

17 p2830 A71-35316

Thermal ground testing of Concorde and Veras, considering static and fatigue testing in heat environment

18 p2899 A71-36464

Static characteristics and free vibration of doubly curved honeycomb sandwich plates, using finite element method

21 p3462 A71-40534

Nonlinear static structural mechanical problems solution, using self correcting initial value formulations

21 p3467 A71-40959

One dimensional structure failure calculation, using mathematical programming static method for load limit approximation

22 p3613 A71-41430

High temperature gas turbine engines rotor blades cooling, deriving generalized dimensionless relations for heat transfer data extension from static tests to operational conditions

23 p3718 A71-44066

STATIC THRUST

Static thrust loss of circular cylinder due to sink effects of turbulent jet discharging along surface line

21 p3317 A71-40012

STATICS

NT ELECTROSTATICS

NT HYDROSTATICS

NT MAGNETOHYDROSTATICS

Reversibility/irreversibility definition application to thermostatics, expressing work by Pfaffian form

15 p2513 A71-31922

German monograph on orthotropic plate equations derivation by kinematics and statics in general coordinates and elasticity relation

15 p2509 A71-32304

Three dimensional solution for statics and dynamics of homogeneous plates, laminates and orthotropic materials in series form, noting Mindlin analysis

21 p3456 A71-40262

Static, kinematic and uniqueness theorems of incremental collapse of frames extended to variable repeated loading

22 p3619 A71-42593

STATIONARY ORBITS

Sudden impulses in geomagnetic field, discussing synchronous equatorial orbit-satellite magnetometer observations

03 p0421 A71-14537

Stationary satellite stationkeeping, considering triaxiality and graphical technique for corrections for luni-solar perturbations and solar pressure

04 p0649 A71-15326

CdS solar cells performance under simulated synchronous orbit conditions, describing test equipment

05 p0702 A71-16081

Heavy solid body motion about stationary point for connected angular velocity vector terminus and trajectory in fixed space

08 p1336 A71-21869

High energy three stage booster system for geostationary orbiter, discussing interstage propellant transfer, apogee impulse system and mission rated payload modular configurations

11 p1838 A71-25574

European geostationary telecommunication satellite stabilization using ion thrusters

16 p2623 A71-32851

Elliptical and circular orbit satellite injection capabilities of Europa 2 launch vehicle, considering geostationary orbit and launcher performance

16 p2645 A71-33364

Heavy solid body motion about stationary point for angular velocity vector extremity moving in fixed and body-connected coordinate systems

20 p3270 A71-39368

STATIONKEEPING

Navigation, inertial guidance and position keeping terms definitions

02 p0280 A71-12897

Pulsed plasma thruster system as secondary propulsion unit for spacecraft attitude, station and trajectory control

04 p0638 A71-15325

Stationary satellite stationkeeping, considering triaxiality and graphical technique for corrections for luni-solar perturbations and solar pressure

04 p0649 A71-15326

Solar radiation pressure acceleration effects on flat satellite in earth synchronous orbit, examining orbital shift and counteracting thrust velocity applications

10 p1671 A71-24333

Communication satellites electric propulsion economic tradeoff studies, considering propellant requirements for north-south stationkeeping, and near-synchronous orbit maneuvers

14 p2292 A71-30746

Satellite communications use of geostationary orbit, considering ground station antennas radiation patterns, signal processing, stationkeeping, etc

17 p2696 A71-34234

ESRO activity in low thrust electric propulsion systems development for attitude stabilization and stationkeeping, using colloid and field emission thruster concepts

[DGLR-71-035] 17 p2794 A71-35541

Dynamic positioning stationkeeping and stability criteria for formation flight systems extended to helicopter and V/STOL transports

18 p2849 A71-35923

STATIONS

NT DEEP SPACE INSTRUMENTATION

NT FACILITY

NT BOSS

NT GLOBAL TRACKING NETWORK

NT GROUND STATIONS

NT ORBITAL SPACE STATIONS

NT ORBITAL WORKSHOPS

NT SPACE DETECTION AND TRACKING

SYSTEM

NT SPACE STATIONS
NT STADAN [SATELLITE TRACKING NETWORK]
NT TRACKING STATIONS
NT WEATHER STATIONS
STATISTICAL ANALYSIS
NT AMPLITUDE DISTRIBUTION ANALYSIS
NT CORRELATION COEFFICIENTS
NT FACTOR ANALYSIS
NT MAXWELL-BOLTZMANN DENSITY FUNCTION
NT MULTIVARIATE STATISTICAL ANALYSIS
NT NONPARAMETRIC STATISTICS
NT NORMAL DENSITY FUNCTIONS
NT PEARSON DISTRIBUTIONS
NT POISSON DENSITY FUNCTIONS
NT PROBABILITY DENSITY FUNCTIONS
NT PROBABILITY DISTRIBUTION FUNCTIONS
NT RAYLEIGH DISTRIBUTION
NT REGRESSION ANALYSIS
NT REGRESSION COEFFICIENTS
NT SEQUENTIAL ANALYSIS
NT STANDARD DEVIATION
NT STATISTICAL CORRELATION
NT STATISTICAL DECISION THEORY
NT STATISTICAL TESTS
NT VARIANCE [STATISTICS]
NT WEIBULL DENSITY FUNCTIONS
Cracked metals brittle fracture statistical analysis, discussing plastic deformation under load
01 p0166 A71-10080
Statistical stability of structurally inhomogeneous material, analyzing weak spots effects on limiting state
01 p0166 A71-10081
Stress fields statistical characteristics in randomly inhomogeneous elastic plate, considering Lomakin solution
01 p0170 A71-10642
Optimal automatic systems statistical theory in relation to sensitivity, identification, invariance and control object dynamic characteristics
01 p0060 A71-10705
Linear dynamic plants in steady state identified via multichannel statistical optimizer
01 p0064 A71-10923
Statistical properties of multimode quantized optical fields, using density matrix in P-representation
02 p0259 A71-11932
Quantum mechanical communication theory of optimal receivers, using statistical detection and estimation theory
02 p0213 A71-12016
A-B-A block copolymers statistical thermodynamics, describing postulated microstructure theoretical model for phase transition prediction
02 p0273 A71-12450
Compact galaxies one-magnitude light outburst near M3, discussing photometric statistical data
02 p0313 A71-12469
Statistical study of microhardness across thickness of gas saturated layer distribution on surface of Ti alloys
02 p0265 A71-12524
Statistical prediction of atmospheric turbulence effects on aeronautical systems
03 p0398 A71-13135
Heat resistant materials long term strength characteristics, determining optimum parameters from creep data statistical analysis by least squares method
03 p0440 A71-13194
Soviet book on gyroscopic devices statistical synthesis covering dynamic characteristics, automatic systems, etc
03 p0423 A71-13371
Launch vehicle under influence of random fin misalignments, predicting roll rate by statistical analysis [AIAA PAPER 70-1382]
03 p0498 A71-13665
Statistical analysis of digital data transmission time error distributions in Polish post office and railroad communications network
03 p0380 A71-14375
Narrow band random processes statistical characteristic relationship derived from upper and lower envelopes
03 p0452 A71-14390
Soviet book on biometry covering correlation coefficients, rectilinear/curvilinear regression, nonparametric statistics, diversity indices, algorithms, dispersion and statistical analysis and probability
04 p0546 A71-15263
PCM telemetry bit error probability confidence intervals and Bayesian posterior distributions derivation, using statistical method
04 p0554 A71-15327
Scalar substance heat transfer characteristics in nonhomogeneous turbulence, using statistical and phenomenological approach
04 p0572 A71-15541
Statistical characteristics of pulsation pressure on surface in turbulent boundary layer of incompressible fluid, discussing effects near smooth flat wall
04 p0575 A71-15607

Statistical method in geodetic surveying including equilibration calculations, error theory, estimation, verification, distributionless tests, etc
04 p0584 A71-15900
Data reduction for badly conditioned systems, describing general classical and modified linear statistical models for parameter determination from erroneous measurements data
[DGLR-70-084]
05 p0726 A71-15950
Antenna aperture random radiation field representation in expansion in eigenfunctions, comparing results with linear antenna statistical theory
05 p0727 A71-15994
Laser light statistical properties including Fokker-Planck equation, photoelectron counting distributions and quantum mechanical equation from Weidlich and Haake theory
05 p0762 A71-16483
Muscle tonus dynamics statistical analysis, obtaining destructive stereotropic influences, therapeutic effects and control mechanisms
05 p0710 A71-16808
Radar receiver dynamic range centering for log-normal target statistics for minimum probability of signal exclusion
05 p0725 A71-17084
Photoelectron count of lognormally fading optical signal, discussing noncentral chi square random variable approximation
05 p0726 A71-17085
Soviet book on statistical antenna theory covering large multielement, mirror, laser and synthetic aperture antennas in optics, acoustics, radio astronomy, radio wave propagation, etc
06 p0872 A71-17447
Automatic computer verification of diurnal temperature and geopotential observations on principal isobaric surfaces by statistical data analysis, describing computer algorithm
06 p0922 A71-17504
French statistical system for civil air transport operations from airport viewpoint
06 p1009 A71-17587
Thin imperfect cylindrical shell stability, considering statistical analysis of initial irregularities
06 p0993 A71-17815
Statistical equilibrium equations solved for atom/ion with complex energy level structure and weak spectral lines, discussing deviations from LTE
06 p0969 A71-17969
Statistical analysis for parabolic approximation of phase dependence observations of integral Mars brightness
06 p0975 A71-18446
Stratified statistical filtering algorithm for numerical simulation of nonlinear systems behavior
07 p1081 A71-18836
Incompressible fluid nonuniform turbulence statistical approach, based on finite number of equations for high order single point correlations
07 p1087 A71-18920
Statistical analysis of neutron induced gain degradation of silicon power transistors, determining failures distribution fit to Weibull function
07 p1070 A71-19063
Mathematical statistics methods application to incorrect problems in mathematical physics, using information theory
07 p1158 A71-19171
Statistical optical measurements of solar scintillation due to atmospheric conditions
07 p1111 A71-19489
Statistical methods for inventory boundary determination and data compression in automatic processing of multispectral scanner remote sensor earth observations from aircraft and spacecraft [AIAA PAPER 71-234]
07 p1068 A71-19711
Statistical information on lightning and static hazards relative to airworthiness
07 p1020 A71-19929
Coupling loss factor estimation, using wave transmission or natural frequency shift methods in statistical energy analysis
07 p1161 A71-19962
Landmark navigation improvement by redundant measurements and statistical data reduction measurement for lunar roving vehicles
07 p1156 A71-20339
Spacecraft orbital elements determination, using statistical analysis in processing observed motion data
08 p1360 A71-21005
Statistical analysis of fiber optics imagery, considering resolution difference between static and dynamically scanned bundles
08 p1334 A71-21180
Statistical analysis of center-limb variations of intensity, spectrum and polarization of solar microwave impulsive bursts
08 p1364 A71-21419
Vector wind shears statistical analysis at various altitudes, using balloon sounding measurements
08 p1327 A71-21457
Observational data statistical evaluation, considering meteorological instrument bias, corresponding in-

strument fluctuations and noise/signal separation by linear algebraic filter
08 p1329 A71-21726
Nonlinear approximation for coherent Green function behavior in randomly fluctuating, unbounded and statistically homogeneous medium, emphasizing large scale fluctuations
08 p1325 A71-21883
Statistical directivity, radiation pattern, drift dispersion of segmented traveling wave antennas
09 p1414 A71-22226
Computer aided statistical model of visual evoked potential in man as normality criterion for pathological indicator
09 p1397 A71-22253
Statistical properties of radio communication system polarization reception coefficient as function of receiving antenna and signal polarization characteristics
09 p1405 A71-22294
Statistics effect of quasi-monochromatic exciting radiation on generated radiation spectrum in nonlinear optics
09 p1461 A71-22396
Oscillographic determination conditions for Co, Ni, and Fe, giving statistical treatment of results
09 p1454 A71-22501
Critique of paper on earth gravitational field correlations to dipole part of magnetic field
09 p1437 A71-22930
Earth gravitational field correlations to dipole part of magnetic field, rejecting modifications to statistical procedures
09 p1437 A71-22931
Book on reliability mathematics covering fundamental statistical concepts, logic diagrams, mathematical models, component reliability prediction, system prediction, reliability growth, assessment methods, etc
09 p1485 A71-22958
Cophase ad hoc statistic for data processing of detectors array sensing signal propagating in uncorrelated noise
09 p1408 A71-23452
Bulk properties effect on adhesive properties of seven epoxy resins, considering stress-strain properties and statistical analysis for tensile shear evaluation
10 p1632 A71-24086
Adhesive bonded joints mechanical behavior relation to materials, processes and experimental techniques, developing statistical analysis and formulas for orthotropic-elastic joints
10 p1614 A71-24087
Aircraft motion and traffic control at air corridors intersections for minimum flight schedule deviation under random disturbance due to weather, using statistical simulation
10 p1639 A71-24158
Cylindrical panel vibration in supersonic flow under random effects, calculating stress-strain statistical properties as function of incident flow velocity
10 p1690 A71-24572
Optimal nonlinear filtering, deriving algorithm based on statistical approximation of system and observer nonlinearities by second order polynomials
10 p1587 A71-24746
Nonlinear dynamic systems phase coordinate variations statistical characteristics, describing data reduction method
11 p1798 A71-25662
Atmospheric thermal sounding problem, using regularization and statistical methods and expanding by empirical orthogonal functions
11 p1795 A71-25920
Galactic clusters statistical analysis for relative sky areas at various distances, discussing inverse apparent diameters and interstellar obscuration effects
11 p1833 A71-26329
Computer aided statistical analysis of irregular quasi-optical transmission lines containing random inhomogeneities
11 p1733 A71-26347
Variance and correlation radius of distortions from transparent dielectric plate, using statistical theory of antennas
11 p1738 A71-26348
Parabolic approximation of total Mars brightness phase dependence observations, using statistical analysis
12 p1955 A71-26596
Statistical nature of time to complete MIL-STD-781 reliability sequential tests for military and space equipment, giving information about MTBF
12 p1908 A71-26656
Experiment dispersion analysis planning, using solution acceptance procedures block diagrams
12 p1988 A71-26711
Statistical estimation in monitoring and control systems analysis, discussing algorithm construction for computer solution of nonlinear differential equations system
12 p1891 A71-26724
Algorithm for nonparametric estimation of random parameters of general exponential family of known

density distributions, investigating empirical estimates convergence to Bayes optimal estimates

12 p1892 A71-27022

Statistical estimation techniques for error probability of digital communication systems

12 p1880 A71-27145

Statistical analysis of gravitational instability for isotropic cosmological models, examining density perturbations as random functions of coordinates and comparing with galactic mass statistics

12 p1965 A71-27178

Statistical analysis of equipment selection for multipurpose scientific laboratory onboard space stations under economic and time constraints

13 p2094 A71-28187

Statistical analyses for tube-annular and annular combustion chamber temperature profiles

13 p2116 A71-28741

RF noise measurement instrumentation using statistical analysis for better interference characterization

13 p2035 A71-28865

Oscillations in system of nonlinear cubic response with narrow-band random excitation, using statistical linearization

13 p2101 A71-29077

Time and frequency statistics of turbulent fluctuations of wind, temperature and humidity in atmospheric surface layer

14 p2266 A71-29706

Atmospheric turbulence statistical models assessment for aircraft design and operation, considering CAT and thunderstorm turbulence data

14 p2266 A71-29751

Noctilucent cloud data statistical treatment by meteor observation double counting method

14 p2233 A71-29966

Noisy image visual discrimination and detection, investigating Bayes criterion ideal statistical method validity for pattern recognition

14 p2197 A71-30815

Atmospheric noise statistical characteristics, investigating short term variations, intensities and application to communications

14 p2237 A71-30964

Defense industry pricing and contracting for inflation, considering statistical analysis and direct cost estimation

14 p2342 A71-31132

Incompressible fluid turbulence theory based on space-time Hopf characteristic functional integral representation for velocity field statistical ensemble

15 p2388 A71-31477

Book on detection of signals in noise covering statistical theory principles and applications in digital communications, radar and sonar

15 p2369 A71-31507

Sonic boom pressure signature laboratory scale measurement after modification by traveling through air jet turbulence, comparing with statistical prediction

[AIAA PAPER 71-618]

15 p2388 A71-31547

Turbulent mixing between parallel incompressible air streams, using statistical investigation of pressure and velocity fields

[AIAA PAPER 71-613]

15 p2389 A71-31582

Conditional distribution density formation for signal-noise mixture based on learning sampling with dependent values

15 p2370 A71-31586

Signal detection in stationary, Markov and other noise background, discussing functional method of statistical and probabilistic representation

15 p2370 A71-31589

Astronomical 4C catalog radio sources statistical analysis, showing mean spectral indices dependence on radio emission fluxes and red shifts

15 p2487 A71-32037

Weak harmonic signal detection in narrow band Gaussian noise, using statistical algorithm

15 p2371 A71-32187

Small scale solid state digital computer for experimental medical data statistical processing

15 p2365 A71-32534

Solar microwave burst frequency occurrence statistical analysis

15 p2495 A71-32687

Statistical analysis of radiometer measurement data of solar emission atmospheric attenuation at 19 GHz

15 p2496 A71-32710

Solar microwave bursts spectrum, calculating maximum radiation fluxes and frequencies from statistical data

15 p2480 A71-32749

Two-parameter statistical theory of material fatigue, considering random and ordered structural nonuniformities in space distributions

16 p2647 A71-32823

Elastic structures stability under randomly fluctuating external loads based on statistical methods

16 p2648 A71-32988

Machine structural elements endurance margin prediction from limited tests, proposing statistical method of integral estimates and tolerance factors

16 p2651 A71-33064

Statistical methods application to buckling of axially loaded columns, considering entire spectrum of elastic, elastoplastic and fully plastic ranges

16 p2654 A71-33123

Statistical procedure for maintainability allocation during early system design to meet specified overall goal

16 p2583 A71-33299

Numerical evaluation for individual samples of random processes obtained from nonstationary engineering experiments

16 p2602 A71-33341

Statistical analysis of durability data of heat resistant alloys for gas turbine engines, using long term mass creep strength tests on industrial melts

16 p2592 A71-33413

German book on problems, mathematical foundations and investigation methods of technical reliability covering Boole model, random variables, distribution functions, failure rates, etc

16 p2583 A71-33524

Materials ultrasonic structural analysis, describing statistical methods for damping data processing

16 p2584 A71-33561

Cracked metals brittle fracture statistical analysis, discussing plastic deformation under loading

16 p2658 A71-33636

Statistical analysis of structurally inhomogeneous material strength, analyzing weak spots effects on limiting state

16 p2658 A71-33637

Statistical microstructural analysis for nucleation and growth kinetics of recrystallization nuclei of metal single crystals

17 p2755 A71-34414

Statistical evaluation of Doppler ultrasonic blood flowmeter, determining correlation between Doppler signal zero crossing density and fluid flow velocity

17 p2689 A71-34448

Instrument calibration, discussing statistical estimation of relationship and experimental design for precision improvement

17 p2738 A71-34526

Statistical behavior of turbulent velocity derivatives in nearly isotropic turbulent field downstream of grid, using high speed digital computing methods

17 p2726 A71-34662

Monograph on statistical theory for weak homogeneous turbulence covering mathematical model, wave correlation functions, Bogoliubov expansion method, kinetic equation, nonlinear interactions, etc

17 p2727 A71-34771

Statistical analysis of polar auroras visual observation, discussing solar activity effects

17 p2733 A71-34836

Galactic clusters characteristics tabulation and statistical analysis, calculating dimensions, luminosity and radial velocities dispersion

17 p2804 A71-34841

Averaging method for nonlinear oscillations in celestial mechanics, radio engineering and electronics and for time lag, random forces and integrodifferential equations

17 p2779 A71-34904

Asymptotic formulas for two point boundary value problem of differential equations system, using averaging method

17 p2765 A71-34905

Periodic or almost periodic small combination vibrations onset conditions by integral equations method and averaging principle

17 p2779 A71-34910

Statistical theory of nonlinear differential equation system with discontinuous trajectory solution, deriving motion stability to first approximation using Liapunov functions

17 p2780 A71-34915

Objective monitoring of human operator, using statistical analysis of EEG based on numerical characteristics of energy spectrum

17 p2692 A71-35168

Lunar surface and soil mechanical properties statistical analysis covering Alphonsus event, cratering and erosion

17 p2805 A71-35179

Fatigue life prediction for structure undergoing random steady Gaussian centered process, determining statistics of absolute maximums

17 p2832 A71-35471

Statistical evaluation of switching elements reliability, considering permanent and temporary failure rates

17 p2718 A71-35627

Statistical analysis of radio structure of quasars, considering red shift and anisotropy in angular size distribution

17 p2811 A71-35746

Statistical analysis of error sources and magnitudes in Boeing 747 weight values obtained by onboard aircraft weighing system and by manual calculations [SAWE PAPER 897]

17 p2676 A71-35813

Space station facilities and launch and prelaunch operations at Kennedy Space Center, discussing statistical analysis for activity optimization and integrated mission management concept

18 p2899 A71-36474

Statistical methods for S-N curve and fatigue limit tests, including iterative method, probit analysis, etc

18 p2936 A71-36695

Concentration broadening of impurity levels in compensated semiconductors, proposing averaging procedure

19 p3117 A71-37262

Nonlinear mechanical system stationary random forcing input and output response data, determining statistical linearization coefficients in Kazakov-Bootton method

19 p3037 A71-37347

Algorithm for nonparametric estimation of random parameters of general exponential family of unknown density distributions, investigating empirical estimates convergence to Bayes optimal estimates

19 p3038 A71-37691

Definitions and axiomatics revision and recommendations for mathematical statistics as applied discipline

19 p3086 A71-37782

Aerosol scattering coefficient in atmosphere, determining statistical characteristics of vertical and spectral structure

19 p3090 A71-37970

Airfield performance evaluation by simulation, providing statistical measures and computer generated motion picture for visual display of simulated future activity

19 p3041 A71-38027

Copper single crystals fatigue as statistical work hardening phenomenon

19 p3081 A71-38072

High temperature creep testing facilities and techniques, evaluating statistically interlaboratory variability and significance of testing and material variables affecting creep results

19 p3081 A71-38132

Radar antenna interference determination based on model using electrical and physical characteristics of reflector type antenna for statistical gain distribution prediction

19 p3021 A71-38458

Location and scale parameters estimation from ordered statistical samples with numerical applications to Gumbel and Weibull distributions

19 p3088 A71-38471

Power balance and statistical analysis of energy flow and response in lightly damped resonant structures

20 p3268 A71-38960

Higher order noisy optical pulse intensity correlations interpretation by statistical model, estimating spike amplitude

20 p3196 A71-39103

Atmospheric thermal sounding problem, using regularization and statistical methods and expanding by empirical orthogonal functions

20 p3256 A71-39211

Statistical investigation of 1500 galaxies in MCG catalog with weak surface brightness, noting sculpture type spheroidal galaxies in Virgo cluster

20 p3289 A71-39299

Statistical processing of phase dependence of Martian integral brightness at 0.3-1.1 microns, noting abrupt reflectivity decrease

20 p3290 A71-39308

Spacecraft orbital elements determination, using statistical analysis in processing observed motion data

20 p3294 A71-39585

Book on statistical mechanics of turbulent fluid flows covering gas oscillations, correlation function, Reynolds equation, laminar flow, particle dispersion, etc

20 p3213 A71-39774

Statistical analysis of microphotometer scan of solar granulation photographs blurring during partial eclipse of 20 May 1966, correcting image for atmospheric and instrument effects

21 p3439 A71-40053

Discrete renewal processes applied to mathematical modeling of physical processes, using statistics of complicated events in reliability analysis

21 p3407 A71-40361

Statistical analysis of endurance limits for castings and forgings of die forged and cast steel, using rotating beam fatigue tests

21 p3388 A71-40754

Statistical methods for calculating cross correlation function integrals of input and output coordinates of automatic control system in presence of random noise at input

22 p3525 A71-41437

Electronic and electrical systems optimization effectiveness through generation of statistical priorities

22 p3525 A71-41438

Statistical analysis of digital automatic control system with unreliable communication channel, determining system mean square error

22 p3525 A71-41439

Probability approach to visual effectiveness of signal flashing lights, showing graphically Broca-Sulzer effect

22 p3498 A71-41485

Extragalactic radio sources polarized radiation intensity statistical analysis, calculating magnetic field scale 22 p3602 A71-42175

Nitrogen, argon and helium viscosity measurements, obtaining density expansion by statistical analysis 22 p3621 A71-42369

Statistical analysis of gravitational instability for isotropic cosmological models, examining density perturbations as random functions of coordinates and comparing with galactic mass statistics 22 p3605 A71-42452

Antenna aperture random radiation field representation in expansion in eigenfunctions, comparing results with linear antenna statistical theory 22 p3524 A71-42743

Actual navigation dispersions, estimation uncertainties and resultant Mars orbit insertion statistical delta V requirements for six Mars approach angles in 1977 Mars window [AAS PAPER 71-323] 23 p3726 A71-42997

Presentation modality as encoding variable in short term memory, obtaining mean recall score as function of trials 23 p3639 A71-43113

Sound transmission through finite closed shells, considering statistical energy analysis, modal coupling and noise reduction 23 p3704 A71-43213

Statistical approach to complex structural vibration under random excitation 23 p3775 A71-43214

Average number of real roots of polynomials consisting of independent random quantities with identical distribution 23 p3699 A71-43571

Least geomagnetic diurnal variation effects period determination by statistical method 23 p3673 A71-43984

Statistical modeling technique for approximate numerical solution of unsteady heat conductivity inverse problem, obtaining foam chamotte and magnesite temperature field data 23 p3782 A71-44059

Point source average signal reflection from conductive plane in random oscillation 23 p3654 A71-44163

Grainy composite material structural analysis, presenting statistical mathematical model 23 p3698 A71-44224

Astronomical observations weighted estimation based on smoothing Pearson curves empirical distribution 23 p3771 A71-44257

Dynamic system optimal weighting function determination, using variational methods for statistical criteria 24 p3813 A71-44677

Nonlinear automatic control system statistical optimization using similarity theory 24 p3813 A71-44681

Nonlinear control system optimal synthesis by statistical criteria, discussing probability and likelihood function 24 p3813 A71-44682

Statistically optimal automatic control system synthesis with phase coordinate vector 24 p3814 A71-44685

Statistical optimization of spherical gyroscope regarded as servomechanism system under random perturbation, using measured values of relative angles between sphere and inner gimbal 24 p3825 A71-44691

Statistical and combined harmonic and statistical linearization methods for piecewise-linear nonlinear system characteristics analysis 24 p3814 A71-44693

Unsteady nonlinear multidimensional feedback control systems characterized by equations in normal form for phase coordinates, investigating solutions accuracy by statistical linearization 24 p3814 A71-44694

Cloud classification from various radar data independent characteristics, using statistical theory of Bayes hypotheses 24 p3844 A71-44878

Stochastically imperfect columns on nonlinear elastic foundations, obtaining approximate asymptotic expression for buckling stresses and lateral displacement autocorrelation 24 p3884 A71-44962

Statistical analysis of spot welded and adhesive joints of high strength Al alloy sheet in aircraft structures 24 p3831 A71-45012

Asteroid belt structure by statistical methods, discussing asteroidal zones and agreement with Kuiper hypothesis and protoplanet theory 24 p3874 A71-45173

Metal hardening by dispersion of spherical ordered and coherent precipitates from statistical theory 24 p3861 A71-45196

Optimum signal processing for distance measurement with lasers, considering propagation, detection and measure process statistical properties, optical radar and sine wave modulation 24 p3834 A71-45206

STATISTICAL COMMUNICATION THEORY U COMMUNICATION THEORY STATISTICAL CORRELATION

Solar X-ray flare activity statistical prediction based on correlation to coronal electron temperature and emission measure [AIAA PAPER 70-1371] 02 p0301 A71-12698

Solar flare forecasting based on statistical correlation to magnetic fields inferred from H alpha filtergrams [AIAA PAPER 70-1372] 02 p0301 A71-12699

Moon free libration second and third mode semiamplitudes from statistical relations 05 p0809 A71-16456

Earthquakes correlation with lunar orbital motions, analyzing lunar perigee and new moon coincidences 05 p0809 A71-16457

Signals statistical parameters and phase space properties, deriving functional relationships for signal processing correlation techniques 09 p1405 A71-22298

Bounded electromagnetic wave propagation in randomly inhomogeneous medium, calculating correlation in amplitude and phase fluctuations 09 p1407 A71-23109

Psychological selection of pupil pilots, discussing statistical correlations between values of some single parameters of Zulliger test and instructional data 10 p1572 A71-24981

Power spectrum symmetry effect on radar signal correlation function and bandwidth 10 p1580 A71-25107

Anisotropic homogeneous two-point double-velocity correlation tensor model for turbulent flow field, deriving relation between micro and macro scale 11 p1748 A71-25153

Pair correlation function for gaseous hydrogen at low density and temperature from quantum mechanical calculation, using Lennard-Jones potential 11 p1801 A71-25367

Optimal impulse correction of linear dynamic system motion based on system phase coordinates statistical information, taking into account correction finite accuracy and power expenditure 12 p1892 A71-27021

Mathematical expectation and correlation function of combined pulse modulator by Monte Carlo method 15 p2382 A71-31983

Subjective fatigue feeling correlation to symptoms based on bank clerks and broadcasting workers work load assessment ratings 17 p2688 A71-34367

Optimal impulse correction of linear dynamic system motion based on system phase coordinates statistical information, taking into account correction finite accuracy and power expenditure 19 p3037 A71-37690

Auroral pulsations physical correlation with cosmic noise absorption, using statistical correlation analysis 20 p3215 A71-38734

Replacement problem in stochastic point processes, obtaining cost over given time period and moments and correlations of replacement number 21 p3407 A71-40367

Martian surface clouds distribution in graph, noting statistical correlation with surface radar altitude 21 p3450 A71-40712

Soviet book on mathematical plasticity theory covering stress/strain flow and deformation, stress/strain tensors statistical averaging methods and hardening conditions 21 p3473 A71-41370

Computer-aided statistical analysis correlation method for prediction of electronic circuit component part variability effects on performance and reliability 22 p3517 A71-42102

Stochastic, random and ordinary Green function relations for two point correlation functions in mathematical physics 23 p3698 A71-43114

STATISTICAL DECISION THEORY

Statistical connection strategies for automatic multiradar air traffic surveillance using track computer 03 p0380 A71-14395

Maximum entropy principle for prior distribution determination in Bayesian reliability estimation, comparing with statistical decision theory 11 p1772 A71-26164

Statistical decision theory in reliability and project management, discussing Venus probe loss 12 p1911 A71-26690

German monograph on experiments with stochastic automata covering noisy sequential nonanticipating channels with finite input/output alphabets, statistical decision functions, etc 17 p2719 A71-34774

Book on synchronous communications theory covering statistical detection, decision and estimation and source and channel encoding 17 p2707 A71-35218

Statistical detection theory applied to images against background of laser produced speckle, using flying-spot type scanning machine 17 p2754 A71-35324

General Stefan problem for heat conduction with melting and free boundary problems occurring in control and statistical decision theories 17 p2841 A71-35794

Numerical solution algorithm for parabolic free boundary problem in statistical decision theory, comparing convergence with asymptotic expansions 18 p2941 A71-36352

Fault detection, diagnosis and prognosis in linear dynamic systems based on statistical decision theory, considering error signal generation and statistics 23 p3682 A71-43945

STATISTICAL DISTRIBUTIONS NT PEARSON DISTRIBUTIONS NT PROBABILITY DISTRIBUTION FUNCTIONS NT RAYLEIGH DISTRIBUTION

Chi-square distributions fitted to observed telecommunication variables distributions 01 p0041 A71-11609

Extensive air shower muons at mountain levels, describing experimental procedure for fluctuation distribution 03 p0476 A71-13856

Antenna aperture random radiation field representation in expansion in eigenfunctions, comparing results with linear antenna statistical theory 05 p0727 A71-15994

Solid solution hardening theories, discussing point obstacles random distribution effect on strength and superposition of multiple hardening mechanisms 08 p1309 A71-21522

Surface pressure field sampled natural functions statistical stability, taking into account eigenvalue magnitudes and rate of decrease 09 p1487 A71-22303

O and B type stars galactic Keplerian parameters statistical distributions based on galaxy point model 11 p1820 A71-25248

Bidirectional reflectance model for randomly rough surface, using distribution function for macroscopic probability of microscopic surface roughness elements with specific slopes 11 p1800 A71-26246

Geminid meteoroids characteristics observation by radio, noting distributions of major semiaxes, plane inclination, elliptic eccentricities and day-by-day number variations 12 p1963 A71-26965

Statistical scatter approximation of creep characteristics using relation to accumulated static damage and time to failure 12 p1979 A71-27352

Log normal random fluctuations of ionospheric electron concentration in F region from vertical sounding and incoherent scatter data 13 p2061 A71-28553

Holograms of physical objects, calculating irradiance statistical distribution from reference-object beam powers ratio 15 p2412 A71-32594

Least squares method effectiveness in nonnormally distributed observation errors compensation 16 p2602 A71-33477

Randomly distributed domain structure of ordered Ni-Cr alloy, using electron microscopy and neutron diffraction 17 p2755 A71-34413

Distributed parameter system measurement optimization devices location for error estimation cost minimization by disturbances statistical characteristics and boundary conditions 17 p2722 A71-35211

Geminid meteoroids characteristics observation by radio, noting distributions of semiaxes, plane inclination elliptic eccentricities and day-by-day number variations 19 p3144 A71-38260

Critique of quasar model of independent random pulse emitting sources conglomeration from incompatibility with light curve 20 p3289 A71-39294

Best linear unbiased estimates for location and scale parameters of extreme value distribution based on given order statistics 21 p3407 A71-40366

Phase distribution randomization in switched antenna array, noting radiation pattern sidelobe compensation application 22 p3522 A71-42312

Two dimensional probabilistic images generation and statistical characteristics determination, noting application to psychophysiological experiments 22 p3518 A71-42422

Digital computer simulation of random disturbances with uniform distribution, determining generated sequence correlation coefficient mean and variance 22 p3518 A71-42492

Extensive air shower muons flux density at mountain altitudes, describing experimental procedure for fluctuation distribution 22 p3595 A71-42657

- Antenna aperture random radiation field representation in expansion in eigenfunctions, comparing results with linear antenna statistical theory 22 p3524 A71-42743
- Normal wave scattering on random permittivity inhomogeneities of stratified waveguide dielectric layer, calculating beam width and energy loss by perturbation procedure 23 p3645 A71-43567
- Average number of real roots of polynomials consisting of independent random quantities with identical distribution 23 p3699 A71-43571
- Astrometrical HF range latitudinal observation error spectrum estimation, showing random dispersion and Chebyshev polynomial expansion parameters for nightly variation 23 p3771 A71-44256
- Interstitial solute carbon distribution in martensite, using generalized perfect lattice gas statistical mechanics 23 p3694 A71-44281
- Accuracy analysis of statistically optimal dynamic system with modulus bounded control for discrete and continuous information input, using Fokker-Planck-Kolmogoroff equation 24 p3814 A71-44689
- Radio echoes from clouds and precipitation, determining detection threshold, station potential and statistical distribution numerical characteristics 24 p3844 A71-44879
- STATISTICAL MECHANICS**
- Computerized statistical simulation of steady state, ergodic, self oscillatory processes in plane magnetron 03 p0386 A71-13811
- Relativistic formulation of thermodynamics and statistical mechanics in special theory of relativity, noting Ott presentation 13 p2102 A71-29324
- Morphological projections in astrophysics, considering single star evolution in terms of Boltzmann-Gibbs statistical mechanics 14 p2318 A71-31020
- Thermodynamics and statistical mechanics of low temperature physics, including entropy, probability, energy spectra and gas liquefaction 20 p3270 A71-39240
- Polymer systems molecular rheology based on statistical mechanics and simplified structural models 24 p3841 A71-44644
- Statistical system formation in fast hadrons collision process and multiple hadron production 24 p3851 A71-45170
- STATISTICAL MOMENTS**
- U DISTRIBUTION MOMENTS**
- STATISTICAL PROBABILITY**
- U PROBABILITY THEORY**
- STATISTICAL TESTS**
- Statistical reliability tests for cosmic ray intensity records from ground stations, stressing time series aspect 06 p0951 A71-18108
- Truncated sequential test for production models based on preproduction testing with allowance for unequal sample sizes 15 p2416 A71-32344
- Statistical tests of solar flares based on maximum likelihood method, discussing longitude distribution, rigid rotation, planetary effects, etc 15 p2480 A71-32751
- Uniform convergence of frequencies of events in independent tests sequence to probabilities of occurrence 17 p2764 A71-34573
- Dynamic system impulse response model for goodness of fit and linearity hypothesis tests by computer simulation 17 p2722 A71-35181
- Creep strength tests planning, discussing minimum necessary tests number and samples distribution to obtain characteristics with accuracy and reliability 19 p3082 A71-38346
- Material fatigue failure under narrow band random vibration effects, deriving fatigue life prediction equation based on composite experimental design and statistical tests 22 p3615 A71-42002
- STATISTICAL WEATHER FORECASTING**
- Soviet papers on statistical and probabilistic weather forecasting covering computerization problems, atmospheric circulation, correlation methods, etc 07 p1150 A71-18870
- Space metric as similarity criterion for meteorological element field synoptic setup, discussing probability for forecasting by analogy 07 p1150 A71-18872
- Atmospheric temperature minima prediction, comparing various correlation methods 07 p1151 A71-18875
- Binomial distribution models for thunderstorm activity at Cape Kennedy 08 p1326 A71-21452
- Statistical method of thunderstorm forecasting, basing algorithm on mathematical techniques 15 p2443 A71-31225

STATOR BLADES

- Axial flow compressors radiated sound reduction by segmented stator blades 03 p0353 A71-13283
- Large axial compressor flow straightening stator blades unsteady pressure measurements with short response time detectors 12 p1945 A71-27469
- Turbomachinery rotor and stator row aerodynamic interaction, describing discrete tone noise generation from far field measurements 15 p2450 A71-32134
- Noise generation due to inlet free stream turbulence incident on isolated stators and rotors, using flat plate cascade blade row model 18 p2956 A71-36498
- Segmented stator vanes performance in axial flow compressor, noting radiated sound reduction 20 p3175 A71-39093
- STATORS**
- Radiometric determination of diametrical distance between rotor and stator of turbomachines 03 p0421 A71-13003
- Rotating blade /rotors/ and stationary /stators/ rows in axial flow molecular pump, deriving overall and individual transmission probabilities 09 p1455 A71-23058
- Symmetrical hysteretic micromotors stator structure with windings around unilateral crowned teeth, calculating maximum EM power in starting mode 13 p1999 A71-28631
- Optimization of mechanical characteristics of asynchronous capacitor microengine designs with asymmetric stator circuit for prolonged continuous operation with negligible steel wear 13 p2002 A71-28929
- Windage data for inert gas in high speed generators rotor-stator gap, investigating turbulent velocity profiles 20 p3181 A71-38915

STAYS**U GUY WIRES****STEADY FLOW**

- NT COUETTE FLOW
- NT HARTMANN FLOW
- Vertical fluid-filled channel with uniform internal heat source, analyzing steady plane-parallel convective motion 01 p0179 A71-10665
- Steady supersonic conducting gas flow in channel with nonconducting walls, calculating electric and gas dynamic parameters for different imposed magnetic field geometries 01 p0133 A71-10791
- Steady isothermal plane gas flow between infinite parallel plates at arbitrary Knudsen numbers, obtaining linear differential equations of mass transfer 01 p0071 A71-11114
- Steady three dimensional ideal dissociative gas flow along stream lines, examining velocity components, pressure gradients, density and mass fraction variable 02 p0239 A71-12124
- Wing computation in steady or unsteady supersonic flow, using network, inverse discrete and numerical inversion methods 03 p0339 A71-13129
- Aerodynamic characteristics of aircraft in steady and unsteady supersonic flow by analog electrical method, including wing-fuselage interactions 03 p0339 A71-13130
- Steady supercritical planar inviscid transonic flows over lifting airfoils, generating unsteady flow by impulsively imposing airfoil boundary condition [AIAA PAPER 70-47] 03 p0341 A71-13433
- Time dependent finite difference solutions of steady state nonequilibrium quasi-one dimensional nozzle flows 03 p0400 A71-13458
- Steady incompressible flow past oblate and prolate spheroids for Reynolds number up to 100, using spherical coordinates and finite difference method 03 p0400 A71-13729
- Viscous incompressible conducting fluid steady flow in rectangular channel under normal external magnetic field 03 p0466 A71-14554
- Viscous incompressible conducting fluid steady laminar flow in rectangular channel with two insulating and two arbitrarily conducting walls under external magnetic field 03 p0466 A71-14556
- One dimensional steady heat transfer in rarefied gas between infinite parallel laws, using Boltzmann kinetic equation 03 p0462 A71-14570
- Steady high power plasma flows using three phase AC generator 04 p0632 A71-14794
- Analog and digital methods for interactions between aircraft lifting elements in steady or unsteady supersonic flow [ONERA-TP-850] 04 p0527 A71-15358
- Tail assembly load distribution in steady uniform flow for nonzero angles of attack, using slender body theory 04 p0527 A71-15367

Longitudinal surface curvature effect on steady two dimensional incompressible laminar thermal boundary layers 04 p0680 A71-15471

Steady two dimensional ideal gas flow past blunt body at incident infinite Mach number, obtaining gas dynamic variable asymptotic expansions as kappa approaches infinity 04 p0528 A71-15553

Stationary flow of viscoplastic liquid in annular gap with temperature dependent viscosity, taking into account energy dissipation 04 p0579 A71-15799

Normal shock waves in one dimensional steady flow of two phase medium, noting phase exchanges and lack of internal equilibrium 04 p0579 A71-15821

Far and near field solutions of plane steady transonic flow past thin airfoil including imbedded shock waves, using small disturbance theory [AIAA PAPER 70-188] 05 p0694 A71-16566

Steady laminar convection in infinite layer of heated homogeneous fluid between constant temperature rigid plate and thermal insulator 05 p0838 A71-16962

Plane steady laminar flow into channel between two semiinfinite parallel plates, constructing asymptotic solution for large Reynolds number 05 p0736 A71-16966

Steady two dimensional flow past flat plate in rectangular channel for low Reynolds number 05 p0738 A71-17249

Steady state mixed subsonic-supersonic flow near blunt leading edge in hypersonic internal flow, using asymptotic solution by time-dependent method [AIAA PAPER 71-85] 06 p0843 A71-18542

Acoustic propagation through variable area duct with steady compressible flow, transforming governing equations into two decoupled linear ordinary differential equations 07 p1160 A71-19952

Two and three dimensional thermals and steady and starting plumes convective fluid motion formulas, using vorticity integration method 07 p1104 A71-20223

Planetary boundary layer stationary air flow over plane homogeneous surface under geostrophic wind conditions, solving for thermal turbulence field stabilization by iterative method 08 p1330 A71-21874

Positive and negative charged particle beam steady one dimensional motion analysis based on continuity, motion and Maxwell equations, allowing for electrostatic particle interactions 09 p1496 A71-22265

Rarefied gas steady and unsteady motions, proposing approximate method for various problems 09 p1382 A71-22372

MHD accelerator in pulsed mode with crossed fields, studying one dimensional steady inviscid flow 09 p1501 A71-22407

Laminar steady flow and heat transfer of viscous heat conducting gas moving between coaxial cylinders, using Runge-Kutta method 09 p1431 A71-22408

Steady boundary layer flow in viscous liquid thin down variable incline for large Reynolds and Froude numbers 09 p1432 A71-22451

Collisionless plasma steady flow past thin symmetrical semiinfinite wedge, considering dispersion due to finite Larmor radius 09 p1504 A71-23052

Axisymmetric steady diabatic flow equations exact solutions 09 p1434 A71-23545

Combustion reactions development with velocity gradient downstream steady shock wave, considering aerodynamic field in supersonic wind tunnel 10 p1694 A71-23813

Steady nonrotational flow around rectilinear profile in finite width uniform current in linear theory, calculating fluid exerted forces 10 p1549 A71-23822

Steady perturbations generated by simple discontinuity in wind field upstream from obstacle in stratified fluid 10 p1638 A71-23840

Vortex layer near circular cone surface in supersonic axisymmetric steady flow of homogeneous inviscid gas 10 p1551 A71-24372

Steady two dimensional MHD laminar flow between two parallel circular porous disks in transverse magnetic field, determining velocity, pressure and shear stress distribution 10 p1649 A71-24408

Closed steady streamline creeping flow in cylindrical cavity applied to bubble or plug train in pulmonary and peripheral capillaries 10 p1571 A71-24614

German monograph on steady toroidal discharges and cylindrical vortex arcs, using electromagnetic gas dynamics equations 10 p1654 A71-25025

Finite difference computer algorithm to solve vertical velocity equation of steady air flow about mesoscale obstacle in stably stratified atmosphere
11 p1793 A71-25169

Galactic wind as steady radial perfect gas flow from stars and central gravitating source
11 p1818 A71-25207

Steady three dimensional subsonic nonviscous flow through turbomachine with arbitrary hub and shroud shapes and finite blade number, using iterative blade to blade procedure
[ASME PAPER 71-GT-2] 11 p1702 A71-25948

Steady transonic flow through two dimensional gas turbine cascades predicted with time dependent formulation of flow equations, giving airflow surface pressure distributions
[ASME PAPER 71-GT-89] 11 p1704 A71-25996

Tangential velocity profile in steady incompressible electrically conducting viscous axial flow between concentric rotating cylinders with radial magnetic field, solving Navier-Stokes equations
11 p1752 A71-26048

Steady barotropic motion of ideal fluid, determining conditions for unit vector serviceability as velocity direction field
11 p1753 A71-26563

Numerical analysis of steady symmetric incompressible flow past elliptical cylinders for Reynolds numbers up to 90
12 p1895 A71-26739

Steady Oseen flow past seminfinit flat plate with force singularity, deriving integral equation solution
12 p1896 A71-26938

Steady supersonic isoelectric flow of thermally and calorically perfect gas past circular cones at zero angle of attack, using dimensional perturbation method
12 p1863 A71-26939

Rectilinear piping system with steady liquid flow, investigating free vibration damping, steady-state amplitudes and stability
12 p1975 A71-27113

Conservation theorem of velocity circulation along moving contours in continuous steady ideal gas flows
12 p1863 A71-27305

Cylindrical duct stationary uniform axial flow effects on propagation of acoustic vibration modes of wavelength smaller than damping length
[ONERA-TP-969] 12 p1981 A71-27479

Hydrodynamic analogy for postulates in special relativity theory, analyzing steady and potential flow of inviscid compressible medium for Chaplygin gas with unreal time
12 p1932 A71-27547

Similarities between ion waves in plasmas and gravity waves in incompressible fluid / steady water flow with allowance for surface tension/
13 p2046 A71-27844

Closed system of macroequations for mass and energy conservation along symmetry axis of steady rarefied supersonic gas flow in front of blunt body
13 p1991 A71-29151

Steady hypersonic nearly free molecular rarefied gas flow about convex body, applying kinetic operator
13 p1991 A71-29152

Three dimensional steady separated liquid and gas flows past low aspect ratio bodies, deriving similarity laws for reduction to two dimensional problem
13 p2049 A71-29169

Flow theory of steady separation zone near body at high Reynolds numbers, determining vortex parameters counterflow inviscid region
13 p2049 A71-29171

Steady flow of electrically conducting incompressible viscous fluid in rotating parallel-plane channel under constant transverse magnetic field
13 p2110 A71-29296

Stationary Gaussian Markovian form randomly fluctuating pressure gradient effects on steady incompressible channel flow velocity
14 p2223 A71-29924

Acoustic wave amplification and attenuation in non-homogeneous steady flows applied to air jet discharging in organ pipe
14 p2224 A71-30208

Method of characteristics application to steady rarefied gas flow from spherical source or sink
14 p2225 A71-30214

Steady state flow of viscous incompressible fluid, proposing difference scheme for numerical solution of Navier-Stokes equations
14 p2226 A71-30437

Methane high temperature oxidation in steady flow system, predicting change rate of species concentrations and gas properties during reaction
14 p2285 A71-30457

Vertical fluid-filled channel with uniform internal heat source, analyzing steady plane-parallel convective motion
14 p2339 A71-30998

Small disturbance equations for steady transonic flows past thin lifting airfoils and slender bodies
[AIAA PAPER 71-566] 15 p2344 A71-31560

Constant density and viscosity fluid steady plane two dimensional flow under no external forces, deriving partial differential equations for vorticity, energy and pressure
15 p2389 A71-31728

Shearing flows in steady vortex around airfoil in perturbed velocity, considering aerodynamic forces torque
15 p2346 A71-31903

Coupled radiative transfer-gas dynamic interactions in unsteady wave propagation, two dimensional steady flows and atmospheric motions
15 p2515 A71-32562

Drag coefficients of bodies of revolution from wind tunnel shock induced steady flow data, considering blast loading experiments in shock tube
16 p2519 A71-32878

Two dimensional steady gas flows with heat addition, using reduction to partial differential equations
16 p2662 A71-33168

Vapor-liquid mixture steady flow from centrifugal injectors, determining kinetic energy loss relationship to phase separation
16 p2624 A71-33608

Steady inhomogeneous axisymmetric nozzle flow, determining pattern by simultaneous solution of radial equilibrium and continuity equations
16 p2521 A71-33614

Perfect incompressible fluid steady rotational linearized three dimensional flows, calculating complex waves system
16 p2560 A71-34056

Steady plasma flow velocity measurements, describing two channel high resolution spectrometer
17 p2787 A71-34390

Navier-Stokes steady nonrectilinear universal complex laminar flow, showing isochoric lamellar or plane motions of constant velocity with streamlines as concentric circles
17 p2727 A71-34695

Numerical solution for two dimensional steady state fluid flow in square cavity by optimum time step formulation
17 p2728 A71-34880

Steady incompressible flow with potential vortex over flat surface under suction
17 p2670 A71-34889

Heat transfer in wall region of steady turbulent flow at large Prandtl numbers, plotting temperature distribution curves
17 p2728 A71-35119

Steady barotropic motion of ideal fluid, determining conditions for unit vector serviceability as velocity direction field
17 p2729 A71-35503

Tubular models sealed at one end with cavity facing oncoming steady gas flow, measuring increased stagnation temperature associated with shock wave formation
17 p2672 A71-35628

Two dimensional steady potential incompressible flow past elastic expandable gas filled envelope fastened to edge of plate normal to flow
17 p2730 A71-35640

Quasi-stationary viscous incompressible liquid flow in porous tube with deforming wall
17 p2694 A71-35641

Shock wave formation in stationary flow adjacent to supersonic flow region, using Friedrich simple wave theory
17 p2673 A71-35645

Two dimensional steady viscous gas transonic flow Navier-Stokes equations, establishing uniqueness of solutions to boundary value problems
17 p2673 A71-35646

Laminar boundary layer structure under seminfinit potential vortex maintained in incompressible steady flow by appropriate conditions at infinity
18 p2906 A71-36317

Two dimensional steady laminar boundary layer theory for incompressible medium, presenting error bounds for Prandtl equation solution
18 p2906 A71-36322

Steady inviscid fluid flows in plane channel and in axially symmetric nozzle, considering external magnetic field effects with electroconductive fluid
18 p2907 A71-36327

Second order accuracy and stability analysis of method of characteristics application to three dimensional steady supersonic flow
18 p2907 A71-36329

Velocity field of viscous steady plane incompressible flow past body, linearizing by Oseen approximation
18 p2910 A71-36946

Stationary plasma flow interaction with axisymmetric spatially periodic magnetic field in presence of Hall effect, determining electric currents structure
19 p3109 A71-37139

Conservation theorem of velocity circulation along moving contours in continuous steady ideal gas flows
19 p3046 A71-38258

Planetary boundary layer stationary air flow over plane homogeneous surface under geostrophic wind

conditions, solving for thermal turbulence field stabilization by iterative method
19 p3091 A71-38468

Slide valve slot fluid flow oscillation frequency range estimate for quasi-stationarity
20 p3183 A71-39168

Short shock wave equations solutions for two dimensional steady flow of ideal gas
20 p3211 A71-39370

Perturbed problem of rotational steady compressible flow in three dimensional channel at upstream infinity / shear flow/, using linearization by current functions
20 p3211 A71-39419

Viscous fluid stirring due to small amplitude rigid circular cylinder rotation, calculating steady flow velocity relationship to Reynolds number
20 p3177 A71-39481

Steady axisymmetric incompressible flow past sphere at low Reynolds numbers, reducing equations of motion to ordinary differential equations
20 p3212 A71-39506

Viscous electrically conducting laminar fluid steady flow through insulated MHD duct under uniform external magnetic field by extended Kantorovich method
20 p3275 A71-39561

Small perturbations of stationary parallel flow with relaxation, considering boundary conditions around slender wings, partial differential equations and similarity law
20 p3213 A71-39569

Acoustic signal pressure mode propagation velocity in infinite rectangular hard-walled duct with steady flow, noting Doppler effect
20 p3271 A71-39765

Elastico-viscous liquid steady secondary flow induced by oblate or prolate spheroid rotating about axis of symmetry from linear partial differential equations solution
20 p3214 A71-39967

Steady and unsteady flow work and energy loss relationships expressed in integral form representing perturbation kinetic energy, internal energy and pressure work
21 p3317 A71-40011

Plane steady irrotational flow of ideal compressible fluid around jet profile, obtaining Kutta-Joukowski theorem
21 p3322 A71-40580

Quasi-steady three dimensional ideal compressible fluid flow between convex and concave sides of neighboring blade profiles in axial flow turbine
21 p3322 A71-40687

German monograph on three dimensional steady hypersonic flow of perfect gas past pyramid shaped bodies of rhombic planform
21 p3323 A71-40774

Steady slow free molecule flow past sphere, obtaining distribution function and surface boundary conditions
21 p3370 A71-40987

Small mesoscale waves development in steady stratified plane parallel flow, assuming mean flow characteristics dependence on vertical coordinate
21 p3412 A71-41391

Kinetic and kinematic properties of steady diabatic complex lamellar gas flows
22 p3530 A71-41696

Steady laminar flame propagation speed prediction computation, applying to hydrazine decomposition
22 p3621 A71-42098

Approximate nonlinear theory of steady incompressible fluid flow about cylindrical bodies from vortex method for thin lifting surfaces
22 p3481 A71-42867

Steady laminar viscous hydromagnetic flow in annulus with porous walls of different permeability, giving wall friction coefficients and velocity distribution
23 p3708 A71-43099

Lifting rectangular thin airfoil in symmetrical incompressible steady uniform orthogonal flow at small angle of attack, deriving Weissinger integral equation
23 p3625 A71-43487

Class of steady viscous incompressible axisymmetric nonrotating flows with axial velocity component dependent on distance along axis from reference point
23 p3663 A71-43489

Rivlin-Ericksen fluid steady flow between parallel plates with uniform suction at lower wall, detailing velocity field, skin friction and flow coefficient
23 p3663 A71-43492

Random fluctuating longitudinal pressure gradient effect on steady incompressible channel flow for arbitrary power spectrum and probability density
23 p3664 A71-43597

Cavities geometry in steady or periodic supercavitating flow from light beam transmission in flow tunnel
23 p3664 A71-44005

Approximate solution for position and strength of shock waves about cones in steady supersonic flow
24 p3790 A71-44624

Natural trihedrons associated with stationary or nonstationary flows in hydrodynamics and MHD, using moving reference theory

24 p3856 A71-44795

Pressure and flow direction defects behind Mach reflected shock near three shock intersection, considering steady flow theoretical model

24 p3820 A71-44953

STEADY STATE

Nonlinear automatic control systems steady random processes approximate analysis by integral linearization of functions and operators

01 p0058 A71-10100

Frequency multipliers and dividers with step-recovery diodes, calculating steady state behavior as function of circuit parameters and input frequency

01 p0052 A71-10322

Linear dynamic plants in steady state identified via multichannel statistical optimizer

01 p0064 A71-10923

Steady state motion equations of multiple unit impact damper attached to periodically excited primary system, developing solution for mathematical model

03 p0505 A71-13547

Differential equations of spherical motion of heavy solid body with ellipsoidal cavity filled with liquid, deriving stationary solutions

03 p0457 A71-13586

Electromagnetic wave absorption in steady state cosmology, considering particle collision and radiation damping effects in plasma model

05 p0806 A71-16167

Hydrogen-oxygen catalytic ignition system steady state model for predicting temperature and concentration profiles

05 p0795 A71-16350

Hydrogen-oxygen reaction kinetics behind steady state shock waves under isothermal branched chain explosion limits

05 p0834 A71-16513

Steady state current-free magnetized plasma generation by microwave discharge, using feedback control to reduce power fluctuations

06 p0938 A71-18458

Unbounded isotropic elastic plate traversed by two parallel cracks, obtaining limiting equilibrium state

07 p1211 A71-19192

Variational approaches to steady state heat conduction, discussing relationship between variational and differential problems

09 p1545 A71-22453

One dimensional steady state performance characteristics of thermomagnetic generators and refrigerators in dimensionless form

09 p1387 A71-23647

Steady state temperature field for infinite space with spherical cavities distributed along straight line, reducing problem to infinite system of algebraic equations

10 p1695 A71-24359

Dynamically symmetrical gyrostad steady state motion stability in force field of two fixed centers, using Raus-Liapunov theorem

10 p1683 A71-24579

Deterministic steady state error model for floated inertial gyroscope, considering lateral or rotational float displacement and temperature distribution variations

11 p1761 A71-25517

Liquid metal cooled, fast spectrum thermionic reactor experiment design based on Fast Reactor Core Test Facility use for dynamic and steady state characteristics determination

11 p1710 A71-25867

Nonlinear hysteretic element narrow band resonant system operating in steady state at fundamental resonance

11 p1743 A71-26538

Forced convection effects on characteristics of steady state cross flow arc in presence of applied transverse magnetic field

12 p1938 A71-27265

Human body thermal behavior modeling, obtaining steady state analytical solution for various boundary conditions and parameters

12 p1875 A71-27563

Heat pipes steady state and dynamic behavior, noting pressure balance, vapor flow, transport capability and applications

12 p1987 A71-27741

Steady state scattering of cylindrical magnetoacoustic waves traveling along axis of rigid ideally conducting static cylinder

13 p2105 A71-28281

Stability of steady states of physical system with respect to finite perturbations

13 p2100 A71-28451

Quantization by levels effect on steady state processes in digital automatic control systems

13 p2044 A71-28918

Gas particle radial reflection model application to hypersonic nearly-free molecular flow about convex bodies, solving steady state problem

13 p1991 A71-29153

Steady state wind driven currents velocity in Lake Erie, using shallow lake level model in numerical calculation

14 p2231 A71-29935

Structural steady state vibration frequency response and resonance testing, investigating nonlinearity effects of large deflections

14 p2326 A71-30065

Velocity-aided Kalman filtering for one dimensional motion under random acceleration, obtaining steady state solution and transit time

14 p2197 A71-30793

Steady state analysis of phase controlled parasitic current, discussing reduction of alternator apparent power requirements and harmonic distortion

15 p2355 A71-32218

Steady state and transient interactions due to thermal integration of isotope Brayton space power and life support systems

15 p2364 A71-32220

Steady state of nonequilibrium Ar-Cs plasma in electric field, attributing instability to plasma radiation effect

15 p2457 A71-32273

Control system stability with nonlinear feedback in steady equilibrium state

16 p2548 A71-32934

Two dimensional axisymmetric shell analytical model for liquid propellant launch vehicle longitudinal vibration modes and steady state response calculation

16 p2653 A71-33092

Plane mirror ruby laser pseudosteady regime, discussing fundamental TEM mode case

16 p2588 A71-34062

Spiral structure of Galaxy, using perturbation method for analysis of steady state interstellar gas with differential rotation due to coupling with stellar gas

16 p2643 A71-34069

Elastic stress waves propagation in photoelastic layered composite materials, indicating wave front steady state

17 p2824 A71-34816

Steady state and transient response of heat source with temperature regulated by electrical feedback controlled variable conductance heat pipe

18 p2868 A71-36394

Two dimensional steady state detonation waves, obtaining generalized Rankine-Hugoniot equations

19 p3045 A71-38126

Steady state thermoelastic mixed boundary value problem for elastic layer with one face stress free and other face resting on rigid frictionless foundation

20 p3309 A71-39495

Ion cyclotron resonance power absorption, deriving expression for average ion kinetic energy at saturation in steady state limit

21 p3418 A71-40231

Steady state performance of two degrees of freedom system consisting of main linear spring mass system under periodic forcing

21 p3459 A71-40298

Transient and steady state flexible rotor dynamics analysis

21 p3461 A71-40325

Fiber reinforced elastic materials steady state plane wave propagation by modeling constituents as continua undergoing individual motions

21 p3469 A71-41004

Mixed and unmixed turbofan engines transient and steady state off-design characteristics, investigating effects of fuel flow rate, nozzle area, inlet pressure, ambient temperature and air bleed

22 p3590 A71-42836

Low thrust interplanetary spacecraft tracking, using spectral factorization for Kalman filtering equations

23 p3732 A71-43063

Digital servo system with signal quantization by level and time, evaluating oscillating motion in steady state mode

23 p3655 A71-43292

Steady state gains and covariance computation for time invariant discretely updated linear systems, demonstrating iterative and algebraic solutions

23 p3660 A71-44116

Parameters steady random variations effect on linear and nonlinear systems steady motion characteristics, using integral equation and averaging methods

24 p3815 A71-44696

Transients determined for Cs vapor discharge phases, observing current fluctuations between steady states in negative resistance zone above 0.2 torr

24 p3858 A71-45246

STEADY STATE CREEP

Anisotropic nonhardenable materials steady creep deformation potential as function of mixed invariant of stress and anisotropy tensor

01 p0172 A71-10797

Matrix stacking fault energy effects on steady state creep rate of recrystallized nickel-cobalt-aluminum oxide alloys, showing stress dependence

08 p1315 A71-21578

Two dimensional stress-strain fields under elastic and elastic-plastic strains and steady state creep, calculating stress distribution around hole in cylindrical shell

09 p1538 A71-22000

Dynamic programming for designing beams and plates under steady creep with minimum weight discussing cantilever beam optimization

11 p1853 A71-26000

Al and Al-Mg alloys average interdislocation internal stress measurement during steady state creep

12 p1916 A71-26000

Torsion creep tests of Al, deriving expressions for steady state creep rate as function of temperature and stress

13 p2083 A71-26000

Transient and steady state creep of circular cylindrical shells loaded by internal pressure, using steady state hardening hypotheses and finite difference methods

14 p2328 A71-32220

Dynamic programming to design beams and plates under steady creep with minimum weight, applying cantilever beam

17 p2832 A71-32273

Recovery-strain hardening rate model for steady state creep

21 p3462 A71-32934

Numerical analysis of steady state creep of simply supported circular cylindrical shells by combining Newton and finite difference methods

21 p3463 A71-33092

Material random temperature and imperfection density effects on 3-bar truss nonlinear steady creep solutions for stress and velocity

22 p3615 A71-34062

Thin soft layer under steady creep conditions, considering axisymmetric problem of simultaneous tension and torsion

24 p3877 A71-34816

Small deflection theory for steady state creep bending of laminated anisotropic rectangular plate under uniform loads, using Galerkin method

24 p3841 A71-34816

STEADY STATE FLOW U EQUILIBRIUM FLOW STEAM

Steam-air mixture viscosity, deriving empirical formula from experimental data

01 p0118 A71-10322

STEAM GENERATORS U BOILERS STEAM TURBINES

Steam turbine blade metal removal rates by repetitive water drop impact, using hydrodynamic model

03 p0405 A71-18458

Cyclic thermal cracking and fatigue analysis in large steam turbine rotors with three dimensional temperature and triaxial stress computation

07 p1216 A71-20000

Axial flow steam and gas turbines performance estimations over ranges of loading, velocity/blade ratio Reynolds number and aspect ratio

15 p2469 A71-31000

Stream lines construction in meridional plane blade nozzle annular cascades of steam and gas turbines in subsonic and supersonic flow

17 p2670 A71-34062

Steam turbine blades induction brazing with programmed cycle, describing coil design

19 p3070 A71-38126

Transonic and supersonic turbine guide vanes, noting air as flow medium in experiment and steam in actual turbine

20 p3176 A71-39495

STEARTHERMOPHILUS

Stearothermophilus spore germination stimulation investigating effects of preheating and amino acid carbohydrate concentration

13 p2010 A71-28918

STEATITE U TALC STEEL STRUCTURES

Steel cylinders with circumferential cracks under repeated impact tensile loads, investigating plain strain fracture toughness index temperature dependence

01 p0166 A71-10797

Tungsten plasma coatings on steel, examining strength dependence on vaporization distance, microstructure and residual stresses

01 p0088 A71-10797

Low temperature steel welded joints resistance brittle fracture, discussing Niblink dynamic loading deep notch static loading and Charpy V tests

03 p0433 A71-14000

Steel-concrete composite beam creep numerical analysis by reduction to elastic problem with initial strains

04 p0669 A71-15000

Steel conical disks two dimensional stressed state determined with deformations at elastic and elastoplastic strains using digital computers

08 p1369 A71-21578

Structural efficiency improvement by materials selection for airframe structures, discussing Al, Ti-Al-V and steel panels 08 p1299 A71-21685

Static friction in steel-polymer couples under vacuum, considering temperature, contact time, normal load and physicomechanical properties effects 09 p1454 A71-22818

Welded steel structures fracture safe design, considering continuity conditions responsible for catastrophes resulting from crack initiation 09 p1458 A71-23453

Light aircraft steel landing gear springs structural design at Cessna, considering certification requirements [SAE PAPER 710400] 10 p1555 A71-24262

Variouly thick standard production heavy plate constructural steels stress condition and elastic energy margin effects on cold brittleness 15 p2414 A71-31652

Steel structural elements resistance reserve to brittle fracture, considering critical temperatures and breaking stresses 15 p2504 A71-31852

Steel cylinders with circumferential cracks under repeated impact tensile loads, investigating plane strain fracture toughness index temperature dependence 16 p2658 A71-33635

Plastic deformation and embrittlement due to stress raisers in steel cylinders from high speed tensile tests at low temperatures 17 p2832 A71-35462

Lubricated friction of steel ball on commercial tempered aluminum plate as function of time 21 p3396 A71-40100

Soviet book on diffusion coatings effects on steel structural elements strength covering cementation, nitriding, sulfidizing, boronizing, siliconizing, chromizing and calorizing processes, etc 23 p3693 A71-44183

STEELS

NT AUSTENITIC STAINLESS STEELS

NT BAINITIC STEEL

NT CARBON STEELS

NT CHROMIUM STEELS

NT HIGH STRENGTH STEELS

NT MARAGING STEELS

NT MARTENSITIC STAINLESS STEELS

NT NICKEL STEELS

NT STAINLESS STEELS

Annealed steels strengthening and structural changes under explosive shock wave 01 p0085 A71-10037

Mechanical properties effect on steels fatigue crack growth rate as function of stress intensity factor 01 p0099 A71-10167

Notched steel bars fatigue strength improvement via compressive self stresses/residual stresses/ 01 p0167 A71-10172

Rapid identification of steels and other metals by chemical, instrumental and organoleptic methods 01 p0183 A71-10256

Prealloyed hot formed Cr-Ni-Mo and Ni-Mo steels manufactured from powders, considering toughness, tensile properties, fatigue and impact strength 01 p0100 A71-10464

Soviet book on boride coatings on iron and steels covering physicochemical interactions and properties 02 p0263 A71-11848

Temperature and plastic deformation rate effects on plasticity and strength of cast iron, Ti and steels 02 p0257 A71-12525

High stress cycles and impact fatigue behavior of common case hardened carburized gear steels under loading 03 p0441 A71-13253

Notched tensile plate steel specimens, investigating temperature and stress state effects on nil ductility transition and fracture strength [SESA PAPER 1735] 03 p0443 A71-13752

Spectrochemical analysis of alloy steels using microspark method 03 p0375 A71-13974

Medium alloy structural steels tempering, investigating Mn, Ni, Cr and Mo effect on activation energy of softening 03 p0445 A71-14338

Steels prior austenite and martensite grain size control by thermal cycling 03 p0446 A71-14492

Physical-metallurgical nature of brittle fracture of steels from phenomenological and atomic /dislocation/ approach 03 p0516 A71-14576

Brittle fracture resistance of mild steel after low cycle fatigue damage 03 p0516 A71-14579

Steel brittle fracture tests using explosive charge stress wave absorption measurements 03 p0517 A71-14583

Steels brittle fracture susceptibility by notch impact bending test, considering plastic deformation zone and crack propagation 04 p0610 A71-14889

Carbide particles mean interparticle spacing and low alloyed steels dislocation density determination by planar and volume methods for metal matrix 04 p0612 A71-15076

Reversible hydrogen brittleness of steels in terms of dislocation theory 04 p0612 A71-15550

Energy dissipation patterns of metal fatigue failure during static and cyclic loading applied to untreated and heat treated steel samples 04 p0671 A71-15637

Sulfide precipitates shape preservation in high strength low alloy hot rolled steel sheets, discussing effects of various additive elements 04 p0614 A71-15782

Martensite formation and fracture toughness in TRIP steels, examining effects of plastic zone ahead of crack tip and triaxiality ahead of notch 04 p0615 A71-15792

Steel wire reinforced Al manufacture and properties, discussing wire-matrix bonding 05 p0764 A71-15922

Cylindrical steel samples with screw type threads, comparing pressed and ground threads effects on tensile strength at low temperatures 05 p0827 A71-16763

TSh-2 hardness test gage, investigating deformation of steel under increasing loads 07 p1106 A71-19141

Industrial Ni alloys and steels fatigue life by short time data extrapolation 07 p1129 A71-19152

Steel under cyclic loads, observing relationship between changes in microstructure and temperature curve shape in fatigue failure process 07 p1211 A71-19194

Steels surface layer strain hardening during diamond smoothing 07 p1117 A71-19364

High temperature ductility of low alloy ferritic steels, correlating tensile elongation values to crack nucleation resistance 07 p1134 A71-19517

Steel coatings produced by boriding, investigating structure and wear resistance properties 07 p1118 A71-19583

Phase transformations during tempering of rhenium steels using X ray, dilatometric and conductivity measurements 07 p1135 A71-19617

Oxide films effect on heat resistant steels hydrogen permeability, using mass spectrometer 07 p1136 A71-19920

Steels fatigue tests, observing crack propagation through weld heat affected zones at two orientations to stress axis 07 p1139 A71-19989

Titanium-steel bimetal part fabrication using explosive and drop forging 08 p1295 A71-20840

Vibrational tumbling effects on steel compressor blades surface roughness, cold hardening, residual stresses and fatigue strength 08 p1295 A71-20842

Forged superhigh density sintered steels strength and fracture mechanism 08 p1304 A71-20995

Multisample test equipment for steels and alloys oxidation resistance at high temperatures in corrosive gaseous atmospheres 08 p1292 A71-21440

Luders bands motion in steel and iron, studying plastic zone velocity dependence on stress, composition, grain size, dislocation substructure and temperature 08 p1308 A71-21517

Guinier-Preston zone formation by mixed substitutional-interstitial solute-atom clustering in bcc metals, considering steel strengthening 08 p1311 A71-21541

Long term creep strengthening by molybdenum in untempered iron and steel 08 p1315 A71-21579

Titanium-steel continuously reinforced composites strength to weight ratings, describing ausforming process and fatigue tests 08 p1316 A71-21587

Cylindrical steel specimens bearing strength under cyclic elastoplastic deformation, investigating stress redistribution effects 08 p1316 A71-21607

Steels in stressed state, determining hydrogen saturation and occlusion 09 p1467 A71-22309

Steels mechanical properties factor analysis, considering Brinell hardness, tensile strength, yield point, relative contraction, elongation and impact strength 09 p1467 A71-22312

Optimum tip vertex angles measurement for determining steels tensile strength and yield point from hardness 09 p1467 A71-22314

Fast brittle crack slowing by mechanical twins in transformer steel and by slip bands in LiF and NaCl crystals 09 p1468 A71-22625

Metallic polycrystalline materials volume changes in plastic deformation from measurements on steel elongation and cross section diameter reduction 09 p1540 A71-22997

Complex alloying of structural steels, stressing structural changes, electron interactions and phase transition changes 09 p1470 A71-23075

Steels, Ni alloys and Ti alloys deformation resistance and deformability, discussing temperature effects on forging rate 09 p1475 A71-23305

Cold prestraining effect on steady state creep strength and rate of precipitation hardened heat resistant steel 09 p1477 A71-23331

Thin cracked steel plate strip necking zone relative opening displacement and strain measurements by moire method 09 p1542 A71-23540

Steel sheet specimens under temperature and stress cycles, studying creep, plastic deformation and service life 10 p1686 A71-24189

Thermal fatigue and service life of thin walled tubular pearlite steel notched specimens in various oxidizing media 10 p1626 A71-24191

Jetting collision effect on structural changes at interface between Ti and steel in explosive bonding, considering plastic deformation and residual stresses 10 p1629 A71-25030

Steel structural transformations under arc melting, cooling and electroslog remelting, noting delta ferrite precipitation with hot stage microscope 11 p1776 A71-25168

Steel alloys solid Cd embrittlement, discussing crack propagation rate temperature dependence and Cd surface diffusion as controlling effect 11 p1777 A71-25447

Low alloy steels and superalloys inertia welding in gas turbine field, discussing microstructure tensile strength and stress rupture [ASME PAPER 71-GT-21] 11 p1770 A71-25965

Quenched and tempered steel, investigating embrittlement as function of temperature in partially dissociated atomic hydrogen environment 11 p1779 A71-26013

Friction and wear of steels, Ti, Al, Cu and copper beryllium in sliding over hardness range of steel plates in vacuum and air 11 p1771 A71-26143

Structural stability degradation mechanisms in welded joint of plain and low alloy steels, deriving equation for carbon diffusing 11 p1771 A71-26158

Al alloys and steel, determining potential and pH changes during stress corrosion crack propagation by microelectrode technique 11 p1783 A71-26497

Plastic deformation and aging effects on fatigue characteristics of steels until rupture under cyclic loads 12 p1916 A71-26945

Boride coated steels and cast iron surfacing with nonconsumable tungsten electrode for higher abrasive wear resistance 12 p1917 A71-27125

Jet fuels deoxygenation effects on steels antiwear properties and critical loading under vibrational and gliding friction 12 p1945 A71-27662

Titanium-containing steels nitriding in ammonia, discussing hydrogen diffusion layers brittleness, cracking, peeling and thickness 12 p1919 A71-27776

Thermal emf measurement of Ti alloy, steel, bronze and duraluminum subjected to fretting corrosion tests 13 p2082 A71-27820

Friction coefficient and wear of steel in vacuum and air at low and room temperatures 13 p2072 A71-27870

Refractory and structural steels and Al alloys, obtaining low cyclic plastic deformation and breaking stress curves 13 p2148 A71-28116

Refractory steels plastic deformation characteristics under isothermal creep 13 p2084 A71-28125

Cyclic strain effects on creep for steel at elevated temperatures, discussing overload frequency effects on plastic strain buildup 14 p2256 A71-29626

Vibration fatigue of metallic materials in vacuum and different gas atmospheres, considering fcc metals, Al alloys and steels [DFVLR-SONDDR-62] 14 p2259 A71-30466

Molybdenum steel annealing, noting carbide phase transformations 15 p2425 A71-31398

Linear plastic deformation of steel under tension, investigating anisotropy in elastic modulus and strength

15 p2503 A71-31478

Hardened low alloy steel ultrasonic attenuation under magnetic field due to thermally introduced residual stresses

15 p2414 A71-31641

Steels resistance to brittle fracture at various temperatures, determining failure stress and transition temperatures for nonuniform stress distribution

15 p2428 A71-31855

Stress distribution during plastic deformation of steel turbine disk from hardness measurements

15 p2505 A71-31863

Multipass low alloy steel weld metal strength dependence on microstructural changes due to thermal effects

15 p2437 A71-32614

Pressed or sintered steel powder joining to wrought mild steel parts, evaluating welded joints with torsion test

15 p2417 A71-32615

Complex alloyed steel under electroslag welding, investigating heat treatment effect on heat affected zone phase composition

15 p2437 A71-32661

Ferritic steels weldability, establishing relations between transition points and cold crack formation

15 p2417 A71-32662

Steel joint weld decay mechanism, observing intergranular corrosion initiation and development in nitric acid solutions

15 p2417 A71-32665

Grade 15 steel vacuum diffusion welding to AMTs alloy or AD1 aluminum, using nickel interlayer in joints

15 p2418 A71-32667

Steels and alloys structure and properties - Conference, Moscow, May 1968

16 p2596 A71-33914

Ti influence on ductility of normalized low alloy steel, considering crack initiation and propagation

16 p2598 A71-33991

Thermostable and heat resistant steels and alloys vibration loading frequency effects on fatigue at high temperatures

16 p2598 A71-33992

Fatigue crack propagation model for explosion bonded titanium-steel system under constant load amplitude conditions

16 p2600 A71-34096

German monograph on structural steels tensile and yield strength, detailing strain rate and testing machine effects

17 p2818 A71-34483

Reversible hydrogen embrittlement mechanism in hydrogenated steels

17 p2757 A71-34496

Circumferential notch effect on distribution of compressive self stresses produced by shallow skin layer expansion in round steel bars, using finite element method

[SESA PAPER 1831]

17 p2819 A71-34529

Heating by thermoelectric damping through sudden removal of stresses on homogeneously strained elastic body, comparing elastic deformation of rubber and steels

17 p2821 A71-34584

Gas turbine engine steels and Al alloys heat resistance, examining fatigue life and creep properties at various temperatures and test durations

17 p2759 A71-35453

Industrial Ni alloys and steels rupture strength by short time data extrapolation

17 p2760 A71-35651

Cylindrical steel and Ni alloy specimens bearing strength in inhomogeneous stress states under cyclic elastoplastic bending and loading to failure

17 p2760 A71-35668

Dynamic yield and absorptivity of steel during brittle fracture propagation under neutron irradiation

18 p2934 A71-35987

Structural steels fatigue resistance, investigating processing technique, chemical composition, plastic and hot working and heat treatment effects

18 p2934 A71-36149

Cutting speed, feed rate, tool geometry and other machining factors effects on surface finishes of face milled steels, titanium and nickel base alloys

[SME PAPER MR-71-146]

18 p2927 A71-36663

Salt bath application to steels and Al alloys heat treatment, discussing carburizing, neutral hardening, austempering, martempering, annealing and brazing

18 p2927 A71-36665

Prestrain directional effects in steel tension and compression test specimens, noting Bauschinger and work hardening effects

18 p2937 A71-36834

Mathematical model for continuous elastoplastic transition stress-strain response of steels and nonferrous metals

18 p2937 A71-36835

Mechanical properties of carburized cermet steel with hypereutectic structure after water quenching and tempering at 300 C

19 p3076 A71-37113

Structural stability and creep properties of heat resistant steel weld joints, considering substitutional and precipitation hardening and dislocation effects

20 p3249 A71-39015

Creep strength extrapolation for high temperature steels, suggesting combined numerical and graphic methods

20 p3249 A71-39017

Creep tests on heat resistant steels, studying elongation/rupture strength and temper hardening

20 p3251 A71-39026

Grain boundary dislocations generation and motion in deformed Nb steel in relation to sliding, using electron microscope analysis

21 p3395 A71-40021

Steels, aluminums and titaniums ultimate and yield strength statistical distributions in Weibull parameter form, presenting stimulus-response potential failure model

[ASME PAPER 71-VIBR-64]

21 p3396 A71-40307

Brittle transition temperature of steels by Vickers hardness testing, comparing with tensile properties and impact fracture process in Charpy impact test

21 p3388 A71-40751

Statistical analysis of endurance limits for castings and forgings of die forged and cast steel, using rotating beam fatigue tests

21 p3388 A71-40754

Cryogenic steels, Al and Ti alloys plane strain fracture toughness at room and subzero temperatures, discussing tensile and notch bend results

21 p3401 A71-40915

Shatter crack incubated nucleation in relation to heat treatment effects on hydrogen elimination in steels, comparing with thermal explosion mechanism

21 p3402 A71-41090

Microhardness, thermo-emf and phase composition of Al coatings on Armco iron and steel under furnace and rapid electric heating

21 p3389 A71-41096

Titanium-containing steels nitriding in ammonia, discussing hydrogen diffusion layers brittleness, cracking, peeling and thickness

21 p3424 A71-41097

Alloy steels supercooled austenite nitriding in ammonia flow, examining diffusion layers by X ray analysis and hardness tests

21 p3404 A71-41164

Diffusion layer structure and phase composition during quenched and annealed steel saturation by Cr at high heating rates

21 p3404 A71-41170

Boridosilicide and boridoaluminide diffusion coatings on iron and steel, investigating formation kinetics structure and properties

21 p3390 A71-41171

Soviet book on steels high temperature elastic stiffness and ductility covering carbon, alloyed and special steels at different temperatures and strain rates

21 p3404 A71-41375

Steels fatigue behavior and cumulative damage effect prediction under strain controlled conditions, comparing with experimental data

22 p3559 A71-41593

Ultrasonic defectoscopy of steel samples, considering grain size effects on SNR

22 p3528 A71-41757

Microhardness and magnetic permeability and viscosity changes during fatigue loading of steel parts, describing electromagnetic fatigue testing method

22 p3554 A71-41771

Fatigue, necked-out and intermediate fracture types observation in load-controlled low-cycle fatigue tests of rolled steel

22 p3617 A71-42496

Thermocouple measurements of thermal gradients in steel during automatic welding

23 p3679 A71-43892

Steel with various intensity stress risers under bending loads, showing difference in crack nucleation and propagation resistance

23 p3778 A71-44036

Heat resistant steels long time strength determination by graph-analytical time-temperature extrapolation

23 p3693 A71-44213

Microalloying effects on phase composition, surface phenomena, fine crystalline structure and microstructure of E1417L steel

24 p3836 A71-44374

Steel silicification in liquid media for high temperature oxidation resistance improvement

24 p3829 A71-44731

Plasma spraying steel coating process, establishing regularity of particle flight velocity variation with distance from burner nozzle

24 p3829 A71-44737

Seizing of flat and flat/spherical steel samples pairs in vacuum as function of temperature, pressure and time of contact, using compression-tension machine

24 p3838 A71-44857

Polyethylene coated machine steel fatigue strength in air, 3 percent NaCl bath and molecular sulfuric acid solution

24 p3841 A71-44863

STEEP GRADIENT AIRCRAFT

U V/STOL AIRCRAFT

STEEPEST ASCENT METHOD

U STEEPEST DESCENT METHOD

STEEPEST DESCENT METHOD

Gradient /steepest ascent/ methods for differential equation systems optimization, discussing convergence acceleration and nonlinear programming

02 p0277 A71-12729

Differential descent method modifications, comparing convergence rates and insensitivity to computer computational errors

05 p0775 A71-1701

Modified steepest descent algorithm for optimum trajectory computation applied to interceptor missile control

14 p2207 A71-30018

Boundary value problems solution in optimal control theory, discussing gradient descent method in state space

19 p3037 A71-37534

Mineral composition optimization of nutrient medium for Hydrogenomonas, using steepest ascent method for mathematical planning of experiments

20 p3193 A71-39236

Elastic trusses optimal design under multiples mechanical constraint conditions, describing steepest descent method with constraint error compensation

21 p3470 A71-41021

Branched space trajectory optimization by steepest descent method with coasting arcs, obviating numerical integration for accuracy increase and computing time reduction

[AAS PAPER 71-309]

23 p3725 A71-42985

Branched trajectory optimization algorithm using steepest descent method applied to space shuttle vehicle mission design

[AAS PAPER 71-326]

23 p3726 A71-43000

Convergence improvement in parallel tangents/penalty function solutions for missile trajectory optimization with terminal constraints, comparing with steepest descent method

23 p3659 A71-44102

STEEPNESS

U SLOPES

STEERABLE ANTENNAS

Steerable 100 m radio telescope design, surface accuracy, receiving installation and cryogenically cooled parametric amplifiers

01 p0068 A71-11342

Communication satellite earth station technology, considering steerable antenna subsystems, high power amplifiers, terminal equipment and frequency bands allocation

02 p0222 A71-12787

Communication satellite earth station steerable antennas drive train resonance and traction drive wheel slippage control by differential velocity feedback, discussing analog simulation

02 p0222 A71-12790

Communication satellite ground station steerable antenna autotracking, evaluating on-line optimal search techniques by digital simulation

02 p0222 A71-12791

Large antenna electrical and mechanical requirements, considering gain/temperature ratio, steerability, housing, design life and erection

02 p0235 A71-12831

Antenna steering systems for satellite communications, discussing tracking, mechanical drives and subreflector servo

02 p0235 A71-12832

Planar microwave array antenna for scan requirement, discussing tilt angle and element arrangement optimization

06 p0876 A71-18097

Planar microwave array antenna for scan requirement, discussing tilt angle and element arrangement optimization

[AJAA PAPER 70-191]

Large steerable radio telescope with equatorially mounted parabolic cylinder for lunar occultation, pulsar and scintillation observations

12 p1894 A71-26930

Wind gust effect on autotracking antenna servosystem tracking error, evaluating torque disturbance admittance

12 p1868 A71-27002

Airborne phased array using computer control for beam steering, investigating row-and-column logic effects on beam shaping and stabilization

14 p2209 A71-31045

L band aircraft antenna array consisting of circularly polarized elements and static electronic steering circuits for synchronous satellites radio links

14 p2273 A71-31074

Dioscures communication satellite system for air traffic control and navigation, discussing aircraft antenna beam electronic scanning by computerized control

17 p2714 A71-34681

Wide angle microwave antenna radiation beam steering with fixed parabolic reflectors, using adaptive primary feed for intercepted field spatial Fourier transformation
17 p2708 A71-35493

Pleumeur-Bodou /France/ ground station steerable parabolic reflector Cassegrain antenna for communication satellites, discussing specifications and radioelectric and mechanical characteristics
17 p2717 A71-35510

Electronic and hydraulic devices for communication satellite ground station steerable antenna servocontrol, driving and pointing, discussing tracking error signals
17 p2724 A71-35511

Three-channel monopulse tracking receiver for automatic steering of satellite tracking antennas, noting gain controlled IF amplifier module
18 p2884 A71-36996

STEERING

Aircraft steering system design, considering oversteering effects in nose wheels, torque for reaction moment balance and tire behavior
16 p2522 A71-33225

Fail operational control moment gyro configuration of four single gimbal gyros, eliminating cross coupling by simple analog steering law
[AIAA PAPER 71-936]
19 p3097 A71-37181

STEFAN-BOLTZMANN LAW

Boundary motion between media during transport phenomena under Stefan conditions, establishing shock front coordinates by Hadamard algorithm
03 p0520 A71-13951

One dimensional two phase Stefan problem solution for melting of heated thin plate, comparing iterative methods
16 p2662 A71-33065

Aircraft ice protection problems, considering one dimensional Stefan method for cyclic deicing system
17 p2838 A71-34850

Approximate solutions to Stefan nonlinear heat and mass transfer problem under various boundary conditions and phase transformation temperature
22 p3622 A71-42687

Temperature distribution in current carrying cylindrical conductor with nonlinear boundary condition of emission by Stefan-Boltzmann law
23 p3783 A71-44070

STELLAR ATMOSPHERES

NT CHROMOSPHERE

NT SOLAR ATMOSPHERE

Rotating stars with partially ionized convective envelopes, investigating general stellar magnetic field production
01 p0150 A71-10060

Stellar atmospheric physics - Conference, University of Queensland, Brisbane, Australia, May 1970
01 p0152 A71-10326

Blue supergiants evolution, discussing chemical composition of atmospheres, mass, binary nature and cluster association
01 p0153 A71-10375

Radiation transfer equation in extended hot stellar atmospheres, discussing scattering effects due to free electrons
01 p0158 A71-10802

Wolf-Rayet star atmospheres, discussing matter density distribution, light pressure effects on particle motion and H and He ionization levels
01 p0158 A71-10803

Hot stellar atmospheres, calculating mean radiation absorption coefficients as function of temperature and electron pressure
01 p0158 A71-10805

M type supergiants atmospheric metals abundances from high dispersion spectrograms analysis
02 p0308 A71-12095

Book on stellar atmospheres covering radiative transfer, opacity, equation of state, LTE, line spectra, atomic levels, etc
03 p0483 A71-13100

MHD parameters in photospheric plasmas of giant and dwarf stars, noting electrical conductivity, Joule dissipation, Reynold and Lundquist numbers
03 p0490 A71-13938

Stellar core evolution from He burning phase to oxygen exhaustion in central region, discussing mixing with envelope under various mass conditions
03 p0493 A71-14196

Convective energy transport in stellar atmospheres, computing hot and cool streams thermal structure based on model
03 p0495 A71-14264

Radiative transfer equation for atmospheres of rotating stars, deriving expression for flux distribution
03 p0495 A71-14381

Mathematical model of stellar atmospheres using radiation emission by elementary cylinder
04 p0647 A71-15236

Close binaries evolution, atmospheres structure and three body problem
04 p0647 A71-15241

UV stellar flux measurements vs theoretical stellar atmosphere models, using rocket and satellite observations
04 p0648 A71-15252

DA and DB white dwarf atmospheres convection effect on structure based on mixing length theory and constant flux model
04 p0658 A71-15841

Be star rarefied gaseous envelopes emitting or absorbing region size determination, noting application to other rotating stellar systems
04 p0659 A71-15843

Hot stars, supergiants and quasars extended and expanding atmospheres, examining resonance line profile formation by coherent scattering
05 p0806 A71-16203

Extended stellar atmospheres production mechanism involving outward acceleration of material in rarefaction wave following shock wave arrival at atmosphere edge
06 p0976 A71-18472

Flux divergence in optically thin outer layers of model moving stellar atmospheres using weighting functions in energy balance equation
07 p1190 A71-18863

Electron scattering effect on emission and absorption lines in stellar atmosphere, considering primary radiation sources uniform distribution and photosphere radiation transmission through electron atmosphere
07 p1192 A71-19291

Magnetic field generation of rotating stars with partially ionized convective envelopes due to emf arising from convective flow Coriolis acceleration
07 p1193 A71-19294

Spectral temporal variations and atmosphere conditions of P Cygnus, including atomic hydrogen densities, electron concentrations, microturbulent velocity and Balmer decrement
07 p1204 A71-20631

Radiation transport equations for stellar atmosphere model with variable depth magnetic field, considering absorption line formation and polarization characteristics
07 p1205 A71-20637

M type supergiants atmospheric metals abundances from high dispersion spectrograms analysis
08 p1362 A71-21145

Lower limit helium abundance envelope models of hydrogen deficient stars, using mixing length theory
08 p1364 A71-21418

Variable stars radii effective temperature and brightness determination from stellar atmosphere models
09 p1523 A71-23021

Planetary nebulae central stars extended atmospheres, calculating gray and nongray models under hydrostatic, radiative and LTE
11 p1818 A71-25203

Spectral line broadening theory applications to qualitative interpretation and quantitative determination of spectrograms from hydrogen line profiles of stellar atmospheric parameters
12 p1969 A71-27667

Helium-rich white dwarfs convective envelopes, acoustic noise generation and corona formation
12 p1970 A71-27746

Pulsar nature and radiation mechanism, examining rotating neutron stars structure and atmospheric dynamics
13 p2140 A71-29041

Super metal rich K giant stars atmospheric model, obtaining abundances and turbulent velocity parameter
14 p2305 A71-29674

Horizontal and post-horizontal branch hydrogen rich stellar atmospheric models, presenting emergent fluxes and H and He line profiles
14 p2314 A71-30645

White dwarf model atmosphere, discussing DA and non-DA spectral types, surface gravity, mass-radius relation, composition and convection effects
14 p2317 A71-31014

White dwarf line spectra, constructing atmospheric models and effective temperatures
14 p2317 A71-31015

Hydrogen deficient white dwarf atmospheres, computing line free flux constant models for He rich compositions with varied metal abundances
14 p2318 A71-31016

White dwarf coronas convection zones thermodynamic calculations, considering high electron degeneracy, and He I and He II ionization
14 p2318 A71-31017

Luminosity curves for eclipsing Algol-type systems with extended atmospheres based on stellar models
17 p2803 A71-34840

Radiative transfer in two-component stellar atmosphere, discussing lines corresponding to solar Ca K-line
17 p2839 A71-35555

Stellar atmospheres mathematical model, considering transfer equation reduction to linear equations set
17 p2808 A71-35556

Non-LTE physics of He atoms in hot stellar atmospheres, presenting numerical results for He I and II line spectra variations explanation
17 p2808 A71-35558

Main sequence A and early F stars with shallow convective envelopes, investigating particle diffusion effects on element abundance data
18 p2960 A71-35939

Cepheid beta Doradus color photometry data, detailing temperature, mean radius, absolute magnitude and surface gravity variations
18 p2971 A71-37070

Variable stars atmospheric radiation, investigating unsteady light reflection
19 p1313 A71-37505

Stellar atmosphere line formation in magnetic fields, considering Milne-Eddington model
19 p1313 A71-37507

Solar and stellar chromospheres and coronas production based on turbulence in granulation, photospheric mechanical flux and supergranular network magnetic field structures
19 p1316 A71-37626

Stellar chromosphere detection through H, K and metastable He lines observation, noting importance for solar physics
19 p1316 A71-37627

Stellar chromosphere characteristics from OAO observation of magnesium II emission in late type stars
19 p1317 A71-37628

Differential line shifts in spectrum of supergiant beta Ori attributed to radial spreading of stellar atmosphere
20 p3290 A71-39302

Photometric and spectroscopic observations of pulsating stars, noting shock waves in atmospheres of W Virginis and RR Lyrae
20 p3292 A71-39446

Crab Nebula pulsar and extar emission from collapsed star magnetosphere, accounting for physical characteristics with nonthermal plasma mechanism
20 p3285 A71-39954

Stellar models with He envelopes and carbon-oxygen cores, discussing internal structures and evolution of helium and R CrB stars
21 p3440 A71-40055

Temperature control bracket energy equation as measure of temperature distribution in pure hydrogen stellar atmosphere, considering electron energy and radiation field
21 p3446 A71-40419

Radiative transfer effects on hydromagnetic stellar atmospheres thermal-convective instability in presence of uniform rotation and uniform magnetic field
21 p3421 A71-40579

Low dispersion luminosity criteria in A and F stars, computing synthetic spectra for atmospheric temperature surface gravity microturbulence and abundance
22 p3601 A71-42166

Pole-on Be star envelope models, comparing H alpha line profiles with line of sight perpendicular to rotation axis
23 p3723 A71-42945

Beta cephei stars atmospheric He and metal abundances, comparing line spectra data with other early B stars sample
23 p3723 A71-42947

Spherical stellar atmosphere radiative transfer equation, using regional averaging method with opacity dependence on layer geometrical radius
23 p3766 A71-43828

M stars atmospheric temperature determination from TiO molecular spectrum by vibrational band intensity measurement
23 p3771 A71-44307

Early stars with extended atmospheres, discussing long term observational programs
24 p3873 A71-45126

STELLAR DOPPLER SHIFT

U DOPPLER EFFECT

U EXTRATERRESTRIAL RADIATION

STELLAR EVOLUTION

Blue supergiants evolution, discussing chemical composition of atmospheres, mass, binary nature and cluster association
01 p0153 A71-10375

Pre-main sequence stellar evolution - Conference, Liege, Belgium, June-July 1969
01 p0157 A71-10757

Solar corona evolution in contraction phase, calculating models based on dissipation theory
01 p0157 A71-10760

Solar system origin, structure and evolution, discussing planet and satellite orbital motion, resonance effects, tides and postaccretional changes
01 p0161 A71-11335

Star origin position in Galaxy, computing meridional galactic orbits for nearby late B types
01 p0161 A71-11385

Stellar nucleosynthesis processes classified into various interior nuclear reactions, discussing stellar evolution role
01 p0131 A71-14422

Semidetached eclipsing binary stars mass exchange, examining stellar evolution, luminosity, mass loss and exchange and Roche limit

02 p0313 A71-12497

Solar-mass star with carbon core and He envelope, constructing evolution model assuming energy losses due to photons with and without neutrinos

02 p0314 A71-12586

Classical Cepheids nature and evolution, discussing relation between periods and luminosity in galaxies, characteristics in scattered clusters, brightness curves

03 p0485 A71-13260

Nonspherical stellar gravitational collapse to black hole state, discussing event horizon concept

03 p0486 A71-13324

Close binary star evolution, discussing mass exchange in system with 7 solar mass primary

03 p0490 A71-13939

Stellar core evolution from He burning phase to oxygen exhaustion in central region, discussing mixing with envelope under various mass conditions

03 p0493 A71-14196

Stellar origin and evolution, discussing interstellar gas heating and condensation, star cluster formation and superdense body decay

04 p0642 A71-14774

Soviet book on stellar physics covering evolution, internal structure, mass, luminosity, radius, density, temperature, bolometric magnitude, energy transfer, etc

04 p0645 A71-15225

Lithium line strength indicator of stellar age, discussing T Tauri, A, carbon, S and Ba II stars

04 p0646 A71-15232

Internal constitution and kinematics of main sequence stars regarding age, evolution and formation place during hydrogen burning phase

04 p0646 A71-15233

Hertzsprung-Russell diagram calibration in terms of age and mass for main sequence B and A stars

04 p0646 A71-15234

Stellar rotation effects on color, magnitude, formation and evolution

04 p0647 A71-15238

Stellar angular momentum, discussing evolution, rotation orbits and relationship between binaries, rotating stars and planetary systems

04 p0647 A71-15240

Close binaries evolution, atmospheres structure and three body problem

04 p0647 A71-15241

Binary star radial velocity measurement, discussing formation, evolution, motion frequency and H-R diagrams

04 p0647 A71-15242

Metal-rich star evolution from main sequence to red giant, examining mass, nuclear reactions and theoretical models

04 p0648 A71-15247

Normal O, blue supergiants and brightest yellow and red supergiant massive stars, considering evolution, luminosity, lifetime mass loss, pulsational instability and supernovae

04 p0648 A71-15248

UV dwarfs observational lifetime, considering progenitor main sequence, red giants and planetary nebulae central stars evolutionary sequence

04 p0648 A71-15249

UV dwarf star evolution, using central and gap star models emphasizing photoneutrino emission

04 p0648 A71-15250

Old subgiant delta Pavonis composition, suggesting metal rich state

04 p0658 A71-15839

Neutron star formation, calculating reimplosion mass fraction of thermonuclear supernovae explosion

05 p0811 A71-16684

Epsilon Aur eclipsing binary primary star mass and evolutionary stage considered to interpret secondary

06 p0970 A71-18032

Stellar chemical composition and structural evolution, discussing mass/luminosity relationship, evolution sequences during hydrogen and helium combustion stages, etc

06 p0970 A71-18200

Interstellar gas and star mass interchange, discussing balance and galactic and stellar evolution models

06 p0972 A71-18334

Stellar mass loss, discussing consequences on interstellar medium and star evolution

06 p0973 A71-18337

Interstellar grain formation relation with stellar evolution in terms of density wave theory of spiral structure origin

06 p0973 A71-18339

Neutral condensations and protostars in H II regions noting original density distributions

06 p0973 A71-18340

Stellar free neutrino and antineutrino emission thermodynamics under hot matter neutronization and hydrodynamic stability during late evolutionary stages

06 p0974 A71-18426

Evolutionary cooling sequences and lifetimes for low mass white dwarfs in Hyades cluster, considering near surface convection in models with hydrogen envelopes

07 p1190 A71-18856

Stability of slowly rotating stars with phase transition in center, determining critical density jump for stability loss

07 p1193 A71-19296

Red giant star s-process and subsequent delayed electron capture, accounting for large Li abundances

07 p1198 A71-19822

He shell burning termination in solar mass stars evolution to white dwarf stage

07 p1198 A71-19823

White dwarfs, neutron stars and black holes origin and characteristics, discussing density, mass radius, gravitation and structure

07 p1199 A71-19999

Population II red giant stars evolution models, investigating relativistic degeneracy, neutrino losses core critical mass and helium flash

08 p1359 A71-20940

Agglomeration process of dust particles growth in primordial solar nebula, considering early evolutionary phase of nearly free contraction and later phase with nebula flattening into gaseous disk rotating about protosun

09 p1523 A71-23045

Star group formation theory, proposing hypothesis on toroidal stages in stellar evolution

09 p1524 A71-23183

Pre-main sequence /T Tauri/ stellar evolution, discussing mass loss rates and star formation by interstellar cloud violent hydrodynamic compression

09 p1528 A71-23592

Mn type peculiar A stars relative abundance from curve of growth analysis, discussing isotope shifts, nucleosynthesis, explosion reactions and structure acceleration

09 p1529 A71-23596

Static relativistic theory of isotropic spherically symmetric star equilibrium stability, assuming certain conditions with respect to mass-energy density and total baryon number

09 p1529 A71-23597

Solar temperature after formation, using isotopic composition differences in terrestrial and extraterrestrial xenon

10 p1668 A71-23871

Nucleosynthesis due to explosive burning in stellar objects for elemental synthesis

10 p1668 A71-24003

German book on variable stars covering supernovae, novae, pulsating variable stars, symbiotic objects, galactic nebulae, stellar and galactic evolution, astronomical photometry, etc

10 p1675 A71-24479

Partial mixing effects on solar neutrino flux and stellar evolution

10 p1662 A71-24497

Massive stars evolutionary models, exploring convective instability effects

11 p1818 A71-25205

Protosun and primordial solar nebula evolution based on dust particles behavior

11 p1819 A71-25221

Dust grain condensation and primordial elements transport into interplanetary space during early stage solar evolution

11 p1819 A71-25222

Star formation angular momentum and magnetic flux problem, investigating collapsing dust cloud theory

11 p1830 A71-26108

Open star cluster NGC 6819 photoelectric and photographic data, indicating age, color magnitude diagram and main sequence turnoff

11 p1831 A71-26134

Neutron star formation from supernova explosion in close binary system

11 p1832 A71-26171

Mass exchange during main sequence evolution of close binaries with shell hydrogen burning

11 p1832 A71-26185

Stellar free neutrino and antineutrino emission thermodynamics under hot matter neutronization and hydrodynamic stability during late evolutionary stages

12 p1954 A71-26576

Prestellar evolution, discussing interstellar medium, star development phases, cloud formation, gravitational/thermal instability and protostars

12 p1960 A71-26783

Stellar evolution, discussing mass loss to interstellar medium, galactic distances determination and supernova explosions

12 p1960 A71-26784

Kinetic equations for particle motion in gravitational fields, discussing stellar configurations evolution

13 p2100 A71-27973

Stellar core evolution of initial mass 1.5 solar mass, starting from He-burning phase

13 p2140 A71-29013

Neutron stars origin and nature, discussing pulsars structure, mass and frequency variations

13 p2143 A71-29297

Horizontal and post-horizontal branch hydrogen rich stellar atmospheric models, presenting emergent fluxes and H and He line profiles

14 p2314 A71-30645

Morphological projections in astrophysics, considering single star evolution in terms of Boltzmann-Gibbs statistical mechanics

14 p2318 A71-31020

Point sources of solar neutrino radiation, explaining negative experimental results without drastic change of main assumptions concerning stellar evolution

15 p2478 A71-31801

Neutrino emission from collapsing stars, discussing possibility of detection by large mass organic scintillator

15 p2478 A71-31802

Extragalactic nebulae, considering galactic formation stages and energy supply problems

15 p2486 A71-31925

Nuclear reactions in high temperature laboratory and stellar plasmas, discussing pinches, thermonuclear burning and star evolution

16 p2613 A71-32972

Subdwarf star data, reviewing spectra, kinematics, nucleosynthesis, interiors, atmospheres, angular momentum, formation, abundances and distribution

16 p2631 A71-33126

Kerr-Newman black hole as generic final state of gravitational collapse developed from Schwarzschild geometry and mass, angular momentum and charge parameters

16 p2631 A71-33177

Main sequence stars hydrogen burning stage, examining neutrino emission and nuclear process effects in stellar evolution

16 p2625 A71-33230

Stellar initial metal content effect on nuclear abundance distributions synthesized under explosive carbon, oxygen and silicon burning conditions

16 p2631 A71-33231

Stars with central He burning and loop occurrence in H-R diagram, suggesting secular instabilities with high stellar mass

16 p2633 A71-33332

Ap and Am stars distribution and ages, considering high proportion in Hyades, Sirius, Praesepe and Coma Berenice clusters

16 p2633 A71-33333

He 4 burning nucleosynthesis, noting Ne 20 buildup in massive stars

16 p2633 A71-33335

Population II stars evolution models from main sequence to supergiant stage, constructing time constant loci in H-R diagram

16 p2635 A71-33432

T Tauri stars Li, Be and B autogenic generation, considering underabundance in surrounding gas

16 p2626 A71-33433

Book on relativistic astrophysics, Volume 1, Stars and relativity, covering stellar dynamics, astronomical models, cosmic objects evolution and star clusters

16 p2635 A71-33481

Wolf-Rayet stars evolution due to stellar matter mixing and escape from nuclei

17 p2800 A71-34571

Star formation at interstellar gas cloud stage, discussing gravitational collapse, Bok dust globules, spectroscopic and IR peculiarities and models

17 p2801 A71-34696

Evolved stellar cores thermonuclear explosion products state, investigating Chapman-Jouguet detonation propagation effects with carbon 12 and oxygen 16 burning under high electron degeneracy

17 p2806 A71-35407

Vela X supernova remnant blast wave model and Gum Nebula formation, discussing kinetic and rotational energy transformation into radiation

17 p2807 A71-35414

Massive pulsationally unstable stars dynamic analysis, formation and upper mass limits

18 p2960 A71-35934

Type II supernovae observations and models, considering photographic light curves and dynamic instabilities in star development, outbursts and ejected matter composition and amounts

18 p2961 A71-35976

Stellar evolution, discussing semiconvective regions, mass loss, red giants and supergiants, He flash structures and globular clusters

18 p2967 A71-36999

Planetary nebulae central stars, considering elementary stellar evolution theory, globular cluster stars and ejection mechanism

18 p2968 A71-37031

Close binary systems evolutionary processes, considering mass transfer and gas dynamics

18 p2968 A71-37033

Degenerate dwarfs theory, discussing stellar structure, stability, evolution and thermal properties

18 p2969 A71-37039

- Rotating isothermic radially pulsating white dwarf evolution, considering neutronization and general relativistic effects
19 p3134 A71-37511
- Missions beyond solar system for studying origin and evolution of life, planets and stars
[AAS PAPER 71-163]
19 p3141 A71-37960
- White dwarfs production in small mass binary systems, deriving formulas for final mass and orbital velocity with application to blue stragglers
19 p3143 A71-38160
- Pulsar periods change rate and radio luminosity decay, discussing magnetic field braking
20 p3286 A71-38762
- Beta processes effect on detonation and postdetonation evolution of degenerate carbon-oxygen core supernovae, using numerical hydrodynamic calculations
20 p3287 A71-39053
- Binary systems formation probability during triple encounters, considering random initial conditions
20 p3290 A71-39301
- Supermassive stars observational data and origin likelihood at center of galaxy or star cluster
20 p3292 A71-39421
- Stellar evolution and cosmic time scales based correlation analysis of star motion and spectral types, considering B stars, A stars, F and G stars and Halo stars
20 p3301 A71-39824
- Energy in universe from stellar and galactic evolution, discussing flow mechanisms, entropy, arresting factors and catastrophic phenomena
20 p3301 A71-39916
- Pulsars luminosity, z-distance and period distribution in Galaxy, comparing supernova remnants
20 p3303 A71-39933
- Timing measurements of pulsar NP 0527 relating frequency, position and transverse velocity with NP 0532, excluding origin in supernova explosion
20 p3303 A71-39936
- Magnetic A stars accretion model, investigating spectra, abundances, ion capture and braking
21 p3439 A71-40051
- Short period variables, considering Scuti stars evolution, pulsations, magnitude and positions in H-R diagram
21 p3440 A71-40054
- Stellar models with He envelopes and carbon-oxygen cores, discussing interior structures and evolution of helium and R CrB stars
21 p3440 A71-40055
- Stellar evolution on horizontal branch and parameters of state of RR Lyrae stars in globular clusters of various ages
21 p3451 A71-40720
- Massive main sequence stars pulsation kinetics, examining amplitude growth, time scale ratios and evolutionary stabilization
22 p3596 A71-41447
- Period-age distribution of pulsars, using radio and optically emitting neutron star model
22 p3599 A71-41925
- Stellar population data, discussing star distribution and galactic evolution
22 p3599 A71-41931
- Internal velocity field role in massive star formation, discussing cloud fragmentation and mass function
23 p3723 A71-42941
- Mg 24 photodisintegration rate in stellar silicon burning process, presenting reactions at low alpha particle energies
23 p3723 A71-42952
- Evolutionary meaning of nitrogen and carbon sequences in Wolf-Rayet stars
23 p3770 A71-44064
- Model computations for Population I star in evolutionary phase from He exhaustion in stellar center up to carbon ignition
24 p3872 A71-45076
- Evolved Cepheid-type stars vibrational stability against nonradial perturbations from quasi-adiabatic approximation of radiative dissipation
24 p3872 A71-45077
- Stars origin theories, discussing stellar associations, young stars, galaxies instability and cosmology and cosmogony
24 p3875 A71-45198
- Shock wave dynamics of brightness curve reflecting supernova outbursts
02 p0307 A71-12088
- H alpha line emission in ionization zones encircling neutron stars, suggesting accretion-induced UV luminosity
02 p0308 A71-12091
- Stellar magnitude equation from corrected catalog data to determine absolute proper motions relative to galaxies
03 p0484 A71-13218
- Classical Cepheids nature and evolution, discussing relation between periods and luminosity in galaxies, characteristics in scattered clusters, brightness curves
03 p0485 A71-13260
- Cepheids in Milky Way spherical component, emphasizing brightness and color curves and spectral characteristics
03 p0485 A71-13261
- Delta Scutum type variable stars, discussing photometric properties, line of sight velocities, color indices, luminosity, chemical composition, etc
03 p0485 A71-13264
- Beta Cepheus type variable stars brightness curves and line of sight velocities graphs, discussing periods, luminosity, spectra, kinematics and spatial characteristics, etc
03 p0486 A71-13266
- Semiregular and irregular variable stars spatial densities and distributions, amplitudes and periods
03 p0486 A71-13268
- Duplex telescope system design and functions for photoelectrical stellar brightness measurements
04 p0588 A71-14829
- Morgan two dimensional stellar spectral system with luminosity classes, comparing to Harvard scheme
04 p0646 A71-15230
- Spectral classification parameters, discussing spectral-type indicators, luminosity indicators, spectra of clusters and galaxies, abundance, population and low metal objects
04 p0646 A71-15231
- Reddening effects in determining intrinsic color of supergiant and cepheid variable stars
04 p0646 A71-15235
- Stellar rotation effects on color, magnitude, formation and evolution
04 p0647 A71-15238
- Extragalactic pulsars visible and X ray detection and luminosity
05 p0801 A71-15928
- Radio pulsars optical counterparts, comparing absolute intensity with Crab Nebula NP 0531
05 p0802 A71-15940
- NGC 7320 as companion galaxy to NGC 7331 rather than member of Stephens quintet, considering red shift texture, lack of distortion and luminosity
05 p0805 A71-16110
- Pulsars optical and X ray luminosity secular decrease, examining emission close to velocity of light radius
05 p0807 A71-16209
- Early type stars radiant flux observation from OGO 6 satellite
06 p0969 A71-17975
- Stellar chemical composition and structural evolution, discussing mass/luminosity relationship, evolution sequences during hydrogen and helium combustion stages, etc
06 p0970 A71-18200
- Strip brightness distribution across Kepler supernova derived from occultation observation by radio telescope
06 p0971 A71-18241
- Sun as variable star, discussing brightness, rotation and magnetic characteristics
06 p0971 A71-18245
- Absorption line blanketing, back warming and blocking effects on B and V magnitudes for F-G stars
07 p1193 A71-19295
- Telescope star photographic magnitude perception maximum capacity, considering effective or equivalent quantum yield and photoemulsion sensitivity
07 p1109 A71-19346
- Eclipsing variable binary stars spectral and luminosity classes determination
07 p1200 A71-20035
- AB Aur light variations in three colors, estimating visual absolute magnitudes free of interstellar absorption and B-V
07 p1201 A71-20433
- Kinescope light characteristics nonlinearity effect of television system penetrating ability for image reproduction of faint stars
07 p1115 A71-20444
- Shock wave dynamics of brightness curve reflecting supernova outbursts
08 p1362 A71-21138
- H alpha line emission in ionization zones encircling neutron stars, suggesting accretion-induced UV luminosity
08 p1362 A71-21141
- Book on dwarf novae covering light variations, spectra, binary systems, absolute magnitude, mass, gas streams, outburst, etc
08 p1363 A71-21165
- Telescope plate scanner automated computerized operation, evaluating faint stars identification and color classification for annual motion surveys
09 p1443 A71-22646
- Variable stars radii effective temperature and brightness determination from stellar atmosphere modes
09 p1523 A71-23021
- Algol secondary component gravity darkening observations, examining IR light curve
09 p1527 A71-23530
- Supernovae light curves theory based on numerical integration of gas dynamics and radiative heat conductivity equations
09 p1528 A71-23591
- Collapsed or neutron star companions of bright binary stars, explaining low luminosity of more massive component
10 p1665 A71-23740
- Empirical solar photosphere continuum models, calculating temperature distribution for absolute intensities at center and limb darkening ratios
10 p1666 A71-23779
- Solar eclipse measurements at 1.18 cm on 11 September 1969, describing limb brightening and center and coronal emission
10 p1666 A71-23790
- Individual M-type red supergiants luminosity, masses and periodicities based on cluster membership and pulsational Q value
10 p1674 A71-24433
- Stellar silicon brightness measurement for evaluating SNR and selecting reference star
10 p1679 A71-24951
- Early stars Vilnius intermediate band and UVB systems comparison for color excess ratios and magnitudes, obtaining reddening line slopes by spectral energy distributions
10 p1682 A71-25131
- Binary alpha Virginis interferometric data, noting distance, luminosity brightness ratio, angular size and diameter, orbits mass, temperature and gravity
11 p1830 A71-26107
- Open star cluster NGC 6819 photoelectric and photographic data, indicating age, color magnitude diagram and main sequence turnoff
11 p1831 A71-26134
- Type I supernovae maximum brightness and occurrence time from photometric analysis
12 p1955 A71-26585
- Cepheids normal color index-spectrum relation, noting brightness variation phases and two-color diagrams reddening lines
12 p1955 A71-26586
- Interstellar dust, investigating starlight reddening by extinction, galactic light, IR star observations and polarization
12 p1959 A71-26775
- C, gM and S spectral type stars, considering distribution, absolute magnitudes and intrinsic colors
12 p1959 A71-26777
- Cepheids period and luminosity relation, using Kraft method
12 p1962 A71-26906
- Cepheids UVB spectrum analysis, examining brightness shapes and color index curves
12 p1962 A71-26907
- Long period Cepheids, obtaining brightness curves distribution for minimum, maximum and fixed phase stellar magnitudes
12 p1962 A71-26908
- Solar Na D lines Doppler width, describing limb darkening data, assuming source function frequency dependent
12 p1970 A71-27748
- Orbital elements and corrected light curve of eclipsing variable star Z Vulpeculae, using FORTRAN 4 program
13 p2137 A71-28513
- Critique on pulsar distance estimates based on dispersion measure, introducing period luminosity function
13 p2137 A71-28592
- German monograph on membership in open star clusters, covering M67, pseudocluster M39 and stellar brightness and motions
13 p2139 A71-28879
- Stellar masses calculation, using dynamical parallaxes, Kepler third law and mass-luminosity relation
14 p2311 A71-30362
- White dwarf discovery method and properties, discussing color, spectra, parallaxes, luminosities, masses, red shifts, cluster and frequency distribution
14 p2316 A71-31005
- Red subluminous stars, presenting catalog identification, proper motions, spectral type, photometric parallax, tangential velocity, UVB photometry, etc
14 p2316 A71-31006
- Subluminous star spectroscopic data, determining temperature and surface gravity
14 p2317 A71-31011

STELLAR MAGNETIC FIELDS

White dwarf stars equilibrium models, discussing vibrational stability and radial pulsations eigenvalues and eigenfunctions 14 p2318 A71-31019

Pleiades flare stars photographic magnitude and brightness data, establishing relation between amplitude and duration 15 p2486 A71-32029

Faint O-B5 type blue stars data, listing absolute spectrophotometric gradients and Balmer series discontinuities 15 p2487 A71-32032

High luminosity G supergiants at 0.4-18 micron wavelengths showing intense silicate emission shell 15 p2497 A71-32764

Young open star cluster NGC 6823 membership based on relative proper motions data and color-magnitude diagram 16 p2631 A71-33180

AO Algol-type variables W Del, T L Mi, RZ Cas, and delta Lib gradient variation and Balmer discontinuity, detailing luminosity and radius ratio effects 16 p2634 A71-33427

NGC 3811 supernova spectrum and light curve data, indicating Type I class 16 p2635 A71-33431

Novas distance determination from estimates of envelope ejection during outburst at maximum brightness, calculating absolute magnitudes 17 p2803 A71-34838

Nova N Her 1963 brightness variations from photometric observations, interpreting data in terms of stellar evolution 17 p2803 A71-34839

Luminosity curves for eclipsing Algol-type systems with extended atmospheres based on stellar models 17 p2803 A71-34840

Variable star brightness measurement, using on-line electronic computer, analog to digital converter and reflector with direct current amplifying photometer 17 p2741 A71-34990

Star counting device, showing stellar fields contribution to total brightness 17 p2742 A71-35004

Position, parallax, distance, visual apparent and absolute magnitude, spectrum and visual luminosity tables for nearby stars 18 p2968 A71-37030

Cepheid beta Doradus color photometry data, detailing temperature, mean radius, absolute magnitude and surface gravity variations 18 p2971 A71-37070

Bolide spectrum on 6 June 1969, determining stellar magnitude and periodic pulsations and asynchronous flares characteristics along trajectory 19 p3132 A71-37381

UV Cet and YZ CMi star flare activity data, noting Poisson distribution of time sequence 19 p3134 A71-37510

Three color photometry of star field in Sagittarius cloud, determining interstellar absorption, density and luminosity for main sequence stars 19 p3144 A71-38169

Transition period for variable stars, considering helium sensitive relationship to luminosity obtained with nonlinear theory 20 p3287 A71-39054

Halos around black holes, showing luminosities caused by synchrotron radiation of magnetized plasma 20 p3289 A71-39295

Gyroscope apparent precession due to reference star light deflection by solar gravitational field 20 p3270 A71-39559

Stellar composition analysis of Small and Large Magellanic clouds using Hertzsprung-Russell, color magnitude and two color diagrams 20 p3301 A71-39823

Short period variables, considering Scuti stars evolution, pulsations, magnitude and positions in H-R diagram 21 p3440 A71-40054

G and K giant stars iron abundances from narrow band indices, using spectrophotometer, red-IR colors and independent luminosity estimates 21 p3444 A71-40240

Bright star at radio source and X ray observations evaluation from optical identification of Cygnus X-1, taking into account spectrum and energy distribution characteristics 21 p3447 A71-40444

Stellar UVB photometric investigation, determining brightness, coordinates, B-V and U-B color indexes of faint blue objects near galactic North Pole 21 p3451 A71-40721

Quasar brightness estimates on celestial photographs, noting variability on time scale 21 p3451 A71-40722

Low dispersion luminosity criteria in A and F stars, computing synthetic spectra for atmospheric temperature surface gravity microturbulence and abundance 22 p3601 A71-42166

Brightness and polarization distributions for supernova remnants IC443 and Puppis A, considering magnetic field orientation and thermal radio emission 22 p3606 A71-42601

Photometric study of light variation and variable stars in luminous supergiants in Large Magellanic Cloud 23 p3723 A71-42940

Globular cluster RR Lyrae horizontal branch stellar models, investigating masses luminosities and compositions 23 p3723 A71-42944

White dwarfs EG 248, GR 289 and EG 250 spectra with circular polarization, detailing violet lines, absolute magnitudes, color and luminosity 23 p3733 A71-43079

Ashen light over Venus nocturnal hemisphere due to reflected earthlight and starlight 23 p3733 A71-43128

Red variable GN Her brightness, color and spectrum, discussing UVB system photoelectric measurements during 1966/68 period 23 p3771 A71-44303

Nova N Vul 1968 UVB system photoelectric observations, noting small amplitude rapid brightness variations during night 23 p3771 A71-44304

Background illumination effect on stellar magnitude photographic measurement, noting stellar image reduction 23 p3680 A71-44309

STELLAR MAGNETIC FIELDS

NT SOLAR MAGNETIC FIELD

Rotating stars with partially ionized convective envelopes, investigating general stellar magnetic field production 01 p0150 A71-10060

Magnetic stars, discussing stellar magnetic fields, Ap stars, crossover effect, period line width correlation, overabundances and models 04 p0648 A71-15245

Nonpulsing pulsar model, discussing idealized neutron star with spin axis aligned with uniform internal magnetic field 04 p0650 A71-15585

Magnetic field generation of rotating stars with partially ionized convective envelopes due to emf arising from convective flow Coriolis acceleration 07 p1193 A71-19294

Radiation transport equations for stellar atmosphere model with variable depth magnetic field, considering absorption line formation and polarization characteristics 07 p1205 A71-20637

Crab Nebula pulsar magnetic field structure, discussing linear polarization modifications and wisps 10 p1668 A71-23870

Pulsar mechanism relation to solar cycle mechanism, discussing magnetic flux correlation to period 10 p1681 A71-25073

Extragalactic radio sources total and linearly polarized radiation one dimensional distributions, noting spectral variations, magnetic fields and rotation measurements 11 p1830 A71-26131

Maximum toroidal magnetic fields of rotating neutron stars dependent on central density, using relativity corrections to plasma hydrodynamic and Maxwell equations 12 p1966 A71-27237

Stellar and interstellar magnetic fields effects on plasma instabilities in Colgate cosmic ray model, using computer simulation 14 p2282 A71-30644

Strong magnetic fields effects on neutron stars or white dwarfs, considering Thomson scattering in fully ionized collisionless plasma 14 p2315 A71-30858

Rapidly rotating early stars and quasars, determining magnetic field generation by turbulent dynamo mechanism 15 p2485 A71-31725

Magnetic stars as cosmic ray generators, considering interstellar gas particle acceleration by EM forces produced by rotating stellar magnetic field 16 p2625 A71-33324

Crab Nebula pulsar rotation and magnetic axes disposition from pulse shape and polarization data at optical and radio wavelengths 16 p2634 A71-33391

White dwarf and neutron stars magnetic field generation, noting system in metastable Lofers state 18 p2963 A71-36242

Solar and stellar chromospheres and coronas production based on turbulence in granulation, photospheric mechanical flux and supergranular network magnetic field structures 19 p3136 A71-37626

Radiative transfer effects on hydromagnetic stellar atmospheres thermal-convective instability in presence of uniform rotation and uniform magnetic field 21 p3421 A71-40579

Static magnetic fields configurations of magnetic and rotating neutron stars, considering general relativistic effects 21 p3450 A71-40714

Brightness and polarization distributions for supernova remnants IC443 and Puppis A, considering magnetic field orientation and thermal radio emission 22 p3606 A71-42601

STELLAR MASS

Quasi-stationary spherical various mass star system, applying ergodic theory in stellar dynamics 01 p0150 A71-10058

Solar-mass star with carbon core and He envelope, constructing evolution model assuming energy losses due to photons with and without neutrinos 02 p0314 A71-12586

Close binary star evolution, discussing mass exchange in system with 7 solar mass primary 03 p0490 A71-13939

Metal-rich star evolution from main sequence to red giant, examining mass, nuclear reactions and theoretical models 04 p0648 A71-15248

Normal O, blue supergiants and brightest yellow and red supergiant massive stars, considering evolution, luminosity, lifetime mass loss, pulsational instability and supernovae 04 p0648 A71-15248

Old subgiant delta Pavonis composition, suggesting metal rich state 04 p0658 A71-15839

Main sequence stars upper mass limit, using linear nonadiabatic analysis for composition dependence and nonlinear hydrodynamic calculations for mass excess 05 p0801 A71-15933

Neutron star formation, calculating reimplosion mass fraction of thermonuclear supernovae explosion 05 p0811 A71-16684

Pulsating stars masses from cepheids and RR Lyrae period, color and luminosity measurements 05 p0814 A71-17094

Stellar chemical composition and structural evolution, discussing mass/luminosity relationship, evolution sequences during hydrogen and helium combustion stages, etc 06 p0970 A71-18200

Cosmic accretion gas dynamics, discussing star, galaxies and galactic cluster effects 06 p0972 A71-18333

Interstellar gas and star mass interchange, discussing balance and galactic and stellar evolution models 06 p0972 A71-18334

Density spatial and temporal fluctuations correlation in stars 06 p0974 A71-18431

Dense /relativistic/ stars structural stability with respect to centrally symmetrical perturbations 09 p1523 A71-23019

Neutron star matter equations of state involving hyperon formation effects for maximal stable mass models, tabulating moments of inertia 10 p1671 A71-24302

Individual M-type red supergiants luminosity, masses and periodicities based on cluster membership and pulsational Q value 10 p1674 A71-24433

Stellar mass relativistic integral theorems and upper and lower bounds for gravitational potential theory 11 p1830 A71-26106

Binary alpha Virginis interferometric data, noting distance, luminosity brightness ratio, angular size and diameter, orbits mass, temperature and gravity 11 p1830 A71-26107

General relativistic von Zeipel theorem providing necessary and sufficient condition for equidensity surfaces coincidence in stationary star axisymmetric rotating mass fluid 11 p1833 A71-26327

Spatial and temporal density fluctuations correlation in stars 12 p1955 A71-26581

Stellar core evolution of initial mass 1.5 solar mass, starting from He-burning phase 13 p2140 A71-29013

Stellar masses calculation, using dynamical parallaxes, Kepler third law and mass-luminosity relation 14 p2311 A71-30362

Visual double stars spectroscopy, discussing stellar mass and parallax determination 14 p2311 A71-30367

White dwarf model atmosphere, discussing DA and non-DA spectral types, surface gravity, mass-radius relation, composition and convection effects 14 p2317 A71-31014

Self gravitating time independent disk-like stellar system model, investigating mass and velocity distributions 16 p2630 A71-33054

Stars with central He burning and loop occurrence in H-R diagram, suggesting secular instabilities with high stellar mass 16 p2633 A71-33332

He 4 burning nucleosynthesis, noting Ne 20 buildup in massive stars 16 p2633 A71-33335

Massive pulsationally unstable stars dynamic analysis, formation and upper mass limits 18 p2960 A71-35934

Spectroscopic binary system with invisible major mass components, considering relativistic companion star 19 p3134 A71-37508

White dwarfs production in small mass binary systems, deriving formulas for final mass and orbital velocity with application to blue stragglers 19 p3143 A71-38160

Supermassive stars observational data and origin likelihood at center of galaxy or star cluster 20 p3292 A71-39421

Nuclear forces effects on maximum mass limit of neutron stars models using V gamma type potentials 20 p3304 A71-39945

BCD Cepheids observations, examining data with quasi-static interpretation approximation for gravity and stellar masses 21 p3441 A71-40065

Massive main sequence stars in rapid differential rotation, investigating structure, energy transport, luminosity and circulation time scale 21 p3444 A71-40241

Spectroscopic radial velocity study of Algol eclipsing variable stars, deriving masses and apsidal motion evidence in short period orbit 21 p3446 A71-40418

Neutron star matter equation of state and models from energy computations, discussing maximum stable mass 21 p3452 A71-41034

Internal velocity field role in massive star formation, discussing cloud fragmentation and mass function 23 p3723 A71-42941

Globular cluster RR Lyrae horizontal branch stellar models, investigating masses luminosities and compositions 23 p3723 A71-42944

Neutron star limiting mass based on soft hadron matter resistance to gravitational collapse in stellar structural stability consideration 23 p3732 A71-43073

Stellar density function outside symmetry plane of galactic phase-space model 24 p3868 A71-44461

STELLAR MASS EJECTION

Semidetached eclipsing binary stars mass exchange, examining stellar evolution, luminosity, mass loss and exchange and Roche limit 02 p0313 A71-12497

Stellar wind effect on accretion, showing critical intensity of particle ejection replacement 03 p0484 A71-13221

Runaway pulsar formation and ejection in supernova collapse, fragmentation, condensation, radiation and disruption 04 p0643 A71-15046

Stellar mass loss, discussing consequences on interstellar medium and star evolution 06 p0973 A71-18337

Novae, symbiotic, T Tauri, U Geminorum and UV Ceti type stars, determining mass loss rate 06 p0973 A71-18338

Double star system with neutron star in pair with matter-losing star, discussing X ray sources variability causes 06 p0976 A71-18455

Zeta Aurigae chromospheric lines observed radial velocities mean variations, taking into account H ion gas acceleration, K star mass ejection and rotation 08 p1364 A71-21417

Pre-main sequence /T Tauri/ stellar evolution, discussing mass loss rates and star formation by interstellar cloud violent hydrodynamic compression 09 p1528 A71-23592

Nucleosynthesis in neutron rich supernova ejecta, performing statistical equilibrium calculations at freeze out temperature and density 10 p1670 A71-24301

M stars mass loss, determining dust shells radii and densities with IR observations of circumstellar emission 11 p1818 A71-25204

Mass exchange during main sequence evolution of close binaries with shell hydrogen burning 11 p1832 A71-26185

Binary system of neutron star paired with matter-losing star, discussing X ray emission variability causes 12 p1956 A71-26605

Stellar evolution, discussing mass loss to interstellar medium, galactic distances determination and supernova explosions 12 p1960 A71-26784

Source count statistics of radio galaxy lifetimes and intergalactic heating, assuming multiple explosions 12 p1968 A71-27540

Plasmoid ejection during flare and condensation by radiative instability, interpreting Simple 3 solar radio bursts in terms of thermal emission 13 p2129 A71-29054

Wolf-Rayet stars evolution due to stellar matter mixing and escape from nuclei 17 p2800 A71-34571

Novas distance determination from estimates of envelope ejection during outburst at maximum brightness, calculating absolute magnitudes 17 p2803 A71-34838

Mass transfer in close binaries, determining gaseous ring formation conditions and properties from ejected particle trajectories computation 17 p2805 A71-35594

Type II supernovae observations and models, considering photographic light curves and dynamic instabilities in star development, outbursts and ejected matter composition and amounts 18 p2961 A71-35976

Stellar evolution, discussing semiconvective regions, mass loss, red giants and supergiants, He flash structures and globular clusters 18 p2967 A71-36999

Planetary nebulae central stars, considering elementary stellar evolution theory, globular cluster stars and ejection mechanism 18 p2968 A71-37031

Cassiopeia A galactic supernova remnant, discussing flocculi formation from material ejected from outer layers before explosion 20 p3304 A71-39941

Planetary formation from sun ejected charged bodies captured in orbit due to electromagnetic effects, considering Sarvajna model 22 p3604 A71-42334

STELLAR MOTIONS

Quasi-stationary spherical various mass star system, applying ergodic theory in stellar dynamics 01 p0150 A71-10058

Star origin position in Galaxy, computing meridional galactic orbits for nearby late B types 01 p0161 A71-11385

Metal poor stars eccentric galactic orbits, considering interstellar medium accretion effect 02 p0312 A71-12468

Computerized simulation of disk galaxies evolution, using doubly periodic model for stellar motions 02 p0318 A71-12925

Circumzenithal micrometric recording of almucantar passages of stars 03 p0422 A71-13011

Galaxies pairs motions, considering disintegrating, rotational and oscillatory types for comparison with observational data 03 p0484 A71-13207

Stellar magnitude equation from corrected catalog data to determine absolute proper motions relative to galaxies 03 p0484 A71-13218

Peculiar velocities nonisotropic distribution in stationary differentially rotating stellar system based on Boltzmann equation solution 03 p0484 A71-13222

RR Lyr type stars kinematic behavior, line of sight velocities, spectral energy distribution and temperature 03 p0485 A71-13263

Delta Scutum type variable stars, discussing photometric properties, line of sight velocities, color indices, luminosity, chemical composition, etc 03 p0485 A71-13264

RR Lyr type dwarf stars, discussing brightness curves, color indices, effective temperatures, line of sight velocities and spectral classes 03 p0485 A71-13265

Beta Cepheus type variable stars brightness curves and line of sight velocities graphs, discussing periods, luminosity, spectra, kinematics and spatial characteristics, etc 03 p0486 A71-13266

Photoelectric device for recording stellar passages, discussing photocascade structure 04 p0592 A71-14858

Photoelectric recording devices for star passages, describing automatic compensation for signal delay instability 04 p0592 A71-14864

Population I Cepheids studies applied to galactic rotation and solar motion parameters estimation, discussing stellar distances inaccuracy effects 04 p0643 A71-14908

Stellar radial velocity measurements using Doppler shifted absorption lines, discussing cluster stars 04 p0646 A71-15227

Proper motions of stars for distance scale of universe using position, relative and fixed reference methods 04 p0646 A71-15228

Stellar angular momentum, discussing evolution, rotation orbits and relationship between binaries, rotating stars and planetary systems 04 p0647 A71-15240

Binary star radial velocity measurement, discussing formation, evolution, motion frequency and H-R diagrams 04 p0647 A71-15242

White dwarfs, investigating spectral classification, clusters, motions and location on H-R diagram 04 p0647 A71-15243

Stellar transit time recording by photoelectric instruments, discussing time constant and slit characteristics 04 p0598 A71-15377

Time lag between actual and measured stellar transit times by photoelectric recording instruments, noting atmospheric, spectral and instrumental factors 04 p0598 A71-15378

Photoelectric stellar transit instrument lens with increased spherical aberration based on light beam passage analysis 04 p0598 A71-15379

Time lag between actual and measured stellar transit times based on photocurrent expansion into Fourier series 04 p0598 A71-15380

Stellar transit time photoelectric instruments time lag measurements by variable flux light source 04 p0599 A71-15382

Resonance phenomena in spiral galaxies, determining stellar orbits, potential and distribution functions 04 p0655 A71-15725

Stellar velocities distribution in nonrotating clusters, examining mass dispersion role in evolution 06 p0974 A71-18430

O-B stars velocity distribution in synergetic association, proposing method for space velocities mean value determination 07 p1192 A71-19289

Stellar intrinsic motions with respect to galaxies, including solar apex coordinates, secular parallax and Oort constants 07 p1194 A71-19331

Planetary nebulae central stars power spectra and HF stellar oscillation observations, using photoelectric time series data 08 p1359 A71-20938

Globular cluster star velocities distribution, examining dynamic evolution models and gravitational effects 08 p1362 A71-21153

Computer simulation model for stars motion in plane of disk-like stellar systems, investigating dynamics of Jeans and gravitational two-stream instability 10 p1670 A71-24181

Star orbit computation in galactic potential fields, using Hamming modified predictor corrector scheme for numerical integration 10 p1678 A71-24927

Stellar velocity distribution in nonrotating clusters, examining mass dispersion role in evolution 12 p1955 A71-26580

Galactic structure historical approach, discussing stellar astronomy foundations, Milky Way, cluster and spiral position, etc 12 p1958 A71-26772

Astronomical catalogs of proper motions and positions, discussing reference systems fundamental declinations and right ascensions measurement principles 12 p1959 A71-26773

Early type stars, open clusters, associations and stellar rings space distribution and state of motion 12 p1959 A71-26776

Stellar orbits for nearby stars, examining short arc statistics and galactic field models 12 p1959 A71-26781

Stellar cluster evolution equations in terms of free particle physics based on Boltzmann equation, describing computerized integrations 12 p1960 A71-26785

Measuring methods for internal velocities of stars and gas within spiral galaxy, considering emission lines and Fabry-Perot interferometer 12 p1960 A71-26786

Equations of motion for single trajectory model of nonspherical stationary rotating stellar systems, assuming phase density dependence on motion integrals 12 p1966 A71-27234

Necessary and sufficient global stability criteria for axisymmetric perturbations of stellar dynamic disk models of galaxies 13 p2138 A71-28775

German monograph on membership in open star clusters, covering M67, pseudocluster M39 and stellar brightness and motions 13 p2139 A71-28879

Double stars astrometry, discussing proper motions, parallaxes and mass ratios of visual binaries 14 p2310 A71-30359

Double and triple stars common proper motion, discussing white dwarf or degenerate components 14 p2310 A71-30360

Double star discovery by common proper motion, using IDS catalog data 14 p2311 A71-30361

Spherical stellar system dynamical evolution model, applying constant point mass technique 14 p2314 A71-30640

White dwarf identification with Lowell proper motion program, detailing color classes, tangential velocity and UVB values 14 p2317 A71-31008

White dwarfs from Catalog of Nearby Stars, indicating radial and tangential velocities, proper motions, positions luminosity and UV spectra
14 p2317 A71-31009

Globular star clusters and spherical galaxies stability, proposing rotating gravitating masses spherically symmetrical system model
15 p2482 A71-31331

Secular parallaxes of reference stars by photometric distances and relative proper motions of open clusters at low galactic latitude
15 p2483 A71-31341

Scorpio-Centaurus association and Gould belt proper motion, discussing convergent point in FK4 catalog with maximum likelihood method
15 p2483 A71-31470

Young open star cluster NGC 6823 membership based on relative proper motions data and color-magnitude diagram
16 p2631 A71-33180

Stellar ring in Aquila, reducing proper motions of stars in all catalogs to General Catalog system and to Brosche FK 4 system
16 p2632 A71-33327

Stellar movement in Galactic field, discussing observational and mathematical techniques for stellar orbits and velocities determination
17 p2801 A71-34697

Newcomb precession determination from Bradley stars proper motions, evaluating neglect of galactic rotation
18 p2961 A71-35942

Stellar proper motions in photographic zenith tubes programs for time service clocks correction, examining catalogs used for astronomical data processing
18 p2962 A71-36110

Correction values to centennial precession, using stellar proper motions
18 p2970 A71-37063

Spectroscopic binary star system with orbital eccentricities less than 5 percent, discussing elliptical or circular orbit possibility
18 p2971 A71-37068

Light curve and apsidal motion of AR Cas from photoelectric photometry
18 p2971 A71-37069

Black holes in binary star systems from orbital eccentricity observations
19 p3142 A71-38006

Stellar proper motion measurement by densitometer automatic scanning of star plates pairs, assessing accuracy
20 p3239 A71-39529

Papers on astronomy covering eclipsing binaries, eclipse functions computations, silicon in sun, Magellanic clouds and stellar kinematics
20 p3300 A71-39819

Stellar evolution and cosmic time scales based correlation analysis of star motion and spectral types, considering B stars, A stars, F and G stars and Halo stars
20 p3301 A71-39824

Observation probability of orbital motion and mass transfer of pulsars in close binary systems, excluding supernova explosion origin for runaway velocities
20 p3304 A71-39943

Total mass density in neighborhood of sun and Galactic force law from stellar motions perpendicular to Galactic plane, using King pseudomoments method
21 p3440 A71-40061

Nearby high velocity stars energy and momentum data, determining orbital properties and integrals of motion
21 p3440 A71-40062

Statistical space velocity distributions, gravitation field strength and vertex deviation for nearby young stars, using density wave theory of galactic spirals
21 p3444 A71-40196

Computer model for dynamical evolution of isolated disks of stars with initial velocity dispersions corresponding to Toomre criterion, noting instability relative to large scale modes
21 p3445 A71-40410

Spectroscopic radial velocity study of Algor eclipsing variable stars, deriving masses and apsidal motion evidence in short period orbit
21 p3446 A71-40418

Thin-shelled ensemble of noncolliding stars surrounding black hole, calculating spectral flux density and brightness
21 p3446 A71-40420

B star in galactic north pole region, noting high radial velocity
21 p3448 A71-40517

Globular star clusters and spherical galaxies stability, modeling as rotating gravitating masses in spherically symmetrical system
22 p3606 A71-42606

Secular parallaxes of reference stars by photometric distances and relative proper motions of open clusters at low galactic latitude
22 p3606 A71-42616

STELLAR OCCULTATION

Strip brightness distribution across Kepler supernova derived from occultation observation by radio telescope
06 p0971 A71-18241

Jupiter occultation of beta Scorpii on 13 May 1971, determining hydrogen/helium ratio
12 p1961 A71-26876

Moon marginal zone charts for determining limb corrections applied to reduction of stellar occultation timing
17 p2797 A71-34185

Double radio emission sources during occultation period, noting structure, angular size components, positional errors and association to quasars
21 p3443 A71-40189

Low cost two channel pulse counter /RUFAS/ for astronomical photoelectric occultation observations, describing resolution, data output and computer interfacing
22 p3542 A71-41932

Fresnel diffraction model appropriateness for stellar occultation by moon
24 p3871 A71-44912

STELLAR RADIATION

NT STELLAR WINDS

High luminosity red variable star radiation, examining degrees of intrinsic polarization
01 p0150 A71-10056

Neutron star in accretion state, investigating generation of relativistic electrons, positrons and X ray and gamma emission
01 p0150 A71-10061

Multicolor polarimetry of Beta Lyrae system, discussing observations instrumentation and reduction
01 p0153 A71-10354

Galactic interstellar grains alignment by starlight, noting photon intrinsic angular momentum role
01 p0159 A71-10865

Sky radiation background in far UV spectral region, calculating stellar component
02 p0304 A71-11913

H alpha line emission in ionization zones encircling neutron stars, suggesting accretion-induced UV luminosity
02 p0308 A71-12091

Optical thickness of reflecting nebula with given brightness illuminated by star, using three dimensional models
02 p0311 A71-12352

Scorpius X-1 X ray and optical variations observation by Vela 5 satellites
02 p0315 A71-12662

Solar line blanketing effect data derivation and analysis for model atmosphere computer programs, considering application to spectrally similar stars
02 p0316 A71-12755

Be stars IR emission, noting thermal free-free radiation superposed upon stellar continuum
03 p0483 A71-13185

Thermal emission from IR star shells calculated from circumstellar graphite dust model
03 p0495 A71-14267

Pulsar NP 0532 average polarization absence due to Crab Nebula depolarization or unpolarized radiation on emission
04 p0643 A71-15047

Mathematical model of stellar atmospheres using radiation emission by elementary cylinder
04 p0647 A71-15236

UV dwarfs observational lifetime, considering progenitor main sequence, red giants and planetary nebulae central stars evolutionary sequence
04 p0648 A71-15249

UV stellar flux measurements vs theoretical stellar atmosphere models, using rocket and satellite observations
04 p0648 A71-15252

Unstable massive main sequence stars nonlinear pulsation, using small amplitude tests of approximation technique
05 p0806 A71-16202

Early type stars radiant flux observation from OGO 6 satellite
06 p0969 A71-17975

Background effects on photographic stellar image photometry
06 p0902 A71-18445

Maserlike pulsar radiation mechanism using Coulomb bremsstrahlung near strong quantizing magnetic field
07 p1190 A71-18858

Alfven waves and magnetosonic radiation by rotating magnetic stars and planets
07 p1193 A71-19293

Continuous optical conversion to IR and directional stellar radiation flow conversion to diffused radiation fields in circumstellar dust envelopes
07 p1187 A71-19821

Variable emission star BD plus 28.637 deg three color photographic observation data evaluation, giving light curves and H-R position
07 p1201 A71-20435

Flare characteristics of UV Cet type stars from statistical analysis of photoelectric light curves
07 p1204 A71-206272

H alpha line emission in ionization zones encircling neutron stars, suggesting accretion-induced UV luminosity
08 p1362 A71-21144

Predicted UV fluxes for main sequence stars, comparing stellar observations with models described by Kucuz, Carbon and Gingerich
09 p1522 A71-22961

Pulsar radiation circular polarization component: Stokes parameter, noting average value different from zero
09 p1522 A71-22971

Stellar X ray sources as close binary stars and novae, calculating radiation by deceleration process
09 p1528 A71-23544

Radiative flux effect on magnetogasdynamical shock in self-gravitating gaseous stars
09 p1506 A71-23589

Background effects in stellar photographic photometry
12 p1903 A71-26595

Periodic variations in circular polarization of continuous radiation of white dwarf G195-19 from 3800 to 45400 A
12 p1956 A71-26610

Time dependent variation of IR polarization of eta Carinae and VY Canis Majoris with separation of interstellar scattering by associated nebula
12 p1956 A71-26611

Star Arcturus chromospheric Lyman alpha emission observation by rocket-borne precision pointing telescope and UV spectrometer
12 p1957 A71-26625

Spacecraft attitude measurement using spatial coherence of laser or star light beam, discussing feasibility and detection equipment
12 p1927 A71-27429

BY Dra stellar flare characteristics by photoelectric observations, noting duration
12 p1971 A71-27750

Fine structure of reddening interstellar extinction curves of stellar radiation, using photographic spectrophotometry
13 p2132 A71-27967

Linear nonadiabatic pulsations of stellar models, discussing numerical method for eigenvalue problem
13 p2132 A71-27968

Blue edge of RR Lyrae instability strip, examining convection, radiation and surface boundary conditions effects
13 p2133 A71-27969

Sky radiation background stellar component in far UV spectral region, determining intensity with Venera instruments
13 p2133 A71-28200

Atmospheric turbulence effects on stellar irradiance and phase, discussing electro-optical recording technique and computer generated statistical data
14 p2270 A71-30016

HF stellar radiation oscillations based on photoelectric monitoring of southern white dwarfs power spectra
14 p2317 A71-31010

Flare star light polarization parameters measurement, describing polarimeter design
15 p2487 A71-32036

Pulsar emission data, presenting average phase shapes and pulse to pulse intensity fluctuations
17 p2797 A71-34372

Soft optical, radio and X ray emission during accretion of interstellar gas by neutron star with magnetic dipole moment
17 p2800 A71-34570

Pulsars electromagnetic radiation, considering bunch of relativistic charged particles
19 p3134 A71-37513

Rotating magnetic white dwarf stars possibility as X ray sources with thermal spectrum, considering evidence based on Sco X-1 emission relationship to bremsstrahlung
19 p3127 A71-38010

Flare stars X ray emission by fast electrons nonthermal bremsstrahlung
19 p3128 A71-38157

Stellar rotation effects on radiation spectral characteristics, calculating He line profiles by LTE method
19 p3143 A71-38158

Crab pulsar NP 0532 low energy gamma radiation emission data, observing flux ratios and pulsations
20 p3278 A71-39109

Cygnus X-1 X ray data with temporal resolution, examining pulsations and flare activity
20 p3278 A71-39110

Monochromatic radio emission from decihertz years distant stars, discussing search experiment by low noise multichannel receivers
20 p3291 A71-39319

Critique of Smith oblique rotator model for Crab pulsar radiation, concerning observation of optical pulse position angle variation and interpulse offset location
20 p3279 A71-39402

Planetary, stellar, galactic, sky and extragalactic UV radiation from OAO-2 spectrophotometric observations, noting interstellar extinction curves

20 p3300 A71-39747

Pulsar radiation from oscillating interface with steady current sheet between rotating radiating magnetic dipole and external plasma

20 p3285 A71-39952

Pulsar radiation beaming due to strong magnetic field, computing Compton scattering and opacity

20 p3285 A71-39953

Crab Nebula pulsar and extar emission from collapsed star magnetosphere, accounting for physical characteristics with nonthermal plasma mechanism

20 p3285 A71-39954

Early stars UV continuum brightness from rocket-borne photoelectric spectrophotometer, estimating total interstellar flux density

21 p3444 A71-40244

Polarization and pulse profiles of pulsars at 410 and 1665 MHz, indicating radiation originating close to star surface

21 p3453 A71-41244

Fluorescence phenomena in celestial bodies, considering atomic lines and molecular bands in stellar and nebulae emissions

22 p3597 A71-41515

Mode changing in pulsar radiation, observing intensity profiles and polarization characteristics

23 p3769 A71-43995

Pulsar 0833-45 LF radiation spectrum decrease explained by pulse broadening due to interstellar scattering

24 p3868 A71-44565

Cyclotron magnetoacoustic wave generation by planets and binary stars in circular orbits, deriving interstellar gas density variations

24 p3869 A71-44804

Stellar UV cut-off by photospheric nacelle recorded on photographic film by Schmidt telescope fitted with objective prism, widening spectrum by scanning

24 p3875 A71-45272

STELLAR REFRACTION

U ATMOSPHERIC REFRACTION

U STELLAR RADIATION

STELLAR ROTATION

NT SOLAR ROTATION

Rotating stars with partially ionized convective envelopes, investigating general stellar magnetic field production

01 p0150 A71-10060

Pulsars characteristics including rotation periods, age, magnetic field strength, gravitational fields and translational motion

01 p0160 A71-11066

Rotating neutron star supernova explosion without nuclear detonation, discussing rotational momentum transfer

02 p0307 A71-12089

Rayleigh, baroclinic and Rossby waves instabilities effects on stellar structure during differential rotation

03 p0486 A71-13322

Pulsar free rotational dynamics accounting for amplitude and time variations in signals, considering non-rigidity and viscosity effects

03 p0493 A71-14211

Radiative transfer equation for atmospheres of rotating stars, deriving expression for flux distribution

03 p0495 A71-14381

Electrical polarization of vacuum around rotating magnetic Newtonian star, evaluating electrostatic potential

04 p0643 A71-14912

Stellar rotation effects on color, magnitude, formation and evolution

04 p0647 A71-15238

Stellar angular momentum, discussing evolution, rotation orbits and relationship between binaries, rotating stars and planetary systems

04 p0647 A71-15240

Normal main sequence B stars, distinguishing features from rapid rotators and supergiants by photometric scheme

05 p0805 A71-16118

Magnetic stars models on possibility of rotational deceleration by hydromagnetic waves radiation without mass loss

07 p1190 A71-18857

Magnetic field generation of rotating stars with partially ionized convective envelopes due to emf arising from convective flow Coriolis acceleration

07 p1193 A71-19294

Rotating neutron star supernova explosion without nuclear detonation, discussing rotational momentum transfer

08 p1362 A71-21139

Zeta Aurigae chromospheric lines observed radial velocities mean variations, taking into account H ion gas acceleration, K star mass ejection and rotation

08 p1364 A71-21417

Pulsar model consisting of rotating neutron star with strong magnetic field

09 p1517 A71-22337

Extragalactic violent events energy from collapsing stars or pulsar bodies rotational energy, producing extended radio sources

09 p1522 A71-22977

Star formation angular momentum and magnetic flux problem, investigating collapsing dust cloud theory

11 p1830 A71-26108

Extragalactic radio sources total and linearly polarized radiation one dimensional distributions, noting spectral variations, magnetic fields and rotation measurements

11 p1830 A71-26131

Periodic rotational LF synchrotron model of magnetic neutron star for pulsar radiation

12 p1947 A71-26649

Relativity and neutronization effects on radial pulsations and density decrease of rotating cold white dwarfs near stability loss, using energetic method

12 p1966 A71-27236

Maximum toroidal magnetic fields of rotating neutron stars dependent on central density, using relativity corrections to plasma hydrodynamic and Maxwell equations

12 p1966 A71-27237

Gravitational waves from rotating relativistic neutron stars [pulsars] in far field region, assuming small velocity and spherical deformation

13 p2133 A71-27971

Rapid differential rotation in completely degenerate white dwarfs, using perturbation method

13 p2135 A71-28300

Rotating Jacobi ellipsoid evolution by gravitational waves emission, discussing triaxial nonaxisymmetrical configurations for rapidly rotating pulsars

13 p2140 A71-29000

Pulsar nature and radiation mechanism, examining rotating neutron stars structure and atmospheric dynamics

13 p2140 A71-29041

Pulsar oblique rotator model wobble and alignment time scales, considering Crab and Vela pulsars precession damping mechanism by internal friction of crust

14 p2313 A71-30428

Pulsed gamma radiation from rotating neutron star, discussing synchrotron emission mechanism based on electron pulses incident on high intensity sharply localized magnetic field

15 p2474 A71-31724

Rapidly rotating early stars and quasars, determining magnetic field generation by turbulent dynamo mechanism

15 p2485 A71-31725

Thermal X ray sources associated with rotating collapsed stars with surrounding plasma shells, discussing plasma density profile and electron distribution in stellar magnetosphere

15 p2497 A71-32762

Equivalent width of metallic lines for pole-on main sequence stars, examining effect of rotational axis inclination with respect to line of sight on washout of lines

16 p2633 A71-33334

Crab Nebula pulsar rotation and magnetic axes disposition from pulse shape and polarization data at optical and radio wavelengths

16 p2634 A71-33391

Pulsars as neutron stars, explaining fast rotation by tendency to conserve angular momentum during compression

17 p2804 A71-34857

Solar-type dwarf star rotation effect on stellar wind structure and thermal regime, obtaining time independent solutions with heat conduction

17 p2796 A71-35577

Scorpius X-1 cocoon pulsar thermal X ray emission model, describing hot gaseous region around rotating neutron star

18 p2969 A71-37043

Temperature limit determination of rotating neutron stars based on heat dissipation due to slowing by frictional forces, noting Crab and Vela pulsars

19 p3131 A71-37337

Rotating isothermic radially pulsating white dwarf evolution, considering neutronization and general relativistic effects

19 p3134 A71-37511

Rotating magnetic white dwarf stars possibility as X ray sources with thermal spectrum, considering evidence based on Sco X-1 emission relationship to bremsstrahlung

19 p3127 A71-38010

Stellar rotation effects on radiation spectral characteristics, calculating He line profiles by LTE method

19 p3143 A71-38158

Theorem proved for monotonic behavior of pressure within relativistic rotating star, assuming stationary axisymmetric gravitational field of Euclidean topology

20 p3293 A71-39447

Crab Nebula optical pulse timing, noting neutron star crust rotation speedup and relaxation, eccentric planetary orbits and sinusoidal effects

20 p3302 A71-39928

Vela pulsar interstellar scattering, studying pulse broadening, rotation measure and radiation origin near magnetic pole

20 p3303 A71-39937

Crab Nebula pulsar magnetosphere, considering model of rotating magnetized neutron star rate of energy generation and rotation law exponent

20 p3305 A71-39948

Massive main sequence stars in rapid differential rotation, investigating structure, energy transport, luminosity and circulation time scale

21 p3444 A71-40241

Radiative transfer effects on hydromagnetic stellar atmospheres thermal-convective instability in presence of uniform rotation and uniform magnetic field

21 p3421 A71-40579

Galaxy active nucleus and quasar fragmentation based on model of rotating supermassive star releasing thermal radiation

21 p3449 A71-40610

Static magnetic fields configurations of magnetic and rotating neutron stars, considering general relativistic effects

21 p3450 A71-40714

Second order rotational effects on stellar nonradial oscillations by perturbation method, taking into account equilibrium configuration distortion by coordinates transformation

22 p3602 A71-42173

Structure and stability of rapidly uniformly rotating supermassive star, using post-Newtonian hydrodynamic equations and standard model

22 p3604 A71-42328

Intrinsic UV color variations of interstellar extinction laws due to stellar rotation, MK spectral type and photometric errors, using rocket observations

22 p3604 A71-42333

Pulsar speedup due to neutron starquakes, deriving self gravitating elastic incompressible sphere model for time prediction

23 p3722 A71-42894

STELLAR SPECTRA

NT SOLAR SPECTRA

Total free electron energy disparity with energy radiated in forbidden O I lines in supernova spectra explained by nova luminescence formation

01 p0151 A71-10067

Ap-type magnetic stars wavelength dependence polarization, discussing polarimetric observations in different spectrum regions

01 p0153 A71-10355

Electric conductivity dependence on optical depth in photospheres of spectral type F, G and K stars for different gravitational acceleration values on surface

01 p0159 A71-10866

Venera probes UV radiation measurement, discussing photometric equipment and spectra for hot stars and Milky Way in L alpha line

02 p0304 A71-11912

Atmospheric turbulence effects on stellar Michelson interferometry

02 p0308 A71-12099

Hydrogen lines of spectrally variable star alpha squared CVn from spectrograms, determining atom concentration, electron density and acceleration of gravity on surface

02 p0311 A71-12357

Wolf-Rayet WN6 stars emission line spectral profiles observation by spectrograms and photoelectric scanning

02 p0314 A71-12584

UV and visual spectra of gamma Cassiopeiae from rocket spectrograph and OAO observations

02 p0314 A71-12585

Cepheids in Milky Way spherical component, emphasizing brightness and color curves and spectral characteristics

03 p0485 A71-13261

RV Tau type stars general and spectral classification, covering color indices, line-of-sight velocities, kinematics and spatial distribution

03 p0485 A71-13262

RR Lyr type stars kinematic behavior, line of sight velocities, spectral energy distribution and temperature

03 p0485 A71-13263

Delta Scutum type variable stars, discussing photometric properties, line of sight velocities, color indices, luminosity, chemical composition, etc

03 p0485 A71-13264

RR Lyr type dwarf stars, discussing brightness curves, color indices, effective temperatures, line of sight velocities and spectral classes

03 p0485 A71-13265

Stellar spectra and spectral types, discussing spectrographs, identification of lines, intensity measurements, absorption lines, Harvard system, etc

04 p0646 A71-15229

Morgan two dimensional stellar spectral system with luminosity classes, comparing to Harvard scheme

04 p0646 A71-15230

Spectral classification parameters, discussing spectral-type indicators, luminosity indicators, spectra of

clusters and galaxies, abundance, population and low metal objects

04 p0646 A71-15231

Lithium line strength indicator of stellar age, discussing T Tauri, A, carbon, S and Ba II stars

04 p0646 A71-15232

White dwarfs, investigating spectral classification, clusters, motions and location on H-R diagram

04 p0647 A71-15243

White dwarf data, examining continuous energy distribution, degenerate star theory, mass-radius relation, spectra, radial velocities and Einstein shift

04 p0648 A71-15244

IR stars, discussing very young stars, circumstellar clouds and IR excesses

04 p0648 A71-15251

Pulsars CP 0328, CP 0834, CP 1133 and CP 1919 radio spectra, examining interstellar scintillation model, transverse velocities and line widths

05 p0802 A71-15939

Technetium stars characteristics, noting MS, S and N spectral types, s process element enhanced abundances and variability

05 p0806 A71-16206

Plutonium in peculiar A stars surfaces as nuclear cosmochronology for determination of r process nuclei age, considering emission line spectra obscurement

05 p0808 A71-16413

Cepheids normal color index-spectrum relation, noting light variation phases and color-color diagrams reddening lines

06 p0975 A71-18436

Absorption line blanketing, back warming and blocking effects on B and V magnitudes for F-G stars

07 p1193 A71-19295

Eclipsing variable binary stars spectral and luminosity classes determination

07 p1200 A71-20035

RW Aur stellar spectrum variation mechanisms

07 p1200 A71-20036

G5-K5 stars 3600-4000 A region, determining forbidden Fe/H lines for G8-K3 giants

07 p1201 A71-20436

Spectral temporal variations and atmosphere conditions of P Cygnus, including atomic hydrogen densities, electron concentrations, microturbulent velocity and Balmer decrement

07 p1204 A71-20631

High dispersion spectrograms of manganese Ap stars alpha And and pi Boo A, estimating electron concentration

07 p1204 A71-20632

Planetary nucleus BD plus 30.3639 degrees and Wolf-Rayet star HD 164270, comparing spectrum and ionization potential

08 p1359 A71-20937

Planetary nebulae central stars power spectra and HF stellar oscillation observations, using photoelectric time series data

08 p1359 A71-20938

Atmospheric turbulence effects on stellar Michelson interferometry

08 p1362 A71-21149

Book on dwarf novae covering light variations, spectra, binary systems, absolute magnitude, mass, gas streams, outburst, etc

08 p1363 A71-21165

All-reflection optical device for stellar spectra automatic widening and concurrent night sky spectrum suppression

09 p1442 A71-22068

Class M supergiants alpha Sco, delta Sge, R Lyr and alpha Her spectra between 7000 and 6000 A wavelengths, tabulating equivalent bandwidths

09 p1524 A71-23189

Total free electron energy disparity with energy radiated in forbidden O I lines in supernova spectra explained by nova luminosity formation

09 p1525 A71-23260

Diffuse interstellar features in spectrum of reddened star in Cygnus OB2 stellar association, tabulating equivalent widths of H alpha and stellar He I line

10 p1665 A71-23749

Atmospheric extinction vs intermediate band color index diagrams, discussing linear correlation and reference star selection

10 p1681 A71-25130

Early stars Vilnius intermediate band and UVB systems comparison for color excess ratios and magnitudes, obtaining reddening line slopes by spectral energy distributions

10 p1682 A71-25131

M stars mass loss, determining dust shells radii and densities with IR observations of circumstellar emission

11 p1818 A71-25204

He I absorption line profiles in normal main sequence B star spectra, discussing He abundance and LTE

11 p1821 A71-25536

Binary alpha Virginis interferometric data, noting distance, luminosity brightness ratio, angular size and diameter, orbits mass, temperature and gravity

11 p1830 A71-26107

He I lines in OB spectra, examining main sequence stars

11 p1830 A71-26111

Extragalactic radio sources total and linearly polarized radiation one dimensional distributions, noting spectral variations, magnetic fields and rotation measurements

11 p1830 A71-26131

Cepheids normal color index-spectrum relation, noting brightness variation phases and two-color diagrams reddening lines

12 p1955 A71-26586

Astronomical photometry and photometric systems, discussing spectral classification, U, V, B, Y, beta system, energy distributions and seven color photography

12 p1903 A71-26774

C, gM and S spectral type stars, considering distribution, absolute magnitudes and intrinsic colors

12 p1959 A71-26777

Pulsars CP 0950 and CP 1133, examining pulse spectra characteristics in 83-111 MHz frequency range

12 p1963 A71-27076

Quasars and X ray sources, observing UVB magnitude variation with photoelectric data

12 p1963 A71-27077

Spectral line broadening theory applications to qualitative interpretation and quantitative determination of spectrograms from hydrogen line profiles of stellar atmospheric parameters

12 p1969 A71-27667

Venera probes UV radiation measurement, discussing photometric equipment and spectra for hot stars and Milky Way in L alpha line

13 p2133 A71-28199

Galactic structure and spectra, examining universe expansion, Hubble law and quasar distances

13 p2142 A71-29129

Rocket-borne Cassegrain telescope system design for stellar spectra in UV region of EM spectrum between 900 and 3300 A

14 p2238 A71-29727

Early type close binary systems AO Cas, HD 47129, HD 190918 and HD 193793 spectral observations

14 p2311 A71-30369

White dwarf discovery method and properties, discussing color, spectra, parallaxes, luminosities, masses, red shifts, cluster and frequency distribution

14 p2316 A71-31005

Red subluminous stars, presenting catalog identification, proper motions, spectral type, photometric parallax, tangential velocity, UVB photometry, etc

14 p2316 A71-31006

White dwarf identification with Lowell proper motion program, detailing color classes, tangential velocity and UVB values

14 p2317 A71-31008

White dwarfs from Catalog of Nearby Stars, indicating radial and tangential velocities, proper motions, positions luminosity and UVB spectra

14 p2317 A71-31009

Spectroscopic criteria for strong lined white dwarf stars identification on low dispersion objective prism plates

14 p2317 A71-31012

White dwarf model atmosphere, discussing DA and non-DA spectral types, surface gravity, mass-radius relation, composition and convection effects

14 p2317 A71-31014

White dwarf line spectra, constructing atmospheric models and effective temperatures

14 p2317 A71-31015

Hydrogen deficient white dwarf atmospheres, computing line free flux constant models for He rich compositions with varied metal abundances

14 p2318 A71-31016

Mu, VV, ST and RW Cephei cold supergiants polarization data, noting spectral dependence

15 p2487 A71-32030

Star EV Lac polarimetric observations during flare, using Cassegrain reflector

15 p2487 A71-32031

Faint O-B5 type blue stars data, listing absolute spectrophotometric gradients and Balmer series discontinuities

15 p2487 A71-32032

High luminosity G supergiants at 0.4-18 micron wavelengths showing intense silicate emission shell

15 p2497 A71-32764

IR stellar object HD 45677, discussing IR spectral energy distribution in terms of black body temperature range

15 p2497 A71-32765

Subdwarf star data, reviewing spectra, kinematics, nucleosynthesis, interiors, atmospheres, angular momentum, formation, abundances and distribution

16 p2631 A71-33126

B and O hot dwarf stars ionic UV line spectra, observing electron and ion damping constants with impact and semiclassical approximations

16 p2633 A71-33338

AO Algol-type variables W Del, T L Mi, RZ Cas, and delta Lib gradient variation and Balmer discontinuity, detailing luminosity and radius ratio effects

16 p2634 A71-33427

NGC 3811 supernova spectrum and light curve data, indicating Type I class

16 p2635 A71-33433

Algol type star AW Peg, determining gradient, temperature, absolute visual magnitudes, equivalent absorption line widths, atmospheric parameters and spectral class

17 p2800 A71-34567

X-Y programmed microdensitometer for stellar spectra analysis, imaging adjustable slit on spectrogram by interchangeable microscope objectives, using Kohler illumination

17 p2742 A71-35001

Digitized microphotometer for star image and stellar spectra detection, describing design, operational principles and applications

17 p2742 A71-35001

Type I supernova broadband identification, examining interstellar medium spectra

17 p2806 A71-35384

Symmetrically distributed nebulae around Wolf-Rayet stars, detailing Nc 7635 and associated star BD 16 plus 60 deg 2522

17 p2806 A71-35410

Pulsating variable star spectral line formation from integral equation solution of radiative transfer and gas flow through shock front

17 p2808 A71-35553

Galactic star cluster K 4 and Ba 10 observations with RGU photographic photometry, noting distances and types

18 p2960 A71-35938

Sunspot forbidden Fe I line spectra, showing high solar iron abundance

18 p2961 A71-35944

Type II supernovae observations and models, considering photographic light curves and dynamic instabilities in star development, outbursts and ejected matter composition and amounts

18 p2961 A71-35976

Position, parallax, distance, visual apparent and absolute magnitude, spectrum and visual luminosity tables for nearby stars

18 p2968 A71-37030

N stars Y CVn, RY Dra and 19 Psc IR synthetic cyanide radial spectrum analysis, determining C 12/C 13 ratio

18 p2969 A71-37044

Pulsars CP 0950 and CP 1133, examining pulse spectra characteristics in 83-111 MHz frequency range

19 p1313 A71-37426

Quasars and X ray sources, observing UVB magnitude variation with photoelectric data

19 p1313 A71-37427

Stellar atmosphere line formation in magnetic fields, considering Milne-Eddington model

19 p1313 A71-37507

Spectroscopic binary system with invisible major mass components, considering relativistic companion star

19 p1314 A71-37508

Emission lines of star S22 in Large Magellanic Cloud, identifying H, Fe II and forbidden Fe II and Ni II lines

19 p1344 A71-38167

Wavelength table for determination of stellar radial velocities in spectral classes F6-M2, including Hyades cluster and Coma Berenices

19 p1344 A71-38168

Differential line shifts in spectrum of supergiant beta Ori attributed to radial spreading of stellar atmosphere

20 p3290 A71-39302

Linear polarization of pulsar PSR 22 18 plus 47 radio emission pulses, attributing periodic fine structure of spectrum to rotation of polarization plane in interstellar medium

20 p3291 A71-39316

IAU Executive Committee, General Assembly and commissions reports on astronomy, including manuscripts preparation guidelines, handbook, etc

20 p3315 A71-39425

Stellar evolution and cosmic time scales based correlation analysis of star motion and spectral types, considering B stars, A stars, F and G stars and Halo stars

20 p3301 A71-39824

BCD Cepheids observations, examining data with quasi-static interpretation approximation for gravity and stellar masses

21 p3441 A71-40065

Wavelength shifts of intensity minima in type I supernova spectra

21 p3449 A71-40606

Close binary stars monochromatic reflection effect calculation, using surface temperature distribution model

22 p3599 A71-41934

Low dispersion luminosity criteria in A and F stars, computing synthetic spectra for atmospheric temperature surface gravity microturbulence and abundance

22 p3601 A71-42166

Interstellar silicate absorption search using VI Cyg No 12 spectrum observations

22 p3605 A71-42349

Pole-on Be star envelope models, comparing H alpha line profiles with line of sight perpendicular to rotation axis

23 p3723 A71-42945

Phase dependent spectra of Cepheids from multi-frequency group calculations in radiative transfer model

23 p3723 A71-42946

White dwarfs EG 248, GR 289 and EG 250 spectra with circular polarization, detailing violet lines, absolute magnitudes, color and luminosity

23 p3733 A71-43079

B stars spectra, calculating C III ions spontaneous electric dipole transitions and oscillator strengths in vacuum UV region

23 p3767 A71-43829

Red variable GN Her brightness, color and spectrum, discussing UVB system photoelectric measurements during 1966/68 period

23 p3771 A71-44303

K and M class stars B and V magnitudes in UVB system based on atomic lines and molecular bands spectral absorption

23 p3771 A71-44306

M stars atmospheric temperature determination from TiO molecular spectrum by vibrational band intensity measurement

23 p3771 A71-44307

Classification method for unwidened low dispersion stellar spectra, giving table for weak stars in region around NGC 6913 cluster

23 p3772 A71-44308

TELLAR SPECTROPHOTOMETRY

Spectrophotometry of star EW Lac, showing variability by H line profiles

02 p0311 A71-12356

Hydrogen lines of spectrally variable star alpha squared CVn from spectrograms, determining atom concentration, electron density and acceleration of gravity on surface

02 p0311 A71-12357

Double beam microphotometer for simultaneous measurement of negatives, reducing processing time and density fluctuations

02 p0251 A71-12358

Open cluster NGC 7789 blue stragglers data acquisition from image tube spectrograms and four color and H beta photometry, obtaining location along main sequence

02 p0314 A71-12583

Stellar spectroscopy by optical heterodyning of laser and star light mixing, using He-Ne laser, high speed photocell and RF power measurement equipment

03 p0487 A71-13331

Stellar spectrograph with image converter, obtaining optimal ratio between telescope and collimator diameters

04 p0589 A71-14833

Stellar spectrometers design features and performance with photomultipliers, emphasizing sensitivity

04 p0589 A71-14834

Iris photometer for star observations, discussing automatic compensation for plate background

04 p0590 A71-14840

UVB photometry of RR Lyrae variables in metal rich globular cluster NGC 6171

04 p0649 A71-15372

Photoelectric photometer measurements of stellar interferometer fringes strength by light modulation

05 p0752 A71-16681

Error allowance of photoelectric sighting grating with incline slits in stellar observations at Pulkovo

07 p1108 A71-19330

Four-color IR photometry of cool carbon, S and M stars

07 p1187 A71-19820

Powerful solar flare H lines spectrophotometric observation, noting hydrogen atom upper energy levels overexcitation

07 p1188 A71-20033

Spectrophotometric observation of solar weak chromospheric flare of 15 June 1964, determining flare origin

07 p1188 A71-20039

Photoelectric UVB observations of variable star AE Aur /November 1963-February 1968/, tabulating and graphing results

07 p1201 A71-20434

Flare characteristics of UV Cet type stars from statistical analysis of photoelectric light curves

07 p1204 A71-20627

Photoelectric and radio observations of flares of UV Cet and YZ CMi stars

07 p1204 A71-20628

Photoelectric observations of EV Lac flares in spectral U, H beta, G and V regions

07 p1204 A71-20629

Three color photoelectric observations of symbiotic star AG Dra in UVB system

07 p1204 A71-20630

Eclipsing variable V701 Cen photoelectric observations in UVB tabulated, fitting Russell model solutions to data

08 p1357 A71-20874

Photoelectric stellar image analyzer for measuring close binary stars separation, collecting data by image coherent superposition

08 p1290 A71-21393

Photon counting stellar photometer for UVB spectra, describing operation and block diagram

09 p1451 A71-23187

Stellar UVB photographic photometry of specific Milky Way oblong region

09 p1527 A71-23525

Quasars or blue stars possibility of radio sources usually identified with galaxies

10 p1674 A71-24448

Book on stellar spectroscopy for peculiar stars covering hot star spectra emission lines, novae, magnetic, metallic line and related stars

10 p1675 A71-24477

Multicolor photographic photometry of flare stars in Orion aggregate based on two UVBR photoelectric sequences

10 p1680 A71-25061

Scattered stellar clusters region stars and interstellar matter from photographic magnitudes diagrams and color indices, determining absorption fluctuations by color excess technique

10 p1681 A71-25127

Intermediate band photometric system for three dimensional star classification based on published stellar spectral energy distribution data

10 p1681 A71-25129

Cepheids broadband photometric study of temperature and blanketing variations as function of turbulent velocity and gravity, using atmospheric models

11 p1818 A71-25206

Interstellar absorption and color excesses in Sco OB-1 from spectral observation and photometry for star cluster and association background

11 p1831 A71-26133

Seyfert galaxy 3C120 photometric behavior, investigating light variations

11 p1831 A71-26168

Cepheids normal color index-spectrum relation, noting brightness variation phases and two-color diagrams reddening lines

12 p1955 A71-26586

Perseus early stars photometry and far UV spectra from Aerobee rocket flight observations

14 p2304 A71-29596

Experimental solar blind photomultipliers for stellar photometry above earth atmosphere at 1450-2800 A, giving spectral response and quantum efficiency

14 p2240 A71-30122

Rocket-borne twin-channel photoelectric stellar photometer for use in 1400-3000 A region, describing nondispersive wavelength isolation methods

14 p2240 A71-30124

Visual binary stars spectroscopic observations, discussing spectra, luminosity, parallax and radial velocities of mass center and individual stars

14 p2311 A71-30365

Visual double stars spectroscopy, discussing stellar mass and parallax determination

14 p2311 A71-30367

Star observation by moon-based telescope for star diameters, multiple components and precise occultation times by distortion and diffraction pattern analysis

14 p2312 A71-30374

Subluminous star spectroscopic data, determining temperature and surface gravity

14 p2317 A71-31011

Faint O-B5 type blue stars data, listing absolute spectrophotometric gradients and Balmer series discontinuities

15 p2487 A71-32032

Photometry and structure of young open cluster NGC 7380, obtaining magnitudes in UVB and positions on Hamburg-Schmidt plates

16 p2632 A71-33321

Computer model of eclipsing binary stars tested with photometric B and V observations and orbital elements of RU Ursae Minoris

16 p2635 A71-33436

Image dissector photomultiplier for acquisition, guiding, focusing and photometric monitoring in telescope control

17 p2741 A71-34992

Automated stellar spectrophotometry, defining possible measurements on crowded spectra

17 p2742 A71-35005

Computerized microphotometry of stellar spectrograms for converting input density data to intensity scales, coding tube sensitizer plates, wedge/strip spectrograms and step wedges

17 p2742 A71-35006

Stellar spectrograms digital filtering for SNR improvement for photographic plate with line widths larger than granulation noise mean period

17 p2743 A71-35008

Radiative transfer in two-component stellar atmosphere, discussing lines corresponding to solar Ca K-line

17 p2839 A71-35555

Solar coronal line photometry eliminating inherent systematic measurement errors of previous methods

17 p2809 A71-35597

Light curve and apsidal motion of AR Cas from photoelectric photometry

18 p2971 A71-37069

High resolution solar UV spectrum observation between 200 and 220 nm by sun-pointed Skylark rocket-borne echelle spectrograph

19 p3135 A71-37611

Three color photometry of star field in Sagittarius cloud, determining interstellar absorption, density and luminosity for main sequence stars

19 p3144 A71-38169

Photoelectric telescope observations of red stars in Cygnus at IR wavelength with threshold brightness detection

20 p3293 A71-39537

Orbital elements of W Ursae Majoris systems, considering radial velocity curves, spectroscopic orbital solution, spectral peculiarities and spectrophotometry

20 p3300 A71-39820

Photoelectric observations of magnetic variable stars with five color photometer, giving light and color curves parallel to main sequence

21 p3440 A71-40057

Spectrophotometric observations of asymptotic giant and red giant branch stars in metal weak globular clusters

21 p3440 A71-40063

Four-color and H beta photometric data tabulation for bright B type stars in Southern Hemisphere

21 p3443 A71-40192

G and K giant stars iron abundances from narrow band indices, using spectrophotometer, red-IR colors and independent luminosity estimates

21 p3444 A71-40240

Early stars UV continuum brightness from rocket-borne photoelectric spectrophotometer, estimating total interstellar flux density

21 p3444 A71-40244

Photographic photometry of M67 to 200-inch telescope limit for main sequence star evolution track

21 p3446 A71-40414

Space distribution of OB stars from revised Victoria H gamma spectrophotometric magnitudes by MK spectral classification

21 p3448 A71-40594

SV Cephei variable photoelectric UVB observation showing existence of quasi-periodic minima with changing characteristics

21 p3451 A71-40715

Stellar UVB photometric investigation, determining brightness, coordinates, B-V and U-B color indexes of faint blue objects near galactic North Pole

21 p3451 A71-40721

Nonlinear photometric effects of limb darkening and gravity darkening dominance in eclipsing variables from light minima observations

22 p3604 A71-42332

Intrinsic UV color variations of interstellar extinction laws due to stellar rotation, MK spectral type and photometric errors, using rocket observations

22 p3604 A71-42333

Orion constellation hot stars UV spectra observation by photography from stratospheric balloon gondola using geomagnetic field for stabilization

23 p3735 A71-43249

Nova N Vul 1968 UVB system photoelectric observations, noting small amplitude rapid brightness variations during night

23 p3771 A71-44304

STELLAR STRUCTURE

Electric conductivity dependence on optical depth in photospheres of spectral type F, G and K stars for different gravitational acceleration values on surface

01 p0159 A71-10866

Quark regions in massive stars internal structure, discussing plasma superconductivity and spectral line emission

01 p0160 A71-11112

General relativistic formulation of massive magnetized rotating conductor, showing electrodynamic properties of surrounding empty space for explanation of stellar structure

01 p0160 A71-11273

Stellar nucleosynthesis processes classified into various interior nuclear reactions, discussing stellar evolution role

01 p0131 A71-11422

Shock wave front propagation instability in decreasing density medium, applying to stellar structure

02 p0241 A71-12510

Solar corona and wind composition, accounting for He flux and heavy elements from diffusion equations solution

02 p0303 A71-12770

Rayleigh, baroclinic and Rossby waves instabilities effects on stellar structure during differential rotation

03 p0486 A71-13322

STELLAR WINDS

Adiabatic temperature gradient requirement for neutral convection mode in general relativity of star in hydrostatic equilibrium 03 p0486 A71-13330

Stellar core evolution from He burning phase to oxygen exhaustion in central region, discussing mixing with envelope under various mass conditions 03 p0493 A71-14196

Soviet book on stellar physics covering evolution, internal structure, mass, luminosity, radius, density, temperature, bolometric magnitude, energy transfer, etc 04 p0645 A71-15225

Internal constitution and kinematics of main sequence stars regarding age, evolution and formation place during hydrogen burning phase 04 p0646 A71-15233

Close binaries evolution, atmospheres structure and three body problem 04 p0647 A71-15241

Stellar structure theory, examining particle aggregates gravitational and pressure forces, energy flow, generation and opacity and equations of state 04 p0648 A71-15246

Models for partially mixed stars at He flash time, determining mixture degree effects, carbon production and total mass 05 p0801 A71-15932

Magnetohydrostatic stellar interior instability, noting magnetic buoyancy 05 p0802 A71-15938

Stellar chemical composition and structural evolution, discussing mass/luminosity relationship, evolution sequences during hydrogen and helium combustion stages, etc 06 p0970 A71-18200

White dwarfs, neutron stars and black holes origin and characteristics, discussing density, mass radius, gravitation and structure 07 p1199 A71-19999

Solar corona structure on 22 September 1968 from radio astronomical and optical eclipse data 09 p1520 A71-22833

Dense /relativistic/ stars structural stability with respect to centrally symmetrical perturbations 09 p1523 A71-23019

Mn type peculiar A stars relative abundance from curve of growth analysis, discussing isotope shifts, nucleosynthesis, explosion reactions and structure acceleration 09 p1529 A71-23596

Soviet book on eruptive stars including U Gem stars, symbiotic stars, R CrB stars, UV Cet stars and alpha squared CVn stars 10 p1677 A71-24732

Massive stars evolutionary models, exploring convective instability effects 11 p1818 A71-25205

Quasar 3C 147 angular structure observations, using long baseline interferometer 11 p1830 A71-26113

Stellar electric charges, determining sign and magnitude by exchange processes between stars and surroundings 12 p1971 A71-27763

K giants, subgiants, M67 and NGC 188 abundances, noting high metallicities 13 p2136 A71-28431

Pulsar nature and radiation mechanism, examining rotating neutron stars structure and atmospheric dynamics 13 p2140 A71-29041

Subluminous star spectroscopic data, determining temperature and surface gravity 14 p2317 A71-31011

White dwarf star gravity mode stability, considering hydrogen-helium transition sorting zone 14 p2318 A71-31018

Hydrogen burning supermassive stars hydrostatic equilibrium models from numerical integration of stellar structure equations 15 p2485 A71-31718

High density degenerate stellar plasma analysis, obtaining phase transition thresholds, elementary particle stability, thermal energy density and interaction model 15 p2487 A71-32038

Evolved stellar cores thermonuclear explosion products state, investigating Chapman-Jouguet detonation propagation effects with carbon 12 and oxygen 16 burning under high electron degeneracy 17 p2806 A71-35407

Book on space science covering celestial coordinates, time and mechanics, planetary atmospheres and interiors, comets, meteors, stellar structure, etc 18 p2963 A71-36246

Solar corona model for structure and dynamic properties, investigating gas-magnetic field interactions 18 p2966 A71-36737

Convective heat transfer in stars from anelastic and Boussinesq approximations, discussing two dimensional solutions, truncated expansions, turbulence and mixing length theories, etc 18 p2968 A71-37038

Degenerate dwarfs theory, discussing stellar structure, stability, evolution and thermal properties 18 p2969 A71-37039

Stellar convective shell plane gas layer, noting time dependence of energy flux 19 p3134 A71-37514

Solar chromosphere and corona manifold structure data, using high resolution filter photography 19 p3136 A71-37616

Neutron star models, discussing crystalline crust, particle superfluid properties, rotational vortices and relation to Crab Nebula pulsar 20 p3304 A71-39944

Stellar models with He envelopes and carbon-oxygen cores, discussing interior structures and evolution of helium and R CrB stars 21 p3440 A71-40055

Errors resulting from linear interpolation use in opacity tables for stellar interior calculations 22 p3599 A71-41923

Solar transition layer and inner corona empirical minimum equator model, using radio, UV, white and monochromatic radiation data 22 p3601 A71-42161

Structure and stability of rapidly uniformly rotating supermassive star, using post-Newtonian hydrodynamic equations and standard model 22 p3604 A71-42328

Neutron star limiting mass based on soft hadron matter resistance to gravitational collapse in stellar structural stability consideration 23 p3732 A71-43073

STELLAR WINDS

Stellar wind effect on accretion, showing critical intensity of particle ejection replacement 03 p0484 A71-13221

Solar wind observations, accounting for cosmic plasma and stellar wind properties 06 p0973 A71-18336

Stellar wind flow models associating energy transport with propagation and dissipation of hydrodynamic waves and heat conduction 14 p2297 A71-29586

Relativistic stellar wind problem, discussing topology solutions 15 p2490 A71-32399

Solar-type dwarf star rotation effect on stellar wind structure and thermal regime, obtaining time independent solutions with heat conduction 17 p2796 A71-35577

Stellar wind equations transformation for reducing parameters number from two to one 24 p3865 A71-44566

STELLARATORS

Thermal insulation and confinement of resistance heated He plasma in Uragan stellarator with large shear 01 p0132 A71-10678

Plasma potential measurement in closed magnetic trap /stellarator/ by electron emitting electrostatic probe 01 p0133 A71-10679

High-beta sharp-boundaried stellarator plasma column feedback stabilization with helical fields 06 p0932 A71-17463

Energetic lifetime, equilibrium and thermal insulation of ohmically heated plasma in stellarator 06 p0937 A71-18350

Confinement and loss mechanisms of ohmically heated plasma in stellarator 06 p0937 A71-18351

Plasma physics and fusion reactor development involving electric conduction, vibration and magnetic effects, stellarator containment, etc 07 p1168 A71-19602

Plasma potential measurement in closed magnetic trap /stellarator/ by electron emitting electrostatic probe 07 p1170 A71-20140

Ohmically heated collision plasma confinement in Uragan racetrack stellarator with large shear, describing magnetic field topography effects and plasma lifetime 17 p2785 A71-34196

Plasma confinement in injector-diverter system of stellarator, measuring radial density distribution 19 p3109 A71-37131

Plasma LF oscillations in Sirius stellarator, showing fundamental frequency dependence on density temperature and magnetic field strength 24 p3853 A71-44504

Ohmic discharge plasma resistance, temperature and oscillations in weak electric fields under electron beam excitation in Sirius stellarator 24 p3854 A71-44518

Energy losses of collisional He plasma with ohmic heating in Uragan stellarator with large shear, comparing plasma lifetime to Bohm confinement time 24 p3855 A71-44664

STEP FUNCTIONS

Time distribution of first passage through fixed level for addecreasing whole number regeneration process with step trajectories 01 p0110 A71-10094

Time distribution of first passage through fixed level for regeneration vector Markov process with step trajectories 01 p0110 A71-10094

Single channel step-type extremal systems with inertial control plants, proposing automatic optimizer 01 p0065 A71-11212

Initial value problems differential equations discontinuities, describing step-size adjustment for fourth order Runge-Kutta methods 02 p0277 A71-12717

Bogoliubov electronic excitations anomalous scattering and tunneling in superconductor intermediate state, noting pair production one direction step function changes 07 p1181 A71-20201

Numerical solution for two dimensional steady state fluid flow in square cavity by optimum time step formulation 17 p2728 A71-34801

STEREOCHEMISTRY

Mass spectroscopic determination of geometric isomers of alpha, beta-unsaturated carboxylic acids noting various modes of fragmentation 01 p0028 A71-113046

Life detection for space missions based on detecting optical asymmetry in biogenic molecules by gas chromatography involving diastereomeric esters synthesis 01 p0029 A71-115626

Remote group interactions after electron impact in 4-substituted cyclohexanones, investigating mass spectrometry in structural and stereochemical problems 02 p0209 A71-125484

Stereoisomeric organic structures in animate nature and life origin on earth 06 p0857 A71-187252

Solid and fluid states oxalyl fluoride vibrational spectra and structure 14 p2191 A71-305751

STEREOGRAPHY

U STEREOPHOTOGRAPHY

Cloud and precipitation boundaries in convective storms studied by stereophotogrammetry and radar, discussing radar echo motion within cloud envelope 01 p0118 A71-10586

Semiautomatic stereophotographic processing of particle interaction data from Wilson chamber 01 p0083 A71-11364

Photogrammetry in precision three dimensional X ray stereoradiography, comparing doses with Kymography, Tomography and Seriescopy 02 p0203 A71-11951

Stereophotogrammetric measurement of plastic deformations of circular Al membrane loaded by pressure pulse, using high speed cameras 03 p0428 A71-13948

Double photographic techniques for meteors and trails, discussing assembly, control and operation 04 p0589 A71-14831

Stereophotogrammetric system for human motion measurement, describing design and operation 04 p0547 A71-15844

Stereo-orthophoto mapping system design and operation 06 p0901 A71-18289

Lunar surface photography, presenting photographs viewed in stereo without telescope 07 p1114 A71-20043

Coherent optical multichannel profiling correlator for increasing automatic stereocompilation speed by X parallax profiles simultaneous measure and display 07 p1114 A71-20209

Star maps for recognition and attitude orientation aids as function of stereographic display realism in manned space flight 07 p1157 A71-20348

Automatic record of terrain profiles from stereoscopic aerial photographs by intersection of ray traces 08 p1288 A71-21252

Aerial photographs point marking by Markov instrument, discussing high precision stereophotogrammetric equipment for photogrammetric work and physical marking 09 p1451 A71-23177

Lunar landing site suitability, using stereoscopic medium and high resolution photography 11 p1836 A71-26533

Hologram mensuration, discussing photogrammetric stereo model differences, close range objects, pointing, geometric fidelity, computerized plate analysis and reconstruction shift 12 p1907 A71-27262

Stereophotogrammetric methods and instruments for studying eye anatomical-optical apparatus and pathological changes 13 p2016 A71-28012

Parallax errors in drawing contour lines on universal stereograph due to aerial photographic images brightness difference 13 p2070 A71-29083

- Instant profile image correlator for coherent optical parallel processing, describing laboratory and aerial stereophotographs results
13 p2071 A71-29351
- Photogrammetric coordinate relation of points on lunar surface and stereopanoramas of scanning photographs by Luna 9 and 13 orbiters
15 p2406 A71-31618
- Automatic coordinate compensation for systematic and random distortions of photographs on stereophotogrammetric devices
15 p2406 A71-31619
- Three dimensional imaginary object reconstruction by holographic stereogram method
22 p3538 A71-41734
- Stereophotogrammetric measurement of body and limb volume changes after prolonged space mission
22 p3502 A71-41861
- Lower atmosphere wind and cloud velocity measurements by combined stereophotogrammetry and balloon visual observation
22 p3542 A71-41862
- Stationary or moving objects spatial coordinates determination by three and four dimensional terrestrial photogrammetry, using phototheodolite stereophotographic pictures
23 p3671 A71-43590
- Stereophotogrammetric measurements of displacements and strains in Al membrane during explosive forming
24 p3825 A71-44755
- TEREOSCOPIC PHOTOGRAPHY**
U STEREOPHOTOGRAPHY
- TEREOSCOPIC VISION**
Stereoscopic depth perception mechanisms, studying stereoaomy in binocular vision for crossed near-zero and uncrossed disparity ranges
08 p1247 A71-21189
- Stereoscopic vision dependent on vertical grating of different spatial frequency of retinal images
09 p1394 A71-23013
- Loci of perceived, equi-, half- and double distance in stereoscopic vision with point source stimuli relative to Vieth-Muller circle
09 p1394 A71-23014
- Stereoscopic effects and apparent shape or position of moving objects at relativistic speeds under binocular observation
16 p2535 A71-33166
- Stereoscopic vision and depth discrimination tests in cats, using conditioned suppression and rod-like shadow disparity stimuli
20 p3191 A71-39958
- Relative size cue for facilitating stereoscopic depth perception in ambiguous disparity stereograms
23 p3638 A71-43110
- Crossed retinal pathways in Siamese cats due to neuroanatomical defect impairing binocular vision and stereoscopic depth perception
23 p3633 A71-43546
- Stereoacuity role in pilot ability to land aircraft at minima, questioning adequacy of Verhoeff depth perception test administration conditions
23 p3637 A71-44244
- STEREOSCOPY**
Information reduction for three dimensional image projection holography, using horizontally direction selective stereoscreen
13 p2068 A71-28710
- Computerized interactive stereographics by treating line identification as primitive, enabling rapid access to stereo pair for speed advantage
21 p3376 A71-40124
- Stereo viewing transmission/reflection display by producing stereopair image on CRT screen with polarizing polaroid sheets
21 p3376 A71-40126
- Perceived distance effect on induced movement from stereoscopic cues
21 p3344 A71-41199
- STEREOTELEVISION**
Cloud base height estimation methods involving vertical radar, laser, stereotelemeter and ceilograph measurements with instrument error analyses
10 p1639 A71-25100
- STERILIZATION**
NT SPACECRAFT STERILIZATION
Mechanical sterilization and cleansing of Goldmann applanation tonometer prisms contaminated with coliphage, comparing with germicidal immersion
13 p2020 A71-29036
- Ammonium perchlorate propellants sterilizability, using medium resolution mass spectrometer and regression analysis of results in thermal stability studies
[AIAA PAPER 71-718]
14 p2286 A71-30769
- STERILIZATION EFFECTS**
NT CHEMICAL EFFECTS
NT CORROSION
NT DECONTAMINATION
NT DEGRADATION
NT THERMAL DEGRADATION
- STERNS**
U AFTERBODIES

- STEROIDS**
NT ALDOSTERONE
NT CHOLESTEROL
NT CORTICOSTEROIDS
NT PENICILLIN
Sterols isolation and identification from Pleistocene sediment by gas-liquid chromatography and combined gas chromatography-mass spectrometry
15 p2366 A71-31367
- Pales /49/ orbit motion analysis for Jupiter mass, noting discrepancies between old and new observations
15 p2488 A71-32198
- Ouabain insensitive effects of metabolism on ion and water content of red blood cells
17 p2681 A71-34943
- STIELTJES INTEGRAL**
Weakly differentiable functional systems related to analytic functions with parametric representation via Stieltjes integral, discussing range theorems
02 p0276 A71-11724
- STIFF STRUCTURES**
U RIGID STRUCTURES
- STIFFENING**
Buckling of eccentrically stiffened multilayered circular cylindrical shells with different orthotropic moduli in tension and compression
12 p1982 A71-27572
- Rectangular plates with unidirectional stiffeners, calculating natural frequencies and mode shapes with approximate method
15 p2507 A71-32128
- STIFFNESS**
Modal coupling in thermally stressed plates, obtaining solution for frequencies and stiffness
02 p0329 A71-12685
- Mathematical model linear in mass and stiffness but nonlinear in damping, considering causal anomalies in hypothetical models and absent in real
05 p0825 A71-16606
- End face frame stiffness effects on cylindrical shell critical pressure
06 p0982 A71-17352
- Bending stiffness matrix for sandwich folded plate, reproducing core shearing deformations
08 p1367 A71-20748
- Nonlinear analysis of cable and truss structures, using computerized stiffness matrix method
08 p1367 A71-20749
- Structural system analysis by partial decomposition of flexibility and stiffness matrices, obtaining coordinate deformations for computer and hand applications
10 p1691 A71-24693
- Numerical solution procedures evaluation for geometrically nonlinear structural analysis by direct stiffness method, noting capability of self correcting initial value formulation
[AIAA PAPER 71-356]
11 p1844 A71-25335
- Stiffness factor in reinforced thermoplastics mechanical properties as function of glass fiber content, working temperature and duration of loading
12 p1920 A71-27012
- Finite element midincrement stiffness matrices in postbuckling analysis of imperfect strut and rectangular plate
15 p2503 A71-31420
- Elastic interaction between specimen and testing machine in mechanical property tests, considering drawbacks to machine stiffness calculation methods
15 p2414 A71-31947
- Rigid framed dome structure stiffness analysis using multiglobal axes and joint equilibrium equations
15 p2507 A71-32105
- Rectangular cylindrical shell finite element, deriving stiffness matrix with stress distribution
15 p2510 A71-32516
- Stiffness matrices determination for flat plate elements under tangential and normal loadings by collocation, using exact polynomial solutions
16 p2652 A71-33083
- Elastic-plastic stiffness matrix methods, applying linear and nonlinear programming techniques to framed structures analysis
16 p2653 A71-33094
- Elastic bar boundary conditions, noting bending stiffness
17 p2825 A71-34886
- High modulus graphite composites application for structural weight reduction and stiffness requirement without strength loss
17 p2762 A71-35202
- Torsion free, rigid and elastic stiffness matrices of thin walled bars, noting transformation to eccentric nodal points
17 p2832 A71-35399
- Constant stiffness beam-columns analysis in pressure piping systems calculations for nuclear industry, using initial parameter method
19 p3102 A71-37073
- Modified Newton-Raphson stiffness matrices and initial value formulations to geometrically nonlinear structural analysis for beam and plane stress triangular elements
20 p3311 A71-39870

- Soviet book on steels high temperature elastic stiffness and ductility covering carbon, alloyed and special steels at different temperatures and strain rates
21 p3404 A71-41375
- Testing machine stiffness determination during strain rate variation and stress relaxation tests for metallic and nonmetallic engineering materials plastic properties assessment
22 p3559 A71-41589
- Rigid rotor whirl dynamics in externally pressurized gas journal bearings, calculating frequencies in terms of stiffness and other parameters
22 p3552 A71-41670
- Stiffness and load capacity control by self compensating flow restrictor for externally pressurized gas lubricated thrust bearing design
22 p3552 A71-41673
- Frequency, density, thickness and structural factors /stiffness/ influence on sound insulation of uncoated and foil coated absorbers
22 p3575 A71-42401
- Stability of edge reinforced circular plate under uniform radial load, considering flexural and extensional stiffness of reinforcing beam
22 p3618 A71-42592
- Stiffness matrix algorithm for triangular plate bending elements using hierarchy of interpolation polynomials
24 p3879 A71-44637
- Hermite polynomials application to stiffness matrix determination in plate finite element method for disk under plane stress, presenting digital computer program flow diagram
24 p3880 A71-44641
- Externally pressurized journal bearings fed with incompressible lubricant, determining feeding system and hydrodynamic effects on bearing stiffness
24 p3830 A71-44949
- Orthogonal experiment plans application to metal elastic stiffness description as function of temperature and strain rate
24 p3840 A71-45375
- STILBENE**
Stimulated emission from stilbenyloxazole solutions under pumping by second harmonic of ruby laser, determining emission thresholds
03 p0434 A71-13502
- STIMULANT**
NT ATROPINE
NT CENTRAL NERVOUS SYSTEM STIMULANTS
NT NORADRENALINE
NT NOREPINEPHRINE
- STIMULATED EMISSION**
Frequency stability of molecular beam laser with stimulated coherent emission
01 p0093 A71-10681
- Stimulated emission of laser output energy using alcohol rodamin-6G solutions under nonuniform pumping conditions
02 p0260 A71-11939
- Stimulated emission from stilbenyloxazole solutions under pumping by second harmonic of ruby laser, determining emission thresholds
03 p0434 A71-13502
- Rare earth polycrystalline powders luminescence stimulation by ruby laser radiation, discussing two photon mechanism, luminous intensities relations and UV radiation
03 p0435 A71-13510
- Semiconductor cadmium sulfide crystal structure changes during high power electron beam and optical pumping, using stimulated emission spectra measurements
03 p0439 A71-13984
- ND and Yb ions stimulated emission from spirally wound glass fibers, comparing activator pumping energy peaks
07 p1122 A71-19135
- Frequency stability of molecular beam laser with stimulated coherent emission
07 p1125 A71-20142
- Erbium ions stimulated emission, spectroscopic properties, pulsed laser action and absorption spectra in yttrium orthoaluminate
07 p1126 A71-20165
- Harmful induced stimulated emission losses in rhodamine unpumped ethyl alcohol and heavy water solutions of various excitation energies
09 p1461 A71-22383
- Frequency and spectral composition effect of incident radiation on stimulated Raman scattering of organic compounds, using ruby laser harmonic emission
09 p1461 A71-22395
- Single mode laser pumping generator of stimulated Brillouin scattering pulse in water
09 p1462 A71-22399
- Stimulated emission of laser oscillation in periodic structures of gelatin films with distributed feedback by backward Bragg scattering
09 p1463 A71-22762
- Intense superradiant emission in HF and DF molecules high gain IR transitions, examining spectral distributions with pneumatically tuned Fabry-Perot interferometer
09 p1498 A71-23478

Continuously tunable stimulated far IR emission in lithium niobate with Q switched ruby laser as pumping agent, discussing power-wavelength characteristics determination

09 p1465 A71-23482

Stimulated Mandelstam-Brillouin, Rayleigh line wing and thermal light scattering, discussing fine structure, glass fracture and components shift

10 p1621 A71-24837

Book on glass lasers covering absorption and fluorescence of glasses, glass structure, energy transfer, nonradiative transitions, quenching, etc

11 p1772 A71-25450

Laser pulse intensity and spectral width effect on measured cross section of stimulated emission

11 p1774 A71-26007

Laser resonator properties with flat outlying mirrors, examining stimulated radiation generation and energy distribution

12 p1916 A71-27764

Gadolinium molybdate neodymium ions stimulated emission, noting luminescence, absorption and spectroscopic properties

13 p2111 A71-28424

Hexamethylindotricarbocyanine iodide ethanol dye solution stimulated fluorescence during excitation by ruby laser radiation in spike generation quasi-continuous monopulse modes

15 p2421 A71-32406

He-Ne lasers stimulated emission, studying optical resonant cavities and discharge tubes construction

15 p2422 A71-32572

Stimulated emission of ZnO laser by electron beam excitation at 82-250 K near A-LO line, considering excitation interactions

16 p2589 A71-34121

Stimulated emission in double heterojunction Al-GaAsP quaternary lasers, considering solution grown crystals advantages

19 p3071 A71-37476

IR pumped stimulated light emission in semiconductors, noting upconversion due to energy transfer between impurity ions

19 p3071 A71-37479

GaAs laser diode junction temperature measurement methods for verification of stimulated emission quenching due to heating

19 p3074 A71-38231

Gadolinium molybdate-neodymium ions stimulated emission, noting luminescence, absorption and spectroscopic properties

21 p3427 A71-40082

Coherent stimulated recombination radiation emission by p-type cadmium silicon arsenide single crystals in liquid nitrogen cryostat under various pumping levels

21 p3431 A71-41229

Stimulated and spontaneous emission from InSe single crystal under focused fast electron beam bombardment

21 p3434 A71-41326

Quantum theory of molecular or atomic spontaneous emission while simultaneously undergoing stimulated emissions or absorptions

21 p3421 A71-41401

Nd positive ion cross section for stimulated emission with glass composition determined by laser and fluorescence measurements

23 p3685 A71-43938

He-Ne laser discharge gap oscillation modes observation, noting applied magnetic field, gas parameters and cathode type effects on stimulated emission

24 p3835 A71-45239

STIMULATED EMISSION DEVICES

NT ARGON LASERS
NT CARBON DIOXIDE LASERS
NT CHEMICAL LASERS
NT GALLIUM ARSENIDE LASERS
NT GAS LASERS
NT GAS MASERS
NT HELIUM-NEON LASERS
NT INFRARED LASERS
NT INJECTION LASERS
NT LASERS
NT LIQUID LASERS
NT MASERS
NT ORGANIC LASERS
NT PULSED LASERS
NT Q SWITCHED LASERS
NT RING LASERS
NT RUBY LASERS
NT SEMICONDUCTOR LASERS
NT SOLID STATE LASERS
NT TRAVELING WAVE MASERS

Stimulated emission wavelength tuning from GaAs and CdSe electron beam pumping laser crystals as function of time and current

07 p1128 A71-20393

STIMULATION

NT AUDITORY STIMULI
NT SENSORY STIMULATION
Analog/hybrid programming of stimulus sequence for cardiac excitation study

04 p0546 A71-15166

Direct and reverse conditioned connections including defense reflexes, response to indifferent stimuli and electrophysiological manifestations

17 p2685 A71-35360

STIMULI

Perceived and responded to discriminative stimuli identification in probability learning, using parameter free model of event pattern association strength

07 p1049 A71-19775

Human nervous system stimulus trace retention in various age groups, using skin galvanic reaction

08 p1240 A71-21788

Human olfactory analyzer, describing equipment for discrete delivery of successive stimuli

09 p1398 A71-22485

Gravitational stimuli due to variations in angular velocity and radius, noting effects on behavioral control

[AIAA PAPER 71-884] 18 p2871 A71-36635

STOCHASTIC PROCESSES

NT MARKOV CHAINS
NT MARKOV PROCESSES
NT RANDOM PROCESSES
NT RANDOM WALK

Optimal prediction of stochastic differential equation solution with Gaussian member and small non-linearity

01 p0110 A71-10098

Autocorrelation function for gravity anomaly stochastic field outside earth spherical surface

01 p0127 A71-10358

Rayleigh wave propagation in stochastically inhomogeneous elastic medium

01 p0169 A71-10637

Stochastic processes applied to loaded redundancy systems reliability analysis

01 p0112 A71-11157

Stochastic model for analysis of track-while-scan technique for aircraft search radar, based on Kalman filter theory

01 p0065 A71-11393

Stochastic wave propagation in continuous randomly inhomogeneous media, surveying analytical methods

02 p0219 A71-12545

Stochastic stability for optimum systems with general search control law for boundary parameters under vector stochastic differential equation

03 p0389 A71-13518

Nonuniform magnetic field cyclotron heating, presenting stochastic criteria in terms of Larmor rotation phase randomization

03 p0462 A71-13928

Nonlinear control laws successive stochastic optimization through nonlinear and subsequent quadratic programming

03 p0392 A71-14403

Radar detection problem, using pseudo Bayes techniques to determine likelihood ratio computational algorithms for stochastic process

04 p0551 A71-15007

Stochastic motion stability of discrete dynamic systems involving Ito equations

04 p0625 A71-15060

Stochastic analysis of wind gusts applied to prediction of long term maximum velocities

04 p0621 A71-15168

Continuous time stochastic optimal control systems necessary and sufficient dynamic programming conditions for optimality

04 p0562 A71-15871

Maximum likelihood identification of stochastic linear dynamic systems using Kalman filter

05 p0731 A71-16554

Queueing model of statistical multiplexer buffer behavior for batch Poisson arrivals and single constant output, applying to time sharing computer buffer design

05 p0724 A71-17063

Digital adaptive spectral filtering canceling undesired power spectra based on measured mean square values ratio and stochastic approximation methods

07 p1082 A71-20408

Buckling loads prediction for conservative elastic systems from vibration data by stochastic and deterministic models, providing nondestructive testing procedure

08 p1368 A71-20804

Book on stochastic processes covering random events, Markov chains, fixed terminal time, discounted cost problem, optimal control and stability theory

08 p1268 A71-21310

Error analysis of adaptive estimators and gradient following algorithms for engineering regression equations, comparing stochastic approximation

08 p1269 A71-21332

Adaptive array processor analysis and optimum design for passive detection of sonar type directional stochastic signals

08 p1256 A71-21602

Regular and stochastic algorithms for efficiency estimation of adaptive predicting filters

08 p1260 A71-22021

Linear optimal stochastic control systems described by covariance matrix correlating errors and estimates of state variables, analyzing instability under parameter variations

[AIAA PAPER 70-36] 09 p1421 A71-22076

Linear optimal stochastic regulator control, using system output instantaneous feedback with minimum quadratic performance measure

09 p1422 A71-22285

Soviet book on navigation and control covering data processing, optimal stochastic self guidance, instrument errors, mean energy consumption and stabilization loop time lag

09 p1491 A71-23145

Stochastic scattering process charged particle flux by Lagrange expansion based on Fokker-Planck equation

09 p1529 A71-23595

Algorithms for optimal control of nonlinear stochastic systems, minimizing control error variance

09 p1425 A71-23684

Scalar wave equation of mutual coherence propagation in turbulent medium with stochastic permittivity using local independence approximation

10 p1641 A71-24398

Two-frequency moving target indicator Doppler radar system, predicting efficiency to clutter drift under stochastic echo and clutter signals

10 p1578 A71-24591

System identification problems, discussing approximation by polynomial integral operators, determinable classes in spectral decompositions, observation noise and stochastic systems stationary in observation time

10 p1587 A71-24742

Optimal stochastic orbit transfer strategy solution by dynamic programming algorithm

10 p1678 A71-24844

Distribution functions of initial and established intervals of stochastic and Poisson sequences in automatic control, reliability and communications theories

10 p1588 A71-24902

Weighted distribution functions of normal processes, calculating stochastic mixture components in Borel sets

10 p1637 A71-24903

Stochastic particle acceleration in random electromagnetic field determination by turbulent plasma motion in external homogeneous magnetic field

10 p1655 A71-25075

Predictive stochastic optimal control model for saccadic eye movements in visual target tracking based on target motion estimate

11 p1723 A71-25142

Structural inference theory applied to stochastic processes class characterized by gamma-distributed interarrival times, deriving conditional probability mass function for process counting variable

11 p1791 A71-25251

Bayesian modeling of nonstationary Poisson process with probabilistic lambda in time

11 p1791 A71-25252

Linear discrete time stochastic system with unknown gain parameters, interpreting open loop feedback optimal control identifier and controller equations

11 p1741 A71-25361

Normality-independence characterization of stochastic integrals in linear processes

11 p1792 A71-26102

Planetary formation, obtaining retrograde orbit probability and distances and masses expectation by stochastic model

11 p1830 A71-26110

Random failure definition based on stochastic processes mutual implication, producing unique characteristic events

11 p1771 A71-26160

Linear estimation with stochastic feedback control to cancel out disturbances or error signals effect, applying to integrated navigation systems involving inertial measurement

12 p1893 A71-27436

Optimal control synthesis of one dimensional stochastic heat and mass transfer processes with distributed parameters

13 p2161 A71-28727

Stochastic discrete time control systems optimization by dynamic programming

13 p2095 A71-28812

Optimal linear feedback for systems governed by differential operational equations, considering stochastic control and cost function

13 p2095 A71-28814

Identification by minimization of Gaussian-Markovian representation of stochastic process, considering positive linear systems and algorithm for matrix calculation

13 p2043 A71-28818

Stochastic identification method for transforming ECG and VCG data to approximate diagnosis, using computerized dipole models

13 p2020 A71-29002

Quantitative performance evaluation of man machine systems in stochastic environments, deriving simulation algorithm

13 p2021 A71-29286

Stochastic modification of binary fluid mixtures hydrodynamic dissipative equations, considering nonequilibrium entropy 13 p2051 A71-29354

Adaptive controller consisting of real time identifier and minimum variance regulator approached through stochastic optimal control theory 14 p2219 A71-29696

Stochastic dynamic meteorological prediction depicted in graphical formats 14 p2269 A71-29947

Biomathematical model and least square estimation from time series data of discrete particle population in stochastic compartmental system 14 p2265 A71-30181

Stochastic signal optimum linear estimation in multiplicative and measurement noises, deriving algorithms 14 p2197 A71-30794

Optimal terminal control stochastic synthesis for linear systems by Bellman second order nonlinear partial differential equations 14 p2220 A71-30872

Nonlinear control systems stochastic stability frequency conditions based on one and multidimensional cases 15 p2379 A71-31293

Probabilistic methods for solving ATC and navigation problems, considering stochastic processes theory 15 p2445 A71-31463

Fluid logic random input, irregularly activated or stochastic control network analysis, using digital control network synthesis technique/DICONESYN III/ 15 p2351 A71-31685

Output probability distributions and covariance functions of nonlinear transformations of Gaussian stochastic processes occurring in signal detection and control theory 15 p2379 A71-31822

Bogoliubov averaging method application to nonlinear stochastic systems described by ordinary and partial differential equations and differential-difference equations 15 p2449 A71-31829

On-line identification of stochastic linear dynamic control systems with applications to Kalman filtering based on statistical correlation technique 15 p2380 A71-31933

Discrete and continuous channel stochastic coding processes and resulting communication system properties 15 p2372 A71-32320

Synchronous data transmission system digital signal harmonic analysis based on stochastic process theory, applying to amplitude and phase modulation 15 p2372 A71-32321

Stochastic wave propagation in continuous randomly inhomogeneous media, surveying analytical methods 15 p2373 A71-32501

Dynamic cryptodeterministic linear systems with random initial state, calculating stochastic response by perturbation scheme 16 p2660 A71-34072

Linear system optimal stochastic control and observation strategies simultaneous determination with quadratic cost by dynamic programming 17 p2719 A71-34742

German monograph on experiments with stochastic automata covering noisy sequential nonanticipating channels with finite input/output alphabets, statistical decision functions, etc 17 p2719 A71-34774

Time ordering operators applications to nonlinear unsteady systems, covering stochastic differential equations solution and phase locked loop phase error probability density calculation 18 p2940 A71-36222

Beam column with probabilistic material and geometric properties, axial loads and boundary conditions, obtaining free vibration and natural frequency stochastic equations 18 p2979 A71-36358

Stochastic character of metal fatigue fracture and fatigue life dependence on stress cycle amplitude, using equiprobability curves 18 p2936 A71-36694

Human operator models parameter estimation by stochastic approximation, considering continuous and sampled data models 19 p3007 A71-37648

Optimality in classification of stochastic processes in recognition system, using predicting filter rms error as discriminating function 19 p3038 A71-37779

Stochastic passband model of tropospheric communications channel, denoting random frequency duration above threshold level 19 p3022 A71-38501

Anomalous distribution in heliocentric longitude of solar injected cosmic radiation, suggesting interplanetary magnetic field lines of force stochastic wandering 19 p3130 A71-38674

Optimal zero-memory regulator for linear system with stochastic jump parameters, considering Bayes and minimax controllers 19 p3039 A71-38711

Optimal control laws existence for stochastic systems with minimized cost functional, considering trajectory information for controller decisions 21 p3360 A71-40254

Machinery failure prediction under high vibration amplitudes using stochastic excursions principles [ASME PAPER 71-VIBR-60] 21 p3460 A71-40305

Replacement problem in stochastic point processes, obtaining cost over given time period and moments and correlations of replacement number 21 p3407 A71-40367

Stochastic model for electron-cyclotron plasma heating by high power microwaves in magnetic mirror 21 p3422 A71-40762

Liapunov-type analysis of linear systems dynamic stability under stochastic parametric excitation, noting application to rectangular flat plates 21 p3469 A71-41008

Dual stochastic relations of optimal control and minimal error observation under random noise, using programming method 21 p3361 A71-41136

Stochastic optimal control of discrete processes with random disturbances 21 p3361 A71-41139

Stochastic ion acceleration in excitation of LF oscillations in second regime of intense pulsed plasma beam discharge 22 p3577 A71-41814

Hydrodynamic equations for dense system fluctuations with stochastic terms in pressure tensor and heat flux vector evaluated for dilute gas 22 p3530 A71-41893

Stochastic ion acceleration by relativistic electron beam in plasma traveling waves with different phase velocities 22 p3578 A71-42065

Book on dynamic programming application to optimal control covering discrete random processes, continuous deterministic and stochastic processes, etc 22 p3567 A71-42428

Single channel queuing system with Poisson input and waiting time dependent mass servicing time, deriving arrival number probabilities generating function 22 p3527 A71-42491

Stochastic, random and ordinary Green function relations for two point correlation functions in mathematical physics 23 p3698 A71-43114

Wave equations for motion in stochastic medium, using linear random operator theory 23 p3699 A71-43115

Space vehicle low thrust minimum terminal variance guidance problem reduced to stochastic bang-bang optimal control system 23 p3702 A71-44101

Stochastic optimal control theory application to airplane rescheduling model, obtaining dynamic programming algorithm for optimal landing and takeoff rules 23 p3702 A71-44104

Jump type behavioral uncertainties in stochastic optimal control problems, considering control of spinning spacecraft 23 p3659 A71-44112

Suboptimal feedback link estimation algorithms for stochastic control, comparing with separation principle 23 p3660 A71-44118

Stochastic properties of probe particle motion in Lorentz plasma, considering interactions and friction and diffusion coefficients 24 p3854 A71-44511

Stochastic process optimal control in presence of constraints, solving two-point boundary value problem by successive approximation method 24 p3814 A71-44688

Nonlinear stochastic systems approximate analysis based on multidimensional nonlinear transforms and distribution functions in Chebyshev-Hermite polynomials, determining dynamic accuracy 24 p3814 A71-44695

Stochastic linear systems stability with random processes coefficients, using differential equations 24 p3815 A71-44698

Galactic stochastic magnetic field lines, deriving dynamic equation for probability density function 24 p3871 A71-44902

Discrete parameter covariance stationary stochastic process in rotation sampling, deriving minimum variance unbiased linear population mean estimator by constrained optimization procedure 24 p3844 A71-45132

Optimal stochastic control law derivation for linear regulator with quadratic performance criterion from limiting form of transfer function 24 p3816 A71-45134

STOICHIOMETRY

Ti-Zr-O alloys cross sections investigation by neutron and X ray diffraction, discussing stoichiometry deviation 06 p0911 A71-17382

Stoichiometric beta NiAl alloy high temperature creep behavior, presenting electron microscopic observations of deformed single crystals dislocation structures 08 p1314 A71-21571

Nickel diffusion in intermetallic compound NiAl as function of temperature and off-stoichiometric composition, noting activation energy changes 11 p1778 A71-25562

Multiple port baffles tests using stoichiometric propane-air mixtures 13 p2116 A71-28746

Stoichiometric hydrogen-oxygen mixture spinning detonation fine structure determination by trace technique and high speed space-time photography 15 p2465 A71-32083

Gallium antimonide synthesis without antimony evaporation stoichiometry disturbances, describing zone refining procedures and quality control 16 p2621 A71-33473

Semiconductor defects, including stoichiometric vacancies in sphalerite lattices, epitaxial interfaces and dislocations in Ge 18 p2953 A71-35870

Buoyant centrifugal force effect on combustion of homogeneous propane-air mixtures at stoichiometric proportions, using steel pipe as centrifuge 19 p3167 A71-38101

STOKES FLOW

Stokes multipliers first approximations for outer expansions of Orr-Sommerfeld flow equation solutions 04 p0570 A71-15096

Turbulent flow of nonlinear Stokes fluids with transverse shear, determining nonlinear properties effects 04 p0575 A71-15605

Hydrodynamic Stokes flow around body of revolution, using least squares method for fluid sticking on wall 10 p1594 A71-24455

Soviet book on MHD flow of incompressible electrically conducting fluid past bodies covering inviscid flows and viscous flows of Stokes and Oseen type 10 p1596 A71-24669

Stokes flow parachute extremely lightweight decelerator for increasing altitude and rocket-borne radiosondes atmospheric data sampling quality [AIAA PAPER 71-401] 11 p1707 A71-25277

Stokes flow equations solutions existence and completeness, considering vector and scalar potentials 14 p2224 A71-30094

Stokes second problem solution, obtaining transient and steady state fluid flow pattern near cylinder executing harmonic rotational oscillations around axis 15 p2393 A71-32263

STOKES LAW

Stokes earth shape formula derivation without removing continental masses for regularization requirement 09 p1438 A71-23181

Milne-Eddington atmosphere, using Unno transfer equations for Stokes parameters 10 p1665 A71-23778

Saturn polarimetric observation, noting rings polarization Stokes parameters, methane absorption bands and continuous spectrum 15 p2482 A71-31336

Saturn polarimetric observation, noting rings polarization, Stokes parameters, methane absorption bands and continuous spectrum 22 p3606 A71-42611

STOL AIRCRAFT

U SHORT TAKEOFF AIRCRAFT

STOMACH

Stomach secretory function and histomorphological changes in dogs under stress 09 p1390 A71-22263

STONES (ROCKS)

U ROCKS

STONY METEORITES

NT ACHONDRITES

NT AUSTRALITES

NT CARBONACEOUS METEORITES

NT CHONDRITES

NT KAPOETA ACHONDRITE

NT MURRAY METEORITE

NT ORGUEIL METEORITE

NT TEKITES

NT TUNGUSK METEORITE

Micrometeorite sputtering in ionosphere producing influx of meteorite atoms and ions in atmosphere, considering temperature dependence of stone meteorite sputtering coefficient 03 p0486 A71-13309

Mg-Cr and Ba-rare earth relationships in stony meteorites and Apollo 11-12 soil and rocks 03 p0487 A71-13335

Stony meteorite fragments, using X ray powder method for diamond detection 06 p0967 A71-17900

STOPPING

Terrestrial and stony meteorite carbon, investigating similarity in isotopic composition 07 p1201 A71-20399

Rock material density, mineral fragments and metallic iron content, indicating part of chondritic stony meteorite 09 p1521 A71-22928

Atmospheric heating effects on thermoluminescence output variations with depth below Ucera meteorite fusion crust, noting nonuniform cosmic rays shielding 10 p1675 A71-24470

Mesosiderites silicate textures and compositions and metal-silicate relationships from mineralogical, petrographical and chemical data 10 p1602 A71-24504

Aubrite radiation age dating for stony meteorites lifetimes as function of collisional destruction, using Ne 21/Al 26 methods 10 p1680 A71-24989

Soviet book on diamonds in meteorites covering abundance and origin in stony and iron meteors, distribution and structure 11 p1833 A71-26326

Iron and stony iron meteorites chemical classification, noting Ni, Ga, Ge and Ir concentrations and metal phases 13 p2134 A71-28290

Stony-iron meteorites composition, considering Ca/Al ratio in mesosiderites 13 p2142 A71-29141

Absolute production rates of He 3 and Ne 21 in average chondrites, determining radiation ages of stony meteorites aged less than two million years 15 p2486 A71-31991

Bibliography and review of meteorites not classified as chondrites, considering achondrites, stony irons and iron meteorites 17 p2798 A71-34453

Stony meteorites relicts in mesozoic formation of central Urals, discussing chemical and mineralogical composition and structure 17 p2800 A71-34517

Stony, stony-iron and iron meteorites magnetic properties relating susceptibility to nickel iron content 17 p2810 A71-35720

Stony meteorite Bushkhof mineral composition data, detailing measured quantities, distribution and appearance 17 p2810 A71-35721

Apollo 11 and 12 lunar rocks and fines, discussing compositional variations and relationships to stony meteorites 23 p3747 A71-43677

STOPPING

NT THRUST TERMINATION
Boeing 737 aircraft takeoff and landing performance, emphasizing high lift systems and stopping capability 07 p1018 A71-19083

Differential circuit for bilateral stopping control of double action piston cylinders, discussing solenoids valves operation 11 p1716 A71-26324

Aircraft accelerate-stop factors and regulations, pilot reaction times and accidents during takeoff 23 p3628 A71-43380

STOPPING POWER

Temperature and velocity dependence of electronic dislocation stopping power in superconductor due to scattering of normal electrons 21 p3432 A71-41268

STORABLE PROPELLANTS

NT AIRCRAFT FUELS

STORAGE

Complex supply system large quantity data handling and cost savings through optimum planning of storage points and transport using linear separable programming 06 p1010 A71-17746

STORAGE BATTERIES

NT NICKEL CADMIUM BATTERIES

NT NICKEL ZINC BATTERIES

NT SILVER ZINC BATTERIES

Solid state electrochemical energy storage device using rubidium silver iodide electrolyte 03 p0350 A71-13031

Soviet book on airplane and helicopter electrical power supply systems covering storage batteries, DC generators, alternators, voltage regulators, current and frequency control, etc 14 p2180 A71-29525

Pulse charging methods for improved storage batteries performance in space power supply systems, noting solar array voltage variations use in spinning satellites 16 p2526 A71-32847

High voltage solid state electrolytic cell battery with Li anodes, testing storage and discharge characteristics 20 p3181 A71-38935

STORAGE STABILITY

Transverse conductivity and temperature dependence of storage time during photographic scanning of astronomical objects with superthion camera 03 p0422 A71-13008

Mercuric oxide-cadmium batteries optimum cell design for low temperature operating conditions and elevated temperature storage life 03 p0351 A71-13038

Unactivated dry charged zinc-silver oxide cells storage life, determining chemical composition changes at various temperatures and time lengths 08 p1235 A71-21100

Activated storage effect on life of secondary Zn-Ag oxide cells, discussing degradation rate of charge retention 08 p1235 A71-21101

Air to air and air to ground missile zinc silver oxide batteries capabilities, including energy density, long storage life and shock and temperature resistance 08 p1236 A71-21104

STORAGE TANKS

Corrosion resistant fiberglass reinforced plastic fluid storage vessels, noting structural characteristics, fabrication techniques, etc 02 p0256 A71-12348

Elastic composite liquid filled shell containers, calculating natural vibration with Ritz method 06 p0992 A71-17809

Cryogenic tanks manufacture from Al alloys 07 p1118 A71-19801

Superinsulation for long term storage of cryogenic propellants in space tanks using double aluminized Mylar with Dacron needles 09 p1546 A71-23009

Aboveground liquid storage tanks design with fiberglass-reinforced composites based on pressure vessels requirements 13 p2157 A71-29307

Cryogenic fluids, considering refrigerants storage vessels, liquid surface detection devices, transfer lines, level gauges 20 p3270 A71-39241

Fluid dynamics in elastic complex geometry tanks, obtaining liquid mass and stiffness matrices for gravitational effects 21 p3467 A71-40948

STORMS

NT CYCLONES

NT HURRICANES

NT IONOSPHERIC STORMS

NT MAGNETIC STORMS

NT NOISE STORMS

NT POLAR SUBSTORMS

NT RAINSTORMS

NT SOLAR STORMS

NT STORMS [METEOROLOGY]

NT SUDDEN IONOSPHERIC DISTURBANCES

NT THUNDERSTORMS

NT TORNADOES

NT TROPICAL STORMS

Snow storms wind field and turbulent region detection, using Doppler VAD pattern and mapping 01 p0117 A71-10576

STORMS [METEOROLOGY]

NT HURRICANES

NT POLAR SUBSTORMS

NT RAINSTORMS

NT THUNDERSTORMS

NT TORNADOES

NT TROPICAL STORMS

Reflectivity and attenuation observations of hail and radar bright band during storms, discussing rain effects 01 p0115 A71-10554

Radar and air flow structure of Alberta hailstorms from radiosonde data, aircraft measured cloud base updrafts and weak echo region concept 01 p0115 A71-10558

Surface and aircraft radar observations of updrafts within weak echo region of Alberta hailstorm, discussing adiabatic flow breakdown into turbulent flow 01 p0115 A71-10559

Dual Doppler radar method of convective storms observation, noting optimization via COPLAN scanning 01 p0117 A71-10574

Storm reflectivity models using weather radar and surface rainfall data correlations 01 p0118 A71-10585

Contour-mapped and digital data field processing and analysis for National Severe Storms Laboratory /NSSL/ radar signal processing and recoding system 01 p0118 A71-10590

Updraft vault dynamic in hailstorms using one dimensional cumulonimbus entraining jet model, observing initial conditions steady state 01 p0119 A71-10744

Severe storm mass and energy convective transport characteristics, using ATS-3 cloud photographs and three layer model 03 p0454 A71-14204

Numerical variational analysis with weak constraint for surface analysis of severe storm gust 05 p0776 A71-16155

Mature severe vortical storm properties, developing atmospheric models for maximum swirling speed and structure [AIAA PAPER 71-53] 06 p0924 A71-18514

Freezing nucleus concentrations in hail and rain from different storms, showing dependence on precipitation type and intensity 08 p1326 A71-21451

Atmospheric vertical particle motion inside convective storms observed by airborne pulse Doppler radar techniques 11 p1794 A71-25374

Wind structure and atmospheric disturbances, noting resolution of pilot-balloon data 11 p1796 A71-26564

Ice forming nuclei in atmosphere during severe convective storms from aged background aerosol and solid particles aerosolized by storm turbulence 12 p1925 A71-27197

Electromagnetic noise pulses generated by convective storms in Iowa during 1970 12 p1881 A71-27200

Storm clouds tops maximum height and vertical velocity calculation, allowing for entrainment and vertical wind shear 15 p2444 A71-31365

Electric charge generation in storm clouds, considering water droplets, ice crystals and air movements role in precipitation and charge separation mechanism 20 p3256 A71-39071

Radar vs visual observation of cloudiness and hazardous weather phenomena, emphasizing storm warnings 24 p3845 A71-44885

STRAIGHT WINGS

U RECTANGULAR WINGS

STRAIN AGING

U PRECIPITATION HARDENING

STRAIN DISTRIBUTION

U STRESS CONCENTRATION

STRAIN ENERGY METHODS

Moire technique calculation of transverse strain directly from longitudinal strain distribution across sections of symmetry in grooved tensile bar 01 p0174 A71-11007

Plastic flow of metal during rolling in T groove, determining particle velocity and strain energy distributions 02 p0257 A71-12565

Metal shaping process during angle steel ream-type rolling, determining metal particles velocity fields, strain energy and total metal pressure on rollers 02 p0257 A71-12566

Cord reinforced elastic homogeneous isotropic cylindrical membrane axisymmetric deformation, using strain energy function 03 p0514 A71-14348

Strain energy curves in generalized coordinates, discussing deformable body state, stress-strain relation, etc 05 p0827 A71-16760

Thickness variation law for plates and shells with minimal elastic strain energy 06 p0982 A71-17358

Element stiffness matrix generator in terms of material and geometric properties by computer algorithm, using displacement functions, transformation matrices and strain energy expression 09 p1542 A71-23281

Strain energy calculation of V notched crack in elastic continuum from finite element computer programs applied to fractures in solid propellant rocket motor cartridges or grains 10 p1693 A71-25056

Error estimate for solution of approximately linear elastic boundary value problems of shells with no strain energy functional, discussing stress-strain relations 12 p1974 A71-26943

Large elastic deformations of incompressible materials shells with inclusion of transverse normal strain, considering thickness change at boundaries 12 p1976 A71-27159

Physically nonlinear bent rod, deriving strain method equations for plasticity with hardening according to broken line law 12 p1978 A71-27336

Cyclic loading failure criteria based on deformation energy concepts 12 p1984 A71-27679

Curved sandwich plate strain and kinetic energy expression derivation for use with finite element displacement method 15 p2508 A71-32136

Strain energy and stability of nonlinear plate and shell bending under Love-Kirchhoff hypothesis, using three dimensional elasticity theory 17 p2815 A71-34296

Fatigue crack propagation dependence on strain energy release rate and crack opening displacement, analyzing data on high yield strength steels, Ti and Al alloys 17 p2826 A71-35152

Strain hardening energy curves in generalized coordinates, discussing deformable body state, stress-strain relation, etc 17 p2832 A71-35459

Molecular bond rupture and strain energy release rates correlation during ozone cracking of rubber from electron paramagnetic resonance and stress elongation measurements
18 p2939 A71-36244

Stress intensity factors and strain energy rate for bonded layered composites with interface flaw/crack/
18 p2983 A71-36846

Structural analysis trends, considering strain and force methods, flutter, dynamic response, atmospheric turbulence and random phenomena problems
20 p3308 A71-39400

Internal pressure deformed star shaped crack, calculating stress intensity factor, crack energy and normal displacement
20 p3310 A71-39866

Lumped parameter models for description of continuous one dimensional and Bernoulli-Euler beam vibration, compared on basis of maximum system strain energy
[ASME PAPER 71-VIBR-5] 21 p3456 A71-40268

Circular cylindrical shells analysis by Koiter strain energy method for small finite deflections, considering simplifying modifications of energy functionals
21 p3468 A71-40976

Elastic shell strain energy calculation, using dimensional analysis and invariance properties for inversion of normal to middle surface
22 p3616 A71-42217

STRAIN FATIGUE

U FATIGUE [MATERIALS]

STRAIN GAGE BALANCES

Frequency response of five component strain gage oscillating balance for dynamic wind tunnel stability testing
14 p2221 A71-30333

Unsteady force and pressure measurements by molecular and parametric transducers including strain gage, drag, moment and piezoelectric balance instruments
15 p2411 A71-32563

STRAIN GAGES

Wind tunnel apparatus for reproducing coning and spinning motions of bodies of revolution, using six-component strain gage balance for aerodynamic forces
01 p0002 A71-10930

Metallic materials semimicroscopic damage in fatigue of S/N gage under constant strain
01 p0104 A71-11396

Boeing 747 flight loads measurements, describing aircraft instrumentation with strain gages and pressure pickups
03 p0348 A71-13766

Elevated temperature strain gages using capacitance changes as indication, discussing design and response tests
03 p0426 A71-13770

Bonded and weldable strain gages for aircraft flight loads measurements at high temperatures, discussing installation, calibration and performance tests
03 p0426 A71-13781

Ni-Cr foil resistance strain gages for high temperature operation, discussing performance test data
03 p0430 A71-14327

Age hardened Ni base material strain-gage cracking phenomenon measurements, using constant strain Gleeble technique
04 p0617 A71-15912

Embedded electrical resistance strain gages for three dimensional stress measurement, describing modifications for internal stresses reduction
05 p0830 A71-17242

Strain gage for in vivo recording of single and tetanic responses of skeletal muscles in mice during work in isometric regime
06 p0855 A71-18378

Strain gage attachment to rat heart ventricle in situ with fine stainless steel pins
06 p0862 A71-18391

Vinoflex glue for Constantan strain gages in low temperature tensometry, showing satisfactory recording at single and multiple loadings
07 p1116 A71-20481

Heating rate effect on parameters of resistance wire strain gages subjected to temperature gradients
09 p1443 A71-22634

Measuring apparatus for cyclic plastic strains at high temperatures, discussing data processing techniques
09 p1443 A71-22636

Transducer design selection for strain gage applications in high nuclear radiation environments based on system requirements
09 p1445 A71-22718

High temperature dynamic strain gage test equipment for evaluating precision, life and environmental limitations
09 p1445 A71-22719

Extensometer for evaluating remote reading strain gage performance at high and rapidly changing temperatures
09 p1445 A71-22720

High temperature thermal null strain gage with sensing unit and electronic control unit to measure mechanical strain in terms of induced thermal strain
09 p1445 A71-22721

Strain level counter monitoring aircraft structural fatigue, describing system components consisting of sensors in critical structure areas and indicator unit with visual display
09 p1445 A71-22725

Materials microstrain determination using automatic capacitance bridge gage and analog or hybrid computer for measurement signal processing
10 p1609 A71-23916

Strain gages of annealed tantalum wire resting on quartz paper base for prolonged tests at high temperatures
12 p1908 A71-27363

Strain gage method for residual stress determination in thin welded brass cylindrical shells produced by deep drawing
13 p2066 A71-28034

Static strain measurements on Ti specimen subjected to different conductive heating rates, testing various gages
14 p2239 A71-29833

Principal axial stresses determination from bonded wire resistance strain gages with known cross sensitivities, deriving expressions from concentric Mohr circles
14 p2239 A71-29834

Aircraft flight load measurements in high temperature environment, determining optimal strain gage installation and calibration
14 p2248 A71-30681

High temperature capacitance strain gage development for aircraft testing, discussing instrument configuration and data reliability
14 p2248 A71-30682

Strain gage torquemeter as primary power indicating instrument in helicopter transmission systems, providing advantages for helicopter designer and operator
[AHS PREPRINT 563] 14 p2250 A71-31110

Bridge circuit for minimizing parasitic electrical disturbances in resistance strain gage measurements of dynamic stresses in impact tests
15 p2408 A71-31865

High temperature stress measurements with electric resistance strain gages, describing test apparatus for gages evaluation
17 p2738 A71-34553

Preencapsulated strain gage measurement during water pressure tests on site built vessels
17 p2744 A71-35238

Strut pressure and axle strain gage systems testing for balance and weighing onboard De Havilland C-7A aircraft
[SAWE PAPER 881] 17 p2676 A71-35827

Real time mechanical strain measurement by optical correlation techniques, using coded matched-filter hologram and incoherent illumination
21 p3377 A71-40229

Electromagnetic stress gage for wave propagation study in nonconducting materials, discussing calibration, design and accuracy
21 p3379 A71-40793

Silicon resistance strain gages sensitivity as function of variable signed load cycles
22 p3550 A71-42880

Automatic measurement of materials nonlinear deformation, considering Morrow mechanical strain gage for plastic deformation
23 p3774 A71-42895

STRAIN HARDENING

Uniaxial strain waves propagation across nonlinear strain hardening slab, deriving expressions for stress, strain, particle velocity and shock path
01 p0175 A71-11013

Shallow shells of revolution of strain-hardening material, deriving stress strain state by rigid plastic body model
01 p0175 A71-11039

Al alloys low cycle fatigue test under axial load, observing hardening behavior and structure by transmission electron microscopy
01 p0104 A71-11397

Fe-Ti alloys at large plastic elongations, investigating strain hardening behavior
01 p0105 A71-11604

Plastic deformation continuum model, including first and second strain gradients
02 p0321 A71-11679

Thermoplasticity plane problems with complex edge loading, deriving algorithm based on theory of flow with translational hardening
02 p0323 A71-11746

Dislocation pinning by interstitial atoms during Cr and Cr-Ce strain aging, using amplitude dependent internal friction technique
02 p0263 A71-11897

Rigid-perfectly plastic model for real materials behavior, considering modification for strain hardening and elastic effects under various load conditions
03 p0509 A71-13780

Stress analysis of thin elastoplastic shells with large displacements loaded into strain hardening range, assuming plastic strain incompressibility
[ASME PAPER 70-WA/PVP-3] 03 p0511 A71-14101

Low strain cyclic hardening and softening in Al-Mg alloy, comparing measurements by monitoring and tensile testing methods
03 p0444 A71-14315

Structural elements carrying capacity increase by strain hardening and nonuniform quenching
05 p0826 A71-16752

Strain hardened plastic cylindrical shells, investigating load bearing capacity
06 p0994 A71-17822

Steels surface layer strain hardening during diamond smoothing
07 p1117 A71-19364

Interstitial solid solution hardening in pure Ni and Ni-C alloys, noting mechanism and C concentration effects
07 p1138 A71-19980

Hardened plasticity zone around circular hole in creep deformed plane under normal forces, determining stress-strain relation and time dependent variations
07 p1219 A71-20647

Short term creep and rupture model, considering strain hardening effect
08 p1371 A71-21610

Plastic strains buildup during thermal cycling, establishing relation between strain interval and cycles number to failure for strain hardening materials
09 p1338 A71-22599

Ni-Al alloy strain hardening, observing high intensity ultrasonic irradiation effect on high temperature creep
09 p1475 A71-23315

Strain effect on ultrasound damping in single W crystals, considering microhardness
09 p1477 A71-23328

Strain hardening and grain size effects on early fatigue damage of polycrystalline metal under fluctuating stress, using micromechanics theory
10 p1685 A71-23933

Prestress vibration hardening of shells of revolution for circumferential 0 and 1 wave number, using VALORS and BALORS programs
11 p1848 A71-25486

Rigid spherical projectile hypervelocity impact with compressible strain-hardening target material, obtaining analytic solution based on dynamic cavity expansion and deep penetration theories
12 p1982 A71-27570

Shells of revolution plastic deformation problem, applying rigid viscoplastic strain hardenable material model
12 p1984 A71-27686

Failure analysis of plastic materials susceptible to cyclic strain hardening under thermal load
13 p2148 A71-28114

Load bearing capacity of thin welded box shaped rod of strain hardening material during bending beyond elastic limit
13 p2153 A71-28294

Polycrystalline Nb cyclic yield point behavior under strain softening and hardening, noting stable hysteresis loop
13 p2087 A71-29123

Transient and steady state creep of circular cylindrical shells loaded by internal pressure, using strain hardening hypotheses and finite difference method
14 p3238 A71-30379

Elastoplastic buckling of structures, considering strain hardening materials, ship and Bauschinger effect
16 p2650 A71-33024

Thin walled rod of strain hardenable material, developing constrained torsion approximation for creep and relaxation
16 p2651 A71-33060

Ordered structure recovery in Fe-Co-V alloy from elasticity limit behavior, studying duration effect on mechanical properties of strain hardened samples
16 p2591 A71-33370

Aging theory application to anisotropic strain hardenable metals creep processes description
16 p2659 A71-33984

Plastic deformation, creep rupture strength, endurance limit and service life of prestressed strain hardenable material
16 p2659 A71-33985

Thermal strain hardening influence on structural changes in coarse grain Ni under creep tests during heat treatment
16 p2598 A71-33990

Square cross section prismatic bars transient creep analysis based on strain, time and combined hardening theories
17 p2815 A71-34188

Strain hardening energy curves in generalized coordinates, discussing deformable body state, stress-strain relation, etc
17 p2832 A71-35459

Composite failure model tested for short term creep and rupture in Mo alloy at constant loads and 785-1400 C, considering strain hardening
17 p2834 A71-35670

STRAIN RATE

- High rate quasi-static dynamic pressure deformation hardening of magnesium single crystals
18 p2934 A71-35990
- Cr-Ni austenitic steels thermomechanical destabilization using cyclic strain hardening
18 p2934 A71-36173
- Nonstationary resonance analysis of forced flexural elastoplastic vibrations of beam of hardening/softening material under cyclic strain
18 p2981 A71-36709
- Recovery-strain hardening rate model for steady state creep
21 p3462 A71-40430
- Strain hardened zirconium alpha tensile stress analysis, explaining inelastic phenomena by dislocation motion blocking with oxygen in lattice structure
21 p3397 A71-40432
- Al alloys tensile deformation and fracture characteristics relation to stress-strain diagrams, discussing strain hardening indices
22 p3560 A71-41642
- Strain hardening effect of Ni, Mn and Mo in Cr steel after high temperature annealing
23 p3693 A71-44216
- Plastic strain hardening media stress-strain relations, discussing rheology, temperature effects, isotropy postulate and deformation processes
24 p3876 A71-44401
- Polycrystalline Ni preloading rate effects on dislocation structure, electrical resistance and flow stress, noting strain hardening mechanism
24 p3837 A71-44675
- Strain hardening narrow strip lateral instability under bending in plane of maximum rigidity, deriving critical moment formula
24 p3883 A71-44854
- Body adaptability to mass forces and surface loads for strain hardening material
24 p3886 A71-45366
- STRAIN RATE**
- Convex functions theory of rigid perfectly plastic structures, formulating strain rate and stress fields relation in subgradients
02 p0326 A71-12339
- Strain rate effects on plastic properties of various metals and alloys
02 p0265 A71-12568
- Mo single crystals polygonization and recrystallization, examining strain rate and deformation conditions effects
02 p0266 A71-12652
- Aluminum compression microstructure under various strain rates and temperatures, discussing dynamic recovery role
02 p0267 A71-12877
- Zr and zircaloy 2 fracture mode, examining grain boundaries and strain rates effects
02 p0268 A71-12887
- Strain rate effect on critical shear and cross slip stresses of Al and Al-Mg single crystals, obtaining stacking fault energy
03 p0442 A71-13364
- Single crystal creep strain rate measurement under cryogenic temperatures by hybrid photoelectric servo system with optical extensometer avoiding physical contact with specimen
03 p0426 A71-13759
- Pressure and strain rate effects on polycrystalline Be shear strength, determining activation energy for dislocation motion
03 p0445 A71-14463
- Thick strips widening by rolling, deriving formula for maximum widening from plastic deformation process description by displacement-rate fields
04 p0602 A71-14608
- Strain ratio measurement of pure sintered molybdenum and boron alloyed molybdenum sheets, discussing deformation anisotropy and texture
04 p0609 A71-14748
- Aluminum bicrystals mechanical properties under high strain rates, considering changes in surface structure, active slip planes and dislocation
04 p0612 A71-15077
- Nickel alloy tensile tests, investigating strain mechanisms dependence on temperature
05 p0765 A71-16189
- Annealed Al bars mechanical properties and stress-strain curves dependence on strain rates under loading
05 p0766 A71-16390
- Shock heating effects due to compression and plastic dissipation on basis of finite one dimensional waves in strain rate sensitive elastic viscoplastic solids
05 p0830 A71-17238
- Recrystallized annealed Ta, examining strain rate effect on mechanical properties
06 p0914 A71-18684
- Strain rate effect on fiber reinforced unidirectional epoxy composites tensile stress, noting steel, boron, beryllium and graphite/epoxy strands
07 p1139 A71-20137
- Loading frequency effect on carbon steel energy dissipation at large stress amplitudes, deriving strain rate relations
07 p1142 A71-20478

- Stress reduction in metal powders compaction at different temperatures and deformation rates
08 p1305 A71-21059
- Self consistent stress relaxation testing, discussing strain rate sensitivity and stress-strain relations
08 p1308 A71-21519
- Titanium single crystal prism slip dislocation dynamics, examining temperature and strain rate effects on shear stress
08 p1309 A71-21521
- Crystalline solids strain rate effects due to simultaneous operation of plastic deformation mechanisms including diffusion controlled creep and dislocation-drag processes
08 p1371 A71-21560
- Strain rate effects on Ta flow stress, examining yield and postyield behavior models and stress-strain diagrams
08 p1313 A71-21562
- Crystal dislocation dynamics at high strain rates, investigating viscous phonon drag
08 p1371 A71-21563
- Al dislocation mobility at high strain rates, plotting true stress vs true strain
08 p1313 A71-21564
- Gamma prime precipitate effects on flow stresses of Ni alloys single crystals at various strain rates and elevated temperatures
08 p1315 A71-21580
- Plastic strains, thermal residual stresses and buckling of rectangular cross section plates and beams subjected to asymmetric heating and cooling
08 p1375 A71-22056
- Uniaxial, equal biaxial and unequal homogeneous biaxial strain rates of viscoelastic materials under isothermal tensile test conditions
09 p1481 A71-22141
- Reference stress parameters for structure creep behavior, using dimensionless stationary state, strain rate and time function
09 p1543 A71-23660
- High strain rate effects on Al single crystals deformation, presenting overall and local strain and lattice rotation measurements in impact tested specimens
11 p1779 A71-26014
- Fracture toughness and critical strain rate measurements in unidirectional glass reinforced plastics as function of resin, hardener, fiber and degree of cure
11 p1790 A71-26387
- Strain rate and temperature effects on flow stress of Ni-Al in polycrystalline and single crystal for activation energies and deformation volumes evaluation
11 p1782 A71-26440
- General dislocation model for high temperature creep of pure metals, discussing strain rate effects
11 p1782 A71-26476
- Monograph on plastic behavior of iron and nickel at high strain rates and at elevated temperatures, discussing thermal effect on deformation characteristics
11 p1783 A71-26489
- Isotropic turbulence three dimensional velocity spectrum function, using absolute mean strain rate constant and variable Reynolds number
12 p1898 A71-27581
- Polycrystalline pure Al and Al-Mg alloy strength, investigating temperature and strain rate effects
13 p2084 A71-28112
- Deformation substructures, strain rates and terminal properties of explosively-formed thin walled stainless steel cylinders, using transmission electron microscopy
13 p2153 A71-28501
- Cr and Cr-Y alloy interstitial residual content and dynamic dislocation-interstitial interactions at various temperatures and strain rates
13 p2085 A71-28578
- Strain and strain rate effect on flow stress and microstructure of Al-Cu eutectic alloy during superplastic deformation, deriving stress-strain diagrams
13 p2086 A71-28624
- Mechanical properties and strain rates determination at high temperature, using automatic loading system with strain gage dynamometer and oscillography
13 p2045 A71-29375
- Compression rolled and hot upset Be sheet stress-strain behavior and deformation dynamics, emphasizing temperature and strain rate effects on polycrystalline flow stress
13 p2088 A71-29404
- Al and Cu dynamic plastic deformation at elevated temperatures, discussing relationship between strain rate sensitivity and activation energy
15 p2428 A71-31972
- Creep deformation during intermittent loading, obtaining strain rate as function of applied stress and stress cycle time
15 p2508 A71-32254
- Annealed stainless steel and Ti alloy in solution heat treated aged condition, detailing elevated temperature and high strain rate effects on fatigue life and tensile properties
15 p2438 A71-32791

- Strain rate effect on crack growth within subcritical load range, deriving expressions for rate-independent and rate-dependent quasi-brittle solids
16 p2590 A71-32946
- Constant load tensile creep tests on polycrystalline ceramics, determining high density alumina applied stress and strain rate
16 p2553 A71-33384
- Large plastic strains in fiber in sheet bending for wide angle range, using Hill theory
17 p2816 A71-34298
- Strain rate effects on composite material tensile and flexural properties measured by load sensors and streak photography
17 p2737 A71-34345
- German monograph on structural steels tensile and yield strength, detailing strain rate and testing machine effects
17 p2818 A71-34483
- Dynamic compressive strength and failure of steel reinforced epoxy composites, discussing strain rate sensitivity
17 p2762 A71-34813
- Consistency examination of thermal activation analysis in Nb, determining strain rate sensitivity of pure Nb and Nb-Mo single crystals subjected to compression at 178 and 273 K
17 p2759 A71-35223
- Thermal and athermal yield stresses of Nb and Nb-Mo single crystals, considering strain rate sensitivity and thermal stress increase with increasing plastic strain
17 p2759 A71-35224
- Test apparatus for studying stress-strain behavior of thin walled metal tubes in torsion, examining strain rate and history effects
18 p2935 A71-36234
- Strain rate dependence of shear stress, plastic cross-slip and stacking fault energy of Al single crystals at 77 K
18 p2937 A71-36749
- Rapid thermal fluctuations effect on Inconel 718 creep rate, noting strain rate decrease under cycling conditions
19 p3080 A71-37716
- High strength metastable austenitic steels fractography, showing alloy composition, strain rate and temperature effects
19 p3080 A71-37717
- Acoustic emission test facility with constant strain rate compressive sample deformation
20 p3208 A71-38823
- Alpha Ti at blue brittle temperature, observing strain rate dependent work hardening effects on necking strain
21 p3398 A71-40464
- Ti-Mo base metastable beta Ti alloy tensile properties anomalies at elevated temperatures, examining strain rate and annealing conditions effect
21 p3399 A71-40699
- Strain rate dependent constitutive relation for shock propagation in porous materials, discussing relaxation time
21 p3465 A71-40794
- Strain rate and temperature effects on polycrystalline Al-Mg alloy strength, considering deformation mechanism
21 p3400 A71-40834
- Temperature and strain rate effects on yield and flow stress of bcc Ti-Mo alloy over 77-824 K range
21 p3404 A71-41414
- Testing machine stiffness determination during strain rate variation and stress relaxation tests for metallic and nonmetallic engineering materials plastic properties assessment
22 p3559 A71-41589
- Woven textile structures tensile strength tests at high strain rates, using unbreakable compact clamp system
22 p3564 A71-41590
- Flexible polyurethane foam plastics under high rate loading, investigating strain rate and structural parameters effects on mechanical properties
22 p3565 A71-41592
- Crack model with strain rate dependent yield stress, calculating stress intensity factor variation with fracture propagation velocity
23 p3774 A71-43145
- Radiation dose effects on polymer strain magnitude under critical cyclic loading
23 p3697 A71-44033
- Closed profile thin walled curvilinear rods, deriving static and strain integrals with Hookes law
24 p3877 A71-44410
- Shear modulus and stress-strain relations for different plastic strain rates
24 p3886 A71-45362
- Orthogonal experiment plans application to metal elastic stiffness description as function of temperature and strain rate
24 p3840 A71-45375

STRAIN SOFTENING
U PLASTIC DEFORMATION

STRANDS

Stress rupture properties of S glass/epoxy single end strands at various load levels, considering distribution functions

07 p1145 A71-20126

STRAPDOWN INERTIAL GUIDANCE

Optimal axis alignment for strapdown inertial guidance system, suggesting alternate method of raised mounting pads and cylindrical alignment pins

02 p0279 A71-12456

Gyro dynamic errors in strapdown inertial guidance system due to body rate

02 p0279 A71-12457

Single degree of freedom strapdown gyroscope performance and drift model, considering steady and vibrational inputs

[DFVLR-SONDDR-80] Strapdown inertial guidance and software technologies for cosmic speed aerospace vehicles and low speed air, marine and ground transport

04 p0623 A71-15301

Orientation vector differential equation formulation for strapdown inertial navigation, applying to rigid body rotation problem

07 p1154 A71-18832

Strapdown inertial navigator alignment by digital filtering techniques, discussing application to aircraft and spacecraft

08 p1331 A71-21170

Strapdown solid state compass based on magnetometer principle, describing gyro feedback correction system and circuitry

08 p1287 A71-21171

German monograph on error analysis in strapdown inertial navigation system covering gimbaled platforms, error propagation, Kalman filtering technique and mathematical equations

14 p2271 A71-30236

Redundant strapdown Inertial Measurement Unit processor recovery requirements, investigating IMU information loss effects during recovery on spacecraft mission

17 p2772 A71-35058

Strapdown or gimbaled inertial measurement units for space shuttle program, considering reliability, redundancy and cost of ownership

17 p2772 A71-35059

Space shuttle guidance, evaluating performance of strapdown and gimbaled systems by nominal and abort trajectories

17 p2773 A71-35061

Skylab strapdown attitude navigation system using components designed for predecessor projects ATM and Saturn I Workshop

17 p2773 A71-35065

Flight test of hybrid strapdown inertial navigator with Doppler radar and occasional position fixes through Kalman filter mechanized in small computer

17 p2776 A71-35765

Strapdown guidance systems computerized test system consisting of minicomputer and cathode ray display tube with keyboard control over all system elements

19 p3040 A71-37208

[AIAA PAPER 71-967] Traversing Infrared Inspection System for C-5 aircraft fail-safe strap panels of bonded Ti-Al laminates, discussing design and application

12 p1911 A71-27327

STRATA

Amplitude curves of reflected wave vertical displacement component in horizontally stratified medium with simple layer velocity pattern

10 p1644 A71-25134

Lunar stratified composition based on electrical conductivity profile from magnetic field fluctuations measurement in terms of two layer model

18 p2961 A71-35993

STRATEGY

Two controlled motions rendezvous problems treated as game between partners using quality criterion as payoff, deriving optimal strategies

03 p0392 A71-14405

N person nonzero sum differential games with linear dynamics, proving existence of equilibrium strategies

04 p0620 A71-15864

Continuous deflection strategies in game problems with motion encounters, discussing absorption sets

05 p0782 A71-16978

Controlled objects convergence game, constructing optimal minimax pursuer strategy

05 p0782 A71-16979

Differential game of convergence, constructing extremal strategy for ensuring motion encounter with given set

05 p0783 A71-17011

Efficient evasion strategies for vehicle pursuit-evasion games with imperfect information, using computer solution

06 p0846 A71-17331

Multistage two player zero-sum games with state determined by difference equations, deriving optimal strategy pair satisfying saddle point condition

10 p1637 A71-24842

Response strategies in two-choice reaction task with continuous cost for time, confirming fast-guess model prediction

12 p1873 A71-27008

Saddle point type differential game problem structure, determining optimal player strategies for fixed point termination

12 p1931 A71-27521

Differential guidance game with aftereffects, investigating extremal strategies

12 p1931 A71-27522

Quandary recognition and referee strategy in digitally controlled modal survey system, noting decision making sources

14 p2208 A71-30314

Optimization of linear tracking strategies, considering time independent and translation invariant N point predictor

15 p2379 A71-31411

Continuous deflection strategies in game problems with motion encounters, discussing absorption sets

18 p2948 A71-36778

Controlled objects convergence game, constructing optimal minimax pursuer strategy

18 p2948 A71-36779

Differential games with deviation from encounter, considering strategies for continuous, programmed and discontinuous control classes to bring motion to given set

19 p3103 A71-37093

Conflict rendezvous, pursuit and deviation game problems, obtaining optimal control strategies approximation by continuous functions

19 p3103 A71-37104

Control strategies for space shuttle transition at 45,000-150,000 ft, emphasizing terminal conditions and stability and control boundaries

19 p3147 A71-37170

Optimal strategies in search of function global maximum

24 p3843 A71-44770

Second order differential guidance game, formulating strategy for optimal feedback control

24 p3849 A71-45338

STRATIFICATION

NT ATMOSPHERIC STRATIFICATION

Mixed ullage heating, convection and conduction models of thermal stratification of cryogenic propellants stored in low gravity environment

11 p1810 A71-26507

Nonuniform sidewall heat flux effect on thermal stratification

13 p2165 A71-29010

STRATIFIED FLOW

Forced plume entrainment of turbulent buoyant jet in stratified fluid as function of Reynolds, similarity and Froude numbers

02 p0278 A71-12704

Incompressible two dimensional inviscid stably stratified fluid flow over vertical step in channel bounded by rigid horizontal lid

03 p0453 A71-14201

Gravity stratified compressible fluid spin-up in sphere, analyzing by increase in container angular velocity and linearization about uniform rotation

06 p0883 A71-18320

Two layer structure of principle air flow over mountain system, noting effect on air waves and rotors formation in leeward region

07 p1149 A71-18795

Turbulent wake shape in stratified medium describing anisotropic diffusion

07 p1088 A71-19190

Two dimensional turbulent wake interaction with linearly stratified main stream, measuring mean and fluctuating temperature and velocity distributions

07 p1092 A71-20277

Laminar mixing region stratified free shear layer stability between two uniform streams from numerical solution of linear sixth order equation for disturbance amplitude function

09 p1432 A71-22851

Steady perturbations generated by simple discontinuity in wind field upstream from obstacle in stratified fluid

10 p1638 A71-23840

Symmetrical airfoil in stratified fluid flow determining camber and incidence effects

10 p1552 A71-24589

Stratified shear flow stability, investigating diffuse interface between two miscible fluids

10 p1595 A71-24623

Phase velocities and vertical amplitude profile of nonsingular mesoscale gravity waves produced in stratified jet flows by floating and deflecting earth rotation forces

11 p1793 A71-25171

Edge waves on sloping beach in exponentially stratified fluid, finding lowest mode/Stokes edge wave/insensitivity to density field

11 p1749 A71-25358

Stabilization effect of rotation on Rayleigh-Taylor instability of stratified compressible inviscid fluid of variable density for noncritical wave numbers

11 p1749 A71-25343

Thermally stratified turbulent shear flow, calculating turbulent energy balance and temperature inhomogeneity spectral equations

12 p1895 A71-26899

Boussinesq stratified fluid zonal flow with vertical and horizontal shear, studying stability to hydrostatic neutral wave perturbations

12 p1925 A71-27194

Horizontal flat plate moving transversely in rotating stratified fluid, calculating boundary layer blocking conditions for entire Rossby and Russell numbers range

12 p1897 A71-27222

Stratified fluid flow over barrier, obtaining stationary solution for initial value problem

13 p2047 A71-28481

Stability theory for thermal stratified viscous parallel flows at Prandtl number of unity, considering atmospheric boundary layer and jet stream mechanisms

13 p2165 A71-29246

Density perturbation effect on transient spin down of incompressible dissipative rotating stratified fluid in cylindrical container

16 p2561 A71-34164

Three level baroclinic model of short range large scale weather prediction at low latitudes, determining background/steering flow in tropical disturbances

17 p2769 A71-34300

Continuously stratified fluid flow into contraction, assuming constant upstream dynamic pressure and density gradient/Long model/

17 p2726 A71-34661

Nonhomogeneous flow stratification in fluid region under thermal and gravitational forces, considering steady state and time dependent density fields

20 p3212 A71-39502

Sloping flat plate impulsively started constant velocity motion through slightly diffusive viscous density-stratified fluid, investigating transient and oscillatory viscous boundary layer flow

20 p3212 A71-39503

Turbulent boundary layer calculation behind surface cusp, taking into account external flow turbulence and thermal stratification

20 p3214 A71-39792

Small mesoscale waves development in steady stratified plane parallel flow, assuming mean flow characteristics dependence on vertical coordinate

21 p3412 A71-41391

Earth rotation effect on mesoscale wave characteristics, considering Coriolis force influence in homogeneous inertly stratified jet stream

21 p3375 A71-41393

STRATIFIED LAYERS

U STRATA

STRATOFORTRESS AIRCRAFT

U B-52 AIRCRAFT

STRATOPAUSE

Stratopause layer atmospheric temperature field characteristics observation, noting association with processes in upper stratosphere and lower mesosphere

15 p2399 A71-31965

Solar eclipse effects on atmospheric structure, circulation and meridional flow, using rocket measured temperature and wind data for pressure and density variations near stratopause

16 p2567 A71-33764

STRATOSPHERE

Thin CAT layer detection in lower stratosphere by L band radar complemented by radiosonde and U-2 aircraft probes

01 p0116 A71-10567

Carbon dioxide band radiances measured by Nimbus 3 satellite IR spectrometer, noting seasonal temperature changes in stratosphere due to meridional circulation

01 p0119 A71-10743

Stratospheric and mesospheric water vapor content by satellite-borne spectral measurements

01 p0120 A71-11103

Commercial SST environmental effects on stratospheric air, water vapor content and earth surface temperature

01 p0074 A71-11178

High altitude aircraft effects on stratospheric ozone due to added water vapor, discussing effects on solar energy transmission, surface temperature and weather

01 p0120 A71-11341

Stratospheric thermal structure and circulation, considering temperature, wind and composition fields

01 p0122 A71-11358

Daytime stratospheric X ray bursts, examining occurrence time, duration, cosmic radio noise and magnetic activity relationship

02 p0299 A71-11775

Upper stratosphere and mesosphere concentrations of Ne, Ar, and Kr from rocket-borne cryogenic air sampler

02 p0246 A71-12701

Atmospheric turbulence at cruise altitudes of supersonic transport aircraft, considering gusts probability, thunderstorms and mountain waves

03 p0346 A71-13137

Venus equatorial stratosphere structure, presenting approximate radiative dynamical calculation for zonal flow mechanism 03 p0488 A71-13552

Troposphere and stratosphere mean annual carbon dioxide cycle measurements, describing aircraft collection equipment and procedure 03 p0418 A71-14205

Aerosols in stratosphere, describing physical appearance, size distribution and concentration 03 p0418 A71-14206

Stratospheric ozone, comparing observations to numerical models of formation, distribution and destruction 04 p0582 A71-15071

Troposphere and stratosphere electric field above Atlantic Ocean, investigating electrode effect role in atmospheric circuit 05 p0738 A71-16220

Tropospheric and stratospheric turbulence, discussing energy sources and sinks and energy spectra pattern at different atmospheric conditions 05 p0741 A71-16625

Rawinsonde reported extreme wind speed in arctic stratosphere at SST altitudes 05 p0777 A71-16700

Vertical behavior of stratospheric optical thickness and dispersion coefficient in red region of spectrum from photometric analysis of Soyuz 3 photographs of daytime horizon 05 p0742 A71-16839

Upper troposphere and lower stratosphere geopotential field short range forecast quasi-geostrophic model 06 p0889 A71-17516

Carbon dioxide and carbon monoxide atmospheric distribution dependence on combined effects of photochemical production, loss and transport in mesosphere and upper stratosphere 06 p0893 A71-17980

Stratospheric soft photon anomalous fluxes associated with May 1967 solar cosmic ray bursts 06 p0959 A71-18157

Charged particle balance equations for stratosphere and mesosphere, noting particle composition investigation and formation and annihilation processes 06 p0963 A71-18261

Upper troposphere-lower stratosphere planetary scale circulation correlation from kinetic energy characteristics analysis 07 p1151 A71-18874

Tropospheric and lower stratospheric radiation balance components vertical profiles, using balloon sounding 07 p1151 A71-18913

Stratospheric small ion density measurements by level flight balloons 07 p1103 A71-19768

Stratospheric and mesospheric water vapor content by satellite-borne spectral measurements 08 p1277 A71-20847

Equatorial region stratospheric and upper tropospheric circulation, examining relationships between time variations of winds at both levels 08 p1327 A71-21455

Mesosphere and stratosphere data from high level observations for supersonic transport and reentering space vehicle operations 08 p1328 A71-21724

Weak ion concentration in stratosphere and mesosphere measured by accumulated capacity amplifier 09 p1443 A71-22676

Supersonic transport air traffic meteorology, considering high altitude and flight velocities, applications technology satellites for lower stratosphere thunderstorms, clear air turbulence, etc 09 p1488 A71-23070

Midlatitude stratosphere and lower ionosphere density model, discussing vertical, diurnal and seasonal variations effects on spacecraft trajectories 09 p1438 A71-23137

Ozone distribution measurements in mesosphere and stratosphere by rocket during seasonal ionospheric disturbance and solar eclipse 09 p1490 A71-23562

Nimbus 4 satellite selective chopper radiometer data on IR radiation emitted by carbon dioxide, considering stratospheric warming 10 p1598 A71-23743

Solar spectrum observations in water band at 1.87 micron by stratospheric balloon sounding 10 p1667 A71-23863

Electrical processes in stratosphere and mesosphere - Conference, Madrid, September 1969 10 p1603 A71-24698

Inferring ionospheric electric fields at stratospheric levels with tropospheric penetration, using balloon measurements and model atmosphere 10 p1603 A71-24700

Stratospheric seasonal wind reversals morphological classification for comparing atmospheric processes over different rocket sounding stations 12 p1900 A71-27065

Stratospheric and mesospheric wind measurements over Leba sounding rocket station 12 p1900 A71-27066

Stratospheric wind seasonal reversals over Polish coast of Baltic Sea in 1967-1969 from rocket sounding and upper air synoptic analysis 12 p1900 A71-27067

Soviet papers on upper atmosphere physics covering thermosphere, dynamic processes and radiative energy transport in stratosphere and mesosphere, and ionospheric parameters radio measurement 13 p2056 A71-28017

Neutral fluctuations of zonal winds in stratosphere and mesosphere from flow equations, noting flow instability role in generation mechanism 13 p2057 A71-28020

Propagation of 26-month oscillations in meridional component of wind velocity in stratosphere at extraequatorial latitudes from hydrothermodynamic equations solution 13 p2057 A71-28021

Seasonal-climatic vertical distributions of radiative heat sources and sinks calculation for Northern Hemisphere stratosphere and lower mesosphere 13 p2057 A71-28023

Stratosphere and lower mesosphere seasonal climatic temperature profiles calculation from radiation transport and balance equations, noting turbulent heat influxes role in stratification formation 13 p2057 A71-28024

Stratospheric air flow patterns and CAT measurements onboard aircraft over and downwind of Western U.S. mountain terrain 14 p2267 A71-29755

Atmospheric models of partially trapped waves propagation in layer above tropopause with large stratospheric Scorer parameter 14 p2268 A71-29763

Stratospheric turbulence correlation to mesoscale horizontal temperature gradient at altitudes flown by SST from Coldscan program 14 p2268 A71-29767

Water vapor contamination long lasting effects on stratospheric measurement during balloon flight 14 p2270 A71-30453

Equatorial upper troposphere and lower stratosphere hurricane and wavelike motions numerical predictions, analyzing heating, friction, cloud physics and ozone dynamics 14 p2270 A71-30500

Electron flux rigidities in polar aurora region, using stratospheric nighttime X ray and cosmic radio noise absorption measurements 14 p2302 A71-30595

Balloon-borne transistorized stratospheric cosmic ray probe, describing simultaneous gas discharge and dual coincidence telescope counters data transmission 14 p2247 A71-30596

Ionospheric absorption winter anomaly including temporal and local variations and frequency dependence, examining possible correlations with stratospheric and mesospheric phenomena 14 p2237 A71-30943

Stratospheric turbulence induced aircraft buffeting dependence on horizontal temperature and wind distribution 15 p2444 A71-31366

Stratospheric circulation synoptic and detailed structure from meteorological rocket network sensors 15 p2396 A71-31614

Soviet papers on processes in upper layers of atmosphere covering troposphere, stratosphere and mesosphere over Northern and Southern Hemispheres 15 p2399 A71-31961

Stratospheric circulation, investigating ozone heating role in temperature field formation by numerical experiment 15 p2399 A71-31963

Northern Hemisphere upper stratospheric temperature pressure field changes during autumn, using isobar surface charts 15 p2400 A71-31966

Northern Hemisphere upper stratosphere and lower mesosphere synoptic meteorological chart construction, using aerological network and rocket radio sounding data 15 p2400 A71-31967

Southern Hemisphere stratosphere and mesosphere meteorological parameters seasonal variation, comparing rocket sounding data with standard models 15 p2400 A71-31968

Radioactive impurities transfer from lower stratosphere into upper troposphere based on vertical air transport data 15 p2400 A71-31970

Altitude and amplitude of winter stratospheric warmings from satellite measured radiance changes, considering radiative transfer equation and variable model of temperature structure 16 p2605 A71-33537

Seasonal temperature and density models for stratosphere and mesosphere from observations by resistance thermometers at Heiss Island Soviet rocket station 16 p2566 A71-33743

Middle stratosphere monthly mean temperature maps based on radiosonde measurements, confirming anomalies with satellite IR spectrometer radiances 16 p2641 A71-33755

Wind and temperature structure in stratosphere at Sonmiani during autumn 1970 from three Dart firings 16 p2567 A71-33765

Belgian report to COSPAR, reviewing experiments with gas release at high altitudes and stratospheric balloons 16 p2667 A71-33870

Stratospheric extraterrestrial particles identification from balloon-collected electron microscope photographs, suggesting cometary origin 16 p2644 A71-34125

Spring and autumn cyclonic circulation in stratosphere and mesosphere up to 95 km, using ionospheric radiosonde and rocket data 17 p2730 A71-34301

Clear air turbulence in midstratosphere, analyzing heat and momentum transports and temperature fluctuations spectra 18 p2943 A71-36008

Stratospheric pressure surfaces height over polar, middle and tropical latitudes as function of long term solar activity 18 p2944 A71-36220

Aerosol layers in stratosphere, determining vertical distribution of electrical conductivity 19 p3047 A71-37335

Short path VLF phase and amplitude measurements during stratospheric warming in February 1969, discussing D region electron density changes 19 p3018 A71-38040

Solar effects contradictory relationships with earth atmosphere, discussing geomagnetic disturbance, annual variations, stratospheric transport and high energy particles 19 p3128 A71-38354

Stratospheric dust effect on electrical conductivity measurements, noting proportionality to ion concentration 20 p3216 A71-38792

Mesosphere and stratosphere ozone vertical density distribution from sounding rocket data, considering photochemical theory and hydrogenic reductions 20 p3221 A71-39694

Seasonal stratospheric wind effects on infrasound propagation to U.S. northeast coast from rockets launched at Cape Kennedy 20 p3306 A71-39762

Stratosphere and mesosphere physics and dynamics, studying composition, radiation fields, temperature, winds, wave phenomena and relations to meteorological theory 20 p3230 A71-39872

E region electron density isopleths height correlation with atmospheric pressure variations, noting sympathetic isobaric surface movements in upper stratosphere 21 p3372 A71-40038

Correlation functions characteristics of wind velocity field in troposphere and stratosphere up to 25 km based on bihourly radiosonde data 21 p3412 A71-41390

Isentropic nature of stratospheric air masses motion from balloon measurements of temperature and radiation 23 p3671 A71-43338

Nitrous oxide dissociation as natural source of stratospheric nitric oxide, noting estimates use as yardstick for artificial source 23 p3642 A71-43347

Earth atmosphere gas composition and electron density variations at F region lower boundary explained by stratospheric explosive and diffusive warmings effect on critical frequency 23 p3671 A71-43578

Stratospheric warmings effect on F 2 region parameters and ionospheric radio wave absorption, assessing time lag 23 p3673 A71-44049

STRATOSPHERE RADIATION

Commercial aviation stratospheric water vapor injections influence on radiation budget, ozone, polar night cloudiness and potential climatic effects 08 p1286 A71-21822

Rocketsonde instrumentation noise separation from stratospheric variability, discussing paired soundings based large scale discrepancies in temperature and wind observations 11 p1794 A71-25386

Stratospheric submillimeter wave emission and water vapor mixing ratios measurements, using Michelson interferometer with phase modulation and Fourier spectroscopy methods 22 p3545 A71-42145

Lower stratosphere submillimeter wavelength radiation measurement using Fourier transform spectroscopy with phase modulation 24 p3822 A71-44448

STRATOTANKER AIRCRAFT U C-135 AIRCRAFT

STRATUS CLOUDS

Aircraft hazards due to frequent low cloud occurrences at Kenya airport, forecasting weather with statistical analysis and radiosounding
13 p2097 A71-29106

Vertical motions, turbulent heat exchange and radiative heat input role in stratus clouds evolution, deriving humidity and heat transfer equations as functions of time
19 p3093 A71-38690

Artificial crystallization and dispersion in supercooled stratus clouds, observing growth, stabilization and disintegration stages in crystallization zones expansion
19 p3093 A71-38691

STREAM FUNCTIONS [FLUIDS]

Compressible gas jet flow from vessel with parallel walls pointing in opposite directions, solving Chaplygin equations for stream functions
01 p0069 A71-10420

Reversible transonic fluid flow through cylindrical blades cascade by hodographic singularities solution of potential and stream function
01 p0003 A71-11023

Downstream boundary condition on stream function, discussing sufficiency conditions in finite difference methods
01 p0071 A71-11162

Constant curvature wing contours in transonic flow, determining stream function by approximation
06 p0842 A71-18227

Multilink approximation of Chaplygin function in subsonic and supersonic flow regions, deriving coupling conditions relative to modified stream function at approximation nodes
07 p1016 A71-20090

Poiseuille pipe flow stability from finite difference equations approximation to nonlinear axisymmetric Navier-Stokes equations under stream function perturbation
07 p1094 A71-20611

Impeller blade loading vorticity on stream surface of revolution for mixed flow compressor, using annular cascade theory
[ASME PAPER 71-GT-17] 11 p1703 A71-25962

Lift and particle displacement around lifting body with stream function as fluid motion equation integral
12 p1866 A71-27577

Pade fractions use in calculation of axisymmetric flow of perfect gas past blunt body of revolution, obtaining stream function Taylor expansion terms
15 p2346 A71-32122

Atmospheric boundary layer circulation dynamic interaction with variable depth barotropic ocean surface, studying stream function during annual cycle
16 p2605 A71-33906

Stream function and velocity of shear flow vortex in infinitely thin profile from linearized Euler equations for boundary value problem
16 p2561 A71-34161

Numerical analysis of laminar recirculating flow between shrouded rotating disks for interaction between vorticity and stream function and swirl-velocity field
18 p2905 A71-36309

Subsonic flow direct and indirect methods including Oswatitch integral equation, thickness parameter expansion, Janzen-Rayleigh method and stream and potential functions in hodograph plane
19 p2992 A71-37453

Nonself-similar problem of developing plane turbulent jet in unbounded space, obtaining second and third terms of asymptotic series of stream function
21 p3368 A71-40692

Transonic nozzle flow with variable stagnation speed of sound across flow, deriving governing equations with stream function as independent variable
21 p3324 A71-40978

Isentropic ideal compressible vortical gas flow in axisymmetric channel, determining stream function and gas density
23 p3625 A71-43549

STREAMLINE FLOW

U LAMINAR FLOW

STREAMLINED BODIES

Singularity carrier auxiliary curves in airfoil cascade design, formulating and proving existence theorem
05 p0693 A71-16397

Boundary layer separation at free streamline attached to body sharp trailing edge, comparing asymptotic solution with numerical analysis of flow on flat plate
12 p1896 A71-27218

Longitudinal space-time correlation function of turbulent near wall pressure pulsations with hydrodynamic wavelength exceeding boundary layer thickness at streamlined model
13 p2049 A71-28846

Acoustical field from streamlined body of revolution moving in homogeneous gaseous medium past semiinfinite rigid screen, using Wiener-Hopf method for diffraction radiation
20 p3175 A71-38809

Critical streamline length in axisymmetric and plane ideal gas flows past conical bodies as function of Mach number and form parameter
24 p3790 A71-45058

STREAMLINING

Inviscid ideally conducting fluid flow past thin foil in transverse magnetic field, using small parameter method
02 p0186 A71-12629

STREAMS

NT GAS STREAMS

STREETS

Aircraft noise propagation in city streets due to intertown V/STOL and helicopter ports, using small scale models
20 p3178 A71-39264

STRENGTH

Machine components resistance to low temperature failure, considering threaded joints, gears and shafts for strength and plasticity characteristics
05 p0827 A71-16764

Dimensionless strength characteristics of convex bodies vs angles of attack in rarefied gas flows by linear regressive analysis using statistical model
13 p1991 A71-29147

Explosively shock strengthened austenitic stainless steel, investigating mechanical properties at elevated temperatures
21 p3398 A71-40462

Strength and plasticity characteristics of hardened multilayer structural steels, investigating layer thickness effect
24 p3837 A71-44729

STRENGTH OF MATERIALS

U MECHANICAL PROPERTIES

STREPTOCOCCUS

Streptococcal flora in pharynx of men during prolonged enclosure noting concomitant hemolytic microbes
06 p0854 A71-18369

Streptococcus mitis bacterium in Apollo 12 lunar retrieved Surveyor 3 TV camera, discussing prelaunch deposition and survival
23 p3633 A71-43815

Pharyngeal streptococcal flora of men confined in sealed chamber, observing microbial transfer
24 p3800 A71-44530

STREPTOMYCETES

Streptomyces sp chitinase purification and properties by column chromatography, noting calcium component
11 p1728 A71-26064

STRESS [BIOLOGY]

Human muscle hardness as isometric stress force indicator
02 p0198 A71-12065

Biological and medical cybernetics approach to closed systems construction for continuous automatic monitoring and control of human physiological processes under harmful conditions
03 p0368 A71-13000

Psychobiological stress of prolonged weightlessness /bed rest/ in man in terms of adaptive homeostatic state and decreased sensory-motor-muscular input
11 p1725 A71-26120

STRESS [PSYCHOLOGY]

NT ACCELERATION STRESSES [PHYSIOLOGY]

NT CENTRIFUGING STRESS

Arterial sclerosis and stenosis physical factors, discussing connective and vascular tissue adaptive responses to mechanical stresses
02 p0200 A71-12415

Muscle simulation by information theory for statistical analysis of behavior based on gas thermodynamics methods, showing stress relation to motor units excitation
03 p0366 A71-12979

Muscle activity control mechanism in animals locked into external feedback loop, relating exciting stimulus to muscles stressed state
03 p0367 A71-12980

Telemetric ECG recordings of workers under high and strongly varying temperature conditions, discussing heart rate variations under heat stress
03 p0370 A71-13065

In-flight EEG recordings telemetry for pilot aptitude testing, showing pilot error relationship to brain oversteering
03 p0370 A71-13067

Autogenic stress effects on susceptibility to cytotoxic and oncogenic virus infections and host defense mechanisms
03 p0359 A71-13152

Personnel selection for emotionally and physically taxing situations by studying physiological responses to anticipated stressors and stress recovery
06 p0851 A71-17607

Photic stimulation at South Pole by EEG, showing no brain stress, undue tension nor anxiety during hypobaric hypoxia acclimatization
06 p0851 A71-17608

Internal osmotic balance and stress induced body fluid osmolality changes due to food or water deprivation, reporting on experimental results with rats
08 p1240 A71-21750

Stomach secretory function and histomorphological changes in dogs under stress
09 p1390 A71-22263

Critical period and habituation in control precision performance response to startle due to pistol shots
11 p1723 A71-25181

Drug effects on LF whole body vibration response of dogs administered with phenobarbital, phenoxylbenzamine and morphine
11 p1720 A71-26121

Space flight factors effects on human physiology and psychology, discussing spacecraft gaseous medium control, food supply, closed ecological systems and weightlessness effects
13 p2016 A71-27876

Heat acclimatization effects on sweat Na concentration over wide sweat rates range, discussing possible mechanisms
13 p2024 A71-29498

High motor stresses effects on muscle acetylcholine content, cholinesterase activity and localization, solitary contractions fusion and pessimal weakening
14 p2186 A71-30553

Systolic and diastolic blood pressures and urinary catecholamines under stress in normotensive and hypertensive subjects
15 p2358 A71-31451

Upright tilt stress effects on cardiac cycle phases in healthy subjects, using noninvasive techniques
15 p2358 A71-31453

German monograph on human mental performance under simultaneous mental and above normal muscular stress involving signal response in double choice reaction problems
15 p2360 A71-32306

Maximal treadmill stress test correlation with postexercise phonocardiogram, ECG and double master test in normal subjects, discussing third and fourth heart sound incidence
15 p2361 A71-32538

Frequency tolerance of vibration stress effects on human performance, considering body resonance, visual acuity, manual tracking and neural capacities
17 p2689 A71-34701

Physiological strains due to industrial heat stress, investigating heart rate and body temperature
18 p2860 A71-36882

Literature survey of nervous-emotional stress effects on pilot during flight, discussing premature fatigue, cardiovascular disorders, psychic disturbances and circadian rhythms
19 p3002 A71-37763

Plasma renin activity in hypertonic and normotonic persons exposed to exogenous stress, comparing with measurements at rest and in orthostasis
20 p3185 A71-38893

Resting and postexercise apexcardiogram correlation with maximal treadmill stress test, noting mean a-wave ratios
21 p3332 A71-40406

Rat plasma creatine phosphokinase activity, hypothermia and stress, considering cold restraint
22 p3486 A71-41938

STRESS [PSYCHOLOGY]

Task difficulty involving simple and choice reaction time under stress of shock, threat of shock and noise
01 p0026 A71-11414

Emotionally induced osmotic pressure and thirst increase of rats during stress, noting eating behavior
02 p0201 A71-12875

Bioelectric activity of cerebral cortex in man under neuroemotional stress, using multichannel radioelectroencephalography
06 p0856 A71-18464

Stress and behavior regulation, investigating pituitary-adrenal system operation
07 p1043 A71-20213

Excretion patterns of air traffic controllers for stress appraisal, using urinalysis
08 p1246 A71-20811

Space flight factors effects on human physiology and psychology, discussing spacecraft gaseous medium control, food supply, closed ecological systems and weightlessness effects
13 p2016 A71-27876

German monograph on human mental performance under simultaneous mental and above normal muscular stress involving signal response in double choice reaction problems
15 p2360 A71-32306

Pilot psychic states in flight, including preliminary demobilization, drowsiness, stunning, euphoria and phobias
16 p2536 A71-33576

Redundancy information effect on human performance in forced pace cognitive tasks under overload stimulus presentation rates
16 p2536 A71-33679

Fatigue and stress measurement on air traffic controllers, using critical fusion frequency methods, tapping tests, self rating and urine catecholamine
17 p2688 A71-34365

Physiological tests for psychic stress effects on aircraft pilot tracking performance, respiration and heart rate
17 p2693 A71-35199

Mental reactive exertion increase phenomenon, investigating achievement under various degrees of carefulness and fatigue
18 p2862 A71-36945

Literature survey of nervous-emotional stress effects on pilot during flight, discussing premature fatigue, cardiovascular disorders, psychic disturbances and circadian rhythms
19 p3002 A71-37763

Psychometric analysis of annoyance by wideband noise with superimposed narrow band component, using multiple regression and scaling method
19 p3008 A71-38061

Human adaptive behavior under psychological stress of astronauts tasks posture-motor characteristics, discussing stabilographic platform test results
22 p3503 A71-42041

Affect adjective checklist assessment of mood changes as function of stress in air traffic controllers
23 p3640 A71-44240

Hematological characteristics of emotional stresses during parachute jump, studying leucocyte, erythrocyte and eosinophil populations changes
24 p3800 A71-44413

Emotional stress of pilots in difficult flight conditions, noting pulse rate increase and biopotentials amplitude changes
24 p3800 A71-44473

STRESS ANALYSIS

NT PHOTOGRAPHIC MEASUREMENT

NT SCHWARTZ METHOD

NT X RAY STRESS ANALYSIS

German monograph on nonlinear flexural-torsional stress analysis of thin walled rods with open profiles covering fork supported and cantilever beam systems
01 p0166 A71-10112

Shells with positive Gaussian curvature, deriving p analytic functions for zero bending stress state and infinitesimal deflections of middle surface
01 p0168 A71-10415

Stability theory of plates beyond elastic limit, discussing elimination of stress variations discontinuity at interface between plastic loading and unloading zones
01 p0170 A71-10648

Variable thickness circular plate uniformly clamped along edge, calculating critical force from eigenfunctions and eigenvalues of equation with one independent variable
01 p0171 A71-10650

Glass fiber reinforced plastics stress and fracture analysis, using approximate and iterative methods for strength estimates and nonlinear stress-strain relationships
01 p0172 A71-10697

Axissymmetric mixed boundary value problem of thermoelasticity for hot stamp penetration into transversely isotropic half space, deriving contact stresses
01 p0175 A71-11036

Transversely isotropic spherical shell of small shear modulus material, deriving stress concentration at circular holes
01 p0175 A71-11038

Stress-strain state of anisotropic inhomogeneous viscoelastic solid fuel charge sphere with annihilating internal boundary
01 p0177 A71-11238

Normal stress analysis at tooth of turbine rotor blade root, taking into account friction force
01 p0143 A71-11247

Simple variable loading and unloading in theory of small elastoplastic deformation under nonuniform heating for residual stress-strain determination
02 p0323 A71-11739

Pressure-bonded trilayer insulator stress analysis, using computer model for explaining alumina component fracturing during fabrication
02 p0256 A71-12249

Temperature fields without induced stress, considering relation between thermal and dislocation stresses in shells of revolution
02 p0325 A71-12283

Equivalence theory applications in three dimensional elasticity, plane deformation and stresses
02 p0328 A71-12534

Matrix algorithm using difference-differential method for thin wall moments of varied thickness anisotropic cylindrical shell
02 p0328 A71-12561

Elastic plate plane stress analysis by Euler variational method for arbitrary geometric shapes and loading, obtaining isotropic and orthotropic solutions
02 p0330 A71-12747

Polish book on limiting load capacity of structural elements covering notched rods and plates with hole under elastoplastic stress
02 p0330 A71-12750

Composite materials interaction stresses by ideal model with linearly elastic isotropic homogeneous inclusions and matrix, solving by finite element method
03 p0505 A71-13536

Elastic and perfectly plastic plane stress problems yield point load lower bounds by finite element method, considering weakened slabs
03 p0505 A71-13541

Strain analysis by moire-rosette method, using fringe patterns from pair of crossed gratings through optical spatial filtering
03 p0423 A71-13549

Isotropic half plane weakened by circular holes normal to boundary, calculating stress-strain state created by concentrated force
03 p0506 A71-13604

Book on fatigue design covering load, stress and stability analyses, fail safe design, damage, residual strength, life, load spectra, structural reliability, etc
03 p0506 A71-13695

Nonhomogeneous strain fields analysis by moire fringe multiplication with full field data reduction by mechanical differentiation
03 p0425 A71-13753

Polymer binder effect photoviscoelastic stress analysis near discontinuous reinforcing fibers, comparing results with finite element method for time dependence
03 p0507 A71-13755

[SESA PAPER 1630] Orthotropic photoelastic analysis of residual stresses in filament-wound composite ring structures, comparing with boring-out and cut-through methods
03 p0508 A71-13773

Scattered light method application to two dimensional plane stress problems, considering fringe spacing and gradient relationship
03 p0426 A71-13779

[SESA PAPER 1718] Two semiinfinite strips joined to form one infinite strip, determining stresses by joint shrinkage
03 p0509 A71-13898

Piecewise linear elastic material three dimensional stress-strain analysis for limiting surfaces between regions with different moduli
03 p0451 A71-13901

Couple stress effects on thermoelastic problem for half space with heat doublet on bounding plane, discussing singularity behavior and order
03 p0510 A71-13910

Elastoplastic stress analysis for samples with notches and holes under tension, discussing boundary condition calculation by finite element method
03 p0510 A71-13949

Stiff rings attached to elastic cylinders, analyzing stresses and deformations under concentrated loads and bending moments about radial and tangential axes
03 p0510 A71-14099

Stress analysis of thin elastoplastic shells with large displacements loaded into strain hardening range, assuming plastic strain incompressibility
03 p0511 A71-14101

[ASME PAPER 70-WA/PVP-3] Finite element program for structural design and stress analysis, introducing creep and plasticity into strain equations
03 p0511 A71-14140

[ASME PAPER 70-WA/DE-4] Laminated circular cylindrical shells under axisymmetric mechanical and thermal loads, including transverse isotropy and shear deformation effects in stress analysis theory
03 p0511 A71-14170

[ASME PAPER 70-WA/APM-53] Stress development in elastic plate with crack under edge loads, estimating plastic zone size at crack ends
03 p0514 A71-14361

German monograph on field equations solution for Cosserat continua in planar strip type regions covering stress analysis
03 p0515 A71-14370

Circular plates strain wave analysis by Laplace transform method, using MacDonald functions approximation
03 p0515 A71-14383

Constant/variable thickness isotropic elastoplastic shallow shells stress analysis and limiting load determination, using numerical method based on successive approximation technique
04 p0664 A71-14603

Shallow spherical shells with periodically spaced holes, discussing stress analysis by least squares method for curved perforated plates
04 p0665 A71-14771

[ASME PAPER 70-PVP-11] Whisker composites mechanical properties analysis, discussing stiffness and strength under static loads, elastic model, stress analysis, statistical tensile failure model, etc
04 p0667 A71-14947

Direct pointwise stress determination in twisted cracked elastic bars under torsion and longitudinal shear by numerical methods
04 p0667 A71-15180

Pressurized isotropic viscoelastic hollow cylinder bonded to elastic casing, analyzing stress during finite deformation
04 p0668 A71-15191

Polarization-optical method of stress analysis problems, explaining high polymers physicochemical properties with Boltzmann-Volterra integral equations
04 p0671 A71-15330

Stress analysis of DC 10 nose landing gear units using photoelastic coating technique
04 p0534 A71-15608

Stress analysis of multilayered composite structures with flaws, emphasizing application to fracture studies
04 p0671 A71-15740

Pure bending and flexure in plane stress with moment stress effects taken into account, considering Saint Venant principle
04 p0672 A71-15760

Ti-Al and Al alloys and Ni maraging steel creep behavior during high stress, elevated temperatures and rapid heating
04 p0617 A71-15909

Aluminum reinforced epoxy model making, testing and stress analysis for aircraft structures, including creep, photoelastic coating and strain gage effects
05 p0821 A71-16340

Photoelastic model stress analysis by holographic interferometry and automatic measurement of light shapes, discussing slicing technique
05 p0752 A71-16733

Fibrous composite materials stress and deformation analysis, using point matching numerical method and boundary point least squares method
05 p0829 A71-17119

Rib reinforced circular cylindrical shells, analyzing elementary and zero bending stress states
06 p0982 A71-17351

Elastic plates and members deformation with constraints on deflections, determining strain state with dynamic programming
06 p0984 A71-17651

Stress analysis of orthotropic twisted bars under tension applied at ends
06 p0985 A71-17740

Stress state analysis in rigidly clamped circular plates bent by edge loads, using three dimensional elasticity theory
06 p0989 A71-17780

Three layer plate with metallic carrier surfaces and plastic foam filler, calculating stress state near applied concentrated moment
06 p0995 A71-17831

Multilayer plates and shells, considering bending, stability, boundary layer stress state, rigid filters theory and local strength
06 p0998 A71-17857

Two and three dimensional photoelasticity, discussing theory and procedures in stress analysis
06 p1001 A71-18063

Main mixed axisymmetric stress for elastic half space with single line separation between boundary conditions, using p-analytic functions
06 p1001 A71-18341

Axissymmetric stress in sphere and space with spherical cavity, using p-analytic functions
06 p1001 A71-18345

Elliptic ring shaped disk with external and internal loading, determining stresses due to uniformly distributed loads
06 p1002 A71-18416

Prismatic shells vibration, buckling and stress analysis, applying computer solutions to complex bodies of revolution
06 p1003 A71-18562

Annealed Mo creep properties and long term strength, observing temperature and stress effects
07 p1130 A71-19165

Electronic encapsulated assemblies thermal stresses due to components expansion coefficients mismatch
07 p1213 A71-19774

Elastic solids fourth order anharmonic equation of state from finite strain theory, resolving ambiguities by Mie-Grüneisen equation
07 p1178 A71-19800

Infinite circular cylindrical shell with elastic stiffener ring, calculating transient axisymmetric bending stress under radial impulse
07 p1213 A71-19907

Stress concentration analysis at arbitrarily oriented cracks in shell, noting curvature influence by single integral equations with Cauchy kernel
07 p1217 A71-20458

Thick-walled toroidal shell under various load distributions, analyzing stress-strain state by network method using computer program
08 p1369 A71-21124

Ta single crystals with interstitial carbon, nitrogen and oxygen, examining Peierls and interstitial hardening stresses additivity
08 p1307 A71-21500

Stress analysis of elastic bending plates by holographic interferometry, comparing results to theory
08 p1373 A71-21757

Stress analysis of anisotropic plate with square holes under tension, using small parameter method 08 p1374 A71-21947

Heat exchanger circular rigid tube sheets calculation by thin plates bending theory, using stepped profile circular plates stress analysis 08 p1374 A71-22053

Shells of revolution under combined thermal and mechanical loading, presenting analytical basis of BOSOR 3 digital stress analysis program 09 p1533 A71-22079

Rumanian book on stress computation in theory of cylindrical median surface plates with arbitrary section and minimal area 09 p1536 A71-22420

Shrouded aircraft engine turbine blades vibration stresses found minimum by setting up paired blades with fixed tension along shroud 09 p1538 A71-22595

Circular cylindrical shell under radial local load, determining maximum stresses in center and boundary 09 p1538 A71-22651

Real time and double exposure holographic interferometry measurements of strain on aluminum cylinder under internal pressure, noting discrepancy with strain gage values 09 p1444 A71-22711

Reference stress parameters for structure creep behavior, using dimensionless stationary state, strain rate and time function 09 p1543 A71-23660

Computerized finite element techniques for stress and structural analysis for space communication and radar applications 10 p1684 A71-23756

Photoelasticity methods applied to model of beam of revolution under simple torsion constructed by stress freezing technique 10 p1684 A71-23837

Euler buckling of hinged slender prismatic bars of rectangular and elliptic cross sections with shear and transverse stress allowance 10 p1685 A71-23959

Binary phase systems stress analytic method for water saturated elastic porous medium 10 p1685 A71-23993

Strength characteristics of machine parts with cracks calculated by graphoanalytic procedure 10 p1686 A71-24192

Transverse strains in solid body due to volumetric stresses counteraction to external load stresses 10 p1687 A71-24198

Bidirectional stress-strain analysis of hinged cylindrical shells crosswise reinforced by rigid ribs using equilibrium equations 10 p1690 A71-24566

Stress state elastic equilibrium of ponderable anisotropic half plane with free and ring reinforced elliptic hole near rectilinear boundary 10 p1690 A71-24567

Plane orthotropic bodies stress analysis by optical polarization method, using models consisting of anisotropic polymer plates fabricated from epoxy resins and woven fiberglass 10 p1690 A71-24573

Spherical shell containing through crack, calculating in-plane and Kirchhoff bending stresses under periodic transverse vibrations 10 p1693 A71-25054

Stress threshold for crack growth in rotating shaft bending fatigue 10 p1693 A71-25058

Infinite thin plate containing circular holes with elastic inclusions under biaxial tension, calculating maximum stresses on common boundaries based on Airy function 11 p1841 A71-25265

Automated optimal weight fully stressed large scale structural design of aircraft, using matrix-mathematical programming technique 11 p1844 A71-25340 [AIAA PAPER 71-361]

Nonhomogeneous variable diameter rods plastic torsion, deriving stress function and distribution 11 p1848 A71-25620

Arbitrary solid cross section frames and arches shakedown analysis including axial forces effects on stress through reduction to linear programming 11 p1849 A71-25678

Incremental plastic analysis under large displacement and physical instabilizing effects, using finite element models and quadratic programming 11 p1849 A71-25679

Soviet book on elasticity theory covering stress and strain tensors, linear closed systems of equations and methods of solution, Saint Venant problem, etc 11 p1850 A71-26097

Conjugate approximations for piecewise functions of stress analysis using finite element method 11 p1792 A71-26103

Mixed boundary value problem for fiber reinforced materials, analyzing shear response in multiply admissible kinematic deformations 11 p1850 A71-26105

Stress analysis near free surfaces in thin composite plates with unidirectionally oriented elastic isotropic fibers, applying boundary point least squares technique 11 p1851 A71-26382

Positive rotational transformations of stress vectors for anisotropic lamina in matrix notation 11 p1852 A71-26393

Creep rate intensity approximate solution as invariant function of stress intensity, determining equivalent stresses under creep 12 p1974 A71-26947

Zero moment stress state realization in thin macrohomogeneous shells by selecting adequate uniform multilayer structures for reinforcement 12 p1975 A71-26963

Transversally isotropic sphere and orthotropic cylinder in symmetrical temperature field, calculating thermal stress equations 12 p1975 A71-27112

Fibrous composite structure stress analysis procedures, considering nonisotropy and brittleness effect [ASME PAPER 71-DE-2] 12 p1977 A71-27321

Static and dynamic stress analysis and limiting loads of plastic shells and plates with temperature field in structural element, using deformation theory 12 p1979 A71-27350

Numerical solution of equations describing stress-strain state of shallow nonuniformly heated shell 12 p1979 A71-27355

Spar box structure under pure bending noting flexural rigidity and stress and stability analysis with Karman nonlinear equations 12 p1981 A71-27498

Inhomogeneous microstructure elastoplastic medium, examining strain and work in plastic deformation 12 p1982 A71-27516

Contact stress between half plane and elastic cover plate, reducing problem to Prandtl type integrodifferential equation with Hilbert kernel 12 p1982 A71-27526

Laminated plates transverse shear effects on deformation and stress distribution, using finite element analysis 12 p1982 A71-27571

Bending stress in conical shell subjected to thermal and pressure loadings with uniform spatial distribution, using perturbation method 12 p1983 A71-27594

Difference equations derivation for flat plates plane stress extension as localized Ritz process, providing common classification of finite difference and finite element methods 13 p2147 A71-27784

Diffused fracture model as basis for plotting delayed fracture curves in space of principal stresses 13 p2149 A71-28119

Multiaxial stress state effects on materials fracture strength, ductility and structural design 13 p2151 A71-28216

Helicopter power transmission failure modes, presenting field experiences correlation with conventional design stress analysis and bench test data [SAE PAPER 710454] 13 p2074 A71-28331

Electron paramagnetic resonance atomic scale stress analysis of high polymer fibers and rubber, measuring chain scission and bond rupture for different loading histories 13 p2091 A71-28440

Suspended hollow cylinder under force of gravity, calculating stresses and displacements by linear elastic theory differential equations 13 p2153 A71-28518

Optimization algorithm for multielement support structure exhibiting minimum deformation energy, comparing Lagrange conditional search method 13 p2101 A71-29186

German monograph on spline functions interpolation for solving integral equations and stress calculation in curvilinear edged disks 13 p2157 A71-29420

Soviet book on space electric rocket engines design and stress analysis covering nuclear reactors, radioactive isotope energy sources and energy converters 13 p2118 A71-29421

Soviet book on stress analysis by optical polarization methods covering theory and practical applications to machine parts and structural components 14 p2321 A71-29528

Critical stress and stability analysis of cylindrical shell with initial indentation of length comparable to radius under axial compression 14 p2321 A71-29536

Stress analysis of thin walled framed structures of variable cross section by second order differential buckling equations, using matrix method 14 p2321 A71-29539

Stress analysis of thin walled framed cylindrical beams under deformation beyond proportionality limit by iteration method 14 p2321 A71-29540

Principal stresses separation in nitrocellulose transparent material with photoelastoplastic properties, using scattered light method 14 p2322 A71-29700

Three dimensional elastic plastic solid, calculating stress and deformation with finite difference procedure 14 p2322 A71-29737

Elastic displacement stress computation in cylindrical systems of isotropic homogeneous material by finite difference method 14 p2323 A71-29744

Linear viscoelastic analysis of two dimensional plane stress model of polyphase composite material with rigid inclusions and voids and polymeric binder 14 p2323 A71-29836

Holographic interferometer for photoelastic stress analysis, eliminating isochromatic pattern interference from isopachic interferogram by double pass object beam and optical rotator 14 p2239 A71-29845

Low ductility materials, considering applications to stress analysis, failure criteria, fatigue, physical metallurgy and polymer mechanics 14 p2251 A71-29893

Nondestructive testing techniques for discrete local materials properties evaluation, allowing nonstatistical analysis of thermomechanical stress behavior 14 p2251 A71-29900

Thermoelastic stress analysis of circular perforated plate under point heat source 14 p2326 A71-30195

Soviet book on glass-reinforced plastic plates and shells covering engineering methods for anisotropic plates and shells stability and stress analysis 14 p2327 A71-30245

Dissimilar elastic half spaces joined over circular region, calculating interfacial traction stresses induced by arbitrary loading from coupled integral equations 14 p2328 A71-30293

Weight effect on large elastic deflection of thin arches, studying stability via nonlinear differential equation using classical approach 14 p2330 A71-30686

Simply supported nearly circular cylindrical shell, calculating nonlinear damped dynamic response due to exponentially decaying radial pressure 14 p2330 A71-30688

Work hardening material planar frame inelastic load deformation and buckling, using finite difference method and variational principle 14 p2330 A71-30693

Internal frictionless contact stress determination for two telescoped cylinders with different diameters, using integrodifferential equation 14 p2331 A71-30845

Dislocation stress analysis in infinite elastic plate with two circular holes under arbitrary steady temperature field 14 p2332 A71-30850

Stability and stress analysis of elastic finned circular cylindrical shells reinforced by stringers 14 p2332 A71-30852

Stress analysis of nonlinearly elastic plate with ring reinforced circular hole 14 p2332 A71-30854

Bending stress of thick laminated plates of isotropic material with variable elasticity modulus 14 p2333 A71-30890

Crack tip strain problem in elastic body, relating fracture energy criterion with mathematical models 14 p2334 A71-31002

Plastic deformation work derivation, taking into account deviation from similarity of stress deviators 15 p2501 A71-31150

Stress analysis by holographic interferometry and automatic light forms analysis 15 p2502 A71-31268

Thermal stresses estimation method based on equivalent stress calculation via use of temperature scale [HEAT EXCH. CONF. PAPER 12] 15 p2504 A71-31634

Interfiber stress model for elastic matrix-fiber reinforced composites under inplane shear and transverse normal loading 15 p2507 A71-32096

Fiber reinforced materials with oriented armoring, calculating stress-strain state under transverse shear 15 p2439 A71-32235

Second order stresses and elastic stability analysis for structures, using supplementary load method 16 p2648 A71-32981

Structural elements residual, principal and total stress determination, using photoelastic coating method 16 p2651 A71-33061

Matrix force analysis, discussing methods for expressing elastic behavior of semiconcave polygon membrane and isotropic polygon bending elements 16 p2652 A71-33082

Stress, slip and damping of clamped elastic plate with finite friction under alternating axial load, using finite element method 16 p2581 A71-33174

Numerical stress analysis of elastic three-dimensional fracture specimen with edge crack, using singular integral equations analogous to Green boundary formula in potential theory

16 p2655 A71-33181

Buckling of axially compressed circular cylindrical shells with localized or random axisymmetric imperfections, deriving asymptotic approximation formulas for stress calculation

16 p2655 A71-33200

[ASME PAPER 71-APM-29]

Orthotropic semiinfinite elastic solid under plane strain, calculating thermal stresses in terms of Green functions

16 p2655 A71-33211

[ASME PAPER 71-APM-18]

Structural reliability predictions using finite element stress program and partial derivative method involving finite approximations

16 p2583 A71-33294

Service life/stress testing, failure analysis and corrective action from technical and cost positions

16 p2583 A71-33315

Neuber elastoplastic analysis of residual notch stresses for improved cumulative damage predictions applied to aluminum alloy under overload

16 p2659 A71-34012

[AIAA PAPER 71-776]

Elastoplasticity shell theory, demonstrating analogy between stresses and strains in three dimensional medium

16 p2660 A71-34067

Displacement field of constant thickness elastic disk with stress boundary conditions, using finite difference technique

17 p2818 A71-34505

Birefringent coating method for stress analysis of fiber-reinforced laminated composites, developing subsurface stress-surface strain relation

17 p2761 A71-34528

[SESA PAPER 1837A]

Holographic interferometer for photoelastic stress analysis by simultaneous acquisition of isochromatic and isopachic fringe patterns without mutual interference, providing increased sensitivity

17 p2738 A71-34541

[SESA PAPER 1792]

Stress analysis through physical modeling, discussing transducing techniques and fabrication-loading analysis

17 p2819 A71-34533

Finite element method stress analysis for evaluating localized stress distributions in thick walled circular tube with step change in thermal expansion

17 p2819 A71-34534

[SESA PAPER 1841A]

Holography applications to complete stress analysis of three dimensional photoelastic models, using double exposure in conjunction with immersion tank

17 p2738 A71-34541

[SESA PAPER 1852]

Strain analysis based on thin metallic film optical measurements, determining principal strain directions from wrinkle and microfracture patterns

17 p2820 A71-34551

[SESA PAPER 1828A]

Limited fatigue strength tests for Al-Mg-Si alloy stress amplitude coefficients under nonuniform loading, defects, strains and creep accumulation

17 p2757 A71-34596

Axissymmetrical elasticity theory for vertical finite length cylinder with mixed boundary conditions on top and bottom end surfaces, obtaining stress and displacement expressions

17 p2822 A71-34779

German monograph on corner singularities in oblique plates calculation with aid of displacement and stress functions, covering bending theory

17 p2823 A71-34796

Three dimensional equilibrium finite element analysis, obtaining approximate stress solutions for symmetric laminates under inplane loading

17 p2824 A71-34812

Stress hybrid finite element model for boundary conditions in solid continua with nodal values as final set of matrix equations

17 p2825 A71-34893

Stress and temperature dependence of diffusional creep, discussing activation energy, grain boundary effects vacancy diffusion and dislocations motion

17 p2758 A71-35220

Stresses and deformation in solid propellants charges under gravitational load, assuming homogeneous isotropic and linearly viscoelastic charge material

17 p2829 A71-35307

Combined brittle and plastic elements model for strain analysis of nonelastic deformed solid

17 p2832 A71-35457

Incompressible fiber reinforced composite materials finite plane deformation continuum theory and stress analysis without restriction concerning elasticity, plasticity or viscoelasticity behavior

18 p2978 A71-36264

[ASME PAPER 71-APM-V]

Cascade displacements and stresses in nozzle ring guide vanes with sectional diaphragm under axial and circumferential flow

18 p2980 A71-36706

Resolved stress formula for shafts under simultaneous tangential bending and torsion acting at dangerous points of cross section

18 p2981 A71-36721

Small strain theory of shells derived from three dimensional equations of equilibrium and compatibility by asymptotic approach

18 p2982 A71-36840

Stress and deflection analysis of plates reinforced with discrete stiffeners in form of simple beams and twisting elements, determining bending moments

18 p2983 A71-36845

Cosserat-type bodies with linear elasticity, obtaining reciprocity theorem and stress solutions under concentrated load

18 p2984 A71-36949

Human heat stress evaluation indices, discussing acclimatization, dehydration, clothing, age, physical fitness, health and sex effects

19 p3006 A71-37483

Zero moment stress state realization in thin macrohomogeneous shells by selecting adequate uniform multilayer structures for reinforcement

19 p3159 A71-38266

Anisotropic material circular rotating disks of various thickness, calculating stress and deformation

19 p3160 A71-38473

Stress analysis of rotating orthotropic disks mounted on elastic shafts, obtaining closed form solution for governing differential equations

20 p3308 A71-39088

Thin shallow spherical shell weakened by circular hole, calculating stressed state from boundary value problem solution

20 p3308 A71-39165

Holographic interferometry application to photoelasticity, interpreting fringe patterns for two dimensional stress analysis

20 p3238 A71-39345

Membrane and bending stresses analysis around elliptic hole in long thin circular cylindrical shell, using perturbation technique

20 p3309 A71-39776

Axissymmetric stress and strain states calculation for linear elastic field in cylindrical tight fits between hub and shaft

21 p3463 A71-40656

German book on static elasticity and theoretical mechanics covering materials stresses and deformations, virtual work principle, linear isotropic elasticity and thermoelasticity

21 p3464 A71-40782

Creep stress and strain analysis in double edged V-shaped notched plates and circumferential V-shaped notched round bars by finite element method

21 p3400 A71-40840

Elastoplastic thermal stress analysis in axisymmetric bodies by finite element method, calculating residual stresses

21 p3466 A71-40841

High strength Al alloys at cryogenic temperatures, presenting plane strain fracture toughness tests results

21 p3401 A71-40916

Nominal stress prediction for plastic tensile instability occurrence in flat orthotropic sheet loaded by biaxial stress system, considering localized and diffuse necking

21 p3469 A71-41005

Micropolar continuum, potential energy, stresses and constitutive relations for buckling of large rectangular grid frameworks under axial load

21 p3469 A71-41009

Stress and contact time calculation for impact of spheres on finite thickness elastic plate overlying rigid foundation

21 p3472 A71-41031

Stress-strain state of rotating viscoelastic hollow cylinder with mobile inner boundary under internal pressure and temperature effects

21 p3472 A71-41145

Soviet book on mathematical plasticity theory covering stress/strain flow and deformation, stress/strain tensors statistical averaging methods and hardening conditions

21 p3473 A71-41370

Curved finite elements application to circular arches, examining convergence properties of various shape functions used in stress resultant calculations

21 p3474 A71-41425

Time harmonic waves oblique propagation in periodically laminated composite, using coupled thermoelasticity theory for plane strain

22 p3613 A71-41433

Open simply supported cylindrical shell internal stresses due to initial deformation based on thin elastic shell linear theory

22 p3613 A71-41563

Quasi-static thermoelasticity and dynamic thermal stress equations solution in matrix form by Fourier transform and Hilbert-Levy method

22 p3614 A71-41567

Optically sensitive epoxy resin based high polymers under pulsed loads, observing deformation and mechanical displacement with high speed photography

22 p3614 A71-41610

Stress analysis of photosensitive coatings and transparent birefringent materials, applying holography to optical polarization method

22 p3537 A71-41614

Buckling for thin stress walled open sections on elastic foundation with constrained direction reinforcement

22 p3614 A71-41693

Thin elastic elliptic plate stress analysis by approximate solution for rectangular plate and parallelepiped equilibrium problems

22 p3616 A71-42212

Nonaxisymmetric boundary value problem solution for transversely isotropic half space with circular separation line between boundary conditions, determining tangential stresses

22 p3617 A71-42576

True stress calculation from automatic diagram plotted in coordinates for cylindrical specimen testing under uniaxial tension

22 p3550 A71-42851

Second order theory of plane plastic flow, investigating characteristic slip lines of perturbed velocity field and stress equations

23 p3774 A71-43144

Homogeneous mountain mass and canyon thermoelastic stress analysis in curvilinear coordinate system by complex variables

23 p3776 A71-43421

Polycrystalline body macrohomogeneous plastic deformation, deriving basic postulates for slippage and plane relationships to tangential stress and shear strength dependence on elastic deformation

23 p3777 A71-43576

Stress and displacement analysis in linear elastic half space consisting of one or two layers bonded to another homogeneous half space

23 p3779 A71-44178

Stress state of arbitrary contour body of revolution under torsion using finite difference method

23 p3779 A71-44218

Thermoviscoelastic problem for semiinfinite plate, determining temperature field and stresses permitting heat propagation

23 p3780 A71-44223

Inelastic transverse strain coefficient and Poisson ratio dependences on plastic and brittle properties

23 p3780 A71-44227

Noncircular cylindrical shells stress and displacement under hydrostatic loads, applying Donnell equations

24 p3879 A71-44618

Fiber reinforced viscoelastic rectangular beam, deriving asymptotic values of stress, curvature and position of neutral axis under constant moment

24 p3879 A71-44630

Convergence and strain accuracy of finite element solutions for nodal displacements in plane elastic mesh

24 p3842 A71-44633

Couple-stress theory application to body model with constrained rotations, discussing elasticity theory modifications in relation to real physical phenomena

24 p3848 A71-44643

Isotropic parabolic elastic cylinder deformation, determining displacements and stresses with Fourier integral and Weber functions

24 p3880 A71-44713

Ring reinforced spherical shell and rib under concentrated normal forces, calculating force factors and displacement by simultaneous deformation analysis allowing moment stresses

24 p3883 A71-44896

Circular cylindrical shell critical stress level leading to stability loss during high speed cogging process based on kinetic energy method

24 p3884 A71-44897

Geometrically nonlinear circular plate under nonuniformly distributed radial force, calculating loading rate and end condition effects on buckling, deflection and stress

24 p3884 A71-44899

Flow and strain analysis and engineering design of porous cylindrical gas film foil bearing at low pressures

24 p3830 A71-44944

Stochastically imperfect columns on nonlinear elastic foundations, obtaining approximate asymptotic expression for buckling stresses and lateral displacement autocorrelation

24 p3884 A71-44962

Stress and displacement solutions to deformation of homogeneous and composite anisotropic near cylindrical bodies, using Almansi algorithm

24 p3885 A71-45061

STRESS CALCULATIONS U STRESS ANALYSIS STRESS CONCENTRATION

Notched metal crack initiation, determining high cyclic loads effects by prior local plastic behavior at stress concentration

01 p0166 A71-10163

Mechanical properties effect on steels fatigue crack growth rate as function of stress intensity factor

01 p0099 A71-10167

Two concentric circular arc parallel cracks interaction in infinite plate under tension, calculating crack tip stress intensity factor based on elastostatics theory

01 p0167 A71-10174

Orthotropic cylindrical shell stress distribution near axial line crack, formulating problem as system of singular integral equations 01 p0167 A71-10175

Heat propagation rate effect on dynamic thermal stress distribution in thin plate, using Hankel and Laplace transforms 01 p0168 A71-10414

Elastic plane with hyperbolic hole under axial tension, determining stress concentration at hole boundary due to irregularities 01 p0168 A71-10424

Stress fields statistical characteristics in randomly inhomogeneous elastic plate, considering Lomakin solution 01 p0170 A71-10642

Stability theory of plates beyond elastic limit, discussing elimination of stress variations discontinuity at interface between plastic loading and unloading zones 01 p0170 A71-10648

Stress concentration and free surface shape at sliding contact for elastic semiinfinite cylinder, discussing mixed boundary value problem 01 p0171 A71-10658

Partially closed Griffith crack shape and stress intensity factor in infinite elastic solid 01 p0172 A71-10842

Nonconservative generalized nodal forces on finitely deformed finite elements 01 p0174 A71-10960

Moire technique calculation of transverse strain directly from longitudinal strain distribution across sections of symmetry in grooved tensile bar 01 p0174 A71-11007

Axial compression of thin circular epoxy resin disks with three dimensional stress state produced by cementing to rigid platens, using triaxial analysis 01 p0109 A71-11008

Stress separation data for axisymmetric and three dimensional data from frozen stress photoelastic model slices 01 p0174 A71-11010

Transversely isotropic spherical shell of small shear modulus material, deriving stress concentration at circular holes 01 p0175 A71-11038

Nonlinear stability of shallow spherical shells under concentrated loads, showing critical loads dependence on shallowness 01 p0177 A71-11239

Numerical method for stress distribution around openings in shells, using orthogonal coordinate system 02 p0321 A71-11649

Elastic elliptic inclusion stress state in plane elastostatics 02 p0321 A71-11680

Shallow spherical shell thermally stressed state produced by temperature gradients 02 p0322 A71-11728

Unsteady axisymmetric temperature and stress distribution in multilayer cylinder in convective heat transfer with temperature-varying medium 02 p0322 A71-11729

Thermal stress concentration around hole in edge-heated elastic strip, using quasi-static formulation 02 p0322 A71-11732

Thermoelastic axisymmetric problem for half space applied to steady temperature field and stress concentration in infinite body with heat conducting plane circular crack 02 p0322 A71-11733

Thermoelasticity problem for stressed state of thin nonaxisymmetric shells with middle surface of revolution 02 p0322 A71-11736

Laminar orthotropic circular cylindrical shell stress state under inversely symmetrical loading 02 p0322 A71-11737

Highly flexible nonlinearly elastic two layer cylinder reinforced by transversely isotropic shell, examining stressed state in axisymmetric temperature field 02 p0323 A71-11742

Disk elongation plastic deformation, determining elastoplastic stressed state for inhomogeneous thermal cycles 02 p0323 A71-11748

Thin shells of revolution local stability during nonuniform stressed state development under heating 02 p0324 A71-11755

Two dimensional stressed state of isotropic plate with elastically reinforced elliptical hole under biaxial tension 02 p0326 A71-12290

Stress concentration at free and reinforced curvilinear holes with random surface roughness applied to plane under hydrostatic tension 02 p0326 A71-12291

Lower bound load carrying capacity of thin walled structures of rods, plates and shells with statistical stable stress field, using plasticity theory 02 p0326 A71-12296

Convex functions theory of rigid perfectly plastic structures, formulating strain rate and stress fields relation in subgradients 02 p0326 A71-12339

Thin circular cylindrical perforated shell, analyzing stress distribution around circular hole by coordinate transformation and partial differential equations 02 p0326 A71-12346

German monograph on arbitrarily distributed internal stresses effect on elastic stability of plates, considering variational problem solution as matrix eigenvalue problem 02 p0327 A71-12375

Stress distribution in gelatin disk and rectangular plate compressed between horizontal slabs, using tangential difference method 02 p0328 A71-12512

Polycrystalline Ni single and overlapping stacking faults production by tensile deformation in premicroyield region, noting stress concentration effects 02 p0268 A71-12888

General nonlinear finite deformation shell and strain membrane theories in terms of reference state quantities by direct physical derivation 03 p0502 A71-13353

Nonlinear elastic effect on stress concentration of incased tubular solid propellant grain 03 p0504 A71-13462

Stresses and deformation in circular matrix subject to internal pressure gradients, assuming cylindrical anisotropy on macroscopic scale 03 p0504 A71-13463

Stress concentration in buckling proof clamped sandwich rod with multilayer rectangular cross section under torsional bending 03 p0504 A71-13527

Distance dependent stress concentration of isotropic plate with two elliptical holes under tension of opposed point forces 03 p0506 A71-13603

Stress distribution around elliptical hole in thin flat rectangular elastic plate under axial in-plane edge loads [ASME PAPER 70-DE-M] 03 p0506 A71-13705

Hollow annular inserts for stress concentration and alternating stress range reduction around holes in thin flat plates, taking friction coefficient into account [ASME PAPER 70-DE-L] 03 p0506 A71-13706

Strain-optical constants determination by ultrasonic technique, using Raman-Nath theory for optical diffraction produced by standing ultrasonic wave 03 p0425 A71-13753

Ring reinforced circular holes in cylindrical shells examining stress concentrations due to internal pressure 03 p0507 A71-13740

Stress intensity factors of hollow notched bars and hydrogen embrittled solid specimens [SESA PAPER 1671] 03 p0443 A71-13751

Nonhomogeneous strain fields analysis by moire fringe multiplication with full field data reduction by mechanical differentiation 03 p0425 A71-13753

Through-thickness fatigue crack growth in polymethyl methacrylate sheets, observing stress intensity factor range, frequency and mean effects [SESA PAPER 1727] 03 p0448 A71-13771

Coupled stresses effect on dynamic stress concentration produced by traveling loads on elastic Cosserat plate 03 p0509 A71-13905

Displacement and stress distribution in infinite elastic medium weakened by Griffith crack 03 p0509 A71-13909

Stress dynamics of optimum high speed piezoelectric pressure probes utilizing backing rod material 03 p0427 A71-13913

Machine screws and metal joints stress distribution, using electric simulation with adaptability to digital computation 03 p0432 A71-13957

Intraluminal pressure effect on stress concentration and deformation of arterial wall in relation to atherosclerosis, using finite element method [ASME PAPER 70-WA/BHF-15] 03 p0373 A71-14113

Optimal design of rotating disks of nonuniform thickness with integral shafts, using two and three dimensional numerical analysis for stress distribution [ASME PAPER 70-WA/DE-6] 03 p0511 A71-14141

Shallow shell theory boundary value problems, calculating stress concentration for domes and shells with holes 03 p0513 A71-14230

Flat sheet under uniform radial tension, varying thickness reinforcement around hole for high stress concentration avoidance 03 p0513 A71-14238

Photoelasticity application for stress-strain state determination around bores made by electron beam, using epoxy models for internal stress distribution 03 p0429 A71-14272

Plastic flow rates in materials under complex loads producing constant stress intensity, considering plastic deformation 03 p0515 A71-14364

Brittle fracture mechanics, discussing shape, stress and dynamic toughness factors, crack-defect interaction and crack barriers 03 p0516 A71-14578

Successive approximation algorithm for stress concentrations at holes in nonlinear shallow shells, applying to cylindrical and spherical shells with circular and elliptical holes 04 p0664 A71-14602

Metallic components strain localization and concentration factors under high pressures or temperatures involving plastic strain, noting static and cyclic load effects 04 p0666 A71-14882

Nonlinear thermoelasticity coupled equations, discussing stress and temperature fields in terms of material response functions 04 p0669 A71-15194

Thermomechanical coupling in axially symmetric viscoelasticity of cylindrical cavity under shear stress, determining stress concentration from temperature distribution 04 p0669 A71-15203

Crack perpendicular to planar interface between isotropic half spaces, noting elastic constants effect on stress components distribution and relative magnitudes 04 p0670 A71-15384

Stress distribution in infinite cracked elastic plate subjected to constant twisting on basis of Reissner thin plates theory 04 p0670 A71-15385

Stress intensity factors for infinite sheet rectangular cut-out with symmetrical edge internal cracks under axial tension 04 p0670 A71-15387

Stress intensity factor of symmetrical notch in apex of triangular plate under concentrated loads 04 p0670 A71-15391

Nb-Mo alloy creep test, determining relationships between steady state creep rate, stress and Mo content 04 p0616 A71-15803

Stress concentration at interface between bonding agent and fuel element in solid propellant grain 05 p0000 A71-15981

German monograph on stress distribution around cutouts in disks, plates and cylindrical shells 05 p0820 A71-16121

Plastic deformation and ductility of Mo alloys under various stress concentrations at room and high temperatures 05 p0765 A71-16175

Molten glass inclusion and stress concentrator /empty hole/ effects on Armo iron electrode potential 05 p0766 A71-16384

Numerical analysis of one dimensional transient temperature fields and elastic thermal stress fields, deriving equations for plate and cylinders with free edges 05 p0823 A71-16494

Bending stress around elliptic elastic inclusions in thin anisotropic plate 05 p0824 A71-16590

Stress distribution in infinite strip weakened by transverse crack under loading at infinity 05 p0825 A71-16612

Beta stabilizers effects on Ti strength, plasticity and stress concentration sensitivity at low temperatures 05 p0767 A71-16766

Austenitic steels and Ti and Al alloys with stress raisers, studying low temperature mechanical properties 05 p0767 A71-16768

Combined deformation of reinforcing elements and polymer binder in monodirectional composite structure, determining stress distribution 06 p0915 A71-17380

Stress distribution at cracks in solid bodies, discussing crack models, plasticity and elasticity theories and continuum mechanical basis of fracture theory 06 p0911 A71-17413

Simply and multiply connected regions in nonlinear media, deriving stress concentration solutions 06 p0987 A71-17772

Local imperfection and stress effects on cylindrical shell stability under various single and combined loads 06 p0991 A71-17803

Elliptical cylindrical shell under internal pressure, investigating stress concentration near surface hole 06 p0994 A71-17821

Stress concentration at holes in plates and shells with multiply connected regions 06 p0999 A71-17863

Stress nonuniformity and initial imperfection influence on cylindrical shell stability 06 p0999 A71-17868

Contact theory of shells under local loads and reinforcing rib interactions 06 p1000 A71-17872

Earthquake correlation to polar motions explained by local stress distribution in lower mantle
06 p0891 A71-17891

Circular and elliptical holes and inclusions effects on stress concentration in elastic beams under uniform compression
06 p1002 A71-18414

Crystalline materials plastic deformation and dynamic yield stress based on elastic shock wave damping
07 p1210 A71-19151

Large inhomogeneous bodies of revolution three dimensional strain state under symmetrical cyclic loads
07 p1210 A71-19159

Physical analogy treating low cycle metal fatigue relation to stress growth in plastic region, discussing cracking mechanisms
07 p1211 A71-19166

Spheroidal cavity effects on elastic medium under axisymmetric stress field, using Legendre potential functions
07 p1212 A71-19253

Antiplane stress distribution around single or collinear cracks in nonwork hardening elastoplastic material under uniform load
07 p1212 A71-19350

Al cast alloys mechanical properties and sensitivity to stress concentration at low temperatures
07 p1311 A71-19366

Tapered cantilevered beams design, determining end deflection and bending stress magnitude by graphical method
07 p1213 A71-19693

Failure theory for anisotropic homogeneous materials, discussing interaction factor, resistance, orthotropism and planar stress
07 p1214 A71-20011

Stress distribution boundary value problem for long isotropic elastic cylinder with strip cracks due to internal pressure
07 p1215 A71-20100

Shallow orthotropic cylindrical shells with weak anisotropy, deriving equations for stress concentration at circular hole
07 p1217 A71-20457

Stress concentration analysis at arbitrarily oriented cracks in shell, noting curvature influence by single integral equations with Cauchy kernel
07 p1217 A71-20458

Stationary temperature field and stresses in infinite body with thermally insulated penny shaped crack, assuming heat source and sink symmetrical distribution
07 p1217 A71-20462

Unsteady temperature field determination in infinite cylindrically anisotropic plate with circular hole, calculating stress by Volterra equations
07 p1218 A71-20463

Stress concentration in planar rectangular shallow shells and plates with polygonal holes
07 p1218 A71-20470

Tensile tests of elastoplastic notched plate in plane stress
07 p1218 A71-20500

Steel conical disks two dimensional stressed state determined with deformations at elastic and elastoplastic strains using digital computers
08 p1369 A71-21116

Aluminum alloy deformations and rupture strength under complex stress at low temperatures, observing anisotropy decrease with temperature
08 p1306 A71-21117

Steady state thermoelastic mixed boundary value problem for elastic layer, obtaining temperature, stresses and displacements in finite integrals through Hankel transforms
08 p1370 A71-21238

Tubular compression members, examining residual stress profile effects on strength reduction
08 p1370 A71-21411

Interstitials role in bcc metals slip anisotropy at low temperatures, examining stress differential effect in Nb-oxygen solid solutions
08 p1307 A71-21505

Cylindrical steel specimens bearing strength under cyclic elastoplastic deformation, investigating stress redistribution effects
08 p1316 A71-21607

Displacement function and principal stress differences in transverse plane of symmetry of axially symmetric photoelastic body
08 p1372 A71-21653

Elastic and elastic-plastic surface strain fields around skewed circular holes in flat plate under uniaxial tension
08 p1372 A71-21654

Stressed state in region of strain raisers around holes in plate subjected to two axial tension associated with plastic yield
08 p1372 A71-21703

Alloy equivalent susceptibility to damage at intermediary service periods and different stress levels under creep conditions at 750 C
08 p1317 A71-21709

Stress distribution and mechanical properties of adhesive bonded metal and plastic lap joints, using statistical analysis
08 p1372 A71-21711

Curved beams bending stress concentration approximate equations for elliptical, circular and rectangular cross sections, providing behavior prediction superior to exact methods
08 p1373 A71-21749

Thermoelastic stress and temperature distribution in doubly connected isotropic plate
08 p1374 A71-21948

Aligned fibers reinforced material hardening rate, taking into account elastic energy and external potential due to internal stress interaction with applied stress
09 p1467 A71-22286

Steels in stressed state, determining hydrogen saturation and occlusion
09 p1467 A71-22309

Al and Mg alloys mechanical properties anisotropy as function of loading conditions, taking into account stress condition effect
09 p1467 A71-22315

Elastic half space two dimensional unsteady temperature and stress fields under induction heating and convective heat transfer
09 p1537 A71-22519

Materials durability in presence of stress concentration under biharmonic loading
09 p1538 A71-22626

Two dimensional stress-strain fields under elastic and elastic-plastic strains and steady state creep, calculating stress distribution around hole in cylindrical shell
09 p1538 A71-22631

Stress effects on electron relaxation time anisotropies in n-type Si, using high temperature piezoresistivity model for population transfer rates
09 p1508 A71-22692

Numerical analysis of winding and heat treatment effects on residual stress distribution in cylindrical glass fiber reinforced plastic products
09 p1482 A71-22816

Stress concentration near hole in transversely isotropic cylindrical and spherical shells made of oriented glass fiber reinforced plastics
09 p1539 A71-22820

Round cross section specimens flexural vibration damping decrement, determining amplitude dependent internal friction with allowance for stressed state
09 p1542 A71-23314

Yield strength theories of heterophase systems with precipitates surrounded by elastic strain fields, considering dislocation precipitation interaction mechanism
09 p1510 A71-23321

Stress corrosion failure prevention in susceptible Al alloys, considering metallurgical structure, environment and stress distribution
09 p1478 A71-23417

Stress concentration correcting factors for fillets in landed aircraft structures
09 p1542 A71-23539

Fracture models of stress field produced by accelerating crack under shear loading, using pulse diffraction method
10 p1684 A71-23932

Temperature stress distribution in infinite plate with time varying heat transfer coefficient
10 p1687 A71-24197

Metal strip with circular hole under tension, calculating plastic strain and stress concentration coefficients
10 p1687 A71-24199

Quasi-static problem of stress-strain distributions in elastic medium with moving crack, calculating arbitrary external force effect on crack
10 p1687 A71-24349

Photometric method for birefringence parameters determination in photoelastic stress distribution measurements, using proposed photosensitivity calibration standards
10 p1611 A71-24354

Linear elastic fracture mechanics in presence of notch stress concentration, considering crack formation and propagation under cyclic stresses
10 p1628 A71-24686

Plate thickness effect on stress distribution around crack, using three dimensional elasticity equations
10 p1693 A71-25055

Stress intensity factor of flat toroidal crack under internal pressure, using approximate solution of axisymmetric problems in fracture mechanics
10 p1693 A71-25057

Simultaneous determination of first and second mode photoelastic maximum shear stress intensity patterns of epoxy model, using computer plotted ellipses
10 p1694 A71-25060

Penny shaped crack in elastic layer bonded to two dissimilar half spaces, investigating stress intensity factors and fracture propagation direction
11 p1841 A71-25301

Dissimilar bonded anisotropic half spaces with flat crack under arbitrary loads, determining stress distribution
11 p1842 A71-25303

Anisotropic bolt bearing specimens failure mode and ultimate load, investigating stress concentration for failure prediction
11 p1844 A71-25325

Slip front mechanisms in clamped or bolted double lap joints from photoelastic analysis of stress environments, discussing fretting fatigue
11 p1845 A71-25348

Carburized steel surface stresses and fatigue behavior, correlating stress distribution measurements and notched bar bending fatigue tests after severe heat treatment steps
11 p1777 A71-25362

Plane stress state determination in laminated local anisotropic elastic solid based on stress functions
11 p1788 A71-25434

Stress and displacement fields in elastic half plane containing edge crack normal to free surface, using integral equations
11 p1847 A71-25444

Stress redistribution and static interlaminar instability of rotating beams and disks of low modulus high yield strength materials
11 p1848 A71-25499

Creep rupture data analysis model based on minimum commitment station function approach generalizing hypothesized time temperature stress relation
11 p1848 A71-25561

Stress-strain states of physically nonlinear anisotropic media, showing boundary value problem equivalent to variational problem
11 p1850 A71-26179

Nodal points stresses determination from finite element solved elastic problems, discussing thin disk stresses as function of mesh pattern regularity
11 p1851 A71-26312

Strain concentration around holes in composite plate by moire techniques
11 p1851 A71-26389

S-shape lines of axial displacement field and interlaminar shear edge effect in laminated composites verified by moire technique
11 p1852 A71-26390

Maximum shear and hoop stress gradients in graphite-epoxy angle-ply laminated composite cylinders for axial and internal pressure loading
11 p1852 A71-26398

Plastic deformation of elliptic inclusion in plane strain of infinite plate, using viscoelastic analogy
11 p1852 A71-26399

Temperature and membrane thermal stress distribution in finite rectangular plate with insulated circular hole, considering steady state heat conduction equation
11 p1852 A71-26404

Dynamic stress and strain concentration in flat plate at sharp change of section, assuming diffuse bending wave field
12 p1973 A71-26703

Stress distribution in infinite elastic solid containing spherical cavity and external crack, discussing displacement components for axisymmetric loading
12 p1974 A71-26740

Boundary value problems of steady state thermoelasticity and axisymmetric Boussinesq stress concentration for half space in linear Cosserat elasticity
12 p1974 A71-26942

Creep rate intensity approximate solution as invariant function of stress intensity, determining equivalent stresses under creep
12 p1974 A71-26947

Loads on compressor, ventilator and turbine rotor disks having large central holes, giving formulas for stress distributions
12 p1945 A71-26952

Anisotropic plate with curvilinear holes, noting stress concentrations
12 p1975 A71-27110

Specimen sample mounting stress effects on fatigue durability scatter in axial load tests
12 p1976 A71-27116

High altitude balloon gore meridional stresses effects on film response by analyzing cylindrical elastic membrane under uniform hydrostatic pressure and axial loads
12 p1976 A71-27121

Plane stress distribution solution for rectangular elastic plastic plate under partial edge loading, using incremental theory
12 p1976 A71-27122

Spherical head projectiles collision with hemispherical shells and square plates with and without protective covering, calculating stress distribution
12 p1976 A71-27160

Residual stress at plate crack determined from elastic stress intensity factor measurements
12 p1977 A71-27311

Nonlinear physical and geometrical thermoelasticity for plane strain and stressed state at circular hole in in

finite space, using approximation in Lagrangian coordinates 12 p1978 A71-27349

Thermal stresses in circular plate with cylindrical orthotropy and reinforced edge, determining temperature and stress distributions 12 p1979 A71-27356

Combined deformation of reinforcing elements and polymer binder in monodirectional composite structure, determining stress distribution 12 p1921 A71-27462

Elastoplastic problem of stress concentration in orthotropic plate with circular notch under tension 12 p1982 A71-27517

Laminated plates transverse shear effects on deformation and stress distribution, using finite element analysis 12 p1982 A71-27571

Axisymmetric stressed-state problem of finite length hollow circular cylinder in Fourier and Fourier-Dini series form 12 p1984 A71-27692

Stress concentrations over smooth perimeters of curvilinear holes in infinite isotropic plates subjected to loads 12 p1984 A71-27694

Stress raisers effect on mechanical properties of fcc materials at cryogenic temperatures 13 p2083 A71-27871

Single fiber reinforced plate initial stress distribution due to linear expansion coefficients difference between matrix and fiber, using optical polarization 13 p2091 A71-28126

Stress concentration due to holes and other stress raisers in plates and shells, taking into account transverse shear strains effects 13 p2149 A71-28127

Stress-strain state induced by concentrated forces in infinite medium with nonlocal rheological deformation law, obtaining particular solutions for quasi-static viscoelastic problems 13 p2149 A71-28128

Stress concentration at circular hole in conical shell, using Bubnov-Galerkin method in conjunction with linear thin shell theory 13 p2150 A71-28135

Stress concentration in variable-modulus perforated plate of isotropic elastic material under hydrostatic pressure 13 p2151 A71-28142

Crack growth and fracture mechanics, discussing linear stress field and plasticity analyses for three dimensional and dynamic problems 13 p2151 A71-28213

Notch analysis of fracture, discussing elasticity theory of stress concentration and applications to brittle inhomogeneous materials and fatigue crack propagation 13 p2151 A71-28215

Multiaxial stress state effects on materials fracture strength, ductility and structural design 13 p2151 A71-28216

Circular cylinder thermal stressed state, considering interaction between temperature and deformation fields 13 p2152 A71-28273

Fatigue crack propagation in thermoplastics, investigating stress intensity effect on factor mean value 13 p2091 A71-28465

Cracks in Cosserat continuum, investigating couple-stress effects on stress concentration 13 p2153 A71-28521

Nonisotropic turbulent stress and viscosity components distributions in noncirculating swirling flow from mean axial and swirl velocities 13 p2161 A71-28622

Optimal design of minimum volume beams of variable height under bilateral restrictions on stresses and displacements 13 p2154 A71-28645

Geometrical parameters of stringer nodes in statically determinate minimum weight equal stress and strength trusses 13 p2154 A71-28647

Friction forces between expansion die sectors and blank, describing effect on closed contour shell stress-strain state and shaping process 13 p2074 A71-28939

Successive approximations method for solving nonlinear elastic problems in transient creep theory, describing stress redistribution 13 p2157 A71-29197

Notch effect on ductile fracture, considering plastic stress and strain concentration in stainless steel, brass, copper and mild steel 13 p2088 A71-29343

Stress concentration for fatigue crack propagation in smooth and notched samples under symmetrical loading 13 p2157 A71-29373

High temperature creep in alpha-Fe, Fe-Mo and Fe-Co alloys, investigating stress dependence and alloying effects in ferromagnetic and paramagnetic temperature ranges 13 p2089 A71-29409

Static load and stress distribution in rolling element bearings, using elastic contact area analysis method [ASLE PREPRINT 71AM 1D-1] 13 p2076 A71-29487

Stress values at arbitrary point of infinite disk loaded by concentrated force acting through rigid slit of circular arc segment 14 p2323 A71-29814

Statically determinate plane strains in plastic solids, establishing geometrical relations between constant normal-shear stresses and principal directions curves 14 p2323 A71-29816

Numerical incremental solution of large deformation elasticity problems at finite rotations and strains 14 p2324 A71-29862

Plate temperature field and stress distribution under thermal pulses, evaluating critical heat load for damage 14 p2325 A71-30049

Elastic sphere equilibrium with penny shaped crack under inner surface pressure, observing stress distribution 14 p2326 A71-30096

Shear stress distribution and local heat flux at surface of axisymmetric bodies for laminar and turbulent boundary layer flow 14 p2170 A71-30219

Geometrical parameters and load carrying capacity of fiberglass reinforced plastic composites with elastoplastic adhesive bonding, deriving relations for stress distribution 14 p2264 A71-30270

Linear isotropic and centro-symmetric second-grade elastic material and special case with coupling stress, calculating stress field of long straight screw and edge dislocations 14 p2327 A71-30290

Monograph on crack problems in mathematical theory of thermoelasticity covering crack effects on stress distribution in circular cylinders, thick plates and infinite solid bodies 14 p2329 A71-30501

Simply supported skew plates buckling under uniform in-plane stresses, obtaining numerical results for various ratios and angles 14 p2331 A71-30698

Circular stresses and concentration coefficient variations in star shaped elastic surface projected onto ring under internal pressure 14 p2287 A71-30853

Momentless axisymmetric stress state and stability loss in thin convex shells of revolution in linear approximation 14 p2333 A71-30891

Stress concentration and free surface shape at sliding contact for elastic semiinfinite cylinder, discussing mixed boundary value problem 14 p2333 A71-30992

Buckling under compressive loads of incompressible neo-Hookean plates for homogeneous initial deformation, using variational principle 14 p2333 A71-30993

Shear stress, eddy viscosity and mixing length distributions in compressible turbulent boundary layers with air and carbon dioxide injection 14 p2228 A71-31025

Finned solid cylinders surface layers, determining residual axial stresses distribution and amount with induction sensor 15 p2503 A71-31480

Probability theory of stresses during random vibrations of flat panel in acoustic field of jet engine exhaust 15 p2504 A71-31704

Thermal buckling of elastic plates exposed to random temperature field producing biaxial stress concentration 15 p2504 A71-31834

Steel structural elements resistance reserve to brittle fracture, considering critical temperatures and breaking stresses 15 p2504 A71-31852

Heat resistant metals long time creep prediction at low stresses or temperatures 15 p2428 A71-31859

Stress distribution during plastic deformation of steel turbine disk from hardness measurements 15 p2505 A71-31863

Elastic-plastic mechanics of steady crack growth under antiplane shear, discussing residual stress effect, plastic zones shape and strain distribution 15 p2428 A71-31974

Circular cylindrical shell with elliptic hole, calculating stress concentration around hole under torsion 15 p2506 A71-32014

Power and exponential time dependences of long term creep strength for wide stress range, assuming linear thermal resistance 15 p2433 A71-32228

Residual stress determination from stress intensity factor measurements, describing application to electron beam welded aluminum plate 15 p2508 A71-32259

German monograph on spatial elasticity problems solution by multidimensional Fourier transformation

covering stress concentration on hollow and solid cones for given load distribution 15 p2509 A71-32300

Rectangular cylindrical shell finite element, deriving stiffness matrix with stress distribution 15 p2510 A71-32516

Vibrationally loaded hollow cylinder with slanted notch, considering fatigue strength behavior as function of rated stress state 15 p2510 A71-32738

Photoelastic determination of stress distribution in thin square plates subjected to gravitational forces multiplied by immersion in Hg 16 p2647 A71-32824

Maximum stress concentration in two dimensional elasticity theory for half plane and circle as function of contour distribution, using Cauchy-Buniakovski inequality in Banach space 16 p2648 A71-32938

Linearly viscoelastic strip with slowly propagating central crack, calculating stress intensity factor and crack opening size 16 p2590 A71-32939

Elastic-plastic finite element analysis of near crack tip stress and strain field structure 16 p2590 A71-32940

Elastic energy release rates and stress intensity from nonlinear load deflection curves as function of crack length to specimen width ratio 16 p2590 A71-32945

Stress intensity history effect on metal fatigue crack growth rate, using closed loop hydraulic testing machine with stepwise increments in sinusoidal tension-tension load cycles 16 p2591 A71-32948

Rods instability with cross sectional stress concentration dependent properties, presenting buckling and bending problems 16 p2648 A71-32990

Finite element analytical technique for calculating stress distribution in elastic body, using minimum potential energy principle 16 p2652 A71-33079

Finite element method application to stress distribution analysis at crack tip of rectangular plate under tension, obtaining elastoplastic response to cyclic loading 16 p2653 A71-33086

Axially symmetric thermal stress distributions in infinite elastic solid containing flat circular external crack 16 p2654 A71-33169

Stress field in elastic strip of finite width under pressure applied to faces of symmetrically situated Griffith crack 16 p2654 A71-33170

Linear elastic body stress field singularities, investigating local geometry and boundary condition effects 16 p2654 A71-33175

Creep tests of admissible stress states in viscoelastic isotropic compressible or incompressible linear and nonlinear solids [ASME PAPER 71-APM-23] 16 p2591 A71-33206

Elastic plate with part-through surface crack, determining stress intensity factor for remote tensile and bending loads [ASME PAPER 71-APM-20] 16 p2655 A71-33209

Dynamic midsurface displacements of thin circular cylindrical shell under uniform membrane stress state and three dimensional surface loads [ASME PAPER 71-APM-12] 16 p2656 A71-33214

Aircraft structures fatigue properties, discussing stresses, life estimates, safety factors and descriptive curves 16 p2656 A71-33343

Isotropic elastic body steady vibrations with moment stresses, solving two dimensional boundary value problem 16 p2658 A71-33716

Isotropic sandwich plates with rigid cores due to shear boundary tractions, considering transverse strain and stress, displacement function and stability 16 p2660 A71-34035

Moment state stability of elastic hinged cylindrical shell and closed ring under pressure and concentrated load, using nonlinear equilibrium theory 16 p2660 A71-34114

Thermal stresses distribution in wedge shaped solids with cracks, solving elastic equilibrium equations 16 p2661 A71-34158

Stress distribution in cylindrical shell with two unequal diametrically opposite reinforced circular holes under internal pressure 16 p2661 A71-34159

Viscous stresses distribution in isothermal incompressible turbulent boundary layer with positive pressure gradient by diffusers in open jet wind tunnel 17 p2725 A71-34209

Nonlinear creep equation of elastoplastic medium under three dimensional stress, assuming elastic, viscoelastic and irreversible plastic deformation 17 p2817 A71-34337

Conical shell with circular hole, determining stress function and normal deflection in torsion
17 p2817 A71-34338

Reinforcing fiber weaknesses, considering stress concentrators, cracks and steps due to handling damage and interaction with contaminants during heat treatment
17 p2817 A71-34343

Deformations and stress concentration on corrugated plate under uniformly distributed load, considering cross section as combination of two cylindrical shells
17 p2818 A71-34401

Stress distribution in isotropic and anisotropic half spaces with crack in interface bonding, reducing boundary value problem to Hilbert problem
17 p2819 A71-34509

Fiber to matrix modulus of elasticity ratio for two dimensional plane stress composite by finite element and moire strain analyses
[SESA PAPER 1826A] 17 p2761 A71-34527

Circumferential notch effect on distribution of compressive self stresses produced by shallow skin layer expansion in round steel bars, using finite element method
[SESA PAPER 1831] 17 p2819 A71-34529

Stress difference elasticity equations from photoelastic data and first stress invariant
[SESA PAPER 1780] 17 p2819 A71-34530

Finite element method stress analysis for evaluating localized stress distributions in thick walled circular tube with step change in thermal expansion
[SESA PAPER 1841A] 17 p2819 A71-34534

Photoelastic determination of crack tip stress intensity factors for various specimen geometries and loading conditions
[SESA PAPER 1825A] 17 p2819 A71-34535

Elastoplastic strain distribution in bent circular Al plate with central hole under concentrated load, giving moire patterns and stress-strain diagram
[SESA PAPER 1822] 17 p2820 A71-34542

Propagating crack arrest capability of circular hole in plate, studying dynamic stress intensity and concentration factors changes
[SESA PAPER 1827A] 17 p2820 A71-34546

Precatastrophic extension effects on local stresses in cracked plates under bending fields, using stress freezing and slicing for photoelastic experiments
[SESA PAPER 1820] 17 p2820 A71-34549

Crack wave loading, investigating dynamic stress intensity factor and time response with photoelastic technique
[SESA PAPER 1835] 17 p2820 A71-34550

Toughness testing for low ductility fracture due to crack development in elastic stress field
17 p2757 A71-34557

Optimal bar design for tangential load transmission into sheet, determining stress distribution
17 p2821 A71-34591

Stress distribution in plates and tubes bonded by stepped joints, assuming generalized plane stress
17 p2824 A71-34814

Circular symmetry stressed state for flat disk with flat circular crack, detailing potential and elasticity theories
17 p2824 A71-34844

Curvature effect on cylindrical shell circumferential crack tip stress intensity, using fatigue crack growth tests
17 p2827 A71-35154

Stresses in smooth circular cylindrical shell under radial local load applied on small area
17 p2828 A71-35303

Thermal stressed state and bending theory of rectangular plate by initial function method, allowing for distributed transverse load
17 p2829 A71-35304

Stress distribution over elements of boss or collar tightened flange joints of circular thin walled shells during bending
17 p2829 A71-35306

Stressed state of nonuniformly heated thermoelastic flexible plates with variable elastic parameters, using integral principle of minimum total potential energy
17 p2829 A71-35310

Thin multilayer pressurized glass fiber-plastic cylindrical shells, calculating stress redistribution due to crack initiation and prestressing effects
17 p2830 A71-35319

Continuous stress distributions across interelement boundaries, using finite element approximations based on displacement assumptions
17 p2831 A71-35352

Hybrid techniques combining boundary and finite element methods, noting application to stress concentration singularities
17 p2831 A71-35354

Plastic deformation and embrittlement due to stress raisers in steel cylinders from high speed tensile tests at low temperatures
17 p2832 A71-35462

Beta stabilizers effects on Ti base binary alloys strength, plasticity and stress concentration sensitivity at low temperatures
17 p2760 A71-35465

Stress variation with varying plastic deformation rate and temperature in tantalum carbide between 1200 and 2200 C
17 p2760 A71-35550

Creep strain separation theory generalization, describing viscous flow strain division into two components
17 p2833 A71-35617

Brittle fracture under stress concentrations, calculating scale factor based on technical cohesive strength statistical theory
17 p2833 A71-35619

Physical analogy treating low cycle metal fatigue relation to stress growth in plastic region, discussing cracking mechanisms
17 p2834 A71-35662

Cylindrical steel and Ni alloy specimens bearing strength in inhomogeneous stress states under cyclic elastoplastic bending and loading to failure
17 p2760 A71-35668

Channel type closed shallow shells stress states calculation, applying asymptotic integration technique to load decomposition
18 p2976 A71-36178

Loaded crack ending at bimaterial composite interface, analyzing crack tip stress field singularity order dependence on material elastic constants
[ASME PAPER 71-APM-O] 18 p2978 A71-36258

Convergent approximations of impulsively loaded stable structures with account of geometry changes and discontinuity interfaces
[ASME PAPER 71-APM-KK] 18 p2978 A71-36267

Two dimensional stress and temperature fields in cooled gas turbine blades with allowance for elasticity, plasticity and creep
18 p2980 A71-36704

Cyclic bending stress distribution in fir tree turbine blade root for arbitrary loading phase
18 p2980 A71-36705

Rib reinforced cylindrical shells deformation under local load, examining stress-strain distribution
18 p2981 A71-36719

Accelerating rotating disks with variable thickness, presenting shear stress distribution
18 p2982 A71-36771

Thin walled beam structures under external torsional loading, calculating distribution of longitudinal and shear stresses
18 p2982 A71-36808

Stress redistribution in laminate composite due to crack normal to interfaces, noting dependence on crack size, layer height and material properties
18 p2982 A71-36841

Minimum weight design of statically determinate elastic truss under multiple stress and displacement constraints, using virtual work of dummy loads
18 p2982 A71-36842

Stress field singularities at interface corners in bonded dissimilar isotropic elastic materials under plane force field applied to wedge subregion
18 p2983 A71-36843

Stress intensity factors and strain energy rate for bonded layered composites with interface flaw/crack
18 p2983 A71-36846

Edge cracked metal sheet elastoplastic strain distribution determination, using optical interference, moire technique and plane stress model finite element method
18 p2983 A71-36848

Photoelastic analysis of maximum stress in wide plate with asymmetrically reinforced circular hole under tension, noting effects of rounded corner at hole edge
18 p2984 A71-37022

Stress wave interaction with macrocrack in elastoplastic and quasi-brittle materials, measuring stress field by optical polarization method and motion picture photography
19 p3154 A71-37086

Variable thickness thin orthotropic spherical shell with hole, calculating stressed state with successive approximation technique
19 p3155 A71-37533

Stress concentration formulas for elliptical hole in spherical shell with or without cap
19 p3156 A71-37540

Stress effect on hydrogen distribution at high temperatures in titanium and Ti-Al-Mo-V alloy
19 p3080 A71-37720

Circular inclusion effects in infinite viscoelastic plate under monotonically increasing uniaxial tension, considering stress distribution
19 p3157 A71-37798

Fracture mechanics for design procedures, producing approximate expressions for stress intensity factors
19 p3158 A71-38019

Elastic field and stress distribution in composite circular rotating disk under constant normal pressure
19 p3159 A71-38187

Rigid disk effect on thermal stress distribution in semiinfinite elastic solid under prescribed surface temperature and heat flux
19 p3159 A71-38188

Stress distribution in cylindrical bodies in internal contact, considering thick elastic plate with elastic disk fitted tightly into hole
19 p3160 A71-38482

Variable thickness plate under cylindrical bending, considering stress concentration around circular hole
19 p3160 A71-38542

Fatigue crack propagation in high yield strength steels at room temperature in air environments, considering primary influence of applied stress intensity range
20 p3248 A71-38769

Deformation and stress distribution three dimensional state around flat parabolic cracks in elastic solids
20 p3307 A71-38777

Corrosion fatigue crack propagation in Ni-Cr-Mo alloy maraging steel in room temperature NaCl solution at various stress intensity ranges
20 p3248 A71-38777

Experimental stress intensity coefficients for contoured double cantilever beams, using Irwin-Kies method based on compliance with respect to crack length
20 p3307 A71-38779

Harmonic stress function and stress intensity factor for elliptical crack embedded in elastic solid and subjected to arbitrary internal pressure
20 p3307 A71-38782

Linear elastic fracture mechanics for design against high cycle fatigue failure, considering stress intensification, crack initiation and propagation
20 p3307 A71-38813

Thin gold films strain distribution determination from X ray diffraction peaks, noting elasticity theory
20 p3276 A71-39012

Stress concentration and defects effect on crack initiation and propagation in austenitic steels thermal fatigue
20 p3307 A71-39022

Internal pressure deformed star shaped crack, calculating stress intensity factor, crack energy and normal displacement
20 p3310 A71-39866

Stress state determination in birefringent elastic material for plane dynamic problems by photoelasticimetric and interferometric techniques
21 p3376 A71-40103

Stress distribution in adhesive lapped joints with emphasis on shear stress
21 p3384 A71-40139

Moire fringe method for direct determination of displacement and strain fields in two and three dimensional surfaces
21 p3377 A71-40230

Straight line vortices in uniform two dimensional straining field, detailing irrotational strain and simple shear
21 p3320 A71-40501

Crack shapes and stress intensity factors for deep edge crack in plate under tension or bending
21 p3467 A71-40907

Thermal stress distribution and temperature profiles in nearly opaque spherical shell under radiant and convective heating flux
21 p3476 A71-40942

Closed form solution for quasi-static thermal stress field due to moving point heat source in circular disk, noting application to welding problems
21 p3467 A71-40966

Cylindrical shell under opposing concentrated outwardly directed radial loads applied to reinforcing ring, presenting stress distributions and displacements
21 p3468 A71-40971

Stress intensity factors of periodically spaced elastic cover plates bonded to elastic half plane, solving contact problem by Fredholm integral equation
21 p3470 A71-41020

Stress concentration in layers of sandwich beams with holes under bending and tension
21 p3473 A71-41156

Stress intensity factors determination for notched structures, using finite element technique
22 p3613 A71-41431

Half space with periodic continuous distributed dislocations and plastic distortions, calculating stress fields and free surface orientation with cartesian coordinate system
22 p3613 A71-41432

Double forces surface distributions, investigating displacement and stress fields singularities of static Lamé equations
22 p3614 A71-41603

Infinite sandwich plate under concentrated torque load on one side, determining stress distribution with double infinite Fourier transform
22 p3614 A71-41604

Stress concentration near holes in high modulus epoxy resin polymer thin plates under pressure wave loads
22 p3614 A71-41611

Finite element method for stress intensity factors calculation in cracked plates under bending
22 p3614 A71-41639

Fracture mechanics analysis of metal fatigue crack growth as function of stress intensity factor 22 p3560 A71-41641

Stress intensity factors analysis of strip with longitudinal crack subject to tension and bending along edges and tension of rectangular plates with central crack 22 p3614 A71-41709

Fracture mode transition under varied mean stress levels in metal fatigue at constant crack growth rate 22 p3561 A71-41711

Computer program for nonuniform thickness ring structure stress distribution under uniform radial line load based on reinforced circular cylindrical shell interaction under hydrostatic pressure 22 p3516 A71-41866

Optically active material photoelastic properties utilization for residual stress distribution determination in machine elements after lathe working 22 p3617 A71-42575

Stress concentration factors of bonded single lap joints by finite element method as functions of dimensionless, geometric and material parameters 22 p3619 A71-42835

Crack model with strain rate dependent yield stress, calculating stress intensity factor variation with fracture propagation velocity 23 p3774 A71-43145

Dynamic three dimensional stress distribution near crack tip in finite plate, using finite difference scheme 23 p3776 A71-43376

Stress concentrations and singularities at interface corners, presenting procedure for standardized mathematical formulation of conditions for different physical problems 23 p3777 A71-43494

Longitudinal shear induced stress field around rigid circular cylindrical inclusion and parallel crack, using Jacobi elliptic function in conformal mapping procedure 23 p3777 A71-43495

Hertzian fracture test for strong solid surface properties measurement based on crack growth in nonuniform stress field due to contact loading 23 p3777 A71-43934

Glass fibers durability in air and vacuum conditions, showing stress concentration coefficients at various tensile stresses 23 p3697 A71-44031

Steel with various intensity stress risers under bending loads, showing difference in crack nucleation and propagation resistance 23 p3778 A71-44036

Nonlinear geometry effects on stress concentration in elastic plates weakened by two circular holes, using complex potential approximations 23 p3778 A71-44041

Thermoelasticity, thermal conductivity and stress distributions in plates with two circular holes under constant contour temperatures, using complex variables theory 23 p3778 A71-44042

Stresses and displacements in elastic half space with variable modulus of elasticity under axisymmetrical shifting load distributed along ring 23 p3778 A71-44045

Fine structure at crack tip expanding in ideally elastoplastic material in plane deformation state and plane stressed state 23 p3778 A71-44061

Fiber reinforced metallic matrix composite under creep, discussing rigidity, stress distribution, rupture strength and failure time 23 p3697 A71-44201

Refractory materials heat resistance criteria, taking into account hollow cylinder thermal stress distribution 23 p3698 A71-44212

Stress state of arbitrary contour body of revolution under torsion using finite difference method 23 p3779 A71-44218

Disk fillets stressed state, determining concentration coefficient and bearing capacity effect 23 p3780 A71-44221

Thermal and mechanical stresses concentration near peripheral notches on ring-shaped graphite, noting notch sensitivity relationship to tip curvature and graphite grain size 23 p3698 A71-44230

Rectangular planform nonshallow spherical and elliptical shells, determining momentless stressed state 24 p3877 A71-44404

Cylindrical shell with elliptical hole, calculating elastic stress concentration due to axial tension based on shallow shell theory 24 p3879 A71-44625

Stress field due to two rigid circular disk inclusions in isotropic homogeneous infinite plate 24 p3879 A71-44627

Finite cylinder forced longitudinal axisymmetric vibrations with prescribed surface stresses, reducing problem to quasi-regular infinite system of linear algebraic equations 24 p3880 A71-44723

Turbulent stress distribution relationship to averaged characteristics of incompressible fluid boundary layer flow with positive pressure gradient 24 p3818 A71-44748

Curvilinear elasticity solutions to stress concentrations at fine necks in cylindrical shaft under torsion, considering semicircle, semiellipse, rectangle, triangle and arc shapes 24 p3882 A71-44846

Thin walled tube under combined bending and torsion, considering stress distribution and curvature behavior 24 p3883 A71-44892

Three dimensional stress field error estimates in linear plate bending, using Prager-Syngé hypercircle elasticity theorem 24 p3884 A71-44964

Thermal stresses relaxation and distribution in infinite anisotropic viscoelastic cylinder 24 p3884 A71-45002

STRESS CORROSION

Vapor phase interaction of methanol and carbon tetrachloride with Ti thin films, discussing Ti stress corrosion cracking implications 01 p0102 A71-10812

Ni maraging steel weldments stress corrosion cracking characteristics in air and pentaborane by electron microscopy 02 p0262 A71-11707

Ti-Al alloy hot salt stress corrosion cracking due to hydrogen production and absorption 02 p0267 A71-12880

Ni maraging steel cantilever beams intergranular stress corrosion cracking in aqueous solutions, noting heat treatment effects 02 p0267 A71-12881

Ti alloy hot salt stress corrosion under simulated engine environmental conditions, presenting threshold data based on residual tensile ductility 02 p0268 A71-12885

High strength stress-corrosion resistant Al alloy forgings fabrication processes, noting chemical composition and physical properties 03 p0441 A71-13255

Al-Zn-Mg alloys intergranular failure due to aqueous stress corrosion cracking, fatigue and exfoliation, analyzing mud-crack pattern 03 p0441 A71-13319

Al-Zn-Mg ternary alloys stress corrosion cracking resistance relation to mechanical strength decrease, quenching rate increase and solution treatment temperature 04 p0609 A71-14772

Al-Zn-Mg ternary alloys stress corrosion cracking resistance relation to heat affected zone postannealing aging and cooling rate decrease 04 p0610 A71-14773

Ti alloys stress corrosion crack propagation in salt water, investigating existence of threshold stress from electrochemical data 04 p0610 A71-14891

Stress corrosion cracking mechanism, considering anodic dissolution, local surface enrichment and hydrogen embrittlement in noble metal species 04 p0610 A71-14892

Al alloys grain boundary precipitation pattern relationship to stress corrosion sensitivity 04 p0613 A71-15746

Microstructure effect on metastable beta Ti alloy strength, toughness, stress corrosion cracking susceptibility 04 p0614 A71-15780

Metal stress corrosion crack propagation rate relationship to electrochemical parameters, considering active and passive regions of potentials 05 p0827 A71-16814

High strength Al alloys stress corrosion resistance testing in various heat treatment conditions, using precracked cantilever beam specimens 06 p0912 A71-18012

Interferometric holography application to elastic stress and surface corrosion of two dimensional objects and metals, discussing stretching 07 p1107 A71-19209

Lattice defect and grain boundary influence on metal dissolution in electrolyte and stress corrosion cracking 07 p1134 A71-19604

High yield strength steel stress corrosion crack tip electrochemical and pH potential conditions, using AgCl reference electrode 07 p1137 A71-19973

Residual stress effects on Al alloys stress corrosion crack growth rates as function of plane strain stress intensity, discussing residual stress elimination methods 07 p1137 A71-19974

Ultrasound effects on Ti alloys Hg embrittlement and stress corrosion cracking by methanol-water-hydrochloric acid mixture 07 p1137 A71-19975

Methanol stress corrosion cracking of Ti-Al-V foil inhibited by pretreatment in aqueous solutions of electrolytes, discussing colloidal character of microcrystallites 07 p1142 A71-20362

Precracked double cantilever beam specimens, measuring resistance to stress corrosion crack propagation as function of overaging in Al alloys 07 p1142 A71-20363

Hydrogen embrittlement in hot salt stress corrosion of Ti alloy 07 p1142 A71-20372

Cold creep effect on stress corrosion testing of metals under uniaxial bending and constant strain 08 p1306 A71-21439

Al-Zn-Mg alloys stress corrosion, using electron transmission microscopy for microstructural investigation 09 p1472 A71-23125

Ti alloys in aircraft industry, considering jet engines applications and structural stability improvements related to fracture toughness, fatigue and stress corrosion 09 p1474 A71-23292

Stress corrosion failure prevention in susceptible Al alloys, considering metallurgical structure, environment and stress distribution 09 p1478 A71-23417

Stress corrosion crack extension in adhesive epoxy joints under combined long term static loads and aggressive action of water 10 p1632 A71-24090

Aluminum-epoxy joints stress corrosion cracking inhibition and crack tip plastic deformation by scanning electron microscopy 10 p1615 A71-24091

Metal plates and sheets stress corrosion cracking velocities, using torsion crack propagation specimen at constant load or deflection 10 p1627 A71-24474

Nondestructive testing method obtaining relaxation modulus and accelerated degradation/stress corrosion of reinforced plastics 11 p1768 A71-25404

Ti-Al-Mo-V alloy stress corrosion cracking, using controlled potential technique in aqueous and methanol environments with and without halogen ions 11 p1777 A71-25448

Computer simulation of stress corrosion cracking, considering electrochemical oxidation mechanism for crack propagation 11 p1847 A71-25449

Ti hot salt stress corrosion, considering effects of oxygen, air velocity, moisture, thermal cycling, fatigue and type of salt 11 p1781 A71-26261

Ti stress corrosion in organic liquids, considering intergranular and transgranular failure 11 p1781 A71-26262

Al alloys and steel, determining potential and pH changes during stress corrosion crack propagation by microelectrode technique 11 p1783 A71-26497

High strength Al alloy forgings processing for stress corrosion cracking prevention, including plane relocation and compressive relief techniques 13 p2073 A71-28146

Stress corrosion cracking, discussing stress effect, environmental and metallurgical factors and electrochemical and sorption theories 13 p2085 A71-28221

Ti-Al binary alloy embrittlement in sea water by notched cantilever beam stress corrosion test, investigating alpha 2 particle precipitation effect on cracking susceptibility 14 p2256 A71-29522

Heat treatment effects on high strength maraging steel tensile, fracture toughness and stress corrosion properties, discussing reversion to austenite 15 p2433 A71-32175

Stress corrosion fatigue crack growth in Ni-Cr-Mo maraging steel, using controlled-potential techniques, pH measurements and fractographic analysis 16 p2590 A71-32942

Tensile properties, plane strain fracture toughness and stress corrosion threshold of high strength precipitation hardening stainless steels 17 p2755 A71-34438

Solution chemistry at stress corrosion crack tips in Al alloys, considering factors affecting pH change with time of initially acidic NaCl solutions 17 p2755 A71-34439

Stress corrosion cracking in high strength steels, showing occurrence along zero isoclinic surfaces 17 p2755 A71-34440

Ti-Al alloys surface film growth and stress corrosion cracking as function of applied potential and environmental pH, presenting results of ellipsometric examination 17 p2756 A71-34489

Crevice effect at stress corrosion crack apex during cathodic polarization of Ti-Al-Mo-V alloy in sulfuric acid, potassium bromide and iodide and methanol solutions 17 p2761 A71-35733

Stress corrosion cracking in Ni maraging steel in NaCl solution, using electrochemical polarization and potential analysis 18 p2934 A71-35989

STRESS CYCLES

Nickel maraging steel in NaCl solution, investigating susceptibility to stress corrosion cracking 18 p2935 A71-36595

Salt solution treated and quenched Mg-Al alloy rods tests in distilled water, investigating transgranular stress corrosion cracking and deformation twinning 19 p3083 A71-38722

Stress corrosion crack branching in high strength steels, considering constant crack velocity and critical stress intensity 20 p3248 A71-38777

Corrosion resistant materials evaluation for suitability in high strength fasteners, considering mechanical properties, stress corrosion cracking and hydrogen embrittlement problems 20 p3251 A71-39340

Aging conditions effect on stress corrosion resistance in short transverse direction of thick sheet Al alloy, using immersion-emersion tests in air and saline solution 20 p3252 A71-39417

Preheating effects on crystal lattice orientation, tensile strength and stress corrosion cracking of Al-Zn-Mg alloy thick plates 22 p3559 A71-41516

Weldable Al-Zn-Mg alloys with cathodic polarization protection, noting decrease in stress corrosion crack propagation rate 22 p3560 A71-41625

Stress corrosion testing of Al alloy in NaCl bath under tensile stress, using Weibull distributions 22 p3560 A71-41627

Scanning electron microscopic observation of fracture surface of austenitic stainless steels for stress corrosion cracking in magnesium chloride and calcium chloride solution 23 p3693 A71-44073

Loading modes effect on stress corrosion cracking of Ni maraging steel in NaCl solution 23 p3693 A71-44074

STRESS CYCLES

Al alloys low cycle fatigue test under axial load, observing hardening behavior and structure by transmission electron microscopy 01 p0104 A71-11397

Reliability prediction for machine parts subjected to cyclic stresses, using statistical analysis of fatigue data for failure rate calculation 02 p0327 A71-12367

High stress cycles and impact fatigue behavior of common case hardened carburized gear steels under loading 03 p0441 A71-13253

Low strain cyclic hardening and softening in Al-Mg alloy, comparing measurements by monitoring and tensile testing methods 03 p0444 A71-14315

Cu-Al alloy, Ti and low carbon steel under LF flexural stress, testing parameters effect on fatigue resistance 03 p0445 A71-14339

Lubricant and ball steel effects on fatigue life / pit formation after repeated stress cycles/ [ASME PAPER 70-LUB-16] 07 p1118 A71-19507

Cyclic stress-strain behavior prediction by mathematical model and computer simulation, applying to Al alloy fatigue 07 p1216 A71-20204

Plastic strains buildup during thermal cycling, establishing relation between strain interval and cycles number to failure for strain hardening materials 09 p1538 A71-22599

Hot strain cycle recording in single and multipass welds for C-Mn steel using welding simulation, surface pressed plug and microscopic techniques 09 p1459 A71-23455

Strain hardening and grain size effects on early fatigue damage of polycrystalline metal under fluctuating stress, using micromechanics theory 10 p1685 A71-23933

Steel sheet specimens under temperature and stress cycles, studying creep, plastic deformation and service life 10 p1686 A71-24189

High temperature fatigue test assembly for symmetric tension compression cycles at 10 kHz 10 p1589 A71-24201

Linear elastic fracture mechanics in presence of notch stress concentration, considering crack formation and propagation under cyclic stresses 10 p1628 A71-24686

Stress cycling effect on creep deformation rate, using recovery creep model [ASME PAPER 71-MET-F] 12 p1977 A71-27315

Polycrystalline Nb cyclic yield point behavior under strain softening and hardening, noting stable hysteresis loop 13 p2087 A71-29123

Soviet book on structural bearing capacity under thermal cycling conditions covering rotating disks, plates and shells calculations 15 p2505 A71-32002

Combined mechanical and cyclic thermal stresses effect on plastic deformation buildup in EI435 alloy preceding breakdown 15 p2433 A71-32236

Surface deformation in polycrystalline Al samples produced by ultrasound generated cyclic stresses, examining slip bands formation by electron microscope 16 p2591 A71-33224

Flight mission severity in cumulative damage flow cycle fatigue and creep stress rupture/ not detected by usual nondestructive testing in aircraft gas turbine industry 16 p2624 A71-33298

Flexural-torsional fatigue fracture of duraluminum, noting dependence on cyclic stress, frequency and medium 16 p2593 A71-33689

Small elastoplastic cyclic strain effects on internal friction and energy dissipation in metals during vibrations 16 p2598 A71-33983

Metal structure, crack nucleation and propagation during fatigue under cyclic stress 18 p2936 A71-36693

Stochastic character of metal fatigue fracture and fatigue life dependence on stress cycle amplitude, using equiprobability curves 18 p2936 A71-36694

Dislocation structures in austenitic steel fatigued at various stress cycles and tensioned at various strains, using transmission electron microscopy 21 p3400 A71-40833

Surface strain cyclic flow growth rates for Al and Ti plates, using end point, flaw opening and striation measurements 22 p3560 A71-41643

Load stress pulse shape and frequency effects on macroscopic dislocations during plastic deformation of crystalline materials 23 p3777 A71-43875

STRESS DISTRIBUTION U STRESS CONCENTRATION STRESS FUNCTIONS

Stress potential for theory of adiabatic reversible processes in nonlinear viscoelastic material undergoing small deformations 01 p0169 A71-10493

Variant function describing long term fatigue strength under complex loads in determining given material damage point during breakdown 01 p0169 A71-10494

Diffusion with convection in flow between parallel walls, using Von Mises transformation 02 p0332 A71-12410

Displacement type equilibrium equations for small deformation imposed on initial finite deformation, estimating elastic energy function based on strong ellipticity condition 03 p0510 A71-13945

Stress-strain function for metal fatigue including mean stress effect 04 p0610 A71-14890

Moment loads and stress functions of orthotropic laminar shells with low shear rigidity 05 p0822 A71-16371

Algorithm for stress functions in elastic region, using variational difference method 05 p0827 A71-16759

Single edge notch tension Al alloy specimens mechanical compliance measurement, solving stress functions for various gage length-sample width combinations 07 p1110 A71-19469

Mechanical properties at different temperatures and allowable design stress for aluminum alloy 07 p1137 A71-19966

Strain continuity equations in statics using equivalent integrodifferential form 07 p1218 A71-20465

Stress equations for thin pyrolytic graphite shells with thermal allowance 09 p1534 A71-22095

Laminated orthotropic plates under transverse loading, developing Navier type solution for Stavsky generalized stress function equation 09 p1534 A71-22101

Flexible elastoplastic shallow shell theory, using mixed variational principle for flexure velocity and stress function 09 p1535 A71-22179

Variational principle for continua dynamic analysis by hybrid finite element method, considering consistent inertia properties of elements obtainable from assumed stress functions 10 p1692 A71-25047

Elastic stress-strain law and internal structure symmetry for three dimensional fibrous composites, including caltrop reinforcement 11 p1852 A71-26396

Minimum volume design of sandwich axisymmetric plates obeying Mises criterion, using calculus of variations 13 p2146 A71-27782

Morera and Maxwell stress functions determination by integrodifferential equations of deformation continuity for bending of thin plates 13 p2148 A71-27791

Stress effects on superconductivity and dislocation cell structure in deformed niobium for compression and tension 13 p2090 A71-29416

Stress intensity factors for deep cracks in single edge cracked bend and compact tension specimens 14 p2322 A71-29739

Shear deformations effect on circular plates from Reissner theory, expressing bending moments and shear forces as functions of lateral deflection and stress function 15 p2507 A71-32112

Linearized shell theory, proposing improvement of Marguerre-Vlasov shallow shell equations in terms of invariant displacement and stress functions 16 p2649 A71-33000

Yield surface approximations for thin shell made of material obeying von Mises yield criterion, considering transverse shear effect 16 p2661 A71-34118

Conical shell with circular hole, determining stress function and normal deflection in torsion 17 p2817 A71-34338

German monograph on corner singularities in oblique plates calculation with aid of displacement and stress functions, covering bending theory 17 p2823 A71-34796

Elastic lattice shells linear theory, deriving stress functions and equations from static-geometric analogy 17 p2831 A71-35396

Algorithm for stress functions in elastic region, using variational difference method based on differentiation of strain energy 17 p2832 A71-35458

Abbreviated testing for material constants determination of equation of fatigue crack propagation from one specimen at different stress amplitudes 18 p2976 A71-35988

Harmonic stress function and stress intensity factor for elliptical crack embedded in elastic solid and subjected to arbitrary internal pressure 20 p3307 A71-38782

Morera and Maxwell stress functions determination by integrodifferential equations of deformation continuity for bending of thin plates 21 p3455 A71-40085

STRESS MEASUREMENT

Ferritic steel with 17 percent Cr, examining dynamic behavior under high speed tension test regarding heterogeneity of plastic deformation, stress peak, etc 01 p0105 A71-11616

Superficial residual stresses measurement in plastic region by Hertzian hardness method, considering indentation by ball and proportionality to load variations 02 p0328 A71-12535

Solid propellants stress measurement using piezoresistive transducer 03 p0501 A71-13172

Thermal cycle stresses at interface of composite glass tape-epoxy casting resin cylinder, using strain gages 03 p0508 A71-13763

Thin web shear test device demonstrated on aluminum foil and glass fiber composites 03 p0508 A71-13765

Recovery rate measurement during creep test by stress drop method 03 p0444 A71-14316

Welded joints triaxial residual stress measurement by scanner 03 p0433 A71-14587

Shock pulse measurements for detecting damage to ball and roller bearings due to fatigue 04 p0604 A71-15673

Principal stresses separation method combining conventional isoclinic parameter and isochromatic fringe order measurements and scattered light method 05 p0822 A71-16373

Elastic plate with heat conducting rectilinear crack, determining steady state temperature field and stresses 05 p0827 A71-16889

Embedded electrical resistance strain gages for three dimensional stress measurement, describing modifications for internal stresses reduction 05 p0830 A71-17242

Residual stress measurement in Hastelloy N gas tungsten arc welds by Sachs boring-out method, permitting stress distribution determination over short distance increments 06 p0912 A71-18043

HF dynamic elastic deformation observation and measurement, including photoelastic method for transient phenomena 06 p1003 A71-18422

Strain field measurement near crack tip in polymethyl methacrylate by holographic interferometry 07 p1209 A71-19043

- Dynamic stress measurement of cantilever beams, frame structures and rings under impulsive loads
07 p1210 A71-19046
- Jet engine rotor strain and temperature data transmission, examining special purpose telemeter design
07 p1062 A71-19628
- Laser thermally generated stress waves measurement errors by comparison with time response predicted from strain theory
07 p1214 A71-19912
- Amplitude dependence of Young modulus defect in metals during large stress HF oscillations
08 p1369 A71-21121
- Luders bands motion in steel and iron, studying plastic zone velocity dependence on stress, composition, grain size, dislocation substructure and temperature
08 p1308 A71-21517
- Nomograms for normal stresses and bending moments in thin circular cylindrical shell under uniformly distributed local load
08 p1374 A71-22054
- Stress profiles measurement in opaque tempered glass and ion exchanged glass-ceramic flat plates from length change during etching
09 p1480 A71-22115
- Mechanical stress amplitude measurement in optically transparent materials during HF vibrations, using polarization method
09 p1535 A71-22188
- Nomograms for thermoelastic stress in plate determined as function of dimensions and heat transfer
09 p1538 A71-22605
- Film thickness effects on stress magnitude in surface layers of bodies under external friction
09 p1455 A71-23078
- Thin cracked steel plate strip necking zone relative opening displacement and strain measurements by moire method
09 p1542 A71-23540
- Stress and structure effects on creep rate of two austenitic steels in quenched state, considering decorated stacking faults
09 p1479 A71-23624
- Weather stress tests for determining optimum adhesive system for bonding reinforced fiberglass panels to Al extrusions held by steel beams
10 p1616 A71-24114
- Direct optical measurements of strains, using spatially coherent light with moire technique
10 p1611 A71-24280
- Cylindrical Duralloy shells critical strain measurement in axial compression under creep conditions
10 p1690 A71-24575
- Nonstationary stress modeling in aircraft structures using random pulse generator applied to jet landing gear break strut fatigue test
10 p1692 A71-24954
- Surface strain measurements in turbine blades by time average holographic interferometry, reviewing resonant modes and holographic fringe patterns [ASME PAPER 71-GT-84]
11 p1762 A71-25992
- Annealed and cold-worked polycrystalline Fe specimens steady state cyclic stress-strain curves and thin films observation by electron microscopy
11 p1780 A71-26024
- Weissenberg rheogoniometer modifications, providing upper cone motion elimination, unsteady/steady state measurements in constant stress field and amplitude/frequency variations
11 p1763 A71-26058
- Temperature dependence of flow stress of cold worked heavily deformed doped W
11 p1781 A71-26296
- Al and Al-Mg alloys average interdislocation internal stress measurement during steady state creep
12 p1916 A71-26895
- Nondestructive magnetic method for measuring longitudinal residual stress in outer portions of ferromagnetic cylindrical bars
12 p1974 A71-26948
- Residual stress at plate crack determined from elastic stress intensity factor measurements [ASME PAPER 71-MET-A]
12 p1977 A71-27311
- Fiber composites monofilament and strand tests, considering fracture, fatigue, stress, corrosion and microstructure
12 p1921 A71-27635
- Strain gage method for residual stress determination in thin walled brass cylindrical shells produced by deep drawing
13 p2066 A71-28034
- Single fiber reinforced plate initial stress distribution due to linear expansion coefficients difference between matrix and fiber, using optical polarization
13 p2091 A71-28126
- Particle-metal matrix interface strength of dispersion strengthened Ni alloys, developing direct tensile stress measurement method
13 p2089 A71-29408
- Soviet book on stress analysis by optical polarization methods covering theory and practical applications to machine parts and structural components
14 p2321 A71-29528
- Static strain measurements on Ti specimen subjected to different conductive heating rates, testing various gages
14 p2239 A71-29833
- Principal axial stresses determination from bonded wire resistance strain gages with known cross sensitivities, deriving expressions from concentric Mohr circles
14 p2239 A71-29834
- Vibrating cantilever beam dynamic stress photoelastic determination based on photomechanics and optic-stress laws
14 p2324 A71-29850
- Stress-strain measurements in inelastic elements by photoelastic, laser, memory, load and plane deformation methods, considering plate with circular hole
14 p2333 A71-30894
- Stresses and deformations of shallow spherical shells with specified edge displacements
15 p2502 A71-31186
- In-plane strain measurement by three beam holography using two incident wave fronts
15 p2404 A71-31267
- Optical methods for measuring mechanical strain by observing shift and deformation of elemental surface areas, using holographic techniques
15 p2404 A71-31269
- Bridge circuit for minimizing parasitic electrical disturbances in resistance strain gage measurements of dynamic stresses in impact tests
15 p2408 A71-31865
- Thermoelastic stress generation in Cu and Ta samples by linear accelerator produced monoenergetic MeV electron pulses, comparing measurements with wave theory predictions
15 p2414 A71-31973
- Residual stress determination from stress intensity factor measurements, describing application to electron beam welded aluminum plate
15 p2508 A71-32259
- Short length strain interferometric measurement from interference patterns of laser light diffracted from adjacent small reflecting surfaces
16 p2576 A71-32864
- Constant load tensile creep tests on polycrystalline ceramics, determining high density alumina applied stress and strain rate
16 p2553 A71-33384
- Residual stress measurement in thin contoured Ti alloy sheets by X ray diffraction, using stress camera in normal incident beam mode
17 p2757 A71-34537
- High temperature stress measurements with electric resistance strain gages, describing test apparatus for gages evaluation
17 p2738 A71-34553
- Anisotropic laminated cylinders under combined axial load, torsion and internal pressure, calculating stresses with Vlasov-Ambartsumyan shell theory
17 p2823 A71-34811
- Holography as nondestructive testing tool, considering application in vibration analysis, stress/strain measurement, bond inspection, internal flaw detection and displacement measurement [SME PAPER IQ-71-121]
18 p2927 A71-36657
- Large deformation stress and mechanical resistance of thin glass circular plates by bending test involving concentric rings
18 p2940 A71-36697
- Turbulent pipe flow dissipation rate, presenting turbulence energy diffusion and stress components spectral distribution measurements
19 p3045 A71-38201
- Stress determination by vibration measurement in cantilever specimens fatigue tests with audio frequency loading, taking into account end restraint elasticity
19 p3160 A71-38347
- Real time mechanical strain measurement by optical correlation techniques, using coded matched-filter hologram and incoherent illumination
21 p3377 A71-40229
- Electromagnetic stress gage for wave propagation study in nonconducting materials, discussing calibration, design and accuracy
21 p3379 A71-40793
- Macroscopic residual stress and strain measurement and crack tip substructure, discussing crystal plastic deformation effect on fatigue crack propagation
21 p3466 A71-40831
- Photoimpact strain measurement errors in tensile tests due to deformation dynamics and quantization in time reduced by scanning along Archimedes spiral
21 p3473 A71-41157
- Epoxy resin plate mechanical stress measurement under impact load, using laser light source three beam interferometric assembly with photographic recorder
22 p3555 A71-41613
- Anisotropic glass fiber plastic material stress, strain and crack formation threshold measurements under long term static and cyclic axial loads
23 p3696 A71-43424
- Stereophotogrammetric measurements of displacements and strains in Al membrane during explosive forming
24 p3825 A71-44755
- STRESS PROPAGATION**
- Cylindrical shells axisymmetric nonlinear strain discontinuities propagation, using Timoshenko equations
03 p0515 A71-14380
- High amplitude stress wave propagation in anisotropic quartz-phenolic composite, noting strong pulse amplitude attenuation [AIAA PAPER 71-179]
06 p1004 A71-18618
- Fracture location in brittle solids, using stress wave propagation in slender rod
09 p1538 A71-22699
- Ultrasonic wave propagation in deformed isotropic elastic materials based on second order theory, examining principal stress axis rotation effect
11 p1849 A71-25682
- Unloading boundary in longitudinal elastic-plastic stress wave propagation, describing response in seminfinites rods [ASME PAPER 71-APM-15]
16 p2655 A71-33212
- Weak discontinuity unloading wave propagation in seminfinites slender prismatic bar of elastoplastic material
16 p2656 A71-33356
- Normal stress discontinuity propagation over expanding circular region below free surface of seminfinites isotropic elastic media
17 p2815 A71-34179
- Elastic stress waves propagation in photoelastic layered composite materials, indicating wave front steady state
17 p2824 A71-34816
- Stress wave propagation in quartz-phenolic composite, measuring particle velocity by velocity interferometer
17 p2762 A71-35207
- Two dimensional cylindrical stress propagation over viscoelastoplastic body arbitrary cylindrical surface under instantaneous compression load, using finite difference method
22 p3613 A71-41564
- Duralumin rods deformation and stress propagation study under dynamic pulse loads, using photosensitive epoxy coatings and high speed photography
22 p3537 A71-41612
- Numerical analysis for flexural stress pulse propagation in nonuniform elastic bars by geometric acoustics
22 p3616 A71-42213
- STRESS RATIO**
- True-torsional stress at plastic strain onset determination in terms of elasticity theory
09 p1536 A71-22323
- STRESS RELAXATION**
- Linear isotropic viscoelastic media, determining stress relaxation and creep properties
01 p0170 A71-10640
- Crack propagation as unstable stress relaxation process, using viscoelastic dislocation model
06 p0984 A71-17557
- Stress relaxation characteristics obtained by compensation principle, force measuring techniques and sample unloading for stress-strain state determination
07 p1210 A71-19160
- Cyclic creep and relaxation of heat resistant alloys at high temperatures, showing inapplicability of static load conditions
07 p1142 A71-20480
- Stress reduction in metal powders compaction at different temperatures and deformation rates
08 p1305 A71-21059
- Self consistent stress relaxation testing, discussing strain rate sensitivity and stress-strain relations
08 p1308 A71-21519
- Isotropic incompressible viscoelastic solid deformation field under uniaxial and equal biaxial relaxation, determining constitutive equation
09 p1534 A71-22142
- Relaxation analysis of strain range, hold time and cycle number in low cycle fatigue testing of annealed stainless steel at 1200 F [ASM PAPER W71-24.1]
09 p1471 A71-23093
- Compression, creep, stress relaxation and overloading effects on delay in fatigue crack growth and structural life predictions
10 p1694 A71-25059
- Mg-Al eutectic alloy and commercial-purity Zr stress relaxation tests and mechanical behavior
11 p1780 A71-26022
- All-beta Ti alloy Ti-V-Cr-Al, testing dynamic behavior of strain aging during stress relaxation period
11 p1780 A71-26026
- Viking rocket heat shield material mechanical properties, examining time-temperature superposition with continuous stress relaxation data measured in vacuum
11 p1791 A71-26518
- Heat resistant alloys strengthened elements, studying high temperatures prolonged exposure effects on surface layers strengthening and residual stresses relaxation
12 p1919 A71-27780
- Cylindrical shell under internal pressure, detailing axial thermal stresses relaxation
15 p2505 A71-31861

- Ring and cylindrical structures comparative stress relaxation at room temperature 15 p2508 A71-32229
- Stress relaxation in rings and rods, discussing errors in data correlation 15 p2508 A71-32230
- Stress relaxation method using compliance measurement of bolted test assembly to determine initial and residual loads after exposure periods 15 p2436 A71-32505
- Heat treatment effectiveness in reducing residual stress from stress relaxation data analysis 15 p2436 A71-32506
- Stress relaxation as source of dimensional instability in precision devices, discussing thermal cycling role in residual stress relief 15 p2436 A71-32507
- Shock produced stress relaxation in thin walled Al tubes, comparing strain-time profiles with thin shell theory 16 p2647 A71-32923
- Saint Venant principle generalization for transient creep and stress relaxation analysis in rectilinear thin walled multiply connected beam under torsion 17 p2833 A71-35612
- Stress relaxation characteristics obtained by compensation principle, force measuring techniques and sample unloading for stress-strain state determination 17 p2834 A71-35656
- Rheological media viscoelastic relaxation theories generalization taking into account thermal stress and conduction 18 p2984 A71-37021
- Stress relaxation in laminated Ti sheet at ambient temperature after vacuum tempering at 800 C, interpreting logarithmic time dependence by activated thermal sliding theory 21 p3399 A71-40527
- High temperatures prolonged exposure effects on surface layers hardening and residual stresses relaxation in heat resistant alloys 21 p3403 A71-41105
- Testing machine stiffness determination during strain rate variation and stress relaxation tests for metallic and nonmetallic engineering materials plastic properties assessment 22 p3559 A71-41589
- Temperature stresses relaxation in transversely isotropic viscoelastic sphere calculated numerically for 500 and 100 hour periods 22 p3616 A71-42486
- Increased microplastic deformation resistance, relaxation stability and aging of beryllium by cyclic heat treatment 23 p3690 A71-43281
- Computer programs based on least squares numerical analysis for complex internal friction spectra due to Snoek and grain boundary relaxation 23 p3648 A71-43927
- Stress relaxation equation for arbitrary initial tensile stresses and pliabilitys applied to machine element design 23 p3778 A71-44044
- Thermal stresses relaxation and distribution in infinite anisotropic viscoelastic cylinder 24 p3884 A71-45002

STRESS RELIEVING

- Aircraft structure fatigue life improvement via material stress coining inside and around holes and slots 01 p0085 A71-10170
- Large Al forgings machining cost reduction via stress relief involving mechanical working following quench 01 p0091 A71-11547
- Nb-sheathed insulators of three coaxial cylinders with ceramic bonding for thermionic converter, discussing pressure bonding techniques and stress relieving properties 02 p0232 A71-12248
- Transverse strains in solid body due to volumetric stresses counteraction to external load stresses 10 p1687 A71-24198
- Stress relief cracking in Cr-Mo steel, considering correlation with embrittlement of water quenched base metal tempered at low temperature 13 p2086 A71-29091
- X ray interference lines widening in Al-Mo alloy foil obtained from melt by rapid cooling attributed to stress relieving 14 p2258 A71-30008
- Stress relaxation as source of dimensional instability in precision devices, discussing thermal cycling role in residual stress relief 15 p2436 A71-32507
- Optimum heat treatment for welds, investigating residual stress relief with higher harmonics method 15 p2417 A71-32664

STRESS RUPTURE STRENGTH

U CREEP RUPTURE STRENGTH

STRESS TENSORS

- Continuum internal thermodynamic constraints effect on materials response, assuming workless stress tensor 03 p0506 A71-13694

Plane nonhomogeneous strain fields deformation tensor determination by moire equations for fringe pitch and angle measurement, considering rectangular block bending 03 p0508 A71-13772

Stationarity of complementary energy in nonlinear elasticity theory, using Piola stress tensor representation for isotropic elastic media 03 p0513 A71-14228

Isotropy postulate experimental verification in case of complex loading involving strain tensor axes turning 06 p0983 A71-17363

Elastic medium residual microstresses probability distribution, noting microdistortion tensor linear and transverse components and tangential and normal stresses relation 06 p1002 A71-18417

Anisotropic materials strength criterion, developing theory from scalar function of two stress tensors 07 p1216 A71-20131

Tensor elasticity relations in linear theory of thin elastic shells in Kirchhoff-Love range 08 p1373 A71-21868

Arbitrary midsurface geometry thin shells nonlinear equations in terms of finite rotation vector and stress resultant tensor component 10 p1684 A71-23761

Linear elastokinetics tensorial field integral representation derivation from reciprocal dynamic theorem for equations of motion 10 p1687 A71-24350

Equilibrium thermodynamics of ideal elastic solids under stress, using Cauchy stress tensor 11 p1799 A71-25740

Isotropic and anisotropic materials stability criteria and boundary surfaces in invariant stress tensor spaces 13 p2149 A71-28120

Stress tensor components partial differential equations solution by method of characteristics, using isochromatic fringes 14 p2328 A71-30377

Structural instability due to cyclic strain accumulation, using plastic deformation constitutive relation with stress tensor and elastic effects 16 p2650 A71-33016

Energy momentum stress tensors for harmonic oscillator model, calculating energetic interaction with plane gravitational wave of same frequency 18 p2946 A71-35982

G structure tensors integrability and fiber extensions, using differential geometry 18 p2976 A71-36097

Two dimensional stress tensor invariants for finite elastic deformations of thin plate using initial complex coordinates 19 p3156 A71-37541

Tensor elasticity relations in linear theory of thin elastic shells in Kirchhoff-Love range 20 p3308 A71-39367

Soviet book on mathematical plasticity theory covering stress/strain flow and deformation, stress/strain tensors statistical averaging methods and hardening conditions 21 p3473 A71-41370

Generalized tensorial equation of motion for stresses in linear elastodynamics, proving limit existence in Sobolev functional space 22 p3614 A71-41607

Stress-strain state of nonlinearly elastic reinforced polymer plate with circular hole, deriving stress tensor components and first approximation solution for pure bending 24 p3882 A71-44838

Microinhomogeneous elastic media with moduli as coordinate random function, investigating stress and strain tensors 24 p3849 A71-45345

STRESS WAVES

Uniaxial strain waves propagation across nonlinear strain hardening slab, deriving expressions for stress, strain, particle velocity and shock path 01 p0175 A71-11013

Photoelastic study of stress wave propagation in composites under fiber matrix strip directed impulsive loading with exploding wire [SESA PAPER 1708] 03 p0507 A71-13758

Exploding wires in photoelastic specimens, examining axially symmetric cylindrical stress wave front with high speed photographs [SESA PAPER 1656] 03 p0459 A71-13769

Mathematical stress wave model for sandwich plates under high velocity impact, considering structural multiple reflections and various material combinations [SESA PAPER 1653] 03 p0508 A71-13774

Circular plates strain wave analysis by Laplace transform method, using MacDonald functions approximation 03 p0515 A71-14383

Fracture of bumper protected fuel tanks subjected to hypervelocity meteoroid impact, applying method of characteristics to stress wave propagation in tank walls [AIAA PAPER 69-369] 03 p0500 A71-14431

Steel brittle fracture tests using explosive charge stress wave absorption measurements 03 p0517 A71-14583

Stress wave scattering in fiber reinforced composite material, using model of parallel elastic cylinders embedded in unbounded elastic medium 05 p0826 A71-16719

Cylindrical structure longitudinal stress wave propagation characteristics, analyzing wave induced structural instability and destruction process 06 p0991 A71-17804

Vibration and wave analysis in dynamic deformation of elastic shells and plates with environmental allowance 06 p1000 A71-17870

Stress wave propagation from spherical cavity in isotropic nonhomogeneous elastic medium in contact with vacuum at infinity, obtaining closed form solution 06 p1001 A71-18250

Photoelastic fringe patterns in double exposure holography interferometric technique for stress wave analysis 07 p1209 A71-19044

Laser thermally generated stress waves measurement errors by comparison with time response predicted from strain theory 07 p1214 A71-19912

Stress wave emission from subcritical crack growth in thin walled Al-V titanium alloy 07 p1137 A71-199676

Stress wave propagation in plates from explosive loading, discussing wave front interaction and scarf formation 07 p1215 A71-200919

Stress waves in elastic spherical shell due to external pressure pulse, approximating near field by saddle point technique 07 p1215 A71-200977

Geometric dispersion of dilatational stress waves propagating in laminated plate composite, comparing transmitted wave forms to code calculations 09 p1538 A71-22687

High strength steel fracture toughness, investigating stress wave emission during crack growth 10 p1627 A71-24534

Transient stresses in heat shield generated by short duration pressure pulses, using method of characteristics for interface stresses [AIAA PAPER 71-351] 11 p1844 A71-25330

Ultrasonic wave propagation in deformed isotropic elastic materials based on second order theory, examining principal stress axis rotation effect 11 p1849 A71-25682

Viscous model for stress wave propagation perpendicular to plates of bilaminate composite material 11 p1851 A71-26381

Impulsive energy deposition generated stress waves in composite media formed by two plane layers with interfacial molecular bond joining 12 p1983 A71-27575

Plane longitudinal stress waves propagation in plane-parallel viscoelastic partition of finite thickness dividing two linear half spaces with different elastic properties 13 p2155 A71-28655

Dynamic damping of plane one dimensional unsteady stress wave passing through viscoelastic layer separating linearly elastic half spaces 13 p2155 A71-28848

Thermomechanical damage by pulsed lasers in metals, discussing energy deposition and stress wave generation for optimal fracture conditions 15 p2422 A71-32555

Periodically laminated elastic half plane response to rapid internal heating, obtaining far field composite stress waves variation due to dispersion [ASME PAPER 71-APM-28] 16 p2663 A71-33201

Ultrasonic pulse technique for plane transverse and longitudinal stress wave dispersion in boron fiber reinforced epoxy composite, determining group velocity dependence on frequency and elastic moduli [ASME PAPER 71-APM-27] 16 p2600 A71-33202

Unloading boundary in longitudinal elastic-plastic stress wave propagation, describing response in semiinfinite rods [ASME PAPER 71-APM-15] 16 p2655 A71-33212

Isotropic elastic circular cylinders longitudinal stress waves, presenting dispersion relation /Pochhammer equation/ numerical solutions 16 p2658 A71-33625

Dynamical thermal expansion effect on plane elastic-plastic stress wave propagation, using classical heat conduction equation 17 p2819 A71-34507

Dynamic polariscope for birefringent materials stress wave low cost analysis 18 p2923 A71-36611

Stress wave interaction with macrocrack in elastoplastic and quasi-brittle materials, measuring stress field by optical polarization method and motion picture photography 19 p3154 A71-37086

Elastic-plastic stress wave attenuation, applying theory of wave propagation in single crystals to flow field numerical solution

21 p3465 A71-40786

Shock stress waves dispersion in laminated composite materials

21 p3465 A71-40790

Pulse attenuation in composite materials, discussing stress waves geometric dispersion and compressive fracturing effects

21 p3465 A71-40791

Dynamic photoelasticity for stress wave propagation in anisotropic fiber reinforced composites, using birefringent models and pulsed ruby laser beam

21 p3471 A71-41027

Stress wave propagation in rod consisting of viscoelastic finite and semiinfinite elastic parts during pulsed sinusoidal load at end

24 p3885 A71-45223

Aerospace materials and structures shock sensitivity from derivation of dynamic fracture propagation relationship to stress wave

24 p3886 A71-45370

STRESS-STRAIN DIAGRAMS

Metal fatigue relationship to cyclic plastic deformation resistance, considering fracture behavior, stress-strain curve, hardening and ductility

01 p0098 A71-10162

Isotropic nonlinearly elastic plate weakened by doubly periodic reinforced curvilinear holes, calculating stress-strain state by Cauchy integrals

01 p0168 A71-10412

Stress-strain relations at plane multiply broken strain trajectories, using local definiteness hypothesis

01 p0171 A71-10653

Shallow shells of revolution of strain-hardening material, deriving stress strain state by rigid plastic body model

01 p0175 A71-11039

Elastic thin walled shells of variable thickness with zero Gaussian curvature, deriving stress strain state with allowance for elastoplasticity

01 p0176 A71-11041

Composite beam of three thin plates reinforced by thin electric ribs, calculating stress strain state by Fourier transforms

01 p0176 A71-11044

Three-layer spherical shell, determining filler effects on stress-strain state at circular hole

01 p0176 A71-11047

Numerical stress-strain calculation for design of high pressure fiberglass-reinforced plastic balloons

01 p0176 A71-11048

German monograph on stress strain state calculation in strengthening material disks

01 p0176 A71-11221

Discontinuous yielding in annealed Al alloy resulting from negative slope in flow stress- strain rate relationship, discussing impurities diffusion role

01 p0105 A71-11606

Stress-strain state variability associated with optimal local heating of shallow shells of revolution

02 p0322 A71-11727

Simple variable loading and unloading in theory of small elastoplastic deformation under nonuniform heating for residual stress-strain determination

02 p0323 A71-11739

Creep effect on cooled blades elastoplastic stress-strain relationship using computer programs

02 p0323 A71-11741

Turbine disks under unsteady and cyclic loads and temperature variations, determining stress and strain by flow theory computer calculation

02 p0323 A71-11745

Turbine disks cyclic nonisothermal deformation with allowance for Bauschinger effect, determining stress-strain state and residual microstresses

02 p0323 A71-11747

Metal fatigue research, examining crack initiation and propagation mechanism, stress-strain relationship and statistical nature

02 p0325 A71-12074

Internal friction measurement under hydrostatic pressure, describing apparatus to determine phase angle between stress and strain

02 p0255 A71-12132

Boundary value problems solution in elasticity theory of isotropic homogeneous body configurations close to ellipsoid of revolution, obtaining stress-strain state by approximate method

02 p0325 A71-12285

Stress-strain state of thin circular plate with variable thickness along circumference under bending due to uniformly distributed load, using small p

02 p0326 A71-12289

Nonlinear quadratic elasticity theory of isotropic tube and hollow sphere under small linear deformations, obtaining stress-strain relation

02 p0326 A71-12294

Thin reinforced viscoelastic isotropic multiconnected plate stress-strain state under bending due to concentrated loads and distributed normal forces

02 p0329 A71-12668

Nb alloys hardening due to interstitial atoms interactions with dislocations, obtaining stress- strain relationship for various impurities, precipitates, strain rates and temperature

02 p0270 A71-12929

Structural design for component low cycle fatigue resistance, emphasizing material cyclic stress- strain behavior

03 p0501 A71-13252

Stress-strain state of plate made from highly elastic polymer containing circular and elliptical holes

03 p0506 A71-13602

Isotropic half plane weakened by circular holes normal to boundary, calculating stress-strain state created by concentrated force

03 p0506 A71-13604

Notched tensile plate steel specimens, investigating temperature and stress state effects on nil ductility transition and fracture strength

[SESA PAPER 1735] 03 p0443 A71-13752

Streak interferometry providing single impact test data for calculating dynamic stress-strain curve

[SESA PAPER 1717] 03 p0509 A71-13777

Piecewise linear elastic material three dimensional stress-strain analysis for limiting surfaces between regions with different moduli

03 p0451 A71-13901

Photoelasticity application for stress-strain state determination around holes made by electron beam, using epoxy models for internal stress distribution

03 p0429 A71-14272

Plastic zone near crack end under forces causing plane deformation, calculating stress-strain state by finite element method

03 p0515 A71-14363

Stress-strain function for metal fatigue including mean stress effect

04 p0610 A71-14890

Annealed Al bars mechanical properties and stress-strain curves dependence on strain rates under loading

05 p0766 A71-16390

Complex modulus of elasticity relation to viscoelastic cantilever beams stress or strain under forced vibration, considering fiber reinforced plastics

05 p0826 A71-16738

Thick plate with circular holes of various sizes, studying stress-strain state

05 p0828 A71-16890

Stress-strain state in elasticity theory of three layer symmetrical plate

05 p0828 A71-16986

Body weakening due to symmetrically expanding crack, discussing internal pressure, elastic equilibrium and stress-strain state

06 p0896 A71-17326

Soviet book on short time creep for designing structural and machine parts operating at high temperatures, analyzing stress-strain state

06 p0983 A71-17432

Composite hollow cylinders of heteromodulus materials, discussing stress-strain state

06 p0984 A71-17650

Boundary conditions of line of symmetry and antisymmetry types for stress-strain state of halved shells

06 p0984 A71-17666

Stress-strain state of isotropic three-layer plates and shells with rigid and light weight fillers, noting weakening by curvilinear holes

06 p0987 A71-17769

Plates and shells under concentrated loads, determining stress-strain state

06 p0988 A71-17773

Multilayer conical and spherical shells of revolution axisymmetric elastic deformation, deriving stress-strain state equations with allowance for transverse shear

06 p0990 A71-17795

Elastic spherical shell three dimensional stress-strain state asymptotic behavior near concentrated force as function of parameter characterizing relative thickness and curvature

06 p0995 A71-17830

Stress-strain state of shallow shells under concentrated heat load, obtaining asymptotic expressions for various parameters

06 p0997 A71-17845

Anisotropic tubular Ti alloy samples, noting yield strength and crystal structure dependence on stress-strain state

06 p0912 A71-17937

Triple integral equations solution based on analytic functions theory, applying to stress- strain state in plate with two equal collinear cracks

06 p1002 A71-18346

Stress-strain state of three-layer polymer plate having different thicknesses, Poisson coefficients and creep functions

06 p1005 A71-18707

Sheet blanks shaping into conical products by rolling, discussing stress-strain state in blank and time dependent rolling process

06 p0906 A71-18711

Stress-strain state of large inhomogeneous bodies of revolution, considering deformation due to arbitrary surface and mass forces in temperature field

07 p1210 A71-19158

Stress relaxation characteristics obtained by compensation principle, force measuring techniques and sample unloading for stress-strain state determination

07 p1210 A71-19160

Ring structure with nonlinear stress-strain law and linear strain-displacement relationship, deriving dynamic response to impulse

07 p1213 A71-19904

Cyclic stress-strain behavior prediction by mathematical model and computer simulation, applying to Al alloy fatigue

07 p1216 A71-20204

Stress-strain state of rectangular transversely isotropic plate with clamped edge under uniformly distributed load, considering bending moments

07 p1218 A71-20473

Electronic recording of cyclic strain diagrams of metals in wide loading frequency range using dynamic hysteresis method

07 p1218 A71-20485

Hydrostatic pressure effects on Al polycrystals stress-strain behavior at room temperature, using magnetostrictive load cell

07 p1143 A71-20490

Hardened plasticity zone around circular hole in creep deformed plate under normal forces, determining stress-strain relation and time dependent variations

07 p1219 A71-20647

Physically nonlinear bodies of revolution, investigating stress-strain state by small parameter and perturbation methods

07 p1219 A71-20650

Stress-strain state of anisotropic circular cylindrical shell with constant thickness, using stepwise linear approximation technique for solving mixed system of partial differential equations

08 p1368 A71-20789

Cylindrical shells with arbitrary cross sectional contour, thickness and longitudinal stiffener spacing under tension or compression, presenting computer algorithm for determining stress-strain state

08 p1368 A71-20790

Composite elongated ellipsoid of revolution under torsion, determining stress-strain state, boundary conditions and elastic displacements

08 p1368 A71-20800

Thick-walled toroidal shell under various load distributions, analyzing stress-strain state by networks method using computer program

08 p1369 A71-21124

Self consistent stress relaxation testing, discussing strain rate sensitivity and stress- strain relations

08 p1308 A71-21519

Strain rate effects on Ta flow stress, examining yield and postyield behavior models and stress- strain diagrams

08 p1313 A71-21562

Al dislocation mobility at high strain rates, plotting true stress vs true strain

08 p1313 A71-21564

Infinite isotropic plate weakened by cracks along circular arcs, calculating stress-strain state and critical loads

09 p1538 A71-22524

Nb alloy high temperature creep and long term strength, determining exponential relations between stress, strain rate and durability

09 p1468 A71-22628

Two dimensional stress-strain fields under elastic and elastic-plastic strains and steady state creep, calculating stress distribution around hole in cylindrical shell

09 p1538 A71-22631

Low temperature tensometry application to stress-strain state of turbine disks

09 p1443 A71-22635

Statically indeterminate rod system design, using linear strengthened materials strain diagrams and Castigliano principle

09 p1538 A71-22650

Reinforced composite materials with curved fibers, considering one dimensional stress-strain relation and misalignment effect

09 p1539 A71-22917

Structural design for low cycle fatigue resistance, considering cyclic stress-strain properties, critical strain and overloads

09 p1541 A71-23097

[ASM PAPER W71-22.3] Crystalline Al stress-strain function parabolic law generalization under combined axial tensile- torsional loading

09 p1480 A71-23700

Stress-strain curves for plastics with or without fiber reinforcements under impulsive compressive loading cycles, using split Hopkinson pressure bar apparatus

10 p1630 A71-23921

Bulk properties effect on adhesive properties of seven epoxy resins, considering stress-strain properties and statistical analysis for tensile shear evaluation

10 p1632 A71-24086

STRESS-STRAIN DISTRIBUTION

Quasi-static problem of stress-strain distributions in elastic medium with moving crack, calculating arbitrary external force effect on crack 10 p1687 A71-24349

Coaxial shells of revolution connected by meridional ribs, deriving elastic equilibrium conditions, stress-strain components and contact forces under thermal and mechanical loads 10 p1688 A71-24358

Cylindrical panel vibration in supersonic flow under random effects, calculating stress-strain statistical properties as function of incident flow velocity 10 p1690 A71-24572

Stress-strain curve and single crystal dislocation structure of Al alloys with coherent precipitates, noting screw dislocations predominance 10 p1629 A71-25033

Fiber reinforced composites, predicting mechanical properties, stress-strain behavior, interface failure, creep and fatigue by mathematical model 11 p1849 A71-25655

Glass fiber reinforced plastics mechanical properties, strain-stress characteristics and anisotropy, deriving orthotropic laminates tensile stiffness under deformation 11 p1849 A71-25656

Surface structure and environment effects on mechanical behavior of crystalline inorganic solids, giving stress-strain diagrams 11 p1808 A71-25999

Annealed and cold-worked polycrystalline Fe specimens steady state cyclic stress-strain curves and thin films observation by electron microscopy 11 p1780 A71-26024

Monograph on turbine blade fir tree roots, calculating stress-strain state of long term static strength under elastic and elastoplastic deformation and unsteady creep 11 p1852 A71-26400

Monograph on plastic behavior of iron and nickel at high strain rates and at elevated temperatures, discussing thermal effect on deformation characteristics 11 p1783 A71-26489

Error estimate for solution of approximately linear elastic boundary value problems of shells with no strain energy functional, discussing stress-strain relations 12 p1974 A71-26943

Numerical solution of equations describing stress-strain state of shallow nonuniformly heated shell 12 p1979 A71-27355

Thin walled stiffened Duralumin box spars bending stress-strain states under unsteady creep 12 p1981 A71-27496

Shear strength effect on axisymmetrical stress-strain state of orthotropic cylindrical shell subjected to nonuniform surface heating 13 p2148 A71-27825

Stress-strain state of strain hardenable rigid-viscoplastic shells of revolution, presenting example calculation for conical shell with uniformly distributed load 13 p2150 A71-28132

Stress-strain state of closed circular cylindrical shells stiffened by longitudinal ribs, analyzing general solution of homogeneous equilibrium equations system 13 p2150 A71-28133

Stress-strain state of circular cylindrical shells in elastic medium, reducing linear problem to solution of single eighth order partial differential equation 13 p2150 A71-28134

Strain and strain rate effect on flow stress and microstructure of Al-Cu eutectic alloy during superplastic deformation, deriving stress-strain diagrams 13 p2086 A71-28624

Stress-strain state of annular billet under local plastic bending by forces in cross sectional plane 13 p2154 A71-28646

Stress-strain state of thin walled ellipsoidal shell of revolution with arbitrarily oriented crack 13 p2156 A71-29069

Longitudinal and transverse rib reinforced plates with parallel cracks extending to edge, obtaining flexural rigidity and stress-strain state 13 p2156 A71-29070

Quasi-stationary one dimensional thermoplastic stress strain state in cylindrical fuel tank during emptying process, allowing for Bauschinger effect 13 p2157 A71-29196

Compression rolled and hot upset Be sheet stress-strain behavior and deformation dynamics, emphasizing temperature and strain rate effects on polycrystalline flow stress 13 p2088 A71-29404

Structural stability in tension and strength tests of thin walled tubes at various stress and strain intensities based on loss of resistance to plastic deformation 14 p2321 A71-29620

Composite materials elastic-plastic behavior under uniaxial loading, determining stress-strain relationships by dislocation theory 14 p2321 A71-29688

Stress-strain state of finite length elastic rod free of bending moments and coupled to semiinfinite plate 14 p2332 A71-30868

Fiber reinforced materials with oriented armoring, calculating stress-strain state under transverse shear 15 p2439 A71-32235

Book on viscoelasticity covering isothermal stress-strain relations, wave propagation, mechanical properties, thermodynamics and nonisothermal effects 15 p2509 A71-32438

Stress-strain state of unclamped thin elastic zero curvature shell under three component surface load and tangential boundary forces 16 p2647 A71-32926

Structural instability due to cyclic strain accumulation, using plastic deformation constitutive relation with stress tensor and elastic effects 16 p2650 A71-33016

Finite element analysis with material nonlinearities, obtaining linear incremental elastoplastic stress-strain relation 16 p2652 A71-33084

Stress-microstrain relationship for metal crystals prestrained in easy glide, obtaining mobile inelastic dislocation density and internal stress 16 p2654 A71-33102

Stress-strain diagrams for oriented fiberglass-reinforced plastic under tension, taking into account temperature and anisotropy effects 16 p2601 A71-33411

Heated tank under axial compression and internal pressure, noting fuel expenditure effects on stress-strain state 16 p2658 A71-33620

Stress-strain diagrams of heat resistant alloys at high temperatures, describing test facility 16 p2598 A71-33988

Stress-strain dependence on surface deflection and nonlinearity during bending of elliptic flat plate under plastic deformation 16 p2659 A71-33994

Stress-strain state of homogeneous and inhomogeneous cylinders and disks with central axial curvilinear hole under internal pressure and thermal loads 17 p2816 A71-34331

Stress-strain state of circular cylindrical shell hinged at edges under local radial loads 17 p2817 A71-34340

Birefringent coating method for stress analysis of fiber-reinforced laminated composites, developing subsurface stress-surface strain relation [SESA PAPER 1837A] 17 p2761 A71-34528

Linear radial loads effect on stress and strain of hyperboloidal rotor disk applied to aircraft engine compressors with two stream flow of working medium 17 p2822 A71-34597

Stress-strain state of thin walled curvilinear frame-type rods of variable cross section with variable elastic moduli along length and contour 17 p2829 A71-35309

Pure and transverse bending of orthotropic cylindrical shell wound with elastic glass plastic filaments, presenting stress-strain diagrams under tension and compression 17 p2830 A71-35318

Three layer trapezoidally corrugated panels with skin under longitudinal compression, determining local stability and stress-strain diagrams 17 p2830 A71-35320

Strain hardening energy curves in generalized coordinates, discussing deformable body state, stress-strain relation, etc 17 p2832 A71-35459

Generalized periodic problem of infinite isotropic plate of constant thickness with periodically arranged groups of holes, determining stress-strain state 17 p2833 A71-35611

Stress relaxation characteristics obtained by compensation principle, force measuring techniques and sample unloading for stress-strain state determination 17 p2834 A71-35656

Stress-strain behavior of tapered circular cylindrical shell, applying equalization calculation to boundary value problem 18 p2976 A71-36179

Test apparatus for studying stress-strain behavior of thin walled metal tubes in torsion, examining strain rate and history effects 18 p2935 A71-36234

Stress-strain state in elasticity theory of three layer symmetrical plate 18 p2982 A71-36786

Mathematical model for continuous elastoplastic transition stress-strain response of steels and nonferrous metals 18 p2937 A71-36835

Orthotropic annular plate plastic flow law, establishing yield conditions with plane stress-strain state equations 19 p3155 A71-37527

Three dimensional orthotropic elastic cylinders symmetric deformations under external loads, calculating stress-strain state with approximate method 19 p3155 A71-37528

Shallow spherical shell under uniform external pressure loads, obtaining boundary conditions effects on stress-strain state 19 p3155 A71-37530

Omega phase embrittlement in aged Ti-Mo alloy, giving tensile properties and load-elongation diagrams 19 p3082 A71-38176

Stress-strain curves of dual slip orientation in Ge single crystals deformed in compression, using interference, optical and electron microscopy 21 p3397 A71-40457

High temperature creep characteristics and strain curves of heat resistant Fe and Ni alloys in turbine components 21 p3403 A71-41155

Al alloys tensile deformation and fracture characteristics relation to stress-strain diagrams, discussing strain hardening indices 22 p3560 A71-41642

Anisotropic glass fiber plastic material stress, strain and crack formation threshold measurements under long term static and cyclic axial loads 23 p3696 A71-43424

Residual stress in closed spherical shell welded along equator, using stress-strain relations 23 p3778 A71-44035

Axisymmetrical elastic deformation of thin helical shell with rectilinear profile, deriving equilibrium equations and stress-strain relationships 23 p3778 A71-44038

Variational stress-strain equation for flexible shallow orthotropic multilayer shells with large deflections under normal pressure and contour loading 23 p3778 A71-44040

Fibers-matrix force interaction effects in metal composites, analyzing stress-strain state of reinforced plate 23 p3697 A71-44202

Diffusive metal coatings stress-strain state effect on composite Mo material strength, deformation and creep characteristics 23 p3697 A71-44206

Ribbed cylindrical shells modeling method for stress-strain state and stability 23 p3780 A71-44219

Stable austenitic stainless steels and fcc metals plastic deformation flow curve model, presenting stress-strain relation 23 p3695 A71-44284

Swaged high purity fine grained Ti stress-strain behavior below 424 K, emphasizing mechanical twinning in plastic deformation 23 p3695 A71-44289

Plastic strain hardening media stress-strain relations, discussing rheology, temperature effects, isotropy postulate and deformation processes 24 p3876 A71-44401

Two layer anisotropic spherical shell of clastohereditary material under uniform pressure, investigating stress-strain state 24 p3880 A71-44710

Stress-strain state of hinged thin multilayer orthotropic cylindrical shells with parameters variable with respect to directrix 24 p3881 A71-44828

Stress-strain state of isotropic elastic plate weakened by cracks, using Fredholm integrals 24 p3881 A71-44832

Edge supported anisotropic elliptic plate with hole under bending by constant lateral edge load, presenting stress-strain state 24 p3882 A71-44837

Stress-strain state of nonlinearly elastic reinforced polymer plate with circular hole, deriving stress tensor components and first approximation solution for pure bending 24 p3882 A71-44838

Wall thickness change to prescribed value by controlling stress-strain state in sheet stamping operations 24 p3831 A71-45013

Cylindrical shell under longitudinal load, examining stress-strain state with semimoment theory 24 p3884 A71-45017

Axisymmetric contact problem of elastic half space stress-strain state, seeking displacements in Hankel integral expansion form 24 p3885 A71-45222

Stress-strain curve of unidirectional fiber reinforced composite Al and N-CI wire under axial compression loads, discussing buckling and shear instabilities 24 p3842 A71-45229

Shear modulus and stress-strain relations for different plastic strain rates 24 p3886 A71-45362

STRESS-STRAIN DISTRIBUTION
U STRESS CONCENTRATION
U STRESS-STRAIN RELATIONSHIPS
U STRESS-STRAIN DIAGRAMS
STRESS-STRAIN-TIME RELATIONS

Glass fiber reinforced plastics strain properties under multiaxial loads, considering long and short time loading, temperature and environmental conditions 01 p0109 A71-10696

Transient creep propagation velocity in dead annealed thin walled Al alloy tubes, using constitutive equation for mean stress-strain-time relationship
03 p0508 A71-13761

High temperature creep comparison of single phase Fe and Ni alloys subjected to constant load tensile tests, measuring strain as function of time
06 p0911 A71-17345

Stress-time superposition creep data for unfilled and coupled glass reinforced polypropylene at 23-80 C
14 p2264 A71-29835

Shock produced stress relaxation in thin walled Al tubes, comparing strain-time profiles with thin shell theory
16 p2647 A71-32923

Plastic stress-strain history at notch roots tested in tensile steel strips under monotonic loads, verifying Hardrath-Ohman theories
22 p3615 A71-42071

Linear viscoelastic stress-strain-time relations for polymethyl methacrylate and epoxy resin
23 p3696 A71-43375

STRESSED-SKIN STRUCTURES
Optimal weight of aerodynamic heat protection layers of stressed skin and optimal efficiency of cooling system for hypersonic aircraft compartments
08 p1375 A71-20836

STRESSES
NT AXIAL STRESS
NT COMBINED STRESS
NT CRITICAL LOADING
NT PHOTOSTRESSES
NT RESIDUAL STRESS
NT SHEAR STRESS
NT TENSILE STRESS
NT THERMAL STRESSES
NT TORSIONAL STRESS
NT TRIAXIAL STRESSES
NT VIBRATIONAL STRESS
Plane micropolar static strain in homogeneous isotropic elastic solid, deriving existence theorems for interior and exterior problems
01 p0172 A71-10841

Aircraft tires mechanical data from small models, discussing mechanical properties, tire stresses and tire temperatures
[AIAA PAPER 71-346] 11 p1707 A71-25325

STRETCHING
Interferometric holography application to elastic stress and surface corrosion of two dimensional objects and metals, discussing stretching
07 p1107 A71-19209

Carbon fibers production by polyacrylonitrile fibers spinning, discussing stretching temperature effects on mechanical properties
[PLASTICS INST. PAPER 12] 08 p1320 A71-20909

Apparatus for rolling and stretching metals at cryogenic temperatures, describing structural features
08 p1300 A71-21810

Snatch force during lines-first deployment of aerodynamic decelerator, including effects of canopy skirt acceleration and suspension wave propagation characteristics
[AIAA PAPER 70-1171] 09 p1385 A71-22915

Stretching, twisting, pure bending and flexure of pretwisted elastic rectangular plates of rectangular cross section
13 p2147 A71-27783

Turbulent hydrodynamic line stretching problem, considering asymptotic rates as application of central limit theorem for dependent random variables sums
19 p3044 A71-37729

Exponential type equation for carbon steel stretched sample necking profile curve
23 p3780 A71-44228

STRIATION
Diffuse reflection from clouds with horizontal surface striations, using Monte Carlo method to follow photons through simplified models
13 p2056 A71-27975

Striated irregularities in ionospheric ion clouds, using model of ionospheric conductivity profile
16 p2573 A71-33957

Externally excited moving striations measurement in low pressure Ar discharge, comparing with ion acoustic wave propagation derivation from model
18 p2948 A71-35859

Drifting whistler frequency cutoff phenomena (striations) observation in low latitude by POGO satellites, discussing interpretation based on propagation effect
20 p3198 A71-39746

Magnetic field aligned striations of Ba ion clouds artificially injected into ionosphere, investigating physical processes based on model
20 p3230 A71-39861

Barium ion cloud release at 194 km, observing striation formation for instability characteristics evaluation
23 p3669 A71-43170

STRINGERS
Axially loaded finite stringer bonded to infinite elastic sheet, considering adhesive shear flow
03 p0514 A71-14350

Circular cylindrical shell with trapezoidal stringers reinforcement system along length, calculating strain during oscillation
03 p0514 A71-14359

Thin circular cylindrical plate reinforced by longitudinal rigid stringers, deriving computer algorithm for calculating forced vibration
03 p0515 A71-14367

Geometrical parameters of stringer nodes in statically determinate minimum weight equal stress and strength trusses
13 p2154 A71-28647

Finite skin-stringer structures natural frequencies determination, using free flexural wave groups
15 p2510 A71-32518

Integrally stiffened panels with bonding material across stringer tops, calculating vibration damping characteristics
17 p2826 A71-35034

Five-span skin-stringer width and damping effects on vibrational response including resonant frequencies and mode shapes by transfer matrix analysis
[ASME PAPER 71-VIBR-101] 21 p3461 A71-40327

STRIP
Two semiinfinite strips joined to form one infinite strip, determining stresses by joint shrinkage
03 p0509 A71-13898

Stress distribution in infinite strip weakened by transverse crack under loading at infinity
05 p0825 A71-16612

Diffraction on strip, investigating for Dirichlet boundary conditions, deriving excited current density and scattered pattern
05 p0722 A71-16869

Elastic deformation of strip, rectangular annulus and cylinder with homogeneous displacement boundary conditions, deriving orthogonality relations for expanded eigenvectors
05 p0828 A71-16993

Tall thin strip rolling in ribbed grooves, determining critical area reductions causing plastic stability loss
08 p1295 A71-20841

Crack propagation model in linearly viscoelastic solid strip based on thermodynamics first law
15 p2506 A71-32011

Stress field in elastic strip of finite width under pressure applied to faces of symmetrically situated Griffith crack
16 p2654 A71-33170

Elastic deformation of strip, rectangular annulus and cylinder with homogeneous displacement boundary conditions, deriving orthogonality relations for expanded eigenvectors
18 p2982 A71-36793

STRIP TRANSMISSION LINES
Cryogenic L band three port stripline circulator, discussing design, construction and applications
01 p0056 A71-11200

Microstrip double down-converter receiver for satellite earth stations, describing thin film integrated circuits and carrier selection
02 p0235 A71-12835

Neuristor pulse propagation analysis for nonlinear distributed circuit of superconductive tunnel junction stripline
03 p0393 A71-14470

Liapunov stability prediction of minimum length for distributed oscillators of superconductive tunnel junction strip line
03 p0388 A71-14475

Gigabit PCM data communications system using functional circuits with microstrip interconnect
05 p0719 A71-16152

Scattering matrix of stripline segment with random change in width of inner strip conductor
11 p1733 A71-26350

Power losses and construction of microwave switch, using orthogonal striplines around thin ferromagnetic film on nonmagnetic substrate
11 p1741 A71-26551

Microwave integrated circuits lumped elements, including microstrip transmission lines configurations and electrical parameters
12 p1886 A71-26988

Microstrip microwave circuit design by complex admittance measurement and computer modeling
12 p1892 A71-27149

Microwave integrated stripline Gunn oscillators with fixed/variable frequency tuning in X band
13 p2039 A71-28911

Rectangular section microstrip lumped capacitance calculation by matrix methods
14 p2210 A71-29571

Phased array pulsed X band microstrip Gunn diode transmitters with temperature stabilization at 9.4 GHz
16 p2547 A71-33555

Continuously variable microwave stripline phase shifter with linear shift vs frequency by dielectric constant variation
18 p2889 A71-36272

Alavalanche diode microwave oscillator design, comparing coaxial lumped, lumped element, microstrip and waveguide circuits
18 p2893 A71-36600

Optimized low loss microstrip microwave filters on silica substrates by photolithographic reduction of LF models
19 p3026 A71-37218

Nonreflecting dielectric support washers design in coaxial-stripline junctions, calculating VSWR as function of dimensions and frequency
19 p3019 A71-38335

Microwave narrow bandpass filters design using microstrip lines
21 p3354 A71-40733

Microstrip line on silicon-silicon oxide system, investigating propagation modes and fringing effect by parallel-plate waveguide model
24 p3809 A71-45091

STRIPPING [DISTILLATION]
Two-phase detonations, discussing importance of stripping mechanism and droplets deformation in reaction zone fuel consumption
05 p0834 A71-16515

STROBOSCOPES
Turbulent wall flow, observing flux and heat transfer conditions with stroboscopic visualization
07 p1105 A71-18782

Holographic stroboscope using ruby laser with passive shutter for HF vibration measurement
14 p2254 A71-30584

Real time stroboscopic vibration analysis technique involving holographic interferometry
15 p2404 A71-31271

Holographic vibration analysis by generalized stroboscopy, combining high reconstruction brightness with time average holograms interpretation
15 p2404 A71-31272

Vibration analysis for static and rotating objects by stroboscopic holography, considering axial flow compressor blades and two-mass system with torsional vibration
15 p2404 A71-31273

Stroboscopic and analytical studies of oscillations and stability regions of gravity gradient satellite in eccentric orbit
18 p2963 A71-36282

Stroboscopic coherent light source for vibrational analysis by holographic interferometry using Pockels cell laser modulator
18 p2923 A71-36610

Strobe lighting for aircraft midair collision hazard reduction, comparing Collision Avoidance System and Pilot Warning Indicator effectiveness
22 p3499 A71-41493

STRONTIUM
NT STRONTIUM ISOTOPES
Apollo 12 igneous rocks and fines from Ocean of Storms, presenting rubidium and strontium chronology and chemistry
23 p3752 A71-43709

STRONTIUM COMPOUNDS
NT STRONTIUM TITANATES
NT STRONTIUM ZIRCONATES
Electron paramagnetic resonance spectral investigation of dynamic Jahn-Teller effect in La doped strontium chloride, discussing structural variations as function of temperature
12 p1942 A71-26743

STRONTIUM ISOTOPES
Apollo 12 lunar rock 12013 rare earth, alkaline and alkali metal and Sr 87/Sr 86 data, discussing light and dark component composition
03 p0494 A71-14221

Rb-Sr isotopic composition in Apollo 12 regolith samples yielding 4.2-5.1 billion year ages
23 p3752 A71-43710

STRONTIUM TITANATES
Vibrational stress induced phase transitions in strontium titanate near transition temperature, using soft mode Raman scattering
17 p2791 A71-34949

Barium strontium lanthanum titanate thermistor bolometer for IR thermal detector, using positive temperature coefficient of resistance
22 p3543 A71-42126

STRONTIUM ZIRCONATES
Electrical conductivity of strontium zirconate and hafnate at 1400-2600 K measured by two-probe method with alternating and direct currents, calculating activation energy
08 p1323 A71-21934

STROUHAL NUMBER
Unsteady flow downwash behind finite span slender wing during supersonic motion at finite Strouhal numbers
12 p1866 A71-27697

Karman vortex street geometry calculation for single circular cylinder, using pressure drag coefficient, Strouhal number and Krouauer criterion
[ASME PAPER 71-VIBR-11] 21 p3457 A71-40273

Karman vortex street induced fluctuating lift forces on tube bundles as function of steady pressure drag coefficient and Strouhal number
[ASME PAPER 71-VIBR-13] 21 p3457 A71-40275

STRUCTURAL ANALYSIS
NT DYNAMIC STRUCTURAL ANALYSIS
NT ENERGY METHODS
NT EQUILIBRIUM METHODS

NT FLUTTER ANALYSIS

NT MATRIX METHODS

NT STRAIN ENERGY METHODS

Structural analysis of invariant automatic control systems characterized by coordinate pairs coupled through disturbed load operator

01 p0058 A71-10406

Glass fiber reinforced plastics stress and fracture analysis, using approximate and iterative methods for strength estimates and nonlinear stress-strain relationships

01 p0172 A71-10697

Eigenvalue errors in applying method of weighted residuals to linear nonself adjoint problems of structural analysis

01 p0174 A71-10944

Kirchhoff triangular shell element design via linear shell theory

01 p0174 A71-10967

Equations of state for materials with memory, discussing derivation methods based on nonlinear functional analysis and applications

01 p0175 A71-11037

Modular ratios effect on structural composites, predicting property values from structural measurements

01 p0103 A71-11276

Papers on LAMS technology for aircraft structural mode control covering B-52 and C-5A aircraft

02 p0187 A71-11658

Elastic half space transient response to normal impulsive surface line load

02 p0321 A71-11677

Rigid plane skeletal structures combinational properties, considering analytic geometry criteria and graphs from algorithm

02 p0327 A71-12395

German monograph on polygonal thin plates calculation by differential equations method for two dimensional boundary value problems solution

02 p0327 A71-12399

Equivalence theory applications in three dimensional elasticity, plane deformation and stresses

02 p0328 A71-12534

Panel flutter structural nonlinearities, discussing shear flexibility, finite curvature and nonlinear inertia effects

[ICAS PAPER 70-29]

03 p0501 A71-13150

General nonlinear finite deformation shell and strain membrane theories in terms of reference state quantities by direct physical derivation

03 p0502 A71-13353

Optimal relaxation time existence for Maxwell solid cylinder bonded to thin casing during forced vibration of rocket assembly, discussing Voigt solid

03 p0497 A71-13469

Beam structures plastic shakedown sufficient conditions derivation in terms of bending moments

03 p0510 A71-13947

Pressurized toroid modified linear membrane theory, presenting approximate solutions for derived boundary value problem by variational calculus methods

[ASME PAPER 70-WA/APM-49]

03 p0512 A71-14168

Multicavity thin walled containers of spheres and intersecting plane partitions, comparing structural properties with single sphere of equal overall volume

03 p0515 A71-14366

Steel-concrete composite beam creep numerical analysis by reduction to elastic problem with initial strains

04 p0669 A71-15198

Papers on structural mechanics covering plates and shells buckling and vibration behavior

05 p0819 A71-15977

Structural design analysis approximation for computational cost and computer storage reduction

05 p0824 A71-16575

Rate sensitive materials impulsively loaded structures by piecewise stationary mode approximate methods

05 p0826 A71-16718

Piecewise linear analysis of two connecting structures including connections with clearance, applying to engine crankshafts and pin-and-eye problems

05 p0829 A71-17116

Stability analysis of structural systems subject to nonconservative forces, using finite element method

05 p0829 A71-17118

Supercritical behavior of metallic plates, using nonlinear equilibrium and strain compatibility equations

06 p0987 A71-17765

Optimal parameter selection for thin walled shell structures, using mathematical programming

06 p0989 A71-17781

Cylindrical sandwich shells with multiple isotropic load carrying and transversely compressible filler layers, deriving local stability equations

06 p0990 A71-17793

Static computations of thin walled shells and honeycombs, examining variational, matrix, finite element, initial function, small parameter and plate bending methods

06 p0999 A71-17867

Matrix displacement /finite element/ method for elastic structures analysis

06 p1001 A71-18050

Flat triangular elements for shell analysis, describing membrane and bending displacements by identical quadratic polynomials

[AIAA PAPER 71-114]

06 p1003 A71-18564

Solid propellant engine structural analysis, examining transient thermal loading and internal pressure effects

[AIAA PAPER 71-115]

06 p1003 A71-18565

Book on computer methods of structural analysis concentrating on frame systems, stiffness matrix techniques and Fortran IV

07 p1210 A71-19099

Nonlinear analysis of cable and truss structures, using computerized stiffness matrix method

08 p1367 A71-20749

Isotropic material structures under static external loads, considering stress rupture strength models

08 p1371 A71-21608

Circular cylindrical shells on coaxial rings coupled by finite number of spokes as structural analytical models for engine casings, deriving formulas for arbitrary loads

08 p1374 A71-22040

Structural element for discrete element idealization of missile and liquid propellant as one composite structure

[AIAA PAPER 70-23]

09 p1430 A71-22087

Plasticity zone changes near circular hole, examining material structure inhomogeneity effects in presence of creep

09 p1535 A71-22183

Linear theory of viscoelasticity, calculating basic relationships based on experimentally determined characteristics under unsteady test conditions

09 p1537 A71-22514

Book on matrix structural analysis covering transformation, structure idealization, displacement method, finite element theory, nonlinear aspects, etc

09 p1539 A71-22873

Statistically indeterminate modified structures automated design reanalysis by displacement method, using matrix formulations, numerical computation and computer operations

09 p1542 A71-23282

Soviet papers on crystalline structure imperfections covering dislocations, structural changes, heating and ultrasound effects, plasticity and substructure disorientation

09 p1475 A71-23311

Soviet papers on structure and properties of metals covering crystal properties, yield strength theories and heterogeneous phase systems

09 p1476 A71-23320

Stress and structure effects on creep rate of two austenitic steels in quenched state, considering decorated stacking faults

09 p1479 A71-23624

Reference stress parameters for structure creep behavior, using dimensionless stationary state, strain rate and time function

09 p1543 A71-23660

Thermal, microstructural and X ray analyses of Al-Ti alloys phase diagrams, measuring hardness and conductivity

09 p1480 A71-23704

Phase diagram isothermal cross sections of Ti-Zr-Nb alloys for various temperatures and heating periods by X ray and microstructural analysis

09 p1480 A71-23705

Computerized finite element techniques for stress and structural analysis for space communication and radar applications

10 p1684 A71-23756

Interactive computer graphics technology industrial applications, emphasizing structural analysis and engineering master drawings

10 p1580 A71-23758

Photochromic paints for nondestructive testing of aerospace materials and structures

10 p1633 A71-24102

Structural system analysis by partial decomposition of flexibility and stiffness matrices, obtaining coordinate deformations for computer and hand applications

10 p1691 A71-24693

Numerical errors in computer programmed structural analysis calculations, using finite element displacement method for exact solutions and error sources identification

10 p1693 A71-25051

Structural inference theory applied to stochastic processes class characterized by gamma-distributed interarrival times, deriving conditional probability mass function for process counting variable

11 p1791 A71-25251

Wing-fuselage-tail interacting low speed flutter, considering mechanical tuning and aerodynamic interference couplings

[AIAA PAPER 71-326]

11 p1842 A71-25306

Retroversion from preferred eigenvalues to determine compatible structural characteristics, deducing

design changes in model configurations from perturbations imposed

[AIAA PAPER 71-345]

11 p1843 A71-25323

Numerical solution procedures evaluation for geometrically nonlinear structural analysis by direct stiffness method, noting capability of self correcting initial value formulation

[AIAA PAPER 71-356]

11 p1844 A71-25331

Elastic collapse analysis of shell structures with variable rectangular grid spacing based on modified finite difference computer program

[AIAA PAPER 71-359]

11 p1844 A71-25333

Composite material structural behavior predictions emphasizing static, dynamic, buckling and post-buckling response of anisotropic plates laminated from unidirectional plies

11 p1846 A71-25429

Managing steel structural analysis under heat treatment, noting age hardening time and temperature

11 p1778 A71-25811

Unijunction transistors operation principles, electrical parameters, structural features and circuit applications

11 p1740 A71-26544

Modified interaction equation for biaxially bent beam columns of hollow tubular sections yielding satisfactory prediction of ultimate strength

12 p1973 A71-26699

Stability analysis of rigid frames and trusses, including effect of bending moments and shear forces before buckling

12 p1976 A71-27161

Specialized version of Jones direct stiffness structural analysis method, deriving functional substitutions in variational formulation for displacement discontinuities

12 p1983 A71-27597

Structural evolution of Ni-Co-Mo maraging steels during martensite reversion at rapid heating, studying heating rate effect on alpha-gamma transformation

12 p2257 A71-29839

Quantitative description of solidification structures of Al-Cu, Al-Cu-Ti, Al-Si, Al-Mg and Al-Si-Cu discussing dendritization index, cooling rate and tensile strength

14 p2257 A71-29843

Force method equations for linear viscoelastic system of incompressible rods obeying small deformation theory

14 p2328 A71-30378

Three dimensional elasticity theory solutions for isotropic axisymmetric bodies of revolution by p-analytic and generalized analytic functions

14 p2333 A71-30885

Stress-strain measurements in inelastic elements by photoelastic, laser, memory, load and plane deformation methods, considering plate with circular hole

14 p2333 A71-30894

Short open noncircular cylindrical shells supported at curvilinear ends, obtaining total values of moments

15 p2507 A71-32103

Rigid framed dome structure stiffness analysis using multiglobal axes and joint equilibrium equations

15 p2507 A71-32105

Stress relaxation in rings and rods, discussing errors in data correlation

15 p2508 A71-32230

Soviet book on plane elasticity theory boundary value problems solution on digital and analog computers

15 p2508 A71-32276

Structural dynamic responses as nonstationary narrow band random process, establishing peak values distribution functions with frequency interpretation

15 p2510 A71-32515

Two-parameter statistical theory of material fatigue, considering random and ordered structural nonuniformities in space distributions

16 p2647 A71-32823

Coupled elastic buckling in continuous systems, determining postbuckling paths for strut, spherical shell and flat plate

16 p2650 A71-33017

Structural elements residual, principal and total stress determination, using photoelastic coating method

16 p2651 A71-33061

Structural strength numerical evaluation, demonstrating effectiveness of regression equations in statistical data processing

16 p2651 A71-33063

Matrix methods of structural analysis and design Conference, Tokyo, August 1969

16 p2651 A71-33076

Dynamic vibration analysis of mechanical structures, considering transfer and stiffness matrix methods

16 p2653 A71-33091

Structural synthesis and analysis concepts discussing design philosophy, failure modes, load conditions, algorithms and computer aided design

16 p2653 A71-33092

- Elastic-plastic stiffness matrix methods, applying linear and nonlinear programming techniques to framed structures analysis 16 p2653 A71-33094
- Manipulation errors in structural systems finite element analyses, examining sources, magnitudes and characteristics 16 p2654 A71-33100
- Small deflection analysis within Cartesian coordinate system applicable to elastic-plastic rectangular plates bending under Tresca yield criterion 16 p2654 A71-33122
- Materials ultrasonic structural analysis, describing statistical methods for damping data processing 16 p2584 A71-33561
- Structure and properties of beryllium compounds from solid state stable electron configuration formation viewpoint, discussing classification based on chemical bond 16 p2597 A71-33920
- Limit analysis of dissipation power and collapse load of rigid perfectly plastic continua with piecewise linear yield surface, using linear programming 17 p2816 A71-34324
- Systems concept formalization, including structural relations on basis of set theory, topological considerations and flow theory 17 p2777 A71-34599
- Monograph on tensile tests of welded joint structural properties as function of introduced heat, applying method to Cu-Ni alloyed steel 17 p2748 A71-34825
- Fracture mechanics, considering toughness /energy absorption/ factor, applied stress, crack size, operating temperature and state of stress 17 p2828 A71-35299
- Shell analysis in curvilinear coordinates, obtaining edge effect equation with canonical kinematic unknowns in plane sections law 17 p2830 A71-35314
- Postbuckling elastic characteristics of structures under combined loading near special critical point 17 p2832 A71-35420
- Sikhote-Alin expedition geological survey, examining crater and pit structural characteristics 17 p2810 A71-35717
- Conformal integrability for symplectic and cosymplectic structures, studying torsion and curvature tensor fields 18 p2976 A71-36126
- Constant stiffness beam-columns analysis in pressure piping systems calculations for nuclear industry, using initial parameter method 19 p3102 A71-37073
- Computer programs for nonlinear finite element analysis with applications to large displacement and small strain problems 19 p3088 A71-38309
- Large stiffness matrices building and manipulation, including structural analysis computer programs input determination, coupling techniques and eigenvalue problems solution 19 p3161 A71-38654
- Holographic interferometry for structure and material deformation measurement, presenting static loading and resonant vibration surveys 20 p3238 A71-39346
- Membrane theory of anisotropic shells, using three dimensional elasticity theory 20 p3308 A71-39366
- Computer aided aircraft design, analysis and production, discussing Numerical Master Geometry program developed by British Aircraft Corporation 20 p3241 A71-39543
- Modified Newton-Raphson stiffness matrices and initial value formulations to geometrically nonlinear structural analysis for beam and plane stress triangular elements 20 p3311 A71-39870
- Viscoelastically damped structures finite element modeling and analyzing methods [ASME PAPER 71-VIBR-36] 21 p3458 A71-40288
- Book on classical theory of structures based on differential equations, covering shear wall behavior and maximum-minimum theorem for frameworks 21 p3466 A71-40890
- Nonlinear static structural mechanical problems solution, using self correcting initial value formulations 21 p3467 A71-40959
- Shell structure computer analysis capability assessment covering U.S. industrial concerns, government agencies and universities research activities 22 p3516 A71-41864
- GWU-FAP computer program for rigid frame elastic-inelastic analysis based on finite element method and plastic initial strain concept 22 p3516 A71-41867
- Bar forces in statically determinate planar truss due to arbitrary loads at joints, describing computer program for sequential solution 22 p3517 A71-41869
- Linear elastic structures analysis by quadratic programming, considering equilibrium equations for forces at joints 22 p3618 A71-42589
- Grainy composite material structural analysis, presenting statistical mathematical model 23 p3698 A71-44224
- Critique of variational formulation approach in finite displacement analysis, considering applicability requirements and limitations 24 p3880 A71-44639
- Thermally loaded rod structures optimization, presenting method for estimating canonical equations influence parameters 24 p3842 A71-44642
- Factorial determinants in solving space contours, considering bending and torsional moments in structural analysis 24 p3881 A71-44800
- Magnetic leakage flux method for nondestructive detection of structural defects 24 p3827 A71-45069
- STRUCTURAL BEAMS**
U BEAMS [SUPPORTS]
STRUCTURAL DESIGN
NT PRESSURE VESSEL DESIGN
Cylindrical shells and circular plates optimal limiting and adaptable loads calculation by Pontryagin maximum principle 01 p0170 A71-10639
- Weight allowance in optimal design of plastic structures under creep 01 p0170 A71-10641
- Lightweight structural elements fabrication from fiber reinforced plastic materials /prepregs/, discussing manufacturing methods, structural design, production and testing of parts, etc 01 p0172 A71-10690
- Papers on bearings covering types, materials, lubricants, applications, etc 01 p0088 A71-10813
- Parametric differentiation method for reducing structural optimization and nonlinear programming problems to solution of simultaneous nonlinear algebraic equations 01 p0174 A71-10951
- Buckling analysis of rectangular waffle plates with multiple sizes of ribs in each stiffening direction, considering stability and design 01 p0178 A71-11583
- Skynet satellites earth stations design, structure, transportation and erection ease, considering operational and stowed position survivability in high velocity winds 02 p0223 A71-12804
- Large antenna electrical and mechanical requirements, considering gain/temperature ratio, steerability, housing, design life and erection 02 p0235 A71-12831
- Optimal design of one end-clamped elastic column subject to conservative concentrated compressive loads 03 p0501 A71-13110
- Structural design for component low cycle fatigue resistance, emphasizing material cyclic stress-strain behavior 03 p0501 A71-13252
- Book on fatigue design covering load, stress and stability analyses, fail safe design, damage, residual strength, life, load spectra, structural reliability, etc 03 p0506 A71-13695
- Truss systems optimal structural design, noting elastic-plastic stability conditions 03 p0509 A71-13897
- Shells and plate disk structures elastoplasticity analysis problems, considering limit loads, large deflections, boundary state theory, optical design, etc 03 p0510 A71-13944
- Finite element program for structural design and stress analysis, introducing creep and plasticity into strain equations [ASME PAPER 70-WA/DE-4] 03 p0511 A71-14140
- Optimal design of rotating disks of nonuniform thickness with integral shafts, using two and three dimensional numerical analysis for stress distribution [ASME PAPER 70-WA/DE-6] 03 p0511 A71-14141
- Six meter reflector telescope construction, discussing design, components and control system 04 p0588 A71-14827
- Minimum weight design for beams and frames with compliance constraints from constitutive relation 04 p0671 A71-15754
- Orthotropic sandwich and homogeneous single layer circular cylindrical shells optimal design 05 p0822 A71-16419
- Structural design analysis approximation for computational cost and computer storage reduction 05 p0824 A71-16575
- Panel with segment-wise constant mass distribution structural optimization design, considering flutter 05 p0824 A71-16577
- Linear programming application to optimum structural design, noting savings in design and price 05 p0825 A71-16610
- Deflection-optimal elastic beams design for distributed dynamic loading 05 p0825 A71-16717
- Structural optimization by concave and piecewise linear programmings, discussing mathematical foundation and iterative method efficiency 05 p0829 A71-17121
- Optimal design with geometric constraints for simply supported Tresca plastic disk and cantilever plate under concentrated force 05 p0830 A71-17223
- Haunched beam design optimization for lightest weight, analyzing failure modes under assumption of elastically rigid perfectly plastic material 06 p0981 A71-17301
- Soviet book on short time creep for designing structural and machine parts operating at high temperatures, analyzing stress-strain state 06 p0983 A71-17432
- Soviet book on fiber reinforced plastics design covering low strength rods, plates and thin walled rings, winding techniques, etc 06 p0983 A71-17435
- Iteration method application to shell design nonlinear differential equations solution 06 p0988 A71-17777
- Cost-optimal zero moment shell geometry, developing digital computer algorithm with dynamic programming 06 p0992 A71-17804
- Reinforced zero moment minimum weight shells strength analysis and optimal design algorithms, using discrete calculation scheme 06 p0998 A71-17854
- Plate and shell designs, considering thin walled structures optimization for minimum weight, volume and cost vs maximum stresses 06 p0998 A71-17858
- General linear shell theory, considering elastic processes in structural design 06 p0998 A71-17860
- Optimal structural design for nonconservative elastic stability of cantilever column, obtaining critical load 07 p1212 A71-19473
- Tapered cantilevered beams design, determining end deflection and bending stress magnitude by graphical method 07 p1213 A71-19693
- Mechanical properties at different temperatures and allowable design stress for aluminum alloy 07 p1137 A71-19966
- Vibrational damping, composition and structural design of cast polyurethane elastomers for Poseidon missile launch tube liner 08 p1367 A71-20694
- Optimal thin walled structures design, using discrete matrix methods for computer programming 08 p1368 A71-20791
- Equatorially mounted parabolic reflector radio telescope, discussing structural design, mechanical drives and electronic control system 08 p1271 A71-21152
- Air cushion vehicle technology, considering economics, propulsion, structures, controllability, flexible skirt systems and R and D [SAE PAPER 710183] 08 p1231 A71-21713
- Complex airframe design for economic and safe operation and long life using fatigue and fracture mechanics [AIAA PAPER 70-512] 08 p1374 A71-22025
- Direct search algorithm for automated optimum structural design with spiral stiffened cylindrical shell application 09 p1533 A71-22077
- Rumanian book on stress computation in theory of cylindrical median surface plates with arbitrary section and minimal area 09 p1536 A71-22420
- Large spaceborne telescope primary mirrors materials under microstructural loads, considering low expansion ceramics and metallics applications 09 p1446 A71-22743
- Floating airport structural design, using hollow concrete blocks filled with polystyrene foam as runway basic unit 09 p1428 A71-22949
- Structural design optimization in rheology, classifying various objectives and constraints 09 p1540 A71-23086
- Structural design for low cycle fatigue resistance, considering cyclic stress-strain properties, critical strain and overloads [ASM PAPER W71-22.3] 09 p1541 A71-23097
- Aircraft wings automated preliminary structural design and weight determination procedures based on external shape, aerodynamic loads and fuel mass interaction 09 p1541 A71-23274
- Statistically indeterminate modified structures automated design reanalysis by displacement method, using matrix formulations, numerical computation and computer operations 09 p1542 A71-23282

STRUCTURAL DYNAMICS

Structural design constraints check by computer single program algorithm, resembling similar human activity

09 p1413 A71-23284

Welded steel structures fracture safe design, considering continuity conditions responsible for catastrophes resulting from crack initiation

09 p1458 A71-23453

Soviet book on aircraft preliminary design specifications as function of performance, aerodynamic and structural parameters, discussing tradeoffs in operational requirements for specific configurations

10 p1554 A71-24012

Variable weight composite materials for aircraft optimal adhesive bonding structural designs, discussing C-5A tow weight saving Ti honeycomb applications

10 p1686 A71-24084

Structural bonding with polyurethane adhesives in missile systems

10 p1615 A71-24094

Light aircraft steel landing gear springs structural design at Cessna, considering certification requirements

[SAE PAPER 710400]

10 p1555 A71-24262

High performance precision shaft and face seal design and applications

10 p1617 A71-24417

Performance-price relations of carbon, boron and glass fiber reinforced resin matrix composites in commercial and aerospace use

10 p1634 A71-24418

Spacecraft deployable booms, discussing structural design, self loading, weight, stowage volume and thermal stability requirements

[AIAA PAPER 71-396]

11 p1841 A71-25272

Large space structures zero backlash deployment mechanism, discussing dynamically scaled model for mechanical and structural design and dynamic analysis

[AIAA PAPER 71-400]

11 p1836 A71-25276

Ti intermediate diagonal tension field shear beam analysis and design for Boeing SST, using Rayleigh-Ritz method

[AIAA PAPER 71-340]

11 p1843 A71-25319

Stability analysis and design optimization with dynamics and aeroelasticity constraints for helicopter rotor blade minimum weight with bending torsion flutter and favorable frequency placements

[AIAA PAPER 71-388]

11 p1846 A71-25352

Prototype graphite fiber/plastic fuselage component design, test and performance prediction, using structural analysis methods

11 p1787 A71-25428

Internal structural design loads for aerospace vehicles subjected to random loads, considering shear, moment and torsion as random components of generalized internal load vector

11 p1838 A71-25516

Metallic diaphragms design, fabrication and testing for cryogenic fluid and positive expulsion systems

[AIAA PAPER 70-683]

11 p1768 A71-25518

Shear deformation effect on optimal design of elastic beams, considering rectangular cross section circular ring by Timoshenko beam theory

11 p1849 A71-25677

Optimal elastic beam structural design for given deflection in presence of body forces, considering rod under centrifugal loads

11 p1849 A71-25680

Fracture-safe design, discussing strength transition, ratio analysis diagram, R-curve resistance, weldability and computer techniques

11 p1778 A71-25747

Dynamic programming for designing beams and plates under steady creep with minimum weight, discussing cantilever beam optimization

11 p1853 A71-26564

Concorde aircraft construction methods, materials and design

12 p1867 A71-26882

Automated low cost structural-mechanical design and optimization of wing pivot systems for variable geometry aircraft

[AIAA PAPER 71-404]

12 p1980 A71-27410

Statically determinate beams optimal design, considering displacement and stress constraints in optimality conditions derivation

12 p1983 A71-27596

Steepest gradient method for optimum structural design, using search for unconstrained maximum or minimum of function with many independent variables

12 p1247 A71-27789

Minimum weight design of statically determinate wide flange beams, using Lagrange multipliers

13 p1251 A71-28210

Multiaxial stress state effects on materials fracture strength, ductility and structural design

13 p1251 A71-28216

Minimum weight design of circular cylindrical shell hinged at ends under axial compression, using random search method with self learning

13 p1252 A71-28280

Structural design effects on air driven two stage ejector supersonic propelling nozzle with conical mixing chamber

13 p1215 A71-28585

Optimal design of minimum volume beams of variable height under bilateral restrictions on stresses and displacements

13 p1254 A71-28645

Optimization algorithm for multielement support structure exhibiting minimum deformation energy, comparing Lagrange conditional search method

13 p1201 A71-29186

Optimal structural design of minimum weight trusses and beam cross sections for given load using computerized nonlinear programming method

14 p1231 A71-29541

Materials and structural design development by high velocity impact testing due to transport and subsonic military aircraft susceptibility to bird collision damage

14 p1221 A71-29642

Aircraft structural design requirements based on statistical analysis of air turbulence intensity and gust loads records from large number of research flights

14 p1213 A71-29784

Materials selection in product design, considering performance, cost, schedule and materials characteristics requirements, with special attention to brittle materials

14 p1230 A71-29899

Exponentially varying thickness thin plate volume minimization for simultaneous stress and deflection constraints under axisymmetric load, using digital computer

14 p1230 A71-30691

L-1011 Tristar antenna arrangement test results, considering weight, aerodynamic and structural design requirements

14 p1221 A71-31060

Radome design and production, considering construction, materials, shape, manufacturing techniques and technological problems

14 p1218 A71-31067

TU-144-Concorde differences, discussing design philosophy engine mounting and thrust, wing span and profiles, gross weight, fuselage cross sections landing gear, droop nose, etc

15 p12349 A71-31873

Optimal rectangular plates with adaptability, using convex programming

15 p12508 A71-32232

Azur satellite structure and mechanism requirements, design and tests, noting damping characteristics and Yo-Yo system

[DGLR-71-014]

15 p12501 A71-32783

Optimal structural design for nonconservative systems under buckling, noting application to minimal weight nonprismatic elastic bar shape determination

16 p12649 A71-33012

Matrix methods of structural analysis and design - Conference, Tokyo, August 1969

16 p12651 A71-33076

Structural synthesis and analysis concepts, discussing design philosophy, failure modes, load conditions, algorithms and computer aided design

16 p12653 A71-33093

Probabilistic approach to prolonged lifetime design and static strength of structures of monocoque and multispar wings, using fatigue characteristics of individual elements

16 p12657 A71-33604

Advanced composites as future aircraft structural materials, discussing design concepts, service experience, manufacturing methods and quality assurance

[AIAA PAPER 71-779]

16 p12660 A71-34014

Optimality condition for statically indeterminate beams minimum deflection design, using principle of stationary mutual complementary energy

16 p12661 A71-34148

Thin walled structure design for critical loading by external force variation, determining carrying capability loss by digital computer matrix methods

17 p12818 A71-34351

Structural design of gyroscope ball bearings, considering additional sliding friction force moment

17 p12739 A71-34561

Aircraft structural parameters optimization satisfying flutter velocity constraint and minimum mass, applying to box beam design

17 p12825 A71-34874

Stiffened panel acoustically induced stress estimation using experimentally determined random S-N curves with various structural parameters

17 p12826 A71-35033

High modulus graphite-boron composites design and application to lightweight structures, illustrating sandwich construction for race boat main boom stiffness and compressive strength

17 p12762 A71-35203

Experimental research at Building Research Station on outdoor sound propagation for building design in relation to aircraft and road traffic noise

17 p12674 A71-35237

Oriented glass fiber-plastics plates and shells design, noting zero moment stress shells and filament overwrapped metallic pressure vessels

17 p12831 A71-35315

Rigid plastic framed structures minimum weight design and analysis formulation by network-topological approach based on yielding concept

17 p12831 A71-35328

Space shuttle with two stage booster and orbiter reusable vehicles, discussing performance, structural design and flight control system

[AIAA PAPER 71-804]

Dynamic programming to design beams and plates under steady creep with minimum weight, applying to cantilever beam

17 p12832 A71-35328

Optimal design of locally orthotropic elastic bodies of fiber reinforced plastics or metals

17 p12763 A71-35628

Optimal design of axisymmetrical annular plate and cylindrical and spherical shells by maximum principle

17 p12833 A71-35628

Book on optimum structural design covering single element optimizations, load transmission, sleded columns, cost-weight tradeoffs and statically indeterminate structures

18 p12977 A71-36240

Composite materials and structures analysis and design, examining elastic constants, thermal expansion coefficients, viscoelastic moduli, conductivity and failure modes

[AIAA PAPER 71-366]

Viking Mars spacecraft pressure vessel design, incorporating linear elastic fracture mechanics for long life

18 p12979 A71-36483

Minimum weight design of statically determinate elastic truss under multiple stress and displacement constraints, using virtual work of dummy loads

18 p12982 A71-36843

High strength Al alloys in structural design, taking into account fracture toughness

18 p12937 A71-36844

Structures with random resistance, calculating upper and lower bounds for safety coefficients average value and variance

19 p13156 A71-37644

Minimum mass design of two dimensional plate-like structure with free vibration fundamental frequency or aeroelastic constraints, using optimal theory for extremum

19 p13158 A71-37877

Fracture mechanics for design procedures, producing approximate expressions for stress intensity factors

19 p13158 A71-38013

Linear elastic fracture mechanics for design against high cycle fatigue failure, considering stress intensification, crack initiation and propagation

20 p13307 A71-38813

Structural support system for large log-periodic antenna, discussing asbestos-cement pressure pipes and fiberglass rods as construction materials for antennas critical electrical characteristic needs

20 p13210 A71-39874

Structural optimization problems involving vibration-weight interactions, using optimal control nonlinear programming transforms

[ASME PAPER 71-VIBR-66]

Dual variational formulation for rigid plastic structure minimum cost design, applying to sandwich and fiber-reinforced plates

[ASME PAPER 71-VIBR-110]

Nonlinear mixed integer programming for automated design and structures optimization, describing penalty function technique and recovery scheme to satisfy integrity requirements

[ASME PAPER 71-VIBR-117]

Direct search penalty function algorithm for treating general mathematical programming form of optimal design problem

[ASME PAPER 71-VIBR-121]

Elastic trusses optimal design under multiple mechanical constraint conditions, describing steepest descent method with constraint error compensation

21 p13470 A71-41021

Stress relaxation equation for arbitrary initial tensile stresses and pliabilitys applied to machine element design

23 p13778 A71-44044

STRUCTURAL DYNAMICS U DYNAMIC STRUCTURAL ANALYSIS STRUCTURAL ENGINEERING

Municipal airport rigid pavements design considering supporting effects of soil subgrade, asphaltic concrete subbase and pavement strength

02 p0237 A71-12165

Flexible pavements design for giant transports considering load repetitions, total systems, environmental effects, etc

02 p0238 A71-12166

Rigid and flexible pavement design and construction in Europe, discussing unreinforced and crack reinforced slabs and CBR method

02 p0238 A71-12167

Aircraft pavements in UK, discussing reinforced and unreinforced concrete, tar-bound bases and surface coatings

02 p0238 A71-12168

Runways, aprons and taxiways strengthening to accommodate higher tire pressures and landing speeds, heavier aircraft and surface riding requirements

02 p0238 A71-12169

Aircraft pavements design and construction problems regarding adverse soil conditions

02 p0238 A71-12170

Carbon fiber composites engineering applications, discussing mechanical properties, weight and economic considerations
[PLASTICS INST. PAPER 30]

08 p1297 A71-20919

Structural efficiency improvement by materials selection for airframe structures, discussing Al, Ti-Al-V and steel panels

08 p1299 A71-21685

Carbon fiber reinforced high interlaminar shear strength composites, noting applications to advanced engineering structures

11 p1785 A71-25408

Book on classical theory of structures based on differential equations, covering shear wall behavior and maximum-minimum theorem for frameworks

21 p3466 A71-40890

STRUCTURAL FAILURE

Metal products structural failure analysis, discussing laboratory equipment and analyst experience and ingenuity

01 p0087 A71-10455

Stress intensity factors of hollow notched bars and hydrogen embrittled solid specimens
[SESA PAPER 1671]

03 p0443 A71-13751

Transmission impending failure detection via lubricating oil monitoring for metal particle content

04 p0532 A71-15415

Energy dissipation patterns of metal fatigue failure during static and cyclic loading applied to untreated and heat treated steel samples

04 p0671 A71-15637

Bearing vibration monitoring for wear and damage detection

04 p0603 A71-15671

Nitrogen tetroxide/hydrazine pulse mode rocket engines structural failure due to chemically reactive gaseous hot spots causing high pressure spiking and detonation initiation
[WSS/CI PAPER 70-24]

06 p0944 A71-17663

Static and kinematic adaptability of plates and shells under progressive structural failure

06 p0989 A71-17784

Cylindrical structure longitudinal stress wave propagation characteristics, analyzing wave induced structural instability and destruction process

06 p0991 A71-17801

Thin metal sheet reinforcements effect on slow stable tear and catastrophic failure
[AIAA PAPER 71-113]

06 p1003 A71-18563

Nonlinear finite difference computer program applied to elliptic cylinder collapse under uniform external pressure, comparing with theoretical bifurcation buckling
[AIAA PAPER 71-146]

06 p1003 A71-18589

Critical dynamic snap-through of shallow clamped arches under concentrated loads, using finite difference method
[AIAA PAPER 71-176]

06 p1004 A71-18615

Geometries and technical specifications deviations effects on service life and fatigue characteristics of thin walled structural components under cyclic loads

06 p1005 A71-18710

Steel under cyclic loads, observing relationship between changes in microstructure and temperature curve shape in fatigue failure process

07 p1211 A71-19194

Martensitic high strength steels composition effect on environmentally induced delayed failure

07 p1139 A71-19990

Bent structure failure under pulse floor acceleration shocks, concerning aircraft seat damage during crash landing

08 p1367 A71-20747

First passage time for snap-through of shallow cylindrical shell subject to stationary random loading, considering numerical solution by Pontryagin-Vitt equation

08 p1369 A71-20809

Materials failure role in Canadian civil aircraft accidents, discussing organized investigation and data flow

08 p1231 A71-21679

Cyclic heating and thermal stresses effect on fatigue strength and durability of turbine blade alloys and structural elements

08 p1372 A71-21702

Variational principle application to stability in failure mechanics of arbitrary linearly elastic bodies, discussing inertia effect on steady state vibrations of cracked bodies

08 p1372 A71-21704

Fatigue crack formation and growth rate relationship, examining variance in cycle number in formation to final failure

09 p1536 A71-22507

Metal sheet failure kinetics, investigating tensile stress and cycle frequency during fatigue crack growth and extension rate effects

09 p1468 A71-22508

Stress corrosion failure prevention in susceptible Al alloys, considering metallurgical structure, environment and stress distribution

09 p1478 A71-23417

Variational formulation for minimum weight of structures with given yield stress, considering homogeneous isotropic material, plasticity condition and collapse mechanism

10 p1685 A71-23977

Unidirectional fibrous composites brittle and ductile failures prediction under tension and torsion, comparing results with tests on glass-epoxy composites

10 p1686 A71-24017

Axisymmetric snap-through of shallow clamped spherical caps under uniform pressure, revealing existence of higher modes as isolated closed loops from approximate solution

10 p1689 A71-24518

Time and temperature effects on epoxy composites mechanical behavior, changing from brittle to ductile to rubbery failure mode

10 p1635 A71-24805

Fiber reinforced plastics/epoxy resins/ electrical effects association with deformation and failure

10 p1635 A71-25013

Anisotropic material failure under combined loading, predicting strength from uniaxial and shear tests
[AIAA PAPER 71-368]

11 p1845 A71-25342

Statistical scatter approximation of creep characteristics using relation to accumulated static damage and time to failure

12 p1979 A71-27352

Cyclic loading failure criteria based on deformation energy concepts

12 p1984 A71-27679

Fractographic analysis of failure kinetics and crack formation in Al alloys, showing microfatigue intrusions and extrusions for various initial stress levels

12 p1919 A71-27682

Compression strength theory for monodirectional reinforced homogeneous anisotropic and piecewise homogeneous materials, using microvolume stability loss failure mechanism

12 p1922 A71-27684

Acoustic emission application to nondestructive testing of materials, manufacturing processes and structural components failures

13 p2073 A71-27939

Linear viscoelastic materials, investigating failure and bending as function of time in response to load under creep conditions

13 p2154 A71-28522

Structure service life and storage failure probability calculation with current load measurements and laboratory fatigue testing

13 p2076 A71-29231

Structural fatigue in aircraft design, discussing twin engine transport tests, crack propagation rate, residual strength, etc

13 p2158 A71-29434

Creep and failure tests for Ti alloys at 500 C and high stresses, discussing work dissipation during creep process

14 p2256 A71-29621

Fretting fatigue test apparatus with load monitoring as function of cycles for relating quantitatively damage to life

14 p2248 A71-30883

Failure and forming limit diagrams in biaxial tension for sheet metal with preexisting inhomogeneities based on Marciniak concept

15 p2505 A71-31945

Notched unidirectional composites failure mechanics under tensile load in fiber direction, considering debonding, plasticity and strength

15 p2428 A71-31971

Reliability prediction of narrow band structures under random excitations, considering catastrophic and fatigue failure modes

15 p2506 A71-32094

Coupling effects between reliability components of integrated circuits by modeling failures in structures

15 p2377 A71-32345

Time dependent fracture and failure criteria for aluminum under stress pulse loading in uniaxial strain, using exploding foil spallation tests in air and vacuum

16 p2590 A71-32943

Atmospheric turbulence prediction, discussing gust sensitive aircraft design for structural overload and fatigue failure decreases
[AIAA PAPER 71-775]

16 p2524 A71-34011

Service failure prediction by photoelastic methods, discussing failure sources and analysis techniques

17 p2820 A71-34554

Anisotropic composite materials failure surface criteria in three dimensional space, using graphical representation

17 p2824 A71-34817

Metal fatigue crack failure prediction for arbitrary uniaxial cyclic loading, discussing method based on

treatment of crack growth as continuous stochastic process

17 p2758 A71-35158

Constrained torsion of spar box fastened along isolated parts of wing span, noting structural failure due to tangential stress distribution

17 p2830 A71-35313

Long time failure modeling of real structure behavior in short times by scale and mathematical models, noting nonaccountability of crack propagation time

17 p2834 A71-35669

Turbine alternating fan failure due to flutter by coupling of vibration modes and effect of mass distribution in blade

18 p2980 A71-36696

Deformation kinetics and failure of high melting Nb and Mo base alloys in plastic state under low cyclic fatigue

18 p2936 A71-36710

Notched fixed-pinned columns under concentric and eccentric compressive loads, presenting failure analysis based on stress intensity concept and methods of limit analysis

18 p2983 A71-36852

S-N curve and structural failure probability due to combined random and primary loads based on mathematical model

19 p3157 A71-37847

Lightweight solar cell structural failure modes under automatic thermal cycling for prolonged period in wide temperature range and by immersion in liquid nitrogen

20 p3179 A71-38852

Fracture testing, discussing fracture toughness, proof testing assemblies, crack identification, growth, catastrophic failure probability, etc

21 p3463 A71-40673

Beryllium reflector plate failure in NASA Plum Brook Reactor, discussing irradiation induced mechanical and physical property changes and internal/external stress effects

21 p3414 A71-40904

One dimensional structure failure calculation, using mathematical programming static method for load limit approximation

22 p3613 A71-41430

Koiter theory for structural snap-through buckling behavior, using discretized matrix procedure based on finite element idealization

22 p3613 A71-41436

Material fatigue failure under narrow band random vibration effects, deriving fatigue life prediction equation based on composite experimental design and statistical tests

22 p3615 A71-42002

Static, kinematic and uniqueness theorems of incremental collapse of frames extended to variable repeated loading

22 p3619 A71-42593

Failure and crack formation in gas turbine engine compressor disks under variable stresses from fatigue tests, considering safety factors

23 p3779 A71-44210

Metal cored cylindrical plastic shells response to transient external pressures, considering failure modes

24 p3878 A71-44610

Rotating disk creep analysis by Van Fo Fi-Ozerov nonlinear equation, obtaining numerical solution for total creep equation and time to failure for two angular velocities

24 p3882 A71-44839

Metal cylindrical shells plastic collapse under axial compression, deriving theoretical load/deflection relationship

24 p3883 A71-44875

STRUCTURAL FATIGUE

U FATIGUE [MATERIALS]

STRUCTURAL FOUNDATIONS

U FOUNDATIONS

STRUCTURAL INFLUENCE COEFFICIENTS

Influence coefficients for thin walled finite length cylindrical shells subjected to uniform internal pressure and edge loads

12 p1983 A71-27586

Direct solution for divergence speed of lifting surface using matrices of structural and static aerodynamic influence coefficients

21 p3456 A71-40171

Frequency, density, thickness and structural factors /stiffness/ influence on sound insulation of uncoated and foil coated absorbers

22 p3575 A71-42401

Inelastic transverse strain coefficient and Poisson ratio dependences on plastic and brittle properties

23 p3780 A71-44227

Thermally loaded rod structures optimization, presenting method for estimating canonical equations influence parameters

24 p3842 A71-44642

STRUCTURAL MATERIALS

U CONSTRUCTION MATERIALS

STRUCTURAL MEMBERS

NT ANISOTROPIC PLATES

- NT ANNULAR PLATES
 NT BEAMS [SUPPORTS]
 NT BOX BEAMS
 NT CANTILEVER BEAMS
 NT CANTILEVER PLATES
 NT CIRCULAR PLATES
 NT COLUMNS [SUPPORTS]
 NT CORRUGATED PLATES
 NT CURVED BEAMS
 NT ELASTIC PLATES
 NT END PLATES
 NT FLAT PLATES
 NT GIRDERS
 NT I BEAMS
 NT LONGERONS
 NT MEMBRANE STRUCTURES
 NT ORTHOTROPIC PLATES
 NT PERFORATED PLATES
 NT PLATES [STRUCTURAL MEMBERS]
 NT POROUS PLATES
 NT RECTANGULAR BEAMS
 NT REINFORCED PLATES
 NT SKIN [STRUCTURAL MEMBER]
 NT STRINGERS
 NT STRUTS
 NT TAPERED COLUMNS
 NT TRUSSES
 NT WING PANELS
- Lightweight structural elements fabrication from fiber reinforced plastic materials /prepregs/, discussing manufacturing methods, structural design, production and testing of parts, etc 01 p0172 A71-10690
- Lower bound load carrying capacity of thin walled structures of rods, plates and shells with statistical stable stress field, using plasticity theory 02 p0326 A71-12296
- Carbon fiber reinforced plastics and metals structural components design, discussing properties, processing and applications 02 p0330 A71-12910
- Polyurethane structural adhesives with excellent tensile shear and T-peel strengths at cryogenic temperatures, long pot lives and good processing characteristics 10 p1630 A71-24068
- Three dimensional reinforced composites for load bearing structural ablator 11 p1789 A71-26037
- Damped mechanical systems sinusoidal vibration analysis, using four pole parameters 12 p1928 A71-26701
- Fiberglass reinforced plastic structural elements heat induced deformation and carrying capacity due to material macroinhomogeneity and rigidities asymmetry 12 p1921 A71-27346
- Aircraft structural elements thermal behavior under aerodynamic heating with linear dependence on initial temperature 12 p1865 A71-27493
- Heat pipe application to OAO as structural isothermizer, considering overall spacecraft thermal network analysis 15 p2512 A71-31594
- Structural materials low temperature testing using cryogenic chambers, high power tensile test machines, semiconductor thermometers and resistance wire strain gauges 15 p2408 A71-31854
- Composite materials fabrication primary and secondary aerospace and aeropropulsion structural components [SME PAPER EM-71-710] 15 p2416 A71-32434
- Structural shapes extrusion technique with superalloy powders, noting fine grain, chemical homogeneity and elevated temperature mechanical properties [ASM PAPER W71-5.4] 16 p2592 A71-33540
- Wing structural elements ballistic damage tolerance and residual fracture strength characteristics, discussing projectile velocity, impact angle and target thickness effects 17 p2827 A71-35161
- Cost-performance tradeoffs of aerospace launch vehicle expandable structural components, investigating program factors, materials and construction technologies [SAWE PAPER 884] 17 p2750 A71-35828
- Extruding complex structural shapes of Ti alloys, considering use of glass as lubricant [SME PAPER MF-71-139] 18 p2927 A71-36662
- Frozen bipropellants as self supporting structural member for booster weight reduction, considering mechanical and thermal properties and melting rate requirement 20 p3276 A71-39609
- STRUCTURAL RELIABILITY**
 Fiberglass reinforced plastics heavy duty structural parts quality control, discussing strength parameters, safety coefficients, testing methods, etc 01 p0088 A71-10689
- Frame structures linear-mode failure probability estimation by reliability analysis 02 p0327 A71-12347

- Construction materials characteristic properties significance for design and structural reliability, discussing weldable Al alloys fatigue strength, internal stresses, inhomogeneity and corrosion behavior 06 p0981 A71-17341
- Complex airframe design for economic and safe operation and long life using fatigue and fracture mechanics [AIAA PAPER 70-512] 08 p1374 A71-22025
- Reliability prediction of narrow band structures under random excitations, considering catastrophic and fatigue failure modes 15 p2506 A71-32094
- Machine design strength criteria in development of formulas for lower bound estimates of mechanical components structural reliability 16 p2582 A71-33293
- Structural reliability predictions using finite element stress program and partial derivative method involving finite approximations 16 p2583 A71-33294
- Combat aircraft vulnerability to projectile impact predicted by model giving target penetration, damage size and structural response [AIAA PAPER 71-777] 16 p2660 A71-34013
- Redundancy method for correct performance of flexible structure with faulty elements prepared from microelectronic information media 17 p2720 A71-34955
- Metal-reinforced glass plastic composite conical shell with positive Gaussian curvature, estimating reliability and stability based on static tests 17 p2830 A71-35316
- Diffusion bonding as economical fabrication process for aerospace applications involving Ti alloys, emphasizing mechanical properties and structural reliability improvement [SME PAPER AD-71-245] 18 p2927 A71-36661
- Static joint wear role in overall machine reliability and service life under working loads from mathematical prediction 22 p3619 A71-42852
- STRUCTURAL RIGIDITY**
U STRUCTURAL STABILITY
STRUCTURAL STABILITY
 NT SHELL STABILITY
- Euler method applicability for finite subcritical deformation stability of isotropically nonlinear elastic body 01 p0165 A71-10065
- Structural stability at low temperatures - Conference, Kiev, February 1970 01 p0097 A71-10076
- Cryogenic pressure vessels carrying capacity, discussing loading types, materials properties, thermal effects, etc 01 p0097 A71-10077
- Statistical stability of structurally inhomogeneous material, analyzing weak spots effects on limiting state 01 p0166 A71-10081
- Bending-torsional flutter stability of cantilevered bar subjected to transverse follower force of fluid jet, using Frobenius method 01 p0166 A71-10125
- Thin elastic orthotropic plate in finite difference formulation, determining natural vibration mode and instability by summary representation method 01 p0168 A71-10410
- Stability theory of plates beyond elastic limit, discussing elimination of stress variations discontinuity at interface between plastic loading and unloading zones 01 p0170 A71-10648
- Circular shallow cylindrical panel stability and creep buckling under hydrostatic pressure 01 p0171 A71-10649
- Buckling in fiber reinforced plastic thin walled shell structures, discussing structural stability problems and methods for prevention of buckling 01 p0172 A71-10698
- Short beams vibrational analysis extended to stability analysis, using Timoshenko theory 01 p0174 A71-10966
- Forced random oscillations of nonholonomic systems about equilibrium positions, deriving stability conditions in white noise disturbances 01 p0176 A71-11042
- Buckling analysis of rectangular waffle plates with multiple sizes of ribs in each stiffening direction, considering stability and design 01 p0178 A71-11583
- LAMS flight control systems for turbulence induced fatigue damage reduction in B-52 and C-5A aircraft, using mathematical models 02 p0188 A71-11660
- Flexural-torsional vibration stability of thin walled elastic bars under longitudinal periodic force, using parametric resonance theory 02 p0321 A71-11687
- Nonlinearly elastic rings and arches under hydrostatic pressure, examining equilibrium with sixth order differential equations 02 p0325 A71-12125

- German monograph on arbitrarily distributed internal stresses effect on elastic stability of plates, considering variational problem solution as matrix eigenvalue problem 02 p0327 A71-12375
- Reinforced plastic laminates structural integrity, describing procedure for mechanical property evaluation 02 p0274 A71-12484
- Stiffened integrally formed panel stability evaluation based on compression structural efficiency and manufacturing costs [AIAA PAPER 69-760] 02 p0329 A71-12686
- Solidified Ni-Mo-Al gas turbine guide vane alloy with improved melting point, creep rupture strength and structural stability 03 p0431 A71-13256
- Elastic instability of transversely isotropic Timoshenko beam, deriving buckling coefficients curves vs parameter measuring shear deformation effect 03 p0504 A71-13452
- Elastic columns under transient loading, ascertaining stability by Liapunov function direct method 03 p0505 A71-13540
- Thin rod deformation by gyrostat motion analysis, deriving anisotropic curved rods equilibrium shapes 03 p0458 A71-13600
- Welded joint structural stability determination by measuring decarburized steel layer thickness after carbon diffusion into lower activity region 03 p0432 A71-13690
- Truss systems optimal structural design, noting elastic-plastic stability conditions 03 p0509 A71-13897
- Al-Mg alloys secondary creep relationship to mechanical instability during tension 03 p0445 A71-14340
- Postbuckling theory and applications covering perfect structure prebuckling state stability, cylindrical shells under axial compression, etc 04 p0664 A71-14734
- Book on flat plate stability covering initial buckling stresses, compressive and shear loads, holes, various reinforcements and shapes, sandwicheing, etc 04 p0667 A71-15074
- Soviet book on perforated plates and shells covering strength, rigidity, lattice tension and bending, stress and strain states, boundary value problems, etc 04 p0671 A71-15398
- Wall stability of parallel elastic plate duct in contact with inviscid compressible liquid flow 04 p0573 A71-15563
- Rotating shafts stability under torsion with two unequal flexural rigidities 04 p0672 A71-15773
- Stability of homogeneous and uniform deformation of isotropic body, using energy criterion 04 p0672 A71-15881
- Thin oval ring noncircularity effect on thermal instability based on small deflection analysis 05 p0820 A71-15983
- Tapered cantilever beam with variable bending rigidity and concentrated mass, investigating nonlinear flexural vibration 05 p0820 A71-15986
- Inhomogeneously reinforced composite structures strengthening by internal stress matching 05 p0771 A71-16365
- Deformation stability of three dimensional body with rheological properties under compression 05 p0824 A71-16591
- Axisymmetric normal loading of lateral surface of finite length elastic solid cylinder 05 p0824 A71-16595
- Structural elements carrying capacity increase by strain hardening and nonuniform quenching 05 p0826 A71-16752
- Aircraft light alloys fatigue characteristics for component endurance evaluation 05 p0767 A71-16757
- Structural stability of incompressible elastic rod of variable rigidity flattened along axis, reducing boundary value problem to equation with continuous operator 05 p0828 A71-16987
- Stability analysis of structural systems subject to nonconservative forces, using finite element method 05 p0829 A71-17118
- Sandwich panels with conical shell or elongated honeycomb fillers, calculating stability and elastic properties 06 p0986 A71-17757
- Elastic plates and shells stability and vibration problems asymptotic solution methods, considering edge effect 06 p0991 A71-17800
- Matrix and round inclusion two component composite equilibrium, considering crack effect on strength 06 p1000 A71-17938
- Brittle plates with statistically distributed cracks, examining limiting equilibrium under tension and compression 06 p1000 A71-17941

- Rigid body stability studies with Hamiltonian as Liapunov function, noting application to flexible compact gravity gradient satellite planar motion
[AIAA PAPER 71-212] 06 p0981 A71-18648
- Apollo lunar module structural integrity for lunar landing verified by Monte Carlo dynamic analysis
07 p1205 A71-18896
- Structural hysteresis in split root fir tree turbine blade attachment under centrifugal forces and cyclic bending moments
07 p1211 A71-19162
- Rapid heating effects on hot pressed TiC cylinders stability, calculating temperature fields and stress distribution
07 p1130 A71-19168
- Unbounded isotropic elastic plate traversed by two parallel cracks, obtaining limiting equilibrium state
07 p1211 A71-19192
- Viscoelastic rectangular thin plate stability under buckling conditions, showing ratio of long term to instantaneous critical loads as function of hereditary properties
07 p1212 A71-19351
- Optimal structural design for nonconservative elastic stability of cantilever column, obtaining critical load
07 p1212 A71-19473
- Tall thin strip rolling in ribbed grooves, determining critical area reductions causing plastic stability loss
08 p1295 A71-20841
- Aircraft turbine engines strength and gas dynamic characteristics improved by vibration decrease using elastic elements
08 p1349 A71-21710
- Beams torsional rigidity under thermal stress due to arbitrary temperature distribution
09 p1534 A71-22103
- General nonlinear elasticity theory including applications, deformation laws, complex nonlinear equations solutions, equilibrium and stability problems, experimental methods and mathematical models
09 p1536 A71-22512
- Theory of plates under finite initial elastic deformation, applying to rectangular plate stability under compressions in two mutually perpendicular directions
09 p1537 A71-22521
- Viscoelastic rectangular sandwich plate bending, stability, deflection and critical load calculation, assuming core stress-strain relation governed by Maxwell-Thompson differential equation
09 p1540 A71-22998
- Euler method applicability for finite subcritical deformation stability of isotropically nonlinear elastic body
09 p1541 A71-23272
- High temperature Ni alloys structural stability, computing gamma prime phase coagulation and average electron vacancy number
09 p1474 A71-23289
- Ti alloys in aircraft industry, considering jet engines applications and structural stability improvements related to fracture toughness, fatigue and stress corrosion
09 p1474 A71-23292
- Cylindrical body stability under axial compression with small elongations and shears, determining critical buckling force
09 p1542 A71-23437
- Plane sandwich plates in supersonic gas flow, investigating aeroelastic stability, transverse shear flexibility and axial loads
09 p1543 A71-23609
- Circular plates with radially symmetric membrane stresses and thickness, investigating stability under peripheral-moving load excitations
10 p1692 A71-24995
- Torsional-flexural stability of stiffened Ti panels for application to supersonic transport, using small deflection energy methods
[AIAA PAPER 71-338] 11 p1843 A71-25317
- B and C polymer laminated film composites efficiency for stability designed structures, considering weight reduction by planar reinforcements
[AIAA PAPER 71-353] 11 p1783 A71-25331
- Inflation of initially spherical balloon of elastic rubber-like material, discussing tensile instability
11 p1707 A71-25445
- Incremental plastic analysis under large displacement and physical instabilizing effects, using finite element models and quadratic programming
11 p1849 A71-25679
- Structural stability degradation mechanisms in welded joint of plain and low alloy steels, deriving equation for carbon diffusing
11 p1771 A71-26158
- Mesoscale gravity waves and jet stream stability in temperature-stratified atmosphere with small wave perturbations, estimating wave phase velocities and amplitude functions
12 p1924 A71-26736
- Stability analysis of rigid frames and trusses, including effect of bending moments and shear forces before buckling
12 p1976 A71-27161
- Three dimensional nonlinear elastic anisotropic body formulating stability at finite subcritical strains with variational principle
12 p1978 A71-27333
- Stability loss in microvolume of laminated composites with small filler concentrations during shrinkage, using three dimensional linearized equations
12 p1978 A71-27344
- Asymmetric structure elastic transversely isotropic sandwich panels bending equations, taking into account transverse shear strain and stability
12 p1981 A71-27497
- Isotropic and anisotropic materials stability criteria and boundary surfaces in invariant stress tensor spaces
13 p2149 A71-28120
- Girder system transverse bending under axial and lateral loads, deriving stability conditions by direct Liapunov method
13 p2153 A71-28519
- Free elastically joined composite rod under tracking forces, calculating stability and oscillations by numerical method
13 p2154 A71-28644
- Cylindrical shell laminar plastic structure effect on stability under hydrostatic pressure, applying Kirchhoff-Love hypothesis
13 p2155 A71-28654
- Dynamically loaded rigid plastic bodies, solving limiting equilibrium problems by extremal principles
13 p2156 A71-29065
- Unbounded orthotropic body with two internal coaxial elliptical cuts, calculating elastic equilibrium
13 p2156 A71-29068
- Biaxial plastic extension stability of anisotropic sheets and cylindrical shells, using Hill plasticity theory of orthotropic materials
13 p2156 A71-29074
- Nonconservative dynamic instability of columns under distributed tangential force, using analog computer
13 p2158 A71-29430
- Instability limit curves for twisted square metal plates under vertical loads with transition from anticlastic to synclastic deformation
13 p2158 A71-29431
- Oscillation and stability of free composite body with elastically suspended masses, simulating liquid sloshing in cavity by equivalent mechanical model
14 p2321 A71-29537
- Structural stability in tension and strength tests of thin walled tubes at various stress and strain intensities based on loss of resistance to plastic deformation
14 p2321 A71-29620
- Nonlinear stability of saddle-like deformed circular and square flat plates and shallow shells under transverse loadings
14 p2322 A71-29692
- Elastic sphere equilibrium with penny shaped crack under inner surface pressure, observing stress distribution
14 p2326 A71-30096
- Stability and longitudinal vibrations of elastic beam under rapid monotonously increasing and impulsive loading assuming free end
14 p2326 A71-30194
- Pin-ended column stability and random behavior under white noise excitation, using analog simulation and application to vertical earthquake and aerospace vibration environments
14 p2330 A71-30683
- Vertically cantilevered column weight and follower force effects on flutter and buckling instabilities respectively
14 p2330 A71-30685
- Weight effect on large elastic deflection of thin arches, studying stability via nonlinear differential equation using elastical approach
14 p2330 A71-30686
- Continuous system nonconservative stability examined by finite element Ritz method with extended Hamilton principle
14 p2330 A71-30687
- Nonuniform cross section tapered, stepped rectangular and I section cantilever beams elastic lateral stability
14 p2330 A71-30689
- Convergent finite element equations for dynamic stability of plates dependent on vibration and buckling modes
14 p2331 A71-30696
- Equilibrium stability of rods, shells and plates during creep due to applied load
14 p2333 A71-30893
- White dwarf star gravity mode stability, considering hydrogen-helium transition sorting zone
14 p2318 A71-31018
- White dwarf stars equilibrium models, discussing vibrational stability and radial pulsations eigenvalues and eigenfunctions
14 p2318 A71-31019
- Al-base alloys granules dimension and shape effects on extruded semifinished product mechanical properties and structural stability
15 p2424 A71-31242
- Multilobed inflated membranes stability under finite deformation, deriving system instability critical conditions
15 p2503 A71-31421
- Thermal buckling of elastic plates exposed to random temperature field producing biaxial stress concentration
15 p2504 A71-31834
- Monograph on rectangular shear elastic plates stability covering Cosserat plane, stress functions, buckling conditions, compressive forces and two dimensional equations
15 p2509 A71-32302
- Elastic rods and rings stability under compression beyond elasticity limit, determining equilibrium branching characteristics near bifurcation point
16 p2647 A71-32927
- Rods stability under nonconservative loads, applying Liapunov functions to boundary value problems
16 p2607 A71-32977
- Second order stresses and elastic stability analysis for structures, using supplementary load method
16 p2648 A71-32981
- Elastic structures stability under randomly fluctuating external loads based on statistical methods
16 p2648 A71-32988
- Elastic stability theory for perfectly elastic materials with couple stresses, deriving exact functional for overall conservative systems of forces and couples
16 p2648 A71-32989
- Rods instability with cross sectional stress concentration dependent properties, presenting buckling and bending problems
16 p2648 A71-32990
- Continuous systems stability analysis under parametric excitation, using time dependent Liapunov functional for frequency response
16 p2607 A71-32992
- Thin plates and shallow shells stability, investigating weak solutions of wall displacement differential equations
16 p2649 A71-32993
- Plastic structures buckling and instability phenomena, using elementary models with limited number of degrees of freedom and associated yield profiles
16 p2649 A71-32999
- Thermoelastic stability of finitely deformed solids under nonconservative surface tractions without body force
16 p2649 A71-33009
- Rigid-plastic solids with viscoplasticity extension, comparing stability with Hill condition
16 p2649 A71-33010
- Yield condition and stability of elastoplastic bodies with large deformations, using Gibbs method of thermodynamics
16 p2650 A71-33015
- Structural instability due to cyclic strain accumulation, using plastic deformation constitutive relation with stress tensor and elastic effects
16 p2650 A71-33016
- Bifurcating systems analysis in structural stability problems, discussing perturbation patterns in nonlinear branching theory
16 p2650 A71-33018
- Structural strength numerical evaluation, demonstrating effectiveness of regression equations in statistical data processing
16 p2651 A71-33063
- Geometrically nonlinear large deflection and structural stability problems, using finite element method
16 p2653 A71-33087
- Stiffened rectangular plates parametric instability under in-plane sinusoidal dynamic forces, using mathematical model with stiffeners as discrete elements
[ASME PAPER 71-APM-26] 16 p2655 A71-33203
- Cryogenic pressure vessels carrying capacity, discussing loading types, materials properties, thermal effects, etc
16 p2593 A71-33633
- Statistical analysis of structurally inhomogeneous material strength, analyzing weak spots effects on limiting state
16 p2658 A71-33637
- Alloying elements effect on structural stability and properties of W and Mo alloys single crystals, studying thermal cycling response
16 p2596 A71-33908
- Isotropic sandwich plates with rigid cores due to shear boundary tractions, considering transverse strain and stress, displacement function and stability
16 p2660 A71-34035
- Eccentrically stiffened thin cylindrical panels instability under uniform axial compression, uniform hoop compression and uniform shear
16 p2661 A71-34150
- Strain energy and stability of nonlinear plate and shell bending under Love-Kirchhoff hypothesis, using three dimensional elasticity theory
17 p2815 A71-34296
- Time dependent bending of circular cross sectioned rod under constant load compression and creep
17 p2821 A71-34564

STRUCTURAL STRAIN

Annular plate stability and postbuckling behavior in steady plane axisymmetric temperature field 17 p2822 A71-34598

Soviet papers on thin walled aircraft structures strength and stability covering bending theory, circular cylindrical shells, thermal stresses of rectangular plates, etc 17 p2828 A71-35301

Three layer trapezoidally corrugated panels with skin under longitudinal compression, determining local stability and stress-strain diagrams 17 p2830 A71-35320

Uniformly rotating thin relativistic disks structure, stability and gravitational fields within general relativity framework 17 p2806 A71-35405

Light alloys fatigue characteristics for aircraft components endurance evaluation 17 p2759 A71-35456

Rotor blade stability, calculating unsteady local lift and effects of blade profile camber and steady angle of attack 17 p2672 A71-35468

Structural stability regions construction for solid body with liquid filled cavities 17 p2730 A71-35607

Structural hysteresis in gas turbine blade herringbone scarf joints under centrifugal forces and cyclic bending moments 17 p2834 A71-35658

Simply supported Bernoulli-Euler beam resting on elastic foundation and carrying equally spaced moving mass particles, calculating lateral response dynamic stability by Galerkin method [ASME PAPER 71-APM-M] 18 p2978 A71-36256

Convergent approximations of impulsively loaded stable structures with account of geometry changes and discontinuity interfaces [ASME PAPER 71-APM-KK] 18 p2978 A71-36267

Elastic beam dynamic buckling stability under transverse follower force, considering force direction dependence on cross sectional twist angle [DFVLR-SONDDR-137] 18 p2980 A71-36679

Structural stability of incompressible elastic rod of variable rigidity flattened along axis, reducing boundary value problem to equation with continuous operator 18 p2982 A71-36787

Clamped oval cylindrical thin walled shells elastic buckling under axial loads, solving stability equations by Fourier method and higher order difference technique 19 p3157 A71-37876

Structural stability and creep properties of heat resistant steel weld joints, considering substitutional and precipitation hardening and dislocation effects 20 p3249 A71-39015

Nonlinear free and forced vibration response and stability of simply supported restrained buckled beams, using analog computer simulation [ASME PAPER 71-VIBR-17] 21 p3458 A71-40277

Flow induced flutter and buckling instability of elastic tube with displacement spring support [ASME PAPER 71-VIBR-39] 21 p3459 A71-40289

Perturbation study of subharmonic rotor instability due to elastic symmetry, obtaining equations of motion [ASME PAPER 71-VIBR-57] 21 p3385 A71-40302

Parametric instability in first spatial and temporal modes of cantilevered elastic columns with longitudinal inertia and end mass 21 p3462 A71-40531

Moderately thick plate transient response stability analysis, using finite difference equation 21 p3467 A71-40957

Nominal stress prediction for plastic tensile instability occurrence in flat orthotropic sheet loaded by biaxial stress system, considering localized and diffuse necking 21 p3469 A71-41005

Elastic stability of prismatic and cantilever bars in torsion 21 p3472 A71-41150

Critical coefficients of axial compressive forces with variable intensity for approximate stability analysis of vertical bars 21 p3472 A71-41151

Maximum vector values for stability and rigidity of elastic systems under modulo limited disturbances, applying to beam deflection and second derivative 21 p3473 A71-41154

Shallow two pinned sinusoidal arches stability under random symmetrically distributed lateral loads, observing deformation, buckling and critical value 22 p3612 A71-41429

Computerized design procedures for externally pressurized flexibly mounted gas lubricated journal bearings, predicting steady state performance, vibration capacity and translational stability 22 p3552 A71-41676

Eigenvalues and eigenvectors error estimation in vibration and stability finite element analysis as function of mesh size, using Birkhoff perturbation method 22 p3617 A71-42541

Nonlinear theory of tensile instability /necking/ of homogeneous isotropic bar obeying Rambert-Osgood law 22 p3618 A71-42588

Stability of edge reinforced circular plate under uniform radial load, considering flexural and extensional stiffness of reinforcing beam 22 p3618 A71-42592

Viking vehicle structural flexibility and propellant sloshing effects on thrust vector control dynamics, obtaining computer simulated responses for hybrid and discrete coordinate models [AAS PAPER 71-348] 23 p3773 A71-43021

Singly and nonsingly connected thin elastic rectangular plate stability analysis under arbitrary compression load on surface 23 p3777 A71-43423

Critical compression loads and stability equations for clamped and hinged circular three layer plates with light filler, using Bessel functions 23 p3778 A71-44043

Material properties, metallurgy, production technology and operational factors effects on machinery structural strength 23 p3779 A71-44207

Gas turbine blades of cast ZrSiO₂ heat resistant alloy, investigating structural strength from fatigue test data 23 p3779 A71-44208

Near equiatomic TiNi thermal martensite transformation premonitory events, discussing crystal structure, mechanical instability and lattice vibrations 23 p3694 A71-44280

Rod buckling under creep conditions, evaluating stability with Shenley model 24 p3877 A71-44405

High temperature aging, structural stability and tensile properties of hot rolled Co-W heat resistant alloy for space applications 24 p3836 A71-44443

Three dimensional incompressible anisotropic body with small deformations, calculating elastic stability theory with variational principle 24 p3880 A71-44708

Geometrically nonlinear integral solutions to equilibrium equations of curvilinear beam under uniform pressure, using Weierstrass functions 24 p3883 A71-44850

Numerical evaluation of structures buckling loads, considering matrix equation application to elastic stability problems 24 p3883 A71-44870

Vertical shaft stability on elastic sliding bearings, considering passage through autooscillations zone 24 p3831 A71-45051

Aerospace materials and structures shock sensitivity from derivation of dynamic fracture propagation relationship to stress wave 24 p3886 A71-45370

STRUCTURAL STRAIN

Circular Al rings under radial impulsive loading by curved magnetically driven Al flyer plates, recording strain-time histories on oscilloscopes [SESA PAPER 1644] 03 p0509 A71-13778

Circular cylindrical shell with trapezoidal stringers reinforcement system along length, calculating strain during oscillation 03 p0514 A71-14359

Shock wave propagation in three dimensional elastic media, calculating finite strains effect on behavior 05 p0828 A71-16988

Side strain reactions of shells of revolution with meridional ribs, integrating equations by Green function 06 p0989 A71-17785

Steel conical disks two dimensional stressed state determined with deformations at elastic and elastoplastic strains using digital computers 08 p1369 A71-21116

Plastic strains buildup during thermal cycling, establishing relation between strain interval and cycles number to failure for strain hardening materials 09 p1538 A71-22599

Gas dynamic test stand analyzing elastoplastic strains in aircraft gas turbine disks and liquid propellant rocket engines turbopumps under alternating nonisothermal loads 09 p1427 A71-22603

Strain level counter monitoring aircraft structural fatigue, describing system components consisting of sensors in critical structure areas and indicator unit with visual display 09 p1445 A71-22725

Variational criterion for stationary mode elastic structural oscillation, considering coincidence with normal modes for materials with stress-strain homogeneous function relationship 10 p1692 A71-25048

Elastic stress-strain law and internal structure symmetry for three dimensional fibrous composites, including caltrop reinforcement 11 p1852 A71-26396

Stresses and deformations of shallow spherical shells with specified edge displacements 15 p2502 A71-31186

Large deflections of thin piecewise prismatic elastic bars by electronic analog computer simulation 16 p2661 A71-3414

Nonlinear creep equation of elastoplastic medium under three dimensional stress, assuming classical viscoelastic and irreversible plastic deformation 17 p2817 A71-3414

Finiteness of deformations and convective terms effect on medium velocity in terms of displacements shock wave propagation in three dimensional elastoplastic medium 18 p2982 A71-36787

Noncircular cylindrical shells stress and displacement under hydrostatic loads, applying Donnell equations 24 p3879 A71-44405

Aircraft fuselage antisymmetric loading strain effects on small aspect delta wing performance 24 p3885 A71-44509

STRUCTURAL VIBRATION

NT BENDING VIBRATION

NT BREATHING VIBRATION

NT FLUTTER

NT LINEAR VIBRATION

NT MISSILE VIBRATION

NT PANEL FLUTTER

NT SELF INDUCED VIBRATION

NT SUPERSONIC FLUTTER

NT TORSIONAL VIBRATION

NT TRANSONIC FLUTTER

Short beams vibrational analysis extended to stability analysis, using Timoshenko theory 01 p0174 A71-10900

Spherical elastic shell axisymmetric vibrations in compressible fluid with free surface 01 p0071 A71-11040

Thin nonlinear elastic bar small longitudinal oscillations, solving boundary value problem for disturbances propagation 01 p0176 A71-11010

Nonautonomous vibrations of self excited catenary beam with tangential force 01 p0177 A71-11220

Book on mechanical vibration and shock measurements covering periodic and random vibration characteristics, instrumentation, control, etc 02 p0251 A71-12170

Free standing tower astronomical telescope discussing vibration problems in pedestal design 02 p0239 A71-12500

Elastic metal thin plates transverse resonant free vibrations, analyzing viscoelastic coatings damping effects [ASME PAPER 70-DE-E] 03 p0506 A71-13760

Elastic metal thin beams transverse resonant free vibrations, analyzing viscoelastic coatings damping effects [ASME PAPER 70-DE-D] 03 p0507 A71-13770

Periodic beam structure vibration response, using formulation for flexural wave propagation groups [ASME PAPER 70-WA/DE-3] 03 p0511 A71-14130

Aircraft fuselage vibration response to turbulent boundary layers, measuring structural wavelengths and phase velocities as functions of frequency [ASME PAPER 70-WA/DE-10] 03 p0348 A71-14140

Structural vibration response to nonhomogeneous random pressure fields based on homogeneous field theory [ASME PAPER 70-WA/DE-11] 03 p0511 A71-14140

Nonlinear partial differential equation solution for natural free-free vibrations of beam structures [ASME PAPER 70-WA/DE-55] 03 p0513 A71-14170

System frequencies and mode shapes characteristics relation to changes in structure, considering matrix approach for equations of motion of undamped vibrations 03 p0516 A71-14420

Monograph on bounds for vibration frequencies and buckling loads of clamped uniform thin elastic plate covering stability, harmonic and biharmonic functions 04 p0667 A71-14890

Axisymmetric free transverse vibration frequencies of centrally clamped spinning membrane disks 04 p0668 A71-15180

Supported rectangular plates HF transverse vibrations by holographic interferometry 04 p0668 A71-15180

Arches and rings in-plane natural vibration frequencies determination based on Newmark numerical integration method for beams 05 p0820 A71-15980

Spherical or conical shells of revolution axisymmetric oscillations, analyzing zero moment equation system spectrum 05 p0822 A71-16370

Double pulse laser holographic interferometry for large noisy vibrating subjects, including demonstration on Al plate 05 p0751 A71-16580

Slender beams transverse vibration, including nonlinear bending inertia in motion equation 05 p0825 A71-16710

Analog periodometer with short response time for helicopter blade vibration studies 05 p0752 A71-16730

Undamped structural vibration problems solution for eigenvalues and eigenvectors using simultaneous iteration method

Long thin circular cylindrical shell circumferential wave functions reduction to beam type transverse vibration equation, including rotatory inertia

Axisymmetric vibration frequencies, form shapes and apparent masses for vertical fluid filled coaxial cylindrical shells resting on shallow spherical shell

Circular cylindrical sandwich shell natural vibrations reduced to shell and filler contact problem, using two and three dimensional models

Elastic plates and shells stability and vibration problems asymptotic solution methods, considering edge effect

Thin elastic shell of revolution with negative Gaussian curvature, discussing free nonaxisymmetric oscillations

Orthotropic plate dynamics, examining plane vibrations with group theory approximate equations

Equidistant multiple span rectangular plates vibration and acoustic radiation under random external forces

Vertical circular cylindrical tank with shallow spherical shell bottom filled partially by ideal incompressible liquid, calculating joint oscillations

Elastic momentless conical tank with spherical bottom partially filled by liquid, calculating axisymmetric oscillation

Critical parameters and vibration frequencies of homogeneous closed circular rings connected to thin shells determined for various boundary conditions

Dynamic stability of cylindrical shell with freely supported edges partly filled with ideal compressible fluid and undergoing steady longitudinal vibrations

Complex form plates bending and oscillations under various boundary conditions, discussing procedure for coordinate sequences construction

Shell-fluid interaction problems, considering liquid filled shells oscillations, acoustic shock waves action, body impact against water, etc

Vibration and wave analysis in dynamic deformation of elastic shells and plates with environmental allowance

Prismatic shells vibration, buckling and stress analysis, applying computer solutions to complex bodies of revolution

Spring supported beam-column n th vibration and buckling eigenvalues, discussing Monte Carlo simulation for evaluating perturbation method accuracy for variance calculation

Holographic interferometric recording of vibration patterns of plexiglass cored construction mirrors

Spacecraft structures vibration testing nonlinear effects, extending asymptotic method for transition through resonance to nonresonant regions

Monte Carlo technique for time domain response analysis of nonlinear structure in random pressure field with large deflection

Forced thickness-stretch vibrations of plated elastic plate, involving time derivatives in boundary conditions

Fluctuating circulation, lift and flow induced structural vibrations of two dimensional bodies, including vortex shedding on sluice gates

Power spectrum analysis of ELDO Europa 1 third stage thrust phase vibrations, using digital filters

Multivariate and multidimensional random processes simulation with specified cross spectral density, applying to nonlinear structural vibration analysis

Spherical sandwich shells free vibration motion equations, taking into account transverse shear deformation and rotatory inertia effects

Space shuttle vibrational characteristics, investigating dynamic models, aeroelasticity, reentry, wing stall flutter and buffet boundaries

Liquid filling effect on oscillation modes of ellipsoidal stainless steel shell in vibrator

Elastic systems vibrations calculated with allowance for amplitude and frequency dependent energy dissipation, using hysteresis loop contour expression

Heterogeneity effects on thin composite cylindrical shells axisymmetric vibration characteristic, considering material and geometric symmetry deviations influence on frequency spectra

Box type structure free vibrations investigation by rectangular finite elements, comparing with natural frequencies and normal modes solution

Energy dissipation-fatigue strength relationships during vibrations for prestrained metals and alloys

Amplitude dependence of Young modulus defect in metals during large stress HF oscillations

First and second frequency harmonics and form shapes of liquid filled cylindrical shell axisymmetric vibrations, analyzing effect of pressure and shell dry portion on vibration frequencies

Symmetric three-layer girder with contact deformations and transverse compression of filler, calculating vibration under elastic impact by numerical analysis

Multilayer plate vibrations calculated with allowance for energy dissipation in material, deriving equations of motion

Electrodynamic transducer design for structural vibration testing system, using low power steering signal converter to generate large scale electromechanical loads

Liquid shell about solid spherical core, analyzing vibrations and sphere gravitational effects on material particle motion

Helicopter vibrational behavior prediction in flight with known aerodynamic loads, using branch modes method

Fourth order boundary problems with discontinuous boundary conditions, considering circular plate transverse vibrations

Vibrational characteristics of pretwisted cantilever beams with uniform rectangular cross section, investigating slenderness ratio effect on natural frequencies

Boundary value problem concerning stability and oscillations of shells of revolution through reduction to Cauchy problem based on direct integration of equilibrium equations

Random vibrations of statistically inhomogeneous elastic systems, using perturbation method

Al alloys one step fatigue tests under combined high temperature and structural vibration conditions

Dynamic analysis of vibrating beams on viscoelastic supports, using Galerkin approximate method

Transform method application to structural dynamic analysis for engineering structure transient response to various vibration modes

Structural system frequency response measurements under environmental noise conditions, discussing autocorrelation function for transient excitation damping

Closed cylindrical shell response to randomly time distributed broadband acoustic excitations, using statistical energy method to compute displacement and interior pressure

Finite element method for stiffness matrix free vibration analysis of thin rectangular plates under central planar loadings

Soviet book on vibrations of deformable systems and computer solutions covering ponderable rods, beams, plane frames, lattice structures, plates, bars, blades, shafts, etc

Apollo spacecraft qualification vibration test program assessment, discussing structural acoustical excitation method

Interchangeable head vibration exciter for 200g large object testing and measurement of structural modes, impedances, transfer functions and calibration

Spherical shallow shell with hole, noting natural vibration frequency

Rotation effects on vibration traveling waves in rotating cylindrical shells, considering Coriolis, centrifugal and torque loads

Heat generation in hinged orthotropic viscoelastic cylindrical shells under transverse vibrations and cyclic surface load

Spherical or conical shells of revolution axisymmetric oscillations, analyzing zero moment equations system spectrum

Vibration natural frequencies and mode shapes of cantilever plate mounted on rotating disk periphery, using finite element technique

Characteristic equation of respiration vibrations of cylindrical ring in incompressible viscous fluid at rest, obtaining damping coefficient for large induced flow Reynolds numbers

Vibration transversely isotropic orthotropic plates, presenting approximate nonlinear dynamic theory

Free elastically joined composite rod under tracking forces, calculating stability and oscillations by numerical method

Vibration amplitudes and transverse acceleration of reentry vehicle during uncontrolled atmospheric descent trajectory

Transverse free vibrations of beam with one end fixed and other supported on bilinear spring and carrying concentrated mass

Vibrating cantilever beam dynamic stress photoelastic determination based on photomechanics and optic-stress laws

Time independent three dimensional streaming secondary motion due to vibrating flexible plate

Imperfect circular disks large amplitude free transverse vibration calculation by Galerkin procedure

Structural steady state vibration frequency response and resonance testing, investigating nonlinearity effects of large deflections

Stability and longitudinal vibrations of elastic beam under rapid monotonously increasing and impulsive loading assuming free end

Approximate similitude relation for vibrating thin shells with scaled surface geometry, using Love equations of motion

Axisymmetric vibrations of heterogeneous isotropic composite clamped circular plates based on Kirchhoff theory

Nonlinear vibrations of clamped and edge supported laminated orthotropic plates, obtaining nonlinear equations of motion solutions by Ritz-Galerkin method

Extensional vibrations of thin cylindrical shell, discussing longitudinal and radial motions coupling and resonant frequency dependence on length/radius ratio

Automated modal data acquisition and processing system/MODAPS/ for real-time modal vibration testing of complex aerospace vehicle structures, describing features, capabilities and utilization

Twist-bending vibration of ring of rectangular cross section for entire range of length-to-diameter ratios, using Rayleigh shell theory

Nonlinear vibration of changing boundaries structures, approximating boundary values by perturbation technique

Missile component vibration environments generation by Minuteman 2 and 3 third stage motors solid propellant oscillatory burning

Nonuniform rotation of nonhomogeneous isotropic elastic cylindrical shell, obtaining steady state axisymmetric vibrations

Free vibrations of beam-like structures, deducing equations of motion

Interferometric holograms of vibrating body via numerical analysis of oscillations amplitude and phases

Longitudinal wave absorbers attenuating resonance vibrations in rods and plates

Nonlinear coupled parametric response of crooked thin walled columns under harmonic longitudinal load

STRUCTURAL WEIGHT

Flutter of thin walled cylindrical shells conveying fluid above critical flow velocity 15 p2508 A71-32135

Nonhomogeneous Helmholtz vibration equation for sectorial annular membranes and plates under arbitrary load, using Fourier method 15 p2508 A71-32231

Energy dissipation in material under complex vibrations, noting role of summary shear stress 15 p2508 A71-32234

Orthotropic layered cylindrical shells, deriving equations of motion for rotationally symmetric vibration 15 p2509 A71-32513

Mathematical techniques of equilibrium states and periodic vibrations in nonlinear elastic systems illustrated by thin plate and shallow cap buckling under uniform pressure 16 p2649 A71-32998

Imperfect circular cylindrical shell under external hydrostatic pressure loads, determining free and resonant vibration modes 16 p2651 A71-33062

Structural vibration and dynamic response analysis, applying finite element motion equations 16 p2653 A71-33090

Dynamic vibration analysis of mechanical structures, considering transfer and stiffness matrix methods 16 p2653 A71-33091

Stationary narrow band Gaussian vibration excursion probability based on Markov point process [ASME PAPER 71-APM-19] 16 p2655 A71-33210

Free vibrations of linear structure with arbitrary support by Rayleigh-Ritz method using unconstrained normal modes [ASME PAPER 71-APM-6] 16 p2656 A71-33218

LF axisymmetric vibrations of spherical completely filled tank with free liquid surface in upper tank and pipeline 16 p2657 A71-33602

Isotropic elastic body steady vibrations with moment stresses, solving two dimensional boundary value problem 16 p2658 A71-33716

Initial interaction phase between thin shallow conical shell vibrating axisymmetrically and ideal incompressible fluid, determining hydrodynamic pressure effects 16 p2560 A71-33901

Energy dissipation of vibrating structures in complex stress state, using generalized stresses and strains as coordinates 16 p2659 A71-33981

Concave thin shell of revolution lowest natural vibration spectra frequency corresponding to simple inflection point 17 p2817 A71-34341

Multicomponent system of elastic plate with hole and built-in viscous-fluid-filled siphon bellows, calculating oscillation by asymptotic methods 17 p2777 A71-34423

German monograph on upper and lower bounds in elastomechanics covering elastostatic, natural vibration and stability problems, elastic states Hilbert space, numerical methods, etc 17 p2818 A71-34480

Freely vibrating supported elastic isotropic oval cylindrical shells natural frequencies and mode shapes 17 p2825 A71-34873

Nonlinear oscillations - Conference, Kiev, August-September 1969 17 p2779 A71-34903

Averaging method for nonlinear oscillations in celestial mechanics, radio engineering and electronics and for time lag, random forces and integrodifferential equations 17 p2779 A71-34904

Slightly nonlinear structures vibration, examining experimental means for mathematical models development and coefficients determination 17 p2779 A71-34906

Asymptotic solution for nonlinear vibrations of mechanical system with slowly varying parameters and strong resistance 17 p2779 A71-34908

Nonlinear vibrations, studying differential equations system in normal form 17 p2779 A71-34909

Periodic or almost periodic small combination vibrations onset conditions by integral equations method and averaging principle 17 p2779 A71-34910

Integration method for second order nonlinear differential equation describing vibrational processes in mechanics, physics and engineering 17 p2766 A71-34913

Integrally stiffened panels with bonding material across stringer tops, calculating vibration damping characteristics 17 p2826 A71-35034

Timoshenko beam transverse vibration with time dependent boundary and normal loads, using Laplace transform method [ASME PAPER 71-APM-F] 18 p2977 A71-36253

Generalized vectorial equation of motion for vibrating nonprismatic thin space beams, discussing boundary conditions, rotary inertia and shear deformation [ASME PAPER 71-APM-F] 18 p2978 A71-36259

Additive damping control of acoustic resonance fatigue of aerospace structures under severe environments, considering materials, tuned devices and layered techniques 18 p2979 A71-36494

Excitation response of oscillatory conservative linear system to transient displacement involving time dependent boundary conditions 18 p2947 A71-36748

Cylindrical shells under uniform external pressure loads, determining boundary conditions effects on natural frequencies and vibration mode shapes 19 p3155 A71-37529

Variable thickness and rigidity cylindrical shells, determining natural frequencies and vibration mode shapes with algorithm based on Ritz method 19 p3155 A71-37531

Edge clamped spherical shell natural vibration frequency determination using Vlasov shell theory equations 19 p3155 A71-37532

Linearly deformable beams with distributed parameters and lumped inclusions, determining natural transverse vibration frequencies and mode shapes 19 p3155 A71-37535

Constitutive equation coefficients determination for nonlinear vibrations of viscoelastic beam by perturbation and optimal linearization method 19 p3158 A71-38060

Power balance and statistical analysis of energy flow and response in lightly damped resonant structures 20 p3268 A71-38960

Transverse waves propagation in vibrating orthotropic rectangular beams, noting inexact information regarding shear distribution 20 p3307 A71-39037

Approximate theory for vibration of nonhomogeneous anisotropic layered plates using asymptotic integration of elasticity equations 20 p3310 A71-39782

Forced and free vibrations of shallow cylindrical shell in rectangular duct filled with ideal fluid 20 p3310 A71-39785

Algorithm for linearly elastic structures vibration natural undamped frequency computation, assuming known dynamic stiffness matrix 20 p3311 A71-39964

Iterative method for linearly elastic structure undamped vibration natural frequency determination with fast convergence 20 p3311 A71-39965

Dynamic influence of isotropic flat plates on spatial vibratory structures containing rigid bodies, considering compatibility and modal coupling [ASME PAPER 71-VIBR-3] 21 p3456 A71-40267

Axial vibration transmission characteristics of shells of revolution, stressing shell mass and thickness, internal damping and edge restraint effects [ASME PAPER 71-VIBR-7] 21 p3457 A71-40270

Von Karman equations analogs solution for nonlinear large amplitude vibrations of circular plate on uniform elastic foundation 21 p3457 A71-40271

Flow induced vibrations of metal bellows with internal cryogenic fluid flow, noting effects of heat transfer, liquid state properties, external damping and condensation [ASME PAPER 71-VIBR-14] 21 p3457 A71-40276

Vibratory amplitudes and stress levels from metal bellows flow induced vibrations, discussing damping and acoustical resonances effects [ASME PAPER 71-VIBR-22] 21 p3458 A71-40279

Structure born noise reduction by viscoelastic coatings, examining effects of thickness, density, bending and shear induced loss factors, moduli and Poisson ratio [ASME PAPER 71-VIBR-29] 21 p3414 A71-40284

Viscoelastically damped structures finite element modeling and analyzing methods [ASME PAPER 71-VIBR-36] 21 p3458 A71-40288

Lumped parameter modeling of fluid elastic vibration response of nonlinear piston driven pneumatic-mechanical system, using finite element control volumes [ASME PAPER 71-VIBR-41] 21 p3459 A71-40291

High load structural dampers evaluation under linear or sinusoidal/triangular displacement control with constant speed testing machines [ASME PAPER 71-VIBR-46] 21 p3459 A71-40295

Viscoelastic materials with varying glass transitions, free and constrained layer damping and damping of LF vibrations in massive structure [ASME PAPER 71-VIBR-47] 21 p3405 A71-40296

Coupled bending-bending vibration of pretwisted tapered cantilever blades, obtaining equations of motion [ASME PAPER 71-VIBR-78] 21 p3460 A71-40315

Transfer matrix and finite element combination technique for plates and shells vibration analysis [ASME PAPER 71-VIBR-85] 21 p3461 A71-40321

Five-span skin-stringer width and damping effects on vibrational response including resonant frequencies and mode shapes by transfer matrix analysis [ASME PAPER 71-VIBR-101] 21 p3461 A71-40322

Cu-rich alloys with high damping capacity at low stress amplitudes for structures and machines, noting damping stability improvement in Mn-Cu alloy by Ca addition [ASME PAPER 71-VIBR-106] 21 p3396 A71-40331

Hybrid electromechanical analog computer real time simulation technique for optimizing vibration response of two degree of freedom system with impact damper [ASME PAPER 71-VIBR-119] 21 p3350 A71-40338

Thin truncated conical shells axisymmetric free vibrations, considering shear deformation and rotary inertia effects 21 p3462 A71-40528

Small deformation dynamic response of vibrating isotropic linearly elastic spherical shell to radial and time dependent body force field 21 p3464 A71-40769

Structural vibrations excited by spatially and temporally random pressure loading, discussing power spectra and vibration measurement 21 p3467 A71-40912

Real time holographic interferometry of steady state mechanical vibrations of engineering structural components applicable to arbitrary small amplitude and large mode numbers 21 p3381 A71-40934

Vibration characteristics of cantilever beam about nonlinear equilibrium state, showing flexibility and prestressed state effect 21 p3468 A71-40968

Clamped circular elastic plate nonlinear free vibrations, obtaining mode shapes and amplitude-frequency relationships 21 p3471 A71-41025

Axisymmetric imperfect conical shells vibration analysis using time average holographic interferometry technique 21 p3382 A71-41028

Paraboloidal shells of revolution inextensional vibrations comparison to Sanders theory, using finite element method 21 p3471 A71-41030

Elastic plates radial vibrations excited by piezoelectric elements, investigating electromechanical coupling coefficient and ultrasonic radiation constants 21 p3473 A71-41365

Parametric and autoparametric instability of aircraft structures 22 p3483 A71-42240

Eigenvalues and eigenvectors error estimation in vibration and stability finite element analysis as function of mesh size, using Birkhoff perturbation method 22 p3617 A71-42541

Statistical approach to complex structural vibration under random excitation 23 p3775 A71-43214

Optimal control of self excited vibration of high speed rotor with thrust magnetic bearing, using analog simulation 23 p3681 A71-43311

Resonance equation for rotating shaft natural vibration, using Timoshenko beam theory and gyroscopic moments 23 p3776 A71-43377

Thin elastic shell of revolution with waves along parallel, considering small free nonaxisymmetric vibrations 24 p3877 A71-44406

Natural vibrations of complex shape plates with clamped edge on resilient base, deriving approximate solution via R functions 24 p3877 A71-44481

Global-local finite element combined Ritz methods for beam and plate vibration analysis 24 p3880 A71-44638

Nonlinear vibrations of circular plate with variable boundary contact on rigid base 24 p3881 A71-44831

Radial thrust bearing balls ovality effect on axial vibration of rapidly rotating turbine engine rotor 24 p3864 A71-45006

STRUCTURAL WEIGHT

German monograph on systems analysis of future jet and fan propulsion systems for VTOL commercial aircraft weight and cost reduction 01 p0142 A71-10115

Weight allowance in optimal design of plastic structures under creep 01 p0170 A71-10641

Elastoplastic zero moment shells weight minimization for given middle surface geometry 01 p0170 A71-10647

Optical communication systems cost and weight optimization by COPTRAN program 02 p0214 A71-12028

Flame-fired thermionic diode service life, output power and voltage efficiency and weight reduction 02 p0196 A71-12269

Optimal cross sectional dimensions of thin walled longeron beams and ribs of skin reinforced delta wings minimizing weight

02 p0329 A71-12562

Subsonic aircraft size effect in conventional design, discussing increased weight increments and economic gain rate

[AIAA PAPER 70-940]

02 p0189 A71-12676

Minimum weight design for beams and frames with compliance constraints from constitutive relation

04 p0671 A71-15754

Lambda rocket motor case weight reduction through use of MB 130 instead of HT 100 steel, presenting structural strength test results

05 p0821 A71-16297

Haunched beam design optimization for lightest weight, analyzing failure modes under assumption of elastically rigid perfectly plastic material

06 p0981 A71-17301

Weight-optimal cylindrical shells of revolution with uniform strength edge reinforcement, discussing pressure vessel design

06 p0982 A71-17356

Reinforced cylindrical minimum weight shells under combined axial compression and internal pressure, examining strength and buckling modes

06 p0982 A71-17357

Reinforced zero moment minimum weight shells strength analysis and optimal design algorithms, using discrete calculation scheme

06 p0998 A71-17854

Aircraft generator service life improvement and weight minimization by close coupling with drive and heat producing components cooling with oil spray and mist

06 p0849 A71-18463

Axially compressed ring and stringer stiffened cylindrical shells minimum weight design, considering configuration instability

[AIAA PAPER 71-147]

06 p1003 A71-18590

Carbon fiber reinforced plastics potential aerospace structural applications, considering weight saving, mechanical properties, thermal expansion, stress concentration, impact resistance, corrosion and lightning problems

[PLASTICS INST. PAPER 43]

08 p1369 A71-20927

Reactor shield weight optimization using FASTER-III Monte Carlo computer program for neutron and gamma ray transport

09 p1539 A71-22810

Variational formulation for minimum weight of structures with given yield stress, considering homogeneous isotropic material, plasticity condition and collapse mechanism

10 p1685 A71-23977

Variable weight composite materials for aircraft optimal adhesive bonding structural designs, discussing C-5A tow weight saving Ti honeycomb applications

10 p1686 A71-24084

Lightweight parabolic antenna model with inflated Mylar tube torus and central mast interconnected by wires, discussing construction, performance tests and tradeoffs

[AIAA PAPER 71-397]

11 p1736 A71-25273

Weight minimization of semiinfinite flat sandwich panel at constant dynamic pressure in supersonic flow subject to flutter constraint, using finite element model

[AIAA PAPER 71-330]

11 p1842 A71-25310

Spacecraft structures weight optimization based on fracture mechanics and reliability cost constraints applied to pressure vessel design

11 p1847 A71-25464

Nuclear thermionic systems conceptual design with converters outside reactor to reduce weight

11 p1710 A71-25874

Thermal control, pressure survival and structural tradeoffs of Jovian atmospheric probe for mission parametric studies

[AIAA PAPER 71-482]

11 p1839 A71-26257

Computerized minimum weight design of elastic redundant trusses under multiple static loads, using algorithms for generating upper and lower bounds for configuration

[AIAA PAPER 71-362]

12 p1980 A71-27409

Minimum weight design of statically determinate wide flange beams, using Lagrange multipliers

13 p2151 A71-28210

Minimum weight design of circular cylindrical shell hinged at ends under axial compression, using random search method with self learning

13 p2152 A71-28280

Geometrical parameters of stringer nodes in statically determinate minimum weight equal stress and strength trusses

13 p2154 A71-28647

Optimized thin walled elements in elastic planar frame structures minimum weight design

14 p2324 A71-29872

Weight effect on large elastic deflection of thin arches, studying stability via nonlinear differential equation using elastical approach

14 p2330 A71-30686

Optimal structural design for nonconservative systems under buckling, noting application to minimal weight nonprismatic elastic bar shape determination

16 p2649 A71-33012

Optimum vertical surface configuration for STOL transports, considering structural weight and performance requirements

[AIAA PAPER 71-769]

16 p2524 A71-34006

Aircraft structural parameters optimization satisfying flutter weight constraint and minimum mass, applying to box beam design

17 p2825 A71-34874

High modulus graphite composites application for structural weight reduction and stiffness requirement without strength loss

17 p2762 A71-35202

High modulus graphite-boron composites design and application to lightweight structures, illustrating sandwich construction for race boat main boom stiffness and compressive strength

17 p2762 A71-35203

Solid state diffusion bonded boron-aluminum composites, discussing mechanical properties, weight and cost reduction and applications

17 p2758 A71-35204

Rigid plastic framed structures minimum weight design and analysis formulation by network-topological approach based on yielding concept

17 p2831 A71-35356

High voltage DC electric power transmission systems with ground return, reducing aircraft wiring weight and energy dissipation

17 p2678 A71-35771

Integrated drive generator for aircraft electrical power systems, improving weight, life and reliability

17 p2678 A71-35781

Administrative techniques of cost/weight tradeoff program for jet transport airplane

[SAWE PAPER 899]

17 p2750 A71-35812

Statistical analysis of error sources and magnitudes in Boeing 747 weight values obtained by onboard aircraft weighing system and by manual calculations

[SAWE PAPER 897]

17 p2676 A71-35813

Composite materials effect on supersonic aircraft weight, design and performance

[SAWE PAPER 888]

17 p2676 A71-35818

Weight reduction potential of composite materials in aerospace structures, proposing weight estimation technique

[SAWE PAPER 887]

17 p2834 A71-35819

Design, analysis and testing of F-111 complex fuselage full scale section of composite materials, noting weight savings

[SAWE PAPER 889]

17 p2835 A71-35825

Composite structures development, discussing wing, fuselage, aeropropulsion and missile development, weight savings of hardware and fighter empennage applications

[AIAA PAPER 71-367]

18 p2979 A71-36275

Premium mechanical properties for materials in space shuttle orbiter project, emphasizing cost and weight reductions

18 p2979 A71-36465

Minimum weight design of statically determinate elastic truss under multiple stress and displacement constraints, using virtual work of dummy loads

18 p2982 A71-36842

Aircraft electronic or fly by wire control systems, discussing aircraft design fuel-structure weight reduction cycle and control system redundancy requirements

[AIAA PAPER 71-959]

19 p3099 A71-37200

Minimum mass design of two dimensional plate-like structure with free vibration fundamental frequency or aeroelastic constraints, using optimal theory for extremum

19 p3158 A71-37877

Pioneer Jupiter spacecraft, noting low weight, radioisotope thermoelectric generators and gyroscopic stabilization by spinning with antenna pointed at earth

[AAS PAPER 71-167]

19 p3141 A71-37964

Real weight formula for shell fuselages based on theoretical similarity considerations

20 p3178 A71-39411

Frozen bipropellants as self supporting structural member for booster weight reduction, considering mechanical and thermal properties and melting rate requirement

20 p3276 A71-39609

Structural optimization problems involving vibration-weight interactions, using optimal control nonlinear programming transforms

[ASME PAPER 71-VIBR-66]

21 p3460 A71-40308

Displacement fields for two dimensional minimum weight frames for load dispositions analogous to perfectly plastic plane flow in metal working

21 p3391 A71-41428

Satellite-borne minimum bulk and weight K-band transmitter and receiver frequency converters design features and performance

22 p3524 A71-42522

Civil transport aircraft and equipment maintenance and reliability problems solutions with best time, cost and weight compromises

24 p3792 A71-44765

Volume-weight characteristics of cross flow heat exchangers for heat regenerating gas turbine engines

24 p3889 A71-45007

Ideal weight of axisymmetric fuselage shells, taking into account load distribution and cabin pressurization

24 p3885 A71-45180

STRUTS

Nonlinear impact buckling of strut, using asymptotic small parameter method

01 p0177 A71-11296

Creep analysis for thermoplastic beams under bending and struts under buckling

10 p1685 A71-23942

Analytical nonlinear landing gear model of flexible aircraft and strut lockup-breakout interaction using digital simulation language /DSL/

[SAE PAPER 710401]

10 p1555 A71-24263

Finite element midincrement stiffness matrices in postbuckling analysis of imperfect strut and rectangular plate

15 p2503 A71-31420

Coupled elastic buckling in continuous systems, determining postbuckling paths for strut, spherical shell and flat plate

16 p2650 A71-33017

Filament wound glass-reinforced plastic struts for cryogenic tank supports in long term planetary missions, testing thermal and mechanical properties

17 p2762 A71-35205

STURM-LIOUVILLE OPERATOR

U STURM-LIOUVILLE THEORY

STURM-LIOUVILLE THEORY

Sturm-Liouville type nonlinear problems solution by Prufer polar coordinate technique, proving equivalency theorem for eigenvalues infinite sequence conversion

22 p3567 A71-42689

STYLUSES

U PENS

STYRENES

NT POLYSTYRENE

Styrene-methyl methacrylate and -acrylonitrile copolymers linear and mass regression rates in hybrid rocket fuels combustion

15 p2464 A71-31640

SUBASSEMBLIES

Experimental flight mechanics in terms of data processing quality, discussing subsystems control

10 p1581 A71-23928

SUBCARRIER WAVES

U CARRIER WAVES

SUBCIRCUITS

U CIRCUITS

U SUBASSEMBLIES

SUBCONTRACTS

Industrial project management, defining functions and responsibilities of program director, contractor, subcontractor and manufacturer

23 p3785 A71-43460

SUBCOOLING

U SUPERCOOLING

SUBCRITICAL FLOW

Critical and near critical two phase flow in venturi tube, applying one dimensional flow equations

[ASME PAPER 71-FE-4]

13 p2051 A71-29447

Subcritical nonlinear potential flows over two dimensional subsonic airfoils by multistrip method of integral relations

18 p2845 A71-36330

SUBGRAVITY

U REDUCED GRAVITY

SUBGROUPS

Commutative nilpotent semigroups, discussing necessary and sufficient conditions for freedom within manifolds

02 p0276 A71-11725

General Markov processes, considering topological space E and semigroup t equal to or greater than zero

12 p1922 A71-26819

Type CS finite groups characterized by nonexpandability into Silov subgroups, defining group order divided into two different prime numbers

24 p3843 A71-44824

SUBHARMONIC GENERATORS

Multioctave microwave frequency synthesizer by subharmonic synthesis and frequency multiplication under digital programmed commands

01 p0054 A71-10972

Subharmonic forced vibrations of one degree of freedom nonlinear mechanical systems, deriving formulas for oscillation amplitude, phase shift and shape factor

09 p1536 A71-22410

Subharmonic oscillations excited by horizontal vibrations of mathematical pendulum suspension

16 p2607 A71-32936

Fluctuations in parametrically excited subharmonic oscillator, deriving steady state probability distribution for amplitude and phase transitions analogous to Brownian motion of particle in potential well

20 p3203 A71-39094

SUBLATTICES

U LATTICES [MATHEMATICS]

U SUBGROUPS

SUBLAYERS

U SUBSTRATES

SUBLIMATION

SUBLIMATION

Resistively heated W-Re wire sublimation characteristics between 1550-1950 C in low pressure oxygen
02 p0264 A71-12255

Reactive molecule and atom attack of refractory materials in dissociated gases at filament temperatures up to sublimation threshold
03 p0374 A71-13124

Chromium steel surface diffusion saturation by sublimated Mo, examining process kinetics
03 p0442 A71-13400

Direct measurement of convective heat transfer coefficient by realizing proportionality to sublimation rate of naphthalene ball near body surface
04 p0545 A71-15158

Two dimensional unsteady heat conduction in solid with subliming surface, replacing original boundary value problem by ordinary integrodifferential equation
14 p2338 A71-30933

Subliming nuclear microthruster design with Monte Carlo study of rarefied gas nozzle flow, noting application to spin stabilization
19 p3103 A71-38351

Oxygen enhanced sublimation of p-type PbTe thermoelectric materials in isothermal and ingradient testing of couples
20 p3266 A71-38953

Aluminum nitride crystals production by sublimation in resistance furnace with graphite heater
22 p3585 A71-41701

Ammonium perchlorate sublimation using simultaneous differential thermal analysis and thermogravimetry
23 p3641 A71-43116

Temperature field measurements above porous surface during ice-water sublimation into vacuum, showing discontinuities due to external heat and mass transfer
23 p3784 A71-44340

SUBMARINE CABLES

International telephone transmission, comparing technical and economic characteristics between submarine cable and satellite systems
10 p1577 A71-24267

SUBMERGED BODIES

NT DIVING (UNDERWATER)

Submerged moving body in nonviscous incompressible fluid, evaluating finite potential flow field momentum with rigid and free far distant outer boundary
06 p0841 A71-17419

Free vibrations of closed spherical shell immersed in ideal incompressible fluid at arbitrary depth
09 p1535 A71-22182

Contact problems of inflated cylindrical membranes with quadrature reduction under normal stress applied to loaded floating and submerged life raft
[ASME PAPER 71-APM-11] 16 p2656 A71-33215

Submerged vehicle drag reduction and turbulence transition damping by MHD boundary layer control, using Lorentz force and optimum magnetic field
20 p3214 A71-39963

SUBMERGING

External respiration, gas exchange and energy expenditures during orthostatic tests involving immersion experiment
01 p0014 A71-11136

Body heat loss in water immersion, using heat transfer model
02 p0207 A71-12387

Long term immersion effects on human water-salt metabolism, noting increased erythrocyte water contents and hematocrit index
13 p2006 A71-28403

Heat balance of human body submerged in water, determining body temperature reduction as function of ambient temperature
13 p2019 A71-28508

Xe 133 elimination from anterior tibial muscles in dry and water immersed sitting subjects, discussing effects of air and oxygen breathing
13 p2022 A71-29358

Photoelastic determination of stress distribution in thin square plates subjected to gravitational forces multiplied by immersion in Hg
16 p2647 A71-32824

Water immersion effect on plasma renin activity, urinary aldosterone excretion and renal sodium and potassium handling in normal man
22 p3485 A71-41720

Healthy males immersion in water containing NaCl, determining modified gravitational field effect on motor functions
22 p3505 A71-42792

Water immersion or bed rest effects on basic metabolism and external respiration under simulated weightlessness
22 p3495 A71-42794

SUBMILLIMETER WAVES

Extra-atmospheric submillimeter astronomy, discussing emission observations between IR and RF region and astrophysical-cosmological applications
01 p0151 A71-10146

Radio astronomy in millimeter and submillimeter ranges, surveying programs and equipment at various observatories
01 p0156 A71-10450

Millimeter and submillimeter radio waves propagation, outlining molecular and aerosol attenuation in real atmosphere together with transmitters and receivers
02 p0212 A71-11872

Quasi-optical waveguide components for millimeter and submillimeter waves, considering couplers, attenuators, isolators, bandpass and bandstop filters
02 p0235 A71-12907

Dispersion equations for complex transmission coefficients of submillimeter EM waves in solid state InSb plasma, applying plasma effects to control elements
03 p0467 A71-13797

Submillimeter wave attenuation measurement over 1 km path during summer rainstorms, comparing results with millimeter waves
05 p0718 A71-15989

Submillimeter and millimeter waves attenuation in rain, comparing calculation results with measurement
05 p0718 A71-15990

Submillimeter wave attenuation in snow, comparing results of calculation based on Mie theory with measurement
05 p0718 A71-15991

Wideband submillimeter range backward wave tubes automatic frequency control system, using combination of passive standard and open cavity
06 p0876 A71-18079

Theoretical submillimeter spectrum of Venusian radiation, determining brightness temperature
07 p1193 A71-19313

Submillimeter wave oscillations possibility by Bloch oscillation of conduction electrons in ideal crystal with periodic energy band structure
08 p1343 A71-21280

Freestanding wire grid manufacture of polarizing films for submillimeter interferometry
08 p1291 A71-21405

Phase regulated AFC system design for millimeter and submillimeter wave backward wave tubes
08 p1267 A71-21805

Fabry-Perot interferometer for dielectrics permittivity and loss measurements in millimeter and submillimeter ranges, discussing design, tests and accuracy
08 p1294 A71-21806

Submillimeter wave extinction in clouds and fogs, using spectrometric results of water optical properties
09 p1408 A71-23375

Symmetric self-calibrating attenuator consisting of rotatable grid between two fixed grids for application at submillimeter wavelengths
09 p1421 A71-23682

Phase modulation application to interferometers for submillimeter waves exceeding 10 microns
12 p1905 A71-26817

Superheterodyne radiometers for millimeter and submillimeter waves, using Mach-Zehnder interferometer frequency mixer for parasitic signal suppression
12 p1886 A71-26847

Radio astronomy in millimeter and submillimeter ranges, surveying programs and equipment at various observatories
12 p1967 A71-27421

Submillimeter wave region solar radiation atmospheric absorption by Fourier spectrometry and double output Michelson interferometer with Goly cell detectors
14 p2307 A71-29740

Night sky submillimeter wave diffuse background radiation telescopic measurements above 120 km
15 p2399 A71-31827

Submillimeter background radiation origin possibility from extragalactic discrete sources based on cosmological models
15 p2478 A71-31828

Theoretical submillimeter spectrum of Venusian radiation, determining brightness temperature
15 p2486 A71-31893

IR and submillimeter wave HCN laser radiation visual observation, using thermal image converter
15 p2420 A71-32385

Frequency response of rainfall attenuation for various drops size distributions, plotting measured values at 890 and 110 GHz
15 p2374 A71-32696

Millimeter wave klystron single-loop phase locking using final 4th-harmonic mixer in reference chain for submillimeter laser frequency measurement
16 p2589 A71-34126

StarLifter borne large aperture astronomical telescope for IR and submillimeter observations, discussing design and operation
20 p3234 A71-39173

Millimeter and submillimeter laser action in symmetric tip molecules optically pumped via parallel absorption bands
20 p3246 A71-39759

Submillimeter plane monochromatic waves propagation in ground layer of turbulent atmosphere, deriving received signals levels fluctuations
20 p3198 A71-39804

Semiconductors submillimeter and far IR reflection spectra and cyclotron resonance measurements
22 p3586 A71-42140

Stratospheric submillimeter wave emission and water vapor mixing ratios measurements, using Michelson interferometer with phase modulation and Fourier spectroscopy methods
22 p3545 A71-42145

Rain and drizzle submillimeter wave attenuation and radar scattering cross section calculation
22 p3515 A71-42737

Submillimeter wave attenuation measurement over 1 km path during summer rainstorms, comparing results with millimeter waves
22 p3515 A71-42738

Submillimeter waves attenuation in rain, comparing calculation with measurement
22 p3515 A71-42739

Submillimeter wave attenuation in snow, comparing results of calculation based on Mie theory with measurement
22 p3515 A71-42740

Quasi-optical waveguide system for measuring electrical properties of dielectric and magnetic materials in submillimeter band
23 p3677 A71-43530

Millimeter and submillimeter wave radiation detection by paramagnetic materials, noting noise equivalent power dependence on various parameters
23 p3717 A71-44293

Lower stratosphere submillimeter wavelength radiation measurement using Fourier transform spectroscopy with phase modulation
24 p3822 A71-44448

Composite quasi-optical-broad waveguide transmission lines for millimeter and submillimeter waves with spectrum phase correction
24 p3810 A71-45258

SUBMINIATURIZATION

Subminiature TV camera with hybrid electronic packaging, providing EIA composite video output format and 450 TVL/RH resolution capability
17 p2747 A71-35788

SUBROUTINES

FORTTRAN-based list processor subroutines for computing Poisson series used in celestial mechanics
04 p0660 A71-15890

NTWO as FORTRAN 4 family of subroutines developed on 7094-7044 system for determining thermodynamic and transport properties of nitrogen
20 p3253 A71-39268

SUBSETS (MATHEMATICS)

U SET THEORY

SUBSONIC AIRCRAFT

Subsonic aircraft size effect in conventional design, discussing increased weight increments and economic gain rate
[AIAA PAPER 70-940] 02 p0189 A71-12676

Subsonic jet engine noise reduction, considering turbojets, turbofans and jet suppressors
08 p1349 A71-21814

Cruising flight range as function of supersonic/subsonic transport fuselage geometrical parameters
12 p1868 A71-27494

Military aviation greases for subsonic commercial airplane lubricants, discussing economic and technical benefits based on service experience and testing
[SAE PAPER 710411] 13 p2091 A71-28304

Economic analysis of subsonic transport airplane design, evaluation and operation
[SAE PAPER 710423] 13 p1995 A71-28310

Large subsonic jet aircraft civil pilots performance under physiological and psychological stresses induced during severe atmospheric turbulence
14 p2188 A71-29783

Fuselage influence on total aircraft drag in subsonic passenger aircraft, considering high aspect ratio cylindrical fuselages
14 p2177 A71-30821

Simulated sonic booms and subsonic jet aircraft noise effects on human subjects of various ages during different sleep stages
15 p2364 A71-32250

Soviet book on subsonic gas turbine passenger planes power supply systems covering Boeing 747, short haul aircraft, DC-10, L-1011, etc
17 p2677 A71-34472

Wing group weight prediction for subsonic aircraft design, taking into account root bending moments due to lift
18 p2976 A71-35925

SUBSONIC FLOW

Three dimensional wings harmonic oscillation with arbitrary frequency in subsonic flow, presenting approximation method for singular integral equation
01 p0173 A71-10844

Lifting surface in unsteady subsonic flow, describing integral equation calculation method including kernel logarithmic singularity
01 p0003 A71-11020

- Small perturbation subsonic flows aerodynamic noise, using matched asymptotic expansions method 02 p0240 A71-12377
- Spanwise distribution of induced drag in subsonic flow by vortex lattice method, noting applicability to arbitrary derivatives in stability analysis 02 p0187 A71-12691
- Sound generation by rotor-stator interaction in subsonic axial flow compressors, using acceleration potential and wake technique 03 p0469 A71-13277
- Contraction coefficient of orifice for subsonic and supersonic flows, including velocity-of-approach and compressibility effects upstream and downstream [ASME PAPER 70-WA/FM-1] 03 p0402 A71-14103
- Compressible subsonic and supercritical flows, developing flowmeter orifice expansion factors [ASME PAPER 70-WA/FM-3] 03 p0402 A71-14105
- Wings with control surfaces in unsteady subsonic flow, applying lifting surface theory [ONERA-TP-889] 04 p0526 A71-15355
- Temperature distribution and heat transfer across transitional separated shear layer under subsonic air flow, using interferometric measurements 04 p0679 A71-15470
- Supersonic jet-bounded subsonic wake interactions, determining recirculation zone boundaries 05 p0694 A71-16848
- Subsonic compressible flow equations solution in terms of velocity potential, obtaining reliable convergence 05 p0737 A71-17115
- Subsonic fan noise, using helicopter rotor noise theory for analysis of phase related and randomly time varying flow distortions 05 p0796 A71-17161
- Pressure distribution singularity at tip of thin lifting parabolic wing in subsonic flow [AIAA PAPER 71-10] 06 p0842 A71-18484
- Optical crossed-beam measurements of turbulence intensities in cold subsonic air jet shear layer [AIAA PAPER 71-137] 06 p0902 A71-18580
- Noise-producing subsonic jet turbulence eddies hot-wire anemometer measurements of convection velocity as functions of frequency [AIAA PAPER 71-154] 06 p0884 A71-18596
- High subsonic jet near-field acoustic energy flux distribution calculation from pressure gradient measurements [AIAA PAPER 71-155] 06 p0884 A71-18597
- Jet plume in subsonic cross flow, calculating counter-rotating vortices as function of distance along trajectory from semiempirical model 07 p1090 A71-19901
- Approximation of Chaplygin equation for subsonic ideal gas plane adiabatic flow, applying to discharge from flat channel with contraction 07 p1016 A71-20083
- Multilink approximation of Chaplygin function in subsonic and supersonic flow regions, deriving coupling conditions relative to modified stream function at approximation nodes 07 p1016 A71-20090
- Prandtl-Glauert pressure distribution rule improvement subsonic planar flow 07 p1017 A71-20312
- Elastic swept wing subsonic aerodynamic characteristics, taking into account aerodynamic load redistribution due to aeroelastic deformations 08 p1229 A71-22035
- Oscillations generating mechanism in resonance tube fed by subsonic gas jet, determining oscillations amplitude and frequency at resonance 09 p1382 A71-22406
- Pressure distribution on arbitrary finite symmetrical wings with rounded leading edges at zero incidence in subsonic flow 09 p1383 A71-22945
- Supersonic and subsonic jets coexistence in rectilinear constant section duct, characterizing flow boundaries by pressure readings and Schlieren flow visualization 09 p1384 A71-23605
- Aerodynamic forces on harmonically oscillating wing in subsonic flow of ideal gas 09 p1384 A71-23615
- Turbulent characteristics of circular subsonic free jet impinging normal to flat plate, measuring heat transfer rates 10 p1694 A71-23951
- Unsteady inward and outward velocities of subsonic radial air flow between two disks, using hot-wire anemometer and cylindrical wave equation 10 p1550 A71-24000
- Turbulent wakes from subsonic-hypersonic bodies for downstream mean flow predictions analysis, considering eddy viscosity function 10 p1550 A71-24338
- Air and carbon dioxide intensive injection effect on turbulent boundary layer of subsonic channel air flow 10 p1551 A71-24378
- Subsonic turbulent boundary layer noise generation and acoustic pressure on aircraft surface, using Lighthill theory 10 p1553 A71-24952
- Compressibility correction for subsonic flows past bluff bodies, considering boundary distortion and pressure distribution shift 11 p1701 A71-25149
- Loads induced on infinite aspect ratio wing by straight infinite free vortex in subsonic compressible freestream, using planar lifting surface theory 11 p1702 A71-25474
- Steady three dimensional subsonic nonviscous flow through turbomachine with arbitrary hub and shroud shapes and finite blade number, using iterative blade to blade procedure [ASME PAPER 71-GT-2] 11 p1702 A71-25948
- High subsonic flow two dimensional turbine cascade design by approximate hodograph method, noting pressure distribution measurements [ASME PAPER 71-GT-34] 11 p1704 A71-25971
- Supersonic and subsonic combustion ramjet engines inlet calibration, using gun tunnel to establish hypersonic throat flow 11 p1860 A71-26271
- Noise field from subsonic air jets by velocity dependence and radiation intensity directivity determination 11 p1753 A71-26445
- Subsonic turbulent jet flow optical measurement by quantitative schlieren technique to overcome hot-body anemometry difficulties due to temperature and velocity fluctuations 12 p1896 A71-27215
- Unsteady large particle numerical solutions to vortical equations of plane and axisymmetric inviscid gas flow past blunt body for subsonic and hypersonic velocities 13 p1989 A71-27901
- Heat transfer within resonant cavities at subsonic and supersonic flow, discussing wind tunnels, test procedures and data reduction [ASME PAPER 71-FE-9] 13 p2166 A71-29450
- Pressure recovery performance of straight-wall two dimensional diffusers with subsonic air-water mixtures, studying gas volume flow ratio and diffuser geometry effects [ASME PAPER 71-FE-20] 13 p2052 A71-29458
- Acoustic tone radiation from subsonic rotor near potential field by interaction with nonuniform inlet flow based on Lighthill aerodynamic sound equation 14 p2225 A71-30210
- Average and pulsating velocity distributions during subsonic air jet interaction with plane baffle, describing jet dissipation geometrical pattern 14 p2225 A71-30223
- Surface curvature effects in nonsimilar second order boundary layer solutions for subsonic plane flow over cylinder with separation 14 p2170 A71-30442
- Rarefied gas Poiseuille flow in parallel plates, cylindrical tube and annulus geometries, deriving subsonic flow velocity profiles by third order constitutive relations 14 p2227 A71-30574
- Supersonic to subsonic solar corona transition, using supersonic solution for solar wind inviscid equations 14 p2302 A71-30648
- Pisa University Aeronautical Institute activities /1960-1970/, considering supersonic and subsonic flow research, thin stiffened shells fatigue under compressive or tensile loads, etc 14 p2222 A71-30822
- Book on pressure losses in ducted flows covering subsonic flow in straight or curved ducts, constrictions flow characteristics, etc 15 p2386 A71-31149
- Two dimensional subsonic irrotational isentropic flow around thick profiles, using coordinate perturbation method 15 p2343 A71-31167
- Heterogeneous detonations literature review, indicating need for research on heat transfer processes in subsonic and supersonic flows 15 p2511 A71-31387
- Film cooling studies in subsonic and supersonic flows, using shock tunnel for gas turbine conditions simulation 16 p2551 A71-32882
- Shock wave propagation in junction of straight duct with side branch for subsonic flow, analyzing reflected and transmitted waves 16 p2555 A71-32886
- Oscillating thin wing with control surfaces in two dimensional compressible subsonic flow, calculating aerodynamic forces based on kernel function method [DFVLR-SONDDR-132] 16 p2519 A71-33013
- Cascading turbomachine blades vibrations measurement in subsonic and sonic high temperature gas flows, describing test facility 16 p2553 A71-33993
- Subsonic turbulent jets acoustic emission, calculating noise intensity in far field for various Mach numbers 17 p2725 A71-34213
- Stream lines construction in meridional plane of blade nozzle annular cascades of steam and gas turbines in subsonic and supersonic flow 17 p2670 A71-34446
- Wall pressure spectra and rms wall pressure levels measurements in subsonic separated flows, postulating model for pressure fluctuation estimation 17 p2728 A71-35037
- Mach number effects on flow field in gas bearings at high subsonic and supersonic tangential speeds based on perturbation theory [ASME PAPER 71-APM-U] 18 p2926 A71-36263
- High subsonic potential flow calculation past circular cylinder by integral relations method 18 p2844 A71-36326
- Subcritical nonlinear potential flows over two dimensional subsonic airfoils by multistrip method of integral relations 18 p2845 A71-36330
- Iterated double integrals for subsonic flow patterns bounded by segments of straight lines and free boundaries, using FORMAC 18 p2909 A71-36703
- Critique of paper on spanwise distribution of induced drag in subsonic flow by vortex lattice method, noting infinities in downwash across all vortex lines 19 p2991 A71-37297
- Subsonic flow direct and indirect methods including Oswatitch integral equation, thickness parameter expansion, Janzen-Rayleigh method and stream and potential functions in hodograph plane 19 p2992 A71-37453
- Compressor blade hodography and profile equations for subsonic two dimensional flow calculated on graphic visualization console 20 p3176 A71-39420
- Three dimensional nonlinear subsonic flow over finite wings of arbitrary planform, solving transonic small disturbance equation by integral method 20 p3177 A71-39568
- Inlet circulation and swirl effect and optimum vane angle for maximum efficiency of subsonic straight conical diffusers 20 p3177 A71-39875
- Two dimensional jet flapped symmetric wing in subsonic flow, assuming irrotational flow inside jet bounded by vortex sheets 21 p3318 A71-40172
- Spanwise lift distribution over wings and wake formation in thin airfoils of finite aspect ratio in linear subsonic potential flow 21 p3319 A71-40495
- Plane acoustic wave transmission problem through finite chord plate array in subsonic gas flow, using factorization method in diffraction theory 21 p3322 A71-40686
- Pitot tube interaction with subsonic rarefied gas flow, considering impact pressure 21 p3323 A71-40695
- Sound wave propagation from two dimensional acoustic source in subsonic fluid moving between two reflecting parallel walls 21 p3323 A71-40695
- Resultant aerodynamic forces on circular arc profile with normal jet in subsonic steady compressible flow, using Imai-Lamla approximation method 23 p3705 A71-44145
- Streamline curvature analysis of compressible subsonic, transonic and supersonic cascade flows in axial turbine blades 23 p3627 A71-44271
- Acoustic noise output from round interfering subsonic jets, considering suppressor nozzle attenuation 23 p3665 A71-44347
- Two dimensional potential flow model of Pitot static probe and subsonic free jet interaction, using conformal mapping and hodograph method [AIAA PAPER 71-998] 24 p3817 A71-44589
- Subsonic force effect calculations on rectangular wings, using downwash velocity potential method 24 p3817 A71-44613

SUBSONIC SPEED

- Aerodynamic forces on control surfaces in subsonic range, investigating pressure distribution on harmonically oscillating wing 03 p0344 A71-14347
- Subsonic tactical missile hydraulic and fluidic autopilot systems for directional control, considering costs, reliability, vulnerability, maintainability, weight and mobility [SME PAPER MS-70-524] 07 p1024 A71-20547
- Trajectories prediction for subsonic spin stabilized projectiles via water tunnel tests, considering blunt nose and tail and rounded nose right circular cylinders [AIAA PAPER 71-296] 08 p1275 A71-22016
- Subsonic velocities erosion behavior of polymeric coatings and composites, considering void content and reinforcement influence on composite structure 09 p1483 A71-23425
- Subsonic and supersonic airline operations, restraints, considering noise, air pollution and inadequate airport facilities 12 p1927 A71-26870
- Transonic wind tunnel testing of air intake and afterbody of double flux engine nacelle at high subsonic Mach numbers and high Reynolds numbers [ONERA-TP-943] 18 p2956 A71-36021

SUBSONIC WIND TUNNELS

Subsonic flight characteristics of LB 21 reentry vehicle, discussing lateral directional stability and lifting fuselage

18 p2972 A71-36436

Flow around obstacle in plasma with ions cold relative to electrons and with directed subsonic, considering relative density measurement

19 p3115 A71-38207

Nonreversible hydraulic control design and emergency maintenance for Tu 154 aircraft subsonic cruising at 11 km altitude

23 p3627 A71-42927

Divergence behavior of flat rectangular panel at subsonic speeds, discussing boundary conditions, natural vibration modes and temperature effects

24 p3878 A71-44611

SUBSONIC WIND TUNNELS

Pulsed subsonic wind tunnel, calculating instantaneous flow velocity with allowance for boundary layer thickness at walls

10 p1549 A71-23855

Nonlinear aerodynamic stability coefficients from free angular motion of rigid bodies, using three degrees of freedom subsonic wind tunnel tests on Apache model

11 p1837 A71-25515

Skin friction drag and velocity profile measurements on flat plate in two phase circular pipe flow in subsonic wind tunnel for gas-solid media, using photographic technique

[ASME PAPER 71-FE-32] 13 p2053 A71-29467

Fan-produced sound pressure fluctuation in very low speed subsonic wind tunnel test stream, noting resulting anemometer calibration errors

14 p2275 A71-30526

Lee side air flow from cone-cylinder model, determining vortex core regions from subsonic wind tunnel smoke visualization techniques

15 p2346 A71-32117

Sting-free aerodynamic drag measurement on ellipsoidal cylinders in subsonic wind tunnel at transition Reynolds numbers

18 p2843 A71-36037

Heated jet interaction with deflecting flow in subsonic wind tunnel, presenting flow visualization and temperature and velocity profiles

[ASME PAPER 71-HT-2] 19 p3163 A71-37980

Turbulence measurement in subsonic wind tunnel gas jet flows containing dust particles, using Doppler difference laser velocimeter

21 p3392 A71-40397

Low speed wind tunnel air velocity measurement with laser velocimeter, using dark background illumination detection of particles scattering across fringe pattern

21 p3378 A71-40398

Low speed wind tunnel measurements correction for acoustic effects due to fan noise propagation

24 p3790 A71-44763

SUBSTRATES

High efficiency epitaxial growth of GaAs by system using substrates oriented along [111]/Ga face

01 p0137 A71-10314

Glass substrates for thin film circuits compared to other materials for properties and suitability, emphasizing surface properties

02 p0230 A71-11816

Fog phenomena systematics, describing physical classification according to substrate and function

02 p0277 A71-12371

Two layer antireflection coatings on glass for He-Ne lasers, calculating optimal film thicknesses for various substrates and wavelengths

06 p0907 A71-18038

Wall turbulence Prandtl-Karman constant calculation, using friction law for viscous sublayer degeneration with infinitely increasing Reynolds number

07 p1085 A71-18754

Epitaxial boron phosphides single crystals growth, using thermal decomposition and reduction for deposition on hexagonal silicon carbide substrates basal plane

07 p1180 A71-20174

Integrated microwave circuits substrate materials, discussing fabrication techniques with attention to mechanical, thermal and electrical characteristics

09 p1418 A71-23059

Epitaxial deposition of discrete separated p- and n-type silicon on single sapphire substrate, considering technique for MOS devices fabrication

09 p1509 A71-23116

Single metal system Al beam leaded chips, substrates and crossovers for multilead packaging, describing fabrication techniques

09 p1509 A71-23119

Substrate materials for microwave integrated circuits, comparing dielectric constants, surface finishes and thermal conductivity for alumina, sapphire, magnesium titanite, YIG and beryllium oxides

09 p1418 A71-23156

Reflectance measurements of dielectric coating on metallic substrate, comparing with analytical model

11 p1799 A71-26233

Substrate materials thermal characteristics determination for thin films resistance thermometers calibration, using pulse heating technique

12 p1908 A71-27593

Coplanar-guide and slot-guide junction circulators on ferrite substrate magnetized perpendicular to surface

13 p2037 A71-28473

Substrates, films and laser mirrors production, discussing material combinations and evaporation processes

13 p2080 A71-29087

Porous carbon and graphite substrates chemical vapor deposition carbon infiltration process, discussing isothermal and thermal and pressure gradients techniques

14 p2262 A71-29652

Substrate emitter monolithic inverted transistor structure for low-power high-current gain application

15 p2375 A71-31474

Fence guide waveguide on dielectric substrate for millimeter wave, applying to power dividers, directional couplers, hybrid rings and resonators

17 p2713 A71-34444

High density MOS memory circuits, using multilayer ceramic substrate board for demonstration

17 p2712 A71-35787

IC applications to microwave frequencies, relating circuit performance to substrate roughness and thickness of thin film metal adhesion layers

18 p2895 A71-36981

Ion beam deposition of insulating carbon thin films on room temperature substrates, considering transparency, index of refraction, insulating capacity, glass scratching ability, etc

20 p3241 A71-39011

Thin dielectric films on germanium substrates, using oxygen diffusion through silicon dioxide

20 p3205 A71-39435

Substrate influence on circuit board conformal coatings electrical insulation resistance, discussing test results with epoxy/glass and ceramic substrates and various coating materials

21 p3353 A71-40438

Surface acoustic waves in layered substructure of piezoelectric epitaxial film of cadmium sulfide on germanium substrate

21 p3429 A71-41208

Hg condensation characteristics on Cs substrate in high velocity nitrogen carrier gas, formulating one dimensional flow model based on two phase three component gas dynamics

22 p3620 A71-41876

Substrate effect on MOSFET noise and y-parameters using wave equation

24 p3862 A71-45354

SUBSTRUCTURES

Al-Ti alloys segregation substructures, studying nucleant particles relationship to crystal solidification

04 p0615 A71-15791

SUBTRACTION

Periodic subtraction and multiplication systems under amplitude limitation, analyzing detection characteristics at arbitrary correlation coefficients

09 p1405 A71-22464

Spatial filter synthesis for real time combined subtraction and correlation in coherent optical data processing system

12 p1905 A71-26808

SUBTRACTORS

U ADDING CIRCUITS

SUBTROPICAL REGIONS

U TEMPERATE REGIONS

U TROPICAL REGIONS

SUCTION

Incompressible fluid laminar flow between stationary and rotating porous disks with equal suction and injection

02 p0240 A71-12337

Wing upper surface air suction influence on aircraft longitudinal controllability, considering control stick forces for deflected flaps and angle of attack

04 p0528 A71-14594

Axisymmetrical, optically thick nonNewtonian, power law boundary layer with injection and suction, obtaining similarity transformations for simultaneous convection and radiation

04 p0685 A71-15516

Plane incompressible boundary layer stability in presence of pressure gradient and suction

05 p0736 A71-16851

Turbulent boundary layer on porous plate with suction and heating, measuring mean velocity and temperature profiles at various locations along wall as function of suction rate

07 p1219 A71-18759

Viscous conducting fluid MHD fluctuating flow over porous flat plate with time dependent suction, determining skin friction and transient velocity profiles

07 p1169 A71-20028

Plasma blowing and suction through channel wall electrodes in two dimensional stationary flow, taking into account Hall effect

09 p1502 A71-22537

Blowing and suction effects on laminar boundary layer flow of quiet fluid over permeable rotating cone, discussing skin friction and heat transfer

10 p1594 A71-24404

High Reynolds numbers asymptotic suction boundary layer linear stability analysis for viscous flow, using transformations to hypergeometric functions

12 p1896 A71-26915

Boundary layer suction optimization to achieve normal velocity component distribution for local Reynolds number equal to critical value at transition point

12 p1896 A71-26915

Laminar source flow between rotating parallel porous disks with equal suction/injection rates solved for infinite radius series, discussing radial velocity and shear stress distributions

12 p1896 A71-27051

Pressure fluctuations in acoustic field of boundary layer under slot suction, considering vortex formation and separation on edges

15 p2389 A71-31713

Variable suction effects on two dimensional fluctuating slip flow of incompressible rarefied gas past infinite flat plate

20 p3211 A71-39466

Rectangular wind tunnel study of suction effect on velocity profiles and characteristics of turbulent boundary layer

20 p3213 A71-39788

Velocity profiles of plane turbulent flow of incompressible fluid on porous surface in presence of suction

20 p3213 A71-39790

Rivlin-Ericksen fluid steady flow between parallel plates with uniform suction at lower wall, detailing velocity field, skin friction and flow coefficient

23 p3663 A71-43492

SUD AVIATION AIRCRAFT

NT ALOUETTE HELICOPTERS

NT CONCORDE AIRCRAFT

NT SE-210 AIRCRAFT

SUD AVIATION SE-210 AIRCRAFT

U SE-210 AIRCRAFT

SUDDEN ENHANCEMENT OF ATMOSPHERICS

Initial phase duration of geomagnetic storms inverse dependence on sudden commencement amplitude in accord with solar wind-magnetosphere interaction

14 p2231 A71-29724

SUDDEN IONOSPHERIC DISTURBANCES

Simultaneous sudden magnetospheric compressions and geomagnetic bay onsets correlation, using IGY data

02 p0245 A71-11967

Conjugate observations of ionospheric absorption associated with electron precipitation during sudden commencement of magnetic storm

03 p0419 A71-14520

Geomagnetic storm disturbance fields measurement by ATS 1 satellite compared with simultaneous low altitude observation, noting cavity sudden commencement compression effect

06 p0887 A71-17259

Ionospheric electron density and reflection height during sudden phase anomaly in solar X-ray flare

08 p1355 A71-21222

Generation mechanism of 27-day recurrent geomagnetic disturbances sudden commencements, analyzing interrelationship between recurrent disturbances, solar data and solar plasma physical parameter

10 p1607 A71-25119

Generation mechanism of magnetohydrodynamic shock waves associated with sudden commencements of 27-day recurrent geomagnetic disturbances

10 p1608 A71-25120

Sudden geomagnetic storm effects on low ionosphere state, discussing solar X-ray and particle radiation

11 p1815 A71-25581

Sudden commencements occurrence frequency diurnal and seasonal variations from worldwide magnetic storms data

11 p1758 A71-25793

Magnetic storms sudden commencements (SSC) occurrence over 1949-1968 period based on original magnetogram observation

12 p1900 A71-26891

VLF and LF time and frequency international comparison, noting diurnal shifts and SID constant magnitude ratio

14 p2204 A71-30972

Sudden phase anomalies relation to solar flares, radio bursts and X radiation from severe worldwide ionospheric storm observation

17 p2796 A71-35345

Sudden commencements occurrence frequency diurnal and seasonal variations from worldwide magnetic storms data

22 p3533 A71-41561

Ionospheric responses to solar flares, correlating sudden frequency deviations with sudden total electron content enhancement

22 p3592 A71-42222

- IGY interplanetary field independent storm sudden commencement triggered magnetospheric polar substorms, indicating sympathetic flare analogy
23 p3668 A71-43164
- GARS
NT GALACTOSE
NT GLUCOSE
NT HEXOSES
NT MONOSACCHARIDES
NT PENTOSE
NT RIBOSE
Catalytic effect of lanthanide hydroxides on formaldehyde conversion to pentoses and hexoses at 110 C in life support systems
13 p2018 A71-28408
Dietary effects of formose sugars ingestion, investigating toxic mechanisms involved
19 p3011 A71-37573
Glucose and fructose extraction from formose sugar mixtures by enzymatic methods using hexokinase reaction
19 p3011 A71-37574
Food utility calculation for various formose sugar treatments as valid qualitative measure of relative effects of dietary materials
19 p3007 A71-37575
Bound sugar content in marine sediments by capillary gas chromatographic-mass spectrometric analysis of trimethylsilyl derivatives
19 p3055 A71-38146
- UGGESTION
Human biomechanical and vegetative reactions to hypnotic suggestion of gravitational effects
08 p1243 A71-21971
- SUITS
NT PRESSURE SUITS
NT SPACE SUITS
- SULFATES
NT HYDROXYLAMINE SULFATE
Chromatographic paper extraction of residual thiosulfate in processed photographic film
19 p3062 A71-37247
- SULFATION
Co-Cr-W alloy sulfidation at high temperatures, performing weight gain, metallographic X ray and electron probe analysis
17 p2758 A71-35149
Ni-Cr alloys sulfidation at 700 C from inert and radioactive marker techniques
18 p2938 A71-37003
Sodium role in accelerated oxidation behavior /sulfidation/ of Ni-base superalloys and binary alloys coated with sodium sulfate or carbonate
23 p3695 A71-44288
- SULFIDES
NT CADMIUM SULFIDES
NT CARBON DISULFIDE
NT COPPER SULFIDES
NT DISULFIDES
NT HYDROGEN SULFIDE
NT INDIUM SULFIDES
NT LEAD SULFIDES
NT MOLYBDENUM DISULFIDES
NT MOLYBDENUM SULFIDES
NT POLYSULFIDES
NT TROLITE
NT ZINC SULFIDES
NT ZINCBLLENDE
Sulfide precipitates shape preservation in high strength low alloy hot rolled steel sheets, discussing effects of various additive elements
04 p0614 A71-15782
Presulfidized Ni alloys and Cr oxidation rates
04 p0615 A71-15787
Powdered W, Mo, Nb and Ta sulfides and compacts thermal vacuum behavior, examining phase compositions and transformations
05 p0769 A71-16861
TiS vaporization thermodynamics by high temperature mass spectrometry, considering ionic fragmentation and ionization cross section errors
07 p1054 A71-19368
Hafnium and zirconium sulfides, determining partial molar free energy of sulfur at metal saturation with electromotive force cell
09 p1387 A71-23129
Sulfide formation process from solar composition cooling gas, examining constrained equilibrium theory
10 p1676 A71-24505
Antimony trisulfide semiconductor films, noting chemical composition effects on photosensitive properties
15 p2461 A71-31286
Chromium sesquisulfide instability towards oxygen at high temperature, using spring thermobalance
18 p2937 A71-36763
Interstellar carbonyl sulfide transition at 109.5 GHz, noting column density
21 p3447 A71-40447
Hologram storage in evaporated thin films of arsenic trisulfides, considering simple diffraction gratings and complex data masks
22 p3542 A71-41811
- Nondestructive detection of hot corrosion- sulfidation in U.S. Navy aircraft turbine engines
24 p3865 A71-45280
- SULFONES
Difunctional epoxy resins from dihydroxydiphenyl sulfone /bisphenol S/, obtaining increased heat resistance and thermal stability
11 p1787 A71-25424
- SULFUR
NT SULFUR ISOTOPES
Fe-S condensates structure and phase transformations during heating, noting importance for antifriction materials synthesis
08 p1322 A71-21062
Hafnium and zirconium sulfides, determining partial molar free energy of sulfur at metal saturation with electromotive force cell
09 p1387 A71-23129
Sulfur effervescing molten slag/gas systems causing planetary vulcanism, examining patterns on earth, moon and Mars
15 p2496 A71-32708
- SULFUR COMPOUNDS
NT CADMIUM SULFIDES
NT CARBON DISULFIDE
NT COPPER SULFIDES
NT CYSTEINE
NT DISULFIDES
NT HYDROGEN SULFIDE
NT HYDROXYLAMINE SULFATE
NT INDIUM SULFIDES
NT LEAD SULFIDES
NT MOLYBDENUM DISULFIDES
NT MOLYBDENUM SULFIDES
NT POLYSULFIDES
NT SULFATES
NT SULFIDES
NT SULFONES
NT SULFUR FLUORIDES
NT SULFUR OXIDES
NT SULFURIC ACID
NT THIOLS
NT TROLITE
NT ZINC SULFIDES
NT ZINCBLLENDE
Sulphydryl cysteamine and disulfide cystamine effect on bacteriophage survival rate at high anaerobic doses
07 p1033 A71-18938
Sulfur containing organic chelating compounds as radiation protective agents
07 p1034 A71-18941
Age dependent changes in mammalian cells radiosensitivity, emphasizing endogenous nonprotein sulphydryl effects
07 p1034 A71-18945
Metabolic effects of sulphur containing cysteamine, cystamine and cysteine radioprotective drugs on oxygen uptake in rats
07 p1039 A71-18982
Interstellar SH search for ground state main line transitions at 111 MHz
14 p2313 A71-30433
- SULFUR FLUORIDES
Sulfur hexafluoride effects on equilibrium electron concentrations in air and argon plasmas, discussing earth reentry simulation applications
01 p0133 A71-10957
Sulfur hexafluoride absorption lines observation by inverted Lamb dip high resolution spectroscopy, using heterodyne methods
02 p0209 A71-12731
CW carbon dioxide laser beam IR absorption by sulfur hexafluoride, investigating saturation parameter relationship to pressure, temperature and relaxation time
03 p0437 A71-13879
Sawtooth structure of convective plasma column in sulfur hexafluoride at cross flow Mach numbers, using thermionic rail accelerator
09 p1498 A71-22096
Cross-excited electrically pulsed carbon dioxide laser investigating self mode locking as function of cavity length, operating pressure and bleachable absorber sulfur hexafluoride
10 p1620 A71-24152
Sulfur hexafluoride equilibrium composition, thermodynamic functions, transport properties and application to simplified enthalpy flow arc model
12 p1939 A71-27267
Thermal boundary layer equation for sulfur hexafluoride steady arc constriction effects in nozzle throat
12 p1939 A71-27268
Radial distribution of electric potential in Penning discharge based on relation between sulfur hexafluoride negative ions transit time and initial energy
13 p2107 A71-28852
Excited state absorption in sulfur hexafluoride traversed by carbon dioxide laser beam
18 p2933 A71-37014
Radial distribution of electric potential in Penning discharge based on relation between sulfur hexafluoride negative ions transit time and initial energy
21 p3425 A71-41281
- Spacecraft communication cut-off during atmospheric reentry due to thermal ionization of gas boundary layer, discussing sulfur hexafluoride injection alleviation and electrostatic probe
22 p3583 A71-41998
- SULFUR ISOTOPES
Carbon and sulfur isotope content in Apollo 12 lunar fines
23 p3751 A71-43702
- SULFUR OXIDES
Sulfur trioxide catalytic formation in gases from fuel-rich propane-air flames containing sulfur
03 p0376 A71-14279
Vibrational and rotational relaxation in sulfur dioxide, measuring relaxation time as function of temperature by ultrasonic absorption
07 p1054 A71-19370
IR laser action at 2-3 microns by low pressure discharge and gas mixtures containing molecular oxygen and sulfur dioxide
08 p1301 A71-21190
Franck-Condon factors, r-centroids and absolute band transition probabilities of NH, SiH, molecular sulfur and SO
10 p1645 A71-24544
Low resolution measurements of IR absorption of sulfur dioxide at room temperature
[ASME PAPER 70-WA/HT-4]
Benzene, benzene-d sub 6 and sulfur dioxide radiative lifetime measurement comparison, investigating internal conversion behavior
13 p2025 A71-28979
Nitrogen and sulfur dioxide reactions in isolation, determining rate by concentration measurements using light absorption technique
15 p2465 A71-32082
Red fuming nitric acid-sulfur dioxide as oxidizer for auxiliary ignition in liquid rocket motors
15 p2465 A71-32110
Far IR sulfur dioxide laser line prediction from transitions involving irregular Fermi interactions between molecular energy levels
15 p2422 A71-32587
Hydrogen sorption capacity by sulfur dioxide frost from cryodeposit formation on stainless steel sphere in vacuum chamber and equilibrium isotherms measurement
17 p2695 A71-35142
- SULFURIC ACID
Heat treatment effect on electrochemical behavior of Ni-Co-Mo maraging steel in sulfuric acid aqueous solution, studying anodic polarization
14 p2257 A71-29840
Titanium alloys analysis by dissolution in sulfuric acid and aerosol injection into spark discharge, discussing standard solution preparation
15 p2367 A71-31650
Titanium carbide powder corrosion resistance to sulphuric acid-hydrogen peroxide system at various temperatures
24 p3838 A71-44739
- SUM RULES
Sum rule functions for expressions of atomic or molecular quantum mechanical properties
16 p2603 A71-33527
- SUMMER
F 1 region unsteady model, examining vertical distribution profile of electron concentration on summer day
06 p0895 A71-18273
Spatial-temporal harmonics of noctilucent cloud occurrences during IQSY with maximum displays after summer solstice in both hemispheres
14 p2233 A71-29965
Summertime meridional wind component profile construction and hydrodynamic model for semi-diurnal fluctuations in upper atmosphere
15 p2399 A71-31962
Latitudinal distribution of electron temperature in F 2 layer during summer daytime period of low solar activity from electron density profile geometrical parameters
19 p3057 A71-38369
- SUMS
Generalized Watson sums calculation with application to magnetization of anisotropic ferromagnet for Callen type decoupling schemes
09 p1506 A71-22149
Fourier coefficients and integral operators S numbers of summable functions
17 p2765 A71-34864
Feinman integral definition and relation to Schroedinger equation for square summable potentials with lower bound
17 p2765 A71-34866
Weak row sum criterion for nonlinear equation systems, applying to discrete two point boundary value problems and linear equation systems
22 p3567 A71-42374
- SUN
Radar astronomy principles, applications and types of measurements, discussing solar, lunar, planetary and meteor observations
02 p0313 A71-12490

SUN SENSORS

- Dicke-Goldenberg solar oblateness measurement explained by equatorial temperature excess smoothly distributed 05 p0812 A71-16691
- Sun as variable star, discussing brightness, rotation and magnetic characteristics 06 p0971 A71-18245
- Soviet papers on sun and stars covering atmospheric structure and physics, nonstationary stars, evolution and galaxies 09 p1524 A71-23182
- Mercury transit across solar disk on 9 May 1970, using photographic micrometeorments 10 p1677 A71-24587
- Quiet sun and new moon brightness temperatures simultaneous measurements as function of frequency and wavelength 12 p1969 A71-27648
- Sun and interplanetary medium, considering pure atomic physics, radio emission, IR excess, solar wind, sunspots and solar radio astronomy 15 p2486 A71-31924
- Data processing technique for radio mapping of sun, discussing unwanted harmonics elimination and noise reduction 15 p2491 A71-32447
- Sun as flattened ellipsoid of revolution, showing flatness effects on planet motion in relativity theory framework 16 p2612 A71-33567
- Mercury transit across solar disk, discussing visual and photographic observations with Repsold and sun refractors and coronagraphs 17 p2809 A71-35579
- Ephemerical times of ingress and egress times of Mercury transit across solar disk 17 p2809 A71-35580
- Solar disk photographs taken by Skylark rocket in EUV and soft X ray region 20 p3293 A71-39534
- Ephemerides of sun, moon, planets and minor planets for October through December 1971 21 p3442 A71-40153
- ³⁵Cl abundance in sun, discussing low noise photoelectric scan 23 p3767 A71-43833
- Precision pointing correction /boresight calibration/ of microwave antennas, using sun as test source 23 p3654 A71-44158

SUN SENSORS

U SOLAR SENSORS

SUNLIGHT

- Polarization of sunlight multiply scattered by atmosphere and cloud particles of Venus from UV to IR 07 p1204 A71-20622
- Sunlight pressure forces and moments on complex shape artificial earth satellites, assuming uniform incident flux 09 p1492 A71-22374
- Intensity and polarization of diffusively transmitted sunlight, taking into account various aerosols distributions and normal molecular contributions 12 p1902 A71-27198
- Cloud layer role in formation of light and heat regime of two layer Venus atmosphere model, considering sunlight reflection 13 p2131 A71-27808
- Inhomogeneous planetary atmosphere resonantly scattered sunlight, calculating intensities with frequency redistribution functions 13 p2100 A71-28346
- Night vision and dark adaptation of eye, noting sunlight effects on visual acuity 13 p2017 A71-28392
- Artificial satellite illumination by sun, calculating height, time and position of earth shadow by nomogram 13 p2145 A71-28511
- Calculational method for predicting angular distribution of sunlight upwelling flux scattered by atmosphere and reflected by ground, using Monte Carlo data 16 p2562 A71-33130
- Sunlight photodetachment rates and energy dependent cross sections for ozone ions, using photon beam excitation in buffer gas 16 p2574 A71-33962
- Daylight photometric flux derivation from filtered measurements of global sun and sky radiant energy, using natural illumination and short wave radiation relationship 20 p3234 A71-39175
- Sunlight scattering by dust in upper atmosphere from primary twilight intensities investigations 20 p3219 A71-39647
- Cloud layer role in formation of light and heat regime of two layer Venus atmosphere model, considering sunlight reflection 21 p3441 A71-40077

SUNRISE

- Ozone screening heights from sunrise effects on D region VLF wave reflection 02 p0212 A71-11968

- Sunrise behavior of midlatitude topside ionosphere at low sunspot numbers from Alouette I electron density and plasma scale height profiles 13 p2055 A71-27920
- Modal interference spacing in frequency range 13.6-22.3 kHz during sunrise transitions on middle latitude east-west propagation paths 15 p2369 A71-31432
- Upper ionosphere electron density scale height data, noting conjugate point sunrise heating effects from Alouette I data 17 p2731 A71-34313
- Ozone concentration measurements near sunrise by balloon-borne electrochemical ozonesonde, noting scattered radiation effect 23 p3667 A71-43074

SUNSPOT CYCLE

- Interplanetary magnetic sector structure near sunspot maximum 01 p0163 A71-11521
- Long range prediction of minimum and maximum of sunspot cycle, including Wolf number 02 p0303 A71-11715
- Wolf numbers monthly fluctuations, giving histogram of fluctuation amplitude distribution 03 p0484 A71-13211
- Night airglow, discussing spectrum, latitudinal dependency, diurnal variation, time and space correlations and sunspot cycle and solar activity effects 03 p0417 A71-14071
- Sunspot cycle period relationship to planetary orbital periods 03 p0493 A71-14210
- Meridional solar magnetic field shape determination, discussing latitude drift of spot forming zones, coronal penetrations and 80 year sunspot periodicity 08 p1358 A71-20887
- Cosmic rays amplitude hysteresis dependence on sunspot mean heliographic latitude and cluster number 08 p1353 A71-20979
- Surges and drops in sunspot cycle from 1832 to 1964, considering minima and maxima of diurnal relative numbers 12 p1962 A71-26957
- Atmospheric neutron production by cosmic radiation over sunspot cycle, measuring energy spectrum with airplanes and balloon-borne instruments 12 p1950 A71-27382
- Earth plasmasphere annual and sunspot cycle variations, considering observations with respect to whistler paths and Pc4 pulsations mean period variations 12 p1902 A71-27669
- Solar sunspot activity cycles, correlating intensities with duration 13 p2142 A71-29119
- Low latitude topside plasma temperature, electron content and ion production/loss rates during sunspot minimum to maximum 17 p2731 A71-34316
- Sunspot cycle effect on solar and lunar daily geomagnetic variations 18 p2966 A71-36745
- Extrasolar influence on solar activity, considering north-south asymmetry of sunspots distribution and annual June/December sunspots incidence extremes 20 p3294 A71-39540

SUNSPOTS

- Nonrecurrent sunspot clusters latitudinal motion speed correlation with solar activity cycle phase 01 p0149 A71-10052
- Solar magnetic fields configuration and evolution, discussing sunspots and white light faculae 01 p0152 A71-10330
- Sunspot and photosphere electric conductivity relationships based on Michard, Mattig and Fricke-El-sasser models 01 p0159 A71-10867
- Solar Li abundance determined from selected sunspot spectra observations 01 p0161 A71-11382
- Solar local SHF emission sources circular polarization, discussing sunspot clusters effects 02 p0306 A71-12076
- Sunspot observation of 22 June 1959, discussing two MgO bands spectrographic analysis 02 p0313 A71-12536
- Quiescent and sunspot prominences line of sight velocity measurements on limb, investigating statistical properties of velocity field 02 p0316 A71-12759
- Sunspots initial appearance east-west asymmetry interpretation by conical atmospheric model, including foreshortening and absorption effects 03 p0483 A71-13188
- Sunspots surface layers azimuthal electric current density, assuming specific magnetic force distribution 03 p0484 A71-13209
- Sunspot spectrograms analysis, observing wavelength shift in Zeeman triplet circular components and magnetic splitting inequality under different circular polarizations 03 p0484 A71-13210
- Sunspot areas and chromospheric flares relationship to distance from central meridian, noting Earth negative influence on solar activity and geometrical observational conditions 03 p0490 A71-13936
- Oppositely polarized maximal magnetic field strengths in sunspot regions during proton flares 03 p0478 A71-13937
- German monograph on molecules in sunspots, discussing molecular absorption lines in umbral spectra recorded in 1969 04 p0643 A71-14974
- Sunspots visual observations in 1969, giving Wolf numbers and rotational means by Carrington elements 04 p0644 A71-15079
- Solar eclipse of 22 September 1968 radio astronomical observations, examining sunspot groups during lunar occultation 04 p0650 A71-15559
- Deizner magnetostatic sunspot model enhancement by surface boundary condition derivation for horizontal pressure difference effect of photosphere 05 p0801 A71-15934
- Sunspot region birth and growth, noting arch filament systems with H alpha time lapse movies 05 p0801 A71-15935
- Line formation calculations for different spot models and arbitrary depth dependence of magnetic field vector, interpreting pi component anomalous splitting 05 p0803 A71-16021
- Eu II and La II line profiles in sunspots and undisturbed photosphere 05 p0803 A71-16022
- Swan band intensity upper limits in spectrum of 18 September 1966 sunspot 06 p0967 A71-17907
- CuH lines in sunspot spectra and solar isotopic ratio of Cu obtained from Cu I lines 06 p0969 A71-17971
- Sunspot heliographic latitude role in 11 year galactic cosmic ray modulation 06 p0955 A71-18133
- Solar cosmic ray activity near sunspot maximum, discussing events of 18 November 1968 and 11 April 1969 06 p0959 A71-18158
- Sunspot lithium abundance observation by high resolution interferometric spectrometer, using line formation theory applicable to medium strength lines 07 p1190 A71-18861
- Sunspot observations on 3 July and 14 September 1967, examining transverse magnetic field distribution and radial gas velocities and motion with magnetograph 07 p1195 A71-19338
- Solar radio waves varying component local sources relationship with sunspots development, describing characteristics based on thermal bremsstrahlung and cyclotron/synchrotron fast electrons radiation 07 p1195 A71-19339
- Solar radio emission constant and slowly varying components, investigating sunspots, activity cycle and flux rate 07 p1195 A71-19340
- Solar optical flares association with type 3 bursts from OGO-3 observations, suggesting temporary creation or enhancement of electron stream propagation by filament or sunspot structure change 07 p1187 A71-19724
- Sunspot boundary displacement toward limb in Fe I, Ti I and H alpha lines in passing from continuum to absorption line observations, discussing Wilson effect 07 p1205 A71-20635
- Eleven year galactic cosmic ray amplitude variation, determining modulation by sunspot groups and latitude 08 p1352 A71-20972
- Nonrecurrent sunspot clusters latitudinal motion speed correlation with solar activity cycle phase 08 p1361 A71-21046
- Solar local SHF emission sources circular polarization, discussing sunspot clusters effects 08 p1361 A71-21126
- Sunspot activity and 107 mm solar flux 27 day variations during 11 year solar cycle 09 p1513 A71-22792
- Midlatitude spread F, sunspot activity and geomagnetic activity variations related, discussing fast solar particles 09 p1437 A71-22938
- Pc and Pi micropulsations, correlating magnetospheric cavity eigenmodes with sunspot activity 09 p1440 A71-23637
- Sunspot molecular lines and rotational temperatures of MgH, CaH and TiO using model umbral atmospheres and photographic spectrograms 10 p1666 A71-23784
- Sunspots umbrae spectrum analysis in 4000-8000 A region, identifying molecular absorption lines photoelectrically 10 p1666 A71-23785
- Unusual sunspot rotation from 30 September to 8 October 1969 in plage region No. 10344, noting flare activity and rotational motion 10 p1666 A71-23786

Sunspot umbra empirical model, deriving temperature and optical depth relationship from IR continuous limb darkening

10 p1666 A71-23787

Sunspot group magnetic field distribution and radial velocities, investigated at H alpha and 6302.499 A atmospheric levels

10 p1666 A71-23788

Magnetostatic sunspot model with twisted field showing radial dependence of azimuthal component

10 p1666 A71-23789

Solar impulsive microwave bursts, showing association with types D, E and F sunspots

10 p1667 A71-23792

Solar cycle large sunspot groups as function of heliographic longitude, noting structure/distribution stability responsible for phenomena

10 p1674 A71-24459

Sunspots forbidden Fe I lines, calculating magnetic dipole and electric quadrupole transition probabilities

11 p1830 A71-26112

Eleven year solar activity cycles interrelationship, giving empirical expression for Wolf numbers in consecutive events

12 p1961 A71-26903

Twenty-two year solar cycles, relating Wolf numbers with minima and maxima in secular cycle

12 p1961 A71-26904

Electromagnetic interference, discussing man-made, inherent and natural types including atmospheric electrical disturbance, precipitation static, sunspots, etc

12 p1879 A71-27059

Type 3 radio bursts at hectometric wavelengths from 13 to 25 August 1968, noting effect of large active sunspot groups

12 p1969 A71-27652

Magnetic field strength measurements from Zeeman splittings of sunspots molecular lines, considering saturation effects

13 p2140 A71-29047

Sunspot deep subphotospheric layer structure, noting evolution, velocity field, visibility and model formulation

13 p2142 A71-29115

Sunspot groups frequency as function of mean area, comparing distributions in Northern and Southern Hemispheres for 11 year cycles

13 p2143 A71-29329

Sunspot penumbra displacements, emphasizing fine structure elements velocity and directional motion

14 p2308 A71-29972

Unipolar sunspot magnetic field and electric currents, comparing chromosphere and photosphere total field vector

14 p2298 A71-29978

Sunspot umbra, calculating vertical magnetic field strength distribution from Fraunhofer lines

14 p2308 A71-29979

Sunspots with proton flares of 7 July and 2 September 1969, examining longitudinal and transverse magnetic field components and total field vector

14 p2298 A71-29980

Gas pressure gradient and transmittance of sunspots, obtaining contours of D2 Na I and 5173 A Mg I lines

14 p2309 A71-29983

Solar radio emission at 3.15 cm wavelength via 22-meter radio telescope, determining relation between source brightness and areas of sunspot groups

14 p2299 A71-29990

Sunspot butterfly diagram interpretation based on heliographic latitude drift relation to gradient of solar rotational velocity

15 p2495 A71-32707

Scattered light effects on sunspot intensities observations during Mercury occultation and near solar limb

15 p2496 A71-32739

Sunspot umbrae and penumbrae, plotting period and amplitude curves for oscillatory velocity field

15 p2497 A71-32744

Solar flare activity and sunspot distribution over central meridian from optical data by NASA solar particle alert network 1967-69

16 p2635 A71-33437

Solar flares forecasting based on group total sunspot area, largest spot area and spots number observations

16 p2627 A71-33903

Sunspot convective heat transfer in terms of magnetic field convection theory, considering motion in photosphere

17 p2802 A71-34826

Sunspot forbidden Fe I line spectra, showing high solar iron abundance

18 p2961 A71-35944

Polarized solar millimeter emission associated with sunspot magnetic field compatible with multiple sources from chromosphere

18 p2966 A71-36762

Sunspot relative number observation accuracy test by least squares method for solar observatories

19 p3130 A71-37226

Stray-light and sunspot intensity measurements of sunspot umbra and aureole during Mercury transit

19 p3147 A71-38668

Sunspot intensity during 9 May 1970 Mercury transit with corrections for scattered light from solar limb observations

19 p3147 A71-38669

Sunspot number relationship with solar radio flux, using cross spectral method for high and moderate activity periods

20 p3279 A71-39324

MHD models of photospheric layers of sunspots emphasizing magnetic forces distribution

20 p3292 A71-39444

Astronomical models relating sunspots to solar magnetic field existence

20 p3293 A71-39530

Extrasolar influence on solar activity, considering north-south asymmetry of sunspots distribution and annual June/December sunspots incidence extremes

20 p3294 A71-39540

Nonflare solar X-ray emission from Cosmos 230 observation, noting presence of sunspot groups with complicated magnetic fields during enhanced short wave emission

20 p3283 A71-39749

Spiral topology of chromospheric fibrils and filaments in H alpha near sunspots, noting similarity with axisymmetric force free magnetic field configuration

22 p3597 A71-41458

Sunspot umbrae molecular line spectra, observing equivalent widths, isotopic abundances and band intensities

22 p3602 A71-42174

Ionospheric propagation hysteresis relationship to secular variation in F region response to sunspot number, noting differences in succeeding solar cycles

22 p3536 A71-42419

Polarized solar radio emission at millimeter wavelength in active regions associated with sunspot magnetic fields

23 p3733 A71-43125

Mg isotopes in solar atmosphere, analyzing absorption bands in sunspot spectrum

23 p3767 A71-43837

Two dimensional velocity field observations in and around sunspots from Doppler spectroheliograms

23 p3767 A71-43838

Molecular gas dissociation equilibrium and carbon monoxide overtone line widths dependences on magnetic field strength in sunspots

24 p3868 A71-44459

Transverse magnetic field measurement over sunspot in chromosphere, noting fan-shaped field line divergence

24 p3870 A71-44817

SUPER SABRE AIRCRAFT

U F-100 AIRCRAFT

SUPERALLOYS

U HEAT RESISTANT ALLOYS

SUPERCAVITATING FLOW

Finite supercavitating wings numerical calculation using acceleration potential method

04 p0526 A71-15210

Supercavitating flow past straight cascade with arbitrary blade shapes, considering lift and drag coefficients, cavitation number, cavity shape and exit flow conditions

[ASME PAPER 71-FE-6]

13 p1995 A71-29448

Water tunnel walls effect on supercavitating flows past slender bodies

20 p3213 A71-39786

Supercavitating bounded flow of weightless fluid past slender bodies, deriving singular integral equations in terms of pressure gradient and cavern thickness derivative

20 p3213 A71-39787

Cavities geometry in steady or periodic supercavitating flow from light beam transmission in flow tunnel

23 p3664 A71-44005

SUPERCAVITATION

U SUPERCAVITATING FLOW

SUPERCARGERS

Air cooled opposed 4, 6 and 8 cylinder light aircraft engines with or without turbosupercharging, considering horsepower improvement and torsional vibration control

[SAE PAPER 700205]

01 p0142 A71-10129

Axial flow turbines comparative performance tests under steady and pulse flow conditions for turbocharger application

14 p2169 A71-29819

Performance test facility for pulsed axial flow gas turbine of turbocharger unit on large diesel engines

15 p2469 A71-31943

Centrifugal superchargers high pressure wheels efficiency improvement, considering blade profiling

23 p3626 A71-43556

SUPERCARGING

U SUPERCARGERS

SUPERCANDING MAGNETS

Filamentary metal matrix composite superconductors for magnet construction

05 p0769 A71-16926

Supersonic wind tunnel electromagnetic balance with superconducting coils

07 p1084 A71-20151

Radiation cooled MPD thruster with permanent and superconducting magnets, describing test facilities and measurement techniques for performance tests

14 p2293 A71-30755

Cosmic ray rigidities spectra measurements above geomagnetic cutoff using balloon-borne emulsion plates in superconducting magnet field

15 p2407 A71-31805

Electrical DC collector machines and MHD magnetic systems design using superconductors, describing models

15 p2355 A71-32274

Superconducting magnetic systems for traveling wave quantum paramagnetic amplifiers, considering minimum weight maser systems

15 p2376 A71-32275

Paramagnetic cycles for low temperature superconducting magnet cooling, discussing refrigerator, cryogenic pumps, regenerators and adjustable heat source and sink

21 p3476 A71-40898

Cu clad Nb-Ti wire wound superconducting solenoids with large fields at 1.6-5.2 K

24 p3809 A71-45105

SUPERCONDUCTIVITY

Physical properties of Nb-Al-Ge alloys with maximum superconducting transition temperature close to boiling hydrogen

01 p0103 A71-11070

Quark regions in massive stars internal structure, discussing plasma superconductivity and spectral line emission

01 p0160 A71-11112

Superconductivity in physical metallurgy, discussing flux line structure and lattices, grain boundaries, stacking faults, etc

02 p0266 A71-12876

Vapor deposited niobium nitride superconducting thin films on fused silica substrates, measuring transition temperature

05 p0792 A71-16236

Acoustic and surface plasma waves in superconducting semiconductor metal films and laminates

05 p0793 A71-16826

Superconducting thin film bridges by vacuum deposition of tin, measuring current-voltage and resistance at SHF and critical temperatures

05 p0793 A71-16828

Spherical superconducting geomagnetic field generating layer under ultrahigh pressure in earth center

06 p0889 A71-17734

Superconducting tunnel junctions radiation emission, discussing superconductivity theory

07 p1178 A71-19777

Superconducting Nb experimental tests for hypothesis concerning relations between anisotropic critical field and dislocation cell structure

07 p1138 A71-19988

Time linear increase of magnetic flux flow through superconducting Nb-Zr wall, inferring empirical critical current density model agreement with measured flow rate

07 p1179 A71-20156

Noise thermometry by Josephson effect, demonstrating self excitation random frequency modulation with thermal noise and thermometer having microkelvin noise temperature measurement capability

07 p1114 A71-20157

Superconducting transition effects on metal and alloy single and polycrystals plasticity

08 p1344 A71-21520

Dislocation pinning point flow stress decrease in superconducting-normal transition

08 p1345 A71-21536

Electron concentration and superconducting characteristics of Nb-Sn alloys from optical measurements

09 p1507 A71-22234

Superconductivity transition of Nb-Ti solid solutions with varying Ti content, using specific heat measurements between 2.5 and 20 K

10 p1628 A71-24890

Neutron star nuclear matter superfluidity and superconductivity possibility from energy gap and critical temperature and magnetic field calculation

11 p1821 A71-25565

X band reflex klystron oscillator with frequency stability comparable to high quality quartz clock by coupling to superconducting cavity

11 p1739 A71-26368

Superconducting alloys order parameter spatial variation and resonance scattering near nonmagnetic impurity at critical temperature, using Heinrich perturbation theory expansion solutions

12 p1942 A71-26744

Superconducting state physics and macroscopic coherent states in superconductors, considering Josephson effect and technology utilization

13 p2110 A71-27888

Nb-Zr-Hf alloys superconductivity properties, determining critical current, critical magnetic field and

SUPERCONDUCTORS

- transition temperature in cold worked and tempered samples 13 p2083 A71-27961
- Nb-Ti-Zr-Hf alloys superconductivity properties, obtaining improved critical current values in tempered vs cold worked samples 13 p2083 A71-27962
- Stress effects on superconductivity and dislocation cell structure in deformed niobium for compression and tension 13 p2090 A71-29416
- Josephson and IC type superconducting tunneling junction neuristor devices performance tests, presenting bibliography 15 p2377 A71-32317
- Binary and ternary metal compounds superconductivity parameters comparison, considering crystal structure, valence electron concentration, component position and processing techniques 16 p2622 A71-33925
- Superconducting transition temperature measurement of cast and solution treated Nb-Zr alloys, substantiating dependence on density of states at Fermi surface 17 p2759 A71-35221
- Superconducting phase transition temperature measurements as function of magnetic field in thin film hollow Al and In cylinders 17 p2791 A71-35742
- Structure, superconductivity transition temperature, microhardness and electrical resistivity of V-Ta-Ti cast alloys 19 p3078 A71-37468
- Phase transformations in superconducting Nb-Ti alloys with Zr during heating or isothermal annealing 19 p3078 A71-37469
- Superconductivity in molybdenum disulfide laminate intercalated with sodium or potassium 19 p3119 A71-37842
- Superconductivity, reviewing critical current/field concepts, Meissner effect, negative surface tension, zero resistance and applications 20 p3276 A71-39247
- Electron concentration and superconducting characteristics of Nb-Sn alloys from optical measurements 21 p3428 A71-41114
- Superconductivity transition of Nb-Ti solid solutions with varying Ti content, using specific heat measurements at 2.5-20 K 21 p3432 A71-41266
- Niobium carbonitride thin film deposition temperature effects on superconducting properties, considering transition temperature and critical currents and fields 23 p3717 A71-44141
- SUPERCONDUCTORS**
- L-alpha X ray spectral band and K absorption edges in vanadium silicides and high temperature superconductors, obtaining energy bands electron distribution 02 p0294 A71-11893
- Differential energy losses of alpha particles traversing materials in superconducting and normal states 03 p0468 A71-14414
- Neuristor pulse propagation analysis for nonlinear distributed circuit of superconductive tunnel junction stripline 03 p0393 A71-14470
- Superconducting niobium aluminide and niobium aluminide-Ge films formation on Nb substrate 05 p0792 A71-16238
- Filamentary metal matrix composite superconductors for magnet construction 05 p0769 A71-16926
- Superconductors applications, noting low cost reliable closed cycle He refrigerators 06 p0941 A71-18017
- Oscillatory magnetic field superimposition effects on flux flow properties of superconducting metal foils 07 p1177 A71-19596
- High transition temperature superconducting materials thin films composition control by sputtering from hot pressed powder mixture ingots targets 07 p1178 A71-19849
- Levitated superconducting ring in Princeton Sphera for plasma physics, describing Dewar, coil and feedback control systems 07 p1170 A71-20152
- Josephson superconducting devices electrical characteristics 07 p1079 A71-20153
- Sn additives effect on In thin film superconducting transmission lines, comparing with Pippard nonlocal theory for mean free path reduction 07 p1179 A71-20155
- Single fluxon drift through superconductors, describing observation technique 07 p1179 A71-20158
- AC superconducting cables design for utilities underground power transmission lines, discussing superconductor and cryogenic envelope configuration and characteristics 07 p1024 A71-20159

- Low temperature material properties analyzer with superconducting microwave resonant cavity 07 p1179 A71-20160
- Superconducting microstrip microwave resonators with high Q, using vacuum deposited lead on alumina substrate 07 p1079 A71-20162
- Bogoliubov electronic excitations anomalous scattering and tunneling in superconductor intermediate state, noting pair production one direction step function changes 07 p1181 A71-20207
- Nonlinear effects in superconductors in electromagnetic field with constant and alternating components 07 p1181 A71-20535
- Voltage induction in superconductors by superimposed AC and DC magnetic fields 08 p1343 A71-20881
- Superconductivity based cryogenic electronics, considering thin film IC, miniaturization, microwave circuits, memory elements, etc 08 p1263 A71-21067
- Electromagnetic device with superconducting elements for magnetic monopole detection in Apollo lunar samples, describing operation principle, amplifier, sample container and transport system 09 p1446 A71-22733
- Thermal conductivity anomalies in thin superconducting metal foils in contact with two superfluid He basins at low temperatures, examining surface electron phonon interactions 10 p1640 A71-23832
- Arc melted ingot high field superconductor, combining critical density and resistive critical field 10 p1655 A71-24042
- Graphite lubricants superconducting properties under high pressures and low temperatures, suggesting new superconductors developments and metal free electron model modification 10 p1656 A71-24299
- Current induced flow of superconducting domains in superconductor intermediate state, presenting theoretical analysis of motion of domains of arbitrary topology 12 p1942 A71-26745
- Thermal noise measurement of superconducting coaxial lambda/2 resonator at 2.46 GHz with ruby traveling wave maser and tunnel diode amplifier setup 12 p1887 A71-27010
- Fluctuation enhanced conductivity of superconductor, considering Maki graph evaluation 13 p1211 A71-28454
- Flux flow noise spectra measurement in pairs of magnetically coupled superconducting films, noting frequency response 13 p1211 A71-28502
- Superconductive Nb-Al alloy critical temperature as function of chemical composition and heat treatment 13 p2085 A71-28576
- Superconducting thin films nonlinear excess current near transition temperature, deriving expression from Tsuzuki microscopic basic equations 13 p1212 A71-29012
- Theorem proving impossibility of stabilizing unstable MHD configuration with nondissipative plasma in vacuum surrounded by superconducting wall by means of finite electrical conductivity wall 14 p2282 A71-30557
- Superconducting Nb-Sn intermetallic compound synthesis from elemental powders by converging shock waves 15 p2461 A71-32378
- Pure superconducting Al wire surface inductance measurement as function of temperature, noting penetration depth value 16 p2621 A71-33425
- Critical current density in niobium alloy with disperse superconducting phase as function of transverse magnetic field strength 16 p2593 A71-33653
- Superhigh cooling rate effects during crystallization of solidified binary alloys, achieving superconductive properties 16 p2598 A71-33998
- Magnetoplasma reflection coefficient for nonzero angle of incidence in Voigt configuration in superconducting coil, calculating effective intervening mass 17 p2789 A71-35348
- Temperature dependence of electrical resistance in mixed superconducting-normal systems, solving transport equation 18 p2954 A71-36746
- Superconducting microjunctions I-V characteristic at critical temperature, investigating voltage fluctuations effects in external circuit 19 p3119 A71-37860
- Diffraction by perfectly conducting plane screens solved by Hilbert space formulation of EM diffraction 19 p3018 A71-38192
- Superconductors intermediate state interrelated electrodynamic and thermal effects, calculating resistivity, heat conduction and thermoelectricity tensors 21 p3432 A71-41267

- Temperature and velocity dependence of electronic dislocation stopping power in superconductor due to scattering of normal electrons 21 p3432 A71-41268
- Electron scattering magnetic impurities effect in insulator layer of tunnel junction on superconductor current 22 p3585 A71-41818
- Superconductors application to electric energy storage and discharge 23 p3630 A71-43106
- Kinetic equations for electron density matrix of superconductors, describing two phase relaxation process 23 p3715 A71-43413
- Critical current of ideally homogeneous second class superconducting film, noting lattice resistance to small displacements 23 p3715 A71-43414
- Objective lens with superconductive winding for high voltage electron microscope, describing optical properties and vibration reduction system 23 p3679 A71-44008
- Anomalous ultrasonic attenuation in pure superconducting Nb from pulse echo amplitude measurements 24 p3860 A71-44751
- Abrikosov vortex lattice in superconductors, calculating resonance linewidth and vacancy formation energy 24 p3860 A71-45119
- SUPERCOOLING**
- Fine structure and lattice constants of Al-W, Al-Mo and Al-Mn alloys at high cooling rates 01 p0101 A71-10675
- Solute core redistribution and dendritic refinement in highly undercooled Fe-Ni alloy, using metallographic and electron microprobe analyses 03 p0442 A71-13365
- Subcooled nitrogen tube flow film boiling, investigating heat transfer and hydraulic resistance 04 p0687 A71-15530
- Superhigh cooling rate effects during crystallization of solidified binary alloys, achieving superconductive properties 16 p2598 A71-33998
- Al-Cu-Mg monovariant alloys directional solidification, considering criterion for plane front growth breakdown based on constitutional supercooling 19 p3078 A71-37701
- Precipitation formation and regulation from supercooled and frontal clouds, noting crystalline cloud seeding effects 19 p3092 A71-38689
- Artificial crystallization and dispersion in supercooled stratus clouds, observing growth, stabilization and disintegration stages in crystallization zones expansion 19 p3093 A71-38691
- Pressure, subcooling and diameter effects on heat transfer and circumferential flow transition of thin wire film boiling of liquid nitrogen in pool 20 p3313 A71-39284
- Alloy steels supercooled austenite nitriding in ammonia flow, examining diffusion layers by X ray analysis and hardness tests 21 p3404 A71-41164
- SUPERCritical FLOW**
- Steady supercritical planar inviscid transonic flows over lifting airfoils, generating unsteady flow by impulsively imposing airfoil boundary condition [AIAA PAPER 70-77] 03 p0341 A71-13433
- Compressible subsonic and supercritical flows, developing flowmeter orifice expansion factors [ASME PAPER 70-WA/FM-3] 03 p0402 A71-14105
- Transonic supercritical flow past arbitrary airfoils, using integral relations method 06 p0844 A71-18553
- Pressure drag and cross flow force coefficients of inclined circular cylinder in supercritical flow 09 p1382 A71-22098
- Aerodynamic noise produced by supercritical jets, using high speed flash photography for schlieren and shadowgraph studies 13 p2069 A71-28767
- Heat transfer and pressure drop characteristics of He in two phase and supercritical flow, calculating He heat exchangers for superconductive devices [HEAT EXCH. CONF. PAPER 24] 15 p2513 A71-31638
- Mesh method for supercritical transonic flow calculation with normal or oblique shock wave at trailing edge 17 p2674 A71-35799
- Turbulent forced-convection heat transfer coefficient for supercritical fluid, extending Prandtl mixing length concept [ASME PAPER 71-HT-26] 19 p3165 A71-37996
- Supercritical carbon dioxide free convective heat transfer, investigating heater surface material and flow effects [ASME PAPER 71-HT-27] 19 p3165 A71-37997
- SUPERCritical PRESSURES**
- Cs and Hg vapors compressibility factor in supercritical range as function of density, considering

charged particles and atoms polarization interactions in ionized metal vapors
19 p3111 A71-37590
N-heptane, carbon dioxide and Freon 13 droplet vaporization measurements at supercritical pressure, comparing with film theory calculation
24 p3890 A71-45072

SUPERFLUID FLOW
U SUPERFLUIDITY
SUPERFLUIDITY

Superfluid gyroscope for general relativity tests, using resonant phonon force field for drift reduction
02 p0248 A71-11943
Superfluid flow through parallel channel, obtaining critical velocity measurements by phase coupling
03 p0404 A71-14199
Thermal conductivity anomalies in thin superconducting metal foils in contact with two superfluid He basins at low temperatures, examining surface electron phonon interactions
10 p1640 A71-23832
Neutron star nuclear matter superfluidity and superconductivity possibility from energy gap and critical temperature and magnetic field calculation
11 p1821 A71-25565
Liquid He containment in space zero-g environment, proposing use of high thermal conductivity porous plug operating in superfluid regime
20 p3184 A71-39280

SUPERGIANT STARS

Blue supergiants evolution, discussing chemical composition of atmospheres, mass, binary nature and cluster association
01 p0153 A71-10375
M type supergiants atmospheric metals abundances from high dispersion spectrograms analysis
02 p0308 A71-12095
Reddening effects in determining intrinsic color of supergiant and cepheid variable stars
04 p0646 A71-15235
Normal O, blue supergiants and brightest yellow and red supergiant massive stars, considering evolution, luminosity, lifetime mass loss, pulsational instability and supernovae
04 p0648 A71-15248
Normal main sequence B stars, distinguishing features from rapid rotators and supergiants by photometric scheme
05 p0805 A71-16118
Blue and red supergiants ratio as function of radial distance from Galactic center, noting distribution in M33
05 p0805 A71-16119
Hot stars, supergiants and quasars extended and expanding atmospheres, examining resonance line profile formation by coherent scattering
05 p0806 A71-16203
M type supergiants atmospheric metals abundances from high dispersion spectrograms analysis
08 p1362 A71-21145
Continuous energy distribution around light maximum of Nova Serpentis 1970 represented by yellow supergiant model, correcting observations for interstellar reddening
08 p1364 A71-21416
Class M supergiants alpha Sco, delta Sge, R Lyr and alpha Her spectra between 7000 and 6000 A wavelengths, tabulating equivalent bandwidths
09 p1524 A71-23189
Individual M-type red supergiants luminosity, masses and periodicities based on cluster membership and pulsational Q value
10 p1674 A71-24433
Mu, VV, ST and RW Cephei cold supergiants polarization data, noting spectral dependence
15 p2487 A71-32030
High luminosity G supergiants at 0.4-18 micron wavelengths showing intense silicate emission shell
15 p2497 A71-32764
Stellar evolution, discussing semiconvective regions, mass loss, red giants and supergiants, He flash structures and globular clusters
18 p2967 A71-36999
Radio stars classes, discussing red dwarf flare, red supergiants, blue dwarf companion, novae, pulsars and X ray stars
21 p3448 A71-40582
M supergiants hot corona base density determination from radio emissions observations, noting equivalence to solar type 4 microwave bursts
22 p3598 A71-41916
Photometric study of light variation and variable stars in luminous supergiants in Large Magellanic Cloud
23 p3723 A71-42940

SUPERHARMONICS
Superharmonic resonance in piecewise linear systems with unsymmetrical characteristics, investigating stability properties by Fourier series method
17 p2781 A71-34926

SUPERHEATING

High performance superheated subliming solid ammonium carbamate thruster using resistojet technology for specific impulse increase
[WSS/CI PAPER 70-210] 15 p2469 A71-32048
SUPERHETERODYNE RECEIVERS
Microwave electromagnetic emission in theta pinch hydrogen plasma by sensitive superheterodyne receivers, noting discharge azimuthal current
08 p1339 A71-21477
Superheterodyne radiometers for millimeter and submillimeter waves, using Mach-Zehnder interferometer frequency mixer for parasitic signal suppression
12 p1886 A71-26847
Amplitude modulated optical band signal detection, comparing optimal direct photodetection and superheterodyne receivers sensitivities
13 p2029 A71-28365
Azimuthal current growth and microwave radiation in theta pinch hydrogen plasma discharge from sensitive superheterodyne receivers
14 p2282 A71-30663
Integrated wideband low-noise X-band sweeping superheterodyne receiver, demonstrating advantages of microwave IC techniques application
16 p2547 A71-33553
Superheterodyne wideband microwave receiver requirements, design and performance
17 p2699 A71-34607
Microwave acoustic delay device incorporated in phase discriminator for AFC, FM noise meters and pseudo-superheterodyne receivers
18 p2893 A71-36599
Oscilloscope and automatically tuned superheterodyne receiver panoramic display units for 10 kHz-60 MHz, considering design, circuits, performance and mechanical arrangement
21 p3353 A71-40518
Millimeter band plasma microwave radiation receivers for emission measurement, presenting schematic diagrams for superheterodyne
24 p3825 A71-44507

SUPERHIGH FREQUENCIES

YIG C band microwave amplifier using longitudinal pumping, comparing to other systems
02 p0228 A71-11692
Solar local SHF emission sources circular polarization, discussing sunspot clusters effects
02 p0306 A71-12076
Two stage parametric SHF amplifier for Skynet V Naval receiver system
02 p0234 A71-12812
Broadband mini ferrite T circulator and isolator for X band
03 p0384 A71-13274
Spatial statistical coherence of X band propagation over path near ground
04 p0552 A71-15211
Radiometeorological measurements of atmospheric structure, using SHF troposcatter synchronously offset beams on great circle propagation path
04 p0584 A71-15545
S band transponder for vehicle-space-ground link subsystem [VSGLS] of USAF integrated telemetry, tracking and command system
05 p0719 A71-16151
H II regions compact radiation sources flux densities observation at centimeter wavelengths
05 p0812 A71-16690
S band pulsed cotal radar transponder for ground base Centaur rocket trajectory tracking from takeoff to splashdown
06 p0870 A71-18475
X band gas tube attenuator for ruby maser saturation protection in pulsed high power radar
07 p1070 A71-18866
X band IMPATT oscillator, discussing frequency stability, rms noise deviation, admittance characteristics, output power loss, temperature effects and power stability
07 p1073 A71-19111
Broadband pulling cavity stabilized X band Gunn oscillator, using measured circuit and diode admittance
07 p1073 A71-19112
One watt CW high efficiency X band avalanche diode amplifier with in-band and second harmonic impedance control
07 p1073 A71-19117
Thermocompensated cavity resonator for SHF wavelength measurements
07 p1075 A71-19302
X band radar system to compare electrical lengths in 100 m range with 10 to minus 6 accuracy, noting applications in geodetic and radio waves phase fluctuation measurements
07 p1075 A71-19345
SHF electric fields effects on free carrier redistribution in semiconductors and surface effect influence on sample conductivity
07 p1177 A71-19496
Wideband X band microstrip image rejection balanced mixer design
08 p1263 A71-20772

Radio telescope measurements of circular polarization and total flux of Jupiter at 13.1 cm wavelength
08 p1357 A71-20871
Solar local SHF emission sources circular polarization, discussing sunspot clusters effects
08 p1361 A71-21126
Biotelemetric contactless recording of animal movements using centimeter band standing waves
09 p1397 A71-22216
External SHF signal effects on multifrequency spectrum of reflex klystron coupled with long waveguide
09 p1414 A71-22221
Trapezoidal and Killian distributions profile parameters at S band in plasma column, noting electron density
09 p1501 A71-22306
Electronically tunable compact X band triplexer, consisting of four port nonreciprocal directional YIG filters in cascade
09 p1418 A71-23416
Varactor tuned X band Gunn oscillator with lumped thin film microwave circuits, discussing GaAs materials, output powers and bandwidths
09 p1421 A71-23722
X band Schottky barrier diodes RF impedance mismatch and noise factor, calculating dependence on microwave oscillator voltage-standing wave ratio
09 p1421 A71-23723
Pulsed ion laser electron density measurement by cavity method in S band, evaluating relaxation time
10 p1623 A71-25021
Microwave amplification using negative resistance device in prototype filter equalization networks, permitting realization of wideband amplifiers for C band and superhigh frequencies
11 p1736 A71-25140
Supernova remnant HB 21 linear polarized radiation observed at 6 cm wavelength, correlating optical nebula shape with radio mappe d contours
11 p1819 A71-25216
X band reflex klystron oscillator with frequency stability comparable to high quality quartz clock by coupling to superconducting cavity
11 p1739 A71-26368
High sensitivity S band meteorological radar detecting clear air echoes from low horizontal layers and high altitude turbulence
12 p1880 A71-27156
Microwave integrated stripline Gunn oscillators with fixed/variable frequency tuning in X band
13 p2039 A71-28911
Interstellar 21 cm and Na D lines comparison in directions of 30 stars at intermediate and high galactic latitudes
14 p2304 A71-29595
High power 10 cm radar as CAT detector, comparing with radar and aircraft data coincident in space and time
14 p2267 A71-29761
Solar radio emission at 3.15 cm wavelength via 22-meter radio telescope, determining relation between source brightness and areas of sunspot groups
14 p2299 A71-29990
M87 nucleus radio flux density variations observation at 5 GHz
14 p2301 A71-30451
Optimal omnidirectional antenna array located on cylindrical head section of sounding rocket for L band telemetry
14 p2216 A71-31035
Multiple planar Luneburg lens circular array for airborne electronically scanned X band narrow beam antenna mounted under aircraft nose or fuselage
14 p2216 A71-31038
Miniature 20-watt CW TWT with samarium cobalt focusing magnets for fitting X-band waveguide, comparing performance, size and weight with conventional design
15 p2375 A71-31206
Superhigh frequency microwave absorption region localization in collisionless plasmas by plasma parameters measurement in toroidal magnetic field
15 p2370 A71-31737
Varactor tuned FM pulsed Gunn oscillator for testing X band delay lines for pulse compression radar
16 p2546 A71-33415
Integrated wideband low-noise X-band sweeping superheterodyne receiver, demonstrating advantages of microwave IC techniques application
16 p2547 A71-33553
Phased array pulsed X band microstrip Gunn diode transmitters with temperature stabilization at 9.4 GHz
16 p2547 A71-33555
Ku band monopulse receiver with electronically tunable Gunn oscillator, discussing negative resistance diodes dynamic impedance properties
16 p2547 A71-33557
SHF low noise IC mixer, considering effects of series resistance and barrier capacitance in diode and internal resistance of local oscillator
16 p2548 A71-33558
Centimeter TEM waves excitation in Fabry-Perot cavity of cyclotron resonance maser by helical electron beam
17 p2750 A71-34263

Scintillation fading of signals in SHF band due to electron density irregularities in F region
17 p2699 A71-34624

Transponder configurations for communication satellites using frequencies above 10 GHz, discussing service type, modulation method and equipment
17 p2705 A71-35092

Temperature and bias circuit frequency modulation in CW X band Gunn oscillators
18 p2888 A71-36132

Apollo lunar surface S band communications and TV systems and equipment, including ground commanded TV assembly
18 p2878 A71-36519

Italian SIRIO experimental SHF telecommunications satellite, noting trapped radiation and high energy electron experiments
18 p2974 A71-36521

Italian SIRIO synchronous satellite for SHF communication, analyzing thermoelastic deformations effect on antenna radiation patterns
18 p2882 A71-36575

Simple type centimeter solar radio bursts identification and relation to flare position, noting radio spectrum over sunspot
18 p2958 A71-36741

Design and fabrication of frequency multipliers from 10 to 30 GHz on silica substrates by scaling and integrated circuit processing
19 p3026 A71-37219

Contact materials effects on X band FM noise and current fluctuations of Gunn elements
19 p3029 A71-38073

X band output power and FM noise of parallel multicontact Gunn oscillators
19 p3029 A71-38074

Rain attenuation measurements, noting limitations on microwave transmission at SHF
19 p3024 A71-38612

Double refracting dielectric microwave lenses design for horn antennas in SHF applications
19 p3036 A71-38643

Methyl alcohol transitions in Orion at 1 cm noting emission source coincidence with IR nebula
21 p3447 A71-40445

Italian Sirio synchronous satellite for SHF propagation and communication experiments on fading statistics, frequency dependence, path diversity and TV transmission
21 p3347 A71-40474

Small scale structure of extragalactic compact radio sources at 6 and 18 cm, obtaining magnetic field strengths and maximum brightness temperatures
22 p3598 A71-41912

X band GaAs diffused IMPATT diodes for high CW efficiencies
22 p3523 A71-42483

Microwave planar Gunn oscillators performance in X band, giving pulsed and CW I-V characteristics
23 p3649 A71-42913

Waveguide system for measuring semiconductor electrical and photoelectric properties at SHF, observing temperature effects
23 p3652 A71-43531

SUPERIMPOSITION [MATHEMATICS]

U SUPERPOSITION [MATHEMATICS]

SUPERMAGNETS

U HIGH FIELD MAGNETS

SUPERNOVAE

Total free electron energy disparity with energy radiated in forbidden O I lines in supernova spectra explained by nova luminescence formation
01 p0151 A71-10067

Supernovae positrons and low energy cosmic rays flux, determining ejected matter plasma properties
01 p0145 A71-11338

Shock wave dynamics of brightness curve reflecting supernova outbursts
02 p0307 A71-12088

Rotating neutron star supernova explosion without nuclear detonation, discussing rotational momentum transfer
02 p0307 A71-12089

Supernova remnant X ray and radio emission secular behavior, considering hot plasma and synchrotron models and continuous injection
04 p0640 A71-14874

Runaway pulsar formation and ejection in supernova collapse, fragmentation, condensation, radiation and disruption
04 p0643 A71-15046

Supernovae high energy gamma rays detection by extensive air shower arrays
04 p0641 A71-15830

Supernova remnant kinematic distance estimates, using molecular absorption line velocities with Schmidt model
05 p0805 A71-16107

Nonthermal extended radio source in pulsar CP 1919 area, proposing as supernova remnant
05 p0805 A71-16117

Neutron star formation, calculating reimplosion mass fraction of thermonuclear supernovae explosion
05 p0811 A71-16684

Strip brightness distribution across Kepler supernova derived from occultation observation by radio telescope
06 p0971 A71-18241

Supernovae expansion, investigating hydrodynamic model with interstellar magnetic fields and relativistic particles effects
06 p0973 A71-18335

Type I supernovae brightness curves analysis by photometry
06 p0975 A71-18435

Gum Nebula-fossil Stromgren sphere of Vela X supernova, deriving ionization model from interstellar measurements
07 p1191 A71-18865

Supernovae as indicators of distances to galaxy clusters based on Karpowicz and Rudnicki catalog and angular measurement
07 p1192 A71-19288

Soft X rays from supernova remnants Pup A and Vela X complex observed by X ray astronomy payload on Nike-Tomahawk rocket
07 p1187 A71-19817

Superheavy elements formation due to fast neutron capture during supernova outbursts, discussing meteorites fission produced noble gases
08 p1337 A71-20959

Shock wave dynamics of brightness curve reflecting supernova outbursts
08 p1362 A71-21138

Rotating neutron star supernova explosion without nuclear detonation, discussing rotational momentum transfer
08 p1362 A71-21139

Decoupled nucleochronological isotopic equations for element age yielding solar system formation interval and supernova galactic distribution
08 p1251 A71-21694

Pulsar association with supernova remnants as energy source for supernova explosions, considering Crab Nebula, Vela X, Cas A and eta Car observations
09 p1518 A71-22350

Explosive nucleosynthesis in Galaxy, discussing carbon detonation, uniform density models, supernova rates and massive stars
09 p1521 A71-22929

Cosmic X ray astronomy, discussing supernova, variable and extragalactic radiation sources, diffuse background radiation and Crab Nebula measurements
09 p1522 A71-22976

Total free electron energy disparity with energy radiated in forbidden O I lines in supernova spectra explained by nova luminescence formation
09 p1525 A71-23260

Supernovae light curves theory based on numerical integration of gas dynamics and radiative heat conductivity equations
09 p1528 A71-23591

Nucleosynthesis due to explosive burning in stellar objects for elemental synthesis
10 p1668 A71-24003

Nucleosynthesis in neutron rich supernova ejecta, performing statistical equilibrium calculations at freeze out temperature and density
10 p1670 A71-24301

Supernova explosion or solar outburst theory of climatic effects on mass extinction of organisms at Cretaceous-Tertiary boundary
10 p1673 A71-24422

Supernovae detonation model, examining nucleosynthesis for solar system abundances
10 p1675 A71-24492

Supernova remnant HB 21 linear polarized radiation observed at 6 cm wavelength, correlating optical nebula shape with radio mapped contours
11 p1819 A71-25216

Neutron star formation from supernova explosion in close binary system
11 p1832 A71-26171

Type I supernovae maximum brightness and occurrence time from photometric analysis
12 p1955 A71-26585

Milky Way Galaxy X ray sources, discussing bremsstrahlung, synchrotron radiation, Compton effect optical objects, supernova remnants and X ray astronomy
12 p1959 A71-26780

Stellar evolution, discussing mass loss to interstellar medium, galactic distances determination and supernova explosions
12 p1960 A71-26784

Galaxy nuclei and quasars model, considering supernova explosions, neutron stars matter accretion and energy radiation
12 p1968 A71-27541

Soft X ray background source, discussing north polar galactic spur as supernova outburst remnant
14 p2298 A71-29732

Pulsars origin from type 2 supernovae, deriving characteristics of exploding massive stars
14 p2313 A71-30436

Pulsars 0527 and 0531 as remnants of binary star supernova explosion, considering mass exchange and measured proper motion of 0531 and Crab Nebula
14 p2315 A71-30657

NGC 3811 supernova spectrum and light curve data, indicating Type I class
16 p2635 A71-33431

Supernovae outburst remnant radio emission from Crab Nebula, discussing synchrotron mechanism and connection with pulsars
16 p2635 A71-33472

Exploding universe phenomena, considering supernovae, exploding galaxies, Crab Nebula, pulsars, quasars and radio galaxies
16 p2643 A71-34036

Type I supernova broadband identification, examining interstellar medium spectra
17 p2806 A71-35384

Gum Nebula size, density and electron temperature data from RAE-1 and OGO-5 satellites and ground based telescopes observations, correlating with Vela X supernova outburst
17 p2806 A71-35409

Vela X supernova remnant blast wave model and Gum Nebula formation, discussing kinetic and rotational energy transformation into radiation
17 p2807 A71-35414

Type II supernovae observations and models, considering photographic light curves and dynamic instabilities in star development, outbursts and ejected matter composition and amounts
18 p2961 A71-35976

Cyg X-1 X ray pulsar age determination and emission model speculations based on observation data for supernova remnant and radio counterpart absence explanation
18 p2962 A71-36151

Contour maps of radio source CTB 1 at UHF, suggesting supernova remnant superimposed on broad faint H II region
18 p2962 A71-36153

H II region formation from type II supernovae explosion, detecting with fluorescence model
20 p3287 A71-39052

Beta processes effect on detonation and postdetonation evolution of degenerate carbon-oxygen core supernovae, using numerical hydrodynamic calculations
20 p3287 A71-39053

Gum Nebula conceived as hydrogen gas mass ionized by UV radiation from supernova explosion related to Vela X remnant, discussing fossil Stromgren sphere model
20 p3294 A71-39572

Pulsars luminosity, z-distance and period distribution in Galaxy, comparing supernova remnants
20 p3303 A71-39933

Timing measurements of pulsar NP 0527 relating frequency, position and transverse velocity with NP 0532, excluding origin in supernova explosion
20 p3287 A71-39936

Cassiopeia A galactic supernova remnant, discussing flocculi formation from material ejected from outer layers before explosion
20 p3304 A71-39941

Continuous injection models for secular X ray and radio emission from supernova remnants in Crab Nebula, Cas A and Tycho
20 p3304 A71-39942

Observation probability of orbital motion and mass transfer of pulsars in close binary systems, excluding supernova explosion origin for runaway velocities
20 p3304 A71-39943

Multiple pulsar ejection in supernova core collapse and neutron star formation energy loss
20 p3305 A71-39947

Interstellar medium time dependent model, investigating supernovae and hot stars UV ionization effects on ion production and heating and cloud formation
21 p3445 A71-40248

Wavelength shifts of intensity minima in type I supernova spectra
21 p3449 A71-40606

Gum Nebula ionization and heating by energetic particles from Vela X supernova
22 p3598 A71-41917

Small circle geometry of Galactic continuum loops, noting consistency with neutral hydrogen and supernova remnant hypothesis
22 p3601 A71-42168

Supernova shell fragmentation as basis for solar system formation model, considering meteoritic materials heavy elements formation by nucleosynthesis followed by r-process event
22 p3604 A71-42192

Cosmic rays origin, discussing nuclear, electron and electromagnetic components, supernovae, pulsars, white dwarfs and gas motions in Galactic Center
22 p3594 A71-42550

Brightness and polarization distributions for supernova remnants IC443 and Puppis A, considering magnetic field orientation and thermal radio emission
22 p3606 A71-42601

SUPEROXIDES

U INORGANIC PEROXIDES

SUPERPOSITION [MATHEMATICS]

Existence theorem and optimal approximation of functions of many variables by superimposing sums of smaller number of variables in complex region
07 p1146 A71-19039

SUPERSATURATION

- Liquid-phase nucleus condensation of supersaturated vapor in drawer, using statistical method
01 p0180 A71-11089
- Al alloy rapidly crystallized film structure, studying atomic diffusion mobility effects on formation of supersaturated solid solutions
07 p1130 A71-19299
- Spinodal decay of supersaturated solid solutions with nonenergetic phase nucleus formation
07 p1135 A71-19616
- Ar condensation onset location in supersonic nozzles for nuclear space propulsion systems, using supercooled vapor pressure measurements beyond saturation point
10 p1593 A71-24328
- Cloud condensation nuclei supersaturation spectrum and aerosol particle concentration variations with height
19 p3092 A71-38683

SUPERSONIC AIRCRAFT

- NT B-70 AIRCRAFT
- NT BOEING 2707 AIRCRAFT
- NT CONCORDE AIRCRAFT
- NT F-4 AIRCRAFT
- NT F-8 AIRCRAFT
- NT F-14 AIRCRAFT
- NT F-15 AIRCRAFT
- NT F-100 AIRCRAFT
- NT F-104 AIRCRAFT
- NT F-111 AIRCRAFT
- NT JAGUAR AIRCRAFT
- NT MIRAGE 3 AIRCRAFT
- NT SAAB 37 AIRCRAFT
- NT SUPERSONIC COMMERCIAL AIR TRANSPORT
- NT SUPERSONIC TRANSPORTS
- NT TSR-2 AIRCRAFT
- NT TU-144 AIRCRAFT
- NT X-15 AIRCRAFT

Mach 2 Mirage Milan ground attack fighter, noting lift aid moustache, low speed and steep approach handling from short airstrips

Heavy supersonic aircraft controllability, noting irreversible boost control system and stability

Aircraft construction materials for 1990s, discussing need for high temperature resistant materials for supersonic and hypersonic airframe and engine structural components

Supersonic aircraft turbojet engine exhaust noise suppressor research program, predicting full scale noise spectra from model suppressor tests
[AIAA PAPER 68-1023]

Supersonic aircraft electrification measurements using projectile frictional charging in ice-gel cloud

Supersonic airplane minimum time turns at constant altitude, determining thrust, bank angle and angle of attack programs with optimal control theory

Aerodynamic heating effects on fatigue and creep properties of supersonic aircraft alloys at high temperatures, considering deformation mechanisms interaction

Long term exposure effects on high temperature resistant supersonic aircraft fuel tank sealants

Transonic aircraft jet exhaust wave structure, examining reflection geometry at shear layer and shock diamond train

Weather influence on long range radio navigation aids, considering supersonic aircraft operation and inertial navigation

Performance testing of fluorosilicone hydraulic fluid in high temperature supersonic aircraft piston pumps

Minimum drag surface shape of thick lifting delta wing integrated with conical fuselage for supersonic cruising speed
[ONERA-TP-947]

V/STOL and supersonic commercial aircraft developments, comparing man and machine performance as information processing systems for aircraft control and navigation

Minimum drag wing-fuselage combination for supersonic speeds and prescribed lifting force, longitudinal moment and volume, using method of successive approximations

Energy state approximation and supersonic aircraft minimum fuel fixed range trajectory optimization, noting not convex velocity set

Altitude, bank angle and thrust program for minimizing time required by supersonic aircraft to turn through specified heading angle and reach required energy

[AIAA PAPER 71-796]

Thyristor power conditioning application to high voltage DC electric power system, presenting SST aircraft sample load profiles

Composite materials effect on supersonic aircraft weight, design and performance
[SAWE PAPER 888]

Strategic bomber B-1A program, discussing airframe and engine contractors, design, characteristics performance, electronic equipment and armament

Three dimensional minimum fuel turns for supersonic aircraft by energy state approximation
[AIAA PAPER 71-913]

Supersonic aircraft shape for shock waves minimization based on channel configuration with converging inlet and diverging outlet section

SUPERSONIC BOUNDARY LAYERS

Supersonic laminar boundary layer structure near convex corners for large turning angles

Plate critical surface temperature in case of stabilization by supersonic boundary layer cooling

Soviet book on supersonic turbulent boundary layer covering gas flow molecular theory, heat and mass transfer at porous surfaces, etc

Supersonic turbulent boundary layer separation on flat plate by forward facing step, measuring mean flow field characteristics
[AIAA PAPER 71-127]

Interaction theory for supersonic separated and reattaching turbulent boundary layers, comparing to real flow past compression ramp
[AIAA PAPER 71-128]

Supersonic turbulent boundary layer measurements in moderate adverse pressure gradient region along two dimensional ramp model
[AIAA PAPER 71-162]

Boundary layer pressure distributions for supersonic fluidics bistable devices

Supersonic turbulent boundary layer density profile over flat plate at single Reynolds number, using Mach-Zender interferometer

Supersonic boundary layer flow profile distortion due to oblique shock during separation

Heat and mass transfer in supersonic laminar boundary layers with light gas injection, deriving approximate solution for binary mixture flow with variable fluid properties

Interaction theory for supersonic separated and reattaching turbulent boundary layers, comparing to real flow past compression ramp
[AIAA PAPER 71-128]

Reattachment angle of supersonic laminar mixed boundary layer, using revolution model with Reynolds number allowance

Supersonic boundary layer transition on adiabatic wall, discussing wind tunnel size, surface roughness and freestream disturbances effects
[AIAA PAPER 70-586]

Inviscid transonic rotational flow expansion around convex corner, applying to supersonic boundary layer over flat plate ending at sharp corner

Supersonic turbulent two dimensional boundary layer flows wall flux and velocity/temperature profiles prediction

Linear stability equations for two dimensional compressible supersonic boundary layer with three dimensional disturbances including thickness growth term

Two dimensional supersonic turbulent free shear layer recompression process from flow model numerical calculation

SUPERSONIC COMBUSTION

Supersonic and subsonic combustion modes in constant area ramjet combustors, deriving dimensionless parameter for varying flow ratios as combustion stability criterion
[ASME PAPER 70-WA/AV-4]

Supersonic combustion thermogasdynamic analysis, presenting combustion processes via pressure-velocity diagram

Supersonic combustion process heat transfer, using momentum integral method for turbulent boundary layer equations

Supersonic combustion ramjet engine with liquid fuel injection, considering atomization process and ignition criteria

Two dimensional supersonic turbulent burning mixing layer, measuring physical properties and growth rate
[WSS/CI PAPER 70-16]

Two dimensional inviscid heated flows in terms of pressure, density, speed, direction and heating rate applied to supersonic duct combustion chambers

Supersonic staggered gutter colander combustion system for plenum chamber burning on high bypass Pegasus turbofan engine of Harrier VTOL aircraft, noting performance improvement

Monograph on hypersonic shock tunnel supersonic combustion research techniques covering test facilities, optical and electromagnetic flow measurement methods, etc

Supersonic hydrogen combustion in vitiated air stream with stepped wall injection, considering temperature, pressure and composition measurements
[AIAA PAPER 71-721]

Ignition and combustion tests of storable boron/magnesium/hexane slurry injected directly in high speed air stream
[AIAA PAPER 71-723]

Supersonic combustion flowfield transverse hydrogen jet injection into Mach 2.5 airstream, discussing recirculation region upstream
[WSS/CI PAPER 71-15]

Supersonic hydrogen diffusion flames ignition aids at near-thermal self ignition point, discussing catalytically-induced preexcitations
[DFVLR-SONDDR-118]

Air-methane supersonic diffusion flame in duct, comparing pressure measurement and gas sampling data with two dimensional combustion analysis
[ONERA-TP-961]

Gaseous hydrogen and methane injection into supersonic air stream heated by plasma burner, studying combustion effects on flow field

SUPERSONIC COMBUSTION RAMJET ENGINES

Composite propulsion systems including Turbo-Ram-Scramjet, Ejector Ramjet, Hyperjet and Bi-liquid Ramjet Rocket

Double oblique shock inlet scramjet model development as test bed for instrumentation and hydrogen fuel supersonic combustion experiments

Shock tunnel extremely high enthalpy and pressure for scramjet engine combustion research

Supersonic and subsonic combustion ramjet engines inlet calibration, using gun tunnel to establish hypersonic throat flow

Heater and nozzle design of ONERA/S4MA hypersonic wind tunnel for supersonic combustion ramjet tests
[ONERA-TP-924]

Hypersonic air transportation based on supersonic combustion ramjet development, discussing economic feasibility

Kalman filter for computerized optimal SRAM air to surface missile alignment, discussing design, digital simulation and flight tests
[AIAA PAPER 71-948]

SUPERSONIC COMBUSTION RAMJET MISSILE

U SUPERSONIC COMBUSTION RAMJET ENGINES

SUPERSONIC COMMERCIAL AIR TRANSPORT

Free wave reflection measurements of normal acoustic impedance of ground surfaces in relation to shock waves from large supersonic commercial aircraft

Commercial supersonic flight, investigating air pollution and alleged climate and weather modification effects due to principal exhaust products

Meteorological problems of operation of commercial supersonic aircraft, including sonic boom intensity and extent
[CASI PAPER 72/7]

SUPERSONIC COMPRESSORS

Supersonic compressor performance, discussing shock and dump losses and wave structure model errors

Analytical model of compressor sensitivity to transient and distorted transient flows, considering inlet duct, compressor stages and combustor up to turbine nozzles
[AIAA PAPER 71-670]

Supersonic cylindrical freon compressor with low blade height for elementary compression and flow visualization aerodynamic and thermodynamic tests

Normal shock existence in blade spacings of rotor and guide vanes of axial flow supersonic compressor as function of pressure nonuniformity

SUPERSONIC DIFFUSERS

Pseudoshock mechanism model, explaining supersonic diffuser main flow static pressure increase and decrease alternately and wall increase monotonously
02 p0239 A71-11870

Started supersonic axisymmetric parallel diffuser, examining wall static pressure and heat transfer
04 p0528 A71-15489

Air inlet for simulation of shock wave separated flow in supersonic diffusers, deriving pressure variation profile along free boundary
13 p1992 A71-29175

Viscous slipstream flow downstream of triple shock wave intersection in supersonic diffuser air flow, using Pitot and static pressure probe measurements
21 p3324 A71-40981

Vacuum water-air ejector with cylindrical mixing chamber and multibarrel nozzle feed, showing increased efficiency by supersonic diffuser substitution
22 p3480 A71-41852

SUPERSONIC FLIGHT

Statics and aerodynamics of lifting decelerators /parawings and sailwings/ at supersonic and hypersonic speeds
01 p0002 A71-10927
[AIAA PAPER 68-945]

Soviet book on meteorological conditions and supersonic aircraft flight covering atmospheric composition and structure, temperature distribution, wind effects, etc
02 p0278 A71-12840

Radiological risks of cosmic radiation during high altitude supersonic flights, considering galactic, solar and incident particles in aircraft atmosphere
03 p0473 A71-13099

Jet engine contribution to lift at supersonic flight velocities via air mass heating, studying three dimensional flow with heat supply and stream deflection
07 p1014 A71-19746

Concorde airworthiness requirements and Air Registration Board participation in flight test program, considering supersonic flight characteristics
09 p1385 A71-23579

Physical and physiopathological effects of high altitude supersonic flight in TF-104G aircraft told by flight surgeon
10 p1572 A71-24980

Supersonic flight path curvature effects on local shock wave production, considering no boom zone and ground rules
11 p1708 A71-26310

Subsonic and supersonic airline operations, restraints, considering noise, air pollution and inadequate airport facilities
12 p1927 A71-26870

Annular vaporizing combustion chamber with film cooling, determining flame temperature under supersonic flight conditions
13 p2117 A71-28749

Supersonic aircraft propulsion by external heat addition, discussing numerical method for suitable caret wing design
17 p2793 A71-35398

SUPERSONIC FLOW

Supersonic overexpanded jet flow past cone, determining impingement point by method of characteristics
01 p0002 A71-10613

Wing-body interference in supersonic inviscid flow, extending Stewartson approach to arbitrary smooth convex cylinder
01 p0002 A71-10774

Steady supersonic conducting gas flow in channel with nonconducting walls, calculating electric and gas dynamic parameters for different imposed magnetic field geometries
01 p0133 A71-10791

Supersonic and transonic flow including effects of pressure oscillations within cavity, predicting rectangular cavities drag from mathematical model
01 p0002 A71-10931

Skew panels with in-plane forces under yawed supersonic flow, calculating flutter by matrix displacement methods
01 p0173 A71-10939

Supersonic electrically conducting gas flow in flat channel with dielectric walls in inhomogeneous magnetic field
02 p0289 A71-11926

Circular cone with cross shaped wings in supersonic flow, determining flow characteristics, velocities and pressure
02 p0185 A71-11958

Skin friction effect on cylindrical shell critical loads at various supersonic gas flow velocities, noting application to flutter analysis
02 p0329 A71-12666

Wing computation in steady or unsteady supersonic flow, using network, inverse discrete and numerical inversion methods
03 p0339 A71-13129
[ONERA-TP-896]

Aerodynamic characteristics of aircraft in steady and unsteady supersonic flow by analog electrical method, including wing-fuselage interactions
03 p0339 A71-13130

Fluid mechanics of interaction of shock wave and turbulent boundary layer at transonic-supersonic speeds
03 p0399 A71-13138

Film cooling effectiveness with He and refrigerant 12 injection into two dimensional turbulent boundary layer of supersonic airflow
03 p0517 A71-13453

Contraction coefficient of orifice for subsonic and supersonic flows, including velocity-of-approach and compressibility effects upstream and downstream
[ASME PAPER 70-WA/FM-1] 03 p0402 A71-14103

Thin plane wings with mixed leading edges, applying linearized supersonic flow theory
03 p0344 A71-14241

Supersonic inviscid flow fields associated with conical premixed flame sheet
03 p0521 A71-14242

Soviet papers on working processes in aircraft engines covering gas flow, liquid injection, nozzles, gas turbines and supersonic flow
03 p0471 A71-14251

Vaporization rate of liquid injected into high temperature supersonic gas flow, considering relation to static pressure and distillation process
03 p0521 A71-14253

Liquid/gas repeated injection into ideal gas plane supersonic flow, determining resultant shock wave radius relation to Mach number and temperature
03 p0404 A71-14254

Plane and wedge shaped airfoil profiles of variable thickness, deriving stability in bilateral supersonic air flow
03 p0515 A71-14365

Turbulent base pressure on conical afterbodies in supersonic axisymmetric flow, including initial direction effect
[AIAA PAPER 70-555] 03 p0344 A71-14450

Inviscid binary gas mixture steady supersonic two dimensional flow past convex corner, taking into account spontaneous condensation
03 p0345 A71-14559

Interaction between supersonic flow and transverse sonic or supersonic jet blown perpendicular to main stream through circular hole in wall
03 p0345 A71-14572

Laser power from carbon monoxide supersonic expansion in nitrogen and argon mixtures, comparing to carbon dioxide gas dynamic lasers
04 p0608 A71-15042

Analog and digital methods for interactions between aircraft lifting elements in steady or unsteady supersonic flow
[ONERA-TP-850] 04 p0527 A71-15358

Two dimensional and axisymmetric flow film cooling effectiveness in supersonic turbulent boundary layer, using Eckert reference enthalpy method
04 p0571 A71-15496

Supersonic compressible turbulent boundary layer on porous cylinder with air injected through wall, investigating heat transfer
04 p0571 A71-15498

Supersonic flow past notch in lateral body surface or in two closely lying coaxial bodies, applying turbulent jet theory to separation zone
04 p0528 A71-15626

Supersonic blunt body flow relaxation processes, calculating bow shock for various flow regimes and reaction rates
05 p0835 A71-16525

Steady state supersonic flow of combustible gas mixture around solid blunt bodies
05 p0836 A71-16530

Supersonic reactive gas flow free expansion over sharp corner into region of constant pressure, using linearized theory and numerical method of characteristics
05 p0836 A71-16535

Energy deposition by MHD into supersonic argon plasma flow in shock tube
05 p0787 A71-16537

Turbulent boundary layer separation at low supersonic Mach numbers based on blowdown wind tunnel tests
05 p0735 A71-16582

Supersonic flow field around flat plate at various angles of attack, comparing Brieden and Lighthill approximations
05 p0694 A71-16713

German monograph on ignition and combustion processes in rapidly flowing gas mixtures covering supersonic flow, ramjet parameters, flow heating, etc
05 p0838 A71-16900

Supersonic flow field downstream of turbofan aircraft engine fan nozzle over bodies of revolution, using boundary layer theory and method of characteristics
05 p0796 A71-17150

Initial structure of wing-body interaction in steady inviscid supersonic flow, obtaining asymptotic expansion from canonical problem solution
05 p0696 A71-17219

Slender, conical, plane and cambered wing-body combinations with different volume distributions in

supersonic flow, comparing experimental with theoretical aerodynamic characteristics
[DFVLR-SONDDR-86] 06 p0841 A71-17418

Shock wave bisector rule improvement, applying to asymptotic behavior of bow shock attached to airfoils in two dimensional supersonic flow
06 p0841 A71-17420

Supersonic flow of rarefied plasma around plane bodies, allowing for electric field effect on ion motion
06 p0842 A71-18252

Chemically reacting viscous supersonic laminar flow in two dimensional divergent plane channel, developing approximate system of parabolic partial differential equations
[AIAA PAPER 71-44] 06 p0866 A71-18505

Supersonic axisymmetric wake-like and two dimensional shear nonuniform free stream flows effects of inviscid flow fields and aerodynamic coefficients of sharp and spherically blunted cones
[AIAA PAPER 71-51] 06 p0843 A71-18515

Three dimensional inviscid supersonic flow fields with primary and embedded shock and expansion waves determined over and behind wings and wing-body configurations
[AIAA PAPER 71-99] 06 p0844 A71-18554

Negatively charged conical electrostatic probe characteristics determination in supersonic plasma stream, using shock tube
[AIAA PAPER 71-143] 06 p0939 A71-18586

Unsteady supersonic aerodynamic coefficients evaluation to desired kinematic consistency level using finite element method
[AIAA PAPER 71-177] 06 p0845 A71-18616

Underexpanded plasma jet supersonic outflow simulation, using laser irradiation of absorbent target materials
07 p1166 A71-19133

One dimensional steady supersonic motion of partially ionized two temperature argon-cesium plasma in disk type Hall MHD generator channel
07 p1023 A71-19728

Intensified molecular diffusion during turbulent mixing of supersonic slipstreams in cylindrical mixing chamber, using optical Prudnikov method
07 p1089 A71-19733

Shock wave interaction with wedge moving at supersonic speed, calculating geometry of regions formed intersecting wavefronts
07 p1014 A71-19741

Viscosity effects on three dimensional supersonic flow around circular half cones on flat plate, examining turbulent boundary layer separation
07 p1014 A71-19744

Supersonic air flow pattern over rectangular indentations on plane and axisymmetric surfaces, examining static pressure and adiabatic temperature distributions
07 p1014 A71-19744

Jet engine contribution to lift at supersonic flight velocities via air mass heating, studying three dimensional flow with heat supply and stream deflection
07 p1014 A71-19746

Supersonic molecular beams with cycling-pressure sources, investigating mass flow rate effects on skimmer interference
07 p1164 A71-19900

Inverse boundary value problems in hydroaeromechanics, involving profile construction from given velocity or pressure distribution and supersonic flow boundaries determination
07 p1091 A71-20078

Surface construction of body of revolution in supersonic gas flow from distribution of velocity vector modulus along generatrix of body, using Frankl method of characteristics
07 p1016 A71-20089

Multilink approximation of Chaplygin function in subsonic and supersonic flow regions, deriving coupling conditions relative to modified stream function at approximation nodes
07 p1016 A71-20090

Axial Mach number distribution of supersonic flow in rocket nozzle with Rao optimum contour
07 p1093 A71-20366

Two dimensional supersonic fluidic amplifier flow field density and characteristics determined by differential interferometry
07 p1028 A71-20588

Supersonic fluidic bistable switch, developing improved pressure recovery
07 p1029 A71-20590

Supersonic pitot fluidistor in bistable mode, investigating improved pressure and flow recovery at large expansion ratios
07 p1029 A71-20591

Similarity criterion for volute centrifugal pumps via supersonic model, considering cavitation parameters influence throughout angular velocities range at flow separation
08 p1347 A71-20784

Flutter analysis of stressed flat simply supported skew panels in supersonic flow, using small deflection thin plate theory
08 p1370 A71-21302

- Electric breakdown in supersonic Ar or air flow behind shock wave, determining threshold discharge currents 08 p1276 A71-21485
- Particle motion behind oblique shock wave in two phase supersonic wedge flow, deriving expressions for particle trajectories and velocity equalization time 08 p1227 A71-21754
- Hanging shock wave in small supersonic flow past profile with broken generatrix in plane ideal gas 08 p1228 A71-21872
- Laser Doppler velocimetric technique for supersonic flow particle trajectory and density measurements, noting particle lag [AIAA PAPER 71-287] 08 p1303 A71-22010
- Convective heat transfer coefficient for supersonic flow past sphere, considering kinetic heating by flow 08 p1378 A71-22047
- Flow lines construction in two dimensional supersonic flow region with rarefaction waves interaction from several disturbance sources 08 p1230 A71-22052
- Three dimensional laminar boundary layer on cone at incidence in supersonic flow evaluated by pressure distribution technique, comparing heat transfer, Pitot probe measurements, etc [AIAA PAPER 70-48] 09 p1381 A71-22088
- Liquid properties effect on secondary injection from spray nozzle, determining jet penetration in supersonic stream by scattered light and schlieren photographs 09 p1381 A71-22089
- Interaction flowfield of two dimensional supersonic airstream with transversely injected jets of various gases, presenting wall static pressure, gas concentration and temperature measurements 09 p1382 A71-22111
- Supersonic collisionless plasma flow around flat plate and expansion into vacuum, using Poisson equation 09 p1500 A71-22233
- Turbulence properties in supersonic flow, considering modes with vorticity, entropy and acoustic aspects 09 p1383 A71-23603
- Supersonic flow separation around cross shaped horizontal tail plane with subsonic leading edge, obtaining pressure distribution and aerodynamic characteristics 09 p1384 A71-23608
- Plane sandwich plates in supersonic gas flow, investigating aeroelastic stability, transverse shear flexibility and axial loads 09 p1543 A71-23609
- Mach cones reflection at thin wing subsonic leading edges in supersonic flow, considering axial disturbance velocity and pressure distributions 09 p1384 A71-23616
- Delta wing of symmetrical thickness and optimum variable geometry for two supersonic cruising speeds 09 p1384 A71-23617
- Turbulent supersonic flow measured by laser anemometry, stressing advantages over optical heterodyning 09 p1453 A71-23693
- Gas dynamic CW laser with supersonic hot moist carbon dioxide-nitrogen as working fluid, discussing laser gain vs water content 10 p1619 A71-23760
- Vortex layer near circular cone surface in supersonic axisymmetric steady flow of homogeneous inviscid gas 10 p1551 A71-24372
- Linear theory of weakly perturbed supersonic plane axisymmetric flows of gas-particles mixture, deriving partial differential equation for perturbation potential 10 p1551 A71-24373
- Cylindrical panel vibration in supersonic flow under random effects, calculating stress-strain statistical properties as function of incident flow velocity 10 p1690 A71-24572
- Backward facing step in confined supersonic two dimensional flow, investigating turbulent shear layer reattachment 10 p1552 A71-24622
- Nonlinear forced vibrations of aeroelastic plate in two dimensional supersonic flow under harmonic pressure near critical Mach number 10 p1690 A71-24643
- Collisionless ion exosphere kinetic and hydrodynamic models comparison for polar wind supersonic flow characteristics 10 p1605 A71-24796
- Perturbation theory of supersonic flow with nonequilibrium radiative heat transfer, investigating pressure, density, temperature and velocity as function of relaxation time 10 p1697 A71-24943
- Acoustic and shock waves propagation in quasi-steady supersonic flow in duct with varying cross section 10 p1598 A71-25083
- Cylindrical shells panel flutter analysis for internal stress and supersonic flow, considering still air buckling data useful for determining buckling loads [AIAA PAPER 71-328] 11 p1842 A71-25308
- Breakup mechanism of liquid sheets and jets in supersonic gas stream, using spark photomicrographs and high speed movies 11 p1750 A71-25471
- Shielded fine wire probe for total temperature rapid measurement in high speed flows, discussing construction and theoretical considerations 11 p1761 A71-25528
- Electrostatic probe measurements of charged particles and thermal ionization relaxation in shock heated low density supersonic monatomic gas flows 11 p1766 A71-26286
- Steady supersonic isoenergetic flow of thermally and calorically perfect gas past circular cones at zero angle of attack, using dimensional perturbation method 12 p1863 A71-26939
- Two phase supersonic barotropic flow with solid particles around thin profile with allowance for elastic particle collisions 12 p1864 A71-27450
- Turbomachine blade cascades in supersonic flow, noting wave configurations, entropy and counter pressure variations 12 p1864 A71-27475
- Particle interaction with wedge surface in supersonic two phase flow, determining incidence coordinates and collision frequency as function of initial conditions 12 p1866 A71-27665
- Unsteady flow downwash behind finite span slender wing during supersonic motion at finite Strouhal numbers 12 p1866 A71-27697
- Supersonic flow around porous-wall conical body with uniform gas injection through wall, deriving equations for pressure at contact surface 13 p1990 A71-28182
- Discrete ionospheric model of supersonic two dimensional low density plasma flow past large bodies, using quasi-neutrality condition 13 p1990 A71-28532
- Chemical reactions occurrence during gas supersonic expansion into vacuum, calculating gas temperature, pressure and density 13 p2025 A71-28774
- Closed system of macroequations for mass and energy conservation along symmetry axis of steady rarefied supersonic gas flow in front of blunt body 13 p1991 A71-29151
- Flow and heat transfer measurements in dihedrons simulating patterns about supersonic conical edge and shock wave interaction line, using thermoincandescence coating technique 13 p1992 A71-29174
- Air stream injection from circular hole in flat plate into supersonic flow, measuring heat transfer 13 p1992 A71-29184
- Wing thickness optimal distribution for minimum wave drag in supersonic flow at zero angle of attack for given planform, using Ritz method at lower Mach numbers 13 p1994 A71-29222
- Chemical nonequilibrium flows in supersonic nozzle for mixture of dissociated gases and inert diluent [ASME PAPER 71-FE-8] 13 p2166 A71-29449
- Heat transfer within resonant cavities at subsonic and supersonic flow, discussing wind tunnels, test procedures and data reduction 13 p2166 A71-29450
- Interaction between viscous mixing shear layer induced by tangential injection and external supersonic flow field, obtaining spark schlieren photographs and wall pressure distributions [ASME PAPER 71-FE-24] 13 p2053 A71-29461
- Turbulent skin friction and heat transfer prediction on flat plates and wind tunnel walls at supersonic and hypersonic Mach numbers, using Van Driest theory 14 p2334 A71-29868
- Linear nonequilibrium shock tunnel driven supersonic MHD generator operation under large scale power extraction and strong electromagnetic-rare gas interactions 14 p2287 A71-29879
- Supersonic mass flux probe description, discussing inlet geometry, angle of attack and Reynolds and Mach numbers effects on performance 14 p2239 A71-29925
- Inert and reactive gas injection in near wake behind afterbodies in supersonic flow, considering influence on base pressure and temperature 14 p2336 A71-30213
- High velocity boundary layer on flat plate, deriving equations analytical solution by flow variables expansion in powers of inversely squared Mach numbers 14 p2226 A71-30441
- Supersonic to subsonic solar corona transition, using supersonic solution for solar wind inviscid equations 14 p2302 A71-30648
- Electrical breakdown of supersonic Ar and air stream behind shock wave, determining threshold discharge currents 14 p2227 A71-30672
- Nonreacting gases supersonic turbulent mixing flowfields, calculating turbulent kinetic energy as function of injection angle and jet velocity [AIAA PAPER 71-725] 14 p2295 A71-30774
- Flowfield production by fluid injection into supersonic crossflow, occurring with liquid/gas jet control of vehicle with combustion ramjets [AIAA PAPER 71-728] 14 p2295 A71-30775
- Two dimensional sonic nonreacting gaseous secondary injection into supersonic primary stream with turbulent boundary layer for application to thrust vector control [AIAA PAPER 71-750] 14 p2227 A71-30786
- Pisa University Aeronautical Institute activities /1960-1970/, considering supersonic and subsonic flow research, thin stiffened shells fatigue under compressive or tensile loads, etc 14 p2222 A71-30822
- Slender body interaction with interface forming after bursting of membrane separating low and high pressure gas supersonic flow in shock wave tube 15 p2386 A71-31162
- Supersonic potential flow at large distance from slender body of revolution at angle of attack, deriving nonlinear partial differential equations system 15 p2343 A71-31170
- Holographic interferometry for observing transparent media in supersonic gas flow, comparing results with Mach-Zehnder interferometry 15 p2404 A71-31275
- Heterogeneous detonations literature review, indicating need for research on heat transfer processes in subsonic and supersonic flows 15 p2511 A71-31387
- Supersonic arc-heated Ar flow, measuring heavy particle temperature and velocity and electron density profiles by pressure scanned Fabry-Perot interferometer [AIAA PAPER 71-589] 15 p2454 A71-31534
- Viscous flow fields around pointed cones at angle of attack in nonuniform supersonic flow, using axisymmetric analog for three dimensional boundary layer [AIAA PAPER 71-624] 15 p2344 A71-31552
- Near field flow pattern of inclined slender body of revolution, using Whitham far field theory of supersonic flow [AIAA PAPER 71-626] 15 p2344 A71-31554
- Inviscid supersonic flow field structure over blunt delta wing, determining attack angle effects on shock layer surface pressure distributions and streamline patterns [AIAA PAPER 71-596] 15 p2512 A71-31576
- Light beam diffraction by supersonic waves, calculating amplitudes with difference-differential equations 15 p2450 A71-32075
- Slipstream due to supersonic source in hypersonic stream, determining shape of limiting surface 15 p2346 A71-32116
- Supersonic flow base pressure correlation based on reduced Reynolds number in mixing region 15 p2346 A71-32121
- Plate excitation by supersonic turbulent and shock boundary layers, measuring wall pressure fluctuation and panel displacement 15 p2507 A71-32132
- Transverse liquid injection into supersonic airstreams, using photographic techniques to determine jet penetration and spreading for various dynamic pressure and density ratios [AIAA PAPER 71-724] 15 p2393 A71-32287
- Surface liquid film wave motion effect on air supersonic turbulent boundary layer flow field, discussing film thickness, heat transfer rates and wall temperatures [AIAA PAPER 71-623] 15 p2515 A71-32544
- Sonic boom phenomena, discussing supersonic flow near aircraft, atmospheric propagation, distortion, focusing, caustics, turbulence effects and reduction 15 p2350 A71-32566
- Shock tunnel investigation of two dimensional supersonic turbulent mixing with and without combustion, using Mach-Zehnder interferometer and piezoelectric transducers 16 p2554 A71-32881
- Film cooling studies in subsonic and supersonic flows, using shock tunnel for gas turbine conditions simulation 16 p2551 A71-32882
- Ionospheric disturbances due to supersonic shock from missile exhaust plume, noting F region compressions and undulations 16 p2563 A71-33358
- Two vortex model for downwash variations in supersonic flow past thin delta wing with separation at leading edges 17 p2669 A71-34190
- Stream lines construction in meridional plane of blade nozzle annular cascades of steam and gas turbines in subsonic and supersonic flow 17 p2670 A71-34446
- Negative pressure gradient effect on separation of supersonic flow over notches, comparing theory with wind tunnel determination 17 p2671 A71-34898

Flow distribution behind laminar boundary layer separation point in supersonic flow, calculating plateau region pressure 17 p2672 A71-35629

Turbulent boundary layer interaction with supersonic outflow behind step, calculating pressure distribution, momentum thickness and friction 17 p2672 A71-35631

Finite difference method application to three-dimensional boundary layer calculation on sphere-segment surfaces in supersonic flow 17 p2672 A71-35632

Fluid jets and droplets deformation in transverse supersonic two phase gas flow 17 p2673 A71-35638

Shock wave formation in stationary flow adjacent to supersonic flow region, using Friedrich simple wave theory 17 p2673 A71-35645

Supersonic flow past V-shaped wings with leading edges, applying method of establishment to space variable for pressure distribution 17 p2673 A71-35647

Pressures, velocities and aerodynamic characteristics of supersonic flow around slender delta wings with forced asymmetry and separation at leading edges 18 p2843 A71-36134

Supersonic flow past thin delta wings with finite velocities at leading edges, noting wing deformation to avoid corner vortices appearance 18 p2843 A71-36181

Mach number effects on flow field in gas bearings at high subsonic and supersonic tangential speeds based on perturbation theory [ASME PAPER 71-APM-U] 18 p2926 A71-36263

Supersonic flow field computation for wing-body combinations by shock-capturing finite difference techniques, discussing improvement based on Runge-Kutta method 18 p2844 A71-36303

Dynamic parameters of supersonic flow incident on conical bodies at large angles of attack, considering flow field and entropy distribution 18 p2845 A71-36328

Second order accuracy and stability analysis of method of characteristics application to three dimensional steady supersonic flow 18 p2907 A71-36329

Secondary floating shock generation in supersonic ideal gas flow about blunt bodies, investigating body configuration and flight regime effects 18 p2845 A71-36331

V shaped conical wing in supersonic and hypersonic flow with shock attached to leading edge, investigating complex wave system with time dependent and analytical methods 18 p2845 A71-36339

Slender wing lift in supersonic flow, analyzing suction force on leading edge and viscosity and nonlinear effects [DFVLR-SONDDR-138] 18 p2848 A71-36677

Supersonic spherical viscous heat conducting gas discharge into vacuum, solving Navier-Stokes equations by buildup method 19 p3042 A71-37087

Shock layer parameters of supersonic viscous gas flow past blunt bodies of heat insulated and cooled surfaces, using Navier-Stokes equations 19 p2991 A71-37089

Kernel function for nonplanar oscillating surfaces in supersonic flow, using finite element method for interfering configurations 19 p2991 A71-37295

Supersonic flow past steady and oscillating blunt bodies of revolution, using singularity transformation and series truncation methods 19 p2993 A71-37878

Injection conditions effect on ignition temperature of methane and hydrogen in hot Mach 2 air stream 19 p3163 A71-37889

French monograph on laminar boundary layer on circular cone at angle of incidence in supersonic stream, calculating separation from parabolic equations by numerical integration 19 p2994 A71-38647

French monograph on similar solutions of laminar boundary layer problem in supersonic flow covering finite difference methods and convective heat flux 19 p2994 A71-38648

Linear theory of weakly perturbed supersonic plane axisymmetric flows of gas-particles mixture, deriving partial differential equation for perturbation potential 20 p3175 A71-38898

Hanging compression shock wave in plane supersonic ideal gas flow past body with broken generatrix 20 p3176 A71-39371

Two dimensional supersonic base flow with small Mach number recirculation zone, determining jet line by variational principle of Poisson equation 20 p3176 A71-39414

Transonic and supersonic turbine guide vanes, noting air as flow medium in experiment and steam in actual turbine 20 p3176 A71-39455

Aerodynamic approximations for unsteady supersonic flow of perfect inviscid gas through flexible duct of revolution 21 p3458 A71-40280

Supersonic and hypersonic viscous gas flows with boundary layer induced pressure gradients, investigating disturbance upstream propagation by asymptotic theory 21 p3322 A71-40680

Nonablating inelastic deformable material surface interaction with external supersonic turbulent boundary layer, observing crosshatch patterns 21 p3323 A71-40941

Two dimensional supersonic moist air expansion around sharp corner, investigating water vapor condensation by homogeneous nucleation 21 p3369 A71-40952

Slender body of revolution in supersonic and subsonic air flow, calculating boundary conditions with Lagrange formulation 21 p3323 A71-40963

Supersonic collisionless plasma flow around flat plate and expansion into vacuum, using Poisson equation 21 p3424 A71-41113

Nonlinear flutter of hinged closed cylindrical shells in supersonic gas flow, comparing with wind tunnel tests on panels 21 p3473 A71-41155

Flat supported plate in plane supersonic oscillating flow, calculating forced vibration with potential flow theory 21 p3473 A71-41367

Two dimensional supersonic flow pattern, velocity and loss in shock waves in front of blade cascade 22 p3479 A71-41842

Conical nozzle roughness on heat transfer in supersonic region 22 p3622 A71-42785

Windward injection into supersonic stream at angle of attack, minimizing vortex disruption 22 p3481 A71-42787

Sonic line position measurement in supersonic flow behind detached shock wave preceding axisymmetric or plane blunt bodies 23 p3625 A71-43092

Plane supersonic ionizing shock wave in magnetic field under small wave plane perturbation from equilibrium position, calculating stability from linearized equations 23 p3663 A71-43575

Carbon dioxide additions effect on electron temperature relaxation and electron concentration distribution in expanding supersonic flow of low temperature Ar plasma 23 p3713 A71-44065

Chemically reacting gas mixture supersonic flow characteristics around blunt body, using differential equations 23 p3784 A71-44336

Supersonic plasma flow interaction with mirror field studied by changing ion-ion collision mean free path in BSG-1A device 24 p3852 A71-44489

Flow angularity prediction near supersonic fuselage forebody with arbitrary cross section and zero sideslip, using small perturbation theory [AIAA PAPER 71-996] 24 p3789 A71-44588

Flare induced laminar boundary layer/shock wave interactions on axisymmetric bodies at zero incidence in supersonic flow under adiabatic conditions 24 p3789 A71-44604

Approximate solution for position and strength of shock waves about cones in steady supersonic flow 24 p3790 A71-44624

Laminar-turbulent boundary layer transition at Mach number 2-10, observing stabilizing effect of transition Reynolds number at increasing heat transfer intensity 24 p3818 A71-44745

Nonlinear theory of wave resistance in supersonic ideal gas flow past finite flat axisymmetric bodies, establishing drag relation to flow rate deficit 24 p3790 A71-44773

Dynamic behavior of dissociating gas supersonic flow past blunt bodies at angle of attack 24 p3790 A71-44775

Particle interaction with wedge surface in supersonic two phase flow, determining incidence coordinates and collision frequency as function of initial conditions 24 p3790 A71-44930

Perturbations generated by two dimensional supersonic channel flows with walls oscillating with harmonic time dependence and small pressure amplitude computed, using linearized method of characteristics 24 p3819 A71-44951

Flat face cylinders in rarefied supersonic gas flow, investigating perturbed region evolution 24 p3790 A71-45096

Mach number distribution along critical streamline in compressed layer in front of cylinder in supersonic flow 24 p3790 A71-45101

**SUPERSONIC FLOW INLETS
U SUPERSONIC INLETS
SUPERSONIC FLUTTER**

Skew panels with in-plane forces under yawed supersonic flow, calculating flutter by matrix displacement methods 01 p0173 A71-10939

Rotary inertia effect on critical dynamic pressure parameters and supersonic flutter of in-plane loaded sandwich plates 07 p1213 A71-19887

Lifting surfaces supersonic-hypersonic flutter at angle of attack determined by shock expansion, Newtonian flow and local flow piston theory [AIAA PAPER 71-327] 11 p1842 A71-25307

Weight minimization of semiinfinite flat sandwich panel at constant dynamic pressure in supersonic flow subject to flutter constraint, using finite element model [AIAA PAPER 71-330] 11 p1842 A71-25310

Flutter analysis of clamped thin skew panels with midplane forces in supersonic flow, using Galerkin method 12 p1974 A71-26766

Supersonic flutter of two dimensional flat plate in presence of chordwise tensile in-plane stresses 12 p1983 A71-27585

Supersonic flutter analysis of clamped skew panels with in-plane forces by Galerkin method, using two dimensional static approximation for aerodynamic loading 14 p2177 A71-30607

Cylindrical membrane aeroelastic stability and flutter analysis at high supersonic or low hypersonic Mach numbers 15 p2506 A71-32019

SUPERSONIC HEAT TRANSFER

Wall static pressure and convective heat transfer measurements in subsonic, transonic and supersonic regions in heated air turbulent flow through variable cross section channel 04 p0680 A71-15476

Supersonic combustion process heat transfer, using momentum integral method for turbulent boundary layer equations 04 p0683 A71-15485

Conical body laminar boundary layer heat transfer problem in supersonic flow, using quasi-linearization and implicit finite difference method 04 p0527 A71-15487

Heat transfer on cylindrical antenna in supersonic high temperature gas flow, noting electromagnetic wave damping due to ablation 13 p1990 A71-28296

SUPERSONIC INLETS

Double oblique shock inlet scramjet model development as test bed for instrumentation and hydrogen fuel supersonic combustion experiments 10 p1590 A71-24862

Supersonic conical inlet additive drag formula, using flow data in freestream 10 p1553 A71-24866

Supersonic and subsonic combustion ramjet engines inlet calibration, using gun tunnel to establish hypersonic throat flow 11 p1860 A71-26271

Supersonic inlet turbojet engine compatibility tests in wind tunnels, using light panels and Summation Device analysis 13 p2114 A71-28032

Engine surge pressure transients in mixed-compression supersonic inlet, describing scale wind tunnel model simulation and measurement techniques [AIAA PAPER 71-671] 14 p2291 A71-30735

Supersonic aircraft shape for shock wave minimization based on channel configuration with converging inlet and diverging outlet section 24 p3791 A71-44572

SUPERSONIC JET FLOW

Plane supersonic overexpanded jet interaction with obstacle, using hodographs for flow pattern construction 01 p0001 A71-10425

Laser schlieren crossed beam measurements in shear layer of shock free Mach 2.46 jet 01 p0094 A71-10953

Supersonic underexpanded jet-plane obstacle flow interaction patterns, discussing pressure and distance effects 02 p0186 A71-12643

Parallel nonuniform supersonic flow of two coaxial gas jets past sphere 03 p0345 A71-14562

Interaction between supersonic flow and transverse sonic or supersonic jet blown perpendicular to main stream through circular hole in wall 03 p0345 A71-14572

Axisymmetric supersonic overexpanded ideal gas jet calculation, using finite difference method based on buildup principle 03 p0346 A71-14573

Variable density turbulent jets, discussing compressible, high temperature gas, cryogenic and supersonic jets, Reynolds equations, etc 04 p0577 A71-15620

- 1 Solid metal plates breakdown mechanism at high temperatures and supersonic plasma jet action
05 p0768 A71-16778
- 2 Supersonic jet-bounded subsonic wake interactions, determining recirculation zone boundaries
05 p0694 A71-16848
- 3 Two dimensional supersonic surface jet-hypersonic bow interaction with axial symmetry
[AIAA PAPER 71-131] 06 p0845 A71-18575
- 4 Supersonic jet noise problem, discussing eddy-ach wave radiation source mechanism from non-linear streamwise development of inviscid instability waves in turbulent mixing layer
[AIAA PAPER 71-150] 06 p0884 A71-18592
- 5 Finite amplitude waves from supersonic jet, discussing pressure fluctuations measurement for examining wave patterns visible on spark shadowgraphs
[AIAA PAPER 71-151] 06 p0845 A71-18593
- 6 Near and far noise fields from coaxial interacting supersonic jet flows
[AIAA PAPER 71-152] 06 p0884 A71-18594
- 7 Supersonic jet noise suppressor with tubes and orifices, examining flow and acoustic characteristics
[AIAA PAPER 71-153] 06 p0884 A71-18595
- 8 Twin tube gas heating resonator using bistable air all attaching supersonic power jet
07 p1028 A71-20582
- 9 Closing shock position in supersonic underexpanded single and two phase jets, determining fluid phase concentration effects on Mach number and nozzle pressure in wind tunnel
08 p1228 A71-21925
- 10 Electron density profiles in supersonic plasma jet, using immersed microwave probe
[AIAA PAPER 71-272] 08 p1342 A71-21998
- 11 Supersonic and subsonic jets coexistence in sublinear constant section duct, characterizing flow boundaries by pressure readings and Schlieren flow visualization
09 p1384 A71-23605
- 12 Screech noise generation by supersonic jet impingement on flat plate, discussing jet disintegration mechanism with resultant shock wave oscillations
11 p1751 A71-25521
- 13 Directional acoustic radiation from supersonic jet, discussing generation mechanism theory based on shear layer instability close to nozzle
12 p1945 A71-27221
- 14 Base flow prediction for axially symmetric cylindrical vehicle with supersonic single central jet by two stream interaction model, comparing Thor flight data
[AIAA PAPER 71-643] 14 p2290 A71-30720
- 15 Analytical predictions of supersonic jet noise, considering acoustic intensity, directivity, refraction, convection and peak Strouhal number
[AIAA PAPER 71-584] 15 p2468 A71-31572
- 16 Colliding supersonic rarefied argon-helium jet flows diffusive separation in low density wind tunnel with electron beam diagnostics apparatus
16 p2554 A71-32800
- 17 Solid metal plates erosion mechanism at high temperatures under supersonic plasma jet action, noting dependence on specific heat and latent heat of fusion
16 p2591 A71-33030
- 18 Supersonic jet expansion in variable geometry channels, obtaining pressure dependence on injection rate and similarity parameters
17 p2669 A71-34216
- 19 Supersonic underexpanded submerged gas jet at various Mach and Knudsen numbers and pressure ratios, observing trailing shock wave geometry
17 p2669 A71-34218
- 20 Closing shock position in supersonic underexpanded single and two phase jets, determining fluid phase concentration effects on Mach number and nozzle pressure in wind tunnel
17 p2671 A71-35269
- 21 Supersonic jet interaction with turbulent wake, calculating plane and axisymmetric flow behind body butt face
17 p2672 A71-35630
- 22 Method of characteristics application to supersonic jet and nozzle gas flow with allowance for equilibrium and nonequilibrium condensation
17 p2673 A71-35636
- 23 Approximate method for hydrodynamic parameters of supersonic ideal-gas jet, considering isentropic region and theoretical boundary of underexpanded jet
18 p2902 A71-36114
- 24 Theoretical and photographic study of underexpanded air jets ejected simultaneously from several mutually interacting nozzles near origin
18 p2903 A71-36115
- 25 Photographic study of colliding underexpanded and normally expanded supersonic jets in two-wind-tunnel assembly with atmospheric static working pressure
18 p2903 A71-36118
- 26 Supersonic jets expansion in variable cross section channel, emphasizing boundary layer behavior
18 p2903 A71-36119
- 27 Complex wave structure development upon underexpanded jet impact on plane obstruction at small incidence angles, determining gas dynamics parameters of supersonic jet
18 p2903 A71-36120
- 28 Acoustic radiation of supersonic jet toward nozzle exit section, plotting pressure pulsations vs active/passive pressure ratio
18 p2903 A71-36122
- 29 Main parameters of free supersonic jets of ideal compressible fluid, comparing with numerical calculations and experimental data
19 p2991 A71-37081
- 30 German monograph on flow and combustion changes during hydrogen and methane transverse injection into hot supersonic air jet
21 p3475 A71-40750
- 31 Supersonic Ar, He and molecular nitrogen jets, determining electron temperature and concentration and atomic state population in shock waves region by spectroscopic measurement
23 p3712 A71-43916
- 32 Reflected shock wave interaction with tangential discontinuity curve for supersonic incompressible jets, examining flow instability
23 p3665 A71-44337
- 33 Gas density distributions in argon and carbon dioxide supersonic jets with low angular divergence in vacuum, using Laval supersonic nozzle
24 p3858 A71-45241
- 34 **SUPERSONIC NOZZLES**
Turbulent boundary layer air flow through supersonic convergent-divergent nozzle with heat transfer, considering relationship between temperature and velocity profiles
01 p0180 A71-10950
- 35 Kinetic equations of quasi-steady homogeneous condensation of water vapor in supersonic nozzle two phase flow
01 p0182 A71-11443
- 36 Secondary gas injection at right angles into supersonic rocket nozzle, investigating side force characteristics
03 p0470 A71-13736
- 37 Jet engine liquid fuel wall layer combustion stimulation by repeated oxidizer injection into supersonic section of nozzle
03 p0472 A71-14256
- 38 Pulsed supersonic nozzle source molecular beam for shock tube target, detecting viscous effects from transient flux observation
04 p0600 A71-15596
- 39 Supersonic axisymmetric annular nozzle design, presenting analytical method for selective design optimization
[AIAA PAPER 71-43] 06 p0946 A71-18504
- 40 Small curvature radius/throat radius ratio supersonic nozzles mass flow rate coefficients at high Reynolds numbers, appraising isentropic flow prediction methods
07 p1015 A71-19877
- 41 Condensed water vapor in supersonic nozzle flow, describing dispersion coefficient measurement
08 p1275 A71-21269
- 42 Optimal design of rigid unadjustable contour for supersonic nozzle, taking into account vehicle flight conditions
08 p1227 A71-21865
- 43 Reentry environment simulation at vehicle stations away from stagnation point, using arc heater with supersonic nozzle duct
[AIAA PAPER 71-261] 08 p1274 A71-21988
- 44 Ar condensation onset location in supersonic nozzles for nuclear space propulsion systems, using supercooled vapor pressure measurements beyond saturation point
10 p1593 A71-24328
- 45 Supersonic gas turbine nozzles with condensed particles, determining optimal contour geometries by direct variational procedures
10 p1551 A71-24379
- 46 Nonequilibrium recombination of dissociated combustion products of hydrogen in oxygen enriched heated air in supersonic nozzle
10 p1696 A71-24381
- 47 Supersonic propelling nozzle optimal parameters for maximum thrust coefficient, discussing nozzle control and efficiency
12 p1865 A71-27504
- 48 Viscous flow in supersonic de Laval nozzle, measuring gas density and rotational temperatures by electron beam techniques
[AIAA PAPER 70-810] 12 p1865 A71-27555
- 49 Structural design effects on air driven two stage ejector supersonic propelling nozzle with conical mixing chamber
13 p2115 A71-28585
- 50 Gas dynamic test assemblies experiments for demonstrating theoretical basis of supersonic nozzle design with radial flow section
13 p1992 A71-29173
- 51 Supersonic gas ejector characteristics of mixing gases with different adiabatic exponents, heat capacities and stagnation temperatures
13 p1994 A71-29233
- 52 Carbon dioxide free jet plumes issuing from supersonic nozzle into high vacuum, measuring densities and temperature
13 p2026 A71-29355
- 53 Exit stream velocity increase in propulsion units by adding latent heat of vaporization by condensation in supersonic nozzle
17 p2728 A71-34882
- 54 Method of characteristics application to supersonic jet and nozzle gas flow with allowance for equilibrium and nonequilibrium condensation
17 p2673 A71-35636
- 55 Discharge coefficient formula for supersonic nozzles at low throat Reynolds numbers, investigating boundary layer thickness for various nozzle geometries
19 p2993 A71-37896
- 56 Optimal design of rigid unadjustable contour for supersonic nozzle, taking into account aircraft flight conditions variation
20 p3176 A71-39364
- 57 Thermal protection of two dimensional supersonic nozzle fed with hot air by tangentially injected cold gaseous films for convergent and constant section ducts
20 p3314 A71-39415
- 58 Inviscid gas flow from supersonic nozzle into submerged region, considering specific heat ratio effect on dimensionless parameters, jet boundaries and suspended shock profiles
21 p3322 A71-40693
- 59 Backflow region and shock interaction in rotating and swirling gas streams and jets in supersonic nozzle with separation and thrust effects
22 p3480 A71-42682
- 60 Electrically excited gas dynamic CO laser using glow discharge in supersonic nozzle plenum
23 p3683 A71-42958
- 61 Supersonic propulsion system inlet, engine and exhaust nozzle in wind tunnel and flight tests, discussing boundary layer effects on performance
23 p3718 A71-43599
- 62 Two dimensional supersonic variable area nozzle geometry calculation as function of Mach number
23 p3626 A71-44071
- 63 Two dimensional reflection supersonic nozzle shock wave initiated unsteady starting process, presenting shadowgraphs from shock tube investigation
24 p3821 A71-45367
- 64 **SUPERSONIC PRESSURE DISTRIBUTION**
U PRESSURE DISTRIBUTION
U SUPERSONIC FLOW
SUPERSONIC SPEEDS
Turbulent separation and reattachment at turbomachine blade trailing edge at supersonic speeds, discussing various flow models
03 p0340 A71-13142
- 65 Plastic, elastomeric, ceramic glass, metallic and composite materials rain erosion resistance at supersonic speeds, examining rate-velocity dependence
03 p0444 A71-14288
- 66 Strong blast wave interaction and transient pressure on conical slender supersonic bodies
04 p0525 A71-14979
- 67 Short rotor blade span supersonic fan for pressure wave forward propagation elimination, obtaining acoustic and aerodynamic characteristics
[AIAA PAPER 71-182] 06 p0885 A71-18621
- 68 Magnus effects on Apache sounding rocket at supersonic speeds, discussing spinning model and static tests
[AIAA PAPER 70-207] 07 p1205 A71-18893
- 69 Horizontally coherent supersonic velocity LF sound signals from Apollo rocket vehicles at high elevations
07 p1208 A71-20149
- 70 Turbulent wakes from subsonic-hypersonic bodies for downstream mean flow predictions analysis, considering eddy viscosity function
10 p1550 A71-24338
- 71 Shock wave incidence on wedge moving at supersonic speed, considering uniform flow region on upper wedge surface for specific values of Mach number and vertex angle
12 p1897 A71-27445
- 72 Axisymmetric flow effects on surface mass injection at supersonic and hypersonic speeds, streamline inclinations and surface pressures generation by turbulent viscous dissipation
14 p2223 A71-29874
- 73 Flat plate span effects on ramp induced adiabatic laminar boundary layer separation at supersonic and hypersonic speeds, measuring surface pressure distribution
[AIAA PAPER 71-559] 15 p2344 A71-31557
- 74 Plane oblique shock wave diffraction on wedge moving in homogeneous gas flow at supersonic speed, reducing boundary value problem to Hilbert problem
16 p2519 A71-32930
- 75 S shock wave and magnetic field interaction at supersonic speed, using shock tube and MHD channel with sectioned electrodes
17 p2790 A71-35643
- 76 Interference loading linear prediction on aircraft stores at supersonic speeds, considering flow field due to jet fighter bomber
19 p2996 A71-37290
- 77 Shock layer pressure distribution for axisymmetric bodies moving at supersonic velocity in gas at rest,

deriving nonstationary analog of Newton-Busemann formula 22 p3481 A71-42864

SUPERSONIC STRIKE AIRCRAFT
 U ATTACK AIRCRAFT
 U SUPERSONIC AIRCRAFT
SUPERSONIC TRANSPORTS
 NT BOEING 2707 AIRCRAFT
 NT CONCORDE AIRCRAFT
 NT SUPERSONIC COMMERCIAL AIR TRANSPORT

Commercial SST environmental effects on stratospheric air, water vapor content and earth surface temperature 01 p0074 A71-11178

SST program relation to airline operations, comparing production configuration, performance, economics and operation with subsonics [AIAA PAPER 70-1217] 01 p0005 A71-11248

Electrohydraulic thrust control system for supersonic transport aircraft engines, considering reliability, performance and weight 01 p0143 A71-11546 [SAE PAPER 700819]

air conditioning of passenger cabin in SST, noting heat exchanges due to radiation, convection and evaporation 03 p0371 A71-13094

Heat tolerance for resting subjects in event of air conditioning system failure in SST passenger cabin 03 p0371 A71-13095

Ozone atmospheric concentration, dissociation in SST air conditioning systems and biochemical poisoning 03 p0358 A71-13096

Physiopathological and otolaryngological repercussions of supersonic flight on SST passengers 03 p0371 A71-13098

Atmospheric turbulence at cruise altitudes of supersonic transport aircraft, considering gusts probability, thunderstorms and mountain waves 03 p0346 A71-13137

Rawinsonde reported extreme wind speed in arctic stratosphere at SST altitudes 05 p0777 A71-16700

Supersonic jet transport legal aspects in land overflight, discussing ground noise and sonic boom effects on persons and property 06 p0846 A71-17644

SST noise suppression research, discussing engine noise suppressor conceptual designs and test results with installed devices 07 p1184 A71-20302

Mesosphere and stratosphere data from high level observations for supersonic transport and reentering space vehicle operations 08 p1328 A71-21724

Supersonic transport air traffic meteorology, considering high altitude and flight velocities, applications technology satellites for lower stratosphere thunderstorms, clear air turbulence, etc 09 p1488 A71-23070

Supersonic transport fuel tank environments and sealant requirements, describing Boeing laboratory environment approach 09 p1385 A71-23424

Supersonic transport inlet-engine-airframe compatibility programs, noting exhaust nozzle installation effects, distortions and noise [AIAA PAPER 68-993] 01 p0659 A71-24854

ATC regulations considered for Concorde introduction to passenger service, discussing landing and takeoff characteristics 11 p1706 A71-25232

Torsional-flexural stability of stiffened Ti panels for application to supersonic transport, using small deflection energy methods [AIAA PAPER 71-338] 11 p1843 A71-25317

Wind tunnel evaluation of analytical method for predicting longitudinal stability and aerodynamic characteristics of large flexible aircraft applied to supersonic transport configuration [AIAA PAPER 71-343] 11 p1707 A71-25322

SST problems, including adequate instrumentation and fuel tank immunization to explosion 12 p1867 A71-26883

Reinforced plastics components in supersonic transport nose radome and missile radar antennas, discussing molding, sandwich materials and computer controlled spraying techniques 12 p1887 A71-27016

Cruising flight range as function of supersonic/subsonic transport fuselage geometrical parameters 12 p1868 A71-27494

SST in relation to U.S. world leadership in air transportation, discussing federal funding needs for technological capability assurance 13 p1998 A71-29387

Stratospheric turbulence correlation to mesoscale horizontal temperature gradient at altitudes flown by SST from Coldscan program 14 p2268 A71-29767

Uneven runway taxiing vibration effects on supersonic transport aircraft, comparing calculation with measurement 14 p2175 A71-30305

SST sonic boom minimization, discussing cross-country flight 14 p2177 A71-30820

Commercial SST aircraft engine noise during takeoff, discussing exhaust geometries for suppression 15 p2468 A71-31595

SST stability augmentation system, discussing performance, operational safety and reliability benefits [AIAA PAPER 71-785] 16 p2525 A71-34015

SST sonic booms, investigating intensity and transonic aircraft supersonic flight feasibility 16 p2525 A71-34100

Environmental effects on SST structural materials fatigue, discussing Ti alloys studies involving temperature effects, crack propagation and residual strength 17 p2821 A71-34556

Stratospheric ozone reduction through catalytic action of nitrogen oxides from SST exhaust, discussing degrading effect on atmospheric radiation shield 18 p2874 A71-36922

Environmental radiation exposure in air travel, comparing integral radiation dosages for conventional jet transport aircraft and SST 20 p3192 A71-38976

SST sonic boom generation, discussing aircraft design and atmospheric conditions effects and property damage 21 p3325 A71-40705

Atmospheric wind, temperature, turbulence, hydrometeors, ozone, cosmic radiation and radio activity effects on commercial SST Concorde flight 21 p3325 A71-40829

Sonic boom minimization including front and rear shocks, exemplifying by SST aircraft 21 p3324 A71-40972

SST handling qualities, takeoff speeds and performance evaluation on six degree of freedom flight simulator 23 p3627 A71-42922

Supersonic transports and ATC, discussing taxiing, takeoff, landing and terminal area operations 24 p3845 A71-44352

SST operation climatic impact assessment program, considering carbon dioxide, water vapor, contrails, particulates, nitrogen oxides and carbon monoxide 24 p3823 A71-44982

SUPERSONIC TURBINES
 Supersonic gas turbine nozzles with condensed particles, determining optimal contour geometries by direct variational procedures 10 p1551 A71-24379

Supersonic turbine design, presenting performance data for film cooled blunt leading edge rotor blades measured in two dimensional cascade experiments [ASME PAPER 71-GT-76] 11 p1704 A71-25990

Transonic and supersonic turbine guide vanes, noting air as flow medium in experiment and steam in actual turbine 20 p3176 A71-39455

SUPERSONIC WAKES
 Gas ionization in supersonic wake at throat, transition and breakthrough points in hyperballistic firing tunnel for atmospheric reentry study 03 p0462 A71-13131

Base pressure variation by mass injection in turbulent supersonic axisymmetric near wake at high Mach numbers 03 p0399 A71-13457

Boundary layer turbulence decay in slender body supersonic near wake expansion region, using linear theory for assessment of change in fluctuation level and turbulent scale size [AIAA PAPER 71-200] 06 p0845 A71-18638

Large angle cones supersonic aerodynamic and wake characteristics at low Reynolds numbers, including model support interference effects [AIAA PAPER 71-264] 08 p1228 A71-21990

Mean flow measurement of cone laminar supersonic wake 09 p1381 A71-22091

Aerodynamic characteristics and flow pattern in wake behind star-shaped body at supersonic speed, determining drag and shock waves location 10 p1551 A71-24371

Magnetically suspended laminar supersonic cone wake stability from hot wire fluctuation and spectral components amplitude/phase measurements 11 p1702 A71-25475

Compressible viscous gas supersonic flow, observing near wake region behind perpendicular trailing face of plate with motion, state, energy and continuity equations 13 p2047 A71-28421

Planar supersonic near wake flow field problem with variable viscosity and base injection, investigating boundary errors spatial decay rate 18 p2906 A71-36321

Compressible viscous gas supersonic flow, observing near wake region behind perpendicular trailing face of rectangular plate with motion, state, energy and continuity equations 21 p3318 A71-40081

Blunt and hemispherical base axisymmetric bodies in Mach 4 free stream, investigating turbulent near wakes generation 21 p3324 A71-40999

Two dimensional and three dimensional wakes of supersonic and hypersonic rarefied gas wind tunnels comparing cone and dihedral configurations 23 p3625 A71-43377

SUPERSONIC WIND TUNNELS
 Spark ignited hydrogen-oxygen detonations in supersonic wind tunnel, using schlieren photographs 05 p0835 A71-16500

Unsteady processes in starting period of supersonic Ludwieg tube, initiating flow by quick opening diaphragm downstream of nozzle 05 p0734 A71-16300

Supersonic wind tunnel design, discussing flexible nozzle flow aspects 06 p0880 A71-17708

Sonic boom problem, investigating pressure signature of large models in supersonic wind tunnels [AIAA PAPER 71-184] 06 p0886 A71-18622

Multiple source schlieren system for flow visualization in Canadian transonic wind tunnel, using integrated logic circuitry for control 07 p1083 A71-19924

Wind tunnel history, evolution and use, covering low speed variable density, high speed transonic, supersonic, hypersonic and hypervelocity wind tunnels 08 p1272 A71-21664

Single and multiple sting support evaluation for unmodified interference free wind tunnel data over 0.8 to 2.2 M range using image method [AIAA PAPER 71-267] 08 p1274 A71-21992

Launch and data reduction in supersonic wind tunnel free flight testing of high fineness ratio bodies [AIAA PAPER 71-278] 08 p1228 A71-22003

Combustion reactions development with velocity gradient downstream steady shock wave, considering aerodynamic field in supersonic wind tunnel 10 p1694 A71-23811

Supersonic boundary layer transition on adiabatic wall, discussing wind tunnel size, surface roughness and freestream disturbances effects [AIAA PAPER 70-586] 12 p1865 A71-27554

Schlieren visualization for supersonic annular fin cascade and freon compressor wind tunnels, using vane holding cylinder devices [ONERA-TP-948] 12 p1867 A71-27711

Ballistic wind tunnel for drag measurement on models during free flight at supersonic speeds 13 p2045 A71-29200

Time variant distortions in supersonic inlet on J-85 GE-13 turbojet engine from wind tunnel test, considering instantaneous distortion amplitudes and contours [AIAA PAPER 71-667] 14 p2290 A71-30737

Negative pressure gradient effect on separation of supersonic flow over notches, comparing theory with wind tunnel determination 17 p2671 A71-34890

Photographic study of colliding underexpanded and normally expanded supersonic jets in two-wind-tunnel assembly with atmospheric static working pressure 18 p2903 A71-36111

Rocket propulsion system equipped space shuttle dynamics, discussing aerodynamic forces and moments measurement in supersonic wind tunnels 19 p3151 A71-37311

High speed wind tunnels air heating system optimization, considering pebble bed air heater for intermittent operations 20 p3209 A71-39068

Stationary collisional shock observation in continuous supersonic plasma wind tunnel involving Q device modified into magnetic de Laval nozzle 21 p3426 A71-41400

SUPINE POSITION
 Sitting and supine position effect on exercise tolerance, heart rate, systolic pressure and respiration rate in male subjects with coronary insufficiency, noting onset of angina pectoris 13 p2014 A71-29300

SUPPORT INTERFERENCE
 Comparative sting supported and free flight tests in hypersonic wind tunnel on modified Apollo launch configuration [AIAA PAPER 71-265] 08 p1274 A71-21992

Single and multiple sting support evaluation for unmodified interference free wind tunnel data over 0.8 to 2.2 M range using image method [AIAA PAPER 71-267] 08 p1274 A71-21992

Aerodynamic support interference in wind tunnel testing of configurations involving bulbous base, mass addition, transition near base and hypersonic low density flows [AIAA PAPER 71-277] 08 p1228 A71-22000

Critical load and elastic base one-sided contact effects on cylindrical shell stability under uniform external pressure, using nonlinear programming 10 p1689 A71-24560

Mechanical support system role in determination of aeroelastic stability of leeward cylinder immersed in wake using undamped flutter theory 14 p2334 A71-31012

Specimen support effects on three point bending tests of fiber-plastic composites, suggesting small diameter roller 21 p3405 A71-40596

SUPPORT SYSTEMS

GROUND OPERATIONAL SUPPORT SYSTEM

GROUND SUPPORT SYSTEMS

PORTABLE LIFE SUPPORT SYSTEMS

USAF weapons and support systems, discussing military R and D funding and resulting constraints 05 p0839 A71-16285

Support systems relative efficiency in external pumping free-free configuration production for flexing ramp 05 p0828 A71-16967

Tracking and data relay satellite system / TDRSS / impact on spacecraft mission support information management [AIAA PAPER 71-224] 07 p1197 A71-19704

Weapons systems design for logistics supportability, discussing operational availability at minimal life cycle cost as function of reliability, maintainability and MIL Spec documentation 09 p1429 A71-23476

Service support for hardware engineering models from breadboard to preproduction stages, determining spare parts location, quantity and cost requirements 09 p1430 A71-23477

Integrated logistics support program for F-14 aircraft maximum maintainability, reliability and operational readiness at optimum cost 16 p2553 A71-34154

Structural support system for large log-periodic antenna, discussing asbestos-cement pressure pipes and fiberglass rods as construction materials for antenna critical electrical characteristic needs 20 p3210 A71-39871

SUPPORTS

Circular cylindrical shell stability under uniform tension, taking into account support flexibility and temperature difference 06 p0990 A71-17794

UK 3 spacecraft support stinging for solar simulation and thermal vacuum testing in 2.5 meter test chamber, describing design and construction 06 p0881 A71-18720

Soviet book on supports and suspensions of aircraft gyroscopic devices covering accuracy, reliability and lifetime factors related to quality and operational conditions 07 p1115 A71-20299

Buckling by torsion of straight circular cylindrical elastically supported bars, using initial parameters method based on matrix calculus 09 p1536 A71-22412

Optimization algorithm for multielement support structure exhibiting minimum deformation energy, comparing Lagrange conditional search method 13 p2101 A71-29186

SUPPRESSORS

SST noise suppression research, discussing engine noise suppressor conceptual designs and test results with installed devices 07 p1184 A71-20302

Acoustic noise output from round interfering subsonic jets, considering suppressor nozzle attenuation 24 p3864 A71-44560

SURFACE CHEMISTRY

SURFACE REACTIONS

SURFACE COATINGS

COATING

SURFACE COOLING

Flat cooling wall optimum thickness for minimum steady state temperature at point exposed to local heating 03 p0520 A71-13955

Steady state thermal stresses and deformations in infinite hollow circular cylinder by sinusoidal internal heat source and Newtonian radiation boundary condition outer surface cooling 07 p1214 A71-20026

Hydrogen condensation and evaporation on liquid helium cooled surfaces in cryopump with reduced thermal radiation loading 09 p1546 A71-23008

Skin cooling effect on awake exercising dog ventilation, noting carbon dioxide response curve, arterial partial pressure and hyperpnea 09 p1396 A71-23366

Coolant combustion effects in transpiration cooling of gas turbine components, using hydrogen, ammonia and nitrogen coolants [ASME PAPER 71-GT-72] 11 p1855 A71-25986

Shock layer parameters of supersonic viscous gas flow past blunt bodies of heat insulated and cooled surfaces, using Navier-Stokes equations 19 p2991 A71-37089

Impact craters crustal thickness and forms relationship to changing physical state of planetary surface during once-molten cooling 19 p3051 A71-37669

SURFACE CRACKS

High strength and plasticity managing steels of Fe-Ni-Co-Mo system, noting surface crack sensitivity in tension 01 p0103 A71-11071

Cross and single polarized light techniques revealing coarse grained fractures cleavage facets 07 p1111 A71-19582

Stress distribution boundary value problem for long isotropic elastic cylinder with strip cracks due to internal pressure 07 p1215 A71-20100

Applied transducer signals from surface and internal fractures of various lengths, depths and positions 09 p1450 A71-22896

Thin cracked steel plate strip necking zone relative opening displacement and strain measurements by moire method 09 p1542 A71-23540

Room temperature curing rubber for detection of cracks and other surface flaws in magnetic materials, revealing cracks in specimen by distinct dark lines 10 p1615 A71-24100

Elastic-plastic fracture behavior engineering model based on surface flaw severity by crack length dimensions measurements [AIAA PAPER 71-371] 11 p1845 A71-25345

Gas turbine wheel design fracture mechanics, discussing buried and surface flaws analysis for rotor failure prediction applications [ASME PAPER 71-GT-10] 11 p1811 A71-25956

Stress distribution in infinite elastic solid containing spherical cavity and external crack, discussing displacement components for axisymmetric loading 12 p1974 A71-26740

Image distortion technique for viewing deformation zones at crack tips on highly polished surface 14 p2323 A71-29849

Dilatometric measurement for crazing rate in rubber-toughened plastics during tensile creep tests 15 p2438 A71-31369

Elastic plate with part-through surface crack, determining stress intensity factor for remote tensile and bending loads [ASME PAPER 71-APM-20] 16 p2655 A71-33209

Surface cracking resistance of polymethyl methacrylate glass in vacuum, air and nitrogen, noting humidity effect 16 p2601 A71-33690

Semiempirical modification of Irwin fracture analysis for semielliptical surface crack in metal plate 20 p3248 A71-38781

Crack shapes and stress intensity factors for deep edge crack in plate under tension or bending 21 p3467 A71-40907

Rayleigh wave reflection from crack tip after propagation along open crack faces in elastic solid, determining surface wave energy loss 21 p3468 A71-41003

SURFACE DEFECTS

Surface flaws in metallurgical products for aircraft building, welds and castings, noting material faults-failure relation and acceptance criteria 03 p0431 A71-13251

Hydrogen outgassing from proton irradiated aluminum samples, determining gas evolution and blister formation during annealing 07 p1139 A71-20173

Moving thin walled tubes surface and internal defects detection based on three dimensional thermal field surface distribution 08 p1300 A71-21899

Eddy current nondestructive tests for surface defects detection, determining optimum test parameters based on calculation 09 p1454 A71-22213

Imperfect thin walled circular cylindrical shells under axial compression with relaxed boundary conditions, determining deformations with differential equations 09 p1541 A71-23089

Brittle alumina ceramic tensile and flexural strengths comparison based on statistical surface flaw distribution theory of fracture 09 p1484 A71-23699

Perturbed magnetic surfaces topology in quadrupole, estimating local imperfections size for plasma control 10 p1652 A71-24661

EPR study of electron irradiated LiF surface defects, emphasizing F-centers generation possibility 11 p1807 A71-25557

Rolling contact spalling fatigue failure incidence in subsurface defects, using engineering model based on crack growth rate 14 p2251 A71-29828

Magnetic field perturbation and electric current injection techniques for characterizing high strength alloys fatigue microcracks 16 p2581 A71-32865

Thin infinite isotropic elastic plate on nonlinear elastic foundation under uniform two dimensional hydrostatic pressure, detailing imperfection effects on initial postbuckling behavior 16 p2648 A71-32979

Surface deformation in polycrystalline Al samples produced by ultrasound generated cyclic stresses, examining slip bands formation by electron microscope 16 p2591 A71-33224

Composite materials reinforced by brittle sapphire and ductile copper whisker crystals, noting surface defects effect on mechanical properties 16 p2601 A71-33917

Surface/volume damage induced by Nd-YAG laser irradiation to LiNbO and KDP crystals in frequency doublers and Pockels cells, using scanning electron micrographs 17 p2790 A71-34376

Axisymmetric imperfect conical shells vibration analysis using time average holographic interferometry technique 21 p3382 A71-41028

Surface strain cyclic flow growth rates for Al and Ti plates, using end point, flaw opening and striation measurements 22 p3560 A71-41643

Eddy current field formation of defect on extended surface crack in ferromagnetic and nonferromagnetic metals, investigating superposed transformer detector inductor coil effects 22 p3529 A71-41770

Monograph on hypersonic low temperature ablation covering cross hatched surface patterns, flow field, turbulent boundary layer, angle of attack, etc [VKI-TN-64] 22 p3621 A71-42031

Machining effects on martensitic stainless steels corrosion resistance, showing formation of defects and internal stresses in surface layers 23 p3692 A71-44028

Stability under uniform external pressure of closed spherical shell with axisymmetric initial imperfection in equatorial region, using finite difference technique 24 p3883 A71-44853

Circular cylindrical laminated anisotropic shells with axisymmetric shape imperfections, investigating upper bound buckling loads 24 p3841 A71-44958

Dielectric and semiconductor crystals surface defects, considering electric polarization structures 24 p3860 A71-45098

SURFACE DIFFUSION

Discrete coatings, surface diffusion and thermomechanical surface treatments for metal fatigue strengthening 01 p0099 A71-10169

Refractory metal thermionic emitter-support systems, measuring surface interdiffusion at high temperatures 02 p0264 A71-12242

Chromium steel surface diffusion saturation by sublimated Mo, examining process kinetics 03 p0442 A71-13400

Zr surface nitriding process in purified and high purity nitrogen respectively, comparing results 04 p0616 A71-15806

Holographic interferometry of diffusely reflecting surfaces, analyzing homologous rays concept 05 p0747 A71-16192

MOS transistors for high digital logic speed and microwave performance, discussing fabrication by double diffusion through mask opening 07 p1078 A71-19998

Cs ions surface diffusion / migration / in presence of blocking electric field on emitter surface, examining contact-ionization ion sources 08 p1342 A71-21914

Steel alloys solid Cd embrittlement, discussing crack propagation rate temperature dependence and Cd surface diffusion as controlling effect 11 p1777 A71-25447

Thermionic emitter CVD W layer on Mo, investigating work function change due to Mo diffusion and crystal structure dependence on heat treatment 11 p1808 A71-25863

Diffusion processes in Mo-W thermionic emitters of massive couple type and piece of Mo substrate with vapor-deposited W layer respectively 11 p1709 A71-25864

Molecular hydrogen sorption pumping by cold carbon dioxide cryodeposits, showing adsorbed molecules surface diffusion into disordered frost structure 17 p2695 A71-35138

Cs ions surface diffusion / migration / in presence of retarding electric field on emitter surface, showing temperature effects 17 p2789 A71-35258

Bulk and surface diffusion roles in clean and contaminated Cu-Ni surfaces adhesion 19 p3080 A71-37713

Insulator surface ion migration effects on MOS and bipolar integrated circuits, describing inversion voltage and surface conductivity and recombination velocities 19 p3033 A71-38505

Cryosorption vacuum pumping, discussing physical and chemical adsorption, adsorbents, surface migration and diffusion, reactivation, deposits, cryopanel adhesion, pump design, etc 20 p3270 A71-39249

Molybdenum hemicarbid layer as diffusion barrier between metal and disilicide, investigating system thermal stability 21 p3399 A71-40526

Mathematical description by Gaussian error function for metals diffusive saturation and diffusion constants determination 21 p3403 A71-41160

Carbon and stainless steels chemical composition effects on diffusion layer structure and fatigue strength after diffusive boring 21 p3403 A71-41162

Austenitic stainless steels diffusion layer formation and structure by gaseous carburization with FeAl-ammonium chloride powder mixture, describing elements redistribution 21 p3390 A71-41166

Boridosilicide and boridoaluminide diffusion coatings on iron and steel, investigating formation kinetics structure and properties 21 p3390 A71-41171

SURFACE DISTORTION

Cylindrical shell compression stability in presence of creep, determining initial surface dent effects 06 p0992 A71-17805

Variable curvature cylindrical shells elastic post-buckling configurations, showing buckle pattern tessellation discontinuity 13 p2157 A71-29126

Thermal distortion effect on heat flow between two contacting semiinfinite solids of different materials 17 p2837 A71-34691

Mean curvature of deformed spherical surface in study of equilibrium configuration of water drops under surface tension, using differential geometry 19 p3045 A71-37899

Half space with periodic continuous distributed dislocations and plastic distortions, calculating stress fields and free surface orientation with cartesian coordinate system 22 p3613 A71-41432

Telescope wave optical imaging performance, deriving point spread function, radial energy integral and modulation transfer functions for different wave front surface deviations 24 p3849 A71-45204

SURFACE ENERGY

Single crystal facet angles and surface energy planes by light reflection for W emitter in vacuum, Cs and iodine 02 p0251 A71-12208

Solid/vapor surface energies of metals at melting point related to heat of sublimation 07 p1134 A71-19518

Temperature variations of effective fracture surface energy of metals and alloys and relation to crack growth in high temperature creep 13 p2085 A71-28505

Ultrasonic vibration energy surface and volume effects, obtaining static forces reduction, processing rate increases, technique shortening and surface finish improvement in manufacturing processes 13 p2075 A71-28949

Metallic body motion in strongly rarefied plasma, determining compensating surface current distribution 13 p1991 A71-29158

Surface state energy positions determination in high-energy gap semiconductors by photovoltage spectral distribution 14 p2284 A71-30404

Monatomic gas interaction with solid phase surface, deriving three dimensional theoretical model including hard spheres collision and surface energy 15 p2451 A71-31675

SURFACE EROSION

U EROSION

SURFACE FINISHING

Discrete coatings, surface diffusion and thermomechanical surface treatments for metal fatigue strengthening 01 p0099 A71-10169

Electropolished and single crystal surface effects on work function of macroscopic tungsten emitter in cesiated converter 02 p0295 A71-12204

Glow discharge cleaning for surface contaminants removal from hydrodynamic gas bearing components, discussing equipment application to thin film lubricant vapor deposition 02 p0256 A71-12461

Carbon fiber surface treatment for reinforced plastic composites interlaminar strength increase, using wet oxidation process based on hypochlorous acid 02 p0274 A71-12485

Metal microfinishing technique, evaluating surface integrity degrading effects and total time requirements 05 p0739 A71-16464

Adhesive resin metal bond stability, examining surface finish and atmospheric moisture effects at various temperatures on exfoliation 06 p0904 A71-17944

Semiconductor thermocell junction polishing effects on bilateral layers tensile strength and electrical contact resistance 07 p1023 A71-19145

N-type Si surface barriers and finishing effects on photoconductivity and photoelectric effect 07 p1179 A71-19921

Fatigue limit of titanium alloy machine parts after finishing mechanical treatment under resonance testing 07 p1142 A71-20484

Axial compressor blades surface finish and fatigue strength restoration by vibrational tumbling 08 p1295 A71-20843

Electroerosion and electrochemical combined effects on machining surface removal, discussing optimal anodic removal rates and electrolyte concentrations 08 p1296 A71-20852

Polished surface quality control using laser divergent coherent beam 09 p1460 A71-22310

Surface treatment effects on high shear strength adhesive bonding of fiber reinforced plastics to metal substructures 10 p1630 A71-24069

Airport runway surface strengthening, discussing overlaying additional rigid or flexible layers, replacing used sections and reinforcement problems 10 p1589 A71-24756

Handbook on adhesive bonding covering adhesive materials, properties selection and compatibility, bonded assembly requirements and joints design, surface preparation, processing, trade sources, etc 11 p1788 A71-25451

Boride coated steels and cast iron surfacing with nonconsumable tungsten electrode for higher abrasive wear resistance 12 p1917 A71-27125

Hand/machine sanded surfaces moderate environment exposure time effects on adhesive bonding of glass fiber reinforced plastic joints 12 p1921 A71-27411

Milling, band grinding, final manual polishing and tumbling polishing effect on fatigue life and surface finish of steel compressor blades 12 p1912 A71-27680

Metal finishing tests on bronze in presence and absence of surface active agents, considering abrasive working 13 p2072 A71-27816

Helicopter component surface finish smoothness and residual stress requirements, using abrasive grinding belt machines with gear link mechanisms 13 p2075 A71-28943

Chromium carbides or borides high melting wear resistant surfacing material for machine components subjected to abrasive wear 15 p2418 A71-32669

Cutting speed, feed rate, tool geometry and other machining factors effects on surface finishes of face milled steels, titanium and nickel base alloys [SME PAPER MR-71-146] 18 p2927 A71-36663

Laser beam applications in drilling, shaping and surface finishing of miniature journal and step-type friction bearings, deriving regression equations for optimal process parameters 24 p3834 A71-45162

SURFACE GEOMETRY

Shells with positive Gaussian curvature, deriving p analytic functions for zero bending stress state and infinitesimal deflections of middle surface 01 p0168 A71-10415

Epitrochoidal profile machining methods and tools for chamber surface in Wankel engine 02 p0257 A71-12560

Geometrical conditions for contact without interference in internal gear stages with small tooth number differences 03 p0431 A71-13024

External-internal gear stages contact ratio on basis of gear wheels working drawing geometrical quantities 03 p0431 A71-13025

Nonlinear free surface effects in low gravity tank draining, finding domains of validity for linearized and nonlinear analysis [AIAA PAPER 69-680] 03 p0399 A71-13439

Level ampoule inner surface curvature nonuniformity, noting correction determination in level scale division 04 p0592 A71-14857

High precision large optical component surface visual monitoring with aid of small size etalons 04 p0593 A71-14869

High strength steel butt welds surface geometry effect on fatigue durability under cyclic loads, using photoelastic analysis 04 p0602 A71-14881

Longitudinal surface curvature effect on steady two dimensional incompressible laminar thermal boundary layers 04 p0680 A71-15471

Local radiative heat transfer and equilibrium temperature between identical uniform surface geometry

planes, discussing directional dependent emittance and absorbance effects [AIAA PAPER 71-76] 06 p1008 A71-18531

Approximate determination of complex geometrical aircraft surfaces in form of discrete points, comparing efficiency to other methods 06 p0848 A71-18171

Fabry-Perot resonator with anisotropic medium deriving reflection mirror shape for optimizing diffraction loss and resonant conditions for extraordinary waves 08 p1289 A71-21212

Rumanian book on stress computation in theory of cylindrical median surface plates with arbitrary section and minimal area 09 p1536 A71-22122

Surface geometry effect of polycentric gas bearing on rotor stability in dynamic equilibrium without radial load 09 p1454 A71-22767

Distribution functions of errors in earth and moon horizon sighting due to planetary surface unevenness 09 p1523 A71-23141

Arbitrary midsurface geometry thin shells nonlinear equations in terms of finite rotation vector and stress resultant tensor component 10 p1684 A71-23767

Wall jets over concave surfaces, obtaining average velocity profiles 10 p1591 A71-23846

Compressible laminar boundary layer flow including second order longitudinal surface curvature effects deriving flow equations from Navier-Stokes equations 11 p1750 A71-25474

Axisymmetric ablating graphite nosetip analysis code, demonstrating shape change, heating distribution and internal conduction coupling [AIAA PAPER 71-413] 11 p1856 A71-26203

Longitudinal solid surface curvature effects on heat transfer, calculating velocity and temperature fields by similarity analysis via boundary layer equations 12 p1987 A71-27734

Edge geometries and aperture distributions of physically realizable planar antennas 13 p2027 A71-27918

Complex geometry surface light pressure moment determination by body image projection onto photometric wedge and linear edge sliding screen procedure respectively, considering errors 13 p2071 A71-29155

Photoelectric, bolometric and photographic recording assembly for measurement of light pressure aerodynamic forces on complex shape body in free molecular flow 13 p2071 A71-29155

Surface curvature effects in nonsimilar second order boundary layer solutions for subsonic plane flow over cylinder with separation 14 p2170 A71-30444

Circular stresses and concentration coefficients variations in star shaped elastic surface projected onto ring under internal pressure 14 p2287 A71-30855

Aspherization coordinates and error corrections of optical systems with nonspherical surfaces by collimating beam method on digital computer 15 p2406 A71-31622

Slipstream due to supersonic source in hypersonic stream, determining shape of limiting surface 15 p2346 A71-32111

Combined finite element method and Rayleigh-Ritz procedure for geometrically nonlinear problems solution of elastic plates with arbitrary shape, boundary and load distribution 16 p2653 A71-33088

Stress-strain dependence on surface deflection and nonlinearity during bending of elliptic flat plate under plastic deformation 16 p2659 A71-33999

Holographic diffraction gratings on plane or concave spherical surface photographic plate, investigating interference fringes and aberration properties 17 p2745 A71-35558

Analog analysis of shape history of ablating graphite nose tips of reentry vehicle, eliminating geometrical instabilities 18 p2984 A71-35955

Laminar boundary layer flow theory for arbitrary curved surfaces, predicting shear stress, thickness and velocity and pressure distributions 18 p2844 A71-36311

Canard space shuttle reusable launch vehicle wing geometry variations effect on flyback systems weight noting influence of aspect ratio and wing area 18 p2974 A71-36488

Low speed angular contact bearings surface geometry effects on friction perturbation torque ripple frequency 18 p2928 A71-36766

Surface relief effect on radiative properties of solid body with random surface roughness distribution 19 p3162 A71-37588

Transparent sample surfaces parallelism interferometric measurement using laser produced two beam nonlocalized fringes 20 p3245 A71-39181

Three dimensional surface displacement measurement by hologram interferometry, applying to cantilever 20 p3235 A71-39187

Holographic interferometry application to two step static displacement measurement of diffusely reflecting surface of rigid body in motion 21 p3377 A71-40227

Existence theorem derivation for moving surface one dimensional geometrical and kinematic compatibility condition 21 p3415 A71-40658

Incompressible inviscid fluid free droplet surface layer tension determination as function of curvature from mechanical moment model 22 p3613 A71-41565

Computerized screen construction for surfaces with net characterized by singularity-free and curve-edges properties 22 p3518 A71-42395

Trapped surface existence conditions and occurrence in strongly curved space-times 22 p3576 A71-42403

Characteristic initial data for gravitational vacuum fields invariant of two initial null hypersurfaces and space-like section sigma 22 p3576 A71-42404

SURFACE INTERACTIONS

U SURFACE REACTIONS

SURFACE IONIZATION

Electron transfer in ion microscope field ionization, analyzing band and periodic surface structure effects, ionization probability and collision formalism 02 p0288 A71-12734

Surface ionization effects on planar silicon bipolar transistors, considering damage reduction by device exposure to high ionizing radiation dose 07 p1174 A71-19057

Sudden thermionic emission in surface ionization at near threshold temperatures of cesium activated tungsten single crystals 09 p1494 A71-22879

Temperature field influence on hysteresis in Cs surface ionization on metal surfaces, observing adsorption phase fine structure and ion current density increase 10 p1657 A71-24542

Mass spectrometric investigation of high power laser beam plasma on solid target, determining multicharged ion yield, energy, angular distribution and recombination effect 15 p2418 A71-31191

SURFACE LAYERS

Mercury planet average dark side temperature indicating top surface layer similarity with moon 01 p0148 A71-10004

Laser heated surface layer fragmentation taking into account particles dispersion due to vaporization, reactive force and mechanical recoil moment 01 p0070 A71-10796

Statistical study of microhardness across thickness of gas saturated layer distribution on surface of Ti alloys 02 p0265 A71-12524

Sunspots surface layers azimuthal electric current density, assuming specific magnetic force distribution 03 p0484 A71-13209

Machine part surface layers properties effect on vibration decrement 03 p0503 A71-13414

Space charge hypersurface layer conductance in semiconductors, allowing for three dimensional surface impurity fields 03 p0467 A71-13976

Industrial and biological polymer compounds active surface layers, discussing thermodynamic aspects, molecular dynamics, energy conversion and boundary layer entropy 06 p0915 A71-17585

Steels surface layer strain hardening during diamond smoothing 07 p1117 A71-19364

Steady state thermoelastic mixed boundary value problem for elastic layer, obtaining temperature, stresses and displacements in finite integrals through Hankel transforms 08 p1370 A71-21238

Ozone flux measurement in atmospheric surface layer by profile method as function of destruction coefficient, friction velocity and concentration 09 p1438 A71-23023

Film thickness effects on stress magnitude in surface layers of bodies under external friction 09 p1455 A71-23078

Metal surface layers structural changes during fretting corrosion, analyzing strain effects 09 p1455 A71-23081

Crystal structure alterations in work hardened surface layers of W, Nb and Mo during thermocyclic treatment, using X ray micrography 09 p1477 A71-23329

Surface layer-bulk body interaction and Rayleigh wave propagation in elastic solid, using two dimensional continuum theory 10 p1691 A71-24645

Physical model describing mechanism of recording through surface corrugation of thermoplastic viscofluid layer by electron beam 10 p1613 A71-24873

Dielectric layer surface electric charge movement determination by measuring metal-insulator-semiconductor (MIS)/capacity response at very low frequency 12 p1942 A71-26829

Optical properties and relative density of lunar surface layer, deriving light reflection and scattering formulas 12 p1964 A71-27089

Heat resistant alloys strengthened elements, studying high temperatures prolonged exposure effects on surface layers strengthening and residual stresses relaxation 12 p1919 A71-27780

Thin solid films on ball bearing surfaces, measuring electrical conductivity 13 p2072 A71-27817

Interferometric studies of focused Nd laser radiation interaction with thin graphite absorbing surface layer, discussing time behavior of plasma expansion and density distribution 13 p2078 A71-28446

Vertical variations of Reynolds stress and heat flux in atmospheric surface layer attributed to sub-mesoscale circulations, using sonic, thermometer and drag measurements 13 p2097 A71-28724

Land-sea drag, Ekman parametrization and Monin-Obukhov transfer process in surface boundary layer of atmospheric circulation model 13 p2097 A71-28725

Laser emission absorption in surface layer of optical glass, determining surface temperature dependence on emission energy density 13 p2079 A71-28859

Time variable effect on synthetic wind speed and air temperature profiles based on sensible heat flux density and stress at surface layer 14 p2266 A71-29705

Thermal emissivity and solar absorptivity of Al coated with surface layers of aluminum oxide and silicon oxide, describing fabrication techniques and performance measurements 14 p2335 A71-30128

Characteristics of field effect and surface barrier GaAs transistor (MESFET) operating at 4.2 K, noting very low temperature hyperfrequency amplifier application 14 p2212 A71-30439

Liquid KCl and LiF surface films effect on combustion rate of ammonium perchlorate mixtures with polystyrene or polymethyl methacrylate for various initial temperatures 15 p2462 A71-31371

Finned solid cylinders surface layers, determining residual axial stresses distribution and amount with induction sensor 15 p2503 A71-31480

Heated or cooled wall surface layers temperature anomaly, noting fluid-wall heat exchange coefficients 15 p2513 A71-31905

Logarithmic decrement of flexural, longitudinal and torsional vibration damping of various size rods, taking into account surface layer energy loss 16 p2659 A71-33979

Anisotropic carrier redistribution near semiconductor charged surface with energy band bending, discussing relaxation rate 17 p2790 A71-34197

Heat and mass transfer during deposition on heated surfaces in nonisothermal gas flow with suspended solid particles, using motion of continuous Newtonian medium 17 p2836 A71-34305

Lateral surface heat transfer effect on thermophysical characteristics in thin layer coatings, discussing temperature gradients in corundum and zirconium oxide on copper 17 p2836 A71-34308

Ti-Al alloys surface film growth and stress corrosion cracking as function of applied potential and environmental pH, presenting results of ellipsometric examination 17 p2756 A71-34489

Machine part surface layers properties effect on internal friction from transverse vibration decrement measurement 17 p2826 A71-35021

Copper on copper friction coefficient dependence on oxygen pressure, investigating exoelectron emission from differently oxidized copper surface layers 18 p2928 A71-36750

Optical properties and relative density of lunar surface layer, deriving light reflection and scattering formulas 19 p3133 A71-37439

Bulk and surface hydrogen concentration comparison in NBS hydrogen-in-titanium standards 19 p3080 A71-37718

Lunar surface layer density and dielectric permeability from radio wave scattering data from automatic spacecraft radar measurements 20 p3295 A71-39616

Dynamic derivation of surface layer representation of lunar gravitational field from Doppler observations on polar and equatorial lunar orbiters 21 p3449 A71-40643

High temperatures prolonged exposure effects on surface layers hardening and residual stresses relaxation in heat resistant alloys 21 p3403 A71-41105

Alloy steels supercooled austenite nitriding in ammonia flow, examining diffusion layers by X ray analysis and hardness tests 21 p3404 A71-41164

Austenitic stainless steels diffusion layer formation and structure by gaseous carburization with FeAl-ammonium chloride powder mixture, describing elements redistribution 21 p3390 A71-41166

Cr diffusion into Ni-Cr alloys in presence of colorized layer, noting increased diffusive mobility 21 p3390 A71-41167

Si addition effect on Ni-Cr alloy colorized layer depth, microhardness, phase structure, chemical composition and scaling resistance 21 p3390 A71-41168

Diffusion layer structure and phase composition during quenched and annealed steel saturation by Cr at high heating rates 21 p3404 A71-41170

Laser emission absorption in surface layer of optical glass, determining surface temperature dependence on emission energy density 21 p3394 A71-41297

Semiconductor surface layer noise generation physical model with allowance for relaxation effects due to traps in space charge region 21 p3432 A71-41301

Sn-N-GaAs semiconductor surface barrier structure electrical properties measurement over wide electron density range, determining energy band diagram and current flow mechanism 21 p3433 A71-41313

Macromolecular binding agent effect on electrophotographic properties of high resistance layers containing photoconductive CdS 22 p3586 A71-42405

Photoconductive CdS disintegration effect on heterophase electrophotographic layer electric and photoelectric properties, noting optimal properties relationship to grain diameter 22 p3586 A71-42406

Turbulent energy budget and velocity dissipation spectrum near grass surface as function of atmospheric stability 22 p3569 A71-42546

Laser optical system for hyperballistic range hypervelocity models surface erosion measurement, describing instrumentation of front-lighted, silhouette and stereo stations 23 p3677 A71-43513

Unpaired electrons and oxygen adsorptive capacity of clean lunar rock and soil surfaces, noting decrease of uptake rate at one monolayer coverage 23 p3764 A71-43798

Machining effects on martensitic stainless steels corrosion resistance, showing formation of defects and internal stresses in surface layers 23 p3692 A71-44028

Temperature effects on niobium carbide friction process in vacuum conditions, considering surface layer microhardness and X ray and metallographic analyses 23 p3692 A71-44030

Boron silicide coatings wear resistance in vacuum and air, determining slipping rate and working medium influence on friction process in active surface layers 24 p3830 A71-44859

Surface oxide, organic and lead film effects on friction and plastic deformation of Zn single crystal during sliding (ASLE PREPRINT 71LC-6) 24 p3839 A71-45288

SURFACE NAVIGATION

Lunar surface vehicle navigation system, describing dead reckoning and sun aspect compass for initial gyro alignment 01 p0124 A71-10514

Marine traffic control via satellite telemetry, describing merchant and powered fishing fleet distribution and navigation requirements 01 p0125 A71-10978

Satellite systems for transatlantic simultaneous air and marine navigation, traffic control and rescue, stressing technical and economical factors 06 p0925 A71-18015

Communications, navigation and surveillance for aircraft and marine vessels in North Atlantic region, discussing baseline traffic control model 07 p1153 A71-18808

Landmark navigation improvement by redundant measurements and statistical data reduction measurement for lunar roving vehicles 07 p1156 A71-20339

Surface navigation system and error analysis for Martian roving vehicle, using continuous tracking of pole star and local vertical

08 p1332 A71-21350

Navigation and communication satellites development for civil aviation and shipping, examining technical, organizational, operational and cost problems

17 p2771 A71-34240

Satellite communication application to maritime mobile service and position determination, discussing VHF and UHF space and shipborne equipment and modulation systems

17 p2697 A71-34241

Maritime operational and frequency requirements for satellite system having worldwide coverage

17 p2697 A71-34251

Civil aviation and merchant marine satellites, considering aircraft and surface vessel antenna characteristics and modulation techniques for optimum communication channel frequencies

17 p2775 A71-35582

Autoplotter for radar echoes on CRT screen, using video tape recorder for ship navigation use

19 p3017 A71-37700

Marine navigation and data communications at L band via synchronous satellite, assessing capabilities by tests on ATS-5 satellite

19 p3102 A71-38070

Satellite navigation system for aviation and marine use, examining operational requirements, economic viability and technical solutions

22 p3570 A71-41509

Satellite navigation, surveillance and communication service requirements for maritime transportation industry, discussing initial services

22 p3572 A71-42093

Book on electronic aids for navigation systems for marine and aerospace transport operation covering measuring and display instruments, radio wave properties, etc

23 p3702 A71-43225

German book on adaptive control systems covering flight attitude control, jet engine thrust, marine surface navigation, identification, etc

23 p3660 A71-44187

SURFACE PROPERTIES

NT ADHESION
NT ADSORPTIVITY
NT COEFFICIENT OF FRICTION
NT INTERFACIAL TENSION
NT SPECTRAL REFLECTANCE
NT SURFACE CRACKS
NT SURFACE DEFECTS
NT SURFACE ENERGY
NT SURFACE ROUGHNESS
NT SURFACE STABILITY
NT SURFACE TEMPERATURE
NT WALL TEMPERATURE

Cryogenic fluids nucleate boiling dependence on solid surface characteristics, considering hysteresis, boiling site spreading and radiation effects

01 p0178 A71-10005

Stress concentration and free surface shape at sliding contact for elastic semiinfinite cylinder, discussing mixed boundary value problem

01 p0171 A71-10658

Thermoelastic theory of stressed crystals and higher order elastic constants covering surface electronic and mass transport properties

02 p0294 A71-11799

Glass substrates for thin film circuits compared to other materials for properties and suitability, emphasizing surface properties

02 p0230 A71-11816

Radar observation of planetary surface characteristics, emphasizing albedo, surface roughness and differentiation

02 p0309 A71-12154

Crystal surface orientation of chemical vapor deposited W thermionic emitter by hydrogen reduction of hexafluoride, using etch pits and X ray diffraction

02 p0295 A71-12211

Cs vapor filled cracks breakdown in thermionic trilayer insulators, calculating electron reflection and ion recombination kinetics on surfaces

02 p0232 A71-12239

Surface thermal and electrical stresses effect on bipolar transistors electrical properties, using NDT criteria for components selection

02 p0236 A71-12921

Free wave reflection measurements of normal acoustic impedance of ground surfaces in relation to shock waves from large supersonic commercial aircraft

03 p0347 A71-13278

Machine part surface layers properties effect on vibration decrement

03 p0503 A71-13414

Elasticity theory two dimensional contact problems, examining cohesion or friction in contact area

03 p0513 A71-14229

Radiation heat transfer from parallel plates with grooved surfaces for direction dependent radiation properties

03 p0521 A71-14293

Ta spectral emissivity in red and green and relationship to surface structure change induced by heat treatment

03 p0460 A71-14465

Alpha titanium-oxygen solid solutions surface structure, using low energy electron diffraction for determination of order-disorder transition and superlattice reflections

04 p0610 A71-14895

Surface impedance of thin metal plate excited by RF electromagnetic field as function of external DC magnetic field

04 p0636 A71-14972

Wave functions of image potential induced surface states of insulators

04 p0630 A71-15395

Cryogenic liquids boiling peculiarities concerning heated surface material thermophysical properties effects on cavity stability, density and heat transfer rate

04 p0688 A71-15537

Turbulent boundary layer wall pressure fluctuations on hydrodynamically smooth and rough surfaces, investigating eddies, space-time decay rate and flow structure

05 p0736 A71-16961

Muscovite mica substrate surface composition as function of preparation and processing, using Auger electron spectroscopy

06 p0941 A71-17408

Jupiter surface features motions and changes, discussing planetary fine structure

06 p0971 A71-18247

Hydrogen and nitrogen binding states and desorption kinetics on 100/ plane of Mo, using flash mass spectrometry

06 p0865 A71-18302

Large aspect ratio rectangular duct with nonuniform surface texture, investigating turbulent flow, maximum velocity positions and zero shear stress

07 p1086 A71-18772

Flow between parallel planes of dissimilar surface texture, obtaining mixing length models velocity profiles, skin friction coefficients and zero shear stress position

07 p1086 A71-18773

Ionizing radiation induced surface damage dependence in matched oxide passivated silicon planar epitaxial transistors on junction fringing electric field strength during exposure

07 p1174 A71-19052

Vibration tumbling duration effects on surface quality, fatigue strength and damping properties of titanium alloy structural parts

07 p1130 A71-19169

Interferometric holography application to elastic stress and surface corrosion of two dimensional objects and metals, discussing stretching

07 p1107 A71-19209

Martian radio emission measurements at millimeter wavelength and surface thermal and electric parameters estimation

07 p1193 A71-19314

Scanning electron microscope for surface morphological investigations of materials after laser irradiation

07 p1113 A71-19793

Soviet papers on solid state electronics problems covering semiconductors photoelectric, magnetic, surface properties, autoemission, photoemission, etc

07 p1178 A71-19917

Pyrolytic graphite hemispherical emissivity measurement on surface parallel and perpendicular to deposition surface at 1200-2300 K

08 p1323 A71-21921

Solid metals and alloys electron emission, considering applications in surface phenomena observation

09 p1473 A71-23224

Material thermal removal by electrical discharge, electron beam and laser machining, discussing effects on surface integrity

09 p1458 A71-23411

Al alloys and ferrous metals adhesive bonding, discussing surface preparation and surface exposure time influence on bonded joint strength for various epoxy adhesive types

10 p1615 A71-24095

Graphite fiber surfaces atomic composition data, using Auger electron spectroscopy in ultrahigh vacuum low energy electron diffraction system

11 p1788 A71-25633

Mars surface pressure and elevation differences determined by spectroscopic observation of carbon dioxide band

11 p1825 A71-25714

Thermionic converters surface physics theory, discussing work functions, desorption energy and rates relationship to atomic and crystallographic properties

11 p1711 A71-25878

Surface strain measurements in turbine blades by time average holographic interferometry, reviewing resonant modes and holographic fringe patterns

[ASME PAPER 71-GT-84] 11 p1762 A71-259925

Surface structure and environment effects on mechanical behavior of crystalline inorganic solids, giving stress-strain diagrams

11 p1808 A71-259926

Nongray surface property effects on radiant heat transfer between interacting opaque surfaces, analyzing spectral emittance wavelength and temperature dependence

[AIAA PAPER 71-464] 11 p1859 A71-262450

Spacecraft surface contamination, noting effects on thermal control and optical equipment

[AIAA PAPER 71-457] 11 p1840 A71-264271

Revolving cylindrical surface reflected energy from scanning fixed laser beam, noting signal frequency

13 p2077 A71-279448

Graphite epoxy composites fiber microstructure and surface condition, noting tensile fracture, crack propagation and brittleness

13 p2092 A71-285948

Depressurization extinguishment of composite solid propellants for thrust termination, considering flames structure, surface characteristics and restart capability

[DFVLR-SONDDR-129] 13 p2113 A71-286151

Error in determining pressure and loading distribution on surface of slender bodies of revolution

13 p1994 A71-293232

GaAs single crystals real surface electrical characteristics, using pulsed field effect techniques

14 p2284 A71-304033

Stress concentration and free surface shape at sliding contact for elastic semiinfinite cylinder, discussing mixed boundary value problem

14 p2333 A71-309922

Martian radio emission measurements at millimeter wavelength and surface thermal and electric parameters estimation

15 p2486 A71-318944

Mars microwave spectrum, discussing brightness temperature increase towards short wavelengths in terms of surface material thermal, electrical or chemical properties

15 p2490 A71-32417

Subsurface moisture and frost detection by capacitive measurement of ground permittivity from landed planetary probes and surface vehicles

15 p2411 A71-32473

Surface and subsurface water analysis on moon and planets by combination neutron experiment using epithermal die-away measurements of hydrogen

15 p2411 A71-32477

Refractory tungsten boride with iron or nickel for powdery surfacing mixtures, showing hardness and wear resistance dependence on low melting component

15 p2438 A71-32675

Single mode ruby laser emission on transparent/dielectrics, observing surface luminescence, free electrons production and adsorbed gases heating

16 p2585 A71-32797

Metal matrix composites fractured and cut surfaces analysis using scanning electron microscopy

[ASM PAPER W71-3.4] 16 p2579 A71-33541

Surface effects of transverse slip screw dislocations in metal fatigue crack nucleation, relating stacking fault energy and number of cycles to failure

16 p2593 A71-33681

Polar asymmetry between distribution of surface features on earth, moon, Mars and Mercury

17 p2801 A71-34670

Machine part surface layers properties effect on internal friction from transverse vibration decrement measurement

17 p2826 A71-35021

Pyrolytic graphite hemispherical emissivity measurement on surface parallel and perpendicular to deposition surface at 1200-2300 K

17 p2763 A71-35265

Wall impedance method application to long distance transmission elliptical, parabolic and circular waveguides

17 p2707 A71-35480

Circular contact area in theory of elasticity with allowance for surface structure of bodies in contact, solving Hertz axisymmetrical problem of elastic bodies

17 p2833 A71-35610

Vibrotumbling duration effects on surface quality, fatigue resistance and damping properties of titanium alloy structural parts

17 p2760 A71-35665

MIS structure voltage-farad characteristics, determining surface state densities for silicon compound dielectric films

18 p2954 A71-35875

Peroxide-alkaline polishing solution for GaAs, evaluating optical quality, surface damage, polishing rate and metallic contact resistance

18 p2955 A71-37004

Ribbed surface electrode effects in plasma accelerator producing high speed monoenergetic blobs

19 p3108 A71-37091

- Surface properties and environmental effects on fatigue striations development and crack initiation in Cu single crystals 19 p3077 A71-37412
- Free carrier surface density and mobility in large MOS transistors from conductivity and Hall measurements 19 p3028 A71-37564
- Theoretical model of excess surface current in p-n junctions, based on surface-controlled tetrode transistor experiment for bipolar transistors I-V characteristics explanation 19 p3029 A71-38142
- Surface heat flux for incipient boiling in liquid metal heat pipes, determining nucleation site radius upper limit in Na heat pipes 19 p3171 A71-38349
- Vacuum UV reflecting surfaces deterioration by intermetallic formation, recommending separation by dielectric barrier layer 20 p3236 A71-39196
- Plasticity with noncoincident yield and loading surfaces, noting isothermal isotropic hardening 20 p3309 A71-39565
- Surface patterns of ablating bodies from water jet flow experiment simulation, discussing vortices detection 21 p3317 A71-40019
- Eutectic Al alloys parallel alignment formation by stable isothermal boundary surface, investigating microstructure 21 p3396 A71-40029
- Silicon semiconductor surface passivation with thermally grown silicon dioxide films 21 p3427 A71-40218
- Meteorite falls in Germany, discussing composition, surface properties, microstructure, weights and circumstances of observation and discovery 21 p3448 A71-40521
- Apollo 11 lunar fines and ground terrestrial mafic rock powders effective surface areas and heats of adsorption, using Brunauer-Emmett-Teller Kr adsorption method 21 p3450 A71-40648
- Insulating materials breakdown by surface discharge, determining corona lifetimes by hemisphere-plane configuration and cylinder-plane electrode 21 p3358 A71-41193
- Semiconductor surface state effects on p-n junction photodiode frequency characteristics under short and open circuit conditions, noting nonequilibrium capacitance during illumination 21 p3358 A71-41215
- Semiconductor surface relaxation behavior with allowance for inhomogeneity and charge exchange between slow states and space charge 21 p3434 A71-41322
- Multivalley semiconductors scale effect due to nonuniform electron heating by electric field, determining effective conductivity as function of plate thickness and surface characteristics 22 p3585 A71-42058
- Topological characterization for constant angular momenta and energy surfaces in equal mass planar three body problem 22 p3568 A71-42697
- Surface energy absorption coefficient determination from decaying sound fields, deriving reverberation time and decay rate equations 23 p3703 A71-43201
- Lunar rocks 12063,9 and 12004,11 opaque mineralogy and textural feature, comparing to apollo 11 samples 23 p3745 A71-43661
- Apollo 12 lunar samples halogen and trace element composition, investigating chemical and physical processes affecting surface halides, platinum group metals and Hg 23 p3749 A71-43689
- Thermally stimulated exoelectron emission and surface properties of lunar rocks and soil 23 p3758 A71-43759
- Surveyor 3 surfaces discoloration and lunar dust contamination, noting Apollo 12 lunar module caused disturbances by on-site observation 23 p3766 A71-43816
- X ray probe, scanning electron microscopy and spectral reflectance analysis of lunar environment effects on Apollo 12 returned Surveyor 3 materials surface cratering 23 p3766 A71-43818
- Thermal radiative cooling system characteristics determination allowing surface material thermal conductivity and blackness degree dependence on temperature 23 p3782 A71-43919
- Hertzian fracture test for strong solid surface properties measurement based on crack growth in nonuniform stress field due to contact loading 23 p3777 A71-43934
- Microalloying effects on phase composition, surface phenomena, fine crystalline structure and microstructure of E1417L steel 24 p3836 A71-44374
- Cylindrical space simulation chamber with spherical test subject, deriving molecular incidence rate from integral equations with probability matrix for finite partial surfaces 24 p3816 A71-45138
- Surface segregation, adhesion and friction of monocrystalline Cu-Al, Cu-Sn and Fe-Al alloys from Auger emission spectroscopy and low energy electron diffraction experiments [ASLE PREPRINT 71LC-5] 24 p3839 A71-45287
- Surface electronic conductivity in oxide glasses for microchannel electron multipliers, noting heat treatment and chemical composition effects 24 p3862 A71-45327
- Polycrystalline Nb and Ta and Ta-on-Nb thin film thermionic emission surface barrier analysis from periodic deviations in Schottky effect 24 p3862 A71-45346
- Surface potential barrier models for thermionic and photoelectric emissions from semiconductors in Schottky deviation region 24 p3862 A71-45350
- Luminescence time decay in optically excited thin direct gap semiconductor with surface losses, establishing phase shift method for carrier lifetime and semiconductor surface properties 24 p3863 A71-45360
- SURFACE REACTIONS**
- Crack opening in infinite isotropic elastic solid via displacements applied to crack surface 01 p0167 A71-10292
- Wave propagation in plane neutral electron beam near interface with semiconductor 01 p0139 A71-10782
- Pyrolyzing vinyl polymers thermal degradation kinetics, deriving surface regression rates relationship to temperature 01 p0109 A71-10935
- Surface destruction of glass dielectric by pulsed laser beam, considering plasma clouds, shock waves, ablation and crack formation 02 p0258 A71-11640
- Carbon fiber surface reactivity relationship to various organic compounds using gas-solid chromatography, evaluating molecular absorption enthalpies 02 p0209 A71-12537
- Lunar Module Ag coated stranded Cu wire, analyzing fluorine contamination with proton microprobe 02 p0209 A71-12592
- Nb surface contamination by oxidation during electrolytic polishing and vacuum annealing 02 p0269 A71-12928
- Nb strips siliconization by silicon hydride decomposition and silicide or silicon oxidation, noting Si surface enrichment and bulk diffusion processes 02 p0272 A71-12943
- Surface oxidation kinetics of iron by solid electrolyte techniques, comparing weight gain method 03 p0374 A71-13122
- Molecular hydrogen formation on dust grain surfaces, discussing recombination efficiency as function of surface temperature 05 p0784 A71-16205
- Refractory metal surfaces behavior in ultrahigh vacuum, using LEED and Auger electron spectroscopy 05 p0766 A71-16240
- Refractory metal surface-gas reactions at high temperatures in vacuum, determining activation energies 05 p0766 A71-16241
- Single layer graphite oxidation kinetics evaluated by electron microscopy, discussing removal rate 06 p0915 A71-17302
- Ti alloy deformation through surface oxidation at elevated temperature, considering lattice parameter and alpha concentration effects 06 p0913 A71-18677
- Adsorbed formaldehyde levels from vaporized paraformaldehyde on various surfaces as function of relative humidity and chemical concentration 07 p1055 A71-19593
- Mo fibers surface state and reactions under uniaxial stress from electron work function measurements 09 p1471 A71-23080
- Surface chemical characteristics of monomeric liquid epoxy resins 10 p1632 A71-24085
- Hydrogen recombination and molecule formation by nonactivated chemisorption on iron grains surfaces 10 p1573 A71-25006
- Uniform surface blowing effects on hypersonic boundary layer with viscous interaction, calculating heat transfer on flat plate and slender wedge 10 p1598 A71-25096
- Photographic study of burning metallized composite propellant, noting burning rate augmentation by heat transfer from alumina particles retained on propellant surface 11 p1809 A71-25502
- [AIAA PAPER 69-173] Glass fiber reinforced plastics, discussing adhesion, wetting and adsorption effects on chemical reactions in glass-resin interfaces 11 p1788 A71-25657
- Metastable state gas flow experiment, investigating laminar boundary layer change in presence of flat plate surface catalytic reaction 11 p1705 A71-26276
- Multiple echo of impurity atom during collisions with solid body surface, contributing to vaporization from layer 12 p1932 A71-27034
- Elementary particle recombination probabilities on solid body surface, using reactive gas model in form of quantum mechanics three body problem 12 p1934 A71-27546
- Classical and quantum mechanical theories of gas atom-solid surface scattering with applications to different physical regimes 14 p2276 A71-30405
- Metals bulk ignition temperature in oxygen atmospheres, emphasizing preignition surface oxidation effects 14 p2337 A71-30456
- Triatomic hydrogen positive ion surface crossing effects in chemical reactions based on potential energy surfaces calculation using diatomics-in-molecules approach 14 p2191 A71-30573
- Monatomic gas interaction with solid phase surface, deriving three dimensional theoretical model including hard spheres collision and surface energy 15 p2451 A71-31675
- Redistribution of carbon, copper, nickel and chromium on friction surfaces of powder metallurgy antifriction cermet slide bearings by spectral analysis 15 p2418 A71-32673
- Low pressure shock tubes performance, investigating wave and contact surface trajectories and ideal velocity deviations 16 p2556 A71-32915
- Temperature fields and mass and heat transfer at surface of solid spherical particle in laminar viscous fluid flow 16 p2557 A71-32931
- Carbon fiber surface reactivity from gas chromatographic measurement, discussing adsorption isotherm of various vapors 16 p2541 A71-34049
- Vapor bubble growth on heated surface with random temperature distribution and liquid microfilm for water and boiling potassium 17 p2836 A71-34306
- Tungsten-oxygen system surface reactions in vacuum, emphasizing interfacial geometry variations, faceting and oxide nucleation 17 p2694 A71-34667
- Kinetic models for gas-surface interactions, considering distribution functions of molecules at solid wall 18 p2874 A71-35900
- Reflected shock wave interaction with shock tube contact surface 18 p2903 A71-36123
- Molecular beam scattering at solid surfaces, outlining scattered particles angular and velocity distribution measurement 18 p2848 A71-36439
- Small scale flow and surface effects in multiphase media hydromechanics, obtaining entropy production in mixture for interphase transformations characterization 19 p3042 A71-37098
- Thermal creep slip velocity expression in power series for arbitrary fraction of molecules diffusely reflected from surface by Bhatnagar-Gross-Krook model solution 19 p3163 A71-37734
- Boron powder combustion at elevated pressures, observing preignition metastable surface reactions, self sustained diffusion burning and decay 19 p3170 A71-38116
- Silicon reactions with aluminum surfaces, using low energy electron diffraction technique 20 p3194 A71-38882
- Metal deformation processing in solid mechanics, discussing plastic idealization for viscous behavior theorems, Ekstein paradox, free surface problems and incremental forging 21 p3389 A71-40983
- Lead oxide pigment photoconductivity, investigating surface processes effects on spectral sensitivity and absorption spectrum 21 p3434 A71-41329
- Intergranular corrosion of chromium carbide sensitized Ni base alloys, noting surface effect during solution heat treatment 22 p3560 A71-41626
- Nitrogen ions surface interactions with Al surfaces at and above earth satellite speeds, measuring normal and tangential momentum accommodation coefficients 22 p3577 A71-41980
- Thermal combustion produced biocomplex vegetable waste mineralization effect on furnace working surface oxide film 22 p3507 A71-42821

SURFACE ROUGHNESS

SURFACE ROUGHNESS

- Transparent solids unpolished samples refractive index and dispersion measurement using Abbe refractometer 01 p0128 A71-10837
- Stress concentration at free and reinforced curvilinear holes with random surface roughness applied to plane under hydrostatic tension 02 p0326 A71-12291
- W and thortiated W grain boundaries topography by trace analysis and field evaporation, observing curved surface with ledges, protrusions and serrations 02 p0266 A71-12737
- Heat transfer correlations for turbulent flow in ducts with rough surfaces 04 p0674 A71-14778
- Coolants Prandtl number effect on pressure drop, heat transfer and friction of rough surfaces 04 p0675 A71-14779
- Leidenfrost film boiling for various liquids over velocity, plate temperature and surface roughness range, noting velocity effect on vaporization rate 04 p0687 A71-15529
- Surface roughness determination by spatially coherent laser light speckles correlation and spectral distribution on film records 04 p0609 A71-15689
- Nonadiabatic compressible turbulent boundary layer heat transfer to rough surfaces under arbitrary pressure gradient [AIAA PAPER 71-166] 06 p0885 A71-18608
- High velocity liquid flow past rough plate surface, investigating boundary layer cavitation effects on convective heat and mass transfer 07 p1086 A71-18774
- Flow field behind two dimensional roughness element in rectangular channel, discussing wall effects, reattachment point position, velocity distribution and turbulence intensity 07 p1086 A71-18775
- Nonuniform feed effects on height of electrospray surface machining microasperities, investigating linear elliptical interpolator pulse sequence 08 p1296 A71-20851
- Pipe flow turbulent friction, describing pressure drop measurements and flow visualization studies on wall roughness effects 09 p1431 A71-22275
- Planetary surface smoothness factor determination by disk brightness, Mars red light and phase curves methods, indicating superiority of visual observation 09 p1520 A71-22828
- Rough circular rod effective surface impedance and propagation constant, discussing guided electromagnetic wave attenuation on structure 10 p1578 A71-24399
- Rail track roughness and irregularities evaluation by railcar vibration measurements, using portable LF low amplitude acceleration measuring and recording system [AIAA PAPER 71-384] 11 p1845 A71-25349
- Handbook on radar cross sections, Volume 2, covering scattering from planar surfaces, complex bodies, rough surfaces, ionized media, plasmas, radar targets and various objects 11 p1733 A71-26009
- Microwave emission from North Sea and North Atlantic at surface wind speeds of 5-25 m/sec, measuring brightness temperature 12 p1902 A71-27199
- Laminar boundary layer perturbation by sinusoidal wall roughness, analyzing effect on transition nature and position 12 p1864 A71-27470
- Surface roughness of 304 stainless steel by Brunauer-Emmett-Teller measurements, using ethylene as adsorbate 14 p2284 A71-30073
- Fresnel diffraction on opaque absorbing screen half planes with small rough surfaces, deriving field attenuation factor and structure/correlation functions 14 p2194 A71-30099
- Mobility capability of lunar roving vehicles relative to terrain roughness, computing power requirements 15 p2494 A71-32496
- Quantitative measurement of speckle contrast for illumination with laser oscillating simultaneously in multilongitudinal modes on rough surface, determining coherence length 16 p2589 A71-34130
- Plastic deformation resistance of rough metal surfaces under heavy loads, discussing mechanical contact changes due to asperities reactions as coherent block 18 p2926 A71-36186
- IC applications to microwave frequencies, relating circuit performance to substrate roughness and thickness of thin film metal adhesion layers 18 p2895 A71-36981
- Heat and mass transfer calculation in turbulent boundary layer on rough surface 20 p3315 A71-39793
- Size classification of limonite Mars simulation samples, noting surface roughness of 0.02-10 microns 21 p3449 A71-40642

Rough metal surface smoothing through annealing in vacuum, deriving governing equations from Mullins theory of thermal grooving and solid surface capillary morphology 22 p3554 A71-42424

Thermal conductivity of elastic, elastoplastic and plastic contact area between two compressed rough surfaces 22 p3622 A71-42686

SURFACE ROUGHNESS EFFECTS

- Free fall speed characteristics of simulated hailstones measured by tracking radar, discussing roughness effects on speed and drag 01 p0115 A71-10556
- Shape and surface roughness effects on turbulent ablation of reentry body nose tip, noting recession rate [AIAA PAPER 69-717] 01 p0071 A71-10934
- Body radiative properties, examining degree of blackness dependence on surface roughness factor 02 p0331 A71-12188
- Erosive burning resulting from nonplanar surface structure of solid propellant 02 p0334 A71-12858
- Plane potential incompressible fluid flow in channel with rough bottom and variable surface pressure, allowing for gravitational and surface tension forces 03 p0406 A71-14567
- Coherence matrix of elliptically polarized radio signal scattered by statistically rough conductive surface 04 p0550 A71-14619
- Surface roughness effects on gas to wall heat transfer in conical converging diverging nozzles, using heated air 04 p0675 A71-14780
- Surface roughness and contamination, drop volume and liquid subcooling effects on Leidenfrost temperature 04 p0675 A71-14783
- Radiative heat transfer between opaque interacting surfaces, investigating surface roughness effects 04 p0684 A71-15513
- Semiempirical turbulence theory generalization to flows near rough surfaces, obtaining unified dependences for wall flows 04 p0575 A71-15610
- Velocity distribution equation for steady incompressible two dimensional turbulent flow, taking pressure gradients and surface roughness effects into account 04 p0578 A71-15764
- Surface roughness and thermal radiation effects on rural and urban boundary layer turbulence and diffusion by wind fluctuations observations 05 p0777 A71-16665
- VHF/UHF satellite transmission, predicting multiple ground reflection effects on signal fading and effective antenna gain by computerized method 06 p0868 A71-17732
- Conductivity of films with surface roughness dimensions large in proportion to screening radius and carrier free path length, presenting refined analysis 07 p1175 A71-19223
- Viscous incompressible slow unsteady flow through circular tube with small axial roughness, obtaining velocity components by integral transform technique 07 p1092 A71-20093
- Vector solution for electromagnetic wave scattering from rough surface of arbitrary dielectric constant 07 p1064 A71-20316
- Multimass system oscillations due to viscous friction factor and kinematic random disturbances, considering dynamic behavior of wheeled vehicle on rough roadbed 07 p1162 A71-20469
- Penetration model of thin solid film lubricant friction on sliding surfaces of finite roughness [ASLE PREPRINT 70LC-15] 08 p1298 A71-21159
- Sound field interaction with sinusoidally corrugated surface, considering aircraft noise measurement implications 08 p1333 A71-21162
- Pressure gradient and roughness effects on laminar, transition and turbulent boundary layer in hypersonic shock tunnel 08 p1377 A71-22031
- Surface roughness ensuring turbulent reattachment at low Reynolds numbers on airfoil sections with separation near leading edge resulting in bubbles [ONERA-TP-923] 10 p1549 A71-23762
- Radiatively interacting adjacent plates in presence of collimated solar flux, considering surface roughness effects on equilibrium temperature distribution [AIAA PAPER 70-817] 11 p1854 A71-25511
- Surface roughness and surface area effect on UV stability of zinc orthotitanate pigments, using electron microscopy and BET nitrogen adsorption [AIAA PAPER 71-451] 11 p1790 A71-26235
- Bidirectional reflectance model for randomly rough surface, using distribution function for macroscopic probability of microscopic surface roughness elements with specific slopes [AIAA PAPER 71-465] 11 p1800 A71-26246

- Supersonic boundary layer transition on adiabatic wall, discussing wind tunnel size, surface roughness and freestream disturbances effects [AIAA PAPER 70-586] 12 p1865 A71-27597
- Laser interference patterns recorded on photosensitive surface of test sample before and after deformation tests, considering irregularly shaped objects with rough surfaces 13 p2067 A71-28449
- Electromagnetic wave reflection by rough surfaces, based on geometrical optics, discussing reflectance power density reflection coefficient and frequency limit 13 p2033 A71-29242
- Uneven runway taxiing vibration effects on supersonic transport aircraft, comparing calculation with measurement 14 p2175 A71-30301
- Electromagnetic wave scattering from rough surfaces, discussing radar return differences for different polarizations 14 p2203 A71-30969
- Body radiative properties, examining degree of blackness dependence on surface roughness factor 15 p2512 A71-31454
- Surface roughness effects on heat transfer to ablating cones, using calculation method adaptable to computer routines for smooth wall 15 p2514 A71-32040
- Surface roughness causes and effects in planar fluidic elements, using large scale models 15 p2351 A71-32030
- Epitaxial Ag thin film with controlled surface roughness on mica, measuring electrical resistivity as function of temperature, thickness and surface specularly in vacuum 15 p2461 A71-32375
- Wall roughness effects on laminar boundary layer velocity profile and Reynolds number, using Hankel functions and integrals 17 p2725 A71-34181
- Optical homodyne detection of light signal waves front scattered by moving surface with normally distributed roughness, calculating conditions for optimum SNR 18 p2930 A71-36092
- Surface renewal and penetration heat transfer model for turbulent flow in smooth and rough tubes 18 p2986 A71-36599
- Two dimensional turbulent boundary layer in incompressible fluid on smooth and rough impermeable wall surfaces under arbitrary pressure gradients 19 p3042 A71-37080
- Surface relief effect on radiative properties of solubility with random surface roughness distribution 19 p3162 A71-37580
- Brazing roughness effects on rectangular plate fin heat exchanger surfaces heat transfer and flow friction characteristics, noting fin surface geometry influence [ASME PAPER 71-HT-29] 19 p3166 A71-37990
- Electromagnetic waves depolarization by rough terrain backscatter, applying theory of surface current perturbation due to surface irregularities 19 p3021 A71-38444
- Bistatic radar scattering cross section from slightly rough perfectly conducting infinite surface, using Fourier transform 19 p3024 A71-38606
- Turbulent boundary layer response to step change in surface roughness, discussing wind tunnel measurements of pressure and velocity profiles 20 p3212 A71-39508
- Stepwise change in wall roughness effects on turbulent shear flow through two dimensional channel, measuring mean velocity, turbulent intensity and shear stress 21 p3365 A71-40014
- Surface roughness and mass transfer influence on boundary layer and friction coefficient for turbulent flow over flat plate 21 p3371 A71-40999
- Roughness role in liquid He-solid boundary thermal resistance, calculating heat transfer coefficient 21 p3416 A71-41121
- Coherence matrix of elliptically polarized radio signal scattered by statistically rough conductive surface 22 p3510 A71-42251
- Turbulent flow of incompressible fluid in rough pipe, determining skin friction coefficient variations with Reynolds number 22 p3531 A71-42291
- Lunik 14 spacecraft radio signal reflection from lunar surface, showing energy spectrum dependence on surface roughness 22 p3511 A71-42301
- Interstellar spherical grains surface roughness: model, noting far UV radiation extinction enhancement 22 p3605 A71-42344
- Conical nozzle roughness on heat transfer in supersonic region 22 p3622 A71-42781

Frequency dependence of Rayleigh wave propagation velocity along rough surfaces, based on smooth surface mass loading

23 p3703 A71-43203

PAM signal transmission through statistically rough waveguide, calculating wall roughness effects on transient response by multiple scattering theory

23 p3645 A71-43566

Rough spheres, cylinders and annuli in contact, determining surface roughness and waviness effects on surface geometry under elastic and plastic deformations

23 p3682 A71-43928

Materials thermal accommodation coefficient and emissivity dependence on surface roughness, noting correlation

24 p3888 A71-44934

Airborne radar sea return averaged pulse shape measurements over various water surfaces, noting clear distinction between specular and scattered reflection components

24 p3824 A71-45083

Quartz crystal mass monitor study of monolayer oxygen adsorption on Al films, noting surface roughness variation with deposition temperature

24 p3803 A71-45348

SURFACE STABILITY

High work function stable faceted W thermionic emitter surface preparation by electroetching and vapor deposition

02 p0295 A71-12209

Mechanical stability of self healing viscous glass layer in porous oxidation protection coating on Ni under high acceleration

02 p0272 A71-12945

Mechanical stability of liquid phase in porous oxidation protective coating on Ni turbine blades under acceleration

02 p0272 A71-12946

Far IR cryogenic black paints absorptive throughout IR with surface stability at liquid He temperature and resistance to abrasion and flaking

08 p1335 A71-21383

Tenzaloy Al mirrors for IR astronomy, discussing results of Hartmann tests for optical stability

14 p2241 A71-30144

Fluid surface instability under perpendicular acceleration, presenting singular perturbation problem solution by successive approximations method

16 p2561 A71-34160

SURFACE TEMPERATURE

NT WALL TEMPERATURE

Mercury planet average dark side temperature indicating top surface layer similarity with moon

01 p0148 A71-10004

Laminar boundary layer free convection at vertical plate with exponentially decreasing surface temperature, determining thermal flux and shear stress

01 p0179 A71-10610

Initial surface superheating effects on high temperature oxidation of titanium in oxygen or dynamic air atmosphere

01 p0101 A71-10672

Commercial SST environmental effects on stratospheric air, water vapor content and earth surface temperature

01 p0074 A71-11178

Lunar surface thermal characteristics revised from analysis of error sources in daytime lunar surface temperatures derived from Surveyor 5 compartment data [AIAA PAPER 69-594]

01 p0163 A71-11582

Thermionic emitter work function extrapolation and interpolation, noting correlation to surface temperature and Cs pressure

02 p0294 A71-12202

Vaporization heat transfer mechanism from capillary wick covered heated surface, considering applicability to heat pipes

03 p0353 A71-13615

Magnetic suspension apparatus for temperature measurement near interface of sliding bodies in vacuum

03 p0397 A71-13914

Lifting body leeward surface maximum heat transfer coefficient in hypersonic flow, considering Reynolds number, incidence and shape effects

04 p0527 A71-15486

Nonuniform blowing and surface temperature turbulent boundary layer, investigating heat transfer

04 p0684 A71-15502

Lunar microwave emission effects and local surface temperature variations due to outward heat flow and low thermal conductivity

05 p0809 A71-16459

Plate critical surface temperature in case of stabilization by supersonic boundary layer cooling

05 p0695 A71-16852

Surface temperature of metal target heated by single laser pulse or pulse sequences, relating various parameters

05 p0764 A71-17042

Inertial grade floated rate integrating gyroscope surface temperature control by closed loop feedback controller

06 p0983 A71-17362

Sea surface temperature estimation by spatially scanning spaceborne systems operating in thermal IR atmospheric window spectral regions

06 p0898 A71-17560

Heat transfer in turbulent boundary layer for arbitrary surface temperature with fluid injection and pressure gradient

07 p1220 A71-18765

Surface temperature radiation interaction between two solid half spaces using Green function reduction method

07 p1223 A71-19254

Downward atmospheric radiation fluxes incident on Martian surface horizontal plane, tabulating atmospheric composition, surface pressures and temperatures and effective sky temperatures

07 p1199 A71-19874

Tropical hurricane central pressure drop to maximal wind velocity ratio, discussing thermal to mechanical energy transfer as function of ocean surface temperature

08 p1330 A71-21873

Moving thin walled tubes surface and internal defects detection based on three dimensional thermal field surface distribution

08 p1300 A71-21899

Defective resistors physical processes during thermal control method, appraising quality from surface temperature distribution

08 p1300 A71-21901

Surface heating and pressure distribution on Lunar Module from rocket exhaust plume impingement tests in vacuum [AIAA PAPER 71-256]

08 p1377 A71-21985

Metallic and nonmetallic objects phase separation and honeycomb structures adhesion lack, analyzing defects by surface temperatures distribution determination

09 p1450 A71-22893

Infrared radiometer sea surface temperature measurements during oceanographic survey, examining inclination angle effect

09 p1440 A71-23590

Periodic rotation reversal effect on hollow cylinder surface temperature distribution in space simulation testing of spin stabilized orbiting satellites

09 p1430 A71-23733

Thermoluminescence glow curve and decay characteristics of Apollo 12 fines and soil samples, suggesting lower mean daytime surface temperature at site

10 p1672 A71-24395

Pulsating incompressible two dimensional laminar boundary layer flow past insulated plate at zero incidence, calculating skin friction and surface temperature

10 p1697 A71-25084

Axisymmetric incompressible boundary layer flow, temperature distribution and heat exchange near critical point of rotating body with varying surface temperature

11 p1854 A71-25239

Experimental method for determining condensed phase heat of reaction of deflagrating double-base propellant, defining minimum surface temperature at solid surface without heat feedback

11 p1809 A71-25493

Mass spectrometric studies of laser beams interaction with solids, discussing surface temperature reached by solid during irradiation

11 p1775 A71-26081

Entry vehicle carbon vapor thermochemistry uncertainties effects on nose tip ablation response concerning stagnation point surface recession and temperature levels [AIAA PAPER 71-414]

11 p1857 A71-26207

Surface evaporation and condensation effects on stability of thin liquid film flowing down heated inclined plane at critical Reynolds number

13 p2160 A71-28596

Laser emission absorption in surface layer of optical glass, determining surface temperature dependence on emission energy density

13 p2079 A71-28859

Earth surface temperature measurement by airborne IR radiometers, discussing accuracy provided by narrow and wideband filters

14 p2240 A71-30126

Surface temperature discrepancy during flameless vacuum burning of trinitrolycerin gunpowder due to vaporization of volatile components

15 p2462 A71-31373

Monsoonal response of Somali Current in Indian Ocean, using spacecraft IR observations of sea surface horizontal temperature gradients

16 p2562 A71-33068

Surface temperature measurements with contact thermometers, discussing sensor design, cost and efficiency

16 p2579 A71-33474

Dynamic bubble growth and diameter at detachment during liquid boiling at heating surfaces, using force equilibrium, laser Mach-Zehnder interferometer and temperature measurements

16 p2663 A71-34038

Global temperature effects on atmospheric carbon dioxide and aerosols density based on atmospheric model, noting earth surface temperature decrease

16 p2575 A71-34047

Thermal equilibrium achievement by highly rarefied gas in closed container with space and time varying surface temperature, deriving gas particle distribution

17 p2784 A71-34195

Vortex boundary layer with dissipative viscous wall and isentropic sublayers, calculating adiabatic surface temperature

17 p2669 A71-34217

Atlantic Ocean surface temperature distribution data for Gulf Stream meanders and eddies, using Ito 1 satellite direct readout IR images

17 p2734 A71-35216

Cs ions surface diffusion/migration in presence of retarding electric field on emitter surface, showing temperature effects

17 p2789 A71-35258

Orography, cloudiness and surface temperature effects in six-layer global atmospheric circulation model, giving January simulation data

17 p2770 A71-35804

Surface temperatures and ablation mechanism of combustion protective plastics reinforced by silica under intense heating measured by IR micropyrometer [ONERA-TP 962]

18 p2984 A71-36028

NASA-SRI Round Robin Ablation Program summary, discussing dimensional analysis, Teflon, nylon and surface temperature

18 p2985 A71-36279

Gas and surface temperature distributions for laminar flow in circular tube, considering conduction, convection and radiation effects [ASME PAPER 71-HT-17]

19 p3164 A71-37988

Rigid disk effect on thermal stress distribution in semiinfinite elastic solid under prescribed surface temperature and heat flux

19 p3159 A71-38188

Laser pulse heated target with thermal plasma production, obtaining target surface temperature as function of time and vaporization rate

20 p3242 A71-38845

Venus lower atmosphere model based on surface pressure and temperature from radio astronomical and radar observations

20 p3296 A71-39626

Inert gases energy accommodation coefficients dependence on clean metal surface temperature based on lattice theory

21 p3415 A71-40538

Laser emission absorption in surface layer of optical glass, determining surface temperature dependence on emission energy density

21 p3394 A71-41297

Oscillatory free convection laminar boundary flow from semiinfinite vertical flat plate, investigating surface temperature variations as distance function from leading edge

22 p3619 A71-41602

Finite element method application to convective heat transfer between parallel planes for arbitrary surface temperatures and Nusselt number

22 p3619 A71-41874

Close binary stars monochromatic reflection effect calculation, using surface temperature distribution model

22 p3599 A71-41934

Thermal radiation effect on laminar boundary layer of nonabsorbing fluid for plane heat emitting surface under natural and forced convection

22 p3622 A71-42680

Enthalpy change between atmospheric carbon dioxide and Venus surface rocks for damping short term lower atmosphere temperature excursions

23 p3736 A71-43344

Forced convection steady heat transfer across laminar incompressible constant-property boundary layers over wedges with step discontinuity in surface temperature

23 p3784 A71-44196

Mars surface soil thermophysical properties, temperature and thermal emission from Mariner spacecraft IR radiometer data, correlating with visual images

24 p3867 A71-44439

SURFACE TENSION U INTERFACIAL TENSION SURFACE TO AIR MISSILES

Hybrid computer simulation of three degree of freedom surface to air missile trajectory, obtaining cluster of points for position errors

04 p0642 A71-14798

Crotale low altitude ground to air missile, discussing target acquisition and fire control units, maintenance and operation

06 p0979 A71-17567

Interceptor missiles minimum flight time control, describing modified steepest descent algorithm for optimal trajectories [AIAA PAPER 71-19]

06 p0979 A71-18486

SURFACE TO SURFACE MISSILES

Air-to-air, air-to-ground and USN surface-to-air guided weapons operational assessment in military environment 09 p1532 A71-22991

SURFACE TO SURFACE MISSILES
 NT ANTITANK MISSILES
 NT INTERCONTINENTAL BALLISTIC MISSILES
 NT MINUTEMAN ICBM
 NT SHILLELAGH MISSILES
 NT SHORT RANGE BALLISTIC MISSILES
 French National Strategic Force sea-ground and ground-ground ballistic missiles characteristics and performances 16 p2646 A71-34099

SURFACE TREATMENT
 U SURFACE FINISHING
SURFACE VEHICLES
 NT AIRCRAFT CARRIERS
 NT CARGO SHIPS
 NT LUNAR ROVING VEHICLES
 NT LUNAR SURFACE VEHICLES
 NT NUCLEAR POWERED SHIPS
 NT ROCKET PROPELLED SLEDS
 NT SATELLITE COMMUNICATIONS SHIPS
 Strapdown inertial guidance and software technologies for cosmic speed aerospace vehicles and low speed air, marine and ground transport 04 p0623 A71-15301

Single mode unmanned Mars roving vehicle with flexible metal toroidal hoop-spoked wheels, discussing remote controlled scale model design for simulation on earth 04 p0566 A71-15333

Solar aspect sensors as navigation components for rolling vehicle heading angle determination 07 p1137 A71-20415

Multimass system oscillations due to viscous friction factor and kinematic random disturbances, considering dynamic behavior of wheeled vehicle on rough roadbed 07 p1162 A71-20469

Urban transit and ATC vehicle identification and position determination system, considering surface and airborne traffic real time information communication 08 p1331 A71-21169

Surface navigation system and error analysis for Martian roving vehicle, using continuous tracking of pole star and local vertical 08 p1332 A71-21350

Experimental research at Building Research Station on outdoor sound propagation for building design in relation to aircraft and road traffic noise 17 p2674 A71-35237

Roving vehicle design for 1979 Mars mission 18 p2898 A71-36445

Injection laser range finder with avalanche photodiode for Mars rover obstacle sensing, discussing range data processing methods 22 p3529 A71-42772

Liquid hydrogen as future replacement for hydrocarbon fuels in surface and air transportation, noting advantages in energy per unit weight and pollution-free combustion 24 p3863 A71-44365

SURFACE WAVES
 NT BAROCLINIC WAVES
 NT CAPILLARY WAVES
 NT GRAVITY WAVES
 NT RIPPLES

Transverse surface wave propagation in piezosemiconducting body with electron damping, formulating boundary conditions 01 p0140 A71-11287

YIG with thin piezosemiconductor coating, investigating transverse surface wave amplification and velocity 01 p0140 A71-11288

Acoustic surface wave amplification using accumulation layer on Si in MOS structures 02 p0249 A71-12039

Far field diffraction of unidirectional surface wave by conducting rectangular wedge in cold anisotropic plasma, showing frequency dependent transmission coefficient 03 p0465 A71-13953

Interdigital converter for excitation and reception of acoustic surface waves on piezoelectric materials in bandpass filter design 03 p0388 A71-14574

Piezoelectric surface waves physical characteristics, examining excitation relationship to construction of microwave devices 04 p0550 A71-14742

Surface tension effect on dispersion of Rayleigh waves in elastic body 04 p0673 A71-15882

Acoustic and surface plasma waves in superconducting semiconductor metal films and laminates 05 p0793 A71-16826

One conduction band semiconductor surface drift waves in presence of current carrier drift 05 p0794 A71-16836

Surface wave filters, tapped delay line pulse compression networks and amplifiers, discussing design and applications 05 p0728 A71-16915

Rayleigh wave propagation in anisotropic substrates, using light diffraction by surface acoustic waves 05 p0783 A71-17078

Charged particle beam interaction with electrostatic surface waves in plasma layer 06 p0929 A71-17317

Surface wave conversion to longitudinal oscillations near strong discontinuity in resonant cold magnetoelective plasma 06 p0937 A71-18355

Concentric shield for surface wave propagation loss at bend in open waveguide, using Airy function 09 p1410 A71-23570

HF and VHF radio propagation on earth surface, describing launchers used for generation and detection 10 p1579 A71-24950

Surface waves propagation in initially deformed elastic body, using elastic potential to define half space mechanical properties 13 p2150 A71-28131

Interdigital broadband hybrid junction transducer terminated in negative resistances for acoustic surface waves amplification 13 p2037 A71-28476

Piezoelectric substrate dependent differences between in-line and crossed field three port circuit models for interdigital surface wave transducers 13 p2038 A71-28612

Surface wave velocity at interface between liquid He 4 and saturated vapor 13 p2101 A71-28769

Traveling wave negative resistance amplifier with corrugated surface wave structure, deriving gain equation 14 p2209 A71-29546

Radiation patterns from piezoelectric transducers on Y face of lithium niobate, using Green function analysis 14 p2283 A71-29795

High coupling low diffraction loss cut for acoustic surface wave propagation on lithium niobate 14 p2283 A71-29796

Monograph on instabilities in ion beam-plasma system covering surface wave propagation, magnetic effect and ion cyclotron radiation characteristics 14 p2281 A71-30507

Magnetized plasma and vacuum plane interface, deriving dispersion equation for electromagnetic surface waves propagating at arbitrary angles 15 p2456 A71-31744

Surface liquid film wave motion effect on air supersonic turbulent boundary layer flow field, discussing film thickness, heat transfer rates and wall temperatures [AIAA PAPER 71-623] 15 p2515 A71-32544

Aperture field distribution for excitation of surface waves with high efficiency and gain 15 p2378 A71-32627

Ultrasonic surface wave generation by infinite interdigital electrode array on piezoelectric material, predicting behavior from equivalent circuit by variational principle 17 p2717 A71-35491

Two-stream instability for magnetically confined pure electron gas column resulting from surface wave interaction 18 p2950 A71-35864

Surface wave patterns created by constant velocity pressure point on inviscid plasma bounded by magnetic field 19 p3111 A71-37637

Thermoelastic plane harmonic and Rayleigh surface waves in elastic solids with thermal relaxation, using Maxwell heat conduction equation 20 p3310 A71-39779

Magnetic fluid sloshing in solenoidal magnetic field, describing fluid free surface waves similarity to ordinary liquid waves in reduced gravity field [ASME PAPER 71-VIBR-24] 21 p3366 A71-40281

Viscous fluid layer surface waves nonlinear theory, analyzing surface friction and gravity force angle effects on wave characteristics 21 p3367 A71-40682

Surface wave digital and analog signal processing filters for time delayed, frequency or phase coded transmission and reception applications 21 p3357 A71-40811

Surface acoustic waves in layered substructure of piezoelectric epitaxial film of cadmium sulfide on germanium substrate 21 p3429 A71-41208

Quasi-static surface waves in Fermi electron plasma with Maxwellian electron velocity distribution 21 p3425 A71-41277

Surface waves at Fermi electron plasma boundary, using kinetic theory of plasma electromagnetic oscillations 21 p3425 A71-41278

HF electric signal detection, using acoustoelectric surface wave field in piezo semiconducting crystal 21 p3436 A71-41363

Elastic continuous medium with nonlocal interactions, calculating surface waves dispersion equations with boundary solutions 21 p3417 A71-41366

Waveguide simulator study of blindness/resonance for surface wave/effect in phased array antennas 22 p3509 A71-41633

Transverse surface wave amplification in piezosemiconductor, considering cases of total or drift current in thin near-surface semiconducting layer 22 p3585 A71-41707

Surface wave delay lines with near octave bandwidth using lithium niobate interdigital ultrasonic transducer with lumped element impedance inverter network 22 p3521 A71-42202

Elastic surface waves bi-phase modulated encoding and decoding at 10 Mbit/sec using Y-cut quartz 23 p3645 A71-43436

Upstream influence and interfacial waves in open channel two fluid small perturbation flow 23 p3663 A71-43446

Fully ionized plasma particle collision effects on surface oscillation stability 23 p3711 A71-43558

Elastic surface wave amplitude and propagation velocity in lunar rocks, calculating Poisson ratio 23 p3761 A71-43784

Frequency shift in air-coupled surface waves during Saturn 5 launches, computing apparent phase velocity experienced by ground 23 p3672 A71-43883

Dielectric permeability tensor of relativistic plasma stream, considering collisionless damping of surface waves in semiinfinite isotropic plasma 23 p3713 A71-44148

Dispersion equation for electromagnetic surface wave propagation along plane boundary of adjacent hot plasma streams 23 p3713 A71-44149

Azimuthal guiding surface wave attenuation with curvature applied to dielectric clad circular cylinder, including impedance tables 24 p3804 A71-44991

SURFACES
 Minimum suction rate preventing laminar boundary layer separation from curvilinear porous surface in jet flow 02 p0186 A71-12553

Space communication reflector surface positioning and optical measuring techniques for best fit 02 p0234 A71-12805

Lifting surfaces supersonic-hypersonic flutter at angle of attack determined by shock expansion, Newtonian flow and local flow piston theory [AIAA PAPER 71-327] 11 p1842 A71-25307

Three dimensional jet flap and lifting line/surface theories application to STOL aerodynamic systems with externally blown flaps and augmentor wing [AIAA PAPER 71-578] 15 p2345 A71-31568

SURFACTANTS
 Wave motions in viscous fluid layer in presence of surfactant elastic substances adjoining solid surface or gas, using Navier-Stokes equations 19 p3042 A71-37084

SURGENS
 NT FLIGHT SURGEONS

SURGERY
 NT LABYRINTHECTOMY

Ultrasonics applications in surgery, therapy and diagnosis, discussing physical principles, piezoelectric transducers, tissue acoustic properties and measurement methods 03 p0372 A71-13351

Cryogenics applications to cryosurgery and long term low temperature storage of living cells and tissues 20 p3189 A71-39252

SURGES
 Automatic antisurge control of axial compressor using partial gas recycling bypass method 03 p0469 A71-13370

Pure impulse two stage turbocompressor, preventing surge with automatic adjustment to air flow rate 05 p0796 A71-16798

Surge voltages produced by transient currents on signal conductors in shielded cables 07 p1022 A71-19946

Compressor surge effect on mixed compression inlet flow from numerical solution of one dimensional unsteady inviscid flow equations in variable area duct [AIAA PAPER 69-484] 10 p1553 A71-24855

Analytical model of compressor sensitivity to transient and distorted transient flows, considering inlet duct, compressor stages and combustor up to turbine nozzles [AIAA PAPER 71-670] 14 p2291 A71-30734

SURVEILLANCE
 Communications, navigation and surveillance for aircraft and marine vessels in North Atlantic region, discussing baseline traffic control model 07 p1153 A71-18808

Airborne surveillance for environmental management, discussing earth resources program, aerial sensors for thermal water pollution, crop disease, salinity and geological structure
07 p1018 A71-19080

Tethered, ground supplied, rotor-borne, self stabilized surveillance platform /Kiebitz/ system, discussing reconnaissance tasks, fire and communication control and data acquisition transmission and evaluation
15 p2347 A71-31212

Aircraft ILS signal reception system, obtaining category III reliability performance by circuit redundancy and automatic incoming information surveillance
15 p2446 A71-31912

Air navigation, surveillance and traffic control technology effects on land and airspace uses at airports
17 p2774 A71-35371

Remote control and surveillance equipment for communication satellite ground station, discussing console and engineering service circuit designs
17 p2709 A71-35518

SURVEILLANCE RADAR
Soviet book on monopulse radar covering surveillance and target tracking systems, antennas, angular resolution, directional sensitivity, etc
01 p0038 A71-11300

Optimum VTOL aircraft landing maneuverability, using short range three dimensional surveillance system and ground computer
03 p0454 A71-13574

Statistical connection strategies for automatic multiradar air traffic surveillance using track computer
03 p0380 A71-14395

Integrated electro-optical microwave radar and laser /lidar/ systems for earth oriented, environmental and domestic applications
07 p1095 A71-18827

Analog surveillance radar signal analysis by digital storage and evaluation methods
08 p1252 A71-20745

Secondary surveillance radar in ATC systems, discussing advantages and implications for controllers
09 p1406 A71-22955

Vertical plane dual beam properties of doubly curved shaped reflector, considering surveillance radar antenna modification to improve performance with ground clutter
13 p2028 A71-27990

Target trajectory detector optimization, using surveillance radar data and Markovian chain apparatus
13 p2033 A71-28993

Cumulative probability of target detection for pulse surveillance radars, relating target cross section, velocity and radar frame
20 p3199 A71-39901

Optical correlation for surveillance and pulse Doppler radar receivers signal processing
20 p3200 A71-39910

ATC height and plan position indicator composite picture display system design and operation, combining functions of primary and secondary surveillance radars
21 p3413 A71-40128

SURVEYOR LUNAR PROBES
NT SURVEYOR 1 LUNAR PROBE
NT SURVEYOR 3 LUNAR PROBE
NT SURVEYOR 5 LUNAR PROBE
Surveyor lunar probes alpha scattering chemical analysis technique tested on rocks of known composition
02 p0305 A71-11984

Optimal model of pressurization system for liquid propellant on Surveyor lunar landing spacecraft
03 p0472 A71-14447

Elastic properties of lunar surface material from Surveyor spacecraft strain gage data
04 p0644 A71-15129

Chemical element composition and mineralogy of powdered lunar surface material, comparing Surveyor, Apollo and Lunik missions data
23 p3748 A71-43682

Alpha radioactivity in Surveyor 3 camera visor, calculating upper limit of Po 210 at equilibrium of Oceanus Procellarum
23 p3765 A71-43812

SURVEYOR 1 LUNAR PROBE
Gray tone differences between undisturbed lunar surface and darker ejecta around Surveyor 1 footpads based on footprint photometry and albedo
15 p2493 A71-32482

SURVEYOR 3 LUNAR PROBE
Surveyor 3 spacecraft TV camera surface discoloration patterns caused by lunar soil blown by Apollo 12 exhaust
08 p1363 A71-21219

Solar particle tracks in clear filter glass from Surveyor 3 spacecraft, comparing with lunar rocks track results
09 p1529 A71-23655

Energy spectrum of iron group solar cosmic ray particles determined from glass removed from Surveyor 3 spacecraft, considering lunar erosion implications
09 p1515 A71-23656

Trapped solar wind He and Ne in Surveyor 3 unpainted Al tube, comparing with Apollo 11 and 12 solar wind composition
10 p1672 A71-24390

Surveyor 3 thermal control surfaces analysis from Apollo 12 samples collection, discussing spectral reflectance and lunar dust effects on surface finishes optical properties
12 p1920 A71-26759

[AIAA PAPER 71-479]
Lunar dust reflectance degradation of thermal control paint on Surveyor 3 TV camera, separating solar radiation effects by analytical model
12 p1920 A71-26760

[AIAA PAPER 71-478]
Surveyor 3 spacecraft attitude change on lunar surface, examining Apollo 12 mission photographs
13 p2145 A71-28699

Apollo 12 returned Surveyor 3 component materials analysis for lunar exposure effects by nondestructive and destructive tests
23 p3765 A71-43811

Interplanetary energy spectrum of solar flare Fe nuclei from tracks in Surveyor 3 glass filter and rock 12022
23 p3765 A71-43813

Microbiological analysis for surviving terrestrial microorganisms from Apollo 12 retrieved Surveyor 3 spacecraft electrical cabling
23 p3633 A71-43814

Streptococcus mitis bacterium in Apollo 12 lunar retrieved Surveyor 3 TV camera, discussing prelaunch deposition and survival
23 p3633 A71-43815

Surveyor 3 surfaces discoloration and lunar dust contamination, noting Apollo 12 lunar module caused disturbances by on-site observation
23 p3766 A71-43816

Apollo 12 returned Surveyor 3 surface sampler examination for micrometeorite pits and soil, glassy spheres and other granular materials adhesion to paint
23 p3766 A71-43817

X ray probe, scanning electron microscopy and spectral reflectance analysis of lunar environment effects on Apollo 12 returned Surveyor 3 materials surface cratering
23 p3766 A71-43818

Apollo 12 returned Surveyor 3 samples examination for meteoroid and lunar ejecta impacts evidence by optical and electron microscopy
23 p3766 A71-43819

Micrometeoroid flux determination from impact sites on Surveyor 3 TV camera optical filter surfaces, noting agreement with Pioneer, Cosmos and Pegasus spacecraft measurements
23 p3766 A71-43820

Surveyor 3 unpainted Al tubing examination by replication electron microscopy for surface damage due to particle impact and ion bombardment in lunar environment
23 p3766 A71-43821

SURVEYOR 5 LUNAR PROBE
Lunar surface thermal characteristics revised from analysis of error sources in daytime lunar surface temperatures derived from Surveyor 5 compartment data [AIAA PAPER 69-594]
01 p0163 A71-11582

SURVEYS
NT GEODETIC SURVEYS
SURVIVAL
Helicopter pilot and passengers emergency survival, considering gravitation force, human tolerances, design factors, etc
01 p0026 A71-11376

Dormancy and survival - Conference, England, September 1968
07 p1041 A71-19521

Algae survival and growth under adverse conditions, considering high and low temperatures, desiccation and halophilism
07 p1048 A71-19522

Survival and rescue medical aspects, discussing water and food intake, dehydration, hygiene, sanitation, rest, injuries, heat and cold exposure, illnesses, rescue operations, etc
08 p1245 A71-20718

Germ survival and transport possibility in outer space, discussing spore survival under UV radiation
13 p2010 A71-28691

Space transport systems, discussing spaceship earth survival problem from cosmocephic criteria
19 p3149 A71-37304

Bacterial spores survival under simulated lunar surface conditions, comparing results with vegetable cells experiments
21 p3334 A71-40567

Simulated Martian environment effects on terrestrial microorganisms survival
22 p3487 A71-42227

Streptococcus mitis bacterium in Apollo 12 lunar retrieved Surveyor 3 TV camera, discussing prelaunch deposition and survival
23 p3633 A71-43815

SURVIVAL EQUIPMENT
Cylindrical transparent plastic antismoke hood with metallized dome, noting respiratory volume and air supply
01 p0028 A71-11599

Cargo aircraft crew safety and survival, describing restraint, escape, flight deck interior doors, fire and smoke hazards and personnel environmental protection [SAE-ARP-1139]
07 p1019 A71-19643

Space shuttle operation phases hazards, emphasizing propellant loading, fire suppression systems, survival equipment and self contained life support devices
17 p2813 A71-34784

Space flight safety, discussing escape, rescue and survival design approaches for astronauts
22 p3611 A71-42037

SUSCEPTIBILITY [MAGNETISM]
U MAGNETIC PERMEABILITY
SUSPENDING [HANGING]
NT MAGNETIC SUSPENSION
Astatic gyroscope with viscous friction at suspension system axes, noting free nonlinear vibrations and motion
03 p0423 A71-13411

Decaying oscillations of sensitive element in ground based gyrocompasses with suspension system permitting Euler angle and translational displacement
07 p1108 A71-19304

Elastic suspension energy dissipation effect on three degrees of freedom gyroscope drift
07 p1108 A71-19307

Soviet book on supports and suspensions of aircraft gyroscopic devices covering accuracy, reliability and lifetime factors related to quality and operational conditions
07 p1115 A71-20299

Gyroscopic drift in gimbal suspension on moving base in presence of friction force proportional to dynamic reactions
10 p1612 A71-24578

Single isolated solid particle irradiation in vacuum, using electrical suspension system with electric field produced by six electrodes on solid cube surface
11 p1806 A71-26087

Suspended hollow cylinder under force of gravity, calculating stresses and displacements by linear elastic theory differential equations
13 p2153 A71-28518

Stationary motions of holonomous five degree of freedom mechanical system of rod suspended homogeneous symmetrical body in central gravitational field
13 p2100 A71-28730

Elastically suspended gyroscope dynamics, using Euler equations of motion allowing for casting rotation
15 p2410 A71-32455

Gas dynamic elastically mounted bearing, describing stability analysis of unloaded rotor central equilibrium position
15 p2417 A71-32457

Nonlinear free oscillations of astatic gyroscope with viscous friction at suspension system axes
17 p2743 A71-35019

SUSPENDING [MIXING]
Spark ignition of polystyrene suspensions during free fall in air, investigating ignition mechanism by high speed photography
12 p1986 A71-26967

SUSPENSION SYSTEMS [VEHICLES]
Harmonic vibration analysis methods, discussing mathematical model, ground tests, structure suspension exciter and pickup location eigenvalue measurement and mode research
14 p2175 A71-30058

SUSPENSIONS
Ultrasonic sound velocity dispersion in various hydro and gas suspensions, considering viscosity and heat conduction effects
01 p0127 A71-10618

Aerosol powder suspensions for spectrochemical objectives in plasma jets
03 p0465 A71-13971

Nonlinear elastic suspension springs with symmetrically hardened behavior for shock and vibration isolation of aerospace instruments and controls
17 p2825 A71-34890

Rapid scanning dual wavelength spectrophotometer for recording oxidation-reduction and membrane bound reactions in turbid suspensions of biological materials
18 p2922 A71-36580

Speed of sound measurement in solid and liquid phase suspensions, considering dense phase inertia forces and particles thermal retardation effects
24 p3827 A71-45019

SWAGING
Swaged high purity fine grained Ti stress-strain behavior below 424 K, emphasizing mechanical twinning in plastic deformation
23 p3695 A71-44289

SWAN BANDS
Swan band intensity upper limits in spectrum of 18 September 1966 sunspot
06 p0967 A71-17907

SWEAT

SWEAT

Water intake effects on human thermal sweat rate and composition in environmental chamber at specific temperature and humidity 02 p2020 A71-11670

Proprioceptive thermoregulatory mechanism of sweat secretion during positive and negative work in man 09 p1401 A71-23369

Heat acclimatization effects on sweat Na concentration over wide sweat rates range, discussing possible mechanisms 13 p2024 A71-29498

Human body temperature regulation under various hydration regimes during exercise, noting changes related to sweating 16 p2530 A71-33243

Maximal sweat evaporative heat loss and permitted work load measurements as function of temperature and clothing insulation 18 p2872 A71-36861

Human body weight and skin sweat gland water loss rates effects on thermoregulation 18 p2858 A71-36864

Human sweat gland duct filling and skin epidermal hydration behavior by analysis of time delays between sweat emergence and steady state, using electrical stimulation 18 p2858 A71-36865

SWEAT COOLING

Atomic and molecular transport coefficients for various species injected into boundary layer on ablating or transpiration cooled surface 01 p0130 A71-10958

High temperature tests of gas turbine engine with transpiration air cooled blades, discussing blade design, fabrication, ductility and oxidation resistance [ASME PAPER 70-WA/GT-1] 03 p0470 A71-14115

Transpiration cooling heat transfer in incompressible turbulent boundary layer, using Couette flow model, boundary layer model and combinations of both 07 p1219 A71-18758

Turbulent boundary layers transpiration cooling prediction with coolant fluid serving as heat sink within structure wall and as protective film 07 p1220 A71-18768

Transpiration cooling of reentry vehicle nosetips, noting two dimensional aspects of porous wall coolant flow and matrix-coolant energy exchange [AIAA PAPER 69-96] 07 p1223 A71-19869

MHD effects on transpiration cooled Couette flow through porous wall, considering magnetic drag produced pressure differential and shear recovery rates 10 p1649 A71-24404

Coolant combustion effects in transpiration cooling of gas turbine components, using hydrogen, ammonia and nitrogen coolants [ASME PAPER 71-GT-72] 11 p1855 A71-25986

Body temperature regulation and heat dissipation responses during continuous and intermittent exercise in man 11 p1721 A71-26354

Radiant heat transfer measurements on sintered gauzes, considering mathematical model of porous wall with sweat cooling 13 p2161 A71-28750

Heat shields for space applications, reviewing heat sinks, double wall cooling techniques and radiative, transpiration and ablation cooling systems 18 p2848 A71-36433

Chill level index for skin temperature effects on rate of evaporative heat loss and thermal information to central controller during heavy work 18 p2860 A71-36876

Heat transfer in transpiration cooled porous heat sources, deriving dimensionless temperature profiles 24 p3891 A71-45185

SWEATING

U PERSPIRATION

SWEAT ANGLE

NT SWEEPBACK

Vortex breakdown on slender sharp edged and modified delta wings with varying sweep angles investigated in wind tunnel using schlieren system for flow visualization [AIAA PAPER 69-778] 08 p1229 A71-22028

Sweep and dihedral geometry effects on blade to blade and meridional flows in turbomachinery blade rows, using actuator disk theory 19 p2994 A71-38274

SWEAP EFFECT

Slave sweep plane-parallel mirror systems design for maximum picture taking rates in high speed cameras 11 p1767 A71-26467

SWEEP FREQUENCY

Quadratic sawtooth voltage and sweep frequency generators design based on periodic parabolic pulse phase modulation of quartz oscillators HF output 04 p0559 A71-15568

Dynamic frequency characteristics of built-up structures by transient rapid sweep testing 11 p1841 A71-25178

Data reading function synchronized digital mass spectrometer with incremental scan by magnetic field sweeping, describing method for polynomial fitting of data 11 p1762 A71-25663

Variable sweep rate frequency response and vibration testing for test time reduction, using closed loop controller for sweep rate modulation 22 p3537 A71-41635

Swept frequency or chirp signals for data transmission and pulse compression, considering long range air ground communication in HF band 22 p3510 A71-42277

Antenna impedance measurements using frequency sweep generator and oscillograph 24 p3810 A71-45127

SWEEPBACK

Sweepback turboblades in parallel wall channel, investigating thickness, camber and leading edge curvature effects on flow and pressure distributions and vortex movement 02 p0186 A71-12606

SWEEPBACK ANGLES

U SWEEPBACK

SWEEP WINGS

NT DELTA WINGS

NT SWEEPBACK WINGS

Swept wing fighter aircraft transonic buffet onset lift coefficient from camber and trailing edge deflection, considering design variations 02 p0186 A71-12679

Aerodynamic characteristics of jet engine installation above wing of swept wing aircraft, noting large lift dependent drag 05 p0696 A71-15954

Maximum stagnation temperature on swept wing leading edge for equilibrium glide entry of space shuttle 07 p1013 A71-18902

Elastic swept wing subsonic aerodynamic characteristics, taking into account aerodynamic load redistribution due to aeroelastic deformations 08 p1229 A71-22035

Fluid mechanics of atmospheric environment and flow on swept wings in short and medium range aircraft design, concerning STOL capability in India 09 p1383 A71-23199

Numerical calculation of trailing vortex sheet pattern behind unstalled swept wing at low speed, obtaining downwash field 20 p3176 A71-39397

Vortex wakes behind straight and swept wings, noting formation of loops and trails close to ground 21 p3319 A71-40494

SWEEPBACK WINGS

NT DELTA WINGS

Sweepback thin cantilever wing transonic flutter density and velocity coefficients, investigating engine pod shaped concentrated mass location effects 11 p1706 A71-25189

Wing design criteria imposed by high speed requirement for short takeoff aircraft, considering thin swept-back wing with small aspect ratio for lateral control 12 p1867 A71-27471

Straight or moderately sweptback wings tip shape effect on vortex sheet roll, using detachment laws 20 p3176 A71-39418

SWIMMING

Arterial blood and muscle lactates in cold water swimming rats indicating reduced circulation endurance factors 09 p1396 A71-23360

Trained college and recreational swimmers cardiac output and maximum oxygen consumption during tethered swimming and treadmill running 13 p2024 A71-29496

Metabolic, ventilator and cardiovascular response during free swimming and treadmill walking, relating oxygen consumption to work intensity 13 p2024 A71-29500

Water temperature effect on body thermoregulation in swimming, comparing swimmers responses to track man on treadmill at same metabolic rate 18 p2861 A71-36893

Semicircular canal and otolithic organ function in free swimming fish angular orientation behavior 21 p3328 A71-39996

SWINGBY TECHNIQUE

Lunar swingby trajectory analysis with atmospheric reentry, characteristics of geocentric portions of earth-moon and moon-earth transfers 09 p1519 A71-22546

SWIRLING

Swirling flow through multiple nozzles of simulated solid propellant rocket motors, determining thrust and mass flow effects on passage 01 p0072 A71-11592

Swirling flow in short cylindrical combustion chambers with diaphragm-free inlet section, examining momentum loss 03 p0405 A71-14382

Axial and swirling mean flow effects on sound transmission and generation in hard walled ducts 06 p0945 A71-17620

Swirling effects on turbulent flow recirculation zone behavior in gas turbine main burners 06 p0946 A71-18477

Vortex breakdown in swirling conical flows, determining swirl angle distribution, flow rates and Reynolds number effects 06 p0843 A71-18513

Mature severe vortical storm properties, developing atmospheric models for maximum swirling speed and structure [AIAA PAPER 71-53] 06 p0924 A71-18514

Conical diffusers swirling inlet flow effects on pressure recovery and outlet flow profile [AIAA PAPER 71-84] 06 p0883 A71-18541

Laminar swirling jet flow through virtual circular cone, assuming velocity singularities on axis 07 p1092 A71-20092

Viscous core of incompressible swirling flow through nozzle using momentum-integral equations [AIAA PAPER 70-51] 11 p1750 A71-25468

Nonisotropic turbulent stress and viscosity components distributions in nonrecirculating swirling flow from mean axial and swirl velocities 13 p2161 A71-28622

Aerodynamics of axial and axial tangential blade swirler twisted jet near nozzle, testing effectiveness of equivalent problem of heat conduction theory 15 p2388 A71-31522

Turbulent swirling flames nonisotropic exchange coefficients determination from time mean velocity, pressure, temperature and concentration distributions 15 p2514 A71-32087

Swirling flow in gas turbine engine combustion chamber forward part, considering air flow characteristics behind blade swirler 16 p2624 A71-33606

Liquid spray steady evaporation and mixing in gaseous swirl, using continuum mechanics 17 p2727 A71-34693

Rotationally symmetric quasi-cylindrical viscous incompressible vortex flows at high swirl, discussing numerical integration with exponential functions 18 p2908 A71-36342

Swirling flow problem in boundary layer theory, proving existence theorem and asymptotic formula for differential equations solution 18 p2910 A71-36815

Inviscid swirling nozzle flow equations from Crocco relation 19 p2993 A71-37890

Swirl flow augmented heat transfer to liquid nitrogen in dispersed film boiling, using twisted tape inserts 20 p3313 A71-39285

Inlet circulation and swirl effect and optimum vane angle for maximum efficiency of subsonic straight conical diffusers 20 p3177 A71-39875

Time dependent analysis of swirling flow boundary layers in rotating container using modified Oseen method 21 p3367 A71-40639

Laminar and rotationally symmetrical flow of viscous incompressible fluid in circular pipe of constant temperature, considering inlet swirl effects and heat transfer to wall 21 p3368 A71-40756

Conical diffusers outlet flow profile and performance, investigating swirling inlet flow effects on pressure recovery 21 p3323 A71-40950

Centrifugal wheel flow swirl effect on pressure/flow rate characteristic in input zone 23 p3626 A71-43555

Heat transfer characteristics of two phase nitrogen film boiling in tubes with tape-generated swirl flow 23 p3783 A71-44195

Mass flow function diagram for axisymmetric isentropic compressible swirling flow in annular duct 24 p3820 A71-44960

SWIRLING WAKES

U TURBULENT WAKES

SWITCHES

NT CAPACITANCE SWITCHES

NT CRYOTRONS

NT ELECTRIC RELAYS

NT ELECTRIC SWITCHES

NT FLUID SWITCHING ELEMENTS

NT SWITCHING CIRCUITS

NT THERMOSTATS

Simple pressure selector switch for measurement up to 40 input pressures 06 p0900 A71-18055

SWITCHING

NT BEAM SWITCHING

NT MICROWAVE SWITCHING

Multilayer structures dynamic phenomena during switching, examining similarity theory with simple p-n junctions 03 p0388 A71-14387

Positive-negative feedback control system optimum switching conditions, deriving simple algebraic formula for nth order system switching equation coefficients 06 p0878 A71-17339

Complex automatic systems with random switch-off, developing failure sequence models
09 p1422 A71-22119

Laser triggered switching, considering theory of laser induced voltage breakdown of gas filled spark gap
12 p1915 A71-27283

Complex automatic systems with random switch-off, developing failure sequence models
14 p2220 A71-29997

Switching on p-n-p-n structure under high injection level in both bases, noting current concentration and voltage steady state buildup
16 p2546 A71-33496

Gas laser triggered switching causing propagating streamer to close by laser pulse introduction into gap
20 p3244 A71-39102

SWITCHING CIRCUITS

NT FLUID SWITCHING ELEMENTS

Aircraft electric systems control by solid state switching, discussing reliability, service life, versatility and compatibility
01 p0007 A71-11627

Microelectronic remanent type latching/ circulating, switching and phase-shifting microwave devices design and performance
02 p0228 A71-11654

Inner FET and FET static and dynamic inverters in digital IC, discussing switching characteristics, gates, memory cells, etc
02 p0228 A71-11812

MOS transistors as high speed switches in magnetic film memory selection matrix, discussing requirements for drive current pulse yield, signal power and dissipation
02 p0229 A71-11815

Space shuttle integrated electronic onboard and ground reusable systems design, considering data flow management, checkout, computer decentralization, electronic switching and redundancy
02 p0231 A71-11978

Cs vapor thermionic diodes with low temperature dual mode characteristics applicable as switching elements in DC to AC power conditioner
02 p0196 A71-12267

Transistor multistable switching circuits, considering construction principles, applications and advantages
03 p0387 A71-13818

Canonic synthesis of electronic relays, considering cascade connected isolation box, analog to digital converter and switch
03 p0393 A71-14469

Periodically reverse switched capacitor network theory, deriving equivalent resonant transfer circuit and expression for voltage transfer ratio
04 p0561 A71-15699

Tunnel diode trigger circuit, calculating effect of junction capacitance variation and small inductance on switching time
05 p0730 A71-17082

Switched binary-weighted resistor network combined with operational amplifier to construct current-summing digital to analog converter
07 p1070 A71-18850

Short-slot waveguide latching ferrite switch structure, operation principle, phase constants calculation and isolation characteristics
08 p1262 A71-20756

Current-switching digital to analog converters based on resistance ladder networks, discussing operation principles, problems and error sources
08 p1258 A71-20988

Space-DMA or space-TDMA techniques conserving spectrum and increasing communication satellite channel capacity, discussing spot beams and switchings
08 p1254 A71-21326

Bilateral switching networks synthesis by topological technique, tracing truth table optimum path by visual pattern detection
08 p1270 A71-21665

Magnetically coupled tunnel diode oscillator with square loop core, calculating leakage and source inductances effect on switching pattern
09 p1416 A71-22593

[IEEE PAPER 11.4]

Approximate optimal control synthesis, eliminating use of nonlinear functional converter for switching units design
09 p1423 A71-22607

Pulse rise time effect on nanosecond magnetic thin film switching with flux reversal and stray field interaction
09 p1508 A71-22704

Analog type semiconductor switches for aircraft and spacecraft automatic checkout systems, discussing component transistor types, optoelectronic devices and materials
09 p1418 A71-23041

Distortion effects in switching diode modulators due to local oscillator interference
09 p1420 A71-23681

Wideband gas discharge duplexer as transmitter receiver microwave antenna switch in H/01/ mode circular waveguide
10 p1584 A71-24720

Switch series data checking and sequence identification in program controlled computer systems, exemplifying tape reading procedure
11 p1734 A71-25637

Viscous fluid flows determination by network calculator consisting of hybrid resistor with electronically switching active nodes
11 p1744 A71-25849

Switched power limitation in p-n-p-n devices turned off by control current pulse, discussing thermal signal level
11 p1808 A71-25916

Laser triggered switching, discussing ability to trigger high voltage spark gaps with nsec delay and subnsec jitter
11 p1775 A71-26083

Junction thermal behavior and energy losses in active contactless bipolar transistor switch loaded by capacitive impedance
11 p1739 A71-26377

Linear sawtooth generator, using MOS unijunction transistors to switch and maintain constant discharge current from timing capacitor
11 p1740 A71-26549

Automaton concept in cybernetics, emphasizing synchronous switching circuit operation with asynchronous input data
12 p1884 A71-27045

Ovonic systems involving electrothermal switching effects on semiconductor glasses, discussing threshold voltage characteristics as function of temperature distribution and glass thickness
12 p1944 A71-27638

Engineering method for synthesizing and calculating AC correcting devices with synchronous switches, deriving equivalent transfer function
13 p2041 A71-27949

Sb and As base chalcogenide diode structures, determining switching and memory characteristics
13 p2110 A71-27956

Low temperature space charge mechanism of threshold switching, using pulse measurements on thin layer multicomponent chalcogenide glasses
13 p2110 A71-28044

Current oscillations and switching effect in amorphous chalcogenide compound films sputtered thermally on unheated glass and pyroceram substrates
13 p2111 A71-28173

Tunnel diode switching forward and reverse non-regenerative delay, examining external load resistance and diode characteristic nonlinearity effects on non-regenerative delay
13 p2038 A71-28717

Driving modes and operation characteristics of reed switches with permanent magnets
13 p2001 A71-28844

Solid state vs electrical-mechanical relay switching and isolation technology
13 p2001 A71-28845

Interface IC circuits for driving high voltage transistor switches from low level logic inputs, noting avionics application
13 p2039 A71-28910

Algorithms for constructing minimized abstract automatic subunits and two switch types as basis for arbitrary linear block encoder
13 p2035 A71-28915

I-V and capacitance characteristics of chalcogenide-glass based matrix-film diode sandwich and film-face switching structures with/without memory
13 p2112 A71-28922

Carrier mobility, conductivity and optical absorption in strong electric fields of chalcogenide glasses for switching and memory effect amorphous semiconductors
13 p2112 A71-28926

Failures detection in combinational digital switching circuits due to component malfunction
13 p2036 A71-29291

Modular digital TDM switch for radially distributed clock synchronization, discussing design and control
13 p2034 A71-29318

Asynchronous digital node combination into synchronous multiplex with data traffic routing functions through switch from remote terminals
14 p2201 A71-30928

Plasma potentials spatial distribution measurement, describing switching circuit and probe design
16 p2620 A71-33905

German monograph on plane realizations of switching circuits, covering crossover points minimization in electric lines interconnecting component parts
17 p2716 A71-34773

French monograph on variable-structure automatic control systems covering algorithms, stability, nonlinear hypersurface slip, minimum time, switching elements, analog simulation, etc
17 p2767 A71-35249

Statistical evaluation of switching elements reliability, considering permanent and temporary failure rates
17 p2718 A71-35627

Synchronization of high-speed digital data communication systems with continentwide interconnected switching centers, discussing elastic storage buffering to compensate for transmission time delay variations
17 p2712 A71-35784

Overcritically doped Gunn diode I-V characteristics stability under constant voltage, discussing use as subnanosecond switching element
18 p2895 A71-36989

Nanosecond ruby laser pulse generation using electro-optic shutter switching circuit external to Q-spoiled cavity
21 p3391 A71-40179

Timer devices and applications, discussing timing and power functions, switching cycles, mechanisms, ratings and life/cost evaluation
21 p3379 A71-40672

Reliable thin film switching circuits fabrication by deposition on suitable substrates
21 p3354 A71-40732

Fast read only memory design implemented in MOS and bipolar technology, noting low access times
21 p3355 A71-40735

Amorphous semiconductors electrical switching effects and applications covering computer memory, visual display control and printing
21 p3355 A71-40740

Thermal switching and negative resistance model and measurements of amorphous semiconductor thin films of Ge, Si and chalcogenide glasses
21 p3428 A71-40741

Glass switching elements with storage properties for electronically controlled flip-flop circuitry, noting composition and fabrication
21 p3355 A71-40742

Signal processing circuits for 1000 MS/S optical communication link using multiplier/signal switch, bit synchronizer and data regenerator
21 p3357 A71-40807

Switching effects in diode structure formed by two tungsten point contacts on glassy cadmium germanium arsenide surface
21 p3358 A71-41207

Switched power limitation due to thermal processes in p-n-p-n devices turned off by gate current pulse
21 p3430 A71-41219

I-V and capacitance characteristics of chalcogenide-glass based matrix-film diode sandwich and film-face switching structures with/ without memory
21 p3433 A71-41317

Carrier mobility, conductivity and optical absorption in strong electric fields of chalcogenide glasses for switching and memory effect amorphous semiconductors
21 p3434 A71-41323

Glassy antimony and arsenic chalcogenide diode structures, determining switching and memory characteristics
21 p3435 A71-41343

Phase distribution randomization in switched antenna array, noting radiation pattern sidelobe compensation application
22 p3522 A71-42312

Analog transistor model for IC simulation, discussing static characteristics and switching times
23 p3650 A71-43350

MINSK 22M computer modifications, discussing peripheral switching, interrupt, timing, operation termination and storage, readout, etc
23 p3648 A71-43355

Reduced switch-off time high voltage p-n-p-n structures using diode blocking coincident with thyristor collector junction
23 p3716 A71-43483

Joule heating effect on static negative differential resistance and switching of chalcogenide thin films
24 p3862 A71-45353

SWITCHING ELEMENTS

U SWITCHING CIRCUITS

SWITCHING FUNCTIONS

U BOOLEAN FUNCTIONS

U SWITCHING

SWITCHING THEORY

Book on fluid power circuits and systems covering switching theory, closed loop systems, pneumatic circuits, servo systems and pressure control
02 p0190 A71-11871

German book on switching theory of linear microwave networks, covering waveguides for n-port network, network modeling, interconnections, etc
02 p0215 A71-12315

Optimal piecewise constant control of continuous time systems with time varying delay, deriving restrictive condition on Hamiltonian integrated between switching instants
03 p0389 A71-14075

Switching analysis for high order vehicle systems with magnitude and direction constraints in attitude control for Saturn rocket with sloshing motion
08 p1269 A71-21331

- Chow parameters of switching functions in threshold logic, discussing basic properties and alternative definitions 13 p2035 A71-28975
- SYLLABLES**
Electronic apparatus isolating temporal segments from spoken syllable for speech analysis 09 p1408 A71-23383
- SYMBOLIC PROGRAMMING**
Information organizer system of symbolic manipulation on model data structures, providing row and column creation, sorting and indexing 22 p3516 A71-41865
- SYMBOLS**
Successive block decoding procedure for reduction of operations required for single information symbol decoding, noting substantial gains at equal error probabilities 17 p2702 A71-34970
Large character set display terminal for public information service system, describing design, construction, components and operating characteristics for nonalpha languages 21 p3350 A71-40129
Character size, case and symbol generation effects on CRT display search time 22 p3503 A71-42195
- SYMMETRICAL BODIES**
NT AXISYMMETRIC BODIES
NT BODIES OF REVOLUTION
NT CELESTIAL SPHERE
NT CONICAL BODIES
NT CYLINDRICAL BODIES
NT ELLIPSOIDS
NT LENTICULAR BODIES
NT PARABOLIC BODIES
NT POINCARÉ SPHERES
NT ROTATING CYLINDERS
NT ROTATING SPHERES
NT SLENDER CONES
NT SPHERES
NT STREAMLINED BODIES
NT TORUSES
Symmetric airfoil profiles with sharp and rounded leading edges in inviscid gas unbounded uniform adiabatic transonic flow, solving by nonlinear approximation 04 p0525 A71-14591
Nonuniform transonic shear compressible flow past symmetric airfoil, using linearized small disturbance theory 10 p1552 A71-24761
Stationary motions of holonomous five degree of freedom mechanical system of rod suspended homogeneous symmetrical body in central gravitational field 13 p2100 A71-28730
Plane motion stability of rapidly rotating symmetric rigid body in atmosphere, deriving short-cut equations system by Bogoliubov-Zubarev method 24 p3847 A71-44416
- SYMMETRY**
Crystal time reversal symmetry for macroscopic laws determination, discussing spontaneous electric and magnetic moments and magnetically ordered systems 01 p0138 A71-10348
Boundary conditions of line of symmetry and antisymmetry types for stress-strain state of halved shells 06 p0984 A71-17666
Elastic stress-strain law and internal structure symmetry for three dimensional fibrous composites, including caltrop reinforcement 11 p1852 A71-26396
Igneous and metamorphic rocks as simulated lunar rocks, determining elastic and attenuation symmetry by quasi-longitudinal pulse velocity and amplitude measurements on spherical specimens 11 p1834 A71-26454
Symmetry properties of equation of motion, considering restrictions on force functions form of particles system due to covariance 12 p1929 A71-26959
- SYMPATHETIC NERVOUS SYSTEM**
Phospholipid dynamics of blood entering and leaving brain during unilateral desympathectomy in dogs 03 p0362 A71-13238
Epinephrine infusion in man, examining systolic time intervals and sympathetic stimulation in cardiovascular dynamics 06 p0850 A71-17440
Intrarenal vascular pattern in carbon dioxide death of rhesus monkeys and dogs, observing sympathetic vasoconstriction 06 p0851 A71-17610
Asphyxia induced changes in regional cutaneous and visceral sympathetic activity in anesthetized rabbits, noting relationship with ear blood flow increase 06 p0854 A71-18324
Myocardium enzyme activity after sympathetic denervation of heart in cats and mice 06 p0857 A71-18726

- Adrenergic neurons in intramural cardiac ganglia in rabbits, using histochemical luminescent microscopy 09 p1391 A71-22533
Intraocular pressure self regulating nervous system components, discussing fluctuation sensors, cortical centers to eye impulse conveyors and glaucoma diagnostic applications 11 p1716 A71-25199
Vago sympathetic nerve trunk stimulation effects on pulmonary blood volume changes magnitudes and pattern in isolated perfused lungs 14 p2187 A71-31135
DC magnetic field effect on organism sympathetic-adrenal system, noting hypokinesia reduction of noradrenalin in hypothalamus and myocardium 15 p2357 A71-31311
Vagus nerve effects on cardiac output adaptation to exercise in sympathectomized dogs 15 p2360 A71-32001
Sympathetic nervous system in short term adaptation to cold, observing oxygen consumption, urinary noradrenaline proportion and excretion 17 p2681 A71-34698
Sympathetic response in renal and splanchnic nerves to induced fall and rise of arterial blood pressure in anesthetized rabbits, investigating baroreceptor reflex effect 17 p2685 A71-35367
Bulbar and baroreceptor inhibition of spinal and supraspinal sympathetic reflex discharges recorded in cats from renal nerve 18 p2857 A71-36689
Renin, plasma norepinephrine and epinephrine responses to work loads of various intensities, evaluating sympathetic nervous system as stimulus for secretion 19 p3008 A71-38551
Parasympathetic inhibition effects on hyperkinetic borderline hypertension, measuring cardiac output, resting heart rate and intraarterial blood pressure 21 p3332 A71-40407
Hypoxia and hypercapnia induced asphyctic differentiation of cutaneous and visceral sympathetic activity in anesthetized paralyzed rabbits 21 p3334 A71-40629
Cardiac sympathetic nervous control of right ventricular pressure-flow dynamics in outflow tract in anesthetized dogs 22 p3484 A71-41522
Vasomotor effects of vagus nerve on canine lung blood content in response to electrical stimulation of vagosympatheticus 22 p3490 A71-42581
- SYMPATHOMIMETICS**
U ADRENERGICS
SYMPTOMOLOGY
Clinical value of electroencephalogram following sleep deprivation in detecting abnormalities in neurological patients 09 p1395 A71-23248
Hyperventilation syndrome in flying personnel, discussing symptoms of paresthesia and extremities contraction, psychoemotional causes and control mechanism 22 p3500 A71-41569
- SYMPTOMS**
U SIGNS AND SYMPTOMS
SYNAPSES
Latency fluctuations and quantal transmitter release influence on end plate potential amplitude distribution, using frog muscle synaptic delays 07 p1045 A71-20445
Extraprimary (briefly latent) postsynaptic negative component of evoked visual potential in cortex of nembutal anesthetized rabbits, using Alvar biophase oscillator 13 p2004 A71-27894
Rat irradiated spinal cord, detailing orthodromic ventral root and monosynaptic reaction to rhythmic and increasing frequency stimulation 15 p2362 A71-32735
Mathematical fatigue models based on permeability variations in synaptic membranes and feedback regulation due to working organ metabolic changes 17 p2687 A71-34354
Physicochemical aspects of conditioned reflexes, including membrane mechanisms, effectiveness of synapses, mediation processes, ribonucleotides function and subcellular structures dynamics 17 p2685 A71-35364
Integral operating mode of nerve paths representation by linear diffusion channel with electrochemically active synapses, deriving complementary partial differential equations 19 p3001 A71-37250
Postsynaptic potentials in adjacent synaptic regions of tonic fiber of rabbit external eye muscle 24 p3798 A71-45066
- SYNCHRONISM**
NT BIT SYNCHRONIZATION
NT FREQUENCY SYNCHRONIZATION
Circadian rhythms synchronization changes in human biological and physiological functions during transmeridian flights 01 p0020 A71-11568

- Time-synchronized approach control combining aircraft precision navigation and guidance with ATOT equipment 02 p0280 A71-12898
Single mode locked Nd-glass laser pulse timing synchronization with Q switched ruby laser 03 p0438 A71-13898
Precision timing system implementation and operation, considering synchronization maintenance by cesium beam clocks, satellite, VLF and LORAN techniques 03 p0429 A71-14298
Comparative national time standards by overflight synchronization method 04 p0585 A71-14655
Atomic clock synchronization with high accuracy 04 p0596 A71-15281
Papers on optics, Volume 8, covering synthetic apertures, light beating spectroscopy, multilayer antireflection coatings, interference microscopy, photoelectron counting, human eye performance laser light, etc 05 p0713 A71-16481
Adaptive/self synchronizing PSK receivers with common power and bandwidth, discussing analytical and numerical investigations of performance characteristics 05 p0723 A71-17054
Coherent communication link pseudonoises synchronization error due to white Gaussian noise and amplitude jitter produced by reference carrier phase error, discussing digital simulation 05 p0725 A71-17072
DCS TDM/DCS TDMA synchronous operation, examining rate buffering, slaved clocks and constant feedback approaches 07 p1058 A71-18823
Satellites for time dissemination, discussing clock synchronization and signal propagation 07 p1154 A71-19011
Monostable multivibrator tunnel diode synchronization bandwidth as function of circuit parameters and junction I-V characteristics 08 p1264 A71-21071
Motion synchronization of objects with single degree of freedom and weak coupling interactions, using small parameter method 08 p1336 A71-21862
Harmonic oscillations frequency dividers with small asynchronous component of nonlinear element conductance, showing self excitation and wide synchronization bandwidth 09 p1413 A71-22152
Beat and synchronization modes of opposed waves in rotating gas ring laser, examining frequency response asymptotic behavior 09 p1460 A71-22222
Mode synchronization in laser with uniform broadening by asymmetrical internal frequency modulation 09 p1462 A71-22397
Haag synchronization theory application to HF vacuum tube oscillators, considering LF perturbation 10 p1609 A71-23852
Mode multiplicity effect on ring laser independent beat and synchronized beat regimes 11 p1774 A71-26004
Binary pulse sequences correlation and synchronization, developing effectiveness criteria with two stage measures 14 p2201 A71-30927
Asynchronous digital node combination into synchronous multiplex with data traffic routing functions through switch from remote terminals 14 p2201 A71-30928
Computer communication asynchronous time division multiplexing, studying communication channel sharing, data buffering and demultiplexing design 14 p2201 A71-30929
Microsecond time synchronization potential through cycle identification of VLF multiple frequency transmissions 14 p2204 A71-30974
Synchronization time of nine solid state lasers as function of frequency alignment 15 p2375 A71-31226
Ultrasonic effects on synchronization of ruby laser radiation, investigating emission pulse structure and peak sequence 15 p2419 A71-31712
Vector synchronism for interaction between ordinary and extraordinary wave during second harmonic emission and frequency mixing in He-Ne laser 17 p2752 A71-34408
Book on synchronous communications theory covering statistical detection, decision and estimation and source and channel encoding 17 p2707 A71-35218
Ground acquisition of digital rate synchronization during experiments in French Dioscours project 18 p2946 A71-36512
Cadence synchronization of multichannel communications systems using orthogonal signals with overlapping transmission spectra 19 p3022 A71-38493

Message distortions analysis in PCM communication systems due to phase fluctuations of synchronization signal

19 p3022 A71-38494

Motion synchronization of objects with one degree of freedom and weak coupling interactions, using small parameter method

20 p3270 A71-39361

One way UHF clock synchronization, using geostationary communication satellites with propagation delays calculated from orbital elements

20 p3239 A71-39460

Tunnel diode harmonic relaxation frequency divider, obtaining large division factors and wide synchronization bands with sinusoidal output signal

20 p3206 A71-39818

Sum and difference frequencies in vibration incident on gas turbine engine, considering synchronous and asynchronous excitation

[ASME PAPER 71-VIBR-103] 21 p3462 A71-40329

Quantitative characterization of unit time response in visual system, mapping latency and synchronicity as functions of stimulus position

23 p3640 A71-43870

Frequency and losses differences of modes as necessary conditions for multimode lasers transverse modes self synchronization

23 p3687 A71-44176

SYNCHRONIZATION

U SYNCHRONISM

SYNCHRONIZED OSCILLATORS

Oscillator frequency synchronization by injection locking, considering nonlinear oscillation model

02 p0230 A71-11818

Widely separated microwave oscillators phase synchronization via satellite transponder

02 p0216 A71-12330

Locking characteristics of automatic phase control circuits in noisy environment

03 p0391 A71-14311

Synchronous digital communication system with each station clock rate established by phase locked oscillator input average, calculating two-station network dynamic stability

05 p0729 A71-17051

Power amplifier klystron self excitation in linear electron accelerators, describing tunable driver circuit with quartz reference oscillator

12 p1889 A71-27754

Phase locked loop model configuration derivation to yield same locking signatures as driven oscillators with FM feedback

13 p2037 A71-28605

Locking in time of phase locked loop with sawtooth comparator for synchronizing two oscillators

14 p2210 A71-29808

Coupled oscillator circuits simultaneous tuning by plane relationship between circuit currents/voltages/

16 p2548 A71-34034

Phase locked loop oscillator applications in communication and instrumentation, discussing tracking receivers, FM and FSK detection, laser modes, pulse width modulation, etc

18 p2884 A71-36997

Fluctuation in synchronized reflex klystron oscillators due to shot noise in electron beams

22 p3521 A71-42264

Dynamic frequency and phase response of digital communications system of synchronized oscillators from time-incremental computer simulation

22 p3523 A71-42376

Combined injection locking with indirect synchronization for FM signals in noisy environment with allowance for bias oscillator LF time constant effect

22 p3514 A71-42393

Signal AM-PM conversion by locking oscillator with single external injection

22 p3523 A71-42480

German monograph on Gunn oscillators frequency stabilization by synchronization with external oscillator emitting HF signals

23 p3649 A71-43045

Microwave power distributed self excited oscillator synchronization using elements insensitive to external disturbances

23 p3655 A71-44318

SYNCHRONIZERS

Digital communication system frame synchronizer performance analysis, using mean time formula and state transition matrices

14 p2201 A71-30925

Probability density function of optimum phase locked loop synchronizer of sinusoidal signal with white Gaussian noise in partially coherent receiver

20 p3195 A71-38858

Signal shape matched suboptimum self bit synchronizer for high SNR and timing error variance, reducing jitter

20 p3203 A71-38862

SYNCHRONOUS COMMUNICATION SATELLITES

U SYNCOM SATELLITES

SYNCHRONOUS DETECTORS

U CORRELATORS

SYNCHRONOUS METEOROLOGICAL SATELLITE

Synchronous meteorological satellite mission goals and system design, describing imaging, data collection, facsimile, space environment, trilateration, ranging and transmission

07 p1067 A71-18807

Synchronous meteorological satellite data collection and transmission system error control, considering design tradeoffs for radio sets and coding techniques

14 p2198 A71-30899

Performance and cost design tradeoff between HF and synchronous meteorological satellite data collection systems, considering platform transmitting power and SNR

14 p2198 A71-30900

Synchronous meteorological satellite programs, noting earth imaging, data transmission, collection and relay and space environment monitoring

17 p2812 A71-34612

Meteorological and instrumental options for atmospheric vertical temperature soundings from geosynchronous satellites, noting Nimbus 3 and ATS measurements of cloud cover and radiance levels

20 p3240 A71-39674

SYNCHRONOUS MOTORS

Stabilized image movement control by mounting object in electric synchronous motor and rotating eccentrically

10 p1567 A71-23989

Soviet book on synchronous reluctance motors covering operation principles, design features and starting characteristics

15 p2354 A71-32200

Adjustable speed drive with brushless DC synchronous motor using rotor position sensor and three phase bridge inverter

23 p3630 A71-43499

SYNCHRONOUS SATELLITES

NT AEROS SATELLITE

NT EARLY BIRD SATELLITES

NT SYNCHRONOUS METEOROLOGICAL SATELLITE

NT SYNCOM SATELLITES

Geostationary communication satellites system with timed orbital motions for avoiding serial sun transit outages and eclipses

01 p0030 A71-10471

Quiet day magnetic field variations at geosynchronous satellite ATS 1, comparing magnetospheric models

03 p0419 A71-14522

Passive mode navigation satellite position fixing, using synchronous satellite and Loran type chart with correction tables

04 p0622 A71-15004

Earth gravitational environment critical parameters at synchronous altitudes by satellite drift observation, discussing geopotential field determination

04 p0583 A71-15306

Large multipurpose synchronous communication satellite, discussing design versatility, applications and operating characteristics

04 p0663 A71-15311

Orbit determination accuracy using synchronous satellite system for tracking near earth spacecraft

04 p0553 A71-15312

Air traffic control using collision risk equations, noting data handling automation, airborne collision avoidance devices and geostationary satellites

04 p0624 A71-15646

Solar cell and coverslide degradations measurement from telemetry data on satellites at near-synchronous altitudes

05 p0702 A71-16086

Sirio synchronous orbit satellite configuration, emphasizing attitude control system, telemetry encoders and electric power supply

05 p0816 A71-16404

Synchronous orbit satellite links in tandem for government and military telephone communications, discussing subjective evaluation for acceptability

05 p0725 A71-10707

Electric microthrusters for geostationary satellites orbit corrections, discussing orbital perturbations and operational characteristics of ammonia electrothermal and ion thrusters

07 p1207 A71-19528

Synchronous satellites orbit and attitude control systems for correcting orbital errors due to launch inaccuracies, solar and lunar effects and terrestrial potential anisotropy

07 p1207 A71-19532

Quiet day geomagnetic field measurements at synchronous orbit ATS 1, calculating equatorial component of interaction force between solar wind and earth

07 p1102 A71-19664

Electron trapping in dielectrics, providing effective light and inexpensive spacecraft bremsstrahlung shield and lower average radiation energy at synchronous altitudes

07 p1164 A71-20625

Meteorological satellites remote sensing advanced instruments and techniques, discussing retrograde polar and synchronous satellite orbits

08 p1366 A71-21744

SERT 2 solar array power system in sun synchronous orbit, considering power conditioning and deployment technique

[AIAA PAPER 70-1159] 09 p1387 A71-22901

Latent heat convective transport from lower to tropical upper troposphere, noting periodic energy fluctuations from time lapse synchronous satellite cloud photographs

09 p1489 A71-23553

Solar radiation pressure acceleration effects on flat satellite in earth synchronous orbit, examining orbital shift and counteracting thrust velocity applications

10 p1671 A71-24333

Optimal synchronous plane accuracy for space triangulation as function of geometrical position of artificial satellite relative to earth sphericity

11 p1758 A71-25812

Geodetic azimuth between two remote points on earth surface based on synchronous satellites positions and photographs

11 p1759 A71-25817

North Atlantic communications, navigation and ATC systems requirements for geostationary satellite operation, considering lifetime rated data and voice channels transmissions volume

11 p1839 A71-26332

Lunar gravitational field application for placing spacecraft into static earth satellite orbit with standing position with respect to rotating earth

12 p1957 A71-26627

Direction of chord in space from synchronous photographic satellite observations, considering optimum satellite altitude

12 p1900 A71-26969

Translation of geodetic geographical coordinates and ellipsoidal altitudes by synchronous photographic satellite observations and satellite-distance measurements from two ground stations

12 p1903 A71-27753

German-French Symphony synchronous communication satellites, discussing frequency and time division multiple access subsystems characteristics

14 p2193 A71-29824

Nationwide man machine remote employment/personal services system including synchronous communication satellite, information and control network and remote terminals

14 p2199 A71-30914

L band aircraft antenna array consisting of circularly polarized elements and static electronic steering circuits for synchronous satellites radio links

14 p2273 A71-31074

Symphonic geostationary satellite fuel-optimal injection problem, employing Tschauner-Hempel differential equations and Monte Carlo simulation

15 p2498 A71-31157

High energy solid propellants use in Europa 2 launch vehicle perigee-apogee motor, considering synchronous satellite payload increase

16 p2645 A71-33365

Very long baseline interferometry of radio emissions from geostationary satellites, determining orbital elements and inertial position

16 p2544 A71-33845

ESRO report to COSPAR on sounding rockets and geostationary satellites development, orbits and decay during extraterrestrial gamma radiation

16 p2667 A71-33867

Time division multiplexing system for ATS, discussing surveillance geostationary satellite feasibility, delta modulation for data transmission and aircraft equipment

17 p2772 A71-34680

Specular reflecting passive radiators for synchronous satellite radiation detectors cooling

[ASME PAPER 71-AV-30] 18 p2869 A71-36397

Radio tracking of aircraft by two geostationary satellites, discussing measurement, navigation and position errors

18 p2945 A71-36508

Large synchronous communication satellite launching by propulsion stages assembling in orbit through automatic rendezvous maneuvers

18 p2975 A71-36526

Italian SIRIO synchronous satellite for SHF communication, analyzing thermoelastic deformations effect on antenna radiation patterns

18 p2882 A71-36575

Synchronous three-axes stabilized communication satellites attitude control system with double gimbaled reaction wheel control actuator, obtaining 0.1 degree pointing accuracy with pitch and roll sensors

[AIAA PAPER 71-949] 19 p3098 A71-37190

ELDO studies of interorbital space tug for transfer of satellites in geosynchronous orbits

19 p3151 A71-37327

Synchronous satellite transmission Faraday rotation conversion into total electron content, removing n_{pi} ambiguity

19 p3128 A71-38032

Marine navigation and data communications at L band via synchronous satellite, assessing capabilities by tests on ATS-5 satellite

19 p3102 A71-38070

Radio frequency interference environment measurement in VHF range by subsynchronous Lincoln experimental satellites 5 and 6

19 p3021 A71-38452

Rechargeable cylindrical hydrogen-oxygen fuel cell for synchronous satellites, determining energy density as function of current, pressure and electrolytes with computer model

20 p3182 A71-38947

Cosmic rays cutoff daily variations at ATS geostationary satellite altitude, noting role of magnetospheric tail in lowering cutoff below calculated value

20 p3282 A71-39739

Italian Sirio synchronous satellite for SHF propagation and communication experiments on fading statistics, frequency dependence, path diversity and TV transmission

21 p3347 A71-40474

Technical characteristics, capabilities and applications of future geostationary communication satellites for U.S. internal commercial communications services

21 p3448 A71-40475

Dual-spin vs three-axis stabilization and control systems for synchronous communication satellite design

21 p3454 A71-40477

Three-axis and dual-spin stabilization systems for future synchronous communication satellites, considering reliability, mission flexibility and growth potential

21 p3455 A71-40479

Synchronous communication satellites stabilization for implementation in 1970-1975 time frame, considering antenna size, power system capacity and vehicle pointing

21 p3348 A71-40480

Attitude stiffness and pointing accuracy of three-axis and dual-spin stabilization system for future synchronous communication satellites

21 p3455 A71-40481

Narrow beam acquisition and angle tracking for spaceborne laser communication links between low earth orbiting and synchronous satellite

21 p3348 A71-40805

Scientific objectives and satellite design of ESRO sponsored geostationary space mission, describing Europa II launcher design and operation

22 p3608 A71-41952

Altitude dynamics and motion stability analysis of gravity oriented synchronous satellite under perturbation effects of environmental forces due to sun, earth, albedo and cosmic rays

22 p3612 A71-42050

Geostationary satellite oceanic automated ATC center design, estimating cost

22 p3572 A71-42095

Atmospheric wind speed estimation, using ATS geostationary satellite cloud photographs

22 p3535 A71-42411

Circular sun synchronous earth satellites, investigating swathing patterns control by orbit selection and modification

23 p3728 A71-43025

Low cost TV ground receiving systems for signals transmitted from synchronous satellites, describing reception techniques, manufacturing and performance characteristics

23 p3646 A71-43594

High energy particle environment model at synchronous altitudes during quiet geomagnetic periods from satellite observation, establishing outer radiation belt distribution function

23 p3722 A71-43978

Point motion in random error region applied to synchronous satellite trajectory control by single impulse correction

24 p3846 A71-45307

SYNCHROTRON NOISE

U ELECTROMAGNETIC NOISE

U SYNCHROTRON RADIATION

SYNCHROTRON RADIATION

Moving type IV solar bursts polarization and rapid fadeout, considering relativistic electrons synchrotron radiation intensity

01 p0152 A71-10331

Neutrino synchrotron radiation for relativistic gas applied to white dwarfs and neutron stars

01 p0145 A71-11337

Quasars radio spectra in 1-5 GHz frequency range, examining emission from expanding clouds due to synchrotron radiation with self absorption

05 p0805 A71-16112

X ray source Sco X-1 gamma radiation due to Compton synchrotron process, comparing flux observation for synchrotron origin validity

05 p0799 A71-16476

Radio background in universe due to synchrotron radiation, X ray and photon backgrounds due to cosmic electrons inverse Compton effect

08 p1351 A71-20960

Magnetic mirror confined plasma diagnostics, considering hot electron density, X ray pulse height and synchrotron radiation measurement techniques

10 p1651 A71-24651

Criticism of paper on synchrotron sources energy spectra formation, examining time dependent spectrum on boundary conditions

11 p1832 A71-26170

Periodic rotational LF synchrotron model of magnetic neutron star for pulsar radiation

12 p1947 A71-26649

Milky Way Galaxy X ray sources, discussing bremsstrahlung, synchrotron radiation, Compton effect optical objects, supernova remnants and X ray astronomy

12 p1959 A71-26780

X ray flux variability of massive elliptical galaxy M87 from rocket flight measurement, considering synchrotron, inverse Compton and thermal bremsstrahlung

12 p1962 A71-26931

Type 2 and 3 solar radio burst generation, proposing coherent synchrotron electron deceleration mechanism

12 p1954 A71-27710

Solar and geophysical morphology of radio burst of active sun, treating bremsstrahlung, gyro, synchrotron and Cerenkov radiation and plasma waves

13 p2137 A71-28514

Galactic LF nonthermal radio emission origin, considering mechanisms of synchrotron radiation from cosmic ray electrons and enhanced bremsstrahlung

14 p2304 A71-29593

Crab Nebula model, discussing electromagnetic field time variation and electron acceleration and synchrotron emission

14 p2304 A71-29632

Energetic electron power spectrum effect on synchrotron radiation from magnetosphere

14 p2298 A71-29722

Quasars circular polarization measurements at 21 cm, noting synchrotron self absorption

14 p2307 A71-29867

Electron gyro and synchrotron radiation from vacuum and isotropic plasma, deriving approximate general formula for power spectrum and polarization

14 p2282 A71-30661

Moving type 4 solar radio burst, describing bipolar magnetic structure and origin in synchrotron radiation from relativistic electrons

15 p2473 A71-31692

Circular polarization and fadeout of moving solar type 4 burst related to magnetic arch and synchrotron emitting electrons deceleration

15 p2473 A71-31693

Light and radio emission from Orion nebula flare stars in meter waveband, discussing coherent mechanisms of plasma oscillations and gyro/synchrotron radiation amplification

15 p2485 A71-31696

Pulsed gamma radiation from rotating neutron star, discussing synchrotron emission mechanism based on electron pulses incident on high intensity sharply localized magnetic field

15 p2474 A71-31724

Supernovae outburst remnant radio emission from Crab Nebula, discussing synchrotron mechanism and connection with pulsars

16 p2635 A71-33472

Gamma rays in Crab Nebula pulsar, considering synchrotron radiation and inverse Compton scattering as production mechanisms

17 p2796 A71-35335

Compton synchrotron spectra of gamma rays produced in Crab Nebula by photons scattered by relativistic electrons, assuming magnetic field due to pulsar

18 p2963 A71-36154

Inhomogeneous synchrotron source model calculation for correlation between linear and circular polarization, comparing with quasars observation

18 p2963 A71-36157

Synchrotron radiation reabsorption in inhomogeneous sources, considering IR spectra of quasars and galactic nuclei

18 p2963 A71-36158

Halos around black holes, showing luminosities caused by synchrotron radiation of magnetized plasma

20 p3289 A71-39295

Crab Nebula and pulsar gamma ray emission from synchrotron or inverse Compton mechanism

20 p3301 A71-39919

Radio pulses from pulsars based on model of coherent synchrotron radiation from magnetosphere trapped charged particles

20 p3285 A71-39951

Ambient medium, reabsorption and Faraday rotation effects on circular polarization degree of synchrotron radiation, using transfer equation

22 p3593 A71-42335

Magnetic fields, bremsstrahlung and synchrotron emission in impulsive flare of 24 October 1969

23 p3721 A71-43849

Nonlinear theory for synchrotron emission of tubular electron flux in cylindrical waveguide, discussing wave-electron interactions optimization

23 p3653 A71-44055

Steady state problem of energy spectrum of variable magnetic field accelerated electrons, considering synchrotron X ray emission of Crab Nebula and pulsar

24 p3869 A71-44801

SYNCHROTRONS

Negative pion elastic scattering differential cross section measurements from 1.71 to 5.53 GeV/c, using zero gradient synchrotron beam on liquid hydrogen target

02 p0286 A71-116478

Supernova remnant X ray and radio emission secular behavior, considering hot plasma and synchrotron models and continuous injection

04 p0640 A71-148747

SYNCOM SATELLITES

NT EARLY BIRD SATELLITES

Satellite communications use of geostationary orbit, considering ground station antennas radiation patterns, signal processing, stationkeeping, etc

17 p2696 A71-34234

SYNCOPE

NT BLACKOUT (PHYSIOLOGY)

Syncope as temporary suspension of consciousness due to cerebral blood supply failure, considering cardiac rhythm disturbances, blood flow obstructions and heart disease

04 p0541 A71-15915

Sudden death and syncope mechanism in aortic valve stenosis, noting presence of baroreceptors in left ventricular wall

13 p2014 A71-29301

Unconsciousness, confusion, amnesia, syncope and sudden death of pilots in flight due to silent ischemic heart diseases

18 p2855 A71-36216

SYNDROMES

U SIGNS AND SYMPTOMS

SYNOPTIC MEASUREMENT

Venus photographs analysis during synoptic periods, noting inconclusive results on cloud layer and planetary surface structures

09 p1521 A71-22845

Stratospheric circulation synoptic and detailed structure from meteorological rocket network sensors

15 p2396 A71-31614

Steady state magnetospheric convection pattern from synoptic maps of magnetic disturbance and auroral motions

20 p3230 A71-39879

SYNOPTIC METEOROLOGY

Synoptic and moisture content charts from Kosmos-243 satellite measurements of escaping thermal RF flux

01 p0073 A71-10540

Global atmospheric circulation, discussing surface irregularities and variable heating role in disturbances

01 p0121 A71-11352

Tropics role in global circulation from satellite photography, discussing convection, cloud clusters, momentum fluxes, etc

01 p0121 A71-11356

Global Atmospheric Research Program (GARP), discussing atmospheric motions, data acquisition, satellite networks, etc

01 p0122 A71-11361

Soviet book on nephanalysis for synoptic forecasting covering meteorological satellite observations and network characteristics, photointerpretation, data processing, cloud identification, weather charts, etc

02 p0278 A71-12842

Urban heat island induced circulation without synoptic winds, using two dimensional atmospheric model

03 p0453 A71-13232

Space metric as similarity criterion for meteorological element field synoptic setup, discussing probability for forecasting by analogy

07 p1150 A71-18872

Upper troposphere-lower stratosphere planetary scale circulation correlation from kinetic energy characteristics analysis

07 p1151 A71-18874

Algorithms for continuous indirect sequential observations utilization with real time synoptic measurements in objective analysis

08 p1328 A71-21725

Tornado producing thunderstorms upper level outflow synoptic and dynamic processes from ATS 3 pictures, discussing convective warming effects

11 p1794 A71-25381

Soviet papers on aviation and synoptic meteorology problems covering vertical motions near cold fronts, cloud development, latitude effect, temperature conditions above mountains, etc

11 p1795 A71-26557

Stratospheric wind seasonal reversals over Polish coast of Baltic Sea in 1967-1969 from rocket sounding and upper air synoptic analysis

12 p1900 A71-27067

Synoptic scale processes effect on high level clear air turbulence production, considering Kelvin-Helmholtz instability role in flow transition
14 p2268 A71-29762

Atmospheric synoptic and mesoscale motions dynamic theory, including baroclinic instabilities, gravity/planetary waves, tides and sea breezes
14 p2236 A71-30493

World Weather Watch global telemetry system including observing stations, and rockets, balloons and satellite-borne sensors, determining atmospheric states on ground and sea
14 p2199 A71-30913

Synoptic climatology of Euroatlantic blocking situations, investigating geographic location and duration
14 p2271 A71-30937

Vertical wind shears distribution in atmospheric boundary layer, noting features due to differences in synoptic processes
15 p2444 A71-31364

Northern Hemisphere upper stratosphere and lower mesosphere synoptic meteorological chart construction, using aerological network and rocket radio sounding data
15 p2400 A71-31967

Objective subsynoptic upper level analysis optimizing smaller scale radiosonde data over U.S.
16 p2604 A71-33533

Nondeveloping synoptic weather systems description by isentropic structural analysis, studying particle motion and dynamic behavior using models
18 p2944 A71-36219

Worldwide data acquisition and tracking of meteorological balloon stations by flyby gravity stabilized satellite
18 p2878 A71-36528

Artificial depression structure from general circulation model synoptic development, reproducing real depression features
19 p3089 A71-37504

Synoptic-aerological conditions of CAT under jet streams, using aircraft measurements
19 p3090 A71-37752

Synoptic and microscale variance spectrum of horizontal wind velocity at 50 m above ground, comparing with perturbations models
20 p3257 A71-39439

Synoptic climatology of blocking situations over European-Atlantic region, obtaining middle troposphere circulation patterns by statistical analysis
21 p3411 A71-40826

Gulf Stream and Middle Atlantic Bight complex synoptic sea surface temperature distribution fromITOS 1 satellite high resolution IR imagery
22 p3536 A71-42885

SYNTAX
NT SYLLABLES
NT WORDS [LANGUAGE]
Synactical characterization of tautologies for deductive systems and theories based on formalized algorithmic languages
18 p2942 A71-36822

SYNTHESIZERS
U CHEMICAL REACTORS
SYNTHETIC ARRAYS
Synthetic endfire hologram radar for small target and clear air turbulence detection
03 p0381 A71-14476

Ground based coherent radar synthetic aperture procedure against uniform velocity targets, discussing airborne holographic synthetic gain applications to stationary antennas
09 p1405 A71-22697

Synthetic aperture Doppler free coherent bistatic radar for high resolution maps of tropospheric radio scatterers
12 p1881 A71-27286

Microwave quasi-holographic techniques, discussing synthetic aperture, chirp radar, rotating target imaging system and beam forming method
22 p3546 A71-42477

SYNTHETIC FIBERS
NT GLASS FIBERS
NT NYLON [TRADEMARK]
NT RAYON
Carbon fiber surface reactivity relationship to various organic compounds using gas-solid chromatography, evaluating molecular absorption enthalpies
02 p0209 A71-12537

Zirconium carbide fiber insulating materials, examining heat conductivity coefficient
05 p0838 A71-16781

Heat conductivity coefficient of thermal insulation material made from zirconium carbide fibers, giving measurement procedure
16 p2662 A71-33033

Synthetic fibers and plastics development, chemical composition, physical and mechanical properties, production growth rates and applications
23 p3696 A71-43107

SYNTHETIC RESINS
NT ACRYLIC RESINS
NT EPOXY RESINS
NT NYLON [TRADEMARK]
NT PHENOLIC RESINS

NT POLYAMIDE RESINS
NT POLYESTER RESINS
NT POLYETHER RESINS
NT POLYMETHYL METHACRYLATE
NT THERMOPLASTIC RESINS
NT THERMOSETTING RESINS
NT VINYL COPOLYMERS
Elastic characteristics of graphite plastics and graphite materials impregnated with synthetic resins, considering aging effect on elastic modulus
09 p1483 A71-22824

Microencapsulation of bonded reactive resins in packaging, logistics and adhesive applications at room and elevated temperatures
10 p1634 A71-24120

Synthetic elastomers, including polymer chain growth, monomer sequence distribution, structural compatibility effects and commercial products development
18 p2939 A71-35886

Synthetic materials technology development, discussing macromolecular materials synthesizing methods and properties
19 p3085 A71-38144

SYNTHETIC RUBBERS
NT ELASTOMERS
SYSTEM EFFECTIVENESS
Hierarchical systems effectiveness estimation algorithm, taking into account reliability
05 p0731 A71-16796

Complex digital computer systems effectiveness measurement, using simulation program with programming language SIMSCRIPT [AIAA PAPER 71-229]
07 p1068 A71-19707

Information model for simulating systems reliability estimates uncertainty, noting state transition matrix, methodology and sensitivity analysis of effectiveness
16 p2583 A71-33304

System effectiveness tasks of producibility analysis, maintainability evaluation and tradeoff studies
16 p2664 A71-33316

Fault tree, failure mode and effect analysis, prediction apportionment and assessment, discussing system effectiveness
16 p2664 A71-33317

Statistical limits on reliability, informativeness, controllability and self organization of complex systems, determining minimum redundancy requirements for suppressing interfering factors
17 p2720 A71-34953

Intelsat communications satellite system network operation, describing reliability outages, maintenance and economy
17 p2705 A71-35101

Aircraft electric power system design with reliability, simplicity, low cost, weight and size, discussing automatic circuit protection and energy power
17 p2678 A71-35780

Aerospace data bus for multiplexed transmission within vehicles, considering control and sequencing methods terminal concepts, capability noise reduction and reliability
17 p2712 A71-35785

Fluid amplifiers in logic circuits and control and monitoring systems, discussing operating principles and performance features
18 p2850 A71-36137

Radar systems performance constraints, discussing environmental effects, carrier frequency, aerial directivity, clutter echoes, transmitter power, etc
22 p3509 A71-42199

Control system effectiveness improvement, using redundancy and self adaptive techniques
23 p3655 A71-43291

SYSTEM FAILURES
Digital systems intermittent failures effects and detection, using system simulation
01 p0046 A71-10204

Single repairable unit system with spares deterioration in storage, calculating long-run availability and time to system failure
02 p0258 A71-12590

Heat tolerance for resting subjects in event of air conditioning system failure in SST passenger cabin
03 p0371 A71-13095

First passage failure probabilities for single degree of freedom systems under random vibration [ASME PAPER 70-WA/APM-14]
03 p0512 A71-14155

Aircraft equipment failures detection and warning systems
04 p0601 A71-15901

Computer aided automatic fault data logging, classification, analysis and reporting methods in integrated ATC system
07 p1155 A71-19556

Complex automatic systems with random switch-off, developing failure sequence models
09 p1422 A71-22119

Time optimal hierarchical failure-search systems by varying structure for four different search algorithms
10 p1585 A71-24161

Computerized system evaluation and feedback data for assurance at hardware level, including reject and failure report documentation
12 p1890 A71-26673

Economic formulation in reliability engineering, expressing cost of failure and reliability improvement in comparable terms
12 p1987 A71-26678

OA0 2 thermal test reliability analysis, using filtering process to eliminate component and subsystem level failures
12 p1971 A71-26681

Manned spacecraft maintenance simulation model, applying complex systems operational availability assessments
12 p1894 A71-26689

Force springs flexural pivots and miniature incandescent lamp tests failure distribution analysis for comparing mechanical vs electrical components [ASME PAPER 71-DE-34]
12 p1911 A71-27326

Complex automatic systems with random switch-off, developing failure sequence models
14 p2220 A71-29997

Markov process models of failure times of repairable systems, using lumping and decomposing techniques
15 p2415 A71-32340

Large nonrepairable systems reliability analysis by partitioning possible states into subsets
15 p2415 A71-32342

Young pilot performance in emergency situations including communication system failure and other equipment breakdowns, noting emotional reactions
16 p2534 A71-32831

Redundancy verification of parallel systems related to element MTBF and decision maker perspective involving acceptance risk of system failure
16 p2582 A71-33292

Allocation, assessment and demonstration of system mean-time-to-repair in complex multiple failure situations
16 p2583 A71-33300

Producer risk determination and tables for Method 4 maintainability demonstration plan of MIL-STD-471
16 p2583 A71-33303

Cost distribution theory for various costs of failure, using probability distribution functions for modeling maintainability and reliability
16 p2583 A71-33305

System safety evaluation model with state-space network for representation of mission phase and hazard degradation
16 p2602 A71-33308

Maintenance replacement sequence selection for minimizing equipment repair time, noting dependence on failure rate
16 p2552 A71-33310

Complex systems with n independently failing subsystems, minimizing expected cost per unit usage by assigning replacement age
16 p2552 A71-33312

Binary relation algebra application to diagnostics tests for system involving redundant subsystems
17 p2720 A71-34960

Reliability analysis of redundant information systems, deriving formulas for risk of failure and faultless operation probability
17 p2721 A71-34966

Machine components resistance to low temperature brittle failure, considering threaded joints, gears and shafts for strength and plasticity characteristics
17 p2832 A71-35463

Performance monitor for aircraft automatic landing systems safety control [AIAA PAPER 71-958]
19 p3099 A71-37199

Systems oriented components selection optimization technique by reliability/quality levels, considering repair and failure cost, storage time and mission duty cycle
19 p3034 A71-38518

Reliability controlled maintenance plan for avionics equipment based on mean time between failures
20 p3203 A71-39087

ATC display device man-computer interaction faults and delays effects on operator performance
21 p3413 A71-40119

Machinery failure prediction under high vibration amplitudes using stochastic excursions principles [ASME PAPER 71-VIBR-60]
21 p3460 A71-40305

Priority standby redundant system consisting of two repairable units, considering preemptive and non-preemptive repair for system failure
21 p3386 A71-40364

Conditional failure density evaluation from hazard rate, considering failure time distribution function, reliability function and conditional failure distribution
21 p3408 A71-40370

SYSTEM LIFE
U RELIABILITY
SYSTEMIZATION
U SYSTEMS ENGINEERING
SYSTEMS ANALYSIS
Dwell time of semiMarkov system in given state with mixed Erlang and exponential distribution functions
01 p0110 A71-10096

German monograph on systems analysis of future jet and fan propulsion systems for VTOL commercial aircraft weight and cost reduction
01 p0142 A71-10115

Gyropendulum and two-rotor gyrocompass equations equivalence conditions, formulating and proving theorem

01 p0080 A71-10627

Optimal automatic systems statistical theory in relation to sensitivity, identification, invariance and control object dynamic characteristics

01 p0060 A71-10705

Automatic control systems analysis and synthesis, applying invariance conditions second form

01 p0061 A71-10711

Complex servo systems with feedback loop and anticipating path, demonstrating equivalence to systems based on error measurements

01 p0062 A71-10719

Pulsed analog and digital control systems invariance conditions at discrete times, using Laplace transform method

01 p0063 A71-10726

Extremal control systems operation, analyzing search and scanning phases

01 p0064 A71-10840

Stochastic processes applied to loaded redundancy systems reliability analysis

01 p0112 A71-11157

Direct thermoelectric conversion systems thermodynamic analysis

01 p0007 A71-11228

Nonlinear precision attitude control system stability analysis algorithm based on quadratic Liapunov function

02 p0278 A71-11648

Thermionic system transient behavior analysis by digital simulation using one diode model

02 p0196 A71-12261

Thermionic reactor analytical model for systems analysis, considering complex interactions between reactor physics, thermionics and thermal/hydraulics

02 p0281 A71-12265

Pulse frequency modulated pulsed control systems, deriving sufficient conditions for limit boundedness/dissipativity

02 p0236 A71-12621

Systems analysis application to stability of aerodynamic cross coupling in flight vehicle motions with steady sideslip, using feedback and root locus techniques

02 p0190 A71-12687

Second order relay system with piecewise constant control, using phase plane analysis technique

03 p0451 A71-13964

Optimal piecewise constant control of continuous time systems with time varying delay, deriving restrictive condition on Hamiltonian integrated between switching instants

03 p0389 A71-14075

Sound and vibration disorder measure for choosing statistical or deterministic models for system/response situation

[ASME PAPER 70-WA/DE-1] 03 p0459 A71-14138

Flight simulators simulation width and parameter sensitivity analysis by state vector feedback method, using multiparameter control root-locus technique

05 p0733 A71-15970

Inertial instruments system-level tests under final use environment, discussing cost reduction

[AGARDGRAPH-128] 05 p0750 A71-16308

Maximum likelihood identification of stochastic linear dynamic systems using Kalman filter

05 p0731 A71-16554

Continual systems analytical mechanics, discussing least constraint variational and Ostrogradskii-Hamilton principle applications in shell stability, filtration, plasticity and dislocation theories

05 p0828 A71-16895

Dynamic systems oscillation period doubling in presence of C bifurcations

05 p0782 A71-16985

Multicomputer system with preparatory and processing subsystems, discussing algorithm for distributing problems flow among processors

05 p0726 A71-17018

Control system synthesis and analysis, using time and frequency domain methods

06 p0878 A71-17427

Optimality criteria for communication systems, considering data transmission rate

06 p0867 A71-17496

State space constrained linear optimal control systems, using cutting plane algorithm for convex programs in Banach spaces

06 p0918 A71-17598

Block decomposition of linear time invariant multivariable control systems

08 p1269 A71-21328

First order digital phase locked loops analysis for single channel command system, using random walk techniques

08 p1270 A71-21351

Vibrating systems with amplitude dependent resistance, determining damping characteristics

08 p1372 A71-21616

Nonstationary automatic control systems analysis using frozen coefficients and weighting functions

08 p1270 A71-21978

Liapunov function construction for linear dynamical systems, applying condition of agreement with eigenvalue analysis

09 p1484 A71-22102

Book on stability theory of dynamical systems covering invariant sets and trajectories, limit sets, minimal sets, Liapunov functions, asymptotic stability of closed sets, etc

09 p1492 A71-22347

Adaptive control systems state variables and nonstationary parameters estimation in presence of random disturbance and measurement noise, using nonlinear filtering theory

09 p1423 A71-22612

Electromechanical systems digital simulation, discussing reticulation, bigraph reduction, mathematical modeling, etc

09 p1428 A71-22774

Book on reliability mathematics covering fundamental statistical concepts, logic diagrams, mathematical models, component reliability prediction, system prediction, reliability growth, assessment methods, etc

09 p1485 A71-22958

Biped locomotion machines dynamic analysis and synthesis by minimum energy criteria for prosthetic-orthotic equipment design and human locomotion analysis

09 p1399 A71-22971

Mathematical model system analysis methods for reliability assurance, discussing worst case and Monte Carlo techniques

09 p1423 A71-23040

Design optimization of aircraft starting and generating systems, identifying information required and system analysis methods

[SAE PAPER 710392] 10 p1558 A71-24256

N body system variables evolution, discussing complete scattering based on mean quadratic and harmonic distances

10 p1642 A71-24432

Nonconservative force system eigenvalues and eigenvectors reproduction by related conservative system

10 p1689 A71-24513

System identification, considering input signals classification, model structure, linear/nonlinear systems identifying and on-line/real time techniques

10 p1586 A71-24736

Second order system with structure perturbation affected parameter value, studying identification and autoadaptation by sign functions

10 p1586 A71-24740

Differential equations of root loci motions for stationary linear automatic control design by hodograph and Evan method

10 p1637 A71-24906

Nonstationary linear systems analysis over finite time interval and graphical method for differential equation, comparing exact and approximate solutions for free oscillations

10 p1643 A71-24908

Laplace transforms for nonlinear systems analysis

11 p1791 A71-25185

Linear continuous time delay feedback systems stability analysis, using root-locus and frequency response techniques

11 p1742 A71-26423

Nonlinear control systems dominating oscillation modes, investigating parameter variations effect by root locus technique

11 p1743 A71-26425

Lunar Roving Vehicle, discussing crew, mobility, power, deployment and navigation subsystems, environment and radio interference problems

11 p1747 A71-26527

Tabular system reliability analysis based on integration of fault tree, state variable and failure modes techniques

12 p1910 A71-26674

Reliability analysis method for systems cyclic operation, demonstrating application for satellite power subsystem

12 p1910 A71-26676

Adaptive control systems probability characteristics in presence of random inputs, discussing improvements by coefficients and interpolation methods

12 p1891 A71-26727

Criterion for fixed adjustment adaptive control systems comparison with self adjusting systems, using frequency range of plant information required for synthesis of correcting devices

12 p1891 A71-26730

Broadband FM systems behavior, calculating transmission deviations via transfer functions obtained from measurements and linear network analysis

12 p1878 A71-26993

French book on practical methods for nonlinear oscillations analysis covering linear and nonlinear systems, autonomous systems, forced harmonics, nonautonomous oscillating systems, etc

13 p2041 A71-28151

Solid nontrivial trajectory existence conditions in connected set of strong bilateral attraction, examining dynamic system in connected noncompact space

13 p2094 A71-28151

Modal control systems with confluent eigenvalues using system mode controllability matrix

13 p2042 A71-28151

Nonlinear multivariable sampled data systems synthesis and analysis in first harmonic approximation, introducing function arbitrary order difference equation

13 p2042 A71-28151

Control of distributed parameter systems, presenting analysis method using arbitrary set of space modes with time dependent coefficients

13 p2042 A71-28151

Listening method for hydraulic drive systems, using vibration signature analysis with rolling, sliding, impact and flow

13 p2000 A71-28151

Dynamic systems conservative by bits and governed by differential equation with discontinuous second member, obtaining limiting cycle existence conditions

14 p2265 A71-29651

Class structure of system identification problems with input and output signals and transform H, applying to stochastic operators

14 p2219 A71-29651

Nuclear space power systems computer simulation for preliminary system and mission analysis, considering Brayton, Rankine and thermionic systems

[AIAA PAPER 71-689] 14 p2208 A71-30771

Gaussian input signal nonlinear sampled data systems analysis using linear components and transfer function

14 p2220 A71-30801

Nonlinear ordinary first order differential equation solution for mechanical system motion, constructing asymptotic representation

14 p2266 A71-30801

High rotor advance ratio from multiblade general coordinates method in linear analysis of lifting rotor dynamic stability and gust ratio

[AHS PREPRINT 512] 14 p2178 A71-31011

Book on dynamic probabilistic systems, Volume 1 covering Markov models, linear processes, systems analysis, statistics, recurrent events, population models, time variations, etc

15 p2440 A71-31111

Decomposing method for linear transfer function identification from frequency or time response, using Caier form continued fraction expansion

15 p2379 A71-31111

Soviet book on discrete control systems covering linear and nonlinear systems synthesis and analysis, digital computer techniques, one and multidimensional systems optimization, etc

15 p2381 A71-31911

Closed loop system analysis of triangular wave generator consisting of integrator, on-off element with hysteresis and multiplier

15 p2376 A71-32011

PAM data transmission systems timing recovery discussing maximum likelihood estimation method for timing parameter from random data

15 p2377 A71-32311

Availability and failure frequency of systems of independent repairable units, using representation by network or reliability block diagram

15 p2415 A71-32311

Gyroscopic system nonstationary operation mode analysis, utilizing asymptotic method with linear matrix equation

15 p2410 A71-32411

Continuous systems stability analysis and parametric excitation, using time dependent Liapunov functional for frequency response

16 p2607 A71-32911

Bifurcating systems analysis in structural stability problems, discussing perturbation patterns in nonlinear branching theory

16 p2650 A71-33011

Allocation, assessment and demonstration of system mean-time-to-repair in complex multiphase failure situations

16 p2583 A71-33311

System safety evaluation model with state-space network for representation of mission phase and hazard degradation

16 p2602 A71-33311

Weighted finite incidence systems constructed using nonnegative integer functions and column vectors

16 p2603 A71-33511

Transverse vibrations of beam with bilinear support spring and nonlinear constraint, using single degree freedom system analysis

[SESA PAPER 1745] 17 p2820 A71-34511

Medical screening techniques, discussing sensitivity specific, reliable, fail-safe and self calibrating instrumentation systems

17 p2689 A71-34611

Generalized ordinary nonlinear differential equations, considering systems with impulses acting on surfaces

17 p2764 A71-34611

- Two level Kalman filter for high order interconnected systems states estimation, deriving coordination algorithm with one step convergence by multilevel systems theory
17 p2718 A71-34735
- Distributed parameter systems described by parabolic differential equations in Hilbert space, discussing existence of optimal control based on quadratic cost criteria
17 p2719 A71-34738
- Nonautonomous nonlinear dynamical systems with simultaneous fast and slow time response, basing analysis method on previous work of Malkin, Massera, Bogoliubov and Mitropolsky
17 p2782 A71-34932
- Time delayed systems periodic and quasi-periodic solutions
17 p2782 A71-34937
- Reliability analysis of universal computer system with identical elementary computers interconnected by communication channels
17 p2710 A71-34958
- Control reliability in automated system of discrete production management
17 p2721 A71-34961
- Redundant algorithms and structures, analyzing anisotropic systems described by continuous differentiable functions
17 p2710 A71-34962
- Soviet papers on exact analytical methods for studying nonlinear automatic control systems covering synthesis, stability, quality and dynamics problems
17 p2783 A71-35126
- Parameter space sections method for nonlinear automatic control systems analysis, reducing initial system by linear transformation of variables to first and second order equations
17 p2783 A71-35127
- French monograph on topological classification and identification of nonlinear systems by structural decomposition method covering general systems theory fundamentals
17 p2767 A71-35230
- Binary and quaternary PSK systems performance with intersymbol, interchannel and cochannel interferences and fading
17 p2707 A71-35478
- Vibrating systems with amplitude dependent resistance, determining damping characteristics logarithmic decrement
17 p2834 A71-35676
- Systems approach to airfield pavement for future aircraft, integrating design, construction, operation and maintenance
18 p2897 A71-36346
- Space station, shuttle and tug as post-Apollo space program, discussing objective, designs and systems analysis
19 p3149 A71-37303
- Analysis and synthesis of linear optical systems involving polarization effects by Pauli algebra of complex second order matrices
20 p3267 A71-38775
- Multicell thermionic fuel element consisting of six thermionic converters, considering reactor and systems analysis
20 p3265 A71-38950
- Decomposition matrix Cauer model for multivariable control systems analysis and design
20 p3207 A71-38995
- Mixed decomposition and convergence of gradient type coordinating algorithm for two-level complex control system using interconnection variables and Lagrange parameters
20 p3208 A71-39472
- Variational methods application to high order dynamic systems resonance boundary value problem
20 p3309 A71-39487
- Probabilistic behavior of repairable two-state systems, assuming reliability measurability by operating time
21 p3407 A71-40362
- Generalized reliability function for systems of arbitrary configurations, using path enumeration approach based on probability theory
21 p3407 A71-40369
- Monograph on satellite airport system modeling for large metropolitan areas covering systems analysis methodology and computer algorithms for optimization [SU-TR-71-1]
21 p3365 A71-40799
- System quality analysis by reliability measures /mean time between failures/, using distribution free evaluation models
22 p3566 A71-42114
- Hazard rate functions of systems with identically distributed subsystem failure times in sequential or simultaneous operation
22 p3566 A71-42118
- Fault detection, diagnosis and prognosis in linear dynamic systems based on statistical decision theory, considering error signal generation and statistics
23 p3682 A71-43945
- Optimal control of time delay systems described by linear differential difference equations
23 p3658 A71-44087
- Analysis and stability of multiloop attitude control systems for flexible spacecraft
23 p3773 A71-44091
- Algorithm for dual compromise control problems arising from each subsystem of inner level in multilevel static hierarchical system
24 p3812 A71-44393
- Integral quadratic control quality estimates in terms of system coefficients with allowance for system oscillation characteristics
24 p3812 A71-44483
- Spatially distributed systems with random parameters, determining random output signals statistical moments
24 p3813 A71-44678
- Statistical and combined harmonic and statistical linearization methods for piecewise-linear nonlinear system characteristics analysis
24 p3814 A71-44693
- Nonlinear stochastic systems approximate analysis based on multidimensional nonlinear transforms and distribution functions in Chebyshev-Hermite polynomials, determining dynamic accuracy
24 p3814 A71-44695
- Dynamic characteristics of self oscillating systems from response to sinusoidal test signals, using Abel integral equations
24 p3881 A71-44835
- Weakly damped nonstationary linear systems analysis by modified sensitivity function method, evaluating solution error
24 p3816 A71-45001
- Systems synthesis by Liapunov direct method, developing vector-matrix equations for systems classes satisfying specified Liapunov scalar functions [ASME PAPER 70-WA/AUT-3]
24 p3816 A71-45135
- ### SYSTEMS DESIGN
- #### U SYSTEMS ENGINEERING
- #### SYSTEMS ENGINEERING
- Time shared computer display system design with analog drive signal generator and digital information channeling processor
01 p0045 A71-10196
- Real time systems design principles for processor organization, logic circuits, fault detection and diagnostic tests to facilitate high degree of reliability and maintainability
01 p0046 A71-10203
- Man machine considerations in all-weather low level navigation system design, noting off-course error reduction by command information display to pilot
01 p0125 A71-10515
- Design principles for sensitive elements of capacitive sensors for distance measurement via electrostatic induction effects
01 p0079 A71-10527
- Multiloop discrete automatic control system invariant with respect to external perturbations
01 p0060 A71-10704
- Nonminimal phase feedback control system synthesis by frequency methods, discussing invariance characteristics
01 p0061 A71-10709
- Invariant automatic control structure for nonlinear plant, using inverse method
01 p0061 A71-10710
- Automatic control systems analysis and synthesis, applying invariance conditions second form
01 p0061 A71-10711
- Automatic feedback control systems performance correction for errors due to weakly damped components effects
01 p0061 A71-10712
- Quasi-invariant automatic feedback control system, deriving basis for determination of perturbation compensating components parameters
01 p0061 A71-10713
- Elastic flight vehicles feedback control systems synthesis by invariance theory
01 p0163 A71-10714
- Rapid-response automatic control systems synthesis, using compensation signals based on external disturbances
01 p0063 A71-10722
- Invariance in nonminimum phase complex combined control systems synthesis, using root hodograph method
01 p0063 A71-10724
- Digital control system for azimuthal optical telescope, using invariance techniques and photoelectric system to compensate for position and program errors
01 p0081 A71-10727
- Data transmission/acquisition/processing systems engineering project management using digital simulation models
01 p0184 A71-10885
- Scientific data transmission systems signal design considerations for Apollo lunar exploration missions
01 p0035 A71-10915
- Manned space flight network telemetry system modification for Skylab, ERTS and Apollo J missions, giving data flow diagrams and equipment electrical characteristics
01 p0035 A71-10917
- Lunar communications relay unit, discussing system design, capability and tradeoffs
01 p0035 A71-10919
- Design concepts providing high plate efficiency in high power injected beam crossed field amplifier capable of CW operation with conduction or liquid cooling
01 p0054 A71-10975
- Design criteria for implantable biotelemetry systems, discussing RF signal transmission through conductive body tissue
01 p0024 A71-10982
- Mission requirements in decision processes for guidance and control system design of aerospace vehicles [AIAA PAPER 70-1231]
01 p0126 A71-11301
- Steerable 100 m radio telescope design, surface accuracy, receiving installation and cryogenically cooled parametric amplifiers
01 p0068 A71-11342
- Thermal design of space experiment by analytical model for temperature regime acceptable to all experimental elements
01 p0017 A71-11454
- Airport system planning from environmental viewpoint, discussing travel market, airport accessibility, airspace utilization and control and land use
02 p0334 A71-11642
- RB 211 turbofan engine design, emphasizing modular construction, systems integration, maintainability and noise reduction
02 p0298 A71-11682
- Satellite system design digital simulation model in GPSS language for performance interrelationships between subsystems and reliability gain in orbit from redundancy
02 p0318 A71-11782
- Clear turbulent atmosphere effects on optical transmission characteristics and communication system design
02 p0213 A71-12010
- Optical /and IR/ communication systems design, considering effects of atmospheric turbulence, molecular absorption and aerosol scattering
02 p0214 A71-12023
- Ultrawide bandwidth optical data relay link between earth satellites, discussing system design concept
02 p0214 A71-12024
- Ultrawide bandwidth laboratory laser communication link for high fidelity signal transmission, discussing system configuration, components and preliminary test results
02 p0214 A71-12025
- Optical communication systems cost and weight optimization by COPTAN program
02 p0214 A71-12028
- Operational laser communication systems performance characteristics review, considering various modulation techniques, heterodyne detection, IR applications, etc
02 p0260 A71-12030
- Digital optimal feedback control device, discussing design requirements, algorithm, block diagram, flow chart and measurement results
02 p0236 A71-12150
- Thermionic converter performance improvement methods, using digital computer for evaluation
02 p0194 A71-12230
- High voltage thermionic module eliminating power conditioning and multiple units series connection, discussing design and coating technologies
02 p0195 A71-12244
- Skyнет project UK and U.S. cooperation, discussing system scope, coordination, contract placing and PERT critical path analysis in management planning
02 p0337 A71-12427
- Skyнет satellite communications system configuration and specifications, discussing geostationary satellite multiple access, SSMA transmission system, power budgets, reliability and repeater specifications
02 p0217 A71-12428
- Skyнет ground stations design, equipment and operations, discussing antennas movement control, Cassegrain reflectors, receiving system amplifier noise temperature and tracking demodulator
02 p0233 A71-12432
- Skyнет type 3 and 4 transportable ground stations, describing antenna, radio cabin with IF and control equipment and channeling cabin with baseband equipment
02 p0217 A71-12437
- Dynamic systems synthesis by exponential power input packet
02 p0285 A71-12670
- Model performance index /Pi/ providing criterion for approximating one dynamic flight control system by another based on geometrical representation of linear autonomous systems [AIAA PAPER 69-885]
02 p0189 A71-12682
- Large antenna electrical and mechanical requirements, considering gain/temperature ratio, steerability, housing, design life and erection
02 p0235 A71-12831

Soviet book on gyroscopic devices statistical synthesis covering dynamic characteristics, automatic systems, etc

03 p0423 A71-13371

Dynamic automatic control and servo systems with distributed parameters, discussing synthesis and precision

03 p0389 A71-13373

He-Ne laser with hemispherical nontunable internal cavity resonator formed by mirrors bonded to discharge tubes

03 p0439 A71-13999

Precision timing system implementation and operation, considering synchronization maintenance by flying cesium beam clocks, satellite, VLF and LF techniques

03 p0429 A71-14270

Intelsat system earth station on-site planning considerations for integration with existing wideband communication system and traffic growth demand

03 p0380 A71-14343

Optimum synthesis of mechanical systems using effort functions

04 p0625 A71-15061

Book on electrical, microwave and digital filter systems and design covering approximations, phase shift, ladder networks, frequency transformation, time domain, etc

04 p0560 A71-15075

Space base biomedical center based on Integrated Medical and Behavioral Laboratory Measurement System (IMBLMS) concept

04 p0546 A71-15280

Aerospace contractor management program projected through 1975 in terms of system engineering, configuration and financial management, with Minuteman Missile as example

04 p0691 A71-15291

Optimal design of low noise multistage microwave oscillator, discussing quartz master oscillator frequency effects

05 p0727 A71-16001

One chamber vacuum furnace for dewax, presinter and sinter of cemented carbides, referring to Cox chart for system design

05 p0758 A71-16248

Closed control loop system design using direct time domain synthesis

05 p0731 A71-16394

Automatic systems design, describing optimization method for nonlinear nonstationary system acted upon by fluctuation signals and disturbances

05 p0731 A71-16793

Optimal control system design quality, using generalized performance characteristics as principal parameter

05 p0732 A71-17022

Control system synthesis for asymptotically stable systems, using Liapunov functions for feedback laws

05 p0732 A71-17023

Earth resources satellite systems R and D planning, using case study approach in economic benefit analysis for parametric requirements determination [AIAA PAPER 68-1077]

05 p0840 A71-17050

Nonlinear dynamic systems synthesis by integral linearization, obtaining gain coefficients and graphs for work reduction

05 p0732 A71-17171

Onboard aircraft refractometer, design, operation principles and effectiveness

05 p0756 A71-17195

Optimum design of dominant type adaptive control systems with large parameter variations, using fourth order approximation

06 p0878 A71-17449

Teleautomatic data processing systems with computer control, synthesizing optimal structure

06 p0871 A71-17495

Automated design system producing wire format data for cabling avionics subsystem of light attack aircraft

[AIAA PAPER 69-976]

06 p0874 A71-17698

Communication satellite systems for long distance telephone connections, comparing transmission possibilities between links and terrestrial extensions

06 p0869 A71-18013

Intelsat 3 global satellite communication system design and performance

06 p0870 A71-18393

Common module series for NASA candidate experiment program for manned space stations in 1975-1985 era, discussing configuration and subsystem design

[AIAA PAPER 71-70]

06 p0980 A71-18528

Synchronous meteorological satellite mission goals and system design, describing imaging, data collection, facsimile, space environment, trilateration, ranging and transmission

07 p1067 A71-18807

Avionics subsystem design improvements for aeronautical systems, considering standardization, weight impact, environmental control, maintainability and equipment growth

07 p1069 A71-18829

F-104D aircraft side stick control system design and function, curriculum maneuvers and component reliability

07 p1018 A71-19092

Saturn launch vehicle navigation, guidance and control system, discussing optimal system design for flight path optimization

07 p1155 A71-19527

Low data rate m-ray frequency shift keyed (MFSK) modulation system design

07 p1061 A71-19534

Extendable Computer System Simulator, discussing simulators as tools for integrated information systems design

[AIAA PAPER 71-228]

07 p1068 A71-19706

Representative data of actual forces and moments applicable to large spacecraft attitude control system for typical crew activities obtained through simulation programs

[AIAA PAPER 69-1006]

07 p1208 A71-19866

Satellite communication system parameters optimization based on economical and technical constraints, applying to Intelsat 3

07 p1063 A71-20040

Man-machine considerations in all-weather low-altitude navigation system design, discussing computer generation of roll command guidance, visual display and pilot modeling

07 p1157 A71-20344

Digital on-off predictive adaptive control system feasibility analysis

07 p1082 A71-20407

Digital active fluid amplifiers static and dynamic behavior, defining complex parameters for system engineering

07 p1026 A71-20564

System sciences - Conference, Honolulu, January 1971

08 p1268 A71-21312

Liapunov design technique for model reference adaptive control systems with feedback and prefilter adjustable gains

08 p1270 A71-21669

Meteorological instrument design, discussing response, errors, accuracy, range and standardization

08 p1293 A71-21733

Meteorological instrument design, emphasizing reliability and maintainability

08 p1293 A71-21734

MOSFET data systems evolution for IMP, discussing effects on system design and reliability approach

08 p1267 A71-21844

Spacecraft computer centered data systems with standby redundancy, automated flexibility and LSI devices for grand tour mission

08 p1260 A71-21846

Multistage rockets terminal control synthesis based on linear functionals

09 p1532 A71-22660

Transducer design selection for strain gage applications in high nuclear radiation environments based on system requirements

09 p1445 A71-22718

Hybrid coordinate formulation for flexible space vehicle attitude control system design

[AIAA PAPER 70-20]

09 p1532 A71-22907

Biped locomotion machines dynamic analysis and synthesis by minimum energy criteria for prosthetic-orthotic equipment design and human locomotion analysis

09 p1399 A71-22971

Direct broadcast television service by satellite transmission, calculating trees and woods effects on attenuation and suggesting receiving system design modification

09 p1408 A71-23384

Single parameter linear physically realizable stable system with lumped parameters, estimating identification process solution uniqueness and stability

09 p1425 A71-23568

Continuous identification algorithm for system containing two delays for signal represented by stationary random process with autocorrelation function approximation

10 p1585 A71-24160

Design optimization of aircraft starting and generating systems, identifying information required and system analysis methods

[SAE PAPER 710392]

10 p1558 A71-24256

Elementary component constant failure rate for systems with prolonged operation without maintenance, determining mathematical model for confidence levels and dependability figures

10 p1617 A71-24266

International telephone transmission, comparing technical and economic characteristics between submarine cable and satellite systems

10 p1577 A71-24267

ATC automation system design, considering controllers decision time savings

10 p1640 A71-24271

Skylab workshop as orbital manned platform for scientific investigation, discussing system details and technical evaluation

10 p1682 A71-24272

Book on digital computers in engineering covering systems, man machine communication, numerical analysis, network analysis program, circuits, device control, etc

10 p1581 A71-24273

Soviet book on design of self guidance systems aerodynamically controlled rockets

10 p1640 A71-24274

Systems approximation by incontinuous orthogonal Haar functions, discussing dynamic properties of input signal synthesis with minimal errors in estimating parameters

10 p1587 A71-24275

System identification problems, discussing approximation by polynomial integral operators, determining classes in spectral decompositions, observation noise and stochastic systems stationary in observation time

10 p1587 A71-24276

Dynamical nonlinear systems observability definition and necessary and sufficient criterion for checking

10 p1587 A71-24277

Nonlinear systems parameter identification schemes using first and second order extended Kalman-Bucy linear filters and sensitivity functions comparing performance by two examples

10 p1587 A71-24278

System design and optimization computer subroutines based on biological mutation and selection principles, using random number generator

11 p1734 A71-25663

Conceptual design of nuclear thermionic power plant for Space Base application, discussing plant efficiency, radiator area requirements, launch weight and shielding

11 p1710 A71-25811

Out of core design of reactor heated thermionic power plant for manned space station, discussing temperature distribution, shielding characteristics and power conversion

11 p1710 A71-25812

Design and operation of split fueled cores with axial heat pipes for 350 kwe out-of-core thermionic power converter system

11 p1712 A71-25813

Parametric performance of quasi-vacuum monothermionic multicell space power generator, discussing surface parameters, fuel form, emission geometry, helium management and generator reliability

11 p1714 A71-25966

Double ended full length external fuel thermionic converter, describing component fabrication, assembly sequence, joining methods, vacuum test procedures and converter load control

11 p1715 A71-25967

Out-of-core heat pipe heated and cooled thermionic converter module mechanical design, fabrication and subcomponent performance evaluation

11 p1715 A71-25968

Design, calibration and computer control of orbital heating simulator, using heat flux sensor feedback for ATM thermal vacuum tests

11 p1745 A71-26223

ATM for manned solar observation, discussing thermal design, thermal vacuum test philosophy, mathematical models and analytical and test data correlation

11 p1838 A71-26224

System and component models for spacecraft thermal control design, considering materials, environmental degradation, measurement errors, manufacturing and quality assurance

11 p1859 A71-26225

Sun sensor design accuracy and stability parameters for spacecraft ultrafine guidance, comparing bias errors with solar simulator measurements

11 p1767 A71-26333

Unijunction transistors operation principles, electrical parameters, structural features and circuit applications

11 p1740 A71-26354

French monograph on nonlinear recurrences solutions and applications to sampled data systems

12 p1928 A71-26505

Design analogies of aerospace and commercial systems, describing computerized simulation methods for system design evaluation and reliability improvement

12 p1909 A71-26666

Reliability analysis as essential input in trade studies for selecting system component designs, emphasizing NERVA program

12 p1928 A71-26667

Mission reliability calculations for systems with redundant units, considering design of airborne warning and control system and other radar control systems

12 p1885 A71-26668

Electronic communication system critical design evaluation, concerning electromechanical components and packaging impact on overall reliability and cost

12 p1878 A71-26669

Manned spacecraft maintenance simulation model, applying complex systems operational availability assessments

12 p1894 A71-26689

Standard transfer function choice method for self adjusting automatic control system design, establishing relations between transient properties and poles and zeros distribution

12 p1891 A71-26725

Marks searchless self adjusting control system calculation, using method of total motion separation into characteristic components

12 p1891 A71-26726

Flight vehicles nonsearching self adjusting control systems synthesis, using gradient method with simplified sensitivity models

12 p1926 A71-26729

Criterion for fixed adjustment adaptive control systems comparison with self adjusting systems, using frequency range of plant information required for synthesis of correcting devices

12 p1891 A71-26730

Airborne radio communication systems, stressing electronic equipment design reliability

12 p1878 A71-26880

Hydraulically powered duplex input servos for flight control system of VFW-Fokker V/STOL fighter aircraft

12 p1867 A71-26884

Laser designs with thermal pumping, obtaining electron states phototransition probability, cooling rates for population inversion and laser action threshold for diatomic gas molecules

12 p1914 A71-27029

Reliable brushless direct-drive system design for controlling position and rate of solar power arrays on orbiting spacecraft

12 p1869 A71-27432

Kalman filtering for complex systems, deriving algorithms for dynamic modeling and bias errors effects in discrete-time state optimum estimation

12 p1893 A71-27435

Wired monitoring system for continuous interference-free twelve-lead ECG recording before, during and after exercise

12 p1876 A71-27630

Optimal control synthesis analog for nonlinear problem, using trial and error method based on Pontryagin maximum principle

13 p2040 A71-27834

Time optimal control system design with lag, determining phase coordinate prediction unit structure

13 p2041 A71-27944

Onboard aircraft refractometer design, operation and effectiveness

13 p2067 A71-28250

Variable structure automatic control system synthesis, giving roots distribution of characteristic equation for fluttering mode

13 p2041 A71-28636

Permanent magnet system design, deriving optimal field configurations and maximum magnetic energy

13 p1999 A71-28637

Optimal control systems design with random parameters and initial state, considering open loop and feedback correction terms

13 p2042 A71-28708

Personnel training in airline operations technology at Friedrich List Transportation Institute for aircraft pilots, flight safety engineers and systems engineers

13 p2021 A71-29143

Acquisition system consisting of positioning of local station burst signal in time slot for PCM-TDMA satellite communication system, discussing design and performance tests

13 p2034 A71-29393

German monograph on spacecraft systems launch readiness prediction covering reliability requirements, configuration analysis, tradeoffs, failure analysis, mathematical techniques, etc

13 p2146 A71-29482

Rocket-borne Cassegrain telescope system design for stellar spectra in UV region of EM spectrum between 900 and 3300 Å

14 p2238 A71-29727

Heuristic signal design for digital communication over fast-fading Gaussian channels, stressing nonorthogonal signaling schemes

14 p2193 A71-30010

Optical aperture configurations effect on image performance, discussing large telescope systems design criteria

14 p2242 A71-30147

Flowfields calculation in inlet design, using flow variable gradients from equations of motion

14 p2170 A71-30608

Engine condition monitoring systems, discussing engineering design requirements with respect to accessibility, accuracy, economics, effectiveness, reliability and maintainability

[AIAA PAPER 71-652]

Performance and cost design tradeoff between HF and synchronous meteorological satellite data collection systems, considering platform transmitting power and SNR

14 p2198 A71-30900

Heavy lift helicopter flight control system design, emphasizing fly by wire electrical analog

[AHS PREPRINT 503] 14 p2178 A71-31079

Electromechanical control system synthesis for compound hingeless rotor helicopter, using root locus method with transfer functions from airframe motion linear model

[AHS PREPRINT 536] 14 p2179 A71-31096

Weapons R and D flexible economical response to defense needs by emphasis on component and subsystem experimentation

14 p2341 A71-31130

Aeros satellite active magnetic attitude control system design, operation and testing

15 p2499 A71-31210

Skylab program organization and management, system design, operations and equipment

15 p2499 A71-31457

Apollo Lunar Module design evolution, considering mission requirements, reliability objectives, environmental factors, manned operation, weight and configuration

15 p2500 A71-31603

Heat pipes design and applications, examining pressure losses in steam and liquid phases and capillarity and gravity effects

[HEAT EXCH. CONF. PAPER 23]

Nonlinear system design based on generalized Popov stability criterion

15 p2513 A71-31637

Operating characteristics of high performance vortex amplifiers, discussing turndown ratios, noise reduction, linearity and stability

15 p2352 A71-32062

Helical induction boiler feed electromagnet pump design, fabrication and testing for potassium Rankine cycle space power system

[GESP-455] 15 p2415 A71-32202

Electrical DC collector machines and MHD magnetic systems design using superconductors, describing models

15 p2355 A71-32274

Gas dynamic elastically mounted bearing, describing stability analysis of unloaded rotor central equilibrium position

15 p2417 A71-32457

Minimum redundancy high resolution radio interferometer for observing H II, planetary nebulae, nonthermal supernova remnants, radio galaxies and solar features

15 p2385 A71-32463

Astronomical mirror mass balancing system, discussing counterweights and levers arrangement and error and temperature compensation

15 p2411 A71-32526

Statistical procedure for maintainability allocation during early system design to meet specified overall goal

16 p2583 A71-33299

Optimal control of distributed parameter systems described by integral and partial differential equations, providing theory and bibliography

16 p2549 A71-33354

Book on fluidic systems design covering analog and digital control, application to aircraft, spacecraft, computers, tracking devices and equivalent circuits

16 p2526 A71-33475

Algebraic structure and design of automatic systems using partitions in set of states of finite automation

16 p2545 A71-33705

Book on space suit evolution covering balloon flight, tropopause, stratosphere, astronautics, astrotrops, astronauts, etc

16 p2537 A71-33872

Communication satellite TV and sound broadcasting system design without unreasonable cost

17 p2697 A71-34237

Radio communication system optimization from viewpoints of global synthesis including economics and partial synthesis based on noise stability, precision and reliability

17 p2698 A71-34392

Soviet book on space radio telemetry systems characteristics, design, requirements and operation conditions covering noise stability, reliability and redundant codes

17 p2699 A71-34521

ATC system models, covering surface movement, runway utilization, terminal areas and enroute traffic

17 p2771 A71-34523

Systems concept formalization, including structural relations on basis of set theory, topological considerations and flow theory

17 p2777 A71-34599

Millimeter wave systems applications to plasma probes, radar, radiometry and communications

17 p2699 A71-34602

Advanced communications satellites system engineering, including configuration based on active body stabilization, rechargeable hydrogen oxygen fuel cells and ion engines

[AIAA PAPER 71-843] 17 p2812 A71-34710

Lunar surface base concept synthesis, considering program objectives and hardware operational approaches

[AIAA PAPER 71-819] 17 p2723 A71-34725

Redundancy approach to information systems synthesis

17 p2720 A71-34952

Redundant information optimizer design, using non-linear elements

17 p2720 A71-34957

Redundancy utilization in automatic control systems synthesis, considering dynamic characteristics sensitivity

17 p2721 A71-34965

GALAXY machine for measuring image position and brightness and converting Schmidt telescope photographic data into computer form, outlining design and development

17 p2741 A71-34996

Earth stations operating in Intelsat System, discussing mandatory performance requirements and design approaches

17 p2705 A71-35100

Queueing theory approach to communication satellite network design, applying to ocean air traffic control and worldwide military broadcast systems

17 p2721 A71-35106

Optimal state regulator approximate design for nonlinear system with quadratic performance index, determining suboptimal feedback law

17 p2722 A71-35212

Spacecraft system design with long life reliability for outer planet exploration missions

[AIAA PAPER 71-831] 17 p2814 A71-35428

Itos I and Noaa I meteorological satellite systems design and operation, outlining attitude and thermal control, sensors, power supply and orbital performance

[AIAA PAPER 71-836] 17 p2814 A71-35432

Technological environment for international communications law, examining system design, radio spectrum resource management and communication satellites

18 p2986 A71-36164

Three day mission biosatellite environmental thermal control system design and flight performance

[ASME PAPER 71-AV-33] 18 p2869 A71-36400

System engineering techniques application to end-to-end space shuttle cargo handling system

18 p2899 A71-36466

Franco-German Symphonic communication satellite, discussing missions and subsystems design features

18 p2974 A71-36522

Architectural and environmental design tools for space system habitability, discussing work and living areas, hygienic facilities, etc

[AIAA PAPER 71-879] 18 p2871 A71-36632

Astronomical telescopes design and characteristics, reviewing electromagnetic radiation properties

18 p2925 A71-36769

Nuclear power station design for optimal reliability levels, noting maintainability requirements

18 p2928 A71-36807

Discrete time digital flight control systems design resulting in closed loop aircraft response characteristics approximation to prescribed flying quality specifications

[AIAA PAPER 71-955] 19 p3024 A71-37196

USAF total in-flight simulator model-following feedback control system, discussing conceptual design and flight test results

[AIAA PAPER 71-961] 19 p2995 A71-37202

Satellite docking systems, discussing laser radar feasibility and device design

19 p3149 A71-37307

Space shuttle structural heat problems, discussing shield design configurations and cooling systems

19 p3150 A71-37311

Systems planning and operation of European applications satellites, noting Sirio and Symphonic programs

19 p3172 A71-37329

TOPS spacecraft parts and technology development, reliability and contribution to long life system design

[AAS PAPER 71-159] 19 p3152 A71-37928

Controllable overhead arc spark gap discharger system design and characteristics for high power research, communication or industrial electrical installations

19 p3000 A71-38642

Nuclear reactor Brayton cycle space power system design point characteristics, discussing cycle parameters, working fluid, turbine inlet temperature, operating pressure level, etc

20 p3262 A71-38913

Multihundred watt radioisotope thermoelectric generator for spacecraft power supply, discussing system design, performance and safety requirements

20 p3263 A71-38927

Viking Lander power system design, discussing functional requirements by mission and science objectives and reliability features

20 p3181 A71-38940

Suboptimal design of closed loop least upper bound fuel control for dynamic systems, minimizing fuel consumption on basis of fixed ultimate error
20 p3206 A71-38971

Multivariable control system design and applications - IEE Conference, Manchester, England, September 1971
20 p3207 A71-38988

Interaction measure for optimal multivariable feedback control system design for complex blending processes, noting paradoxical solution
20 p3207 A71-38993

Computerized design of large multivariable control systems using inverse Nyquist array method
20 p3202 A71-38994

Decomposition matrix Caue model for multivariable control systems analysis and design
20 p3207 A71-38995

Frequency domain computer graphics technique for linear time-invariant multivariable feedback control system design
20 p3207 A71-38997

Boeing 747 aircraft hydraulic system design, discussing thin wall high pressure tubing, swaged sleeves and welded joints
20 p3183 A71-39148

L-1011 aircraft hydraulic system design modifications and improvements, discussing gas turbine power source, fluids evaluation, filters, welded steel tubing and maintenance procedures
20 p3183 A71-39149

Power by wire actuators and fly by wire flight controls, discussing systems configuration, reliability, economy and durability
20 p3183 A71-39150

Holographic interferometry equipment design for NDT and vibrational and deformation analysis, discussing apparatus construction, optical quality and industrial applications
20 p3238 A71-39344

Ultrasonic radar simulator to produce data for radar system performance evaluation, describing automated short range and manual long range systems
20 p3196 A71-39376

Mixed decomposition and convergence of gradient type coordinating algorithm for two-level complex control system using interconnection variables and Lagrange parameters
20 p3208 A71-39472

Adaptive reception of weak repetitive signals on background of intense fluctuating noise, synthesizing adaptive detection system for multipath propagation and small SNR
20 p3199 A71-39809

Computer use in automatic tracking radar systems design, describing adaptive radar hardware
20 p3200 A71-39902

Terrain and atmospheric parameters affecting radar system design at microwave frequencies, discussing radar backscatter cross section and attenuation
20 p3200 A71-39904

Computerized tabular data display with cross-bar addressed glow discharge panel, discussing system details
21 p3350 A71-40115

Mechanical elements and systems optimal design, discussing variational and programming techniques application to machine elements design optimization [ASME PAPER 71-VIBR-62]
21 p3385 A71-40306

Linear multidegree of freedom shock isolation system optimum design, masses, spring and damping coefficients, using mathematical programming [ASME PAPER 71-VIBR-81]
21 p3461 A71-40317

Radiative-conductive heat transfer systems optimum thermal design, using nonlinear programming with mathematical model based on nodal analysis [ASME PAPER 71-VIBR-120]
21 p3474 A71-40339

Optimal design for system reliability and maintainability, using dynamic programming model
21 p3407 A71-40363

Papers on communication satellites for 1970s covering various national domestic systems, aeronautical service, ERTS data transmission and collection problems, etc
21 p3347 A71-40473

Attitude stiffness and pointing accuracy of three-axis and dual-spin stabilization system for future synchronous communication satellites
21 p3455 A71-40481

Instrument servomechanisms with spring-coupled inertial dampers, evaluating dimensional design parameters from analytical root locus
21 p3326 A71-40616

Linear multivariate sampled-data control systems optimal design based on deadbeat performance
21 p3360 A71-40618

Cybernetics and automatic control of space systems with pursuit process, using trajectory approximation with mathematical model graphs
21 p3452 A71-40857

Cold gas rocket propulsion systems design parameters, determining performance and weight formulae
21 p3437 A71-41050

High resolution astronomical radiointerferometry, discussing radio telescope system design
21 p3452 A71-41052

Design and technological calculations in machine building, analyzing flow, creep and elastoplastic deformation theories
21 p3472 A71-41144

Soviet book on high pressure centrifugal pumps design and calculation covering industrial applications, systems engineering, components, etc
21 p3391 A71-41371

Soviet book on multivariable automatic control system synthesis with adaptation to computer covering methodology, algorithms, transfer function approximation and stability problem
22 p3525 A71-41799

Analytical model for air navigation and ATC system design, demonstrating system parameters effects on lateral separation standards for parallel flight lanes
22 p3571 A71-42083

Relcomp conversational time-sharing computer program for rapid calculation of reliability and MTBF of systems with serial and redundant units
22 p3517 A71-42103

Computerized algorithm for redundant configuration system reliability function generation from Boolean algebra transmission function
22 p3517 A71-42107

Large telescope design - Conference, Geneva, March 1971, covering telescope projects, optical properties, mountings and control and drive systems
22 p3542 A71-42120

Design technique based on frequency response loci associated with characteristic transfer functions for linear time-invariant multivariable feedback control system
22 p3526 A71-42284

Optimal design of low noise multistage microwave oscillator, discussing quartz master oscillator frequency effects
22 p3524 A71-42750

Discrete system high order optimality sufficient conditions and methods for singular and nonsingular controls study
22 p3527 A71-42854

Control system synthesis from transient process estimates with Liapunov functions, proposing optimality criteria based on Gaussian minimum constraint principle extension
22 p3527 A71-42855

Synthesis models and methods for large scale automated control systems with human elements, discussing mathematical models and computerized design
22 p3528 A71-42858

Aircraft pitot static systems design with removable drain plug, noting line installation problems
23 p3675 A71-43387

Program management techniques, discussing organization, planning, systems engineering and personnel selection
23 p3785 A71-43453

NASA NHB reliability engineering provisions for aeronautical and space system contractors, considering criteria for program management, system engineering, manufacturing and facilities
23 p3682 A71-43497

Nonlinear discrete system optimal feedback controller synthesis for low sensitivity to parameter variations by difference equations quasilinearization and dynamic programming
23 p3656 A71-43855

Deterministic system optimal control with single control and several cost functionals by Pontryagin maximum principle
23 p3656 A71-43858

Synthesis procedure for feedback parameter adaptive control systems, discussing computer simulation data
23 p3658 A71-44081

Pole placement design of dynamic compensators for linear time invariant multivariable systems, using transfer function matrices
23 p3660 A71-44119

German book on adaptive control systems covering decision processes and application examples
23 p3660 A71-44188

Electrohydraulic stand for vibration strength testing, discussing system design, specifications, frequency-amplitude characteristics and applications
23 p3662 A71-44235

Data transmitting and receiving instruments and systems development problems covering signal shaping and converters and information channel and data reception theories
24 p3806 A71-44375

Optimum design of linear multivariate sampled data systems, using deadbeat and integral performance criteria and output response error
24 p3812 A71-44451

Nonlinear and multivariate optimal sampled data control systems design with bounded control and state variables, using dynamic programming and divisional technique
24 p3812 A71-44452

Earth resources technology satellites image processing system including electron beam recorder,
24 p3806 A71-44454

image corrector, electro-optical systems and digital processors as design features
24 p3825 A71-44510

Future transportation technology impact, considering system design evaluation criteria and civil aviation and urban mass transit systems contributions
24 p3892 A71-44580

Computer systems design for complex process control, constructing models with differential equations and Boolean functions
24 p3806 A71-44581

Earth observation system design decision making considering data needs, technology readiness, man role in earth resources programs and space program schedule
24 p3892 A71-44582

Flow and strain analysis and engineering design of porous cylindrical gas film foil bearing at low pressures
24 p3830 A71-44583

SYSTEMS STABILITY

Nonlinear pulsed automatic control systems at solute stability with unsteady linearity by Pontryagin principle, considering forced and free motions
01 p0058 A71-10454

Optimal multiimpulse compensation for dynamic system external disturbances by minimax differential game approach, restricting impulse number and magnitude
01 p0059 A71-10454

Lipschitz functional differential equations systems uniform asymptotic stability under diminishing perturbations
01 p0111 A71-10474

Modulo value influence on computer operation reliability, allowing for supplementary verification equipment reliability
01 p0049 A71-10595

Nonlinear single-degree of freedom mechanical system vibration under small random perturbations
01 p0127 A71-10545

Automatic control and information systems epsilon invariance, generalizing Kotelnikov theorem on continuous signals reduction
01 p0060 A71-10709

Nonlinear feedback control systems invariance, investigating coordinate and parametric disturbances compensation
01 p0063 A71-10725

Single channel step-type extremal systems with inertial control plants, proposing automatic optimizer
01 p0065 A71-11231

Relay corrector for widening automatic control systems stability via jump-change in signal amplification factor
01 p0065 A71-11231

Stability conditions of Liapunov function for system of ordinary differential equations with prescribed phase flow
01 p0113 A71-11294

Neural pulse frequency modulation model limitations and modification for error sampled control system stability analysis
01 p0038 A71-11311

Hydraulic servomechanism with piston-type control valve, examining oil compressibility and sustained oscillations effects on system stability
01 p0007 A71-11377

Nonlinear networks interconnected by lossless transmission lines, deriving global asymptotic stability condition
01 p0065 A71-11577

Self locked He-Cd 114 laser pulse velocity behavior, discussing stability
02 p0260 A71-11949

Cesium consumption rates and content in thermionic converter components affecting system performance indicated via integral adsorption reservoir
02 p0195 A71-12244

Incore thermionic diode reactor stability review and evaluation, discussing reactivity feedback mechanisms, analytical models and results
02 p0280 A71-12265

Control system for resonant mechanical loads with feedback, examining stability conditions and oscillation damping by Coulomb friction
03 p0431 A71-13074

Lagrange theorem inversion for two degrees of freedom systems, emphasizing Liapunov assumption regarding mechanical systems stability
03 p0449 A71-13114

Linear ordinary differential equations system with random coefficients, proving mean stability theorem
03 p0450 A71-13119

Dynamic polysystems stability and optimization, discussing minimality and recurrence in state space set
03 p0450 A71-13120

Nonlinear time varying discrete feedback systems input-output properties, deriving stability criteria by generalized small gain and passivity theorems
03 p0389 A71-13327

Vibrationally stressed elastic system stability, considering vibration rate amplitude as criterion
03 p0503 A71-13408

Stochastic stability for optimum systems with general search control law for boundary parameters under vector stochastic differential equation 03 p0389 A71-13518

Navier-Stokes equations numerical solution method, considering stability and convergence of scheme and system of difference equations 03 p0452 A71-14175

Neural pulse frequency modulated error sampled control system stability, considering model limitations and modifications 03 p0390 A71-14307

Stability of linear time invariant discrete systems including multiple poles 03 p0393 A71-14471

RC active filter with lumped-distributed components, discussing system stability at transition region between extreme electrical lengths 04 p0560 A71-14744

Interfacial wetting, bonding and chemical and mechanical stabilities in whisker composites, discussing system stability 04 p0611 A71-14948

Stochastic motion stability of discrete dynamic systems involving Ito equations 04 p0625 A71-15060

Spacecraft attitude control system with inertia wheels, determining stability by decomposition method 04 p0663 A71-15300

Parametric resonance and first order instability region of Mathieu equation in nonlinear systems 04 p0620 A71-15737

Oscillations of nonlinear system with conditions for main amplitude equations 05 p0780 A71-16179

Liapunov function time derivative for autonomous system asymptotic stability tests by exact differential method 05 p0774 A71-16579

Nonlinear systems stability conditions, determining system coordinates absolute values upper bounds under initial and parametric disturbance conditions 05 p0731 A71-16792

Control system synthesis for asymptotically stable systems, using Liapunov functions for feedback laws 05 p0732 A71-17023

Automatic systems multipositional elements reliability, analyzing output errors and transition states stability 05 p0729 A71-17039

Absolute stability of closed automatic control system with nonlinear components, discussing frequency criterion 05 p0732 A71-17172

Soviet book on Liapunov functions covering autonomous linear and nonlinear systems, asymptotic and absolute stability, etc 06 p0916 A71-17442

Second order nonlinear systems with limited state variables, determining structural stability regions 06 p0928 A71-18233

Stability, stationarity and amplitude damping of random parametric vibration system, using nonlinear differential equations 07 p1147 A71-19591

Laser operation instability with nonlinear filter, deriving electrons differential velocity distribution functions on inhomogeneous emitter 07 p1126 A71-20197

Dynamic system stability criterion under constantly acting perturbations over finite time interval 07 p1161 A71-20267

System with aftereffect along programmed trajectory, studying controlled motion stability and accuracy 07 p1161 A71-20269

Equilibrium position stability of Hamiltonian systems with one and two degrees of freedom in resonance 08 p1336 A71-21859

Action reproduction accuracy of nonlinear controlled systems with constraints and delays, considering stability degree 08 p1336 A71-21861

Optimal asymptotic stability laws of control systems with unstable plant, using piecewise coordinate functions 08 p1270 A71-21949

Liapunov matrix equation for linear and nonlinear automatic control systems stability 08 p1325 A71-21976

Nonlinear automatic control systems stabilization by seeking Liapunov function satisfying certain integral relationships 08 p1270 A71-21977

Nonlinear automatic control system stability with random stationary parameters 08 p1271 A71-22024

Linear optimal stochastic control systems described by covariance matrix correlating errors and estimates of state variables, analyzing instability under parameter variations [AIAA PAPER 70-36] 09 p1421 A71-22076

Nonlinear control systems absolute instability, establishing general frequency criteria 09 p1421 A71-22117

Self adaptive systems with dynamic characteristics stabilization, obtaining algorithm for adaptive loop optimization 09 p1422 A71-22120

Nonlinear control systems absolute stability range in parameter space 09 p1422 A71-22121

Thermodynamic system with concentrated loads due to heat and mass transfer or chemical reactions, analyzing wave processes and system stability 09 p1544 A71-22269

Book on stability theory of dynamical systems covering invariant sets and trajectories, limit sets, minimal sets, Liapunov functions, asymptotic stability of closed sets, etc 09 p1492 A71-22347

Soviet papers on differential equations and applications covering control and system stability, elastic theory, boundary value problems, etc 09 p1495 A71-23428

Differential equations system theorems for conditions of solution stability in presence of large initial perturbation 09 p1495 A71-23429

Conservative systems of differential equations with single degree of freedom, considering periodic solutions existence, determination and stability 09 p1495 A71-23436

Ordinary differential equations invariance properties, considering applications to stability problems 09 p1486 A71-23470

Liapunov functions generation for input-output stability of dynamical systems, using causal operator and state space realization 09 p1425 A71-23471

Stable system identification by equivalent structure model on analog computer with standard rectangular pulse input signal 09 p1413 A71-23567

Single parameter linear physically realizable stable system with lumped parameters, estimating identification process solution uniqueness and stability 09 p1425 A71-23568

Linear differential equations stability analysis by implicit equations applied to resonance phenomena, using Weierstrass theorem 10 p1640 A71-23803

Numerical integration of perturbed linear systems of differential equations by step method comparing power series 10 p1636 A71-23960

Reliability of redundant repairable systems with preventive maintenance, determining mean time between failures 11 p1769 A71-25660

Linear continuous time delay feedback systems stability analysis, using root-locus and frequency response techniques 11 p1742 A71-26423

Adaptive control systems components stability and accuracy requirements, demonstrating functional multipliers and quorum elements operation by functional diagrams, transient equations and signal waveforms 12 p1890 A71-26717

Approximate stability criteria-system parameter relationships facilitating higher order adaptive systems synthesis 12 p1890 A71-26722

Stability of RLC networks with negative resistances, applying Liapunov functions 12 p1891 A71-26998

Spacecraft nonlinear stabilization system phase space structure, transient processes and system stability domain, using point-to-point transformation method 12 p1972 A71-27018

Automatic control systems with nonlinear hysteresis characteristics, deriving frequency conditions for absolute system stability 12 p1892 A71-27025

Critical stability solutions to ordinary second order differential equations including holomorphic functions with series expansions 12 p1930 A71-27238

Theorems of instability for differential equation in linear normalized spaces, using Liapunov second method 12 p1930 A71-27239

Stability and coarseness of one- and two-channel invariant control systems for various forms of parameter deviations 12 p1893 A71-27340

Stability of first order gain model reference adaptive control system with sinusoidal input 12 p1973 A71-27580

Nonlinear closed loop control system with PFM and PWM, obtaining asymptotic stability condition by Liapunov and La Salle theorems 12 p1893 A71-27726

Piecewise-linear approximation of nonlinear friction effect on interferometric servosystem stability, deriving formulas for harmonic linearization coefficient of linearity 13 p2041 A71-28375

Stability of steady states of physical system with respect to finite perturbations 13 p2100 A71-28451

Girder system transverse bending under axial and lateral loads, deriving stability conditions by direct Liapunov method 13 p2153 A71-28519

Stability of feedback systems with backlash, deriving stability criterion in form of existence theorem for multiplier function 13 p2042 A71-28703

Stability criteria for nonlinear time-varying feedback systems, using passivity theorem 13 p2042 A71-28705

Liapunov stability of gyroscopic stabilizers as electromechanical systems, assuming nonrigidity of rotor, gimbal and platform suspension 13 p2069 A71-28726

Soviet book on multiloop automatic control systems covering matrix notation, stability and accuracy, invariance principle, compensating cross couplings, etc 14 p2218 A71-29527

Distributed parameter systems with transfer function as ratio of output and input multiple transforms, deriving open and closed loop stability criteria 14 p2265 A71-29602

Difference equations system trivial solution stability condition existence and uniqueness theorems 14 p2265 A71-29628

Nonlinear systems stability analysis for arbitrary disturbances, using semistochastic technique 14 p2219 A71-29735

Nonlinear control systems absolute instability, establishing general frequency criteria 14 p2219 A71-29995

Self adaptive systems with dynamic characteristics stabilization, obtaining algorithm for adaptive loop optimization 14 p2220 A71-29998

Nonlinear control systems absolute stability range in parameter space, using system of inequalities 14 p2220 A71-29999

Nonlinear multiple component automatic control systems equations and frequencies for absolute stability 15 p2378 A71-31292

Nonlinear control systems stochastic stability frequency conditions based on one and multidimensional cases 15 p2379 A71-31293

Sufficient stability of difference approximations for initial boundary value problems 15 p2441 A71-31354

Multilobed inflated membranes stability under finite deformation, deriving system instability critical conditions 15 p2503 A71-31421

Zero solution stability of nonlinear system of differential equations with constantly acting perturbations 15 p2449 A71-31830

Stability criterion for cross coupled symmetrical two dimensional nonlinear control systems allowing different slopes for Popov lines 15 p2380 A71-31938

Pulse frequency modulated control systems stability analysis by Liapunov method, introducing discrete correction into modulation law 15 p2381 A71-31979

Linearly increasing input signal tracking in nonlinear control systems with pulse frequency modulation, discussing error determination, asymptotic stability and equations of motion 15 p2381 A71-31980

Nonconservative elastic system involving standard double pendulum model under retarded follower load, calculating damping, time delay and parameter variations effects on stability 15 p2449 A71-32012

Hamilton-Jacobi equation application to forces selection for mechanical systems asymptotic stabilization, minimizing functional by Euler-Lagrange equations 16 p2602 A71-32814

Minimum dimensionality determination for control process stabilizing linear mechanical system, obtaining necessary and sufficient conditions for stabilization 16 p2607 A71-32933

Control system stability with nonlinear feedback in steady equilibrium state 16 p2548 A71-32934

Continuous systems stability and instability - Conference, Herrenab, West Germany, September 1969 16 p2648 A71-32976

Hilbert space valued systems and elliptic boundary value problems stability, employing circle criterion 16 p2549 A71-32978

Static stability criterion dynamic extension for nonlinear continua under conservative loads, using Liapunov functions 16 p2607 A71-32980

Gravity waves over flow with nonuniform velocity distribution, investigating neutral stability problem of generation and momentum transport

16 p2557 A71-32984

Closed circuit electrical, mass and heat flow stability analysis, showing capacities or inductances trace effects

16 p2607 A71-32991

Continuous systems stability analysis under parametric excitation, using time dependent Liapunov functional for frequency response

16 p2607 A71-32992

Stability of governing parameters critical values (Taylor, Rayleigh or Reynolds numbers) and periodic solutions in fluid mechanics

16 p2558 A71-33002

Thermoelastic stability as function of thermodynamic properties of elastic materials, applying invariance principle to dynamical systems on Banach space

16 p2649 A71-33004

Feedback stabilization of linear distributive systems in form of second-order evolutionary equation in Hilbert space, applying to plasma stabilization

16 p2618 A71-33006

Mechanical continuous system equilibrium stability under follower forces, discussing viscous damping destabilizing effects

16 p2608 A71-33007

Holder stability and logarithmic convexity as special case of Liapunov function applied to linear elastic systems without body force

16 p2608 A71-33008

Stability of linear viscoelastic systems under non-conservative forces, obtaining equations for perturbed motion for equilibrium or creep state

16 p2650 A71-33020

Equilibrium state instability in system with two degrees of freedom, using Liapunov method

16 p2608 A71-33026

Digital filters, describing transfer function, frequency response, stability and design

16 p2546 A71-33478

Two dimensional linear communication system with crossed channels with different amplification factors and time constant, examining stability with root trajectory method

16 p2549 A71-33569

Closed linear systems optimal stabilization, determining transfer function from Wiener Hopf equation

16 p2550 A71-33900

Linear single loop sampled data time delay feedback systems stability analysis

16 p2550 A71-34168

Multiple mass rheonomic vibrational systems dynamic stability, presenting approximate solution and critical dissipation level for damping parametric resonances

17 p2777 A71-34346

Linear comparison systems stability condition proved with Kotlianskii and Bailey theorems

17 p2764 A71-34510

Logarithmic frequency characteristics in stable nonlinear pulsed systems synthesis

17 p2718 A71-34558

Periodic surface concept application to restricted three body problem of dynamical systems through averaging method, presenting stability theorem

17 p2804 A71-34918

Linear differential equations solutions stability in Banach space for finite and infinite dimensional cases, generalizing Liapunov theorems

17 p2781 A71-34922

Superharmonic resonance in piecewise linear systems with unsymmetrical characteristics, investigating stability properties by Fourier series method

17 p2781 A71-34926

Vibrationally stressed elastic system stability, considering vibration rate amplitude as criterion

17 p2826 A71-35017

Atomic clocks on manned space stations, discussing stability in aerospace environment, techniques for earth based timer calibration, reference device, maintenance and corrections

17 p2743 A71-35056

Second order and degenerate third order nonlinear automatic control systems analysis by point mapping method, considering global stability and self oscillation mode

17 p2783 A71-35128

Frequency criteria for absolute stability of equilibrium states and processes in nonlinear automatic control systems

17 p2783 A71-35130

Nonlinear automatic control systems stability under large modulus-limited deviations based on method of sections and direct Liapunov method

17 p2783 A71-35131

Nonlinear automatic control systems sensitivity to changes in prescribed operating conditions and component parameters

17 p2784 A71-35136

Soviet book on self adjusting systems dynamics with frequency stabilization characteristics, covering

linearized motion equations, narrow band processes, etc

17 p2722 A71-35175

Discrete-time optimal linear systems structure and stability, assuming quadratic costs and perfect observability

17 p2722 A71-35180

Cascade connection of nonlinear block and time invariant finite dimensional system, discussing stabilization by controlled state variable feedback

17 p2722 A71-35213

Co-Ge-Si alloys phase equilibria, evaluating long term stability of junctions between thermoelectric batteries conducting series connectors

17 p2759 A71-35337

Bounded plane circular three body problem stability, analyzing Jacobi integral and canonical equations

17 p2807 A71-35496

Bounded circular three body problem stability, deriving Jacobi integral and canonical equations with Poincare variables

17 p2807 A71-35498

Linear neutral differential equation uniform asymptotic stability relation to perturbed differential equation containing bounded linear operators

17 p2767 A71-35523

Bounded integral manifolds existence for perturbed system of nonlinear differential equations near critical point, periodic orbit or periodic surface

17 p2769 A71-35795

Unstable nonlinear systems transient behavior analysis with two-time perturbation method applied to Bernard and Taylor flow problems

17 p2730 A71-35797

Book on stability theory covering Liapunov functions, variable structure automatic control systems and differential equations solutions in Banach space

18 p2947 A71-36250

Linear functional equations bounded solutions stability by reflexive Banach space mapping, applying to elliptical and parabolic differential equations ill-posed problems

18 p2941 A71-36351

Numerical stability of extended Kantorovich method for single term variational approximation of torsional problem

18 p2980 A71-36702

Hamiltonian systems equilibrium position stability conditions in presence of resonances, assuming neutrality in linear approximation

19 p3103 A71-37096

Discrete closed loop system stability with Kalman filter by determining z plane poles of special augmented transition matrix

19 p3036 A71-37235

Stability theorem for predictor-corrector methods for differential equations systems solution using computer

19 p3085 A71-37421

Absolute instability of nonlinear control systems, applying circular criterion to systems with nonstationary nonlinearities

19 p3037 A71-37568

Spacecraft nonlinear stabilization system phase space structure, transient processes and system stability domain, using point-to-point transformation method

19 p3152 A71-37688

Automatic control systems with nonlinear hysteresis characteristics, deriving frequency conditions for absolute system stability

19 p3038 A71-37694

Wave growth for distributed parameter dynamic system independent of time and coordinates, investigating stability with linear approximation

19 p3103 A71-37757

Linear system stability via Liapunov method and square integral, establishing continuous and discrete time systems equivalence

19 p3086 A71-37885

Book on active and nonlinear wave propagation in electronics covering transmission lines, wave systems stability, quasi-harmonic active propagation, equivalent circuits, etc

19 p3029 A71-38018

Nonlinear instability theory for wave system in plane Poiseuille flow, deriving asymptotic solution for initial value problem

19 p3046 A71-38203

Finite Larmor radius equations for collisionless plasmas in magnetic fields, noting application to axisymmetric systems stability

19 p3115 A71-38209

Monograph on strong signal behavior of control systems containing multiphase rectifier, covering stability of high power sources

19 p3039 A71-38550

Frequency domain stability criteria for dynamical systems with random parameters, considering open loop stability, stochastic gain element rms value and linear element effective bandwidth

19 p3039 A71-38710

Liapunov direct method for transient multimachine power-system stability analysis using multivariable control modeling

20 p3207 A71-38949

Exponential absolute stability of nonlinear discrete systems of Lure type, deriving modified frequency condition

20 p3255 A71-39028

Checking method for reflection-type holographic system behavior, emphasizing critical stability of glass plate

20 p3236 A71-39191

Nonlinear autonomous oscillation systems stability conditions derivation by Kamenkov method for quasi-linear systems

20 p3269 A71-39107

Liapunov stability of rigorous particular solutions /corresponding to libration points/ of three body problem, determining motions of satellite influenced by two spherical bodies

20 p3291 A71-39317

Equilibrium position stability of Hamiltonian systems with one and two degrees of freedom in resonance

20 p3270 A71-39322

Action reproduction accuracy of nonlinear controlled systems with constraints and delays, estimating maximum error and stability degree

20 p3208 A71-39363

Liapunov functions application to Stability of systems described by nonlinear second-order ordinary differential equations, considering feedback control loops construction

20 p3255 A71-39454

Lagrange-Dirichlet and Routh systems stability theorems inversion, proving motion instability in case of potential energy maximum in solutions to differential equations

21 p3414 A71-40050

Cyclic discrete holonomic mechanical system Liapunov stability analysis, developing matrix formalism for kinetic energy, Routhian, Hamiltonian and dynamic potential energy quadratic approximation

21 p3454 A71-40097

Stability characteristics and general transient motion of vertical finite width three lobe journal bearings assuming incompressible fluid with cavitation [ASME PAPER 71-VIBR-76]

21 p3385 A71-40330

Critical evaluation of Schur-Cohn condition test for stability of multilevel finite difference schemes

21 p3408 A71-40859

Liapunov-type analysis of linear systems dynamic stability under stochastic parametric excitation, noting application to rectangular flat plates

21 p3469 A71-41000

Axially loaded slender beam mass and deformation effect on constrained bending motion system stability and dynamic response

21 p3469 A71-41010

Stability and quality diagrams of linear discrete automatic control systems with time constant parameter

21 p3361 A71-41114

Modulation instability of dispersion type NMR stabilizer of resonance conditions, determining critical frequency of self excitation and maximum amplification

22 p3519 A71-41444

Externally pressurized gas journal bearing whirl instability stabilization system, predicting whirl onset threshold speed

22 p3551 A71-41664

Spiral grooved thrust and spherical gas bearings predicting stability and frequency response by Newton-Raphson and orthonormalization methods

22 p3551 A71-41664

Soviet book on multivariable automatic control system synthesis with adaptation to computer covering methodology, algorithms, transfer function approximation and stability problem

22 p3525 A71-41791

French monograph on extrapolation type extremum control systems speed and stability performance improvement based on Jacob step duration modulation method

22 p3526 A71-42060

Stability of finite difference approximation to mixed initial boundary value problems for linear parabolic system of equations

22 p3567 A71-42229

Quasi-optical transmission line stability improvement, investigating pulsating light beam concept

22 p3512 A71-42301

Flip-flop circuits nonlinear distributed network mathematical model, investigating oscillations nonexistence

22 p3527 A71-42627

Single cavity multiple device microwave oscillated with 12 IMPATT diodes combined output power presenting proof for circuit configuration stable operation free from moding problems

22 p3524 A71-42638

Telemetry systems with discrete compression-expansion function, calculating noise stability improvement

ment as compared to linear and nonlinear signal conversion operations

22 p3515 A71-42859

Axial flow compressors stable operation, using rotating guide vanes regulation

23 p3626 A71-43554

Small autooscillations of high order differential equations system, investigating bifurcation occurrence relationship to zero equilibrium position stability change

23 p3699 A71-43572

Singular optimal control theory generalization using appropriate transformations, considering stability results for bang-bang solutions

23 p3657 A71-43941

Stability conditions of linear discrete system with periodic feedback from spectrum location of bounded linear operator acting in Banach space

23 p3657 A71-44078

Asymptotic stability domain determination for nonlinear distributed parameter system, deriving coupling coefficients

23 p3699 A71-44079

Analysis and stability of multiloop attitude control systems for flexible spacecraft

23 p3773 A71-44091

Adaptive guaranteed cost control for systems with parametric variation, demonstrating system stability and airframe pitch control

23 p3659 A71-44111

Single- and multivariable discrete nonlinear control systems with pulse amplitude modulation, deriving frequency criteria for stochastic stability in mean

24 p3812 A71-44397

Stochastic linear systems stability with random processes coefficients, using differential equations

24 p3815 A71-44698

Linear systems with randomly varying parameters, deriving stability conditions from one dimensional distribution functions

24 p3815 A71-44699

Vibrational systems stability in presence of time dependent random parametric disturbances, using frequency analysis methods

24 p3848 A71-44851

Unstable systems dynamic stabilization, deriving conditions from second order linear differential equations with variable coefficients

24 p3849 A71-45048

SYSTOLE

Abnormal left ventricular contour with late systolic murmur at apex preceded by click and with abnormal T waves in electrocardiogram

02 p0197 A71-11694

Epinephrine infusion in man, examining systolic time intervals and sympathetic stimulation in cardiovascular dynamics

06 p0850 A71-17440

Mitral valve systolic prolapse aggravation due to G acceleration and aeromedical significance

09 p1395 A71-23246

SYSTOLIC PRESSURE

Right and left ventricular systolic time intervals from high fidelity pulmonary arterial pulse wave measurements

06 p0852 A71-17875

Transthoracic measurements of left and right ventricular systolic pressures in anesthetized mice, using fiber optics and strain gage manometer techniques

09 p1401 A71-23371

Baroreflex regulation of pulse interval during bicycling exercise, using systolic pressure-pulse relation to express reflex sensitivity

13 p2012 A71-28951

Sitting and supine position effect on exercise tolerance, heart rate, systolic pressure and respiration rate in male subjects with coronary insufficiency, noting onset of angina pectoris

13 p2014 A71-29303

Systolic and diastolic blood pressures and urinary catecholamines under stress in normotensive and hypertensive subjects

15 p2358 A71-31451

Heart myocardium contractility assessment based on pressure rise rate relation to intraventricular pressure during isovolumic systole

17 p2681 A71-35039

Myocardial inotropism index, using left ventricle time varying pressure/volume ratio in systole

17 p2683 A71-35121

Heart rate and systolic pressure variability control through visual feedback of physiological information, obtaining respiratory measurements and ECG

21 p3344 A71-41037

Cardiac sympathetic nervous control of right ventricular pressure-flow dynamics in outflow tract in anesthetized dogs

22 p3484 A71-41522

Mid-systolic clicks and papillary muscle dysfunction evidence in arteriosclerotic heart disease from ECG, carotid pulse tracing and phonocardiography

23 p3635 A71-44126

Early systolic clicks shown due to mitral valve prolapse by phonocardiography, cardiac catheterization and angiography

23 p3635 A71-44127

T

T SHAPE

Rectangular composite prismatic bar with T shaped cross section, calculating torsion with summary representation method

17 p2824 A71-34847

Rectangular waveguide with T shaped pedestal, deriving characteristic impedance, maximum power and damping constant

22 p3515 A71-42746

Ultrasonic method for measuring poor root penetration zone width in welded T joints without reference standard, suggesting practical applications

24 p3829 A71-44785

T TAIL SURFACES

Aircraft response to atmospheric gust, discussing spectral analysis procedures and calculation results on T-tail aircraft design

01 p0005 A71-10752

T tail flutter analysis, considering dihedral, angle of attack and aerodynamic force effects

11 p1706 A71-25188

Aircraft with T tail configuration, examining dynamic response to lateral gusts

14 p2174 A71-29786

Experimental and theoretical aeroelastic analysis of Fokker F-28 T tail, using flutter model and flight flutter tests

17 p2676 A71-35649

T TAURI STARS

Novae, symbiotic, T Tauri, U Geminorum and UV Ceti type stars, determining mass loss rate

06 p0973 A71-18338

Pre-main sequence /T Tauri/ stellar evolution, discussing mass loss rates and star formation by interstellar cloud violent hydrodynamic compression

09 p1528 A71-23592

T Tauri stars Li, Be and B autogenic generation, considering underabundance in surrounding gas

16 p2626 A71-33433

Hydroxyl emission at T Tauri stars positions in Taurus-Auriga region, discussing radial velocities of stars and dust clouds

19 p3144 A71-38172

T-33 AIRCRAFT

Lateral-directional handling qualities and roll control power requirements for executive jet and military class II airplanes in landing approach flight phase [AIAA PAPER 71-771]

16 p2524 A71-34007

TABLES [DATA]

NT CONVERSION TABLES

Orbital elements of spectroscopic binary Zeta Scuti by computer program and spectrograph observations, tabulating results

01 p0152 A71-10353

Mie extinction parameters tabulation for computed signal transmission through rain at microwave and visible frequencies

01 p0029 A71-10469

Program and auxiliary tables for stellar azimuth determination by observations near elongation

01 p0159 A71-10810

Solar constant and zero air mass spectrum, discussing new standard values

01 p0159 A71-10861

Solar chromospheric flares observations tabulation /1969/ and H alpha line width curves graph

01 p0144 A71-10870

Extragalactic radio source 3CR catalog, analyzing emission spectra

02 p0300 A71-12087

Visual information industrial processing rates correction tables with digits, letters, Landholdt fringes and geometrical figures

03 p0364 A71-13525

Minor planets precise position tabulations, correcting previously published data

03 p0493 A71-14195

Compressed liquid and gaseous fluorine constant volume specific heat measurements, tabulating results

04 p0674 A71-14729

Corrections derived for Labs-Neckel 1968 solar radiation tables transformation into 1968 International Practical Temperature Scale

05 p0797 A71-16018

Arsenic first spark line spectra using high resolution grating spectrograph and Fabry-Perot interferometer

05 p0717 A71-16910

Pulsar data tabulation of positions, dispersion measures, and class I pulse periods and widths

06 p0966 A71-17676

Zodiacal light brightness measurement in three mutually perpendicular directions, tabulating data

06 p0966 A71-17677

Soviet book of gas dynamic function tables for two and three dimensional flows past blunt bodies

07 p1013 A71-19050

Photoelectric UVB observations of variable star AE Aur /November 1963-February 1968/, tabulating and graphing results

07 p1201 A71-20434

Eclipsing variable V701 Cen photoelectric observations in UVB tabulated, fitting Russell model solutions to data

08 p1357 A71-20874

Extragalactic radio source 3CR catalog, analyzing emission spectra

08 p1362 A71-21137

Book of tables and graphs for circular cylindrical shells free vibrations

08 p1370 A71-21234

Rotating cantilever beams flexural vibrations, developing tables for frequency equation determination

08 p1370 A71-21306

Lunar reverse side, tabulating reference points on western libration zone and eastern sector

08 p1366 A71-21777

Distributed gain amplifiers synthesis technique permitting use of filter and transmission line design tables

09 p1413 A71-22158

Approximate determination of 44 minor planets orbits, tabulating orbital elements

09 p1526 A71-23344

Italian book on mixed plasmas equilibrium compositions and thermodynamic properties, covering numerical values tabulation for nitrogen mixtures with He, Ar and Xe

09 p1505 A71-23353

Equilibrium compositions and thermodynamic properties tabulated for argon-oxygen plasmas at 0.01 to 10 atm and up to 35,000 K

12 p1986 A71-27187

Saturnicentric latitude measurements tabulation for use with standard drawings

13 p2136 A71-28388

Solar chromospheric flares in 1969, constructing tables of observation data commencement and end time and H alpha line maximum width

13 p2128 A71-28480

Tables of scattering functions and albedo for semiinfinite atmospheres according to nonconservative Rayleigh phase matrix for diffuse radiation computation

14 p2274 A71-30059

Supplementary tables to SI nomenclature for radiometry and photometry including photon flux

14 p2242 A71-30157

Normal gravity field parameters from harmonic coefficients and satellite observation data

15 p2492 A71-32468

Beam foil excited Ar spectrum between 500 and 1000 A, tabulating lines with ionization stages based on line intensity variation with beam energy

15 p2368 A71-32601

Producer risk determination and tables for Method 4 maintainability demonstration plan of MIL-STD-471

16 p2583 A71-33303

Meteor spectrum analysis presenting tables for Soviet observations

16 p2639 A71-33694

Galactic clusters characteristics tabulation and statistical analysis, calculating dimensions, luminosity and radial velocities dispersion

17 p2804 A71-34841

Mars, Uranus and Jupiter observations with Sao Paulo Observatory Danjon astrolabe, presenting east and west transits right ascension and declination tables

18 p2961 A71-35943

Truth table analysis of models of Jupiter Great Red Spot, suggesting chromophores welling from below

18 p2967 A71-36926

Position, parallax, distance, visual apparent and absolute magnitude, spectrum and visual luminosity tables for nearby stars

18 p2968 A71-37030

Two dimensional structures of 76 extragalactic radio sources at 1425 MHz in tabular and graphical forms

18 p2970 A71-37064

Radio sources position data table based on high accuracy telescope observation including calibration uncertainties and measurement random errors

19 p3142 A71-38008

Mars motion 1751-1969, comparing Clemence theory and Newcomb Tables of sun with meridian and radar ranging Mars observations

19 p3144 A71-38166

Wavelength table for determination of stellar radial velocities in spectral classes F6-M2, including Hyades cluster and Coma Berenices

19 p3144 A71-38168

Book on antenna characteristics covering tabulated data for cylindrical dipoles and monopoles, imperfectly conducting dipoles, circular loop antennas and broadside and endfire arrays

20 p3196 A71-39200

Cold climate clothed human windchill tables, considering various heat transfer modes and skin temperature

20 p3192 A71-39205

Computerized tabular data display with cross-bar addressed glow discharge panel, discussing system details
21 p3350 A71-40115

Solar activity tabulation and review covering International Geophysical Year and International Quiet Sun Year
21 p3442 A71-40151

Solar radioelectric activity in 1966, tabulating mean daily density and variability of solar flux
21 p3442 A71-40152

Four-color and H beta photometric data tabulation for bright B type stars in Southern Hemisphere
21 p3443 A71-40192

Tabular listing of frequency allocations for space services and radio astronomy made at Extraordinary Administrative Radio Conference
21 p3348 A71-40476

Errors resulting from linear interpolation use in opacity tables for stellar interior calculations
22 p3599 A71-41923

Glass fiber reinforced flame retardant thermoplastic resins, tabulating flammability resistance and mechanical properties
22 p3565 A71-42076

Geomagnetic index Kp frequency distribution tables /1932-1970/
23 p3670 A71-43192

Persistent and semipersistent thick and dense fog visibility definitions and tabulated data for London/Heathrow Airport and Kingsway/Holborn during 1950-1969
23 p3701 A71-43890

Tables for aurora correlation with solar radio bursts at 185 MHz
23 p3769 A71-43908

Quasars light curves and intensity-time tables
23 p3769 A71-43993

Tables of Crab Nebula pulsar radio pulse arrival times at Arecibo observatory
24 p3867 A71-44435

TABS [CONTROL SURFACES]

Jet tab thrust vector control system for tactical missile applications, describing operational principles, design details and performance characteristics [AIAA PAPER 71-752]
18 p2956 A71-36773

TABULATION

U. TABULATION PROCESSES

Computer program for selected gases outgassing rates calculation, tabulating and plotting for NERVA fuel elements gas evaluation
09 p1492 A71-23348

TACAN

Navigator role in TACAN of reconnaissance and fighter aircraft, noting Weapon System Officer functions
01 p0123 A71-10503

L band DME and TACAN improvements, emphasizing use of static broadband amplifiers
02 p0235 A71-12905

U.S. domestic ATC airspace enroute and terminal area navigation system effects on pilot workload, projecting future FAA requirements
07 p1157 A71-20347

Technical aspects of tactical all-weather instrument landing system of Swedish STOL aircraft Saab 37 Viggen
11 p1796 A71-25233

U.S. Army ATC cost-effective system developments for high density low altitude helicopter tactical operations to avoid enemy radar under near-all weather conditions
22 p3571 A71-42084

TACHISTOSCOPES

Digital tachystoscope functions, operating principles and designs, discussing tests of visual perception related functions
05 p0714 A71-16924

TACHYCARDIA

Digital-induced bundle branch ventricular tachycardia from electrode catheter recordings of dogs specialized conducting tissues
06 p0852 A71-17873

TACHYONS

Gravitational shock waves from tachyons, considering capability for Weber gravitational radiation detection apparatus excitation across astronomical distances
11 p1798 A71-25591

Tachyons in cosmic ray showers, investigating occurrence frequency relative to electrons
15 p2474 A71-31731

TACTICAL AIR NAVIGATION

U. TACAN

TACTICS

Zero sum differential game solution for aerial combat problem, applying direct gradient methods
23 p3699 A71-44103

TACTILE DISCRIMINATION

Visual-tactile dominance relationship as function of tactical judgment accuracy
07 p1045 A71-20385

Vibrotactile information transmission, discussing skin mechano-receptive systems and similarities or differences between auditory and tactile characteristics
10 p1563 A71-24231

Performance differences between tactile and visual localization and temporal ordering ability, using sequential presentation of high rate point stimuli
15 p2363 A71-31948

Functional ability of human tactual analyzer by measuring minimum interval between two discrete controlled stimuli
21 p3344 A71-41064

TACTILE SENSATION

U. TOUCH

TAGGING

U. MARKING

TAIL ASSEMBLIES

Carbon fiber reinforced epoxy composites, evaluating application as helicopter tail rotor blade material
02 p0273 A71-12477

Tail assembly load distribution in steady uniform flow for nonzero angles of attack, using slender body theory
04 p0527 A71-15367

Round cold jet inclination effects on VTOL aircraft tail assembly lift and longitudinal stability in transition region [DGLR-70-053]
05 p0693 A71-15967

Aft vs canard horizontal tail locations for fighter/attack configuration at sub and supersonic speeds, observing lift coefficient, L/D and longitudinal stability [AIAA PAPER 71-8]
06 p0848 A71-18482

Composite structures development, discussing wing, fuselage, aeropropulsion and missile development, weight savings of hardware and fighter empennage applications [AIAA PAPER 71-367]
18 p2979 A71-36275

TAIL MOUNTINGS

U. TAIL ASSEMBLIES

TAIL PLANES

U. HORIZONTAL TAIL SURFACES

TAIL SURFACES

NT. HORIZONTAL TAIL SURFACES

Inclined engine cold circular jet effects on tail control surfaces aerodynamic characteristics, considering aircraft longitudinal stability [DFVLR-SONDDR-104]
10 p1552 A71-24593

Sailplanes tail load static derivation for instantaneous unchecked longitudinal maneuver, considering aperiodic response
11 p1708 A71-26486

Sailplanes control, deriving incremental aerodynamic load on horizontal tail produced by instantaneous elevator deflection
11 p1708 A71-26487

Flight test measurements of shock cell noise loading of aircraft tail planes, noting alleviation by nozzle and mirror structural modifications
19 p2998 A71-38467

TAILLESS AIRCRAFT

NT. MIRAGE 3 AIRCRAFT

TAILORING

U. DESIGN

TAILS [ASSEMBLIES]

U. TAIL ASSEMBLIES

TAKEOFF

NT. VERTICAL TAKEOFF

All-weather aircraft operations, discussing takeoff, landing, safety and forecasting
06 p0847 A71-17923

Boeing 737 aircraft takeoff and landing performance, emphasizing high lift systems and stopping capability
07 p1018 A71-19083

Aircraft optimum minimum noise takeoff profile, solving by equations of motion system for jet aircraft
08 p1331 A71-20779

Soviet book on aircraft flight with incomplete and asymmetrical thrust covering probabilistic characteristics, stability, landing and takeoff with partial engine failures, etc
10 p1554 A71-24013

Mutual aerodynamic effects of SM-1 helicopters during simultaneous takeoff and landing, determining minimum distances between helicopters
12 p1867 A71-26953

Jet engines with afterburners, describing exhaust nozzle control, takeoff and landing advantages and thrust variations
21 p3437 A71-40858

SST handling qualities, takeoff speeds and performance evaluation on six degree of freedom flight simulator
23 p3627 A71-42922

Low thrust vehicle optimal takeoff calculations from orbit about oblate planet, using two variable asymptotic expansion technique [AAS PAPER 71-367]
23 p3729 A71-43037

TAKEOFF RUNS

STOL and boundary layer control aircraft takeoff and landing distance, considering jet suction action influence on lift and drag coefficients
04 p0529 A71-14595

French disengageable silencer for jet engine noise attenuation during aircraft takeoff
15 p2471 A71-32696

Supercooled fog dissipation by liquid propane determining effectiveness in providing operational support to aircraft landing and takeoff
16 p2604 A71-33546

Trailing wake hazards of large transports in takeoff and landing, examining configuration stability of vortices pair in ground effect
17 p2674 A71-35759

Aircraft noise reduction in takeoffs/operations procedures and by land use planning
20 p3209 A71-39394

Aircraft accelerate-stop factors and regulations pilot reaction times and accidents during takeoff
23 p3628 A71-43386

TAKEOFF SYSTEMS

U. AIRCRAFT LAUNCHING DEVICES

TALC

Van der Waal bound lamellar solids interlayer binding energy computational model, discussing talc and pyrophyllite equilibrium stacking arrangements and force constants
10 p1573 A71-24541

Statites replicas electron microscopy for microstructure variations with composition and firing conditions differences, discussing protoenstatite crystallization and glass phase formation
13 p2093 A71-28664

TALKING

NT. SYLLABLES

NT. WORDS [LANGUAGE]

TANDEM ROTOR HELICOPTERS

NT. CH-46 HELICOPTER

NT. CH-47 HELICOPTER

TANK GEOMETRY

Nonlinear large vibrations of ideal incompressible homogeneous fluid in cylindrical sector tanks, determining hydrodynamic equations coefficients and relation to tank geometry
03 p0405 A71-14564

Computerized sloshing frequencies of tilting two dimensional tank of flat free surfaces with respect to effective gravity
11 p1752 A71-26198

TANKS [CONTAINERS]

NT. CYLINDRICAL TANKS

NT. FUEL TANKS

NT. PROPELLANT TANKS

NT. SPHERICAL TANKS

NT. STORAGE TANKS

NT. WING TANKS

Dynamic behavior of liquids in partially filled mobile tanks under almost centrifugal force fields
01 p0069 A71-10398

Liquid-vapor system in closed container, investigating transient pressure rise under heat and mass transfer interactions including incipient and nucleate boiling
04 p0687 A71-15535

Elastic momentless conical tank with spherical bottom partially filled by liquid, calculating axisymmetric oscillation
06 p0995 A71-17826

Model and glass tank furnaces for earth upper mantle convection movements simulation, studying fluid dynamics and geodynamic processes
07 p1105 A71-20448

TANTALUM

Ta thermal properties at high temperature in case of cylinder, powder and wire specimens
01 p0100 A71-10547

Chemisorption layer kinetics of oxygen on thin Ta films at room temperature and low pressures
03 p0441 A71-13359

Chemisorption and sticking probability of nitrogen on Ta films, considering relationship to temperature and pressure
03 p0441 A71-13360

Chemisorption rate and physical adsorption of nitrogen on Ta films as function of temperature
03 p0441 A71-13361

Ta spectral emissivity in red and green and relationship to surface structure change induced by heat treatment
03 p0460 A71-14465

Ta single crystals solution hardening, discussing interstitial impurities effects on bcc metals flow stress temperature dependence
05 p0765 A71-16162

Nitrogen chemisorption and absorption on polycrystal Ta ribbons, using static method in ultrahigh vacuum
06 p0940 A71-17299

Nitrogen chemisorption on Ta by field emission microscopy, taking into account work function changes
06 p0940 A71-17299

Recrystallized annealed Ta, examining strain rate effect on mechanical properties
06 p0914 A71-18684

Ta single crystals with interstitial carbon, nitrogen and oxygen, examining Peierls and interstitial hardening stresses additivity
08 p1307 A71-21503

Ta and W single crystals yield stress temperature dependence, confirming asymmetric Peierls barrier
08 p1307 A71-21507

Slip asymmetry in Ta and Ta alloys, discussing effects of temperature and alloying elements
08 p1308 A71-21518

Strain rate effects on Ta flow stress, examining yield and postyield behavior models and stress-strain diagrams
08 p1313 A71-21562

Corrosion mechanism in Ta-Li high temperature heat pipes by ion analysis, demonstrating oxygen and yttrium diffusion into heating zone
12 p1916 A71-26974

Boron modifications and carbides formation by vapor deposition on tantalum filaments
12 p1943 A71-27093

W, Mo, Ta and W-Mo alloys hardness integrity, using high temperature microhardness tester
13 p2084 A71-28113

Tantalum disilicide kinetic interaction with Ta, investigating formation rate at various temperatures
13 p2089 A71-29415

Ta nitriding temperature and duration effects on tensile strength, elongation and surface hardness
15 p2424 A71-31240

Fifth group transition elements V, Nb and Ta, showing most stable metal dioxide gaseous compounds
15 p2424 A71-31391

Thermoelastic stress generation in Cu and Ta samples by linear accelerator produced monochromatic MeV electron pulses, comparing measurements with wave theory predictions
15 p2414 A71-31973

Unalloyed tantalum as containment material in mercury Rankine cycle SNAP 8 system boiler for 5 year service life
15 p2448 A71-32221

Thermionic emission and adsorption characteristics of Ta single crystal faces in cesium atom streams, using thermoelectronic and surface ionization methods
15 p2453 A71-32643

Thermal characteristics of emission and work functions of spherical Ta single crystal faces by Martin microscope measurements
15 p2453 A71-32644

Sputtered tantalum films oxygen content determination by anodization current efficiency measurements
16 p2621 A71-33187

Thermophysical properties of Ta, W and Ta-W alloy at high temperatures, using automatic high vacuum facility
20 p3247 A71-38764

Low temperature proton irradiation damage and recovery in discontinuous Ta films sputtered in oxygen and nitrogen
22 p3585 A71-41804

Interconnection Ta thin films and silicon encapsulation for solid state components in hybrid IC under high humidity
23 p3656 A71-43431

Polycrystalline Nb and Ta and Ta-on-Nb thin film thermionic emission surface barrier analysis from periodic deviations in Schottky effect
24 p3862 A71-45346

TANTALUM ALLOYS

Ta alloys single crystals elastic compliance constants over temperature range, deriving bulk and shear moduli and anisotropy factor
01 p0100 A71-10373

Cu compatibility with refractory Ta-W alloy interface at high temperature, noting eutectic formation
01 p0100 A71-10374

Crystalline structural changes during decomposition of supersaturated solid solution of Ta in Co
01 p0101 A71-10608

Hardening effects of various Ta proportions in Fe-Ni-Ta alloys, noting austenitic nature after homogenization and quenching at high temperature
01 p0105 A71-11619

Precipitation reactions in concentrated Ta-Hf and Nb-Hf alloys at 600-1400 C from X ray diffraction and transmission microscopy, discussing phase relations
06 p0914 A71-18679

Slip asymmetry in Ta and Ta alloys, discussing effects of temperature and alloying elements
08 p1308 A71-21518

Solid solution hardening of Ta base alloys as function of elastic interaction between dislocations and solute atoms
08 p1309 A71-21523

Protective coatings of Ta, Nb and TD alloys for high performance thermal protection systems, discussing space shuttle reentry heat shield
11 p1778 A71-25554

W-Mo-Ta system alloys investigated along four radial sections from tungsten corner, establishing Ta additions effect on maximal strength
11 p1782 A71-26473

Nb-N and Ta-N alloys, calculating electrical resistivity and solid solutions lattice constants at various temperatures
12 p1917 A71-27295

Silicidization on Nb-Ta alloys, considering formation of niobium disilicide phase with hexagonal lattice
15 p2425 A71-31401

Phase diagrams of ternary systems Ta-Fe-B and Ta-Ni-B using X ray and metallographic analyses
16 p2592 A71-33575

High temperature tensile strength of Ta-W-Hf alloy sheet with protective Si-Ti coating in vacuum and air
18 p2933 A71-35951

Ti-W-B, Hf-Ta-B and Ta-W-B alloys isothermal phase diagrams at 1400 C, using X ray analysis and metallographic techniques
19 p3076 A71-37112

Structure, superconductivity transition temperature, microhardness and electrical resistivity of V-Ta-Ti cast alloys
19 p3078 A71-37468

Concentration effects of Nb and Ta on strengthening in tetrahedral section of W-Mo-Nb-Ta system at temperatures from 20 to 1100 C
19 p3078 A71-37473

Thermophysical properties of Ta, W and Ta-W alloy at high temperatures, using automatic high vacuum facility
20 p3247 A71-38764

Ta-W polycrystals and single crystals oxidation at 850-1100 C, noting anisotropic scale-fracture morphologies
20 p3252 A71-39373

Solid solution hardening in Ta alloy single crystals, investigating temperature effects on interstitial impurities scavenging and lattice mechanism
21 p3395 A71-40027

Monocrystalline and polycrystalline Ta-Hf oxidation at 750-1050 C, noting orientation
22 p3563 A71-42363

Tensile and creep rupture strength and microstructure of Co-Fe-Ta alloys at elevated temperatures
24 p3836 A71-44442

TANTALUM CARBIDES

Metals and alloys strengthening by in situ grown transition metal carbide fibers, noting whisker-like characteristics
08 p1315 A71-21586

Co-Cr and Ni-Cr eutectic alloys with single crystal TaC fiber reinforcement, discussing unidirectional solidification
09 p1479 A71-23623

Polycrystalline NbC and TaC Young, shear and bulk moduli determination at high temperature, noting porosity and temperature effects
11 p1781 A71-26294

Ta-V-C ternary system solidus surface and equilibrium diagram determination by metallographic techniques and X ray and thermal analyses
15 p2430 A71-32147

Heat content measurement of tantalum carbide in homogeneity range at high temperatures by mixing method using bulk calorimeter
15 p2431 A71-32155

Stress variation with varying plastic deformation rate and temperature in tantalum carbide between 1200 and 2200 C
17 p2760 A71-35550

High temperature four point bending vacuum furnace machine testing thin refractory sheets, noting strain rate, velocity jump and relaxation on tantalum carbide
19 p3063 A71-37554

Eutectoidal decomposition of tantalum dicarbide, noting X ray phase identification during carburization of tantalum ribbons
20 p3252 A71-39961

TaC-WC, ZrC-WC and refractory compounds thermal expansion coefficient measurements
24 p3838 A71-44738

TANTALUM COMPOUNDS

NT TANTALUM CARBIDES

NT TANTALUM OXIDES

Tantalum and niobium disilicides enthalpy and heat capacity temperature dependences
02 p0263 A71-12198

Tantalum and niobium disilicides enthalpy and specific heat temperature dependences in 1200-2100 K range
15 p2426 A71-31504

Minimum voltages and limiting frequencies for oblique cut longitudinal octahedral crystal modulators with large electro-optic coefficients, including lithium niobates and tantalates
15 p2461 A71-32606

TANTALUM OXIDES

SHF lithium tantalum oxide optical modulator for optical detector evaluation, discussing bandwidth and phase modulation characteristics
12 p1903 A71-26790

Thermal diffusion in tantalum-oxygen and columbium-oxygen mixed crystals, investigating temperature and concentration effects
16 p2599 A71-34092

Simultaneous degassing and thermal diffusion phenomena in annealed tantalum-oxygen mixed crystals, investigating maximum temperature effect
16 p2599 A71-34094

Tantalum and niobium ternary oxides recovery from liquid potassium solution, determining composition and crystallographic modifications by chemical and X ray diffraction analyses
20 p3194 A71-39372

TAPE MERGING

U DATA PROCESSING

U MAGNETIC TAPES

TAPE RECORDERS

Magnetic tape recording system FM distortion derivation from head-to-tape spacing transfer function
01 p0033 A71-10892

Instrumentation magnetic tape recorder reproduce systems equalization using active circuits and signal processing to develop required transfer function
01 p0082 A71-10894

Machine-to-machine compatibility in wideband magnetic tape recording, discussing record-head gap width variations effects on record transfer characteristics
01 p0033 A71-10895

Instrumentation tape recorder time base error effects on signal carrier amplitude and spectral purity
01 p0033 A71-10896

Notch power ratio noise tests on magnetic tape recorder/reproducer using direct recording in baseband
01 p0034 A71-10910

Very long baseline interferometry (VLBI)/one-bit instrumentation using videotape recorders in geodetic and geophysical measurements
02 p0251 A71-12332

FM data recording system with transducers for converting varying parameters into frequency and tape recorder capable of playback for computer analysis
03 p0383 A71-14344

Photoelectric automatic logger with perforated tape recorder, discussing block diagram
04 p0589 A71-14837

FM converter for tape recording of LF biological data
04 p0545 A71-15163

Analog transducers and tape recorders measurement sensitivity and conversion factor stabilization using push-pull signals
05 p0747 A71-16144

Signals measurement distortions in FM recording-reproducing channel due to recorder magnetic tape speed fluctuations, discussing compensation methods
05 p0752 A71-16724

Long life spacecraft tape recorders, considering digital and analog equipment and life and reliability testing of components and complete units
07 p1106 A71-18812

Magnetic tape recording systems nonlinear amplitude distortion in terms of transfer function characteristics applied to analog instrumentation
09 p1449 A71-22786

Random vibration laboratory equalization by multiple taping of noise signals on recorder and manual processing
11 p1746 A71-26513

Video tape recorder (VTR) for onboard storage of wideband analog and high rate digital sensor outputs of ERTS
14 p2249 A71-30901

Field testing for radio telemetry receiving systems calibration, including tape recorder degradation effects during data processing
14 p2198 A71-30903

Tape recorder equalization techniques effects on attainable bit error probability in digital communication, considering asymptotic prediction recording PCM/FM case
14 p2249 A71-30918

Autoplotter for radar echoes on CRT screen, using video tape recorder for ship navigation use
19 p3017 A71-37700

Spacecraft tape recorder design for five years minimum continuous unattended reliable operation, describing quality control and environmental/life testing procedures
22 p3608 A71-41507

TAPER

U TAPERING

TAPERED COLUMNS

Tapered cantilevered beams design, determining end deflection and bending stress magnitude by graphical method
07 p1213 A71-19693

TAPERED WINGS

U SWEPT WINGS

TAPERING

Tapered distributed RC low pass network configuration with voltage-controlled sources for sensitivity reduction low and high Q factors
21 p3361 A71-41409

TARE (DATA REDUCTION)

U DATA REDUCTION

TARGET ACQUISITION

Information feedback distortion and countertraining effects on learning and performance in lever displacement-target test
01 p0026 A71-11415

Target detection facilitation by adjacent border control involving distance between inducing visual fields and duration of presentation

01 p0026 A71-11416

Radar energy loss estimate over space targets, considering various energy distributions in given search volume, target acquisition probability, signal to noise ratio, etc

02 p0212 A71-11879

Optical design of image selector for Cassegrain telescope recording difference spectrum of targets in focal plane

03 p0425 A71-13646

Proportional navigation vs optimally evasive constant speed target in two dimensions, considering lateral acceleration and time constraints in pursuer control

03 p0455 A71-14438

Radar target optimal detection algorithms in cloud of passive reflectors, noting space surveillance regularities

05 p0722 A71-16870

Crotale low altitude ground to air missile, discussing target acquisition and fire control units, maintenance and operation

06 p0979 A71-17567

High target geodetic coordinates determination by measuring vertical angles without using azimuth

06 p0889 A71-17675

Fluctuating radar target detection in clutter by sidelobe blanking system, discussing false alarm adaptive threshold procedure

07 p1154 A71-18842

Free and systematic horizontal visual search target detection times, testing human subjects with mixed stimulus schedules on high and low contrast targets

07 p1047 A71-19463

Target aiming function /TAF/ susceptibility to vagotonic vegetative imbalance in male subjects after experimental kinesis

07 p1047 A71-19464

Airborne night vision system performance, determining maximum range for ground target acquisition

08 p1286 A71-20692

Target detection improvement in reconnaissance by black and white TV system, using narrow band filters for conversion to multispectral sensor system

08 p1287 A71-21240

Satellite carrier tracking and phase lock carrier loops, evaluating lock and reacquisition performance loss by linear model and Monte Carlo digital simulation

08 p1270 A71-21352

Mean retinal threshold gradient along horizontal meridian for dark and light adapted eyes, considering dynamic neural mechanism

10 p1566 A71-24807

Optimal nonlinear control with fixed time and compact convex target set, using gradient method

12 p1923 A71-27728

Radarscope net for target azimuth and distance and for direct altitude readout through beacon numerics

13 p2033 A71-28886

Instantaneous frequency statistical characteristics of passive noise spectra and fluctuating signals reflected from nonpoint moving radar targets

14 p2195 A71-30111

Electromagnetic inverse scattering model of electrical radius of conducting spherical radar target employing expansion of scattered field in vector wave functions

14 p2196 A71-30564

Airborne ECM receiver, determining conditions for detecting victim radar signal before signal reflection from aircraft

15 p2368 A71-31207

Speed and accuracy relation of hand movement aimed at target, showing error as function of length of uncontrolled terminal phase

16 p2536 A71-33372

Low level target locating by monopulse and conical scanning radar, solving balance equation

17 p2708 A71-35482

Q switched laser range finders, discussing programmed ephemeris guided, divergence data utilizing and semiautomatic tracking systems with emphasis on target acquisition [ONERA-TP-964]

18 p2945 A71-36029

Light detection and ranging /LIDAR/ system in airborne and ground applications for moving target location and tracking

18 p2882 A71-36615

Five-gate automatic acquisition star and satellite TV tracker with video signal from vidicon or image orthicon, using line-to-line correlation for SNR improvement

18 p2882 A71-36904

Optical target detection and position error signal system for boost phase missiles, using TV with digital computer controlled dual tracking electronics

18 p2883 A71-36911

Extraretinal correction and memory for target position, suggesting corrective tendency of eye movements in dark

19 p3004 A71-38286

Proportional navigation for trajectory control of missile homing on target in planar pursuit

20 p3261 A71-38856

Recursive algorithms for detection probabilities of fluctuating targets in Gaussian noise, including cell averaging constant false alarm rate /CFAR/ extension

20 p3195 A71-38860

Cumulative probability of target detection for pulse surveillance radars, relating target cross section, velocity and radar frame

20 p3199 A71-39901

Binary moving-window integrator radar target azimuth measurement error determination, presenting target detection probability curves obtained by digital simulation

21 p3348 A71-40725

Noise equivalent irradiance evaluation of passive IR scanners for target thermal mapping systems operating in earth atmosphere, determining figure of merit

22 p3545 A71-42150

Visual performance in simulated target acquisition tasks as function of flare-ignition altitude

22 p3503 A71-42196

Linear regression optimal filtering application to aircraft target tracking

23 p3659 A71-44094

TARGET PENETRATION U TERMINAL BALLISTICS

TARGET RECOGNITION

IR flying spot telescope with CW laser beam scanning and target motion sensing capabilities

01 p0081 A71-10830

Eye movements in dark during attempt to maintain ocular position defined by prior viewing of fixation target

01 p0016 A71-11388

Truncated periodic targets modulation in partially coherent light, deriving diffraction image formulas

02 p0260 A71-12146

Human performance in continuous pursuit tracking with temporary target obscurations, noting positional and velocity control systems

07 p1047 A71-19461

Target field luminance, interstimulus interval and target-mask spatial separation effects on visual backward masking, estimating inhibitory region radius

07 p1051 A71-20218

Target detection performance in simulated real time airborne reconnaissance mission, taking into account search time and image type, contrast and rate of motion

08 p1248 A71-21227

Coherent optical target recognition through phase distorting medium, using holography, Fourier transform and autocorrelation functions

08 p1335 A71-21377

Optimum antenna array processing design for target detection in nonuniform clutter background, using decision-theoretic processor with digital computer

08 p1256 A71-21604

Saccadic and smooth pursuit eye movements modification to visual targets instantaneous velocity changes at varying intervals

10 p1560 A71-23988

Intermittent noise effects on performance of visual search tasks of varying complexity, measuring test subjects target detection time under various noise/time ratio conditions

10 p1562 A71-24206

Algorithm for using presence indicator context and test for target recognition system, discussing simulation technique for use without hardware target recognizer

11 p1734 A71-25143

In-flight target reporting, analyzing quantitative meaning of ambiguous general modifier terminology as used by pilots in verbal sighting reports

12 p1875 A71-27251

Target trajectory detector optimization, using surveillance radar data and Markovian chain apparatus

13 p2033 A71-28993

Emitter location techniques for airborne passive ECM, discussing accuracies in terms of geometry, sample number, random and bias errors

15 p2375 A71-31205

Visual movement aftereffect storage absence of patterned surround for fixated visible target

15 p2364 A71-31984

Target and nontarget processing equivalence in visual search for item recognition and forced choice task, questioning Neisser hypothesis of preattentive screening

15 p2364 A71-31985

Autokinetic motion of luminous target, relating apparent visual movement to experienced displacement

17 p2694 A71-35739

Automatic classification of targets characterized by radar returns at discrete set of frequencies in Rayleigh region and first resonance range

17 p2747 A71-35773

Digital processing for automatic extraction of information from reconnaissance images, discussing target and terrain configurations pattern recognition technique

17 p2747 A71-35774

Noise equivalent irradiance equation for airborne IR scanner at peak response detector wavelength, involving target scene radiance and hot iridome emittance

18 p2917 A71-36608

Target value and exposure duration effects on results in visual search tasks, discussing results in relation to previously reported inconsistencies

18 p2854 A71-36440

Prefrontal cortex lesions effect on trained anticipatory visual target fixation in cats, noting performance impairment in voluntary eye movement control

21 p3329 A71-40701

Radar data video extractor adaptive thresholding device synthesis criteria to quantize echoes for ensuring constant false alarm rate and target visibility

22 p3508 A71-41515

ATC integrated communication, navigation and identification system, discussing design, economic technology and flexibility

22 p3571 A71-42080

TARGET SIMULATORS

Complex dielectric structure simulation for microwave scattering purposes using rotating target and zone technique

01 p0051 A71-10220

TARGET THICKNESS

Electron energy spectra construction from Al, Si and Au target layers transmission angular distribution measurements, using computer calculated spectra for comparison

09 p1497 A71-22680

TARGETS

NT RADAR TARGETS

TASK COMPLEXITY

Task difficulty involving simple and choice reaction time under stress of shock, threat of shock and noise

01 p0026 A71-11414

Performance decrement during bimodal vigilance task, discussing arousal and selective attention constructs

04 p0541 A71-14747

Alcohol effects on complex task performance including monitoring, compensatory tracking and mental arithmetic

04 p0547 A71-15896

Subjective and electromyographic estimation of fatigue and muscle activity physiological levels, considering isometric muscle contraction task endurance

07 p1047 A71-19496

Complex psychomotor task time duration relation to subtask performance and psychological measures

07 p1047 A71-19496

Human performance in pursuit tracking task with realistic structured and blank backgrounds

07 p1047 A71-19496

Relevant cue placement effects in concept identification tasks employing enforced verbal encoding

07 p1048 A71-19575

Engineering task and computing devices cost effectiveness matching, methodology improvements and penalties for less effective device spectrum utilization

09 p1412 A71-23272

Intermittent noise effects on performance of visual search tasks of varying complexity, measuring test subjects target detection time under various noise/time ratio conditions

10 p1562 A71-24206

Mental load physiological parameters determination by binary choice task, noting changes in heart and respiratory rates and systolic and diastolic pressure

17 p2688 A71-34393

Tasks with subject guiding vehicle at arbitrary speed along tolerance band defined course, considering prediction model for velocity-bandwidth relationship

17 p2693 A71-35493

Distributed Fetch sequencing computer techniques discussing system speeds, throughput rates, bus requirement and arithmetic processor demand reduction and task performing capability

17 p2712 A71-35773

Human performance as function of task and environmental factors, using psychological and physiological references

22 p3503 A71-42196

Alpha activity parameters during human performance of motor tasks with open and closed eyes

23 p3631 A71-43101

Short term central fatigue as causal factor of delayed psychological refractory period in multiple choice visual signal tasks

23 p3634 A71-43860

TASK SEQUENCERS

U CONTROL EQUIPMENT

U SEQUENTIAL CONTROL

TASKS

NT AUDITORY TASKS

NT VISUAL TASKS

Three phase code transformation task reliability and correlation, representing general factor analytic intellectual abilities and personality characteristics

20 p3192 A71-39070

Aircraft noise effects on hearing acuity and perceptual and intellectual judgment tasks

21 p3342 A71-40351

TASTE

- Evoked cortical responses to taste solutions of acid and salt applied to human tongue surface, using averaging technique 13 p2012 A71-28887
- Taste modalities identification by factor analysis technique based on correlation matrix between independent stimuli 21 p3341 A71-40073

TAURUS CONSTELLATION

- Taurus dust cloud magnetic field line of sight component observations and M17 and Cyg A absorption spectra data noting Zeeman splitting at 21 cm H lines 12 p1957 A71-26623
- Aries-Taurus region as soft X ray source, determining energy flux and source 14 p2301 A71-30426
- Hydroxyl emission at T Tauri stars positions in Taurus-Auriga region, discussing radial velocities of stars and dust clouds 19 p3144 A71-38172
- Taurus X-1 X ray emission polarization from rocket-borne polarimeter measurements, utilizing incoherent scattering 20 p3302 A71-39921

TAXIING

- Taxiing aircraft position and wheel trajectories for specific nose wheel path 02 p0187 A71-11641
- Power spectral density analysis of aircraft structural response to taxiing produced random vibrations involving landing gear orifice damping and Coulomb friction 11 p1708 A71-26311
- Uneven runway taxiing vibration effects on supersonic transport aircraft, comparing calculation with measurement 14 p2175 A71-30305
- Powered landing gear wheel system requirements for parking and taxiing of commercial jet transport airplanes [SAE PAPER 710446] 14 p2176 A71-30530
- Aircraft random heave-pitch response to taxiing on rough runways, analyzing dynamic loads and fatigue damage by power spectral techniques 18 p2850 A71-36675

TAXONOMY

- Human performance reliability data system using taxonomic structure for classifying behavioral studies and predicting man-machine performance 16 p2536 A71-33318

TAYLOR INSTABILITY

- Conducting fluids Rayleigh-Taylor instability in vertical magnetic field, taking into account Hall currents 03 p0463 A71-13473
- Collisional effects on Taylor and Kelvin instabilities in composite medium, considering longitudinal wave propagation mode 05 p0788 A71-16627
- Turbulent diffusion coefficients in isothermal and nonisothermal pipe flow, comparing with Bory and Taylor theories 07 p1222 A71-18994
- MHD Rayleigh-Taylor instability in galvanic approximation, demonstrating Hartmann number stabilizing effect 07 p1167 A71-19188
- Stabilization effect of rotation on Rayleigh-Taylor instability of stratified compressible inviscid fluid of variable density for noncritical wave numbers 11 p1749 A71-25434
- Fluid interface Rayleigh-Taylor type instability, considering control as optimal regulator problem 11 p1742 A71-26413
- Nonlinear global strong cellular branching solutions stability of Navier-Stokes equations 16 p2558 A71-32997
- Momentum transfer secondary flow between rotating cylinders in terms of effective/molecular viscosity ratio as function of Taylor number [ASME PAPER 71-APM-30] 16 p2559 A71-33199
- Fixed sphere on axis of unbounded rotating fluid/R greater than unity/, suggesting flow of Taylor column type 17 p2726 A71-34576
- Unstable nonlinear systems transient behavior analysis with two-time perturbation method applied to Bernard and Taylor flow problems 17 p2730 A71-35797
- Smallest Taylor number corresponding to Couette flow stability between two rotating cylinders subjected to rotationally symmetrical perturbation 18 p2902 A71-36093
- Taylor vortex flow stability between rotating concentric cylinders, using fifth order amplitude expansions in matrix form 24 p3817 A71-44420

TAYLOR SERIES

- Hybrid computers solution of linear differential equations, analyzing Taylor series /derivatives/ use for compensation 01 p0048 A71-10224

Convex Taylor series truncations minimization by iterative method based on approximating initial functional 03 p0452 A71-14058

Electron collision frequency energy dependence influence on electrical conductivity of weakly ionized plasmas, considering Taylor series expansion around probable plasma electron velocity 10 p1623 A71-23875

Microwave tunnel diode oscillator, representing nonlinear characteristics with Taylor series 11 p1737 A71-25666

Jacobi polynomial series analytic continuity properties based on relation with corresponding Taylor series 17 p2764 A71-34421

Semiempirical Taylor formula application to asymptotic turbulent boundary layer formed in mixing jet region 17 p2728 A71-35118

Automatic control system output signal changes due to finite variations, noting expansion into Taylor series 17 p2723 A71-35344

Three dimensional bounded circular three body problem solution in form of Taylor power series of time and vicinity values for canonical elliptical elements 17 p2807 A71-35497

Celestial body mass determination in many body problem, using Kalman-Bucy filtering for Taylor series approximation linearized problem 18 p2960 A71-35935

Compiler program generation for ordinary differential equations system automatic numerical solution by Taylor series method 20 p3254 A71-38754

Combined radiative and conductive heat transfer prediction in semitransparent solids by Taylor series expansion, defining radiative conductivity 22 p3620 A71-41883

Piecewise polynomial Taylor methods to numerically solve first order ordinary differential equations 23 p3698 A71-42901

TAYLOR THEOREM

U TAYLOR SERIES

TEA LASERS

U CARBON DIOXIDE LASERS

TEACHING

U EDUCATION

TEAMS

Social factors of labor organization and control in scientific teams for industry 02 p0335 A71-11856

TEARING

Geomagnetic tail tearing instability nonlinear evolution, discussing quasi-linear theory 05 p0742 A71-16630

Thin metal sheet reinforcements effect on slow stable tear and catastrophic failure [AIAA PAPER 71-113] 06 p1003 A71-18563

TECHNETIUM

Technetium stars characteristics, noting MS, S and N spectral types, s process element enhanced abundances and variability 05 p0806 A71-16206

TECHNIQUES

U METHODOLOGY

TECHNOLOGICAL FORECASTING

Future air transportation concepts, discussing short haul travel market, economic, environmental, safety, convenience and reliability aspects 18 p2989 A71-36671

Low speed aerodynamics, detailing relevance tree technological forecasting method of Canadian science council national goals list 22 p3481 A71-42766

TECHNOLOGIES

NT BIOTECHNOLOGY

NT MARINE TECHNOLOGY

Science and technology trend forecasting for planning, organization and program selection 02 p0335 A71-11852

Social quantitative benefit vs risk assessment of new technologies, considering atomic power safety 02 p0336 A71-12120

Technology assessment effects on science and engineering progress 02 p0336 A71-12121

TECHNOLOGY ASSESSMENT

Advanced technology influence on world meteorological service requirements 08 p1328 A71-21720

Meteorological equipment development and test program, discussing technical objectives, feasibility and user requirements 08 p1330 A71-21736

Aircraft noise abatement control on international basis by setting acoustic technological capability compulsory standards of quietness 08 p1379 A71-21826

Low noise microwave transistor amplifiers technology, discussing performance levels in frequency coverage, SNR, gain flatness and power output 17 p2714 A71-34604

Electrical power systems for spacecraft, reviewing solar cells, batteries, fuel cells and radioisotope thermoelectric generators 19 p3121 A71-37122

Synthetic materials technology development, discussing macromolecular materials synthesizing methods and properties 19 p3085 A71-38144

Cryogenic rocket propulsion technology covering propellant selection, pumping, cavitation, starting, tank stratification, instrumentation, hydrogen uses, nuclear propulsion, cost, availability, toxicity and storability 20 p3306 A71-39250

Aircraft high temperature turbine engine design, reviewing technological advances coupled with laboratory engine and component tests 20 p3277 A71-39399

German book on metallurgy, production and application of rare metals, discussing high vacuum technology 21 p3399 A71-40783

Air freight economics and growth forecast, discussing rates, cost and technological aspects 22 p3623 A71-41840

Recovery, launch and landing operations of earth orbital shuttle vehicles, discussing space rescue capabilities 22 p3609 A71-41989

Technology developments in rotor, drive, flight controls and cargo handling systems of heavy lift helicopter system, noting military and commercial applications [AIAA PAPER 71-994] 24 p3792 A71-45296

TECHNOLOGY TRANSFER

Technology gap between thermionic converter physics and reactor engineering, emphasizing language problem 02 p0281 A71-12272

Information and technology transfer in multinational corporate R and D, discussing mechanisms of communication, use of common technical language and impediments due to attitude differences 07 p1225 A71-19450

Space research impact on general economy and ecology, noting royalty-free licensing to private industry by NASA 14 p2341 A71-30257

Satellite communication role in disseminating information and promoting technology in underdeveloped countries 18 p2987 A71-36168

Technology transfer management, distinguishing between active and passive pursuit of technology, catalyst and vertical and horizontal transfer [AIAA PAPER 71-1008] 24 p3891 A71-44593

TECHNOLOGY UTILIZATION

Flight simulator visual systems, discussing improvement objectives in terms of current technology, image quality, system reliability and maintainability 01 p0066 A71-10016

Air traffic control by satellite, discussing CNES-SGAC and ESRO experiments within Discours project test program 01 p0125 A71-10748

Ducting materials and joints technology fallout from aerospace projects, discussing reliability in terms of corrosion resistance, fatigue strength and thrust compensating duct design 01 p0007 A71-11431

Laser systems for metal working, discussing operation modes, workpiece properties and optical systems 02 p0259 A71-11697

Materials science and manufacturing in space, discussing potential technologies and laboratory techniques using vacuum, weightlessness, temperature and radiation environment 02 p0255 A71-11973

Communication satellite earth station technology, considering steerable antenna subsystems, high power amplifiers, terminal equipment and frequency bands allocation 02 p0222 A71-12787

Carbon fiber reinforced plastics and metals structural components design, discussing properties, processing and applications 02 p0330 A71-12910

Satellites applications in French space programs, discussing telecommunication, meteorology, air navigation aids, space geodesy and earth resources 02 p0337 A71-12918

Microelectronics technology effects on electronics engineer education, considering data processing applications and circuit types 03 p0388 A71-13005

Orbital space stations for earth studies, considering atmospheric, hydrological and meteorological observations, astronomy, medico-biological and technological experiments and interplanetary spacecraft bases construction 03 p0497 A71-13418

Radioisotopes technical applications in industrial and aerospace sciences, discussing radioactive gas 03 p0497 A71-13418

penetrants, radiation interaction and geometrical measurements

03 p0455 A71-13533

Space research benefits from applications technology satellites and materials utilization, reviewing satellite communication networks, meteorology geodesy, navigation, geology and agriculture

03 p0524 A71-14245

Communication technology development relation to NASA programs, discussing receivers, microwave tubes, solid state transmitters, lasers, information retrieval and frequency sharing

03 p0388 A71-14412

Ultrasonic Doppler techniques in medical diagnosis, measuring ultrasonic probes directivities by echo amplitudes from various target configurations

03 p0373 A71-14422

Glass laser types, properties and applications, noting welding and cutting, plasma generation, controlled thermonuclear reactions, neutron generation, intense short duration X ray fields, etc

04 p0605 A71-14709

Laser applications in biology and medicine covering surgery, ophthalmology, microorganisms, viruses, tissue culture, tumor eradication, radiation hazards, etc

04 p0541 A71-14722

NASA qualitative reliability technology applications to chemical industry

04 p0602 A71-14802

Space technology and earth problems - AAS Conference, Las Cruces, New Mexico, October 1969

04 p0579 A71-14817

Space technology utilization in weather problems, considering tornado and other meteorological phenomena similarity to swirling vortex formation during missile flight

04 p0621 A71-14818

NASA Office of Technology Utilization, examining publications, information sources, data processing and dissemination facilities

04 p0690 A71-14938

Whisker composites applications, considering aerospace technology, turbine components, deep submergence structures, dental ceramics, electronics and wear resistant materials

04 p0611 A71-14952

Army avionics technology transfer to civil aviation, discussing communication systems, flight control and landing aids

04 p0557 A71-15017

Navy X ray research and utilization, discussing generation and interaction, radiography, radiation damage, dosimetry, spectroscopy, fluorescence analysis, etc

04 p0625 A71-15095

NASA program for aerospace technology application to medicine

04 p0546 A71-15281

Aerospace technology application to oceanic instrumentation and communication requirements

04 p0583 A71-15307

Nimbus AVCS imagery applied to studies of bedrock geology, geomorphology and climate

04 p0597 A71-15309

Minuteman missile technology application as boosters for near earth spacecraft launching, emphasizing tradeoff between reliability and cost

04 p0663 A71-15313

Aerospace technology direct and derived benefits for public, discussing earth resources program, communication satellites and NASA effect on nonaerospace activities and economy

04 p0691 A71-15315

Space sciences future applications for mankind - Conference, Santa Maria, California, October 1970

04 p0553 A71-15316

Electrical power generation from sunlight without pollution, using solar cell elevated rug technology

05 p0704 A71-16100

Si solar cell technology, discussing contacts, low temperature performance and conversion efficiency

05 p0757 A71-16103

Holography applications, recording and reconstructing three dimensional objects by split laser beam interference technique

05 p0747 A71-16194

USAF technology programs providing near term particular capability needs and long term fundamental incremental gains

05 p0839 A71-16286

Semiconductor laser diodes structural and operational characteristics, discussing applications in aircraft and construction machines guidance systems

05 p0761 A71-16328

R and D management decision making process structural model, discussing technological forecasting based on organized technical information, quantized judgments, optimum resource allocation and hybrid technique

05 p0840 A71-16744

Microwave integrated circuit technology, discussing substrates, conductors, dielectrics and resistors materials and design data and fabrication techniques

05 p0728 A71-16914

Scientific applications of satellite photometric observations, considering geomagnetic effects on spacecraft rotation, satellite size and reflection properties, etc

05 p0723 A71-16970

Data reduction for information retrieval, considering electron beams application for electronic circuit ultraminiaturization

06 p0871 A71-17525

Superconductors applications, noting low cost reliable closed cycle He refrigerators

06 p0941 A71-18017

Lasers applications to materials working including welding, cutting, machining, etc

06 p0908 A71-18069

Avionics subsystem design improvements for aeronautical systems, considering standardization, weight impact, environmental control, maintainability and equipment growth

07 p1069 A71-18829

True vertical laser application for precision vertical alignment of large structures, using mercury mirror

07 p1122 A71-19206

Laser systems for biomedical applications, considering ophthalmology, dermatology, surgery, biological and cellular research, analytical and diagnostic medicine

07 p1049 A71-19782

Laser microbeam welding, drilling and trimming of electronic devices

07 p1118 A71-19787

Laser applications in chemical research, exploring fast chemical processes, isotope enrichment and molecular reactions and structure observations

07 p1124 A71-19790

Fluidics applications noting liquid level regulation, press control, alarm, windshield wiper, hydrofoil stabilization, pneumatic conveyor belt, respirator, stepping motor and tape centering control

07 p1023 A71-20003

Rhenium in modern technology - Conference, Moscow, October 1968, Part 2

07 p1140 A71-20231

Phototechnology for phase holograms recording and information storage in hardened gelatin

07 p1116 A71-20620

Carbon fiber composites utilization problems for product and tool designers, considering mechanical properties anisotropy, fiber alignment and bundle strength

[PLASTICS INST. PAPER 42]

08 p1322 A71-20931

Laser technology R and D with respect to high average and/or peak power and chemical to coherent light energy conversion

09 p1462 A71-22584

Interactive computer graphics technology industrial applications, emphasizing structural analysis and engineering master drawings

10 p1580 A71-23758

Holography utilization to data processing, discussing factors affecting recording and matched filters creation for pattern recognition

10 p1581 A71-23917

Book on aviation technology and market structure covering technological and scientific effects on industry innovative behavior, R and D programs, operating costs, etc

10 p1698 A71-23982

Soviet papers on physical foundations of ultrasonic technology covering applications in machining, welding, cleansing, and drying

10 p1616 A71-24132

NASA aerodynamic research applicable to business aircraft concerning wind tunnel and flight tests, STOL performance and high speed cruise technology

[SAE PAPER 710378]

10 p1554 A71-24244

Space research utilization in medicine, discussing remote blood pressure measurements, seismocardiography visual analysis, sterilization procedures and equipment for physically handicapped

10 p1571 A71-24754

Carbon fiber reinforced plastics industrial engineering applications, noting cost effectiveness, strength and elasticity

11 p1861 A71-25407

Soviet laser spectroscopy applications including microsample chemical analysis, superhigh resolution problem, nonlinear optics devices, interferometric seismometer and air pollution analyzer

11 p1776 A71-26351

Structural dynamics test simulation technology, discussing criteria, techniques, equipment, combined environments and relationship between testing and analysis

11 p1745 A71-26493

Complementary symmetry MOS technology for logic circuit design of inverters, gates, flip-flops, switches and storage units

12 p1883 A71-27044

Superconducting state physics and macroscopic coherent states in superconductors, considering Josephson effect and technology utilization

13 p2110 A71-27888

Technical, sales/marketing and management - Conference, Coronado, California, May 1971

13 p2091 A71-28161

MAC malfunction detection, analysis and recording system applications in commercial airlines, emphasizing real time response for maintenance function

[SAE PAPER 710425]

13 p1995 A71-28313

Orbital space stations for earth studies, considering atmospheric, hydrological and meteorological observations, astronomy, medico-biological and technological experiments and interplanetary spacecraft based construction

14 p2319 A71-29602

Ion and electron beams technology application to microelectronics, discussing limitations imposed by electron/ion optical effects

14 p2277 A71-30700

Solid propellant rocket engine design, discussing combustion instability technology applications in damping and driving mechanisms influence determination

[AIAA PAPER 71-754]

14 p2296 A71-30780

Interrogation, recording and location system satellite techniques for wildlife tracking and monitoring, describing collar antenna, battery pack and solar cells

14 p2200 A71-30922

Commercial spinoff from government sponsored R and D, considering productivity and industry benefits

14 p2342 A71-31131

Holography applications - Conference, Besancon, France, July 1970

15 p2402 A71-31252

Satellite IR photography, discussing camera systems, photointerpretation, applications in glaciology, hydrology, oceanography, geology, volcanology and environmental protection

15 p2408 A71-31832

Pilot training efficiency increase through advanced simulation technology utilization, discussing computerized flight simulators, CRT display systems and automated briefings

15 p2384 A71-31880

Education satellite technology, discussing transmission levels, low cost high sensitivity receiver design, and TV broadcasting

16 p2638 A71-33581

Space applications to world needs, emphasizing potential major agricultural production improvements

16 p2665 A71-33585

Space program economics, discussing applications, benefits, spending and byproduct effects cost planning, funding and organization

16 p2665 A71-33590

Potential benefits accruing to air superiority fighters by integrating automatic feedback control systems technology into design, using F-4 as baseline configuration

[AIAA PAPER 71-764]

16 p2523 A71-34002

Satellite communication technology in next decades covering Intelsat 4 characteristics, meteorological satellites, navigation aids, multichannel telephone and TV circuits and frequency assignment

17 p2699 A71-34677

Space shuttle applications and utilization, discussing payloads, performance modes, Mission Support Module, ancillary equipment, system interfaces and related profiles

[AIAA PAPER 71-816]

17 p2812 A71-34720

Cockpit display, discussing aircraft operators displays in use of head-up displays, area map navigation, CRT and electroluminescent readouts

17 p2691 A71-35110

Small satellite role in meteorological, earth observation, communications and navigation missions, discussing orbit, weight, electrical power, attitude control, data handling and modular design concepts

17 p2805 A71-35331

Lunar Orbiter photographs utilization in earth science courses, illustrating geologic features, stratigraphy and historical geology

18 p2915 A71-35888

Technological environment for international communications law, examining system design, radio spectrum resource management and communications satellites

18 p2986 A71-36164

Hybrid circuits thick film technology, discussing printed circuits fabrication processes and electrical and mechanical properties

18 p2888 A71-36224

Side-looking airborne radars and image recording scanners design for geoscience applications, discussing gray scale improvement, multispectral sensing, target discrimination, etc

18 p2875 A71-36366

High intensity molecular beams properties, measurement and production methods, considering kinetic energy, chemical composition and technology applications

18 p2908 A71-36438

Space technology - Conference, Cocoa Beach, Florida, April 1971, Volumes 1 and 2

18 p2972 A71-36442

European space programs, presenting post-Apollo utilization views
[AIAA PAPER 71-817] 18 p2988 A71-36500

Semifinished product production technology influence on heat resistant alloys mechanical properties, considering forging, rolling, casting, melting, diffusion welding and powder metallurgy
18 p2937 A71-36725

French space programs, discussing European and international activities, telecommunication, meteorology, data collecting, natural resources and air and sea traffic control
18 p2975 A71-36753

NASA technology utilization program, discussing technical information, spin-off benefits and various applications
19 p3173 A71-38408

Holography applications in science and technology, considering plasma diagnostics, particle motion pictures, stress and vibration measurements, flow visualization, data processing and aeronautical navigation
19 p3068 A71-38725

Thermionic reactor technology, including insulator seal, nuclear fuel, emitter, tri-layer structure and interelectrode plasma
20 p3265 A71-38949

Pulsed Nd laser source mass spectroscopy application to geological material analysis, tabulating assessed limits of detection for various elements
20 p3245 A71-39422

Beam-lead technology application to complementary MOS IC processing
21 p3357 A71-40814

Holography review covering photon, grain and speckle noises limitations, large 3D picture production and various applications
21 p3381 A71-40930

High vacuum mass spectrometric hazardous gas detection system used during cryogenic loading of Saturn vehicles, discussing application to environmental pollution detection
22 p3542 A71-41988

Manned orbital operations economy for space station utilization, discussing laboratory equipment, on-orbit supervision, maintenance and remote communications limitations
[MDAC-WD-1746] 22 p3611 A71-42030

Space technology applications to earth environment and resources management, discussing satellite-borne remote sensor systems and data processing techniques
[SD-71-734] 22 p3535 A71-42047

Book on space technology for developing countries covering economic, social and educational reform, solar system exploration and extraterrestrial civilizations
22 p3623 A71-42066

Sintered metals and powder metallurgy technology, discussing methods and materials available to widen applications
22 p3562 A71-42225

Holography, covering thin, thick, transmission, reflection, amplitude and phase type holograms principles and applications in interferometry, microscopy, imaging, optical data processing, etc
22 p3546 A71-42476

Acoustic holography imaging technology, discussing sound field visualization and applications in nondestructive testing, medical diagnostics, ultrasonic microscopy, seismology and underwater viewing
22 p3546 A71-42478

Book on thick film microelectronics covering microcircuit design, fabrication, packaging and applications
23 p3650 A71-43224

High power laser characteristics for large scale industrial applications
23 p3685 A71-43516

Physical and technological aspects of holographic recording including optical data processing, Fourier hologram reconstruction and random structure information determination
23 p3679 A71-43896

Stability augmentation system for aircraft elastic modes control, discussing active flutter suppression technology
23 p3629 A71-44107

Digital computer applications to physics problems, giving examples of plasma research and methane molecule properties determination based on quantum mechanics
24 p3847 A71-44355

Future transportation technology impact, considering system design evaluation criteria and civil aviation and urban mass transit systems contributions
[AIAA PAPER 71-1010] 24 p3892 A71-44594

Environment degradation relation to technology, discussing priorities
[AIAA PAPER 71-1016] 24 p3892 A71-44597

Ion implantation technique utilization for reducing MOSFET devices threshold voltage and gate drain capacitance
24 p3808 A71-44725

Earth observation system design decision making, considering data needs, technology readiness, man role in earth resources programs and space program schedule
24 p3892 A71-44867

Physics and technology discoveries utilization in industrial control, considering semiconductors, thin films, lasers, holography, cryogenics, etc
24 p3827 A71-45071

Laser beam applications in drilling, shaping and surface finishing of miniature journal and step-type friction bearings, deriving regression equations for optimal process parameters
24 p3834 A71-45162

TECTONIC MOVEMENT
U TECTONICS
TECTONICS
Critique of Ethiopian Afar depression formation as oceanic crust resulting from Arabia drift, considering plate tectonics analysis for bifurcated spreading zones
04 p0582 A71-15126

Earth-moon tectonic relationships and structural similarity, analyzing earthquake frequency dependence on lunar phase and distance based on Middlehurst catalogs
15 p2492 A71-32478

Lunar crust tectonic analysis, using mosaic pattern technique based on eightfold division of spherical surface
15 p2493 A71-32486

Lunar near-side tectonic patterns, including mare ridges, rills, highland ridges and crater walls features within maria from Lunar Orbiter photographs
19 p3052 A71-37676

Lunar volcano-tectonic processes, considering primary circular or polygonal surface features evolution
19 p3052 A71-37678

TEE
U T SHAPE
TEFLON (TRADEMARK)
Oxygen reduction on Teflon bonded Pt electrodes, eliminating concentrated overvoltage
02 p0210 A71-12955

LES 6 satellite solid Teflon pulsed plasma thruster performance, determining energy balance thrust and circuit parameters
[AIAA PAPER 70-179] 03 p0472 A71-14429

Si solar cell cover glass assembly and packaging improvements using Teflon
05 p0702 A71-16079

Laminar ablating air-Teflon boundary layers with carbon difluoride and atomic fluorine constituents, using UV thermal radiation measurements
[AIAA PAPER 71-39] 06 p1008 A71-18500

Solid Teflon fuel pulsed plasma thruster optical measurements, showing different exhaust velocities for neutral, singly, doubly and triply ionized atoms
[AIAA PAPER 71-194] 06 p0948 A71-18632

NASA-SRI Round Robin Ablation Program summary, discussing dimensional analysis, Teflon, nylon and surface temperature
18 p2985 A71-36279

Optical properties of metallized fluorinated ethylene propylene Teflon films with various thicknesses, discussing suitability as spacecraft thermal control surface
[ASME PAPER 71-AV-35] 18 p2869 A71-36402

Carbon difluoride in ablating air-TEFLON laminar boundary layers by spectrally and spatially resolved UV thermal radiation measurements
19 p3163 A71-37881

Reflecting and ablating Teflon heat shields for radiative environment of outer planets atmosphere
[AAS PAPER 71-147] 19 p3084 A71-37950

Teflon insulated LT type electrical conductors for 203-493 K, including chemical, ozone, UV and fuel resistance tests
22 p3520 A71-41694

TEKTITE PROJECT
Blood plasma volume decrease, red cell mass and survival measurements in aquanauts of Tektite I at prolonged habitation
11 p1720 A71-26123

Emergency surface decompression and treatment procedures for project Tektite aquanauts, determining safe interval and schedules for return to habitat on ocean floor
16 p2535 A71-33110

Tektite II program of underwater research as future manned space flight operations model, discussing mission structure, crew selection and communications
[AIAA PAPER 71-828] 17 p2690 A71-34718

TEKTITES
NT AUSTRALITES
Elemental abundances of microtektites and tektites, noting differences from Apollo samples
02 p0312 A71-12363

Tektite age correction factor determination through annealing of fission tracks, describing experimental technique with reference to etching conditions
05 p0808 A71-16300

Tektites earth vs possible lunar or cometary origins, taking into account chemical composition
06 p0968 A71-17963

Lunar vs terrestrial origin of tektites, discussing meteoritic impact craters, age factor and properties
16 p2637 A71-33517

Long range thermoluminescent dating of meteorites and tektites, discussing dependence on thermal release of trapped carriers, radiation saturation and instrumental errors
16 p2638 A71-33518

Cuban tektite classification based on age, discussing physical properties and chemical composition
17 p2797 A71-34275

Meteoritics, covering impact on earth, craters, astrometres, tektites, carbonaceous chondrites properties, collisions, fragmentation, etc
17 p2809 A71-35714

Tektites atmospheric and geological history, noting fragmentation and surface sculpturing processes
17 p2811 A71-35728

Refractive index changes by shock compression metamorphism of tektite, soda lime and silica glasses
19 p3084 A71-37661

Uranium content correction for Ivory Coast microtektites, discussing effects on age values and correlation between tektite falls, geomagnetic reversals and faunal changes
20 p3292 A71-39405

Geographic distribution pattern of Australasian tektites, considering origin and crater theory of tektite events
21 p3450 A71-40646

Physical chemistry of Aouelloul impact crater glass, suggesting meteoritic origin of tektites
21 p3450 A71-40647

Lunar glassy objects and mineral grains surface microstructure by optical and scanning electron microscopy, comparing with tektites and terrestrial volcanic analogs
23 p3745 A71-43664

Tektite organic constituents evidence from high temperature mass spectrometry, investigating relation to formation process and terrestrial contamination
23 p3769 A71-43926

TELECHIRICS
U REMOTE HANDLING
TELECOMMUNICATION
NT AIRCRAFT COMMUNICATION
NT AUTOMATIC PICTURE TRANSMISSION
NT BIOTELEMETRY
NT BROADCASTING
NT CLOSED CIRCUIT TELEVISION
NT COLOR TELEVISION
NT DATA LINKS
NT DEFENSE COMMUNICATIONS SATEL-LITE SYSTEM
NT EDUCATIONAL TELEVISION
NT FACSIMILE COMMUNICATION
NT GROUND-AIR-GROUND COMMUNICA-TIONS
NT INTERPLANETARY COMMUNICATION
NT LUNAR COMMUNICATION
NT MULTICHANNEL COMMUNICATION
NT OPTICAL COMMUNICATION
NT PULSE COMMUNICATION
NT PULSE FREQUENCY MODULATION
NT TELEMETRY
NT RADIO COMMUNICATION
NT RADIO RELAY SYSTEMS
NT RADIO TELEGRAPHY
NT RADIO TELEMETRY
NT REENTRY COMMUNICATION
NT SPACE COMMUNICATION
NT SPACECRAFT ANTENNAS
NT SPACECRAFT COMMUNICATION
NT TELEMETRY
NT TELEPHONY
NT TRANSOCEANIC COMMUNICATION
NT VIDEO COMMUNICATION
NT VOICE COMMUNICATION
NT VOICE DATA PROCESSING
NT WIDEBAND COMMUNICATION
NT WIRELESS COMMUNICATIONS
Chi-square distributions fitted to observed telecommunication variables distributions
01 p0041 A71-11609

Skyнет satellites in orbit communications, repeaters testing, describing test facilities, spacecraft communication subsystems operation, terminals calibration and atmospheric losses
02 p0218 A71-12440

INTELSAT earth station operations via SPADE demand-assignment system, discussing interference requirements, frequency stability, gain flatness, etc
02 p0221 A71-12780

Communication satellite systems ground stations operating personnel training, outlining basic and specialized study and on-job training program
02 p0224 A71-12826

Radio frequency interference project control responsibilities and teamwork, noting communication transmitter design example
03 p0383 A71-13177

Army avionics technology transfer to civil aviation, discussing communication systems, flight control and landing aids
04 p0557 A71-15017

Lunar far side communication, discussing libration point and lunar orbit relay system for high bit rate telemetry, TV and astronaut backpack communication
04 p0555 A71-15339

Broadband radiated man-made electromagnetic noise measurement for communication systems performance determination, noting instrumentation problems
05 p0721 A71-16468

Human vision in communication system analysis, discussing psychophysical investigation, brightness functions, spatial frequency response and modulation transfer function
05 p0713 A71-16484

Field amplitude distribution parameter in long distance tropospheric communications based on fading depth
05 p0722 A71-16866

PSK pseudonoise/spread spectrum communication systems with SNR reduction, examining phase nonlinearities effect
05 p0725 A71-17074

Optimality criteria for communication systems, considering data transmission rate
06 p0867 A71-17496

Book on earth satellite telecommunications systems and international law covering historical, scientific, economic, legal and political background
06 p1010 A71-18020

ATS F and G, discussing communications experimental program with deployable 30 ft parabolic antenna [SAE PAPER 700759]
08 p1366 A71-21368

Computer processing in communications - Conference, Polytechnic Institute of Brooklyn, April 1969
08 p1255 A71-21590

Satellite communications earth station antennas, describing antenna elements and subsystems analysis, design and performance
09 p1418 A71-23099

Satellite, rocket and Thomson scatter data application to communications - IEE Conference, London, January 1971
10 p1575 A71-23864

Electronic communication system critical design evaluation, concerning electromechanical components and packaging impact on overall reliability and cost
12 p1878 A71-26688

Airborne radio communication systems, stressing electronic equipment design reliability
12 p1878 A71-26688

Communication satellites telephone, telex and high speed data transmission systems engineering, discussing intercontinental TV, synchronous orbit injection and solar panel deployment
12 p1973 A71-27610

Coding for feedback communication system with additive white Gaussian noise, using mean-square estimation error
13 p2034 A71-29379

Sensing and communications technologies for short wayside headways, considering applicable equipment for personal rapid transit systems, modulation, coding and data transmission techniques
14 p2195 A71-30337

Atmospheric noise statistical characteristics, investigating short term variations, intensities and application to communications
14 p2237 A71-30964

IMPATT diode oscillator for CW Doppler radar, microwave detection and communications systems, emphasizing cost reduction
15 p2377 A71-32522

Intelsat 4 satellite Spade communication system, using common reserve circuits and repeaters
15 p2373 A71-32640

Two dimensional linear communication system with crossed channels with different amplification factors and time constant, examining stability with root trajectory method
16 p2549 A71-33569

Rumanian space research, reviewing participation in socialist nations programs in physics, meteorology, communications and biology
16 p2665 A71-33854

Space research system telecommunications, considering telemetry, tracking and telecommand systems
17 p2696 A71-34229

Satellite telecommunication systems, considering standard and small transportable ground stations and Intelsat system
17 p2696 A71-34233

Communication satellite systems integration into general telecommunication network, considering telephone circuit data transmission characteristics, routing and signal processing
17 p2696 A71-34235

Communication satellite systems vs conventional terrestrial methods, emphasizing economic comparison
17 p2697 A71-34236

First generation domestic communications satellite system, discussing various proposals for FCC authorization [AIAA PAPER 71-842]
17 p2700 A71-34711

Communications - IEEE Conference, Montreal, June 1971
17 p2703 A71-35076

Electromagnetic coupling measurement between two antennas in cluttered communications system, emphasizing scale model prediction technique
17 p2703 A71-35078

Book on synchronous communications theory covering statistical detection, decision and estimation and source and channel encoding
17 p2707 A71-35218

HEOS A-1 satellite telecommunication system, describing command, telemetry and ranging subsystems
18 p2875 A71-35984

Papers on international communications law, covering technological environment, broadcasting control and satellite transmitted TV programs content
18 p2986 A71-36162

International communications law development, discussing capital investment, information dissemination, 1967 space treaty and Intelsat program
18 p2986 A71-36163

Technological environment for international communications law, examining system design, radio spectrum resource management and communication satellites
18 p2986 A71-36164

Satellite telecommunications problems, discussing frequency assignment and power efficiency
18 p2877 A71-36515

European 12 GHz regional satellite telecommunications systems, discussing band assignment limitation and frequency reuse
18 p2877 A71-36517

Telecommunications satellite data acquisition from automatic beacons, discussing Eole program
18 p2988 A71-36543

Book on communication satellites technology covering satellite transponders, spacecraft antennas and subsystems, high power transmission, launch vehicles, digital techniques, earth stations, etc
19 p3149 A71-37271

Telecommunication developments covering coaxial cables, waveguides, error elimination, information theory, sound transmission and radars
19 p3016 A71-37340

Telecommunications satellites, discussing Intelsat series, multiple access, radio navigation, weather satellites and earth resources satellites
19 p3017 A71-37493

International Telecommunication Union report on telecommunication and peaceful uses of outer space, covering space programs, communication satellites, UN role, etc
19 p3172 A71-37517

Book on electronic components covering radio, cathode ray and microwave tubes, telecommunication, ceramic materials, light conversion to electricity, integrated circuits, etc
20 p3205 A71-39775

Transmission characteristics of communication systems with incoherent carriers through fading and nonfading media, showing advantage of PFM-AM with clipped noise carrier
20 p3201 A71-39913

Incoherent carrier communications system, obtaining message SNR of 60-70 dB for analog signals with compound pulse modulation and carrier clipping
21 p3347 A71-40375

French R and D Directorate exhibits at 29th Le Bourget air show, discussing laser applications, telecommunication, navigation-guidance, energy conversion, test facilities and environmental studies
24 p3816 A71-44764

TELEGRAPH SYSTEMS

European telecommunications satellite project, discussing INTELSAT and telephony-telegraphy-telex system
06 p1010 A71-17999

Telegraphy binary data transmission through channels with frequency-selective fading, investigating noise stability improvement by programmed carrier frequency variation and receiver passband shifting
17 p2698 A71-34394

TELEGRAPHY

U TELEGRAPH SYSTEMS

TELEMETERS

U TELEMETRY

TELEMETRY

NT BIOTELEMETRY

NT PCM TELEMETRY

NT PULSE FREQUENCY MODULATION

TELEMETRY

NT RADIO TELEMETRY

Telemetry - Conference, Los Angeles, October 1970
01 p0031 A71-10876

Algorithm and computer program generating formats and logic equations for addressable remote multiplexed time division telemetry systems
01 p0050 A71-10880

Instrumentation System Margin Analysis Program /ISMAP/ for ICBM telemetry data acquisition systems performance tests
01 p0032 A71-10882

Field tests for telemetry receiving systems solid calibration, describing antenna pointing
01 p0033 A71-10881

Manned space flight network telemetry system modification for Skylab, ERTS and Apollo J missions, giving data flow diagrams and equipment electronic characteristics
01 p0035 A71-10900

Telemetry and communications roles in Apollo flight operations, describing data system management
01 p0035 A71-10900

Telemetering - IEEE Conference, Los Angeles April 1970
01 p0036 A71-10900

Marine traffic control via satellite telemetry, describing merchant and powered fishing fleet distribution and navigation requirements
01 p0125 A71-10900

Output format coding for telemetry data compression channel and frame identification
01 p0036 A71-10900

Antenna and telemetry system for spherical shape ICBM reentry vehicles data link to ground
01 p0036 A71-10900

Remote modules for spacecraft analog/digital telemetry distributing multiplexer input gates
01 p0036 A71-10900

Telemetry demodulation system using linguistic and statistical methods in pattern recognition
01 p0036 A71-10900

Equatorial ionosphere correlation distance regarding VHF telemetry disturbances and satellite tracking, determining antenna ground spacing
01 p0074 A71-11314

Skyнет satellite mission profile, onboard equipment and control system, discussing communications, command/telemetry processing equipment, electronic power sources, and secondary propulsion
02 p0320 A71-12474

Small scientific spacecraft onboard computers, discussing integration into satellite telemetry system and relationship with ground based data processing facilities
03 p0382 A71-13240

MITOL problem-oriented compiler language for real time and postflight telemetry data processing
04 p0556 A71-15274

Flexible telemetry systems for space flight applications, considering component exchangeability and electric connections variability by mechanical and electronic means
05 p0718 A71-15944

Solid state circuit digital frequency discrimination with low pass filter in ESRO stations telemetry receivers AFC and antisideband system
05 p0720 A71-16320

Sirio synchronous orbit satellite configuration, emphasizing attitude control system, telemetry encoders and electric power supply
05 p0816 A71-16464

Solar X-ray radiation measurements using real time telemetry from SOLRAD satellites
05 p0799 A71-17080

Nimbus 4 satellite telemetry information processing with data sampling and formatting flexibility
05 p0726 A71-17110

NASA Data Processing Facility for earth resource technology satellite telemetry
05 p0818 A71-17140

Geometrical and physical distance measurement for laser telemetry, involving time and speed factors, emission and receiver beams
06 p0869 A71-18040

Intelsat 3 Ground Control System functions, describing operation of tracking, telemetry and command stations subsystems
06 p0870 A71-18300

Jet engine rotor strain and temperature data transmission, examining special purpose telemeters design
07 p1062 A71-19620

Parachute ejectable rocket-borne instrument package with telemetry system for lower ionosphere measurements, describing electrical and mechanical design and operation
07 p1208 A71-19800

Directional antenna with parabolic reflector for missile tracking in telemetry band, considering radiation diagrams and design approach
07 p1078 A71-20010

Deep space probes telemetry system a priori data compression ratio evaluation using channel activities under unknown output signals cross correlation [AIAA PAPER 71-231]
08 p1258 A71-20790

N-channel PSK/PM digital telemetry system modulation scheme for space exploration
08 p1254 A71-21300

Flexibly programmable spacecraft data handling system, considering computer aided telemetry system for data acquisition and transmission
08 p1258 A71-21300

Binary pseudorandom codes sequences correlation properties in PSK telemetry
09 p1404 A71-22140

Guiana Space Center facilities and equipment, describing computerized and automated real time

telemetering and data processing systems for spacecraft tracking

09 p1425 A71-22274

Artificial earth satellites orientation determined by onboard telemetric measurements, constructing model for rotational motion around center of mass

09 p1531 A71-22569

Telemetry system for control data transmission, noting pulse comparison with feedback signal

13 p2031 A71-28633

Digital FM techniques for combined time and frequency division multiplexing, improving telemetry sampling channel bandwidth utilization

14 p2193 A71-30020

Self contained lightweight airborne data acquisition system for atmospheric and meteorological research, using analog recorder and telemetry system

14 p2243 A71-30311

Integrated flight test data system combining digital airborne data acquisition/recording system with telemetry/microwave link to computerized ground station

14 p2243 A71-30318

Unsteady controlled object dynamic characteristics evaluation for search-free self adjusting systems and telemetric information processing improvements

14 p2220 A71-30814

Telemetering - IEEE Conference, Washington, D.C., April 1971

14 p2197 A71-30896

Omnidirectional broadband telemetry antenna array for spacecraft providing near isotropic circular polarized radiation with open line microstrip feed

14 p2199 A71-30907

Walsh orthogonal functions application in signal processing and as carrier waves in telemetry data transfer systems

14 p2199 A71-30909

Satellite telemetry systems for data transmission to developing nations ground stations decoding equipment

14 p2199 A71-30910

Microwave responders in FM or AM modes with cavity resonator, considering use in medium distance telemetering or telemonitoring

14 p2215 A71-30911

Optimal omnidirectional antenna array located on cylindrical head section of sounding rocket for L band telemetry

14 p2216 A71-31035

Telemetry polarization diversity combiners for data dropout elimination, considering input signal characteristics and propagation

15 p2370 A71-31642

Error estimates in transmission of pulse code telemetering signals by nonredundant binary code through asymmetric channel

16 p2543 A71-33706

Space research system telecommunications, considering telemetry, tracking and telecommand systems

17 p2696 A71-34229

Optimum and suboptimum decision rules for two-channel deep space telemetry system with modulation consisting of PM with two orthogonal phase functions

17 p2704 A71-35088

Digital filtering in PCM communication systems with active repeater satellites and space vehicle telemetry

18 p2881 A71-36569

Grand Tour missions centralized data handling, describing computer aided telemetry system and self testing and repairing control computer

19 p3025 A71-37954

Automatic ATC display systems, discussing electronic flight progress strip for telemetry reproduction

19 p3102 A71-38300

Base triangle determination by geometric geodesy, using laser telemetry and satellite optical observations with cataphotic reflecting prisms

20 p3220 A71-39661

Miniature biopotential transmitter suitable for telemetry, giving EEG and circuit and performance characteristics

21 p3342 A71-40184

Transistorized high power telemetry amplifier design, describing test equipment for input and collector load impedance

22 p3519 A71-41632

AM crosstalk in unified carrier telemetry system, studying implications for carrier false lock and tracking

22 p3514 A71-42390

TELEMETRY AUTO REDUCTION SYSTEM

U DATA REDUCTION

U TELEMETRY

TELEOPERATORS

Book on human factors application in teleoperator design and operation covering aerospace environments, transportation, remote control, sensors and actuator subsystems

09 p1399 A71-22613

Man-teleoperator-robot teams for space exploration facilities construction and operation, discussing lunar programs

17 p2723 A71-34722

Astronaut teleoperators use for space operations cost reduction and future experiments productivity increase

22 p3503 A71-42033

TELEPHONES

NT RADIOTELEPHONES

TELEPHONY

Satellite regional broadcasting and telephony/data services cost model

02 p0221 A71-12781

Linear low noise wideband frequency modulator for Intelsat 4 satellite telephony communication, considering channel capacity

02 p0234 A71-12819

Earth station communication system planning for Intelsat 4, discussing telephony and TV transmission

02 p0225 A71-12830

Synchronous orbit satellite links in tandem for government and military telephone communications, discussing subjective evaluation for acceptability

05 p0725 A71-17070

European telecommunications satellite project, discussing INTELSAT and telephony-telegraphy-telex system

06 p0101 A71-17999

Communication satellite systems for long distance telephone connections, comparing transmission possibilities between links and terrestrial extensions

06 p0869 A71-18013

Multichannel laser telephone communication link experimental operation results in U.S.S.R.

07 p0108 A71-18838

Telephone channel phase-frequency distortions effects on discrete signal transmission quality from phase-delay-time frequency characteristics criterion

08 p1253 A71-20774

International telephone transmission, comparing technical and economic characteristics between submarine cable and satellite systems

10 p1577 A71-24267

Sirio B European communication satellite, discussing electronic equipment for simultaneous multichannel telephony and color TV transmission

14 p2319 A71-29820

European telecommunication and TV distribution satellite system, including telephony, telegraphy, telex and wideband data transmission

17 p2696 A71-34232

Communication satellite systems integration into general telecommunication network, considering telephone circuit data transmission characteristics, routing and signal processing

17 p2696 A71-34235

Single sideband mechanical filters for voice multiplex transmission in radio and telephone systems, discussing material characteristics

17 p2714 A71-34608

Comparison of demand assignment multiple access/modulation techniques for satellite communication using high quality telephone channels

17 p2706 A71-35103

Satellite communication ground station center in conjunction with Intelsat 3 satellites system for transcontinental telephone links

17 p2708 A71-35508

Communication satellite ground station terminal equipment, discussing carrier current telephone, video and sound TV apparatus

17 p2717 A71-35516

Internal commutation of telephonic channels with variable destination in time division multiple access system

18 p2880 A71-36547

Laser development and applications in telephone communications, manufacturing and holographic memory

21 p3393 A71-40877

Trigonometric synthesizers with nonuniformly sectioned tapped delay line and summation circuit for signal distortion correction in telephone channel

23 p3650 A71-43288

TELESCOPES

NT APOLLO TELESCOPE MOUNT

NT ASTRONOMICAL TELESCOPES

NT HELIOMETERS

NT MANNED ORBITAL TELESCOPES

NT PARTICLE TELESCOPES

NT PYROHELIOMETERS

NT RADIO TELESCOPES

NT REFLECTING TELESCOPES

NT REFRACTING TELESCOPES

NT SCHMIDT CAMERAS

NT SPACEBORNE TELESCOPES

NT SPECTROSCOPIC TELESCOPES

NT X RAY TELESCOPES

IR flying spot telescope with CW laser beam scanning and target motion sensing capabilities

01 p0081 A71-10830

Intercept Ground Optical Recording telescope and Mobile Optical Tracking System for electro-optical photography, discussing measurement and system errors and CAMDAT computer program

04 p0554 A71-15320

Image recording system low light /IRSILL/ camera design for long range attitude and events /LORAE/ telescopes in short missile instrumentation

18 p2919 A71-36086

Autoexposure system for tracking telescopes, describing photometer and camera shuttle automatic control subsystems

18 p2919 A71-36088

Ten cm aperture penta and roof-penta mirror assemblies for telescope internal optical alignment

22 p3549 A71-42553

Telescope wave optical imaging performance, deriving point spread function, radial energy integral and modulation transfer functions for different wave front surface deviations

24 p3849 A71-45204

TELETYPEWRITER SYSTEMS

Remote area voice, teletype and data communication using satellites for providing links with central terminals, considering economic feasibility by cost analysis

04 p0555 A71-15338

TELETYPEWRITERS

Human fingers coordination during teletype operation, examining temporal characteristics

02 p0205 A71-12055

TELEVISION CAMERAS

Space TV systems using SEC /secondary electron conduction/ camera tube

04 p0597 A71-15289

Mariner Mars 1969 TV cameras instrument design and calibration techniques

06 p0898 A71-17632

Surveyor 3 spacecraft TV camera surface discoloration patterns caused by lunar soil blown by Apollo 12 exhaust

08 p1363 A71-21219

Minor planet Icarus earth approach observations with reflector and TV camera, determining spherical coordinates by comparison with reference stars

14 p2309 A71-29993

Direct spectra analysis system using refrigerated image isocoon TV camera as detector for astronomical spectrograph

17 p2741 A71-34993

Subminiature TV camera with hybrid electronic packaging, providing EIA composite video output format and 450 TVL/RH resolution capability

17 p2747 A71-35788

Five-gate automatic acquisition star and satellite TV tracker with video signal from vidicon or image orthicon, using line-to-line correlation for SNR improvement

18 p2882 A71-36904

Mariner 6 and 7 Mars color TV recording of craters, chaotic terrain and canals, using wide and narrow angle cameras

20 p3297 A71-39628

High performance image isocoon camera tube, noting resolution, contrast, service life, cost and TV applications

22 p3548 A71-42510

Interplanetary navigation TV camera in-flight calibration, discussing instrument error sources elimination

22 p3573 A71-42771

Alpha radioactivity in Surveyor 3 camera visor, calculating upper limit of Po 210 at equilibrium of Oceanus Procellarum

23 p3765 A71-43812

Streptococcus mitis bacterium in Apollo 12 lunar retrieved Surveyor 3 TV camera, discussing prelaunch deposition and survival

23 p3633 A71-43815

TELEVISION EQUIPMENT

NT IMAGE DISSECTOR TUBES

NT TELEVISION CAMERAS

NT TELEVISION RECEIVERS

Automatic testing of electro-optical systems including TV, IR and laser applications

03 p0395 A71-13082

Astronomical telescope efficiency improvement, using TV kinescope equipment with superorthicons and videofrequency amplifiers

04 p0589 A71-14832

TV techniques for solar optical image, describing equipment for recording and conversion

04 p0589 A71-14835

TV systems for earth resources survey satellites, discussing high resolution return beam vidicon tubes, laser beam image reproducer and electron beam recorder systems

05 p0816 A71-16143

TV spectrophotometer with photographic and photoelectric measurement techniques advantages for measuring astronomical telescope spectral passbands

07 p1109 A71-19349

TV display eye movement monitor with automatic coordinate digital printout for permanent record

07 p1053 A71-20402

Granular features of solar surface, describing television equipment used aboard balloon for image in 1.2-2 microns region

10 p1680 A71-25004

Thick film flat spiral inductor filter design for television signals, using linear analysis computer program
13 p2039 A71-28913

Optical readout system for analysis of laser Doppler velocimeter signals displayed on TV screen and recorded photographically
18 p2931 A71-36587

TELEVISION RECEIVERS

Optokinetic nystagmus device, combining TV set and bar generator with controllable frame desynchronization for moving image and electrical control of stimulus parameters
09 p1399 A71-22973

Direct broadcast television service by satellite transmission, calculating trees and woods effects on attenuation and suggesting receiving system design modification
09 p1408 A71-23384

Low cost TV ground receiving systems for signals transmitted from synchronous satellites, describing reception techniques, manufacturing and performance characteristics
23 p3646 A71-43594

TELEVISION RECEPTION

Small scale spatially periodic auroral arc distortion observations, using low light level TV reception
06 p0893 A71-17981

Satellite TV broadcasting development in European community, giving cost estimation procedure and program reception methods
18 p2876 A71-36504

TELEVISION SYSTEMS

NT ADVANCED VIDICON CAMERA SYSTEM [AVCS]
NT CLOSED CIRCUIT TELEVISION

NT COLOR TELEVISION

NT EDUCATIONAL TELEVISION

Dog blood flow telemetric measurement with TV system using ultrasonic signals Doppler effect
01 p0024 A71-11059

Two channel 450 mm TV telescope at Pulkovo Observatory, investigating atmospheric turbulence deformations of stellar images
04 p0588 A71-14828

TV systems for earth resources survey satellites, discussing high resolution return beam vidicon tubes, laser beam image reproducer and electron beam recorder systems
05 p0816 A71-16143

TV holography systems, discussing camera and reproducer resolution and operation methods at real time scan rates
07 p1109 A71-19452

Simple nerve system receptor field organization in visual analyzer simulated by TV circuit with scanning beam control focusing
07 p1051 A71-20210

TV monitoring and digital data recording of human corneal reflection during voluntary eye movements, considering visual perception studies application
07 p1051 A71-20210

Kinescope light characteristics nonlinearity effect of television system penetrating ability for image reproduction of faint stars
07 p1115 A71-20444

Target detection improvement in reconnaissance by black and white TV system, using narrow band filters for conversion to multispectral sensor system
08 p1287 A71-21240

TV and silver halide emulsion application to planetary photography from space orbit, providing film system immediate information storage and high resolution
09 p1447 A71-22746

Black and white television scanning ability of color differentiation and gray tone identification by signal fluctuations in aerial imagery
12 p1907 A71-27261

Equatorward moving fast auroral waves recorded with image intensifier-TV system
14 p2229 A71-29660

Distant artificial cosmic objects coordinate determination by image converter/closed TV system screen photography and TV observations of space probes
14 p2309 A71-29992

Satellite systems for educational TV program distribution, discussing orbit utilization, ground stations and ATS program
16 p2645 A71-33588

Automatic data reduction system for TV images of star fields acquired from OAO
17 p2743 A71-35009

Optical target detection and position error signal system for boost phase missiles, using TV with digital computer controlled dual tracking electronics
18 p2883 A71-36911

Information producing capabilities of various combinations of SNR, bandwidth and contrast in simulated digital encoding TV systems
21 p3347 A71-40130

Sampled video data technique with information redundancy for processing and narrow-band transmission, discussing TV display, noting applications in corporate communications and teaching
22 p3547 A71-42508

Low light level TV system using Plumbicon tube and 3-stage image intensifiers
22 p3548 A71-42511

TV data acquisition system for auroral and ionospheric research, noting visual and subvisual detection sensitivity
23 p3677 A71-43515

TELEVISION TRANSMISSION

Earth station communication system planning for Intelsat 4, discussing telephony and TV transmission
02 p0225 A71-12830

Meteorological satellite systems, discussing earth image transmission by TV cameras IR photography, data processing and cloud pictures
05 p0817 A71-16641

Intelsat 3 satellite Communication, Telemetry, and Command system using transponders for multichannel voice and TV transmission
06 p0870 A71-18398

PCM TV photographic data communication for grand tour of outer planets, emphasizing adaptive information-preserving data compression system for optimal performance
08 p1254 A71-21346

Incore thermionic reactor as low cost power supply for direct-to-home TV satellite, converting thermal power to electrical without moving masses
16 p2526 A71-32853

Education satellite technology, discussing transmission levels, low cost high sensitivity receiver design and TV broadcasting
16 p2638 A71-33581

Communication satellite ground station terminal equipment, discussing carrier current telephone, video and sound TV apparatus
17 p2717 A71-35516

Airborne vidiconer visual communication system for transmitting single frame TV information in digital form from air to ground over narrow and wideband circuits
17 p2709 A71-35760

Juridical and institutional aspects of problems raised by TV programs content transmitted by communication satellites, noting applicability of international law
18 p2986 A71-36166

Satellite broadcasting of TV programs, assessing cost for European community
18 p2876 A71-36503

Mixed satellite TV broadcasting system for France, estimating cost
18 p2988 A71-36505

Pilot system of satellite transmitted educational TV involving lines reduction on TV screen
18 p2988 A71-36506

TV broadcasting by satellite to isolated users via cable transmission, estimating cost and satellite optimal radiating power
18 p2877 A71-36507

Stabilizing system for retransmission beam of direct TV broadcast satellite, considering rebroadcast antenna, electronic sensor and antenna pointing subsystem
18 p2892 A71-36576

Direct broadcast satellite TV communications, discussing international regulations and legal aspects
18 p2989 A71-36578

Italian Sirio synchronous satellite for SHF propagation and communication experiments on fading statistics, frequency dependence, path diversity and TV transmission
21 p3347 A71-40474

TV multiplexing and broadband multichannel real time telemetry data transmission without loss between Kennedy Space Center and ground station for computer operation
23 p3645 A71-43519

TELLEGEN THEORY

U GYRATORS

U NETWORK ANALYSIS

U NETWORK SYNTHESIS

TELLURIC CURRENT MICROPULSATIONS

U MICROPULSATIONS

TELLURIC FIELDS

U ELECTRIC FIELDS

TELLURIC LINES

Telluric lines from 6327.5 to 6330.0 Å in solar spectrum from photoelectric observations
09 p1525 A71-23196

Solar spectra of far IR absorption of atmosphere above 4.2 km, using interferometer and cryogenic bolometer measurements
09 p1490 A71-23557

Oxygen telluric lines contours shape analysis, allowing for atmospheric nonisothermicity and inhomogeneity
19 p3090 A71-37978

TELLURIDES

NT BISMUTH TELLURIDES

NT CADMIUM TELLURIDES

NT INDIUM TELLURIDES

NT LEAD TELLURIDES

NT MERCURY TELLURIDES

NT TIN TELLURIDES

NT ZINC TELLURIDES

Zinc arsenide-zinc telluride ternary system phase diagram investigation by X ray, differential thermal

and microstructural analyses and microhardness measurements
16 p2621 A71-33591

Rhenium tellurides phase transformation during decomposition in Ar
16 p2621 A71-33591

GeTe alloyed with Zn, Cd or Hg, measuring electrical conductivity and thermoelectric power temperature dependence
21 p3435 A71-41212

TiTe thin films phase composition and structural properties as functions of component content, deposition conditions and annealing parameters, using X ray diffractometer and IR microscope
24 p3862 A71-41523

TELLURIUM

Te-doped In Sb single crystal growth in transverse magnetic fields, using Czochralski crystal puller
01 p0100 A71-10300

Carbon dioxide laser frequency doubling by crystal reflector output element, discussing shortcomings for conversion efficiency enhancement at power density increase
05 p0761 A71-16200

Carbon dioxide laser radiation frequency doubling using Te for second harmonic generation
18 p2933 A71-37070

Te coefficient for frequency doubling with pulsed carbon dioxide lasers, considering peak second harmonic generation conversion efficiency due to absorption of fundamental
18 p2933 A71-37070

Tellurium concentrations and photocurrent spectra in Te-doped InSb single crystal samples, determining Te diffusion after annealing
21 p3430 A71-41212

Evaporated tellurium thin films electric properties, discussing fabrication techniques, temperature dependence, field effect and Hall mobilities, threshold voltage and stability
23 p3715 A71-43440

TELLURIUM ALLOYS

PbTe-GeTe-PbSe solid solution alloyed by lead chloride, investigating structure, composition and distribution of basic elements
15 p2460 A71-31210

Thermoelectric properties of quaternary Sb-Bi-Te-Se solid solutions, noting low thermal conductivity
22 p3584 A71-41610

TELLURIUM COMPOUNDS

NT BISMUTH TELLURIDES

NT CADMIUM TELLURIDES

NT INDIUM TELLURIDES

NT LEAD TELLURIDES

NT MERCURY TELLURIDES

NT TELLURIDES

NT TIN TELLURIDES

NT ZINC TELLURIDES

Thin films of Te compounds with Zn and Ga and group metals - Conference, Vilnius, U.S.S.R., December 1969, Part 3
24 p3861 A71-45240

TELSTAR SATELLITES

Second Pleumeur-Bodou /France/ ground station for Telstar satellite communication, discussing equipment specifications, Cassegrain antenna and parabolic reflector
17 p2708 A71-35500

TEMPER [METALLURGY]

Phosphorus segregation to prior austenite grain boundaries in ferrite, considering effect on Ni-Cr-C steel temper embrittlement
09 p1471 A71-23131

High strength stainless steel dislocation structure and mechanical properties, discussing tempering, tensile strength, precipitation hardening and temperature effects
11 p1776 A71-25100

Low carbon high chromium steel, emphasizing nitrogen content effects on temper brittleness
15 p2427 A71-31520

Chromium stainless steels fine structure, noting quenching and tempering temperatures effects
19 p3076 A71-37131

Creep tests on heat resistant steels, studying elongation/rupture strength and temper hardening
20 p3251 A71-39020

Stress relaxation in laminated Ti sheet at ambient temperature after vacuum tempering at 800 C, interpreting logarithmic time dependence by activated thermal sliding theory
21 p3399 A71-40520

High strength stainless steel dislocation structure and mechanical properties, discussing tempering, tensile strength, precipitation hardening and temperature effects
21 p3402 A71-41080

TEMPERATE REGIONS

Directional cosmic ray cut-off and loop-cone folding distribution at geomagnetic midlatitude sites
01 p0146 A71-11400

Forbush midlatitude microdecreases effects on diurnal cosmic ray intensity, using neutron monitor
05 p0799 A71-16620

Pc 1 pulsations occurrence frequency diurnal annual and 11 year variations at midlatitudes, relating distribution with carrier frequencies of perturbation
06 p0894 A71-18266

Northern Hemisphere midlatitude numerical weather prediction, investigating effects of tropic and southern regions by wall insertion model
07 p1152 A71-19754

Geomagnetic field quiet solar diurnal variations, examining dynamo theory in lower ionosphere at middle latitudes
07 p1104 A71-20045

Thomson scatter measurements of F region ionization drifts vertical velocity at midlatitudes, studying electric field influence
08 p1279 A71-21204

Midlatitude VLF discrete emissions generation regions location by dispersion analysis of ground station observations, determining plasma density along path for events
08 p1282 A71-21634

Geomagnetic activity winter-summer difference in Northern and Southern Hemisphere middle latitudes
08 p1283 A71-21645

Second order longitudinal variations of vertical ionospheric drift by middle latitude horizontal neutral air winds, showing maxima at universal time
11 p1754 A71-25604

Midlatitude F layer electron concentration increase during magnetic storm, assuming auroral zone heating of horizontal winds
11 p1754 A71-25607

Universal time effect on E region critical frequency at large solar zenith angles, considering ionization source at midlatitude range
11 p1757 A71-25785

Concentration and transport from auroral zone of minor constituents in mesosphere and lower thermosphere during anomalous midlatitude radio absorption periods
14 p2230 A71-29711

Transmission loss measurements at HF over 960 km temperate latitude path for wave polarization calculations and ionospheric absorption estimation
14 p2196 A71-30468

Modal interference spacing in frequency range 13.6-22.3 kHz during sunrise transitions on middle latitude east-west propagation paths
15 p2369 A71-31432

Mass spectroscopy of upper atmosphere neutral composition at equatorial, middle and polar latitudes from meteorological rockets
16 p2566 A71-33758

Large scale traveling ionospheric disturbances at midlatitudes related to polar substorms on statistical basis
16 p2573 A71-33955

VHF wave transhorizontal propagation correlation with daytime E layers in temperature zone, noting height dependence and seasonal and diurnal variations
17 p2707 A71-35445

Circadian rhythms of human renal excretions in polar, temperate and equatorial regions
20 p3190 A71-39477

Midlatitude ionospheric data comparison to F 2 critical frequency from continuity equation and neutral air winds
21 p3372 A71-40043

Universal time effect on E region critical frequency at large solar zenith angles, considering ionization source at midlatitude range
22 p3532 A71-41553

Semiannual variation in F 2 layer peak height and critical frequencies at midlatitudes, considering vertical ionospheric drifts effects
23 p3665 A71-42973

TEMPERATURE

NT AMBIENT TEMPERATURE
NT ATMOSPHERIC TEMPERATURE
NT AURORAL TEMPERATURE
NT BODY TEMPERATURE
NT BRIGHTNESS TEMPERATURE
NT COMBUSTION TEMPERATURE
NT CRITICAL TEMPERATURE
NT CURIE TEMPERATURE
NT FLAME TEMPERATURE
NT FLASH POINT
NT GAS TEMPERATURE
NT HIGH TEMPERATURE
NT IGNITION TEMPERATURE
NT ION TEMPERATURE
NT IONOSPHERIC TEMPERATURE
NT LOW TEMPERATURE
NT LUNAR TEMPERATURE
NT NOISE TEMPERATURE
NT OPERATING TEMPERATURE
NT PLANETARY TEMPERATURE
NT PLASMA TEMPERATURE
NT ROOM TEMPERATURE
NT SATELLITE TEMPERATURE
NT SKIN TEMPERATURE (BIOLOGY)
NT SOLAR TEMPERATURE
NT STAGNATION TEMPERATURE
NT SURFACE TEMPERATURE
NT TRANSITION TEMPERATURE

NT WALL TEMPERATURE
Thermoelectric materials thermodynamic properties, developing coldness as universal function of viscous heat conducting fluids
17 p2837 A71-34694

TEMPERATURE COMPENSATION
Temperature compensated semiconductor transducers for dynamic pressure measurements, using Si Zener diodes
01 p0057 A71-11289

Inertial instruments temperature compensation vs control
02 p0253 A71-12460

Temperature compensated Zener diodes noise voltage measurements in ELF domain
05 p0729 A71-17000

Semiconductor laser threshold current temperature dependence, considering maximum power gain and compensation techniques
06 p0908 A71-18424

Thermocompensated cavity resonator for SHF wavelength measurements
07 p1075 A71-19302

Varactor capacitance variations compensation for temperature dependent diffusion potentials and dielectric constants changes
08 p1265 A71-21299

Temperature compensation for frequency changes stabilization of avalanche transit time diode microwave oscillator, using loop circuits and high dielectric constant ceramics
13 p2036 A71-27938

Low-power long-life high-accuracy digital inertial reference assembly, using dual voltage spinmotor operated pulse rebalanced temperature compensated gas bearing gyroscopes
14 p2272 A71-30803

Crystal oscillator temperature compensation using hyperabrupt junction varactor diode as reactance modulator and thermistor for temperature sensitive voltage control
14 p2215 A71-30902

Astronomical mirror mass balancing system, discussing counterweights and levers arrangement and error and temperature compensation
15 p2411 A71-32526

Gravimeters calibration by inclination method with astronomical theodolite, tabulating relative errors and temperature corrections
24 p3826 A71-44767

Passive gas flow control with compensation for ambient temperature and supply pressure variations, using choked orifice with area variation linearly proportional to diaphragm deflection [ASME PAPER 70-WA/AUT-14]
24 p3828 A71-45137

TEMPERATURE CONTROL

Automatic temperature monitor and proportional solid state DC controller for electrophysiological use
01 p0022 A71-10247

Combat aircraft cockpit temperature control system design and operation
01 p0004 A71-10270

Thermal design of space experiment by analytical model for temperature regime acceptable to all experimental elements
01 p0017 A71-11454

Inertial instruments temperature compensation vs control
02 p0253 A71-12460

Temperature controlled zinc-silver oxide reserve battery, describing design for high power/energy density, broad operating temperature range and high altitude environmental capability
03 p0352 A71-13044

Spacecraft structural design and thermal control, discussing requirements and responsibilities of designer
03 p0499 A71-13741

Flat cooling wall optimum thickness for minimum steady state temperature at point exposed to local heating
03 p0520 A71-13955

Liquid cooled space suit fluidic temperature control, using pressure differential variations across garment for cooling level modulation [ASME PAPER 70-WA/FLCS-19]
03 p0355 A71-14092

Cylindrical shell spacecraft thermal control coating system optimization, using truncated series representation [ASME PAPER 70-WA/AUT-13]
03 p0499 A71-14151

Automatic temperature control for cryostats operating at 1-300 K, describing mechanical, electrical and combined devices
03 p0429 A71-14302

Vacuum UV degradation of thermal control coatings on ATS-1 satellite, comparing with laboratory simulation
04 p0618 A71-14896

Ascending pathways from spinal thermosensitive region to hypothalamic temperature control center, considering spinothalamic tract impulse frequency temperature response and bilateral RF coagulations
04 p0539 A71-15094

ITOS-1 meteorological satellite launch and operational sequences in orbit, discussing thermal and attitude control, power and communications and sensor equipment
04 p0663 A71-15314

Space shuttle systems structural joints thermal control, discussing contact conductance with and without interstitial fillers
04 p0676 A71-15334

Heat pipe operating principle, design and applications, discussing liquids for different temperature ranges, heat flux density and temperature control
04 p0689 A71-15816

Polymorphic nucleus leukocytes pyrogenic protein fraction effects on rabbits hypothalamus thermal control structures
05 p0707 A71-16386

Inertial grade floated rate integrating gyroscope surface temperature control by closed loop feedback controller
06 p0983 A71-17362

Thermal control surfaces experiment onboard Black Arrow X3 satellite
06 p0981 A71-18675

Phase change solidification phenomena in n-hexadecane for spacecraft thermal control systems, considering two or three dimensional models
07 p1223 A71-19876

Equation derived for operation of turboprop engine with high pressure compressor controlling gas temperature at turbine front
08 p1347 A71-20831

Precision temperature controller using resistive sensor and Wheatstone bridge in heater loop, discussing prototype design for gyroscope application
08 p1287 A71-20986

Defective resistors physical processes during thermal control method, appraising quality from surface temperature distribution
08 p1300 A71-21901

Temperature analyzer function under ambient temperatures in children
08 p1242 A71-21961

Molybdenite oxidation kinetics by thin layer technique with close temperature and gas composition control, measuring temperature, gas composition and particle size effects
09 p1472 A71-23128

Apollo spacecraft and lunar landing module thermal control surfaces, considering inorganic silicate bonded paint
09 p1533 A71-23426

Concorde thermal fatigue test installation, controlling temperature by transfer temperature variation in single heat exchanger block
09 p1430 A71-23580

Time optimal control for massive solids heating or cooling from initial into prescribed finite state with constraints
10 p1695 A71-24159

Airborne electronics reliability testing in temperature controlled chamber
10 p1589 A71-24604

Life prolongation during high intensity microwave exposures with ambient air temperature control for radiation bioeffects studies
11 p1717 A71-25291

Papers on heat transfer and spacecraft thermal control covering solid-vacuum interfaces thermal and visible radiation properties, multilayer insulation, thermal control devices, etc
11 p1854 A71-25360

Heat pipe applications for space vehicle thermal control, discussing spacecraft radiators, thermal exchangers and structure isothermalization [AIAA PAPER 71-410]
11 p1856 A71-26205

Noncondensable gas temperature controlled heat pipe systems design, considering working fluid, reservoir wicks and ambient thermal environment [AIAA PAPER 71-420]
11 p1857 A71-26211

Variable conductance heat pipes feedback mechanisms for spacecraft electrical temperature control system design, using steady state analysis based performance model [AIAA PAPER 71-421]
11 p1857 A71-26212

Variable conductance inert gas type heat pipe for spacecraft electronic equipment fine temperature control, noting design to eliminate start-up problems [AIAA PAPER 71-422]
11 p1857 A71-26213

Manned space station optimal thermal control design, investigating heat pipe and semipassive/air cooled concepts [AIAA PAPER 71-431]
11 p1838 A71-26220

Space station thermal control system design, verifying radiator adequacy by parametric computer analysis with allowance for thermal coating degradation, vehicle attitude and other variables [AIAA PAPER 71-435]
11 p1858 A71-26223

Space shuttle thermal protection system optimal weight by numerical parameterization, discussing temperature constraints and material rearrangement effects [AIAA PAPER 71-444]
11 p1839 A71-26229

Paint absorbance values effect on passive thermal control system primary component, using calibrated computer satellite model
[AIAA PAPER 71-455] 11 p1859 A71-26238

Reflectance restoration of proton and UV degraded spacecraft thermal control coatings by low temperature oxygen plasma treatment applied to Surveyor 3
[AIAA PAPER 71-463] 11 p1800 A71-26244

Spacecraft surface contamination, noting effects on thermal control and optical equipment
[AIAA PAPER 71-457] 11 p1840 A71-26421

Thermal control coating materials, measuring separate and combined electron and UV radiation effects on reflectance and emittance in vacuum
11 p1800 A71-26519

Space stable thermal control coatings, noting reflectance optical spectroscopy of zinc oxide based paints and zinc orthotitanate
11 p1747 A71-26520

Surveyor 3 thermal control surfaces analysis from Apollo 12 samples collection, discussing spectral reflectance and lunar dust effects on surface finches optical properties
[AIAA PAPER 71-479] 12 p1920 A71-26759

Solar energy absorbance changes in spacecraft thermal control surfaces exposed to particulate radiation at simulated synchronous altitude, using computerized model
[AIAA PAPER 71-453] 12 p1928 A71-26761

Vanadium containing high strength low alloy steel thermomechanical processing by last hot mill pass temperature control
[ASME PAPER 71-MET-1] 12 p1918 A71-27320

Multiple circumferential heat pipes construction and tests for spacecraft thermal control, using simulated space environment
[AIAA PAPER 71-412] 12 p1972 A71-27408

IR radiation role in limiting central heater maximum temperature and heat transfer to high density oxygen in cryogenic storage systems
13 p2166 A71-29505

Temperature control in presence of varying heat sources or sinks through thermal conductance
16 p2576 A71-32973

Temperature stabilization with self controlled water and radiation cooled heat pipes using argon in addition to K heat transfer medium
16 p2663 A71-34039

Environmental thermal control/life support system for manned space station, discussing maintenance, weight, power and volume
[AIAA PAPER 71-827] 17 p2690 A71-34719

Densely packaged microelectronics thermal control, using immersion cooling in dielectric fluids
17 p2718 A71-35786

Space station prototype environmental thermal control and life support systems, considering maintainability, reliability, weight penalties and fault detection and isolation
[ASME PAPER 71-AV-22] 18 p2867 A71-36389

Thermal design, analysis, testing and flight performance of ITOS-1 spacecraft, noting fail-safe temperature regulation
[ASME PAPER 71-AV-23] 18 p2868 A71-36390

Steady state and transient response of heat source with temperature regulated by electrical feedback controlled variable conductance heat pipe
[ASME PAPER 71-AV-27] 18 p2868 A71-36394

Thermal control using nitrogen, circuit board, switching, flexible, transformer and segmented evaporator heat pipes
[ASME PAPER 71-AV-29] 18 p2868 A71-36396

Three day mission biosatellite environmental thermal control system design and flight performance
[ASME PAPER 71-AV-33] 18 p2869 A71-36400

Prototype space station environmental thermal control and life support system digital simulation for transient design and performance prediction
[ASME PAPER 71-AV-34] 18 p2869 A71-36401

Space station thermal control systems design, discussing pumped loop, air cooled semipassive and heat pipe systems
[ASME PAPER 71-AV-36] 18 p2869 A71-36403

Thermomodulation method instrument using cold indicator depot with heat exchanger for standardization of heart-time-volume measurements
18 p2872 A71-36692

Gas controlled variable conductance heat pipe for OAO-C onboard processor temperature stabilization, describing thermal performance tests under simulated flight conditions
[AIAA PAPER 71-411] 18 p2975 A71-36775

Temperature regulation during exercise by proportional control, investigating skin temperature effect on set point temperature, sweat rate and skin thermal conductance
18 p2860 A71-36879

On-off temperature control system with distributed parameters under boundary conditions, investigating symmetric self oscillation
19 p3163 A71-37780

Gravity induced free convection effects in melting phenomena for thermal control, predicting tempera-

ture distributions and solid-liquid interface profiles by two dimensional model
20 p3314 A71-39354

Infrared and thermal evaluation of tactical aircraft phased array radar antenna design with cooling air distribution for steady state operating temperature maintenance
21 p3352 A71-40434

Pulsed ruby laser holography improvement by coherence length increase with temperature controlled multitalons and beam uniformity through ruby crystals improvement
21 p3393 A71-40925

Distributed parameter system optimal feedback control with quadratic performance indices dependence on discrete point states, applying to uniform bar temperature control
23 p3656 A71-43853

Riccati equation reduction for optimal control of linear quadratic distributed parameter systems applied to temperature and heat flow regulation
23 p3653 A71-43969

TEMPERATURE DIFFERENCES U TEMPERATURE GRADIENTS TEMPERATURE DISTRIBUTION

Real vortices velocity, density and temperature distribution determination, discussing flow measurements by hot-wire anemometer, multiple spark camera interferography and smoke visualization techniques
01 p0069 A71-10107

Laser active element temperature field nonuniformity, calculating thermal stresses
01 p0093 A71-10614

Turbulent boundary layer air flow through supersonic convergent-divergent nozzle with heat transfer, considering relationship between temperature and velocity profiles
01 p0180 A71-10950

Time, temperature and transformation curves for Ti alloy by dilatometry, hardness measurements, X rays and micrography, discussing martensite and beta-alpha transformations
01 p0105 A71-11620

Spatial-temporal distribution of laser spark plasma electron density and temperature based on holographic interferometry
02 p0258 A71-11639

Unsteady axisymmetric temperature and stress distribution in multilayer cylinder in convective heat transfer with temperature-varying medium
02 p0322 A71-11729

Thermoelastic axisymmetric problem for half space applied to steady temperature field and stress concentration in infinite body with heat conducting plane circular crack
02 p0322 A71-11733

Highly flexible nonlinearly elastic two layer cylinder reinforced by transversely isotropic shell, examining stressed state in axisymmetric temperature field
02 p0323 A71-11742

Fiberglass reinforced plastic materials in steady temperature fields, determining creep and load carrying capacity
02 p0272 A71-11753

Charged particle temperature distribution in outer ionosphere, disregarding collisional energy exchange
02 p0244 A71-11920

Argon plasma column inductive discharge parameters at atmospheric pressure from radial temperature distribution measurements
02 p0290 A71-12181

Temperature fields without induced stress, considering relation between thermal and dislocation stresses in shells of revolution
02 p0325 A71-12283

Thermodynamic similarity laws for rocket fuel tanks with cryogenic propellants, using dimensional analysis for unsteady temperature distributions
02 p0332 A71-12526

Cylindrical wall with variable heat conductivity coefficient, solving temperature distribution by asymptotic method
02 p0333 A71-12540

Mean and pulsation characteristics of velocity and temperature in turbulent conducting jets under longitudinal and transverse magnetic fields
02 p0292 A71-12626

Rectangular parallelepiped and solid cylinder temperature distributions under time dependent ambient heating or cooling, solving thermal conductivity equation
02 p0333 A71-12647

Solar chromosphere model, investigating radiative transfer effect on temperature structure of plane slab heated by thermal conduction
03 p0483 A71-13186

Temperature distribution in heat conducting cylindrical laser rod at large pumping pulse repetition rates
03 p0435 A71-13512

Laminar flow of liquid in duct with zero heat resistance of walls, calculating temperature distribution during radiative convective heating
03 p0519 A71-13745

Temperature field of radiation heated bodies, using analytic method based on backradiation law approximation by linear function with limit error in Stat range
03 p0519 A71-13745

Cylindrical sample longitudinally isothermal zone, unsteady temperature field calculation from heat conduction equation with allowance for temperature dependence of thermodynamic properties
03 p0520 A71-13749

Ionospheric electron temperature global pattern from satellite observations
03 p0415 A71-14060

Heated glass free jet characteristics at low Reynolds numbers, evaluating temperature distribution and two dimensional fluid dynamic effects
[ASME PAPER 70-WA/FE-3] 03 p0521 A71-14100

Electron beam welding and boring, considering temperature distribution relation to pulse duration
03 p0433 A71-14200

Reciprocal thermal influence, temperature and conduction distance of electronic components in compact circuits
03 p0387 A71-14310

UV scanning polychromator spectroheliometer on Apollo Telescope Mount, examining temperature distribution on sun
03 p0430 A71-14410

Thermal variations of all-glass and air-gap Fabry-Perot etalons for radial velocities measurement, discussing resolution
04 p0593 A71-14910

Cathode tip shape influence on temperature and velocity fields in gas tungsten arc welding, noting effect on weldment area and penetration
04 p0603 A71-14920

Ionized gas flow temperature distribution effects on half width of H beta line
04 p0633 A71-15060

Nonlinear thermoelasticity coupled equations, discussing stress and temperature fields in terms of material response functions
04 p0669 A71-15110

Transient heat transfer in fins undergoing phase transformation, obtaining approximate solution of temperature distribution and interface motion by perturbation technique
04 p0678 A71-15410

Temperature distribution and heat transfer across transitional separated shear layer under subsonic air flow, using interferometric measurements
04 p0679 A71-15410

Heated jet injection into isothermal turbulent boundary layer, investigating temperature distribution downstream with conduction model
04 p0572 A71-15410

Free convection temperature field about isothermal spheres in air, using interferometer for axisymmetric field
04 p0686 A71-15510

German monograph on open turbulent methane-oxygen flame temperature and concentration distribution, determination from jet density measurements, using radiometric method
05 p0831 A71-16120

Temperature gradients and cooling rates of Ti alloy sheet moving arc weld pools, discussing instantaneous solidification
05 p0757 A71-16210

Hydrogen-oxygen catalytic ignition system steady state model for predicting temperature and concentration profiles
05 p0795 A71-16310

Numerical analysis of one dimensional transient temperature fields and elastic thermal stress fields, deriving equations for plate and cylinders with free edges
05 p0823 A71-16410

Strong shock wave Mach reflection, determining pressure and temperature at wedge surface by shock tube experiment
05 p0835 A71-16520

Plasma boundary layer temperature distribution near conducting surfaces by measuring current voltage characteristics
05 p0790 A71-16770

Fe 57 nuclei longitudinal and transverse relaxation in yttrium iron oxide sublattices at various temperatures and magnetic field strengths
05 p0794 A71-16870

Elastic plate with heat conducting rectilinear crack, determining steady state temperature field and stresses
05 p0827 A71-16880

German monograph on hot-wire anemometry in fluids, taking into account partial differential equation solution for temporal and spatial temperature distribution along wire
05 p0753 A71-16880

Vertical temperature distribution measurements by meteorological satellites distribution measurements applied to numerical weather forecasting
05 p0778 A71-17040

Polycrystalline Al alloys inelastic deformation under combined stress at elevated temperatures, observing time dependent behavior

05 p0830 A71-17237

Homogeneous rod heat transfer inverse problem, considering temperature distribution determination

06 p1005 A71-17325

Automatic computer verification of diurnal temperature and geopotential observations on principal isobaric surfaces by statistical data analysis, describing computer algorithm

06 p0922 A71-17504

Soviet papers on satellite meteorology covering atmospheric radiation fields, wind determination, temperature distribution transformations and cloud forms identification

06 p0922 A71-17507

Atmospheric radiating gas components contribution to thermal balance at various altitudes, geographic latitudes and seasons

06 p0923 A71-17509

Radiation temperature fields and cloud distributions seasonal and latitude characteristics by meteorological earth satellite data

06 p0924 A71-17517

Global radiation temperature distribution inhomogeneities in underlying surfaces, atmosphere and radiation absorbing areas

06 p0924 A71-17518

Monte Carlo calculations of intrinsic radiation and blackness degree of nonisothermal cavities with non-specific temperature profile

06 p0897 A71-17529

Critique of paper on lithosphere thermal regime descending into mantle

06 p0889 A71-17636

Nonstationary temperature fields and thermal stresses in plates and shells for discontinuous boundary conditions

06 p0991 A71-17799

Unsteady heat conduction in thermally coupled spherical regions, discussing duration, penetration depth and temperature histories

06 p1006 A71-18071

MHD oscillating flow along infinite unmagnetized conducting plane porous wall, deriving temperature field in boundary layer

06 p0937 A71-18231

Tangential velocity and total temperature distribution axial and radial gradients from secondary flow functions and turbulent energy equations

06 p0883 A71-18321

Unsteady temperature fields in thin anisotropic plates with variable coefficient of heat exchange from side surfaces

06 p1009 A71-18730

Wall flow boundary layer, observing external turbulent field effect on velocity and temperature distribution and heat exchange

07 p1086 A71-18771

Boiling layer microcharacteristics, investigating temperature pulsations near wall attachment and subcooled liquid two phase boundaries

07 p1221 A71-18788

One dimensional nonstationary temperature field in solid body with linearly related heat conductivity and capacity

07 p1221 A71-18921

Stress-strain state of large inhomogeneous bodies of revolution, considering deformation due to arbitrary surface and mass forces in temperature field

07 p1210 A71-19158

Steel under cyclic loads, observing relationship between changes in microstructure and temperature curve shape in fatigue failure process

07 p1211 A71-19194

Supersonic air flow pattern over rectangular indentations on plane and axisymmetric surfaces, examining static pressure and adiabatic temperature distributions

07 p1014 A71-19744

Viscous incompressible fluid flow between two cofocal elliptic cylinders, discussing temperature distribution and heat transfer in annulus

07 p1224 A71-20029

Pulsed ruby laser radiation energy characteristics relation to crystal temperature distribution, thermal deformation and compensating lens focal length

07 p1126 A71-20188

Two dimensional turbulent wake interaction with linearly stratified main stream, measuring mean and fluctuating temperature and velocity distributions

07 p1092 A71-20277

Rock forming monomineralic aggregates thermal conductivity at ordinary temperature and pressure in relation to density, crystal structure and chemical composition

07 p1105 A71-20448

Stationary temperature field and stresses in infinite body with thermally insulated penny shaped crack, assuming heat source and sink symmetrical distribution

07 p1217 A71-20462

Unsteady temperature field determination in infinite cylindrically anisotropic plate with circular hole, calculating stress by Volterra equations

07 p1218 A71-20463

Evaporated Rh films preparation at various substrate temperatures in vacuum UV, determining reflectance and optical constants

08 p1343 A71-21183

Steady state thermoelastic mixed boundary value problem for elastic layer, obtaining temperature, stresses and displacements in finite integrals through Hankel transforms

08 p1370 A71-21238

Buckling of thin elastic circular plates under steady state axisymmetric temperature distribution

08 p1370 A71-21304

Moving thin walled tubes surface and internal defects detection based on three dimensional thermal field surface distribution

08 p1300 A71-21899

Defective resistors physical processes during thermal control method, appraising quality from surface temperature distribution

08 p1300 A71-21901

Thermoelastic stress and temperature distribution in doubly connected isotropic plate

08 p1374 A71-21948

Temperature distributions and heat flux for gray gas in radiative equilibrium bounded by walls with different temperatures, using differential approximation [AIAA PAPER 70-834]

09 p1516 A71-22094

Beams torsional rigidity under thermal stress due to arbitrary temperature distribution

09 p1534 A71-22103

Thermal field calculation theory for complex shape electronic devices

09 p1414 A71-22185

Hybrid integral microcircuits with thin film resistor heat sources, determining temperature fields on substrate and boundaries

09 p1416 A71-22495

Elastic half space two dimensional unsteady temperature and stress fields under induction heating and convective heat transfer

09 p1537 A71-22519

Closed spherical shell, calculating optimal internal temperature fields for keeping thermal stresses at low level under local axisymmetric heating

09 p1537 A71-22520

Adiabatic and melting point gradients in earth core, discussing temperature distribution inhibition to convection radial components

09 p1436 A71-22642

Turbulent air flow velocity and temperature fluctuations, determining mean fields, Prandtl number distributions and correlation moments and coefficients

09 p1432 A71-22729

Spatially uniform dense partially ionized plasmas asymptotic thermochemical relaxation processes due to heavy particle density, temperature or superimposed electric field changes

09 p1502 A71-22859

Metallic and nonmetallic objects phase separation and honeycomb structures adhesion lack, analyzing defects by surface temperatures distribution determination

09 p1450 A71-22893

IC quality control by temperature fields contactless measurement, using microthermographs

09 p1450 A71-22894

Thermal conductivity measurement of cryopumped solid gas deposits in thin walled stainless steel cylinder with temperature gradients

09 p1546 A71-23007

Shallow conical shells local heat treatment, determining optimal temperature fields

09 p1546 A71-23084

Steady one dimensional temperature field of cylindrical shell spacecraft, allowing for heat conduction and convective and radiative heat transfer within shell

09 p1546 A71-23148

Book on atmospheric boundary layer dynamics considering theoretical models of vertical distribution of wind velocity, temperature and humidity

09 p1488 A71-23175

Atmospheric surface layer shear/buoyant production, flux divergence and dissipation in terms of turbulent kinetic energy and transport in temperature variance budget

09 p1490 A71-23555

Periodic rotation reversal effect on hollow cylinder surface temperature distribution in space simulation testing of spin stabilized orbiting satellites

09 p1430 A71-23733

Temperature stress distribution in infinite plate with time varying heat transfer coefficient

10 p1687 A71-24197

Elastic half space with plane boundary subjected to transient temperature field, calculating temperature distribution and thermoelastic strain through Laplace transform

10 p1688 A71-24351

Steady state temperature field for infinite space with spherical cavities distributed along straight line,

reducing problem to infinite system of algebraic equations

10 p1695 A71-24359

Thermoviscoelasticity approximate method for materials with nonstationary nonuniform temperature distribution dependent mechanical properties, using time-temperature analogy principle

10 p1688 A71-24360

E and F region positive ion composition, electron concentration and thermal balance vertical profile, discussing ionizing radiation spectrum, plasma cooling, primary chemical reaction rates and ionospheric formation

10 p1573 A71-24550

Temperature distribution in composite media sections involving solid interfacial sources, using Vodicica orthogonality equations

10 p1697 A71-24694

Light scattering from gas thermal fluctuations, deriving density-density correlation function over various pressures

10 p1642 A71-24836

German monograph on thermal shock experimental analysis covering derivation of method for determining temperatures and thermal stresses in nuclear reactor structures

10 p1697 A71-25036

Temperature distribution inside solid sphere rotating in viscous incompressible liquid with constant strength heat source at center, discussing flow field around sphere

11 p1853 A71-25146

Axisymmetric incompressible boundary layer flow, temperature distribution and heat exchange near critical point of rotating body with varying surface temperature

11 p1854 A71-25239

Electromagnetic fields induction in biological tissues, recording energy absorption temperature distribution in phantom models with thermograph camera

11 p1717 A71-25289

Radiatively interacting adjacent plates in presence of collimated solar flux, considering surface roughness effects on equilibrium temperature distribution [AIAA PAPER 70-817]

11 p1854 A71-25511

Deterministic steady state error model for floated inertial gyroscope, considering lateral or rotational float displacement and temperature distribution variations

11 p1761 A71-25517

Vibrational and rotational temperature diurnal variations of upper atmospheric OH emissions from IR spectroscopic measurements, discussing earth shadow effects on mean intensity

11 p1753 A71-25541

Thermosphere diurnal variations two dimensional model atmosphere characteristic waves, separating density and temperature variations

11 p1756 A71-25649

Diurnal temperature variations in middle ionosphere by rocket probes, noting solar activity changes influence

11 p1759 A71-25823

Thermionic converters performance in ignited mode from transport equations for diffusion region, determining electron concentration, potential and temperature

11 p1711 A71-25879

Incore thermionic cell power output limitation and thermal/electrical data determination at steady state operation, considering temperature distribution

11 p1713 A71-25894

Thermal and electrical characteristics of two nuclear type cylindrical converters with nonuniform emitter temperature

11 p1714 A71-25903

Axisymmetric ablating graphite nosetip analysis code, demonstrating shape change, heating distribution and internal conduction coupling [AIAA PAPER 71-413]

11 p1856 A71-26206

Temperature and membrane thermal stress distribution in finite rectangular plate with insulated circular hole, considering steady state heat conduction equation

11 p1852 A71-26404

Temperature distribution in metal sheets due to point and circular surface heat sources for laser welding applications, using power supply approximation model

12 p1985 A71-26571

Solar corona active regions thermal model, considering X ray emission and temperature distribution

12 p1946 A71-26589

Transversally isotropic sphere and orthotropic cylinder in symmetrical temperature field, calculating thermal stress equations

12 p1975 A71-27112

Thermal buckling and snapping of flat rings and of shallow conical rings under axisymmetric temperature distribution [ASME PAPER 71-DE-B]

12 p1977 A71-27317

Thermal stresses in circular plate with cylindrical orthotropy and reinforced edge, determining temperature and stress distributions

12 p1979 A71-27356

Gas field nonuniformity as function of turbine engine combustion chamber design parameters, discussing hot tube circumferential holes total area effect

12 p1945 A71-27501

Ovonic systems involving electrothermal switching effects on semiconductor glasses, discussing threshold voltage characteristics as function of temperature distribution and glass thickness

12 p1944 A71-27638

Annular solid state microwave diodes temperature distribution at diode/heat sink interface, presenting closed form solution for calculation of absolute temperature rise

12 p1889 A71-27699

Longitudinal solid surface curvature effects on heat transfer, calculating velocity and temperature fields by similarity analysis via boundary layer equations

12 p1887 A71-27737

Upper atmosphere neutral components temperature differences estimates from gas hydrodynamic equations solution by disturbances method

13 p2057 A71-28019

Charged particle temperature distribution in outer ionosphere, disregarding collisional energy exchange

13 p2058 A71-28207

Circular cylinder thermal stressed state, considering interaction between temperature and deformation fields

13 p2152 A71-28273

Laminar free convection heat transfer in vertical rectangular corner, considering velocity and temperature distribution

13 p2161 A71-28621

Approximation procedures for quasi-static problems solution in thermoviscoelasticity theory, considering time-variable boundaries and inhomogeneous temperature fields

13 p2154 A71-28648

Atmospheric frontogenesis models with air velocity fields acting on initially large scale temperature distributions

13 p2097 A71-28722

Frequency and temperature variations of active diode region in pulsed GaAs laser, using Fabry-Perot interferometer

13 p2079 A71-28923

Gas turbine engine combustion chamber outlet, noting gas flow temperature field peripheral nonuniformity

13 p2118 A71-28972

Computational efficiency comparison between finite element and finite difference methods for temperature distribution calculations

[ASME PAPER 69-WA/HT-38] 13 p2155 A71-28977
Temperature dependent thermophysical properties effect on temperature distribution in step-heated semiinfinite solid, deriving time limited perturbation solution

13 p2164 A71-28988

Nonuniform sidewall heat flux effect on thermal stratification

13 p2165 A71-29010

Scott effect observation of superrotation of upper atmosphere, relating temperature gradient, magnetic field and gas rotation

13 p2063 A71-29095

Relativistic thermo-magnetoelastic wave propagation, considering elastic solid under magnetic and thermal fields

13 p2101 A71-29105

Honeycomb cell multilayer and reinforced structures, examining temperature field radiative heat transport and thermal conductivity and emissivity

13 p2165 A71-29180

Interstellar grain temperatures, considering radiant energy distribution and optical properties effects

14 p2305 A71-29679

Interstellar grain temperatures, determining shape effects on emissivities

14 p2305 A71-29680

Heat exchange and temperature distribution between two liquids divided by plate, discussing possible errors

14 p2335 A71-30948

Plate temperature field and stress distribution under thermal pulses, evaluating critical heat load for damage

14 p2325 A71-30049

Turbine blade profiles nonstationary temperature fields during thermal fatigue tests, measuring surface temperature via thin film thermocouples

14 p2252 A71-30265

Equilibria of molybdenum-nitrogen solid solutions at various temperatures

14 p2260 A71-30474

Meteorological research on upper atmosphere energy sinks/sources, composition, density, turbulence, winds and thermal structure

14 p2236 A71-30494

Stratospheric turbulence induced aircraft buffeting dependence on horizontal temperature and wind distribution

15 p2444 A71-31366

Air cooling methods for aircraft engine turbine rotor blades, considering heat distribution in rotor disk

15 p2467 A71-31461

Argon plasma column inductive discharge parameters at atmospheric pressure from radial temperature distribution measurements

15 p2454 A71-31489

Noise and spectral analysis for measuring fluid flow with random temperature fluctuations by transit times

15 p2406 A71-31596

Thermal buckling of elastic plates exposed to random temperature field producing biaxial stress concentration

15 p2504 A71-31834

Stratospheric circulation, investigating ozone heating role in temperature field formation by numerical experiment

15 p2399 A71-31963

Stratopause layer atmospheric temperature field characteristics observation, noting association with processes in upper stratosphere and lower mesosphere

15 p2399 A71-31965

Mo sheet electron beam penetration during welding, calculating heat-affected zone temperature distribution

15 p2435 A71-32466

Crystallization temperatures of lunar gabbroid rocks from Tranquility base, comparing with dry silicate melts

15 p2401 A71-32498

Solar atmosphere vertical temperature and density distribution measurements, using spatially averaged H and K resonance line profiles central reversals

15 p2496 A71-32742

Solar wind outflow from active regions by numerical integration of hydrodynamics equations, using corona temperature distribution

15 p2480 A71-32753

Radiation flux calculation and divergence in regions with stepwise temperature and chemical composition distribution

16 p2661 A71-32798

Gas cooled porous plate unsteady temperature field during high temperature action, considering thermoradiative, convective and mixed radiative-convective heat transfer

16 p2662 A71-32833

Temperature fields and mass and heat transfer at surface of solid spherical particle in laminar viscous fluid flow

16 p2557 A71-32931

Plasma boundary layer temperature distribution near conducting surfaces from I-V characteristics of gas gap

16 p2618 A71-33028

Thermal stresses in gas turbine rotor blade with two dimensional temperature field, using closed /Saint Venant/ plate solutions

16 p2657 A71-33543

Gas turbine engine combustion chamber outlet gas temperature field peripheral nonuniformity, detailing jets disruptive capacity effects in mixing zone

16 p2625 A71-33609

Middle stratosphere monthly mean temperature maps based on radiosonde measurements, confirming anomalies with satellite IR spectrometer radiances

16 p2641 A71-33755

Lunar interior thermal history models for setting radioactive heat sources upper limits consistent with proposed temperature distribution

16 p2642 A71-33797

Thermal equilibrium achievement by highly rarefied gas in closed container with space and time varying surface temperature, deriving gas particle distribution

17 p2784 A71-34195

Complex form plates with energy sources in combined cooling system, calculating temperature field

17 p2836 A71-34422

Annular plate stability and postbuckling behavior in steady plane axisymmetric temperature field

17 p2822 A71-34598

Monograph on flame form and temperature field at burners with nozzle for oxygen addition, using water model

17 p2837 A71-34795

Heat transfer in wall region of steady turbulent flow at large Prandtl numbers, plotting temperature distribution curves

17 p2728 A71-35119

Atlantic Ocean surface temperature distribution data for Gulf Stream meanders and eddies, using Ito's 1 satellite direct readout IR images

17 p2734 A71-35216

Supersonic turbulent two dimensional boundary layer flows wall flux and velocity/temperature profiles prediction

17 p2729 A71-35283

Combustion products and temperature distributions along axis of hexane/air diffusion flame

18 p2984 A71-35867

Clear air turbulence in midstratosphere, analyzing heat and momentum transports and temperature fluctuations spectra

18 p2943 A71-36008

Temperature distribution from line sources and sinks in infinite medium during finite time

18 p2986 A71-36595

Two dimensional stress and temperature fields in cooled gas turbine blades with allowance for elastoplasticity and creep

18 p2980 A71-36595

Thermal effects of continuously tungsten iodine lamp pumped Nd-YAG laser, measuring rod temperature distribution by microprobe beam

18 p2932 A71-37007

Temperature distribution in space shuttle during short radius reentry

19 p3161 A71-37371

Nonlinear radiative heat transfer in hydrocarbon plasma gas, obtaining temperature distributions

19 p3161 A71-37400

Solar photosphere and low chromosphere model temperature-height profile

19 p3135 A71-37607

Binary alloy solidification in electroslag remelting process, determining temperature distribution and solidus, mushy and liquidus zones by heat transfer analysis

19 p3079 A71-37707

Translational freezing in free expanding jets of N_2 , nitrogen and carbon dioxide from molecular beam intensity measurements, deriving perpendicular temperature

19 p3045 A71-37880

Velocity and temperature pulsations as function of stratification parameter in atmospheric boundary layer

19 p3090 A71-37970

Gas and surface temperature distributions for laminar flow in circular tube, considering conduction, convection and radiation effects

19 p3164 A71-37985

Plasma radiation effects in gas tube electric arc heating, obtaining temperature and heat flux profiles and I-V characteristics from energy transport mathematical model

19 p3164 A71-37995

Radiation heat transfer volume interchange factor approximation for gases with nonuniform temperature, composition or pressure, comparing with exact numerical computations

19 p3164 A71-37995

Spontaneous hot zone formation in oil flow through small pipes, showing significance in pressure losses and plain bearings calculations

19 p3046 A71-38275

Self induced thermal distribution due to laser beam discussing effects on refractive index inhomogeneities and second harmonic generation

20 p3196 A71-39100

Viscoelastic polar materials thermomechanical behavior, deriving stress tensor, couple stress tensor, entropy density and linear constitutive equations

20 p3309 A71-39560

Earth surface effective temperature map from meteorological satellites IR imagery interpretation

20 p3260 A71-39680

Lower thermosphere vertical temperature distribution measurements, using ionization and heat manometers

20 p3222 A71-39700

Upper atmospheric temperature and soft solar X-ray time scale fluctuation data, using satellite drag observations and statistical analysis

20 p3280 A71-39700

Stratosphere and mesosphere physics and dynamics, studying composition, radiation fields, temperature, winds, wave phenomena and relations to meteorological theory

20 p3230 A71-39870

Cooled film anemometer techniques for hypersonic wake temperature and velocity distribution measurements for projectiles in free flight range

21 p3363 A71-40380

Temperature control bracket energy equation as measure of temperature distribution in pure hydrogen stellar atmosphere, considering electron energy and radiation field

21 p3446 A71-40401

Plane waves propagation in viscoelastic bodies representing parallel union of Kelvin and Maxwell bodies in magneto-thermal field

21 p3463 A71-40570

Temperature distribution along short heated wire cooled by flowing liquid with parabolic velocity distribution, using power series for differential equation solution

21 p3378 A71-40580

Thin skewed plates bending and twisting at constant temperature moment, obtaining angle skew effects on torque-twist relation

21 p3463 A71-40595

Parametric differentiation solution accuracy and stability for temperature profile and heat flux behind one dimensional hypersonic shock, including thermal radiation

21 p3409 A71-41010

Generalized radiation cooling of convex solid demonstrating existence of unique stable positive

solution to boundary value problem related to temperature distribution

21 p3477 A71-41184

Integral and pointwise estimates of insulated cylinder temperature field spatial decay for semilinear parabolic equations

21 p3473 A71-41186

Frequency and temperature variation with time in active region of pulsed GaAs laser diode, using Fabry-Perot interferometer

21 p3394 A71-41318

Algorithms for calculating temperature fields of electronic devices on computers, considering solid body in shape of bounded cylinder

22 p3519 A71-41442

Temperature field of thermochemical sensor in automatic control systems, developing thermal energy transport models for circular disk with energy source at center

22 p3537 A71-41443

Slow toroidal theta-Z pinch experiment, describing measurements temperature distribution with emphasis on transitions between stable and unstable states

22 p3580 A71-41588

Multilayer printed circuit boards defects detection by temperature field monitoring

22 p3520 A71-41764

Heat transfer and temperature field calculation in turbulent flows through channels of noncircular cross sections, allowing for secondary flow

22 p3619 A71-41871

Spalding-Patankar numerical integration for heat transfer from air cooled disk rotating near stator, considering frictional heating, disk temperature distribution and nonunity Prandtl numbers

22 p3620 A71-41878

Plane Couette flow temperature and velocity fields for Newtonian fluid with temperature dependent viscosity under locally and temporally constant wall temperature

22 p3620 A71-41881

Close binary stars monochromatic reflection effect calculation, using surface temperature distribution model

22 p3599 A71-41934

Electromagnetic radiation in stagnation flow region, determining temperature distribution absorption coefficient of carbon dioxide at rest between two parallel plates

22 p3621 A71-42024

Material random temperature and imperfection density effects on 3-bar truss nonlinear steady creep solutions for stress and velocity

22 p3615 A71-42211

Convective cloud dissipation after rainfall, calculating temporal behavior of temperature fields, water content, moisture and air motion rate

22 p3569 A71-42847

Gulf Stream and Middle Atlantic Bight complex synoptic sea surface temperature distribution fromITOS 1 satellite high resolution IR imagery

22 p3536 A71-42885

Horizontal velocity and temperature spectra at high wavenumbers in three dimensional quasi-geostrophic turbulent flow

23 p3701 A71-43346

Translational and rotational temperature and density variations through shock waves in oxygen and nitrogen, using Monte Carlo scheme

23 p3781 A71-43444

Statistical modeling technique for approximate numerical solution of unsteady heat conductivity inverse problem, obtaining foam chamotte and magnesite temperature field data

23 p3782 A71-44059

Nonsteady heat conduction of multilayer cylindrical and conical shells in periodic radiation flux, calculating temperature distribution

23 p3783 A71-44067

Vertical heat transfer coefficient of flat and cylindrical walls in fluidized bed from wall vertical temperature distribution

23 p3783 A71-44069

Temperature distribution in current carrying cylindrical conductor with nonlinear boundary condition of emission by Stefan-Boltzmann law

23 p3783 A71-44070

Heat exchange between two fluid streams in concurrent, countercurrent, laminar or turbulent boundary layer flow separated by flat plate, determining temperature distribution

23 p3783 A71-44193

Forced convection steady heat transfer across laminar incompressible constant-property boundary layers over wedges with step discontinuity in surface temperature

23 p3784 A71-44196

Thermoviscoelastic problem for semifinite plate, determining temperature field and stresses permitting heat propagation

23 p3780 A71-44223

Heat generating granular layer tube, obtaining temperature distribution across cross section and boundary conditions

23 p3719 A71-44338

Temperature field measurements above porous surface during ice-water sublimation into vacuum, showing discontinuities due to external heat and mass transfer

23 p3784 A71-44340

Dense discharge plasma temperature and ionization distributions in He, H and Ar, investigating pulsed arc emission dependence on current and pressure

24 p3855 A71-44520

Free convection heat transfer from vertical flat plate with sinusoidal wall temperature distribution [AIAA PAPER 71-988]

24 p3887 A71-44583

Conductive heat transfer and temperature jump in polyatomic gas between parallel plates evaluated by variational principle based on linearized integro-differential equation

24 p3889 A71-44969

Space vehicle radiative cooling system rib temperature field calculation, taking into account material heat conductivity temperature dependence

24 p3889 A71-45023

Two dimensional stationary temperature fields calculation for temperature independent heat conduction

24 p3890 A71-45068

Thermomolecular pressure gradients and temperatures in flow between parallel plates for statistical gas models at arbitrary Knudsen numbers

24 p3891 A71-45242

TEMPERATURE EFFECTS

Cr-Ni steel elastic properties under intercrystalline corrosion, examining temperature effects on internal friction, electric resistivity and vibration frequency

01 p0096 A71-10038

Steel cylinders with circumferential cracks under repeated impact tensile loads, investigating plain strain fracture toughness index temperature dependence

01 p0166 A71-10079

Two-phase composites stability at various temperatures, noting failure regularities dependence on components mechanical properties relationship

01 p0106 A71-10083

Anomalous temperature dependent silver halides photoemission related to lattice vibrationally dependent hybridization of valence states

01 p0137 A71-10148

Anodic temperature effect on Cs thermionic converter operation under arc regime, obtaining potential jump electron temperature relation near anode

01 p0005 A71-10158

High temperature annealing effect on sapphire single whiskers structure, using electron microscopy

01 p0106 A71-10276

Isotactic polypropylene and high pressure polyethylene in contact with steel, examining temperature effect on friction and adhesion

01 p0106 A71-10299

Ta alloys single crystals elastic compliance constants over temperature range, deriving bulk and shear moduli and anisotropy factor

01 p0100 A71-10373

Cr-Tb alloys phase transformations and diagrams dependence on temperature and composition, using physicochemical analysis

01 p0100 A71-10418

Millimeter waves attenuation in fog, showing strong temperature dependence and correlation with visibility

01 p0117 A71-10580

Temperature effects on heat transfer in turbulent boundary layer on cooled plate at various Reynolds numbers

01 p0179 A71-10609

Laminar boundary layer free convection at vertical plate with exponentially decreasing surface temperature, determining thermal flux and shear stress

01 p0179 A71-10610

Cylindrical shell stability under combined axial compression and heating, using finite difference method

01 p0170 A71-10646

Similar gas discharges for carbon dioxide lasers, including thermal effects and particle distributions over energy levels

01 p0093 A71-10682

Edge dislocations in deformed single crystals of Nb-Mo and Nb-Re alloys at various temperatures

01 p0101 A71-10738

Porous Ti thermal and electrical properties from room to high temperatures

01 p0102 A71-10785

TiC and ZrC samples with different porosities, examining bending strength at various temperatures

01 p0102 A71-10786

High electron temperature H and He I and II, calculating partition functions

01 p0158 A71-10806

Maraging steel welded plates edge displacements under linear multiflame burner heating, determining temporal deformations by heat distribution from additional source

01 p0088 A71-11098

Foamy properties at various temperatures of nonaqueous hydroliquids based on petroleum fractions and organic silicon and phosphorus oligomers

01 p0088 A71-11107

Temperature dependence curves and X ray spectrum analyses of different ferrite compositions, indicating absorption band K-edge shift toward shorter wave region

01 p0139 A71-11111

Optically pumped rubidium maser short term frequency instability caused by thermal noise and resonator temperature and pumping power fluctuation

01 p0095 A71-11211

Global atmospheric circulation, discussing surface irregularities and variable heating role in disturbances

01 p0121 A71-11352

Electron mobility in gallium arsenide phosphide solid solutions, discussing temperature effects

01 p0141 A71-11465

Hall electron mobility in cadmium arsenide as function of concentration and temperature

01 p0141 A71-11466

F region reflected radio wave heating effect, considering electron temperature, collision frequency and heat conductivity

01 p0400 A71-11531

Biological clocks self oscillating mechanism as temperature dependent component of circadian clocks in multicellular organisms, assuming small enzyme concentrations

01 p0020 A71-11566

Quenched Al-Mg alloys, investigating dislocation mechanisms for plastic flow by creep tests at various temperatures

01 p0105 A71-11605

Homogenization and dehomogenization phenomena at high temperature of Cr-Ni austenitic steels, discussing electron microscope microstructural examinations after heat treatment

01 p0105 A71-11617

Water intake effects on human thermal sweat rate and composition in environmental chamber at specific temperature and humidity

02 p0202 A71-11670

Cutaneous blood flow in anesthetized pig forelimb modified by brain temperature changes

02 p0197 A71-11671

Turbine disks under unsteady and cyclic loads and temperature variations, determining stress and strain by flow theory computer calculation

02 p0323 A71-11745

Metal hardening under cyclic thermal loads, determining deformation, breakdown, creep and stress-strain relation

02 p0324 A71-11752

Fiberglass reinforced plastic cylindrical shells, investigating rheological effects during heating and concentrated radial loads

02 p0324 A71-11754

Thin shells of revolution local stability during nonuniform stressed state development under heating

02 p0324 A71-11755

High purity Nb and Nb-O solid solution single crystals, investigating temperature dependence of yield stress

02 p0263 A71-11866

Heat transfer and friction drag calculation for turbulent boundary layer of gas with temperature dependent physical properties

02 p0185 A71-11884

Thin exploding wire restrike channels, examining temperature, electron density and thermal conductivity temporal behavior

02 p0284 A71-11941

Apollo 11 lunar samples dielectric constants, losses and electrical conductivities as function of temperature and frequency, comparing with terrestrial and simulated lunar rocks

02 p0305 A71-11985

Nonrelativistic cosmic particles spectrum and chemical composition changes, examining ionization and heating energy loss effect

02 p0300 A71-12093

Q switched laser wave birefringence thermal variations in liquids, calculating optical anisotropy temperature dependence

02 p0261 A71-12172

Chemically interacting gases transfer properties at varying temperatures, determining collision parameters by viscosity, diffusion coefficients, molecular beam scattering and vibrational relaxation time

02 p0286 A71-12186

Tantalum and niobium disilicides enthalpy and heat capacity temperature dependences

02 p0263 A71-12198

Maximum efficiency of cylindrical thermionic converters with Mo emitter and collector over temperature range

02 p0194 A71-12224

Volt-ampere characteristics dependence on collector temperature in thermionic converters compared with collector work function

02 p0195 A71-12235

Resistively heated W-Re wire sublimation characteristics between 1550-1950 C in low pressure oxygen

02 p0264 A71-12255

Sintered W rolling in vacuum over reduction and temperature ranges

02 p0256 A71-12514

Temperature effect on ductility of thin sheet sintereed or vacuum melted Mo during deep drawing 02 p0257 A71-12517

Composition and annealing temperature effects on recrystallization of vacuum melted thin wire and rod Mo alloys 02 p0265 A71-12521

Temperature and plastic deformation rate effects on plasticity and strength of cast iron, Ti and steels 02 p0257 A71-12525

Thermally induced helical inversion absence in single component cholesteric liquid crystals indicating impurity compensation 02 p0296 A71-12571

Magnetic field effect on boundary temperature in axisymmetric MHD flow in vortex chamber, using dissipationless approximation 02 p0293 A71-12633

Glass fiber reinforced plastics tensile strength under various continuous loading rates and elevated temperatures 02 p0275 A71-12667

Titanium dichromide phase modifications under hardening at various temperatures, using thermal and X ray analysis 02 p0266 A71-12674

Solar flare trigger mechanism, proposing inner corona thermal runaway of radiative power function 02 p0302 A71-12761

IR radiation effect on gas molecular dissociation, showing dissociation temperature decrease due to IR photon absorption 02 p0288 A71-12850

Aluminum compression microstructure under various strain rates and temperatures, discussing dynamic recovery role 02 p0267 A71-12877

Si-Fe fatigue crack growth in vacuum at various temperatures, discussing stress intensity, cleavage and ductility effects 02 p0267 A71-12882

Surface thermal and electrical stresses effect on bipolar transistors electrical properties, using NDT criteria for components selection 02 p0236 A71-12921

Niobium mechanical properties temperature dependence from plastic deformation tests, taking into account interstitial and substitutional impurity concentrations 02 p0271 A71-12936

Niobium alloys for gas turbine blades, examining working temperatures, protective coatings and ductility 02 p0271 A71-12939

Niobium aluminide pest, investigating oxidation effects on Nb-Al protective coatings from 600 to 1400 C 02 p0271 A71-12942

Silane for polycrystalline films deposition on oxidized silicon wafers, noting substrate temperature effects on preferred orientation of deposits 02 p0297 A71-12958

Telemetric ECG recordings of workers under high and strongly varying temperature conditions, discussing heart rate variations under heat stress 03 p0370 A71-13065

Rabbit hypothalamic neuron stimulation by changes in ambient temperature 03 p0361 A71-13225

Urban heat island induced circulation without synoptic winds, using two dimensional atmospheric model 03 p0453 A71-13232

Thin glass fibers relaxation characteristics, discussing shear modulus, internal friction and temperature effects 03 p0448 A71-13298

Chemisorption rate and physical adsorption of nitrogen on Ta films as function of temperature 03 p0441 A71-13361

Corrosion rate of Nb in aqueous solutions as function of temperature, using electrochemical potential measurements 03 p0442 A71-13363

Neodymium glass laser with intracavity emission polarization, determining thermally induced double refraction effect on energy characteristics 03 p0435 A71-13505

High strength steels fracture toughness, investigating loading rate and temperature effects 03 p0442 A71-13625

Ultrasonic absorption in hydrogen sulfide, measuring vibrational and rotational relaxation times as function of temperature 03 p0459 A71-13718

Buoyancy effect on boundary layer flow over heated horizontal circular cylinder immersed in uniform axial free stream, considering successively greater displacements 03 p0519 A71-13731

Notched tensile plate steel specimens, investigating temperature and stress state effects on nil ductility transition and fracture strength [SESA PAPER 1735] 03 p0443 A71-13752

Pulsed laser threshold measurements in YAG activated by Ho, Er and Tm isotopes, noting temperature dependence 03 p0438 A71-13890

Cylindrical sample longitudinally isothermal zone unsteady temperature field calculation from heat conduction equation with allowance for temperature dependence of thermodynamic properties 03 p0520 A71-13960

Thermal conductivity rapid measurement in 300-1200 K range using traversing thermocouple technique [ASME PAPER 70-WA/ENER-2] 03 p0429 A71-14107

Variational equation of motion for thin walled open section bars coupled flexure and torsion, considering thermal effects [ASME PAPER 70-WA/APM-51] 03 p0513 A71-14169

Shivering and heat polynoma threshold temperature shift in guinea pigs, considering thermal adaptation under cool environment exposure 03 p0364 A71-14250

Accelerated cavitation damage in Na, examining pressure and temperature effects 03 p0443 A71-14286

Temperature effect on slip- and spark-induced crack propagation in polycrystalline Mo 03 p0444 A71-14317

Calorimetric measurements determining total hemispheric emittance of thin gold films as function of temperature, demonstrating film thickness effect [AIAA PAPER 70-63] 03 p0522 A71-14456

Ultrafine grain metals strength properties at cryogenic temperatures and near melting point, discussing grain boundaries 03 p0446 A71-14487

Plastic zone effects on notch effect on crack initiation, analyzing ductile-brittle transition temperature relation to sample size 04 p0666 A71-14883

Al-Zn-Mg alloys hardness and conductivity behavior as function of aging time and temperature 04 p0610 A71-14884

Clear potting polymers, investigating temperature and ionizing particle irradiation effects on properties 04 p0618 A71-14898

Thermal diffusivity measurements over 40 to 1400 C range using pulsed electron beam 04 p0595 A71-14963

Diffusion and solubility of thermally induced acceptors in indium antimonide single crystals 04 p0636 A71-15085

Phonon-magnon absorption bands temperature dependences in Ni, Co and Li ferrimagnetic spinels, giving graphical data for Curie points 04 p0637 A71-15106

Pressure-temperature equivalences in elasticity problems, considering applications to case bonded solid propellant rocket grains 04 p0638 A71-15197

Pilot performance under helicopter cabin high temperature and humidity 04 p0547 A71-15422

Army rotorcraft hot day standard design hover criterion, developing analytical models for hovering aircraft, cost, climatology and environmental features 04 p0533 A71-15431

Round cylinder in viscous fluid asymmetrically disturbed flow, calculating dynamic and temperature conditions with difference method 04 p0571 A71-15492

Carbon monoxide fundamental band spectral absorptivity distributions at various high temperatures and optical densities 04 p0549 A71-15512

Two phase mixtures thermally induced flow oscillations, discussing scaling criteria, phase change numbers and stability boundaries 04 p0687 A71-15532

Conditioned reflex gas exchange shifts in persons under repeated local thermal stimuli 04 p0540 A71-15572

Deformation pattern, interstitial impurities and alloying elements effects on temperature dependence of elasticity modulus of Nb and alloys 04 p0613 A71-15641

Pressure and temperature variation effects on vibratory cavitation damage tests conducted in water 04 p0604 A71-15767

Stationary flow of viscoplastic liquid in annular gap with temperature dependent viscosity, taking into account energy dissipation 04 p0579 A71-15799

Mo wire annealing with degassing, investigating temperature effect on mechanical properties 04 p0616 A71-15802

Ti-Al and Al alloys and Ni maraging steel creep behavior during high stress, elevated temperatures and rapid heating 04 p0617 A71-15909

Liquid fuel drop evaporation under pressure on hot surface, measuring lifetime and transient interface temperature at subcritical and supercritical conditions 04 p0689 A71-15919

Magnetic and thermal pressures in solar wind from Explorer 34 data 05 p0797 A71-16050

Ti-Ag and Ti-Pd-Ag solar cell contacts structure and degradation dependence on high temperature and humidity environmental exposure 05 p0699 A71-16060

Temperature effects on Si solar cell short circuit currents, considering solar spectrum, photon absorption coefficient and diffusion length 05 p0700 A71-16060

Si solar cell low temperature low solar illumination intensity I-V performance deficiencies, considering corrective design modifications 05 p0701 A71-16060

Li doped Si solar cells recovery after irradiation, examining temperature dependence 05 p0704 A71-16100

Plastic deformation and ductility of Mo alloys under various stress concentrations at room and high temperatures 05 p0765 A71-16157

Pure Fe and Fe-Ni alloys thermal stress component temperature dependence measurement, investigating Ni addition effect on alloy softening 05 p0765 A71-16180

Nickel alloy tensile tests, investigating strain mechanisms dependence on temperature 05 p0765 A71-16180

Molecular hydrogen formation on dust grain surfaces, discussing recombination efficiency as function of surface temperature 05 p0784 A71-16200

Transistors and Zener diodes temperature dependence and normal and accelerated life tests 05 p0728 A71-16280

Density and temperature dependences of viscosities and thermal conductivity of dense fluids 05 p0831 A71-16400

CdS laser wavelength and relative threshold excitation levels as function of temperature based on band edge absorption effects 05 p0763 A71-16490

Shock tube diaphragm bursting by passing heavy current through overlapping heated wire under pressure 05 p0734 A71-16590

Doped tungsten high temperature behavior, discussing hypotheses regarding doping agents microstructural effects 05 p0767 A71-16590

Dicke-Goldenberg solar oblateness measurements explained by equatorial temperature excess smoothly distributed 05 p0812 A71-16690

Machine components resistance to low temperature failure, considering threaded joints, gears and shafts for strength and plasticity characteristics 05 p0827 A71-16760

Be impact strength temperature dependence and fracture structure, noting grain boundaries cohesion role 05 p0768 A71-16770

Muscular heat production effect on contraction during cold adaptation tests 05 p0710 A71-16800

Al single crystals creep deformation, noting thermally activated mechanism at cryogenic temperatures 05 p0769 A71-16870

Logic circuitry materials physical properties changes effects on performance-controlling parameters at low temperatures 05 p0732 A71-17070

Shock heating effects due to compression and plastic dissipation on basis of finite one dimensional waves in strain rate sensitive elastic viscoplastic solid 05 p0830 A71-17230

High temperature diffusion controlled transient creep, considering unimolecular reaction kinetics stress and temperature dependence 05 p0830 A71-17230

Monte Carlo evaluation of molecular transport property integrals temperature dependence 06 p0917 A71-17550

Flight personnel green protection system from nuclear weapons high intensity thermal effects 06 p0858 A71-17600

Water cooled head cap for heat stress amelioration in subjects working in warm environments 06 p0859 A71-17610

Nonlinear unsteady heat conduction problems, investigating thermophysical property dependence on temperature and body coordinates by half space approximate methods 06 p1006 A71-17740

Variational methods application to optimal heating of thin elastic shells, using elastic-energy functional minimization as optimality criterion 06 p1006 A71-17760

Circular cylindrical shell stability under uniform tension, taking into account support flexibility and temperature difference 06 p0990 A71-17790

- Flexible plates and shallow shells supercritical deformation in high temperature field, taking into account modulus of elasticity and thermal expansion coefficient temperature dependence 06 p0990 A71-17796
- Thin orthotropic shells thermocreeper in variable temperature field reduced to integration of linear partial differential equation system 06 p0997 A71-17852
- Cured epoxy polymer, determining diffusion coefficients, solubility, permeability and equilibrium water absorption as function of curing agent and temperature 06 p0915 A71-17943
- Cr-Ni stainless steel tensile and compressive stresses effect on hydrogen permeability at elevated temperatures 06 p0912 A71-17946
- Solar cosmic ray intensity yearly variation by pressure corrected neutron monitor, discussing atmospheric temperature effects, coronal emission heliographic distribution and annual wave amplitude 06 p0953 A71-18117
- Resistor characteristics temperature dependence, considering platinum resistor and thermistor with negative temperature coefficient 06 p0900 A71-18186
- Venomotor responses of forearm veins to local and remote thermal stimuli to skin in exercising man 06 p0862 A71-18383
- Semiconductor laser threshold current temperature dependence, considering maximum power gain and compensation techniques 06 p0908 A71-18424
- Ti alloy deformation through surface oxidation at elevated temperature, considering lattice parameter and alpha concentration effects 06 p0913 A71-18677
- Explosive metal welding bond interface, investigating heat treatment effect on microstructure 06 p0914 A71-18680
- Ti alloy embrittlement by prolonged high temperature exposure, using substandard fracture mechanics test for time-temperature dependence 06 p0915 A71-18686
- Temperature stratification effects on free atmosphere turbulence structure under Archimedean forces, noting energy dissipation buoyancy forces and adiabatic gradients 07 p1150 A71-18796
- Long wave radiation balance components vertical profiles, showing temperature stratification effect 07 p1151 A71-18914
- Temperature effect in sodium fluoroacetate protective action mechanism for mice irradiation 07 p1037 A71-18968
- Frequency variation with temperature in coaxial cavity avalanche transit time microwave oscillators explained by diode junction capacitance and cavity length changes with temperature 07 p1074 A71-19120
- Annealed Mo creep properties and long term strength, observing temperature and stress effects 07 p1130 A71-19165
- Rapid heating effects on hot pressed TiC cylinders stability, calculating temperature fields and stress distribution 07 p1130 A71-19168
- Thermally induced modifications of high power CW laser beam, considering heat losses by forced and free convection 07 p1122 A71-19207
- Cadmium arsenide alpha and beta phases Hall constant temperature dependence, studying photoelectric and optical properties 07 p1177 A71-19279
- Zr solid state solubility in Mo as function of quenching temperature, using optical microscopy and microhardness testing techniques 07 p1130 A71-19300
- Mg alloys mechanical properties and microstructure changes under static tension in temperature range 20-293 K 07 p1131 A71-19363
- Mg-Cd single crystals deformation by prismatic slip as function of testing temperature and state of order 07 p1132 A71-19437
- Notch geometry and temperature effects on Ti-Al-Mo-V alloy creep rupture behavior 07 p1134 A71-19470
- Electrical conductivity measurement for thorium oxide at 1000-1600 C and at low oxygen partial pressures, discussing Seebeck coefficient behavior 07 p1177 A71-19569
- Laser beam propagation through atmosphere, measuring phase variation dependence on turbulent temperature structure for comparison with prediction 07 p1123 A71-19574
- Mechanical and plastic properties of Ni-Mo alloys subjected to hot working, determining tensile strength as function of test temperature 07 p1136 A71-19635
- Frequency shift in hydrogen maser due to atomic collisions with storage bulb surface /wall shift/, investigating temperature dependence 07 p1124 A71-19686
- Au-Ba intermetallic compound electron work function temperature dependence 07 p1179 A71-19922
- Intrinsic stacking fault energy temperature dependence in austenitic Fe-Cr-Ni alloys determination from dislocation mode measurements by high temperature transmission electron microscopy 07 p1138 A71-19984
- Steels fatigue tests, observing crack propagation through weld heat affected zones at two orientations to stress axis 07 p1139 A71-19989
- Multistage axial flow turbine off-design performance prediction, exploring inlet temperature and pressure and exit pressure variation effects [ASME PAPER 70-PWR-2] 07 p1184 A71-20199
- Re hot rollability under low vacuum conditions as function of temperature, comparing with cold rolling 07 p1120 A71-20240
- W-Re alloy microstructure creep, long term strength and plastic properties as function of temperature, using electron microscopy 07 p1141 A71-20241
- Mo-Re alloy wire structure and properties, observing heat treatment effect with metallographic techniques and X ray analysis 07 p1141 A71-20242
- Etchant type, concentration and temperature effect on various plastics track etching ratio and sensitivity 07 p1145 A71-20272
- Free-space focused microwave system for determining materials complex permittivity to temperatures over 2000 C 07 p1115 A71-20357
- Laser beam self induced thermal distortion in near field absorbing moving medium by theoretical model based on geometrical optics 07 p1128 A71-20389
- Fiberglass reinforced plastic strength and deformability under tension as function of loading rate and test temperature 07 p1145 A71-20466
- Temperature dependence of Vickers pyramid hardness for Ti, Zr and Hf carbides at wide temperature range in vacuum 07 p1142 A71-20483
- Thermal recovery effects on electrical resistivity in deformed polycrystalline Nb samples tested at varying strain rates and 263-509 R temperatures 07 p1144 A71-20496
- Ce, Pr and Nd solubility in Cr, investigating temperature dependence, microhardness, deoxidation and alpha phase by X ray, metallographic and durometric analyses 07 p1144 A71-20652
- Microwave dual mode reciprocal ferrite phase shifters, deriving insertion phase variations as function of ambient temperature and high average power heating 08 p1262 A71-20760
- Air temperature effects on internal combustion engines intake process, using similarity theory 08 p1347 A71-20782
- Carbon fiber and carbon fiber-polyester composites chemical resistance to acid and alkaline solutions at various concentrations and temperatures [PLASTICS INST. PAPER 32] 08 p1320 A71-20903
- Carbon fibers, light metal alloys and composites, studying moduli of elasticity and shear thermal variations [PLASTICS INST. PAPER 16] 08 p1320 A71-20904
- Carbon fibers production by polyacrylonitrile fibers spinning, discussing stretching temperature effects on mechanical properties [PLASTICS INST. PAPER 12] 08 p1320 A71-20909
- Resonance line formation in multidimensional media, applying to non-LTE line transfer for two dimensional temperature variations 08 p1359 A71-20942
- Maraging steels thermal embrittlement, discussing austenite grain boundaries inclusions, carbide networks precipitation and carbon concentration 08 p1305 A71-21027
- Vacuum-melted and deformed Mo alloys tests, showing long term strength decrease under cyclic heating 08 p1305 A71-21030
- Mo microstructure changes at high temperatures noting polygonization, grain migration and crack propagation during failure 08 p1305 A71-21032
- Al-Be-Mg alloys under solution treatment, noting aging and prolonged heating effects on mechanical properties from solid solution decomposition diagram 08 p1305 A71-21034
- W and Mo single crystals metallographic microanalysis for temperature cycles effects on microstructure 08 p1305 A71-21056
- Stress reduction in metal powders compaction at different temperatures and deformation rates 08 p1305 A71-21059
- Zinc electrodes performance improvement, discussing electrochemical corrosion rate, current density and temperature effects 08 p1233 A71-21082
- Unactivated dry charged zinc-silver oxide cells storage life, determining chemical composition changes at various temperatures and time lengths 08 p1235 A71-21100
- Temperature effects on energy dissipation during vibration in ferromagnetic and nonferromagnetic metals, comparing damping capabilities for homologous temperatures 08 p1306 A71-21119
- Nonrelativistic cosmic particles spectrum and chemical composition changes, examining ionization and heating energy loss effect 08 p1355 A71-21143
- Carbon dioxide laser Ge windows thermal runaway characteristics 08 p1302 A71-21391
- Nonlinear theory of intrinsic semiconductor electromagnetic wave transmission under skin effect conditions, determining reflectance and carrier temperature 08 p1344 A71-21442
- Interstitial nitrogen effects on thermally activated flow in Nb single crystals, determining yield and flow stresses and strain-rate sensitivity dependences on temperature 08 p1307 A71-21504
- Ta and W single crystals yield stress temperature dependence, confirming asymmetric Peierls barrier 08 p1307 A71-21507
- Slip asymmetry in Ta and Ta alloys, discussing effects of temperature and alloying elements 08 p1308 A71-21518
- Titanium single crystal prism slip dislocation dynamics, examining temperature and strain rate effects on shear stress 08 p1309 A71-21521
- Li and temperature effects on mechanical properties of Mg base single crystals in basal and prismatic slip 08 p1309 A71-21525
- Al microstructure and strength, investigating prior deformation and temperature effects 08 p1313 A71-21561
- Gamma prime precipitate effects on flow stresses of Ni alloys single crystals at various strain rates and elevated temperatures 08 p1315 A71-21580
- Refractory materials at normal and high temperatures, describing cyclic shear test methods 08 p1372 A71-21612
- Gas turbine blades design and exploitation processes, discussing long time fatigue strength, static durability and heating effects at elevated temperatures 08 p1299 A71-21708
- Satellite-borne Ge radiation detectors, investigating design criteria and performance at elevated temperatures 08 p1267 A71-21847
- High temperature nitrogen plasma, calculating thermodynamic and electrical parameters dependence on pressure and temperature 08 p1342 A71-21917
- Dark adaptation in humans under Arctic conditions, noting role of physiological disorders 08 p1242 A71-21958
- Temperature dependent ionic domain for yttrium oxide doped thoria as solid electrolytes at low oxygen activities 09 p1480 A71-22114
- Liquid crystals of cholesteryl nonanoate with cholesteryl chloride or cholesteryl propionate, examining color dependence on temperature 09 p1442 A71-22270
- Friction and wear tests on materials of various speeds, loads and temperatures at high relative humidity 09 p1426 A71-22325
- Temperature induced spectral line widening of trivalent positive Pr ions in lanthanum niobate crystals 09 p1507 A71-22391
- Integrated circuits semiconductor components, determining effects of heat energy production/withdrawal and strong field on electric current carriers mobility and concentration 09 p1416 A71-22496
- Ultrasound propagation velocity dependence on high pressure and temperature in carbon dioxide, considering Rao rule applicability to highly compressed gases 09 p1492 A71-22529
- Yield point temperature dependence in heat resistant austenitic alloys, showing tendency to brittle failure under short term overloads 09 p1468 A71-22598
- Heating rate effect on parameters of resistance wire strain gages subjected to temperature gradients 09 p1443 A71-22634

Shock reheated chondrites metal phases, discussing postshock cooling thermal histories by metallographic and electron microprobe studies

09 p1519 A71-22643

Stress effects on electron relaxation time anisotropies in n-type Si, using high temperature piezoresistivity model for population transfer rates

09 p1508 A71-22692

Measuring instrument for amorphous and polycrystalline materials resistivity and Seebeck coefficient as function of temperature and pressure

09 p1446 A71-22737

Martensitic transformation of Fe-Ni-Si alloys under tensile plastic strains at 233-373 K

09 p1469 A71-22849

Burning rate temperature sensitivity of composite solid propellants, using granular diffusion flame model

09 p1510 A71-22911

Aqueous HCl refractive indices measured for room temperature to Venus cloud temperature and various concentrations

09 p1522 A71-22937

Si Read diode computer simulated large-signal operation, determining temperature effect on microwave oscillating efficiency

09 p1417 A71-22966

GaAs junction laser continuous operation, investigating reflectivity dependence of temperature rise, stimulated light output and power efficiency

09 p1464 A71-22988

Molybdenite oxidation kinetics by thin layer technique with close temperature and gas composition control, measuring temperature, gas composition and particle size effects

09 p1472 A71-23128

Directionally solidified Ni base superalloys, determining stress and temperature effect on primary creep strain

09 p1472 A71-23130

Temperature and pressure effects on phase transformations, structural changes and related processes in metals, comparing thermographic and calorimetric methods

09 p1547 A71-23227

Annealed Al-Mg alloys mechanical measurement, noting low temperature tensile strength and yield point variations with specimen composition and temperature

09 p1473 A71-23230

Thin glass fibers relaxation characteristics, discussing shear modulus, internal friction and temperature effects

09 p1483 A71-23271

Steels, Ni alloys and Ti alloys deformation resistance and deformability, discussing temperature effects on forging rate

09 p1475 A71-23305

Molybdenum alloy under annealing and heating by AC electric current, investigating structure change effects on strength properties

09 p1475 A71-23312

Ni-Co strained alloy, examining coercive force as function of annealing time at various temperatures

09 p1475 A71-23313

Nickel under slow loading conditions at various temperatures, examining disorientation angles of substructure

09 p1476 A71-23317

Thermal reduction methods for refractory metal powders of W, Mo, Zr, V, Hf, Nb, Ta and Ti

09 p1457 A71-23389

Laser thermal energy-materials interaction, discussing excess heat buildup, power generation, reflectivity and repetition rates

09 p1458 A71-23406

Material thermal removal by electrical discharge, electron beam and laser machining, discussing effects on surface integrity

09 p1458 A71-23411

Umkehr inversion system for vertical ozone distribution observation, calculating error due to ignorance of temperature dependence of ozone absorption

09 p1489 A71-23447

Wave propagation in elastoviscoplastic medium in temperature field under complex dynamic and thermal conditions, considering mathematical models and mechanical properties changes

09 p1543 A71-23611

Pulmonary vasoconstrictor response to temperature dependent acute hypoxia, using isolated rat lungs with heparinized homologous blood under constant volume pulsatile inflow

10 p1561 A71-24124

Metals ultrasonic welding, discussing welded elements interactions in terms of thermal and diffusive phenomena, sample preparation, transducers, electric generators and process control systems

10 p1617 A71-24134

Carrier concentration, radiation dose and temperature effects on radiation defect formation in Si and Ge during gamma irradiation

10 p1655 A71-24138

Ambient temperature effects on flicker fusion threshold, using constant stimuli and forced choice methods for determination of test subjects sensory sensitivity to heat and cold exposure

10 p1568 A71-24184

Temperature induced bending of rectangular plate, obtaining stress-strain state

10 p1687 A71-24196

High pressure ratio centrifugal compressors for small gas turbine engines, investigating power and specific fuel consumption variation with pressure and temperature

10 p1658 A71-24218

He-Ne laser 0.63 micron line collisional broadening dependence on gas temperature

10 p1620 A71-24342

Thin isotropic plates with time and temperature dependent surface heat exchange coefficients, presenting heat conduction equations

10 p1695 A71-24361

Nb-Ti alloy oxidation kinetics at various temperatures and pressures, noting linear patterns and oxide formation

10 p1626 A71-24403

Atmospheric heating effects on thermoluminescence output variations with depth below Uceru meteorite fusion crust, noting nonuniform cosmic rays shielding

10 p1675 A71-24470

Book on electrical equipment deterioration in adverse environments covering climatic action, excessive heat, atmospheric temperature variations, water vapor adsorption and condensation, etc

10 p1583 A71-24478

Weld heat affected zone transient thermal stresses examined by weld joint model constrained system

10 p1617 A71-24533

Temperature field influence on hysteresis in Cs surface ionization on metal surfaces, observing adsorption phase fine structure and ion current density increase

10 p1657 A71-24542

Metal-metal adhesive bonds temperature effects, long term static loads, dynamic strength and aging behavior

10 p1618 A71-24684

Time and temperature effects on epoxy composites mechanical behavior, changing from brittle to ductile to rubbery failure mode

10 p1635 A71-24805

German monograph on absorbed anions effect on Ni and Ni-Mo alloys anodic behavior covering temperature dependence, electrons interaction, sulfide ions activation and magnetic properties

10 p1628 A71-24874

Pathophysiological aspects of microwave irradiation, considering thermal response of human and animal organisms to electromagnetic radiation exposure

10 p1573 A71-25079

Heated mirrors and hot plasma column effects on diffraction losses and power output of gas lasers

10 p1623 A71-25093

Aircraft tires mechanical data from small models, discussing mechanical properties, tire stresses and tire temperatures

11 p1707 A71-25325

Rate constant temperature dependence for ozone reaction with oxygen, considering airglow features due to singlet molecular oxygen

11 p1801 A71-25370

Nighttime airflow deviations over urban areas from radar tracked tetron flights, discussing effects as function of atmospheric wind and temperature

11 p1793 A71-25377

Steel alloys solid Cd embrittlement, discussing crack propagation rate temperature dependence and Cd surface diffusion as controlling effect

11 p1777 A71-25447

Extinction parameters of submicron carbon, tungsten and Si particles in hydrogen measured at various temperatures, discussing scattering amplitude functions and Monte Carlo calculations

11 p1854 A71-25507

Creep rupture data analysis model based on minimum commitment station function approach, generalizing hypothesized time temperature stress relation

11 p1848 A71-25561

Nickel diffusion in intermetallic compound NiAl as function of temperature and off-stoichiometric composition, noting activation energy changes

11 p1778 A71-25562

Cast cobalt base superalloys extrusion and forging, noting hot deformation effects on tensile properties, stress rupture strength and ductility

11 p1778 A71-25854

BeO reflected-fast-spectrum liquid-metal-cooled thermionic reactor, discussing two dimensional transport perturbation theory computer code for temperature coefficients evaluation

11 p1712 A71-25887

Quenched and tempered steel, investigating embrittlement as function of temperature in partially dissociated atomic hydrogen environment

11 p1779 A71-26017

Ordered Ti-Al lattice parameters measurement in low and high temperature diffractometer attachment

11 p1780 A71-26025

Proteins hydrolysis, investigating temperature effect on reaction, determining optimum conditions for maximum amino acids yields

11 p1728 A71-26066

Air- and vacuum-melted Hastelloy-Ni-based alloy/creep-rupture properties dependence on irradiation temperature

11 p1781 A71-26077

Thermal environment effect on human skin temperature and final temperature and tolerance time prediction from early exposure

11 p1725 A71-26173

Mechanical waves propagation in elastic-viscoplastic medium in presence of temperature field, using mechanical and mathematical models

11 p1850 A71-26177

Thermal contact resistance measurements between sliding contacts after load application under various temperatures, using transient pulse technique

11 p1858 A71-26226

Nongray surface property effects on radiant heat transfer between interacting opaque surfaces, analyzing spectral emittance wavelength and temperature dependence

11 p1859 A71-26245

Low temperature and composition effects on alloy softening in group 6A metals alloyed with Re

11 p1781 A71-26293

Polycrystalline NbC and TaC Young, shear and bulk moduli determination at high temperature, noting porosity and temperature effects

11 p1781 A71-26294

Temperature dependence of flow stress of cold-worked heavily deformed doped W

11 p1781 A71-26296

Body temperature regulation and heat dissipation responses during continuous and intermittent exercise in man

11 p1721 A71-26354

Temperature-respiration relations from isolated rat skeletal muscle mitochondria oxygen consumption measurements

11 p1723 A71-26408

Strain rate and temperature effects on flow stress of Ni-Al in polycrystalline and single crystal for activation energies and deformation volumes evaluation

11 p1782 A71-26440

Radiating laminar convective flow in vertical heated channel, noting radiation effects on temperature and velocity

11 p1860 A71-26446

Lunar surface properties, noting shock effects from impact induced pressures and temperatures

11 p1834 A71-26453

Long duration high temperatures rated stress effects on Ti beta alloy IVT-1, correlating creep with beta granular boundaries migration

11 p1782 A71-26471

LiF single crystals temperature, strain rate and positive Mg ionic impurity effects on work hardening characteristics

11 p1809 A71-26478

Monograph on plastic behavior of iron and nickel at high strain rates and at elevated temperatures, discussing thermal effect on deformation characteristics

11 p1783 A71-26489

Corrosive contaminants, oxygen, humidity and temperature environment simulation

11 p1746 A71-26496

Thermosensitive quartz anemometer operating in vibrational mode, discussing design and applications in low airflow velocity measurement

12 p1906 A71-26826

Photomagnetic effect in ferric borate, noting photoinduced change, radiation sensitivity and temperature effects

12 p1943 A71-26857

Thermally stratified turbulent shear flow, calculating turbulent energy balance and temperature inhomogeneity spectral equations

12 p1895 A71-26899

Heat conduction effects on small amplitude plane harmonic wave propagation in transversely isotropic elastic Zn single crystals

12 p1985 A71-26925

Astronaut selection and training, considering acceleration, hypoxia, weightlessness and temperature variation tolerance

12 p1873 A71-26951

Thermal transient effects in optically pumped pulsed lasers, presenting approximate calculation of temperature distribution and laser rod distortion effect on collimated light beam

12 p1914 A71-26979

Temperature gradients effect on density distribution in material near critical point, using classical and scaling-law theories and Ising model

12 p1929 A71-27031

Current controlled unstable pulse oscillator, discussing depletion layer transistors and upper frequency limit as function of thermal loads and switching times

12 p1887 A71-27043

Alternating acceleration and increased ambient temperatures effects on time interval perception and muscular effort estimation

12 p1874 A71-27164

Amorphous semiconductors, including electrical conductivity, temperature dependence, germanium/silicon structural model and mobility energy

12 p1944 A71-27244

Wall-stabilized arc column optimization from energy balance solutions, considering temperature and pressure effects on Ar arcs

12 p1939 A71-27275

High temperature tensile strength, creep rupture behavior and high temperature exposure effects on subsequent room temperature properties of maraging steel plates and welds

12 p1918 A71-27314

Fiberglass reinforced plastic structural elements heat induced deformation and carrying capacity due to material macroinhomogeneity and rigidities asymmetry

12 p1921 A71-27346

Perpendicularly woven fiberglass reinforced plastics stability, elasticity and viscoelasticity as function of temperature

12 p1921 A71-27347

Small deformation theory of thermoplasticity with medium mechanical characteristics dependent on temperature, noting use in nonmechanical structural transformations and radioactive irradiation

12 p1978 A71-27348

Axisymmetrically strained thin elastic shells of revolution with temperature dependent random elastic characteristics

12 p1979 A71-27358

Axisymmetric deformation of thin elastic shell of revolution under combined effect of static surface load and nonuniform heating

12 p1979 A71-27359

Aircraft structural elements thermal behavior under aerodynamic heating with linear dependence on initial temperature

12 p1865 A71-27493

Pressure and wall temperature gradients effects on equilibrium enthalpy profiles and heat transfer coefficients of incompressible turbulent boundary layers, using eddy conductivity model

12 p1986 A71-27553

Metallographic equipment for metal surface microstructure observations of samples under tensile loads at temperatures from 4.2 to 300 K

12 p1908 A71-27757

Heat resistant alloys strengthened elements, studying high temperatures prolonged exposure effects on surface layers strengthening and residual stresses relaxation

12 p1919 A71-27780

Fatigue corrosion resistance of duraluminum anodized at various temperatures

13 p2082 A71-27823

Torsion creep tests of Al, deriving expression for steady state creep rate as function of temperature and stress

13 p2083 A71-27963

Fast neutron irradiation effect on Ni-Cr alloy electrical resistivity as function of temperature and initial composition

13 p2083 A71-27964

Thermally induced torque of circular thin walled open section booms, predicting steady state behavior

13 p2148 A71-27980

Metallic materials static to dynamic transition in creep noting temperature and purity effects

13 p2084 A71-28110

Polycrystalline pure Al and Al-Mg alloy strength, investigating temperature and strain rate effects

13 p2084 A71-28112

Thermally activated crystal microcrack initiation by fusion of leading and following dislocations

13 p2149 A71-28118

Alloying elements isomorphous and valence-electron localization effects on Ti alpha/beta transformation temperature

13 p2085 A71-28223

Hall effect measurements and electron microscope examination of Te-doped gallium arsenide crystals annealed at various temperatures

13 p2111 A71-28503

Temperature variations of effective fracture surface energy of metals and alloys and relation to crack growth in high temperature creep

13 p2085 A71-28505

Heat balance of human body submerged in water, determining body temperature reduction as function of ambient temperature

13 p2019 A71-28508

Temperature dependent isophote wavelength in Brill and Planck formulas, comparing uvby and UVB photometric systems

13 p2068 A71-28512

Cr and Cr-Y alloy interstitial residual content and dynamic dislocation-interstitial interactions at various temperatures and strain rates

13 p2085 A71-28578

Thermal relaxation effects on thermal adjustment between gas and wall, comparing with thermograms from shock tube experiments

13 p2161 A71-28619

Liquid and gaseous Hg thermoelectric power measurements at sub and supercritical temperatures and various pressures

13 p2000 A71-28676

Mars physical conditions compared to earth, simulating Martian conditions and low temperature and UV effects on proteins

13 p2009 A71-28688

Thermal suppression of photoconductivity in crystals with two impurity types, showing carrier concentration decrease in conduction band in narrow temperature range

13 p2112 A71-28924

Gasoline-air combustion zone extent as function of inlet temperature for plane turbulent flame in square-section channel

13 p2163 A71-28960

Thermal unimolecular processes falloff data calculation based on Rice-Ramsperger-Kassel or Rice-Ramsperger-Kassel-Marcus theories

13 p2025 A71-29037

Cosmic ray microvariations during thunderstorm perturbations, considering total ionizing, soft and hard components and local temperature effect

13 p2130 A71-29124

Adrenocortical function in garden dormouse during autumnal preparation for hibernation, considering environmental temperature factors

13 p2014 A71-29315

Microwave exposure effects on organisms and biological functions responses and thermal stresses as function of specific frequencies, power density and environmental temperature

13 p2021 A71-29325

Asymmetric synthesis of alanine by hydrogenolytic asymmetric transamination, noting temperature effect

13 p2026 A71-29376

Compression rolled and hot upset Be sheet stress-strain behavior and deformation dynamics, emphasizing temperature and strain rate effects on polycrystalline flow stress

13 p2088 A71-29404

Tantalum disilicide kinetic interaction with Ta, investigating formation rate at various temperatures

13 p2089 A71-29415

Temperature effects on cosmic rays muon component variations during cold fronts passage

13 p2131 A71-29485

Three body ion-neutral association reactions of NO ions with oxygen, nitrogen and carbon dioxide, noting temperature effect on rate constant

13 p2026 A71-29507

Temperature dependence and mechanical properties of Mo materials with various diffusive protective base coatings based on continuity and density

14 p2256 A71-29623

Static strain measurements on Ti specimen subjected to different conductive heating rates, testing various gages

14 p2239 A71-29833

Structural evolution of Ni-Co Mo maraging steel during martensite reversion at rapid heating, studying heating rate effect on alpha-gamma transformation

14 p2257 A71-29839

Zirconium oxidation kinetics at 500-1200 C under low oxygen pressure

14 p2257 A71-29843

Thermodynamic equilibrium constants of Fe-MgO-SiO₂-O₂ system reactions at one atmosphere and 900-1300 C

14 p2190 A71-29875

Thermally activated plastic deformation of metals at low temperatures, determining stress flow, creep properties and upper yield limit

14 p2258 A71-30007

Temperature dependent absorption line width and secondary moments of nuclear magnetic resonance spectra of Ti-Zr-H system

14 p2258 A71-30009

W and Mo single crystals metallurgical microanalysis for thermal cycling effects on microstructure

14 p2259 A71-30172

Proteinoids self assembly into primitive cell from observations of polypeptide generation during amino acid heating

14 p2190 A71-30179

Potentiometric measurement of temperature effects on electrical resistance and Hall effect in Ni-Co alloys

14 p2259 A71-30188

Skin temperature sensitivity factors, discussing neural correlates of thermal sensation and skin receptors causing thermal stimulation sensitivity

14 p2183 A71-30253

Al-Li alloys precipitation characteristics and time-temperature-transformation curves after solution treatment, water quenching and aging

14 p2259 A71-30393

Nitrogen-carbon dioxide system molecular resonant energy exchange vibration-vibration probability measurement by shock tube and IR emission monitoring, noting temperature effects

14 p2276 A71-30399

Large circular plate residual stresses due to local spot heating and cooling, investigating effects of yield strain, heat input rate and peak temperature

14 p2329 A71-30462

Equilibria of molybdenum-nitrogen solid solutions at various temperatures

14 p2260 A71-30474

Temperature, odor mixing and stimulation frequency effects on olfactory receptor potential of fly *Lucilia sericata*

14 p2186 A71-30568

Temperature dependence of current gain in p-n-p transistors due to increased surface recombination rate

14 p2123 A71-30623

Silicon planar transistors at low injection levels, showing current transfer function temperature dependence

14 p2123 A71-30624

Heat sink requirements in transistor devices, examining temperature dependence of thermal resistivity and electrical capacitance

14 p2284 A71-30631

Low flame temperature propellants, investigating temperature and humidity aging effects on physical and ballistic properties

14 p2286 A71-30732

Liquid hydrazine catalytic reactor startup characteristics as function of catalyst adsorbed gas condition and temperature by high speed motion picture observation

14 p2294 A71-30760

X-type hot-wire probe thermal turbulent wake interference, discussing wind tunnel investigation of wire distance effect on pitch angle sensitivity

14 p2339 A71-31022

Aviation oils high temperature viscometry, describing test equipment and measurement results at 200-300 C

14 p2264 A71-31128

Ta nitriding temperature and duration effects on tensile strength, elongation and surface hardness

15 p2424 A71-31240

Liquid KCl and LiF surface films effect on combustion rate of ammonium perchlorate mixtures with polystyrene or polymethyl methacrylate for various initial temperatures

15 p2462 A71-31371

Turbulent gas flame length in motionless air of various ambient temperatures, comparing calculation with measurement

15 p2511 A71-31380

Molten Co-Cr alloy structural transitions at increasing temperatures, relating to change in solid state with increasing Cr content

15 p2425 A71-31393

Zirconium iodide vapor deposition kinetics, determining activation temperature

15 p2425 A71-31395

Molybdenum steel annealing, noting carbide phase transformations

15 p2425 A71-31398

Oxidation kinetics of pure Al in dry oxygen as function of pressure and temperature, using manometric method

15 p2426 A71-31408

Metals dynamic fracture model, discussing critical incubation time and temperature dependence

15 p2503 A71-31446

Integrable multivibrators insensitive to supply voltages and temperature variations, determining pulse widths from passive components

15 p2375 A71-31475

Metal specific work breakdown during crack propagation, investigating thermal effect of plastic deformation with thermocouples

15 p2413 A71-31479

Chemically interacting gases transfer properties at various temperatures, determining collision parameters and interaction cross sections and energies

15 p2451 A71-31494

Tantalum and niobium disilicides enthalpy and specific heat temperature dependences in 1200-2100 K range

15 p2426 A71-31504

Magnetostriction in cobalt and nickel-cobalt ferrites from room temperature to 300 C

15 p2426 A71-31514

Thermal dissociation rate of undiluted nitrogen in shock tube over 5700 to 12,000 K range, using pressure measurements

15 p2451 A71-31549

Heating effects on wing tip vorticity diffusion rate in gas vortex, causing outward radial convection and increased kinematic viscosity

15 p2512 A71-31556

Temperature and shock structure effects on choked jet noise characteristics, using axisymmetric convergent and convergent-divergent nozzles for radiated noise fields investigation [ALAA PAPER 71-192] 15 p2468 A71-31570

Boron combustion characteristics as function of temperature, pressure and gaseous fuel mixture ratio, using color photography [WSS/CI PAPER 71-19] 15 p2464 A71-31628

Temperature dependence of H-beta emission from hot hydrogen-helium plasmas, calculating production rate at 10,000-100,000,000 K 15 p2455 A71-31722

Steels resistance to brittle fracture at various temperatures, determining failure stress and transition temperatures for nonuniform stress distribution 15 p2428 A71-31855

Low temperature and tensile loading rates effects on static and dynamic strength of steel rods with ground and rolled threads 15 p2505 A71-31862

Sheet metal fatigue test method for transverse 100-1000 Hz bending at normal and high temperatures, applying to 1.5 mm Ti alloy sheet 15 p2505 A71-31864

Metallic Ni trace effects on oxygen chemisorption forms on nickel oxide in various temperature regions 15 p2367 A71-31901

Ni-Co alloys electrical resistivity dependence on temperature after mechanical and thermal treatments 15 p2429 A71-31994

Recrystallization nuclei linear growth rate activation energy relationship to Ni plastic deformation magnitude, temperature and purity 15 p2429 A71-31995

Time dependence of peak emission energy shift due to junction temperature rise in GaAs junction lasers operated with flat topped current pulse 15 p2420 A71-32027

Pressure and velocity distributions in gas filled cavity undergoing resonant acoustic oscillations due to heat addition 15 p2392 A71-32126

Thermal coefficient of resistivity of carbides and solid solutions of Ti, Zr, Hf, V and Nb, noting inverse dependence of covalent bond in Mo-Me band 15 p2430 A71-32154

Niobium and zirconium carbides enthalpy and specific heat dependence on temperature and composition 15 p2431 A71-32156

Zirconium monocarbide congruent vaporization rate and temperature dependence for nonstoichiometric compositions 15 p2431 A71-32157

Truncated-cone hot-pressed silicon carbide samples, measuring enthalpy and heat capacity as temperature function at high temperatures 15 p2431 A71-32160

Thermally induced residual stresses effect on yield behavior of unidirectionally solidified eutectic composites 15 p2432 A71-32171

Thermodynamic properties of dilute solutions of oxygen in liquid Fe-Co and Fe-Ni binary mixtures, obtaining Gibbs energy variation with temperature 15 p2432 A71-32174

Nickel sponge preparation by liquid nickel sulfide reaction with NiO under reduced pressure at various temperatures 15 p2433 A71-32178

Dispersion hardened Co strength and plasticity temperature dependence, determining Ti and Nb carbides additives effects 15 p2434 A71-32237

Creep rupture behavior and high temperature exposure effects on room temperature properties of Ni-Cr-Mo maraging steel plates and welds 15 p2434 A71-32256

Epitaxial Ag thin film with controlled surface roughness on mica, measuring electrical resistivity as function of temperature, thickness and surface specularity in vacuum 15 p2461 A71-32376

Electric field effect of epitaxial thin silver films on mica in vacuum as function of temperature, thickness and surface specularity 15 p2461 A71-32377

Thermal conductivity, diffusion and viscosity of gases and multicomponent gaseous mixtures at high temperatures 15 p2515 A71-32450

Sigma phase intergranular precipitation in low carbon Ni-Co-Cr-Mo alloys, noting temperature effect on morphology 15 p2436 A71-32546

Multipass low alloy steel weld metal strength dependence on microstructural changes due to thermal effects 15 p2437 A71-32614

Niobium-zirconium system alloys Debye-Waller factor temperature and concentration dependence, noting nonmonotonicities due to phonon spectra 15 p2437 A71-32625

Unijunction transistor peak point voltage stabilization, giving formula for interbase resistance multiplier variation with temperature 15 p2378 A71-32636

Complex alloyed steel under electroslog welding, investigating heat treatment effect on heat affected zone phase composition 15 p2437 A71-32661

Temperature effects on service life of cermet bronze-graphite bearings using different lubricants 15 p2418 A71-32674

Annealed stainless steel and Ti alloy in solution heat treated aged condition, detailing elevated temperature and high strain rate effects on fatigue life and tensile properties 15 p2438 A71-32791

Plasma jet chemical reactions, discussing temperature and quenching effects, molecular and gas decomposition and endothermic compounds formation 15 p2540 A71-32967

Periodically laminated elastic half plane response to rapid internal heating, obtaining far field composite stress waves variation due to dispersion [ASME PAPER 71-APM-28] 15 p2663 A71-33201

Stress-strain diagrams for oriented fiberglass-reinforced plastic under tension, taking into account temperature and anisotropy effects 15 p2601 A71-33411

Pure superconducting Al wire surface inductance measurement as function of temperature, noting penetration depth value 15 p2621 A71-33425

Laser light pulses in anisotropic crystal, investigating nonlinear thermal rotation of polarization plane 15 p2587 A71-33570

Antiwear properties of jet fuels as function of dissolved oxygen, resin and heteroorganic compound content and temperature, considering antioxidant additives 15 p2623 A71-33579

Heated tank under axial compression and internal pressure, noting fuel expenditure effects on stress-strain state 15 p2658 A71-33620

Mechanical and plastic properties of Ni-Mo alloys subjected to hot working, determining tensile strength as function of test temperature 15 p2593 A71-33631

Steel cylinders with circumferential cracks under repeated impact tensile loads, investigating plane strain fracture toughness index temperature dependence 15 p2658 A71-33635

Cold hardened Cr-Si steels strength/plasticity thermal dependence and brittleness from short torsion and compression tests, identifying low temperature failure mechanisms 15 p2593 A71-33638

Two-phase composites stability at various temperatures, studying mechanical properties dependence on second phase proportion 15 p2593 A71-33639

Welded joints ductile and brittle static tensile strength at low temperatures, allowing for mechanical inhomogeneities 15 p2584 A71-33641

Nonlinear dependence of resistance in metals on impurity concentration and temperature due to umklapp electron phonon interaction and anisotropy of phonon spectrum 15 p2593 A71-33654

Anisotropic carbon-graphite materials and metals temperature dependence of thermal expansion coefficients, noting approximation by Debye heat capacity function 15 p2601 A71-33710

Thermospheric hydrogen density and temporal variations from Explorer 32 measurements, discussing dependence on exospheric temperature 15 p2565 A71-33731

Physical conditions leading to deuterium enhancement in earth upper atmosphere as function of thermopause temperature and eddy diffusion 15 p2569 A71-33809

Thermospheric dynamics, including global compositional structure, winds and temperature response to solar radiation and vertical mass diffusion 15 p2571 A71-33838

Deformation conditions and annealing temperature effects on fine structure of Mo single crystals, noting polygonization 15 p2595 A71-33884

Cyclic heat treatment effect on fine structure and properties of Mo single crystals in He atmosphere 15 p2595 A71-33885

Mo single crystals physicomechanical and microstructural anisotropy under tension at different temperatures, noting strength and plasticity dependence on crystallographic orientation 15 p2596 A71-33888

Polymers mechanical losses temperature-frequency dependence, using nonlinear viscoelastic theory 15 p2602 A71-33982

Superhigh cooling rate effects during crystallization of solidified binary alloys, achieving superconductive properties 16 p2598 A71-33998

Cadmium doped silicon diodes I-V curve sinusoidal relaxation oscillations frequency and amplitude dependence on temperature 16 p2548 A71-34020

Electroconductivity and Hall effect in doped GaAs at low temperatures, studying temperature dependence of electron concentration, mobility and localization 16 p2623 A71-34030

Global temperature effects on atmospheric carbon dioxide and aerosols density based on atmospheric model, noting earth surface temperature decrease 16 p2575 A71-34040

Temperature dependent electron structure model of free energy decomposition of beta phase in Ti alloys 16 p2599 A71-34085

Thermal diffusion in tantalum-oxygen and columbium-oxygen mixed crystals, investigating temperature and concentration effects 16 p2599 A71-34092

Simultaneous degassing and thermal diffusion phenomena in annealed tantalum-oxygen mixed crystals, investigating maximum temperature effect 16 p2599 A71-34094

Temperature effects on photoelectric photometry, considering photomultiplier tube and electronics black box with photons and electric pulses 16 p2548 A71-34097

Temperature effects on spontaneous electrical and contractile activity of smooth muscle cells of portal vein in rats 16 p2533 A71-34110

Optically pumped rubidium maser short term frequency instability caused by thermal noise and resonator temperature and pumping power fluctuations 17 p2750 A71-34262

Deformation temperature effects on microstructure and mechanical properties of low alloy Mo, considering cold brittleness temperature and associated plasticity 17 p2755 A71-34418

Maximum temperature engine concept, definition and application to future aircraft propulsion system performance [SAE PAPER 710461] 17 p2792 A71-34498

Monograph on tensile tests of welded joint structural properties as function of introduced heat, applying method to Cu-Ni alloyed steel 17 p2748 A71-34825

Time dependent corrections to one component monatomic systems equilibrium rate of reactions and temperature change, using moment method for integrating nonlinear Boltzmann equation 17 p2785 A71-34945

Sound velocity in real gases as function of pressure and temperature, deriving by van Itterbeek result generalization for higher pressures 17 p2783 A71-35038

Curve power factors and radiation induced changes in silicon photovoltaic solar cells, considering junction depth, bulk resistivity, temperature and illuminating light intensity 17 p2677 A71-35049

Nonlinear unsteady heat conduction problems, investigating thermophysical property dependence on temperature and body coordinates by half space and approximate methods 17 p2838 A71-35115

Iron based Cr-Co-Mo alloys equilibrium diagrams and phase transformations at various temperatures, emphasizing intermetallic compounds effects on mechanical properties 17 p2758 A71-35148

Stress and temperature dependence of diffusional creep, discussing activation energy, grain boundary effects vacancy diffusion and dislocations motion 17 p2758 A71-35220

Semiconductor behavior of zirconium oxide formed on Zr substrate with n-type below 685 C and p-type above 17 p2759 A71-35222

Cs ions surface diffusion/migration in presence of retarding electric field on emitter surface, showing temperature effects 17 p2789 A71-35258

High temperature nitrogen plasma, calculating thermodynamic and electrical parameters dependence on pressure and temperature 17 p2789 A71-35262

Electrical insulation behavior of MHD generator channel having Ar-K plasma, noting temperature dependence of surface conductivity 17 p2789 A71-35274

Temperature and pressure effects on viscosity and thermal conductivity of dissociating air at high temperatures 17 p2785 A71-35277

- Plate temperature fluctuations effect on convective flow and heat transfer from horizontal plate, presenting solutions for LF and HF 17 p2838 A71-35419
- Machine components resistance to low temperature brittle failure, considering threaded joints, gears and shafts for strength and plasticity characteristics 17 p2832 A71-35463
- Ultrasound propagation velocity dependence on high pressure and temperature in carbon dioxide, considering Rao rule applicability to highly compressed gases 17 p2784 A71-35506
- Stress variation with varying plastic deformation rate and temperature in tantalum carbide between 1200 and 2200 C 17 p2760 A71-35550
- Photopolymer recording materials fixing by flashing holograms with Xe light or deactivating catalyst with thermal methods 17 p2745 A71-35591
- Thermal, turbulent and macroscopic motions in solar loop prominence of 4 May 1960, using spectral line composition by Gaussian profiles 17 p2809 A71-35596
- Annealed Mo creep and stress rupture at high temperatures for typical deformation 17 p2760 A71-35661
- Hot pressed TiC cylinder thermal shock resistance from tests to failure after heat cycling at 1000-1200 C 17 p2760 A71-35664
- Orography, cloudiness and surface temperature effects in six-layer global atmospheric circulation model, giving January simulation data 17 p2770 A71-35804
- Water vapor effects on shock compressed air in thermodynamic equilibrium by computer program, noting temperature and electron concentration reduction 18 p2984 A71-35857
- Impure GaAs and InP semiconductors compensation by introducing diffusible temperature dependent impurities 18 p2953 A71-35871
- Large scale atmospheric turbulence, considering anisotropy, thermal stratification, pressure and Coriolis forces effects 18 p2944 A71-36009
- Thermal emf changes for noble and refractory metal thermocouples, determining drift in high temperature air, Ar and vacuum environments for long time periods 18 p2916 A71-36049
- Temperature and bias circuit frequency modulation in CW X band Gunn oscillators 18 p2888 A71-36132
- Al distribution in gallium aluminum arsenide films obtained by epitaxial growth from liquid phase, showing temperature variation dependence during deposition 18 p2954 A71-36161
- Cr-Ni austenitic steels thermomechanical destabilization using cyclic strain hardening 18 p2934 A71-36173
- Static feed water electrolysis system of life support system, discussing current density, operating time and temperature effects on voltage for various electrochemical cell sizes [ASME PAPER 71-AV-25] 18 p2868 A71-36392
- Hot water vapor total emissivity charts at various temperatures, using band model parameters with spectroscopic data 18 p2985 A71-36592
- Temperature dependent directional differences of modulus of elasticity of Mo sheet, using resonance technique 18 p2936 A71-36711
- Profile changes of magnetically non-split lines in faculae, explaining observations by outer layers temperature increase 18 p2965 A71-36731
- Temperature dependence of electrical resistance in mixed superconducting-normal systems, solving transport equation 18 p2954 A71-36746
- Transistors life testing for temperature and voltage dependence of failure rates 18 p2893 A71-36805
- Squirrel monkeys midbrain reticular formation direct thermal stimulation effects on physiological or behavioral thermoregulatory responses 18 p2858 A71-36860
- Maximal sweat evaporative heat loss and permitted work load measurements as function of temperature and clothing insulation 18 p2872 A71-36861
- Hypothalamic unit activity relation to thermoregulation, investigating preoptic area response to local and peripheral temperature changes 18 p2859 A71-36869
- Preoptic anterior hypothalamic area temperature sensitive neurons, showing integrative center for thermoregulation 18 p2859 A71-36870
- Male and female physiological responses to heat stress, discussing sweating, skin and body temperature, heart rate and metabolism 18 p2859 A71-36871
- Chill level index for skin temperature effects on rate of evaporative heat loss and thermal information to central controller during heavy work 18 p2860 A71-36876
- Impulse skin temperature encoding in primate cutaneous thermoreceptors in dynamic thermal conditions 18 p2860 A71-36877
- Temperature regulation during exercise by proportional control, investigating skin temperature effect on set point temperature, sweat rate and skin thermal conductance 18 p2860 A71-36879
- Brain temperature change effects on cardiovascular responses, examining heart rate and systemic arterial blood pressure 18 p2860 A71-36880
- Cats preoptic and skin temperature change effects on posterior hypothalamic neurons 18 p2861 A71-36888
- Pilocarpine induced synchronous sweat expulsions, noting frequency linear dependence on ambient temperature with and without generalized sweating 18 p2861 A71-36889
- Temperature effects on spinal excitation and inhibition in cats, investigating spinal motoneurons discharge frequency 18 p2861 A71-36890
- Water temperature effect on body thermoregulation in swimming, comparing swimmers responses to track man on treadmill at same metabolic rate 18 p2861 A71-36893
- Spinal cord ascending neurons temperature sensitivity, comparing data from cats experiments with hypothalamic temperature sensors sensitivity 18 p2861 A71-36894
- Cutaneous circulation control by venous thermoregulatory reactions to temperature variations, using dog saphenous veins perfused with autologous blood or Krebs-Ringer solution 18 p2862 A71-36898
- Heat transfer coefficients calculation for human body in cold water from heat balance equations, comparing with free convection coefficients in cross-flowing water 18 p2862 A71-36900
- MHD systems equilibrium and stability involved in quiescent prominences, considering temperature dependence of heat conductivity, magnetic field and initial gas compression 18 p2967 A71-36927
- Electric power and efficiency of thermoelements with temperature dependent thermoelectric properties by heat balance technique 18 p2852 A71-36965
- IMPATT diode microwave oscillator temperature effect on operation, comparing with Read diode small signal admittance characteristics 18 p2895 A71-36986
- Temperature variations effect on TRAPATT microwave oscillator parameters, considering upper temperature limit dependence on heat dissipated in diode and heat sink thermal resistance 18 p2895 A71-36988
- Mo, W and Mo-W alloys chlorination kinetics, investigating temperature and pressure effects on reaction rate from electron micrographs 18 p2938 A71-37002
- Thermal effects of continuously tungsten iodine lamp pumped Nd-YAG laser, measuring rod temperature distribution by microprobe beam 18 p2932 A71-37009
- Temperature effects on wear and failure of titanium and niobium carbides, using electron microscopy 18 p3076 A71-37114
- Vacuum deposited thin Cr films on glass, investigating substrate temperature and inert gas pressure effects on texture 18 p3076 A71-37117
- Chromium stainless steels fine structure, noting quenching and tempering temperatures effects 18 p3076 A71-37118
- Deformation rate and temperature effects on optimum strength and ductility of die forged and extruded Mo-Ti alloys 18 p3077 A71-37269
- Unsteady approach to nonisothermal flow theory for Couette flow, making general assumptions concerning rheological law and temperature dependence of fluidity 18 p3043 A71-37386
- Nitrous oxide internal and rotational partition functions for temperature range 200 to 350 K, using molecular constants tabulated by Pliva 18 p3106 A71-37408
- Hypersonic flow theory evolution, considering friction and high temperature effects and flows about slender, blunt and bluff bodies 18 p2992 A71-37455
- Plastic deformation and fracture of beta Ti alloy under tensile tests at room and low temperatures 19 p3077 A71-37464
- Phase diagram of Ti-Cr alloys for temperatures from 800 to 1600 C 19 p3077 A71-37466
- Temperature dependence of ionization rates in aluminum gallium arsenides for samples with varying Al contents 19 p3117 A71-37486
- Thin film Au-CdS-Al type metal-semiconductor barriers, determining barrier height from temperature dependence measurements of I-V characteristics 19 p3118 A71-37488
- Aerodynamic compensation for ambient medium temperature effect on fluidic standard components and timing devices 19 p2998 A71-37570
- Test facility for studying temperature dependence of thermal diffusivity and true heat capacity of metals between minus 150 and plus 400 C 19 p3063 A71-37588
- Plastic deformation effects on austenite thermal stabilization in Fe-Ni-C alloy, considering temperature dependence 19 p3079 A71-37704
- High strength Cr-Mo-Co stainless steels with improved toughness and ductility by austenitizing temperature selection 19 p3079 A71-37707
- Rapid thermal fluctuations effect on Inconel 718 creep rate, noting strain rate decrease under cycling conditions 19 p3080 A71-37716
- High strength metastable austenitic steels fractography, showing alloy composition, strain rate and temperature effects 19 p3080 A71-37717
- Thermal creep slip velocity expression in power series for arbitrary fraction of molecules diffusely reflected from surface by Bhatnagar-Gross-Krook model solution 19 p3163 A71-37734
- Temperature effects in incompressible elastic materials, adapting Adkins-Green isothermal successive approximation technique to thermoelasticity problems 19 p3157 A71-37800
- Electron density inhomogeneity behavior, examining thermal electron motion and collisionless plasma initial condition effects 19 p3114 A71-37857
- Atmospheric pressure and temperature inhomogeneities effects on thermal radiation transmission function of water vapor 19 p3090 A71-37973
- Air and jet fuel-air mixtures, calculating temperature dependent laminar and turbulent heat transfer parameters and transport properties [ASME PAPER 71-HT-41] 19 p3166 A71-38002
- Far IR collision induced spectrum in carbon dioxide, observing temperature and pressure dependence in gas phase and absorption in liquid 19 p3106 A71-38051
- Slow and explosive gas phase oxidation of carbon suboxide and monoxide over various pressure and temperature ranges, noting branching reactions 19 p3167 A71-38088
- Calculation method for standard potentials and enthalpies of metals during oxidation and chlorination, representing molar functions dependence on temperature 19 p3082 A71-38153
- Thermal behavior simulation of cooling biological system, describing heat generation and transfer at normothermic to hibernating body temperatures with mathematical model 19 p3003 A71-38199
- Hypergolic rocket propellant system gas phase ignition, measuring ambient pressure, flow parameters and propellant temperature effects on delay characteristics 19 p3123 A71-38297
- Atmospheric temperature effect on solar diurnal variation of muon component, considering asymptotic characteristics of cosmic ray anisotropy 19 p3129 A71-38378
- Ni-Cd battery cell with third electrode for charge control, testing thermal and electrical performance as function of charge and discharge rate 20 p3179 A71-38905
- Solar array technology for lunar surface applications including silicon cells, cadmium sulphide thin films, temperature effects, prototype module and radiation degradation 20 p3181 A71-38941
- Creep tests evaluation for stress and temperature effects on apparent activation energy 20 p3250 A71-39018
- Solution temperature and Ti/C ratio effects on Cr-Ni-Ti austenitic steels creep properties, including precipitation, deformation, rupture and coalescence 20 p3250 A71-39025

Temperature dependent extracavity and intracavity etalon effects in optical materials for carbon dioxide lasers

20 p3245 A71-39178

Corresponding states fluids film boiling with cylindrical heaters, studying pressure and diameter effects

20 p3312 A71-39283

Nonhomogeneous flow stratification in fluid region under thermal and gravitational forces, considering steady state and time dependent density fields

20 p3212 A71-39502

Axisymmetric small Rossby number flow driven by axially distributed heat sources, examining core multiboundary layer structure

20 p3212 A71-39507

Homogeneous temperature changes and radial temperature gradients effects on optical lens system, obtaining Bessel type differential equation

20 p3239 A71-39532

Apollo 11 lunar crystalline igneous rock samples electrical conductivity temperature dependence, noting age of moon

20 p3295 A71-39619

Turbulent boundary layer calculation behind surface cusp, taking into account external flow turbulence and thermal stratification

20 p3214 A71-39792

Nighttime hydroxyl airglow emission intensity and excitation temperature measurements, noting seasonal and nocturnal variations

20 p3227 A71-39834

Solid solution hardening in Ta alloy single crystals, investigating temperature effects on interstitial impurities scavenging and lattice mechanism

21 p3395 A71-40027

Pure Fe phase transformation plasticity as function of material, stress, temperature interval and change rate, cycle number and experiment duration

21 p3396 A71-40028

Mo and high temperature Mo alloys thermally activated deformation mechanisms from flow stress athermal component and effective stress temperature dependence observation

21 p3396 A71-40030

Cosmic ray variations due to atmospheric pressure disturbances and ionizing component variations due to temperature effects, estimating ground observation errors

21 p3437 A71-40074

Atomic hydrogen maser wall shift elimination by operating at temperature to obtain zero average phase shift per atomic collision

21 p3391 A71-40201

Activation energy and temperature dependence of radiation induced free radical destruction in N-acetyl-DL-valine, using Arrhenius plots

21 p3345 A71-40203

Physiological responses to head and neck vs trunk and leg cooling under hyperthermic stress

21 p3331 A71-40356

High density packaging effects on multilayer interconnection board reliability tested in thermal environments

21 p3352 A71-40437

Fe-C alloys martensitic transformation, investigating high quench rate effects

21 p3397 A71-40451

Explosively shock strengthened austenitic stainless steel, investigating mechanical properties at elevated temperatures

21 p3398 A71-40462

Alpha Ti at blue brittle temperature, observing strain rate dependent work hardening effects on necking strain

21 p3398 A71-40464

Charpy impact test measurement of maraging steel thermal embrittlement, observing fracture mode and toughness changes with heat treatment

21 p3398 A71-40467

Dislocation structures of polycrystalline tungsten after deformation and recovery annealing, observing temperature dependence of critical strain for recrystallization

21 p3399 A71-40472

Inert gases energy accommodation coefficients dependence on clean metal surface temperature based on lattice theory

21 p3415 A71-40538

Self induced transparency in ruby attenuator, detailing phase relaxation effects at various temperatures

21 p3427 A71-40546

Sensory transmission of spinal heat and cold sensitivity in ascending spinal neurons of anesthetized cats

21 p3334 A71-40630

Cutaneous and intestinal blood flow differentiation during hypothalamic heating and cooling in anesthetized dogs

21 p3335 A71-40632

Ti-Mo base metastable beta Ti alloy tensile properties anomalies at elevated temperatures, examining strain rate and annealing conditions effect

21 p3399 A71-40699

Reflecting telescope Schmidt camera photographic color system temperature dependency from cluster NGC 103 photographs

21 p3379 A71-40717

Thermal switching and negative resistance model and measurements of amorphous semiconductor thin films of Ge, Si and chalcogenide glasses

21 p3428 A71-40741

Optical phonons and temperature dependent phase transitions in paraelectric antimony and ferroelectric sulfoiodide semiconductors, using polarized IR and Raman spectra measurements

21 p3428 A71-40775

Temperature effect on fatigue strength of Ni steel by tension-compression fatigue test at low temperatures

21 p3400 A71-40832

Strain rate and temperature effects on polycrystalline Al-Mg alloy strength, considering deformation mechanism

21 p3400 A71-40834

Low temperature effects on succinate oxidase activity of mitochondrial membranes in hibernating squirrels

21 p3336 A71-40854

Liquid metal elevated temperature time dependent corrosion effects on immersed structural materials, discussing blocked two level factorial experiment design for multiply telescoping sequences

21 p3400 A71-40880

Ni-steels toughness improvement at cryogenic temperatures by accelerated cooling, using Charpy V-notch and static and dynamic fracture tests at 139.7-671.7 R

21 p3400 A71-40881

HD rotational relaxation collision number temperature dependence calculation from excitation probability, comparing with experiment

21 p3419 A71-40911

Cryogenic steels, Al and Ti alloys plane strain fracture toughness at room and subzero temperatures, discussing tensile and notch bend results

21 p3401 A71-40915

Specimen design effects on Al and Ti alloy plane strain fracture toughness at room and cryogenic temperatures, discussing crack propagation and rolling directions orientations

21 p3401 A71-40917

Buckling load reduction for axially compression loaded geometrically perfect cylindrical shells by wall temperature gradients induced partial yielding

21 p3469 A71-41006

High temperatures prolonged exposure effects on surface layers hardening and residual stresses relaxation in heat resistant alloys

21 p3403 A71-41105

Stress-strain state of rotating viscoelastic hollow cylinder with mobile inner boundary under internal pressure and temperature effects

21 p3472 A71-41145

Microwave photoconductivity of boron single crystals under pulsed illumination, determining temperature effects on carrier mobility, recombination coefficients and relaxation times

21 p3428 A71-41202

Fabrication and I-V characteristics of S-type negative resistance alloyed diodes prepared from sulfur-doped n-type Si, outlining temperature dependence of turnoff time

21 p3358 A71-41203

Temperature, magnetic field and pressure dependence of electrical conductivity, thermal emf, Hall effect and transverse Nernst-Ettingshausen effect in indium-doped lead telluride

21 p3429 A71-41210

Impurity photoconductivity, generation-recombination noise and temperature dependences of Hall coefficient and equilibrium carrier mobility in p-type cobalt-doped germanium

21 p3429 A71-41213

Temperature dependence of impurity photoluminescence of Cr-doped GaAs single crystals, measuring activation energy

21 p3430 A71-41214

Current-voltage characteristics of n-i-GaAs epitaxial structures at various temperatures, indicating use in memory devices and high power switches

21 p3430 A71-41223

Pure and doped Ge dumbbell p and n type samples at liquid helium temperatures, investigating electric breakdown

21 p3430 A71-41224

High resistance undoped GaAs samples at different temperatures, investigating energy spectra, Hall effect and electron conductivity

21 p3431 A71-41227

Penning process for small ionization probability per atomic collision, obtaining ion production constant relationship to temperature

21 p3420 A71-41252

Mn-Ge solid solutions coercive force and magnetization, investigating temperature dependence and heat treatment effects

21 p3432 A71-41264

Superconductors intermediate state interrelated electrodynamic and thermal effects, calculating resistivity, heat conduction and thermoelectricity tensors

21 p3432 A71-41268

Temperature and velocity dependence of electron dislocation stopping power in superconductor due to scattering of normal electrons

21 p3432 A71-41269

Electrical conductivity and thermoelectric power measurements for polycrystalline beta-SiC heavily doped with nitrogen, estimating electron effective mass and carrier mobility at high temperatures

21 p3433 A71-41304

Cyclotron resonance measurement for holes in uniaxially compressed Si, determining pressure and temperature effects on relative half width of hole line by relaxation time

21 p3433 A71-41304

Bismuth telluride single crystals thermal conductivity and thermoelectric power temperature dependence 2.3-100 K, discussing magnetic field effects

21 p3433 A71-41313

Thermal suppression of photoconductivity crystals with two impurity types, showing carrier concentration decrease in conduction band in narrow temperature range

21 p3434 A71-41321

Cr-doped n-type semiinsulating GaAs single crystal photoconductivity measurement, noting spectral peaks dependence on temperature

21 p3434 A71-41321

Copper gallium diselenide point contact diodes I-V characteristics temperature and illumination dependence, considering high temperature and photoelectric devices applications

21 p3434 A71-41328

GeTe alloyed with Zn, Cd or Hg, measuring electrical conductivity and thermoelectric power temperature dependence

21 p3435 A71-41349

Soviet book on steels high temperature elastic stiffness and ductility covering carbon, alloyed and special steels at different temperatures and strain rates

21 p3404 A71-41378

X band Gunn diode oscillator pulsed operation stability delay time relationship to CW operation frequency/temperature characteristics, suggesting contact resistance role

21 p3359 A71-41414

Temperature and strain rate effects on yield and flow stress of bcc Ti-Mo alloy over 77-824 K range

21 p3404 A71-41414

Edge dislocations mobility in zone refined alpha Ti single crystals in bending, using etch pit techniques at 77, 200 and 300 K

21 p3404 A71-41414

Thermal effects in loop prominences formation after solar flares from model computer simulation

22 p3597 A71-41454

Cryogenic liquids thermal behavior under operational conditions, discussing Europa 3 second stage liquid hydrogen and oxygen engine

22 p3588 A71-41504

Polymer materials for aerospace construction, considering behavior in cryogenic and high temperature environments

22 p3564 A71-41514

Preheating effects on crystal lattice orientation, tensile strength and stress corrosion cracking of Al-Zn-Mg alloy thick plates

22 p3559 A71-41514

Laminar collisionless shock propagation perpendicular to magnetic field into hot plasma, calculating temperature effects on leading edge growth rate

22 p3579 A71-41580

Intense ionizing radiation and thermal treatment effects on electrical parameters of Si semiconductor devices

22 p3584 A71-41619

Intergranular corrosion of chromium carbide sensitized Ni base alloys, noting surface effect during solution heat treatment

22 p3560 A71-41626

Transition metal/particularly Ti/ carbide hardness temperature dependence explained from dislocation theory viewpoint, relating hardness to electronic structure

22 p3565 A71-41657

Temperature dependent threshold current density and doping gradient at p-n junction in epitaxial GaAs injection laser diodes

22 p3555 A71-41686

Temperature effects on tungsten lattice and Gruisen parameters and thermal expansion coefficients at low temperatures by X ray method

22 p3561 A71-41724

Heat resistant Ni alloys hot strength level and temperature dependence as function of gamma-prime phase particle size, discussing aging effect on creep rate

22 p3561 A71-41841

- Inhomogeneous high-beta collisionless plasma temperature gradient effects on ion-acoustic and Alfvénic drift instabilities 22 p3583 A71-41907
- Balloon Sonde I experiment, discussing telemetry from flying body and temperature effects on earth IR radiation measurement 22 p3535 A71-42053
- Crystal lattice vibration and molecular libration effects on solid carbon tetrachloride heat capacity at 0-20 and 200-230 K 22 p3585 A71-42059
- Solar cycle variation effects on interstellar hydrogen within solar system, discussing thermal motion, density, far UV ionization and charge transfer reactions 22 p3601 A71-42169
- Two temperature region oxidation of zirconium diboride, showing formation of continuous surface film and quadratic crystallized discontinuous layer 22 p3563 A71-42246
- Microstructure, yield point and creep rupture strength of Nb-Ti alloy, investigating oxygen concentration and temperature effects 22 p3563 A71-42365
- Oxygen concentration and heat treatment effects on structure and mechanical properties of Nb-Zr alloys 22 p3563 A71-42366
- Electrical resistivity and thermoelectric power sensitivity for simple liquid metals near melting temperature, determining temperature effects from pseudopotential models 22 p3586 A71-42370
- Inconel superalloy microscopic observation of local melting and hot ductility behavior during weld thermal cycles to clarify cracking cause in heat affected zone 22 p3564 A71-42494
- Pure Al annealed polycrystal electron microscopic observation for fatigue deformation at room and elevated temperatures, noting dislocation loop role in crack initiation and propagation 22 p3564 A71-42497
- Ambient temperature effects on spontaneous rewarming of ground squirrels during awakening after hibernation 22 p3491 A71-42582
- Temperature and frequency dependence of electron phonon interaction maxima in rhenium, explaining transverse and longitudinal waves ultrasonic attenuation by two band theory 22 p3578 A71-42597
- Laminar Couette flow between parallel plates with mechanical energy dissipation and temperature dependent viscosity, determining velocity and temperature distribution 22 p3531 A71-42683
- Linear and nonlinear models for computer aided circuit design involving Zener diodes, providing for thermal effects 22 p3524 A71-42762
- Gaseous medium composition and multiple freezing temperature effects on catalase activity 22 p3497 A71-42831
- Laser radiation destruction of transparent dielectrics, proposing electronic excitations conversion to heat and thermal explosion 22 p3682 A71-42891
- Oxygen interaction with polycrystalline W, calculating sticking probabilities and desorption spectra at various temperatures 22 p3641 A71-42906
- Bipolar junction transistor doping effects on bandgap decrease and emitter efficiency, explaining current gain temperature dependence 22 p3648 A71-42911
- Temperature effects on fatigue response and tensile properties of coarse grained alpha Ti containing 0.085 wt pct oxygen 22 p3688 A71-42924
- Delta-zirconium hydride hydrogen engassing experiment, investigating hydrogen absorption rate and diffusion constant temperature dependence 22 p3688 A71-42929
- Thermal feedback modification of Si JFETs AC and DC characteristics at low operating temperatures 22 p3649 A71-43070
- Glass particles crystallization in sintered metal matrix glass materials, examining microcracks and temperature and cyclic heating effects 22 p3696 A71-43251
- High temperature sintering kinetics of tungsten, observing heating rate effects 22 p3690 A71-43257
- Carbon dioxide absorption temperature dependence in 1750-1200 A region, calculating electron densities and transition moments 22 p3641 A71-43326
- Mn-Zn ferrite for pulse transformers, discussing permeability and temperature range 22 p3650 A71-43348
- Ni-based alloy strength characteristics dependence on heat treatment during melting and casting in vacuum and in air 22 p3691 A71-43425
- Polycrystalline thin film CdSe-CdS and CdSe-CdTe solid solution semiconductor alloys Hall mobility and carrier concentration dependence on substrate temperature 22 p3715 A71-43433
- Gunn oscillator frequency stabilization at minus 10 to 60 C by high Q single tuned oscillator circuit, considering requirements for 20 GHz radio relay system 22 p3651 A71-43438
- Temperature effects on long wavelength photon frequency and linewidth in diamond, using Raman scattering techniques 22 p3715 A71-43471
- Room temperature GaAlAs close confinement /single heterojunction/ laser diode performance and applications 22 p3684 A71-43503
- Alkali metals vaporization from heated lunar samples, suggesting lunar rock erosion by localized heating due to volcanism or meteorite impact 22 p3741 A71-43636
- Apollo 11 and 12 devitrified glass fragments temperature histories indicating broad range of subsolidus crystallization temperatures 22 p3746 A71-43667
- Apollo 12 lunar glass spherules chemical composition, homogeneity, densities and thermal histories, using electron probe analysis 22 p3758 A71-43758
- Thermally stimulated exoelectron emission and surface properties of lunar rocks and soil 22 p3758 A71-43759
- Specific heat of Apollo 11 breccia and Apollo 12 olivine dolerite at 95-340 K 22 p3762 A71-43786
- Dielectric properties of Apollo 12 samples and lunar interior as function of frequency and temperature 22 p3762 A71-43788
- Apollo 12 lunar soil samples magnetic resonance properties, determining temperature, frequency and thermal annealing dependence 22 p3763 A71-43796
- Lunar glass spheres cratering origin hypothesis from target temperature effects on crater morphology in targets impacted by high velocity Al projectiles 22 p3765 A71-43808
- Material distribution as function of temperature in postflare loop system after east limb proton flare of 12 August 1970 22 p3768 A71-43847
- Thermal radiative cooling system characteristics determination allowing surface material thermal conductivity and blackness degree dependence on temperature 22 p3782 A71-43919
- SbSI crystal reflection spectra anisotropy and band structure at 90, 273 and 300 K, comparing experimental data with group analysis 22 p3717 A71-43947
- Electron microscopic study of antiphase domains size and shape in Ni-Mn alloy after annealing 22 p3692 A71-44009
- Zirconium monocarbide electrical conductivity, Hall coefficient, thermal emf and magnetic susceptibility measurements for temperature dependence at 500-1000 C in homogeneity region 22 p3692 A71-44021
- Temperature effects on niobium carbide friction process in vacuum conditions, considering surface layer microhardness and X ray and metallographic analyses 22 p3692 A71-44030
- Niobium carbonitride thin film deposition temperature effects on superconducting properties, considering transition temperature and critical currents and fields 22 p3717 A71-44141
- Thermal history of universe traced from assumption of photon and plasma turbulence for galactic formations, discussing thermal instability and heating effects 22 p3770 A71-44181
- Gas turbine blade models of heat resistant ZrSiO₄ alloy under operational temperature variations, observing fatigue strength 22 p3779 A71-44209
- Postoperative states of turbine disk alloys at 280-500 and 550-630 C, noting lower durability values 22 p3779 A71-44211
- Heat resistant steels long time strength determination by graph-analytical time-temperature extrapolation 22 p3693 A71-44213
- Combined heat, noise and vibration stress effects on human performance and physiological functions including heart rate, body temperature and mental arithmetic 22 p3637 A71-44247
- Swaged high purity fine grained Ti stress-strain behavior below 424 K, emphasizing mechanical twinning in plastic deformation 22 p3695 A71-44289
- Preoptic and environmental temperature effects on hibernator thermoregulatory responses, noting changes in metabolic rates 22 p3637 A71-44301
- Large volume liquid oxygen pool boiling, investigating heat exchange coefficient dependence on flux density and pressure 22 p3705 A71-44339
- Temperature and frequency effects on permittivity and dielectric loss angle tangent in glasses and pyroceramics 22 p3859 A71-44379
- I-V characteristics and temperature responses of negative S and N-type resistances in niobium-niobium oxide-indium structures, considering use as active elements in membrane circuits 22 p3859 A71-44380
- Gas lasers application to length measurement technology, discussing temperature, air pressure and vibration effects on laser frequency stabilization 22 p3833 A71-44449
- Fuel droplet burning rate variation with ambient temperature and oxygen concentration in combustion gas environment 22 p3887 A71-44606
- Divergence behavior of flat rectangular panel at subsonic speeds, discussing boundary conditions, natural vibration modes and temperature effects 22 p3878 A71-44611
- IR spectra temperature dependence of CsI crystals doped with sulfate and carbonate anions and Pb and Cd cations, observing intensive absorption bands 22 p3860 A71-44665
- Barium titanate single crystal solid solution electro-optic characteristics at 6328 A and temperatures above Curie point, determining temperature dependences 22 p3860 A71-44667
- Mo-W, Ta-W and Nb-W alloys X ray analysis at various temperatures, calculating interdiffusion coefficients and temperature effects on W concentration 22 p3836 A71-44671
- High purity Be single crystal transverse bending tests, plotting yield stress and bending angle vs temperature 22 p3836 A71-44673
- Recrystallized metalceramic W plastic deformation effects on brittleness temperature threshold, revealing relationship to impurity segregations at grain boundaries 22 p3837 A71-44674
- Kinetic parameters and conditions for optimal epitaxial growth of GaAs from liquid phase, observing solution cooling rate effect on p-n junction quality 22 p3808 A71-44724
- Platinoid boride production, determining reaction sintering temperature with thermal metallographic and X ray analysis 22 p3838 A71-44735
- Titanium, niobium and tungsten carbides microhardness temperature dependence at 77-1973 K, discussing activation energy and deformation mechanism 22 p3838 A71-44741
- Slip, surface permeability and temperature gradient effects on surface friction and heat transfer in boundary layer near cylinder critical point 22 p3887 A71-44743
- Local and central body temperature effects on human cutaneous venomotor reflexes, monitoring venous wall tension by measuring hand dorsal veins pressure during temporary arrest of hand circulation 22 p3797 A71-44777
- Seizing of flat and flat/spherical steel samples pairs in vacuum as function of temperature, pressure and time of contact, using compression-tension machine 22 p3838 A71-44857
- Temperature dependence of external friction coefficient between high-melting carbides in vacuum at constant normal load and slipping rate 22 p3830 A71-44863
- Hydrogen fluoride vibrational relaxation times behind incident shock waves at various temperatures 22 p3802 A71-44922
- Speed of sound measurement in solid and liquid phase suspensions, considering dense phase inertia forces and particles thermal retardation effects 22 p3827 A71-45019
- Working gas parameter determination for valve supply main system during feed opening, explaining heating effect for second valve by shock wave theory 22 p3793 A71-45021
- Thermal contact resistance of adhesive joints as function of adhesive solidification pressure and temperature and of joint surface physicochemical and geometrical parameters 22 p3831 A71-45024
- Low temperature kinetics of metastable He atom pair collisions, investigating temperature dependence of plasma ionization 22 p3856 A71-45054
- Stress and magnetic field induced spin density wave polarization vectors rotation in Cr single crystals, accounting for Young modulus temperature and magnetic field dependence 22 p3861 A71-45131

Ni-base superalloys metallography, investigating catastrophic cracking in weld heat affected zones by electron microscopy 24 p3839 A71-45139

Self similar solution for unsteady powder combustion rate with decreasing pressure, generalizing to rate dependence on pressure and initial temperature 24 p3891 A71-45217

Inhomogeneous high-collision finite-pressure plasma stability, finding thermal instability development under uniform temperature and arbitrary pressure 24 p3858 A71-45243

InTe thin films formation, growth kinetics and physical properties, determining vapor deposited film thickness dependence on glass substrate temperature 24 p3861 A71-45249

Orthogonal experiment plans application to metal elastic stiffness description as function of temperature and strain rate 24 p3840 A71-45375

TEMPERATURE FIELDS

U TEMPERATURE DISTRIBUTION

TEMPERATURE GRADIENTS

Elastic boundary value problem of viscoelastic cylindrical body with temperature and time variations and relaxation kernel 01 p0169 A71-10492

Heat transfer between rarefied monatomic gas and porous wall, examining temperature jump with model kinetic equation for Knudsen layer 01 p0179 A71-10612

Global atmospheric circulation theory relation to flow pattern of free thermal convection in rotating fluid subjected to horizontal temperature gradient 01 p0122 A71-11359

Light beam deflection due to temperature gradient in laminar gas flow in shielding pipe for laser communication, considering beam waveguide design 02 p0284 A71-11869

Cepheid radius-temperature variation functions phase shift 02 p0308 A71-12101

Free convection in compressible viscous heat conducting liquid near critical point, discussing temperature gradients, layer heights, density distribution and inhomogeneity effect 02 p0331 A71-12190

Adiabatic temperature gradient requirement for neutral convection mode in general relativity of star in hydrostatic equilibrium 03 p0486 A71-13330

Planetary atmosphere circulation kinetic energy, energy transformation and driving temperature gradients, using similarity, dimensional and thermodynamic approaches 03 p0488 A71-13551

Schlieren device for visualization of thermal gradients in boundary layer of any orientation, replacing natural astigmatism with arbitrarily adjustable one 05 p0749 A71-16266

Lunar microwave emission effects and local surface temperature variations due to outward heat flow and low thermal conductivity 05 p0809 A71-16459

Rigid heat conductors, using controllable states for heat flux-temperature gradient materials response function measurements 05 p0837 A71-16721

NonNewtonian liquids with arbitrary surface temperature and pressure gradients, solving dynamic and thermal boundary layers equations 06 p1006 A71-18008

Heat resistant alloys low cycle fatigue tests at 20-800 C, establishing residual strain change patterns as function of stress and temperature 09 p1468 A71-22600

Heating rate effect on parameters of resistance wire strain gages subjected to temperature gradients 09 p1443 A71-22634

Rarefied gas flow along boundary wall with temperature gradient, determining thermal creep and temperature slip effects 09 p1547 A71-23167

Fluid rotational stability between coaxial cylinders rotating at same angular velocity in presence of radial temperature gradient 10 p1696 A71-24374

Organic thermoregulator control signal generation as function of body peripheral to central temperature ratios, using skin temperature rise measurements 10 p1564 A71-24485

Rotating plane layer viscous incompressible conducting fluid flow between two parallel walls with temperature gradient subject to perpendicular gravitational and magnetic fields 11 p1757 A71-25767

Cold front zone meteorological elements, calculating temperature gradients, dew point deficit, and wind vector vertical distribution 11 p1795 A71-26558

Optical beam side refraction, determining physical conditions for vertical air temperature gradients at line of sight altitude above earth surface 12 p1902 A71-27484

Local heat transfer in tubes under nonstationary conditions, calculating coefficients from wall temperature gradient at surface 13 p2160 A71-28587

Gas flow in plane channel due to longitudinal temperature gradient at arbitrary Knudsen number, using linearized Boltzmann kinetic model equation 13 p1993 A71-29194

Stability theory for thermal stratified viscous parallel flows at Prandtl number of unity, considering atmospheric boundary layer and jet stream mechanisms 13 p2165 A71-29246

Spatial variations in cosmic He abundance attributed to primordial temperature fluctuations at early epochs in Friedmann universe 14 p2303 A71-29587

Stratospheric turbulence correlation to mesoscale horizontal temperature gradient at altitudes flown by SST from Coldsap program 14 p2268 A71-29767

Convection stability in arbitrarily shaped fluid containers heated from below with temperature gradient above critical value 14 p2337 A71-30408

Plane horizontal fluid film convective stability with free boundaries in vertical circular cylinder for periodic modulation of vertical temperature gradient or gravitational field 14 p2338 A71-30873

Free convection in compressible viscous heat conducting liquid near critical point, discussing temperature gradients, layer heights, density distribution and inhomogeneity effect 15 p2512 A71-31497

Monsoonal response of Somali Current in Indian Ocean, using spacecraft IR observations of sea surface horizontal temperature gradients 16 p2562 A71-33068

Hot-wire anemometers design and operation in fluidics, discussing temperature gradient due to heat transfer effects 16 p2579 A71-33435

Magnetic drift wave instabilities in plasmas with nonuniform density and temperature gradient 16 p2572 A71-33949

Microwave amplifiers gain fluctuations effect on Dicke radiometers minimum detectable temperature difference, considering traveling wave tubes and tunnel diode and mixer IF amplifiers 16 p2548 A71-34133

Lateral surface heat transfer effect on thermophysical characteristics in thin layer coatings, discussing temperature gradients in corundum and zirconium oxide on copper 17 p2836 A71-34308

Cylindrical nonuniform plasma with radial temperature and emitter density gradients, analyzing molecular rotational levels intensity distribution and Doppler widths 17 p2787 A71-34587

Time constant for perspiration onset in humans exposed to stepwise increase in external heat load 18 p2862 A71-36897

Crystal growth method based on controlled power reduction under stabilizing thermal gradients, eliminating chemical heterogeneities 19 p3077 A71-37416

Lunar interior thermal radiation measurement in meter wavelength range during period of solar radio image behind limb, showing inverse temperature gradient with depth 19 p3138 A71-37756

Longitudinal vortex rolls onset for laminar forced convection between two horizontal flat plates subjected to uniform axial wall temperature gradient [ASME PAPER 71-HT-1] 19 p3163 A71-37979

Non-Newtonian liquids with arbitrary surface temperature and pressure gradients, solving dynamic and thermal boundary layers equations 20 p3311 A71-38975

Temperature decay method for determining superinsulation thermal conductivity, equating insulation heat transfer rate to calorimeter plate heat loss 20 p3312 A71-39273

Shuttle convective heat transfer involving similar axial temperature gradients in piston and cylinder, calculating interaction with wall conduction by finite difference computer program 20 p3312 A71-39281

Temperature gradients measurements in transit instrument pavilion and errors in time determination for two year period 20 p3237 A71-39314

Homogeneous temperature changes and radial temperature gradients effects on optical lens system, obtaining Bessel type differential equation 20 p3239 A71-39532

Exact solutions for cord reinforced materials with thermomechanical constraints of incompressibility and inextensibility and thermal constraint on temperature gradient 20 p3310 A71-39869

Rotating plane layer viscous incompressible conducting fluid flow between two parallel walls with temperature gradient subject to perpendicular gravitational and magnetic fields 22 p3532 A71-41539

Inhomogeneous high-beta collisionless plasma temperature gradient effects on ion-acoustic and Alfvén drift instabilities 22 p3583 A71-41907

Buckling thermal gradients for rotating orthotropic annular plates under edge pull load 22 p3619 A71-42841

Venusian atmosphere circulation modeling, calculating temperature differences, thermal inertia and wind velocity 23 p3735 A71-43298

Enthalpy change between atmospheric carbon dioxide and Venus surface rocks for damping short term lower atmosphere temperature excursions 23 p3736 A71-43348

Apollo 12 lunar core sample thermoluminescence dependence on radiation dose rates, detecting temperature gradients in regolith by differential thermal analysis 23 p3760 A71-43776

Thermocouple measurements of thermal gradients in steel during automatic welding 23 p3679 A71-43892

Variational formulation for stability of parallel flows with imposed temperature gradient 23 p3783 A71-44180

Cepheid sequence interpretation on gradient diagram based on model atmosphere photometric data 23 p3771 A71-44305

TEMPERATURE INDICATORS

U INDICATING INSTRUMENTS

U TEMPERATURE MEASURING INSTRUMENTS

TEMPERATURE INVERSIONS

NT CENTRIFUGING STRESS

Breaking waves and resulting CAT characteristics from ultrahigh resolution FM-CW radar observation, using model of unstable waves at sheared inversion layer 01 p0116 A71-10565

Annual and diurnal variations of temperature inversion over antarctic plateau, discussing wind field structure and ice crystal precipitation 05 p0778 A71-17043

Vertical velocities in atmosphere measured by acoustic Doppler during diurnal thermal plumes and breaking wave occurrence within nocturnal inversion 10 p1574 A71-23746

Meteorological tower high resolution CW-FM radar measurements for studies of temperature inversions, waves, thermal plumes and convection in atmospheric boundary layer 14 p2192 A71-29707

Upper temperature inversion as condition producing pollutants turbulent diffusion in atmospheric boundary layer 22 p3568 A71-41648

TEMPERATURE MEASUREMENT

Radiometric temperature measurement via source radiated power/photon flux ratio, using Planck equation variation 01 p0178 A71-10140

Gas temperature measurement behind strong shocks in diaphragmless electric shock tube by spectral line inversion method, noting application to gas dynamics 01 p0078 A71-10156

Thermistor bridges for temperature measurement, discussing linearity conditions 01 p0079 A71-10250

Heat conduction approximate averaging equation, determining mean unstationary temperature of arbitrary nuclear fuel element 01 p0179 A71-10617

Interstellar dust grains temperature as intracloud position function under assumed radiative heating and cooling, discussing hydrogen formation 01 p0157 A71-10759

Mammalian hair effectiveness as insulation, using biotelemetry for deep body temperature measurement 01 p0023 A71-10886

Rotational temperature and density measurements in rarefied flow over sharp leading edge flat plate, obtaining shock layer static pressure 01 p0082 A71-10955

Temperature telemetry for pyrogenic drugs testing on dogs 01 p0023 A71-10977

Natural convection turbulent boundary layer temperature profile measurements along isothermal vertical plate, indicating temperature distribution independence of altitude in fully developed turbulent region 01 p0180 A71-10994

Quiet corona temperature from solar equator soft X ray flux measurement by satellite-borne heliograph 02 p0300 A71-12077

Nitrogen inductive low pressure discharge, determining vibrational and rotational temperatures, ionization 02 p0300 A71-12077

ion degree, electron temperature and energy balance by spectroscopic technique

02 p0286 A71-12178

Gain/temperature measurement test set for earth station receiving system by radio sources program tracking unit, noting antenna power ratios determination by attenuator

02 p0222 A71-12797

Gain/temperature measurement for earth station antenna and receiving subsystem by FM method, determining Y-factor/noise power proportional increase/

02 p0222 A71-12798

Stainless steel sputter deposits equilibrium phases, determining deposition temperature ranges for austenite and ferrite formation

02 p0267 A71-12884

Solar photosphere temperature constancy in thin CO layer from equivalent spectral line width determination

03 p0484 A71-13208

Tower turbulence characteristics, using surface wind and temperature measurements to estimate horizontal velocity and dissipation rate variances at top

03 p0452 A71-13226

Six channel selective chopper radiometer design and construction for carbon dioxide emission monitoring for remote atmospheric temperature sounding by Nimbus 4

03 p0423 A71-13356

Temperature sensitive paint and thermocouple techniques comparison for boundary layer transition data, considering aerodynamic heating and transition Reynolds numbers

03 p0518 A71-13468

Fabry-Perot spectrometer systems for solar corona emission spectra and temperature measurements during eclipses

03 p0489 A71-13629

Magnetic thermometry below 3 K using stable AC mutual inductance bridge

03 p0427 A71-13915

Rugged stable differential Pt resistance thermometer for Lunar Heat Flow Program, discussing construction, calibration and environmental test

03 p0427 A71-13917

Left ventricular volume and cardiac work evaluation by thermolindium technique, employing thermocatheter for temperature measurement [ASME PAPER 70-WA/TEMP-2]

03 p0372 A71-14102

Metal oxide particle temperature determination in flames

03 p0376 A71-14283

Single thermocouple temperature measurement, discussing millivoltmeters wiring method with resistance matching to ensure accuracy

03 p0430 A71-14329

Air plasmas temperature measurements behind reflected shock wave, examining radiative cooling effects and total radiant energy

04 p0632 A71-14704

Remote determination of temperature by operating and etalon thermistors resistances measurement with DC bridge

04 p0591 A71-14855

Emissivity and temperature measurement of assembled microscopic particles in black body cavity

04 p0676 A71-14954

Mach-Zehnder interferometer measurements of average temperature and heat transfer rate in free convection on heated vertical flat plate

04 p0599 A71-15522

Measuring instrument for lunar surface layer heat flow, temperature and thermal conductivity

04 p0599 A71-15543

Hydrodynamic and thermal measurements in turbulent boundary layer of liquid drop flow past plate for mineral oil-water mixtures

04 p0576 A71-15617

Airborne radiation thermometry corrections for intervening atmospheric absorption and emission and ocean surface nonblackness

04 p0601 A71-15762

Ti alloy plate multipass welding process, describing temperature measurement techniques for multiple thermal cycles

04 p0604 A71-15910

Plasma temperature measurement in local thermodynamic equilibrium using total continuum emitted during seeding with hydrogen

05 p0786 A71-16171

Temperature measurements for xenon plasma diagnostics in high output pulsed mode

05 p0786 A71-16223

Plasma temperature determination in Hg high pressure discharge with TII addition

05 p0786 A71-16224

Vapor deposited niobium nitride superconducting thin films on fused silica substrates, measuring transition temperature

05 p0792 A71-16236

Sea surface temperature estimation by spatially scanning spaceborne systems operating in thermal IR atmospheric window spectral regions

06 p0898 A71-17560

Umbral rotational temperatures determined from equivalent widths of molecular lines

06 p0967 A71-17906

Laser produced plasma temperature measurements using X ray detectors

06 p0938 A71-18459

High sensitivity portable two channel apparatus for brain temperature measurements using small glass insulated thermistors

06 p0863 A71-18469

Resistance thermometer for temperature measurement in turbulent boundary layer near wall, giving expression for correction factor

07 p1106 A71-18786

Jet engine rotor strain and temperature data transmission, examining special purpose telemeters design

07 p1062 A71-19628

Temperature measurement inaccuracies in 30 to 40 km region by balloonsensors sensors, involving IR cooling of thermistor

08 p1277 A71-20989

Quiet corona temperature from solar equator soft X ray flux measurement by satellite-borne heliograph

08 p1361 A71-21127

Injected air cooled turbine blade trailing edges temperature, calculating thermal distribution with differential equations

08 p1348 A71-21265

Combustion chamber radiant heat transfer measurements, describing radiometer

08 p1288 A71-21270

Hydrogen fluid phase and temperature measurement by single sensor with fluid phase discrimination circuit for transient response sampling

08 p1293 A71-21697

Radioisotope with radiation sensor, minimizing temperature measurement errors in free atmosphere

08 p1293 A71-21745

Molecular and atomic oxygen properties in nonequilibrium flows, determining vibrational temperature and number density by electron beam fluorescence technique

08 p1338 A71-21997

Velocity components, species densities and temperature local measurements, using laser Doppler velocimeters, Raman scattering and tunable lasers

08 p1303 A71-22008

Gunn diodes temperature, calculating power density dissipation by simple domain mode models and accumulation mode operation

09 p1414 A71-22249

Upper atmosphere neutral component temperature measurement from thermal spread of charged particles beam

09 p1437 A71-22679

High temperature measurement by photographic technique using radiation-sensitive color film for unpredictable exposure conditions

09 p1444 A71-22712

Resistance thermometer using amorphous Pd-Si-Cr alloy for enhancing sensitivity at cryogenic temperatures

09 p1444 A71-22714

High accuracy temperature measurements using type K thermocouples

09 p1445 A71-22724

High gas temperatures calorimetric measurement, providing probes with industrial temperature range capability

09 p1449 A71-22791

Venus atmospheric temperature and pressure measurements during and after Venera 7 soft landing

09 p1528 A71-23560

Infrared radiometer sea surface temperature measurements during oceanographic survey, examining inclination angle effect

09 p1440 A71-23590

Gas agent temperature measurement by sodium spectral line reversal method using MHD generators experimental research

09 p1512 A71-23671

Unlit lunar limb observations at IR wavelengths, presenting temperature charts and thermal abnormalities

09 p1530 A71-23716

Resistance thermometry measurements near wall in turbulent flow, considering error causes

10 p1591 A71-23847

Book on heat transfer measurement techniques, discussing cryogenic temperature measurements, optical, spectroscopic and probe methods

10 p1695 A71-24187

Temperature measurement techniques annual progress survey including contact and radiation thermometers, IR thermography, microwave radiometry, fluidic sensors, and liquid crystals

10 p1612 A71-24685

Hot-wire anemometry for measuring velocity-temperature coefficients in turbulent flow with heat transfer

10 p1597 A71-25016

TEMPERATURE MEASUREMENT

Flame plasma temperature determination by microwave attenuation measurements, discussing measured values comparison with predictions by thermal ionization equation

11 p1804 A71-25193

Internal combustion engine gas temperature measurement, using ultrasonic wave frequency shift method

11 p1810 A71-25269

Shielded fine wire probe for total temperature rapid measurement in high speed flows, discussing construction and theoretical considerations

11 p1761 A71-25528

Spectroscopic measurement of high temperatures for ionized gases / plasmas/ in local thermodynamic equilibrium

11 p1761 A71-25571

Rocket propellant performance improvement with boron, giving boiling temperature vs pressure and calculation methods for combustion products composition

11 p1809 A71-25573

Graphite arc radiance temperature measurements with submillisecond resolution, using high speed photoelectric and photographic pyrometers

12 p1905 A71-26812

Temperature measurement methods using thermocouples and hot-wire anemometers for rapidly changing hot gases

12 p1906 A71-26990

Rocket sonde prototype for wind and temperature measurements, discussing electrical circuits, mechanical design and operation

12 p1972 A71-27064

Viscous flow in supersonic de Laval nozzle, measuring gas density and rotational temperatures by electron beam techniques

12 p1865 A71-27555

Radar based values of neutral night exospheric temperature, discussing dominant effect of annual variation

13 p2055 A71-27921

Ionospheric ion temperature measurement method by exploring transverse velocity distribution, discussing surface pollution and spurious effects

13 p2055 A71-27929

Ion temperature measurement for plasma focus, using laser light scattering

13 p2079 A71-28673

Metal temperatures in rotating cooled gas turbine blades, discussing coolant flow aerodynamics

13 p2117 A71-28748

Gas temperature measurement in aircraft combustion chambers, using calorimetric probe

13 p2117 A71-28757

Temperature and radical concentration measurements for high temperature flowing gas streams in rig simulating conditions in ramjet combustion chamber and nozzle

13 p2162 A71-28758

Computerized use of transient thermal resistance and power pulses superposition to calculate instantaneous transistor junction temperatures for various pulse conditions

13 p2038 A71-28770

Upper atmosphere temperature measurements using red emission Doppler contour width data of atomic oxygen at 6300 A

14 p2229 A71-29673

Aircraft instrumentation and data analysis for clear air turbulence, including orthogonal components and temperature and wind distributions

14 p2267 A71-29753

Earth surface temperature measurement by airborne IR radiometers, discussing accuracy provided by narrow and wideband filters

14 p2240 A71-30126

Temperature and thermal flux measurement with calorimetric heat receivers during gas dynamic processes, determining physical properties and geometry effects on errors

14 p2335 A71-30184

Turbine blade profiles nonstationary temperature fields during thermal fatigue tests, measuring surface temperature via thin film thermocouples

14 p2252 A71-30265

Electron temperature and density measurement apparatus using Thomson scattering of laser light for collisionless MHD shock waves

14 p2280 A71-30424

In-flight base heating and thermal environment measurements from Thor Delta launch vehicle using six strap-on solid propellant motors

14 p2320 A71-30721

Supersonic hydrogen combustion in vitiated air stream with stepped wall injection, considering temperature, pressure and composition measurements

14 p2286 A71-30772

Satellite atmospheric temperature sounding by radiometric measurements, obtaining vertical temperature profile by mathematical inversion process

14 p2236 A71-30938

Hertzian radiometry experimental aspects covering background and medium temperature measurements,

sky radiometry and absorbing gas total pressure measurements

14 p2204 A71-30969

White dwarf stars effective temperature measurements, matching absolute spectral energy distributions with fluxes from model atmospheres

14 p2317 A71-31013

Burning gunpowder temperature measurement in gaseous phase, describing thermocouple method

15 p2463 A71-31388

Nitrogen inductive low pressure discharge, determining vibrational and rotational temperatures, ionization degree, electron temperature and energy balance by spectroscopic technique

15 p2451 A71-31487

Supersonic arc-heated Ar flow, measuring heavy particle temperature and velocity and electron density profiles by pressure scanned Fabry-Perot interferometer [AIAA PAPER 71-589]

15 p2454 A71-31534

Flat plate surface film cooling by two dimensional tangent slot injection in hypersonic turbulent flow, measuring equilibrium temperatures and skin friction [AIAA PAPER 71-599]

15 p2343 A71-31541

Rotational temperature and density measurements in high speed gas flow by electron beam fluorescence technique

15 p2406 A71-31544

Jet edge tone sensor and internal feedback fluidic oscillator for temperature measurement, using dependence of sound speed in gas

15 p2352 A71-32065

Snake IR receptor sense organs tested by IR stimulus from carbon dioxide laser, suggesting receptor operation on thermal principle

15 p2360 A71-32296

Mercury, Mars, Venus, Jupiter and Saturn temperatures at 9.55 mm wavelength, calibrating antenna gain with radio sources

15 p2490 A71-32414

Temperature measurements in shock heated carbon monoxide by IR emission-absorption technique

15 p2411 A71-32554

Plane shock front collapse through logarithmic spiral contraction, obtaining pressure and temperature conditions downstream of front

16 p2556 A71-32919

Plasma temperature determination errors from relative g_f -values, noting effects on absolute transition probabilities

16 p2618 A71-33154

Ammonium perchlorate combustion characteristics as function of initial temperature by miniature thermocouple measurements

16 p2623 A71-33361

Solar wind velocity and ion temperature measurement by modulation-type ion trap onboard interplanetary Venera 3 satellite

16 p2626 A71-33456

Surface temperature measurements with contact thermometers, discussing sensor design, cost and efficiency

16 p2579 A71-33474

Nimbus 3 and 4 satellite observation data comparison with sounding rocket and rawinsondes based on temperature as function of pressure measurements

16 p2572 A71-33846

Superconducting transition temperature measurement of cast and solution treated Nb-Zr alloys, substantiating dependence on density of states at Fermi surface

17 p2759 A71-35221

Flame temperature measurement by radiation and gas dynamic methods

17 p2745 A71-35440

Remote sounding of earth atmosphere temperature and composition

17 p2736 A71-35565

Superconducting phase transition temperature measurements as function of magnetic field in thin film hollow Al and In cylinders

17 p2791 A71-35742

Temperature measurement by electron beam, using rarefied gas probing for determination of molecule distribution at various vibrational and rotational levels [ONERA-TP-960]

18 p2915 A71-36026

Thermal mapping performance of passive airborne IR scanners for remote environmental sensing, estimating SNR and noise equivalent irradiance

18 p2921 A71-36364

Mean dry bulb temperature estimation during daylight hours by subtracting proportion of average daily range from daily maxima average

18 p2944 A71-36961

Temperature limit determination of rotating neutron stars based on heat dissipation due to slowing by frictional forces, noting Crab and Vela pulsars

19 p3131 A71-37337

Test facility for thermal diffusivity measurements in solids by method of plane temperature waves using periodic optical heating at 1500 K

19 p3063 A71-37589

Solar brightness temperature measurements using balloon-borne Michelson interferometer

19 p3135 A71-37613

Carbon dioxide IR radiation measurements of duration of constant reflected shock temperature in over-tailored shock tunnel

19 p3041 A71-37893

Interlaboratory program to evaluate thermocouple pyrometric practices in metals high temperature testing

19 p3065 A71-38136

GaAs laser diode junction temperature measurement methods for verification of stimulated emission quenching due to heating

19 p3074 A71-38231

Meteorological rocket nose portion thermal regime, determining housing, insulation coating and compartments temperature

19 p3172 A71-38632

Venera 7 satellite data during descent through Venus atmosphere and activity after soft landing on 15 December 1970, noting temperature and pressure measurements

20 p3289 A71-39130

Atmospheric thermal sounding problem, using regularization and statistical methods and expanding by empirical orthogonal functions

20 p3256 A71-39211

Thermodynamic measurement of cryogenic temperatures based on gases at low pressures or platinum electrical resistance

20 p3270 A71-39243

Capacitive thermometry characteristics of dielectric crystallized titanate-containing glass ceramic at cryogenic temperatures

20 p3253 A71-39279

E region wind and temperature measurements from Nancy incoherent scatter experiments, observing prevailing semidiurnal oscillation with phase propagating downwards

21 p3372 A71-40041

Evaporated Permalloy films deposition temperature measurement by vacuum evaporated Chromel-constantan thin film thermocouple, noting temperature difference between film and glass substrate

21 p3384 A71-40220

Turbulent hypersonic wake density and temperature measurement for slender cone model in shock tunnel, using dual electron beam excitation technique

21 p3364 A71-40396

Transient pressure, temperature and density measurement of dense hot gas

21 p3364 A71-40402

Cholesterol liquid crystals technique for thermal analysis of microcircuits, multilayer circuit boards, semiconductor devices and other electronic components

21 p3355 A71-40738

Jet flame stability characteristics of propane-air mixture ejected into counter air stream by temperature and concentration measurements and visual observation

21 p3475 A71-40758

Air temperature measurement errors, comparing thermometers with and without meteorological screening

21 p3383 A71-41240

Temperature pulsation measurements by high altitude aircraft in presence of lower troposphere convection elements

21 p3412 A71-41389

Global three dimensional atmospheric temperature mapping by selective chopper radiometer on Nimbus 4 satellite, measuring carbon dioxide IR emission

22 p3533 A71-41629

Mean body temperature computation in neutral and hot environments from rectal and skin temperatures

22 p3485 A71-41723

Interferometric measurement of gas temperature in positive column of discharges used for carbon dioxide lasers

22 p3574 A71-41725

Radiative and turbulent heat transfer in atmospheric surface layer, measuring radiative heat flux divergence and temperature fluctuations at different heights

22 p3534 A71-41860

Jupiter disk temperature measurement at eight frequencies in 20.5-35.5 GHz range, comparing with saturated ammonia model calculations

22 p3599 A71-41922

Remote sensing of chlorophyll and temperature in marine and fresh waters by spectroradiometer and differential and IR filter radiometers onboard airplane

22 p3534 A71-41986

Contactless determination of low temperatures by IR radiation thermometers, applying to measurement on transparent materials

22 p3546 A71-42158

Upper atmospheric temperature and density measurements from artificial cloud observations

23 p3667 A71-43139

Ientropic nature of stratospheric air masses motion from balloon measurements of temperature and radiation

23 p3671 A71-43338

Equilibrium phase relations in lunar rocks and synthesized analogs, determining liquidus and solidus temperatures

23 p3742 A71-43742

Liquid crystals structural, elastic and optical properties, noting application to measurements of temperatures, pressures and electric and magnetic fields

23 p3717 A71-43742

Laser pulse produced plasma in freely expanding high density nitrogen gas jets, measuring electron temperature and light-plasma interaction time

23 p3687 A71-44041

Local thermodynamic equilibrium deviation theory, and application in low density Ar plasma, noting interference in Langmuir probe and spectroscopic electron temperature measurements

23 p3714 A71-44041

Temperature and electron density measurements of free jet of ionized nitrogen at atmospheric pressure by plasma spectroscopy, estimating Prandtl numbers

23 p3664 A71-44041

Total temperature thermocouple probe based on spherical cylinder recovery temperature with combined advantages of hot wire and shielded probe, discussing design and applications

24 p3826 A71-44041

Balloon measurement of solar flux and brightness temperature in 12-24 micron range

24 p3873 A71-45104

Gaseous media parameters in wave energy exchanger, examining compression cycles, temperature ratios and flow velocities for maximum conversion efficiency

24 p3891 A71-45104

Thermal resistance, junction temperature and minimum power meter for semiconductor transistors as diodes with/without heat sinks

24 p3810 A71-45304

TEMPERATURE MEASURING INSTRUMENTS

NT PNEUMATIC PROBES

NT RADIATION PYROMETERS

NT RESISTANCE THERMOMETERS

NT TEMPERATURE PROBES

NT THERMOCOUPLE PYROMETERS

NT THERMOMETERS

Thermal pattern visualizing and interpretation in imaging in far IR, noting equipment and uses of thermography in medicine, science and technology

01 p0078 A71-10704

Magnetic suspension apparatus for temperature measurement near interface of sliding bodies in vacuum

03 p0397 A71-13914

Fast multiple point measurement of fluid temperature and flow speed fields using bead thermistors and digital system

03 p0427 A71-13914

Human body thermography for studying physiological changes due to exercise, anoxia or accelerations

06 p0860 A71-18494

Electromagnetic fields induction in biological tissues, recording energy absorption temperature distribution in phantom models with thermograph camera

11 p1717 A71-25274

Electric current heated thin resistance film thermoelectric transducer, measuring temperature with thermocouple

12 p1888 A71-27574

Thermal relaxation effects on thermal adjustment between gas and wall, comparing with thermograms from shock tube experiments

13 p2161 A71-28664

Wheatstone bridge with thermistors, discussing linearity, sensitivity and applications for temperature difference and flow velocity measurements/anemometers

13 p2071 A71-29204

Continuous recording of human rectal temperature under extreme environmental conditions, using battery powered thermographs with thermistor probes

20 p3192 A71-39004

Fluid phase discrimination temperature measurement system, using thin carbon film resistance thermometer with electrical power pulse sensing liquid/gas phase discrimination

20 p3237 A71-39224

Calibrated IR thermographic camera development and applications in medicine, X ray beam energy reactor cooling rod measurements

22 p3545 A71-42104

TEMPERATURE PHOTOMETERS

U PHOTOMETERS

U TEMPERATURE MEASURING INSTRUMENTS

NT PNEUMATIC PROBES

NT PNEUMATIC PROBES

Reverse flow temperature probe design and calibration for vertical soundings from aircraft, comparing radiosonde method

02 p0247 A71-11814

Hot wire total temperature probe at hypersonic speeds for flow field measurements [AIAA PAPER 71-273]

08 p1377 A71-21994

Rocketsonde instrumentation noise separation from atmospheric variability, discussing paired soundings and large scale discrepancies in temperature and wind observations

11 p1794 A71-25386

Shielded fine wire probe for total temperature rapid measurement in high speed flows, discussing construction and theoretical considerations

11 p1761 A71-25528

High enthalpy flow temperature probe, determining ignition temperature of combustion gases by chromel-alumel thermocouple

11 p1765 A71-26277

Detailed wind velocities and temperature profile measurements by FPS-14 radar/Jimsphere technique for space vehicle and SST applications

22 p3569 A71-42543

Sporadic E layer observation by reference electrode electron temperature probe on sounding rocket, determining electron density below 85 km in D region

23 p3671 A71-43367

TEMPERATURE PROFILES

Atmospheric temperature profile in cloud presence, discussing remote sounding techniques with maximum probability method

01 p0120 A71-10854

Natural convection turbulent boundary layer temperature profile measurements along isothermal vertical plate, indicating temperature distribution independence of altitude in fully developed turbulent region

01 p0180 A71-10994

Wind speed difference quotient conversion to gradients at atmospheric surface layer geometric mean height, considering wind and temperature profiles

03 p0452 A71-13229

Lower atmosphere vertical temperature profiles by optical refraction measurements from photographs of equally spaced illuminated targets

03 p0453 A71-13233

Spiral plate heat exchanger temperature-length profile calculation by Runge-Kutta technique

04 p0678 A71-15464

Skin friction, Stanton numbers, velocity and temperature profiles in accelerating turbulent boundary layer flows, using Prandtl mixing length

04 p0680 A71-15478

Temperature profiles in high velocity compressible turbulent boundary layer over flat plate without pressure gradients

04 p0681 A71-15480

Single disk rotating in still air, calculating temperature profiles and local heat transfer coefficients

04 p0683 A71-15494

Thermal radiation-conduction interaction in horizontal fluid layer, obtaining temperature profiles with Mach-Zehnder interferometer

04 p0685 A71-15515

Unstable atmospheric surface layer wind speed and temperature profiles mathematical representation

05 p0777 A71-16664

Nimbus 3 and 4 satellites IR grating spectrometers for remote sensing of vertical temperature and humidity profiles of stratosphere and troposphere near Philippines

05 p0818 A71-17137

Neutral ionospheric temperature profile diurnal variation at Arecibo from incoherent scatter measurements, considering relevance to 1400 hour density maximum

06 p0887 A71-17271

Kinetic theory calculation of partially ionized plasma near-electrode electron temperature profiles

06 p0939 A71-18583

Large diameter tube high Reynolds number air flow temperature profiles, using chromel-alumel thermocouple

07 p1220 A71-18762

Earth atmosphere thermal sounding problems, considering indirect temperature profile determination, various degrees of cloudiness and Planck function dependence on pressure

07 p1151 A71-18909

Planetary atmospheres structure and dynamics, discussing composition and vertical temperature profile models

07 p1191 A71-18915

Fredholm integral equation stabilization methods for atmospheric IR transfer in vertical temperature profile determination

08 p1286 A71-21877

Atmospheric surface layer wind and temperature profile measurements over horizontally uniform flat terrain

09 p1489 A71-23554

Low Prandtl number laminar compressible boundary layer flow over flat plate, obtaining recovery temperature profile and heat transfer by matched asymptotic expansions method

10 p1597 A71-25066

Velocity, temperature and concentration profiles correlation for compressible turbulent boundary layer along porous flat plate, with carbon dioxide injection, discussing cooling applications

10 p1598 A71-25095

Multilayered spherical model induced fields and static heating patterns, approximating primate cranial structure EM plane wave irradiation

11 p1717 A71-25287

Upper atmosphere neutral temperature profiles in auroral zone, using aluminum and barium oxide clouds fluorescent emission

11 p1753 A71-25547

Wind speed and potential temperature vertical profile in day/night planetary atmospheres estimated by similarity theory of boundary layer parameters

11 p1826 A71-25719

Temperature, concentration and heat conductivity profiles of chemically reacting gas mixtures with thermal gradient, using classical transfer equations

13 p2025 A71-27884

Heat exchange during stabilized laminar flow of incompressible liquid in circular pipe with radiative cooling, deriving temperature profile and Nusselt number dependence

13 p2046 A71-28180

Statistical analyses for tube-annular and annular combustion chamber temperature profiles

13 p2116 A71-28741

Vertical distribution of small ion density and of electric polar conductivity and ion temperature profiles in atmosphere at 1.5-19 km from balloon measurements

13 p2065 A71-29425

Time variable effect on synthetic wind speed and air temperature profiles based on sensible heat flux density and stress at surface layer

14 p2266 A71-29705

Least squares method for inversion of radiative transfer equation, considering atmospheric temperature profiles determination from outgoing radiance

14 p2337 A71-30296

IR scanning vertical temperature profile radiometer forITOS meteorological satellites, describing electronic signal processing

14 p2200 A71-30916

Satellite atmospheric temperature sounding by radiometric measurements, obtaining vertical temperature profile by mathematical inversion process

14 p2236 A71-30938

Internal gravity waves vertical propagation in lower ionosphere from temperature and wind profiles measurements

16 p2561 A71-32802

Turbulent flow in circular duct, determining asymptotic temperature profiles and Nusselt number values from Prandtl numbers and velocity distribution

16 p2554 A71-32836

Altitude and amplitude of winter stratospheric warmings from satellite measured radiance changes, considering radiative transfer equation and variable model of temperature structure

16 p2605 A71-33537

Thermosphere and exosphere static models with empirical thermal profiles, giving temperature, density and composition as function of height

16 p2564 A71-33722

Seasonal temperature and density models for stratosphere and mesosphere from observations by resistance thermometers at Heiss Island Soviet rocket station

16 p2566 A71-33743

Wind and temperature structure in stratosphere at Sonmiani during autumn 1970 from three Dart firings

16 p2567 A71-33763

Atmospheric stability at 30-90 km based on wind and temperature data from grenade experiments

16 p2568 A71-33788

Electron temperature profiles in ionosphere from rocket probes, noting correlation with geomagnetic activity indexes

16 p2569 A71-33798

Thermospheric circulation and temperature changes due to global scale winds flow through F region ionization anomalies, using time independent dynamic model

16 p2571 A71-33836

Laminar boundary layer flow at stagnation point with intensive injection of different absorbing medium, calculating temperature profiles and thermal fluxes

17 p2725 A71-34215

F region plasma phenomena discoveries by U.S. researchers /1967-1970/, considering thermal structure, ion composition, conjugate photoelectrons effects, wind effects, etc

17 p2732 A71-34465

Spectral scanning method for determining temperature profile of jet- or rocket-engine exhaust stream by gas radiation and transmittance measurements, discussing radiometric errors effects

18 p2916 A71-36048

Radial temperature profiles of long induction discharge in argon at atmospheric pressure

19 p3111 A71-37579

Heated jet interaction with deflecting flow in subsonic wind tunnel, presenting flow visualization and temperature and velocity profiles

19 p3163 A71-37980

[ASME PAPER 71-HT-2]

Gravity effect on developing laminar flow with forced convection in vertical isothermal tube, investigating velocity and temperature profiles and heat transfer rate

19 p3164 A71-37983

Velocity and temperature profiles at near-critical point of nitrogen turbulent boundary layer flow over heated flat plate by thermocouple/pitot-static probe

19 p3165 A71-37994

Chlorine-fluorine flame, determining adiabatic propagation speed, refractive index field, temperature profile, composition distribution and atom concentrations

19 p3168 A71-38105

Radial temperature profiles in low pressure oxygen-calcium wire diffusion flames from optical measurements based on radiative transfer equation

19 p3170 A71-38115

Fredholm integral equation stabilization methods for atmospheric IR transfer in vertical temperature profile determination

19 p3060 A71-38470

Step-change single blow transient temperature response synthesis by data reduction with aid of operational calculus and half-line convolution integral equation theory

20 p3314 A71-39488

Vertical temperature profiles from Nimbus 3 satellite spectral radiance measurements, stressing importance for atmospheric circulation prediction

20 p3258 A71-39666

Atmospheric thermal sounding radiation data interpretation, determining integral Fredholm equation solution, absorption characteristics and temperature profiles

20 p3258 A71-39670

Exospheric evening temperature behavior data, using Fabry-Perot interferometer measurements of atomic oxygen line Doppler broadening

20 p3222 A71-39703

Auroral excitation and ionization intensity and rotational and Doppler temperature vertical profiles measurements, emphasizing emission rate profiles

20 p3227 A71-39839

Steady propagation of plane laminar flame through uniform mixture of hydrogen and bromine gases, obtaining temperature and concentration profiles

21 p3474 A71-40524

Thermal stress distribution and temperature profiles in nearly opaque spherical shell under radiant and convective heating flux

21 p3476 A71-40942

Temperature pulsation measurements by high altitude aircraft in presence of lower troposphere convection elements

21 p3412 A71-41389

Turbulence energy balance and temperature pulsations in free atmosphere in presence of water phase transformation in clouds of given microstructure

21 p3412 A71-41394

Conductive and radiative axial heat transfer in packed/stagnant beds at 20-750 C, giving temperature profiles

22 p3620 A71-41877

IR atmospheric temperature profiles sounding by selective chopper radiometer launched into polar orbit on Nimbus 4 satellite

22 p3544 A71-42144

Differential equations system for convective incompressible fluid flow boundary layer temperature profile description, analyzing solution existence and uniqueness

23 p3781 A71-43306

High Prandtl/Schmidt/ number fluids turbulent flow temperature profile derivation by turbulent transport mathematical model

23 p3664 A71-44199

Heat exchange during stabilized laminar flow of incompressible liquid in circular pipe with radiative cooling, deriving temperature profile and Nusselt number dependence

24 p3888 A71-44933

Liquid droplet vaporization under exposure to hot gas, obtaining time dependent temperature and concentration profiles in vicinity from coupled diffusion equations

24 p3888 A71-44963

Temperature field profiling along radius in front of gas turbine stage, applying to regeneratively cooled turbine engine

24 p3864 A71-45011

Heat transfer in transpiration cooled porous heat sources, deriving dimensionless temperature profiles

24 p3891 A71-45185

Ionospheric and neutral atmospheric temperature profile, composition and electron density and energy measurements by MR-12 rocket

24 p3824 A71-45310

Vertical electron concentration and temperature profiles at 80-170 km measured by rocket launched on 10 July 1969 at Volgograd

24 p3824 A71-45322

TEMPERATURE SCALES

TEMPERATURE SCALES

Convective velocity and temperature scales deduced numerically and observationally for unstable planetary boundary layer and for turbulent Rayleigh convection

03 p0453 A71-13613

Corrections derived for Labs-Neckel 1968 solar radiation tables transformation into 1968 International Practical Temperature Scale

05 p0797 A71-16018

Thermal stresses estimation method based on equivalent stress calculation via use of temperature scale

[HEAT EXCH. CONF. PAPER 12]

15 p2504 A71-31634

TEMPERATURE SENSORS

NT THERMISTORS

Atmospheric temperature remote sounding from satellites using radiometer with selective chopper for carbon dioxide emission

03 p0422 A71-13355

Atmospheric temperature remote sounding via balloon-borne selective chopper radiometer

03 p0423 A71-13357

Transducer with single crystal Ge for high heat flux measurement, noting calibration by direct conduction

04 p0599 A71-15589

High performance fighter aircraft engine pressure ratio and turbine inlet temperature measurement, using fluidic sensors

07 p1028 A71-20586

Hydrogen fluid phase and temperature measurement by single sensor with fluid phase discrimination circuit for transient response sampling

[NAS PAPER M-3]

08 p1293 A71-21697

Upper air sounding systems problems, discussing aerodynamic heat transfer between temperature sensor and ambient air

08 p1330 A71-21739

High temperature thermal null strain gage with sensing unit and electronic control unit to measure mechanical strain in terms of induced thermal strain

09 p1445 A71-22721

Centerline loss, transient sink temperature and thermal conductivity design constant considerations for thin foil copper-Gardon heat flux sensors

[AIAA PAPER 71-470]

11 p1764 A71-26251

Aerodynamic heating tests of cone flap reentry vehicle using temperature sensitive paint

20 p3311 A71-39197

Meteorological rocketsonde film mounted thermistor bead temperature sensor, developing mathematical model for thermometric correction formulas in automatic data processing

20 p3236 A71-39208

Fluid phase discrimination temperature measurement system, using thin carbon film resistance thermometer with electrical power pulse sensing for liquid/gas phase discrimination

20 p3237 A71-39278

Woomera /Australia/ meteorological rocket firings, using temperature and wind profiles to assess sensors and parachutes performance

20 p3221 A71-39691

Resistance wire temperature sensor spatial resolution calculation, considering sensor length and isotropic turbulence effects on temperature spectrum and dissipation

22 p3542 A71-41904

Fluid amplifiers theory and use as temperature and pressure sensors, discussing applications in chemical and ammunition industries and jet aircraft control

[IEEE PAPER 70-TP-120-IGA]

23 p3630 A71-42921

TEMPERATURE TRANSDUCERS

U TEMPERATURE MEASURING INSTRUMENTS

U TEMPERATURE SENSORS

TEMPERING

Medium alloy structural steels tempering, investigating Mn, Ni, Cr and Mo effect on activation energy of softening

03 p0445 A71-14338

Potentiokinetic study of anodic polarization in maraging Fe alloys, considering relationship to structural transformations during tempering

05 p0765 A71-16200

Phase transformations during tempering of rhodium steels using X ray, dilatometric and conductivity measurements

07 p1135 A71-19617

Stress relief cracking in Cr-Mo steel, considering correlation with embrittlement of water quenched base metal tempered at low temperature

13 p2086 A71-29091

Mechanical properties of carburized cermet steel with hypereutectic structure after water quenching and tempering at 300 C

19 p3076 A71-37113

Alloying elements effects on martensite decomposition and carbide phase formation during tempering of chromium steels

21 p3401 A71-41085

Transformation zones of Ti alloy in isothermal conditions after tempering, showing martensite decomposition and omega phase detection by hardness measurements

22 p3560 A71-41624

Tempering anomalies of austenitic stainless steels partially transformed into martensite, using dilatometry, resistivity and internal friction measurements

22 p3562 A71-42244

High purity Ni wire hardening by lucinae agglomeration during tempering, using comparative tension curves

22 p3562 A71-42245

Thermoelastic coefficient development by tempering for Ni-Fe alloy containing Be

22 p3563 A71-42325

TENSILE CREEP

Al-Mg alloys secondary creep relationship to mechanical instability during tension

03 p0445 A71-14340

Matrix stacking fault energy effect on tensile creep deformation modes in gamma prime precipitation hardened nickel-base alloys

19 p3080 A71-37721

Al alloy tensile tests at high temperature and constant elongation and loading rates, noting creep strain

20 p3251 A71-39167

TENSILE DEFORMATION

Deformation and strength of pipes manufactured from oriented glass fiber reinforced plastics under axial tension

01 p0177 A71-11237

Polycrystalline Zr extremely low temperature tensile deformation, discussing prestraining effects, stress-displacement relations, strain distribution, twinning, etc

02 p0267 A71-12878

Polycrystalline Ni single and overlapping stacking faults production by tensile deformation in premicroyield region, noting stress concentration effects

02 p0268 A71-12888

Elastoplastic stress analysis for samples with notches and holes under tension, discussing boundary condition calculation by finite element method

03 p0510 A71-13949

Crack opening displacement concept in fracture mechanics, considering crack tip radius as measure of extension potential

04 p0670 A71-15392

High temperature ductility of low alloy ferritic steels, correlating tensile elongation values to crack nucleation resistance

07 p1134 A71-19517

Fiberglass reinforced plastic strength and deformability under tension as function of loading rate and test temperature

07 p1145 A71-20466

Recrystallized and nitrided Mo alloy microstructure under plastic deformation by tension at high temperatures

08 p1305 A71-21029

Electrochemical polarization effects on Ni single crystals mechanical behavior under tensile deformation

08 p1310 A71-21539

Stacking fault formation and mechanical twinning in Ni base superalloy during tensile deformation at high temperature

08 p1315 A71-21581

Inflation of initially spherical balloon of elastic rubber-like material, discussing tensile instability

11 p1707 A71-25445

Load-deformation characteristics in tension, compression and bending of two thin cement laminates reinforced with short random glass fibers, discussing stiffness and residual strain

11 p1790 A71-26384

Kinetics of Ti single crystals tensile deformation by prismatic gliding, studying moving dislocations interactions with metal impurities

14 p2257 A71-29844

Optical methods for measuring mechanical strain by observing shift and deformation of elemental surface areas, using holographic techniques

15 p2404 A71-31269

Aluminum single crystals tensile deformation and annealing to produce polygonized substructure

15 p2432 A71-32172

Iron single crystals plastic deformation under tension, studying ductile/brittle fractures mechanisms and transition temperature

16 p2591 A71-33369

Cell structure development during room temperature tensile deformation of beryllium after prism slip by combined X ray diffraction-transmission electron microscopy

20 p3249 A71-39002

Al alloys tensile deformation and fracture characteristics relation to stress-strain diagrams, discussing strain hardening indices

22 p3560 A71-41642

Bending strain diagram conversion into tensile strain diagram, considering elastic limit values correction for Cu-Ni-Al alloy

22 p3561 A71-41644

Nonlinear theory of tensile instability /necking/ of homogeneous isotropic bar obeying Ramberg-Osgood law

22 p3618 A71-42248

Heat treatment specifications selection for Ni alloys by mathematical method based on cylindrical specimens elongation under tensile loads

23 p3691 A71-41249

Width/thickness ratio effect on steel, brass and molybdenum sheet specimens plasticity and deformation under tension at room temperature

23 p3694 A71-41249

TENSILE PROPERTIES

Prealloyed hot formed Cr-Ni-Mo and Ni-Mo alloys manufactured from powders, considering toughness, tensile properties, fatigue and impact strength

01 p0100 A71-10000

Ni coated carbon fibers tensile properties, examining thickness, stress-strain curve, plasticity and grain size

03 p0448 A71-14110

Whisker composites tensile and fatigue properties fracture toughness and mechanical properties at high temperatures

04 p0611 A71-14940

Aging effect on tensile mechanical properties as hardness of high purity binary Ni-Cr alloys at 290-500 C

07 p1138 A71-19900

Thermally stable fibers fabricability and properties relation to polymer chemical structure and tensile strength

09 p1481 A71-22225

Hydrogen peroxide immersion effects on dimethyl silicone seal rubber tensile properties and tear strength

10 p1631 A71-24000

Forgeability and tensile properties of spark sintered unstrained Ti-Al-V preforms from prealloyed powder in uncontrolled atmosphere

13 p2084 A71-28100

Explosive and isostatic forming effects on commercial precipitation-hardenable Al-Cu alloy microstructure, tensile properties and fatigue life

15 p2433 A71-32100

Annealed stainless steel and Ti alloy in solution heat treated aged condition, detailing elevated temperature and high strain rate effects on fatigue life and tensile properties

15 p2438 A71-32700

Strain rate effects on composite material tensile and flexural properties measured by load sensors and streak photography

17 p2737 A71-34400

Tensile properties, plane strain fracture toughness and stress corrosion threshold of high strength precipitation hardening stainless steels

17 p2755 A71-34400

Omega phase embrittlement in aged Ti-Mo alloys giving tensile properties and load-elongation diagrams

19 p3082 A71-38100

Ti alloys heat resistant properties evaluation for long service under various heat treatment conditions considering tensile properties, fracture toughness and microstructure

19 p3082 A71-38400

Hydrogen content effect on annealed and work hardened palladium wire tensile properties, determining yield/tensile stress and elongation

20 p3247 A71-38700

Tensile properties and notch toughness of Al alloys at low temperature, considering fracture toughness and weld strength

20 p3251 A71-39200

Precipitation hardened Ti-Nb alloy, correlating room temperature tensile properties with microstructure from step aging

21 p3387 A71-40400

Ti-Mo base metastable beta Ti alloy tensile properties anomalies at elevated temperatures, examining strain rate and annealing conditions effect

21 p3399 A71-40600

Brittle transition temperature of steels by Vickers hardness testing, comparing with tensile properties and impact fracture process in Charpy impact test

21 p3388 A71-40700

Nominal stress prediction for plastic tensile instability occurrence in flat orthotropic sheet loaded in biaxial stress system, considering localized and diffuse necking

21 p3469 A71-41000

TENSILE STRENGTH

Welded joints ductile and brittle static tensile strength at low temperatures, allowing for mechanical inhomogeneities

01 p0085 A71-10000

Fiberglass-reinforced plastics loading conditions effects on tensile strength, determining creep rupture strength from test data

01 p0107 A71-10400

- Reinforced polymers strength and deformation under tensile loads applied across fibers
01 p0107 A71-10496
- Anisotropic polycrystalline carbon fiber tensile strength and bending behavior, interpreting inelastic characteristics from single filament experiments
02 p0273 A71-11945
- Multilayer composites preparation by cold rolling stacks of alternating Al and Sn foils, determining tensile strength relation to layer thickness
02 p0264 A71-12278
- Glass fiber reinforced plastics tensile strength under various continuous loading rates and elevated temperatures
02 p0275 A71-12667
- Nitriding effects on short time tensile strength, plastic properties and hardness of niobium
04 p0612 A71-15549
- Strengthening curve determination by tensile tests for plastic yield limit, strength and elongation at rupture
04 p0673 A71-15898
- Glass textolite materials strength during cooling under tensile, high rate tension and impact loads
05 p0771 A71-16362
- Cylindrical steel samples with screw type threads, comparing pressed and ground threads effects on tensile strength at low temperatures
05 p0827 A71-16763
- Graphite fiber reinforced Al-Si alloy composite tensile strength and microstructure, observing tension failure modes
06 p0914 A71-18678
- Semiconductor thermocell junction polishing effects on bilateral layers tensile strength and electrical contact resistance
07 p1023 A71-19145
- Fiberglass reinforced plastic strength and deformability under tension as function of loading rate and test temperature
07 p1145 A71-20466
- Carbon fiber reinforced Al composites fabrication and evaluation by metallographic examination, considering tensile strength
[PLASTICS INST. PAPER 17]
08 p1322 A71-20930
- Al microstructure and strength, investigating prior deformation and temperature effects
08 p1313 A71-21561
- Cylindrical steel specimens bearing strength under cyclic elastoplastic deformation, investigating stress redistribution effects
08 p1316 A71-21607
- Cast Mo alloy at low temperatures, investigating plasticity, plasticity and tensile strength characteristics
08 p1316 A71-21615
- Theoretical model of elastic medium with diverse tensile and compression resistances under finite deformation
08 p1373 A71-21944
- Transverse bending of hinged or clamped rectangular plates with different tensile and compressive resistance
08 p1373 A71-21945
- Tensile data for dispersion hardened iron containing thoria spherulites analyzed in terms of Orowan theory, considering bcc materials yield strength
09 p1466 A71-22172
- Optimum tip vertex angles measurement for determining steels tensile strength and yield point from hardness
09 p1467 A71-22314
- Specimen width effect on ultimate fiberglass tensile strength for specimens cut from tubes and oriented at certain angle to symmetry axes
09 p1482 A71-22504
- Mechanical strength and elastic properties under tension and bending of boron fibers, noting dependence on surface defects
09 p1482 A71-22823
- Prolonged storage effect on polycarbonates mechanical properties, measuring tensile strength, elastic modulus, yield point and breakdown strains under uniaxial tension
09 p1483 A71-22825
- Annealed Al-Mg alloys mechanical measurement, noting low temperature tensile strength and yield point variations with specimen composition and temperature
09 p1473 A71-23230
- High temperature Fe, Co and Ni alloys for gas turbine components, considering tensile and creep rupture strength increase by thermal mechanical processing
09 p1475 A71-23298
- Molybdenum alloy under annealing and heating by AC electric current, investigating structure change effects on strength properties
09 p1475 A71-23312
- Microstructural defects responsible for tensile strength reduction in carbon fibers subjected to high temperature graphitization, using transmission electron microscopy
09 p1483 A71-23653
- Brittle materials tensile strength testing method, using thermal contraction loading device
09 p1479 A71-23698
- Brittle alumina ceramic tensile and flexural strengths comparison based on statistical surface flaw distribution theory of fracture
09 p1484 A71-23699
- Tensile yield and ultimate strength and elongation of Al after unidirectional and reversed torsional prestrain
10 p1624 A71-23940
- Polyurethane structural adhesives with excellent tensile shear and T-peel strengths at cryogenic temperatures, long pot lives and good processing characteristics
10 p1630 A71-24068
- Deformability and strength of soft fiber reinforced plastics under biaxial tension, determining low temperature critical tensile stresses and elongation ratios
10 p1634 A71-24194
- Anisotropic material failure under combined loading, predicting strength from uniaxial and shear tests
[AIAA PAPER 71-368]
11 p1845 A71-25342
- Failure analysis of notched unidirectional composites under tensile load parallel to fiber, considering Griffith-Irwin-Orowan fracture theory applicability
[AIAA PAPER 71-369]
11 p1784 A71-25343
- Fiber length, diameter, bundle size, glass content and sizing effects on fiberglass reinforced plastic systems flexural, tensile and impact strength
11 p1784 A71-25395
- Carboxyl terminated butadiene-acrylonitrile/epoxy carbon fiber composites fracture energy, noting fracture strength, short beam shear strength and tensile strength at cryogenic temperatures
11 p1785 A71-25403
- Longitudinal tensile strength of unidirectional fibrous glass/polymeric matrix composites under high loading rates
11 p1785 A71-25405
- Carbon fiber reinforcement in carbon fiber/glass fiber mat sandwich beams increasing tensile and compressive strength
11 p1846 A71-25412
- Impact composite materials with reactive resins as binders for polyester fabric, determining peel resistance, tensile shear strength and high temperature aging effect
11 p1786 A71-25416
- Low alloy steels and superalloys inertia welding in gas turbine field, discussing microstructure tensile strength and stress rupture
[ASME PAPER 71-GT-21]
11 p1770 A71-25965
- High temperature tensile strength, creep rupture behavior and high temperature exposure effects on subsequent room temperature properties of maraging steel plates and welds
[ASME PAPER 71-MET-E]
12 p1918 A71-27314
- Hereditary elastic body model with various tensile and compressive strengths, using elasticity theory with differing moduli
12 p1982 A71-27518
- Tensile strength and plasticity of hot rolled maraging steel at low temperatures
13 p2082 A71-27869
- Tensile strength and fracture toughness of carbon fiber polyester composites, using mechanical testing and scanning electron microscopy
13 p2092 A71-28625
- Hybrid boron-graphite filaments in epoxy matrix composite, describing increased tensile strength and modulus of elasticity
14 p2261 A71-29638
- Quantitative description of solidification structures of Al-Cu, Al-Cu-Ti, Al-Si, Al-Mg and Al-Si-Cu, discussing dendritization index, cooling rate and tensile strength
14 p2257 A71-29842
- Al-Mg-Si alloy development with low quenching sensitivity and high tensile strength
14 p2259 A71-30471
- Ta nitriding temperature and duration effects on tensile strength, elongation and surface hardness
15 p2424 A71-31240
- Niobium fine structure, examining annealing in vacuum effects on strength
15 p2425 A71-31400
- High tensile strength maraging steels aging, discussing dispersed precipitates formation by homogeneous nucleation
15 p2427 A71-31525
- Co-Mo and Co-Mo-Ti stainless maraging steels tensile strength after quenching, establishing Mo and Co alloying limits
15 p2427 A71-31526
- Polyacrylonitrile and rayon precursor graphite fibers diameter relation to Young modulus and tensile strength
15 p2438 A71-31817
- Molybdenum and tungsten alloys, detailing strengthening with hafnium carbide
15 p2428 A71-31840
- Low temperature and tensile loading rates effects on static and dynamic strength of steel rods with ground and rolled threads
15 p2505 A71-31862
- Heat treatment effects on high strength maraging steel tensile, fracture toughness and stress corrosion properties, discussing reversion to austenite
15 p2433 A71-32175
- Radiation effects on epoxy adhesive mechanical properties including compressive shear stress, modulus of elasticity and tensile strength
15 p2439 A71-32510
- Stress-strain diagrams for oriented fiberglass-reinforced plastic under tension, taking into account temperature and anisotropy effects
16 p2601 A71-33411
- Welded joints ductile and brittle static tensile strength at low temperatures, allowing for mechanical inhomogeneities
16 p2584 A71-33641
- Al-Mg alloy with Ti, Zr, Mo and B additions under tensile and impact loads, investigating mechanical properties, strength and crack formation
16 p2594 A71-33712
- Fibrous composites with multiple and variable shear strength interfaces to improve longitudinal shear and transverse tensile strengths and toughness
17 p2817 A71-34342
- Monograph on fiber-resin composites covering glass, boron and carbon fibers and epoxy matrix materials tensile and thermoelastic properties
17 p2761 A71-34469
- German monograph on structural steels tensile and yield strength, detailing strain rate and testing machine effects
17 p2818 A71-34483
- Bunched parallel reinforcing fibers of equal size and varying tensile strength, deriving critical loads and stresses under gradual failure
17 p2763 A71-35451
- Cylindrical steel and Ni alloy specimens bearing strength in inhomogeneous stress states under cyclic elastoplastic bending and loading to failure
17 p2760 A71-35668
- Vacuum melted Mo alloy low temperatures elasticity, plasticity and tensile strength characteristics
17 p2760 A71-35675
- High temperature tensile strength of Ta-W-Hf alloy sheet with protective Si-Ti coating in vacuum and air
18 p2933 A71-35951
- Fiber volume content, fiber-matrix bonding, heat treatment and age hardening effects on transverse modulus and tensile strength of unidirectional Al matrix fibrous composites
18 p2935 A71-36597
- Intermetallic formation in Au-Al systems via diffusion couples, determining activation energy, silicon effect and tensile strength
19 p3119 A71-38513
- Steels, aluminum and titanium ultimate and yield strength statistical distributions in Weibull parameter form, presenting stimulus-response potential failure model
[ASME PAPER 71-VIBR-64]
21 p3396 A71-40307
- Retained lattice strain and substructure domain size effects on tensile strength at room and elevated temperature in dispersion strengthened Ni alloys
21 p3397 A71-40453
- Tensile, impact and fatigue properties of welded Ti alloys, determining joint quality and friction welding sensitivity in highly stressed gas turbine components
21 p3387 A71-40619
- Preheating effects on crystal lattice orientation, tensile strength and stress corrosion cracking of Al-Zn-Mg alloy thick plates
22 p3559 A71-41516
- Woven textile structures tensile strength tests at high strain rates, using unbreakable compact clamp system
22 p3564 A71-41590
- Tensile fracture in grip section of fiber reinforced reduced cross section plastic composite specimens
22 p3564 A71-41591
- Heat resistant Ni alloys hot strength level and temperature dependence as function of gamma-prime-phase particle size, discussing aging effect on creep rate
22 p3561 A71-41841
- Quenching effects on glazed and unglazed alumina rods in various media, noting improved flexural and tensile strength, thermal shock resistance and impact resistance
22 p3565 A71-42342
- Theoretical estimation of tensile strength, elastic modulus and deformation of cubical diamond specimens under tension and compression
22 p3565 A71-42873
- Graphite high modulus fiber material tensile strength, modulus of elasticity and elongation measurement method and equipment
23 p3696 A71-42898
- Temperature effects on fatigue response and tensile properties of coarse grained alpha Ti containing 0.085 wt pct oxygen
23 p3688 A71-42924
- Mo and Co alloying effects on high temperature chromium ball bearing steels contact strength
23 p3692 A71-44037

- Heat treatment effect on tensile and bending fatigue strength of Al alloy thin sheet 23 p3693 A71-44217
- Solid powder metallurgy tungsten alloys, determining scale factor effect on bending strength and fatigue limit 23 p3693 A71-44226
- Lutetium strength and plastic deformation characteristics under tension, presenting temperature and strain rate effects 23 p3693 A71-44229
- Tensile and creep rupture strength and microstructure of Co-Fe-Ta alloys at elevated temperatures 24 p3836 A71-44442
- High temperature aging, structural stability and tensile properties of hot rolled Co-W heat resistant alloy for space applications 24 p3836 A71-44443
- Prestraining effect on D16 duraluminum corrosion fatigue and tensile strengths 24 p3838 A71-44856

TENSILE STRESS

- Two concentric circular arc parallel cracks interaction in infinite plate under tension, calculating crack tip stress intensity factor based on elastostatics theory 01 p0167 A71-10174
- Reinforced cylindrical shells under external pressure, investigating longitudinal tensile stresses effect on stability 01 p0175 A71-11040
- Al fatigue testing by cyclic uniaxial tensile load, examining deformation, internal friction ductility and plastic strain 02 p0262 A71-11683
- Static tension effect on damping capacity of drawn rods under flexural vibrations, considering materials with strong magneto-mechanical hysteresis 03 p0503 A71-13413
- Flat sheet under uniform radial tension, varying thickness reinforcement around hole for high stress concentration avoidance 03 p0513 A71-14238
- Thermal fatigue cracks in gas turbine blade models under simultaneous thermal cycling and static tensile loads simulating pulsed regimes 04 p0671 A71-15638
- Stress analysis of orthotropic twisted bars under tension applied at ends 06 p0985 A71-17747
- Circular cylindrical shell stability under uniform tension, taking into account support flexibility and temperature difference 06 p0990 A71-17794
- Thin plates and shell with various yield stress materials, observing limiting equilibrium under tension and compression loads 06 p0992 A71-17810
- Cr-Ni stainless steel tensile and compressive stresses effect on hydrogen permeability at elevated temperatures 06 p0912 A71-17946
- Cr alloys endurance and dynamic creep under HF tension-compression loads at room temperature 07 p1129 A71-19154
- Tubular Mg and Ti alloy samples under tension and compression load, observing creep properties 07 p1211 A71-19195
- Mg alloys mechanical properties and microstructure changes under static tension in temperature range 20-293 K 07 p1131 A71-19363
- Single edge notch tension Al alloy specimens mechanical compliance measurement, solving stress functions for various gage length-sample width combinations 07 p1110 A71-19469
- Strain rate effect on fiber reinforced unidirectional epoxy composites tensile stress, noting steel, boron, beryllium and graphite/epoxy strands 07 p1139 A71-20137
- Thermal fatigue testing apparatus for material longevity, simulating tensile stresses due to centrifugal forces on gas turbine engine blade during thermal load 08 p1271 A71-20837
- Static tensile stresses effect on magnetized ferromagnetic materials damping properties explained by anisotropic microplastic strains dissipating energy during bending vibration 08 p1306 A71-21120
- Bolted joint assemblies under sustained loading, examining joint and fastener coating, bolt design and strength level and shear and tension stress effects 08 p1371 A71-21412
- Hot extruded W-Cu pseudoalloys under tension and compression, determining impact strength and plasticity 08 p1316 A71-21614
- Stress analysis of anisotropic plate with square holes under tension, using small parameter method 08 p1374 A71-21947
- Apparatus for fatigue testing under tensile stress in vacuum at frequencies of 15-30 Hz with 500 kg maximum load 09 p1426 A71-22505

- Metal sheet failure kinetics, investigating tensile stress and cycle frequency during fatigue crack growth and extension rate effects 09 p1468 A71-22508
- Materials bending fatigue strength calculations for biaxial tension compared with experiments, showing agreement 09 p1538 A71-22596
- Crystalline Al stress-strain function parabolic law generalization under combined axial tensile-torsional loading 09 p1480 A71-23700
- Climbing drum peel adhesion test anomaly in spacecraft adhesive bonded honeycomb structure under lap shear and flatwise tension 10 p1614 A71-24075
- Infinite thin plate containing circular holes with elastic inclusions under biaxial tension, calculating maximum stresses on common boundaries based on Airy function 11 p1841 A71-25265
- Composites under transverse normal tensile loading micromechanics failure criteria based on distortion energy theory, taking into account multiaxial stress concentration 11 p1784 A71-25334
- Supersonic flutter of two dimensional flat plate in presence of chordwise tensile in-plane stresses 12 p1983 A71-27585
- Metallographic equipment for metal surface microstructure observations of samples under tensile loads at temperatures from 4.2 to 300 K 12 p1908 A71-27757
- Low alloy alpha Ti alloy ignition during breaking in oxygen containing gases, considering partial oxygen pressure and tensile loads 13 p2082 A71-27815
- Complex loading history effect on elastoplastic deformation trajectories delay trail characteristic angles and length variation, determining plastic strain vector components in Euclidean space 13 p2155 A71-28652
- Particle-metal matrix interface strength of dispersion strengthened Ni alloys, developing direct tensile stress measurement method 13 p2089 A71-29408
- Al matrix-stainless steel composites under tensile loading parallel to reinforcement direction, noting creep behavior at ambient temperature 13 p2089 A71-29413
- Polycrystalline Hf under tension at various temperatures, determining H effects on fracture, operative deformation modes and hydride habit planes 13 p2090 A71-29417
- Plasticity theory for materials with different mechanical properties in tension and compression, deriving yield criteria and flow rules by tensorial expansions 14 p2322 A71-29736
- Linear plastic deformation of steel under tension, investigating anisotropy in elastic modulus and strength 15 p2503 A71-31478
- Brittle plates with stochastic distribution of cracks under biaxial tensile-compressive stresses, obtaining critical load 15 p2504 A71-31853
- Failure and forming limit diagrams in biaxial tension for sheet metal with preexisting inhomogeneities based on Marciniak concept 15 p2505 A71-31945
- Tensile stress and compressive effects on grain boundary precipitate morphology in Ni-base superalloy during creep 15 p2433 A71-32179
- Age hardenable Inconel X-750 superalloy mechanical response to tensile loads for identifying microstructural changes due to deformation 15 p2437 A71-32616
- Elastoplastic analysis by matrix displacement method, discussing perforated plate under tension and bar thermal stress due to rapid heating 16 p2652 A71-33085
- Elastic plate with part-through surface crack, determining stress intensity factor for remote tensile and bending loads 16 p2655 A71-33209
- Uniformly extended elastic circular plate with rectilinear slot under normal tensile loads at boundary 16 p2660 A71-34115
- Tensional thermoelasticity theory of continuum media, analyzing material particle interactions by stress tensor and equations of motion 17 p2815 A71-34187
- Low temperature tensile prestressing effect on recrystallization kinetics of polycrystalline large grain Ni by isothermal annealing method 17 p2755 A71-34194
- Metal strips with holes under tensile loads, determining plastic region boundaries with photostress method 17 p2821 A71-34592
- Optimal cross section of minimum volume rotating shaft with complex fatigue strength, accounting for tension and shear effects 17 p2822 A71-34595

- Static tension effect on damping capacity of stretched rods under flexural vibrations, considering materials with strong magneto-mechanical hysteresis 17 p2826 A71-35472
- Center cracked tension panels residual strength evaluation and prediction, deriving analysis technique based on stress intensity factor 17 p2827 A71-35189
- Al alloy sheet fatigue crack closure under cyclic tensile loading, deriving expression for crack propagation rate in terms of effective stress amplitude 17 p2828 A71-35166
- Low rigidity stretched prismatic beam bending under tension by force couple 17 p2831 A71-35346
- Hot pressed W-Cu pseudoalloys strength and ductility under tension and compression 17 p2760 A71-35616
- Nonheat treated extruded Mo alloy under tension and vacuum conditions at various temperatures, investigating cylindrical samples dimensions effects 18 p2936 A71-36770
- Photoelastic analysis of maximum stress in wide plate with asymmetrically reinforced circular hole under tension, noting effects of rounded corner at hole edge 18 p2984 A71-37020
- Maximum yielding tensile stress envelope curves as function of structural load index based on compression tests of Al alloy stiffened plane panels 20 p3309 A71-39570
- Strain hardened zirconium alpha tensile stress analysis, explaining inelastic phenomena by dislocation motion blocking with oxygen in lattice structure 21 p3397 A71-40434
- Tensile strain response for spallation fracture in metals by impact and electron beam heating of Al, Cu and Ti alloys 21 p3466 A71-40799
- Crack shapes and stress intensity factors for deep edge crack in plate under tension or bending 21 p3467 A71-40906
- Plastic stress-strain history at notch roots tested in tensile steel strips under monotonic loads, verifying Hardrath-Ohman theories 22 p3615 A71-42076
- Glass fibers durability in air and vacuum conditions showing stress concentration coefficients at various tensile stresses 23 p3697 A71-44047
- Stress relaxation equation for arbitrary initial tensile stresses and pliabilitys applied to machine element design 23 p3778 A71-44023
- Cylindrical shell with elliptical hole, calculating elastic stress concentration due to axial tension based on shallow shell theory 24 p3879 A71-44622
- Crack propagation kinetics in organic glass subjected to monotonically increasing tension perpendicular to crack plane, examining crack contour prior to spontaneous rupture 24 p3883 A71-44858
- Elastoplastic deformation of Zn single crystals under uniaxial tensile loads, noting critical stresses relationship to current pulses 24 p3838 A71-45100

TENSILE TESTERS
U TENSILE TESTS
TENSILE TESTS

- Tensile and stress rupture tests of Co base alloy bars extruded from prealloyed powders made by Ar gas atomization 01 p0100 A71-10488
- Ferritic steel with 17 percent Cr, examining dynamic behavior under high speed tension test regarding heterogeneity of plastic deformation, stress peak, etc 01 p0105 A71-11616
- Fiber reinforced thermoplastics deformation characteristics, using uniaxial tensile test 02 p0274 A71-12480
- Reduction-elongation relation in plastic deformation of tensile test samples of Ti alloys subject to thermomechanical treatment 02 p0265 A71-12523
- Low strain cyclic hardening and softening in Al-Mg alloy, comparing measurements by monitoring and tensile testing methods 03 p0444 A71-14315
- Notched tensile tests for measuring metal ductile brittle transition temperature, deriving proportionality law 04 p0666 A71-14877
- Tungsten wire reinforced brass composites, studying multiple necking phenomena during tensile tests 04 p0615 A71-15794
- Strengthening curve determination by tensile tests for plastic yield limit, strength and elongation at rupture 04 p0673 A71-15896
- Nickel alloy tensile tests, investigating strain mechanisms dependence on temperature 05 p0765 A71-16189
- Glass fiber reinforced plastic plates static tensile and low cycle fatigue tests under pulsating tension 05 p0772 A71-16739

Tensile test equipment for fiberglass reinforced plastics strength measurement under shear
05 p0772 A71-16888

High temperature creep comparison of single phase Fe and Ni alloys subjected to constant load tensile tests, measuring strain as function of time
06 p0911 A71-17345

W fiber reinforced Al strain distribution under tensile load, using moire grid method
07 p1144 A71-20495

Tensile tests of elastoplastic notched plate in plane stress
07 p1218 A71-20500

High modulus graphite fiber reinforced composites tensile and compressive test methods and results [PLASTICS INST. PAPER 23]
08 p1321 A71-20913

Low alloy Mo mechanical characteristics relation to structural states obtained during tensile and bending tests
08 p1316 A71-21613

Uniaxial, equal biaxial and unequal homogeneous biaxial strain rates of viscoelastic materials under isothermal tensile test conditions
09 p1481 A71-22141

Comparative tensile and creep tests of reinforced thermoplastics for performance/cost selection [PLASTICS INST. PAPER 4]
09 p1481 A71-22340

Tensile-compressive testing apparatus for low cycle load at high temperatures
09 p1426 A71-22499

High temperature tensile strength testers for metallic and carbon filaments
09 p1446 A71-22735

TiNi martensitic transformations-fatigue strength relation at room temperature, observing hysteresis in tensile compressive loading cycle to maximum stress
09 p1477 A71-23349

Ferrous and nonferrous sheet metals neck formation prevention for increasing elongation in tensile tests, using continuous plastic bending method
09 p1479 A71-23697

Brittle materials tensile strength testing method, using thermal contraction loading device
09 p1479 A71-23698

Fine structure and heat resistance of thin Ni-Cr alloys specimens after prolonged exposure to high temperatures under tensile loads
09 p1480 A71-23703

Cruciform biaxial fatigue under alternate tensile and compressive forces, using finite element analysis and photoelastic-coating techniques
10 p1685 A71-23941

Zr effect on Ti-Mo beta alloy stability, considering Zr suppression and retardation of omega precipitation on basis of TTT diagram and tensile tests
10 p1625 A71-24007

Stress rupture behavior of S glass/epoxy multifilament strands, developing tensile and creep test apparatus installed in controlled environment building
11 p1784 A71-25397

Graphite epoxy composites fatigue testing, including loaded and unloaded shear, hardness and tensile strength in wet and dry environments
11 p1785 A71-25402

Elastic characteristics of multilayer structures with honeycomb fillers, discussing deflection, tensile and compression tests
12 p1980 A71-27362

Structural stability in tension and strength tests of thin walled tubes at various stress and strain intensities based on loss of resistance to plastic deformation
14 p2321 A71-29620

Pisa University Aeronautical Institute activities /1960-1970/, considering supersonic and subsonic flow research, thin stiffened shells fatigue under compressive or tensile loads, etc
14 p2222 A71-30822

Dilatometric measurement for crazing rate in rubber-toughened plastics during tensile creep tests
15 p2438 A71-31369

Deformation work for strained copper during tensile testing until fracture as function of slenderness in neck
15 p2427 A71-31700

Notched unidirectional composites failure mechanics under tensile load in fiber direction, considering debonding, plasticity and strength
15 p2428 A71-31971

Constant load tensile creep tests on polycrystalline ceramics, determining high density alumina applied stress and strain rate
16 p2553 A71-33384

Tension test for filamentary composites, employing hardened Al alloy wedges adhesive bonded to gripping edges
17 p2739 A71-34818

Monograph on tensile tests of welded joint structural properties as function of introduced heat, applying method to Cu-Ni alloyed steel
17 p2748 A71-34825

Plastic deformation and embrittlement due to stress raisers in steel cylinders from high speed tensile tests at low temperatures
17 p2832 A71-35462

Molybdenum mechanical characteristics relation to structural states obtained during tensile and bending tests
17 p2760 A71-35673

Prestrain directional effects in steel tension and compression test specimens, noting Bauschinger and work hardening effects
18 p2937 A71-36834

Plastic deformation and fracture of beta Ti alloy under tensile tests at room and low temperatures
19 p3077 A71-37464

Testing apparatus contribution to bending in tension specimens, noting instrument errors role
19 p3065 A71-38133

Thermocouple drift effect on creep and tension rupture life at high temperature
19 p3065 A71-38137

Gripping method for short length tubing during high temperature tensile tests
19 p3069 A71-38139

Al alloy tensile tests at high temperature and constant elongation and loading rates, noting creep strain
20 p3251 A71-39167

Inconel-600 under heat treatment and tension tests, examining grain boundaries slip interaction
21 p3397 A71-40458

Orientation dependent microhardness and columnar and feather crystal structures of directionally cast Al alloys in tensile test bars
21 p3399 A71-40471

Heat treatment for weldability and formability improvement of Udimet 700, evaluating by bend, hardness and tensile tests
21 p3388 A71-40622

Dislocation structures in austenitic steel fatigued at various stress cycles and tensioned at various strains, using transmission electron microscopy
21 p3400 A71-40833

Photoimpact strain measurement errors in tensile tests due to deformation dynamics and quantization in time reduced by scanning along Archimedes spiral
21 p3473 A71-41157

Tensile fracture in grip section of fiber reinforced reduced cross section plastic composite specimens
22 p3564 A71-41591

Stress corrosion testing of Al alloy in NaCl bath under tensile stress, using Weibull distributions
22 p3560 A71-41627

Stress intensity factors analysis of strip with longitudinal crack subject to tension and bending along edges and tension of rectangular plates with central crack
22 p3614 A71-41709

True stress calculation from automatic diagram plotted in coordinates for cylindrical specimen testing under uniaxial tension
22 p3550 A71-42851

Cylindrical and weakly concave shells, testing critical pressure relationship to axial tension load with celluloid models
24 p3884 A71-44898

TENSION

Composition and composition inhomogeneity effects on plated wire memory elements strain sensitivity, considering tension and torsion sensitivities
09 p1509 A71-23115

Stress intensity factors for deep cracks in single edge cracked bend and compact tension specimens
14 p2322 A71-29739

Lutetium strength and plastic deformation characteristics under tension, presenting temperature and strain rate effects
23 p3693 A71-44229

Thin soft layer under steady creep conditions, considering axisymmetric problem of simultaneous tension and torsion
24 p3877 A71-44409

TENSION TESTERS

U TENSILE TESTS

TENSOMETERS

Tensometer for measuring strain rate effects on composites mechanical properties
05 p0734 A71-16930

Vinoflex glue for Constantan strain gauges in low temperature tensometry, showing satisfactory recording at single and multiple loadings
07 p1116 A71-20481

Low temperature tensometry application to stress-strain state of turbine disks
09 p1443 A71-22635

TENSOR ANALYSIS

Book on applied matrix and tensor analysis covering coordinate systems, vectors, transformations, etc
03 p0450 A71-13569

Computer program TENSOR for numerical solutions of shell theory
03 p0515 A71-14396

Anisotropic materials strength criterion, developing theory from scalar function of two stress tensors
07 p1216 A71-20131

German monograph on nonnumerical transformation of tensor equations by computers, applying to shallow shell theory
10 p1692 A71-25038

Plasticity theory for materials with different mechanical properties in tension and compression, deriving yield criteria and flow rules by tensorial expansions
14 p2322 A71-29736

German monograph on thermally stressed shear soft shells with finite deformation covering tensor analysis, thermoelasticity, temperature fields and two dimensional bodies
15 p2509 A71-32305

Landau-Lifshitz pseudotensor analogs of ten mechanical conservation laws in Einstein theory of gravitation
16 p2611 A71-33275

Identities required for classification of Newman-Penrose formalism equations, using tensor description
16 p2612 A71-34068

Action-at-a-distance theory of gravitation generalized to tensor interactions of all orders, considering special relativity demands and perihelion advance of Mercury
17 p2797 A71-34368

Moller gravitational field energy-momentum pseudotensor comparison with Einstein canonical and Landau-Lifshitz pseudotensors and Mizkewitsch quasitensor, noting chronometric invariance
17 p2778 A71-34638

G structure tensors integrability and fiber extensions, using differential geometry
18 p2976 A71-36097

Deformation field of continuous medium in Minkowski space-time, defining tensor in Euclidean space of initial configuration
18 p2947 A71-36191

Space-time model of torsion tensor effect on geodetic lines under Schwarzschild metric, evaluating orbital perihelion motion of planets and light ray bending
18 p2967 A71-36826

Generalized continuum of interleafed microstructures coupled by forces, investigating equations of motion, tensor indices and asymmetrical effects
20 p3399 A71-39566

Yield conditions and flow rules derivation from hypoelasticity, regarding constitutive equation as linear transformation on six dimensional inner product space of symmetrical tensors
21 p3455 A71-40090

Rigidly plastic shell theory Lagrangian formulation for moderately large deflections, defining kinematic and dynamic tensors for field equations
24 p3880 A71-44640

TENSOR FIELDS

U TENSORS

TENSORS

NT STRESS TENSORS

Coleman-Noll inequality, examining validity for all tensors G
05 p0826 A71-16720

Quasi-stationary permittivity tensor corrections for smoothly nonuniform electron plasma in absence of magnetic field, using geometrical optics methods
09 p1500 A71-22240

Anisotropy tensor and figurative vector components relation with eigenvector correspondence to eigenstate and eigenmodulus in similitude ratio
10 p1688 A71-24451

Tensor inertia conversion from principal to rotated coordinates system, obtaining negative products in aircraft [DFVLR-SONDDR-111]
10 p1557 A71-24949

Neutron transport equation in five dimensional tensor form, applying finite differencing by integration method via use of divergence theorem
11 p1791 A71-25741

Gravitational potential tensor and equations of motion of relativistic mechanics for isolated system of masses
15 p2481 A71-31187

Elastic properties relativistic theory, defining deformation tensor and constitutive laws
15 p2442 A71-31904

Classification of curvature tensor of relativistic Riemann space-time gravitational metric field
16 p2611 A71-33276

Scalar-tensor field self consistent interaction theory eliminating Einstein gravitational model paradox
17 p2801 A71-34629

Difficulties in using Richter and Noll symbolism in theory of nonlinear deformation, involving representation of tensors as double fields
18 p2976 A71-36095

Conformal integrability for symplectic and cosymplectic structures, studying torsion and curvature tensor fields
18 p2976 A71-36126

Green tensor function for waveguides, resonators and radiating devices with boundaries coinciding with orthogonal cylindrical coordinate systems surfaces
19 p3104 A71-38339

Tensors in relativistic asymmetrical field theory, generalizing Einstein gravitation and Maxwell electromagnetic equations for electrogravitational fields
19 p3105 A71-38580

Invariant characteristics of Einstein spaces according to Petrov classification, determining gravitational fields described by covariant equation involving space curvature tensor and arbitrary scalar
19 p3105 A71-38585

Cosserat continuum elastic tensor potentials applied to Kirchhoff theory of wave diffraction
20 p3269 A71-39033

Continuum dislocation theory, discussing initial stress couple problem, slip motion and dislocation rate tensor
21 p3468 A71-41000

Quasi-stationary permittivity tensor corrections for smoothly nonuniform electron plasma in absence of magnetic field, using geometrical optics methods
21 p3424 A71-41129

Finite Fourier transforms from finite dimensional algebraic viewpoint, deriving fast Fourier transform algorithm via tensor products induced matrix factorization
23 p3698 A71-42920

Gravitational shock waves study by tensor distribution technique including Einstein equations solution
23 p3770 A71-44006

Dielectric permeability tensor of relativistic plasma stream, considering collisionless damping of surface waves in seminfinit isotropic plasma
23 p3713 A71-44148

TERBIUM

Cr-Tb alloys phase transformations and diagrams dependence on temperature and composition, using physicochemical analysis
01 p0100 A71-10418

Compact optical Faraday rotation isolator using terbium-aluminum garnet and high field permanent magnets of rare earth alloys
22 p3559 A71-42566

TERMINAL BALLISTICS

Ballistic projectile velocity measurement using condenser charged thin wire circuit
03 p0422 A71-13273

Projectile impacts into laminated targets consisting of plastic layers backed by Al substrates using SHAPE code with hydrodynamic elastoplastic distortion model
03 p0504 A71-13431

Hybrid simulation to increase hit possibility of rocket fired from military tanks at moving targets
11 p1735 A71-25848

Rigid spherical projectile hypervelocity impact with compressible strain-hardening target material, obtaining analytic solution based on dynamic cavity expansion and deep penetration theories
12 p1982 A71-27570

Combat aircraft vulnerability to projectile impact predicted by model giving target penetration, damage size and structural response
16 p2660 A71-34013

Wing structural elements ballistic damage tolerance and residual fracture strength characteristics, discussing projectile velocity, impact angle and target thickness effects
17 p2827 A71-35161

Armored cockpit for attack aircraft combat effectiveness, including mold line tumbling plates, terminal ballistic kinematics and integral structural armor
17 p2675 A71-35530

Switched mode adaptive terminal control for propulsive landing of nonlifting gravity turn ballistic vehicle under uncertain atmospheric conditions
19 p3095 A71-37154

Bonding conditions effect on wave mode formation at explosive bonded interface in bullet experiments on thin metal targets
22 p3617 A71-42495

TERMINAL FACILITIES

Digital simulation program in GPSS language for airline operations including aircraft maintenance, flight scheduling, terminal space, equipment, work forces utilization, etc
02 p0227 A71-11809

Skyнет system small communications terminal specifications and equipment for ship to shore telegraphic traffic, considering small dish antenna for shipboard installation
02 p0217 A71-12436

Test terminal for Skyнет satellite communications, describing parabolic antenna, computer, receiver system, calibration program, etc
02 p0218 A71-12441

Shipborne satellite communications terminal, describing antenna, control and monitoring systems and performance characteristics
02 p0221 A71-12785

Helicopter operations integration into civil air traffic system, noting special requirements for mixed fixed and rotary wing terminal environments
02 p0279 A71-12892

V/STOL aircraft operations, considering terminals, landing and approach aids, air traffic, noise and pollution control, performance, airworthiness regulations and licensing
03 p0347 A71-13572

Air transport development, examining capital investment, traffic volume and facilities
03 p0524 A71-14246

Airport planning and terminal facilities operation in 1970s, considering impact on developing countries
04 p0566 A71-14994

Helicopters, heliports and helistops, discussing need for public facilities
04 p0692 A71-15440

Public-use ground level and rooftop helicopter and STOL aircraft landing facilities for city and suburban traffic
04 p0567 A71-15442

Optimum flight paths for V/STOL aircraft operating in short haul transportation near city centers
04 p0624 A71-15443

Airport adaptation to large capacity aircraft, considering terminal installations, infrastructures, runways, roads and traffic areas
06 p0879 A71-17589

Lyons-Satolas /France/ International Airport project, discussing layout, facilities and noise control problem
06 p0880 A71-17590

Hovering and low speed flight capabilities of tilt wing VTOL aircraft in terminal area under near-zero visibility instrument landing conditions
06 p0847 A71-18481

System automation evolutionary process in terminal Air Traffic Control environment
07 p1155 A71-19717

ATC automated systems, discussing National Airspace System En Route Stage A and Advanced Radar Terminal System
07 p1156 A71-19719

U.S. domestic ATC airspace enroute and terminal area navigation system effects on pilot workload, projecting future FAA requirements
07 p1157 A71-20347

Airport lighting facilities in Japan, considering fixtures, marker and obstruction lights and apron floodlight
07 p1084 A71-20355

ATC automation program for en route and terminal centers, discussing combined nationwide system features, IFR volume and video digitizer data links
08 p1332 A71-21659

Boeing 747 aircraft passenger handling measures in Frankfurt airport, discussing loading, unloading, baggage claim and customs control
09 p1430 A71-23696

Air cargo volume development trends, examining worldwide airport terminal capacities and pallet/ containerization systems modular design and operation
10 p1699 A71-24824

Airport terminal building design and construction, noting economy and expansibility core requirements
13 p2044 A71-28307

Optimum functional integration and performance requirements of navigation aids and ATC in terminal area
13 p2098 A71-28333

Roissy-en-France airport, describing construction, passenger handling, terminal facilities, traffic volume and runway system
13 p2045 A71-29309

Melbourne/Tullamarine airport, describing facilities, capacity, road system, cargo and passenger handling areas and runway layout
13 p2045 A71-29310

Frankfurt terminal baggage conveyor system, describing passenger capacity and luggage handling equipment
13 p2045 A71-29312

Ultra Compact Airport Terminal, describing landside, terminal and airside elements
13 p2045 A71-29313

ATC system models, covering surface movement, runway utilization, terminal areas and enroute traffic
17 p2771 A71-34523

Satellite voice communications system for small terminals in remote areas, discussing feasibility, design, cost and frequency allocation
17 p2706 A71-35123

Communication satellite ground station terminal equipment, discussing carrier current telephone, video and sound TV apparatus
17 p2717 A71-35516

Binational Basle-Mulhouse airport, discussing traffic structure, buildings and runway development
18 p2897 A71-35996

Narita site Tokyo international airport, discussing transportation, runways, ground handling, navigation aids, lighting, etc
18 p2897 A71-35997

Airport system utilization, discussing aircraft noise, capacity problems
19 p0304 A71-37594

Airport facilities operational planning, discussing computer simulation parking systems and arrivals building
19 p0304 A71-38026

International air cargo handling through runways, terminals, parking and maintenance areas, noting facilities planning
20 p3209 A71-39358

Airport design for passenger and baggage handling efficiency, considering choice between continuous and batching type intra-airport transit system
22 p3529 A71-42072

STOL aircraft system, discussing ground installations, runways, three dimensional area navigation aids, noise reduction, air traffic and short haul productivity
24 p3791 A71-44572

TERMINAL GUIDANCE

Space rescue operations, discussing notification, emergency location, terminal guidance systems and techniques application, international codes, etc
01 p0164 A71-11431

Second order variational endpoint condition numerical application used for low thrust minimum fuel orbital transfer problems
03 p0450 A71-13445

Optimum automatic flight control techniques in horizontal guidance of aircraft at terminal
07 p1156 A71-20306

Multistage rockets terminal control synthesis based on linear functionals
09 p1532 A71-22660

Terminal area control, discussing geographically grouped visual information displays, controllers coordination, plan position indicators and telecommunication
10 p1639 A71-23945

Optimal terminal control stochastic synthesis for linear systems by Bellman second order nonlinear partial differential equations
14 p2220 A71-30872

Night rescue terminal navigation, considering design, development and tests of Limited Night Recovery System for HH-53 helicopter
14 p2273 A71-31095

Precision landing guidance system using microwave scanning beam technique, stressing application to aerospace transportation
15 p2446 A71-32723

Switched mode adaptive terminal control for propulsive landing of nonlifting gravity turn ballistic vehicle under uncertain atmospheric conditions
19 p3095 A71-37154

Lifting entry and terminal phase system optimization for 1975 Mars Viking lander, considering graphical tradeoff approach including design parameter and atmospheric model variations
19 p3148 A71-37171

Integrated test concept for terminal guidance: subsystems and components evaluation, laboratory calibration and simulation tests
19 p3040 A71-37210

Terminal guidance sensing from spinning spacecraft in swifby mission to outer planets
19 p3101 A71-37916

Space vehicle low thrust minimum terminal variance guidance problem reduced to stochastic bang-bang optimal control system
23 p3702 A71-44101

Convergence improvement in parallel tangent/penalty function solutions for missile trajectory optimization with terminal constraints, comparing with steepest descent method
23 p3659 A71-44102

Control strategies for space shuttle transition at 45,000-150,000 ft, emphasizing terminal conditions and stability and control boundaries
19 p3147 A71-37170

Craters produced by high speed hardened spherical particles, investigating depth and diameter relationship to impact speed
24 p3885 A71-45324

TERMINAL VELOCITY

Control strategies for space shuttle transition at 45,000-150,000 ft, emphasizing terminal conditions and stability and control boundaries
19 p3147 A71-37170

Craters produced by high speed hardened spherical particles, investigating depth and diameter relationship to impact speed
24 p3885 A71-45324

TERMINALS

Multichannel on-line data terminals using minicomputer for communication control, error detection and data buffering
05 p0727 A71-17068

Large character set display terminal for public information service system, describing design, construction, components and operating characteristics for nonalpha languages
21 p3350 A71-40129

TERMINATING

U STOPPING

TERMINATOR LINES

VLF electromagnetic propagation, calculating mode conversion efficiency at solar terminator on angle based on flat model with finite wall conductivities
09 p1411 A71-23576

TERMINOLOGY

Navigation, inertial guidance and position keeping terms definitions
02 p0280 A71-12897

In-flight target reporting, analyzing quantitative meaning of ambiguous general modifier terminology as used by pilots in verbal sighting reports
12 p1875 A71-27251

Planetological terminology for geological processes and features of earth, moon and planets
15 p2516 A71-32499

German glossary of commercial air traffic with english equivalents
18 p2989 A71-36962

ERNARY ALLOYS

Nb-Fe-Al and Nb-Co-Al alloys phase equilibrium by X ray and microstructural analyses
01 p0100 A71-10417

Physical properties of Nb-Al-Ge alloys with maximum superconducting transition temperature close to boiling hydrogen
01 p0103 A71-11070

Alloying effects on room temperature mechanical properties of vacuum melted Mo-C-Ti, Mo-C-Zr and Mo-Ti-Zr under plastic deformation and recrystallization
02 p0265 A71-12520

Al-Zn-Mg alloys intergranular failure due to aqueous stress corrosion cracking, fatigue and exfoliation, analyzing mud-crack pattern
03 p0441 A71-13319

Ni-Fe-Cr alloys microduplex structure, describing mechanical properties and workability
03 p0447 A71-14499

Al-Zn-Mg ternary alloys stress corrosion cracking resistance relation to mechanical strength decrease, quenching rate increase and solution treatment temperature
04 p0609 A71-14772

Al-Zn-Mg ternary alloys stress corrosion cracking resistance relation to heat affected zone postannealing aging and cooling rate decrease
04 p0610 A71-14773

Al-Zn-Mg alloys low temperature mechanical properties dependence on aging treatment
05 p0767 A71-16769

Overload and underload effects on Al-Mg-Si creep deformation and damage accumulation under single load change
05 p0768 A71-16800

Ti-Zr-O alloys cross sections investigation by neutron and X ray diffraction, discussing stoichiometry deviation
06 p0911 A71-17382

Nb-V-Mo alloys lattice structure, examining continuous solid solutions with X ray and metallographic analysis
07 p1129 A71-19144

Ni-transition element ternary alloys with bcc and fcc lattices, examining electron structure and ordering processes
07 p1163 A71-19429

Ordered phases precipitation in ternary and quaternary ferritic alloys, investigating morphology, structure, distribution, coarsening kinetics and mechanical properties
07 p1133 A71-19443

Phase equilibria of Mo-Nb-Hf alloys using metallographic durometric and X ray tests
07 p1135 A71-19614

Mo-Re-Hf ternary alloys physical and mechanical properties, considering workability, electrical resistivity and expansion coefficient
07 p1140 A71-20237

Ternary Mo-Hf-C alloys thermomechanical and mechanical property relationship, obtaining yield strength at various temperatures
08 p1313 A71-21557

Ternary systems Hf-W-B, Hf-Re-B and Nb-Re-B isothermal sections phase diagrams at high temperature, using X ray analysis
08 p1317 A71-21858

Anomalous electrical resistivity during decomposition of supersaturated solid solution of Fe-Co-Mo alloy
09 p1468 A71-22359

V-Mn-B, Mo-Mn-B and W-Mn-B systems phase equilibria, describing diagrams isothermal sections at specific temperature
09 p1470 A71-23065

Fe-Cr-Zr ternary alloys, investigating Zr effect on high temperature hardness and heat resistance
09 p1473 A71-23228

Phase diagram isothermal cross sections of Ti-Zr-Nb alloys for various temperatures and heating periods by X ray and microstructural analysis
09 p1480 A71-23705

Phase diagram of Ti-Ta-Mo alloy system, obtaining solubility and electrical conductivity for various cross sections
09 p1480 A71-23706

Comparative isothermal oxidation of Fe-Cr-Al, Ni-Cr-Al and Co-Cr-Al alloys with protective scales
10 p1624 A71-23971

Ternary compositions for high temperature alloys Ni-Cr-Al and Co-Cr-Al, using superimposed oxidation data on phase diagrams /oxide mapping/
10 p1625 A71-23972

Mo-Ti-C ternary alloy, examining solid state solubility, equilibrium conditions and microhardness
10 p1628 A71-24647

Mo-Fe-C ternary system, investigating various concentrations, microhardness measurements, solid state solubility and ductility
10 p1628 A71-24648

Powders and torch techniques for brazing, including Mn-Ni-Co, Cu-Mn-Ni, Zr-Ti-Be, Ti-Cu-Ni and Zr-Be alloys
11 p1769 A71-25746

Mo-Zr-Cr alloy samples cast annealed and quenched at 1500 C, calculating phase equilibrium diagram
12 p1918 A71-27528

Addition effects on ordering kinetics in Ni-Mn based ternary alloys, using Raman neutronography
12 p1918 A71-27543

Nb-Zr-Hf alloys superconductivity properties, determining critical current, critical magnetic field and transition temperature in cold worked and tempered samples
13 p2083 A71-27961

Hf-W-B, Hf-Re-B and Nb-Re-B ternary systems isothermal phase diagrams at high temperature, using X ray analysis
14 p2261 A71-30837

Mo-Ni-C ternary alloy X ray analysis, determining solidus temperature from phase diagrams
15 p2424 A71-31237

Ti-Al-V alloys heat resistance relationship to phase structure from bending test at high temperature
15 p2426 A71-31404

Ternary Co-Cr-Al alloy oxidation data, detailing kinetics, products, mechanisms, resistance behavior and rate
16 p2589 A71-32870

Ternary Co-Cr-Al alloy oxidation resistant composition selection, using oxide maps superimposed on phase diagram
16 p2590 A71-32872

Phase diagrams of ternary systems Ta-Fe-B and Ta-Ni-B using X ray and metallographic analyses
16 p2592 A71-33575

Anomalous electrical resistivity variation during decomposition of supersaturated solid solution of Fe-Co-Mo alloy
16 p2593 A71-33632

Binary and ternary metal compounds superconductivity parameters comparison, considering crystal structure, valence electron concentration, component position and processing techniques
16 p2622 A71-33925

Co-Ge-Si alloys phase equilibria, evaluating long term stability of junctions between thermoelectric batteries conducting series connectors
17 p2759 A71-35337

Al-Cu-Mg monovariant alloys directional solidification, considering criterion for plane front growth breakdown based on constitutional supercooling
19 p3078 A71-37701

Ternary solid solutions with substitutional and interstitial solute atoms, developing statistical mechanical interaction model
20 p3194 A71-38805

Elements distribution in ternary alloy system during simultaneous saturation and burning-out of two components and successive diffusion into third
21 p3403 A71-41161

TERNARY SYSTEMS

Mo-Ti-C Ti system phase equilibria at 1400 C, considering two phase region tie lines direction by metallographic and X ray analyses
02 p0264 A71-12279

Three-stable parametrons ternary logic circuits synthesis by topological method, realizing Post algebra basic operators
03 p0382 A71-13521

Ternary Al-B-Ti system, investigating Al corner and B effect on grain refinement
07 p1138 A71-19981

Groups IV-VIII transition metals reaction with Re and B, studying ternary compounds formation by X ray and metallographic analyses
07 p1140 A71-20233

Phase equilibria in Zr-Mo-Re and Zr-W-Re systems, studying isothermal section diagrams via X ray and metallographic techniques
07 p1140 A71-20234

W-Re-Ir ternary system phase diagrams, studying physicochemical properties via X ray and metallographic techniques
07 p1140 A71-20235

C solubility in Mo-W solid solution at various temperatures
08 p1306 A71-21063

Monovariant eutectic Co-Cr-C ternary systems, determining pseudobinary and near-pseudobinary phases by differential thermal and microprobe analyses and optical microscopy
11 p1780 A71-26025

Curie point of solid solutions in ternary system of zirconate-titanate and lead metaniobate, using maxima on temperature dependence curve of permittivity
13 p2111 A71-28152

Sodium oxide-titanium dioxide-water ternary system, determining sodium titanates formation regions in equilibria in 300 C isotherm
15 p2367 A71-31902

Ti-Mo-C ternary system phase diagram
15 p2430 A71-32146

Ta-V-C ternary system solidus surface and equilibrium diagram determination by metallographic techniques and X ray and thermal analyses
15 p2430 A71-32147

Nb-Re-C system, investigating polythermal NbC-Re cross section structure by metallographic chemical and X ray analyses and microhardness and melting point measurements
15 p2430 A71-32148

Isothermal sections at 1400 C of systems niobium-titanium-boron and niobium-molybdenum-boron by X ray analysis
15 p2437 A71-32672

Zinc arsenide-zinc telluride ternary system phase diagram investigation by X ray, differential thermal and microstructural analyses and microhardness measurements
16 p2621 A71-33564

Si-B-C alloy phase diagram near SiC-B cross section, noting B solubility limit, microhardness and electrical resistivity
16 p2592 A71-33565

Ternary systems chemical composition of contacting and equilibrium states due to directional flow in multicomponent diffusion layer, noting relationship to phase diagrams
16 p2541 A71-33929

Partial configurational thermodynamic functions of interstitial species in ternary solid solutions containing substitutional and interstitial solute atoms
20 p3194 A71-38804

Nonstoichiometric zirconium niobium carbide thermodynamic properties, deriving components activity equations from statistical considerations based on pairwise interaction energies
20 p3252 A71-39554

Zirconium uranium carbide and zirconium hafnium carbide thermodynamic properties, using time-of-flight mass spectrometer
20 p3252 A71-39555

TERRAIN ANALYSIS

Ground relief representation by contour lines and by profiles, noting error possibilities
01 p0074 A71-11328

Terrain and frictionally induced vertical velocity analysis for local and regional forecasting operations, considering low level air flow effects
05 p0777 A71-16674

Mars surface TV pictures from Mariner 6 and 7, including cratered and uncratered terrains, light and dark markings and south polar cap
06 p0965 A71-17628

Terrain backscatter characteristics in EHF band, establishing average radar cross sections for various incidence angles
06 p0867 A71-17713

Terrain altitude evaluation in orthoprojectors, using off-line systems for contour lines approximation
06 p0901 A71-18290

Seasonal and year-to-year crop radar sensing in agriculture for socioeconomic applications
07 p1095 A71-18825

Computer plotting of living units, business and industrial plant location for public utilities planning
08 p1280 A71-21246

Department of Defense data processing equipment for all weather airborne terrain imaging radar mapping sensor
08 p1288 A71-21250

Automatic record of terrain profiles from stereoscopic aerial photographs by intersection of ray traces
08 p1288 A71-21252

Natural image computer for terrain pattern recognition and delineation from aerial photographic inputs
08 p1281 A71-21255

Forested area landscape characteristics from remote sensed imagery, establishing base line information for vegetation mapping
09 p1438 A71-23209

Cumulative frequency curves of terrain slopes by radar shadow frequency method
09 p1439 A71-23216

Aerial photographic measurements of terrain spectral reflectance and analysis of water resource color and quality by scene color standard technique
09 p1439 A71-23218

Mars atmosphere optical thickness by polarimetric /ground and spacecraft/ observations, considering light areas roughness /smoothness/ factor variation with wavelength
12 p1964 A71-27086

Color and color IR films for soil identification, performing optical density measurements on film transparencies with densitometer
13 p2071 A71-23994

Passive mapping of terrain with sidelooking radiometry by storing received signals from various elements over extended flight path
17 p2746 A71-35763

Digital processing for automatic extraction of information from reconnaissance images, discussing target

and terrain configurations pattern recognition technique
17 p2747 A71-35774

Remote sensors for hydrogeologic prospecting in arid terrains, recommending vertical and horizontal polarized microwave radiometers
18 p2913 A71-36362

Operational calibration of airborne IR spectrometer over hydrogeologically significant terrains, obtaining radiance spectra
18 p2920 A71-36363

Vegetation penetration with K-band side-looking airborne imaging radars, noting multifrequency multipolarization system application for terrain reconnaissance
18 p2875 A71-36365

Mars atmosphere optical thickness by polarimetric /ground and spacecraft/ observations, considering light areas roughness /smoothness/ factor variation with wavelength
19 p3133 A71-37436

IR linescan technique for airborne terrain mapping, discussing choice of waveband, system parameters and display techniques with emphasis on film recording
22 p3546 A71-42425

Arctic ocean pack ice terrain profiling by airborne laser altimeter and coincident photography, analyzing data for ice development stages interpretation
24 p3833 A71-44986

TERRAIN FOLLOWING AIRCRAFT

NT TSR-2 AIRCRAFT

Terrain following radar for airborne guidance of low flying military aircraft
12 p1927 A71-26881

TERRESTRIAL DUST BELT

Light scattering and polarization measurements in upper atmosphere by modulated searchlight, indicating dust layers
03 p0414 A71-14018

Near earth motion equations for electrically charged dust particles in gravitating dipole magnetic fields, using zero-relative-velocity surfaces and energy integral
09 p1437 A71-22832

Skylight scattering components from zenith for intensity/polarization variation during twilight and upper atmosphere dust sounding
10 p1607 A71-25114

Circumterrestrial meteoroid dust cloud properties based on night sky brightness photometric observation
12 p1964 A71-27090

Laser radar investigation of upper atmosphere dust layer, obtaining evidence for Silverberg cometary micrometeoroid shower hypothesis
16 p2641 A71-33760

Circumterrestrial cosmic dust clouds properties determination by optical methods, using twilight observations at solar vertical symmetric points
17 p2810 A71-35725

Circumterrestrial meteoroid properties based on night sky brightness photometric observation
19 p3133 A71-37440

Circumterrestrial dust cloud characteristics from night sky brightness photometric measurements, noting seasonal changes
20 p3219 A71-39646

TERRESTRIAL MAGNETISM

U GEOMAGNETISM

TERRESTRIAL RADIATION

Kamchatka volcanic mantles and lunar surface radiation polarization characteristics similarities
01 p0149 A71-10049

Global ozone distribution from inverted radiance measurements by IR interferometer spectrometer /IRIS/ on Nimbus 3 satellite
01 p0074 A71-11249

Earth radiation latitude nonuniformity effect on error in onboard satellite local vertical determinations, using Cosmos satellite data
02 p0304 A71-11915

Earth radiation measurement at 10-12 microns by Cosmos 243 satellite-borne radiometer, comparing temperatures for boundary air layers in cloudless conditions
02 p0246 A71-12115

Escaping-earth radiation actinometric measurement by meteorological satellites, discussing seasonal thermal radiation variations in Southern Hemisphere polar regions
04 p0579 A71-14637

Actinometric network for monthly sums of overall solar radiation and earth surface radiative balance, estimating random errors mean square values
04 p0621 A71-14640

Solar wind parameters-terrestrial electromagnetic field micropulsations relation based on interplanetary probes and time correlated ground observations
05 p0800 A71-17170

IR horizon sensors design, taking into account earth radiation properties
06 p0892 A71-17965

Kamchatka volcanic mantles and lunar surface radiation polarization characteristics similarities
08 p1361 A71-21043

Earth intrinsic radiation flux incident angular coefficient, examining effect on partially screened flat spacecraft elements
09 p1546 A71-23154

Terrestrial spectroscopy by cryogenic gravity meter with hollow superconducting niobium sphere in cylindrically symmetric magnetic field, detecting earth spheroidal oscillations
10 p1598 A71-23737

Soviet book on earth radiation belts and cosmic rays covering space-borne experiments, Van Allen belt, charged particle motion, origin hypotheses, etc
11 p1818 A71-26525

Earth surface thermal radio emission measurements by UHF radiometry onboard Cosmos 243 satellite, showing brightness profiles of water, ice and land areas
12 p1899 A71-26639

Earth radiation budget measurements, noting planetary albedo, IR radiant emittance and net balance
12 p1901 A71-27191

Earth radiation latitude nonuniformity effect on error in onboard satellite local vertical determinations, using Cosmos satellite data
13 p2133 A71-28202

German book on radiation climate of earth covering EM, corpuscular IR radiation sources, spectral composition, biological effects, etc
14 p2298 A71-29941

Michelson interferometer onboard Nimbus 4 satellite for recording earth IR emission spectrum
14 p2241 A71-30140

Cosmic and telluric radiation biological effects on parametria, discussing relationship between dosage and growth rate
16 p2532 A71-33757

Earth radiance analysis by IR interferometric spectrometer of Nimbus 3 satellite, noting cloud cover as dominant variable
18 p2912 A71-36065

Earth IR radiance at 5-20 microns from interferometric spectrometer /IRIS/ aboard NIMBUS 3 satellite
18 p2912 A71-36101

Earth upper atmosphere outgoing thermal radiation radiance calculation in near IR spectrum
19 p3054 A71-37968

Earth radiation flux spectral intensity measurements, noting latitudinal distributions, day and night variations and oceanic and continental curves
19 p3056 A71-38355

Earth-atmosphere system radiation budget, comparing meteorological satellites actinometric data with calculated climatological maps of planetary long wave radiation distribution
20 p3259 A71-39678

Microwave emission measurement of earth surface from Cosmos 243 satellite, detecting radio brightness temperature dependence on latitude and local features
20 p3260 A71-39685

Solar and terrestrial IR reflected radiation from Cosmos satellites measurements, determining clouds upper boundary height
20 p3261 A71-39688

Balloon Sonde I experiment, discussing telemetry from flying boat and temperature effects on earth IR radiation measurement
22 p3535 A71-42053

Ashen light over Venus nocturnal hemisphere due to reflected earthlight and starlight
23 p3733 A71-43128

ITOS meteorological satellite scanning radiometer using point detector optical system for earth imaging
23 p3676 A71-43511

TESSERAL HARMONICS

Geocentric coordinates from dynamic satellite geodesy, using gravimetric Stokes and Venning-Meinesz functions
03 p0406 A71-13010

Satellite orbital period variation under earth gravitational potential tesseral and sectorial harmonics
09 p1526 A71-23341

TEST BEDS

U TEST EQUIPMENT

TEST CHAMBERS

NT ANECHOIC CHAMBERS

NT HYPERBARIC CHAMBERS

NT PRESSURE CHAMBERS

NT VACUUM CHAMBERS

Space environment simulation chamber shrouds, developing mathematical expressions for temperature distributions in flat plates and trapezoidal fins
05 p0733 A71-16137

Free molecular flow on cryosurface in cylindrical space simulation chamber with spherical test object
09 p1433 A71-23005

Airborne electronics reliability testing in temperature controlled chamber
10 p1589 A71-24604

Dynamic Test Chamber for sounding rocket or spacecraft functional testing in simulated flight environment
11 p1746 A71-26508

Fatigue measurements in hot working conditions on subjects wearing self contained breathing apparatus in heat chamber
17 p2688 A71-34368

Manned 90 day test of closed chamber regenerative life support system simulator, describing subsystem crew nutrition, hygiene, maintenance and leisure activities
22 p3503 A71-42043

TEST EQUIPMENT

Metal products structural failure analysis, discussing laboratory equipment and analyst experience and ingenuity
01 p0087 A71-10428

Chairs, stands and swings for vestibular and visual analyzer tests
01 p0024 A71-11070

Machine for measuring inertial and structural responses to shock in single degree of freedom and more complex systems having dominant resonant frequency
01 p0068 A71-11548

Laser radial-shear common path interferometer for lens testing
02 p0250 A71-12144

Solar energy thermionic converter life test program and equipment, noting failure due to loss of intraelectrode Cs
02 p0194 A71-12223

Test terminal for Skynet satellite communications, describing parabolic antenna, computer, receiver system, calibration program, etc
02 p0218 A71-12441

Gain/temperature measurement test set for earth station receiving system by radio sources program, tracking unit, noting antenna power ratios determination by attenuator
02 p0222 A71-12797

RB 211 turbofan engine development testing, describing test program, test facilities, equipment and instrumentation
02 p0299 A71-12912

Versatile Avionic Shop Test /VAST/ general purpose digital tester, discussing hardware and software
03 p0395 A71-13084

Test equipment for damping ability of vibration absorbing coatings on prismatic rods under pure bending, using electromagnetic vibration induction system and optical recorder
03 p0396 A71-13417

Test equipment with axial mode closed loop machine for cyclic deformation and fatigue in pure bending [SESA PAPER 1726]
03 p0507 A71-13756

Universal endurance test machine for tubular samples torsion testing under hydrostatic pressure
04 p0673 A71-15894

CdS solar cells performance under simulated synchronous orbit conditions, describing test equipment
05 p0702 A71-16081

Precision gyro and accelerometer testing evolution, noting instrument performance and electrical and mechanical equipment [AGARDOGRAPH-128]
05 p0749 A71-16303

Tensile test equipment for fiberglass reinforced plastics strength measurement under shear
05 p0772 A71-16888

Universal testing machines dynamic load errors due to testing speed
05 p0734 A71-17247

UK 3 spacecraft support sting for solar simulations and thermal vacuum testing in 2.5 meter test chamber, describing design and construction
06 p0881 A71-18720

TSh-2 hardness test gage, investigating deformation of steel under increasing loads
07 p1106 A71-19141

Test equipment for elasticity modulus measurements of neutron irradiated materials, noting u-c nuclear fuels and alloy samples
07 p1084 A71-20356

Laboratory test set for integration of data compression and error correction encoding of digital communications system
07 p1065 A71-20424

Thermal fatigue testing apparatus for material longevity, simulating tensile stresses due to centrifugal forces on gas turbine engine blade during thermal load during
08 p1271 A71-20837

Multisample test equipment for steels and alloys oxidation resistance at high temperatures in corrosive gaseous atmospheres
08 p1292 A71-21440

Performance test methods and equipment for aircraft avionics and weapons systems, discussing computer integration with radar and phototheodolite range instrumentation system
08 p1260 A71-21660

Low temperature creep testing apparatus providing for microstructural examination of materials without distortions due to specimen temperature change to room temperature
09 p1426 A71-22318

Materials mechanical properties measurement methods and equipment at cryogenic temperatures including microscopes, X ray cameras, microhardness tester, fatigue and impact strength testing machines
09 p1468 A71-22329

Tensile-compressive testing apparatus for low cycle load at high temperatures
09 p1426 A71-22499

Device for rapid direct analysis of beryllium ores and concentrates in transport containers, using radiometric method
09 p1427 A71-22506

Real time low frequency narrow band spectrum analyzer using time compression technique for vibrating machinery diagnosis and prognosis
09 p1443 A71-22708

F-111 airframe static test instrumentation, describing computerized processing of simultaneous inputs from 400 channels of tape recorded strain, load and deflection data
09 p1444 A71-22717

High temperature dynamic strain gage test equipment for evaluating precision, life and environmental limitations
09 p1445 A71-22719

Special purpose analog and digital data acquisition systems for test and instrumentation requirements
09 p1449 A71-22789

High temperature fatigue test assembly for symmetric tension compression cycles at 10 kHz
10 p1589 A71-24201

High temperature testing assembly for reinforced plastics and binders in oxidizing and inert media under tension, compression, bending and cleavage loads
10 p1589 A71-24202

Measurement system for communication satellite ground station equipment including parametric amplifier, wideband receiver, power oscillators, and radio transmitters and receivers
10 p1590 A71-25103

Glass fiber reinforced plastics fatigue tests, discussing closed loop hydraulic servomechanism equipment, testing methods and materials and mean stress effects
11 p1789 A71-25658

Interchangeable head vibration exciter for 200g large object testing and measurement of structural modes, impedances, transfer functions and calibration
11 p1746 A71-26495

Automatic equalizer-analyzer system for random or shock vibration testing, including narrow-band equalization, simplified display techniques and self-calibrating procedures
11 p1747 A71-26514

Calibration test rig for high accuracy liquid hydrogen flowmeter, discussing design and operation
12 p1906 A71-26836

Traversing Infrared Inspection System for C-5 aircraft fail-safe strap panels of bonded Ti-Al laminates, discussing design and application
12 p1911 A71-27327

Explosive shock loading effect on materials properties, describing test equipment
12 p1895 A71-27689

Metallographic equipment for metal surface microstructure observations of samples under tensile loads at temperatures from 4.2 to 300 K
12 p1908 A71-27757

EMC susceptibility test equipment consisting of portable buzzing relay noise generator
13 p2045 A71-28874

Machine for corrosion testing materials under various static and dynamic axial tension, torsion and bending loads
13 p2045 A71-29374

Concorde SST flight test equipment installation with PCM recording and visual instruments
14 p2174 A71-30055

Low cost go/no-go portable aircraft engine tester connected to engine mounted sensors
14 p2221 A71-30327

Automated modal data acquisition and processing system /MODAPS/ for real-time modal vibration testing of complex aerospace vehicle structures, describing features, capabilities and utilization
14 p2245 A71-30341

Shock wave caused chemical reactions between solids and cryogenic liquids, discussing shock sensitivity tester for liquid propellant- structural material systems
14 p2222 A71-30546

Impact sensitivity tester for engineering materials in liquid and gaseous oxygen at high pressures
14 p2222 A71-30548

Design provisions for captive fired testing of solid rocket motors, describing equipment and procedures for monitoring motor phenomena during testing
14 p2292 A71-30742

Test equipment for radiometric analysis of impurities concentration distribution in semiconductors, using thin plane-parallel layers continuous removal method
15 p2383 A71-31657

Pulse type ultrasonic flaw detecting apparatus based on reflected echo size estimation
15 p2409 A71-32194

Low temperature creep deformation recorder with liquid He coolant, discussing Al and Pb single crystal tests
15 p2385 A71-32239

F-15 aircraft integrated data system for flight test program information, discussing development and major elements
16 p2524 A71-34010

German monograph on electron motion in cesium plasma covering Boltzmann equation, radiative transfer, mathematical model, electron velocity distribution, etc
17 p2787 A71-34485

High temperature stress measurements with electric resistance strain gages, describing test apparatus for gages evaluation
17 p2738 A71-34553

Batch unit for investigation of injectors in vapor-liquid flows, discussing measurement system and energy dissipation
17 p2724 A71-35275

Test apparatus for mechanical/thermal fatigue and vibration strength of turbine blades in high temperature gas flow
17 p2724 A71-35461

Test equipment for acoustic fatigue of materials and structural elements
17 p2724 A71-35663

Cyclic torsional shear testing of refractory materials at normal and high temperatures, describing test equipment
17 p2834 A71-35672

Strut pressure and axle strain gage systems testing for balance and weighing onboard De Havilland C-7A aircraft
17 p2676 A71-35827

[SAWE PAPER 881] Weightlessness simulation for aerospace mechanisms, using tower release and gyrometric system for testing stage separation, satellite perturbation, yo-yo, probes and mast development
18 p2971 A71-36018

Test apparatus for studying stress-strain behavior of thin walled metal tubes in torsion, examining strain rate and history effects
18 p2935 A71-36234

Strapdown guidance systems computerized test system consisting of minicomputer and cathode ray display tube with keyboard control over all system elements
19 p3040 A71-37208

Neutron radiography of Apollo ordnance, describing test facility and equipment
19 p3063 A71-37449

Test equipment for evaluating human higher nervous activity, noting use for radiotelegraphist selection
19 p3007 A71-37775

Testing apparatus contribution to bending in tension specimens, noting instrument errors role
19 p3065 A71-38133

Creep testing machines load axiality, investigating bending strains allowable limits excess as function of tensile stress and temperature
19 p3082 A71-38134

Automated test capability for digital modules, describing test generation, circuit analysis and simulation programs
19 p3030 A71-38406

Pulsed ruby laser holographic instrumentation for materials tests, detailing reflected wave front complex amplitude characterization
20 p3245 A71-39347

High load structural dampers evaluation under linear or sinusoidal /triangular/ displacement control with constant speed testing machines
21 p3459 A71-40295

[ASME PAPER 71-VIBR-46] Specimen support effects on three point bending tests of fiber-plastic composites, suggesting small diameter roller
21 p3405 A71-40596

Fracture testing, discussing fracture toughness, proof testing assemblies, crack identification, growth, catastrophic failure probability, etc
21 p3463 A71-40673

Abbreviated test language for avionic systems, discussing program organization, statement formats, vocabulary and syntax diagrams
21 p3351 A71-40812

Solid body contact interaction devices at high temperatures in vacuum, gas and air for evaluation of surface coatings, adhesion, diffusion, mechanical properties, etc
21 p3382 A71-41174

Soviet papers on meteorological observation and instrument testing covering precipitation gages, hygrometers, humidity gages, anemometer testing, mobile monitoring, pyrheliometers, etc
21 p3383 A71-41376

Testing machine stiffness determination during strain rate variation and stress relaxation tests for metallic and nonmetallic engineering materials plastic properties assessment
22 p3559 A71-41589

Superhigh vacuum apparatus for creep and long term strength tests on metals at high temperatures, giving results for niobium alloys
22 p3538 A71-41699

Vacuum apparatus for fatigue tests at room and low temperatures, giving results for annealed copper
22 p3538 A71-41700

Radiation flaw detection by fast neutrons, monitoring thick lead plates and three-layer articles
22 p3528 A71-41761

Ultrasonic inspection apparatus for defects detection in metal pipes, using immersion echo mode with two piezoelectric scanning heads rotating about pipe
22 p3529 A71-41774

Test bed engine studies of overall excess air ratio permissible deviation, obtaining diagram for constraints calculation
24 p3864 A71-45022

Apparatus for dynamically equivalent ground tests of satellite instrumentation and attitude control system
24 p3817 A71-45273

Single channel electron multiplier manufacture and performances, discussing test equipment and procedures
24 p3811 A71-45331

TEST FACILITIES

NT ANECHOIC CHAMBERS
NT BALLISTIC RANGES
NT BLOWDOWN WIND TUNNELS
NT CASCADE WIND TUNNELS
NT ENGINE TESTING LABORATORIES
NT ENVIRONMENTAL LABORATORIES
NT HYPERVELOCITY WIND TUNNELS
NT LOW DENSITY WIND TUNNELS
NT LOW SPEED WIND TUNNELS
NT MISSILE RANGES
NT PLASMA JET WIND TUNNELS
NT RECTANGULAR WIND TUNNELS
NT ROCKET TEST FACILITIES
NT SHOCK TUNNELS
NT SLOTTED WIND TUNNELS
NT SUBSONIC WIND TUNNELS
NT SUPERSONIC WIND TUNNELS
NT TEST RANGES
NT TEST STANDS
NT TRANSIENT REACTOR TEST FACILITY
NT TRANSONIC WIND TUNNELS
NT WIND TUNNELS

German book on Goettingen Aerodynamic Research Institute /1945-1969/
01 p0068 A71-11406

Skyнет satellites in orbit communications, repeaters testing, describing test facilities, spacecraft communication subsystems operation, terminals calibration and atmospheric losses
02 p0218 A71-12440

Test laboratory for Skyнет spacecraft communications subsystems at microwave frequencies
02 p0238 A71-12443

RB 211 turboprop engine development testing, describing test program, test facilities, equipment and instrumentation
02 p0299 A71-12912

Laboratory facilities for DC-10 structural test program using fatigue test machines and computer controlled servo loading systems
03 p0397 A71-13724

[SAE PAPER 700829] Fluid mechanical and gas dynamic experimentation by Slingshot aerodynamic test facility
04 p0564 A71-14675

Ground and airborne aircraft flight simulation methods, discussing simulator layouts and application to Concorde project
04 p0566 A71-15206

Electro-optical solar simulator, describing system design, performance and applications for spacecraft testing
04 p0567 A71-15366

Test rail system of Les Landes Testing Center, discussing optical and electromagnetic observation, measurement and test coordination and control facilities and equipment
04 p0567 A71-15817

Jet noise suppressor development test techniques and facilities, discussing model tests at hydrodynamic ONERA wind tunnel
04 p0639 A71-15819

Test facility for fatigue and thermal fatigue of turbine blades in high temperature gas flow
05 p0734 A71-16762

Aircraft engine double-reverberant chamber duct lining test facility, discussing noise fields, air flow, layout, performance, insertion and transmission losses, etc
06 p0880 A71-17619

Test facility for acoustic fatigue of materials and structural elements
07 p1083 A71-19167

Magnetic annular arc accelerator for high pressure high enthalpy flow test facility
07 p1083 A71-19880

Artificial lightning generation facilities for aircraft component developmental testing by manufacturer
07 p1020 A71-19931

USAF Camera Calibration Facility, describing precision multibank collimator for measuring focal length, distortion, prism effect, fiducial center and other camera parameters

08 p1272 A71-21258

Large space vehicle acoustic environment test facility, investigating combined direct and/or reverberant sound field effects

08 p1272 A71-21430

Two phase Hg tunnel for shock wave visualization by RF discharge between test model body and external ring, comparing measurements with supersonic flow theory

08 p1272 A71-21751

Combined radiative-convective heating test facility for atmospheric entry simulation

[AIAA PAPER 71-255]

08 p1273 A71-21984

Water cooled channel flow test device for arc jet material ablation studies, simulating reentry environment of high energy turbulent boundary layer flow

[AIAA PAPER 71-260]

08 p1273 A71-21987

Altitude rate generation for aircraft instruments testing

09 p1448 A71-22770

High thrust aircraft engines test facility design

09 p1428 A71-22956

Two dimensional test facility in blowdown wind tunnel transonic section, discussing porous sidewall boundary layer control effects on airfoils geometric characteristics

[AIAA PAPER 71-293]

09 p1428 A71-22957

Arc heated duct facilities providing high temperature supersonic turbulent boundary layer flows over large samples for orbital logistic vehicle thermal protection tests

[AIAA PAPER 71-262]

09 p1429 A71-23060

Space shuttle vehicles and assembly flow manufacturing, development and operations requirements, including ground rules, verification test facilities, cost reduction and interrelationships

[AIAA PAPER 71-316]

10 p1590 A71-24831

Military aircraft flight test establishments, discussing airframe, engine, flight control and weapons delivery systems tests work flow integration requirements

11 p1708 A71-26315

Automated facility for electronic equipment production reliability environmental testing, discussing human engineering and test and failure mode designs

11 p1746 A71-26512

ONERA test facility for thrust measurement, describing test bed installation and operation and procedure for calculating thrust coefficients

12 p1945 A71-27472

Airline engine performance testing from operator perspective, using automated test cell data acquisition system

[SAE PAPER 710451]

13 p2044 A71-28329

Neutron radiography facility using TRIGA reactor source, discussing design and performance

13 p2044 A71-28523

High temperature gas turbine alloys corrosion tests, describing laboratory facilities for preliminary screening

13 p2086 A71-28752

Gas dynamic test assemblies experiments for demonstrating theoretical basis of supersonic nozzle design with radial flow section

13 p1992 A71-29173

AEDC test facilities laser instrumentation for flow field diagnostics by Doppler velocimeter, holographic flow visualization and particle studies

14 p2245 A71-30332

Simulated altitude test facilities selection for Space Shuttle Orbiter Engine

[AIAA PAPER 71-679]

14 p2292 A71-30743

Radiation cooled MPD thruster with permanent and superconducting magnets, describing test facilities and measurement techniques for performance tests

[AIAA PAPER 71-696]

14 p2293 A71-30755

Chronic and acute gamma irradiation facilities used in animal experiments simulating steady cosmic radiation and powerful solar flare radiation expected in prolonged space flight

15 p2357 A71-31313

Performance test facility for pulsed axial flow gas turbine of turbocharger unit on large diesel engines

15 p2469 A71-31943

Facility for signal noise measurement in proportional fluidic amplifiers, discussing stored sweep spectra interpretation

15 p2351 A71-32053

Test facility and performance predictions for Rankine cycle power system components, including lithium heater, potassium boiler, condenser and preheater

[GESP-451]

15 p2448 A71-32223

Thermal stability test assembly for refractory materials cylindrical specimens, using argon plasma jet

15 p2385 A71-32238

French shock tube test facility for reproducing and investigating effects of sonic booms on vision and physiological processes

16 p2552 A71-33350

Stress-strain diagrams of heat resistant alloys at high temperatures, describing test facility

16 p2598 A71-33988

Cascading turbomachine blades vibrations measurement in subsonic and sonic high temperature gas flows, describing test facility

16 p2553 A71-33993

Flight test program, facilities and instrumentation for F-14 aircraft structural, powerplant, avionics, performance and carrier suitability evaluation

16 p2526 A71-34153

Lens test facility calibrating Mipir radar boresight lenses by measuring deviations due to gravitational effects

18 p2897 A71-36072

Space station regenerative life support system 90-day manned test in simulator, discussing objectives, facilities and procedures

[ASME PAPER 71-AV-38]

18 p2870 A71-36405

Hyperballistic free flight test facilities using light gas guns, considering wake of flight vehicle at hypersonic velocity and aerothermal phenomena

18 p2898 A71-36411

Low temperature test facility for cryogenic and rocket materials under combined tension and torsion

18 p2900 A71-36726

Integrated test concept for terminal guidance subsystems and components evaluation, laboratory calibration and simulation tests

[AIAA PAPER 71-969]

19 p3040 A71-37210

Full mission engineering simulator/flight controls integration laboratory utilization in Apollo program, describing equipment for control systems testing, monitoring and troubleshooting

[AIAA PAPER 71-970]

19 p3040 A71-37211

Neutron radiography of Apollo ordnance, describing test facility and equipment

19 p3063 A71-37449

Test facility for studying temperature dependence of thermal diffusivity and true heat capacity of metals between minus 150 and plus 400 C

19 p3063 A71-37588

Test facility for thermal diffusivity measurements in solids by method of plane temperature waves using periodic optical heating at 1500 K

19 p3063 A71-37589

Vaporization heat transfer in saturated liquid capillary flow through wick structure, describing test facility and procedure

[ASME PAPER 71-HT-35]

19 p3166 A71-38000

High temperature creep testing facilities and techniques, evaluating statistically interlaboratory variability and significance of testing and material variables affecting creep results

19 p3081 A71-38132

Motion measurements applications to facility design and inertial navigation hardware performance test problems concerning test platform response to ground motion, forces and disturbances

[AIAA PAPER 71-923]

19 p3102 A71-38327

Acoustic emission test facility with constant strain rate compressive sample deformation

20 p3208 A71-38823

Component performance of three loop Rankine cycle test rig using lithium, potassium and NaK-78 as working fluids

20 p3263 A71-38923

Instrumentation in aerospace simulation facilities - Conference, Rhode-Saint-Genese, Belgium, June 1971

21 p3362 A71-40380

High speed aerodynamic test facilities development over past 25 years, discussing deficiencies and improvements

22 p3529 A71-41984

TEST FIRING

ELDO test firings failure analysis program, considering self destruction charges and vibration environmental load

[DGLR-70-060]

05 p0815 A71-15964

Design provisions for captive fired testing of solid rocket motors, describing equipment and procedures for monitoring motor phenomena during testing

[AIAA PAPER 71-678]

14 p2292 A71-30742

Self regulating steady state cryopump system for simulated altitude testing during rocket engine firings

20 p3184 A71-39198

TEST METHODS

U TESTS

TEST PILOTS

Flight tests - Conference, Beverly Hills, September 1970

07 p1017 A71-19076

TEST PROGRAMS

U TESTS

TEST RANGES

NT BALLISTIC RANGES

NT MISSILE RANGES

Earth-moon test range for testing earth environmental characteristics in cislunar space, discussing administrative benefits

04 p0649 A71-15296

Geodetic satellite data utilization for test range specific point positioning, control densification, earth

gravitational model determination and tracking station locations

18 p2913 A71-36492

TEST STANDS

Altitude engine test stands evolution in Germany, discussing design

04 p0566 A71-14984

Test stand for endurance and creep testing of plastics, glazed ceramics and other brittle materials

04 p0567 A71-15645

Gas dynamic test stand for cyclic thermal load testing of gas turbine engine materials and components at variable heating and cooling rates and mechanical loads

08 p1271 A71-20835

Gas dynamic test stand analyzing elastoplastic strains in aircraft gas turbine disks and liquid propellant rocket engines turbopumps under alternating nonisothermal loads

09 p1427 A71-22603

Optimal phase trajectories of coordinates of electrodynamic vibration test stand, analyzing motion of moving part and optimal control signal along coil

15 p2353 A71-32190

Pneumatic isolation system for inertial instrument testing, using computer simulation model to evaluate physical parameter variation effect on pad suspension dynamic behavior

[AIAA PAPER 71-910]

19 p3040 A71-37161

Inertial devices test pads geokinetic reference systems definition, using astronomical data

[AIAA PAPER 71-911]

19 p3046 A71-37162

Two dimensional seismic mathematical and scale techniques appropriate to inertial navigation devices test pads noise isolation examination

[AIAA PAPER 71-912]

19 p3056 A71-38326

Electrohydraulic stand for vibration strength testing, discussing system design, specifications, frequency-amplitude characteristics and applications

23 p3662 A71-44235

TEST VEHICLES

NT FLIGHT TEST VEHICLES

TESTERS

U TEST EQUIPMENT

TESTING

U TESTS

TESTING MACHINES

U TEST EQUIPMENT

TESTING TIME

Spectrophotometric instrumentation in physics and chemistry, discussing developments in automation accuracy and measurement time

03 p0429 A71-14326

Incident shock test time and reflected pressure for turbulent boundary layer at high Mach numbers in air and nitrogen

04 p0563 A71-14663

Nonreflected shock tunnels hypersonic air flow, determining beginning and end times for optimum testing periods

04 p0563 A71-14666

Product test duration and extent from reliability theory viewpoint

05 p0759 A71-16725

Aircraft gas turbine engine components equivalent testing by shortening testing time required to increase service life

05 p0796 A71-16761

Statistical nature of time to complete MIL-STD-781 reliability sequential tests for military and space equipment, giving information about MTBF

12 p1908 A71-26656

Computer program for prediction of repair time elements for versatile avionic ship test

16 p2545 A71-33314

Aircraft gas turbine engine components equivalent testing by shortening testing time required to increase service life

17 p2793 A71-35460

High performance electric arc driven shock tube for shock velocities to 45 km/sec and test times over 4 microseconds, using 80/20 helium-hydrogen mixture

21 p3365 A71-40975

Variable sweep rate frequency response and vibration testing for test time reduction, using closed loop controller for sweep rate modulation

22 p3537 A71-41635

Establishment time measurement for laminar separated flow, using shock tunnel driver section to give long test time at low incident Mach number

24 p3818 A71-44628

TESTS

NT SALT SPRAY TESTS

NT THERMAL VACUUM TESTS

Cascade flow test data, considering blade section performance in transonic and supersonic axial flow compressors

03 p0343 A71-13829

Inertial quantity sensors testing, discussing environmental control, calibration, inspection, etc

[AGARDOGRAPH-128]

05 p0749 A71-16302

TETHERLINES

Parachute decelerator towline energy absorber shock attenuation characteristics, discussing drop test results
[AIAA PAPER 70-1202] 11 p1708 A71-25527

TETRACHLORIDES

Titanium and silicon tetrachlorides oxygen-containing impurities determination without hydrolysis, describing measuring device design
15 p2383 A71-31659

TETRACHLOROMETHANE

U CARBON TETRACHLORIDE

TETRAD THEORY

Gauge equations in general relativity theory for tetrad gravitational potential formulation, based on algebraic invariants method
17 p2778 A71-34636

TETRAGONS

NT RECTANGLES

NT TRAPEZOIDS

TETRAHEDRONS

Tetra-Core structural composite material, discussing fabrication techniques, test results, potential and applications
08 p1369 A71-21225

TETRANITROTETRAZACYCLOCTANE

U HMX

TETRAPHENYLS

Emission spectra of solutions of oxazole and axadiazole derivatives and of tetraphenylbutadiene as effective active media for liquid phase lasers
11 p1774 A71-26001

TETRODES

P-channel MOSFET tetrodes static and dynamic characteristics compared to conventional MOS triode, considering transfer and gate threshold voltage
02 p0229 A71-11811

Phase shift and attenuation measurements in high power microwave ferrite tetrodes circuits, using semiconductor transducers (digadectors)
24 p3809 A71-44871

TEXTBOOKS

NASA and Army Research Office /ARO/ instruction monographs applications for classroom and self study use
04 p0691 A71-15279

German book on static elasticity and theoretical mechanics covering materials stresses and deformations, virtual work principle, linear isotropic elasticity and thermoelasticity
21 p3464 A71-40782

TEXTILES

NT COTTON FIBERS

NT RAYON

Woven textile structures tensile strength tests at high strain rates, using unbreakable compact clamp system
22 p3564 A71-41590

TEXTS

Information content and digital storage of aerial photography using assessing entropy of written English text
02 p0248 A71-11953

TEXTURES

Automatic pattern recognition, discussing texture as discriminant of crops on radar imagery
05 p0743 A71-17145

Roller metals crystallographic texture and pole figure determination using X ray diffractometer
09 p1467 A71-22307

Fe-Si alloy with pronounced texture and large grain size, determining lattice period from X ray diffractogram obtained by reverse response method
09 p1467 A71-22308

Fiber textures formation in polycrystalline Zr from cold forging and cold drawing, observing fully developed recrystallization
10 p1629 A71-25028

German monograph on Mo sheets textures and plastic anisotropy covering recrystallization processes, crystallography, etc
14 p2256 A71-29580

Vacuum-melted low-carbon low-manganese steel, investigating Ni and Cr additions effects on recrystallization textures
19 p3079 A71-37703

TFX AIRCRAFT

U F-111 AIRCRAFT

THALAMUS

Midbrain reticular neurons discharges in response to electrical stimulation of posterior ventral nucleus of thalamus
01 p0008 A71-10072

Brain stem mechanisms underlying visual discrimination in rhesus monkeys subjected to bilateral lesions of the inferotemporal cortex, posterior thalamus or midbrain
13 p2011 A71-28807

Cat thalamus ventrolateral nucleus neuronal discharges during waking and slow and fast wave sleeps
17 p2680 A71-34689

Visual and auditory evoked potentials enhancement in cats using cryogenic blockage of nonspecific

thalamo-cortical system in inferior thalamic peduncle region
17 p2682 A71-35112

Arousal and activation in nonspecific reticulo-thalamo-cortical systems due to underlying emotion expressed through cortical, visceral and somatomotor channels
21 p3330 A71-40247

Posterolateral thalamus nucleus neurons response to visual, acoustic and somatic stimuli in cats with microelectrodes
22 p3490 A71-42578

Postsynaptic de- and hyperpolarization potential development mechanisms in wakeful cats cortical neurons during LF thalamic structure stimulation
24 p3797 A71-44720

THALLIUM

NT THALLIUM COMPOUNDS

Glass fibers and rods from thallium-sodium ion exchanging, investigating flexibility, focusing and light conduction without distortion
16 p2588 A71-34120

Spatiotemporally coherent pulsed Ne and Ti vapor lasers superradiation, showing coherence time dependence on pulse length and gas pressure
23 p3683 A71-43395

THALLIUM COMPOUNDS

Optical and photoelectrical properties of thin amorphous thallium arsenic sulfide, thallium antimony sulfide and thallium bismuth sulfide films obtained by vacuum deposition
05 p0794 A71-16835

Heat treated thallium bismuth sulfide, selenide and telluride amorphous and polycrystalline thin films electrical conductivity, differential thermal emf and forbidden bandwidth
20 p3276 A71-39076

Anisotropic transport coefficients valence band model of TlSe, measuring electric conductivity, Hall effect and thermo-emf as function of temperature
21 p3434 A71-41328

TlTe thin films phase composition and structural properties as functions of component contents, deposition conditions and annealing parameters, using X ray diffractometer and IR microscope
24 p3862 A71-45252

THAWING

U MELTING

THEMIS PROJECT

Themis project automatic navigation program, examining optimum stochastic feedback error analysis and sensitivity algorithms
01 p0125 A71-10525

THEODOLITES

Prelaunch automatic azimuth alignment theodolites for Saturn 1B and Saturn 5 space vehicles inertial guidance system, discussing return images separation and error signal generation
08 p1289 A71-21375

Stationary or moving objects spatial coordinates determination by three and four dimensional terrestrial photogrammetry, using phototheodolite stereophotographic pictures
23 p3671 A71-43590

Gravimeters calibration by inclination method with astronomical theodolite, tabulating relative errors and temperature corrections
24 p3826 A71-44767

THEODORSEN TRANSFORMATION

Low speed airfoil characteristics calculation by digital computer, using Theodorsen conformal transformation method for potential flow pressure distribution
[SAE PAPER 710389] 10 p1550 A71-24253

THEOREM PROVING

Automatic computer program synthesis based on theorem proving approach for construction of recursive and iterative programs operating on natural numbers, lists and trees
10 p1581 A71-23968

Theorems of instability for differential equation in linear normalized spaces, using Liapunov second method
12 p1930 A71-27239

Theorem proving impossibility of stabilizing unstable MHD configuration with nondissipative plasma in vacuum surrounded by superconducting wall by means of finite electrical conductivity wall
14 p2282 A71-30557

Nonreversibility of Marachkov theorem on asymptotic stability, using scalar equation
16 p2612 A71-33595

Chinese remainder theorem for noncommutative rings with divisors of zero and without two-sided unity element in number theory
18 p2976 A71-36096

Asymptotic expansion for hyperbolic Cauchy problem solution, proving correctness
21 p3409 A71-41079

Nonlinear differential equations with retarded argument, proving asymptotic and oscillatory solutions theorems
22 p3568 A71-42692

Validity theorems derived for complex parameter elasticity theory equations by vector functions expansion
23 p3777 A71-43583

THEOREMS

NT ADDITION THEOREM

NT BAYES THEOREM

NT CASTIGLIANO VARIATIONAL THEOREM

NT EXISTENCE THEOREMS

NT GAUSS-MARKOV THEOREM

NT LAGRANGE SIMILARITY HYPOTHESIS

NT LEBESGUE THEOREM

NT LIOUVILLE THEOREM

NT POYNTING THEOREM

NT RECIPROCAL THEOREMS

NT SCHAUDER FIXPOINT THEOREM

NT SIMILARITY THEOREM

NT UNIQUENESS THEOREM

Qualitative behavior for classical dynamical systems, discussing various theorems
06 p0918 A71-17641

Theorems concerning relaxation in point total and single step iterative solution for Hammerstein type nonlinear equations
06 p0920 A71-18212

Differential equations system theorems for conditions of solution stability in presence of large initial perturbation
09 p1495 A71-23429

Two theorems on minimax transversal filter equalization at receiver for digital communication systems distortion reduction
14 p2193 A71-30012

Joseph type theorems derivation for parallel fluid flow with wave perturbation stability governed by Orr-Sommerfeld equation
18 p2902 A71-36041

Theorem proved for monotonic behavior of pressure within relativistic rotating star, assuming stationary axisymmetric gravitational field of Euclidean topology
20 p3293 A71-39447

THEORETICAL PHYSICS

NT NEWTON THEORY

NT QUANTUM THEORY

Initial value or boundary value problems in mathematical physics, solving by process of condition elimination
05 p0780 A71-16178

Mathematical physics multidimensional boundary value problems seminumerical solution, using differential-difference method and integral transformations
05 p0783 A71-17014

Mathematical statistics methods application to incorrect problems in mathematical physics, using information theory
07 p1158 A71-19171

Physics laws and simplifications, discussing Newtonian mechanics, electrodynamics, relativity, atomic physics and quantum theory
07 p1163 A71-19603

Theoretical physics - NSF Conference, University of Notre Dame, South Bend, Indiana, April 1970
08 p1333 A71-21172

Soviet book on variational methods in mathematical physics covering energy method, Ritz process, Bubnov-Galerkin method and least squares method
12 p1931 A71-27292

Relativistic formulation of thermodynamics and statistical mechanics in special theory of relativity, noting Ott presentation
13 p2102 A71-29324

Cosmological constant role in relativistic cosmology, considering retention for additional freedom in linking relativity theory with other parts of physical theory
22 p3607 A71-42882

THERAPY

NT CHEMOTHERAPY

NT PSYCHOTHERAPY

NT RADIATION THERAPY

Ultrasonics applications in surgery, therapy and diagnosis, discussing physical principles, piezoelectric transducers, tissue acoustic properties and measurement methods
03 p0372 A71-13351

THERMAL ABSORPTION

NT POLAR CAP ABSORPTION

Transient thermal laminar boundary layer, investigating absorbing-emitting gas effects
04 p0685 A71-15520

Reentry spherical vehicles with variable wall thickness, determining heat flux absorption without surface ablation and wake contamination
[AIAA PAPER 71-424] 11 p1858 A71-26215

Airlock thermal capacitor for radiator performance augmentation by absorbing heat on orbit hot side and rejecting on cold, providing coolant temperature level damping
[AIAA PAPER 71-429] 11 p1858 A71-26218

Plane thermal waves in heat conducting and radiating/emitting and absorbing/ medium occupying half space x greater than zero
[DFVLR-SONDDR-133] 16 p2664 A71-34141

Thermal control using nitrogen, circuit board, switching, flexible, transformer and segmented evaporator heat pipes
[ASME PAPER 71-AV-29] 18 p2868 A71-36396

Low temperature plasma radiation flux heated absorbing fluid, investigating convective heat transfer to semitransparent wall 24 p3856 A71-44893

THERMAL ACCOMMODATION COEFFICIENTS

U ACCOMMODATION COEFFICIENT

THERMAL AGITATION

U THERMAL ENERGY

THERMAL BATTERIES

Semiconductor thermoelectric battery p-n cell elements joining with mercury amalgam for commutating 14 p2181 A71-29953

Actinometer thermobatteries surface sensitivity distribution effect on solar radiation flux measurement accuracy 20 p3237 A71-39330

THERMAL BOUNDARY LAYER

Magnetic field effect on boundary temperature in axisymmetric MHD flow in vortex chamber, using dissipationless approximation 02 p0293 A71-12633

Natural convection inside horizontal cylindrical cylinder, selecting fluid, geometry and thermal boundary condition for high Prandtl and Grashof numbers 03 p0519 A71-13732

Shock-reflection interferometry of electron and mass density profiles of ionized argon end wall thermal layer 04 p0674 A71-14701

Longitudinal surface curvature effect on steady two dimensional incompressible laminar thermal boundary layers 04 p0680 A71-15471

Thermal boundary layer thickness and momentum in turbulent flow over film cooled surface 04 p0680 A71-15473

Prandtl number measurement in turbulent thermal boundary layer along flat plate with stepwise wall temperature variation 04 p0680 A71-15477

Transient thermal laminar boundary layer, investigating absorbing-emitting gas effects 04 p0685 A71-15520

Schlieren device for visualization of thermal gradients in boundary layer of any orientation, replacing natural astigmatism with arbitrarily adjustable one 05 p0749 A71-16266

NonNewtonian liquids with arbitrary surface temperature and pressure gradients, solving dynamic and thermal boundary layers equations 06 p1006 A71-18008

Heat transfer and thermal entrance length in annular channel with rounded and sharp inlet edges 07 p1220 A71-18763

Boiling layer microcharacteristics, investigating temperature pulsations near wall attachment and subcooled liquid two phase boundaries 07 p1221 A71-18788

Boiling in two-phase layer on heated wall in relation to thermal exchange mechanisms 07 p1221 A71-18790

Thermal boundary layer flattening influence on atmospheric cellular convection from satellite observations 07 p1104 A71-20219

Two layer thermal and velocity model of gaseous film cooling with constant turbulent step slot flow [ASME PAPER 71-GT-3] 11 p1855 A71-25949

Thermal boundary layer equation for sulfur hexafluoride steady arc constriction effects in nozzle throat 12 p1939 A71-27268

Modified heat conductivity solutions for region with moving boundary, applying to crystallization front or crack propagation 13 p2159 A71-28037

Thermal boundary layer instability near heated vertical flat plate in poorly conducting liquid under horizontal DC electric field 14 p2337 A71-30407

Non-Newtonian liquids with arbitrary surface temperature and pressure gradients, solving dynamic and thermal boundary layers equations 20 p3311 A71-38975

Boundary vorticity method for finite amplitude convection in plane Poiseuille flow with isothermally heated and cooled plates, using Boussinesq approximation 21 p3477 A71-40993

Thermal conductivity determination of Ar at extremely high temperatures, using temporal development of thermal boundary layer at shock tube wall 22 p3619 A71-41523

Laminar heat transfer losses effects on piston gas heater performance, computing heat transfer rate and thermal boundary layer thickness 24 p3887 A71-44603

THERMAL BUCKLING

Flutter analysis of plates with inplane boundary support flexibility exposed to transverse pressure loading or buckled by uniform thermal expansion 01 p0173 A71-10940

Thin circular cylindrical shell stability subjected to axisymmetric thermal pulse, describing buckling process by mathematical model 05 p0820 A71-16186

Buckling of thin elastic circular plates under steady state axisymmetric temperature distribution 08 p1370 A71-21304

Thermal deflection tests of fused silica mirror blanks by holographic interferometry 09 p1447 A71-22745

Thermal buckling and snapping of flat rings and of shallow conical rings under axisymmetric temperature distribution [ASME PAPER 71-DE-B] 12 p1977 A71-27317

Thermal buckling of elastic plates exposed to random temperature field producing biaxial stress concentration 15 p2504 A71-31834

Thermal buckling prediction for ring-stiffened cylinders, taking into account ring out-of-plane bending stiffness 17 p2825 A71-34896

Buckling thermal gradients for rotating orthotropic annular plates under edge plow load 22 p3619 A71-42842

THERMAL COMFORT

Antixposure suits physiological evaluation for subjective comfortableness, oral and skin temperatures and pulse rate, determining optimum environmental temperature 17 p2692 A71-35195

Humid operative temperature as index for biophysical thermometry and thermal comfort sensation prediction 18 p2861 A71-36887

Skylab life support, habitability and thermal comfort system, discussing ventilation, humidity, carbon dioxide and odor control and water, food and waste management 22 p3609 A71-41976

THERMAL CONDUCTIVITY

Carbon dioxide laser vs electron beam welding, examining weldability of high thermal conductivity metals 01 p0087 A71-10452

Boron additive effects on Ti thermal conductivity and expansion 01 p0102 A71-10787

Three dimensional ablation calculated for reentry sphere-cone taking into account shape changes and internal heat conduction [AIAA PAPER 70-199] 01 p0180 A71-10952

Thermal conductivity and diffusivity determination of powders by introducing dispersed metal particles 01 p0182 A71-11447

Longitudinal electrical and thermal conductivities of fully ionized plasma in strong external magnetic field 01 p0136 A71-11473

Thin exploding wire restrike channels, examining temperature, electron density and thermal conductivity temporal behavior 02 p0284 A71-11941

Apollo 11 lunar rocks excess heat capacity and thermal conductivity at liquid He temperatures due to peaks in vibrational frequency distribution 02 p0306 A71-11989

Multicomponent plasma electrical and thermal conductivities from quantum mechanical scattering cross sections 02 p0289 A71-12176

Rectangular parallelepiped and solid cylinder temperature distributions under time dependent ambient heating or cooling, solving thermal conductivity equation 02 p0333 A71-12647

Symmetrical solar wind model solutions with thermal conductivity, showing constant mass and total energy flux conditions relationship to critical line 02 p0303 A71-12771

Solar chromosphere model, investigating radiative transfer effect on temperature structure of plane slab heated by thermal conduction 03 p0483 A71-13186

Thermoelectric transport properties of ionospheric electron gas above 100 km 03 p0406 A71-13301

Temperature field of radiation heated bodies, using analytic method based on backradiation law approximation by linear function with limit error in Stark range 03 p0519 A71-13746

Thermal conductivity of binary gas mixtures with/without hydrogen to 1100 K, using molecular kinetic theory and structure model 03 p0520 A71-13749

Reciprocal thermal influence, temperature areas and conduction distance of electronic components in compact circuits 03 p0387 A71-14325

Thermal conductivity determination for materials by pulsed laser or flash lamp energy absorption 04 p0595 A71-149619

Space shuttle systems structural joints thermal control, discussing contact conductance with and without interstitial fillers 04 p0676 A71-15334

Composite materials of highly conductive metallic fibers randomly distributed in low conductivity matrices, investigating parameters affecting thermal conductivity from stochastic models 04 p0678 A71-15434

Thermal conductance of contacts between dissimilar solids with interstitial fluids, calculating heat flow direction effect by double constriction model 04 p0678 A71-15454

Thermal conductive liquid hydrodynamic stabilization of Hartmann flow in rectangular canal with transverse field, examining magnetic effect on heat transfer 04 p0635 A71-15506

Measuring instrument for lunar surface layer heat flow, temperature and thermal conductivity 04 p0599 A71-15543

Thermal conductivity and emittance of arc and powdered W at 1800-2800 K 04 p0612 A71-15579

Density and temperature dependences of viscosity and thermal conductivity of dense fluids 05 p0831 A71-16408

Austenite-martensite transformation effects on Fe-Ni-Co alloys low temperature thermal conductivity 05 p0768 A71-16771

Zirconium carbide fiber insulating materials, examining heat conductivity coefficient 05 p0838 A71-16781

Unsteady heat conductivity problems with nonlinear boundary conditions, using perturbation method 05 p0838 A71-16782

Dilatometric thermal expansion method for determining cylindrical solid body thermal conductivity coefficient 05 p0838 A71-16790

Low electrical conductivity semiconductor melts thermal conductivity, discussing energy quasi-gap existence 05 p0794 A71-16881

Polyatomic gases thermal conductivity coefficient, examining magnetic field effect 06 p1005 A71-17316

Diffusion coefficient and thermal conductivity dependence on plasma parameters in Tokamak installation 06 p0930 A71-17397

Combined continuity and force equations for sound attenuation as function of thermal and viscous losses in liquid gases, taking into account fcc and bcc packing 06 p0927 A71-17569

Parabolic equation for plate unsteady thermal conductivity during nonuniform heating, analyzing finite difference solution accuracy 06 p1006 A71-18007

N and CO thermal conductivity shock tube measurements, discussing pressure distribution and high temperature effects 06 p1007 A71-18075

Nonstoichiometric VC, studying thermal and electrical conductivities, thermoelectric properties and Hall coefficient 06 p0912 A71-18085

Fully ionized quasi-one dimensional magnetic nozzle flow analysis, including effects of unequal electron and ion temperatures and electron thermal conductivity [AIAA PAPER 71-141] 06 p0939 A71-18584

Thermal contact resistance as function of time during static load 07 p1116 A71-18917

Vision mathematical model based on homogeneous medium thermal conductivity equation 07 p1043 A71-20112

Rock forming monomineralic aggregates thermal conductivity at ordinary temperature and pressure in relation to density, crystal structure and chemical composition 07 p1105 A71-20448

Finite and large pressure inhomogeneous plasma with finite electron heat conduction, calculating instability 07 p1173 A71-20534

Thermal conductivity coefficients of heat conducting pastes in transistor application 08 p1318 A71-20845

Soviet book on thermal conductivity of monatomic and polyatomic gases and hot and cold mixtures, comparing molecular kinetic theory collision integral formulas with experimental data 08 p1375 A71-21656

Hg vapor thermal conductivity measurement at 300-900 K and atmospheric pressure, using hot wire method 08 p1376 A71-21919

Single crystal W thermal conductivity measurement at 1200-2500 K, discussing apparatus and error sources 08 p1318 A71-21920

Thermal conductivity of Li and Na carbonates alone and combined in mixture with magnesia at various temperatures

08 p1377 A71-21933

One dimensional nonstationary motion of compressible electrically conducting gas with allowance for heat conduction and viscosity, solving MHD equations

09 p1499 A71-22129

Semiconductor thermoelectric materials in intercrystalline boundaries porosity effects on electrical and thermal conductivity

09 p1506 A71-22162

Thermal conductance measurement in electroexplosive device by self balancing wire bridge, considering quality control or design applications

09 p1493 A71-22732

Interlayer shear modulus relation to thermal conductivity coefficient in oriented glass fiber reinforced plastics

09 p1482 A71-22814

Shock wave interaction with evaporating aerosol for diffusive and ablative models taking into account thermal conductivity

09 p1433 A71-22856

Thermal conductivity measurement of cryopumped solid gas deposits in thin walled stainless steel cylinder with temperature gradients

09 p1546 A71-23007

Thermal conductivity of Ar binary mixtures with He, N and Ne, using secondary concentric cylinders cell

09 p1547 A71-23463

Heat conductivity anomalies of thin metallic plates at very low temperatures, discussing secondary phonons angular distribution and electron energy flux

10 p1640 A71-23816

Thermal conductivity anomalies in thin superconducting metal foils in contact with two superfluid He basins at low temperatures, examining surface electron phonon interactions

10 p1640 A71-23832

Edge losses effects on thermal conductivity of thermal insulations at high temperature measured by guarded hot plate method

10 p1694 A71-23907

Thermal conductivity, electrical resistivity and specific heat of hot pressed beryllium

10 p1624 A71-23908

Ti thermal conductivity, electrical resistivity and total emittance at high temperatures in ultrahigh vacuum, discussing phase transformation effect

10 p1624 A71-23910

Thin metal foils total energy flux, electron/phonon temperatures and thermal conductivity anomalies at liquid He temperatures

10 p1657 A71-24457

Dutch monograph on nonstationary hot-wire method determining thermal conductivity coefficient of gases, using recorded temperature vs time relation

10 p1697 A71-24677

Electrical and thermal conductivity coefficients and energy diffusion coefficient in lower ionosphere, assuming weak ionization of ionospheric plasma

10 p1607 A71-24998

Thermal conductivity prediction during ablation of phenolic-carbon and phenolic-graphic composites for heating and cooling conditions

11 p1783 A71-25304

Carbon fiber-epoxy resin composites Young modulus, thermal and electrical conductivities as function of fiber alignment and porosity

11 p1784 A71-25399

Cesium vapor thermal conductivity measurements with miniature vacuum mode thermionic diode, investigating net accommodation coefficient dependence on surface temperature

11 p1714 A71-25901

Various configuration thermal contacts, examining conductance with electric analog

11 p1858 A71-26225

Centerline loss, transient sink temperature and thermal conductivity design constant considerations for thin foil copper-Gardon heat flux sensors

11 p1764 A71-26251

Thermal conductivity of Apollo 11 lunar fines as function of temperature, pressure and bulk density

11 p1833 A71-26255

Lunar crust regolith thermophysical properties concerning particle size and mass, specific heat and thermal conductivity from Luna 16 automatic station sampler

12 p1963 A71-26964

Atmospheric pressure electrical and thermal conductivities on nitrogen and hydrogen up to 26,000 K from argon arc measurements

12 p1939 A71-27271

Shock heated Ar thermal conductivity measurements by following temperature boundary layer with time resolved interferograms with HF laser stroboscope light source

12 p1986 A71-27578

Ferromagnetic and antiferromagnetic single crystals thermal conductivity at 193-673 K, analyzing anomalies on basis of magnetic and structural characteristics

12 p1944 A71-27661

Dissimilar metals welding, emphasizing melting point, linear expansion coefficient, thermal conductivity, electrical resistivity and polymorphic transformation

13 p2072 A71-27887

Cerebrum temperature variations and tissue insulating and heat conducting properties in ether anesthetized dogs with heads cooled by water stream

13 p2004 A71-28029

Equation for calculating thermal conductivity of gases and liquids, comparing calculations with experiments

13 p2159 A71-28183

Rarefied collisionless plasma, obtaining hydrodynamic equations for magnetic viscosity and thermal conductivity

13 p2106 A71-28564

Boundary value problems solution for composite cylinder consisting of three different layers with no-ideal thermal contacts

13 p2165 A71-29086

Radiative capacity of materials with low thermal conductivity at high temperatures determination from reflectivity measurements for oblique light incidence

14 p2240 A71-30051

Gravitational instability of heat conducting compressible fluid relative to class of axisymmetric perturbations, considering viscosity, magnetic field and uniform rotation

14 p2226 A71-30397

Extended flat body thermal conductivity determination by local heating at constant heater helix temperature

14 p2338 A71-30622

Multicomponent plasma electrical and thermal conductivities from Debye potential quantum mechanical scattering cross sections

15 p2454 A71-31485

Thermal conductivity and coating emittance measurements by stationary substrate heater method suitable for materials applied by flame vaporization

15 p2512 A71-31501

Nitrogen plasma electrical and thermal conductivities and radiative source strength at atmospheric pressure and 9,000-12,500 K, using Hall probe and optical methods

15 p2454 A71-31535

Thermal conductivity, diffusion and viscosity of gases and multicomponent gaseous mixtures at high temperatures

15 p2515 A71-32450

Thermal properties of solar wind plasma, determining electron and proton temperature distributions, proton heating rate, electron thermal conductivity and energy exchange rates

15 p2480 A71-32754

Temperature control in presence of varying heat sources or sinks through thermal conductance

16 p2576 A71-32973

Heat conductivity coefficient of thermal insulation material made from zirconium carbide fibers, giving measurement procedure

16 p2662 A71-33033

Perturbation method for solving nonstationary heat conduction problems with nonlinear boundary conditions

16 p2662 A71-33034

Minima and maxima in composition dependence of thermal diffusion factor and conductivity of gas mixtures

16 p2614 A71-33104

Molybdenum single crystals isotropic thermal conductivity, electrical resistivity and total hemispheric degree of blackness at high temperatures

16 p2595 A71-33882

High porosity carbon-graphite materials thermal and electrical conductivities at high temperatures by potentiometric method

17 p2761 A71-34208

Composite rocket engine casing thermal flux approximation from multilayer plate heat conductivity

17 p2837 A71-34568

Hydrostatic, dynamic, hydrodynamic and two-component corona models and solar corpuscular radiation, considering heat conductivity and viscosity effects on solar wind dynamic characteristics

17 p2795 A71-34828

Polyatomic gases thermal conductivity and rotational relaxation number from thermomolecular pressure differences across capillary tubes

17 p2785 A71-34946

Single crystal W thermal conductivity measurement at 1200-2500 K, discussing apparatus and error sources

17 p2759 A71-35264

Temperature and pressure effects on viscosity and thermal conductivity of dissociating air at high temperatures

17 p2785 A71-35277

German monograph on high temperature measurement of thermal and electrical conductivity of W and Mo single crystals

18 p2915 A71-35960

Ceramic fibrous materials for high temperature insulation, discussing practical approach to obtain lower thermal conductivity

18 p2939 A71-36668

MHD systems equilibrium and stability involved in quiescent prominences, considering temperature dependence of heat conductivity, magnetic field and initial gas compression

18 p2967 A71-36927

Metals and alloys thermal conductivity prediction using Lorentz ratio and electrical resistivity measurements

18 p2938 A71-36991

Rheological media viscoelastic relaxation theories generalization taking into account thermal stress and conduction

18 p2984 A71-37021

Electroconductivity, thermal conductivity and diffusivity, specific heat and emissivities of Ti at 1000-1700 K

19 p3078 A71-37582

Viscous relativistic fluid plane laminar flow, discussing incompressible thermally nonconducting case and stationary models

19 p3044 A71-37640

Thermal conductivity anomalous behavior prediction for carbon dioxide, argon, nitrogen, oxygen and methane in critical region

19 p3165 A71-37998

Variable thermal conductance wall based on working fluid evaporation and condensation

19 p3166 A71-38001

Porous material slab pyrolysis, studying density and thermal conductivity changes and reaction kinetics

19 p3170 A71-38117

Nonlinear coupling between thermal conduction and radiative transfer in solar chromosphere by iterative method

19 p3143 A71-38159

Lunar crust regolith thermophysical properties concerning particle size and mass, specific heat and thermal conductivity from Luna 16 automatic station sampler

19 p3144 A71-38259

Lateral heat transfer measurements in cryogenic multilayer insulation, considering effective thermal conductivity

20 p3312 A71-39272

Temperature decay method for determining superinsulation thermal conductivity, equating insulation heat transfer rate to calorimeter plate heat loss

20 p3312 A71-39273

Ni-Cd cells thermal conductivity measurements for heat balance and dissipation calculations for space vehicle power supply systems, describing experimental apparatus

20 p3184 A71-39556

Radial energy contours of pulsed ruby laser beam in direct determination of thermal conductivity by flash technique, using heat flux transducer

21 p3391 A71-40180

Bismuth telluride single crystals thermal conductivity and thermoelectric power temperature dependence 2.3-100 K, discussing magnetic field effects

21 p3433 A71-41314

Solid and liquid Ge thermal conductivity measurement at high temperatures by coaxial cylinder and flat layer methods

21 p3435 A71-41334

Thin bismuth films thermal and electrical conductivities and thermoelectric power measurements, examining preparation methods

21 p3435 A71-41338

Thermal conductivity determination of Ar at extremely high temperatures, using temporal development of thermal boundary layer at shock tube wall

22 p3619 A71-41523

Thermal conductivity of elastic, elastoplastic and plastic contact area between two compressed rough surfaces

22 p3622 A71-42686

Apollo 12 lunar fines 12001, 19 thermal conductivity vacuum measurements, using line heat source method

23 p3761 A71-43781

Apollo 11 and 12 rocks specific heat and thermal conductivity at 2-5 K, comparing elastic properties

23 p3761 A71-43785

Thermal radiative cooling system characteristics determination allowing surface material thermal conductivity and blackness degree dependence on temperature

23 p3782 A71-43919

Thermoelectricity, thermal conductivity and stress distributions in plates with two circular holes under constant contour temperatures, using complex variables theory

23 p3778 A71-44042

Statistical modeling technique for approximate numerical solution of unsteady heat conductivity inverse

problem, obtaining foam chamotte and magnesite temperature field data

23 p3782 A71-44059

Inverse problem for heat conductivity equation in semimfinite region with Tikhonov specific initial and boundary conditions

23 p3782 A71-44062

Porous fiber reinforced composite low density heat insulating materials thermal conductivity measurements, showing energy transport by heat transfer mechanisms

23 p3784 A71-44341

Composition effects on binary gas mixtures thermal conductivity coefficient, considering Hirschfelder-Eucken formula

24 p3886 A71-44369

Polycrystals thermoelastic characteristics, determining thermal expansion and conductivity macroscopic coefficients

24 p3840 A71-44402

Thermal conductivities of pure and mixed ortho- and parahydrogen and/or deuterium at temperatures with no molecular internal energy exchange

24 p3850 A71-44553

Previous plastic loading deformation effect on contact area, print number, size distribution and thermal conductivity for flat surfaces

24 p3830 A71-44943

Space vehicle radiative cooling system rib temperature field calculation, taking into account material heat conductivity temperature dependence

24 p3889 A71-45023

Plasma perturbations in curved magnetic field due to electron thermal conductivity finiteness

24 p3856 A71-45053

Thermal conductivity, diffusivity and specific heat of lunar soil and basalt analogs, using Luna 16 samples

24 p3873 A71-45103

THERMAL CONDUCTIVITY GAGES

Thermal conductivity rapid measurement in 300-1200 K range using traversing thermocouple technique [ASME PAPER 70-WA/ENER-2]

03 p0429 A71-14107

Hg vapor thermal conductivity measurement at 300-900 C and atmospheric pressure, using hot wire method

08 p1376 A71-21919

Single crystal W thermal conductivity measurement at 1200-2500 K, discussing apparatus and error sources

08 p1318 A71-21920

Single crystal W thermal conductivity measurement at 1200-2500 K, discussing apparatus and error sources

17 p2759 A71-35264

Solid and liquid Ge thermal conductivity measurement at high temperatures by coaxial cylinder and flat layer methods

21 p3435 A71-41334

THERMAL CONDUCTORS

Nonlinear heat conduction of contacting bars with boundary conditions of fourth kind, using small parameter method

02 p0332 A71-12529

Rigid heat conductors, using controllable states for heat flux-temperature gradient materials response function measurements

05 p0837 A71-16721

Plasma boundary layer temperature distribution near conducting surfaces by measuring current voltage characteristics

05 p0790 A71-16776

Hydrodynamic equations for behavior of thermally conducting viscous compressible fluid in first post-Newtonian approximation to general relativity, obtaining conservation laws

09 p1518 A71-22338

Various configuration thermal contacts, examining conductance with electric analog

11 p1858 A71-26225

Thermal contact resistance measurements between sliding contacts after load application under various temperatures, using transient pulse technique

11 p1858 A71-26226

Plasma boundary layer temperature distribution near conducting surfaces from I-V characteristics of gas gap

16 p2618 A71-33028

Plane thermal waves in heat conducting and radiating/emitting and absorbing/medium occupying half space x greater than zero

16 p2664 A71-34141

Thermoelastic materials thermodynamic properties, developing coldness as universal function of viscous heat conducting fluids

17 p2837 A71-34694

Heat transfer by radiation, conduction and convection, including various types of thermal insulation

20 p3311 A71-39244

THERMAL CONTROL COATINGS

Lunar dust deposition and brushing effects on spectral solar reflectance of thermal control materials in vacuum

11 p1799 A71-26241

Vacuum UV phototube module for degradation measurement of optical components, including mirrors, windows, lenses and thermal control surfaces

[AIAA PAPER 71-461] 11 p1800 A71-26243

Solar absorptance sensitivity to thermal surface particulate contamination as function of particle composition, quantity, size and linearity with obscured area

[AIAA PAPER 71-473] 11 p1800 A71-26253

Lunar dust reflectance degradation of thermal control paint on Surveyor 3 TV camera, separating solar radiation effects by analytical model

[AIAA PAPER 71-478] 12 p1920 A71-26760

Optical properties of metallized fluorinated ethylene propylene Teflon films with various thicknesses, discussing suitability as spacecraft thermal control surface

[ASME PAPER 71-AV-35] 18 p2869 A71-36402

THERMAL CONVECTION

U FREE CONVECTION

THERMAL CURRENTS

U CONVECTIVE FLOW

THERMAL CYCLING TESTS

Thermal cycling effect on Al-B composites, considering surface roughening and crack initiation

01 p0103 A71-11279

Turbine disks under unsteady and cyclic loads and temperature variations, determining stress and strain by flow theory computer calculation

02 p0323 A71-11745

Disk elongation plastic deformation, determining elastoplastic stressed state for inhomogeneous thermal cycles

02 p0323 A71-11748

Metal hardening under cyclic thermal loads, determining deformation, breakdown, creep and stress-strain relation

02 p0324 A71-11752

Photoelastoplastic analysis of creep and stress of aluminum notched bars and cracked plates under thermal cycle using epoxy resin simulation

03 p0507 A71-13757

Thermal cycle stresses at interface of composite glass tape-epoxy casting resin cylinder, using strain gages

03 p0508 A71-13763

Thermal fatigue cracks in gas turbine blade models under simultaneous thermal cycling and static tensile loads simulating pulsed regimes

04 p0671 A71-15638

Al alloys thermal fatigue resistance measurement using testing apparatus involving HF induction heating

07 p1142 A71-20325

Thermal fatigue testing apparatus for material longevity, simulating tensile stresses due to centrifugal forces on gas turbine engine blade during thermal loading

08 p1271 A71-20837

Gas dynamic test stand for cyclic thermal load testing of gas turbine engine materials and components at variable heating and cooling rates and mechanical loads

08 p1271 A71-20839

Vacuum-melted and deformed Mo alloys tests, showing long term strength decrease under cyclic heating

08 p1305 A71-21030

W and Mo single crystals metallographic microanalysis for temperature cycles effects on microstructure

08 p1305 A71-21056

Creep enhancement by additional microplastic deformation in refractory alloys during thermal cycling

08 p1317 A71-21618

Cyclic heating and thermal stresses effect on fatigue strength and durability of turbine blade alloys and structural elements

08 p1372 A71-21702

Plastic strains buildup during thermal cycling, establishing relation between strain interval and cycles number to failure for strain hardening materials

09 p1538 A71-22599

Heat resistant alloys low cycle fatigue tests at 20-800 C, establishing residual strain change patterns as function of stress and temperature

09 p1468 A71-22600

Crystal structure alterations in work hardened surface layers of W, Nb and Mo during thermocyclic treatment, using X ray micrography

09 p1477 A71-23329

Hot strain cycle recording in single and multipass welds for C-Mn steel using welding simulation, surface pressed plug and microscopic techniques

09 p1459 A71-23455

Steel sheet specimens under temperature and stress cycles, studying creep, plastic deformation and service life

10 p1686 A71-24189

Ni-based superalloy stress cycle frequency effect on elevated temperature fatigue life

11 p1779 A71-26012

Hot salt stress corrosion, considering effects of oxygen, air velocity, moisture, thermal cycling, fatigue and type of salt

11 p1781 A71-26261

Aircraft power plants sealing materials, emphasizing porous cermet seals heat resistance under thermal cyclic loads

12 p1895 A71-27687

Gas turbine blades fatigue crack development and failure analysis under thermal cycling tests, considering chemical processes and thermal and mechanical stresses

13 p2149 A71-28111

Gas turbine blades thermal fatigue test and analysis investigating static tensile loading effects on heat resistance under thermal cycling

13 p2149 A71-28131

W and Mo single crystals metallographic microanalysis for thermal cycling effects on microstructure

14 p2259 A71-30171

Soviet book on structural bearing capacity under thermal cycling conditions covering rotating disks, plates and shells calculations

15 p2505 A71-32001

Stress relaxation as source of dimensional instability in precision devices, discussing thermal cycling relief in residual stress relief

15 p2436 A71-32503

Cyclic heat treatment effect on fine structure and properties of Mo single crystals in He atmosphere

16 p2595 A71-33881

Alloying elements effect on structural stability and properties of W and Mo alloys single crystals, studying thermal cycling response

16 p2596 A71-33901

Gas turbine blades dynamic characteristics determination, investigating vibrational stresses, thermal cycles, alloy physicomechanical properties and coatings effects

16 p2659 A71-33981

Creep rate enhancement by additional microplastic deformation in refractory alloys during thermal cycling

17 p2761 A71-35675

Rapid thermal fluctuations effect on Inconel 718 creep rate, noting strain rate decrease under cycling conditions

19 p3080 A71-37717

Lightweight solar cell structural failure modes under automatic thermal cycling for prolonged period in wide temperature range and by immersion in liquid nitrogen

20 p3179 A71-38851

Pure Fe phase transformation plasticity as function of material, stress, temperature interval and change rate, cycle number and experiment duration

21 p3396 A71-40021

Environmental rationale behind thermal shock testing, discussing approaches for temperature cycling provision

23 p3682 A71-43901

Zirconium carbide eutectic and supraeutectic alloy preparation with graphite addition, determining heat resistance under thermal cycling tests

23 p3697 A71-44021

THERMAL DECOMPOSITION

U PYROLYSIS

THERMAL DEGRADATION

Pyrolyzing vinyl polymers thermal degradation kinetics, deriving surface regression rates relationships to temperature

01 p0109 A71-10931

Polyphenylene thermal degradation and curing, discussing pyrolytic effects of chlorine and polynuclear structure

11 p1855 A71-26031

Pyrolysis-gas chromatography locating degradation front in phenolic ablative plastics, giving percent phenolic resin vs distance normal to surface

11 p1728 A71-26044

Spacecraft thermal control coatings for long duration exposure to near-earth orbital conditions, determining optical properties degradation and solar absorptance

11 p1859 A71-26237

Thermal oxidation and metal evaporation effects on electrical properties of silicon-silicon dioxide wafer interface in MOS structures

12 p1944 A71-27091

Plate temperature field and stress distribution under thermal pulses, evaluating critical heat load from damage

14 p2325 A71-30041

Polymer thermal degradation theory of pressure-sensitive hybrid combustion, calculating linear regression rates

19 p3170 A71-38121

Hybrid circuit heat sensitive semiconductor chip mounting methods for preventing thermal degradation

21 p3356 A71-40744

Solar energy degradation heat trapping-dissipating walls for inhabited living space on lunar surface

22 p3529 A71-42844

THERMAL DIFFUSION

Calculated dispersion in decaying grid turbulence, showing agreement with test results for diffusion of heat from line source

01 p0072 A71-11484

- Refractory metal thermionic emitter-support systems, measuring surface interdiffusion at high temperatures 02 p0264 A71-12242
- Electron thermal diffusion effects during light interference patterns exposure, generating strong electric fields and holographic storage in electro-optic materials 06 p0940 A71-17309
- Low density monatomic gases mixtures multicomponent thermal diffusion coefficients, demonstrating for heat conductivity and dissociated air equations 06 p0929 A71-18072
- Deformation-thermal diffusion processes relation for thin coated composite materials under variable thermal stresses 07 p1210 A71-19156
- Two dimensional thermal convection through shallow layer with vertical shear using numerical model 07 p1152 A71-19752
- Prograde and retrograde 4 day circulation in Boussinesq fluid layer by traveling thermal waves in Venus upper atmosphere 09 p1526 A71-23446
- Nb-Pd system concentration profiles and thermal diffusion coefficients, investigating phase formations by electron probe microanalysis 10 p1629 A71-25035
- Diffusion and thermal mechanism ignition theories, applying to altitude relighting of gas turbine engine combustors 13 p2116 A71-28745
- Thermal diffusion effect on gas flow velocity measurements with anemometers with heat convection signals 14 p2239 A71-29815
- Temperature dependent diffusion coefficient of yttrium in refractory metal single crystals of Mo, W, Nb and Ta, using radiometric analysis 14 p2258 A71-30005
- Industrial Ti and beta-Ti alloy hydrogen thermidiffusion and effects on brittleness 15 p2424 A71-31238
- Minima and maxima in composition dependence of thermal diffusion factor and conductivity of gas mixtures 16 p2614 A71-33104
- Richardson number relationship to vertical heat diffusion coefficients in boundary layer 16 p2605 A71-34070
- Thermal diffusion in tantalum-oxygen and columbium-oxygen mixed crystals, investigating temperature and concentration effects 16 p2599 A71-34092
- Heat transfer in interstitial solid solutions, interpreting thermal diffusion measurements in transition metals mixed crystals 16 p2599 A71-34093
- Simultaneous degassing and thermal diffusion phenomena in annealed tantalum-oxygen mixed crystals, investigating maximum temperature effect 16 p2599 A71-34094
- Uniform shear flow past seminfinit flat plate, studying diffuse and heat transfer near leading edge 16 p2561 A71-34162
- Deformation-thermal diffusion processes relation for thin coated composite materials under variable thermal stresses 17 p2834 A71-35654
- Boron powder combustion at elevated pressures, observing preignition metastable surface reactions, self sustained diffusion burning and decay 19 p3170 A71-38116
- Diffusion layer structure and phase composition during quenched and annealed steel saturation by Cr at high heating rates 21 p3404 A71-41170
- Au diffusion parameters in CdS determined under Cd and sulfur vapor atmospheres at 540-1000 C, explaining profile difference by dissociative mechanism 21 p3433 A71-41315
- Metallic polycrystal deformation equations, obtaining creep, Norton law dependences and thermally dissipated energy 22 p3560 A71-41606
- Mo-W, Ta-W and Nb-W alloys X ray analysis at high temperatures, calculating interdiffusion coefficients and temperature effects on W concentration 24 p3836 A71-44671
- THERMAL DIFFUSIVITY**
- Thermal conductivity and diffusivity determination of powders by introducing dispersed metal particles 01 p0182 A71-11447
- Apparatus for thermal diffusivity measurements under gas atmosphere at high temperature, using flash method 04 p0595 A71-14962
- Thermal diffusivity measurements over 40 to 1400 C range using pulsed electron beam 04 p0595 A71-14963
- Computer simulation of thermal diffusivity measurements by flash method, considering errors due to boundary conditions 04 p0607 A71-14964
- Heat conduction equation for thermal diffusivity measurements by flash method in two layer composites 04 p0595 A71-14965
- Thermal diffusivity and total emissivity measurements of solids between 1500 K and melting point, using arc image furnace 04 p0595 A71-14966
- Diffusion and solubility of thermally induced acceptors in indium antimonide single crystals 04 p0636 A71-15085
- Thermal diffusivity in disks and rods irradiated by sinusoidally modulated thermal radiation beam, measuring temperature phase difference across front and back faces 07 p1223 A71-19622
- Anomalous thermal diffusivity measurements of Hf, Nb and Zircalloys, using modulated electron beam technique 10 p1624 A71-23909
- Tungsten high temperature thermal diffusivity at 1000-2500 K by flash technique 10 p1624 A71-23911
- Electroconductivity, thermal conductivity and diffusivity, specific heat and emissivities of Ti at 1000-1700 K 19 p3078 A71-37582
- Test facility for studying temperature dependence of thermal diffusivity and true heat capacity of metals between minus 150 and plus 400 C 19 p3063 A71-37588
- Test facility for thermal diffusivity measurements in solids by method of plane temperature waves using periodic optical heating at 1500 K 19 p3063 A71-37589
- Composite materials thermal diffusivity at high temperatures by quasi-stationary and monotonic methods, determining validity domain of differential heat conduction equation without heat sources 24 p3889 A71-44967
- THERMAL DISSOCIATION**
- LiOH dissociation energy in acetylene-air flames 03 p0376 A71-14281
- Population inversions in shock induced dissociation of alkali halides in 2000 to 7000 K range, considering rate constants and molecular relaxation 04 p0629 A71-14694
- Laser torch plasma dispersion gas dynamics from motion and kinetics of ionization processes 05 p0760 A71-16181
- Quenched and tempered steel, investigating embrittlement as function of temperature in partially dissociated atomic hydrogen environment 11 p1779 A71-26013
- Dissociation and particle velocity in shock heated molecular beams of oxygen or hydrogen and argon mixtures, using mass spectroscopic measurements 11 p1765 A71-26282
- Thermal dissociation rate of undiluted nitrogen in shock tube over 5700 to 12,000 K range, using pressure measurements [AIAA PAPER 71-620] 15 p2451 A71-31549
- ZrC vaporization at high temperatures, investigating dissociation into components by mass spectroscopy 15 p2431 A71-32158
- Oxygen dissociation and recombination rate constants at high temperatures from gas density interferometric measurement in relaxation zone of normal shock waves 15 p2367 A71-32570
- Graphitizing and nongraphitizing substances carbonization, observing cokes chemical structure changes and thermal decomposition 15 p2368 A71-32733
- Shock tube investigation of cyanogen and CN molecule dissociation at high temperatures, considering kinetics of CN decomposition 16 p2538 A71-32891
- Pure carbon monoxide dissociation rate behind incident shock wave in high temperature environment, using two wavelength IR emission data 16 p2539 A71-32909
- Low temperature plasma reactions, discussing electron impact and collisions, ion formation, molecular excitation and thermal dissociation, vibrational relaxation, recombination, etc 16 p2539 A71-32964
- Sodium superoxide isothermal decomposition, detailing metallic oxide effects with differential thermal analysis, thermogravimetry and differential thermogravimetry 17 p2694 A71-34672
- Thermal dissociation rate of excited CsF, calculating ion-ion recombination rates 21 p3346 A71-40888
- Thermal dissociation rates of alkali chlorides interpreted in terms of chloride ion collisional detachment rate 21 p3346 A71-40889
- Hydrogen and helium thermal dissociation and ionization at Jupiter and Saturn adiabatic atmospheric models conditions 24 p3850 A71-44809
- Carbonyl fluoride thermal decomposition in excess Ar behind incident and reflected shock waves, analyzing reaction rate variation with temperature and total pressure 24 p3802 A71-44941
- Thermal dissociation reactions and radiation effects on flow variables in front of and behind strong normal shock, using gray gas approximation 24 p3822 A71-45368
- THERMAL EFFECTS**
- U TEMPERATURE EFFECTS**
- THERMAL EFFICIENCY**
- U THERMODYNAMIC EFFICIENCY**
- THERMAL EMISSION**
- NT THERMIONIC EMISSION**
- Fusibility and thermal emf of ternary intermetallic TiFe-TiCo-TiNi system 01 p0103 A71-11090
- Thermoemissive and adsorptive properties of Nb single crystals in Cs atomic beam at various temperatures 01 p0139 A71-11100
- Titanium and niobium monocarbides electron work function relation to homogeneity region composition, considering electron structure and thermal emission 02 p0263 A71-12199
- Computer controlled eclipse telescope for coronal thermal emission IR spectrum observation 03 p0424 A71-13633
- Thermal emission from IR star shells calculated from circumstellar graphite dust model 03 p0495 A71-14267
- Transient thermal laminar boundary layer, investigating absorbing-emitting gas effects 04 p0685 A71-15520
- Stimulated thermal Rayleigh scattering with picosecond pulses, discussing contributory processes 07 p1164 A71-19779
- Refractory transition metals diborides thermoemissive properties for use in cathode materials 07 p1144 A71-20653
- Solar flare model, computing thermal X ray emission 08 p1350 A71-20945
- Soft X ray bursts involving solar flares from satellite observations, discussing thermal nature and total activity related H-alpha emission rates 10 p1660 A71-23794
- Galactic X ray thermal emission model, discussing origin and location of sources 10 p1662 A71-24675
- Venus, Mars, Jupiter and lunar thermal emission data in 7-25 micron region 11 p1824 A71-25698
- Thermal and electrical characteristics of two nuclear type cylindrical converters with nonuniform emitter temperature 11 p1714 A71-25903
- Directional thermal emission from rough lunar surface as function of crater frequency, aspect ratio and solar deviation angle, comparing to Lambertian behavior [AIAA PAPER 71-480] 11 p1833 A71-26256
- Earth surface thermal radio emission measurements by UHF radiometry onboard Cosmos 243 satellite, showing brightness profiles of water, ice and land areas 12 p1899 A71-26639
- Microwave emission from North Sea and North Atlantic at surface wind speeds of 5-25 m/sec, measuring brightness temperature 12 p1902 A71-27199
- Plasmoid ejection during flare and condensation by radiative instability, interpreting Simple 3 solar radio bursts in terms of thermal emission 13 p2129 A71-29054
- Solar corona XUV resonance line spectrum interpretation, using thermal emission from inhomogeneous regions 14 p2297 A71-29678
- Interstellar grain temperatures, determining shape effects on emissivities 14 p2305 A71-29680
- Thermal emissivity and solar absorptivity of Al coated with surface layers of aluminum oxide and silicon oxide, describing fabrication techniques and performance measurements 14 p2335 A71-30128
- Thermal emission analysis method for studying phase transformations and chemical conversion kinetics in multicomponent systems, applying to liquid evaporation rate measurement 14 p2338 A71-30618
- Galactic nebula YM 29 radiometric observations showing thermal source, mass and Balmer line fluxes comparable to planetary nebula 14 p2314 A71-30643
- Pressure-induced absorption in planetary atmospheres from hydrogen-methane collisions, stressing resulting thermal opacity 14 p2315 A71-30659
- Point defects relation to thermoelectric emission at high temperatures in yttrium oxide 15 p2462 A71-32714

Thermal imaging devices scanning systems for producing televisionlike images, noting alternate line scanning

15 p2412 A71-32759

Galactic nucleus thermal emission due to dirty ice or silicate grains, explaining far IR radiation power output and spectral dependence

15 p2498 A71-32773

Plane thermal waves in heat conducting and radiating /emitting and absorbing/ medium occupying half space x greater than zero [DFVLR-SONDDR-133]

16 p2664 A71-34141

IR study of thermal anomalies during lunar night, discussing ages and distribution on terrain

17 p2797 A71-34184

Papers on astronomy and astrophysics, Volume 8, covering lunar microwave thermal emission observation and origin

17 p2804 A71-35176

Lunar microwave thermal emission observation and theoretical predictions based on lunar surface models

17 p2804 A71-35177

Thermal radio emission of Jovian planets atmospheres, deriving brightness temperature [AAS PAPER 71-109]

19 p3139 A71-37909

Interplanetary medium thermal emission detection, presenting diffuse background radiation upper limits in intermediate IR from sounding rocket data

20 p3288 A71-39114

Atmospheric moisture from Cosmos 243 satellite measurements of intrinsic atmospheric radiothermal emission

20 p3218 A71-39587

Microwave sounding of ocean and earth surface thermal emission and atmospheric water vapor content by Cosmos 243 satellite-borne radiometers

20 p3259 A71-39672

Solar low energy X-ray spectra observation during impulsive bursts, discussing thermal and nonthermal emission properties

21 p3438 A71-40425

Solar thermal radio component observations at 169 MHz with east-west radioheliograph related to helmet and active coronal streamers

22 p3597 A71-41461

Brightness and polarization distributions for supernova remnants IC443 and Puppis A, considering magnetic field orientation and thermal radio emission

22 p3606 A71-42601

Mars surface soil thermophysical properties, temperature and thermal emission from Mariner spacecraft IR radiometer data, correlating with visual images

24 p3867 A71-44439

Raman microwave scattering on Langmuir oscillations, showing suprathermal emission origin in theta pinch plasma

24 p3853 A71-44505

Materials thermal accommodation coefficient and emissivity dependence on surface roughness, noting correlation

24 p3888 A71-44934

THERMAL ENERGY

Shock induced exothermic reactions on boundary layer transition in shock tube, investigating free stream thermal energy release effects

04 p0572 A71-15503

Electromagnetic and thermal energy fluxes during magnetic storms, using interplanetary spacecraft and D variation data

07 p1099 A71-19397

Lunar two cycle interior thermal history influence on maria and crater morphology, noting active and passive phase roles

09 p1520 A71-22836

Laser thermal energy-materials interaction, discussing excess heat buildup, power generation, reflectivity and repetition rates

09 p1458 A71-23406

Small amplitude resonant thermal acoustic oscillations of inviscid polytropic gas contained in finite length tube

11 p1798 A71-25446

Laser quantum theoretical analysis, considering atomic thermal motion, photon emission and absorption induced recoil effects on lasing threshold and operating frequency

14 p2253 A71-29574

Equatorial electrojet as supplementary heat source for tropical region upper atmosphere based on thermal energy release calculation

15 p2399 A71-31964

Particle collision effects on electrostatic probe electron or ion current collection in transition regime as function of relative thermal energy

15 p2409 A71-32107

Laser-induced retinal damage model based on energy interaction modes, including thermal and acoustic transients, vaporization and dielectric breakdown

18 p2863 A71-35955

Integrated waste collection and purification system using radioisotopes for thermal energy in 180-day space mission life support system [ASME PAPER 71-AV-4]

18 p2865 A71-36371

Heat and fictitious forces in variable rest mass relativistic particle dynamics for thermal energy conservation laws interpretation

19 p3162 A71-37641

Electromagnetic and thermal energy fluxes during magnetic storms, using interplanetary spacecraft and D variation data

19 p3053 A71-37821

Thermal or chemical energy conversion to electromagnetic radiation by laser, discussing atomic or molecular processes and thermodynamic limitations

20 p3242 A71-38939

MHD power generator for converting heat into electricity by interacting magnetic field with flowing electrically conducting fluid

21 p3436 A71-40020

Temperature field of thermochemical sensor in automatic control systems, developing thermal energy transport models for circular disk with energy source at center

22 p3537 A71-41443

ATS power supply concepts, considering growth capability, control, reliability, thermal dissipation and weight minimization

22 p3588 A71-41958

Thermal energy requirement for homogeneous solid propellant ignition, measuring flame formation time and temperature

24 p3863 A71-44762

THERMAL ENVIRONMENTS

Thermal environment loads in lunar ambulation, discussing Apollo EVA suit system and internally produced heat

02 p0207 A71-12386

Human tolerances to thermal environment extremes in aerospace activities

02 p0207 A71-12388

Ablative materials performance in high radiative heat flux environments produced by CW carbon dioxide laser [AIAA PAPER 70-864]

03 p0449 A71-14437

QAO 2 design and performance features concerning pointing accuracy and stability, command capability, data handling, thermal environment, orbit constraints, ultraviolet spectroscopy, etc

05 p0818 A71-17128

UK 3 spacecraft support sting for solar simulation and thermal vacuum testing in 2.5 meter test chamber, describing design and construction

06 p0881 A71-18720

Thermal environment effect on human skin temperature and final temperature and tolerance time prediction from early exposure

11 p1725 A71-26117

Temperature uncertainties determination in spacecraft thermal analysis, using influence coefficients obtained from steady state heat balance equation [AIAA PAPER 71-430]

11 p1858 A71-26219

Manned space station optimal thermal control design, investigating heat pipe and semipassive/ air cooled concepts [AIAA PAPER 71-431]

11 p1838 A71-26220

Space station thermal control system design, verifying radiator adequacy by parametric computer analysis with allowance for thermal coating degradation, vehicle attitude and other variables [AIAA PAPER 71-435]

11 p1858 A71-26223

Space shuttle vehicle models, calculating surface flow patterns and pressure and aerodynamic heating distributions for comparison with test data [AIAA PAPER 71-594]

15 p2343 A71-31539

Thermal ground testing of Concorde and Veras, considering static and fatigue testing in heat environment

18 p2899 A71-36464

Human temperature tolerance during exposure to hot and cold environments, using skin temperature as indicator

18 p2859 A71-36875

Respiratory aspects of hyperbaric thermal environments, considering heat exchange by convection

18 p2860 A71-36878

Time constant for perspiration onset in humans exposed to stepwise increase in external heat load

18 p2862 A71-36897

THERMAL EXPANSION

NT THERMAL BUCKLING

Boron additive effects on Ti thermal conductivity and expansion

01 p0102 A71-10787

Be mirrors thermal dimensional instabilities dependence on crystalline anisotropy, discussing X ray quality control technique

03 p0424 A71-13637

Thermal expansion of dilute binary composites concerning ceramic-glass, glass-metal, metal-metal and organic-metal systems

03 p0449 A71-14458

Thermal expansion of unidirectional, angle-ply and complex laminated graphite-epoxy composites, considering fiber orientation, hysteresis and interlayer stress relaxation

03 p0449 A71-14459

Reduced pressure effects on thermal expansion and fragmentation of rocks

03 p0418 A71-14444

Thermal lattice expansion measurements on carbon powders up to graphitization temperatures, using X ray diffraction

04 p0618 A71-14444

Boron fiber-Al alloy composites linear thermal expansion as function of fiber volume fraction and orientation

04 p0615 A71-15154

Group 4 and 5 transition metal carbides thermal expansion determined on quartz dilatometer at various temperatures

05 p0768 A71-16788

Dilatometric thermal expansion method for determining cylindrical solid body thermal conductivity coefficient

05 p0838 A71-16789

Laser produced plasma expansion into vacuum, discussing ion energy angular distributions measurement

06 p0938 A71-18446

Electronic encapsulated assemblies thermal stresses due to components expansion coefficients mismatch [AIAA PAPER 71-109]

07 p1213 A71-19770

Laminate analogy predicting elastic and thermal expansion properties of short fiber reinforced composites, extending to two and three dimensional woven fabric composites

07 p1215 A71-20120

Thermal expansion of gas breakdown plasma in argon under heating by high voltage transient pumped carbon dioxide laser

09 p1463 A71-22788

Materials with prescribed magnetic properties and expansion coefficients developed using relationships between solid solutions structure and physical properties

10 p1623 A71-23904

Spherical plasma ball thermokinetic expansion model, considering solid state laser irradiation

11 p1806 A71-26090

Dissimilar metals welding, emphasizing melting point, linear expansion coefficient, thermal conductivity, electrical resistivity and polymorphic transformation

13 p2072 A71-27888

Physical processes and variations in polar F region, discussing solar photoionization, particle ionization, thermal expansion, electric fields, neutral air wind erosion drag, etc

14 p2234 A71-30038

Coupled thermoelastic disturbances in half space due to thermal shock incident on surface at finite heat expansion rates

14 p2335 A71-30199

Critical parameters in two component thermal ignition system based on Bowes computer evaluation of dimensionless temperature formula

14 p2337 A71-30458

Anisotropic carbon-graphite materials and metal temperature dependence of thermal expansion coefficients, noting approximation by Debye heat capacity function

16 p2601 A71-33710

Welded, bearing and interlocking joints and adhesive bonding in carbon fiber reinforced plastics, discussing anisotropy, thermal expansion and electrochemical corrosion problems

17 p2748 A71-34344

Dynamical thermal expansion effect on plane elastic-plastic stress wave propagation, using classical heat conduction equation

17 p2819 A71-34503

Finite element method stress analysis for evaluating localized stress distributions in thick walled circular tube with step change in thermal expansion [SESA PAPER 1841A]

17 p2819 A71-34534

Composite materials and structures analysis and design, examining elastic constants, thermal expansion coefficients, viscoelastic moduli, conductivities and failure modes [AIAA PAPER 71-366]

18 p2979 A71-36274

Temperature effects on tungsten lattice and Gruisen parameters and thermal expansion coefficients at low temperatures by X ray method

22 p3561 A71-41724

Magnetostriction in antiferromagnetic, spin flopped and paramagnetic phases of hydrated cesium manganese trichloride, studying volume changes and thermal expansion near phase transition

22 p3585 A71-41885

Thermal expansion coefficient and bulk modulus of lunar rocks 10020, 10046, 10057 and 12022.95

23 p3761 A71-43782

Polycrystals thermoelastic characteristics, determining thermal expansion and conductivity macroscopic coefficients

24 p3840 A71-44402

Vertical laminar natural convection boundary layer stability during thermal expansion at large Prandtl number

24 p3886 A71-44422

- Ta-C-WC, Zr-C-WC and refractory compounds thermal expansion coefficient measurements
24 p3838 A71-44738
- THERMAL FATIGUE**
Thermal cycling effect on Al-B composites, considering surface roughening and crack initiation
01 p0103 A71-11279
Superalloy turbine engine guide vane thermal fatigue cracks repair by plasma arc fusion method
03 p0432 A71-13257
Optimal firing temperature schedule during gas turbine loading for minimal thermal fatigue of hot gas path components, considering hollow stationary airfoils
ASME PAPER 70-WA/GT-2] 03 p0470 A71-14116
Thermal fatigue cracks in gas turbine blade models under simultaneous thermal cycling and static tensile loads simulating pulsed regimes
04 p0671 A71-15638
Test facility for fatigue and thermal fatigue of turbine blades in high temperature gas flow
05 p0734 A71-16762
Refractory alloys elastoplastic deformation under cyclic loading, deriving thermal fatigue equations
07 p1129 A71-19155
Thermal fatigue testing apparatus for material longevity, simulating tensile stresses due to centrifugal forces on gas turbine engine blade during thermal loading
08 p1271 A71-20837
Automatic materials testing device for thermal fatigue and strength under programmed loading
08 p1271 A71-20838
Heat resistant materials strength characteristics with long service periods, formulating equation for time dependence of rupture resistance
08 p1306 A71-21111
Thermal fatigue testing of materials under static load with allowance for creep
09 p1426 A71-22497
Thermal fatigue tests of high temperature Ni and Co base alloys by fluidized bed technique
09 p1469 A71-22812
Concorde thermal fatigue test installation, controlling temperature by transfer temperature variation in single heat exchanger block
09 p1430 A71-23580
Thermal fatigue and service life of thin walled tubular pearlite steel notched specimens in various oxidizing media
10 p1626 A71-24191
Gas turbine blades fatigue crack development and failure analysis under thermal cycling tests, considering chemical processes and thermal and mechanical stresses
13 p2149 A71-28117
Low cyclic failure resistance at elevated temperatures and static defects calculation, based on fatigue and empirical endurance curves
13 p2149 A71-28122
Gas turbine blades thermal fatigue test and analysis, investigating static tensile loading effects on heat resistance under thermal cycling
13 p2149 A71-28124
Turbine blade profiles nonstationary temperature fields during thermal fatigue tests, measuring surface temperature via thin film thermocouples
14 p2252 A71-30265
Refractory metals fatigue testing under nonstationary thermal loads, considering test data reliability improvement
14 p2259 A71-30268
Thermal fatigue cracking of gas turbine blades in fuel combustion product flow, investigating surface composition, microhardness and structure under simulated loads
15 p2469 A71-32227
Simulated turbine blade thermal fatigue testing under transient and steady state heating and spanwise loading, obtaining crack initiation and propagation data
[SAE PAPER 710459] 17 p2792 A71-34500
Test apparatus for mechanical/thermal fatigue and vibration strength of turbine blades in high temperature gas flow
17 p2724 A71-35461
Refractory alloys elastoplastic deformation under cyclic loading, deriving thermal fatigue equations
17 p2760 A71-35653
Male and female physiological responses to heat stress, discussing sweating, skin and body temperature, heart rate and metabolism
18 p2859 A71-36871
Stress concentration and defects effect on crack initiation and propagation in austenitic steels thermal fatigue
20 p3307 A71-39022
- THERMAL INSTABILITY**
Thermally induced preload changes in roller bearings due to temperature gradients measured, using strain gage bridges and thermocouples
01 p0088 A71-11006
- Thermal instabilities in rapidly rotating fluids with buoyancy force and depth gradient, noting geophysical analogy of self gravitating sphere
03 p0409 A71-13727
Fuel rod bundle boundary layer in longitudinal fluid flow, investigating turbulent temperature and pressure pulsations
04 p0684 A71-15504
Tokamak copper shell as feedback control device for toroidal plasma, considering stabilization of thermal instability
06 p0932 A71-17462
Nonlinear subgrid scale eddy viscosity formulation for turbulence generated by mean shear or thermal instability at large Reynolds number
07 p1094 A71-20615
Ventilation rates and thermal factors of sensitive elements in radiosondes, using wind tunnel tests
11 p1761 A71-25382
Thermal fluctuations in earth upper atmosphere, related to satellite deceleration and X ray solar radiation changes by autocorrelation and cross correlation analyses
11 p1817 A71-25822
Adversely heated fluid flow layers between rigid boundaries, studying thermal instability due to formation of stationary secondary rolls
[ASME PAPER 71-APM-00] 18 p2985 A71-36269
Unstable thermal stratification and critical Reynolds number effects on dynamic instability of Ekman boundary layer vortex rolls
20 p3257 A71-39438
- THERMAL INSULATION**
Thermal insulation and confinement of resistance heated He plasma in Uragan stellarator with large shear
01 p0132 A71-10678
Mammalian hair effectiveness as insulation, using biotelemetry for deep body temperature measurement
01 p0023 A71-10886
Nonsupporting aerodynamic foam material thermal insulation system with reliability for cryogenic rocket propellant tank, considering polyurethane and polyvinylchloride
01 p0164 A71-11541
Zirconium carbide fiber insulating materials, examining heat conductivity coefficient
05 p0838 A71-16781
Steady laminar convection in infinite layer of heated homogeneous fluid between constant temperature rigid plate and thermal insulator
05 p0838 A71-16962
Energetic lifetime, equilibrium and thermal insulation of ohmically heated plasma in stellarator
06 p0937 A71-18350
Iterative solution for radiation-dominated heat balance about heat shield or superinsulation nodes, testing performance in thermal analyzer program
07 p1221 A71-18905
Stationary temperature field and stresses in infinite body with thermally insulated penny shaped crack, assuming heat source and sink symmetrical distribution
07 p1217 A71-20462
Multilayer insulation systems for cryogenics protection aboard spacecraft, considering mechanical properties, radiation shielding, component evacuation rate and outgassing
08 p1375 A71-21748
Optical-electrical analogy of thermal radiation impedance of thin dielectric films in low temperature insulation
09 p1494 A71-23003
Superinsulation for long term storage of cryogenic propellants in space tanks using double aluminized Mylar with Dacron needles
09 p1546 A71-23009
Edge losses effects on thermal conductivity of thermal insulations at high temperature measured by guarded hot plate method
10 p1694 A71-23907
Ablative thermal insulation materials testing for naval missile propulsion system application
11 p1789 A71-26032
Numerical and scale modeling interaction for spacecraft thermal design verification
[AIAA PAPER 71-439] 11 p1838 A71-26227
Reradiative and high temperature insulative space shuttle thermal protection systems with actively cooled, passively cooled and uncooled substructures
[AIAA PAPER 71-443] 11 p1838 A71-26228
Ceramic fiber external insulation thermal protection systems for space shuttles, considering use with Al and Ti
[AIAA PAPER 71-442] 12 p1985 A71-26763
Cryogenic propellant tank thermal insulation system based on polypropylene oxide, polyurethane polyvinylchloride and polymethacrylimide foams, discussing design, technology and model tests
12 p1985 A71-26834
High energy hydrogen-oxygen launch vehicle thermal insulation system, discussing closed cell rigid polyvinyl chloride foam mechanical characteristics, use and tests
12 p1985 A71-26835
- Space shuttle comparison with transport aircraft, discussing high thermal resistant and cryogenic insulator material concepts, with application to Concorde structural computations
12 p1973 A71-27605
NASA space station design, describing operational procedures, structure, meteoroid, thermal and radiation insulation and living quarters
15 p2498 A71-31137
Liquid hydrogen rocket propellant tanks insulation problems in space shuttle and orbiter
15 p2499 A71-31216
Heat conductivity coefficient of thermal insulation material made from zirconium carbide fibers, giving measurement procedure
16 p2662 A71-33033
Neutron irradiated and unirradiated Ta sheathed BeO insulated grounded junction thermocouples drift measurement
18 p2916 A71-36046
Thin thermally insulating film on metallic sample, showing vapor layer elimination during liquid nitrogen quenching
18 p2934 A71-36172
Ceramic fibrous materials for high temperature insulation, discussing practical approach to obtain lower thermal conductivity
18 p2939 A71-36668
Maximal sweat evaporative heat loss and permitted work load measurements as function of temperature and clothing insulation
18 p2872 A71-36861
Meteorological rocket nose portion thermal regime, determining housing, insulation coating and compartments temperature
19 p3172 A71-38632
Meteorological rocket nose thermal shield, discussing design and effectiveness
19 p3172 A71-38636
Heat transfer by radiation, conduction and convection, including various types of thermal insulation
20 p3311 A71-39244
Polyvinyl chloride foam insulation system for liquid hydrogen-liquid oxygen space vehicles tested under groundhold and simulated flight conditions
20 p3253 A71-39269
Spray foam insulation for Saturn S-2 stage, consisting of phenolic honeycomb core composite purged with helium
20 p3312 A71-39270
Open cell lightweight cryogenic insulation for reusable liquid hydrogen fueled vehicles including space shuttle
20 p3312 A71-39271
Lateral heat transfer measurements in cryogenic multilayer insulation, considering effective thermal conductivity
20 p3312 A71-39272
Temperature decay method for determining superinsulation thermal conductivity, equating insulation heat transfer rate to calorimeter plate heat loss
20 p3312 A71-39273
Elastomeric rocket motor thermal insulants ablation, considering composite properties, heat transfer, compounding and tests
21 p3406 A71-40603
Integral and pointwise estimates of insulated cylinder temperature field spatial decay for semilinear parabolic equations
21 p3473 A71-41186
Low temperature thermal insulation using diffraction effects of multilayer perforated reflecting screens
22 p3622 A71-42678
Insulators normalized theory application to selective transparent insulators photosynthesis operation
22 p3484 A71-42843
Porous fiber reinforced composite low density heat insulating materials thermal conductivity measurements, showing energy transport by heat transfer mechanisms
23 p3784 A71-44341
- THERMAL NEUTRONS**
GaAs transmutational doping by slow neutrons irradiation, using Cd and In screens for impurities distribution control
07 p1175 A71-19219
Endurance limit of construction materials under fast and thermal neutron irradiation in reactor channel
16 p2598 A71-33986
- THERMAL NOISE**
Optically pumped rubidium maser short term frequency instability caused by thermal noise and resonator temperature and pumping power fluctuation
01 p0095 A71-11211
Variable microwave thermal noise temperature standard generator with output ranging from below 40 to above 370 K
02 p0250 A71-12139
Earth station equipment for Intelsat 4, discussing thermal noise, transmitters, wideband receivers and demodulators
02 p0224 A71-12829

Thermal DC noise generated in plasma at electron-ion collisions, using quantum mechanics for noise frequencies in EM radiation RF spectra

03 p0463 A71-13345

Oscillator signal frequency instability relationship with spectral purity based on thermal noise effects [ONERA-TP-912]

05 p0722 A71-16706

Thermal noise perturbed oscillator RF spectrum determination from frequency instability in time domain

[ONERA-TP-927] 07 p1075 A71-19265

Noise behavior of Schottky barrier gate FET at microwave frequencies, discussing effects of carrier velocity saturation and parasitic resistances on noise parameters and measurement method

08 p1261 A71-20741

Zero point fluctuations measurement standards for thermal and quantum noise, considering microwave network analytic application

11 p1733 A71-26366

Thermal noise measurement of superconducting coaxial lambda/2 resonator at 2.46 GHz with ruby traveling wave maser and tunnel diode amplifier setup

12 p1887 A71-27010

Thermal noise in space charge limited solid state diodes with field dependent mobility and hot carriers

14 p2284 A71-30502

Primary and secondary standardization and precision measurement of thermal noise power at various radio frequencies and temperatures

14 p2204 A71-30977

Optically pumped rubidium maser short term frequency instability caused by thermal noise and resonator temperature and pumping power fluctuations

17 p2750 A71-34262

Computer simulation of error probability performances of binary coherent PSK system under thermal noise and intersymbol and interchannel radio interferences effects

17 p2707 A71-35476

Turbulence growth during parametric wave excitation, observing thermal noise effects

19 p3104 A71-37852

Distributed tunnel diode traveling wave amplifier load noise thermal and shot components, noting impedance boundaries

20 p3206 A71-39814

Input admittance, drain noise and induced gate noise measurements in search for excess gate noise in large geometry MOSFET

24 p3863 A71-45355

THERMAL PLASMAS

Ray tracing in warm collisionless magnetoplasmas based on wave dispersion relation, discussing satellite communication

01 p0137 A71-11612

Thermal magnetospheric plasma densities from hydromagnetic whistlers dispersion characteristics by normalized dispersion curve method

03 p0419 A71-14521

Supernova remnant X ray and radio emission secular behavior, considering hot plasma and synchrotron models and continuous injection

04 p0640 A71-14874

Short dipole antenna impedance in warm isotropic plasma using Vlasov theory

04 p0553 A71-15221

Thermal Ar plasma with gas additives as standard intensity light source of optically thick spectral lines, using interpolation and Kirchhoff-Planck function

07 p1168 A71-19323

Center fed dipole antenna with displaced feed points in warm plasma medium, calculating radiation patterns

08 p1264 A71-21221

Admittance of aperture antenna radiating into lossy warm overdense plasma half space, considering electron energy

09 p1505 A71-23521

Electrostatic field second order penetration into Vlasov warm electron plasma, using electron velocity distribution models

10 p1647 A71-23890

Photoelectron energy loss rate to ambient electrons in thermal plasma, noting geomagnetic field influence

10 p1662 A71-24558

Nitric oxide ion two body recombination with nitrogen dioxide and trioxide molecular ions, examining ionic neutralization reactions in decaying dilute thermal plasma at 300 degrees K

11 p1801 A71-25297

Anomalous dispersion and instability in solar wind plasma with thermal anisotropy and high beta ratio, applying magnetosonic wave-particle interactions

11 p1816 A71-25754

Satellite square loop antennas radiation resistance in warm plasma, comparing calculated values with Ariel 3 satellite measurements

12 p1883 A71-27700

Computer simulated semiinfinite uniform plasma expansion in vacuum, showing inapplicability of thermal velocity burst ion model

13 p2104 A71-27846

Electric field angular distribution of short radio frequency probe in warm anisotropic plasma under magnetic field

13 p2104 A71-27852

Magnetospheric two component plasma model, considering thermal and suprathermal spectra

13 p2060 A71-28432

Diffusion measurement of highly ionized thermal Cs plasma in magnetic field by Langmuir probe, determining density profile

13 p2106 A71-28450

Optimal thermonuclear plasma confinement considering external electromagnetic field as control variable, based on Boltzmann-Vlasov model

13 p2107 A71-28832

Radiation resistance of Alford loop antenna immersed in warm plasma, comparing theoretical values with measurements from Ariel 3 satellite experiment

13 p2034 A71-29290

Far zone field and radiated power equations for corner driven traveling wave loop antenna in warm plasma, comparing data for Ariel 3 satellite

14 p2283 A71-31040

Warm plasmas impedances and power transfer near lower hybrid resonance, including electron pressure effects in full electromagnetic treatment

15 p2456 A71-31923

Thermal electron density fluctuations in weakly ionized gas from viewpoint of particle diffusion in single charged particle phase space, considering incoherent scattering

15 p2458 A71-32392

Current distribution on grid type dipole antenna in warm isotropic plasma, using direct source approach and boundary value analysis

17 p2698 A71-34430

Thermal electrodeless plasma generation below RF range through magnetic induction heating, applying to argon glow and arc discharges

17 p2788 A71-34869

Far field radiation patterns and optimum design of horizontal rhombic antenna in warm plasma, using linearized hydrodynamic theory

18 p2875 A71-35969

Laser pulse heated target with thermal plasma production, obtaining target surface temperature as function of time and vaporization rate

20 p3242 A71-38845

Plasmasphere evening ionization anomalies observations from spherical electrostatic analyzers onboard OV3-1 polar orbiting satellite, noting thermal plasma depletion during orbit night sector

20 p3225 A71-39741

Particle model measurements of collision and heating times in two dimensional thermal computer plasma

21 p3423 A71-40843

Solar radio bursts and noise storms frequency band spectra, investigating warm plasma wave propagation and mode coupling theories

22 p3579 A71-41462

THERMAL POLLUTION

Global environmental monitoring and remote sensing from satellites, considering thermal, air and water pollution

22 p3534 A71-41961

ERTS remote sensing techniques, discussing objectives for southeastern U.S. in terms of agriculture, forestry, strip mine land reclamation and thermal pollution

22 p3534 A71-41967

THERMAL POWER

U TURBOGENERATORS

THERMAL PROPERTIES

U THERMODYNAMIC PROPERTIES

THERMAL PROTECTION

Thermal design of space experiment by analytical model for temperature regime acceptable to all experimental elements

01 p0017 A71-11454

Blunt body nose protection from radiation-convective heat transfer, using porous injection of radiation absorbing substance

04 p0685 A71-15518

Heat transfer boundary conditions determination in studying heat protective coatings effectiveness, discussing measurement methods for stagnation temperatures and heat fluxes from exhaust gases

04 p0600 A71-15643

Antihat protective clothing effectiveness for aircraft crews, discussing outer coating reflectivity and emissivity, insulating layer and internal surface

05 p0715 A71-16934

Flight personnel green protection system from nuclear weapons high intensity thermal effects

06 p0858 A71-17609

Temperature profile similarity and thermal protective coating thickness for single reentered spacecraft [AIAA PAPER 71-37]

06 p0916 A71-18498

Flammability and heat transfer characteristics of flame retardant cotton, Nomex and polybenzimidazole (PBI) protective fabrics

07 p1145 A71-19573

Space shuttle structures and materials, considering booster arrangements thermal protection, high temperature metals and composite materials

07 p1216 A71-20722

Optimal weight of aerodynamic heat protective layers of stressed skin and optimal efficiency of cooling system for hypersonic aircraft components

08 p1375 A71-20474

Space transportation vehicles thermal protection systems, discussing reusable ceramic and oxidation resistant carbon-carbon composite materials properties and weight saving potential [SAE PAPER 700771]

08 p1375 A71-21374

Arc heated duct facilities providing high temperature supersonic turbulent boundary layer flows over large samples for orbital logistic vehicle thermal protection tests

[AIAA PAPER 71-262] 09 p1429 A71-23069

Organo-ceramic composites for thermal protection of aerospace vehicles, discussing heat sink property

09 p1483 A71-23207

Thermal louvers radiative heat transfer characteristics with solar irradiation effects, using Monte Carlo method

11 p1854 A71-25194

Thermal louver models in space simulation chambers, determining heat dissipation, optical efficiencies, blade geometry and solar radiation effects

11 p1854 A71-25194

Protective coatings of Ta, Nb and TD alloys for high performance thermal protection systems, discussing space shuttle reentry heat shield

11 p1778 A71-25554

Ablative polymers for thermal protection of aerodynamic surfaces, propulsion structures and ground equipment, discussing energy absorption of various polymeric materials

11 p1789 A71-26030

Ablative thermal insulation materials testing for naval missile propulsion system application

11 p1789 A71-26030

Reradiative and high temperature insulative space shuttle thermal protection systems with actively cooled, passively cooled and uncooled structures [AIAA PAPER 71-443]

11 p1838 A71-26228

Space shuttle thermal protection system optimization by numerical parameterization, discussing temperature constraints and material rearrangement effects

[AIAA PAPER 71-444] 11 p1839 A71-26229

Performance prediction of fixed wing leading edges: radiative, ablative and active cooling thermal protection systems and system weights comparison for space shuttle entry mission [AIAA PAPER 71-445]

11 p1839 A71-26230

Lightweight oxidation resistant carbon-carbon composites for space shuttle leading edge component thermal protection [AIAA PAPER 71-446]

11 p1790 A71-26231

Spacecraft thermal control coatings for long duration exposure to near-earth orbital conditions, determining optical properties degradation and solar absorptance [AIAA PAPER 71-454]

11 p1859 A71-26237

System and component models for spacecraft thermal control design, considering materials, environmental degradation, measurement errors, manufacturing and quality assurance [AIAA PAPER 71-456]

11 p1859 A71-26238

Thermal control, pressure survival and structural tradeoffs of Jovian atmospheric probe for mission parametric studies [AIAA PAPER 71-482]

11 p1839 A71-26257

Ceramic fiber external insulation thermal protection systems for space shuttles, considering use with Al and Ti [AIAA PAPER 71-442]

12 p1985 A71-26763

Space shuttle thermal protection systems, discussing design requirements and constraints, materials selection, tradeoff and cost effectiveness studies

12 p1971 A71-26984

Modified low density polyisocyanurate foams for low heating rate thermal protection, considering high char yield with reduced surface recession

13 p2091 A71-28178

Radioisotope heat sources protection from reentry ablation and thermal stress with outer anisotropic pyrolytic graphite shield

13 p2099 A71-29259

Film cooling as solid surfaces protection in high temperature environments, considering two and three dimensional secondary compressible and incompressible flow geometries

14 p2337 A71-30244

Porous refractory materials for thermochemical protection against high temperature plasma flow, discussing effectiveness in erosive wear reduction

15 p2432 A71-32164

Niobium alloy use for space shuttle thermal protection, examining oxidation and mechanical properties

17 p2757 A71-34495

Reusable space shuttle optimization, discussing earth-to-orbit transportation, economic aspects,

Booster vehicles design, propellant cryogenic tanks and thermal protection
[AIAA PAPER 71-805] 17 p2814 A71-35430

Surface temperatures and ablation mechanism of combustion protective plastics reinforced by silica under intense heating measured by IR micropyrometer [ONERA-TP-962] 18 p2984 A71-6028

Mechanical design of frictionless bimetal actuator power system for spacecraft thermal control [ASME PAPER 71-AV-39] 18 p2870 A71-36406

Multilayer insulation systems development and selection for cryogenics thermal protection on space vehicles, considering mechanical properties, radiation shielding, components, evacuation rate and outgassing 19 p3171 A71-38547

Thermal protection and electrical and mechanical evaluation of SNAP 19 radioisotope thermoelectric generator for integration with Viking Mars lander 20 p3267 A71-38964

Thermal protection of two dimensional supersonic nozzle fed with hot air by tangentially injected cold gaseous films for convergent and constant section ducts 20 p3314 A71-39415

Space transportation orbiter design covering thermal protection, aerodynamics and cross range problems during earth reentry 22 p3609 A71-41979

Pressure sensors thermal protection by porous Zr disk as heat shield, considering acoustic transparency, linearity, transient response and air flow resistance [ONERA-TP-957] 22 p3547 A71-42501

THERMAL RADIATION

Thermal pattern visualizing and interpretation by imaging in far IR, noting equipment and uses of thermography in medicine, science and technology 01 p0078 A71-10135

Rayleigh-Gans-Born approximation application to thermal radiation of reflecting convex plasma sphere, cylinder and ellipsoid 02 p0288 A71-11633

Satellite sounding of atmospheric pollution by spectral analysis of outgoing thermal radiation 02 p0241 A71-11689

Planetary and lunar thermal radio emission and brightness temperature measurements using sensitive receivers and large aperture radio telescopes 02 p0309 A71-12155

Thermal radiation effects on M-2 double base solid propellant ignition, deflagration and burning rate 02 p0298 A71-12851

Earth surface and atmosphere thermal radio emission measurement by radio telescope on Cosmos 243 satellite 03 p0409 A71-13420

Thermal radiation from hot water vapor and carbon dioxide imbedded in cool atmosphere, using extended molecular band models 03 p0518 A71-13649

Steady state node simplification technique for thermal radiation in gray enclosures, including computer program 03 p0522 A71-14446

Escaping-earth radiation actinometric measurement by meteorological satellites, discussing seasonal thermal radiation variations in Southern Hemisphere polar regions 04 p0579 A71-14637

Thin metallic films thermal radiation properties at cryogenic temperatures, calculating spectral normal emissivity as temperature wavelength and thickness function 04 p0684 A71-15510

Thermal radiation absorbing and emitting medium in flow between parallel plates, examining heat transfer for simultaneous radiation and convection 04 p0685 A71-15517

Nongray thermal radiation effect on laminar forced convection over heated horizontal flat plate, determining temperature profiles for optically thin and thick boundary layers 04 p0688 A71-15741

Soviet monograph on thermal sounding of atmosphere by satellite covering moisture content, cloud surfaces and stratosphere temperatures and thermal radiation distribution 05 p0738 A71-16197

Surface roughness and thermal radiation effects on rural and urban boundary layer turbulence and diffusion by wind fluctuations observations 05 p0777 A71-16665

Self similar thermal wave in two-temperature plasma under laser heating for different pulse duration and energy absorption values 06 p0936 A71-17689

Spacecraft sterilization by microbial inactivation, comparing thermoradiation and dry heat methods 06 p0853 A71-17959

Thermal radiation from finite cylindrical particle cloud, determining far field angular distribution by Monte Carlo method [AIAA PAPER 71-78] 06 p1008 A71-18535

Thermal and bleaching waves as diffusion phenomena in opposite limits, discussing laser heating [AIAA PAPER 71-109] 06 p0928 A71-18559

Solid propellant combustion instability, considering burning propellant mass flux response to periodic thermal radiation 06 p0948 A71-18645

[AIAA PAPER 71-209] Soviet book on thermal radiation sensing covering system functional circuits, radar conversion, military application and personnel training 07 p1060 A71-19100

Surface temperature radiation interaction between two solid half spaces using Green function reduction method 07 p1223 A71-19254

Thermal diffusivity in disks and rods irradiated by sinusoidally modulated thermal radiation beam, measuring temperature phase difference across front and back faces 07 p1223 A71-19622

Phonon excitations radiated from thermal source in He II below 0.3 K, using carbon film detectors 09 p1497 A71-22418

Optical-electrical analogy of thermal radiation impedance of thin dielectric films in low temperature insulation 09 p1494 A71-23003

Ground water flow into Lehigh River, Pennsylvania identification by thermal IR imagery 09 p1439 A71-23217

Balloonborne radiometric instrumentation for solar and thermal radiations upward and downward flux measurements, discussing net radiation balance as function of solar elevation 09 p1515 A71-23558

Matter and antimatter separation mechanism in universe based on thermal radiation thermodynamic properties 10 p1665 A71-23739

Venusian atmosphere subcloud layers intrinsic outgoing thermal radiation and IR spectrum transmissivity from satellite temperature, pressure, moisture content and chemical composition data 10 p1681 A71-25128

Extinction parameters of submicron carbon, tungsten and Si particles in hydrogen measured at various temperatures, discussing scattering amplitude functions and Monte Carlo calculations [AIAA PAPER 70-838] 11 p1854 A71-25507

Venus thermal radiation limb darkening measurements, indicating complex atmospheric structure 11 p1824 A71-25699

Airlock thermal capacitor for radiator performance augmentation by absorbing heat on orbit hot side and rejecting on cold, providing coolant temperature level damping [AIAA PAPER 71-429] 11 p1858 A71-26218

Turbulent boundary layer thermal flux fluctuation spectral distribution determination by applying fluctuation diagram method to filtered signals 12 p1985 A71-26828

Periodic disturbances propagation in radiating gray gas, using singular eigenfunction expansions 13 p2165 A71-29356

Nuclear light bulb engine based on thermal radiation energy transfer from gaseous uranium fuel through internally cooled transparent wall to seeded hydrogen [AIAA PAPER 71-642] 14 p2274 A71-30719

Thermal X ray sources associated with rotating collapsed stars with surrounding plasma shells, discussing plasma density profile and electron distribution in stellar magnetosphere 15 p2497 A71-32762

IR line radiation from galactic center thermal radio sources, determining element abundances 16 p2633 A71-33336

Long range thermoluminescent dating of meteorites and tektites, discussing dependence on thermal release of trapped carriers, radiation saturation and instrumental errors 16 p2638 A71-33518

Plane thermal waves in heat conducting and radiating/ emitting and absorbing/ medium occupying half space x greater than zero [DFVLR-SONDDR-133] 16 p2664 A71-34141

Thermal radiation effect on normal shock wave structure in gas-particle flows, deriving approximate closed-form solution for gray absorbing particle cloud 17 p2727 A71-34879

IR astronomy review covering semiconductor detectors and astronomical radiation sources including thermal and nonthermal sources 18 p2959 A71-35909

Wide heat load range space radiator design for space mission environmental control/life support system, using stagnation control [ASME PAPER 71-AV-5] 18 p2865 A71-36372

Gas flow energy transport, discussing thermal radiation, radiant flux density, planetary atmosphere entry, thermodynamic equilibrium and differential approximations 18 p2847 A71-36426

Greenhouse effect in gray planetary atmosphere, showing thermal radiation generation and scattering with principles of invariance 18 p2970 A71-37049

Lunar interior thermal radiation measurement in meter wavelength range during period of solar radio

image behind limb, showing inverse temperature gradient with depth 19 p3138 A71-37756

Indirect reduction of vertical atmospheric water vapor profile from measured outgoing thermal radiation by regularization method 19 p3090 A71-37966

Earth upper atmosphere outgoing thermal radiation radiance calculation in near IR spectrum 19 p3054 A71-37968

Atmospheric pressure and temperature inhomogeneities effects on thermal radiation transmission function of water vapor 19 p3090 A71-37973

Radiation energy density and radiation heat flux in small rectangular cavity, assuming modes excitation spectrum according to Planck distribution function [ASME PAPER 71-HT-16] 19 p3164 A71-37987

Optical characteristics of thermal IR scanners, using mirrors and prisms in parallel or converging ray pencils and rotating wedges 19 p3068 A71-38709

Radiometric measurement of total normal emittances of real surfaces at cryogenic temperatures 20 p3313 A71-39289

Surface cover materials thermal radiation characteristics and radiation resistance of plastics and solar cells, discussing friction in vacuum and spacecraft surface contamination by outgassing 20 p3210 A71-39453

Normal emission factors of dielectric materials at 1000-1500 C, using black bodies in study of thermal radiation of refractory materials 20 p3254 A71-39960

German monograph on plasma layer temperature distribution in optical resonator covering spectral distribution of thermal radiation 21 p3379 A71-40749

Parametric differentiation solution accuracy and stability for temperature profile and heat flux behind one dimensional hypersonic shock, including thermal radiation 21 p3409 A71-41016

Aircraft heat viewer for underlying surfaces radiation properties, suggesting qualitative survey type thermal aerial photo combination with simultaneous radiometric measurements 21 p3383 A71-41300

Pyroelectric detector linear arrays for IR thermal imaging at room temperature 22 p3543 A71-42131

Thermal radiation effect on laminar boundary layer of nonabsorbing fluid for plane heat emitting surface under natural and forced convection 22 p3622 A71-42680

Midlatitude ionosphere and magnetosphere thermal protons dynamic behavior, investigating magnetic storm effects 23 p3720 A71-43129

Thermal radiative cooling system characteristics determination allowing surface material thermal conductivity and blackness degree dependence on temperature 23 p3782 A71-43919

Nonstationary radiative heat transfer between cylindrical body and ambient medium, determining regular heating condition region 23 p3782 A71-43921

Thermal radiation hemi-ellipsoidal and hemispherical collectors efficiency characteristics from Monte Carlo simulation for focusing photon bundle trajectories 23 p3783 A71-44191

Two dimensional radiative heat transfer in absorbing-emitting medium bounded by nonisothermal gray walls from Monte Carlo simulation, showing gas emissive power distribution 23 p3784 A71-44276

Thermal and nonequilibrium microwave emission from colliding plasma beams in transverse magnetic mirror field 24 p3854 A71-44517

Radiative thermal flux model of Venus atmosphere, using Venera data and greenhouse effect 24 p3870 A71-44822

Surface of revolution annular elements thermal radiation and heat exchange for propellant schematization, attachment to missile wall and opening into ambient medium 24 p3889 A71-44970

THERMAL RADIO EMISSION

U RADIO EMISSION

U THERMAL EMISSION

THERMAL REACTORS

Compact fast reactor design for space power with rotating fuel drums, Mo alloy reflectors and honeycomb support structure 16 p2606 A71-33252

THERMAL RESISTANCE

Junction-casing and junction-ambient medium thermal resistance determined in power transistors and diodes 01 p0055 A71-11125

Gas turbine engine Ni alloys heat resistance, examining fatigue life and creep properties at various temperatures and test durations

05 p0767 A71-16754

Thermal resistance of thermal p-n junction semiconductor microwave limiter diodes in continuous and pulsed mode operation

06 p0873 A71-17543

Thermal resistance to heat transfer at interface between hard smooth flat surface and softer turned surface

[AIAA PAPER 71-80]

06 p1008 A71-18537

Heat resistant extended life carbon fiber/polyimide resin composites, noting aerospace applications

[PLASTICS INST. PAPER 34]

08 p1321 A71-20920

Air to air and air to ground missile zinc silver oxide batteries capabilities, including energy density, long storage life and shock and temperature resistance

08 p1236 A71-21104

Heat resistance in air of Co-Cr alloys as function of chemical composition

08 p1317 A71-21763

Kovpak method for estimating and extrapolating heat resistance characteristics, considering alloy long term strength

09 p1538 A71-22627

Fe-Cr-Zr ternary alloys, investigating Zr effect on high temperature hardness and heat resistance

09 p1473 A71-23228

Aluminum high temperature resistant diffusion type coatings structure and chemical composition, outlining turbine blades testing for thermal shock, oxidation and sulfur and sea salt corrosion

09 p1474 A71-23287

Prediction of metals heat resistance increase by thermomechanical treatment, considering Ni-Al alloy

09 p1477 A71-23332

Fine structure and heat resistance of thin Ni-Cr alloys specimens after prolonged exposure to high temperatures under tensile loads

09 p1480 A71-23703

Degradation rate tests on adhesive bonded sandwich panels of temperature resistant composite structural materials at varying atmospheric pressures

10 p1614 A71-24073

Long term exposure effects on high temperature resistant supersonic aircraft fuel tank sealants

10 p1631 A71-24081

Thermal resistance estimation for machine parts of heat resistant alloys under real working conditions

10 p1686 A71-24190

Heat resistant plastics, considering thermal endurance characteristics and use of high strength fillers in aerospace industry

10 p1634 A71-24580

Difunctional epoxy resins from dihydroxydiphenyl sulfone/bisphenol S, obtaining increased heat resistance and thermal stability

11 p1787 A71-25424

Thermal contact resistance measurements between sliding contacts after load application under various temperatures, using transient pulse technique

[AIAA PAPER 71-438]

11 p1858 A71-26226

Nb and Mo doped Ni-Al alloy with Ni-Nb additions, obtaining diagrams of composition versus heat resistance in high temperature bending tests

12 p1916 A71-26968

Space shuttle comparison with transport aircraft, discussing high thermal resistant and cryogenic insulator material concepts, with application to Concorde structural computations

12 p1973 A71-27605

Aircraft power plants sealing materials, emphasizing porous cermet seals heat resistance under thermal cyclic loads

12 p1895 A71-27688

Low cyclic failure resistance at elevated temperatures and static defects calculation, based on fatigue and empirical endurance curves

13 p2149 A71-28122

Gas turbine blades thermal fatigue test and analysis, investigating static tensile loading effects on heat resistance under thermal cycling

13 p2149 A71-28124

Computerized use of transient thermal resistance and power pulses superposition to calculate instantaneous transistor junction temperatures for various pulse conditions

13 p2038 A71-28770

Heat sink requirements in transistor devices, examining temperature dependence of thermal resistivity and electrical capacitance

14 p2284 A71-30631

Ti-Al-V alloys heat resistance relationship to phase structure from bending test at high temperature

15 p2426 A71-31404

Heat resistant metals long time creep prediction at low stresses or temperatures

15 p2428 A71-31859

Nonporous polycrystalline silicon carbide production by reaction sintering, applying to high temperature technology

15 p2430 A71-32142

Optimum temperature for Zr and Mo soldering of graphite materials with formation of carbide interlayer for ensuring maximum heat resistance

15 p2439 A71-32145

Power and exponential time dependences of long term creep strength for wide stress range, assuming linear thermal resistance

15 p2433 A71-32228

Al-Cu-Li-Mn and magnesium/rare-earth-element alloys heat resistance and microhardness, determining strengthening by intermetallics

16 p2597 A71-33926

Gas turbine engine steels and Ni alloys heat resistance, examining fatigue life and creep properties at various temperatures and test durations

17 p2759 A71-35453

Temperature variations effect on TRAPATT microwave oscillator parameters, considering upper temperature limit dependence on heat dissipated in diode and heat sink thermal resistance

18 p2895 A71-36988

Ti alloys heat resistant properties evaluation for long service under various heat treatment conditions, considering tensile properties, fracture toughness and microstructure

19 p3082 A71-38420

High density packaging effects on multilayer interconnection board reliability tested in thermal environments

21 p3352 A71-40437

Roughness role in liquid He-solid boundary thermal resistance, calculating heat transfer coefficient

21 p3416 A71-41122

X ray analysis of scale formation in precipitation hardened nickel, investigating thermal resistance and oxidation rates

23 p3691 A71-43520

High power semiconductor devices in pulsed operation mode for transient thermal resistance and p-n junction temperature estimation

23 p3652 A71-43584

Zirconium carbide eutectic and supereutectic alloys preparation with graphite addition, determining heat resistance under thermal cycling tests

23 p3697 A71-44025

Refractory materials heat resistance criteria, taking into account hollow cylinder thermal stress distribution

23 p3698 A71-44212

Thermal contact resistance of adhesive joints as function of adhesive solidification pressure and temperature and of joint surface physicochemical and geometrical parameters

24 p3831 A71-45024

Thermal resistance, junction temperature and maximum power meter for semiconductor transistors and diodes with/without heat sinks

24 p3810 A71-45203

THERMAL SHIELDING U HEAT SHIELDING THERMAL SHOCK

Physiological effects of heat exchange between human organism and ambient medium by evaporation, radiation, conduction and convection

01 p0028 A71-11597

Thermal shock physiological effects, determining skin-air convective heat exchange coefficient

06 p0860 A71-18190

Aluminum high temperature resistant diffusion type coatings structure and chemical composition, outlining turbine blades testing for thermal shock, oxidation and sulfur and sea salt corrosion

09 p1474 A71-23287

Concorde environmental testing, considering endurance tests, thermal shock rigs and plant for simulating air supply from compressor stages of aircraft gas turbine engines

09 p1430 A71-23583

German monograph on thermal shock experimental analysis covering derivation of method for determining temperatures and thermal stresses in nuclear reactor structures

10 p1697 A71-25036

Lunar surface properties, noting shock effects from impact induced pressures and temperatures

11 p1834 A71-26453

Collisionless plasma thermal shock wave, showing heat in electron component transportable along magnetic field at lower rates than thermal velocity

13 p2106 A71-28425

Coupled thermoelastic disturbances in half space due to thermal shock incident on surface at finite heat expansion rates

14 p2335 A71-30191

Mechanical properties of composites consisting of Al matrix reinforced by boron fibers, considering high temperature creep, corrosion and thermal shock resistivity

14 p2259 A71-30473

Aging of cast iron components by thermal shocks, considering heat treatment for machine elements dimensional stabilization

15 p2414 A71-31527

Crack propagation in brittle solids under constant deformation or thermal shock, verifying behavior of results with polycrystalline aluminum oxides

16 p2590 A71-32321

Hot pressed TiC cylinder thermal shock resistance from tests to failure after heat cycling at 1000-1200°C

17 p2760 A71-33421

Isotropic viscoelastic plates of variable thickness subjected to mechanical and thermal stress, considering circular and rectangular plates vibration by external thermal shock

19 p3160 A71-36441

Collisionless plasma thermal shock wave, showing heat in electron component transportable along magnetic field at lower rates than thermal velocity

21 p3421 A71-40041

Quenching effects on glazed and unglazed aluminum rods in various media, noting improved flexural and tensile strength, thermal shock resistance and impact resistance

22 p3565 A71-42322

Environmental rationale behind thermal shock testing, discussing approaches for temperature cycling provision

23 p3682 A71-43901

THERMAL SIMULATION

Gas flame heater for heat resistant samples under fatigue tests, simulating gas turbine engine operating conditions

01 p0067 A71-10041

Inverse problems for parameters and optimal heat transfer model in thermophysical processes

02 p0331 A71-11732

Model and glass tank furnaces for earth upper mantle convection movements simulation, studying fluid dynamics and geodynamic processes

07 p1105 A71-20441

Stored arc heated air true temperature, flight and altitude simulation facility in Mach number 8 to 10 range for air breathing propulsion research

08 p1273 A71-21981

Free molecular flow on cryosurface in cylindrical space simulation chamber with spherical test object

09 p1433 A71-23001

Convective heat flow simulation in lower troposphere, using water-heated plate model and shadowgraph photography

10 p1638 A71-23871

Design, calibration and computer control of orbital heating simulator, using heat flux sensor feedback for ATM thermal vacuum tests

11 p1745 A71-26221

Mixed ullage heating, convection and conduction models of thermal stratification of cryogenic propellants stored in low gravity environment

11 p1810 A71-26501

Thermal/vacuum space simulation assembly level testing for prelaunch confidence of Mariner spacecraft

12 p1893 A71-26631

Simulated turbine blade thermal fatigue testing under transient and steady state heating and spanwise loading, obtaining crack initiation and propagation data

17 p2792 A71-34501

High enthalpy plasma jet wind tunnels, considering arc heaters and simulation range extension to higher adiabatic static pressures to avoid nonequilibrium expansion in nozzle

18 p2898 A71-36411

Semiconductor materials compensated trapping levels analysis, applying thermally simulated capacitance discharge technique

21 p3431 A71-41231

THERMAL STABILITY

Medications stability regarding high temperature humidity, ambient gas composition, increased oxygen content, radiation, vacuum, vibrations and accelerations

01 p0025 A71-11141

Trilayer niobium-alumina-niobium sheath insulator thermal stability test under electrical load

02 p0232 A71-12252

Inertial instruments temperature compensation verification control

02 p0253 A71-12401

Imide-pyrrone copolymers preparation by solution polymerization, considering base/acid degradation resistance and thermal stability in air and vacuum

04 p0549 A71-15749

Thin oval ring noncircularity effect on thermal instability based on small deflection analysis

05 p0820 A71-15983

CdS solar cells thermal stability and performance, discussing satellite applications

05 p0699 A71-16056

CdTe thin film solar cell characterization, showing low carrier concentration of base layer and improved stability at elevated temperatures

05 p0772 A71-16385

Dispersion medium effects on thermal hardening of lubricating oils with Na or Li additives

05 p0838 A71-16782

Unsteady heat conductivity problems with nonlinear boundary conditions, using perturbation method

05 p0838 A71-16782

Thin film cermet resistive elements physical controls electrical properties, physical controls, thermal and radiation stability

07 p1071 A71-19075

Rapid heating effects on hot pressed TiC cylinders stability, calculating temperature fields and stress distribution

07 p1130 A71-19168

Jet fuels thermal stability and corrosive properties during prolonged storage

07 p1182 A71-19492

Polytropic models second order pulsations, evaluating stellar pulsational stability and thermal imbalance

08 p1359 A71-20941

Long time static strength, durability and thermal stability relations determined for heat resistant alloys at operational temperatures

08 p1306 A71-21112

Papers on polymers thermal stability, Volume 1, covering molecular structure, reaction kinetics, scission, thermosetting resins, etc

08 p1323 A71-21474

Thermally stable fibers fabricability and properties relation to polymer chemical structure and tensile strength

09 p1481 A71-22247

Transparent radiating gas thermal instability criteria derivation from gasdynamic equations

09 p1519 A71-22528

Nonhomogeneous cosmological model with equations describing universe relative density variation, demonstrating thermal instability role in galaxies formation

10 p1667 A71-23856

Low cost directly coupled differential amplifier with thermodynamic drift stabilization for biological studies

10 p1570 A71-24444

Shallow spherical shell thermal stability, investigating factors affecting Galerkin method validity

10 p1690 A71-24574

Difunctional epoxy resins from dihydroxydiphenyl sulfone /bisphenol S/, obtaining increased heat resistance and thermal stability

11 p1787 A71-25424

Thermal stability of cylindrical laminated fiberglass reinforced plastic shells, solving by linear shell stability theory

11 p1790 A71-26175

High temperature plastic lubricants thermal stability, discussing thickening agent-dispersed medium interaction effects

12 p1922 A71-27663

Olympus 593 supersonic engine lubricants tests, defining requirements in terms of bulk thermal stability, resistance to hot bearing breakdown, oil mist coking, etc

14 p2250 A71-29826

Shape instabilities for eutectic alloys composite microstructure at elevated temperatures

14 p2259 A71-30413

Ammonium perchlorate propellants sterilizability, using medium resolution mass spectrometer and regression analysis of results in thermal stability studies

14 p2286 A71-30769

Solar prominences formation, discussing coronal thermal instability, chromospheric heat balance, magnetic field and gas heating

15 p2482 A71-31334

Stratospheric turbulence induced aircraft buffeting dependence on vertical wind shear, Richardson number and thermal stability change from underlying to overlying layer

15 p2444 A71-31365

Fifth group transition elements V, Nb and Ta, showing most stable metal dioxide gaseous compounds

15 p2424 A71-31391

Thermal stability test assembly for refractory materials cylindrical specimens, using argon plasma jet

15 p2385 A71-32238

Thermoelastic stability as function of thermodynamic properties of elastic materials, applying invariance principle to dynamical systems on Banach space

16 p2649 A71-33004

Acoustic vibrations generation and transmission in nonadiabatic gas containing heat sources, taking into account conductive and radiative heat transfer and momentum loss

16 p2662 A71-33029

Perturbation method for solving nonstationary heat conduction problems with nonlinear boundary conditions

16 p2662 A71-33034

Thermospheric convective instability as interpretation of north polar cap high speed winds observed by satellite at 200 km altitude during magnetic storm of May 1967

16 p2572 A71-33847

Materials stability testing in high temperature propane-butane combustion product flow, selecting compact silicon carbide for structural use in redox medium

17 p2761 A71-34310

Broadband varactor tuned X band Gunn oscillator, investigating output power and temperature stability

17 p2717 A71-35340

Ganymede thermal inertia data from simultaneous visual photometry and IR radiometry observations during 17 March 1971 eclipse

17 p2807 A71-35418

Transparent radiating gas thermal instability criteria derivation from gasdynamic equations

17 p2807 A71-35504

Thermal stability and oxidation and corrosion resistance of lubricating oil based on trimethyl propane ester [ONERA-TP-930]

18 p2939 A71-36016

Thermally stabilized volcanic rock magnetic properties and coupling hysteresis effect changes due to reheating in weak magnetic field

18 p2912 A71-36197

MHD systems equilibrium and stability involved in quiescent prominences, considering temperature dependence of heat conductivity, magnetic field and initial gas compression

18 p2967 A71-36927

Perfluoropolyether fluid lubricant physical and chemical properties at high and low temperatures, explaining metals effects on thermal stability by topochemical reaction mechanism

19 p3083 A71-37424

Plastic deformation effects on austenite thermal stabilization in Fe-Ni-C alloy, considering temperature dependence

19 p3079 A71-37704

Polyamides reinforced with finely chopped glass fiber, noting mechanical strength, Martens yield temperature and heat stability

19 p3085 A71-38476

Aluminum-aluminum nickelide rod eutectic composite elevated temperature stability, presenting coarsening kinetic analysis

21 p3398 A71-40469

Molybdenum hemicarbide layer as diffusion barrier between metal and disilicide, investigating system thermal stability

21 p3399 A71-40526

Radiative transfer effects on hydromagnetic stellar atmospheres thermal-convective instability in presence of uniform rotation and uniform magnetic field

21 p3421 A71-40579

Solar prominences formation, discussing coronal thermal instability, chromospheric heat balance, magnetic field and gas heating

22 p3606 A71-42609

Thermal stability of naphthenes up to 1000 F, considering hypersonic aircraft fuel applications

22 p3588 A71-42837

Sintered construction material with high SiC content, investigating thermal stability in nitrogen, air, carbon dioxide and water vapor above 2000 K

23 p3696 A71-44020

Curie point region automatic thermal stabilization effectiveness of cylindrical/disk shaped segnetoceramic elements in electrostrictive constant magnetic field converters

24 p3828 A71-45164

Inhomogeneous high-collision finite-pressure plasma stability, finding thermal instability development under uniform temperature and arbitrary pressure

24 p3858 A71-45243

THERMAL STRESSES

Heat propagation rate effect on dynamic thermal stress distribution in thin plate, using Hankel and Laplace transforms

01 p0168 A71-10414

Heat conductivity equations for thermal stresses of thin cylindrically anisotropic plates made of reinforced laminar plastics

01 p0169 A71-10499

Laser active element temperature field nonuniformity, calculating thermal stresses

01 p0093 A71-10614

Thermal stresses on curved surface of initially stressed circular cylinder with smooth rigid insulated cover

01 p0172 A71-10839

Thermally induced preload changes in roller bearings due to temperature gradients measured, using strain gage bridges and thermocouples

01 p0088 A71-11006

Axisymmetric mixed boundary value problem of thermoelasticity for hot stamp penetration into transversely isotropic half space, deriving contact stresses

01 p0175 A71-11036

Micropolar elastic body with spherical inclusion, investigating thermal and couple stresses

01 p0181 A71-11286

Stress-strain state variability associated with optimal local heating of shallow shells of revolution

02 p0322 A71-11727

Shallow spherical shell thermally stressed state produced by temperature gradients

02 p0322 A71-11728

Unsteady axisymmetric temperature and stress distribution in multilayer cylinder in convective heat transfer with temperature-varying medium

02 p0322 A71-11729

Thermal stress concentration around hole in edge-heated elastic strip, using quasi-static formulation

02 p0322 A71-11732

Thermoelastic stresses in closed laminar orthotropic shells of revolution subjected to axisymmetric loads and temperature gradients

02 p0322 A71-11735

Thermal prestress effect on natural vibrations of hinge supported isotropic cylindrical shell, integrating equations of motion by Bubnov-Galerkin method

02 p0322 A71-11738

Simple variable loading and unloading in theory of small elastoplastic deformation under nonuniform heating for residual stress-strain determination

02 p0323 A71-11739

Elastoplastic unsteady thermally stressed state of square and rectangular planform bodies by calculated theory of small deformations, using strain compatibility equations with Airy stress function

02 p0323 A71-11743

Thin cylindrical work hardening shell under nonuniform heating and external stresses, determining elastoplastic deformation by flow theory

02 p0323 A71-11744

Thermoelastic theory of stressed crystals and higher order elastic constants covering surface electronic and mass transport properties

02 p0294 A71-11799

Temperature fields without induced stress, considering relation between thermal and dislocation stresses in shells of revolution

02 p0325 A71-12283

Stability loss of cylindrical and spherical shells under heating and external force, determining critical temperature and loads

02 p0325 A71-12286

Modal coupling in thermally stressed plates, obtaining solution for frequencies and stiffness

02 p0329 A71-12685

Surface thermal and electrical stresses effect on bipolar transistors electrical properties, using NDT criteria for components selection

02 p0236 A71-12921

Thin walled circular cylindrical shells creep buckling under radial pressure and thermal gradients [ASME PAPER 70-WA/APM-8]

03 p0512 A71-14152

Critique of thermoelastic problem solution for thermal stress in semiinfinite body under step heat input

04 p0669 A71-15193

Rectangular and circular thin orthotropic plates thermal buckling approximate solution using Rayleigh-Ritz energy method

05 p0819 A71-15978

Pure Fe and Fe-Ni alloys thermal stress component temperature dependence measurement, investigating Ni addition effect on alloy softening

05 p0765 A71-16188

Numerical analysis of one dimensional transient temperature fields and elastic thermal stress fields, deriving equations for plate and cylinders with free edges

05 p0823 A71-16494

Gas turbine engine nozzle guide vanes under pulsed thermal operation, discussing service life evaluation and increase

05 p0827 A71-16756

Circular disks or cylinders with temperature boundary conditions, discussing iterative solution and computer program for transient thermoelastic stresses

05 p0829 A71-17117

Thin isotropic plate nonstationary coupled thermoelasticity problem, obtaining recursion equation system for thermal stresses

06 p0983 A71-17367

Nonstationary temperature fields and thermal stresses in plates and shells for discontinuous boundary conditions

06 p0991 A71-17799

Stress-strain state of shallow shells under concentrated heat load, obtaining asymptotic expressions for various parameters

06 p0997 A71-17845

Infinite elastic plate with rectilinear crack, determining heat exchange effect on thermoelastic stresses

06 p1000 A71-17939

Turbine blades thermal stresses due to nonlinearities, using computerized simulation

06 p1000 A71-18003

Solid propellant engine structural analysis, examining transient thermal loading and internal pressure effects

06 p1003 A71-18565

Thermal stresses in annular plate of fiberglass reinforced epoxy resin

07 p1209 A71-18919

Deformation-thermal diffusion processes relation for thin coated composite materials under variable thermal stresses

07 p1210 A71-19156

Electronic encapsulated assemblies thermal stresses due to components expansion coefficients mismatch 07 p1213 A71-19774

Steady state thermal stresses and deformations in infinite hollow circular cylinder by sinusoidal internal heat source and Newtonian radiation boundary condition outer surface cooling 07 p1214 A71-20026

Cyclic thermal cracking and fatigue analysis in large steam turbine rotors with three dimensional temperature and triaxial stress computation [ASME PAPER 70-PWR-1] 07 p1216 A71-20198

Laser beam self induced thermal distortion in near field absorbing moving medium by theoretical model based on geometrical optics 07 p1128 A71-20389

Cyclic heating and thermal stresses effect on fatigue strength and durability of turbine blade alloys and structural elements 08 p1372 A71-21702

Thermoelastic stress and temperature distribution in doubly connected isotropic plate 08 p1374 A71-21948

Temperature and pressure discontinuity stresses in compact heat exchangers, considering tubes as elastic foundation underneath tube plate 08 p1374 A71-22034

Plastic strains, thermal residual stresses and buckling of rectangular cross section plates and beams subjected to asymmetric heating and cooling 08 p1375 A71-22056

Beams torsional rigidity under thermal stress due to arbitrary temperature distribution 09 p1534 A71-22103

Thermal stresses in finite circular cylinder heated axisymmetrically over curved surface, constructing thermoelastic displacement potential and biharmonic Love function 09 p1536 A71-22452

Finite length rotating cylinder, calculating axisymmetric creep under thermal effects in power series from theory of small elastoplastic deformation 09 p1537 A71-22516

Closed spherical shell, calculating optimal internal temperature fields for keeping thermal stresses at low level under local axisymmetric heating 09 p1537 A71-22520

Nomograms for thermoelastic stress in plate determined as function of dimensions and heat transfer 09 p1538 A71-22605

High temperature thermal null strain gage with sensing unit and electronic control unit to measure mechanical strain in terms of induced thermal strain 09 p1445 A71-22721

Approximate trigonometric solution to thermoelastic boundary value problem of plane with doubly periodic system of holes, deriving unsteady temperature and thermstress fields 10 p1687 A71-24195

Temperature stress distribution in infinite plate with time varying heat transfer coefficient 10 p1687 A71-24197

Weld heat affected zone transient thermal stresses examined by weld joint model constrained system 10 p1617 A71-24533

Three dimensional composite reinforcement principles, discussing thermal strain reduction and mechanical properties 10 p1691 A71-24772

German monograph on thermal shock experimental analysis covering derivation of method for determining temperatures and thermal stresses in nuclear reactor structures 10 p1697 A71-25036

Thin circular cylindrical shells thermoelastic behavior under one directional radiant heating, comparing measured displacements and strains with calculated values based on measured temperature distributions 11 p1841 A71-25187

Dynamic response of rotationally symmetric open ended thin shells of revolution under transient impulsive and thermal loadings, using FORTRAN 4 finite difference program 11 p1847 A71-25466

Soviet book on thermal stresses in bodies of revolution of arbitrary shape covering energy conservation equations and heat equations solutions 11 p1850 A71-26096

Soviet book on thermoelasticity covering thermal stresses in disks, plates, shells and bodies of revolution in steady and unsteady temperature fields 11 p1850 A71-26100

Temperature and membrane thermal stress distribution in finite rectangular plate with insulated circular hole, considering steady state heat conduction equation 11 p1852 A71-26404

Microcrack formation in carbon fiber-resin matrix composites under thermal stress 12 p1920 A71-27013

Transversally isotropic sphere and orthotropic cylinder in symmetrical temperature field, calculating thermal stress equations 12 p1975 A71-27112

Thermal buckling and snapping of flat rings and of shallow conical rings under axisymmetric temperature distribution [ASME PAPER 71-DE-B] 12 p1977 A71-27317

Plastic conical shell with variable thickness, calculating load carrying capacity under cyclic mechanical and thermal loads 12 p1979 A71-27353

Thermal stresses in circular plate with cylindrical orthotropy and reinforced edge, determining temperature and stress distributions 12 p1979 A71-27356

Thermal stress analysis of hinged thin circular cylindrical shells of variable thickness by computerized discrete orthogonalization method 12 p1979 A71-27357

Initial thermal stresses effect on natural vibrations of orthotropic cylindrical shells 12 p1979 A71-27360

Bending stress in conical shell subjected to thermal and pressure loadings with uniform spatial distribution, using perturbation method 12 p1983 A71-27594

Shear strength effect on axisymmetrical stress-strain state of orthotropic cylindrical shell subjected to nonuniform surface heating 13 p2148 A71-27825

Failure analysis of plastic materials susceptible to cyclic strain hardening under thermal load 13 p2148 A71-28114

Circular cylinder thermal stressed state, considering interaction between temperature and deformation fields 13 p2152 A71-28273

Thermal stresses in infinite viscoelastic plate due to external heat source 13 p2152 A71-28278

Radioisotope heat sources protection from reentry ablation and thermal stress with outer anisotropic pyrolytic graphite shield 13 p2099 A71-29259

Thermal load capacity and nozzle shape for guiding and constricting high current plasmas from electric arc data, using Ar as discharge gas 14 p2279 A71-29851

Plate temperature field and stress distribution under thermal pulses, evaluating critical heat load for damage 14 p2325 A71-30049

Thermoelastic stress analysis of circular perforated plate under point heat source 14 p2326 A71-30195

Thermal stresses in multilayer anisotropic fiberglass wound conical shell under axisymmetric gradients applicable to structural missile nose cone design 14 p2330 A71-30694

Reinforced toroidal shells stability under critical local loads, edge moment and heating, using finite difference method 14 p2332 A71-30847

Dislocation stress analysis in infinite elastic plate with two circular holes under arbitrary steady temperature field 14 p2332 A71-30850

Thermal stresses estimation method based on equivalent stress calculation via use of temperature scale [HEAT EXCH. CONF. PAPER 12] 15 p2504 A71-31634

Hardened low alloy steel ultrasonic attenuation under magnetic field due to thermally introduced residual stresses 15 p2414 A71-31641

Cylindrical shell under internal pressure, detailing axial thermal stresses relaxation 15 p2505 A71-31861

Soviet book on structural bearing capacity under thermal cycling conditions covering rotating disks, plates and shells calculations 15 p2505 A71-32002

Surface melting, spallation and stress response prediction for metals under pulsed electron beam heating, using one dimensional finite difference computer program 15 p2390 A71-32005

Pulsed electron beam heating of metals, determining surface melting, spallation and induced stresses with one dimensional computer programs 15 p2429 A71-32006

Combined mechanical and cyclic thermal stresses effect on plastic deformation buildup in E1435 alloy preceding breakdown 15 p2433 A71-32236

German monograph on thermally stressed shear soft shells with finite deformation covering tensor analysis, thermoelasticity, temperature fields and two dimensional bodies 15 p2509 A71-32305

Elastoplastic analysis by matrix displacement method, discussing perforated plate under tension and bar thermal stress due to rapid heating 16 p2652 A71-33085

Axially symmetric thermal stress distributions in infinite elastic solid containing flat circular external crack 16 p2654 A71-33169

Orthotropic semiinfinite elastic solid under plane strain, calculating thermal stresses in terms of Green functions [ASME PAPER 71-APM-18] 16 p2655 A71-33211

Thermal stresses in gas turbine rotor blade with two dimensional temperature field, using closed /Saint Venant/ plate solutions 16 p2657 A71-33543

Thermal stresses in anisotropic infinite elastic orthotropic laminated cylinder with arbitrary number of layers under axisymmetric heating 16 p2657 A71-33596

Thermoelastic critical equilibrium of plate with rectilinear crack under heat transfer from edge surface and tensile stress 16 p2658 A71-33686

Enthalpy probe heat response dependence on surface thermal load amplitude 16 p2581 A71-34032

Thermal stresses distribution in wedge shaped solids with cracks, solving elastic equilibrium equations 16 p2661 A71-34158

Stress-strain state of homogeneous and inhomogeneous cylinders and disks with central axial curvilinear hole under internal pressure and thermal loads 17 p2816 A71-34331

Thermal stresses in plane strain of isotropic micropolar elastic solids without heat sources, reducing thermoelastic to isothermal problem 17 p2821 A71-34583

Thermal and athermal yield stresses of Nb and Nb-Mo single crystals, considering strain rate sensitivity and thermal stress increase with increasing plastic strain 17 p2759 A71-35224

Thermal stressed state and bending theory of rectangular plate by initial function method, allowing for distributed transverse load 17 p2829 A71-35304

Turbine disks failure under radial temperature drop, studying effects on load bearing capacity for thermal stresses 17 p2832 A71-35454

Gas turbine engine nozzle guide vanes under pulsed thermal operation, discussing service life evaluation and increase 17 p2832 A71-35455

Deformation-thermal diffusion processes relation for thin coated composite materials under variable thermal stresses 17 p2834 A71-35654

Transient thermal stresses in infinite cylinder of rectangular cross section with heat sources, using integral transforms 18 p2976 A71-36127

Two dimensional dynamic thermal stresses in Al plate, allowing for Newtonian surface heat exchange 18 p2981 A71-36720

Rheological media viscoelastic relaxation theories generalization taking into account thermal stress and conduction 18 p2984 A71-37021

Human heat stress evaluation indices, discussing acclimatization, dehydration, clothing, age, physical fitness, health and sex effects 19 p3006 A71-37483

Neodymium-glass lasers active elements thermal-stress-induced birefringence effects on energetic and polarization characteristics 19 p3072 A71-37767

Rigid disk effect on thermal stress distribution in semiinfinite elastic solid under prescribed surface temperature and heat flux 19 p3159 A71-38188

Thermoelastic axisymmetric equilibrium of elastic semiinfinite two dimensional medium with Griffith crack under prescribed heat flux 19 p3159 A71-38189

Isotropic viscoelastic plates of variable thickness subjected to mechanical and thermal stress, considering circular and rectangular plates vibration by external thermal shock 19 p3160 A71-38480

Heat stresses in elastic compressible material plate strip subjected to finite deformation 20 p3308 A71-39038

Thermal stresses and couples in micropolar elastic solid cavity and rigid inclusion during uniform heat flow 20 p3309 A71-39560

Mo and high temperature Mo alloys thermally activated deformation mechanisms from flow stress athermal component and effective stress temperature dependence observation 21 p3396 A71-40030

Thermal stresses in infinite elastic plate with circular hole and single heat source, considering steady state heat conduction 21 p3464 A71-40753

Numerical analysis for transient elastoplastic thermal stresses on turbine disks at variable rotation speeds 21 p3466 A71-40836

elastoplastic thermal stress analysis in axisymmetric bodies by finite element method, calculating residual stresses 21 p3466 A71-40841

Thermal stress distribution and temperature profiles of nearly opaque spherical shell under radiant and convective heating flux 21 p3476 A71-40942

Closed form solution for quasi-static thermal stress due to moving point heat source in circular disk, finding application to welding problems 21 p3467 A71-40966

Quasi-static thermoelasticity and dynamic thermal stress equations solution in matrix form by Fourier transform and Hilbert-Levy method 22 p3614 A71-41567

Validity study of mathematical models representing temperature rate variations of electronic components, considering thermal and electrical stresses 22 p3517 A71-42109

Temperature stresses relaxation in transversely isotropic viscoelastic sphere calculated numerically for 500 and 100 hour periods 22 p3616 A71-42486

Two-component composite cylindrical body thermoelastic stresses near junction-surface edge under none deformation conditions 23 p3776 A71-43420

Homogeneous mountain mass and canyon thermoelastic stress analysis in curvilinear coordinate system by complex variables 23 p3776 A71-43421

Solid circular plate with diverse elastic moduli in different directions and hole at center, calculating thermoelastic stresses 23 p3777 A71-43422

Refractory materials heat resistance criteria, taking into account hollow cylinder thermal stress distribution 23 p3698 A71-44212

Thermal and mechanical stresses concentration near peripheral notches on ring-shaped graphite, noting notch sensitivity relationship to tip curvature and graphite grain size 23 p3698 A71-44230

Thermally loaded rod structures optimization, presenting method for estimating canonical equations influence parameters 24 p3842 A71-44642

Cyclic symmetrical deformation of thin elastic conical shells of revolution of variable thickness with meridional ribs under physical and thermal loads 24 p3882 A71-44843

Photoelastic analysis of thermal stresses in polyurethane rubber ring reinforced polymers, ceramets and rubber-metal composites 24 p3883 A71-44895

Thermal stresses relaxation and distribution in infinite anisotropic viscoelastic cylinder 24 p3884 A71-45002

Thermal stresses produced by steady heat flow in two layer plate simply supported at contour 24 p3886 A71-45363

THERMAL VACUUM TESTS

Nb-W-Hf-Y creep rupture properties in thermal vacuum, achieving strength improvement by pretest annealing 05 p0766 A71-16242

Powdered W, Mo, Nb and Ta sulfides and compacts thermal vacuum behavior, examining phase compositions and transformations 05 p0769 A71-16861

Temperature dependence of Vickers pyramid hardness for Ti, Zr and Hf carbides at wide temperature range in vacuum 07 p1142 A71-20483

Titanium diboride contact interaction with Ti, Zr and V in vacuum at various temperatures 09 p1471 A71-23083

GAO 2 thermal test reliability analysis, using filtering process to eliminate component and subsystem level failures 12 p1971 A71-26681

Apollo program all-up spacecraft thermal vacuum tests, considering component and subsystem reliability analysis, thermal model verification and certification requirements 12 p1894 A71-26682

ATS F and G thermal control, discussing heat pipe, coupler and model tests 18 p2868 A71-36395

Multiple channel fringe counting interferometer for remote monitoring of large diameter microwave antenna under test in simulated solar thermal and vacuum environment 20 p3235 A71-39186

Solid body contact interaction devices at high temperatures in vacuum, gas and air for evaluation of surface coatings, adhesion, diffusion, mechanical properties, etc 21 p3382 A71-41174

THERMALIZATION [ENERGY ABSORPTION]

Noncoherent scattering, considering redistribution in continuous absorption and frequency dependent thermalization lengths 04 p0658 A71-15840

Thermalization processes in earth bow shock with emphasis on ion heating, using electromagnetic dispersion relation for ion-ion streaming instability 13 p2054 A71-27908

Thermalization and diffusion of electron cloud injected into afterglow cylindrical plasma, calculating steady state distribution as function of position and velocity 14 p2280 A71-30175

Solar wind ion thermalization in earth bow shock by counterstreaming instability related to interplanetary magnetic field 15 p2399 A71-31774

Partially thermalized model of stellar system, considering potential and density distribution 21 p3439 A71-40052

THERMIONIC CATHODES

Thermionic dispenser cathodes with emitter surfaces covered and replenished from inside by high work function material 02 p0295 A71-12213

In-pile tests of multielement thermionic converter with Mo- and W-based alloy cathodes, noting output electric power dependence on internal heat release 11 p1711 A71-25877

Hollow cathodes as main and neutralizer cathodes in Kaufman electrostatic propulsion system, discussing test installation and results [DGLR-71-045] 17 p2794 A71-35542

THERMIONIC CONVERSION SYSTEMS

U THERMIONIC POWER GENERATION

THERMIONIC CONVERTERS

Anode sheath width for collisionless thermionic converter with Ba plus Cs filler, assuming linear potential variation 01 p0005 A71-10157

Anodic temperature effect on Cs thermionic converter operation under arc regime, obtaining potential jump electron temperature relation near anode 01 p0005 A71-10158

Dense plasma high current density effects on low voltage arc in thermionic converter 01 p0005 A71-10159

Book on direct energy conversion principles and methods covering fusion, fuel cells, MHD, thermoelectric, thermionic, photovoltaic, electrohydrodynamic, piezoelectric and ferroelectric power generation 01 p0006 A71-11193

Electropolished and single crystal surface effects on work function of macroscopic tungsten emitter in cesiated converter 02 p0295 A71-12204

Bare and cesiated work function of covapor deposited tungsten-rhenium electrodes from vacuum emission vehicle Schottky plots 02 p0295 A71-12205

Vacuum work function of thermionic converter using planar monocrystalline rhenium emitter over temperature range 02 p0192 A71-12206

Electron emission formulation for cesiated metal surfaces in thermionic converter in terms of work function, using Swanson-Strayer correlation 02 p0295 A71-12210

Thermionic converter with single crystal 110 W emitter surfaces and Nb collector, measuring I-V performance 02 p0193 A71-12212

Thermionic converter tests, discussing W emitter with Nb and Mo-on-Nb collectors, surface and electrode combinations 02 p0193 A71-12214

Thermionic converter with oriented W electrodes, discussing computerized data acquisition system for mapping I-V performance 02 p0193 A71-12215

Life, efficiency and electrical stability tests of cylindrical thermionic converters with various emitter and collector materials 02 p0193 A71-12216

Performance tests of identical cylindrical thermionic converters with W emitters and Nb collectors, using X ray diffraction and work function measurements 02 p0193 A71-12217

Long term stability and post test analysis of vapor deposited W emitters in high performance cylindrical thermionic converters 02 p0193 A71-12218

Low temperature cylindrical thermionic converters with CVD Re electrodes, discussing design, fabrication and performance 02 p0193 A71-12219

Sirene 311 cylindrical thermionic converter in pile life testing in Triton swimming pool nuclear reactor 02 p0193 A71-12220

THERMIONIC CONVERTERS

Cylindrical thermionic converter for Incore Thermionic Reactor, discussing diodes engineering problems and performance test for lifetime 02 p0194 A71-12221

Solar energy thermionic converter life test program and equipment, noting failure due to loss of intraelectrode Cs 02 p0194 A71-12223

Maximum efficiency of cylindrical thermionic converters with Mo emitter and collector over temperature range 02 p0194 A71-12224

Three component two temperature plasma model of thermionic converter, including volume ionization-recombination processes 02 p0194 A71-12225

Thermionic converter Cs plasmas electron temperature and density gradients spectroscopic measurements compared with prediction from energy transport analysis and ionization coefficients 02 p0194 A71-12226

Thermionic converter electron-cesium atom momentum transfer collision probability, considering scattering cross sections 02 p0287 A71-12227

Thermionic converter performance improvement methods, using digital computer for evaluation 02 p0194 A71-12230

Space charge problem for thermionic converter emitter sheath for electrons and ions with half-Maxwellian distribution 02 p0291 A71-12234

Volt-ampere characteristics dependence on collector temperature in thermionic converters compared with collector work function 02 p0195 A71-12235

Transport analysis of collision dominated relaxation plasma in ignited mode thermionic converter 02 p0291 A71-12237

Thermionic converter spectroscopic measurements in several regions of I-V characteristics, noting plasma radiation intensity periodic waveform 02 p0195 A71-12238

Cylindrical thermionic converter irradiation tests under Incore Thermionic Reactor (ITR) Project, discussing postmortem examinations 02 p0195 A71-12243

High voltage thermionic module eliminating power conditioning and multiple units series connection, discussing design and coating technologies 02 p0195 A71-12244

Cesium consumption rates and content in thermionic converter components affecting system performance indicated via integral adsorption reservoir 02 p0195 A71-12245

Hydride thermionic reactor system transient behavior dynamic mathematical model and digital simulation 02 p0281 A71-12262

Heat balance measurements at collector of heat pipe thermionic converter 02 p0196 A71-12268

Thermionic converter integrated Cs reservoir module power efficiency and service life, considering diode technology 02 p0196 A71-12270

Liquid Cs graphite integral reservoir effect on thermionic converter performance 02 p0196 A71-12271

Technology gap between thermionic converter physics and reactor engineering, emphasizing language problem 02 p0281 A71-12272

Nuclear reactors for space power supply with turboelectric, thermoelectric and thermionic converters 02 p0282 A71-12305

Energy converters for satellite nuclear power plants, discussing rotating, MHD, thermionic and thermoelectric systems 02 p0282 A71-12306

Thermionic converter output improvement by Ar injection at low Cs pressures, noting electron space charge neutralization 08 p1340 A71-21490

Thermionic conversion - IEEE Conference, Miami Beach, October 1970 11 p1709 A71-25856

Electron beam welding machine reducing number of fabrication variables during final assembly procedure in thermionic converters fabrication, discussing UHV systems 11 p1709 A71-25866

Liquid metal cooled, fast spectrum thermionic reactor experiment design based on Fast Reactor Core Test Facility use for dynamic and steady state characteristics determination 11 p1710 A71-25867

Nuclear thermionic systems conceptual design with converters outside reactor to reduce weight 11 p1710 A71-25874

Out-of-core thermionic converter system using heat pipes as electrical resistive elements, discussing design and performance 11 p1710 A71-25875

Design optimization of out-of-core cylindrical thermionic converter module with heat pipes and integral finned radiator

11 p1711 A71-25876

In-pile tests of multielement thermionic converter with Mo- and W-based alloy cathodes, noting output electric power dependence on internal heat release

11 p1711 A71-25877

Thermionic converters surface physics theory, discussing work functions, desorption energy and rates relationship to atomic and crystallographic properties

11 p1711 A71-25878

Thermionic converters performance in ignited mode from transport equations for diffusion region, determining electron concentration, potential and temperature

11 p1711 A71-25879

Thermionic converter performance from theoretical model, considering transport, ionization-recombination, and electrostatic sheath phenomena

11 p1711 A71-25880

Thermionic reactor core design for undersea conditions based on neutron data and calculation related with diode materials

11 p1711 A71-25882

Design and operation of split fueled cores with axial heat pipes for 350 kwe out-of-core thermionic power converter system

11 p1712 A71-25884

Thermionic reactor parametric criticality studies, evaluating fuel element and core design variations effects

11 p1712 A71-25885

BeO reflected-fast-spectrum liquid-metal-cooled thermionic reactor, discussing two dimensional transport perturbation theory computer code for temperature coefficients evaluation

11 p1712 A71-25887

Measured and calculated comparison of thermionic converter cesium plasma electron densities, using rate equations taking into account collision, diffusion and photoabsorption processes

11 p1712 A71-25889

Thermionic energy converter, calculating behavior of transition regions between collisionless region adjacent to electrodes and plasmas

11 p1712 A71-25890

Thermionic converter electrostatic sheath analysis, using discontinuous distribution functions for emitted, plasma and trapped particles, and computer program

11 p1713 A71-25891

In-core thermionic reactor network reliability analysis, assuming component failures as equally probable stochastic events

11 p1713 A71-25893

Radioisotope thermionic power supply for unmanned electric propulsion missions to outer planets, using 69 modules consisting of thermionic converter and emitter heat pipe

11 p1811 A71-25897

Quasi-vacuum mode thermionic converter for space and remote terrestrial power supplies, describing computer codes for design optimization

11 p1713 A71-25899

Thermal and electrical characteristics of two nuclear type cylindrical converters with nonuniform emitter temperature

11 p1714 A71-25903

Variable spacing thermionic converter consisting of fluoride vapor deposited W emitter and Nb collector, considering cesiated work function of electrode pair

11 p1714 A71-25905

Chemically vapor deposited deep etched tungsten emitter for high performance cylindrical thermionic converter

11 p1714 A71-25906

Long term performance stability of two unfueled out-of-pile thermionic converters

11 p1714 A71-25908

Thermionic integrated Cs reservoir converter for in-pile applications, discussing design for various coolant temperatures

11 p1715 A71-25909

Double ended full length external fuel thermionic converter, describing component fabrication, assembly sequence, joining methods, vacuum test procedures and converter load control

11 p1715 A71-25910

Out-of-core heat pipe heated and cooled thermionic converter module mechanical design, fabrication and subcomponent performance evaluation

11 p1715 A71-25912

Thermionic converter 9000 hour endurance test, performing metallographic, spectrographic and chemical analysis on emitter, collector, metal ceramic seal, brazing and alumina spacers

11 p1715 A71-25913

Soviet book on thermionic and MHD energy conversion covering gas ionization, converter operation and low temperature plasma physics

11 p1715 A71-26099

Equations system describing parametric distribution of ionized plasma in thermionic converter gap,

discussing current density effects on low voltage arc discharge

12 p1938 A71-27210

Near anode surface electrode potential region width measurement in Knudsen thermionic converter with Ba-Cs interelectrode medium

14 p2181 A71-29954

Thermionic converter output improvement by Ar injection at low Cs pressures

14 p2182 A71-30679

Plasma state and IV characteristics of thermionic converter, discussing cathode emitting area increases and patchiness effects

14 p2182 A71-30680

Out-of-core nuclear thermionic converter system design feature concerning heat pipes, vapor-cooled radiators, modularity and reliability

15 p2448 A71-32224

Propulsion systems evaluation for Mars and Jupiter missions, using bundled ESKA 28 electrostatic ion thrusters and incore thermionic reactors

[DGLR-71-046] 17 p2794 A71-35545

Charged particles transport in thermionic converter near-emitter plasma, determining potential and electron density profiles

18 p2953 A71-36968

Low pressure Cs vapor thermionic converter with lanthanum boride cathode, investigating arc conditions and I-V characteristics

19 p2999 A71-38254

Thermionic converters experimental testing, developing kinetic theory of plasma diodes in steady state Knudsen mode for uniform potential distribution

19 p2999 A71-38256

Equations system describing parametric distribution of ionized plasma in thermionic converter gap, discussing current density effects on low voltage arc discharge

19 p3000 A71-38622

Interelectrode spacing effects on nonequilibrium cesium plasmas in close spaced thermionic converters

20 p3179 A71-38876

Multicell thermionic fuel element consisting of six thermionic converters, considering reactor and systems analysis

20 p3265 A71-38950

Self magnetic field effect on I-V characteristics of Cs-Ba thermionic converter, noting effects of pressure differential due to ponderomotive forces action

21 p3326 A71-41294

THERMIONIC DIODES

NT CESIUM DIODES

Cylindrical Xe filled thermionic diodes breakdown and low voltage arcs at various pressures and interelectrode distances

02 p0190 A71-11942

Cylindrical thermionic converter for Incore Thermionic Reactor, discussing diodes engineering problems and performance test for lifetime

02 p0194 A71-12221

Thermionic stability life tests of cylindrical diodes with W emitters at constant current and optimal Cs and collector temperatures

02 p0194 A71-12222

Reactor gammas effects on thermionic diode output simulated in electron accelerator

02 p0238 A71-12228

Double sheath emission barrier existence criterion at thermionic diode emitter based on ion trapping effect

02 p0290 A71-12232

Ignited mode theory applied to wide-spaced thermionic diodes, verifying LTE plasma column development

02 p0291 A71-12233

Thermionic diode with integral guard ring, measuring emitter and collector work functions and heat transfer

02 p0195 A71-12236

Thermionic Diode Kinetics Experiment with on-line analog computer simulation, investigating thermionic reactor powerplant dynamics and control by non-nuclear means

02 p0195 A71-12258

Thermionic Diode Kinetics Experiment analog simulation results concerning coupling, burnout, startup, etc

02 p0196 A71-12259

Incore thermionic diode reactor stability review and evaluation, discussing reactivity feedback mechanisms, analytical models and results

02 p0280 A71-12260

Thermionic system transient behavior analysis by digital simulation using one diode model

02 p0196 A71-12261

Cs vapor thermionic diodes with low temperature dual mode characteristics applicable as switching elements in DC to AC power conditioner

02 p0196 A71-12267

Flame-fired thermionic diode service life, output power and voltage efficiency and weight reduction

02 p0196 A71-12269

Thermionic converter nonsaturation effect in diode I-V characteristics from computerized analysis for

plasma transport phenomena and sheath-electrode plasma interactions

11 p1713 A71-25876

Open loop transient analysis of thermionic diode kinetics experiment with analog computer nuclear reactor simulator

11 p1797 A71-25876

Computer acquired performance mapping of a spaced planar diode with etched Re emitter and Nb collector over wide operating temperature range

11 p1737 A71-25876

Design, fabrication and testing of electrically heated externally configured thermionic diodes with emitter using mandrel side of CVD fluoride tungsten for anode surface

11 p1715 A71-25876

Computer acquired I-V characteristics of thermionic fixed spaced planar diodes

23 p3630 A71-25876

THERMIONIC EMISSION

Langmuir S curves for W /110/-Cs and Mo /100/-adsorption determined by thermionic electron emission microscope, noting minimum work function

02 p0295 A71-12232

Double sheath emission barrier existence criterion at thermionic diode emitter based on ion trapping effect

02 p0290 A71-12232

Cs vapor filled cracks breakdown in thermionic tri-layer insulators, calculating electron reflection and ion recombination kinetics on surfaces

02 p0232 A71-12232

Sudden thermionic emission in surface ionization near threshold temperatures of cesium activated tungsten single crystals

09 p1494 A71-25876

Thermionic emission and adsorption characteristics of Ta single crystal faces in cesium atom stream using thermoelectronic and surface ionization methods

15 p2453 A71-38254

Thermal characteristics of emission and work functions of spherical Ta single crystal faces by Mass microscope measurements

15 p2453 A71-38254

Noise equivalent resistance of thermionic tube stability and reliability criterion

16 p2545 A71-38254

Polycrystalline Nb and Ta and Ta-on-Nb thin film thermionic emission surface barrier analysis for periodic deviations in Schottky effect

24 p3862 A71-45876

Surface potential barrier models for thermionic photoelectric emissions from semiconductors with Schottky deviation region

24 p3862 A71-45876

THERMIONIC EMITTERS

Thermionic emitter work function extrapolation by interpolation, noting correlation to surface temperature and Cs pressure

02 p0294 A71-12232

Vacuum work function of thermionic converters using planar monocrystalline rhenium emitter over temperature range

02 p0192 A71-12232

Cesiated work functions of directed monocrystalline Re thermionic emitter from saturated electron emission currents over temperature range

02 p0295 A71-12232

Single crystal facet angles and surface energy plane by light reflection for W emitter in vacuum, Cs and iodine

02 p0251 A71-12232

High work function stable faceted W thermionic emitter surface preparation by electroetching and vapor deposition

02 p0295 A71-12232

Crystal surface orientation of chemical vapor deposited W thermionic emitter by hydrogen reduction of hexafluoride, using etch pits and X ray diffraction

02 p0295 A71-12232

Thermionic converter with single crystal 110° emitter surfaces and Nb collector, measuring I-V performance

02 p0193 A71-12232

Thermionic dispenser cathodes with emitter surfaces covered and replenished from inside by low work function material

02 p0295 A71-12232

Thermionic converter tests, discussing W emitters with Nb and Mo-on-Nb collectors, surface and electrode combinations

02 p0193 A71-12232

Performance tests of identical cylindrical thermionic converters with W emitters and Nb collectors using X ray diffraction and work function measurements

02 p0193 A71-12232

Long term stability and post test analysis of vapor deposited W emitters in high performance cylindrical thermionic converters

02 p0193 A71-12232

Thermionic stability life tests of cylindrical diodes with W emitters at constant current and optimal Cs collector temperatures

02 p0194 A71-12222

Maximum efficiency of cylindrical thermionic converters with Mo emitter and collector over temperature range

02 p0194 A71-12224

Thermionic emitter metal surface adsorption, investigating impurities and additives effects by analytical model

02 p0295 A71-12231

Thermionic diode with integral guard ring, measuring emitter and collector work functions and heat transfer

02 p0195 A71-12236

Refractory metal thermionic emitter-support systems, measuring surface interdiffusion at high temperatures

02 p0264 A71-12242

Carbon vapor deoxidized W on thermionic converter emitters, investigating deposition parameters effect on microporosity

11 p1807 A71-25860

Thermionic emitter CVD W layer on Mo, investigating work function change due to Mo diffusion and crystal structure dependence on heat treatment

11 p1808 A71-25863

Diffusion processes in Mo-W thermionic emitters of massive couple type and piece of Mo substrate with vapor-deposited W layer respectively

11 p1709 A71-25864

Chemically vapor deposited deep etched tungsten emitter for high performance cylindrical thermionic converter

11 p1714 A71-25906

Computer acquired performance mapping of fixed spaced planar diode with etched Re emitter and Nb collector over wide operating temperature range

11 p1737 A71-25907

Thermionic reactor technology, including insulator seal, nuclear fuel, emitter, tri-layer structure and inner-electrode plasma

20 p3265 A71-38949

Thermionic Power Generation

Thermionic conversion - IEEE Conference, Carmel, October 1969

02 p0191 A71-12201

Thermionic Diode Kinetics Experiment with on-line analog computer simulation, investigating thermionic reactor powerplant dynamics and control by non-nuclear means

02 p0195 A71-12258

Low power thermionic reactors, comparing four types design, characteristics and performance estimates for power plants

02 p0281 A71-12263

Operating experience with miniature thermionic radioisotope-fueled batteries, using thermal-thermionic models

02 p0196 A71-12273

Thermionic conversion - IEEE Conference, Miami Beach, October 1970

11 p1709 A71-25856

In-core thermionic power system for manned space station application, discussing driver fuel elements, nuclear radiation shield, heat rejection and coolant outlet temperature

11 p1710 A71-25869

In-core thermionic reactor flight system for space base applications, providing electric power and thermal shielding

11 p1710 A71-25870

Conceptual design of nuclear thermionic power plant for Space Base application, discussing plant efficiency, radiator area requirements, launch weight and shielding

11 p1710 A71-25871

Out of core design of reactor heated thermionic power plant for manned space station, discussing temperature distribution, shielding characteristics and power conversion

11 p1710 A71-25873

Driver terrestrial in-core thermionic reactor dynamic behavior, discussing computerized simulation with respect to coolant loop

11 p1711 A71-25883

In-core thermionic cell power output limitation and thermal/electrical data determination at steady state operation, considering temperature distribution

11 p1713 A71-25894

Space base 100 kw thermionic reactor power plant featuring interchange core replacement package

11 p1713 A71-25895

Externally fueled thermionic reactor power plant incorporation into unmanned ion propulsion spacecraft

11 p1811 A71-25896

Radioisotope thermionic power supply for unmanned electric propulsion missions to outer planets, using 69 modules consisting of thermionic converter and emitter heat pipe

11 p1811 A71-25897

Parametric performance of quasi-vacuum mode thermionic multicell space power generator,

discussing surface parameters, fuel form, emitter geometry, helium management and generator reliability

11 p1714 A71-25900

In-core thermionic reactor as low cost power supply for direct-to-home TV satellite, converting thermal power to electrical without moving masses

16 p2526 A71-32853

Multicell thermionic fuel element consisting of six thermionic converters, considering reactor and systems analysis

20 p3265 A71-38950

Thermionic Reactors

U Ion Engines

U Nuclear Rocket Engines

Thermistors

Thermistor bridges for temperature measurement, discussing linearity conditions

01 p0079 A71-10250

Fast multiple point measurement of fluid temperature and flow speed fields using bead thermistors and digital system

03 p0427 A71-13921

Remote determination of temperature by operating and etalon thermistors resistances measurement with DC bridge

04 p0591 A71-14855

Ventilation rates and thermal factors of sensitive elements in radiosondes, using wind tunnel tests

11 p1761 A71-25382

Wheatstone bridge with thermistors, discussing linearity, sensitivity and applications for temperature difference and flow velocity measurements

13 p2071 A71-29278

Crystal oscillator temperature compensation using hyperabrupt junction varactor diode as reactance modulator and thermistor for temperature sensitive voltage control

14 p2215 A71-30902

Validity and reproducibility of cardiac output determination by thermomodulation, using dual thermistor catheter introduced in pulmonary artery

16 p2531 A71-33366

Thermistor bolometer characteristics, considering resistance-performance relationship, radiation and Wheatstone bridge potentials

20 p3233 A71-38969

Continuous recording of human rectal temperature under extreme environmental conditions, using battery powered thermographs with thermistor probes

20 p3192 A71-39041

Meteorological rocketsonde film mounted thermistor bead temperature sensor, developing mathematical model for thermometric correction formulas in automatic data processing

20 p3236 A71-39208

Barium strontium lanthanum titanate thermistor bolometer for IR thermal detector, using positive temperature coefficient of resistance

22 p3543 A71-42126

Thermo-Photovoltaic Generators

U Photoelectric Generators

U Thermoelectric Generators

Thermo-Aeroelasticity

U Aeroelasticity

U Thermoelasticity

Thermobalances

Thermobalance for studying high temperature silicon-carbon reaction kinetics, incorporating HF current, coaxial shielding of electrical connections and electromagnetic balance

17 p2838 A71-35475

Thermochemical Properties

NT Heat of Combustion

NT Heat of Dissociation

NT Heat of Formation

NT Heat of Vaporization

Venus atmosphere and lithosphere thermochemical composition, examining various models

06 p0966 A71-17898

Computer calculation of phase diagrams from thermochemical data for Cr-Mo and Mg-Cd systems

07 p1034 A71-19519

Spatially uniform dense partially ionized plasmas asymptotic thermochemical relaxation processes due to heavy particle density, temperature or superimposed electric field changes

09 p1502 A71-22859

High performance ablative composites thermal physical characteristics from differential equations, describing thermochemical ablation-in depth and boundary layer transport processes

11 p1856 A71-26041

Ar arc plasma thermochemical nonequilibrium, using finite difference techniques for nonlinear integrodifferential equations

15 p2455 A71-31538

Thermochemistry data changes influence in form of heat of formation, partition functions, specie free energy or specific heat on high temperature gas mixtures composition

15 p2514 A71-32097

Temperature field of thermochemical sensor in automatic control systems, developing thermal energy transport models for circular disk with energy source at center

22 p3537 A71-41443

Thermochemistry

NT Aerothermochemistry

Concentrated elongation dependence on cross sectional area reduction in industrial Ti alloys undergoing thermomechanical treatment

09 p1468 A71-22324

Entry vehicle carbon vapor thermochemistry uncertainties effects on nose tip ablation response concerning stagnation point surface recession and temperature levels

[AIAA PAPER 71-414]

11 p1857 A71-26207

Soviet book on aircraft materials science and treatment covering steel/cast iron processing, metallography, heat/thermochemical conditioning, surface protection and corrosion prevention

14 p2256 A71-29529

Thermocompression

U Compressing

U Heating

Thermocouple Pyrometers

Interlaboratory program to evaluate thermocouple pyrometric practices in metals high temperature testing

19 p3065 A71-38136

Thermocouples

Technological development of thermoelectric radionuclide batteries for space applications using Ge-Si thermocouples

02 p0282 A71-12304

Left ventricular volume and cardiac work evaluation by thermomodulation technique, employing thermocatheter for temperature measurement

[ASME PAPER 70-WA/TEMP-2]

03 p0372 A71-14102

Thermal conductivity rapid measurement in 300-1200 K range using traversing thermocouple technique

[ASME PAPER 70-WA/ENER-2]

03 p0429 A71-14107

Single thermocouple temperature measurement, discussing millivoltmeters wiring method with resistance matching to ensure accuracy

03 p0430 A71-14329

Large diameter tube high Reynolds number air flow temperature profiles, using chromel-alumel thermocouple

07 p1220 A71-18762

Mechanical, heat resistant and thermoelectric properties of W-Re alloys for thermocouples

07 p1114 A71-20250

High accuracy temperature measurements using type K thermocouples

09 p1445 A71-22724

High enthalpy flow temperature probe, determining stagnation temperature of combustion gases by chromel-alumel thermocouple

11 p1765 A71-26277

Temperature measurement methods using thermocouples and hot-wire anemometers for rapidly changing hot gases

12 p1906 A71-26990

Electric current heated thin resistance film thermoelectric transducer, measuring temperature rise with thermocouple

12 p1888 A71-27158

Burning gunpowder temperature measurement in gaseous phase, describing thermocouple method

15 p2463 A71-31388

Metal specific work breakdown during crack propagation, investigating thermal effect of plastic deformation with thermocouples

15 p2413 A71-31479

Hybrid thermocouple with PbTe and SiGe thermoelectric materials, discussing development status and performance prediction

15 p2355 A71-32225

French monograph on thermal microflowmeters covering anemometers, fluid mechanics, Nusselt number, thermocouple flowmeters

17 p2744 A71-35228

Neutron irradiated and unirradiated Ta sheathed BeO insulated grounded junction thermocouples drift measurement

18 p2916 A71-36046

Thermal emf changes for noble and refractory metal thermocouples, determining drift in high temperature air, Ar and vacuum environments for long time periods

18 p2916 A71-36049

Laboratory method assessing homogeneity and interchangeability of thermocouple wires, considering thermoelectric properties of widely separated wire from same spool

18 p2852 A71-36990

Thermocouple drift effect on creep and tension rupture life at high temperature

19 p3065 A71-38137

Grand tour missions radioisotope thermoelectric generator power source, presenting optimization technique for hot thermocouple junction operation

20 p3264 A71-38932

Evaporated Permalloy films deposition temperature measurement by vacuum evaporated Chromel-constantan thin film thermocouple, noting temperature difference between film and glass substrate
21 p3384 A71-40220

Pyroelectric, pneumatic and thermocouple detectors comparison, discussing IR detectors availability for use in spectrophotometers in 2-20 micron region
22 p3544 A71-42142

Thermocouple measurements of thermal gradients in steel during automatic welding
23 p3679 A71-43892

Total temperature thermocouple probe based on circular cylinder recovery temperature with combined advantages of hot wire and shielded probe, discussing design and applications
24 p3826 A71-44971

THERMODYNAMIC COUPLING

German monograph on network method application for conductive and radiative energy transfer coupling problems
14 p2336 A71-30231

High power microwave phase shifter, using beryllium oxide filler ceramic dielectrics to obtain thermal coupling between ferrite element and waveguide wall
17 p2713 A71-34396

Nonlinear coupling between thermal conduction and radiative transfer in solar chromosphere by iterative method
19 p3143 A71-38159

Finite amplitude entropic waves with propagated acoustic radiation-fluid particle motion energy coupling, using thermodynamic f function methods
20 p3315 A71-39772

Non-LTE picket fence model in radiative equilibrium solutions for thermal coupling and line strength parameter
21 p3438 A71-40243

THERMODYNAMIC CYCLES

NT BRAYTON CYCLE

NT CARNOT CYCLE

NT RANKINE CYCLE

Heat rejection radiator influence on space nuclear power system as function of mass/area for Brayton, Rankine, thermoelectric and thermionic conversion schemes
13 p1999 A71-28597

Turbo-MHD cycle technology of nuclear electric power systems with high temperature reactor for space and terrestrial applications
[AIAA PAPER 71-638]
14 p2273 A71-30716

Gas generator with high thrust-weight ratio, discussing thermodynamic cycles, mass flow rates and combustion chamber
15 p2471 A71-32571

THERMODYNAMIC EFFICIENCY

Rotor loss coefficients for prediction of radial gas turbine performance using one dimensional analysis
01 p0143 A71-11016

Reinforced tube bundles thermal efficiency and convective heat transfer, discussing inter-rib cavity depth effects
01 p0181 A71-11229

Nozzle parameters effects on conical vortex heat exchanger characteristics, considering optimal area in critical cross section for maximum energy and temperature efficiency
08 p1233 A71-20835

Optimal weight of aerodynamic heat protection layers of stressed skin and optimal efficiency of cooling system for hypersonic aircraft compartments
08 p1375 A71-20836

Soviet book on theory of aircraft bladed machines covering axial flow, centrifugal and composite turbines and compressors, thermodynamic efficiency, control turbocompressor matching, etc
11 p1814 A71-26401

Continuous combustion gas turbine with stepwise heat release, investigating ideal thermal efficiency cycle of gas overexpansion, cooling and compression
13 p2115 A71-28583

Approximate method for calculating film cooling effectiveness of flat plate in presence of turbulent boundary layer with injection ratios less than unity
13 p2166 A71-29368

Approximate method for calculating film cooling effectiveness of flat plate at injection ratios exceeding 3.0
13 p2166 A71-29369

THERMODYNAMIC EQUILIBRIUM

Thermodynamic calculation of chemical equilibrium of rocket propellants and gun powders using computer program in Fortran IV
01 p0141 A71-10343

Saha equilibrium deviations in wall stabilized rare gas arc plasmas under normal pressure, describing numerical method for temperature and density distributions evaluation
01 p0133 A71-10746

Book on stellar atmospheres covering radiative transfer, opacity, equation of state, LTE, line spectra, atomic levels, etc
03 p0483 A71-13100

High melting point metal systems with nitrogen or oxygen, discussing engassing and degassing reactions kinetics and thermodynamic equilibrium
03 p0442 A71-13362

Electron temperature measurement in electromagnetic shock tube by spectroscopy and ruby laser light scattering in plasma, examining validity of local thermal equilibrium assumption
04 p0632 A71-14688

Shock tube spectroscopic and reaction kinetic research, considering studies before LTE
04 p0547 A71-14692

Argon plasma jet local thermodynamic equilibrium at various electron densities, examining Boltzmann excitation and ionization temperatures
04 p0633 A71-14902

Solar atmosphere semiempirical models taking into account non-LTE conditions
04 p0651 A71-15667

Plasma temperature measurement in local thermodynamic equilibrium using total continuum emitted during seeding with hydrogen
05 p0786 A71-16171

Shock waves in nitrogen, carbon dioxide and mixtures, measuring Mach number for deviation evaluation from vibrational and dissociation equilibria
05 p0835 A71-16522

Statistical equilibrium equations solved for atom/ion with complex energy level structure and weak spectral lines, discussing deviations from LTE
06 p0969 A71-17969

Local radiative heat transfer and equilibrium temperature between identical uniform surface geometry planes, discussing directional dependent emittance and absorptance effects
[AIAA PAPER 71-76]
06 p1008 A71-18533

Ionizational and electron thermal nonequilibrium effects in insulator boundary layer of potassium-seeded nitrogen MHD accelerator
[AIAA PAPER 71-138]
06 p0939 A71-18581

Shock waves with high equilibrium temperature, calculating structure during multiple ionization of atoms
07 p1087 A71-19186

Earth macroclimate mean zonally averaged state equilibrium solution, using thermohydrodynamic equations
08 p1325 A71-20882

Resonance line formation in multidimensional media, applying to non-LTE line transfer for two dimensional temperature variations
08 p1359 A71-20942

Quantum mechanical relation for magnetized electron gas in constant magnetic field and thermal equilibrium
08 p1337 A71-21192

Static relativistic theory of isotropic spherically symmetric star equilibrium stability, assuming certain conditions with respect to mass-energy density and total baryon number
09 p1529 A71-23597

Radiatively interacting adjacent plates in presence of collimated solar flux, considering surface roughness effects on equilibrium temperature distribution
[AIAA PAPER 70-817]
11 p1854 A71-25511

He I absorption line profiles in normal main sequence B star spectra, discussing He abundance and LTE
11 p1821 A71-25536

Spectroscopic measurement of high temperatures for ionized gases /plasmas/ in local thermodynamic equilibrium
11 p1761 A71-25571

Equilibrium thermodynamics of ideal elastic solids under stress, using Cauchy stress tensor
11 p1799 A71-25740

Photon emission-absorption probabilities relation in thermodynamically quasi-equilibrium state as function of photo transition excitation frequency, temperature and chemical potential
12 p1931 A71-27303

Transient thermodynamic processes of two phase vapor-liquid emulsion emptying at subcritical temperature in heat engines
12 p1944 A71-27500

Thermodynamic equilibrium constants of Fe-MgO-SiO₂-O₂ system reactions at one atmosphere and 900-1300 C
14 p2190 A71-29875

Jet mixing control of thermodynamic state of space stored cryogenic fluids, minimizing mass penalties resulting from equilibrium departures
[AIAA PAPER 71-646]
14 p2285 A71-30723

Plasma physics measurement objectives in terms of deviations from thermodynamic equilibrium, discussing relationship between measuring device calibration and experimental data interpretation
15 p2453 A71-31200

Equilibrium constant and heat of dissociation from dynamic viscosity of dissociating gas, noting dependence on composition and temperature
15 p2366 A71-31484

Reversibility/irreversibility definition application to thermostatics, expressing work by Pfaffian form
15 p2513 A71-31922

Diffuse interstellar medium hydrogen radio recombination lines radiation transfer, investigating their thermodynamic equilibrium effects
15 p2498 A71-32772

Plasma local thermodynamic equilibrium relation to continuum, molecular band, atomic lines intensity and absorption line reversal/equivalent widths measurements
16 p2617 A71-32822

Thermal equilibrium achievement by highly rarefied gas in closed container with space and time varying surface temperature, deriving gas particle distribution
17 p2784 A71-34394

German book on noise covering electrical fluctuation phenomena, thermodynamic equilibrium, electromechanical systems, semiconductors and ferromagnetic fields, diodes, etc
17 p2713 A71-34470

Non-LTE problems computation based on integro-equation approach, using discrete operator for radiative transfer equation solution
17 p2808 A71-35539

Non-LTE physics of He atoms in hot stellar atmospheres, presenting numerical results for He I and II line spectra variations explanation
17 p2808 A71-35539

Water vapor effects on shock compressed air thermodynamic equilibrium by computer program, noting temperature and electron concentration reduction
18 p2984 A71-35858

Gas flow energy transport, discussing thermal radiation, radiant flux density, planetary atmosphere energy thermodynamic equilibrium and differential approximations
18 p2847 A71-36424

Normal and oblique shock thermodynamic equilibrium state variables calculation, taking into account dissociation and ionization
18 p2909 A71-36674

Electric fields effects on ionization and recombination rate in non-LTE Cs plasma
18 p2852 A71-36964

Localized deformation effect on common-emitter transistor current gain, giving equations system defining band diagram configuration of p-n junction in thermal equilibrium
19 p3027 A71-37490

Gas and electron temperature and thermal nonequilibrium in argon plasma jet from electrodeless induction discharge
19 p3111 A71-37577

Deuterium Balmer line intensities and overpopulation measurements relationship to thermal equilibrium in pinch discharges
21 p3421 A71-40142

Non-LTE picket fence model in radiative equilibrium solutions for thermal coupling and line strength parameter
21 p3438 A71-40243

Radiant monatomic gas flux boundary conditions derivation, considering all points in local thermodynamic equilibrium
21 p3475 A71-40666

Thermodynamic equilibrium calculation and demonstration of Mo siliciding by circulation method in hydrogen-free gaseous medium containing silicon chlorides
21 p3390 A71-41169

Equilibrium neutral gas and plasma electron number density fluctuation determination, deriving correlation functions from Liouville equation
22 p3530 A71-41890

Gas-metal reactions in refractory metals purification, discussing reaction kinetics, thermodynamic equilibria and dissolved gases induced mechanical properties changes
22 p3564 A71-42423

Thermodynamics of irreversible processes extended to nonlinear systems remote from equilibrium, considering Onsager reciprocity relations
23 p3780 A71-43100

Tunnel MOS diode oxide thickness and thermal equilibrium considerations, emphasizing reverse bias case AC conductance, capacitance and DC I-V characteristics
23 p3652 A71-43937

Local thermodynamic equilibrium deviation theory and application in low density Ar plasma, noting difference in Langmuir probe and spectroscopic electron temperature measurements
23 p3714 A71-44154

Transient thermodynamic processes of two phase vapor-liquid emulsion draining at subcritical temperature in heat engines
24 p3819 A71-44928

THERMODYNAMIC PROPERTIES

NT CRITICAL POINT

NT CRITICAL PRESSURE

NT CRITICAL TEMPERATURE

NT EMISSIVITY

NT ENTHALPY

NT ENTROPY

NT FREE ENERGY

NT FUSIBILITY

NT GIBBS FREE ENERGY

NT HEAT OF COMBUSTION
NT HEAT OF FORMATION
NT HEAT OF SOLUTION
NT HEAT OF VAPORIZATION
NT MELTING POINTS
NT PYROELECTRICITY
NT SPECIFIC HEAT
NT SUPERCRITICAL PRESSURES
NT SURFACE ENERGY
NT THERMAL BUCKLING
NT THERMAL CONDUCTIVITY
NT THERMAL DIFFUSION
NT THERMAL DIFFUSIVITY
NT THERMAL EXPANSION
NT THERMAL INSTABILITY
NT THERMAL STABILITY
NT THERMOCHEMICAL PROPERTIES
NT THERMOPHYSICAL PROPERTIES
NT VAPOR PRESSURE
NT VOLATILITY

Visual cells outer segments structure and retinal photoreception characteristics, describing open thermodynamic system

Molybdenum borocarbide synthesis and properties, discussing melting temperature, electrical and heat conductivity, thermal emf, microhardness, etc

Algorithm for nonstationary thermal regime of electronic equipment using heat balance method for variation in thermal coefficients and source power

Ta thermal properties at high temperature in cast cylinder, powder and wire specimens

Porous Ti thermal and electrical properties from room to high temperatures

High temperature calorimetry of solids for heat capacity and thermal processes thermodynamic and thermokinetic characteristics, considering calorimeter design engineering

Direct thermoelectric conversion systems thermodynamic analysis

Nonideal plasma thermodynamics data, discussing particle interactions, Coulomb potential, stability, etc

Molecular hydrogen thermodynamic properties in ideal state from spectroscopic data, using WKB method

Simple gases and liquids thermodynamic properties, calculating isotopic effects by corresponding states law with quantum corrections

Nitrogen austenite solute-solute binding energy derivation from experimental data for comparison with carbon austenite

Fermion system phase transition model thermodynamic behavior near critical point region for various interactions

Continuum internal thermodynamic constraints effect on materials response, assuming workless stress tensor

Radiative properties of construction properties and working media, noting importance to radiative heat transfer calculation

Cylindrical sample longitudinally isothermal zone unsteady temperature field calculation from heat conduction equation with allowance for temperature dependence of thermodynamic properties

Heat capacity and thermodynamic properties of alpha beryllium nitride from 20 to 315 K, using precision calorimeter

Beta-Li hexafluoroaluminate heat capacity and thermodynamic properties from 15 to 380 K

Multiproperty apparatus for high temperature determination of tungsten thermal properties, using direct electrical heating methods

Human legs thermal response during cooling for refrigeration anesthesia, deriving analytical model for temperature level prediction as function of time

Cryogenic liquids boiling peculiarities concerning heated surface material thermophysical properties effects on cavity stability, density and heat transfer rate

Fluorine liquid-vapor coexistence boundary and critical point parameters, considering thermodynamic and transport properties

Single chamber plasmatron with rising arc I-V characteristics, obtaining electrical and thermal properties in dimensionless form

Liquid hydrogen, oxygen and water droplets histories in space, examining size and temperature

Shock tube research instrumentation with fast response time for data on thermodynamic and transport properties, relaxation times and kinetics of high temperature gases

Industrial and biological polymer compounds active surface layers, discussing thermodynamic aspects, molecular dynamics, energy conversion and boundary layer entropy

Human organ thermal properties prediction by measuring water content of equal fat/protein tissues

Interstellar medium characteristics, examining H I and II regions thermal properties and shock waves

Elastic and thermodynamic properties of transition metal carbides, comparing Debye temperatures obtained from elastic constant to those obtained from specific heat data

Shock formation and chemical activation in solid secondary explosives detonation, considering propagation acceleration by pressure rise in terms of reaction products thermodynamic properties

Ordered intermetallic CsCl compounds thermodynamic properties determination, noting linear relationship between intrinsic disorder and formation heat

Austenitic stainless steel intergranular corrosion model for thermodynamic analysis leading to grain boundary diffusion and Cr concentration profiles determination

Undoped and Nd doped synthetic fluorapatite single crystals heat capacity, thermal expansion and thermal conductivity measurements, yielding Debye temperature

Mo-Re alloys thermal and electrical properties from X ray analysis of two phase structure

Liquid Al binary systems thermodynamic properties, using emf, improved dew point and distribution methods

Zinc-silver oxide batteries thermodynamic characteristics obtained from silver-silver oxide and zinc-zinc hydroxide electrodes data

Rocket engine thermodynamic characteristics and parameters determination, using extrapolation formulas with initial fuel composition

Ternary Mo-Hf-C alloys thermomechanical and mechanical property relationship, obtaining yield strength at various temperatures

High temperature nitrogen plasma, calculating thermodynamic and electrical parameters dependence on pressure and temperature

Turbulent hot gas motion in round pipes from semiempirical turbulence theory, accounting for energy dissipation and thermodynamic parameter variability

Models for nonferromagnetic solid body mechanics allowing for relationships among mechanical, thermal and electromagnetic processes

Thoria containing Ni and Co base powders reduction in hydrogen atmosphere for precipitation hardened materials production, determining optimal thermodynamic and reaction kinetic factors

Italian book on mixed plasmas equilibrium compositions and thermodynamic properties, covering numerical values tabulation for nitrogen mixtures with He, Ar and Xe

Matter and antimatter separation mechanism in universe based on thermal radiation thermodynamic properties

Monograph on dense gases state parameters measurement at high temperatures, applying to nitrogen

Thermodynamic properties of interstitial solid solutions with fcc metals from atomically discrete model by computer simulation

Heisenberg ferromagnet with applied external magnetic field, investigating thermodynamic properties near Curie point

Incore thermionic cell power output limitation and thermal/electrical data determination at steady state operation, considering temperature distribution

Switched power limitation in p-n-p-n devices turned off by control current pulse, discussing thermal signal level

Thermodynamic calculation of silicon chloride gas for high temperature two stage molybdenum silicification in glowing discharge under vacuum conditions

High performance ablative composites thermal physical characteristics from differential equations, describing thermochemical ablation-in- depth and boundary layer transport processes

Expanding laser generated plasma self similarity model from hydrodynamic equations, describing thermokinetic properties

Design, calibration and computer control of orbital heating simulator, using heat flux sensor feedback for ATM thermal vacuum tests

ATM for manned solar observation, discussing thermal design, thermal vacuum test philosophy, mathematical models and analytical and test data correlation

High velocity plasma jet accelerator operation, plotting heat and electromagnetic forces vs arc current, mass flow rate and nozzle diameter

Thermodynamical properties computation for binary mixture in equilibrium at constant pressure and temperature based on Gibbs free energy

Probability theory application to entropy and conductivity matrices

Equilibrium compositions and thermodynamic properties tabulated for argon-oxygen plasmas at 0.01 to 10 atm and up to 35,000 K

Sulfur hexafluoride equilibrium composition, thermodynamic functions, transport properties and application to simplified enthalpy flow arc model

Thermal scale modeling limitations for radiation-conduction system of unmanned spacecraft, discussing material thermal properties, model dimensions, instrumentation effects and environment simulation

Modified heat conductivity solutions for region with moving boundary, applying to crystallization front or crack propagation

Refractory materials production using chemical deposits from gaseous phase, discussing mechanical, physical and thermal properties of obtained coatings

Dense liquid thermodynamic model, using approximate equation of state

Thermodynamic properties prediction for liquefied natural gas and other cryogenic fluids, using two fluid method

Binary interstitial solid solutions thermodynamic properties calculation with Kirkwood expansion, allowing crystal first order partition function measurement without degeneracy error

Hadron matter thermodynamical properties at high temperatures, developing dual resonance dynamic model of high energy particle interactions

Mechanical and thermal properties of chemical vapor deposited carbon composite felt material for reentry heat shielding

Heat transfer near critical point, examining continuity, momentum and energy equations for variable thermodynamic and transport properties effects

Optical, mechanical, thermal and electrical properties of IR sensor materials at low operating temperatures

Solid helium and molecular/metallic hydrogen thermodynamic properties and phase diagrams as functions of pressures corresponding to Jupiter and Saturn

Molecular hydrogen thermodynamic properties in ideal state from spectroscopic data, using WKB method

Thermodynamic properties effects on transverse acceleration wave propagation in inhomogeneous isotropic elastic bodies with internal state variables

Thermodynamic properties of titanium carbide of variable composition at high temperature, considering

enthalpy, specific heat and entropy change due to thermal vacancies 15 p2431 A71-32159

Thermodynamic properties of dilute solutions of oxygen in liquid Fe-Co and Fe-Ni binary mixtures, obtaining Gibbs energy variation with temperature 15 p2432 A71-32174

Book on viscoelasticity covering isothermal stress-strain relations, wave propagation, mechanical properties, thermodynamics and nonisothermal effects 15 p2509 A71-32438

Thermomechanical damage by pulsed lasers in metals, discussing energy deposition and stress wave generation for optimal fracture conditions 15 p2422 A71-32555

Electronic excitation contribution to thermodynamic properties of high temperature gases according to partition function cutoff criteria 15 p2515 A71-32647

Thermal properties of solar wind plasma, determining electron and proton temperature distributions, proton heating rate, electron thermal conductivity and energy exchange rates 15 p2480 A71-32754

Nonequilibrium and equilibrium plasmas thermodynamic properties and molecular, atomic and ionic internal partition functions and relaxation times 16 p2617 A71-32955

Continuous media nonlinear thermomechanical behavior, presenting finite element formulation of deformation and irreversible thermodynamics problems 16 p2654 A71-33095

Coolant thermophysical properties effect on heat transfer intensity in porous metals, analyzing differential equations 17 p2835 A71-34204

Triple Knudsen cell method to determine thermodynamic activity of Cu in bcc solid solution of Ti-Cu alloys 17 p2756 A71-34488

Thermoelectric materials thermodynamic properties, developing coldness as universal function of viscous heat conducting fluids 17 p2837 A71-34694

High temperature nitrogen plasma, calculating thermodynamic and electrical parameters dependence on pressure and temperature 17 p2789 A71-35262

Degenerate dwarfs theory, discussing stellar structure, stability, evolution and thermal properties 18 p2969 A71-37039

Light elements thermodynamic state variables at high pressure, calculating electron density distribution as function of ion configuration with linear response theory 18 p2970 A71-37047

Interstitial solute thermomigration of C in Ti, V, Fe, Co, Ni and Pd, using radioactive tracer technique 19 p3079 A71-37710

Mg-Ge alloys liquid and two phase mixtures thermodynamic properties at 660-1130 C, using galvanic cell with magnesium chloride electrolyte 19 p3080 A71-37715

Artificial fog thermodynamic conditions and evolution data, using scattered laser beam angular distribution measurements 19 p3091 A71-38586

Dissolved and mixed water vapor condensation aerosol nuclei thermodynamic properties from aircraft and ground-based cloud measurement data 19 p3092 A71-38686

Partial configurational thermodynamic functions of interstitial species in ternary solid solutions containing substitutional and interstitial solute atoms 20 p3194 A71-38804

Semiconductor lasers, discussing laser action concepts, optical waveguiding, power conversion efficiency, thermal properties, reliability, crystal imperfections, GaAs laser properties, transient phenomena, etc 20 p3243 A71-39066

Soviet book on unsteady motions of continuous media covering gas dynamics, thermodynamics, shock and plane detonation waves, three dimensional gas motions, etc 20 p3211 A71-39144

NTWO as FORTRAN 4 family of subroutines developed on 7094-7044 system for determining thermodynamic and transport properties of nitrogen 20 p3253 A71-39268

Nonstoichiometric zirconium niobium carbide thermodynamic properties, deriving components activity equations from statistical considerations based on pairwise interaction energies [ECS PAPER 120] 20 p3252 A71-39554

Zirconium uranium carbide and zirconium hafnium carbide thermodynamic properties, using time-of-flight mass spectrometer 20 p3252 A71-39555

Viscoelastic polar materials thermomechanical behavior, deriving stress tensor, couple stress tensor, entropy density and linear constitutive equations 20 p3309 A71-39562

Frozen bipropellants as self supporting structural member for booster weight reduction, considering mechanical and thermal properties and melting rate requirement 20 p3276 A71-39609

Viscoelastic materials property inequalities as consequence of Gibbs free energy minimum, disproving interpretation as indication of second order phase transition 20 p3310 A71-39867

Exact solutions for cord reinforced materials with thermomechanical constraints of incompressibility and inextensibility and thermal constraint on temperature gradient 20 p3310 A71-39869

Refractory diborides in oxidizing environments, considering mechanical strength, thermal stability, oxidation resistance, heat conductivity, thermal expansion, specific heat and electrical resistance 21 p3405 A71-40138

Thermodynamic ion current ratios of solid solution V-Ti alloys, using Knudsen effusion and time of flight mass spectrometric methods 21 p3398 A71-40463

Thermodynamic activities of Ti and Al in bcc beta phase of Ti-Al system 21 p3398 A71-40465

Helium, neon, nitrogen, oxygen, argon, carbon dioxide and monoxide and methane thermodynamic and transport properties calculation using computer program for state equations 21 p3351 A71-40893

Heisenberg ferromagnet magnetic and thermodynamic properties in random phase approximation, determining magnetization and susceptibility with Green function theory 21 p3476 A71-40897

Stainless steels nitriding in presence of halogen compounds with heat treatment, observing thermodynamic potential shift 21 p3389 A71-41099

Switched power limitation due to thermal processes in p-n-p-n devices turned off by gate current pulse 21 p3430 A71-41219

Solid helium and molecular metallic hydrogen thermodynamic properties and phase diagrams as functions of pressures corresponding to Jupiter and Saturn interiors 22 p3606 A71-42613

Nonstationary thermal behavior of thermoelectric cooling device for coolant temperature disturbances, proposing transfer function determination method 23 p3664 A71-44072

Thermodynamic properties of Ti-Mo alloys, using triple Knudsen cell technique 23 p3694 A71-44279

Thermodynamic properties and nozzle flow calculations for high temperature and pressure hydrogen, presenting results in Mollier diagram 24 p3887 A71-44629

Liquid Mg-Al alloys thermodynamic properties determination by electrochemical and barometric methods 24 p3840 A71-45372

THERMODYNAMICS

NT AEROTHERMODYNAMICS

NT COMBUSTION PHYSICS

Entropy-disorder concepts relation in teaching thermodynamics, urging treatment as macroscopic theory 01 p0126 A71-10134

Chronometrically invariant formulation of relativistic thermodynamics second law distinguishing between three dimensional space and time 01 p0156 A71-10550

Kinetic theory of gas mixtures and thermodynamic laws of irreversible processes, deriving hydrodynamic equations and Onsager relations 01 p0130 A71-10793

Acceleration waves propagation in elastoplastic materials based on nonlinear thermodynamic theory 01 p0173 A71-10873

Inverse problems for parameters and optimal heat transfer model in thermophysical processes 02 p0331 A71-11731

Thermodynamic equations of state for dissociating and ionizing high temperature air applied to vertical and oblique compression shocks 02 p0331 A71-12067

Thermodynamic calculations simplification, using identical transformation of differential expressions 02 p0332 A71-12320

Elastoplastic, viscoelastic and directed elastic continuous media kinematic and thermodynamic description based on intermediate state of reference concept 02 p0326 A71-12335

A-B-A block copolymers statistical thermodynamics, describing postulated microstructure theoretical model for phase transition prediction 02 p0273 A71-12450

Thermodynamic similarity laws for rocket fuel tanks with cryogenic propellants, using dimensional analysis for unsteady temperature distributions 02 p0332 A71-12526

Nonlinear heat conduction of contacting bars with boundary conditions of fourth kind, using small parameter method 02 p0332 A71-12529

Plasticity theory simplified via revision based on thermodynamics 03 p0501 A71-13109

Thermodynamical theories and differential equations of thermoelectricity, generalizing energy and variational theorems 03 p0501 A71-13127

Differential equations of thermodynamics presentation to engineering students in form suitable for programmed study 03 p0518 A71-13526

Elastoviscoplastic materials infinitesimal theory extension to thermodynamic processes by limit transition, deriving constitutive equations 03 p0510 A71-13946

Dissipative structures in thermodynamics of irreversible processes of hydrodynamics and chemical kinetics 04 p0675 A71-14792

Lorentz invariants in relativistic fluid dynamics and thermodynamics in nonvacuo, suggesting determination through earth-moon space flight experiments 04 p0661 A71-14872

Supersonic combustion thermogasdynamics analysis, presenting combustion processes via pressure-velocity diagram 04 p0676 A71-14986

Fluctuation-dissipation thermodynamics with variables changing sign during time reversal 04 p0676 A71-15118

Soviet book on continuous media covering dynamic, thermodynamic and electrodynamic equations mechanic problems, three dimensional space, internal degrees of freedom, etc 04 p0626 A71-15373

Book on nonequilibrium /irreversible/ thermodynamics covering field theories, balance equations, continua, variational principles, energy dissipation, entropy, etc 04 p0626 A71-15600

Air, helium and carbon dioxide injection effect on turbulent boundary layer thermodynamic behavior by wind tunnel experiments 04 p0576 A71-15615

Soviet book on fundamentals of heat transfer theory covering thermodynamic equations, steady, unsteady, turbulent, incompressible and MHD flows, etc 05 p0831 A71-16196

Orthogonality principle in irreversible thermodynamics, proving generalization for Onsager nonlinear symmetry relations 05 p0837 A71-16708

Iron meteorites microstructure investigation by light and transmission electron microscopy, determining plastic deformation and cooling rate from thermomechanical history 06 p0964 A71-17343

Powder combustion unsteady processes equations, taking into account nonadiabatic flame front and chemical reactions incompleteness 06 p1005 A71-17389

Soviet book on fundamentals of thermoviscoelasticity mathematical theory covering deformable media mechanics and thermodynamics, fatigue defects, etc 06 p0984 A71-17437

Metal fretting corrosion energy analysis in terms of thermodynamics of irreversible process 06 p0904 A71-17942

Rh alloys thermodynamic reactions with fluorinating agents including fluorine, bromine, pentafluoride and chlorine trifluoride 06 p0904 A71-17949

Stellar free neutrino and antineutrino emission thermodynamics under hot matter neutronization and hydrodynamic stability during late evolutionary stages 06 p0974 A71-18426

TiS vaporization thermodynamics by high temperature mass spectrometry, considering ionic fragmentation and ionization cross section errors 07 p1054 A71-19368

Nonideal plasma thermodynamically complete equation of state based on shock wave experiments 07 p1173 A71-20533

Free boundary problems for heat equation involving interface coinciding initially with fixed face, proving existence, uniqueness and continuous dependence theorems 08 p1324 A71-20879

Book on plasma physics, Volume 1, covering electromagnetic fields, fluid mechanics and theory, mathematical analysis and thermodynamics 08 p1341 A71-21892

Compressed nitrogen thermodynamic calculations, determining virial equation of state applicability 08 p1376 A71-21905

Thermodynamic system with concentrated loads due to heat and mass transfer or chemical reactions, analyzing wave processes and system stability 09 p1544 A71-22269

- Nonlinear fluctuation-dissipation thermodynamics
time-even and time-odd parameters concerning
index relations for nonquantum Markovian case
09 p1544 A71-22366
- French book on thermodynamics and gas dynamics
covering theoretical and applied thermodynamics, air
compressors, combustion, internal combustion en-
gines, water vapor, compressible fluid cooling, etc
09 p1545 A71-22965
- Entropy-free thermodynamics second law based on
reversible expansion, using homogeneous nonstatic
thermological models
10 p1674 A71-24468
- Soviet papers on heat and mass transfer covering
diffusion, transport in capillary and dispersed
media, irreversible thermodynamics, material dry-
ness, etc
10 p1696 A71-24481
- Thermodynamics - Conference, Cardiff, Wales,
April 1970
11 p1828 A71-25733
- Cosmic evolution and thermodynamic irreversibil-
ity: discussing definitions and relationships of ther-
modynamic, historical and cosmological arrows of
time
11 p1828 A71-25736
- Earth atmospheric zonal circulation model, using
hydrothermodynamic equations with Newton law for
radiative heat sources
11 p1795 A71-25919
- Soviet book on thermal stresses in bodies of revolu-
tion of arbitrary shape covering energy conservation
equations and heat equations solutions
11 p1850 A71-26096
- Stellar free neutrino and antineutrino emission ther-
modynamics under hot matter neutronization and
thermodynamic stability during late evolutionary stages
12 p1954 A71-26576
- Transport coefficients interrelations, using irrever-
sible process thermodynamics
13 p2161 A71-28620
- Relativistic formulation of thermodynamics and
statistical mechanics in special theory of relativity,
Qing Ott presentation
13 p2102 A71-29324
- Iterative solution for quasi-linear heat equation, ex-
amining convergence for equation describing self
similar heat wave from instantaneous plane source
14 p2334 A71-29564
- Local short term mesoscale weather forecasting by
finite difference solution of hydrothermodynamic
equations
15 p2443 A71-31222
- Hydrometeorological fields derivatives transforma-
tion in hydrothermodynamic equations numerical in-
tegration
15 p2443 A71-31224
- Initial value problem in quasi-static thermoelastic-
ity using heat equation and Somiglian tensor
15 p2504 A71-31698
- Crack propagation model in linearly viscoelastic
solid strip based on thermodynamics first law
15 p2506 A71-32011
- German textbook on fundamentals of ther-
modynamics covering energy conversion, reversible/
irreversible processes, chemical/molecular ther-
mophysics, statistical analysis, probability theory, etc
15 p2516 A71-32767
- Vaporization thermodynamics of lanthanum car-
bides from Knudsen effusion mass spectrometry
16 p2538 A71-32812
- Chemical equilibria susceptibility to gravitational
field effects, suggesting coincidence with conditions
derived from relativistic thermodynamics
16 p2540 A71-33257
- General Stefan problem for heat conduction with
melting and free boundary problems occurring in con-
trol and statistical decision theories
17 p2841 A71-35794
- Critical point anomaly in saturation curves of
reduced temperature-compressibility planes of pure
substances, using metric differential geometry and
thermodynamics
18 p2985 A71-36452
- Instrumentation and techniques of torsional pendu-
lum and braid analyses, studying trace moisture and
are cycle effects on thermomechanical spectra of
polymeric materials
18 p2939 A71-36596
- First law of thermodynamics implications to general
theory of work and energy for material systems
18 p2986 A71-36811
- Thermodynamics axioms for work and energy under
volume-area continuity conditions, discovering local
over density in velocity field
18 p2948 A71-36812
- Alternating-direction Galerkin methods application
to parabolic and hyperbolic differential equations for
obtaining efficient iterative solution of heat equation
on rectangle
19 p3087 A71-38305
- Heat conduction equation coupling to wave equa-
tion in adjacent regions from operational method solution
of Volterra equation reduced problem
19 p3171 A71-38532
- Fronts and frontal clouds evolution theory as non-
stationary two dimensional problem with allowance for
dynamics and thermodynamics
19 p3091 A71-38682
- Error analysis for stable implicit difference methods
for heat equation with derivative boundary condition
20 p3254 A71-38758
- Earth atmospheric zonal circulation model, using
hydrothermodynamic equations with Newton law for
radiative heat sources
20 p3256 A71-39210
- Thermodynamics and statistical mechanics of low
temperature physics, including entropy, probability,
energy spectra and gas liquefaction
20 p3270 A71-39240
- Thermodynamics second law restrictions on con-
stitutive equations of electromagnetic theory for non-
linear materials with long-range gradually fading
memory, considering dissipation principle conse-
quences
20 p3270 A71-39485
- Finite elastoplastic deformation thermodynamic
theory based on isotropic work hardening, excluding
Bauschinger effect or localized modification of yield
surface due to plastic flow
20 p3308 A71-39486
- Molecular chaos breakdown under shear flow, cal-
culating thermodynamic fluctuation formula for un-
limited Reynolds number increase
21 p3418 A71-40628
- Fundamental derivative γ and other ther-
modynamic variables in gas dynamics, considering
transonic passage variation, Prandtl-Meyer wave,
adiabatic flow and nonlinear wave propagation
22 p3530 A71-41887
- Thermodynamic systems generalized topological
representation providing real system conceptual
reticulation into elements from ideal lumped param-
eter components
22 p3621 A71-42674
- Analytical transformations of variational conditions
in nonequilibrium thermodynamics, using mechanical
analogies similar to dLambert principle
22 p3622 A71-42688
- Thermodynamics of irreversible processes extended
to nonlinear systems remote from equilibrium, con-
sidering Onsager reciprocity relations
23 p3780 A71-43104
- Nonlocal thermodynamics constitutive theory of
continuous systems with global energy balance in
terms of classical thermostatics
23 p3782 A71-43868
- Inverse problem for heat conductivity equation in
semiinfinite region with Tikhonov specific initial and
boundary conditions
23 p3782 A71-44062
- Solid fuel combustion in presence of unsteady heat
propagation in heated layer, solving fuel heat conduc-
tion equation for sudden combustion rate change
24 p3891 A71-45218
- THERMOELASTICITY**
- Boundary value problems in thermoelastic equilib-
rium of unbounded isotropic plate with slits and foreign
circular inclusion
01 p0170 A71-10643
- Axissymmetric mixed boundary value problem of
thermoelasticity for hot stamp penetration into trans-
versely isotropic half space, deriving contact stresses
01 p0175 A71-11036
- Thermoelastic axisymmetric problem for half space
applied to steady temperature field and stress concen-
tration in infinite body with heat conducting plane cir-
cular crack
02 p0322 A71-11733
- Coupled Riemann-Hilbert boundary value problems
for thermoelastic state near thermally insulated crack
in inhomogeneous elastic medium
02 p0322 A71-11734
- Thermoelastic stresses in closed laminar orthotropic
shells of revolution subjected to axisymmetric loads
and temperature gradients
02 p0322 A71-11735
- Thermoelasticity problem for stressed state of thin
nonaxisymmetric shells with middle surface of revolu-
tion
02 p0322 A71-11736
- Elastoplastic unsteady thermally stressed state of
square and rectangular planform bodies by calculated
theory of small deformations, using strain compati-
bility equations with Airy stress function
02 p0323 A71-11743
- Homogeneous and composite polycrystalline
materials macroscopic thermoelastic characteristics
determination based on structural model
02 p0324 A71-11750
- Thermoelastic theory of stressed crystals and higher
order elastic constants covering surface electronic and
mass transport properties
02 p0294 A71-11799
- Thermodynamical theories and differential equa-
tions of thermoelasticity, generalizing energy and
variational theorems
03 p0501 A71-13127
- Couple stress effects on thermoelastic problem for
half space with heat doublet on bounding plane,
discussing singularity behavior and order
03 p0510 A71-13910
- Thermoelastic deformation of elastic media with
stochastically inhomogeneous microstructure, charac-
terizing physical properties as steady random vari-
ables
03 p0514 A71-14358
- Critique of thermoelastic problem solution for ther-
mal stress in semiinfinite body under step heat input
04 p0669 A71-15193
- Nonlinear thermoelasticity coupled equations,
discussing stress and temperature fields in terms of
material response functions
04 p0669 A71-15194
- Thermomechanical coupling in axially symmetric
viscoelasticity of cylindrical cavity under shear stress,
determining stress concentration from temperature
distribution
04 p0669 A71-15203
- Rectangular thin elastic plate with circular holes
under heat flow, solving thermoelastic problem by
point matching
05 p0823 A71-16492
- Dynamic thermoelastic response of rapidly heated
plate elements, developing variational principle
05 p0824 A71-16560
- Thin isotropic plate nonstationary coupled ther-
moelasticity problem, obtaining recursion equation
system for thermal stresses
06 p0983 A71-17367
- Thermoelastic equilibrium of multiply connected
plate during convective heat exchange
06 p0989 A71-17788
- Thin circular cylindrical shell thermoelastic vibra-
tions, deriving differential equations of motion with al-
lowance for shear, rotatory and translational inertia
06 p0996 A71-17840
- Thermoelasticity, mechanical and thermal
processes in deformation of elastic plates and shells
06 p0999 A71-17866
- Infinite elastic plate with rectilinear crack, deter-
mining heat exchange effect on thermoelastic stresses
06 p1000 A71-17939
- Steady state thermoelastic mixed boundary value
problem for elastic layer, obtaining temperature,
stresses and displacements in finite integrals through
Hankel transforms
08 p1370 A71-21238
- Thermoelastic stress and temperature distribution in
doubly connected isotropic plate
08 p1374 A71-21948
- Thermoelasticity equations solutions for special
cases
09 p1535 A71-22259
- Thermal stresses in finite circular cylinder heated
axisymmetrically over curved surface, constructing
thermoelastic displacement potential and biharmonic
Love function
09 p1536 A71-22452
- Nomograms for thermoelastic stress in plate deter-
mined as function of dimensions and heat transfer
09 p1538 A71-22605
- Elastic half space with plane boundary subjected to
transient temperature field, calculating temperature
distribution and thermoelastic strain through Laplace
transform
10 p1688 A71-24351
- Variational principles for initial boundary value
problem of fully coupled linear thermoelasticity for in-
homogeneous anisotropic materials with microstruc-
ture
10 p1689 A71-24512
- Thin circular cylindrical shells thermoelastic
behavior under one directional radiant heating, com-
paring measured displacements and strains with cal-
culated values based on measured temperature distribu-
tions
11 p1841 A71-25187
- Environmental effects on laminated anisotropic
plates thermoelasticity for critical swelling strains,
using Hookes law extension of Duhamel-Neumann
equations
11 p1783 A71-25332
- Thermoelastic heat release in muscular twitch final
phase, discussing energy storage as function of active
or passive muscular tension
11 p1718 A71-25626
- Soviet book on thermoelasticity covering thermal
stresses in disks, plates, shells and bodies of revolu-
tion in steady and unsteady temperature fields
11 p1850 A71-26100
- Boundary value problems of steady state ther-
moelasticity and axisymmetric Boussinesq stress con-
centration for half space in linear Cosserat elasticity
12 p1974 A71-26942
- Coupled thermoelasticity, bending and stability of
thin walled shells and plates of oriented fiberglass
reinforced plastics with low shear rigidity, using
Timoshenko theory
12 p1978 A71-27345
- Nonlinear physical and geometrical thermoelasticity
for plane strain and stressed state at circular hole in in-

THERMOELECTRIC CONVERSION SYSTEMS

finite space, using approximation in Lagrangian coordinates 12 p1978 A71-27349

Axisymmetric problem solution in theory of elasticity and thermoelasticity for semiinfinite circular cones truncated along spherical surface 12 p1980 A71-27361

Thin walled elastic isotropic shallow shell with thermal boundary conditions, obtaining thermoelastic solution in series form 12 p1984 A71-27687

Steady thermoelastic equilibrium of infinite isotropic plate containing imbedded circular inclusion with cuts along circumference 12 p1984 A71-27693

Consistent discrete models of continuous bodies electrothermoelastic behavior, using finite element formulations for general energy balance equations derivation 13 p2099 A71-27785

One dimensional wave propagation at low temperatures in thermoelastic half space under step strain at free surface 13 p2148 A71-27828

Coupled thermoelastic disturbances in half space due to thermal shock incident on surface at finite heat expansion rates 14 p2335 A71-30191

Thermoelastic stress analysis of circular perforated plate under point heat source 14 p2326 A71-30195

Thermoelastic shells and plates approximate linear theory, detailing uniqueness theorem for initial mixed boundary value problem 14 p2329 A71-30446

Monograph on crack problems in mathematical theory of thermoelasticity covering crack effects on stress distribution in circular cylinders, thick plates and infinite solid bodies 14 p2329 A71-30501

Fe-Ni alloys with Cr, investigating heat treatment effect on thermoelastic coefficient 15 p2426 A71-31482

Initial value problem in quasi-static thermoelasticity, using heat equation and Somigliana tensor 15 p2504 A71-31698

Thermoelastic stress generation in Cu and Ta samples by linear accelerator produced monochromatic MeV electron pulses, comparing measurements with wave theory predictions 15 p2414 A71-31973

German monograph on thermally stressed shear soft shells with finite deformation covering tensor analysis, thermoelasticity, temperature fields and two dimensional bodies 15 p2509 A71-32305

Thermoelastic stability as function of thermodynamic properties of elastic materials, applying invariance principle to dynamical systems on Banach space 16 p2649 A71-33004

Thermoelastic stability of finitely deformed solids under nonconservative surface tractions without body force 16 p2649 A71-33009

Dynamic uncoupled thermoelasticity analysis using integration by Goodier method in five dimensional space 16 p2662 A71-33171

Thermoelastic critical equilibrium of plate with rectilinear crack under heat transfer from edge surface and tensile stress 16 p2658 A71-33686

Tensional thermoelasticity theory of continuum media, analyzing material particle interactions by stress tensor and equations of motion 17 p2815 A71-34187

Monograph on fiber-resin composites covering glass, boron and carbon fibers and epoxy matrix materials tensile and thermoelastic properties 17 p2761 A71-34469

Thermal stresses in plane strain of isotropic micropolar elastic solids without heat sources, reducing thermoelastic to isothermal problem 17 p2821 A71-34583

Heating by thermoelastic damping through sudden removal of stresses on homogeneously strained elastic body, comparing elastic deformation of rubber and steels 17 p2821 A71-34584

Thermoelastic Cosserat plate with insulated un-stressed circular hole under uniform temperature gradient at infinity 17 p2822 A71-34675

Thermoelastic materials thermodynamic properties, developing coldness as universal function of viscous heat conducting fluids 17 p2837 A71-34694

Stressed state of nonuniformly heated thermoelastic flexible plates with variable elastic parameters, using integral principle of minimum total potential energy 17 p2829 A71-35310

Italian SIRIO synchronous satellite for SHF communication, analyzing thermoelastic deformations effect on antenna radiation patterns 18 p2882 A71-36575

Rheological media viscoelastic relaxation theories generalization taking into account thermal stress and conduction 18 p2984 A71-37021

Nonlinear differential equations and boundary conditions describing behavior of electrically polarizable finitely deformable heat conducting continuum interacting with electric field 19 p3118 A71-37793

Temperature effects in incompressible elastic materials, adapting Adkins-Green isothermal successive approximation technique to thermoelasticity problems 19 p3157 A71-37800

Rigid disk effect on thermal stress distribution in semiinfinite elastic solid under prescribed surface temperature and heat flux 19 p3159 A71-38188

Thermoelastic axisymmetric equilibrium of elastic semiinfinite two dimensional medium with Griffith crack under prescribed heat flux 19 p3159 A71-38189

Steady state thermoelastic mixed boundary value problem for elastic layer with one face stress free and other face resting on rigid frictionless foundation 20 p3309 A71-39495

Thermoelastic plane harmonic and Rayleigh surface waves in elastic solids with thermal relaxation, using Maxwell heat conduction equation 20 p3310 A71-39779

Ti-Ni alloy martensitic thermoelastic transformation and memory effect, using optical microscopy to examine change in lattice discontinuity 21 p3398 A71-40459

Time harmonic waves oblique propagation in periodically laminated composite, using coupled thermoelasticity theory for plane strain 22 p3613 A71-41433

Coupled thermoelastic problem of homogeneous isotropic elastic half space with embedded spherical cavity 22 p3613 A71-41566

Quasi-static thermoelasticity and dynamic thermal stress equations solution in matrix form by Fourier transform and Hilbert-Levy method 22 p3614 A71-41567

One dimensional propagation and multiple reflection of plane thermoelastic wave in Lamé elastic isotropic plate with finite heat transmission 22 p3615 A71-41911

Thermoelastic coefficient development by tempering for Ni-Fe alloy containing Be 22 p3563 A71-42325

Micropolar elasticity plane problems equilibrium equations system solution, considering elastic half space deformation and steady thermoelasticity 23 p3775 A71-43316

Two-component composite cylindrical body thermoelastic stresses near junction-surface edge under plane deformation conditions 23 p3776 A71-43420

Homogeneous mountain mass and canyon thermoelastic stress analysis in curvilinear coordinate system by complex variables 23 p3776 A71-43421

Solid circular plate with diverse elastic moduli in different directions and hole at center, calculating thermoelastic stresses 23 p3777 A71-43422

Thermoelasticity, thermal conductivity and stress distributions in plates with two circular holes under constant contour temperatures, using complex variables theory 23 p3778 A71-44042

Polycrystals thermoelastic characteristics, determining thermal expansion and conductivity macroscopic coefficients 24 p3840 A71-44402

Thin isotropic shells with terminal shear rigidity, deriving complex version of classical theory of thermoelasticity for plastic shells with low shear resistance 24 p3878 A71-44482

Asymptotic design formulas for thermoelastic supercritical strains in thin elastic shallow spherical shells under external pressure 24 p3881 A71-44827

THERMOELECTRIC CONVERSION SYSTEMS

U THERMOELECTRIC POWER GENERATION

THERMOELECTRIC COOLING

Cascade thermoelectric cooler/heat pump/transient response for various geometries, materials and environmental conditions 03 p0355 A71-14320

Ettingshausen refrigerator dynamic behavior mathematical models, using current density and potential gradient as controlling variables 04 p0678 A71-15465

Nonstationary thermal behavior of thermoelectric cooling device for coolant temperature disturbances proposing transfer function determination method 23 p3664 A71-44344

THERMOELECTRIC GENERATORS

NT SNAP 15
NT SNAP 19
NT SNAP 21
NT SNAP 23
NT SNAP 27

Book on direct energy conversion principles and methods covering fusion, fuel cells, MHD, thermoelectric, thermionic, photovoltaic, electrodynodynamic, piezoelectric and ferroelectric power generation 01 p0006 A71-11111

Technological development of thermoelectric radionuclide batteries for space applications using Si thermocouples 02 p0282 A71-12311

Nuclear reactors for space power supply with thermoelectric, thermoelectric and thermionic converters 02 p0282 A71-12311

Energy converters for satellite nuclear power plants, discussing rotating, MHD, thermionic and thermoelectric systems 02 p0282 A71-12311

Limited reliability mathematical model of radioisotopic thermoelectric generators semiconductor couples based on catastrophic failures 11 p1715 A71-26101

Cost optimization for solar generator thermoelectricities by selecting temperature, contact resistance material parameters and fabrication technology 15 p2351 A71-31611

Reliability analysis of solar thermoelectric generator module as function of individual photocells, circuit design and redundancy 15 p2351 A71-31611

Long life radioisotope thermoelectric generators for space missions, discussing power degradation mechanisms and design trends 19 p3102 A71-37979

Radioisotope thermoelectric generators integration for Pioneer 6/7 program, discussing design requirements 19 p3103 A71-37979

Pioneer Jupiter spacecraft, noting low weight radioisotope thermoelectric generators and gyroscope stabilization by spinning with antenna pointed at earth 19 p3141 A71-37979

Radioisotope thermoelectric generators in micro milliwatt power range for biomedical applications 20 p3192 A71-38911

Long life performance predictions for lead telluride and silicon germanium radioisotope thermoelectric generators for deep space missions 20 p3263 A71-38911

Multihundred watt radioisotope thermoelectric generator for JPL outer planet missions, discussing vacuum/xenon filled performance and response to thermal/electrical transients 20 p3263 A71-38911

Multihundred watt radioisotope thermoelectric generator for spacecraft power supply, discussing system design, performance and safety requirements 20 p3263 A71-38911

Performance tests of high temperature silicon-germanium alloy thermoelectric generator for outer planet mission spacecraft 20 p3264 A71-38911

Cascaded thermoelectric generator using Si-Ge and Pb-Te elements with heat pipe interstage coupling 20 p3264 A71-38911

Multihundred watt radioisotope thermoelectric generator heat source survivability in multiple skin reentry 20 p3264 A71-38911

Grand tour missions radioisotope thermoelectric generator power source, presenting optimization technique for hot thermocouple junction operation 20 p3264 A71-38911

Radioisotope thermoelectric generator safety analysis operations considerations for users of large nuclear space power systems 20 p3264 A71-38911

Protective xenon atmospheres in sealed silicon-germanium alloy thermoelectric generators, discussing leakage and pressure levels 20 p3265 A71-38911

Tubular compact air cooled thermoelectric module endurance and performance tests and computer simulation for space reactor power system 20 p3266 A71-38911

Long term performance of lead telluride thermoelectric generators tested under SNAP 21, 23A and 27 programs 20 p3266 A71-38911

Long life radioisotope thermoelectric generators discussing mathematical model to simulate expected performance profiles 20 p3266 A71-38911

Nuclear characteristics of plutonium fuel for thermoelectric generators and required shield thickness 20 p3266 A71-38911

for sensitive radiation experiment in outer planet spacecraft
22 p3592 A71-42300

THERMOELECTRIC MATERIALS

Aging process effects on thermoelectric semiconductors physical stability for cryogenic applications
05 p0793 A71-16799

Semiconductor thermocell junction polishing effects on bilateral layers tensile strength and electrical contact resistance
07 p1023 A71-19145

Semiconductor thermoelectric materials intercrystalline boundaries porosity effects on electrical and thermal conductivity
09 p1506 A71-22162

Hybrid thermocouple with PbTe and SiGe thermoelectric materials, discussing development status and performance prediction
15 p2355 A71-32225

Physicomechanical properties of cermet sintered thermoelectric materials, considering n- and p-type samples of Si-Ge alloys
19 p3075 A71-37111

Cascaded thermoelectric generator using Si-Ge and Pb-Te elements with heat pipe interstage coupling
20 p3264 A71-38929

Oxygen enhanced sublimation of p-type PbTe thermoelectric materials in isothermal and ingradient testing of couples
20 p3266 A71-38953

SNAP 19 TAGS thermoelectric generator life tests at high temperature in Ar, predicting long term performance including thermoelectric material and isotope fuel decay effects
20 p3266 A71-38963

SNAP 19 Radioisotope Thermoelectric Generator (RTG) for advanced space missions, using lead telluride and silver antimony germanium telluride as conversion materials
20 p3267 A71-38965

THERMOELECTRIC OUTER PLANET SPACECRAFT

U TOPS (SPACECRAFT)

THERMOELECTRIC POWER GENERATION

Direct thermoelectric conversion systems thermodynamic analysis
01 p0007 A71-11228

Cs thermoelectric power near critical temperature and pressure, determining dense plasma electron-neutral elements interaction effects
11 p1715 A71-26153

Co-Ge-Si alloys phase equilibria, evaluating long term stability of junctions between thermoelectric batteries conducting series connectors
17 p2759 A71-35337

Reactor power systems for earth orbital space station, considering thermoelectric and Brayton cycle power conversion modules
20 p3262 A71-38919

Isotope Brayton four module adaptable compact power system for space station, using plutonium 238 fuel and lithium hydride shielding for neutron attenuation
20 p3263 A71-38922

PbTe thermoelectric converter for ZrH reactor space power supply, discussing operational performance, design and materials technology
20 p3265 A71-38951

Electrical conductivity and thermoelectric power measurements for polycrystalline beta-SiC heavily doped with nitrogen, estimating electron effective mass and carrier mobility at high temperatures
21 p3433 A71-41307

Bismuth telluride single crystals thermal conductivity and thermoelectric power temperature dependence 2.3-100 K, discussing magnetic field effects
21 p3433 A71-41314

GeTe alloyed with Zn, Cd or Hg, measuring electrical conductivity and thermoelectric power temperature dependence
21 p3435 A71-41345

Te-doped n-type GaSb semiconductor negative magnetoresistance and magnetothermoelectric power dependence on longitudinal magnetic field
21 p3436 A71-41349

n-type cadmium germanium arsenide single crystal semiconductor electron and hole effective mass determination from thermoelectric power measurement
21 p3436 A71-41350

Electrical resistivity and thermoelectric power sensitivity for simple liquid metals near melting temperature, determining temperature effects from pseudopotential models
22 p3586 A71-42370

THERMOELECTRIC SPACECRAFT

U TOPS (SPACECRAFT)

THERMOELECTRICITY

Liquid sodium and potassium thermoelectric potentials, calculating Seebeck coefficients to 600 C
01 p0141 A71-11602

Photoelectrical and thermoelectrical properties of CdS, CdS-CdSe and CdSe single crystals epitaxial films
05 p0793 A71-16823

Radioelectric /Hall/ effect due to electromagnetic wave propagation in semiconductors, noting longitudinal electric field generation by thermoelectric forces
05 p0794 A71-16882

Nonstoichiometric VC, studying thermal and electrical conductivities, thermoelectric properties and Hall coefficient
06 p0912 A71-18085

Composition and annealing effects on mechanical and thermoelectric properties of sintered wire W-Re alloys
07 p1143 A71-20493

Thermoelectric microwave radiation sensors with small area n-n junctions, investigating carrier heating effects on I-V characteristics
10 p1584 A71-24723

Spontaneous magnetic fields in laser produced plasmas explained as thermoelectric currents
11 p1807 A71-26406

Electric current heated thin resistance film thermoelectric transducer, measuring temperature rise with thermocouple
12 p1888 A71-27158

Consistent discrete models of continuous bodies electrothermoelastic behavior, using finite element formulations for general energy balance equations derivation
13 p2099 A71-27785

Thermal emf measurement of Ti alloy, steel, bronze and duraluminum subjected to fretting corrosion tests
13 p2082 A71-27820

Liquid and gaseous Hg thermoelectric power measurements at sub and supercritical temperatures and various pressures
13 p2000 A71-28676

Semiconductor thermoelectric battery p-n cell elements joining with mercury amalgam for commutating
14 p2181 A71-29953

Thermoelectric and thermomagnetic phenomena in semiconductors with impurity ions, solving electric conductivity and diffusion and Poisson equations for weak magnetic fields
16 p2622 A71-34027

Electric power and efficiency of thermoelements with temperature dependent thermoelectric properties by heat balance technique
18 p2852 A71-36965

Nonlinear differential equations and boundary conditions describing behavior of electrically polarizable finitely deformable heat conducting continuum interacting with electric field
19 p3118 A71-37793

Life tested thermoelements postoperative diagnostic analysis, using thermoelectric techniques
20 p3182 A71-38952

Heat treated thallium bismuth sulfide, selenide and telluride amorphous and polycrystalline thin films electrical conductivity, differential thermal emf and forbidden bandwidth
20 p3276 A71-39076

Microhardness, thermo-emf and phase composition of Al coatings on Armcro iron and steel under furnace and rapid electric heating
21 p3389 A71-41096

Thin bismuth films thermal and electrical conductivities and thermoelectric power measurements, examining preparation methods
21 p3435 A71-41338

Thermoelectric properties of quaternary Sb-Bi-Te-Se solid solutions, noting low thermal conductivity
22 p3584 A71-41618

Zirconium monocarbide electrical conductivity, Hall coefficient, thermal emf and magnetic susceptibility measurements for temperature dependence at 500-1000 C in homogeneity region
23 p3692 A71-44021

Nd-Bi phase diagrams from thermal differential, metallographic and X ray analyses, discussing carrier concentration and mobilities, Hall coefficients, conductivity and thermal emf
23 p3692 A71-44022

Vacuum fusion sintered rhodium borides melting point, microhardness and conductivity and thermal emf temperature dependences determination by thermal metallographic and X ray analyses
23 p3717 A71-44024

THERMOGRAMS

U RECORDING INSTRUMENTS

U TEMPERATURE MEASURING INSTRUMENTS

THERMOGRAPHS

U RECORDING INSTRUMENTS

U TEMPERATURE MEASURING INSTRUMENTS

THERMOGRAVIMETRY

Thermogravimetric analysis of goethite-rich sample of Mars type limonite, considering sorption process relation to Mars environment and polar caps
04 p0644 A71-15131

Temperature and pressure effects on phase transformations, structural changes and related processes in metals, comparing thermographic and calorimetric methods
09 p1547 A71-23227

High heating rate thermogravimetric analyzer for ablative plastics, predicting response with semiempirical analytical model
11 p1744 A71-26042

Ammonium perchlorate sublimation using simultaneous differential thermal analysis and thermogravimetry
23 p3641 A71-43116

THERMOLUMINESCENCE

CdS single crystals with Cu and Cl additives, observing optical flash and thermoluminescence in IR band
03 p0468 A71-14385

Thermoluminescence glow curve and decay characteristics of Apollo 12 fines and soil samples, suggesting lower mean daytime surface temperature at site
10 p1672 A71-24395

Atmospheric heating effects on thermoluminescence output variations with depth below Uceram meteorite fusion crust, noting nonuniform cosmic rays shielding
10 p1675 A71-24470

Thermoluminescent phosphorus films irradiation by electrons with energies up to 15 keV in vacuum chamber
12 p1942 A71-26648

Long range thermoluminescent dating of meteorites and tektites, discussing dependence on thermal release of trapped carriers, radiation saturation and instrumental errors
16 p2638 A71-33518

Thermoluminescent dosimeter for skin basal layer dose measurement in mixed beta and gamma radiation fields
17 p2693 A71-35450

Luminescence, thermoluminescence and spectral reflectance of lunar samples from Oceanus Procellarum and Mare Tranquillitatis
23 p3760 A71-43775

Apollo 12 lunar core sample thermoluminescence dependence on radiation dose rates, detecting temperature gradients in regolith by differential thermal analysis
23 p3760 A71-43776

Natural and X ray excited thermoluminescence in Apollo 12 lunar samples and terrestrial plagioclases
23 p3761 A71-43778

THERMOMAGNADYNAMICS

U THERMOMAGNETIC EFFECTS

THERMOMAGNETIC COOLING

One dimensional steady state performance characteristics of thermomagnetic generators and refrigerators in dimensionless form
09 p1387 A71-23647

THERMOMAGNETIC EFFECTS

Thermomagnetic gas torque within kinetic theory framework for collinear static and alternating magnetic fields
02 p0291 A71-12316

Ancient geomagnetic intensity in Japan by comparing natural remanent magnetization with known thermoremanent magnetization induction, using stepwise heating method on antique pottery
04 p0582 A71-15127

Soviet book on kinetic effects in semiconductors covering galvanoresistive and thermomagnetic effects, energy bands, quantum theory, oscillation theory, etc
06 p0941 A71-17431

Thermal and electrical transport in tungsten crystal for strong magnetic fields and liquid helium temperatures
08 p1344 A71-21365

Boundary condition effects on thermomagnetic torque from moment method solution for Boltzmann equation for diatomic molecular gas in magnetic field and cylindrical geometry
09 p1502 A71-22853

Thermomagnetic modulated Kerr effect readout and magneto-optical laser recording at high output on cobalt base metallic films
10 p1613 A71-25108

Magnetoactive plasma layer in strong constant magnetic field, computing dispersion equation for large amplitude thermomagnetic wave propagation
15 p2456 A71-31745

Thermoelectric and thermomagnetic phenomena in semiconductors with impurity ions, solving electric conductivity and diffusion and Poisson equations for weak magnetic fields
16 p2622 A71-34027

Thermomagnetic modulated Kerr effect readout and magneto-optical laser recording at high output on cobalt base metallic films
10 p1613 A71-25108

Magnetoactive plasma layer in strong constant magnetic field, computing dispersion equation for large amplitude thermomagnetic wave propagation
15 p2456 A71-31745

Thermoelectric and thermomagnetic phenomena in semiconductors with impurity ions, solving electric conductivity and diffusion and Poisson equations for weak magnetic fields
16 p2622 A71-34027

Thermoelectric and thermomagnetic phenomena in semiconductors with impurity ions, solving electric conductivity and diffusion and Poisson equations for weak magnetic fields
16 p2622 A71-34027

THERMOMAGNETISM

U THERMOMAGNETIC EFFECTS

THERMODYNAMICS

U THERMODYNAMICS

THERMOMETERS

NT RESISTANCE THERMOMETERS

Yaw sphere and thermometer combination, examining proportional vertical heat flux
03 p0422 A71-13231

Magnetic thermometry below 3 K using stable AC mutual inductance bridge
03 p0427 A71-13915

Geothermometer based on plagioclase-magmatic liquid equilibrium
05 p0751 A71-16411

Errors from multiple reflections between target environment viewed by IR thermometer or radiometer and background environment
05 p0752 A71-16672

High altitude radiosonde thermometer and pressure sensor construction, discussing radiation error and wire lag
08 p1293 A71-21740

Temperature measurement techniques annual progress survey including contact and radiation thermometers, IR thermography, microwave radiometry, fluidic sensors, and liquid crystals
10 p1612 A71-24685

Simple sensitive multichannel servo system thermobarometer for volume changes corrections, noting adaptation to five channel closed circuit respiratory apparatus
12 p1874 A71-27138

Surface temperature measurements with contact thermometers, discussing sensor design, cost and efficiency
16 p2579 A71-33474

Air temperature measurement errors, comparing thermometers with and without meteorological screening
21 p3383 A71-41240

Contactless determination of low temperatures by IR radiation thermometers, applying to measurement on transparent materials
22 p3546 A71-42158

THERMOMETRY

U TEMPERATURE MEASUREMENT

THERMONUCLEAR ENERGY

U THERMONUCLEAR POWER GENERATION

THERMONUCLEAR EXPLOSIONS

Thermonuclear microbombs for manned spacecraft propulsion to solar system boundary, describing system design and performance
04 p0625 A71-15647

Neutron star formation, calculating reimplosion mass fraction of thermonuclear supernovae explosion
05 p0811 A71-16684

Night D region ion kinetics data during thermonuclear detonation, discussing formation and conversion rates, electron concentration and recombination
08 p1278 A71-21009

Collapsing white dwarf stars, investigating detonation wave formation for thermonuclear explosion
16 p2631 A71-33228

Evolved stellar cores thermonuclear explosion products state, investigating Chapman-Jouguet detonation propagation effects with carbon 12 and oxygen 16 burning under high electron degeneracy
17 p2806 A71-35407

Cosmos satellite data on mainland China thermonuclear explosion of 27 December 1968, observing radiation effects on particles in natural radiation belts
20 p3278 A71-39128

High altitude thermonuclear explosion fission fragments locating method, considering magnetogravitational trap as potential well for heavy charged fragments
20 p3279 A71-39143

Night D region ion kinetics data during thermonuclear detonation, discussing formation and conversion rates, electron concentration and recombination
20 p3219 A71-39589

THERMONUCLEAR POWER GENERATION

Fusion energy technology, discussing controlled reactor construction and operation
07 p1169 A71-20000

THERMONUCLEAR PROPULSION

U NUCLEAR PROPULSION

THERMONUCLEAR REACTIONS

NT CONTROLLED FUSION

NT NUCLEAR FUSION

Controlled thermonuclear reactions produced by exposing LiD target to short pulses of Nd-glass laser, measuring neutrons number and plasma temperature
10 p1620 A71-24208

Calorimetric determination of reactor gamma source heating as function of specimens thickness and atomic number, discussing slab and cylindrical geometrical effects
11 p1797 A71-26078

Optimal thermonuclear plasma confinement considering external electromagnetic field as control variable, based on Boltzmann-Vlasov model
13 p2107 A71-28832

Enhanced low energy nuclear resonance reaction cross section estimation, finding Be 9 isotope reaction with proton for clean controlled thermonuclear reactor
24 p3847 A71-44495

Tokamak T-3A plasma neutron emission, confirming thermonuclear nature of radiation
24 p3856 A71-45113

THERMOPHILES

Thermophilic, mesophilic and psychrophilic anaerobes fatty acid composition, discussing results obtained by mass spectral analysis
15 p2360 A71-32050

THERMOPHILIC PLANTS

NT BLUE GREEN ALGAE

THERMOPHYSICAL PROPERTIES

NT CRITICAL POINT

NT CRITICAL PRESSURE

NT CRITICAL TEMPERATURE

NT EMISSIVITY

NT FUSIBILITY

NT HEAT OF SOLUTION

NT MELTING POINTS

NT PYROELECTRICITY

NT SPECIFIC HEAT

NT SUPERCRITICAL PRESSURES

NT THERMAL CONDUCTIVITY

NT THERMAL DIFFUSION

NT THERMAL DIFFUSIVITY

NT THERMAL STABILITY

NT VAPOR PRESSURE

NT VOLATILITY

Soviet book on oxide and silicate materials chemistry and technology covering corrosion, thermophysical properties shear stress, drying, etc
02 p0272 A71-11825

High temperature thermophysical properties of vanadium, establishing heat conductivity coefficient, electric resistivity, Lorentz number, monochromatic and total hemispherical emission coefficients
02 p0263 A71-12189

Mercury microwave and IR observations interpreted for thermophysical models for planetary subsurface, discussing rotation and heating
03 p0492 A71-14069

Thermophysical properties of methane, considering virial coefficients, vapor and melting pressures
04 p0674 A71-14728

Thermophysical properties of solids at high temperatures - Conference, Salford, England, July-September 1970, Part I
04 p0594 A71-14953

High speed measurements of thermophysical properties at high temperatures, including photoelectric and photographic methods
04 p0595 A71-14957

Thermophysical properties of solids at high temperatures concerning zirconium carbide, corundum, metals and Ba-Cs system
04 p0612 A71-15578

Nonlinear unsteady heat conduction problems, investigating thermophysical property dependence on temperature and body coordinates by half space and approximate methods
06 p1006 A71-17749

Oxygen-kerosene fuel combustion products, calculating thermal and physical constants
08 p1346 A71-21263

Thermophysical properties of solids at high temperatures - Conference, University of Salford, England, April 1970
10 p1624 A71-23906

Heat resistance, thermal stability, thermal conductivity coefficient and specific heat measured in cylindrical hollow specimens of corundum materials
10 p1634 A71-24200

System and component models for spacecraft thermal control design, considering materials, environmental degradation, measurement errors, manufacturing and quality assurance
11 p1859 A71-26239

Temperature dependent thermophysical properties effect on temperature distribution in step-heated semiinfinite solid, deriving time limited perturbation solution
13 p2164 A71-28988

Nb single and polycrystalline thermal conductivity/diffusivity, specific heat, electrical resistivity and monochromatic/integrated degree of blackness at high temperatures
14 p2258 A71-30052

High temperature thermophysical properties of vanadium, establishing heat conductivity coefficient, electric resistivity, Lorentz number, monochromatic and total hemispherical emission coefficients
15 p2426 A71-31496

Nonlinear unsteady heat conduction problems, investigating thermophysical property dependence on temperature and body coordinates by half space and approximate methods
17 p2838 A71-35115

High speed system for thermophysical properties measurement of electrical conductors above 2000 K in subsecond experiments
19 p3062 A71-37246

Thermophysical properties of Ta, W and Ta-W alloy at high temperatures, using automatic high vacuum facility
20 p3247 A71-38764

Convective heat transfer between laminar fluid flow and circular flat tubes, considering wall thermophysical properties effect
22 p3619 A71-41873

Mars surface soil thermophysical properties, temperature and thermal emission from Mariner spacecraft IR radiometer data, correlating with visual images
24 p3867 A71-44439

THERMOPHYSICS

U THERMODYNAMICS

THERMOPLASTIC FILMS

U POLYMERIC FILMS

THERMOPLASTIC RESINS

Glass fiber reinforced thermoplastics application possibilities and limitations, considering physical and mechanical properties
01 p0108 A71-10695

Fiber reinforced thermoplastics deformation characteristics, using uniaxial tensile test
02 p0274 A71-12480

Injection molded thermoplastics with fiberglass reinforcement, examining mechanical properties and thermal and stress cracking resistance
05 p0773 A71-17123

Glass fiber reinforced thermoplastics with increased room temperature mechanical properties, noting effect of heat, aging and chemical environment exposure
07 p1145 A71-19692

Optimal design and manufacture of wall attachment fluidic devices, noting thermoplastics injection molding followed by ultrasonic bonding
07 p1121 A71-20565

Organofunctional silane interfacial coupling for high strength glass reinforced thermoplastics
08 p318 A71-20695

Thermosetting and thermoplastic carbon fiber composites fabrication molding techniques, forms provisions and new uses
[PLASTICS INST. PAPER 33]
08 p1321 A71-20916

Comparative tensile and creep tests of reinforced thermoplastics for performance/cost selection
[PLASTICS INST. PAPER 4]
09 p1481 A71-22340

Reinforcement theory fiber filled thermoplastics, considering fiber strength and length
[PLASTICS INST. PAPER 2]
09 p1481 A71-22341

Deformation and strength characteristics of fiber composite thermoplastic resins in terms of stiffness and reinforcement factors
[PLASTICS INST. PAPER 3]
09 p1481 A71-22343

Tribological characteristics of carbon fiber reinforced thermoplastics, noting improved sliding wear against metal surfaces
[PLASTICS INST. PAPER 12]
09 p1481 A71-22344

Thermoplastics reinforcement with carbon, silicon nitride and silicon carbide fibers, noting fiber aspect ratio
[PLASTICS INST. PAPER 5]
09 p1482 A71-22345

Fiber reinforced thermoplastics fabrication by fluidized bed techniques, fusing powder matrix to fiber surface for continuous coating
11 p1768 A71-25415

Stiffness factor in reinforced thermoplastics mechanical properties as function of glass fiber content, working temperature and duration of loading
12 p1920 A71-27012

Fatigue crack propagation in thermoplastics, investigating stress intensity effect on factor mean value
13 p2091 A71-28465

Glass fiber reinforced flame retardant thermoplastic resins, tabulating flammability resistance and mechanical properties
22 p3565 A71-42076

THERMOPLASTICITY

Elastoplastic unsteady thermally stressed state of square and rectangular planform bodies by calculated theory of small deformations, using strain compatibility equations with Airy stress function
02 p0323 A71-11743

Thermoplasticity plane problems with complex edge loading, deriving algorithm based on theory of flow with translational hardening
02 p0323 A71-11746

Creep analysis for thermoplastic beams under bending and struts under buckling
10 p1685 A71-23942

Physical model describing mechanism of recording through surface corrugation of thermoplastic viscofluid layer by electron beam
10 p1613 A71-24873

Small deformation theory of thermoplasticity with medium mechanical characteristics dependent on temperature, noting use in nonmechanical structural transformations and radioactive irradiation
12 p1978 A71-27348

Static and dynamic stress analysis and limiting loads of plastic shells and plates with temperature field in structural element, using deformation theory
12 p1979 A71-27350

Quasi-stationary one dimensional thermoplastic stress strain state in cylindrical fuel tank during emptying process, allowing for Bauschinger effect
13 p2157 A71-29196

THERMORECEPTORS

Human temperature control computer simulation, considering sudomotor, vasomotor and metabolic as

error signals from hypothalamic and cutaneous thermoreceptors

07 p1048 A71-19585

Temperature analyzer function under ambient temperatures in children

08 p1242 A71-21961

Impulse skin temperature encoding in primate cutaneous thermoreceptors in dynamic thermal conditions

18 p2860 A71-36877

HERMOREGULATION

Automatic temperature monitor and proportional solid state DC controller for electrophysiological use

01 p0022 A71-10247

Human heat exchange and body overheating mechanism at high ambient temperatures at sea level and lowered pressures

01 p0013 A71-11134

Human thermoregulatory response to ambient temperature variations, considering deep body and skin temperature interrelations

02 p0202 A71-11667

Human body temperature regulation feedback control system model by electric circuit analog, discussing digital simulation for static and dynamic responses

02 p0203 A71-11805

Conditioned reflex gas exchange shifts in persons under repeated local thermal stimuli

04 p0540 A71-15572

Water cooled garments, discussing human thermoregulation, developments and current suits

06 p0859 A71-17957

Human temperature control computer simulation, considering sudomotor, vasomotor and metabolic as error signals from hypothalamic and cutaneous thermoreceptors

07 p1048 A71-19585

Human body temperature regulation, investigating mild exercise dehydration effects

07 p1044 A71-20349

Gas exchange and muscular thermoregulation activity in rats under environmental oxygen deficiency

08 p1242 A71-21963

Proprioceptive thermoregulatory mechanism of sweat secretion during positive and negative work in man

09 p1401 A71-23369

Electroretinogram b-wave slope reduction by cooling of dark adapted frogs during serial flash stimulation

10 p1564 A71-24442

Organic thermoregulator control signal generation as function of body peripheral to central temperature ratios, using skin temperature rise measurements

10 p1564 A71-24485

Chemical thermoregulation muscular electricity activity during shivering and thermoregulation tonus change after cold adaptation, discussing oxygen consumption rise

10 p1564 A71-24486

Chronic inability of succinate for protection against paralysis of rats exposed to hyperbaric oxygen toxicity, correlating thermocontrol response

11 p1720 A71-26124

Human body thermal behavior modeling, obtaining steady state analytical solution for various boundary conditions and parameters

12 p1875 A71-27563

Local cutaneous heat regulation in man, using thermoelectrode method in analyzing response to constant temperature thermode application to small skin surface

13 p2014 A71-29314

Mathematical and mechanical models of human thermal system thermodynamic/transport processes and external regulation devices for single elements and entire body

13 p2023 A71-29400

Gas exchange, thermoregulatory muscle tone and electrical activity in rat muscles in hyperoxic atmosphere

15 p2360 A71-32533

Human body temperature regulation under various hydration regimes during exercise, noting changes related to sweating

16 p2530 A71-33243

Human sweating regulation at rest, evaluating thermal inputs effects on thermoregulatory center and internal hypothalamic and skin temperatures

17 p2683 A71-35146

Human thermoregulator set point under physical exercise, using behavioral indicator

17 p2686 A71-35388

Behavioral thermoregulation - Conference, Lyons, France, September 1970

18 p2858 A71-36859

Squirrel monkeys midbrain reticular formation direct thermal stimulation effects on physiological or behavioral thermoregulatory responses

18 p2858 A71-36860

Young guinea pigs thermal adaptation tests at different temperatures and environmental conditions, observing threshold temperature shifting for shivering and heat polypnea

18 p2858 A71-36863

Human body weight and skin sweat gland water loss rates effects on thermoregulation

18 p2858 A71-36864

Human thermoregulation, discussing experimental determination of equation for mean body temperature calculation in neutral and warm environments

18 p2858 A71-36866

Local skin thermoregulation mechanism in man controlled by cooperative bradykinin biosynthesis, using IR thermometry recording of thermal stimulus

18 p2859 A71-36868

Hypothalamic unit activity relation to thermoregulation, investigating preoptic area response to local and peripheral temperature changes

18 p2859 A71-36869

Preoptic anterior hypothalamic area temperature sensitive neurons, showing integrative center for thermoregulation

18 p2859 A71-36870

Brown fat thermogenesis regulation, emphasizing adipose tissue and afferent nerves control by experimental system approach, using intact unanesthetized unrestrained animals

18 p2859 A71-36872

Skin temperature and perspiration role in metabolic heat elimination, considering evaporation coefficient relationship to convection coefficient

18 p2859 A71-36873

Chill level index for skin temperature effects on rate of evaporative heat loss and thermal information to central controller during heavy work

18 p2860 A71-36876

Temperature regulation during exercise by proportional control, investigating skin temperature effect on set point temperature, sweat rate and skin thermal conductance

18 p2860 A71-36879

Thyroidectomy and cold adaptation effects on hibernating hamsters thermoregulation and heat transfer coefficient

18 p2860 A71-36881

Physiological control of local sweating rate

18 p2860 A71-36884

Thermoregulation under stringent low temperature conditions, considering internal body temperature maintenance by homeothermic organism

18 p2861 A71-36891

Water temperature effect on body thermoregulation in swimming, comparing swimmers responses to track man on treadmill at same metabolic rate

18 p2861 A71-36893

Skeletal muscles shivering thermogenesis during cold adaptation, investigating thermoregulation effects on organ and system heat production

18 p2862 A71-36895

Squirrel monkey physiological and behavioral thermoregulation elements interrelationships, considering mean skin and medial preoptic hypothalamic temperatures

18 p2862 A71-36896

Cutaneous circulation control by venous thermoregulatory reactions to temperature variations, using dog saphenous veins perfused with autologous blood or Krebs-Ringer solution

18 p2862 A71-36898

Guinea pig thermoregulation of shivering and nonshivering thermogenesis, showing intrahypothalamic noradrenaline injection effects on threshold temperature elevation

18 p2862 A71-36901

Thermal behavior simulation of cooling biological system, describing heat generation and transfer at normothermic to hibernating body temperatures with mathematical model

19 p3003 A71-38199

Ambient temperature effects on spontaneous rewarming of ground squirrels during awakening after hibernation

22 p3491 A71-42582

Arterial blood pressure spontaneous fluctuations due to cutaneous circulation adjustments by thermoregulatory system

23 p3632 A71-43142

Hyperoxia effects on thermoregulation and neurochemical functions, showing temperature increases in cerebrum and decreases in cortical and subcortical formations

23 p3633 A71-43582

Preoptic and environmental temperature effects on hibernator thermoregulatory responses, noting changes in metabolic rates

23 p3637 A71-44301

THERMOSETTING RESINS

NT EPOXY RESINS

NT NYLON (TRADEMARK)

NT PHENOLIC RESINS

NT POLYAMIDE RESINS

Cured thermosetting polymers, investigating water effect on microstructure and mechanical properties

06 p0916 A71-17945

Carbon fiber reinforced carbon base composites manufacture by thermal decomposition of carbon fiber reinforced thermosetting resins, discussing polymer matrix shrinkage control

[PLASTICS INST. PAPER 36]

08 p1319 A71-20894

Thermosetting and thermoplastic carbon fiber composites fabrication molding techniques, forms provisions and new uses

[PLASTICS INST. PAPER 33]

08 p1321 A71-20916

Fractography of thermoset resins toughened with Hycar carboxyl terminated butadiene acrylonitrile, using electron microscope

11 p1785 A71-25406

Thermosetting acryl modified epoxy resin, stressing adhesive bonding strength, workability and curing characteristics

11 p1787 A71-25423

Thermosetting polyphenylene resins synthesis and use in reinforced ablative composites, discussing polymerization and curing

11 p1789 A71-26036

THERMOSIPHONS

Two phase heat transfer in thermosiphon counterflow under simulated gravities of 0.1 to 100 earth gravity, measuring critical heat flow rates and convection coefficients

04 p0687 A71-15531

Liquid flow and heat transfer in thermosiphons in centrifugal and Coriolis force fields

24 p3888 A71-44931

Open cylindrical thermosiphon for laminar flow, predicting heat transfer performance by finite difference solution for comparison with Lighthill analysis

24 p3889 A71-44973

THERMOSPHERE

Space research on thermosphere H and He properties - COSPAR Conference, Prague, May 1969

03 p0410 A71-14002

Thermospheric neutral particle molecular nitrogen density and temperature measurements by rockets, noting correlations with diurnal, solar cycle and other variations

03 p0414 A71-14020

Lyman alpha radiation scattering observation by satellites, obtaining geocoronal atomic hydrogen distribution in thermosphere and exosphere

03 p0415 A71-14028

Mesosphere and lower thermosphere probing, noting electron and ion densities distributions, collision frequencies and ionospheric loss rates

05 p0740 A71-16427

Mesosphere and lower thermosphere heat input rates and circulation, calculating worldwide average eddy diffusion coefficient

06 p0892 A71-17978

Upper atmosphere hydroxyl emission mechanism, discussing absorption band, energy balance, atomic hydrogen and ozone in lower thermosphere and nitrogen oxides

08 p1277 A71-21006

Thermospheric heating by solar radiation in Schumann-Runge continuum, taking into account height and atmospheric components distribution

09 p1435 A71-22431

Thermospheric gas density determined from solar UV absorption measurement at grazing ray and near vertical incidence

10 p1676 A71-24551

Thermosphere heating due to auroral electrojets, discussing thermospheric variations and eddy viscosity

10 p1602 A71-24554

Atomic oxygen and carbon dioxide measurement in lower thermosphere by mass spectroscopy

10 p1606 A71-24803

Thermosphere diurnal variations two dimensional model atmosphere characteristic waves, separating density and temperature variations

11 p1756 A71-25649

Thermosphere daily variations consisting of diurnal oscillations excited by ozone and EUV heating

12 p1925 A71-27729

Turbopause oxygen/nitrogen decrease effect on ion and neutral composition changes in thermospheric region during magnetic storm, using simultaneous ionospheric and atmospheric equations

14 p2229 A71-29665

Concentration and transport from auroral zone of minor constituents in mesosphere and lower thermosphere during anomalous midlatitude radio absorption periods

14 p2230 A71-29711

Incoherent scatter measurements for ionospheric bulk velocity, thermospheric dynamics, F region gravity wave, photoelectron flux, ionic collision frequency and magnetic field direction

14 p2202 A71-30945

Thermospheric density response to auroral heating during geomagnetic disturbances simulation assuming impulse heat input into small latitude band within auroral ovals

15 p2398 A71-31770

Thermosphere and exosphere static models with empirical thermal profiles, giving temperature, density and composition as function of height

16 p2564 A71-33722

Thermospheric hydrogen density and temporal variations from Explorer 32 measurements, discussing dependence on exospheric temperature

16 p2565 A71-33731

Thermospheric electron heating rate and ion chemistry above Wallops Island during 7 March 1970 solar eclipse, measuring ion composition and concentration 16 p2565 A71-33732

Thermospheric wind measurement by chemical releases, observing artificial cloud motion and growth 16 p2565 A71-33735

Tidal theory comparison with lower thermospheric wind observations, taking into consideration dissipation and excitation effects 16 p2565 A71-33736

Diurnal variation of atmospheric parameters in thermosphere deduced from incoherent scatter and satellite drag, discussing atmospheric model correspondence to observed data 16 p2566 A71-33742

Thermospheric composition determination from satellite drag derived densities, comparing with data computed from mass spectroscopic observations 16 p2566 A71-33750

Thermospheric dynamics three dimensional model in terms of atmospheric system eigenfunctions, deriving formulas for solar XUV and corpuscular heating during geomagnetic storms 16 p2567 A71-33781

Chemical trimethyl aluminum releases in lower thermosphere for temperature, density, winds, turbulence, diffusion coefficients and atomic oxygen content measurements 16 p2568 A71-33792

Seasonal density variations in thermosphere and exosphere, obtaining model from Explorers 19 and 39 drag measurements for comparison with OGO-6 mass spectroscopy 16 p2569 A71-33802

Air density observation near 150 km heights from Cosmos 316 orbit, noting geomagnetic disturbance effects and semiannual variation 16 p2569 A71-33806

Neutral lower thermosphere density variations at high and middle latitude in Southern Hemisphere from OVI-15 /SPADES/ satellite accelerometer measurements 16 p2570 A71-33824

Thermospheric circulation and temperature changes due to global scale winds flow through F region ionization anomalies, using time independent dynamic model 16 p2571 A71-33836

Thermospheric dynamics, including global compositional structure, winds and temperature response to solar radiation and vertical mass diffusion 16 p2571 A71-33838

Thermosphere structure and motion from neutral atmospheric density data, noting correlation with enhanced geomagnetic activity 16 p2571 A71-33840

Lower thermosphere and ionosphere upper limits of positively ionized water molecules number density, considering desorption and recombination processes 16 p2571 A71-33842

Lower thermosphere atomic nitrogen concentration during maximum solar activity, using rocket-borne radio frequency and time of flight mass spectrometers 16 p2572 A71-33843

Thermospheric convective instability as interpretation of north polar cap high speed winds observed by satellite at 200 km altitude during magnetic storm of May 1967 16 p2572 A71-33847

Neutral thermosphere and exosphere structure, discussing density, temperature, composition and diurnal and seasonal variations 17 p2732 A71-34461

Bibliography on neutral atmosphere dynamics covering waves, winds, turbulence and disturbances in thermosphere and ionospheric effects 17 p2732 A71-34462

Atmospheric energy balance and transfer in lower thermosphere in terms of population temperatures and degrees of freedom [translational, rotational, vibrational, electronic, chemical, etc] 18 p2910 A71-35841

Thermospheric density determination from ESRG rocket flight produced artificial fluorescent AIO clouds 18 p2914 A71-37060

Thermospheric winds measurement during geomagnetic storms with Fabry-Perot interferometer from Doppler shift of two 6300 A fringe profiles 19 p3047 A71-37366

Semiannual amplitude variations in F 2 region for estimating oxygen density dissociation and temperature ratios in lower thermosphere 19 p3048 A71-37398

Thermospheric atomic oxygen and molecular nitrogen number densities, discussing earth atmospheric absorption of solar UV lines 20 p3214 A71-38727

Thermospheric wind induction by auroral electrojet heating, considering effects of Joule dissipation of magnetospheric electric fields 20 p3215 A71-38744

Earth thermosphere models, discussing shortwave solar radiation as major energy source during quiet conditions, diurnal variations of structure, neutral-charged components interconnection, etc 20 p3216 A71-39117

Upper atmosphere hydroxyl emission mechanism, discussing absorption band, energy balance, atomic hydrogen and ozone in lower thermosphere and nitrogen oxides 20 p3218 A71-39586

Winds and diffusion measurements in lower thermosphere using sodium vapor cloud release from Centaur IIB rocket 20 p3221 A71-39692

Lower thermosphere and mesosphere water vapor and neutral composition spectrometric measurements, estimating hydrogen and oxygen atom recombination coefficient limits with mass analyzers 20 p3221 A71-39696

Lower thermosphere neutral composition fine structure data from rocket-borne time of flight mass spectrometer, emphasizing atomic nitrogen vertical distribution 20 p3222 A71-39697

High Arctic latitude thermospheric helium and hydrogen rocket-borne mass spectrometric measurements, showing concentrations and winter bulge 20 p3222 A71-39698

Lower thermospheric density and molecular nitrogen partial density rocket measurements, obtaining neutral gas temperature vertical distribution and ion density profile 20 p3222 A71-39699

Midlatitude lower thermosphere atomic and molecular oxygen rocket measurements, presenting concentration and vertical distribution data 20 p3222 A71-39700

Lower thermosphere vertical temperature distribution measurements, using ionization and heat manometers 20 p3222 A71-39702

Thermospheric atomic hydrogen concentration temporal variations in situ measurement by Explorer 32 satellite 20 p3232 A71-39898

Lower thermosphere eddy diffusion coefficient effects on height variations in ionospheric composition 21 p3372 A71-40044

Venusian thermosphere, observing dayside solar radiation absorption generated upward dayside and downward nightside vertical motions 23 p3735 A71-43333

THERMOSTABILITY

U THERMAL STABILITY

THERMOSTATS

Sweat and time constant response of human thermostat to linear gradient heat load, using analog computer experiment 18 p2859 A71-36874

THERMOTROPISM

U ANISOTROPY

U TEMPERATURE EFFECTS

THERMOVISCOELASTICITY

Soviet book on fundamentals of thermoviscoelasticity mathematical theory covering deformable media mechanics and thermodynamics, fatigue defects, etc 06 p0984 A71-17437

Thermoviscoelasticity approximate method for materials with nonstationary nonuniform temperature distribution dependent mechanical properties, using time-temperature analogy principle 10 p1688 A71-24360

Mechanical waves propagation in elastic viscoplastic medium in presence of temperature field, using mechanical and mathematical models 11 p1850 A71-26177

Approximation procedures for quasi-static problems solution in thermoviscoelasticity theory, considering time-variable boundaries and inhomogeneous temperature fields 13 p2154 A71-28648

Thermoviscoelastic problem for semiinfinite plate, determining temperature field and stresses permitting heat propagation 23 p3780 A71-44223

THETA PINCH

Corrugated theta pinch stabilization, considering variable axial HF current and quadrupole magnetic field 03 p0464 A71-13930

Theta pinch plasma enhanced radiation at far IR wavelengths, observing emission exceeding thermal bremsstrahlung 03 p0465 A71-14189

MHD continua z-theta pinch stabilization, discussing analytical models for determining feedback spatial and temporal resolution 06 p0931 A71-17458

Dyaamic stabilization of instability in bumpy theta pinch by generalization of energy principle 06 p0934 A71-17480

Atomic processes in plasmas including excitation, deexcitation, ionization, recombination, charge

transfer, free-free transitions and spectral line broadening for theta pinch parameters determination 07 p1172 A71-20505

Collisionless shock waves generation in theta pinches, plasma formation, experimental devices, diagnostic methods and magnetic probes 07 p1172 A71-20507

High theta plasmas instabilities, discussing collisionless bounce model of theta pinch and diagnostic measurements 07 p1173 A71-20511

Microwave electromagnetic emission in theta pinch hydrogen plasma by sensitive superheterodyne receivers, noting discharge azimuthal current 08 p1339 A71-21477

Azimuthal current growth and microwave radiation in theta pinch hydrogen plasma discharge from sensitive superheterodyne receivers 14 p2282 A71-30663

Theta pinch deuterium plasma heating by carbon dioxide laser as function of pulse duration and energy 16 p2587 A71-33188

Equilibrium state linear theta pinch plasma confinement dependence on magnetic force lines curvature radius 17 p2786 A71-34278

Plasma losses in high current plasma configuration due to inverse skin effect by observation for discharge regimes in theta pinch, zeta and Tokamak systems 21 p3422 A71-40763

Three frame pulsed holographic interferometry of plasma radial density profiles and helical displacement for use with theta pinch device 21 p3423 A71-40937

Slow toroidal theta-Z pinch experiment, describing measurements temperature distribution with emphasis on transitions between stable and unstable states 22 p3580 A71-41588

Raman microwave scattering on Langmuir oscillations, showing suprathermal emission origin in theta pinch plasma 24 p3853 A71-44505

Rarefied theta pinch plasma collective interactions, examining kinetic instability, electron energy distribution, anisotropy, suprathermal microwave emission, cyclotron harmonics and oscillations 24 p3854 A71-44513

THIAMINE

Solid and liquid diets during thiamine deficiency, noting hunger dependence on novelty 13 p2011 A71-28808

THICK FILMS

Thick film flat spiral inductor filter design for television signals, using linear analysis computer program 13 p2039 A71-28913

Thick film microcircuit DC-TO-DC converter electronics design for TOPS spacecraft power subsystem 14 p2214 A71-30801

Hybrid circuits thick film technology, discussing printed circuits fabrication processes and electrical and mechanical properties 18 p2888 A71-36224

Wireless assembly methods for thin and thick film hybrid and monolithic IC, emphasizing flip-chip elements microelectronic devices fabrication and interconnection 22 p3525 A71-41714

Thick film hybrid microcircuits for spacecraft electronic systems component reliability 23 p3650 A71-43123

Book on thick film microelectronics covering microcircuit design, fabrication, packaging and applications 23 p3650 A71-43224

Thick film technology and tests for hybrid microcircuits and semiconductor packaging 23 p3651 A71-43430

THICK WALLS

Perforated thick shallow spherical shell, solving boundary value problem for external loads 02 p0329 A71-12671

Thick walled noncircular cylinders shape showing full plasticization at collapse 04 p0673 A71-15885

Thick plate with circular holes of various sizes, studying stress-strain state 05 p0828 A71-16890

Thick-walled toroidal shell under various load distributions, analyzing stress-strain state by networks method using computer program 08 p1369 A71-21124

Solid profile wing motion near solid wall or free surface, using acceleration potential method 12 p1863 A71-27174

Finite element method stress analysis for evaluating localized stress distributions in thick walled circular tube with step change in thermal expansion [SESA PAPER 1841A] 17 p2819 A71-34534

THICKENED LEADING EDGES

U LEADING EDGES

THICKNESS

NT FILM THICKNESS

NT TARGET THICKNESS

boundary layer thickness measurement behind wave front using oscillogram of electrostatic current 01 p0078 A71-10160

thickness variation law for plates and shells with elastic strain energy 06 p0982 A71-17358

all thickness measurement by ultrasonic tests in presence of corrosion, discussing instruments development 06 p0897 A71-17416

transversally isotropic spherical shell with constant stress, calculating equation system for equilibrium 12 p1975 A71-27105

large elastic deformations of incompressible materials shells with inclusion of transverse normal stress, considering thickness change at boundaries 12 p1976 A71-27159

variously thick standard production heavy plate structural steels stress condition and elastic energy margin effects on cold brittleness 15 p2414 A71-31652

thickness effect on fracture toughness and crack propagation of Al alloy sheets used for aircraft skins 17 p2758 A71-35153

ages using X radiation for measuring thickness, linearity and response time, noting application of absorption and fluorescence techniques 17 p2744 A71-35287

ultrasonic immersion echo pulse thickness meter single side access measurement in Al and Zr alloys 22 p3528 A71-41759

poradic E layer thickness measurement by Phase Resonance, measuring phase advance on F region 23 p3666 A71-42975

THICKNESS RATIO

ing thickness optimal distribution for minimum drag in supersonic flow at zero angle of attack given planform, using Ritz method at lower Mach numbers 13 p1994 A71-29222

inviscid incompressible flow past thin circular arc foil at zero incidence, expanding for complex potential or velocity in powers of thickness ratio 17 p2670 A71-34674

Width/thickness ratio effect on steel, brass and bismuth sheet specimens plasticity and deformation under tension at room temperature 23 p3694 A71-44233

AIRFOILS

INFINITE SPAN WINGS

THIN WINGS

Monograph on plane shock wave interactions covering supersonically moving two dimensional thin airfoils, slender bodies of revolution and thin wings 01 p0003 A71-11227

inviscid ideally conducting fluid flow past thin foil transverse magnetic field, using small parameter method 02 p0186 A71-12629

Numerical analysis of flow field around thin airfoil two dimensional nonuniform stream, using finite difference method 02 p0187 A71-12680

Varying electrical resistivity incompressible fluid with Hall effect in presence of thin airfoil 03 p0343 A71-13903

Far and near field solutions of plane steady incompressible flow past thin airfoil including imbedded shock waves, using small disturbance theory 05 p0694 A71-16565

IAA PAPER 70-1887

Thin airfoils theory in nonequilibrium magnetohydrodynamics with nonuniform nonequilibrium free stream, using Green function technique 09 p1383 A71-23200

Electrical resistive incompressible fluid motion past in airfoils in oblique field, showing inverse dependence of lift on magnetic Reynolds number 10 p1648 A71-23956

Laminar incompressible boundary layer flow over in Joukowski, parabolic and slender wedge airfoils, using small perturbation and quasi-similar theories 10 p1549 A71-23957

Small surface curvature effect on unsteady hypersonic flow over thin oscillating wedge, using perturbation theory 11 p1705 A71-26197

Three dimensional jet flapped wing matched asymptotic expansion solution for high aspect ratios based in thin airfoil theory assuming inviscid and incompressible flow 12 p1863 A71-27217

Two phase supersonic barotropic flow with solid particles around thin profile with allowance for elastic particle collisions 12 p1864 A71-27450

Small disturbance equations for steady transonic flows past thin lifting airfoils and slender bodies 15 p2344 A71-31560

IAA PAPER 71-5661

Inviscid incompressible flow past thin circular arc foil at zero incidence, expanding for complex potential or velocity in powers of thickness ratio 17 p2670 A71-34674

Gust loading on two dimensional thin airfoil in compressible flow, deriving closed-form lift expression 17 p2671 A71-35285

Spanwise lift distribution over wings and wake formation in thin airfoils of finite aspect ratio in linear subsonic potential flow 21 p3319 A71-40495

Lifting rectangular thin airfoil in symmetrical incompressible steady uniform orthogonal flow at small angle of attack, deriving Weissinger integral equation 23 p3625 A71-43487

THIN BODIES

Hypersonic perfect gas flow past thin three dimensional body with strong viscous interaction, obtaining aerodynamic characteristics and drag and heat coefficients 03 p0345 A71-14563

Thin shallow annular radiating fins for heat removal from sphere or polyhedron with isothermal surfaces, determining optimal weight and geometrical parameters 12 p1986 A71-27331

Thin metallic body of revolution under electromagnetic pulse, predicting transient induced currents with radiation condition in finite difference solution 15 p2372 A71-32368

Large deflections of thin piecewise prismatic elastic bars by electronic analog computer simulation 16 p2661 A71-34117

Uniformly rotating thin relativistic disks structure, stability and gravitational fields within general relativity framework 17 p2806 A71-35405

Generalized vectorial equation of motion for vibrating nonprismatic thin space beams, discussing boundary conditions, rotary inertia and shear deformation [ASME PAPER 71-APM-P] 18 p2978 A71-36259

Rayleigh scattering by obliquely oriented uniform thin cylindrical particles /needles/, using dielectric needle approximation 20 p3196 A71-39406

Ti-Al-Sn and Al alloys thin sectioned specimens cryogenic fracture strength, discussing surface crack fracture behavior 21 p3401 A71-40918

THIN FILMS

NT FERROMAGNETIC FILMS

Irreversible processes during formation of contact between indium telluride thin film and metal in vacuum at high temperature 01 p0137 A71-10150

Electrical resistivity and structure of thin films of W, Mo and Cr evaporated in vacuum by neodymium laser 01 p0101 A71-10674

Thin film lumped element microwave integrated circuits from concept to final functional devices 01 p0053 A71-10735

Thin film methods applied to microwave integrated circuits for compactness, reliability and low cost 01 p0053 A71-10736

Field effect photocurrent maximum in thin film semiconductors below Debye radius associating hole capture by recombination centers 01 p0139 A71-10781

Vapor phase interaction of methanol and carbon tetrachloride with Ti thin films, discussing Ti stress corrosion cracking implications 01 p0102 A71-10812

Glass substrates for thin film circuits compared to other materials for properties and suitability, emphasizing surface properties 02 p0230 A71-11816

Metallized capacitors types and properties, considering extra thin dielectric films and high field strength 02 p0230 A71-11817

Fuel cell electrodes preparation by sputtering thin Ta and Pt layers on porous Vycor 03 p0353 A71-13056

Vacuum deposited Bi thin films on glass substrates at liquid He temperature, investigating characteristics of critical thickness 03 p0466 A71-13291

Solid state traveling wave amplifier using thin n-type epitaxial GaAs layer 03 p0384 A71-13316

Physical, chemical and electrical properties of silicon nitride thin films deposited pyrolytically on Si substrates, analyzing deposition process effects 03 p0468 A71-14001

Computer controlled laser machining system for cutting integrated circuit masks in thin films deposited as fused silica substrates 03 p0433 A71-14342

Thin metallic films thermal radiation properties at cryogenic temperatures, calculating spectral normal emissivity as temperature wavelength and thickness function 04 p0684 A71-15510

CdS thin film grain boundaries and stacking faults effects on electrical resistivity 05 p0791 A71-16055

Copper sulfide-cadmium disulfide thin film solar cells degradation under simulated orbital conditions, determining electrochemically induced copper filament growth as electric shorts causes 05 p0699 A71-16057

CdTe thin film solar cell characterization, showing low carrier concentration of base layer and improved stability at elevated temperatures 05 p0699 A71-16059

Solar cell R and D in France, emphasizing thin film improvement 05 p0704 A71-16101

Apparatus for thin film solid state devices fabrication under ultrahigh vacuum 05 p0733 A71-16233

Vapor deposited niobium nitride superconducting thin films on fused silica substrates, measuring transition temperature 05 p0792 A71-16236

Thin CdS condensate layer formation mechanism during films slow vacuum deposition onto glass or polystyrene sublayer bases 05 p0793 A71-16821

Superconducting thin film bridges by vacuum deposition of tin, measuring current-voltage and resistance at SHF and critical temperatures 05 p0793 A71-16828

Optical and photoelectrical properties of thin amorphous thallium arsenic sulfide, thallium antimony sulfide and thallium bismuth sulfide films obtained by vacuum deposition 05 p0794 A71-16835

Light scattering from ultrathin free liquid films, calculating irradiance optical functions variation with geometry and film thickness 05 p0763 A71-16906

Supercritical Permalloy thin films thickness effect on magnetic domain structure 06 p0941 A71-17401

Metal coatings and thin films wetting by soldering materials, emphasizing oxide removal 06 p0903 A71-17426

Organic thin film layer semiconductors photoconductivity, developing semiempirical theory of pulse formation 06 p0941 A71-17735

Light emitting film /LEF/ displays, discussing physical principles, construction and applications of electroluminescent thin film devices 07 p1105 A71-18737

Thin film cermet resistive elements physical controls electrical properties, physical controls, thermal and radiation stability 07 p1071 A71-19075

Ruby laser passive Q switching by phototropic thin film shutter, outlining advantages over bleachable dyes 07 p1122 A71-19140

Holographic lens used with pulsed ruby laser for machining single and multiple spots on Ti thin film on glass 07 p1122 A71-19205

Dielectric thin optical film waveguides excitation for integrated optical circuitry by Gaussian laser beams 07 p1123 A71-19213

CdTe thin film anomalous photovoltaic effect and piezoelectric dependence on real state 07 p1176 A71-19271

Thin polycrystalline CdTe film photovoltaic effect dependence on monochromatic light incidence angle 07 p1176 A71-19272

Light effect on dielectric constant of thin hardened dichromated gelatin films for holographic recordings 07 p1110 A71-19482

Thin oxide films on solution grown single crystals of cubic beta-silicon carbide, discussing physical and electronic properties measurements 07 p1177 A71-19571

High transition temperature superconducting materials thin films composition control by sputtering from hot pressed powder mixture ingots targets 07 p1178 A71-19849

Cadmium telluride epitaxial films on potassium bromide, investigating external gases effects on photovoltaic properties 07 p1179 A71-19919

Oxide films effect on heat resistant steels hydrogen permeability, using mass spectrometer 07 p1136 A71-19920

Niobium nitride thin films very high critical current and field characteristics, noting deposition by sputtering 07 p1179 A71-20154

Sn additives effect on In thin film superconducting transmission lines, comparing with Pippard nonlocal theory for mean free path reduction 07 p1179 A71-20155

Amorphous semiconducting thin films quenching fabrication techniques and electrical properties 07 p1181 A71-20410

Penetration model of thin solid film lubricant friction on sliding surfaces of finite roughness [ASLE PREPRINT 70LC-15] 08 p1298 A71-21159

Sliding load history effects on friction of thin burnished films of molybdenum disulfide in vacuum [ASLE PREPRINT 70LC-18] 08 p1298 A71-21161

Wave interference effects and energy transfer in coupled thin film optical waveguides 09 p1460 A71-22159

Metal friction surface oxide thin films and secondary structures thickness determination using electron microscope method 09 p1454 A71-22311

Hybrid integral microcircuits with thin film resistor heat sources, determining temperature fields on substrate and boundaries 09 p1416 A71-22495

Pulse rise time effect on nanosecond magnetic thin film switching with flux reversal and stray field interaction 09 p1508 A71-22704

Optical-electrical analogy of thermal radiation impedance of thin dielectric films in low temperature insulation 09 p1494 A71-23003

Pyrolytic aluminum oxide thin films on Si substrate by thermodecomposition, measuring vapor deposition parameters and Si surface preparation effects on dielectric and interface properties 09 p1509 A71-23117

Pulse echo ultrasonic measurement of thin film layer between thick media, using real time computation 09 p1458 A71-23439

Radar backscattering from thin metallic conductive films, giving results for Al and Ni from anechoic chamber measurements 09 p1410 A71-23517

Varactor tuned X band Gunn oscillator with lumped thin film microwave circuits, discussing GaAs materials, output powers and bandwidths 09 p1421 A71-23722

Lubricating oil thin films interfacial Newtonian flow elastohydrodynamics, studying transient effects on contact load damping parameters 10 p1614 A71-23981

Conductivity in microwave Permalloy thin films without external magnetic field comparing Fuchs-Sondheimer theory 10 p1656 A71-24213

Tangential body forces and pressure perturbation interactions in thin liquid film, considering destabilizing effect impairing film cooling efficiency 11 p1751 A71-25491

Monolayer submicron self supporting particle film samples preparation for sintering by transmission electron microscopy 11 p1763 A71-26150

Resistance increases in thin film Evanoth resistors due to hydrogen gas absorption and desorption 11 p1738 A71-26162

Vanadium oxide thin vapor transport films on single crystal aluminum oxide, using RF sputtering of powdered targets 11 p1809 A71-26397

Longitudinal and transverse differential permeabilities of discrete regions in thin ferromagnetic films, accounting for material inhomogeneities 11 p1809 A71-26546

Modified Landau-Lipschitz equation of thin ferromagnetic film for slowly reversing magnetic fields solved by interpolation, discussing magnetization curve subrelaxation segment 11 p1809 A71-26547

Thin gallium films metastable gamma and delta phase ring diagrams using electron diffraction techniques 12 p1942 A71-26821

Epitaxial garnet films magnetic anisotropic models, describing mobile cylindrical domains 12 p1943 A71-26854

Polycrystalline copper and magnetic films thin intermediate layers, showing prevention of epitaxial growth 12 p1943 A71-26855

Magnetic field detection by magnetometer with coherent magnetization rotation in thin magnetic film 12 p1906 A71-26856

Electric current heated thin resistance film thermoelectric transducer, measuring temperature rise with thermocouple 12 p1888 A71-27158

Thin film compound Au-Al intermetallic structure of CaCl_2 type with lattice period of 3.140 plus or minus 0.003 Å from electronographic measurement 12 p1917 A71-27308

Substrate materials thermal characteristics determination for thin films resistance thermometers calibration, using pulse heating technique 12 p1908 A71-27593

Thin solid films on ball bearing surfaces, measuring electrical conductivity 13 p2072 A71-27817

Low temperature space charge mechanism of threshold switching, using pulse measurements on thin layer multicomponent chalcogenide glasses 13 p2110 A71-28044

Fluctuation enhanced conductivity of superconductor, considering Maki graph evaluation 13 p2111 A71-28454

Flux flow noise spectra measurement in pairs of magnetically coupled superconducting films, noting frequency response 13 p2111 A71-28502

Thin film hybrid IC microwave component development, noting market and consumer applications 13 p2039 A71-28909

Superconducting thin films nonlinear excess current near transition temperature, deriving expression from Tsuzuki microscopic basic equations 13 p2112 A71-29012

Ion migration direction in thin Ag, Cu and Au films under direct current effect from resistance radioactive tracer measurements and scanning electron micrographs 13 p2112 A71-29333

Molybdenum disulfide bonded solid film lubricants performance characteristics, considering load, speed and temperature effects [ASLE PREPRINT 71AM 2D-1] 13 p2076 A71-29486

Fast burning rates in thin film solid composite propellants composed of McCormick-Selph 510, 164 monopropellant, oxidizer and polyvinyl chloride binder [AIAA PAPER 71-655] 14 p2285 A71-30730

Resonant excitation of thin film dielectric optical waveguide through supercritical layer by limited light beam with arbitrary amplitude-phase distribution 15 p2375 A71-31227

Crosshatched wave patterns in liquid films, discussing supersonic wind tunnel experiments aimed at elimination of sublimation or vaporization as pattern generating mechanisms 15 p2389 A71-31551

Epitaxial Ag thin film with controlled surface roughness on mica, measuring electrical resistivity as function of temperature, thickness and surface specularly in vacuum 15 p2461 A71-32376

Electric field effect of epitaxial thin silver films on mica in vacuum as function of temperature, thickness and surface specularly 15 p2461 A71-32377

Gas-solid interaction by shock tube method, determining thickness and thermal accommodation effects on thin metal film resistance thermometer response 16 p2576 A71-32922

Energy spectrum parameters from Burstein-Moss effect observation in thin CdO layers, explaining absorption edge shape at various electron concentrations 16 p2622 A71-34029

Lateral surface heat transfer effect on thermophysical characteristics in thin layer coatings, discussing temperature gradients in corundum and zirconium oxide on copper 17 p2836 A71-34308

Strain analysis based on thin metallic film optical measurements, determining principal strain directions from wrinkle and microfracture patterns [SESA PAPER 1828A] 17 p2820 A71-34551

Superconducting phase transition temperature measurements as function of magnetic field in thin film hollow Al and In cylinders 17 p2791 A71-35742

Lande g factors measurement of excited electronic states in Ne 20 II and III, using alignment of radiating particles in beam foil light source 18 p2949 A71-35978

Thin thermally insulating film on metallic sample, showing vapor layer elimination during liquid nitrogen quenching 18 p2934 A71-36172

Thickness monitoring technique for thin films, using silicon solar cell mounted adjacent to substrate with ion deposition 18 p2922 A71-36591

Combinational possibilities of special application modules based on thin-film hybrid integrated circuits in standardized encapsulations 18 p2893 A71-36625

Magnetic thin films - Conference, Prague, September 1970 18 p2954 A71-36936

EuO , YIG , GdIG and ferrite magnetic oxide thin films growth techniques and magnetic properties comparison with bulk materials 18 p2954 A71-36937

Magnetic thin film domain wall velocity dependence on magnetic field intensity as function of film thickness, discussing nonlinearity causes 18 p2955 A71-36938

Mossbauer effect applications to magnetic thin films, discussing electric and magnetic hyperfine interactions and experimental difficulties 18 p2955 A71-36939

LF ferromagnetic resonance in anisotropic polycrystalline thin magnetic films, noting dependence on magnetization inhomogeneity 18 p2955 A71-36940

Transcritical Permalloy thin film domain structure investigating external field effect on powder deposition and proposing model 18 p2955 A71-36941

IC applications to microwave frequencies, relating circuit performance to substrate roughness and thickness of thin film metal adhesion layers 18 p2895 A71-36942

Vacuum deposited thin Cr films on glass substrate describing hydrogen adsorption effects 19 p3076 A71-37000

Vacuum deposited thin Cr films on glass, investigating substrate temperature and inert gas pressure effects on texture 19 p3076 A71-37001

Laser Curie point writing characteristics and fraction efficiencies of MnBi thin films for graphic recording 19 p3062 A71-37002

High quality continuous tone micromachining image recording on metal thin films by low power pulsed gas laser heating 19 p3071 A71-37003

Ring laser formed by single mode light guiding in film, using nitrogen laser for pump source 19 p3071 A71-37004

Thin film Au-CdS-Al type metal-semiconductor barriers, determining barrier height from temperature dependence measurements of I-V characteristics 19 p3118 A71-37005

MOS transistors thin monocrystalline silicon layer formation by epitaxial growth and substrate selective electrochemical etching 19 p3028 A71-37006

Vacuum deposition of silica and alumina thin film on silicon substrate MOS diodes, using CW carbon dioxide laser 19 p3074 A71-37007

Mass transport at high current densities in Al-Mo thin film conducting stripes, noting effect on life 19 p3119 A71-37008

Ni-Cr thin film resistors reliability, describing deposits on silicon dioxide, intermetallic formation and electromigration 19 p3034 A71-37009

Hybrid thin film radiosonde transmitter design atmospheric temperature and humidity data transmission from meteorological sounding balloon to ground station 19 p3035 A71-37010

Ion bombardment thinning apparatus for preparing electron microscope foils of inorganic nonmetallic samples including ceramics, minerals and rocks 20 p2333 A71-38000

Thin layers shear strength and friction under high pressure, describing rotating-anvil shear press with high sensitivity strain gage equipped load and torque cells 20 p3241 A71-38001

Solar array technology for lunar surface applications including silicon cells, cadmium sulphide films, temperature effects, prototype module and radiation degradation 20 p3181 A71-38002

Copper sulfide-cadmium sulfide thin film solar cell under simulated orbital conditions, including thermal cycling, constant illumination and temperature effects 20 p3182 A71-38003

Ion beam deposition of insulating carbon thin film on room temperature substrates, considering transparency, index of refraction, insulating capacity, glass scratching ability, etc 20 p3241 A71-38004

Thin gold films strain distribution determined from X ray diffraction peaks, noting elasticity effects 20 p3276 A71-38005

Heat treated thallium bismuth sulfide, selenide and telluride amorphous and polycrystalline thin film electrical conductivity, differential thermal emf and forbidden bandwidth 20 p3276 A71-38006

Ga spreading over Ag and Au thin films surface from electronographic and optical experiments, noting volume heterodiffusion 20 p3276 A71-38007

Fluid phase discrimination temperature measurement system, using thin carbon film resistance thermometer with electrical power pulse sensing liquid/gas phase discrimination 20 p3237 A71-38008

Flat thin films in stripline cavity resonator v TEM mode, expressing bandwidth and resonance frequency difference 20 p3239 A71-38009

Thin dielectric films on germanium substrates, measuring oxygen diffusion through silicon dioxide 20 p3205 A71-38010

Thin single crystalline film deposition by molecular beam epitaxy of GaAs, describing surface structure observation with high energy electron diffraction 21 p3427 A71-40000

Reliable thin film switching circuits fabrication deposition on suitable substrates 21 p3354 A71-40001

- Thermal switching and negative resistance model and measurements of amorphous semiconductor thin films of Ge, Si and chalcogenide glasses
21 p3428 A71-40741
- Electron elastic scattering in thin films by impurities, noting conductivity dependence on film thickness
21 p3428 A71-41126
- Thin bismuth films thermal and electrical conductivities and thermoelectric power measurements, examining preparation methods
21 p3435 A71-41338
- Wireless assembly methods for thin and thick film and monolithic IC, emphasizing flip-chip elements microelectronic devices fabrication and interconnection
22 p3525 A71-41714
- Thin film optical waveguide TE-TM mode converters, using gyrotropic or anisotropic substrate material
22 p3556 A71-41806
- Hologram storage in evaporated thin films of arsenic trisulfides, considering simple diffraction patterns and complex data masks
22 p3542 A71-41811
- Thin liquid films under simultaneous shear and gravity forces, noting data incorporation into transport equations for heat and mass transfer
22 p3620 A71-41884
- Thermoremanent recording by Curie point writing in manganese-bismuth films for magneto-optic mass memories
22 p3587 A71-42473
- Experimental observation of 10.6 micron guided waves in Ge thin films, noting application to carbon dioxide laser communication
22 p3587 A71-42568
- Thin nickel films elastoresistance properties, examining magnetic state effects
23 p3691 A71-43361
- Bulk metal electromigration and crack failure in Al film conductors, considering purity, glassing and nucleation
23 p3651 A71-43426
- Termination and interface aging resistance of thin film resistors under corrosion, noting Ti-Pd-Au materials
23 p3651 A71-43429
- Thin film silicide resistors in monolithic IC for high sheet resistance or radiation hardness using sputtering deposition without protective overlayer
23 p3655 A71-43428
- Thin film oxide, ferroelectric and bismuth titanate dielectrics for high capacitance microwave IC technology
23 p3651 A71-43429
- Interconnection Ta thin films and silicon encapsulation for solid state components in hybrid IC under high humidity
23 p3656 A71-43431
- Polycrystalline thin film CdSe-CdS and CdSe-CdTe solid solution semiconductor alloys Hall mobility and carrier concentration dependence on substrate temperature
23 p3715 A71-43433
- Silicon thin film on sapphire for bipolar and MOSFET transistors for microwave IC and subnanosecond switching circuits
23 p3715 A71-43434
- Evaporated tellurium thin films electric properties, discussing fabrication techniques, temperature dependence, field effect and Hall mobilities, threshold voltage and stability
23 p3715 A71-43435
- Electron energy spectrum in periodic semiconductor structures of super thin p-n junction layers
23 p3716 A71-43485
- Silicon Schottky tunnel MOS diodes, discussing effect of thin interfacial film between metal and semiconductor on I-V characteristics
23 p3652 A71-43936
- Wideband phase-matched carbon dioxide laser second harmonic generation in GaAs thin film waveguide through dielectric dispersion
23 p3687 A71-44136
- Niobium carbonitride thin film deposition temperature effects on superconducting properties, considering transition temperature and critical currents and fields
23 p3717 A71-44141
- Phase composition and defect structure of thin film CdTe islet compensates on NaCl and KBr cleavage faces
23 p3718 A71-44316
- Thin film circuit microstructures and integrated microcircuits with distributed parameters, discussing analytical determination of microcell parameters
24 p3807 A71-44378
- Thin soft layer under steady creep conditions, considering axisymmetric problem of simultaneous tension and torsion
24 p3877 A71-44409
- W and Mo thin films phase diagrams, determining surface energies and heats for transformations
24 p3860 A71-44718
- Liquid properties and ambient pressure effects on cavitation erosion in thin film
24 p3819 A71-44946
- Excess minority carrier diffusion length measurement in thin silicon wafers, using light-spot and dark-spot methods
24 p3861 A71-45202
- Thin films of Te compounds with Zn an Ga subgroup metals - Conference, Vilnius, U.S.S.R., December 1969, Part 3
24 p3861 A71-45247
- Cd doped thin polycrystalline CdTe films rectification mechanism and DC conductivity, discussing light, electric field and temperature effects
24 p3861 A71-45248
- InTe thin films formation, growth kinetics and physical properties, determining vapor deposited film thickness dependence on glass substrate temperature
24 p3861 A71-45249
- InTe thin films with 60-75 percent Te content, investigating phase composition and physical properties
24 p3862 A71-45250
- HgTe-CdTe thin films structural and optical properties, measuring absorption spectra in UV, IR and visible regions to determine Te contents effect
24 p3862 A71-45251
- TiTe thin films phase composition and structural properties as functions of component contents, deposition conditions and annealing parameters, using X ray diffractometer and IR microscope
24 p3862 A71-45252
- Polycrystalline Nb and Ta and Ta-on-Nb thin film thermionic emission surface barrier analysis from periodic deviations in Schottky effect
24 p3862 A71-45346
- Electron microscopic investigation of Au thin film deposits on Si single crystals in ultrahigh vacuum, noting semiconductor-like resistance/temperature behavior at liquid He temperatures
24 p3862 A71-45347
- Joule heating effect on static negative differential resistance and switching of chalcogenide thin films
24 p3862 A71-45353
- THIN LAYER CHROMATOGRAPHY**
Thin layer silica gel chromatography applied to cosmic dust chemical composition
17 p2811 A71-35730
- THIN PLATES**
Thin elastic plates generalized variational equations derivation from virtual displacements and forces principles for arbitrary subdomains, observing node displacement continuity condition
01 p0166 A71-10124
- Heat propagation rate effect on dynamic thermal stress distribution in thin plate, using Hankel and Laplace transforms
01 p0168 A71-10414
- High speed light gage Al welding, discussing plasma arc system
01 p0087 A71-10454
- Heat conductivity equations for thermal stresses of thin cylindrically anisotropic plates made of reinforced laminar plastics
01 p0169 A71-10499
- Axial compression of thin circular epoxy resin disks with three dimensional stress state produced by cementing to rigid platens, using triaxial analysis
01 p0109 A71-11008
- Composite beam of three thin plates reinforced by thin electric ribs, calculating stress strain state by Fourier transforms
01 p0176 A71-11044
- Interference patterns obtained in transmitted light, determining surface parallelism of thin plates transparent in IR region using carbon dioxide laser
02 p0259 A71-11936
- Stress-strain state of thin circular plate with variable thickness along circumference under bending due to uniformly distributed load, using small p
02 p0326 A71-12289
- German monograph on polygonal thin plates calculation by differential equations method for two dimensional boundary value problems solution
02 p0327 A71-12399
- Plastic deformation rate effect on deep drawing of sintered and vacuum melted thin sheet Mo
02 p0256 A71-12516
- Temperature effect on ductility of thin sheet sintered or vacuum melted Mo during deep drawing
02 p0257 A71-12517
- Thin reinforced viscoelastic isotropic multiconnected plate stress-strain state under bending due to concentrated loads and distributed normal forces
02 p0329 A71-12668
- Circular plates forced vibrations, considering internal damping and free and supported boundaries in thin plate wave equation solutions
03 p0502 A71-13300
- Transverse oscillations determination in cyclically deformed thin plate under plane stress by energy dissipation calculation using Hooke law
03 p0502 A71-13401
- Thin reinforced laminates configurations with elastic behavior of homogeneous orthotropic or isotropic material, considering flat plates and thin shells constitutive equations
03 p0505 A71-13537
- Stress distribution around elliptical hole in thin flat rectangular elastic plate under axial in-plane edge loads
03 p0506 A71-13705
- Elastic metal thin plates transverse resonant free vibrations, analyzing viscoelastic coatings damping effects
03 p0506 A71-13709
- Launching intermediate velocity thin plastic sheets for short duration pressure pulse studies of dynamic materials properties
03 p0427 A71-13916
- Thin circular cylindrical plate reinforced by longitudinal rigid stringers, deriving computer algorithm for calculating forced vibration
03 p0515 A71-14367
- Thin Al and plexiglass sheets biaxial stress field effect on fatigue and fracture
04 p0665 A71-14768
- Monograph on bounds for vibration frequencies and buckling loads of clamped uniform thin elastic plates covering stability, harmonic and biharmonic functions
04 p0667 A71-14899
- Surface impedance of thin metal plate excited by RF electromagnetic field as function of external DC magnetic field
04 p0636 A71-14972
- Uniform thin orthotropic skew flat plates free undamped vibration based on classical plate theory, using Rayleigh-Ritz method
05 p0820 A71-15987
- Heat conduction three dimensional problem in radiation heated thin crystalline plates with temperature dependent thermophysical characteristics
05 p0831 A71-16184
- Rectangular thin elastic plate with circular holes under heat flow, solving thermoelastic problem by point matching
05 p0823 A71-16492
- Bending stress around elliptic elastic inclusions in thin anisotropic plate
05 p0824 A71-16590
- Maximal deflection of square and rectangular thin plates with small initial concavities, using dynamic relaxation method for lateral and postbuckling in-plane edge loads
05 p0830 A71-17225
- Thin isotropic plate nonstationary coupled thermoelasticity problem, obtaining recursion equation system for thermal stresses
06 p0983 A71-17367
- Elastic rectangular and thin plates design under dynamic loading, using Bubnov-Galerkin method for computer solutions
06 p0992 A71-17808
- Thin plates and shell with various yield stress materials, observing limiting equilibrium under tension and compression loads
06 p0992 A71-17810
- Thin metal sheet reinforcements effect on slow stable tear and catastrophic failure
06 p1003 A71-18563
- Unsteady temperature fields in thin anisotropic plates with variable coefficient of heat exchange from side surfaces
06 p1009 A71-18730
- Thin plate impact and plastic nonpenetrating deformation by blunt projectiles
07 p1209 A71-19045
- Viscoelastic rectangular thin plate stability under buckling conditions, showing ratio of long term to instantaneous critical loads as function of hereditary properties
07 p1212 A71-19351
- Transient and turbulent flow structure in wake behind thin plates in wind tunnel, noting velocity fields, temperature and initial boundary layers
07 p1089 A71-19750
- Flutter analysis of stressed flat simply supported skew panels in supersonic flow, using small deflection thin plate theory
08 p1370 A71-21302
- Buckling of thin elastic circular plates under steady state asymmetric temperature distribution
08 p1370 A71-21304
- Heat exchanger circular rigid tube sheets calculation by thin plates bending theory, using stepped profile circular plates stress analysis
08 p1374 A71-22053
- Twirl vortex development in unsteady separated flow past thin flat plate, using flow visualization
09 p1432 A71-22582
- Thin metallic disk radar cross sections for near resonance frequencies backscatter, comparing experimental and computer results
09 p1410 A71-23518
- Thin cracked steel plate strip necking zone relative opening displacement and strain measurements by moire method
09 p1542 A71-23540
- Heat conductivity anomalies of thin metallic plates at very low temperatures, discussing secondary phonons angular distribution and electron energy flux
10 p1640 A71-23816

THIN WALLED SHELLS

Thin simply supported polygonal and rhombic plates critical hydrostatic buckling loads and free vibration frequency calculation by conformal mapping and power series expansion

10 p1686 A71-24018

Thin isotropic plates with time and temperature dependent surface heat exchange coefficients, presenting heat conduction equations

10 p1695 A71-24361

Thin metal foils total energy flux, electron/phonon temperatures and thermal conductivity anomalies at liquid He temperatures

10 p1657 A71-24457

Dynamic plastic bending theory of thin circular annular plate with central hole under uniform impulse

10 p1689 A71-24519

Limiting equilibrium of thin rigid plastic plate with piecewise smooth contour under skew symmetric load

10 p1690 A71-24568

Thin flexible panel acoustic power radiation due to turbulent boundary layer wall pressure fluctuations excitation

10 p1596 A71-24814

Infinite thin plate containing circular holes with elastic inclusions under biaxial tension, calculating maximum stresses on common boundaries based on Airy function

11 p1841 A71-25265

Finite element method for stiffness matrix free vibration analysis of thin rectangular plates under central planar loadings

[AIAA PAPER 71-334]

11 p1842 A71-25313

Initially curved thin elastic plates, predicting large deflection and postbuckling behavior with finite element procedure

[AIAA PAPER 71-357]

11 p1844 A71-25336

Stress analysis near free surfaces in thin composite plates with unidirectionally oriented elastic isotropic fibers, applying boundary point least squares technique

11 p1851 A71-26382

Flutter analysis of clamped thin skew panels with midplane forces in supersonic flow, using Galerkin method

12 p1974 A71-26766

Savart plates use in grating interferometers, deriving expressions for phase retardations for arbitrary angles between optical axis and plate normal

12 p1904 A71-26798

Rayleigh wave propagation along edge of thin plate, calculating velocity dependence on frequency

12 p1929 A71-26929

Coupled thermoelasticity, bending and stability of thin walled shells and plates of oriented fiberglass reinforced plastics with low shear rigidity, using Timoshenko theory

12 p1978 A71-27345

Morera and Maxwell stress functions determination by integrodifferential equations of deformation continuity for bending of thin plates

13 p1248 A71-27891

Edge restraint effects on postbuckling behavior of thin flat plates under uniformly distributed compressive loads, noting buckling load and stiffness increase

13 p1253 A71-28466

Exponentially varying thickness thin plate volume minimization for simultaneous stress and deflection constraints under axisymmetric load, using digital computer

14 p2330 A71-30691

Dynamic response and perforation of thin plates subjected to projectile impact, measuring plastic deformation, dynamic strain and displacement with high speed camera

15 p2503 A71-31422

Photoelastic determination of stress distribution in thin square plates subjected to gravitational forces multiplied by immersion in Hg

16 p2647 A71-32824

Magnetoelastic oscillations of thin conducting plate in magnetic field, solving electrodynamic equations

16 p2647 A71-32928

Thin infinite isotropic elastic plate on nonlinear elastic foundation under uniform two dimensional hydrostatic pressure, detailing imperfection effects on initial postbuckling behavior

16 p2648 A71-32979

Thin plates and shallow shells stability, investigating weak solutions of wall displacement differential equations

16 p2649 A71-32993

Mathematical techniques of equilibrium states and periodic vibrations in nonlinear elastic systems illustrated by thin plate and shallow cap buckling under uniform pressure

16 p2649 A71-32998

One dimensional two phase Stefan problem solution for melting of heated thin plate, comparing iterative methods

16 p2662 A71-33065

Thin plate theory approach with discrete triangular approximation of moment and displacement surfaces for plate bending analysis

16 p2652 A71-33081

Infinite length rectangular thin plate bent by uniform load, presenting exact solutions for stresses and displacements from couple-stresses plane strain elasticity theory

17 p2818 A71-34441

Residual stress measurement in thin contoured Ti alloy sheets by X ray diffraction, using stress camera in normal incident beam mode

17 p2757 A71-34537

Dugdale mathematical model for cylindrical bending of thin plates, finding resulting plastic zone dependence on applied moment and normal coordinate

[SESA PAPER 1854A]

17 p2819 A71-34538

Sloshing liquid natural frequencies change in cylindrical shell by movable devices, considering immersed thin elastic plate effect

17 p2726 A71-34579

Axisymmetric nonlinear buckling equations for composite thin circular elastic plates of isotropic or orthotropic layers under radial compression

17 p2821 A71-34580

Transverse oscillations determination in cyclically deformed thin plate under plane stress by energy dissipation calculation using Hookes law

17 p2825 A71-35012

Thin circular disk rotating at constant angular velocity, solving three dimensional elasticity problem with formal power series of thickness-diameter ratio

[ASME PAPER 71-APM-Q]

18 p2978 A71-36260

Wrinkled flat membranes analogy to very thin plates in flexure

18 p2982 A71-36836

Fatigue crack propagation in thin aluminum plates under fluctuating tensile loads, concerning Forman model

18 p2938 A71-36851

Plastic zones and stable crack growth at notches in thin high strength sheet alloys, using replication technique

18 p2938 A71-36853

Free vibrations frequencies and mode shapes of anisotropic elastic thin plates, using Galerkin method

18 p2983 A71-36931

Two dimensional stress tensor invariants for finite elastic deformations of thin plate using initial complex coordinates

19 p3156 A71-37541

High temperature four point bending vacuum furnace machine testing thin refractory sheets, noting strain rate, velocity jump and relaxation on tantalum carbide

19 p3063 A71-37554

Thin circular annular Al plate buckling under uniform radial compression

19 p3157 A71-37872

Pressure pulse shape effect on final plastic deformation of simply supported thin circular plate

19 p3158 A71-38181

Electromagnetic plane wave monostatic scattering incident to thin circular metallic disk, calculating spectral and transient response from far field amplitude and phase data

19 p3036 A71-38608

Free and forced nonlinear vibrations of rigidly clamped thin circular plate, deriving ordinary differential equations

20 p3307 A71-38795

Morera and Maxwell stress functions determination by integrodifferential equations of deformation continuity for bending of thin plates

21 p3455 A71-40085

Peak resonant response of thin rectangular plate with elastic edge restraint under concentrated load

[ASME PAPER 71-VIBR-6]

21 p3456 A71-40269

Thin skewed plates bending and twisting at constant temperature moment, obtaining angle skew effects on torque-twist relation

21 p3463 A71-40592

Free and forced finite amplitude nonlinear oscillations of thin elastic annular plate with free inner and clamped immovable boundaries

21 p3471 A71-41026

Thin elastic plate under dynamic loading, applying asymptotic expansion techniques to three dimensional dynamic elasticity theory

22 p3613 A71-41435

Stress concentration near holes in high modulus epoxy resin polymer thin plates under pressure wave loads

22 p3614 A71-41611

Plane wave propagation following thin elastic rectangular plate impact against smooth rigid obstacle, using difference scheme

22 p3531 A71-41910

Thin elastic elliptic plate stress analysis by approximate solution for rectangular plate and parallelepiped equilibrium problems

22 p3616 A71-42212

Irregularly shaped thin elastic plates under uniform transverse or point loads with singularities resulting from loading or corner conditions

22 p3618 A71-42591

Aerodynamic nonstationary conjugate heat transfer of thin plate with heat sources in incompressible fluid flow

22 p3622 A71-42300

Singly and nonsingly connected thin elastic rectangular plate stability analysis under arbitrary compression load on surface

23 p3777 A71-43000

THIN WALLED SHELLS

German monograph on nonlinear flexural-torsion stress analysis of thin walled rods with open profile covering fork supported and cantilever beam systems

01 p0166 A71-10100

Buckling in fiber reinforced plastic thin walled structures, discussing structural stability problems and methods for prevention of buckling

01 p0172 A71-10600

Elastic thin walled shells of variable thickness with zero Gaussian curvature, deriving stress strain relations with allowance for elastoplasticity

01 p0176 A71-11000

Thermoelasticity problem for stressed state of thin nonaxisymmetric shells with middle surface of revolution

02 p0322 A71-11700

Thin cylindrical work hardening shell under nonuniform heating and external stresses, determining elastoplastic deformation by flow theory

02 p0323 A71-11700

Thin shells of revolution local stability during nonuniform stressed state development under heating

02 p0324 A71-11700

Soviet book on engineering theory of ideally plastic thin shells covering elastoplastic equilibrium, bearing capacity, material anisotropy, etc

02 p0324 A71-11800

Bending of thin elastic orthotropic shallow shells taking into account large deflections, temperature distribution and material nonuniformities

02 p0325 A71-12200

Thin circular cylindrical perforated shell, analyzing stress distribution around circular hole by coordinate transformation and partial differential equations

02 p0326 A71-12300

Optimal cross sectional dimensions of thin walled longeron beams and ribs of skin reinforced delta wing minimizing weight

02 p0329 A71-12500

Thin walled lipped-channel and trapezoidal section beams under end moment loading, deriving differential equations and strain energy for end plates

02 p0330 A71-12900

Doubly curved thin shallow shells nonlinear stability, using piecewise linearization for postbuckling load-displacement curves

03 p0501 A71-13000

Thin reinforced laminates configurations with elastic behavior of homogeneous orthotropic isotropic material, considering flat plates and thin shells constitutive equations

03 p0505 A71-13500

Thin walled prismatic body resistance to torque extension of solution for rectangular bars, considering shearing stresses and transverse forces

03 p0505 A71-13500

Transient creep propagation velocity in dead annealed thin walled Al alloy tubes, using constitutive equation for mean stress-strain-time relationship

03 p0508 A71-13700

Finite element method for composite materials anisotropic behavior, considering flat sheets plate stress and thin shells membrane and bending deformations

03 p0508 A71-13700

Stress analysis of thin elastoplastic shells with large displacements loaded into strain hardening range, assuming plastic strain incompressibility

[ASME PAPER 70-WA/PVP-3]

03 p0511 A71-14100

Thin walled circular cylindrical shells creep buckling under radial pressure and thermal gradients

[ASME PAPER 70-WA/APM-8]

03 p0512 A71-14100

Variational equation of motion for thin walled open section bars coupled flexure and torsion, considering thermal effects

[ASME PAPER 70-WA/APM-51]

03 p0513 A71-14100

Thin walled cylindrical shells with filler, determining stability under axial compression by computer calculation

03 p0514 A71-14300

Multicavity thin walled containers of spheres and intersecting plane partitions, comparing structural properties with single sphere of equal overall volume

03 p0515 A71-14300

Thin shells of revolution formed of closed box sections, using numerical integration and stiffness matrices for solution

[ASME PAPER 70-PVP-12]

Absorption coefficient of plane wave scattering from thin spherical resistive shell for broadband RF radiation monitoring

04 p0558 A71-15100

Eccentrically stiffened thin spherical shell instability under uniform external pressure

04 p0669 A71-15100

- Nondestructive test with high resolution instrumentation for observing long thin walled cylinder lateral displacements prior to buckling under axial compression 04 p0669 A71-15297
- Thin convex shell of evolution bounded by two valleys minimum vibration frequency using asymptotic method of integration 04 p0671 A71-15556
- Thin elastic orthotropic oval cylindrical shells nonlinear flexural vibration based on assumed modes, using Galerkin method 05 p0819 A71-15979
- Thin circular cylindrical shell stability subjected to axisymmetric thermal pulse, describing buckling process by mathematical model 05 p0820 A71-16186
- Static thin shells and disks gravitational fields in general relativity 05 p0781 A71-16447
- Staticogeometrical relations of thin torus shaped shell and closed curvilinear rods 05 p0824 A71-16594
- Thin shallow shell theory boundary value problem, discussing reduction to Fredholm integral equations system 05 p0828 A71-16893
- Thin walled shell free linear vibrations frequency analysis calculation using asymptotic method 05 p0829 A71-16994
- Thin orthotropic shallow elastic shells with initial effects, analyzing critical pressure states 06 p0982 A71-17355
- Thin elastic shallow spherical dome nonlinear motion under uniformly distributed external pressure 06 p0982 A71-17360
- Buckling of cold formed Al alloy thin walled columns under compression, investigating longitudinal half wave formation 06 p0985 A71-17748
- Thin cylindrical shell in ideal compressible fluid, calculating longitudinal resonance waves for acoustic excitation 06 p0985 A71-17755
- Variational methods application to optimal heating of thin elastic shells, using elastic-energy functional minimization as optimality criterion 06 p1006 A71-17767
- Axisymmetric stability loss of thin long cylindrical shell with elastic filler under uniformly distributed compressive forces over shell ends 06 p0987 A71-17770
- Thin shallow shell theory, describing asymptotic method for nonlinear equations integration 06 p0988 A71-17776
- Geometrically nonlinear thin nonshallow shells of revolution, deriving axisymmetrical elastic deformation equations 06 p0988 A71-17780
- Optimal parameter selection for thin walled shell structures, using mathematical programming 06 p0989 A71-17781
- Thin walled prismatic shell constrained torsion problem, applying Reissner mixed variational method 06 p0992 A71-17806
- Thin plates and shell with various yield stress materials, observing limiting equilibrium under tension and compression loads 06 p0992 A71-17810
- Thin elastic shell of revolution with negative Gaussian curvature, discussing free nonaxisymmetric oscillations 06 p0992 A71-17811
- Thin imperfect cylindrical shell stability, considering statistical analysis of initial irregularities 06 p0993 A71-17815
- Thin elastic partially liquid filled shells of revolution, applying asymptotic integration method to free vibrations case 06 p0995 A71-17834
- Thin circular cylindrical shell thermoelastic vibrations, deriving differential equations of motion with allowance for shear, rotary and translational inertia 06 p0996 A71-17840
- Critical parameters and vibration frequencies of homogeneous closed circular rings connected to thin shells determined for various boundary conditions 06 p0996 A71-17844
- Thin orthotropic shells thermocreeper in variable temperature field reduced to integration of linear partial differential equation system 06 p0997 A71-17852
- Thin walled two layer bimetallic shells of revolution under large deformation, analyzing equilibrium by zero moment theory 06 p0998 A71-17856
- Thin walled flexible shell theory and equilibrium under large deformation 06 p0999 A71-17862
- Numerical algorithms of elastic stability solutions for thin walled axisymmetrically loaded shells of revolution with finite difference schemes 06 p0999 A71-17864
- Static computations of thin walled shells and honeycombs, examining variational, matrix, finite element, initial function, small parameter and plate bending methods 06 p0999 A71-17867
- Nonlinear statics of thin walled cylindrical and spherical shells, including buckling under various end conditions 06 p0999 A71-17869
- Thin elastic toroidal shells under nonsymmetric harmonic loadings, reducing problem to membrane and edge effect linear solutions 06 p1002 A71-18415
- Design criteria for buckling prediction of elliptical and circular cylindrical shells under axial compression from asymmetric and axisymmetric shape imperfections distribution 06 p1003 A71-18588
- Dynamic response of pressurized thin circular cylindrical shells under moving loads [AIAA PAPER 71-175] 06 p1004 A71-18614
- Thin paraboloidal shells of revolution under external hydrostatic pressure loading, analyzing free vibrations by finite element method [AIAA PAPER 71-214] 06 p1004 A71-18650
- Strength characteristics of thin walled anisotropic shells, using difference-differential method to reduce partial differential equations 06 p1005 A71-18709
- Thin shallow elastic shells boundary value problem, deriving existence and multiplicity of equilibrium state critical points for bending and buckling 07 p1213 A71-19639
- Thin shallow spherical shell vertical impact against ideal incompressible liquid surface, calculating axisymmetric deformation and hydrodynamic load distribution 07 p1089 A71-19738
- Thin single layer orthotropic circular cylindrical shell shear coupled traveling wave reflections, determining stresses in terms of particle velocities 07 p1216 A71-20134
- Thin cylindrical shell of revolution delaminations detection model, using free vibration natural frequency parameter under clamped-clamped conditions 07 p1216 A71-20135
- Thin spherical roller supported domes stability and axisymmetric deformation under apex point loads, investigating plastic buckling and inelastic strain effects 07 p1216 A71-20222
- Stiffened long cylinder with time variable thickness and strengthening thin shell system elastic displacements due to nonstationary vibrations and nonuniform pressure distribution 07 p1217 A71-20459
- Thin shallow shells under surface loads with allowance for electric field induced body forces and moments, deriving four equations system 08 p1368 A71-20788
- Heterogeneity effects on thin composite cylindrical shells axisymmetric vibration characteristic, considering material and geometric symmetry deviations influence on frequency spectra 08 p1368 A71-20805
- Tensor elasticity relations in linear theory of thin elastic shells in Kirchhoff-Love range 08 p1373 A71-21868
- Moving thin walled tubes surface and internal defects detection based on three dimensional thermal field surface distribution 08 p1300 A71-21899
- Nomograms for normal stresses and bending moments in thin circular cylindrical shell under uniformly distributed local load 08 p1374 A71-22054
- Flutter analysis of rotating thin cylindrical shell with outer surface exposed to inviscid helical air flowfield 09 p1533 A71-22078
- Stress equations for thin pyrolytic graphite shells with thermal allowance 09 p1534 A71-22095
- Torsional oscillation of hollow isotropic elastic cylinder encased in thin elastic shell, deriving representation satisfying equation of motion and initial and boundary conditions 09 p1539 A71-22918
- Imperfect thin walled circular cylindrical shells under axial compression with relaxed boundary conditions, determining deformations with differential equations 09 p1541 A71-23089
- Thin cylindrical shell deformation under concentrated transverse loads applied through rigid boss, determining displacement variations as function of applied loads and edge constraints 09 p1543 A71-23659
- Arbitrary midsurface geometry thin shells nonlinear equations in terms of finite rotation vector and stress resultant tensor component 10 p1684 A71-23761
- Thin spherical shell under uniform normal pressure using dynamic stability criterion and energy method for asymptotic nonlinear shell equations 10 p1685 A71-23937
- Thermal fatigue and service life of thin walled tubular pearlite steel notched specimens in various oxidizing media 10 p1626 A71-24191
- Low temperature plasticity of Al alloy thin walled tubular specimens under axial tension and internal pressure 10 p1626 A71-24193
- Limit load carrying capacity of thin walled tube under combined forces, including pressure effects by variational method of plasticity theory 10 p1688 A71-24384
- Approximate solution for limit load carrying capacity of thin walled tube under combined loadings, deriving formulas describing boundary surface 10 p1688 A71-24385
- Critical speeds for inviscid compressible potential flow past thin elastic cylindrical shells, using long wave approximation 10 p1689 A71-24565
- German monograph on basic equations for isotropic elastic homogeneous thin shell subjected to infinitesimal displacements, determining work of form change 10 p1692 A71-25037
- Thin circular cylindrical shells thermoelastic behavior under one directional radiant heating, comparing measured displacements and strains with calculated values based on measured temperature distributions 11 p1841 A71-25187
- Elastic boundary conditions effect on natural frequencies and resonant displacement of thin isotropic circular cylindrical shell under concentrated load with harmonic time history [AIAA PAPER 71-335] 11 p1843 A71-25314
- High precision finite element for static analysis of loaded thin elastic shells of revolution including shear deformations [AIAA PAPER 71-360] 11 p1844 A71-25339
- Flutter analysis of long thin cylindrical shells rotating in circular helical air flow field [AIAA PAPER 71-373] 11 p1845 A71-25346
- Dynamic response of rotationally symmetric open-ended thin shells of revolution under transient impulsive and thermal loadings, using FORTRAN 4 finite difference program 11 p1847 A71-25466
- Buckling load scatter reduction in axially compressed thin walled circular shells as function of manufacturing accuracy [DFVLR-SONDDR-92] 12 p1974 A71-26869
- Oscillation theorem for natural vibrations of thin shells of revolution, considering boundary value problem eigenvalues 12 p1977 A71-27304
- Coupled thermoelasticity, bending and stability of thin walled shells and plates of oriented fiberglass reinforced plastics with low shear rigidity, using Timoshenko theory 12 p1978 A71-27345
- Thermal stress analysis of hinged thin circular cylindrical shells of variable thickness by computerized discrete orthogonalization method 12 p1979 A71-27357
- Axisymmetrically strained thin elastic shells of revolution with temperature dependent random elastic characteristics 12 p1979 A71-27358
- Axisymmetric deformation of thin elastic shell of revolution under combined effect of static surface load and nonuniform heating 12 p1979 A71-27359
- Thin walled stiffened Duralumin box spars bending stress-strain states under unsteady creep 12 p1981 A71-27496
- Influence coefficients for thin walled finite length cylindrical shells subjected to uniform internal pressure and edge loads 12 p1983 A71-27586
- Thin walled elastic isotropic shallow shell with thermal boundary conditions, obtaining thermoelastic solution in series form 12 p1984 A71-27687
- Strain gage method for residual stress determination in thin walled brass cylindrical shells produced by deep drawing 13 p2066 A71-28034
- Stress concentration at circular hole in conical shell, using Bubnov-Galerkin method in conjunction with linear thin shell theory 13 p2150 A71-28135
- Load bearing capacity of thin walled box shaped rod of strain hardening material during bending beyond elastic limit 13 p2153 A71-28294
- Deformation substructures, strain rates and terminal properties of explosively-formed thin walled stainless steel cylinders, using transmission electron microscopy 13 p2153 A71-28501
- Magnetic shielding of various shaped enclosures such as rectangular or cylindrical cross sections in terms of normalized parameters 13 p2039 A71-28870

Stress-strain state of thin walled ellipsoidal shell of revolution with arbitrarily oriented crack

13 p2156 A71-29069

Load capacity and transient creep of thin walled rod under free torsion, using successive approximations

13 p2157 A71-29212

Circular cylindrical thin walled shells buckling, determining postbuckling patterns development by high speed cinematography

13 p2157 A71-29305

Structural stability in tension and strength tests of thin walled tubes at various stress and strain intensities based on loss of resistance to plastic deformation

14 p2321 A71-29620

Thin hyperelastic tube forced large amplitude radial oscillations, deriving exact solution for general forcing function

14 p2322 A71-29690

Thin shallow initially curved sheets fracture theory, extending Griffith analysis

14 p2322 A71-29738

Thin shell isotropic clamped free elliptical cylindrical shells with various cross sectional eccentricities, measuring frequencies and mode shapes by vibration analysis

14 p2324 A71-29869

Soviet book on stability of thin walled reinforced and multilayer shells with various designs and boundary conditions

14 p2325 A71-29939

Critical loads and stability loss equations near edge of thin convex clamped elliptical shell of revolution under uniform external compression loads

14 p2325 A71-30024

Thin walled cylindrical elastic shell with rectangular holes at equal intervals along straight line, deriving boundary conditions expression by R-functions

14 p2326 A71-30190

Approximate similitude relation for vibrating thin shells with scaled surface geometry, using Love equations of motion

14 p2327 A71-30204

Extensional vibrations of thin cylindrical shell, discussing longitudinal and radial motions coupling and resonant frequency dependence on length/radius ratio

14 p2327 A71-30209

Generalized elastic thin shell nonlinear theory, deriving equilibrium equations and boundary conditions from shape dependent energy considerations

14 p2329 A71-30448

Pisa University Aeronautical Institute activities /1960-1970/, considering supersonic and subsonic flow research, thin stiffened shells fatigue under compressive or tensile loads, etc

14 p2222 A71-30822

Perturbed motion linear equations of body rigidly coupled to thin walled elastic shell partially filled with heavy compressible fluid

14 p2227 A71-30867

Momentless axisymmetric stress state and stability loss in thin convex shells of revolution in linear approximation

14 p2333 A71-30891

Isotropic elastic thin oval rings nonlinear free and forced flexural vibrations calculation by Galerkin method

15 p2503 A71-31436

Thin walled tubes under external and internal pressures axial loads and torques, showing load capacity limit dependence

15 p2428 A71-31860

Arbitrarily shaped thin shell elastic-plastic deformation transient response prediction, using improved finite difference method

15 p2505 A71-32008

Thin conical shell under longitudinal impact, deriving theory for transverse and rotary inertias and transverse shear deformation effects

15 p2506 A71-32017

Nonlinear coupled parametric response of crooked thin walled columns under harmonic longitudinal load

15 p2507 A71-32095

Flutter of thin walled cylindrical shells conveying fluid above critical flow velocity

15 p2508 A71-32135

Shock produced stress relaxation in thin walled Al tubes, comparing strain-time profiles with thin shell theory

16 p2647 A71-32923

Stress-strain state of unclamped thin elastic zero curvature shell under three component surface load and tangential boundary forces

16 p2647 A71-32926

Asymptotic eigenvalue density estimates for edge-hinged thin elastic rectangular shell, determining shell stability linear equation solution conditions

16 p2647 A71-32937

Thin plates and shallow shells stability, investigating weak solutions of wall displacement differential equations

16 p2649 A71-32993

Cosserat surface static stability, considering construction of direct theories of thin shells

16 p2649 A71-33001

Convective motions in differentially rotating thin spherical shells, explaining solar differential rotation

16 p2630 A71-33055

Thin walled rod of strain hardenable material, developing constrained torsion approximation for creep and relaxation

16 p2651 A71-33060

Thin elastic shells Koiter-Sanders mathematical model finite element analysis using Ritz method

[ASME PAPER 71-APM-32] 16 p2655 A71-33197

Dynamic midsurface displacements of thin circular cylindrical shell under uniform membrane stress state and three dimensional surface loads

[ASME PAPER 71-APM-12] 16 p2656 A71-33214

Integral containing Heaviside and Dirac delta function in integrand with minus and plus infinity limits, computing value using thin spherical shells in general relativity

16 p2656 A71-33263

Initial interaction phase between thin shallow conical shell vibrating axisymmetrically and ideal incompressible fluid, determining hydrodynamic pressure effects

16 p2560 A71-33901

Yield surface approximations for thin shell made of material obeying von Mises yield criterion, considering transverse shear effect

16 p2661 A71-34118

Error estimates in thin elastic shell linear theory, modifying three dimensional displacement field

17 p2815 A71-34224

Concave thin shell of revolution lowest natural vibration spectra frequency corresponding to simple inflection point

17 p2817 A71-34341

Finite length thin circular cylindrical shells with clamped or simply supported edges, calculating flexural free vibration natural frequencies

17 p2822 A71-34643

Book on asymptotic approximation in three dimensional thin and thick elastic shell theory including interior and Kirchhoff edge zone equations

17 p2822 A71-34770

Finite length heterogeneous thin layered cylindrical shell axisymmetric free vibration frequency spectrum analysis

17 p2826 A71-35035

Soviet papers on thin walled aircraft structures strength and stability covering bending theory, circular cylindrical shells, thermal stresses of rectangular plates, etc

17 p2828 A71-35301

Stress distribution over elements of boss or collar tightened flange joints of circular thin walled shells during bending

17 p2829 A71-35306

Stress-strain state of thin walled curvilinear frame-type rods of variable cross section with variable elastic moduli along length and contour

17 p2829 A71-35309

Thin elastic spherical shells reinforced by stringers and frames and loaded by internal or external uniform pressure, calculating by energy method

17 p2829 A71-35311

Thin multilayer pressurized glass fiber-plastic cylindrical shells, calculating stress redistribution due to crack initiation and prestressing effects

17 p2830 A71-35319

Saint Venant principle generalization for transient creep and stress relaxation analysis in rectilinear thin walled multiply connected beam under torsion

17 p2833 A71-35612

Test apparatus for studying stress-strain behavior of thin walled metal tubes in torsion, examining strain rate and history effects

18 p2935 A71-36234

Spinning centrally clamped thin shallow spherical shell free vibration numerical analysis by considering perturbation about equilibrium configuration

[ASME PAPER 71-APM-G] 18 p2977 A71-36254

Thin walled shell free linear vibrations frequency density calculation using asymptotic method

18 p2982 A71-36794

Inertial effects induced by rotating thin walled shell of finite thickness, considering general relativity equations of motion for test particle

18 p2970 A71-37059

Prestressed thin shells elastic deformation, using Kirchhoff hypothesis of shell theory

19 p3154 A71-37072

Natural axisymmetric vibration of thin elastic shell of revolution, deriving eigenvalues convergence to spectrum lower bound by asymptotic method

19 p3154 A71-37097

Variable thickness thin orthotropic spherical shell with hole, calculating stressed state with successive approximation technique

19 p3155 A71-37533

Prestressing effect on yield surfaces of Al and Cu thin walled tubes

19 p3079 A71-37705

Clamped oval cylindrical thin walled shells elastic buckling under axial loads, solving stability equations

by Fourier method and higher order difference technique

19 p3157 A71-37876

Externally pressurized thin walled elastic spherical shells influence coefficients singularity

19 p3158 A71-37886

Buckling and initial postbuckling behavior of clamped thin shallow spherical sandwich shells under axisymmetrical loads

19 p3159 A71-38185

Oscillation theorem for natural vibrations of thin shells of revolution, considering boundary value problem eigenvalues

19 p3159 A71-38264

Zero moment stress state realization in thin macrohomogeneous shells by selecting adequate uniform multilayer structures for reinforcement

19 p3159 A71-38266

Thin shallow spherical shell weakened by circular hole, calculating stressed state from boundary value problem solution

20 p3308 A71-39163

Tensor elasticity relations in linear theory of thin elastic shells in Kirchhoff-Love range

20 p3308 A71-39367

Dynamo theory for ionospheric thin shell model, considering wind fields determination from diurnal geomagnetic variations

20 p3218 A71-39522

Nonassociated constitutive equations for rigid viscoplastic plates and thin rotationally symmetric shells under dynamic loading with Huber-Mises yield condition

20 p3310 A71-39777

Asymptotic geometric optics methods application to thin shell theory, reducing transport equation to ordinary differential equation

20 p3310 A71-39863

Thin truncated conical shells axisymmetric free vibrations, considering shear deformation and rotary inertia effects

21 p3462 A71-40528

Shallow spherical cap and deep thin spherical shell buckling, solving integral equations by iterative procedure

21 p3463 A71-40542

German monograph on creep buckling tests of finned and unfinned thin walled pipes of heat resistant breeder reactor cladding materials

21 p3464 A71-40781

Thin elastic shell of revolution under asymmetric loads, calculating time dependent transient response with implicit backward and explicit central differencing schemes

21 p3467 A71-40960

Interlaminar shear stress and midsurface displacement of thin orthotropic laminated cylindrical shells, using linear deformation theory

21 p3470 A71-41018

Nonlinear periodically oscillating motions in shell theory, examining buckling characteristics of thin walled structures under dynamic and shock loads action

21 p3473 A71-41152

Open simply supported cylindrical shell internal stresses due to initial deformation based on thin elastic shell linear theory

22 p3613 A71-41563

Elastic and inelastic thin shell nonlinear theory derivation by integrating material continuity equations of motion over shell thickness

23 p3775 A71-43318

Axisymmetrical elastic deformation of thin helicoidal shell with rectilinear profile, deriving equilibrium equations and stress-strain relationships

23 p3778 A71-44038

Thin closed circular cylindrical shell under arbitrary loading

23 p3778 A71-44039

Thin elastic shell of revolution with waves along parallel, considering small free nonaxisymmetric vibrations

24 p3877 A71-44406

Closed profile thin walled curvilinear rods, deriving static and strain integrals with Hookes law

24 p3877 A71-44410

Thin isotropic shells with terminal shear rigidity, deriving complex version of classical theory of thermoelasticity for plastic shells with low shear resistance

24 p3878 A71-44482

Curved finite element for elastic-plastic analysis of thin toroidal shells of revolution with discontinuous meridional slope under axisymmetric loadings

24 p3879 A71-44634

Asymptotic design formulas for thermoelastic supercritical strains in thin elastic shallow spherical shells under external pressure

24 p3881 A71-44827

Stress-strain state of hinged thin multilayer orthotropic cylindrical shells with parameters variable with respect to directrix

24 p3881 A71-44828

Axisymmetric elastic deformation of layered thin anisotropic shells of revolution, using computer integration for arbitrary loads and boundary conditions 24 p3882 A71-44841

Cyclic symmetrical deformation of thin elastic conical shells of revolution of variable thickness with meridional ribs under physical and thermal loads 24 p3882 A71-44843

Buckling stability and critical loads of thin elastic cylindrical shells with hollow core in axial compression 24 p3882 A71-44844

Thin walled tube under combined bending and torsion, considering stress distribution and curvature behavior 24 p3883 A71-44892

THIN WALLS

Coupled vibrations of thin walled beams of open cross section using finite element method 01 p0175 A71-11015

Flexural-torsional vibration stability of thin walled elastic bars under longitudinal periodic force, using parametric resonance theory 02 p0321 A71-11687

Lower bound load carrying capacity of thin walled structures of rods, plates and shells with statistical stable stress field, using plasticity theory 02 p0326 A71-12296

Plate and shell designs, considering thin walled structures optimization for minimum weight, volume and cost vs maximum stresses 06 p0998 A71-17858

Geometries and technical specifications deviations effects on service life and fatigue characteristics of thin walled structural components under cyclic loads 06 p1005 A71-18710

Optimal thin walled structures design, using discrete matrix methods for computer programming 08 p1368 A71-20791

Wideband microwave absorbing wall using dielectric material of foamed polystyrol powder coated with graphite, discussing design procedure and thickness reduction 08 p1253 A71-21297

Curved beams deformation with open thin walled cross section, using equilibrium and energy methods 11 p1848 A71-25579

Finite element for torsion of thin walled open tubes, applying to matrix force analysis 12 p1974 A71-26871

Thermally induced torque of circular thin walled open section booms, predicting steady state behavior 13 p2148 A71-27980

Center of rigidity position determination in cross section of thin walled beam under nonuniform temperature due to creep 13 p2154 A71-28642

Transient creep of thin walled composite beam under bending and tensile loads in nonuniform temperature field by increment method 14 p2321 A71-29538

Stress analysis of thin walled framed structures of variable cross section by second order differential buckling equations, using matrix method 14 p2321 A71-29539

Stress analysis of thin walled framed cylindrical beams under deformation beyond proportionality limit by iteration method 14 p2321 A71-29540

Optimized thin walled elements in elastic planar frame structures minimum weight design 14 p2324 A71-29872

Thin walled structure design for critical loading by external force variation, determining carrying capability loss by digital computer matrix methods 17 p2818 A71-34351

Orthotropic thin walled bars with rigidly connected rectangular elements, applying displacement under torsion with allowance for shear to H beam 17 p2823 A71-34782

Torsion free, rigid and elastic stiffness matrices of thin walled bars, noting transformation to eccentric nodal points 17 p2832 A71-35399

Thin walled beam structures under external torsional loading, calculating distribution of longitudinal and shear stresses 18 p2982 A71-36808

Buckling for thin stress walled open sections on elastic foundation with constrained direction reinforcement 22 p3614 A71-41693

Dynamic response of thin walled structures natural frequency analyzed for formulating potential and kinetic energy for stiffness and mass matrices by minimization principle 24 p3878 A71-44555

Elasticity theory for rectangular region with thin-walled inclusion under symmetrical external forces, reducing to three quasi-regular infinite systems of linear algebraic equations 24 p3880 A71-44722

THIN WINGS
NT INFINITE SPAN WINGS

Thin delta wing with leading edge separation, obtaining drag lift and rolling moment coefficients and pressure distribution 02 p0185 A71-12408

Thin plane wings with mixed leading edges, applying linearized supersonic flow theory 03 p0344 A71-14241

Pressure distribution singularity at tip of thin lifting parabolic wing in subsonic flow [AIAA PAPER 71-10] 06 p0842 A71-18484

Cavitation flow of fluid with free surface past underwater wing with jet flap, solving equations of motion for thin foil with jet emergent from trailing edge 07 p1092 A71-20086

Thin rectangular wing load distribution in nonstationary incompressible flow, using downwash integral equation Fourier transform 09 p1383 A71-22946

Mach cones reflection at thin wing subsonic leading edges in supersonic flow, considering axial disturbance velocity and pressure distributions 09 p1384 A71-23616

Sweptback thin cantilever wing transonic flutter density and velocity coefficients, investigating engine pod shaped concentrated mass location effects 11 p1706 A71-25189

Thin delta wing in hypersonic inviscid flow at small angles of attack, calculating motion equations and boundary conditions at small perturbations 12 p1863 A71-27330

Wing design criteria imposed by high speed requirement for short takeoff aircraft, considering thin swept-back wing with small aspect ratio for lateral control 12 p1867 A71-27471

Oscillating thin wing with control surfaces in two dimensional compressible subsonic flow, calculating aerodynamic forces based on kernel function method [DFVLR-SONDDR-132] 16 p2519 A71-33013

Supersonic flow past thin delta wings with finite velocities at leading edges, noting wing deformation to avoid corner vortices appearance 18 p2843 A71-36181

Total lift data correlation for thin sharp edged low aspect ratio delta wings at low speeds, noting trailing edge effects in incompressible flow 20 p3176 A71-39398

THIOLS
NT CYSTEINE

Chemical protection against ionizing radiation by thiols and disulfides, discussing hydrogen transfer 07 p1032 A71-18930

Structure-function studies of aminothiol radioprotectants on *Escherichia coli* B/r, discussing radiation response at 274 and 77 K 07 p1033 A71-18936

Thiol and disulphide compounds radiation protection capacity at cellular level in tissue culture, using reproductive integrity as protection criteria 07 p1034 A71-18948

Biochemical mechanism of radioprotective action of aminothiols in mammals 07 p1039 A71-18979

Radioprotective mercaptoethylamine /MEA/ effect on aerobic resynthesis of ATP in thymus nuclei and oxidative phosphorylation in rat liver mitochondria 07 p1039 A71-18984

Jet fuel antiwear properties relation to viscosity and adsorption tar and mercaptans content 15 p2464 A71-31678

Mercaptoalkylamine group radiation protection preparations on resistance of rats and mice to lateral acceleration rate 22 p3491 A71-42700

Aminothiol group radioprotective drugs effect on guinea pigs cardiac function during lateral acceleration 22 p3491 A71-42702

Aminothiol class radiation protector influence on tissue damage of white rats under single and two-fold gamma irradiation at various test conditions 22 p3494 A71-42729

THIURONIUM

Radioprotective effectiveness of cystamine and S beta-aminoethylthiuronium in mice under combined gamma irradiation and transverse acceleration loads 22 p3494 A71-42730

THOMAS-FERMI MODEL

Atomic scale elastic structure equations of state for Thomas-Fermi model extension to high pressures, considering earth core iron-silicates composition 11 p1802 A71-25572

THOMAS-FERMI THEORY
U THOMAS-FERMI MODEL
THOMSON EFFECT
U THERMOELECTRICITY
THOMSON SCATTERING

Thomson scattering role in solar corona electrons cooling 06 p0976 A71-18454

Thomson scatter measurements of F region ionization drifts vertical velocity at midlatitudes, studying electric field influence 08 p1279 A71-21204

Two fluid continuum theory of Thomson scattering extended to uniform DC magnetic field and electron drift, finding backscattered power dependent on magnetism 08 p1283 A71-21640

Satellite, rocket and Thomson scatter data application to communications - IEE Conference, London, January 1971 10 p1575 A71-23864

Poloidal magnetic field measurements in toroidal pinch by Thomson scattered carbon dioxide laser beam 10 p1651 A71-24631

Thomson light diffusion in laser diagnostics, deducing electron density/temperature and ion temperature 11 p1776 A71-26274

Plasma diagnostics covering magnetic, electron beam, electrostatic, laser, holography, interferometry, Thomson scattering, microwave and electroacoustic techniques 11 p1766 A71-26287

Solar corona electrons cooling by Thomson scattering, calculating electron energy loss 12 p1955 A71-26604

Strong magnetic fields effects on neutron stars or white dwarfs, considering Thomson scattering in fully ionized collisionless plasma 14 p2315 A71-30858

Daytime rocket and ground based radar Thomson scatter measurements of electron densities and temperatures in lower ionosphere 15 p2399 A71-31772

Low density plasma diagnostics using Thomson scattering of laser light 16 p2618 A71-33161

Lasers as light sources, discussing Rayleigh, Tyndall, Raman and Thomson scatterings from various media 16 p2612 A71-33373

Electron distribution functions construction from spectrum of laser light Thomson scattering by rarefied plasma 19 p3074 A71-38215

THOR DELTA LAUNCH VEHICLE

In-flight base heating and thermal environment measurements from Thor Delta launch vehicle using six strap-on solid propellant motors [AIAA PAPER 71-644] 14 p2320 A71-30721

THOR LAUNCH VEHICLES
NT THOR DELTA LAUNCH VEHICLE

Base flow prediction for axially symmetric cylindrical vehicle with supersonic single central jet by two stream interaction model, comparing Thor flight data [AIAA PAPER 71-643] 14 p2290 A71-30720

THORAL LAUNCH VEHICLES
NT THOR DELTA LAUNCH VEHICLE
THORAX

Moulting of *Calpodex ethlius* larvae head and thorax isolated with prothoracic glands dependent on molting hormone injection 01 p0016 A71-11347

Isopotential maps comparison of thorax with vectorcardiograms from superficial potential distribution zones 02 p0207 A71-12111

Trans thoracic measurements of left and right ventricular systolic pressures in anesthetized mice, using fiber optics and strain gage manometer techniques 09 p1401 A71-23371

Renal hemodynamic factors in whole kidney glomerulotubular balance in anesthetized dogs by manipulating filtration rate through constriction of aorta, thoracic vena cava, etc 16 p2529 A71-33194

Diaphragm mechanics, discussing thoracic pressure-lung volume and air flow relationships of respiratory system during electrophrenic stimulation in men and cats 16 p2530 A71-33239

THORIUM
NT THORIUM ISOTOPES

Thorium wavelength measurements by interferometry, noting weighted averages as secondary standards of length 04 p0627 A71-15692

Lunar rocks 12040 and 12013 and anorthositic, determining U-Th distributions with induced fission track maps 23 p3752 A71-43712

THORIUM ALLOYS

Oxidation kinetics and scale morphology of chromium oxide forming thoriated and unthoriated Ni alloys, discussing rate controlling processes effects 16 p2590 A71-32871

THORIUM COMPOUNDS
NT THORIUM OXIDES

High temperature vaporization of titanium, zirconium, hafnium and thorium carbides by Knudsen effusion mass spectrometry, measuring ion intensities, formation enthalpies and dissociation energies 16 p2540 A71-33251

Diffusion coefficients determination in planetary boundary layer with radon and ThB, using vertical distribution profile of concentration 18 p2912 A71-36193

THORIUM ISOTOPES

- U-Pb and Th-Pb age discrepancy in lunar dust, proposing Rn-222 emanation in decay chains 14 p2307 A71-29733
- Isotopic abundances and composition of U and Th in Apollo 12 soil and breccia samples, using mass spectroscopy 23 p3753 A71-43716
- Isotopic composition of U and Th in Apollo 12 lunar rock samples from mass and alpha spectroscopy 23 p3753 A71-43717

THORIUM OXIDES

- Thoria dispersed Ni-Cr alloy hypersonic entry ablation model, accounting for Cr oxidation [AIAA PAPER 71-34] 06 p1009 A71-18654
- Electrical conductivity measurement for thorium oxide at 1000-1600 C and at low oxygen partial pressures, discussing Seebeck coefficient behavior 07 p1177 A71-19569
- Phase equilibria, microstructure and physical properties of high temperature vacuum sintered oxygen deficient zirconia and thorium 08 p1304 A71-20697
- Ni-Cr thorium dispersion strengthened alloys, determining tensile effects on high temperature mechanical properties 08 p1311 A71-21545
- Temperature dependent ionic domain for yttrium oxide doped thorium as solid electrolytes at low oxygen activities 09 p1480 A71-22114
- Tensile data for dispersion hardened iron containing thorium spherulites analyzed in terms of Orowan theory, considering bcc materials yield strength 09 p1466 A71-22172
- Thorium containing Ni and Co base powders reduction in hydrogen atmosphere for precipitation hardened materials production, determining optimal thermodynamic and reaction kinetic factors 09 p1475 A71-23306
- Protective coatings of Ta, Nb and Ti alloys for high performance thermal protection systems, discussing space shuttle reentry heat shield 11 p1778 A71-25554
- TD NiCr nickel based alloy high temperature oxidation control, discussing thorium dispersion effect on Ni-Cr oxidation properties 11 p1779 A71-26015
- Recrystallization behavior of thorium dispersion hardened W-Re alloy compared to pure W by X ray diffraction, hardness tests, metallographic and electron microscopy methods 20 p3247 A71-38763

THORIUM 232

U THORIUM ISOTOPES

THORIUM 230

U THORIUM ISOTOPES

THORIUM 234

U THORIUM ISOTOPES

THORON

U RADON

THREADS

- Soviet book on bolting and coupling elements threads used in aircraft industry covering configurations selection, cutting, tolerance requirements and quality control 02 p0258 A71-12723
- Cylindrical steel samples with screw type threads, comparing pressed and ground threads effects on tensile strength at low temperatures 05 p0827 A71-16763
- Low temperature and tensile loading rates effects on static and dynamic strength of steel rods with ground and rolled threads 15 p2505 A71-31862

THREE BODY PROBLEM

- Gravitating point motion under attraction by two fixed centers, investigating hyperbolic case 01 p0156 A71-10449
- Three body gravitational capture of interstellar dust in solar system, examining zodiacal cloud 01 p0158 A71-10771
- Numerical analysis of Hill limiting case of restricted three body problem regarding quasi-periodic, ergodic and escape orbits for natural and artificial satellites 01 p0161 A71-1380
- Lagrange points role in three body problem, discussing applications to space probe positioning 02 p0316 A71-12739
- Satellite translational motion in circular problem of three bodies, discussing existence of equations integral 03 p0484 A71-13223
- Nonlinear stability of triangular points in restricted problem of three bodies, using second order expansions, Lie transform and multiple scale method 03 p0487 A71-13448
- Triangular libration points stability in elliptic restricted three body problem, determining parametric resonance region 03 p0495 A71-14226
- Nonplanar moon-earth trajectories, determining restricted three body problem analytical solution accuracy [AIAA PAPER 70-1060] 03 p0495 A71-14274

Close binaries evolution, atmospheres structure and three body problem 04 p0647 A71-15241

Three body plane restricted problem axisymmetric periodic solutions, establishing linear equations of variation 04 p0652 A71-15703

Resonance in planar elliptic restricted three body problem, noting primaries eccentricity and long term effects 04 p0653 A71-15710

Trojan asteroid planar motion considered within restricted circular three body problem framework, discussing singularities 04 p0655 A71-15722

Three body stellar problem libration calculation using nonlinear mechanics methods, and application to lunar satellite perturbation by earth and lunar gravitational effects 04 p0655 A71-15728

Periodic orbits in general three body problem with nonzero angular momenta 04 p0656 A71-15730

Periodic orbit families in planar Pythagorean three body problem 04 p0656 A71-15731

Stability and resonances in restricted three body problem, using method of surface-of-section 04 p0656 A71-15732

Restricted three body problem of asteroid orbital motion in solar and Jupiter field in three dimensional space 04 p0656 A71-15734

Existence of Lagrangian and Eulerian solutions of generalized three body problem, discussing applications 04 p0660 A71-15888

General elliptic three body problem, discussing triangular Lagrangian point stability 05 p0809 A71-16472

Canonical linear Hamiltonian systems normalization algorithm, applying to restricted three body problem 05 p0810 A71-16547

Particle nonlinear motion near equilateral libration points in restricted three body problem [AIAA PAPER 70-98] 05 p0810 A71-16553

Hard-sphere gas three-particle collision integrals, using binary collision expansion 05 p0785 A71-16704

Restricted three body problem, discussing secular variations equilibrium solutions stability 05 p0814 A71-17093

Libration points of generalized restricted three body problem, using Lagrangian solutions 06 p0976 A71-18450

Nanosecond laser produced lithium hydride spherical plasma expansion model, taking into account three body and radiative recombinations 06 p0938 A71-18457

Planetary diurnal rotation, discussing motion of small particle in solar and planet gravitational fields 07 p1201 A71-20437

Resonances stability and development in restricted three body problem with two degrees of freedom 07 p1202 A71-20514

Minor planets mean motions commensurability with Jupiter in restricted three body problem 07 p1202 A71-20515

Three body problem stability investigation, using Liapunov perturbation function 08 p1361 A71-21052

Media resistance effects on three body problem three dimensional periodic orbits, discussing implications to solar system formation from surrounding nebula 09 p1527 A71-23534

Restricted three body problem involving two spherical bodies and elongated artificial satellite, considering equations of motion and positions stability 10 p1667 A71-23830

Restricted three body problem with variable thrust particle motion in Newtonian field 10 p1672 A71-24337

Infinitesimal body motion near triangular points of elliptic restricted three body problem, dividing equations of motion into two independent components by transformation 10 p1679 A71-24930

Stability conditions of three body problem constant libration solutions by Routh, presenting geometrical interpretation for locus of mass centers 10 p1679 A71-24932

Libration points in generalized restricted three body problem, discussing Lagrangian solutions 12 p1955 A71-26600

Zero relative velocity surfaces in bounded circular three body problem in presence of magnetic dipole, deriving Jacobi integral 12 p1947 A71-26634

Generalization of restricted three body problem in formulation with principal gravitating body constituting flattened ellipsoid 12 p1964 A71-27177

Planar elliptic restricted three body problem, calculating variational equations separation with matrix approach 13 p2136 A71-28359

Equations of motion of infinitesimal particles attracted by Newtonian gravitation of two mutual revolving masses in circular orbits 13 p2101 A71-29114

Three body problem stability investigation, using Liapunov perturbation function 14 p2310 A71-30169

Three particle elastic scattering amplitudes calculation using local Yukawa potentials 14 p2277 A71-30862

Plane photogravitational restricted circular three body problem symmetrical periodic orbits closing on rotating plane after revolutions 15 p2483 A71-31340

Papers on mathematical methods in astrodynamics and celestial mechanics for earth-moon trajectories computation, satellite orbit determination and three body problem 16 p2630 A71-33056

Elliptic restricted three body problem, calculating fictitious retrograde Jovian satellites orbits in rotating-pulsating axes for sun-Jupiter case 16 p2633 A71-33337

Periodic surface concept application to restricted three body problem of dynamical systems through averaging method, presenting stability theorem 17 p2804 A71-34918

Bounded plane circular three body problem stability, analyzing Jacobi integral and canonical equations 17 p2807 A71-35496

Three dimensional bounded circular three body problem solution in form of Taylor power series of time and vicinity values for canonical elliptical elements 17 p2807 A71-35497

Bounded circular three body problem stability, deriving Jacobi integral and canonical equations with Poincare variables 17 p2807 A71-35498

Periodic orbits around Lagrange libration points of restricted three body problem disturbed by gravitational and radiative influences 17 p2809 A71-35599

Planetary capture in restricted three body problem and bridge formation between galaxies 20 p3286 A71-38761

Excising neighborhood of singularity from manifold with vector field definition, making possible regularization of two and three body problems 20 p3254 A71-38900

Satellite capture by Jupiter, calculating satellite orbits based on aphelion and perihelion conditions derived from planetary elliptical orbit three body problem 20 p3287 A71-38978

Liapunov stability of rigorous particular solutions /corresponding to libration points/ of three body problem, determining motions of satellite influenced by two spherical bodies 20 p3291 A71-39315

Mass changes in restricted quasi-circular variable mass three body problem with particle equations of motion having Jacobi integral 20 p3291 A71-39320

Existence theorem of quasi-periodic solutions with two degrees of freedom for planar three body problem 21 p3441 A71-40093

Two dimensional elliptic restricted three body problem, considering regularization mechanism and periodic collision orbits 21 p3441 A71-40095

Numerical power series integration of differential equations of special three body problem with truncation errors elimination to fifth order 21 p3450 A71-40654

Three body problem involving large mass ratio by backward numerical integration in constant density resisting medium 22 p3601 A71-42164

Plane photogravitational restricted circular three body problem symmetrical periodic orbits closing on rotating plane after revolutions 22 p3606 A71-42615

Topological characterization for constant angular momenta and energy surfaces in equal mass planar three body problem 22 p3568 A71-42697

Energy transfer between in-plane and out-of-plane motions in L4 neighborhood for restricted three body problem [AAS PAPER 71-313] 23 p3725 A71-42989

Out-of-plane motion about libration points within framework of elliptic restricted three body problem, using Mathieu and Hill equation 23 p3727 A71-43009

Earth-moon and other trajectories calculation in planar elliptic restricted three body problem by slowly varying Jacobi function [AAS PAPER 71-381] 23 p3731 A71-43051

Three body problem of two heavy mass particles oscillatory motion in periodic orbits on straight line under Newtonian attraction 23 p3734 A71-43241

Bounded circular-space three body problem, obtaining Lagrangean solutions for triangular motion configuration stability 24 p3870 A71-44816

THREE DIMENSIONAL BOUNDARY LAYER

Axial turbomachine rotating blades, calculating three dimensional boundary layer thickness for laminar flow 01 p0069 A71-10337

Three dimensional numerical model of unstable planetary boundary layer integrated for convecting and turbulent region height, mean lateral shear and Reynolds flux direction 03 p0453 A71-13612

Three dimensional boundary layer with Pohlhausen velocity distribution, examining stability on yawing wing 05 p0736 A71-16850

Slender cone hypersonic laminar three dimensional boundary layer separation at angle of attack, proposing helical vortex model [AIAA PAPER 71-129] 06 p0845 A71-18573

Numerical integration of equations of three dimensional laminar boundary layer on spreading lines 07 p1087 A71-19182

Three dimensional laminar boundary layer on cone at incidence in supersonic flow evaluated by pressure distribution technique, comparing heat transfer, Pitot probe measurements, etc [AIAA PAPER 70-48] 09 p1381 A71-22088

Convective heat transfer in three dimensional stagnation point boundary layer flow characterized by real gas properties 10 p1698 A71-25098

Three dimensional turbine end wall boundary layer with shear term, using momentum integral analysis and cross flow velocity profiles [ASME PAPER 71-GT-6] 11 p1751 A71-25952

Three dimensional boundary layer flow and velocity profiles in mixed diffuser with equal angle walls [ASME PAPER 71-GT-40] 11 p1704 A71-25973

Three dimensional turbulent boundary layer calculations, using two dimensional method based on turbulent energy equation empirical conversion into shear stress transport equation 11 p1753 A71-26443

Equilibrium air boundary layer flows at three dimensional stagnation points, discussing flow characteristics and real gas heat transfer parameters [AIAA PAPER 70-809] 12 p1866 A71-27582

Hodograph models family for cross flow velocity component of three dimensional turbulent boundary layers, applying integral method to curved rectangular channels data [ASME PAPER 71-FE-1] 13 p2051 A71-29445

Finite difference scheme for calculating three dimensional incompressible turbulent boundary layer development on infinite yawed cylinder [ASME PAPER 71-FE-19] 13 p2052 A71-29457

Three dimensional boundary layers on axisymmetric bodies with large positive and negative crossflows, using finite difference method 17 p2727 A71-34875

Prandtl three dimensional boundary layer equations in orthogonal curvilinear coordinates, applying implicit finite difference scheme to solution 18 p2906 A71-36318

Compressible three dimensional nonsimilar laminar boundary layers numerical analysis using two layer heuristic model 18 p2845 A71-36336

THREE DIMENSIONAL COMPOSITES

General solution to three dimensional problem in elasticity theory for cylindrical transverse isotropic medium, applying results to thick walled shells stress-strain 02 p0329 A71-12563

Elastic stress-strain law and internal structure symmetry for three dimensional fibrous composites, including caltrop reinforcement 11 p1852 A71-26396

Phase velocity for three dimensional structures of impedance elements, using approximate solution methods and dispersion equation 14 p2194 A71-30080

THREE DIMENSIONAL FLOW

Poincare hydrodynamic analogy in celestial mechanics, relating differential equations for dynamic systems with two degrees of freedom and two and three dimensional flow 01 p0154 A71-10383

Three dimensional attached compressible laminar boundary layer on slender cones in hypersonic flight at high angles of attack derived by numerical integration 01 p0070 A71-10926

Steady three dimensional ideal dissociative gas flow along stream lines, examining velocity components, pressure gradients, density and mass fraction variable 02 p0239 A71-12124

Sound radiation from finite span airfoil in three dimensional turbulent flow, considering lift function effect 03 p0399 A71-13280

Three dimensional cascade flow, discussing potential flow, shear flow, flow disturbances and flow approximations for annular cascades 03 p0342 A71-13827

Three dimensional turbulent jet reattachment, investigating wall attachment distance with aspect and offset ratio and Reynolds number variations [ASME PAPER 70-WA/FLCS-5] 03 p0401 A71-14081

Three dimensional nonboundary layer laminar radially inward incompressible Newtonian fluid flow between corotating disks, using integral method [ASME PAPER 70-WA/FE-4] 03 p0402 A71-14126

Flows on 3-manifolds near isolated invariant sets 04 p0620 A71-15727

Three dimensional inviscid compressible flow past sharp shouldered blunt bodies at angle of attack, presenting time dependent finite difference technique [AIAA PAPER 71-56] 06 p0843 A71-18515

Three dimensional transonic shear flow structure in turbomachine cascade, using time dependent numerical solution [AIAA PAPER 71-83] 06 p0843 A71-18540

Three dimensional inviscid supersonic flow fields with primary and embedded shock and expansion waves determined over and behind wings and wing-body configurations [AIAA PAPER 71-99] 06 p0844 A71-18554

Jet engine contribution to lift at supersonic flight velocities via air mass heating, studying three dimensional flow with heat supply and stream deflection 07 p1014 A71-19746

Three dimensional axisymmetric flows in tornado-like vortex boundary layer, determining nonlinear radial and vertical velocity distribution components 07 p1152 A71-19753

Two and three dimensional thermals and steady and starting plumes convective fluid motion formulas, using vorticity integration method 07 p1104 A71-20223

Aerodynamic characteristics of conical and pyramidal configurations with various planforms by slender body theory, replacing three dimensional flow by two dimensional flow 08 p1227 A71-20776

Three dimensional nonlinear heat conduction problem solving by perturbation theory and finite integral transform 08 p1377 A71-21927

Three dimensional end effects on MHD flow in rectangular channel with nonconducting walls 09 p1499 A71-22133

Incompressible viscous fluid nonsteady three dimensional flow, obtaining velocity field and pressure distribution in boundary layer 09 p1433 A71-23092

Conditional instability of second kind /CISK/ in three dimensional quasi-geostrophic low latitude flow, examining Yamasaki model 09 p1490 A71-23561

Axial turbomachine three dimensional cascade flow calculation from dynamics vector equations 09 p1383 A71-23601

Three dimensional unsteady irrotational flow in variable cross section duct, reducing Navier-Stokes equation to Euler equation 10 p1591 A71-23850

Underexpanded transverse sonic jet-hypersonic stream three dimensional flowfield based on inviscid rotational flow model 11 p1701 A71-25472

Asymmetric three dimensional aerodynamic density fields from holographic interferograms, applying to supersonic flow from free jet 11 p1762 A71-25802

Steady three dimensional subsonic nonviscous flow through turbomachine with arbitrary hub and shroud shapes and finite blade number, using iterative blade to blade procedure [ASME PAPER 71-GT-2] 11 p1702 A71-25948

Nonstationary three dimensional weakly ionized incompressible viscous gas plasma flow in homopolar device, noting effects on ionization-diffusion balance 12 p1935 A71-26753

Three dimensional MHD flows with strong transverse magnetic fields variable area rectangular ducts with conducting sides 12 p1938 A71-27216

Three dimensional jet flapped wing matched asymptotic expansion solution for high aspect ratios based on thin airfoil theory assuming inviscid and incompressible flow 12 p1863 A71-27217

Three dimensional incompressible flow about slender foil in perfect fluid, stressing vortex field effect 12 p1865 A71-27477

Three dimensional steady separated liquid and gas flows past low aspect ratio bodies, deriving similarity laws for reduction to two dimensional problem 13 p2049 A71-29169

Numerical study of three dimensional structure and energetics of unstable disturbances in pure baroclinic and barotropic zonal currents, using eigenvalue technique 14 p2269 A71-29949

Three dimensional spatial unsteady hypersonic gas flow about bodies behind strong shock wave front 14 p2169 A71-30182

MHD three dimensional flow between rotating and stationary disks in transverse magnetic field with uniform suction at stationary disk 14 p2283 A71-30839

Discrete tone noise generation by high speed fans and compressor blades, using McCune analysis for linearized three dimensional compressible flow in finite annulus [AIAA PAPER 71-617] 15 p2468 A71-31555

MHD rectilinear two dimensional flows at high Hartmann number, including extension to three dimensional problems 15 p2459 A71-32560

Perfect incompressible fluid steady rotational linearized three dimensional flows, calculating complex waves system 16 p2560 A71-34056

Three dimensional nonlinear heat conduction problem solving by perturbation theory and finite integral transformation method 17 p2838 A71-35271

Weak shock propagation in three dimensional unsteady flow, obtaining shock construction rule 17 p2729 A71-35423

Finite difference method application to three dimensional boundary layer calculation on sphere-segment surfaces in supersonic flow 17 p2672 A71-35632

Reynolds differential equations for three dimensional gas lubrication flows, noting linear velocity at rotating cylinder surface 17 p2749 A71-35639

Boundary velocity and temperature field of unsteady natural periodic convection over three dimensional obstacle for arbitrary Prandtl numbers 18 p2984 A71-35950

Hyperbolic and parabolic system three dimensional boundary layer equations, discussing characteristics and subcharacteristics roles in influence and dependence zones determination 18 p2902 A71-36039

Numerical integration of Euler equations for three dimensional time dependent unsteady flow by extension of method of characteristics 18 p2904 A71-36302

Second order accuracy and stability analysis of method of characteristics application to three dimensional steady supersonic flow 18 p2907 A71-36329

Three dimensional rotational gas flows, using Berker compatibility equations 19 p3045 A71-37795

French monograph on laminar boundary layer on circular cone at angle of incidence in supersonic stream, calculating separation from parabolic equations by numerical integration 19 p2994 A71-38647

Soviet book on unsteady motions of continuous media covering gas dynamics, thermodynamics, shock and plane detonation waves, three dimensional gas motions, etc 20 p3211 A71-39144

Complex three dimensional shock waves about space shuttle configuration, visualizing hypersonic nitrogen flow with electron beams 20 p3211 A71-39356

Perturbed problem of rotational steady compressible flow in three dimensional channel at upstream infinity/shear flow/, using linearization by current functions 20 p3211 A71-39419

Vortex flow through axial, axially radial and other three dimensional axisymmetric channels, using finite difference model for flow equations solution 20 p3211 A71-39465

Three dimensional nonlinear subsonic flow over finite wings of arbitrary planform, solving transonic small disturbance equation by integral method 20 p3177 A71-39568

Hot split-film anemometer sensors for three dimensional air velocity vector measurement 21 p3378 A71-40487

MHD flow stability under arbitrary three dimensional disturbances, considering energy estimate for interaction between magnetic field and velocity field at critical Reynolds number 21 p3422 A71-40676

Boundary layer disturbances influence on three dimensional hypersonic flow about infinite triangular flat plate, investigating pressure effects on heat transfer and friction coefficients 21 p3322 A71-40681

Quasi-steady three dimensional ideal compressible fluid flow between convex and concave sides of neighboring blade profiles in axial flow turbine 21 p3322 A71-40687

THREE DIMENSIONAL MOTION

German monograph on three dimensional steady hypersonic flow of perfect gas past pyramid shaped bodies of rhombic planform

21 p3323 A71-40774

Numerical model of three dimensional convection in atmosphere with vertical wind shear, solving system of differential equations

21 p3411 A71-41385

Inlet conditions for centrifugal compressor impeller covering pressure, temperature and velocity measurements on quasi-three dimensional model

22 p3480 A71-42035

Two dimensional and three dimensional wakes in supersonic and hypersonic rarefied gas wind tunnels, comparing cone and dihedron configurations

23 p3625 A71-43357

Potential two and three dimensional flows past body in presence of rigid wall, using matched asymptotic expansions

23 p3625 A71-43369

THREE DIMENSIONAL MOTION

NT THREE DIMENSIONAL FLOW

Continuous thrust spacecraft optimal trajectory regularization, obtaining differential equations for three dimensional motion

01 p0154 A71-10381

Weakly ionized gas discharge three dimensional unsteady motion of viscous incompressible gas discharge plasma in homopolar device curvilinear channel, emphasizing secondary overflow during acceleration

07 p1167 A71-19235

Three degree of freedom gas bearing for wind tunnel dynamic measurements, allowing models simultaneous spin, pitch and yaw motions

08 p1275 A71-22004

Flight path optimization with multiple time scales, discussing decoupling of high order three dimensional aircraft flight problem into several low order problems

10 p1556 A71-24858

Time independent three dimensional streaming secondary motion due to vibrating flexible plate

14 p2325 A71-30061

Thin circular disk rotating at constant angular velocity, solving three dimensional elasticity problem with formal power series of thickness-diameter ratio

18 p2978 A71-36260

Elastic circular plate with hole traversed by tube filled with viscous fluid, studying system motion

19 p3043 A71-37539

Stationary or moving objects spatial coordinates determination by three and four dimensional terrestrial photogrammetry, using phototheodolite stereophotographic pictures

23 p3671 A71-43590

THRESHOLD CURRENTS

Threshold currents of injection lasers with heterojunctions providing correction for optical thickness in terms of electromagnetic theory

01 p0094 A71-10779

TWT microwave amplifier parameters effect on power threshold for electron beam signal control loss

03 p0385 A71-13790

Emission threshold current in semiconductor heterojunction p-p-n laser

03 p0439 A71-13977

AlAs-GaAs heterojunction laser threshold currents and CW operation at room temperature as function of p- and n-type emitter regions

03 p0439 A71-13987

Quantum statistical analogy between laser threshold region and second order phase transition of ferromagnets

03 p0440 A71-14197

Semiconductor laser threshold current temperature dependence, considering maximum power gain and compensation techniques

06 p0908 A71-18424

Electric breakdown in supersonic Ar or air flow behind shock wave, determining threshold discharge currents

08 p1276 A71-21485

GaAs lasers p-n junction active region thickness from minority carrier mobility and spontaneous emission measurements in threshold current determination

09 p1460 A71-22305

Sensitivity threshold of optical heterodyne receiver as function of laser amplitude spectrum, using photodetector output noise

10 p1622 A71-24882

Ovonic systems involving electrothermal switching effects on semiconductor glasses, discussing threshold voltage characteristics as function of temperature distribution and glass thickness

12 p1944 A71-27638

Gunn diode operation at below threshold bias voltage, investigating microwave oscillations amplification

13 p2036 A71-27953

Low temperature space charge mechanism of threshold switching, using pulse measurements on thin layer multicomponent chalcogenide glasses

13 p2110 A71-28044

Threshold SNR for signal frequency meter based on zero number count method, determining reliability

14 p2194 A71-30088

Electrical breakdown of supersonic Ar and air stream behind shock wave, determining threshold discharge currents

14 p2227 A71-30672

Ions acceleration during current passage through plasma, discussing maximum energies, threshold current and electron beam flux density

17 p2787 A71-34284

Electrical medical apparatus with electrodes and intracardiac catheters, considering electric current danger threshold, electrocution hazards and safety precautions

17 p2693 A71-35486

Neutron irradiation effects on radiative, nonradiative and threshold currents in epitaxial GaAs laser diodes at room temperature

20 p3275 A71-38785

Semiconducting plasma carrier density gradient instability, investigating threshold curve for n-type germanium

21 p3434 A71-41330

Gunn diode operation at below threshold bias voltage, investigating microwave oscillations amplification

21 p3358 A71-41339

Temperature dependent threshold current density and doping gradient at p-n junction in epitaxial GaAs injection laser diodes

22 p3555 A71-41686

Indium gallium phosphide p-n junction laser operation at 4.2 and 77 K, considering threshold currents magnitude

23 p3687 A71-44138

Ion implantation technique utilization for reducing MOSFET devices threshold voltage and gate drain capacitance

24 p3808 A71-44725

THRESHOLD DETECTORS [DOSIMETERS]

Omnidirectional intensity of atmospheric gamma rays at balloon altitudes at various energy thresholds, noting integral spectrum flattening at lower energies

03 p0473 A71-13306

Neutron spectra measurement in epithermal energy range by activation of threshold and resonance foils, using expansion in orthonormal polynomials

04 p0594 A71-14915

Optimal radiant source power for photoelectric two axis autocollimation angle trackers, considering detector threshold sensitivity

19 p3067 A71-38659

THRESHOLD GATES

Low power nanosecond threshold logic gates for LSI multiplier

01 p0046 A71-10208

P-channel MOSFET tetrodes static and dynamic characteristics compared to conventional MOS triode, considering transfer and gate threshold voltage

02 p0229 A71-11811

Threshold logic gates, discussing inputting weighting and summing principle, applicability, IC approach and various logic designs

13 p2034 A71-28771

Room temperature ionic instability on p channel silicon gate MOS devices due to processing method, noting threshold voltage change

19 p3033 A71-38506

THRESHOLD LOGIC

Low power nanosecond threshold logic gates for LSI multiplier

01 p0046 A71-10208

Error correction coding/decoding techniques integration, discussing convolutional and block coding and Viterbi, Sequential and Threshold decoding algorithms

07 p1066 A71-20425

Chow parameters of switching functions in threshold logic, discussing basic properties and alternative definitions

13 p2035 A71-28975

Majority-logic decodable block codes construction by combining shorter length codes, obtaining correctable error bounds

20 p3201 A71-38873

Radar data video extractor adaptive threshold device synthesis criteria to quantize echoes for ensuring constant false alarm rate and target visibility

22 p3508 A71-41525

THRESHOLD SHIFT

U THRESHOLDS

THRESHOLDS

Dynamic FM demodulator with tracking filter for threshold extension

02 p0235 A71-12821

Pulsed laser threshold measurements in YAG activated by Ho, Er and Tm isotopes, noting temperature dependence

03 p0438 A71-13890

Impulse-noise human ear damage-risk criterion correction factor for single impulse, studying temporary threshold shift

05 p0712 A71-16284

Threshold and power relations for optical radars in pure and turbid atmospheres, determining visibility range for object detection

13 p2027 A71-27856

Energy level threshold gradients for steady and unsteady lasing in four-level lasers, obtaining power output and pulse duration

13 p2077 A71-28155

THRESHOLDS [PERCEPTION]

Visual threshold dependence on retinal location for various colors under conditions of scotopic, mesopic and photopic adaptation

01 p0009 A71-10203

Cat retina ganglion cell /YCC-1/ threshold intensity, obeying reversed Weber law

01 p0009 A71-10203

Monochromatic light glare effect on human eye as function of wavelength, using visual threshold variation as criterion

01 p0016 A71-11388

Inner ear basilar membrane motions estimation for lower hearing threshold, using nonlinear model

02 p0201 A71-12471

Quantitative relation between temporary threshold shift and peripheral circulatory effects of sound, using finger pulse amplitude strain gauge

03 p0359 A71-13156

Peak diameter differences of sensitization by annular surrounds in subjects, concerning scotopic increment threshold and retinal illuminance

03 p0365 A71-14376

Human rotation perception, discussing man-carrying rotation device, angular acceleration threshold, etc

04 p0541 A71-14756

Suprathreshold vision retinal image contrast loss measurement, suggesting role of balance between optical unsharpness and neural oversharpness

04 p0540 A71-15833

Acoustic intensity and exposure time duration for threshold lesion in cat brain

05 p0712 A71-16283

Human skin analyzer excitability test, discussing threshold response

05 p0710 A71-16809

Nervous and muscular elements above threshold excitation on potential subthreshold stimulation background by electronic analog model

07 p1050 A71-20114

Nervous and muscular tissues excitability during subthreshold rhythmic stimulation, discussing mathematical model for compounding polarization induced electrotonic fluctuations

07 p1050 A71-20115

Retinal threshold along horizontal meridian for dark and light adapted eyes for stray light from small foveally fixated high luminance target

08 p1247 A71-21000

Human visual analyzer excitability shifts due to short duration point light stimuli

08 p1243 A71-21972

Foveal vision absolute thresholds for various duration light pulses and flash pairs at different separations

10 p1560 A71-23992

Ambient temperature effects on flicker fusion threshold, using constant stimuli and forced choice methods for determination of test subjects sensory sensitivity to heat and cold exposure

10 p1568 A71-24184

Cortical potentials evoked by weak acoustic signals below hearing threshold in man

10 p1564 A71-24440

Thresholds comparison for angular acceleration derived by subjective cupulometry and by staircase method, determining thresholds for rotation perception and oculogyral illusion

10 p1570 A71-24605

Peripheral visual resolution measurements, determining acuity thresholds at fovea and various points on temporal retina horizontal meridian over range of luminance values

10 p1564 A71-24608

Mean retinal threshold gradient along horizontal meridian for dark and light adapted eyes, considering dynamic neural mechanism

10 p1566 A71-24807

Visual suppression and intensity threshold changes during voluntary eye saccades with different luminance regions in visual field, discussing inhibition processes

11 p1718 A71-25583

Two flash threshold measurement of comparison stimulus duration of Bloch law for anticollision strobe lights

11 p1725 A71-26116

Dark adapted albino rats behavioral assessment, measuring absolute visual thresholds to white and colored light

13 p2008 A71-28457

Vertical translational acceleration perception threshold of aircraft pilot seated in upright position

14 p2188 A71-29780

Fly *Lucilia sericata* olfactory receptor and unit action potentials response to odor stimulation by homologous compounds

14 p2186 A71-30569

Gundefender earplug evaluation tests, using temporary threshold shift reduction and modified rhyme

Techniques for speech intelligibility measurement in noise 15 p2364 A71-32196

Beta inflection in darkness adaptation curve, postulating stimulus thresholds in mono and binocular examinations for perception time and sensitivity 16 p2527 A71-32866

Spectral sensitivities of discrete slow potentials and threshold level nerve spikes in *Limulus* ommatidium as function of hyperpolarizing current 16 p2527 A71-32869

Anatomical load sensing method, determining torso strain thresholds by sensitivity tests [NASA PAPER 1823A] 17 p2689 A71-34539

Frequency and level dependent discrepancy between free field and pressure thresholds at low frequencies due to physiological noise produced under earcap 17 p2681 A71-34699

Human central fovea theoretical model for target stimuli threshold detection performance prediction 17 p2693 A71-35325

Young guinea pigs thermal adaptation tests at different temperatures and environmental conditions, observing threshold temperature shifting for shivering and heat polynea 18 p2858 A71-36863

Threshold electrical phosphene dependence on impulse duration and stimulation frequency in subjects adapted to darkness 19 p3002 A71-37444

Image visual observation in coherent diffuse illumination, discussing human eye angular resolution deterioration and depth vision threshold dependence on light characteristics 19 p3074 A71-38195

Increment thresholds for foveally viewed square and circular visual stimuli, suggesting availability of more than one spatial integration pattern 19 p3003 A71-38277

Readout systems light emitting numerals legibility, determining threshold values from response categorization into correct responses, misreadings and missed signals 21 p3376 A71-40125

Visual processes involved in flash perception, considering attention attraction at suprathreshold levels, unreliability at threshold levels and latency effects 22 p3497 A71-41477

Subjective brightness of flashing light stimulus within fovea as function of stimulus size, noting edge effects contribution at suprathreshold levels 22 p3497 A71-41478

Flash threshold perception in relation to flicker, showing flicker/flash sensitivity ratio constancy over large intensity level range 22 p3497 A71-41479

Absolute foveal thresholds as function of flashes pulse length and null period 22 p3497 A71-41480

Flashing lights effective intensity at threshold and suprathreshold levels, discussing Broca-Sulzer effect observance conditions 22 p3498 A71-41484

Flashing lights vision threshold systematic variations, using quadrant adaptometer for continuous tracking of sensitivity fluctuations 22 p3500 A71-41498

Visual information discernibility measurement for suprathreshold transfer in display to observer system, noting use for color contrast scaling and disturbance evaluation 22 p3547 A71-42504

Human auditory adaptation to medium intensity noise complex action under relative isolation and hypokinesia conditions from monaural hearing threshold measurement 24 p3799 A71-44400

Correlation coefficients between sensitivity thresholds of cupula-endolymphatic system to angular and Coriolis accelerations with human resistance to motion sickness 24 p3795 A71-44532

Polymer odor threshold determination for hygienic considerations in sealed/pressurized chamber construction, comparing static and dynamic methods 24 p3800 A71-44539

Increment threshold for monoptic and dichoptic vision, showing spatial and luminance effects 24 p3801 A71-44979

THROMBOSIS

Thrombosis and coronary heart disease - Conference, Porvoo, Finland, September 1969 02 p0199 A71-12413

Antithrombotic agent search, finding anticoagulants useful for Venous system 02 p0200 A71-12418

THROTTLING

Hydrodynamic forces on pistons in sharp-edged spool valves with double throttling gaps at Reynolds numbers from 60 to 240 09 p1434 A71-23664

High thrust throttleable monopropellant hydrazine catalytic reactors for planetary landing vehicles, considering engine designs, dynamic characteristics and response to commanded duty cycles [AIAA PAPER 71-705] 14 p2294 A71-30762

Throttleable bipropellant rocket engine, discussing cryogenic and space storable propellants and injection system optimization based on combustion mechanism photographic observation [AIAA PAPER 71-740] 14 p2296 A71-30783

THRUST

NT HIGH THRUST

NT JET THRUST

NT LOW THRUST

NT MICROTHRUST

NT RETROTHRUST

NT ROCKET THRUST

NT STATIC THRUST

NT VARIABLE THRUST

Aircraft propulsive thrust moment effect on phugoid motion, examining angle of attack and flight path variations with resulting instability 03 p0347 A71-13340

Maximum thrust plug nozzle design for fixed inlet geometry, using calculus of variations for optimum contour determination [AIAA PAPER 71-40] 06 p0946 A71-18501

Propulsion system and fuel regulator design effect on thrust change during air ejection for VTOL aircraft stabilization in hovering flight 10 p1659 A71-24753

THRUST AUGMENTATION

Irreversibility control in two gas flows mixture, discussing jet engines thrust increase by air-exhaust gases admixture 06 p0945 A71-18051

Book on aircraft gas turbine engine technology covering combustion chambers, exhaust systems, lubricating oils, thrust augmentation, inlet ducts and overhaul procedures 08 p1348 A71-21625

Turbopropulsion systems thrust augmentor combustion instability, discussing physical causes due to various pressure oscillation modes [AIAA PAPER 71-697] 14 p2293 A71-30756

Turbojet and turbofan augmentors combustion instability, discussing pressure oscillations elimination by screech liner and flameholder design [AIAA PAPER 71-698] 14 p2294 A71-30757

Analytical model of oscillatory combustion in aircraft engine augmentors [AIAA PAPER 71-700] 15 p2466 A71-31324

Low area ratio ejectors internal flow phenomena synthesis, increasing thrust augmentation by mixing and diffusion [AIAA PAPER 71-576] 15 p2468 A71-31566

Turbojet engines thrust and fuel economy improvement by gas-air jet mixing, discussing efficiency increase and noise reduction 15 p2472 A71-32717

Optimal gas temperature in bypass and turbojet engines afterburners ensuring minimum fuel flow rate dependence on thrust augmentation 16 p2624 A71-33607

F 101 30,000 lb thrust augmented turbofan engine for B-1 bomber, considering maintainability and bird ingestion tolerance 19 p3122 A71-37491

Performance prediction and evaluation of propulsion-augmented high lift systems for STOL aircraft, considering weight, thrust and wing loading [AIAA PAPER 71-990] 24 p3791 A71-44585

THRUST BEARINGS

Externally pressurized gas thrust bearings, examining performance and pressure distribution in film 02 p0256 A71-12412

Finite wall conductance effect on performance /pressure and load capacity/ of MHD hydrostatic thrust bearings [ASME PAPER 70-LUB-1] 07 p1117 A71-19503

Thermohydrodynamic equations for viscous incompressible lubricant flow in hydrostatic thrust bearings, considering inertia and temperature effects 10 p1617 A71-24482

NaK lubricated segmented hydrodynamic fluid film tilting pad type journal bearings and Kingsbury type self aligning thrust bearings 15 p2447 A71-32210

Compliant surface fluid film thrust and journal bearing analysis, using coupled flow-elasticity model and load tests 17 p2747 A71-34192

Rotating inertia effects on step-type MHD hydrostatic thrust bearing characteristics, discussing disk shape and operating conditions for improvement 17 p2748 A71-34641

Book on lubrication systems selection, application, handling and maintenance covering journal and thrust bearings, nuclear reactors and machine tools 19 p3069 A71-37523

Quasi-static pressure characteristics of gas lubricated thrust bearing with shrouded Rayleigh step pads, solving nonlinear equation of motion [ASME PAPER 71-VIBR-75] 21 p3385 A71-40313

Automatic control theory application to pneumatic self vibration /hammer/ occurrence criteria derivation

for externally-pressurized gas-lubricated thrust collar bearings 22 p3551 A71-41660

Centrally-fed circular inherently-compensated aerostatic gas thrust bearing flow behavior in inlet region, obtaining graphs for design optimization 22 p3551 A71-41663

Spiral grooved thrust and spherical gas bearings, predicting stability and frequency response by Newton-Raphson and orthonormalization methods 22 p3551 A71-41668

Computerized step-jump and time-transient dynamic analysis application to gimbal mounted Rayleigh-step gas-lubricated thrust bearing design 22 p3552 A71-41672

Stiffness and load capacity control by self compensating flow restrictor for externally pressurized gas lubricated thrust bearing design 22 p3552 A71-41673

Plain externally pressurized thrust air bearings with porous inserts and high supply pressures, comparing with discrete orifice feed 22 p3553 A71-41679

Externally pressurized double thrust bearings with variable gas film laminar restrictor increasing stiffness at low eccentricity ratios 22 p3553 A71-41680

Optimal control of self excited vibration of high speed rotor with thrust magnetic bearing, using analog simulation 23 p3681 A71-43311

Pneumatic hammer /self oscillation/ occurrence in gas lubricated externally pressurized annular thrust bearing, comparing experimental and theoretical stability data 24 p3830 A71-44948

Radial thrust bearing balls ovality effect on axial vibration of rapidly rotating turbine engine rotor 24 p3864 A71-45006

THRUST CHAMBER PRESSURE

Rocket propulsion systems local heat transfer investigation, comparing experimental data to Bartz formula estimates over wide combustion chamber pressure range 12 p1945 A71-26983

THRUST CHAMBERS

Oxygen difluoride/diborane propellant thrust chamber and injector technology, discussing engine duty cycles and performance [AIAA PAPER 70-717] 07 p1183 A71-18890

Regeneratively cooled stainless steel thrust chamber failure related to internal carburization by fuel decomposition and propellant combustion 11 p1810 A71-25505

Cooling effectiveness of liquid film barrier injected into rocket thrust chamber with vortex motion, considering heat transfer and performance [AIAA PAPER 71-676] 14 p2291 A71-30740

Combustion instability with wave motion coupling in solid propellant rocket motors due to energy gain and loss mechanisms within chamber [AIAA PAPER 71-753] 14 p2296 A71-30787

THRUST CONTROL

NT THRUST VECTOR CONTROL

Electrohydraulic thrust control system for supersonic transport aircraft engines, considering reliability, performance and weight [SAE PAPER 700819] 01 p0143 A71-11546

Thrust-minus drag optimization by base bleed and/or boattailing, using computer program 01 p0004 A71-11589

Soviet book on maneuvering of spacecraft covering trajectory calculation, thrust control, translunar and interplanetary flights, atmospheric reentry, orbital rendezvous, optimal control, etc 02 p0321 A71-12725

Minimum propellant deterministic guidance law for bounded-thrust constant jet exhaust velocity spacecraft, using neighboring extremal theory [AIAA PAPER 71-118] 06 p0978 A71-18568

Satellite rendezvous programmed control with allowance for thrust limitation by free trajectories method, determining impulse duration, magnitude and time 09 p1531 A71-22571

Soviet book on aircraft flight with incomplete and asymmetrical thrust covering probabilistic characteristics, stability, landing and takeoff with partial engine failures, etc 10 p1554 A71-24013

Aircraft with automatic thrust controller, calculating transfer functions characterizing speed and attitude control modes 10 p1640 A71-24910

Closed form formula for plasma thrust from arc jets with self induced magnetic fields, predicting electrode erosion and entrainment 11 p1810 A71-25457

Optimal flight of material point in central field of forces subject to controlled small thrust 12 p1957 A71-26632

Thrust and flow rate control in choked convergent nozzles by potential vortex generation, verifying swirling nozzle flow analytical model 15 p2391 A71-32061

- Altitude, bank angle and thrust program for minimizing time required by supersonic aircraft to turn through specified heading angle and reach required energy [AIAA PAPER 71-796] 16 p2525 A71-34021
- On-line radar tracking of six orbital elements of thrust maneuvering spacecraft, obtaining discrete nonlinear measurement and dynamical equations [AIAA PAPER 71-902] 19 p3095 A71-37153
- Jet engines with afterburners, describing exhaust nozzle control, takeoff and landing advantages and thrust variations 21 p3437 A71-40858
- Minimum propellant guidance laws comparison for impulsive and bounded thrust spacecraft, considering jump and controllability conditions for one burn trajectory 22 p3611 A71-42025
- Valentine technique difficulty in testing stationary solution for control optimality, discussing overcoming method for problem of sounding rocket thrust control in vacuo 23 p3773 A71-43856

THRUST LOADS

- Circular shallow prestressed arches with fixed ends, considering initial thrust effect on snap buckling 03 p0505 A71-13545

THRUST MEASUREMENT

- Thrustmeter for direct in-flight measurement of aircraft engine jet thrust 03 p0422 A71-13332
- Instantaneous aerodynamic force measurements and flow visualization on flapping wing, showing increase of thrust force mean value over maximum steady state value 10 p1550 A71-24362
- Thrust measurement of aircraft and rocket propulsion systems, comparing cost and characteristics of mechanical, electrical and hydraulic systems 12 p1894 A71-26991
- ONERA test facility for thrust measurement, describing test bed installation and operation and procedure for calculating thrust coefficients 12 p1945 A71-27472
- Thrust measurement of aircraft propulsion systems, considering hydraulic piston device, edge clearance, oil quantity and calibration 14 p2251 A71-29860
- Aircraft engine in-flight thrust determination, discussing indirect and direct measurement methods [DFVLR-SONDDR-119] 15 p2350 A71-32720
- Direct thrust measurement on electrostatic ion engine ESKA 18 P, comparing with values calculated from applied voltage and ionic current [DGLR-71-043] 17 p2793 A71-35538
- Pulsed plasma rail mercury propellant thruster for satellite attitude control, measuring thrust and exhaust velocity with balance and Langmuir probe respectively 18 p2956 A71-36243

THRUST POWER

U THRUST

THRUST PROGRAMMING

- Krylov-Bogoliubov averaging method in optimal satellite motion programming of transfer orbit and low thrust correction 10 p1587 A71-24843
- Optimal thrust programming for rocket near spherical planet, transfer between circular orbits and lunar landing at predicted point 10 p1683 A71-24847
- Propulsive lift augmentation for horizontal landing of low and medium L/D reentry vehicles, determining optimum thrust program 22 p3612 A71-42046

THRUST TERMINATION

- Depressurization extinguishment of composite solid propellants for thrust termination, considering flame structure, surface characteristics and restart capability [DFVLR-SONDDR-129] 13 p2113 A71-28615

THRUST VECTOR CONTROL

- Thrust vector control system of reduced impact dispersion of Skylark sounding rocket [AIAA PAPER 70-1375] 03 p0497 A71-13658
- Jet deviation by secondary gas injection, predicting lateral thrust performance 04 p0525 A71-14793
- Spacecraft launch trajectory optimization, combining thrust vector, inclination constraints and final adjustment parameters 07 p1207 A71-19529
- Lift/cruise engine design and thrust vector control influence on VTOL transport aircraft transition characteristics and ground acoustic field [DGLR-70-040] 10 p1556 A71-24749
- Beam vector control from ion bombardment thrusters with dual grid electrostatic, movable screen electrode and discharge chamber extraction systems [AIAA PAPER 71-691] 14 p2293 A71-30751
- Auxiliary propulsion system using low power MPD thrusters, discussing feasibility of thrust vectoring with skewed magnetic coil arrangement [AIAA PAPER 71-695] 14 p2293 A71-30754
- Two dimensional sonic nonreacting gaseous secondary injection into supersonic primary stream with turbulent boundary layer for application to thrust vector control [AIAA PAPER 71-750] 14 p2227 A71-30786
- Optimal trajectory analysis for constant thrust optimal-coast minimum propellant control of rocket powered space vehicle 15 p2488 A71-32091
- V/STOL aircraft with vectored thrust propulsion systems, noting weight and center of gravity-lift-thrust relationship changes effect on performance [SAWE PAPER 894] 17 p2676 A71-35817
- Jet tab thrust vector control system for tactical missile applications, describing operational principles, design details and performance characteristics [AIAA PAPER 71-752] 18 p2956 A71-36773
- Viking vehicle structural flexibility and propellant sloshing effects on thrust vector control dynamics, obtaining computer simulated responses for hybrid and discrete coordinate models [AAS PAPER 71-348] 23 p3773 A71-43021

THRUST-WEIGHT RATIO

- Aircraft propulsion, discussing piston, turbojet, turboprop and turboprop engines in terms of thrust to weight ratio, specific fuel consumption and propulsive efficiency 04 p0638 A71-14977
- Low modulus solid propellants family for low thrust-to-mass ratio fully case bonded end-burning motors, using polymer network theory for binder formulation [AIAA PAPER 71-654] 14 p2285 A71-30729
- Gas generator with high thrust-weight ratio, discussing thermodynamic cycles, mass flow rates and combustion chamber 15 p2471 A71-32571

THRUSTORS

U ROCKET ENGINES

THUNDERSTORMS

- Convective thunderstorm propagation from Doppler radar velocities at leading edges 01 p0117 A71-10571
- Severe thunderstorm warning by single pulse Doppler radar plan shear indicator 01 p0117 A71-10572
- Wind flow patterns in severe thunderstorms structures, using Doppler radar 01 p0117 A71-10573
- Traffic radar generated weather contours for air traffic controller in helping aircraft avoid thunderstorms 01 p0118 A71-10587
- Anticyclonic eddy formation and emergence within severe thunderstorm observed by radar and surface data, noting wave development along pseudocold front 01 p0118 A71-10588
- Thunderstorms anvil cloud high level outflow mapping by Doppler radar at various heights and elevation angles 05 p0721 A71-16669
- Polarization of thunderstorm IF electromagnetic noise, taking into account earth electrical conductivity under detector 07 p1063 A71-19758
- Roughrider F-100F aircraft flights in thunderstorms and Apollo 12 launch electric field measurements, comparing patterns and magnitudes of lightning strikes to vehicles 07 p1208 A71-19927
- Binomial distribution models for thunderstorm activity at Cape Kennedy 08 p1326 A71-21452
- Thunderstorms environment analysis from radar and aircraft scannings, determining cumulonimbus cloud air kinematic properties for three dimensional circulation model 09 p1488 A71-23252
- Power spectra and electrostatic mechanism of thunder from intercloud and cloud to ground lightning using analog and digital methods 09 p1489 A71-23444
- F2 region ionospheric disturbances association with severe thunderstorms from radio observations 09 p1490 A71-23559
- Radiation measurements near thunderstorms and tornadoes, testing hypothesis of meteoritic matter-antimatter annihilation mechanism for ball lightning 10 p1599 A71-23752
- Solar and lunar modulation of geophysical parameters, atmospheric electricity and thunderstorms in complex space-meteorology scope 10 p1604 A71-24706
- Tornado producing thunderstorms upper level outflow synoptic and dynamic processes from ATS 3 pictures, discussing convective warming effects 11 p1794 A71-25381
- VLF noise spectra in earth-ionosphere cavity due to thunderstorm discharges, noting resonance level splitting by geomagnetic field 13 p2030 A71-28542
- Solar flares effect on potential gradient and earth current characteristics, suggesting solar triggered increase in thunderstorm frequency 13 p2130 A71-29107

- Cosmic ray microvariations during thunderstorm perturbations, considering total ionizing, soft and hard components and local temperature effect 13 p2130 A71-29124

- Oklahoma and Malaysia thunderstorms comparison based on weather reconnaissance aircraft measurements, considering turbulence patches 14 p2266 A71-29752

- Thunderstorm gust fronts from Oklahoma surface mesonet and weather radar data, considering hazard to aircraft 14 p2267 A71-29751

- Thunderstorm, CAT, weather and mountain wave induced turbulence forecasting and analysis for transport aircraft 14 p2268 A71-29764

- Charge generating mechanism based on charge separation from falling precipitation particles effect on thunderstorm electrification 14 p2269 A71-29951

- Thunderstorms and lightning flashes location determination by ground based and satellite measurements of disturbance induced RF noise, using atmospheric spectral characteristics for range estimating methods 14 p2203 A71-30958

- Statistical method of thunderstorm forecasting, basing algorithm on mathematical techniques 15 p2443 A71-31225

- Nonadiabatic convection parameters calculation allowing for vertical wind shear, determining effect on thunderstorm maximum possible duration, gusts and precipitation quantity 15 p2444 A71-31361

- Lightning observation by OSO-E satellite, suggesting maximum thunderstorm incidence over North Atlantic Ocean 19 p3061 A71-38675

- Sporadic E layer ionization relation to thundersquall surface pressure disturbance, considering gravity wave propagation 23 p3670 A71-43322

- Thunderclouds and torrential clouds classification from radar data, developing algorithm model with Bayes method 24 p3845 A71-44884

THYMIDINE

- Tritiated thymidine effects on splenic lymphocytes regeneration, discussing DNA synthesis, cycle completion and resident populations 11 p1719 A71-26055

THYMINE

- Possible prebiotic synthesis of thymine by heating uracil, paraformaldehyde and hydrazine in ammoniacal solution for three days at 70 C 18 p2855 A71-36231

THYRATRONS

- High power hydrogen thyatron grid-anode structure without gradient grids, discussing design and performance tests 23 p3649 A71-42916

THYRISTORS

- Thyristor circuitry for AC controllers and single phase frequency converter 01 p0051 A71-10262
- Variable voltage and frequency thyristor inverter, describing series commutation power stage 03 p0352 A71-13047
- Thyristors junction area current rise time extension, discussing emitter field regional delay times as function of p-n-p-n structural properties 12 p1886 A71-26849
- Book on thyristor phase-controlled converters and cycloconverters covering operation, control and performance 13 p1998 A71-27941
- Thyristor power conditioning application to high voltage DC electric power system, presenting SST aircraft sample load profiles 17 p2678 A71-35770
- Reduced switch-off time high voltage p-n-p-n structures using diode blocking coincident with thyristor collector junction 23 p3716 A71-43483

THYROID GLAND

- Enzyme activity reduction in thyroid gland tissue of albino rats under deep hypothermia 01 p0012 A71-11057
- Cellular mitosis role in daily mitotic activity in albino rats intestinal crypts and thyroid gland 01 p0012 A71-11058
- K, Na, Ca and I electrolytes content in thyroid gland and blood during experimental hypothyroidism in rabbits 06 p0852 A71-17668
- Thyroidectomized vitamin A deficient rats, noting visual sensitivity loss not correlated to thyroid 13 p2008 A71-28455
- Diurnal variations of mitotic activity in thyroid epithelial cells of different follicle size 15 p2356 A71-31290
- Ascorbic acid reduction in organs due to thyroid hormones saturation under hypothermia 17 p2680 A71-34646

Thyroidectomy and cold adaptation effects on operating hamsters thermoregulation and heat transfer coefficient 18 p2860 A71-36881

Rat thyroid gland changes during acclimatization to simulated high altitude environments, observing high hormone stimulation 23 p3637 A71-44300

THYROXINE

Human kidney cell generation and life cycle parameters, considering thyroxine effects 07 p1041 A71-19594

Thyroxine effects on brain glutamine isoenzymes interaction and deamidation in mitochondrial fractions, comparing with sodium phosphate, bicarbonate and aspartate 21 p3338 A71-41069

A

Bending and torsional oscillations in rectangular specimens of femur and tibia, calculating elastic and shear moduli of compact bone tissues 13 p2019 A71-28658

Xe 133 elimination from anterior tibial muscles in dry and water immersed sitting subjects, discussing effects of air and oxygen breathing 13 p2022 A71-29358

TRAVELING **IONOSPHERIC**

DISTURBANCES

AL OSCILLATION

TIDES

ATMOSPHERIC TIDES

LUNAR TIDES

Earth tide and nutation correlation, examining internal structure 08 p1285 A71-21779

Earth rotation slowing, discussing observations of earth and lunar time variations and methods of computing tidal effects 10 p1603 A71-24691

Earth tide and nutation correlation, examining internal structure based on model with liquid center and solid inner core 15 p2401 A71-32684

Tidal analysis of sea surface elevations from satellite-borne altimeter as function of instrument errors and orbital determinations 22 p3536 A71-42549

Planetary tidal forces correlation with solar activity distribution, observing Ca flocculi spectrum 23 p3768 A71-43851

WELDING

GAS TUNGSTEN ARC WELDING

ATTITUDE (INCLINATION)

WING AIRCRAFT

XC-142 AIRCRAFT

VC 400 tilt wing VTOL cargo and passenger transport aircraft, discussing component and system development and testing phase 01 p0004 A71-10466

Hovering and low speed flight capabilities of tilt wing VTOL aircraft in terminal area under near-zero visibility instrument landing conditions 06 p0847 A71-18481

AIAA PAPER 71-7]

Automated low cost structural-mechanical design and optimization of wing pivot systems for variable geometry aircraft 12 p1980 A71-27410

AIAA PAPER 71-404]

Propeller blade structures for high speed tilt wing turboprop V/STOL aircraft, considering materials selection, weight control, cyclic pitch control, noise reduction, etc 15 p2350 A71-32785

DGLR-71-018]

Helicopter, tilt wing and jet lift hovering aircraft outflow measurements to determine suitability as rescue vehicles 24 p3791 A71-44586

AIAA PAPER 71-992]

LTD PROPELLERS

Flightworthy 25-foot diameter propotor wind tunnel test, considering civil and military need for VTOL transportation 14 p2177 A71-31077

[AHS PREPRINT 501]

LTING

U ATTITUDE (INCLINATION)

LTING ROTORS

Tilt-rotor VTOL aircraft design, discussing ground proximity effects on blade bending moments and flying qualities 04 p0531 A71-15404

Flightworthy 25-foot diameter propotor wind tunnel test, considering civil and military need for VTOL transportation 14 p2177 A71-31077

[AHS PREPRINT 501]

Tilt-fold-propotor VTOL aircraft stability and control, emphasizing pylon tilt and rotor stop-fold effects on flying qualities 19 p2998 A71-38652

IMBER IDENTIFICATION

Forested area landscape characteristics from remote sensed imagery, establishing base line information for vegetation mapping 09 p1438 A71-23209

Space photos for land use and forestry, considering IR color photographs from Apollo 9 flight 13 p2064 A71-29398

Satellite remote sensing for crops and timber identification/detection, surface moisture measurements, soil mapping, marine hazard evaluation, etc 17 p2730 A71-34245

Aerial color photography in forestry for species identification, reforestation areas development, watershed studies and land planning 17 p2737 A71-34272

Multispectral color aerial photography for identification of farm crops and tree species, using broadband camera filters 17 p2737 A71-34274

TIMBER INVENTORY

Airborne remote sensing application to agriculture and forestry for crop forecasting, soil mapping, insect infestation detection and range surveys 06 p0896 A71-18406

User requirements for Earth Resources Satellite data, considering information dissemination and forest inventory application 07 p1106 A71-18802

TIME

NT ACCESS TIME

NT BURNING TIME

NT EPHEMERIS TIME

NT FLIGHT TIME

NT MTBF

NT REACTION TIME

NT RELAXATION TIME

NT RESPONSE TIME [COMPUTERS]

NT TESTING TIME

NT TRANSIT TIME

NT UNIVERSAL TIME

Thermodynamic, electrodynamic and cosmological time asymmetry, discussing arrow-of-time concept as fundamental to physical space/time relationships 11 p1828 A71-25735

Cosmic evolution and thermodynamic irreversibility, discussing definitions and relationships of thermodynamic, historical and cosmological arrows of time 11 p1828 A71-25736

Time between noontime and evening maxima in F2 layer critical frequency compared with evening maximum period, showing dependence on noontime solar zenith angle 13 p2062 A71-28559

Reversible and irreversible processes and arrow of time concept, considering direct interaction of two charges without field 13 p2101 A71-28766

TIME CONSTANT

MOSFET transistors instabilities due to charge exchange near oxide-silicon interface states, determining energy levels distribution and time constants 05 p0791 A71-16165

Single loop automatic control system with lag, determining time constant and transfer functions critical values for real positive first and second derivative elements 06 p0879 A71-17520

Time constant for collateral ventilation in human, dog and pig lungs under various physiological conditions 06 p0856 A71-18385

Multicomponent exponential curves analysis by Post-Widder equation, providing continuous distribution function of time constants in inhomogeneous systems 12 p1870 A71-27129

Population II stars evolution models from main sequence to supergiant stage, constructing time constant loci in H-R diagram 16 p2635 A71-33432

Two dimensional linear communication system with crossed channels with different amplification factors and time constant, examining stability with root trajectory method 16 p2549 A71-33569

Time constant dependence of hybrid rocket combustion chamber on engine parameters and structure 16 p2625 A71-33619

Four phase reluctance motor design for electromagnetic torque variation, examining function of commutation frequency and phase time constants 17 p2677 A71-35710

Sweat and time constant response of human thermostat to linear gradient heat load, using analog computer experiment 18 p2859 A71-36874

Time constant for perspiration onset in humans exposed to stepwise increase in external heat load 18 p2862 A71-36897

TIME DELAY

U TIME LAG

TIME DEPENDENCE

Elastic boundary value problem of viscoelastic cylindrical body with temperature and time variations and relaxation kernel 01 p0169 A71-10492

Weather radar signals decorrelation times due to vertical wind shear and azimuth scanning 01 p0030 A71-10598

Hydromagnetic waves interaction with time dependent inhomogeneous background fluid, using Hamilton principle 01 p0136 A71-11475

Time, temperature and transformation curves for Ti alloy by dilatometry, hardness measurements, X rays and micrography, discussing martensite and beta-alpha transformations 01 p0105 A71-11620

Regular and stochastic oscillations in plasma beam discharge produced by beam instability from observing time dependent variations in spectral line luminescence intensities 02 p0288 A71-11634

Auroral absorption classification of cosmic noise at 32 MHz, plotting time and amplitude distribution diagrams 02 p0243 A71-11769

Explosion shock wave induced short wave radio emission, deriving time related gas ionization state of wave front 02 p0284 A71-11927

Venusian exospheric temperature local time dependence from heat conduction equation for instantaneous heating during Mariner 5 observation 02 p0304 A71-11971

Electron charge dependence on universe age, considering possible gravitational constant dependence on time 02 p0313 A71-12547

Rectangular parallelepiped and solid cylinder temperature distributions under time dependent ambient heating or cooling, solving thermal conductivity equation 02 p0333 A71-12647

Zn deposition on Zn single crystals in KOH solution, examining time and potential effects on deposit morphology 02 p0210 A71-12956

D region electron density time variations, using partial radio reflection technique during solar eclipse of 20 May 1966 03 p0407 A71-13379

Time dependent finite difference solutions of steady state nonequilibrium quasi-one dimensional nozzle flows 03 p0400 A71-13458

Polymer binder effect photoviscoelastic stress analysis near discontinuous reinforcing fibers, comparing results with finite element method for time dependence [SESA PAPER 1630] 03 p0507 A71-13755

Plane nonsteady gas dynamic flows, reducing to system of time dependent equations system, presenting Chaplygin equation generalization 03 p0401 A71-13908

Projectile entry into water vertically from air, predicting cavity shape as function of time based on hydraulic flow model [ASME PAPER 70-WA/FE-8] 03 p0402 A71-14129

Sonic boom wave pressure history prediction on arbitrarily oriented plane walls by explicit fixed mesh time dependent numerical method [ASME PAPER 70-WA/APM-9] 03 p0349 A71-14153

Homogeneous turbulence decay formulation using multipoint velocity correlations, initial time derivatives and time evolution 03 p0405 A71-14415

Integral relation between boundary conditions and aerodynamic loads on straight and inverted wings, using reversibility theory for arbitrary time dependences 03 p0345 A71-14566

Al-Zn-Mg alloys hardness and conductivity behavior as function of aging time and temperature 04 p0610 A71-14884

Laser radiation metal fracture, using pulsed X ray metallography and high speed photography for cavity depth and material ejection time dependences 04 p0608 A71-15116

Pulsar radiation intensity time variations at radio frequencies, noting observations of CP 1133 04 p0649 A71-15273

Numerical weather forecasting model using time dependent boundary values for restricting to acceptable error limits 04 p0622 A71-15676

Nonlinear time varying systems global and local controllability, deriving conditions related to linear systems controllability 04 p0561 A71-15867

Lagrangian methods yielding relativistically covariant formalism for wave packets in weakly inhomogeneous and time dependent plasma dynamics, obtaining motion equations from Euler-Lagrange equations 05 p0789 A71-16657

Geomagnetic field secular variation subdivision based on time effect, noting harmonic processes with 20 year period 05 p0745 A71-17191

TIME DEPENDENCE

Self-consistent polycrystalline model for combined stress state time dependent creep, examining flow potential existence 05 p0830 A71-17236

Polycrystalline Al alloys inelastic deformation under combined stress at elevated temperatures, observing time dependent behavior 05 p0830 A71-17237

Finite difference methods for time dependent Fokker-Planck equation conserving total system mass, energy and momentum 06 p0936 A71-17556

Continuous monotonic nonlinear controlled systems with time dependent, phase coordinates and nonnegative parameter disturbances, considering Chetaev estimate for restricted approximate solution 06 p0879 A71-17670

Time structure of auroral radio absorption from magnetically conjugate and closely spaced observations 06 p0892 A71-17977

Phenomenological one dimensional model of solar cosmic ray propagation for anisotropy and intensity as function of time during early phases of events 06 p0950 A71-18102

Particle flux energy spectra and time dependence of 25 February 1969 solar proton event 06 p0959 A71-18156

Cosmic ray multiple neutron intensities time variations measurements at Syowa Station [Antarctica], considering Forbush decrease, diurnal variations, solar protons and storm time increase 06 p0960 A71-18163

Inviscid mixed subsonic-supersonic gas flows with shocks, developing time dependent numerical method [AIAA PAPER 71-45] 06 p0883 A71-18506

Steady state mixed subsonic-supersonic flow near blunt leading edge in hypersonic internal flow, using asymptotic solution by time-dependent method [AIAA PAPER 71-85] 06 p0843 A71-18542

Monte Carlo technique for time domain response analysis of nonlinear structure in random pressure field with large deflection [AIAA PAPER 71-213] 06 p1004 A71-18649

Ti alloy embrittlement by prolonged high temperature exposure, using substandard fracture mechanics test for time-temperature dependence 06 p0915 A71-18686

Thermal contact resistance as function of time during static load 07 p1116 A71-18917

X irradiation induced currents across aluminum oxide films sandwiched between thin metal electrodes as function of voltage and time 07 p1174 A71-19056

Time-altitude diurnal variations in molecular and atomic oxygen concentrations at 65-200 km from continuity equations 07 p1099 A71-19391

Human work load assessments by time study of officers and physiologists, noting disagreeing values 07 p1047 A71-19466

Plasma frequency resonance time duration-local electron cyclotron frequency relationship by oblique echo model 07 p1168 A71-19681

On-off control system with crew motion caused random disturbing torques on spacecraft, determining waiting time, jet firing frequency and fuel consumption rate 07 p1208 A71-19885

Time linear increase of magnetic flux flow through superconducting Nb-Zr wall, inferring empirical critical current density model agreement with measured flow rate 07 p1179 A71-20156

Stiffened long cylinder with time variable thickness and strengthening thin shell system elastic displacements due to nonstationary vibrations and nonuniform pressure distribution 07 p1217 A71-20459

Heat resistant materials strength characteristics with long service periods, formulating equation for time dependence of rupture resistance 08 p1306 A71-21111

Test results extrapolation for heat resistant alloys long time strength using exponential relation between time to rupture and value for initial stress decrease 08 p1306 A71-21114

Pulsed discharge path in He at 100 atm and air atmosphere pressures, determining electrical conductivity dependence on discharge time by high speed photography 08 p1341 A71-21497

Atmospheric pressure pulsation time spectra on earth surface as function of stratification conditions 08 p1286 A71-21876

Exponentially decaying intensity averaging time and introscope inertia effect on image unsharpness during object uniform or harmonic motion 08 p1294 A71-21902

Unsteady scattering patterns analysis, determining atmospheric extinction coefficient by reflected light

oscillograms, formulas or signal amplitude time recording 09 p1487 A71-22385

Polarization of short period oscillations Pc_2 - Pc_4 dependence on time of day, oscillation type and geomagnetic field activity 09 p1436 A71-22449

Numerical solution of quasi-one dimensional viscous heat conducting compressible Laval nozzle flows by time dependent finite difference scheme 09 p1545 A71-22454

Soft electron fluxes spatial distribution and temporal variations in magnetosphere based on Elektron 2 charged particle trap data 09 p1513 A71-22573

Time dependent dispersion simulation by random number generator, introducing horizontal and vertical shear, buoyancy and anisotropic turbulence 09 p1488 A71-23027

Image restoration from random fluctuations, developing analog procedure from time dependent functions of spatial frequencies and approximation 09 p1407 A71-23048

Thick walled anisotropic nonhomogeneous elastic cylinder or plate under axial symmetric time dependent pressure, investigating transient response 09 p1540 A71-23087

Rapidly quenched CuAu ordered state development on low temperature annealing, presenting Young modulus variation as function of heat treatment time 09 p1477 A71-23350

Electromagnetic wave propagation in anisotropic ionospheric plasma with time-varying random electron density irregularities 09 p1506 A71-23586

Auroral zone electron energy spectra local time dependence from polar satellite observations 09 p1515 A71-23632

Gravitational instability of nonhomogeneous cosmological model, establishing density perturbation growth as function of time for model containing matter and radiation 10 p1667 A71-23851

Temperature stress distribution in infinite plate with time varying heat transfer coefficient 10 p1687 A71-24197

Thin isotropic plates with time and temperature dependent surface heat exchange coefficients, presenting heat conduction equations 10 p1695 A71-24361

Artificial satellite orbital velocity tangential component time variation from variational calculus direction law 10 p1674 A71-24441

Morphology, dynamics and time variations of auroral zone electron precipitation events from balloon measurements of bremsstrahlung X rays 10 p1662 A71-24535

Heat transfer in cylindrical cavity with circulating flow as function of time and Peclet number 10 p1696 A71-24615

One dimensional Gaussian electrostatic wave packet nonlinear time development due to weak resonant broad beam introduction into cold uniform plasma 10 p1652 A71-24658

Solar cycle time variations in trapped radiation belt proton flux, deriving proton transport equation from Boltzmann equation 10 p1663 A71-24785

Ionospheric dynamic behavior, describing time dependent continuity and ion, electron and neutral particle motion equations 10 p1606 A71-24914

Q switched ruby laser time dependent spectrum analysis by high speed camera with Fabry-Perot interferometer, noting holographic interferometry application 10 p1622 A71-24962

Fully ionized gas under electric and magnetic fields, calculating electron velocity distribution and runaway rate as function of time from Boltzmann equation 10 p1654 A71-24975

Inviscid model for flow field within plumes of two-dimensional underexpanded jets calculated by time dependent finite difference method 11 p1853 A71-25160

Linear discrete time stochastic system with unknown gain parameters, interpreting open loop feedback optimal control identifier and controller equations 11 p1741 A71-25361

Creep rupture data analysis model based on minimum commitment station function approach, generalizing hypothesized time temperature stress relation 11 p1848 A71-25561

Time dependence of atmospheric ionization at polar cap absorption event, obtaining relativistic and non-relativistic solar cosmic rays ionization equations 11 p1754 A71-25586

Angular, spectral and temporal properties of Cerenkov radiation in cosmic ray extensive air showers 11 p1815 A71-25594

Mean neutron monitor multiplicity time variations for solar cosmic ray events and Forbush decrease with modulation spectrum allowance 11 p1816 A71-25732

Coupled and uncoupled versions of Hartree-Fock theory, calculating atomic system linear response to external time dependent perturbation and Green function 11 p1802 A71-26029

Criticism of paper on synchrotron sources energy spectra formation, examining time dependent spectrum on boundary conditions 11 p1832 A71-26170

Hankle cascade effects on atomic lifetime reliability from collisional excitation experiments 11 p1803 A71-26171

Fracture mechanics and time dependent strength of elastic or viscoelastic solids adhesively jointed by polymeric bonding layer 11 p1851 A71-26301

Partly time invariant and periodically time varying gain equations based on Banach algebras spectral mapping theorem and higher order circle criteria 11 p1742 A71-26411

Short term frequency stability of precision oscillators and frequency generators, discussing conversion from frequency to time domain and among time domain measures 11 p1739 A71-26425

Time dependent variation of IR polarization of ethyl Carinae and VY Canis Majoris with separation of interstellar scattering by associated nebula 12 p1956 A71-26611

Nonstatic random isotropic medium geometrical optics, considering refractive index temporal fluctuations [ONERA-TP-970] 12 p1929 A71-26821

Time and space variable echo waves in electron plasma by wave packets interaction, considering spectral line width finiteness influence 12 p1937 A71-27039

Photography date effects on intensive study site airphoto interpretations, using color and color IR films 12 p1907 A71-27259

Hand/machine sanded surfaces moderate environment exposure time effects on adhesive bonding of glass fiber reinforced plastic joints 12 p1921 A71-27411

Diaphragm opening time influence on gas flow shock tubes 12 p1897 A71-27455

Temporal and spectral stimuli combinations effects on judged noisiness of aircraft sounds by college students 12 p1868 A71-27533

Crack extension criterion for time dependent spallation, correlating simple mechanistic model with Al alloys data 12 p1919 A71-27777

Unsteady one dimensional time-dependent diabatic gas flow equations reduced to single partial differential equation, deriving solutions for entropy distribution 13 p2158 A71-27821

Frequency vs time spectral shapes of magnetospheric VLF discrete emissions for field line and electron stream parameters 13 p2027 A71-27911

Sporadic E wind shear theory, discussing time variation in metallic ion content 13 p2055 A71-27921

Solid bodies crack development theory, emphasizing crack tip fine and hyperfine structures concept and time dependent effects 13 p2149 A71-28121

Crack kinematics for bodies with time dependent deformation and strength characteristics in brittle fracture, discussing tip region, crack models and energy equation 13 p2149 A71-28121

Geomagnetic field secular variation subdivision based on time effect, noting harmonic processes with 20 year period 13 p2059 A71-28241

Western frequency drift effects on spectrum time evolution azimuthal asymmetry in decreasing period geomagnetic pulsation intervals 13 p2060 A71-28261

Cavity cross sections deformation in heavy ideal liquid, deriving nonlinear system of equations for time dependence within framework of small perturbation theory 13 p2047 A71-28271

Sintering time effect on initial permeability of Ni-Fe-Cu-Mo alloy made by powder metallurgy 13 p2086 A71-28621

Control of distributed parameter systems, presenting analysis method using arbitrary set of space modes with time dependent coefficients 13 p2042 A71-28701

Time domain solution of coupling to two wire transmission line, determining coefficients by steady state measurements 13 p2001 A71-28801

- Combustion process in mixing zone of kerosene-air mixture and hot combustion products, deriving optimum time relation to characteristic temperature in burning region 13 p2163 A71-28964
- German monograph on time dependent gas temperature in decaying plasmas, using frequencies of standard acoustic wave stimulated by pulsed discharges in confined gases 13 p2110 A71-29423
- Computational technique for finding bang-bang time optimal controls of nonlinear time-varying systems with bounded control function inputs 14 p2219 A71-29699
- Time variable effect on synthetic wind speed and air temperature profiles based on sensible heat flux density and stress at surface layer 14 p2266 A71-29705
- Solar active region photospheric radial velocity field variations, using magnetograph in Fe I line 14 p2308 A71-29977
- Random ergodic process extremal behavior, determining mean time to reach original maximum or minimum 14 p2194 A71-30087
- Stable oscillation development time in phantatron oscillator, using linearization of nonlinear term 14 p2211 A71-30114
- Time dependent clearance changes effects on aerodynamic characteristics of sectorially grooved gas bearings, describing lift and drag coefficients calculation 14 p2252 A71-30227
- Time dependent problems involving parabolic and hyperbolic differential equations, discussing formulation for approximate solution by Galerkin methods 14 p2265 A71-30294
- Al-Li alloys precipitation characteristics and temperature-transformation curves after solution treatment, water quenching and aging 14 p2259 A71-30393
- Time dependence of signal emf induced in toroidal rotation precession magnetometer sensor with elliptical cross section 14 p2246 A71-30481
- General atmospheric circulation mean time distribution, kinetic energy, regional interactions and mathematical simulation 14 p2236 A71-30492
- Cosmic ray modulation by solar wind, developing model with time variations based on magnetic bending power 14 p2302 A71-30647
- Digital communication system frame synchronizer performance analysis, using mean time formula and state transition matrices 14 p2201 A71-30925
- Normal time average holography amplitude range extension by integration over vibration cycle fraction 15 p2404 A71-31270
- Time dependent partial differential equations solutions, considering hopscotch class algorithms, Galerkin type methods and finite difference schemes 15 p2441 A71-31352
- Optimization of linear tracking strategies, considering time dependence and translation invariant N point predictor 15 p2379 A71-31411
- Metals dynamic fracture model, discussing critical incubation time and temperature dependence 15 p2503 A71-31446
- Plasma jet electron temperature and distribution between pulsed coaxial electromagnetic accelerator exit section, studying time variation 15 p2454 A71-31490
- Propagation angle effect on time harmonic wave dispersion in periodically laminated medium, using two dimensional equations of elasticity [ASME PAPER 70-WA/APM-47] 15 p2506 A71-32010
- Time dependence of peak emission energy shift due to junction temperature rise in GaAs junction lasers operated with flat topped current pulse 15 p2420 A71-32027
- Nonequilibrium dissociating gas flow past blunt body using time dependent shock layer analysis 15 p2346 A71-32049
- Power and exponential time dependences of long term creep strength for wide stress range, assuming linear thermal resistance 15 p2433 A71-32228
- Electron charge dependence on universe age, considering possible gravitational constant dependence on time 15 p2494 A71-32503
- Type 3 solar emission bursts, investigating time profiles and quasi-oscillatory decay 15 p2480 A71-32750
- Continuous holographic recording of wave front temporal variations for nonstationary processes 15 p2413 A71-32788
- Polycrystalline graphite total creep time dependent effects based on mathematical model of nonlinear hereditary theory 16 p2600 A71-32799
- Shock wave reflection process model in magnetic fields, describing time development of interaction process 16 p2616 A71-32901
- Time dependent fracture and failure criteria for aluminum under stress pulse loading in uniaxial strain, using exploding foil spallation tests in air and vacuum 16 p2590 A71-32943
- Continuous systems stability analysis under parametric excitation, using time dependent Liapunov functional for frequency response 16 p2607 A71-32992
- Self gravitating time independent disk-like stellar system model, investigating mass and velocity distributions 16 p2630 A71-33054
- Weakly nonlinear single degree of freedom cubic system under simultaneous time varying force and parametric excitation, presenting resonance frequencies classification [ASME PAPER 71-APM-24] 16 p2655 A71-33205
- Synthesis method for combining individual part repair time distributions for maintainability prediction using computer 16 p2552 A71-33301
- Maintenance replacement sequence selection for minimizing equipment repair time, noting dependence on failure rate 16 p2552 A71-33310
- Complex systems with n independently failing subsystems, minimizing expected cost per unit usage by assigning replacement age 16 p2552 A71-33312
- Upper atmosphere density fluctuations associated with solar activity and local time values, using Cosmos 14 satellite drag data 16 p2564 A71-33666
- Thermospheric hydrogen density and temporal variations from Explorer 32 measurements, discussing dependence on exospheric temperature 16 p2565 A71-33731
- Upper atmospheric composition and density variations with latitude and local time, using OV3-6 satellite measurements 16 p2566 A71-33756
- Upper atmospheric neutral composition diurnal variations as function of altitude, local time and solar activity 16 p2570 A71-33829
- Atmospheric density variation response time measurement to geomagnetic activity by satellites-borne low-G accelerometer calibration system, considering atmospheric heating mechanism 16 p2571 A71-33839
- Fluid droplet collapse in two phase system gas flows, noting time dependence 16 p2663 A71-33893
- Time variations of magnetotail plasma sheet from electron energy spectral measurements on Vela satellites 16 p2629 A71-33945
- Temporal and spatial relations between impulsive Pi bursts near midnight at polar substorms onset and IPDP micropulsation events in afternoon-evening hours 16 p2573 A71-33952
- Short light pulse evolution from noise, considering time dependence of pulse duration and peak intensity 16 p2589 A71-34137
- Transfer function and temporal behavior interrelations for linear network, characterizing circuit delay and rise time by center of gravity and inertial moment of pulse response 16 p2550 A71-34139
- Time variation of electron density and temperature in pulsed lasers operating on nitrogen band transitions, using charged particle balance equation 17 p2751 A71-34382
- Quasar internal kinematics and fine structure rapid time variations from radio interferometry 17 p2799 A71-34502
- Time dependent bending of circular cross sectioned rod under constant load compression and creep 17 p2821 A71-34564
- Cosmological upper limit on gravitational constant time variation, extending Dicke theoretical bound to pressure filled cosmologies in flat space 17 p2801 A71-34651
- Electromagnetic wave propagation into time varying medium, considering boundary value transmission problems 17 p2701 A71-34760
- Impulsive time variation plane wave reflection from ionospheric sech squared electron density profile, comparing full wave and WKB solutions 17 p2701 A71-34769
- Two dimensional compressible turbulent boundary layer with time dependent mean velocity and density fields, deriving momentum and kinetic energy integral equations 17 p2727 A71-34876
- Numerical solution for two dimensional steady state fluid flow in square cavity by optimum time step formulation 17 p2728 A71-34880
- Velocity determination in hypersonic low density wind tunnel based on high energy electron beam produced nitrogen ions time of flight 17 p2670 A71-34887
- Time dependent corrections to one component monatomic systems equilibrium rate of reactions and temperature change, using moment method for integrating nonlinear Boltzmann equation 17 p2785 A71-34945
- Dynamic response as function of time of nonlinear nonautonomous second order control system to external disturbances, using moving phase plane method 17 p2721 A71-35135
- Time decrease of acoustically irradiated aerosol concentration involving coagulation processes 17 p2784 A71-35347
- Transversely excited carbon dioxide lasers gain measurements for linear and helical electrodes at various gas mixtures and pressures as function of time 17 p2754 A71-35404
- Time dependent multidimensional axisymmetric computations for extended extragalactic radio sources propagation into intergalactic media having different densities and temperatures 17 p2806 A71-35411
- Asteroids 457-Alleghania, 649-Josepha, 1038-Tuckia, 1161-Thessalia, 1162-Larissa and 1297-Quadea orbital elements and ephemerides, taking into account planetary perturbations 17 p2809 A71-35581
- Time dependent multiple backscattering of pulsed light for linearly polarized incident radiation 17 p2709 A71-35809
- Anharmonic effects in time dependent vibrational relaxation of diatomic molecules in rapidly expanding flows, considering N-CO-Ar mixtures 17 p2948 A71-35837
- Time resolution enhancement in laser photography, recording fast events with long pulse length laser without auxiliary shutters 18 p2914 A71-35851
- Local time dependence of auroral zone electron precipitation X ray events from balloon measurements of bremsstrahlung 18 p2911 A71-35894
- Dynamic properties of modulating and mixing nonlinear systems consisting of time dependent impedance controlled by pumping source 18 p2875 A71-35975
- Space time structure of acoustic waves propagating in cylindrical duct with weakly absorbing walls and axial inviscid time dependent fluid flow [ONERA-TP-965] 18 p2946 A71-36030
- Space-time correlation measurements in grid-generated isotropic turbulence, determining full- and narrow-band velocity signals Eulerian time correlation 18 p2902 A71-36035
- Impulsively started time-dependent rotational Couette flow stability analysis by initial value problem and quasi-steady approaches 18 p2902 A71-36038
- Nonlinear time varying systems digital integration simulation techniques by variational equations approach, discussing accuracy, execution time and limitations 18 p2884 A71-36141
- Timoshenko beam transverse vibration with time dependent boundary and normal loads, using Laplace transform method [ASME PAPER 71-APM-F] 18 p2977 A71-36253
- Numerical integration of Euler equations for three dimensional time dependent unsteady flow by extension of method of characteristics 18 p2904 A71-36302
- Numerical solution of time dependent incompressible flow differential transport equations including turbulence effects 18 p2905 A71-36312
- Time dependent calculation of mixed two dimensional or axisymmetric transonic flows in nozzle, writing equations of motion with transformed spatial variables 18 p2906 A71-36323
- Time dependent rotating laminar flow of viscous incompressible fluid in closed cylindrical container, presenting numerical solutions to Navier-Stokes equations 18 p2908 A71-36343
- Implicit continuous fluid Eulerian time dependent multidimensional fluid flows calculation at arbitrary Mach number based on finite difference approximation 18 p2908 A71-36345
- Frictionless hypersonic flow around body by time dependent numerical processes and method of characteristics 18 p2846 A71-36423
- Temperature distribution from line sources and sinks in infinite medium during finite time 18 p2986 A71-36594
- Balloon observations of solar protons on 29-30 September 1968 over Iceland with GM telescopes and scintillation detectors, considering energy spectrum and time behavior 18 p2958 A71-36744

Optimal control of linear time varying neutral system, solving differential equations set 19 p3037 A71-37238

Second approximation estimates of spatial-temporal signals parameters 19 p3015 A71-37260

Dissipative fluid motion, discussing approaches to analysis of real fluids time dependent complex flow equations 19 p3089 A71-37499

UV Cet and YZ CMi star flare activity data, noting Poisson distribution of time sequence 19 p3134 A71-37510

Stellar convective shell plane gas layer, noting time dependence of energy flux 19 p3134 A71-37514

Time-altitude diurnal variations in molecular and atomic oxygen concentrations at 65-200 km from continuity equations 19 p3053 A71-37815

Ergodic boundary in time evolution of two dimensional incompressible Navier-Stokes equations solution at large Reynolds numbers 19 p3045 A71-37841

Homogeneous collisionless plasma in external electric field, considering evolution in time of charged particles distribution functions 19 p3114 A71-37858

Ionospheric neutral composition variations as function of height, local time and solar activity 19 p3056 A71-38356

F 2 region electron density spatial and temporal distribution, investigating plasma vertical drift effects 19 p3058 A71-38384

Atmospheric pressure pulsation time spectra on earth surface as function of stratification conditions 19 p3060 A71-38469

Solar limb H alpha spicules spectrograms, noting oscillations and time intervals 19 p3147 A71-38665

Plasma sheath formation near absorbing wall, calculating electric potential and current variations in space and time 19 p3117 A71-38723

Horizontal cosmic ray muon component intensity measurement and time studies for solar and sidereal variations 20 p3277 A71-38839

Laser pulse heated target with thermal plasma production, obtaining target surface temperature as function of time and vaporization rate 20 p3242 A71-38845

Finite thickness infinite slab with radiation from time dependent source, solving nonhomogeneous boundary value problem for linear transport equation 20 p3269 A71-39079

Cygnus XR-1 X ray intensity fluctuations, discussing time scales and periodicities 20 p3278 A71-39111

Time variation of average values of magnetic field strength and size in solar polar regions, noting field element decrease before solar activity maximum 20 p3291 A71-39322

Gamma ray production by pulsar-emitted particles interaction with surrounding nebula matter, investigating radiation intensity time variation 20 p3279 A71-39325

One way UHF clock synchronization, using geostationary communication satellites with propagation delays calculated from orbital elements 20 p3239 A71-39460

Viscoelastic polar materials thermomechanical behavior, deriving stress tensor, couple stress tensor, entropy density and linear constitutive equations 20 p3309 A71-39562

Infinite elastic plate forcing by time varying radial pressure in circular hole at center 20 p3309 A71-39563

General relativistic time delay and moon-earth masses and Mars mass-ephemeris ratios from S-band range and Doppler tracking 20 p3296 A71-39623

Geopotential temporal variations from earth Baker-Nunn satellite observations 20 p3219 A71-39658

Upper atmospheric temperature and soft solar X-ray time scale fluctuation data, using satellite drag observations and statistical analysis 20 p3280 A71-39705

Electron flux time dependence, observing flare increases, Forbush decreases, counting rate changes and intensity variations 20 p3281 A71-39733

Speech intelligibility prediction in time varying aircraft noise based on test score relationship to articulation index for steady state noise 20 p3271 A71-39766

Dayglow and twilight emission data, discussing atomic excitation mechanisms, particle production rates, height profiles and temporal variations 20 p3227 A71-39835

Auroral conjugacy and time dependent geometry via all sky cameras and image orthicon TV onboard conjugate-flying aircraft 20 p3228 A71-39840

Auroral electrons temporal and spatial structure from ground based optical observations and rocket-borne electron detector measurements 20 p3228 A71-39849

Time dependent plasmopause motion after increase and decrease in magnetic activity based on analytical model of plasma flow 20 p3232 A71-39897

Thermospheric atomic hydrogen concentration temporal variations in situ measurement by Explorer 32 satellite 20 p3232 A71-39898

Crab Nebula pulsar radio properties, observing energy release due to increase in period, multipath propagation effects, intensity and time dependence 20 p3302 A71-39923

Lubricated friction of steel ball on commercial tempered aluminum plate as function of time 21 p3396 A71-40100

Interstellar medium time dependent model, investigating supernovae and hot stars UV ionization effects on ion production and heating and cloud formation 21 p3445 A71-40248

Young adult males split-period sleep regimes dependence on intervening wakefulness time interval, periods length and onset sidereal time 21 p3330 A71-40348

Airloads and moments changes of aircraft flying over trailing vortices, investigating time dependent aerodynamic forces 21 p3321 A71-40508

Stress relaxation in laminated Ti sheet at ambient temperature after vacuum tempering at 800 C, interpreting logarithmic time dependence by activated thermal sliding theory 21 p3399 A71-40527

Sonic booms loudness as function of peak overpressures and rise times, using semiempirical formulae 21 p3325 A71-40530

Rotating viscous fluid flow between concentric circular cylinders, predicting velocity field dependence on position and time during inner cylinder sudden stop 21 p3366 A71-40543

Transversally excited and atmospheric carbon dioxide laser, measuring time behavior of refraction index profile and lensing effects on resonator 21 p3392 A71-40547

Seyfert galaxy micron photometry measurements, determining IR radiation flux changes with time 21 p3449 A71-40611

Pulsed argon ion laser data, presenting excitation mechanisms and time resolved gain measurements 21 p3392 A71-40625

Time dependent analysis of swirling flow boundary layers in rotating container using modified Oseen method 21 p3367 A71-40639

Time periodic convection development in incompressible viscous fluid with distributed heat sources 21 p3475 A71-40689

Time-space description of steady and homogeneous turbulence in incompressible fluid flow 21 p3367 A71-40690

Time varying aircraft noise effect on speech intelligibility, discussing test for relation to articulation index 21 p3343 A71-40709

Incompressible flow hydrodynamic time dependent problems for moving walls and free surfaces, using Marker-Cell computing method 21 p3368 A71-40849

Liquid metal elevated temperature time dependent corrosion effects on immersed structural materials, discussing blocked two level factorial experiment design for multiply telescoping sequences 21 p3400 A71-40880

Penny shaped crack under time dependent impact wave loads, investigating transient response with integral transformations 21 p3468 A71-41002

Charged particles acceleration in homogeneous magnetic field varying periodically with time /Alfven magnetic pumping/ 21 p3424 A71-41117

Frequency and temperature variation with time in active region of pulsed GaAs laser diode, using Fabry-Perot interferometer 21 p3394 A71-41318

Time harmonic waves oblique propagation in periodically laminated composite, using coupled thermoelasticity theory for plane strain 21 p3613 A71-41433

Massive main sequence stars pulsation kinetics, examining amplitude growth, time scale ratios and evolutionary stabilization 21 p3596 A71-41447

Thermal conductivity determination of Ar at extremely high temperatures, using temporal development of thermal boundary layer at shock tube wall 21 p3619 A71-41523

Temporal frequency spectra for spherical wave propagating through atmospheric turbulence, using covariance functions and Taylor hypothesis 21 p3575 A71-41788

Spectral line intensity measurement errors due to electron-temperature fluctuations averaging in continuous plasma sources 22 p3581 A71-41741

Linear time-varying system state space representation determination based on scalar differential equation, considering advantages 22 p3566 A71-41811

GaAs lasers filamentary coupling, investigating various mode perturbations in temporal output 22 p3558 A71-42311

Probabilistic system observation at random times calculating Markov renewal processes optimal long-run control 22 p3527 A71-42611

Convective cloud dissipation after rainfall, calculating temporal behavior of temperature fields, water content, moisture and air motion rate 22 p3569 A71-42811

Equatorial F 2 region lattice model with curved field line geometry for plane stratified atmosphere and time dependent problem solution 23 p3667 A71-43137

Electron velocity distribution relaxation in time dependent weakly ionized plasma within electric field solving Boltzmann equation 23 p3708 A71-43151

Transient response of electroacoustic transducer arrays, computing time dependent velocities for prescribed electrical inputs 23 p3704 A71-43211

Time dependence of radial mechanical driving point impedance of Al cylindrical shell immersed in two anechoic tanks related to chemical reaction 23 p3662 A71-43215

Rocket and radio wave wind profiles from 60 km to E region near 53N, presenting partial reflections and zonal winds time cross section 23 p3700 A71-43343

Time dependent progress of vibrational rotational transitions in chemical laser using hydrogen-fluorine mixture investigated by oscillography with IKM-1 monochromator 23 p3684 A71-43405

Gas laser power gain time dependence on molecular rotational relaxation under light pulse excitation 23 p3684 A71-43415

Transient pressure measurement in plasma exhaust flow of 500 microsec duration, discussing discharge temporal behavior and cold gas pressure front existence 23 p3711 A71-43598

Lunar cosmogenic radionuclides production time and spatial dependence calculations, comparing Apollo 11 and 12 measurements 23 p3754 A71-43729

Nitrogen and neon cations number density time dependence during plasma decay in neon-nitrogen mixtures 23 p3711 A71-43881

Flicker adaptation effect on visual sensitivity to temporal fluctuations of light intensity 23 p3635 A71-43974

Duralumin fatigue process in air and corrosive medium, showing loading frequency and time dependence effects 23 p3692 A71-44027

Transverse mode locking by cylindrically symmetric laser, noting time varying spot size with spacing frequency 23 p3688 A71-44295

Electron motion in plasma under stochastic electric field, emphasizing distribution function dependence on velocity and time 24 p3853 A71-44510

Classical Poincare-von Zeipel canonical perturbation theory extension to adiabatically perturbed systems with slow dependence on time or dynamic variables 24 p3848 A71-44790

Vibrational systems stability in presence of time dependent random parametric disturbances, using frequency analysis methods 24 p3848 A71-44855

Perturbations generated by two dimensional supersonic channel flows with walls oscillating with harmonic time dependence and small pressure amplitude computed, using linearized method of characteristics 24 p3819 A71-44951

Laser radiation intensity modulation by time varying magnetic field 24 p3834 A71-45055

Seyfert galaxies optical polarization, investigating time and wavelength dependences by multicolor polarimetric and photometric observations 24 p3873 A71-45071

Minimal order linear time-invariant systems description by smallest possible number of parameters, deriving differential or difference equations based on input/output parameters [DFVLR-SONDDR-135] 24 p3816 A71-45121

TIME DISCRIMINATION

Optimal temporal and spatial temporal resolution for unknown parameter of interfering signal on white noise background 09 p1404 A71-22211

Signals temporal uncertainty and sensory modality influence on watchkeeping performance, discussing signal density effect on pulses duration increments detection

10 p1568 A71-24183

Human time estimation tests, describing methods of production, verbal estimation and production in randomized blocks of trials

10 p1562 A71-24207

Brief light flash duration discrimination, discussing magnitude and time between flashes

10 p1570 A71-24607

Human vision spatial and temporal resolution relationship, examining image contrast sensitivity and target size, viewing distance and luminance reduction effects

10 p1572 A71-25000

Time variation in phase transitions at output of arbitrary band limiting channel in differential phase modulation system, using calculation method

11 p1733 A71-26340

Alternating acceleration and increased ambient temperatures effects on time interval perception and muscular effort estimation

12 p1874 A71-27164

Spatio-temporal patterns in visual contrast sensitivity, noting exaggerated eye movements effects

13 p2018 A71-28462

Intramodal and crossmodal sensory transfer of visual and auditory temporal patterns in normal young adults

13 p2022 A71-29326

Spatial and temporal discrimination functions in vision, audition and touch, establishing and controlling stimuli by vibrators

14 p2188 A71-30252

Time duration judgment under visual stimulus, noting numerosity effects

18 p2863 A71-37018

Time sense modifications among human groups isolated in underground environment and deprived of timekeeping means, evaluating average individual behavior

22 p3500 A71-41577

Time resolved tropospheric scatter layers from simultaneous bistatic and monostatic radar detection

23 p3646 A71-44174

TIME DIVISION MULTIPLEXING

Physiological data telemetry link using time division multiplex method

01 p0024 A71-10981

Injection lasers as logic elements in optical communication systems with time division multiplexing, examining optimal switching and pulse duration reduction

02 p0259 A71-11875

Time division multiplexing methods for optical communications systems, considering error performance of digital formats used with mode-locked laser sources

02 p0214 A71-12021

Time division multiple access techniques for Defense Satellite Communications System

07 p1057 A71-18819

Computer controlled time division multiple access control system for U.S. Army Satellite Communications Agency, discussing tests and operational details

07 p1057 A71-18820

Time division multiple access/TDMA/ hardware for military communication satellite systems

07 p1057 A71-18821

DCS TDM/DCS TDMA synchronous operation, examining rate buffering, slaved clocks and constant feedback approaches

07 p1058 A71-18823

Digital transmission in Defense Communications System, discussing data requirements, converter and TDM involving terrestrial and satellite links

07 p1066 A71-20432

Space-DMA or space-TDMA techniques conserving spectrum and increasing communication satellite channel capacity, discussing spot beams and switchings

08 p1254 A71-21326

Multiuser satellite communications system transmission capacity, comparing time division with Walsh multiplexing

08 p1269 A71-21334

Satellite communication earth stations time division multiple access systems, discussing operational principles and configurations

12 p1895 A71-27000

Modular digital TDM switch for radially distributed clock synchronization, discussing design and control

13 p2034 A71-29318

Transmitter clock phase lock loop for PCM-TDMA satellite communication system, applying to control system design having time lag

13 p2034 A71-29392

Acquisition system consisting of positioning of local station burst signal in time slot for PCM-TDMA satellite communication system, discussing design and performance tests

13 p2034 A71-29393

German-French Symphony synchronous communication satellites, discussing frequency and time division multiple access subsystems characteristics

14 p2193 A71-29824

Digital FM techniques for combined time and frequency division multiplexing, improving telemetry sampling channel bandwidth utilization

14 p2193 A71-30020

Computer communication asynchronous time division multiplexing, studying communication channel sharing, data buffering and demultiplexing design

14 p2201 A71-30929

Time division multiplexing system for ATS, discussing surveillance geostationary satellite feasibility, delta modulation for data transmission and aircraft equipment

17 p2772 A71-34680

PSK signals time division multiplexing and frequency multiplexed subcarrier systems equivalence and efficiency for digital communications

17 p2706 A71-35107

German TDMA system based on satellite repeater, discussing network configuration, transmission parameters, control, frame/burst format and field trial

18 p2875 A71-36050

Bit and scanning field synchronizations of time multiplex for air traffic control

18 p2946 A71-36513

Range and range rate measuring equipment for PCM-TDMA satellite communications system data feed and orbit observation

18 p2879 A71-36533

Multiple access to communication satellites by time division multiplexing

18 p2879 A71-36544

Pulse bursts phase regulation subassembly modules, noting use for time division multiple access system control

18 p2879 A71-36545

Quadruphase modem development in time division multiple access system

18 p2880 A71-36546

Internal commutation of telephonic channels with variable destination in time division multiple access system

18 p2880 A71-36547

Time division multiple access system with narrow beam coverage

18 p2880 A71-36548

Digital speech interpolation technique application to PCM-TDMA demand assignment system, noting traffic handling capacity and cost reduction

18 p2880 A71-36549

PSK modem for PCM-TDMA system, discussing performance tests on INTELSAT 3

18 p2880 A71-36551

Two spot beam switching without storage at satellite for time division multiple access system in satellite communication, giving switching algorithm

22 p3514 A71-42482

Common channel signaling system for demand assigned multiple access satellite communication, discussing design features and applications to PCM-TDMA

22 p3514 A71-42520

TIME FUNCTIONS

Time distribution of first passage through fixed level for nondecreasing whole number regeneration process with step trajectories

01 p0110 A71-10094

Time distribution of first passage through fixed level for regeneration vector Markov process with step trajectories

01 p0110 A71-10095

Compression shock wave development in compressible media, deriving wave amplitude/time relationship via velocity distribution approximation by discontinuous Mach wave series

01 p0069 A71-10122

Optimal piecewise constant control of continuous time systems with time varying delay, deriving restrictive condition on Hamiltonian integrated between switching instants

03 p0389 A71-14075

Discrete and analog electrical differentiators accuracy for input functions time derivatives determination, considering systematic errors and application suitability

04 p0599 A71-15567

Time interval maximum transmittable energy under spectral limitation, deriving time limited pulse functions for minimum energy loss

05 p0720 A71-16393

Multiple acoustic evoked responses coherence time course using mathematical correlation and Fourier transforms

05 p0714 A71-16922

Nonlinear fluctuation-dissipation thermodynamics with time-even and time-odd parameters concerning four index relations for nonquantum Markovian case

09 p1544 A71-22366

Image restoration from random fluctuations, developing analog procedure from time dependent functions of spatial frequencies and approximation

09 p1407 A71-23048

Reference stress parameters for structure creep behavior, using dimensionless stationary state, strain rate and time function

09 p1543 A71-23660

Flow with time harmonic function velocity in wind tunnel, controlling rate by sonic striction of varying cross section

10 p1552 A71-24454

Equivalence relationship between state space defined parameter and difference order of time-variable scalar differential equation

[DFVLR-SONDDR-79] 12 p1922 A71-27006

Simplified EEG time domain procedure, using method of period analytic estimates of power spectrum moments

15 p2364 A71-31960

PAM data transmission systems timing recovery, discussing maximum likelihood estimation method for timing parameter from random data

15 p2377 A71-32314

Lunar seismic energy diffusion, calculating transmitted and reflected acoustic wave intensities as time function after explosion

16 p2637 A71-33511

Temporal distribution of photons radiated by He-Ne laser operating in five modes

17 p2750 A71-34202

Orbital transfer time equation reformulation, discussing various orbit constraints accommodation and rapid convergence in rendezvous orbit iterative determination

[AAS PAPER 71-335] 23 p3727 A71-43008

Necessary and sufficient conditions for optimal control problems equivalence, considering time functions for disturbing influence of external forces

23 p3656 A71-43861

TIME LAG

Dwell time of semiMarkov system in given state with mixed Erlang and exponential distribution functions

01 p0110 A71-10096

Mechanical systems free motion, comparing effects of external and delayed action internal forces

01 p0155 A71-10446

Cauchy problem for nonlinear integrodifferential equations with time lag argument, estimating iterative solution existence and uniqueness

01 p0112 A71-10491

Liapunov stability of neutral first order nonlinear differential equations solutions with time lag

01 p0112 A71-10655

Turbulent jet noise estimation taking into account retarded time effect on acoustic radiation

01 p0072 A71-14688

Group delay measurements accuracy, using Nyquist method as function of FM and response characteristics of measured two-terminal pair network

03 p0386 A71-13814

Shape effect of compressed solid fuel on thermal ignition delay time in heated gas flow for pyroxyline

03 p0520 A71-13993

Linear integrodifferential time lag systems quick response problem approximate iterative solution, considering convergence and controllability conditions

03 p0452 A71-14060

First and second order lag system frequency response to pulse width modulated input signals [ASME PAPER 70-WA/AUT-8] 03 p0380 A71-14149

Beam-plasma mechanism of very long delayed radio echoes from ionosphere

03 p0381 A71-14552

Photoelectric recording devices for star passages, describing automatic compensation for signal delay instability

04 p0592 A71-14864

Time lag between actual and measured stellar transit times by photoelectric recording instruments, noting atmospheric, spectral and instrumental factors

04 p0598 A71-15378

Time lag between actual and measured stellar transit times based on photocurrent expansion into Fourier series

04 p0598 A71-15380

Stellar transit time photoelectric instruments time lag measurements by variable flux light source

04 p0599 A71-15382

Feedback control circuits with delay time, examining overshoot diagrams

05 p0730 A71-16127

Gravitational constant time variation based on planetary radar echo time delay in comparison with atomic time, discussing accuracy limits

05 p0807 A71-16227

Relativity and solar quadrupole moment effects in time delay measurements of signal traveling from earth to artificial satellites

05 p0808 A71-16446

Differential games with information lag, considering pursuit problems and capture conditions

05 p0782 A71-16980

Initial conditions selection for optimal control of systems with time lag

05 p0782 A71-16982

Noise stability during complex signals reception and lag measurement on fluctuating noise background

06 p0866 A71-17371

Invariant control system with optimum gain and time lag adjustment for compensating parameter changes under random disturbance

06 p0879 A71-17519

Optimal process control with various delay times, discussing maximum principle variant and calculus of variations

06 p0879 A71-17671

Cosmic rays transient north-south polar asymmetry, confirming time lag between Forbush decrease onsets

06 p0956 A71-18140

Solar flare delayed relativistic electron appearance, comparing radio, optical and X ray data for particle intensities

06 p0961 A71-18171

Delay time between beams reflected from different parts of meteor trail, using phase invariant and frequency scanning methods

06 p0869 A71-18263

Group delay times criterion of multibeam propagation of ionospheric radio echoes for communications systems

06 p0869 A71-18281

Saturn launch vehicle gust penetration loads, presenting separated flow and associated time lag effects

06 p1004 A71-18617

Linear delay input effects on analog cross correlator mean performance, plotting output SNR vs integration time

07 p1059 A71-18851

Ionospheric total electron content specification for satellite transponders time delay error reduction

07 p1095 A71-19002

Nonlinear control systems with transport lag, obtaining parameter plane equations for stability analysis

07 p1082 A71-20369

Experimental arrangement for delay times in propeller/rpm controller system

08 p1271 A71-20832

Closed loop systems with odd-symmetrical nonlinear components and distributed delay, calculating self oscillations

09 p1422 A71-22367

Soviet book on navigation and control covering data processing, optimal stochastic self guidance, instrument errors, mean energy consumption and stabilization loop time lag

09 p1491 A71-23163

Meteor trails distance determination by radar pulses reflection observation, estimating reflected signal delay dispersion and plotting mean square errors

10 p1576 A71-24037

Ignition delay times behind reflected shock wave of alkanes methane through pentane in stoichiometric argon simulated air mixture

10 p1657 A71-24047

Continuous identification algorithm for system containing two delays for signal represented by stationary random process with autocorrelation function approximation

10 p1585 A71-24160

Displaced and delayed retinal feedback adaptation theory for human factors problems in man machine systems

10 p1571 A71-24825

Riser whistlers observed at low latitude ground station, noting time delay increase with frequency

10 p1579 A71-25009

Compression, creep, stress relaxation and overload effects on delay in fatigue crack growth and structural life predictions

10 p1694 A71-25059

Time delay in pulsed optical carbon dioxide laser pumping mechanism in high current gaseous discharge

11 p1773 A71-25796

Linear continuous time delay feedback systems stability analysis, using root-locus and frequency response techniques

11 p1742 A71-26423

Rigid plastic media dynamic model, showing yielding time delay effect on residual deflection as function of load duration

12 p1982 A71-27515

Time optimal control system design with lag, determining phase coordinate prediction unit structure

13 p2041 A71-27944

Quarks search near extensive air shower cores, discussing apparatus and results for detection of long delayed particles

13 p2120 A71-28052

Muons arrival times distribution in extensive air showers, examining delay as function of particle production heights

13 p2126 A71-28095

Diffused fracture model as basis for plotting delayed fracture curves in space of principal stresses

13 p2149 A71-28119

Smith method for radio wave propagation time lag calculation, assessing maximum error by comparing calculated with measured distance/frequency characteristics

13 p2030 A71-28561

Time optimal systems with control lag, showing elimination of self oscillations

13 p2042 A71-28640

Optimality conditions for initial functions of time lag control systems onboard flight vehicles with transient response dependent on preceding trajectory coordinates

13 p2043 A71-28733

Neutral particle gas integral kinetic equations numerical solution without integration on lag parameter

13 p1991 A71-29157

Millimeter wave waveguide time delay distortion characteristics equalization using directional filter cascades

14 p2210 A71-29572

Aerospace pressure vessels delayed time failure, discussing flaws growth rate in context of linear elastic crack tip stress intensity factors

14 p2325 A71-29898

Visual sensation time theory validity investigation, discussing time elapsed between retinal receptor stimulation and perceptory sensation

14 p2189 A71-30406

Collector current delay and rise times in transistor common emitter configuration for linear, sine and exponential input signals

14 p2213 A71-30630

Sampled data delay-lock loop for tracking biphasic modulated pulsed-envelope RF signal arrival time

14 p2197 A71-30796

Atmospheric sources spectral amplitude ratios and group delay times correlation, obtaining VLF ionospheric propagation characteristics from single station observations

14 p2237 A71-30957

Group delay time differences in locating sources of atmospheric dependent on arrival azimuth, time of day and season

14 p2237 A71-30959

Liapunov stability of neutral first order nonlinear differential equations solutions with time lag

14 p2266 A71-30989

Ethane-oxygen-argon mixtures ignition behind reflected shock wave, deriving composition temperature dependences correlation

15 p2463 A71-31625

Transistorized long time delay relay for power supply circuits with constant function on reenergization after interruption

15 p2376 A71-32021

Active all-pass networks with shaped group-frequency delay characteristics, discussing design based on automatic synthesis

15 p2372 A71-32323

Photon dwell time in one dimensionally isotropically scattering medium, assuming absorbed state as arbitrary function of optical thickness

15 p2492 A71-32460

Pulsed output, delay time and rotational-vibrational transitions of high pressure transverse discharge CO laser

15 p2424 A71-32613

Individual liquid fuel droplets ignition factors, introducing heating-up and evaporation delay

15 p2516 A71-32709

Energy dependence of collisional time delay functions computed for H/IS/ atoms interacting via hydrogen potential, determining scattering cross sections

16 p2613 A71-32811

Electrical discharge plasmas, investigating electron multiplication, secondary processes, Paschen law, pressure effects and formation time lag

16 p2617 A71-32957

General relativistic time delay of electromagnetic radiation propagation due to solar gravitational field measured from Mariner 6 and 7 range and Doppler data

16 p2640 A71-33737

Linear single loop sampled data time delay feedback systems stability analysis

16 p2550 A71-34168

Time delayed systems periodic and quasi-periodic solutions

17 p2782 A71-34937

Perturbation free delay time measurement in digital data processing system, using Schmitt triggers or tunnel diode discriminators

18 p2885 A71-36225

Differential games with information lag, considering pursuit problems and capture conditions

18 p2948 A71-36780

Initial conditions selection for optimal control of systems with time lag

18 p2948 A71-36782

Perspiration delay times characterizing potohydrotic reflex, analyzing neurophysiological mechanism

18 p2861 A71-36885

Atmospheric rotation on Venus, examining Gierasch model based on radiative drive coupled with response time lags

18 p2967 A71-36930

Secondary visual tracking tasks utility in assessing lag effect in simulated combat aircraft dynamics

18 p2873 A71-36973

Human response to auditory stimuli start and cessation, noting time lag and perception duration

19 p3001 A71-37283

Ignition delays of propane-oxygen-argon mixtures in shock tubes from pressure and heat flux measurements in reflected region

19 p3169 A71-38106

Hypergolic rocket propellant system gas phase ignition, measuring ambient pressure, flow parameter and propellant temperature effects on delay characteristics

19 p3123 A71-38297

Controller design for linear closed loop system with transport delay, discussing simplified procedure with correction by zero-pole cluster outside bandpass

19 p3040 A71-38717

Auroral zone ionosphere time lag observations, noting delay in cosmic noise absorption pulsations to fast bremsstrahlung X rays, luminosity and micropulsations

20 p3215 A71-38740

Solar high energy cosmic ray proton burst observations, examining maximum flux delay time with Venus 6 satellite

20 p3281 A71-39734

ATC display device man-computer interaction faults and delays effects on operator performance

21 p3413 A71-40119

Bicarbonate requirement for elimination of lag period of chemoautotrophically grown *Hydrogenomonas eutropha*

21 p3329 A71-40213

Distributed RC network application as microelectronic delay line, discussing delay response improvement by compensating network

21 p3353 A71-40589

Emitted signal delay time effect on operational precision of semiconductor laser radar for measuring lower cloud boundary heights

21 p3394 A71-41239

Electrical breakdown initiation in high vacuum by electron beam, investigating discharge delay time dependence on beam parameters

21 p3420 A71-41292

X band Gunn diode oscillator pulsed operation starting delay time relationship to CW operation frequency/temperature characteristics, suggesting contact resistance role

21 p3359 A71-41411

Graph-analytical method of determining optimal adjustment of real differentiating units and components introduced into single loop automatic control system with time lag

22 p3525 A71-41440

Aircraft response to pilot or autopilot command during altitude control maneuver, calculating lag magnitudes

22 p3482 A71-41691

Hold time effects on plastic deformation and fracture in high temperature low cycle metal fatigue

22 p3561 A71-41942

Dynamic frequency and phase response of digital communications system of synchronized oscillators from time-incremental computer simulation

22 p3523 A71-42376

Human eye-tracking phase lags representation by time delays depending on target motion class

22 p3490 A71-42451

Sampled data control systems with pulse frequency modulation and time lag element, determining error response

22 p3527 A71-42493

Unsteady pressure gradient reduction effect on airfoil dynamic stall delay

22 p3481 A71-42841

Interplanetary time delay and light deflection measurements anomalies, investigating gravitational and electromagnetic fields interaction

23 p3766 A71-43824

Heliographic longitude effect on delay time between solar proton observation and flare occurrence from HEOS A1 data, noting magnetic field influence

23 p3768 A71-43852

Optimal control of time delay systems described by linear differential difference equations

23 p3658 A71-44087

Joint phase locked and delay tracking system dynamics for pseudorandom radio signal detection

23 p3646 A71-44267

Dual control theory for distributed systems with time lag described by partial differential equations, considering controller and algorithms synthesis

24 p3814 A71-44686

Transportation lag simulation by fluidic transmission lines and bubble tubes

24 p3793 A71-45086

TIME LAPSE PHOTOGRAPHY

U CHRONOPHOTOGRAPHY

TIME MEASUREMENT

NT CLOCK PARADOX

Pulsar pulse arrival times measurement for general relativity theory test, determining positions and period change rates

02 p0315 A71-12660

Pagcos 1 balloon satellite rotation observation over two years, determining period as time function

03 p0379 A71-14005

- Precision timing system implementation and operation, considering synchronization maintenance by flying cesium beam clocks, satellite, VLF and LF techniques
03 p0429 A71-14270
- Resonant self tuning narrow band amplifier, considering transient processes by time domain quantization for differential equations with constant coefficients
04 p0559 A71-15569
- Gravitational constant time variation based on planetary radar echo time delay in comparison with atomic time, discussing accuracy limits
05 p0807 A71-16227
- Physiological interaction between conscious and unconscious trace processes during time count by pairing acoustic, tactile, proprioceptive and photic stimuli
06 p0850 A71-17599
- Time judgment error as function of angular velocity during body rotation
07 p1043 A71-20216
- Navigational precision timing from earth rotation based pendulum to atomic second based quartz oscillator clocks
07 p1156 A71-20341
- Carbon dioxide laser molecular upper level vibrational relaxation time measurement
07 p1128 A71-20527
- Gas-liquid fluidic timing control device, discussing media combination, oscillator complete clock, bubble counter and pressure gages
07 p1031 A71-20605
- Optimal time determination for using radioactive isotope as radiation source in nondestructive testing
08 p1332 A71-21898
- Laser applications in physics research, discussing nonlinear optics and spectroscopy, time and distance measurements and Raman and Rayleigh light scattering
09 p1462 A71-22585
- Orbit transfer time of low thrust propulsion systems, assuming constant acceleration and thrust tangential to trajectory
10 p1670 A71-24273
- Planetary mass system as pulsar timing error sources, noting change in barycenter of solar system
10 p1675 A71-24493
- Earth rotation slowing, discussing observations of earth and lunar time variations and methods of computing tidal effects
10 p1603 A71-24691
- Atmospheric turbulence effects on sonic boom rise times by statistical theory
10 p1556 A71-24817
- Time unit definition by atomic clocks, taking into account relativistic effects
11 p1762 A71-25622
- Rat 24 hour clock inborn nature, discussing dependence on alternating light-dark periods for time measurement
13 p2010 A71-28801
- Crab pulsar optical time of arrival measurements from four observatories, discussing errors in data reduction to inertial reference frame
14 p2315 A71-30658
- VLF and LF time and frequency international comparison, noting diurnal shifts and SID constant magnitude ratio
14 p2204 A71-30972
- Microsecond time synchronization potential through cycle identification of VLF multiple frequency transmissions
14 p2204 A71-30974
- Aircraft flyby effective noise duration calculations, examining observation points and analysis methods
15 p2350 A71-32519
- Atomic clocks on manned space stations, discussing stability in aerospace environment, techniques for earth based timer calibration, reference device, maintenance and corrections
17 p2743 A71-35056
- Perturbation free delay time measurement in digital data processing system, using Schmitt triggers or tunnel diode discriminators
18 p2885 A71-36225
- Crab Nebula pulsar timing measurement leading to model involving inflation of closed magnetosphere with explosively released plasma
19 p3142 A71-38007
- Earth clock precision and rotation retardation effects on ephemeris time, comparing with atomic clock
19 p3060 A71-38529
- Pressure, time and attenuation measurements of high explosive driven air shock in steel pipe, comparing with numerical simulation
20 p3208 A71-38787
- Time-of-flight measurements for relationship between velocity, mass and temperature in molecular gas motion and electron-atom collision kinematics
20 p3271 A71-38789
- Temperature gradients measurements in transit instrument pavilion and errors in time determination for two year period
20 p3237 A71-39314
- Universal time and atomic clock earth rotation irregularities measurements checked for Chandler period
20 p3216 A71-39479
- Clock paradox problem resolution in relativity theory, considering space travel effects on time measurement and aging process
20 p3271 A71-39571
- Crab Nebula pulsar timing observations, correcting arrival times to solar system barycenter and dispersion effect
20 p3302 A71-39929
- Time arrival measurements of optical pulses from Crab Nebula pulsar correlated to solar system barycenter
20 p3303 A71-39931
- Timing measurements of pulsar NP 0527 relating frequency, position and transverse velocity with NP 0532, excluding origin in supernova explosion
20 p3303 A71-39936
- Stationary signal space topology concept in special relativity, considering points neighborhoods as independent of signal sending time
21 p3346 A71-40091
- Chronobiology purposes, techniques and applications, discussing rhythmic or cyclic variation calculation, biological rhythms spectra and classification and time structure alteration of organisms
21 p3329 A71-40149
- Ionized carbon monoxide in cometary tails, estimating time scale in recombination of ions into C and O atoms
21 p3442 A71-40155
- Longitude corrections in standard time service transfer from Greenwich to Herstmonceux, discussing precision requirements
21 p3443 A71-40163
- Stress and contact time calculation for impact of spheres on finite thickness elastic plate overlying rigid foundation
21 p3472 A71-41031
- Loran-C pulse hyperbolic navigation system application to time and frequency measurements, evaluating errors
22 p3570 A71-41524
- Cosmic ray sidereal time period, using neutron monitors, meson telescope and various ion chambers
23 p3719 A71-43126
- Unknown parameter identification in nonlinear dynamic systems from state variable time history measurement
23 p3660 A71-44114
- Tables of Crab Nebula pulsar radio pulse arrival times at Arecibo observatory
24 p3867 A71-44435
- Establishment time measurement for laminar separated flow, using shock tunnel driver section to give long test time at low incident Mach number
24 p3818 A71-44628
- Atomic time standards, discussing Cs 133, hydrogen maser, ammonia maser and rubidium gas cell equipment
24 p3827 A71-44994
- Time scale and time interval characteristics for scientific use, tabulating associated units
24 p3827 A71-44995
- ## TIME MEASURING INSTRUMENTS
- NT ATOMIC CLOCKS
- NT CHRONOMETERS
- NT CLOCKS
- NT TIMING DEVICES
- Mayer formula time determinations from meridian passage instrument, using star program and equalization observations
03 p0422 A71-13009
- Electronic time scale converters for frequency synthesizers
04 p0592 A71-14861
- McDonald Observatory lunar ranging station including telescope matching optics, guiding, timing equipment, pulsed ruby laser system and calibration procedures
16 p2553 A71-33780
- ## TIME OF FLIGHT SPECTROMETERS
- Carbon dioxide photodissociation in vacuum UV, using time-of-flight spectroscopy and metastable photofragment detection by electron emission from metal surfaces
14 p2190 A71-30571
- Mass and charge dependent ion discrimination in linear pulsed time of flight mass spectrometer, using electric field for source storage and count enhancement
18 p2922 A71-36590
- ## TIME OPTIMAL CONTROL
- Optimal control discrete time matrix Riccati equation, establishing convergence, uniqueness and stability properties
02 p0275 A71-11673
- ATA Collision Avoidance System based on time and frequency synchronization via ground stations or other aircraft
02 p0280 A71-12895
- Nonlinear control synthesis based on minimum duration of transient processes leading to system stabilization, using Pontryagin maximum principle
03 p0392 A71-14406
- Time optimal control for system described by linear differential equations, discussing two-step sequential synthesis
03 p0392 A71-14407
- Nonlinear time optimal off-on feedback control system synthesis, deriving algorithms
03 p0392 A71-14410
- Nonlinear stabilization systems time and energy optimal control syntheses using Pontryagin maximum principle
03 p0393 A71-14411
- Satellite time optimal attitude control, using gravity gradient technique with active libration damping
03 p0500 A71-14434
- Proportional navigation vs optimally evasive constant speed target in two dimensions, considering lateral acceleration and time constraints in pursuer control
03 p0455 A71-14438
- Single phase static inverter module with voltage waveform synthesis by time optimal response (bang-bang/ closed loop technique
04 p0535 A71-15287
- Bellman function for time optimal problem under Lipschitz condition
05 p0782 A71-16981
- Time optimal control of systems with magnitude and impulse limited constraints on control forces
05 p0782 A71-16983
- Interceptor missiles minimum flight time control, describing modified steepest descent algorithm for optimal trajectories [AIAA PAPER 71-19]
06 p0979 A71-18486
- Stratified statistical filtering algorithm for numerical simulation of nonlinear systems behavior
07 p1081 A71-18836
- Two body pursuit problem minimax and optimum absorption time control algorithm
07 p1082 A71-20642
- Time varying multivariable system transformation to phase variable canonical form
08 p1324 A71-21329
- Nonlinear plants time optimal control
09 p1422 A71-22122
- Adaptive time optimal control for inertial system with air jet attitude control
09 p1423 A71-22611
- Automatic generator for finite rectangular/isoparametric element stiffness and mass matrices, discussing memory requirements and computation time optimization
09 p1542 A71-23280
- Time optimal control for massive solids heating or cooling from initial into prescribed finite state with constraints
10 p1695 A71-24159
- Time optimal hierarchical failure-search systems by varying structure for four different search algorithms
10 p1585 A71-24161
- Optimal control law for regulating energy distribution of emitted radar signals in multichannel system for minimizing target search duration
10 p1579 A71-24722
- Bayesian modeling of nonstationary Poisson process with probabilistic lambda in time
11 p1791 A71-25252
- Time optimal phase locked AFC system synthesis based on Pontryagin maximum principle, comparing computerized and experimental transient response
12 p1882 A71-27514
- Optimal nonlinear control with fixed time and compact convex target set, using gradient method
12 p1923 A71-27728
- Time optimal control problem solution for linear and nonlinear piecewise continuous systems by penalty function method
13 p2040 A71-27897
- Time optimal control system design with lag, determining phase coordinate prediction unit structure
13 p2041 A71-27944
- Time optimal systems with control lag, showing elimination of self oscillations
13 p2042 A71-28640
- Optimality conditions for initial functions of time lag control systems onboard flight vehicles with transient response dependent on preceding trajectory coordinates
13 p2043 A71-28733
- Stochastic discrete time control systems optimization by dynamic programming
13 p2095 A71-28812
- Minimum time low thrust rocket transfer between elliptic orbits in strong gravity field, using averaging method
13 p2139 A71-28816
- Minimum time profiles for F-104 aircraft by Balakrishnan epsilon technique, comparing solutions with energy method
13 p1996 A71-28831

- Jet-supported VTOL aircraft fuel-time-optimal landing control, using mathematical model, Pontryagin maximum principle and analog computer solution
13 p1997 A71-29281
- Computational technique for finding bang-bang time optimal controls of nonlinear time-varying systems with bounded control function inputs
14 p2219 A71-29699
- Series connected nonlinear systems time optimal control by n interval theorem or optimization with restricted phase coordinates
14 p2220 A71-30000
- Hybrid computer solutions for optimal control of time varying systems with parameter uncertainties, exemplifying minimax load relief for large launch vehicles
14 p2319 A71-30019
- VTOL aircraft minimum climb-to-cruise time transition optimal open loop and suboptimal closed loop control synthesis
14 p2220 A71-30799
- Constant-thrust trajectory problem with gravitational acceleration as linear function of radius vector, obtaining minimum fuel solution in integrals
15 p2488 A71-32043
- Nonoscillating and quasi-oscillating conditions of time optimal second order nonlinear control systems with piecewise-continuous right hand sides
15 p2482 A71-32620
- Optimal stabilization of self adjusting control system for nonstationary plant in limited time by linear model using Lagrange multipliers
15 p2382 A71-32622
- Discrete-time optimal linear systems structure and stability, assuming quadratic costs and perfect observability
17 p2722 A71-35180
- Bellman function for time optimal problem under Lipschitz condition
18 p2942 A71-36781
- Time optimal control of systems with magnitude and impulse limited constraints on control forces
18 p2896 A71-36783
- Time optimal control for distributed systems with random properties, considering n integral relations and flying wing vehicle torsional vibration problems
19 p2994 A71-37094
- Optimality criterion for convergence of iterative solution of linear time optimal problem in reflective Banach space
19 p3088 A71-38414
- Satellite circular orbit trajectory plane time optimal relocation, examining turn angle angular position and modulus of maximum lateral acceleration
20 p3288 A71-39121
- Time optimal transfer trajectory in central Newtonian force field between two arbitrary points under jet acceleration
20 p3289 A71-39135
- Time optimal control synthesis for linear integration-type system described by n -order differential equations, using operational calculus
21 p3359 A71-40165
- Minimal time function of optimal feedback controls for normal and semidynamical systems
21 p3359 A71-40252
- Time optimal self alignment methods for inertial platforms, using mathematical model based on torque iteration and bang bang misalignment angles control
21 p3413 A71-40544
- Minimal time climb velocity optimization for stratospheric and tropospheric jet aircraft flights
22 p3482 A71-41972
- Time optimal semiautomatic attitude control for circular orbiting satellite pitch motion, using gravitational and aerodynamic torques
22 p3570 A71-42001
- High and low propulsion for optimal transfers between coplanar coaxial elliptic orbits, determining impulse number and timing
23 p3729 A71-43038 [AAS PAPER 71-368]
- Optimal singular control conditions for intermediate rocket thrust arc nonoptimality in Newtonian gravitational field for minimum fuel fixed time trajectory
23 p3718 A71-43378
- Optimal timing for interplanetary midcourse guidance maneuvers for realistic cost function, indicating first and last maneuver sensitivity
23 p3702 A71-43939
- Optimal linear final parameter control synthesis for dynamic systems with given accuracy, using multivariate statistical analysis
24 p3814 A71-44690
- TIME RESPONSE**
Long period atmospheric fluctuations, investigating large scale disturbance structure from observed data
01 p0119 A71-10852
- Digital hybrid systems simulator (DIHYSYS) program, examining subsystems sampling and execution time and applications
02 p0226 A71-11780
- Thin exploding wire restrike channels, examining temperature, electron density and thermal conductivity temporal behavior
02 p0284 A71-11941

- Time interval tracking in humans during steady and transient performance of homogeneous discrete motor acts sequence
02 p0205 A71-12056
- Sound duration effect on brain activity of cats, studying EEG and behavioral responses
03 p0361 A71-13189
- Circular Al rings under radial impulsive loading by curved magnetically driven Al flyer plates, recording strain-time histories on oscilloscopes [SESA PAPER 1644]
03 p0509 A71-13778
- Real time oscilloscope observation of ultrafast photodiode response to mode locked laser pulses
03 p0438 A71-13886
- Light-dark cycle strength as Zeitgeber for circadian rhythms in isolated man
03 p0364 A71-14249
- Time zone change effects on worldwide schedule flight crews sleep patterns, considering biological functions Circadian rhythm changes
04 p0544 A71-15057
- Sunspot region birth and growth, noting arch filament systems with H alpha time lapse movies
05 p0801 A71-15935
- Metal microfinishing technique, evaluating surface integrity degrading effects and total time requirements
05 p0759 A71-16464
- Planetary nebulae and H II region dust density perturbation e-folding time, examining Lyman continuum radiation
05 p0812 A71-16689
- Tunnel diode trigger circuit, calculating effect of junction capacitance variation and small inductance on switching time
05 p0730 A71-17082
- MOSFET inverter pulse response analysis using hyperbolic functional description
05 p0726 A71-17086
- Solar flare on 9 June 1968, observing proton energy spectra and flux variation with time profiles
06 p0958 A71-18155
- Solar flare electrons at 10-200 MeV region, discussing energy spectra and time history
06 p0961 A71-18170
- Ar-oxygen mixture in undiluted nitrogen, discussing relaxation time change during adiabatic excitation and molecule oscillations deactivation
07 p1163 A71-19276
- Scorpius X-1 X ray emission temporal behavior on 3 March 1969
07 p1198 A71-19831
- Martensitic high strength steels composition effect on environmentally induced delayed failure
07 p1139 A71-19990
- Human conditioned reflexes to time and EEG responses under acute hypoxia
08 p1243 A71-21970
- Threshold distribution of time intervals between atmospherics contradicting Poisson law
09 p1435 A71-22445
- Delayed e-wave like electrical response to light and inhibition in developing frog retina
09 p1393 A71-23011
- Decoding computational work and time, discussing cost increases related to communication reliability
09 p1407 A71-23102
- Perfectly plastic and viscoplastic materials relation between permanent deflection and response time in boundary value problems
10 p1684 A71-23931
- Pulse response of unsheathed coaxial umbilical cable connector mounted flush with missile skin
10 p1585 A71-25072
- Destabilizing buoyancy forces effect on weak homogeneous shear flow turbulence in gases, discussing turbulence decay with time and turbulence energy growth
12 p1896 A71-26940
- Design charts relating time response characteristics to parameters of closed loop transfer functions possessing conjugate pair of poles
13 p2042 A71-28706
- Simply supported normal mode plate time response to traveling wave at oblique incidence, using numerical analysis
14 p2326 A71-30068
- Ar-oxygen mixture in undiluted nitrogen, discussing relaxation time change during adiabatic excitation and molecule oscillations deactivation
14 p2276 A71-30170
- Time coordinate compensator for time variable spectrometers operating on long plastic scintillators with two terminal photomultipliers
14 p2247 A71-30579
- Triangular pulse shaper using transistors and dynistors, obtaining pulse duration, rise time and maximum repetition frequency
14 p2213 A71-30581
- Sonic boom wave interaction with topographic models, measuring surface pressure time history [AIAA PAPER 71-619]
15 p2389 A71-31548
- Decimeter solar radio bursts time splitting data, presenting high time and frequency resolution on double bursts
15 p2473 A71-31720

- Decomposing method for linear transfer functions identification from frequency or time response, using Cauchy form continued fraction expansion
15 p2379 A71-31821
- Performance differences between tactile and visual localization and temporal ordering ability, using sequential presentation of high rate point stimuli
15 p2363 A71-31948
- Random time variation in sound radiation far field of point sources in subsonic circular rotational motion
15 p2450 A71-32129
- Arbitrary shape pulsed AM systems prediction technique improvement, using time-domain signal
15 p2373 A71-32371
- Spectroscopic plate emulsion with excellent signal to noise characteristics, investigating baking time response in controlled nitrogen atmosphere
16 p2577 A71-33137
- Optical parametric oscillation internal to laser cavity, including temporal response effects of laser population inversion
17 p2751 A71-34377
- Crack wave loading, investigating dynamic stress intensity factor and time response with photoelastic technique [SESA PAPER 1835]
17 p2820 A71-34550
- Payload cost and response time reductions for shuttleborne space experiments, examining NASA Ames airborne research program management technique [AIAA PAPER 71-808]
17 p2813 A71-34731
- Nonautonomous nonlinear dynamical systems with simultaneous fast and slow time response, basing analysis method on previous work of Malkin, Massera, Bogoliubov and Mitropolsky
17 p2782 A71-34932
- Recognition response time experiments for word number effects in target set, discussing familiarity judgment and response decision
17 p2683 A71-35250
- Gages using X radiation for measuring thickness range, linearity and response time, noting application of absorption and fluorescence techniques
17 p2744 A71-35287
- Linear array antenna far field transient time response formulation, using concise vector field integral equations and generalization
17 p2717 A71-35584
- Explosive instability effect on plasma distribution function, field energy level and time response
18 p2950 A71-35863
- Finger freezing time correlation with cooling rate discussing effects of indeterminate skin supercooling
18 p2860 A71-36883
- Straight-line orbit approximation for plasma response function in system with periodic particle orbits
19 p3113 A71-37750
- Cygnus X-1 X ray data with temporal resolution, examining pulsations and flare activity
20 p3278 A71-39110
- Compensation pyrheliometers and thermoelectric actinometers response lag and irregular operation after instantaneous shadowing, discussing techniques for determining instrument inertial characteristics
20 p3237 A71-39332
- Hypoxia effects on response time to peripheral visual signals, noting direct relation to exposure severity and duration
22 p3499 A71-41495
- Continuous signal representations in time and frequency domains by Fourier series
23 p3644 A71-43284
- Analog transistor model for IC simulation discussing static characteristics and switching times
23 p3650 A71-43350
- Closed loop response speed evaluation for model reference adaptive control system, using sinusoidal test signal
23 p3656 A71-43860
- Quantitative characterization of unit time response in visual system, mapping latency and synchronicity as functions of stimulus position
23 p3640 A71-43870
- Multiple Walsh function generator design for improved time response relative to digital components, comparing with Rademacher device
23 p3646 A71-43962
- Random processes overshoots, determining probability distributions of overshoot duration and time of first attainment of given level for random sequences
24 p3815 A71-44703
- TIME SERIES ANALYSIS**
Local invariants under axial rotation, deriving recurrence relations for time series expansions and perturbation methods
01 p0154 A71-10387
- Lunar and solar periodic magnetic variations, using time series analysis based on discrete Fourier transforms for frequency spectrum lines
04 p0582 A71-15097
- Parameter estimation of mixed autoregressive moving-average (ARMA) time series using output data
06 p0878 A71-17332

Statistical reliability tests for cosmic ray intensity
records from ground stations, stressing time series
model

06 p0951 A71-18108

Time series approximation of acceleration functions
analytical solution of low thrust interplanetary
transfers, treating flyby and rendezvous mission
sides

06 p0977 A71-18566

Planetary nebulae central stars power spectra and
stellar oscillation observations, using photoelec-
tric time series data

08 p1359 A71-20938

Time series analysis techniques concerning correla-
tion, auto and cross power spectral density, amplitude
and period histograms, real time pattern recognition
and filtering

09 p1405 A71-22783

Direct digital control system for random excitation
environmental testing, discussing interfacing of
ME/DATA time series processor and minicomputer

11 p1736 A71-26500

Atmospheric turbulence space-time relationships
measurements, discussing computerized time series,
spatial and phase spectral analysis for sensors data

14 p2267 A71-29754

Biomathematical model and least square estimation
from time series data of discrete particle population in
stochastic compartmental system

14 p2265 A71-30181

Simplified EEG time domain procedure, using
method of period analytic estimates of power spec-
trum moments

15 p2364 A71-31960

Summation dial vectorial representation of stationa-
ry and nonstationary time series data, relating rhythms
to bed rest study

20 p3190 A71-39480

TIME SHARING

Batch/Time-Sharing Monitor for achieving balance
of digital computer systems efficiency and responsive-
ness, discussing performance modeling and empirical
measurements

01 p0043 A71-10178

Multiprogrammed and time shared multiaccess
digital computers operating systems design, discussing
dynamic memory protection structures

01 p0043 A71-10179

Time sharing executive component of general pur-
pose operating system for digital computers,
discussing architecture and construction

01 p0043 A71-10180

Operational memory share supervisor program with
storage protection feature for real time multitask
digital process control and teleprocessing of electrical
power utility system

01 p0043 A71-10181

ADEPT-50 resource sharing system for classified
data processing, describing time sharing security con-
trol model

01 p0044 A71-10188

Time shared computer display system design with
analog drive signal generator and digital information
channeling processor

01 p0045 A71-10196

Real time graphic display monitoring of time sharing
computer systems operational state

01 p0046 A71-10207

Missiles and aircraft trajectories computation time
reduced via time sharing and hybridization

02 p0227 A71-11794

Time sharing program for digital logic circuits simu-
lation

05 p0726 A71-16959

All-digital multichannel narrow band FSK data
receiver with time-shared arithmetic processor,
discussing prototype design and performance
[IEEE PAPER 70-TP-49-COM]

05 p0724 A71-17064

Time shared FSK FM modulator using second order
digital filter with one variable multiplier

05 p0725 A71-17066

Time shared digital computer-based data acquisition
and control system for multiple remote laboratories,
using modular programming, multiprocessing and lan-
guage processors

08 p1260 A71-21851

Man oriented program system for industrial facili-
ties engineering design with modular structure, operat-
ing in time sharing mode

09 p1412 A71-23275

Civil Engineering Systems Laboratory remote ter-
minal interactive time sharing computer facility,
discussing consulting engineer design office ex-
periences and computing center management

09 p1412 A71-23277

Problem Oriented Languages for consulting and
construction engineering problem solving by transla-
tor-generator for time shared system

09 p1412 A71-23278

Optimal models for time shared computer systems
with real time multiprogramming

10 p1581 A71-24727

Time sharing digital computers busy period task
completions modeling as semi-Markov process

13 p2035 A71-28974

Distributed computer system at McDonald observa-
tory, discussing experience with IBM 1800 process
control computer time shared operation

17 p2711 A71-35011

Optimal models for time shared computer systems
with real time multiprogramming

19 p3025 A71-37692

Time sharing technique application to RF inter-
ference with ATC resulting from transmitting and
receiving antennas collocation

19 p3102 A71-38436

Interactive computerized design system for un-
dergraduate aerospace engineering, using remote time
sharing computer terminals

22 p3517 A71-41991

Microwave scanning beam guidance receiver design
for aircraft landing aid, discussing time sharing and
flight control

22 p3572 A71-42091

Relcomp conversational time-sharing computer pro-
gram for rapid calculation of reliability and MTBF of
systems with serial and redundant units

22 p3517 A71-42103

Waiting time distribution in computer controlled
queueing system with Poisson input, deriving formulas
on basis of total probability and Markov chain theory

24 p3806 A71-44654

TIME SIGNALS

Comparative national time standards by overflight
synchronization method

04 p0585 A71-14653

Quartz clock nonsystematic and frequency fluctua-
tion statistical properties compared with GBR radio
station

04 p0600 A71-15664

Satellites for time dissemination, discussing clock
synchronization and signal propagation

07 p1154 A71-19011

Error reduction in reconstructions of time concen-
trated band limited signals from given set of linear
measurements

09 p1407 A71-23101

Stretch technique for pulse time transformation in-
cluding signal slowdown, speedup or time reversal
performed within window with duration determined
by time-bandwidth product

12 p1881 A71-27427

Satellite time and frequency dissemination,
discussing deficiencies of HF broadcasts for naviga-
tion and communication systems

18 p2878 A71-36530

Standard frequency and UTC time signal trans-
mission coherent with SI atomic second

22 p3509 A71-42087

Phase discontinuity transmitter-receiver system for
VLF/LF time signals

24 p3804 A71-44997

TIMERS

U TIMING DEVICES

TIMING

U TIME MEASUREMENT

TIMING DEVICES

Pendulum clock with contactless drive for
isochronal autooscillation period, outlining pulse am-
plitude and duration stabilization

04 p0592 A71-14863

Sampled data delay-lock loop for tracking biphasic
modulated pulsed-envelope RF signal arrival time

14 p2197 A71-30796

Serial edge absolute coded and parallel alphanumeric
time on engineering sequential films, discussing
frame selection, marking, offset, pull down and expo-
sure correction

18 p2919 A71-36085

Aerodynamic compensation for ambient medium
temperature effect on fluidic standard components
and timing devices

19 p2998 A71-37570

Signal shape matched suboptimum self bit
synchronizer for high SNR and timing error variance,
reducing jitter

20 p3203 A71-38862

Timer devices and applications, discussing timing
and power functions, switching cycles, mechanisms,
ratings and life/cost evaluation

21 p3379 A71-40672

TIN

Multilayer composites preparation by cold rolling
packets of alternating Al and Sn foils, determining ten-
sile strength relation to layer thickness

02 p0264 A71-12278

Sn additives effect on In thin film superconducting
transmission lines, comparing with Pippard nonlocal
theory for mean free path reduction

07 p1179 A71-20155

Sn-N-GaAs semiconductor surface barrier structure
electrical properties measurement over wide electron
density range, determining energy band diagram and
current flow mechanism

21 p3433 A71-41313

TIN ALLOYS

Electron concentration and superconducting
characteristics of Nb-Sn alloys from optical measure-
ments

09 p1507 A71-22234

Molten Co-Sn alloys, detailing vaporization rate,
vapor pressure and partial and integral isothermal and
isobaric formation potentials

15 p2425 A71-31394

Sn-Pb alloy solidification point analysis around
liquid-solid front with interface visualization by elec-
tron microprobe

20 p3238 A71-39416

Electron concentration and superconducting
characteristics of Nb-Sn alloys from optical measure-
ments

21 p3428 A71-41114

TIN COMPOUNDS

NT NIOBIUM STANNIDES

NT TIN OXIDES

NT TIN TELLURIDES

Laser parameters of Nd-doped hydrated
phosphorus oxychloride-stannic chloride liquid
system compared with YAG and Nd-doped glass, stu-
dying optical evolution and losses

13 p2078 A71-28400

Superconducting Nb-Sn intermetallic compound
synthesis from elemental powders by converging
shock waves

15 p2461 A71-32378

Cadmium-tin-arsenide conduction and valence band
structure parameter refinement from Faraday effect
and absorption spectra of single crystals in polarized
light

21 p3433 A71-41319

TIN OXIDES

Magneto-optical oscillatory absorption spectrum of
tin oxide crystal at 1.3 K observed beyond band-band
absorption edge with peaks as function of magnetic
field

21 p3431 A71-41235

TIN TELLURIDES

Multiple layer liquid epitaxial growth of lead tin tel-
lurides from Pb-Sn solution, determining low carrier
concentrations by Hall effect and capacitance mea-
surements

22 p3585 A71-41810

Diffused slice Pb-Sn-Te photodiode arrays for IR
detection and thermal imaging, evaporating Pb-Sn
contacts onto n and p type surfaces

22 p3543 A71-42130

TIP DRIVEN ROTORS

Do-132 light five seat tip drive turbine helicopter,
discussing applications, flight testing, design and
major components

01 p0004 A71-10465

Optimum rotor/jet thrust ratio determination
procedure for tip jet driven rotors, considering per-
formance upper bound

19 p2998 A71-38653

TIP SPEED

Tip vortex effects on rotor blade flutter in hovering
flight, discussing compressibility and oscillation
frequency

05 p0694 A71-16564

Flow field velocity distribution at rotating wing
devices tip vortices

[AHS PREPRINT 522] 14 p2172 A71-31088

Size effects on large rotor systems design, consider-
ing weight, blade loading, tip speed, etc

[AHS PREPRINT 552] 14 p2180 A71-31104

High speed neutral buoyancy bubble generators for
aerodynamic flow visualization, investigating tip vor-
tex from wing or helicopter rotor blade

19 p3064 A71-37725

Wing tip vortex control device, discussing design,
operation and effectiveness

20 p3175 A71-39084

Peak velocity vectors in transverse plane of jet
transport aircraft wake, measuring tip vortices core
size

21 p3319 A71-40491

TIP VORTICES

U TIP SPEED

U VORTICES

TIPS

NT BLADE TIPS

NT WING TIPS

Sword shaped tip on plastic sphere front portion,
detailed hydrodynamic drag reduction at various
Reynolds numbers

24 p3818 A71-44711

TIRES

NT AIRCRAFT TIRES

Flexible tires theoretical models application to
wheel shimmy analysis, examining stretched string
and point contact theories validity

10 p1557 A71-24864

Two dimensional effects of cylinders rolling on
elastic half space, investigating inflated tire shear
stress and slip region

11 p1850 A71-26101

Shimmying wheel with elastic tire, investigating motion equations for wobble and forces exerted by ground

13 p1997 A71-29230

TIROS SATELLITES

NT TOS I

International cooperation in space radio science, considering real time telemetry application via Solrad, Tiros and Alouette satellites

17 p2697 A71-34252

TISSUES (BIOLOGY)

NT ENDOTHELIUM

NT EPITHELIUM

NT NEUROGLIA

NT PERITONEUM

Pt electrode oxygen diffusion and consumption systematic errors effect on oxygen partial pressure measurement in perfused tissues

01 p0021 A71-10073

Enzyme activity reduction in thyroid gland tissue of albino rats under deep hypothermia

01 p0012 A71-11057

Free radical activity in white mice tissues under hyperbaric oxygenation, examining antioxidants effects

01 p0012 A71-11075

Comparative radiation damage at different depth-dose tissue distributions in dogs

01 p0013 A71-11132

Arterial sclerosis and stenosis physical factors, discussing connective and vascular tissue adaptive responses to mechanical stresses

02 p0200 A71-12415

Antiarrhythmic drugs choice based on excitable tissues biophysics, considering contrast between cardiac muscle and nerve

02 p0201 A71-12419

Tissue cooling with liquid nitrogen, determining film boiling transition temperature and heat transfer rates [ASME PAPER 70-WA/HT-16]

03 p0372 A71-14096

Absorbed dose equivalent from high energy neutrons and protons incident on tissue, using nucleon-meson cascade calculations

04 p0624 A71-14804

Living human tissue thermal behavior analytical modeling including internal heat generation and blood flow effects

04 p0539 A71-15460

Decaborane effects on amino acid metabolic patterns of various rat tissues, considering holoenzyme inactivation

05 p0706 A71-16294

Metabolic processes in bone tissues as basis for fighting bone disease, emphasizing enzymes role

05 p0710 A71-16858

Human organ thermal properties prediction by measuring water content of equal fat/protein tissues

06 p0851 A71-17603

Digitalis-induced bundle branch ventricular tachycardia from electrode catheter recordings of dogs specialized conducting tissues

06 p0852 A71-17873

Gas bubble statics in physical systems and organism tissues during decompression

06 p0855 A71-18374

Computer applications in analysis of biological structures, considering tissues, cells, chromosomes, proteins and lipids

06 p0863 A71-18691

Thiol and disulphide compounds radiation protection capacity at cellular level in tissue culture, using reproductive integrity as protection criteria

07 p1034 A71-18948

Tissue typing instrumentation with fluorochromatic cytotoxicity assay for quantitative data analysis, eliminating visual counting

07 p1050 A71-20050

Nervous and muscular tissues excitability during subthreshold rhythmic stimulation, discussing mathematical model for compounding polarization induced electrotonic fluctuations

07 p1050 A71-20115

Skin tissues autoecoflora composition and natural immunity indices changes after 18 day orbital flight from microbiological and immunological examinations

09 p1389 A71-22204

Biological learning, considering EEG wave activity association with structural change underlying information storage in cerebral tissue

10 p1562 A71-24226

Electromagnetic fields induction in biological tissues, recording energy absorption temperature distribution in phantom models with thermograph camera

11 p1717 A71-25289

Tissue respiration and hemopoiesis in heterothermic and homotheimic rodents under hypoxia

11 p1719 A71-25670

Biological tissues ultra-weak chemiluminescence, discussing nature, characteristics and measurement

11 p1724 A71-25672

Human heart, kidneys, liver and spleen tissues antigen composition analysis by isolation of pure antibodies

12 p1872 A71-27723

Dietary pyridoxal deficiency causing amino acid content reduction in liver, kidney, brain and heart tissues

13 p2003 A71-27837

Cerebrum temperature variations and tissue insulating and heat conducting properties in ether anesthetized dogs with heads cooled by water stream

13 p2004 A71-28029

Reduced diaphragmatic muscle tissue resistance in rats during prolonged hypokinesia, showing sorption of basic vital neutral red stain

13 p2007 A71-28417

Human tissues neutron induced physical doses calculation

13 p2021 A71-29260

Heat transfer through human peripheral tissue based on one dimensional steady state continuum model combining effects of conduction, convection, vascular heat exchange and metabolism

13 p2025 A71-29502

Hypothermia effect on lipid synthesis of hamster tissue following intravenous injection of acetate-C 14

14 p2182 A71-29582

Pyruvate and lactate concentrations in muscle tissue and blood at rest and during exercise

14 p2187 A71-31136

Dietary antioxidant vitamin level effects on fine structure of proximal convoluted tubules in rats, studying changes due to oxygen toxicity

16 p2528 A71-33116

Human alveolar wall tissue length-tension characteristics, noting age, sex and expiratory flow relationships

16 p2530 A71-33246

Turtles organs and tissues responses during Zond 5 and 7 lunar probes circumlunar flight

16 p2532 A71-33678

Nitrogen and oxygen exit rate from subcutaneous gas pockets in rats during tissue blood flow elevation due to cobalt chloride injection

17 p2678 A71-34174

Factors affecting tissue oxygen supply in old people, showing capillary circulation disturbance role in hypoxia development during aging

17 p2679 A71-34220

Hemopoiesis and anoxybiotic processes comparative characteristics in brain and muscular tissues of heterothermal and homoiothermal rodents during prolonged hypoxia

17 p2679 A71-34221

Increased oxygen concentrations effect on mice pulmonary tissues during prolonged exposure

17 p2679 A71-34222

Neutron radiography and dosimetry as clinical diagnostic tool, calculating resolution through tissues for simulated human arm

17 p2693 A71-35449

Book on biological effects of radiation covering ionizing radiation properties and effects at molecular, cellular and tissue levels

19 p3002 A71-38048

Daily endurance exercise influence on key tissues resting aerobic metabolism, using Warburg technique to determine rats heart, skeletal muscle and liver tissue oxygen consumption

20 p3185 A71-38886

Cholesterol and esterified cholesterol distribution in human skin from analysis on fat, epidermis, corium, subcutaneous tissue and serum by chromatographic/colorimetric methods

20 p3185 A71-38892

Postexercise elevated tissue temperatures contributions to oxygen consumption in rats, suggesting hypothalamic adjustment

20 p3186 A71-38981

Tissular and cellular biological resistance as indices for organism resistance to adverse effects, noting increase due to muscular training and cold adaptation

20 p3187 A71-39219

Cryogenics applications to cryosurgery and long term low temperature storage of living cells and tissues

20 p3189 A71-39252

Ultrasound absorption in liver tissue due to macromolecular relaxation processes

20 p3191 A71-39770

Simultaneous measurement of transverse and longitudinal bioelectric potential differences in plants without direct contact with tissues, using vibrating reed electrometer

21 p3375 A71-39985

Central nervous tissue sensitivity, considering direct sensing of gravitational stimuli of vibratory character

21 p3328 A71-39997

Internal short chain alkane populations of paraffinic hydrocarbons in tobacco teratoma and habituated tissue cultures

21 p3345 A71-40204

Intracellular pH and carbon dioxide combining curve of muscle tissue in dogs, using DMO method

21 p3355 A71-40631

Cat and human eye movement control system measurements, studying isolated oculomotorary muscles and globe restraining tissues dynamics

22 p3489 A71-42441

Optical second harmonic generation in excited tissues by Q switched ruby laser irradiation, observing narrow band emission line in collagenous tissues

22 p3559 A71-42567

Aminothiols class radiation protector influence on tissue damage of white rats under single and two-folys gamma irradiation at various test conditions

22 p3494 A71-42779

Composite tissue blocks method for comparative pathomorphological investigation of radiation pathology

22 p3505 A71-42779

Hyperoxic medium effects on experimental animal cells, tissues and organs morphology, ultrastructure and histochemistry

22 p3495 A71-42804

Ultrasonic evaluation of heart anatomical abnormalities in congenital and acquired heart diseases including myocardium hypertrophy and tissue degeneration

23 p3639 A71-43118

Manned spacecraft radiation protection against cosmic rays, considering proton attenuation in shielded materials and dose formation in body tissues

24 p3801 A71-44889

TITANATES

NT BARIUM TITANATES

NT ILMENITE

NT LEAD TITANATES

NT PEROVSKITES

NT STRONTIUM TITANATES

High purity hafnium titanate, discussing preparations and DTA, electron microscopy wet chemical and X-ray analyses

02 p0275 A71-12599

Surface roughness and surface area effect on UV stability of zinc orthotitanate pigments, using electron microscopy and BET nitrogen adsorption

11 p1790 A71-26233

Space radiation environmental effects on reactively encapsulated zinc orthotitanates and paints

12 p1920 A71-26764

Curie point of solid solutions in ternary system of zirconate-titanate and lead metaniobate, using maximum on temperature dependence curve of permittivity

13 p2111 A71-28152

Sodium oxide-titanium dioxide-water ternary system, determining sodium titanates formation regions in equilibria in 300 C isotherm

15 p2367 A71-31900

Capacitive thermometry characteristics of dielectrically crystallized titanate-containing glass ceramic at cryogenic temperatures

20 p3253 A71-39275

TITANIUM

NT TITANIUM ISOTOPIES

Oxygen diffusion coefficient during metal/Ti oxidation in unsteady high temperature region, allowing for interfacial phase boundary shift

01 p0101 A71-10677

Porous Ti thermal and electrical properties from room to high temperatures

01 p0102 A71-10783

Vapor phase interaction of methanol and carbon tetrachloride with Ti thin films, discussing Ti stress corrosion cracking implications

01 p0102 A71-10812

Metallurgical and structural production of diffusion-bonded titanium honeycomb sandwich panels for aerospace hardware weight saving

01 p0090 A71-11276

Soviet book on chemistry of titanium covering intermetallic compounds, hydroxides, dioxide, titanates, halides, sulfates, titanium ores, deposit sites, etc

02 p0209 A71-11843

Bending of plate of nonuniform elasticity over thickness due to gas surface layer saturation during heating prior to rolling

02 p0328 A71-12511

Temperature and plastic deformation rate effects on plasticity and strength of cast iron, Ti and steels

02 p0257 A71-12522

Groove depth/residual deformation/in vibration rolling of Ti cylindrical samples, considering impression force, cylinder and steel spheres diameters

02 p0258 A71-12644

Cu-Al alloy, Ti and low carbon steel under L.F. flexural stress, testing parameters effect on fatigue resistance

03 p0445 A71-14335

Alpha titanium-oxygen solid solutions surface structure, using low energy electron diffraction for determination of order-disorder transition and superlattice reflections

04 p0610 A71-14899

Spectral emittance of Ti at high temperatures in visible region under vacuum

04 p0611 A71-14956

Soviet book on oxidation in Ti and Ti alloys covering physical, chemical and crystallographic characteristics

teristics of Ti-O system, Ti component manufacture, etc

04 p0612 A71-15374

Sponge titanium quality improvement involving chlorination, tetrachloride purity, magnesium and thermal reduction

04 p0616 A71-15824

Rushing effects on fractional composition and quality of sponge titanium, including optimum end size of pieces

04 p0616 A71-15825

Ti microcrystals on single crystal tungsten substrate, discussing phase transformations

05 p0768 A71-16854

Ni and Ti cutting, examining wear for various microcutter refractory materials

05 p0759 A71-16862

Ti-Bc composites produced by powder coextrusion, discussing microprobe studies to determine microstructure thermal stability

[ASME PAPER F-70-3] 05 p0000 A71-17104

Hydrogen solubility in alpha Ti, using electrical resistivity measurement at liquid nitrogen temperature

07 p1139 A71-19991

Titanium-steel bimetal part fabrication using explosive and drop forging

08 p1295 A71-20840

Bcc Ti-V single crystals deformation modes and resolved shear stresses as function of temperature and composition

08 p1307 A71-21510

Titanium single crystal prism slip dislocation dynamics, examining temperature and strain rate effects on shear stress

08 p1309 A71-21521

Ti effects on Ni-Mo-Cr alloy strengthening, correlating microstructures and mechanical properties

08 p1311 A71-21542

Titanium-steel continuously reinforced composites strength to weight ratings, describing ausforming process and fatigue tests

08 p1316 A71-21587

Ti thermal conductivity, electrical resistivity and total emittance at high temperatures in ultrahigh vacuum, discussing phase transformation effect

10 p1624 A71-23910

Prior deformation and subsequent annealing influence on fatigue response of coarse grained alpha Ti, evaluating relative effects of dislocation locking and mechanical twinning

10 p1626 A71-24445

Jetting collision effect on structural changes at interface between Ti and steel in explosive bonding, considering plastic deformation and residual stresses

10 p1629 A71-25030

Torsional-flexural stability of stiffened Ti panels for application to supersonic transport, using small deflection energy methods

[AIAA PAPER 71-338] 11 p1843 A71-25317

Ti intermediate diagonal tension field shear beam analysis and design for Boeing SST, using Rayleigh-Ritz method

[AIAA PAPER 71-340] 11 p1843 A71-25319

Solid circular Ti shaft torsion boundary value problem solution, using elastic-viscoplastic materials thermodynamics and constitutive relations

11 p1849 A71-25801

Ti hot salt stress corrosion, considering effects of oxygen, air velocity, moisture, thermal cycling, fatigue and type of salt

11 p1781 A71-26261

Ti, B and graphite fiber composites application to aircraft design, discussing mechanical properties and market competition

12 p1918 A71-27676

Structural characteristics of Ti subjected to high speed deformation rates, examining formation of crystallographic glide lines and twins as function of deformation degree and rate

13 p2085 A71-28226

Static strain measurements on Ti specimen subjected to different conductive heating rates, testing various gages

14 p2239 A71-29833

Kinetics of Ti single crystals tensile deformation by prismatic gliding, studying moving dislocations interactions with metal impurities

14 p2257 A71-29844

Cooling during welding of Ti for prevention of deleterious overheating, discussing safe temperature range for water cooling during butt welding of tubes

15 p2413 A71-31221

Fatigue crack propagation model for explosion bonded titanium-steel system under constant load amplitude conditions

16 p2600 A71-34096

Titanium and composite fabrication for F-14 aircraft, discussing hot forming, chemical milling and electron beam welding

16 p2585 A71-34156

Ti adsorption on W and Re, measuring field emission average work function at various Ti layer thicknesses

17 p2791 A71-34855

Oxygen sorption rate by Ti at low pressure from measurement in stainless steel ultrahigh vacuum chamber

17 p2695 A71-35139

Titanium and superalloy radiative heat shield design for space shuttle booster, recommending postsupported honeycomb configuration

18 p2973 A71-36462

Electroconductivity, thermal conductivity and diffusivity, specific heat and emissivities of Ti at 1000-1700 K

19 p3078 A71-37582

Stress effect on hydrogen distribution at high temperatures in titanium and Ti-Al-Mo-V alloy

19 p3080 A71-37720

Low cost Ti substitutions for Ni and alloys in corrosion resistant applications, prosthetic devices and pollution control equipment

20 p3251 A71-39339

Steels, aluminums and titaniums ultimate and yield strength statistical distributions in Weibull parameter form, presenting stimulus-response potential failure model

[ASME PAPER 71-VIBR-64] 21 p3396 A71-40307

Alpha Ti at blue brittle temperature, observing strain rate dependent work hardening effects on necking strain

21 p3398 A71-40464

Stress relaxation in laminated Ti sheet at ambient temperature after vacuum tempering at 800 C, interpreting logarithmic time dependence by activated thermal sliding theory

21 p3399 A71-40527

Intermittent stress creep tests on low carbon steel, commercially pure iron, Cr-Mo steel and commercially pure tantalum, noting static-to- dynamic transition

21 p3400 A71-40835

Oxygen diffusion coefficient during metal/titanium/oxidation in unsteady high temperature region, allowing for interfacial phase boundary shift

21 p3401 A71-41054

Edge dislocations mobility in zone refined alpha Ti single crystals in bending, using etch pit techniques at 77, 200 and 300 K

21 p3404 A71-41415

Temperature effects on fatigue response and tensile properties of coarse grained alpha Ti containing 0.085 wt pct oxygen

23 p3688 A71-42924

High energy proton spallation cross sections for several radionuclides from Ti targets, discussing application to lunar materials and meteorites analysis

23 p3706 A71-43199

Swaged high purity fine grained Ti stress-strain behavior below 424 K, emphasizing mechanical twinning in plastic deformation

23 p3695 A71-44289

Diffusion acceleration in bcc Ti due to imperfections of fine structure created during polymorphous transformation

24 p3840 A71-45379

TITANIUM ALLOYS

Periodically modulated phase structure transformations in decomposition of Cu-Ti and Cu-Ti-Al alloys during aging at different temperatures

01 p0101 A71-10670

Boron additive effects on Ti thermal conductivity and expansion

01 p0102 A71-10787

Materials for spacecraft design requirements, considering composite and refractory metals, Ti and heat resistant alloys

01 p0102 A71-10816

Fusibility and thermal emf of ternary intermetallic TiFe-TiCo-TiNi system

01 p0103 A71-11090

Ti and Ti-Al alloys machinability, discussing physical properties, dynamic deformation behavior and optimal cutting, milling and drilling

[SME PAPER EM-70-101] 01 p0089 A71-11254

Ti alloys isothermal forging, using precision-cast superalloy dies

[SME PAPER MF-70-122] 01 p0089 A71-11255

Hot forming/die quenching of aluminum and titanium alloy integrally stiffened panels

[SME PAPER EM-70-178] 01 p0089 A71-11259

Fe-Ti alloys at large plastic elongations, investigating strain hardening behavior

01 p0105 A71-11604

Ti-Al-V alloy transformations under continuous cooling, using TTT diagram to describe kinetics

01 p0105 A71-11618

Time, temperature and transformation curves for Ti alloy by dilatometry, hardness measurements, X rays and micrography, discussing martensite and beta-alpha transformations

01 p0105 A71-11620

Ni-Al-Ti alloys strength, investigating matrix precipitate lattice parameter mismatch effects

02 p0263 A71-11865

Decomposition of unstable beta solid solution of Ti-V alloy, using X ray and microscopic analyses

02 p0263 A71-11929

Mo-TiC-Ti system phase equilibria at 1400 C, considering two phase region tie lines direction by metallographic and X ray analyses

02 p0264 A71-12279

Mechanical properties of Ti alloys subjected to rolling and heat treatment

02 p0265 A71-12522

Reduction-elongation relation in plastic deformation of tensile test samples of Ti alloys subject to thermomechanical treatment

02 p0265 A71-12523

Statistical study of microhardness across thickness of gas saturated layer distribution on surface of Ti alloys

02 p0265 A71-12524

Alpha and beta Ti alloys metastable phases decomposition behavior, using electrical resistance measurements and X ray analysis

02 p0266 A71-12651

Ti-Al alloy hot salt stress corrosion cracking due to hydrogen production and absorption

02 p0267 A71-12880

Ti alloy hot salt stress corrosion under simulated engine environmental conditions, presenting threshold data based on residual tensile ductility

02 p0268 A71-12885

Ti-Al-V hydrogen induced fatigue crack growth at room temperature under sustained load

02 p0268 A71-12891

Ti alloys crack initiation by solid Cd coating under tensile stress with intimate contact, noting time and temperature effects

03 p0441 A71-13318

Titanium, Inconel and stainless steel alloys deep drawing press loads under various lubrication and temperature conditions, considering work hardening, friction and anisotropic coefficients

[ASME PAPER 70-WA/PROD-26] 03 p0433 A71-14114

Water impact erosion on stainless steel, Ni and Al and Ti alloys, observing impact velocity relationship with number

03 p0444 A71-14287

Ni-Ti system electrocatalysts for fuel cell and accumulator electrodes

03 p0355 A71-14318

Titanium alloy turbine disks creep rupture strength and service life, considering pressing and forming manufacturing technology

04 p0664 A71-14604

Ti alloys stress corrosion crack propagation in salt water, investigating existence of threshold stress from electrochemical data

04 p0610 A71-14891

Soviet book on oxidation in Ti and Ti alloys covering physical, chemical and crystallographic characteristics of Ti-O system, Ti component manufacture, etc

04 p0612 A71-15374

Near equiatomic Ta-Ru alloys phase transformations by resistance and susceptibility changes and X ray powder patterns of cooled structure

04 p0614 A71-15777

Microstructure effect on metastable beta Ti alloy strength, toughness, stress corrosion cracking susceptibility

04 p0614 A71-15780

Al-Ti alloys segregation substructures, studying nucleant particles relationship to crystal solidification

04 p0615 A71-15791

Binary Ti alloys hydrogenation-dehydrogenation treatment effect on alloying element activity

04 p0615 A71-15801

Ti-Ir alloy equilibrium diagram in entire concentration range, emphasizing phase stabilization at room temperature

04 p0616 A71-15805

Ti alloy research, describing transparent atmosphere chamber design and dilatometer control modifications

04 p0604 A71-15908

Ti-Al and Al alloys and Ni maraging steel creep behavior during high stress, elevated temperatures and rapid heating

04 p0617 A71-15909

Ti alloy plate multipass welding process, describing temperature measurement techniques for multiple thermal cycles

04 p0604 A71-15910

Titanium alloys for drop and press forged airframe, engine, rocket and spacecraft components, presenting physical and mechanical properties for various alloys and applications

05 p0757 A71-16136

Ti and Ni base high temperature alloys welded joints efficiency, discussing fatigue, storage, long time heat and corrosion tests

05 p0765 A71-16172

Ti alloys welded joints in annealed state and after heat treatment strengthening, noting welding conditions, filler wire composition and edge preparation

05 p0757 A71-16173

Heat, solution and cooling treatment of Ti-Al-V-Sn alloy for high strength and plastic properties

05 p0765 A71-16199

TITANIUM ALLOYS

Temperature gradients and cooling rates of Ti alloy sheet moving arc weld pools, discussing instantaneous solidification

05 p0757 A71-16212

Ti-Al-V foils by electron beam vapor deposition, discussing metallurgical characteristics

05 p0765 A71-16237

Abnormal microstructure in hot rolled plates and sheets of alpha plus beta Ti alloys

05 p0766 A71-16349

Beta stabilizers effects on Ti strength, plasticity and stress concentration sensitivity at low temperatures

05 p0767 A71-16766

Austenitic steels and Ti and Al alloys with stress raisers, studying low temperature mechanical properties

05 p0767 A71-16768

Ti alloys beta phase solid solution decomposition during cooling and plastic deformation at low temperatures

05 p0767 A71-16770

Co-ti alloy hardness recovery, noting dependence on solid solution structure after low temperature aging

05 p0768 A71-16855

Ti-Zr-O alloys cross sections investigation by neutron and X ray diffraction, discussing stoichiometry deviation

06 p0911 A71-17382

Soviet book on machinability of titanium alloys covering microstructure, physical properties, surface finish and fatigue properties, tooling for industrial machining operations, etc

06 p0903 A71-17444

Anisotropic tubular Ti alloy samples, noting yield strength and crystal structure dependence on stress-strain state

06 p0912 A71-17937

Ti alloy deformation through surface oxidation at elevated temperature, considering lattice parameter and alpha concentration effects

06 p0913 A71-18677

Ti alloy embrittlement by prolonged high temperature exposure, using substandard fracture mechanics test for time-temperature dependence

06 p0915 A71-18686

Vibration tumbling duration effects on surface quality, fatigue strength and damping properties of titanium alloy structural parts

07 p1130 A71-19169

Tubular Mg and Ti alloy samples under tension and compression load, observing creep properties

07 p1211 A71-19195

Dissolved hydrogen effects on mechanical properties, modulus of elasticity, lattice constants and X ray lines of Ti alloys, showing cold brittleness at high strain rates

07 p1130 A71-19298

TiNi antiphase boundaries direct observation using transmission electron dark field imaging technique

07 p1131 A71-19431

Binary Ti-Al and ternary Ti-Al-X alloys precipitation strengthening, investigating structure, mechanical properties and deformation behavior

07 p1133 A71-19444

Notch geometry and temperature effects on Ti-Al-Mo-V alloy creep rupture behavior

07 p1134 A71-19470

Oxygen effect on mechanical properties of Ti alloys with V and V-Al content, showing strengthening up to 400 C

07 p1136 A71-19631

Transition metals effect on Ti alloys grain size, suggesting La, Y, Ni, Pd and Pt effectiveness in crystal structure refinement

07 p1136 A71-19632

Stainless steel coatings vacuum deposition on Ti alloy plates, considering product cryogenic and mechanical properties

07 p1118 A71-19853

Mechanical and interface reaction properties of alumina reinforced Ti-Al-V alloy composites fabricated by vacuum diffusion bonding

07 p1137 A71-19965

Stress wave emission from subcritical crack growth in thin walled Al-V titanium alloy

07 p1137 A71-19967

Strength, toughness and hardness of gas tungsten arc multipass welds in titanium alloy plates

07 p1119 A71-19970

Ultrasound effects on Ti alloys Hg embrittlement and stress corrosion cracking by methanol-water-hydrochloric acid mixture

07 p1137 A71-19975

Ternary Al-B-Ti system, investigating Al corner and B effect on grain refinement

07 p1138 A71-19981

Metastable beta phase Ti-Mo and Ti-V alloys ternary additions effect on decomposition

07 p1138 A71-19982

Microstructural variables effects on fracture stress in alpha beta Ti alloy having Widmanstatten structure

07 p1139 A71-19992

Methanol stress corrosion cracking of Ti-Al-V foil inhibited by pretreatment in aqueous solutions of elec-

trolytes, discussing colloidal character of microcrystallites

07 p1142 A71-20362

Hydrogen embrittlement in hot salt stress corrosion of Ti alloy

07 p1142 A71-20372

Fatigue limit of titanium alloy machine parts after finishing mechanical treatment under resonance testing

07 p1142 A71-20484

V-Ti alloys high temperature behavior dependence on Ti content, examining interstitial impurities effects on mechanical properties

08 p1310 A71-21532

High strength martensite beta Ti alloy microstructure, discussing ductility and age hardening

08 p1312 A71-21552

Thermomechanical treatment effects on microstructure and fracture toughness of extruded Beta III titanium alloy

08 p1313 A71-21558

Paired dislocations after high temperature deformation in precipitation hardened Co-Ti alloy

08 p1315 A71-21582

Plasma arc welding of jet engine components of Ti and Ni alloys, comparing to gas tungsten arc and electron beam processes

08 p1299 A71-21684

Structural efficiency improvement by materials selection for airframe structures, discussing Al, Ti-Al-V and steel panels

08 p1299 A71-21685

Complex Al brazing alloy for honeycomb core joining to Ti alloy face sheets, discussing fillet formation and strength optimization

08 p1299 A71-21686

X ray analysis of oxide film structure, oxygen concentration and residual stresses at surface of oxidized Ti and Ti alloy

08 p1317 A71-21760

Ti alloy powders and Ti-base refractory compounds production from Ti alloys wastes

08 p1317 A71-21856

Ti-Mo alloys porous materials for work in hot solutions of nonoxidizing acids, discussing production technology and corrosion resistance

08 p1317 A71-21857

Concentrated elongation dependence on cross sectional area reduction in industrial Ti alloys undergoing thermomechanical treatment

09 p1468 A71-22324

Multicomponent Ti alloys mechanical properties for cryogenics applications, describing alloying advantages with tantalum

09 p1468 A71-22601

Stacking faults and fcc precipitation of Ti beta alloys after high temperature heating

09 p1469 A71-22850

Continuous seam diffusion bonding of Ti alloy thin gage and sandwich structures in air, considering joint types

[ASM PAPER W71-23.4]

09 p1455 A71-23094

Beta Ti alloy sheet and foil mechanical property tests, honeycomb core fabrication, forming and welding evaluations

[ASM PAPER W71-23.1]

09 p1455 A71-23095

Fatigue life and crack propagation of sheet, plate, extrusions and forgings in annealed and solution treated aged Ti-Al-V-Sn alloy

[ASM PAPER W71-22.5]

09 p1471 A71-23096

Fracture toughness relationship to microstructure in alpha-beta Ti alloy heat treated to constant yield strength, considering crack propagation

09 p1472 A71-23126

Ti-6Al-4V and solution treated and aged Ti-6Al-6V-2Sn alloys, investigating relationship between alpha grain size and crack initiation fatigue strength

09 p1472 A71-23131

Ti alloys in aircraft industry, considering jet engines applications and structural stability improvements related to fracture toughness, fatigue and stress corrosion

09 p1474 A71-23292

Chromium and titanium alloyed austenitic steels, examining short and long time application as turbine engine parts

09 p1475 A71-23295

Quality assurance in Ti and Ti alloys processing, discussing smelting, ingot homogenization staging, costs and facilities

09 p1456 A71-23303

Forging conditions effects on Ti alloys mechanical properties, considering ingot conversion to semifinished product

09 p1475 A71-23304

Steels, Ni alloys and Ti alloys deformation resistance and deformability, discussing temperature effects on forging rate

09 p1475 A71-23305

Full penetration argon arc welding of titanium alloy plates without edge preparation

09 p1457 A71-23357

Impact strength decrease of welded joints in Ti alloys due to air cooling rate after aging

09 p1478 A71-23421

Ti alloys structural high temperature applications in fighter aircraft, considering fabrication and assembly methods

09 p1458 A71-23422

Grain size influence on deformation characteristics of commercial Ti with oxygen and Fe impurities, discussing test results on various mechanical properties

09 p1479 A71-23423

Precision forging and pressing of Al alloy and alloy parts of aircraft structures at cost effective prices

09 p1459 A71-23424

Thermal, microstructural and X ray analyses of Ti alloys phase diagrams, measuring hardness and conductivity

09 p1480 A71-23425

Phase diagram isothermal cross sections of Ti-Nb alloys for various temperatures and heating periods by X ray and microstructural analysis

09 p1480 A71-23426

Phase diagram of Ti-Ta-Mo alloy system, obtaining solubility and electrical conductivity for various compositions

09 p1480 A71-23427

Ti-Nb alloys constitution, discussing alpha-beta phase dissolution and undercooled beta phase decomposition

10 p1623 A71-23428

Isothermal transformation of metastable beta Ti-Mo alloys, considering contraction start point coincidence with point of quenched omega transformation to aged omega in TTT diagram

10 p1625 A71-23429

Zr effect on Ti-Mo beta alloy stability, considering Zr suppression and retardation of omega precipitation on basis of TTT diagram and tensile tests

10 p1625 A71-23430

Internal friction from hydrogen dissolved in Ti alloys, considering solute interstitial atoms causing asymmetrical distortion decrease with increased concentration

10 p1625 A71-23431

Recrystallization of V and V-Ti alloy, discussing hardness measurements, tensile tests, X ray diffraction, optical and electron microscopy

10 p1625 A71-23432

Alloy and heat treatment effect on Ti bondability, adhesive bonded aircraft structure, using annealed aged Ti-6Al-4V and Ti-6Al-6V-2Sn alloys for testing

10 p1615 A71-23433

Ti-Ti5S13 eutectic oriented solidification structure showing unidirectional growth faceted silicide film and disorientation

10 p1626 A71-23434

Nb-Ti alloy oxidation kinetics at various temperatures and pressures, noting linear patterns and oxide formation

10 p1626 A71-23435

Ti-Al-Cr-Fe alloys microstructure, investigating alpha and beta phases with X ray diffraction

10 p1627 A71-23436

Ni-Cr-Ti-Al-Mo system equilibrium conditions, conducting phase analysis by X ray and optical and electron microscopy

10 p1627 A71-23437

Ti-V alloys electrolytic deposition, discussing electrolyte composition, current density, temperature coating thickness

10 p1627 A71-23438

Mo-Ti-C ternary alloy, examining solid state solubility, equilibrium conditions and microhardness

10 p1628 A71-23439

Powder metallurgy parts application in aircraft illustrating flareless-sleeve coupling nut of pressurized sintered Ti-6Al-4V alloy

10 p1618 A71-23440

Superconductivity transition of Nb-Ti solid solutions with varying Ti content, using specific heat measurements between 2.5 and 20 K

10 p1628 A71-23441

Liquid and solid phase relations in Be-Al-Ti system by chemical, thermal, microscopic and X ray investigation, discussing solubility range of ternary phase and intermetallic compounds

10 p1629 A71-23442

Ti-Al-Mo-V alloy stress corrosion cracking, using controlled potential technique in aqueous methanol environments with and without halogen ions

11 p1777 A71-23443

Intermetallic compound precipitation processes in Ti-Cu alloys for high yield strengths, using electron microscopy

11 p1779 A71-23444

Ordered Ti-Al lattice parameters measurement at low and high temperature diffractometer attachment

11 p1780 A71-23445

All-beta Ti alloy Ti-V-Cr-Al, testing dynamic behavior of strain aging during stress relaxation process

11 p1780 A71-23446

Ti-Zr alloy phase diagram from vacuum melting using high purity wafers and apparatus similar to McQuillan

11 p1780 A71-23447

Coated abrasive grinding of Ti alloys using water, various soluble cutting oils and inorganic phosphate solutions as coolants and lubricants

11 p1771 A71-26142

Ti stress corrosion in organic liquids, considering intergranular and transgranular failure

11 p1781 A71-26262

Nb-Ti alloys internal friction spectra due to oxygen content, applying graphical decomposition method

11 p1781 A71-26322

Ti-Zr alloying in for microstructural hardness and mechanical strength increases, discussing Zr concentrations at Nb granular boundaries

11 p1782 A71-26470

Long duration high temperatures rated stress effects on Ti beta alloy IVT-1, correlating creep with beta granular boundaries migration

11 p1782 A71-26471

Fast heated titanium-vanadium martensite beta-phase transformations comparison with slow heated structures

11 p1782 A71-26472

Ti-V alloys, observing as-quenched omega phase and transition to aged form by selected-area diffraction and dark-field electron microscopy

11 p1783 A71-26479

Predeformation effects on metastable Ni base Ti alloys precipitation aging at extrinsic stacking faults, using thin foil microscopy

12 p1916 A71-26894

Ti alloys aging, noting hardness increase and fine structure alpha phase coherent with beta solid solution matrix

12 p1917 A71-27296

Aged beta Ti alloy microstructure and mechanical properties, examining initial dislocation structure and interstitial concentration effects

12 p1917 A71-27297

Titanium-containing steels nitriding in ammonia, discussing hydrogen diffusion layers brittleness, cracking, peeling and thickness

12 p1919 A71-27776

Low alloy alpha Ti alloy ignition during breaking in oxygen containing gases, considering partial oxygen pressure and tensile loads

13 p2082 A71-27815

Thermal emf measurement of Ti alloy, steel, bronze and duraluminum subjected to fretting corrosion tests

13 p2082 A71-27820

Fatigue crack growth rate in plates of anisotropic materials, considering Al and Ti alloys under cyclic loads

13 p2082 A71-27826

Mechanical properties and heat treatment of Ti-V and Ti-V-Al alloys in quenched and quenched-aged states

13 p2083 A71-27872

Mechanical properties of Ti-Al-Cr and Ti-Al-Cr-Mo alloys annealed below solidus temperatures

13 p2083 A71-27873

Beta stabilizers effect on mechanical properties of alpha structure Ti-Al-V alloys subjected to different heat treatments

13 p2083 A71-27874

Mechanical properties of welded joints in Ti alloys with high oxygen content

13 p2072 A71-27875

Ti-Co-B and Ti-Re-B systems diagrams of isothermal sections at 800 and 1400 C

13 p2083 A71-28008

Forgeability and tensile properties of spark sintered unstrained Ti-Al-V preforms from prealloyed powders in uncontrolled atmosphere

13 p2084 A71-28147

Alloying elements isomorphous and valence-electron localization effects on Ti alpha/beta transformation temperature

13 p2085 A71-28223

Mechanical properties, hardness and dislocation structure of Ti bearing maraging steels, considering Mo role in strength and plastic properties improvement

13 p2086 A71-28581

Fe/Ti pair diffusion coefficients at various temperatures, showing thin central and two single phase zone formation

13 p2087 A71-29263

Ti-Al binary alloy embrittlement in sea water by notched cantilever beam stress corrosion test, investigating alpha 2 particle precipitation effect on cracking susceptibility

14 p2256 A71-29522

Creep and failure tests for Ti alloys at 500 C and high stresses, discussing work dissipation during creep process

14 p2256 A71-29621

Discontinuous phase decomposition increase in Co-Ni-Ti alloys by plastic deformation and Al additions, indicating grain boundary diffusion control

14 p2258 A71-30003

Temperature dependent absorption line width and secondary moments of nuclear magnetic resonance spectra of Ti-Zr-H system

14 p2258 A71-30009

Cutting angle effect on service life of broaching tools for Ti alloys annealed forgings, using high-speed P18 tool steel

14 p2259 A71-30271

Shape-memory effect in equiatomic Ti-Nb alloys with reversible martensitic transformation

14 p2259 A71-30392

Local shielding chambers for welding circumferential and longitudinal seams in Ti alloys with minimum residual oxygen concentrations

14 p2253 A71-30489

Beta stabilizing Mo and Cr effects on mechanical properties of welded and heat treated Ti alloys

14 p2260 A71-30490

Ti alloy powders and Ti-based refractory compounds production from Ti alloy scrap, describing electrorefining, hydrogenation and carburization processing

14 p2260 A71-30835

Porous Ti-Mo alloy materials for operation in hot solutions of nonoxidizing acids, discussing production technology and corrosion resistance

14 p2260 A71-30836

Ti-Al-V alloy forgings fatigue strength improvements, discussing surface finish, heat treatments and alpha and beta grain size

14 p2261 A71-31105

Ti alloys inert gas shielded welding, determining relationship between welding current, electrode feed rate and electrode wire protruding length and diameter

15 p2413 A71-31219

Industrial Ti and beta-Ti alloy hydrogen thermodynamic effects on brittleness

15 p2424 A71-31238

Microstructure and mechanical properties of Ti-rich alloys of Ti-W system, constructing phase diagram

15 p2425 A71-31402

Ti-Al-V alloys heat resistance relationship to phase structure from bending test at high temperature

15 p2426 A71-31404

Titanium alloys analysis by dissolution in sulfuric acid and aerosol injection into spark discharge, discussing standard solution preparation

15 p2367 A71-31650

Titanium alloy durability under cyclic torsion in vacuum at various temperatures, investigating fatigue life and tensile strength

15 p2428 A71-31856

Unidirectionally and cross rolled titanium alloys elastic properties anisotropy during cooling, discussing Young modulus distribution

15 p2428 A71-31857

Sheet metal fatigue test method for transverse 100-1000 Hz bending at normal and high temperatures, applying to 1.5 mm Ti alloy sheet

15 p2505 A71-31864

Unidirectionally solidified Ti-base eutectic composites and alloys strength and microstructural stability under heat treatment

15 p2432 A71-32170

High strength steels and Ti alloys machining, discussing hardness levels, cutting speeds, tool chip contact area, and reasonable production rates

15 p2416 A71-32426

Ti alloys argon TIG welding to Nb alloys, detailing joint impact strength, fusion zone ductility and bending tests

15 p2418 A71-32668

Isothermal sections at 1400 C of systems niobium-titanium-boron and niobium-molybdenum-boron by X ray analysis

15 p2437 A71-32672

Annealed stainless steel and Ti alloy in solution heat treated aged condition, detailing elevated temperature and high strain rate effects on fatigue life and tensile properties

15 p2438 A71-32791

Fatigue limits of Ti alloy by Wohler and Locati loading methods

16 p2592 A71-33406

Scale factor effect on brittle fracture strength for Ti and Al alloys and high strength steels

16 p2657 A71-33409

Oxygen effect on mechanical properties of Ti alloys with V and V-Al content, showing strengthening up to 400 C

16 p2593 A71-33627

Transition metals effect on Ti alloys grain size, suggesting La, Y, Ni, Pd and Pt effectiveness in crystal structure refinement

16 p2593 A71-33628

Airframe structural uses of Al, Ti and Be alloys, discussing need for structural efficiency improvements by proper heat treatment and stress relieving techniques

16 p2594 A71-33875

Ti influence on ductility of normalized low alloy steel, considering crack initiation and propagation

16 p2598 A71-33991

Equiatomic TiNi martensite crystal structure and internal defects investigation by electron microscopy and electron and X ray diffractions

16 p2598 A71-34045

Temperature dependent electron structure model of free energy decomposition of beta phase in Ti alloys

16 p2599 A71-34085

Triple Knudsen cell method to determine thermodynamic activity of Cu in bcc solid solution of Ti-Cu alloys

17 p2756 A71-34488

Ti-Al alloys surface film growth and stress corrosion cracking as function of applied potential and environmental pH, presenting results of ellipsometric examination

17 p2756 A71-34489

Ti alloys metastable omega phase precipitation effect on mechanical properties, using thin film microscopy

17 p2756 A71-34492

Residual stress measurement in thin contoured Ti alloy sheets by X ray diffraction, using stress camera in normal incident beam mode

17 p2757 A71-34537

Environmental effects on SST structural materials fatigue, discussing Ti alloys studies involving temperature effects, crack propagation and residual strength

17 p2821 A71-34556

Corrosion resistance of Ar TIG welded joints in Ti alloys, discussing chemical and mechanical slag film removal effects

17 p2757 A71-34804

Ti alloys electroslog welding with consumable and nonconsumable electrode combinations, presenting W electrode consumption and weld mechanical properties

17 p2748 A71-34805

High temperature Ti alloys welding, discussing strength, ductility, beta stabilizing elements and chemical compositions

17 p2758 A71-34806

Wrought precipitation hardened Co-base alloy, investigating Ti and Al additives effects on tensile and stress rupture strengths, microstructure and fabricability

17 p2758 A71-35147

Beta stabilizers effects on Ti base binary alloys strength, plasticity and stress concentration sensitivity at low temperatures

17 p2760 A71-35465

Vibrotumbling duration effects on surface quality, fatigue resistance and damping properties of titanium alloy structural parts

17 p2760 A71-35665

Crevice effect at stress corrosion crack apex during cathodic polarization of Ti-Al-Mo-V alloy in sulfuric acid, potassium bromide and iodide and methanol solutions

17 p2761 A71-35733

Beta Ti-Pu solid solution, constructing diffusion phase diagrams from electron beam microprobe analysis and autoradiography

18 p2935 A71-36174

Ti alloys diffusion bonding and forging, discussing joints testing and material utilization improvement through die forging process

18 p2927 A71-36656

Diffusion bonding as economical fabrication process for aerospace applications involving Ti alloys, emphasizing mechanical properties and structural reliability improvement

18 p2927 A71-36661

Extruding complex structural shapes of Ti alloys, considering use of glass as lubricant

18 p2927 A71-36662

Cutting speed, feed rate, tool geometry and other machining factors effects on surface finishes of face milled steels, titanium and nickel base alloys

18 p2927 A71-36663

Blue edge anodize technique for revealing segregation in Ti alloys without affecting mechanical properties

18 p2938 A71-37058

Ti-W-B, Hf-Ta-B and Ta-W-B alloys isothermal phase diagrams at 1400 C, using X ray analysis and metallographic techniques

19 p3076 A71-37112

High temperature strengthening of vacuum melted W-Ti alloys with Mo and Zr additions

19 p3076 A71-37267

Deformation rate and temperature effects on optimum strength and ductility of die forged and extruded Mo-Ti alloys

19 p3077 A71-37269

Plastic deformation and fracture of beta Ti alloy under tensile tests at room and low temperatures

19 p3077 A71-37464

Phase diagram of Ti-Cr alloys for temperatures from 800 to 1600 C

19 p3077 A71-37466

Intermediary eutectic delta phase in Ti-Os equilibrium diagram based on microstructural, X ray and differential thermal analyses

19 p3078 A71-37467

Structure, superconductivity transition temperature, microhardness and electrical resistivity of V-Ta-Ti cast alloys

19 p3078 A71-37468

- Phase transformations in superconducting Nb-Ti alloys with Zr during heating or isothermal annealing 19 p3078 A71-37469
- Vertical phase diagrams of Ti-Al-Zr-Mo-Fe alloy system at varying Fe concentrations, showing structural hardening after quenching 19 p3078 A71-37471
- Isothermal phase diagrams and composition effects on plasticity in Mo-Ti-Zr-C system in Al-rich region 19 p3078 A71-37472
- Martensite-type omega phase formation in Ti alloys during grinding by abrasive wheels and tapes, noting dependence on plastic deformation 19 p3078 A71-37474
- Stress effect on hydrogen distribution at high temperatures in titanium and Ti-Al-Mo-V alloy 19 p3080 A71-37720
- Omega phase embrittlement in aged Ti-Mo alloy, giving tensile properties and load-elongation diagrams 19 p3082 A71-38176
- Metallurgical and mechanical properties of Ti-Al-V joints produced by thin film diffusion brazing with copper 19 p3070 A71-38316
- Ti alloys heat resistant properties evaluation for long service under various heat treatment conditions, considering tensile properties, fracture toughness and microstructure 19 p3082 A71-38420
- Argon arc welding of Ti VTS-L alloy to Ti VTS-L and to wrought alloys OT4 and OT4-1, noting ductility, tough and stress raiser insensitive joints 19 p3070 A71-38421
- Ti alloys semiautomatic pulsed arc MIG welding, showing increased productivity and reduced distortion 19 p3070 A71-38423
- Solution temperature and Ti/C ratio effects on Cr-Ni-Ti austenitic steels creep properties, including precipitation, deformation, rupture and coalescence 20 p3250 A71-39025
- Commercial Ti alloys homogeneity as function of ingot diameter, noting mechanical properties of semifinished products 20 p3252 A71-39544
- Intermetallic compound Ti-Ni phase transformations, relating martensite crystal structure with premartensitic instability 21 p3397 A71-40433
- Ti-Ni alloy martensitic thermoelastic transformation and memory effect, using optical microscopy to examine change in lattice discontinuity 21 p3398 A71-40459
- Precipitation hardened Ti-Nb alloy, correlating room temperature tensile properties with microstructure from step aging 21 p3387 A71-40461
- Thermodynamic ion current ratios of solid solution V-Ti alloys, using Knudsen effusion and time of flight mass spectrometric methods 21 p3398 A71-40463
- Thermodynamic activities of Ti and Al in bcc beta phase of Ti-Al system 21 p3398 A71-40465
- Tensile, impact and fatigue properties of welded Ti alloys, determining joint quality and friction welding sensitivity in highly stressed gas turbine components 21 p3387 A71-40619
- Resistance NOR Ti BOND joining of Ti shapes, forming Ti-Cu eutectic at Cu plated Ti joint interface 21 p3387 A71-40620
- Ti-Mo base metastable beta Ti alloy tensile properties anomalies at elevated temperatures, examining strain rate and annealing conditions effect 21 p3399 A71-40699
- Tensile strain response for spallation fracture in metals by impact and electron beam heating of Al, Cu and Ti alloys 21 p3466 A71-40798
- Cryogenic steels, Al and Ti alloys plane strain fracture toughness at room and subzero temperatures, discussing tensile and notch bend results 21 p3401 A71-40915
- Specimen design effects on Al and Ti alloy plane strain fracture toughness at room and cryogenic temperatures, discussing crack propagation and rolling directions orientations 21 p3401 A71-40917
- Ti-Al-Sn and Al alloys thin sectioned specimens cryogenic fracture strength, discussing surface crack fracture behavior 21 p3401 A71-40918
- Titanium-containing steels nitriding in ammonia, discussing hydrogen diffusion layers brittleness, cracking, peeling and thickness 21 p3424 A71-41097
- Superconductivity transition of Nb-Ti solid solutions with varying Ti content, using specific heat measurements at 2.5-20 K 21 p3432 A71-41266
- Temperature and strain rate effects on yield and flow stress of bcc Ti-Mo alloy over 77-824 K range 21 p3404 A71-41414
- Transformation zones of Ti alloy in isothermal conditions after tempering, showing martensite decomposition and omega phase detection by hardness measurements 22 p3560 A71-41624
- Ti alloy microarea alloying element concentration quantitative analysis by EPMA program, obtaining working curves for Al, Fe, Cr, Mo and V 22 p3561 A71-41944
- Ti-Fe and Ti-Cr binary alloys microsegregation genetic trend measurement by electron probe microanalysis, observing critical cooling rate from beta phase 22 p3562 A71-41945
- Beta eutectoid and solid solution Ti binary alloys omega phase morphology observation by transmission electron microscopy, noting elliptical and cubic types hexagonal crystal structure 22 p3562 A71-41946
- Metastable beta type Ti binary alloys isothermal transformation microstructure observation by microscopic and X ray diffraction methods 22 p3562 A71-41947
- Microstructure, yield point and creep rupture strength of Nb-Ti alloy, investigating oxygen concentration and temperature effects 22 p3563 A71-42365
- High temperature Ti-Ni alloy stacking variation stability, studying size, shear and valence electron concentration effects 22 p3586 A71-42367
- Austenitic Fe-Ni-Ti steel strengthening by precipitation hardening and subsequent aging at 600 C 23 p3690 A71-43282
- Fatigue strength of two phase Ti alloys, considering work hardening, electrochemical finishing, electropolishing and protective media 23 p3694 A71-44232
- Thermodynamic properties of Ti-Mo alloys, using triple Knudsen cell technique 23 p3694 A71-44279
- Near equiatomic TiNi thermal martensite transformation premonitory events, discussing crystal structure, mechanical instability and lattice vibrations 23 p3694 A71-44280
- Hydrogen solubility in alpha phase Ti-Al alloys, using resistometric technique and electron microscopy 23 p3694 A71-44282
- Phase and microstructure changes during nitriding process of Fe-Ti alloys, stressing Ti concentration effect 24 p3837 A71-44733
- ### TITANIUM BORIDES
- Titanium diboride contact interaction with Ti, Zr and V in vacuum at various temperatures 09 p1471 A71-23083
- Hot pressed boron carbide and titanium diboride for use as indenter materials for tungsten carbide hardness measurements at high temperatures 15 p2409 A71-32165
- ### TITANIUM CARBIDES
- TiC and ZrC samples with different porosities, examining bending strength at various temperatures 01 p0102 A71-10786
- Titanium and niobium monocarbides electron work function relation to homogeneity region composition, considering electron structure and thermal emission 02 p0263 A71-12199
- Mo-TiC-Ti system phase equilibria at 1400 C, considering two phase region tie lines direction by metallographic and X ray analyses 02 p0264 A71-12279
- Titanium carbide ingots production for laminar and flake precipitation of graphite, using electric arc furnace with consumable electrode 02 p0238 A71-12281
- Secondary recrystallization of Ti, Zr and Nb carbides within homogeneity ranges, determining activation energies as function of carbon deficiency in carbide lattice 04 p0609 A71-14749
- Fused titanium carbide structure and property changes during annealing 05 p0769 A71-16863
- Rapid heating effects on hot pressed TiC cylinders stability, calculating temperature fields and stress distribution 07 p1130 A71-19168
- Temperature dependence of Vickers pyramid hardness for Ti, Zr and Hf carbides at wide temperature range in vacuum 07 p1142 A71-20483
- Solid solution reactions analysis for Ti/TiC powder formation 08 p1304 A71-20993
- Cemented carbides based on TiC-molybdenum carbide-Ni, studying properties as function of molybdenum carbide and C contents in primary solid solution 08 p1304 A71-20994
- Metals and alloys strengthening by in situ grown transition metal carbide fibers, noting whisker-like characteristics 08 p1315 A71-21586
- Single crystal TiC-VC alloys mechanical properties, considering room temperature hardness, high temperature deformation and brittle to ductile transitional temperature 08 p1316 A71-21589
- Ultrasonic vibration effects on TiC sintering during isothermal heating with and without pressure 09 p1470 A71-23080
- Solid state reaction of titanium carbide with Ti, Zr and V in vacuum at high temperatures 13 p2082 A71-27828
- Mechanical properties of carbon fibers thinly coated with TiC by chemical vapor deposition from hydrogen, methane and titanium tetrachloride vapor mixture 13 p2092 A71-28625
- Ceramic rod supported helix derived traveling wave tubes, considering titanium carbide for internal attenuators due to zero temperature coefficient of resistivity 14 p2214 A71-30700
- Titanium carbide based cermet materials with Al-Ni steel binder, investigating production conditions, hardness, machining and quenching properties 15 p2429 A71-32133
- ### Ti-Mo-C ternary system phase diagram
- High resolution energy spectra and valence band structure vs carbon content in homogeneous titanium carbides 15 p2430 A71-32154
- Neutron irradiation effect on lattice parameters and distortion energy of titanium and chromium carbides using X ray analysis 15 p2430 A71-32155
- Thermodynamic properties of titanium carbide of variable composition at high temperature, considering enthalpy, specific heat and entropy change due to thermal vacancies 15 p2431 A71-32159
- High temperature vaporization of titanium, zirconium, hafnium and thorium carbides by Knudsen effusion mass spectrometry, measuring ion intensities, formation enthalpies and dissociation energies 16 p2540 A71-33255
- Abrasive capability, shape and strength of refractory powders of fused titanium and niobium carbides and calcium boride compared with synthetic corundum 16 p2592 A71-33574
- Plastic deformation in hot compressed Ti, Zr and Nb carbides during diamond grinding, studying fine structure on diffractometer 16 p2584 A71-33896
- Hot pressed TiC cylinder thermal shock resistance from tests to failure after heat cycling at 1000-1200 C 17 p2760 A71-35664
- Temperature effects on wear and failure of titanium and niobium carbides, using electron microscopy 19 p3076 A71-37114
- Age hardening of Mo alloys with titanium and zirconium carbides at high temperatures after quenching 19 p3077 A71-37264
- WC and TiC-Co solid solution phase after sintering inhomogeneous structure, investigating grain growth and phase decomposition behavior at various temperatures 23 p3689 A71-43105
- Complex TiC-WC carbides under homogenizing annealing, noting defects, solubility, lattice constant and grain growth 23 p3689 A71-43255
- Ti, Zr and Nb carbides alloying effects on deformed and annealed Mo alloys cellular structure and mechanical properties 24 p3836 A71-44672
- Titanium carbide powder corrosion resistance to sulphuric acid-hydrogen peroxide system at various temperatures 24 p3838 A71-44739
- Homogenizing annealed TiC-WC carbides properties at room temperature, investigating microhardness, microbrittleness and resistivity 24 p3838 A71-44740
- Titanium, niobium and tungsten carbides microhardness temperature dependence at 77-1973 K, discussing activation energy and deformation mechanism 24 p3838 A71-44741
- ### TITANIUM COMPOUNDS
- NT BARIUM TITANATES
- NT ILMENITE
- NT LEAD TITANATES
- NT PEROVSKITES
- NT RUTILE
- NT STRONTIUM TITANATES
- NT TITANATES
- NT TITANIUM BORIDES
- NT TITANIUM CARBIDES
- NT TITANIUM NITRIDES
- NT TITANIUM OXIDES
- Titanium dichloride phase modifications under hardening at various temperatures, using thermal and X ray analysis 02 p0266 A71-12674

Ni maraging steels weld heat-affected zone, showing liquid grain boundary film formation due to titanium sulfide inclusions constitutional liquidation 04 p0603 A71-14921

Apollo 11 and 12 lunar rock opaque oxides differences in titanium contents 05 p0807 A71-16298

TiS vaporization thermodynamics by high temperature mass spectrometry, considering ionic fragmentation and ionization cross section errors 07 p1054 A71-19368

TiH metallographic and lattice parameters variation with hydrogen content 07 p1139 A71-19993

TiNi martensitic transformations-fatigue strength relation at room temperature, observing hysteresis in tensile compressive loading cycle to maximum stress 09 p1477 A71-23349

Cu-Ti-Al system intermediate phases crystallization from melt in large concentration areas, discussing four-phase reactions 10 p1627 A71-24597

Galvanomagnetic properties of solid refractory zirconium and titanium compounds in two-band representation, measuring Hall effect and reluctance vs external magnetic field 15 p2426 A71-31512

Titanium and silicon tetrachlorides oxygen-containing impurities determination without hydrolysis, describing measuring device design 15 p2383 A71-31659

Titanium, vanadium and niobium carbohydrides, investigating electronic structure effects on atomic behavior 15 p2429 A71-32140

Chemical properties of titanium, zirconium and hafnium germanides exposed to acids, oxidizers, complex salts, alkaline solutions and water 19 p3075 A71-37106

Bulk and surface hydrogen concentration comparison in NBS hydrogen-in-titanium standards 19 p3080 A71-37718

Titanium dihydride room temperature polymorphic transition from fcc to body centered tetragonal, noting different transition temperatures 22 p3563 A71-42368

TITANIUM DIOXIDE
U TITANIUM OXIDES
TITANIUM ISOTOPES
Li, B, Mg and Ti isotopic abundances and search for trapped solar wind Li in Apollo 11 and 12 rocks 23 p3752 A71-43708

TITANIUM NITRIDES
Grain growth inhibition in niobium diboride by TiN addition 07 p1144 A71-19390

Titanium nitride sintering in vacuum, noting strain by grain sliding to pore center under surface tension force effects 12 p1918 A71-27527

Nitrogen solubility in Ni-Mo and Ni-W melts, detailing Ti and pressure effects 15 p2424 A71-31392

Hall effect and reluctance of TiN and ZrN specimens obtained by hot compression 15 p2427 A71-31515

TITANIUM OXIDES
NT ILMENITE
NT RUTILE
Initial surface superheating effects on high temperature oxidation of titanium in oxygen or dynamic air atmosphere 01 p0101 A71-10672

Si solar cells with titanium oxide antireflection coatings, discussing environmental test results 05 p0700 A71-16064

Si solar cells with antireflection titanium dioxide layer, comparing performance with conventional adhesive cover system 05 p0700 A71-16065

X ray analysis of oxide film structure, oxygen concentration and residual stresses at surface of oxidized Ti and Ti alloy 08 p1317 A71-21760

Ti dioxide-opacified porcelain enamel reflectance spectra analysis, deriving scattering cross sections and dispersed particle sizes and distribution 09 p1480 A71-22116

Elemental analysis for lunar rocks and regolith, comparing silicon oxide and titanium oxide composition in Apollo 12 and Apollo 11 samples 10 p1672 A71-24389

Alumina and titania codeposition from acid copper electrolyte as function of oxide crystalline form, discussing addition agents effects 11 p1779 A71-26011

Sodium oxide-titanium dioxide-water ternary system, determining sodium titanates formation regions in equilibriums in 300 C isotherm 15 p2367 A71-31902

M stars atmospheric temperature determination from TiO molecular spectrum by vibrational band intensity measurement 23 p3771 A71-44307

TITRATION

Aircraft turbine oils acid number potentiometric determination, discussing automatic titration procedure and apparatus and solvents influence on titration curve and inflection point 18 p2940 A71-36680

TNT [TRINITROTOLUENE]
U TRINITROTOLUENE
TOBACCO
Isolated tobacco chloroplasts disintegration, measuring simultaneous particle size and photochemical reduction rate changes by electron microscopy 04 p0539 A71-15269

TOLERANCES [MECHANICS]
Soviet book on bolting and coupling elements threads used in aircraft industry covering configurations selection, cutting, tolerance requirements and quality control 02 p0258 A71-12723

Group and form classification of production errors and tolerances in aircraft construction 04 p0602 A71-14610

Monograph on tolerance effects and performance degradation in microwave acials covering axial displacement, active array, radiation pattern prediction and mutual coupling 13 p2037 A71-28495

Tasks with subject guiding vehicle at arbitrary speed along tolerance band defined course, considering prediction model for velocity-bandwidth relationship 17 p2693 A71-35437

Hydraulic servo equipment filtration systems design, discussing contamination effects and servo components physical characteristics effects on tolerance level 19 p2999 A71-38320

TOLERANCES [PHYSIOLOGY]
NT ACCELERATION TOLERANCE
NT ALTITUDE TOLERANCE
NT COLD TOLERANCE
NT HEAT TOLERANCE
NT HUMAN TOLERANCES
NT RADIATION TOLERANCE
Hypoxia tolerance of aircrew with previous impaired flight consciousness in high altitude high performance aircraft 06 p0859 A71-17617

Simulated high altitude chronic hypoxia and long term sideropenic anemia adapted animals, investigating acute anoxia tolerance of myocardium 07 p1044 A71-20331

Carbon dioxide tolerance after hypercarbia adaptation of rhesus monkeys in upright position 09 p1395 A71-23250

Rats hypoxia tolerance, noting smoke effects on survival, respiratory rate, body temperature and glycolytic parameters 09 p1396 A71-23364

Dynamics of increasing organism resistance to hypoxia, considering reactions occurring in various tissues during adaptation 12 p1869 A71-26653

Tolerance tests including EEG, glucose test, thermal stress and G stress for aircrew fitness assessment after cranio-cerebral incidents 12 p1871 A71-27633

Ar, N and Ne partial pressure tolerance in dogs, plotting saturation curves 13 p2005 A71-28038

Simple organisms resistance and adaptation to low pressure, anoxia, intense cooling, UV irradiation and Mars conditions 13 p2009 A71-28687

Rabbit tolerance to pulmonary edema by lung exposure to low ozone dosage 19 p3009 A71-38558

Lateral accelerations effect on mice tolerance to toxic doses of aminothiols and indolylalkylamine-series radiation protection drugs 22 p3491 A71-42706

Healthy males immersion in water containing NaCl, determining modified gravitational field effect on motor functions 22 p3505 A71-42792

Toxic gaseous compounds effects on low pressure tolerance of rats under hypoxic hypoxia in atmosphere containing polymer decomposition products 22 p3506 A71-42806

Animal tolerance to carbon monoxide, nitrogen oxide, triethylamine and freon-12 toxic effects after adaptation to hypoxia from tests on albino mice 22 p3496 A71-42810

TOLLMEIN-SCHLICHTING WAVES
Tollmien-Schlichting waves in flow field of mixed coaxial laminar air diffusion flames, using flow visualization and hot-wire anemometry 19 p3167 A71-38094

Laminar boundary layer transition prediction techniques, evaluating empirical formulations and Schlichting-Tollmien stability methods [AJAA PAPER 71-985] 24 p3817 A71-44581

TOLUENE
Toluene and aniline-methylcyclohexane and toluene-aniline nonideal liquid systems, measuring

molecular diffusion coefficients as function of concentration by Savart plate birefringent interferometer 24 p3820 A71-45074

TONE

U PITCH

TONGUE

Evoked cortical responses to taste solutions of acid and salt applied to human tongue surface, using averaging technique 13 p2012 A71-28887

TONOMETRY

U INTRAOCULAR PRESSURE
U PRESSURE MEASUREMENTS

TONUS

U MUSCULAR TONUS

TOOLING

Ni and Fe alloys for tooling materials, examining die life and wear at elevated temperatures [SME PAPER MF-70-121] 01 p0900 A71-11266

Epitrochoidal profile machining methods and tools for chamber surface in Wankel engine 02 p0257 A71-12560

Three dimensional isostatic pressing process, discussing equipment, tooling and forging preforms and finished parts production 10 p1618 A71-24764

Tools production and shaping for extrusion of light metal profiles 10 p1619 A71-25032

TOOLS

NT BORING MACHINES
NT GRINDING MACHINES
NT LATHES
NT MACHINE TOOLS

Carbon fiber composites utilization problems for product and tool designers, considering mechanical properties anisotropy, fiber alignment and bundle strength [PLASTICS INST. PAPER 42] 08 p1322 A71-20931

Ni-base alloys machining, discussing special tools and manufacturing methods with special reference to machinability of Inconel 718, Rene 41 and 95 [SME PAPER MR-71-825] 15 p2416 A71-32427

TOPOGRAPHY

NT LUNAR TOPOGRAPHY

Side-looking airborne radar (SLAR) imagery and site selection for soil pattern topography 02 p0244 A71-11952

EEG topography continuous recording for signal analysis based on regression theory 05 p0713 A71-16321

Interactive computer graphics in cartography, considering on-line updating of digital topographic map file by human decision making 08 p1281 A71-21248

Forested area landscape characteristics from remote sensed imagery, establishing base line information for vegetation mapping 09 p1438 A71-23209

Mars surface harmonics and continental drift from radar and spectroscopic topographic height determination 16 p2638 A71-33519

Impact craters and depressions on earth, examining meteoritic origin, characteristic features, energy release and cryptovolcanism 17 p2805 A71-35376

Martian surface topography effects on mean wind from time independent and frictionless thermal wind equation solution for radiative-convective atmospheres at scaling analysis level 18 p2964 A71-36287

Australian Liverpool and Strang way craters as probable meteoritic impact origin from topographic and petrographic data 19 p3049 A71-37653

Ries structure in southern Germany, considering complicated crater geometry revealed by surface topography and geophysical investigations 19 p3049 A71-37654

Astronomical telescopic observations of Mars for map updating, discussing surface colors 19 p3145 A71-38570

Externally pressurized gas-lubricated foil bearing rotation speed effects on gap topography and clearance variation 22 p3552 A71-41671

Amplitude prediction for terrestrial radar echoes from ground using topographical data 22 p3514 A71-42469

TOPOLOGY

NT FIXED POINTS [MATHEMATICS]
NT IMBEDDINGS [MATHEMATICS]
NT INVARIANT IMBEDDINGS
NT METRIC SPACE

Charged particle motion in magnetic dipole field, investigating singularity and topological flow nature 01 p0127 A71-10382

Bilateral switching networks synthesis by topological technique, tracing truth table optimum path by visual pattern detection 08 p1270 A71-21665

TOPS [SPACECRAFT]

- Universe models topology, examining relation between CT and CP invariance 08 p1366 A71-21786
- Perturbed magnetic surfaces topology in quadrupole, estimating local imperfections size for plasma control 10 p1652 A71-24661
- Topological unistor graph solutions to linear equations of electronic circuits by structural conjugate numbers on digital computer 11 p1792 A71-26376
- Topological methods of linear electric circuits analysis, considering Kirchhoff, Maxwell and Mason methods 11 p1743 A71-26464
- General Markov processes, considering topological space E and semigroup t equal to or greater than zero 12 p1922 A71-26819
- Relativistic stellar wind problem, discussing topology solutions 15 p2490 A71-32399
- Universe models topology, examining relation between CT and CP invariance 16 p2638 A71-33547
- Systems concept formalization, including structural relations on basis of set theory, topological considerations and flow theory 17 p2777 A71-34599
- French monograph on topological classification and identification of nonlinear systems by structural decomposition method covering general systems theory fundamentals 17 p2767 A71-35230
- Polynomial Hamiltonian for type VIII and IX vacuum cosmologies, suggesting quantized versions involving fluctuations of 3-space signature and topology 18 p2946 A71-35983
- Active network analysis by topological formulation, eliminating k-trees 19 p3038 A71-38489
- Physical constraints on universe topology near collapsed ordinary stars interaction in general relativity theory 19 p3105 A71-38583
- Stationary signal space topology concept in special relativity, considering points neighborhoods as independent of signal sending time 21 p3346 A71-40091
- Crystal lattice drag by conduction electrons and Onsager relationship between electroacoustic coefficients valid for arbitrary topology of Fermi surface 21 p3428 A71-41127
- Spiral topology of chromospheric fibrils and filaments in H alpha near sunspots, noting similarity with axisymmetric force free magnetic field configuration 22 p3597 A71-41458
- Thermodynamic systems generalized topological representation providing real system conceptual reticulation into elements from ideal lumped parameter components 22 p3621 A71-42674
- Topological characterization for constant angular momenta and energy surfaces in equal mass planar three body problem 22 p3568 A71-42697
- Relationships among topologies definable on commutative algebraic ring 24 p3843 A71-44798

TOPS [SPACECRAFT]

- Catalytic hydrazine thruster design, fabrication and testing for TOPS spacecraft single-axis attitude control simulation program [AIAA PAPER 71-706] 14 p2294 A71-30763
- Thick film microcircuit DC-TO-DC converter electronics design for TOPS spacecraft power subsystem [AAS PAPER 71-153] 19 p3153 A71-37955
- TOPS spacecraft parts and technology development, reliability and contribution to long life system design [AAS PAPER 71-159] 19 p3152 A71-37928
- Jupiter entry probe integration on TOPS and Pioneer outer planet spacecraft for flyby missions, discussing design feasibility and spacecraft modification requirements [AAS PAPER 71-153] 19 p3153 A71-37955

TORCHES

- Powders and torch techniques for brazing, including Mn-Ni-Co, Cu-Mn-Ni, Zr-Ti-Be, Ti-Cu-Ni and Zr-Be alloys 11 p1769 A71-25746

TORNADOES

- Maximum wind speed estimation in tornadoes and waterspouts, using cloud deck height and funnel cloud photographs 03 p0453 A71-14203
- Space technology utilization in weather problems, considering tornado and other meteorological phenomena similarity to swirling vortex formation during missile flight 04 p0621 A71-14818
- Rocket probe launched by aircraft for measuring pressure, temperature, magnetic field and wind

velocity around tornado vortex through radio telemetry 05 p0778 A71-17140

Radiation measurements near thunderstorms and tornadoes, testing hypothesis of meteoritic matter-antimatter annihilation mechanism for ball lightning 10 p1599 A71-23752

Tornado producing thunderstorms upper level outflow synoptic and dynamic processes from ATS 3 pictures, discussing convective warming effects 11 p1794 A71-25381

Tornado and waterspouts, using concentrated vortices produced in laboratory rotating tanks and mathematical models 17 p2726 A71-34657

TOROIDAL DISCHARGE
NT RING DISCHARGE

German monograph on steady toroidal discharges and cylindrical vortex arcs, using electromagnetic gas dynamics equations 10 p1654 A71-25025

TOROIDAL PLASMAS

Plasma rotation effects on toroidal systems diffusion, considering pressure gradient, rotational velocity, transverse electric field and path lengths 03 p0464 A71-13931

Plasma ring vortex formation in atmospheric crossed electric discharges, analyzing photographs of vortex onset and development 04 p0631 A71-14600

Tokamak copper shell as feedback control device for toroidal plasma, considering stabilization of thermal instability 06 p0932 A71-17462

Low pressure toroidal plasma confinement with flow in axially symmetric configurations, using numerical model 06 p0935 A71-17554

Stable ellipsoidal plasma configurations in alternating electrode annular system, considering longitudinal magnetic field strength, electrode voltage and gas discharge chamber pressure 07 p1171 A71-20185

Plasma ring vortices in crossed electrical discharges attributed to shock wave induced plasma flow across lines of force of azimuthal magnetic field 08 p1338 A71-20785

Current carrying plasma in toroidal trap, studying instability and equilibrium due to captured and escaping particles 08 p1339 A71-21476

Star group formation theory, proposing hypothesis on toroidal stages in stellar evolution 09 p1524 A71-23183

Electromagnetic extraordinary wave propagation in toroidal plasma with sheared magnetic field, discussing ordinary component generation at upper hybrid frequency 10 p1650 A71-24629

Poloidal magnetic field measurements in toroidal pinch by Thomson scattered carbon dioxide laser beam 10 p1651 A71-24631

Plasma jet drift stabilization in toroidal magnetic field with diverter producing 180 degree field line rotation 12 p1941 A71-27548

Fast plasma ions energy distributions in toroidal accelerators with quasi-stationary discharge 13 p2108 A71-28854

Equilibrium of current carrying plasma in toroidal system, studying instabilities due to trapped and slowly drifting particles 14 p2282 A71-30662

Equilibrium diffusion of rotating plasma in toroidal systems, deriving two fluid hydrodynamic equations with allowance for ion temperature perturbation 19 p3109 A71-37140

Finite-beta stabilization of collisionless trapped particle mode in toroidal plasma confinement devices, using magnetic well dug by plasma diamagnetism 19 p3112 A71-37742

Tokamak T-3A device plasma electron temperature measurements, using Thomson scattering with electric, microwave, laser and diamagnetic data 19 p3113 A71-37854

Shearless magnetic fields discontinuities in marginal stabilization of MHD instabilities for constant pinch force free fields, including toroidal effects 20 p3275 A71-39463

HF plasma heating in Tokamak torus device by magnetosonic wave energy absorption in high density region via Buchsbaum hybrid resonance 21 p3422 A71-40764

Hot plasma fast ions energy distributions in toroidal accelerators with quasi-stationary discharge 21 p3426 A71-41286

Plasma/magnetic field pressure ratio and inductance per unit length in Tokamak plasma pinch with arbitrary cross section 22 p3579 A71-41583

Slow toroidal theta-Z pinch experiment, describing measurements temperature distribution with emphasis on transitions between stable and unstable states 22 p3580 A71-41588

Plasma acceleration of low pressure toroidal discharge, measuring plasma velocity as function of radial magnetic field for different pressures 23 p3711 A71-41458

Stationary toroidal plasma under external magnetic field, investigating classical resistive diffusion velocity with one fluid MHD equations 23 p3713 A71-41458

Plasma diffusion lifetime and electron concentration measurements in Tokamak-3 by pulsed neon hydrogen injection and microwave multichord probe 24 p3852 A71-41458

Multispecies high temperature Tokamak pinch heating by energetic particle injection, using Bales-Lenard kinetic equation 24 p3852 A71-41458

Tokamak T-3A plasma neutron emission, considering thermonuclear nature of radiation 24 p3856 A71-41458

Quasi-stationary electric field in toroidal magnetization chamber with meridional and equatorial slots, deriving formulas for components as function of coordinates 24 p3857 A71-41458

TOROIDAL SHELLS

Staticgeometrical relations of thin torus shell and closed curvilinear rods 05 p0824 A71-14140

Thin elastic toroidal shells under nonsymmetric loading, reducing problem to membrane edge effect linear solutions 06 p1002 A71-14140

Thick-walled toroidal shell under various load distributions, analyzing stress-strain state by network method using computer program 08 p1369 A71-20785

Reinforced toroidal shells stability under critical loads, edge moment and heating, using finite difference method 14 p2332 A71-30662

Toroidal shell stability analysis for asymmetric buckling based on small deflection theory linear relations, deriving upper critical pressure by Bubner-Galerkin method 17 p2831 A71-30662

Curved finite element for elastic-plastic analysis of thin toroidal shells of revolution with discontinuous meridional slope under axisymmetric loadings 24 p3879 A71-41458

TOROIDS

Optimal design of toroidal inductors with DC without repetitive trials 01 p0053 A71-14140

Pressurized toroid modified linear membrane theory, presenting approximate solutions for derating boundary value problem by variational calculation methods [ASME PAPER 70-WA/APM-49] 03 p0512 A71-14140

Micro pulsations dynamic properties and resonance cavity modes, obtaining coupled toroidal and poloidal modes solution 06 p0969 A71-14140

Purely azimuthal magnetic toroidal-meridional component poloidal field conversion by slow precession motion superimposition on rotating fluid uniform current distribution 06 p0894 A71-14140

Coaxial plasma beam polarization interaction in toroidal magnetic field with diverter, showing stream trapping in hollow plasma cylinder 15 p2453 A71-30662

Consecutive toroidally circulating buoyant element interactions by numerical simulation, including vortex formation process effects 18 p2901 A71-30662

Magnetic induction by HF current passing over conducting torus enclosed by larger torus, obtaining vector potential, current density and inductance expressions 24 p3857 A71-41458

TORPEDO ENGINES

NT ULLAGE ROCKET ENGINES

TORQUE

Thermomagnetic gas torque within kinetic theory framework for collinear static and alternating magnetic fields 02 p0291 A71-12040

Permanent magnet torque generator reaction torque effect in precision gyros and accelerometers 02 p0279 A71-12040

Unwanted gimbal rotation friction torques in gimbal wheel bearings due to lubrication viscous friction, wedging and contamination 02 p0253 A71-12040

Helicopters safe antitorque control, describing Fenestron ducted fan design 04 p0532 A71-15140

Synthesized hydrocarbon oil antiwear and extreme pressure additives effects on bearing spinning torque and endurance 06 p0904 A71-17140

Solar wind torque on earth magnetic dipole based magnetosphere model analytic solution in rotating reference frame 06 p0891 A71-17140

- Control of time varying mechanical torque normal to ball bearing pair common spin axis by cross torque control through misalignment coupling
[ASLE PREPRINT 70LC-9] 08 p1298 A71-21156
- Aerodynamic forces and hinge moments of delta cruciform control surface in blunt-nosed canard configuration for subsonic, transonic and supersonic flows
11 p1701 A71-25161
- Thermally induced torque of circular thin walled open section booms, predicting steady state behavior
13 p2148 A71-27980
- Pulse width modulation controlled DC motors, deriving formulas for speed and torque characteristics
13 p1999 A71-28630
- Differential rotational equations of motion for triaxial rigid body about center of mass under arbitrary torque
14 p2307 A71-29882
- Solar wind torque on geomagnetic cavity by rotational unipolar induction currents, including Joule heating of ionospheric plasma and directional magnetic fields
15 p2474 A71-31773
- Thin walled tubes under external and internal pressures axial loads and torques, showing load capacity limit dependence
15 p2428 A71-31860
- Turbulent gaseous nonmagnetic protogalaxies under external torques, calculating angular velocity distribution
15 p2490 A71-32400
- Free and enclosed disks rotation resistance at high Reynolds numbers, calculating fluid induced torque with logarithmic velocity profiles for turbulent boundary layer flow
[ASME PAPER 71-APM-25] 16 p2520 A71-33204
- Low speed angular contact bearings surface geometry effects on friction perturbation torque ripple frequency
18 p2928 A71-36764
- Transfer function system relating cornering force and aligning torque of rolling pneumatic aircraft tire to yaw angle and lateral displacement
21 p3324 A71-40167
- Transient torsional vibration due to suddenly applied torque, deriving transfer function for systems with four degrees of freedom
[ASME PAPER 71-VIB-99] 21 p3461 A71-40326
- Thin skewed plates bending and twisting at constant temperature moment, obtaining angle skew effects on torque-twist relation
21 p3463 A71-40592
- Infinite sandwich plate under concentrated corner torque load on one side, determining stress distribution with double infinite Fourier transform
22 p3614 A71-41604
- Mathematical model of solar radiation pressure force and torque acting on spacecraft surface intercepting solar photon stream
[AAS PAPER 71-352] 23 p3728 A71-43024
- TORQUE MEASURING APPARATUS**
- TORQUEMOTORS**
- Four phase reluctance motor design for electromagnetic torque variation, examining function of commutation frequency and phase time constants
17 p2677 A71-35710
- TORQUEMETERS**
- Strain gage torque meter as primary power indicating instrument in helicopter transmission systems, providing advantages for helicopter designer and operator
[AHS PREPRINT 563] 14 p2250 A71-31110
- TORQUES**
- Permanent magnet torque generator reaction torque effect in precision gyros and accelerometers
02 p0279 A71-12452
- Magnetic torquer for satellite attitude control consisting of solenoid with hard magnetic material core
18 p2973 A71-36463
- TORSION**
- Torsion computation for bar with rectangular cross section by analogy with electrical networks, comparing with Saint Venant results
01 p0167 A71-10340
- Torsion of solid bounded by one sheet of hyperboloid of two sheets of revolution under mixed boundary conditions, using Legendre transform
01 p0173 A71-10843
- Variational equation of motion for thin walled open section bars coupled flexure and torsion, considering thermal effects
[ASME PAPER 70-WA/APM-51] 03 p0513 A71-14169
- Rotating shafts stability under torsion with two unequal flexural rigidities
04 p0672 A71-15773
- Universal endurance test machine for tubular samples torsion testing under hydrostatic pressure
04 p0673 A71-15899
- Torsional wave propagation in elastic circular composite cylinders, introducing correction factors for approximate theory
07 p1214 A71-19955
- Composition and composition inhomogeneity effects on plated wire memory elements strain sensitivity, considering tension and torsion sensitivities
09 p1509 A71-23115
- Epoxy resin fatigue behavior from double torsion technique, considering stable crack movement in brittle materials
11 p1785 A71-25401
- Orthotropic conical shell subjected to torsion, using Ritz approximate energy method for linear stability problem solution
11 p1848 A71-25618
- Nonhomogeneous variable diameter rods plastic torsion, deriving stress function and distribution
11 p1848 A71-25620
- Solid circular Ti shaft torsion boundary value problem solution, using elastic-viscoplastic materials thermodynamics and constitutive relations
11 p1849 A71-25801
- Axisymmetric bodies torsion problems solution by superimposing elasticity equations, using point matching technique
14 p2329 A71-30463
- Orthotropic thin walled bars with rigidly connected rectangular elements, applying displacement under torsion with allowance for shear to H beam
17 p2823 A71-34782
- Rectangular composite prismatic bar with T shaped cross section, calculating torsion with summary representation method
17 p2824 A71-34847
- Torsion problem of inhomogeneous anisotropic viscoelastic rod transformation, using area variation coefficient for modeling
17 p2828 A71-35240
- Conformal integrability for symplectic and cosymplectic structures, studying torsion and curvature tensor fields
18 p2976 A71-36126
- Numerical stability of extended Kantorovich method for single term variational approximation of torsional problem
18 p2980 A71-36702
- Torsion of hollow beam consisting of two homogeneous isotropic rods with different elastic properties and simply connected cross sections, solving by conformal mapping
19 p3155 A71-37387
- Function construction procedure for ring-shaped structure conformal mapping onto doubly connected regions with simple contours, applying to prismatic rod torsion problem
23 p3776 A71-43419
- Thin soft layer under steady creep conditions, considering axisymmetric problem of simultaneous tension and torsion
24 p3877 A71-44409
- Algorithm for pure torsion of doubly connected square profile prismatic bars with hole, using R functions and variational technique
24 p3881 A71-44834
- TORSIONAL STRESS**
- German monograph on nonlinear flexural-torsional stress analysis of thin walled rods with open profiles covering fork supported and cantilever beam systems
01 p0166 A71-10112
- Repeated bending and torsion of viscoplastic bars and circular cylinders, using hereditary nonlinear integral equations
02 p0322 A71-11688
- Stress concentration in buckling proof clamped sandwich rod with multicut rectangular cross section under torsional bending
03 p0504 A71-13527
- Mechanical model for orthotropic elastoplastic plates with clamped torsion susceptible ribs
03 p0504 A71-13528
- Thin walled prismatic body resistance to torque by extension of solution for rectangular bars, considering shearing stresses and transverse forces
03 p0505 A71-13542
- Thin walled prismatic shell constrained torsion problem, applying Reissner mixed variational method
06 p0992 A71-17806
- Composite elongated ellipsoid of revolution under torsion, determining stress-strain state, boundary conditions and elastic displacements
08 p1368 A71-20800
- Beams torsional rigidity under thermal stress due to arbitrary temperature distribution
09 p1534 A71-22103
- True torsional stress at plastic strain onset determination in terms of elasticity theory
09 p1536 A71-22323
- Buckling by torsion of straight circular cylindrical elastically supported bars, using initial parameters method based on matrix calculus
09 p1536 A71-22412
- Electromagnetic testing machine for torsion fatigue characteristics under steady and programmed cyclic loading conditions
09 p1426 A71-22498
- Stability characteristics of glass fiber reinforced plastic orthotropic cylindrical shell with elastic filler under torsion
09 p1539 A71-22821
- Torsional oscillation of hollow isotropic elastic cylinder encased in thin elastic shell, deriving representation satisfying equation of motion and initial and boundary conditions
09 p1539 A71-22918
- Crystalline Al stress-strain function parabolic law generalization under combined axial tensile-torsional loading
09 p1480 A71-23700
- Photoelasticity methods applied to model of beam of revolution under simple torsion constructed by stress freezing technique
10 p1684 A71-23837
- Tensile yield and ultimate strength and elongation of Al after unidirectional and reversed torsional prestrain
10 p1624 A71-23940
- Metal plates and sheets stress corrosion cracking velocities, using torsion crack propagation specimen at constant load or deflection
10 p1627 A71-24474
- Torsional-flexural stability of stiffened Ti panels for application to supersonic transport, using small deflection energy methods
[AIAA PAPER 71-338] 11 p1843 A71-25317
- Room temperature rated coercive force measurements of Ni sheet specimens in torsional bending cycles for saturation value, using ballistic method
11 p1778 A71-25563
- Reinforced plates flexural and torsional rigidity characteristics for stiffeners design, considering oblique angular coordinates system
12 p1982 A71-27509
- Torsion creep tests of Al, deriving expression for steady state creep rate as function of temperature and stress
13 p2083 A71-27963
- Uniform torsion of elastic body weakened by spherical cut in form of rigid inclusion
13 p2150 A71-28139
- Load capacity and transient creep of thin walled rod under free torsion, using successive approximations
13 p2157 A71-29212
- Torsion of circular composite rods of sectors with different shear moduli and radial cracks
14 p2326 A71-30193
- Titanium alloy durability under cyclic torsion in vacuum at various temperatures, investigating fatigue life and tensile strength
15 p2428 A71-31856
- Fatigue testing machine for axial and torsional loadings at low temperatures in vacuum
15 p2384 A71-31858
- Circular cylindrical shell with elliptic hole, calculating stress concentration around hole under torsion
15 p2506 A71-32014
- Displacements produced by impulsive torsional body force situated within elastic half space bonded to half space of different material properties
16 p2647 A71-32859
- Thin walled rod of strain hardenable material, developing constrained torsion approximation for creep and relaxation
16 p2651 A71-33060
- Flexural-torsional fatigue fracture of duraluminum, noting dependence on cyclic stress, frequency and medium
16 p2593 A71-33689
- Constrained torsion of spar box fastened along isolated parts of wing span, noting structural failure due to tangential stress distribution
17 p2830 A71-35313
- Saint Venant principle generalization for transient creep and stress relaxation analysis in rectilinear thin walled multiply connected beam under torsion
17 p2833 A71-35612
- Cyclic torsional shear testing of refractory materials at normal and high temperatures, describing test equipment
17 p2834 A71-35672
- Test apparatus for studying stress-strain behavior of thin walled metal tubes in torsion, examining strain rate and history effects
18 p2935 A71-36234
- Resolved stress formula for shafts under simultaneous tangential bending and torsion acting at dangerous points of cross section
18 p2981 A71-36721
- Thin walled beam structures under external torsional loading, calculating distribution of longitudinal and shear stresses
18 p2982 A71-36808
- Elastic stability of prismatic and cantilever bars in torsion
21 p3472 A71-41150
- Regular and singular perturbation solutions for beam bending under axial forces and shaft warping in torsion
22 p3616 A71-42214
- Effective shear modulus of multilayered rectangular elastic isotropic member in uniform torsion
22 p3618 A71-42587

Strength and deformation characteristics of glass plastic under torsional and compressive shear loads, investigating temperature effects on elastic modulus 23 p3697 A71-44204

Stress state of arbitrary contour body of revolution under torsion using finite difference method 23 p3779 A71-44218

Factorial determinants in solving space contours, considering bending and torsional moments in structural analysis 24 p3881 A71-44800

Curvilinear elasticity solutions to stress concentrations at fine necks in cylindrical shaft under torsion, considering semicircle, semiellipse, rectangle, triangle and arc shapes 24 p3882 A71-44846

Thin walled tube under combined bending and torsion, considering stress distribution and curvature behavior 24 p3883 A71-44892

TORSIONAL VIBRATION

Natural frequencies of cantilever turbine blade with asymmetric aerofoil under coupled bending-torsion vibrations, using Ritz-Galerkin method for equations of motion 01 p0143 A71-11014

Flexural-torsional vibration stability of thin walled elastic bars under longitudinal periodic force, using parametric resonance theory 02 p0321 A71-11687

Turbomachine blades torsional-bending vibrations aerodynamic damping, noting natural frequency shift 03 p0340 A71-13141

Energy dissipation during torsional and flexural vibrations of steel and duralumin specimens subjected to plastic deformation, accounting for discrepancies due to methodical errors 04 p0671 A71-15640

Transverse and torsional vibrations of fuselage-wing combination with wing tip fuel tanks, calculating mass and stiffness matrix for elastic beam 07 p1022 A71-20364

Contained cross sectional deformation effects on turbine blades natural torsional vibration frequencies 08 p1372 A71-21617

Energy dissipation during independent flexural-torsional vibrations of rods, noting alternating shear stress superposition effect on damping 09 p1538 A71-22629

Elastic media damping effects on rigid bodies HF vertical and rotational vibrations, considering approximate solution for structural amplitude response 09 p1541 A71-23088

Lumped parameter torsional and flexural system synthesis for vibratory characteristics, using transfer matrices 10 p1692 A71-24925

Thermal flutter of satellite storable tubular extendible members, determining static flexural and torsional vibrations due to solar radiation 12 p1984 A71-27736

Bending and torsional oscillations in rectangular specimens of femur and tibia, calculating elastic and shear moduli of compact bone tissues 13 p2019 A71-28658

Twist-bending vibration of ring of rectangular cross section for entire range of length-to-diameter ratios, using Rayleigh shell theory 14 p2328 A71-30414

Torsionally oscillating disk in steadily rotating incompressible second order fluid, calculating transverse and radial shear stress 15 p2387 A71-31185

Vibration analysis for static and rotating objects by stroboscopic holography, considering axial flow compressor blades and two-mass system with torsional vibration 15 p2404 A71-31273

Circular rings coupled twist bending vibrations, considering rotatory inertia and shearing deformation effects 15 p2510 A71-32517

Rotary inertia and shear deformation effects on three dimensional flexural vibrations of circular ring on elastic foundation 16 p2657 A71-33421

Logarithmic decrement of flexural, longitudinal and torsional vibration damping of various size rods, taking into account surface layer energy loss 16 p2659 A71-33799

Cross sectional warpage effects on turbine blades natural torsional vibration frequencies 17 p2834 A71-35677

Instrumentation and techniques of torsional pendulum and braid analyses, studying trace moisture and cure cycle effects on thermomechanical spectra of polymeric materials 18 p2939 A71-36596

Time optimal control for distributed systems with random properties, considering integral relations and flying wing vehicle torsional vibration problems 19 p2994 A71-37094

Viscous torsional vibrations inadequacy for interpreting solar activity cycles relative to magnetic field 20 p3290 A71-39303

Torsional natural frequencies in coupled turbine and reciprocating engine system driving common propeller, using matrix techniques [ASME PAPER 71-VIBR-83] 21 p3461 A71-40319

Transient torsional vibration due to suddenly applied torque, deriving transfer function for systems with four degrees of freedom 21 p3461 A71-40326

Free axisymmetric torsional vibrations of thick hollow conical frustums cantilevered at small end, considering conicity and cone thickness effects 22 p3618 A71-42590

TORSO

Anatomical load sensing method, determining torso pain thresholds by sensitivity tests [SESA PAPER 1823A] 17 p2689 A71-34539

TORUSES

Dynamic systems toroidal manifolds disturbance, discussing invariant torus preservation 08 p1336 A71-22017

TOUCH

NT TACTILE DISCRIMINATION

Spatial and temporal discrimination functions in vision, audition and touch, establishing and controlling stimuli by vibrators 14 p2188 A71-30252

Computerized touch display for ATC tasks compared to conventional keyboard tabular display performance 21 p3413 A71-40114

TOUCHDOWN

Helicopter optimal autorotation landing parameters for touchdown at zero speed, including rotor rpm drop due to flow separation on blades 23 p3627 A71-43090

TOUGHNESS

NT NOTCH SENSITIVITY

Prealloyed hot formed Cr-Ni-Mo and Ni-Mo steels manufactured from powders, considering toughness, tensile properties, fatigue and impact strength 01 p0100 A71-10464

Fabrication, texture, alloying, substructure and fracture effects on bend ductility and toughness of beryllium sheet 15 p2436 A71-32509

Fibrous composites with multiple and variable shear strength interfaces to improve longitudinal shear and transverse tensile strengths and toughness 17 p2817 A71-34342

Toughness testing for low ductility fracture due to crack development in elastic stress field 17 p2757 A71-34557

Damage tolerant aircraft structures material toughness and residual strength, presenting fracture test results on precracked panels reinforced with crack stoppers 17 p2827 A71-35157

High strength Cr-Mo-Co stainless steels with improved toughness and ductility by austenitizing temperature selection 19 p3079 A71-37707

Linear-elastic fracture mechanics limits concerning toughness based on elastic-plastic rupture model for yielding materials 19 p3161 A71-38726

Ni-steels toughness improvement at cryogenic temperatures by accelerated cooling, using Charpy V-notch and static and dynamic fracture tests at 139.7-671.7 R 21 p3400 A71-40881

TOWED BODIES

Rigid towed and free flight glider, considering loads and turbulent atmosphere effects 09 p1385 A71-23669

Longitudinal stability of plate-like load towed beneath helicopter in horizontal forward flight 23 p3630 A71-44346

TOWED TARGETS

U TOWED BODIES

TOWERS

Optimum positioning and structure of light hogged antenna masts for radio communications and broadcasting networks 01 p0068 A71-11085

Free standing tower astronomical telescope, discussing vibration problems in pedestal design 02 p0239 A71-12500

Tower turbulence characteristics, using surface wind and temperature measurements to estimate horizontal velocity and dissipation rate variances at top 03 p0452 A71-13226

Wind speed measurement by cup and sonic anemometers, considering errors due to tower structure effect 05 p0752 A71-16663

TOWING

Nonlinear mathematical model for dynamical behavior of extensible towing cable subjected to aerodynamic forces generated by uniform flow field, discussing system stability 14 p2171 A71-31026

TOWNSEND DISCHARGE

NT GAS DISCHARGES

NT RING DISCHARGE

NT TOROIDAL DISCHARGE

Fast luminous fronts /ionizing waves/ in Kaufman streamer and Townsend discharges in nitrogen, discussing optical space and time resolved measurements 15 p2459 A71-32102

Molecular hydrogen primary ionization coefficients measurement in non-self sustained Townsend discharge, using light detection method based on radiant flux vs electron density proportionality 24 p3850 A71-44800

TOXIC DISEASES

NT CARBON MONOXIDE POISONING

Vitamin B6 protection against asymmetric dimethylhydrazine poisoning, administering B6 alone and with cortical phospholipids in mice 10 p1572 A71-24100

Toxic biological effects of life functions gases and products in albino rats 22 p3506 A71-42800

TOXIC HAZARDS

Sanitary, chemical and toxic properties of polymeric materials in isolation chamber with contaminated outgassing atmosphere at moderate temperature 01 p0024 A71-11111

Ozone atmospheric concentration, dissociation in SST air conditioning systems and biochemical poisoning 03 p0358 A71-13000

Intensive Chlorella cultivation for controlling toxic gaseous contaminants in atmosphere 06 p0861 A71-18300

Tannic acid and water washing effects on prevention of monomethylhydrazine absorption through skin in dogs 16 p2535 A71-33110

Time of useful function after mice exposure to life threatening toxic mixtures of carbon monoxide, carbon dioxide and ammonia produced by combustion 22 p3486 A71-41830

Toxic gaseous compounds effects on low pressure tolerance of rats under hypoxic hypoxia in atmosphere containing polymer decomposition products 22 p3506 A71-42800

Physiological effects on mice of air pollution with gaseous toxic substances from urine and feces, noting increased respiration rate and choline esterase activity 22 p3506 A71-42800

TOXICITY

NT CARBON MONOXIDE POISONING

Prophylactic radiation protection through lipid toxicants reduction in white rats tissues by high efficiency chemical radioprotectors 06 p0849 A71-17390

Plastics thermal decomposition, investigating combustion products and toxicity 06 p0916 A71-18000

Toxicity reduction of aminomethylisothiourea compounds through n-substitution with amino acids, noting slight decrease in radioprotective effectiveness 07 p1037 A71-18900

Acute inhalation toxicity of monomethylhydrazine vapor on rats, mice, beagles, squirrels and rhesus monkeys, considering hematology and blood chemistry tests 07 p1046 A71-19000

Toxic substances absorption, metabolism, excretion by man, discussing role of solubility, transfer through membrane tissue, liver and kidney in metabolizing and excreting organs 07 p1042 A71-19700

Pulmonary oxygen toxicity, considering composition of endobronchial saline extracts of rats and edema development 13 p2015 A71-29360

Dietary effects of formose sugars ingestion, investigating toxic mechanisms involved 19 p3011 A71-37570

Preservative phenol derivative effects on toxic gas evolution from stored urine in sealed vessels 22 p3506 A71-42800

Animal tolerance to carbon monoxide, nitrogen oxide, triethylamine and freon-12 toxic effects after adaptation to hypoxia from tests on albino mice 22 p3496 A71-42810

Indole vapor inhalation and direct injection into mice, rats and rabbits, examining toxic qualities 22 p3506 A71-42810

Human expired air toxicity effect on mice neurohumoral changes stimulating inhibitory reactions in central nervous system 22 p3506 A71-42810

TOXICITY AND SAFETY HAZARD

Unsymmetrical dimethylhydrazine /UDMH/ effect on canine blood coagulation, blood-aqueous barrier and cornea 02 p0199 A71-12380

Safe escape from toxic combustion products environment, discussing time of environmental dependence dependence on consolidated biokinetic forces 04 p0543 A71-15050

Jet aircraft flight decks pressurization, tobacco smoking and carbon monoxide levels, discussing potential dangers 09 p1400 A71-23240

TOXICOLOGY

Toxicology in aerospace vehicles design and operation, discussing occupational exposures, propellant operations, medical aspects, hazards, etc

08 p1244 A71-20712
Aircraft accidents investigation toxicological aspects, discussing drugs, alcohol and carbon monoxide involvement
[SAE PAPER 710395] 10 p1569 A71-24259
Toxicological evaluation of CO in humans and other mammals, considering pilot performance prediction for aircraft environment

TOXINS AND ANTITOXINS

NT ENDOTOXINS

TRACE CONTAMINANTS

Trace impurities effect on oxygen adsorption by Mo, using low energy electron diffraction, Auger electron spectroscopy and flash desorption mass spectrometry

17 p2694 A71-34856
Flame atomic fluorescence-atomic emission DC spectrometer for trace wear metals analysis in jet engine oils, covering spectral wavelengths below and above 3500 Å

17 p2695 A71-35150
Composition and daily fluctuations of trace contaminants during 90-day space station simulator test [ASME PAPER 71-AV-17] 18 p2867 A71-36384

Atmospheric trace and pollutant molecules global survey, using airborne/spaceborne high resolution Fourier interference IR spectrometer

22 p3542 A71-41963

TRACE ELEMENTS

Apollo 12 lunar core and soil samples indicating meteoritic trace elements abundance

01 p0148 A71-10003
Trace element patterns of Apollo 12 lunar rock 12013 light and dark portions, discussing Rb-Sr age and Li, K, Rb, Sr, Ba and rare earth concentrations

03 p0494 A71-14222
Ar-Ag arc, microwave discharge and plasma torch techniques in emission spectroscopy of trace elements in biological materials

03 p0377 A71-14421
Archaeological volcanics geochemistry and modern basalts chemical and geographic characteristics, considering trace element model

06 p0892 A71-17895
Hypertensive effects and tissue metal levels due to Cd, Hg and Zn intraperitoneal injection in rats

09 p3197 A71-23543
Earth and meteorites evolution, discussing material transport between lower and upper mantles and crust based on model of trace elements

11 p1820 A71-25226
Chemical fractionations in meteorites, considering trace elements abundance in L chondrites and implications for cosmochemistry

13 p2141 A71-29097
Fluorine and other trace elements in lunar plagioclase concentrates from Apollo 11 fines, and anorthosite inclusion from Apollo 12 breccia

20 p3292 A71-39383
Rare earth trace elements abundance of Apollo 14 lunar soil samples from Fra Mauro, comparing with chondrites

23 p3735 A71-43248
Minor element concentrations and population sources of Apollo 11 and 12 olivine and plagioclase, using microprobe analyses

23 p3738 A71-43614
Neutron activation data on Zn, Ga, Ge, Cd, In and Ir trace elements for Apollo 12 lunar rock and soil sample

23 p3747 A71-43673
Trace element abundances in Apollo 12 lunar rock and fine samples and mineral separates from Ocean of Storms

23 p3747 A71-43675
Meteoritic material characterization from trace elements in Apollo lunar soil, core samples, breccia and anorthositic fragments by neutron activation analysis

23 p3747 A71-43678
Trace elements concentration and metallic particles analysis from Apollo 12 lunar igneous rocks, soils and breccias, noting relation to sample location and exposure age

23 p3748 A71-43681
Apollo 12 lunar soils and igneous rocks from Ocean of Storms, determining major, minor and trace element composition with chemical, X ray fluorescence and spectrographic techniques

23 p3748 A71-43683
Apollo 11 and 12 lunar fines 10084 and 12070 trace element determination, using multielement neutron activation analysis

23 p3749 A71-43690
Rare earth elements and trace elements abundance in Apollo 12 igneous rocks, breccia and lunar soil

23 p3750 A71-43695

TRACERS

Field effect transistors internal source and drain resistances measurement, using characteristic tracer

04 p0558 A71-15084

UV absorber dyes in fluorescent tracers, discussing theory of dimensional sensitivity and use in liquid-film developers to quench background fluorescence

23 p3681 A71-43194

TRACKERS

U TRACKING [POSITION]

TRACKING [POSITION]

NT COMPENSATORY TRACKING

NT MISSILE TRACKING

NT OPTICAL TRACKING

NT PHOTOGRAPHIC TRACKING

NT PURSUIT TRACKING

NT RADAR TRACKING

NT RADIO TRACKING

NT RANGE AND RANGE RATE TRACKING

NT SATELLITE TRACKING

NT SPACE DETECTION AND TRACKING

SYSTEM

NT SPACECRAFT TRACKING

NT STAR TRACKERS

Time interval tracking in humans during steady and transient performance of homogeneous discrete motor acts sequence

02 p0205 A71-12056
Soviet radio telescope tracking control system, describing feedback sensors, digital computer, servomotors, actuators and control panels

04 p0565 A71-14848
Ships and aircraft position finding method based on satellite radio signals Doppler measurements, analyzing ionospheric influences

07 p1154 A71-19036
Surface navigation system and error analysis for Martian roving vehicle, using continuous tracking of pole star and local vertical

08 p1332 A71-21350
Tracking loops coherent reference signal with data aided demodulator, using power in modulation and carrier

12 p1879 A71-27071
Optimal control and tracking problems duality in cases of bounded coordinates and continuously acting perturbations respectively

14 p2220 A71-30870
Linearly increasing input signal tracking in nonlinear control systems with pulse frequency modulation, discussing error determination, asymptotic stability and equations of motion

15 p2381 A71-31980
ATC satellites providing communications channels between aircraft and ground control stations and aircraft localization

16 p2605 A71-32849
Book on fluidic systems design covering analog and digital control, application to aircraft, spacecraft, computers, tracking devices and equivalent circuits

16 p2526 A71-33475
Autonomous unknown landmark tracking space shuttle navigation system performance assessment by digital computer program providing error analysis and Monte Carlo simulation

17 p2773 A71-35067
Physiological tests for psychic stress effects on aircraft pilot tracking performance, respiration and heart rate

17 p2693 A71-35199
Autoexposure system for tracking telescopes, describing photometer and camera shuttle automatic control subsystems

18 p2919 A71-36088
Antenna tracking, RF and bore-sight alignment on ships and ground stations using Apollo lunar surface experiments package [ALSEP]

18 p2876 A71-36473
Worldwide data acquisition and tracking of meteorological balloon stations by flyby gravity stabilized satellite

18 p2878 A71-36528
Secondary visual tracking tasks utility in assessing lag effect in simulated combat aircraft dynamics

18 p2873 A71-36973
Computerized automatic estimation techniques application to real time aircraft tracking in ATC system design

19 p3096 A71-37172
[AIAA PAPER 71-926]
Rapidly converging second order optimal tracking algorithms for adaptive equalization on basis of estimated bounds for eigenvalues of signal plus noise correlation matrix

20 p3201 A71-38872
Human perceptual motor skill development in tracking performance, using feedback control system gain and effective time delay as measures

21 p3343 A71-40909
Mathematical models for computerized ATC automatic aircraft flight tracking logics without tracks smoothing

22 p3573 A71-42396
Error insensitive proportional integral derivative (P-I-D) tracking controller design using optimal linear regulator theory

23 p3657 A71-43946
Joint phase locked and delay tracking system dynamics for pseudorandom radio signal detection

23 p3646 A71-44267

TRACKING ANTENNAS

U DIRECTIONAL ANTENNAS

TRACKING FILTERS

Dynamic FM demodulator with tracking filter for threshold extension

02 p0235 A71-12821
Differential radiometer with ultranarrow interference filter for daytime tracking of high altitude chemical vapor trails

03 p0424 A71-13636
Sampled phase lock loop filter for tracking short pulses, deriving frequency stability criterion and margins

05 p0725 A71-17080
Earth based orbit determination for Mars orbiting spacecraft, comparing batch and sequential tracking filter data processing methods

06 p0978 A71-18657
[AIAA PAPER 71-119]
Real time tracking filter candidates for implementation in systems tracking maneuvering vehicles compared in terms of accuracy and computer requirements for tactical applications

07 p1069 A71-18837
Fokker-Planck boundary value solutions to transient phase error response of nonlinear phase locked tracking systems

07 p1082 A71-20428
FM demodulator system with parametric tracking filters for threshold improvement, discussing reception performance

08 p1265 A71-21279
Stability of model tracking adaptive control systems with reduced state feedback and measurement noise

08 p1269 A71-21336
Iterative processing technique for limited measurement sets, discussing Kalman filter reaching steady state during ballistic target tracking

08 p1269 A71-21340
Maneuvering vehicles behavior model selection for real time Kalman filter tracking algorithm, based on accuracy predictions and empirical performance

08 p1270 A71-21349
On-line closed loop adaptive control for tracking filter with several inputs and outputs

10 p1586 A71-24739
Slip vs static error offset for first and passive second order phase locked loop as function of signal to noise ratio via computer simulation

12 p1892 A71-27073
Transfer function optimization for linear tracking filter model with controlled resonant frequency, analyzing noise band performance

14 p2194 A71-30089
Sinusoidal vibration tests using narrowband tracking filters, considering automatic servocontrols and feedback loop optimum matching

14 p2175 A71-30310
Lock-loop loop technique with pulled oscillator for feedback frequency demodulation and tracking filter operation

14 p2220 A71-30920
Intelsat 3 and 4 RF demodulator design with tracking filters, using varactor for frequency control and discriminator for frequency drift compensation

18 p2890 A71-36558
Aerospace vehicles high resolution photography, introducing phase rate image tracking sensors for forward motion compensation

18 p2883 A71-36909
Optimal tracking feedback filter for closed loop systems with irrational transfer function, using heuristic method

21 p3359 A71-40251

TRACKING NETWORKS

NT DEEP SPACE NETWORK

NT GLOBAL TRACKING NETWORK

NT MANNED SPACE FLIGHT NETWORK

NT SPACE DETECTION AND TRACKING

SYSTEM

Manual tracking systems identification and real time display, developing software system

01 p0027 A71-11437
Satellite triangulation network adjustment based on simultaneous errors observations, using filtering equations for matrix manipulations reduction

03 p0413 A71-14009
NASA Office of Tracking and Data Acquisition mission support and ground and spacecraft communication networks

04 p0551 A71-14936
Satellite systems for transatlantic simultaneous air and marine navigation, traffic control and rescue, stressing technical and economical factors

06 p0925 A71-18015
Geodetic system with satellites and automatic radio beacons, establishing network on earth surface to track isolated points

18 p2913 A71-36529

TRACKING RADAR

Free fall speed characteristics of simulated hailstones measured by tracking radar, discussing roughness effects on speed and drag

01 p0115 A71-10556

- Soviet book on monopulse radar covering surveillance and target tracking systems, antennas, angular resolution, directional sensitivity, etc
01 p0038 A71-11300
- Acquisition and processing of aircraft search radar data obtained by track-while-scan technique, using off-line digital computer
01 p0040 A71-11392
- Automated radar calibration system using star tracker and computerized control
04 p0554 A71-15318
- C-band radar network calibration, using GEOS 2 satellite worldwide tracking data
04 p0554 A71-15319
- Frequency agile waveforms effects on detection and tracking radars performance, decorrelating distributed clutter echoes
08 p1253 A71-20798
- Omnidirectional radar moving target detection from clutter, using Doppler filter system
09 p1407 A71-23047
- Radar target direction variation (glint) sensed by amplitude monopulse tracking antenna receiving nonuniform waves
14 p2214 A71-30807
- Three dimensional ATC radar supplying simultaneous range, azimuth and elevation information for indefinite number of targets by continuous searching
15 p2371 A71-32167
- Computer use in automatic tracking radar systems design, describing adaptive radar hardware
20 p3200 A71-39902
- Doppler tracking radar systems, obtaining probability density function of Doppler signal amplitude
20 p3200 A71-39907
- National Aviation System stage A ATC displaying digitized radar data positions together with automatic track positions
22 p3570 A71-41634
- TRACKING STATIONS**
NT DEEP SPACE INSTRUMENTATION FACILITY
NT GLOBAL TRACKING NETWORK
NT SPACE DETECTION AND TRACKING SYSTEM
NT STADAN [SATELLITE TRACKING NETWORK]
Antenna gain of Space Communications and Tracking terminal from feedhorn radiation pattern and reflector geometry
02 p0219 A71-12448
- High efficiency feeds for large satellite autotracking earth station antennas, using focal plane distribution
02 p0223 A71-12808
- Radar station-satellite contact times using horizon crossing, lunar occultation and keyhole constraints
02 p0280 A71-12898
- Satellite geodesy for determining tracking station coordinates and gravity field
08 p1285 A71-21801
- Guiana Space Center facilities and equipment, describing computerized and automated real time telemetry and data processing systems for spacecraft tracking
09 p1425 A71-22274
- Satellite communication earth stations tracking receiver, describing operational principles with special attention to down-converter and demodulator circuits
12 p1887 A71-27001
- Earth gravity field and satellite tracking stations positions geodetic parameters in geocentric reference frame
17 p2733 A71-35027
- Geodetic satellite data utilization for test range specific point positioning, control densification, earth gravitational model determination and tracking station locations
18 p2913 A71-36492
- Communication satellites automatic tracking system, noting low cost
18 p2881 A71-36555
- NASA Stadan and Speopt optical and laser tracking sites dynamic position estimations from GEOS 1 and 2 observations, analyzing model error effects
20 p3220 A71-39662
- Nikolajev-Helwan space direction determination between satellite tracking stations at long distances, using simultaneous circle method
21 p3374 A71-41051
- Earth based radio tracking data types involving simultaneous or near simultaneous spacecraft tracking from widely separated tracking
[AAS PAPER 71-399]
23 p3643 A71-43066
- TRACKING STUDIES**
U TRACKING [POSITION]
TRACTION
High traction fluid effect on high speed roller bearing cage skidding, comparing with military specification oil
[ASME PAPER 70-LUB-E]
03 p0432 A71-13707
- Dissimilar elastic half spaces joined over circular region, calculating interfacial traction stresses induced by arbitrary loading from coupled integral equations
14 p2328 A71-30293

TRACTS

U SITES
TRADEOFFS

- Space transportation system performance risks due to design parameter uncertainties, presenting analysis method for tradeoff studies based on figure of merit calculation
04 p0663 A71-15335
- Monopulse receiver design system and image band noise factors tradeoffs, discussing preselector and integrated front end trends
11 p1737 A71-25676
- Response strategies in two-choice reaction task with continuous cost for time, confirming fast-guess model prediction
12 p1873 A71-27008
- Performance and cost design tradeoff between HF and synchronous meteorological satellite data collection systems, considering platform transmitting power and SNR
14 p2198 A71-30900
- System effectiveness tasks of producibility analysis, maintainability evaluation and tradeoff studies
16 p2664 A71-33316
- Administrative techniques of cost/weight tradeoff program for jet transport airplane
[SAWE PAPER 899]
17 p2750 A71-35812
- TRAFFIC**
NT AIR TRAFFIC
TRAFFIC CONTROL
NT AIR TRAFFIC CONTROL
NT RADAR APPROACH CONTROL
Marine traffic control via satellite telemetry, describing merchant and powered fishing fleet distribution and navigation requirements
01 p0125 A71-10978
- Satellite systems for transatlantic simultaneous air and marine navigation, traffic control and rescue, stressing technical and economical factors
06 p0925 A71-18015
- Communications, navigation and surveillance for aircraft and marine vessels in North Atlantic region, discussing baseline traffic control model
07 p1153 A71-18808
- Urban transit and ATC vehicle identification and position determination system, considering surface and airborne traffic real time information communication
08 p1331 A71-21169
- TRAILING EDGES**
Boundary layer separation at free streamline attachment to sharp trailing edge of flat plate, deducing terminal velocity profile for two dimensional flow
02 p0185 A71-12376
- Turbulent separation and reattachment at turbomachine blade trailing edge at supersonic speeds, discussing various flow models
03 p0340 A71-13142
- Stability theory for pair of trailing vortices, investigating induced field convection, modes, amplification, cut-off distance, etc
[AIAA PAPER 70-53]
03 p0341 A71-13436
- Vortex sheet behavior in inviscid subsonic flow of lifting wing with nonzero trailing edge angle
03 p0342 A71-13738
- Lateral vibration effects on heaving airfoil blunt trailing edge vortex shedding flows, examining base cavity damping by flow visualization
06 p0984 A71-17621
- Phantom and Buccaneer aircraft boundary layer control, examining lift from trailing and leading edges
06 p0847 A71-17953
- Cavitation flow of fluid with free surface past underwater wing with jet flap, solving equations of motion for thin foil with jet emergent from trailing edge
07 p1092 A71-20086
- Injected air cooled turbine blade trailing edges temperature, calculating thermal distribution with differential equations
08 p1348 A71-21265
- Flat plate trailing edge problem solution consistent with second order boundary layer theory, establishing laminar wake evolution nature and upstream influence
11 p1701 A71-25469
- Hele-Shaw flow viscous tails from airfoil, observing high Reynolds number trailing edge flow for separation and initiation of Kutta condition
11 p1705 A71-26447
- Boundary layer separation at free streamline attached to body sharp trailing edge, comparing asymptotic solution with numerical analysis of flow on flat plate
12 p1896 A71-27218
- Compressible viscous gas supersonic flow, observing near wake region behind perpendicular trailing face of plate with motion, state, energy and continuity equations
13 p2047 A71-28421
- Transverse flow in cavity ensurance by air exhaust cooling of trailing edges of gas turbine blades with deflector
16 p2624 A71-33544

- Skin friction, trailing edge boundary profiles and tuft flow patterns on model F-4D aircraft in transonic flow
[AIAA PAPER 71-762]
16 p2521 A71-34004
- Constant velocity flow past semiinfinite flat plate trailing edge, emphasizing wake region structure
16 p2560 A71-34144
- Transonic flow fields in slender symmetric profile incorporating shock relations at trailing edge
16 p2522 A71-34146
- Compressible viscous gas supersonic flow, observing near wake region behind perpendicular trailing face of rectangular plate with motion, state, energy and continuity equations
21 p3318 A71-40086
- Acoustic resonance excitation by vortex shedding from flat plate trailing edge in low speed wind tunnel
24 p3848 A71-44523
- Vortex shedding from blunt trailing edge of flat plate spanning wind tunnel under oscillating flap arm acoustic resonance excitations
24 p3848 A71-44523
- TRAILING-EDGE FLAPS**
Trailing edge flap automatic control for glider performance improvement
03 p0346 A71-13020
- Shock interaction effects on flapped delta wing in hypersonic speed, presenting method for estimating reflected expansion wave impingement boundaries and resulting aerodynamic coefficients
12 p1868 A71-27593
- TRAINERS**
U TRAINING DEVICES
TRAINING
U EDUCATION
TRAINING AIRCRAFT
NT JAGUAR AIRCRAFT
NT T-33 AIRCRAFT
Alpha jet trainer, describing design, configuration, power plants, landing gear maintainability and mission duration
15 p2347 A71-31202
- TRAINING DEVICES**
Airline flight simulators and associated pilot training equipment, discussing improvements in flying control systems, computers, visual systems and power supplies
01 p0066 A71-10014
- Motion simulation in flight training device, discussing basic phenomena, minimum requirements and methods of mechanization with regard to equipment design features and maintainability
01 p0066 A71-10014
- Planetaria as celestial navigation instruction aids, discussing astronomical simulation capabilities, celestial coordinate systems, special effect projectors, etc
01 p0022 A71-10513
- Aircraft navigator training, examining flight around trainer balance from cost effectiveness standpoint
01 p0022 A71-10513
- Shadow projector creating visual illusion of space surrounding flying aircraft for aviation training, relating perceived distortions to system parameters
06 p0864 A71-18711
- Ground based flight equipment evaluation in routine primary pilot training
12 p1875 A71-27244
- Flight training program for twin-engine transition using commercially available training device
[SAE PAPER 710480]
13 p2017 A71-28344
- Monkeys trained to observe and report two-member serial position sequences with delayed matching-sample procedure
14 p2187 A71-29511
- DC 10 flight crew individualized ground training program, emphasizing hands-on equipment and instruction hardware
[SAE PAPER 710472]
14 p2176 A71-30533
- Aircraft-simulating cockpit procedure training statistical data and development problems concerning safety, economy and efficiency performance
15 p2384 A71-31881
- Pilot training efficiency increase through advanced simulation technology utilization, discussing computerized flight simulators, CRT display systems and automated briefings
15 p2384 A71-31884
- Aircraft pilot learning process with C-8 trainee determining effective evaluation indexes including error ratio, control numbers, pulse rate and reaction time
17 p2692 A71-35194
- Lunar Orbiter photographs utilization in earth science courses, illustrating geologic features, stratigraphy and historical geology
18 p2915 A71-35884
- Training cycle in altitude chamber for human adaptation to hypoxia, high temperatures and transverse myogenic loads
22 p3505 A71-42803
- TRAINING SIMULATORS**
NT COCKPIT SIMULATORS
NT FLIGHT SIMULATORS

NT SPACECRAFT CABIN SIMULATORS

Flight training simulators - Conference, London, October 1970

01 p0065 A71-10012

Flight simulation in various degrees of environmental realism by visual and other physiological cues, discussing available devices and techniques relative to specific training tasks

01 p0066 A71-10020

Simulated low visibility landing training, discussing airborne and ground based simulators

01 p0067 A71-10022

Flight training simulator use in airline operations, discussing economics of various simulator types with projection toward ultimate simulator

01 p0183 A71-10023

Air navigational training simulators, discussing navigation aids, civilian navigator use, visual simulation and land-mass radar

01 p0125 A71-10526

Real time solar flare image production for Skylab astronaut training, using films of H alpha, XUV and X ray solar images
[AIAA PAPER 71-73]

06 p0902 A71-18530

Link 747 simulator design and operation, describing cockpit layout, motion picture system and malfunction insertion and display unit

06 p0881 A71-18665

Apollo simulator navigation and docking training techniques, discussing manned LM and CSM key role performance

07 p1156 A71-20342

Radar analog simulators for Polish air traffic controllers training, describing optical and electronic equipment

09 p1428 A71-22950

Digital simulator for training ATC officers, considering authenticity and working and geographical environments

09 p1428 A71-22954

Six degree of freedom hybrid digital computer program for complex flight control and associated mode logic design and training

11 p1736 A71-25852

Training simulators as substitutes for airborne training, considering limitations and future developments
[SAE PAPER 710476]

13 p2044 A71-28341

Flight crew training ground school programs, featuring automated instruction in cockpit classroom with audio visual machines
[SAE PAPER 710478]

13 p2017 A71-28343

Visual devices for training simulators, discussing film and closed circuit TV systems and components

15 p2385 A71-31889

TRAJECTORIES

NT ABORT TRAJECTORIES
NT ASCENT TRAJECTORIES
NT BALLISTIC TRAJECTORIES
NT CIRCULUNAR TRAJECTORIES
NT DESCENT TRAJECTORIES
NT EARTH-MARS TRAJECTORIES
NT EARTH-MOON TRAJECTORIES
NT ELECTRON TRAJECTORIES
NT HYPERBOLIC TRAJECTORIES
NT INTERPLANETARY TRAJECTORIES
NT LUNAR TRAJECTORIES
NT MIDCOURSE TRAJECTORIES
NT MISSILE TRAJECTORIES
NT MOLECULAR TRAJECTORIES
NT MOON-EARTH TRAJECTORIES
NT PARTICLE TRAJECTORIES
NT REENTRY TRAJECTORIES
NT RENDEZVOUS TRAJECTORIES
NT ROUND TRIP TRAJECTORIES
NT SPACECRAFT TRAJECTORIES

TRAJECTORY ANALYSIS

Lunar gravitational field parameters from Lunar Orbiters trajectory measurement, discussing theoretical basis

01 p0149 A71-10048

Time distribution of first passage through fixed level for nondecreasing whole number regeneration process with step trajectories

01 p0110 A71-10094

Time distribution of first passage through fixed level for regeneration vector Markov process with step trajectories

01 p0110 A71-10095

Stress-strain relations at plane multiply broken strain trajectories, using local definiteness hypothesis

01 p0171 A71-10653

Laser beam trajectory changes due to asymmetrical shading with circular absorbing diaphragm, noting characterization by energy distribution over cross section

01 p0095 A71-11216

Taxiing aircraft position and wheel trajectories for specific nose wheel path

02 p0187 A71-11641

Missiles and aircraft trajectories computation time reduced via time sharing and hybridization

02 p0227 A71-11794

Reference trajectory and additional phase variable methods for motion equations integration applied to vehicle in atmosphere

02 p0304 A71-11904

Soviet book on maneuvering of spacecraft covering trajectory calculation, thrust control, translunar and interplanetary flights, atmospheric reentry, orbital rendezvous, optimal control, etc

02 p0321 A71-12725

Solid body motion about fixed point on pseudoeuclidean Lobachevskii plane under external forces, using Euler angle analogy

03 p0457 A71-13423

Neighboring optimum feedback guidance to motivate min-distance lookup parameter determined by minimizing metric function of perturbed state and reference trajectory
[AIAA PAPER 69-888]

03 p0454 A71-13446

Indirect, linear and nonlinear optimal guidance schemes from precomputed reference trajectory, using iterative techniques for boundary equations

03 p0454 A71-13449

Sounding rocket-moving target spatial relationship trajectory modeling by digital simulation, applying to vehicle launching during solar eclipse of March 1970
[AIAA PAPER 70-1374]

03 p0497 A71-13657

Postflight analysis including six degree of freedom trajectory digital simulation of Aerobee 350 sounding rocket behavior under large thrust misalignment
[AIAA PAPER 70-1380]

03 p0498 A71-13663

Wind compensation method for launching sounding rockets susceptible to nonlinear wind effects, using data generated by six degree of freedom trajectory digital simulation program
[AIAA PAPER 70-1390]

03 p0498 A71-13672

Charged particle trajectory under dipole magnetic field, deriving Stoermer orbit existence and uniqueness proof

04 p0625 A71-15081

N interval trajectory estimation computer program minimum variance adjustment technique, discussing airborne astrophotographic camera system for reentry bodies position determination

04 p0556 A71-15330

Analytical techniques for invariant properties of families of moon-earth trajectories

04 p0660 A71-15891

Nonguided finned rocket initial stability problem, evaluating axis and tangent trajectory

05 p0817 A71-16638

Numerical and graphic drive shaft motion trajectories in dynamic gyroscopic system with four degrees of freedom

06 p0928 A71-18232

Free-fall periodic orbits /interplanetary trajectories/ connecting earth and Mars, using patched conic analysis
[AIAA PAPER 71-92]

06 p0977 A71-18547

Mars lander deorbit trajectory sensitivity analysis for fixed flight path and communications angles at atmospheric entry, comparing with Monte Carlo simulation
[AIAA PAPER 71-190]

06 p0978 A71-18628

Multiple interplanetary flyby trajectories precision targeting, using sequence of alternate heliocentric and planetocentric trajectory segments with position and time matching constraints
[AIAA PAPER 71-191]

06 p0978 A71-18629

Space vehicle motion on planetary flyby trajectories, using Chebyshev polynomial series and Picard successive approximations method to solve two point boundary value problem
[AIAA PAPER 71-192]

06 p0978 A71-18630

Space vehicle landing trajectories calculation from visual and radio observations of orbital parameters

07 p1196 A71-19495

Normalized hodographic mapping for constrained trajectory families, discussing mapping concepts, information content and applications
[AIAA PAPER 69-924]

07 p1199 A71-19884

Lunar gravitational field parameters from Lunar Orbiters trajectory measurement, discussing theoretical basis

08 p1361 A71-21042

Newton inverse square law of gravitation in solar system, considering closed orbit trajectories

08 p1363 A71-21320

Heavy solid body motion about stationary point for connected angular velocity vector terminus and trajectory in fixed space

08 p1336 A71-21869

Trajectories prediction for subsonic spin stabilized projectiles via water tunnel tests, considering blunt nose and tail and rounded nose right circular cylinders
[AIAA PAPER 71-296]

08 p1275 A71-22016

Angle of attack vertical variations of free flight trajectory missile, estimating missile, trajectory and atmospheric parameters effects on fluctuations relative to center of mass

08 p1367 A71-22051

Lunar swingby trajectory analysis with atmospheric reentry, characteristics of geocentric portions of earth-moon and moon-earth transfers

09 p1519 A71-22546

Circumplanar trajectories with return to earth atmosphere, comparing various methods

09 p1519 A71-22662

Satellite path geometry along Keplerian elliptical orbit, taking earth flattening into consideration

09 p1520 A71-22664

Nomograms for meteor geocentric velocity and trajectory with correction for zenith attraction and radiant

09 p1520 A71-22831

Small meteor streams trajectories and radiants from epsilon-Lyrids, alpha-Coronids and phi-Draconids observations by amateur astronomers

09 p1520 A71-22841

NASA pulsed laser ranging systems for scientific satellite tracking, determining accuracy by trajectory and long arc orbital comparison

10 p1576 A71-24051

Second and higher order perturbation theory for two body trajectories, using recursive formulas
[AIAA PAPER 70-1056]

11 p1820 A71-25459

Skipping entry trajectories up to fifth extremal points in planetary atmosphere, using matched asymptotic solution

11 p1837 A71-25483

Southern Hemisphere general atmospheric circulation data, using constant volume balloons dispersion

11 p1755 A71-25641

Topocentric satellite trajectory approximation along circular orbit by n-degree equation, using coordinate-time relation

11 p1829 A71-25809

Dynamic systems with singular trajectories, analyzing orbital stability in locally compact space

11 p1799 A71-26157

Spacecraft flight trajectory parameters estimation from unknown second moment matrix of navigation measurement errors

12 p1957 A71-26628

Maximum likelihood method for accuracy of spacecraft trajectory determination by complex expressions in multidimensional geometric representation

12 p1957 A71-26629

Equations of motion for single trajectory model of nonspherical stationary rotating stellar systems, assuming phase density dependence on motion integrals

12 p1966 A71-27234

Roll rate variation and lift effect on reentry vehicle impact, comparing analytic treatment with six degree of freedom trajectory simulation

13 p2144 A71-27977

Reference trajectory and additional phase variable methods for motion equations integration applied to vehicle in atmosphere

13 p2133 A71-28191

Solid nontrivial trajectory existence conditions near connected set of strong bilateral attraction, examining dynamic system in connected noncompact space

13 p2094 A71-28497

Longitudinal proper motions of flight vehicle based on equivalent dynamic systems for trajectory coincident with nonsingular transformation in phase space

13 p2145 A71-28731

Target trajectory detector optimization, using surveillance radar data and Markovian chain apparatus

13 p2033 A71-28993

Quasi-stationary gliding trajectories of aircraft in planetary atmosphere during constant control of attack and bank angles

13 p2143 A71-29185

Trajectory analysis of geocentric phase and selenospheric motion of space vehicle leaving lunar surface and returning to earth atmosphere

13 p2143 A71-29209

Wind tunnel model trajectory simulation system with closed loop control by digital computer, describing instrumentation, system servoamplifiers and testing procedures

14 p2208 A71-30334

Daniel comet collision frequency calculations with asteroids and microasteroids based on trajectory analysis

15 p2481 A71-31299

Lost City /Oklahoma/ meteorite photometric and trajectory data, comparing flight characteristics with other fireballs

15 p2489 A71-32360

Goddard trajectory determination system, discussing attitude dynamics, data preparation, differential correction and orbit information

15 p2495 A71-32645

Low pressure shock tubes performance, investigating wave and contact surface trajectories and ideal velocity deviations

16 p2556 A71-32915

Laser beam trajectory changes due to asymmetrical shading with circular absorbing diaphragm, noting characterization by energy distribution over cross section

17 p2750 A71-34267

Normal mode vibrations of system with trajectories of unit mass in Euclidean space, determining modal subspaces by potential function

17 p2776 A71-34295

Quasi-closed Einstein universe model, showing orbits rotation similar to perihelions in Schwarzschild field

17 p2778 A71-34630

Statistical theory of nonlinear differential equation system with discontinuous trajectory solution, deriv-

ing motion stability to first approximation using Liapunov functions

17 p2780 A71-34915

Space shuttle guidance, evaluating performance of strapdown and gimbaled systems by nominal and abort trajectories

17 p2773 A71-35061

Cost effective high speed projectile trajectory plotting system for gunnery range instrumentation, applying to aircraft path recording during automatic landing control

18 p2924 A71-36613

Closed loop control of nonlinear systems in potentially large neighborhood of nominal trajectory, reducing nonlinear differential equations to related canonical linear form

19 p3037 A71-37239

Autonomous two dimensional system with given trajectory and singular points, describing differential equations construction

19 p3085 A71-37350

Close binary star systems U Gem, VV Pup and UX UMa, calculating gas streams trajectory movement

19 p3134 A71-37509

Finite radius rotating cylinder stability analysis, using equilibrium functions of distribution with trajectory integration method

19 p3134 A71-37512

Navigation, orbit and trajectory analysis of 1979 Jupiter-Uranus-Neptune Grand Tour mission, assuming deep space network tracking

[AAS PAPER 71-117] 19 p3101 A71-37936

Radio signal group trajectory in ionosphere expressed as series expansion in terms of increasing power of beam reflection height

19 p3020 A71-38371

Two body orbits problem concerning satellite flightpath transfer possibility to orbit touching cyclic or elliptical trajectories

20 p3287 A71-38849

Interplanetary single impulse flight trajectories optimization and computation, determining geometrical and kinematic characteristics

20 p3288 A71-39120

Heavy solid body motion about stationary point for angular velocity vector extremity moving in fixed and body-connected coordinate systems

20 p3270 A71-39368

Space shuttle optimal lifting trajectory analysis, examining boost launch system performance increase

22 p3608 A71-41955

Low gravity field phenomena, discussing vertical jump on moon, ball trajectories launched from asteroid and voyage to neutron star

22 p3600 A71-41983

Space shuttle operations analysis for cislunar space, including transfer trajectory inclination and long term effects

[AAS PAPER 71-300] 23 p3724 A71-42976

Herrick-Gibbs preliminary orbit determination method in matrix form for spacecraft extended to process greater than three inertial position vectors

[AAS PAPER 71-317] 23 p3725 A71-42991

Relay data link and trajectory design integration for Viking orbiter 1975 mission

[AAS PAPER 71-320] 23 p3726 A71-42994

Bi-injection earth departure mode analysis for combined flyby/orbiter Jupiter-Saturn-Pluto and Jupiter-Uranus-Neptune Grand Tour missions

[AAS PAPER 71-322] 23 p3726 A71-42996

Earth-Jupiter-Saturn-earth trajectories, determining mission planning parameters

[AAS PAPER 71-361] 23 p3729 A71-43031

N-body integrated reference trajectories and navigation requirements for extended Venus/Mercury 1973 mission midcourse correction

[AAS PAPER 71-362] 23 p3729 A71-43032

Solar electric propulsion application to Halley Comet flythrough and rendezvous missions, describing trajectory characteristics and payload capabilities

[AAS PAPER 71-363] 23 p3729 A71-43033

Fast spacecraft trajectory computation in n-body inverse square force field, developing closed form recurrence formula for onboard computers

[AAS PAPER 71-382] 23 p3731 A71-43052

Solar system escape trajectory analysis for Jupiter-Saturn-Pluto and Jupiter-Uranus-Neptune Grand Tour missions, presenting flyby characteristics and heliocentric postencounter directions

[AAS PAPER 71-383] 23 p3731 A71-43053

Mariner 9 Mars 71 mission orbit determination, trajectory and maneuver strategy for near earth, cruise, planetary approach and satellite phases, using in-flight tracking data

[AAS PAPER 71-391] 23 p3732 A71-43059

Objects motion analysis by dynamical photogrammetric methods, integrating optical image points differential motion for trajectory equations

23 p3678 A71-43589

Analytic solution to range deviations along descending branch of free flight trajectory of ballistic vehicle in planetary atmosphere

24 p3872 A71-45015

Two step spacecraft reentry guidance involving skip trajectory at parabolic speeds, proposing algorithm for running coordinate and speed vector components values

24 p3846 A71-45301

Trajectory correction problem optimal measurement set, showing solution by linear programming simplex algorithm method

24 p3846 A71-45306

TRAJECTORY CONTROL NT TRAJECTORY OPTIMIZATION

Cassiopee attitude control device for sounding rocket impulse trajectory correction, discussing spinning nose cones, corrective algorithm and final impact accuracy

[AIAA PAPER 70-1378] 03 p0498 A71-13661

Space vehicle trajectories, discussing programming method to control motion for prescribed boundary conditions

03 p0495 A71-14236

Pulsed plasma thruster system as secondary propulsion unit for spacecraft attitude, station and trajectory control

04 p0638 A71-15325

Complete system associated with given control, discussing trajectories uniform approximation and nonlinear controllability conditions based on linear partial differential equation

04 p0620 A71-15865

Numerical integration for continuously thrusting spacecraft optimal trajectory, considering rectangular Cartesian and polar cylindrical coordinates characteristics

[AIAA PAPER 69-903] 07 p1191 A71-18891

Apollo 12 Lunar Module high landing accuracy, discussing control actions, trajectory error sources and power descent

07 p1206 A71-19086

Impact dispersion reduction of uncontrolled sounding rocket ZENITH with CUCKOO booster by canard control, noting flight path angle error by tracking radar

09 p1533 A71-23598

Propulsion, guidance and stability of ground effect vehicle with perimetric Coanda fluid boundary

13 p1997 A71-29308

Soviet book on long range rocket ballistics covering control system, dynamics, firing distance, motion equations, stage separation and nominal trajectories

13 p1246 A71-29438

Dynamic stability of controlled spacecraft with liquid propellant rocket engines, considering acceleration and braking sections of trajectory

16 p2646 A71-33656

Orbital elements determination for Osumi Japanese satellite, describing trajectory correction for atmospheric effect

17 p2802 A71-34746

Soviet book on radio control of various flight vehicles covering closed loop synthesis, missile guidance, spacecraft trajectory correction and air traffic control

17 p2775 A71-35403

Proportional navigation for trajectory control of missile homing on target in planar pursuit

20 p3261 A71-38856

Spacecraft interplanetary guidance trajectory correction, deriving algorithm for optimal accuracy and minimum fuel expenditure

20 p3288 A71-39124

Optimal control laws existence for stochastic systems with minimized cost functional, considering trajectory information for controller decisions

21 p3360 A71-40254

Gradient algorithm for optimal trajectory control with inequality and singular arcs, using nonlinear programming and Euler-Lagrange equations

23 p3658 A71-44085

Point motion in random error region applied to synchronous satellite trajectory control by single impulse correction

24 p3846 A71-45307

TRAJECTORY MEASUREMENT

Lunar gravitational field parameters from Lunar Orbiters trajectory measurement, discussing theoretical basis

01 p0149 A71-10048

External stores separation induced aerodynamic interactions, using high speed cinematographic recording of drop trajectories and/or store loads weighing in aircraft flow field

[ONERA-TP-849] 04 p0527 A71-15357

Soviet book on radio measurement methods and mathematical data processing in space trajectory measurements

04 p0555 A71-15375

Soviet book on spacecraft motion parameters measurements accuracy covering electronic systems error sources and reduction in design and data processing

08 p1251 A71-20675

Trajectory measurement program optimization, constructing algorithm for variational problems

08 p1360 A71-21001

Trajectory measurement optimal program, using least squares method

08 p1360 A71-21002

Lunar gravitational field parameters from Lunar Orbiters trajectory measurement, discussing theoretical basis

08 p1361 A71-21001

Captive trajectory techniques for six degree-of-freedom external store separation wind tunnel testing, noting capability for missile guidance system simulation

[AIAA PAPER 71-282] 08 p1275 A71-23598

Sounding rocket flight accurate trajectory determination cost effective radar tracking system

10 p1610 A71-24000

Optimal measurement programs for instrument controlled spacecraft trajectory sections, using maximum likelihood method

12 p1957 A71-29308

Lunar orbiter earth-moon-earth optimal trajectory geocentric section calculations from low circumlunar flight procedures

13 p2142 A71-29900

Meteors light curves, showing maximum brightness distribution in visible trajectory

16 p2639 A71-33140

Airborne astrophotographic camera system for simultaneous determination of multiple object reentry trajectories at Air Force test range

18 p2918 A71-36613

Reentry vehicles trajectory reconstruction by computer program and Kalman filter estimation techniques, analyzing instrument errors

[AIAA PAPER 71-933] 19 p3097 A71-37350

Radar measurements of vertical structure and motion trajectories of cumulus-rain clouds, studying vertical flows velocities and radar echo characteristics

19 p3094 A71-38371

Trajectory measurement method optimization, determined by algorithm, applying to radial velocities of artificial satellite orbit around Mars

20 p3294 A71-39368

Trajectory measurement optimal program, using least squares method

20 p3294 A71-39368

Earth-moon and other trajectories calculation n-planar elliptic restricted three body problem by slow varying Jacobi function

[AAS PAPER 71-381] 23 p3731 A71-43031

Io passage in front of binary star beta Scorpii on May 1971, presenting satellite trajectory calculation and appulse time

23 p3733 A71-43199

TRAJECTORY OPTIMIZATION

Continuous thrust spacecraft optimal trajectory regularization, obtaining differential equations three dimensional motion

01 p0154 A71-10300

Recurrent Lagrange multipliers coordinate transformation for optimal low thrust Earth-Jupiter trajectories

01 p0160 A71-10900

Tactical missile flight test planning using digital simulation data reduction techniques for fast cost effective trajectory synthesis

02 p0226 A71-11700

Optimal two impulse correction with minimum energy for planetary approach trajectory and subsequent satellite orbit transfer

02 p0304 A71-11900

Control programs realizability for optimal escape trajectories of low thrust vehicles with motion about mass of center and with or without artificial gravity

02 p0319 A71-11900

Optimal control of exhaust velocity for plane motion of variable mass point along trajectory under gravitational and resisting forces

02 p0284 A71-12200

Pursuit game strategy based on Hamilton-Jacobi formalism, considering internal and external potential fields, optimum trajectories and gravitational and electromagnetic fields

03 p0483 A71-13100

Multistage rocket propelled strategic ballistic missiles and space boosters design and trajectory optimization, using SWORD computer program

04 p0556 A71-15200

Linear functional differential equations trajectory optimization, proving maximal principle

04 p0620 A71-15800

Interceptor missiles minimum flight time control describing modified steepest descent algorithm for optimal trajectories

[AIAA PAPER 71-19] 06 p0979 A71-18400

Optimal vacuum rocket trajectories over spherically earth, deriving nonlinear differential equations for position and velocity

[AIAA PAPER 71-20] 06 p0976 A71-18400

Multiple impulsive spacecraft trajectory optimization technique application to comet rendezvous problem, using computer program

[AIAA PAPER 71-93] 06 p0977 A71-18500

Numerical integration for continuously thrusting spacecraft optimal trajectory, considering rectangular Cartesian and polar cylindrical coordinates characteristics

[AIAA PAPER 69-903] 07 p1191 A71-18800

Trajectory optimization, using Pontryagin maximum principle for differential inclusions
07 p1146 A71-19178

Saturn launch vehicle navigation, guidance and control system, discussing optimal system design for flight path optimization
07 p1155 A71-19527

Spacecraft launch trajectory optimization, combining thrust vector, inclination constraints and final adjustment parameters
07 p1207 A71-19529

Spacecraft minimum impulse /or fuel/ ellipse-ellipse transfer, discussing computer survey results of 650 trajectories
07 p1199 A71-19899

Numerical results for optimal trajectory control and filtering using Kalaba method
08 p1269 A71-21327

Atmospheric reentry trajectories optimization by differential dynamic programming
08 p1363 A71-21347

Two stage rocket trajectory optimization for prescribed flight range, maximizing hit probability for given number of launches
08 p1367 A71-22036

Winged lifting body quasi-optimal reentry trajectory for minimum flight time, taking into account angle of attack control and angular motion inertia
08 p1367 A71-22038

Selection of uncorrelated measurement composition ensuring optimal accuracy of space vehicle trajectory
09 p1519 A71-22541

Optimal trajectory measurement program for orbit parameter determination, assuming random errors and nondegenerate weighting matrix of normal equations
09 p1519 A71-22542

Minimal characteristic velocity of single impulse transfer between coplanar elliptical orbits with allowance for thrust action finite time
09 p1519 A71-22544

Optimal acceleration from earth orbit to hyperbolic velocities of low thrust space vehicle, constructing asymptotic expansions near and far from central field
09 p1519 A71-22545

Coplanar transfer orbits optimal trajectories in central Newtonian gravitational field, using Krotov sufficient criteria
09 p1519 A71-22566

Space vehicle trajectories power-optimal single parameter nonlinear correction, assuming ideal impulse performance
09 p1523 A71-23136

Rectilinear trajectory optimization of second order nonlinear system, formulating existence and uniqueness theorems of optimal control
09 p1424 A71-23433

Two-impulse optimal transfers between Keplerian orbits, deriving expression for switching conditions in explicit form
09 p1529 A71-23602

Low thrust minimum fuel space vehicle transfer from initial circular orbit to coplanar elliptic orbit of given energy and angular momentum
10 p1671 A71-24334

Minimum propellant optimal rendezvous maneuver of two cosmic vehicles on circular orbits, considering tracking vehicle motion equations
10 p1672 A71-24335

Space shuttle application to periodic interplanetary orbit making flyby without stopping, discussing trajectory requirements and relative orientation of earth, Venus and Mars
10 p1676 A71-24515

Optimal thrust programming for rocket near spherical planet, transfer between circular orbits and lunar landing at predicted point
10 p1683 A71-24847

Minimum N-impulse time free transfers between elliptic orbits for Lawden primer vector, using state and adjoint variables during firing
11 p1820 A71-25460

Soviet book on dynamics of spacecraft descent to earth covering reentry vehicles trajectory optimization, with allowance for atmospheric perturbation effects
11 p1840 A71-26375

Thrust power optimization for spacecraft earth-planet round trip trajectories
12 p1957 A71-26633

Weierstrass condition for optimality in coplanar elliptic orbit transfer involving velocity impulse control variables, discussing switching relations at corner of optimal trajectory
12 p1963 A71-27061

Optimal lunar springboard effect for maximum characteristics velocity savings on interplanetary missions utilizing gravitational field by departing spacecraft
12 p1970 A71-27718

Optimal nonlinear control with fixed time and compact convex target set, using gradient method
12 p1923 A71-27728

Optimal two impulse correction with minimum energy for planetary approach trajectory and subsequent satellite orbit transfer
13 p2133 A71-28188

Control programs reliability for optimal escape trajectories of low thrust vehicles with motion about mass of center and with or without artificial gravity
13 p2144 A71-28192

Optimality conditions for initial functions of time lag control systems onboard flight vehicles with transient response dependent on preceding trajectory coordinates
13 p2043 A71-28733

Optimal transfers in central gravitational field, using perturbation formulas of osculating Keplerian orbit elements and corresponding linearized equations
13 p2139 A71-28825

Satellite launcher flight plan maximizing mass in orbit or apogee for rocket trajectories optimal control
13 p2139 A71-28827

Fuel optimal noncoplanar orbital transfers of thrust limited rocket
13 p2139 A71-28828

Spacecraft landing trajectory minimization for lower reentry maneuver space bound at orbital speeds and fixed point coordinates
13 p2145 A71-29177

Lunar orbiter earth-moon-earth optimal trajectories geocentric section calculations from low circumlunar flight procedures
13 p2142 A71-29178

Spacecraft trajectory optimization during atmospheric reentry with allowance for total-load restriction, using Pontryagin maximum principle
13 p2143 A71-29195

Spacecraft optimal atmospheric reentry trajectory for minimum flight distance, investigating angle of attack control with allowance for load constraints
13 p2143 A71-29229

Spacecraft motion during flight toward planet, including trajectory correction energy loss, autonomous angular measurements and attractive forces
13 p2146 A71-29237

Modified steepest descent algorithm for optimum trajectory computation applied to interceptor missile control
14 p2207 A71-30018

Optimal two impulse minimum thrust transfer of particle between coplanar circular orbits under perturbations in flight plane
14 p2310 A71-30187

German monograph on linear theory of optimization problems for low thrust rockets covering orbital calculations, flight characteristics and Coast Arc problem
14 p2319 A71-30233

Energy state approximation and supersonic aircraft minimum fuel fixed range trajectory optimization, noting not convex velocity set
14 p2177 A71-30609

Symphonie geostationary satellite fuel-optimal injection problem, employing Tschauner-Hempel differential equations and Monte Carlo simulation
15 p2498 A71-31157

Optimization of linear tracking strategies, considering time independent and translation invariant N point predictor
15 p2379 A71-31411

Constant-thrust trajectory problem with gravitational acceleration as linear function of radius vector, obtaining minimum fuel solution in integrals
15 p2488 A71-32043

Optimal trajectory analysis for constant thrust optimal-coast minimum propellant control of rocket powered space vehicle
15 p2488 A71-32091

Optimal phase trajectories of coordinates of electrodynamic vibration test stand, analyzing motion of moving part and optimal control signal along coil
15 p2353 A71-32190

Optimality conditions for trajectory in Banach space, considering generalized controls
18 p2896 A71-36188

Reentry glider approximate optimal atmospheric entry trajectories for maximizing function of terminal velocity, altitude, flight path and heading angle under terminal nonlinear constraints
19 p3096 A71-37168

Explicit procedure for discrete approximations to general nonlinear fixed-time continuous optimal control problems without intermediate trajectory constraints
19 p3037 A71-37556

Onboard approach guidance instrument for Grand Tour to outer planets missions reducing fuel for corrective maneuvers by estimating trajectories
19 p3101 A71-37914

Optimal control with minimax cost for systems of n first-order state equations with performance measured by Chebyshev type functional over state trajectory
19 p3039 A71-38716

Energy optimal single impulse transfer from hyperbolic trajectory to circular orbit
20 p3288 A71-39119

Interplanetary single impulse flight trajectories optimization and computation, determining geometrical and kinematic characteristics
20 p3288 A71-39120

Satellite circular orbit trajectory plane time optimal relocation, examining turn angle angular position and modulus of maximum lateral acceleration
20 p3288 A71-39121

Spacecraft reentry into random medium atmosphere, determining optimal control procedure for prescribed arrival region and time with simulation equation
20 p3269 A71-39123

Time optimal transfer trajectory in central Newtonian force field between two arbitrary points under jet acceleration
20 p3289 A71-39135

Space tug optimal round trip trajectories for payload earth escape injection missions, obtaining boundary value problem solution by Newton-Raphson iteration technique
21 p3452 A71-40908

Space shuttle optimal lifting trajectory analysis, examining boost launch system performance increase
22 p3608 A71-41955

Optimal fuel trajectories involving intermediate thrust arcs, considering strong thrust variations, mid-course guidance and numerical results
22 p3600 A71-41959

Space shuttle trajectory design optimization by nonlinear programming, proposing mathematical model to handle equality and inequalities constants
22 p3600 A71-42013

Minimum propellant guidance laws comparison for impulsive and bounded thrust spacecraft, considering jump and controllability conditions for one burn trajectories
22 p3611 A71-42025

KC-135 aircraft climb trajectories for optimum constant lift coefficient, range and fuel amount
22 p3481 A71-42834

Trajectory aiming plane in optimum satellite orbit selection for planetary flyby and orbiter missions
[AAS PAPER 71-305] 23 p3724 A71-42981

Fuel optimal analytic multiburn transfer trajectories and shuttle rendezvous, assuming gravity vector linear dependence on position vector for burn arcs
[AAS PAPER 71-306] 23 p3724 A71-42982

Minimum norm and gradient projection constrained optimization techniques as mathematical procedures for iterative solutions of trajectory optimization problems
[AAS PAPER 71-307] 23 p3724 A71-42983

Iterative solution of least squares programming problem for finite thrust rocket trajectory optimization
[AAS PAPER 71-308] 23 p3724 A71-42984

Branched space trajectory optimization by steepest descent method with coasting arcs, obviating numerical integration for accuracy increase and computing time reduction
[AAS PAPER 71-309] 23 p3725 A71-42985

Minimum propellant deterministic guidance law for bounded thrust constant jet exhaust velocity rocket guidance law, comparing to minimum propellant impulsive thrust guidance law
[AAS PAPER 71-310] 23 p3725 A71-42986

Viking Mars 1975 mission analysis software system for trajectory optimization, describing condensed format print and contour plot program
[AAS PAPER 71-311] 23 p3725 A71-42987

Branched trajectory optimization algorithm using steepest descent method applied to space shuttle vehicle mission design
[AAS PAPER 71-326] 23 p3726 A71-43000

Optimal ascent trajectories for delta wing space shuttle flight, using accelerated gradient methods
[AAS PAPER 71-328] 23 p3726 A71-43001

Space tug assist to escape branched trajectories optimization
[AAS PAPER 71-330] 23 p3727 A71-43003

Low thrust vehicle optimal takeoff calculations from orbit about oblate planet, using two variable asymptotic expansion technique
[AAS PAPER 71-367] 23 p3729 A71-43037

High and low propulsion for optimal transfers between coplanar coaxial elliptic orbits, determining impulse number and timing
[AAS PAPER 71-368] 23 p3729 A71-43038

Impulsive trajectory optimization for asteroid Eros round trip sample return mission using chemical propulsion
[AAS PAPER 71-369] 23 p3730 A71-43039

Reusable space tug payload injection missions, determining optimal round trip trajectories at earth escape energy levels
[AAS PAPER 71-370] 23 p3730 A71-43040

Optimal singular control conditions for intermediate rocket thrust arc nonoptimality in Newtonian gravitational field for minimum fuel fixed time trajectory
23 p3718 A71-43378

Second variation for general space trajectories in terms of pseudo-Hamiltonian of Pontryagin, applying

to singular arc optimality in space vehicle escape maneuver 23 p3768 A71-43857

Vector functionals optimization, programming optimal trajectories 23 p3657 A71-44017

Convergence improvement in parallel tangents/penalty function solutions for missile trajectory optimization with terminal constraints, comparing with steepest descent method 23 p3659 A71-44102

Trajectory correction problem optimal measurement set, showing solution by linear programming simplex algorithm method 24 p3846 A71-45306

TRANQUILIZERS

Benzodiazepine series tranquilizers effect on mice resistance to hypoxia and lifetime, noting diazepam as most effective 12 p1872 A71-27722

Psychological and neurophysiological definitions of vigilance, considering alcohol and tranquilizers effects 16 p2533 A71-34040

TRANSCENDERS

U TRANSMITTER RECEIVERS

TRANSCENDENTAL FUNCTIONS

NT EXPONENTIAL FUNCTIONS

NT LOGARITHMS

NT PERIODIC FUNCTIONS

NT SINE SERIES

NT TRIGONOMETRIC FUNCTIONS

Asynchronous spatial harmonics effect on O-type interaction in comb-type slow wave structure, obtaining transcendental dispersion equation 05 p0728 A71-16011

Periodic motions stability in purely imaginary characteristic indices pairs transcendental critical case 07 p1161 A71-20266

Asynchronous spatial harmonics effect on O-type interaction in comb-type slow wave structure, obtaining transcendental dispersion equation 22 p3524 A71-42759

Longitudinal rib reinforced cylindrical shell under axial compression loads, determining equilibrium stability with approximation of transcendental equations 23 p3780 A71-44222

Elasticity and acoustic theory eigenvalues determination in spherical coordinates using transcendental equation 24 p3882 A71-44836

TRANSDUCERS

NT DIGITAL TRANSDUCERS

NT ELECTROACOUSTIC TRANSDUCERS

NT ELECTRONIC TRANSDUCERS

NT IMAGE TRANSDUCERS

NT MAGNETIC TRANSDUCERS

NT MICROPHONES

NT MODE TRANSFORMERS

NT PIEZOELECTRIC GAGES

NT PIEZOELECTRIC TRANSDUCERS

NT PIEZORESISTIVE TRANSDUCERS

NT PRESSURE SENSORS

NT QUARTZ TRANSDUCERS

NT SOUND TRANSDUCERS

NT TORQUERS

NT ULTRASONIC WAVE TRANSDUCERS

Human respiratory parameters telemetry, discussing transducer development for ventilatory volume measurement 03 p0370 A71-13068

Transistorized displacement meter with variable frequency oscillator and inductive transducer as sensing element 03 p0387 A71-13816

FM data recording system with transducers for converting varying parameters into frequency and tape recorder capable of playback for computer analysis 03 p0383 A71-14344

Pneumatic resistance transducer for fluidic measurement of mechanical quantities 07 p1030 A71-20598

Electrodynamic transducer design for structural vibration testing system, using low power steering signal converter to generate large scale electromechanical loads 09 p1386 A71-22606

Accelerometer for direct measurements of angular acceleration of rotating shafts, using semiconductor transducers 09 p1443 A71-22706

Transducer design selection for strain gage applications in high nuclear radiation environments based on system requirements 09 p1445 A71-22718

Variable capacitance signal transducers characteristics, circuitry and pulse width modulation 09 p1448 A71-22771

Viking Mars 1975 surface meteorological transducers, discussing measurements, environment and mission constraints 09 p1448 A71-22773

Fluidic inertial instruments, describing sensor or transducer components, flight control systems, rate damper systems and attitude control systems 09 p1387 A71-22785

Applied transducer signals from surface and internal fractures of various lengths, depths and positions 09 p1450 A71-22896

Hall effect mechanical vibration transducer with indium arsenide semiconductors and elastically suspended magnets 10 p1612 A71-24639

Frequency response of velocity and acceleration transducers for oscillatory environments instrumentation 11 p1762 A71-25935

Electric current heated thin resistance film thermoelectric transducer, measuring temperature rise with thermocouple 12 p1888 A71-27158

Electropneumatic transducer system linearization, matching nonlinearities in EM and pneumatic subsystems 13 p1999 A71-28638

Fluidic devices with combined pneumatic and hydraulic components, describing jet-siphon liquid flow frequency transducer with pneumatic pulse counting device 15 p2353 A71-32071

Electro-pneumatic transducer for conversion of electrical into fluidic signals, using temperature dependence of laminar gas jet deflection angle in flow along heated curved wall 15 p2353 A71-32072

Response nonlinearity of multiple turn transformer type transducer for angular displacement magnitudes conversion to electrical signals, noting relationship to turning angle and instrument dimensions 24 p3810 A71-45152

TRANSEQUATORIAL PROPAGATION

Ionospheric propagation prediction accuracy problems, considering numerical mapping, horizontal gradients, absorption, scatter, maximum usable frequency and transequatorial propagation 14 p2202 A71-30949

TRANSFER FUNCTIONS

Imaging with partially coherent light, generalizing optical transfer function in Fresnel approximation 01 p0078 A71-10144

Automatic feedback control systems steady dynamic error reduction by introducing control action forward loop, determining transfer function 01 p0062 A71-10721

Magnetic tape recording system FM distortion derivation from head-to-tape spacing transfer function 01 p0033 A71-10892

Instrumentation magnetic tape recorder reproduce systems equalization using active circuits and signal processing to develop required transfer function 01 p0082 A71-10894

Saturn V second stage longitudinal oscillation from structure and propulsion system interaction examined by transfer function simulator subroutine /TRANSIM/ computer program 02 p0318 A71-11888

Isotropic photoptical channels transfer functions analysis, using two dimensional Fourier transforms 02 p0211 A71-11829

Qualitative theory of unknown parameters selection electronic circuit synthesis, considering polynomial coefficients of transfer function 02 p0230 A71-11838

Discrete values of inverse diffusion length occurring in solutions of anisotropic transfer equations 04 p0642 A71-14904

Coordinatograph control system transfer function and interpolation error calculation 05 p0732 A71-17040

Dynamic data processing systems with feedback and internal noise, evaluating carrying capacities, limiting parameters and optimal transfer function 05 p0732 A71-17164

Single loop automatic control system with lag, determining time constant and transfer functions critical values for real positive first and second derivative elements 06 p0879 A71-17520

Flexible aircraft to atmospheric turbulence transfer functions, discussing in-flight measurements [ONERA-TP-894] 06 p0847 A71-18021

Signal cross correlation processing in unstable and turbulent plasmas, comparing correlational and spectral analyses of plasma dispersion and transfer function measurements 06 p0938 A71-18456

Linear sequential circuits feedforward inverse transfer function matrix existence condition and construction procedure 07 p1081 A71-18735

Transfer function voltage controlled transistorized amplifier using silicon carbide nonlinear resistance element 07 p1075 A71-19301

Pulse width controlled, regulated DC-DC converter with passive low pass filtering, discussing open loop transfer functions, stability analysis and linear models 07 p1024 A71-20413

Internally ported vortex amplifier, presenting dynamic equivalent circuit with transfer functions 07 p1025 A71-20555

Transfer function synthesis by RC fluidic circuit presenting transfer function element circuits analysis and experimental verification 07 p1026 A71-20598

Photographic materials holographic exposure improvement due to increased sensitometric speed and macroscopic transfer characteristics 08 p1290 A71-21411

Resistance and reactance network transfer function determination using poles and zeros method 09 p1423 A71-22585

Optical transfer function measurement and comparison test applications to aerial camera wide angle lens standard design, using interlaboratory comparisons 09 p1494 A71-23011

Amplitude characteristic polynomial Chebyshev approximation by linear phase nonrecursive digital filter transfer function 09 p1417 A71-23418

Adder transfer characteristics, demonstrating summation method for signal to noise ratio improvement 09 p1407 A71-23065

Milne-Eddington atmosphere, using Unno transfer equations for Stokes parameters 10 p1665 A71-23774

Photoelectric imaging devices resolution performance, considering modulation transfer function and measurement methods 10 p1610 A71-24004

Model theory identification application to aeronautical systems, discussing transfer function representation, state variable and direct methods 10 p1587 A71-24711

Stability indices of automatic control system from open circuit logarithmic frequency characteristics determining poles of transfer function 10 p1588 A71-24949

Aircraft with automatic thrust controller, calculating transfer functions characterizing speed and attitude control modes 10 p1640 A71-24988

Linear automatic flight control systems synthesized based on transfer functions and logarithmic amplitude characteristics of open systems 10 p1588 A71-24949

Correlation, transfer and coherence functions measurements, using digital signal analysis 11 p1731 A71-25555

Isotropic MHD turbulence in incompressible flow by diagrammatic representation, obtaining approximation with transfer functions and scalar equations for correlation 11 p1805 A71-25666

Collisionless motion of solar wind ions in heliographic magnetic field, giving transfer function of charged particles 12 p1947 A71-26646

Standard transfer function choice method for selecting adjusting automatic control system design, establishing relations between transient properties and poles and zeros distribution 12 p1891 A71-26777

Fiber optics for spectroscopic illumination, discussing absolute and angular transmission measurements and optical angular transfer function calculations 12 p1905 A71-26888

Dynamic data processing systems with feedback and internal noise, evaluating carrying capacities, limiting parameters and optimal transfer function 12 p1893 A71-27446

Spring loaded intermittent contact devices vibration system parameters for computer programmed transfer function matrix solution, noting gravity loaded variant 12 p1931 A71-27474

Engineering method for synthesizing and calculating AC correcting devices with synchronous switches deriving equivalent transfer function 13 p2041 A71-27946

Multichannel scaler as interface between edge scan unit and calculator to generate optical transfer functions 13 p2066 A71-28121

Design charts relating time response characteristics to parameters of closed loop transfer functions possessing conjugate pair of poles 13 p2042 A71-28705

Eigenvalue problem for transfer matrix of two dimensional Ising lattice with free boundaries perpendicular to transfer direction, calculating correlation function between spins 13 p2094 A71-28777

Distributed parameter systems with transfer function as ratio of output and input multiple transform deriving open and closed loop stability criteria 14 p2265 A71-29605

Transfer function optimization for linear tracking filter model with controlled resonant frequency, analyzing noise band performance 14 p2194 A71-30088

Acoustooptic deflector modulation transfer function calculated from autocorrelation theorem 14 p2241 A71-30141

- Mathematical model for short term adaptation to vestibular stimuli, deriving transfer function relating angular velocities of nystagmus and head rotation
14 p2182 A71-30250
- Gust transfer functions relating lift and moments to upwash in single sinusoidal wave for large aspect ratio rectangular wings in turbulent incompressible flow
14 p2176 A71-30604
- Silicon planar transistors at low injection levels, showing current transfer function temperature dependence
14 p2213 A71-30624
- Gaussian input signal nonlinear sampled data systems analysis using linear components and transfer function
14 p2220 A71-30800
- RC analog fluidic circuits design for arbitrary transfer functions generation
15 p2351 A71-31682
- Decomposing method for linear transfer functions identification from frequency or time response, using Cauer form continued fraction expansion
15 p2379 A71-31821
- German monograph on photographic masks as position frequency filters covering pattern recognition, transfer functions, etc
15 p2410 A71-32309
- Aspect ratio influence on instability and non-minimum phase effects of longitudinal motion of aircraft relative to negative lift-drag expression transfer functions
[DFVLR-SONDDR-127] 16 p2523 A71-33405
- Digital filters, describing transfer function, frequency response, stability and design
16 p2546 A71-33478
- Closed linear systems optimal stabilization, determining transfer function from Wiener Hopf equation
16 p2550 A71-33900
- Transfer function and temporal behavior interrelations for linear network, characterizing circuit delay and rise time by center of gravity and inertial moment of pulse response
16 p2550 A71-34139
- Gray radiative transfer equations, bridging Planck and Rosseland mean absorption coefficients
17 p2839 A71-35557
- Computer algorithm determining transfer function of linear electronic circuit in autonomous quadrupole form with zero initial conditions
18 p2887 A71-35884
- Parametric resonant circuit with low pumping frequency and transfer function variation according to arbitrary complex periodic law
18 p2896 A71-36623
- Pulse transfer functions for aperiodic and weakly oscillating control objects identification
19 p3039 A71-38640
- Transfer function for transmission through maser medium, cancelling signal distortions due to propagation
20 p3242 A71-38877
- Pseudotransfer function for interference contrast of coherent illuminated phase edge object
20 p3245 A71-39427
- Frequency response of nonlinear feedback control systems, using modified polar plot of open loop transfer function
20 p3208 A71-39914
- Transfer function system relating cornering force and aligning torque of rolling pneumatic aircraft tire to yaw angle and lateral displacement
21 p3324 A71-40167
- Optimal tracking feedback filter for closed loop systems with irrational transfer function, using heuristic method
21 p3359 A71-40251
- Transient torsional vibration due to suddenly applied torque, deriving transfer function for systems with four degrees of freedom
[ASME PAPER 71-VIBR-99] 21 p3461 A71-40326
- Envelope process transfer function calculation for self adaptive systems parametric control dynamic characteristics
21 p3361 A71-41138
- Exposing light and resulting density distribution and granularity in lower photographic emulsion layer, investigating modulation transfer function and power spectrum
22 p3538 A71-41733
- Optical transfer function measurement by holographic techniques, describing Fourier transform method useful for lens production testing
22 p3539 A71-41738
- Holographic image reconstruction analysis based on two beam interferometry by spatially incoherent light source, obtaining optical transfer function
22 p3539 A71-41740
- Branch points of root locus curves for rational transfer functions and transfer functions with recovery time
[DFVLR-SONDDR-110] 22 p3566 A71-41854
- Design technique based on frequency response locus associated with characteristic transfer functions for linear time-invariant multivariable feedback control system
22 p3526 A71-42284
- Computer program for on-line determination of minimal realizations of transfer function matrices, using Rosenbrock system matrix formulation
22 p3526 A71-42285
- Image detail reproduction quality and resolution, describing signal to noise and modulation transfer function effects
22 p3547 A71-42505
- Defocused optical system imaging properties and optical transfer function improvement by shaded aperture, discussing necessary conditions and light absorption effect
22 p3548 A71-42551
- Flat modulation transfer functions obtained by spatial filtering of high aspect ratio annular apertures images in coherent optical processor
22 p3549 A71-42552
- Transfer equation formulation for radiation field determination in anisotropically scattering medium
22 p3621 A71-42598
- Linear digital interpolator in program controlled metal cutting tool circuit, determining transfer function with z transforms
22 p3525 A71-42876
- FET nonlinear and cross modulation characteristics, basing performance prediction on power series approximation to measured LF transfer characteristics
23 p3649 A71-43068
- Primary sensor transfer function selection to minimize rms error in information transmission over telemetry channel for subsequent digital processing
23 p3648 A71-43294
- Optimal gyroscopic servosystems feasibility analysis, using approximation technique for finite memory optimal filter transfer function
23 p3675 A71-43296
- Spherical stellar atmosphere radiative transfer equation, using regional averaging method with opacity dependence on layer geometrical radius
23 p3766 A71-43828
- Mach-Zehnder interferometric measurement of modulation transfer function of optical instrument disturbed by turbulent atmosphere
23 p3679 A71-43893
- Nonstationary thermal behavior of thermoelectric cooling device for coolant temperature disturbances, proposing transfer function determination method
23 p3664 A71-44072
- Pneumatic passive lead networks for fluidic systems, presenting transfer functions, equivalent circuits and design information
23 p3631 A71-44096
- Pole placement design of dynamic compensators for linear time invariant multivariable systems, using transfer function matrices
23 p3660 A71-44119
- Sequential zero-pole placement technique for multivariable control systems, developing algorithm for computing closed loop transfer function matrix
23 p3660 A71-44120
- Soviet book on rational, irrational and transcendental transfer functions electronic modeling covering mathematical theory and applications to control plants
23 p3648 A71-44185
- Optimal stochastic control law derivation for linear regulator with quadratic performance criterion from limiting form of transfer function
24 p3816 A71-45134
- Telescope wave optical imaging performance, deriving point spread function, radial energy integral and modulation transfer functions for different wave front surface deviations
24 p3849 A71-45204
- TRANSFER OF TRAINING**
Flight training by simulator, discussing justification and effectiveness criteria, transfer of learning to real flight situations, information flow models, full mission simulation, etc
01 p0066 A71-10019
- Communication satellite systems ground stations operating personnel training, outlining basic and specialized study and on-job training program
02 p0224 A71-12826
- Overtraining reversal effect on attention process, using choice response and eye fixations compared to criterion trained group
10 p1562 A71-24204
- Learning sets development relation to transfer suppression, discussing previously learned discriminations retention
13 p2011 A71-28803
- Monkeys trained to observe and report two-member serial position sequences with delayed matching-to-sample procedure
14 p2187 A71-29519
- TRANSFER ORBITS**
NT INTERPLANETARY TRANSFER ORBITS
Optimal two impulse correction with minimum energy for planetary approach trajectory and subsequent satellite orbit transfer
02 p0304 A71-11901
- Orbiting vehicle state variables at ballistic transfer termination for known injection errors, calculating fuel consumption for final adjustments
03 p0485 A71-13249
- Second order variational endpoint condition numerical application used for low thrust minimum fuel orbital transfer problems
03 p0450 A71-13445
- Television satellites orbital transfer from low to geostationary orbit using ion propulsion
03 p0378 A71-13742
- Geometrical solutions to central motion and space vehicle dynamics, including Chaplygin problem, position and velocity transfer and comet tail separation
05 p0810 A71-16584
- Optimal orbital transfer problem by numerical integration of Contensou singular alternating arcs, solving second order differential system followed by quadrature
05 p0812 A71-16730
- Two impulse rendezvous between coplanar circular planetary orbits, considering mono-impulsive interception /flyby/ problem for optimality
05 p0812 A71-16731
- Mars 1971 orbiter mission, investigating orbit determination accuracy during approach phase
[AIAA PAPER 71-189] 06 p0978 A71-18627
- Spacecraft minimum impulse /or fuel/ ellipse-ellipse transfer, discussing computer survey results of 650 trajectories
07 p1199 A71-19899
- Minimal characteristic velocity of single impulse transfer between coplanar elliptical orbits with allowance for thrust action finite time
09 p1519 A71-22544
- Lunar swingby trajectory analysis with atmospheric reentry, characteristics of geocentric portions of earth-moon and moon-earth transfers
09 p1519 A71-22546
- Coplanar transfer orbits optimal trajectories in central Newtonian gravitational field, using Krotov sufficient criteria
09 p1519 A71-22566
- Two-impulse optimal transfers between Keplerian orbits, deriving expression for switching conditions in explicit form
09 p1529 A71-23602
- Orbit transfer time of low thrust propulsion systems, assuming constant acceleration and thrust tangential to trajectory
10 p1670 A71-24273
- Trans-Mars launch window problem, discussing minimum delta-V three-impulse noncoplanar transfer from circular parking orbit onto asymptotic velocity vector
10 p1671 A71-24331
- Low thrust minimum fuel space vehicle transfer from initial circular orbit to coplanar elliptic orbit of given energy and angular momentum
10 p1671 A71-24334
- Krylov-Bogoliubov averaging method in optimal satellite motion programming of transfer orbit and low thrust correction
10 p1587 A71-24843
- Optimal stochastic orbit transfer strategy solution by dynamic programming algorithm
10 p1678 A71-24844
- Optimal transfer programming for rocket near spherical planet, transfer between circular orbits and lunar landing at predicted point
10 p1683 A71-24847
- Minimum N-impulse time free transfers between elliptic orbits for Lawden primer vector, using state and adjoint variables during firing
11 p1820 A71-25460
- Kaufman ion thruster providing electric propulsion for satellite spiraling from parking to synchronous orbit
[AIAA PAPER 70-1101] 11 p1810 A71-25501
- Logistics system for synchronous orbit space stations supply, discussing parking to synchronous orbit transfer of reusable and disposable logistics vehicles
11 p1838 A71-25530
- Weierstrass condition for optimality in coplanar elliptic orbit transfer involving velocity impulse control variables, discussing switching relations at corner of optimal trajectory
12 p1963 A71-27061
- Optimal two impulse correction with minimum energy for planetary approach trajectory and subsequent satellite orbit transfer
13 p2133 A71-28188
- Minimum time low thrust rocket transfer between elliptic orbits in strong gravity field, using averaging method
13 p2139 A71-28816
- Optimal transfers in central gravitational field, using perturbation formulas of osculating Keplerian orbit elements and corresponding linearized equations
13 p2139 A71-28825
- Fuel optimal noncoplanar orbital transfers of thrust limited rocket
13 p2139 A71-28828

Optimal two impulse minimum thrust transfer of particle between coplanar circular orbits under perturbations in flight plane 14 p2310 A71-30187

Symphonic geostationary satellite fuel-optimal injection problem, employing Tschauner-Hempel differential equations and Monte Carlo simulation 15 p2498 A71-31157

Solar electric propulsion and transfer system for higher payloads of SECOM communication satellites, using Europa 2 launcher 16 p2644 A71-32855

Optimal maneuvers of axisymmetrical rotating satellite, minimizing orbital transfer 17 p2815 A71-35603

Optimal transfer in central field between coplanar circular orbits, allowing for errors in velocity changes and phase variables 18 p2962 A71-36107

European space tug orbit to orbit autonomous shuttle system, discussing participation in post-Apollo programs 18 p2988 A71-36489

Right ascension and declination accuracy for Sirius satellite attitude determination in transfer orbit, describing computer program 19 p3150 A71-37312

ELDO studies of interorbital space tug for transfer of satellites in geosynchronous orbits 19 p3151 A71-37327

Balance function concept extension to optimal control problem for finding numerical iterative solutions, considering low thrust orbit transfer problem 19 p3037 A71-37557

Optimality of Contensou singular alternating arcs in time-free central-field orbital transfer problem, using succession of infinitely small impulses 19 p3134 A71-37558

Two body orbits problem concerning satellite flightpath transfer possibility to orbit touching cyclic or elliptical trajectories 20 p3287 A71-38849

Energy optimal single impulse transfer from hyperbolic trajectory to circular orbit 20 p3288 A71-39119

Satellite circular orbit trajectory plane time optimal relocation, examining turn angle angular position and modulus of maximum lateral acceleration 20 p3288 A71-39121

Time optimal transfer trajectory in central Newtonian force field between two arbitrary points under jet acceleration 20 p3289 A71-39135

Orbit-to-orbit shuttles as earth capture systems for round trip planetary missions, using hyperbolic rendezvous technique with returning interplanetary spacecraft 22 p3600 A71-41954

Optimal impulsive transfer of minimum characteristic velocity between hyperbolic asymptotes associated with real planet 22 p3600 A71-41969

Fuel optimal analytic multiburn transfer trajectories and shuttle rendezvous, assuming gravity vector linear dependence on position vector for burn arcs [AAS PAPER 71-306] 23 p3724 A71-42982

Orbital transfer time equation reformulation, discussing various orbit constraints accommodation and rapid convergence in rendezvous orbit iterative determination [AAS PAPER 71-335] 23 p3727 A71-43008

Fuel optimal transfer from circular orbit space station to rendezvous with vehicles in different circular orbits [AAS PAPER 71-365] 23 p3729 A71-43035

Low thrust vehicle optimal takeoff calculations from orbit about oblate planet, using two variable asymptotic expansion technique [AAS PAPER 71-367] 23 p3729 A71-43037

High and low propulsion for optimal transfers between coplanar coaxial elliptic orbits, determining impulse number and timing [AAS PAPER 71-368] 23 p3729 A71-43038

TRANSFORM INTEGRALS

U INTEGRAL TRANSFORMATIONS

TRANSFORMATION TENSORS

U TENSORS

TRANSFORMATIONS

Torsion problem of inhomogeneous anisotropic viscoelastic rod transformation, using area variation coefficient for modeling 17 p2828 A71-35240

TRANSFORMATIONS [MATHEMATICS]

NT COORDINATE TRANSFORMATIONS

NT LAPLACE TRANSFORMATION

Linear homogeneous nth order ordinary differential equations reduction to equations with constant coefficients by transformation of independent variables 01 p0110 A71-10317

Transform for hydrogen ion exchange perturbation problem, involving first order partial differential equations and method of characteristics 01 p0130 A71-10368

Keplerian orbit numerical integration, considering Runge-Kutta method and transformations 01 p0154 A71-10377

Canonical theory of dynamics, examining independent variable transformations for perturbed two body problem 01 p0154 A71-10379

Nonaffine similarity laws and transformations subject to limitations of Newtonian impact theory for two dimensional bodies, obtaining aerodynamic coefficients 01 p0002 A71-10948

Thermodynamic calculations simplification, using identical transformation of differential expressions 02 p0332 A71-12320

Celestial mechanics, Volume 1, Dynamical principles and transformation theory covering quasi-periodic motions, many body problems, Lie groups, etc 02 p0316 A71-12774

Partial differential equation approximate solution by matrix transformation, reducing boundary or mixed problem to n independent linear ordinary differential equations 03 p0449 A71-13117

Modified Coles compressibility transformation scaling for wake mapping with Howarth-Dorodnitsyn scaling suppression 03 p0400 A71-13460

Symmetric sparse matrices transformation to triple diagonal form, giving algorithms for nonzero elements growth minimization 03 p0450 A71-13623

Inhomogeneous elasticity theory under spherical symmetry, using linear differential equations transformation into constant coefficient equations 03 p0507 A71-13714

Boundary value problems transformation into initial value problems, obviating homogeneity in boundary conditions 03 p0451 A71-13715

First order nonlinear nonautonomous systems equivalence to second order linear autonomous systems through governing differential equations variables integral transformation 03 p0390 A71-14076

Laminar and turbulent mixing of two parallel streams of dissimilar fluids, using similarity transformation [ASME PAPER 70-WA/APM-37] 03 p0403 A71-14162

Gaussian probability density functions covariance matrices dimension-reducing mapping using confidence spaces 04 p0619 A71-15331

Steady heat conduction with generation, discussing boundary value problem transformation by change of variables 04 p0677 A71-15453

Generalized von Zeipel treatment of lunar and artificial satellite theories, generating single canonical transformation by variable separation technique 04 p0654 A71-15719

Corrections derived for Labs-Neckel 1968 solar radiation tables transformation into 1968 International Practical Temperature Scale 05 p0797 A71-16018

Novozhilov complex transformation method extended to Timoshenko theory of elastic shells constructed with allowance for transverse shear deformation 05 p0820 A71-16187

Fast transformations algorithm for generalized spectral analysis 05 p0774 A71-16415

Recursive triangular algorithm for Lie transformation from introduction of small parameter into generating function and Hamiltonian 05 p0774 A71-16543

Perturbation theory using Lie transforms, discussing reformulation leading to algorithm 05 p0774 A71-16545

Power series uniformization by transformations of perturbation functions irregular part, considering compatibility problem 06 p0919 A71-18197

Minimum-sensitivity network synthesis using continuously equivalent transformations and weighted sum of sensitivities square magnitudes as criterion 08 p1268 A71-21272

Self oscillatory system behavior under sinusoidal external force, using nonlinear differential equations transformation 08 p1334 A71-21292

Orthogonal transforms and feature selection using pattern, Harr, Walsh, Fourier and Karhunen-Loeve spaces for providing efficient classification algorithms in pattern recognition 08 p1258 A71-21354

Bessel transform and corresponding inversion formula, showing relationship to Fourier, Watson and Kontorovich-Lebedev transforms for boundary value problems solution 08 p1324 A71-21355

Transform coding techniques using orthogonal matrices to implement bandwidth or dimension reduction for image processing in digital communication systems 08 p1259 A71-21356

PCM signal encoding redundancy reduction using discrete code transformation, considering telephal implementation 08 p1255 A71-21357

Matrix multiplication algorithm based on degree of freedom analysis for various transformations and spectral analysis 08 p1260 A71-21358

Book on matrix structural analysis covering transformation, structure idealization, displacement method, finite element theory, nonlinear aspects, etc 09 p1539 A71-21359

Linear antenna arrays synthesis with Z transform permitting sidelobe reduction and nulls in antenna radiation patterns 09 p1419 A71-21360

Growth minimization of nonzero elements in sparse matrix during reduction to Hessenberg triangular form by Gaussian similarity transformations 10 p1635 A71-21361

One dimensional linear stationary system described by linear differential equations, discussing identification procedure with transformation into integral equations 10 p1585 A71-24362

Asymptotic transformations and stability criteria for nonstationary linear automatic control systems using Krylov-Bogoliubov slow time concept 10 p1588 A71-24363

Infinitesimal body motion near triangular points of elliptic restricted three body problem, dividing equations of motion into two independent components in transformation 10 p1679 A71-24364

German monograph on nonnumerical transformation of tensor equations by computers, applying to shallow shell theory 10 p1692 A71-25030

Transform method application to structural dynamics analysis for engineering structure transient response to various vibration modes 11 p1841 A71-25031

Numerical methods solutions of implicit differential equations systems, discussing first order implicit and second order explicit systems transformation 11 p1791 A71-25032

Lenslike media with parabolic index profiles, describing equivalent transformation theorem for distributed optical systems design 12 p1928 A71-26030

Stretch technique for pulse time transformation including signal slowdown, speedup or time reversal performed within window with duration determined by time-bandwidth product 12 p1881 A71-27430

WKB wave functions for one dimensional nonrelativistic problems by simple transformation derivation, solving by application of Liouville substitution and Schrodinger equation 12 p1923 A71-27600

Hill-Brown differential equations for satellite coordinates transformed for integration with analytical programming language 13 p2135 A71-28230

Explicit recursive algorithms for construction of Hill and von Zeipel transformations 13 p2135 A71-28231

Distributed parameter systems with transfer function as ratio of output and input multiple transformations deriving open and closed loop stability criteria 14 p2265 A71-29030

Class structure of system identification problems with input and output signals and transform H, applying to stochastic operators 14 p2219 A71-29031

Langer transformation effects on radial equation of internuclear potential curves calculation by Rydberg-Klein-Rees method 14 p2277 A71-30230

German monograph on similarity transformation application to MGD channel flows covering mechanical, electromagnetic and thermodynamic equations 14 p2283 A71-30830

Output probability distributions and covariance functions of nonlinear transformations of Gaussian stochastic processes occurring in signal detection and control theory 15 p2379 A71-31830

Controlled motion dynamics of spacecraft performing maneuvers, applying point transformation to third order nonlinear system moving about center of mass lateral motion 16 p2646 A71-33630

Uniqueness theorem for second order differential equation associated with inverse problem of spectral analysis, developing operator transformation procedure 16 p2603 A71-33830

- Steady and linear systems discretization by Laguerre transformation and isomorphism between continuous and discrete signals 16 p2550 A71-34058
- Unbounded linear operator in Hilbert space, constructing characteristic function for transformation 17 p2765 A71-34865
- Stroboscopic method of differential equations transformation, considering application to linear and nonlinear Mathieu equations 17 p2781 A71-34928
- Conformal transformation of multiply connected plane domain of Poincare standardization 17 p2672 A71-35469
- Frictionless hypersonic flows by transforming partial differential equations into ordinary, noting detonation wave analogy 18 p2846 A71-36424
- Hadamard transform source encoding application to Apollo unified S-band telemetry links, considering possible system performance improvement 18 p2876 A71-36470
- High order optimality conditions, considering multidimensional control and transformation in space of states 19 p3037 A71-37567
- Model-reference feedback control system, investigating effects of equivalence lack between reference and plant on iterative process convergence by linear transformation 19 p3038 A71-37778
- Computer aided digital transform natural image processing, using Fourier, Hadamard and Haar matrix algebra 19 p3026 A71-38404
- Sequence convergence of similarity transformations in matrix balancing for accurate eigenvalues computation 20 p3254 A71-38756
- Nonlinear hydrodynamic field equations transformations into complex wave equations for application to ideal compressible fluids 20 p3211 A71-39031
- Generalized finite Hankel transform method for engineering problems with complicated boundary conditions 20 p3255 A71-39034
- Walsh function imagery analysis by Hadamard-Walsh transform and eigenvector expansion technique 20 p3197 A71-39610
- Walsh functions in image processing, rotational feature selection and pattern recognition, defining set of orthogonal transformations 20 p3255 A71-39611
- Generalized hodograph transformation with velocity potential as function of continuous second derivatives 21 p3406 A71-40154
- Relativistic behavior of uniformly accelerated translational observer motion relative to inertial observer from space-time transformation 21 p3415 A71-40653
- Geophysical cartesian coordinate system transformation, using vector-matrix formalism 21 p3375 A71-41355
- Analytical transformations of variational conditions in nonequilibrium thermodynamics, using mechanical analogies similar to dAlambert principle 22 p3622 A71-42688
- Singular optimal control theory generalization using appropriate transformations, considering stability results for bang-bang solutions 23 p3657 A71-43941
- Stellar wind equations transformation for reducing parameters number from two to one 24 p3865 A71-44566
- Kruskal transformation canonization of perturbed periodic systems with Hamiltonian 24 p3843 A71-44789
- ## TRANSFORMERS
- NT INSTRUMENT TRANSFORMERS
- NT MODE TRANSFORMERS
- Aeronautical electronic equipment, discussing static transformer, radiotelephone sets, angle of approach meter, etc 03 p3083 A71-13018
- High power regulated energy transfer by inductor-transformers with single and multiple stages using trapezoidal current waveshapes 03 p3052 A71-13048
- Elliptic-function low pass microwave filters and other C sections applications including broadband impedance transformers 08 p1262 A71-20766
- Transistorized pulsed amplifier stage in common base configuration with transformer coupling 11 p1739 A71-26466
- Transforming network conditions for two state one port terminations Q factor existence from Mobius transformations and invariance properties 14 p2209 A71-29545
- French monograph on system reliability of particle detection device covering methodology, functional models, Monte Carlo simulation, spectrometers and DC/DC converters 17 p2767 A71-35231
- French monograph on DC/DC transformers with controllable output voltage covering ion beam electrostatic deviation during attitude control, equivalent transformer circuits, etc 17 p2677 A71-35234
- ## TRANSFORMS
- U TRANSFORMATIONS [MATHEMATICS]
- ### TRANSIENT HEATING
- NT PULSE HEATING
- NT SHOCK HEATING
- One dimensional transient heat conduction analysis by iterative isotherm migration method, discussing boundary conditions, stability, truncation error and relative efficiency 04 p0677 A71-15452
- Transient heat transfer in fins undergoing phase transformation, obtaining approximate solution to temperature distribution and interface motion by perturbation technique 04 p0678 A71-15457
- Transient thermal laminar boundary layer, investigating absorbing-emitting gas effects 04 p0685 A71-15520
- Transient heat flow mean and first moments prediction by discontinuous linear or quadratic trial functions and variations 05 p0831 A71-16491
- Unsteady heat conduction in thermally coupled spherical regions, discussing duration, penetration depth and temperature histories 06 p1006 A71-18071
- Elastic half space with plane boundary subjected to transient temperature field, calculating temperature distribution and thermoelastic strain through Laplace transform 10 p1688 A71-24351
- Weld heat affected zone transient thermal stresses examined by weld joint model constrained system 10 p1617 A71-24533
- Thermal transients in composite cylinders, solving diffusion equation by Laplace transform technique 13 p2164 A71-28987
- High power semiconductor devices in pulsed operation mode for transient thermal resistance and p-n junction temperature estimation 23 p3652 A71-43584
- ## TRANSIENT LOADS
- NT BLAST LOADS
- NT GUST LOADS
- NT IMPACT LOADS
- NT LANDING LOADS
- NT SHOCK LOADS
- Elastic columns under transient loading, ascertaining stability by Liapunov function direct method 03 p0505 A71-13540
- Solid propellant engine structural analysis, examining transient thermal loading and internal pressure effects [AIAA PAPER 71-115] 06 p1003 A71-18565
- Dynamic response of rotationally symmetric open-ended thin shells of revolution under transient impulsive and thermal loadings, using FORTRAN 4 finite difference program 11 p1847 A71-25466
- Transient thermal stresses in infinite cylinder of rectangular cross section with heat sources, using integral transforms 18 p2976 A71-36127
- Elastic beam-columns with initial curvature and pinned or clamped ends under transient axial and distributed lateral loads, deriving upper displacement bounds 19 p3159 A71-38184
- Hypersonic flat plate under impulsive loads, calculating time dependent transient wall shear stress and boundary layer induced pressure 21 p3369 A71-40964
- Complex structural systems response characteristics under steady state sinusoidal, transients and random loadings, developing hybrid elastodynamic equations 21 p3470 A71-41011
- ## TRANSIENT OSCILLATIONS
- Nonlinear systems near steady state oscillation transient behavior analysis by linear differential equations with periodic coefficients 03 p0451 A71-13817
- Solid state laser oscillation transient features analysis by dynamic rate equations, taking into account electric field phase variations in mode locking 08 p1301 A71-21277
- Nature and average magnitude of lightning discharges causing transient excitation of earth-ionosphere cavity resonance 13 p2054 A71-27795
- Power line and signal line transients in digital systems 13 p2032 A71-28863
- Self excited and transient oscillations parameters determination in nonlinear control systems, using control area concept 15 p2383 A71-32697
- Excitation response of oscillatory conservative linear system to transient displacement involving time dependent boundary conditions 18 p2947 A71-36748
- Nonlinear vibrating system characteristics relationship to transient process, deriving Abel integral equations for damping coefficient and restoring force 19 p3104 A71-38483
- Transient torsional vibration due to suddenly applied torque, deriving transfer function for systems with four degrees of freedom [ASME PAPER 71-VIBR-99] 21 p3461 A71-40326
- Scorpius X-1 optical and X ray flux transient short period oscillations correlation from Aerobee sounding rocket data 23 p3733 A71-43077
- ## TRANSIENT PRESSURES
- Strong blast wave interaction and transient pressure on conical slender supersonic bodies 04 p0525 A71-14979
- Liquid-vapor system in closed container, investigating transient pressure rise under heat and mass transfer interactions including incipient and nucleate boiling 04 p0687 A71-15535
- Transient pressures in spacecraft and volume compartments with outgassing for ambient pressure decrease and low pressures unattainable with large chambers 11 p1840 A71-26398
- Engine surge pressure transients in mixed-compression supersonic inlet, describing scale wind tunnel model simulation and measurement techniques [AIAA PAPER 71-671] 14 p2291 A71-30735
- Static and transient pressure measurement in turbulent boundary layers, using transducer with piezoelectric sensing element 20 p3233 A71-38822
- Transient pressure measurement in plasma exhaust flow of 500 microsec duration, discussing discharge temporal behavior and cold gas pressure front existence 23 p3711 A71-43598
- ## TRANSIENT REACTOR TEST FACILITY
- Small fast spectrum thermionic reactor experiment open loop dynamics and control, discussing nonlinear transient simulation studies on closed loop plant 11 p1712 A71-25886
- ## TRANSIENT RESPONSE
- Transient response of pulse frequency modulation automatic control systems for zero or nonzero initial conditions, using signal Laplace transforms 01 p0059 A71-10528
- Transient heat conduction of solids obeying Fourier law, deriving numerical solution for boundary value problem by Laplace transformation 01 p0180 A71-10937
- Transient processes in transistor with strong input signal, using substitution parameter for nonlinear differential equation 01 p0055 A71-11155
- Transient effects due to electromagnetic cascades in lead during copper wall passage in ionization chamber 01 p0084 A71-11370
- Elastic half space transient response to normal impulsive surface line load 02 p0321 A71-11677
- Q switched ruby laser facility for measuring light pulse transmission spatial and temporal response through clouds 02 p0213 A71-12013
- Transient response measurements of multiple scattered laser radiation from clouds as function of view field 02 p0260 A71-12032
- Low level optical signal transient response measuring instrument with nsec resolution and automatic photomultiplier current gain control 02 p0249 A71-12131
- Thermionic system transient behavior analysis by digital simulation using one diode model 02 p0196 A71-12261
- Hydride thermionic reactor system transient behavior dynamic mathematical model and digital simulation 02 p0281 A71-12262
- Transient creep propagation velocity in dead annealed thin walled Al alloy tubes, using constitutive equation for mean stress-strain-time relationship 03 p0508 A71-13761
- Polar orbiting satellite observed transient plasma density enhancements relation to geomagnetic activity 03 p0417 A71-14042
- Fluid lines transient response to frequency modulated signal inputs, considering Newtonian fluids or perfect gases [ASME PAPER 70-WA/FLCS-1] 03 p0354 A71-14078
- Fluid lines transient response obtained in infinite series form [ASME PAPER 70-WA/FE-22] 03 p0403 A71-14132
- Buoyancy effects on transient free convection heat transfer in revolving tube for zero to 100 g centrifugal acceleration [ASME PAPER 70-HT-10] 03 p0521 A71-14292

Cascade thermoelectric cooler/heat pump/transient response for various geometries, materials and environmental conditions

03 p0355 A71-14320

Acoustic plane waves transient interaction with cylindrical elastic shell, using Volterra integral equations

04 p0668 A71-15189

Mechanical oscillator mean square response to nonstationary random excitation

04 p0669 A71-15200

Transient waveform distortion of arbitrarily modulated signal propagating through ideal waveguide

04 p0553 A71-15219

Numerical analysis of one dimensional transient temperature fields and elastic thermal stress fields, deriving equations for plate and cylinders with free edges

05 p0823 A71-16494

Transient response of solid propellant combustion to pressure variations and sudden depressurization

05 p0795 A71-16540

Semiinfinite simply supported cylindrical shell transient response due to axisymmetrically engulfing step pressure wave, investigating moving load critical velocity

05 p0823 A71-16556

Coaxial cone antenna transient response to incident field along ground plane, using signal generated as step function in time

06 p0875 A71-17717

Log periodic dipole array transient radiation, obtaining radiated pulse envelope time dependence as function of antenna admittance and input pulse frequency spectrum

06 p0875 A71-17720

Cylindrical anisotropic shells transient deformation processes under external pressure, discussing equations of motion integration

06 p0996 A71-17838

Optimal discrete signal filters with finite duration transient process, describing approximation procedure to restore noise distorted signals

06 p0876 A71-17928

Cylindrical Langmuir probe RF transient response characteristics in transition regime

06 p0902 A71-18585

Microcircuits component vulnerability, deriving time independent nonlinear terminal I-V characteristics, electrical switching response and ionizing radiation induced transient response

07 p1070 A71-19059

Zirconium droplet combustion in oxygen-rare gas mixtures, observing transient burning phenomena, oxidation conditions and luminosity-time records

07 p1223 A71-19623

Infinite circular cylindrical shell with elastic stiffener ring, calculating transient axisymmetric bending stress under radial impulse

07 p1213 A71-19907

Transient signal generation by propagation of large amplitude pulses, discussing angular dependence in water

07 p1063 A71-19960

Transient stabilization analysis for electronic circuits containing diverse components with variable parameters, considering active low pass filter example

07 p1078 A71-20061

Fokker-Planck boundary value solutions to transient phase error response of nonlinear phase locked tracking systems

07 p1082 A71-20428

Transients estimation for measuring lines of LF pressure sensors, taking into account hydraulic resistance in inlet channel

08 p1286 A71-20834

Hydrogen fluid phase and temperature measurement by single sensor with fluid phase discrimination circuit for transient response sampling

08 p1293 A71-21697

Thick walled anisotropic nonhomogeneous elastic cylinder or plate under axial symmetric time dependent pressure, investigating transient response

09 p1540 A71-23087

Lubricating oil thin films interfacial Newtonian flow elastohydrodynamics, studying transient effects on contact load damping parameters

10 p1614 A71-23981

Transient electromagnetic wave propagation in lossy directionally anisotropic time varying stratified plasma, using characteristics method

10 p1648 A71-24296

Soviet book on liquid propellant rocket engines nonstationary operation covering dynamic processes, transient conditions, component elements, fuel delivery, etc

10 p1659 A71-24649

Hydrodynamic lubrication temporary breakdown during initiation of extrusion process

10 p1618 A71-24924

Transform method application to structural dynamic analysis for engineering structure transient response to various vibration modes

11 p1841 A71-25150

Dynamic frequency characteristics of built-up structures by transient rapid sweep testing

11 p1841 A71-25178

Structural system frequency response measurements under environmental noise conditions, discussing autocorrelation function for transient excitation damping

11 p1797 A71-25182

Transient mean square response of simple structural systems to forcing function representing rocket engine noise, comparing with stationary mean square response for each launch stage

11 p1837 A71-25327

Transient stresses in heat shield generated by short duration pressure pulses, using method of characteristics for interface stresses

11 p1844 A71-25330

Initially spherical liquid droplet transient response under surface tension accelerated by external gas flow

11 p1749 A71-25355

Transient resonance response of slender entry vehicles in rolling trim at spin-pitch intersection for offset coplanar and orthogonal leading models

11 p1837 A71-25480

Transient ion sheath effects on spherical metallic plasma probe complex admittance at different frequencies, comparing numerical results with experiment

11 p1805 A71-25803

Open loop transient analysis of thermionic diode kinetics experiment with analog computer nuclear reactor simulator

11 p1797 A71-25904

Retinal sine wave flicker transient response obtained with circular uniform field and counterphase grating targets

11 p1799 A71-26141

Mutual coherence effects in time varying radiation fields on two beam interferometric optical discrimination response

11 p1800 A71-26306

Transient dynamics of ventilation and heart rate following positive and negative sustained step changes in work load initiated from different load levels

11 p1722 A71-26357

Transient characteristics of MOS channel transistors, solving nonlinear differential equations describing current and potential distribution

12 p1886 A71-26850

Plasma plate under vacuum conditions, examining transient radiation and spatial dispersion

12 p1937 A71-27118

Plate and acoustic finite elements simulation of window-room system coupled transient response to sonic booms, discussing equations of motion and cavity depth effect

12 p1981 A71-27481

Transient nature of fuel droplet combustion, discussing burning rates and flame to drop diameter ratio

13 p2161 A71-28614

Optimality conditions for initial functions of time lag control systems onboard flight vehicles with transient response dependent on preceding trajectory coordinates

13 p2043 A71-28733

Computerized use of transient thermal resistance and power pulses superposition to calculate instantaneous transistor junction temperatures for various pulse conditions

13 p2038 A71-28770

Successive approximations method for solving nonlinear elastic problems in transient creep theory, describing stress redistribution

13 p2157 A71-29197

Semiconductor injection laser output transient response, analyzing stepshaped impressed current by differential rate equations

13 p2081 A71-29391

Transient creep of thin walled composite beam under bending and tensile loads in nonuniform temperature field by increment method

14 p2321 A71-29538

Pulsed GaAs point contact diodes quick response performance, obtaining contact electrical characteristics and Schottky-type rectifying barriers by half period currents

14 p2211 A71-30093

Transient and steady state creep of circular cylindrical shells loaded by internal pressure, using strain hardening hypotheses and finite difference method

14 p2328 A71-30379

Collector current delay and rise times in transistor common emitter configuration for linear, sine and exponential input signals

14 p2213 A71-30630

Analytical model of compressor sensitivity to transient and distorted transient flows, considering inlet duct, compressor stages and combustor up to turbine nozzles

14 p2291 A71-30734

Transient response and design formulas for microwave power stabilizer with nonlinear inertial feedback containing semiconductor attenuator

15 p2378 A71-31230

Gunpowder unsteady burning as closed dynamic system, studying frequency characteristics transient processes

15 p2462 A71-3111

Arbitrarily shaped thin shell elastic-plastic deformation transient response prediction, using implicit finite difference method

15 p2505 A71-3111

Steady state and transient performance of Brayton cycle alternator and electronic controls for space power

15 p2355 A71-3111

Steady state and transient interactions due to thermal integration of isotope Brayton space power life support systems

15 p2364 A71-3111

Unified raindrop breakup theory, examining special liquid drop transient response under surface acceleration by uniform external gas flow

16 p2557 A71-3111

Transient response of water drops to shock waves reduced accelerations at near critical Weber number

16 p2557 A71-3111

Density perturbation effect on transient spin down of incompressible dissipative rotating stratified fluid cylindrical container

16 p2561 A71-3111

Transient matrix heat transfer test data reduction: discussing direct curve matching methods implementation by distance function minimization

17 p2835 A71-3111

Square cross section prismatic bars transient creep analysis based on strain, time and combined hardening theories

17 p2815 A71-3111

Digital computer techniques for transient processing and test control

17 p2709 A71-3111

Impulsively loaded expanding cylindrical shell transient elastic-plastic response, using linearized assumption on plastic flow behavior

17 p2821 A71-3111

Unstable nonlinear systems transient behavior analysis with two-time perturbation method applied to hard and Taylor flow problems

17 p2730 A71-3111

Transient laminar two dimensional boundary layer induced pressures due to suddenly accelerated hypersonic semiinfinite flat plate

18 p2901 A71-3111

Steady state and transient response of heat source with temperature regulated by electrical feedback controlled variable conductance heat pipe

18 p2868 A71-3111

Simple structures large elastic-plastic transient deformations, using finite element method

19 p3157 A71-3111

Transient response of Euler-Bernoulli and Timoshenko beams and cylindrical shells with moving loads

19 p3158 A71-3111

Filter design for optimal transient performance: comparing with steady state frequency response

19 p3038 A71-3111

Electromagnetic plane wave monostatic scattering incident to thin circular metallic disk, calculating spectral and transient response from far field amplitude and phase data

19 p3036 A71-3111

Transient RF pulse dispersion along plasma lossy coaxial gas discharge, noting group delay

20 p3272 A71-3111

Transient performance of phase locked loop aboard tumbling satellite, noting relation to time, S and fade modulation

20 p3196 A71-3111

Liapunov direct method for transient multimachine power-system stability analysis using multivariable control modeling

20 p3207 A71-3111

Single and double pass traveling wave electro-optical modulator phase retardation transient response calculation

20 p3235 A71-3111

Step-change single blow transient temperature response synthesis by data reduction with aid of operational calculus and half-line convolution integral equation theory

20 p3314 A71-3111

Lunar interior electrical conductivity and temperature three-layer model from magnetic transient response measurement in solar wind

20 p3301 A71-3111

Gravity receptors in *Phycomyces sporangiotheca* considering transient and long term geotropic responses

21 p3339 A71-3111

Vibration isolation system performance under transient conditions, deriving equations of motion with and without inertia torque effect

21 p3458 A71-3111

Transient and steady state flexible rotor dynamic analysis

21 p3461 A71-3111

Nonlinear autonomous systems transient response, obtaining approximate solutions by generalized averaging technique based on ultraspherical polynomial expansions 21 p3415 A71-40532

Moderately thick plate transient response stability analysis, using finite difference equation 21 p3467 A71-40957

Thin elastic shell of revolution under asymmetric loads, calculating time dependent transient response with implicit backward and explicit central differencing schemes 21 p3467 A71-40960

Penny shaped crack under time dependent impact wave loads, investigating transient response with integral transformations 21 p3468 A71-41002

Rectangular plate under lateral and inplane pressure pulses, examining transient response with Mathieu equation 21 p3471 A71-41023

Computerized step-jump and time-transient dynamic analysis application to gimbal mounted Rayleigh-step gas-lubricated thrust bearing design 22 p3552 A71-41672

Electronic broad banding of VLF/LF antennas for PSK radio communication through switched magnetically coupled reactor, determining antenna transient response 22 p3513 A71-42388

Vergence eye movements control, discussing transient and frequency responses 22 p3489 A71-42446

Mixed and unmixed turbofan engines transient and steady state off-design characteristics, investigating effects of fuel flow rate, nozzle area, inlet pressure, ambient temperature and air bleed 22 p3590 A71-42836

Control system synthesis from transient process estimates with Liapunov functions, proposing optimality criteria based on Gaussian minimum constraint principle extension 22 p3527 A71-42855

Three dimensional transient interaction of spherical acoustic waves with cylindrical elastic shell, using integral transform techniques 23 p3775 A71-43207

Transient response of electroacoustic transducer arrays, computing time dependent velocities for prescribed electrical inputs 23 p3704 A71-43211

Bandpass filter harmonic signal phase shift distortion effect on transient response in PSK of multichannel transmission 23 p3644 A71-43286

PAM signal transmission through statistically rough waveguide, calculating wall roughness effects on transient response by multiple scattering theory 23 p3645 A71-43566

Fluidic element input impedance measurement, noting aperiodic nature of transient response in input channel 23 p3631 A71-44019

Electromagnetic pulses scattering by conducting wedge in uniaxially anisotropic plasma, obtaining electric dipole radiation fields transient time for various plasma frequencies 23 p3646 A71-44171

Metal cored cylindrical plastic shells response to transient external pressures, considering failure modes 24 p3878 A71-44610

Transient dynamic characteristics of aircraft under unsteady flight, using Laplace-Carson integral transforms 24 p3792 A71-45016

Transients determined for Cs vapor discharge phases, observing current fluctuations between steady states in negative resistance zone above 0.2 torr 24 p3858 A71-45246

TRANSIENTS [SURGES]
U SURGES
TRANSISTOR AMPLIFIERS
 Push-pull power amplifiers with class B complementary transistors, describing driver stage 02 p0229 A71-11693

Transistor amplifiers automatic gain control open loop amplitude characteristics, discussing output level stabilization relation to signal source coupling and negative feedback 02 p0233 A71-12544

FET chopper amplifier for low level DC signals from thermocouples, strain gauge bridge circuits and weak transducer sources 03 p0384 A71-13275

Transistorized amplifiers synthesis with multiloop feedback 05 p0728 A71-16871

C band field effect transistor amplifiers with stable power gain, discussing circuit analysis, design parameters and test results 05 p0729 A71-16917

Photodetector-transistor amplifier coupling for maximum SNR in optical communication systems 06 p0866 A71-17370

Spacecraft phased arrays design, considering solid state amplifiers effect on total array performance and transistors and varactors output power efficiency 07 p1069 A71-18813

Transfer function voltage controlled transistorized amplifier using silicon carbide nonlinear resistance element 07 p1075 A71-19301

Combined HF compensation of single stage transistor amplifier with RC feedback in emitter circuit 07 p1079 A71-20262

Scatter effects of transistor parameters on maximum undistorted output-voltage amplitude of single stage amplifier 07 p1080 A71-20263

Transistorized DC amplifiers operational characteristics, discussing principal electrical parameters and application in phase lock AFC loops 08 p1263 A71-20786

Microwave multistage transistor amplifier with IC configuration, discussing design and performance 08 p1265 A71-21287

MOS transistor cascade amplifiers, discussing monolithic integrated circuits 09 p1416 A71-22492

Transistorized pulsed amplifier stage in common base configuration with transformer coupling 11 p1739 A71-26466

Wideband transistor amplifier frequency response at low frequencies, discussing gain increase, thermal pull-in effect, barrier layer geometry and switching control functions 12 p1887 A71-27042

LF transistor power amplifier protection from power overloads in case of short circuit at output 12 p1889 A71-27625

Two transistor emitter follower DC amplifier, using simplified equivalent circuit 13 p1999 A71-28628

Transistorized microwave amplifier/limiter for upper part of decimeter wave range, suggesting limitation in automatic gain control transistors 16 p2547 A71-33499

Low noise microwave transistor amplifiers technology, discussing performance levels in frequency coverage, SNR, gain flatness and power output 17 p2714 A71-34604

Low noise FET amplifiers for earth station radio receivers 17 p2715 A71-34687

German monograph on field effect transistors as controllable resistors with applications in adjustable amplifiers and dampers, covering nonlinear harmonic distortion and control dynamics 18 p2887 A71-35961

General purpose pulsed microwave radar receiver, describing balanced mixer and transistorized IF amplifier design and construction 18 p2887 A71-36015

Gyrator circuit design with two antiparallel transistor amplifier stages for minimal DC current reception 18 p2888 A71-36223

Emission transistor for Eole balloon transmitter power amplifier, discussing trouble-free emission, high output, wide temperature range, lightweight and reliability features 18 p2891 A71-36563

Gain and stability of MOS transistor small signal amplifier as function of frequency, using lumped element equivalent circuit 19 p3028 A71-37563

Microwave transistor amplifier dynamic range performance, comparing low noise and high power capabilities with traveling wave tubes 19 p3029 A71-38295

Linearization techniques for multiple signal interference reduction in broadband transistor power amplifiers in 225-400 MHz range 19 p3030 A71-38434

Transistorized microwave amplifiers with dissipative equalizing networks, describing transistor equivalent circuit 20 p3205 A71-39810

Transistorized high power telemetry amplifier design, describing test equipment for input and collector load impedance 22 p3519 A71-41632

Emitter-base W metallized contacts RF power transistors for improved hot spotting and breakdown reliability, comparing with Al 23 p3651 A71-43441

Transistorized amplifier circuit for measuring power of CW emission from He-Ne laser 23 p3685 A71-43532

Operational principles and circuit diagram of transistorized preamplifier for Si p-n gamma quanta radiant flux detector, noting noise properties and possible improvements 24 p3810 A71-45151

Optimal number of parallel connections of transistors in amplifier for improving SNR 24 p3810 A71-45260

Low temperature noise in p and n channel MOST amplifiers 24 p3812 A71-45361

TRANSISTOR CIRCUITS
 High input impedance wideband frequency measurement probe with bipolar and unipolar transistor circuits 01 p0051 A71-10284

Pulse-fed transistorized discrete devices reliability properties estimation by model, taking into account structural properties 01 p0057 A71-11232

Switching bipolar transistor dynamic model equivalent circuit diagram characterization by parameters 02 p0228 A71-11655

MOS transistor inverters static and dynamic characteristics in IC assemblies 02 p0228 A71-11656

MOS transistors as high speed switches in magnetic film memory selection matrix, discussing requirements for drive current pulse yield, signal power and dissipation 02 p0229 A71-11815

Double balanced cross coupled transistor mixer, predicting conversion gain and inter and cross modulation distortion performances 02 p0233 A71-12345

Transistorized displacement meter with variable frequency oscillator and inductive transducer as sensing element 03 p0387 A71-13816

Transistor multistable switching circuits, considering construction principles, applications and advantages 03 p0387 A71-13818

Oscillator for guiding clock mechanism of 400 mm photographic telescope, using high stability transistorized multivibrator 04 p0591 A71-14847

Automatic amplitude control of transistorized quartz clock master oscillator 04 p0592 A71-14860

Microwave transistor circuit simplified noise figure expression including feedback and parasitics effects 05 p0719 A71-16164

Transistorized transmitters constant phase low distortion AM system based on Chireix method, generating AM from two push-pull phase modulated signals 05 p0720 A71-16392

Transistorized four-quadrant control signals voltage multiplier, analyzing operation and circuit diagrams 06 p0879 A71-17493

RF distributed transistors for high reliability and power operation, discussing failure physics 07 p1076 A71-19559

Planar transistors operating conditions effects on current gain degradation following emitter-base reverse biasing 07 p1076 A71-19560

Transistorized ultrasonic oscillator active conductances and other circuit parameters effects on self oscillation frequency stability 07 p1078 A71-20060

Polarizing phase shifter for quasi-optical transmission lines, describing varistor network operation 08 p1264 A71-21068

Transistor circuit constant current technique for wave generation and shaping involving triangular, trapezoid and staircase waveforms 08 p1264 A71-21223

Transistorized gas laser discharge current stabilizer using double feedback circuit, discussing schematic diagram and operation principles 08 p1303 A71-21807

Transistorized amplitude limiter with series connected nonlinear element and filter tuned to input signal first harmonic, describing amplitude characteristics calculation method 09 p1415 A71-22299

Emitter coupled integrated transistorized logic elements, improving steady state noise stability by hysteresis in transfer characteristics 09 p1416 A71-22467

Integrated circuit components equivalent circuits, considering transistor logic circuits and admissible noise 09 p1416 A71-22491

External and transistor noise temperature effects on SNR of transistorized microwave receiving antennas 09 p1417 A71-23038

Analog type semiconductor switches for aircraft and spacecraft automatic checkout systems, discussing component transistor types, optoelectronic devices and materials 09 p1418 A71-23041

Temporary nonlinear feedback effect on stability of triggering potential and output pulse repetition rate of transistor self relaxing blocking oscillator 09 p1424 A71-23169

Junction thermal behavior and energy losses in active contactless bipolar transistor switch loaded by capacitive impedance 11 p1739 A71-26377

TRANSISTOR LOGIC

- Series resonant transistor circuit exhibiting response nonlinearity caused by conductance and charge storing capacitance of p-n junction 11 p1740 A71-26544
- Detection characteristics of transistor input circuit with automatic bias 11 p1740 A71-26545
- Transistorized multichannel registers for optical oscillograph records, discussing frame storage and digital processing circuitry 12 p1889 A71-27755
- Dual phase asynchronous or hysteretic micromotors powering with two transistorized static DC to AC voltage converter circuits 13 p1999 A71-28629
- Interface IC circuits for driving high voltage transistor switches from low level logic inputs, noting avionics application 13 p2039 A71-28910
- Metal oxide semiconductor digital circuit supply voltage, load capacitance and standby power drain 14 p2206 A71-29547
- Active antennas for frequency range 100 kHz to 250 MHz, discussing transistor circuitry optimization with respect to noise and linearity 14 p2210 A71-29822
- Triangular pulse shaper using transistors and dynistors, obtaining pulse duration, rise time and maximum repetition frequency 14 p2213 A71-30581
- Balloon-borne transistorized stratospheric cosmic ray probe, describing simultaneous gas discharge and dual coincidence telescope counters data transmission 14 p2247 A71-30596
- Equivalent circuit parameters of microwave planar power transistors at high injection levels, indicating parameters frequency dependence determination 14 p2213 A71-30627
- Preliminary circuit-stage alignment procedures in multistable triggers manufacture with counter input based on tunnel diodes and transistors 14 p2213 A71-30632
- Transistorized trigger generator with improved commutation, using inductor circuit limiting collector voltage front durations 15 p2375 A71-31234
- LF white Gaussian noise generator with continuously variable output, describing transistorized circuitry and output characteristics 15 p2371 A71-31851
- Transistorized long time delay relay for power supply circuits with constant function on reenergization after interruption 15 p2376 A71-32021
- Pulse detection equipment by peak voltage and current value sampling, using avalanche transistors 15 p2377 A71-32324
- Transistor minimum noise figure in low noise microwave amplifier circuit 15 p2378 A71-32635
- Solid state voltage regulator with hybrid tunnel-diode/transistor circuit discriminator for overload protection, discussing operation, circuit diagram and performance 17 p2716 A71-34786
- Transistorized analog multiplication circuit for automatic control system requiring controller input proportional to product of two values 17 p2719 A71-34787
- Transistor circuit driven hydrogen-oxygen fuel cell, testing internal impedance effect on power supply noise for comparison with lumped parameter model 19 p3000 A71-38463
- Beam-lead devices, discussing comparison to conventional transistor chip, reliability, applications and assembly techniques 21 p3357 A71-40815
- Transistorized amplifier circuit for measuring power of CW emission from He-Ne laser 23 p3685 A71-43532
- Wideband transistorized active dipole antenna for reception at 100-1000 MHz, calculating impedance and effective height by linear theory 24 p3807 A71-44360
- Transistorized AGC circuit for use with ultrasonic Doppler-cardiogram recording system to retain signal characteristics under strong fluctuations 24 p3801 A71-44543
- Phase sensitive magnetic semiconductor pulse width modulator with diode bridge consisting of single saturable-core choke input and transistor circuit output arms 24 p3810 A71-45155
- Two component 1/f noise measurements in p-channel MOS transistors 24 p3812 A71-45352
- TRANSISTOR LOGIC**
- Basic digital circuits with integrated TTL and MOS structural elements, giving diagrams for dual counters, frequency dividers, adders and shift registers 02 p0231 A71-11862
- MOS transistors for high digital logic speed and microwave performance, discussing fabrication by double diffusion through mask opening 07 p1078 A71-19998

- Integrated digital emitter coupled logic /ECL/ circuits with transistors in nonsaturated mode 18 p2896 A71-36799
- Cellular array for multiplication and division of two binary numbers, discussing implementation with transistor-transistor logic integrated circuits 18 p2894 A71-36833

TRANSISTORS

- NT FIELD EFFECT TRANSISTORS**
- NT JUNCTION TRANSISTORS**
- NT SILICON TRANSISTORS**
- Transistor collector pulse response characteristics measurement at high voltages in avalanche multiplication region, considering dissipated power curve 01 p0051 A71-10282
- Planar diffused transistor characterization by equivalent circuit model using input impedance and amplification measurements 01 p0051 A71-10310
- Junction-casing and junction-ambient medium thermal resistance determined in power transistors and diodes 01 p0055 A71-11125
- Transient processes in transistor with strong input signal, using substitution parameter for nonlinear differential equation 01 p0055 A71-11155
- Carrier mobility dependence on channel transverse electric field in MOS transistor 02 p0231 A71-11841
- Nomograms predicting transistors transition frequencies as function of geometric and physical characteristics 02 p0235 A71-12920
- Surface thermal and electrical stresses effect on bipolar transistors electrical properties, using NDT criteria for components selection 02 p0236 A71-12921
- Automatic transistor noise factor measurement equipment consisting of noise source, signal amplifier, synchronizing oscillator, controllable attenuator and automatic control circuits 04 p0557 A71-15078
- MOS transistor and circuits in digital applications, presenting current-voltage characteristics, conduction resistance, transconductance, etc 04 p0557 A71-15083
- Voltage distribution in transistor base for forward and reverse biases, discussing nonuniform potential distribution 05 p0728 A71-16007
- Transistors and Zener diodes temperature dependence and normal and accelerated life tests 05 p0728 A71-16289
- Modified Ebers-Moll equivalent circuit model for saturation characteristics of high voltage transistors 07 p1174 A71-19058
- Failure criteria percentages for bipolar transistors, determining adequacy of Weibull distribution for low gamma ray dose survival probability 07 p1071 A71-19064
- RF distributed transistors for high reliability and power operation, discussing failure physics 07 p1076 A71-19559
- Charging carriers of MOS structure interface states, considering effect on static transistor characteristics 08 p1265 A71-21291
- Nonlinear planar transistor model, analyzing majority carrier current flow fields in base due to injection of emitter and collector p-n junctions 12 p1888 A71-27612
- Semiconductor materials technologies, discussing optoelectronic and microwave components, photodiode arrays, HF diodes and transistors and IC Doppler radar units 13 p2111 A71-28908
- Current constriction-resistance variations relations in transistors, discussing current redistribution 14 p2213 A71-30629
- Collector current delay and rise times in transistor common emitter configuration for linear, sine and exponential input signals 14 p2213 A71-30630
- Heat sink requirements in transistor devices, examining temperature dependence of thermal resistivity and electrical capacitance 14 p2284 A71-30631
- Transistor resistances difference measurement under reversed polarities during quality control testing 14 p2214 A71-30635
- Substrate emitter monolithic inverted transistor structure for low-power high-current gain application 15 p2375 A71-31474
- Microwave transistor case design, considering RF parasitics, thermal dissipation, environmental mechanical factors, ceramic technology and sealing 15 p2377 A71-32500
- Commercial production of high reliability components in plane transistors, bipolar integrated circuits and printed circuits technologies 18 p2889 A71-36535
- Low noise microwave transistor, describing geometry and diffusions optimization, power gain, reliability and base resistance 18 p2892 A71-36564

- Transistors life testing for temperature and voltage dependence of failure rates 18 p2893 A71-36885
- Equivalent circuits for planar devices behavior under ionizing radiation, considering bipolar and MOS transistors 19 p3034 A71-38460
- Collector/base current ratio degradation in bipolar transistors, describing mechanisms characteristics and protective techniques 19 p3034 A71-38510
- Transistor fed active radiating array antennas showing dependence on elemental mutual coupling 19 p3035 A71-38610
- Impurity diffusion self aligned MOS and lateral transistors used in IC 21 p3354 A71-40710
- Microwave communication transistors, considering power, low noise, digital and CATV types 21 p3358 A71-40810
- Emitter-base junction degradation by avalanche breakdown in planar transistors with low doping/epitaxial/ base region 22 p3520 A71-41614
- Distributed gate multicollector MOS transistor presenting negative resistance operation mode 22 p3520 A71-41614
- Analog data computation with hybrid and logic operational elements, applying to periodic functional arithmetic mean determination and transistor characteristics representation 22 p3518 A71-42424
- Voltage distribution in transistor base for forward and reverse biases, discussing nonuniform potential distribution 22 p3524 A71-42750
- Microwave bipolar transistors computer aided design, describing optimization and synthesis procedures and RF performance 23 p3649 A71-43060
- Conventional components in hybrid circuits, using leadless inverted device, SOT-23 transistor and multilayer ceramic capacitors 23 p3655 A71-43348
- Analog transistor model for IC simulations discussing static characteristics and switching times 23 p3650 A71-43350
- HF and LF transistors suitability for integrated high Q LC circuits, studying inductivity, Q and component frequency dependence 24 p3807 A71-44370
- Transistor current gain as function of emitter current for low injection levels 24 p3807 A71-44380
- Transistor compensation stabilizers design and fabrication with enhanced voltages 24 p3807 A71-44380
- MOS transistors operating in unsaturated region discussing source and drain series resistance measurement techniques 24 p3808 A71-44650
- TRANSIT**
- Mercury transit across solar disk on 9 May 1970 using photographic micromasurements 10 p1677 A71-24581
- Mercury and Venus transit periodicity before solar disk, examining celestial mechanics and solar system distances determination 10 p1680 A71-25001
- Satellite orbit period variation data for PERLO program visual observations, calculating topocentric celestial equator transits 11 p1732 A71-25824
- Photographic quasi-draconitic period measurements from satellite transit across topocentric celestial equator tested on Echo 2 and Pages A 11 p1732 A71-25824
- TRANSIT TIME**
- Stellar transit time recording by photoelectric instruments, discussing time constant and slit characteristics 04 p0598 A71-15377
- Time lag between actual and measured stellar transits by photoelectric recording instruments, noting atmospheric, spectral and instrumental factors 04 p0598 A71-15378
- Time lag between actual and measured stellar transits times based on photocurrent expansion into Fourier series 04 p0598 A71-15380
- Stellar transit time photoelectric instruments time lag measurements by variable flux light source 04 p0599 A71-15382
- Singly tuned IMPATT diodes, examining noise and power saturation 05 p0729 A71-16915
- Large signal oscillation mode model for GaAs devices operational prediction, including space charge and intervalley transfer time effects 07 p1070 A71-18867
- Avalanche transit time devices operational model principles and characteristics, giving data on experimental circuits 07 p1072 A71-19101

- Large signal microwave equivalent circuits analysis of IMPATT diodes, allowing carrier multiplication by impact ionization at every point in diode 07 p1072 A71-19108
- Avalanche diodes TRAPATT mode initial conditions by computer analysis 07 p1072 A71-19109
- X band IMPATT oscillator, discussing frequency stability, rms noise deviation, admittance characteristics, output power loss, temperature effects and power stability 07 p1073 A71-19111
- Microwave oscillator circuit with cap structures for testing millimeter wave IMPATT diodes 07 p1073 A71-19119
- Frequency variation with temperature in coaxial cavity avalanche transit time microwave oscillators explained by diode junction capacitance and cavity length changes with temperature 07 p1074 A71-19120
- Phase locked avalanche transit time oscillators FM noise spectra 07 p1074 A71-19124
- X band multiple IMPATT oscillator combining 12 packaged diodes in waveguide cavity for 10.5 watt CW output at 9.1 GHz, noting clean spectrum 07 p1075 A71-19266
- IMPATT and Gunn microwave oscillators injection phase locking, discussing stationary state synchronization theory and phase vs frequency deviation measurements 08 p1263 A71-20990
- Epitaxial InP three level oscillators in K and Q bands /18-40 GHz/, suggesting optimum operating frequency determined by defined transit velocity 09 p1421 A71-23719
- Si p-n-n junction avalanche diode, investigating experimental evidence of microwave generation at subharmonics of transit time excitation and trapped-plasma mode 12 p1887 A71-27047
- Temperature compensation for frequency changes stabilization of avalanche transit time diode microwave oscillator, using loop circuits and high dielectric constant ceramics 13 p2036 A71-27938
- Velocity-aided Kalman filtering for one dimensional motion under random acceleration, obtaining steady state solution and transit time 14 p2197 A71-30793
- Noise and spectral analysis for measuring fluid flow with random temperature fluctuations by transit times 15 p2406 A71-31596
- Time domain model of device-circuit characteristics of TRAPATT diode microwave oscillator 15 p2378 A71-32699
- Reflex klystron repeller space analysis of potential distribution, electron trajectories, transit time and admittance, taking into account space charge effect 17 p2713 A71-34432
- Ephemerical times of ingress and egress times of Mercury transit across solar disk 17 p2809 A71-35580
- Silicon IMPATT microwave oscillators, calculating CW power as function of frequency by scaling approximation 18 p2888 A71-36129
- Self consistent one dimensional large signal analysis of Read type IMPATT diode oscillator, taking into account device-circuit interaction 18 p2888 A71-36130
- IMPATT diode amplifiers and oscillators AM and FM noise spectra and SNR prediction for comparison with experiment 18 p2888 A71-36271
- Automatic fringe counting pulsed ultrasonic interferometer for transit time measurement, using phase sensitive multiple echo detection 18 p2922 A71-36586
- Harmonic generation in trapped-plasma-mode IMPATT diode microwave oscillators with waveguide-coaxial cavity 18 p2894 A71-36828
- Microwave avalanche diodes, considering drift velocity and power efficiency limitations of IMPATT mode 18 p2894 A71-36976
- IMPATT diode microwave oscillator temperature effect on operation, comparing with Read diode small signal admittance characteristics 18 p2895 A71-36986
- One- and two-sided abrupt junction IMPATT diodes, investigating Si junction type effects on avalanche region and diode design 18 p2895 A71-36987
- High peak power microwave oscillators, discussing pulsed limited space charge accumulation and TRAPATT diodes pulsed radiation sources performance 19 p3029 A71-38294
- Two phase flow speed transit time measurements by correlation methods with randomly fluctuating signals, noting use in small bore tubes and strip steel production 19 p3067 A71-38658
- Time-of-flight measurements for relationship between velocity, mass and temperature in molecular gas motion and electron-atom collision kinematics 20 p3271 A71-38789
- Temperature gradients measurements in transit instrument pavilion and errors in time determination for two year period 20 p3237 A71-39314
- Numerical integration of element T /transit time through perihelion/ in perturbations of near parabolic comet orbits 20 p3291 A71-39321
- GaAs and silicon IMPATT diodes applications and performance, discussing power levels, amplifier applications, injection locked oscillators and microwave signal source 21 p3357 A71-40818
- Si Pt-n-p transit time microwave diode source noise measurement, noting low noise characteristics and suitability for local oscillator applications 21 p3359 A71-41413
- X band GaAs diffused IMPATT diodes for high CW efficiencies 22 p3523 A71-42483
- IMPATT diodes noise performance lower limits, deriving optimization theorem for GaAs diodes under assumption of equal ionization coefficients for electrons and holes 22 p3524 A71-42632
- IMPATT diode development for millimeter wave applications including oscillators, sweep generators and Doppler radar 22 p3524 A71-42763
- Reactive impedance matching of Gunn or IMPATT diodes for microwave oscillators by dielectric tuning 23 p3650 A71-43071
- Large amplitude high efficiency TRAPATT oscillation mode in Si avalanche diodes, using resonant cavity for voltage and current waveforms analysis 23 p3650 A71-43352
- P times least squares analysis complications by systematic earthquake location errors and azimuthal station anomalies variation 23 p3672 A71-43884
- TRANSITION**
- Transition period for variable stars, considering helium sensitive relationship to luminosity obtained with nonlinear theory 20 p3287 A71-39054
- TRANSITION FLOW**
- Two dimensional wake laminar-turbulent transition by single and double frequency sounds imposition and wind tunnel natural disturbance, inducing velocity fluctuations 01 p0001 A71-10132
- Surface and aircraft radar observations of updrafts within weak echo region of Alberta hailstorm, discussing adiabatic flow breakdown into turbulent flow 01 p0115 A71-10559
- Spherical particle motion investigation in plane Couette flow, predicting critical Reynolds number for transition to turbulent flow 03 p0398 A71-13112
- Free and impinging axisymmetric turbulent jet characterization model providing continuous transition from nozzle exit through fully developed region [ASME PAPER 70-WA/FLCS-6] 03 p0401 A71-14082
- Heat transfer and fluid friction of hydrogen and helium gas flows undergoing turbulent to laminar flow transition in heated pipe [ASME PAPER 69-HT-54] 03 p0405 A71-14291
- Laminar flow stability and transition to turbulent flow, giving nonlinear theory for perturbations development 04 p0574 A71-15602
- Laminar to turbulent transition in pipes, using scattered light method 04 p0578 A71-15635
- Two dimensional wake laminar-turbulent transition, emphasizing velocity fluctuation nonlinear interaction 05 p0695 A71-16964
- Channel flow and flow past bodies turbulent/ laminar reverse transition for friction drag and heat transfer reduction 06 p0881 A71-17584
- Two dimensional hypersonic laminar wakes incipient transition region calculation based on boundary layer approximation and von Karman integral formulation 06 p0846 A71-18640
- Boundary layer nonlinear stability theory, considering hydrodynamic problems associated with laminar flow transition into turbulent flow 07 p1086 A71-18777
- Approximate bridging relations for heat transfer, surface shear and drag in transitional regime between free molecule and continuous flows 07 p1087 A71-18894
- Laminar-turbulent bounded jet stability, examining transition zone shift with smoke visualization 07 p1029 A71-20594
- Numerical simulation of developing and decaying two dimensional isotropic turbulence consistent with Batchelor predictions 10 p1595 A71-24619
- Pipe flow hot wire measurements at turbulence onset Reynolds numbers, exhibiting axisymmetric laminar velocity profile distortion 11 p1748 A71-25155
- Variational formulation for hydrodynamic stability based on local potential motion, determining transition from laminar to turbulent flow 11 p1749 A71-25441
- Streamwise vortices of distinct periodicity in laminar transitional turbulent reattaching flows over wide Mach number range 11 p1751 A71-25496
- Laminar boundary layer perturbation at sinusoidal wall roughness, analyzing effect on transition nature and position 12 p1864 A71-27470
- Emmons spot theory extension for boundary layer flow on blunt bodies, deducing spot formation rate dependence on transition Reynolds and Mach numbers 12 p1865 A71-27557
- Flow visualization of free convection laminar-to-turbulent transition along vertical heated plate in water induced by two dimensional forced disturbances [DFVLR-SONDDR-116] 12 p1987 A71-27739
- Aerodynamic characteristics similarity and variation in hypersonic flow transition region from free molecular flow to solid medium 13 p1991 A71-29172
- Flow transition to laminar drag law for thin cylinder freely suspended in Hg in rotating vertical cylindrical MHD channel 14 p2279 A71-29615
- Synoptic scale processes effect on high level clear air turbulence production, considering Kelvin-Helmholtz instability role in flow transition 14 p2268 A71-29762
- Density distribution of neutral matter in cometary atmosphere in transition region between hydrodynamic and free molecular flow 15 p2484 A71-31662
- Flow stability in differentially heated inclined rectangular box of small depth/length ratio, examining thermal convection and transition to turbulent flow as function of inclination angle 15 p2513 A71-31930
- Conical converging nozzle flow of perfect monatomic gas in rarefied near continuum, transition and near free molecular regimes, using finite difference methods 15 p2390 A71-32045
- Sphere drag in hypersonic jet transition flow near free molecule limit, using magnetic suspension method 15 p2347 A71-32124
- Aperture angle effect on flow separation in inlet section of diffuser with cylindrical to conical channel transition 16 p2521 A71-33611
- Gas and liquid drop laminar, transition and turbulent flows heat transfer intensification in circular tubes, applying to hydraulic resistance design 17 p2835 A71-34205
- Plane Poiseuille flow at constant rate, developing numerical simulation of transition and turbulence 18 p2845 A71-36337
- Laminar-turbulent inverse transition in divergent radial flow between two parallel flat disks 21 p3366 A71-40101
- Hartmann number for velocity pulsation free transition from turbulent MHD flow to laminar, noting difference relative to linear stability theory 24 p3856 A71-45059
- Liquid transition through critical value, considering self oscillation mode frequency 24 p3821 A71-45340
- TRANSITION LAYERS**
- Total particle number changes, evaluating approximate methods for transition effect calculation 03 p0426 A71-13870
- Topside ionosphere O-H ions transition level altitude variation due to atmosphere winds 03 p0416 A71-14030
- Temperature distribution and heat transfer across transitional separated shear layer under subsonic air flow, using interferometric measurements 04 p0679 A71-15470
- Eclipse observations interpretation for transition region between extreme limb and low chromosphere 06 p0967 A71-17905
- Thermionic energy converter, calculating behavior of transition regions between collisionless region adjacent to electrodes and plasmas 11 p1712 A71-25890
- Radio model of brightness temperature and electron density in transition layer of solar active regions, using Laplace transformation and hydrostatic equilibrium equation 13 p2141 A71-29050
- Plastic scintillators anomalous pulse spectra in sea level transition region attributed to EM cascades single particles /muons/ production 14 p2301 A71-30425

White dwarf star gravity mode stability, considering hydrogen-helium transition sorting zone

14 p2318 A71-31018

UV studies of solar atmosphere in quiet and active regions, considering low and high chromosphere, transition zone, quiet corona and inhomogeneity

18 p2968 A71-37034

Charged particles interaction with geomagnetic field, discussing plasma equations of motion, ionospheric current induction, transition layer and magnetotail rotation

20 p3216 A71-39118

Transition layer structure formation of epitaxial semiconducting films, discussing model for dislocation origin

21 p3427 A71-40727

Photocurrent for two stage transition in space charge layer in p-n junctions of germanium with radiation defects

21 p3435 A71-41333

Solar transition layer and inner corona empirical minimum equator model, using radio, UV, white and monochromatic radiation data

22 p3601 A71-42161

Steady state transition layer between cold solar plasma flow and geomagnetic field in one dimensional model

22 p3536 A71-42622

Total particle number changes, evaluating approximate methods for transition effect calculation

22 p3550 A71-42671

Bimetallic plated high strength steel, noting transition zone effects on mechanical properties

23 p3692 A71-44026

TRANSITION METALS

NT CADMIUM
NT CHROMIUM
NT COBALT
NT COBALT ISOTOPES
NT COBALT 60
NT GOLD
NT HAFNIUM
NT IRIIDIUM
NT IRON
NT IRON 57
NT MANGANESE
NT MANGANESE ISOTOPES
NT MOLYBDENUM
NT NICKEL
NT NIOTBIUM
NT OSMIUM
NT PALLADIUM
NT PLATINUM
NT REFRACTORY METALS
NT RHENIUM
NT RHENIUM ISOTOPES
NT RHODIUM
NT SCANDIUM ISOTOPES
NT TANTALUM
NT TECHNETIUM
NT TITANIUM
NT TUNGSTEN
NT VANADIUM
NT YTTRIUM
NT ZIRCONIUM

Transition metals powders and carbides sintering by high temperature hot pressing in homogeneity region, determining optimum conditions and activation energy

02 p0236 A71-12276

Transition metals carbides and nitrides homogeneity regions relation to nonlocalized valence electrons in lattice and configuration stabilizing ability

02 p0264 A71-12280

Transition metal carbides and nitrides, observing metallic and nonmetallic sublattice dynamic characteristics by X ray diffraction

02 p0266 A71-12672

Group 4 and 5 transition metal carbides thermal expansion determined on quartz dilatometer at various temperatures

05 p0768 A71-16789

Transition metal diborides X ray emission K alpha band, establishing asymmetry index, bandwidth and maximum power shift deviations from B

05 p0770 A71-17169

Elastic and thermodynamic properties of transition metal carbides, comparing Debye temperatures obtained from elastic constant to those obtained from specific heat data

06 p0915 A71-18687

Ni-transition element ternary alloys with bcc and fcc lattices, examining electron structure and ordering processes

07 p1163 A71-19429

Binary A15 phases transition elements compositional variations effects on atomic ordering

07 p1163 A71-19430

Transition metals effect on Ti alloys grain size, suggesting La, Y, Ni, Pd and Pt effectiveness in crystal structure refinement

07 p1136 A71-19632

Groups IV-VIII transition metals reaction with Re and B, studying ternary compounds formation by X ray and metallographic analyses

07 p1140 A71-20233

Re intermetallic compounds structure and physical properties, examining chemical reactivity with transition metals as function of elements periodic table position

07 p1140 A71-20236

Refractory transition metals diborides thermoemissive properties for use in cathode materials

07 p1144 A71-20653

Electron paramagnetic resonance and optical absorption spectra of transition metal ions in zoisite crystal

08 p1343 A71-20658

Machining electrode materials, investigating high melting transition metals electroerosive stability and bending strength on basis of electronic theory

08 p1296 A71-20853

Hf alloys containing transition metals, discussing phase transformations and solid solutions

09 p1473 A71-23225

Transition metals hydrides electrical resistance calculation based on theory of hydrogen electrodiffusion/oclusion/into incomplete d-states

09 p1473 A71-23232

Oxygen and nitrogen thermotransport in transition metals by microindentation hardness testing for concentration determination

11 p1778 A71-25533

Electron structure of transition metals defects, using self consistent method to match resonance and drift integrals to cohesion energy

11 p1808 A71-26342

Transition metal diborides chemical stability after treatment with oxygenless acid in nitrogen and air atmosphere

12 p1877 A71-27124

Electrical conductivity, thermal emf, expansion and Hall coefficient of hot compressed powdered diborides of group IV and V transition metals

13 p2084 A71-28036

Transition metals addition effects on cast Zr grain size, microhardness and electrical resistivity, explaining results in terms of solid state electron theory

15 p2424 A71-31239

D-transition metal carbides properties based on electron configuration localization model

15 p2429 A71-32138

Carbon K alpha band measurements in transition metal carbides, graphite and diamond, using X ray spectrometer with diffraction grating

15 p2430 A71-32149

Thermal coefficient of resistivity of carbides and solid solutions of Ti, Zr, Hf, V and Nb, noting inverse dependence of covalent bond in Me-Me band

15 p2430 A71-32154

Hot pressed transition metal carbide samples microhardness measurement, interpreting results in terms of atomic electron configurations

15 p2431 A71-32162

Surfacing materials based on transition metal borides with boron carbide additions, testing brittleness, hardness and abrasive wear resistance

15 p2431 A71-32163

Transition metals classification according to effect on structure and physical properties of deformable Al alloys

15 p2434 A71-32331

Low temperature heat capacities from 1.5 to 15 K for transition metal borides and solid solutions

15 p2437 A71-32649

Transition metals effect on Ti alloys grain size, suggesting La, Y, Ni, Pd and Pt effectiveness in crystal structure refinement

16 p2593 A71-33628

Transition metal carbides and nitrides ordered structures, determining C and N atoms positions with electron and neutron diffractions

16 p2597 A71-33921

Transition metals monocarbides and mononitrides electronic structure, investigating electrical, thermoelectrical and galvanomagnetic properties

16 p2597 A71-33922

Heat transfer in interstitial solid solutions, interpreting thermal diffusion measurements in transition metals mixed crystals

16 p2599 A71-34093

Quantum counter action in various media including trivalent and divalent rare earth ions, Fe group transition metal ions, semiconductors and gases

18 p2930 A71-36145

Transition metals addition effect on W sintering behavior in 1000-2000 C range, explaining by electron exchange between alloy components

21 p3396 A71-40031

Transition metal/particularly Ti carbide hardness temperature dependence explained from dislocation theory viewpoint, relating hardness to electronic structure

22 p3565 A71-41657

Transition metal physicochemical properties explanation by many-electron effects in Hubbard model

23 p3714 A71-42932

Noble and transition metals dilute alloys electronic structure in hybridized tight binding nearly free elec-

tron representation, using Harrison-Kanamori pseudopotential theory

24 p3860 A71-45111

Noble or transition metals based dilute alloys electronic structure, describing pure metal band structure by interpolation scheme of hybridized tight binding and nearly free electron orbitals

24 p3860 A71-45112

TRANSITION POINTS

Laminar-turbulent boundary layer transition point on wing, using hot-wire anemometer and oscilloscope

02 p0186 A71-12277

Notched tensile tests for measuring metal ductile brittle transition temperature, deriving proportional law

04 p0666 A71-14811

Cylindrical Langmuir probe LF transient response characteristics in transition regime

[ALAA PAPER 71-142] 06 p0902 A71-18555

Boundary layer suction optimization to achieve normal velocity component distribution for low Reynolds number equal to critical value at transition point

12 p1896 A71-26995

Ferritic steels weldability, establishing relationship between transition points and cold crack formation

15 p2417 A71-32622

Upper atmosphere minor component distribution rearrangement, investigating transition time to diffusion equilibrium

24 p3823 A71-45066

TRANSITION PROBABILITIES

Limit theorems for spacewise inhomogeneous random walks on straight line with Markov chain transition probabilities

01 p0110 A71-10000

Argon ion CW lasers, discussing design, inverted population, plasma, radiative transition probabilities, pumping, frequency spectra and active medium

01 p0092 A71-10111

Nomograms predicting transition probabilities, frequencies as function of geometric and physical characteristics

02 p0235 A71-12999

Rare gases interaction with focused multimode switched laser beam, measuring orders of nonlinear and multiphoton ionization probabilities

05 p0761 A71-16313

Halogens atomic transition probabilities spectroscopic measurements in visible and near IR spectrum using gas driven shock tube

07 p1163 A71-19648

Hydrogen and deuterium oscillator strengths and transition probabilities for Lyman and Werner series individual bands by electronic dipole moment functions

07 p1164 A71-20011

Triatomic molecules relaxation process, considering translational-vibrational energy exchange in atomic collisions and transition probabilities for carbon dioxide-helium system

08 p1337 A71-20606

Eigenfunction expansions of reduced nonGaussian phase error transition probability density function for first order tracking loop, analyzing spectral properties of Fokker-Planck equation

08 p1324 A71-21345

Franck-Condon factors, r-centroids and absolute band transition probabilities of NH, SiH, molecular sulfur and SO

10 p1645 A71-24545

Laser designs with thermal pumping, obtaining electron states phototransition probability, cooling rate for population inversion and laser action threshold for diatomic gas molecules

12 p1914 A71-27002

Hartree-Fock energy levels, transition probabilities and wave functions for highly ionized atoms in B isoelectronic sequences, including spin-orbit interactions

15 p2452 A71-32555

Radiative mean life measurements by low energy beam foil excitation, considering branching ratio of transition probabilities equal to unity

16 p2576 A71-33090

Plasma temperature determination errors from relative g-f values, noting effects on absolute transition probabilities

16 p2618 A71-33133

Transition probabilities of random processes with rapid variability, using continuous Markov smoothness under Fokker-Planck equation

16 p2612 A71-33522

Quantum mechanical considerations underlying calculations of two-photon transition probabilities, discussing experiments on semiconductors, ionic crystals and organic compounds

18 p2930 A71-36244

Transition probabilities for Ar I, using Coulomb approximation values of radial wave function integrals

20 p3271 A71-38777

Close coupling calculation for low energy hydrogen atom-molecule collision, discussing cross section transition probabilities and elastic scattering

20 p3272 A71-39577

Absolute transition probabilities derivation for excitation of atmospheric nitrogen molecules and positive ion systems by electrons impact from optical measurement

24 p3850 A71-44371

TRANSITION TEMPERATURE

High transition temperature superconducting materials thin films composition control by sputtering from hot pressed powder mixture ingots targets

07 p1178 A71-19849

Glassy state beta transition temperatures in cured epoxy resins, showing diglycidyl ether of bisphenol A (DGEBA) dependence

08 p1323 A71-21475

Superconductivity transition of Nb-Ti solid solutions with varying Ti content, using specific heat measurements between 2.5 and 20 K

10 p1628 A71-24890

Impurity lifetime broadening due to scattering at Fermi surfaces, calculating Dingle temperature in noble metals

11 p1808 A71-26145

Superconducting thin films nonlinear excess current near transition temperature, deriving expression from Tsuzuki microscopic basic equations

13 p2112 A71-29012

CW gain measurements on rotation-vibration P branch transitions of CO molecular laser, calculating gas temperature, Einstein coefficient and population densities

15 p2423 A71-32609

Iron single crystals plastic deformation under tension, studying ductile/brittle fractures mechanisms and transition temperature

16 p2591 A71-33369

Vibrational stress induced phase transitions in strontium titanate near transition temperature, using soft mode Raman scattering

17 p2791 A71-34949

Superconducting transition temperature measurement of cast and solution treated Nb-Zr alloys, substantiating dependence on density of states at Fermi surface

17 p2759 A71-35221

Transition temperature behavior in plane strain fracture toughness tests on A517-F steel, comparing with Charpy tests

20 p3248 A71-38770

Glass transition temperature and specific heat of Apiezon N and T greases used as thermal bonding agent at cryogenic temperatures

20 p3253 A71-39267

Brittle transition temperature of steels by Vickers hardness testing, comparing with tensile properties and impact fracture process in Charpy impact test

21 p3388 A71-40751

Superconductivity transition of Nb-Ti solid solutions with varying Ti content, using specific heat measurements at 2.5-20 K

21 p3432 A71-41266

Titanium dihydride room temperature polymorphic transition from fcc to body centered tetragonal, noting different transition temperatures

22 p3563 A71-42368

Niobium carbonitride thin film deposition temperature effects on superconducting properties, considering transition temperature and critical currents and fields

23 p3717 A71-44141

OH transitions excitation temperatures in absorbing cloud from observations of W12

24 p3871 A71-44906

TRANSITS

NT THEODOLITES

TRANSLATING

NT MACHINE TRANSLATION

TRANSLATIONAL MOTION

NT THREE DIMENSIONAL FLOW

NT THREE DIMENSIONAL MOTION

Radially deforming sphere dynamic behavior during translational motion in infinite incompressible static medium

02 p0241 A71-12669

Satellite translational motion in circular problem of three bodies, discussing existence of equations integral

03 p0484 A71-13223

Translational vs deformation displacement motion in sensitivity of double exposure holographic interferometry

03 p0429 A71-14181

Translatory vapor bubbles motion in binary liquid mixtures under heat and mass transfers

04 p0687 A71-15534

Air lubricated bearing elements lifting force, restoring moment and translational rigidity, considering dependence on minimum clearance, sliding rate, pressing force and geometric parameters

05 p0758 A71-16351

Decaying oscillations of sensitive element in ground based gyrocompasses with suspension system permitting Euler angle and translational displacement

07 p1108 A71-19304

Moon shape, translational and rotational motion determination by optical tracking, discussing possible

refinements as function of distance measurement accuracy

09 p1525 A71-23337

Planetary rotational and translational motion interaction in Einstein gravitation theory, describing orbital elements secular disturbances in two body problem

09 p1526 A71-23339

Translation-rotation motion of elongated body in Vinti potential field

10 p1667 A71-23814

Cavitation microstreaming near spherical drop or bubble performing translational harmonic oscillations in liquid at rest

11 p1749 A71-25183

Boundary layer equation for free convective diffusion on flat vertical plate in translation motion in viscous incompressible fluid

11 p1854 A71-25240

Longitudinal proper motions of flight vehicle based on equivalent dynamic systems for trajectory coincident with nonsingular transformation in phase space

13 p2145 A71-28731

Vertical translational acceleration perception threshold of aircraft pilot seated in upright position

14 p2188 A71-29780

Two spheroid rigid bodies rotational and translational motion, using linear and Hill type differential equations for angular variables and coordinates

14 p2312 A71-30384

Gyrocompass stability during circulations and arbitrary periodic maneuvers, taking into account translational motion vertical inertia component

17 p2746 A71-35604

Ideally incompressible fluid with free surface, analyzing interfacial tension forces effects on rotational-translational motion stability

17 p2730 A71-35648

Relativistic behavior of uniformly accelerated translational observer motion relative to inertial observer from space-time transformation

21 p3415 A71-40653

Laser speckle interferometry for translational motions and vibrations detection, considering applications in radar and acoustics analysis

21 p3393 A71-40932

Deformation and translation measurements with holographic interferometry, considering flat surface moved with precision differential screw micrometer

21 p3381 A71-40933

Rotating space station simulator for translational and rotational motion determination under gravity gradient torque action and control under input state conditions

22 p3529 A71-41970

Three body problem of two heavy mass particles oscillatory motion in periodic orbits on straight line under Newtonian attraction

23 p3734 A71-43241

Translational and rotational vibrational motion correlation of solid body mass center in Newtonian force field

24 p3872 A71-45047

TRANSLATORS

Programming language translator system, describing syntactic specifications for input-output relationships

01 p0045 A71-10190

TRANSUNAR SPACE

U INTERPLANETARY SPACE

TRANSMISSION

NT AERODYNAMIC HEAT TRANSFER

NT AUTOMATIC PICTURE TRANSMISSION

NT CONDUCTIVE HEAT TRANSFER

NT CONVECTIVE HEAT TRANSFER

NT DATA TRANSMISSION

NT DIFFRACTION PROPAGATION

NT DOUBLE SIDEBAND TRANSMISSION

NT ELECTRIC POWER TRANSMISSION

NT ELECTROMAGNETIC WAVE TRANSMISSION

NT GROUND WAVE PROPAGATION

NT HEAT TRANSFER

NT HEAT TRANSMISSION

NT HYPERSONIC HEAT TRANSFER

NT IONOSPHERIC F-SCATTER PROPAGATION

NT IONOSPHERIC PROPAGATION

NT LAMINAR HEAT TRANSFER

NT LIGHT SCATTERING

NT LIGHT TRANSMISSION

NT MICROWAVE TRANSMISSION

NT MULTIPATH TRANSMISSION

NT RADAR TRANSMISSION

NT RADIATIVE HEAT TRANSFER

NT RADIO TRANSMISSION

NT SATELLITE TRANSMISSION

NT SCATTER PROPAGATION

NT SHOCK WAVE PROPAGATION

NT SHORT WAVE RADIO TRANSMISSION

NT SINGLE SIDEBAND TRANSMISSION

NT SOUND TRANSMISSION

NT STRESS PROPAGATION

NT SUPERSONIC HEAT TRANSFER

NT TELEVISION TRANSMISSION

NT TRANSEQUATORIAL PROPAGATION

NT TURBULENT HEAT TRANSFER

NT WAVE PROPAGATION

Transmission impending failure detection via lubricating oil monitoring for metal particle content

04 p0532 A71-15415

TRANSMISSION CIRCUITS

Broadband IMPATT diode multistage transmission amplifiers computer aided design and X band performance

07 p1073 A71-19114

Radio propagation and antennas transmission formulas, discussing fundamental circuit elements with inductors and capacitors

11 p1798 A71-25596

Intelsat 4 satellite Spade communication system, using common reserve circuits and repeaters

15 p2373 A71-32640

Independent sideband transmitter checkout and maintenance for maximum communication circuit performance

21 p3353 A71-40519

TRANSMISSION EFFICIENCY

Antenna gain, transmission efficiency and receiving cross sections in dissipative isotropic medium

01 p0041 A71-11614

Medium speed data transmission systems tested for quality and functional characteristics

02 p0228 A71-11819

Skyнет project earth station effective radiated power and gain by dual satellite access measurements

02 p0218 A71-12445

Microwave radiometry for earth terminal and communication satellite performance measurements, including gain, tracking, noise temperature, radome attenuation, power and transfer characteristics

02 p0218 A71-12446

Hybrid mode flare feed horns for parabolic antennas, discussing horn parameters and angular aperture effects on gain factor or aperture transmission efficiency

02 p0234 A71-12807

Traffic capacity of Gaussian communications channel with Rayleigh fading, examining code transmission coefficient under discrete control mode

03 p0378 A71-13394

Catastrophic error propagation and minimum weight codewords in convolutional codes

07 p1069 A71-20417

Reproduction quality of information transmitted by error correcting codes for stationary symmetrical channel without storage

08 p1251 A71-20732

Information transmission rate and error probability in analog feedback systems, showing normalized maximum transmission speed dependence on signal to noise ratio

08 p1268 A71-21283

Efficiency evaluation of large parabolic antenna reflector by frequency scaling

09 p1409 A71-23496

Radio communication accuracy characteristics in calculation of maximum frequency, skip distance and emission angle by transmission curves for midlatitude ionosphere

13 p2030 A71-28544

Antenna radiation resistance and efficiency in dissipative medium, using concept of modified power density

17 p2701 A71-34764

Optimum pulse transmission through thin exponentially inhomogeneous plasma region for maximum amplitude signal reception, using matched filter theory

17 p2788 A71-34768

Transmission performance of thin route satellite communication system for northern Canada, comparing FM, PCM and delta modulation techniques

17 p2703 A71-35081

Total diffraction efficiency of transmittance storage holograms, using space dependent contrast function

18 p2915 A71-35902

TRANSMISSION LINES

NT BEAM WAVEGUIDES

NT COAXIAL CABLES

NT COMMUNICATION CABLES

NT FLUID TRANSMISSION LINES

NT PLASMAGUIDES

NT POWER LINES

NT STRIP TRANSMISSION LINES

NT SUBMARINE CABLES

NT WAVEGUIDES

Nonlinear networks interconnected by lossless transmission lines, deriving global asymptotic stability condition

01 p0065 A71-11574

Electronic equipment shielding against spurious signals, determining minimum metal thickness for desired effectiveness based on transmission line theory

03 p0383 A71-13178

Fluidic ID transmission line characteristic impedance measurement as function of signal frequency, noting correlation with Nichols theory

[ASME PAPER 70-WA/FLCS-14]

03 p0354 A71-14089

Optical transmission lines design techniques with thermal gas lenses, calculating system parameters by geometrical optics, wave, electrodynamic and Fourier transfer methods

04 p0628 A71-15810

Sn additives effect on In thin film superconducting transmission lines, comparing with Pippard nonlocal theory for mean free path reduction

07 p1179 A71-20155

Slot transmission line bandpass and bandstop filters and hybrid couplers for microwave IC applications, presenting experimental performance data

08 p1262 A71-20761

Polarizing phase shifter for quasi-optical transmission lines, describing varistor network operation

08 p1264 A71-21068

Multiple reflections method for complex reflection and transmission coefficients of microwave transmission line permitting use of digital computers

09 p1413 A71-22151

Distributed gain amplifiers synthesis technique permitting use of filter and transmission line design tables

09 p1413 A71-22158

Backscatter from nonuniform dielectric coated cylinders in terms of inner surface admittance, using transmission line approach

09 p1410 A71-23515

Microwave devices with transmission lines excited by curvilinear electron beams, deriving dispersion equations for TWT with allowance for space charge effect

10 p1584 A71-24717

Ferrite resonator coupled to microwave transmission line, deriving instability effects threshold power level for comparison with measurement

10 p1584 A71-24725

Gas turbine exhaust silencer performance prediction by transmission line theory, considering LF requirements effect on size and cost

[ASME PAPER 71-GT-8] 11 p1811 A71-25954

Computer aided statistical analysis of irregular quasi-optical transmission lines containing random inhomogeneities

11 p1733 A71-26347

Electromagnetic wave propagation on uniform transmission line network, discussing passivity and stability notions concerning energy exchange between waves and material

12 p1879 A71-27039

Antenna analysis method based on transmission line theory, yielding current distribution and input impedance of finite conical antenna

12 p1880 A71-27154

Electric and magnetic fields of fundamental modes in cylindrical and rectangular dielectric microwave resonators, classifying transmission lines connections

12 p1888 A71-27613

Lumped inhomogeneities reflections effect on characteristics of AM signal along transmission line

12 p1883 A71-27624

Self- and mutual admittances for axial rectangular slots in inhomogeneous cylindrical plasma layer, giving coupled radial transmission line model for propagation

13 p2105 A71-28002

Time domain solution of coupling to two wire transmission line, determining coefficients by steady state measurements

13 p2001 A71-28868

Digital wire line system data bus design, calculating transmission performance of noise environment shielded twisted pair cable by linear filter model

14 p2198 A71-30904

Spectral theory of linear differential operators for microwave oscillatory systems synthesis from inhomogeneous line segments, determining line characteristic impedances and local reflection function

15 p2369 A71-31233

Book on microwave fields and circuits covering waveguides, transmission lines, impedance matching, sources, resonators, antennas, etc

17 p2716 A71-34772

Ground noise reduction with balancing units, discussing transmission line driving and receiving end applications

17 p2716 A71-34859

Optimized low loss microstrip microwave filters on silica substrates by photolithographic reduction of LF modes

19 p3026 A71-37218

Broadband compensation of HF tunnel diode traveling wave amplifier using separate stages in transmission line

19 p3026 A71-37256

Book on active and nonlinear wave propagation in electronics covering transmission lines, wave systems stability, quasi-harmonic active propagation, equivalent circuits, etc

19 p3029 A71-38018

Coupling coefficients in set of connected cavity-type transmission lines, analyzing effects of individual elements, slot geometries and conducting walls

19 p3019 A71-38337

Multiple scattering of VHF and UHF radio waves from bundle conductor high voltage power transmission lines

19 p3021 A71-38446

Dipole antenna bandwidth extension by conjugate reactance loading based on periodically loaded transmission line theory

19 p3036 A71-38602

Numerical solution of two dimensional scattering by waveguide bifurcation, using transmission line matrix impulse analysis

22 p3511 A71-42282

Quasi-optical transmission line stability improvement, investigating pulsating light beam concept

22 p3512 A71-42309

Pulsed signal secondary forward scattering in optical fiber transmission lines

23 p3646 A71-43968

Shunt driven circular loop antenna effective length, current distribution and input admittance, comparing to transmission lines

23 p3655 A71-44169

Spectral representation and propagation mode of microwave transmission line on circular waveguides at great distance

24 p3803 A71-44361

Electromagnetic fields in moving anisotropic medium, using network formulation based on radial transmission line representation

24 p3805 A71-45092

TEM mode hybrid networks analysis extension to tapered transmission lines, indicating design limitations on VSWR and isolation characteristics

24 p3816 A71-45094

Composite quasi-optical-broad waveguide transmission lines for millimeter and submillimeter waves with spectrum phase correction

24 p3810 A71-45258

End line matching for high gain traveling wave amplifier constructed from heterogeneous transmission line with negative resistance

24 p3810 A71-45262

TRANSMISSION LOSS

Time interval maximum transmittable energy under spectral limitation, deriving time limited pulse functions for minimum energy loss

05 p0720 A71-16393

Antarctic terrain dielectric and loss properties effects on VLF attenuation and phase constants of earth-ionosphere waveguide paths over ice covered regions

06 p0868 A71-17733

Gas laser gain and loss coefficients measurement, using resonator staged calibrator plate for optimal and nonoptimal conditions

07 p1122 A71-19139

Light attenuation and depolarization measurements on glass fibers in index matching oil

07 p1159 A71-19212

Information loss in transmission by group error correcting codes in stationary symmetric channel without storage

08 p1252 A71-20733

Ribbed aluminum panels airborne sound transmission loss, evaluating structural damping effects

08 p1231 A71-21431

Dielectric constant and loss tangent measurements at 60 and 90 GHz for Teflon, polystyrene and Lucite sheets, using Fabry-Perot interferometer

09 p1418 A71-23415

Concentric shield for surface wave propagation loss at bend in open waveguide, using Airy function

09 p1410 A71-23570

Power losses and construction of microwave switch, using orthogonal striplines around thin ferromagnetic film on nonmagnetic substrate

11 p1741 A71-26551

Wire grid simulation of electron density, transmission and reflection of lossless and lossy reentry plasma sheath under microwave radiation at X and K bands

12 p1935 A71-26767

Local and sequential propagation characteristics of electromagnetic fields and waves in inhomogeneous lossy medium

13 p2028 A71-27995

Transmission loss measurements at HF over 960 km temperate latitude path for wave polarization calculations and ionospheric absorption estimation

14 p2196 A71-30468

Power density prediction based on electromagnetic compatibility analysis of radar environments, comparing predicted propagation losses with measurements

19 p3021 A71-38455

Conversion losses as function of signal power and circuit impedance in narrow band triode frequency converter

19 p3022 A71-38499

Diffraction loss equality in field distribution at confocal laser resonator mirrors with circular coupling holes

20 p3242 A71-38850

Computer programming for on-line correction of microwave measurements of loss and reflection ef-

fects between network analyzer and device/circuit under test

20 p3205 A71-3935

Frequency dependent conductor coating matrix for lossy cylindrical conductors with circular section using diffusion equation

20 p3197 A71-3946

Reflection and transmission coefficients of lossy single-wave waveguide line with random inhomogeneities

20 p3198 A71-3980

Wave polarization and midpath ground reflection effects on power loss of two hop radio signal propagation through ionosphere

22 p3511 A71-4222

TV multiplexing and broadband multichannel real time telemetry data transmission without loss between Kennedy Space Center and ground station for computer operation

23 p3645 A71-4359

TRANSMISSIVITY

F 2 layer transmission coefficient, describing altitude linear dependence of electron density maximum

02 p0244 A71-1177

Cloud drop size distribution from spectral transmission measurements, using spectroradiometer

04 p0621 A71-1500

Gas mixture transmission function, determining multiplication method accuracy

07 p1151 A71-1897

Liquid water far IR absorption spectrum, presenting transmission coefficients table

07 p1158 A71-1897

MHD waves incident at density step, calculating reflection, refraction and transmission coefficients and coupling modes

11 p1807 A71-2642

Radio reflection and transmission coefficients for thin highly ionized layers under earth magnetic field, based on numerical integration of differential equations

23 p3665 A71-4296

Transmission coefficient calculations for infinite grating of conducting circular cylinders, considering parallel and perpendicular polarizations

23 p3655 A71-4417

TRANSMITTANCE

Carbon dioxide IR absorption bands at elevated pressures, deriving transmission function

01 p0130 A71-1110

Transparent dielectrics sheet radiation absorptance, emittance and transmittance determination by Monte Carlo method

01 p0183 A71-1156

Double beam spectrophotometer for small transmission changes, discussing measurement range and uncertainty

02 p0247 A71-1172

In vivo green soybean and corn leaves bidirectional IR reflection and transmission distribution functions

05 p0739 A71-16255

Atmospheric boundary layer IR transmittance spectra compared to spectrum calculated from transmittance functions

07 p1152 A71-1914

Carbon dioxide IR absorption bands at elevated pressures, deriving transmission function

08 p1337 A71-2084

Multilayer interference optical minus filters low ripple transmittance design, using equivalent layer concept

08 p1334 A71-2118

Spectral transmittance of pressure induced and intrinsic absorption of IR energy by carbon dioxide and water due to Fermi bands and asymmetric molecules

10 p1644 A71-2395

Atmospheric transmittance vertical structure, using aerosol attenuation and optical densities from aircraft sounding under cloudless conditions

11 p1795 A71-2592

Venus-Mercury flyby vehicle solar cells, cover glasses, adhesives and Kapton film, investigating space radiation effects on solar absorptance and transmittance

11 p1859 A71-2623

Normally incident electromagnetic wave propagation in inhomogeneous gyration medium, obtaining reflection and transmission coefficients and discussing resonance

13 p2108 A71-2908

Spectral luminance and transmittance of noctilucent clouds for spaceborne photometric observation, using American-Swedish rocket particle experiment

14 p2232 A71-29962

Gas pressure gradient and transmittance of sunspots, obtaining contours of D2 Na I and 5173 A Mg lines

14 p2309 A71-2998

Searchlight problem with isotropic scattering for semiinfinite and finite geometries, computing transmission functions for Fourier intensity components by kernel approximation method

17 p2839 A71-3557

Reflection and transmission coefficients for electromagnetic propagation across magnetic field in parabolic plasma layer, determining EM-plasma wave conversion efficiency
19 p3014 A71-37079

Absorption of anisotropically scattering medium compared with measured hemispherical reflectances and transmittances
[ASME PAPER 71-HT-20] 19 p3165 A71-37991

Reflection and transmission coefficients of nonresonant slots in rectangular waveguide antenna with comb type slow wave structure
19 p3019 A71-38334

Automatic single beam recording spectroradiometer system for measurements of spectral irradiance, radiance, transmittance and reflectance
20 p2325 A71-39176

Atmospheric transmittance vertical structure, using aerosol attenuation and optical densities from aircraft sounding under cloudless conditions
20 p2327 A71-39215

Atmospheric transmittance measurement errors in determining temperature, water vapor and ozone distributions from satellite remote sensing
20 p2328 A71-39671

Reflection and transmission coefficients of long lossy single-wave waveguide line with random inhomogeneities
20 p3198 A71-39805

Atmospheric optical transmission coefficient measurements using steerable laser radar system
21 p3372 A71-40040

Isotropic light scattering in unsteady plane layer of finite optical thickness, obtaining reflection and transmission coefficients for radiative transfer
22 p3607 A71-42869

Ionospheric propagation penetrating and nonpenetrating modes full wave reflection and transmission coefficients determination for height and frequency variation by thin film optical method
23 p3643 A71-42972

TRANSMITTER RECEIVERS

Radio telemetry transmitter receiver systems notch noise testing for relationships between spectral power density, video and IF bandwidths and peak deviation
01 p0034 A71-10908

Wideband gas discharge duplexer as transmitter receiver microwave antenna switch in H/01/ mode circular waveguide
10 p1584 A71-24720

Polarization distortion of partially polarized wave emission and reception by two channel horn antennas, noting radio astronomy, radar and optics applications
10 p1584 A71-24876

Remote controlled automatically tuned 1-kw short wave transmitter with zero power tuning mode of power stage and drive unit frequency generation
12 p1887 A71-26989

Airborne communications with AN/ARC-154 transceiver in single radio, discussing extended frequency coverage, multimode operation, navigation and input/output provisions
17 p2775 A71-35758

Minimum spacing between two base station antennas for mobile radio diversity reception
19 p3014 A71-37217

Geometrical optics convergence coefficient in earth ionosphere waveguide for arbitrary transmitter receiver location
19 p3017 A71-37866

Co-site analysis model automated for evaluation EM compatibility of single site employing large number of transmitting and receiving equipments
19 p3032 A71-38457

AN/ARC-144 solid state ultrareliable UHF multimode aircraft transceiver, discussing tuning, frequency synthesis and broadband power amplifier
20 p3196 A71-39209

Signal reception noise stability by superregenerative transceiver in meteorological system
21 p3383 A71-41242

Mathematical model of emission spectrum for PKZ radiosonde and radiosondes using superregenerative transceivers
21 p3383 A71-41243

TRANSMITTERS

NT IONOSONDES

NT RADIO BEACONS

NT RADIO TRANSMITTERS

NT RADIOSONDES

NT RADIOTELEPHONES

NT RAWINSONDES

NT REPEATERS

NT TRANSMITTER RECEIVERS

Ionospheric modification of F region through high power HF transmitter heating
01 p0040 A71-11529

Transmitter system for Skynet spacecraft performance tests using calibrated automatic level control and microwave calorimeters
02 p0218 A71-12442

Earth station equipment for Intelsat 4, discussing thermal noise, transmitters, wideband receivers and demodulators
02 p0224 A71-12829

Radio frequency interference project control responsibilities and teamwork, noting communication transmitter design example
03 p0383 A71-13177

Optimal algorithmic coordination of spaceborne computer-transmitter coupling, using SIMSCRIPT language simulation
08 p1259 A71-21599

Intelsat 4 satellite transponder, examining receivers, transmitters, mechanical stability and heat transfer
10 p1578 A71-24509

Millimeter broadband high power traveling wave transmitter tubes with stub voltage tuning for ground stations of satellite communication systems
16 p2545 A71-32975

Phased array pulsed X band microstrip Gunn diode transmitters with temperature stabilization at 9.4 GHz
16 p2547 A71-33555

Miniature biopotential transmitter suitable for telemetry, giving EEG and circuit and performance characteristics
21 p3342 A71-40184

Optimal power transfer through atmospheric turbulence by adaptive laser transmitter using beacon waveform to probe channel state
22 p3512 A71-42378

TRANSMUTATION

GaAs transmutational doping by slow neutrons irradiation, using Cd and In screens for impurities distribution control
07 p1175 A71-19219

TRANSCOCEANIC COMMUNICATION

North Atlantic communications, navigation and ATC systems requirements for geostationary satellite operation, considering lifetime rated data and voice channels transmissions volume
11 p1839 A71-26332

TRANSCOCEANIC SYSTEMS

NT TRANSCOCEANIC COMMUNICATION

Satellite systems for transatlantic simultaneous air and marine navigation, traffic control and rescue, stressing technical and economical factors
06 p0925 A71-18015

Trapped waveguide mode frequency of whispering gallery propagation in F region explaining round world echoes and long distance satellite observations
10 p1577 A71-24292

TRANSONIC AIRCRAFT

U SUPERSONIC AIRCRAFT

TRANSONIC COMPRESSORS

Transonic compressor rotors blade camberline shape optimization by various tip diffusion factor-ratio combinations
07 p1184 A71-20200

Transonic compressor shock wave noise generation and decay rates at multiple tones, using sonic boom analysis
11 p1703 A71-25953

Mach number effects on axial flow transonic compressor characteristics, using empirical corrections based on measured three dimensional grid characteristics
15 p2471 A71-32715

Multiple tone generation by axial flow transonic compressors, considering shock waves production and propagation associated with supersonic elements of blading
18 p2848 A71-36497

TRANSONIC FLIGHT

SST sonic booms, investigating intensity and transonic aircraft supersonic flight feasibility
16 p2525 A71-34100

Cone-cylinder-cone missile type body in transonic buffeting environment determining static and fluctuating wall pressure distribution
18 p2843 A71-36020

Sonic boomless transonic transports design, performance, economics and airline routes at Mach 1.2 and 0.98
19 p2996 A71-37598

TRANSONIC FLOW

Transonic flow through planar cylinder lattices, discussing flow pattern visualization and recording techniques by high speed camera
01 p0001 A71-10108

Supersonic and transonic flow including effects of pressure oscillations within cavity, predicting rectangular cavities drag from mathematical model
01 p0002 A71-10931

Fredholm method for reversible transonic flow in computing aircraft wing and turbomachine or helicopter blade airfoils for compressibility law
01 p0003 A71-11022

Reversible transonic fluid flow through cylindrical blades cascade by hodographic singularities solution of potential and stream function
01 p0003 A71-11023

Impulsively started time dependent transonic flow of ideal compressible gas past circular cylinder, using finite difference method
01 p0003 A71-11160

Swept wing fighter aircraft transonic buffet onset lift coefficient from camber and trailing edge deflection, considering design variations
02 p0186 A71-12679

Fluid mechanics of interaction of shock wave and turbulent boundary layer at transonic-supersonic speeds
03 p0399 A71-13138

Flow characteristics in turbomachine blade cascades with transonic regime, emphasizing shock-boundary layer interaction phenomena
03 p0340 A71-13140

Steady supercritical planar inviscid transonic flows over lifting airfoils, generating unsteady flow by impulsively imposing airfoil boundary condition
03 p0341 A71-13433

Transonic flow equations for chemically inert gases binary mixture, considering diffusion effect on dissipative process
03 p0401 A71-13906

Lifting and side force distributions acting on body in transonic flow
03 p0344 A71-14232

Plane transonic flow with curved compression shock wave between subsonic and supersonic regions
03 p0345 A71-14560

Interaction between supersonic flow and transverse sonic or supersonic jet blown perpendicular to main stream through circular hole in wall
03 p0345 A71-14572

Symmetric airfoil profiles with sharp and rounded leading edges in inviscid gas unbounded uniform adiabatic transonic flow, solving by nonlinear approximation
04 p0525 A71-14591

Hydrodynamic equations for discontinuity problems of origin and disruption of vortices, transonic gas flow and shock wave formation, using Lagrange equations
04 p0579 A71-15813

Transonic flow with chemical reactions, analyzing one and two dimensional problem by small perturbation method
05 p0717 A71-16534

Far and near field solutions of plane steady transonic flow past thin airfoil including imbedded shock waves, using small disturbance theory
05 p0694 A71-16565

Transonic jets pressure and density fluctuations dependence on air humidity, discussing flow field measurements by differential and Mach-Zehnder interferometry and wall pressure distributions
05 p0737 A71-17153

Constant curvature wing contours in transonic flow, determining stream function by approximation
06 p0842 A71-18227

Three dimensional transonic shear flow structure in turbomachine cascade, using time dependent numerical solution
06 p0843 A71-18540

Transonic supercritical flow past arbitrary airfoils, using integral relations method
06 p0844 A71-18553

Transonic gas flows in axisymmetric small throat curvature radius Laval nozzle with appreciable flow parameters variation in transverse direction
07 p1014 A71-19732

Monograph on transonic shock free potential flow around quasi-elliptical airfoil sections, investigating flow stability under unsteady disturbances
07 p1015 A71-19773

Two dimensional flow field in secondary sonic transverse jet injection port vicinity, studying free stream Mach number, total pressure and specific heats ratio
07 p1090 A71-19896

Ideal gas jet sonic flow past wedge according to Kirchhoff scheme, testing sine series solution for convergence
07 p1016 A71-20085

Computerized transonic airfoil design from predetermined supercritical velocity distribution, obtaining equivalent incompressible flow through streamline and potential line network transformation
07 p1017 A71-20304

Dissipative fluid sonic flow and shock conditions downstream of symmetrical plane barrier
10 p1549 A71-23824

Body profile low frequency oscillations in transonic gas flow, investigating nonlinear differential equation boundary value problem by approximation method
10 p1550 A71-24363

Nonuniform transonic shear compressible flow past symmetric airfoil, using linearized small disturbance theory
10 p1552 A71-24761

Underexpanded transverse sonic jet-hypersonic stream three dimensional flowfield based on inviscid rotational flow model
11 p1701 A71-25472

Two dimensional analysis of isentropic perfect gas flow fields in axisymmetric nozzles for transonic two phase flow initial values, calculating particle trajectories
11 p1751 A71-25508

Time dependent asymptotic solution for transonic flows in hyperbolic nozzle and turbine cascades with oblique shock
11 p1704 A71-25975

[ASME PAPER 71-GT-42]

- Steady transonic flow through two dimensional gas turbine cascades predicted with time dependent formulation of flow equations, giving airfoil surface pressure distributions
[ASME PAPER 71-GT-89] 11 p1704 A71-25996
- Transonic airfoil testing techniques in two dimensional flow, discussing wind tunnel conditions at various Reynolds numbers 12 p1864 A71-27467
- Uniform transonic ideal gas flow past finite bodies approximated by Karman equation 13 p1989 A71-27902
- Transonic gas flow measurement during sudden expansion from circular nozzle into coaxial cylindrical channel, emphasizing flow attachment 13 p1993 A71-29192
- Transonic gas flow around profile, proving uniqueness of Frankl solution 13 p1993 A71-29221
- Low thrust jet effect on base pressures on boat-tailed afterbodies in Mach number 0.8-1.2 flow 14 p2169 A71-29889
- Two dimensional transonic potential flow near convex corner 14 p2225 A71-30215
- Inviscid transonic rotational flow expansion around convex corner, applying to supersonic boundary layer over flat plate ending at sharp corner 14 p2226 A71-30444
- Pressure distribution and drag prediction over slender axisymmetric fuselages and afterbodies and exhaust nozzles at transonic Mach numbers 14 p2170 A71-30771
- Transonic flow past bodies of revolution, using finite difference scheme 14 p2171 A71-30876
- Gas dynamic and irrotational flow equations system transformation into Cauchy-Riemann equations via Beltrami coordinate transformation for simple representation of transonic flows [DFVLR-SONDDR-124] 14 p2228 A71-31127
- Density and velocity profiles of transonic flow past wavy wall at various channel heights, using Mach-Zehnder interferometer 15 p2386 A71-31165
- Finite element method application to transonic viscous flow through cascades and channels [AIAA PAPER 71-602] 15 p2388 A71-31542
- Shock and pressure gradient induced turbulent transonic flow separation, using two dimensional circular arc model for flow field investigation [AIAA PAPER 71-565] 15 p2344 A71-31559
- Small disturbance equations for steady transonic flows past thin lifting airfoils and slender bodies [AIAA PAPER 71-566] 15 p2344 A71-31560
- Compressible transonic flow about two dimensional airfoils, developing inviscid nonlinear potential equations by relaxation procedures [AIAA PAPER 71-569] 15 p2345 A71-31562
- Inviscid compressible transonic flow field equations for perfect gas in conical rocket nozzles, measuring wall and center line pressures 15 p2390 A71-32040
- Book on hodograph equations covering plane transonic flow, Tricomi boundary value problems, weak shocks and pressure density relations 15 p2394 A71-32766
- Skin friction, trailing edge boundary profiles and tuft flow patterns on model F-4D aircraft in transonic flow [AIAA PAPER 71-762] 16 p2521 A71-34001
- Transonic flow fields in slender symmetric profiles, incorporating shock relations at trailing edge 16 p2522 A71-34163
- Hypothetical gases transonic flow higher approximation, expressing flow solutions by Airy functions 17 p2726 A71-34508
- Two dimensional steady viscous gas transonic flow Navier-Stokes equations, establishing uniqueness of solutions to boundary value problems 17 p2673 A71-35646
- Mesh method for supercritical transonic flow calculation with normal or oblique shock wave at trailing edge 17 p2674 A71-35799
- Transonic flow numerical analysis, discussing initial conditions and imbedded shocks choice for computational efficiency 18 p2905 A71-36307
- Time dependent calculation of mixed two dimensional or axisymmetric transonic flows in nozzle, writing equations of motion with transformed spatial variables 18 p2906 A71-36323
- Generalized relaxation methods application to transonic flow problems, combining with numerical integration theory for ordinary differential equations 18 p2906 A71-36324
- Small disturbance transonic flows potential equations numerical solutions, using mixed finite difference theory 18 p2844 A71-36325
- Plane transonic gas flows through Laval nozzle and symmetrical wedge-shaped profile, solving boundary value problem by reduction to singular integral equation 19 p2991 A71-37101
- Axisymmetric plane transonic flow past convex corner point, obtaining characteristics by mapping into hodograph plane 19 p2991 A71-37103
- Transonic flow theory and experiment, considering hodograph method, integral equation method, parabolic method and method of characteristics 19 p2992 A71-37454
- Numerical analysis of plane transonic flows past shock free airfoils without boundary layer separation using inverse method of complex characteristics 19 p2994 A71-38307
- Transonic and supersonic turbine guide vanes, noting air as flow medium in experiment and steam in actual turbine 20 p3176 A71-39455
- Three dimensional nonlinear subsonic flow over finite wings of arbitrary planform, solving transonic small disturbance equation by integral method 20 p3177 A71-39568
- Shock free transonic deceleration of solar wind due to ionizing interactions, discussing plasma flow 21 p3438 A71-40604
- V shaped notches drag coefficients behavior in transonic regime, observing inviscid-viscid interaction controlling flow separation and reattachment 21 p3323 A71-40954
- Transonic nozzle flow with variable stagnation speed of sound across flow, deriving governing equations with stream function as independent variable 21 p3324 A71-40978
- Streamline curvature analysis of compressible subsonic, transonic and supersonic cascade flows in axial turbine blades 23 p3665 A71-44347
- Transonic flows about two dimensional airfoils, calculating far field boundary conditions with coordinate transformation 24 p3789 A71-44620
- Transonic airfoil cascade analytical design, determining efficiency from velocity distribution 24 p3791 A71-45381
- ### TRANSONIC FLUTTER
- F-8D aircraft transonic flight and wind tunnel tests for buffet onset prediction, considering effects of g level and fluctuation amplitude and frequency [AIAA PAPER 70-341] 10 p1557 A71-24863
- Sweepback thin cantilever wing transonic flutter density and velocity coefficients, investigating engine pod shaped concentrated mass location effects 11 p1706 A71-25189
- ### TRANSONIC INLETS
- #### U SUPERSONIC INLETS
- ### TRANSONIC SPEED
- Transonic wing profiles analog determination by hodograph method 05 p0694 A71-16735
- Gliding guided ribbon parachute for transonic speed deployment, investigating turn capability, opening reliability, structural integrity and effective drag 10 p1557 A71-24868
- Shock wave strength for laminar boundary layer separation at transonic speeds with external flow freestream Mach number near one 14 p2324 A71-29883
- ### TRANSONIC TURBINES
- #### U SUPERSONIC TURBINES
- ### TRANSONIC WIND TUNNELS
- Wind tunnel history, evolution and use, covering low speed variable density, high speed transonic, supersonic, hypersonic and hypervelocity wind tunnels 08 p1272 A71-21666
- Single and multiple sting support evaluation for unmodified interference free wind tunnel data over 0.85 to 2.2 M range using image method [AIAA PAPER 71-267] 08 p1274 A71-21993
- Transonic wind tunnel wall interference effects experimental determination, investigating porous and slotted walls 08 p1229 A71-22013
- Two dimensional test facility in blowdown wind tunnel transonic section, discussing porous sidewall boundary layer control effects on airfoils geometric characteristics [AIAA PAPER 71-293] 09 p1428 A71-22957
- Static aerodynamic data correlation for high subsonic speed transport aircraft model in transonic wind tunnels, including relative buoyancy and turbulence effects [AIAA PAPER 71-291] 09 p1429 A71-23423
- High Reynolds number transonic wind tunnel need in U.S., discussing wing maximum lift and pitching moment, shock induced flow separation, etc 10 p1589 A71-24174
- Lift correction in perforated two dimensional transonic wind tunnels, considering incidence angle and streamline curvature effects on airfoil models 10 p1590 A71-24953
- Transonic wind tunnel testing of air intake and afterbody of double flux engine nacelle at high subsonic Mach numbers and high Reynolds numbers [ONERA-TP-943] 18 p2956 A71-36021
- Dual scatter laser Doppler velocimeters for transonic wind tunnel measurements and calibrated applied to simulated helicopter downwash, high lift wing and jet crossflow 21 p3364 A71-40980
- ### TRANSONICS
- #### U TRANSONIC FLOW
- ### TRANSPARENCY
- Transparent solids unpolished samples refractive index and dispersion measurement using Abbe refractometer 01 p0128 A71-10840
- Transparent dielectrics sheet radiation absorptance, emittance and transmittance determination by Monte Carlo method 01 p0183 A71-11555
- Semitransparent spherical dielectric shell under diffuse incident radiation, determining absorptance and reflectance by Monte Carlo method 03 p0518 A71-13644
- Holographic interferometry with both beams traversing transparent object, providing variable sensitivity and directional phase detection 03 p0425 A71-13620
- Radiation energy deposition profiles in transparent liquids, using holographic interferometer 05 p0748 A71-16262
- Two wavelength nondiffuse holography for interference metrology of transparent media 05 p0748 A71-16262
- Mathematical analysis of eye transparency, discussing light scattering from normal cornea, stroma, swollen opaque corneas and cataractous lens 08 p1240 A71-21373
- Mechanical stress amplitude measurement in optically transparent materials during HF vibrations, using polarization method 09 p1535 A71-22181
- Transparent radiating gas thermal instability criteria derivation from gasdynamic equations 09 p1519 A71-22525
- Mars border-disk brightness comparison noting atmospheric transparency effects 09 p1520 A71-22834
- Corneal transparency in metabolic activity absence using acid mucopolysaccharide depletion and prolonged gamma irradiation 09 p1393 A71-22950
- Two wavelength holographic interferometry for transparent media with high or low sensitivity, using diffraction grating 12 p1904 A71-26750
- Rapid scan astronomical spectrophotometer with 1024 channel for signal averaging on slow change in sky transparency for improving accuracy 12 p1904 A71-26800
- Principal stresses separation in nitrocellulose transparent material with photoelastic properties using scattered light method 14 p2322 A71-29700
- Transparency of extragalactic space to very high energy photons, considering background gamma ray effects 15 p2472 A71-31190
- Holographic interferometry for observing transparent media in supersonic gas flow, comparing results with Mach-Zehnder interferometry 15 p2404 A71-31270
- Transparent polymer dielectric luminescence and destruction under Q switched laser radiation with subthreshold power and picosecond pulses 16 p2588 A71-33650
- Method of producing transparent model composites materials for photo-orthotropic-elastic studies, allowing preparation of larger laminates 17 p2820 A71-34540
- Picosecond duration coherent light pulse propagation in resonant medium, discussing basic equations self induced transparency, Bloch equations, soliton model and higher conservation laws 17 p2754 A71-35371
- Transparent radiating gas thermal instability criteria derivation from gasdynamic equations 17 p2807 A71-35500
- Two dimensional objects three dimensional images, possibility based on self-reproduction effect for arbitrary periodic distribution function of transparencies using coherent light source 19 p3064 A71-37770
- Calcium difluoride powder under sintering, examining optical transparency and morphological features 19 p3069 A71-38040
- Polycarbonates transparency applications in aircraft windshield design, discussing heat resistance, mechanical, chemical and optical properties 20 p3253 A71-38751
- Transparent scandium oxide powder development by hot pressing, plotting IR transmission vs wavelength 20 p3253 A71-38811
- Ion beam deposition of insulating carbon thin film on room temperature substrates, considering transparency, index of refraction, insulating capacity, glass scratching ability, etc 20 p3241 A71-39001

Transparent sample surfaces parallelism interferometric measurement using laser produced two beam nonlocalized fringes

20 p3245 A71-39181

Laser-drilled transparent material hole geometry dependence on beam focus and intensity, computing laser power, mode and work positioning

20 p3246 A71-39492

Self induced transparency in ruby attenuator, detailing phase relaxation effects at various temperatures

21 p3427 A71-40546

Reflected shadow method for constrained zone photoelastic observation around cracks in birefringent transparent plate under plane stress

22 p3549 A71-42555

Laser radiation destruction of transparent dielectrics, proposing electronic excitations conversion to heat and thermal explosion

23 p3682 A71-42891

Photoactivated electric field effects in nematic liquid crystals for recording real time transparent phase holograms

23 p3674 A71-42955

Heating dynamics of transparent dielectrics exposed to pulsed laser beam operating in free laser mode

23 p3683 A71-43270

TRANSPARENT MATERIALS U TRANSPARENCY TRANSPARATION

Heat transfer to transpired turbulent boundary layer, reviewing theoretical models and experimental results for friction coefficient and Stanton number

[ASME PAPER 71-HT-44] 19 p3166 A71-38003

Ideal gases and binary monatomic gas mixtures beats of transport derivation from kinetic theory expressions for thermal transpiration

24 p3891 A71-45384

TRANSPARATION COOLING U SWEAT COOLING TRANSPONDERS

Widely separated microwave oscillators phase synchronization via satellite transponder

02 p0216 A71-12330

Radar information digital extractors for processing signals from airborne transponder

03 p0382 A71-13570

S band transponder for vehicle-space-ground link subsystem /VSGLS/ of USAF integrated telemetry, tracking and command system

05 p0719 A71-16151

Intelsat 3 satellite Communication, Telemetry, and Command system using transponders for multichannel voice and TV transmission

06 p0870 A71-18398

S band pulsed cotal radar transponder for ground base Centaur rocket trajectory tracking from takeoff to splashdown

06 p0870 A71-18475

Ionospheric total electron content specification for satellite transponders time delay error reduction

07 p1095 A71-19002

Intelsat 4 satellite transponder, examining receivers, transmitters, mechanical stability and heat transfer

10 p1578 A71-24509

Carrier suppression in angle modulated transponding telemetry by first order stationary stochastic processes

12 p1880 A71-27074

ATS 1 and 3 satellite VHF transponders for ships and aircraft location, communication and remote sensing, discussing performance test results

14 p2198 A71-30898

Microwave responders in FM or AM modes with cavity resonator, considering use in medium distance telemetering or telemonitoring

14 p2215 A71-30911

Transponder configurations for communication satellites using frequencies above 10 GHz, discussing service type, modulation method and equipment

17 p2705 A71-35092

Intelsat 4 transponder for broadband multicarrier operation with frequency and pulse modulation, considering TWT, tunnel diode amplifiers, filters, equalizers, mixers, multiplexers and antennas

17 p2705 A71-35099

Distance measurement system with onboard transponder, discussing subcarrier and pseudorandom code signal techniques synthesis

18 p2879 A71-36532

Performance prediction model for electromagnetic compatibility of ATC radar beacon system, testing interrogator-transponder links along air route

19 p3102 A71-38435

TRANSPORT AIRCRAFT

NT AN-24 AIRCRAFT

NT BAC 111 AIRCRAFT

NT BOEING 737 AIRCRAFT

NT BOEING 747 AIRCRAFT

NT BOEING 7207 AIRCRAFT

NT C-5 AIRCRAFT

NT C-130 AIRCRAFT

NT C-131 AIRCRAFT

NT C-135 AIRCRAFT

NT CARGO AIRCRAFT

NT CH-3 HELICOPTER

NT CH-46 HELICOPTER

NT CH-47 HELICOPTER

NT CH-54 HELICOPTER

NT CONCORDE AIRCRAFT

NT DC 10 AIRCRAFT

NT DH 121 AIRCRAFT

NT DHC 4 AIRCRAFT

NT DO-31 AIRCRAFT

NT F-28 TRANSPORT AIRCRAFT

NT H-53 HELICOPTER

NT H-56 HELICOPTER

NT L-1011 AIRCRAFT

NT SHORT HAUL AIRCRAFT

NT TU-144 AIRCRAFT

NT VC-10 AIRCRAFT

NT XC-142 AIRCRAFT

Commercial transport aircraft maintenance simulation Monte Carlo Modeling techniques, considering application to airline operations
[SAE PAPER 700345] 01 p0067 A71-10128

VC 400 tilt wing VTOL cargo and passenger transport aircraft, discussing component and system development and testing phase

01 p0004 A71-10466

Aladin 2 interurban Stol transport design with blown wings and jet deflection by wing flaps, emphasizing engine noise reduction

01 p0005 A71-10749

Hypersonic conventional and rocket transport aircraft, discussing costs and air and noise pollution
[AIAA PAPER 70-1218] 01 p0184 A71-11302

Transport aircraft tire pressure and multiwheeled landing gear limitations regarding pavement design

02 p0189 A71-12163

Direct lift V/STOL transport aircraft design, discussing environmental factors in relation to noise, air pollution, jet interference and safety

04 p0530 A71-15403

Navigation and traffic control of VTOL commercial transport aircraft, discussing noise, G forces, turbulent wakes, approach profiles and V-ports

04 p0624 A71-15429

Supersonic aircraft turbojet engine exhaust noise suppressor research program, predicting full scale noise spectra from model suppressor tests
[AIAA PAPER 68-1023] 06 p0945 A71-17693

Draw-through cooling of electronic equipment in subsonic and supersonic commercial jet transports, discussing internal circulation system design
[SAE-AIR-64A] 07 p1077 A71-19642

Design objectives for subsonic, transonic and supersonic civil transport flying characteristics based on MIL-F-8785, considering aircraft control
[SAE-ARP-842B] 07 p1019 A71-19645

Static aerodynamic data correlation for high subsonic speed transport aircraft model in transonic wind tunnels, including relative buoyancy and turbulence effects
[AIAA PAPER 71-291] 09 p1429 A71-23423

Lift/cruise engine design and thrust vector control influence on VTOL transport aircraft transition characteristics and ground acoustic field
[DGLR-70-040] 10 p1556 A71-24749

Medium weight NAMC C-1A tactical transport aircraft technical specifications

11 p1706 A71-25231

Validity range of response prediction methods for large flexible aircraft to continuous atmospheric turbulence, discussing power spectral densities and fatigue life
[AIAA PAPER 71-342] 11 p1707 A71-25321

European airbus, considering flight trials of first A.300B high capacity transport aircraft

12 p1867 A71-26921

Space shuttle comparison with transport aircraft, discussing high thermal resistant and cryogenic insulator material concepts, with application to Concorde structural computations

12 p1973 A71-27605

Economic analysis of subsonic transport airplane design, evaluation and operation
[SAE PAPER 710423] 13 p1995 A71-28310

Transport aircraft all weather automatic landing operation, examining guidance system and independent monitors
[SAE PAPER 710441] 13 p2098 A71-28323

Military/commercial STOL transport design, discussing performance, payload and equipment requirements with emphasis on production cost benefits
[SAE PAPER 710468] 13 p1996 A71-28336

Cost efficient sound limit expenditures per parameter unit in commercial transport aircraft design

13 p2167 A71-28945

Commercial V/STOL and jet VTOL transport, discussing Do-31 test results, landing approach, air traffic control automation and electronic control

13 p1997 A71-29131

Structural fatigue in aircraft design, discussing twin engine transport tests, crack propagation rate, residual strength, etc

13 p2158 A71-29434

Atmospheric turbulence effect on turbine powered transport aircraft, discussing gust accelerations, avoidance, detection, forecasting and pilot control

14 p2172 A71-29750

Thunderstorm, CAT, weather and mountain wave induced turbulence forecasting and analysis for transport aircraft

14 p2268 A71-29764

Jet transport aircraft stability and controllability under atmospheric turbulence conditions, discussing longitudinal and lateral-directional characteristics with particular attention to unstable spiral mode

14 p2173 A71-29772

Jet transport aircraft design for safety under air turbulence conditions, considering cruise altitude limitations and pitch and g excursion reduction by special autopilot mode

14 p2173 A71-29777

Normal accelerations experienced by transport aircraft fleet from fatigue load meter data analysis, discussing counting rates seasonal variations

14 p2174 A71 29788

Computer aided design program for civil transport aircraft configuration, performance, propulsion, weight and costs to meet given specifications

14 p2175 A71-30398

Transport aircraft JT9D high bypass ratio engine development, noting maintainability and stability improvements

[SAE PAPER 710419] 14 p2289 A71-30527

Powered landing gear wheel system requirements for parking and taxiing of commercial jet transport airplanes

[SAE PAPER 710446] 14 p2176 A71-30530

Commercial vs military design criteria for STOL transport aircraft, noting landing and takeoff distances and noise levels

[SAE PAPER 710465] 14 p2176 A71-30536

Aladin II four-jet engine STOL intercity transport aircraft, noting low noise characteristics and passenger capacity

15 p2347 A71-31412

V/STOL lift fan airliner project HS 141 for intercity transport, describing features, weight and performance data, noise characteristics and reliability criteria

15 p2348 A71-31413

Large variable sweep wing maneuver load relief system with ailerons reducing resulting bending moment at pivot

15 p2348 A71-31600

European Airbus automatic pilot and flight control system, including computers in electromechanical subassemblies

15 p2446 A71-31914

Optimum vertical surface configuration for STOL transports, considering structural weight and performance requirements

[AIAA PAPER 71-769] 16 p2524 A71-34006

Automatic landing systems using internal navigation derived translational state information, discussing evaluation by simulation of transport aircraft operating with conventional instrument landing system

[AIAA PAPER 71-795] 16 p2605 A71-34020

VTOL transport optimal airframe/propulsion systems design, discussing thrust requirements, performance, control, cruise functions, fuel consumption and fan characteristics

[AIAA PAPER 71-744] 17 p2792 A71-34225

Aircraft for international long haul transportation, discussing criteria for selection based on environmental, operational, budgetary and policy considerations

17 p2674 A71-35208

Gulfstream 2 acoustics program for cabin noise level reduction, compliance with FAA takeoff and landing noise certification and structure qualification against sonic fatigue

17 p2675 A71-35527

Large jet transport aircraft trailing vortices, studying velocity fields, core diameters and logarithmic variations of circulation

17 p2674 A71-35755

Trailing wake hazards of large transports in takeoff and landing, examining configuration stability of vortex pair in ground effect

17 p2674 A71-35757

Administrative techniques of cost/weight tradeoff program for jet transport airplane
[SAE PAPER 899] 17 p2750 A71-35812

Hypersonic aircraft design usable as transport or space shuttle, determining aerodynamic behavior in viscous flow

18 p2847 A71-36431

Feasibility assessment of hypersonic transports with actively cooled airframe structure, considering liquid hydrogen fuel use as coolant

19 p2995 A71-37123

Sonic boomless transonic transports design, performance, economics and airline routes at Mach 1.2 and 0.98

[CASI PAPER 72/8] 19 p2996 A71-37598

European airbus development, discussing basic, long range and stretched capacity versions and aerodynamic and structural design features

20 p3177 A71-38749

Convertible rotor transport aircraft, considering ATC, mass transportation systems, safety, noise and socio-economics 20 p3178 A71-39387

Flight tests for hazard evaluation to other aircraft from wake turbulence generated by large jet transport airplanes 21 p3321 A71-40506

Book on fatal civil aircraft accidents medical and pathological investigation covering transport, light and glider aircraft case histories and statistics 23 p3638 A71-42910

Civil transport aircraft and equipment maintenance and reliability problems solutions with best time, cost and weight compromises 24 p3792 A71-44765

TRANSPORT COEFFICIENTS

U COEFFICIENTS

U TRANSPORT PROPERTIES

TRANSPORT EQUATION

U BOLTZMANN TRANSPORT EQUATION

TRANSPORT PROPERTIES

NT ATMOSPHERIC CONDUCTIVITY

NT CARRIER MOBILITY

NT DIFFUSION COEFFICIENT

NT EDDY VISCOSITY

NT ELECTRICAL RESISTIVITY

NT ELECTRON MOBILITY

NT GAS VISCOSITY

NT GASEOUS DIFFUSION

NT HOLE MOBILITY

NT IONIC MOBILITY

NT IONOSPHERIC CONDUCTIVITY

NT MAGNETORESISTIVITY

NT PHOTOCONDUCTIVITY

NT PLASMA CONDUCTIVITY

NT SUPERCONDUCTIVITY

NT THERMAL CONDUCTIVITY

NT THERMAL DIFFUSIVITY

NT VISCOSITY

Atomic and molecular transport coefficients for various species injected into boundary layer on ablating or transpiration cooled surface 01 p0130 A71-10958

Chemically interacting gases transfer properties at various temperatures, determining collision parameters by viscosity, diffusion coefficients, molecular beam scattering and vibrational relaxation time 02 p0286 A71-12186

Thermoelectric transport properties of ionospheric electron gas above 100 km 03 p0406 A71-13301

Multicomponent ionized gases mixture transport coefficients for field-free and strong magnetic field cases 03 p0463 A71-13471

Transport mechanism for holes in polycrystalline Ge films based on Matthiessen rule, considering surface scattering and dislocation 03 p0468 A71-14464

Fluorine liquid-vapor coexistence boundary and critical point parameters, considering thermodynamic and transport properties 05 p0831 A71-16409

Shock tube research instrumentation with fast response time for data on thermodynamic and transport properties, relaxation times and kinetics of high temperature gases 06 p0897 A71-17430

Monte Carlo evaluation of molecular transport property integrals temperature dependence 06 p0917 A71-17551

Turbulent shear flows transport properties, computing atmospheric and vortex motions by invariant modeling of Reynolds stress term in boundary layer momentum equation [AIAA PAPER 71-217] 06 p0886 A71-18653

Intermetallic III-V compound semiconducting films and layers charge carrier transport phenomena and optical properties 07 p1178 A71-19850

Ionized gases quantum transport cross sections and collision integrals, considering energy and temperature ranges for attractive and repulsive screened Coulomb potentials 07 p1224 A71-20283

Hydromagnetic shock wave structure, treating plasma in two fluid approximation with collisional transport coefficients in changing density and temperature 10 p1596 A71-24657

Mixed plasmas transport properties at one atmosphere and 5000-35,000 K, considering helium-nitrogen, argon-nitrogen and xenon-nitrogen plasmas 12 p1986 A71-27188

Sulfur hexafluoride equilibrium composition, thermodynamic functions, transport properties and application to simplified enthalpy flow arc model 12 p1939 A71-27267

Heat transfer near critical point, examining continuity, momentum and energy equations for variable thermodynamic and transport properties effects 14 p2336 A71-30241

Chemically interacting gases transfer properties at various temperatures, determining collision parameters and interaction cross sections and energies 15 p2451 A71-31494

Plasma heat transport associated with matter, momentum, energy and electrical charges transfer 16 p2617 A71-32956

Moment and heat transfer coefficients for disks rotating in rarefied environment, noting transport characteristics decrease with increasing rarefaction 19 p3161 A71-37292

Particle size-frequency distributions of volcanic pyroclastic tuffs for transport and deposit evaluation 19 p3051 A71-37672

Air and jet fuel-air mixtures, calculating temperature dependent laminar and turbulent heat transfer parameters and transport properties [ASME PAPER 71-HT-41] 19 p3166 A71-38002

NTWO as FORTRAN 4 family of subroutines developed on 7094-7044 system for determining thermodynamic and transport properties of nitrogen 20 p3253 A71-39268

Auxin transport and geotropic response of roots and shoots, discussing plant growth mechanisms under stimulation-inhibition conditions 21 p3340 A71-39980

MnSe-CdSe mixed crystals growth investigation by elements, binary compounds and solid solutions vapor transport properties 21 p3427 A71-40214

Quasi-fluid mechanical formulation generation for ionized gases dispersive transport coefficients by linear dynamic response function technique 21 p3423 A71-40800

Helium, neon, nitrogen, oxygen, argon, carbon dioxide and monoxide and methane thermodynamic and transport properties calculation using computer program for state equations 21 p3351 A71-40893

Anisotropic transport coefficients valence band model of TiSe, measuring electric conductivity, Hall effect and thermo-emf as function of temperature 21 p3434 A71-41328

Transport properties of low density gas of rotating diatomic molecules, deriving quantum mechanical expression for relaxation time via restricted distorted wave approximation method 23 p3706 A71-42908

Hydrodynamic model of momentum, heat and mass transport for turbulent flow in straight circular pipes, tabulating velocity profiles and eddy diffusivity 23 p3780 A71-43091

Shock initiation problem collisionless solution for transport properties of gas flow, considering departure from Navier-Stokes solution 24 p3819 A71-44791

Transportation lag simulation by fluidic transmission lines and bubble tubes 24 p3793 A71-45086

TRANSPORT THEORY

NT CHAPMAN-ENSKOG THEORY

NT EYRING THEORY

NT MIXING LENGTH FLOW THEORY

Neutron linear transport theory boundary value problems, using Green function approach 01 p0111 A71-10333

Turbulent transport equations derivation for incompressible fluid unsteady flow in arbitrary geometry, considering application to flow between parallel plates 01 p0072 A71-11469

Multicomponent gaseous mixtures and plasmas transport analysis improved formalism consisting of N moment Boltzmann equation and N parameter distribution function representation 02 p0290 A71-12229

Turbulent plasma radio emission theory of photon production and transport, considering application to quasars 02 p0292 A71-12587

Boundary motion between media during transport phenomena under Stefan conditions, establishing shock front coordinates by Hadamard algorithm 03 p0520 A71-13951

German monograph on radiative transport in freely expanding gas clouds covering analytical and numerical calculations and experiments 03 p0418 A71-14369

Low temperature confined cesium plasma, observing ion-acoustic oscillation excitation effects on transfer process and ionization 07 p1167 A71-19236

Atmospheric surface layer shear/buoyant production, flux divergence and dissipation in terms of turbulent kinetic energy and transport in temperature variance budget 09 p1490 A71-23555

Spherical harmonics differential approximation generalized from one dimensional radiation specific intensity angular dependence Jacobi polynomial expansion 10 p1696 A71-24536

Linearized relativistic transport equation for mixture of isobaric Maxwellian molecules, solving in

terms of eigenfunctions and eigenvalues of collision operators 10 p1645 A71-2402

BeO reflected-fast-spectrum liquid-metal-cooled thermionic reactor, discussing two dimensional transport perturbation theory computer code for temperature coefficients evaluation 11 p1712 A71-2502

Cosmic ray propagation in interplanetary space deriving steady state transport equation with energy losses 11 p1817 A71-2602

Spherically symmetric radiative transfer problem constructing model with neutron transport theory [AIAA PAPER 71-466] 11 p1859 A71-2602

Low temperature confined Cs plasma, observing ion-acoustic oscillation excitation effects on transport process and ionization 12 p1935 A71-2602

Transport phenomena in rarefied gases, discussing sound dispersion in helium, weak shock wave acoustic propagation in monatomic gases and kinetics in alternating fields 12 p1930 A71-27188

Transport coefficients interrelations, using irreversible process thermodynamics 13 p2161 A71-28002

Angular momentum meridional transport flux wave number-frequency spectral characteristics in mid-troposphere of Southern Hemisphere 13 p2063 A71-29102

Reactor shielding problems solutions involving removal-diffusion theory, two dimensional transport theory and Monte Carlo method 13 p2099 A71-29202

Quantum-theoretical transport equation for diatomic gases with internal degrees of freedom, generalizing for arbitrary spacing between internal energy levels 14 p2275 A71-30002

Two dimensional jet interaction flow field, investigating gas dynamic and transport phenomena [AIAA PAPER 71-561] 15 p2514 A71-32222

Scalar material transport in incompressible homogeneous turbulent fluid based on one point correlations equations 17 p2835 A71-34202

Transport theory applications - Conference, Oxford University, September 1970 17 p2808 A71-35502

Dense fluids linearized general transport equation solution, obtaining explicit expressions for shear viscosity 18 p2950 A71-37002

Hydrodynamic equations for anisotropic plasmas magnetic fields, considering collisionless and collisional transport effects 19 p3111 A71-37602

Splitting-up method with variational optimization for time independent nonstationary hydrodynamic transfer equations for use in meteorology, oceanography, etc 19 p3088 A71-38002

Finite thickness infinite slab with radiation free time dependent source, solving nonhomogeneous boundary value problem for linear transport equation 20 p3269 A71-39002

Plasma transport processes role in E region from midlatitude nocturnal and auroral ionospheric modes in terms of transport equations 20 p3232 A71-39802

Cosmic ray transport in random magnetic fields deriving coupled integrodifferential equations for field intensity and flux 22 p3592 A71-41912

TRANSPORTATION

NT AIR TRANSPORTATION

NT RAIL TRANSPORTATION

NT RAPID TRANSIT SYSTEMS

NT SPACE TRANSPORTATION

NT URBAN TRANSPORTATION

Book on human factors application in teleoperator design and operation covering aerospace environments, transportation, remote control, sensors and actuator subsystems 09 p1399 A71-22602

Airport design for passenger and baggage handling efficiency, considering choice between continuous and batching type intra-airport transit system 22 p3529 A71-42012

TRANSURANUM ELEMENTS

NT CALIFORNIUM ISOTOPES

NT PLUTONIUM

NT PLUTONIUM 238

Superheavy transuranic elements in meteorites and lunar dust by fossil track microscopy 10 p1673 A71-24422

Radioisotopes as energy source for power conversion systems, discussing future availability of fission products and transuranium elements from commercial nuclear power reactors 20 p3265 A71-38902

TRANSVERSE ACCELERATION

Hypothalamus supraoptic nucleus morphological changes in rats under prolonged transverse acceleration

09 p1388 A71-22195

Transverse impact resistive graphite fiber reinforced plastic /GFRP/ lightweight sandwich panels and beam structures, using thin inner core facings

11 p1846 A71-25417

Vibration amplitudes and transverse acceleration of ventral vehicle during uncontrolled atmospheric descent trajectory

13 p2146 A71-29208

Dogs peripheral blood reaction to complex action of transverse accelerations and gamma irradiation

22 p3494 A71-42727

Transverse accelerations effect on human speech features

24 p3795 A71-44471

Transverse acceleration effect on aspartic aminotransferase activity in humans and rats

24 p3795 A71-44528

Morphological changes in dogs brain vessels under transverse accelerations

24 p3796 A71-44546

TRANSVERSE OSCILLATION

IN H WAVES

Transverse oscillations determination in cyclically deformed thin plate under plane stress by energy dissipation calculation using Hooke law

03 p0502 A71-13401

Console rod free and forced transverse vibrations amplitude dependent damping, considering longitudinal tensile force effect and hysteresis

03 p0502 A71-13405

Natural transverse vibrations of beam with variable cross section and parameters exhibiting small random deviations

06 p0983 A71-17368

Evanescent electromagnetic waves quantization by creating transverse triplet wave modes as noninteracting harmonic oscillator, discussing atomic excitation

07 p1159 A71-19548

Transverse and torsional vibrations of fuselage-wing combination with wing tip fuel tanks, calculating mass and stiffness matrix for elastic beam

07 p1022 A71-20364

Transverse free vibrations of beam with one end fixed and other supported on bilinear spring and carrying concentrated mass

14 p2323 A71-29847

Plasma-electron beam system relaxation oscillations due to threshold excitation of transverse ionic oscillations by HF vibrations

15 p2460 A71-32706

Transversely excited atmospheric pressure pulsed carbon dioxide laser with helical electrode, discussing diverging lens effect due to cavity transverse electric discharges

17 p2750 A71-34370

Transverse vibrations of beam with bilinear support spring and nonlinear constraint, using single degree of freedom system analysis

17 p2820 A71-34543

Transverse oscillations determination in cyclically deformed thin plate under plane stress by energy dissipation calculation using Hooke law

17 p2825 A71-35012

Cantilever bar free and forced transverse vibrations amplitude dependent damping, considering longitudinal tensile force effect and hysteresis

17 p2825 A71-35015

Timoshenko beam transverse vibration with time dependent boundary and normal loads, using Laplace transform method

18 p2977 A71-36253

Wake formation behind circular cylinders undergoing self excited and forced transverse oscillations

21 p3458 A71-40282

Transversely vibrating hollow cylindrical beam sound radiation and response to acoustic excitation, predicting resonant frequencies

21 p3461 A71-40320

Elastic plates transverse vibrations fundamental frequency from constant deflection lines method

22 p3617 A71-42537

Motion equations derived for slender beam transverse vibrations on continuous viscoelastic foundation, considering nonlinearities from external couplings, longitudinal displacements and curvature

22 p3617 A71-42539

Transverse mode locking by cylindrically symmetric laser, noting time varying spot size with spacing frequency

23 p3688 A71-44295

TRANSVERSE VIBRATION

IN TRANSVERSE WAVES

IN H WAVES

Longitudinal acceleration and distinct transverse waves propagation in Hadamard and Green hypoelastic materials

01 p0165 A71-10025

Longitudinal oscillations excitation by transverse electromagnetic wave in collision-magnetized plasma, noting LF wave buildup

01 p0134 A71-11030

Transverse surface wave propagation in piezosemiconducting body with electron damping, formulating boundary conditions

01 p0140 A71-11287

YIG with thin piezosemiconductor coating, investigating transverse surface wave amplification and velocity

01 p0140 A71-11288

Quasi-transverse extraordinary wave interaction with density fluctuations in inhomogeneous magnetized plasma, using modulation measurement for instability diagnosis

01 p0136 A71-11440

Transverse wave instability of unmagnetized collisionless plasma subjected to shear flow

01 p0136 A71-11477

Sunward magnetosheath magnetic field fluctuations, noting power levels spatial variations, transverse shock aligned fields and longitudinal waves

01 p0075 A71-11493

Electrical measuring device error caused by longitudinal instability of frame held in tensile suspension during casing transverse vibration

02 p0253 A71-12635

Carbon steel specimens size effect on energy dissipation and damping characteristics under transverse flexural vibrations

03 p0503 A71-13412

Cyclotron electron beam transverse waves interaction in microwave amplifier resonant coupling element with double spiral

03 p0385 A71-13795

Axissymmetric free transverse vibration frequencies of centrally clamped spinning membrane disks

04 p0668 A71-15186

Supported rectangular plates HF transverse vibrations by holographic interferometry

04 p0668 A71-15188

Multidimensional detonation wave structure, presenting spacing prediction by transverse wave strength

05 p0834 A71-16509

Excited waves due to transverse disturbance normal to boundary in dielectric half of isotropic Vlasov plasma with Cerenkov instability

05 p0789 A71-16658

Slender beams transverse vibration, including nonlinear bending inertia in motion equation

05 p0825 A71-16716

Microwave circuit with coupled TEM bars for L band Si avalanche diodes

05 p0729 A71-16920

Long thin circular cylindrical shell circumferential wave functions reduction to beam type transverse vibration equation, including rotatory inertia

06 p0984 A71-17618

Optimum design of high peak power transversely excited atmospheric pressure carbon dioxide laser using ballast resistor energy measurements

07 p1121 A71-18749

Rolling contact body displacement effect on bearings rigidity with allowance for inner ring transverse vibration

08 p1295 A71-20689

Natural potential and nonpotential electron oscillations excitation in plasma by transverse wave field, determining wave amplitude threshold and excitation instability

09 p1500 A71-22239

Fourth order boundary problems with discontinuous boundary conditions, considering circular plate transverse vibrations

09 p1543 A71-23614

Parametric excitation of transverse waves in inhomogeneous electron plasma driven by oscillating electric field, using multimode perturbation method

10 p1647 A71-23891

Spherical shell containing through crack, calculating in-plane and Kirchhoff bending stresses under periodic transverse vibrations

10 p1693 A71-25054

Transverse EM field in plasma, deriving closed equation for distribution function

11 p1804 A71-25500

Transverse electromagnetic wave penetration in semibounded plasma with specular electron reflection

12 p1878 A71-26958

Transverse excitation of elastic ultrasonic waves in CdS piezoelectric plates, considering conductivity effect on damping

12 p1944 A71-27544

Transverse acoustic wave amplification in solid propellant rocket motor, using discrete mass injection as excitation source

12 p1946 A71-27565

Circular waveguides containing pure dielectrics, examining propagation mode inversion criteria via TE and TM characteristic equations

13 p2037 A71-28606

Laser resonator with selector for Hermite-Gaussian TEM/22/ mode, obtaining integral equation solutions for eigenmodes and eigenvalues on digital computer

13 p2078 A71-28608

Imperfect circular disks large amplitude free transverse vibration calculation by Galerkin procedure

14 p2326 A71-30064

Thermodynamic properties effects on transverse acceleration wave propagation in inhomogeneous isotropic elastic bodies with internal state variables

15 p2504 A71-31729

External off-axis TEM wave transformation into natural oscillation modes in Fabry-Perot resonator under axiality disturbance and impinging-excited wave mismatch

15 p2410 A71-32401

Relativistic kinetic theory of large amplitude transverse Alfvén wave, discussing propagation in collisionless plasma

15 p2459 A71-32653

Magnetic stabilization of transverse plasma instabilities, considering waves propagating transversely to plasma direction in presence of uniform external magnetic field

15 p2460 A71-32658

Pulsed laser double exposure holographic interferometry for measuring transverse wave propagation in beams

15 p2413 A71-32790

Transverse shock waves fine structure and saturation of ion-acoustic turbulence in collisionless plasma, using magnetic field probe and MHD equations

16 p2619 A71-33649

Plane mirror ruby laser pseudosteady regime, discussing fundamental TEM mode case

16 p2588 A71-34062

Machine part surface layers properties effect on internal friction from transverse vibration decrement measurement

17 p2826 A71-35021

Transverse wave structure of two-dimensional detonation waves propagating in narrow channel, considering longitudinal instabilities

17 p2841 A71-35708

Transverse wave tubes with cyclotron and synchronous wave interactions as microwave amplifiers, analyzing energy exchange mechanism and axial beam velocity spread

18 p2888 A71-36128

Double exposure pulsed laser holographic interferometry application to transverse wave propagation in Al plate

18 p2977 A71-36233

Lecher waves, line waves and TEM waves, demonstrating advantage of solving diffusion equation within transversal plane for determination of line parameters

19 p3014 A71-37075

Nonthermal electrons interaction with electron plasma oscillations and HF transverse waves in upstream solar wind

19 p3125 A71-37353

Transverse waves and electromagnetic instabilities propagating along magnetic field in homogeneous plasma, discussing ions and electrons energy losses and plasma dispersion

19 p3114 A71-38206

Nonlinear equations for traveling wave amplifiers using transverse wave interaction modes /cyclotron and synchronous electron beam waves/, calculating saturation characteristics

20 p3203 A71-39003

Transverse waves propagation in vibrating orthotropic rectangular beams, noting inexact information regarding shear distribution

20 p3307 A71-39037

Transverse hydromagnetic shock structure in partially ionized gas, calculating ions, electrons and atoms temperatures, velocities and momentum

21 p3444 A71-40239

Transversally excited and atmospheric carbon dioxide laser, measuring time behavior of refraction index profile and lensing effects on resonator

21 p3392 A71-40547

Natural potential and nonpotential electron oscillations excitation in plasma by transverse wave field, determining wave amplitude threshold and excitation instability

21 p3424 A71-41125

Electromagnetic HF wave field pressure effects on slow transverse magnetic wave propagation along plasma layer, noting dispersion equations difference from linear theory

21 p3426 A71-41400

Transverse surface wave amplification in piezosemiconductor, considering cases of total or drift current in thin near-surface semiconducting layer

22 p3585 A71-41707

Magnetospheric VLF transverse wave propagation along geomagnetic field, examining dispersion relation

22 p3533 A71-41797

Thin film optical waveguide TE-TM mode converters, using gyrotropic or anisotropic substrate material

22 p3556 A71-41806

Transverse acoustic wave amplification due to mass injection around submerged nozzle in solid propellant rocket engines, noting annular flow role

22 p3589 A71-42034

Double-heterostructure injection laser radiation transverse polarization from reflectivity analysis of GaAs-air interface vs TE and ME mode incidence angle

22 p3558 A71-42201

Ideally conducting and dielectric coaxial bodies of revolution, investigating joint excitation by TM wave

22 p3522 A71-42304

Exact test particle propagator of Lenard-Bernstein equation for magnetoplasma, applying to transverse plasma echoes

22 p3584 A71-42466

Millimeter transverse electric wave diffraction by spherical plasma, interpreting interferometric measurements of electron density

23 p3708 A71-43085

Frequency and losses differences of modes as necessary conditions for multimode lasers transverse modes self synchronization

23 p3687 A71-44176

High order transverse cavity mode selection and propagation in homojunction and heterojunction GaAs injection lasers, using five layer dielectric model

24 p3832 A71-44432

RF power absorption by magnetized uniform hot electron-ion plasma column submitted to TE and TM waves

24 p3852 A71-44498

Plane TEM wave propagation in free space using rectangular waveguide partially filled with two dielectric slabs

24 p3809 A71-45093

TEM mode hybrid networks analysis extension to tapered transmission lines, indicating design limitations on VSWR and isolation characteristics

24 p3816 A71-45094

TRAPEZOIDS

Trapezoidal and Killian distributions profile parameters at S band in plasma column, noting electron density

09 p1501 A71-22306

TRAPPED MAGNETIC FIELDS

Neutral current sheets in slow moving plasma with frozen-in magnetic field with null force line

16 p2638 A71-33651

Two dimensional magnetospheric model, investigating magnetic line dipole field confinement in empty cavity by tail-like infinitely conducting plasma at constant pressure

20 p3286 A71-38732

TRAPPED PARTICLES

NT INNER RADIATION BELT
NT MAGNETICALLY TRAPPED PARTICLES
NT OUTER RADIATION BELT
NT PROTON BELTS
NT RADIATION BELTS

Double sheath emission barrier existence criterion at thermionic diode emitter based on ion trapping effect

02 p0290 A71-12232

Stability of finite pressure plasma trapped by magnetic field, discussing trapped particle effects

03 p0463 A71-13296

Solar flare particles effects on magnetospheric energetic particle population, discussing magnetic activity effects on trapped particles

03 p0473 A71-13578

Radiation intensity produced by inverse Compton effect between solar flux and Van Allen belt trapped high energy electrons

04 p0640 A71-14875

Primary auroral electron flux angular distribution measurement by rocket probe, showing particle precipitation and trapping by electrostatic double layers in ionosphere

04 p0584 A71-15896

Copper sulfide-cadmium disulfide heterojunctions photocapacitance effects, discussing current generating mechanism and modulation by trapped charge with heat treatment effects taken into account

05 p0699 A71-16054

Si solar cells electron spectrum irradiation, simulating space environment synchronous altitude trapped electrons omnidirectional and flux/energy characteristics

05 p0702 A71-16083

Solar electrons access to closed field lines in geomagnetosphere quasi-trapping region from satellite observation

06 p0949 A71-17257

Avalanche diodes TRAPATT mode initial conditions by computer analysis

07 p1072 A71-19109

Electron trapping in MIS transistor, discussing thermal annealing process activation energy and trap production by radiation

07 p1076 A71-19499

Dawn to dusk magnetospheric electric field effect on energetic stably trapped particle drift shell pitch angle degeneracy

07 p1103 A71-19675

Noncollisional plasma LF instabilities, discussing flute-like, drift wave and trapped particle modes from spatially confined plasma Vlasov equation

07 p1173 A71-20509

Electron trapping in dielectrics, providing effective light and inexpensive spacecraft bremsstrahlung shield and lower average radiation energy at synchronous altitudes

07 p1164 A71-20625

Electron diffusion in trap with magnetic mirrors under pulsed field perturbations, determining coefficients by numerical integration of drift equation

09 p1513 A71-22551

Elongation characteristics of modulation type charged particle traps and analyzers, discussing ions and electrons trapping

09 p1513 A71-22668

One dimensional plasma wave nonlinear dispersion relation, stability and harmonic generation from statistical properties of trapped particle orbits in random potential

09 p1503 A71-22862

Stability of finite pressure plasma trapped by magnetic field, discussing trapped particle effects

09 p1504 A71-23269

Geomagnetically trapped particles radial diffusion across L shells, considering influence on steady state structure and dynamics of radiation belts

09 p1514 A71-23460

Trapped solar wind He and Ne in Surveyor 3 unpainted Al tube, comparing with Apollo 11 and 12 solar wind composition

10 p1672 A71-24390

Magnetic field and trapped electron/proton correlated pulsations due to magnetospheric field line resonance, using model based on Maxwell equation two dimensional solution

10 p1664 A71-24786

Meteoritic Xe isotopes production mechanism covering spallation, neutron absorption, extinct ¹²⁹I and ²⁴⁴Pu radiative decay and Xe component trapping

11 p1819 A71-25223

P-i-n avalanche diode trapped plasma avalanche triggered transit (TRAPATT) oscillations characteristics and voltage waveform under square wave driving current, using computer program

12 p1887 A71-27046

Si p-n-n junction avalanche diode, investigating experimental evidence of microwave generation at subharmonics of transit time excitation and trapped-plasma mode

12 p1887 A71-27047

Long term storage of relativistic energetic electrons and protons in solar corona from IMP 4 and Pioneer 8 observations related to delayed emission from flares

12 p1969 A71-27657

Magnetospheric electron echo probe experiment, using sounding rocket and injecting gun for controlled particle trapping investigation

12 p1953 A71-27674

Stability of trapped particle equilibrium, considering contribution to plasma wave dispersion

13 p2104 A71-27847

High energy cosmic ray components, investigating tracks and trapped magnetic monopoles

13 p2120 A71-28051

Trapped charged particle cyclotron, bounce and drift motion in distorted geomagnetic field

14 p2300 A71-30033

Equilibrium of current carrying plasma in toroidal system, studying instabilities due to trapped and slowly drifting particles

14 p2282 A71-30662

Hydrogen atoms trapped in gamma irradiated calcium phosphates, studying radiation yields, electron paramagnetic resonance line widths, dose saturation and relaxation

16 p2538 A71-32873

Exact charge neutral magnetopause equilibrium, discussing microinstabilities as trapped particle flow cause

16 p2563 A71-33233

Charged particles distribution in magnetosphere beyond radiation belts, proposing unstable radiation zone model containing auroral and semitrapped particles

16 p2626 A71-33450

Long range thermoluminescent dating of meteorites and tektites, discussing dependence on thermal release of trapped carriers, radiation saturation and instrumental errors

16 p2638 A71-33518

Northern high latitude electron trapping boundary position diurnal, seasonal and geomagnetic Kp variations based on ESRO 1/Aurora polar satellite observations

16 p2627 A71-33753

Plasmopause position during stormtime increase in trapped energetic electrons, measuring near prime geomagnetic meridian by whistler techniques

16 p2629 A71-33969

Helium-cadmium laser discharge, discussing possible He trapping mechanisms and improved tube design to eliminate He cleanup

18 p2933 A71-37013

Cyclotron resonance energization of trapped electrons in magnetosphere from plasma pseudoparticle shape calculation, noting geophysical effect

19 p3117 A71-20509

Trapped protons flux vs L profile measurement on board sounding rocket near equator, comparing with calculation from neutron albedo source atmospheric losses

20 p3284 A71-20625

Radio pulses from pulsars based on noncoherent synchrotron radiation from magnetospheric trapped charged particles

20 p3285 A71-20625

Trapping of neutrals from fast atom beam impinging on molecular hydrogen influx fed electron-cyclotron plasma target

21 p3422 A71-20625

Ring current location in magnetosphere, noting magnetospheric ion cyclotron instability region as a proton trapping boundary

22 p3332 A71-20625

Large amplitude high efficiency TRAPATT operation in Si avalanche diodes, using resonance frequency for voltage and current waveforms analysis

23 p3650 A71-20625

Coulomb interaction effect between charged particles in amorphous semiconductor, noting state of reduction at Fermi energy

23 p3715 A71-20625

Longitudinal magnetic field inhomogeneity influence on inhomogeneous plasma Alfvén instability considering magnetic field pressure and trapped particles

23 p3713 A71-20625

Trapped hydrogen atoms detection in proton irradiated KCl and NaCl single crystals at 77 K by electron paramagnetic resonance spectroscopy

24 p3650 A71-20625

Manned spacecraft hazard from charged particle radiation during solar flares and trapped particle geomagnetic field, recommending protection measures

24 p3865 A71-20625

TRAPPED RADIATION

U RADIATION BELTS

U TRAPPED PARTICLES

TRAPPING

NT CRYOTRAPPING

Solid state single injection diodes with surface traps, calculating trapping noise

06 p0872 A71-13296

TRAPS

NT COLD TRAPS

NT ION TRAPS (INSTRUMENTATION)

Spontaneous oscillations in semiconductor deep traps, deriving conditions for soft or hard transition

07 p1176 A71-20625

Nonuniform trap distribution effect on I-V characteristics of dielectric diodes, allowing for field line ionization

13 p2040 A71-20625

Nonuniform trap distribution effect on I-V characteristics of dielectric diodes, allowing for field line ionization

21 p3358 A71-20625

TRAVELING IONOSPHERIC DISTURBANCES

Traveling ionospheric disturbances at magnetic equator, determining electron concentration profile by incoherent scatter radar

15 p2398 A71-20625

Traveling ionospheric disturbances dynamic properties, calculating horizontal phase velocity from ionogram data

16 p2568 A71-20625

Neutral winds in F region from traveling ionospheric disturbance data, investigating gravity wave hypothesis

16 p2570 A71-20625

Large scale traveling ionospheric disturbances at midlatitudes related to polar substorms on statistical basis

16 p2573 A71-20625

Traveling ionospheric disturbances due to gravity wave interactions during solar eclipse of 7-1970, confirming electron content variations from ATS 3 polarization data

16 p2575 A71-20625

Traveling ionospheric perturbations investigated by vertical sounding with interference method, predicting group path difference measurements as function of frequency and time

19 p3058 A71-20625

Traveling ionospheric disturbances excitation mechanism by passing acoustic gravity waves

23 p3665 A71-20625

TRAVELING WAVE AMPLIFIERS

Solid state traveling wave amplifier using thin type epitaxial GaAs layer

03 p0384 A71-13296

Multisignal characteristics of high power modulated microwave traveling wave tube amplifiers

07 p1080 A71-19499

Unilateral GaAs traveling wave microwave amplifier based on space charge growth in domain-stable

transferred electron semiconductors, considering power, noise, gain and efficiency 11 p1736 A71-25234

TWT amplifiers in radar and communication systems, investigating AM and FM noise theory and reduction 11 p1734 A71-26435

Traveling wave negative resistance amplifier with corrugated surface wave structure, deriving gain equation 14 p2209 A71-29546

Superconducting magnetic systems for traveling wave quantum paramagnetic amplifiers, considering minimum weight maser systems 15 p2376 A71-32275

Output characteristics of three different segmented M-type crossed field TWT amplifiers in large signal operation from field amplitude distribution along interaction space 15 p2378 A71-32628

Gain improvement in TWT parametric amplifiers based on slow space charge waves interaction with slow wave structure field by electron beam modulation 15 p2378 A71-32629

Soviet book on microwave quantum amplifiers covering traveling wave and multicavity masers calculation, design, tests, applications and basic components 17 p2753 A71-34474

Traveling wave tube for reflex type amplifier on-board space communication satellite, discussing prototype reliability and performance 17 p2714 A71-34682

Broadband compensation of HF tunnel diode traveling wave amplifier using separate stages in transmission line 19 p3026 A71-37256

Microwave transistor amplifier dynamic range performance, comparing low noise and high power capabilities with traveling wave tubes 19 p3029 A71-38295

Nonlinear equations for traveling wave amplifiers using transverse wave interaction modes (cyclotron and synchronous electron beam waves), calculating saturation characteristics 20 p3203 A71-39003

Three-frequency parametric traveling wave amplifier amplification and conversion factors calculation by numerical method with allowance for fast and slow space charge wave effects 20 p3206 A71-39812

Distributed tunnel diode traveling wave amplifier load noise thermal and shot components, noting impedance boundaries 20 p3206 A71-39814

TWT off-transmission band area exponentially fading wave effects on electron beam modulation and amplification 22 p3522 A71-42316

End line matching for high gain traveling wave amplifier constructed from heterogeneous transmission line with negative resistance 24 p3810 A71-45262

TRAVELING WAVE MASERS

Nd glass traveling wave laser single frequency emission luminescence stability as function of pumping power, using dispersive ring resonator 07 p1122 A71-19136

Optimal location of nonreciprocal disk shaped YIG element of traveling wave quantum ruby paramagnetic amplifier for weak magnetic field levels 10 p1585 A71-24883

Thermal noise measurement of superconducting coaxial lambda/2 resonator at 2.46 GHz with ruby traveling wave maser and tunnel diode amplifier setup 12 p1887 A71-27010

Radio source 3C 273 observation at 8.2 mm wavelength, using traveling wave maser on radio telescope for tenfold sensitivity improvement 14 p2253 A71-29989

TRAVELING WAVE MODULATION

Optical PCM communications system with lithium tantalate traveling wave modulator capable of one gigabit/sec transmission and detection rate 02 p0215 A71-12042

Traveling wave phototube for demodulating pulse amplitude modulated laser emission, investigating equivalent resistance 06 p0900 A71-18184

Single and double pass traveling wave electro-optic light modulator phase retardation transient response calculation 20 p3235 A71-39180

TWT off-transmission band area exponentially fading wave effects on electron beam modulation and amplification 22 p3522 A71-42316

Single mode ruby laser spatiotemporal coherence characteristics with emission moment controlled by Q switch operating on modulated ultrasonic traveling waves 23 p3683 A71-43394

TRAVELING WAVE TUBES

Helical TWT direct wave propagation constants calculation method 01 p0052 A71-10475

TWT and klystron intermodulation reduction by amplitude and phase correction device 02 p0223 A71-12811

TWT microwave amplifier parameters effect on power threshold for electron beam signal control loss 03 p0385 A71-13790

Interelectrode focusing voltage effect on electron beam and tube efficiency in TW and backward wave tubes with electrostatic focusing systems 03 p0385 A71-13793

Current interception in TWT electron beam affecting minimum noise factor level 03 p0386 A71-13803

Traveling wave tubes electric simulation, giving block diagram for circuit model 03 p0386 A71-13806

Nonlinear M-type traveling wave tube equations for large signal mode, discussing electron precipitation 04 p0556 A71-14623

Solid state transferred electron broadband amplifiers in electronic countermeasure memory systems for radar pulse replica retransmission, comparing with low noise traveling wave tubes 04 p0558 A71-15361

Cylindrical electromagnetic wave amplification in TWT with radial line and diverging electron flux 05 p0727 A71-16003

TWT noise level minimization in 8 mm band with circular spiral slow wave structure and five electrode gun 05 p0723 A71-16874

Microwave devices with transmission lines excited by curvilinear electron beams, deriving dispersion equations for TWT with allowance for space charge effect 10 p1584 A71-24717

Hybrid M-type microwave oscillators including backward and traveling wave tubes with crossed fields in large amplitude mode, considering power efficiency and frequency control 12 p1888 A71-27620

Traveling wave tube magnetic field focusing and accelerating voltage effects on power output 12 p1889 A71-27627

Optical and microwave multifrequency autooscillatory drift and reflex klystrons, TWT and electronic oscillators, comparing to He-Ne lasers 14 p2211 A71-30091

Ceramic rod supported helix derived traveling wave tubes, considering titanium carbide for internal attenuators due to zero temperature coefficient of resistivity 14 p2214 A71-30702

Hysteresis loop measurements and functional measurements correlation on periodic permanent magnet stacks of TWT ring magnets of Sm-Co alloy 14 p2285 A71-30705

Miniature 20-watt CW TWT with samarium cobalt focusing magnets for fitting X-band waveguide, comparing performance, size and weight with conventional design 15 p2375 A71-31206

Millimeter broadband high power traveling wave transmitter tubes with stub voltage tuning for ground stations of satellite communication systems 16 p2545 A71-32975

Low noise TWT amplifiers, performance, reliability and cost reduction 17 p2714 A71-34605

Traveling wave tube for reflex type amplifier on-board space communication satellite, discussing prototype reliability and performance 17 p2714 A71-34682

Nonlinear gain and AM/PM conversion in FDMA communication through satellite repeater, using traveling wave tubes plus postional filter 17 p2703 A71-35082

Traveling wave plasma accelerator, discussing use for spacecraft propulsion 19 p3122 A71-37321

Nonlinear M-type traveling wave tube equations for large signal mode, discussing electron trajectories 22 p3521 A71-42263

TWT off-transmission band area exponentially fading wave effects on electron beam modulation and amplification 22 p3522 A71-42316

Cylindrical electromagnetic wave amplification in TWT with radial line and diverging electron flux 22 p3524 A71-42752

TRAVELING WAVES

Clear air radar structures temperature, wind components and true gust velocities combined with radar data for observed traveling wave features 01 p0030 A71-10560

Hydrodynamic equations for isothermal atmosphere stratified by uniform gravitational field, obtaining traveling wave solutions 04 p0570 A71-15030

Thin single layer orthotropic circular cylindrical shell shear coupled traveling wave reflections, determining stresses in terms of particle velocities 07 p1216 A71-20134

Incompressible equilibrium plasma ellipsoid stability in electromagnetic traveling wave field 08 p1341 A71-21500

Statistical directivity, radiation pattern, drift dispersion of segmented traveling wave antennas 09 p1414 A71-22226

Traveling wave antenna arrays of mismatched elements, calculating element resistances and spacings 09 p1408 A71-23488

Traveling shock waves interaction with orifice inside ducts, noting anomalous phenomena probably due to unsteady boundary layer growth or time lag 10 p1596 A71-24923

Pulsar oblique magnetic rotorator model, noting large amplitude EM traveling wave effects on electron motion 10 p1679 A71-24956

Handbook on radar cross section, Volume 1, covering scattering theory, edge/tip diffraction, creeping/traveling waves and various geometric shapes 11 p1733 A71-26008

Traveling wave propagation, modal vibrations and elastic transmission medium studies from theoretical seismograms for realistic gravitating heterogeneous spherical earth model 11 p1760 A71-26148

Rotation effects on vibration traveling waves in rotating cylindrical shells, considering Coriolis, centrifugal and torque loads [ASME PAPER 71-DE-A] 12 p1977 A71-27316

Plane traveling electromagnetic wave existence, propagation and refraction in nonlinear dispersive nonmagnetic isotropic lossless medium 13 p2027 A71-27899

Simply supported normal mode plate time response to traveling wave at oblique incidence, using numerical analysis 14 p2326 A71-30068

Frequency equations for trains of axisymmetric harmonic waves traveling in infinitely long three layered elastic circular cylindrical shells and rods 14 p2327 A71-30202

Arbitrary gravitational field effects on natural frequencies of rotating ring laser with traveling electromagnetic wave 15 p2421 A71-32408

Incompressible equilibrium plasma ellipsoid stability in electromagnetic traveling wave field 16 p2618 A71-33048

Traveling waves propagation in elastic shell of revolution subjected to bending moment 17 p2833 A71-35618

Modulated electron beam interaction with plasma, showing amplitude growth and traveling wave profile distortion 19 p3114 A71-37856

Traveling wave power resonances in ring laser with nonlinearly absorbing cell, noting role of absorbing component lamb saturation 21 p3394 A71-41257

Vacuum UV traveling wave excitation by high voltage pulse and hydrogen laser technology 23 p3684 A71-43502

Traveling wave laser with confocal, plane and semiconcentric resonators, calculating emission field spatial-temporal structure and inversion distribution 23 p3685 A71-43561

Traveling wave laser emission phase and amplitude fluctuations and spectral line width determination from single-mode distributed parameter model 23 p3685 A71-43563

Sandwich wire traveling wave antenna radiation patterns, obtaining attenuation constant 23 p3654 A71-44157

External, HF, traveling wave field interactions with homogeneous electron plasma longitudinal oscillations under magnetic field 24 p3853 A71-44503

Traveling wave pair interaction with three energy level medium at resonance frequencies, deriving coupled differential equations for amplitude variations 24 p3833 A71-44662

TREADMILLS

Human work level adjustment to specific energy expenditures during hard work on servocontrolled treadmill 02 p0202 A71-11665

Human steady and unsteady state treadmill exercise, comparing cardiac output, heart rate and oxygen uptake interrelationships 09 p1401 A71-23367

Maximal treadmill stress test correlation with postexercise phonocardiogram, ECG and double master test in normal subjects, discussing third and fourth heart sound incidence 15 p2361 A71-32538

Resting and postexercise apexcardiogram correlation with maximal treadmill stress test, noting mean a-wave ratios 21 p3332 A71-40406

TREAT [TEST FACILITY]

U TRANSIENT REACTOR TEST FACILITY
TREES [MATHEMATICS]

Automatic computer program synthesis based on theorem proving approach for construction of recursive and iterative programs operating on natural numbers, lists and trees

10 p1581 A71-23968

Fault tree, failure mode and effect analysis, prediction apportionment and assessment, discussing system effectiveness

16 p2664 A71-33317

Adaptive algorithm designing minimum expected cost test trees for detection and isolation of single faults in systems

19 p3069 A71-38287

Active network analysis by topological formulation, eliminating k-trees

19 p3038 A71-38489

Low speed aerodynamics, detailing relevance tree technological forecasting method of Canadian science council national goals list

22 p3481 A71-42766

TREES [PLANTS]

Direct broadcast television service by satellite transmission, calculating trees and woods effects on attenuation and suggesting receiving system design modification

09 p1408 A71-23384

TREMORS

Stop test method to study acceleration in movement control processes in man, considering elbow joint movements in normal and pathological tremors in Parkinson disease afflicted subjects

19 p3007 A71-37569

Aquanuts tremor response measurement by muscle force transducer during compression and decompression in 520-foot saturation dive, noting differences among individuals

21 p3331 A71-40350

TRENDS

Science and technology trend forecasting for planning, organization and program selection

02 p0335 A71-11852

TRESCA FLOW

Optimal design with geometric constraints for simply supported Tresca plastic disk and cantilever plate under concentrated force

05 p0830 A71-17223

Plastic spherical shell containing cylindrical section under Tresca yield conditions, obtaining upper critical load limits

11 p1850 A71-25943

Load carrying capacity of edge clamped spherical shells of revolution with Tresca yield condition under uniform internal pressure

14 p2332 A71-30848

Strength analysis of shells of revolution and plates under axisymmetrical loads for rigidly plastic material with Tresca yield condition

14 p2332 A71-30849

Small deflection analysis within Cartesian coordinate system applicable to elastic-plastic rectangular plates bending under Tresca yield criterion

16 p2654 A71-33122

TRIANGLES

Cubature formulas for plane triangular domain, giving leading error terms

05 p0726 A71-16958

TRIANGULAR WINGS

U DELTA WINGS

TRIANGULATION

Triangulation position fix techniques employing lines of bearing, n-locus, least square fits and resection by intersection method

02 p0280 A71-12900

Satellite triangulation network adjustment based on simultaneous errors observations, using filtering equations for matrix manipulations reduction

03 p0413 A71-14009

Integrated data processing of stereotriangulation system providing automatic map plotting

08 p1281 A71-21249

Aerial photographic block aerotriangulation error analysis, discussing block configuration, perimeter and vertical controls, premarking, overlapping, etc.

08 p1288 A71-21260

Favorable construction of elementary figures of cosmic triangulation in three dimensional Cartesian coordinates, determining errors

09 p1404 A71-22272

Optimal synchronous plane accuracy for space triangulation as function of geometrical position of artificial satellite relative to earth sphericity

11 p1758 A71-25812

Variation coefficient and corrections to dependent observations for space triangulation leveling by least squares method, comparing closing directions

11 p1759 A71-25815

Satellite geodetic global networks employing triangulation, trilateration and height measurements, deriving dominant point observation stations /Hazay-Tarczy method/

11 p1759 A71-25816

Space triangulation corrections of equatorial topocentric coordinates and radius vector of Jupiter in Baker-Nunn net, using Geos A satellite optical and laser observations

11 p1732 A71-25819

Aerial and block triangulation error analysis accuracy dependence on reference point number, introducing camera internal orientation improvement

13 p2062 A71-28903

Soviet geodetic network construction and compensation, noting triangulation of first and second class in each polygon

15 p2395 A71-31464

Differential refraction elimination in stellar triangulation measurements for reference stars catalog and flash coordinates

16 p2642 A71-33801

Nonlinear compensation for film deformation in aerial photography correcting spatial phototriangulation grids

19 p3063 A71-37270

Base triangle determination by geometric geodesy, using laser telemetry and satellite optical observations with cataphotic reflecting prisms

20 p3220 A71-39661

Stable auroral red and hydrogen arcs simultaneous spectrographic triangulation, noting correlation

20 p3232 A71-39895

Space triangulation and orbital methods of geodetic surveying of earth with satellites, using simultaneous observations from two and three stations

21 p3374 A71-40584

TRIATOMIC MOLECULES

Triatomic molecules relaxation process, considering translational-vibrational energy exchange in atomic collisions and transition probabilities for carbon dioxide-helium system

08 p1337 A71-20669

Triatomic hydrogen positive ion surface crossing effects in chemical reactions based on potential energy surfaces calculation using diatomics-in-molecules approach

14 p2191 A71-30573

Helium plasma afterglow at low temperatures, describing triatomic ion recombination and dissociation

15 p2460 A71-32730

Helium plasma afterglow at low temperatures, describing triatomic ion recombination and dissociation

23 p3710 A71-43301

TRIAxIAL STRESSES

Welded joints triaxial residual stress measurement by scanner

03 p0433 A71-14587

TRIAxIALITY

U TRIAXIAL STRESSES

TRICHLORIDES

U CHLORIDES

TRIDENT AIRCRAFT

U DH 121 AIRCRAFT

TRIGGER CIRCUITS

High acceleration resistant electronic trigger fuse for in-flight gun launched projectile payloads ignition and ejection

[AIAA PAPER 70-1389] 03 p0468 A71-13671

Imploding wire trigger technique for high shock velocity electric arc drivers in shock tubes

04 p0564 A71-14671

Photodetector triggered single pulse selection from mode locked ruby laser

04 p0608 A71-15595

Tunnel diode trigger circuit, calculating effect of junction capacitance variation and small inductance on switching time

05 p0730 A71-17082

Temporary nonlinear feedback effect on stability of triggering potential and output pulse repetition rate of transistor self relaxing blocking oscillator

09 p1424 A71-23169

Laser triggered switching, discussing ability to trigger high voltage spark gaps with nsec delay and subnsec jitter

11 p1775 A71-26083

Tunnel diode driven multivibrator, noting triggering signal amplitude and duration effects on output pulse width

11 p1740 A71-26550

Laser triggered switching, considering theory of laser induced voltage breakdown of gas filled spark gap

12 p1915 A71-27283

Preliminary circuit-stage alignment procedures in multistage triggers manufacture with counter input based on tunnel diodes and transistors

14 p2213 A71-30632

High speed pulse response and power-delay product of planar Gunn diodes, noting delay time and power delay product

14 p2215 A71-30834

Transistorized trigger generator with improved commutation, using inductor circuit limiting collector voltage front durations

15 p2375 A71-31234

Perturbation free delay time measurement in digital data processing system, using Schmitt triggers or tunnel diode discriminators

18 p2885 A71-36222

Harmonic extraction from high power efficient avalanche diodes, discussing circuit in terms of multiple reflection triggering process

18 p2895 A71-36985

Intercavity scanning for mode selection of carbon dioxide laser in transversely degenerate resonator by localized electron-beam-trigger excitation

23 p3687 A71-44111

TRIGGERS

U ACTUATORS

TRIGONOMETRIC FUNCTIONS

NT SINE SERIES

Periodicity solutions of Whittaker-Hill equation; trigonometric series form by three term recurrence relations

03 p0450 A71-13322

Periodic orbits representation in trigonometric series with numerical coefficients and truncation for applications

04 p0654 A71-15172

Rectangular plate bending with mixed boundary conditions, using paired trigonometric series

06 p1005 A71-18702

Mean periodic exponential functions with certain trigonometric properties, proving summation and equiconvergence theorems

08 p1325 A71-22010

Approximate trigonometric solution to the inelastic boundary value problem of plane with doubly periodic system of holes, deriving unsteady temperature and thermostress fields

10 p1687 A71-24158

Rectangular plate bending elements displacement functions representation by trigonometric expressions, using finite element method

13 p2147 A71-27757

Viscous fluid flow past circular cylinder, using trigonometric representation of vorticity based on truncated Stokes-Picard and Oseen-Picard methods

18 p2844 A71-36312

Exponential continually discrete analytic function of complex variable in explicit form, obtaining addition theorem for trigonometric functions

19 p3089 A71-38411

TRIM [BALANCE]

U AERODYNAMIC BALANCE

TRIMETHYL COMPOUNDS

Mass spectral properties of alkoxy-cyclohexan-trimethylsilyl ethers and alkoxy-cyclohexyl trimethylsilanes, using deuterium labeling

02 p0209 A71-12572

Esters synthesis from cyclic trimethylolpropane butyral and monobasic saturated acids mixtures

15 p2438 A71-31672

Thermal stability and oxidation and corrosion resistance of lubricating oil based on trimethyl propyl ester

18 p2939 A71-36010

Bound sugar content in marine sediments by capillary gas chromatographic-mass spectrometric analysis of trimethylsilyl derivatives

19 p3055 A71-38141

Low pressure trimethylaluminum vapor and oxygen flat diffusion flame structure, observing separation formation and growth

19 p3121 A71-38255

TRINITROTOLUENE

Critique of paper on explosive hazards of large solid rocket motors, suggesting extrapolation of fraction TNT equivalent

18 p2955 A71-36281

TRIODES

P-channel MOSFET tetrodes static and dynamic characteristics compared to conventional MOS triodes considering transfer and gate threshold voltage

02 p2229 A71-11856

Time-pulse converter for semiconductor triodes D.C. amplification factor measurement

02 p0230 A71-11832

Conversion losses as function of signal power and circuit impedance in narrow band triode frequency converter

19 p3022 A71-38450

Frequency and power limits of field effect triodes noting application to gridistor for millimeter waves

23 p3653 A71-43959

TRIPLET EXCITATION

U ATOMIC ENERGY LEVELS

TRIPLET STATE

U ATOMIC ENERGY LEVELS

TRIPROPELLANTS

U LIQUID ROCKET PROPELLANTS

TRITIUM

Tritium and He-3 nuclei measurements in Al target from Soyuz spacecraft observation

08 p1354 A71-21022

Net fusion energy from laser heated deuterium-tritium particles dependent on plasma temperature, electrical energy and electron-ion thermalization through collisions

11 p1805 A71-25794

- Tritiated thymidine effects on splenic lymphocytes regeneration, discussing DNA synthesis, cycle completion and resident populations 11 p1719 A71-26055
- Soyuz observation of tritium and He-3 nuclei in Al targets exposed to space radiation 20 p3280 A71-39601
- Vacuum package with Ti bulk sublimator/ion pump combination for 150 kv neutron generator tritium decontamination 21 p3414 A71-40900
- D-T plasma cumulation laser heating problem, considering similarity theory for electron conductivity and bremsstrahlung 21 p3395 A71-41360
- Expanding D-T plasma laser heating equations derivation, allowing for heat produced by associated thermonuclear fusion 23 p3710 A71-43320
- Tritium activity measurement in Apollo 11 fines, breccia and crystalline rock, comparing with meteoritic values 23 p3755 A71-43735
- Radioactive rare gases and tritium in Apollo 12 lunar rocks and in sample return container, noting relationship to solar flare event 23 p3755 A71-43736
- Tritium and argon radioactivities and depth variations in Apollo 12 rocks, discussing solar flare and cosmic ray exposure ages 23 p3755 A71-43737
- TROCHIDS**
U PIVOTS
TROILITE
Troilite rich Ni-Fe particle /mini-moon/ from lunar surface, discussing different theories of origin 07 p1196 A71-19543
- Opaque mineral compositions in Apollo 12 lunar rocks, noting ilmenite, spinels, native iron and troilite 23 p3739 A71-43620
- TROJAN ORBITS**
Trojan periodic orbits interpretation to establish manifolds evolution for mass ratio variations 04 p0652 A71-15702
- Elliptic restricted problem periodic Trojan librations about equilateral points, analyzing stability 04 p0652 A71-15704
- Trojan asteroid planar motion considered within restricted circular three body problem framework, discussing singularities 04 p0655 A71-15722
- TROPICAL METEOROLOGY**
Dynamics of tropical disturbances on Intertropical Convergence Zone /ITCZ/, using model covering entire hemisphere 01 p0120 A71-10856
- Equatorial ring current asymmetry and change during magnetic storms studied by DR indices 08 p1279 A71-21212
- Equatorial region stratospheric and upper tropospheric circulation, examining relationships between time variations of winds at both levels 08 p1327 A71-21455
- Atmospheric wave dynamics in equatorial region, obtaining approximate solution with Coriolis force within perturbation theory 11 p1795 A71-25921
- Spectral statistics of seasonal tropospheric wave disturbances in tropical Western Pacific, observing synoptic and planetary scale wind field 21 p3374 A71-41177
- Vertical equatorial ozone distribution, incorporating oxygen hydrogen reactions and diffuse and advective transport in time dependent meridional model 23 p3673 A71-43987
- TROPICAL REGIONS**
Tropics role in global circulation from satellite photography, discussing convection, cloud clusters, momentum fluxes, etc 01 p0121 A71-11356
- C, N and O nuclei abundances in radiation belt near geometric equator, using data obtained by OGO-5 satellite in 1968 03 p0473 A71-13475
- Triplet O I excitation in night sky of tropical regions, using photometric measurements of line spectra 03 p0409 A71-13789
- VLF emissions at low latitudes by transverse and longitudinal resonance electron energies calculations 05 p0721 A71-16441
- Ionspheric transmission model vs current model for examination of low latitude geomagnetic pulsation origin 05 p0743 A71-17002
- Equatorial zone daytime F 2 maximum height diurnal variation latitude change with decreasing solar activity from vertical sounding 07 p1100 A71-19401
- Equatorial electric field generation by ionsphere dynamo region neutral wind meridional component 07 p1101 A71-19409
- Ionspheric low energy electron and proton fluxes near equator from Isis 1 satellite soft particle spectrometer observations, considering energy spectra and pitch angle distribution 07 p1187 A71-19679
- Multiple magnetopause crossings in equatorial plane by OGO 5, showing magnetopause motion composed of two oscillations 08 p1282 A71-21631
- Latent heat convective transport from lower to tropical upper troposphere, noting periodic energy fluctuations from time lapse synchronous satellite cloud photographs 09 p1489 A71-23553
- Low latitude DS ionspheric current component and auroral electrojet intensity for intense geomagnetic storms, considering particle observations by ATS 5 synchronous satellite 10 p1605 A71-24790
- Daytime lower ionosphere electron density profiles over equator, using rocket-borne Langmuir and plasma noise probes 10 p1606 A71-24913
- Riser whistlers observed at low latitude ground station, noting time delay increase with frequency 10 p1579 A71-25009
- VLF propagation in low latitude ionosphere from FR-1 satellite observations, obtaining electron density model of equatorial anomaly 11 p1755 A71-25642
- Three dimensional quasi-stationary problem of local winds in neutrally stratified atmosphere in low latitudes, analyzing Coriolis force role 13 p2096 A71-28016
- Nonzonal atmospheric motion effects on meteorological elements 26-month oscillations stability in equatorial zone from linear hydrothermodynamic equations 13 p2057 A71-28022
- Microbiological contamination of jet aircraft fuel tanks in tropical regions, considering maintenance [SAE PAPER 710438] 13 p1996 A71-28320
- Quasi-biennial oscillation in low latitude geomagnetic Sq field, showing larger amplitude under equatorial electrojet by harmonic analysis 14 p2231 A71-29719
- Faraday rotation of Transit 4A satellite signals recorded at three stations within Southeast Asian equatorial zone, showing latitudinal variation of ionspheric electron content at sunspot minimum 14 p2235 A71-30249
- Nimbus 4 Interrogation Recording and Location System meteorological experiment for tropical region upper atmosphere information 14 p2200 A71-30917
- Earth gravitational field anomalies relation to atmospheric circulation and tropical perturbations 15 p2443 A71-31223
- Equatorial electrojet as supplementary heat source for tropical region upper atmosphere based on thermal energy release calculation 15 p2399 A71-31964
- Proton measurements in ring current by OGO-3 satellite compared with geomagnetic field data at low and high latitudes 16 p2626 A71-33663
- Mass spectroscopy of upper atmosphere neutral composition at equatorial, middle and polar latitudes from meteorological rockets 16 p2566 A71-33758
- Low and midlatitude ionspheric motion determination using barium ion cloud release technique 16 p2570 A71-33827
- Solar particle flux profile and low latitude cut-off observation by low altitude satellite during March 1969 to July 1970 events 16 p2628 A71-33936
- Three level baroclinic model of short range large scale weather prediction at low latitudes, determining background /steering flow/ in tropical disturbances 17 p2769 A71-34300
- Low latitude topside plasma temperature, electron content and ion production/loss rates during sunspot minimum to maximum 17 p2731 A71-34316
- Atmospheric ozone data in tropical regions from Nimbus 3 IR interferometer spectrometer measurements, indicating easterly jet stream existence during summer monsoon period 17 p2771 A71-35810
- Equatorial zone daytime F 2 maximum height diurnal variation latitude change with decreasing solar activity from vertical sounding 19 p3053 A71-37825
- Equatorial electric field generation by ionsphere dynamo region neutral wind meridional component 19 p3053 A71-37833
- Quiet sun diurnal variations of intertropical F 2 ionization in true heights over Tamanrasset meridian 19 p3054 A71-37863
- Tropical cumulus clouds seeding experiments with silver iodide smoke, discussing cloud growth and precipitation increase 19 p3093 A71-38693
- Circadian rhythms of human renal excretions in polar, temperate and equatorial regions 20 p3190 A71-39477
- Equatorial ionspheric density measurements on quiet and perturbed days, using San Marco 2 satellite balance 21 p3373 A71-40047
- Low latitude whistler propagation characteristics associated with magnetic storms in March 1970 at Sugadaira /Japan/ 23 p3644 A71-43364
- Equatorial convective cloud mesosystems formation from Apollo 6 data, investigating Hadley circulation energy generation 23 p3701 A71-44011
- TROPICAL STORMS**
NT HURRICANES
Dynamics of tropical disturbances on Intertropical Convergence Zone /ITCZ/, using model covering entire hemisphere 01 p0120 A71-10856
- Tropical storms and cyclones development numerical simulation with ten-level model, considering radiational cooling and physical parameters effects 03 p0453 A71-14202
- Conditional instability of second kind /CISK/ in three dimensional quasi-geostrophic low latitude flow, examining Yamasaki model 09 p1490 A71-23561
- TROPICS**
U TROPICAL REGIONS
TROPISM
NT GEOTROPISM
NT GYROTROPISM
Plants behavioral reactions to continuous gravitational field directional reorientation by clinostat, discussing gravity compensation effects on tropism and forces required for geotropic response 21 p3341 A71-40004
- Pinto beans circadian leaf movements in simulated weightless environment, relating rotational treatment time to rhythm phase 21 p3341 A71-40006
- TROPOPAUSE**
Computer estimation of correctness of tropopause determination from singular points based on criteria from global meteorological network 06 p0922 A71-17505
- Carbon dioxide concentrations in tropopause, investigating flux from northern troposphere into stratosphere 13 p2063 A71-29112
- Atmospheric models of partially trapped waves propagation in layer above tropopause with large stratospheric Scorer parameter 14 p2268 A71-29763
- Venusian polar tropopause and cloud layer from IR spectral recording in carbon dioxide band near inferior conjunction for crescent regions 20 p3290 A71-39306
- TROPOSPHERE**
Nitrous oxide tropospheric abundance from IR solar spectrum altitude variation 01 p0073 A71-10139
- EM pulse distortion in resonant and nonresonant gases, discussing applications to homogeneous tropospheric propagation 01 p0040 A71-11608
- Long wave radiation fluxes calculation in troposphere based on principal radiant heat transfer components separation 02 p0277 A71-12117
- Ionspheric and tropospheric effects on differential phase path in very long baseline interferometry, using ray tracing computer program 02 p0251 A71-12331
- Tropospheric positive and negative ions mobility distribution measurement from converging channel chamber data 02 p0247 A71-12849
- Troposphere and stratosphere mean annual carbon dioxide cycle measurements, describing aircraft collection equipment and procedure 03 p0418 A71-14205
- Tropospheric diffraction fields computation in atmospheres with modified refractive index increasing monotonically with height, discussing IF and LF ground wave propagation 04 p0552 A71-15020
- German monograph on ozone recording device and temporal and spatial variations of tropospheric ozone in Northern Hemisphere 04 p0582 A71-15100
- Wind foot cirrus cloud pattern relationship to tropospheric jet streams based on high resolution satellite color photographs 04 p0621 A71-15275
- Troposphere and stratosphere electric field above Atlantic Ocean, investigating electrode effect role in atmospheric circuit 05 p0738 A71-16220
- Tropospheric and stratospheric turbulence, discussing energy sources and sinks and energy spectra pattern at different atmospheric conditions 05 p0741 A71-16625
- Lidar observations of visually clear troposphere compared with simultaneous rawinsonde data for relationship between lidar echoes and atmospheric winds aloft 05 p0721 A71-16670

Field amplitude distribution parameter in long distance tropospheric communications based on fading depth

05 p0722 A71-16866

Upper troposphere and lower stratosphere geopotential field short range forecast quasi-geostrophic model

06 p0889 A71-17516

Upper troposphere-lower stratosphere planetary scale circulation correlation from kinetic energy characteristics analysis

07 p1151 A71-18874

Tropospheric and lower stratospheric radiation balance components vertical profiles, using balloon sounding

07 p1151 A71-18913

Troposphere effects on radio wave propagation and satellite communication

07 p1059 A71-19010

Mesoscale relative diffusion estimates in low troposphere from tetron /constant volume balloon/ flights at Nevada Test Site

08 p1326 A71-21449

Equatorial region stratospheric and upper tropospheric circulation, examining relationships between time variations of winds at both levels

08 p1327 A71-21455

Long range tropospheric radio wave propagation, calculating signal impulse function and time lag between diffraction and reflection

09 p1404 A71-22217

Latent heat convective transport from lower to tropical upper troposphere, noting periodic energy fluctuations from time lapse synchronous satellite cloud photographs

09 p1489 A71-23553

Tropospheric temperature and aerosol/molecule ratio determination by optical radar measurements, using Doppler broadening in spectral analysis of laser radar echoes

09 p1466 A71-23628

Diurnal variations of meridional winds by dynamo electric field in troposphere, comparing with Thomson scattering

09 p1490 A71-23646

Convective heat flow simulation in lower troposphere, using water-heated plate model and shadowgraph photography

10 p1638 A71-23879

Tropospheric ionization mechanism for gas to particle condensation embryos existence, using positive and negative ions ground level and altitude profile

10 p1604 A71-24704

Sensible heat meridional transport frequency spectra wavenumber in Southern Hemisphere midtroposphere

13 p2063 A71-29108

Angular momentum meridional transport flux wave number-frequency spectral characteristics in mid-troposphere of Southern Hemisphere

13 p2063 A71-29109

Radio waves tropospheric refraction based on far field of vertical electrical dipole on impedance sphere

14 p2191 A71-29510

Equatorial upper troposphere and lower stratosphere hurricane and wavelike motions numerical predictions, analyzing heating, friction, cloud physics and ozone dynamics

14 p2270 A71-30500

Soviet papers on processes in upper layers of atmosphere covering troposphere, stratosphere and mesosphere over Northern and Southern Hemispheres

15 p2399 A71-31961

Radioactive impurities transfer from lower stratosphere into upper troposphere based on vertical air transport data

15 p2400 A71-31970

Tropospheric range error in EM signal arriving at earth zenith, measuring integral of refractivity through atmosphere from height, pressure, temperature and humidity

16 p2569 A71-33800

Lidar soundings of troposphere, investigating multilayer echo structure of haze layers, clouds and rainstorms

17 p2770 A71-34706

Tropospheric stratification structure from high resolution FM/CW radar sounder, comparing with internal gravity wave atmospheric models

17 p2771 A71-35808

Atmospheric structure near large amplitude Kelvin-Helmholtz billows in upper troposphere, deriving static stability, vertical wind shear and Richardson number

19 p3089 A71-37498

Physical interpretation of electromagnetic waves at attenuation function HF singularity during diffraction over spherical surface, applying to short wave diffraction in tropospheric model

20 p3198 A71-39802

Synoptic climatology of blocking situations over European-Atlantic region, obtaining middle troposphere circulation patterns by statistical analysis

21 p3411 A71-40826

Laser remote sensing technique for tropospheric refractivity fluctuation profile measurement with tethered balloon-borne retroreflector tracking by ground based tracker

21 p3374 A71-40977

Soviet monograph on radio wave propagation in fluctuating parameters media covering ionosphere /fluctuating electron concentration/ and troposphere /fluctuating inhomogeneities and refractive index values/

21 p3349 A71-41372

Temperature pulsation measurements by high altitude aircraft in presence of lower troposphere convection elements

21 p3412 A71-41389

Correlation functions characteristics of wind velocity field in troposphere and stratosphere up to 25 km based on bihourly radiosonde data

21 p3412 A71-41390

Size distribution and concentration of magnetic spherules in troposphere from electron and optical microscopy

23 p3665 A71-42965

TROPOSPHERIC SCATTERING

Long range troposcatter, evaluating antenna directivity effects on signal fading rate and fluctuation

01 p0037 A71-11087

Tropospheric layers radio reflectivity as function of refractivity index and thickness/wavelength ratio

01 p0040 A71-11607

Radiometeorological measurements of atmospheric structure, using SHF troposcatter synchronously off-set beams on great circle propagation path

04 p0584 A71-15545

Data transmission via FDM/FM troposcatter channels, predicting system performance in error rate terms

05 p0723 A71-17052

Path intermodulation data distortion derivation from noise power ratio measurements over five tropospheric scatter paths during system acceptance tests

05 p0723 A71-17055

Tropospheric height integral of refractivity for predicting atmospheric electromagnetic range at arbitrary elevation angle from surface weather data

08 p1257 A71-21881

ATC station ground to air communication via VHF tropospheric scatter, discussing high power radio transmitters and low noise over the horizon receivers combination

10 p1576 A71-24175

Synthetic aperture Doppler free coherent bistatic radar for high resolution maps of tropospheric radio scatterers

12 p1881 A71-27286

Multichannel modular tropospheric scatter equipment as economic solution for medium range HF communication

13 p2034 A71-29317

Low elevation angle tropospheric fading relationship to satellite communications and broadcasting at frequencies between 1 and 20 GHz

17 p2703 A71-35083

Tropospheric refraction effects and field strength dependence on height at frequencies below 10 MHz

19 p3017 A71-37862

Stochastic passband model of tropospheric communications channel, denoting random frequency duration above threshold level

19 p3022 A71-38501

Time resolved tropospheric scatter layers from simultaneous bistatic and monostatic radar detection

23 p3646 A71-44174

TROPOSPHERIC WAVES

Infrasonic shock wave generation in troposphere by powerful earthquakes, causing upper atmosphere density rise due to heating

08 p1278 A71-21019

Energy flux of tropospheric mesoscale waves and heat influx into upper mesosphere caused by energy absorption, discussing wavelength and latitude effects

12 p1924 A71-26735

Infrasonic shock wave generation in troposphere by powerful earthquakes, causing upper atmosphere density rise due to heating

20 p3219 A71-39599

Spectral statistics of seasonal tropospheric wave disturbances in tropical Western Pacific, observing synoptic and planetary scale wind field

21 p3374 A71-41177

Receiving and transmitting antennas directional gain effect on microwave long range tropospheric propagation

23 p3644 A71-43289

TROUBLESHOOTING

U MAINTENANCE

TRUNCATION [MATHEMATICS]

U APPROXIMATION

TRUNCATION ERRORS

Bits round-off and approximate division error effects in data compressor design, suggesting best maximum error criteria

01 p0050 A71-10878

Long term atmospheric circulation prediction model, considering horizontal grid resolution effect of truncation error

14 p2269 A71-29906

Finite difference technique for convective flow equations involving shock wave propagation, discussing heuristic analysis for truncation error

18 p2907 A71-36352

Numerical power series integration of differential equations of special three body problem with truncation errors elimination to fifth order

21 p3450 A71-40496

Error evaluation for incomplete gamma function calculated by truncated asymptotic series

21 p3408 A71-40895

TRUNKS [LINES]

U TRANSMISSION LINES

TRUNNIONS

U SHAFTS [MACHINE ELEMENTS]

TRUSSES

Truss systems optimal structural design, noting elastic-plastic stability conditions

03 p0509 A71-13894

Nonlinear analysis of cable and truss structures using computerized stiffness matrix method

08 p1367 A71-20740

Stability analysis of rigid frames and trusses, including effect of bending moments and shear forces before buckling

12 p1976 A71-27164

Computerized minimum weight design of elastic redundant trusses under multiple static loads, using algorithms for generating upper and lower bounds for configuration

12 p1980 A71-27400

Geometrical parameters of stringer nodes in statically determinate minimum weight equal stress and strength trusses

13 p2154 A71-28642

Optimal structural design of minimum weight trusses and beam cross sections for given load using computerized nonlinear programming method

14 p2321 A71-29544

Snap-through buckling of three hinged deep trusses and wire restrained column under critical quasi-static loading based on elastica theory of prismatic bars

17 p2815 A71-34295

German monograph on plane, arbitrarily curved and bending resistant trusses calculations allowing for elastic and plastic deformation

17 p2823 A71-34800

Minimum weight design of statically determinate elastic truss under multiple stress and displacement constraints, using virtual work of dummy loads

18 p2982 A71-36840

Elastic trusses optimal design under multiple mechanical constraint conditions, describing steepest descent method with constraint error compensation

21 p3470 A71-41022

Bar forces in statically determinate planar truss due to arbitrary loads at joints, describing computer program for sequential solution

22 p3517 A71-41869

Material random temperature and imperfection density effects on 3-bar truss nonlinear steady creep solutions for stress and velocity

22 p3615 A71-42210

TRYPTAMINES

Pyridoxine and serotonin metabolism changes and vestibular disorders observation in space flight

16 p2532 A71-33677

Prolonged hypokinesia effect on rats serotonin /5-HT/ metabolism, noting pronounced blood content deviation from normal during first to third and thirteenth to fifteenth day

20 p3187 A71-39218

Serotonin and gamma-aminobutyric acid loss and interaction in rat midbrain slices incubated in media containing Na, K and Ca ions

21 p3338 A71-41079

Serotonin /5-oxytryptamine/ extraction from rat whole blood in series analysis, using acidic butanol instead of ordinary butanol

24 p3801 A71-44541

TRYPTOPHAN

Brain polysomes disaggregation and tryptophan elevation in immature rats and adult animals after L-dopa administration

20 p3186 A71-38979

TSR-2 AIRCRAFT

Terrain-following radar for TSR-2 aircraft, discussing reliability trials and improvement

07 p1062 A71-19557

TU-134 AIRCRAFT

D-30 bypass engine hydraulic control system for Tu-134 aircraft, discussing fuel flow regulator assembly and operation

09 p1511 A71-22947

TU-144 AIRCRAFT

TU-144-Concorde differences, discussing design philosophy engine mounting and thrust, wing span and profiles, gross weight, fuselage cross sections landing gear, droop nose, etc

15 p2349 A71-31873

UBE ANODES

Plasma anode tube in metal-ceramic envelope with improved capabilities for electron emission studies, considering movable Langmuir probe
11 p1806 A71-25902

UBE CATHODES

COLD CATHODE TUBES
COLD CATHODES
HOT CATHODES
PHOTOCATHODES
PHOTOMULTIPLIER TUBES
THERMIONIC CATHODES

UBE GRIDS

Facility backspattered material effect on performance of glass-coated accelerator grids for Kaufman electron bombardment thrusters
[AIAA PAPER 71-156] 06 p0947 A71-18598

UBE HEAT EXCHANGERS

Temperature and pressure discontinuity stresses in compact heat exchangers, considering tubes as elastic foundation underneath tube plate
08 p1374 A71-22034

Heat exchanger circular rigid tube sheets calculation by thin plates bending theory, using stepped profile circular plates stress analysis
08 p1374 A71-22053

Liquid Na heat exchanger fabrication, using electron beam welding technique for stainless steel components assembly
11 p1768 A71-25390

Heat transfer surfaces performance measurements, considering tube bundles with fluid flow perpendicular to tube generatrices
[HEAT EXCH. CONF. PAPER 25] 15 p2383 A71-31639

Heat transfer and hydraulic resistance in cross flow heat exchanger with slitlike channels
17 p2836 A71-34212

Surface renewal and penetration heat transfer model for turbulent flow in smooth and rough tubes
18 p2986 A71-36593

UBERCULOSIS

Chromosome mapping of Pasteurella pseudotuberculosis by interrupted mating, indicating chromosome transfer in more than one linkage group
09 p1396 A71-23474

UBES

Nonlinear quadratic elasticity theory of isotropic tube and hollow sphere under small linear deformations, obtaining stress-strain relation
02 p0326 A71-12294

Tubular compression members, examining residual stress profile effects on strength reduction
08 p1370 A71-21411

Finite element for torsion of thin walled open tubes, applying to matrix force analysis
12 p1974 A71-26871

Structural stability in tension and strength tests of thin walled tubes at various stress and strain intensities based on loss of resistance to plastic deformation
14 p2321 A71-29620

Thin hyperelastic tube forced large amplitude radial oscillations, deriving exact solution for general forcing function
14 p2322 A71-29690

Thin walled tubes under external and internal pressures axial loads and torques, showing load capacity limit dependence
15 p2428 A71-31860

Stress distribution in plates and tubes bonded by stepped joints, assuming generalized plane stress
17 p2824 A71-34814

German monograph on free convective heat transfer from heated tubes in air in presence of bounding walls parallel to tube axis
20 p3311 A71-39043

UBING

U PIPES [TUBES]

UMBLING MOTION

Vibrational tumbling effects on steel compressor blades surface roughness, cold hardening, residual stresses and fatigue strength
08 p1295 A71-20842

Axial compressor blades surface finish and fatigue strength restoration by vibrational tumbling
08 p1295 A71-20843

Tumbling triaxial satellite in elliptical orbit about spherical planet, determining resonant and nonresonant gravity gradient perturbations
13 p2145 A71-28356

Vibrotumbling duration effects on surface quality, fatigue resistance and damping properties of titanium alloy structural parts
17 p2760 A71-35665

Transient performance of phase locked loop on-board tumbling satellite, noting relation to time, SNR and fade modulation
20 p3196 A71-38871

Docking with passive orbiting spinning or tumbling objects for space debris elimination and space rescue operations, describing remotely controlled despinning and retrieval methods
22 p3610 A71-42005

UMORS

NT CANCER

NT LEUKEMIAS

Long term hypoxia effects on granuloma and various organs in rats, noting collagen and noncollagenous proteins formation stimulation and/or inhibition
05 p0706 A71-16293

Radiosensitizers indanetrione, menadione Synkavit and N-ethylmaleimide, noting effects on murine ascitic tumor
07 p1035 A71-18950

Polycation effect on tumor cells, describing growth rate inhibitions, X ray sensitivity and DNA interference
07 p1035 A71-18951

L-erythro-alpha, beta-dihydroxybutyraldehyde radiosensitizing effect on adrenocarcinoma Ehrlich ascites tumor cells
07 p1035 A71-18952

Mouse Ehrlich ascites tumor cells, examining Co-60 gamma ray influence in presence of radiosensitizing 5,8-dihydroxypsoralen
07 p1035 A71-18953

Radioprotective drugs relationship to modification of glycolysis in Ehrlich ascites tumor cells
07 p1035 A71-18954

Methylhydrazine radiosensitization of Ehrlich ascites tumor cells, investigating X radiation enhanced cell killing effect via deoxyribonucleic acid strand breakage
07 p1035 A71-18955

Ehrlich ascites tumor cell membrane potassium and electrophoretic mobility loss, investigating radiation effects under radiosensitizing and radioprotecting drugs
07 p1036 A71-18956

Radiosensitizing effect of iodine compounds in dilute solution on Ehrlich ascites tumor cells and SH enzymes
07 p1036 A71-18957

Tumor DNA increase of halogenated pyrimidines incorporation compared to normal tissue DNA, discussing infraarterial infusion of radiosensitizing agents
07 p1040 A71-18989

Bromouridine as radiosensitizing agent improving effectiveness of radiation therapy of malignant brain tumor cells
07 p1040 A71-18990

TUNERS

NT WAVEGUIDE TUNERS

TUNGSTEN

Tungsten plasma coatings on steel, examining shear strength dependence on vaporization distance, microstructure and residual stresses
01 p0088 A71-10788

Tungsten exploding wires electron emission during vacuum melting
02 p0284 A71-11881

Tungsten cathode current partitioning in dense Ar plasma, noting electron emitter work function reduction due to ion space charge field
02 p0289 A71-11940

Ceramic fibers formation by particles mechanical deformation by extrusion in W matrix, describing grain structure of various extruded metal oxides
02 p0273 A71-12149

Langmuir S curves for W /110/-Cs and Mo /100/-Sr adsorption determined by thermionic electron emission microscope, noting minimum work function
02 p0295 A71-12203

Electropolished and single crystal surface effects on work function of macroscopic tungsten emitter in cesiated converter
02 p0295 A71-12204

Single crystal facet angles and surface energy planes by light reflection for W emitter in vacuum, Cs and iodine
02 p0251 A71-12208

High work function stable faceted W thermionic emitter surface preparation by electroetching and vapor deposition
02 p0295 A71-12209

Crystal surface orientation of chemical vapor deposited W thermionic emitter by hydrogen reduction of hexafluoride, using etch pits and X ray diffraction
02 p0295 A71-12211

Thermionic converter with single crystal 110 W emitter surfaces and Nb collector, measuring I-V performance
02 p0193 A71-12212

Thermionic converter tests, discussing W emitter with Nb and Mo-on-Nb collectors, surface and electrode combinations
02 p0193 A71-12214

Performance tests of identical cylindrical thermionic converters with W emitters and Nb collectors, using X ray diffraction and work function measurements
02 p0193 A71-12217

Long term stability and post test analysis of vapor deposited W emitters in high performance cylindrical thermionic converters
02 p0193 A71-12218

Thermionic stability life tests of cylindrical diodes with W emitters at constant current and optimal Cs and collector temperatures
02 p0194 A71-12222

Vapor deposited W impurities effect on crystal structure and preferred orientation, considering work function increase
02 p0296 A71-12241

W, W-Re and Re-Mo creep rupture properties investigation for selection of optimum materials for isotope containment for thermionic capsules
02 p0195 A71-12254

W and W-Mo alloy creep properties during interaction with low pressure oxygen, simulating cladding-oxide fuel interaction in thermionic device
02 p0264 A71-12257

Desorption and migration of Cs adsorbed on W surface under electric field, using field emission microscope
02 p0296 A71-12340

Sintered W rolling in vacuum over reduction and temperature ranges
02 p0256 A71-12514

W and thoriated W grain boundaries topography by trace analysis and field evaporation, observing curved surface with ledges, protrusions and serrations
02 p0266 A71-12737

Doped W wire core porosity and anomalous recrystallization behavior microstructural observation by electron microscopy
02 p0268 A71-12890

Multiproperty apparatus for high temperature determination of tungsten thermal properties, using direct electrical heating methods
04 p0595 A71-14967

Thermal conductivity and emittance of arc cast and powdered W at 1800-2800 K
04 p0612 A71-15579

Tungsten, molybdenum and rhenium single crystals hemispherical emissivity at high temperatures by electron beam heating, considering grain boundary contribution
04 p0613 A71-15581

Nitrogen diffusion and solubility in W, deriving expression for permeation constant
04 p0614 A71-15784

Tungsten wire reinforced brass composites, studying multiple necking phenomena during tensile tests
04 p0615 A71-15794

Doped tungsten high temperature behavior, discussing hypotheses regarding doping agents microstructural effects
05 p0767 A71-16599

Pure W monochromatic emissivity measurements at 0.4 to 4 microns and at high temperatures
05 p0767 A71-16600

Ti microcrystals on single crystal tungsten substrate, discussing phase transformations
05 p0768 A71-16854

Reinforced Ni-based composites, discussing barrier coating for tungsten fibers
05 p0769 A71-16860

Mo and W residual outgassing partial fluxes, considering process duration and impurities identification
05 p0754 A71-16947

Hydrogen and nitrogen chemisorbed species interactions on /100/ tungsten crystals, using flash desorption methods
07 p1056 A71-19846

Be films evaporated in vacuum on W single crystals, investigating adsorption and electron emission by field emission microscopy
07 p1178 A71-19918

Rhenium effect on tungsten sensitivity to brittle fracture, measuring amplitude dependence of internal friction at temperatures from 77 to 1273 K
07 p1141 A71-20247

W fiber reinforced Al strain distribution under tensile load, using moire grid method
07 p1144 A71-20495

W and Mo single crystals metallographic microanalysis for temperature cycles effects on microstructure
08 p1305 A71-21056

Thermal and electrical transport in tungsten crystal for strong magnetic fields and liquid helium temperatures
08 p1344 A71-21365

Tungsten crystal Fermi surface galvanomagnetic coefficients in scattering process by semiempirical scheme
08 p1344 A71-21366

Ta and W single crystals yield stress temperature dependence, confirming asymmetric Peierls barrier
08 p1307 A71-21507

Single crystal W thermal conductivity measurement at 1200-2500 K, discussing apparatus and error sources
08 p1318 A71-21920

Secondary ion component on tungsten target surface during sputtering by alkali metal ions
09 p1494 A71-22878

Sudden thermionic emission in surface ionization at near threshold temperatures of cesium activated tungsten single crystals
09 p1494 A71-22879

Primary, secondary and combinatory recrystallization kinetics and textures in tungsten wire of different compositions over 900-2300 C using X ray analysis and metallography

09 p1476 A71-23323

Subgrain growth kinetics for tungsten deformed by rolling and polygonizing annealing, using metallography, X ray microradiography and crystal spectrometry

09 p1476 A71-23324

Ultrasonic irradiation effect on single tungsten crystals deformation characteristics and structure

09 p1477 A71-23327

Strain effect on ultrasound damping in single W crystals, considering microhardness

09 p1477 A71-23328

Crystal structure alterations in work hardened surface layers of W, Nb and Mo during thermocyclic treatment, using X ray micrograph

09 p1477 A71-23329

Tungsten high temperature thermal diffusivity at 1000-2500 K by flash technique

10 p1624 A71-23911

Low temperature sintering of Ni-P alloy coated tungsten, discussing diffusion phenomena

10 p1625 A71-23999

Electron beam welding of tungsten to tungsten/rhenium and tungsten/rhenium to niobium, discussing techniques for assembly of thermionic converter fuel elements

11 p1769 A71-25858

Carbon vapor deoxidized W on thermionic converter emitters, investigating deposition parameters effect on microporosity

11 p1807 A71-25860

Macroscopic working model for CVD tungsten assuming change of substrate work function and preferential crystal orientation by impurity adsorbed molecules

11 p1808 A71-25861

Thermionic emitter CVD W layer on Mo, investigating work function change due to Mo diffusion and crystal structure dependence on heat treatment

11 p1808 A71-25863

Diffusion processes in Mo-W thermionic emitters of massive couple type and piece of Mo substrate with vapor-deposited W layer respectively

11 p1709 A71-25864

Chemically vapor deposited deep etched tungsten emitter for high performance cylindrical thermionic converter

11 p1714 A71-25906

Temperature dependence of flow stress of cold worked heavily deformed doped W

11 p1781 A71-26296

Gravitational constant determination, using rotating mounted W sphere and gas tight chamber with cylinder suspended from quartz fiber

12 p1931 A71-27245

Pure W single crystals grown by electron beam zone melting technique, noting rolling workability

12 p1919 A71-27761

Mo and W single crystals mechanical properties, considering C and iron group additions influence

14 p2255 A71-29516

Uniaxially reinforced W-Cu matrix composite material dynamic compressive load properties, considering strain rates and yield stress

14 p2257 A71-29643

Critical aspect ratio of W fibers in metal matrix composites for stress rupture applications

14 p2258 A71-29921

W and Mo single crystals metallographic microanalysis for thermal cycling effects on microstructure

14 p2259 A71-30172

Nitrogen solubility in W at high temperature, using metal high vacuum apparatus and mass filter partial pressure measuring instrument

14 p2260 A71-30475

Nickel alloys susceptibility to pores formation in tungsten inert gas welding in argon-nitrogen mixture, considering influence of Cr, Mo and W

14 p2260 A71-30487

Chromatographic separation of molybdenum, niobium and tungsten based on metal ions absorption by aluminum oxide

15 p2367 A71-31647

Binding states, adsorbate densities and desorption kinetics of hydrogen on crystal planes of tungsten

15 p2367 A71-31676

Be, U and W shear strength measurements, detailing strain, strain rate and pressure effects [ASME PAPER 70-WA/PT-2]

15 p2434 A71-32260

Tensile strength of boron, silicon carbide coated boron, silicon carbide, stainless steel and tungsten fibers after exposure to air, argon and aluminum at high temperatures

15 p2435 A71-32440

Tungsten single crystals under deuteron bombardment, noting structural defects formation as function of irradiation energy

16 p2595 A71-33883

Crystal structure defects of W samples containing small and large angle grain boundaries, using field ion emission microscopes

16 p2580 A71-33927

Tungsten-oxygen system surface reactions in vacuum, emphasizing interfacial geometry variations, faceting and oxide nucleation

17 p2694 A71-34667

Single crystal W thermal conductivity measurement at 1200-2500 K, discussing apparatus and error sources

17 p2759 A71-35264

Ionizer, neutralizer and ion optics of cesium contact ion thruster, examining porous W materials technology [DGLR-71-033]

17 p2793 A71-35535

German monograph on high temperature measurement of thermal and electrical conductivity of W and Mo single crystals

18 p2915 A71-35960

Oxygen adsorption study on polycrystalline W through work function variation and adhesion coefficient measurements, using mass spectrometry

18 p2874 A71-35974

Microcrystal orientation in recrystallized tungsten structure by charged particles channelography

18 p2954 A71-36804

Bubble formation during annealing of W doped with K, Al and Si compounds, using electron microscopy with thin foil and fracture replication techniques

19 p3079 A71-37708

Thermophysical properties of Ta, W and Ta-W alloy at high temperatures, using automatic high vacuum facility

20 p3247 A71-38764

Field induced changes in W specimens during field ion microscope operation, considering behavior of dislocations and grain boundaries

21 p3395 A71-40024

Transition metals addition effect on W sintering behavior in 1000-2000 C range, explaining by electron exchange between alloy components

21 p3396 A71-40031

Dislocation structures of polycrystalline tungsten after deformation and recovery annealing, observing temperature dependence of critical strain for recrystallization

21 p3399 A71-40472

Nitrogen adsorption on single crystal W planes by flash desorption experiment, noting work function change dependence on planes

21 p3345 A71-40539

Quasi-equilibrium prediction of rate of volatilization/erosion/ of solid tungsten by reaction with gaseous oxygen at high temperature and low pressure

21 p3404 A71-41419

Temperature effects on tungsten lattice and Grueneisen parameters and thermal expansion coefficients at low temperatures by X ray method

22 p3561 A71-41724

Oxygen interaction with polycrystalline W, calculating sticking probabilities and desorption spectra at various temperatures

23 p3641 A71-42906

High temperature sintering kinetics of tungsten, observing heating rate effects

23 p3690 A71-43257

Emitter-base W metallized contacts RF power transistors for improved hot spotting and breakdown reliability, comparing with Al

23 p3651 A71-43441

Li-filled vacuum-deposited W heat pipes for efficient heat extraction from nuclear reactors, discussing design, fabrication and testing

23 p3682 A71-43595

Heat resistant Ni-base composite stiffened with W wires, investigating interaction between alloy and fibers from metallographic and X ray diffraction microscopy data

23 p3693 A71-44214

Recrystallized metalceramic W plastic deformation effects on brittleness temperature threshold, revealing relationship to impurity segregations at grain boundaries

24 p3837 A71-44674

W and Mo thin films phase diagrams, determining surface energies and heats for transformations

24 p3860 A71-44718

W and Mo single and polycrystals structural changes by ion bombardment in Li vapor atmosphere at 1500 C, using mass spectrometer

24 p3838 A71-44862

TUNGSTEN ALLOYS

Bare and cesiated work function of covapor deposited tungsten-rhenium electrodes from vacuum emission vehicle Schottky plots

02 p0295 A71-12205

W, W-Re and Re-Mo creep rupture properties investigation for selection of optimum materials for isotope containment for thermionic capsules

02 p0195 A71-12254

Resistively heated W-Re wire sublimation characteristics between 1550-1950 C in low pressure oxygen

02 p0264 A71-12255

W and W-Mo alloy creep properties during interaction with low pressure oxygen, simulating clad oxide fuel interaction in thermionic device

02 p0264 A71-12255

W-Mo alloy enthalpy and specific heat measurement at high temperatures by drop calorimetry

04 p0613 A71-12255

Nb-W single crystal deformation, discussing thermal solid solution strengthening

06 p0914 A71-12255

Ni-W eutectic alloy unidirectional solidification, obtain composite structure in Ni-W solid solution

06 p0915 A71-12255

Phase equilibria in Zr-Mo-Re and Zr-W-Re systems, studying isothermal section diagrams via X ray metallographic techniques

07 p1140 A71-23323

W-Re-Ir ternary system phase diagrams, studying physicochemical properties via X ray and metallographic techniques

07 p1140 A71-23323

Re based W alloys for electronic tube hot cathode, discussing reduction and annealing effects on mechanical and plastic properties

07 p1140 A71-23323

W-Re alloy ingot nonmetallic inclusions composition, phase structure, using electron probe, metallography and electrolytic techniques

07 p1141 A71-23323

W-Re alloy microstructure creep, long term strength and plastic properties as function of temperature, using electron microscopy

07 p1141 A71-23323

W-Mo-Re high temperature alloys, discussing strength, elastic properties, creep, thermal resistance and expansion coefficient

07 p1141 A71-23323

Optimal recrystallization of thin wire cast W alloy subject to high size reduction

07 p1141 A71-23323

Mechanical, heat resistant and thermoelectric properties of W-Re alloys for thermocouples

07 p1114 A71-23323

Composition and annealing effects on mechanical and thermoelectric properties of sintered wire W alloys

07 p1143 A71-23323

Hot extruded W-Cu pseudoalloys under tension and compression, determining impact strength and plasticity

08 p1316 A71-23323

Discontinuous decomposition and aging kinetics of supersaturated solid solutions of tungsten in cobalt, comparing to precipitation theories

09 p1469 A71-23323

Shape and size variations of dispersed particles of Ta, Zr, La and Y in tungsten during sintering

10 p1624 A71-23323

Chemical vapor deposition process for preparing W-Re alloys having uniform Re content and defining coherent grain structure

11 p1797 A71-23323

W-Mo-Ta system alloys investigated along C phase diagram from tungsten corner, establishing additions effect on maximal strength

11 p1782 A71-23323

Dutch monograph on Cr-W interdiffusion in solid state concerning Kirkendall effect and relationship between chemical and self diffusion

11 p1783 A71-23323

Boron solubility in Mo-W solid solution, discussing microstructure, electrical and mechanical properties for range of alloying ratios

12 p1918 A71-23323

Ni-Cr and Ni-W alloys high temperature strength properties, considering stacking fault energy, dislocation velocity, Young modulus and dislocation locking

12 p1919 A71-23323

W, Mo, Ta and W-Mo alloys hardness integrated with high temperature microhardness tester

13 p2084 A71-23323

Nitrogen solubility in Ni-Mo and Ni-W melts, determining Ti and pressure effects

15 p2424 A71-31313

Comparative creep rupture properties of tungsten-rhenium consolidated by arc melting and powder metallurgy, considering rupture life and rupture ductility

15 p2427 A71-31313

Creep rupture properties of W-Re arc melted powder metallurgy materials at 1650 and 2200 C as function of time, void and grain size

15 p2428 A71-31313

Molybdenum and tungsten alloys, detailing strengthening with hafnium carbide

15 p2428 A71-31313

Hot compaction of tungsten and pseudoalloys powders in terms of volumetric-viscous flow dependence on isothermal exposure time, using Kovalchenko-Samsonov equation

16 p2592 A71-33883

Addition effects on polygonization of deformed single crystals of Mo and W with Re, using X ray analysis

16 p2596 A71-33883

Alloying elements effect on structural stability and properties of W and Mo alloys single crystals, studying thermal cycling response

16 p2596 A71-33908

Co-Cr-W alloy sulfidation at high temperatures, performing weight gain, metallographic X ray and electron probe analysis

17 p2758 A71-35149

Hot pressed W-Cu pseudoalloys strength and ductility under tension and compression

17 p2760 A71-35674

High temperature tensile strength of Ta-W-Hf alloy sheet with protective Si-Ti coating in vacuum and air

18 p2933 A71-35951

High temperature tests of short time strength, hardness, moduli of elasticity of W-Mo alloys subject to plastic deformation and annealing

18 p2936 A71-36712

Carbon effects on strength, ductility, brittle transition and plastic strains of tungsten at high temperatures

18 p2936 A71-36713

Mo, W and Mo-W alloys chlorination kinetics, investigating temperature and pressure effects on reaction rate from electron micrographs

18 p2938 A71-37002

Ti-W-B, Hf-Ta-B and Ta-W-B alloys isothermal phase diagrams at 1400 C, using X ray analysis and metallographic techniques

19 p3076 A71-37112

High temperature strengthening of vacuum melted W-Ti alloys with Mo and Zr additions

19 p3076 A71-37267

Concentration effects of Nb and Ta on strengthening in tetrahedral section of W-Mo-Nb-Ta system at temperatures from 20 to 1100 C

19 p3078 A71-37473

Recrystallization behavior of thorium dispersion hardened W-Re alloy compared to pure W by X ray diffraction, hardness tests, metallographic and electron microscopy methods

20 p3247 A71-38763

Arc melting consolidated W-Re-Hf-C alloy mechanical properties from tensile, creep and bend tests

20 p3247 A71-38766

Ta-W polycrystals and single crystals oxidation at 850-1100 C, noting anisotropic scale-fracture morphologies

20 p3252 A71-39373

Chemical vapor deposited tungsten or other refractory metal alloys mechanical properties evaluation at high temperature, describing hoop stress measurement apparatus for induction heated specimens

20 p3252 A71-39553

Tungsten and tungsten alloys weldability by gas tungsten arc, electron beam and chemical vapor deposition techniques

21 p3388 A71-40624

Solid powder metallurgy tungsten alloys, determining scale factor effect on bending strength and fatigue limit

23 p3693 A71-44226

High temperature aging, structural stability and tensile properties of hot rolled Co-W heat resistant alloy for space applications

24 p3836 A71-44443

Mo-W, Ta-W and Nb-W alloys X ray analysis at high temperatures, calculating interdiffusion coefficients and temperature effects on W concentration

24 p3836 A71-44671

Tungsten filaments as reinforcing agent of heat resistant composite chromium alloy, investigating long term high temperature effects

24 p3837 A71-44728

TUNGSTEN CARBIDES

Submicron sectioning apparatus for studying slow carbon self diffusion in dense polycrystalline tungsten carbide

03 p0429 A71-14187

Hard metals and WC-Co alloy stress and heat treatment effect on coercive force, crack formation energy and abrasive resistance

06 p0911 A71-17342

Solid solution reactions analysis for W Ti/C powder formation

08 p1304 A71-20993

WC-Co system binder phase composition and properties, studying W content as function of initial carbide grain size, Co content, sintering and quenching time

09 p1466 A71-22170

Tungsten carbide advantages in hard metals structure, including high pressure strength, high elasticity modulus and plastic properties

14 p2255 A71-29517

Hot pressed boron carbide and titanium diboride for use as indenter materials for tungsten carbide hardness measurements at high temperatures

15 p2409 A71-32165

Zirconium dioxide reactions with chromium, molybdenum and tungsten carbides, studying reaction products, phase composition, sintering temperatures and chemical separation

15 p2432 A71-32166

Tungsten carbide-cobalt alloys, investigating binder metal mechanical properties relationship to composition by chemical analysis and X ray inspection

19 p3083 A71-38475

WC and TiC-Co solid solution phase after sintering inhomogeneous structure, investigating grain growth and phase decomposition behavior at various temperatures

23 p3689 A71-43103

Complex TiC-WC carbides under homogenizing annealing, noting defects, solubility, lattice constant and grain growth

23 p3689 A71-43253

TaC-WC, ZrC-WC and refractory compounds thermal expansion coefficient measurements

24 p3838 A71-44738

Homogenizing annealed TiC-WC carbides properties at room temperature, investigating microhardness, microbrittleness and resistivity

24 p3838 A71-44740

Titanium, niobium and tungsten carbides microhardness temperature dependence at 77-1973 K, discussing activation energy and deformation mechanism

24 p3838 A71-44741

TUNGSTEN COMPOUNDS

NT TUNGSTEN CARBIDES

NT TUNGSTEN FLUORIDES

NT TUNGSTEN OXIDES

Tungsten boride sintering bonds with molten Ni as function of wettability low dihedral angle, discussing cermet porosity range

07 p1130 A71-19297

Tungsten or molybdenum disulfide formation discussing tribolytic deposition process

10 p1635 A71-25010

Refractory tungsten boride with iron or nickel for powdery surfacing mixtures, showing hardness and wear resistance dependence on low melting component

15 p2438 A71-32675

Raman and IR reflection spectra of zinc tungstate single crystals

17 p2790 A71-34201

TUNGSTEN FLUORIDES

Design, fabrication and testing of electrically heated externally configured thermionic diodes with emitter using mandrel side of CVD fluoride tungsten for electrode surface

11 p1715 A71-25911

TUNGSTEN HALIDES

NT TUNGSTEN FLUORIDES

TUNGSTEN INERT GAS WELDING

U GAS TUNGSTEN ARC WELDING

TUNGSTEN OXIDES

Corrosive oxide layer formation kinetics during interaction of oxygen with polycrystalline W at 500-1000 K, using desorption mass spectrometry

23 p3641 A71-42907

Tungsten and molybdenum oxide crystals shape and size during annealing in various gas atmospheres and vacuum conditions

23 p3690 A71-43255

TUNGUSK METEORITE

Optical anomalies associated with Tungusk meteorite fall in 1908, noting volcanic activity and noctilucent cloud formations

14 p2233 A71-29964

Tunguska explosion of 30 June 1908, determining air waves propagation velocity

16 p2639 A71-33696

TUNING

Upper frequency limit to mechanical tuning range of waveguide-mounted transferred electron oscillators due to transverse resonance

01 p0055 A71-11173

Optimal gain tuning elements of cryogenically cooled parametric amplifiers

02 p0235 A71-12833

Measuring instruments for hyperabrupt varactor tuning diodes in RF, VHF and UHF ranges

05 p0728 A71-16396

Laser tuning techniques, noting acoustooptic, Doppler, oscillator and dye cell methods

07 p1124 A71-19794

Microwave oscillators with Gunn effect device resonant circuit and YIG tuning, discussing design and performance

08 p1263 A71-20992

Accurate single-sideband radio receiver tuning, observing reconstitution of harmonic tones in human speech strong vowel sounds

08 p1254 A71-21318

Bulk effect microwave oscillators energy source design, considering operation mode and circuit tuning control parameters

08 p1266 A71-21623

Temperature dependent wavelength tuning of Pb-Sn-Te diode lasers, noting air pollution detection use

09 p1463 A71-22764

High power magnetically tunable microwave interference filters based on spin waves magnetic field dependent dispersion in ferrimagnetic materials

09 p1421 A71-23721

Wing-fuselage-tail interacting low speed flutter, considering mechanical tuning and aerodynamic interference couplings

[AIAA PAPER 71-326] 11 p1847 A71-25306

Tunable Gunn oscillator obtained by semiconductor surface loading, discussing oscillation frequency as function of anode to edge distance

11 p738 A71-26365

Remote controlled automatically tuned l-kw short wave transmitter with zero power tuning mode of power stage and drive unit frequency generation

12 p1887 A71-26989

Parameters optimization for increasing tuning range of resonator with contactless piston based on numerical solution of transcendental equation

12 p1889 A71-27623

Double cavity tuning of Gunn oscillators at mm wavelengths achieving output power improvements

14 p2215 A71-30831

Continuously tunable pulsed UV source using broadband dye laser emission input to rotatable KDP crystal

16 p2586 A71-33141

Coupled oscillator circuits simultaneous tuning by plane relationship between circuit currents/voltages/

16 p2548 A71-34034

Tuning range extension of doubly resonant lithium iodate parametric oscillator by upconversion, using simultaneous pumping by single ruby laser beam

19 p3071 A71-37477

Interference of transferred electron device operation involving harmonic tuning, considering EMC aspects

19 p3032 A71-38461

Damped isolation and undamped vibration absorber model for dynamic control, discussing frequency response and tuning and damping performance

[ASME PAPER 71-VIBR-45] 21 p3459 A71-40294

Tunable CW optical parametric oscillator optimum operating conditions, using barium, sodium and lithium niobate crystals parametric fluorescence tuning curves for comparison

22 p3557 A71-41863

Tunable spin-flip magneto-Raman IR laser, describing indium antimonide scattering, tuning range and applications

22 p3557 A71-42133

Human visual system color and edge-sensitive channels confirmation by psychological tests of tuning for orientation

23 p3640 A71-43548

Wideband microwave amplifier with two antiparallel high efficiency avalanche diode pairs, presenting fishbone shaped tuning plate for bandwidth widening

23 p3653 A71-43961

Spectral properties and tunability of far IR from ZnTe and lithium niobate crystals from difference-frequency mixing of mode-locked Nd glass laser pulses

23 p3686 A71-43997

Dye laser electronic tuning by inserting calcium-molybdenum oxide acousto-optic filter into cavity

23 p3687 A71-44137

TUNNEL DIODES

Self excited cavity oscillators with tunnel and parametric diodes and nonequilibrium medium, noting single and multimodes, energy capabilities and frequency interactions

02 p0231 A71-11874

Tunnel diode frequency multiplier circuit, analyzing harmonic I-V characteristics by equivalent network method

03 p0384 A71-13396

Neuristor pulse propagation analysis for nonlinear distributed circuit of superconductive tunnel junction stripline

03 p0393 A71-14470

Large signal mode tunnel diode amplifier amplitude and phase characteristics by computer study

04 p0556 A71-14622

Tunnel diode trigger circuit, calculating effect of junction capacitance variation and small inductance on switching time

05 p0730 A71-17082

Asynchronous tunnel diode microwave detector, considering frequency properties and sensitivity

06 p0874 A71-17547

Superconducting tunnel junctions radiation emission, discussing superconductivity theory

07 p1178 A71-19777

Tunnel diode output voltage converter circuit diagram and waveforms

07 p1080 A71-20360

Low noise C band beam lead tunnel diode amplifiers characteristics and application in low cost microstrip reflection amplifiers

08 p1262 A71-20759

Microwave amplifier resonant gain frequencies as function of tunnel diode circuit, proposing low input design formulas

08 p1264 A71-21069

Monostable multivibrator tunnel diode synchronization bandwidth as function of circuit parameters and junction I-V characteristics

08 p1264 A71-21071

Microwave diode technology, discussing Schottky barrier, p-n junction, varactor, tunnel, bulk effect and avalanche diodes performance and applications
08 p1266 A71-21622

Autoparametric oscillator with tunnel diode and variable capacitors, considering effective frequency range extension
09 p1414 A71-22528

Tunnel diode microwave oscillator design, discussing fixed frequency or varactor tuned operation, power instabilities and load variations
09 p1415 A71-22457

Magnetically coupled tunnel diode oscillator with square loop core, calculating leakage and source inductances effect on switching pattern
[IEEE PAPER 11.4] 09 p1416 A71-22593

Metal-oxide-metal tunnel diode properties, discussing parametric effects on small and large signals detector operation
09 p1416 A71-22684

Amplitude discriminating Goto circuit with four tunnel diodes operating on negative and positive half periods as amplitude distribution analyzer at 40 MHz
10 p1582 A71-23954

Microwave tunnel diode oscillator, representing nonlinear characteristics with Taylor series
11 p1737 A71-25666

Differential phase frequency characteristics of low noise or tunnel diode regenerative amplifiers
11 p1738 A71-25941

Malfunction probabilities in presence of wideband noise for tunnel diode binary logic element /flip-flop/ pulse triggered into either of two output states
11 p1740 A71-26543

Tunnel diode driven multivibrator, noting triggering signal amplitude and duration effects on output pulse width
11 p1740 A71-26550

Thermal noise measurement of superconducting coaxial lambda/2 resonator at 2.46 GHz with ruby traveling wave maser and tunnel diode amplifier setup
12 p1887 A71-27010

Tunnel diode microwave oscillator design, using circle diagrams of operational and load characteristics
12 p1888 A71-27513

Tunnel diode switching forward and reverse non-regenerative delay, examining external load resistance and diode characteristic nonlinearity effects on non-regenerative delay
13 p2038 A71-28717

Microwave frequency mixer using two inverted tunnel diodes in series connection
14 p2211 A71-30116

Preliminary circuit-stage alignment procedures in multistable triggers manufacture with counter input based on tunnel diodes and transistors
14 p2213 A71-30632

Solid state voltage regulator with hybrid tunnel-diode/transistor circuit discriminator for overload protection, discussing operation, circuit diagram and performance
17 p2716 A71-34786

Perturbation free delay time measurement in digital data processing system, using Schmitt triggers or tunnel diode discriminators
18 p2885 A71-36225

Tunnel diode oscillator equivalent circuits with frequency variance by changing load susceptance
19 p3026 A71-37145

Broadband compensation of HF tunnel diode traveling wave amplifier using separate stages in transmission line
19 p3026 A71-37256

Relaxation time model of solid state diodes based on equations for electrons of given energy, including p-n junction and tunnel diodes
19 p3027 A71-37495

Differential phase frequency characteristics of low noise or tunnel diode regenerative amplifiers
20 p3205 A71-39261

Distributed tunnel diode traveling wave amplifier load noise thermal and shot components, noting impedance boundaries
20 p3206 A71-39814

Tunnel diode harmonic relaxation frequency divider, obtaining large division factors and wide synchronization bands with sinusoidal output signal
20 p3206 A71-39818

Large signal mode tunnel diode amplifier amplitude and phase characteristics by computer study
22 p3521 A71-42262

Range finder receiver based on Si avalanche detector coupled to tunnel diode circuit, with automatic gain control through tunnel diode bias control
23 p3677 A71-43518

Silicon Schottky tunnel MOS diodes, discussing effect of thin interfacial film between metal and semiconductor on I-V characteristics
23 p3652 A71-43936

Tunnel MOS diode oxide thickness and thermal equilibrium considerations, emphasizing reverse bias case AC conductance, capacitance and DC I-V characteristics
23 p3652 A71-43937

Series stabilization reflection type tunnel diode microwave amplifier synthesis with allowance for real circulator reactance
24 p3810 A71-45259

TUNNEL RESISTORS U ELECTRON TUNNELING U RESISTORS TUNNELING

One dimensional acoustic tunnel effect for incident wave normal to barrier analogous to macroscopic spin waves and quantum mechanics
15 p2449 A71-31703

TUPOLEV AIRCRAFT NT TU-134 AIRCRAFT

Tu-154 responsibilities of three-man crews, considering flight plan, refueling, cargo loading and unloading
11 p1744 A71-25258

Nonreversible hydraulic control design and emergency maintenance for Tu 154 aircraft subsonic cruising at 11 km altitude
23 p3627 A71-42927

TUPOLEV TU-124 AIRCRAFT U TU-144 AIRCRAFT

TUPOLEV TU-134 AIRCRAFT U TU-134 AIRCRAFT

TURBIDITY

Unsteady light field spatial moments in turbid medium boundary layer with intense anisotropic scattering during illumination by narrow beam
02 p0277 A71-12116

Radiative transfer in nonuniform turbid medium with constant absorption coefficient
05 p0742 A71-16840

Threshold and power relations for optical radars in pure and turbid atmospheres, determining visibility range for object detection
13 p2027 A71-27856

Aerosol power law distribution exponent and particle limiting radii from turbid atmosphere outgoing visible radiation polarization high altitude measurements
13 p2063 A71-29111

Short narrow light pulse reflection from thick turbid medium with strong anisotropic scattering, obtaining backscattering signal power from unsteady transport equation solution
16 p2544 A71-34105

Rapid scanning dual wavelength spectrophotometer for recording oxidation-reduction and membrane bound reactions in turbid suspensions of biological materials
18 p2922 A71-36580

Solid state linear array piezoelectric hydroacoustic image transducer for underwater viewing in turbid oceanic environments
20 p3233 A71-38828

Circumsolar radiation and atmospheric turbidity effects on readings of compensation type pyroheliometers with allowance for receiver sensitivity
21 p3384 A71-41382

Atmospheric aerosol stratification, turbidity, stratospheric layer and purification zone from optical sounding data
24 p3823 A71-44821

TURBINE BLADES

Turbine blades coupled bending vibrations in centrifugal field, deriving vibration equations including previously neglected centrifugal coupling terms
01 p0166 A71-10120

Axial turbomachine rotating blades, calculating three dimensional boundary layer thickness for laminar flow
01 p0069 A71-10337

Natural frequencies of cantilever turbine blade with asymmetric aerofoil under coupled bending-torsion vibrations, using Ritz-Galerkin method for equations of motion
01 p0143 A71-11014

Pressure fluctuations on fixed blades of axial flow compressor, determining sensor dynamic characteristics
01 p0003 A71-11024

Normal stress analysis at tooth of turbine rotor blade root, taking into account friction force
01 p0143 A71-11247

Turbine and compressor blade profiles grinding, formulating mathematical rules for shaping links adaptable to programmed control
02 p0258 A71-12569

Blade bound vortex system mathematical model for optimum heavily loaded ducted fans, including thrust, power and efficiency design parameters
02 p0299 A71-12677

Niobium alloys for gas turbine blades, examining working temperatures, protective coatings and ductility
02 p0271 A71-12939

Mechanical stability of liquid phase in porous oxidation protective coating on Ni turbine blades under acceleration
02 p0272 A71-12946

Engine turbine blades aerodynamic oscillation damping calculation procedure
03 p0503 A71-13416

High temperature tests of gas turbine engine with transpiration air cooled blades, discussing blade design, fabrication, ductility and oxidation resistance
[ASME PAPER 70-WA/GT-1] 03 p0470 A71-14115

Turbine blades with high aspect ratios, calculating behavior at small Reynolds number
[ASME PAPER 70-WA/GT-11] 03 p0343 A71-14119

Steam turbine blade metal removal rates by repetitive water drop impact, using hydrodynamic model
03 p0405 A71-14290

Heat transfer through phase change in metallic heat carrier exposed to strong centrifugation encountered in turbine blades
04 p0639 A71-15462

Film cooling of flat plates by angled cold air injection for turbine blade applications
04 p0639 A71-15472

Thermal fatigue cracks in gas turbine blade models under simultaneous thermal cycling and static tensile loads simulating pulsed regimes
04 p0671 A71-15638

Heat flow in unidirectional solidification of vacuum cast alloy turbine blades, using analog thermal model
05 p0758 A71-16244

Turbine blades flexural vibration modes, noting frequency parameter dependence on angular velocity, disk radius and stagger angle
05 p0796 A71-16648

Test facility for fatigue and thermal fatigue of turbine blades in high temperature gas flow
05 p0734 A71-16762

Gas-particle mixture cascade flow over turbine blades, considering momentum/heat transfer and particle trajectories
06 p0841 A71-17701

Turbine blades thermal stresses due to nonlinearities, using computerized simulation
06 p1000 A71-18003

Structural hysteresis in split root fir tree turbine blade attachment under centrifugal forces and cyclic bending moments
07 p1211 A71-19162

Gas-particle mixture cascade flow over turbine blades, considering momentum/heat transfer and particle trajectories
07 p1017 A71-20311

Thermal fatigue testing apparatus for material longevity, simulating tensile stresses due to centrifugal forces on gas turbine engine blade during thermal loading
08 p1271 A71-20837

Injected air cooled turbine blade trailing edges temperature, calculating thermal distribution with differential equations
08 p1348 A71-21265

Contained cross sectional deformation effects on turbine blades natural torsional vibration frequencies
08 p1372 A71-21617

Solidification process for unidirectionally cast airfoil shaped turbine components from Ni superalloys, discussing mold withdrawal
08 p1299 A71-21682

Composition, microstructure, heat treatment and properties of Ni alloy with high rupture strength and hot corrosion resistance for turbine blade applications
08 p1299 A71-21687

Gas turbine blades design and exploitation processes, discussing long time fatigue strength, static durability and heating effects at elevated temperatures
08 p1299 A71-21708

Shrouded aircraft engine turbine blades vibration stresses found minimum by setting up paired blades with fixed tension along shroud
09 p1538 A71-22595

Low temperature tensometry application to stress-strain state of turbine disks
09 p1443 A71-22635

Gas turbine blades local heat transfer, correlating experimental surface temperature, heat transfer coefficient and internal coolant temperature with theoretical estimates
09 p1547 A71-23658

Coupled vibration modes for nonrotating blade-disk system in axial flow turbines and fans calculated by finite element method
[AIAA PAPER 71-375] 11 p1845 A71-25348

Air cooled turbine blades activated diffusion brazing and gas pressure welding, using composite finned configuration model
[ASME PAPER 71-GT-32] 11 p1770 A71-25969

Flow patterns within centrifugal and mixed flow impeller channel, examining velocity distributions, blade surface pressure and flow behavior
[ASME PAPER 71-GT-41] 11 p1704 A71-25974

Metal matrix composite fabrication procedures for gas turbine engine fan blades, stressing diffusion bonding process susceptibility to blades volume producibility
[ASME PAPER 71-GT-46] 11 p1770 A71-25979

Supersonic turbine design, presenting performance data for film cooled blunt leading edge rotor blades measured in two dimensional cascade experiments
[ASME PAPER 71-GT-76] 11 p1704 A71-25990

Surface strain measurements in turbine blades by time average holographic interferometry, reviewing resonant modes and holographic fringe patterns [ASME PAPER 71-GT-84] 11 p1762 A71-25992

Axisymmetrical incompressible and compressible fluid flow inverse problem formulation and solution with application to turbine blade design 11 p1752 A71-26051

Monograph on turbine blade fir tree roots, calculating stress-strain state of long term static strength under elastic and elastoplastic deformation and unsteady creep 11 p1852 A71-26400

Cascade approximation of unsteady forces acting on blades of axial flow turbomachines, using perturbation potential combined with slip condition [ONERA-TP-944] 12 p1946 A71-27713

Quasi-axisymmetric and superposed fine fluctuating structure of ideal incompressible vortex flows in axial flow turbines, assuming infinite mutual blade proximity [ONERA-TP-945] 12 p1866 A71-27714

Gas turbine blades cast heat treated superalloys high temperature mechanical properties during aging 12 p1919 A71-27778

Gas turbine blades fatigue crack development and failure analysis under thermal cycling tests, considering chemical processes and thermal and mechanical stresses 13 p2149 A71-28117

Gas turbine blades thermal fatigue test and analysis, investigating static tensile loading effects on heat resistance under thermal cycling 13 p2149 A71-28124

Aerofoil cascades with axial velocity change in incompressible flow, determining turbine blade force dependence on circulation 13 p1990 A71-28467

Metal temperatures in rotating cooled gas turbine blades, discussing coolant flow aerodynamics 13 p2117 A71-28748

Vortex induced shear and secondary flow through row of spheres, curved channel, turbine blades, rotating impeller, suction pipe and upstream boundary layers 14 p2224 A71-30176

Turbine blade profiles nonstationary temperature fields during thermal fatigue tests, measuring surface temperature via thin film thermocouples 14 p2252 A71-30265

Flexible blades cascade at various pitch angles and Reynolds numbers 15 p2343 A71-31203

Stress distribution during plastic deformation of steel turbine disk from hardness measurements 15 p2505 A71-31863

Thermal fatigue cracking of gas turbine blades in fuel combustion product flow, investigating surface composition, microhardness and structure under simulated loads 15 p2469 A71-32227

End play influence on dynamic bending vibration stresses induced by aerodynamic forces in axial flow turbine rotor blades in case of resonant vibrations 15 p2508 A71-32298

Gas turbine blades effusion cooling effectiveness, using boundary layer theory to calculate blade profile local heat transfer 15 p2472 A71-32716

Program parameters effects on fatigue life of turbine blade heat resistant alloys at high temperatures under cyclic loading 16 p2592 A71-33407

Thermal stresses in gas turbine rotor blade with two dimensional temperature field, using closed/Saint Venant/plate solutions 16 p2657 A71-33543

Transverse flow in cavity ensurance by air exhaust cooling of trailing edges of gas turbine blades with deflector 16 p2624 A71-33544

Swirling flow in gas turbine engine combustion chamber forward part, considering air flow characteristics behind blade swirler 16 p2624 A71-33606

Axial flow gas turbines blade cascades forming arrays with convergent channels, discussing contours design 16 p2521 A71-33615

Gas flow behind cylindrical nozzles at roots and along periphery for narrow blades, using radial equilibrium equation 16 p2521 A71-33617

Gas turbine blades dynamic characteristics determination, investigating vibrational stresses, thermal cycles, alloy physicomechanical properties and coatings effects 16 p2659 A71-33987

Simulated turbine blade thermal fatigue testing under transient and steady state heating and spanwise loading, obtaining crack initiation and propagation data [SAE PAPER 710459] 17 p2792 A71-34500

Runner and cavitation characteristics of hydraulic machine with finite blade number and ideal frictionless incompressible working fluid determination by potential theory 17 p2727 A71-34668

Engine turbine blades aerodynamic vibration damping calculation procedure 17 p2826 A71-35023

Pretwisted cantilever airfoil cross section turbine and compressor blades vibration natural frequencies and mode shapes 17 p2828 A71-35282

Dirichlet problem in hodograph plane of compressible fluid flow from aircraft, helicopter blades or turbine blade airfoils 17 p2672 A71-35470

Structural hysteresis in gas turbine blade herringbone scarf joints under centrifugal forces and cyclic bending moments 17 p2834 A71-35658

Cross sectional warpage effects on turbine blades natural torsional vibration frequencies 17 p2834 A71-35677

Fan jet first stage turbine blade air cooling, describing design, heat transfer data, efficiency and temperature distribution 18 p2956 A71-35904

Siren wail in turbine axial stage due to nonuniform pressure fields behind blade cascades 18 p2843 A71-36180

Book on external corrosion and deposits on boiler tubes and gas turbine blades covering mineral matter in fuels, oxidation, additives, etc 18 p2935 A71-36247

Turbine alternating fan failure due to flutter by coupling of vibration modes and effect of mass distribution in blade 18 p2980 A71-36696

Two dimensional stress and temperature fields in cooled gas turbine blades with allowance for elasticity, plasticity and creep 18 p2980 A71-36704

Cyclic bending stress distribution in fir tree turbine blade root for arbitrary loading phase 18 p2980 A71-36705

On-design performance characteristics of radial gas turbines, investigating blade geometry, rotor losses and pressure ratio effects 19 p3123 A71-38269

Steam turbine blades induction brazing with programmed cycle, describing coil design 19 p3070 A71-38315

Holographic interferometry application to vibration mode pattern analysis of steam turbine and centrifugal compressor blades and disks 19 p3067 A71-38419

Condensate removal devices for potassium vapor Rankine space power turbines to prevent blade erosion and efficiency degradation 20 p3262 A71-38918

Gas turbine blades cast heat treated superalloys high temperature mechanical properties during aging 21 p3403 A71-41103

Gas turbine engine turbine blades service life increase by Cr and Al vacuum diffusion metallization, presenting full scale endurance test results 21 p3390 A71-41173

Centrifugal superchargers high pressure wheels efficiency improvement, considering blade profiling 23 p3626 A71-43556

Gas turbine blades of cast Zr56K heat resistant alloy, investigating structural strength from fatigue test data 23 p3779 A71-44208

Gas turbine blade models of heat resistant Zr56K alloy under operational temperature variations, observing fatigue strength 23 p3779 A71-44209

Streamline curvature analysis of compressible subsonic, transonic and supersonic cascade flows in axial turbine blades 23 p3665 A71-44347

TURBINE ENGINES

NT BRISTOL-SIDDELEY OLYMPUS 593 ENGINE 23 p3779 A71-44208

NT DUCTED FAN ENGINES 23 p3779 A71-44209

NT GAS TURBINE ENGINES 23 p3779 A71-44209

NT J-57 ENGINE 23 p3779 A71-44209

NT J-85 ENGINE 23 p3779 A71-44209

NT JET ENGINES 23 p3779 A71-44209

NT RAMJET ENGINES 23 p3779 A71-44209

NT SUPERSONIC COMBUSTION RAMJET ENGINES 23 p3779 A71-44209

NT TURBOFAN ENGINES 23 p3779 A71-44209

NT TURBOJET ENGINES 23 p3779 A71-44209

NT TURBOPROP ENGINES 23 p3779 A71-44209

NT TURBORAMJET ENGINES 23 p3779 A71-44209

Aircraft turbine engine development, considering mismatch reduction between engine and airframe in flight tests 01 p0143 A71-11180

Superalloy turbine engine guide vane thermal fatigue cracks repair by plasma arc fusion method 03 p0432 A71-13257

L-1011 aircraft auxiliary power unit with lightweight free turbine engine, giving fuel economy and lower pneumatic pressures [SAE PAPER 700814] 03 p0353 A71-13725

Turbine engine vibration dampers viscous resistance calculation based on equations of motion for incompressible and unheated Navier-Stokes liquid 03 p0470 A71-13956

VTOL aircraft turbine engine vibration criteria, discussing measurement methods, engine design, bending frequency and dynamic characteristics 04 p0532 A71-15419

Helicopter turbine engine protection device design guidelines 04 p0533 A71-15434

High temperature turbine parts protective coatings, discussing aluminum diffusion prevention and crack and oxidation resistance 09 p1456 A71-23290

Chromium and titanium alloyed austenitic steels, examining short and long time application as turbine engine parts 09 p1475 A71-23295

High speed photographic assembly with turbine drive for continuous recording and frame photography 10 p1613 A71-24872

Superalloy dispersion strengthened and fused slurry silicide coatings for aircraft gas turbine engines and space shuttle heat shields 11 p1778 A71-25555

Optimum weight protective system against uncontained rotor failure with radial fragment passage through turbine engine casing [ASME PAPER 71-GT-70] 11 p1813 A71-25985

Turbine engine fuel control stability on CH-47C helicopter, using flight tests and lag damper simulation [AHS PREPRINT 560] 14 p2297 A71-31107

VTOL turboshaft engine powered propulsion system development, detailing design requirements, program planning, component research and system integration [AHS PREPRINT 562] 14 p2297 A71-31109

Aircraft high temperature turbine engine design, reviewing technological advances coupled with laboratory engine and component tests 20 p3277 A71-39399

Turbine propulsion system smoking and exhaust gas emission, discussing aircraft and automobile pollution emission 20 p3277 A71-39452

Torsional natural frequencies in coupled turbine and reciprocating engine system driving common propeller, using matrix techniques [ASME PAPER 71-VIBR-83] 21 p3461 A71-40319

In-flight monitoring of aircraft turbine engine reliability 23 p3718 A71-43233

Operating variables effect on pollutant exhaust from jet aircraft turbine engines, discussing combustor design techniques for emissions reduction 23 p3718 A71-43600

Radial thrust bearing balls ovality effect on axial vibration of rapidly rotating turbine engine rotor 24 p3864 A71-45006

Nondestructive detection of hot corrosion-sulfidation in U.S. Navy aircraft turbine engines 24 p3865 A71-45280

TURBINE EXHAUST NOZZLES

Gas turbine exhaust silencer performance prediction by transmission line theory, considering LF requirements effect on size and cost 11 p1811 A71-25954

Time dependent asymptotic solution for transonic flows in hyperbolic nozzle and turbine cascades with oblique shock [ASME PAPER 71-GT-42] 11 p1704 A71-25975

TURBINE INSTRUMENTS

Turbine flowmeters for liquids with different viscosity and wide range of flow rates, calculating static characteristics 03 p0428 A71-13958

Optimum calibration of turbine flow sensors AC voltage signals with volume proportional frequency by weighted least squares techniques 11 p1762 A71-25934

Heading reference system feedback linear control circuits containing fluidic vortex rate sensor applied to turbine drive 15 p2353 A71-32070

TURBINE PUMPS

Flexible laminated cam ring for high speed variable displacement vane pumps [SAE PAPER 700792] 01 p0091 A71-11544

Gas dynamic test stand analyzing elastoplastic strains in aircraft gas turbine disks and liquid propellant rocket engines turbopumps under alternating nonisothermal loads 09 p1427 A71-22603

High speed vane type main engine fuel pump for small gas turbine engines [ASME PAPER 71-GT-24] 11 p1812 A71-25966

TURBINE WHEELS

Turbine disks and shafts for low temperature operation, examining brittle fracture tendency by acceleration testing

01 p0098 A71-10078

Turbine disks under unsteady and cyclic loads and temperature variations, determining stress and strain by flow theory computer calculation

02 p0323 A71-11745

Turbine disks cyclic nonisothermal deformation with allowance for Bauschinger effect, determining stress-strain state and residual microstresses

02 p0323 A71-11747

Radiometric determination of diametrical distance between rotor and stator of turbomachines

03 p0421 A71-13003

Titanium alloy turbine disks creep rupture strength and service life, considering pressing and forming manufacturing technology

04 p0664 A71-14604

Thin gas turbine disk strength under axisymmetric flexural vibrations, noting agreement of calculated and experimental rotor rpm danger zone

04 p0671 A71-15639

Turbine disks failure under nonuniform heating, deriving expression for critical rpm

05 p0826 A71-16755

Cyclic thermal cracking and fatigue analysis in large steam turbine rotors with three dimensional temperature and triaxial stress computation

[ASME PAPER 70-PWR-1] 07 p1216 A71-20198

Gas turbine rotor axial load determination, using static pressure distribution

08 p1348 A71-21268

Radial flow energy losses in rotating cylindrical cascade of inward-flow turbine wheel, determining profile losses and exit blade angle

08 p1349 A71-22044

Gas turbine wheel design fracture mechanics, discussing buried and surface flaws analysis for rotor failure prediction applications

[ASME PAPER 71-GT-10] 11 p1811 A71-25956

Variable elasticity algorithm for axial flow turbine disks with allowance for plasticity, creep and loading history

12 p1979 A71-27351

Nonlinear limit rotation velocity and circulation induced by wheel in axial flow turbomachine for incompressible ideal fluid, using iterative numerical algorithm

[ONERA-TP-946] 12 p1866 A71-27715

Turbine wheels and shafts for low temperature operation, examining brittle fracture by acceleration testing

16 p2593 A71-33634

Linear radial loads effect on stress and strain of hyperboloidal rotor disk applied to aircraft engine compressors with two stream flow of working medium

17 p2822 A71-34597

Rupturing rotations estimates for turbine disks, considering failure modes and load bearing capacity

17 p2829 A71-35305

Turbine disks failure under radial temperature drop, studying effects on load bearing capacity for thermal stresses

17 p2832 A71-35454

Dynamic properties of turbine wheels under bending vibrations, classifying resonant frequencies on basis of vibration modes

18 p2981 A71-36722

Holographic interferometry application to vibration mode pattern analysis of steam turbine and centrifugal compressor blades and disks

19 p3067 A71-38419

Graphical display of digital computer simulated steady state unbalanced turborotor response for lumped and distributed parameter models, using GATRAN language

[ASME PAPER 71-VIBR-42] 21 p3459 A71-40292

Distributed mass and elastic damping finite element model for turborotor system on fluid film bearings

[ASME PAPER 71-VIBR-56] 21 p3385 A71-40301

Lumped parameter simulation model for flexible turbine rotor dynamics in nonspinning coordinate system, discussing bearing constraints modeling methods and eigenanalysis applicability

[ASME PAPER 71-VIBR-71] 21 p3385 A71-40309

Vibration analysis of simulated axial flow turbine disks by holography, illustrating advantages of full field modal and deflection information

[ASME PAPER 71-VIBR-105] 21 p3377 A71-40330

Axially coupled turborotors, calculating coupling characteristics, disk inertia and gyroscopic effects on dynamic response, by transfer matrix techniques

[ASME PAPER 71-VIBR-108] 21 p3462 A71-40332

Numerical analysis for transient elastoplastic thermal stresses on turbine disks at variable rotation speeds

21 p3466 A71-40836

Circumferential flow direction nonuniformity effect in front of compressor wheel on intensity spread and resonant rotor blade vibrations

22 p3615 A71-41847

Flow acceleration coefficient effect at inlet on centrifugal compressor wheel characteristics during axial-radial rotation

23 p3626 A71-43553

Centrifugal wheel flow swirl effect on pressure/flow rate characteristic in input zone

23 p3626 A71-43555

Centrifugal superchargers high pressure wheels efficiency improvement, considering blade profiling

23 p3626 A71-43556

Postoperative states of turbine disk alloys at 280-500 and 550-630 C, noting lower durability values

23 p3779 A71-44211

TURBINES

NT AXIAL FLOW TURBINES

NT GAS TURBINES

NT SHROUDED TURBINES

NT STEAM TURBINES

NT SUPERSONIC TURBINES

NT TWO STAGE TURBINES

Channel form determination from circles family envelopes, discussing turbine duct geometries

06 p0841 A71-18009

Maximum efficiency of turbine for driving auxiliary equipment, noting design constraints

08 p1349 A71-22046

Three dimensional turbine end wall boundary layer with shear term, using momentum integral analysis and cross flow velocity profiles

[ASME PAPER 71-GT-6] 11 p1751 A71-25952

Cooling air injection effect on turbine efficiency, presenting experimental results for single stage air driven turbine with cylindrical stator and rotor blades

12 p1946 A71-27503

Performance tests of two identical Brayton cycle heat exchanger units consisting of recuperator, heat sink exchanger and ducting in combination with turbine

15 p2355 A71-32213

Compressors and turbines centripetal stages operational characteristics, investigating airflow rate and pressure ratio effects on power

24 p3790 A71-45380

TURBOALTERNATORS

U AC GENERATORS

U TURBOGENERATORS

TURBOCHARGERS

U SUPERCHARGERS

U TURBOCOMPRESSORS

TURBOCOMPRESSORS

Pressure fluctuations on fixed blades of axial flow compressor, determining sensor dynamic characteristics

01 p0003 A71-11024

Rotating stall in axial flow compressor high pressure stages, taking into account boundary layer separation

01 p0003 A71-11063

Guide vanes small aspect ratio effect on high pressure stages of axial flow compressors

02 p0186 A71-12558

Casing/end wall/ boundary layers in multistage axial flow compressors, discussing velocity distributions

03 p0340 A71-13144

Sound generation by rotor-stator interaction in subsonic axial flow compressors, using acceleration potential and wake technique

03 p0469 A71-13277

Axial flow compressors radiated sound reduction by segmented stator blades

03 p0353 A71-13283

Automatic antisurge control of axial compressor using partial gas recycling bypass method

03 p0469 A71-13370

Axial flow compressor design emphasizing component efficiency

03 p0470 A71-13825

Axial compressor flow characteristics by computerized calculation methods, considering annular duct swirling flow model

03 p0342 A71-13828

Cascade flow test data, considering blade section performance in transonic and supersonic axial flow compressors

03 p0343 A71-13829

Low speed two dimensional axial flow compressor cascade data, considering lift drag ratio and minimum loss coefficient

[ASME PAPER 70-WA/GT-10] 03 p0343 A71-14118

Fan/compressor noise research covering vane/blade ratio and geometry effects on transmission through blade rows

[ASME PAPER 70-WA/GT-12] 03 p0471 A71-14120

Single stage axial flow turbocompressor with trips, examining viscosity effects on flow velocity profiles

[ASME PAPER 70-WA/FE-24] 03 p0343 A71-14133

Two stage compressors with subsonic and supersonic air velocity and high camber rotor blades, discussing strength against centrifugal force

05 p0796 A71-16647

Pure impulse two stage turbocompressor, preventing surge with automatic adjustment to air flow rate

05 p0796 A71-16798

Turbocharged diesel engine precompressed intake cooling by evaporation cooling, considering water injection effects on centrifugal compressor

08 p1347 A71-21268

Axial compressor blades surface finish and fatigue strength restoration by vibrational tumbling

08 p1295 A71-21268

Multistage gas turbine design optimization, using parameter and component analysis with computer calculations

08 p1348 A71-21268

Velocity and static pressure redistribution in distorted flow field upstream of axial flow compressor

[AIAA PAPER 69-485] 10 p1553 A71-24242

Axial compressor subsonic stages theoretical experimental investigation, discussing blade design calculation and experimental methods and results

10 p1554 A71-24242

Sound radiation and wake turbulence spectra for axial compressor single airfoils, including double circular arc profiles

[ASME PAPER 71-GT-4] 11 p1703 A71-25952

Soviet book on theory of aircraft bladed machines covering axial flow, centrifugal and composite turbines and compressors, thermodynamic efficiency control turbocompressor matching, etc

11 p1814 A71-26242

Large axial compressor flow straightening stator blades unsteady pressure measurements with short response time detectors

12 p1945 A71-27351

Measurement errors in testing single stage air driven axial flow compressors and turbines

13 p2115 A71-28115

Multistage axial flow compressors on digital computer, testing gas dynamic design in final adjustment phase

13 p2115 A71-28115

Monograph on potential flow interaction between blade rows in axial flow compressors covering mathematical model, numerical analysis and experiment

13 p1990 A71-28115

Circumferential traversing probe technique for multistage analysis of axial flow compressors, considering mass flow averaging data reduction technique

[ASME PAPER 71-FE-33] 13 p2118 A71-29442

Axial flow turbines comparative performance tests under steady and pulse flow conditions for turbocharger application

14 p2169 A71-29442

Vibration analysis for static and rotating objects by stroboscopic holography, considering axial flow compressor blades and two-mass system with torsional vibration

15 p2404 A71-31124

Dynamic stress on rotor blades of aircraft engine axial compressor stages with low hub/diameter ratios

16 p2624 A71-33124

Noise research facility for fan and multistage compressor sound radiation, discussing anechoic chamber power drive, test control, recording and real time analysis system

16 p2553 A71-33124

Gas turbine with high velocity combustor, pure pulse compressor and turbine and isothermal burner

17 p2793 A71-34124

Multiple tone generation by axial flow transonic compressors, considering shock waves production and propagation associated with supersonic elements

18 p2848 A71-36424

Segmented stator vanes performance in axial flow compressor, noting radiated sound reduction

20 p3175 A71-39024

Higher pressure ratios trend in aircraft gas turbine leading to higher exit temperatures from compressor noting real gas effects

21 p3437 A71-40124

Normal shock existence in blade spacings of rotor and guide vanes of axial flow supersonic compressor as function of pressure nonuniformity

22 p3479 A71-41824

Streamline calculation of gas flow in bypass compressor with flow area divided by longitudinal partition

22 p3479 A71-41824

Circumferentially nonuniform flow in front of axial compressor stage with stepwise two zone pressure velocity distribution resulting in increased guide vane losses

22 p3479 A71-41824

Circumferential flow direction nonuniformity effect in front of compressor wheel on intensity spread and resonant rotor blade vibrations

22 p3615 A71-41824

Axial flow compressors stable operation, using rotating guide vanes regulation

23 p3626 A71-43553

TURBOCONVERTERS

U TURBOGENERATORS

TURBOELECTRIC CONVERSION

U TURBOGENERATORS

TURBOFAN AIRCRAFT

NT A-7 AIRCRAFT

NT BAC 111 AIRCRAFT
NT BOEING 737 AIRCRAFT
NT CONCORDE AIRCRAFT
NT DH 121 AIRCRAFT
NT DO-31 AIRCRAFT
NT F-28 TRANSPORT AIRCRAFT
NT F-111 AIRCRAFT
NT IL-62 AIRCRAFT
NT SAAB 37 AIRCRAFT
NT SE-210 AIRCRAFT
NT TU-134 AIRCRAFT
NT TU-144 AIRCRAFT

Turbofan STOL transport application to air transportation congestion, discussing conditioning landing field length, navigational/control problems and jet flap concepts

12 p1868 A71-27602

Quiet turbofan STOL feasibility, discussing structural, propulsive and technical aspects, economy, passenger comfort and performance estimates

15 p2348 A71-31605

TURBOFAN ENGINES

High lift systems for four-engine Mach 0.8 turbofan STOL aircraft, discussing propulsion, aerodynamics and design trends

[SAE PAPER 700811] 01 p0003 A71-11545

RB 211 turbofan engine design, emphasizing modular construction, systems integration, maintainability and noise reduction

02 p0298 A71-11682

M49 Larzac turbofan engine, describing design, development, performance data, manufacturing techniques, operation and maintenance

02 p0299 A71-12607

RB 211 turbofan engine development testing, describing test program, test facilities, equipment and instrumentation

02 p0299 A71-12912

High bypass ratio fan engine design for low noise, discussing acoustic treatment, turbine noise and modulation tones

[ASME PAPER 70-WA/GT-14] 03 p0471 A71-14122
Turbojet and turbofan engines state of art statistical compilation, presenting graphs of interrelationship of characteristic values and design parameters

05 p0839 A71-16139

Supersonic flow field downstream of turbofan aircraft engine fan nozzle over bodies of revolution, using boundary layer theory and method of characteristics

05 p0796 A71-17150

Low velocity and coaxial jet noise data and correlations for noise prediction of turbofan engines

05 p0796 A71-17155

Turbofan engine noise reduction, using acoustic liners in inlet and exhaust ducts

[AIAA PAPER 71-183] 06 p0947 A71-18622

Subsonic jet engine noise reduction, considering turbojets, turbofans and jet suppressors

08 p1349 A71-21814

Design point selection on fan characteristic curve of turbofan engines, discussing bypass ratio effect on specific impulse, flight velocity and turbine inlet temperature

08 p1349 A71-22042

Turbofan VTOL or STOL intercity aircraft, examining high bypass lift engine design

10 p1557 A71-24861

Discrete frequency rotor interaction noise from lifting fans, using force harmonics acting on blades

[ASME PAPER 71-GT-12] 11 p1812 A71-25958

Design and fabrication of Borsic aluminum composite fan blades for supersonic turbofan engines, considering 430 F application without severe vibratory stress

[ASME PAPER 71-GT-90] 11 p1771 A71-25997

Convertible fan/shaft engine for V/STOL tactical and transport aircraft, detailing mechanical arrangement, design and performance

11 p1813 A71-26054

PT6A-6 turboprop engine technology leading to turboprop, turboshaft and turbofan engines development

[SAE PAPER 710385] 12 p1946 A71-27536

CF6 turbofan engine development, discussing performance and endurance tests and design changes for reliable low cost operation

[SAE PAPER 710421] 13 p2114 A71-28308

Supersonic staggered gutter colander combustion system for plenum chamber burning on high bypass Pegasus turbofan engine of Harrier VTOL aircraft, noting performance improvement

13 p2116 A71-28743

Afterburning turbofan engine thrust calculation by gas generator method, using F-111A for comparison tests

[AIAA PAPER 71-680] 14 p2292 A71-30744

Turbojet and turbofan augmentors combustion instability, discussing pressure oscillations elimination by screech liner and flameholder design

[AIAA PAPER 71-698] 14 p2294 A71-30757

Combination tone noise generation from turbofans with supersonic fan blade tip speed, determining sound power distribution among engine rotation frequency harmonics

[AIAA PAPER 71-730] 14 p2295 A71-30777

Acoustic linings for attenuation of fan generated noise in turbofan engines, considering interaction between analytical lining performance prediction and flow duct testing

[AIAA PAPER 71-731] 14 p2295 A71-30778

Optimal turbofan engine and reaction drive rotor combinations for helicopter design

[AHS PREPRINT 561] 14 p2297 A71-31108

Fan induced low speed jet noise from turbofan engines, discussing results of far field sound measurements for simulated nacelle configurations with and without acoustic liners

[AIAA PAPER 71-586] 15 p2467 A71-31533

French SNECMA M56 turbofan engine design for medium capacity airliners, featuring low specific fuel consumption and low noise level

15 p2471 A71-32692

Fan jet first stage turbine blade air cooling, describing design, heat transfer data, efficiency and temperature distribution

18 p2956 A71-35904

F 101 30,000 lb thrust augmented turbofan engine for B-1 bomber, considering maintainability and bird ingestion tolerance

19 p3122 A71-37491

Aircraft structures sonic fatigue due to high frequency noise from turbofan engines, discussing case histories, failure diagnosis and precautionary design measures

19 p2997 A71-37843

Low noise levels of DC-10 aircraft with CF6-6D turbofan engines, discussing design, flyover tests and FAA requirements

[CASI PAPER 72/5] 20 p3178 A71-39424

Mixed and unmixed turbofan engines transient and steady state off-design characteristics, investigating effects of fuel flow rate, nozzle area, inlet pressure, ambient temperature and air bleed

22 p3590 A71-42836

TURBOFANS

Fan/compressor noise research covering vane/blade ratio and geometry effects on transmission through blade rows

[ASME PAPER 70-WA/GT-12] 03 p0471 A71-14120

Fan propulsion power plants with mechanical and gas dynamical energy distribution systems for commercial VTOL aircraft

09 p1511 A71-22964

Coupled vibration modes for nonrotating blade-disk system in axial flow turbines and fans calculated by finite element method

[AIAA PAPER 71-375] 11 p1845 A71-25348

Tip turbine driven lift fan noise reduction tests, considering design parameters effects

[AIAA PAPER 71-743] 14 p2296 A71-30784

Turbine alternating fan failure due to flutter by coupling of vibration modes and effect of mass distribution in blade

18 p2980 A71-36696

Multiple pure tone and broadband noise generation in high speed turbofans, noting analytical model

20 p3277 A71-39773

TURBOGENERATORS

Nuclear reactors for space power supply with turboelectric, thermoelectric and thermionic converters

02 p0282 A71-12305

Soviet handbook of aircraft electrical equipment covering DC and turbine powered generators, lubrication materials, electromagnetic interference countermeasures, etc

14 p2181 A71-29330

SNAP 8 turbine-alternator as nuclear-electric space power converter, discussing rotating machinery components design and 10,000 hr endurance testing results

15 p2447 A71-32208

Rankine cycle turboelectric nuclear space power conversion system with liquid K as working fluid, discussing current technology status

16 p2526 A71-33525

TURBOJET AIRCRAFT

U JET AIRCRAFT

TURBOJET ENGINE CONTROL

Optimal synthesis of selective multidimensional invariant control systems applied to turboprop engine with differential reductor

01 p0062 A71-10718

Two-spool turbojet engine nozzle diameter adjustment system for increasing thrust, fuel economy and reliability, describing automatic clamshell shutter control mechanism

15 p2471 A71-32527

TURBOJET ENGINES

NT BRISTOL-SIDDELEY OLYMPUS 593 ENGINE

NT DUCTED FAN ENGINES

NT J-57 ENGINE

NT J-85 ENGINE

NT TURBOFAN ENGINES

NT TURBOPROP ENGINES

Turbojet engine design for methane element of liquefied natural gas as aircraft fuel, discussing supersonic transport applications

01 p0141 A71-10485

Two-spool turbojet engines matching by rapid superposition method

01 p0142 A71-10821

Air transportation reliability through turbojet engine performance monitoring

02 p0298 A71-12368

Two shaft turbojet engine parameter plot techniques effectiveness, varying low pressure cascade rpm or nozzle system passage cross sections

03 p0472 A71-14259

Turbojet and turbofan engines state of art statistical compilation, presenting graphs of interrelationship of characteristic values and design parameters

05 p0839 A71-16139

Subsonic jet engine noise reduction, considering turbojets, turbofans and jet suppressors

08 p1349 A71-21814

Twin spool turbojet engine dynamic response, discussing simulator predictions, digital computer control, nozzle area variations and operating trajectories

[ASME PAPER 71-GT-14] 11 p1812 A71-25960

Low cost short life gas turbine design based on parametric performance and component selection, outlining turbojet production

[ASME PAPER 71-GT-69] 11 p1813 A71-25984

Vertical straight lift turbojet engine design and development, presenting component material properties/weights, endurance tests and performance data

[ASME PAPER 71-GT-75] 11 p1813 A71-25989

Supersonic inlet turbojet engine compatibility tests in wind tunnels, using light panels and Summation Device analysis

13 p2114 A71-28032

RB 162 turbojet engine combustors for VTOL aircraft, achieving ignition by two pressure jet atomizers operative during starting cycle

13 p2116 A71-28742

Subsonic and supersonic turbojet aircraft engines development, discussing design, operation, reliability, weight, fuel consumption and cost

14 p2287 A71-29811

Absorbent materials for sound attenuation in turbine ducts, examining flow velocity, absorbent structure and cladding effects

14 p2288 A71-30518

Turbojet and turbofan augmentors combustion instability, discussing pressure oscillations elimination by screech liner and flameholder design

[AIAA PAPER 71-698] 14 p2294 A71-30757

Turbojet engine combustor nitric oxide formation prediction based on adiabatic micromixed perfectly stirred reactor model analysis

[AIAA PAPER 71-713] 15 p2470 A71-32286

Jet engine high pressure turbine high temperature alloy blades and vanes grinding operation, discussing testing, operating conditions and coolant application

[SME PAPER MR-71-802] 15 p2416 A71-32432

Linear two shaft turbojet model development and conditions for stability, observability, controllability and feedback loop parameters

15 p2383 A71-32711

Turbojet engines thrust and fuel economy improvement by gas-air jet mixing, discussing efficiency increase and noise reduction

15 p2472 A71-32717

Optimal gas temperature in bypass and turbojet engines afterburners ensuring minimum fuel flow rate dependence on thrust augmentation

16 p2624 A71-33607

TURBOMACHINE BLADES

NT COMPRESSOR BLADES

NT ROTOR BLADES [TURBOMACHINERY]

NT STATOR BLADES

NT TURBINE BLADES

Sweptback turboblades in parallel wall channel, investigating thickness, camber and leading edge curvature effects on flow and pressure distributions and vortex movement

02 p0186 A71-12606

Flow characteristics in turbomachine blade cascades with transonic regime, emphasizing shock-boundary layer interaction phenomena

03 p0340 A71-13140

Turbomachine blades torsional-bending vibrations aerodynamic damping, noting natural frequency shift

03 p0340 A71-13141

Turbulent separation and reattachment at turbomachine blade trailing edge at supersonic speeds, discussing various flow models

03 p0340 A71-13142

Pressure distribution over blade in cascade nozzle for incompressible and compressible particulate gas flow

[AIAA PAPER 71-82] 06 p0883 A71-18539

Three dimensional transonic shear flow structure in turbomachine cascade, using time dependent numerical solution

[AIAA PAPER 71-83] 06 p0843 A71-18540

Rotating low aspect ratio turbomachinery blades natural frequencies and mode shapes, using finite element method for equilibrium equations eigenvalue problem

[AIAA PAPER 71-374] 11 p1845 A71-25347

- Steady three dimensional subsonic nonviscous flow through turbomachine with arbitrary hub and shroud shapes and finite blade number, using iterative blade to blade procedure
[ASME PAPER 71-GT-2] 11 p1702 A71-25948
- Two dimensional flow in radial turbomachine bladed impeller, comparing numerical solution based on potential theory with experimental results
[ASME PAPER 71-GT-20] 11 p1703 A71-25964
- Cascading turbomachine blade row coupled flutter, correlating camber angle, cascade condition and elasticity
13 p2157 A71-29128
- Supercavitating flow past straight cascade with arbitrary blade shapes, considering lift and drag coefficients, cavitation number, cavity shape and exit flow conditions
[ASME PAPER 71-FE-6] 13 p1995 A71-29448
- Sound radiation and pressure fields inside vibrating turbomachine blades, using miniaturized microphones and compact capacitive detectors
14 p2288 A71-30517
- Cascading turbomachine blades vibrations measurement in subsonic and sonic high temperature gas flows, describing test facility
16 p2553 A71-33993
- Stagnation pressure changes in unsteady flow downstream of turbomachine blades with fluctuating circulation related to vortex sheets
17 p2671 A71-35279
- Incompressible potential cascade flow interaction, presenting approximate method based on blade profile flow expression by power series with distance between cascades as parameter
21 p3322 A71-40685
- TURBOMACHINERY**
- NT AXIAL FLOW TURBINES
NT CENTRIFUGAL COMPRESSORS
NT CENTRIFUGAL PUMPS
NT GAS TURBINES
NT SHROUDED TURBINES
NT STEAM TURBINES
NT SUPERSONIC TURBINES
NT TURBINE PUMPS
NT TURBINES
NT TURBOCOMPRESSORS
NT TURBOFANS
NT TURBOGENERATORS
NT TWO STAGE TURBINES
- Radiometric determination of diametrical distance between rotor and stator of turbomachines
03 p0421 A71-13003
- Internal aerodynamics /turbomachinery/ - Conference, Cambridge University, England, July 1967
03 p0342 A71-13823
- Turbomachinery R and D to improve components and engine performance
03 p0470 A71-13824
- Compressible flow similarity parameters, establishing dimensionless relations for radial turbomachines design
03 p0343 A71-13830
- Turbine machine elements approximation by difference equations of axisymmetrical elasticity theory problem
04 p0671 A71-15644
- Tilting pad hydrodynamic and porous hydrostatic gas lubricated journal bearings for miniature cryogenic turbomachinery
[ASLE PREPRINT 70LC-10] 08 p1298 A71-21158
- Axial turbomachine three dimensional cascade flow calculation from dynamics vector equations
09 p1383 A71-23601
- Entropy production in adiabatic flow in turbomachines, based on momentum equations for inviscid flow
[ASME PAPER 71-FE-3] 13 p1994 A71-29446
- True time averaged oscillating pressure measurements and testing in turbomachinery, including hydraulic, mechanical and evaluation methods
[ASME PAPER 71-FE-28] 13 p1995 A71-29464
- Turbomachinery rotor and stator row aerodynamic interaction, describing discrete tone noise generation from far field measurements
15 p2450 A71-32134
- Turbomolecular vacuum pump impeller theoretical efficiency with allowance for diffuse law of interaction between gas molecules and interblade channel walls
20 p3183 A71-39170
- Uniform inlet flow inside centrifugal turbomachinery diffusers with flat parallel side walls, measuring pressure distribution and boundary layer velocity profiles
21 p3323 A71-40757
- TURBOPROP AIRCRAFT**
- NT AN-24 AIRCRAFT
NT C-130 AIRCRAFT
- Propeller blade structures for high speed tilt wing turboprop V/STOL aircraft, considering materials selection, weight control, cyclic pitch control, noise reduction, etc
[DGLR-71-018] 15 p2350 A71-32785

- Soviet book on practical aerodynamics of aircraft with turboprop engines covering piloting, forces and moments, stability, controllability, takeoff, landing, etc
19 p2994 A71-38534
- TURBOPROP ENGINES**
- Optimal synthesis of selective multidimensional invariant control systems applied to turboprop engine with differential reductor
01 p0062 A71-10718
- Universal mini carrier UMC-120 light turboprop STOL transport
05 p0696 A71-16133
- Equation derived for operation of turboprop engine with high pressure compressor controlling gas temperature at turbine front
08 p1347 A71-20831
- Turboprop aircraft engine service life extension, correcting deficiencies via accelerated tests based on relation between failure rate and usage
09 p1511 A71-22633
- Turboprop and turboshaft engine control requirements, showing torque and power dependence on engine speed and control block diagrams
10 p1659 A71-24755
- PT6A-6 turboprop engine technology leading to turboprop, turboshaft and turbofan engines development
[SAE PAPER 710385] 12 p1946 A71-27536
- Reduction gearbox reliability problems from development and service experience with PT6A turboprop engine
[SAE PAPER 710433] 13 p2073 A71-28318
- TURBOPUMPS**
- U TURBINE PUMPS
- TURBORAMJET ENGINES**
- Axisymmetric inlet design for turboramjet powered hypersonic cruise vehicle, examining effects of spillage and cowl drags on air flow characteristics
16 p2521 A71-34149
- TURBOROTORS**
- U TURBINE WHEELS
- TURBOSHAPTS**
- Turbine disks and shafts for low temperature operation, examining brittle fracture tendency by acceleration testing
01 p0098 A71-10078
- Turboprop and turboshaft engine control requirements, showing torque and power dependence on engine speed and control block diagrams
10 p1659 A71-24755
- PT6A-6 turboprop engine technology leading to turboprop, turboshaft and turbofan engines development
[SAE PAPER 710385] 12 p1946 A71-27536
- VTOL turboshaft engine powered propulsion system development, detailing design requirements, program planning, component research and system integration
[AHS PREPRINT 562] 14 p2297 A71-31109
- Linear two shaft turbojet model development and conditions for stability, observability, controllability and feedback loop parameters
15 p2383 A71-32711
- Turbine wheels and shafts for low temperature operation, examining brittle fracture by acceleration testing
16 p2593 A71-33634
- TURBOSUPERCHARGERS**
- U SUPERCHARGERS
U TURBOCOMPRESSORS
- TURBULENCE**
- NT ATMOSPHERIC TURBULENCE
NT CLEAR AIR TURBULENCE
NT GUSTS
NT HOMOGENEOUS TURBULENCE
NT ISOTROPIC TURBULENCE
NT LOW LEVEL TURBULENCE
NT LOW TURBULENCE
NT MAGNETOHYDRODYNAMIC TURBULENCE
NT PLASMA TURBULENCE
- Acoustic turbulence spectrum in compressible fluid with potential motion, using complex traveling wave amplitudes in hydrodynamic equations
02 p0239 A71-11924
- Turbulence intensity in combustion zone of stabilized air-kerosene flame from annular burner, using He diffusion measurements
03 p0520 A71-13994
- Two dimensional wall jet and wall wake flow turbulence characteristics, considering mean and fluctuating flow properties
[ASME PAPER 70-WA/APM-35] 03 p0403 A71-14161
- Decay time of low Reynolds number weak turbulence generated by single and multistage grids, considering three dimensional energy spectrum
04 p0569 A71-15026
- Elliptical and spiral galactic angular momentum and velocity dispersion relations, considering cosmological turbulence during formation
06 p0971 A71-18244
- High beta collisionless shock wave turbulence, discussing frequency and wavenumber spectra and

- turbulence level measurements by light scattering technique
09 p1504 A71-23221
- Turbulence research retrospective and new developments, reviewing contributions by Reynolds, Rayleigh, Prandtl, Taylor and Tollmien
11 p1751 A71-25449
- Electromagnetic backscatter cross section for irregular turbulent dielectric media by rigorous heuristic derivations
13 p2028 A71-27575
- Inertial range transfer in two and three dimensional turbulence, using almost-Markovian Galilean-invariant model
15 p2445 A71-31958
- Real turbulent fluctuations superimposed on mean and satisfying free space Einstein equations, basic model on oscillating gravitation and elementary particles as excitons
17 p2777 A71-34950
- Self generated turbulence in insulating liquids during unipolar charge carrier injection, describing charge transport by Lagrangian diffusion process
19 p3044 A71-37770
- Turbulence growth during parametric wave excitation, observing thermal noise effects
19 p3104 A71-37871
- Kinematic dynamo equations for turbulent generation of large scale magnetic and small scale turbulent fields, presenting exact treatment of fluctuation as ordered field equations
21 p3416 A71-41111
- Book on turbulence covering measurement techniques, equations of motion, Newtonian viscous fluids, Reynolds stresses, flow visualization, random processes, turbulent energy, boundary layers, etc
21 p3371 A71-41221
- TURBULENCE EFFECTS**
- Mountain-size atmospheric eddies on leeward slopes of Carpathian and Low Tatra mountains, discussing turbulence effects on air navigation
01 p0113 A71-10343
- Frequency correlation between amplitude and phase fluctuations of different-frequency spherical waves propagating in turbulent medium
01 p0073 A71-10545
- Nonlinear single-degree of freedom mechanical system vibration under small random perturbations
01 p0127 A71-10549
- Turbulent diffusion role in magnetic fields origin in sun, planets and galactic gaseous disk
01 p0162 A71-11414
- LAMS flight demonstration, discussing instrumentation, flutter boundary and dynamic responses, aerodynamic testing and structural response to turbulence
02 p0188 A71-11664
- Clear turbulent atmosphere effects on optical transmission characteristics and communication systems design
02 p0213 A71-12018
- Atmospheric turbulence effects reduction in optical communication by statistical communication theory, considering digital system and waveform estimation
02 p0213 A71-12018
- Optical heterodyne receiver design, using nonlinear recursive techniques to estimate atmospheric fluctuation effects on IF signal characteristics
02 p0249 A71-12023
- Galaxies dynamic parameters formation associated with cosmological turbulence in expanding universe
02 p0307 A71-12081
- Atmospheric turbulence effects on stellar Michelson interferometry
02 p0308 A71-12095
- German monograph on differential solar rotation resulting from anisotropic turbulent viscosity in hydrogen convection zone
02 p0317 A71-12844
- Statistical prediction of atmospheric turbulence effects on aeronautical systems
03 p0398 A71-13133
- Clear air turbulence effects on flight and structural response of aircraft, using gust loads model
[ONERA-TP-867] 03 p0346 A71-13136
- Turbulence level effects on aerodynamic losses of axial flow turbomachines, discussing boundary layer of blades
03 p0340 A71-13143
- Tower turbulence characteristics, using surface wind and temperature measurements to estimate horizontal velocity and dissipation rate variances at top
03 p0452 A71-13222
- Two channel 450 mm TV telescope at Pulkovo Observatory, investigating atmospheric turbulence deformations of stellar images
04 p0588 A71-14828
- Free stream turbulence enhanced stagnation line heat and mass transfer on two dimensional blunt body
04 p0681 A71-15481

Air flow turbulence effect on heat transfer and boundary layer growth around flat plate, aerodynamic profile and cylinder

04 p0681 A71-15483

Various free stream turbulence levels at nonconverging and converging walls, investigating foreign gas film cooling

04 p0683 A71-15501

Optical beam scintillation dependence on wavelength in strong refractive index turbulence

04 p0609 A71-15694

Hydrogen plasma turbulent heating, simulating ion-acoustic instability

05 p0786 A71-16226

Thermoanemometer frequency characteristic determination, simulating turbulent oscillations by plane acoustic waves

05 p0753 A71-16845

Heat transfer from rotating disk to parallel nonrotating disk, investigating turbulence effect from air flow pattern observation

06 p1007 A71-18315

Solar photosphere macroturbulence effects on Fraunhofer lines and central intensities of various absorption lines

06 p0975 A71-18443

Gaseous film cooling effectiveness under varying conditions of free stream turbulence intensity, hot gas acceleration, Mach number and film coolant flow rate

07 p1219 A71-18760

Wall flow boundary layer, observing external turbulent field effect on velocity and temperature distribution and heat exchange

07 p1086 A71-18771

Hot-wire anemometer calibration, measuring shear stress and turbulence distributions in circular channel

07 p1106 A71-18785

Laser beam propagation through atmosphere, measuring phase variation dependence on turbulent temperature structure for comparison with prediction

07 p1123 A71-19574

Galaxies dynamic parameters formation associated with cosmological turbulence in expanding hot universe

08 p1362 A71-21135

Atmospheric turbulence effects on stellar Michelson interferometry

08 p1362 A71-21149

Magnetic field generation in acoustically turbulent medium, deriving spectral function equation

08 p1341 A71-21795

Rotor blade random vibrations in response to turbulence

[AIAA PAPER 70-548]

09 p1381 A71-22081

Turbulence properties in supersonic flow, considering modes with vorticity, entropy and acoustic aspects

09 p1383 A71-23603

Surface roughness ensuring turbulent reattachment at low Reynolds numbers on airfoil sections with separation near leading edge resulting in bubbles

[ONERA-TP-923]

10 p1549 A71-23762

Scalar wave equation of mutual coherence propagation in turbulent medium with stochastic permittivity using local independence approximation

10 p1641 A71-24398

Atmospheric turbulence effects on sonic boom rise times by statistical theory

10 p1556 A71-24817

Binary on-off laser communication channels, calculating atmospheric turbulence effect on Poisson detection error probability

11 p1730 A71-25198

Comparative vertical turbulence and loss restrictive stochastic models for threshold crossing rotor blade flapping vibrations at low lift high advance ratio

[AIAA PAPER 71-389]

11 p1846 A71-25351

Solar photosphere macroturbulence effects on Fraunhofer lines and central intensities of various absorption lines

12 p1955 A71-26593

Optical beam propagation, determining turbulent medium effects with holographic wave front reconstruction technique

12 p1904 A71-26795

Condenser microphones aerodynamically induced noise, investigating acoustic pressure lower limit dependence on air flow velocity and turbulence

12 p1888 A71-27063

Ice forming nuclei in atmosphere during severe convective storms from aged background aerosol and soil particles aerosolized by storm turbulence

12 p1925 A71-27197

Atmospheric turbulence effects on focused coaxial carbon dioxide and He-Ne laser beam propagation

13 p2078 A71-28525

Grid-induced turbulence effect on flameout characteristics of kerosene-air flames stabilized by bluff bodies of different sizes

13 p2163 A71-28961

Turbulence level effects on mixing of three plane parallel slipstreams with equal velocities and temperature from smoke visualization

13 p2163 A71-28962

Wind noise reduction by windshields, considering effect of mean flow velocity, turbulence, flow direction, windscreen shape and size, covering material and microphone location

13 p2040 A71-29283

Fluctuations of Gaussian light beams due to turbulence in lenslike medium, using perturbation method

13 p2102 A71-29388

Atmospheric turbulence effect on turbine powered transport aircraft, discussing gust accelerations, avoidance, detection, forecasting and pilot control

14 p2172 A71-29750

Air turbulence primary and secondary effects on aircraft flight and avoidance criteria considerations

14 p2268 A71-29768

Flight characteristics under atmospheric turbulence conditions, analyzing analog trace records of airspeed, normal acceleration, altitude, air temperature, control surface and flight attitude parameters

14 p2173 A71-29771

Automatic aircraft landing system modification for improvement of response to air turbulence effects

14 p2271 A71-29773

Atmospheric turbulence effects on stellar irradiance and phase, discussing electro-optical recording technique and computer generated statistical data

14 p2270 A71-30016

Linear antenna radiation pattern broadening due to atmospheric turbulence

14 p2194 A71-30074

Atmospheric turbulence effect on far field diffraction pattern of annular aperture

14 p2275 A71-30465

Asymptotic intensity fluctuations of plane light wave propagating in turbulent medium, using parabolic equation and Markov model

15 p2387 A71-31190

Sonic boom pressure signature laboratory scale measurement after modification by traveling through air jet turbulence, comparing with statistical prediction

[AIAA PAPER 71-618]

15 p2388 A71-31547

Grid induced turbulence effects on air flow around enclosed diffusion flame

[WSS/CI PAPER 71-14]

15 p2463 A71-31623

Rapidly rotating early stars and quasars, determining magnetic field generation by turbulent dynamo mechanism

15 p2485 A71-31725

Structural panel under acoustic loading by supersonic convected turbulence, deriving responses with finite Fourier transforms

15 p2507 A71-32131

Sonic boom phenomena, discussing supersonic flow near aircraft, atmospheric propagation, distortion, focusing, caustics, turbulence effects and reduction

15 p2350 A71-32566

Galaxy formation in expanding universe, discussing primordial plasma and photon gas turbulent medium for magnetic field amplification by dynamo mechanism

16 p2625 A71-33052

Galaxy formation by weak and strong primeval turbulence in relation to velocity and density perturbation

16 p2631 A71-33232

Magnetic field generation in acoustically turbulent MHD medium, deriving spectral function equation and eigenvectors

16 p2619 A71-33545

Refraction, terrain, air attenuation, fog and rain, turbulence and shielding effects on acoustic propagation in lower atmosphere

17 p2734 A71-35235

Solar oblateness and Li abundance interpretation by model of thermally driven turbulence terminated at rotating core surface containing partial mass

17 p2806 A71-35385

Direct numerical integration for equation of radiative transfer in turbid atmosphere with allowance for scattering on molecules and aerosols

17 p2736 A71-35564

Numerical solution of time dependent incompressible flow differential transport equations including turbulence effects

18 p2905 A71-36312

Kinematic-dynamo theory with turbulent diffusivity effect, discussing resistivity as random function of position

18 p2969 A71-37045

Flight investigation of turbulence effects on aircraft longitudinal flying qualities, evaluating pilot ratings for ILS approach task

[AIAA PAPER 71-905]

19 p2995 A71-37156

Laser light beam attenuation, considering turbulent pulsation effects in closed channel fluid flow axial region

19 p3071 A71-37279

Collisions or weak turbulence caused noise effects on broadening of echo pulses in magnetically trapped particles, using propagator formalism

19 p3113 A71-37746

Free stream turbulence effects on local heat transfer from sphere situated in forced convection air flow

[ASME PAPER 71-HT-8]

19 p3164 A71-37985

Milky Way galaxy internal small scale magnetic field generation, relating strength to cyclonic turbulence properties and large scale shear

20 p3287 A71-39055

Solar magnetic field generation by gyrotropic turbulence, noting inadequacy of Steenbeck explanation for quantitative estimates of solar cycle parameters

20 p3291 A71-39317

Upper atmospheric anomalous molecular oxygen distribution, discussing turbulent theory with autocorrelation of density fluctuations

20 p3222 A71-39701

Turbulent shear effect on isolated trailing single vortex decay behind aircraft

21 p3320 A71-40503

Momentum transfer between gas and condensed phase in metallized solid propellant rocket motors, measuring noncontinuum and turbulence effects on sphere drag

21 p3437 A71-40861

Resistance wire temperature sensor spatial resolution calculation, considering sensor length and isotropic turbulence effects on temperature spectrum and dissipation

22 p3542 A71-41904

Variable stability aircraft lateral directional flying qualities, investigating turbulence effects

22 p3483 A71-42833

Aircraft wake turbulence and trailing vortices, investigating physical characteristics, hazard potential and avoidance techniques

23 p3628 A71-43234

Review of papers at EUROMECH 23 colloquium on finite amplitude and diffusive effects in acoustics, covering acoustic damping by relaxation, dust and moisture, turbulence effects, etc

23 p3704 A71-43447

Centrifugal wheel flow swirl effect on pressure/flow rate characteristic in input zone

23 p3626 A71-43555

Narrow light beam transmission in weakly nonlinear turbulent atmosphere, calculating large scale permittivity inhomogeneity effect on average intensity by model

23 p3645 A71-43564

Thermal history of universe traced from assumption of photon and plasma turbulence for galactic formations, discussing thermal instability and heating effects

23 p3770 A71-44181

Turbulent defocusing and displacement fluctuations of focused He-Ne laser beam in atmosphere over paths near ground

23 p3688 A71-44329

TURBULENCE METERS

Liquid flow velocity fluctuations measuring methods based on liquid-electrode contact potential dependence on flow velocity-electrolyte conductivity temperature relationship

01 p0072 A71-11225

Turbulence measurement by electrothermoanemometry, discussing method errors

05 p0753 A71-16846

Atmospheric turbulence measurement and detection using non-Doppler radar

07 p1058 A71-18845

Hot wire signal interpretation using universal calibration law, studying yaw and incidence angles effects

09 p1453 A71-23694

Structure constant of jet exhaust turbulence of J-57 with afterburner by laser beam probing compared with scintillation and hot-wire anemometer measurements

11 p1766 A71-26304

Miniature aerodynamic turbulence gage using axisymmetric lifting body sensor

13 p2066 A71-28158

Dynamic small perturbation calibration of constant temperature hot-wire anemometers for turbulence measurements in Karman vortex streets, comparing static method

16 p2581 A71-34166

TURBULENT AIR CURRENTS

U AIR CURRENTS

U TURBULENT FLOW

TURBULENT BOUNDARY LAYER

Temperature effects on heat transfer in turbulent boundary layer on cooled plate at various Reynolds numbers

01 p0179 A71-10609

Fluid flow turbulent boundary layer development in channel inlet under injection, obtaining friction coefficient and dynamic characteristics at subsonic velocities

01 p0070 A71-10794

Adiabatic compressible turbulent boundary layer equations for two dimensional and axisymmetric flow, discussing methods of solution based on eddy viscosity formulation

[AIAA PAPER 69-687]

01 p0071 A71-10933

Turbulent boundary layer air flow through supersonic convergent-divergent nozzle with heat transfer, considering relationship between temperature and velocity profiles

01 p0180 A71-10950

Natural convection turbulent boundary layer temperature profile measurements along isothermal vertical plate, indicating temperature distribution independence of altitude in fully developed turbulent region

01 p0180 A71-10994

Axisymmetric hypersonic wind tunnel nozzle design by determining inviscid contour and correcting for turbulent boundary layer growth

[AIAA PAPER 69-337]

01 p0003 A71-11578

Heat transfer and friction drag calculation for turbulent boundary layer of gas with temperature dependent physical properties

02 p0185 A71-11884

Heat and gas curtain efficiency in turbulent boundary layer on flat plate, including heat transfer data

02 p0331 A71-11886

Laminar-turbulent boundary layer transition point on wing, using hot-wire anemometer and oscilloscope

02 p0186 A71-12555

Film cooling in gaseous medium, assuming turbulent boundary layer at blowing point

02 p0333 A71-12645

Compressible turbulent boundary layers with fluid injection, considering transpiration cooling, skin friction coefficient, etc

03 p0398 A71-13128

Fluid mechanics of interaction of shock wave and turbulent boundary layer at transonic-supersonic speeds

03 p0399 A71-13138

Turbulent boundary layer structure and prediction, considering various turbulence onset theories

03 p0340 A71-13147

Three dimensional incompressible wake behind blunt obstacle at leading edge of flat plate compared with mathematical model by Oseen linearization

[AIAA PAPER 69-747]

03 p0341 A71-13434

Turbulent boundary layer recovery factor for wedge model in hypersonic helium flow at high Reynolds and Mach numbers

03 p0517 A71-13461

Compressible turbulent boundary layer skin friction measurements on adiabatic flat plate, discussing drag balance calibration

[ASME PAPER 70-WA/FE-26]

03 p0403 A71-14134

Aircraft fuselage vibration response to turbulent boundary layers, measuring structural wavelengths and phase velocities as functions of frequency

[ASME PAPER 70-WA/DE-10]

03 p0348 A71-14144

Fluid-loaded rectangular plates and membranes random vibration excitation by turbulent boundary layer flow

[ASME PAPER 70-WA/DE-15]

03 p0511 A71-14147

Incident shock test time and reflected pressure for turbulent boundary layer at high Mach numbers in air and nitrogen

04 p0563 A71-14663

Laminar and turbulent boundary layer effects on flow velocity and Mach number behind shock front

04 p0567 A71-14664

Soviet book on friction and heat transfer covering interaction of bodies with internal/external liquid/gas laminar/turbulent boundary layer flows

04 p0571 A71-15264

Skin friction, Stanton numbers, velocity and temperature profiles in accelerating turbulent boundary layer flows, using Prandtl mixing length

04 p0680 A71-15478

Turbulent boundary layer equations for heat and mass transfer in incompressible and compressible flows, using eddy viscosity formulation

04 p0680 A71-15479

Temperature profiles in high velocity compressible turbulent boundary layer over flat plate without pressure gradients

04 p0681 A71-15480

Turbulent compressible two dimensional boundary layer flows with heat transfer, pressure gradients and wall blowing or suction

04 p0681 A71-15482

Two dimensional and axisymmetric flow film cooling effectiveness in supersonic turbulent boundary layer, using Eckert reference enthalpy method

04 p0571 A71-15496

Supersonic compressible turbulent boundary layer on porous cylinder with air injected through wall, investigating heat transfer

04 p0571 A71-15498

Heated jet injection into isothermal turbulent boundary layer, investigating temperature distribution downstream with conduction model

04 p0572 A71-15499

Uniformly blown turbulent boundary layer on flat plate, investigating unheated solid starting length effect on heat transfer

04 p0572 A71-15500

Nonuniform blowing and surface temperature turbulent boundary layer, investigating heat transfer

04 p0684 A71-15502

Incompressible fluid turbulent boundary layer equations, examining approximate semiempirical calculations

04 p0573 A71-15555

Semiempirical differential equation derived for turbulence scale behavior and turbulent boundary layer on flat plate

04 p0575 A71-15606

Statistical characteristics of pulsation pressure on surface in turbulent boundary layer of incompressible fluid, discussing effects near smooth flat wall

04 p0575 A71-15607

Turbulent fluid flow past surfaces, calculating pressure pulsations at boundary layer

04 p0576 A71-15612

Turbulent pressure pulsations at surface of floating body of revolution moving unsteadily in sea water during boundary layer development

04 p0576 A71-15613

Aqueous acid solution turbulent boundary layer characteristics during alkali solution injection through porous surface in presence of positive pressure gradient

04 p0576 A71-15614

Air, helium and carbon dioxide injection effect on turbulent boundary layer thermodynamic behavior by wind tunnel experiments

04 p0576 A71-15615

Pulsed velocity longitudinal component in water flow turbulent boundary layer, investigating intensity, spectral characteristics and drag reduction

04 p0576 A71-15616

Hydrodynamic and thermal measurements in turbulent boundary layer of liquid drop flow past plate for mineral oil-water mixtures

04 p0576 A71-15617

Friction, mass and heat transfer in turbulent boundary layers of fluid flows past obstacles

04 p0577 A71-15619

Microsensor measurement of spatial correlation between pressure fluctuations of turbulent boundary layer

04 p0600 A71-15636

Turbulent boundary layer development and heat transfer in parallel wall passage entrance region, comparing measurement results with computer solution

04 p0689 A71-15920

Incompressible turbulent boundary layer flow over steadily rotating flat plate blade, discussing centrifugal pumping and shear stress

05 p0694 A71-16581

Turbulent boundary layer separation at low supersonic Mach numbers based on blowdown wind tunnel tests

05 p0735 A71-16582

Surface roughness and thermal radiation effects on rural and urban boundary layer turbulence and diffusion by wind fluctuations observations

05 p0777 A71-16665

Air injection into turbulent boundary layer flow through porous plate, examining heat transfer and shielding efficiency

05 p0838 A71-16783

Turbulent energy balance equation terms for atmospheric boundary layer

05 p0778 A71-16837

Turbulent boundary layer wall pressure fluctuations on hydrodynamically smooth and rough surfaces, investigating eddies, space-time decay rate and flow structure

05 p0736 A71-16961

Soviet book on supersonic turbulent boundary layer covering gas flow molecular theory, heat and mass transfer at porous surfaces, etc

06 p0841 A71-17439

Wave number/phase velocity spectrum of wall pressure measurements beneath two dimensional turbulent boundary layer

06 p0882 A71-18317

Supersonic turbulent boundary layer separation on flat plate by forward facing step, measuring mean flow field characteristics

[AIAA PAPER 71-127]

06 p0844 A71-18571

Interaction theory for supersonic separated and reattaching turbulent boundary layers, comparing to real flow past compression ramp

[AIAA PAPER 71-128]

06 p0844 A71-18572

Supersonic turbulent boundary layer measurements in moderate adverse pressure gradient region along two dimensional ramp model

[AIAA PAPER 71-162]

06 p0884 A71-18604

High temperature gaseous flow, discussing approximate methods of calculation of turbulent boundary layer

[AIAA PAPER 71-163]

06 p0885 A71-18605

Two dimensional turbulent boundary layer flows numerical methods with simplicity and accuracy

[AIAA PAPER 71-164]

06 p0885 A71-18606

Finite difference calculation for two dimensional compressible turbulent boundary layer flow with heat transfer, using mixing length concept

[AIAA PAPER 71-165]

06 p0885 A71-18607

Nonadiabatic compressible turbulent boundary layer heat transfer to rough surfaces under arbitrary pressure gradient

[AIAA PAPER 71-166]

06 p0885 A71-18608

Turbulent skin friction and boundary layer velocity measurements on nonadiabatic flat plates at hypersonic Mach numbers

[AIAA PAPER 71-167]

06 p0885 A71-18609

Boundary layer turbulence decay in slender body supersonic near wake expansion region, using linear theory for assessment of change in fluctuation level and turbulent scale size

[AIAA PAPER 71-200]

06 p0845 A71-18639

Separated turbulent eddy viscosity models incompressible similar reverse flow velocity profiles from Falkner-Skan equations

[AIAA PAPER 71-203]

06 p0886 A71-18641

Heat and mass transfer in turbulent boundary layers - Conference, Herceg Novi, Yugoslavia, September 1968, Volume 1

07 p1219 A71-18751

Turbulent boundary layer theories and classification according to prediction ability relative to heat transfer rates, shear stress distribution and fields of concentration

07 p1085 A71-18752

Turbulent boundary layer in incompressible fluid with vanishing viscosity, analyzing degeneration of isothermal boundary layer, viscous sublayer and density pulsations

07 p1085 A71-18753

Wall turbulence Prandtl-Karman constant calculation, using friction law for viscous sublayer degeneration with infinitely increasing Reynolds number

07 p1085 A71-18754

Turbulent boundary layer approximate analytical method based on momentum and energy integral correlations and limiting laws of friction and heat transfer

07 p1085 A71-18756

Transpiration cooling heat transfer in incompressible turbulent boundary layer, using Couette flow model, boundary layer model and combinations of both

07 p1219 A71-18758

Turbulent boundary layer on porous plate with suction and heating, measuring mean velocity and temperature profiles at various locations along wall as function of suction rate

07 p1219 A71-18759

Turbulent boundary layer asymptotic theory, taking into account boundary conditions effect on friction and transfer factor laws

07 p1085 A71-18761

Prediction method for turbulent boundary layer development using shear work integral for range from wall jet to adverse pressure gradient flow

07 p1085 A71-18764

Heat transfer in turbulent boundary layer for arbitrary surface temperature with fluid injection and pressure gradient

07 p1220 A71-18765

Turbulent boundary layer laminarization prediction in moderate accelerations, using Pathankar-Spalding finite difference formulation and experimental results for shear stress model selection

07 p1085 A71-18767

Turbulent boundary layers transpiration cooling prediction with coolant fluid serving as heat sink within structure wall and as protective film

07 p1220 A71-18768

Spalding-Pathankar finite difference method application to combined free and forced convection turbulent boundary layer with variable fluid properties and chemical reaction

07 p1054 A71-18769

Positive pressure gradient turbulent boundary layer local characteristics in plane diffuser, using Reynolds stress change equations

07 p1086 A71-18770

Resistance thermometer for temperature measurement in turbulent boundary layer near wall, giving expression for correction factor

07 p1106 A71-18786

Heat and mass exchange coefficients and critical separation for turbulent boundary layer during nonuniform blowing under nonisothermal conditions

07 p1087 A71-18918

Turbulent cylindrical boundary layer velocity distribution, determining power law functional relationship by wind and water tunnel experimental measurements

07 p1088 A71-19420

Equations systems for free turbulent boundary layer in incompressible fluid, deriving semiempirical formulas for turbulent viscosity coefficient

07 p1089 A71-19735

Viscosity effects on three dimensional supersonic flow around circular half cones on flat plate, examining turbulent boundary layer separation

07 p1014 A71-19743

Skewed turbulent boundary layer and incompressible laminar flow on rotating disk, considering effective viscosity relations and applications domain

07 p1090 A71-19889

Compressible turbulent boundary layers integral solution based on entrainment theory

07 p1090 A71-19903

Turbulent boundary layer skin friction measurement by dual pitot tube, taking into account mean velocity profile 08 p1275 A71-21309

Turbulent boundary layer pressure fluctuations in-flight measurements on Boeing 737 aircraft, obtaining power spectral densities and RMS pressure fluctuations for various Mach numbers 08 p1231 A71-21426

Pressure gradient and roughness effects on laminar, transition and turbulent boundary layer in hypersonic shock tunnel 08 p1377 A71-22031

Cross flow profiles for compressible turbulent boundary layers with and without flow reversal via hodograph models family 08 p1229 A71-22033

Uniform two dimensional incompressible turbulent boundary layer with uniformly distributed surface mass injection, correlating results on basis of turbulent kinetic energy equation 09 p1430 A71-22105

Arc heated duct facilities providing high temperature supersonic turbulent boundary layer flows over large samples for orbital logistic vehicle thermal protection tests [AIAA PAPER 71-262] 09 p1429 A71-23060

Mathematical model for secondary flow in turbulent boundary layer in corners and salients, confirming existence of transversal pressure gradient variation 10 p1592 A71-23979

Supersonic turbulent boundary layer density profile over flat plate at single Reynolds number, using Mach-Zender interferometer 10 p1593 A71-24270

Air and carbon dioxide intensive injection effect on turbulent boundary layer of subsonic channel air flow 10 p1551 A71-24378

Thin flexible panel acoustic power radiation due to turbulent boundary layer wall pressure fluctuations excitation 10 p1596 A71-24814

Subsonic turbulent boundary layer noise generation and acoustic pressure on aircraft surface, using Lighthill theory 10 p1553 A71-24952

Velocity, temperature and concentration profiles correlation for compressible turbulent boundary layer along porous flat plate, with carbon dioxide injection, discussing cooling applications 10 p1598 A71-25095

Interaction theory for supersonic separated and reattaching turbulent boundary layers, comparing to real flow past compression ramp [AIAA PAPER 71-128] 11 p1702 A71-25476

Compressible turbulent boundary layer interaction with wedge or corner induced oblique shock waves, using transformation methods 11 p1750 A71-25481

Shear stress and eddy viscosity distribution in Mach 20 compressible turbulent boundary layer, using mixing length flow theory 11 p1751 A71-25499

Atmospheric boundary layer refractive index fluctuation isotropy for small turbulence, using intensity distribution photography over collimated laser beam cross section 11 p1762 A71-25923

Two dimensional incompressible turbulent boundary layer, determining velocity distribution with Cole law of wake 11 p1752 A71-26259

Three dimensional turbulent boundary layer calculations, using two dimensional method based on turbulent energy equation empirical conversion into shear stress transport equation 11 p1753 A71-26443

Turbulent boundary layer thermal flux fluctuation spectral distribution determination by applying fluctuation diagram method to filtered signals 12 p1985 A71-26828

Plane and circular turbulent jet boundary layer expansion in slipstream, comparing analytical with experimental results 12 p1898 A71-27505

Pressure and wall temperature gradients effects on equilibrium enthalpy profiles and heat transfer coefficients of incompressible turbulent boundary layers, using eddy conductivity model [AIAA PAPER 69-689] 12 p1986 A71-27553

Nozzle wall hypersonic turbulent boundary layers at free stream Mach number, using pitot, hot wire, wall pressure fluctuation and static pressure measurements [AIAA PAPER 70-746] 12 p1898 A71-27558

Turbulent boundary layers calculation downstream of compressible relaxing slot injection flows, using finite difference method based on eddy viscosity model 13 p2046 A71-27986

Multicomponent turbulent boundary layer calculation for partially ionized gases 13 p2046 A71-28185

Blowing angle effect on heat protection effectiveness of flat wall in slit injected low speed air flow with turbulent boundary layer in wind tunnel 13 p2159 A71-28420

Two dimensional turbulent boundary layer before rectangular step, investigating heat exchange in separation regions 13 p2048 A71-28572

Turbulent boundary layer friction and heat transfer under longitudinal pressure gradient 13 p2048 A71-28590

Thermal turbulence at infinite Prandtl number of horizontally infinite fluid layer heated from below, using Boussinesq equations 13 p2162 A71-28776

Longitudinal space-time correlation function of turbulent near wall pressure pulsations with hydrodynamic wavelength exceeding boundary layer thickness at streamlined model 13 p2049 A71-28846

Monograph on heat transfer from rotating heated surface with induced turbulent boundary layers covering disk, cone and sphere geometries 13 p2162 A71-28882

Turbulent flame boundaries and maximum brightness surface position in gasoline-air mixtures, using photography and gas analysis measurements of carbon dioxide concentrations 13 p2162 A71-28955

Approximate method for calculating film cooling effectiveness of flat plate in presence of turbulent boundary layer with injection ratios less than unity 13 p2166 A71-29368

Diffusion coefficient as function of height in turbulent atmospheric boundary layer, considering similarity laws between wind tunnel and field data 13 p2051 A71-29432

Separation control of two dimensional air flow with turbulent boundary layer along circular cylindrical wall by jets or suction 13 p2051 A71-29433

Hodograph models family for cross flow velocity component of three dimensional turbulent boundary layers, applying integral method to curved rectangular channels data [ASME PAPER 71-FE-1] 13 p2051 A71-29445

Turbulent boundary layer parameters changes across normal shock wave, integrating energy integral equation [ASME PAPER 71-FE-16] 13 p2052 A71-29455

Finite difference scheme for calculating three dimensional incompressible turbulent boundary layer development on infinite yawed cylinder [ASME PAPER 71-FE-19] 13 p2052 A71-29457

Properties of arbitrarily thick turbulent boundary layer for incompressible axial flow past long cylinder [ASME PAPER 71-FE-25] 13 p1995 A71-29462

Transformation of compressible turbulent and laminar boundary layers with and without wall blowing [ASME PAPER 71-FE-37] 13 p2166 A71-29472

Atmospheric turbulent shear layer model, giving velocity, stable, unstable and neutral profiles 14 p2267 A71-29759

Shear stress distribution and local heat flux at surface of axisymmetric bodies for laminar and turbulent boundary layer flow 14 p2170 A71-30219

Approximate calculation of turbulent boundary layers with adverse pressure gradient, using empirical auxiliary and momentum integral equations and skin friction formula 14 p2226 A71-30400

Two dimensional sonic nonreacting gaseous secondary injection into supersonic primary stream with turbulent boundary layer for application to thrust vector control [AIAA PAPER 71-750] 14 p2227 A71-30786

Gray air flow in turbulent optically thin boundary layer, determining radiant energy transport by Patankar-Spalding finite difference procedure 14 p2338 A71-30932

Surface renewal and penetration model in heat and momentum transfer analogy for incompressible turbulent boundary layer flow 14 p2227 A71-30935

Shear stress, eddy viscosity and mixing length distributions in compressible turbulent boundary layers with air and carbon dioxide injection 14 p2228 A71-31025

Compressible turbulent boundary layers closed form solution by extending Buri momentum integral analysis of incompressible turbulent boundary layers 14 p2228 A71-31129

Friction in compressible turbulent boundary layers at isothermal adiabatic wall 15 p2510 A71-31163

Dyson integral equation describing generalized field of normal waves in plane randomly inhomogeneous turbulent layer 15 p2388 A71-31513

Nonreacting and equilibrium chemically reacting gas turbulent boundary layer flows through hyper-

velocity nozzles, comparing calculation with experiment [AIAA PAPER 71-597] 15 p2512 A71-31577

Turbulent wall jet with initial boundary layer, calculating growth and separation in arbitrary pressure gradient by integral method [AIAA PAPER 71-612] 15 p2389 A71-31581

Error analysis of Corcos hypothesis concerning cross spectra of pseudoacoustic LF turbulent pressure pulsations on flat plate 15 p2389 A71-31708

Plate excitation by supersonic fluids heat transfer boundary layers, measuring wall pressure fluctuation and panel displacement 15 p2507 A71-32132

German monograph on viscous fluids heat transfer in pipes covering Prandtl number dependence, turbulent boundary layer flow and transition areas 15 p2514 A71-32375

Airfoils with turbulent boundary layers, calculating acoustic radiation from surface distribution of pressure fluctuations 15 p2347 A71-32520

Surface liquid film wave motion effect on air supersonic turbulent boundary layer flow field, discussing film thickness, heat transfer rates and wall temperatures [AIAA PAPER 71-623] 15 p2515 A71-32544

Turbulent boundary layer growth over flat plate and compression corner model in hypersonic gun tunnels, measuring pressure and heat transfer rate distributions 16 p2554 A71-32880

Air injection into turbulent boundary layer flow through porous plate, examining heat transfer and shielding efficiency 16 p2662 A71-33035

Free and enclosed disks rotation resistance at high Reynolds numbers, calculating fluid induced torque with logarithmic velocity profiles for turbulent boundary layer flow [ASME PAPER 71-APM-25] 16 p2520 A71-33204

Integral analysis of incompressible turbulent boundary layer with mass transfer and pressure gradient, including Stevenson velocity profiles and skin friction law [ASME PAPER 71-APM-2] 16 p2559 A71-33221

Turbulent boundary layer transition in shock tube with thickness inhomogeneity regions, using schlieren photographs 16 p2559 A71-33404

Viscous stresses distribution in isothermal incompressible turbulent boundary layer with positive pressure gradient by diffusers in open jet wind tunnel 17 p2725 A71-34209

Vortex boundary layer with dissipative viscous wall and isentropic sublayers, calculating adiabatic surface temperature 17 p2669 A71-34217

Two dimensional compressible turbulent boundary layer with time dependent mean velocity and density fields, deriving momentum and kinetic energy integral equations 17 p2727 A71-34876

Incompressible turbulent boundary layers at low Reynolds numbers, using eddy viscosity and mixing length concepts for computation 17 p2728 A71-34884

Semiempirical Taylor formula application to asymptotic turbulent boundary layer formed in mixing jet region 17 p2728 A71-35118

Supersonic turbulent two dimensional boundary layer flows wall flux and velocity/temperature profiles prediction 17 p2729 A71-35283

Interior region of incompressible turbulent boundary layer with pressure gradient on permeable wall, discussing local similitude hypothesis 17 p2729 A71-35346

Turbulent boundary layer interaction with supersonic outer flow behind step, calculating pressure distribution, momentum thickness and friction 17 p2672 A71-35631

Unsteady laminar boundary layers flow around three dimensional bodies, using finite difference techniques and power series expansion of time square root [ONERA-TP-941] 18 p2901 A71-36019

Bursting phenomenon measurement in turbulent boundary layer by hot wire, noting spottiness, HF intermittency and energy balance dynamics 18 p2985 A71-36036

Numerical integration of turbulent boundary layer equations, using mixing length concept 18 p2902 A71-36112

Electric and magnetic fields effect on turbulent boundary layer of conducting gas near electrode in MHD channel with insulated walls 18 p2951 A71-36113

Incompressible turbulent shear boundary layer equations of motion, developing integrodifferential formulation of Navier-Stokes theory 18 p2904 A71-36184

Adverse pressure gradient effects on compressible turbulent boundary layer flow in parallel duct at Mach 4 and high Reynolds number

18 p2904 A71-36297

Incompressible two dimensional turbulent hyper-sonic boundary layer flow velocity, pressure, temperature and density distributions

18 p2908 A71-36429

Elastic boundary interaction with viscous sublayer of turbulent boundary layer for Reynolds stresses and drag reduction possibility

19 p3042 A71-37082

Two dimensional turbulent boundary layer in incompressible fluid on smooth and rough impermeable wall surfaces under arbitrary pressure gradients

19 p3042 A71-37088

Turbulent boundary layer jet flow calculation using equivalent heat conduction theory

19 p3161 A71-37128

In-flight noise radiation by wing-mounted jet engines on aircraft fuselage based on correlation with turbulent boundary layer pressure fluctuations

19 p2997 A71-37846

Streamwise wall curvature and transition effects in turbulent boundary layers, using modified eddy viscosity and mixing length concepts

19 p3045 A71-37891

Turbulent boundary layer and heat transfer measurements along cooled conical convergent-divergent nozzle

19 p2993 A71-37982

Heat and mass transfer through porous plate into turbulent two dimensional incompressible boundary layer, using van Driest damped mixing length

19 p3045 A71-37986

Velocity and temperature profiles at near-critical point of nitrogen turbulent boundary layer flow over heated flat plate by thermocouple/pitot-static probe

19 p3165 A71-37994

Heat transfer to transpired turbulent boundary layer, reviewing theoretical models and experimental results for friction coefficient and Stanton number

19 p3166 A71-38003

Predicted flow nonuniformities due to laminar and turbulent boundary layer buildup in shock tubes, studying effects on dissociation rates of bromine in argon mixture

19 p3046 A71-38225

Laminar-turbulent transition zone in boundary layer about bodies moving in gas at high Reynolds number, using statistical physics methods

19 p3046 A71-38481

Static and transient pressure measurement in turbulent boundary layers, using transducer with piezoelectric sensing element

20 p3233 A71-38822

Heat and mass exchange coefficients and critical separation for turbulent boundary layer with secondary fluid injection under nonisothermal conditions

20 p3210 A71-38897

Incompressible turbulent boundary layer with pressure gradients, calculating Clauser equilibrium model and flow with constant wall shear stress

20 p3210 A71-39030

Atmospheric boundary layer refractive index fluctuation isotropy for small turbulence, using intensity distribution photography over collimated laser beam cross section

20 p3236 A71-39214

Turbulent boundary layer response to step change in surface roughness, discussing wind tunnel measurements of pressure and velocity profiles

20 p3212 A71-39505

Rectangular wind tunnel study of suction effect on velocity profiles and characteristics of turbulent boundary layer

20 p3213 A71-39788

Water tunnel study of turbulent boundary layers structure in incompressible fluid with longitudinal pressure gradient at inlet section of converging and diverging nozzles

20 p3213 A71-39789

Plane equilibrium turbulent boundary layer with longitudinal pressure gradient

20 p3214 A71-39791

Turbulent boundary layer calculation behind surface cusp, taking into account external flow turbulence and thermal stratification

20 p3214 A71-39792

Heat and mass transfer calculation in turbulent boundary layer on rough surface

20 p3315 A71-39793

Submerged vehicle drag reduction and turbulence transition damping by MHD boundary layer control, using Lorentz force and optimum magnetic field

20 p3214 A71-39963

Compressible circular free jet instability allowing for turbulent boundary layer thickness, considering influence of axisymmetry on spatial growth rate and disturbance phase velocity

21 p3365 A71-40013

Mean velocity profile and wall friction coefficients of perturbed turbulent boundary layer on flat plate

21 p3366 A71-40511

Noise sources in axial flow fans, considering radiation from turbulent boundary layers, scattering of incident turbulence and secondary flow influence

21 p3323 A71-40710

Nonablating inelastic deformable material surface interaction with external supersonic turbulent boundary layer, observing crosshatch patterns

21 p3323 A71-40941

Unsteady state boundary layer equations solution in laminar flow systems with free surface and transfer of heat or mass

21 p3370 A71-40990

Two dimensional supersonic turbulent free shear layer recompression process from flow model numerical calculation

21 p3371 A71-40998

Resonant oscillations effect on heat transfer across mixing length in cavities spanned by low speed turbulent shear layers

21 p3371 A71-41033

Monograph on hypersonic low temperature ablation covering cross hatched surface patterns, flow field, turbulent boundary layer, angle of attack, etc

22 p3621 A71-42031

Diffusion from continuous line source in turbulent boundary layer, comparing calculation based on Lagrangian similarity with measurements

23 p3664 A71-44200

Heat transfer in turbulent boundary layer separation zones ahead of step, using local flow parameters at wall boundary layer limit

24 p3887 A71-44746

Incompressible turbulent boundary layer with suction and surface injection computation by implicit finite difference method and turbulent kinetic energy equation for mixing length flow

24 p3820 A71-44954

TURBULENT DIFFUSION

Enclosed diffusively turbulent flames, determining area of maximum ion concentration

01 p0178 A71-10338

Maximum ion concentration zone in diffusively turbulent flames in fuel gas free jets, using mass exchange processes analysis

01 p0178 A71-10341

Turbulent diffusion gas jet length in transverse flow and in stationary air medium

01 p0181 A71-11147

Turbulent diffusion role in magnetic fields origin in sun, planets and galactic gaseous disk

01 p0162 A71-11419

Calculated dispersion in decaying grid turbulence, showing agreement with test results for diffusion of heat from line source

01 p0072 A71-11484

Altitude distribution of oxygen in atmosphere with eddy diffusion allowance from ARCAS 2 rocket photometric observations

01 p0077 A71-11528

Turbulent diffusion of impurity from infinite line source in clouds and fog, allowing for particle entrainment

05 p0776 A71-16422

Artificially produced holes closing in clouds, investigating role of water vapor and droplets turbulent diffusion by mathematical model

05 p0777 A71-16668

Galaxy gaseous disk as low mode dynamo, calculating turbulent diffusion coefficient for passive magnetic fields

05 p0811 A71-16688

Mesosphere and lower thermosphere heat input rates and circulation, calculating worldwide average eddy diffusion coefficient

06 p0892 A71-17978

Turbulent diffusion coefficients in isothermal and nonisothermal pipe flow, comparing with Bory and Taylor theories

07 p1222 A71-18994

Turbulent wake shape in stratified medium describing anisotropic diffusion

07 p1088 A71-19190

Gas bubble growth and dissolution due to pressure fluctuations in turbulent diffusion liquid flow

07 p1094 A71-20475

Eddy diffusivities and turbulent diffusion characteristics in atmospheric surface layer, using universal function based on similarity theory

09 p1487 A71-22639

Turbulent diffusion in stationary thermally stratified atmospheric boundary layer, considering gravitational sedimentation and impurities lifetime

11 p1795 A71-25585

Cloud height distribution pattern, developing analogy between diffusion and quantum motions

12 p1924 A71-26737

Turbulent diffusion Langevin model with pressure-viscous stress interaction, calculating particle dispersion, Reynolds number, Richardson law time span and Eulerian-Lagrangian relations

12 p1898 A71-27730

Eddy diffusivity of mass in air measurement discrepancies in circular duct, considering axial concentration and radial distributions

14 p2339 A71-30934

Physical conditions leading to deuterium enhancement in earth upper atmosphere as function of theopause temperature and eddy diffusion

16 p2569 A71-33808

Kinematic-dynamo theory with turbulent diffusivity effect, discussing resistivity as random function of position

18 p2969 A71-37040

Eddy viscosity in barotropic planetary boundary layer, finding turbulent diffusion coefficient dependence on turbulent kinetic energy

20 p3257 A71-39498

Lower thermosphere eddy diffusion coefficient effects on height variations in ionospheric composition

21 p3372 A71-40040

Upper temperature inversion as condition producing pollutants turbulent diffusion in atmospheric boundary layer

22 p3568 A71-41646

Turbulent energy budget and velocity dissipation spectrum near grass surface as function of atmospheric stability

22 p3569 A71-42546

Diffusion from continuous line source in turbulent boundary layer, comparing calculation based on Lagrangian similarity with measurements

23 p3664 A71-44200

TURBULENT FLOW

NT CAVITATION FLOW

NT SUPERCAVITATING FLOW

Uniformly turbulent incompressible heavy fluid sloshing and free oscillations in rigid rotating vessel using linear surface wave theory

01 p0069 A71-10411

Snow storms wind field and turbulent region detection, using Doppler VAD pattern and mapping

01 p0117 A71-10570

Viscosity model application to turbulent planetary Couette flow velocity profile and shear stress values obtaining skin friction relation

01 p0071 A71-10954

Film cooling effectiveness in hypersonic turbulence flow from downstream surface equilibrium temperature measurement

01 p0180 A71-10964

Locally isotropic hydrodynamic turbulent field statistical properties for kinetic energy and temperature dissipation fluctuations

01 p0120 A71-11104

Heat transfer in nongray radiating gas turbulence flow in circular tube

01 p0181 A71-11440

Turbulent transport equations derivation for incompressible fluid unsteady flow in arbitrary geometry considering application to flow between parallel plates

01 p0072 A71-11464

Arc discharge plasma response to turbulent gas flow covering wide range of Reynolds numbers measured with Langmuir probes

01 p0136 A71-11478

Microwave scattering from plasma fluctuation produced by forcing gas in turbulent flow through discharge tube, investigating frequency spectrum broadening

01 p0136 A71-11480

Pipe bends effects on heat transfer coefficient on turbulent forced convection

02 p0330 A71-11650

Shear flow turbulent friction in boundary layer deriving Navier-Stokes equation integrodifferential formulation

02 p0241 A71-12411

Uniform magnetic field effects on electroconducting fluids turbulent flow and heat transfer characteristics

02 p0293 A71-12648

Plastic impact principle of hydraulic losses in turbulent viscous flow, using Navier-Stokes equation with friction term

03 p0397 A71-13006

Variational problem for turbulent liquid flow mass transport on inclined flat plate, using plane Poiseuille flow solution

03 p0398 A71-13108

Spherical particle motion investigation in plane Couette flow, predicting critical Reynolds number for transition to turbulent flow

03 p0398 A71-13112

Turbulent separation and reattachment at turbomachine blade trailing edge at supersonic speeds, discussing various flow models

03 p0340 A71-13142

Sound radiation from finite span airfoil in three dimensional turbulent flow, considering lift function effect

03 p0399 A71-13280

Turbulent flow near porous wall with pressure gradient, calculating velocity and shear distribution by modified Van Driest theory

03 p0399 A71-13432

High pressure arc heater data correlation for laminar and turbulent flows, examining radiation and thermal and electrical conduction effects

03 p0517 A71-13443

- Correlation measurements by laser in turbulent gas flow, determining phase structure velocity distributions and coherence lengths 03 p0435 A71-13529
- Plane Couette flow turbulence, discussing wall region shear and core homogeneity 03 p0400 A71-13546
- Hess solution for heavy body rotating about fixed point, considering cavities filled with ideal incompressible fluid in turbulent and irrotational motion and linear invariant relation 03 p0458 A71-13591
- Symmetry axis motion of solid body with ellipsoidal cavity filled with ideal incompressible uniformly turbulent fluid 03 p0458 A71-13596
- Convective velocity and temperature scales deduced numerically and observationally for unstable planetary boundary layer and for turbulent Rayleigh convection 03 p0453 A71-13613
- Turbulent flow mean velocity beyond rotating disk edge, using momentum integral method [ASME PAPER 70-FT-1] 03 p0400 A71-13702
- Turbulent fluid flow through pipe, measuring circumferential velocity component close to wall by electrochemical techniques 03 p0400 A71-13733
- Heat transfer and fluid friction of hydrogen and helium gas flows undergoing turbulent to laminar flow transition in heated pipe [ASME PAPER 69-HT-54] 03 p0405 A71-14291
- Downstream heat transfer and wall friction predictions for quasi-developed strongly heated turbulent pipe flow, using mixing length model [ASME PAPER 70-HT-8] 03 p0405 A71-14294
- Nuclear rocket nozzle cooling passages, discussing heat transfer and friction correlations for single-phase hydrogen turbulent flow [AIAA PAPER 70-661] 03 p0456 A71-14444
- Turbulent base pressure on conical afterbodies in supersonic axisymmetric flow, including initial direction effect [AIAA PAPER 70-555] 03 p0344 A71-14450
- Shock tube run time in acceleration region at turbulent regime for air, using pitot pressure measurements 04 p0563 A71-14668
- Heat transfer correlations for turbulent flow in ducts with rough surfaces 04 p0674 A71-14778
- Heat transfer and pressure drop in air flowing in square tube with two dimensional discrete turbulence promoters applied to opposite walls 04 p0675 A71-14781
- Flow patterns modification through space charges, demonstrating laminarization of turbulent flow and boundary layer separation prevention 04 p0569 A71-14985
- Third order correlations in grid turbulence, investigating high pass filtering effect at small cut-off frequencies 04 p0569 A71-15027
- Heat transfer to concentric annular turbulent mercury flow, determining wetting effect, velocity profiles, eddy diffusivity of momentum transfer and friction factors 04 p0570 A71-15172
- Soviet monograph on atmospheric boundary layer covering compressible turbulent air flow, diurnal fluctuations, fog, air pollution and lower atmosphere electric field 04 p0621 A71-15399
- Thermal boundary layer thickness and momentum in turbulent flow over film cooled surface 04 p0680 A71-15473
- Wall static pressure and convective heat transfer measurements in subsonic, transonic and supersonic regions in heated air turbulent flow through variable cross section channel 04 p0680 A71-15476
- Scalar substance heat transfer characteristics in nonhomogeneous turbulence, using statistical and phenomenological approach 04 p0572 A71-15541
- Error estimates for turbulent flow characteristics determination by visualization and solid particle photography 04 p0573 A71-15562
- Prewhitening technique for acoustic turbulent flow data recording and analysis 04 p0600 A71-15598
- Turbulent flows - Conference, Kiev, June 1967 04 p0573 A71-15601
- Laminar flow stability and transition to turbulent flow, giving nonlinear theory for perturbations development 04 p0574 A71-15602
- Wyld diagram method extended to turbulence decay, considering operators expressed as integrals with kernels 04 p0575 A71-15604
- Turbulent flow of nonlinear Stokes fluids with transverse shear, determining nonlinear properties effects 04 p0575 A71-15605
- Closed system of differential equations derived for kinematic characteristics of turbulent flow in pressurized smooth pipe 04 p0575 A71-15608
- Semiempirical turbulence theory generalization to flows near rough surfaces, obtaining unified dependences for wall flows 04 p0575 A71-15610
- Turbulent flow structure and properties near flat wall, confirming turbulent friction damping by statistical analysis 04 p0576 A71-15611
- Turbulent fluid flow past surfaces, calculating pressure pulsations at boundary layer 04 p0576 A71-15612
- Air flow turbulence generating grids at nozzle outlet in wind tunnel for measuring turbulence levels 04 p0577 A71-15618
- Turbulent pressurized and open channel flows analysis by flow visualization, using solid particles and dynamic ball rate sensors 04 p0578 A71-15627
- Laminar to turbulent transition in pipes, using scattered light method 04 p0578 A71-15635
- Velocity distribution equation for steady incompressible two dimensional turbulent flow, taking pressure gradients and surface roughness effects into account 04 p0578 A71-15764
- German monograph on open turbulent methane-oxygen flame temperature and concentration distribution determination from jet density measurements, using radiometric method 05 p0831 A71-16123
- Soviet book on fundamentals of heat transfer theory covering thermodynamic equations, steady, unsteady, turbulent, incompressible and MHD flows, etc 05 p0831 A71-16196
- Expanding universe magnetic field origin, examining Batchelor condition for spontaneous appearance in turbulent conducting fluid motion 05 p0809 A71-16470
- Gaseous mixtures turbulent combustion, considering turbulent flame propagation velocity 05 p0836 A71-16536
- Small surface elements local skin friction sensor measurements near wall during laminar and turbulent flow, making direct shear force measurements 05 p0752 A71-16734
- Longitudinal turbulent air flow past plate, applying heat transfer and drag calculations 05 p0838 A71-16784
- Laminar or turbulent chemically reacting gas mixture flow in circular tube, examining heat transfer with enthalpy equation 05 p0838 A71-16791
- Streamwise vorticity formation by wall turbulence nonuniformities, deducing secondary currents direction 05 p0736 A71-16963
- Two dimensional wake laminar-turbulent transition, emphasizing velocity fluctuation nonlinear interaction 05 p0695 A71-16964
- Grid turbulence interaction with uniform mean shear flow, examining initial disturbance length scale effects 05 p0695 A71-16965
- Inlet turbulence interaction with rotor potential flow as noise source in axial flow fans, developing expression for sound power radiated 05 p0738 A71-17163
- Submerged moving body in nonviscous incompressible fluid, evaluating finite potential flow field momentum with rigid and free far distant outer boundary 06 p0841 A71-17419
- Channel flow and flow past bodies turbulent/laminar reverse transition for friction drag and heat transfer reduction 06 p0881 A71-17584
- Tangential velocity and total temperature distribution axial and radial gradients from secondary flow functions and turbulent energy equations 06 p0883 A71-18321
- Swirling effects on turbulent flow recirculation zone behavior in gas turbine main burners [AIAA PAPER 71-2] 06 p0946 A71-18477
- Hypersonic flight test base pressure results at high Reynolds numbers for slender cone in turbulent flow, noting implications for ground test simulation [AIAA PAPER 71-134] 06 p0883 A71-18578
- Optical crossed-beam measurements of turbulence intensities in cold subsonic air jet shear layer [AIAA PAPER 71-137] 06 p0902 A71-18580
- Turbulent shear flows transport properties, computing atmospheric and vortex motions by invariant modeling of Reynolds stress term in boundary layer momentum equation 06 p0886 A71-18653
- Turbulent flow main characteristics calculation based on maximum stability hypothesis with respect to most dangerous perturbation, presenting numerical solutions by digital computer 07 p1085 A71-18755
- Large diameter tube high Reynolds number air flow temperature profiles, using chromel-alumel thermocouple 07 p1220 A71-18762
- Large aspect ratio rectangular duct with nonuniform surface texture, investigating turbulent flow, maximum velocity positions and zero shear stress 07 p1086 A71-18772
- Boundary layer nonlinear stability theory, considering hydrodynamic problems associated with laminar flow transition into turbulent flow 07 p1086 A71-18777
- Flame propagation process, investigating transfer in turbulent flow, combustion times and burning in channel 07 p1220 A71-18778
- Free convection turbulent flow under supercritical conditions, investigating convection heat transfer and flow patterns 07 p1220 A71-18780
- Turbulent wall flow, observing flux and heat transfer conditions with stroboscopic visualization 07 p1105 A71-18782
- Two dimensional turbulent channel flow, determining local mean wall shear stress from velocity gradient 07 p1087 A71-18784
- Incompressible fluid nonuniform turbulence statistical approach, based on finite number of equations for high order single point correlations 07 p1087 A71-18920
- Turbulent velocity field in noncircular cross section rectilinear duct, determining relation between viscosities ratio and dimensionless velocity by integral transformation 07 p1087 A71-18992
- Turbulent diffusion coefficients in isothermal and nonisothermal pipe flow, comparing with Bory and Taylor theories 07 p1222 A71-18994
- Incompressible turbulent circulatory fluid flow in plane curvilinear channel, deriving energy balance equations 07 p1088 A71-19199
- Turbulent flame propagation at high Reynolds numbers, discussing nonthermal hydrodynamic mechanism, laminar front and fine structure 07 p1223 A71-19249
- Atmospheric meteor zone turbulent motions under Archimedes forces based on radio observations 07 p1101 A71-19412
- Compressibility effect on turbulent pipe flow shear stress distribution, presenting high subsonic Mach number theoretical results from Kjellstroem-Hedberg momentum equation integration 07 p1088 A71-19423
- Compressible turbulent flows free mixing based on two dimensional viscous flow equations [AIAA PAPER 71-4] 07 p1088 A71-19701
- Transient and turbulent flow structure in wake behind thin plates in wind tunnel, noting velocity fields, temperature and initial boundary layers 07 p1089 A71-19750
- Turbulent transfer model in wall region, estimating mean surface renewal frequency for mass momentum and heat transfer rates and velocity, temperature and concentration profiles 07 p1092 A71-20224
- Turbulent pipe, channel and plane Couette flow by Prandtl model equations, comparing with experimental data 07 p1092 A71-20278
- Turbulent pipe flow, developing analogy between momentum and heat transfer 07 p1224 A71-20371
- Digital turbulence amplifiers, investigating dynamic switching response 07 p1024 A71-20552
- Fluidic diverting valve independent of turbulent reattachment, examining large scale model and digital element characteristics in closed loop system 07 p1024 A71-20553
- Turbulence amplifier optimal dimensioning for maximum fan-out factor and minimal signal transport time 07 p1024 A71-20554
- Nonlinear subgrid scale eddy viscosity formulation for turbulence generated by mean shear or thermal instability at large Reynolds number 07 p1094 A71-20615
- Local turbulent friction factors and heat transfer coefficients for fluid flows through ducts of arbitrary cross section with prescribed wall heat flux distribution 07 p1224 A71-20654
- Locally isotropic hydrodynamic turbulent fields statistical properties for kinetic energy and temperature dissipation fluctuations 08 p1325 A71-20850
- Random solution of stochastic integral equation of tagged point in continuous turbulent flow 08 p1276 A71-21357
- Stationary longitudinal turbulent flow of air with equilibrium ionization and dissociation around plate, calculating heat exchange and frictional drag 08 p1228 A71-21922

Hydrodynamically stabilized turbulent viscous incompressible fluid flow in circular tube, examining nonstationary convective heat transfer by numerical methods

08 p1276 A71-21923

Turbulent air flow in cooled tubes, studying local heat transfer and hydraulic resistance

08 p1377 A71-21924

Velocity profile in viscous sublayer at wall based on maximum stability principle applied to Karman constant for turbulent channel flow

08 p1277 A71-21950

High turbulent flow simulation in hypervelocity wind tunnel for reentry vehicles operational testing, discussing nozzle gas dynamic and mechanical design [AIAA PAPER 71-253]

08 p1273 A71-21982

Static pressure port errors in hypersonic turbulent flow, using approximate shear layer momentum balance for pressure increase derivation

08 p1228 A71-21996

Flow in channel with abrupt asymmetric widening, calculating expanding flow velocity profile by Prandtl semiempirical turbulence theory

08 p1277 A71-22041

Turbulent velocity pulsations measurement by conduction anemometer with three-electrode sensor

09 p1499 A71-22132

Pipe flow turbulent friction, describing pressure drop measurements and flow visualization studies on wall roughness effects

09 p1431 A71-22275

Turbulent hot gas motion in round pipes from semiempirical turbulence theory, accounting for energy dissipation and thermodynamic parameter variability

09 p1431 A71-22370

Turbulent flow in initial section of convergent axisymmetric nozzle based on logarithmic velocity law

09 p1431 A71-22409

Turbulent air flow velocity and temperature fluctuations, determining mean fields, Prandtl number distributions and correlation moments and coefficients

09 p1432 A71-22729

Heat transfer to slender bodies in hypersonic flow, comparing wind tunnel measurements with modified reference enthalpy method predictions for laminar and turbulent flow

09 p1545 A71-22941

Turbulence properties in supersonic flow, considering modes with vorticity, entropy and acoustic aspects

09 p1383 A71-23603

Turbulent supersonic flow measured by laser anemometry, stressing advantages over optical heterodyning

09 p1453 A71-23693

Resistance thermometry measurements near wall in turbulent flow, considering error causes

10 p1591 A71-23847

Air jet velocity and turbulence measurements by modified Doppler technique, using CW lasers

10 p1609 A71-23874

Turbulent flows in diverging cylindrical tube, observing stationary and traveling vortex breakdowns

10 p1592 A71-23952

Phythan perturbation theory for stationary homogeneous turbulence of incompressible fluid

10 p1594 A71-24511

Turbulent incompressible air flow in-stream static pressure fluctuations measurement, describing bleed type pressure transducer theory, design and operational characteristics

10 p1611 A71-24516

Coaxial jets development and mixing in axisymmetric twisted turbulent ring air flow injected through inlets

10 p1594 A71-24560

Circular subsonic free jet impinging on wall, investigating high intensity frequency noise and turbulence spectrum

10 p1594 A71-24594

Backward facing step in confined supersonic two dimensional flow, investigating turbulent shear layer reattachment

10 p1552 A71-24622

Turbulent shear flows, examining zero and negative entrainment in boundary layers

10 p1595 A71-24626

Plane rigid airfoil with fixed center of gravity, discussing motion in turbulent air and gust loads

10 p1557 A71-24947

Laser heating induced turbulence in fluid medium, using dimensional analysis for effective Reynolds number

10 p1622 A71-24960

Hot-wire anemometry for measuring velocity-temperature coefficients in turbulent flow with heat transfer

10 p1597 A71-25016

Mean and fluctuating forces on flat plates normal to turbulent flow, giving power spectral density measurements of drag fluctuating component

10 p1598 A71-25085

Anisotropic homogeneous two-point double-velocity correlation tensor model for turbulent flow field, deriving relation between micro and macro scale

11 p1748 A71-25153

Pipe flow hot wire measurements at turbulence onset Reynolds numbers, exhibiting axisymmetric laminar velocity profile distortion

11 p1748 A71-25155

Variational formulation for hydrodynamic stability based on local potential motion, determining transition from laminar to turbulent flow

11 p1749 A71-25441

Streamwise vortices of distinct periodicity in laminar transitional turbulent reattaching flows over wide Mach number range

11 p1751 A71-25496

Turbulent vortex rings motion empirical model, deriving equations valid at large distances from discharging orifice

11 p1751 A71-25498

Two layer thermal and velocity model of gaseous film cooling with constant turbulent step slot flow [ASME PAPER 71-GT-3]

11 p1855 A71-25949

Turbulent photosphere and chromosphere, investigating finite resistivity effects on solar flare phenomena

11 p1832 A71-26173

Maximum velocity position in turbulent shear flow for differential pressure effect between double pitot tubes, using inductance type transducer

11 p1767 A71-26313

Monograph on bulk flow theory for turbulent lubricant films, discussing flow rates, pressure gradients and shear stresses

11 p1772 A71-26462

One dimensional premixed turbulent flame energy equation as function of heat release rate curve, temperature, velocity, composition and density

12 p1985 A71-26741

Nonviscous fluid isotropic turbulent motion concept, and structural stability role in steady state flow statistical properties

12 p1895 A71-26827

Thermally stratified turbulent shear flow, calculating turbulent energy balance and temperature inhomogeneity spectral equations

12 p1895 A71-26899

Destabilizing buoyancy forces effect on weak homogeneous shear flow turbulence in gases, discussing turbulence decay with time and turbulence energy growth

12 p1896 A71-26940

Smooth annuli correlation equation for friction factor, discussing Prandtl turbulence based Spalding inner velocity profile modification

12 p1896 A71-27053

Spectral density of friction pulsations in turbulent channel wall flow for various length to height ratios and Reynolds numbers, using electrochemical method

12 p1897 A71-27306

Hypersonic cruise vehicles viscous interactions areas, examining compression corners, shock interactions, laminar and turbulent flow, boundary layer separation, etc [AIAA PAPER 70-781]

12 p1865 A71-27551

Flow visualization of free convection laminar-to-turbulent transition along vertical heated plate in water induced by two dimensional forced disturbances [DFVLR-SONDDR-116]

12 p1987 A71-27739

Laminar flow breakdown in circular tubes, noting disturbance level effect on intermittent flow parameters and turbulent zone length distribution

13 p2046 A71-27827

Local and mean heat transfer at initial thermal segment for stabilized turbulent air flow in circular tubes and rectangular channels

13 p2159 A71-28419

Nonhomogeneous turbulent flow with magnetic field, deriving MHD turbulence model neglecting velocity correlation time

13 p2107 A71-28565

Heat shield ablation under high enthalpy chemically active turbulent gas flow in hydrojet engine manifolds

13 p2160 A71-28589

Wall shear stress and static pressure of developing turbulent flow in square ducts with convective accelerating core for various Reynolds numbers

13 p2048 A71-28595

Nonisotropic turbulent stress and viscosity components distributions in nonrecirculating swirling flow from mean axial and swirl velocities

13 p2161 A71-28622

Soviet papers on combustion processes in turbulent and laminar flows of kerosene and gasoline mixtures, stressing gas turbine engines problems

13 p2162 A71-28954

Flame propagation speed, combustion zone extent and distance from front to maximum brightness surface in turbulent gasoline-air flames

13 p2162 A71-28956

Flame propagation rate in gasoline-air flow with tubular and grid-induced turbulence during two-stage burning process

13 p2162 A71-28959

Gasoline-air combustion zone extent as function of inlet temperature for plane turbulent flame in square section channel

13 p2163 A71-28958

Grid-induced turbulence effect on flameout characteristics for kerosene-air flames stabilized by bodies of different sizes

13 p2163 A71-28959

Correlation model of stability and onset of turbulent motions for incompressible fluid, noting inconsistency of Keller-Friedman equations

13 p2050 A71-29270

Turbulent wall jets in presence of main flow longitudinal pressure gradient, using approximate integral method

13 p2050 A71-29271

Acceleration covariance in turbulent flow isotropic homogeneous incompressible viscous conducting fluid

13 p2109 A71-29292

Turbulent gas flow through duct with alternating pressure gradient, considering heat transfer and frictional resistance

13 p2166 A71-29335

Friction factor for low Reynolds number turbulent flow in large aspect ratio rectangular ducts, comparing Blasius and Prandtl relations [ASME PAPER 71-FE-A]

13 p2051 A71-29393

Particle energy spectrum function effect on flow energy spectrum in turbulent gas-solid suspension flow [ASME PAPER 71-FE-15]

13 p2052 A71-29404

Boundary layer equations based on eddy viscosity model for turbulent free shear flow, solving numerically in Crocco coordinate plane [ASME PAPER 71-FE-17]

13 p2052 A71-29405

Properties of arbitrarily thick turbulent boundary layer for incompressible axial flow past long cylinder [ASME PAPER 71-FE-25]

13 p1995 A71-29406

Numerical solution of coupled boundary layer equations describing strongly cooled turbulent flow of gas between parallel plates with property variation [ASME PAPER 71-FE-38]

13 p2166 A71-29407

Axisymmetric flow effects on surface mass injection at supersonic and hypersonic speeds, streamlines inclinations and surface pressures generation by turbulent viscous dissipation

14 p2223 A71-29800

Incompressible planar fluid flow magnitude, direction and turbulent shear stress measurement by hot-wire anemometer

14 p2239 A71-29808

Turbulent flow and high sound level effects on acoustic attenuation in narrow rectangular duct

14 p2224 A71-30023

Nondimensional entrance loss equation for radial turbulent flows without swirl between parallel disks

14 p2226 A71-30040

Nonresonant noise from turbulent nonpremixed flames, discussing burner diameter, impingement angle and equivalence ratio effects on acoustic power radiated [AIAA PAPER 71-732]

14 p2295 A71-30707

Turbulent flow asymmetrical mechanics equation derivation from conservation laws, discussing Navier-Stokes equation, angular momentum and transport theory

14 p2227 A71-30804

Turbulent gas flame length in motionless air of various ambient temperatures, comparing calculation with measurement

15 p2511 A71-31339

Ultrasonic rotameter for turbulent wall velocity calculation measurement, using cylindrical electroacoustic capacitor converter with solid dielectric for radiators and receivers

15 p2444 A71-31404

Incompressible fluid turbulence theory based on space-time Hopf characteristic functional integral representation for velocity field statistical ensemble

15 p2388 A71-31405

Flat plate surface film cooling by two dimensional tangent slot injection in hypersonic turbulent flow measuring equilibrium temperatures and skin friction [AIAA PAPER 71-599]

15 p2343 A71-31515

Shock and pressure gradient induced turbulent transonic flow separation, using two dimensional circular arc model for flow field investigation [AIAA PAPER 71-565]

15 p2344 A71-31515

Airfoils broadband noise generation mechanism in turbulent flow in anechoic chamber [AIAA PAPER 71-587]

15 p2468 A71-31515

Nonreacting and equilibrium chemically reacting gas turbulent boundary layer flows through hypersonic nozzles, comparing calculation with experiment [AIAA PAPER 71-597]

15 p2512 A71-31515

Direct measurement of spatial velocity correlation functions in turbulent flow by conditional probability of scattered light

15 p2449 A71-31818

Laminar square jet from turbulence amplified analyzing centerline velocity distribution and supply pressure recovery

15 p2391 A71-32004

Random turbulent signals from hot wires across pipe flow, studying form, skewness and flatness factors
15 p2391 A71-32108

Turbulent flow field mean velocity components measurements near thin rotating disk
15 p2392 A71-32253

Low Reynolds number turbulent flow in large aspect ratio rectangular ducts, investigating Blasius and Prandtl circular tube friction factor relations
15 p2392 A71-32261

Turbulent gaseous nonmagnetic protogalaxies under external torques, calculating angular velocity distribution
15 p2490 A71-32400

Laser Doppler turbulent and laminar flow velocity measurement model, using optical mixing spectroscopy theory
15 p2423 A71-32589

Turbulent flow in circular duct, determining asymptotic temperature profiles and Nusselt number values from Prandtl numbers and velocity distribution
16 p2554 A71-32836

Intermittence and scale similarity in turbulent flow structure, analyzing eddies distribution inhomogeneity
16 p2557 A71-32932

Heat transfer and drag calculations in longitudinal turbulent air flow around plate with constant or variable physical properties
16 p2662 A71-33036

Laminar or turbulent chemically reacting gas mixture flow in circular tube, examining heat transfer with enthalpy equation
16 p2662 A71-33041

Vertical acceleration effect on gas-hydraulic analogy for turbulent flows with and without jumps with error dependence on Froude number and length to depth ratio
16 p2560 A71-33598

Turbulent combustion stability in rocket engine with allowance for walls reflecting acoustic waves excited by flame
16 p2663 A71-33605

Extension of Heisenberg model for spectral transfer to second order fluids in turbulent shear flow, noting accompanying weakening of anisotropic influences
17 p2725 A71-34181

Detachment prediction in turbulent incompressible plane flows on thick bodies applied to wall with disconnections and flat plate normal to wind
17 p2669 A71-34189

Gas and liquid drop laminar, transition and turbulent flows heat transfer intensification in circular tubes, applying to hydraulic resistance design
17 p2835 A71-34205

Cesium vapor diffusion condensations from laminar argon flows in tubes and turbulent movement on banks, considering boundary layer mist formation effect
17 p2785 A71-34206

Undulating laminar and turbulent liquid film flows down vertical surface, determining velocity fields and local heat transfer coefficients
17 p2725 A71-34210

Scalar material transport in incompressible inhomogeneous turbulent fluid based on one point correlations equations
17 p2835 A71-34211

Statistical behavior of turbulent velocity derivatives in nearly isotropic turbulent field downstream of grid, using high speed digital computing methods
17 p2726 A71-34662

Mass transfer in turbulent flow region downstream of circular pipe sudden enlargement for high Schmidt numbers, using diffusion controlled electrolysis technique
17 p2837 A71-34692

Navier-Stokes steady nonrectilinear universal complex laminar flow, showing isochoric lamellar or plane motions of constant velocity with streamlines as concentric circles
17 p2727 A71-34695

Eddy viscosity model for turbulent pipe flow, yielding velocity distribution, shear, energy production and viscous dissipation rate
17 p2728 A71-34881

Heat transfer in wall region of steady turbulent flow at large Prandtl numbers, plotting temperature distribution curves
17 p2728 A71-35119

Stationary longitudinal turbulent flow of air with equilibrium ionization and dissociation around plate, calculating heat exchange and frictional drag
17 p2671 A71-35266

Hydrodynamically stabilized turbulent viscous incompressible fluid flow in circular tube, examining unsteady convective heat transfer by numerical methods
17 p2729 A71-35267

Turbulent air flow in cooled tubes, studying local heat transfer and hydraulic resistance
17 p2838 A71-35268

Partial differential equations governing second order correlation functions for velocity and magnetic field in isotropic conducting turbulent flow
17 p2789 A71-35443

Thermal, turbulent and macroscopic motions in solar loop prominence of 4 May 1960, using spectral line composition by Gaussian profiles
17 p2809 A71-35596

Turbulent plane flow velocity profile stability characteristics covering parabolic Poiseuille flow under infinitesimal disturbances
18 p2901 A71-35855

Turbulent flow of air film between rotating circular and stationary plane surfaces, determining pressure distributions, inertial forces effects and velocity profiles
18 p2926 A71-36185

Rigid sphere and concentric shells models approximation to turbulent motion in liquid-filled precessing spherical cavity
[ASME PAPER 71-APM-Y] 18 p2904 A71-36265

Singularities of Euler equations in turbulent flow problems, studying design of difference schemes
18 p2907 A71-36335

Plane Poiseuille flow at constant rate, developing numerical simulation of transition and turbulence
18 p2845 A71-36337

Convective heat exchange coefficient determination for human body immersed in turbulent water flow, using fractional calorimetry
18 p2858 A71-36862

Turbulent rotating tube flows kinematic similarities, deriving heat and mass transfer, swirl damping and axial and rotational velocity profile
19 p3043 A71-37127

Air flow in pipe with double screw thread, calculating tangential forces and turbulent viscosity coefficient along isostachs
19 p3043 A71-37266

CAT physical model and formation mechanism, using turbulent zone characteristics and wind velocity spectra
19 p3049 A71-37448

Turbulent hydrodynamic line stretching problem, considering asymptotic rates as application of central limit theorem for dependent random variables sums
19 p3044 A71-37729

Atmospheric meteor zone turbulent motions under Archimedes forces based on radio observations
19 p3054 A71-37836

Combustion dynamics, including fire spread in solid fuels, ignition, turbulent/laminar fields and boundary layer, stagnation point and opposed jet burning
19 p3166 A71-38077

Turbulent pipe flow dissipation rate, presenting turbulence energy diffusion and stress components spectral distribution measurements
19 p3045 A71-38201

Spectral density of friction pulsations in turbulent channel wall flow for various length to height ratios and Reynolds numbers, using electrochemical method
19 p3046 A71-38262

Difference equations derivation for meteorological turbulent flow prediction, considering errors due to finite difference approximations
19 p3087 A71-38306

Turbulent flow stability with respect to small disturbances, applying maximum stability principle to stable averaged flow
20 p3210 A71-38895

Windage data for inert gas in high speed generators rotor-stator gap, investigating turbulent velocity profiles
20 p3181 A71-38915

Flow instability in stagnation point region of circular cylinder in turbulent channel flow, using hydrogen bubble method for flow visualization
20 p3211 A71-39454

Concentrated vorticity regions motion in turbulent flow, calculating mean displacement velocity relationship to turbulent velocity fluctuation
20 p3212 A71-39473

Longitudinal diffusivity of turbulent flows in open channels and circular pipes, discussing experiments
20 p3212 A71-39504

Book on statistical mechanics of turbulent fluid flows covering gas oscillations, correlation function, Reynolds equation, laminar flow, particle dispersion, etc
20 p3213 A71-39774

Laminar and turbulent incompressible viscous flow with spiral vortices between two parallel rotating disks
20 p3213 A71-39778

Velocity profiles of plane turbulent flow of incompressible fluid on porous surface in presence of suction
20 p3213 A71-39790

Turbulent boundary layer calculation behind surface cusp, taking into account external flow turbulence and thermal stratification
20 p3214 A71-39792

Semibounded jets in laminar and turbulent flows, discussing boundary layers skin and stream regions, step flow velocities, temperatures and self similar problems
20 p3214 A71-39794

Turbulent energy variations in unsteadily moving flow with structural shift, emphasizing formation of vortices with various inertia scales
20 p3214 A71-39796

Velocity and resistance profiles for unsteady turbulent flow in rough pressure channels, using Prandtl hypothesis
20 p3214 A71-39797

Turbulent motions in fluids of small viscosity as inviscid flows with vortex sheets and rolled-up cores
21 p3317 A71-40010

Stepwise change in wall roughness effects on turbulent shear flow through two dimensional channel, measuring mean velocity, turbulent intensity and shear stress
21 p3365 A71-40015

Turbulence measurement in subsonic wind tunnel gas jet flows containing dust particles, using Doppler difference laser velocimeter
21 p3392 A71-40397

Turbulence measurement by crossed laser beam attenuation due to scattering from particles in clean or seeded flow, studying damping and transport of matter
21 p3392 A71-40400

Turbulent fluids constitutive equations verification by Truesdell principle of material indifference in incompressible and compressible fluids
21 p3367 A71-40652

Time-space description of steady and homogeneous turbulence in incompressible fluid flow
21 p3367 A71-40690

Turbulent viscosity, energy dissipation and diffusion parameters of steady plane boundary layer flows of incompressible fluids with transverse shift in closed system of differential equations
21 p3368 A71-40691

Spectral density functions of velocity pulsations and frequency dependent stability in turbulent plane and axisymmetric channel air flows at different Reynolds numbers
21 p3368 A71-40697

Coaxial free mixing flow calculations, using turbulent kinetic energy method
21 p3369 A71-40958

Energy method application to inhomogeneous turbulent flow with large eddies as recurrent velocity field structures, considering longitudinal rolls in boundary layer wall region
21 p3370 A71-40985

Numerically simulated turbulent velocity flow field, covering Navier-Stokes and energy conservation equations
21 p3371 A71-40996

Surface roughness and mass transfer influence on boundary layer and friction coefficient for turbulent flow over flat plate
21 p3371 A71-40997

Blunt and hemispherical base axisymmetric bodies in Mach 4 free stream, investigating turbulent near wakes generation
21 p3324 A71-40999

Book on turbulence covering measurement techniques, equations of motion, Newtonian viscous fluids, Reynolds stresses, flow visualization, random processes, turbulent energy, boundary layers, etc
21 p3371 A71-41248

Heat transfer and temperature field calculation in turbulent flows through channels of noncircular cross sections, allowing for secondary flow
22 p3619 A71-41871

Turbulent flow of incompressible fluid in rough pipe, determining skin friction coefficient variation with Reynolds number
22 p3531 A71-42291

Turbulent skin friction drag for tapered wings as function of root chord Reynolds number
22 p3481 A71-42839

Turbulent low Mach number electrostatic ion shocks evolution, correlating turbulence spatial growth with reflected ions distribution
23 p3708 A71-42892

Hydrodynamic model of momentum, heat and mass transport for turbulent flow in straight circular pipes, tabulating velocity profiles and eddy diffusivity
23 p3780 A71-43091

Coherent acoustic wave propagation speed and attenuation coefficient in turbulent flow
23 p3703 A71-43209

Convective heat transfer by laminar and turbulent free convection in air on large horizontal and vertical planes
23 p3781 A71-43324

Horizontal velocity and temperature spectra at high wavenumbers in three dimensional quasi-geostrophic turbulent flow
23 p3701 A71-43346

Aerodynamic combustion noise generation from premixed or diffusion open turbulent flames, using fluid mechanics and Lighthill method
23 p3781 A71-43448

Kraichnan turbulence theory based on exact solution of model equations presenting strong structural similarities with turbulent Navier-Stokes equations
23 p3701 A71-43976

High Prandtl/Schmidt/ number fluids turbulent flow temperature profile derivation by turbulent transport mathematical model

23 p3664 A71-44199

Fluid elements streamwise dispersion in two dimensional turbulent shear open channel flow, using Markovian model for numerical simulation

24 p3817 A71-44421

Turbulent stress distribution relationship to averaged characteristics of incompressible fluid boundary layer flow with positive pressure gradient

24 p3818 A71-44748

Computer program for recirculating fluid flows applied to concentration curves obtained by gas injection on pipe center line with fully developed turbulent flow

24 p3820 A71-44956

Shielded hot-wire probe for mean and rms flow velocities in highly turbulent and rapidly reversing flows

24 p3828 A71-45075

Turbulence spectral function asymptotic behavior with infinitely increasing wave number, using graphic technique

24 p3821 A71-45220

TURBULENT HEAT TRANSFER

Shape and surface roughness effects on turbulent ablation of reentry body nose tip, noting recession rate [AIAA PAPER 69-717]

01 p0071 A71-10934

Turbulent boundary layer air flow through supersonic convergent-divergent nozzle with heat transfer, considering relationship between temperature and velocity profiles

01 p0180 A71-10950

Heat transfer in nongray radiating gas turbulent flow in circular tube

01 p0181 A71-11403

Heat transfer and friction drag calculation for turbulent boundary layer of gas with temperature dependent physical properties

02 p0185 A71-11884

Heat and gas curtain efficiency in turbulent boundary layer on flat plate, including heat transfer data

02 p0331 A71-11886

Turbulent heat transfer in nonNewtonian fluid flow, considering generalized Prandtl number effect

02 p0241 A71-12642

Prandtl number measurement in turbulent thermal boundary layer along flat plate with stepwise wall temperature variation

04 p0680 A71-15477

Turbulent heat and mass exchange intensity at gas screen, investigating nonisothermality and wall penetrability effects

04 p0683 A71-15497

Laminar turbulent tube flow heat transfer, investigating internal radiation exchange and wall heat conduction and generation effects

04 p0685 A71-15519

Differential phenomenological theory for turbulent free convection along heated vertical plate

04 p0686 A71-15524

Scalar substance heat transfer characteristics in nonhomogeneous turbulence, using statistical and phenomenological approach

04 p0572 A71-15541

Turbulent hydrodynamics and heat transfer in rotating flows of incompressible fluid

04 p0578 A71-15631

Heat transfer in exchangers with forced laminar or turbulent flows with linear pressure drop and exponential thermal flux distribution

04 p0688 A71-15740

Turbulent boundary layer development and heat transfer in parallel wall passage entrance region, comparing measurement results with computer solution

04 p0689 A71-15920

Atmospheric diffusion parameters investigated by smoke plumes in atmospheric boundary layer, evaluating turbulent energy dissipation

05 p0778 A71-16838

Turbulent heat transfer measurements on blunt cone in nitrogen flow at high Mach number under various angles of attack

[AIAA PAPER 71-38]

06 p1008 A71-18499

Hypersonic lifting entry vehicle turbulent heat transfer and boundary layer transition at various angles of attack and Reynolds numbers

[AIAA PAPER 71-100]

06 p0844 A71-18555

Heat exchange in turbulent flow at large Prandtl numbers, using Van Driest formula

07 p1223 A71-19747

Anomalous resistance and turbulent heating of strongly nonisothermal plasma in strong magnetic field due to electron scattering by ion-acoustic turbulent pulsations beats

12 p1936 A71-27032

Stratosphere and lower mesosphere seasonal climatic temperature profiles calculation from radiation transport and balance equations, noting turbulent heat influxes role in stratification formation

13 p2057 A71-28024

Turbulent boundary layer friction and heat transfer under longitudinal pressure gradient

13 p2048 A71-28590

Turbulent skin friction and heat transfer prediction on flat plates and wind tunnel walls at supersonic and hypersonic Mach numbers, using Van Driest theory

14 p2334 A71-29868

Flap induced flow deflection effects in hypersonic shock tunnel, obtaining turbulent heating, skin friction and pressure data

[AIAA PAPER 71-598]

15 p2343 A71-31540

Turbulent swirling flames nonisotropic exchange coefficients determination from time mean velocity, pressure, temperature and concentration distributions

15 p2514 A71-32087

Heat transfer in wall region of steady turbulent flow at large Prandtl numbers, plotting temperature distribution curves

17 p2728 A71-35119

Surface renewal and penetration heat transfer model for turbulent flow in smooth and rough tubes

18 p2986 A71-36593

Turbulent boundary layer and heat transfer measurements along cooled conical convergent-divergent nozzle

[ASME PAPER 71-HT-4]

19 p2993 A71-37982

Turbulent forced-convection heat transfer coefficient for supercritical fluid, extending Prandtl mixing length concept

[ASME PAPER 71-HT-26]

19 p3165 A71-37996

Vertical motions, turbulent heat exchange and radiative heat input role in stratus clouds evolution, deriving humidity and heat transfer equations as functions of time

19 p3093 A71-38690

Swirl flow augmented heat transfer to liquid nitrogen in dispersed film boiling, using twisted tape inserts

20 p3313 A71-39285

Radiative and turbulent heat transfer in atmospheric surface layer, measuring radiative heat flux divergence and temperature fluctuations at different heights

22 p3534 A71-41860

Heat exchange between two fluid streams in cocurrent, countercurrent, laminar or turbulent boundary layer flow separated by flat plate, determining temperature distribution

23 p3783 A71-44193

TURBULENT JETS

Turbulent jet noise estimation taking into account retarded time effect on acoustic radiation

01 p0072 A71-11468

Mean and pulsation characteristics of velocity and temperature in turbulent conducting jets under longitudinal and transverse magnetic fields

02 p0292 A71-12626

Forced plume entrainment of turbulent buoyant jet in stratified fluid as function of Reynolds, similarity and Froude numbers

02 p0278 A71-12704

Three dimensional turbulent jet reattachment, investigating wall attachment distance with aspect and offset ratio and Reynolds number variations

[ASME PAPER 70-WA/FLCS-5]

03 p0401 A71-14081

Free and impinging axisymmetric turbulent jet characterization model providing continuous transition from nozzle exit through fully developed region

[ASME PAPER 70-WA/FLCS-6]

03 p0401 A71-14082

Axially symmetrical two phase turbulent air jet, examining small liquid droplets effect on flow structure

[ASME PAPER 70-WA/APM-45]

03 p0404 A71-14166

Variable density turbulent jets, discussing compressible, high temperature gas, cryogenic and supersonic jets, Reynolds equations, etc

04 p0577 A71-15620

Turbulent jet diffusion and vortex models, noting velocity profile in mixing and turbulent boundary layers

04 p0577 A71-15625

Supersonic flow past notch in lateral body surface or in two closely lying coaxial bodies, applying turbulent jet theory to separation zone

04 p0528 A71-15626

Turbulent and laminar jet propagation and mixing in rotor downwash field

[DGLR-70-050]

05 p0795 A71-15961

Aerodynamic sound generation by turbulent circular free jets, presenting solution to inhomogeneous acoustical wave equation by Lighthill

[DFVLR-SONDDR-87]

06 p0881 A71-17421

Noise-producing subsonic jet turbulence eddies hot-wire anemometer measurements of convection velocity as functions of frequency

[AIAA PAPER 71-154]

06 p0884 A71-18596

Turbulent He jet measurements using hot-wire anemometry and digital recording techniques, assessing accuracy

[AIAA PAPER 71-201]

06 p0886 A71-18639

Noise reduction in turbulent jet by repeated air injection at boundary of jet core

06 p0848 A71-18704

Acoustic radiation spectra from turbulent jets, assuming approximate Gaussian statistics and second

order velocity correlation space-time characteristics obtainable from frozen flow

07 p1016 A71-19011

Compressible two dimensional laminar and turbulent free jet characteristics, presenting unitary models with similarity transformation

07 p1029 A71-20009

Laminar-turbulent bounded jet stability, examining transition zone shift with smoke visualization

07 p1029 A71-20009

Fluidic ambient velocity and pressure measurement sensors, using unbounded turbulent jets

07 p1029 A71-20009

Acoustical response of closed flue pipe as function of blowing pressure and air jet turbulence level

08 p1276 A71-21011

Aeroacoustic phenomena in free turbulent gas jet, discussing structure, noise-turbulence correlation and acoustic field generation at subsonic/critical velocities

09 p1384 A71-23401

Turbulent characteristics of circular subsonic flow jet impinging normal to flat plate, measuring heat transfer rates

10 p1694 A71-23911

Turbulent diffusion flame laminarization by perimposed rotating flow field, discussing boundary layer stabilizing effect of external centrifugal force field

10 p1695 A71-24641

Turbulent free jets expansion, presenting method for velocity distribution calculation via suitable correlations between average velocity and turbulent fluctuations

10 p1596 A71-24941

Circular turbulent liquid jet in external stream, considering Reichardt theory, jet expansion law, asymptotic similarity and constant eddy viscosity hypothesis

10 p1597 A71-24941

Curvature effects on laminar and turbulent free boundary between irrotational flow and stagnant fluid, discussing pressure effects

11 p1702 A71-25461

Subsonic turbulent jet flow optical measurement quantitative schlieren technique to overcome hot-wire anemometry difficulties due to temperature and velocity fluctuations

12 p1896 A71-27201

Turbulent submerged wall air jet on ablating graphite surface, examining friction and heat and mass exchange in boundary layer

13 p2160 A71-28511

Circular air jet velocity, turbulence intensity and energy spectra distributions, investigating longitudinal acoustic field influence

14 p2225 A71-30211

Reattachment of single two dimensional turbulent air jet, investigating gas flow characteristics in combustion chambers

14 p2170 A71-30411

Liquid phase evaporation rates in free turbulent air liquid droplet jet, giving droplet dynamic characteristics determination criterion

14 p2227 A71-30611

Aerodynamics of axial and axial tangential blade swirler twisted jet near nozzle, testing effectiveness as equivalent problem of heat conduction theory

15 p2388 A71-31521

Turbulent wall jet with initial boundary layer, calculating growth and separation in arbitrary pressure gradient by integral method

[AIAA PAPER 71-612]

15 p2389 A71-31521

Tube or duct confined submerged turbulent jet expansion angle calculation for various expansion ratios

15 p2390 A71-32011

Proportional fluid amplifier, measuring deflection angle, jet turbulence and noise level

15 p2390 A71-32011

Turbulent compressible underexpanded two dimensional jet interaction with crossflowing free stream, analyzing flow field by numerical solution of Navier-Stokes equations

[AIAA PAPER 71-611]

15 p2514 A71-32271

Divergent semibounded turbulent isothermal jet at constant density emerging from slot, determining length of initial and main sections

16 p2560 A71-33611

Subsonic turbulent jets acoustic emission, calculating noise intensity in far field for various Mach numbers

17 p2725 A71-34211

Flow visualization and hot-wire measurements showing vortex shedding association with turbulent air jet issuing from flat plate into cross wind

17 p2670 A71-34651

Turbulent He jet time resolved velocity and mass fraction measurements, using hot-wire anemometry and digital recording techniques

17 p2670 A71-34871

Noise generation due to inlet free stream turbulence incident on isolated stators and rotors, using flat plate cascade blade row model

18 p2956 A71-36491

Turbulent boundary layer jet flow calculation using equivalent heat conduction theory

19 p3161 A71-37128

Jet turbulence orderly structure enhancement, control and relation to noise, studying response to periodic surging of frequency and amplitude

19 p3056 A71-38204

Atmospheric convective motion model, applying turbulent jet method

19 p3093 A71-38696

Boundary layer approximation for isothermal turbulent plane semibounded jet expanding over porous surface, deriving friction stresses and flow velocity in skin and stream regions

20 p3214 A71-39795

Static thrust loss of circular cylinder due to sink effects of turbulent jet discharging along surface line

21 p3317 A71-40012

Turbulent jet flow concentration, velocity and direction measurements, describing cold and hot wire techniques and data reduction system

21 p3378 A71-40401

Nonself-similar problem of developing plane turbulent jet in unbounded space, obtaining second and third terms of asymptotic series of stream function

21 p3368 A71-40692

Solid particle or droplet admixture effect on turbulent gas jet structure

22 p3530 A71-41872

Microwave scattering noise spectrum from turbulent rocket-exhaust jet illuminated by plane wave

22 p3510 A71-42208

Scattering from turbulent rocket-exhaust jet illuminated by focused microwave beam, calculating noise spectrum by approximate theory

22 p3510 A71-42209

Unbounded turbulent jet transducer element fluidic sensors, measuring ambient velocity and density from pressure data

22 p3531 A71-42768

Flow field generation by coaxial turbulent jets, determining velocity distribution, turbulence intensities and shear stresses by hot-wire anemometers

23 p3627 A71-44198

Free axisymmetric turbulent annular nozzle jet propagation, detailing velocity distribution variation due to momentum loss in stall region

23 p3664 A71-44335

Two dimensional incompressible turbulent wall jet in moving stream, describing viscous flow characteristics and various boundary layer parameters

24 p3818 A71-44605

Generalized eddy viscosity model application to quiescent and coflowing axisymmetric turbulent jets mixing

24 p3818 A71-44626

TURBULENT MIXING

Two free homogeneous turbulent coaxial air jet mixing, showing mass transfer between boundary layers and interface presence

02 p0185 A71-12409

Laminar and turbulent mixing of two parallel streams of dissimilar fluids, using similarity transformation

[ASME PAPER 70-WA/APM-37]

Turbulent mixing of two parallel similar and dissimilar fluid streams, comparing velocity and density profiles measurements with similarity solution

03 p0403 A71-14162

Turbulent pulsation mixing of free gas jets in mechanical vortex generator with turbulization level control

04 p0577 A71-15621

Dispersion model of turbulent mixing of isothermal and nonisothermal slipstreams of air-gasoline combustion products in nozzles

04 p0577 A71-15622

Turbulent mixing at homogeneous wakes boundary, using heat conduction theory equivalence

04 p0578 A71-15628

Minimum mixing losses of axisymmetric turbulent wakes in profiled wall channels

04 p0578 A71-15629

Two dimensional supersonic turbulent burning mixing layer, measuring physical properties and growth rate

[WSS/CI PAPER 70-16]

Centerline velocity and concentration decay predictions of free and confined jet models with/without secondary flows, considering turbulent mixing

06 p0883 A71-18478

Free turbulent mixing of heated high speed central hydrogen jet and cold low speed annular air stream coupled with finite rate chemical reactions

06 p0866 A71-18479

Supersonic jet noise problem, discussing eddy-Mach wave radiation source mechanism from nonlinear streamwise development of inviscid instability waves in turbulent mixing layer

06 p0884 A71-18592

Compressible turbulent flows free mixing based on two dimensional viscous flow equations

07 p1088 A71-19701

Intensified molecular diffusion during turbulent mixing of supersonic slipstreams in cylindrical mixing chamber, using optical Prudnikov method

07 p1089 A71-19733

Reactant-product structure of turbulent multicomponent mixture with first order reactions at large wavenumbers

07 p1091 A71-20020

Turbulent mixing and radiative transfer relationship to micrometeorological temperature structure of atmospheric boundary layer

10 p1638 A71-23878

Mixing layer of turbulent flows in homogeneous nonconducting and conducting incompressible fluids, extending approximate solution to flow in longitudinal magnetic field

10 p1593 A71-24366

Modular concept mathematical model for combustion and pollution formation processes in jet engine combustors, including turbulent mixing and reaction kinetics

[AIAA PAPER 71-714]

14 p2294 A71-30766

Nonreacting gases supersonic turbulent mixing flowfields, calculating turbulent kinetic energy as function of injection angle and jet velocity

[AIAA PAPER 71-725]

14 p2295 A71-30774

Turbulent mixing between parallel incompressible air streams, using statistical investigation of pressure and velocity fields

[AIAA PAPER 71-613]

15 p2389 A71-31582

Shock tunnel investigation of two dimensional supersonic turbulent mixing with and without combustion, using Mach-Zehnder interferometer and piezoelectric transducers

16 p2554 A71-32881

Turbulent homogeneous air-fuel mixtures pulsating combustion in plane chambers with nozzle and plate stabilizers, noting influence of fuel type and mixture composition

16 p2663 A71-33360

Liquid spray steady evaporation and mixing in gaseous swirl, using continuum mechanics

17 p2727 A71-34693

Turbulent multispecies gas mixing measurements using dark field laser schlieren system

18 p2930 A71-36059

Free shear layer similarity flow profiles correlation for turbulent isobaric jet mixing by spread rate parameters, using viscosity models

21 p3371 A71-41032

TURBULENT WAKES

NT PROPELLER SLIPSTREAMS

NT SLIPSTREAMS

Two dimensional wake laminar-turbulent transition by single and double frequency sounds imposition and wind tunnel natural disturbance, inducing velocity fluctuations

01 p0001 A71-10132

Three dimensional incompressible wake behind blunt obstacle at leading edge of flat plate compared with mathematical model by Oseen linearization

[AIAA PAPER 69-747]

03 p0341 A71-13434

Base pressure variation by mass injection in turbulent supersonic axisymmetric rear wake at high Mach numbers

03 p0399 A71-13457

Mean velocity profile measurements in turbulent wake behind single or parallel arbitrarily spaced and sized cylinders with adverse pressure gradient

[ASME PAPER 70-WA/FE-10]

03 p0403 A71-14131

Radar scattering from turbulent underdense ionized wakes, showing relationship between Doppler spectrum and wake characteristics

04 p0551 A71-15011

Axisymmetric turbulent wakes with zero excess momentum, noting mean and pulsation velocity and Reynolds shear stresses

04 p0577 A71-15624

Turbulent mixing at homogeneous wakes boundary, using heat conduction theory equivalence

04 p0578 A71-15628

Minimum mixing losses of axisymmetric turbulent wakes in profiled wall channels

04 p0578 A71-15629

Dynamic model of flow separation of plane fluid past body in channel with eddy wake formation

04 p0578 A71-15630

Wall jet and wake flow prediction, using Prandtl-Kolmogoroff turbulence model

04 p0578 A71-15766

Finned missiles aerodynamics at high angle of attack, examining body vortex wake region interaction with fins

[AIAA PAPER 71-50]

06 p0980 A71-18511

FAA full scale aircraft vortex wake turbulence flight test programs

[AIAA PAPER 71-97]

06 p0848 A71-18552

Turbulent wake shape in stratified medium describing anisotropic diffusion

07 p1088 A71-19190

Transient and turbulent flow structure in wake behind thin plates in wind tunnel, noting velocity fields, temperature and initial boundary layers

07 p1089 A71-19750

Velocity and density measurements in hypervelocity ballistic projectile turbulent wakes, using hot film anemometers

[AIAA PAPER 68-701]

07 p1015 A71-19891

Two dimensional turbulent wake interaction with linearly stratified main stream, measuring mean and fluctuating temperature and velocity distributions

07 p1092 A71-20277

Ionospheric wake spacecraft potential, electron current and temperature observations, using Agena/Gemini manned two body system sensors

09 p1517 A71-22175

Spring supported circular cylinder stability in wake flow of similar cylinder at various spacings using quasi-static aerodynamic derivatives and flutter theory

09 p1539 A71-22942

Cylinder vibration due to wake force in wind tunnel, discussing self exciting force induction

09 p1540 A71-23057

Turbulent wakes from subsonic-hypersonic bodies for downstream mean flow predictions analysis, considering eddy viscosity function

10 p1550 A71-24338

Sound radiation and wake turbulence spectra from axial compressor single airfoils, including double circular arc profiles

[ASME PAPER 71-GT-4]

11 p1703 A71-25950

Wake flow behind two dimensional perforated plates normal to air stream, measuring drag, shedding, velocity and turbulence at Reynolds number 25,000-90,000

11 p1705 A71-26449

Structure and shape of vortex wake associated with oblique flow past multiblade hinged rotor, using cavitation method

13 p1993 A71-29217

X-type hot wire probe thermal turbulent wake interference, discussing wind tunnel investigation of wire distance effect on pitch angle sensitivity

14 p2339 A71-31022

Acoustic wave after passage through turbulent wake, measuring phase fluctuations

15 p2387 A71-31169

Flow measurements in axisymmetric turbulent wake of sphere in low speed wind tunnel

15 p2346 A71-32123

Potential vortex with turbulent viscous core and axial velocity excess or deficiency, using integral method with quasi-cylindrical flow approximations to describe core flow

15 p2393 A71-32278

Holographic interferometry measurements of mean and localized fluctuating wake density field of cones fired at Mach 6 at ballistic range, using pulsed laser

[AIAA PAPER 71-564]

16 p2520 A71-33105

Turbulent wakes flow entrainment mechanism, investigating turbulence spreading near interface between laminar and turbulent regions

17 p2671 A71-34899

Aircraft accident litigation related to wake turbulence concerning pilot or air traffic controller faults

17 p2842 A71-35387

Supersonic jet interaction with turbulent wake, calculating plane and axisymmetric flow behind body butt face

17 p2672 A71-35630

Aircraft vortex wake turbulence including formation, disintegration, hazards reduction, instability and interactions with following vehicles

17 p2673 A71-35753

Aircraft wake turbulence/trailing vortex systems/avoidance during flight, describing procedures for pilots and tower operators

[CASI PAPER 72/6]

19 p2992 A71-37596

Wakes of freely falling water drops, discussing flow patterns, kinetic energy, vorticity decay and velocity profiles

19 p3089 A71-37733

Turbulence and flow pattern in wake of bluff body flame stabilizers, using hot-wire anemometer measurements and Prandtl-Kolmogorov model

19 p1168 A71-38102

Spherical cap bubbles in water and mineral oil at various dynamic viscosities, measuring laminar and turbulent wakes character, rise speed and shape

21 p3365 A71-40017

Mass spectrometer application to gas analysis of samples from turbulent wake of hypervelocity projectiles

21 p3362 A71-40384

Sequential electric spark technique for hypervelocity projectiles turbulent wake velocity measurements at ballistic ranges in free flight regime

21 p3362 A71-40385

Simultaneous CW microwave radiometer and laser probing of hypersonic wake ionization and turbulence, relating radiation temperature, radar echo and mechanical flow field structure

21 p3392 A71-40387

Charge density fluctuation measurements in ionized turbulent hypersonic sphere wakes, using Langmuir and continuum electrostatic probes and microwave interferometric and scattering equipment

21 p3363 A71-40388

Hypersonic turbulent wake density measurements in free flight hypersonic ranges by electron beam fluorescence probe technique

21 p3363 A71-40389

Turbulent hypersonic wake density and temperature measurement for slender cone model in shock tunnel, using dual electron beam excitation technique

21 p3364 A71-40396

Aircraft wake turbulence and detection - Conference, Seattle, September 1970

21 p3318 A71-40482

Aircraft wake turbulence, reviewing aerodynamic vortex research as exemplified by Karman vortex street and edgetone phenomenon

21 p3318 A71-40483

Flight tests for hazard evaluation to other aircraft from wake turbulence generated by large jet transport airplanes

21 p3321 A71-40506

Atmospheric and wake turbulence effects on aircraft from discrete gust and spectral interpretations, discussing load production and uncontrollable rolling moments

21 p3321 A71-40507

Flight test experiment to evaluate mechanized automatic control system to minimize wake turbulence effects on aircraft

21 p3321 A71-40509

Aircraft wake turbulence relation to CAT, discussing flight control loss, jumbo jets trailing vortex wakes breakup and detection and safe aircraft spacing

21 p3325 A71-40704

Aircraft generated vortex wakes and core air motions hazards for encountering light airplane

23 p3628 A71-43381

TURING MACHINES

Algorithm determining sequential machine error partition representing inessential errors

14 p2206 A71-29521

F-bounded erasing operator in abstract family of language for mapping, applying to families defined by tape-bounded Turing acceptors

20 p3201 A71-38846

Time-bounded grammars and languages capable of simulation by Turing acceptors in automata theory

20 p3202 A71-39050

TURNING FLIGHT

Nonlinear proportional navigation guided homing missile and minimum time to turn, developing quadratic equation with close larger positive root approximation

07 p1156 A71-19878

Glider flight mechanics for turning flight, discussing relationships between turning radius, flight speed, sink rate and aerodynamic characteristics

08 p1232 A71-21770

Supersonic airplane minimum time turns at constant altitude, determining thrust, bank angle and angle of attack programs with optimal control theory

08 p1232 A71-22032

Turn rate gyro installation angle and airspeed effects on instrument reliability, presenting in-flight investigation results relative to turn rate information usefulness under various flight conditions

[SAE PAPER 710380]

10 p1610 A71-24245

Spacecraft banking control during reentry, deriving dynamic equations of angular motion

16 p2646 A71-33655

Altitude, bank angle and thrust program for minimizing time required by supersonic aircraft to turn through specified heading angle and reach required energy

[AIAA PAPER 71-796]

16 p2525 A71-34021

Three dimensional minimum fuel turns for supersonic aircraft by energy state approximation

[AIAA PAPER 71-913]

19 p3096 A71-37163

Three dimensional hypervelocity reentry trajectories, using aerodynamic lift and vehicle bank angle as optimal control parameter

[AIAA PAPER 71-920]

19 p3096 A71-37169

TURNSTILE ANTENNAS

Error introduced into coherent two-way Doppler tracking measurements on spinning satellite, using turnstile antenna

12 p1882 A71-27431

TURTLES

Sodium counterflow from serosal to mucosal surface of short-circuited acid-killed turtle bladder

01 p0015 A71-11182

Postflight histological analysis of turtles aboard Zond 7, noting decrease in cell nuclei size due to space flight conditions adaptation

21 p3334 A71-40568

TVC (CONTROL)

U THRUST VECTOR CONTROL

TWENTY-SEVEN DAY VARIATION

Solar wind asymmetric component on basis of 27-day cosmic ray variations

06 p0953 A71-18121

Twenty-seven day variations in cosmic ray intensity and geomagnetic activity index, using filter and power spectrum methods

06 p0953 A71-18122

Sunspot activity and 107 mm solar flux 27 day variations during 11 year solar cycle

09 p1513 A71-22792

Twenty-seven day variation and cosmic ray intensity modulation relationship, examining 11 year variation from superposition of transient decreases

10 p1660 A71-23800

Generation mechanism of 27-day recurrent geomagnetic disturbances sudden commencements, analyzing interrelationship between recurrent disturbances, solar data and solar plasma physical parameter

10 p1607 A71-25119

Generation mechanism of magnetohydrodynamic shock waves associated with sudden commencements of 27-day recurrent geomagnetic disturbances

10 p1608 A71-25120

Cosmic ray intensity diurnal data recorded during maximum and minimum solar activity periods, relating to 27 day and shorter variations

11 p1815 A71-25590

TWILIGHT

U TWILIGHT GLOW

TWILIGHT GLOW

Twilight helium emission diurnal and seasonal variations relationship to geomagnetic activity and solar depression, using Abastumani observations

07 p1099 A71-19389

Morning and evening H alpha hydrogen line in twilight glow, establishing connection with solar activity level

07 p1105 A71-20439

Twilight helium 10,830 A emission observations and calculations, using grille spectrometer

08 p1283 A71-21638

Earth twilight aureole and cloud spectra from satellite photometry

08 p1285 A71-21792

Secondary umkehr effect in solar UV region at twilight, proposing origin mechanism by ozone layer optical properties

08 p1357 A71-21875

Night glow emission post twilight decay rates at different seasons by Chamberlain relation, discussing F layer ionization

09 p1441 A71-23644

Twilight airglow measurements of hydroxyl and molecular oxygen bands by balloon-borne instruments including IR grating spectrometer and filter photometers

10 p1601 A71-24400

Skylight scattering components from zenith for intensity/polarization variation during twilight and upper atmosphere dust sounding

10 p1607 A71-25114

Predawn enhancement structure of oxygen red line airglow at 6300 A from time-latitude isophote diagrams, discussing F region photoelectron recombination role

11 p1755 A71-25611

Meteoroid aerosols optical manifestation from photometric measurements on stratospheric balloons, demonstrating Orionids effects on twilight sky brightness

12 p1960 A71-26832

Photometric analysis of manned spacecraft twilight brightness photographs for spherical atmosphere in single scattering approximation

12 p1901 A71-27103

Earth surface nighttime, twilight and daytime horizons visual observations by Soyuz 9 spacecraft

13 p2060 A71-28426

Twilight OH emission intensity and rotational temperature in mesosphere as function of solar position below horizon

14 p2232 A71-29959

Airglow research review and bibliography covering past four years observations of nightglow, twilight, dayglow and metals in upper atmosphere

17 p2732 A71-34466

Circumterrestrial cosmic dust clouds properties determination by optical methods, using twilight observations at solar vertical symmetric points

17 p2810 A71-35725

Twilight glow spectrophotometry and visual observations from Soyuz 5 spacecraft, determining atmospheric optics and vertical aerosol profile

18 p2911 A71-36006

Twilight aureole visual observation and objective colorimetry from Soyuz spacecraft, noting importance for atmospheric composition determination

18 p2911 A71-36007

Upper atmosphere dust scattering indicatrix from twilight sky brightness at solar vertical, determining total directed scattering coefficient

19 p3132 A71-37390

Twilight helium emission diurnal and seasonal variations relationship to geomagnetic activity and solar depression, using Abastumani observations

19 p3053 A71-37814

Sunlight scattering by dust in upper atmosphere from primary twilight intensities investigations

20 p3219 A71-39647

Spectrophotometry and photography of earth twilight aureole, clouds and underlying surface from manned Soyuz 5 and 7 spacecraft

20 p3240 A71-396759

Dayglow and twilight emission data, discussing atomic excitation mechanisms, particle production rates, height profiles and temporal variations

20 p3227 A71-39838

Search for upper atmosphere MgO content, using modified Ebert spectrometer with photomultiplier detection to measure twilight excited scattered and resonance radiation

23 p3670 A71-43191

Atmospheric transmission functions for twilight airglow of alkalis Na, Li and K

23 p3673 A71-43983

TWINNING

NT MECHANICAL TWINNING

Mo-Re alloy crystallographic features observation by transmission electron microscopy, noting equivalence of twin-slip and twin-twin interactions

11 p1783 A71-26477

Crystal elastic twinning dislocation theory, discussing twins origin and growth, hysteresis effects, crystal development and stability loss

19 p3156 A71-37758

Salt solution treated and quenched Mg-Al alloy rods tests in distilled water, investigating transgranular stress corrosion cracking and deformation twinning

19 p3083 A71-38722

TWISTED WINGS

Lifting line equation inversion for twisted wings of elliptic planform with arbitrary spanwise upwash

22 p3481 A71-42838

TWISTING

Stress distribution in infinite cracked elastic plate subjected to constant twisting on basis of Reissner thin plates theory

04 p0670 A71-15385

Naturally twisted and orthotropic cylindrical beam bending by transverse load

04 p0673 A71-15886

Vibrational characteristics of pretwisted cantilever beams with uniform rectangular cross section, investigating slenderness ratio effect on natural frequencies

09 p1543 A71-23661

Stretching, twisting, pure bending and flexure of pretwisted elastic rectangular plates of rectangular cross section

13 p2147 A71-27783

Instability limit curves for twisted square metal plates under vertical loads with transition from anticlastic to synclastic deformation

13 p2158 A71-29431

Column buckling under initially random bending and twisting, comparing numerical analysis accuracy with Bernoulli-Euler results

14 p2330 A71-30692

Face shear and thickness twist waves in bcc crystal plates, presenting numerical computation results for Fe and W

15 p2426 A71-31418

Coupled natural frequencies in rectangular cross section pretwisted cantilever beams flexural vibrations

15 p2503 A71-31442

Fiberglass shift moduli based on twist tests, using ratio of deformations on adjacent faces

15 p2438 A71-31654

Thin skewed plates bending and twisting at constant temperature moment, obtaining angle skew effects on torque-twist relation

21 p3463 A71-40592

TWITCHING

Thermoelastic heat release in muscular twitch final phase, discussing energy storage as function of active or passive muscular tension

11 p1718 A71-25626

TWO BODY ORBITS

U TWO BODY PROBLEM

TWO BODY PROBLEM

Canonical theory of dynamics, examining independent variable transformations for perturbed two body problem

01 p0154 A71-10379

Two fixed centers problem generalization for case of material point attracted to coordinates origin by force proportional to radius

01 p0155 A71-10445

Motion equations of spherical gyroscope in gravitational field of larger mass derived from Gupta quantum theory of gravitation

01 p0161 A71-11274

Sun and planet system relative motion, using equations of invariant mechanics

03 p0492 A71-14190

Perturbation theory of celestial mechanics, using expansions of negative powers of mutual distances between two bodies

05 p0810 A71-16546

Nomogram construction for graphical solution of two body problem using radius-vector and velocity components applied to solar system

09 p1520 A71-22844

- Planetary rotational and translational motion interaction in Einstein gravitation theory, describing orbital elements secular disturbances in two body problem
09 p1526 A71-23339
- Orbital analysis of two body problem with slowly decreasing mass, constructing limited time interval approximate solutions for three distinct phase domains
10 p1676 A71-24523
- Second and higher order perturbation theory for two body trajectories, using recursive formulas
[AIAA PAPER 70-1056] 11 p1820 A71-25459
- Two spheroid rigid bodies rotational and translational motion, using linear and Hill type differential equations for angular variables and coordinates
14 p2312 A71-30384
- Equilibrium position stability of nonlinear two body satellite system in circular orbits in gravitational central force field, using linearized equations of motion
15 p2499 A71-31176
- Simplified H. A. Newton formula applied to two zero-mass bodies rectilinear motion, using time coordinates power series
15 p2481 A71-31300
- Gravity decrease effects on planetary orbits, considering two bodies in circular and elliptical orbits and many bodies solar system with interaction between planets
16 p2631 A71-33167
- German book on satellite geodesy covering two body problem, perturbation theory, earth gravitational field, gravitational effects of sun and moon, radiation pressure, etc
17 p2799 A71-34470
- Book on linear and ordinary celestial mechanics covering perturbed two body motion, numerical methods, canonical theory and initial value problems
17 p2799 A71-34471
- Orbital elements oscillations in celestial mechanics two body problem with slowly decreasing mass described by nonlinear nonautonomous differential equations system, obtaining approximate solutions
17 p2804 A71-34912
- Three degree of freedom perturbed two body problem, applying theory of redundant variables to Lagrangian equations of motion
19 p3143 A71-38163
- Elliptic parameters of osculating orbits in two body problem with variable mass
20 p3267 A71-38791
- Two body orbits problem concerning satellite flightpath transfer possibility to orbit touching cyclic or elliptical trajectories
20 p3287 A71-38849
- Excising neighborhood of singularity from manifold with vector field definition, making possible regularization of two and three body problems
20 p3254 A71-38900
- German monograph on static fields in general relativity theory covering covariant equilibrium conditions, two body problems, vacuum fields and Newtonian gravity principles
20 p3269 A71-39077
- TWO DIMENSIONAL BODIES**
Nonaffine similarity laws and transformations subject to limitations of Newtonian impact theory for two dimensional bodies, obtaining aerodynamic coefficients
01 p0002 A71-10948
- Curvature matching method for two dimensional flexible plate nozzle contour of trisomic wind tunnel, obtaining overdetermined simultaneous equations
01 p0068 A71-10970
- Monograph on plane shock wave interactions covering supersonically moving two dimensional thin airfoils, slender bodies of revolution and thin wings
01 p0003 A71-11227
- Dynamic problems of two dimensions with semisurface of section, examining charged particles motion in axisymmetric magnetic field
04 p0627 A71-15706
- Unsteady coefficient measurements to corroborate theory for coefficient distribution about little elongated two dimensional wings with control surfaces
05 p0694 A71-16737
- Plane EM waves at two dimensional periodic media boundary, obtaining reflection and refraction for harmonics
05 p0723 A71-17029
- Flow field behind two dimensional roughness element in rectangular channel, discussing wall effects, reattachment point position, velocity distribution and turbulence intensity
07 p1086 A71-18775
- Three-part mixed boundary problem concerning equilibrium of semiinfinite two dimensional elastic medium containing Griffith cracks parallel to free boundary
07 p1214 A71-20021
- Two dimensional rigid wings, investigating response characteristics to gust loads
09 p1383 A71-23440
- Two dimensional contact problem for isotropic body in triangle form on half plane, calculating elastic constants with difference Green function
13 p2156 A71-29071
- Aerodynamic behavior of bodies in wake of two dimensional bluff bodies, discussing loads
13 p1994 A71-29265
- German monograph on thermally stressed shear soft shells with finite deformation covering tensor analysis, thermoelasticity, temperature fields and two dimensional bodies
15 p2509 A71-32305
- Hypersonic small perturbation flow past two dimensional or axisymmetric slender bodies supporting logarithmic shock waves
17 p2670 A71-34658
- Two dimensional jet flapped symmetric wing in subsonic flow, assuming irrotational flow inside jet bounded by vortex sheets
21 p3318 A71-40172
- Two dimensional flow over two dimensional finite wing without correction for downwash, assuming known pressure distribution
21 p3318 A71-40173
- Perturbation velocity of laminar wake downstream of two dimensional body in boundary layer, considering transition behind trip wire
21 p3322 A71-40640
- Transonic flows about two dimensional airfoils, calculating far field boundary conditions with coordinate transformation
24 p3789 A71-44620
- Slender two dimensional wedge wings aerodynamic characteristics in hypersonic strong interaction flow, determining wall shear stress and lift drag ratio effects
24 p3789 A71-44621
- TWO DIMENSIONAL FLOW**
NT COUETTE FLOW
Shock formation in cylindrical and two dimensional tubes investigated numerically by FLIC method for compressible fluid flow
01 p0069 A71-10130
- Two dimensional wake laminar-turbulent transition by single and double frequency sounds imposition and wind tunnel natural disturbance, inducing velocity fluctuations
01 p0001 A71-10132
- Poincare hydrodynamic analogy in celestial mechanics, relating differential equations for dynamic systems with two degrees of freedom and two and three dimensional flow
01 p0154 A71-10383
- Vertical fluid-filled channel with uniform internal heat source, analyzing steady plane-parallel convective motion
01 p0179 A71-10665
- Slowly varying plane flows of highly conducting inviscid quasi-neutral gas plasma in channel with solid metallic walls as electrodes
01 p0133 A71-10790
- Two dimensional potential flow theory for incompressible unsteady flow about multiple lifting bodies in small amplitude motion
01 p0071 A71-10929
- Viscosity model application to turbulent plane Couette flow velocity profile and shear stress values, obtaining skin friction relation
01 p0071 A71-10954
- Steady isothermal plane gas flow between infinite parallel planes at arbitrary Knudsen numbers, obtaining linear differential equations of mass transfer
01 p0071 A71-11114
- Boundary layer separation at free streamline attachment to sharp trailing edge of flat plate, deducing terminal velocity profile for two dimensional flow
02 p0185 A71-12376
- German monograph on plane ideal gas flows calculation with allowance for unsteady gaslight walls and compression shocks using difference methods
02 p0240 A71-12400
- Numerical analysis of flow field around thin airfoil in two dimensional nonuniform stream, using finite difference method
02 p0187 A71-12680
- Axial turbomachines boundary layer flow, describing two dimensional cascade calculation methods
03 p0340 A71-13146
- Plane laminar flow stability along flexible boundary, obtaining numerical and asymptotic solutions
03 p0399 A71-13198
- Plane Couette flow turbulence, discussing wall region shear and core homogeneity
03 p0400 A71-13546
- Uniform flow stability near two dimensional stagnation region formed by blunt body immersion in cross flow
03 p0400 A71-13728
- Two dimensional cascade flow, discussing methods of flow field idealization, nonviscous incompressible flow theoretical methods, compressibility and viscosity effects
03 p0342 A71-13826
- Plane nonsteady gas dynamic flows, reducing to system of time dependent equations system, presenting Chaplygin equation generalization
03 p0401 A71-13908
- Two dimensional annular flow of viscous heat conducting gas between coaxial cylinders, using Navier-Stokes equations
03 p0401 A71-14066
- Low speed two dimensional axial flow compressor cascade data, considering lift drag ratio and minimum loss coefficient
[ASME PAPER 70-WA/GT-10] 03 p0343 A71-14118
- Two dimensional wall jet and wall wake flow turbulence characteristics, considering mean and fluctuating flow properties
[ASME PAPER 70-WA/APM-35] 03 p0403 A71-14161
- Incompressible two dimensional inviscid stably stratified fluid flow over vertical step in channel bounded by rigid horizontal lid
03 p0453 A71-14201
- Lateral drift of solid particles suspended in plane supersonic gas flow along wall with recess step, using successive approximation for equations
03 p0404 A71-14255
- Plane transonic flow with curved compression shock wave between subsonic and supersonic regions
03 p0345 A71-14560
- Boundary layer growth effects on two dimensional flow field in low pressure test gas of circular and rectangular shock tubes
04 p0568 A71-14667
- Two dimensional incompressible laminar boundary layer flow along ablative blunt body in irradiant environment
04 p0679 A71-15467
- Linearized equation for stability and heat transfer of two dimensional incompressible laminar boundary layer in water flow
04 p0679 A71-15469
- Longitudinal surface curvature effect on steady two dimensional incompressible laminar thermal boundary layers
04 p0680 A71-15471
- Two dimensional and axisymmetric flow film cooling effectiveness in supersonic turbulent boundary layer, using Eckert reference enthalpy method
04 p0571 A71-15496
- Steady two dimensional ideal gas flow past blunt body at incident infinite Mach number, obtaining gas dynamic variable asymptotic expansions as kappa approaches infinity
04 p0528 A71-15553
- Two dimensional hypersonic flow field density gradient distribution measurement by space-time resolved laser schlieren system
04 p0600 A71-15592
- Dynamic model of flow separation of plane fluid past body in channel with eddy wake formation
04 p0578 A71-15630
- Linearized shock waves and periodic disturbances propagation by discrete ordinates method in planar radiative gas dynamics
04 p0689 A71-15742
- German monograph on centered two dimensional nonequilibrium hypersonic expansion flow, considering real gas flow with chemical reactions
05 p0693 A71-16124
- Transonic flow with chemical reactions, analyzing one and two dimensional problem by small perturbation method
[ONERA-TP-749] 05 p0717 A71-16534
- Two dimensional wake laminar-turbulent transition, emphasizing velocity fluctuation nonlinear interaction
05 p0695 A71-16964
- Plane steady laminar flow into channel between two semiinfinite parallel plates, constructing asymptotic solution for large Reynolds number
05 p0736 A71-16966
- Plane Poiseuille viscoelastic liquids flow stability, using method of inner and outer expansions based on Chun and Schwarz asymptotic solution of Orr-Sommerfeld equation
05 p0737 A71-17102
- Steady two dimensional flow past flat plate in rectangular channel for low Reynolds number
05 p0738 A71-17249
- Shock wave bisector rule improvement, applying to asymptotic behavior of bow shock attached to airfoil in two dimensional supersonic flow
06 p0841 A71-17420
- Plane Poiseuille flow stability to finite amplitude periodic disturbances, using Orr-Sommerfeld eigenfunctions
06 p0881 A71-17429
- Two dimensional supersonic turbulent burning mixing layer, measuring physical properties and growth rate
[WSS/CI PAPER 70-16] 06 p0943 A71-17657
- Plane incompressible MHD boundary layer on porous plate, considering heat and mass transfer in blowing or suction velocity distribution
06 p0936 A71-17736
- Supersonic flow of rarefied plasma around plane bodies, allowing for electric field effect on ion motion
06 p0842 A71-18252
- Airfoils in two dimensional nonuniformly sheared slipstreams, predicting pressure distribution from mathematical model for comparison with measurement
[AIAA PAPER 71-94] 06 p0843 A71-18549

Two dimensional flow around wing sections with slats and slotted flaps in various positions, presenting surface pressure and boundary layer measurements [AIAA PAPER 71-96] 06 p0844 A71-18551

Two dimensional turbulent boundary layer flows numerical methods with simplicity and accuracy [AIAA PAPER 71-164] 06 p0885 A71-18606

Finite difference calculation for two dimensional compressible turbulent boundary layer flow with heat transfer, using mixing length concept [AIAA PAPER 71-165] 06 p0885 A71-18607

Two dimensional hypersonic laminar wakes incipient transition region calculation based on boundary layer approximation and von Karman integral formulation [AIAA PAPER 71-202] 06 p0846 A71-18640

Friction, heat transfer and mass transfer theory of flow represented by two dimensional parabolic boundary layer equations 07 p1085 A71-18766

Two dimensional turbulent channel flow, determining local mean wall shear stress from velocity gradient 07 p1087 A71-18784

Compressible turbulent flows free mixing based on two dimensional viscous flow equations [AIAA PAPER 71-4] 07 p1088 A71-19701

Two dimensional flow MHD in plasmas with anisotropic pressure, considering weak shock waves parameter changes in linear approximation 07 p1168 A71-19726

Transpiration cooling of reentry vehicle nosetips, noting two dimensional aspects of porous wall coolant flow and matrix-coolant energy exchange [AIAA PAPER 69-96] 07 p1223 A71-19869

Two dimensional flow field in secondary sonic transverse jet injection port vicinity, studying free stream Mach number, total pressure and specific heats ratio 07 p1090 A71-19896

Rarefied gas flow and heat transfer in plane Couette flow using Bhatnagar-Gross-Krook model with ellipsoidal distribution 07 p1224 A71-20024

Two and three dimensional thermals and steady and starting plumes convective fluid motion formulas, using vorticity integration method 07 p1104 A71-20223

Two dimensional turbulent wake interaction with linearly stratified main stream, measuring mean and fluctuating temperature and velocity distributions 07 p1092 A71-20277

Turbulent pipe, channel and plane Couette flow by Prandtl model equations, comparing with experimental data 07 p1092 A71-20278

Prandtl two dimensional time dependent similarity flows with vortex sheets 07 p1093 A71-20279

Finite element solution of plane Poiseuille rarefied gas flow between parallel infinite plates 07 p1093 A71-20284

Prandtl-Glauert pressure distribution rule improvement subsonic planar flow 07 p1017 A71-20312

Two dimensional supersonic fluidic amplifier flow field density and characteristics determined by differential interferometry 07 p1028 A71-20588

Aerodynamic characteristics of conical and pyramidal configurations with various planforms by slender body theory, replacing three dimensional flow by two dimensional flow 08 p1227 A71-20776

Resonance line formation in multidimensional media, applying to non-LTE line transfer for two dimensional temperature variations 08 p1359 A71-20942

Short shock wave equations for two dimensional steady motions of ideal gas 08 p1276 A71-21871

Flow lines construction in two dimensional supersonic flow region with rarefaction waves interaction from several disturbance sources 08 p1230 A71-22052

Uniform two dimensional incompressible turbulent boundary layer with uniformly distributed surface mass injection, correlating results on basis of turbulent kinetic energy equation 09 p1430 A71-22105

Electrohydrodynamic flow in plane channel with conducting walls and axial emitter electrode, determining velocity and pressure profiles distortion 09 p1502 A71-22538

Plane Poiseuille flow bounded by solid walls, applying Fourier expansion method to stability problem 09 p1432 A71-22583

Linear mountain lee wave model with nonlinear lower boundary condition for arbitrary basic flow and two dimensional topography, computing flow field 09 p1487 A71-23024

Pseudo-stationary shock wave in plane MHD flow of conducting gases, deriving existence theorem for linear relations between vorticity and current density 10 p1648 A71-24281

Plane unsteady convective motion of viscous incompressible liquid in infinite horizontal vessel of rectangular cross section due to wall temperature fluctuations 10 p1696 A71-24375

Friction drag and energy losses of steady plane incompressible boundary layer flow of viscous liquid on nonconducting wall in MHD channel 10 p1649 A71-24377

Steady two dimensional MHD laminar flow between two parallel circular porous disks in transverse magnetic field, determining velocity, pressure and shear stress distribution 10 p1649 A71-24408

Villat problem of ideal incompressible two dimensional fluid flow around plate, determining stagnation point location 10 p1594 A71-24452

Numerical simulation of developing and decaying two dimensional isotropic turbulence consistent with Batchelor predictions 10 p1595 A71-24619

Backward facing step in confined supersonic two dimensional flow, investigating turbulent shear layer reattachment 10 p1552 A71-24622

Nonlinear forced vibrations of aeroelastic plate in two dimensional supersonic flow under harmonic pressure near critical Mach number 10 p1690 A71-24643

Solar wind blast wave dependence on initial disturbance energy and angular extent by time dependent two dimensional hydrodynamic flow simulation 10 p1663 A71-24779

Airfoil profiles coupling method for determining complex potential of two dimensional ideal incompressible fluid flow due to arbitrary airfoil section movement near rectilinear wall 10 p1597 A71-25015

Universal equations of two dimensional incompressible unsteady laminar boundary layer 10 p1597 A71-25017

Compressible flow in two dimensional boundary layers in arbitrary pressure gradient, using turbulent energy equation for skin frictions and free stream Mach numbers 10 p1598 A71-25082

Pulsating incompressible two dimensional laminar boundary layer flow past insulated plate at zero incidence, calculating skin friction and surface temperature 10 p1697 A71-25084

Plane unsteady polytropic MHD flow equations reduced to time independent system, using complex variable techniques 11 p1804 A71-25439

Prandtl first order boundary layer equations for two dimensional laminar incompressible flow past circulation controlled circular lifting rotor 11 p1702 A71-25494

Multiphase two dimensional mixing and combustion of flow fields suspended in gaseous medium for propulsion systems problems, obtaining governing equations [AIAA PAPER 70-145] 11 p1854 A71-25509

Two dimensional flow in radial turbomachine bladed impeller, comparing numerical solution based on potential theory with experimental results [ASME PAPER 71-GT-20] 11 p1703 A71-25964

High subsonic flow two dimensional turbine cascade design by approximate hodograph method, noting pressure distribution measurements [ASME PAPER 71-GT-34] 11 p1704 A71-25971

Steady transonic flow through two dimensional gas turbine cascades predicted with time dependent formulation of flow equations, giving airfoil surface pressure distributions [ASME PAPER 71-GT-89] 11 p1704 A71-25996

Lagerstrom mathematical model for two dimensional viscous flow at low Reynolds number, discussing asymptotic solutions for limit process expansions analysis 11 p1752 A71-26010

Time dependent shear stress, temperature and boundary layer pressure in laminar flow over stepwise accelerated flat plate at hypersonic speed 11 p1856 A71-26193

Ideal incompressible fluid flow around fixed obstacle near rectilinear wall, investigating plane motion with profile couple method 11 p1705 A71-26258

Two dimensional incompressible turbulent boundary layer, determining velocity distribution with Cole law of wake 11 p1752 A71-26259

Three dimensional turbulent boundary layer calculations, using two dimensional method based on turbulent energy equation empirical conversion into shear stress transport equation 11 p1753 A71-26443

Plane parallel Couette flow stability with respect to small perturbations, considering positive wave numbers and Reynolds numbers 12 p1897 A71-27307

Transonic airfoil testing techniques in two dimensional flow, discussing wind tunnel conditions at various Reynolds numbers 12 p1864 A71-27308

Two dimensional inviscid heated flows in terms of pressure, density, speed, direction and heating rate applied to supersonic duct combustion chambers 12 p1987 A71-27309

Discrete ionospheric model of supersonic of dimensional low density plasma flow past bodies, using quasi-neutrality condition 13 p1990 A71-28207

Two dimensional turbulent boundary layer bodies rectangular step, investigating heat exchange and separation regions 13 p2048 A71-28208

Two dimensional prediction of adiabatic wall temperature and heat transfer coefficient downstream of film cooling slots, using Prandtl mixing length formula 13 p2160 A71-28209

Plane stationary constant-vorticity incompressible flow region surrounded by potential flow, determining two dimensional velocity distribution by numerical calculation 13 p2050 A71-29229

Numerical method for two dimensional or axisymmetric heated flows allowing for dissipation extending to viscous flow, using Navier-Stokes equations in streamwise coordinates 13 p2118 A71-29229

Compressible electrically conducting liquid two dimensional steady state laminar flow calculations in MHD duct 13 p2109 A71-29229

Two dimensional vortex filament development artificially shed in laminar boundary layer on flat plate without pressure gradient, using hydrogen bubble visualization technique 13 p2051 A71-29406

Separation control of two dimensional air flow over turbulent boundary layer along circular cylindrical wall by jets or suction 13 p2051 A71-29406

Two dimensional jet flap cascades, presenting stream deflection angles as function of jet to main stream momentum flux [ASME PAPER 71-FE-14] 13 p1995 A71-29406

Incompressible conducting fluid plane jet expanded in homogeneous slipstream, deriving partial differential equations for nonconduction approximations 14 p2278 A71-29606

Two dimensional flow research on high lift airfoil for STOL aircraft, using vorticity distribution as wind tunnel wall blowing techniques 14 p2169 A71-29906

Two dimensional transonic potential flow near convex corner 14 p2225 A71-30206

Nonlinear dynamical evolution of two dimensional unstable shear flows, using numerical integration of time dependent incompressible Navier-Stokes equations 14 p2226 A71-30406

Two dimensional sonic nonreacting gaseous secondary injection into supersonic primary stream with turbulent boundary layer for application to thrust vector control [AIAA PAPER 71-750] 14 p2227 A71-30707

Vertical fluid-filled channel with uniform internal heat source, analyzing steady plane-parallel convective motion 14 p2339 A71-30909

Two dimensional hypersonic boundary layer equations solution upper and lower bounds determined as initial value problem 15 p2386 A71-31101

Two dimensional subsonic irrotational isentropic flow around thick profiles, using coordinate perturbation method 15 p2343 A71-31101

Velocity profile of steady two dimensional incompressible laminar boundary layer flow with suction or injection, noting wall shear function 15 p2388 A71-31444

Constant density and viscosity fluid steady plane two dimensional flow under no external forces, deriving partial differential equations for vorticity, energy and pressure 15 p2389 A71-31721

Two dimensional viscous incompressible fluid flow field calculation in fluidic element, giving Navier-Stokes equations solution in finite difference form 15 p2390 A71-32093

Two dimensional wind tunnel tests on airfoils fastened between tunnel walls, investigating variable chord concept applicability in sailplane design 15 p2350 A71-32229

Peristaltic pumping mechanism as progressive wave train of transverse wall displacement in plane two dimensional channel 15 p2366 A71-32559

MHD rectilinear two dimensional flows at high Hartmann number, including extension to three dimensional problems 15 p2459 A71-32556

Coupled radiative transfer-gas dynamic interactions in unsteady wave propagation, two dimensional steady flows and atmospheric motions

15 p2515 A71-32562

Two dimensional viscous hypersonic flow past thin, needle shaped and highly blunted bodies with strong boundary layer interaction on outer stream

15 p2347 A71-32569

Stationary nonparallel plane flow stability with horizontal shear to three dimensional nondivergent disturbances in Boussinesq fluid, using Arnold method

15 p2393 A71-32637

Two dimensional MHD flow past flat plate with magnetic field aligned with flow field, using method of matched asymptotic expansions

16 p2615 A71-32860

Shock tunnel investigation of two dimensional supersonic turbulent mixing with and without combustion, using Mach-Zehnder interferometer and piezoelectric transducers

16 p2554 A71-32881

Heat transfer, density and pressure measurements of hypersonic two dimensional centered nonequilibrium corner expansion oxygen flow with frozen boundary in shock tunnel

16 p2555 A71-32906

Approximation analysis for laminar two dimensional boundary layer behind plane shock wave moving over infinite flat plate

16 p2556 A71-32914

Plane Couette flow with finite disturbances, investigating stability in nonlinear terms

16 p2558 A71-32986

Unstable two dimensional incompressible flow and wake development, using finite difference calculations for Navier-Stokes equations

16 p2558 A71-32996

Oscillating thin wing with control surfaces in two dimensional compressible subsonic flow, calculating aerodynamic forces based on kernel function method [DFVLR-SONDDR-132]

16 p2519 A71-33013

Two dimensional steady gas flows with heat addition, using reduction to partial differential equations

16 p2662 A71-33168

Nonlinear heat transfer in plane rarefied isothermal Couette gas flow, using BGK model

16 p2561 A71-34143

Two dimensional laminar separation bubbles in high Reynolds number flow fields, using finite difference solutions to Navier-Stokes equations

16 p2561 A71-34165

Detachment prediction in turbulent incompressible plane flows on thick bodies applied to wall with disconnections and flat plate normal to wind

17 p2669 A71-34189

Plane laminar two phase jet flow consisting of small spherical particles suspended in incompressible carrier fluid in presence of adjacent parallel moving free stream

17 p2726 A71-34582

Perturbed two dimensional laminar boundary layers of incompressible conducting fluid flow along insulated concave wall in transverse magnetic field, investigating three dimensional instability

17 p2788 A71-34642

Navier-Stokes steady nonrectilinear universal complex laminar flow, showing isochoric lamellar or plane motions of constant velocity with streamlines as concentric circles

17 p2727 A71-34695

Numerical solution for two dimensional steady state fluid flow in square cavity by optimum time step formulation

17 p2728 A71-34880

Supersonic turbulent two dimensional boundary layer flows wall flux and velocity/temperature profiles prediction

17 p2729 A71-35283

Time and space variable magnetic field effects on plane unsteady MHD boundary layer flow separation

17 p2789 A71-35343

Plane Poiseuille flow stability evaluation for finite amplitude periodic disturbances, using harmonic analysis

17 p2729 A71-35389

Supersonic jet interaction with turbulent wake, calculating plane and axisymmetric flow behind body butt face

17 p2672 A71-35630

Two dimensional steady potential incompressible flow past elastic expandable gas filled envelope fastened to edge of plate normal to flow

17 p2730 A71-35640

Two dimensional steady viscous gas transonic flow Navier-Stokes equations, establishing uniqueness of solutions to boundary value problems

17 p2673 A71-35646

Turbulent plane flow velocity profile stability characteristics covering parabolic Poiseuille flow under infinitesimal disturbances

18 p2901 A71-35855

Transient laminar two dimensional boundary layer induced pressures due to suddenly accelerated hypersonic semiinfinite flat plate

18 p2901 A71-35856

Oblique shock-combustion wave polar investigation of stationary two dimensional flow of fuel mixture in compressed gas

18 p2985 A71-36133

Plane laminar flow linear stability problem, using Orr-Sommerfeld equation with Volterra integral equation

18 p2904 A71-36136

Two dimensional flow of non-Newtonian fluids with rigid spherical substructure, solving linear coupled ordinary differential equations for spin and velocity field [ASME PAPER 71-APM-N]

18 p2926 A71-36257

Plane laminar incompressible jet flow along parabola with no external stream, using second order boundary layer theory

[ASME PAPER 71-APM-MM]

18 p2904 A71-36268

Free-Lagrange method for two dimensional flow numerical simulation, covering mesh optimization and equations of motion

18 p2905 A71-36304

Two dimensional laminar incompressible fluid flow past flat plate at various angles of attack, studying vortex shedding characteristics

18 p2844 A71-36311

Planar supersonic near wake flow field problem with variable viscosity and base injection, investigating boundary errors spatial decay rate

18 p2906 A71-36321

Two dimensional steady laminar boundary layer theory for incompressible medium, presenting error bounds for Prandtl equation solution

18 p2906 A71-36322

Time dependent calculation of mixed two dimensional or axisymmetric transonic flows in nozzle, writing equations of motion with transformed spatial variables

18 p2906 A71-36323

Shock wave diffraction propagation through nonuniform fluid, noting application to two dimensional unsteady flows

18 p2907 A71-36332

Plane Poiseuille flow at constant rate, developing numerical simulation of transition and turbulence

18 p2845 A71-36337

Two dimensional flow equations for incompressible viscous fluid in square cavity

18 p2907 A71-36340

Incompressible two dimensional turbulent hypersonic boundary layer flow velocity, pressure, temperature and density distributions

18 p2908 A71-36429

Velocity field of viscous steady plane incompressible flow past body, linearizing by Oseen approximation

18 p2910 A71-36946

Plane MHD Couette flow stability with asymmetric velocity profile shaped by transverse magnetic field, considering Hartmann flow

19 p3108 A71-37077

Plane unsteady gas flow under action of dihedral angle shaped piston traveling at constant velocity

19 p3042 A71-37080

Plane transonic gas flows through Laval nozzle and symmetrical wedge-shaped profile, solving boundary value problem by reduction to singular integral equation

19 p2991 A71-37101

Axisymmetric plane transonic flow past convex corner point, obtaining characteristics by mapping into hodograph plane

19 p2991 A71-37103

Critical forward speed effects on two dimensional peripheral jet ground effect support systems, comparing theoretical analysis with wind tunnel model data [AIAA PAPER 71-908]

19 p2995 A71-37159

Viscous relativistic fluid plane laminar flow, discussing incompressible thermally nonconducting case and stationary models

19 p3044 A71-37640

Ergodic boundary in time evolution of two dimensional incompressible Navier-Stokes equations solution at large Reynolds numbers

19 p3045 A71-37841

Heat and mass transfer through porous plate into turbulent two dimensional incompressible boundary layer, using van Driest damped mixing length [ASME PAPER 71-HT-10]

19 p3045 A71-37986

Nonlinear instability theory for wave system in plane Poiseuille flow, deriving asymptotic solution for initial value problem

19 p3046 A71-38203

Ideally conducting magnetostatic equilibria and associated time dependent resistive flows from two dimensional solution for MHD equations

19 p3115 A71-38211

Plane parallel Couette flow stability with respect to small perturbations, considering positive wave numbers and Reynolds numbers

19 p3046 A71-38263

Numerical analysis of plane transonic flows past shock free airfoils without boundary layer separation using inverse method of complex characteristics

19 p2994 A71-38307

Fronts and frontal clouds evolution theory as nonstationary two dimensional problem with allowance for dynamics and thermodynamics

19 p3091 A71-38682

Short shock wave equations solutions for two dimensional steady flow of ideal gas

20 p3211 A71-39370

Hanging compression shock wave in plane supersonic ideal gas flow past body with broken generatrix

20 p3176 A71-39371

Two dimensional supersonic base flow with small Mach number recirculation zone, determining jet line by variational principle of Poisson equation

20 p3176 A71-39414

Compressor blade holography and profile equations for subsonic two dimensional flow calculated on graphic visualization console

20 p3176 A71-39420

Variable suction effects on two dimensional fluctuating slip flow of incompressible rarefied gas past infinite flat plate

20 p3211 A71-39466

Second order viscoelastic fluid two dimensional stagnation point flow, solving boundary layer equations

20 p3213 A71-39564

Velocity profiles of plane turbulent flow of incompressible fluid on porous surface in presence of suction

20 p3213 A71-39790

Plane equilibrium turbulent boundary layer with longitudinal pressure gradient

20 p3214 A71-39791

Shock fronts diffraction and reflection with vortices generation at discontinuities, predicting wave shape and strength distribution in two dimensional or axisymmetric situations

21 p3365 A71-40016

Two dimensional flow over two dimensional finite wing without correction for downwash, assuming known pressure distribution

21 p3318 A71-40173

Straight line vortices in uniform two dimensional straining field, detailing irrotational strain and simple shear

21 p3320 A71-40501

Plane steady irrotational flow of ideal compressible fluid around jet profile, obtaining Kutta-Joukowski theorem

21 p3322 A71-40580

Nonself-similar problem of developing plane turbulent jet in unbounded space, obtaining second and third terms of asymptotic series of stream function

21 p3368 A71-40692

Two dimensional supersonic moist air expansion around sharp corner, investigating water vapor condensation by homogeneous nucleation

21 p3369 A71-40952

Laminar incompressible plane wall jet, calculating flow characteristics for potential core region with integral method

21 p3370 A71-40988

Boundary vorticity method for finite amplitude convection in plane Poiseuille flow with isothermally heated and cooled plates, using Boussinesq approximation

21 p3477 A71-40993

Two dimensional supersonic turbulent free shear layer recompression process from flow model numerical calculation

21 p3371 A71-40998

Flat supported plate in plane supersonic oscillating flow, calculating forced vibration with potential flow theory

21 p3473 A71-41367

Small mesoscale waves development in steady stratified plane parallel flow, assuming mean flow characteristics dependence on vertical coordinate

21 p3412 A71-41391

Displacement fields for two dimensional minimum weight frames for load dispositions analogous to perfectly plastic plane flow in metal working

21 p3391 A71-41428

Two dimensional supersonic flow pattern, velocity and loss in shock waves in front of blade cascade

22 p3479 A71-41842

Plane Couette flow temperature and velocity fields for Newtonian fluid with temperature dependent viscosity under locally and temporally constant wall temperature

22 p3620 A71-41881

Plane MHD boundary layer growth and separation in viscous incompressible flow past cylinder under abrupt motion and transverse magnetic field

22 p3584 A71-42685

Plane diabatic Prim gas flow, reducing hodograph equations in elliptic regions to Cauchy-Riemann equations via Baeklund transformations

23 p3662 A71-43121

Second order theory of plane plastic flow, investigating characteristic slip lines of perturbed velocity field and stress equations

23 p3774 A71-43144

Plane steady rotational flow of inviscid gas with arbitrary state equation for straight or circular streamlines

23 p3662 A71-43236

Two dimensional and three dimensional wakes in supersonic and hypersonic rarefied gas wind tunnels, comparing cone and dihedral configurations

23 p3625 A71-43357

Potential two and three dimensional flows past body in presence of rigid wall, using matched asymptotic expansions

23 p3625 A71-43369

Two dimensional radiative heat transfer in absorbing-emitting medium bounded by nonisothermal gray walls from Monte Carlo simulation, showing gas emissive power distribution

23 p3784 A71-44276

Fluid elements streamwise dispersion in two dimensional turbulent shear open channel flow, using Markovian model for numerical simulation

24 p3817 A71-44421

Flow instability due to viscosity variation in high pressure two dimensional laminar flow of Newtonian fluid between rigid parallel plates

24 p3819 A71-44945

Two-dimensional asymptotic solutions to Navier-Stokes equations for weak vortex discontinuity flow with vanishing viscosity

24 p3820 A71-45060

Small perturbation development of plane potential motion of ideal incompressible fluid in elliptical region, confirming instability

24 p3821 A71-45219

TWO DIMENSIONAL JETS

Two dimensional free gas jet expansion into quiescent medium, predicting terminal shock position

03 p0400 A71-13466

Simplified two dimensional jet reattachment model, using Goertler profile equation and constant spread parameter

[ASME PAPER 70-WA/FLCS-8]

03 p0401 A71-14084

Two dimensional jets forced and induced switching by vortex flow

[ASME PAPER 70-WA/FLCS-13]

03 p0354 A71-14088

Heated glass free jet characteristics at low Reynolds numbers, evaluating temperature distribution and two dimensional fluid dynamic effects

[ASME PAPER 70-WA/FE-3]

03 p0521 A71-14125

Ideal incompressible fluid plane jets interaction with flow discontinuity at jet boundaries, deriving nonlinear system of integral equations

03 p0405 A71-14564

Plane ideal incompressible fluid jet impact on curvilinear surface, considering flow characteristics near stagnation point

04 p0567 A71-14592

Two dimensional supersonic surface jet-hypersonic flow interaction with axial symmetry

[AIAA PAPER 71-131]

06 p0845 A71-18575

Uniform magnetic field parallel alignment effects on incompressible electrically conducting free two dimensional jet flow stability at large Reynolds number

07 p1084 A71-18745

Compressible two dimensional laminar and turbulent free jet characteristics, presenting unitary method with similarity transformation

07 p1029 A71-20593

Interaction flowfield of two dimensional supersonic airstream with transversely injected jets of various gases, presenting wall static pressure, gas concentration and temperature measurements

09 p1382 A71-22111

Two dimensional discrete fluidic element with Coanda effect, calculating switching discharge, jet gap and circulation zone length

09 p1386 A71-22654

Plane jet in counterflow with vortex shedding control, discussing solid boundary and jet momentum effects

10 p1592 A71-23980

Inviscid model for flow field within plumes of two dimensional underexpanded jets calculated by time dependent finite difference method

11 p1853 A71-25160

Inviscid incompressible two dimensional jet deflection by various dimension segments, investigating potential flow with Schwarz-Christoffel transformation and free streamline theory

11 p1753 A71-26444

Reattachment of single two dimensional turbulent air jet, investigating gas flow characteristics in combustion chambers

14 p2170 A71-30419

Turbulent compressible underexpanded two dimensional jet interaction with crossflowing free stream, analyzing flow field by numerical solution of Navier-Stokes equations

[AIAA PAPER 71-611]

15 p2514 A71-32277

Two dimensional jet interaction flow field, investigating gas dynamic and transport phenomena

[AIAA PAPER 71-561]

15 p2514 A71-32279

Intermittency signals correlation, determining lateral motion of two dimensional jet boundaries

18 p2901 A71-35854

Boundary layer approximation for isothermal turbulent plane semibounded jet expanding over porous surface, deriving friction stresses and flow velocity in skin and stream regions

20 p3214 A71-37975

Two dimensional potential flow model of Pitot static probe and subsonic free jet interaction, using conformal mapping and hodograph method

[AIAA PAPER 71-998]

24 p3817 A71-44589

Two dimensional incompressible turbulent wall jet in moving stream, describing viscous flow characteristics and various boundary layer parameters

24 p3818 A71-44605

TWO FLUID MODELS

Optimum two fluid mixing chamber length for energy efficiency of conical diffusers in straight pipe jet pump systems

03 p0399 A71-13369

Simple two fluid solar wind speed and proton temperature model, discussing nonthermal energy dissipation

03 p0481 A71-14504

Two fluid model solar wind, predicting electron temperature and heat flow

05 p0799 A71-16692

MHD system hydrodynamic stability using propellant and fuel filled reactor cavity to form three region two fluid vortex

06 p0882 A71-18318

Collisional drift plasma wave instability nonlinear analysis, calculating wave amplitude as function of magnetic field based on two fluid theory

07 p1166 A71-18883

Ionospheric irregularities two fluid model, using nonlinear differential equations for longitudinal waves propagating in hot collisional magnetoplasma

10 p1648 A71-24294

Hydromagnetic shock wave structure, treating plasma in two fluid approximation with collisional transport coefficients in changing density and temperature

10 p1596 A71-24657

Capillary pressure and contact angle drop of two fluid flow separated by parallel plate interface

11 p1750 A71-25443

Hydrodynamic instabilities of MHD plasma with current, using two fluid model in crossed magnetic-electric fields

13 p2105 A71-27879

Magnetospheric two component plasma model, considering thermal and suprathermal spectra

13 p2060 A71-28432

Gasdynamic lasers optically active medium two fluid model, deriving solutions for CW generators and quantum amplifiers

17 p2754 A71-35397

Unified linear theory for MHD waves in weakly ionized radiating plasma, deriving two-fluid model set of equations corresponding to magnetoacoustic, thermal, electrothermal and ionization rate waves

21 p3423 A71-40945

Weakly ionized magnetoplasma with no axial drift, investigating collisional drift-type instability by linearized two fluid hydrodynamic numerical analysis

22 p3580 A71-41586

Radial electric field and electrostatic potential in solar wind from two fluid model

22 p3592 A71-41921

Upstream influence and interfacial waves in open channel two fluid small perturbation flow

23 p3663 A71-43446

Heat exchange between two fluid streams in cocurrent, countercurrent, laminar or turbulent boundary layer flow separated by flat plate, determining temperature distribution

23 p3783 A71-44193

TWO PHASE FLOW

Kinetic equations of quasi-steady homogeneous condensation of water vapor in supersonic nozzle two phase flow

01 p0182 A71-11443

One component two phase mixtures critical flow in nozzles, orifices and short tubes, considering interphase heat, mass and momentum transfer

[ASME PAPER 70-WA/HT-5]

03 p0520 A71-14095

Axially symmetrical two phase turbulent air jet, examining small liquid droplets effect on flow structure

[ASME PAPER 70-WA/APM-45]

03 p0404 A71-14166

Heat transfer intensification under forced one and two phase flow in channels

04 p0675 A71-14782

Two phase heat transfer in thermosyphon counterflow under simulated gravities of 0.1 to 100 earth gravity, measuring critical heat flow rates and convection coefficients

04 p0687 A71-15531

Two phase mixtures thermally induced flow oscillations, discussing scaling criteria, phase change numbers and stability boundaries

04 p0687 A71-15532

Normal shock waves in one dimensional steady flow of two phase medium, noting phase exchanges in lack of internal equilibrium

04 p0579 A71-15100

Energy deposition, vacuum expansion and vaporization of barium in two phase jets, using combustion and solid state shock waves

05 p0836 A71-16400

Gas-particle mixture cascade flow over turbine blades, considering momentum/heat transfer and particle trajectories

[AIAA PAPER 70-712]

06 p0841 A71-17171

Boiling layer microcharacteristics, investigating temperature pulsations near wall attachment and cooled liquid two phase boundaries

07 p1221 A71-18180

Boiling in two-phase layer on heated wall in relation to thermal exchange mechanisms

07 p1221 A71-18180

Gas-particle mixtures weak disturbances, applying linearized hydromechanic and phase transformation kinetic equations

07 p1088 A71-19940

Gas-particle mixture cascade flow over turbine blades, considering momentum/heat transfer and particle trajectories

[AIAA PAPER 70-712]

07 p1017 A71-20300

Two phase Hg tunnel for shock wave visualization by RF discharge between test model body and external ring, comparing measurements with supersonic flow theory

08 p1272 A71-21710

Particle motion behind oblique shock wave in transonic supersonic wedge flow, deriving expressions for particle trajectories and velocity equalization time

08 p1227 A71-21710

Closing shock position in supersonic underexpanded single and two phase jets, determining liquid phase concentration effects on Mach number and nozzle pressure in wind tunnel

08 p1228 A71-21900

Apparatus for vapor-liquid flow studies, discussing measurement system and energy dissipation

08 p1273 A71-21940

One component two phase flow in tubes with increasing pressure gradient, investigating flow choking and correlating measurements with analytical results

09 p1434 A71-23400

Linear theory of weakly perturbed supersonic planar axisymmetric flows of gas-particles mixture, deriving partial differential equation for perturbation potentials

10 p1551 A71-24300

Two phase mixture nonequilibrium flow mathematical model with allowance for colliding droplets coagulation and atomization based on high speed photographic studies

10 p1551 A71-24300

Inviscid incompressible two phase concave type corner flows embedded with small spherical particles, examining streamlines, critical collision conditions and approximate viscous effects

10 p1598 A71-25000

Two dimensional analysis of isentropic perfect gas flow fields in axisymmetric nozzles for transonic two phase flow initial values, calculating particle trajectories

[AIAA PAPER 69-572]

11 p1751 A71-25500

Shock tube facility with two-phase system of solid particles and gases as primary driven fluid, applying hypervelocity impact phenomena observation

11 p1745 A71-26200

Two phase supersonic barotropic flow with solid particles around thin profile with allowance for elastic particle collisions

12 p1864 A71-27400

Transient thermodynamic processes of two phase vapor-liquid emulsion emptying at subcritical temperature in heat engines

12 p1944 A71-27500

Particle interaction with wedge surface in supersonic two phase flow, determining incidence conditions and collision frequency as function of initial conditions

12 p1866 A71-27600

Soviet monograph on turbines and jet nozzles for two phase flows covering gas-particle velocity and temperature differences, turbine design, etc

13 p2117 A71-28890

Two phase critical flow of one component mixture in nozzles, orifices and short tubes, considering interphase heat, mass and momentum transfer rates

[ASME PAPER 70-WA/HT-5]

13 p2049 A71-28900

Critical and near critical two phase flow in venturi tube, applying one dimensional flow equations

13 p2051 A71-29440

Phase changes/droplet solidification/effect on two phase nozzle flow, considering perturbation treatment

[ASME PAPER 71-FE-11]

13 p2052 A71-29450

Particle energy spectrum function effect on fluid energy spectrum in turbulent gas-solid suspension flow

[ASME PAPER 71-FE-15]

13 p2052 A71-29450

Pressure recovery performance of straight-wall two dimensional diffusers with subsonic air-water mix

- tures, studying gas volume flow ratio and diffuser geometry effects
[ASME PAPER 71-FE-20] 13 p2052 A71-29458
- Skin friction drag and velocity profile measurements on flat plate in two phase circular pipe flow in subsonic wind tunnel for gas-solid media, using photographic technique
[ASME PAPER 71-FE-32] 13 p2053 A71-29467
- Two component solid gas vortex flows with end wall injection eliminating boundary layer losses for colloid core nuclear rocket engine concept
[AIAA PAPER 71-637] 14 p2273 A71-30715
- Heat transfer and pressure drop characteristics of He in two phase and supercritical flow, calculating He heat exchangers for superconductive devices
[HEAT EXCH. CONF. PAPER 24] 15 p2513 A71-31638
- Air-water flow pressure loss and phase distribution in tube with wire coil swirl generators
[GESP-449] 15 p2354 A71-32209
- One dimensional two phase Stefan problem solution for melting of heated thin plate, comparing iterative methods 16 p2662 A71-33065
- Fluid droplet collapse in two phase system gas flows, noting time dependence 16 p2663 A71-33893
- Plane laminar two phase jet flow consisting of small spherical particles suspended in incompressible carrier fluid in presence of adjacent parallel moving free stream 17 p2726 A71-34582
- Thermal radiation effect on normal shock wave structure in gas-particle flows, deriving approximate closed-form solution for gray absorbing particle cloud 17 p2727 A71-34879
- Closing shock position in supersonic underexpanded single and two phase jets, determining liquid phase concentration effects on Mach number and nozzle pressure in wind tunnel 17 p2671 A71-35269
- Batch unit for investigation of injectors in vapor-liquid flows, discussing measurement system and energy dissipation 17 p2724 A71-35275
- Fluid jets and droplets deformation in transverse supersonic two phase gas flow 17 p2673 A71-35638
- Relaxation effects on velocity and temperature of solid particles in gas flows, emphasizing acoustic propagation, compression shock structure and nozzle flows 18 p2909 A71-36441
- Two phase flow model of water droplets velocity in air stream, using Fresnel biprism and laser differential scheme 19 p3072 A71-37587
- Pressure wave propagation through one and two component annular and mist flows, showing importance of inertial interphase momentum transfer 19 p3171 A71-38293
- Two phase flow speed transit time measurements by correlation methods with randomly fluctuating signals, noting use in small bore tubes and strip steel production 19 p3067 A71-38658
- Liquid jet injection into transverse two-phase vapor-liquid flow, calculating penetration path and depth from semiempirical theory 20 p3210 A71-38896
- Linear theory of weakly perturbed supersonic plane axisymmetric flows of gas-particles mixture, deriving partial differential equation for perturbation potential 20 p3175 A71-38898
- Gas-solid particles flow pseudofluid equations, discussing difference of species and partial density and various flow phases 21 p3365 A71-40018
- Two phase critical flow of saturated and subcooled high pressure liquid nitrogen through convergent-divergent nozzle, comparing with water 21 p3369 A71-40894
- Two phase flow in asymmetrically roughened ducts, investigating secondary flow effects on heat transfer characteristics 21 p3477 A71-40995
- Two phase gas-liquid ejectors with cylindrical mixing chamber, discussing ejection equations, jet flow parameters, operation modes and diffuser substitution 22 p3479 A71-41851
- Vacuum water-air ejector with cylindrical mixing chamber and multibarrel nozzle feed, showing increased efficiency by supersonic diffuser substitution 22 p3480 A71-41852
- Solid particle or droplet admixture effect on turbulent gas jet structure 22 p3530 A71-41872
- Mean void fraction of adiabatic two phase flow by luminescent tracer dispersed in liquid phase 23 p3675 A71-43323
- Heat transfer characteristics of two phase nitrogen film boiling in tubes with tape-generated swirl flow 23 p3783 A71-44195
- Ideal gas and liquid droplets two phase flow continuity and motion one dimensional equations, describing relations between velocity, density, pressure and bulk component concentrations 24 p3818 A71-44709
- Two phase nonequilibrium flow mathematical model with allowance for colliding droplets coagulation and atomization based on high speed photographic studies 24 p3790 A71-44927
- Transient thermodynamic processes of two phase vapor-liquid emulsion draining at subcritical temperature in heat engines 24 p3819 A71-44928
- Particle interaction with wedge surface in supersonic two phase flow, determining incidence coordinates and collision frequency as function of initial conditions 24 p3790 A71-44930
- TWO PHASE SYSTEMS**
U BINARY SYSTEMS [MATERIALS]
TWO REFLECTOR ANTENNAS
Unfurlable spacecraft antenna design and electrical characteristics, using Gregorian geometry with conical main and parabolic subreflector 02 p0232 A71-12324
- Cassegrain system far field radiation pattern and gain loss prediction for beam steering by subreflector tilting 02 p0222 A71-12793
- Multiple beam antenna with fixed spherical reflector and movable dual subreflector feedhorns, comparing with conventional Cassegrain antenna for satellite tracking 02 p0233 A71-12794
- Shaped dual reflector antenna gain prediction based on feedhorn radiation pattern and system geometry 02 p0233 A71-12795
- Shaped dual reflector system phase errors due to feedhorn or subreflector axial displacement, examining effects on gain and secondary radiation pattern 02 p0222 A71-12796
- Two mirror Cassegrain antenna secondary reflector random fluctuations effects on drift in main lobe direction 17 p2713 A71-34397
- Circularly polarized parabolic SHF antenna with plane and parabolic reflectors, testing radiation pattern performance 22 p3515 A71-42521
- TWO STAGE TURBINES**
Two-spool turbojet engines matching by rapid superposition method 01 p0142 A71-10821
- Two stage compressors with subsonic and supersonic air velocity and high camber rotor blades, discussing strength against centrifugal force 05 p0796 A71-16647
- TYPE 2 BURSTS**
Center limb linearized impulsiveness calculations for type 2 solar bursts recorded with circular polarization features 02 p0302 A71-12762
- Type 2 and 3 solar radio bursts, discussing models without reabsorption 08 p1356 A71-21755
- Type 2 and 3 solar radio burst model, examining exciting agent as electron bunch emitting electron plasma waves 08 p1356 A71-21756
- Type 2 and 3 solar radio burst generation, proposing coherent synchrotron electron deceleration mechanism 12 p1954 A71-27710
- Radioheliographic 80 MHz observations of harmonic type 2 solar burst near limb flare 15 p2472 A71-31688
- Culgoora 80 MHz radioheliographic observations of 13 October 1969 harmonic solar type 2 burst attributed to explosive flare behind west limb 15 p2472 A71-31689
- Coronal emission from turbulent plasma excited by shock wave, discussing relation to type 2 radio bursts 15 p2473 A71-31719
- Type 2 radio burst disturbances in coronal magnetic field, considering shock wave travel parallel to magnetic field lines 18 p2957 A71-36159
- TYPE 3 BURSTS**
Type 3 solar radio bursts, examining proton and electron stream exciters 05 p0804 A71-16030
- Type 3 solar radio bursts observed at low frequencies for half rotation, discussing occurrence, drift rates, propagation time and emission 05 p0804 A71-16031
- Type 3 solar radio burst storms at low frequencies, suggesting electron packet exciters propagating with little deceleration 06 p0968 A71-17916
- Solar optical flares association with type 3 bursts from OGO-3 observations, suggesting temporary creation or enhancement of electron stream propagation by filament or sunspot structure change 07 p1187 A71-19724
- Solar burst theories, considering type 3 radiation source model for determination of lower corona plasma waves energy densities 08 p1358 A71-20889
- Type 2 and 3 solar radio bursts, discussing models without reabsorption 08 p1356 A71-21755
- Type 2 and 3 solar radio burst model, examining exciting agent as electron bunch emitting electron plasma waves 08 p1356 A71-21756
- Type 3 solar radio bursts in absence of H alpha flares, noting soft X-ray emission 12 p1946 A71-26619
- Type 3 radio bursts at hectometric wavelengths from 13 to 25 August 1968, noting effect of large active sunspot groups 12 p1969 A71-27652
- Solar type 3 radio bursts polarization measurement by recording and subsequent digital processing 12 p1969 A71-27653
- Type 2 and 3 solar radio burst generation, proposing coherent synchrotron electron deceleration mechanism 12 p1954 A71-27710
- Type 3 solar LF radio burst storms, considering streamer density, inhomogeneities and solar wind speed 13 p2141 A71-29053
- Solar type 3 bursts with fundamental and second harmonic structure for corona reflected and direct rays at 80 MHz observed with Culgoora radioheliograph 15 p2473 A71-31690
- Harmonic type 3 solar bursts radioheliographic observations, discussing polarization characteristics 15 p2473 A71-31691
- Type 3 solar emission bursts, investigating time profiles and quasi-oscillatory decay 15 p2480 A71-32750
- Type 3 solar radio burst instantaneous emission frequency relationship to local plasma frequency in region with subrelativistic particles 18 p2958 A71-36742
- Interplanetary electron associations with type 3 solar bursts, using decametric OGO 3 and solar geophysical observations 23 p3721 A71-43176
- Type 3 solar radio bursts polarization characteristics distribution, determining Faraday rotation dispersion effect by trial and error technique 23 p3768 A71-43850
- TYPE 4 BURSTS**
Moving type IV solar bursts polarization and rapid fadeout, discussing relativistic electrons synchrotron radiation intensity 01 p0152 A71-10331
- Type IV solar radio emission broadband intensity fluctuations explained by MHD pulsations in flux tubes in corona 01 p0162 A71-11387
- Type 4 source movement out to 6 solar radii from solar center based on 80 MHz brightness temperature observations 14 p2306 A71-29694
- Moving type 4 solar radio burst, describing bipolar magnetic structure and origin in synchrotron radiation from relativistic electrons 15 p2473 A71-31692
- Circular polarization and fadeout of moving solar type 4 burst related to magnetic arch and synchrotron emitting electrons deceleration 15 p2473 A71-31693
- Moving type 4 solar radio burst observation on 10 October 1969 with radioheliograph, noting circular polarization, movement direction, speed and structure 15 p2473 A71-31694
- Polarized meandering type 4 burst of solar flare from 80 MHz radioheliographic observations, noting association with plasmoids containing synchrotron emitting relativistic electrons 15 p2473 A71-31695
- TYPEWRITERS**
NT AUTOMATIC TYPEWRITERS
NT TELETYPEWRITERS
- U**
U TUBES
U MANOMETERS
U.S.S.R.
Meteorite craters in U.S.S.R., discussing impact, explosive and complex craters 09 p1520 A71-22842
- Far ionospheric propagation of round-the-world echo signals from Moscow to Antarctic station Molodezhnaia and back to Moscow 11 p1731 A71-25773
- Long term vertical and horizontal variations of long wave radiation field in free atmosphere over U.S.S.R., using actinometric sounding data 22 p3570 A71-42848

U.S.S.R. SPACE PROGRAM

Soviet astronautics with emphasis on Cosmos satellite program, discussing launching bases, booster rocket designs, radio signals and missions

01 p0164 A71-11456

Soyuz 9 scientific and technical experiments during prolonged orbital flight, discussing day and night horizon

03 p0495 A71-14391

Salut 1/Soyuz 10 mission, discussing configuration, size orbits and docking procedure

18 p2975 A71-36685

U.S. and U.S.S.R. space stations with European participation, discussing design, international cooperation and legal and political problems

19 p3149 A71-37305

UBV SPECTRA

Mira Ceti type long period variable giant stars emission spectra, emphasizing UBV photometry and IR electrophotometry

03 p0486 A71-13267

Photoelectric measurements of four comets, discussing instrumental data transformations to international UBV system

03 p0490 A71-13943

UBV photometry of RR Lyrae variables in metal rich globular cluster NGC 6171

04 p0649 A71-15372

Photoelectric UBV observations of variable star AE Aur /November 1963-February 1968/, tabulating and graphing results

07 p1201 A71-20434

Three color photoelectric observations of symbiotic star AG Dra in UBV system

07 p1204 A71-20630

Eclipsing variable V701 Cen photoelectric observations in UBV tabulated, fitting Russell model solutions to data

08 p1357 A71-20874

UBV colors and polarization models for reflection nebulae based on Mie scattering functions for exponential size distribution of silicate particles

09 p1517 A71-22332

Variable stars, quasars and X ray source ScoXR-1 UBV light photoelectric data, examining optical emissions and brightness variations

09 p1524 A71-23186

Photon counting stellar photometer for UBV spectra, describing operation and block diagram

09 p1451 A71-23187

Stellar UBV photographic photometry of specific Milky Way oblong region

09 p1527 A71-23525

WX Cep eclipsing system photoelectric components computed in standard UBV colors, obtaining orbital elements

09 p1527 A71-23526

Early stars Vilnius intermediate band and UBV systems comparison for color excess ratios and magnitudes, obtaining reddening line slopes by spectral energy distributions

10 p1682 A71-25131

Astronomical photometry and photometric systems, discussing spectral classification, U, V, B, Y, beta system, energy distributions and seven color photography

12 p1903 A71-26774

Cepheids UBV spectrum analysis, examining brightness shapes and color index curves

12 p1962 A71-26907

Quasars and X ray sources, observing UBV magnitude variation with photoelectric data

12 p1963 A71-27077

Temperature dependent isophote wavelength in Brill and Planck formulas, comparing uvby and UBV photometric systems

13 p2068 A71-28512

Red subluminal stars, presenting catalog identification, proper motions, spectral type, photometric parallax, tangential velocity, UBV photometry, etc

14 p2316 A71-31006

White dwarf identification with Lowell proper motion program, detailing color classes, tangential velocity and UBV values

14 p2317 A71-31008

Photometry and structure of young open cluster NGC 7380, obtaining magnitudes in UBV and positions on Hamburg-Schmidt plates

16 p2632 A71-33321

Computer model of eclipsing binary stars tested with photometric B and V observations and orbital elements of RU Ursae Minoris

16 p2635 A71-33436

Quasars and X ray sources, observing UBV magnitude variation with photoelectric data

19 p3133 A71-37427

Rhea and Titan UBV photoelectric observations, obtaining light curve magnitude variation

21 p3440 A71-40056

Photoelectric observations of magnetic variable stars with five color photometer, giving light and color curves parallel to main sequence

21 p3440 A71-40057

Narrow band and UBV photoelectric photometry of Uranus geometric albedo and magnitude at unit distance as functions of wavelength

21 p3443 A71-40191

Be star theta Corona Borealis UBVV H alpha filter observations, noting spectroscopic changes of light variation due to particles in stellar atmosphere

21 p3443 A71-40193

H beta and UBV photoelectric photometry of southern galactic cluster, deriving absolute magnitude calibrations and intrinsic color relations

21 p3443 A71-40194

SV Cephei variable photoelectric UBV observation showing existence of quasi-periodic minima with changing characteristics

21 p3451 A71-40715

Stellar UBV photometric investigation, determining brightness, coordinates, B-V and U-B color indexes of faint blue objects near galactic North Pole

21 p3451 A71-40721

Red variable GN Her brightness, color and spectrum, discussing UBV system photoelectric measurements during 1966/68 period

23 p3771 A71-44303

Nova N Vul 1968 UBV system photoelectric observations, noting small amplitude rapid brightness variations during night

23 p3771 A71-44304

K and M class stars B and V magnitudes in UBV system based on atomic lines and molecular bands spectral absorption

23 p3771 A71-44306

UDIMET ALLOYS

Hot working cast nickel based alloy for thin gage sheet, noting electroslog remelting increased temperature range

07 p1136 A71-19964

Udimet 700 superalloy gamma prime precipitate particle size, volume fraction and chemical composition as function of time and temperature

15 p2433 A71-32176

Heat treatment for weldability and formability improvement of Udimet 700, evaluating by bend, hardness and tensile tests

21 p3388 A71-40622

UH-1 HELICOPTER

UH-1B helicopter flight test noise measurements data reduction and analysis, presenting sound pressure vs frequency and time plots

04 p0531 A71-15405

High performance UH-1 compound helicopter high speed flight research, considering rotor loads, stability, control and flying qualities [AHS PREPRINT 570]

14 p2180 A71-31111

UHTRIX [NUCLEAR REACTORS]

U HIGH TEMPERATURE NUCLEAR REACTORS

ULLAGE ROCKET ENGINES

Saturn S-4B continuous vent system for propellant tanks during parking orbit to prevent excessive pressure, requiring liquid settling with auxiliary ullaging rockets

18 p2973 A71-36453

ULM [LIGHT MODULATION]

U ULTRASONIC LIGHT MODULATION

ULTRA SHORT WAVE RADIO EQUIPMENT

U VERY HIGH FREQUENCY RADIO EQUIPMENT

ULTRAHIGH FREQUENCIES

NT P BAND

VHF/UHF telemetry antenna stellar calibration using radio stars

01 p0054 A71-10909

Universal UHF telemetry system for use on artillery projectiles and gun launched probes, describing components

01 p0034 A71-10911

Interference levels in UHF band measured from aircraft altitudes using LES-6 receiver adapted to KC-135 aircraft

01 p0037 A71-11166

Cryogenic L band three port stripline circulator, discussing design, construction and applications

01 p0056 A71-11200

Atmospheric UHF attenuation observations by horn antenna

01 p0039 A71-11381

L band DME and TACAN improvements, emphasizing use of static broadband amplifiers

02 p0235 A71-12905

Microwave circuit with coupled TEM bars for L band Si avalanche diodes

05 p0729 A71-16920

VHF/UHF satellite transmission, predicting multiple ground reflection effects on signal fading and effective antenna gain by computerized method

06 p0868 A71-17732

S band pulsed cotar radar transponder for ground base Centaur rocket trajectory tracking from takeoff to splashdown

06 p0870 A71-18475

Navigation and communication experiment at L band on board S.S. Manhattan using ATS-5 satellite

with biphasic PSK modulation of three tones for ranging

07 p1057 A71-18811

UHF sharing between space and terrestrial services: discussing relationships between frequency choice, satellite relay performance, RF power requirements and system costs

07 p1065 A71-20444

Human gastrointestinal tract functional disturbances after prolonged work in UHF field

08 p1249 A71-21951

Wideband UHF amplification in bulk n-type GaAs during domain generation, comparing cut-off Gunn frequency

09 p1507 A71-22277

Trapezoidal and Killian distributions profiles: parameters at S band in plasma column, noting electron density

09 p1501 A71-22303

Decimeter range diode commutation devices, calculating speed, wideband capability, noise level and maximum power

11 p1741 A71-26550

Intense vacuum UV atomic line source excited by 2450 MHz microwave discharge cavity with cleaved spectrum, noting window deterioration and self absorption

14 p2240 A71-30121

Field strength standards and calibrations for frequencies from audio to 1 GHz range, discussing uncertainties

14 p2205 A71-30980

Low carrier power aircraft antenna module for airborne UHF communications system, considering range/field strength measurements

14 p2216 A71-31040

VHF and UHF ground reflection measurements for antenna site layout, showing feasible operations at short ranges

14 p2217 A71-31050

Positions and flux densities of radio sources from Fourth Cambridge catalog by pencil beam measurements at 408 MHz, using Molonglo telescope

15 p2485 A71-31697

L band microwave IC front end for identification: friend or foe [IFF] receiver, noting environmental and filtering requirements

16 p2547 A71-33550

UHF head for 225-400 MHz AM receiver, emphasizing choice of ring mixer and passband filter switching principle

16 p2548 A71-34120

High power efficiency solid state UHF sources: comparing Gunn and avalanche diodes performance

17 p2715 A71-34685

Percent-of-time distributions of attenuation by rain, clouds and atmospheric gases on earth-space paths at frequencies below 30 GHz

17 p2704 A71-35089

Apollo lunar surface S band communications and TV systems and equipment, including ground command and TV assembly

18 p2878 A71-36519

Marine navigation and data communications at L band via synchronous satellite, assessing capabilities by tests on ATS-5 satellite

19 p3102 A71-38070

RF noise surveys in urban areas for effective space to earth communication link design at UHF

19 p3021 A71-38443

AN/ARC-144 solid state ultrareliable UHF multimode aircraft transceiver, discussing tuning, frequency synthesis and broadband power amplifier

20 p3196 A71-39209

One way UHF clock synchronization, using geostationary communication satellites with propagation delays calculated from orbital elements

20 p3239 A71-39460

ULTRAHIGH VACUUM

Bearing materials for ultrahigh vacuum applications, discussing various metals and alloys friction and wear characteristics

05 p0757 A71-16142

Monte Carlo method for ultrahigh vacuum free molecule flow transmission probability for straight tubes

05 p0785 A71-16395

Ultrahigh vacuum extractor gase design and performance

05 p0753 A71-16946

Ultrahigh vacuum gas analysis by mass spectrometry, discussing quadrupole and omegatron mass spectrometers performance with special reference to reversible adsorption characteristics

11 p1763 A71-26187

Epitaxial deposition of Au on ultrahigh vacuum cleaved mica during early nucleation and growth

14 p2284 A71-30072

Oxygen sorption rate by Ti at low pressure from measurement in stainless steel ultrahigh vacuum chamber

17 p2695 A71-35139

In situ metal-gas secondary standard assembly for ultrahigh vacuum gage calibration, using repeatable

- pressure generation from binary erbium-hydrogen system 17 p2744 A71-35140
- Hydrogen discharge from Fe-C alloys in absolute suction metal mold, finding discharge decrease with increasing carbon content 18 p2926 A71-36300
- Space environment simulation for ultrahigh vacuum effects on crystalline enzymes activity, measuring by chemiluminescence techniques 21 p3334 A71-40573
- Ultrahigh vacuum by condensate pump, defining vacuum level by mass spectrometric determination of residual gas content 23 p3661 A71-43271
- Hydrogen evacuation with He condensation pump in ultrahigh vacuum region 23 p3661 A71-43272
- Vacuum pumped Apollo 12 lunar soil sample (2001.118 gas exposure effects, interface microanalysis and adhesion measurements in ultrahigh vacuum system 23 p3759 A71-43767
- ULTRALOW FREQUENCIES**
- U EXTREMELY LOW RADIO FREQUENCIES**
- ULTRAPURE METALS**
- High purity Ge crystals growth, studying Hall effect and resistivity for semiconductor detector fabrication 08 p1345 A71-21841
- Characterization of high purity metals by residual resistivity ratio, using nondestructive eddy current decay method 18 p2938 A71-36992
- High purity metals residual electrical resistivity, observing impurities, vacancies, dislocations, plastic strain and polycrystalline effects 19 p3076 A71-37115
- Anomalous ultrasonic attenuation in pure superconducting Nb from pulse echo amplitude measurements 24 p3860 A71-44751
- High purity Sb, In and Ag by vacuum distillation, zone melting and electrolytic refining for semiconductor electronics 24 p3861 A71-45201
- ULTRASONIC AGITATION**
- Rana temporaria isolated sciatic nerve excitation process, investigating continuous ultrasound effect 09 p1391 A71-22486
- Ultrasonic vibration effects on TiC sintering during isothermal heating with and without pressure 09 p1470 A71-23063
- Acoustic beam attenuation through liquid medium under ultrasonically excited cavitation, taking into account bubble configuration 09 p1434 A71-23668
- Ultrasonic vibration effects on DNA and RNA content in skin and kidneys of albino rats 15 p2356 A71-31288
- Ultrasonic softening of lens material to facilitate aspiration, using in vivo rabbit lenses for cataracts production 15 p2365 A71-32348
- Residual stress magnitude and distribution in metal strips rolled with ultrasonic vibrations 21 p3389 A71-41093
- ULTRASONIC GRINDING MACHINES**
- U GRINDING MACHINES**
- U ULTRASONIC MACHINING**
- ULTRASONIC INSPECTION**
- U ULTRASONIC TESTS**
- ULTRASONIC LIGHT MODULATION**
- Microwave ultrasonic beam visualization techniques via Bragg diffraction of laser beam, investigating resolution capability 03 p0436 A71-13717
- Optico-acoustical deflector with high resolving capability, using Bragg light diffraction by ultrasonic waves 04 p0604 A71-14627
- Ultrasonic effects on synchronization of ruby laser radiation, investigating emission pulse structure and peak sequence 15 p2419 A71-31712
- Signal processing operation of real time optical correlator, using ultrasonic light modulators 17 p2708 A71-35484
- Acousto-optical effects, materials and devices of laser beam control using diffraction and refraction by ultrasonic waves 18 p2932 A71-36607
- Brillouin scattering effect on noise of Bragg imaging in ultrasonic band at room temperature, using convergent illuminating light beam 22 p3541 A71-41779
- Mode locked transversely excited atmospheric carbon dioxide laser with Ge ultrasonic diffraction cell active loss modulator generating 10.6 micron wavelength pulses 22 p3557 A71-42132
- Optico-acoustical deflector with high resolving capability, using Bragg light diffraction by ultrasonic waves 22 p3558 A71-42267
- Ruby laser radiation modulation by ultrasonic mirror oscillations, discussing mechanism 24 p3836 A71-45269
- ULTRASONIC MACHINING**
- Brittle materials ultrasonic machining, discussing abrasive particle shape, size, temperature and pressure effects on process accuracy, speed, quality and efficiency 10 p1617 A71-24133
- Ultrasonic cleaning by cavitation disintegration of highly adhesive surface coatings, discussing cleansing liquid, field parameters and external static pressure effects on process efficiency 10 p1617 A71-24135
- ULTRASONIC RADIATION**
- Ultrasonic sound velocity dispersion in various hydro and gas suspensions, considering viscosity and heat conduction effects 01 p0127 A71-10618
- High resolution automatic measurement of ultrasonic velocity changes using interferometer and FM oscillator 02 p0250 A71-12134
- Strain-optical constants determination by ultrasonic technique, using Raman-Nath theory for optical diffraction produced by standing ultrasonic wave 03 p0425 A71-13716
- Ultrasonic absorption in hydrogen sulfide, measuring vibrational and rotational relaxation times as function of temperature 03 p0459 A71-13718
- Amino acid content alteration in internal organs in rabbits under HF electromagnetic and ultrasound oscillations 04 p0547 A71-15573
- Ultrasonic position sensor for automatic control, using short pulses for azimuth and range resolution 06 p0896 A71-17321
- Monograph on optical imaging of ultrasonic fields by acoustic Bragg diffraction covering heuristic plane wave and ray approach scattered fields 07 p1111 A71-19575
- Ultrasonic cavitation noise spectra in liquid helium and nitrogen, comparing He I and II 07 p1160 A71-19951
- Ultrasonic effects on Ti alloys Hg embrittlement and stress corrosion cracking by methanol-water-hydrochloric acid mixture 07 p1137 A71-19975
- Transistorized ultrasonic oscillator active conductances and other circuit parameters effects on self oscillation frequency stability 07 p1078 A71-20060
- Pulsed laser schlieren system for ultrasonic wave front imaging in nondestructive testing techniques 08 p1286 A71-20949
- Ultrasonic effects on dislocations and grain boundaries in vacuum annealed polycrystalline Al specimens 09 p1467 A71-22288
- Ultrasonic propagation velocity dependence on high pressure and temperature in carbon dioxide, considering Rao rule applicability to highly compressed gases 09 p1492 A71-22529
- Ni-Al alloy strain hardening, observing high intensity ultrasonic irradiation effect on high temperature creep 09 p1475 A71-23315
- Nondestructive evaluation of ultrasonic wave propagation in adhesively bonded test specimens, using schlieren method 10 p1616 A71-24104
- Soviet papers on physical foundations of ultrasonic technology covering applications in machining, welding, cleansing, and drying 10 p1616 A71-24132
- Ultrasonic cleaning by cavitation disintegration of highly adhesive surface coatings, discussing cleansing liquid, field parameters and external static pressure effects on process efficiency 10 p1617 A71-24135
- Metals crystallization in ultrasonic field, investigating structural change as function of energy and impedance factors and cavitation effects in fine grain formation 10 p1626 A71-24136
- High accuracy deflector and diffraction sensors for optical tracking systems, noting dependence on ultrasonic frequency 10 p1610 A71-24169
- Ultrasonic energy density measurement over various frequencies in liquids, using instrument unperturbed by standing acoustic waves 10 p1612 A71-24682
- Internal combustion engine gas temperature measurement, using ultrasonic wave frequency shift method 11 p1810 A71-25269
- Ultrasonic wave propagation in deformed isotropic elastic materials based on second order theory, examining principal stress axis rotation effect 11 p1849 A71-25682
- Nematic liquid crystal ultrasonic measurements at room temperature, showing anisotropic attenuation dependence on magnetic field orientation 11 p1808 A71-26149
- Light diffraction by superposed parallel ultrasonic waves for diffraction pattern symmetry, using n-th order approximation method 12 p1928 A71-26650
- Transverse excitation of elastic ultrasonic waves in CdS piezoelectric plates, considering conductivity effect on damping 12 p1944 A71-27544
- Heat resistant alloys face polishing with ultrasonically cleaned grinding wheel abrasive rim surface 13 p2075 A71-28942
- Ultrasonic field distribution patterns from metallic and ceramic concave spherical reflectors under excitation by single or multiple piezoelectric elements 13 p2101 A71-29267
- Localized focused ultrasonic beam action on brain portions without skull trepanation in animals and man, visualizing sonic field by Tepler effect 15 p2356 A71-31291
- Surface deformation in polycrystalline Al samples produced by ultrasound generated cyclic stresses, examining slip bands formation by electron microscope 16 p2591 A71-33224
- Ultrasonic reflection from defects, using method of similarity and approximation of ray acoustics 16 p2584 A71-33560
- Ultrasonic propagation velocity dependence on high pressure and temperature in carbon dioxide, considering Rao rule applicability to highly compressed gases 17 p2784 A71-35506
- Automatic fringe counting pulsed ultrasonic interferometer for transit time measurement, using phase sensitive multiple echo detection 18 p2922 A71-36586
- Slow wideband excitation of ultrasonic waves with piezoelectric crystal delay line subject to microwave radiation 19 p3015 A71-37251
- Papers on ultrasonic transducer materials covering magnetostrictive metals and alloys and piezoelectric crystals and ceramics 20 p3236 A71-39253
- Magnetostrictive metals and piezomagnetic ceramics as transducer materials for ultrasonic wave generation, detection and filtration 20 p3236 A71-39254
- Piezoelectric transducer materials and techniques for ultrasonic devices, covering delay lines, light deflectors and modulator operating above 100 MHz 20 p3237 A71-39256
- Ultrasonic absorption in liver tissue due to macromolecular relaxation processes 20 p3191 A71-39770
- Elastic plates radial vibrations excited by piezoelectric elements, investigating electromechanical coupling coefficient and ultrasonic radiation constants 21 p3473 A71-41365
- Electromagnetoacoustic ultrasonic vibrations radiation and reception angular orientation as function of transducer design parameter, frequency and propagation velocity 22 p3528 A71-41756
- Optical holographic detection and measurement of ultrasonic waves, providing practical method of investigating LF sound waves 22 p3541 A71-41785
- Ultrasonic subharmonic waves amplified in standing waves through utilization of propagation medium nonlinearity and cavity reflector induced dispersion 23 p3704 A71-43362
- Single mode ruby laser spatiotemporal coherence characteristics with emission moment controlled by Q switch operating on modulated ultrasonic traveling waves 23 p3683 A71-43394
- Acoustoelectrical current oscillations in GaAs films at low temperature under ultrasonic Rayleigh wave amplification 23 p3716 A71-43477
- Anomalous ultrasonic attenuation in pure superconducting Nb from pulse echo amplitude measurements 24 p3860 A71-44751
- ULTRASONIC SOLDERING**
- Soviet book on microwelding by pressure covering semiconductor-metal bonding, ultrasonic soldering and thermal processes 23 p3682 A71-44125
- ULTRASONIC SPEEDS**
- U SUPERSONIC SPEEDS**
- ULTRASONIC TESTS**
- Ultrasonic frequency characteristics for flaw detection, discussing short and long pulses coupling to test samples 01 p0086 A71-10303
- Metal flaw size measurement, discussing ultrasonic echo amplitude and defect scanning methods 01 p0086 A71-10304
- Electrical resistance spot weld penetration measurement via ultrasonic method using shear waves 01 p0086 A71-10305

Ultrasonic methods for evaluating adhesive bond strength in composites, metal to metal laminates and honeycombs

01 p0086 A71-10306

Reference standards for nondestructive ultrasonic inspection for quality control

01 p0091 A71-11424

Elastic behavior of bone as two phase composite material, using ultrasonically measured hydroxyapatite moduli

[ASME PAPER 70-WA/BHF-3] 03 p0373 A71-14110

Metallographic specimens etching by cavitation damage, testing performance by ultrasonic vibration technique

03 p0445 A71-14420

Ultrasonic Doppler techniques in medical diagnosis, measuring ultrasonic probes directivities by echo amplitudes from various target configurations

03 p0373 A71-14422

Holography developments concerning interferometry, microscopy, display systems, data storage and ultrasonic tests

04 p0587 A71-14724

Ultrasonic viscosimeter for gamma irradiation effects on materials structure, determining fluid viscosity changes from rate of damping of plate vibrations

04 p0594 A71-14918

Fused silica and single crystal NaCl nonlinear parameters from ultrasonic beams mixing studies

05 p0793 A71-16410

Metals and alloys with bcc structure, investigating ductile-to-brittle transition by ultrasonic MHz technique

05 p0770 A71-17251

Isotropic and slightly anisotropic materials elastic constants evaluation from ultrasonic reflection measurement

05 p0771 A71-17252

Wall thickness measurement by ultrasonic tests in presence of corrosion, discussing instruments development

06 p0897 A71-17416

Carbon fibers and composites nondestructive testing, discussing defect detection problems in ultrasonics, X ray diffraction and X radiography methods [PLASTICS INST. PAPER 52]

08 p1296 A71-20918

Metals and alloys internal friction meter based on intense ultrasonic vibration, discussing error compensation

09 p1426 A71-22320

Mechanized ultrasonic inspection probes with high stable dynamic acoustic coupling coefficient, high sensitivity and wear resistance and low coupling fluid expenditure

09 p1450 A71-22897

Elastic ultrasonic vibrations effects on metals and alloys microstructure and elastic and nonelastic properties

09 p1477 A71-23326

Ultrasonic irradiation effect on single tungsten crystals deformation characteristics and structure

09 p1477 A71-23327

Strain effect on ultrasound damping in single W crystals, considering microhardness

09 p1477 A71-23328

Ultrasonic waves propagation in hydraulic and lubricating oils, testing shear resistance

09 p1484 A71-23673

Ultrasonic modulus vs strength of high modulus fiber reinforced epoxy matrix composites in non-destructive testing

09 p1484 A71-23687

Blood pressure measurement with Doppler ultrasonic flowmeter, providing sensitive and accurate noninvasive approach for continuous measurement of systemic arterial pressure

12 p1874 A71-27139

Ultrasonic echocardiograms of anterior cusp of mitral valve in aortic valve disease

13 p2002 A71-27814

Nondestructive testing, discussing visual, liquid penetrant, thermal, X and gamma rays, ultrasonics, magnetic, electrical and eddy currents methods

13 p2073 A71-28218

Ultrasonic/radiographic method for intraocular foreign body localization

13 p2013 A71-29031

Hardened low alloy steel ultrasonic attenuation under magnetic field due to thermally introduced residual stresses

15 p2414 A71-31641

Pulse type ultrasonic flaw detecting apparatus based on reflected echo size estimation

15 p2409 A71-32194

Automated ultrasonic inspection system for L-1011 adhesive bonded fuselage panels using through transmission technique

[SME PAPER IQ-71-746] 15 p2417 A71-32437

Left ventricular posterior wall motion measurements in myocardial infarction, using ultrasonic echogram time-motion data

15 p2365 A71-32536

Focused ultrasonic nondestructive tests search units, describing focal distance, beam diameter and lens/crystal radius optimum ratio

16 p2581 A71-32863

Ultrasonic pulse technique for plane transverse and longitudinal stress wave dispersion in boron fiber reinforced epoxy composite, determining group velocity dependence on frequency and elastic moduli

[ASME PAPER 71-APM-27] 16 p2600 A71-33202

Materials ultrasonic structural analysis, describing statistical methods for damping data processing

16 p2584 A71-33561

Two frequency ultrasonic flaw detector for determination of defects opening widths, examining ultrasonic pulse transmission through thin air layers

16 p2580 A71-33562

Circulation parameters in vascular network by bloodless zonal ultrasonic sphygmography based on acoustic biochocologation

17 p2689 A71-34648

Composite panel of ten-ply unidirectional boron/epoxy laminate adhesively bonded to Al face sheets, discussing ultrasonic inspection technique

17 p2749 A71-35495

Aircraft parts testing by NDT methods, considering ultrasonic system for valve defects and fluorescent particle system for crack detection

18 p2929 A71-37056

Cavitation damage in water to unalloyed metals and Ni superalloy, using ultrasonic vibratory testing with magnetostrictive transducer

19 p3081 A71-37904

Monograph on blood flow rates instantaneous measurement from ultrasound signals of Doppler flowmeter, discussing steady laminar flow test results

20 p3193 A71-39262

Ultrasonic radar simulator to produce data for radar system performance evaluation, describing automated short range and manual long range systems

20 p3196 A71-39376

Nondestructive testing of carbon fiber reinforced composites with resin matrices [CFRP], suggesting ultrasonics for void detection

21 p3387 A71-40598

Acoustical holographic opaque structures visualization techniques and applications, discussing ultrasound qualities, image converters, detector arrays and medical diagnostic utilization

22 p3540 A71-41752

Electroacoustic circuit of ultrasonic resonance thickness gage based on frequency dependence of piezoelectric transducer conductance in multilayered acoustic system

22 p3528 A71-41755

Ultrasonic defectoscopy of steel samples, considering grain size effects on SNR

22 p3528 A71-41757

Ultrasonic time shadow method based on defect detection by sharpness of vibration propagation time change during scanning

22 p3528 A71-41758

Ultrasonic immersion echo pulse thickness meter for single side access measurement in Al and Zr alloys

22 p3528 A71-41759

Ultrasonic inspection apparatus for defects detection in metal pipes, using immersion echo mode with two piezoelectric scanning heads rotating about pipe

22 p3529 A71-41774

Ultrasonics use in physiological and pathophysiological experiments on human organism, considering ultrasonic vibration physical properties

22 p3502 A71-41941

Ultrasonic evaluation of heart anatomical abnormalities in congenital and acquired heart diseases including myocardium hypertrophy and tissue degeneration

23 p3639 A71-43118

Eye and orbit A and B ultrasonography scanning technique, showing minimal echogram distortions in meridional arc scans

24 p3799 A71-44367

Transistorized AGC circuit for use with ultrasonic Doppler-cardiogram recording system to retain signal characteristics under strong fluctuations

24 p3801 A71-44543

Basic parameters of echo and mirror shadow methods for ultrasonic defectoscopy of welded joints, considering standardization principles

24 p3829 A71-44784

Ultrasonic method for measuring poor root penetration zone width in welded T joints without reference standard, suggesting practical applications

24 p3829 A71-44785

Ultrasonic flaw detection analytical and experimental wave propagation procedure including dynamic photoelasticity and elastic wave computer codes in nondestructive testing

24 p3831 A71-45282

ULTRASONIC WAVE TRANSDUCERS

Aircraft ultrasonic altitude and vertical velocity sensor for low flight, discussing VTOL aircraft automatic hovering control and time lag

01 p0084 A71-11624

Glow discharge microphone for acoustic pressure detection and measurement at ultrasonic frequencies

02 p0232 A71-121

Multielectrode ultrasonic transducer with multiplexing circuits for electronic readout scanning, discussing application in rapid inspection of plate or strip isopress heat sources

08 p1287 A71-212

Equivalent electrical circuits of interdigital transducers for piezoelectric generation and detection of ultrasonic Rayleigh waves

09 p1420 A71-238

Metals ultrasonic welding, discussing welded elements interactions in terms of thermal and diffusional phenomena, sample preparation, transducers, electrical generators and process control systems

10 p1617 A71-241

Statistical evaluation of Doppler ultrasonic blood flowmeter, determining correlation between Doppler signal zero crossing density and fluid flow velocity

17 p2689 A71-344

Ultrasonic surface wave generation by infinite interdigital electrode array on piezoelectric material, predicting behavior from equivalent circuit by variational principle

17 p2717 A71-354

Wavefront reconstruction interferometry with acoustical holography using ultrasound camera, surface deformation and mechanically scanned detection methods

18 p2923 A71-3666

Ultrasonic technique for crack and craze velocity measurement in material subjected to stress in liquid environment

20 p3233 A71-3888

Ultrasonic holography in nondestructive testing, using single transducer or separate focussed transducers for transmission and reception

22 p3541 A71-4171

Backward propagation method for ultrasonic image reconstruction, examining resolution in near field of high contrast objects

22 p3541 A71-4171

Surface wave delay lines with near octave bandwidth using lithium niobate interdigital ultrasonic transducer with lumped element impedance inverting network

22 p3521 A71-422

Scanning ultrasonic imaging technique for in vivo monitoring of microscopic bubble formation in decompression sickness, presenting image displays

22 p3504 A71-422

Radiation field profiles and applications of broadband ultrasonic transducers, including thickness and viscosity measurements

23 p3674 A71-429

ULTRASONIC WAVES

U ULTRASONIC RADIATION

ULTRASONIC WELDING

Optimal design and manufacture of wall attachment fluidic devices, noting thermoplastics injection molding followed by ultrasonic bonding

07 p1121 A71-205

Ultrasonic bonding techniques discussing high frequency activated adhesives, equipment and automated processes

10 p1615 A71-240

Metals ultrasonic welding, discussing welded elements interactions in terms of thermal and diffusional phenomena, sample preparation, transducers, electrical generators and process control systems

10 p1617 A71-241

ULTRASONICS

Ultrasonics for industry - Conference, London, October 1970

01 p0086 A71-10306

Ultrasonic flowmeters for unsteady flow, discussing beam deflection method, phase difference systems, etc

01 p0079 A71-10301

Dog blood flow telemetric measurement with TV system using ultrasonic signals Doppler effect

01 p0024 A71-1105

Ultrasonics applications in surgery, therapy and diagnosis, discussing physical principles, piezoelectric transducers, tissue acoustic properties and measurement methods

03 p0372 A71-13351

Ultrasound propagation visualization in solids describing sensitive schlieren apparatus

06 p0903 A71-17323

Pulse echo ultrasonic measurement of thin film layer between thick media, using real time computation

09 p1458 A71-23439

Ultrasonic vibration energy surface and volume effects, obtaining static forces reduction, processing rate increases, technique shortening and surface finish improvement in manufacturing processes

13 p2075 A71-28945

Microcavity parametric oscillations in stationary ultrasonic field

14 p2275 A71-30438

Room temperature ultrasonic frequency fatigue behavior of Ni-base superalloy single crystals 17 p2756 A71-34493

Frequency power and resolution effects on ultrasonic holography for medical diagnosis involving information processing on computer 19 p3066 A71-38240

Differential method of ultrasonic inspection and binary comparative search heads for implementation, combining mirror shadow and echo methods features 22 p3553 A71-41760

Holographic ultrasonic imaging method for flaw detection in aerospace materials and structures 22 p3554 A71-41782

ULTRAVIOLET ABSORPTION

Organic dye laser output and service life enhancement, using filters for absorption of UV pumping radiation photodecomposition of rhodamine 6G alcohol solution 03 p0435 A71-13509

Atmospheric absorption by oxygen, determining metastable molecules absorption cross section at 1095 Å 06 p0888 A71-17290

Gas concentration determination for mixture by UV energy absorption measured in terms of photomultiplier tube output current, describing oxygen sensor 08 p1287 A71-20987

Lutetium effects on UV absorption strength of Nd-YAG laser materials 20 p3244 A71-39104

UV and IR transmissivity and absorption coefficients of fused quartz between room temperature and 1500 C 22 p3565 A71-42559

Carbon dioxide UV absorption and dissociation processes and reaction kinetics of dissociation products 23 p3642 A71-43329

ULTRAVIOLET LIGHT

U ULTRAVIOLET RADIATION

Earth optical radiation environment observation from satellites, reviewing solar spectra, near IR cloud spectra and vacuum UV radiometer scans 09 p1437 A71-22739

Folded all-reflecting Schmidt camera UV image converter system for space astronomy applications, discussing pressure sensitivity effects on UV direct recording emulsion 09 p1447 A71-22751

Solar disk photographs taken by Skylark rocket in EUV and soft X ray region 20 p3293 A71-39534

ULTRAVIOLET PHOTOMETRY

Venera probes UV radiation measurement, discussing photometric equipment and spectra for hot stars and Milky Way in L alpha line 02 p0304 A71-11912

Photoelectric and radio observations of flares of UV Ceti and YZ CMi stars 07 p1204 A71-20628

High resolution UV solar photographs by stratospheric balloon-borne Cassegrain telescope 10 p1680 A71-25018

Venera probes UV radiation measurement, discussing photometric equipment and spectra for hot stars and Milky Way in L alpha line 13 p2133 A71-28199

Visible and UV photometric recording of microorganism reproduction in liquid medium for application to Mars extraterrestrial life detection 13 p2019 A71-28682

SV Cephei variable photoelectric UVB observation showing existence of quasi-periodic minima with changing characteristics 21 p3451 A71-40715

ULTRAVIOLET RADIATION

NT FAR ULTRAVIOLET RADIATION

NT LYMAN ALPHA RADIATION

NT LYMAN BETA RADIATION

NT NEAR ULTRAVIOLET RADIATION

Plant leaves mean effective optical constants from diffuse UV reflectance and transmittance measurements 01 p0073 A71-10834

UV effect on airborne bacteria survival in simulated Martian dust clouds 01 p0019 A71-11557

Martian environment simulator chamber for pressure, visible light, biological objectives UV irradiation and daily temperature cycle 01 p0068 A71-11559

Pentose breakdown photosensitivity from UV irradiation in presence of minerals, considering prebiological period carbohydrates evolution and interaction with purines and pyrimidines 01 p0029 A71-11561

H alpha line emission in ionization zones encircling neutron stars, suggesting accretion-induced UV luminosity 02 p0308 A71-12091

Upper atmospheric gas components vertical distribution by airborne photometric absorption and attenuation measurements in UV spectrum 02 p0246 A71-12118

Frog eye response to UV light stimulation, investigating sensitivity from electroretinogram 03 p0363 A71-13484

X ray effects on dogs with and without UV preexposure, determining blood protein and chemical composition, hemoglobin content and thermostability 03 p0364 A71-13524

Solrad 8 satellite monitoring of Lyman alpha and UV radiation, discussing flux variation at 1080-1350 Å 03 p0479 A71-14043

Solar UV radiation measurements by OSO-3, obtaining flux variation over solar rotation period 03 p0481 A71-14508

Gas laser technology developments, discussing UV CW noble gas ion lasers, high output IR carbon dioxide lasers, metal vapor and pure helium lasers 04 p0605 A71-14711

UV dwarfs observational lifetime, considering progenitor main sequence, red giants and planetary nebulae central stars evolutionary sequence 04 p0648 A71-15249

UV dwarf star evolution, using central and gap star models emphasizing photoneutrino emission 04 p0648 A71-15250

UV stellar flux measurements vs theoretical stellar atmosphere models, using rocket and satellite observations 04 p0648 A71-15252

Electron, proton and UV irradiation effects on CdS solar cell protective plastic films with or without adhesive coatings, measuring transmission changes 05 p0771 A71-16087

Intergalactic gas photoionization by quasars UV radiation, using Friedman cosmological model 05 p0805 A71-16111

Electron temperature anisotropy in lower ionosphere, discussing effects of solar UV radiation propagating along geomagnetic field during daytime 05 p0744 A71-17183

He I 584 Å dayglow radiation measurement by retarding potential photoelectron analyzer on Javelin sounding rocket 06 p0887 A71-17267

UV light starvation prevention, describing biological effects and illumination equipment for working areas 06 p0858 A71-17528

Intergalactic gas ionization and heating by UV radiation 06 p0974 A71-18429

Static solar H II region ionization balance, energy, UV radiation transfer, gravitational equilibrium and interstellar gas temperature 06 p0975 A71-18442

Interstellar silicate extinction related to 2200 Å band from determination of enstatite optical constants 07 p1200 A71-20053

Flare characteristics of UV Ceti type stars from statistical analysis of photoelectric light curves 07 p1204 A71-20627

Si solar cells transparent radiation protective coatings stability and degree of blackness, discussing UV irradiation and proton and electron bombardment 08 p1287 A71-21024

H alpha line emission in ionization zones encircling neutron stars, suggesting accretion-induced UV luminosity 08 p1362 A71-21141

Secondary umkehr effect in solar UV region at twilight, proposing origin mechanism by ozone layer optical properties 08 p1357 A71-21875

Organic compounds biosynthesis in simulated Mars atmosphere, using UV irradiation for photocatalytic production from CO and water mixtures 09 p1403 A71-22647

KCl films exciton-induced photoemission, discussing mechanism of photoelectron emission rise with time under steady UV radiation 09 p1508 A71-22685

Predicted UV fluxes for main sequence stars, comparing stellar observations with models described by Kucsz, Carbon and Gingerich 09 p1522 A71-22962

O I and II resonance transitions radiative lifetimes in vacuum UV, using beam foil method 10 p1676 A71-24501

Radiative lifetimes of UV multiplets in atomic C, N and O, using modified phase shift technique 10 p1645 A71-24547

Thermospheric gas density determined from solar UV absorption measurement at grazing ray and near vertical incidence 10 p1676 A71-24551

Upper Martian atmosphere UV emission spectrum observation noting carbon dioxide photoionization, ion fluorescent scattering and photon/electron dissociative excitation 10 p1604 A71-24776

Vacuum UV phototube module for degradation measurement of optical components, including mirrors, windows, lenses and thermal control surfaces [AIAA PAPER 71-461] 11 p1800 A71-26243

Reentry heating simulation, noting UV radiation effects as shock layer thickness decreases [AIAA PAPER 71-467] 11 p1899 A71-26248

Quantitative UV radiative transfer and photolysis in model Jupiter atmosphere, considering coloration by ammonia and hydrogen sulfide gases in cloud region 11 p1834 A71-26455

High intensity vacuum UV solar simulator, using high pressure jet pinched xenon arc lamp with magnesium fluoride envelope 11 p1747 A71-26515

Thermal control coating materials, measuring separate and combined electron and UV radiation effects on reflectance and emittance in vacuum 11 p1850 A71-26519

Intergalactic gas ionization and heating by UV radiation 12 p1955 A71-26579

Static solar H II region ionization balance and energy, UV radiation transfer, gravitational equilibrium and interstellar gas temperature 12 p1955 A71-26592

UV airglow in 1304 Å line of oxygen from Cosmos 215 satellite observation 12 p1899 A71-26638

Jupiter upper atmosphere extreme UV dayglow, involving resonant scattering and fluorescence of incident solar flux 12 p1961 A71-26888

Universe UV radiation intensity, estimating inverse Compton effect interaction of cosmic relativistic electrons with relict radiation 12 p1948 A71-27079

Electron temperature anisotropy in lower ionosphere, discussing effects of solar UV radiation propagating along geomagnetic field during daytime at middle latitudes 13 p2059 A71-28240

Flash UV photolysis of ozone/water vapor mixtures, noting OH radical nonreaction with ozone 13 p2025 A71-28349

UV photolysis of ozone in presence of molecular oxygen, discussing energy exchange reaction with molecular oxygen 13 p2025 A71-28350

Mars physical conditions compared to earth, simulating Martian conditions and low temperature and UV effects on proteins 13 p2009 A71-28688

Germ survival and transport possibility in outer space, discussing spore survival under UV radiation 13 p2010 A71-28691

Space objects sterilization techniques in Soviet Union and United States, covering hot air, ionizing radiation, UV light, ethylene oxide with or without Freon, etc 13 p2019 A71-28694

Wind transport effect on redistribution of ionization produced by geocoronal and interplanetary UV emissions in nighttime ionosphere, using electron density sounding rocket data 14 p2230 A71-29709

Astrophysical and aeronomic UV molecular photoabsorption cross sections, discussing experimental techniques and associated systematic and random errors 14 p2190 A71-29905

UV radiation sensitive flame sensor for high temperature ambients, consisting of Geiger-Müller tube triggered by photoelectron released from photocathode 14 p2248 A71-30707

Arc heated plasma expansion through nozzle, observing population inversion of neutral carbon self-absorption UV atomic line [AIAA PAPER 71-592] 15 p2454 A71-31537

Solar UV radiation atmospheric absorption during IQSY by ion chamber measurements, considering upper atmosphere oxygen concentration 15 p2396 A71-31616

Chromosphere and solar quiet regions transition zone model, investigating radio and UV emission and height dependence of temperature and density 15 p2497 A71-32745

Continuously tunable pulsed UV source using broadband dye laser emission input to rotatable KDP crystal 16 p2586 A71-33141

Solar UV radiation data during 7 March 1970 eclipse from photometers sensitive to narrow bands, discussing sources, atmospheric absorption and D region ionosphere 16 p2627 A71-33773

UV photoemission measurements on hexagonal ZnO cleaved in vacuum, determining Zn 3d states location 17 p2791 A71-34854

Long wavelength UV photoproduction of amino acids on primitive earth, using hydrogen sulfide as photon acceptor 18 p2855 A71-36229

UV studies of solar atmosphere in quiet and active regions, considering low and high chromosphere, transition zone, quiet corona and inhomogeneity 18 p2968 A71-37034

Universe UV radiation intensity, estimating inverse Compton effect interaction of cosmic relativistic electrons with relic radiation 19 p3126 A71-37429

Light production by 2.5-490 eV helium ion collisions with nitrogen, considering 1200 and 3200 Å emission 19 p3107 A71-38055

Cystine synthesis in simulated primitive conditions by UV irradiation of methane, ethane, ammonia, water vapor and hydrogen sulfide in spherical vessel 19 p3014 A71-38678

Thermospheric atomic oxygen and molecular nitrogen number densities, discussing earth atmospheric absorption of solar UV lines 20 p3214 A71-38727

Electromagnetically driven shock tube with precursor effect due to ionization of impurities by UV radiation from discharge, using gages to tag gas flow 20 p3239 A71-39431

Gum Nebula conceived as hydrogen gas mass ionized by UV radiation from supernova explosion related to Vela X remnant, discussing fossil Stroemgren sphere model 20 p3294 A71-39572

Continuous solar UV and X rays monitoring by SOLRAD 10 satellite, investigating solar activity and flares effect on shortwave communications and manned space travel 20 p3294 A71-39580

Si solar cells transparent radiation protective coatings stability and degree of blackness, discussing UV irradiation and proton and electron bombardment 20 p3240 A71-39604

High altitude aerosol layer effects on atmospheric UV albedo, correcting ozone scale height spaceborne measurements 20 p3221 A71-39695

Planetary, stellar, galactic, sky and extragalactic UV radiation from OAO-2 spectrophotometric observations, noting interstellar extinction curves 20 p3300 A71-39747

UV radiation in space and Venus atmosphere, studying L-alpha lines luminescence hot stars intensity, Milky Way brightness and hydrogen envelope existence 20 p3282 A71-39748

Early stars UV continuum brightness from rocket-borne photoelectric spectrophotometer, estimating total interstellar flux density 21 p3444 A71-40244

UV photochemistry of lower Jovian clouds, using experimental simulation 21 p3447 A71-40427

Photocatalytic stimulation of UV radiation photolysis of amino acids and pentoses in aqueous solutions by metal oxide sols 21 p3345 A71-40574

High power tunable second harmonic and UV sum frequency generation from rhodamine 6G dye laser and ADP crystal 22 p3556 A71-41803

Optical line spectrum and ionization equilibria of hard UV radiation and energetic proton heated hydrogen, helium, nitrogen, oxygen and neon 22 p3601 A71-42160

Intrinsic UV color variations of interstellar extinction laws due to stellar rotation, MK spectral type and photometric errors, using rocket observations 22 p3604 A71-42333

Unicellular organisms increased tolerance to UV radiation, discussing cells repairing ability in dark and pigments and protective compounds screening role 22 p3496 A71-42828

UV radiation effect on amino acids and peptides in different gas atmospheres in presence of salts and metal oxides 22 p3496 A71-42829

Combined and individual effects of UV light, X ray irradiation and freezing-thawing cycles on ribonuclease 22 p3496 A71-42830

Beta Sco occultation by Jupiter, interpreting UV light curve 23 p3733 A71-43124

UV absorber dyes in fluorescent tracers, discussing theory of dimensional sensitivity and use in liquid-film developers to quench background fluorescence 23 p3681 A71-43194

Carbon dioxide photolysis at 1740-2100 Å applied to photochemistry of Mars lower atmosphere 23 p3641 A71-43327

Polyethylene coating physicochemical properties under UV radiation, discussing density and modulus of elasticity, internal stresses, microcrack formation and preventive heat treatment 23 p3697 A71-44032

Optical enhancement of photomultipliers extended to UV wavelengths, using suprasil and spectroil fused silica with high flat transmission curves as optical materials 24 p3829 A71-45212

ULTRAVIOLET REFLECTION

Atmospheric reflection latitude and angular dependence on wavelengths from satellite UV measurements, noting ozone content seasonal variation of ozonosphere 03 p0413 A71-14010

Low energy proton irradiation induced thin polymer contaminant films effect on far UV reflecting mirrors reflectance and scattered light 08 p1290 A71-21382

UV spectral energy distribution of Jupiter from rocket-borne Cassegrain telescope observation, computing planet geometric reflectivity in 2100- 3600 Å range 15 p2491 A71-32422

Vacuum UV reflecting surfaces deterioration by intermetallic formation, recommending separation by dielectric barrier layer 20 p3236 A71-39196

ULTRAVIOLET SPECTRA

Mg I and II vacuum UV emission series, presenting quantum defect plot 01 p0129 A71-10137

Auroral vacuum UV spectra and 3914 Å emission from sounding rocket data 01 p0076 A71-11502

UV and visual spectra of gamma Cassiopeiae from rocket spectrograph and OAO observations 02 p0314 A71-12585

Night airglow spectral components by Cosmos 92 satellite measurements, considering UV region sources and intensity variations 03 p0417 A71-14050

Lunar continent surface microstructure from UV and IR spectra, discussing photometric function determination by geometric shadows and diffraction effects 03 p0492 A71-14055

High pressure rare gas UV emission spectra, examining wavelength cut-offs and flux ratios 04 p0549 A71-15691

Planetary nebulae continuous UV spectrum, discussing glow process, electron temperature and density and Balmer discontinuity 06 p0974 A71-18434

UV absorption line spectra from HI regions, evaluating X ray and photoionization heating models 07 p1190 A71-18853

Photon intensities of UV spectral lines from energetic magnetically confined vacuum carbon arc, using monochromator double ion chamber detector system 09 p1502 A71-22813

Quantum yield of carbon dioxide photolysis at 1470 Å concerning Mars and Venus atmospheres 09 p1403 A71-23377

Atomic and molecular hydrogen yields of propyne photolysis at 1470 Å Xe resonance line 09 p1403 A71-23378

Brightness temperature from solar UV continuum in 1680 to 600 Å in photosphere-chromosphere transition model 10 p1666 A71-23780

Extreme UV spectra of Sc XIV, Ti XV and V XVI, identifying and classifying lines in 18-25 Å range 11 p1729 A71-26140

Planetary nebulae continuous UV spectrum, discussing glow process, electron temperature and density and Balmer discontinuity 12 p1955 A71-26584

Solar vacuum UV spectrum analysis, using echelle grating spectrograph onboard Skylark sounding rockets 13 p2070 A71-29048

Perseus early stars photometry and far UV spectra from Aerobee rocket flight observations 14 p2304 A71-29596

Rocket-borne Cassegrain telescope system design for stellar spectra in UV region of EM spectrum between 900 and 3300 Å 14 p2238 A71-29727

In-flight UV spectrometric measurements of simulated Jupiter atmosphere, using sunlight gas mixture released from Mariner spacecraft in interplanetary space 14 p2308 A71-29914

Experimental solar blind photomultipliers for stellar photometry above earth atmosphere at 1450-2800 Å, giving spectral response and quantum efficiency 14 p2240 A71-30122

Rocket-borne twin-channel photoelectric stellar photometer for use in 1400-3000 Å region, describing nondispersive wavelength isolation methods 14 p2240 A71-30124

Intense vacuum UV atomic line source excited in 2450 MHz microwave discharge cavity with clean spectrum, noting window deterioration and self absorption 14 p2240 A71-30127

Argon ion laser mode locking in UV lines with intracavity acousto-optic modulator, describing pulse duration and average power 15 p2423 A71-32588

B and O hot dwarf stars ionic UV line spectra, observing electron and ion damping constants with impact and semiclassical approximations 16 p2633 A71-33338

Solar extreme UV flash spectrum from spaceborne ultraviolet spectrograph aboard Aerobee 170 rocket launched during March 1970 eclipse, comparing with homogeneous and inhomogeneous temperature models 16 p2640 A71-33771

Mariner 1969 flyby Mars UV spectrum observations, interpreting data in terms of atmospheric, topographic and polar cap adsorptive characteristics 17 p2799 A71-34746

UV Raman remote gas sensors incorporating laser-scattered radiation with high resolution monochromator 17 p2753 A71-35252

High resolution solar UV spectrum observations between 200 and 220 nm by sun-pointed Skylark rocket-borne echelle spectrograph 19 p3135 A71-37034

Far UV solar spectra observations, using OSO-2 5 and 6 spectroheliograms 19 p3136 A71-37074

Lunar surface microstructure inhomogeneity bimodal distribution from IR and UV spectral analysis 20 p3295 A71-39695

Solar far UV Fe and Ni ion lines 23 p3723 A71-42920

Atomic hydrogen dayglow Lyman alpha structure from Mars exosphere from Mariner 6 and 7 UV spectrometric observations 23 p3734 A71-43181

Orion constellation hot stars UV spectra observation by photography from stratospheric balloon gondola using geomagnetic field for stabilization 23 p3735 A71-43238

Photographic far UV solar spectra during eclipse of 7 March 1970, discussing coronal lines, prominences and quiet atmosphere structure 24 p3871 A71-44949

Venus upper atmospheric UV spectra from rocket-borne telescope spectrophotometer, considering O and H I emission features 24 p3872 A71-44949

Identification of 417 Å line in solar EUV spectrum, calculating collision strengths and recombination rates for Fe XV 24 p3873 A71-45114

Stellar UV cut-off by statorpheric nacelle recording on photographic film by Schmidt telescope fitted with objective prism, widening spectrum by scanning 24 p3875 A71-45221

Explorer SAS-D astronomical satellites for UV spectra recording by TV cameras 24 p3876 A71-45221

ULTRAVIOLET SPECTROGRAPHS ULTRAVIOLET SPECTROMETERS ULTRAVIOLET SPECTROMETERS

UV scanning polychromator spectroheliometer on Apollo Telescope Mount, examining temperature distribution on sun 03 p0430 A71-14434

Mariner 6 and 7 UV spectrometers, describing technical details, operating characteristics and calibration of planetary coronagraph and Ebert-Fastie monochromator used for Martian atmosphere analysis 11 p1766 A71-26300

Solar vacuum UV spectrum analysis, using echelle grating spectrograph onboard Skylark sounding rockets 13 p2070 A71-29048

OH emission column density upper limit from rocket-borne UV spectrometer measurement of resonantly scattered sunlight intensity in electronic transition vibrational band 16 p2574 A71-33900

Auroral far UV spectrum and intensity measurements, discussing atmospheric absorption effects on rocket-borne spectrometer sensitivity 21 p3372 A71-40072

ULTRAVIOLET SPECTROSCOPY

Carbon disulfide absorption spectrum measurements in far UV region 01 p0129 A71-10259

Active nitrogen afterglow complex spectrum analysis from vacuum UV to IR, proposing energy transfer mechanism 03 p0460 A71-13359

Rocket UV astronomy, discussing atmospheric and interstellar absorption, equipment design and OAO experiments 04 p0649 A71-15258

Vertical atmospheric ozone distribution from inversion of spectral UV radiation, comparing results with statistical method 05 p0742 A71-16677

OAO 2 design and performance features concerning pointing accuracy and stability, command capability, data handling, thermal environment, orbit constraints, ultraviolet spectroscopy, etc 05 p0818 A71-17121

OAO experiments instrument packages for UV observations from orbit, discussing telescopes pointing accuracy and stability, mission objectives, etc 05 p0755 A71-17121

UV solar spectrum rocket-borne high resolution spectroscopy by Fabry-Perot interferometer and

echelle grating, discussing design parameters and recorded data 06 p0903 A71-18718

Atomic N and C photoionization cross sections by shock tube vacuum UV spectrometry 10 p1646 A71-24990

Carbon dioxide photodissociation in vacuum UV, using time-of-flight spectroscopy and metastable photofragment detection by electron emission from metal surfaces 14 p2190 A71-30571

Rocket observation for spatial distribution of far UV nightglow at Lyman alpha and shorter wavelengths 15 p2398 A71-31764

Spectroscopic measurement of vacuum UV radiation from shock heated krypton plasma, noting self reversed resonance lines indicating cold boundary layer 17 p2787 A71-34589

Vacuum pump fluids spectral absorption coefficient measurement, using variable UV cell 17 p2784 A71-35141

Earth UV dayglow observation by Aerobee rocket-borne scanning spectrometer, noting features due to atomic oxygen and nitrogen and nitrogen oxide gamma band 20 p3226 A71-39830

UMBILICAL CONNECTORS

Pulse response of unshielded coaxial umbilical cable connector mounted flush with missile skin 10 p1585 A71-25072

UMBRA [SHADOWS]

U SHADOWS

UMKEHR EFFECT

Umkehr technique vs Mast-Brewer sondes for ozone vertical distributions 01 p0073 A71-10857

Secondary umkehr effect in solar UV region at twilight, proposing origin mechanism by ozone layer optical properties 08 p1357 A71-21875

Umkehr inversion system for vertical ozone distribution observation, calculating error due to ignorance of temperature dependence of ozone absorption 09 p1489 A71-23447

Vertical ozone distribution estimation by umkehr observations, discussing optimum statistical inversion technique application 11 p1794 A71-25387

UMKLAPP PROCESS

Nonlinear dependence of resistance in metals on impurity concentration and temperature due to umklapp electron phonon interaction and anisotropy of phonon spectrum 16 p2593 A71-33654

UNCAMBERED WINGS

NT RING WINGS

UNCERTAINTY

U PROBABILITY THEORY

UNCONSCIOUSNESS

NT BLACKOUT [PHYSIOLOGY]

NT NARCOSIS

Syncope as temporary suspension of consciousness due to cerebral blood supply failure, considering cardiac rhythm disturbances, blood flow obstructions and heart disease 04 p0541 A71-15915

Unconsciousness, confusion, amnesia, syncope and sudden death of pilots in flight due to silent ischemic heart diseases 18 p2855 A71-36216

Potential epilepsy determination in flight personnel, suggesting systematic EEG with hyperventilation and photic stimulation tests and personal history data of head trauma and unconsciousness 21 p3331 A71-40357

UNCOUPLED MODES

Transition selection with adjustable outcoupling for laser device applied to carbon dioxide 23 p3688 A71-44294

UNDAMPED OSCILLATIONS

System frequencies and mode shapes characteristics relation to changes in structure, considering matrix approach for equations of motion of undamped vibrations 03 p0516 A71-14457

Undamped structural vibration problems solution for eigenvalues and eigenvectors using simultaneous iteration method 05 p0829 A71-17113

Dynamic frequency and phase characteristics of oscillatory circuit dependent linearly on time variable capacitance 10 p1643 A71-24907

Current controlled unstable pulse oscillator, discussing depletion layer transistors and upper frequency limit as function of thermal loads and switching times 12 p1887 A71-27043

Algorithm for linearly elastic structures vibration natural undamped frequency computation, assuming known dynamic stiffness matrix 20 p3311 A71-39964

Iterative method for linearly elastic structure undamped vibration natural frequency determination with fast convergence 20 p3311 A71-39965

Gyrocompass in gyropendulum stabilized Cardan suspension, deriving system undamped oscillations equations 24 p3847 A71-44415

UNDERCARRIAGES

Aircraft multiwheel undercarriage effect on rigid and flexible pavements, examining failure modes 02 p0189 A71-12164

UNDERGROUND COMMUNICATION

Optimum VLF electromagnetic link between underground terminals with emitter-receiver horizontal antennas, calculating radiation pattern 02 p0211 A71-11717

UNDERGROUND NUCLEAR EXPLOSIONS

U NUCLEAR EXPLOSIONS

UNDERWATER ACOUSTICS

Acoustic holography for simultaneous three-dimensional image and internal structure insight, discussing applications to submarine exploration and medical diagnostics 13 p2071 A71-29299

Solid state linear array piezoelectric hydroacoustic image transducer for underwater viewing in turbid oceanic environments 20 p3233 A71-38828

Acoustical holography principles properties and applications, discussing liquid surface levitation, Bragg diffraction and undersea and seismic utilization 21 p3381 A71-40931

UNDERWATER BREATHING APPARATUS

Emergency surface decompression and treatment procedures for project Tekite aquanauts, determining safe interval and schedules for return to habitat on ocean floor 16 p2535 A71-33110

UNDERWATER COMMUNICATION

Tekite II program of underwater research as future manned space flight operations model, discussing mission structure, crew selection and communications [AIAA PAPER 71-828] 17 p2690 A71-34718

UNDERWATER ENGINEERING

Zinc-silver oxide batteries underwater and aerial applications, designing medium high rate long life cells 08 p1236 A71-21102

Thermionic reactor core design for undersea conditions based on neutron data and calculation related with diode materials 11 p1711 A71-25882

UNDERWATER PHOTOGRAPHY

Underwater objects plotted in double projectors, reconstructing water surface optical refraction 01 p0083 A71-11327

UNDERWATER SOUND

U UNDERWATER ACOUSTICS

UNIAxIAL STRAIN

U AXIAL STRAIN

UNIFIED S BAND

Unified S band communication system for manned space flight network ground stations 01 p0035 A71-10916

UNIFORM FLOW

Uniformly blown turbulent boundary layer on flat plate, investigating unheated solid starting length effect on heat transfer 04 p0572 A71-15500

Grid turbulence interaction with uniform mean shear flow, examining initial disturbance length scale effects 05 p0695 A71-16965

Far field sound radiated from steady loading of isolated subsonic rotor, noting dependence on spatial uniformity of flow entering rotor 05 p0697 A71-17160

Eigenvalues of axially uniform fluid waveguide with eccentric annulus cross section and acoustically hard boundaries 12 p1928 A71-26700

Shock wave incidence on wedge moving at supersonic speed, considering uniform flow region on upper wedge surface for specific values of Mach number and vertex angle 12 p1897 A71-27445

Uniform transonic ideal gas flow past finite bodies approximated by Karman equation 13 p1989 A71-27902

Viscous gas jets in uniform oncoming flow, deriving similarity laws by dimensionality theory 13 p1994 A71-29223

Uniform shear flow past semiinfinite flat plate, studying diffuse and heat transfer near leading edge 16 p2561 A71-34162

Poloidal Hall current calculation in hydrodynamic approximation for stationary weakly interacting and conducting cylindrical plasma flow with uniform transverse flow parameter distribution 19 p3109 A71-37138

Highly uniform inlet velocity profile influence on conical diffuser characteristics 20 p3177 A71-39798

Gravitational radiation interaction with uniform incompressible inviscid fluid in simple motion, consider-

ing response in linearized approximation to general relativity 21 p3446 A71-40421

Uniform inlet flow inside centrifugal turbomachinery diffusers with flat parallel side walls, measuring pressure distribution and boundary layer velocity profiles 21 p3323 A71-40757

UNIMOLECULAR STRUCTURES

Incomplete energy equilibration in short lived activated complexes, measuring translational energy of unimolecular ion decomposition fragments 05 p0716 A71-15924

Thermal unimolecular processes falloff data calculation based on Rice-Ramsperger-Kassel or Rice-Ramsperger-Kassel-Marcus theories 13 p2025 A71-29037

UNIONS [CONNECTORS]

Wire connection damage due to high vibration, examining termination and joining techniques 18 p2852 A71-36837

UNIPOLAR TRANSISTORS

U FIELD EFFECT TRANSISTORS

UNIQUENESS THEOREM

Boundary value problem for linear Boltzmann equation in kinetic theory, proving existence and uniqueness theorems 02 p0276 A71-12338

Halley method of tangential hyperbolas in Banach space, deriving local existence, uniqueness and convergence theorems 04 p0620 A71-15668

Uniqueness theorem for sources of electromagnetic fields expressible as magnitude integrable functions of time, considering implications for antenna aperture limitations on radar resolution 06 p0868 A71-17729

Iterative solution of nonlinear operator equations in Banach spaces, proving existence, uniqueness and convergence theorems 06 p0920 A71-18211

Uniqueness theorem for Dirichlet series bounded on real axis 07 p1146 A71-19040

Free boundary problems for heat equation involving interface coinciding initially with fixed face, proving existence, uniqueness and continuous dependence theorems 08 p1324 A71-20879

Rectilinear trajectory optimization of second order nonlinear system, formulating existence and uniqueness theorems of optimal control 09 p1424 A71-23433

Rellich uniqueness theorem for Helmholtz equation for steady state wave propagation in inhomogeneous anisotropic media subject to Sommerfeld radiation 12 p1929 A71-26865

Bending problems of elastoplastic plate rigidly clamped over edges, deriving theorems on existence, uniqueness and convergence of approximate solutions 12 p1974 A71-26962

Potential theory mixed inverse problem and uniqueness theorem concerning body shape and density determination from external potential of bulk masses 12 p1931 A71-27510

Dirichlet problem for degenerate elliptic differential equations, discussing existence and uniqueness of solution by Schwarz alternating method 12 p1923 A71-27512

Existence and uniqueness of solution to Dirichlet boundary value problem of invariant in nonclassical theory of elasticity concerning behavior of media with memory 13 p2154 A71-28651

Transonic gas flow around profile, proving uniqueness of Frankl solution 13 p1993 A71-29221

Difference equations system trivial solution stability condition existence and uniqueness theorems 14 p2265 A71-29628

Thermoelastic shells and plates approximate linear theory, detailing uniqueness theorem for initial mixed boundary value problem 14 p2329 A71-30446

Existence and uniqueness theorem for n-point boundary value problems of nonlinear ordinary differential equations, using Polya condition 15 p2442 A71-31871

Uniqueness of positive solutions to self adjoint elliptic partial differential equations with nonlinear forcing terms under Dirichlet and Neumann boundary conditions 15 p2442 A71-31872

Ionospheric motion boundary value problem, deriving uniqueness of solution 16 p2564 A71-33718

Uniqueness theorem for second order differential equation associated with inverse problem of spectral analysis, developing operator transformation procedure 16 p2603 A71-33890

Existence and uniqueness of generalized weak solution to problem of coupling unsteady partial differential equations 16 p2603 A71-34000

Mixed boundary value problem of hereditary elasticity theory, discussing existence and uniqueness of solution

17 p2818 A71-34425

Soviet book on ordinary differential equations covering basic concepts, existence and uniqueness theorems, linear homogeneous and nonhomogeneous equations with constant coefficients, etc

17 p2768 A71-35626

Two dimensional steady viscous gas transonic flow Navier-Stokes equations, establishing uniqueness of solutions to boundary value problems

17 p2673 A71-35646

Unique linear product approximations of continuous functions of several variables extended to general convex sets

17 p2768 A71-35682

Existence and uniqueness of weak solution of wave equation with nonlinear boundary condition, using Galerkin method

18 p2940 A71-36094

Oblique shock wave incident on plane boundary of nonlinear homogeneous elastic solid, proving wave reflection pattern uniqueness

18 p2982 A71-36813

Compressible boundary layer equations similarity solutions uniqueness proof, using asymptotic behavior

18 p2909 A71-36814

Divergence structure nonlinear elliptic equations, demonstrating smooth solutions uniqueness of Dirichlet problem

18 p2942 A71-36816

Contact problem for elasticity theory taking hereditary deformation into account, proving existence and uniqueness theorems

19 p3156 A71-37538

Theorems on parabolic and hyperbolic differential equations solutions continuous dependence on elliptic operator coefficients, deriving proof by hypothesis of existence and uniqueness

21 p3408 A71-40651

Random analogs of boundary value problems class for biharmonic functions, demonstrating unique solution existence

21 p3410 A71-41189

Uniqueness theorems and boundary conditions for problem related to Navier-Stokes equations

22 p3566 A71-41514

Existence and uniqueness of boundary layer equations similarity solution for viscous incompressible fluid flow past paraboloid

22 p3531 A71-42197

Static, kinematic and uniqueness theorems of incremental collapse of frames extended to variable repeated loading

22 p3619 A71-42593

Viscous hydrodynamic equations functional type boundary value problem, investigating uniqueness theorem for elliptic equations

22 p3531 A71-42629

Differential equations system for convective incompressible fluid flow boundary layer temperature profile description, analyzing solution existence and uniqueness

23 p3781 A71-43306

UNITED NATIONS

Satellite broadcasting defined by UN, discussing community and home direct reception modes and educational TV potentialities and problems

17 p2697 A71-34238

Legal problems in space telecommunications, discussing UN and international nongovernmental organizations solutions for interference protection, pirate space stations and spacecraft distress or emergency

17 p2841 A71-34247

UN leadership in space communications international cooperation, emphasizing communication satellite systems application to educational TV

17 p2841 A71-34249

Global broadcasting from space, suggesting international cooperation and UN role

17 p2841 A71-34250

International Telecommunication Union report on telecommunication and peaceful uses of outer space, covering space programs, communication satellites, UN role, etc

19 p3172 A71-37517

UNITED STATES OF AMERICA

NT CALIFORNIA

NT COLORADO

NT IDAHO

NT MINNESOTA

NT NEW JERSEY

NT OKLAHOMA

Airborne inertial and area navigation systems performance requirements proposed for U.S. domestic airspace, including projection through 1995

01 p0124 A71-10508

Judicial Panel on Multidistrict Litigation of federal district and court of appeals judges with power to transfer cases to single district

22 p3624 A71-42069

Federal Aviation Act amendment prohibiting controlling interest in air carrier without Civil Aeronautics Board approval

22 p3624 A71-42070

UNITS OF MEASUREMENT

Supplementary tables to SI nomenclature for radiometry and photometry including photon flux

14 p2242 A71-30157

Time scale and time interval characteristics for scientific use, tabulating associated units

24 p3827 A71-44995

UNIVERSAL TIME

Wintertime Arctic F region critical frequency secondary maxima, discussing UT control hypothesis

03 p0408 A71-13386

International Time Bureau /Paris/ astronomical and geophysical research based on universal time and latitude observations of earth rotation

06 p0890 A71-17879

Universal time effect on E region critical frequency at large solar zenith angles, considering ionization source at midlatitude range

11 p1757 A71-25785

Universal time and atomic clock earth rotation irregularities measurements checked for Chandler period

20 p3216 A71-39479

Universal time effect on E region critical frequency at large solar zenith angles, considering ionization source at midlatitude range

22 p3532 A71-41553

Standard frequency and UTC time signal transmission coherent with SI/atomic/ second

22 p3509 A71-42087

Comparative north and south polar F layer electron density dependence on universal time and latitude, using ionosonde data

23 p3669 A71-43172

UNIVERSE

Magnetic field generation during radiation era, discussing generating mechanism by angular momentum transfer between ion and electron-photon gases in expanding plasma

01 p0148 A71-10024

Linear MHD theory of inhomogeneities in axisymmetric models of universe with cosmological magnetic field

01 p0160 A71-11093

Static solutions to equations of gravity, showing nonequilibrium universe with negatively determinate time-similar Ricci curvature

01 p0160 A71-11117

Galaxies dynamic parameters formation associated with cosmological turbulence in expanding hot universe

02 p0307 A71-12085

Electron charge dependence on universe age, considering possible gravitational constant dependence on time

02 p0313 A71-12547

Cosmological models with matter and radiation for evolution of universe

03 p0484 A71-13206

Gravitational stresses derived for Friedmann-Lobachevskii and Schwarzschild spaces

03 p0456 A71-13297

Friedman universe model in centrally symmetric reading system

04 p0644 A71-15123

Metagalactic background X rays origin, hypothesizing electron leakage from radio galaxy

04 p0657 A71-15748

Physical and geometrical properties of dust filled universes, using left invariant metrics compatible with Einstein equations

05 p0773 A71-15925

Closed evolving universe by vanishing pressure, considering eight different models including three cyclic models

05 p0813 A71-16811

Black hole model for gravitational collapse of universe according to Einstein theory

05 p0813 A71-16956

World models with antipoles for deriving cosmological density parameter upper bound

05 p0814 A71-17092

NonMarkoffian kinetic theory for hierarchical structure of clusters in expanding universe

06 p0964 A71-17314

Perturbation growth in free particle expanding Universe with critical density, considering Newton gravitation theory

06 p0974 A71-18427

Light propagation in mixmaster universe model based on Einstein equations solution

06 p0974 A71-18428

Einstein equations of gravitational field for universe filled with radiation, obtaining spherical symmetrical inhomogeneous solutions

07 p1203 A71-20530

Galaxies dynamic parameters formation associated with cosmological turbulence in expanding hot universe

08 p1362 A71-21135

Conformally flat universe class with short range scalar gravity, satisfying Einstein field equations

08 p1334 A71-21311

Linear MHD theory of inhomogeneities in axisymmetric models of universe with cosmological magnetic field

08 p1366 A71-21348

Mean luminous cosmic matter density calculations using galaxy counts and mass data eliminating minority functions

09 p1516 A71-22202

Local mean cosmic density from double galaxy data

09 p1516 A71-22202

Mean cosmic density based on galactic cluster masses

09 p1516 A71-22202

Homogeneous isotropic relativistic cosmological model of universe, discussing construction

09 p1523 A71-23040

Book on universe surveying astronomy, measuring tools, solar system, radiation, planets, space exploration, exobiology, astrophysics, Milky Way, galaxies, cosmic evolution, etc

09 p1526 A71-23414

Hot universe model, discussing small scale entropy matter distribution, adiabatic density perturbations, energy balance, formation of galactic clusters, galaxies, globular clusters and quasars

09 p1527 A71-23515

Nonhomogeneous cosmological model with equations describing universe relative density variations demonstrating thermal instability role in galaxies formation

10 p1667 A71-23811

Soviet book on stars, galaxies and metagalaxies covering stellar luminosities, spectra, novae and supernovae

10 p1668 A71-24010

Cosmological enhancement of density perturbations and amplitude variation of acoustic and gravitational waves in anisotropic homogeneous universe

10 p1678 A71-24888

Debye-Huckel gravitational potential in Lemaitre universe

10 p1680 A71-25010

Perturbation growth in free particle expanding universe with critical density, considering Newtonian gravitation theory

12 p1954 A71-26575

Light propagation in mixmaster universe model based on Einstein equations solution

12 p1955 A71-26575

Universe global structure and quasar frequency distribution based on red shifts and cosmological interpretations

12 p1968 A71-27640

Closed universes quantization and gravitational field in general relativity, emphasizing superspace concept and finite-dimensional model quantum theories construction

13 p2100 A71-28399

Early isotropic universe structure evolution, considering non-Friedmannian cosmic expansion stages, metagalactic turbulence and cosmological models

13 p2141 A71-29100

Matter density in universe, comparing delayed galactic growth with observed radio sources and quasars

14 p2305 A71-29677

Gravitation theory with universe reference frame concept consistent with general relativity theory based on equivalence principle

14 p2315 A71-30864

Electron charge dependence on universe age, considering possible gravitational constant dependence on time

15 p2494 A71-32500

Einstein field equations solution for universe filled with perfect fluid of position-dependent density

16 p2611 A71-33277

Mass spectrometric studies of origin of light elements Li, Be and B in universe, considering spallation of stellar and galactic gases by high energy particles

18 p2959 A71-35914

Physical constraints on universe topology near collapsed-ordinary stars interaction in general relativity theory

19 p3105 A71-38583

Entropy generation and survival of protogalaxies in expanding universe, deriving bulk/shear viscosity heat transport and sound waves damping rate in relativistic fluid

20 p3287 A71-39051

Energy in universe from stellar and galactic evolution, discussing flow mechanisms, entropy, arresting factors and catastrophic phenomena

20 p3301 A71-39916

Critical analysis of big bang cosmological theory discussing evidence insufficiency and steady state universe possibility

20 p3305 A71-39995

Expanding metagalaxy closed model with changing gravitational constant, noting matter motion in moving and central reference systems

21 p3441 A71-40077

Cosmological models of universe based on expansion-gravitational interaction, including red shift, radio sources, quasars and background radiation measurements 21 p3451 A71-40776

Cosmological enhancement of density perturbations and amplitude variation of acoustic and gravitational waves in anisotropic homogeneous universe 21 p3453 A71-41251

Dissipative processes role in early universe within chaotic cosmology program 23 p3769 A71-43992

Uniform model universes with matter and black body radiation, obtaining radiation temperature dependence on scale factor 23 p3769 A71-43994

Einstein equations for universes with expansion, rotation, shear and Bianchi type IX spaces, obtaining diagrammatic solutions 23 p3770 A71-44124

Thermal history of universe traced from assumption of photon and plasma turbulence for galactic formations, discussing thermal instability and heating effects 23 p3770 A71-44181

Initial singularity removal in model big bang universe compatible with 3K black body radiation in terms of renormalized gravitational theory 23 p3770 A71-44182

UNKNOWN

U DEPENDENT VARIABLES

U PROBLEM SOLVING

UNLOADING

Solar telescope coelostat and auxiliary mirror hydropneumatic unloading mechanism 04 p0566 A71-14870

Stress relaxation characteristics obtained by compensation principle, force measuring techniques and sample unloading for stress-strain state determination 07 p1210 A71-19160

Army/Navy operational evaluation of offshore containerships discharge by CH-54 helicopters [AHS PREPRINT 573] 14 p2180 A71-31114

UNLOADING WAVES

Elastoplastic loading or unloading wave complex in solids, analyzing stability by breakdown into elastic and plastic components 07 p1217 A71-20461

UNMANNED SPACECRAFT

NT BEACON SATELLITES

NT BIOSATELLITE 2

NT BIOSATELLITE 3

NT BIOSATELLITES

NT ECHO 1 SATELLITE

NT ECHO 2 SATELLITE

NT EXPLORER 22 SATELLITE

NT GEODETIC SATELLITES

NT GEOS 1 SATELLITE

NT GEOS 2 SATELLITE

NT GEOS-C SATELLITE

NT JUPITER PROBES

NT LUNAR PROBES

NT LUNIK LUNAR PROBES

NT LUNIK 14 LUNAR PROBE

NT MARINER SPACE PROBES

NT MARINER SPACECRAFT

NT MARINER VENUS-MERCURY 1973

NT MARINER 5 SPACE PROBE

NT MARINER-MERCURY 1973

NT MARS PROBES

NT NAVIGATION SATELLITES

NT OSO

NT OSO-E

NT OSO-F

NT OSO-G

NT OSO-3

NT PAGEOS SATELLITE

NT PASSIVE SATELLITES

NT PIONEER SPACE PROBES

NT PIONEER 6 SPACE PROBE

NT PIONEER 7 SPACE PROBE

NT PIONEER 8 SPACE PROBE

NT PIONEER 9 SPACE PROBE

NT SOLAR OBSERVATORIES

NT SOLAR PROBES

NT SPACE PROBES

NT SURVEYOR LUNAR PROBES

NT SURVEYOR 1 LUNAR PROBE

NT SURVEYOR 3 LUNAR PROBE

NT SURVEYOR 5 LUNAR PROBE

NT VENERA SATELLITES

NT VENERA 3 SATELLITE

NT VENERA 4 SATELLITE

NT VENERA 6 SATELLITE

NT VENUS PROBES

NT ZOND SPACE PROBES

NT ZOND 3 SPACE PROBE

NT ZOND 5 SPACE PROBE

Single module unmanned Mars roving vehicle with flexible metal toroidal hoop-spoked wheels, discussing remote controlled scale model design for simulation on earth 04 p0566 A71-15333

Unmanned scientific missions to outer planets in late 1970s, discussing instruments requirements, flight paths, spacecraft designs and payloads 04 p0649 A71-15347

Space based reusable manned/unmanned tug, discussing potential missions, system requirements and auxiliary hydrogen oxygen propulsion system [AIAA PAPER 70-719] 09 p1511 A71-22902

Jupiter gravitational potential mapping for Grand Tours spacecraft, discussing Jovian satellites effect on orbit and trajectory perturbations 09 p1525 A71-23222

Externally fueled thermionic reactor power plant incorporation into unmanned ion propulsion spacecraft 11 p1811 A71-25896

Impact resistant power packages for unmanned planetary probe landers, discussing radioisotope thermionic multiconverter array optimal configuration 11 p1713 A71-25898

Thermal scale modeling limitations for radiation-conduction system of unmanned spacecraft, discussing material thermal properties, model dimensions, instrumentation effects and environment simulation 13 p2159 A71-27988

Unmanned flight vehicles recovery system, describing built-in rotor design for navigation and high precision landing [DGLR-71-020] 15 p2351 A71-32787

Unmanned spacecraft first day failures, discussing launch environment, duration tests in simulated space and performance improvement 16 p2645 A71-33296

Planetary quarantine analysis for unmanned Mars orbiter, considering accidental spacecraft impact, loose particles and gases used for attitude control and pressurization 16 p2537 A71-33799

Earth-spacecraft radio communication requirements for future unmanned planetary missions, emphasizing imaging experiments and sensors 18 p2877 A71-36518

European unmanned interorbital tug, investigating configurations, structure, hookup system, docking and propellant supply 19 p3150 A71-37309

Hardware reliability improvement techniques for long life unmanned space missions [AAS PAPER 71-156] 19 p3153 A71-37957

Unmanned spacecraft pursuit of evading manned vehicle by game theory, assuming full information availability to both players 19 p3038 A71-38014

Balanced space programs for 1970s and beyond, discussing unmanned planetary missions, manned Apollo, Skylab and space shuttle projects, private, foreign and international programs [AIAA PAPER 71-1020] 24 p3892 A71-44598

UNSTABLE BURNING

U COMBUSTION STABILITY

UNSTEADY FLOW

NT OSCILLATING FLOW

Multiple spark camera for unsteady compressible flow investigations, considering geometrical optical design, parallax, spark producing electric circuitry, etc 01 p0078 A71-10106

Unsteady cavitation flow, presenting physical mechanism of cavity formation in liquid flow and formulation of governing equations 01 p0069 A71-10110

Arterial branches pulsating flow and wave propagation in large blood vessels, considering flow measurements from simulated model experiments 01 p0008 A71-10111

Unsteady flow theory, describing milestone experiments in aerodynamics 01 p0001 A71-10266

Ultrasonic flowmeters for unsteady flow, discussing beam deflection method, phase difference systems, etc 01 p0079 A71-10302

Ion exchange kinetics during pulsating fluid flow, developing approximate mathematical model 01 p0070 A71-10619

Radiative transfer equations averaging over quantum angles and energies, discussing use for nonsteady gas dynamic problems 01 p0179 A71-10666

One dimensional motion of unsteady incompressible conducting free jet in transverse magnetic field, noting computer solution by characteristics method 01 p0133 A71-10792

Two dimensional potential flow theory for incompressible unsteady flow about multiple lifting bodies in small amplitude motion 01 p0071 A71-10929

Lifting surface in unsteady subsonic flow, describing integral equation calculation method including kernel logarithmic singularity 01 p0003 A71-11020

Linear stability of finite difference approximations to no-slip boundary conditions in nonsteady fluid flow 01 p0071 A71-11161

Turbulent transport equations derivation for incompressible fluid unsteady flow in arbitrary geometry, considering application to flow between parallel plates 01 p0072 A71-11469

Unsteady convective heat transfer in pipes in presence of heat flux density and flow rate aperiodic variations 02 p0331 A71-11885

German monograph on plane ideal gas flows calculation with allowance for unsteady gastight walls and compression shocks using difference methods 02 p0240 A71-12400

Boundary layer solution for unsteady compressible incompressible flow past body, discussing momentum conservation equation solution by series expansion 02 p0241 A71-12848

Initial phase of unsteady laminar flow from cylindrical vessel through circular cylindrical tube 03 p0398 A71-13105

Incompressible elastoviscous unsteady fluid flow past circular cylinder, confining calculations to non-zero vorticity region near cylinder 03 p0398 A71-13108

Wing computation in steady or unsteady supersonic flow, using network, inverse discrete and numerical inversion methods [ONERA-TP-896] 03 p0339 A71-13129

Aerodynamic characteristics of aircraft in steady and unsteady supersonic flow by analog electrical method, including wing-fuselage interactions 03 p0339 A71-13130

Unsteady flow induced by circular cylinder impulsive motions, examining vortices formation and interaction 03 p0399 A71-13197

One dimensional unsteady barotropic fluid flow based on Euler equations, describing rarefied plasma nonlinear motions 03 p0462 A71-13289

Unsteady MHD forced flow of viscous incompressible electrically conducting fluid against rotating disk 03 p0459 A71-13902

Plane nonsteady gas dynamic flows, reducing to system of time dependent equations system, presenting Chaplygin equation generalization 03 p0401 A71-13908

Unsteady flow about solid cylinder falling through viscous fluid in vertical tube, obtaining velocity profiles via solution of Navier-Stokes equation [ASME PAPER 70-WA/FE-9] 03 p0403 A71-14130

Unsteady one dimensional isentropic gas flows, discussing nonlinear pressure waves geometry 03 p0405 A71-14345

German monograph on loss estimation for nonsteady gasdynamic duct-drum pressure exchangers, discussing design and optimization problems 04 p0568 A71-14925

Wings with control surfaces in unsteady subsonic flow, applying lifting surface theory [ONERA-TP-889] 04 p0526 A71-15355

Analog and digital methods for interactions between aircraft lifting elements in steady or unsteady supersonic flow [ONERA-TP-850] 04 p0527 A71-15358

One dimensional unsteady flows of combustible gas mixtures with detonation waves generation, noting electromagnetic effects 05 p0833 A71-16502

Unsteady processes in starting period of supersonic Ludwig tube, initiating flow by quick opening diaphragm downstream of nozzle 05 p0734 A71-16563

Unsteady viscous rotational stagnation point flow, solving vorticity transport equation 05 p0736 A71-16722

Laser Doppler heterodyning system for bidirectional pulsatile fluid flow velocity magnitude and direction measurement 05 p0756 A71-17233

Laminar pulsating ducted flow heat transfer, taking into account velocity distribution time dependence 06 p1005 A71-17682

Pulsating liquid filled hemispherical shell dynamic characteristics, determining hydrodynamic pressure and shell displacements 06 p0882 A71-17837

French book on fluid mechanics, Volume 3, covering nonsteady phenomena, boundary layer and viscous flow 06 p0882 A71-18019

Unsteady heat conduction in thermally coupled spherical regions, discussing duration, penetration depth and temperature histories 06 p1006 A71-18071

Incompressible unsteady viscous fluid flow through circular cross section curved pipe, noting centrifugal effects in interior 06 p0882 A71-18316

Unsteady supersonic aerodynamic coefficients evaluation to desired kinematic consistency level using finite element method [AIAA PAPER 71-177] 06 p0845 A71-18616

Runge-Kutta type difference methods for calculating unsteady gas flow with shock waves 07 p1087 A71-19184

Unsteady viscous incompressible flow over impulsively started rotating disk by acceleration averaging method

07 p1088 A71-19356

Nonstationary isentropic low density flows with axial or central symmetry, suggesting characteristics with flow rate and sound speed variation as in stationary source flow

07 p1014 A71-19729

Unsteady viscous incompressible electrically conducting fluid flow past accelerated conductor or insulator flat plate in uniform transverse magnetic field

07 p1169 A71-20022

Viscous conducting fluid MHD fluctuating flow over porous flat plate with time dependent suction, determining skin friction and transient velocity profiles

07 p1169 A71-20028

Unsteady MHD channel flow between two semi-infinite harmonically oscillating and perfectly conducting solids, determining liquid velocity profile curves

07 p1169 A71-20032

Solid foil small oscillations in unsteady incompressible flow, mapping physical plane and corresponding complex potential region onto curvilinear half strip

07 p1092 A71-20088

Viscous incompressible slow unsteady flow through circular tube with small axial roughness, obtaining velocity components by integral transform technique

07 p1092 A71-20093

Unsteady boundary layers on sphere or cone moving along axis, determining skin friction angular response

07 p1016 A71-20098

Boundary layer separation in unsteady pipe flow, examining velocity profiles under influence of periodic pressure fluctuations

07 p1093 A71-20280

Unsteady incompressible laminar boundary layer equations, obtaining similarity solutions from momentum integral equation

07 p1093 A71-20365

Unsteady analogy for hypersonic flows past blunt bodies with shock deformation

08 p1227 A71-21863

Pulsed air gust generator for sinusoidal streamwise perturbation of wind tunnel test stream, describing upstream blowing air jet array, flow calibration and mathematical model

08 p1275 A71-22005

Rarefied gas steady and unsteady motions, proposing approximate method for various problems

09 p1382 A71-22372

Twin vortex development in unsteady separated flow past thin flat plate, using flow visualization

09 p1432 A71-22582

Thin rectangular wing load distribution in nonstationary incompressible flow, using downwash integral equation Fourier transform

09 p1383 A71-22946

Incompressible viscous fluid unsteady three dimensional flow, obtaining velocity field and pressure distribution in boundary layer

09 p1433 A71-23092

One dimensional unsteady barotropic fluid flow based on Euler equations, describing rarefied plasma nonlinear motions

09 p1504 A71-23265

Three dimensional unsteady irrotational flow in variable cross section duct, reducing Navier-Stokes equation to Euler equation

10 p1591 A71-23850

Pulsed subsonic wind tunnel, calculating instantaneous flow velocity with allowance for boundary layer thickness at walls

10 p1549 A71-23855

Unsteady low Mach number flow calculation by singular perturbation method with matched asymptotic expansions, considering application to aerodynamic noise

10 p1549 A71-23936

Unsteady inward and outward velocities of subsonic radial air flow between two disks, using hot-wire anemometer and cylindrical wave equation

10 p1550 A71-24000

Incompressible fluid plane unsteady laminar boundary layers equations solution through reduction to nonlinear partial differential equation and series expansion

10 p1592 A71-24025

Incompressible fluid plane laminar unsteady boundary layer, obtaining Falkner-Skan equation as special case for similar solutions in steady flow case

10 p1592 A71-24026

Unsteady incompressible laminar boundary layer universal equation form for solution through reduction to ordinary differential equations and series coefficients determination

10 p1593 A71-24027

Plane unsteady convective motion of viscous incompressible liquid in infinite horizontal vessel of rectangular cross section due to wall temperature fluctuations

10 p1696 A71-24375

Universal equations of two dimensional incompressible unsteady laminar boundary layer

10 p1597 A71-25017

Acoustic and shock waves propagation in quasi-steady supersonic flow in duct with varying cross section

10 p1598 A71-25083

Unsteady hypersonic flow around melting axisymmetric blunt bodies of revolution with profile depending on wall temperature, calculating temperature distribution and wall pressure

10 p1698 A71-25087

Viscous liquid unsteady flow in long circular tube as function of mean velocity distribution, discussing radial flow and pressure distribution

11 p1749 A71-25268

Plane unsteady polytropic MHD flow equations reduced to time independent system, using complex variable techniques

11 p1804 A71-25439

Small surface curvature effect on unsteady hypersonic flow over thin oscillating wedge, using perturbation theory

11 p1705 A71-26197

Unsteady solution of simplified atmospheric dynamics equations, reducing to system of Volterra integral equations of second kind for complex horizontal wind velocity

12 p1924 A71-26734

Errors due to air flow pulsation in orifice meters, discussing various diameter ratios

12 p1906 A71-26872

Unsteady mass exchange during laminar MHD free convection on vertical plate, deriving time dependence expression for external magnetic field

12 p1938 A71-27242

Flow in vicinity of stagnation point of sphere and cylinder during pulsating motion in nonuniform stream

12 p1897 A71-27448

Unsteady flow measurement around wing sections during rapid angle of attack variations, emphasizing helicopter rotor blades

12 p1864 A71-27468

Pulsed MPD arc experiment, determining voltage characteristics and rotating current spokes occurrence and behavior

12 p1941 A71-27567

Unsteady flow downwash behind finite span slender wing during supersonic motion at finite Strouhal numbers

12 p1866 A71-27697

Cascade approximation of unsteady forces acting on blades of axial flow turbomachines, using perturbation potential combined with slip condition

12 p1946 A71-27713

Unsteady one dimensional time-dependent diabatic gas flow equations reduced to single partial differential equation, deriving solutions for entropy distribution

13 p2158 A71-27829

Unsteady curvilinear motion of lifting surface, calculating induced gas flow velocities in terms of vortex densities

13 p1992 A71-29188

Unsteady hypersonic self similar gas flow and drag on circular cone accelerated according to power law, using small perturbation theory

13 p1993 A71-29205

Laminar incompressible fully developed pulsating flow between parallel flat plates effects on local time-average heat flux

14 p2334 A71-29603

Three dimensional spatial unsteady hypersonic gas flow about bodies behind strong shock wave front

14 p2169 A71-30182

Viscous gas unsteady flow between harmonically oscillating and nonoscillating walls

14 p2225 A71-30220

Average and pulsating velocity distributions during subsonic air jet interaction with plane baffle, describing jet dissipation geometrical pattern

14 p2225 A71-30223

Nonsteady air flow direction generation and measurement, comparing three-tube probe with hot-wire anemometer data

14 p2244 A71-30326

Radiative transfer equations averaging over quantum angles and energies, discussing use for nonsteady gas dynamic problems

14 p2339 A71-30999

Unsteady incompressible laminar viscous flow past infinite flat plate with arbitrary time dependent velocity, using Laplace transformation

15 p2387 A71-31184

Vibratory stresses in heat exchangers due to pressure pulsation induced acoustic resonances, calculating flow pulsations from Karman vortex streets [HEAT EXCH. CONF. PAPER 13]

15 p2513 A71-31635

Performance test facility for pulsed axial flow gas turbine of turbocharger unit on large diesel engines

15 p2469 A71-31943

Shock wave attenuation along uniform perforated tube, considering rarefaction and compression waves in resulting unsteady flow

16 p2554 A71-32813

Unsteady waves in parallel shear flows, noting viscous and nonlinear effects

16 p2558 A71-33040

Unsteady viscous flow around oscillating cylinder calculating fluctuating lift, drag and moment effects with Navier-Stokes equations

16 p2520 A71-33099

Unsteady compressible flow measurement, determining local lift coefficient from pressure distribution along airfoil

16 p2520 A71-33365

Stagnation pressure changes in unsteady flow downstream of turbomachine blades with fluctuating circulation related to vortex sheets

17 p2671 A71-35272

Time and space variable magnetic field effects on plane unsteady MHD boundary layer flow separation

17 p2789 A71-35348

Weak shock propagation in three dimensional unsteady flow, obtaining shock construction rule

17 p2729 A71-35424

Artificially induced unsteady flows effects on flame stabilization by model opposed jet stabilizer employing premixed propane-air combustible flow and opposed air jet

17 p2840 A71-35707

Boundary velocity and temperature field of unsteady natural periodic convection over three dimensional obstacle for arbitrary Prandtl numbers

18 p2984 A71-35950

Unsteady multispecies gas mixture concentration flow measurement, using Raman scattering of pulsed nitrogen laser light

18 p2930 A71-36060

Numerical integration of Euler equations for three dimensional time dependent unsteady flow by extension of method of characteristics

18 p2904 A71-36302

Shock wave diffraction propagation through nonuniform fluid, noting application to two dimensional unsteady flows

18 p2907 A71-36332

Plane unsteady gas flow under action of dihedral angle shaped piston traveling at constant velocity

19 p3042 A71-37084

Unsteady approach to nonisothermal flow theory for Couette flow, making general assumptions concerning rheological law and temperature dependence of fluidity

19 p3043 A71-37386

Numerical methods for unsteady compressible flows, considering method of characteristics, Lax-Wendroff and particle-in-cell method

19 p2992 A71-37456

Unsteady flow of incompressible micropolar fluid due to sphere oscillations, calculating velocity, drag and stress components

19 p3045 A71-37790

Nonlinear combustion instability in liquid propellant rocket engines, describing unsteady combustor flow with single wave equation

19 p3122 A71-38092

Computer algorithm for simulation of one dimensional unsteady compressible fluid flow in presence of area change, wall friction, heat transfer and entropy gradients

19 p3025 A71-38291

Fronts and frontal clouds evolution theory as nonstationary two dimensional problem with allowance for dynamics and thermodynamics

19 p3091 A71-38682

Soviet book on unsteady motions of continuous media covering gas dynamics, thermodynamics, shock and plane detonation waves, three dimensional gas motions, etc

20 p3211 A71-39144

Unsteady analogy for hypersonic flows past blunt bodies with shock deformation

20 p3176 A71-39362

Variable suction effects on two dimensional fluctuating slip flow of incompressible rarefied gas past infinite flat plate

20 p3211 A71-39466

Turbulent energy variations in unsteadily moving flow with structural shift, emphasizing formation of vortices with various inertia scales

20 p3214 A71-39796

Velocity and resistance profiles for unsteady turbulent flow in rough pressure channels, using Prandtl hypothesis

20 p3214 A71-39797

Steady and unsteady flow work and energy loss relationships expressed in integral form representing perturbation kinetic energy, internal energy and pressure work

21 p3317 A71-40011

Aerodynamic approximations for unsteady supersonic flow of perfect inviscid gas through flexible duct of revolution

21 p3458 A71-40280

Unsteady viscous compressible flow through straight channel with flat porous walls under time varying pressure
21 p3367 A71-40591

Nonstationary ideal gas flow in variable section axisymmetric channel, noting flow disturbances during sudden changes in conditions at outlet section
21 p3368 A71-40696

Spectral density functions of velocity pulsations and frequency dependent stability in turbulent plane and axisymmetric channel air flows at different Reynolds numbers
21 p3368 A71-40697

Soviet monograph on unsteady motion of compressible fluids covering acoustic and shock wave reflection from solid boundaries, impact penetration and pressure propagation
21 p3369 A71-40869

Unsteady laminar flow in polygonal ducts, calculating velocity profiles, friction factors and energy dissipation
21 p3371 A71-40994

Near-normal plane shock wave reflection from rigid impermeable wall, obtaining nonstationary flow parameters in terms of Jacobi polynomials convergent series
22 p3531 A71-42865

Ideal compressible fluid plane unsteady vortex-free selfsimilar flow, obtaining particular solutions families similar to Riemann waves and Prandtl-Meyer flows
22 p3532 A71-42866

Cavities geometry in steady or periodic supercavitating flow from light beam transmission in flow tunnel
23 p3664 A71-44005

Natural trihedrons associated with stationary or nonstationary flows in hydrodynamics and MHD, using moving reference theory
24 p3856 A71-44795

Dynamics of pipelines with nonstationary fluid flow, deriving equations for dynamic instability regions and for resonant vibration amplitudes
24 p3884 A71-45014

Unsteady state MGD equations and Alfvén velocity behavior, examining triple orthogonal curves system formed by magnetic, principal normal and binormal lines
24 p3857 A71-45186

UNSTEADY STATE

Elastoplastic unsteady thermally stressed state of square and rectangular planform bodies by calculated theory of small deformations, using strain compatibility equations with Airy stress function
02 p0323 A71-11743

Partial differential equations mixed boundary value problems with unsteadiness over part of boundary reduced to Cauchy problem
06 p0916 A71-17385

Thermal separator type refrigerating machines design, discussing gas expansion under unsteady conditions
06 p0882 A71-18310

Periodic nonstationary random process spectral representation derivation by applying Loeve harmonizability theorem
08 p1334 A71-21298

Linear theory of viscoelasticity, calculating basic relationships based on experimentally determined characteristics under unsteady test conditions
09 p1537 A71-22514

Approximate analytical formulas for free oscillations of nonstationary linear control systems using canonical transformations
10 p1643 A71-24898

Nonstationary linear systems analysis over finite time interval and graphical method for differential equation, comparing exact and approximate solutions for free oscillations
10 p1643 A71-24908

Unsteady controlled object dynamic characteristics evaluation for search-free self adjusting systems and telemetric information processing improvements
14 p2220 A71-30814

Nonlinear combustion stability problems in liquid propellant rocket engines, describing unsteady combustion response by Crocco time lag hypothesis
15 p2467 A71-31471

Unsteady random processes structural analysis application to nonlinear dynamic systems, evaluating algorithms effectiveness and improvement by self adaptive operators with finite memory
24 p3815 A71-44705

UNSWEPT WINGS

NT RECTANGULAR WINGS

NT RING WINGS

Vortex wakes behind straight and swept wings, noting formation of loops and trails close to ground
21 p3319 A71-40494

UPCONVERTERS

U PARAMETRIC FREQUENCY CONVERTERS

UPDRAFTS

U VERTICAL AIR CURRENTS

UPPER AIR

U UPPER ATMOSPHERE

UPPER ATMOSPHERE

NT D REGION

NT E REGION

NT EXOSPHERE

NT F1 REGION

NT F2 REGION

Upper atmosphere temperature, wind and diffusion measurements using artificial luminous clouds
01 p0074 A71-11088

Large fluxes of energetic neutral atomic hydrogen at 800 km preceding geomagnetic disturbance, using sounding rocket electrostatic analyzer
01 p0148 A71-11526

Upper atmospheric gas components vertical distribution by airborne photometric absorption and attenuation measurements in UV spectrum
02 p0246 A71-12118

Cosmic dust in mesosphere and upper atmosphere during weak noctilucent cloud from rocket collecting flight
02 p0246 A71-12703

Upper atmosphere micrometeorite research with sounding rockets, considering interplanetary particle flux
03 p0485 A71-13250

Thermoelectric transport properties of ionospheric electron gas above 100 km
03 p0406 A71-13301

Semiannual variation in upper atmosphere air density from satellite orbit data
03 p0407 A71-13304

High drag satellite 1968-59A orbits from optical and radar observations, obtaining rotational speed of upper atmosphere
03 p0407 A71-13305

Neutral upper atmosphere response to solar activity variations, discussing temperature, density and helium/oxygen composition
03 p0409 A71-13577

Upper atmosphere meteorological sounding facility for recording position and telemetry data from balloons, rocket payloads and meteor trails
03 p0397 A71-13673

Optical evidence of meteoric aerosols in upper atmosphere at maximum Orionids, showing double red luminosity of sky above Adi Ugrī
03 p0489 A71-13750

Jupiter details rotational periods variations, characterizing dynamic properties of atmosphere upper layers
03 p0490 A71-13940

Light scattering and polarization measurements in upper atmosphere by modulated searchlight, indicating dust layers
03 p0414 A71-14018

Upper atmosphere densities from satellite drag data, noting semiannual variations
03 p0414 A71-14021

Rocket observations of far IR radiation from upper atmosphere
03 p0415 A71-14026

Rocket-borne Na-K vapor release for upper atmosphere winds profiles and diffusion measurements by ballistic camera photography
03 p0415 A71-14027

High atmosphere X ray absorption grazing scale height variations from satellite measurement of solar X-ray flux during sunrise and sunset
03 p0480 A71-14049

Geography of upper atmospheric IR emission layers from Cosmos 65 observation
05 p0738 A71-16045

Bora-Sond rocket for upper atmosphere low cost sounding, describing propulsion system design and chemistry
05 p0816 A71-16417

Upper atmosphere electromagnetic probing - Conference, Calcutta, July 1969
05 p0739 A71-16426

Solar stimulated X ray fluorescence by photoelectric ionization in upper atmosphere, discussing effects on X ray astronomy experiments
06 p0949 A71-17268

Upper atmosphere nitric oxide density measurement by scanning UV spectrometers on Nike-Apache rockets, noting ionization consequences for D region
06 p0888 A71-17273

Geomagnetic storm on 24 March 1969, obtaining upper atmosphere emission data in middle latitude zone
06 p0894 A71-17996

High energy albedo neutron production by cosmic ray collisions, investigating balloon altitude flux variations near atmospheric top
06 p0962 A71-18179

Upper atmosphere investigation by ground based pulsed laser radar
06 p0910 A71-18719

Upper atmosphere H atoms concentration maxima and minima from topside to bottomside ionospheric electron contents ratio, using coupled continuity and thermal equations
07 p1098 A71-19031

Upper atmosphere semidiurnal pressure variations from wind data obtained by radar observation of meteors, discussing seasonal and planetary changes
07 p1151 A71-19147

Upper atmosphere hydroxyl emission mechanism, discussing absorption band, energy balance, atomic hydrogen and ozone in lower thermosphere and nitrogen oxides
08 p1277 A71-21006

Infrasonic shock wave generation in troposphere by powerful earthquakes, causing upper atmosphere density rise due to heating
08 p1278 A71-21019

Upper atmospheric research - Conference, Boulder, Colorado, August 1970
08 p1278 A71-21196

Ionization measurements of high latitude and altitude cosmic rays covering four solar maxima
08 p1355 A71-21628

Horizontal He distribution in upper atmosphere fromOGO 6 mass spectrometric data normalization for altitude by Jacchia model atmosphere
08 p1283 A71-21647

World Weather Watch plan, discussing upper air, surface and satellite observations, telecommunication and data processing
08 p1328 A71-21719

Upper air sounding systems problems, discussing aerodynamic heat transfer between temperature sensor and ambient air
08 p1330 A71-21739

Upper atmosphere wind measurement by meteor trails radar sounding, discussing seasonal variations, amplitudes and phases of harmonic components
09 p1487 A71-22302

Diurnal variation symmetry of upper atmosphere molecular oxygen concentration in terms of ozone photodissociation
09 p1435 A71-22446

Midlatitude upper atmospheric low energy proton intensity obtained from meteorological rocket data
09 p1513 A71-22579

Solar activity effects on midlatitude upper atmosphere corpuscular radiation intensity studied by rocket sounding
09 p1513 A71-22580

Upper atmospheric composition by nitrogen molecules radiative transition analysis, using laser resonance backscattering effect
09 p1436 A71-22581

Upper atmosphere IR emission model with reference to thermal excitation, chemical reactions and electron excitation
09 p1437 A71-22670

Upper atmosphere neutral component temperature measurement from thermal spread of charged particles beam
09 p1437 A71-22679

Upper atmospheric ion composition during Orionid meteor shower activity by rocket-borne RF mass spectrometer
09 p1437 A71-22680

Book on aeronomy covering earth upper atmosphere structure, tidal oscillations, gravity waves, airglow, aurora, ionospheric disturbances, electric currents and turbulence
09 p1437 A71-22778

Differential rotation in sun, giant planets and upper atmospheres of earth and Venus, attributing solar rotation to tides caused by planets
09 p1522 A71-22961

Miniature cryogenic systems for cooling IR detectors in upper atmosphere involving earth surface, airglow and OH emission measurements
09 p1545 A71-23004

Prograde and retrograde 4 day circulation in Boussinesq fluid layer by traveling thermal waves in Venus upper atmosphere
09 p1526 A71-23446

Diborane release into upper atmosphere, considering effectiveness as atmospheric tracer
09 p1489 A71-23450

Upper atmosphere semidiurnal pressure variation calculation from hydrodynamic equations similar to atmospheric tides theory
10 p1600 A71-24038

Atmospheric electric ring current in higher atmosphere with equatorial flow across magnetic lines, using dipole tensor conductivity model
10 p1603 A71-24701

Nitric oxide diurnal variation model in upper atmosphere incorporating solar flux, absorption cross sections and chemical rate constants
10 p1605 A71-24795

Optimum frequency for detection of acoustic sources in upper atmosphere as function of altitude and turbulence
10 p1642 A71-24833

Upper atmosphere statistical structure based on analysis of deviations of satellite-determined air densities from theoretical Jacchia model, noting latitudinal, seasonal and diurnal variations
10 p1607 A71-25024

Skylight scattering components from zenith for intensity/polarization variation during twilight and upper atmosphere dust sounding

10 p1607 A71-25114

Mass spectroscopy applications to neutral and ionized terrestrial upper atmosphere, lunar atmosphere and space research

11 p1726 A71-25218

Vibrational and rotational temperatures diurnal variations of upper atmospheric OH emissions from IR spectroscopic measurements, discussing earth shadow effects on mean intensity

11 p1753 A71-25541

Upper atmosphere neutral temperature profiles in auroral zone, using aluminum and barium oxide clouds fluorescent emission

11 p1753 A71-25547

Oxygen atom deficiency and very low exospheric temperature in Mars and Venus upper atmospheres, considering photochemical processes and molecular diffusion

11 p1826 A71-25723

International coordinated measurements of solar activity geophysical effects in upper atmosphere, discussing synchronized observations of Cosmos 261 satellite and ground based ionospheric station network

11 p1816 A71-25762

Upper atmospheric molecular and atomic N and O diurnal variations correlated to atmospheric heating as function of solar UV radiation from sounding rocket data

11 p1757 A71-25775

Thermal fluctuations in earth upper atmosphere, related to satellite deceleration and X ray solar radiation changes by autocorrelation and cross correlation analyses

11 p1817 A71-25822

Neutral H concentration in upper atmosphere during solar minimum, using ion thermal energies from rocket and satellite mass spectrometric, radio and proton whistler measurements

12 p1898 A71-26637

Latitude dependence of upper atmosphere corpuscular radiation intensity, analyzing sounding data from Indian Ocean area

12 p1947 A71-26645

Solar activity and geomagnetic disturbance effects on upper atmosphere density from ATS 2 satellite orbit observations

12 p1899 A71-26886

Pitch angle distribution effects of auroral electrojet on scattering and absorption of fast precipitated electrons in upper atmosphere, using computerized Monte Carlo technique

13 p2119 A71-27794

Upper atmospheric winds measurements at 160 and 275 km, finding upward motion difficult to relate to intrinsic atmospheric motions

13 p2056 A71-27930

Soviet papers on upper atmosphere physics covering thermosphere, dynamic processes and radiative energy transport in stratosphere and mesosphere, and ionospheric parameters radio measurement

13 p2056 A71-28017

Upper atmosphere neutral components temperature differences estimates from gas hydrodynamic equations solution by disturbances method

13 p2057 A71-28019

Upper atmosphere radiative energy transport equation derivation with allowance for deviations from Kirchhoff law, examining fluorescence mechanism and effect on radiative heating

13 p2057 A71-28025

Venus upper atmosphere retrograde circulation correlation with solar couple effect on thermal semidiurnal atmospheric tide

13 p2134 A71-28286

Scott effect observation of superrotation of upper atmosphere, relating temperature gradient, magnetic field and gas rotation

13 p2063 A71-29095

Monograph on persistent radio meteor echoes fading relation to upper atmosphere wind structure

14 p2192 A71-29579

Spectral lines of O I/S/ generated by oxygen molecule dissociative recombination in upper atmosphere observed in nightglow at geomagnetic equator with Fabry-Perot spectrometer

14 p2229 A71-29663

Upper atmosphere temperature measurements using red emission Doppler contour width data of atomic oxygen at 6300 Å

14 p2229 A71-29673

Upper atmosphere aeronomy historical review, considering meteor trails, radio waves, auroral photography, terrestrial magnetic field and spectroscopy

14 p2229 A71-29704

Low energy electron precipitation effects on upper atmosphere based on polar cap and auroral oval electron spectrum comparison

14 p2300 A71-30035

Meteorological research on upper atmosphere energy sinks/sources, composition, density, turbulence, winds and thermal structure

14 p2236 A71-30494

Upper atmosphere exploration by San Marco 2 satellite, studying diurnal density variations and effects of large geomagnetic storms

14 p2236 A71-30817

Nimbus 4 Interrogation Recording and Location System meteorological experiment for tropical region upper atmosphere information

14 p2200 A71-30917

Solar UV radiation atmospheric absorption during IQSY by ion chamber measurements, considering upper atmosphere oxygen concentration

15 p2396 A71-31616

Summertime meridional wind component profile construction and hydrodynamic model for semidiurnal fluctuations in upper atmosphere

15 p2399 A71-31962

Equatorial electrojet as supplementary heat source for tropical region upper atmosphere based on thermal energy release calculation

15 p2399 A71-31964

Upper atmosphere night sky luminescence observations during IQSY, discussing correlations between night airglow, solar activity, interstellar dust disturbances and meteor phenomena

15 p2400 A71-31987

Dispersal of jet aircraft exhaust emissions near airports and of smoke trails in upper atmosphere, assessing pollutant levels near large urban airports

15 p2349 A71-32244

Spatially periodic static field mass spectrometers for upper atmosphere composition measurements on board satellite and sounding rocket

15 p2400 A71-32350

Upper atmosphere temperatures from barium oxide fluorescence emissions in ion cloud rocket experiments, studying thermal response to geomagnetic disturbances

16 p2562 A71-32808

Atmospheric density measurements at 70 to 115 km altitude range from rocket soundings with accelerometer instrumented inflatable spheres

16 p2562 A71-33066

Spatial and angular distribution of upper atmospheric IR emission layers from Cosmos 65 observation

16 p2563 A71-33449

Objective subsynoptic upper level analysis optimizing smaller scale radiosonde data over U.S.

16 p2604 A71-33533

Upper atmosphere atomic hydrogen H sub alpha emission, correlating intensity and hydroxyl vibration temperature

16 p2564 A71-33665

Upper atmosphere density fluctuations associated with solar activity and local time values, using Cosmos 14 satellite drag data

16 p2564 A71-33666

Upper atmosphere He, Ne, Na and K atoms collisions with molecular oxygen, determining ejected electron energy during fast Na, K, Rb and Cs ionization for meteor phenomena modeling

16 p2639 A71-33695

Joule heating and winds in upper atmosphere due to geomagnetic disturbances at 140 km altitude, deriving set of nonlinear partial differential equations

16 p2564 A71-33726

Neutral upper atmosphere properties, discussing temperature, density and wind variations during disturbed conditions associated with geomagnetic storms

16 p2565 A71-33727

Upper atmosphere heating at high latitudes, analyzing air density variations from Molniya 1K satellite observations over 2 year period

16 p2565 A71-33740

Upper atmospheric composition and density variations with latitude and local time, using OV3-6 satellite measurements

16 p2566 A71-33756

Mass spectroscopy of upper atmosphere neutral composition at equatorial, middle and polar latitudes from meteorological rockets

16 p2566 A71-33758

Laser radar investigation of upper atmosphere dust layer, obtaining evidence for Silverberg cometary micrometeoroid shower hypothesis

16 p2641 A71-33760

Corpuscular flux intensities in upper atmosphere from meteorological rocket measurements in polar arctic region, discussing altitude-time dependence

16 p2627 A71-33777

Upper atmospheric winds viscous damping energy deposition calculation for midlatitude profiles

16 p2568 A71-33789

Upper atmosphere parameters determination by simultaneous positional and photometric satellite observations

16 p2568 A71-33793

Upper atmosphere neutral species latitudinal and seasonal distributions, using turbulent transport coefficients and photochemical reaction rate constants in finite difference solution

16 p2569 A71-33804

Upper atmosphere rotational speed variations from measurements of orbital inclination of satellites

16 p2569 A71-33807

Physical conditions leading to deuterium enhancement in earth upper atmosphere as function of the mopause temperature and eddy diffusion

16 p2569 A71-33808

Upper atmospheric neutral composition diurnal variations as function of altitude, local time and solar activity

16 p2570 A71-33809

Upper atmosphere density determination from Cosmos satellite deceleration data, allowing for diurnal and semiannual variations and solar radio emission intensity effects

16 p2571 A71-33810

Swiss space research, surveying international cooperative scientific activity relative to upper atmosphere satellite geodesy, solar wind, lunar sample analysis, IR and UV astronomy and celestial mechanics

16 p2665 A71-33811

Soviet report to COSPAR on upper atmosphere astronomical science including Soyuz spacecraft, lunar sample recovery and surface vehicle delivery

16 p2666 A71-33804

Secondary electrons and photons energy spectra and depth dependence in upper atmosphere from numerical solution of one dimensional transport equations

16 p2628 A71-33929

Bibliography on upper atmosphere hydrogen covering Lyman alpha and beta and Balmer alpha measurements, non-Maxwellian distribution, diurnal variations and oxygen evolution

17 p2732 A71-34464

Airglow research review and bibliography covering past four years observations of nightglow, twilight, dayglow and metals in upper atmosphere

17 p2732 A71-34464

Upper atmosphere density observation by a switched ruby laser radar

17 p2753 A71-34740

Upper atmosphere mean temperature, pressure, density and wind distributions as functions of altitude, season and latitude, discussing planetary, infrasonic and internal gravity wave effects

17 p2735 A71-35230

Vibrational temperature of nitric oxide in upper atmosphere, computing collisional, radiative and chemiluminescent excitation rates

18 p2910 A71-35840

Earth upper atmosphere superrotation due to zonally averaged magnetospheric electric fields

18 p2911 A71-35999

Upper atmosphere dust scattering indicatrix from twilight sky brightness at solar vertical, determining total directed scattering coefficient

19 p3132 A71-37390

Artificial earth satellite orbital decay rate measurement for upper atmosphere density data, using combined directional observations and orbit data

19 p3048 A71-37390

Upper atmosphere hydroxyl emission nocturnal average vibrational temperature correlation with molecular oxygen emission intensities

19 p3049 A71-37400

Earth upper atmosphere outgoing thermal radiation radiance calculation in near IR spectrum

19 p3054 A71-37960

Whistlers as diagnostic tools in space plasma, measuring electron densities at large distances in earth's outer atmosphere within magnetosphere

19 p3116 A71-38240

Upper atmosphere supplementary electron flux data following geomagnetic disturbance from high altitude balloon experiments

19 p3129 A71-38350

Vibrationally excited oxygen molecules formation and decomposition in upper atmosphere, calculating day and night equilibrium concentrations

19 p3057 A71-38370

Soviet papers on physical processes in upper atmosphere covering ion composition, electron concentration and temperature, luminescent clouds, sporadic E layer, etc

19 p3060 A71-38627

Liquid carbon tetrachloride artificial luminescent cloud formation in upper atmosphere, considering injection conditions for rapid vaporization and required concentration

19 p3061 A71-38633

Seasonal, latitudinal and diurnal variations of upper atmospheric structural parameters including density and temperature

19 p3061 A71-38656

Upper atmosphere hydroxyl emission mechanism, discussing absorption band, energy balance, atomic hydrogen and ozone in lower thermosphere and nitrogen oxides

20 p3218 A71-39586

Sunlight scattering by dust in upper atmosphere from primary twilight intensities investigations

20 p3219 A71-39647

Sounding rockets sampling of cosmic dust in upper atmosphere during and after Zeta Perseid and Arietid meteor showers

20 p3299 A71-39651

Neutral upper atmosphere observations, discussing lower thermospheric density and composition diurnal, seasonal and latitudinal variations and solar activity effects

20 p3220 A71-39690

Upper atmospheric anomalous molecular oxygen distribution, discussing turbulent theory with autocorrelation of density fluctuations

20 p3222 A71-39701

Upper atmospheric temperature and soft solar X-ray time scale fluctuation data, using satellite drag observations and statistical analysis

20 p3280 A71-39705

Diurnal and semiannual variations in upper atmosphere density from Cosmos satellite drag observations, noting calculation systematic errors

20 p3223 A71-39707

Long term upper atmosphere density variations correlated with solar flux, using satellite observations

20 p3223 A71-39708

Upper atmosphere density variations and time lag with respect to geomagnetic disturbances, using satellite drag measurements

20 p3223 A71-39709

Semiannual upper atmosphere density variations near solar maximum from satellite drag data, relating height amplitude profile with exospheric temperatures

20 p3223 A71-39710

Solar radiation effects on upper atmosphere soft electron flux and energy spectrum during day and night

20 p3281 A71-39724

Rapid retrograde rotation of Y shaped cloud formations in Venus upper atmosphere, discussing correlation with slow ground rotation

21 p3441 A71-40106

Upper atmospheric density numerical calculation from draconite period by Perlo program using satellite observation near celestial equator

21 p3374 A71-40655

International coordinated measurements of solar activity geophysical effects in upper atmosphere, discussing synchronized observations of Cosmos 261 satellite and ground based ionospheric station network

22 p3591 A71-41530

Upper atmospheric molecular and atomic nitrogen and oxygen diurnal variations correlated to atmospheric heating as function of solar UV radiation from sounding rocket data

22 p3532 A71-41543

Upper atmospheric primary cosmic ray layer ionization, considering secondary particles, X rays, neutrons, tritons and mesons as ionizing agents

22 p3591 A71-41647

Heat balance effects of acousto-gravitational waves in upper atmosphere, concerning infrasonics from earthquakes, polar auroral arcs and magnetic storms

22 p3533 A71-41656

German Aeros satellite for upper atmosphere aeronomy research, describing objectives regarding atmospheric composition and density

22 p3610 A71-42008

Upper atmospheric temperature and density measurements from artificial cloud observations

23 p3667 A71-43139

Upper atmosphere rotation rate decrease at altitudes above 350 km, determining zonal wind variations by satellite orbits analysis from Hewitt camera observations

23 p3667 A71-43140

Search for upper atmosphere MgO content, using modified Ebert spectrometer with photomultiplier detection to measure twilight excited scattered and resonance radiation

23 p3670 A71-43191

Mars and Venus upper atmospheric electron distribution compared with theoretical ionospheric models, considering solar wind as ionization source

23 p3736 A71-43342

Solar soft X-rays scattering in upper atmosphere, providing background against cosmic X rays

23 p3721 A71-43363

Hydroxyl emission of upper atmosphere, considering atomic hydrogen and ozone near thermosphere base

23 p3673 A71-43982

Venus upper atmospheric UV spectra from rocket-borne telescope spectrophotometer, considering O I and H I emission features

24 p3872 A71-44919

Upper atmosphere minor component distribution rearrangement, investigating transition time to diffusion equilibrium

24 p3823 A71-45031

UPPER IONOSPHERE

NT F REGION

NT F1 REGION

NT F2 REGION

Upper ionosphere electron concentration enhancement in polar cap from satellite probe measurements

03 p0408 A71-13385

Topside ionosphere O-H ions transition level altitude variation due to atmosphere winds

03 p0416 A71-14030

Satellite topside sounders oblique echoes, investigating upper hybrid resonance with WKB technique

03 p0420 A71-14531

Topside ionosphere plasma resonance due to electrostatic wave echoes, comparing electron temperature dependent beat pattern with ray tracing calculations

03 p0421 A71-14540

Average electron density profiles for quiet and disturbed topside ionosphere at high latitudes, tabulating profile numbers

05 p0743 A71-17005

Solar geomagnetic seasonal ionization control of upper ionosphere longitudinal composition variations from polar satellite observations

10 p1602 A71-24555

Far ionospheric propagation of round-the-world echo signals from Moscow to Antarctic station Molodezhnaia and back to Moscow

11 p1731 A71-25773

Midlatitude topside ionospheric electron density mean diurnal and seasonal variations from Alouette 1 satellite observation

11 p1757 A71-25784

N/z/ profiles of upper ionosphere from Alouette 1 vertical sounding data, proposing model for ionosphere shape

11 p1758 A71-25786

Multicomponent whistler spectra due to discrete ionization inhomogeneities and complex structure nonuniformities forming diffuse whistlers in outer ionosphere

11 p1758 A71-25789

Sunrise behavior of midlatitude topside ionosphere at low sunspot numbers from Alouette 1 electron density and plasma scale height profiles

13 p2055 A71-27920

Flight characteristics of ion engine powered automatic laboratories in upper ionosphere

13 p2146 A71-29210

High latitude upper ionospheric structures and plasma flow in magnetosphere from Alouette/ISIS topside sounders, noting solar UV and particle ionization sources

14 p2234 A71-30042

Simultaneous ionospheric electron density measurements from Isis satellite topside and incoherent scatter soundings

15 p2394 A71-31428

Topside ionosphere structure in high latitudes, discussing electron density profile, corpuscular radiation ionizing effects, polar peak and trough

15 p2400 A71-32349

Faraday rotation of satellite signals across transverse region, considering sudden jumps at transverse point in lower and topside ionosphere

16 p2544 A71-33959

Upper ionosphere electron density scale height data, noting conjugate point sunrise heating effects from Alouette 1 data

17 p2731 A71-34313

Upper ionospheric plasma measurements by gyro plasma probe equipped Lambda rocket, deducing electron density profile from plasma resonance effects

20 p3224 A71-39721

Far ionospheric propagation of round-the-world echo signals from Moscow to Antarctic station Molodezhnaia and back to Moscow

22 p3509 A71-41541

Midlatitude topside ionospheric electron density mean diurnal and seasonal variations from Alouette 1 satellite observation

22 p3532 A71-41552

Ionization profiles of upper ionosphere from Alouette 1 vertical sounding data, proposing model for ionosphere shape

22 p3532 A71-41554

Multicomponent whistler spectra due to discrete ionization inhomogeneities and complex structure nonuniformities forming diffuse whistlers in upper ionosphere

22 p3532 A71-41557

UPWASH

Upwash interference on two dimensional jet flap wing in slotted wall tunnel, using small disturbance theory

02 p0187 A71-12690

Lifting line equation inversion for twisted wings of elliptic planform with arbitrary spanwise upwash

22 p3481 A71-42838

URACIL

Possible prebiotic synthesis of thymine by heating uracil, paraformaldehyde and hydrazine in ammoniacal solution for three days at 70 C

18 p2855 A71-36231

URANIUM

NT URANIUM ISOTOPES

NT URANIUM 235

K-U abundance systematics in Apollo 11 and 12 lunar rock suites and earth crust

06 p0968 A71-17961

Apollo 11 and 12 lunar samples compared with deep earth rocks, noting potassium-uranium ratio

14 p2318 A71-31126

Be, U and W shear strength measurements, detailing strain, strain rate and pressure effects

[ASME PAPER 70-WA/PT-2] 15 p2434 A71-32260

Uranium content correction for Ivory Coast microtektites, discussing effects on age values and correlation between tektite falls, geomagnetic reversals and faunal changes

20 p3292 A71-39405

Fission track analyses of uranium enriched phases in Apollo 11 and 12 basaltic rocks

23 p3739 A71-43615

Lexan plastic fission track analysis of uranium distribution in glassy residuum in Apollo 11 rock 10017

23 p3739 A71-43616

Lunar rocks 12040 and 12013 and anorthositic, determining U-Th distributions with induced fission track maps

23 p3752 A71-43712

URANIUM CARBIDES

High temperature neutron irradiation properties of uranium oxides, carbides and nitrides coated with tungsten-rhenium

02 p0296 A71-12246

Zirconium uranium carbide and zirconium hafnium carbide thermodynamic properties, using time-of-flight mass spectrometer

[ECS PAPER 120] 20 p3252 A71-39555

URANIUM COMPOUNDS

NT URANIUM CARBIDES

NT URANIUM OXIDES

Materials technology of Ta-W-Hf clad uranium mononitride fuel for lithium cooled compact fast space power reactor, including irradiation tests

16 p2606 A71-33254

URANIUM ISOTOPES

NT URANIUM 235

U-Pb and Th-Pb age discrepancy in lunar dust, proposing Rn-222 emanation in decay chains

14 p2307 A71-29733

Neutron activation analysis of Apollo 11 lunar fines, determining Pb 204, U, Bi and Tl contents

23 p3753 A71-43715

Isotopic abundances and composition of U and Th in Apollo 12 soil and breccia samples, using mass spectroscopy

23 p3753 A71-43716

Isotopic composition of U and Th in Apollo 12 lunar rock samples from mass and alpha spectrometry

23 p3753 A71-43717

URANIUM OXIDES

Kr 85 disposition following Mo-uranium oxide cermet fuels irradiation in test chamber

02 p0296 A71-12240

High temperature neutron irradiation properties of uranium oxides, carbides and nitrides coated with tungsten-rhenium

02 p0296 A71-12246

Out-of-pile experiment for measuring uranium dioxide fuel redistribution rates, determining vent hole plugging time and thermal cycling

02 p0296 A71-12247

High temperature specific heat of refractory molybdenum and uranium dioxide

04 p0612 A71-14959

URANIUM 235

Thermionic reactor experiment design to evaluate U-235 fueled fast spectrum core dynamic and steady state characteristics, discussing system features

11 p1710 A71-25868

URANUS [PLANET]

Uranus physically self consistent atmosphere model based on spectroscopic, photometric and radio observational data

07 p1198 A71-19828

Uranus radio emission model, considering presence of gaseous ammonia at saturation pressure in atmosphere

09 p1519 A71-22526

Uranus atmospheric molecular hydrogen abundance from pressure induced overtone spectra, using quadrupole moment and polarizability matrix elements theoretical values

11 p1827 A71-25731

Uranus radio emission measurements at 8.22 mm wavelength, noting brightness temperature and atmospheric properties

12 p1965 A71-27226

Magnetospheric tail models for Uranus type planet with viscous and magnetic coupling compared to geomagnetic configuration

14 p2305 A71-29664

Uranus and Neptune microwave emission spectra and atmospheric temperatures, comparing with Jupiter and Mars

15 p2490 A71-32410

Uranus radio emission measurement at 8.22 mm, obtaining brightness temperature

15 p2490 A71-32412

Uranus radio emission model, indicating presence of gaseous ammonia at saturation pressure

17 p2807 A71-35501

Mars, Uranus and Jupiter observations with Sao Paulo Observatory Danjon astrolabe, presenting east and west transits right ascension and declination tables

18 p2961 A71-35943

Uranus radio emission measurements at 8.22 mm wavelength, noting brightness temperature and atmospheric properties 19 p3132 A71-37378

Narrow band and UVB photoelectric photometry of Uranus geometric albedo and magnitude at unit distance as functions of wavelength 21 p3443 A71-40191

Quantitative equivalence model in planet-satellite formation within Jupiter and Uranus systems 22 p3604 A71-42191

URBAN DEVELOPMENT

Airport system planning for natural and urban environment compatibility 08 p1380 A71-21835

Urban housing environment data acquisition from remote sensor imagery, stressing rapid surveys and data timeless attribute 09 p1439 A71-23213

Geographic urban information and change detection systems with remote sensing inputs, discussing data storage and retrieval 09 p1439 A71-23214

Automatic pattern recognition of urban development changes from aerial photographs, using computer program and nonlinear registration technique for cell pairs partitioning 17 p2711 A71-35043

Urban environmental quality analysis using color IR aerial photography, considering film sensitivity and haze penetration 18 p2911 A71-36062

Automated pattern recognition for urban texture and land use assessment by aerial photographs, using digitally scanned optical Fourier transforms 18 p2912 A71-36063

URBAN PLANNING

Community actions for jet aircraft noise reduction, discussing noise environments, nationwide goals, decision making and economic incentives 15 p2516 A71-32249

Site selection and area planning for major airport, illustrating Montreal and Toronto systems [CASI PAPER 72/2] 19 p3040 A71-37593

URBAN TRANSPORTATION

NT RAIL TRANSPORTATION

Aladin 2 interurban Stoll transport design with blown wings and jet deflection by wing flaps, emphasizing engine noise reduction 01 p0005 A71-10749

V/STOL short haul transport systems, discussing interurban applications, all-weather operation, operating costs, noise and atmospheric pollution 03 p0523 A71-13565

Intercity V/STOL air transportation system, discussing traffic movements, cost and terminals 03 p0454 A71-13566

VTOL aircraft IFR airworthiness, noting necessity of higher safety levels for metropolitan air transit systems 04 p0533 A71-15426

Public-use ground level and rooftop helicopter and STOL aircraft landing facilities for city and suburban traffic 04 p0567 A71-15442

Optimum flight paths for V/STOL aircraft operating in short haul transportation near city centers 04 p0624 A71-15443

Urban transit and ATC vehicle identification and position determination system, considering surface and airborne traffic real time information communications 08 p1331 A71-21169

Aircraft capabilities in intraurban transportation for Detroit metropolitan area, considering vehicle design, fleet size, cost and terminal location [AIAA PAPER 71-504] 14 p2172 A71-29548

Helicopter systems operations in, around and between major metropolitan areas, considering performance of New York Airways [AIAA PAPER 71-507] 14 p2339 A71-29549

Integrated short-haul interurban transportation system, considering combination of conventional jet aircraft, STOL aircraft and high-speed ground transportation [AIAA PAPER 71-508] 14 p2221 A71-29550

Aladin II four-jet engine STOL intercity transport aircraft, noting low noise characteristics and passenger capacity 15 p2347 A71-31412

Operating costs and runway lengths for V/STOL in city and suburban short haul air transportation 18 p2987 A71-36347

Monograph on satellite airport system modeling for large metropolitan areas covering systems analysis methodology and computer algorithms for optimization [SU-TR-71-1] 21 p3365 A71-40799

Future transportation technology impact, considering system design evaluation criteria and civil aviation and urban mass transit systems contributions [AIAA PAPER 71-1010] 24 p3892 A71-44594

UREAS

NT THIURONIUM

Reactivity measurements of protective agent selenium toward primary water radiolysis radicals 07 p1033 A71-18934

Urea-inorganic phosphate mixtures as prebiotic nucleoside phosphorylating agents 07 p1055 A71-19544

Urea hydrolysis reaction rates by urease at low water activity, noting use for Mars surface bioassay 22 p3487 A71-42226

URETHANES

Photoelastic compensator of urethane rubber, describing construction and applications 01 p0082 A71-11009

High peel strength epoxy and urethane adhesives for aircraft bonding, discussing high temperature curing and honeycomb panel repair 10 p1630 A71-24064

Coupling agents in urethane and epoxy adhesives, discussing lap shear and T-peel tests on mild and stainless steels, Al and glass cloth substrates 10 p1616 A71-24108

Shelf stable two component urethane adhesives with prepolymer reactive silane coupling agents for high peel strength retention in humid environment 14 p2261 A71-29637

URIDYLIC ACID

Template catalysis of acetyl transfer reactions, showing triple helices formation by polyuridylic acid with adenoside derivatives 13 p2026 A71-29479

URINALYSIS

Pilot nervous-emotional state during flight conditions determined from uropesin excreted in urine 05 p0711 A71-17028

Excretion patterns of air traffic controllers for stress appraisal, using urinalysis 08 p1246 A71-20811

Bone tissue optical density and blood serum and urine calcium content of Soyuz 9 crew members during and after flight 09 p1389 A71-22201

Alloisoleucine configuration in blood serum of maple syrup urine disease patients, using gas liquid chromatography 09 p1403 A71-22477

Urinary metabolites relationship to fatigue, considering excretion of proteins, electrolytes, simple organic compounds and hormones 17 p2679 A71-34357

Sympathetic nervous system in short term adaptation to cold, observing oxygen consumption, urinary noradrenaline proportion and excretion 17 p2681 A71-34698

Urinary protein excretion rates in high altitude inhabitants, showing polycythemia effect on creatinine clearances levels 19 p3009 A71-38561

Biochemical measurements of human urine and blood changes during simulated oxygen-helium dives to 1500 feet 21 p3331 A71-40353

Antidiuretic action of chlorpropamide in mammalian kidney, considering intrarenal infusions effect on urinary concentration, free water clearance, glomerular filtration and sodium excretion 22 p3486 A71-41939

Water-salt metabolism in human blood and urine under high temperature conditions after residence in different climatic zone 24 p3794 A71-44414

URINATION

Dog uropesin excretion dynamics under extremal flight conditions, detailing hypoxia, high temperature radical accelerations and impact G forces effects 15 p2358 A71-31322

Chronic centrifugation effects on food intake and urine output in mice, considering water intake and growth rate 20 p3186 A71-38984

URINE

Glucocorticoid metabolite excretion with urine in healthy people as function of age and sex 06 p0858 A71-18727

Physiological and biochemical characterization of natriuretic hormone in human urine and blood plasma 13 p2013 A71-28952

Automated self sterilizing breadboard unit for potable water reclamation from urine by electrolysis-electrodialysis for long term space missions [ASME PAPER 71-AV-11] 18 p2866 A71-36378

Radiation damage diagnosis in humans, investigating free amino acid excretion with urine by paper chromatography method 22 p3495 A71-42736

Preservative phenol derivative effects on toxic gas evolution from stored urine in sealed vessels 22 p3506 A71-42808

Urine preservatives for urine water recovery system, noting ammonia and organic compound contents in condensate 22 p3506 A71-42809

Decontaminating methods for water regenerated from urine under space flight conditions by filtering water condensate through sorbents 22 p3506 A71-42815

Urine conservation in spacecraft cabin sanitation facilities by phenol-containing preparation emphasizing PNF method for long period operation 22 p3507 A71-42812

UROLOGY

Flight concomitant pathogenetic effects on urinary tract conditions, noting kidney descent, inflammatory episodes and calculosis 10 p1566 A71-24676

Animal urinary bladder mechanical properties from controlled stretch tests, identifying viscoelastic elastostatic and creep elements 14 p2186 A71-30184

Dog uropesin excretion dynamics under extremal flight conditions, detailing hypoxia, high temperature radical accelerations and impact G forces effects 15 p2358 A71-31322

USA [UNITED STATES]

U UNITED STATES OF AMERICA

USNS KINGSPORT

U SATELLITE COMMUNICATIONS SHIPS

UTERUS

Female aircrews under moderate hypoxia, noting uterine rheography modification 06 p0860 A71-18190

UTILITIES

Computer plotting of living units, business and industrial plant location for public utilities planning 08 p1280 A71-21240

UTILITY AIRCRAFT

NT BO-105 HELICOPTER

NT DHC 4 AIRCRAFT

NT UH-1 HELICOPTER

Agricultural information and advisory services: utilizing remote sensing, computer sciences, research programs, educational involvement, satellites and aircraft 06 p1010 A71-18408

Worldwide remote sensing with satellites, high flying aircraft and computer data processing, discussing application in less developed countries 06 p0896 A71-18406

Transavia Airtruk agricultural aircraft, discussing efficiency, work capacity, economics, configuration and performance 08 p1230 A71-21226

Air-photo interpretation to inventory kind of cattle-raising operation practiced on farms of southern Ontario 08 p1282 A71-21437

Commercial business and utility aircraft chemically oxygen generators to satisfy FAA requirements: discussing weight, size and maintenance savings and increased safety [SAE PAPER 710390] 10 p1558 A71-24256

UTILITY AIRCRAFT

NT PIPER AIRCRAFT

UTILIZATION

NT WASTE UTILIZATION

V

V BAND

U EXTREMELY HIGH FREQUENCIES

V GROOVES

V shaped notches drag coefficients behavior in transonic regime, observing inviscid-viscid interaction controlling flow separation and reattachment 21 p3323 A71-40954

V/STOL AIRCRAFT

NT ALOUETTE HELICOPTERS

NT AUTOGYROS

NT BO-105 HELICOPTER

NT CH-3 HELICOPTER

NT CH-46 HELICOPTER

NT CH-47 HELICOPTER

NT CH-54 HELICOPTER

NT COMPOUND HELICOPTERS

NT DHC 4 AIRCRAFT

NT DO-31 AIRCRAFT

NT FLYING PLATFORMS

NT H-53 HELICOPTER

NT H-56 HELICOPTER

NT HELICOPTERS

NT MILITARY HELICOPTERS

NT OH-6 HELICOPTER

NT RIGID ROTOR HELICOPTERS

NT ROTARY WING AIRCRAFT

NT SHORT TAKEOFF AIRCRAFT

NT UH-1 HELICOPTER

NT VERTICAL TAKEOFF AIRCRAFT

Short haul air transportation technological factors for VTOL, STOL, CTOL and light aircraft, considering operating costs, passenger service and environment impact [AIAA PAPER 70-1287] 02 p0188 A71-11700

V/STOL short haul transport systems, discussing interurban applications, all-weather operation, operating costs, noise and atmospheric pollution 03 p0523 A71-13565

Intercity V/STOL air transportation system, discussing traffic movements, cost and terminals 03 p0454 A71-13566

- V/STOL services integration into UK air traffic system 03 p0454 A71-13567
- Intercity V/STOL aircraft transport system, solving congestion problems through all weather superiority, low noise level and separate ATC 03 p0347 A71-13571
- V/STOL aircraft operations, considering terminals, landing and approach aids, air traffic, noise and pollution control, performance, airworthiness regulations and licensing 03 p0347 A71-13572
- Terminal area operations of V/STOL aircraft, considering approaches, approach speeds, wind and velocity effects and noise 03 p0347 A71-13573
- V/STOL aircraft in civil air transportation, discussing safety, reliability, maintainability and propulsion system concepts 03 p0348 A71-13576
- V/STOL aircraft wing-propeller interaction, using mean flow deflection angle in lift and drag characteristics prediction 04 p0526 A71-14988
- Direct lift V/STOL transport aircraft design, discussing environmental factors in relation to noise, air pollution, jet interference and safety 04 p0530 A71-15403
- Helicopter and V/STOL aircraft external noise and downwash measurements during simulated jungle rescue mission 04 p0531 A71-15409
- Optimum flight paths for V/STOL aircraft operating in short haul transportation near city centers 04 p0624 A71-15443
- V/STOL spray generation tests concerning pilot visibility impairment in low altitude overwater hover 04 p0534 A71-15444
- V/STOL aircraft visual aids flight evaluation concerning minimum landing area operations 04 p0534 A71-15445
- Airborne variable stability helicopter flight simulator for V/STOL aircraft design 05 p0697 A71-16954
- Hovering and low speed flight capabilities of tilt wing VTOL aircraft in terminal area under near-zero visibility instrument landing conditions [AIAA PAPER 71-7] 06 p0847 A71-18481
- V/STOL microwave scanning beam approach and landing system, describing ground and airborne station equipment and operation 08 p1332 A71-21680
- Wind tunnel boundary interference on V/STOL model calculated in test section with solid vertical and slotted horizontal walls, using image method and Fourier transforms [AIAA PAPER 70-575] 08 p1229 A71-22029
- V/STOL aircraft automatic flight controls and electronic head down displays, discussing handling qualities, lift effectiveness and autostabilization 10 p1554 A71-23944
- Commercial V/STOL aircraft area navigation system requirements, discussing airborne computer, flight plan data storage and control subsystems and horizontal orientation display 10 p1639 A71-24150
- V/STOL component of unified transportation system, discussing transportation modes, airport locations, noise reduction, cost factors, etc 10 p1556 A71-24274
- V/STOL civil aircraft, considering rotor lift and variable sweep wings 10 p1556 A71-24850
- Convertible fan/shaft engine for V/STOL tactical and transport aircraft, detailing mechanical arrangement, design and performance 11 p1813 A71-26054
- Hydraulically powered duplex input servos for flight control system of VFW-Fokker V/STOL fighter aircraft 12 p1867 A71-26884
- Prop-fan propulsion system for V/STOL short haul transport aircraft, discussing performance, noise and weight characteristics [SAE PAPER 710471] 13 p2115 A71-28338
- V/STOL and supersonic commercial aircraft developments, comparing man and machine performance as information processing systems for aircraft control and navigation 13 p2018 A71-28486
- Commercial V/STOL and jet VTOL transport, discussing Do-31 test results, landing approach, air traffic control automation and electronic control 13 p1997 A71-29131
- V/STOL aircraft instruments, deck display and automatic flight controls for takeoff and landing operation 13 p2098 A71-29132
- V/STOL aircraft gust effects prediction with mathematical models based on nonlinear hybrid simulation at takeoff and landing altitudes 14 p2173 A71-29775
- V/STOL aircraft flight path and attitude controls in turbulence, discussing design based on state variable methods of control theory 14 p2173 A71-29776
- Civil aviation customer /operator, passenger and community/ needs, describing STOL and V/STOL aircraft 14 p2340 A71-30162
- V/STOL propulsion units lift ratings based on aircraft system requirements [SAE PAPER 710471] 14 p2176 A71-30537
- Head- or helmet-mounted display/control system in V/STOL aircraft for pilot workload and training reduction [AHS PREPRINT 532] 14 p2189 A71-31093
- Handling qualities of V/STOL research vehicles during steep terminal area approaches, discussing powered lift fan VTOL aircraft limitations and instrument landing approach [AHS PREPRINT 544] 14 p2179 A71-31101
- Composite materials application to V/STOL prop/rotors, determining material properties parametric effect on frequencies and weight by Southwell coefficients [AHS PREPRINT 554] 14 p2180 A71-31106
- V/STOL lift fan airliner project HS 141 for intercity transport, describing features, weight and performance data, noise characteristics and reliability criteria 15 p2348 A71-31413
- Propeller blade structures for high speed tilt wing turboprop V/STOL aircraft, considering materials selection, weight control, cyclic pitch control, noise reduction, etc [DGLR 71-018] 15 p2350 A71-32785
- Optimum vertical surface configuration for STOL transports, considering structural weight and performance requirements [AIAA PAPER 71-769] 16 p2524 A71-34006
- Harrier aircraft development from flight test viewpoint, discussing conventional flight envelope problems caused by V/STOL concept imposed constraints [AIAA PAPER 71-773] 16 p2524 A71-34009
- Civil V/STOL aircraft projects, discussing design, lift fan engines, weights, flight performance, noise levels, safety and comfort standards 16 p2525 A71-34101
- V/STOL aircraft with vectored thrust propulsion systems, noting weight and center of gravity-lift-thrust relationship changes effect on performance [SAWE PAPER 894] 17 p2676 A71-35817
- Hybrid V/STOL jet lift aircraft design, examining wing area-lift engine bypass ratios relation [AIAA PAPER 71-767] 18 p2850 A71-36273
- Operating costs and runway lengths for V/STOL in city and suburban short haul air transportation 18 p2987 A71-36347
- V/STOL developments at Hawker Siddeley Aviation, noting circulation controlled rotor concept and HS-141 aircraft [CASI PAPER 72/18] 19 p2997 A71-37605
- V/STOL aircraft airworthiness certification, considering standards developed by FAA in cooperation with industry [CASI PAPER 72/21] 19 p2997 A71-37607
- Civil V/STOL aircraft engines requirements, considering noise reduction, thrust, multifunction propulsion/blowing, lift and booster fan engines [CASI PAPER 72/19] 19 p3122 A71-38021
- Aircraft noise propagation in city streets due to intertown V/STOL and helicopter ports, using small scale models 20 p3178 A71-39264
- V/STOL aircraft lift fan aerodynamics, discussing optimum fan pressure ratios, augmentation ratio, noise constraints, wing loading and fan configurations [AIAA PAPER 71-981] 24 p3791 A71-44577
- AIAA members comments on STOL, VTOL and V/STOL aircraft merits and developments [AIAA PAPER 71-1015] 24 p3791 A71-44596
- Flight dynamics of noise optimal flight profiles for V/STOL aircraft, minimization of gust effects on aircraft and nonlinear dynamic stability of parachute-load systems 24 p3792 A71-44761
- VACANCIES [CRYSTAL DEFECTS]**
- NT FRENKEL DEFECTS
- High speed quenching on zone refined molybdenum, considering retained vacancies as contamination effects 05 p0765 A71-16163
- Pure polycrystalline Al under uniaxial tension, noting vacancy rupture mechanism 06 p1000 A71-17940
- Crystal dislocations and vacancy colonies complexes generation, discussing metal fatigue microcracks mechanism 06 p1002 A71-18419
- Nonpairwise van der Waal interactions effects on vacancy formation energies in monatomic solids, using Lorentz oscillator and two body models for comparison 08 p1344 A71-21367
- Binding energies between solute atoms and vacancies in dilute Al alloys measured by quantitative transmission electron microscopy 08 p1310 A71-21530
- Quenched and aged Pt, investigating secondary defects for vacancies clustering modes by transmission electron and field-ion microscopy 11 p1779 A71-26016
- Semiconductor defects, including stoichiometric vacancies in sphalerite lattices, epitaxial interfaces and dislocations in Ge 18 p2953 A71-35870
- Dezincification of Al-Zn alloys, creating loops and dislocations due to vacancies from Zn evaporation 18 p2935 A71-36199
- High purity metals residual electrical resistivity, observing impurities, vacancies, dislocations, plastic strain and polyisotropy effects 19 p0376 A71-37115
- Vacancy absorption model for fatigue crack propagation in Al based on X ray inspection and transmission electron microscopy 21 p3399 A71-40698
- Energy levels and vacancy association of defects in annealed GaAs at 600-1100 C under controlled vapor pressures, using cathodoluminescence measurements 21 p3428 A71-41044
- Vacancies production in pure Ni and V foils by bombardment with high intensity laser pulses 22 p3556 A71-41812
- Weakly diffracted beam observation of small quenching vacancy loops and Guinier-Preston precipitate zones in Al and Al-Cu, using transmission electron microscopy 23 p3691 A71-43359
- Abrikosov vortex lattice in superconductors, calculating resonance linewidth and vacancy formation energy 24 p3860 A71-45119
- Bulk diffusion and glide and self climb mechanisms of vacancy and interstitial loop growth in Mo during neutron postirradiation annealing 24 p3839 A71-45193
- VACUUM**
- NT HIGH VACUUM
- NT ULTRAHIGH VACUUM
- Vacuum-like state of physical medium as initial state of Friedmann cosmology, noting fluctuation instability for conversion into ordinary matter 05 p0806 A71-16180
- Laser produced plasma expansion into vacuum, discussing ion energy angular distributions measurement 06 p0938 A71-18460
- Vacuum science and technology - Conference, Washington, D.C., October 1970 07 p1160 A71-19842
- Electron fluxes hydrodynamic stability in vacuum confined by external electric and magnetic fields and inertia forces, noting electron oscillations possibility 08 p1340 A71-21494
- Cathode material ions acceleration during pulsed discharge in vacuum, discussing experimental investigation results 08 p1341 A71-21496
- Monograph on marginal stability analysis of MHD instabilities by force free magnetic fields in plasma-vacuum systems covering gravitational, pinch and shearless models 12 p1934 A71-26569
- Vacuum symmetry and asymmetry, analyzing physical meaning of Dirac vacuum in quantum field theory 22 p3577 A71-42853
- VACUUM APPARATUS**
- NT CONDENSATION PUMPS
- NT ION PUMPS
- NT IONIZATION GAGES
- NT KNUDSEN GAGES
- NT MOLECULAR PUMPS
- NT PENNING GAGES
- NT VACUUM CHAMBERS
- NT VACUUM FURNACES
- NT VACUUM GAGES
- NT VACUUM PUMPS
- Liquid nitrogen cold trap for oil diffusion pump 05 p0757 A71-16232
- Apparatus for thin film solid state devices fabrication under ultrahigh vacuum 05 p0733 A71-16233
- Matched impedance microwave vacuum feedthrough 05 p0757 A71-16234
- Vacuum merging speed and magnetospheric cross tail electric field inverse proportionality to plasma sheet particle concentration 13 p2056 A71-27934
- Elastomer O ring vacuum device for positive holding of Schumann film for precise microdensitometry during rocket flight in 7 March 1970 solar eclipse 14 p2249 A71-30887
- Vacuum package with Ti bulk sublimator/ion pump combination for 150 kv neutron generator tritium decontamination 21 p3414 A71-40900

VACUUM CHAMBERS

Superhigh vacuum apparatus for creep and long term strength tests on metals at high temperatures, giving results for niobium alloys 22 p3538 A71-41699

Vacuum apparatus for fatigue tests at room and low temperatures, giving results for annealed copper 22 p3538 A71-41700

Vacuum water-air ejector with cylindrical mixing chamber and multibarrel nozzle feed, showing increased efficiency by supersonic diffuser substitution 22 p3480 A71-41852

Vacuum and inert gas TOR-1 device for studying physical properties of lunar soil and terrestrial analogs 24 p3828 A71-45104

VACUUM CHAMBERS

Oil diffusion pumped space simulation vacuum chamber performance improvement methods including water vapor and carbon dioxide desorption, Ti sublimation pumping and 20 K cryopumping 06 p0881 A71-18462

UK 3 spacecraft support sting for solar simulation and thermal vacuum testing in 2.5 meter test chamber, describing design and construction 06 p0881 A71-18720

Plasma fluxes transport in vacuum chamber by quadrupole magnetic field, studying H plasmoids motion 08 p1340 A71-21482

Atmospheric seal leakage control tests for long orbital lifetime space station designs, discussing vacuum chamber monitored pressure shell penetrations [AIAA PAPER 71-337] 11 p1836 A71-25316

Thermoluminescent phosphorus films irradiation by electrons with energies up to 15 keV in vacuum chamber 12 p1942 A71-26648

Hydrogen sorption capacity by sulfur dioxide frost from cryodeposit formation on stainless steel sphere in vacuum chamber and equilibrium isotherms measurement 17 p2695 A71-35142

Intermittent hypersonic wind tunnels, considering pressure and vacuum storage, blowdown tunnels and pressure tubes 18 p2897 A71-36409

Vacuum brazing for nozzle guide vanes repair in aircraft gas turbine engines, noting economic advantages 19 p3069 A71-38313

Light spark plasma in gas cloud, considering directed ejection to vacuum chamber and fireball acceleration 22 p3581 A71-41816

VACUUM DEPOSITION

Mated magnetic film memory design employing continuous vacuum deposition fabrication 01 p0047 A71-10213

Electrical resistivity and structure of thin films of W, Mo and Cr evaporated in vacuum by neodymium laser 01 p0101 A71-10674

Vacuum deposited Bi thin films on glass substrates at liquid He temperature, investigating characteristics of critical thickness 03 p0466 A71-13291

Ultrahigh vacuum deposited Ni, Fe, W and Mo films, determining molecular oxygen adsorption efficiencies 04 p0636 A71-15015

Low stress integral coverslips deposition by high vacuum ion beam sputtering for solar cell manufacturing cost reduction 05 p0702 A71-16078

Thin CdS condensate layer formation mechanism during films slow vacuum deposition onto glass or polystyrene sublayer bases 05 p0793 A71-16821

Superconducting thin film bridges by vacuum deposition of tin, measuring current-voltage and resistance at SHF and critical temperatures 05 p0793 A71-16828

Cohesive strength of metal coatings obtained by simultaneous vacuum condensation of strengthening phase and matrix material vapors 07 p1130 A71-19157

Stainless steel coatings vacuum deposition on Ti alloy plates, considering product cryogenic and mechanical properties 07 p1118 A71-19853

Be films evaporated in vacuum on W single crystals, investigating adsorption and electron emission by field emission microscopy 07 p1178 A71-19918

Vacuum deposited Cr film formation as function of condensation rate 09 p1469 A71-22847

Spectral reflectance of water cryodeposits on liquid nitrogen cooled surfaces in vacuum IR integrating sphere [AIAA PAPER 71-447] 11 p1858 A71-26232

Reflecting Au films deposition on glass substrates by evaporation in vacuo, discussing optical devices, reproduction and bonding improvements 11 p1809 A71-26431

Gas permeability of polymeric foils reduction by vapor metallization in vacuum, noting dependence on surface state, diffusion layer and macroporosity 16 p2601 A71-33684

Adhesive strength of metal coatings obtained by simultaneous vacuum condensation of strengthening phase and matrix material vapors 17 p2760 A71-35655

Vacuum deposited thin Cr films on glass substrate, describing hydrogen adsorption effects 19 p3076 A71-37116

Vacuum deposited thin Cr films on glass, investigating substrate temperature and inert gas pressure effects on texture 19 p3076 A71-37117

Vacuum deposition of silica and alumina thin films on silicon substrate MOS diodes, using CW carbon dioxide laser 19 p3074 A71-38233

Failure analysis of vacuum deposited Al film interconnections at contact windows, considering grain size effect and reliability improvement techniques 19 p3119 A71-38512

Gas turbine engine turbine blades service life increase by Cr and Al vacuum diffusion metallization, presenting full scale endurance test results 21 p3390 A71-41173

IR filters and coatings, describing vacuum deposited layer properties of II/VII, heavy halide and V/VI glass compounds 22 p3544 A71-42135

Electron microscopic investigation of Au thin film deposits on Si single crystals in ultrahigh vacuum, noting semiconductor-like resistance/temperature behavior at liquid He temperatures 24 p3862 A71-45347

Structural and electrical properties of sublimation deposited GaAs films on sapphire and semiinsulating substrate in vacuum 24 p3863 A71-45358

VACUUM EFFECTS

Solid molybdenum disulfide lubricants antifriction properties and performance under atmospheric and high vacuum conditions, noting humidity effects and composition of friction-evolved gases 01 p0106 A71-10036

Human survivability and work capacity in aerospace environments, discussing sudden unprotected exposure to vacuum 01 p0022 A71-10512

Flow field of two dimensional nozzle exhausting to vacuum, describing computer program based on BGK equation and plotting exhaust region density, temperature and velocity [AIAA PAPER 69-658] 01 p0002 A71-10932

Laser vs electron beam welding, examining high and partial vacuum and atmospheric pressure environments, penetration and ionization and dissociation processes [SME PAPER MR-70-523] 01 p0090 A71-11269

Sintered W rolling in vacuum over reduction and temperature ranges 02 p0256 A71-12514

Oxidation potential criterion for metal sticking to rolls during rolling in vacuum, considering Ta, Zr, Mo, W, Ni, Cu, Nb and V 02 p0256 A71-12515

Gear drives operating in vacuum conditions, calculating friction coefficient with dimensional analysis 02 p0258 A71-12598

Sliding friction and wear of metal pairs under vacuum, using gravimetric and electron optical methods 03 p0432 A71-13366

Spectral emittance of Ti at high temperatures in visible region under vacuum 04 p0611 A71-14956

Creep strength of Nb alloys with Mo at high temperatures in vacuum, noting Zr-C complex alloying effect 04 p0613 A71-15642

Pure metal structure effect on friction and lubrication under steady slip in ultrahigh vacuum at low temperatures 05 p0757 A71-16185

Refractory metal surfaces behavior in ultrahigh vacuum, using LEED and Auger electron spectroscopy 05 p0766 A71-16240

Refractory metal surface-gas reactions at high temperatures in vacuum, determining activation energies 05 p0766 A71-16241

Small scale vacuum stream degassing of molten aluminum for hydrogen removal 05 p0758 A71-16247

Energy deposition, vacuum expansion and vaporization of barium in two phase jets, using combustion and solid state shock waves 05 p0836 A71-16538

Ellipsoidal level surface gas cloud expansion into vacuum 05 p0783 A71-16991

Air bearings design for laser scanner high speed rotating mirror in vacuum, describing static and dynamic tests for rotor inversion point [ASME PAPER 70-LUB-15] 07 p1117 A71-195060

Re hot rollability under low vacuum conditions as function of temperature, comparing with cold rolling 07 p1120 A71-202440

Wet and dry lubricated slip ring systems long term application testing in ion pumped vacuum chambers 07 p1120 A71-202740

Friction-wear characteristics of self lubricating composites under sliding conditions in air and vacuum [ASLE PREPRINT 70LC-17] 08 p1298 A71-211600

Sliding load history effects on friction of thin burnished films of molybdenum disulfide in vacuum [ASLE PREPRINT 70LC-18] 08 p1298 A71-211600

Surface heating and pressure distribution on Lunar Module from rocket exhaust plume impingement tests in vacuum [AIAA PAPER 71-256] 08 p1377 A71-219850

Supersonic collisionless plasma flow around flat plate and expansion into vacuum, using Poisson equation 09 p1500 A71-222330

Apparatus for fatigue testing under tensile stress in vacuum at frequencies of 15-30 Hz with 500 kg maximum load 09 p1426 A71-225050

Static friction in steel-polymer couples under vacuum, considering temperature, contact time, normal load and physicochemical properties effects 09 p1454 A71-228180

Service life of solid molybdenum disulfide based plastic coatings with different binders under high vacuum friction investigated by mass spectroscopy 09 p1454 A71-228190

Mo, W and Zr effects on niobium reaction with residual gases during heating in vacuum 09 p1469 A71-228460

O I and II resonance transitions radiative lifetimes in vacuum UV, using beam foil method 10 p1676 A71-245010

Solids evaporation into vacuum, considering interconnected problems of heat conduction and evaporation front boundary conditions 10 p1697 A71-250630

Metals mechanical properties under vacuum conditions, discussing alternate bending tests of Cu and Al specimens under range of oxygen pressures 11 p1777 A71-253890

Long term life test and vacuum tests of high temperature resistojets, using ammonia and hydrogen propellants [AIAA PAPER 70-1136] 11 p1811 A71-255230

Macroscopic working model for CVD tungsten assuming change of substrate work function and preferential crystal orientation by impurity adsorbed molecules 11 p1808 A71-258610

Mo evaporation in vacuum, oxygen and water vapor atmospheres at high temperatures 11 p1709 A71-258650

Long life vacuum tests of dry and wet lubricated slip ring systems for power and signal transfer, discussing wear, noise and contact resistance 11 p1771 A71-260500

Friction and wear of steels, Ti, Al, Cu and copper beryllium in sliding over hardness range of steel plates in vacuum and air 11 p1771 A71-261430

Design, calibration and computer control of orbital heating simulator, using heat flux sensor feedback for ATM thermal vacuum tests [AIAA PAPER 71-432] 11 p1745 A71-262210

Vacuum UV phototube module for degradation measurement of optical components, including mirrors, windows, lenses and thermal control surfaces [AIAA PAPER 71-461] 11 p1800 A71-262430

Electron beam welding of metal-metal and metal-ceramic joints and sapphire sealing under vacuum 11 p1745 A71-263990

Viking rocket heat shield material mechanical properties, examining time-temperature superposition with continuous stress relaxation data measured in vacuum 11 p1791 A71-265180

Plasma plate under vacuum conditions, examining transient radiation and spatial dispersion 12 p1937 A71-271180

Titanium nitride sintering in vacuum, noting strain by grain sliding to pore center under surface tension force effects 12 p1918 A71-275270

Solid state reaction of titanium carbide with Ti, Zr and V in vacuum at high temperatures 13 p2082 A71-278210

Computer simulated semiinfinite uniform plasma expansion in vacuum, showing inapplicability of thermal velocity burst model 13 p2104 A71-278460

Bacteria and yeast strains, fungus specimens and seaweed species high vacuum resistance, noting microorganisms interplanetary transport in outer space 13 p2009 A71-286890

Stage 1 fatigue fracture mechanism in Ni-based superalloy single crystals, observing air and vacuum effects 13 p2088 A71-29405

Optical interferometer with evacuated light paths, describing operating principles, cost efficiency and compactness 14 p2238 A71-29803

Surface temperature discrepancy during flameless vacuum burning of trinitroglycerin gunpowder due to vaporization of volatile components 15 p2462 A71-31373

Niobium fine structure, examining annealing in vacuum effects on strength 15 p2425 A71-31400

Titanium alloy durability under cyclic torsion in vacuum at various temperatures, investigating fatigue life and tensile strength 15 p2428 A71-31856

Optimal radiative capacity of star shaped radiator with mirror reflecting surfaces for vacuum cooling of elongated finned bodies 17 p2836 A71-34311

Tungsten-oxygen system surface reactions in vacuum, emphasizing interfacial geometry variations, faceting and oxide nucleation 17 p2694 A71-34667

Nonheat treated extruded Mo alloy under tension and vacuum conditions at various temperatures, investigating cylindrical samples dimensions effects 18 p2936 A71-36714

Ellipsoidal level surface gas cloud expansion into vacuum 18 p2948 A71-36791

Supersonic spherical viscous heat conducting gas discharge into vacuum, solving Navier-Stokes equations by buildup method 19 p3042 A71-37087

Sealed and vented fusing devices, testing vacuum effects on performance at high and low temperatures 19 p3035 A71-38536

Mass of virtual particle responsible for gravitation of vacuum and expansion of universe, considering correspondence to red shift in quasar spectra 19 p3146 A71-38644

Spherical indium crystal manufacture in space, suspending and positioning weightless containerless melt in air and vacuum by adhesion and cohesion for crystal growth 20 p3247 A71-38767

German monograph on static fields in general relativity theory covering covariant equilibrium conditions, two body problems, vacuum fields and Newtonian gravity principles 20 p3269 A71-39077

Graphite properties in high and ultrahigh vacuum, suggesting use as electrode material in vacuum gages and residual gas analyzers 21 p3405 A71-40221

Space environment simulation for ultrahigh vacuum effects on crystalline enzymes activity, measuring by chemiluminescence techniques 21 p3334 A71-40573

Supersonic collisionless plasma flow around flat plate and expansion into vacuum, using Poisson equation 21 p3424 A71-41113

Apollo 12 lunar fines 12001, 19 thermal conductivity vacuum measurements, using line heat source method 23 p3761 A71-43781

Temperature effects on niobium carbide friction process in vacuum conditions, considering surface layer microhardness and X ray and metallographic analyses 23 p3692 A71-44030

Glass fibers durability in air and vacuum conditions, showing stress concentration coefficients at various tensile stresses 23 p3697 A71-44031

Relativistic electron beam propagation entering vacuum or neutral gas filled region through grounded conducting wall, using one dimensional model 23 p3713 A71-44146

Temperature field measurements above porous surface during ice-water sublimation into vacuum, showing discontinuities due to external heat and mass transfer 23 p3784 A71-44340

Temperature dependence of external friction coefficient between high-melting carbides in vacuum at constant normal load and slipping rate 24 p3830 A71-44863

Gas density distributions in argon and carbon dioxide supersonic jets with low angular divergence in vacuum, using Laval supersonic nozzle 24 p3858 A71-45241

Channel electron multiplier principles and characteristics, discussing secondary electron production probability during electron irradiation of surface in vacuum 24 p3811 A71-45326

VACUUM FURNACES

One chamber vacuum furnace for dewax, presinter and sinter of cemented carbides, referring to Cox chart for system design 05 p0758 A71-16248

Sintered or cast Re refining in vacuum electron beam furnace using water-cooled crystallizer, discussing metal losses during melting 06 p0904 A71-17948

Photon intensities of UV spectral lines from energetic magnetically confined vacuum carbon arc, using monochromator double ion chamber detector system 09 p1502 A71-22813

Vacuum heat treatment of brazed and diffusion bonded jet engine components near melting temperature 13 p2073 A71-28145

VACUUM GAGES

NT IONIZATION GAGES

NT KNUDSEN GAGES

NT PENNING GAGES

Ultrahigh vacuum extractor gage design and performance 05 p0753 A71-16946

Dynamic pressure reduction method errors in vacuum gages calibration 05 p0754 A71-16949

In situ metal-gas secondary standard assembly for ultrahigh vacuum gage calibration, using repeatable pressure generation from binary erbium- hydrogen system 17 p2744 A71-35140

Graphite properties in high and ultrahigh vacuum, suggesting use as electrode material in vacuum gages and residual gas analyzers 21 p3405 A71-40221

Vacuum covered gage measurements in sorption and cryogenic systems with activated pumping surfaces, concerning molecular gas flux leaving specimen 21 p3417 A71-41298

Mullard channel electron multipliers applications to space research, scientific instruments, vacuum devices and mass spectrometers 24 p3811 A71-45332

VACUUM MELTING

Tungsten exploding wires electron emission during vacuum melting 02 p0284 A71-11881

Composition and annealing temperature effects on recrystallization of vacuum melted thin wire and rod Mo alloys 02 p0265 A71-12521

Stainless steel deoxidation by carbon in laboratory scale vacuum induction melting, explaining reaction kinetics 05 p0758 A71-16246

Sintered or cast Re refining in vacuum electron beam furnace using water-cooled crystallizer, discussing metal losses during melting 06 p0904 A71-17948

Ti-Zr alloy phase diagram from vacuum melting, using high purity wafers and apparatus similar to McQuillan 11 p1780 A71-26028

Vacuum melted Ni base superalloys, determining Mo and hardener effects on gamma prime solvus temperature and solutioning rate 13 p2090 A71-29418

Grade 15 steel vacuum diffusion welding to AMTs alloy or AD1 aluminum, using nickel interlayer in joints 15 p2418 A71-32667

Mo single crystal growth by vacuum melting without oil vapors, noting reduced carbon content and increased ductility 16 p2595 A71-33880

Closed die forgings of vacuum remelted carbon and low alloy steels to improve transverse ductility and microcleanness for aircraft industry 17 p2749 A71-35336

Vacuum melted Mo alloy low temperatures elasticity, plasticity and tensile strength characteristics 17 p2760 A71-35675

Vacuum-melted low-carbon low-manganese steel, investigating Ni and Cr additions effects on recrystallization textures 19 p3079 A71-37703

Reduced oxygen effect on structure and mechanical, technological and corrosive properties of stainless steel melted in open and vacuum furnaces 23 p3690 A71-43279

Ni-based alloy strength characteristics dependence on heat treatment during melting and casting in vacuum and in air 23 p3691 A71-43425

VACUUM PUMPS

NT CONDENSATION PUMPS

NT ION PUMPS

NT MOLECULAR PUMPS

Vacuum pump fluids spectral absorption coefficient measurement, using variable UV cell 17 p2784 A71-35141

Turbomolecular vacuum pump impeller theoretical efficiency with allowance for diffuse law of interaction between gas molecules and interblade channel walls 20 p3183 A71-39170

Two stage rotor-piston vacuum pump, determining minimum work of gas compression 20 p3183 A71-39171

Cryosorption vacuum pumping, discussing physical and chemical adsorption, adsorbents, surface migration and diffusion, reactivation, deposits, cryopanel adhesion, pump design, etc 20 p3270 A71-39249

Vacuum covered gage measurements in sorption and cryogenic systems with activated pumping surfaces, concerning molecular gas flux leaving specimen 21 p3417 A71-41298

Pilot vacuum pump with piston-rotor compression action to enhance pumping performance, comparing to single stage pumps 22 p3554 A71-42490

Ultrahigh vacuum by condensate pump, defining vacuum level by mass spectrometric determination of residual gas content 23 p3661 A71-43271

VACUUM SPECTROSCOPY

Vacuum spectrum modification theory for inverse Compton scattering in cold collisionless plasma 07 p1165 A71-18855

Vacuum pump fluids spectral absorption coefficient measurement, using variable UV cell 17 p2784 A71-35141

VACUUM SYSTEMS

Magnetic suspension apparatus for temperature measurement near interface of sliding bodies in vacuum 03 p0397 A71-13914

Clean cryogenic vacuum high speed gas pumping system for calibrating spectrometers for use on Apollo telescope mount 07 p1160 A71-19854

Electron beam welding machine reducing number of fabrication variables during final assembly procedure in thermionic converters fabrication, discussing UHV systems 11 p1709 A71-25866

Physical and mechanical properties of controlled flow vacuum cured glass reinforced polyimide prepreg laminates 22 p3565 A71-42595

VACUUM TUBE OSCILLATORS

NT BACKWARD WAVE TUBES

NT CATHODE RAY TUBES

NT COLD CATHODE TUBES

NT GAS DISCHARGE TUBES

NT MICROWAVE OSCILLATORS

Multicircuit vacuum tube oscillator with delay, calculating self oscillation line width reduction by two external resonators with high Q factor 04 p0558 A71-15121

Haag synchronization theory application to HF vacuum tube oscillators, considering LF perturbation 10 p1609 A71-23852

Single loop quartz vacuum tube oscillators, calculating oscillation spectral line width due to thermal and shot noise and circuit parameters fluctuations 12 p1889 A71-27622

VACUUM TUBES

NT BACKWARD WAVE TUBES

NT CATHODE RAY TUBES

NT COLD CATHODE TUBES

NT GAS DISCHARGE TUBES

NT MICROWAVE OSCILLATORS

NT VACUUM TUBE OSCILLATORS

Vacuum tube launchers and boosters for launching small to medium size meteorological probe rocket into lower atmosphere [AIAA PAPER 70-1393] 03 p0498 A71-13674

Current spectral noise density in nonlinear element transmitter stage, examining vacuum tube frequency multiplier phase and amplitude fluctuations 09 p1405 A71-22469

Energy spectrum minimization of intrinsic phase fluctuations in multistage vacuum tube frequency multiplier, using graphic analysis 11 p1738 A71-25940

Noise equivalent resistance of thermionic tubes as stability and reliability criterion 16 p2545 A71-33073

Energy spectrum minimization of intrinsic phase fluctuations in multistage vacuum tube frequency multiplier, using graphic analysis 20 p3205 A71-39260

VACUUM ULTRAVIOLET RADIATION

U FAR ULTRAVIOLET RADIATION

VALENCE

Anomalous temperature dependent silver halides photoemission related to lattice vibrationally dependent hybridization of valence states 01 p0137 A71-10148

Free hole drag in p-type Ge by photons in optical transitions between valence band subbands, examining magnetic field effects 02 p0296 A71-12613

High resolution energy spectra and valence band structure vs carbon content in homogeneous titanium carbides 15 p2430 A71-32150

Soft X ray spectra measurements of vanadium carbides in homogeneity range on ultralong wave spectrometer, showing three zone energy structure of valence band 15 p2430 A71-32151

VALKYRIE AIRCRAFT

Complex molecules forced vibrations as material points system with quasi-elastic valence bonds 15 p2452 A71-32624

Multiply ionized Ar excited valency and inner shell transitions, investigating emission spectrum and energy levels 15 p2368 A71-32747

Chemical bonds types in intermetallic, metal-like and nonmetallic compounds, stressing model based on valence electrons configuration localization 16 p2622 A71-33919

Diffusion processes electron mechanism in metal-metal and metal-nonmetal systems, using configurational model for valence electrons localization 21 p3403 A71-41159

Anisotropic transport coefficients valence band model of TiSe, measuring electric conductivity, Hall effect and thermo-emf as function of temperature 21 p3434 A71-41328

VALKYRIE AIRCRAFT

U B-70 AIRCRAFT

VALLEYS

Attitude measurements of fractures bounding lunar rilles from systematic increase with height 13 p2134 A71-28289

Hadley Rille origin as lava channel and partly collapsed lava tube, taking into account topographic configuration, terrestrial analogs, geomorphology and meteoroid bombardment 13 p2139 A71-28781

Hadley, Prinz and Schroter lunar sinuous rills morphology from Orbiter photography, discussing rills origin 15 p2493 A71-32489

VALSALVA EXERCISE

Pulse wave velocity measurements in human veins by transcutaneous ultrasonic flow detectors, noting respiration and Valsalva effects 12 p1874 A71-27136

VALSALVA MANEUVER

U VALSALVA EXERCISE

VALUE

NT Q VALUES

VALVES

NT ARTIFICIAL HEART VALVES

NT AUTOMATIC CONTROL VALVES

NT CONTROL VALVES

NT FUEL VALVES

NT PRESSURE REGULATORS

NT SOLENOID VALVES

Mitral valve muscular fibers, investigating pathological changes of myocardium of left heart ventricle 02 p0198 A71-11695

Fluidic diverting valve independent of turbulent reattachment, examining large scale model and digital element characteristics in closed loop system 07 p1024 A71-20553

Aircraft fuel and air conditioning systems vortex valves and diodes, examining flow patterns into and out of chambers 07 p1025 A71-20556

Jet pipe valve characteristics, discussing pressure and flow recovery for various loads, nozzle diameter ratios and spacings 07 p1025 A71-20559

Low pressure air jet sensing power pneumatic and fluidic circuits and interface valves for low pressure signal setup to main line pressure, considering circuit design 07 p1030 A71-20597

Hydrodynamic forces on pistons in sharp-edged spool valves with double throttling gaps at Reynolds numbers from 60 to 240 09 p1434 A71-23664

Liquid fluorine feed system valves, seals and seats, discussing design criteria for flight weight components [AIAA PAPER 70-705] 11 p1709 A71-25519

Aircraft parts testing by NDT methods, considering ultrasonic system for valve defects and fluorescent particle system for crack detection 18 p2929 A71-37056

Slide valve slot fluid flow oscillation frequency range estimate for quasi-stationarity 20 p3183 A71-39168

Working gas parameter determination for valve supply main system during feed opening, explaining heating effect for second valve by shock wave theory 24 p3793 A71-45021

VAN ALLEN RADIATION BELTS

U RADIATION BELTS

VAN DE GRAAFF ACCELERATORS

Beam foil spectroscopy using van de Graaff accelerator, considering applications to atomic physics research and teaching 08 p1272 A71-21667

VAN DER WAAL FORCES

Solar Na I Fraunhofer lines empirical constants and abundance, discussing van der Waal attraction, Stark broadening and radiative damping 06 p0969 A71-17974

Nonpairwise van der Waal interactions effects on vacancy formation energies in monatomic solids, using Lorentz oscillator and two body models for comparison 08 p1344 A71-21367

Van der Waal bound lamellar solids interlayer binding energy computational model, discussing talc and pyrophyllite equilibrium stacking arrangements and force constants 10 p1573 A71-24541

Solar atmosphere line broadening by neutral hydrogen, noting discrepancy in van der Waals interaction 14 p2306 A71-29686

Nonadiabatic effects in van der Waal line broadening, taking into account mixing between degenerate magnetic sublevels in atomic collisions 19 p3106 A71-37409

VANADATES

Ferrimagnetic vanadate garnet IR Faraday rotation as function of wavelengths and temperature, considering ions multivalence and multilattice site modifications 06 p0941 A71-18040

VANADIUM

High temperature thermophysical properties of vanadium, establishing heat conductivity coefficient, electric resistivity, Lorentz number, monochromatic and total hemispherical emission coefficients 02 p0263 A71-12189

EPR spectrum of tetravalent vanadium ions in gamma irradiated corundum at liquid He temperatures, showing equidistant lines width temperature dependence 04 p0637 A71-15105

Manganese, iron and vanadium ion ordering in orthorhombic zoisite structure by electron paramagnetic resonance technique 07 p1053 A71-18741

Bcc Ti-V single crystals deformation modes and resolved shear stresses as function of temperature and composition 08 p1307 A71-21510

Cr and V diffusion plating influence on principal characteristics of highly alloyed martensitic and carbon steels 12 p1912 A71-27690

Solid state reaction of titanium carbide with Ti, Zr and V in vacuum at high temperatures 13 p2082 A71-27821

Fifth group transition elements V, Nb and Ta, showing most stable metal dioxide gaseous compounds 15 p2424 A71-31391

High temperature thermophysical properties of vanadium, establishing heat conductivity coefficient, electric resistivity, Lorentz number, monochromatic and total hemispherical emission coefficients 15 p2426 A71-31496

Vacancies production in pure Ni and V foils by bombardment with high intensity laser pulses 22 p3536 A71-41812

VANADIUM ALLOYS

Nb-V-Mo alloys lattice structure, examining continuous solid solutions with X ray and metallographic analysis 07 p1129 A71-19144

Kinetics of transformation to long range ordering in Ni-V as function of heat treatment 07 p1131 A71-19433

Oxygen effect on mechanical properties of Ti alloys with V and V-Al content, showing strengthening up to 400 C 07 p1136 A71-19631

Ordered states effects on mechanical properties of Va-Co-Ni ternary alloys, considering creep behavior difference between ordered and disordered structures 08 p1309 A71-21526

V-Ti alloys high temperature behavior dependence on Ti content, examining interstitial impurities effects on mechanical properties 08 p1310 A71-21532

Recrystallization of V and V-Ti alloy, discussing hardness measurements, tensile tests, X ray diffraction, optical and electron microscopy 10 p1625 A71-24010

Ti-V alloys electrolytic deposition, discussing electrolyte composition, current density, temperature and coating thickness 10 p1627 A71-24646

Fast heated titanium-vanadium martensite beta-phase transformations comparison with slow heated structures 11 p1782 A71-26472

Nb-V, V-Pd and Pd-Nb systems diffusion coefficient as function of concentration for equilibrium diagrams, using method of diffusion layers 11 p1782 A71-26475

Ti-V alloys, observing as-quenched omega phase and transition to aged form by selected-area diffraction and dark-field electron microscopy 11 p1783 A71-26479

Vanadium containing high strength low alloy steel thermomechanical processing by last hot mill pass temperature control [ASME PAPER 71-MET-1] 12 p1918 A71-27320

Mechanical properties and heat treatment of Ti-V and Ti-V-Al alloys in quenched and quenched-aged states 13 p2083 A71-27872

Ti-Al-V alloy forgings fatigue strength improvements, discussing surface finish, heat treatments and alpha and beta grain size 14 p2261 A71-31111

Oxygen effect on mechanical properties of Ti alloys with V and V-Al content, showing strengthening up to 400 C 16 p2593 A71-33611

Yttrium effect on phase composition of V-Ga alloys from microstructural, X ray structural and microcalorimetric analysis 16 p2622 A71-33941

Fe-Ni-V-C alloy strengthening by cyclic martensite phase transformation 17 p2756 A71-34411

Structure, superconductivity transition temperature, microhardness and electrical resistivity of V-Ti cast alloys 19 p3078 A71-37441

Thermodynamic ion current ratios of solid solution V-Ti alloys, using Knudsen effusion and time of flight mass spectrometric methods 21 p3398 A71-40441

Structure, hardness, density and electrical resistivity of binary alloys V-Ti, V-Cr, V-Al and V-Sn 23 p3691 A71-43261

VANADIUM CARBIDES

Nonstoichiometric VC, studying thermal and electrical conductivities, thermoelectric properties and Hall coefficient 06 p0912 A71-18081

Single crystal TiC-VC alloys mechanical properties considering room temperature hardness, high temperature deformation and brittle to ductile transition temperature 08 p1316 A71-21581

Ta-V-C ternary system solidus surface and equilibrium diagram determination by metallographic techniques and X ray and thermal analyses 15 p2430 A71-32141

Soft X ray spectra measurements of vanadium carbides in homogeneity range on ultralong wave spectrometer, showing three zone energy structure and valence band 15 p2430 A71-32151

Single crystal vanadium carbide magnetic susceptibility decrease with increasing carbon content attributed to orbital paramagnetism 21 p3395 A71-40021

VANADIUM COMPOUNDS

NT VANADATES

NT VANADIUM CARBIDES

NT VANADIUM OXIDES

K-beta and L-alpha X ray spectral emission bands of high melting vanadium compounds, considering chemical bonds 02 p0263 A71-11891

L-alpha X ray spectral band and K absorption edges in vanadium silicides and high temperature superconductors, obtaining energy bands electron distribution 02 p0294 A71-11891

Vanadium and niobium carbides as function of C content, studying lattice constants, microhardness and electrical resistivity 06 p0912 A71-18081

Titanium, vanadium and niobium carbides, investigating electronic structure effects on atomic behavior 15 p2429 A71-32141

Trigonal crystal field and spin-orbit interaction matrices for ion energy levels in vanadium compounds in strong g scheme, using symmetry group tensor operators 21 p3427 A71-40071

VANADIUM ISOTOPES

Apollo 12 lunar samples 12002,128, 12021,496, 12038,43 and 12070,52 vanadium isotopic composition 23 p3751 A71-43701

VANADIUM OXIDES

Vanadium oxide thin vapor transport films on single crystal aluminum oxide, using RF sputtering of powdered targets 11 p1809 A71-26391

VANELESS DIFFUSERS

Centrifugal compressor vaneless diffuser, estimating energy losses with hydrodynamic model 08 p1348 A71-21261

Centrifugal compressor bladeless diffuser parameters, flow kinematics and energy losses, noting effects of friction coefficient and expansion angle 23 p3626 A71-43551

VANES

NT GUIDE VANES

NT JET VANES

Hydraulic vane pumps, including variable displacement, double and compound pumps 01 p0006 A71-10811

High speed vane type main engine fuel pump for small gas turbine engines [ASME PAPER 71-GT-24] 11 p1812 A71-25961

VAPOR DEPOSITION

NT VACUUM DEPOSITION

Vapor phase aluminization in Ar atmosphere furnace, discussing physicochemical aspects, thermal cycles and deposition kinetics

01 p0099 A71-10267

Polycrystalline semiconductors Hall effect by grain structure model for low and high resistivity boundaries, giving vapor deposited cadmium selenide film data

01 p0137 A71-10283

Bare and cesiated work function of covapor deposited tungsten-rhenium electrodes from vacuum emission vehicle Schottky plots

02 p0295 A71-12205

High work function stable faceted W thermionic emitter surface preparation by electroetching and vapor deposition

02 p0295 A71-12209

Crystal surface orientation of chemical vapor deposited W thermionic emitter by hydrogen reduction of hexafluoride, using etch pits and X ray diffraction

02 p0295 A71-12211

Vapor deposited W impurities effect on crystal structure and preferred orientation, considering work function increase

02 p0296 A71-12241

Glow discharge cleaning for surface contaminants removal from hydrodynamic gas bearing components, discussing equipment application to thin film lubricant vapor deposition

02 p0256 A71-12461

Gaseous impurities diffusion into silicon via open tube microelectronic method

02 p0297 A71-12922

Whisker growth by vapor phase reactions, detailing thermodynamics, kinetics and supersaturation in aluminum oxide whisker formation

04 p0635 A71-14942

Vapor deposition rates from liquid binary alloy targets under ion sputtering

05 p0757 A71-16235

Vapor deposited niobium nitride superconducting thin films on fused silica substrates, measuring transition temperature

05 p0792 A71-16236

Ti-Al-V foils by electron beam vapor deposition, discussing metallurgical characteristics

05 p0765 A71-16237

Cosmic accretion gas dynamics, discussing star, galaxies and galactic cluster effects

06 p0972 A71-18333

MOS large scale IC phosphosilicate glass substrate vapor deposits effects, including hardness, pinhole density and electromigration

07 p1070 A71-18868

Permanent IR electron radiation effects on hardened MOS integrated inverter circuits, using units with plasma grown and vapor deposited aluminum oxide

07 p1174 A71-19053

Pyrolytic aluminum oxide thin films on Si substrate by thermodecomposition, measuring vapor deposition parameters and Si surface preparation effects on dielectric and interface properties

09 p1509 A71-23117

Refractory metals coating of various substrates by gaseous phase chemical deposition, discussing diffusion process theoretical analysis, experimental apparatus and coatings mechanical and physical properties

11 p1768 A71-25391

Barium ion cloud experiments for ionospheric vapor release determination from Rubis Rocket trajectory visible markings

11 p1755 A71-25643

Pyrolytic graphite, discussing fabrication by chemical vapor deposition process, mechanical and physical properties, residual stresses, applications in reentry vehicle heat shields, rocket nozzle throats, etc

11 p1789 A71-25743

Carbon vapor deoxidized W on thermionic converter emitters, investigating deposition parameters effect on microporosity

11 p1807 A71-25860

Chemical vapor deposition process for preparing W-Re alloys having uniform Re content and dense coherent grain structure

11 p1797 A71-25862

Variable spacing thermionic converter consisting of fluoride vapor deposited W emitter and Nb collector, considering cesiated work function of electrode pair

11 p1714 A71-25905

Chemically vapor deposited deep etched tungsten emitter for high performance cylindrical thermionic converter

11 p1714 A71-25906

Vacuum arc welding stability in vaporized Mo cathode material as function of current and arc length, describing burner design for material replenishment

11 p1770 A71-25946

Vanadium oxide thin vapor transport films on single crystal aluminum oxide, using RF sputtering of powdered targets

11 p1809 A71-26397

Boron modifications and carbides formation by vapor deposition on tantalum filaments

12 p1943 A71-27093

Refractory materials production using chemical deposits from gaseous phase, discussing mechanical, physical and thermal properties of obtained coatings

13 p2074 A71-28526

Mechanical properties of carbon fibers thinly coated with TiC by chemical vapor deposition from hydrogen, methane and titanium tetrachloride vapor mixture

13 p2092 A71-28627

Electron beam vapor deposited CoCrAlY coating composition optimization with ballistic impact and furnace/long term burner rig oxidation tests

14 p2257 A71-29636

Porous carbon and graphite substrates chemical vapor deposition carbon infiltration process, discussing isothermal and thermal and pressure gradients techniques

14 p2262 A71-29652

Epitaxial deposition of Au on ultrahigh vacuum cleaved mica during early nucleation and growth

14 p2284 A71-30072

Zirconium iodide vapor deposition kinetics, determining activation temperature

15 p2425 A71-31395

Carbide coating formation on graphite from vapor-gas phase, calculating thermodynamics and kinetics by digital computer for comparison with experiment

15 p2438 A71-32143

Spatially periodic inhibition of gold vapor condensation by intense optical standing wave using Q switched laser radiation

20 p3245 A71-39403

Chemical vapor deposited tungsten or other refractory metal alloys mechanical properties evaluation at high temperature, describing hoop stress measurement apparatus for induction heated specimens

[ECS PAPER 384-RPN] 20 p3252 A71-39553

Crystal growth of III-V compound semiconductors from vapor phase, studying deposition processes chemistry by mass spectrometry

21 p3427 A71-40216

Thin single crystalline film deposition by molecular beam epitaxy of GaAs, describing surface structure observation with high energy electron diffraction

21 p3427 A71-40217

Evaporated Permalloy films deposition temperature measurement by vacuum evaporated Chromel-constantan thin film thermocouple, noting temperature difference between film and glass substrate

21 p3384 A71-40220

Tungsten and tungsten alloys weldability by gas tungsten arc, electron beam and chemical vapor deposition techniques

21 p3388 A71-40624

GaAs contacts fabrication by successive metals or alloy evaporation, examining surface distribution by X ray microprobe

22 p3585 A71-41703

Evaporated tellurium thin films electric properties, discussing fabrication techniques, temperature dependence, field effect and Hall mobilities, threshold voltage and stability

23 p3715 A71-43435

InTe thin films formation, growth kinetics and physical properties, determining vapor deposited film thickness dependence on glass substrate temperature

24 p3861 A71-45249

VAPOR GENERATORS

U VAPORIZERS

VAPOR LIQUID EQUILIBRIUM

U LIQUID-VAPOR EQUILIBRIUM

VAPOR PHASES

Damkohler analysis of nitrogen-silica gel absorption isotherm in multimolecular range, noting vapor phase transport and absorbed phase diffusivities

03 p0517 A71-13175

Gas phase atomic hydrogen, nitrogen and oxygen detection by photoelectron spectroscopy of ground state, suggesting application to gas phase kinetics

04 p0548 A71-14799

Gas phase composition effect on CdS deposits crystalline perfection by Knudsen effusion apparatus and mass spectrometry

06 p0942 A71-18084

Gas phase model for ammonium perchlorate deflagration at 20-100 atmospheres

[AIAA PAPER 71-171] 06 p0944 A71-18611

Vapor bubbles radius at heating surface separation moment at boiling under free convection and forced motion through channel

07 p1221 A71-18923

Gas phase ion-molecule phosphine reactions in pure and binary mixtures by ion cyclotron resonance spectroscopy, considering acidity and basicity

08 p1251 A71-21699

Gas phase ignition of solid propellants involving gas phase variable density for constant density based equations by Howarth transformation

10 p1695 A71-24332

Experimental method for determining condensed phase heat of reaction of deflagrating double-base

propellant, defining minimum surface temperature at solid surface without heat feedback

11 p1809 A71-25493

Burning gunpowder temperature measurement in gaseous phase, describing thermocouple method

15 p2463 A71-31388

Heat pipes design and applications, examining pressure losses in steam and liquid phases and capillarity and gravity effects

[HEAT EXCH. CONF. PAPER 23] 15 p2513 A71-31637

Carbon fiber surface reactivity from gas chromatographic measurement, discussing adsorption isotherm of various vapors

16 p2541 A71-34049

Soviet book on gas phase chemical reactions rate constants determination covering elementary processes kinetics empirical methods

17 p2694 A71-34522

Cylindrical powder samples combustion stability, noting gaseous and condensed phase interaction effects on sound emission

17 p2840 A71-35699

Added inert gases effect on gas phase H atoms recombination rate at room temperature, using electron spin resonance spectroscopy

19 p3011 A71-38080

Slow and explosive gas phase oxidation of carbon suboxide and monoxide under various pressure and temperature ranges, noting branching reactions

19 p3167 A71-38088

Hypergolic rocket propellant system gas phase ignition, measuring ambient pressure, flow parameters and propellant temperature effects on delay characteristics

19 p3123 A71-38297

Nitriding process on Nb alloy, presenting gas phase temperature, time and composition effects

24 p3838 A71-44894

VAPOR PRESSURE

Thermophysical properties of methane, considering virial coefficients, vapor and melting pressures

04 p0674 A71-14728

Lithium tetrafluoro-aluminate equilibrium vapor pressure over solid aluminum fluoride plus solid lithium cryolite examined by weight-loss effusion method

07 p1055 A71-19624

Vapor pressure measurements of mineral oils for hydraulic power systems, using transpiration method

09 p1484 A71-23666

Ar condensation onset location in supersonic nozzles for nuclear space propulsion systems, using supercooled vapor pressure measurements beyond saturation point

10 p1593 A71-24328

Venus cloud hypotheses, discussing chemical composition, vapor pressure, temperatures and spectroscopic abundances

11 p1824 A71-25705

Neurospora germination and growth in medium of low water activity due to NaCl or nonelectrolyte addition

11 p1721 A71-26146

Equilibrium temperatures, pressures and oxygen fugacities of equilibrated chondrites in meteorites

13 p1411 A71-29098

Total and vapor pressure sensing and hybrid analog/digital electronic controller for multiburn cryogenic spacecraft propulsion pressurization

[AIAA PAPER 71-647] 14 p2290 A71-30724

Molten Co-Sn alloys, detailing vaporization rate, vapor pressure and partial and integral isothermal and isobaric formation potentials

15 p2425 A71-31394

Hydrogen condensation in interstellar gas clouds onto solid dust grains from vapor pressure measurements of solid hydrogen at low temperatures

16 p2634 A71-33392

Saturated Hg vapor pressure at 650-900 K by boiling point method

19 p3162 A71-37591

Low pressure Cs vapor thermionic converter with lanthanum boride cathode, investigating arc conditions and I-V characteristics

19 p2999 A71-38254

VAPOR TRAILS

U CONTRAILS

VAPORIZATION HEAT

U HEAT OF VAPORIZATION

VAPORIZERS

NT EVAPORATORS

Fuel evaporation in combustion chambers L-shaped and annular vaporizers, determining operational parameters effect on evaporation ratio

10 p1658 A71-25123

Low pressure drop fuel liquid injectors for jet engine combustors, using gas turbine vaporizer design

[ASME PAPER 71-GT-38] 11 p1812 A71-25972

VAPORIZING

NT BOILING

NT EVAPORATION

NT FILM BOILING

NT FLASHING [VAPORIZING]

NT LEIDENFROST PHENOMENON

NT NUCLEATE BOILING

VAPORS

NT PROPELLANT EVAPORATION NT SUBLIMATION NT TRANSPIRATION

Spherical alcohol droplet vaporization in acoustically disturbed medium, considering convective heat and mass transfer

01 p0179 A71-10798

Vaporization and combustion kinetics of condensed single drop kerosene and gasoline thickened by polyisobutylene

01 p0142 A71-11446

Vaporization chemistry in C, Si, Cr, Mo and Nb high temperature oxidation, using thermochemical diagrams

03 p0374 A71-13123

Gas flow parameter changes under partially vaporized fluid injection, considering effects on pressure, temperature and rate of resultant mixture

03 p0521 A71-14252

Vaporization rate of liquid injected into high temperature supersonic gas flow, considering relation to static pressure and distillation process

03 p0521 A71-14253

TiS vaporization thermodynamics by high temperature mass spectrometry, considering ionic fragmentation and ionization cross section errors

07 p1054 A71-19368

IR laser propagation through fog with droplet vaporization, assuming incident electromagnetic radiation as plane harmonic wave

08 p1302 A71-21392

Oxidation/vaporization kinetics of chromium oxide hot pressed and sintered pellets

09 p1480 A71-22113

Meteorite masses evaporation during flare, showing discrepancies for luminosity factors

09 p1520 A71-22830

Multiple echo of impurity atom during collisions with solid body surface, contributing to vaporization from layer

12 p1932 A71-27034

Melting body disintegration in hypersonic gas flow under radiation influence from shock layer, assuming optically thin boundary layer and intense vaporization

14 p2336 A71-30222

Molten Co-Sn alloys, detailing vaporization rate, vapor pressure and partial and integral isothermal and isobaric formation potentials

15 p2425 A71-31394

Thermal conductivity and coating emittance measurements by stationary substrate heater method suitable for materials applied by flame vaporization

15 p2512 A71-31501

ZrC vaporization at high temperatures, investigating dissociation into components by mass spectroscopy

15 p2431 A71-32158

Vaporization thermodynamics of lanthanum carbides from Knudsen effusion mass spectrometry

16 p2538 A71-32812

High temperature vaporization of titanium, zirconium, hafnium and thorium carbides by Knudsen effusion mass spectrometry, measuring ion intensities, formation enthalpies and dissociation energies

16 p2540 A71-33251

Vaporization heat transfer in saturated liquid capillary flow through thick structure, describing test facility and procedure

[ASME PAPER 71-HT-35]

19 p3166 A71-38000

Quasi-equilibrium prediction of rate of volatilization/erosion of solid tungsten by reaction with gaseous oxygen at high temperature and low pressure

21 p3404 A71-41419

Alkali metals vaporization from heated lunar samples, suggesting lunar rock erosion by localized heating due to volcanism or meteorite impact

23 p3741 A71-43636

Knudsen cell-mass spectrometric study of Apollo 12 samples vaporization process

23 p3750 A71-43700

Mass diffusivity effects in film boiling of water droplets vaporizing in air, Ar, N, He and steam

23 p3782 A71-43907

Liquid droplet vaporization under exposure to hot gas, obtaining time dependent temperature and concentration profiles in vicinity from coupled diffusion equations

24 p3888 A71-44963

N-heptane, carbon dioxide and Freon 13 droplet vaporization measurements at supercritical pressure, comparing with film theory calculation

24 p3890 A71-45072

VAPORS

NT CESIUM VAPOR NT MERCURY VAPOR NT METAL VAPORS NT SODIUM VAPOR NT WATER VAPOR

VARACTOR DIODE CIRCUITS

Varactor-tuned Gunn diode oscillators, discussing computerized design, circuit analysis and device characteristics

01 p0054 A71-10974

Semiconductor devices for frequency multiplication including variable capacitance, charge storage effect and composite varactor diodes

06 p0873 A71-17541

Spacecraft phased arrays design, considering solid state amplifiers effect on total array performance and transistors and varactors output power efficiency

07 p1069 A71-18813

Varactor tuned X band Gunn oscillator with lumped thin film microwave circuits, discussing GaAs materials, output powers and bandwidths

09 p1421 A71-23722

Intermodulation distortion in abrupt junction current pumped varactor frequency converter

20 p3202 A71-38848

Regenerative nonlinear RC amplifier oscillations due to series opposed varicap diode capacitance

24 p3810 A71-45261

VARACTOR DIODES

Gallium arsenide devices in microwave communications, discussing Gunn oscillators, FET, varactors and radar applications

02 p0231 A71-12049

Measuring instruments for hyperabrupt varactor tuning diodes in RF, VHF and UHF ranges

05 p0728 A71-16396

Diffusion varactor and Schottky barrier semiconductor diodes for frequency multiplication at millimeter wave frequency range

06 p0873 A71-17545

K band double-tuned nondegenerate parametric amplifier using single-packaged GaAs varactor diode, discussing design and performance

08 p1262 A71-20763

Wide band low noise millimeter wave parametric amplification using wafer varactor diodes with Schottky barrier junctions

08 p1263 A71-20769

Varactor capacitance variations compensation for temperature dependent diffusion potentials and dielectric constants changes

08 p1265 A71-21299

Microwave diode technology, discussing Schottky barrier, p-n junction, varactor, tunnel, bulk effect and avalanche diodes performance and applications

08 p1266 A71-21622

X- to K-band harmonic generator using nonlinear capacitance of varactor diode, deriving maximum efficiency, optimum load and generator impedances

09 p1417 A71-23036

Varactor-tuned avalanche microwave source, using interchangeable iris shims at output cavity for passive stabilization, power output and tuning variability

09 p1418 A71-23155

In-line harmonic tripler with GaAs varactor diode, detailing waveguide mount fabrication, power extraction filter and reverse bias voltage effects

14 p2211 A71-29857

Crystal oscillator temperature compensation using hyperabrupt junction varactor diode as reactance modulator and thermistor for temperature sensitive voltage control

14 p2215 A71-30902

Varactor tuned FM pulsed Gunn oscillator for testing X band delay lines for pulse compression radar

16 p2546 A71-33415

Broadband varactor tuned X band Gunn oscillator, investigating output power and temperature stability

17 p2717 A71-35340

I-V characteristics of plasma varactor formed near central or external conductor surface during coaxial line filling with plasma

23 p3651 A71-43403

VARACTORS

U VARACTOR DIODES

VARIABLE

Long period variable stars cumulative error increase for larger period variability

01 p0150 A71-10059

Variable voltage and frequency thyristor inverter, describing series commutation power stage

03 p0352 A71-13047

Nonlinear partial differential equations solution by variable separation method

03 p0451 A71-13713

[ASME PAPER 70-AUT-A]

VARIABLE AREA WINGS

U TRAILING-EDGE FLAPS

VARIABLE GEOMETRY STRUCTURES

Concorde aircraft Olympus 593 two-spool turbojet engine, discussing variable nozzle and intake assembly, afterburner and control system

07 p1183 A71-19081

Delta wing of symmetrical thickness and optimum variable geometry for two supersonic cruising speeds

09 p1384 A71-23617

Variable geometry external fuel tanks for high performance aircraft with drag reduction upon fuel transfer

[ALAA PAPER 71-395]

11 p1707 A71-25271

Automated low cost structural-mechanical design and optimization of wing pivot systems for variable geometry aircraft

[ALAA PAPER 71-404]

12 p1980 A71-27410

Wind tunnel tests of geometrically compatible airfoils for variable chord sailplane

13 p1994 A71-29257

Two dimensional wind tunnel tests on airfoil fastened between tunnel walls, investigating variable chord concept applicability in sailplane design

15 p2350 A71-32294

Performance evaluation of variable geometry external fuel tank prototypes by static structural tests, wind tunnel tests and flight tests on F-111 aircraft

[ALAA PAPER 71-763]

Supersonic jets expansion in variable cross section channel, emphasizing boundary layer behavior

18 p2903 A71-36111

Variable structure digital control servomechanism flutter mode analysis, using nonlinear differential equation

22 p3528 A71-42871

Extendible, variable profile nozzle for various flow regimes operation, developing numerical design algorithm

24 p3821 A71-45371

VARIABLE LIFT

U LIFT

VARIABLE MASS SYSTEMS

Generalized Hamilton-Jacobi theorem extension to dynamic equations of motion for holonomic mechanical systems of variable mass with impulse connecting multiplier

01 p0128 A71-11151

Optimal control of exhaust velocity for plane motion of variable mass point along trajectory under gravitational and resisting forces

02 p0284 A71-12292

Permanent motion stability of heavy body having variable mass geometry

05 p0783 A71-17030

Equations of motions solution for variable mass point, taking into account drag and velocity

06 p0979 A71-17494

Orbital analysis of two body problem with slowly decreasing mass, constructing limited time interval approximate solutions for three distinct phase domains

10 p1676 A71-24523

Optimal motion of multistage body of variable mass during vertical climb with allowance for weight limitations

10 p1683 A71-24844

Equations of motion for variable mass system of bodies, developing mathematical model of flight vehicle as six degrees of freedom control plant

12 p1926 A71-26772

Graviplane flight theory, spacecraft center of mass motion in central gravitational field with continuous mass geometry variation

16 p2646 A71-33666

Mass changes in restricted quasi-circular variable mass three body problem with particle equations of motion having Jacobi integral

20 p3291 A71-39326

Relativistic equation derivation for dynamics of point with varying rest mass from Newtonian principle

21 p3415 A71-40655

Lagrange equations for variable mass systems with rotational transport and relative motions

23 p3773 A71-43093

VARIABLE STARS

NT CEPHEID VARIABLES

NT NOVAE

NT SUPERNOVAE

NT T TAURI STARS

High luminosity red variable star radiation, examining degrees of intrinsic polarization

01 p0150 A71-10059

Long period variable stars cumulative error increase for larger period variability

01 p0150 A71-10059

Soviet papers on physics of nebulas and variable stars covering luminescence, reflecting and scattering properties, spectrophotometry, computerized simulation, etc

02 p0311 A71-12354

Spectrophotometry of star EW Lac, showing variability by H line profiles

02 p0311 A71-12356

Hydrogen lines of spectrally variable star alpha squared CVn from spectrograms, determining atom concentration, electron density and acceleration of gravity on surface

02 p0311 A71-12357

Soviet papers on pulsating stars covering classical, dwarf and spherical component Cepheids, RV Tau and RR Lyr types, variable stars, etc

03 p0485 A71-12358

Stellar variability emphasizing pulsations, noting role of He II critical ionization zone in maintaining self oscillations

03 p0485 A71-12359

RV Tau type stars general and spectral classification, covering color indices, line-of-sight velocities, kinematics and spatial distribution

03 p0485 A71-13262

Delta Scutum type variable stars, discussing photometric properties, line of sight velocities, color indices, luminosity, chemical composition, etc

03 p0485 A71-13264

Beta Cepheus type variable stars brighter curves and line of sight velocities graphs, discussing periods, luminosity, spectra, kinematics and spatial characteristics, etc

03 p0486 A71-13266

Mira Ceti type long period variable giant stars emission spectra, emphasizing UVB photometry and IR electrophotometry 03 p0486 A71-13267

Semiregular and irregular variable stars spatial densities and distributions, amplitudes and periods 03 p0486 A71-13268

UBV photometry of RR Lyrae variables in metal rich globular cluster NGC 6171 04 p0649 A71-15372

Magnetic stars with brightness variations in visual and blue light, noting method for period determination 04 p0650 A71-15397

Algol type variables, investigating gradient Balmer discontinuity and diameter variations 04 p0651 A71-15662

Variable stars GR 181-202 in galactic cluster IC 1848 field examined by Schmidt telescope 04 p0651 A71-15663

Technetium stars characteristics, noting MS, S and N spectral types, s process element enhanced abundances and variability 05 p0806 A71-16206

Sun as variable star, discussing brightness, rotation and magnetic characteristics 06 p0971 A71-18245

Novae, symbiotic, T Tauri, U Geminorum and UV Ceti type stars, determining mass loss rate 06 p0973 A71-18338

Flare stars in solar neighborhood, obtaining time averaged energy radiation upper bounds 06 p0976 A71-18474

Eclipsing variable binary stars spectral and luminosity classes determination 07 p1200 A71-20035

RW Aur stellar spectrum variation mechanisms 07 p1200 A71-20036

AB Aur light variations in three colors, estimating visual absolute magnitudes free of interstellar absorption and B-V 07 p1201 A71-20433

Photoelectric UVB observations of variable star AE Aur (November 1963-February 1968), tabulating and graphing results 07 p1201 A71-20434

Variable emission star BD plus 28.637 deg three color photographic observation data evaluation, giving light curves and H-R position 07 p1201 A71-20435

Photoelectric and radio observations of flares of UV Ceti and YZ CMi stars 07 p1204 A71-20628

Photoelectric observations of EV Lac flares in spectral U, H beta, G and V regions 07 p1204 A71-20629

Eclipsing variable binary system RR Centauri observed photoelectrically in yellow and blue light 08 p1357 A71-20875

Book on dwarf novae covering light variations, spectra, binary systems, absolute magnitude, mass, gas streams, outburst, etc 08 p1363 A71-21165

Variable stars radii effective temperature and brightness determination from stellar atmosphere modes 09 p1523 A71-23021

Variable stars, quasars and X ray source ScoXR-1 UVB light photoelectric data, examining optical emissions and brightness variations 09 p1524 A71-23186

Eclipsing system GG Cas, presenting photoelectric data 09 p1527 A71-23527

Algol secondary component gravity darkening observations, examining IR light curve 09 p1527 A71-23530

German book on variable stars covering supernovae, novae, pulsating variable stars, symbiotic objects, galactic nebulae, stellar and galactic evolution, astronomical photometry, etc 10 p1675 A71-24479

Soviet book on eruptive stars including U Gem stars, symbiotic stars, R CrB stars, UV Ceti stars and alpha squared CVn stars 10 p1677 A71-24732

Multicolor photographic photometry of flare stars in Orion aggregate based on two UVBR photoelectric sequences 10 p1680 A71-25061

Automated and conventional photometry of short period variable star 14 Aurigae, using automatic telescope 12 p1956 A71-26617

Coma galactic cluster, investigating nuclei oblateness, diagrams and tables of variables 12 p1962 A71-26910

BY Dra stellar flare characteristics by photoelectric observations, noting duration 12 p1971 A71-27750

Linear nonadiabatic pulsations of stellar models, discussing numerical method for eigenvalue problem 13 p2132 A71-27968

Orbital elements and corrected light curve of eclipsing variable star Z Vulpeculae, using FORTRAN 4 program 13 p2137 A71-28513

Pleiades flare stars photographic magnitude and brightness data, establishing relation between amplitude and duration 15 p2486 A71-32029

Flare star light polarization parameters measurement, describing polarimeter design 15 p2487 A71-32036

AO Algol-type variables W Del, T L Mi, RZ Cas, and delta Lib gradient variation and Balmer discontinuity, detailing luminosity and radius ratio effects 16 p2634 A71-33427

Irregular variable BL Lac photographic observations, equating object with radio source VRO 42.22.01 16 p2635 A71-33430

Algol type star AW Peg, determining gradient, temperature, absolute visual magnitudes, equivalent absorption line widths, atmospheric parameters and spectral class 17 p2800 A71-34567

Luminosity curves for eclipsing Algol-type systems with extended atmospheres based on stellar models 17 p2803 A71-34840

Variable star brightness measurement, using on-line electronic computer, analog to digital converter and reflector with direct current amplifying photometer 17 p2741 A71-34990

Pulsating variable star spectral line formation from integral equation solution of radiative transfer and gas flow through shock front 17 p2808 A71-35553

Variable and magnetic stellar model hypothesis concerning long period modulation due to radial and non-radial oscillation mode coupling beat in dipole magnetic field 18 p2962 A71-36152

Variable stars atmospheric radiation, investigating unsteady light reflection 19 p3133 A71-37505

Rotating isothermic radially pulsating white dwarf evolution, considering neutronization and general relativistic effects 19 p3134 A71-37511

Critique of Woodward-Youngrau hypothesis of frequency dependence of light velocity in gravitational fields based on variable stars observations, considering photon rest mass 20 p3286 A71-38836

Transition period for variable stars, considering helium sensitive relationship to luminosity obtained with nonlinear theory 20 p3287 A71-39054

Photometric and spectroscopic observations of pulsating stars, noting shock waves in atmospheres of W Virginis and RR Lyrae 20 p3292 A71-39446

Pulsar pulsed optical radiation search, noting dependence on determination of accurate positions by radio methods 20 p3303 A71-39938

Visible optical pulsars search with Fourier and correlation techniques in X ray sources, supernova remnants, white dwarfs, IR stars, planetary nebulae, etc 20 p3304 A71-39939

Short period variables, considering Scuti stars evolution, pulsations, magnitude and positions in H-R diagram 21 p3440 A71-40054

Photoelectric observations of magnetic variable stars with five color photometer, giving light and color curves parallel to main sequence 21 p3440 A71-40057

OH emission sources associated with long period variable IR stars emitting in 1665-1667 MHz lines 21 p3441 A71-40067

Spectroscopic radial velocity study of Algol eclipsing variable stars, deriving masses and apsidal motion evidence in short period orbit 21 p3446 A71-40418

Nonlinear photometric effects of limb darkening and gravity darkening dominance in eclipsing variables from light minima observations 22 p3604 A71-42332

Photometric study of light variation and variable stars in luminous supergiants in Large Magellanic Cloud 23 p3723 A71-42940

Soviet papers on astrophysics covering variable stars and galactic structure, stellar atmospheres, cometary physics and evolution, stellar and solar spectroscopic observations, etc 23 p3771 A71-44302

Red variable GN Her brightness, color and spectrum, discussing UVB system photoelectric measurements during 1966/68 period 23 p3771 A71-44303

Eclipsing variables period change dependence on spherical coordinate of stellar position in sky from O-C diagrams 24 p3873 A71-45080

VARIABLE SWEEP WINGS

V/STOL civil aircraft, considering rotor lift and variable sweep wings 10 p1556 A71-24850

Variable sweep wing aircraft angular motion mathematical model, analyzing inertial moments influence on control dynamics 11 p1708 A71-25661

Large variable sweep wing maneuver load relief system with ailerons reducing resulting bending moment at pivot 15 p2348 A71-31600

Fighter F-14 podded engine high variable sweep wing design including nozzle, nacelle, fuselage shift, aspect ratio and lift control improvements 16 p2526 A71-34152

Variable geometry B-1A bomber aircraft, discussing size, payloads, speed, altitude range and runway takeoff 19 p2996 A71-37516

Panavia 200 multipurpose military aircraft, describing variable geometry design concept, performance characteristics, engines, armament and electronics 24 p3792 A71-44766

VARIABLE THRUST

Solid propellant rocket motor combustion control by fluidic vortex valve, considering thrust variation [AIAA PAPER 70-643] 07 p1183 A71-18904

Restricted three body problem with variable thrust particle motion in Newtonian field 10 p1672 A71-24337

VARIANCE

Time variant distortions in supersonic inlet on J-85-GE-13 turbojet engine from wind tunnel test, considering instantaneous distortion amplitudes and contours [AIAA PAPER 71-667] 14 p2290 A71-30733

VARIANCE [STATISTICS]

NT MULTIVARIATE STATISTICAL ANALYSIS

Variance estimates and error expectations for satellite coordinates and velocity vectors from star altitude measurements 02 p0278 A71-11903

N interval trajectory estimation computer program minimum variance adjustment technique, discussing airborne astrogographic camera system for reentry bodies position determination 04 p0556 A71-15330

Spring supported beam-column nth vibration and buckling eigenvalues, discussing Monte Carlo simulation for evaluating perturbation method accuracy for variance calculation 06 p1004 A71-18591

Kalman filter application as observer of observable signals derivatives, using gain matrix to minimize variance estimate for instrument landing systems 08 p1269 A71-21343

Frequency counted measurements and phase locking to noisy oscillators, showing counted frequency method sample variance slow convergence to actual variance 10 p1574 A71-23763

Second order experimental plans, obtaining regression analysis for matrix elements and regression coefficients variance 12 p1988 A71-26707

Variance estimates and error expectations for satellite coordinates and velocity vectors from star altitude measurements 13 p2098 A71-28190

Adaptive controller consisting of real time identifier and minimum variance regulator approached through stochastic optimal control theory 14 p2219 A71-29696

Variances and covariances calculation for fluctuating numbers of semiconductor conduction electrons in terms of noise 14 p2211 A71-30292

Structures with random resistance, calculating upper and lower bounds for safety coefficients average value and variance 19 p3156 A71-37643

Noise variance maximum likelihood estimate based on order statistics for first order Reed-Muller code transmission over zero-mean white Gaussian noise channel 20 p3202 A71-38875

Depth perception variability under central and peripheral illumination conditions, using Duncan multiple range test for data analysis 22 p3498 A71-41481

Mathematical models for microorganism exponential die-off rate and variance estimation from decontamination data 22 p3504 A71-42231

Exact and approximate algorithms for computation of modeling and bias errors in linear minimum error variance estimation 23 p3656 A71-43940

Discrete parameter covariance stationary stochastic process in rotation sampling, deriving minimum variance unbiased linear population mean estimator by constrained optimization procedure 24 p3844 A71-45132

Electron multiplier pulse height distribution for single electron input, investigating relative variance correlation with statistical fluctuations of gain
24 p3811 A71-45329

VARIATION METHOD
U CALCULUS OF VARIATIONS
VARIATIONAL PRINCIPLES
Self gravitating fluid spheroid oscillations in hydrostatic equilibrium with magnetic fields using variational principle
01 p0129 A71-11336
Nondissipative micromorphic media field equations derivation, applying variational principle to theory of deformable bodies
01 p0177 A71-11372
Finite element method approximations outside variational principle in elasticity problems, examining convergence to exact solution
[ASME PAPER 70-WA/APM-34]
03 p0512 A71-14160
Geometrically nonlinear shell dynamics, basing equations of motion and compatibility on variational principles
03 p0514 A71-14346
Nonlinear variational analysis theory for weather forecasting
05 p0773 A71-16154
Dynamic thermoelastic response of rapidly heated plate elements, developing variational principle
05 p0824 A71-16560
Variational principle for generalized theory of heat conduction with finite wave speed, reducing nonlinear boundary value problem to ordinary differential equation
05 p0837 A71-16567
Inverse variational principles of brittle body fracture derived by extending inverse variational principles of mechanics and thermodynamics
05 p0825 A71-16609
Continual systems analytical mechanics, discussing least constraint variational and Ostrogradskii-Hamilton principle applications in shell stability, filtration, plasticity and dislocation theories
05 p0828 A71-16895
Composite materials plasticity limit calculation using variational principles
05 p0773 A71-16992
Planetary boundary layer forecast model, determining horizontal and vertical wind components, temperature, pressure and moisture with numerical variational objective analysis
05 p0778 A71-17049
Variational principles for linear initial value problems with sources on and within boundaries, using time convolutions
05 p0776 A71-17218
Variational principle for MHD of ideal fluid, determining canonical variables and Hamiltonian
06 p0929 A71-17378
Rectangular panel acoustic response by variational finite element method, including radiated sound field effects on structural vibration
06 p0984 A71-17622
Elastic shell dynamics under initial and boundary conditions, developing variational principle algorithm
06 p0986 A71-17756
Conductive heat transfer with nonlinear boundary condition, reducing to linear boundary value problem through variational principle
07 p1224 A71-19902
Komkov class of boundary value problems and associated variational principles, discussing necessary conditions for basic functional or potential extremal behavior
08 p1323 A71-20878
Variational principle application to stability in failure mechanics of arbitrary linearly elastic bodies, discussing inertia effect on steady state vibrations of cracked bodies
08 p1372 A71-21704
Flexible elastoplastic shallow shell theory, using mixed variational principle for flexure velocity and stress function
09 p1535 A71-22179
Variational and boundary value problems in regular regions containing manifolds with dimensionalities lower than n minus one
09 p1485 A71-22289
Iterative computation of variational optimization problems by analog computers with digital logic control /hybrid computers/
09 p1413 A71-23665
Pluto orbit integration over 4.5 million years by variation of parameters technique and confirming Neptune-Pluto orbital resonances
10 p1669 A71-24179
Boltzmann equation for shock wave structure, comparing errors of variational principles and moment methods of approximation
10 p1593 A71-24279
German book on optimization for variational problems with ordinary differential equations as secondary conditions
10 p1636 A71-24480

Variational principles for initial boundary value problem of fully coupled linear thermoelasticity for inhomogeneous anisotropic materials with microstructure
10 p1689 A71-24512
Polygonal elastic plates natural frequencies investigation by conformal mapping and variational method, transforming holomorphic function into equivalent problem of circular boundary plate
10 p1691 A71-24813
Variational principle for continua dynamic analysis by hybrid finite element method, considering consistent inertia properties of elements obtainable from assumed stress functions
10 p1692 A71-25047
Duality in doubly curved shells analysis by finite element method, applying Kirchhoff-Love shells boundary conditions and energy variational principle
10 p1693 A71-25049
Structural dynamics motion matrix Newmark generalized acceleration operator, Wilson averaging variant and Gurtin variational principle investigations for stability and approximation viscosity
10 p1693 A71-25050
Analytical lunar ephemeris, comparing variational and parallax inequalities with various theories
11 p1831 A71-26137
Shallow laminated shells nonlinear bending equations, using variational principle with allowance for transverse shear strain of layers
12 p1975 A71-27104
Three dimensional nonlinear elastic anisotropic body formulating stability at finite subcritical strains with variational principle
12 p1978 A71-27333
Variational principle for ideal fluid MHD, determining canonical variables and Hamiltonian
12 p1940 A71-27456
Specialized version of Jones direct stiffness structural analysis method, deriving functional substitutions in variational formulation for displacement discontinuities
12 p1983 A71-27597
Planar elliptic restricted three body problem, calculating variational equations separation with matrix approach
13 p2136 A71-28359
Grid refinement technique generating sequences of approximate solutions to two-point variational problems defined on continuous flows
13 p2096 A71-29380
Buckling under compressive loads of incompressible neo-Hookean plates for homogeneous initial deformation, using variational principle
14 p2333 A71-30993
Variational principles and finite element method in partial differential equations, emphasizing basis functions fundamental to Galerkin procedure
15 p2441 A71-31351
Variational principles application to continuum mechanics boundary and initial value problems, discussing examples in elastostatics, piezoelectricity and hydroelasticity
15 p2441 A71-31416
Finite element method theory, discussing variational principle use, continuity requirements on interelement boundaries and incremental formulations of nonlinear problem in solid mechanics
16 p2651 A71-33077
Variational principles in solid continua mechanics, describing finite element models
16 p2651 A71-33078
Mixed finite element formulation for shallow shells, discussing element matrix generation phase and governing variational principle
16 p2652 A71-33080
Nonlinear elastic incompressible bodies with small deformations, obtaining three dimensional static and dynamic stability variational equation
17 p2816 A71-34328
Direct variational methods for solving parabolic boundary value problems of arbitrary order in space variables, considering Dirichlet problem solution
17 p2764 A71-34640
Ultrasonic surface wave generation by infinite interdigital electrode array on piezoelectric material, predicting behavior from equivalent circuit by variational principle
17 p2717 A71-35491
Variational principle with reflectivity extremum for inhomogeneous planetary atmospheric line spectra profile calculation from radiative transfer equation
18 p2964 A71-36286
Dynamic response of oddly stiffened circular cylindrical shells, using modified variational method
18 p2980 A71-36495
Numerical stability of extended Kantorovich method for single term variational approximation of torsional problem
18 p2980 A71-36702
Composite materials plasticity limit calculation using variational principles
18 p2940 A71-36792

Complementary variational principles, noting application to differential, integral and matrix equations
18 p2943 A71-36957
Nonlinear elasticity theory variational principles modification for finite deformation of elastic body
19 p3154 A71-37095
Inelastic buckling process of axially compressed cylindrical shells with edge constraints, using variational principle and Rayleigh-Ritz method
19 p3158 A71-38182
Splitting-up method with variational optimization for time independent nonstationary hydrodynamic transfer equations for use in meteorology, oceanology, etc
19 p3088 A71-38313
Energy and variational principles, studying local stability of equilibrium of elastic body subjected to conservative and gyroscopic forces
20 p3232 A71-38795
Error bounds and variational principles for nonlinear differential and integral equations, exemplifying by Liouville and Poisson-Boltzmann equations
20 p3255 A71-39495
Variational principle for obtaining upper and lower bounds on minimum drag on body of given volume in slow viscous flow
20 p3177 A71-39500
Mechanical elements and systems optimal design, discussing variational and programming techniques application to machine elements design optimization
[ASME PAPER 71-VIBR-62]
21 p3385 A71-40306
Multibeam holographic interference Gabor theory construction, using variational principle and potential theory
21 p3379 A71-40626
Elastic shells of revolution displacement analysis, using incremental variational theory with finite element method
22 p3613 A71-41434
Multibeam holographic interferometry, using variational principle and potential theory
22 p3574 A71-41786
Analytical transformations of variational conditions in nonequilibrium thermodynamics, using mechanical analogies similar to d'Alembert principle
22 p3622 A71-42688
Conservative Hamiltonian systems with infinitely deep potential wells, obtaining periodic solutions with variational technique
23 p3698 A71-43008
Lunar orbit space station lifetime, using averaged variational equations numerical integration for terrestrial, solar and lunar gravitational field effects
23 p3730 A71-43047
Invariance theory for nonlocal variational principles, covering energy forms and identities, weak coordinate invariance, integral balance and conservation laws
23 p3700 A71-44179
Three dimensional incompressible anisotropic body with small deformations, calculating elastic stability theory with variational principle
24 p3880 A71-44708
Conductive heat transfer and temperature jump in polyatomic gas between parallel plates evaluated by variational principle based on linearized integro-differential equation
24 p3889 A71-44969

VARIATIONS
NT ALTERNATIONS
NT ANNUAL VARIATIONS
NT DIURNAL VARIATIONS
NT GEOMAGNETIC MICROPULSATIONS
NT GEOMAGNETIC PULSATIONS
NT MAGNETIC VARIATIONS
NT NOCTURNAL VARIATIONS
NT PERIODIC VARIATIONS
NT TWENTY-SEVEN DAY VARIATION
NT WIND VARIATIONS

VARIOMETERS
Balloon and glider vertical speed indicators, considering barometric devices and electric variometer
06 p0901 A71-18248
Geomagnetic field variations recording by two variometers, correcting for variation components effects by instruments orientation
06 p0901 A71-18284
Quartz magnetic variometer allowing simultaneous recording of magnetic field variations and suspension axis inclination changes
06 p0901 A71-18285

VARIATORS
Polarizing phase shifter for quasi-optical transmission lines, describing variator network operation
08 p1264 A71-21068
Gamma irradiation effect on conductivity of variators made of p-type black SiC
12 p1886 A71-26897
Black SiC variators IV characteristics and conductivity, investigating fast neutron irradiation and isochronal annealing effects
12 p1886 A71-26898

- Gamma radiation induced changes in parameters of black silicon carbide nonlinear semiconductor resistors/varistors/ 16 p2546 A71-33464
- VASCULAR SYSTEM**
- NT AORTA
- NT ARTERIES
- NT BLOOD VESSELS
- NT CAPILLARIES [ANATOMY]
- NT GLOMERULUS
- NT VEINS
- Eating and digestion effects on conscious dog coronary and visceral vasoactivity 01 p0015 A71-11183
- Arterial sclerosis and stenosis physical factors, discussing connective and vascular tissue adaptive responses to mechanical stresses 02 p0200 A71-12415
- Natural or endogenous fibrinolysis and its pharmacological enhancement as possible approach to prophylaxis of vascular occlusions 02 p0200 A71-12417
- Blood pressure and velocity waveform recording for patients during cardiac catheterization, interpreting relationships to vascular impedance 02 p0201 A71-12915
- Antigenic properties of human vascular wall layers in atherosclerosis, using agar precipitation and immunoelectrophoretic measurements 04 p0540 A71-15574
- Lung volume direction and change rate effects on pulmonary vascular conductance and arterial flow in isolated dog lung lobe 05 p0711 A71-16952
- Intrarenal vascular pattern in carbon dioxide death of rhesus monkeys and dogs, observing sympathetic vasoconstriction 06 p0851 A71-17610
- Acute pulmonary embolism diagnoses, using vascular angiography 07 p1042 A71-19838
- Vascular effector structure in orientation reaction of peripheral vessels to sound, using plethysmogram and rheoencephalogram indications 08 p1242 A71-21962
- Argyrophil sphincter formations in intraorganic vascular channels of hearing organ 08 p1243 A71-21967
- Stroke-pulmonary blood volume relation and vascular recruitment and distensibility in dogs, allowing independent control of flow, heart rate and left atrial pressure 10 p1561 A71-24123
- Heart rate and diastolic inflow coronary resistance extravascular component, discussing heart artificial stimulation and pharmacological maximal dilation effects 10 p1565 A71-24679
- Hypertensive heart and pulmonary vascular disease, examining chronic alveolar hypoxia effects 11 p1719 A71-25931
- Blood liquid state control in sanguiferous canal as function of humoral feedback in coagulation, fibrinolytic and anticoagulation systems 13 p2010 A71-28718
- Coronary blood flow response to acute and chronic hypoxia, observing vascular smooth muscle relaxation relation to released adenosine 14 p2184 A71-30281
- Coronary vasculature development under hypoxia and pulmonary hypertension as possible cause of right ventricle phasic flow contour changes 14 p2184 A71-30282
- Hypothermia effects on cat and dog vascular tonus vasomotor reflex regulation, suggesting role of inhibition due to changed afference from cooled tissues 16 p2533 A71-34111
- Circulation parameters in vascular network by bloodless zonal ultrasonic sphymography based on acoustic bioecholocation 17 p2689 A71-34648
- Nasal vascular system reactions during 120-day bed rest hypokinesia under drug affected metabolism 20 p3188 A71-39229
- Active vasodilation in gracilis muscle vascular bed due to perfusion pressure changes 20 p3189 A71-39378
- Potassium concentrations and osmolality levels changes effects on vascular resistance in subcutaneous adipose tissue blood flow 20 p3189 A71-39379
- Human vascular and extravascular fluid changes during six days bedrest based on fluid volume and ideal body weight from individual heights 21 p3331 A71-40354
- VASOCONSTRICTION**
- Sexual behavior of male cats after parachlorophenylalanine injections, noting unchanged or diminished performance and serotonin lowering in brain 02 p0199 A71-12365
- Plethysmographical study of noise effects on hearing and peripheral vasoconstriction in man and animals 03 p0359 A71-13155
- Carotid sinus hypotension in dogs under fasting/digestion conditions, considering effect on splanchnic circulation and vasoconstrictor response 04 p0538 A71-15090
- Traumatic vasospastic disease in forest workers with Raynaud phenomena, considering cold vasodilation and occupational vibration vasoconstriction by finger blood circulation tests 05 p0708 A71-16616
- Intrarenal vascular pattern in carbon dioxide death of rhesus monkeys and dogs, observing sympathetic vasoconstriction 06 p0851 A71-17610
- Myocardial ventricle contraction in high altitude hypoxia adaptation, using barochamber trained rats 06 p0857 A71-18467
- Hypoxemia reflex neurogenic vasoconstrictor factors competition with local vasodilator mechanisms in skeletal muscle 08 p1237 A71-20680
- Pulmonary vasoconstrictor response to temperature dependent acute hypoxia, using isolated rat lungs with heparinized homologous blood under constant volume pulsatile inflow 10 p1561 A71-24124
- Pulmonary arterial system impedance and transmission properties, noting hypoxia and serotonin infusion vasoconstrictor effects 11 p1719 A71-25929
- Hypoxia effects on cardiovascular reflexes during hypoxia, measuring response of heart rate to lower body negative pressure 16 p2529 A71-33191
- VASOCONSTRICTOR DRUGS**
- Central nervous system reactions to vasopressin and oxytocin presence in cerebrospinal fluid and blood, discussing respiratory frequency and antidiuretic tests 03 p0363 A71-13485
- Cold pressor response tests under altitude acclimatization and simultaneous hypoxic acclimatization and cold in man 22 p3502 A71-41831
- VASODILATION**
- Vasodilator, oxygen, potassium and osmolality effects on exercise hyperemia in dog gracilis muscle 01 p0015 A71-11184
- Human skin blood flow and venous tone in middle finger and forearm during leg muscle exercise to exhaustion 01 p0016 A71-11410
- Traumatic vasospastic disease in forest workers with Raynaud phenomena, considering cold vasodilation and occupational vibration vasoconstriction by finger blood circulation tests 05 p0708 A71-16616
- Hypoxemia reflex neurogenic vasoconstrictor factors competition with local vasodilator mechanisms in skeletal muscle 08 p1237 A71-20680
- Active vasodilation in gracilis muscle vascular bed due to perfusion pressure changes 20 p3189 A71-39378
- Coronary dilating substances of low molecular weight separated through dialysis from hypothalamus protein carriers 21 p3338 A71-41072
- VASOMOTOR NERVOUS SYSTEM**
- U NERVOUS SYSTEM
- VC-10 AIRCRAFT**
- VC-10 aircraft ILS electronic equipment reliability tests 04 p0559 A71-15873
- VECTOR ANALYSIS**
- NT COLLINEARITY
- NT COPLANARITY
- NT CURL [VECTORS]
- NT VORTICITY
- Time vector method for aircraft flight test data evaluation, discussing control deflections effects on phugoid motion, lateral stability derivatives and error estimation 03 p0347 A71-13341
- Book on applied matrix and tensor analysis covering coordinate systems, vectors, transformations, etc 03 p0450 A71-13569
- Spatial vector calculations using laser distance measurement and optical observations 03 p0380 A71-14191
- Optimal control systems, using vector analysis in definition of envelope contact test 05 p0774 A71-16644
- Kincaid iterative solution for multidimensional systems of nonlinear equations, noting quadratic convergence as function of initial vectors 05 p0775 A71-17046
- Orientation vector differential equation formulation for strapdown inertial navigation, applying to rigid body rotation problem 07 p1154 A71-18832
- Vector wind shears statistical analysis at various altitudes, using balloon sounding measurements 08 p1327 A71-21457
- Inequality constraints in primer optimal N impulse solutions, introducing penalty function and its gradient with respect to control variables 11 p1791 A71-25497
- Comet orbits correction, including differential coefficients perturbations based on Kulikov equation for difference between computed and true radius vector 11 p1833 A71-26328
- Ectopic right atrial rhythms in ECG vectorial analysis 12 p1870 A71-27289
- Newton gravitation theory, showing extension by relativistic mass and vector gravitation potential addition 14 p2305 A71-29682
- General nonorthogonal coordinate systems operation techniques, modifying matrix theory for vector equations handling in classical mechanics 15 p2442 A71-32111
- Weighted finite incidence systems construction using nonnegative integer functions and column vectors 16 p2603 A71-33591
- Nonlinear resonance problems analysis by averaging schemes, considering Volosov and Morgunov stability conditions 17 p2781 A71-34929
- Linear array antenna far field transient time response formulation, using concise vector field integral equations and generalization 17 p2717 A71-35584
- Generalized vectorial equation of motion for vibrating nonprismatic thin space beams, discussing boundary conditions, rotary inertia and shear deformation [ASME PAPER 71-APM-P] 18 p2978 A71-36259
- Third basic problem solution in elasticity theory satisfying boundary condition and Lamé equation system with two arbitrary vectors 19 p3160 A71-38484
- Maximum vector values for stability and rigidity of elastic systems under modulo limited disturbances, applying to beam deflection and second derivative 21 p3473 A71-41154
- Vector functionals optimization, programming optimal trajectories 23 p3657 A71-44017
- Earth angular velocity of rotation vector, discussing rotation rate and polar motion variations 23 p3674 A71-44260
- Systems synthesis by Liapunov direct method, developing vector-matrix equations for systems classes satisfying specified Liapunov scalar functions [ASME PAPER 70-WA/AUT-3] 24 p3816 A71-45135
- VECTOR CALCULUS**
- U VECTOR SPACES
- VECTOR CONTROL**
- U DIRECTIONAL CONTROL
- VECTOR CURRENTS**
- Geomagnetic solar quiet field and terrestrial currents diurnal variations, discussing interrelations and vector polarization 07 p1104 A71-20047
- VECTOR SPACES**
- NT ADJOINTS
- NT BANACH SPACE
- NT CANONICAL FORMS
- NT EIGENVALUES
- NT EIGENVECTORS
- NT HILBERT SPACE
- NT JORDAN FORM
- NT MATRICES [MATHEMATICS]
- NT STATE VECTORS
- NT VECTORS [MATHEMATICS]
- NT VORTICITY
- Schwarz-Neumann method for Dirichlet problem of elliptic differential equations describing regions intersection in n-dimensional Euclidean space 01 p0109 A71-10031
- Dual methods for calculating minimum of convex function on intersection of convexes, considering reflexive Banach space and normalized vector space 13 p2095 A71-28822
- Optimal control problems solution using linear vector space of continuous operators with constraints in Volterra integral and functional differential equations 13 p2043 A71-28829
- Gravitational field equations derivation from least action principle, interpreting additional vector field in generalization as vector potential of electromagnetic field 17 p2778 A71-34632
- Periodic solutions existence for autonomous system of ordinary differential equations, modifying parameter functionalization of vector fields in phase spaces 17 p2766 A71-34934
- Vehicle attitude determination and guidance sensor orientation by vector space matrix method, minimizing errors by weighted least squares affine transformation technique 23 p3773 A71-43064
- VECTORCARDIOGRAPHY**
- Equilateral tetrahedral and Frank systems compared for standard reference system applications in spatial vectorcardiography 01 p0022 A71-10400

- Adapted multichannel analyzer for cardiology visualizing vectorcardiographic loops
02 p0206 A71-12107
- Medical data processing techniques in electrocardiography and effort vectorcardiography facilitating clinical observations
02 p0207 A71-12110
- Isopotential maps comparison of thorax with vectorcardiograms from superficial potential distribution zones
02 p0207 A71-12111
- Vectorcardiograms comparison recorded with different electrode leads or amplification systems based on spatial points coordinates correlation coefficients
03 p0371 A71-13115
- Hyperventilation and isoproterenol infusion, investigating T wave abnormalities, arterial blood gases and plasma electrolyte concentration
07 p1042 A71-19837
- Primary T wave derived from ECG waveform dependent intrinsic ventricular recovery properties
07 p1050 A71-19840
- Left ventricular enlargements, comparing vectorcardiographic spatial magnitude and electrocardiographic precordial QRS voltage measurements
11 p1725 A71-26428
- Digital computer analysis of orthogonal ECG and VCG from patients with myocardial infarction
12 p1875 A71-27287
- Stochastic identification method for transforming ECG and VCG data to approximate diagnosis, using computerized dipole models
13 p2020 A71-29002
- Spatial T-area vectors dependence on RR distances for exact examination of healthy and sick heart muscles
15 p2362 A71-32660
- Patients with selective cine coronary arteriography, statistically correlating vectorcardiographic diagnoses of myocardial infarcts with changes in arteries
18 p2854 A71-36139
- Vectorcardiographic analysis of patients with ECG diagnosed inferior atrial rhythm
22 p3490 A71-42519
- Diagnostic import of QRS notching in HF ECG of living subjects with heart disease, noting notch count correlation with ventricular enlargement
23 p3636 A71-44130
- VECTORS [MATHEMATICS]**
NT EIGENVECTORS
NT STATE VECTORS
NT VORTICITY
- Time vector method extension to equations of motion with real roots, noting applications to aircraft flight control problems
06 p0925 A71-18049
- Noninferior performance index vectors in multicriteria optimal control theory
07 p1147 A71-19472
- Book on electromagnetic fields and waves covering vectors, current density, flux integral, Coulomb law, Laplace equation, magnetomotive force, waveguides, etc
08 p1335 A71-21459
- Planet rotation vector determination, using satellite stellar observations and planetary surface reference points
08 p1365 A71-21776
- Balance equation solution in spherical coordinate form, applying vector alterations to geostrophic wind field from pressure-height observations grid point analysis
10 p1638 A71-23964
- Anisotropy tensor and figurative vector components relation with eigenvector correspondence to eigensate and eigenmodulus in similitude ratio
10 p1688 A71-24451
- Helical motions with vorticity-velocity and conduction current-free force magnetic vectors parallelisms
11 p1804 A71-25177
- Steady barotropic motion of ideal fluid, determining conditions for unit vector serviceability as velocity direction field
11 p1753 A71-26563
- Liquid propellant rockets with rotating reactive force vectors, improving equations of motion
12 p1972 A71-27492
- Computer phase hologram synthesis simplified modification, using EM field vector transformation for points
13 p2070 A71-29029
- Planet intrinsic rotation vector determination, using satellite stellar observations and planetary surface reference points
15 p2495 A71-32681
- Rectangular plate with two adjacent sides clamped and two supported, solving bending problems with linear algebraic vector equations
17 p2824 A71-34846
- Steady barotropic motion of ideal fluid, determining conditions for unit vector serviceability as velocity direction field
17 p2729 A71-35503

- Covariant definition of radius vector in Riemann space, studying position operator in general relativity theory
19 p3105 A71-38582
- Excising neighborhood of singularity from manifold with vector field definition, making possible regularization of two and three body problems
20 p3254 A71-38900
- Nonrandom measurement error analysis in vector form for mutually dependent and independent errors
21 p3383 A71-41241
- Varying magnetic field disturbance by eddy currents in conductive elliptical cylinder, obtaining field vector potential and magnetic induction vector
22 p3528 A71-41769
- Validity theorems derived for complex parameter elasticity theory equations by vector functions expansion
23 p3777 A71-43583
- VEGARD-KAPLAN BANDS**
Nitrogen Vegard-Kaplan and second positive band systems emission, using rocket-borne spectrometer in UV aurora
07 p1102 A71-19670
- VEGETABLES**
Thermal combustion produced biocomplex vegetable waste mineralization effect on furnace working surface oxide film
22 p3507 A71-42821
- VEGETATION**
Remote sensing systems for vegetation analysis, discussing machine-aided photointerpretation methods for data analysis [AIAA PAPER 70-308]
01 p0084 A71-11590
- Vegetation penetration with K-band side-looking airborne imaging radars, noting multifrequency multipolarization system application for terrain reconnaissance
18 p2875 A71-36365
- Earth surface characteristics measurements with remote sensors, proposing overland albedo measurements for clues as to ground type/clouds, vegetation, sand and snow/
20 p3260 A71-39684
- VEHICLE WHEELS**
NT NOSE WHEELS
Aircraft multiwheel undercarriage effect on rigid and flexible pavements, examining failure modes
02 p0189 A71-12164
- Single module unmanned Mars roving vehicle with flexible metal toroidal hoop-spoked wheels, discussing remote controlled scale model design for simulation on earth
04 p0566 A71-15333
- Flexible tires theoretical models application to wheel shimmy analysis, examining stretched string and point contact theories validity
10 p1557 A71-24864
- Shimmying wheel with elastic tire, investigating motion equations for wobble and forces exerted by ground
13 p1997 A71-29230
- Powered landing gear wheel system requirements for parking and taxiing of commercial jet transport airplanes [SAE PAPER 710446]
14 p2176 A71-30530
- VEHICULAR TRACKS**
Rail track roughness and irregularities evaluation by railcar vibration measurements, using portable LF low amplitude acceleration measuring and recording system [AIAA PAPER 71-384]
11 p1845 A71-25349
- VEINS**
Renin level in renal venous and peripheral blood in patients with renovascular hypertension
01 p0010 A71-10391
- Human skin blood flow and venous tone in middle finger and forearm during leg muscle exercise to exhaustion
01 p0016 A71-11410
- Mixed venous oxygen tension oxide determination by nitrogen-carbon rebreathing method, considering pulmonary blood flow and oxygen carrying capacity
03 p0360 A71-13182
- Local cooling effects on responsiveness of muscular and cutaneous arteries and veins in dogs, noting blood flow redistribution
04 p0538 A71-15091
- Venomotor responses of forearm and hand veins to rapid changes in skin temperature in exercising man
06 p0861 A71-18382
- Venomotor responses of forearm veins to local and remote thermal stimuli to skin in exercising man
06 p0862 A71-18383
- Pulse wave velocity measurements in human veins by transcutaneous ultrasonic flow detectors, noting respiration and Valsalva effects
12 p1874 A71-27136
- Calcium ions effects on electrophysiological properties of portal vein muscle cells in rats
16 p2533 A71-34109
- Temperature effects on spontaneous electrical and contractile activity of smooth muscle cells of portal vein in rats
16 p2533 A71-34110

- Cutaneous circulation control by venous thermoregulatory reactions to temperature variations using dog saphenous veins perfused with autologous blood or Krebs-Ringer solution
18 p2862 A71-36899
- Small pressure wave transmission in abdominal venae cavae of dogs in mathematical model development for viscoelastic behavior of large veins
20 p3187 A71-38990
- Inspired oxygen concentrations effects on arterial and mixed venous pH, carbon dioxide uptake and oxygen partial pressure in normal subjects
20 p3189 A71-39400
- Local and central body temperature effects on human cutaneous venomotor reflexes, monitoring venous wall tension by measuring hand dorsal vein pressure during temporary arrest of hand circulation
24 p3797 A71-44777
- VELA SATELLITES**
Critique of Vela 4 scattered Lyman alpha experiment, discussing maximum flux region and radiation intensity
17 p2805 A71-35386
- Solar wind angular momentum calculation from short term directional, density and velocity fluctuations, using Vela 3 satellite data
22 p3592 A71-42162
- Interplanetary plasma and magnetic field observations by Vela 3 and Imp 3 satellites
23 p3708 A71-43154
- Vela 4A and 4B satellite observation of impulsive energetic electron fluxes in distant magnetotail associated with magnetospheric polar substorms
23 p3670 A71-43184
- VELOCITY**
NT ACOUSTIC VELOCITY
NT AIRSPEED
NT ANGULAR VELOCITY
NT CRITICAL VELOCITY
NT ESCAPE VELOCITY
NT EXHAUST VELOCITY
NT FLOW VELOCITY
NT GROUP VELOCITY
NT HIGH SPEED
NT HYPERSONIC SPEED
NT LIGHT SPEED
NT LOW SPEED
NT ORBITAL VELOCITY
NT PHASE VELOCITY
NT PROPAGATION VELOCITY
NT RADIAL VELOCITY
NT RELATIVISTIC VELOCITY
NT ROTOR SPEED
NT SOLAR VELOCITY
NT SUBSONIC SPEED
NT SUPERSONIC SPEEDS
NT TERMINAL VELOCITY
NT TIP SPEED
NT TRANSONIC SPEED
NT WIND VELOCITY
- Velocity transposition theory based on velocity perception constancy effects, noting importance for human engineering guidance in sea, land, air and space traffic fields [DFVLR-SONDDR-107]
18 p2863 A71-35828
- VELOCITY DISTRIBUTION**
Real vortices velocity, density and temperature distribution determination, discussing flow measurements by hot-wire anemometer, multiple spark camera interferography and smoke visualization techniques
01 p0069 A71-10100
- Compression shock wave development in compressible media, deriving wave amplitude/time relationship via velocity distribution approximation by discontinuous Mach wave series
01 p0069 A71-10122
- Turbulent boundary layer air flow through supersonic convergent-divergent nozzle with heat transfer, considering relationship between temperature and velocity profiles
01 p0180 A71-10950
- Clamped rectangular metal plates dynamic plastic behavior under uniformly distributed impulsive velocities
02 p0321 A71-11678
- Ionization gage detector signal interpretation as function of reflected molecule velocity distribution, noting shutter speed errors
02 p0286 A71-12128
- Boundary layer separation at free streamline attachment to sharp trailing edge of flat plate, deducing terminal velocity profile for two dimensional flow
02 p0185 A71-12376
- Lifting oscillatory reentry trajectories, developing equation method to consider density and velocity distributions
02 p0320 A71-12403
- Plastic flow of metal during rolling in T groove, determining particle velocity and strain energy distributions
02 p0257 A71-12565
- Mean and pulsation characteristics of velocity and temperature in turbulent conducting jets under longitudinal and transverse magnetic fields
02 p0292 A71-12626

Standard deviation of atmospheric turbulence velocity components over flat arid terrain

02 p0278 A71-12707

Electron velocity distribution in fully ionized plasma under crossed electric and magnetic fields, assuming Fokker-Planck expression for Lorentz gas

02 p0293 A71-12743

Solar granules velocity profiles, establishing horizontal outflow and vertical upflow from filtergrams at 6569.2 Å absorption

02 p0316 A71-12754

Casing/end wall/ boundary layers in multistage axial flow compressors, discussing velocity distributions

03 p0340 A71-13144

Peculiar velocities nonisotropic distribution in stationary differentially rotating stellar system based on Boltzmann equation solution

03 p0484 A71-13222

Turbulent flow near porous wall with pressure gradient, calculating velocity and shear distribution by modified Van Driest theory

03 p0399 A71-13432

Instantaneous deflection and velocity distribution curves of cantilever beam with uniformly varying length in constant gravity field by numerical methods

03 p0504 A71-13465

Jet fluid dynamics under various boundary conditions and velocity distributions

03 p0341 A71-13579

Centrifugal compressor impeller exit flow velocity distribution distortion based on equations of motion involving entropy gradient terms

03 p0343 A71-13831

Boltzmann equation solution for isotropic heat velocity distribution in molecular gas kinetics

03 p0401 A71-13907

Unsteady flow about solid cylinder falling through viscous fluid in vertical tube, obtaining velocity profiles via solution of Navier-Stokes equation [ASME PAPER 70-WA/FE-9]

03 p0403 A71-14130

Mean velocity profile measurements in turbulent wake behind single or parallel arbitrarily spaced and sized cylinders with adverse pressure gradient [ASME PAPER 70-WA/FE-10]

03 p0403 A71-14131

Single stage axial flow turbocompressor with trips, examining viscosity effects on flow velocity profiles [ASME PAPER 70-WA/FE-24]

03 p0343 A71-14133

Rarefied gas low speed slip flow over wedge, solving for velocity profiles and skin friction [ASME PAPER 70-WA/APM-26]

03 p0344 A71-14158

Turbulent mixing of two parallel similar and dissimilar fluid streams, comparing velocity and density profiles measurements with similarity solution [ASME PAPER 70-WA/APM-38]

03 p0404 A71-14163

Laminar corner boundary layer secondary flow, taking into account velocity and skin friction distributions

03 p0404 A71-14239

Homogeneous turbulence decay formulation using multipoint velocity correlations, initial time derivatives and time evolution

03 p0405 A71-14415

Cathode tip shape influence on temperature and velocity fields in gas tungsten arc welding, noting effect on weldment area and penetration

04 p0603 A71-14924

Plasmoid mass and velocity distribution in pulsed plasma accelerators, using mass spectrometers and platinum thermal probe

04 p0634 A71-15111

Skin friction, Stanton numbers, velocity and temperature profiles in accelerating turbulent boundary layer flows, using Prandtl mixing length

04 p0680 A71-15478

Tubular powder channel gas velocity distribution and pressure buildup during burning

04 p0638 A71-15680

Velocity distribution equation for steady incompressible two dimensional turbulent flow, taking pressure gradients and surface roughness effects into account

04 p0578 A71-15764

Small elliptical galaxy associated with radio source 3C 386, noting luminosity, internal velocity dispersion and low metal abundance

05 p0805 A71-16109

Main pulmonary artery velocity profiles in dogs and man, using thin-film resistance anemometer

05 p0706 A71-16324

Nonuniformly rotating Hg fluid, noting hydromagnetic stability and velocity control by imposed radial current distribution between coaxial ring shaped electrodes

05 p0788 A71-16608

Velocity profiles of steady axial flow of homogeneous incompressible Newtonian liquid between infinitely long parallel eccentric circular cylinders

05 p0735 A71-16611

Plasma jet radial velocity distribution measurement by probe technique, calculating current density from azimuthal magnetic field via Maxwell equation [DFVLR-SONDDR-88]

05 p0788 A71-16643

Terrain and frictionally induced vertical velocity analysis for local and regional forecasting operations, considering low level air flow effects

05 p0777 A71-16674

Incompressible fluid boundary layer with negative pressure gradient near separation point, discussing stability characteristics and velocity profiles

05 p0736 A71-16847

Incompressible boundary layers with specific velocity distribution, studying stability on straight and yawing wings

05 p0736 A71-16849

Three dimensional boundary layer with Pohlhausen velocity distribution, examining stability on yawing wing

05 p0736 A71-16850

Asymptotic formulas for vortex and velocity field far from body in plane viscous incompressible fluid flow

05 p0737 A71-16990

Inviscid incompressible flow velocity distribution in conical configurations with water as working fluid, using method of integral relations

05 p0737 A71-17103

Oceanic rise crest heat flow model, examining vertical velocity distribution of mass transport

06 p0889 A71-17635

Laminar pulsating ducted flow heat transfer, taking into account velocity distribution time dependence

06 p1005 A71-17682

Moving condensate film effect on velocity profile and mass transfer rate from gas-vapor mixture by Crank-Nicholson method

06 p1006 A71-18070

Forced convective heat transfer in laminar flow fluid of vanishing viscosity in constant wall temperature pipe, discussing velocity distribution effects

06 p0882 A71-18073

Elliptical and spiral galactic angular momentum and velocity dispersion relations, considering cosmological turbulence during formation

06 p0971 A71-18244

Solid propellant rocket chamber unstable motion, discussing pressure and velocity coupling

06 p0946 A71-18297

Tangential velocity and total temperature distribution axial and radial gradients from secondary flow functions and turbulent energy equations

06 p0883 A71-18321

Stellar velocities distribution in nonrotating clusters, examining mass dispersion role in evolution

06 p0974 A71-18430

Laminar incompressible flow heat transfer in inlet between parallel plates at constant temperature, considering pressure gradient effect on boundary layer velocity profile

06 p1008 A71-18497

Separated turbulent eddy viscosity models incompressible similar reverse flow velocity profiles from Falkner-Skan equations [AIAA PAPER 71-203]

06 p0886 A71-18641

Wall flow boundary layer, observing external turbulent field effect on velocity and temperature distribution and heat exchange

07 p1086 A71-18771

Flow between parallel planes of dissimilar surface texture, obtaining mixing length models velocity profiles, skin friction coefficients and zero shear stress position

07 p1086 A71-18773

Two dimensional turbulent channel flow, determining local mean wall shear stress from velocity gradient

07 p1087 A71-18784

Turbulent velocity field in noncircular cross section rectilinear duct, determining relation between viscosities ratio and dimensionless velocity by integral transformation

07 p1087 A71-18992

O-B stars velocity distribution in synthetic association, proposing method for space velocities mean value determination

07 p1192 A71-19289

Turbulent cylindrical boundary layer velocity distribution, determining power law functional relationship by wind and water tunnel experimental measurements

07 p1088 A71-19420

Three dimensional axisymmetric flows in tornado-like vortex boundary layer, determining nonlinear radial and vertical velocity distribution components

07 p1152 A71-19753

High latitude E region plasma irregularities based on wind velocity shear fields

07 p1153 A71-19760

Unsteady MHD channel flow between two semi-infinite harmonically oscillating and perfectly conducting solids, determining liquid velocity profile curves

07 p1169 A71-20032

Inverse boundary value problems in hydroaeromechanics, involving profile construction from given velocity or pressure distribution and supersonic flow boundaries determination

07 p1091 A71-20078

Surface construction of body of revolution in supersonic gas flow from distribution of velocity vector

modulus along generatrix of body, using Frankl method of characteristics

07 p1016 A71-20089

Flow-through carbon dioxide lasers population inversion relation to individual gas components and electron velocity distribution functions

07 p1126 A71-20187

Two dimensional turbulent wake interaction with linearly stratified main stream, measuring mean and fluctuating temperature and velocity distributions

07 p1092 A71-20277

Boundary layer separation in unsteady pipe flow, examining velocity profiles under influence of periodic pressure fluctuations

07 p1093 A71-20280

Computerized transonic airfoil design from predetermined supercritical velocity distribution, obtaining equivalent incompressible flow through streamline and potential line network transformation

07 p1017 A71-20304

Low density plasma flow past bodies, measuring disturbed zone velocity, density and temperature distributions by Langmuir probes

07 p1173 A71-20528

Velocity distribution and Reynolds number relation to thickness in liquid films using turbulent viscosity

07 p1094 A71-20545

Two axisymmetric jets impingement in fluid amplifiers, discussing velocity profiles of radial jet

07 p1029 A71-20592

Solar disk active region gas development radial velocities on two levels /4 July 1966/, using double magnetograph

07 p1205 A71-20636

Stagnation point flow flame sheet model, showing density-viscosity product variation for injection rate effect on velocity profile

08 p1375 A71-20865

Homogeneous Newtonian cosmological model, constructing ellipsoidal velocity distributions and kinetic theory

08 p1358 A71-20932

Globular cluster star velocities distribution, examining dynamic evolution models and gravitational effects

08 p1362 A71-21153

Thomson scatter measurements of F region ionization drifts vertical velocity at midlatitudes, studying electric field influence

08 p1279 A71-21204

Turbulent boundary layer skin friction measurement by dual pitot tube, taking into account mean velocity profile

08 p1275 A71-21309

Solar wind speed distributions /1962-1970/ as function of solar cycle

08 p1356 A71-21641

Velocity profile in viscous sublayer at wall based on maximum stability principle applied to Karman constant for turbulent channel flow

08 p1277 A71-21950

Flow in channel with abrupt asymmetric widening, calculating expanding flow velocity profile by Prandtl semiempirical turbulence theory

08 p1277 A71-22041

Turbulent velocity pulsations measurement by conduction anemometer with three-electrode sensor

09 p1499 A71-22132

Friction and wear tests on materials of various speeds, loads and temperatures at high relative humidity

09 p1426 A71-22325

Low temperature plasma electron velocity distribution function perturbation due to exothermal chemical reactions

09 p1501 A71-22389

Turbulent flow in initial section of convergent axisymmetric nozzle based on logarithmic velocity law

09 p1431 A71-22409

Electrohydrodynamic flow in plane channel with conducting walls and axial emitter electrode, determining velocity and pressure profiles distortion

09 p1502 A71-22538

Velocity distribution measurement of Cs gas flow from orifice in near-free molecule regime, using apparatus based on time of flight method

09 p1432 A71-22682

Ground based coherent radar synthetic aperture procedure against uniform velocity targets, discussing airborne holographic synthetic gain applications to stationary antennas

09 p1405 A71-22697

Turbulent air flow velocity and temperature fluctuations, determining mean fields, Prandtl number distributions and correlation moments and coefficients

09 p1432 A71-22729

Electron gun diode design for beam-collisionless plasma interaction nonlinear evolution, studying delta function beam velocity distribution

09 p1502 A71-22754

Normal shock wave in He, comparing measured and predicted molecular velocity distribution functions

09 p1433 A71-22857

- Incompressible viscous fluid nonsteady three dimensional flow, obtaining velocity field and pressure distribution in boundary layer
09 p1433 A71-23092
- Solar photosphere turbulent velocity, taking into account instrumental profile effects
09 p1524 A71-23193
- Electromagnetic waves reflection and transmission from weakly ionized moving plasma, noting dependence on medium velocity and nonlinearity effect
09 p1505 A71-23519
- Mach cones reflection at thin wing subsonic leading edges in supersonic flow, considering axial disturbance velocity and pressure distributions
09 p1384 A71-23616
- Combustion reactions development with velocity gradient downstream steady shock wave, considering aerodynamic field in supersonic wind tunnel
10 p1694 A71-23813
- Wall jets over concave surfaces, obtaining average velocity profiles
10 p1591 A71-23842
- Orr-Sommerfeld hydrostatic stability equation derivation for nonparallel flow in wake from Goldstein velocity distribution, noting lateral direction velocity component magnitude
10 p1592 A71-24024
- Sporadic meteors geocentric velocity distribution over celestial sphere by photographic observation and oblique radio sounding, noting annual variations
10 p1668 A71-24029
- Charged particles velocity distribution effect on plasma flow in transverse nonuniform magnetic field, observing configuration/trajectory distortion and particle dispersion
10 p1649 A71-24319
- Turbulent wakes from subsonic-hypersonic bodies for downstream mean flow predictions analysis, considering eddy viscosity function
10 p1550 A71-24338
- Cylindrical shock wave in solid body rotating gas for angular variation effects on shock velocity, using similarity method
10 p1593 A71-24405
- Superthermal ions velocity distribution in nonisothermal plasma, comparing real velocity distribution to Maxwellian distribution
10 p1651 A71-24630
- Velocity and static pressure redistribution in distorted flow field upstream of axial flow compressors
[AIAA PAPER 69-485] 10 p1553 A71-24856
- Turbulent free jets expansion, presenting method for velocity distribution calculation via suitable correlations between average velocity and turbulent fluctuations
10 p1596 A71-24939
- Fully ionized gas under electric and magnetic fields, calculating electron velocity distribution and runaway rate as function of time from Boltzmann equation
10 p1654 A71-24975
- Velocity profiles for flows with laminar heat transfer in circular tube and rectangular duct inlet region with wall suction and injection
10 p1597 A71-25064
- Velocity, temperature and concentration profiles correlation for compressible turbulent boundary layer along porous flat plate, with carbon dioxide injection, discussing cooling applications
10 p1598 A71-25095
- Amplitude curves of reflected wave vertical displacement component in horizontally stratified medium with simple layer velocity pattern
10 p1644 A71-25134
- Pipe flow hot wire measurements at turbulence onset Reynolds numbers, exhibiting axisymmetric laminar velocity profile distortion
11 p1748 A71-25155
- Velocity distributions in axisymmetric air jets submerged in coaxial oscillating stream measured by hot-wire anemometer
11 p1748 A71-25156
- Finite difference computer algorithm to solve vertical velocity equation of steady air flow about mesoscale obstacle in stably stratified atmosphere
11 p1793 A71-25169
- Forced convection in atmosphere boundary layer, considering nonlinear unsteady vertical airflow velocity increments over temperature spot on earth surface
11 p1793 A71-25170
- Ideal compressible fluid slow motion in permanent and nonpermanent regime, discussing velocity field geometrical interpretation
11 p1748 A71-25173
- Helical motions with vorticity-velocity and conduction current-free force magnetic vectors parallelisms
11 p1804 A71-25177
- Viscous liquid unsteady flow in long circular tube as function of mean velocity distribution, discussing radial flow and pressure distribution
11 p1749 A71-25268
- Dust devil vortex model, considering boundary layer velocity profiles and thickness and integrated radial and vertical mass flows
11 p1794 A71-25470
- Static pressure recovery and core region velocity profile in rectangular wall diffusers with uniform shear flow
[ASME PAPER 71-GT-5] 11 p1751 A71-25951
- Flow variation effect on velocity and flow angle distribution at exit of shrouded radial flow impeller with backward swept blades, using streamline curvature method
[ASME PAPER 71-GT-15] 11 p1703 A71-25961
- Three dimensional boundary layer flow and velocity profiles in mixed diffuser with equal angle walls
[ASME PAPER 71-GT-40] 11 p1704 A71-25973
- Flow patterns within centrifugal and mixed flow impeller channel, examining velocity distributions, blade surface pressure and flow behavior
[ASME PAPER 71-GT-41] 11 p1704 A71-25974
- Tangential velocity profile in steady incompressible electrically conducting viscous axial flow between concentric rotating cylinders with radial magnetic field, solving Navier-Stokes equations
11 p1752 A71-26048
- Two dimensional incompressible turbulent boundary layer, determining velocity distribution with Cole law of wake
11 p1752 A71-26259
- Spherical celestial bodies with linear equatorial velocities, deriving anomalous rotation law
11 p1833 A71-26260
- Maximum velocity position in turbulent shear flow for differential pressure effect between double pitot tubes, using inductance type transducer
11 p1767 A71-26313
- Anisotropic instability in velocity distribution of ions in plasmas under external RF electric field
12 p1934 A71-26572
- Stellar velocity distribution in nonrotating clusters, examining mass dispersion role in evolution
12 p1955 A71-26580
- Radial velocity fields-magnetic fields relationship in solar atmosphere active and quiet regions
12 p1955 A71-26587
- Large amplitude wave propagation in arteries, deriving aorta mathematical model consistent with heart pressure and flow pulses and wavefront velocity
12 p1870 A71-26937
- Boundary layer suction optimization to achieve normal velocity component distribution for local Reynolds number equal to critical value at transition point
12 p1896 A71-26973
- Smooth annuli correlation equation for friction factor, discussing Prandtl turbulence based Spalding inner velocity profile modification
12 p1896 A71-27053
- Isotropic turbulence three dimensional velocity spectrum function, using absolute mean strain rate constant and variable Reynolds number
12 p1898 A71-27581
- Downward moving large scale surface velocity fields of solar atmosphere from magnetograph data
12 p1968 A71-27645
- Photospheric layers supergranular motion and oscillations as function of solar atmosphere height and sun position, investigating velocity fields two dimensional structure
12 p1970 A71-27701
- Longitudinal solid surface curvature effects on heat transfer, calculating velocity and temperature fields by similarity analysis via boundary layer equations
12 p1987 A71-27737
- Parametric dissipative plasma instability in HF electric field, showing plateau formation in velocity distribution function causes Cerenkov dissipation decrease
12 p1941 A71-27765
- Laminar boundary layer centrifugal Gortler instability over concave wall, depending on velocity profile inflection points
13 p2046 A71-27840
- Ionospheric ion temperature measurement method by exploring transverse velocity distribution, discussing surface pollution and spurious effects
13 p2055 A71-27929
- Spiral galaxy NGC 4569 member of Virgo cluster, using measurements of central velocity field, rotation and density estimates
13 p2132 A71-27965
- Boundary layers velocity distribution measurements, using scattered laser radiation Doppler shift
13 p2078 A71-28574
- Laminar free convection heat transfer in vertical rectangular corner, considering velocity and temperature distribution
13 p2161 A71-28621
- Nonisotropic turbulent stress and viscosity components distributions in noncirculating swirling flow from mean axial and swirl velocities
13 p2161 A71-28622
- Atmospheric frontogenesis models with air velocity fields acting on initially large scale temperature distributions
13 p2097 A71-28727
- Combustion, reaction and flame propagation during gas mixtures burning, allowing for disruption of Maxwell-Boltzmann molecular velocity distribution
13 p2162 A71-28971
- Sunspot deep subphotospheric layer structure, noting evolution, velocity field, visibility and model formulation
13 p2142 A71-29171
- Pressure, velocity and potential distribution of flow around arbitrarily shaped body of revolution during arbitrary motion in perfect liquid
13 p1992 A71-29181
- Plane stationary constant-vorticity incompressible flow region surrounded by potential flow, determining two dimensional velocity distribution by numerical calculation
13 p2050 A71-29278
- Helicopter rotor vortex system and induced velocity field for various angles of attack, flight conditions and unit loads, using smoke visualization technique
13 p1994 A71-29235
- MHD flow abrupt widening and narrowing, considering M shaped velocity profiles
14 p2278 A71-29606
- MHD flow in rectangular channel with two conducting walls, investigating velocity structure
14 p2278 A71-29607
- Argon plasma jet velocity distribution at MHD channel exit with magnetic quadrupole, using calorimetric plasma velocity measurements and Doppler shift observations
14 p2278 A71-29611
- Incompressible liquid laminar boundary layer flow velocity profile and normal friction stress calculation by successive approximation method
14 p2169 A71-29630
- Atmospheric turbulent shear layer model, giving velocity, stable, unstable and neutral profiles
14 p2267 A71-29755
- Solar active regions velocity field at different levels and discussing transition region from photosphere to chromosphere
14 p2308 A71-29972
- Solar limb flare evolution on 11 July 1966, observing filament structure, vertical velocity and branching
14 p2298 A71-29977
- Solar active region photospheric radial velocity field time variations, using magnetograph in Fe I line
14 p2308 A71-29977
- Supersonic plasma flow effects on neutral hydrogen, helium and charged particle density and velocity profiles in polar ionosphere
14 p2234 A71-30040
- Average and pulsating velocity distributions during subsonic air jet interaction with plane baffle, describing jet dissipation geometrical pattern
14 p2225 A71-30223
- German monograph on particle motion in symmetric rotation flow velocity covering potential vorticity, track curves, resistance laws, transition region, drag and pressure effects
14 p2170 A71-30234
- Curved wall jet pressure distribution numerical calculation for given velocity profiles
14 p2328 A71-30306
- Flow field velocity distribution at rotating wings devices tip vortices
[AHS PREPRINT 522] 14 p2172 A71-31088
- Boltzmann equation approximate solution for molecular velocity distribution function perturbations by inelastic collisions
15 p2386 A71-31158
- Density and velocity profiles of transonic flow past wavy wall at various channel heights, using Mach-Zehnder interferometer
15 p2386 A71-31165
- Ion beam collisionless relaxation in hot electron plasma, observing oscillation spectra and velocity distributions
15 p2453 A71-31245
- Velocity profile of steady two dimensional incompressible laminar boundary layer flow with suction or injection, noting wall shear function
15 p2388 A71-31441
- Incompressible fluid turbulence theory based on space-time Hopf characteristic functional integral representation for velocity field statistical ensemble
15 p2388 A71-31477
- Recirculating cells and entrance conditions influence on confined heterogeneous jets laminar mixing, measuring velocity and concentration profiles
[AIAA PAPER 71-601] 15 p2389 A71-31578
- Velocity profiles of oscillating flow in wake of blunt based body, using finite difference solutions of vorticity transport and Poisson equations
[AIAA PAPER 71-603] 15 p2345 A71-31579
- Turbulent mixing between parallel incompressible air streams, using statistical investigation of pressure and velocity fields
[AIAA PAPER 71-613] 15 p2389 A71-31582

Interference analysis of wing with overlapping multipropellers in uniform velocity stream confined in elliptical cross section cylinder
[AIAA PAPER 71-614] 15 p2346 A71-31583

Flow velocity field in main plastic deformation zone during orthogonal cutting from continuity equation 15 p2415 A71-31986

Attaching jet flow on inclined flat plate with small offset, obtaining centerline shape and velocity profile 15 p2391 A71-32058

Hydromechanical analysis of jet spreading in low pressure planar fluid amplifiers for low Reynolds numbers and finite aspect ratios, deriving velocity distribution equations 15 p2391 A71-32058

Pressure and velocity distributions in gas filled cavity undergoing resonant acoustic oscillations due to heat addition 15 p2392 A71-32126

Slip flow development in parallel plate channel entrance, discussing center line velocity and excess pressure distributions 15 p2393 A71-32262

Turbulent gaseous nonmagnetic protogalaxies under external torques, calculating angular velocity distribution 15 p2490 A71-32400

Plasma oscillations growth rates for symmetrical double-humped velocity distributions, comparing with distribution functions without infinite tails 15 p2460 A71-32657

Sunspot umbrae and penumbrae, plotting period and amplitude curves for oscillatory velocity field 15 p2497 A71-32744

Temporal and spatial flow velocity profiles produced by shock tube generated pressure wave propagation in open-end pipe 16 p2556 A71-32921

Hydrodynamic stability, determining velocity field bounds in laminar boundary layer by Nagumo-Westphal theory of parabolic differential operators [DFVLR-SONDDR-131] 16 p2557 A71-32982

Gravity waves over flow with nonuniform velocity distribution, investigating neutral stability problem of generation and momentum transport 16 p2557 A71-32984

Self gravitating time independent disk-like stellar system model, investigating mass and velocity distributions 16 p2630 A71-33054

Free and enclosed disks rotation resistance at high Reynolds numbers, calculating fluid induced torque with logarithmic velocity profiles for turbulent boundary layer flow [ASME PAPER 71-APM-25] 16 p2520 A71-33204

Integral analysis of incompressible turbulent boundary layer with mass transfer and pressure gradient, including Stevenson velocity profiles and skin friction law [ASME PAPER 71-APM-2] 16 p2559 A71-33221

Short convergents without risk of detachment, deducing corresponding distribution on provisional wall from velocity field 16 p2521 A71-34054

Viscous incompressible fluid flow between two rotating nonconcentric cylinders, presenting transverse velocity profiles 17 p2725 A71-34177

Wall roughness effects on laminar boundary layer velocity profile and Reynolds number, using Hankel functions and integrals 17 p2725 A71-34180

Undulating laminar and turbulent liquid film flows down vertical surface, determining velocity fields and local heat transfer coefficients 17 p2725 A71-34210

German monograph on electron motion in cesium plasma covering Boltzmann equation, radiative transfer, mathematical model, electron velocity distribution, etc 17 p2787 A71-34485

Galactic clusters characteristics tabulation and statistical analysis, calculating dimensions, luminosity and radial velocities dispersion 17 p2804 A71-34841

Two dimensional compressible turbulent boundary layer with time dependent mean velocity and density fields, deriving momentum and kinetic energy integral equations 17 p2727 A71-34876

Supersonic turbulent two dimensional boundary layer flows wall flux and velocity/temperature profiles prediction 17 p2729 A71-35283

Partial differential equations governing second order correlation functions for velocity and magnetic field in isotropic conducting turbulent flow 17 p2789 A71-35443

Large jet transport aircraft trailing vortices, studying velocity fields, core diameters and logarithmic variations of circulation 17 p2674 A71-35755

Turbulent plane flow velocity profile stability characteristics covering parabolic Poiseuille flow under infinitesimal disturbances 18 p2901 A71-35855

Turbulent flow of air film between rotating circular and stationary plane surfaces, determining pressure distributions, inertial forces effects and velocity profiles 18 p2926 A71-36185

Two dimensional flow of non-Newtonian fluids with rigid spherical substructure, solving linear coupled ordinary differential equations for spin and velocity field [ASME PAPER 71-APM-N] 18 p2926 A71-36257

Molecular beam scattering at solid surfaces, outlining scattered particles angular and velocity distribution measurement 18 p2848 A71-36439

Spectroheliogram Doppler movies of solar velocity fields showing oscillatory and slowly varying components 18 p2965 A71-36728

Solar photospheric velocity field measurements, using balloon-borne sodium resonance cell with diffraction limited telescope 18 p2965 A71-36729

Doppler velocity field recording method over two dimensional solar active region image, using narrow band filter with video photographic subtraction technique 18 p2924 A71-36730

Asymptotic formulas for vortex and velocity field far from body in plane viscous incompressible fluid flow 18 p2909 A71-36790

Thermodynamics axioms for work and energy under volume-area continuity conditions, discovering local power density in velocity field 18 p2948 A71-36812

Velocity field of viscous steady plane incompressible flow past body, linearizing by Oseen approximation 18 p2910 A71-36946

Plane MHD Couette flow stability with asymmetric velocity profile shaped by transverse magnetic field, considering Hartmann flow 19 p3108 A71-37077

Air injection into trailing vortex core, noting jet flow effect on circumferential velocity 19 p2991 A71-37291

Friction velocity in stably stratified constant flux layer with known heat flux, using log-linear velocity profile with fixed Monin-Obukhov parameter value 19 p3089 A71-37502

Wakes of freely falling water drops, discussing flow patterns, kinetic energy, vorticity decay and velocity profiles 19 p3089 A71-37733

Low density plasma electron velocity distribution deviation due to Maxwellian photon radiation resulting from inelastic collisions with atoms 19 p3112 A71-37739

Bounded nonthermal plasma radiation temperature variations relationship to electron velocity distribution functions 19 p3113 A71-37747

Continuum mechanical approach to velocity dispersion of longitudinal plane waves in elastic solid containing dislocations 19 p3118 A71-37794

Velocity and temperature pulsations as function of stratification parameter in atmospheric boundary layer 19 p3090 A71-37971

Heated jet interaction with deflecting flow in subsonic wind tunnel, presenting flow visualization and temperature and velocity profiles [ASME PAPER 71-HT-2] 19 p3163 A71-37980

Gravity effect on developing laminar flow with forced convection in vertical isothermal tube, investigating velocity and temperature profiles and heat transfer rate [ASME PAPER 71-HT-6] 19 p3164 A71-37983

Velocity and temperature profiles at near-critical point of nitrogen turbulent boundary layer flow over heated flat plate by thermocouple/pitot-static probe [ASME PAPER 71-HT-23] 19 p3165 A71-37994

Solar velocity field decomposition into oscillatory and slowly varying components by spectroheliograms with high spatial resolution 19 p3146 A71-38662

Windage data for inert gas in high speed generators rotor-stator gap, investigating turbulent velocity profiles 20 p3181 A71-38915

Integrodifferential difference equation for isotropic portion of velocity distribution function resulting from electron excitation and Coulomb interaction 20 p3274 A71-39048

Turbulent boundary layer response to step change in surface roughness, discussing wind tunnel measurements of pressure and velocity profiles 20 p3212 A71-39505

Rectangular wind tunnel study of suction effect on velocity profiles and characteristics of turbulent boundary layer 20 p3213 A71-39788

Velocity profiles of plane turbulent flow of incompressible fluid on porous surface in presence of suction 20 p3213 A71-39790

Velocity and resistance profiles for unsteady turbulent flow in rough pressure channels, using Prandtl hypothesis 20 p3214 A71-39797

Highly uniform inlet velocity profile influence on conical diffuser characteristics 20 p3177 A71-39798

Circular conical diffuser inlet velocity profile effect on efficiency, presenting experimental results for different cone angles and expansion ratios 20 p3177 A71-39799

Generalized hodograph transformation with velocity potential as function of continuous second derivatives 21 p3406 A71-40154

Statistical space velocity distributions, gravitation field strength and vertex deviation for nearby young stars, using density wave theory of galactic spirals 21 p3444 A71-40196

Cooled film anemometer techniques for hypersonic wake temperature and velocity distribution measurements for projectiles in free flight range 21 p3363 A71-40386

Computer model for dynamical evolution of isolated disks of stars with initial velocity dispersions corresponding to Toomre criterion, noting instability relative to large scale modes 21 p3445 A71-40410

Viscous vortex rings of small cross section, considering velocity in ideal fluid with arbitrary vorticity in core and arbitrary circumferential velocity 21 p3366 A71-40484

Peak velocity vectors in transverse plane of jet transport aircraft wake, measuring tip vortices core size 21 p3319 A71-40491

Fog formation and dispersal by velocity field induced by helicopter trailing vortices, presenting dynamic model with droplet depletion, evaporation and condensation 21 p3321 A71-40510

Mean velocity profile and wall friction coefficients of perturbed turbulent boundary layer on flat plate 21 p3366 A71-40511

Hot-wire anemometer measurement of free oscillation damping of viscous and sluggish fluid in U tube, determining velocity distribution 21 p3366 A71-40512

Rotating viscous fluid flow between concentric circular cylinders, predicting velocity field dependence on position and time during inner cylinder sudden stop 21 p3366 A71-40543

Temperature distribution along short heated wire cooled by flowing liquid with parabolic velocity distribution, using power series for differential equation solution 21 p3378 A71-40581

Lunar near surface seismic velocity distribution for cold accretion and meteorite impact models, comparing travel times 21 p3450 A71-40645

MHD flow stability under arbitrary three dimensional disturbances, considering energy estimate for interaction between magnetic field and velocity field at critical Reynolds number 21 p3422 A71-40676

Spectral density functions of velocity pulsations and frequency dependent stability in turbulent plane and axisymmetric channel air flows at different Reynolds numbers 21 p3368 A71-40697

Rotationally symmetric quasi-cylindrical viscous incompressible vortex flow, using method of weighted residuals approximating axial velocity and circulation profiles by series of exponentials 21 p3369 A71-40951

Energy method application to inhomogeneous turbulent flow with large eddies as recurrent velocity field structures, considering longitudinal rolls in boundary layer wall region 21 p3370 A71-40985

Numerically simulated turbulent velocity flow field, covering Navier-Stokes and energy conservation equations 21 p3371 A71-40996

Quasi-static surface waves in Fermi electron plasma with Maxwellian electron velocity distribution 21 p3425 A71-41277

Miniature wind tunnel velocity field calibration for testing anemometers, using null method with spherical probe 21 p3384 A71-41380

Correlation functions characteristics of wind velocity field in troposphere and stratosphere up to 25 km based on bihourly radiosonde data 21 p3412 A71-41390

Mesoscale perturbations in wind velocity field in jet streams, interpreting data in terms of hydrodynamic stability theory 21 p3412 A71-41392

- Fluid velocity gradient measurement by laser-Doppler techniques based on signal spectrum bandwidth or frequency shift corresponding to position shift near wall 22 p3541 A71-41792
- Circumferentially nonuniform flow in front of axial compressor stage with stepwise two zone pressure and velocity distribution resulting in increased guide vane losses 22 p3479 A71-41845
- Plane Couette flow temperature and velocity fields for Newtonian fluid with temperature dependent viscosity under locally and temporally constant wall temperature 22 p3620 A71-41881
- Kinetic theory of optically pumped gas, incorporating atomic line radiation effects on spatial and time evolution of velocity distribution 22 p3530 A71-41888
- Solid propellant rocket motor stable operation region, describing propellant response function to pressure and velocity fluctuations [ONERA-TP-1016] 22 p3588 A71-41956
- Velocity profiles of heavy viscous fluid free oscillatory motion in U-tube by hot-wire anemometry 22 p3531 A71-42242
- Internal velocity field role in massive star formation, discussing cloud fragmentation and mass function 23 p3723 A71-42941
- Shock wave attenuation in two diaphragm tube, obtaining velocity profiles with microwave phase detector system 23 p3674 A71-43086
- Second order theory of plane plastic flow, investigating characteristic slip lines of perturbed velocity field and stress equations 23 p3774 A71-43144
- Electron velocity distribution relaxation in time dependent weakly ionized plasma within electric field, solving Boltzmann equation 23 p3708 A71-43151
- Plasma conductivity dependence on electron velocity distribution function in distorted Maxwellian form 23 p3709 A71-43259
- Minimum drag and lifting line characteristics of large aspect ratio wing in uniform shear flow with velocity variations along span 23 p3625 A71-43312
- Horizontal velocity and temperature spectra at high wavenumbers in three dimensional quasi-geostrophic turbulent flow 23 p3701 A71-43346
- Two dimensional velocity field observations in and around sunspots from Doppler spectroheliograms 23 p3767 A71-43838
- Knudsen effusion problem in thermal molecular gas jet mixing, using moment method based on velocity distribution function 24 p3817 A71-44354
- Subsonic force effect calculations on rectangular wings, using downwash velocity potential method 24 p3789 A71-44613
- Plasma spraying steel coating process, establishing regularity of particle flight velocity variation with distance from burner nozzle 24 p3829 A71-44737
- Pressure and mass velocity profiles behind two dimensional shock wave generation on Al flat plates explosive surface 24 p3839 A71-45228
- VELOCITY ERRORS**
- Variance estimates and error expectations for satellite coordinates and velocity vectors from star altitude measurements 02 p0278 A71-11903
- Instrument orientation optimization for ballistic missile applications, emphasizing acceleration induced velocity and position errors 11 p1796 A71-26410
- Variance estimates and error expectations for satellite coordinates and velocity vectors from star altitude measurements 13 p2098 A71-28190
- Combined inertial and instrument landing aircraft navigation systems with reduced cross runway position and velocity errors, using optimal linear estimation 14 p2272 A71-30606
- Speed overestimation in intermittent illumination of moving bars and textures as function of frequency, using Piaget and brightness enhancement phenomena 15 p2366 A71-32713
- Low pressure shock tubes performance, investigating wave and contact surface trajectories and ideal velocity deviations 16 p2556 A71-32915
- Speed and accuracy relation of hand movement aimed at target, showing error as function of length of uncontrolled terminal phase 16 p2536 A71-33372

- Kalman filter in preflight postflight analysis of velocity increment by spin rocket plume impingement at preentry altitudes 19 p3148 A71-37179
- [AIAA PAPER 71-934]
- Light velocity measurements by optical and microwave techniques, noting electromagnetic constant error and role in distance measurement and physical theories development 24 p3827 A71-44996

VELOCITY FIELDS

U VELOCITY DISTRIBUTION

VELOCITY MEASUREMENT

NT WIND VELOCITY MEASUREMENT

- Convective thunderstorm propagation from Doppler radar velocities at leading edges 01 p0117 A71-10571

- Mass and phase spectrometry in modulated molecular beam experiment for neutral particles velocity measurement prior to ionization 01 p0028 A71-11303

- Aircraft ultrasonic altitude and vertical velocity sensor for low flight, discussing VTOL aircraft automatic hovering control and time lag 01 p0084 A71-11624

- Projectile velocity measurement by laser and Fabry-Perot interferometer using Doppler effect 02 p0258 A71-11657

- Meteor particle speed and size estimation using accelerated glass microsphere bombardment in plasmoid 02 p0304 A71-11914

- Spectrograph design for simultaneous measurement of velocity spectra and charge-to-mass ratios of ions, using magnetic and electric fields deflection effects 02 p0249 A71-12126

- High resolution automatic measurement of ultrasonic velocity changes using interferometer and FM oscillator 02 p0250 A71-12134

- Quiescent and sunspot prominences line of sight velocity measurements on limb, investigating statistical properties of velocity field 02 p0316 A71-12759

- Ballistic projectile velocity measurement using condenser charged thin wire circuit 03 p0422 A71-13273

- Venus atmosphere wind velocity calculation based on radial velocity fluctuations measurements of instrument packages parachuted from Venera 5 and 6 satellites 03 p0486 A71-13288

- Turbulent fluid flow through pipe, measuring circumferential velocity component close to wall by electrochemical techniques 03 p0400 A71-13733

- Fast multiple point measurement of fluid temperature and flow speed fields using bead thermistors and digital system 03 p0427 A71-13921

- Ascending aorta blood flow sequential velocity measurement using conical hot-film probe with linearized constant temperature anemometer circuit [ASME PAPER 70-WA/BHF-13] 03 p0373 A71-14111

- Superfluid flow through parallel channel, obtaining critical velocity measurements by phase coupling 03 p0404 A71-14199

- Hot-wire anemometer velocity measurement in slow air flow 03 p0430 A71-14374

- Fabry-Perot etalon and focal reducer parameters for extragalactic radial velocities measurement, comparing optical mountings 04 p0593 A71-14909

- Thermal variations of all-glass and air-gas Fabry-Perot etalons for radial velocities measurement, discussing resolution 04 p0593 A71-14910

- Ghost images due to reflection between interference filters and Fabry-Perot etalons during measurement of radial velocities 04 p0593 A71-14911

- H II region high velocity observations by two etalon, propane scanned photoelectric Fabry-Perot spectrometer with reflecting telescope 04 p0581 A71-15044

- Binary star radial velocity measurement, discussing formation, evolution, motion frequency and H-R diagrams 04 p0647 A71-15242

- Doppler radar velocity sensors and altimeters for lunar and planetary spacecraft instruments soft landing 04 p0597 A71-15324

- Solar wind velocity and ion temperature measurement by modulation-type ion trap onboard interplanetary Venera 3 satellite 05 p0798 A71-16052

- Gas and liquid flows local velocity measurements, using Doppler frequency shifts due to wave scattering at solid microparticles suspended in flow 05 p0753 A71-16786

- Changing rotational velocity recording device for vestibular apparatus tests, examining stimulus reaction speed 05 p0714 A71-16810

- Laser Doppler heterodyning system for bidirectional pulsatile fluid flow velocity magnitude and direction measurement 05 p0756 A71-17233

- Frequency domain and time domain methods analysis of signal from laser velocimeter 06 p0900 A71-18055

- Laser Doppler velocimeter, describing simplified stable optical arrangement 06 p0900 A71-18055

- Ionospheric drift velocity fluctuations by similar fading method, discussing applicability and errors 06 p0894 A71-18262

- Noise-producing subsonic jet turbulence eddies hot-wire anemometer measurements of convection velocity as functions of frequency [AIAA PAPER 71-154] 06 p0884 A71-18594

- Turbulent skin friction and boundary layer velocity measurements on nonadiabatic flat plates at hypersonic Mach numbers [AIAA PAPER 71-167] 06 p0885 A71-18609

- Velocity and density measurements in hypersonic velocity ballistic projectile turbulent wakes, using hot-film anemometers [AIAA PAPER 68-701] 07 p0105 A71-19891

- Fluidic ambient velocity and pressure measurement sensors, using unbounded turbulent jets 07 p0129 A71-20595

- Galactic optical radial velocity measurements compared to 21 cm red shifts derived velocity 08 p1357 A71-20873

- Ephemeride and atomic uniform time scales comparison for earth rotation velocity changes, estimating diurnal and semidiurnal tides effect 08 p1284 A71-21673

- Velocity components, species densities and temperature local measurements, using laser Doppler velocimeters, Raman scattering and tunable lasers [AIAA PAPER 71-283] 08 p1303 A71-22008

- Laser Doppler system for subsonic and supersonic jet flow velocity measurements, discussing calibration and measurement errors 08 p1303 A71-22009

- Laser Doppler velocimetric technique for supersonic flow particle trajectory and density measurements, noting particle lag [AIAA PAPER 71-287] 08 p1303 A71-22010

- Laser Doppler velocimeter, determining basic operational parameters including required particle density, number, type, size, output signal to noise ratio, etc [AIAA PAPER 71-288] 08 p1304 A71-22011

- Centrifugal pump channels flow velocity measurement by optical method, noting flow separation near blade exits 08 p1230 A71-22048

- Turbulent velocity pulsations measurement by conduction anemometer with three-electrode sensor 09 p1499 A71-22132

- Velocity distribution measurement of Cs gas flow from orifice in near-free molecule regime, using apparatus based on time of flight method 09 p1432 A71-22682

- Shock wave free surface velocity measurement using moire method for photographic recording with image converter streak camera 09 p1444 A71-22715

- Satellite-borne sensor for ionospheric ions velocity measurement, describing design and operation principles 09 p1438 A71-23141

- Ionospheric ions drift velocity horizontal and vertical components distribution, using satellite-borne sensor 09 p1438 A71-23142

- Venus atmosphere wind velocity calculation based on radial velocity fluctuations measurements of instrument packages parachuted from Venera 5 and 6 satellites 09 p1525 A71-23261

- Noise reduction in Rudd type laser velocimeter by conversion to light scattering system 09 p1453 A71-23695

- Laser fluid flow velocimeter pulse output resolution approximation, using spectrum analyzer or discriminator measurements 09 p1453 A71-23726

- Velocity measurements for slowly moving pendulum bob with incandescent filament lamp, detecting Doppler shifted beam interference beat frequency with photomultiplier 10 p1574 A71-23738

- Vertical velocities in atmosphere measured by acoustic Doppler during diurnal thermal plumes and breaking wave occurrence within nocturnal inversion 10 p1574 A71-23746

- Power density spectrum of longitudinal velocity fluctuations in pretransition pulsed boundary layer 10 p1591 A71-23836

- Air jet velocity and turbulence measurements by modified Doppler technique, using CW lasers 10 p1609 A71-23874

- Sporadic meteors geocentric velocity distribution over celestial sphere by photographic observation and oblique radio sounding, noting annual variations 10 p1668 A71-24029

Horizontal and vertical trace velocities of traveling ionospheric disturbances, interpreting in terms of atmospheric gravity waves

10 p1602 A71-24462

Flow visualization and velocity measurements in repeatedly branching tube systems representative of human lung, estimating viscous dissipation and pressure drop

10 p1571 A71-24625

Variable shear interferometer for infinite fringe operation and velocity measurement, discussing refractive index distributions in stationary and moving media

10 p1613 A71-24994

Hot-wire anemometry for measuring velocity-temperature coefficients in turbulent flow with heat transfer

10 p1597 A71-25016

Frequency response of velocity and acceleration transducers for oscillatory environments instrumentation

11 p1762 A71-25935

Directional laser Doppler velocimeter measurements in perturbed circular flow, noting use in cardiovascular research

11 p1766 A71-26303

Measuring methods for internal velocities of stars and gas within spiral galaxy, considering emission lines and Fabry-Perot interferometer

12 p1960 A71-26786

Thermosensitive quartz anemometer operating in vibrational mode, discussing design and applications in low airflow velocity measurement

12 p1906 A71-26826

Subsonic turbulent jet flow optical measurement by quantitative schlieren technique to overcome hot-body anemometry difficulties due to temperature and velocity fluctuations

12 p1896 A71-27215

Signals single set synthesis for simultaneous target information transmission and range and velocity measurement

12 p1883 A71-27617

Velocity and magnetic field measurements in solar active regions, using fine scan simultaneous Doppler and magnetogram observations

12 p1968 A71-27646

Sound velocity measurements in superheated Cs vapors, using least squares method for analytic relationships on saturation line and isobars

13 p2099 A71-27881

Spiral galaxy NGC 4569 member of Virgo cluster, using measurements of central velocity field, rotation and density estimates

13 p2132 A71-27965

Meteor particle speed and size estimation using accelerated glass microsphere bombardment in plasmoid

13 p2133 A71-28201

Boundary layers velocity distribution measurements, using scattered laser radiation Doppler shift

13 p2078 A71-28574

Fluid velocity measurements by electroacoustic transducers using phase difference relation

13 p2069 A71-28901

Velocity measurements in gas mixtures by hot-wire and hot-film anemometers, inferring transport properties from direct calibrations

13 p2069 A71-29008

Solar wind speed data, investigating variations in satellite observations

13 p2130 A71-29062

Ion probe measurements of very low fluid velocities, improving accuracy by marking technique

14 p2223 A71-29745

Frequency-length relationship for bulk InP microwave oscillators in 10-100 micron thickness range, obtaining threshold field and average transit velocity

14 p2210 A71-29791

Thermal diffusion effect on gas flow velocity measurements with anemometers with heat convection signals

14 p2239 A71-29815

Sunspot penumbra displacements, emphasizing fine structure elements velocity and directional motion

14 p2308 A71-29972

Laser Doppler velocimetry accuracy degrading factors, considering light beam focus phase anomaly and distortions due to density fluctuations

14 p2245 A71-30331

AEDC test facilities laser instrumentation for flow field diagnostics by Doppler velocimeter, holographic flow visualization and particle studies

14 p2245 A71-30332

Transient ground motion velocity measurement system, using piezoresistive acceleration transducers, electronic integrator and digital zeroing circuit

14 p2245 A71-30340

Inertial instruments with outputs indicative of time integral and time double integral of vehicle acceleration for velocity and distance determination

14 p2245 A71-30343

Planetary nebula NGC 7009 narrow band filter photographs and spectra, detailing emission lines, intensity and velocity variations and model

14 p2313 A71-30430

Storm clouds tops maximum height and vertical velocity calculation, allowing for entrainment and vertical wind shear

15 p2444 A71-31362

Shock wave splitting in KBr, determining shock profiles and velocities by electromagnetic method

15 p2463 A71-31385

Casing material effects on velocity of low speed phase prior to detonation onset of high density PETN, testing steel, Plexiglas, Duralumin and brass

15 p2511 A71-31390

Supersonic arc-heated Ar flow, measuring heavy particle temperature and velocity and electron density profiles by pressure scanned Fabry-Perot interferometer

[AIAA PAPER 71-589] 15 p2454 A71-31534

Direct measurement of spatial velocity correlation functions in turbulent flow by conditional probability of scattered light

15 p2449 A71-31866

Burning velocity measurement of laminar conical hydrogen-air flames on 10.3 mm diam water cooled nozzle burner, using schlieren and particle tracking techniques

15 p2465 A71-32085

Large gas bubble migration in rotating liquid without gravity, noting velocity dependence on stagnation point distance and radius of curvature

15 p2392 A71-32119

Solution concentration, solid content, specific gravity and bulk modulus measurements by sound velocity measurement

15 p2409 A71-32197

Turbulent flow field mean velocity components measurements near thin rotating disk

15 p2392 A71-32253

Laser Doppler turbulent and laminar flow velocity measurement model, using optical mixing spectroscopy theory

15 p2423 A71-32589

Low speed testing of VTOL models in wind tunnels, describing method for estimating free air approach velocity and angle of attack

15 p2386 A71-32724

Ionizing shocks in argon produced by pressure driven shock tube, measuring velocity and ionization within and behind nozzle

16 p2616 A71-32904

Gas and liquid flows local velocity measurements, using Doppler frequency shifts due to wave scattering at solid microparticles suspended in flow

16 p2576 A71-33038

Oscillating circular cylinder wake fluctuating velocity measurement at low Reynolds numbers, using hot-wire anemometer

[ASME PAPER 71-APM-33] 16 p2520 A71-33196

Earth velocity vector right ascension, declination and magnitude determination from cosmic 3 K background radiation anisotropy

16 p2563 A71-33402

Solar wind velocity and ion temperature measurement by modulation-time ion trap onboard interplanetary Venera 3 satellite

16 p2626 A71-33456

Meteoroid velocity measurement by satellite-borne meteoroid detectors, giving Geminid meteor shower measurements results

16 p2639 A71-33724

Geminid meteoroid dust particles detection, determining velocity and orbital elements from OGO 3 flux measurements

16 p2640 A71-33741

Upper atmosphere rotational speed variations from measurements of orbital inclination of satellites

16 p2569 A71-33807

Velocity and magnetic field equations of electroconductive fluid vortex motion due to annular receptacle insulating walls rotation

16 p2620 A71-34057

Molecular jet velocity measurement, using periodic spatial variation modulation of radio frequency field

16 p2614 A71-34063

Cold plasma flow rate determination from emission inhomogeneities, using time of flight method and high speed streak photography for instantaneous velocity measurements

17 p2787 A71-34286

Steady plasma flow velocity measurements, describing two channel high resolution spectrometer

17 p2787 A71-34390

Precision area navigation system, considering position and velocity continuous measurement in three dimensional space, system components and simulation program

17 p2771 A71-34616

Turbulent He jet time resolved velocity and He mass fraction measurements, using hot-wire anemometry and digital recording techniques

17 p2670 A71-34878

Velocity determination in hypersonic low density wind tunnel based on high energy electron beam produced nitrogen ions time of flight

17 p2670 A71-34887

Point target horizontal speed determination with circular beam radar for measuring signal intensity and

range, noting application to insects in atmospheric waves

17 p2706 A71-35122

Stress wave propagation in quartz-phenolic composite, measuring particle velocity by velocity interferometer

17 p2762 A71-35207

Vortex laser Doppler velocimeter system for aircraft wake turbulence velocity profile mapping, describing optical arrangements, back and forward scattering modes and prototype design

17 p2754 A71-35756

Airborne Doppler velocity sensors, considering hydrometeors effects on HF signal attenuation and reflection

17 p2747 A71-35768

Flow velocity measurement by laser differential Doppler heterodyning, obtaining SNR from frequency difference between shifted beams

18 p2914 A71-35848

Random noise effects on oscillator short term frequency stability and velocity measurement by Doppler effect

18 p2879 A71-36531

Optical readout system for analysis of laser Doppler velocimeter signals displayed on TV screen and recorded photographically

18 p2931 A71-36587

Laser velocity measuring system for tracking high speed rocket sleds on Holloman test track

18 p2932 A71-36616

Laser velocimeter for wide range velocity measurement, using photodetector to observe light scattering by particles flowing across fringe pattern

18 p2932 A71-36618

Solar photospheric velocity field measurements, using balloon-borne sodium resonance cell with diffraction limited telescope

18 p2965 A71-36729

Gas flow velocity measurements in channel, using electromagnetic technique

19 p3061 A71-37090

Two phase flow model of water droplets velocity in air stream, using Fresnel biprism and laser differential scheme

19 p3072 A71-37587

Seismic wave velocity measurements in pahoehoe basalt flows in lava beds, comparing with laboratory dilatational velocities

19 p3052 A71-37685

Altitude dependent vertical drift velocity of small scale ionospheric inhomogeneities, using correlation of signal time lag scanning in frequency domain

19 p3058 A71-38391

Monograph on electron drift rate measurement in low pressure arc discharge using microwave dragging technique

19 p3116 A71-38549

Radar equipment for meteor velocity and radiants measurement at VHF by pulse diffraction method

19 p3067 A71-38635

Swedish monograph on low air flow velocity measurement with hot-wire anemometer under free and forced convection, using schlieren method

19 p3172 A71-38645

Two phase flow speed transit time measurements by correlation methods with randomly fluctuating signals, noting use in small bore tubes and strip steel production

19 p3067 A71-38658

Solar velocity field decomposition into oscillatory and slowly varying components by spectroheliograms with high spatial resolution

19 p3146 A71-38662

Ultrasonic technique for crack and craze velocity measurement in material subjected to stress in liquid environment

20 p2333 A71-38817

Laser Doppler holographic technique for fluid velocity field visualization and quantitative two dimensional vector velocity measurement

20 p2335 A71-39183

Monograph on blood flow rates instantaneous measurement from ultrasound signals of Doppler flowmeter, discussing steady laminar flow test results

20 p3193 A71-39262

Flow velocity measurement in electromagnetically driven unsteady shock tube from charged particles extraction, using ionization gases

20 p2339 A71-39432

Real time multitrack half tone recorder for displaying three dimensional information on instantaneous blood velocity measurement by Doppler effect

21 p3377 A71-40132

Sequential electric spark technique for hypervelocity projectiles turbulent wake velocity measurements at ballistic ranges in free flight regime

21 p3362 A71-40385

Low speed wind tunnel air velocity measurement with laser velocimeter, using dark background illumination detection of particles scattering across fringe pattern

21 p3378 A71-40398

Dual scatter laser Doppler velocimeters for transonic wind tunnel measurements and calibration applied to simulated helicopter downwash, high lift wing and jet crossflow

21 p3364 A71-40399

Solar wind angular momentum flux transport from nonradial velocity components measurements by Mariner 5, noting agreement with comet tail observations

21 p3438 A71-40428

Hot split-film anemometer sensors for three dimensional air velocity vector measurement

21 p3378 A71-40487

Pre- and post-exposure recording in holographic measurement of high object velocities for enhanced image reconstruction

22 p3537 A71-41597

Fluid velocity gradient measurement by laser-Doppler techniques based on signal spectrum bandwidth or frequency shift corresponding to position shift near wall

22 p3541 A71-41792

Velocity and frequency drifting measurement apparatus developed for rotating machinery study

22 p3523 A71-42474

Atmospheric self-aligning dual-scatter laser Doppler velocimeter, calculating backscattered power, range, wavelength and scatter centers number relationships

22 p3559 A71-42564

Unbounded turbulent jet transducer element fluidic sensors, measuring ambient velocity and density from pressure data

22 p3531 A71-42768

Transient response of electroacoustic transducer arrays, computing time dependent velocities for prescribed electrical inputs

23 p3704 A71-43211

Pressure altimeter, airspeed and vertical velocity instruments, discussing selection, installation, pilot verification, error identification, repair and use

23 p3675 A71-43385

Liquid flow rate measurement by determining fall time of cmf generated in sensor coil by fluid nuclei precessing freely in magnetic field

23 p3678 A71-43536

Power spectrum analysis of solar granular intensity fluctuations and velocities, noting asymmetry behavior of Ba II line in individual convection cells

23 p3677 A71-43834

Plasma acceleration of low pressure toroidal gas discharge, measuring plasma velocity as function of radial magnetic field for different pressures

23 p3711 A71-43874

Optical anemometers for local nondestructive flow velocity measurements, discussing signal analysis possibilities

23 p3679 A71-43952

Speed of sound measurement in solid and liquid phase suspensions, considering dense phase inertia forces and particles thermal retardation effects

24 p3827 A71-45019

Shielded hot-wire probe for mean and rms flow velocities in highly turbulent and rapidly reversing flows

24 p3828 A71-45075

VELOCITY POTENTIALS

U FLOW DISTRIBUTION

U VELOCITY DISTRIBUTION

VELOCITY PROBES

U PITOT TUBES

U SPEED INDICATORS

VELOCITY PROFILES

U VELOCITY DISTRIBUTION

VENERA SATELLITES

NT VENERA 3 SATELLITE

NT VENERA 4 SATELLITE

NT VENERA 6 SATELLITE

Venera probes UV radiation measurement, discussing photometric equipment and spectra for hot stars and Milky Way in L alpha line

02 p0304 A71-11912

Venusian atmosphere adiabatic and isothermal models from Venera automatic stations data, discussing temperature, pressure, density and cloud layer thickness

05 p0804 A71-16041

Venera satellites and Mariner 5 radio wave fluctuations and discontinuities of refractive index in Venusian atmosphere, considering atmospheric turbulence

05 p0719 A71-16042

Venera probes UV radiation measurement, discussing photometric equipment and spectra for hot stars and Milky Way in L alpha line

13 p2133 A71-28199

Venusian atmosphere adiabatic and isothermal models from Venera automatic stations data, discussing temperature, pressure, density and cloud layer thickness

16 p2635 A71-33445

Venera satellites and Mariner 5 radio wave fluctuations and discontinuities of refractive index in Venusian atmosphere, considering atmospheric turbulence

16 p2542 A71-33446

Venera 7 satellite data during descent through Venus atmosphere and activity after soft landing on 15 December 1970, noting temperature and pressure measurements

20 p3289 A71-39130

Radio wave propagation characteristics in Venusian atmosphere and interplanetary plasma from Venera 7 probe data

24 p3805 A71-45312

VENERA 3 SATELLITE

Solar wind velocity and ion temperature measurement by modulation-type ion trap onboard interplanetary Venera 3 satellite

05 p0798 A71-16052

Solar wind velocity and ion temperature measurement by modulation-type ion trap onboard interplanetary Venera 3 satellite

16 p2626 A71-33456

VENERA 4 SATELLITE

Galactic cosmic rays and interplanetary magnetic field flux measurements onboard Venera 4 space probe, noting lack of correspondence with Forbush decrease

20 p3282 A71-39737

VENERA 6 SATELLITE

Solar high energy cosmic ray proton burst observations, examining maximum flux delay time with Venus 6 satellite

20 p3281 A71-39734

VENTILATION

Tidal volume and respiratory rate changes at start and end of exercise, considering ventilation control and neurogenic respiratory reflexes

04 p0545 A71-15161

Oxygen intake, ventilation and heart rate during various intensity and duration tests

05 p0708 A71-16615

Time constant for collateral ventilation in human, dog and pig lungs under various physiological conditions

06 p0856 A71-18385

Carbohydrate ingestion produced respiratory gas exchange ratio and alveolar ventilation effects on arterial oxygen tension in normal men

07 p1052 A71-20333

High altitude submaximal and maximal work by humans, noting time required for steady state oxygen consumption, ventilation and heart rate

09 p1401 A71-23368

Ventilation rates and thermal factors of sensitive elements in radiosondes, using wind tunnel tests

11 p1761 A71-25382

Pressure effects on human ventilation and gas exchange, determining stratified inhomogeneity during deep diving

12 p1873 A71-27126

Muscular fatigue of healthy Bengali males with increasing work loads under varying environmental conditions, considering ventilation, heart rate and oxygen consumption

17 p2688 A71-34360

Oxygen metabolic rate in isolated canine lungs at various static inflation levels and cyclic ventilation, examining mechanical deformation effects

17 p2683 A71-35145

Monograph on peripheral chemoreceptors and central chemosensitive area control of ventilation during chronic blood acid base changes and hypoxia in mammals

18 p2852 A71-35869

Phrenic nerve activity correlation with ventilation in anesthetized cats, analyzing relationship between phrenic impulse rate and integrated electrical activity

20 p3192 A71-38983

VENTILATION FANS

Acoustic measurement of rotor tones in duct of four blade ventilation fan

19 p3000 A71-38655

VENTILATORS

Loads on compressor, ventilator and turbine rotor disks having large central holes, giving formulas for stress distributions

12 p1945 A71-26952

VENTING

Out-of-pile experiment for measuring uranium dioxide fuel redistribution rates, determining vent hole plugging time and thermal cycling

02 p0296 A71-12247

Dynamics and thermodynamics of water and oxygen particles ejected into space by Apollo during translunar flight, using ground based photographic observations

11 p1833 A71-26254

Saturn S-4B continuous vent system for propellant tanks during parking orbit to prevent excessive pressure, requiring liquid settling with auxiliary ullaging rockets

18 p2973 A71-36453

Orbital nonpropulsive vent system to remove excess or residual propellant vapors and waste gases with minimum impulse imbalances imparted to vehicle

18 p2973 A71-36454

VENTRAL SECTIONS

Ventral spinocerebellar tract cellular level contrast transmission to motoneurons, considering monitoring of inhibitory interneurons output against excitatory input

12 p1869 A71-26701

VENTURI TUBES

Small gas discharge coefficient of venturi tubes

02 p0253 A71-12575

Computer programmable flow coefficient formulas for standard constrictions, orifice gages and Venturi nozzles

10 p1595 A71-24644

Critical and near critical two phase flow in venturi tube, applying one dimensional flow equations [ASME PAPER 71-FE-4]

13 p2051 A71-29441

VENUS (PLANET)

Venus spectra 10488 A carbon dioxide band from high dispersion spectroscopy

03 p0488 A71-13556

Venus low retrograde spin rate explained as result of capture of moonlike object from retrograde orbit transforming planet rotational energy into heat

04 p0642 A71-14822

Venus surface alteration for human habitation

04 p0539 A71-15340

Venus high resolution spectra interpretation for sub-II band of carbon dioxide isotope

04 p0659 A71-15859

Shock structure at Venus and Mars dependence on interplanetary magnetic field orientation from Mariner 4 and 5 data, indicating magnetosheaths existence

05 p0810 A71-16636

Mariner mission to Venus and Mercury in 1973/74, discussing special opportunity characteristics, mission options, real time TV picture transmission, trajectory analysis, etc

05 p0814 A71-17230

Theoretical submillimeter spectrum of Venusian radiation, determining brightness temperature

07 p1193 A71-19313

Radar scattering law derivation method for small regions of Venus surface, synthesizing CW spectra

08 p1357 A71-20877

Interplanetary plasma disturbances in Venus proximity from Venera measurements

09 p1520 A71-22664

Venus motion, mass, dimensions, shape, topography and atmosphere

09 p1520 A71-22819

Venus photographs analysis during synoptic periods, noting inconclusive results on cloud layer and planetary surface structures

09 p1521 A71-22845

Venus inferior conjunctions tables from 1960 to 2023, presenting geocentric latitude at conjunction time

09 p1528 A71-23549

Hydrogen isotopes around terrestrial planets: discussing H and deuterium dynamic behavior in Venus and Mars coronas

10 p1668 A71-24000

IR polarization of Venus, providing Venus atmosphere effective particle size estimate

10 p1675 A71-24489

Mercury and Venus transit periodicity before solar disk, examining celestial mechanics and solar system distances determination

10 p1680 A71-25000

Venus, Mars, Jupiter and lunar thermal emission data in 7-25 micron region

11 p1824 A71-25695

Venus water, discussing polar seas, acidity, temperature, wind patterns and clouds

11 p1824 A71-25700

Venus life forms, describing algae grown in pure carbon dioxide under pressure in acidic nutrient media at high temperatures

11 p1724 A71-25700

Hydrogen plasma simulation of solar wind-planetary body interaction, showing electric fields behind moon and Venus

11 p1816 A71-25755

Venus-Mercury flyby vehicle solar cells, cover glasses, adhesives and Kapton film, investigating space radiation effects on solar absorbance and transmittance

11 p1859 A71-26236

Venus retrograde rotation, showing consistency with Laplacian theory of cosmology and Fesenkov theory

12 p1961 A71-26901

Venus polarimetric observational data comparison with polarization characteristics of radiation scattered at gamma-distribution particle sizes, determining refractivity and particle radius

12 p1964 A71-27088

Venus Schrotter effect, noting phase deviations from ephemeris values

13 p2136 A71-28387

Space vehicle observation effect on Mars and Venus conceptions, considering origins of life, ru-

- away greenhouse effect on earth and atmospheric circulation 14 p2308 A71-29909
- Theoretical submillimeter spectrum of Venusian radiation, determining brightness temperature 15 p2486 A71-31893
- Polarimetric observations of Venus during 1969 inferior conjunction, showing no evident halo effect due to hexagonal ice crystals 15 p2491 A71-32424
- Venus L alpha emission, negating deuterium origin 18 p2970 A71-37055
- Venus polarimetric observational data comparison with polarization characteristics of radiation scattered at gamma-distribution particle sizes, determining refractivity and particle radius 19 p3133 A71-37438
- Soviet papers on terrestrial planets, discussing Mercury, Venus and Mars atmosphere, surface, internal structure and physical conditions 21 p3452 A71-40882
- Venus survey, discussing mass, radius, rotation, internal structure, magnetic field, radiation belts, surface properties, atmospheric composition, cloud layer, etc 21 p3452 A71-40884
- Artificial illumination for Venus surface pictures from landed space vehicle 22 p3608 A71-41953
- Ashen light over Venus nocturnal hemisphere due to reflected earthlight and starlight 23 p3733 A71-43128
- High dispersion spectroscopic observations of Venus, finding carbon dioxide band rotational temperature 24 p3873 A71-45079
- VENUS ATMOSPHERE**
- Venera-borne gas analyzers for parachute descent probing of Venus atmosphere, describing design and operation 02 p0248 A71-11916
- Venusian exospheric temperature local time dependence from heat conduction equation for instantaneous heating during Mariner 5 observation 02 p0304 A71-11971
- Venus lower atmosphere structure and brightness temperature spectrum analysis for composition, temperature and pressure profiles 03 p0484 A71-13212
- Venus atmosphere wind velocity calculation based on radial velocity fluctuations measurements of instrument packages parachuted from Venera 5 and 6 satellites 03 p0486 A71-13288
- Venus equatorial stratosphere structure, presenting approximate radiative dynamical calculation for zonal flow mechanism 03 p0488 A71-13552
- High dispersion spectroscopic observations of Venus carbon dioxide bands for deriving rotational temperature 03 p0488 A71-13557
- Venus atmosphere rotational model, considering nonlinear instability due to wind shear from solar heat induced convection 03 p0489 A71-13607
- Venus high dispersion spectra used for line positions and constants of carbon dioxide 7820 and 7883 A bands 04 p0629 A71-14806
- Balloon position determination in Venusian atmosphere, using ranging measurement and radiated signal polarization 04 p0623 A71-15014
- Venus halo as photometric evidence for hexagonal ice in cloudtops 04 p0660 A71-15862
- Decimeter radio wave propagation in Venusian atmosphere, determining refraction and absorption coefficients height dependence based on Venera spacecraft data 05 p0718 A71-15993
- Venusian atmosphere adiabatic and isothermal models from Venera automatic stations data, discussing temperature, pressure, density and cloud layer thickness 05 p0804 A71-16041
- Venera satellites and Mariner 5 radio wave fluctuations and discontinuities of refractive index in Venusian atmosphere, considering atmospheric turbulence 05 p0719 A71-16042
- Layer boundaries and critical concentrations of anomalous increase of radiation in earth and Venus atmospheres along tangential directions 05 p0738 A71-16044
- Venus planetary science, discussing radar and space probe measurements as basis for different atmospheric models 05 p0814 A71-17226
- Venus atmosphere and lithosphere thermochemical composition, examining various models 06 p0966 A71-17898
- Escape mechanisms examined to explain liquid water absence on Venus surface, considering hot acidic hydrosphere consequences for biological activity 06 p0968 A71-17955
- Venusian atmospheric cloud cover, determining nature of particles by optical reflective properties 07 p1191 A71-18907
- Radio signal refractive index fluctuations in Venus atmosphere from Mariner 5 data 07 p1197 A71-19762
- Radiative heat transfer during entry into shocked Venus model atmosphere 07 p1199 A71-19870
- Polarization of sunlight multiply scattered by atmosphere and cloud particles of Venus from UV to IR 07 p1204 A71-20622
- Carbon dioxide 7883 and 7820 A band strengths compared in Venus atmosphere 08 p1338 A71-21396
- Venusian atmospheric models of troposphere, stratosphere and thermosphere based on satellites observation data 09 p1519 A71-22527
- Venus motion, mass, dimensions, shape, topography and atmosphere 09 p1520 A71-22835
- Energy distribution in dark and light details on Venus spectrograms, considering relation to clouds in upper atmosphere 09 p1520 A71-22838
- Aqueous HCl refractive indices measured for room temperature to Venus cloud temperature and various concentrations 09 p1522 A71-22937
- Differential rotation in sun, giant planets and upper atmospheres of earth and Venus, attributing solar rotation to tides caused by planets 09 p1522 A71-22961
- Venusian atmosphere carbon dioxide, water, molecular oxygen and nitrogen contents from Venera 5 and 6 data 09 p1523 A71-23144
- Venus atmosphere wind velocity calculation based on radial velocity fluctuations measurements of instrument packages parachuted from Venera 5 and 6 satellites 09 p1525 A71-23261
- Prograde and retrograde 4 day circulation in Boussinesq fluid layer by traveling thermal waves in Venus upper atmosphere 09 p1526 A71-23446
- Venus atmospheric temperature and pressure measurements during and after Venera 7 soft landing 09 p1528 A71-23560
- Venus atmosphere determinations by Mariner 5 radio occultation measurements, deriving altitude profiles of refractivity, molecular number density, pressure, temperature and radio frequency absorption 10 p1669 A71-24176
- Aqueous HCl solutions refractive index calculation from concentration dependence for Venus clouds composition 10 p1680 A71-25012
- Venusian atmosphere subcloud layers intrinsic outgoing thermal radiation and IR spectrum transmittivity from satellite temperature, pressure, moisture content and chemical composition data 10 p1681 A71-25128
- Venus atmosphere chemical composition, determining N, O, water and carbon dioxide concentrations, temperature and pressure 11 p1823 A71-25691
- Mariner 5 Venus exospheric Lyman alpha measurements for dayside temperature value, using molecular hydrogen photodissociation model 11 p1823 A71-25692
- Venus daytime ionospheric models using electron, ion and neutral gas heat conduction with momentum and chemical equations for charged particle densities 11 p1823 A71-25693
- Venus atmosphere composition and structure from microwave spectrum, noting surface pressure and temperature and water vapor 11 p1823 A71-25694
- Venus atmosphere mm and cm radio wave propagation calculated from temperature, pressure and chemical composition data 11 p1823 A71-25695
- Venus atmosphere critical refraction model, examining optical effects and ray paths 11 p1823 A71-25696
- Venus atmosphere spectra, emphasizing line and continuum absorption coefficients relative to scattering 11 p1823 A71-25697
- Venus thermal radiation limb darkening measurements, indicating complex atmospheric structure 11 p1824 A71-25699
- Venus cloud pattern contrast, using photoelectric scans with narrow band interference filter sequences 11 p1824 A71-25702
- Venus cloud composition, noting partially hydrated iron chloride as principal constituent 11 p1824 A71-25703
- Venus ferrous chloride hydrate cloud production, examining geochemical problems 11 p1824 A71-25704
- Venus cloud hypotheses, discussing chemical composition, vapor pressure, temperatures and spectroscopic abundances 11 p1824 A71-25705
- Oxygen atom deficiency and very low exospheric temperature in Mars and Venus upper atmospheres, considering photochemical processes and molecular diffusion 11 p1826 A71-25723
- Carbon dioxide cations emission bands in Mars and Venus dayglows, suggesting fluorescent scattering and photoionization as main excitation sources 11 p1827 A71-25724
- Atmospheric modeling for earth and Venus heterosphere structure using multicomponent radiative hydrodynamic equations, determining atmospheric temperature and constituents height variation 11 p1828 A71-25764
- Venus maps from high resolution radio telescope observations, investigating surface pressure/temperature, planetary atmosphere and water vapor presence 11 p1830 A71-26109
- Line formation effective pressure from Venus atmosphere spectra, discussing phase angle variations 11 p1835 A71-26457
- Venusian atmosphere heat transfer processes, calculating radiant fluxes and convective motion model 12 p1958 A71-26640
- Venus subcloud layer, investigating radiant heat transfer in convective lower atmosphere 12 p1958 A71-26646
- Venus atmosphere adiabatic and isothermal models, investigating water vapor content, pressure and temperature 12 p1964 A71-27085
- Cloud layer role in formation of light and heat regime of two layer Venus atmosphere model, considering sunlight reflection 13 p2131 A71-27808
- Venus atmospheric turbulence from Venera 4, 5, 6 and Mariner 5 observations, discussing scaling laws and normalized signal-amplitude standard deviation 13 p2132 A71-27928
- Venera-borne gas analyzers for parachute descent probing of Venus atmospheric composition, describing design and operation 13 p2067 A71-28203
- Venus upper atmosphere retrograde circulation correlation with solar couple effect on thermal semidiurnal atmospheric tide 13 p2134 A71-28286
- Venus carbon dioxide spectrum, observing spatial and temporal variation in abundance 13 p2134 A71-28287
- Venus rotation observations during 1964 eastern spring elongation, noting weather period and wind velocities 13 p2136 A71-28386
- Venus cloud height at equatorial and polar latitudes, using carbon dioxide band distribution intensity 13 p2138 A71-28593
- Ionic and thermal structure model of daytime Venus ionosphere with solar wind heating based on Mariner 5 flyby mission 14 p2305 A71-29661
- Venusian atmosphere RF refractive attenuation height dependence, field strength measurements comparison, inversion layer influence and surface echoes effects 14 p2309 A71-30098
- Jupiter Red Spot, zonal wind and banded appearance, Venus vertical temperature structure and atmospheric motions, and Mars circulation, dust phenomena and atmosphere stratification 14 p2313 A71-30499
- URSI-IAU-COSPAR Woods Hole Conference on lunar emission and Mercury surface temperature from radiometry, discussing Mars and Venus atmosphere measurements 14 p2316 A71-30967
- Radiative heat transfer equilibrium in earth, Venus and Mars atmospheres, taking into account interaction with ground 15 p2395 A71-31448
- Venusian atmosphere circulation modeling, calculating temperature differences, thermal inertia and wind velocity 15 p2496 A71-32729
- Venusian atmosphere adiabatic and isothermal models from Venera automatic stations data, discussing temperature, pressure, density and cloud layer thickness 16 p2635 A71-33445
- Venera satellites and Mariner 5 radio wave fluctuations and discontinuities of refractive index in Venusian atmosphere, considering atmospheric turbulence 16 p2542 A71-33446
- Layer boundaries and critical concentrations of anomalous increase of radiation in earth and Venus atmospheres along tangential directions 16 p2635 A71-33448

Diurnal variation of Venus and Mars exospheric temperatures, using neutral heating efficiency calculation based on molecular theory

16 p2641 A71-33769

Refutation of greenhouse model of Venus atmosphere from Venus 4 and Mariner 5 data, proposing volcanic activity burst hypothesis

17 p2803 A71-34835

Venusian atmospheric models from troposphere, stratosphere and thermosphere models based on satellites data

17 p2807 A71-35502

Doubling method application to multiple scattering of polarized light, studying Venus visible disk reflection of sunlight

17 p2784 A71-35569

Venus surface temperature dependence on incident solar flux based on runaway greenhouse nongray calculation, considering water vapor as IR opacity source in models

18 p2964 A71-36285

Venus atmospheric model based on Mariner 5 and Venera satellites observation, comparing with optical observation from earth

18 p2965 A71-36293

Atmospheric rotation on Venus, examining Gierasch model based on radiative drive coupled with response time lags

18 p2967 A71-36930

Mars, Venus and earth atmospheres, considering abundance of volatiles such as carbon dioxide, water, oxygen, nitrogen, argon, carbon monoxide, chlorine and fluorine

18 p2968 A71-37032

Venus atmosphere adiabatic and isothermal models, investigating water vapor content, pressure and temperature

19 p3133 A71-37435

Spectral composition of emitted radiation, emissivity and absorptivity of Venus atmosphere at high temperatures

19 p3135 A71-37580

Venus atmosphere chemical composition, temperature and pressure, discussing model cloud layer, circulation and upper atmospheric structure

19 p3138 A71-37759

Venera 7 satellite data during descent through Venus atmosphere and activity after soft landing on 15 December 1970, noting temperature and pressure measurements

20 p3289 A71-39130

Venusian polar tropopause and cloud layer from IR spectral recording in carbon dioxide band near inferior conjunction for crescent regions

20 p3290 A71-39306

Mars and Venus atmospheres, considering energetics, mean winds, temperature differences, circulations and climates

20 p3296 A71-39624

Venus atmosphere chemical composition from gas analysers onboard Venera automatic stations, determining element abundance, water vapor density and cloud layer structure

20 p3296 A71-39625

Venus lower atmosphere model based on surface pressure and temperature from radio astronomical and radar observations

20 p3296 A71-39626

Venus atmosphere decimeter wave field intensity fluctuations and refraction coefficient variations

20 p3297 A71-39627

UV radiation in space and Venus atmosphere, studying L-alpha lines luminescence hot stars intensity, Milky Way brightness and hydrogen envelope existence

20 p3282 A71-39748

Cloud layer role in formation of light and heat regime of two layer Venus atmosphere model, considering sunlight reflection

21 p3441 A71-40077

Rapid retrograde rotation of Y shaped cloud formations in Venus upper atmosphere, discussing correlation with slow ground rotation

21 p3441 A71-40106

Venus 3-4 micron region continuum absorption from high resolution spectra of Venus and sun

21 p3448 A71-40448

Height variations of Venusian cloud tops at planet equatorial and polar regions

21 p3449 A71-40608

Atmospheric modeling for earth and Venus heterosphere structure using multicomponent radiative hydrodynamic equations for atmospheric temperature and constituents height variation determination

22 p3598 A71-41532

Venus water ice clouds existence possibility from high altitude IR spectra and ground based spectroscopic observations

22 p3603 A71-42189

Decimeter radio wave propagation in Venusian atmosphere, determining refraction and absorption coefficients height dependence based on Venera spacecraft data

22 p3515 A71-42742

Photochemical mechanism of atomic carbon production in Mars and Venus atmospheres, comparing dayglow emissions with Mariner results

23 p3734 A71-43157

Venusian atmosphere circulation modeling, calculating temperature differences, thermal inertia and wind velocity

23 p3735 A71-43298

Mariner S-band occultation experimental data compared with theory for accuracy of physical characteristics of Mars and Venus atmosphere, reviewing data reduction and error analysis

23 p3735 A71-43331

Venusian thermosphere, observing dayside solar radiation absorption generated upward dayside and downward nightside vertical motions

23 p3735 A71-43333

Mars and Venus carbon dioxide atmospheres, covering solar EUV heating efficiency, upper atmosphere temperature and chemical recombinations

23 p3735 A71-43334

Governing equations numerical integration for Venusian atmosphere circulation, calculating solar heating distribution in spherical polar coordinates

23 p3735 A71-43340

Venusian photochemistry, discussing hydrogen source from HCl, loss of water in relation to HCl, carbon dioxide stability and COS and hydrogen sulfide in visible clouds

23 p3736 A71-43341

Mars and Venus upper atmospheric electron distribution compared with theoretical ionospheric models, considering solar wind as ionization source

23 p3736 A71-43342

Enthalpy change between atmospheric carbon dioxide and Venus surface rocks for damping short term lower atmosphere temperature excursions

23 p3736 A71-43344

Numerical modeling of Venus atmosphere taking into account short wave radiation absorption, boundary layer, mesoscale convection and horizontal friction

24 p3870 A71-44819

Radiative thermal flux model of Venus atmosphere, using Venera data and greenhouse effect

24 p3870 A71-44822

Venus upper atmospheric UV spectra from rocket-borne telescope spectrophotometer, considering O I and H I emission features

24 p3872 A71-44919

Radio wave propagation characteristics in Venusian atmosphere and interplanetary plasma from Venera 7 probe data

24 p3805 A71-45312

VENUS PROBES

NT MARINER 5 SPACE PROBE

NT VENERA SATELLITES

NT VENERA 3 SATELLITE

NT ZOND 3 SPACE PROBE

NT ZOND 5 SPACE PROBE

Venus planetary science, discussing radar and space probe measurements as basis for different atmospheric models

05 p0814 A71-17226

Interplanetary magnetic field intensity and geomagnetic activity level correlation with 27-day solar activity cycle based on Venera 4 and Mariner 5 data comparison

09 p1519 A71-22577

Statistical decision theory in reliability and project management, discussing Venus probe loss

12 p1911 A71-26690

Venus planetology missions, discussing objectives, experimental packages, payloads, costs and entry/lander configurations

17 p2802 A71-34717

VENUS RADAR ECHOES

Radar interferometric mapping of Venus surface reflectivity in polarized mode at 70 cm wavelength

03 p0490 A71-13782

Radar reflection from Mercury and Venus, discussing observations of echo times predicted relativistic increase

12 p1967 A71-27419

VERBAL COMMUNICATION

Auditory illusions, investigating phonemic restorations, verbal transformations and perceptual organization

07 p1051 A71-20212

VERTEBRAE

Cancellous bones mechanical properties from compression testing of human femora, vertebrae and cranial bones

[AIAA PAPER 71-111]

06 p0863 A71-18561

Cervical vertebral distortion during acrobatic flight, discussing clinical and medico-legal aspects and preventive measures

23 p3632 A71-43219

VERTEBRAL COLUMN

Lower vertebral column forces and moments in seated human under seat-to-head acceleration

04 p0542 A71-14788

Manned aerospace vehicular escape systems, discussing human vertebral column structural limits under vertical gravity acceleration

06 p0863 A71-18587

Spinal column radiographic examination after pilot ejection, discussing vertebral injuries detection

13 p2019 A71-28516

VERTEBRATES

NT BATS

NT BIRDS

NT CATS

NT CATTLE

NT CHICKENS

NT CHIMPANZEES

NT DOGS

NT FISHES

NT FROGS

NT GUINEA PIGS

NT HAMSTERS

NT HUMAN BEINGS

NT MAMMALS

NT MICE

NT MONKEYS

NT PIGEONS

NT PRIMATES

NT RABBITS

NT RATS

NT RODENTS

NT SHARKS

NT SNAKES

NT TURTLES

Vertebrate retina receptive field structure, suggesting interaction between receptor, horizontal and bipolar cells

07 p1046 A71-20622

Electrophysiological studies of olfaction in vertebrates, describing role in orientation, sexual behavior and population control

08 p1241 A71-21942

Functional anatomy of vertebrate gravity receptor system in spatial orientation, discussing otolith organs, sensory cells and hair cell topography in the elasmobranch labyrinth

21 p3327 A71-39994

Nonactomyosin component differentiation in potassium chloride insoluble myofilaments in vertebrate smooth muscle cells

24 p3794 A71-44420

VERTICAL AIR CURRENTS

Comparative convection levels and energy instabilities in vertical motion, using particle and layer methods

01 p0113 A71-10538

Surface and aircraft radar observations of updrafts within weak echo region of Alberta hailstorm, discussing adiabatic flow breakdown into turbulent flow

01 p0115 A71-10559

Aircraft measurement of vertical and horizontal structures of temperature, moisture, refractivity and turbulence for atmospheric convection patterns, comparing radar structure to meteorological soundings

01 p0116 A71-10564

Updraft vault dynamic in hailstorms using one-dimensional cumulonimbus entraining jet model, observing initial conditions steady state

01 p0119 A71-10748

Scale lengths in atmospheric turbulence from spectra and autocorrelation of vertical air velocity component measured in low flying aircraft

01 p0120 A71-10859

Free nonlinear air convective motion in two-dimensional cloud banks along vertical wind shift

02 p0277 A71-11690

Mountainous region vertical air flow research, describing superpressure balloon and precise pressure radiosonde system

02 p0189 A71-12420

Atmospheric air columns centers of gravity, determining height from vertically integrated equations of motion

02 p0278 A71-12749

Terrain and frictionally induced vertical velocity analysis for local and regional forecasting operations, considering low level air flow effects

05 p0777 A71-16674

Mesoscale orographic inhomogeneities in vertical air flows past surfaces, noting leeward air waves and upper/lower boundary layers

07 p1149 A71-18793

Vertical air motions velocity in rainfall from Doppler spectrum total radar reflectivity and median velocity

07 p1150 A71-18798

Two dimensional thermal convection through shallow layer with vertical shear using numerical model

07 p1152 A71-19752

Glider flight in thermal air currents, discussing aircraft behavior, pilot sensory perceptions and reactions and use of variometers for ascent rate determination

08 p1230 A71-20685

Diagnostic numerical model of frontal vertical circulation in atmospheric boundary layer using local parameters

08 p1326 A71-21448

Vertical velocity effects on ionospheric horizontal wind magnitude and direction, solving integral equations system by successive approximations

09 p1435 A71-22428

- Atmospheric vertical particle motion inside convective storms observed by airborne pulse Doppler radar techniques
11 p1794 A71-25378
- Vertical air motions measurement by balloon radar tracking, discussing method of radar noise error reduction by ascent rate smoothing technique
11 p1794 A71-25385
- Radioactive impurities transfer from lower stratosphere into upper troposphere based on vertical air transport data
15 p2400 A71-31970
- Northern Hemisphere atmospheric vertical velocity computation for all seasons compatible with climatological heating functions, using time averaged thermodynamic energy equation
17 p2770 A71-34803
- Wind velocity vertical component determination through meteor trail drift observation, presenting mean diurnal measurements data
19 p3059 A71-38393
- Subequatorial ionospheric upward moving irregularities during high sunspot activity, explaining phenomenon at F 2 region level by Hall drift from daytime west-east electric field
23 p3665 A71-42971
- Venusian thermosphere, observing dayside solar radiation absorption generated upward dayside and downward nightside vertical motions
23 p3735 A71-43333
- VERTICAL DISTRIBUTION**
- Umkehr technique vs Mast-Brewer sondes for ozone vertical distributions
01 p0073 A71-10857
- Planetary scale Rossby waves, examining vertical structure for zonal flow blocking and polar stratosphere warming
01 p0120 A71-10860
- Ionospheric columnar electron content perturbation by plane atmospheric waves
01 p0077 A71-11509
- Lower ionosphere partially reflecting regions, describing vertical thickness distribution based on 1.75 MHz backscatter soundings
01 p0040 A71-11525
- Altitude distribution of oxygen in atmosphere with eddy diffusion allowance from ARCAS 2 rocket photometric observations
01 p0077 A71-11528
- ELF and VLF radio attenuation for propagation below inhomogeneous isotropic ionosphere with realistic vertical variation models for electron density and collision frequency
02 p0212 A71-11964
- Upper atmospheric gas components vertical distribution by airborne photometric absorption and attenuation measurements in UV spectrum
02 p0246 A71-12118
- Ionospheric electron concentration enhancement at different heights during solar flare, using incoherent scatter radar technique
02 p0300 A71-12471
- Yaw sphere and thermometer combination, examining proportional vertical heat flux
03 p0422 A71-13231
- Lower atmosphere vertical temperature profiles by optical refraction measurements from photographs of equally spaced illuminated targets
03 p0453 A71-13233
- Ionospheric electron collision frequency and concentration height distribution during annular solar eclipse of 20 May 1966
03 p0407 A71-13378
- Midlatitude topside ionosphere electron density diurnal variations, discussing F 2 layer seasonal anomaly altitudinal extension
03 p0409 A71-13390
- Ionospheric measurements by rocket-borne HF capacitance probe during solar flare of 26 February 1969, determining electron density vertical stratification
03 p0416 A71-14032
- High atmosphere X ray absorption grazing scale height variations from satellite measurement of solar X-ray flux during sunrise and sunset
03 p0480 A71-14049
- Visual alignment task performance for marks with vertical separation under various illuminations
04 p0547 A71-15849
- Atmospheric aerosol vertical distribution by lidar system, describing ruby Q switched giant pulse laser design and operation
05 p0720 A71-16221
- Atmospheric aerosol vertical distribution by lidar system, discussing backscatter function, relative humidity, wind velocity, visibility, etc
05 p0720 A71-16222
- Vertical atmospheric ozone distribution from inversion of spectral UV radiation, comparing results with statistical method
05 p0742 A71-16671
- Vertical behavior of stratospheric optical thickness and dispersion coefficient in red region of spectrum from photometric analysis of Soyuz 3 photographs of daytime horizon
05 p0742 A71-16839
- Atmospheric ionization by vertical gamma and alpha radiation of natural radioactive products, comparing to vertical behavior of conductivity
05 p0799 A71-16843
- Vertical temperature distribution measurements by meteorological satellites distribution measurements applied to numerical weather forecasting
05 p0778 A71-17044
- Nimbus 3 and 4 satellites IR grating spectrometers for remote sensing of vertical temperature and humidity profiles of stratosphere and troposphere near Philippines
05 p0818 A71-17137
- Atmospheric ion concentration at 100-200 km related to solar zenith angle, describing diurnal and vertical behavior by photochemical theory
05 p0744 A71-17182
- Sunset and sunrise vertical displacement rate of lower ionosphere from spectral analysis of field intensities at 236, 557 and 1277 kHz
05 p0744 A71-17184
- Vertical NO profile at 100-220 km from 1968 Cosmos 224 measurement of atmospheric glow near horizon
05 p0744 A71-17186
- Vertical electron density profiles correction coefficients, noting computational work decrease and F region frequency discrepancy due to ionization
05 p0746 A71-17207
- Forced convection over infinite periodically overheated plane on basis of mesometeorological vertical wind velocity
06 p0923 A71-17515
- Oceanic rise crest heat flow model, examining vertical velocity distribution of mass transport
06 p0889 A71-17635
- Vertical structure of solar faculae from spectroscopic method for three dimensional information derivation
06 p0967 A71-17908
- Ambipolar diffusion coefficient noting vertical variations
06 p0893 A71-17993
- High energy albedo neutron production by cosmic ray collisions, investigating balloon altitude flux variations near atmospheric top
06 p0962 A71-18179
- F 1 region unsteady model, examining vertical distribution profile of electron concentration on summer day
06 p0895 A71-18273
- Vertical electron density profile variations during ionospheric perturbations in years of solar activity maximum and minimum
06 p0895 A71-18277
- Electron concentration vertical profile in ionosphere as function of altitude of radio wave reflection and group refraction and velocity characteristics
06 p0895 A71-18278
- Vertical profile of electron collisions effective frequencies in auroral ionosphere E region
06 p0895 A71-18279
- Tropospheric and lower stratospheric radiation balance components vertical profiles, using balloon sounding
07 p1151 A71-18913
- Long wave radiation balance components vertical profiles, showing temperature stratification effect
07 p1151 A71-18914
- Planetary atmospheres structure and dynamics, discussing composition and vertical temperature profile models
07 p1191 A71-18915
- Time-altitude diurnal variations in molecular and atomic oxygen concentrations at 65-200 km from continuity equations
07 p1099 A71-19391
- Quasi-exponential model of electron vertical profile in D region for aeronomic and ionizing radiation characteristics during solar flare of 30 October 1969
07 p1195 A71-19393
- Underlying and interlayer N/b₁ ionization distribution in unobservable region, discussing single and multilayer approximation
07 p1101 A71-19410
- Oxygen and nitrogen metastable constituents in daytime atmosphere airglow, obtaining altitude density distributions
07 p1103 A71-19764
- He ion vertical concentration profiles from space probe mass spectrometer measurements
08 p1278 A71-21020
- Fredholm integral equation stabilization methods for atmospheric IR transfer in vertical temperature profile determination
08 p1286 A71-21877
- Low latitude atmospheric vertical density variations, comparing solar and geomagnetic activities effects
09 p1436 A71-22578
- Cosmic ray and radiation belt data from vertical probes, determining radiation in instantaneous cross section of atmosphere
09 p1513 A71-22666
- Altitude spectrum of ion formation in interaction of proton flux with atmosphere, using Bragg dissipation function
09 p1514 A71-23153
- Book on atmospheric boundary layer dynamics considering theoretical models of vertical distribution of wind velocity, temperature and humidity
09 p1488 A71-23175
- Umkehr inversion system for vertical ozone distribution observation, calculating error due to ignorance of temperature dependence of ozone absorption
09 p1489 A71-23447
- Motion effects on atmospheric density altitude distribution, discussing vertical waves, gravity, temperature and winds
09 p1441 A71-23645
- Tropospheric ionization mechanism for gas to particle condensation embryos existence, using positive and negative ions ground level and altitude profiles
10 p1604 A71-24704
- Midlatitude D region considering electron concentration height distribution, ionization process and solar activity effects
10 p1606 A71-24916
- D and E region electron density height distribution profiles, using multifrequency absorption data
10 p1606 A71-24920
- Phase velocities and vertical amplitude profile of nonsingular mesoscale gravity waves produced in stratified jet flows by floating and deflecting earth rotation forces
11 p1793 A71-25171
- Vertical ozone distribution estimation by umkehr observations, discussing optimum statistical inversion technique application
11 p1794 A71-25387
- Wind speed and potential temperature vertical profile in day/night planetary atmospheres estimated by similarity theory of boundary layer parameters
11 p1826 A71-25719
- Atmospheric transmittance vertical structure, using aerosol attenuation and optical densities from aircraft sounding under cloudless conditions
11 p1795 A71-25924
- Visual dominance in body and object verticality judgments as function of nonvisual information, considering modal system interaction and contact
11 p1724 A71-26076
- Cloud height distribution pattern, developing analogy between diffusion and quantum motions
12 p1924 A71-26737
- Optical beam side refraction, determining physical conditions for vertical air temperature gradients at line of sight altitude above earth surface
12 p1902 A71-27484
- Seasonal-climatic vertical distributions of radiative heat sources and sinks calculation for Northern Hemisphere stratosphere and lower mesosphere
13 p2057 A71-28023
- Atmospheric ion concentration at 100-200 km related to solar zenith angle, describing vertical and diurnal density pattern by photochemical theory
13 p2059 A71-28239
- Sunset and sunrise vertical displacement rate of lower ionosphere from spectral analysis of field strength at 236, 557 and 1277 kHz
13 p2059 A71-28241
- Vertical NO profile at 100-220 km from 1968 Cosmos 224 measurement of atmospheric glow near horizon
13 p2059 A71-28243
- Vertical electron density profiles correction coefficients, noting computational work decrease and F region frequency discrepancy due to ionization
13 p2060 A71-28262
- Vertical distribution of small ion density and of electric polar conductivity and ion temperature profiles in atmosphere at 1.5-19 km from balloon measurements
13 p2065 A71-29425
- Sunspot umbra, calculating vertical magnetic field strength distribution from Fraunhofer lines
14 p2308 A71-29979
- Altitude size distribution of atmospheric aerosol from sky radiance measurements in sun aureole region, calculating sunlight forward single scattering
14 p2310 A71-30125
- Atmospheric neutron data at various altitudes, relating densities, fluxes and spectra to solar activity
14 p2301 A71-30589
- IR scanning vertical temperature profile radiometer for Ilos meteorological satellites, describing electronic signal processing
14 p2200 A71-30916
- Satellite atmospheric temperature sounding by radiometric measurements, obtaining vertical temperature profile by mathematical inversion process
14 p2236 A71-30938
- Height sign change prediction for lower cloud boundary from pressure Laplacian sign at earth surface
15 p2443 A71-31359

Vertical wind shear calculation in atmospheric surface layer, studying layer thickness effect
15 p2444 A71-31363

Vertical wind shears distribution in atmospheric boundary layer, noting features due to differences in synoptic processes
15 p2444 A71-31364

Stratospheric turbulence induced aircraft buffeting dependence on vertical wind shear, Richardson number and thermal stability change from underlying to overlying layer
15 p2444 A71-31365

Height variations of ionospheric absorption of downgoing whistler waves during nighttime at moderate and low latitudes
15 p2369 A71-31426

Wind profile determinations at 90-100 km from meteor trail drift and ionosphere inhomogeneity radar data, noting semidiurnal harmonics in wind components
15 p2395 A71-31450

Vertical muon spectra and charge ratio in energy range 30-800 GeV at sea level from Kiel cosmic ray spectrometry
15 p2474 A71-31778

Vertical intensity of cosmic ray muons in Mont Blanc tunnel, describing apparatus and experimental site
15 p2477 A71-31795

Vertical intensity and angular distribution of cosmic ray muons from observations using scintillator neon flash tube telescopes at three depths
15 p2477 A71-31796

Solar atmosphere vertical temperature and density distribution measurements, using spatially averaged H and K resonance line profiles channel reversals
15 p2496 A71-32742

Thermosphere and exosphere static models with empirical thermal profiles, giving temperature, density and composition as function of height
16 p2564 A71-33722

Semiannual density variation in heterosphere as function of height based on satellite drag and atmospheric models
16 p2564 A71-33723

Upper atmospheric neutral composition diurnal variations as function of altitude, local time and solar activity
16 p2570 A71-33829

Earth upper mantle electrical conductivity as function of depth based on geomagnetic variation field spatial distribution data
16 p2572 A71-33907

Secondary electrons and photons energy spectra and depth dependence in upper atmosphere from numerical solution of one dimensional transport equations
16 p2628 A71-33937

Heterosphere semiannual density variation with amplitude as function of height, noting dependence on temperature distribution and sunspot cycle
16 p2574 A71-33963

Oceanic masses vertical gravity gradient, noting slight decrease with depth
16 p2575 A71-34065

Richardson number relationship to vertical heat diffusion coefficients in boundary layer
16 p2605 A71-34070

Atmospheric short wave radiation angular and vertical distribution relation to aerosol scattering parameters, using transport equation
16 p2605 A71-34104

Twilight glow spectrophotometry and visual observations from Soyuz 5 spacecraft, determining atmospheric optics and vertical aerosol profile
18 p2911 A71-36006

Diffusion coefficients determination in planetary boundary layer with radon and ThB, using vertical distribution profile of concentration
18 p2912 A71-36193

Atmospheric radiant heat influx spectral distribution, evaluating vertical profiles of short wave radiation and aerosol effects
19 p3047 A71-37281

Aerosol layers in stratosphere, determining vertical distribution of electrical conductivity
19 p3047 A71-37335

Atmospheric structure near large amplitude Kelvin-Helmholtz billows in upper troposphere, deriving static stability, vertical wind shear and Richardson number
19 p3089 A71-37498

Time-altitude diurnal variations in molecular and atomic oxygen concentrations at 65-200 km from continuity equations
19 p3053 A71-37815

Quasi-exponential model of electron vertical profile in D region for aerodynamic and ionizing radiation characteristics during solar flare of 30 October 1969
19 p3127 A71-37817

Underlying and interlayer N₂/ionization distribution in unobservable region, discussing single and multilayer approximation
19 p3053 A71-37834

Indirect reduction of vertical atmospheric water vapor profile from measured outgoing thermal radiation by regularization method
19 p3090 A71-37966

Radionuclides depth distribution gradient in lunar samples, suggesting solar proton medium flux constancy over last million years
19 p3127 A71-38004

Ionospheric neutral composition variations as function of height, local time and solar activity
19 p3056 A71-38356

F 2 region electron density spatial and temporal distribution, investigating plasma vertical drift effects
19 p3058 A71-38384

Altitude dependent vertical drift velocity of small scale ionospheric inhomogeneities, using correlation of signal time lag scanning in frequency domain
19 p3058 A71-38391

Fredholm integral equation stabilization methods for atmospheric IR transfer in vertical temperature profile determination
19 p3060 A71-38470

Cloud condensation nuclei supersaturation spectrum and aerosol particle concentration variations with height
19 p3092 A71-38683

Atmospheric transmittance vertical structure, using aerosol attenuation and optical densities from aircraft sounding under cloudless conditions
20 p3257 A71-39215

He ion vertical concentration profiles from space probe mass spectrometer measurements
20 p3219 A71-39600

Vertical temperature profiles from Nimbus 3 satellite spectral radiance measurements, stressing importance for atmospheric circulation prediction
20 p3258 A71-39666

Altitude variation of atmospheric air scattering coefficient from Soyuz 3 spacecraft measurements, considering aerosol stratification
20 p3259 A71-39676

Mesosphere and stratosphere ozone vertical density distribution from sounding rocket data, considering photochemical theory and hydrogenic reductions
20 p3221 A71-39694

Lower thermosphere neutral composition fine structure data from rocket-borne time of flight mass spectrometer, emphasizing atomic nitrogen vertical distribution
20 p3222 A71-39697

Lower thermospheric density and molecular nitrogen partial density rocket measurements, obtaining neutral gas temperature vertical distribution and ion density profile
20 p3222 A71-39699

Midlatitude lower thermosphere atomic and molecular oxygen rocket measurements, presenting concentration and vertical distribution data
20 p3222 A71-39700

Lower thermosphere vertical temperature distribution measurements, using ionization and heat manometers
20 p3222 A71-39702

Gravity waves effects on ionospheric columnar electron content data, using Faraday rotation and differential Doppler measurements of geostationary satellite radio signals
20 p3224 A71-39717

Exospheric ion composition determination by vertical space probe mass spectrometer measurements, obtaining H, He, N, O and NO ion concentration vertical profiles
20 p3280 A71-39720

Ionospheric heating Q calculation of electron gas, evaluating heat inflow at various altitudes
20 p3281 A71-39725

Dayglow emissions for OH, molecular oxygen, sodium, lithium, potassium, atomic oxygen and nitrogen, considering height profiles and diurnal variations
20 p3226 A71-39828

Atmospheric neutral and singly ionized He extreme UV emission altitude distribution measurement by sounding rocket-borne thin film photon counters
20 p3231 A71-39891

E region electron density isopleths height correlation with atmospheric pressure variations, noting sympathetic isobaric surface movements in upper stratosphere
21 p3372 A71-40038

Lower thermosphere eddy diffusion coefficient effects on height variations in ionospheric composition
21 p3372 A71-40044

Brewer bubbler as continuous surface ozone sensor, measuring ozone vertical distribution in atmosphere
21 p3377 A71-40181

Height variations of Venusian cloud tops at planet equatorial and polar regions
21 p3449 A71-40608

Longitudinal, transverse and vertical wind distribution microstructure during convection from airborne experiments
21 p3412 A71-41388

Seasonal variations in vertical distribution of ozone at high latitudes, using Murgatroyd model of looped meridional atmospheric circulation
21 p3375 A71-41398

Ionization profiles of upper ionosphere from Alouette 1 vertical sounding data, proposing model for ionosphere shape
22 p3532 A71-41550

Sporadic E layer initial height seasonal variations as mean geographic latitudes, considering solar zenith angle and activity effects
22 p3533 A71-41646

Cosmic ray muons absolute intensity determination using Durham vertical spectrograph
22 p3593 A71-42350

Primary and secondary cosmic ray muon variations in vertical and zenith angles, determining coupling coefficients
22 p3593 A71-42357

Nimbus 3 satellite IR spectrometer atmospheric pressure height profiles, comparing with nearby radiosonde data
22 p3535 A71-42410

Solar chromosphere spectrum analysis, measuring H alpha line relative shifts variation with altitude
22 p3607 A71-42872

Ionospheric propagation penetrating and nonpenetrating modes full wave reflection and transmission coefficients determination for height and frequency variation by thin film optical method
23 p3643 A71-42972

Vertical equatorial ozone distribution, incorporating oxygen hydrogen reactions and diffuse and advective transport in time dependent meridional model
23 p3673 A71-43987

Vertical atmospheric humidity profile variations relationship to clouds water vapor content from thermal radio emission measurements onboard Cosmos 243 satellite
23 p3673 A71-44048

Vertical heat transfer coefficient of flat and cylindrical walls in fluidized bed from wall vertical temperature distribution
23 p3783 A71-44069

Atmospheric vertical humidity profile determination by measuring microwave radiation from satellite
24 p3822 A71-44350

Atmospheric vertical humidity profile from ground measurements of radio wave absorption at 1.35 cm water vapor line
24 p3822 A71-44820

F 2 region magnetic disturbances conjugacy mechanisms, considering vertical ionization profiles
24 p3823 A71-45029

Radio absorption in lower ionosphere, determining vertical distribution of electron density and production rates from solar protons energy spectrum
24 p3867 A71-45041

Mass spectrometer measurements of hydrogen, helium, nitrogen, oxygen and nitrogen oxide ion concentrations vertical profiles in ionosphere at midlatitudes
24 p3824 A71-45311

Vertical electron concentration and temperature profiles at 80-170 km measured by rocket launched on 10 July 1969 at Volgograd
24 p3824 A71-45322

VERTICAL FINIS
U FINIS
VERTICAL FLIGHT

Aircraft ultrasonic altitude and vertical velocity sensor for low flight, discussing VTOL aircraft automatic hovering control and time lag
01 p0084 A71-11624

Mathematical simulation of visual distance perception capacity of man from ground reference landmarks observation during vertical flight
07 p1051 A71-20121

VERTICAL LANDING

V/STOL aircraft instruments, deck display and automatic flight controls for takeoff and landing operation
13 p2098 A71-29132

VTOL and STOL aircraft comparative study covering site area, cost and noise and toxic gas production
14 p2175 A71-30163

Long term prospects of air traffic development in competition with other modes, estimating VTOL service demand
14 p2340 A71-30164

VTOL turboshaft engine powered propulsion system development, detailing design requirements, program planning, component research and system integration
14 p2297 A71-31109

[AHS PREPRINT 562]
Low speed testing of VTOL models in wind tunnels, describing method for estimating free air approach velocity and angle of attack
15 p2386 A71-32724

Aerodynamic design of VTOL propellers, demonstrating possibility of cyclic control of XC-142 experimental propeller
15 p2347 A71-32784

Helicopter optimal autorotation landing parameters for touchdown at zero speed, including rotor rpm drop due to flow separation on blades 23 p3627 A71-43090

VERTICAL MOTION

Object constant speed motion in terrestrial orthodromy, examining Shuler vertical small oscillations stability 01 p0125 A71-10628

Vertical fluid-filled channel with uniform internal heat source, analyzing steady plane-parallel convective motion 01 p0179 A71-10665

Ionospheric vertical wind role in anomaly of quiet sun diurnal geomagnetic variation at magnetic equator 02 p0243 A71-11764

Stratospheric wind field determination at extreme vertical velocity, noting baric field asymmetry 06 p0923 A71-17512

General aviation aircraft accidents involving seat belt and shoulder harness restrained occupants, discussing vertical force effects on survivability and injuries in severe crashes [SAE PAPER 710399] 10 p1555 A71-24261

Amplitude curves of reflected wave vertical displacement component in horizontally stratified medium with simple layer velocity pattern 10 p1644 A71-25134

R region layers vertical drift from phase paths of radio waves reflected from constant electron density surfaces 11 p1756 A71-25646

F layer vertical drifts due to winds at midlatitudes, computing longitudinal variations 13 p2054 A71-27793

Upper atmospheric winds measurements at 160 and 275 km, finding upward motion difficult to relate to intrinsic atmospheric motions 13 p2056 A71-27930

Vertical translational acceleration perception threshold of aircraft pilot seated in upright position 14 p2188 A71-29780

Vertical fluid-filled channel with uniform internal heat source, analyzing steady plane-parallel convective motion 14 p2339 A71-30998

Elastically mounted gyroscope stability under parameter excited vertical vibrations, using vector differential equation and multichannel oscillograph 15 p2502 A71-31173

Storm clouds tops maximum height and vertical velocity calculation, allowing for entrainment and vertical wind shear 15 p2444 A71-31362

Solid disk supported above flat plate by thin layer of gas flowing from central orifice, studying vertical motion equilibrium and dynamic data [ASME PAPER 71-APM-3] 16 p2559 A71-33220

F region vertical drift velocities at Millstone Hill, deriving ion velocity along magnetic field lines in upper part of F2 region from continuity equation 17 p2732 A71-34427

Vertical motions, turbulent heat exchange and radiative heat input role in stratus clouds evolution, deriving humidity and heat transfer equations as functions of time 19 p3093 A71-38690

Atmospheric stratification effects on downward motion of aircraft vortex wakes, developing approximate model 21 p3318 A71-40486

Film boiling liquid hydrogen vertical flow system, determining buoyancy effects on hydrodynamic and heat transfer characteristics 21 p3476 A71-40895

VERTICAL PERCEPTION

Satellite onboard local vertical detection, emphasizing IR horizon sensors role 06 p0892 A71-17964

Horizontal-vertical velocity illusions relationship, noting independent determinants 17 p2691 A71-35109

VERTICAL STABILIZERS

U STABILIZERS [FLUID DYNAMICS]

VERTICAL TAILS

U STABILIZERS [FLUID DYNAMICS]

U TAIL ASSEMBLIES

VERTICAL TAKEOFF

Helicopter rotor inertial system kinetic energy, examining takeoff advantages 09 p1385 A71-23670

VTOL and STOL aircraft comparative study covering site area, cost and noise and toxic gas production 14 p2175 A71-30163

Long term prospects of air traffic development in competition with other modes, estimating VTOL service demand 14 p2340 A71-30164

Low speed testing of VTOL models in wind tunnels, describing method for estimating free air approach velocity and angle of attack 15 p2386 A71-32724

Aerodynamic design of VTOL propellers, demonstrating possibility of cyclic control of XC-142 experimental propeller [DGLR-71-017] 15 p2347 A71-32784

Jet engine thrust induced nonconservative effects in aeroelastic analysis of vertical takeoff, using cantilever beam torsion and bending differential equations 16 p2650 A71-33019

VERTICAL TAKEOFF AIRCRAFT

NT FLYING PLATFORMS

NT XC-142 AIRCRAFT

German monograph on systems analysis of future jet and fan propulsion systems for VTOL commercial aircraft weight and cost reduction 01 p0142 A71-10115

VC 400 tilt wing VTOL cargo and passenger transport aircraft, discussing component and system development and testing phase 01 p0004 A71-10466

Optimum VTOL aircraft landing maneuverability, using short range three dimensional surveillance system and ground computer 03 p0454 A71-13574

VTOL systems for commercial short haul air transportation, discussing large helicopters and compound aircraft applications for system capacity profitability and efficiency increases 03 p0347 A71-13575

Compound and VTOL aircraft and prototype compact downtown V-ports for short haul air transportation improvement and expansion 03 p0348 A71-13619

Environmental effects on VTOL design - Conference, Arlington, Texas, November 1970 04 p0529 A71-15401

Tilt-rotor VTOL aircraft design, discussing ground proximity effects on blade bending moments and flying qualities 04 p0531 A71-15404

VTOL aircraft turbine engine vibration criteria, discussing measurement methods, engine design, bending frequency and dynamic characteristics 04 p0532 A71-15419

VTOL aircraft IFR airworthiness, noting necessity of higher safety levels for metropolitan air transit systems 04 p0533 A71-15426

VTOL handling qualities criteria for civil IFR qualifications, taking into account pilot abilities 04 p0533 A71-15427

Three axis flight director for precise helicopter control, deflected slipstream STOL or VTOL attitude and power under low ceiling and visibility landing 04 p0624 A71-15428

Navigation and traffic control of VTOL commercial transport aircraft, discussing noise, G forces, turbulent wakes, approach profiles and V-ports 04 p0624 A71-15429

VTOL aircraft engine air particle separator development, examining airframe and engine design 04 p0533 A71-15433

Sand and dust erosion on small VTOL gas turbine engines, discussing effects on inlets, compressor housing and blades 04 p0639 A71-15436

VTOL operation under snow and ice conditions, discussing adhesion, radiation absorption and electrical properties of ice 04 p0533 A71-15437

VTOL and STOL port federal design criteria, outlining planning and construction 04 p0567 A71-15441

Attitude and velocity control for VTOL aircraft takeoff and landing operations in hovering flight, discussing simulation devices and testing operations [DGLR-70-073] 05 p0779 A71-15948

Round cold jet inclination effects on VTOL aircraft tail assembly lift and longitudinal stability in transition region [DGLR-70-053] 05 p0693 A71-15967

Rotary wing and VTOL aircraft controllability requirements definition through in-flight simulation of visual and kinetic impressions and environmental conditions by BO-105 helicopter 05 p0696 A71-16135

VTOL aircraft avionics systems, discussing automatic flight control and navigation systems integration 06 p0925 A71-17925

Lift fan propulsion for civil VTOL transports, considering applicability, attitude control, system design, fan transition and cross flow noise 07 p1022 A71-20373

Fluidic pressure ratio control for vertical takeoff aircraft lift engine fuel system, describing breadboard circuit, test bed and flight standard 07 p1028 A71-20587

VTOL aircraft gear systems, discussing bearings, shaft connection, Ti alloy components, etc 09 p1454 A71-22963

Fan propulsion power plants with mechanical and gas dynamical energy distribution systems for commercial VTOL aircraft 09 p1511 A71-22964

Lift/cruise engine design and thrust vector control influence on VTOL transport aircraft transition characteristics and ground acoustic field [DGLR-70-040] 10 p1556 A71-24749

VTOL lift fan engine design for minimum noise levels, noting silencers application 10 p1659 A71-24750

VTOL heat engine and propulsion system design and performance, citing Pegasus jet lift engine as compromise between takeoff and cruise function 10 p1659 A71-24751

VTOL propulsion systems safety requirements, considering single and double breakdowns 10 p1659 A71-24752

Propulsion system and fuel regulator design effect on thrust change during air ejection for VTOL aircraft stabilization in hovering flight 10 p1659 A71-24753

Turbofan VTOL or STOL intercity aircraft, examining high bypass lift engine design 10 p1557 A71-24861

VTOL propulsion, discussing gas turbine pressure ratio inlet temperature and lifting and high bypass fans 13 p2114 A71-27838

Optimization of military VTOL aircraft secondary power systems, considering alternate power source for aircraft hydraulics, pneumatic drives, etc [SAE PAPER 710445] 13 p1998 A71-28326

RB 162 turbojet engine combustors for VTOL aircraft, achieving ignition by two pressure jet atomizers operative during starting cycle 13 p2116 A71-28742

Supersonic staggered gutter colander combustion system for plenum chamber burning on high bypass Pegasus turbofan engine of Harrier VTOL aircraft, noting performance improvement 13 p2116 A71-28743

Commercial V/STOL and jet VTOL transport, discussing Do-31 test results, landing approach, air traffic control automation and electronic control 13 p1997 A71-29131

Jet-supported VTOL aircraft fuel-time-optimal landing control, using mathematical model, Pontryagin maximum principle and analog computer solution 13 p1997 A71-29281

Helicopter systems operations in, around and between major metropolitan areas, considering performance of New York Airways [AIAA PAPER 71-507] 14 p2339 A71-29549

VTOL aircraft minimum climb-to-cruise time transition optimal open loop and suboptimal closed loop control synthesis 14 p2220 A71-30799

Flightworthy 25-foot diameter propotor wind tunnel test, considering civil and military need for VTOL transportation [AHS PREPRINT 501] 14 p2177 A71-31077

Handling qualities of V/STOL research vehicles during steep terminal area approaches, discussing powered lift fan VTOL aircraft limitations and instrument landing approach [AHS PREPRINT 544] 14 p2179 A71-31101

VTOL turboshaft engine powered propulsion system development, detailing design requirements, program planning, component research and system integration [AHS PREPRINT 562] 14 p2297 A71-31109

Wing installed VTOL coaxial drive lift fan model in wind tunnel test, investigating performance in crosswind environment [AIAA PAPER 71-742] 15 p2469 A71-32284

Propeller driven VTOL aircraft performance improvement, comparing variable camber/diameter counterrotating and blowing device equipped propellers [DGLR-71-023] 15 p2350 A71-32786

Rotorcraft and VTOL aircraft noise characteristics, noting implications of reduction to acceptable levels 16 p2523 A71-33419

VTOL aircraft gross weight and direct operating costs penalties from additionally installed control power [AIAA PAPER 71-768] 16 p2524 A71-34005

VTOL transport optimal airframe/propulsion systems design, discussing thrust requirements, performance, control, cruise functions, fuel consumption and fan characteristics [AIAA PAPER 71-744] 17 p2792 A71-34225

Low disk-loading propotor application to propeller and fanjet STOL and fanjet VTOL short haul aircraft [AIAA PAPER 71-781] 17 p2674 A71-34481

Near field noise measurement on quarter-scale model to estimate fuselage pressure in VTOL aircraft for conventional, short and vertical takeoff configurations 19 p2997 A71-37844

Tilt-fold-propotor VTOL aircraft stability and control, emphasizing pylon tilt and rotor stop-fold effects on flying qualities 19 p2998 A71-38652

Central terminal rapid processing and high speed VTOL aircraft effects on airport design, flight time, cost and ATC 20 p3210 A71-39394

VTOL and fan lift STOL aircraft, discussing simulation and head-up displays for roll demand, vertical speed and ILS beam

21 p3413 A71-40134

German VAK 191B combat VTOL aircraft development program, describing prototype ground tests, autopilot preoptimization and hover flight tests

22 p3482 A71-41517

Rotor performance and design for hover and cruise VTOL flights

22 p3482 A71-42238

VTOL air system for automobile travel replacement noting noise, cost, pollution and traffic congestion reduction

22 p3624 A71-42527

AIAA members comments on STOL, VTOL and V/STOL aircraft merits and developments

[AIAA PAPER 71-1015] 24 p3791 A71-44596

Prop rotor and lift fan VTOL aircraft ground noise level reduction, using flight trajectory management

[AIAA PAPER 71-991] 24 p3792 A71-45295

VERTICAL TAKEOFF AND LANDING

U VERTICAL LANDING

U VERTICAL TAKEOFF

VERTICES

U APEXES

VERTIGO

USAF aeromedical consultation service experience on vertigo cases covering symptoms and related diseases

21 p3331 A71-40358

Alcohol ingestion effects on vertigo and nystagmic vestibular responses to angular acceleration, considering visual fixation and alertness control

22 p3501 A71-41827

Vertigo due to increased middle ear pressure, discussing etiology from experience of aeromedical consultation service

22 p3502 A71-41833

VERTOL MILITARY HELICOPTERS

U BOEING AIRCRAFT

VERY HIGH FREQUENCIES

NT P BAND

VHF radiation from plasma during electron beam interaction with fast magnetoacoustic wave stimulated by external spatially periodic currents

01 p0132 A71-10155

VHF/UHF telemetry antenna stellar calibration using radio stars

01 p0054 A71-10909

Normal mode helix antenna with rectangular and tapered Al strip conductors, measuring impedance variation with frequency at VHF range

03 p0387 A71-13820

VHF radar measurements of scattering by field aligned irregularities associated with equatorial spread F

03 p0420 A71-14532

Automated precision polarimeter for HF-VHF range

04 p0586 A71-14654

Low distortion gain-controlled 140 MHz IF main amplifiers for 2700-channel microwave repeaters, discussing design and performance

05 p0730 A71-17069

Pulsar MP 0628 meter wave radiation, noting linear polarization and frequency dependence of pulse rate

06 p0965 A71-17387

Atmospheric propagation errors of satellite tracking system in VHF region

07 p1059 A71-19028

Ionospheric scintillation effects on fading of oppositely circularly polarized VHF signals in space communications

09 p1410 A71-23522

Phase sector direction finder for VHF range, using log periodic dipole arrays

11 p1738 A71-26338

Holographic narrow beam VHF antenna design and testing, using X band scale model

13 p2036 A71-27999

Feasibility of VHF aeronautical satellite system frequency sharing band used by ATC service, employing spatial separation, antenna directivity and frequency offset

13 p2032 A71-28873

Type 4 source movement out to 6 solar radii from solar center based on 80 MHz brightness temperature observations

14 p2306 A71-29694

Pulsar MP 0628 meter wave radiation, noting linear polarization and frequency dependence of pulse rate

14 p2310 A71-30166

ATS 1 and 3 satellite VHF transponders for ships and aircraft location, communication and remote sensing, discussing performance test results

14 p2198 A71-30898

VHF and UHF ground reflection measurements for antenna site layout, showing feasible operations at short ranges

14 p2217 A71-31050

Computer program for processing of UHF radiation patterns of ESRO 4 scientific satellite omnidirectional antenna systems

14 p2217 A71-31051

VHF wave transhorizontal propagation correlation with daytime E layers in temperature zone, noting height dependence and seasonal and diurnal variations

17 p2707 A71-35445

Radio frequency interference environment measurement in VHF range by subsynchronous Lincoln experimental satellites 5 and 6

19 p3021 A71-38452

Radar equipment for meteor velocity and radiants measurement at VHF by pulse diffraction method

19 p3067 A71-38635

Radio and optical aurora correlation and control by polar electrojet, using VHF backscatter and geomagnetic recordings

20 p3229 A71-39853

VERY HIGH FREQUENCY RADIO EQUIPMENT

Receiving equipment for navigation satellites of Naval Weapons Laboratory, considering 150 MHz channel

07 p1205 A71-19015

Lightning flash-ground strokes VHF radio pictures by hyperbolic position fixing system, obtaining three dimensional series fixes as function of time

08 p1325 A71-20880

ATC station ground to air communication via VHF tropospheric scatter, discussing high power radio transmitters and low noise over the horizon receivers combination

10 p1576 A71-24175

VOR antenna system with Alford loops above circular conducting ground plate, investigating radiation fields

18 p2894 A71-36827

High Q micropower filters for VHF applications based on conditionally stable negative resistance operation, describing computer-aided design, construction and performance

21 p3361 A71-40822

VERY LOW FREQUENCIES

Proton Flare Project 1969 observation of VLF radio wave propagation, detecting sudden phase anomaly events due to solar activity

01 p0144 A71-10288

Optimum VLF electromagnetic link between underground terminals with emitter-receiver horizontal antennas, calculating radiation pattern

02 p0211 A71-11717

Annular solar eclipse effects on VLF transmissions phase delay

02 p0212 A71-11969

VLF emissions at low latitudes by transverse and longitudinal resonance electron energies calculations

05 p0721 A71-16441

Convective cyclotron instability in whistler mode, discussing magnetosphere as generation mechanism and taking into account magnetospheric plasma inhomogeneity

05 p0743 A71-17003

Polar chorus background hiss generation, investigating VLF wave characteristics responsible for harder electron precipitation from magnetosphere

05 p0743 A71-17004

Antarctic terrain dielectric and loss properties effects on VLF attenuation and phase constants of earth-ionosphere waveguide paths over ice covered regions

06 p0868 A71-17733

Enhanced ionization density duct propagation of VLF radio waves in magnetosphere

07 p1062 A71-19578

VLF electric field data in interplanetary medium from Pioneer 8 space probe observation

07 p1196 A71-19655

Particle diffusion modulation by simultaneous VLF and ULF electromagnetic waves during rocket experiment

07 p1062 A71-19680

VLF hiss directions from Injun 5 Poynting flux observations, proposing propagation across plasmapause boundary

08 p1282 A71-21633

Midlatitude VLF discrete emissions generation regions location by dispersion analysis of ground station observations, determining plasma density along path for events

08 p1282 A71-21634

Whistlers with harmonic bands caused by multiple stroke lightning, using Injun 5 VLF data

08 p1283 A71-21649

Earth-ionosphere waveguide model of VLF signals propagation with perturbed ionosphere, considering magnetic dipole transmitting antenna array

09 p1410 A71-23575

VLF electromagnetic propagation, calculating mode conversion efficiency at solar terminator on angle based on flat model with finite wall conductivities

09 p1411 A71-23576

Solar particle effects on polar cap VLF radio propagation along polar and transpolar paths, considering short term phase effects

10 p1577 A71-24313

Magnetospheric VLF banded emissions spectral analysis, investigating OGO-5 data by high time resolution spectral techniques

10 p1579 A71-24788

Attenuation and phase velocity of ELF and VLF radio waves propagating under anisotropic ionosphere, discussing geomagnetic field effect

11 p1731 A71-25603

Midlatitude VLF hiss distinction from discrete emissions /chorus/ based on event tape recording analysis spectrum analysis

12 p1878 A71-26837

F region ion and temperature effects on VLF and ELF wave absorption in whistler mode propagation at midlatitudes during solar minimum

12 p1879 A71-27044

Transient ELF electromagnetic disturbance propagation in earth-ionosphere cavity, determining waveguide source-observer separation and attenuation constant

13 p2027 A71-27794

Color frequency-time spectrograms of VLF electric and magnetic field Poynting flux data from Injun 5 satellite

13 p2054 A71-27914

Frequency vs time spectral shapes of magnetospheric VLF discrete emissions for field line and electron stream parameters

13 p2027 A71-27910

Geomagnetic field effects on directional propagation of LF and VLF radio waves in ionosphere, taking into account ion types effects

13 p2029 A71-28026

VLF noise spectra in earth-ionosphere cavity due to thunderstorm discharges, noting resonance level splitting by geomagnetic field

13 p2030 A71-28542

VLF band signal daytime propagation phase anomalies in earth-ionosphere waveguide, using models with geomagnetic field effect

14 p2191 A71-29509

Ionospheric VLF signal propagation paths based on earth atmospheric simulation and mathematical models

14 p2228 A71-29513

Ionospheric VLF and ELF wave observations, noting ion cyclotron resonance and harmonics effects on propagation

14 p2202 A71-30940

Atmospheric VLF electromagnetic emissions and electron instabilities data from satellite observation in detailing source regions, large amplitude electrostatic waves and wave-particle correlation

14 p2202 A71-30952

VLF and LF time and frequency international comparison, noting diurnal shifts and SID constant magnitude ratio

14 p2204 A71-30972

VLF signal propagation during low and high solar activity, discussing equipment precision, diurnal and seasonal phase variations and phase anomalies correlation

14 p2204 A71-30977

Microsecond time synchronization potentials through cycle identification of VLF multiple frequency transmissions

14 p2204 A71-30974

Modal interference spacing in frequency range 13.6-22.3 kHz during sunrise transitions on middle latitude east-west propagation paths

15 p2369 A71-31432

Internal reflection of VLF whistlers incident from above on model nighttime lower ionosphere

15 p2369 A71-31433

VLF radio signals phase anomalies due to solar X-ray flares, monitoring by detectors onboard OSO-4 satellite

15 p2369 A71-31434

Stable auroral red arcs on 29 September 1967, 30 October and 1 November 1968, comparing OGO 2 and OGO 4 VLF data on plasmapause crossings

15 p2397 A71-31757

VLF atmospheric integrated intensities changes probably due to ionization by meteors

15 p2371 A71-31839

Linear and nonlinear whistler mode cyclotron instability, discussing VLF emissions generation mechanism in magnetosphere

16 p2615 A71-32803

Normal angle determination by rocket observations for whistler mode waves propagation through magnetosphere and ionosphere from conjugate VLF ground station signals

16 p2569 A71-33809

Laboratory model for ionospheric perturbations effects on long range VLF paths

19 p3017 A71-37863

Short path VLF phase and amplitude measurements during stratospheric warming in February 1969, discussing D region electron density changes

19 p3018 A71-38040

VLF fields of horizontal dipole in waveguide formed between ice covered ground and anisotropic ionosphere of Antarctica

19 p3024 A71-38595

VLF wave excitation, noting ratios between vertically and horizontally polarized sources

19 p3024 A71-38613

- Lunar crust exploration by VLF surface waves, discussing frequency dependent depth penetration, conducting layers detection and communication or navigation use
20 p3291 A71-39313
- High latitude VLF radio emissions rate of occurrence at all magnetic times, noting diurnal variations
20 p3198 A71-39745
- ELF and VLF emissions during PCA, correlating data with particle and photometer recordings from ground based, satellite and rocket-borne observations
20 p3229 A71-39856
- Broadband electrostatic VLF wave observation in polar magnetosphere by OV3-3 satellite, noting emission power spectra density relationship to frequency
20 p3199 A71-39889
- VLF ion wave instabilities in polar wind based on plasma kinetic theory, comparing with electrostatic wave observation by OV3-3 satellite
20 p3231 A71-39890
- Magnetospheric VLF waves growth rate variations, calculating frequency spectrum and intensity with self consistent solution
21 p3346 A71-40046
- Ionospheric geomagnetic field effect on ELF/VLF radio propagation
23 p3643 A71-42967
- Atmospheric triggered VLF emissions theory, examining magnetospheric whistler Morse pulses
23 p3645 A71-43135
- VLF day and night waveguide modes attenuation coefficients and phase velocities, using moving secondary source formed by mode conversion at sunrise and sunset shadow line
24 p3803 A71-44650
- Phase discontinuity transmitter-receiver system for VLF/LF time signals
24 p3804 A71-44997
- VESTA ASTEROID**
Photoelectric polarization curve, reflectivity and absolute diameter of Vesta, comparing with Lyot curve
22 p3602 A71-42177
- VESTIBULAR TESTS**
Guinea pigs head and eye movements produced by vestibular apparatus stimulation via static pressure changes
01 p0010 A71-10347
- Cortical vestibular projection zones in formation of conditioned reflexes and spatial orientation of cats
01 p0012 A71-11054
- Guinea pigs vestibular adaptation to repeated angular acceleration dependent on acceleration direction
01 p0012 A71-11056
- Chairs, stands and swings for vestibular and visual analyzer tests
01 p0024 A71-11073
- Head spatial position effects on vestibular compensation rates in rabbits
01 p0012 A71-11074
- Neuron network modeling by stable rhythmic impulsion system, considering vestibular nystagmus
01 p0025 A71-11137
- Space mission reflex vestibular disturbance and motion sickness prevention, examining artificial gravity and drugs
02 p0198 A71-11979
- Vestibular nystagmus and display luminance effects on hand-eye coordination in compensatory tracking of aircraft instrument
02 p0207 A71-12381
- Biocybernetic model of vestibular control system for spatial orientation, considering semicircular canals fluid motion angular velocity sensors and linear displacement perception
03 p0367 A71-12982
- Heat rotation induced eye movements in cats by neuron level determination, considering vestibular apparatus of signal transmission loop for mathematical model
03 p0356 A71-12983
- Vestibular function on earth and in space - Conference, Uppsala, May 1968
04 p0536 A71-14751
- Vestibular physiology, discussing endolymph chemical composition, cupola structure and function and hair cells
04 p0536 A71-14752
- Vestibular problems in long manned space flight, discussing weightlessness and rotating environment for artificial gravity
04 p0541 A71-14753
- Astronaut visual acuity under angular acceleration, considering vestibular stimulus direction and nystagmus upbeating or downbeating
04 p0536 A71-14754
- Gravity effects on experimental nystagmus in rabbits under electrical, rotatory and caloric vestibular stimulation, taking into account semicircular canals and otolith organs
04 p0536 A71-14758
- Extraterrestrial vestibular research, discussing geocentric and heliocentric otolithic regulation and gravitation theory
04 p0542 A71-14759
- Labyrinth destruction, Meniere disease, labyrinthectomy and vestibular neuritis effects on eyes counter-rolling, discussing otolith organ damage determination
04 p0537 A71-14762
- Ascending neuron vestibulo-ocular reflex arc, emphasizing medial longitudinal fasciculus
04 p0537 A71-14763
- Vestibular habituation retention, showing nystagmic response reduction to repetitive rotatory and caloric tests
04 p0537 A71-14764
- Vestibular nerve projection to association fields of cerebral cortex in Rhesus monkey under alpha chloralose and without anesthetic agent
04 p0537 A71-14765
- Transganglionic degeneration in vestibular nerve resulting from transection of peripheral sensory nerve branch of bipolar neurone
04 p0537 A71-14766
- Vestibular system semicircular canals mathematical model determination of galvanic stimulation and directional preponderance, considering visual, postural and vehicle orientation feedback loops
04 p0543 A71-14790
- Space motion sickness causes and prevention, discussing syndromes, psychophysiological factors, vestibular mechanics and adaptation
04 p0539 A71-15283
- Vestibular apparatus cortical zone projections on striopallidal complex in cats
05 p0707 A71-16387
- Changing rotational velocity recording device for vestibular apparatus tests, examining stimulus reaction speed
05 p0714 A71-16810
- Electrically rotating chair transmitting medicobiological information of functional state of vestibular analyzer and statokinetic stability
05 p0715 A71-17027
- Unilateral labyrinthectomy model for evaluating antinotion drug effects on vestibular function in guinea pigs
06 p0854 A71-18361
- Gastric and rectal mechanoreceptor stimulation influences on vestibular rotation nystagmus in rabbits
06 p0856 A71-18466
- Coriolis vestibular reaction testing of pilot trainees, evaluating brief vestibular disorientation test validity and reliability at 10 and 15 rpm test conditions
08 p1247 A71-20823
- Linear acceleration effects on human otolithic and vestibular apparatus, discussing vestibulovegetative motion sickness syndrome and nystagmus index activation
08 p1242 A71-21956
- Vestibular stimulation effects on bioelectrical activity in retina, optic tract, geniculus, visual cortex and ectosylvian gyrus in anesthetized cats
09 p1390 A71-22215
- Weightlessness, high acceleration and aerospace vehicle maneuvering effects on cardiovascular and vestibular systems, discussing disorientation, space sicknesses and blood circulation
09 p1398 A71-22357
- Optokinetic and vestibular effects on human operator reliability in aircraft control systems
09 p1399 A71-22681
- Vestibular system functions physical analog model, predicting responses to motion inputs and possible problems for flight situations
10 p1569 A71-24237
- Cochlear/vestibular apparatus, ganglion cells, spinal roots and nerve trunk damage from ionizing radiation based on neural elements transirradiation in neoplasms
10 p1566 A71-25039
- Neural transmission to vestibular nuclei of semicircular canal response to rotational stimulation, discussing test methods and results with decerebrated or anesthetized cats
10 p1566 A71-25042
- Humans and animals vestibular stimuli effect on external respiration function and respiration center neuron activity
13 p2007 A71-28413
- Somatic and autonomic responses in vestibular tolerance of human subjects, using Coriolis acceleration test
13 p2007 A71-28414
- Soviet book on vestibular reactions covering functional relationship between stimulus parameters and labyrinth nonauditory part, adaptation to Coriolis forces and response to ionizing radiation
13 p2008 A71-28672
- Rotation perception in dark and oculogravimetric illusion, using power law to describe subjective vestibular sensation relation to angular acceleration stimulus pulses
13 p2022 A71-29327
- Hybrid computer program for data reduction or on-line analysis of nystagmus during closed loop experiment involving visual and/or vestibular function
13 p2022 A71-29359
- Mathematical model for short term adaptation to vestibular stimuli, deriving transfer function relating angular velocities of nystagmus and head rotation
14 p2182 A71-30250
- Pigeon vestibular apparatus fluids and structures physical properties, detailing specific gravity and viscosity of endolymph, perilymph and cupola
14 p2185 A71-30467
- Cortical neurodynamics during vestibular afferent activity and associated cardiovascular and respiratory reactions, noting EEG correlation to hemodynamics
16 p2527 A71-32828
- Pyridoxine and serotonin metabolism changes and vestibular disorders observation in space flight
16 p2532 A71-33677
- Stroke number and vestibular nystagmus duration and frequency under successively increasing angular acceleration from tests on guinea pigs
20 p3189 A71-39238
- Vestibular apparatus effect on brain stem somatic activity
21 p3328 A71-39998
- Weightlessness effect on vestibular apparatus from bullfrogs vestibular nerve single fibers spike train data during orbital flight
22 p3598 A71-41689
- Bull frog activity at rest and response to centripetal acceleration by on-board centrifuge in vestibular space experiment OFO-A
22 p3484 A71-41690
- Vestibulo-colic reflex control of head movement in seated man under sinusoidal and stepwise rotational velocity stimulation, comparing with ocular stabilization
22 p3501 A71-41822
- Habituation and suppression of vestibulo-ocular vertical nystagmic responses to Coriolis stimulation in pentathlon athletes, comparing to pilots and airman trainees
22 p3501 A71-41826
- Alcohol ingestion effects on vertigo and nystagmic vestibular responses to angular acceleration, considering visual fixation and alertness control
22 p3501 A71-41827
- Central pathway connection between vestibular and oculomotor nuclei through pons responsible for horizontal eye movements induced by visual and vestibular stimuli
22 p3488 A71-42436
- Vestibular and proprioceptive stabilization of eye movements
22 p3489 A71-42448
- Human orthostatic and vestibular stability responses to weightlessness during extended space flights noting acceleration tolerance, physical efficiency, infection resistance and medication sensitivity
22 p3495 A71-42790
- Visual and vestibular analyzers interaction, noting reduction in duration of counterrotation illusion and postrotation nystagmus in humans
22 p3505 A71-42797
- Prolonged small radiation dosage effects on vestibular analyzer in normal and antiradiation drug protected dogs
22 p3495 A71-42798
- Stabilographic indices and excitability curves of vestibular response to galvanic currents, using van Egmond cupulometry method
24 p3796 A71-44544
- Coordination structure of human hand arbitrary movements during stimulation of horizontal semicircular canals in vestibular apparatus by negative angular acceleration
24 p3796 A71-44545
- VESTIBULES**
Vestibular sensory epithelial cells form and organization, discussing morphological polarization
04 p0536 A71-14760
- Motor and vestibular analyzers and frontal hypothalamus role in gravitational loads compensation during orthostasis, noting respiration, arterial pressure and brain bioelectric activity changes
20 p3188 A71-39223
- Gravity sensing mechanism of inner ear, discussing statoceptors existence in vestibule
21 p3327 A71-39995
- VFR [RULES]**
U VISUAL FLIGHT RULES
VHF OMNIRANGE NAVIGATION
VOR/DME ground station oriented aircraft area navigation horizontal guidance capability, discussing digital input/output flight control
08 p1331 A71-21166
- Converter-indicator direct digital readout design, using photodiodes for LSI VOR area navigation display systems low power operation
09 p1491 A71-22610
- Large scale MOS IC digital VOR navigation converter, comparing accuracy, size, weight and cost with standard design
17 p2776 A71-35789
- Navigational accuracy improvement by combining VOR/DME information with airspeed and heading

VIABILITY

- data via maximum likelihood filter, using small airborne computer
[AIAA PAPER 71-928] 19 p3097 A71-37174
- Concorde aircraft navigation system comprising triple inertial systems, dual VOR/DME, dual ILS and dual ADF
[CASI PAPER 72/9] 19 p3100 A71-37599
- Combined inertial navigation and VOR/DME systems contribution to area navigation accuracy and efficiency
22 p3571 A71-42080
- VOR/DME air navigation equipment using Kalman-Bucy filter and airborne air data system (ADS)
22 p3573 A71-42289

VIABILITY

- Probability theory for viable microorganism exposure in fractured contaminated solid, using quantal response model
07 p1048 A71-19600
- Chlorella viability and mutability aboard Soyuz and Zond spacecraft, noting trend toward growth of anomalies in autosporeulation
21 p3343 A71-40566

VIBRATION

- NT BENDING VIBRATION
NT BREATHING VIBRATION
NT COMBUSTION VIBRATION
NT FLUTTER
NT FORCED VIBRATION
NT FREE VIBRATION
NT LATTICE VIBRATIONS
NT LINEAR VIBRATION
NT MISSILE VIBRATION
NT PANEL FLUTTER
NT POGO EFFECTS
NT RANDOM VIBRATION
NT RESONANT VIBRATION
NT SELF INDUCED VIBRATION
NT STRUCTURAL VIBRATION
NT SUPERSONIC FLUTTER
NT TORSIONAL VIBRATION
NT TRANSONIC FLUTTER

Single mass vibrational impact system optimal periodic motions, analyzing vibrators productivity optimization via analog of sphere bouncing down staircase

German monograph on vibration fields representation by superposition of planar waves with complex wave vectors, considering convergent series of Hankel and Bessel functions

Simplified characteristic equation for plane piezoelectric vibrations of lithium niobate and lithium tantalate crystals, using perturbation methods

Linear second order multidegree of freedom vibrational system with singular mass matrix, determining response to excitation
[ASME PAPER 71-VIBR-10] 21 p3457 A71-40272

Vibrational systems stability in presence of time dependent random parametric disturbances, using frequency analysis methods

VIBRATION DAMPERS

U VIBRATION ISOLATORS

VIBRATION DAMPING

Dissipative mechanical filter for rocket self excited vibrations to eliminate oscillatory instability, describing transfer function and modal characteristics

Nonlinear stabilization of beam instability during electron beam interaction with decay plasma, determining distribution function in damping dynamics of HF vibrations

Control system for resonant mechanical loads with feedback, examining stability conditions and oscillation damping by Coulomb friction

Turbomachine blades torsional-bending vibrations aerodynamic damping, noting natural frequency shift

Circular plates forced vibrations, considering internal damping and free and supported boundaries in thin plate wave equation solutions

Console rod free and forced transverse vibrations amplitude dependent damping, considering longitudinal tensile force effect and hysteresis

Vibration dampers optimization, considering viscous and inelastic resistance effect on sensitivity of harmonically moving system response

Carbon steel specimens size effect on energy dissipation and damping characteristics under transverse flexural vibrations

Static tension effect on damping capacity of drawn rods under flexural vibrations, considering materials with strong magneto-mechanical hysteresis

Machine part surface layers properties effect on vibration decrement

Logarithmic damping of flexural oscillations produced by residual fretting stresses in circular plates

Engine turbine blades aerodynamic oscillation damping calculation procedure

Test equipment for damping ability of vibration absorbing coatings on prismatic rods under pure bending, using electromagnetic vibration induction system and optical recorder

Elastic metal thin plates transverse resonant free vibrations, analyzing viscoelastic coatings damping effects
[ASME PAPER 70-DE-E] 03 p5056 A71-13709

Elastic metal thin beams transverse resonant free vibrations, analyzing viscoelastic coatings damping effects
[ASME PAPER 70-DE-D] 03 p5057 A71-13710

Turbine engine vibration dampers viscous resistance calculation based on equations of motion for incompressible and unheated Navier-Stokes liquid

Gas flow past straight airfoil, analyzing damped natural oscillations

Space vehicle attitude stabilization system, using sensor with hysteresis relay characteristic for vibration damping

Mathematical model linear in mass and stiffness but nonlinear in damping, considering causal anomalies in hypothetical models and absent in real

Medical transportation by ambulance, helicopter and fixed wing aircraft, considering vibration damping and acceleration

Support systems relative efficiency in external damping free-free configuration production for flexing beam

Random Gaussian noise driven damped nonlinear oscillator, discussing Duffing equation, consolidated expansions for response spectrum and common factors

Defense of damping theory applications in flutter analysis, discussing energy dissipation

Quarter wave tube in off- and near-resonance regimes, dissipating energy by jet formation during flow emergence from cavity into duct
[AIAA PAPER 71-87] 06 p0881 A71-18543

Discrete linear vibration systems viscous damping local modifications effect on eigenvalues and vectors, using Weissenburgers procedure in matrix form
[AIAA PAPER 71-215] 06 p0928 A71-18651

Stability, stationarity and amplitude damping of random parametric vibration system, using nonlinear differential equations

Alloying elements, mechanical working and heat treatment effects on vibration damping of Mg-Zr alloys, using Fastov device

Martensitic stainless steels structure related to energy dissipation capability, obtaining damping mechanism as magnetomechanical hysteresis

Vibrational damping, composition and structural design of cast polyurethane elastomers for Poseidon missile launch tube liner

Vibrating systems with amplitude dependent resistance, determining damping characteristics

Viscous layer damping effect on liquid surface oscillations in vessel, satisfying boundary conditions and obtaining frequency equation

Aircraft turbine engines strength and gas dynamic characteristics improved by vibration decrease using elastic elements

Periodically supported and damped closed circular beam structure, determining frequency response matrix

Energy dissipation during independent flexural-torsional vibrations of rods, noting alternating shear stress superposition effect on damping

Damped vibrations logarithmic decrement determination during automatic recording of number of cycles, emphasizing error analysis

Elastic media damping effects on rigid bodies HF vertical and rotational vibrations, considering approximate solution for structural amplitude response

09 p1541 A71-23088

Round cross section specimens flexural vibration damping decrement, determining amplitude dependence internal friction with allowance for stressed state

Light general aviation airplanes flying qualities in a flight simulation, considering longitudinal short period frequency and damping, pitch control sensitivity and lift curve slope

Passive nutation damping of spin stabilized orbiting satellites with mechanical and pendulum dampers involving nonlinear interaction of vibrational and rotational motions

Structural system frequency response measurements under environmental noise conditions, discussing autocorrelation function for transient excitation damping

Spring coupled inertially damped instrument servomechanisms design, applying phase margin maximization criterion

Damped mechanical systems sinusoidal vibration analysis, using four pole parameters

Satellite pitching oscillations optimal stabilization, obtaining approximate solution for finite time

Rectilinear piping system with steady liquid flow, investigating free vibration damping, steady-state amplitudes and stability

Helicopter blades inherent vibration damping, comparing theoretical and semiempirical predictions to experimental results

Vibration damping of simply supported sandwich beam with viscoelastic core, using energy method
[ASME PAPER 71-DE-C] 12 p1977 A71-27181

Tacsat 1 telecommunications relay system, discussing UHF-SHF antenna radiation patterns, ground terminal equipment, nutation dampers and attitude and orbital correction procedures

Fretting corrosion relationship to mechanical vibrations damping capacity for Fe and Cu alloys, noting energy dissipation

Gimbal suspended gyroscope in elastically damped frame with dynamically unbalanced rotor, noting oscillations and drifts

Characteristic equation of respiration vibrations of cylindrical ring in incompressible viscous fluid at rest, obtaining damping coefficient for large induced flow Reynolds numbers

Adaptive automatic control systems, determining damping coefficient and natural oscillation frequencies with second order differential equations

Damping characteristics (absorption coefficient) of dissipative systems, defining authentic value of energy dissipation characteristic determination from forced and free vibrations

Nonlinear damped vibratory system with two degrees of freedom excited by two external harmonic forces of different frequencies, investigating summation tones stability

Nonlinear/mixed/damping forces on forced vibration system response, developing recursion procedure for equation of motion coefficients

Damped gravity orientated satellite linearized analysis for vibrational response to large amplitude motion

Solid propellant rocket engine design, discussing combustion instability technology applications in damping and driving mechanisms influence determination
[AIAA PAPER 71-754] 14 p2296 A71-30788

Asymptotic stability of equilibrium position of vibrating linear mechanical systems with semidefinite damping matrix applicable to satellite attitude stabilization

Forced vibration damping of satellites in elliptical orbits by variable cantilevers and rotor

Space vehicle attitude stabilization system, using sensor with hysteresis relay characteristic for vibration damping

Open microwave resonators self oscillations damping, using Sommerfeld radiation conditions

Alloying elements, mechanical working and heat treatment effects on vibration damping of Mg-Zr alloys

Earth satellite plane periodic oscillations damping with respect to center of mass in orbital plane during motion on elliptical Kepler orbit

16 p2646 A71-33659

Forced transverse vibration damping of end loaded elastic cantilever beam, determining hysteresis loop contour from resonance curves

16 p2658 A71-33977

Logarithmic decrement of flexural, longitudinal and torsional vibration damping of various size rods, taking into account surface layer energy loss

16 p2659 A71-33979

Multiple mass rheonomic vibrational systems dynamic stability, presenting approximate solution and critical dissipation level for damping parametric resonances

17 p2777 A71-34346

Cantilever bar free and forced transverse vibrations amplitude dependent damping, considering longitudinal tensile force effect and hysteresis

17 p2825 A71-35015

Vibration dampers optimization, considering viscous and inelastic resistance effect and sensitivity of harmonically moving system response

17 p2826 A71-35018

Static tension effect on damping capacity of stretched rods under flexural vibrations, considering materials with strong magneto-mechanical hysteresis

17 p2826 A71-35020

Machine part surface layers properties effect on internal friction from transverse vibration decrement measurement

17 p2826 A71-35021

Logarithmic damping of bending oscillations produced by residual fretting stresses in circular plates

17 p2826 A71-35022

Engine turbine blades aerodynamic vibration damping calculation procedure

17 p2826 A71-35023

Clamped-clamped sandwich beam with thin face sheets and soft viscoelastic core, investigating forced, damped, nonlinear and LF flexural vibrations

17 p2826 A71-35032

Integrally stiffened panels with bonding material across stringer tops, calculating vibration damping characteristics

17 p2826 A71-35034

Vibrating systems with amplitude dependent resistance, determining damping characteristics logarithmic decrement

17 p2834 A71-35676

Friction role in impact shock absorbers for elastic systems out of static equilibrium and resonance excitation in vibrations, noting harmful effects

17 p2834 A71-35679

Viscous layer damping of liquid surface oscillations in vessel, satisfying boundary conditions and obtaining frequency equation

17 p2730 A71-35681

Dynamic flexibility method based on Green resolvent, presenting applications to linear damped/undamped forced/free harmonic/periodic vibration

18 p2947 A71-36177

Nutation damping and vibration isolation in dual spin spacecraft, using flexible dissipative coupling between platform and rotor

18 p2971 A71-36276

Additive damping control of acoustic resonance fatigue of aerospace structures under severe environments, considering materials, tuned devices and layered techniques

18 p2979 A71-36494

Artificial gravity Skylab wobble damping, using ATM control moment gyros

18 p2975 A71-36650

Damping characteristics of Ni base refractory alloys at high temperatures, showing increase with cyclic strain amplitude

18 p2936 A71-36708

Vertical statically unbalanced rotating shaft with two degrees of freedom, investigating internal damping, flexural vibrations and equation of motion

19 p3154 A71-37348

Vibration control methods, discussing oscillation and acoustic noise reduction

19 p3069 A71-37518

Vibrating systems behavior under combined parametric excitation and self oscillation mechanism, investigating damping and generation control

19 p3155 A71-37526

Satellite pitching oscillations optimal stabilization, obtaining approximate solution for finite time

19 p3152 A71-37695

Nonlinear vibrating system characteristics relationship to transient process, deriving Abel integral equations for damping coefficient and restoring force

19 p3104 A71-38483

Attitude control of gravity orientated satellite in arbitrary orbit by solar pressure, showing libration damping characteristics of radiation force

20 p3306 A71-39396

Four layer sandwich damping with viscoelastic material, noting frequency dependent effectiveness

[ASME PAPER 71-VIBR-20] 21 p3458 A71-40278

Flow induced vibration suppression by perforated concentric shroud around circular cylinder, investigating porosity and shroud/cylinder diameter ratio effects

[ASME PAPER 71-VIBR-28] 21 p3458 A71-40283

Beams with multiple constrained viscoelastic layer coatings, presenting damped vibrational response prediction for various materials, geometries, wavelengths and temperatures

[ASME PAPER 71-VIBR-40] 21 p3459 A71-40290

High load structural dampers evaluation under linear or sinusoidal/triangular displacement control with constant speed testing machines

[ASME PAPER 71-VIBR-46] 21 p3459 A71-40295

Viscoelastic materials with varying glass transitions, free and constrained layer damping and damping of LF vibrations in massive structure

[ASME PAPER 71-VIBR-47] 21 p3405 A71-40296

Single mass flexible rotor in elastic bearings mounted on damped flexible supports, analyzing dynamic unbalance response and transient motions

[ASME PAPER 71-VIBR-72] 21 p3460 A71-40310

Five-span skin-stringer width and damping effects on vibrational response including resonant frequencies and mode shapes by transfer matrix analysis

[ASME PAPER 71-VIBR-101] 21 p3461 A71-40327

Optimum geometry and vibration damping ability of laminated three layer elastic-viscoelastic-elastic beam at resonance

[ASME PAPER 71-VIBR-102] 21 p3461 A71-40328

Cu-rich alloys with high damping capacity at low stress amplitudes for structures and machines, noting damping stability improvement in Mn-Cu alloy by Cd addition

[ASME PAPER 71-VIBR-106] 21 p3396 A71-40331

Hot-wire anemometer measurement of free oscillation damping of viscous and sluggish fluid in U tube, determining velocity distribution

21 p3366 A71-40512

Acoustic damping of clamped and hinged rectangular panel at natural frequency, noting dependence on aspect ratio

21 p3416 A71-41200

Extinguishing parametric vibrations, changing equivalent natural frequency from resonant state by supplementary load

21 p3473 A71-41368

Air pressurized bearing mounted rotor with vertical shaft, discussing elastically suspended foundation mass and damping effect on self excited vibration

22 p3550 A71-41659

Longitudinal electron oscillations damping in ionized plasma, obtaining wave dispersion relation from BGK model

22 p3583 A71-42372

Forced vibration of internally damped circular and annular plates with clamped boundaries, obtaining driving point and transfer impedances and force transmissibility

23 p3775 A71-43204

Review of papers at EUROMECH 23 colloquium on finite amplitude and diffusive effects in acoustics, covering acoustic damping by relaxation, dust and moisture, turbulence effects, etc

23 p3704 A71-43447

Objective lens with superconductive winding for high voltage electron microscope, describing optical properties and vibration reduction system

23 p3679 A71-44008

Trap states existence in OSO type satellites, considering damping mechanism and computer results

23 p3773 A71-44092

Stability augmentation system for aircraft elastic modes control, discussing active flutter suppression technology

23 p3629 A71-44107

Control surfaces and direct jet force flutter suppression system shown to increase flutter speed of wing

23 p3630 A71-44108

Lifting rotors aerodynamic damping in forward flight, describing methods for blade response variance matrix computation

24 p3789 A71-44559

Stability of gyropendulum damped by astatic gyroscope

24 p3828 A71-45158

Structural materials ability for irreversible conversion of mechanical to thermal energy from free longitudinal vibrations attenuation measurements in rod

24 p3817 A71-45200

VIBRATION EFFECTS

NT POGO EFFECTS

Motor and sensory nerve conduction impairment in upper extremities in vibration disease

01 p0010 A71-10394

Vibrational degrees of freedom effects on capture cross sections and ion-molecule complexes formation in ion-dipole collisions

01 p0130 A71-10477

Opposed wave synchronization mode stability in gas laser undergoing torsional vibrations

01 p0093 A71-10604

Cardan suspension axes nonperpendicularity and misalignment effects on precision of gyroscope motion in presence of system angular vibrations

01 p0083 A71-11043

He-Ne discharge regular oscillations effect on laser output power

02 p0259 A71-11930

Random vibrations nonlinear effects on gas bearing pendulous-integrating gyroscopic accelerometer response, using digital simulation

02 p0252 A71-12454

Oscillatory motion effects on bonded solid film lubricants wear life, discussing oscillation arc and frequency, surface finish and load

02 p0258 A71-12593

Electrical measuring device error caused by longitudinal instability of frame held in tensile suspension during casing transverse vibration

02 p0253 A71-12635

Law of motion for two degrees of freedom integrating gyro mounted on oscillating base, using averaging method

02 p0253 A71-12637

Soviet book on mechanical oscillator threshold sensitivity to small moment of forces, covering light friction and radiometric oscillatory instability effects and estimates

02 p0285 A71-12839

Sound and vibration disorder measure for choosing statistical or deterministic models for system/response situation

[ASME PAPER 70-WA/DE-1] 03 p0459 A71-14138

Vibration effects on free convection heat transfer from fluid filled horizontal cylinder

04 p0675 A71-14784

Quantitative acoustic vibration effects on cooldown rate of bodies from room temperature to liquid nitrogen or helium temperature

04 p0686 A71-15525

ELDO test firings failure analysis program, considering self destruction charges and vibration environmental load

[DGLR-70-060] 05 p0815 A71-15964

Traumatic vasospastic disease in forest workers with Raynaud phenomena, considering cold vasodilation and occupational vibration vasoconstriction by finger blood circulation tests

05 p0708 A71-16616

Redundant structure dynamic analysis for forced and free vibrations, using finite element rank force method

05 p0829 A71-17120

Lateral vibration effects on heaving airfoil blunt trailing edge vortex shedding flows, examining base cavity damping by flow visualization

06 p0984 A71-17621

LF vibration effects on human beings, discussing circulatory reactions

06 p0859 A71-18188

Patients transportation pathology, discussing accelerations and vibrations in ambulances, helicopters and fixed wing aircraft

06 p0860 A71-18191

Quartz astatic galvanometer resistant to geomagnetic field variations, vibrations or microseismic noise

06 p0901 A71-18286

Short term creep effect on high speed air flows, investigating material behavior under vibration loads, corrosion and erosion

07 p1130 A71-19163

Vibration tumbling duration effects on surface quality, fatigue strength and damping properties of titanium alloy structural parts

07 p1130 A71-19169

Fringe interferogram variable visibility control, eliminating vibration effects

07 p1109 A71-19467

Eye motion phase and amplitude measurement concerning visual acuity during whole body vibration

07 p1053 A71-20338

Stiffened long cylinder with time variable thickness and strengthening thin shell system elastic displacements due to nonstationary vibrations and nonuniform pressure distribution

07 p1217 A71-20459

Vibration and buffeting effects on man, discussing aerospace environments, biomechanics, human tolerances and performance, etc

08 p1244 A71-20709

Vibrational tumbling effects on steel compressor blades surface roughness, cold hardening, residual stresses and fatigue strength

08 p1295 A71-20842

Axial compressor blades surface finish and fatigue strength restoration by vibrational tumbling

08 p1295 A71-20843

Mechanical, physiological and psychological responses of man to sinusoidal whole body vibration

08 p1248 A71-21230

Small natural vibrations effect of solar sail-propelled system on heliocentric orbit motion

09 p1531 A71-22559

Ultrasonic vibration effects on TiC sintering during isothermal heating with and without pressure

09 p1470 A71-23063

Space travel genetic effects, discussing radiation, weightlessness, vibration and acceleration

09 p1394 A71-23149

Vibrational effects on capture cross sections and ion-molecule complexes formation based on ion-dipole collisions, noting multiple reflection probabilities and collision lifetimes

09 p1498 A71-23662

Nitrogen molecules vibrational excitation effect on elastic collisions frequency in nitrogen plasma

10 p1646 A71-23819

Vibrational nonequilibrium influence on IR radiative energy transfer in nongray nonisothermal gases

10 p1643 A71-24967

Far field sound radiation pattern from vibrating circular piston set in nonrigid baffle for sonar detectors

11 p1798 A71-25186

Arbitrary direction harmonic vibration effects on kinetic friction coefficient between sliding bodies

11 p1767 A71-25267

Prestress vibration hardening of shells of revolution for circumferential 0 and 1 wave number, using VALORS and BALORS programs

11 p1848 A71-25486

Drug effects on LE whole body vibration response of dogs administered with phenobarbital, phenoxymepazine and morphine

11 p1720 A71-26121

Inertial navigation system consisting of gyro horizon compass, directional gyro and computer, considering errors due to compass vibrations

12 p1927 A71-27169

Vibration effects on image resolution and acutance of Zeiss RMK AR 15/23 aerial camera, using aircraft vibration simulator for testing

12 p1907 A71-27263

Ultrasonic vibration energy surface and volume effects, obtaining static forces reduction, processing rate increases, technique shortening and surface finish improvement in manufacturing processes

13 p2075 A71-28949

Vibration effect on heat transfer by natural convection from oscillating horizontal wire in air

13 p2164 A71-28984

Atmospheric turbulence induced aircraft vibrations effects on aircrew performance, discussing physiological and psychological responses

14 p2187 A71-29778

Time independent three dimensional streaming secondary motion due to vibrating flexible plate

14 p2325 A71-30061

Uneven runway taxiing vibration effects on supersonic transport aircraft, comparing calculation with measurement

14 p2175 A71-30305

Vibration fatigue of metallic materials in vacuum and different gas atmospheres, considering fcc metals, Al alloys and steels

14 p2259 A71-30466

Camera vibration, and refraction anomaly effects on error of designated position for star or satellite

14 p2250 A71-31120

Elastically mounted gyroscope stability under parameter excited vertical vibrations, using vector differential equation and multichannel oscillograph

15 p2502 A71-31173

Ultrasonic vibration effects on DNA and RNA content in skin and kidneys of albino rats

15 p2356 A71-31288

Iodine vapor bleaching under molecular electronic-vibrational transition due to ruby laser intense monochromatic radiation

15 p2421 A71-32409

Man machine system dynamic properties and biomechanical model concepts, determining random vibration effects on sitting and working human body

15 p2366 A71-32728

Subharmonic oscillations excited by horizontal vibrations of mathematical pendulum suspension

16 p2607 A71-32936

Small elastoplastic cyclic strain effects on internal friction and energy dissipation in metals during vibrations

16 p2598 A71-33983

Thermostable and heat resistant steels and alloys vibration loading frequency effects on fatigue at high temperatures

16 p2598 A71-33992

Two mirror Cassegrain antenna secondary reflector random fluctuations effects on drift in main lobe direction

17 p2713 A71-34397

Frequency tolerance of vibration stress effects on human performance, considering body resonance, visual acuity, manual tracking and neural capacities

17 p2689 A71-34701

Stiffened panel acoustically induced stress estimation using experimentally determined random S-N curves with various structural parameters

17 p2826 A71-35033

Integrally stiffened panels with bonding material across stringer tops, calculating vibration damping characteristics

17 p2826 A71-35034

Vibration and corrosion-erosion damage effects on material behavior during short term creep in high speed air flows

17 p2760 A71-35659

Vibrotumbling duration effects on surface quality, fatigue resistance and damping properties of titanium alloy structural parts

17 p2760 A71-35665

Vibrational combustion study of powder, using Helmholtz resonators with connected auxiliary combustion chamber

17 p2839 A71-35697

Excitation response of oscillatory conservative linear system to transient displacement involving time dependent boundary conditions

18 p2947 A71-36748

Wire connection damage due to high vibration, examining termination and joining techniques

18 p2852 A71-36837

Stability of uncontrolled space vehicles with on-board masses vibrating at small amplitude

19 p3152 A71-37537

Combined action of vibration and gamma irradiation on sporulation dynamics, survival rate and mutability of *Chlorella*

20 p3193 A71-39237

Free convective heat transfer in cryogenic liquid filled enclosure, studying effects of vibration near resonant frequency

20 p3314 A71-39292

Vibration effects on human body, discussing neurophysiological data, safe exposure limits, therapeutic applications, motion sickness, muscular responses and biomechanical effects

21 p3342 A71-40147

Flow induced vibrations of metal bellows with internal cryogenic fluid flow, noting effects of heat transfer, liquid state properties, external damping and condensation

[ASME PAPER 71-VIBR-14] 21 p3457 A71-40276

Machinery failure prediction under high vibration amplitudes using stochastic excursions principles

[ASME PAPER 71-VIBR-60] 21 p3460 A71-40305

Structural optimization problems involving vibration-weight interactions, using optimal control nonlinear programming transforms

[ASME PAPER 71-VIBR-66] 21 p3460 A71-40308

Sum and difference frequencies in vibration incident on gas turbine engine, considering synchronous and asynchronous excitation

[ASME PAPER 71-VIBR-103] 21 p3462 A71-40329

Rotational and vibrational effects in ion dipole collisions

21 p3419 A71-40905

Vibration induced paroxysmal and cardiovascular hazards during patients transport to hospital by air or ambulance, discussing therapeutic and preventive treatments

22 p3500 A71-41573

Material fatigue failure under narrow band random vibration effects, deriving fatigue life prediction equation based on composite experimental design and statistical tests

22 p3615 A71-42002

Mice under combined gamma radiation and vibration and acceleration dynamic factors, studying radioresistance recovery rate

22 p3494 A71-42725

Vibration influence on peripheral blood reaction to gamma radiation in dogs, using clinico-hematological indices

22 p3494 A71-42728

Man machine system dynamic properties and biomechanical model concepts, determining random vibration effects on sitting and working human body

23 p3639 A71-43299

Printed circuit board components and connections survival under severe vibration and G forces, considering resonant frequency, mounting methods and lead wire strain relief

23 p3652 A71-43538

Human reaction to externally induced body vibration, discussing vibration exposure limits

23 p3640 A71-43901

Mechanical vibrations effects on mouse embryos growth and development, investigating critical frequencies and accelerations

23 p3637 A71-44246

Combined heat, noise and vibration stress effects on human performance and physiological functions including heart rate, body temperature and mental arithmetic

23 p3637 A71-44247

Gas lasers application to length measurement technology, discussing temperature, air pressure and vibration effects on laser frequency stabilization

24 p3833 A71-44449

Motion equations of statically unbalanced two degree of freedom gyroscope excited by base linear vibrations, determining instrument errors as function of casing/body coupling

24 p3828 A71-45159

Unlubricated instrument ball bearing axial vibration frequency and amplitude effect on fretting corrosion at constant temperature and humidity

[ASLE PREPRINT 71LC-7] 24 p3832 A71-45289

VIBRATION ISOLATORS

Low cost multichannel peak/average sine vibration control system with acceleration selector and averager

01 p0067 A71-10864

Single degree of freedom vibration isolation systems, examining nonlinear damping range

[ASME PAPER 70-DE-B] 03 p0432 A71-13711

Turbine engine vibration dampers viscous resistance calculation based on equations of motion for incompressible and unheated Navier-Stokes liquid

03 p0470 A71-13956

Cascaded inertial vibration isolation systems, using rigid masses interconnected by air spring type isolator elements

11 p1853 A71-26492

Vibration absorbers optimization for multiple degree of freedom systems with random excitations, applying optimal control theory in frequency domain

13 p2158 A71-29427

Helicopter fuselage vertical and in-plane main rotor head vibratory forces isolation with hydrodynamic servocentered system at transmission/airframe interface

[AHS PREPRINT 514] 14 p2253 A71-31085

Longitudinal wave absorbers attenuating resonance vibrations in rods and plates

15 p2504 A71-31707

Nonlinear elastic suspension springs with symmetrically hardened behavior for shock and vibration isolation of aerospace instruments and controls

17 p2825 A71-34890

Nutation damping and vibration isolation in dual spin spacecraft, using flexible dissipative coupling between platform and rotor

18 p2971 A71-36276

Pneumatic isolation system for inertial instrument testing, using computer simulation model to evaluate physical parameter variation effect on pad suspension dynamic behavior

[AIAA PAPER 71-910] 19 p3040 A71-37161

Blower suction line random vibrations due to distributed random pressure, investigating various isolation arrangements for vibration reduction

20 p3308 A71-39085

Vibration isolation system performance under transient conditions, deriving equations of motion with and without inertia torque effect

[ASME PAPER 71-VIBR-33] 21 p3458 A71-40287

Damped isolation and undamped vibration absorber model for dynamic control, discussing frequency response and tuning and damping performance

[ASME PAPER 71-VIBR-45] 21 p3459 A71-40294

VIBRATION MEASUREMENT

Book on mechanical vibration and shock measurements covering periodic and random vibrations characteristics, instrumentation, control, etc

02 p0251 A71-12175

Engine vibration high temperature transducer, discussing piezoelectric materials properties and design considerations relative to temperature, pressure, acoustic noise, humidity environment

02 p0255 A71-12911

Cantilever beam bending vibration, measuring driving point impedance and natural frequencies at low strain amplitudes for Mg alloy, Mn-Cu and coated Al beams

03 p0502 A71-13299

Nonlinear system with one degree of freedom under HF and velocity dependent force, determining quasi-periodic vibrations with two frequencies by averaging method

03 p0502 A71-13406

Aircraft fuselage vibration response to turbulent boundary layers, measuring structural wavelengths and phase velocities as functions of frequency

[ASME PAPER 70-WA/DE-10] 03 p0348 A71-14144

Mechanical vibrations recording and measurement by photographing motions of points and lines on tested surface

03 p0430 A71-14330

Accelerometer design for nuclear reactor vibration measurements, considering environmental effects

04 p0587 A71-14824

Star image vibration trail amplitude, determining rms deviation with automatic system

04 p0590 A71-14843

Portable photoelectric recorder for solar limb vibration frequency spectrum and amplitude measurements

04 p0590 A71-14844

VTOL aircraft turbine engine vibration criteria, discussing measurement methods, engine design, bending frequency and dynamic characteristics

04 p0532 A71-15419

Air transportation systems ride vibration environments in relation to human comfort

04 p0532 A71-15421

Bearing vibration monitoring for wear and damage detection

04 p0603 A71-15671

Piezoelectric ceramic transducer vibration measurement under mechanical loading, noting displacement as function of thickness and time

04 p0601 A71-15835

Book on vibration measurements covering resonant and self excitation patterns, aeroengines, machine parts, transducers and engineering techniques

05 p0820 A71-16275

Precision systems oscillations measurement by transistorized two channel photoelectric image converter, discussing circuit diagram

05 p0751 A71-16356

Analog periodometer with short response time for helicopter blade vibration studies

05 p0752 A71-16736

Thin cylindrical shell in ideal compressible fluid, calculating longitudinal resonance waves for acoustic excitation

06 p0985 A71-17755

Optimal contactless kinetocardiography recording LF patient chest vibrations, comparing short wave method

06 p0863 A71-18468

Electro-optical method for energy dissipation characteristics of mechanical systems subject to attenuating vibration

07 p1107 A71-19170

Buckling loads prediction for conservative elastic systems from vibration data by stochastic and deterministic models, providing nondestructive testing procedure

08 p1368 A71-20804

Rotating cantilever beams flexural vibrations, developing tables for frequency equation determination

08 p1370 A71-21306

Rubidium viscosity near solidification point from thin immersed plate forced vibrations amplitude

09 p1508 A71-22540

Damped vibrations logarithmic decrement determination during automatic recording of number of cycles, emphasizing error analysis

09 p1443 A71-22630

Piezoelectric accelerometers for high temperature vibration measurements, examining materials critical characteristics, design minimal weights and vibration system test methods

09 p1443 A71-22707

Finite element method for stiffness matrix free vibration analysis of thin rectangular plates under central planar loadings

11 p1842 A71-25313

Rail track roughness and irregularities evaluation by railcar vibration measurements, using portable LF low amplitude acceleration measuring and recording system

11 p1845 A71-25349

Piezotron accelerometer for vibration measurement, combining quartz sensing element with subminiature solid state electrostatic amplifier

11 p1767 A71-26442

Vibration analysis by holography, discussing recording media, maximum light utilization, stroboscopic and time-averaged techniques and alterations in sensitivity

13 p2067 A71-28396

Holographic stroboscope using ruby laser with passive shutter for HF vibration measurement

14 p2254 A71-30584

Digital laser interferometer for vibration measurements, describing theory, transistorized circuitry and performance characteristics

15 p2401 A71-31138

Real time stroboscopic vibration analysis technique involving holographic interferometry

15 p2404 A71-31271

Holographic vibration analysis by generalized stroboscopy, combining high reconstruction brightness with time average holograms interpretation

15 p2404 A71-31272

Vibration analysis for static and rotating objects by stroboscopic holography, considering axial flow compressor blades and two-mass system with torsional vibration

15 p2404 A71-31273

Cascading turbomachine blades vibrations measurement in subsonic and sonic high temperature gas flows, describing test facility

16 p2553 A71-33993

Nonlinear system with one degree of freedom under HF and velocity dependent forces, determining two-frequency quasi-periodic vibrations by averaging method

17 p2826 A71-35016

Electro-optical method for energy dissipation characteristics determination for mechanical systems subject to attenuating vibration

17 p2746 A71-35666

Stroboscopic coherent light source for vibrational analysis by holographic interferometry using Pockels cell laser modulator

18 p2923 A71-36610

Holography as nondestructive testing tool, considering application in vibration analysis, stress/strain measurement, bond inspection, internal flaw detection and displacement measurement

18 p2927 A71-36657

Hysteresis loop analysis with allowance for material imperfect elasticity in mechanical vibration problems, using strain amplitude decrement relation

18 p2981 A71-36707

Gyroscope rotor axial moment of inertia of measurement by connection to small vibrator device

19 p3062 A71-37148

Stress determination by vibration measurement in cantilever specimens fatigue tests with audio frequency loading, taking into account end restraint elasticity

19 p3160 A71-38347

Soviet monograph on vibration method for fluid viscosity measurement covering Newtonian fluids, low and high frequency viscosimeters, materials coefficients, temperature and pressure factors, etc

20 p3234 A71-39146

Vibration analysis of simulated axial flow turbine disks by holography, illustrating advantages of full field modal and deflection information

[ASME PAPER 71-VIBR-105] 21 p3377 A71-40330

Structural vibrations excited by spatially and temporally random pressure loading, discussing power spectra and vibration measurement

21 p3467 A71-40912

Laser speckle interferometry for translational motions and vibrations detection, considering applications in radar and acoustics analysis

21 p3393 A71-40932

Real time holographic interferometry of steady state mechanical vibrations of engineering structural components applicable to arbitrary small amplitude and large mode numbers

21 p3381 A71-40934

Electromagnetoacoustic ultrasonic vibrations radiation and reception angular orientation as function of transducer design parameter, frequency and propagation velocity

22 p3528 A71-41756

Elastic plates transverse vibrations fundamental frequency from constant deflection lines method

22 p3617 A71-42537

Holographic method for investigating piston type oscillations with phase modulated reference light beam

24 p3829 A71-45270

VIBRATION METERS

NT LUNAR SEISMOGRAPHS

NT SEISMOGRAPHS

On-line digital dampometer for free oscillation wind tunnel model study under varying Mach number and stagnation pressure avoiding flutter destruction

21 p3363 A71-40391

VIBRATION MODE

NT UNCOUPLED MODES

Thin elastic orthotropic plate in finite difference formulation, determining natural vibration mode and instability by summary representation method

01 p0168 A71-10410

Elastic body-vibrating surface interaction, examining friction coefficient under various modes

01 p0088 A71-10626

Laser image speckle interferometer design for observing vibrational modes on diffusely reflecting surfaces as alternative to holographic methods

02 p0254 A71-12718

System frequencies and mode shapes characteristics relation to changes in structure, considering matrix approach for equations of motion of undamped vibrations

03 p0516 A71-14457

Thin elastic orthotropic oval cylindrical shells nonlinear flexural vibration based on assumed modes, using Galerkin method

05 p0819 A71-15979

Multilayered anisotropic cylindrical shells free vibration modes

05 p0819 A71-15982

Air lubricated mechanical oscillator dynamics and modes of operation as function of system parameters, using analog computer

05 p0758 A71-16352

Three mass vibrational impact system analysis by mathematical electronic analogs, examining system and excitation parameters influence on vibrational modes and dissipative properties

05 p0821 A71-16357

Turbine blades flexural vibration modes, noting frequency parameter dependence on angular velocity, disk radius and stagger angle

05 p0796 A71-16648

Orthotropic plate dynamics, examining plane vibrations with group theory approximate equations

06 p0993 A71-17818

Holographic interferometric recording of vibration patterns of plexiglass cored construction mirrors

[AIAA PAPER 71-180] 06 p0903 A71-18619

Large signal oscillation mode model for GaAs devices operational prediction, including space charge and intervalley transfer time effects

07 p1070 A71-18867

Plasma instabilities under radial magnetic field effect across homogeneous field, considering oscillation modes

07 p1167 A71-19231

Cylindrical, conical and spherical shells natural frequencies and vibration modes determination using matrix series

07 p1212 A71-19365

Vibrational and rotational relaxation in sulfur dioxide, measuring relaxation time as function of temperature by ultrasonic absorption

07 p1054 A71-19370

Oscillation mode selection method applied to Fabry-Perot interferometer using Faraday effect

07 p1109 A71-19454

Coupling loss factor estimation, using wave transmission or natural frequency shift methods in statistical energy analysis

07 p1161 A71-19962

Box type structure free vibrations investigation by rectangular finite elements, comparing with natural frequencies and normal modes solution

08 p1369 A71-20807

Natural frequencies approximation for vibration modes of stiffened and singly curved panel structures

08 p1369 A71-20810

Electrochemical cell interelectrode planar spacing regulator system, discussing electrode constant vibration amplitude to current ratio

08 p1296 A71-20855

Bulk effect microwave oscillators energy source design, considering operation mode and circuit tuning control parameters

08 p1266 A71-21623

First and second frequency harmonics and form shapes of liquid filled cylindrical shell axisymmetric vibrations, analyzing effect of pressure and shell dry portion on vibration frequencies

08 p1374 A71-22055

Nonlinear sampled data feedback control systems periodic mode of oscillations, using state variable approach

09 p1423 A71-23033

Helicopter vibrational behavior prediction in flight with known aerodynamic loads, using branch modes method

09 p1385 A71-23606

Inhomogeneous rotating self-gravitating system kinetic theory, linearizing collisionless Boltzmann equation to two dimensional linear integral equation for obtaining small oscillation modes

10 p1641 A71-24278

Lumped parameter torsional and flexural system synthesis for vibratory characteristics, using transfer matrices

10 p1692 A71-24925

Earth eigen vibrations excitation by gravity waves, tabulating energy content of even and odd harmonics overtones

10 p1607 A71-25005

Variational criterion for stationary mode elastic structural oscillation, considering coincidence with normal modes for materials with stress-strain homogeneous function relationship

10 p1692 A71-25048

Transform method application to structural dynamic analysis for engineering structure transient response to various vibration modes

11 p1841 A71-25150

Coupled vibration modes for nonrotating blade-disk system in axial flow turbines and fans calculated by finite element method

[AIAA PAPER 71-375] 11 p1845 A71-25348

Vibration modes of objects and light scattering from rough surfaces, using laser speckle changes

11 p1776 A71-26138

Traveling wave propagation, modal vibrations and elastic transmission medium studies from theoretical seismograms for realistic gravitating heterogeneous spherical earth model

11 p1760 A71-26148

Plasma instabilities under radial magnetic field effects across homogeneous field, considering oscillation modes

12 p1934 A71-26749

Unsteady vibrations of rotating free solid body entering atmosphere at hypersonic velocity, taking into account nonlinearity of aerodynamic moments

12 p1972 A71-27171

Free vibrations of three dimensional system of rods subjected to transverse vibrations in two planes of symmetry

12 p1930 A71-27172

Optimal estimate of spectral density of vibration process over finite time interval, using spectral analyzer

12 p1930 A71-27175

RAE satellite flexible boom vibration, obtaining antenna boom static deflection, natural frequencies and thermal bending effects

[ASME PAPER 71-DE-J] 12 p1977 A71-27319

Cylindrical duct stationary uniform axial flow effects on propagation of acoustic vibration modes of wavelength smaller than damping length

[ONERA-TP-969] 12 p1981 A71-27479

Kane-Mindlin differential equations solved by perturbation techniques for free extensional vibrations in elastic plates

12 p1981 A71-27483

Frequencies and modes of natural vibrations of closed cylindrical shell with elastic filler

12 p1981 A71-27508

Vibration natural frequencies and mode shapes of cantilever plate mounted on rotating disk periphery, using finite element technique

13 p2147 A71-27788

Vibration mode patterns of acoustoelectric oscillators, describing detecting apparatus

13 p2036 A71-28469

Regenerative system reliability, examining oscillation mode selector

13 p2040 A71-28995

TM, TE and combination cavity modes choice for plasma column electron density distribution determination by perturbation methods

14 p2279 A71-29859

Automated modal data acquisition and processing system (MODAPS) for real-time modal vibration testing of complex aerospace vehicle structures, describing features, capabilities and utilization

14 p2245 A71-30341

Convergent finite element equations for dynamic stability of plates dependent on vibration and buckling modes

14 p2331 A71-30696

Transferred electron microwave oscillators high efficiency operation mode with more severe limitation than limited space charge accumulation mode

14 p2215 A71-30826

Normal time average holography amplitude range extension by integration over vibration cycle fraction

15 p2404 A71-31270

Rectangular plates with unidirectional stiffeners, calculating natural frequencies and mode shapes with approximate method

15 p2507 A71-32128

Annular ducts finite amplitude spinning acoustic modes propagation and subsonic choking, allowing for nonlinear effects in perturbation procedure

15 p2450 A71-32133

Orthotropic layered cylindrical shells, deriving equations of motion for rotationally symmetric vibration

15 p2509 A71-32513

Time average holographic interferometric fringes of circular plate vibrating in two rationally related modes

15 p2412 A71-32593

Rocket body longitudinal autooscillation modes, taking into account pipeline fluid discontinuous cavitation oscillations

16 p2644 A71-32834

Two dimensional axisymmetric shell analytical model for liquid propellant launch vehicle longitudinal vibration modes and steady state response calculation

16 p2653 A71-33092

Free vibrations of linear structure with arbitrary support by Rayleigh-Ritz method using unconstrained normal modes

16 p2656 A71-33218

Dynamic characteristics of weakly damped elastic body, considering complex natural modes generation for vibration tests in aircraft design

16 p2657 A71-33403

Normal mode vibrations of system with trajectories of unit mass in Euclidean space, determining modal subspaces by potential function

17 p2776 A71-34295

Elastic spherical shell coupled to rigid body, calculating asymmetric free vibration natural frequencies and mode shapes from boundary conditions

17 p2817 A71-34339

Multiple mass rheonomic vibrational systems dynamic stability, presenting approximate solution and critical dissipation level for damping parametric resonances

17 p2777 A71-34346

Friction force moment in ball bearing without lubrication in presence of angular vibrations of one race

17 p2748 A71-34563

Freely vibrating supported elastic isotropic oval cylindrical shells natural frequencies and mode shapes

17 p2825 A71-34873

Asymptotic methods for distributed system nonlinear time and space vibrations, discussing system dispersion effect on resonance conditions

17 p2780 A71-34914

Functional analytic methods for periodic and quasi-periodic solution of differential equations in nonlinear oscillation theory

17 p2780 A71-34921

Functional analytical iteration methods for calculating nonlinear vibrations of several degrees of freedom and error estimation improvement, considering uniformly converging Fourier series expansion

17 p2782 A71-34939

Spheroidal oscillations attenuation, considering discrepancy between theory and experiment due to earth interior dissipation

17 p2735 A71-35244

Pretwisted cantilever airfoil cross section turbine and compressor blades vibration natural frequencies and mode shapes

17 p2828 A71-35282

Exhaust pipe or diffusion kinetic flame type relaxation autooscillatory fuel combustion system, calculating vibration frequency, amplitude and mode

17 p2839 A71-35695

French book on linear vibrations covering systems with one or more degrees of freedom in free and forced vibration, propagation in discontinuous and continuous media, etc

17 p2784 A71-35737

High efficiency avalanche diode microwave oscillator design guidelines based on oscillation mode theory, covering CW and pulsed operations

18 p2888 A71-36131

Turbine alternating fan failure due to flutter by coupling of vibration modes and effect of mass distribution in blade

18 p2980 A71-36696

Dynamic properties of turbine wheels under bending vibrations, classifying resonant frequencies on basis of vibration modes

18 p2981 A71-36722

Dynamic piecewise-continuous linear systems oscillation period doubling in presence of C bifurcations

18 p2948 A71-36785

Harmonic generation in trapped-plasma-mode IMPATT diode microwave oscillators with waveguide-coaxial cavity

18 p2894 A71-36828

Free vibrations frequencies and mode shapes of anisotropic elastic thin plates, using Galerkin method

18 p2983 A71-36931

Cylindrical shells under uniform external pressure loads, determining boundary conditions effects on natural frequencies and vibration mode shapes

19 p3155 A71-37529

Variable thickness and rigidity cylindrical shells, determining natural frequencies and vibration mode shapes with algorithm based on Ritz method

19 p3155 A71-37531

Linearly deformable beams with distributed parameters and lumped inclusions, determining natural transverse vibration frequencies and mode shapes

19 p3155 A71-37535

Rectangular cantilever plate free vibration under in-plane acceleration loads, calculating frequencies and mode shapes by Ritz method and computer technique

19 p3157 A71-37850

Holographic interferometry application to vibration mode pattern analysis of steam turbine and centrifugal compressor blades and disks

19 p3067 A71-38419

Higher order approximation for normal vibration modes in nonlinear two degree of freedom systems

20 p3267 A71-38799

Oscillatory modes of perturbation in onset of flow instability for Newtonian liquid between concentric rotating cylinders with transverse pressure gradient

20 p3212 A71-39484

Gas dynamic model for coupled vibrational and radiative nonequilibrium in carbon dioxide, obtaining macroscopic collisional and radiative transfer equations

21 p3418 A71-40233

Dynamic influence of isotropic flat plates on spatial vibratory structures containing rigid bodies, considering compatibility and modal coupling

[ASME PAPER 71-VIBR-3] 21 p3456 A71-40267

Five-span skin-stringer width and damping effects on vibrational response including resonant frequencies and mode shapes by transfer matrix analysis

[ASME PAPER 71-VIBR-101] 21 p3461 A71-40327

Automatic balance control device for regulating vibration caused by rotating ill-balanced mass system

21 p3388 A71-40755

Natural frequencies and vibration mode shapes of missile with idealized air friction force tangent to instantaneous neutral axis

21 p3455 A71-41012

Clamped circular elastic plate nonlinear free vibrations, obtaining mode shapes and amplitude-frequency relationships

21 p3471 A71-41025

Gas bearing ground clearance effects on pivoted pad resonance, pitching vibration mode, static journal displacement and friction

22 p3551 A71-41661

Ultrasonic time shadow method based on defect detection by sharpness of vibration propagation time change during scanning

22 p3528 A71-41758

Holographic spectral analysis to determine modes oscillating in multilongitudinal and multitransverse mode laser

22 p3541 A71-41791

Vibration amplitudes and phases (excitation modes) during flutter for weakly inhomogeneous annular cascade flow with blade interaction and random inhomogeneity

22 p3615 A71-41846

Natural frequencies and vibration modes of perforated cylindrical, conical and spherical shells of revolution, using Ritz method

22 p3617 A71-42488

Digital servo system with signal quantization by level and time, evaluating oscillating motion in steady state mode

23 p3655 A71-43292

Large amplitude high efficiency TRAPATT oscillation mode in Si avalanche diodes, using resonant cavity for voltage and current waveforms analysis

23 p3650 A71-43352

Active flutter mode control system synthesis for flight test, showing mass balancing as possible artificial symmetrical wing destabilization

23 p3629 A71-44106

Divergence behavior of flat rectangular panel at subsonic speeds, discussing boundary conditions, natural vibration modes and temperature effects

24 p3878 A71-44611

Boundary value problems eigenvalues determination with differential equations for lifting surfaces vibration theory

24 p3818 A71-44706

Poloidal magnetic field effects on polytrope oscillation modes, using second order tensor virial equations

24 p3871 A71-44905

Translational and rotational vibrational motion correlation of solid body mass center in Newtonian force field

24 p3872 A71-45047

Evolved Cepheid-type stars vibrational stability against nonradial perturbations from quasi-adiabatic approximation of radiative dissipation

24 p3872 A71-45077

Liquid transition through critical value, considering self oscillation mode frequency

24 p3821 A71-45340

VIBRATION PERCEPTION

Human skin vibratory sensibility consideration as analyzer receptor for stimuli conversion into nervous processes

07 p1043 A71-20116

Vibrotactile information transmission, discussing skin mechano-receptive systems and similarities or differences between auditory and tactile characteristics

10 p1563 A71-24231

VIBRATION PICKUPS

U TRANSDUCERS

U VIBRATION METERS

VIBRATION PROTECTION

U VIBRATION ISOLATORS

VIBRATION SIMULATORS

Aircraft structures fatigue testing device using programmed control of electrical inputs to electrodynamic vibration stand, noting load cycle effects and damage accumulation

01 p0168 A71-10409

Interchangeable head vibration exciter for 200g large object testing and measurement of structural modes, impedances, transfer functions and calibration

11 p1746 A71-26495

Random vibration laboratory equalization by multiple taping of noise signals on recorder and manual processing

11 p1746 A71-26513

Automatic equalizer-analyzer system for random or shock vibration testing, including narrow-band equalization, simplified display techniques and self-calibrating procedures

11 p1747 A71-26514

Boeing 347 helicopter program consisting of analysis, vibration simulation, wind tunnel, whirl tower and bench tests

[AHS PREPRINT 571] 14 p2180 A71-31112

Vibration simulation of elastohysteric systems on analog computers using photocurrent-voltage relationship of polycrystalline photoresistors

16 p2658 A71-33978

Vibration analysis of simulated axial flow turbine disks by holography, illustrating advantages of full field modal and deflection information

[ASME PAPER 71-VIBR-105] 21 p3377 A71-40330

VIBRATION TESTING MACHINES

U VIBRATION SIMULATORS

VIBRATION TESTS

NT DAMPING TESTS

Phase-plane motion of engine assembly, using graphoanalytic delta method

01 p0128 A71-11241

Dynamic aeroelastic calculations for aircraft, using ground vibration test data

03 p0501 A71-13134

Mirror-coupled oscillations of open resonant cavities for arbitrary coupling coefficients

03 p3385 A71-13799

Automatic excitation forces generation for aircraft structure ground vibration tests using digital computer [ONERA-TP-870] 04 p0669 A71-15352

Spacecraft structures vibration testing nonlinear effects, extending asymptotic method for transition through resonance to nonresonant regions

[AIAA PAPER 71-211] 06 p1004 A71-18647

Vibration decrement amplitude dependence study using internal friction method of freely attenuated transverse vibrations, considering energy dissipation

08 p1317 A71-21761

Electrodynamic transducer design for structural vibration testing system, using low power steering signal converter to generate large scale electromechanical loads

09 p1386 A71-22606

Real time low frequency narrow band spectrum analyzer using time compression technique for vibration machinery diagnosis and prognosis

09 p1443 A71-22708

Aircraft continuous elastomechanical system parameters determination by ground vibration tests, using integral equation, phase resonance and separation technique

[DFVLR-SÖNDR-103] 10 p1692 A71-24946

Apollo spacecraft qualification vibration test program assessment, discussing structural acoustical excitation method

11 p1745 A71-26441

Two-shaker single input sinusoidal and random vibration tests, considering Hunter-Helmuth solution with constant cross coupling compensation in frequency band

11 p1745 A71-26491

LF vibration qualification tests for Mariner Mars 1971 propellant tanks

11 p1746 A71-26494

User-oriented conversational language computer program for Jet Propulsion Laboratory digital control random excitation environmental test system for spacecraft

11 p1736 A71-26498

Computer programs for random noise vibration test digital control, describing data base and logic programs

11 p1736 A71-26499

MODAPS real time data processing system for modal vibration testing consisting of analog subsystems, digital interfaces and on-line mimic computer

11 p1746 A71-26502

Modal characteristic pick-up system for vibration tests of rockets or aircraft on ground, using small size accelerometers with individual electronic circuit

12 p1895 A71-27719

Thin shell isotropic clamped free elliptical cylindrical shells with various cross sectional eccentricities, measuring frequencies and mode shapes by vibration analysis

14 p2324 A71-29869

Yak 40 aircraft flight test program, discussing airworthiness requirements, static structural, vibration and wind tunnel tests

14 p2174 A71-29911

Mobility definition and measurement methods, discussing portable instrument and vibration testing application

14 p2252 A71-30056

Vibration data analysis of analog and digital methods for cost comparisons

14 p2221 A71-30057

Harmonic vibration analysis methods, discussing mathematical model, ground tests, structure suspension exciter and pickup location eigenvalue measurement and mode research

14 p2175 A71-30058

Sinusoidal vibration tests using narrowband tracking filters, considering automatic servocontrols and feedback loop optimum matching

14 p2175 A71-30310

Automated modal data acquisition and processing system /MODAPS/ for real-time modal vibration testing of complex aerospace vehicle structures, describing features, capabilities and utilization

14 p2245 A71-30341

Fincap communication antennas design and environmental tests for vibration, acceleration, waterproofing, salt corrosion, ice formation and compass safe distance

14 p2216 A71-31047

Optimal phase trajectories of coordinates of electrodynamic vibration test stand, analyzing motion of moving part and optimal control signal along coil

15 p2353 A71-32190

Dynamic characteristics of weakly damped elastic body, considering complex natural modes generation for vibration tests in aircraft design

16 p2657 A71-33403

Vibration response NDT for fatigue crack damage in laminated filament-reinforced epoxy composites

17 p2824 A71-34815

Test apparatus for mechanical/thermal fatigue and vibration strength of turbine blades in high temperature gas flow

17 p2724 A71-35461

Cavitation damage in water to unalloyed metals and Ni superalloy, using ultrasonic vibratory testing with magnetostrictive transducer

19 p3081 A71-37904

Holographic interferometry equipment design for NDT and vibrational and deformation analysis, discussing apparatus construction, optical quality and industrial applications

20 p3238 A71-39344

Random vibration testing digital computer control system and experiment design, considering discrete Fourier transform techniques application

21 p3360 A71-40285

Vibration tests of instruments, machines and apparatus, allowing for functional reliability

22 p3536 A71-41441

Variable sweep rate frequency response and vibration testing for test time reduction, using closed loop controller for sweep rate modulation

22 p3537 A71-41635

Electrohydraulic stand for vibration strength testing, discussing system design, specifications, frequency-amplitude characteristics and applications

23 p3662 A71-44235

VIBRATIONAL FREEZING

Nonequilibrium nozzle flow determination for vibrationally relaxing gas, describing sudden freeze approximation method validity

16 p2556 A71-32907

VIBRATIONAL FREQUENCIES

U VIBRATIONAL SPECTRA

VIBRATIONAL RELAXATION

U MOLECULAR RELAXATION

VIBRATIONAL SPECTRA

Initial vibrational energy level distribution of hydrogen fluoride formed in reaction between atomic fluorine and molecular hydrogen, using IR chemiluminescence

03 p0375 A71-13495

Vibrational relaxation behind incident shock waves in pure nitrogen, using end wall pressure measurements

03 p0375 A71-13496

Vibrational transition matrix elements for diatomic molecules, using semiempirical Cashion method for potential functions

03 p0460 A71-13497

Computer design of magnetron gun forming electron beam of specific pervance and oscillatory energy in converging magnetic field

03 p0385 A71-13796

Sodium atom excitation by high energy particle collisions behind shock waves, measuring electron and vibrational temperatures

03 p0376 A71-13992

IR microwave double resonance of ammonia during IR vibration-rotation transitions induced by pumping of nitrous oxide laser

03 p0440 A71-14198

Shock tube measurements of vibrational energy transfer in molecular carbon dioxide-nitrogen-water system

04 p0629 A71-14693

Nocturnal intensity and excitation temperature variation of hydroxyl vibrational rotational band in air-glow

04 p0581 A71-15050

Thin convex shell of evolution bounded by two parallel minimum vibration frequency using asymptotic method of integration

04 p0671 A71-15556

Oxygen molecule vibrational excitation by electron impact, measuring elastic and inelastic processes

04 p0630 A71-15653

Gas dynamic coupling effect on vibrational deexcitation of carbon monoxide at 1400 to 2200 K range in shock tube

05 p0835 A71-16523

Radiatively driven acoustic waves, studying radiative transfer-gas motion interaction under local molecular equilibrium for vibrational rate processes

05 p0836 A71-16532

Laser emission from helium-air-methane mixture identification by comparing with vibrational rotational transition

06 p0906 A71-17307

Chemical energy conversion in lasers, discussing vibrational inversions in diatomic and multiaxial molecules and chain reactions

07 p1121 A71-19098

Electronically excited molecule mean vibrational energy relaxation, discussing deactivation during collisions

07 p1162 A71-19132

Circular membranes and plates with arbitrary hole distribution, deriving natural vibrations frequency characteristic equations by infinite determinants

07 p1218 A71-20464

Heterogeneity effects on thin composite cylindrical shells axisymmetric vibration characteristic, considering material and geometric symmetry deviations influence on frequency spectra

08 p1368 A71-20805

Carbon dioxide laser population inversion using chemical reaction of burning with gas combustion products of vibrationally excited polyatomic molecules

08 p1302 A71-21499

Inelastic collision effects on vibrational excitation of diatomic molecules with conserved energy

08 p1338 A71-21781

Laser modulator with multilayer dielectric mirror coating on piezoelectric substrate, investigating vibration distribution and maximum frequency deviation

08 p1303 A71-21808

Gaseous 3-oxetanone ring compound, investigating IR and vibrational spectra and molecular structure

09 p1403 A71-22473

Nonresonance vibrational exchange in molecular binary harmonic and one component anharmonic oscillators with beam laser applications

10 p1622 A71-24888

IR and Raman spectra vibrational analysis of crystalline and fluidic oxalyl bromide, explaining observations by two geometrical isomers existence

11 p1727 A71-25363

Ground state dissociation energies and long range internuclear potentials of diatomic molecules of halogens from spectroscopic vibrational spacings

11 p1728 A71-26065

Atomic bond strength of solid solution hardening as function of composition for calcium/strontium difluorides, using vibrational IR and laser Raman spectra

12 p1877 A71-26804

Solar photosphere vibrational temperature determination, using Franck-Condon factor with equivalent line widths for five CN vibrational bands

12 p1963 A71-27081

Natural frequencies of finite circular cylinders in axially symmetric longitudinal vibration, using Rayleigh-Ritz method to derive differential equations for expansion functions coefficients

12 p1981 A71-27482

Collision induced hydrogen spectra for overtone absorptions by gas mixtures under temperature and density conditions matching planetary atmospheres

13 p2138 A71-28773

Fluorochlorosilane preparation and identification by Raman laser spectroscopy, establishing line to vibration mode relation

14 p2189 A71-29746

Franck-Condon factors, densities and r-centroids for diatomic molecules, computing vibrational wave functions by FORTRAN V

14 p2276 A71-30297

Solid and fluid states oxalyl fluoride vibrational spectra and structure

14 p2191 A71-30575

Coupled natural frequencies in rectangular cross section pretwisted cantilever beams flexural vibrations

15 p2503 A71-31442

Automatic system for random vibration spectra control, consisting of spectrum shaper/analyzer and multidimensional controller

15 p2379 A71-31845

Mathematical model of multidimensional system stability for random vibration spectra control, including white noise generators, spectrum shaper/analyzer and summator

15 p2380 A71-31847

Carbon monoxide gas dynamic laser oscillation generation, observing maximum power and vibrational exchange among single diatomic species states

15 p2422 A71-32583

Gaseous, liquid and polycrystalline biacetyl vibrational spectra and structure, noting mutual exclusion between IR and Raman radiation

16 p2538 A71-32874

Vibrational relaxation of CO by Fe atoms in Ar shock tube following iron pentacarbonyl decomposition

16 p2539 A71-32897

Carbon dioxide laser population inversion based on chemical combustion reaction producing gas of vibrationally excited polyatomic molecules

16 p2585 A71-33047

Concave thin shell of revolution lowest natural vibration spectra frequency corresponding to simple inflection point

17 p2817 A71-34341

Population inversion damping on vibrational-rotational transitions of carbon dioxide molecule during interaction with monochromatic radiation pulse, using two level model

17 p2752 A71-34387

IR and Raman vibrational spectra and structure of tetrafluorocyclobutane

17 p2695 A71-35520

Vibrational population distribution in high power liquid nitrogen cooled CO laser by emission spectroscopy

17 p2754 A71-35751

Vibrational energy distribution and emission lines of fluorine atoms plus chloroform reactions in chemical laser, using equal gain measurements

19 p3071 A71-37331

Solar photosphere vibrational temperature determination, using Franck-Condon factor with equivalent line widths for five CN vibrational bands

19 p3133 A71-37431

Gaseous and solid polycrystalline HNCS and DNCS IR and Raman spectra, studying LF of lattice vibrations

19 p3118 A71-37649

Organic dyes pulse emission spectra shifts during pumping by ruby and neodymium-glass lasers, discussing vibrational relaxations role in mechanism

19 p3072 A71-37766

Pressure induced hydrogen collisions vibrational spectra absorption coefficients at high temperatures and local thermodynamic equilibrium

19 p3108 A71-38720

Kinetic modeling of vibrational state populations in high power direct discharge excited CO laser, using iterative technique

20 p3243 A71-39005

Low vibrational level CO transitions of flowing electrochemically excited liquid nitrogen cooled helium-air-methane-carbon monoxide laser in Q switched operation

20 p3244 A71-39100

Materials behavior at low temperatures, investigating lattice vibrational spectra relation to specific heat, conducting electron energies, thermal expansion, etc

20 p3270 A71-39242

Associative ionization and dissociative recombination cross sections of hydrogen molecular ions as function of vibrational coupling restricted to Rydberg states

20 p3272 A71-39577

Dayglow neutral and ionized diatomic nitrogen band system emission excitation mechanism from vibrational and rotational intensity distributions observations

20 p3226 A71-39829

Nonresonant vibrational exchange in molecular binary harmonic and one component anharmonic oscillators with beam laser applications

21 p3394 A71-41255

Hydrogen autoionization rates for molecular vibrational transitions near threshold, using internal conversion model

22 p3578 A71-42464

Electrical CO laser performance prediction from pumping mechanism based on vibrational energy exchange under thermal nonequilibrium conditions

23 p3683 A71-42954

Absorption spectra of benzene, naphthalene and anthracene crystals, noting resonance coupling type effect on vibrational spectrum

24 p3851 A71-45171

VIBRATIONAL STRESS

Vibrationally stressed elastic system stability, considering vibration rate amplitude as criterion

03 p0503 A71-13408

Helicopter pilot and passenger comfort/vibration tolerance criteria

04 p0532 A71-15420

Monocular and binocular vision comparison under moderate whole body Gz sinusoidal vibration stress environments

06 p0858 A71-17606

Mechanical stress amplitude measurement in optically transparent materials during HF vibrations, using polarization method

09 p1535 A71-22188

Variational criterion for stationary mode elastic structural oscillation, considering coincidence with normal modes for materials with stress-strain homogeneous function relationship

10 p1692 A71-25048

Dynamic analysis of vibrating beams on viscoelastic supports, using Galerkin approximate method

10 p1694 A71-25088

Design and fabrication of Borisic aluminum composite fan blades for supersonic turbofan engines, considering 430 F application without severe vibratory stress

[ASME PAPER 71-GT-90] 11 p1771 A71-25997

Vibratory stresses in heat exchangers due to pressure pulsation induced acoustic resonances, calculating flow pulsations from Karman vortex streets

[HEAT EXCH. CONF. PAPER 13] 15 p2513 A71-31635

End play influence on dynamic bending vibration stresses induced by aerodynamic forces in axial flow turbine rotor blades in case of resonant vibrations

15 p2508 A71-32298

Energy dissipation of vibrating structures in complex stress state, using generalized stresses and strains as coordinates

16 p2659 A71-33981

Gas turbine blades dynamic characteristics determination, investigating vibrational stresses, thermal cycles, alloy physicochemical properties and coatings effects

16 p2659 A71-33987

Al-Mg-Si alloy vibration creep endurance under single step loading, emphasizing strain and defect accumulation

17 p2757 A71-34593

Vibrational stress induced phase transitions in strontium titanate near transition temperature, using soft mode Raman scattering

17 p2791 A71-34949

Vibrationally stressed elastic system stability, considering vibration rate amplitude as criterion

17 p2826 A71-35017

Axial flow turbines, calculating effects of axial clearance between stator and rotor bladings on rotor impulse blades bending vibration strength

18 p2979 A71-36299

Two-mirror optical system to study energy dissipation in elastic systems subjected to cyclic straining

18 p2924 A71-36727

Vibratory amplitudes and stress levels from metal bellows flow induced vibrations, discussing damping and acoustical resonances effects

[ASME PAPER 71-VIBR-22] 21 p3458 A71-40279

Cu-rich alloys with high damping capacity at low stress amplitudes for structures and machines, noting damping stability improvement in Mn-Cu alloy by Cd addition

[ASME PAPER 71-VIBR-106] 21 p3396 A71-40331

VIBRATORS

U ELECTRIC CHOPPERS

VIBRATORY LOADS

Coupled vibrations of thin walled beams of open cross section using finite element method

01 p0175 A71-11015

Dynamic stability of cantilever under pulsating scanning load

07 p2128 A71-20474

Spring loaded intermittent contact devices vibrating system parameters for computer programmed transfer matrix solution, noting gravity loaded variant

12 p1931 A71-27480

Vibrationally loaded hollow cylinder with slanted notch, considering fatigue strength behavior as function of rated stress state

15 p2510 A71-32738

Hinged bar dynamic buckling under harmonic axial load, using Timoshenko beam theory with longitudinal vibration effects

17 p2832 A71-35400

VIBROCARDIOGRAPHY

U PHONOCARDIOGRAPHY

VIBROMETERS

U VIBRATION METERS

VICKERS VC-10 AIRCRAFT

U VC-10 AIRCRAFT

VICKERS 1100 AIRCRAFT

U VC-10 AIRCRAFT

VIBRO COMMUNICATION

High reliability low energy camera tubes for video communication in space missions, considering vidicons with photoconducting layer with large time constant

17 p2739 A71-34683

Communication satellite ground station terminal equipment, discussing carrier current telephone, video and sound TV apparatus

17 p2717 A71-35516

Visual displays preview, noting miniature eight-character alphanumeric, tabular, video, telephone and graphical displays

18 p2924 A71-36619

Sampled video data technique with information redundancy for processing and narrow-band transmission, discussing TV display, noting applications in corporate communications and teaching

22 p3547 A71-42508

TV multiplexing and broadband multichannel real time telemetry data transmission without loss between Kennedy Space Center and ground station for computer operation

23 p3645 A71-43519

VIDEO DATA

Straight and curved edges produced vidiosignal amplitude spectra discrimination in TV image scanning of nuclear particle path photographs, using filtering device

02 p0248 A71-11827

Rectilinear edge aperture filtration, examining mismatch angle effects on vidiosignal amplitude

02 p0248 A71-11828

Astronomical objects light polarization recording on magnetic video tape, providing digitized data for computer input

03 p0424 A71-13631

Digital computer techniques for Mars surface imagery systematic video data distortions quantification and correction onboard Mariner 6 and 7

06 p0871 A71-17631

ATC automation program for en route and terminal centers, discussing combined nationwide system features, IFR volume and video digitizer data links

08 p1332 A71-21659

VIDEO EQUIPMENT

Queueing model for analyzing video scan converter

01 p0047 A71-10215

Weather radar automatic data processing system for digitizing echo reflectivity by Video Integrator and Processor

01 p0050 A71-10594

Very long baseline interferometry (VLBI) one-bit instrumentation using videotape recorders in geodetic and geophysical measurements

02 p0251 A71-12332

Videotype sampling in electromechanical equilibria feedback stabilization of hydromagnetically contained plasmas

06 p0932 A71-17460

Video MTI pulse radar Doppler filter optimum symmetrical weighting factors in clutter-plus-noise environment

07 p1059 A71-18847

Optokinetic nystagmus device, combining TV sensor and bar generator with controllable frame desynchronization for moving image and electrical control of stimulus parameters

09 p1399 A71-22973

Video tape recorder (VTR) for onboard storage of wideband analog and high rate digital sensor outputs of ERTS

14 p2249 A71-30904

Videometer instrument for solar flares quantitative measurement, eliminating red sensitive vidicon for real time operation in H alpha region

17 p2742 A71-35003

Subminiature TV camera with hybrid electronic packaging, providing EIA composite video output format and 450 TVL/RH resolution capability

17 p2747 A71-35708

Five-gate automatic acquisition star and satellite TV tracker with video signal from vidicon or image orthicon, using line-to-line correlation for SNR improvement

18 p2882 A71-36904

Image intensifiers for color conversion, image deflection and scanning, shuttering and recording defining information gain criterion for comparison with unaided photography

18 p2925 A71-36907

Autoplotter for radar echoes on CRT screen, using video tape recorder for ship navigation use

19 p3017 A71-37700

Radar data video extractor adaptive threshold device synthesis criteria to quantize echoes for ensuring constant false alarm rate and target visibility

22 p3508 A71-41523

VIDICONS

NT RETURN BEAM VIDICONS

High reliability low energy camera tubes for video communication in space missions, considering vidicons with photoconducting layer with large time constant

17 p2739 A71-34683

Videometer instrument for solar flares quantitative measurement, eliminating red sensitive vidicon for real time operation in H alpha region

17 p2742 A71-35003

Two dimensional isophotes of extreme solar coronae from integrated vidicon pictures taken from moon surface by Surveyors 6 and 7

19 p3147 A71-38670

VIEW EFFECTS

Sight of body and active locomotion effects on perceptual adaptation to tilted vision in male subjects

01 p0010 A71-10398

Mathematical model of visual information of edge contrast effects in human eye as functions of image brightness and viewing angle

07 p1051 A71-20123

Visual recognition process for simple achromatic image confined within simultaneous-perception viewing angles, deriving hypothetical model based on psychological factors

10 p1567 A71-24162

Optical communication system combining heterodyne noise suppression and direct detection advantages concerning spatial coherence and wide field-of-view receiver optics

12 p1903 A71-26789

Neurophysiological investigation of visual tilt aftereffect, comparing judgment precision at vertical and horizontal to oblique orientation with/without gravity cue

21 p3335 A71-40671

Savart plate Francon modification at arbitrary angles to optic axis, examining view field limiting factors and fringe patterns

22 p3549 A71-42554

VIKING LANDER SPACECRAFT

Biological instrumentation and soil sampler aboard Viking lander for 1975 mission to Mars

16 p2537 A71-33808

Automated lunar landing missions with modified Mars Viking spacecraft, discussing propulsion and subsystems modifications, science payload and lunar exploration capabilities

[AIAA PAPER 71-822] 17 p2812 A71-34724

Lifting entry and terminal phase system optimization for 1975 Mars Viking lander, considering graphical tradeoff approach including design parameter and atmosphere model variations

[AIAA PAPER 71-922] 19 p3148 A71-37171

Viking Lander power system design, discussing functional requirements by mission and science objectives and reliability features

20 p3181 A71-38940

Thermal protection and electrical and mechanical evaluation of SNAP 19 radioisotope thermoelectric generator for integration with Viking Mars lander

20 p3267 A71-38964

Mars Viking Lander camera system with solid state focus switching, radiometry and solar imaging survivability

23 p3677 A71-43517

VIKING MARS PROGRAM

Biological instrumentation and soil sampler aboard Viking lander for 1975 mission to Mars

16 p2537 A71-33808

Viking Mars spacecraft pressure vessel design, incorporating linear elastic fracture mechanics for long life 18 p2979 A71-36487

Thermal protection and electrical and mechanical evaluation of SNAP 19 radioisotope thermoelectric generator for integration with Viking Mars lander 20 p3267 A71-38964

Unified procedure for detection of life on Mars by Viking program missions, using mass spectrometer for remote biologically oriented experiments 23 p3376 A71-43541

VIKING ORBITER SPACECRAFT

NT VIKING ORBITER 1975

Viking vehicle structural flexibility and propellant sloshing effects on thrust vector control dynamics, obtaining computer simulated responses for hybrid and discrete coordinate models [AAS PAPER 71-348] 23 p3773 A71-43021

VIKING ORBITER 1975

Viking Mars 1975 surface meteorological transducers, discussing measurements, environment and mission constraints 09 p1448 A71-22773

Viking Mars 1975 mission analysis software system for trajectory optimization, describing condensed format print and contour plot program [AAS PAPER 71-311] 23 p3725 A71-42987

Relay data link and trajectory design integration for Viking orbiter 1975 mission [AAS PAPER 71-320] 23 p3726 A71-42994

VIKING ROCKET VEHICLE

Viking rocket heat shield material mechanical properties, examining time-temperature superposition with continuous stress relaxation data measured in vacuum 11 p1791 A71-26518

VINTI THEORY

Translation-rotation motion of elongated body in Vinti potential field 10 p1667 A71-23814

VINYL COPOLYMERS

Electrical properties, chemical resistance and reinforced plastics applications of telechelic ultrahigh vinyl polybutadiene resins 11 p1786 A71-25422

VINYL CYANIDE

U ACRYLONITRILES

VINYL ETHYLENE

U BUTADIENE

VINYL POLYMERS

Pyrolyzing vinyl polymers thermal degradation kinetics, deriving surface regression rates relationship to temperature 01 p0109 A71-10935

VIOLENCE

NT ATTACKING [ASSAULTING]

VIROGO STAR CLUSTER

M87, Cen A NGC 5128 and 3C 273 X ray emission observations in Virgo cluster, using Uhuru satellite 11 p1814 A71-25215

Virgo XR-1 X rays observation with rocket-borne proportional counters, noting photo index or bremsstrahlung temperature consistency with spectrum 18 p2959 A71-37050

Statistical investigation of 1500 galaxies in MCG catalog with weak surface brightness, noting sculpture type spheroidal galaxies in Virgo cluster 20 p3289 A71-39299

Absolute spectral energy distribution and K-corrections for giant elliptical galaxies in Virgo cluster 23 p3722 A71-42935

VIRIAL THEOREM

Compressed nitrogen thermodynamic calculations, determining virial equation of state applicability 08 p1376 A71-21905

Computerized least squares fit of second virial coefficients vs critical temperature to Lennard-Jones potential function for hydrocarbons, halides, alcohols and cyclic compounds 13 p2103 A71-29005

Galaxies clusters mass determination with aid of virial theorem based on velocity dispersion, emphasizing black holes existence 21 p3450 A71-40713

Poloidal magnetic field effects on polytropic oscillation modes, using second order tensor virial equations 24 p3871 A71-44909

VIRTUAL WORK

U EQUILIBRIUM

VIRUSES

NT BACTERIOPHAGES

Active bacterial immunity development in long term space flights, discussing natural and nonspecific resistance to viruses and recurrent infections 21 p3332 A71-40552

VISCERA

NT ADRENAL GLAND

NT BLADDER

NT ENDOCRINE GLANDS

NT ESOPHAGUS

NT INTESTINES

NT KIDNEYS

NT LIVER

NT LUNGS

NT ORGANS

NT PANCREAS

NT PINEAL GLAND

NT PITUITARY GLAND

NT RECTUM

NT SPLEEN

NT STOMACH

NT THYROID GLAND

Eating and digestion effects on conscious dog coronary and visceral vasoactivity 01 p0015 A71-11183

Carotid sinus hypotension in dogs under fasting/digestion conditions, considering effect on splanchnic circulation and vasoconstrictor response 04 p0538 A71-15090

Somatosensory and viscerosensory stimulation effects on cortex neuron amygdala complex and convergent interrelations 06 p0849 A71-17384

Asphyxia induced changes in regional cutaneous and visceral sympathetic activity in anesthetized rabbits, noting relationship with ear blood flow increase 06 p0854 A71-18324

Cerebellum efferent visceral field functional organization in cats 08 p1240 A71-21794

Visceral system regulation processes investigation in human organism during manual labor and environmental adaptation, using multichannel biotelemetry and computer processing 08 p1241 A71-21941

Instrumental learning of cardiovascular and visceral responses and behavioral, physiological and biochemical consequences in relation to psychosomatic therapy 20 p3190 A71-39548

VISCOELASTIC CYLINDERS

Hollow circular cylinder with variable inner radius, solving nonlinear viscoelasticity dynamic load problem 01 p0168 A71-10422

Elastic boundary value problem of viscoelastic cylindrical body with temperature and time variations and relaxation kernel 01 p0169 A71-10492

Thick walled slowly rotating viscoelastic cylinder deformation under varying gravitational loads, using theory of elasticity 01 p0169 A71-10500

Pressurized isotropic viscoelastic hollow cylinder bonded to elastic casing, analyzing stress during finite deformation 04 p0668 A71-15191

Elastic and viscoelastic multilayer reinforced circular cylindrical shells stability, determining transverse shear stress role 06 p0996 A71-17841

Longitudinal waves propagation in viscoelastic semi-infinite rod under constant velocity impact, solving by characteristics and finite difference methods 11 p1850 A71-26178

Heat generation in hinged orthotropic viscoelastic cylindrical shells under transverse vibrations and cyclic surface load 12 p1978 A71-27343

Torsion problem of inhomogeneous anisotropic viscoelastic rod transformation, using area variation coefficient for modeling 17 p2828 A71-35240

Thermal stresses relaxation and distribution in infinite anisotropic viscoelastic cylinder 24 p3884 A71-45002

VISCOELASTIC DAMPING

U ELASTIC DAMPING

U VISCOUS DAMPING

VISCOELASTIC FLOW

U VISCOELASTICITY

VISCOELASTICITY

NT PHOTOVISCOELASTICITY

NT THERMOVISCOELASTICITY

Nonlinear viscoelastic material with stress dependent properties, solving for thick walled shells deformation under internal pressure 01 p0168 A71-10423

Viscoelastic behavior of boron fiber-epoxy resin composites at high temperature from torsion pendulum study, proposing linear model for damping peak effect 01 p0107 A71-10460

Stress potential for theory of adiabatic reversible processes in nonlinear viscoelastic material undergoing small deformations 01 p0169 A71-10493

Nonlinear viscoelastic beam with hereditary properties, analyzing forced harmonic vibration propagation 01 p0169 A71-10638

Linear isotropic viscoelastic media, determining stress relaxation and creep properties 01 p0170 A71-10640

Fatigue effects on metallic materials elastoviscoplasticity properties 01 p0175 A71-11025

Shear wave propagation into heat conducting viscoelastic fluids, considering steady one dimensional flow stability 01 p0181 A71-11188

Stress-strain state of anisotropic inhomogeneous viscoelastic solid fuel charge sphere with annihilating internal boundary 01 p0177 A71-11238

Free lateral vibration of viscoelastic metallic beam under axial creep, considering elastic deformation 02 p0324 A71-11996

Elastoplastic, viscoelastic and directed elastic continuous media kinematic and thermodynamic description based on intermediate state of reference concept 02 p0326 A71-12335

German monograph on displacement elimination method in viscoelastic shell theory covering shearing loads derivation from stress functions 02 p0327 A71-12398

Thin reinforced viscoelastic isotropic multiconnected plate stress-strain state under bending due to concentrated loads and distributed normal forces 02 p0329 A71-12668

Incompressible elastoviscous unsteady fluid flow past circular cylinder, confining calculations to non-zero vorticity region near cylinder 03 p0398 A71-13108

Elastic metal thin plates transverse resonant free vibrations, analyzing viscoelastic coatings damping effects [ASME PAPER 70-DE-E] 03 p0506 A71-13709

Elastic metal thin beams transverse resonant free vibrations, analyzing viscoelastic coatings damping effects [ASME PAPER 70-DE-D] 03 p0507 A71-13710

Covering plate steady state response to acoustic vibrations in viscoelastic half space, calculating interface displacement frequency spectra under zero shear stress assumption 03 p0459 A71-13719

Composite viscoelastic materials fracture energy determination using equations for line crack in linear materials from spherical flaw theory and Griffith concept [SESA PAPER 1647] 03 p0508 A71-13764

Creep failure in elastoviscoplastic media from time and load-path dependent processes near axisymmetric fissure prior to cracking 03 p0509 A71-13874

Polyvinyl chloride nonlinear viscoelastic behavior by multiple integral representation, determining kernel functions for mixed time parameters from tension/torsion creep experiments [ASME PAPER 70-WA/APM-21] 03 p0512 A71-14156

Plane wave propagation in layer direction in fiber reinforced viscoelastic materials 04 p0669 A71-15202

Thermomechanical coupling in axially symmetric viscoelasticity of cylindrical cavity under shear stress, determining stress concentration from temperature distribution 04 p0669 A71-15203

Transient axisymmetrical rotary shear wave propagation in nonhomogeneous viscoelastic media with cylindrical hole 04 p0671 A71-15752

Liquid-solid viscoelastic motion equations derived from conservation laws and nonequilibrium processes phenomenological theory 05 p0821 A71-16359

Viscoelastic fluids flow stability between arbitrary spaced concentric cylinders, noting critical Taylor number dependence on gap size 05 p0735 A71-16715

Complex modulus of elasticity relation to viscoelastic cantilever beams stress or strain under forced vibration, considering fiber reinforced plastics 05 p0826 A71-16738

Plane Poiseuille viscoelastic liquids flow stability, using method of inner and outer expansions based on Chun and Schwarz asymptotic solution of Orr-Sommerfeld equation 05 p0737 A71-17102

Viscoelastic rectangular thin plate stability under buckling conditions, showing ratio of long term to instantaneous critical loads as function of hereditary properties 07 p1212 A71-19351

Elastico-viscous liquid laminar free convection flow along nonuniformly heated vertical flat plate, using momentum integral method for boundary layer velocity and temperature distributions 07 p1091 A71-20031

Viscoelastic plates forced motion under dynamic loads by Valani method, considering elastic and layered elastic-viscoelastic circular plates 08 p1368 A71-20801

Elastic solutions convergence in nonlinear problems of viscoelastic incompressible media, formulating and proving uniqueness theorem for certain conditions 08 p1369 A71-21053

Uniaxial, equal biaxial and unequal homogeneous biaxial strain rates of viscoelastic materials under isothermal tensile test conditions 09 p1481 A71-22141

Quasi-static problems in nonlinear viscoelasticity theory, comparing integral operator and variable

- moduli methods for convergence and accuracy of successive approximations 09 p1537 A71-22513
- Linear theory of viscoelasticity, calculating basic relationships based on experimentally determined characteristics under unsteady test conditions 09 p1537 A71-22514
- Viscoelastic rectangular sandwich plate bending, stability, deflection and critical load calculation, assuming core stress-strain relation governed by Maxwell-Thompson differential equation 09 p1540 A71-22998
- Dynamic analysis of vibrating beams on viscoelastic supports, using Galerkin approximate method 10 p1694 A71-25088
- French book on macromolecular chemistry covering solid state polymers, polymerization reactions involving free radicals, linear viscoelasticity, vitreous transition of macromolecular polymers, electrical conductivity, etc 11 p1729 A71-26152
- Unidirectional glass fiber epoxy composite material nonlinear viscoelastic behavior, using isothermal uniaxial creep and recovery tests with thermodynamic constitutive equations 11 p1851 A71-26385
- Perpendicularly woven fiberglass reinforced plastics stability, elasticity and viscoelasticity as function of temperature 12 p1921 A71-27347
- Soviet papers on wave propagation in viscoelastic and elastoplastic media covering shock wave interaction, magnetoelastic waves, etc 12 p1980 A71-27444
- Two dimensional periodic and doubly periodic boundary value problems solution in theory for stable oscillations of elastic and viscoelastic bodies perforated by circular holes 12 p1980 A71-27447
- Circular viscoelastic plate under in-plane forces, determining increase in curvature as function of time 12 p1983 A71-27574
- Stress-strain state induced by concentrated forces in infinite medium with nonlocal rheological deformation law, obtaining particular solutions for quasi-static viscoelastic problems 13 p2149 A71-28128
- Solids continuum mechanics and fracture criteria, emphasizing intermixed elastic, plastic or viscoelastic types materials behavior idealization 13 p2151 A71-28214
- Thermal stresses in infinite viscoelastic plate due to external heat source 13 p2152 A71-28278
- Linear viscoelastic materials, investigating failure and bending as function of time in response to load under creep conditions 13 p2154 A71-28522
- Plane longitudinal stress waves propagation in plane-parallel viscoelastic partition of finite thickness dividing two linear half spaces with different elastic properties 13 p2155 A71-28655
- Viscoelastic and elastic shells boundary value problems relation, studying natural and forced oscillations of isotropic viscoelastic shells 13 p2155 A71-28656
- Linear viscoelastic analysis of two dimensional plane stress model of polyphase composite material with rigid inclusions and voids and polymeric binder 14 p2323 A71-29836
- Force method equations for linear viscoelastic system of incompressible rods obeying small deformations theory 14 p2328 A71-30376
- Particle displacements during resonance motion of shear and compression waves in linearly viscoelastic flat plate of finite thickness 14 p2332 A71-30851
- Dispersion and attenuation of plane longitudinal waves in laminated medium of elastic and viscoelastic layers, showing effect of composite parameters variations [ASME PAPER 70-WA/APM-40] 15 p2505 A71-32009
- Crack propagation model in linearly viscoelastic solid strip based on thermodynamics first law 15 p2506 A71-32011
- Book on viscoelasticity covering isothermal stress-strain relations, wave propagation, mechanical properties, thermodynamics and nonisothermal effects 15 p2509 A71-32438
- Linearly viscoelastic strip with slowly propagating central crack, calculating stress intensity factor and crack opening size 16 p2590 A71-32939
- Stability of linear viscoelastic systems under non-conservative forces, obtaining equations for perturbed motion for equilibrium or creep state 16 p2650 A71-33020
- Creep tests of admissible stress states in viscoelastic isotropic compressible or incompressible linear and nonlinear solids [ASME PAPER 71-APM-23] 16 p2591 A71-33206
- Polymers mechanical losses temperature-frequency dependence, using nonlinear viscoelastic theory 16 p2602 A71-33982
- Stresses and deformation in solid propellants charges under gravitational load, assuming homogeneous isotropic and linearly viscoelastic charge material 17 p2829 A71-35307
- Composite materials and structures analysis and design, examining elastic constants, thermal expansion coefficients, viscoelastic moduli, conductivities and failure modes [ALAA PAPER 71-366] 18 p2979 A71-36274
- Rheological media viscoelastic relaxation theories generalization taking into account thermal stress and conduction 18 p2984 A71-37021
- Polyethylene, polypropylene and copolymers sliding friction viscoelastic nature, obtaining relationship between sliding force, adhesion bond shear strength and contact area 19 p3068 A71-37425
- Circular inclusion effects in infinite viscoelastic plate under monotonically increasing uniaxial tension, considering stress distribution 19 p3157 A71-37798
- Forced axisymmetric motion of circular viscoelastic plate, including effects of rotatory inertia, transverse shear and time dependent boundary conditions 19 p3157 A71-37848
- Constitutive equation coefficients determination for nonlinear vibrations of viscoelastic beam by perturbation and optimal linearization method 19 p3158 A71-38060
- Isotropic viscoelastic plates of variable thickness subjected to mechanical and thermal stress, considering circular and rectangular plates vibration by external thermal shock 19 p3160 A71-38480
- Rigid body longitudinal impact against free end of variable cross sectioned viscoelastic cantilever beam, obtaining solution as rapidly converging Fourier series 19 p3160 A71-38485
- Small pressure wave transmission in abdominal venae cavae of dogs in mathematical model development for viscoelastic behavior of large veins 20 p3187 A71-38987
- Viscoelastic polar materials thermomechanical behavior, deriving stress tensor, couple stress tensor, entropy density and linear constitutive equations 20 p3309 A71-39562
- Second order viscoelastic fluid two dimensional stagnation point flow, solving boundary layer equations 20 p3213 A71-39564
- Viscoelastic materials property inequalities as consequence of Gibbs free energy minimum, disproving interpretation as indication of second order phase transition 20 p3310 A71-39867
- Four layer sandwich damping with viscoelastic material, noting frequency dependent effectiveness [ASME PAPER 71-VIBR-20] 21 p3458 A71-40278
- Structure born noise reduction by viscoelastic coatings, examining effects of thickness, density, bending and shear induced loss factors, moduli and Poisson ratio [ASME PAPER 71-VIBR-29] 21 p3414 A71-40284
- Viscoelastically damped structures finite element modeling and analyzing methods [ASME PAPER 71-VIBR-36] 21 p3458 A71-40288
- Beams with multiple constrained viscoelastic layer coatings, presenting damped vibrational response prediction for various materials, geometries, wavelengths and temperatures [ASME PAPER 71-VIBR-40] 21 p3459 A71-40290
- Viscoelastic materials with varying glass transitions, free and constrained layer damping and damping of LF vibrations in massive structure [ASME PAPER 71-VIBR-47] 21 p3405 A71-40296
- Plane waves propagation in viscoelastic body representing parallel union of Kelvin and Maxwell bodies in magneto-thermal field 21 p3463 A71-40577
- Elastic viscous plastic effects calculation in materials, describing method permitting constitutive equations introduction into computer programs for continuum mechanics equations solution 21 p3465 A71-40787
- Elastic viscous plastic waves profiles of finite uniaxial strain, obtaining constitutive equations 21 p3465 A71-40788
- Viscoelastic boundary layer flow solutions, using second order constitutive equation 21 p3370 A71-40989
- Stress-strain state of rotating viscoelastic hollow cylinder with mobile inner boundary under internal pressure and temperature effects 21 p3472 A71-41145
- Two dimensional cylindrical stress propagation over viscoelastoplastic body arbitrary cylindrical surface under instantaneous compression load, using finite difference method 22 p3613 A71-41564
- Temperature stresses relaxation in transversely isotropic viscoelastic sphere calculated numerically for 500 and 100 hour periods 22 p3616 A71-42486
- Motion equations derived for slender beam transverse vibrations on continuous viscoelastic foundation, considering nonlinearities from external couplings, longitudinal displacements and curvature 22 p3617 A71-42534
- Linear viscoelastic stress-strain-time relations for polymethyl methacrylate and epoxy resin 23 p3696 A71-43376
- Rivlin-Ericksen fluid steady flow between parallel plates with uniform suction at lower wall, detailing velocity field, skin friction and flow coefficient 23 p3663 A71-43499
- Fiber reinforced viscoelastic rectangular beam deriving asymptotic values of stress, curvature and position of neutral axis under constant moment 24 p3879 A71-44630
- Stress wave propagation in rod consisting of viscoelastic finite and semiinfinite elastic parts during pulsed sinusoidal load at end 24 p3885 A71-45223
- Non-Newtonian film thickness, load capacity and maximum viscoelastic stress effect in point contact with second order fluid lubricant for slide/roll ratio [ASLE PREPRINT 71LC-16] 24 p3832 A71-45293
- VISCOMETERS**
- Ultrasonic viscosimeter for gamma irradiation effects on materials structure, determining fluid viscosity changes from rate of damping of plate vibrations 04 p0594 A71-14918
- Viscosity measurement apparatus for molten materials, presenting block diagram of logic circuit for recording pendulum behavior 05 p0754 A71-16968
- Fluidic viscometer using laminar impedance element for output signal amplification 17 p2677 A71-35289
- Soviet monograph on vibration method for fluid viscosity measurement covering Newtonian fluids, low and high frequency viscosimeters, materials coefficients, temperature and pressure factors, etc 20 p2324 A71-39146
- VISCOMETRY**
- Aviation oils high temperature viscosimetry, describing test equipment and measurement results at 200-300 C [DFVLR-SONDDR-123] 14 p2264 A71-31128
- Viscometric motions of continuous bodies, studying kinematics and dynamics of d'Alembert, homogeneous and circulation preserving groups 20 p3309 A71-39567
- Radiation field profiles and applications of broadband ultrasonic transducers, including thickness and viscosity measurements 23 p3674 A71-42919
- VISCOPLASTIC FLOW**
- U VISCOPLASTICITY**
- VISCOPLASTICITY**
- Repeated bending and torsion of viscoplastic bars and circular cylinders, using hereditary nonlinear integral equations 02 p0322 A71-11688
- Nonstationary rotating MHD viscoplastic medium between coaxial cylinders in crossed electric and magnetic fields, determining zone interface position and stress distribution 03 p0464 A71-13601
- Elastoviscoplastic materials infinitesimal theory extension to thermodynamic processes by limit transition, deriving constitutive equations 03 p0510 A71-13946
- Stationary flow of viscoplastic liquid in annular gap with temperature dependent viscosity, taking into account energy dissipation 04 p0579 A71-15799
- Deformation time and displacement bound theorems for impulsive loading of plastic and viscoplastic materials 04 p0673 A71-15883
- Shock heating effects due to compression and plastic dissipation on basis of finite one dimensional waves in strain rate sensitive elastic viscoplastic solids 05 p0830 A71-17238
- Wave propagation in elastoviscoplastic medium in temperature field under complex dynamic and thermal conditions, considering mathematical models and mechanical properties changes 09 p1543 A71-23611
- Perfectly plastic and viscoplastic materials relation between permanent deflection and response time in boundary value problems 10 p1684 A71-23931
- Solid circular Ti shaft torsion boundary value problem solution, using elastic-viscoplastic materials thermodynamics and constitutive relations 11 p1849 A71-25801
- Mechanical waves propagation in elastic viscoplastic medium in presence of temperature field, using mechanical and mathematical models 11 p1850 A71-26177

Elastoplastic and elastic-viscoplastic waves propagation, considering longitudinal wave resonance, plane load waves and loading and unloading criteria 12 p1980 A71-27446

Shells of revolution plastic deformation problem, applying rigid viscoplastic strain hardenable material model 12 p1984 A71-27686

Stress-strain state of strain hardenable rigid-viscoplastic shells of revolution, presenting example calculation for conical shell with uniformly distributed load 13 p2150 A71-28132

Viscoplastic cylindrical shell dynamic buckling during axial impact of rigid mass, discussing constitutive equations 14 p2331 A71-30841

Rigid-plastic solids with viscoplasticity extension, comparing stability with Hill condition 16 p2649 A71-33010

Viscoplastic elastic medium behavioral relations, considering instantaneous and nonretarded plastic deformation 16 p2660 A71-34066

Viscoplastic elastic medium behavior, breaking down elastoplastic deformation into plastic and elastic deformations 18 p2977 A71-36187

Elastoviscoplastic system with components undergoing effects of external, resistance and attraction forces, determining motion 18 p2977 A71-36194

Nonassociated constitutive equations for rigid viscoplastic plates and thin rotationally symmetric shells under dynamic loading with Huber-Mises yield condition 20 p3310 A71-39777

Elastic viscous plastic effects calculation in materials, describing method permitting constitutive equations introduction into computer programs for continuum mechanics equations solution 21 p3465 A71-40787

Elastic viscous plastic waves profiles of finite uniaxial strain, obtaining constitutive equations 21 p3465 A71-40788

Soviet book on hydrodynamics of nonstationary motions of viscoplastic media covering mechanical properties of clay, mortar, cement, lubricating oil, petroleum and disperse media, etc 21 p3369 A71-40872

Two dimensional cylindrical stress propagation over viscoelastoplastic body arbitrary cylindrical surface under instantaneous compression load, using finite difference method 22 p3613 A71-41564

VISCOSITY
NT EDDY VISCOSITY
NT GAS VISCOSITY

Ultrasonic sound velocity dispersion in various hydro and gas suspensions, considering viscosity and heat conduction effects 01 p0127 A71-10618

Viscosity model application to turbulent plane Couette flow velocity profile and shear stress values, obtaining skin friction relation 01 p0071 A71-10954

Variable viscosity effect on laminar forced convective heat transfer in rectangular duct, using ethylene glycol and aqueous solutions 03 p0518 A71-13616

Stationary flow of viscoplastic liquid in annular gap with temperature dependent viscosity, taking into account energy dissipation 04 p0579 A71-15799

Nitrogen plasma viscosity at atmospheric pressure, using moving sphere resistance measurement 05 p0786 A71-16225

Density and temperature dependences of viscosity and thermal conductivity of dense fluids 05 p0831 A71-16408

Viscosity measurements for saturated liquid state of Ne, Ar, H, N, O, CO and methane 06 p0929 A71-17315

Turbulent velocity field in noncircular cross section rectilinear duct, determining relation between viscosity ratio and dimensionless velocity by integral transformation 07 p1087 A71-18992

Equations systems for free turbulent boundary layer in incompressible fluid, deriving semiempirical formulas for turbulent viscosity coefficient 07 p1089 A71-19735

Viscosity effects on three dimensional supersonic flow around circular half cones on flat plate, examining turbulent boundary layer separation 07 p1014 A71-19743

Plane steady state MHD shock wave structure in infinitely conducting fluid under magnetic field perpendicular to shock velocity, introducing quadratic artificial viscosity factor 07 p1174 A71-20616

Rubidium viscosity near solidification point from thin immersed plate forced vibrations amplitude 09 p1508 A71-22540

Motion perturbation equations for guided space vehicles, allowing for sloshing liquid propellant viscosity effects 09 p1532 A71-22657

Age effects on whole blood viscosity with Wells-Brookfield microviscometer, investigating role of hematocrit and plasma protein 11 p1722 A71-26362

Disperse systems dynamic behavior, considering density ratio, discontinuity diameter, viscosity and shear modulus 14 p2256 A71-29518

Gravitational instability of heat conducting compressible fluid relative to class of axisymmetric perturbations, considering viscosity, magnetic field and uniform rotation 14 p2226 A71-30397

Pigeon vestibular apparatus fluids and structures physical properties, detailing specific gravity and viscosity of endolymph, perilymph and cupula 14 p2185 A71-30467

Aviation oils high temperature viscosimetry, describing test equipment and measurement results at 200-300 C [DFVLR-SONDDER-123] 14 p2264 A71-31128

Jet fuel antiwear properties relation to viscosity and adsorption tar and mercaptans content 15 p2464 A71-31678

Mathematical theory of planetary atmosphere oscillations, considering coriolis, magnetic and viscous forces effects 16 p2561 A71-32804

Momentum transfer secondary flow between rotating cylinders in terms of effective/molecular viscosity ratio as function of Taylor number [ASME PAPER 71-APM-30] 16 p2559 A71-33199

Dense fluids linearized general transport equations solution, obtaining explicit expressions for shear viscosity 18 p2950 A71-37061

Soviet monograph on vibration method for fluid viscosity measurement covering Newtonian fluids, low and high frequency viscosimeters, materials coefficients, temperature and pressure factors, etc 20 p3234 A71-39146

Turbulent viscosity, energy dissipation and diffusion parameters of steady plane boundary layer flows of incompressible fluids with transverse shift in closed system of differential equations 21 p3368 A71-40691

Plane Couette flow temperature and velocity fields for Newtonian fluid with temperature dependent viscosity under locally and temporally constant wall temperature 22 p3620 A71-41881

Laminar Couette flow between parallel plates with mechanical energy dissipation and temperature dependent viscosity, determining velocity and temperature distribution 22 p3531 A71-42683

Spherical projectile hypervelocity impact on compressible fluid, showing viscosity effects on velocity and stress distribution behind shock front 24 p3877 A71-44426

Aviation fuels lubricating characteristics, discussing refining methods, viscosity, service performance and load testing 24 p3864 A71-45383

VISCOUS DAMPING

Finite amplitude sound interaction with Helmholtz resonator, attributing losses to viscous damping and orifice jet flow kinetic energy dissipation 03 p0456 A71-13279

Single degree of freedom vibration isolation systems, examining nonlinear damping range [ASME PAPER 70-DE-B] 03 p0432 A71-13711

Turbine engine vibration dampers viscous resistance calculation based on equations of motion for incompressible and unheated Navier-Stokes liquid 03 p0470 A71-13956

Optimal viscous damping effect of cylindrical filled fuel tanks on satellite nutations 06 p0979 A71-17417

Combined continuity and force equations for sound attenuation as function of thermal and viscous losses in liquid gases, taking into account fcc and bcc packing 06 p0927 A71-17569

Discrete linear vibration systems viscous damping local modifications effect on eigenvalues and vectors, using Weissengubers procedure in matrix form [AIAA PAPER 71-215] 06 p0928 A71-18651

Subdomain magnetic particles ferrofluid colloidal dispersions, for energy conversion devices, viscous dampers, accelerometers, gyroscope supports and specific gravity meters [IEEE PAPER 27.2] 07 p1178 A71-19611

Viscous layer damping effect on liquid surface oscillations in vessel, satisfying boundary conditions and obtaining frequency equation 08 p1276 A71-21621

Linear damping in piston type liquid damped accelerometers, using porous glass materials 09 p1451 A71-23173

Structural materials dynamic analysis, considering viscous, hysteresis and viscoelastic damping [AIAA PAPER 71-349] 11 p1843 A71-25328

Vibration damping of simply supported sandwich beam with viscoelastic core, using energy method [ASME PAPER 71-DE-C] 12 p1977 A71-27318

Dynamic damping of plane one dimensional unsteady stress wave passing through viscoelastic layer separating linearly elastic half spaces 13 p2155 A71-28848

Mechanical continuous system equilibrium stability under follower forces, discussing viscous damping destabilizing effects 16 p2608 A71-33007

Upper atmospheric winds viscous damping energy deposition calculation for midlatitude profiles 16 p2568 A71-33789

Viscous layer damping of liquid surface oscillations in vessel, satisfying boundary conditions and obtaining frequency equation 17 p2730 A71-35681

Turbulent rotating tube flows kinematic similarities, deriving heat and mass transfer, swirl damping and axial and rotational velocity profile 19 p3043 A71-37127

Destabilization phenomenon in nonconservative systems, considering simultaneous operation of damping mechanisms and critical load calculation 20 p3269 A71-39036

Four layer sandwich damping with viscoelastic material, noting frequency dependent effectiveness [ASME PAPER 71-VIBR-20] 21 p3458 A71-40278

Viscoelastically damped structures finite element modeling and analyzing methods [ASME PAPER 71-VIBR-36] 21 p3458 A71-40288

Optimum geometry and vibration damping ability of laminated three layer elastic-viscoelastic-elastic beam at resonance [ASME PAPER 71-VIBR-102] 21 p3461 A71-40328

VISCOUS DRAG

Vibration dampers optimization, considering viscous and inelastic resistance effect on sensitivity of harmonically moving system response 03 p0503 A71-13409

Astatic gyroscope with viscous friction at suspension system axes, noting free nonlinear vibrations and motion 03 p0423 A71-13411

Longitudinal turbulent air flow past plate, applying heat transfer and drag calculations 05 p0838 A71-16784

Crystal dislocation dynamics at high strain rates, investigating viscous phonon drag 08 p1371 A71-21563

Friction drag and energy losses of steady plane incompressible boundary layer flow of viscous liquid on nonconducting wall in MHD channel 10 p1649 A71-24377

Hipp pendulum controller electromechanical clock, considering dry and viscous friction dynamic models 12 p1932 A71-27525

Asymptotic limiting viscous flow pattern and drag on flat plate with stationary separation zones at large Reynolds numbers 13 p2050 A71-29204

Heat transfer and drag calculations in longitudinal turbulent air flow around plate with constant or variable physical properties 16 p2662 A71-33036

Approximate calculation of pressure distribution, separation points and drag on circular cylinder in viscous liquid flow, using ideal fluid jet model 16 p2560 A71-33597

Vibration dampers optimization, considering viscous and inelastic resistance effect and sensitivity of harmonically moving system response 17 p2826 A71-35018

Nonlinear free oscillations of astatic gyroscope with viscous friction at suspension system axes 17 p2743 A71-35019

Centrifugal compressor bladeless diffuser parameters, flow kinematics and energy losses, noting effects of friction coefficient and expansion angle 23 p3626 A71-43551

Compressible flow across shaft face seals and narrow slots, examining fluid inertia, viscous friction and entrance losses 23 p3663 A71-43592

Sword shaped tip on plastic sphere front portion, detailing hydrodynamic drag reduction at various Reynolds numbers 24 p3818 A71-44711

VISCOUS FLOW

NT BOUNDARY LAYER FLOW
NT BOUNDARY LAYER SEPARATION
NT COUETTE FLOW
NT REATTACHED FLOW
NT SECONDARY FLOW
NT SEPARATED FLOW
NT STOKES FLOW
 Unsteady MHD forced flow of viscous incompressible electrically conducting fluid against rotating disk 03 p0459 A71-19302

Hypersonic viscous air flow past blunt bodies with radiation, obtaining solution for Navier-Stokes equations by finite difference scheme

03 p0343 A71-14062

Two dimensional annular flow of viscous heat conducting gas between coaxial cylinders, using Navier-Stokes equations

03 p0401 A71-14066

Single stage axial flow turbocompressor with trips, examining viscosity effects on flow velocity profiles [ASME PAPER 70-WA/FE-24]

03 p0343 A71-14133

Viscous heating effects on laminar combined free and forced convection through vertical circular tubes

04 p0676 A71-15177

Viscous incompressible MHD fluid steady laminar flow past semiinfinite flat plate, noting heat transfer characteristics

04 p0635 A71-15508

Dynamic characteristics of submerged twisted jet flow of incompressible viscous fluid

04 p0573 A71-15560

Ring flow expansion of incompressible viscous fluid in cylindrical channel

04 p0573 A71-15561

Pulsed supersonic nozzle source molecular beam for shock tube target, detecting viscous effects from transient flux observation

04 p0600 A71-15596

Free convective flow in plane channel by boundary layer approximation, deriving continuity equations for viscous stress tensor

04 p0689 A71-15814

Unsteady viscous rotational stagnation point flow, solving vorticity transport equation

05 p0736 A71-16722

Viscous incompressible fluid flow with free boundary at large Reynolds numbers, deriving asymptotic expansion solution for wave motion

05 p0737 A71-16989

Asymptotic formulas for vortex and velocity field far from body in plane viscous incompressible fluid flow

05 p0737 A71-16990

Variable viscosity fluid laminar flow, measuring tube resistance at critical Reynolds numbers as function of energy dissipation

05 p0737 A71-17037

Viscous incompressible flow problems, using finite difference methods for solving Navier-Stokes equations

06 p0917 A71-17564

French book on fluid mechanics, Volume 3, covering nonteady phenomena, boundary layer and viscous flow

06 p0882 A71-18019

Forced convective heat transfer in laminar flow fluid of vanishing viscosity in constant wall temperature pipe, discussing velocity distribution effects

06 p0882 A71-18073

Chemically reacting viscous supersonic laminar flow in two dimensional divergent plane channel, developing approximate system of parabolic partial differential equations

[AIAA PAPER 71-44]

06 p0866 A71-18505

Turbulent boundary layer in incompressible fluid with vanishing viscosity, analyzing degeneration of isothermal boundary layer, viscous sublayer and density pulsations

07 p1085 A71-18753

Wall turbulence Prandtl-Karman constant calculation, using friction law for viscous sublayer degeneration with infinitely increasing Reynolds number

07 p1085 A71-18754

Viscous incompressible axisymmetrical flow, examining vortices near stagnation point of infinite flat obstacle

07 p1089 A71-19737

Viscous gas flow interaction on delta wing and oblique airfoil at Mach number of infinity

07 p1014 A71-19739

Viscous incompressible jet flow impinging on plane wall, considering negligibility of ambient medium viscosity within boundary layer equations framework

07 p1089 A71-19749

Landau viscous incompressible boundary layer separation formula comparison with Chudov finite difference method

07 p1090 A71-19751

Unsteady viscous incompressible electrically conducting fluid flow past accelerated conductor or insulator flat plate in uniform transverse magnetic field

07 p1169 A71-20022

Viscous conducting fluid MHD fluctuating flow over porous flat plate with time dependent suction, determining skin friction and transient velocity profiles

07 p1169 A71-20028

Viscous incompressible fluid flow between two cofocal elliptic cylinders, discussing temperature distribution and heat transfer in annuli

07 p1224 A71-20029

Viscous incompressible slow unsteady flow through circular tube with small axial roughness, obtaining velocity components by integral transform technique

07 p1092 A71-20093

Cylindrical viscous jet surrounded by flowing gas, investigating flow stability by linear perturbation theory

07 p1093 A71-20281

Computer calculation of high Reynolds number viscous and inviscid flow over arbitrary shaped two dimensional bodies and airfoils

07 p1017 A71-20313

Hydrodynamically stabilized turbulent viscous incompressible fluid flow in circular tube, examining nonstationary convective heat transfer by numerical methods

08 p1276 A71-21923

Velocity profile in viscous sublayer at wall based on maximum stability principle applied to Karman constant for turbulent channel flow

08 p1277 A71-21950

Viscous similitude reduction to Mach number independent Birkhoff binary scaling for hypersonic flow over slender bodies

[AIAA PAPER 71-252]

08 p1377 A71-21981

Laminar steady flow and heat transfer of viscous heat conducting gas moving between coaxial cylinders, using Runge-Kutta method

09 p1431 A71-22408

Laminar boundary layer interaction with shock wave in viscous supersonic flow near concave compression corner

09 p1384 A71-23618

Numerical solution of axisymmetric minimum drag bodies in hypersonic viscous gas flow, obtaining coefficient of friction by local variations method

10 p1551 A71-24370

Plane unsteady convective motion of viscous incompressible liquid in infinite horizontal vessel of rectangular cross section due to wall temperature fluctuations

10 p1696 A71-24375

Thermohydrodynamic equations for viscous incompressible lubricant flow in hydrostatic thrust bearings, considering inertia and temperature effects

10 p1617 A71-24482

Point matching technique applied to two dimensional solidification of viscous flow over semiinfinite flat plate, transforming moving free boundary problem to stationary domain

[ASME PAPER 70-APM-R]

10 p1596 A71-24733

Uniform surface blowing effects on hypersonic boundary layer with viscous interaction, calculating heat transfer on flat plate and slender wedge

10 p1598 A71-25096

Small cross section viscous vortex ring velocity in ideal fluid with arbitrary vorticity distribution in core

11 p1749 A71-25357

Viscous core of incompressible swirling flow through nozzle using momentum-integral equations [AIAA PAPER 70-51]

11 p1750 A71-25468

Viscous fluid flows determination by network calculator consisting of hybrid resistor with electronically switching active nodes

11 p1744 A71-25849

Lagerstrom mathematical model for two dimensional viscous flow at low Reynolds number, discussing asymptotic solutions for limit process expansions analysis

11 p1752 A71-26010

Asymptotic expansions for viscous flow along right angle corner, satisfying layer equations and boundary conditions

11 p1752 A71-26104

Nonstationary three dimensional weakly ionized incompressible viscous gas plasma flow in homopolar device, noting effects on ionization-diffusion balance

12 p1935 A71-26753

High Reynolds numbers asymptotic suction boundary layer linear stability analysis for viscous flow, using transformations to hypergeometric functions

12 p1896 A71-26923

Atmospheric viscous dissipation energy relationships, calculating Martian atmosphere thermal structure

12 p1965 A71-27192

Hypersonic cruise vehicles viscous interactions areas, examining compression corners, shock interactions, laminar and turbulent flow, boundary layer separation, etc

[AIAA PAPER 70-781]

12 p1865 A71-27551

Viscous convergent-divergent nozzle flow slender channel approximation, discussing nozzle geometry, Reynolds number and wall temperature effects

[AIAA PAPER 69-654]

12 p1865 A71-27556

Radiative emission effects on viscous flow in shock structure of low density hypersonic flow around blunt body

12 p1986 A71-27583

Compressible viscous gas supersonic flow, observing near wake region behind perpendicular trailing face of plate with motion, state, energy and continuity equations

13 p2047 A71-28421

Viscous dissipation effects on Nusselt number in combined free and forced convection through vertical concentric annuli

13 p2160 A71-28601

Asymptotic limiting viscous flow pattern and drag on flat plate with stationary separation zones at large Reynolds numbers

13 p2050 A71-29255

Viscous gas jets in uniform oncoming flow, deriving similarity laws by dimensionality theory

13 p1994 A71-29256

Wind tunnel simulation of viscous hypersonic parallel laminar boundary layer interactions, presenting similarity parameter effects on aerodynamic characteristics

13 p1994 A71-29257

Stability theory for thermal stratified viscous parallel flows at Prandtl number of unity, considering atmospheric boundary layer and jet stream mechanisms

13 p2165 A71-29258

Rotational effects on laminar subsonic compressible viscous flow across shaft face seals, noting leakage rates and pressure profiles

14 p2251 A71-29944

Viscous gas flow past semiinfinite porous plate with gas injection or suction and identical composition on outer flow

14 p2224 A71-30000

Multicomponent gas nonequilibrium viscous flow near blunt body stagnation point, presenting shock layer parameter variations effects on heat exchange

14 p2336 A71-30200

Spinning sphere impulsively starting rotation from rest in compressible viscous fluid, calculating boundary layer growth by matched asymptotic expansion method

14 p2225 A71-30201

Steady state flow of viscous incompressible fluid proposing difference scheme for numerical solution of Navier-Stokes equations

14 p2226 A71-30400

Asymptotic behavior of boundary layer equation solution for viscous incompressible flow past curved linear obstacle

14 p2227 A71-30800

Pitching stability derivatives of sharp oscillating wedges at zero incidence in viscous hypersonic flow from perturbation method, including thickness and wave reflection effects

14 p2171 A71-31000

Unsteady incompressible laminar viscous flow past infinite flat plate with arbitrary time dependent velocity, using Laplace transformation

15 p2387 A71-31100

Finite element method application to transonic viscous flow through cascades and channels [AIAA PAPER 71-602]

15 p2388 A71-31500

Viscous flow fields around pointed cones at angle of attack in nonuniform supersonic flow, using axisymmetric analog for three dimensional boundary layer

15 p2344 A71-31500

Separation controlled transonic drag rise modification for V-shaped notches attributed to inviscid/viscous interaction controlling flow separation and reattachment

15 p2345 A71-31500

Constant density and viscosity fluid steady planar two dimensional flow under no external forces, deriving partial differential equations for vorticity, energy and pressure

15 p2389 A71-31700

Two dimensional viscous incompressible fluid flow field calculation in fluidic element, giving Navier-Stokes equations solution in finite difference form

15 p2390 A71-32000

Viscous boundary layer induced shock decay from analysis of disturbances generated by power law bodies in otherwise uniform two dimensional flow

15 p2392 A71-32100

Potential vortex with turbulent viscous core and axial velocity excess or deficiency, using integral method with quasi-cylindrical flow approximations describe core flow

15 p2393 A71-32200

Two dimensional viscous hypersonic flow past thin needle shaped and highly blunted bodies with strong boundary layer interaction on outer stream

15 p2347 A71-32500

Incompressible viscous fluid flow between disks oscillating about state of rigid rotation, studying spin up time effects

16 p2607 A71-32800

Temperature fields and mass and heat transfer surface of solid spherical particle in laminar viscous fluid flow

16 p2557 A71-32900

Viscous incompressible flow stability between concentric rotating cylinders, developing nonlinear model of two disturbance interaction

16 p2558 A71-32900

Unsteady waves in parallel shear flows, noting viscous and nonlinear effects

16 p2558 A71-33000

Unsteady viscous flow around oscillating cylinder calculating fluctuating lift, drag and moment effects with Navier-Stokes equations

16 p2520 A71-33000

Viscous fluid flow velocities instantaneous potential based on continuous medium, energy conservation and classic kinetic matter theories

16 p2560 A71-34055

Viscous incompressible fluid flow between two rotating nonconcentric cylinders, presenting transverse velocity profiles

17 p2725 A71-34177

Viscous trailing vortices decay downstream of non-free axial flow fan, assuming steady axisymmetric incompressible laminar flow

17 p2725 A71-34191

Viscous stresses distribution in isothermal incompressible turbulent boundary layer with positive pressure gradient by diffusers in open jet wind tunnel

17 p2725 A71-34209

Viscous incompressible flow along right angle corner, using algebraic nature of asymptotic flow field for numerical analysis boundary conditions

17 p2726 A71-34504

Viscous incompressible fluid flow downstream of paraboloid of revolution described by matching boundary layer approximations to potential flow solutions

17 p2727 A71-34673

Monograph on dynamic viscous pressure interaction in hypersonic flow covering boundary layer effect on oscillating body unsteady pressure distribution in continuum hypersonic flow

17 p2671 A71-35217

Hydrodynamically stabilized turbulent viscous incompressible fluid flow in circular tube, examining unsteady convective heat transfer by numerical methods

17 p2729 A71-35267

Hypersonic viscid-inviscid internal flow field interaction with laminar boundary layer in circular ducts, using method of characteristics and implicit finite difference scheme

17 p2671 A71-35281

Creep strain separation theory generalization, describing viscous flow strain division into two components

17 p2833 A71-35617

Viscous relaxing gas hypersonic flow around sphere in presence of nonequilibrium chemical reactions in shock layer

17 p2673 A71-35637

Quasi-stationary viscous incompressible liquid flow in porous tube with deforming wall

17 p2694 A71-35641

Asymptotic solution of viscous incompressible flow past uniformly heated paraboloid of revolution with constant surface temperature

17 p2730 A71-35800

Viscous fluid flow past circular cylinder, using trigonometric representation of vorticity based on truncated Stokes-Picard and Oseen-Picard methods

18 p2844 A71-36316

Rotationally symmetric quasi-cylindrical viscous incompressible vortex flows at high swirl, discussing numerical integration with exponential functions

18 p2908 A71-36342

Viscous compressible flow around slender body in hypersonic slip flow regime, using finite difference method

18 p2908 A71-36344

Hypersonic aircraft design usable as transport or space shuttle, determining aerodynamic behavior in viscous flow

18 p2847 A71-36431

Asymptotic expansions for solution of wave motions of viscous incompressible fluid flow with free boundary at large Reynolds number

18 p2909 A71-36789

Asymptotic formulas for vortex and velocity field far from body in plane viscous incompressible fluid flow

18 p2909 A71-36790

Viscous incompressible conducting fluid at constant flow rate under magnetic field variation, investigating laminar unsteady MHD Couette flow problem with approximate solution

19 p3108 A71-37092

Air flow in pipe with double screw thread, calculating tangential forces and turbulent viscosity coefficient along isochors

19 p3043 A71-37266

Initial viscous heat conducting gas dynamic state one dimensional decay problem solution, using kinetic theory with Boltzmann equation

19 p3046 A71-38541

Variational principle for obtaining upper and lower bounds on minimum drag on body of given volume in slow viscous flow

20 p3177 A71-39500

Viscous electrically conducting laminar fluid steady flow through insulated MHD duct under uniform external magnetic field by extended Kantorovich method

20 p3275 A71-39561

Laminar and turbulent incompressible viscous flow with spiral vortices between two parallel rotating disks

20 p3213 A71-39778

Compressible viscous gas supersonic flow, observing near wake region behind perpendicular trailing

face of rectangular plate with motion, state, energy and continuity equations

21 p3318 A71-40081

Viscous vortex rings of small cross section, considering velocity in ideal fluid with arbitrary vorticity in core and arbitrary circumferential velocity

21 p3366 A71-40484

Rotating viscous fluid flow between concentric circular cylinders, predicting velocity field dependence on position and time during inner cylinder sudden stop

21 p3366 A71-40543

Unsteady viscous compressible flow through straight channel with flat porous walls under time varying pressure

21 p3367 A71-40591

Supersonic and hypersonic viscous gas flows with boundary layer induced pressure gradients, investigating disturbance upstream propagation by asymptotic theory

21 p3322 A71-40680

Viscous incompressible flow past semiinfinite slender body with upper and lower surface forced vibrations, solving ideal fluid and boundary layer equations by Shkadov method

21 p3367 A71-40683

Laminar viscous flow past semiinfinite flat plate to second Oseen type approximation, obtaining shear stress on plate

21 p3368 A71-40707

Rotationally symmetric quasi-cylindrical viscous incompressible vortex flow, using method of weighted residuals approximating axial velocity and circulation profiles by series of exponentials

21 p3369 A71-40951

Viscous slipstream flow downstream of triple shock wave intersection in supersonic diffuser air flow, using Pitot and static pressure probe measurements

21 p3324 A71-40981

Second order viscous liquid pulsating flow superposed on steady laminar flow through circular pipe, examining non-Newtonian effects on flow characteristics

22 p3530 A71-41562

Existence and uniqueness of boundary layer equations similarity solution for viscous incompressible fluid flow past paraboloid

22 p3531 A71-42197

Steady laminar viscous hydromagnetic flow in annulus with porous walls of different permeability, giving wall friction coefficients and velocity distribution

23 p3708 A71-43099

Circle, half plane and cylinder theorems for slow viscous flows involving hydrodynamic singularities under rigid boundary

23 p3625 A71-43237

Viscous heating and non-Newtonian behavior of incompressible steady pipe flow with variable transport properties, using perturbation method

23 p3662 A71-43370

Viscous incompressible flow between concentric rotating spheres, investigating hydrodynamic stability

23 p3663 A71-43443

Class of steady viscous incompressible axisymmetric nonrotating flows with axial velocity component dependent on distance along axis from reference point

23 p3663 A71-43489

Navier-Stokes equations solutions for incompressible laminar viscous fluid flow produced by vortex filament placed on cone axis

23 p3664 A71-44004

Boundary layer solution for initial flow around impulsively started sphere in viscous fluid at high Reynolds numbers

23 p3664 A71-44144

Two dimensional incompressible turbulent wall jet in moving stream, describing viscous flow characteristics and various boundary layer parameters

24 p3818 A71-44605

Compressible viscous flow calculation, deriving finite element analog of Navier-Stokes and energy equations

24 p3818 A71-44617

Flow instability due to viscosity variation in high pressure two dimensional laminar flow of Newtonian fluid between rigid parallel plates

24 p3819 A71-44945

Two-dimensional asymptotic solutions to Navier-Stokes equations for weak vortex discontinuity flow with vanishing viscosity

24 p3820 A71-45060

Hydraulic resistance of laminar isothermal flow of fluid with structural viscosity in circular cylindrical rigid channel

24 p3821 A71-45227

VISCOUS FLUIDS

Free convection in compressible viscous heat conducting liquid near critical point, discussing temperature gradients, layer heights, density distribution and inhomogeneity effect

02 p0331 A71-12190

Plastic impact principle of hydraulic losses in turbulent viscous flow, using Navier-Stokes equation with friction term

03 p0397 A71-13006

Unsteady flow about solid cylinder falling through viscous fluid in vertical tube, obtaining velocity profiles via solution of Navier-Stokes equation

[ASME PAPER 70-WA/FE-9] 03 p0403 A71-14130

Free convection in compressible viscous heat conducting fluid, determining parameters leading to onset

03 p0521 A71-14233

Round cylinder in viscous fluid asymmetrically disturbed flow, calculating dynamic and temperature conditions with difference method

04 p0571 A71-15492

Viscous fluid laminar periodic flow in constant cross section circular pipe, noting Kelvin functions, flow profile, wall forces and Reynolds number

06 p0881 A71-17411

Anomalous viscous fluid in channel with nonconducting walls, considering magnetic field effect on heat transfer

06 p0937 A71-17738

Incompressible unsteady viscous fluid flow through circular cross section curved pipe, noting centrifugal effects in interior

06 p0882 A71-18316

Hydrodynamic stability of viscous conducting fluid plane Couette-Poiseuille flow in transverse magnetic field by linear theory, considering complete spectrum of small disturbances

07 p1169 A71-19727

Viscous fluid horizontal motion due to moving heat source and boundary

07 p1091 A71-20030

Viscous incompressible fluid partly filling rotating cylindrical cavity, considering motion under centrifugal forces in adjoining unperturbed free surface region

07 p1093 A71-20467

Incompressible viscous liquid forced oscillations stability, developing linearization procedure for non-linear operator equation of perturbations

08 p1275 A71-21051

Free fall of sphere in viscous fluid, expressing fluctuations frequency as function of interfacial tension, sphere density and diameter

08 p1276 A71-21878

Laminar flow of viscous electrically conducting fluid in traveling magnetic field, examining channel flow in traveling wave field of one directional and two directional inductor

09 p1499 A71-22134

Hydrodynamic equations for behavior of thermally conducting viscous compressible fluid in first post-Newtonian approximation to general relativity, obtaining conservation laws

09 p1518 A71-22338

Steady boundary layer flow in viscous liquid thin down variable incline for large Reynolds and Froude numbers

09 p1432 A71-22451

Concentration profile in incompressible viscous fluid flow across plane plate in oscillating motion, considering gravity diffusion

09 p1434 A71-23729

Induced electrostatic field in forced Hg vortex of ideal viscous electrically conducting fluid under axial magnetic field

10 p1649 A71-24456

Viscous compressible fluid response to incident gravitational wave, deriving governing equations in linearized approximation to general relativity

10 p1676 A71-24496

Temperature distribution inside solid sphere rotating in viscous incompressible liquid with constant strength heat source at center, discussing flow field around sphere

11 p1853 A71-25146

Boundary layer equation for free convective diffusion on flat vertical plate in translation motion in viscous incompressible fluid

11 p1854 A71-25240

Viscous liquid unsteady flow in long circular tube as function of mean velocity distribution, discussing radial flow and pressure distribution

11 p1749 A71-25268

Viscous fluid flows determination by network calculator consisting of hybrid resistor with electronically switching active nodes

11 p1744 A71-25849

Bifurcation solutions of Navier-Stokes equations for time periodic motions of viscous incompressible fluid at critical Reynolds number

12 p1922 A71-26867

Soviet book on MHD flows in channels covering one dimensional theory, viscous fluids, boundary layers, electric fields, laminar flow, etc

12 p1940 A71-27294

Characteristic equation of respiration vibrations of cylindrical ring in incompressible viscous fluid at rest, obtaining damping coefficient for large induced flow Reynolds numbers

13 p2047 A71-28397

Acceleration covariance in turbulent flow of isotropic homogeneous incompressible viscous conducting fluid

13 p2109 A71-29295

Steady flow of electrically conducting incompressible viscous fluid in rotating parallel-plane channel under constant transverse magnetic field

13 p2110 A71-29296

Interaction between viscous mixing shear layer induced by tangential injection and external supersonic flow field, obtaining spark schlieren photographs and wall pressure distributions

13 p2053 A71-29461

Couette flow two point boundary value problem solution using Navier-Stokes and Barnett viscous gas equations

14 p2224 A71-30185

Axisymmetrical three component flow equations for incompressible viscous fluid in cylinder with rotating disk

14 p2227 A71-30855

Vertical magnetic field and Coriolis forces effect on equilibrium of heavy viscous incompressible infinitely conducting rotating fluid

15 p2453 A71-31183

Free convection in compressible viscous heat conducting liquid near critical point, discussing temperature gradients, layer heights, density distribution and inhomogeneity effect

15 p2512 A71-31497

Energy dissipation in harmonically oscillating spherical annulus filled with viscous fluid

15 p2391 A71-32104

German monograph on viscous fluids heat transfer in pipes covering Prandtl number dependence, turbulent boundary layer flow and transition areas

15 p2514 A71-32375

Two dimensional flow equations for incompressible viscous fluid in square cavity

18 p2907 A71-36340

Initial flow past circular cylinder in viscous incompressible fluid calculation by numerical integration using boundary layer coordinates

18 p2908 A71-36341

Time dependent rotating laminar flow of viscous incompressible fluid in closed cylindrical container, presenting numerical solutions to Navier-Stokes equations

18 p2908 A71-36343

Velocity field of viscous steady plane incompressible flow past body, linearizing by Oseen approximation

18 p2910 A71-36946

Wave motions in viscous fluid layer in presence of surfactant elastic substances adjoining solid surface or gas, using Navier-Stokes equations

19 p3042 A71-37084

Elastic circular plate with hole traversed by tube filled with viscous fluid, studying system motion

19 p3043 A71-37539

Viscous relativistic fluid plane laminar flow, discussing incompressible thermally nonconducting case and stationary models

19 p3044 A71-37640

Solid cylindrical particles interaction under entrainment in pipe by viscous incompressible fluid, obtaining numerical solution by reduction to flow past moving body

19 p3046 A71-38418

Viscous fluid stirring due to small amplitude rigid circular cylinder rotation, calculating steady flow velocity relationship to Reynolds number

20 p3177 A71-39481

Sloping flat plate impulsively started constant velocity motion through slightly diffusive viscous density-stratified fluid, investigating transient and oscillatory viscous boundary layer flow

20 p3212 A71-39503

Elastico-viscous liquid steady secondary flow induced by oblate or prolate spheroid rotating about axis of symmetry from linear partial differential equations solution

20 p3214 A71-39967

Hot-wire anemometer measurement of free oscillation damping of viscous and sluggish fluid in U tube, determining velocity distribution

21 p3366 A71-40512

Viscous fluid layer surface waves nonlinear theory, analyzing surface friction and gravity force angle effects on wave characteristics

21 p3367 A71-40682

Time periodic convection development in incompressible viscous fluid with distributed heat sources

21 p3475 A71-40689

Laminar and rotationally symmetrical flow of viscous incompressible fluid in circular pipe of constant temperature, considering inlet swirl effects and heat transfer to wall

21 p3368 A71-40756

Velocity profiles of heavy viscous fluid free oscillatory motion in U-tube by hot-wire anemometry

22 p3531 A71-42242

Approximate analytic solution for nonstationary heat transfer for viscous incompressible laminar fluid flow in annular cylindrical ducts

22 p3622 A71-42679

Generalized solutions existence proof for viscous incompressible fluids free convection, investigating

smoothness properties dependence on initial values and forces

22 p3622 A71-42863

Mgd shock propagation in viscous heat conducting gas, investigating radiation escape effect

23 p3708 A71-43100

VISIBILITY

NT LOW VISIBILITY

Aircraft compartment glare minimization for flight crew visibility conditions and visual performance improvement

01 p0004 A71-10028

Monograph on visibility of satellite in elliptic orbit covering probabilistic aspects, communication, navigation, weather, reconnaissance and scientific satellites

02 p0319 A71-11970

Runway visual range automatic assessment, discussing data handling, digital display and error sources

04 p0623 A71-15023

Poor visual flight meteorological conditions, discussing instrumental and visual aids, airport landing and approach, holding patterns and overshoots

06 p0847 A71-17922

Fringe interferogram variable visibility control, eliminating vibration effects

07 p1109 A71-19467

Threshold and power relations for optical radars in pure and turbid atmospheres, determining visibility range for object detection

13 p2027 A71-27856

Horizontal visibility range determination of lights on landing strip

15 p2443 A71-31360

Standard visibility and scattering coefficient changes due to humidity variation from maritime aerosol particles equilibrium radii calculations

16 p2605 A71-34084

Visual conspicuity measurements, determining effects of directed attention and relation to visibility

18 p2854 A71-36002

Concorde droop nose for takeoff and landing visibility improvement, describing design and operation

19 p2997 A71-38343

Spectral density modulation visibility at Michelson interferometer exit illuminated with white light parallel beam

21 p3375 A71-40072

Light sources selection and design for visibility range sensors employing backscattering

21 p3382 A71-41236

Light wave attenuation in fog, mist, rainfall and snowfall during propagation through atmosphere, deriving semiempirical formulas for attenuation rate relationship to visibility

22 p3569 A71-42523

Atmospheric visibility /light extinction/ measurement from modulated CW laser backscattered signal

22 p3549 A71-42565

Wind velocities and directions, air temperature and visibility range in atmospheric boundary layer under fog conditions

22 p3569 A71-42846

Laser technique for runway and slant visibility range, lower cloud boundary and atmospheric damping coefficient

23 p3701 A71-43889

Persistent and semipersistent thick and dense fog visibility definitions and tabulated data for London/Heathrow Airport and Kingsway/Holborn during 1950-1969

23 p3701 A71-43890

American development in automatic flight control, noting FAA requirements, pilot involvement and visibility enhancement

24 p3846 A71-44455

VISIBLE RADIATION

U LIGHT [VISIBLE RADIATION]

VISIBLE SPECTRUM

U LIGHT [VISIBLE RADIATION]

VISION

NT BINOCULAR VISION

NT COLOR VISION

NT MONOCULAR VISION

NT NIGHT VISION

NT STEREOSCOPIC VISION

Salmonid fishes from Great Britain and southern Germany, analyzing visual pigments and liver retinols

01 p0008 A71-10229

Rudd vision mechanism, considering daylight effect on spectral sensitivity and visual pigment retinal extract proportions

01 p0009 A71-10271

Human vision in communication system analysis, discussing psychophysical investigation, brightness functions, spatial frequency response and modulation transfer function

05 p0713 A71-16484

Visual mathematical model based on homogeneous medium thermal conductivity equation

07 p1043 A71-20112

Helium and nitrogen breathing effects upon intratracheal pressure during and after near vacuum exposure in anesthetized and unanesthetized dogs

09 p1400 A71-23359

Unanesthetized rabbits visual cortex cells neuronal activity during sound-rhythmic light flashes association

12 p1871 A71-27488

Dark adapted albino rats behavioral assessment measuring absolute visual thresholds to white and colored light

13 p2008 A71-28475

Near and intermediate vision in civil aircraft crews, presenting statistical evaluation of age factor effect on visual acuity in professional and nonprofessional personnel

13 p2019 A71-28505

Spatial and temporal discrimination functions in vision, audition and touch, establishing and controlling stimuli by vibrators

14 p2188 A71-30252

Light brightness and duration effect on central vision response time during dark adaptation

24 p3795 A71-44533

VISIOPLASTICITY

U FLOW VISUALIZATION

U PLASTIC FLOW

VISUAL ACCOMMODATION

Mathematical model for eye crystalline lens accommodation control interaction with pupil, deriving dynamic equations from human/cat experiments with/without neurological control

03 p0356 A71-12984

Accommodation model concerning nervous control of ciliary muscle

03 p0373 A71-14378

Visual accommodation measurement based on apparent motion of laser specular reflection pattern

04 p0609 A71-15697

Optical perception constancy of object size, developing mathematical models of accommodation, convergence and retinal image size

07 p1051 A71-20120

Visual accommodation mechanism, discussing microinterval nerve interaction role

09 p1391 A71-22488

Flight stress effects on blood pressure and eye accommodation from frequent takeoffs and landing of AN-24 aircraft

11 p1723 A71-25261

Eye accommodation range limiting for increased adjustment accuracy of optico-mechanical instruments, considering spectacle lens, telescope, magnifying glass and microscope

14 p2189 A71-30416

Visual field displacement, examining directed attention and maladaptive adaptation

15 p2363 A71-31949

Visually evoked cortical responses and visual acuity, discussing ocular convergence and accommodation effects

15 p2359 A71-31955

Aircraft pilot physical examination for regression curves on near vision and eye accommodation, noting age effect

17 p2692 A71-35197

Risk additivity in portfolios from experiments on accommodation role in binocular rivalry control

17 p2684 A71-35254

Accommodometer for automatic measurement of eye response to accommodation stimulus

18 p2863 A71-35849

Peripheral visual field and perceptual factors effect on accommodation under conflicting cues, using laser scintillation measurement

21 p3338 A71-41198

VISUAL ACUITY

NT HYPEROPIA

Astronaut visual acuity under angular acceleration, considering vestibular stimulus direction and nystagmus upbeating or downbeating

04 p0536 A71-14754

Human eye optical performance, noting retina anatomy and physiology, visual acuity, resolving power and reflectometry

05 p0713 A71-16482

Eye motion phase and amplitude measurement concerning visual acuity during whole body vibration

07 p1053 A71-20338

Atmospheric ions effects on human visual performance, taking into account ozone concentration and humidity

09 p1493 A71-22741

Dynamic visual acuity-horizontal eye movements correlation in man and monkeys, discussing fovea, parafovea and oculomotor control

10 p1560 A71-23984

Chromatic visual acuity measurement for gratings with bars of equal luminance and different colors

10 p1560 A71-23985

Peripheral visual resolution measurements, determining acuity thresholds at fovea and various points on temporal retina horizontal meridian over range of luminance values

10 p1564 A71-24608

Night vision and dark adaptation of eye, noting sun-light effects on visual acuity 13 p2017 A71-28392

Acuity-dark adaptation in strabismic amblyopia, discussing mechanisms for defects 13 p2012 A71-28833

Visually evoked cortical responses and visual acuity, discussing ocular convergence and accommodation effects 15 p2359 A71-31955

Visual system image blur and lateral inhibition effects on visual performance, convolving luminance profiles of targets with point spread functions 19 p3007 A71-38059

Wavelength discrimination from color naming by young adults with normal visual acuity and color vision 19 p3004 A71-38285

Flashing light stimuli application to clinical instrument design for detection and quantitative assessment of early pathological visual loss based on minimum discernible luminance difference 22 p3498 A71-41482

VISUAL AIDS

Electronic control indicator for human pilot capability enhancement using color coded cathode ray display, presenting information from seven different instruments 01 p0081 A71-10750

Visual information industrial processing rates correction tables with digits, letters, Landolt fringes and geometrical figures 03 p0364 A71-13525

Flight simulation requirements and design, considering analog computers, motion platforms and visual systems 04 p0566 A71-14996

Poor visual flight meteorological conditions, discussing instrumental and visual aids, airport landing and approach, holding patterns and overshoots 06 p0847 A71-17922

Aircraft visual warning indicating system, outlining design criteria, color and brightness recommendations [SAE-ARP-1088] 07 p1019 A71-19644

Terminal area control, discussing geographically grouped visual information displays, controllers coordination, plan position indicators and telecommunication 10 p1639 A71-23945

Night vision visual systems with image intensifiers, noting effect on human eye performance at low light levels 10 p1641 A71-24057

Concorde economic flight testing methods, discussing Bagnac flight simulator mobile cabin visualization and color TV terrain model 12 p1868 A71-27608

VISUAL CONTROL

Dynamic visual acuity-horizontal eye movements correlation in man and monkeys, discussing fovea, parafovea and oculomotor control 10 p1560 A71-23984

Risk additivity in portfolios from experiments on accommodation role in binocular rivalry control 17 p2684 A71-35254

VISUAL CUES

U CUES

U VISUAL PERCEPTION

VISUAL DISCRIMINATION

Eye wavelength /color/ discrimination ability measurements for linear dispersion spectra 01 p0016 A71-11390

Binocular synchronization data, suggesting visual coordination dependent on continuous eye movement and retinal feedback timing 05 p0712 A71-16218

Mariner near encounter pictures with maximum discriminability, applying algorithms for contrast and resolution enhancement and noise removal 06 p0898 A71-17634

Free and systematic horizontal visual search target detection times, testing human subjects with mixed stimulus schedules on high and low contrast targets 07 p1047 A71-19463

Linear mathematical model for human visual edge contrast by delineating and emphasizing image contours 07 p1043 A71-20101

Visual-tactile dominance relationship as function of tactual judgment accuracy 07 p1045 A71-20385

Chromatic visual acuity measurement for gratings with bars of equal luminance and different colors 10 p1560 A71-23985

Absolute and relative visual movement perception quantitative models relevant to length perception theory 10 p1570 A71-24603

Human vision spatial and temporal resolution relationship, examining image contrast sensitivity and target size, viewing distance and luminance reduction effects 10 p1572 A71-25000

Psychophysical evaluation of glide slope detection accuracy by diamond vs square shape in runway centerline stripping as aircraft landing aid 12 p1875 A71-27252

Human visual geometrical illusions and figural aftereffects, determining mechanism locations for spatial patterns physical and phenomenal properties 13 p2018 A71-28464

Visual discrimination learning by monkeys with inferotemporal cortex lesions, using positive reinforcers and electric shock punishments 13 p2011 A71-28804

Behavioral effects of electrically induced EEG abnormalities in inferotemporal and occipital cortex in monkeys on visual pattern discrimination and successive spatial reversals 13 p2011 A71-28806

Brain stem mechanisms underlying visual discrimination in rhesus monkeys subjected to bilateral lesions of the inferotemporal cortex, posterior thalamus or midbrain 13 p2011 A71-28807

Luminance and luminous flux discrimination in light and dark reared rats after early visual deprivation 13 p2011 A71-28810

Electroencephalographic and evoked cortical potential correlates of reaction time and visual discrimination in humans 13 p2022 A71-29345

Monkeys trained to observe and report two-member serial position sequences with delayed matching-to-sample procedure 14 p2187 A71-29519

Noisy image visual discrimination and detection, investigating Bayes criterion ideal statistical method validity for pattern recognition 14 p2197 A71-30815

Performance differences between tactile and visual localization and temporal ordering ability, using sequential presentation of high rate point stimuli 15 p2363 A71-31948

Visual movement aftereffect storage absence of patterned surround for fixated visible target 15 p2364 A71-31984

Aircraft pilot physical examination for regression curves on near vision and eye accommodation, noting age effect 17 p2692 A71-35197

Stimulus control during conditional discrimination development at various training stages, using two key situation and two visual dimensions 17 p2686 A71-35499

Autokinetic motion of luminous target, relating apparent visual movement to experienced displacement 17 p2694 A71-35739

Visual signal detection from noise, investigating mental images effects in six sense modalities 18 p2862 A71-37016

Wavelength discrimination from color naming by young adults with normal visual acuity and color vision 19 p3004 A71-38285

Stereoscopic vision and depth discrimination tests in cats, using conditioned suppression and rod-like shadow disparity stimuli 20 p3191 A71-39958

Neurophysiological investigation of visual tilt aftereffect, comparing judgment precision at vertical and horizontal to oblique orientation with/without gravity cue 21 p3335 A71-40671

Successively presented flashing lights detection, discrimination and brightness measurements with four channel binocular Maxwellian viewing system 22 p3498 A71-41488

Test field size, brightness and retinal location effect on observer assessment of stimulus at subfusal frequencies flicker suggesting inherent clock mechanism within human brains 22 p3499 A71-41497

Visual information discernibility measurement for suprathreshold transfer in display to observer system, noting use for color contrast scaling and disturbance evaluation 22 p3547 A71-42504

VISUAL DISPLAYS

U DISPLAY DEVICES

VISUAL FIELDS

Target detection facilitation by adjacent border control involving distance between inducing visual fields and duration of presentation 01 p0026 A71-11416

Transient response measurements of multiple scattered laser radiation from clouds as function of view field 02 p0260 A71-12032

Brightness field spatial structure of solar radiation reflected from earth by Cosmos 149 satellite, discussing homogeneity and isotropy 02 p0246 A71-12114

Unsteady light field spatial moments in turbid medium boundary layer with intense anisotropic scattering during illumination by narrow beam 02 p0277 A71-12116

Sensitivity, size and receptive fields position in cat retina ganglion cells 05 p0706 A71-16341

Three electrode image translator with electrostatic electron beam focusing, rendering high uniform resolution over entire viewfield 06 p0897 A71-17531

Spatial field of vision in healthy subjects and glaucoma patients, noting age effect 06 p0853 A71-17950

Mathematical model for perpendicular coordinate transformation from pattern to sensation in central visual field 07 p1050 A71-20106

Simple nerve system receptor field organization in visual analyzer simulated by TV circuit with scanning beam controlled focusing 07 p1050 A71-20108

Vertebrate retina receptive field structure, suggesting interaction between receptor, horizontal and bipolar cells 07 p1046 A71-20623

Monocular vision field structural color in violet and yellow region under increasing light frequency and periodic electric stimulation 10 p1560 A71-23990

Positive/latero-lateral accelerations and acute hypoxic hypoxia effects on central visual fields behavior in simulated flight 10 p1571 A71-24978

Cat single optic nerve fibers receptive field, observing functional organization and conduction velocity 13 p2008 A71-28458

Human visual system gate type lateral interaction to luminous intensity, noting visual field response to monocular viewing 13 p2018 A71-28460

Visual field displacement, examining directed attention and maladaptive adaptation 15 p2363 A71-31949

Flash field size effect on flash blindness of aircraft crews, measuring recovery time 16 p2535 A71-33113

Holographic display for blind landing system with variable image perspective over wide field of view, using collimated or cylindrical laser beam 18 p2945 A71-36061

Foveal perceptive fields for human vision, using measurements of contrast illusions in grids and bars 18 p2857 A71-36687

Spaceborne astronomical telescope image stabilization system, utilizing field splitting technique 18 p2925 A71-36903

Aircraft head-up display systems for providing pilot information focused at infinity within pilot normal field of view 21 p3413 A71-40131

Inhibitory binocular receptive fields in dorsal nucleus of lateral geniculate body for dominant and nondominant eye in cats, using moving slit and flash spot stimulation 21 p3335 A71-40669

Peripheral visual field and perceptual factors effect on accommodation under conflicting cues, using laser scintillation measurement 21 p3338 A71-41198

Flashing light stimuli application to clinical instrument design for detection and quantitative assessment of early pathological visual loss based on minimum discernible luminance difference 22 p3498 A71-41482

Hypoxia effects on response time to peripheral visual signals, noting direct relation to exposure severity and duration 22 p3499 A71-41495

Test field size, brightness and retinal location effect on observer assessment of stimulus at subfusal frequencies flicker suggesting inherent clock mechanism within human brains 22 p3499 A71-41497

Hologram recording by optical wave field scanning with arbitrary aperture and point source at center of entrance pupil and photoreceiver 23 p3675 A71-43398

VISUAL FLIGHT

Poor visual flight meteorological conditions, discussing instrumental and visual aids, airport landing and approach, holding patterns and overshoots 06 p0847 A71-17922

Vision loss from windshield tinting in night visual flying accident 08 p1247 A71-20824

Pilot vision during final approach and landing in turbojet transport operations 08 p1247 A71-20826

Visual flight simulation devices, considering high resolution photographic films and digital memories 13 p2046 A71-29483

Air transport accident research in night approach simulators, noting visual information null in descent path and delay in relative motion supplement data 15 p2363 A71-31602

VISUAL FLIGHT RULES

VFR flying under adverse weather conditions, discussing radio navigational aid equipment and communication with ground stations

08 p1330 A71-20683

VFR flying under bad weather conditions, discussing flight through and above cloud layers, need for radiotelephone communication and ground radar support

08 p1231 A71-21767

Commercial ATC, considering VFR, flight control and inertial navigation

22 p3570 A71-42078

European automatic flight control systems for landing in category IIIA conditions, discussing triplex system in Trident and simplex in Caravelle

24 p3846 A71-44456

VISUAL OBSERVATION

High precision large optical component surface visual monitoring with aid of small size etalons

04 p0593 A71-14869

Jupiter Great Red Spot continuous changes on basis of observational records of South Equatorial Belt disturbances

04 p0643 A71-15000

Lower atmosphere thermal microfluctuation measurement to examine solar seeing area and dome effect

04 p0622 A71-15658

Celestial bodies position determination, discussing optical observation, interferometry, radar, lasers and applications

05 p0811 A71-16650

Meteor atmospheric paths, relating appearance height, maximal brightness and disappearance to velocity, mass, path inclination and ablation coefficient

07 p1194 A71-19317

Space vehicle landing trajectories calculation from visual and radio observations of orbital parameters

07 p1196 A71-19495

Orienting response and apparent motion toward and away from observer, using galvanic skin response and finger pulse volume studies

07 p1048 A71-19515

Mathematical simulation of visual distance perception capacity of man from ground reference landmarks observation during vertical flight

07 p1051 A71-20121

Stellar image quality at Abastumani on Mount Kanouli, considering image diffraction picture at 755 magnification

07 p1201 A71-20440

Materials fatigue disintegration process visual examination for crack development kinetics, using fiber optics

09 p1454 A71-22316

Planetary surface smoothness factor determination by disk brightness, Mars red light and phase curves methods, indicating superiority of visual observation

09 p1520 A71-22828

Small meteor streams trajectories and radiants from epsilon-Lyrids, alpha-Coronids and phi-Draconids observations by amateur astronomers

09 p1520 A71-22841

Airborne multispectral remote sensing of forests, describing previsual detection of damage from insect infestations, disease organisms and oxidant air pollution

09 p1438 A71-23210

Comets structural features via visual observations, emphasizing inner coma structures and expanding envelopes surrounding nucleus

09 p1526 A71-23351

Simulated artificial satellite position determination, using experienced and inexperienced observers

09 p1528 A71-23547

Visual dominance in body and object verticality judgments as function of nonvisual information, considering modal system interaction and contact

11 p1724 A71-26076

Cloud shape data, comparing meteorological satellite measurements and ground based visual observations

11 p1795 A71-26559

Radiation induced visual phosphores observed by dark adapted human subjects in fast neutron, X ray and positive pion beams at Berkeley comparative to primary cosmic ray effects

12 p1871 A71-27675

Nondestructive testing, discussing visual, liquid penetrant, thermal, X and gamma rays, ultrasonics, magnetic, electrical and eddy currents methods

13 p2073 A71-28218

Auroral color variations and human color perception, noting visual appearance agreement with calculations based on normal spectrum

13 p2060 A71-28348

Iapetus magnitude variations due to orientation changes in poles, comparing visual and photometric observations

13 p2136 A71-28389

Optical effects observation by air traveler during takeoff, including haze or cloud droplet scattering,

halos, shock wave shadows, shallow watercolors and twilight wedge

13 p2022 A71-29350

Externally blown flap powered transport high lift wind tunnel model visual flow field investigation with multiple filament smoke streamlines

[AIAA PAPER 71-577] 15 p2345 A71-31567

Physical characteristics of comet Encke from visual observations, indicating nucleus of porous refractory material and ice structure

15 p2484 A71-31664

Meteor atmospheric paths, relating appearance, height, maximal brightness and disappearance to velocity, mass, path inclination and ablation coefficient

15 p2486 A71-31897

IR and submillimeter wave HCN laser radiation visual observation, using thermal image converter

15 p2420 A71-32385

Stereoscopic effects and apparent shape or position of moving objects at relativistic speeds under binocular observation

16 p2535 A71-33166

Jupiter systematic visual observations during 1968-1969 apparition, noting Red Spot conspicuousness, south temperate zone white spots, etc

16 p2635 A71-33429

Meteor showers of March 1969, noting delta Lyrids, gamma Cygnids and beta Ursa Minorids observations

16 p2639 A71-33699

High angular resolution of astronomical objects by ground telescopes, considering slowly and rapidly variable defects, atmospheric defects and their reduction

16 p2641 A71-33766

Honda 1968 comet activity from photographic and visual brightness observations, establishing relation between brightness fluctuations and solar activity

17 p2803 A71-34831

Visual integral brightness estimates of Ikeya-Seki 1967n comet observed at Dyushambe from 9 January to 18 April 1968

17 p2803 A71-34833

Statistical analysis of polar auroras visual observation, discussing solar activity effects

17 p2733 A71-34836

Polar auroras visual observations, plotting diurnal changes in height and occurrence frequency

17 p2803 A71-34837

Automation in optical astrophysics - Conference, Edinburgh, August 1970

17 p2740 A71-34980

Visual adaptation mathematical model, studying relation of brightness static transformation into luminance

17 p2692 A71-35174

Mercury transit across solar disk, discussing visual and photographic observations with Repsold and sun refractors and coronagraphs

17 p2809 A71-35579

Twilight aureole visual observation and objective colorimetry from Soyuz spacecraft, noting importance for atmospheric composition determination

18 p2911 A71-36007

Phase object visualization by Hilbert transformation, noting image properties evolution as function of various experimental parameters

18 p2947 A71-36043

Aerospace imagery enhancement for visual interpretation, considering ERTS applications

18 p2919 A71-36084

Photometric and spectroscopic study of NGC 3627 galaxy nucleus through optical observation of radio point galaxies

18 p2963 A71-36192

Visual detection of stars in spacecraft environment, considering window cleanliness and antireflection coating effect on light scattering

18 p2864 A71-36278

Optically identified B2 radio sources at 5 GHz, presenting flux density measurements, spectral index and visual identity

18 p2970 A71-37066

Optical space observations need in solar physics, stressing 0.2 sec angular resolution for extreme UV and magnetic field measurement

19 p3136 A71-37619

Jovian satellite eclipse observations, reviewing simultaneous narrow band multichannel visual and near IR studies

[AAS PAPER 71-107] 19 p3139 A71-37908

Image visual observation in coherent diffuse illumination, discussing human eye angular resolution deterioration and depth vision threshold dependence on light characteristics

19 p3074 A71-38195

Artificial satellites optical characteristics from amateur observers, discussing brightness and absolute magnitude

20 p3305 A71-38731

Cloud cover charts for North Atlantic-European-North African region, comparing satellite and ground station visual observations

20 p3258 A71-39552

Sporadic and shower meteoroids mass distribution temporal variations as function of magnitude and solar longitude from visual and radio echo measurements

20 p3298 A71-39643

X ray rocket observations of Sco X-1 on 7-8 August 1969 compared to simultaneous optical observation interpreting in terms of hot plasma model

20 p3283 A71-3975

Bright star at radio source and X ray observations evaluation from optical identification of Cygnus X-1 taking into account spectrum and energy distribution characteristics

21 p3447 A71-4044

Jet flame stability characteristics of propane-air mixture ejected into counter air stream by temperature and concentration measurements and visual observation

21 p3475 A71-40751

Telescopic observations of Apollo 8-14 spacecraft suggesting addition of specular reflecting surfaces or transmitters radiating at optical frequencies

21 p3349 A71-4140

Fingerprint identification by holographic correlator pattern recognition techniques, discussing reconstructed image visual observation and photoelectric measurement

22 p3539 A71-41748

Human observer performance in imaging systems, detailing contrast, ambient illumination, resolution, exposure time, display size, field of view and image blur and enhancement

22 p3547 A71-42503

TV data acquisition system for auroral and ionospheric research, noting visual and subvisual detection sensitivity

23 p3677 A71-43515

Radar vs visual observation of cloudiness and hazardous weather phenomena, emphasizing storm warnings

24 p3845 A71-44885

VISUAL PERCEPTION

NT AUTOKINESIS

NT CRITICAL FLICKER FUSION

NT SPACE PERCEPTION

NT VISUAL DISCRIMINATION

Flight simulator visual systems, discussing improvement objectives in terms of current technology, image quality, system reliability and maintainability

01 p0066 A71-10016

Line segment orientation visual perception relation to horizontal, vertical and oblique planes, considering induction effect susceptibility and visual illusions

01 p0010 A71-10274

Sight of body and active locomotion effects on perceptual adaptation to tilted vision in male subjects

01 p0010 A71-10398

Temporary connection of neurons in visual and associative cortical regions of hemispheres in cats

01 p0012 A71-11053

Figural noise and rotation effects on visual form perception, using random and redundancy figures in figure cancellation task

01 p0026 A71-11417

Visual images induced in aircraft crew members, during pressure chamber experiments, discussing latent period and persistence of sequences

02 p0198 A71-11899

Extraauditory effects of sound on senses, concerning visual functions, nystagmus, galvanic skin response and audioanalgesic use

03 p0359 A71-13158

Frog eye response to UV light stimulation, investigating sensitivity from electroretinogram

03 p0363 A71-13484

Soviet book on visual image formation on retina covering perception, stabilization, manipulative ability, etc

03 p0364 A71-13692

Neural activities during simultaneous contrast and information processing in visual system

03 p0364 A71-14188

Neurophysiological aspects of human optical and acoustical perception, discussing pattern recognition and cognizance role in optical image evaluation

03 p0373 A71-14331

Suprathreshold vision retinal image contrast loss measurement, suggesting role of balance between optical unsharpness and neural oversharpness

04 p0540 A71-15833

Rotation direction perception by three cue system for polar projection of dotted line, considering differential retinal velocity relative to axis of rotation

05 p0713 A71-16550

Nervous system activity changes relation to physical exercise type and extent, measuring visual response time

05 p0708 A71-16620

Digital tachystoscope functions, operating principles and designs, discussing tests of visual perception related functions

05 p0714 A71-16924

Visual pattern perception learning, recognition upon subsequent encountering and unfavorable conditions

05 p0716 A71-17243

Visual cortex inhibitory neurons, examining pause discharges in rabbits during light stimulation 06 p0849 A71-17383

Book on visual perception covering physics of light, rods and cones, color vision, brightness psychophysiology, stimulus generalization, etc 06 p0850 A71-17409

Shadow projector creating visual illusion of space surrounding flying aircraft for aviation training, relating perceived distortions to system parameters 06 p0864 A71-18716

Automated vision tester for evaluating space environment effects and multiphasic health screening 07 p1046 A71-18805

Perception - Conference, New York, October 1970 07 p1042 A71-19694

Space-time interactions and associated input-output mismatches from overprinting, sequential blanking and displacement visual perceptual information processing 07 p1049 A71-19695

Human eye optimum information reception assessment by Weber-Fechner law, threshold amount constancy and minimum continuous signal energy 07 p1043 A71-20110

Optical perception constancy of object size, developing mathematical models of accommodation, convergence and retinal image size 07 p1051 A71-20120

Mathematical model of visual information of edge contrast effects in human eye as functions of image brightness and viewing angle 07 p1051 A71-20123

TV monitoring and digital data recording of human corneal reflection during voluntary eye movements, considering visual perception studies application 07 p1051 A71-20210

Average minimum time for incorrect movement amendment, based on performer ability to process visual feedback 07 p1045 A71-20386

Pilot visual perception time of instrument readings after viewing external features and landmarks 07 p1053 A71-20540

Vestibular stimulation effects on bioelectrical activity in retina, optic tract, geniculate, visual cortex and ectosylvian gyrus in anesthetized cats 09 p1390 A71-22215

Darkness adapted human eye, investigating absolute light perception threshold dependence on light stimulus gradient 09 p1391 A71-22487

Optokinetic and vestibular effects on human operator reliability in aircraft control systems 09 p1399 A71-22681

Temporal masking effects with perception of color matching double flashes 09 p1394 A71-23015

Nonius horopter theory and mathematical model, discussing binocular disparity and monocular visual direction criterion 09 p1399 A71-23016

Reduction or disappearance of visual aftereffect of movement without patterned surrounding consisting of dots, concentric circles, grid pattern or vertical bars 10 p1558 A71-23744

Phi movement/pure motion/perception between successively presented, granular, moving objects, dichoptic and random dot Julesz patterns 10 p1567 A71-23987

Saccadic and smooth pursuit eye movements modification to visual targets instantaneous velocity changes at varying intervals 10 p1560 A71-23988

Foveal vision absolute thresholds for various duration light pulses and flash pairs at different separations 10 p1560 A71-23992

Visual recognition process for simple achromatic image confined within simultaneous-perception viewing angles, deriving hypothetical model based on psychological factors 10 p1567 A71-24162

Visual image propagation from retina to higher level formations in multichannel system of cat visual analyzer 10 p1561 A71-24163

Information processing in biological and artificial brains, analyzing visual perceptual system 10 p1568 A71-24224

Eye movement tendencies, investigating rectilinear, horizontal or vertical and center of gravity fixation effects on visual perception 10 p1570 A71-24602

Absolute and relative visual movement perception quantitative models relevant to length perception theory 10 p1570 A71-24603

Proximal changes and stimulus patterns associated with rotation direction evoking visually perceived oscillation 10 p1570 A71-24606

Brief light flash duration discrimination, discussing luminance and time between flashes 10 p1570 A71-24607

Human visual system response to moving spatially periodic stimuli, developing mathematical model for motion perception 10 p1572 A71-24999

Cosmic rays visual perception by Apollo astronauts during lunar flight, discussing human eye as Cerenkov radiation detector 11 p1716 A71-25237

Visual suppression and intensity threshold changes during voluntary eye saccades with different luminance regions in visual field, discussing inhibition processes 11 p1718 A71-25583

Forced choice visual signal detection tasks scanning strategies and differential sensitivity to various target locations 11 p1724 A71-26075

Visual dominance in body and object verticality judgments as function of nonvisual information, considering modal system interaction and contact 11 p1724 A71-26076

Comparative contrast and cues for illumination effects on perception of surface lightness, using target cast shadow experiments 12 p1872 A71-26613

Visual contrast sensitivity and fundus oculi pattern changes due to accelerations in pelvis-head axis 12 p1870 A71-27165

Thyroidectomized vitamin A deficient rats, noting visual sensitivity loss not correlated to thyroid 13 p2008 A71-28455

Human visual system gate type lateral interaction to luminous intensity, noting visual field response to monocular viewing 13 p2018 A71-28460

Intramodal and crossmodal sensory transfer of visual and auditory temporal patterns in normal young adults 13 p2022 A71-29326

Visual perception theoretical models for liminal contrast prediction 13 p2023 A71-29442

Eye movements and visual perception, describing scan path for memory traces 14 p2188 A71-29801

Visual sensation time theory validity investigation, discussing time elapsed between retinal receptor stimulation and perceptory sensation 14 p2189 A71-30406

Readiness potential, vertex positive wave and contingent negative variation recordings for evaluation of neural events associated with visually stimulated perception 15 p2359 A71-31953

Visual latencies at photopic levels as function of binocular differences in retinal illuminance, using Limulus adaptation model and ERG correspondence 16 p2527 A71-32867

Light adaptation and visual latency, discussing temporal resolving properties of eye as function of binocular differences and target background contrast 16 p2527 A71-32868

Spectral sensitivities of discrete slow potentials and threshold level nerve spikes in Limulus ommatidium as function of hyperpolarizing current 16 p2527 A71-32869

Isolated lower case letters visual recognition, investigating perceptual similarities and common properties serving as cues 17 p2680 A71-34655

Human visual perception response to brightness under sinusoidal current, suggesting interaction with retinal neural structures 17 p2680 A71-34656

Human visual depth impression by gradient patterns, discussing experimental verification for hypothesis concerning perceptual economy principle 17 p2684 A71-35252

Neural network hypothesis for mechanism of backward masking and disinhibition in visual perception 17 p2684 A71-35253

Human visual system differential luminance sensitivity tests using simultaneous stimuli in yes-no procedure 17 p2684 A71-35256

Human central fovea theoretical model for target stimuli threshold detection performance prediction 17 p2693 A71-35325

Human visual system biological model for pattern recognition based on spatial filtering covering Fourier transform modification for application to discrete case 17 p2694 A71-35793

Visual conspicuity measurements, determining effects of directed attention and relation to visibility 18 p2854 A71-36002

Subjects with strabismic amblyopia, investigating defects in cone or rod mechanisms of dark adaptation by using colored filters 18 p2854 A71-36011

Foveal perceptive fields for human vision, using measurements of contrast illusions in grids and bars 18 p2857 A71-36687

Zoellner illusion as function of inducing and test lines intersect angle and lines density, deriving error functions 18 p2863 A71-37019

Human visual mental imagery for oscillation rate estimation of subfusional light, using critical flicker frequency test 18 p2863 A71-37020

Functional relation of primary responses and unit spike activity at subcortical visual centers in cats 19 p3001 A71-37443

Visual target pursuit tracking test confirming error amending by central mechanism without sensory feedback 19 p3007 A71-37545

Visual system image blur and lateral inhibition effects on visual performance, convolving luminance profiles of targets with point spread functions 19 p3007 A71-38059

Increment thresholds for foveally viewed square and circular visual stimuli, suggesting availability of more than one spatial integration pattern 19 p3003 A71-38277

Visual sensations produced by cosmic ray muons passing in different directions through human eyes and head 19 p3005 A71-38677

Human retinal blood circulation changes and vision disturbance under transversely directed acceleration, using dark chamber teleophthalmoscopy 20 p3188 A71-39228

Visual attention automatization due to repeated stimulus experience, noting fixation rate habituation concomitance with fixations spatial distribution uncertainty reduction 20 p3193 A71-39545

Visual perceptual masking under binocular and dichoptic conditions separating peripheral and central interference effects 21 p3342 A71-40225

Visual projection, magnification and retina overlap on dorsal lateral geniculate nucleus in cats measured by random scatter in receptive field 21 p3335 A71-40668

Retinal directional effect measurements confirming mathematical model based on Gaussian distribution of retinal cones orientation, explaining brightness stimuli effectiveness and hue shift 21 p3335 A71-40670

Light flux spatial coherence in visual reception, considering aventurine spots perception as point light source 21 p3344 A71-41065

Peripheral visual field and perceptual factors effect on accommodation under conflicting cues, using laser scintillation measurement 21 p3338 A71-41198

Flashing lights perception and application - Conference, London, April 1971 22 p3497 A71-41476

Visual processes involved in flash perception, considering attention attraction at suprathreshold levels, unreliability at threshold levels and latency effects 22 p3497 A71-41477

Flash threshold perception in relation to flicker, showing flicker/flash sensitivity ratio constancy over large intensity level range 22 p3497 A71-41479

Depth perception variability under central and peripheral illumination conditions, using Duncan multiple range test for data analysis 22 p3498 A71-41481

Flash light angular size, adaptation luminance, pulse shape and color effects on Blondel-Rey constant tested on observers with good binocular vision 22 p3498 A71-41483

Flashing lights attention attraction classification based on experimental results conversion into psychometric scale 22 p3498 A71-41486

Apparent motion effects associated with stationary flashing lights configurations, noting frequency response characteristics analogous to real motion effects in human visual system model 22 p3498 A71-41487

Successively presented flashing lights detection, discrimination and brightness measurements with four channel binocular Maxwellian viewing system 22 p3498 A71-41488

Color defective vision and aviation color signal light flashes recognition, indicating Farnsworth Lantern performance prediction test superiority 22 p3499 A71-41490

Effective flashes by scintillating Xe arc flash tube, considering perception by human eye 22 p3499 A71-41492

Flashing lights vision threshold systematic variations, using quadrant adaptometer for continuous tracking of sensitivity fluctuations 22 p3500 A71-41498

Visual performance and retinal vascular changes under hypobaric elevation and hypoxia, noting stereopsis, binocular depth perception, critical flicker fusion, dark adaptation, etc 22 p3485 A71-41719

VISUAL PHOTOMETRY

Eye movement effect on visual system input and information use in perception

22 p3489 A71-42440

Human visual system color and edge-sensitive channels confirmation by psychological tests of tuning for orientation

23 p3640 A71-43548

Visual pigments in color blind subjects, using retinal densitometry

24 p3794 A71-44464

Mach bands appearance in red/green triangular wave intensity distributions generated on CRT, quantifying perceived brightness distribution by matching with variously positioned light slit

24 p3800 A71-44468

Increment threshold for monoptic and dichoptic vision, showing spatial and luminance effects

24 p3801 A71-44979

Visual masking effects in cat striate cortex single cell activity, using moving slit and diffuse flashing light stimuli

24 p3799 A71-45140

VISUAL PHOTOMETRY

Visible and UV photometric recording of microorganism reproduction in liquid medium for application to Mars extraterrestrial life detection

13 p2019 A71-28682

Photoelectric scanning photometer for visual binaries measurement, using on-line computer for data sampling and acquisition from three photon counters

14 p2246 A71-30357

Photometric measurements of light attenuation on baffles in visible, considering sensor location and surface coating

20 p2324 A71-39174

Daylight photometric flux derivation from filtered measurements of global sun and sky radiant energy, using natural illumination and short wave radiation relationship

20 p2324 A71-39175

VISUAL SIGNALS

Human tracking of external targets and body point projections, examining visual feedback role

02 p0205 A71-12057

Holographic twin image elimination by nonlinear method based on statistical differences in objects and diffraction fields

03 p0425 A71-13656

Forced choice visual signal detection tasks scanning strategies and differential sensitivity to various target locations

11 p1724 A71-26075

Mathematical model of human visual system light adaptive signal transformation

17 p2692 A71-35171

Visual signal detection from noise, investigating mental images effects in six sense modalities

18 p2862 A71-37016

Probability approach to visual effectiveness of signal flashing lights, showing graphically Broca-Sulzer effect

22 p3498 A71-41485

Hypoxia effects on response time to peripheral visual signals, noting direct relation to exposure severity and duration

22 p3499 A71-41495

VISUAL STIMULI

Visual threshold dependence on retinal location for various colors under conditions of scotopic, mesopic and photopic adaptation

01 p0009 A71-10233

Ocular pursuit movement evocation by visual and proprioceptive stimulation

01 p0009 A71-10235

Stimulus transretinal velocity effects on human torsional eye movements

01 p0009 A71-10236

EEG dynamics and visual cortex neuron responses in cats to conditioned optical stimulus during defensive reflex formation

01 p0011 A71-11052

Reaction time diurnal variations to optical and acoustic stimuli, investigating disturbed natural sleep-waking rhythm effects

02 p0197 A71-11684

Eye movements frequency and slow phase displacement in response to optokinetic stimulation of parrots and cats

02 p0199 A71-12385

Peak diameter differences of sensitization by annular surrounds in subjects, concerning scotopic increment threshold and retinal illuminance

03 p0365 A71-14376

Retinal neurons receptive field center, examining excitation and direct inhibition interaction

05 p0707 A71-16596

EEG wave phase durations over human brain surface, examining asymmetry distribution level

05 p0709 A71-16801

Visual analyzer functional state during latent motion sickness on rocking devices simulating moving aircraft

05 p0711 A71-17026

Photic stimulation at South Pole by EEG, showing no brain stress, undue tension nor anxiety during hypobaric hypoxia acclimatization

06 p0851 A71-17608

Free and systematic horizontal visual search target detection times, testing human subjects with mixed stimulus schedules on high and low contrast targets

07 p1047 A71-19463

Figural change perception in apparent motion, considering resolving capabilities and visual stimuli for plastic deformation and shape rotation

07 p1048 A71-19516

Perceptron learning systems with cross connections in single functional elements class, discussing visual patterns training schemes

07 p1068 A71-20103

Space vehicle apparent distance magnitude estimation judgments, investigating stimulus range effects on response range and Stevens type power function exponent

07 p1051 A71-20217

Target field luminance, interstimulus interval and target-mask spatial separation effects on visual backward masking, estimating inhibitory region radius

07 p1051 A71-20218

Human visual analyzer excitability shifts due to short duration point light stimuli

08 p1243 A71-21972

Rhodopsin dissociation and retina photochemical and bioelectrical processes after light flashes of various intensity

09 p1388 A71-22124

Computer aided statistical model of visual evoked potential in man as normality criterion for pathological indicator

09 p1397 A71-22253

Biophysical nature of human memory, investigating electrosensitivity phase modulators and variations by suprainensitive light stimulus to eye and adjustment reflex

09 p1391 A71-22484

Optokinetic nystagmus device, combining TV set and bar generator with controllable frame desynchronization for moving image and electrical control of stimulus parameters

09 p1399 A71-22973

Delayed e-wave like electrical response to light and inhibition in developing frog retina

09 p1393 A71-23011

W-formed summated evoked potential to light stimulus in healthy subjects significant to Wilcoxon test

09 p1393 A71-23012

Loci of perceived, equi-, half- and double distance in stereoscopic vision with point source stimuli relative to Vieth-Muller circle

09 p1394 A71-23014

World four dimensional and space three dimensional characters and psychophysical sensations dependence on Weber-Fechner law and tristimulus principle in psychology

09 p1530 A71-23730

Contour density effects on evoked critical response, discussing improved photopic visibility, spatial summation area and retina interaction

10 p1559 A71-23983

Spectral sensitivity by stimulus control and presentation in barred pattern alternatives and photopic system monitoring by visual evoked responses

10 p1560 A71-23986

Monocular vision field structural color in violet and yellow region under increasing light frequency and periodic electric stimulation

10 p1560 A71-23990

Postexcitatory inhibition of monochromatic flickering potentials on electroretinogram in man under intensive dazzling stimuli

10 p1564 A71-24443

Two flash threshold measurement of comparison stimulus duration of Bloch law for anticollision strobe lights

11 p1725 A71-26116

Human color vision investigation by psychophysical methods, discussing spectral sensitivity, pigment absorption and defective color vision as function of stimulus wavelength

12 p1873 A71-26863

Anesthetized cats visual cortex responses to prolonged light stimuli, studying dependence on photopic retina cone and rod apparatus

12 p1871 A71-27489

Extraprimary /briefly latent/ postsynaptic negative component of evoked visual potential in cortex of nembutal anesthetized rabbits, using Alvar biophase oscillator

13 p2004 A71-27894

Visual cortex neurons impulse activity and postsynaptic potential changes due to light stimuli from quasi-intracellular recordings

13 p2005 A71-28381

Grating pattern vision models, examining single neural network and multiple channel stimulus information processing

13 p2018 A71-28461

Human afterimage and pupillary activity in darkness after strong light exposure, noting dependence on stimulus intensity and duration

13 p2018 A71-28463

Visual evoked cortical response in man related to rate, spatial frequency and wavelength of alternating barred pattern with background illumination

13 p2012 A71-28888

Distinctive visual evoked response potential field patterns resulting from human retina stimulation, using electrode array on occipital scalp

13 p2012 A71-28892

Multiple starlike flashes and short streaks reported by subjects exposed to neutrons under 25 mev, discussing interaction with retinal rods by proton recoils

13 p2022 A71-29355

Readiness potential, vertex positive wave and contingent negative variation recordings for evaluation of neural events associated with visually stimulated perception

15 p2359 A71-31953

Visually evoked cortical responses and visual acuity, discussing ocular convergence and accommodation effects

15 p2359 A71-31955

Beta inflection in darkness adaptation curve, postulating stimulus thresholds in mono and binocular examinations for perception time and sensitivity

16 p2527 A71-32866

Redundancy information effect on human performance in forced pace cognitive tasks under overload stimulus presentation rates

16 p2536 A71-33679

Human visual evoked cortical potential spectral sensitivity measurement, comparing results with psychophysical data

17 p2680 A71-34652

Cat pupillary system static and dynamic response determination under light and electrical stimulation, using TV pupillometer and on-line computer

17 p2691 A71-35044

Visual and auditory evoked potentials enhancement in cats using cryogenic blockage of nonspecific thalamo-cortical system in inferior thalamic peduncle region

17 p2682 A71-35112

Visual evoked potentials and cortical recovery cycle data for normal and psychiatric subjects of various ages

17 p2682 A71-35113

Visual evoked brain potential amplitude and detection efficiency relationship, discriminating between arousal and attention effects

17 p2682 A71-35114

Stimulus familiarization effects on visual selection patterns during exposure to banal and incongruous paired stimuli

17 p2683 A71-35251

Orientation reflexes neuronal activity due to various stimuli, noting hippocampus reaction to sound and light

17 p2685 A71-35361

Conjugate eye movement stimulator and monitor for human experimentation in closed loop, open loop and variable feedback modes of operation

17 p2693 A71-35392

Reaction times distributions in visual or auditory mode single and multiple motor response units

17 p2686 A71-35433

Stimulus control during conditional discrimination development at various training stages, using two key situation and two visual dimensions

17 p2686 A71-35499

Multiple positive off effects in human electroretinogram, recording rhythmic wavelets due to intense stimuli with averaging computer and short time constant amplifier

17 p2687 A71-35802

Colored light sources luminosity determination by Helmholtz-Kohlrausch effect, discussing brilliant and fluorescent stimulus

18 p2854 A71-36003

Time duration judgment under visual stimulus, noting numerosity effects

18 p2863 A71-37018

Threshold electrical phosphene dependence on impulse duration and stimulation frequency in subjects adapted to darkness

19 p3002 A71-37444

Increment thresholds for foveally viewed square and circular visual stimuli, suggesting availability of more than one spatial integration pattern

19 p3003 A71-38277

Detectability measurement of foveal stimulus, suggesting nonuniformity of retinal illuminance in visual task

19 p3003 A71-38278

Human visual cerebral cortex potentials evoked by sinusoidally modulated field under stabilized and unstabilized conditions

19 p3004 A71-38279

Stimulus patterns spatial intervals and line thickness effects on stabilized retinal images

19 p3004 A71-38280

Visual evoked potential relationship to apparent size reduction of invariant retinal image

19 p3004 A71-38281

- Visually evoked cerebral cortex responses to on- and offset of patterned light and contour density and sharpness in humans
19 p3004 A71-38282
- Hue shifts by intermittent stimulation, suggesting interaction between stimulus intermittency and temporal color coding in visual system
19 p3004 A71-38283
- Visual sensations produced by cosmic ray muons passing in different directions through human eyes and head
19 p3005 A71-38677
- Surround luminance effect on relative perceptual latency of response, using test stimuli confined to rod free area of fovea
20 p3184 A71-38774
- Visual attention automatization due to repeated stimulus experience, noting fixation rate habituation concomitance with fixations spatial distribution uncertainty reduction
20 p3193 A71-39545
- Stereoscopic vision and depth discrimination tests in cats, using conditioned suppression and rod-like shadow disparity stimuli
20 p3191 A71-39958
- Subjective brightness of flashing light stimulus within fovea as function of stimulus size, noting edge effects contribution at suprathreshold levels
22 p3497 A71-41478
- Flashing light stimuli application to clinical instrument design for detection and quantitative assessment of early pathological visual loss based on minimum discernible luminance difference
22 p3498 A71-41482
- Test field size, brightness and retinal location effect on observer assessment of stimulus at subfusal frequencies flicker suggesting inherent clock mechanism within human brains
22 p3499 A71-41497
- Visual stimulus control removal and restoration in rhesus monkeys, analyzing test errors
22 p3497 A71-42860
- Quantitative characterization of unit time response in visual system, mapping latency and synchronicity as functions of stimulus position
23 p3640 A71-43870
- Flicker adaptation effect on visual sensitivity to temporal fluctuations of light intensity
23 p3635 A71-43974
- Bioelectrical activity of monkeys cortex and deep cerebral structures under lasting rhythmic photostimuli
24 p3793 A71-44411
- HF signals adaptation dependence from human cornea potential measurements by presenting narrow band chromatic stimuli to subjects under photopic, mesopic and scotopic adaptation conditions
24 p3794 A71-44467
- Afterimage induced smooth eye movements despite absence of moving visual stimulus, suggesting retinal image stabilization and saccadic behavior inhibiting processes
24 p3794 A71-44469
- Retinal image stabilization variables, noting whole fade characteristics sensitivity to stimulus pattern variations
24 p3795 A71-44470
- Averaged evoked potentials of human cortex in response to visual stimuli
24 p3796 A71-44549
- Simultaneous recordings of ERG and visually evoked cortical potential to stimuli of differing luminance and pattern, comparing spatial frequency characteristics
24 p3801 A71-44977
- Averaged potentials in vertex and occipital region of human cranium evoked by emotional visual stimuli
24 p3798 A71-45057
- Visual masking effects in cat striate cortex single cell activity, using moving slit and diffuse flashing light stimuli
24 p3799 A71-45140
- VISUAL TASKS**
Visual task vigilance deterioration under hypoxia, considering work-rest schedule effect and IQ scores
01 p0017 A71-11418
- Human vigilance performance in brightness discrimination task under hypoxia, considering reaction time in signal detection
04 p0541 A71-14740
- V/STOL spray generation tests concerning pilot visibility impairment in low altitude overwater bover
04 p0534 A71-15444
- Practice effects on visual vigilance task performance with and without search
04 p0540 A71-15845
- Visual alignment task performance for marks with vertical separation under various illuminations
04 p0547 A71-15849
- Target field luminance, interstimulus interval and target-mask spatial separation effects on visual backward masking, estimating inhibitory region radius
07 p1051 A71-20218
- Kundt optical illusion rule experimental testing under variable conditions with respect to monocular vision bisecting of horizontal straight lines, rectangles and squares
10 p1562 A71-24205
- Intermittent noise effects on performance of visual search tasks of varying complexity, measuring test subjects target detection time under various noise/time ratio conditions
10 p1562 A71-24206
- Pretask instructions effect on vigilance task performance, measuring time related signal detection correct and incorrect response percentages
10 p1571 A71-24808
- Forced choice visual signal detection tasks scanning strategies and differential sensitivity to various target locations
11 p1724 A71-26075
- Multiple suprathreshold visual and auditory monitoring tasks, evaluating vigilance decrement, individual differences, intertask relationships and channel capacity
12 p1874 A71-27248
- Sensomotor activity tests of operator perceiving high speed stimuli in broad visual field for psychological selection of aircraft and spacecraft pilots
13 p2018 A71-28416
- Target and nontarget processing equivalence in visual search for item recognition and forced choice task, questioning Neisser hypothesis of preattentive screening
15 p2364 A71-31985
- Optical tracking task performance and nystagmus during angular acceleration in yaw and pitch, comparing differences due to vertical and horizontal canal response
16 p2535 A71-33107
- Partial reinforcement effect in visual vigilance task, varying knowledge of results as incentive
16 p2537 A71-33680
- Weibull distribution analysis of saccadic eye movements interval during visual task
17 p2688 A71-34366
- Visual search performance as function of color coding for information location tested on aeronautical charts
17 p2689 A71-34703
- Magnification level for optimum performance at microminiature inspection with binocular microscope, minimizing time
17 p2689 A71-34704
- Long duration brightness change in electroluminescent panel detection during monitoring task, discussing role of payoffs and signal ratios
17 p2690 A71-34705
- Stimulus familiarization effects on visual selection patterns during exposure to banal and incongruous paired stimuli
17 p2683 A71-35251
- Psychological correlates of pattern identification tasks and invariance of pattern recognition under rotation, using Kabrisky model of human visual system
17 p2694 A71-35792
- Target value and exposure duration effects on recall in visual search tasks, discussing results in relation to previously reported inconsistencies
18 p2854 A71-36103
- Secondary visual tracking tasks utility in assessing lag effect in simulated combat aircraft dynamics
18 p2873 A71-36973
- Detectability measurement of foveal stimulus, suggesting nonuniformity of retinal illuminance in visual task
19 p3003 A71-38278
- Prefrontal cortex lesions effect on trained anticipatory visual target fixation in cats, noting performance impairment in voluntary eye movement control
21 p3329 A71-40174
- Character size, case and symbol generation effects on CRT display search time
22 p3503 A71-42195
- Visual performance in simulated target acquisition tasks as function of flare-ignition altitude
22 p3503 A71-42196
- Central panel luminance effect on peripheral visual detection time in search tasks
23 p3638 A71-42899
- Short term central fatigue as causal factor of delayed psychological refractory period in multiple choice visual signal tasks
23 p3634 A71-43864
- Low grade hypoxia effects on human physiological responses and performance in vigilance/display monitoring tasks
23 p3636 A71-44238
- VISUAL TRACKING**
U OPTICAL TRACKING
U VISUALIZATION OF FLOW
U FLOW VISUALIZATION
VITAMIN A
U RETINENE
VITAMIN B
U THIAMINE
VITAMIN B COMPLEX
U BIOTIN
- VITAMIN B 06**
U PYRIDOXINE
VITAMIN C
U ASCORBIC ACID
VITAMIN K
U PHYLLUQUINONE
VITAMINS
NT ASCORBIC ACID
NT BIOTIN
NT PHYLLUQUINONE
NT PYRIDOXINE
NT RETINENE
NT THIAMINE
Biological radioprotectants in space flights including amino acids, bacterial polysaccharides, hormones and vitamins
06 p0861 A71-18358
- Dietary antioxidant vitamin level effects on fine structure of proximal convoluted tubules in rats, studying changes due to oxygen toxicity
16 p2528 A71-33116
- VITREOUS MATERIALS**
Percutaneous vitreous carbon electrodes long term effects, considering mechanical stability, bioelectrical signal receptivity, low interface impedance and surrounding epidermis growth
01 p0021 A71-10238
- Apollo 11 and 12 devitrified glass fragments temperature histories indicating broad range of subsolidus crystallization temperatures
23 p3746 A71-43667
- VLASOV EQUATIONS**
Charged particle motion in self consistent continuous wave spectrum from Vlasov and Poisson equations solution
02 p0289 A71-11955
- Electrostatic waves linear dispersion relation in Maxwellian unmagnetized ions and magnetized electrons Vlasov plasma
03 p0789 A71-16656
- Excited waves due to transverse disturbance normal to boundary in dielectric half of isotropic Vlasov plasma with Cerenkov instability
05 p0789 A71-16658
- Supraluminous waves modes in field free two component anisotropic plasma by linearized relativistic Vlasov equation
05 p0791 A71-16939
- Plasma stabilization, considering feedback loop system with Maxwell-Vlasov equations
06 p0931 A71-17452
- Noncollisional plasma LF instabilities, discussing flute-like, drift wave and trapped particle modes from spatially confined plasma Vlasov equation
07 p1173 A71-20509
- Plasma configurations kinetic description by differential equations based on Vlasov and Maxwell equations, obtaining boundary layer distribution between plasma and magnetic field
08 p1340 A71-21492
- Plasma decay turbulence in spatially homogeneous ensemble of undamped dispersive waves in macroscopic and Vlasov terms, using time asymptotic perturbation method
10 p1647 A71-23887
- Electrostatic field second order penetration into Vlasov warm electron plasma, using electron velocity distribution models
10 p1647 A71-23890
- Electron thermal anisotropy effect on oblique whistlers preceding strong collisionless shock waves, using linear Vlasov theory
13 p2064 A71-29168
- Flat galaxies dynamics via linearized Vlasov equation integration and Poisson equation exact solution
14 p2303 A71-29590
- Plasma configurations kinetic description by differential equations based on Vlasov and Maxwell equations, obtaining boundary layer distribution between plasma and magnetic field
16 p2618 A71-33043
- Vlasov theory application to nonshallow shells, suggesting discretization procedure with quadrilateral finite elements for calculation by finite differences
17 p2816 A71-34325
- Vlasov-Poisson equations of collisionless plasma flow around conducting cylinder without magnetic effects, using nonrestrictive hybrid simulation techniques
18 p2951 A71-36025
- Edge clamped spherical shell natural vibration frequency determination using Vlasov shell theory equations
19 p3113 A71-37749
- Collisionless plasma Vlasov and Poisson equations numerical solution based on Fourier-Fourier transform, comparing with particle motion simulation
19 p3113 A71-37748
- Digital simulation of pseudowaves and plasma sheath formation about grid by computer solution of ion Vlasov equation for ion distribution function time evolution

Nonlinear Vlasov equation numerical integration methods, discussing Hermite expansion, characteristic function transform and truncation techniques 21 p3408 A71-40844

VLF EMISSION RECORDERS

Whistler indicator generation, relating VLF emissions to iono-acoustic oscillations in magnetosphere 07 p1099 A71-19387

Whistler indicator generation, relating VLF emissions to iono-acoustic oscillations in magnetosphere 19 p3052 A71-37812

Auroral ELF and VLF emission at high latitudes, discussing chorus and hiss generation regions and noise mechanism 20 p3229 A71-39854

VOICE

Human voice imitation of tonal signals pitch interval 02 p2026 A71-12061

VOICE COMMUNICATION

NT TELEPHONY

NT VOICE DATA PROCESSING

Speech signals digital encoding with adaptive linear predictor for reducing redundancy, discussing digital simulation results and subjective comparison with log-PCM encoder 01 p0030 A71-10472

Apollo lunar surface communications, discussing VHF system for voice and telemetry and TV hardware and techniques 01 p0035 A71-10914

Remote area voice, teletype and data communication using satellites for providing links with central terminals, considering economic feasibility by cost analysis 04 p0555 A71-15338

Satellite voice communication by suppressed clock pulse duration modulation technique, using optimum digital modulation and processing for maximum traffic and cost effectiveness 04 p0555 A71-15340

Quantized multiple access voice communications, comparing QPPM-AM and FM performances concerning transmitter power, RF bandwidth, circuit complexity, etc [IEEE PAPER 69-TP-448-COM] 05 p0724 A71-17056

Computer for speaking and answering verbal questions, using continuous frequency spectrum analysis and phonemes spectra in memory storage 06 p0871 A71-18057

Intelsat 3 satellite Communication, Telemetry, and Command system using transponders for multichannel voice and TV transmission 06 p0870 A71-18398

Multichannel laser telephone communication link experimental operation results in U.S.S.R. 07 p1058 A71-18838

Data communication role in National Airspace System, concerning radar and flight data acquisition, intersystem transfer and voice control [AIAA PAPER 71-248] 07 p1063 A71-19722

Unique word detection in digital burst communication, determining effects on voice quality from analytic study and digital simulation 08 p1255 A71-21595

International telephone transmission, comparing technical and economic characteristics between submarine cable and satellite systems 10 p1577 A71-24267

Flight helmets speech intelligibility evaluation using in-flight manikin recording 10 p1572 A71-25069

Computer simulation of automatic voice communication link intelligibility measurement, using speech recognition techniques 13 p2032 A71-28872

Apollo 14 communications support by USAF, discussing voice and data relay between spacecraft and control center, global weather support, cartographic and geodetic services, etc 16 p2541 A71-33178

Single sideband mechanical filters for voice multiplex transmission in radio and telephone systems, discussing material characteristics 17 p2714 A71-34608

Space station communications systems, discussing data relay satellites transmission paths to ground, multiple voice channels, two way color TV and onboard telephones 17 p2699 A71-34610

European regional satellite communication system, discussing TV coverage, spot beam antennas, frequency reuse, speech interpolation and circuits allocation 17 p2700 A71-34679

Satellite voice communications system for small terminals in remote areas, discussing feasibility, design, cost and frequency allocation 17 p2706 A71-35123

ESRO part of joint ATC communication experiment for L band satellite use, giving voice and data transmission and distance measurement techniques tests results 18 p2945 A71-36510

European regional satellite communication system, discussing TV coverage, spot beam antennas, frequency reuse, speech interpolation and circuits allocation 18 p2877 A71-36516

Trigonometric synthesizers with nonuniformly sectioned tapped delay line and summation circuit for signal distortion correction in telephone channel 23 p3650 A71-43288

VOICE DATA PROCESSING

Satellite voice communication by suppressed clock pulse duration modulation technique, using optimum digital modulation and processing for maximum traffic and cost effectiveness 04 p0555 A71-15340

Electronic apparatus isolating temporal segments from spoken syllable for speech analysis 09 p1408 A71-23383

FDMA single channel per carrier satellite communication system voice processing and modulation techniques, discussing analog frequency modulation and phase shift keying 17 p2704 A71-35086

VOID RATIO

Subsonic velocities erosion behavior of polymeric coatings and composites, considering void content and reinforcement influence on composite structure 09 p1483 A71-23425

Long term oxidative aging effects on interlaminar shear strength retention of low void graphite/ boron reinforced polyimide resin composites 11 p1785 A71-25410

Mean void fraction of adiabatic two phase flow by luminescent tracer dispersed in liquid phase 23 p3675 A71-43323

VOIDS

Nondestructive testing of carbon fiber reinforced composites with resin matrices (CFRP), suggesting ultrasonics for void detection 21 p3387 A71-40598

VOIGT EFFECT

Magnetoplasma electric and magnetic resonances by Voigt configuration, noting similarity to single particle scattering and particle size dependence 05 p0787 A71-16497

Mars atmospheric CO abundances and rotational temperature from Voigt line profiles 10 p1646 A71-24993

Optimal parameters of Fabry-Perot etalon for error minimization in Doppler and dispersion portions determination of Voigt profile width 17 p2737 A71-34410

VOLATILITY

Terrestrial basalts and lunar rocks volatile element concentrations comparison, noting relationship to abundance in chondrites 16 p2633 A71-33348

Lunar rock volatile and siderophile elements, comparing with terrestrial and meteoritic basalts 23 p3746 A71-43672

Lead isotopes volatile transfer in Apollo 11 and 12 lunar soil samples, discussing lunar age estimates 23 p3752 A71-43714

VOLATILIZATION

U VAPORIZING

VOLCANICS

U VOLCANOLOGY

VOLCANOLOGY

Lunar crater origin determination by terrestrial volcanic and meteoritic craters and maars geological criteria application to Lunar Orbiter 5 photographs 02 p0313 A71-12549

Precambrian and Cambrian stromatolites used for determination of nearest lunar approach to earth 04 p0583 A71-15141

Archaean volcanics geochemistry and modern basalts chemical and geographic characteristics, considering trace element model 06 p0892 A71-17895

Pulverized volcanogenic products and chemicals polarizing properties determination, applying to lunar surface layer 07 p1107 A71-19201

Volcanic petrochemical differences of Ethiopian rift and plateaus 09 p1436 A71-22645

Lunabase regions origin, suggesting volcanic dust masses fluidized by volcanic gases 09 p1528 A71-23550

Geomagnetic reversals in volcanic flows, computing paleomagnetic pole positions similar to Tertiary rocks 10 p1601 A71-24397

Marine sediment age by fission track dating of volcanic glass shards, noting agreement with K-Ar, paleomagnetic and paleontological ages 10 p1601 A71-24430

Normal albedo and polarization maximum degree wavelength dependence from terrestrial volcanic pulverized samples 14 p2305 A71-29677

Lunar transients in Aristarchus region with respect to tidal, sunrise, illumination, magnetic tail, bow shock and solar activity hypotheses 15 p2492 A71-32479

Lunar craters formation impact vs volcanic theories, using lunar probes for recognizing moon surface shocked materials 15 p2493 A71-32481

Glazing lunar craterlet interiors in Apollo 11 observations, comparing solar flash heating and volcanic bomb impact formation 15 p2493 A71-32484

Lunar-Martian craters relationship, discussing volcanic model of lava infilling, caldera floors and magmatic pressure 15 p2494 A71-32494

Sulfur effervescing molten slag/gas systems causing planetary vulcanism, examining patterns on earth moon and Mars 15 p2496 A71-32708

Refutation of greenhouse model of Venus atmosphere from Venus 4 and Mariner 5 data, proposing volcanic activity burst hypothesis 17 p2803 A71-34835

Thermally stabilized volcanic rock magnetic properties and coupling hysteresis effect changes due to reheating in weak magnetic field 18 p2912 A71-36197

Meteorite impact and vulcanism - Conference, Houston, October 1970 19 p3049 A71-37651

Capelinhos and Taal volcanoes base surges and deposits 19 p3051 A71-37670

Tuff rings from Fort Rock-Christmas Lake Valley basin, investigating morphologic and volcanic features for surface water role in genesis 19 p3051 A71-37671

Particle size-frequency distributions of volcanic pyroclastic tuffs for transport and deposit evaluation 19 p3051 A71-37672

Small lunar and terrestrial craters, determining impact or volcanic origin by depth-diameter ratio 19 p3137 A71-37677

Lunar volcano-tectonic processes, considering primary circular or polygonal surface features evolution 19 p3052 A71-37678

Morphologic variations and locations of terraced depressions in lunar maria, indicating drained lava lakes 19 p3137 A71-37679

Cauldron subsidence in lunar post-mare crater contiguous pair, discussing compatibility with volcanic origin hypothesis 19 p3137 A71-37680

Morphological features of crater Copernicus as lunar caldera, observing agreement with volcanic origin 19 p3137 A71-37681

Lunar soils structural-mechanical properties and composition, discussing volcanic origin and terrestrial analogs 20 p3295 A71-39618

Dribble spires in Snake River Plain, Idaho, discussing basalt lava features and remnants in lunar areas 22 p3533 A71-41839

Cascade mountains volcanic ash deposits elemental abundances correlation by computerized gamma ray spectra analysis of TRIGA reactor activated glass separates 22 p3533 A71-41855

Geothermic processes determination and registration in volcanic activity range by satellite IR measurements 22 p3534 A71-42004

VOLT-AMPERE CHARACTERISTICS

I-V characteristics of low and high resistance p(SiC)-n(CdS) junctions prepared by different methods 01 p0139 A71-11116

Microwave Gunn diodes I-V characteristics as function of carrier concentration 01 p0057 A71-11213

GaAs strongly doped p-n junctions, examining I-V characteristics changes under electron bombardment and mixed reactor field irradiation 01 p0140 A71-11458

Gunn diodes I-V characteristics width as function of carrier concentration/mobility and diode length, noting role of impact ionization in strong electric field 02 p0231 A71-11877

Thermionic converter with single crystal 110 W emitter surfaces and Nb collector, measuring I-V performance 02 p0193 A71-12212

Thermionic converter with oriented W electrodes, discussing computerized data acquisition system for mapping I-V performance 02 p0193 A71-12215

Volt-ampere characteristics dependence on collector temperature in thermionic converters compared with collector work function 02 p0195 A71-12235

Thermionic converter spectroscopic measurements in several regions of I-V characteristics, noting plasma radiation intensity periodic waveform 02 p0195 A71-12238

End layers role in forward I-V characteristics of P-I-N power diodes, ensuring minority carrier current continuity

02 p0235 A71-12919

Rapid mass transport to Pt electrodes in foamed electrolytes, examining current density-anode overpotential relationship

02 p0210 A71-12957

Copper oxide-magnesium thermal cells open circuit voltage drop in latter discharge stages, discussing cuprous ion activity at cathode

02 p0197 A71-12959

Tunnel diode frequency multiplier circuit, analyzing harmonic I-V characteristics by equivalent network method

03 p0384 A71-13396

Noise-induced current fluctuations on S-shaped I-V curve in Cr-doped GaAs diodes

03 p0387 A71-13982

Pulsed semiconductor devices with S-shaped current-voltage curve, considering relaxation oscillator and voltage generator circuits

04 p0558 A71-15565

Gold and Aquadag contacts with single crystal nickel oxide surfaces, determining I-V characteristics

04 p0637 A71-15588

Si solar cell low temperature low solar illumination intensity I-V performance deficiencies, considering corrective design modifications

05 p0701 A71-16073

Solar cells for Jupiter mission, discussing radiation and environmental tests concerning I-V characteristics

05 p0701 A71-16074

Si solar cells I-V characteristics measurement at low temperature

05 p0701 A71-16075

Dynamic I-V characteristics of megawatt pulsed MPD-arc plasma thruster under various axial magnetic fields given for Ar and hydrogen propellants

05 p0796 A71-16574

Plasma boundary layer temperature distribution near conducting surfaces by measuring current voltage characteristics

05 p0790 A71-16776

Single chamber plasmatron with rising arc I-V characteristics, obtaining electrical and thermal properties in dimensionless form

05 p0790 A71-16844

Ge diodes double injection experiments, measuring I-V characteristics, AC small signal admittance and noise

06 p0876 A71-18037

Resistor characteristics temperature dependence, considering platinum resistor and thermistor with negative temperature coefficient

06 p0900 A71-18186

Silicon dioxide space charge distribution dependence on photoinjected currents in MOS structures, showing charge effects on I-V characteristics

07 p1174 A71-19055

Microcircuits component vulnerability, deriving time independent nonlinear terminal I-V characteristics, electrical switching response and ionizing radiation induced transient response

07 p1070 A71-19059

Microwave frequency measuring techniques extension into IR, developing Si point contact diode with nonlinear I-V characteristics

07 p1125 A71-19797

Avalanche transistor emitter current voltage characteristics, using Kirchhoff equations for equivalent circuit

07 p1077 A71-19798

Current-voltage characteristics of Josephson junction, discussing noise effect at near transition temperature of superconductor and external signal driving

07 p1079 A71-20170

Volt-ampere characteristics of exploding Cu, Nichrome, Al and Ni wires during explosions induced by pulsed current in air

07 p1161 A71-20194

Volt-ampere characteristics of dual base n-type semiconductors as function of input p-n junctions

08 p1264 A71-21070

Monostable multivibrator tunnel diode synchronization bandwidth as function of circuit parameters and junction I-V characteristics

08 p1264 A71-21071

Pulsed MHD generator model with nonequilibrium plasma, obtaining I-V characteristics

08 p1237 A71-21929

Flush-mounted electrostatic probe for plasma properties measurement, calculating negative ions effect on I-V characteristics

09 p1442 A71-22073

I-V and capacitance characteristics of silicon diodes prepared by diffusive melting, considering recombination processes in p-n junctions

09 p1414 A71-22290

Balloon flight instrumentation for solar cell I-V measurements, using semiconductor selection circuits and RF telemetry

09 p1446 A71-22734

AlN insulating films electrical characteristics for use in charge storage devices, presenting Al-AlN-Au capacitor current-voltage-insulator thickness relationships

09 p1509 A71-23118

Annealing and white light illumination effect on I-V characteristics of long Ge diodes irradiated by 5 MeV electrons at 77 K

10 p1583 A71-24144

Pinch effect in nondegenerate intrinsic inhomogeneous semiconductors under nonuniform spatial volume recombination, resulting in nonlinear I-V characteristics

10 p1656 A71-24321

Quasi-one dimensional approximation equations derivation for electrohydrodynamic channel flows with small interaction parameter, obtaining I-V characteristics

10 p1649 A71-24365

Thermoelectric microwave radiation sensors with small area n-n junctions, investigating carrier heating effects on I-V characteristics

10 p1584 A71-24723

Pulse rate and pumping power effects on emission spectra and I-V characteristics of multielement GaAs injection lasers

10 p1622 A71-24884

Electrical conduction in cholesteryl acetate, propionate and stearate in solid, liquid crystal and isotropic liquid states characterized by I-V measurements

11 p1807 A71-25564

Josephson junction I-V characteristics self resonant current peaks calculation by finite difference scheme simulation, comparing results with perturbation technique and experiment

11 p1742 A71-25800

Thermionic collector work function measurements, considering error sources and I-V characteristics

11 p1711 A71-25881

Thermionic converter nonsaturation effect in diode I-V characteristics from computerized analysis for plasma transport phenomena and sheath-electrode-plasma interactions

11 p1713 A71-25892

MOS transistors on P substrates, investigating ionizing radiation effects on I-V characteristics

12 p1885 A71-26830

Black SiC varistors IV characteristics and conductivity, investigating fast neutron irradiation and isochronal annealing effects

12 p1886 A71-26898

Multilayered semiconductor structures with p-n junctions, discussing I-V characteristics, noninjection component effects, carrier transport and negative resistance

13 p2111 A71-28920

Electron-hole scattering effect on carrier heating and I-V characteristics in semiconductors, using relaxation time and self consistent analysis

13 p2111 A71-28921

I-V and capacitance characteristics of chalcogenide-glass based matrix-film diode sandwich and film-face switching structures with/without memory

13 p2112 A71-28922

Nonuniform trap distribution effect on I-V characteristics of dielectric diodes, allowing for field ionization

13 p2040 A71-28927

Physical process causing negative differential resistance segment on I-V curve of single junction transistor, describing thyristor-triggered relaxation oscillator

14 p2214 A71-30633

Plasma state and IV characteristics of thermionic converter, discussing cathode emitting area increases and patchiness effects

14 p2182 A71-30680

Spherical free-molecular electrostatic probe surrounded by finite sheath, calculating I-V characteristic saturation current regimes

15 p2409 A71-32100

Electric arc burning in contracted Ar plasma between two plates, calculating normal current density and I-V characteristic

15 p2457 A71-32271

Plasma boundary layer temperature distribution near conducting surfaces from I-V characteristics of gas gap

16 p2618 A71-33028

Computer algorithm for diode detector static and dynamic I-V characteristics calculation by trial and error process with piecewise linear approximation

16 p2546 A71-33399

Vibration simulation of elastohysteric systems on analog computers using photocurrent-voltage relationship of polycrystalline photoresistors

16 p2658 A71-33978

Cadmium doped silicon diodes I-V curve sinusoidal relaxation oscillations frequency and amplitude dependence on temperature

16 p2548 A71-34026

I-V characteristics of compensated semiconductors during nonequilibrium carrier injection from contacts

16 p2622 A71-34028

VOLT-AMPERE CHARACTERISTICS

Microwave Gunn diodes I-V characteristics as function of carrier concentration and power efficiency

17 p2713 A71-34264

Pulsed MHD generator model with nonequilibrium plasma, obtaining I-V characteristics

17 p2677 A71-35273

Continuous flush electrostatic probe for weakly ionized flowing gas surface density gradient and charged particle free stream density determination, obtaining I-V characteristics

18 p2950 A71-35858

Si p-n junctions microplasmas I-V characteristics, discussing avalanche breakdown, temperature dependence and light emission

18 p2953 A71-35872

Tunnelling conductance anomaly in metal-insulator-metal junctions containing paramagnetic impurities, analyzing I-V characteristics during switching effect

18 p2954 A71-36802

Overcritically doped Gunn diode I-V characteristics stability under constant voltage, discussing use as subnanosecond switching element

18 p2895 A71-36989

Thin film Au-CdS-Al type metal-semiconductor barriers, determining barrier height from temperature dependence measurements of I-V characteristics

19 p3118 A71-37488

MOS field effect transistors operation and DC characteristics including threshold voltage and substrate doping effects

19 p3027 A71-37562

Superconducting microjunctions I-V characteristic at critical temperature, investigating voltage fluctuations effects in external circuit

19 p3119 A71-37860

Plasma radiation effects in gas tube electric arc heating, obtaining temperature and heat flux profiles and I-V characteristics from energy transport mathematical model

19 p3164 A71-37989

Noise, admittance and I-V characteristics of hot holes in space charge limited Ge diodes at high voltage and frequencies to 22 MHz

19 p3029 A71-38141

Theoretical model of excess surface current in p-n junctions, based on surface-controlled tetrode transistor experiment for bipolar transistors I-V characteristics explanation

19 p3029 A71-38142

Low pressure Cs vapor thermionic converter with lanthanum boride cathode, investigating arc conditions and I-V characteristics

19 p2999 A71-38254

Electron removal from neutralizing emitter in cylindrical ion beam, determining I-V characteristics of plane diode with positive charge distribution

20 p3272 A71-39152

High power continuous electron-optical beam formation in electron gun, determining cathode and leakage current and I-V characteristics as function of pressure

20 p3204 A71-39158

Fabrication and I-V characteristics of S-type negative resistance alloyed diodes prepared from sulfur-doped n-type Si, outlining temperature dependence of turnoff time

21 p3358 A71-41203

N-type negative resistance, photoconductivity and I-V characteristics of sulfur-doped p-type Si, showing hole capture cross section dependence on electric field

21 p3429 A71-41204

Negative differential conductance of anthracene single crystals in electrolytes, observing N-shaped I-V characteristics

21 p3430 A71-41221

Ge and Si point contact semiconductor diodes anisotropic deformation, investigating pressure effects on current and negative resistance in forward branch of I-V characteristics

21 p3430 A71-41222

Current-voltage characteristics of n-i GaAs epitaxial structures at various temperatures, indicating use in memory devices and high power switches

21 p3430 A71-41223

Oscillations in He, Ne and Ar glow discharges, obtaining I-V characteristics

21 p3426 A71-41290

Self magnetic field effect on I-V characteristics of Cs-Ba thermionic converter, noting effects of pressure differential due to ponderomotive forces action

21 p3326 A71-41294

Multilayered semiconductor structure with p-n junctions, discussing I-V characteristics, noninjection current component effects, carrier transport and negative resistance

21 p3433 A71-41306

Electron-hole scattering effect on carrier heating and I-V characteristics in semiconductors, using relaxation time and self consistent analysis

21 p3433 A71-41308

I-V and capacitance characteristics of chalcogenide-glass based matrix-film diode sandwich and film-face switching structures with/ without memory

21 p3433 A71-41317

Nonuniform trap distribution effect on I-V characteristics of dielectric diodes, allowing for field ionization 21 p3358 A71-41325

Copper gallium diselenide point contact diodes I-V characteristics temperature and illumination dependence, considering high temperature and photoelectric devices applications 21 p3434 A71-41327

Acoustic wave detection in K-seeded methane-oxygen flame plasma, using I-V characteristic modulation of fixed electrostatic probe 22 p3580 A71-41622

Current-voltage hysteresis and memory properties of silicon-silicon nitride capacitors as function of oxide layer and stacking fault traps 22 p3586 A71-41684

Neutron irradiation effects on Si p-n junction field effect transistors I-V characteristics, charge distribution in space charge region and transconductance 22 p3586 A71-41684

Early effect incorporation in Ebers-Moll simulation model for junction transistor large signal behavior to obtain current gain and conductance dependence on voltage 22 p3523 A71-42484

I-V characteristics of weakly ionized cold plasma plane layer with electron-atom collisions 22 p3584 A71-42875

Multilayer epitaxial InP transferred electron microwave oscillator I-V characteristics and frequency dependence on layer thickness 23 p3649 A71-42912

Microwave planar Gunn oscillators performance in X band, giving pulsed and CW I-V characteristics 23 p3649 A71-42913

Thermal feedback modification of Si JFETs AC and DC characteristics at low operating temperatures 23 p3649 A71-43070

I-V characteristics of plasma varactor formed near central or external conductor surface during coaxial line filling with plasma 23 p3651 A71-43403

Computer acquired I-V characteristics of thermionic fixed spaced planar diodes 23 p3630 A71-43596

Silicon Schottky tunnel MOS diodes, discussing effect of thin interfacial film between metal and semiconductor on I-V characteristics 23 p3652 A71-43936

Tunnel MOS diode oxide thickness and thermal equilibrium considerations, analyzing reverse bias case AC conductance, capacitance and DC I-V characteristics 23 p3652 A71-43937

I-V characteristics and temperature responses of negative S and N-type resistances in niobium-niobium oxide-indium structures, considering use as active elements in membrane circuits 24 p3859 A71-44380

Nondiffusion theory for I-V characteristics of monolayer and quasi-monolayer photosensitive semiconductors with various carrier injection levels 24 p3859 A71-44385

VOLTAGE

U ELECTRICAL POTENTIAL

VOLTAGE AMPLIFIERS

Transistorized four-quadrant control signals voltage multiplier, analyzing operation and circuit diagrams 06 p0879 A71-17493

Scatter effects of transistor parameters on maximum undistorted output-voltage amplitude of single stage amplifier 07 p1080 A71-20263

Programmable solid state pulse generator for charge-sensitive amplifier excitation at high pulse repetition rates, discussing circuit elements and applications 08 p1267 A71-21850

VOLTAGE BREAKDOWN

U ELECTRICAL FAULTS

VOLTAGE GENERATORS

NT PHOTOVOLTAIC CELLS

Satellite static inverter for voltage wave form synthesis by time optimal response closed loop technique, providing input insensitive AC output 02 p0190 A71-11675

Pulse rise, fall times and peak current values in sawtooth-voltage generator relaxation circuits with avalanche transistors 03 p0387 A71-13998

Pulsed semiconductor devices with S-shaped current-voltage curve, considering relaxation oscillator and voltage generator circuits 04 p0558 A71-15565

Quadratic sawtooth voltage and sweep frequency generators circuit based on periodic parabolic pulse phase modulation of quartz oscillators HF output 04 p0559 A71-15568

AC signal amplitude measurements, describing circuit design with DC voltage generation proportional to input AC voltage 06 p0899 A71-17926

Linear sawtooth voltage phantatron type generator, presenting operation time diagrams and circuit advantages 12 p1906 A71-26900

Radioactive decay energy conversion of beta particle emitting cerium 144 into high voltage electricity in coaxial cylinder cell 15 p2447 A71-32211

Step voltage generator design based on periodic release of prespecified charge fractions by storage condenser using dosing capacitor 18 p2893 A71-36624

Multijunction functional devices for operation as decade digital counter, step voltage generator, analog/digital converter, binary counter, neuristor line, etc 22 p3520 A71-41706

VOLTAGE MEASUREMENT

U ELECTRICAL MEASUREMENT

VOLTAGE REGULATORS

Electrochemical cell interelectrode planar spacing regulator system, discussing electrode constant vibration amplitude to current ratio 08 p1296 A71-20855

Automatic control circuits for millimeter wave backward wave tube frequency tuning and supply voltage regulation 08 p1267 A71-21804

Symphonic communication satellite power supply system voltage control, discussing controlled system properties based on closed circuit frequency characteristics 10 p1683 A71-24642

Voltage regulating diodes, discussing development and principal characteristics of Epi-Z family of Zener diodes 13 p2037 A71-28575

Soviet book on airplane and helicopter electrical power supply systems covering storage batteries, DC generators, alternators, voltage regulators, current and frequency control, etc 14 p2180 A71-29525

Pulse width modulated output voltage analysis in autonomous inverters, using Fourier series and digital computer 15 p2353 A71-32078

Optimum L shaped quadrupole filter for controlled valve voltage inverters 15 p2353 A71-32079

Unijunction transistor peak point voltage stabilization, giving formula for interbase resistance multiplier variation with temperature 15 p2378 A71-32636

Solid state voltage regulator with hybrid tunnel-diode/transistor circuit discriminator for overload protection, discussing operation, circuit diagram and performance 17 p2716 A71-34786

Spurious effects on stabilizing circuits with loaded Zener diodes for reference voltage source 18 p2893 A71-36800

Microelectronics high power hybrid circuit design, discussing application of packaging techniques to 10 Amp series regulator 21 p3353 A71-40440

Background LF noise of semiconducting diode voltage regulators with breakdown due to avalanche effect 22 p3523 A71-42472

Current controlled diodes used as voltage variable capacitors in oscillators 23 p3652 A71-43832

VOLTAGE VARIATION INDICATORS

U VOLTMETERS

VOLTERRA EQUATIONS

Almost periodic solutions of two nonlinear Volterra integral equations 07 p1147 A71-19256

Contact heat conduction boundary value problems, applying parabolic potentials method to Volterra singular integral equation systems 09 p1545 A71-22876

Unsteady solution of simplified atmospheric dynamics equations, reducing to system of Volterra integral equations of second kind for complex horizontal wind velocity 12 p1924 A71-26734

Optimal control problems solution using linear vector space of continuous operators with constraints in Volterra integral and functional differential equations 13 p2043 A71-28829

General adjoint relation between linear functional differential equations and Volterra integral equations 13 p2096 A71-29381

Differentiability of nonlinear Volterra integral equations of second kind with convolutional weakly singular kernels 15 p2442 A71-31870

Asymptotic solution of nonlinear Volterra integral equation, examining nonlinear heat conduction and boundary layer heat transfer 18 p2942 A71-36747

Heat conduction equation coupling to wave equation in adjacent regions from operational method solution of Volterra equation reduced problem 19 p3171 A71-38532

Asymptotic behavior of nonlinear Volterra integrodifferential equation solution, noting applications to nuclear reactor dynamics 21 p3409 A71-41077

Nonlinear Volterra integral equation system solution using almost periodic forced oscillations 21 p3409 A71-41086

Boundedness theorem for Volterra equations, discussing applications 22 p3568 A71-42696

VOLTMETERS

NT MILLIVOLTMETERS

Radio signals fine structure examination by instantaneous pulsed voltage measurements, describing fast response digital voltmeter circuit with memory element 15 p2409 A71-32181

VOLUME

NT BODY VOLUME (BIOLOGY)

Metallic polycrystalline materials volume changes in plastic deformation from measurements on steel elongation and cross section diameter reduction 09 p1540 A71-22997

Exponentially varying thickness thin plate volume minimization for simultaneous stress and deflection constraints under axisymmetric load, using digital computer 14 p2330 A71-30691

Myocardial inotropism index, using left ventricle time varying pressure/volume ratio in systole 17 p2683 A71-35121

Cell volume analyzer for sensing individual blood cells and plotting number as function of size 20 p3191 A71-38824

Extragalactic radio sources counts for proportional space volume determination, comparing various cosmological models 22 p3596 A71-41445

VOLUMETRIC ANALYSIS

Liquid silicate systems density calculation from partial molar volumes of oxide components 05 p0716 A71-16407

Volume spectra during heat treatment in metallic systems, using automatic dilatometry 07 p1112 A71-19613

Volume variations detection by Hartmann air jet fluidic oscillator 07 p1030 A71-20602

Volume, compliance and flow resistance of pulmonary vascular compartments of dogs 10 p1560 A71-24122

Fluorometric microvolumetric test for unconjugated 11-hydroxycorticosteroids distribution in plasma, noting concentrations in capillary and venous blood 11 p1718 A71-25627

Radiation heat transfer volume interchange factors approximation for gases with nonuniform temperature, composition or pressure, comparing with exact numerical computations 19 p3164 A71-37990

Physiological responses of burro Equus asinus to oxygen lack in mountain altitudes, studying red blood cell and plasma volumes 19 p3005 A71-38560

Epoxy-alumina trihydrate composite system fracture energy data, noting interdependence of surface topography, phase dispersion volume fraction, particle size and spacing 23 p3696 A71-43102

VOLUMETRIC STRAIN

Ground effect vehicles limiting volumetric dissipations from air cushion and propulsion systems with fluid boundary by Coanda effect 07 p1019 A71-19923

Transverse strains in solid body due to volumetric stresses counteraction to external load stresses 10 p1687 A71-24198

Compression strength theory for monodirectional reinforced homogeneous anisotropic and piecewise homogeneous materials, using microvolume stability loss failure mechanism 12 p1922 A71-27684

VON KARMAN EQUATION

Kolmogoroff and von Karman constants relationship, using atmospheric model 03 p0452 A71-13227

Free flexural vibrations of orthotropic rectangular plates subjected to large amplitude free or forced oscillations, using von Karman nonlinear equations 08 p1370 A71-21307

Von Karman equations analogs solution for nonlinear large amplitude vibrations of circular plate on uniform elastic foundation 21 p3457 A71-40271

VON MISES THEORY

U STRESS FUNCTIONS

VON ZEIPPEL METHOD

Generalized von Zeipel treatment of lunar and artificial satellite theories, generating single canonical transformation by variable separation technique 04 p0654 A71-15719

Von Zeipel procedure convergence for proving theorem pertaining to conditionally periodic motion equations with small change in Hamiltonian 04 p0661 A71-15892

Canonical perturbation theory formulation applied to Poincare-von Zeipel method

10 p1679 A71-24935

General relativistic von Zeipel theorem providing necessary and sufficient condition for equidensity surfaces coincidence in stationary star axisymmetric rotating mass fluid

11 p1833 A71-26327

Analytic theories in celestial mechanics, checking by exact differential equations form based on Von Zeipel method

13 p2135 A71-28353

Classical Poincare-von Zeipel canonical perturbation theory extension to adiabatically perturbed systems with slow dependence on time or dynamic variables

24 p3848 A71-44790

VOR SYSTEMS

U VHF OMNIRANGE NAVIGATION

VORTEX BREAKDOWN

Rotating inviscid incompressible fluids in tubes, investigating axisymmetric nonlinear waves motion in relation to vortex breakdown

01 p0072 A71-11224

Vortex breakdown in swirling conical flows, determining swirl angle distribution, flow rates and Reynolds number effects

[AIAA PAPER 71-52]

06 p0843 A71-18513

Vortex breakdown on slender sharp edged and modified delta wings with varying sweep angles investigated in wind tunnel using schlieren system for flow visualization

[AIAA PAPER 69-778]

08 p1229 A71-22028

Turbulent flows in diverging cylindrical tube, observing stationary and traveling vortex breakdowns

10 p1592 A71-23952

Heat transfer to airfoil in oscillating flow at large angles of attack, showing vortex shed reattachment and Nusselt numbers increase

[ASME PAPER 71-GT-18]

11 p1703 A71-25963

Flow visualization and hot-wire measurements, showing vortex shedding association with turbulent air jet issuing from flat plate into cross wind

17 p2670 A71-34659

Karman vortex street breakdown under deceleration, noting vortices distortion and annihilation followed by vortex street formation of different frequency

19 p3046 A71-38202

Vortices motion and decay, constructing asymptotic solution to Navier-Stokes equations

21 p3366 A71-40485

Vortex wakes transport and decay for various aircraft types, flight modes and meteorological conditions

21 p3320 A71-40499

Windward injection into supersonic stream at angle of attack, minimizing vortex disruption

22 p3481 A71-42787

VORTEX COLUMNS

U VORTICES

VORTEX DISTURBANCES

U VORTICES

VORTEX FLOW

U VORTICES

VORTEX GENERATION

U VORTEX GENERATORS

VORTEX GENERATORS

Anticyclonic eddy formation and emergence within severe thunderstorm observed by radar and surface data, noting wave development along pseudocold front

01 p0118 A71-10588

Magnetic field effect on boundary temperature in axisymmetric MHD flow in vortex chamber, using dissipationless approximation

02 p0293 A71-12633

Vorticity generation or suppression using scale analysis with vorticity equation, considering wind shear in jet stream

02 p0241 A71-12744

Discrete vortex formation above perforated flat plate in wind tunnel, examining unsteady boundary layer

03 p0345 A71-14568

Plasma ring vortex formation in atmospheric crossed electric discharges, analyzing photographs of vortex onset and development

04 p0631 A71-14600

Photographic study of early vortex formation in flow started by shock diffracting over edge

04 p0586 A71-14702

Trailing vortex generation behind jet flapped wing at high wing lift coefficients

04 p0527 A71-15413

Couette flow between rotating cylinders and Taylor vortex formation by Liapunov-Schmidt method and spectrum perturbation theory, discussing secondary flow determination accuracy

04 p0575 A71-15603

Twin vortex development in unsteady separated flow past thin flat plate, using flow visualization

09 p1432 A71-22582

Two dimensional vortex filament development artificially shed in laminar boundary layer on flat plate without pressure gradient, using hydrogen bubble visualization technique

13 p2051 A71-29428

Pressure fluctuations in acoustic field of boundary layer under slot suction, considering vortex formation and separation on edges

15 p2389 A71-31713

Thrust and flow rate control in choked convergent nozzles by potential vortex generation, verifying swirling nozzle flow analytical model

15 p2391 A71-32061

Consecutive toroidally circulating buoyant elements interactions by numerical simulation, including vortex formation process effects

18 p2901 A71-35954

VORTEX INJECTORS

Cooling effectiveness of liquid film barrier injected into rocket thrust chamber with vortex motion, considering heat transfer and performance

[AIAA PAPER 71-676]

14 p2291 A71-30740

Windward injection into supersonic stream at angle of attack, minimizing vortex disruption

22 p3481 A71-42787

VORTEX RINGS

Vortex layer near circular cone surface in supersonic axisymmetric steady flow of homogeneous inviscid gas

10 p1551 A71-24372

Small cross section viscous vortex ring velocity in ideal fluid with arbitrary vorticity distribution in core

11 p1749 A71-25357

Turbulent vortex rings motion empirical model, deriving equations valid at large distances from discharging orifice

11 p1751 A71-25498

Viscous vortex rings of small cross section, considering velocity in ideal fluid with arbitrary vorticity in core and arbitrary circumferential velocity

21 p3366 A71-40484

Effective momentum ratio for Lamb circular cylinder double vortex, Hill spherical vortex, Thomson straight line paired vortices and Helmholtz circular ring vortex

21 p3321 A71-40541

VORTEX SHEETS

Vortex wakes behind STOL operations high lift wings, discussing height above ground and various wind tunnel dimensions effects

13 p1990 A71-28033

Stagnation pressure changes in unsteady flow downstream of turbomachine blades with fluctuating circulation related to vortex sheets

17 p2671 A71-35279

Numerical calculation of trailing vortex sheet pattern behind unstalled swept wing at low speed, obtaining downwash field

20 p3176 A71-39397

Straight or moderately sweptback wings tip shape effect on vortex sheet roll, using detachment laws

20 p3176 A71-39418

Turbulent motions in fluids of small viscosity as inviscid flows with vortex sheets and rolled-up cores

21 p3317 A71-40010

Two dimensional jet flapped symmetric wing in subsonic flow, assuming irrotational flow inside jet bounded by vortex sheets

21 p3318 A71-40172

Subscale modeling of aircraft trailing vortices in controllable laboratory environment

21 p3318 A71-40488

Aircraft wing tip vortex air motion measurements, utilizing Doppler radar techniques

21 p3318 A71-40489

Drooped wing tip effects on trailing vortex sheet structure and position from spanwise load distribution determination by vortex lattice theory

21 p3319 A71-40493

Trailing vortices behind wing tip with vortex dissipator, using wind tunnel flow visualization and flight tests

21 p3319 A71-40496

Airloads and moments changes of aircraft flying over trailing vortices, investigating time dependent aerodynamic forces

21 p3321 A71-40508

Plane vortex sheet in inviscid incompressible finitely conducting fluid under uniform magnetic field, considering hydromagnetic stability

23 p3663 A71-43490

VORTEX STREETS

NT KARMAN VORTEX STREET

Vortex streets behind circular cylinders at Reynolds numbers 50-160, discussing transition

06 p0842 A71-18322

Plane jet in counterflow with vortex shedding control, discussing solid boundary and jet momentum effects

10 p1592 A71-23980

Propeller vortex theory, calculating vortex streets pitch distributions and wake configuration

14 p2170 A71-30443

Aircraft wake turbulence /trailing vortex systems/ avoidance during flight, describing procedures for pilots and tower operators

[CASI PAPER 72/6]

19 p2992 A71-37596

Aircraft trailing vortex pair linear stability, obtaining flow field near curved vortex filament with swirl and axial velocities

21 p3320 A71-40500

Trailing vortex pair behind aircraft, presenting equilibrium characteristics and effects on safety

21 p3321 A71-40504

Aircraft wake turbulence relation to CAT, discussing flight control loss, jumbo jets trailing vortex wakes breakup and detection and safe aircraft spacing

21 p3325 A71-40704

Aircraft generated vortex wakes and core air motions hazards for encountering light airplane

23 p3628 A71-43381

Acoustic resonance excitation by vortex shedding from flat plate trailing edge in low speed wind tunnel

24 p3848 A71-44557

VORTEX TUBES

U VORTICES

VORTICES

Real vortices velocity, density and temperature distribution determination, discussing flow measurements by hot-wire anemometer, multiple spark camera interferography and smoke visualization techniques

01 p0069 A71-10107

Mountain-size atmospheric eddies on leeward slope of Carpathian and Low Tatra mountains, discussing turbulence effects on air navigation

01 p0113 A71-10349

Atmospheric boundary layer nonlinear equations of motion numerical integration for eddies structure and wind direction and latitude effects on turbulence intensities

01 p0113 A71-10351

Sweptback turboblasts in parallel wall channel, investigating thickness, camber and leading edge curvature effects on flow and pressure distributions and vortex movement

02 p0186 A71-12606

Blade bound vortex system mathematical model for optimum heavily loaded ducted fans, including thrust, power and efficiency design parameters

02 p0299 A71-12677

Unsteady flow induced by circular cylinder impulsive motions, examining vortices formation and interaction

03 p0399 A71-13197

Stability theory for pair of trailing vortices, investigating induced field convection, modes, amplification, cut-off distance, etc

[AIAA PAPER 70-53]

03 p0341 A71-13436

Vortex sheet behavior in inviscid subsonic flow of lifting wing with nonzero trailing edge angle

03 p0342 A71-13738

Two dimensional jets forced and induced switching by vortex flow

[ASME PAPER 70-WA/FLCS-13]

03 p0354 A71-14088

Nonvented vortex fluid amplifier receiver tubes flow and performance characteristics

[ASME PAPER 70-WA/FLCS-18]

03 p0354 A71-14091

Vortex angular rate sensor flow characteristics, solving Navier-Stokes equations by numerical technique

[ASME PAPER 70-WA/FE-5]

03 p0402 A71-14127

Turbulent jet diffusion and vortex models, noting velocity profile in mixing and turbulent boundary layers

04 p0577 A71-15625

Setting spherical particle into rotation in fluid characterized by uniform rotational motion far from particle

05 p0735 A71-16159

Asymptotic formulas for vortex and velocity field far from body in plane viscous incompressible fluid flow

05 p0737 A71-16990

Steady diabatic inviscid gas flow properties, emphasizing vortex lines geometry

05 p0839 A71-17047

Lateral vibration effects on heaving airfoil blunt trailing edge vortex shedding flows, examining base cavity damping by flow visualization

06 p0984 A71-17621

Gas turbine aircraft engine compressor blades foreign object ingestion control by inlet vortex flow suppression jets, indicating wind tunnel air intake applications

06 p0945 A71-17696

Laminar flow convective heat and mass transfer on end walls of vortex chambers

06 p1005 A71-17737

Slender bodies of revolution with cylindrical aerobodies in subsonic wind tunnel, examining vortex systems and aerodynamic forces

06 p0842 A71-18048

MHD system hydrodynamic stability using propellant and fuel filled reactor cavity to form three region two fluid vortex

06 p0882 A71-18318

Finned missiles aerodynamics at high angle of attack, examining body vortex wake region interaction with fins

[AIAA PAPER 71-50] 06 p0980 A71-18511

Wing-canard configurations nonlinear vortex interactions, using Sacks method of vortex sheet simulation with discrete vortices distribution

[AIAA PAPER 71-95] 06 p0844 A71-18550

FAA full scale aircraft vortex wake turbulence flight test programs

[AIAA PAPER 71-97] 06 p0848 A71-18552

Slender cone hypersonic laminar three dimensional boundary layer separation at angle of attack, proposing helical vortex model

[AIAA PAPER 71-129] 06 p0845 A71-18573

Supersonic jet noise problem, discussing eddy-Mach wave radiation source mechanism from nonlinear streamwise development of inviscid instability waves in turbulent mixing layer

[AIAA PAPER 71-150] 06 p0884 A71-18592

Noise-producing subsonic jet turbulence eddies hot-wire anemometer measurements of convection velocity as functions of frequency

[AIAA PAPER 71-154] 06 p0884 A71-18596

Vortex flow theory, developing computer program for various separation flows

07 p1086 A71-18776

Equilibrium positions of multiple pairs of vortices in wakes of circular and elliptic bodies

07 p1087 A71-18901

Vortex perturbations in Friedman cosmological model near zero time, showing perturbation growth associated with increasing Hubble expansion anisotropy

07 p1192 A71-19285

Fluctuating circulation, lift and flow induced structural vibrations of two dimensional bodies, including vortex shedding on sluice gates

07 p1014 A71-19592

Viscous incompressible axisymmetrical flow, examining vortices near stagnation point of infinite flat obstacle

07 p1089 A71-19737

Three dimensional axisymmetric flows in tornado-like vortex boundary layer, determining nonlinear radial and vertical velocity distribution components

07 p1152 A71-19753

Jet plume in subsonic cross flow, calculating counter-rotating vortices as function of distance along trajectory from semiempirical model

07 p1090 A71-19901

Wind tunnel experiments on vortex shedding from circular cylinders in oscillating free stream

07 p1090 A71-19908

Prandtl two dimensional time dependent similarity flows with vortex sheets

07 p1093 A71-20279

Internally ported vortex amplifier, presenting dynamic equivalent circuit with transfer functions

07 p1025 A71-20555

Aircraft fuel and air conditioning systems vortex valves and diodes, examining flow patterns into and out of chambers

07 p1025 A71-20556

Plasma ring vortices in crossed electrical discharges attributed to shock wave induced plasma flow across lines of force of azimuthal magnetic field

08 p1338 A71-20785

Sound generation by frontal collision of double pair vortices, showing pressure proportional to Mach number

10 p1641 A71-24346

German monograph on steady toroidal discharges and cylindrical vortex arcs, using electromagnetic gas dynamics equations

10 p1654 A71-25025

Centrifugal particle separation limit in free vortex, stressing particle interference with vortex flow and viscous effects

11 p1750 A71-25467

Dust devil vortex model, considering boundary layer velocity profiles and thickness and integrated radial and vertical mass flows

11 p1794 A71-25470

Loads induced on infinite aspect ratio wing by straight infinite free vortex in subsonic compressible freestream, using planar lifting surface theory

11 p1702 A71-25474

Streamwise vortices of distinct periodicity in laminar transitional turbulent reattaching flows over wide Mach number range

11 p1751 A71-25496

Rotationally symmetric flow above infinite rotating disk by nonexistence proof and uniqueness theorem

12 p1896 A71-26924

Vortex shedding characteristics of circular cylinders at low Reynolds numbers from experiment on tapered models wake structure

12 p1897 A71-27220

Marginal vortex effects on aerodynamics of helicopter lifting surfaces, considering blade form and noise spectrum tested in hydrodynamic tunnel

12 p1864 A71-27473

Three dimensional incompressible flow about slender foil in perfect fluid, stressing vortex field effect

12 p1865 A71-27477

Flow field model for steady asymmetric vortex system shed from slender body of revolution in coning motion

[AIAA PAPER 70-52] 12 p1865 A71-27552

Quasi-axisymmetric and superposed fine fluctuating structure of ideal incompressible vortex flows in axial flow turbines, assuming infinite mutual blade proximity

[ONERA-TP-945] 12 p1866 A71-27714

Trailing vortices shed by aircraft lifting surfaces, noting wake effects importance at low speeds

13 p1995 A71-28176

Monograph on free and confined vortex gas burner flow characteristics covering pressure distribution, velocity, power law, mass flow in boundary layers, etc

13 p2047 A71-28496

Gas flow in nozzle, stages and gas dynamic systems, discussing motion in cross sectional plane

13 p'990 A71-28588

Flow theory of steady separation zone near body at high Reynolds numbers, determining vortex parameters counterflow inviscid region

13 p2049 A71-29171

Structure and shape of vortex wake associated with oblique flow past multiblade hinged rotor, using cavitation method

13 p1993 A71-29217

Air flow past small aspect ratio thick-section wing at small angles of attack, investigating vortex system effect on flow characteristics in absence of lift

13 p1994 A71-29234

Helicopter rotor vortex system and induced velocity field for various angles of attack, flight conditions and unit loads, using smoke visualization technique

13 p1994 A71-29235

Vortex induced shear and secondary flow through row of spheres, curved channel, turbine blades, rotating impeller, suction pipe and upstream boundary layers

14 p2224 A71-30176

Two component solid gas vortex flows with end wall injection eliminating boundary layer losses for colloid core nuclear rocket engine concept

[AIAA PAPER 71-637] 14 p2273 A71-30715

Laminar boundary layer of free vortex and source flow, obtaining similarity transform of Navier-Stokes equation

14 p2228 A71-31027

Flow field velocity distribution at rotating wing devices tip vortices

[AHS PREPRINT 522] 14 p2172 A71-31088

Equation for motion of buoyant free vortices in inviscid fluid subjected to gravity

[AIAA PAPER 71-604] 15 p2388 A71-31543

Shearing flows in steady vortex around airfoil in perturbed velocity, considering aerodynamic forces torque

15 p2346 A71-31903

Operating characteristics of high performance vortex amplifiers, discussing turn-down ratios, noise reduction, linearity and stability

15 p2352 A71-32062

Vortex type pneumatic angular rate sensor with vanes and hydrodynamic viscous coupling, determining differential pressure outputs

15 p2352 A71-32063

Constant speed vortex rate sensor, calculating angular momentum dissipation due to shear stresses and response to step signal input

15 p2352 A71-32064

Lee side air flow from cone-cylinder model, determining vortex core regions from subsonic wind tunnel smoke visualization techniques

15 p2346 A71-32117

Potential vortex with turbulent viscous core and axial velocity excess or deficiency, using integral method with quasi-cylindrical flow approximations to describe core flow

[AIAA PAPER 71-615] 15 p2393 A71-32278

Intermittence and scale similarity in turbulent flow structure, analyzing eddies distribution inhomogeneity

16 p2557 A71-32932

Aerodynamic free vortex loading on two dimensional wing at zero incidence at low speeds in incompressible flow

16 p2521 A71-33420

Aerodynamic characteristics of arbitrary planform wing moving near screen, ground or water surface, using vortex model

16 p2521 A71-33596

Perfect incompressible fluid steady rotational linearized three dimensional flows, calculating complex waves system

16 p2560 A71-34056

Stream function and velocity of shear flow vortex in infinitely thin profile from linearized Euler equations for boundary value problem

16 p2561 A71-34161

Two vortex model for downwash variations in supersonic flow past thin delta wing with separation at leading edges

17 p2669 A71-34190

Viscous trailing vortices decay downstream of non-free axial flow fan, assuming steady axisymmetric incompressible laminar flow

17 p2725 A71-34191

Vortex boundary layer with dissipative viscous wall and isentropic sublayers, calculating adiabatic surface temperature

17 p2669 A71-34217

Jet induced secondary flow interaction with circular plate, showing ring vortex effects on pressure distribution

17 p2669 A71-34334

Tornado and waterspouts, using concentrated vortices produced in laboratory rotating tanks and mathematical models

17 p2726 A71-34657

Steady incompressible flow with potential vortex over flat surface under suction

17 p2670 A71-34889

Flow field induced by aircraft trailing vortices near ground during takeoff and landing, noting experimental departure from theory

17 p2671 A71-34900

Magnetic annular arc continuous operation at atmospheric pressure, determining arc velocity and rotational frequency as functions of magnetic flux density and arc current

17 p2788 A71-34901

Aircraft vortex wake turbulence including formation, disintegration, hazards reduction, instability and interactions with following vehicles

17 p2673 A71-35753

Jumbo jet trailing vortex mathematical model for studying effect on penetrating aircraft

17 p2673 A71-35754

Large jet transport aircraft trailing vortices, studying velocity fields, core diameters and logarithmic variations of circulation

17 p2674 A71-35755

Vortex laser Doppler velocimeter system for aircraft wake turbulence velocity profile mapping, describing optical arrangements, back and forward scattering modes and prototype design

17 p2754 A71-35756

Trailing wake hazards of large transports in takeoff and landing, examining configuration stability of vortex pair in ground effect

17 p2674 A71-35757

Two dimensional laminar incompressible fluid flow past flat plate at various angles of attack, studying vortex shedding characteristics

18 p2844 A71-36311

Laminar boundary layer structure under semi-infinite potential vortex maintained in incompressible steady flow by appropriate conditions at infinity

18 p2906 A71-36317

Rotationally symmetric quasi-cylindrical viscous incompressible vortex flows at high swirl, discussing numerical integration with exponential functions

18 p2908 A71-36342

Asymptotic formulas for vortex and velocity field far from body in plane viscous incompressible fluid flow

18 p2909 A71-36790

Helicopter rotor noise due to blade-vortex interaction, using linear gust model

18 p2849 A71-36934

Turbulent rotating tube flows kinematic similarities, deriving heat and mass transfer, swirl damping and axial and rotational velocity profile

19 p3043 A71-37127

Air injection into trailing vortex core, noting jet flow effect on circumferential velocity

19 p2991 A71-37291

Critique of paper on spanwise distribution of induced drag in subsonic flow by vortex lattice method, noting infinities in downwash across all vortex lines

19 p2991 A71-37297

Relativistic hydrodynamic solution for gravitational interaction of vortex and potential motion of homogeneous medium

19 p3134 A71-37515

High speed neutral buoyancy bubble generators for aerodynamic flow visualization, investigating tip vortex from wing or helicopter rotor blade

19 p3064 A71-37725

Vortex-induced heating alleviation to lee side of slender wings in hypersonic flow by contouring leading edge planform

19 p2993 A71-37892

Hypersonic lee surface vortex heating alleviation on delta wing by apex alignment with free stream

19 p2993 A71-37895

Longitudinal vortex rolls onset for laminar forced convection between two horizontal flat plates subjected to uniform axial wall temperature gradient

19 p3163 A71-37979

- Wing tip vortex control device, discussing design, operation and effectiveness 20 p3175 A71-39084
- Simultaneous radar and instrumented aircraft observations in clear air turbulent layer for eddy dissipation rates calculation 20 p3256 A71-39207
- Perturbed problem of rotational steady compressible flow in three dimensional channel at upstream infinity (shear flow), using linearization by current functions 20 p3211 A71-39419
- Unstable thermal stratification and critical Reynolds number effects on dynamic instability of Ekman boundary layer vortex rolls 20 p3257 A71-39438
- Vortex flow through axial, axially radial and other three dimensional axisymmetric channels, using finite difference model for flow equations solution 20 p3211 A71-39465
- Laminar and turbulent incompressible viscous flow with spiral vortices between two parallel rotating disks 20 p3213 A71-39778
- Gortler-Taylor vortices visualization in liquids between rotating concentric cylinders using pulverized aluminum 20 p3213 A71-39781
- Turbulent energy variations in unsteadily moving flow with structural shift, emphasizing formation of vortices with various inertia scales 20 p3214 A71-39796
- Turbulent motions in fluids of small viscosity as inviscid flows with vortex sheets and rolled-up cores 21 p3317 A71-40010
- Surface patterns of ablating bodies from water jet flow experiment simulation, discussing vortices detection 21 p3317 A71-40019
- Vortex flow over helicopter rotor square tips, using visualization technique with ammonia vapor boundary layer flow over diazonium salt solution 21 p3318 A71-40169
- Vortices motion and decay, constructing asymptotic solution to Navier-Stokes equations 21 p3366 A71-40485
- Atmospheric stratification effects on downward motion of aircraft vortex wakes, developing approximate model 21 p3318 A71-40486
- Peak velocity vectors in transverse plane of jet transport aircraft wake, measuring jet vortices core size 21 p3319 A71-40491
- Free vortices from slender wings, controlling strength, position, core stability and thickness on basis of one dimensional flow model 21 p3319 A71-40492
- Vortex wakes behind straight and swept wings, noting formation of loops and trails close to ground 21 p3319 A71-40494
- Vortex wake development and aircraft dynamics, using computer graphics and flow visualization techniques 21 p3319 A71-40497
- Boeing 747, Lockheed C-5A and other aircraft vortex wake characteristics by tower flyby technique 21 p3320 A71-40498
- Vortex wakes transport and decay for various aircraft types, flight modes and meteorological conditions 21 p3320 A71-40499
- Straight line vortices in uniform two dimensional straining field, detailing irrotational strain and simple shear 21 p3320 A71-40501
- Self induction function and stability for vortex with finite core at aircraft wing, confirming Crow theory 21 p3320 A71-40502
- Turbulent shear effect on isolated trailing single vortex decay behind aircraft 21 p3320 A71-40503
- Flow visualization of aircraft trailing vortex wakes in towing tank with electrochemically activated dye, noting flow instability 21 p3321 A71-40505
- Fog formation and dispersal by velocity field induced by helicopter trailing vortices, presenting dynamic model with droplet depletion, evaporation and condensation 21 p3321 A71-40510
- Effective momentum ratio for Lamb circular cylinder double vortex, Hill spherical vortex, Thomson straight line paired vortices and Helmholtz circular ring vortex 21 p3321 A71-40541
- Propeller vortex noise analysis by on-line 1/3 octave band resolution, discussing characteristic results from noise measurements on various propeller configurations 21 p3325 A71-40868
- Rotationally symmetric quasi-cylindrical viscous incompressible vortex flow, using method of weighted residuals approximating axial velocity and circulation profiles by series of exponentials 21 p3369 A71-40951
- Fluctuating lift and drag forces on accelerating free falling sphere, discussing relation to asymmetrical wake vortex shedding 21 p3324 A71-40970
- Energy method application to inhomogeneous turbulent flow with large eddies as recurrent velocity field structures, considering longitudinal rolls in boundary layer wall region 21 p3370 A71-40985
- Numerical computation of potential vortex induced laminar boundary layer on circular disks, using two layer asymptotic expansion 22 p3530 A71-41886
- Approximate nonlinear theory of steady incompressible fluid flow about cylindrical bodies from vortex method for thin lifting surfaces 22 p3481 A71-42867
- Aircraft wake turbulence and trailing vortices, investigating physical characteristics, hazard potential and avoidance techniques 23 p3628 A71-43234
- Vortice generation in laminar boundary layer of water flow under hydraulic pressure reduction, proposing mathematical model 23 p3662 A71-43315
- Heat transfer measurements in differentially heated fluid annulus for nonrotating and rotating flow 23 p3781 A71-43335
- Gas dynamics nonstationary linearized equation solutions based on nonstationary source- and vortex-like singularities 23 p3663 A71-43491
- Isentropic ideal compressible vortical gas flow in axisymmetric channel, determining stream function and gas density 23 p3625 A71-43549
- Navier-Stokes equations solutions for incompressible laminar viscous fluid flow produced by vortex filament placed on cone axis 23 p3664 A71-44004
- Taylor vortex flow stability between rotating concentric cylinders, using fifth order amplitude expansions in matrix form 24 p3817 A71-44420
- Vortex shedding from blunt trailing edge of flat plate spanning wind tunnel under oscillating flap and acoustic resonance excitations 24 p3848 A71-44558
- Two-dimensional asymptotic solutions to Navier-Stokes equations for weak vortex discontinuity flow with vanishing viscosity 24 p3820 A71-45060
- VORTICITY**
- Boundary layer theory extended to cross vorticity transport in outer flow approaching two dimensional stagnation point 03 p0398 A71-13103
- Vorticity amplification in stagnation flow by stretching, discussing effects on average boundary layer profile 03 p0398 A71-13104
- Macroscale atmospheric vorticity model, using nonlinear system hydrodynamic and addsends free motion equations 06 p0923 A71-17513
- Stationary Navier-Stokes equations solution vorticity asymptotic behavior in three and two dimensional neighborhoods of infinity 07 p1147 A71-19640
- Turbulence properties in supersonic flow, considering modes with vorticity, entropy and acoustic aspects 09 p1383 A71-23603
- Pseudo-stationary shock wave in plane MHD flow of conducting gases, deriving existence theorem for linear relations between vorticity and current density 10 p1648 A71-24281
- Helical motions with vorticity-velocity and conduction current-free force magnetic vectors parallelisms 11 p1804 A71-25177
- Impeller blade loading vorticity on stream surface of revolution for mixed flow compressor, using annular cascade theory [ASME PAPER 71-GT-17] 11 p1703 A71-25962
- Plane stationary constant-vorticity incompressible flow region surrounded by potential flow, determining two dimensional velocity distribution by numerical calculation 13 p2050 A71-29220
- Heating effects on wing tip vorticity diffusion rate in gas vortex, causing outward radial convection and increased kinematic viscosity [AIAA PAPER 71-616] 15 p2512 A71-31556
- Nonlinear stability theory, considering velocity and vorticity perturbations in circular Couette plane Poiseuille and shear layer flows 15 p2393 A71-32568
- Navier-Stokes steady nonrectilinear universal complex laminar flow, showing isochoric lamellar or plane motions of constant velocity with streamlines as concentric circles 17 p2727 A71-34695
- Numerical analysis of laminar recirculating flow between shrouded rotating disks for interaction between vorticity and stream function and swirl-velocity field 18 p2905 A71-36309
- Viscous fluid flow past circular cylinder, using trigonometric representation of vorticity based on truncated Stokes-Picard and Oseen-Picard methods 18 p2844 A71-36316
- Concentrated vorticity regions motion in turbulent flow, calculating mean displacement velocity relationship to turbulent velocity fluctuation 20 p3212 A71-39473
- Modified asymptotic perturbation expansion method application to free flow rotation effect on boundary layer for hypersonic flow about blunt body 20 p3177 A71-39483
- VORTICITY EQUATIONS**
- Vorticity generation or suppression using scale analysis with vorticity equation, considering wind shear in jet stream 02 p0241 A71-12744
- Unsteady viscous rotational stagnation point flow, solving vorticity transport equation 05 p0736 A71-16722
- Streamwise vorticity formation by wall turbulence nonuniformities, deducing secondary currents direction 05 p0736 A71-16963
- Two and three dimensional thermals and steady and starting plumes convective fluid motion formulas, using vorticity integration method 07 p1104 A71-20223
- Unsteady large particle numerical solutions to vortical equations of plane and axisymmetric inviscid gas flow past blunt body for subsonic and hypersonic velocities 13 p1989 A71-27901
- Boundary vorticity method for finite amplitude convection in plane Poiseuille flow with isothermally heated and cooled plates, using Boussinesq approximation 21 p3477 A71-40993
- Convergence proof for chordwise vorticity equation for discrete panel wing loading 22 p3481 A71-42840
- VORTICITY TRANSPORT HYPOTHESIS**
- Gortler instability of laminar boundary layer flow on concave wall with finite length effect for perturbation vortices 10 p1592 A71-23958
- VOSTOK SPACECRAFT**
- NT VOSTOK 2 SPACECRAFT
- VOSTOK 2 SPACECRAFT**
- Voshkod 2 cosmonauts physiological data, presenting heart beat, respiration rates, oculomotor activity and blood composition 22 p3495 A71-42791
- VOWELS**
- Isolated synthesized vowel fundamental tone duration, intensity and frequency imitation by human voice 02 p0205 A71-12060
- Accurate single-sideband radio receiver tuning, observing reconstitution of harmonic tones in human speech strong vowel sounds 08 p1254 A71-21318
- VOYAGEUR HELICOPTER**
- U CH-46 HELICOPTER
- VTO FIGHTER AIRCRAFT**
- U FIGHTER AIRCRAFT
- U VERTICAL TAKEOFF AIRCRAFT
- VTOL**
- U VERTICAL LANDING
- U VERTICAL TAKEOFF
- VTOL AIRCRAFT**
- U VERTICAL TAKEOFF AIRCRAFT
- VULCANIZATES**
- U VULCANIZED ELASTOMERS
- VULCANIZED ELASTOMERS**
- Low compression set and volume swell of vulcanizates of fluoroelastomer at elevated temperatures for sealing applications 10 p1632 A71-24099
- VULNERABILITY**
- Lightning hazards for helicopters, discussing components vulnerability and protective design requirements 04 p0531 A71-15412

W

W WINGS
U VARIABLE SWEEP WINGS
WAFERS

- Silane for polycrystalline films deposition on oxidized silicon wafers, noting substrate temperature effects on preferred orientation of deposits 02 p0297 A71-12958
- Radiation hardened semiconductor device technique by irradiating silicon wafers on lot to lot basis 07 p1071 A71-19065
- Semiconductor wafers examination with He-Ne IR laser scan microscope, producing oscilloscope

shadowgraph displays of IR transmission variations in wafers

11 p1763 A71-26186

Thermal oxidation and metal evaporation effects on electrical properties of silicon-silicon dioxide wafer interface in MOS structures

12 p1944 A71-27096

Excess minority carrier diffusion length measurement in thin silicon wafers, using light-spot and dark-spot methods

24 p3861 A71-45202

WAKEFULNESS

Neuron pairs discharge sequence temporal correlation in cats association cortex during natural sleep and wakefulness

01 p0011 A71-10849

Biosatellite 3 monkey sleep and wake states based on visual and computer analysis of telemetered EEG data from earth orbital flight

09 p1395 A71-23242

Natural sleep and wakefulness stages neurophysiology based on bioelectric activity spectral and correlation analyses

13 p2005 A71-28380

Heart rate variability in REM sleep, stage 4 sleep and wakeful state from ECG of normal males, calculating coefficient of temporal variability for each state

13 p2014 A71-29319

Cat thalamus ventrolateral nucleus neuronal discharges during waking and slow and fast wave sleeps

17 p2680 A71-34689

Young adult males: split-period sleep regimes dependence on intervening wakefulness time interval, periods length and onset sidereal time

21 p3330 A71-40348

WAKES

NT AIRCRAFT WAKES

NT HELICOPTER WAKES

NT HYPERSONIC WAKES

NT LAMINAR WAKES

NT PROPELLER SLIPSTREAMS

NT SLIPSTREAMS

NT SUPERSONIC WAKES

NT TURBULENT WAKES

Modified Coles compressibility transformation for wake mapping with Howarth-Dorodnitsyn scaling suppression

03 p0400 A71-13460

Supersonic jet-bounded subsonic wake interactions, determining recirculation zone boundaries

05 p0694 A71-16848

Flat plate wake displacement sources in potential flow, considering high Reynolds numbers outside boundary layer

05 p0695 A71-16960

Two dimensional wake laminar-turbulent transition, emphasizing velocity fluctuation nonlinear interaction

05 p0695 A71-16964

Far wake asymptotic structure in rarefied plasma flow past charged bodies

07 p1165 A71-18878

Equilibrium positions of multiple pairs of vortices in wakes of circular and elliptic bodies

07 p1087 A71-18901

Wakes in Ar plasma beam, discussing obstacle geometry effects and plasma drift velocity

07 p1169 A71-19805

Axissymmetric wake diffusion flame response to HF periodic velocity oscillations at combustor boundaries

08 p1375 A71-20863

Oscillating airfoil wake interaction with fixed cascade, considering two dimensional incompressible inviscid small perturbation flow theory

09 p1511 A71-22943

Orr-Sommerfeld hydrostatic stability equation derivation for nonparallel flow in wake from Goldstein velocity distribution, noting lateral direction velocity component magnitude

10 p1592 A71-24024

Two dimensional incompressible turbulent boundary layer, determining velocity distribution with Cole law of wake

11 p1752 A71-26259

Wake flow behind two dimensional perforated plates normal to air stream, measuring drag, shedding, velocity and turbulence at Reynolds number 25,000-90,000

11 p1705 A71-26449

Ionospheric plasma drift from rockets wake measurements at high latitude, discussing plasma rarefaction

12 p1899 A71-26889

Vortex shedding characteristics of circular cylinders at low Reynolds numbers from experiment on tapered models wake structure

12 p1897 A71-27220

Aerodynamic behavior of bodies in wake of two dimensional bluff bodies, discussing loads

13 p1994 A71-29265

Inert and reactive gas injection in near wake behind afterbodies in supersonic flow, considering influence on base pressure and temperature

14 p2336 A71-30213

Mechanical support system role in determination of aeroelastic stability of leeward cylinder immersed in wake using undamped flutter theory

14 p2334 A71-31021

Velocity profiles of oscillating flow in wake of blunt based body, using finite difference solutions of vorticity transport and Poisson equations

15 p2345 A71-31579

Unstable two dimensional incompressible flow and wake development, using finite difference calculations for Navier-Stokes equations

16 p2558 A71-32996

Oscillating circular cylinder wake fluctuating velocity measurement at low Reynolds numbers, using hot-wire anemometer

16 p2520 A71-33196

Constant velocity flow past semiinfinite flat plate trailing edge, emphasizing wake region structure

16 p2560 A71-34140

Flow processes around body of hypersonic velocity, studying plasma diagnostics in ionized wake

18 p2952 A71-36421

Wake formation behind circular cylinders undergoing self excited and forced transverse oscillations [ASME PAPER 71-VIBR-25]

21 p3458 A71-40282

Plasma flow around disk in single ended Q machine with magnetic field parallel to flow velocity, measuring density profile for wake structure

22 p3580 A71-41587

WALKING

Walking effects on body composition and cardiovascular function of middle aged men

06 p0862 A71-18388

Metabolic energy cost prediction equation for level or grade walking with/without loads

09 p1401 A71-23372

Lower extremities interlink angles correlation and cross correlation functions during walking for locomotor functions analysis in man

13 p2006 A71-28382

Metabolic, ventilator and cardiovascular response during free swimming and treadmill walking, relating oxygen consumption to work intensity

13 p2024 A71-29500

WALL FLOW

Pseudoshock mechanism model, explaining supersonic diffuser main flow static pressure increase and decrease alternately and wall increase monotonously

02 p0239 A71-11870

Gas and fluid flow through flat and cylindrical porous cermet walls, determining permeation energy loss and radial flow hydraulic resistance

02 p0240 A71-12277

German monograph on plane ideal gas flows calculation with allowance for unsteady gastight walls and compression shocks using difference methods

02 p0240 A71-12400

Casing /end wall/ boundary layers in multistage axial flow compressors, discussing velocity distributions

03 p0340 A71-13144

Plane Couette flow turbulence, discussing wall region shear and core homogeneity

03 p0400 A71-13546

Turbulent fluid flow through pipe, measuring circumferential velocity component close to wall by electrochemical techniques

03 p0400 A71-13733

Two dimensional wall jet and wall wake flow turbulence characteristics, considering mean and fluctuating flow properties [ASME PAPER 70-WA/APM-35]

03 p0403 A71-14161

Lateral drift of solid particles suspended in plane supersonic gas flow along wall with recess step, using successive approximation for equations

03 p0404 A71-14255

Downstream heat transfer and wall friction predictions for quasi-developed strongly heated turbulent pipe flow, using mixing length model [ASME PAPER 70-HT-8]

03 p0405 A71-14294

Turbulent compressible two dimensional boundary layer flows with heat transfer, pressure gradients and wall blowing or suction

04 p0681 A71-15482

Various free stream turbulence levels at nonconverging and converging walls, investigating foreign gas film cooling

04 p0683 A71-15501

Inviscid nonheat conducting gas flow parameters behind shock wave reflection from solid wall at obtuse angle using linear approximation from variable separation method

04 p0572 A71-15554

Semiempirical turbulence theory generalization to flows near rough surfaces, obtaining unified dependences for wall flows

04 p0575 A71-15610

Turbulent flow structure and properties near flat wall, confirming turbulent friction damping by statistical analysis

04 p0576 A71-15611

Convective mass transfer, velocity and concentration fields during nonNewtonian fluid motion in circular pipe with diffusion flow at wall

04 p0579 A71-15798

Small surface elements local skin friction sensor measurements near wall during laminar and turbulent flow, making direct shear force measurements

05 p0752 A71-16754

Streamwise vorticity formation by wall turbulence nonuniformities, deducing secondary current direction

05 p0736 A71-16964

Laminar flow convective heat and mass transfer over end walls of vortex chambers

06 p1005 A71-17734

Anomalous viscous fluid in channel with nonconducting walls, considering magnetic field effect on heat transfer

06 p0937 A71-17738

MHD oscillating flow along infinite unmagnetized conducting plane porous wall, deriving temperature field in boundary layer

06 p0937 A71-182312

Nozzle wall hypersonic boundary layers in helium tunnel, presenting skin friction measurements and heat transfer rates

06 p0884 A71-186030

Thermal creep velocity in rarefied gas over infinite plane wall, using linearized Boltzmann-Krook equation

07 p1084 A71-187464

Wall turbulence Prandtl-Karman constant calculation, using friction law for viscous sublayer degeneration with infinitely increasing Reynolds number

07 p1085 A71-187545

Wall flow boundary layer, observing external turbulent field effect on velocity and temperature distribution and heat exchange

07 p1086 A71-187717

Flow field behind two dimensional roughness element in rectangular channel, discussing wall effects, reattachment point position, velocity distribution and turbulence intensity

07 p1086 A71-187757

Turbulent wall flow, observing flow and heat transfer conditions with stroboscopic visualization

07 p1105 A71-187824

Two dimensional turbulent channel flow, determining local mean wall shear stress from velocity gradient

07 p1087 A71-187844

Resistance thermometer for temperature measurement in turbulent boundary layer near wall, giving expression for correction factor

07 p1106 A71-187864

Cavitation flow of fluid with free surface past flat plate between parallel walls

07 p1092 A71-20081

MHD Couette flow at stationary plate under transverse magnetic field, discussing effect on heat transfer between electrically conducting walls

07 p1170 A71-200994

Turbulent transfer model in wall region, estimating mean surface renewal frequency for mass momentum and heat transfer rates and velocity, temperature and concentration profiles

07 p1092 A71-20224

Fluidic coincidence position sensors, using wall attachment amplifiers and nozzle displacement

07 p1030 A71-20601

Fluidic OR-NOR element multiple regression analysis, investigating wall attachment, hysteresis switch pressure and percentage recovery

07 p1031 A71-20607

Wall attachment jet control volume model, examining flow momentum with restrictive force

07 p1031 A71-20609

Continuous flow past plate located perpendicular to wall with inviscid incompressible fluid having linear variation of velocity with height

08 p1227 A71-20828

Velocity profile in viscous sublayer at wall based on maximum stability principle applied to Karman constant for turbulent channel flow

08 p1277 A71-21950

Plane Poiseuille flow bounded by solid walls, applying Fourier expansion method to stability problem

09 p1432 A71-22583

Rarefied gas flow along boundary wall with temperature gradient, determining thermal creep and temperature slip effects

09 p1547 A71-23167

Incompressible inviscid fluid flow in presence of two homogeneous porous layers, examining hydrodynamic instability

10 p1591 A71-23754

Heterogeneous chemical reaction for visualization of wall streamlines on moving obstacle, discussing boundary layer structure at large Prandtl and Schmidt numbers

10 p1591 A71-23835

Resistance thermometer measurements near wall in turbulent flow, considering error causes

10 p1591 A71-23847

Pulsed subsonic wind tunnel, calculating instantaneous flow velocity with allowance for boundary layer thickness at walls

10 p1549 A71-23855

Gortler instability of laminar boundary layer flow on concave wall with finite length effect for perturbation vortices

10 p1592 A71-23958

Wall conductivity effects in MHD rectangular duct flow at high Hartmann numbers with uniform magnetic field applied parallel to one pair of duct sides

10 p1649 A71-24419

Hydrodynamic Stokes flow around body of revolution, using least squares method for fluid sticking on wall

10 p1594 A71-24455

Laminar incompressible boundary layer flow stability, emphasizing wall curvature and flexibility effects

10 p1594 A71-24548

Circular subsonic free jet impinging on wall, investigating high intensity frequency noise and turbulence spectrum

10 p1594 A71-24594

Airfoil profiles coupling method for determining complex potential of two dimensional ideal incompressible fluid flow due to arbitrary airfoil section movement near rectilinear wall

10 p1597 A71-25015

Compressible similar laminar boundary layer equations for zero wall shear and mass addition, describing heat transfer reduction and boundary layer growth by asymptotic analysis

11 p1750 A71-25479

Rotating plane layer viscous incompressible conducting fluid flow between two parallel walls with temperature gradient subject to perpendicular gravitational and magnetic fields

11 p1757 A71-25767

Three dimensional turbine end wall boundary layer with shear term, using momentum integral analysis and cross flow velocity profiles

11 p1751 A71-25952

Three dimensional convergence for spherical shock wave by linear pinch wall shaping based on Whitham ray-shock theory

11 p1752 A71-26191

Ideal incompressible fluid flow around fixed obstacle near rectilinear wall, investigating plane motion with profile couple method

11 p1705 A71-26258

Heat transfer in laminar free-convection boundary layers adjacent to plane and axisymmetric walls at constant temperature, deriving skin friction and mass flow rate

12 p1985 A71-26941

Spectral density of friction pulsations in turbulent channel wall flow for various length to height ratios and Reynolds numbers, using electrochemical method

12 p1897 A71-27306

Supersonic boundary layer transition on adiabatic wall, discussing wind tunnel size, surface roughness and freestream disturbances effects

12 p1865 A71-27554

Heat exchange at large Prandtl numbers near porous flat wall with liquid injection, calculating Stanton number

13 p2046 A71-28181

Eigenvalue, shooting and parallel shooting methods for solving Falkner-Skan boundary layer equation with positive or negative wall shear

13 p2047 A71-28230

Blowing angle effect on heat protection effectiveness of flat wall in slit injected low speed air flow with turbulent boundary layer in wind tunnel

13 p2159 A71-28420

Wall shear stress and static pressure of developing turbulent flow in square ducts with convective accelerating core for various Reynolds numbers

13 p2048 A71-28595

Blowing and wall curvature effects on gas flow separation and critical pressure gradient in Couette flow examples

13 p1993 A71-29193

Compressible rarefied gas Couette flow over plane wall, calculating mean free path with Boltzmann equation relaxation model

13 p2051 A71-29357

Separation control of two dimensional air flow with turbulent boundary layer along circular cylindrical wall by jets or suction

13 p2051 A71-29433

Spatial MHD flow in diffuser bounded by two diverging and two parallel walls, showing solutions with axial symmetry in cylindrical and spherical coordinate systems

14 p2278 A71-29605

MHD flow in rectangular channel with two conducting walls, investigating velocity structure

14 p2278 A71-29607

Viscous gas unsteady flow between harmonically oscillating and nonoscillating walls

14 p2225 A71-30220

Numerical heat transfer and wall friction results, demonstrating gas transport property variation effects on three laminar flow situations

14 p2338 A71-30931

Friction in compressible turbulent boundary layers at isothermal adiabatic wall

15 p2510 A71-31163

Density and velocity profiles of transonic flow past wavy wall at various channel heights, using Mach-Zehnder interferometer

15 p2386 A71-31165

Laminar boundary layer growth along moving flat plate wall, obtaining series solution relating shear stress to velocity ratio

15 p2390 A71-32018

Fluid jets along curved or straight walls with non-zero external potential flow, analyzing Coanda effect

15 p2390 A71-32055

Shock wave diffraction patterns on plane walled convex corners in air, nitrogen and carbon dioxide at various Mach numbers

16 p2556 A71-32918

Pipe Poiseuille flow instability with respect to finite amplitude disturbances, calculating Reynolds stress by linear wall mode

16 p2558 A71-33021

Wall shear stress, momentum and displacement thickness of shock induced boundary layer interaction in tube and over flat plate, using integral method [ASME PAPER 71-APM-21]

16 p2559 A71-33208

Velocity and magnetic field equations of electroconductive fluid vortex motion due to annular receptacle insulating walls rotation

16 p2620 A71-34057

Laminar boundary layer past continuous moving surface with constant wall velocity, deriving perturbation solution in terms of Green function

16 p2560 A71-34074

Wall roughness effects on laminar boundary layer velocity profile and Reynolds number, using Hankel functions and integrals

17 p2725 A71-34180

Detachment prediction in turbulent incompressible plane flows on thick bodies applied to wall with disconnections and flat plate normal to wind

17 p2669 A71-34189

Vortex boundary layer with dissipative viscous wall and isentropic sublayers, calculating adiabatic surface temperature

17 p2669 A71-34217

Laminar flow in incompressible fluid between rotating disk and fixed wall at small distances with radial mass stream, using finite difference method for Navier-Stokes equations

17 p2726 A71-34581

Perturbed two dimensional laminar boundary layers of incompressible conducting fluid flow along insulated concave wall in transverse magnetic field, investigating three dimensional instability

17 p2788 A71-34642

Heat transfer in wall region of steady turbulent flow at large Prandtl numbers, plotting temperature distribution curves

17 p2728 A71-35119

Supersonic turbulent two dimensional boundary layer flows wall flux and velocity/temperature profiles prediction

17 p2729 A71-35283

Parabolic boundary layer equations for heat convection problems with unknown wall boundary conditions, noting solution by deterministic and nondeterministic optimization methods

17 p2838 A71-35355

Weakly interacted laminar MHD flow growth in entrance region of plane channel with wall conductances investigated by momentum integral method

18 p2951 A71-36251

Two dimensional turbulent boundary layer in incompressible fluid on smooth and rough impermeable wall surfaces under arbitrary pressure gradients

19 p3042 A71-37088

Plane Couette-Poiseuille flow stability between porous walls with fluid injection and suction causing uniform crossflow

19 p3044 A71-37728

Streamwise wall curvature and transition effects in turbulent boundary layers, using modified eddy viscosity and mixing length concepts

19 p3045 A71-37891

Spectral density of friction pulsations in turbulent channel wall flow for various length to height ratios and Reynolds numbers, using electrochemical method

19 p3046 A71-38262

Incompressible turbulent boundary layer with pressure gradients, calculating Clauser equilibrium model and flow with constant wall shear stress

20 p3210 A71-39030

Water tunnel walls effect on supercavitating flows past slender bodies

20 p3213 A71-39786

Stepwise change in wall roughness effects on turbulent shear flow through two dimensional channel, measuring mean velocity, turbulent intensity and shear stress

21 p3365 A71-40015

Mean velocity profile and wall friction coefficients of perturbed turbulent boundary layer on flat plate

21 p3366 A71-40511

Diffusing gas mixtures slipping rate along wall at arbitrary accommodation coefficients, deriving expression based on molecule distribution functions from linearized Boltzmann equations solution

21 p3418 A71-40678

Incompressible flow hydrodynamic time dependent problems for moving walls and free surfaces, using Marker-Cell computing method

21 p3368 A71-40849

Rotating plane layer viscous incompressible conducting fluid flow between two parallel walls with temperature gradient subject to perpendicular gravitational and magnetic fields

22 p3532 A71-41535

Convective heat transfer between laminar fluid flow and circular flat tubes, considering wall thermophysical properties effect

22 p3619 A71-41873

Potential two and three dimensional flows past body in presence of rigid wall, using matched asymptotic expansions

23 p3625 A71-43369

Wall effects and correction rules for cavitation flow past wedge in closed water tunnel, deriving drag coefficient from various theoretical models

23 p3663 A71-43442

Rivlin-Ericksen fluid steady flow between parallel plates with uniform suction at lower wall, detailing velocity field, skin friction and flow coefficient

23 p3663 A71-43492

Sound wave propagation from two dimensional acoustic source in subsonic fluid moving between two reflecting parallel walls

23 p3705 A71-44145

Heat transfer in turbulent boundary layer separation zones ahead of step, using local flow parameters at wall boundary layer limit

24 p3887 A71-44746

Gas concentration measurement at wall with argon and helium injection at pipe entrance, investigating protecting film cooling efficiency

24 p3819 A71-44929

WALL JETS

Wall jet and wake flow prediction, using Prandtl-Kolmogoroff turbulence model

04 p0578 A71-15766

Prediction method for turbulent boundary layer development using shear work integral for range from wall jet to adverse pressure gradient flow

07 p1085 A71-18764

Optimal design and manufacture of wall attachment fluidic devices, noting thermoplastics injection molding followed by ultrasonic bonding

07 p1121 A71-20565

Wall jets over concave surfaces, obtaining average velocity profiles

10 p1591 A71-23842

High velocity airstream interaction with multiple gas jets from single row multihole wall injectors, discussing jet penetration and mixing in cross flow

11 p1750 A71-25478

Optimal blowing wall jet prediction for suppressing separation from high lift aerofoils with incomplete mixing of upstream boundary layer

11 p1704 A71-26196

Turbulent submerged wall air jet on ablating graphite surface, examining friction and heat and mass exchange in boundary layer

13 p2160 A71-28569

Turbulent wall jets in presence of main flow longitudinal pressure gradient, using approximate integral method

13 p2050 A71-29225

Curved wall jet pressure distribution numerical calculation for given velocity profiles

14 p3238 A71-30306

Turbulent wall jet with initial boundary layer, calculating growth and separation in arbitrary pressure gradient by integral method

15 p2389 A71-31581

Gas stream-wall interaction for Maxwell model by scattering element-detector system with specular reflection and diffusion separation

15 p2389 A71-31702

Laminar and turbulent incompressible entry flows in channel with jets along walls, determining filling length

18 p2904 A71-36135

Laminar incompressible plane wall jet, calculating flow characteristics for potential core region with integral method

21 p3370 A71-40988

Two dimensional incompressible turbulent wall jet in moving stream, describing viscous flow characteristics and various boundary layer parameters

24 p3818 A71-44605

Strongly curved wall jets development in thick boundary layer upstream of blowing slot, discussing calculation method, correction for shear stresses and comparison with experimental results

24 p3819 A71-44952

WALL PRESSURE

Wall static pressure and convective heat transfer measurements in subsonic, transonic and supersonic regions in heated air turbulent flow through variable cross section channel

04 p0680 A71-15476

Started supersonic axisymmetric parallel diffuser, examining wall static pressure and heat transfer

04 p0528 A71-15489

Turbulent boundary layer wall pressure fluctuations on hydrodynamically smooth and rough surfaces, investigating eddies, space-time decay rate and flow structure

05 p0736 A71-16961

Wave number/phase velocity spectrum of wall pressure measurements beneath two dimensional turbulent boundary layer

06 p0882 A71-18317

Plane normal shock wave reflection in relaxing gas for shock tube endwall upstream and downstream dynamic pressures, using method of characteristics

09 p1546 A71-23166

Thin flexible panel acoustic power radiation due to turbulent boundary layer wall pressure fluctuations excitation

10 p1596 A71-24814

Nozzle wall hypersonic turbulent boundary layers at free stream Mach number, using pitot, hot wire, wall pressure fluctuation and static pressure measurements [AIAA PAPER 70-746]

12 p1898 A71-27558

Flowfields behind reflected shock waves, predicting end-wall pressure, radiative heat transfer and radiative gas dynamic coupling effects

12 p1986 A71-27562

Longitudinal space-time correlation function of turbulent near wall pressure pulsations with hydrodynamic wavelength exceeding boundary layer thickness at streamlined model

13 p2049 A71-28846

Interaction between viscous mixing shear layer induced by tangential injection and external supersonic flow field, obtaining spark schlieren photographs and wall pressure distributions

13 p2053 A71-29461

Plate excitation by supersonic turbulent and shock boundary layers, measuring wall pressure fluctuation and panel displacement

15 p2507 A71-32132

Wall pressure spectra and rms wall pressure levels measurements in subsonic separated flows, postulating model for pressure fluctuation estimation

17 p2728 A71-35037

Cone-cylinder-cone missile type body in transonic buffeting environment determining static and fluctuating wall pressure distribution [ONERA-TP-942]

18 p2843 A71-36020

Pressure and heat flux measurements at wall of nose cone in hypersonic wind tunnel flow with high generatrix enthalpy

18 p2844 A71-36182

WALL TEMPERATURE

Mean heat transfer coefficients determination at surface front of built-in alpha calorimeter from wall temperature data

01 p0179 A71-10611

Resonance tube heat losses, discussing thermal exchange mechanism and wall temperature limits

01 p0180 A71-10993

Circular pipe gas laminar flow at constant wall temperature, determining heat exchange and drag by motion and energy equations integration in boundary layer approximations

02 p0240 A71-12192

Laminar boundary layer convective heat transfer with constant wall temperature, using Gaussian quadrature formulas

02 p0332 A71-12394

Cylindrical wall with variable heat conductivity coefficient, solving temperature distribution by asymptotic method

02 p0333 A71-12540

Flat plate film boiling heat transfer under forced boundary layer convection, examining nonstationary wall temperature effects

02 p0333 A71-12646

Flat cooling wall optimum thickness for minimum steady state temperature at point exposed to local heating

03 p0520 A71-13955

Hemispherical imploding shock wave reflection, noting cold wall presence and gas density effects

04 p0568 A71-14682

Pressure gradients and slot Reynolds number effects on impervious wall film cooling effectiveness in constant density flow

04 p0680 A71-15474

Prandtl number measurement in turbulent thermal boundary layer along flat plate with stepwise wall temperature variation

04 p0680 A71-15477

Hypersonic laminar cavity heat transfer, including upstream boundary layer thickness, unequal core and wall temperature effects

04 p0528 A71-15491

Laminar turbulent tube flow heat transfer, investigating internal radiation exchange and wall heat conduction and generation effects

04 p0685 A71-15519

Leidenfrost film boiling for various liquids over velocity, plate temperature and surface roughness range, noting velocity effect on vaporization rate

04 p0687 A71-15529

Compression waves produced in viscous heat conducting gas by impulsive one dimensional piston start and by wall temperature change

05 p0831 A71-16477

Convective heat transfer in coolant with constant velocity in ring channel with heat sources, deriving expressions for flow and wall temperature

06 p1006 A71-18004

Boiling in two-phase layer on heated wall in relation to thermal exchange mechanisms

07 p1221 A71-18790

Temperature distributions and heat flux for gray gas in radiative equilibrium bounded by walls with different temperatures, using differential approximation [AIAA PAPER 70-834]

09 p1516 A71-22094

Exact numerical solution for laminar compressible boundary layers with nonuniform wall temperatures compared with Luxton-Frion approximate method results, noting skin friction effects

09 p1545 A71-22940

Incident thermal flux parameters and wall temperature effects on flow characteristics in prepreparation zone of laminar boundary layer and separation point location

10 p1551 A71-24368

Plane unsteady convective motion of viscous incompressible liquid in infinite horizontal vessel of rectangular cross section due to wall temperature fluctuations

10 p1696 A71-24375

Unsteady hypersonic flow around melting axisymmetric blunt bodies of revolution with profile depending on wall temperature, calculating temperature distribution and wall pressure

10 p1698 A71-25087

Pressure and wall temperature gradients effects on equilibrium enthalpy profiles and heat transfer coefficients of incompressible turbulent boundary layers, using eddy conductivity model

12 p1986 A71-27553

Viscous convergent-divergent nozzle flow slender channel approximation, discussing nozzle geometry, Reynolds number and wall temperature effects

12 p1865 A71-27556

Laminar boundary layers with large wall heating and flow acceleration, considering heat transfer parameter increase

12 p1987 A71-27589

Local heat transfer in tubes under nonstationary conditions, calculating coefficients from wall temperature gradient at surface

13 p2160 A71-28587

Two dimensional prediction of adiabatic wall temperature and heat transfer coefficient downstream of film cooling slots, using Prandtl mixing length forms

13 p2160 A71-28598

Nonuniform sidewall heat flux effect on thermal stratification

13 p2165 A71-29010

Heat exchange and temperature distribution between two liquids divided by plate, discussing possible errors

14 p2335 A71-30048

Circular pipe gas laminar flow at constant wall temperature, determining heat exchange and drag by motion and energy equations integration in boundary layer approximations

15 p2388 A71-31498

Heated or cooled wall surface layers temperature anomaly, noting fluid-wall heat exchange coefficients

15 p2513 A71-31905

Plate temperature fluctuations effect on convective flow and heat transfer from horizontal plate, presenting solutions for LF and HF

17 p2838 A71-35419

Pressure and heat flux measurements at wall of nose cone in hypersonic wind tunnel flow with high generatrix enthalpy

18 p2844 A71-36182

Longitudinal vortex rolls onset for laminar forced convection between two horizontal flat plates subjected to uniform axial wall temperature gradient

19 p3163 A71-37979

Gas nature effect on wall temperature and heat transfer in Hartmann-Sprenger tube

21 p3366 A71-40102

Macroscopic values of energy exchange between polyatomic gas and solid wall, considering heat transfer rate and wall temperature change

23 p3781 A71-43105

Vertical heat transfer coefficient of flat and cylindrical walls in fluidized bed from wall vertical temperature distribution

23 p3783 A71-44069

Free convection heat transfer from vertical flat plate with sinusoidal wall temperature distribution [AIAA PAPER 71-988]

24 p3887 A71-44583

Low temperature plasma radiation flux heated absorbing fluid, investigating convective heat transfer to semitransparent wall

24 p3856 A71-44893

WALL TEMPERATURE DISTRIBUTION

U TEMPERATURE DISTRIBUTION

U WALL TEMPERATURE

WALLOPS ISLAND

Land breeze fronts observed by X and S band radars at Wallops Island

01 p0116 A71-10567

Mesoscale meteorological structure during radar CAT detection at Wallops Island during January-March 1968 and 1969

01 p0116 A71-10567

Solar eclipse sounding rocket study of totality path over Wallops Station for 7 March 1970 event, discussing payload launch, ground support equipment, planning, etc

03 p0397 A71-13676

[AIAA PAPER 70-1395]

WALLS

NT BULKHEADS

NT NOZZLE WALLS

NT POROUS WALLS

NT THICK WALLS

NT THIN WALLS

NT WIND TUNNEL WALLS

Wall thickness measurement by ultrasonic tests in presence of corrosion, discussing instruments development

06 p0897 A71-17416

Frequency shift in hydrogen maser due to atomic collisions with storage bulb surface /wall shift/, investigating temperature dependence

07 p1124 A71-19686

Normal shock wave interaction with deformable solid walls, determining explosion or sonic booms effects on elastic structures and protection devices

10 p1556 A71-24483

WALSH FUNCTION

Orthogonal signal analysis and synthesis with Walsh functions, giving practical implementations of required operations

09 p1406 A71-23030

Walsh orthogonal functions application in signal processing and as carrier waves in telemetry data transfer systems

14 p2199 A71-30909

Walsh function imagery analysis by Hadamard-Walsh transform and eigenvector expansion technique

20 p3197 A71-39610

Walsh functions in image processing, rotational feature selection and pattern recognition, defining set of orthogonal transformations

20 p3255 A71-39611

Multiple Walsh function generator design for improved time response relative to digital components, comparing with Rademacher device

23 p3646 A71-43962

WANKEL ENGINES

Internal mixing scheme for continuous fuel injection in Wankel engine via swirl nozzle during intake-compression cycle

02 p0298 A71-12559

Epitrochoidal profile machining methods and tools for chamber surface in Wankel engine

02 p0257 A71-12560

Wankel engine chamber gas leakage determination based on exit slot sample gas analysis, considering air to working fluid ratio

04 p0638 A71-14598

Motorized glider equipped with Wankel engine for self powered takeoff, describing prototype design and flight test data

08 p1232 A71-21769

WAR GAMES

On-line real time optimal control computations for aerial combat games between two aircraft, assessing airborne computer requirements

16 p2525 A71-34022

WARFARE

NT ANTISUBMARINE WARFARE

NT COMBAT

Electronic warfare technology, discussing airborne platforms, battlefield surveillance, jamming devices, homing and warning systems

04 p0557 A71-15019

WARHEADS

NT NUCLEAR WARHEADS

Ballistic reentry warheads atmospheric interception, investigating defensive nuclear bursts effects

01 p0163 A71-10268

WARMING

U HEATING

U WARNING DEVICES

U WARNING SYSTEMS

U WARNING SIGNALS

U WARNING SYSTEMS

U WARNING SYSTEMS

Severe thunderstorm warning by single pulse Doppler radar plan shear indicator

01 p0117 A71-10572

ATA Collision Avoidance System based on time and frequency synchronization via ground stations or other aircraft

02 p0280 A71-12895

Solar radio bursts at 19 GHz, investigating single frequency proton warning technique
03 p0481 A71-14506

Aircraft equipment failures detection and warning systems
04 p0601 A71-15901

Aircraft visual warning indicating system, outlining design criteria, color and brightness recommendations [SAE-ARP-1088]
07 p1019 A71-19644

Human role in Aerospace Defense Command navigation, discussing Airborne Warning And Control System and navigational aspects of ADC mission
07 p1157 A71-20346

Aircraft aquaplaning skidding prevention by runway resurfacing and water depth sensor warning indicators
10 p1609 A71-23946

Mission reliability calculations for systems with redundant units, considering design of airborne warning and control system and other radar control systems
12 p1885 A71-26675

Concorde power plant fire protection system, describing prototype engine bay overheat detection system and additional UV optical fire detection system
14 p2288 A71-30300

Aircraft angle of attack limiter parameters, describing automatic warning system for impending stall
16 p2523 A71-33621

Recursive algorithms for detection probabilities of fluctuating targets in Gaussian noise, including cell averaging constant false alarm rate /CFAR/ extension
20 p3195 A71-38860

Comparative detection performance of Siebert and Dicke-fix constant false alarm rate /CFAR/ radar detectors for signals in Gaussian noise
20 p3195 A71-38866

Probability functional formulas for quasi-determinate signal on unsteady normal noise background for use in false alarm and correct detection
20 p3199 A71-39815

Canadian Forces experiments on aircraft flashing lights covering warning signals, navigation and anticollision displays and autokinetic phenomenon
22 p3499 A71-41491

Strobe lighting for aircraft midair collision hazard reduction, comparing Collision Avoidance System and Pilot Warning Indicator effectiveness
22 p3499 A71-41493

WARPAGE
Cross sectional warpage effects on turbine blades natural torsional vibration frequencies
17 p2834 A71-35677

Regular and singular perturbation solutions for beam bending under axial forces and shaft warping in torsion
22 p3616 A71-42214

WASHERS [SPACERS]
Wet and dry lubricated slip ring systems long term application testing in ion pumped vacuum chambers
07 p1120 A71-20274

Nonreflecting dielectric support washers design in coaxial-stripline junctions, calculating VSWR as function of dimensions and frequency
19 p3019 A71-38335

WASHING
Tannic acid and water washing effects on prevention of monomethylhydrazine absorption through skin in dogs
16 p2535 A71-33119

WASHOUT [RADIOACTIVITY]
U FALLOUT

WASTE DISPOSAL
Space shuttle life support, protective and crew system interfaces, discussing food and waste management and accident procedures
07 p1052 A71-20230

Feeding systems, potable water and waste disposal in space cabins
08 p1245 A71-20730

Liquid wastes venting into space environment, producing ice particle clouds interference with spacecraft optical instruments
11 p1753 A71-26506

Integrated waste collection and purification system using radioisotopes for thermal energy in 180-day space mission life support system
[ASME PAPER 71-AV-4] 18 p2865 A71-36371

Waste management subsystem for 90-day space station simulator test of regenerative life support system
[ASME PAPER 71-AV-7] 18 p2865 A71-36374

Skylab life support systems design and performance prediction covering thermal and humidity control, atmospheric supply, carbon dioxide removal, water and waste management
[ASME PAPER 71-AV-14] 18 p2866 A71-36381

Space shuttle environmental control and life support system design covering atmospheric pressure, composition, humidity, temperature, water and waste management
[ASME PAPER 71-AV-16] 18 p2867 A71-36383

Orbital nonpropulsive vent system to remove excess or residual propellant vapors and waste gases with minimum impulse imbalances imparted to vehicle
18 p2973 A71-36454

Spacecraft housekeeping relation to logistics elements of maintenance and up and down cargo supply
18 p2899 A71-36467

Housekeeping systems for manned modular space station and shuttle, discussing steward duties and waste control
[AIAA PAPER 71-880] 18 p2871 A71-36633

Engineering aspects of zero gravity personal hygiene and waste management systems, noting controlled air flows, surface tension and artificial gravity use
[AIAA PAPER 71-865] 18 p2872 A71-36653

Urine conservation in spacecraft cabin sanitation facilities by phenol-containing preparations, emphasizing PNF method for long period operation
22 p3507 A71-42822

WASTE UTILIZATION
Regenerated nutrients as foods for long duration space missions, discussing physicochemical methods for metabolic waste products conversion into safe synthetic nutrient compounds
01 p0026 A71-11250

Astronaut space nutrition, discussing Apollo mission short range nonregenerative mode, long range closed loop regenerative cycles and waste recycling
01 p0027 A71-11572

Potential foods synthesis for long duration space missions by physicochemical methods, discussing regeneration of carbohydrates from metabolic waste carbon dioxide and electrolytic byproduct hydrogen
07 p1056 A71-20375

Ti alloy powders and Ti-base refractory compounds production from Ti alloys wastes
08 p1317 A71-21856

Concentric tube resistojet tested on hydrogen and ammonia propellants for use with biowaste propellants
[AIAA PAPER 70-1133] 09 p1387 A71-22908

Biowaste resistojet propulsion system for NASA space station orbit-keeping, describing design and operation
[AIAA PAPER 71-686] 14 p2293 A71-30748

Ti alloy powders and Ti-based refractory compounds production from Ti alloy scrap, describing electrorefining, hydrogenation and carbidization processing
14 p2260 A71-30835

Biowaste resistojet engine design and performance for various propellants and propellant mixtures
[AIAA PAPER 71-687] 15 p2470 A71-32293

Resistojet power and specific impulse performance, investigating biowaste derived propellant chemical nonequilibrium effects
[AIAA PAPER 71-688] 17 p2696 A71-35534

Integrated waste collection and purification system using radioisotopes for thermal energy in 180-day space mission life support system
[ASME PAPER 71-AV-4] 18 p2865 A71-36371

Space station life support prototype vapor diffusion water reclamation system for pure and sterile water distillation from urine process stream
[ASME PAPER 71-AV-31] 18 p2869 A71-36398

Skylab habitability considerations in Orbital Workshop design, discussing waste management, food management and sleeping compartments
[AIAA PAPER 71-872] 18 p2870 A71-36628

Housekeeping systems for manned modular space station and shuttle, discussing steward duties and waste control
[AIAA PAPER 71-880] 18 p2871 A71-36633

Engineering aspects of zero gravity personal hygiene and waste management systems, noting controlled air flows, surface tension and artificial gravity use
[AIAA PAPER 71-865] 18 p2872 A71-36653

Oxidation of water in regeneration under spacecraft conditions, measuring organic impurities degree of oxidation in inhabited cabin atmospheric vapor condensates
22 p3506 A71-42814

Decontaminating methods for water regenerated from urine under space flight conditions by filtering water condensate through sorbents
22 p3506 A71-42815

Biologically mineralized human waste products utilization in nutrient solutions for higher and lower autotrophs cultivation
22 p3507 A71-42819

Human waste product utilization possibility through mineralization by wet combustion method
22 p3507 A71-42820

Group analysis of impurities in water regenerated from liquid human wastes
24 p3800 A71-44529

WASTES
NT HUMAN WASTES
NT METABOLIC WASTES
NT URINE

Physiological effects on mice of air pollution with gaseous toxic substances from urine and feces, noting increased respiration rate and choline esterase activity
22 p3506 A71-42807

Thermal combustion produced biocomplex vegetable waste mineralization effect on furnace working surface oxide film
22 p3507 A71-42821

WATCHES
U CLOCKS

WATER
NT COLD WATER
NT HEAVY WATER
NT POTABLE WATER
NT SEA WATER

Explosive boiling of water and organic liquids around pulse heated Pt wire, discussing vaporization process, fluctuating nucleation and temperature behavior
02 p0331 A71-12193

Acoustic velocity in water, examining air bubble effects on pressure pulse attenuation
03 p0459 A71-13720

Liquid hydrogen, oxygen and water droplets released in space, examining size and temperature histories
06 p0964 A71-17277

Cured epoxy polymer, determining diffusion coefficients, solubility, permeability and equilibrium water absorption as function of curing agent and temperature
06 p0915 A71-17943

Cured thermosetting polymers, investigating water effect on microstructure and mechanical properties
06 p0916 A71-17945

Escape mechanisms examined to explain liquid water absence on Venus surface, considering hot acidic hydrosphere consequences for biological activity
06 p0968 A71-17955

Liquid water far IR absorption spectrum, presenting transmission coefficients table
07 p1158 A71-18911

Submillimeter wave extinction in clouds and fogs, using spectrometric results of water optical properties
09 p1408 A71-23375

Spectral transmittance of pressure induced and intrinsic absorption of IR energy by carbon dioxide and water due to Fermi bands and asymmetric molecules
10 p1644 A71-23950

Normal shock wave acceleration of water droplets by external pressure, observing distortion and breakup through shadowgraph techniques
[AIAA PAPER 71-325] 11 p1749 A71-25305

Water drops deformation and fragmentation due to shock wave impact in high velocity air stream
[AIAA PAPER 71-392] 11 p1749 A71-25354

Spectroscopic search for water on Mars during 1963-1970, summarizing conclusions concerning quantity and variations with location, season and from year to year
11 p1826 A71-25715

Liquid water natural occurrence on Martian surface, considering possibility of ice melting by sunlight or other heat sources
11 p1826 A71-25718

Spectral reflectance of water cryodeposits on liquid nitrogen cooled surfaces in vacuum IR integrating sphere
[AIAA PAPER 71-447] 11 p1858 A71-26232

Spectral analysis methods for detection of water on celestial bodies, considering possible abundance on planets and stars
12 p1962 A71-26956

Critical Rayleigh numbers for natural convection of water confined in square cells, noting heat transfer modes
[ASME PAPER 70-WA/HT-7] 13 p2164 A71-28981

Ions association constant with water in propylene carbonate from proton magnetic resonance measurements
13 p2026 A71-29040

Galactic H II regions 35 cm water source emission line profile observation, noting frequency and intensity variations
14 p2304 A71-29594

Water diluent effect on molten hydrazine mononitrate critical diameter and condensed explosive detonation stability
15 p2463 A71-31383

Explosive boiling of water and organic liquids around pulse heated Pt wire, discussing vaporization process, fluctuating nucleation and temperature behavior
15 p2512 A71-31499

Sodium oxide-titanium dioxide-water ternary system, determining sodium titanates formation regions in equilibria in 300 C isotherm
15 p2367 A71-31902

Subsurface water detection on lunar traverse by tilt angle electromagnetic depth sounding
15 p2492 A71-32475

Lunar subsurface water detection from satellite in polar orbit around moon by electromagnetic measurement
15 p2492 A71-32476

Surface and subsurface water analysis on moon and planets by combination neutron experiment using epithermal die-away measurements of hydrogen
15 p2411 A71-32477

Water, carbon and rare gases in lunar crater breccias based on meteorites nature
15 p2494 A71-32490

Lunar and Martian subsurface liquid water under porous rock layers and permafrost, using terrestrial hydrogeology analogs

15 p2494 A71-32491

Existence conditions for liquid water on Mars, considering freezing depression, condensation, capillary evaporation and permafrost melting

15 p2494 A71-32492

Water distribution in space, natural satellites and terrestrial planets, discussing Clarke abundance values and hydrochlorosphere concept

15 p2494 A71-32493

Transient response of water drops to shock wave induced accelerations at near critical Weber numbers

16 p2557 A71-32925

Polymethyl methacrylate lifetime tested in water and heptane, showing increase with orientation degree

16 p2601 A71-33683

Lower thermosphere and ionosphere upper limits of positively ionized water molecules number density, considering desorption and recombination processes

16 p2571 A71-33842

Cometary dissociative recharging and recombination dissociation of water and hydrogen peroxide molecules in comets, giving empirical relation for effective cross sections

17 p2803 A71-34830

Mars, Venus and earth atmospheres, considering abundance of volatiles such as carbon dioxide, water, oxygen, nitrogen, argon, carbon monoxide, chlorine and fluorine

18 p2968 A71-37032

Tuff rings from Fort Rock-Christmas Lake Valley basin, investigating morphologic and volcanic features for surface water role in genesis

19 p3051 A71-37671

Reactions of H and O with hydrogen peroxide and water in discharge flow systems, measuring rate coefficients

19 p3012 A71-38083

Hamster body fat, water and density measurements by dilution method and air displacement technique, comparing to determination by direct chemical analysis upon sacrificing

19 p3005 A71-38555

Water aerosol flux interaction and drop capture with particles of solid reagent, considering agaroid films and precipitation on thin wires

19 p3094 A71-38699

Spherical cap bubbles in water and mineral oil at various dynamic viscosities, measuring laminar and turbulent wakes character, rise speed and shape

21 p3365 A71-40017

Microwave water emission in Comet Bennett, deriving column density for various temperatures of cometary gas

21 p3443 A71-40190

Water radiolysis measurement in nuclear reactor tests, discussing experiment design as doubly telescoping sequences of blocks

21 p3345 A71-40202

Radio telescopic search for extraterrestrial oxygen 18 containing water microwave emission, suggesting water vapor maser pumping mechanism dependence on isotopic species

21 p3444 A71-40223

Room temperature evaporating water drop shape history on cooper, lucite, stainless steel and Teflon, observing wetting dynamics effects

21 p3476 A71-40903

Urea hydrolysis reaction rates by urease at low water activity, noting use for Mars surface bioassay

22 p3487 A71-42226

Nonaqueous biosystems unlikelihood from consideration of enzymatic activity possibility and liquid water unique ability for complexity required by carbonaceous biosystems

22 p3487 A71-42229

Mass diffusivity effects in film boiling of water droplets vaporizing in air, Ar, N, He and steam

23 p3782 A71-43907

WATER BALANCE

Long term lunar surface environment, discussing radiation, thermal and meteoroid protection, water budget, carbon dioxide removal and air lock design

11 p1726 A71-26534

Long term immersion effects on human water-salt metabolism, noting increased erythrocyte water contents and hematocrit index

13 p2006 A71-28403

Human body water metabolism during acute high altitude exposure with heavy physical activity and high food intakes

16 p2530 A71-33240

Human nitrogen and water-salt metabolism and respiratory activity during prolonged confinement in small volume chamber with cyclic varying hypoxic air

22 p3495 A71-42799

WATER CONSUMPTION

Water intake effects on human thermal sweat rate and composition in environmental chamber at specific temperature and humidity

02 p0202 A71-11670

Pressure increase, dry air consumption and power requirements effects of water quantity fed into centrifugal compressor

08 p1347 A71-20833

Secretory function intensity of salivary glands, liver and stomach of animals and humans with different water-salt metabolism conditions

11 p1719 A71-25669

Food and water intake changes associated with interruption of hypothalamus anterior or posterior fiber connections

13 p2011 A71-28802

Chronic centrifugation effects on water intake and urine output in mice, considering food intake and growth rate

20 p3186 A71-38984

WATER CONTENT

U MOISTURE CONTENT

WATER COOLED REACTORS

NT BOILING WATER REACTORS

NT PLUM BROOK REACTOR

Iron corrosion product deposition on pipe wall from aqueous stream dependent on shear rate, using radioactive tracer technique

03 p0442 A71-13368

Transient flow measurement with sharp-edged orifices, considering pump trip accidents simulation in water cooled nuclear reactors

[ASME PAPER 71-FE-30] 13 p2053 A71-29465

Water cooled reactor Zircaloy brazing filler metals, investigating corrosion resistance, joint strength and brazing capability

18 p2928 A71-36856

WATER DEPRIVATION

Prolonged water deprivation effects on hypothalamic self stimulation of rats with electrodes chronically implanted in posterior lateral hypothalamus

05 p0711 A71-17087

Internal osmotic balance and stress induced body fluid osmolality changes due to food or water deprivation, reporting on experimental results with rats

08 p1240 A71-21750

WATER EROSION

Metals erosion by cavitation and liquid impingement, discussing test methods and resistance prediction

03 p0404 A71-14174

Water impact erosion on stainless steel, Ni and Al and Ti alloys, observing impact velocity relationship with number

03 p0444 A71-14287

Plastic, elastomeric, ceramic glass, metallic and composite materials rain erosion resistance at supersonic speeds, examining rate-velocity dependence

03 p0444 A71-14288

Rain and sand erosion materials tests, considering temperature and atmosphere pressure effects and relation between fatigue behavior and erosion/cavitation strength

03 p0444 A71-14289

Steam turbine blade metal removal rates by repetitive water drop impact, using hydrodynamic model

03 p0405 A71-14290

Subsonic velocities erosion behavior of polymeric coatings and composites, considering void content and reinforcement influence on composite structure

09 p1483 A71-23425

Polyurethane coatings development for subsonic rain erosion protection for aircraft structures, using whirling arm apparatus with simulated rainfall

10 p1632 A71-24101

Circular lead specimens in water flow, determining external magnetic field effects on cavitation and erosion

14 p2278 A71-29613

Materials and processing methods for rain erosion resistant ceramic coated plastic structures for supersonic aircraft, considering fiberglass reinforced polyimide radomes with alumina coating

14 p2262 A71-29645

WATER FLOW

Critical heat release in water film on vertical pipe with inside cooling

01 p0181 A71-11244

Projectile entry into water vertically from air, predicting cavity shape as function of time based on hydraulic flow model

[ASME PAPER 70-WA/FE-8] 03 p0402 A71-14129

Linearized equation for stability and heat transfer of two dimensional incompressible laminar boundary layer in water flow

04 p0679 A71-15469

Heat transfer measurements in thin water films on brass tube, using electrically heated elements

04 p0680 A71-15475

Pulsed velocity longitudinal component in water flow turbulent boundary layer, investigating intensity, spectral characteristics and drag reduction

04 p0576 A71-15616

Inviscid incompressible flow velocity distribution in conical configurations with water as working fluid, using method of integral relations

05 p0737 A71-17103

Natural convection heat transfer between two isothermal concentric spheres, using water and silicone oils as convective fluids

07 p1222 A71-18995

Membrane separate systems ion and water mass transport, noting effect on anolyte concentration and alkaline battery performance

08 p1234 A71-21092

Similarities between ion waves in plasmas and gravity waves in incompressible fluid/steady water flow with allowance for surface tension

13 p2046 A71-27844

Lake Erie steady state wind driven currents numerical solutions, using shallow lake model for velocity as function of depth and horizontal position

13 p2054 A71-27857

Circular lead specimens in water flow, determining external magnetic field effects on cavitation and erosion

14 p2278 A71-29613

Air-water flow pressure loss and phase distribution in tube with wire coil swirl generators

15 p2354 A71-32209

Convective heat exchange coefficient determination for human body immersed in turbulent water flow, using fractional calorimetry

18 p2858 A71-36862

Heat transfer coefficients calculation for human body in cold water from heat balance equations, comparing with free convection coefficients in cross-flowing water

18 p2862 A71-36900

Vortice generation in laminar boundary layer of water flow under hydraulic pressure reduction, proposing mathematical model

23 p3662 A71-43315

Wall effects and correction rules for cavitation flow past wedge in closed water tunnel, deriving drag coefficient from various theoretical models

23 p3663 A71-43442

Thermally driven motion of water with free surface in rotating annulus, investigating steady wave flow by three dimensional nonlinear Navier-Stokes equations numerical integration

24 p3844 A71-44417

WATER INJECTION

Turbocharged diesel engine precompressed inlet air cooling by evaporation cooling, considering water injection effects on centrifugal compressor

08 p1347 A71-20781

Hollow cone water spray from pressure jet swirl atomizer into uniform air stream, observing drop velocities and trajectories by high speed photography

13 p2049 A71-28753

WATER INTAKES

Diurnal water and food intake and body weight changes pattern in rats with hypothalamic lesions

22 p3486 A71-41936

WATER JETS

U HYDRAULIC JETS

WATER LANDING

NT DITCHING [LANDING]

Axially symmetric bodies impact landing on water surface, deriving acceleration for comparison with measurement

01 p0178 A71-11398

Sea trials with dummy payloads of sounding rocket recovery systems, using parachutes, flotation torus, radio beacons, fluorescent dyes and smoke generators

06 p0881 A71-18674

Two stage parachute system RESY for water and land recovery of sounding rocket payloads

09 p1533 A71-23599

WATER LOSS

Valeraldehyde o-nitrophenylhydrazone mass spectrum with low intensity peak due to combined hydroxyl and water loss from molecular ion

02 p0209 A71-12573

Voluntary body water and salt deficits decreasing human heat tolerance

05 p0708 A71-16597

Human body weight and skin sweat gland water loss rates effects on thermoregulation

18 p2858 A71-36864

Moderate heat exposure effects on human circadian variations in body temperature, heart and metabolic rates and water loss

24 p3797 A71-44779

WATER MANAGEMENT

Ground wave propagation over nonuniform overburden with arbitrarily varying complex dielectric coefficient and depth, discussing application to water table mapping

09 p1436 A71-22644

Ground water flow into Lehigh River, Pennsylvania identification by thermal IR imagery

09 p1439 A71-23217

Aerial photographic measurements of terrain spectral reflectance and analysis of water resource color and quality by scene color standard technique

09 p1439 A71-23218

Aerial and orbital remote sensing of water quality, considering waste materials effect on coastal marine environment

11 p1760 A71-26504

Mineral and water resources remote sensing, discussing sensor systems and data interpretation techniques with special reference to Colorado Bonanza project
11 p1760 A71-26531

Remote sensors for hydrogeologic prospecting in arid terrains, recommending vertical and horizontal polarized microwave radiometers
18 p2913 A71-36362

Life support water management subsystem 4-man 90-day test in space station simulator with closed water and oxygen loops and no resupply
[ASME PAPER 71-AV-6] 18 p2865 A71-36373

Skylab life support systems design and performance prediction covering thermal and humidity control, atmospheric supply, carbon dioxide removal, water and waste management
[ASME PAPER 71-AV-14] 18 p2866 A71-36381

Space shuttle environmental control and life support system design covering atmospheric pressure, composition, humidity, temperature, water and waste management
[ASME PAPER 71-AV-16] 18 p2867 A71-36383

Aerial and satellite environmental water quality control surveillance, discussing remote sensing techniques and objectives
19 p3059 A71-38402

Oxidation of water in regeneration under spacecraft conditions, measuring organic impurities degree of oxidation in inhabited cabin atmospheric vapor condensates
22 p3506 A71-42814

WATER POLLUTION

Aerial and orbital remote sensing of water quality, considering waste materials effect on coastal marine environment
11 p1760 A71-26504

Environmental water pollution observation by remote sensing, discussing aerial photography
19 p3059 A71-38403

Global environmental monitoring and remote sensing from satellites, considering thermal, air and water pollution
22 p3534 A71-41961

WATER PRESSURE

Preencapsulated strain gage measurement during water pressure tests on site built vessels
17 p2744 A71-35238

WATER PURIFICATION

U WATER TREATMENT

WATER RECLAMATION

Cosmonaut water supply and regeneration in spacecraft using self contained biological cycle
01 p0025 A71-11150

Artificial mineralization of water regenerated from human waste products in space flight
15 p2362 A71-31309

Reverse osmosis application to wash water recovery in manned space mission life support systems, emphasizing membranes development
[ASME PAPER 71-AV-1] 18 p2864 A71-36368

Closed cycle life support water electrolysis system using solid plastic sheet electrolyte/ion exchange membrane/sulfonated perfluoro polymer
[ASME PAPER 71-AV-9] 18 p2866 A71-36376

Automated self sterilizing breadboard unit for potable water reclamation from urine by electrolysis-electrodialysis for long term space missions
[ASME PAPER 71-AV-11] 18 p2866 A71-36378

Space station life support prototype vapor diffusion water reclamation system for pure and sterile water distillation from urine process stream
[ASME PAPER 71-AV-31] 18 p2869 A71-36398

Urine preservatives for urine water recovery system, noting ammonia and organic compound contents in condensate
22 p3506 A71-42809

Decontaminating methods for water regenerated from urine under space flight conditions by filtering water condensate through sorbents
22 p3506 A71-42815

Group analysis of impurities in water regenerated from liquid human wastes
24 p3800 A71-44529

WATER RECOVERY

U WATER RECLAMATION

WATER TAKEOFF AND LANDING AIRCRAFT

NT SEAPLANES

U AMPHIBIOUS AIRCRAFT

WATER TREATMENT

Water cooled head cap for heat stress amelioration in subjects working in warm environments
06 p0859 A71-17611

WATER TUNNELS

U HYDRAULIC TEST TUNNELS

WATER VAPOR

Stratospheric and mesospheric water vapor content by satellite-borne spectral measurements
01 p0120 A71-11103

Commercial SST environmental effects on stratospheric air, water vapor content and earth surface temperature
01 p0074 A71-11178

High altitude aircraft effects on stratospheric ozone due to added water vapor, discussing effects on solar energy transmission, surface temperature and weather
01 p0120 A71-11341

Water vapor emission measurement, using shock tube for gas heating and black body calibrated optical system for radiation measurement
01 p0028 A71-11348

Kinetic equations of quasi-steady homogeneous condensation of water vapor in supersonic nozzle two phase flow
01 p0182 A71-11443

Photochemistry, diffusion and escape of atomic and molecular hydrogen on Mars, noting water vapor spectroscopy consistent with temperature profiles
01 p0162 A71-11488

Energetic electron precipitation effects on upper D region water cluster ion population at various vapor mixing ratios
02 p0245 A71-11961

Hydroxyl and water vapor emission properties in interstellar medium attributed to maser action
02 p0313 A71-12498

Atmospheric water vapor dimers absorption of microwaves, computing total absorption coefficient
03 p0378 A71-13295

Martian atmospheric water vapor latitude distribution, evaluating high dispersion spectroscopic observations
03 p0488 A71-13555

Mars atmosphere carbon dioxide condensate cloud layer implications, considering temperature lapse rate and water condensation at lower levels
03 p0489 A71-13608

Thermal radiation from hot water vapor and carbon dioxide imbedded in cool atmosphere, using extended molecular band models
03 p0518 A71-13649

Mars atmospheric water vapor detection during Southern Hemisphere spring and summer season
04 p0645 A71-15139

Artificially produced holes closing in clouds, investigating role of water vapor and droplets turbulent diffusion by mathematical model
05 p0777 A71-16668

IR radiation absorption by water vapor in atmospheric transmittance windows, discussing fine structure of absorption spectrum
05 p0778 A71-16841

Water vapor condensation due to heterogeneous nucleation in nozzles, considering flows seeded with inorganic smoke and metallic ions
[ASME PAPER 70-FE-22] 05 p0737 A71-16974

Mars atmospheric data from Mariner flights, discussing north polar haze, bright surface features morphology, multiring structures and water vapor exchange
06 p0965 A71-17627

Electronic compensation of water vapor effects in respiratory mass spectrometry
07 p1052 A71-20335

Stratospheric and mesospheric water vapor content by satellite-borne spectral measurements
08 p1277 A71-20847

Condensed water vapor in supersonic nozzle flow, describing dispersion coefficient measurement
08 p1275 A71-21269

Commercial aviation stratospheric water vapor injections influence on radiation budget, ozone, polar night cloudiness and potential climatic effects
08 p1286 A71-21822

Water vapor condensation effects on methane-air combustion gases for aerodynamic test medium
[AIAA PAPER 71-258] 08 p1377 A71-21986

French book on thermodynamics and gas dynamics covering theoretical and applied thermodynamics, air compressors, combustion, internal combustion engines, water vapor, compressible fluid cooling, etc
09 p1545 A71-22965

Atmospheric water vapor dimers microwave absorption, computing total absorption coefficient
09 p1408 A71-23268

Single to triplet transitions of water vapor as function of scattering angle in electron impact detection
09 p1498 A71-23381

Solar spectrum observations in water band at 1.87 micron by stratospheric balloon sounding
10 p1667 A71-23863

Book on electrical equipment deterioration in adverse environments covering climatic action, excessive heat, atmospheric temperature variations, water vapor adsorption and condensation, etc
10 p1583 A71-24478

High resolution measurement of carbon dioxide broadened half widths for water vapor lines in fundamental band
10 p1645 A71-24965

Half widths calculation for carbon dioxide broadened water vapor absorption lines in nu sub 2 fundamental, considering dipole-quadrupole interactions
10 p1645 A71-24966

Daytime atmospheric water vapor measurements at IR astronomy mountain sites in southwestern U.S.
11 p1793 A71-25243

Comparative accuracies of vertical atmospheric water vapor profiles by radiosonde and laser backscatter Raman component
11 p1794 A71-25383

Water vapor latitude variation on Mars from Coude spectrograph of 107 inch telescope
11 p1826 A71-25716

Martian atmospheric water vapor abundance during 10 February-25 April 1969 Mars opposition by spectroscopic observations
11 p1826 A71-25717

Mo evaporation in vacuum, oxygen and water vapor atmospheres at high temperatures
11 p1709 A71-25865

Hot water vapor curve of growth, using statistical band model with exponential line intensity distribution yielding spectral absorption coefficients
12 p1904 A71-26793

Water vapor dimer effects on atmospheric brightness temperature in cm and mm radiometric investigations from satellites above ocean areas
12 p1901 A71-27099

Flash UV photolysis of ozone/water vapor mixtures, noting OH radical nonreaction with ozone
13 p0205 A71-28349

Noctilucent cloud formation from water vapor concentrations in mesosphere and lower thermosphere of arctic and midlatitude regions measured by rocket-borne RF mass spectrometers
14 p2232 A71-29957

Water vapor contamination long lasting effects on stratospheric measurement during balloon flight
14 p2270 A71-30453

Cloud control and modification through seeding with hygroscopic compounds
14 p2271 A71-30611

CW 28 micron signal resonant regenerative amplification in pulsed water vapor laser, showing pulse to pulse frequency coherence
14 p2255 A71-30832

Water vapor emission map at 22 GHz from W 49, using three-station long baseline radio interferometer data
16 p2631 A71-33179

Vapor bubble growth on heated surface with random temperature distribution and liquid microfilm for water and boiling potassium
17 p2836 A71-34306

Water vapor effects on shock compressed air in thermodynamic equilibrium by computer program, noting temperature and electron concentration reduction
18 p2984 A71-35857

Venus surface temperature dependence on incident solar flux based on runaway greenhouse nonray calculation, considering water vapor as IR opacity source in models
18 p2964 A71-36285

Water vapor electrolysis for oxygen generation and humidity control in long term manned space flight
[ASME PAPER 71-AV-24] 18 p2868 A71-36391

Hot water vapor total emissivity charts at various temperatures, using band model parameters with spectroscopic data
18 p2985 A71-36592

Indirect reduction of vertical atmospheric water vapor profile from measured outgoing thermal radiation by regularization method
19 p3090 A71-37966

Atmospheric pressure and temperature inhomogeneities effects on thermal radiation transmission function of water vapor
19 p3090 A71-37973

Surface layer humidity correlation to height of atmosphere emitting in IR spectral region, determining water vapor content by recording earth radiation angular distribution
19 p3054 A71-37974

Water vapor effect on vibrational relaxation of CO in shock tubes, measuring IR emissions
19 p3012 A71-38084

Atmospheric water vapor effects on microwave frequencies refraction index structure
19 p3024 A71-38611

Dissolved and mixed water vapor condensation aerosol nuclei thermodynamic properties from aircraft and ground-based cloud measurement data
19 p3092 A71-38686

Cloud elements evolution, investigating electrical charges effects on ice crystal growth rate in water vapor by laboratory experiment
19 p3092 A71-38688

Amino silica gels absorption properties with respect to carbon dioxide, hydrogen sulfide and water vapor, comparing affinity
20 p3193 A71-39233

Nimbus 2 satellite observed 6.7 micron water vapor radiation, compared to calculated radiances
21 p3373 A71-40224

Water vapor dimer effects on atmospheric brightness temperature in cm and mm radiometric investigations from satellites above oceans
22 p3533 A71-41654

HCN and water vapor submillimeter and far IR laser frequency measurement against fundamental frequen-

cy standard by harmonic generation and beat frequency detection

22 p3557 A71-42152

Hydrous analog stability in lunar amphibole Apollo samples as function of water vapor pressure and temperature

23 p3743 A71-43648

Gas interaction with lunar fines, investigating carbon monoxide, nitrogen, oxygen, argon and water vapor adsorption

23 p3758 A71-43754

Vertical atmospheric humidity profile variations relationship to clouds water vapor content from thermal radio emission measurements onboard Cosmos 243 satellite

23 p3673 A71-44048

Temperature field measurements above porous surface during ice-water sublimation into vacuum, showing discontinuities due to external heat and mass transfer

23 p3784 A71-44340

Radio-optical dispersometer for atmospheric water vapor density measurement with increased sensitivity

24 p3809 A71-44985

Absorption spectrum of atmospheric gases from laser spectrometer based on tunable ruby laser, measuring water vapor absorption coefficients in multipass cell

24 p3834 A71-45207

WATER VEHICLES

NT AIRCRAFT CARRIERS

NT CARGO SHIPS

NT NUCLEAR POWERED SHIPS

NT SATELLITE COMMUNICATIONS SHIPS

NT SHIPS

WATER WAVES

Thermally driven motion of water with free surface in rotating annulus, investigating steady wave flow by three dimensional nonlinear Navier-Stokes equations numerical integration

24 p3844 A71-44417

WATTMETERS

Acoustic wattmeter with piezometric electric signal sensor and amplifier for measuring elastic wave intensity in liquids

07 p1114 A71-20059

AC power meters using electronic multiplier for overcoming limitations concerning frequency ranges, response times, power factor and distortion

10 p1609 A71-23918

Radio frequency power meters comparison, reducing mismatch and directivity errors with directional coupler

14 p2205 A71-30984

WAVE ATTENUATION

NT ACOUSTIC ATTENUATION

NT RADAR ATTENUATION

NT RADIO ATTENUATION

NT SHOCK WAVE ATTENUATION

Collisionless damping of electromagnetic waves in regions with strong homogeneity of cold plasma

02 p0291 A71-12509

Visible and IR radiation attenuation in rain and snow, comparing calculation based on Mie diffraction formulas with measurement

05 p0718 A71-15992

Electromagnetic wave absorption in steady state cosmology, considering particle collision and radiation damping effects in plasma model

05 p0806 A71-16167

Electromagnetic wave absorption in Einstein-de Sitter cosmology, considering collision and radiation damping effects for radiated angular frequencies

05 p0806 A71-16168

High amplitude stress wave propagation in anisotropic quartz-phenolic composite, noting strong pulse amplitude attenuation

06 p1004 A71-18618

Dissipation and nonlinearity effects on linear three dimensional wave front, obtaining Burger equation for gas dynamics

09 p1433 A71-23053

Submillimeter wave extinction in clouds and fogs, using spectrometric results of water optical properties

09 p1408 A71-23375

Italian book on microwave propagation covering electromagnetic wave attenuation, rainfall space-time structure and radioelectrical/meteorological data recording

11 p1731 A71-25650

Nonlinear skin effects in gas discharge plasma during electromagnetic wave propagation with dissipation, obtaining wave amplitude and carrier temperature dependence on reflection parameters

13 p2108 A71-29042

Helical wave deceleration with inhomogeneous plasma approximated by anisotropically conducting plane

14 p2279 A71-30115

Longitudinal waves correlation damping in high temperature plasma under magnetic field, calculating dielectric constant by quantum statistical method

14 p2280 A71-30450

Longitudinal wave absorbers attenuating resonance vibrations in rods and plates

15 p2504 A71-31707

Dispersion and attenuation of plane longitudinal waves in laminated medium of elastic and viscoelastic layers, showing effect of composite parameters variations

[ASME PAPER 70-WA/APM-40]

15 p2505 A71-32009

Radiation from electrostatic waves in thin current sheet in geomagnetic tail into cold magnetized plasma, noting wave damping for wide frequency range

16 p2562 A71-32805

Pressure histories due to weak shock wave propagation through dividing flow junction, describing wave decay in side branch duct

16 p2555 A71-32887

Elastic seismic waves attenuation in polycrystalline ceramics and rocks by grain boundary relaxation, noting strong frequency dependence of earth mantle internal friction

17 p2735 A71-35390

Detonation wave with dual front structure, calculating attenuation in Chapman-Jouquet regime by boundary shock layer method

17 p2839 A71-35635

Dissipative wave motion asymptotic theory, considering initial boundary value problems for linear partial differential equations

18 p2910 A71-36819

Turbulence measurement by crossed laser beam attenuation due to scattering from particles in clean or seeded flow, studying damping and transport of matter

21 p3392 A71-40400

Elastic-plastic stress wave attenuation, applying theory of wave propagation in single crystals to flow field numerical solution

21 p3465 A71-40786

Pulse attenuation in composite materials, discussing stress waves geometric dispersion and compressive fracturing effects

21 p3465 A71-40791

Light wave attenuation in fog, mist, rainfall and snowfall during propagation through atmosphere, deriving semiempirical formulas for attenuation rate relationship to visibility

22 p3569 A71-42523

Temperature and frequency dependence of electron phonon interaction maxima in rhenium, explaining transverse and longitudinal waves ultrasonic attenuation by two band theory

22 p3578 A71-42597

Ion acoustic waves dispersion relation, presenting attenuation and phase velocity tables

23 p3667 A71-43138

Plastic work hardening produced by pressure application to spherical cavity surface in infinite elastoplastic medium, considering spherical elastic wave attenuation

23 p3775 A71-43147

Coherent acoustic wave propagation speed and attenuation coefficient in turbulent flow

23 p3703 A71-43209

Azimuthal guiding surface wave attenuation with curvature applied to dielectric clad circular cylinder, including impedance tables

24 p3804 A71-44991

WAVE DIFFRACTION

Shock wave diffraction at sharp edges, discussing physical principles, angle and pressure ratio effects

01 p0001 A71-10109

Plane shock wave diffraction at wedge, analyzing role of gas specific heats ratio

01 p0070 A71-10664

Horizontal shear wave diffraction by finite crack and rigid ribbon in elastic medium

01 p0173 A71-10845

Plane acoustic wave diffraction by dense periodic grating, using crimped surface scattering with Neumann and mixed boundary conditions

01 p0128 A71-11120

Diffraction of cylindrical wave on thin infinite weakly reflecting cylindrical shell

01 p0128 A71-11121

Plane acoustic wave diffraction and acting force on sphere in low viscosity medium, obtaining asymptotic formulas for pressure, velocity and intensity

01 p0128 A71-11123

Diffraction on smooth convex body, constructing convergent series for homogeneous wave equation solution

01 p0038 A71-11203

Polarization structure of paraboloid mirror antennas circular emission by geometrical diffraction theory of spherical edge waves

01 p0056 A71-11204

Diffraction properties of three dimensional asymmetric gratings for reflected and transmitted E-polarized waves

01 p0038 A71-11215

Two dimensional diffraction of plane wave by perfectly conducting wedge using straightforward scattering approach

03 p0456 A71-13347

Far field diffraction of unidirectional surface wave by conducting rectangular wedge in cold anisotropic plasma, showing frequency dependent transmission coefficient

03 p0465 A71-13993

Vertical dipole electromagnetic field diffraction by circular aperture in opaque screen with coaxial concentric conducting disk

03 p0379 A71-13967

Plane acoustic wave diffraction at thin semiinfinite elastic plate, reducing to Riemann boundary problems for Helmholtz equation in half space

03 p0459 A71-14067

Soviet book on electromagnetic waves diffraction and propagation covering numerical analysis, media and asymptotic theory based on local field principle

03 p0380 A71-14407

Plane electromagnetic wave diffraction on infinite system of parallel metallic strips, determining natural frequencies

04 p0549 A71-14611

Electromagnetic wave glancing incidence on ideally conducting screen of infinitely thin strips by geometrical optics approximation

04 p0625 A71-14646

Plane wave diffraction by double grating of thin circular cylinders, determining field polarization in x directions parallel and perpendicular to axis

05 p0718 A71-15995

He-Ne laser beam parameters and diffraction field measurement by holography

05 p0760 A71-16260

Bragg diffracted light intensity increase from standing resonating acoustic wave, considering applicability for laser communication multiplexing and demultiplexing

05 p0720 A71-16269

Far field characteristics for diffraction of plane harmonic electromagnetic wave obliquely incident on rectangular wedge in uniaxially anisotropic medium

05 p0781 A71-16144

Crack extension by incident elastic wave diffraction for specific shear stress character at wave front

05 p0825 A71-16709

Diffraction on strip, investigating for Dirichlet boundary conditions, deriving excited current density and scattered pattern

05 p0722 A71-16869

Structural information propagation in optical wave fields arising in diffraction and scattering of quasis-monochromatic light by fixed objects

05 p0753 A71-16903

German monograph on shock wave diffraction wedge angular changes in ideal gas region, comparing experimental with perturbation theoretical results

05 p0737 A71-17107

Complex incident fields analysis by ray diffraction method, using set of simple sources with same amplitude and phase characteristics as actual incident field

06 p0868 A71-17728

Fourier resonance associated with electromagnetic wave diffraction from multilayer gratings

06 p0870 A71-18349

Electromagnetic wave diffraction by multielement and multilayer arrays, discussing asymptotic solution, error estimate and convergence

07 p1060 A71-19180

Shock wave diffraction by two dimensional weak disturbances, using aerodynamics blast method

07 p1223 A71-19255

Arbitrary strength and shape shock front propagation past ocean surface, calculating diffraction at interface

07 p1094 A71-20614

Field intensity of plane electromagnetic wave diffracted at conducting sphere

08 p1252 A71-20735

Three diffracting light beams parametric interaction, applying variational method to theory of backward wave parametric oscillator

08 p1334 A71-21181

Electromagnetic wave diffraction by variable curvature and surface impedance cylindrical structure

08 p1254 A71-21356

Long range tropospheric radio wave propagation, calculating signal impulse function and time lag between diffraction and reflection

09 p1404 A71-22217

Artificial dielectric refractive index with diffraction allowance as function of multilayer geometry, wave frequency, polarization and propagation direction

09 p1406 A71-22884

Book on applied diffraction theory covering scalar and vector wave theory, radio wave propagation, linear integral equations, microwave lens, Fabry-Perot interferometers, etc

09 p1494 A71-22959

Electric field equations of plane EM wave diffraction at lattice of conducting cylinders, using Hankel function

09 p1408 A71-23113

Near field asymptotic solution for electromagnetic wave diffraction by perfectly conducting wedge, using steepest descent method

09 p1411 A71-23679

Stiles-Crawford effect interpretation by geometrical optics interferences, microwaves and diffraction scalar theory, calculating retinal cones mean diameters

10 p1560 A71-23991

Laboratory model for radio star scintillation and other diffraction phenomena by thin weak random phase changing screen including earth atmosphere or solar wind

10 p1678 A71-24797

Short N wave refraction and diffraction by gas-filled soap bubble, discussing measurements to explain peaking and rounding in sonic boom pressure signature

10 p1642 A71-24811

Electromagnetic wave diffraction on arbitrary spheres, including scattering and attenuation by four water droplets

10 p1579 A71-24877

Doppler geodetic measurements, discussing ionospheric wave diffraction errors, refractive index and electromagnetic wave propagation

11 p1732 A71-25831

Handbook on radar cross section, Volume 1, covering scattering theory, edge/tip diffraction, creeping/traveling waves and various geometric shapes

11 p1733 A71-26008

Diffraction of spherical wave on triangular prism, using reduction by group theory of point sources

12 p1878 A71-26838

Cylindrical cavities in infinite series, examining shear wave diffraction

12 p1975 A71-27109

Elastic plane shear wave diffraction on elliptical cylinders in half space, using elliptical wave function series and linear algebraic equations

12 p1978 A71-27332

E- and H-polarized waves diffraction on three antenna arrays crossing at arbitrary angles

12 p1882 A71-27615

Uniform asymptotic diffraction of plane wave from ideally reflecting cylinder, using parabolic equation method

13 p2027 A71-27900

Inverse diffraction of plane wave by periodic and doubly periodic arrays, calculating velocity potential and pressure distributions for Neumann and Dirichlet problems

13 p2027 A71-27905

Elastic wave diffraction in infinite series of spherical cavities with centers on straight line

13 p2100 A71-28275

Electromagnetic wave diffraction by ideally conducting wedge of finite radius, deriving asymptotic formula for plane wave scattering

13 p2029 A71-28360

HF diffraction of plane electromagnetic waves by ideally conducting iris diaphragm, developing boundary value problem asymptotic solution

13 p2029 A71-28448

Diffraction-limited electromagnetic theory of image formation for point reference arbitrary shape hologram

13 p2072 A71-29440

Reflection, diffraction and transmission of plane microwave incident on conducting screen perforated periodically with circular holes, using transmission line analysis and dipole moments method

14 p2192 A71-29568

Electromagnetic wave diffraction coefficients for discontinuity in curvature from surface field asymptotic description near singularity

14 p2192 A71-29794

High coupling low diffraction loss cut for acoustic surface wave propagation on lithium niobate

14 p2283 A71-29796

Plane electromagnetic waves diffraction by moving periodic metal strip grating, taking into account relativistic effects

14 p0000 A71-30076

Stationary saddle points phase method for wave diffraction problems in inhomogeneous medium, deriving asymptotic expansion for surface integrals

14 p2194 A71-30078

Electromagnetic wave diffraction at multilayer wire grating, discussing computer program for diffraction field calculation

14 p2194 A71-30086

Plane shock wave diffraction at wedge, analyzing role of gas specific heats ratio

14 p2228 A71-30997

Light beam diffraction by supersonic waves, calculating amplitudes with difference-differential equations

15 p2450 A71-32075

Circular aperture microwave antenna near field calculations based on ray diffraction theory in geometrical optics

15 p2372 A71-32366

Matched/mismatched crossed beam interference field combination with sinusoidal holographic diffraction grating, studying metric properties and moire-obtured bands

15 p2410 A71-32404

Interferometric observation of photon fluctuation during Fraunhofer diffraction by small round hole, considering light granular structure at low intensities

15 p2421 A71-32405

Fabry-Perot interferometer laser beam diffraction effects on fringe pattern formation, deriving field distributions in near and far zones

15 p2421 A71-32459

Shock wave diffraction patterns on plane walled convex corners in air, nitrogen and carbon dioxide at various Mach numbers

16 p2556 A71-32918

Plane oblique shock wave diffraction on wedge moving in homogeneous gas flow at supersonic speed, reducing boundary value problem to Hilbert problem

16 p2519 A71-32930

Light diffraction by holographic gratings in pink ruby due to absorption coefficient spatial variations

16 p2578 A71-33149

Plane electromagnetic wave diffraction on ideally conducting convex body of large electrical dimensions, obtaining Maxwell equations asymptotic solution

16 p2542 A71-33485

Diffraction on smooth convex body, constructing convergent series for homogeneous wave equation solution

17 p2697 A71-34255

Polarization structure of parabolic reflector antennas circular radiation by geometrical diffraction theory of spherical edge waves

17 p2697 A71-34256

Diffraction properties of three dimensional asymmetric arrays for reflected and transmitted H- and E-polarized waves

17 p2698 A71-34266

Electromagnetic wave diffraction by moving wedge with surface impedance, evaluating Doppler shifts and scattered field in shadow region

17 p2698 A71-34429

Book on optical holography covering basic concepts, Fourier transform, propagation and diffraction, pulsed lasers, interferometry, geometric analysis of point source hologram, etc

17 p2738 A71-34450

Arbitrary cross sectional semiinfinite conductor, investigating electromagnetic wave diffraction

17 p2701 A71-34754

Total diffraction efficiency of transmittance storage holograms, using space dependent contrast function

18 p2915 A71-35902

Nonlinear diffraction of weak shock waves near rigid wall with sharp bend, obtaining approximate solution by matched asymptotic expansion method

19 p3043 A71-37100

Diffraction by perfectly conducting plane screens solved by Hilbert space formulation of EM diffraction

19 p3018 A71-38192

Wave diffraction at step junction of two rectangular waveguides and symmetrical diaphragm with dielectric fillers

19 p3019 A71-38332

Plane electromagnetic wave diffraction by dense periodic array with Dirichlet and mixed boundary conditions, determining solution asymptotic behavior

19 p3104 A71-38416

Plane electromagnetic wave diffraction by circular cylinder with longitudinal slot, determining scattered field by Riemann-Hilbert method

19 p3020 A71-38417

Free space diffraction of E-polarized plane electromagnetic wave by slit in thick conducting screen, deriving approximate solution from Wiener Hopf equation by matrix techniques

19 p3023 A71-38592

Diffraction loss equality in field distribution at confocal laser resonator mirrors with circular coupling holes

20 p3242 A71-38850

Physical interpretation of electromagnetic waves attenuation function HF singularity during diffraction over spherical surface, applying to short wave diffraction in tropospheric model

20 p3198 A71-39802

Shock fronts diffraction and reflection with vortices generation at discontinuities, predicting wave shape and strength distribution in two dimensional or axisymmetric situations

21 p3365 A71-40016

Far field light diffraction due to circular plane wave apertures rendered partially coherent by atmospheric turbulence

21 p3415 A71-40635

Shock wave diffraction at symmetric lenticular wing profile with free stream critical Mach number of 0.87, using Godunov difference scheme

21 p3322 A71-40679

Plane acoustic wave transmission problem through finite chord plate array in subsonic gas flow, using factorization method in diffraction theory

21 p3322 A71-40686

CdS single crystal acoustoelectric domain determination, using light diffraction method

21 p3436 A71-41364

Plane electromagnetic wave diffraction by infinite system of parallel metallic strips, determining natural frequencies and eigenfunctions

22 p3510 A71-42251

Wave diffraction by air gap multilayered dielectric coated sphere with azimuthal slot for low loss transmission, obtaining radiation pattern

22 p3522 A71-42283

Plane electromagnetic wave diffraction on periodic arbitrary profile array, presenting near and far field asymptotic characteristics

22 p3511 A71-42306

Low temperature thermal insulation using diffraction effects of multilayer perforated reflecting screens

22 p3622 A71-42678

Plane wave diffraction by double grating of thin circular cylinders, determining field polarization in directions parallel and perpendicular to axis

22 p3515 A71-42744

Millimeter transverse electric wave diffraction by spherical plasma, interpreting interferometric measurements of electron density

23 p3708 A71-43085

Dual integral equations solutions to electromagnetic wave diffraction at plane conducting slotted screen

23 p3644 A71-43258

Light modulator based on Doppler effect and diffraction, providing spatially separated beams with different wavelengths

23 p3678 A71-43535

Plane electromagnetic wave diffraction on dense periodic array at conducting screen, showing far field asymptotic behavior for E and H polarization

23 p3647 A71-44331

Plane electromagnetic wave diffraction by infinitely conductive grating at nonorthogonal incidence angles, using conformal mapping technique

24 p3847 A71-44357

Electromagnetic wave diffraction properties by ribbon metallic lattice in optically active media using Riemann-Hilbert method

24 p3804 A71-44716

Convolution integral equation unique solution in second kind Fredholm equation form, applying to plane polarized electromagnetic wave diffraction on infinitely thin band

24 p3804 A71-44769

Numerical analysis of electromagnetic wave diffraction on inhomogeneous transmitting bodies, reducing Maxwell equations boundary value problem to differential equations solution

24 p3804 A71-44772

Two sided error estimates for electrodynamic impedance, admittance and scattering matrices in diffraction theory

24 p3805 A71-45256

Nonlinear equations of compressible medium motion near point of contact between shock and diffraction waves

24 p3821 A71-45365

WAVE DISPERSION

Plasma beam systems dispersion equation with allowance for electron collisions with heavy particles

01 p0132 A71-10154

Wave dispersion and evanescent modes in rectangular waveguides filled with transversely inhomogeneous dielectric rod

01 p0056 A71-11196

Trapped LF ion wave propagation along warm plasma cylinder imbedded in dielectric, obtaining dispersion relation

01 p0136 A71-11476

Ray tracing in warm collisionless magnetoplasmas based on wave dispersion relation, discussing satellite communication

01 p0137 A71-11612

Laser channel multipath dispersion due to atmospheric inhomogeneities for point and nonzero-area apertures under clear weather conditions

02 p0214 A71-12034

Dispersion relation for LF quasi-static ion acoustic waves in finite geometry plasma

03 p0464 A71-13933

Nonpotential ion cyclotron waves propagation at very large angles to unperturbed magnetic field, obtaining dispersion relation numerical solutions

03 p0420 A71-14530

Spectral analysis increased sensitivity for dispersion systems, using optimum filtering of spatial frequencies

04 p0590 A71-14838

Electrostatic waves linear dispersion relation in Maxwellian unmagnetized ions and magnetized electrons Vlasov plasma

05 p0789 A71-16656

Vertical behavior of stratospheric optical thickness and dispersion coefficient in red region of spectrum

from photometric analysis of Soyuz 3 photographs of daytime horizon

05 p0742 A71-16839

Similarity methods, partial differential numerical analysis, dispersive wave and perturbation theory applications to mechanics

06 p0920 A71-18220

Uniaxial compression effect on dispersion of helicon wave in n-type semiconductors, considering strain potential constants determination

07 p1176 A71-19269

Wave dispersion in transversely isotropic rods, discussing phase velocities, spectral lines and cut-off frequencies

07 p1214 A71-19957

Dielectric loaded waveguide electromagnetic field and coupling matrix derivation by finite element computer program, presenting dispersion curves and field plots

08 p1262 A71-20765

Plane light wave interactions with moving dispersive dielectric medium, considering electron UV or ion IR resonant oscillation in regions of anomalous dispersion

08 p1253 A71-21278

Geometric dispersion of dilatational stress wave propagating in laminated plate composite, comparing transmitted wave forms to code calculations

09 p1538 A71-22687

One dimensional plasma wave nonlinear dispersion relation, stability and harmonic generation from statistical properties of trapped particle orbits in random potential

09 p1503 A71-22862

Dispersion equations of plane parallel waveguide filled with hot magnetized plasma, using linear approximation

09 p1503 A71-22883

High power magnetically tunable microwave interference filters based on spin waves magnetic field dependent dispersion in ferrimagnetic materials

09 p1421 A71-23721

Plasma decay turbulence in spatially homogeneous ensemble of undamped dispersive waves in macroscopic and Vlasov terms, using time asymptotic perturbation method

10 p1647 A71-23887

Microwave devices with transmission lines excited by curvilinear electron beams, deriving dispersion equations for TWT with allowance for space charge effect

10 p1584 A71-24717

Tunable organic dye laser with dispersion prism for increased radiation spectral density and luminescence band smooth frequency control

12 p1912 A71-26757

Two beam interferometry, measuring phase shift and dispersion at slit by channeled spectra

12 p1904 A71-26797

Nonlinear waves in weakly dispersing media, discussing packet self-focusing and -compression, electromagnetic radiation with acoustic oscillations, geometric optics and HF-LF interactions

12 p1929 A71-27166

Sound dispersion in monatomic gases from viewpoint of linearized hydrodynamic, Boltzmann and model equations

12 p1930 A71-27190

Stability of trapped particle equilibrium, considering contribution to plasma wave dispersion

13 p2104 A71-27847

Plane traveling electromagnetic wave existence, propagation and refraction in nonlinear dispersive nonmagnetic isotropic lossless medium

13 p2027 A71-27899

Ion wave frequency shift and instability suppression by RF electric field, examining wave-field coupling

13 p2110 A71-29334

Dispersion and boundary equation concerning space-charge wave propagation under diffusion effect in Gunn semiconductors with anisotropic conductivity and finite thickness

14 p2283 A71-29793

Phase velocity for three dimensional structures of impedance elements, using approximate solution methods and dispersion equation

14 p2194 A71-30080

Magnetized plasma and vacuum plane interface, deriving dispersion equation for electromagnetic surface waves propagating at arbitrary angles

15 p2456 A71-31744

Magnetoactive plasma layer in strong constant magnetic field, computing dispersion equation for large amplitude thermomagnetic wave propagation

15 p2456 A71-31745

Dispersion and attenuation of plane longitudinal waves in laminated medium of elastic and viscoelastic layers, showing effect of composite parameters variations

[ASME PAPER 70-WA/APM-40]

15 p2505 A71-32009

Propagation angle effect on time harmonic wave dispersion in periodically laminated medium, using two dimensional equations of elasticity

[ASME PAPER 70-WA/APM-47]

Collisionless small amplitude shocks in plasmas, considering wave dispersion and critical Mach number effects

15 p2506 A71-32010

Gases refractive behavior, discussing constitutive properties, wave propagation, Lorentz electron theory of dispersion, spectral interferometry and hook method

15 p2459 A71-32561

Ultrasonic pulse technique for plane transverse and longitudinal stress wave dispersion in boron fiber reinforced epoxy composite, determining group velocity dependence on frequency and elastic moduli

[ASME PAPER 71-APM-27]

16 p2600 A71-33202

Isotropic elastic circular cylinders longitudinal stress waves, presenting dispersion relation /Pochhammer equation/ numerical solutions

16 p2658 A71-33625

Electron beam nonlinear interaction with plasma, considering electrostatic wave propagation, instability and dispersion equation

17 p2786 A71-34261

Anisotropy instabilities of hydromagnetic wave propagation at small angle perpendicular to magnetic field above ion cyclotron frequency, calculating dispersion relation

17 p2788 A71-34664

Long distance FM signal pulse propagation and maximum compression synthesis in dispersive media, using asymptotic theory for mathematical treatment

17 p2701 A71-34761

Hall fields effect on interaction of MHD waves in inhomogeneous plasma, considering MHD wave dispersion

19 p3109 A71-37134

Transmitted and reflected waves dispersion and structure in waveguide loaded by semiinfinite series of equidistant homogeneous scattering bodies

19 p3019 A71-38329

Transient RF pulse dispersion along plasma loaded coaxial gas discharge, noting group delay

20 p3272 A71-38783

Pressure anisotropy effects on plasma wave coupling and modification for dispersion in collisionless beam-plasma systems

20 p3273 A71-39045

Dispersion equation determining periodic structures natural modes propagation constants, using induced electromotive and magnetomotive forces method

20 p3198 A71-39806

Time variable dispersion of Crab Nebula pulsar, showing coincidence with occultation by solar corona

20 p3302 A71-39927

E x B plasma instability in auroral arcs, deriving dispersion relation

21 p3373 A71-40045

Cosmic plasma electron thermal motions effects on cosmic electromagnetic absorption, taking into account electron-electron collision effects in electromagnetic waves dispersion relationships

21 p3442 A71-40162

Shock stress waves dispersion in laminated composite materials

21 p3465 A71-40790

Pulse attenuation in composite materials, discussing stress waves geometric dispersion and compressive fracturing effects

21 p3465 A71-40791

Spiral wave dispersion, wave number and amplitude relationship in Galaxy near inner Lindblad resonance, noting correlation with ionized hydrogen density

21 p3451 A71-40855

Sound wave dispersion in metals in inclined magnetic field, noting sound velocity deviation

21 p3417 A71-41265

Elastic continuous medium with nonlocal interactions, calculating surface waves dispersion equations with boundary solutions

21 p3417 A71-41366

Electromagnetic wave dispersion in interstellar plasma, noting indistinguishable form from natural dispersion of photons with nonzero rest mass

22 p3574 A71-41598

Homogeneous positive plasma column perturbation analysis in axial magnetic field, deriving model for ionization waves dispersion characteristics

22 p3582 A71-41898

LF wave propagation in weakly ionized plasma under magnetic field, observing forward and backward waves dispersions near cathode

22 p3582 A71-41905

Longitudinal electron oscillations damping in ionized plasma, obtaining wave dispersion relation from BGK model

22 p3583 A71-42372

Three-receiver radio wave dispersion analysis application to ionospheric drift records to assess effects of velocity variation with time

22 p3515 A71-42599

Nonlinear waves in weakly dispersing media, discussing packet self-focusing and -compression, electromagnetic radiation with acoustic oscillations, geometric optics and HF-LF interactions

22 p3576 A71-42621

Uniform progressing wave expansions solutions, using comparison equation method for hyperbolic and mixed type equations

22 p3567 A71-42630

Ion acoustic waves dispersion relation, presenting attenuation and phase velocity tables

23 p3667 A71-43138

Pulsar CP 0950 radio emission intensity variations measurement, using dispersion removal technique for interstellar medium signal distortion

24 p3871 A71-44908

Radio-optical dispersometer for atmospheric water vapor density measurement with increased sensitivity

24 p3809 A71-44981

Dispersion characteristics of He-Ne laser at 3.3 microns

24 p3834 A71-45041

HF dispersion, power and energy storage in periodic slow wave waveguides of resonator chains coupled through openings

24 p3805 A71-45253

WAVE DRAG

NT INTERFERENCE DRAG

Induction and wave drag due to Alfvén waves on long cylindrical satellite in ionosphere, investigating radiated power integral

12 p1973 A71-27576

Wing thickness optimal distribution for minimum wave drag in supersonic flow at zero angle of attack for given planform, using Ritz method at lower Mach numbers

13 p1994 A71-29222

Electromagnetic wave propagation in uniform simple medium, demonstrating drag effects relative to inertial and accelerated frame

17 p2699 A71-34431

Nonlinear theory of wave resistance in supersonic ideal gas flow past finite flat axisymmetric bodies, establishing drag relation to flow rate deficit

24 p3790 A71-44773

WAVE EQUATIONS

NT DIRAC EQUATION

NT EIKONAL EQUATION

NT KLEIN-GORDON EQUATION

NT SCHRÖDINGER EQUATION

Diffraction on smooth convex body, constructing convergent series for homogeneous wave equation solution

01 p0038 A71-11203

Weak periodic solutions of hyperbolic partial differential equation with quadratic dissipative term for biharmonic waves

02 p0276 A71-12000

Point source acoustic radiation field in presence of absorbing plane, presenting solutions and approximations based on plane wave reflection and modified image method

03 p0456 A71-13276

Circular plates forced vibrations, considering internal damping and free and supported boundaries in thin plate wave equation solutions

03 p0502 A71-13300

Coupled wave equations for magnetoplasma with anisotropic pressure

03 p0463 A71-13346

Periodicity solutions of Whittaker-Hill equation in trigonometric series form by three term recurrence relations

03 p0450 A71-13372

Papers on hyperbolic equations and waves covering Cauchy problem, Feynman integrals, general relativistic hydrodynamics, flow stability, etc

04 p0626 A71-15575

Adiabatic invariant of nonlinear periodic wave described by partial differential equations in weakly inhomogeneous medium

05 p0780 A71-16177

German monograph on vibration fields representation by superposition of planar waves with complex wave vectors, considering convergent series of Hankel and Bessel functions

05 p0782 A71-16898

Classical many component plasma dynamics with collective particle interactions in self consistent longitudinal electric field, deriving complex wave equations

06 p0937 A71-18062

Macroscopic dynamics of many-component plasmas in electromagnetic fields, discussing formulation in scalar complex wave equations containing pressure and electromagnetic potentials

07 p1168 A71-19688

Bessel equation solutions for electromagnetic and acoustic wave equations in form of Hankel functions

08 p1333 A71-20740

Short shock wave equations for two dimensional steady motions of ideal gas

08 p1276 A71-21871

Higher dimensional wave equation boundary value control, investigating hyperbolic problems in several space dimensions with application of Holmgren and John uniqueness theorems

09 p1424 A71-23467

Scalar wave equation of mutual coherence propagation in turbulent medium with stochastic permittivity using local independence approximation
10 p1641 A71-24398

Two dimensional sound wave equation solution in terms of time retarded arguments, deriving analytical expressions for aircraft noise intensity and power
11 p1797 A71-25144

Sound waves propagation and scattering in moving media, deriving wave equation for acoustical pressure by iterative process
11 p1747 A71-25147

Stable limit cycles and triggering limits of first radial mode in nonlinearly unstable liquid propellant rocket motors, using wave equation and Galerkin method
11 p1836 A71-25162

Longitudinal wave propagation in ideal elastic bar with viscous stress, calculating approximation to non-linear wave equations
13 p2153 A71-28483

Dirichlet, neumann and mixed boundary value problems relative to wave equation for rectangle, discussing solution based on singularity theorem
14 p2266 A71-30810

Matrix solution for wave equation with mode coupling of VLF and ELF radio waves in horizontally stratified layer of anisotropic ionosphere plasma
15 p2373 A71-32444

Forced oscillations of system governed by one dimensional nonlinear wave equations, using perturbation procedure for solutions near linear resonant frequencies
16 p2606 A71-32857

Nonlinearity effects on slow variation of small amplitude constant profile periodic sound waves propagating in radiating gas, deriving nonlinear model wave equations
16 p2607 A71-32858

Constant profile solutions stability for nonlinear wave equations with convection and dissipation
16 p2608 A71-33023

Diffraction on smooth convex body, constructing convergent series for homogeneous wave equation solution
17 p2697 A71-34255

Quasi-linear wave equations approximate solution construction by asymptotic methods
17 p2777 A71-34420

Existence and uniqueness of weak solution of wave equation with nonlinear boundary condition, using Galerkin method
18 p2940 A71-36094

Nonlinear combustion instability in liquid propellant rocket engines, describing unsteady combustor flow with single wave equation
19 p3122 A71-38093

Heat conduction equation coupling to wave equation in adjacent regions from operational method solution of Volterra equation reduced problem
19 p3171 A71-38532

Wave and elementary particles equations invariance properties relationship with respect to Lie group and conservation laws
19 p3105 A71-38579

Nonlinear hydrodynamic field equations transformations into complex wave equations for application to ideal compressible fluids
20 p3211 A71-39031

Short shock wave equations solutions for two dimensional steady flow of ideal gas
20 p3211 A71-39370

Convergence of progressive shock wave solutions for higher order equations of conservation laws with dissipation and dispersion terms, proving shock curves existence
21 p3414 A71-40141

Approximate controllability for boundary value control of higher dimensional wave equation
21 p3360 A71-40253

Kinetic wave equation matrix elements for three resonantly coupled electrostatic plasma waves noting application to electron plasma coupling with ion sound waves
22 p3582 A71-41900

Electrostatic mode wave equations for low beta plasma microinstabilities in axisymmetric magnetic mirror machines, including effects of particle cyclotron, bouncing and drift motions
22 p3582 A71-41902

Wave equations for motion in stochastic medium, using linear random operator theory
23 p3699 A71-43115

Nonlinear wave packet and modulated beam propagation description in approximate heuristic theories, considering chimeras as neoclassical approximation for equations solution
23 p3705 A71-44122

WAVE EXCITATION
NT ACOUSTIC EXCITATION
NT HARMONIC EXCITATION
Nonlinear resonance excitation of ion acoustic plasma waves by weak external electric field, using partial differential equations
01 p0134 A71-11027

Longitudinal oscillations excitation by transverse electromagnetic wave in collision-magnetized plasma, noting LF wave buildup
01 p0134 A71-11030

Plane infinite horn antenna with small aperture angle coupled to waveguide, considering wave excitation
01 p0038 A71-11207

Resonance excitation of high amplitude waves in plasma cylinder by HF azimuthally axially periodic current flowing through coil encircling plasma
02 p0291 A71-12504

Resonant excitation of plane dielectric waveguide by plane monochromatic wave
03 p0378 A71-13798

Polarization control of emission from cross-shaped slots on square and circular waveguide walls via phase and amplitude adjustment
03 p0386 A71-13809

Piezoelectric surface waves physical characteristics, examining excitation relationship to construction of microwave devices
04 p0550 A71-14742

Thin spherical shell with circular cutout under HF axisymmetric excitation by concentrated radial force
04 p0667 A71-15181

Symmetrical wave excitation by electric dipole of conical surface ideally conducting along hyperbolic spirals, obtaining solution by integral transformation
05 p0727 A71-15996

Excited waves due to transverse disturbance normal to boundary in dielectric half of isotropic Vlasov plasma with Cerenkov instability
05 p0789 A71-16658

Plasma electron cyclotron heating, observing wave excitation at 100 MHz and decay after initial wave
06 p0930 A71-17396

Helicon wave resonance excitation and indication in intermediate magnetic fields in semiconductors
07 p1176 A71-19274

Cs ion beam space charge and current neutralization by electron capture for partially ionized plasma formation, investigating longitudinal electrostatic wave excitation
07 p1171 A71-20193

Infinitely long dielectric rod waveguide HE sub 11 surface wave mode launching efficiency, using Fourier integral
08 p1262 A71-20754

Scattering structures of two parallel elliptical cylinders, tapes or combinations, deriving surface current density distribution under plane TM wave excitation
09 p1407 A71-23107

Azimuthal surface waves launching on cylindrical impedance boundary using waveguide open end as excitation aperture
09 p1410 A71-23571

High efficiency gas chamber for obtaining Raman spectra of corrosive gases at atmospheric pressure by He-Ne laser excitation
10 p1619 A71-23857

Parametric excitation of transverse waves in inhomogeneous electron plasma driven by oscillating electric field, using multitime perturbation method
10 p1647 A71-23891

Mode hopping due to GaAs lasers longitudinal mode inhomogeneous sequential excitations perpendicular to junction at injection levels above threshold
10 p1619 A71-24039

EM wave excitation in plane parallel waveguide by rotating relativistic electron flux, deriving dispersion relation and interaction solutions
10 p1577 A71-24323

Quasi-linear theory of inhomogeneities generation in equatorial jet, considering space charge waves excitation by electric current perpendicular to geomagnetic field
11 p1757 A71-25772

Quasi-stationary three dimensional array excitation by large phase shift calculated for circular conducting elements
12 p1885 A71-26840

Plasma turbulent electron and ion heating by large amplitude whistler resonant excitation, investigating mechanisms
12 p1937 A71-27182

Weakly ionized plasma instabilities in high frequency field exceeding electron collision frequency, considering waves parametric excitations
12 p1937 A71-27204

Transverse excitation of elastic ultrasonic waves in CdS piezoelectric plates, considering conductivity effect on damping
12 p1944 A71-27544

Soviet book on detonation waves in condensed media covering excitation and propagation in compacted explosives, liquid/solid explosives and pulsations
13 p2161 A71-28737

Finite antenna arrays excitation patterns, yielding electromagnetic parameters approaching preselected optimal values
14 p2192 A71-29807

Earth-ionosphere waveguide excitation by satellite-borne horizontal dipole antenna, deriving fields at earth surface based on idealized model
14 p2196 A71-30562

ULF geomagnetic pulsations interpretation based on Kelvin-Helmholtz magnetospheric instability mechanism and bounce resonance wave excitation, considering energy exchange with energetic protons
14 p2202 A71-30954

Convectively cooled carbon dioxide-nitrogen-helium electric discharge laser theory based on excitation and relaxation processes, comparing with experiment [AIAA PAPER 71-588]
15 p2419 A71-31574

Longitudinal ionic wave excitation by grid in collisionless Q machine plasma
15 p2456 A71-31820

External off-axis TEM wave transformation into natural oscillation modes in Fabry-Perot resonator under axially disturbance and impinging-excited wave mismatch
15 p2410 A71-32401

Gases high resolution Raman spectroscopy, using mirror system for exciting laser beam multiplication
15 p2423 A71-32600

Aperture field distribution for excitation of surface waves with high efficiency and gain
15 p2378 A71-32627

Plane infinite horn antenna with small aperture angle coupled to waveguide, discussing wave excitation and field strength
17 p2697 A71-34259

Centimeter TEM waves excitation in Fabry-Perot cavity of cyclotron resonance maser by helical electron beam
17 p2750 A71-34263

Coherent electromagnetic excitation of optical transition levels by fluorescence measurement, obtaining dipole moment and relaxation times
18 p2929 A71-35903

Corner reflector excitation by vertical or horizontal log-periodic dipole antenna for unidirectional wide-band radiation, deriving far field expression
18 p2895 A71-36994

Slow wideband excitation of ultrasonic waves with piezoelectric crystal delay line subject to microwave radiation
19 p3015 A71-37251

Turbulence growth during parametric wave excitation, observing thermal noise effects
19 p3104 A71-37852

Auroral radio noise from electrostatic oscillations excited by fast proton beams
19 p3018 A71-38046

Longitudinal wave interaction and excitation by current instability in equatorial jet, considering energy transfer mechanism
19 p3057 A71-38363

Monostatic plane wave scattering by semimfinite perfectly conducting wedge with rounded edge for line source excitation in far field
19 p3023 A71-38593

Line source excitation for maximum aperture efficiency with given side lobe level
19 p3035 A71-38596

Excitation asymmetry effects on current distribution and far field of thin dipole radiators
19 p3036 A71-38604

VLF wave excitation, noting ratios between vertically and horizontally polarized sources
19 p3024 A71-38613

Weakly ionized plasma instabilities in high frequency field exceeding electron collision frequency, considering waves parametric excitations
19 p3117 A71-38616

Electrostatic oscillations excitation in magnetized homogeneous plasma by electromagnetic waves nonlinear interactions, deriving expression for induced fluctuations spectral density
20 p3273 A71-38966

Parametric excitation of ionic waves in ionosphere by irradiation with electromagnetic wave at characteristic electron frequency
20 p3218 A71-39546

Electron oscillation induced longitudinal standing wave excitation and suppression in beam-plasma system by passing electron beam through axially bounded plasma
20 p3275 A71-39864

Shear layers acoustic excitation, considering coupling between sound waves and rotational excited shear waves in flow detachment line
21 p3317 A71-40014

Natural potential and nonpotential electron oscillations excitation in plasma by transverse wave field, determining wave amplitude threshold and excitation instability
21 p3424 A71-41125

Electron beam modulation at optical frequencies, calculating excited radiation characteristics with quantum theory
21 p3420 A71-41254

Finite amplitude monochromatic wave self modulation in nonlinear medium, showing excitation process dependence on initial conditions
21 p3417 A71-41261

- Sound waves excitation and amplification in weakly ionized plasma within alternating electric field
21 p3425 A71-41282
- LF oscillations excitation and resonance amplification in mercury vapor plasma discharge
21 p3425 A71-41283
- Gravitational wave impingement upon static magnetic field, noting EM waves excitation
21 p3417 A71-41397
- Quasi-linear theory of inhomogeneities generation in equatorial jet, considering space charge waves excitation by electric current perpendicular to geomagnetic field
22 p3532 A71-41540
- Stochastic ion acceleration in excitation of LF oscillations in second regime of intense pulsed plasma beam discharge
22 p3577 A71-41814
- Ideally conducting and dielectric coaxial bodies of revolution, investigating joint excitation by TM wave
22 p3522 A71-42304
- Plasma turbulent electron and ion heating by large amplitude whistler resonant excitation, investigating mechanisms
22 p3583 A71-42459
- Nonlinear effects on spatial growth of cesium plasma wave excited by electron beam of varying density and velocity
22 p3584 A71-42535
- Symmetrical wave excitation by electric dipole of conical surface ideally conducting along hyperbolic spirals, obtaining solution by integral transformation
22 p3524 A71-42745
- Traveling ionospheric disturbances excitation in F2 layer by passing acoustic gravity waves
23 p3665 A71-42966
- Electric field induced current distribution on cylindrical antenna, considering delta generator and electromagnetic waves excitations
23 p3643 A71-43122
- Wave phenomena in space chamber rarefied plasma, clarifying spontaneously excited noise wave properties by passive experiment
23 p3710 A71-43365
- Vacuum UV traveling wave excitation by high voltage pulse and hydrogen laser technology
23 p3684 A71-43502
- Magnetosonic wave excitation and electron heating in magnetically confined hydrogen plasma hybrid resonance region
24 p3853 A71-44502
- Electromagnetic waves excitation in coaxial resonator by relativistic electron beam, assuming presence of steady longitudinal magnetic field
24 p3833 A71-44663

WAVE FRONT DEFORMATION

- Laser beam phase front distortion by atmospheric turbulence, discussing interferometric measurements
04 p0608 A71-15137
- Hologram imagery and aberrations computer based analysis, considering hologram geometries and nonchromatic aberrations
08 p1290 A71-21387
- Variance and correlation radius of distortions from transparent dielectric plate, using statistical theory of antennas
11 p1738 A71-26348
- Wavefront overturning in rarefied quasi-neutral plasma, investigating kinetic equations self similar solutions stability
19 p3114 A71-37859
- Pulsed ruby laser holographic instrumentation for materials tests, detailing reflected wave front complex amplitude characterization
20 p3245 A71-39347
- Laser beams amplitude-phase correction by holographic method, obtaining beams with plane fronts and Gaussian amplitude distribution
20 p3245 A71-39413
- Interference patterns from hologram interferometer related to aberration theory
24 p3826 A71-44980

WAVE FRONT RECONSTRUCTION

- NT KINOFORM
- Spatial and temporal coherence effects in holography, giving general formula for reconstructed virtual image
02 p0251 A71-12148
- Three dimensional hologram reconstruction and recording, using extended source
03 p0428 A71-14057
- Image contrast limits in thin phase hologram reconstruction of diffuse objects with large reference-object irradiance ratios
04 p0601 A71-15687
- Nomographs for point source holographic imaging, discussing recording and reconstruction geometry
05 p0753 A71-16913
- Holography development, discussing three dimensional images, fine grain recording emulsions and beam switching during reconstruction
06 p0897 A71-17369
- Faraday and polar Kerr reconstruction effects in stored magnetic holography
[IEEE PAPER 8.1] 07 p1112 A71-19609

- Holographic recording intermodulation noise suppression by image wave field distortion and retrieval, considering signal to noise ratio
08 p1287 A71-21187

- Photographic emulsion model for signal to average noise irradiance ratio analysis in hologram reconstruction
08 p1287 A71-21188

- Hologram imagery and aberrations computer based analysis, considering hologram geometries and nonchromatic aberrations
08 p1290 A71-21387

- Image reconstruction from three dimensional holograms
08 p1292 A71-21488

- Holography of focused images, using arbitrarily shaped off-axis reference wave and white light for image restoration
09 p1442 A71-22393

- Holography principles, discussing formation and reconstruction for in-line, off-axis and Fourier transform type holographic systems
09 p1449 A71-22787

- Constant period discrete holograms features, investigating laser visualization, recording, reconstruction and image focusing
10 p1608 A71-23810

- Holographic image recording and reconstruction in two and three dimensions, including light wavelike nature, Huygens principle, wavefront reproduction and spectral composition
10 p1613 A71-24849

- Holography principles development, history, wave field recording, processing and reconstructing techniques for image quality improvement, laser applications, etc
11 p1767 A71-26352

- Aberration reduction and optimal in-line and off-axis recording geometry in acoustical holography
12 p1904 A71-26794

- Optical beam propagation, determining turbulent medium effects with holographic wave front reconstruction technique
12 p1904 A71-26795

- Fresnel hologram focusing method, considering Leith and Upatnieks wave front reconstruction with diffused illumination
12 p1907 A71-27212

- Hologram mensuration, discussing photogrammetric stereo model differences, close range objects, pointing, geometric fidelity, computerized plate analysis and reconstruction shift
12 p1907 A71-27262

- Plane wave holographic recording and reconstruction, investigating effects of photosensitive medium as three dimensional diffractive pupil
13 p2068 A71-28711

- Aberration-free wave front reconstruction from holograms illuminated at wavelengths differing from forming wavelength
14 p2240 A71-30130

- Hologram size and film type limitations effects on resolution of reconstructed image in edgeline holography
14 p2241 A71-30131

- Photographic emulsion thickness variation effect on wave front recording and reconstruction on holographic plate
14 p2241 A71-30132

- Recorded wave front aperture sharing technique for space division multiplexing of small holograms
14 p2242 A71-30151

- Plane wave and virtual image reconstruction from three dimensional holograms
14 p2248 A71-30676

- Two beam holographic interferometer based on spherical mirrors with laser beam splitting by semitransparent plate and image reconstruction in monochromatic and nonmonochromatic light
15 p2402 A71-31257

- Holographic interferometry, discussing deformation second derivatives mapping and fringes formation and visibility
15 p2403 A71-31262

- In-plane strain measurement by three beam holography using two incident wave fronts
15 p2404 A71-31267

- Optical wave reconstruction from microwave holograms and application to interferometry, considering resolving power and visible images of microwave transparencies
15 p2405 A71-31281

- Continuous holographic recording of wave front temporal variations for nonstationary processes
15 p2413 A71-32788

- Insufficient spatial and temporal coherence effects on holographic image reconstruction by injection laser, noting application to optical data processing
16 p2577 A71-33142

- Pulse laser holographic interferometry for refractivity measurement, considering wave front reconstruction principles
16 p2578 A71-33160

- Three dimensional hologram recording and reconstruction, discussing image geometry, reference beam intensity, size finiteness, transition limits and photosensitive materials
16 p2580 A71-33623

- Red blood cell image hologram reconstruction and superresolution based on coherent physical optics, using computer program
17 p2693 A71-35586

- Phase-only complex valued spatial filter for holographic wave front construction involving amplitude and phase modulations, investigating performance
17 p2745 A71-35590

- Minimum aberrations in image wave front due to wavelength shift between recording and reconstruction beams in holography, using computer program
18 p2914 A71-35846

- Wavefront reconstruction interferometry with acoustical holography using ultrasound camera, surface deformation and mechanically scanned detector methods
18 p2923 A71-36609

- Acoustic or microwave hologram reconstruction into visible three dimensional image in real time
19 p3066 A71-38412

- Fresnel hologram focusing method, considering Leith and Upatnieks wave front reconstruction with diffused illumination
19 p3067 A71-38624

- Long object photography with lens array in non-coherent light and subsequent integrated image focus holography in laser beam for reconstruction in white light
19 p3068 A71-38708

- Multicolor images with volume dielectric holograms in photopolymer materials, reconstructing complex three dimensional images with high resolution in white light
20 p3236 A71-39192

- Pre- or postexposure effect in holographic recording and reconstruction in reference to object beam intensity ratio
20 p3236 A71-39193

- Wave reconstruction from gaseous flow hologram analysis with differential interferometry in polarized light and schlieren techniques with phase filter defocusing
20 p3239 A71-39461

- IR holography with cholesteric liquid crystals as recording medium and carbon dioxide laser as light source, discussing demagnification and image reconstruction
21 p3379 A71-40703

- French book on optical holography covering interference phenomena, image reconstruction from interferograms, geometrical and mathematical aspects, image quality and color holography
21 p3379 A71-40778

- Hologram recording materials within and outside visible spectrum, considering sensitivity, reconstruction efficiency, resolution limitations, nonlinear and noise effects
21 p3380 A71-40920

- Pre- and post-exposure recording in holographic measurement of high object velocities for enhanced image reconstruction
22 p3537 A71-41597

- Holographic electron microscopy, discussing speckle-free illuminated plane object reconstruction from holograms
22 p3538 A71-41732

- Three dimensional imaginary object reconstruction by holographic stereogram method
22 p3538 A71-41734

- Hologram interference fringes formation and location using grating model of diffusely reflecting surface
22 p3539 A71-41739

- Holographic image reconstruction analysis based on two beam interferometry by spatially incoherent light source, obtaining optical transfer function
22 p3539 A71-41740

- Backward propagation method for ultrasonic image reconstruction, examining resolution in near field for high contrast objects
22 p3541 A71-41784

- Digital computer holography, discussing generation, reconstruction, applications in optical spatial filtering and surface testing and sampling and quantization effects
22 p3546 A71-42479

- Millimeter wave holographic imaging for concealed weapon detection by phase-only hologram, discussing recording and reconstruction systems configurations
22 p3546 A71-42485

- Noise-free linear wave front reconstruction from nonlinearly recorded holograms, noting importance of amplitude transfer function
22 p3550 A71-42571

- Hologram recording by optical wave field scanning with arbitrary aperture and point source at center of entrance pupil and photoreceiver
23 p3675 A71-43398

- Physical and technological aspects of holographic recording including optical data processing, Fourier

hologram reconstruction and random structure information determination 23 p3679 A71-43896

WAVE FRONTS

NT SHOCK FRONTS

Exploding wires in photoelastic specimens, examining axially symmetric cylindrical stress wave front with high speed photographs [SESA PAPER 1656] 03 p0459 A71-13769

Detonation waves in gases and two phase systems with nonideal wave front, calculating acetylene explosion parameters for different initial pressures 03 p0520 A71-13991

EEG wave phase durations over human brain surface, examining asymmetry distribution level 05 p0709 A71-16801

Radial direction shearing interferometry, considering wave front radial phase derivative display by axicon or circular grating arrangements 07 p1110 A71-19477

Dissipation and nonlinearity effects on linear three dimensional wave front, obtaining Burger equation for gas dynamics 09 p1433 A71-23053

Metrological holographic interferometry, discussing speckle pattern application for wavefront phase samples 10 p1613 A71-25092

Galaxy M33 density wave velocity and detection, discussing star distribution, H II regions red and blue supergiant and hot stars 11 p1821 A71-25540

Quasi-point type radar target angular motion simulation by controlling electromagnetic wave phase front in receiving field 14 p2193 A71-29825

Fast luminous fronts /ionizing waves/ in Kanal streamer and Townsend discharges in nitrogen, discussing optical space and time resolved measurements 15 p2459 A71-32648

Argon gas ionization behind reflected shock wave front investigation by double probe method with HF multistep pulse voltage 16 p2576 A71-32911

Wave fronts in Einstein-Maxwell theory, showing perturbation propagation along background spacetime metric field 16 p2609 A71-33261

Elastic stress waves propagation in photoelastic layered composite materials, indicating wave front steady state 17 p2824 A71-34816

Detonation wave with dual front structure, calculating attenuation in Chapman-Jouquet regime by boundary shock layer method 17 p2839 A71-35635

One-dimensional numerical model of nonisothermal plasma, showing soliton separation from leading front by ion-acoustic shock waves after reversal stage 19 p3042 A71-37076

Approximate motion equations of gas flow behind detonation front in flat explosive plate covered by inert coating 23 p3781 A71-43358

Multicomponent signal arrival angles wave front analysis from antenna array phase and amplitude measurements for radio direction finding 24 p3803 A71-44647

Telescope wave optical imaging performance, deriving point spread function, radial energy integral and modulation transfer functions for different wave front surface deviations 24 p3849 A71-45204

WAVE FUNCTIONS

NT MOLECULAR ORBITALS

NT PAULI EXCLUSION PRINCIPLE

MF, LF and VLF ionospheric radio wave propagation theory using spherical wave functions for computer simulation 04 p0552 A71-15215

Wave functions of image potential induced surface states of insulators 04 p0630 A71-15395

Spiral waves in galaxies, using crossed stream inclined wave model 04 p0658 A71-15842

Projected Hartree-Fock energy spectra using basis wave functions with harmonic oscillator and Wood-Saxon radial dependence 06 p0929 A71-17577

Nucleus energy spectra projection from Hartree-Fock intrinsic wave functions model space, using coupled orbital matrix elements 06 p0929 A71-17578

Laser resonator mode representation with oblate spheroidal vector wave function through boundary value problem formulation 08 p1301 A71-21293

Partial wave method for nonspherical quantum scatterer, applying to electron elastic scattering by molecules 09 p1496 A71-22237

Wave structure and mutual coherence functions of optical wave propagating in turbulent atmosphere, considering signal to noise ratio 10 p1641 A71-23948

Density matrix components for multiconfiguration wave functions, constructing N electron /spin free/ Hamiltonian configuration interaction matrix 11 p1802 A71-26056

WKB wave functions for one dimensional non-relativistic problems by simple transformation derivation, solving by application of Liouville substitution to Schroedinger equation 12 p1923 A71-27666

Radiation intensity spatial dependence on laser polarization, giving three dimensional model for wave function phase calculation 13 p2077 A71-28046

Electron energy spectra of amorphous semiconductors by cell method, replacing conditions for splicing wave functions by extremum integral 13 p2112 A71-28925

Franck-Condon factors, densities and r-centroids for diatomic molecules, computing vibrational wave functions by FORTRAN V 14 p2276 A71-30297

Electromagnetic inverse scattering model of electrical radius of conducting spherical radar target employing expansion of scattered field in vector wave functions 14 p2196 A71-30564

Hartree-Fock energy levels, transition probabilities and wave functions for highly ionized atoms in B I isoelectronic sequences, including spin-orbit interactions 15 p2452 A71-32597

Electromagnetic absorption cross sections from wave function of free carriers in semiconductors with point defects 16 p2623 A71-34031

Transition probabilities for Ar I, using Coulomb approximation values of radial wave function integral 20 p3271 A71-38776

German monograph on comparison between quantum mechanical approximate methods through projection of approximated eigenfunctions covering Schroedinger equation, wave functions, Born-Oppenheimer approximation, etc 20 p3271 A71-39042

Partial wave method for nonspherical quantum scatterer, applying to electron elastic scattering by molecules 21 p3420 A71-41119

Electron energy spectra of amorphous semiconductors by cell method, replacing wave functions condition extremum integral 21 p3434 A71-41321

Filippov-Ovcharenko wave functions in form of interaction constant inverse power series for calculating two and three nucleon ground state binding energies 22 p3578 A71-42056

WAVE GENERATION

Midlatitude atmospheric gravity waves generation by auroral heating during magnetic substorms 02 p0245 A71-11965

Propagation modes and circularly polarized wave production in circular waveguides with anisotropic walls 03 p0384 A71-13317

Pulsar radio wave generation, discussing emission theory and frequency independence of beam width and polarization 03 p0493 A71-14208

Ionospheric and exospheric ELF magnetic waves generation by high altitude nuclear explosions, discussing hydromagnetic waves propagation 04 p0581 A71-14981

Electromagnetic wave generation by interaction in plasma stream resonator, considering Coulomb friction and boundary reflection coefficients 04 p0633 A71-15110

Wave formation behavior on melting surface of flat plate in heated air stream 04 p0678 A71-15455

Convective cyclotron instability in whistler mode, discussing magnetosphere as generation mechanism and taking into account magnetospheric plasma inhomogeneity 05 p0743 A71-17003

Transition radiation generation zones, determining physical cause 05 p0786 A71-17030

Ion-acoustic waves generation mechanism in outer space by strong electromagnetic radiation, considering quasars, supernovae shells, pulsars and solar supercorona 05 p0800 A71-17196

Ruby laser driven luminous waves during breakdown and heating within freely expanding gas jet observed with streak photography 07 p1126 A71-20168

Transistor circuit constant current technique for wave generation and shaping involving triangular, trapezoid and staircase waveforms 08 p1264 A71-21223

Magnetosonic waves generation by interaction of bow shock with frozen tangential discontinuities in solar wind 09 p1521 A71-22866

Equivalent electrical circuits of interdigital transducers for piezoelectric generation and detection of ultrasonic Rayleigh waves 09 p1420 A71-23680

Waves generated by obstacle steady motion along axis of uniformly rotating electrically conducting homogeneous fluid, using Lighthill technique 10 p1595 A71-24624

Soviet book on nonstationary waves covering gravity waves development, moving periodic pressure systems, seismic disturbances and nonhomogeneous ideal liquids 10 p1595 A71-24650

Soviet book on physics of interaction between atmosphere and ocean covering heat transfer, wave formation, vertical mixing in upper sea layer, etc 10 p1639 A71-24671

HF and VHF radio propagation on earth surface, describing launchers used for generation and detection 10 p1579 A71-24950

Generation mechanism of magnetohydrodynamic shock waves associated with sudden commencements of 27-day recurrent geomagnetic disturbances 10 p1608 A71-25120

Linear sawtooth generator, using MOS unijunction transistors to switch and maintain constant discharge current from timing capacitor 11 p1740 A71-26549

Impulsive energy deposition generated stress waves in composite media formed by two plane layers with interfacial molecular bond joining 12 p1983 A71-27575

Ion-acoustic waves generation in outer space by strong electromagnetic radiation, considering quasars, supernovae shells, pulsars and solar supercorona 13 p1228 A71-28251

Factors affecting respiratory waves formation, modulating arterial blood pressure recordings and photoplethysmograms 14 p2185 A71-30411

Closed loop system analysis of triangular wave generator consisting of integrator, on-off element with hysteresis and multiplier 15 p2376 A71-32026

Acoustical wave generation measurement during iris and retina photocoagulation and ruby laser burns, noting intraocular pressure surge simultaneous with ocular tissue explosion 15 p2365 A71-32346

Unsteady one dimensional MHD shock wave evolution and separation in shock tube, using single fluid continuum equations with numerical dissipation 15 p2457 A71-32389

Magnetospheric resonator properties bounded by ionosphere/earth system lines of force, examining nonuniform plane wave generation and standing wave pulsation period 15 p2401 A71-32731

Collapsing white dwarf stars, investigating detonation wave formation for thermonuclear explosion 16 p2631 A71-33228

Bounded sources gravitational waves generation and propagation, noting refraction phenomenon in matter presence 16 p2612 A71-33282

Wave formation during metals explosive welding, indicating process of wave freezing by acoustic equations analysis 17 p2749 A71-35369

Shock wave formation in stationary flow adjacent to supersonic flow region, using Friedrich simple wave theory 17 p2673 A71-35645

Pulsar radiation generation by charged particles nonlinear Thomson scattering of strong LF electromagnetic wave and nonthermal radio emission 18 p2960 A71-35940

Hypothetical analogy between wave formation during explosive welding and Karman vortex street arising in liquid flow around cylinder 19 p3068 A71-37083

Photographic observations of plasma eruptions from metal and opaque dielectric targets subjected to neodymium laser pulses, discussing successive shock wave formation 19 p3070 A71-37085

Wave growth for distributed parameter dynamic system independent of time and coordinates, investigating stability with linear approximation 19 p3103 A71-37577

Nonuniform sampling procedure for linear transversal filters synthesis, obtaining phase-sampled impulse response filters suitable for AM and FM waveforms generation and matched filtering 20 p3203 A71-38859

Polar mesosphere internal gravity waves generation and propagation, using temperature and wind profiles from rocket grenade method 20 p3221 A71-39693

Magnetospheric VLF waves growth rate variations, calculating frequency spectrum and intensity with self consistent solution

21 p3346 A71-40046

Small mesoscale waves development in steady stratified plane parallel flow, assuming mean flow characteristics dependence on vertical coordinate

21 p3412 A71-41391

High Mach number turbulent magnetosonic shocks generation by driving reflecting piston into plasma, simulating by electromagnetic particle code

23 p3708 A71-42893

Cyclotron magnetoacoustic wave generation by planets and binary stars in circular orbits, deriving interstellar gas density variations

24 p3869 A71-44804

Whistling atmospheric generation mechanism, showing ionic sound excitation by hydromagnetic wave propagation through magnetospheric rapid plasma concentration change regions

24 p3823 A71-45035

Pressure and mass velocity profiles behind two dimensional shock wave generation on Al flat plates explosive surface

24 p3839 A71-45228

WAVE INTERACTION

NT SHOCK WAVE INTERACTION

VHF radiation from plasma during electron beam interaction with fast magnetoacoustic wave stimulated by external spatially periodic currents

01 p0132 A71-10155

Nonlinear interaction between long planetary waves and zonal circulation in atmospheric model with negative viscosity

01 p0113 A71-10537

Bar impact against rigid obstacle, using method of characteristics for elastoplastic waves propagation and interaction

01 p0171 A71-10651

Quasi-transverse extraordinary wave interaction with density fluctuations in inhomogeneous magnetized plasma, using modulation measurement for instability diagnosis

01 p0136 A71-11440

Hydromagnetic waves interaction with time dependent inhomogeneous background fluid, using Hamilton principle

01 p0136 A71-11475

Bounded plasma wave interaction matrix elements calculation from orthogonal system formation by normal waveguide modes

02 p0289 A71-11891

Coherent light wave propagation in two level system, discussing wave periodicity, deviation from sinusoidal form, interaction with medium and energy loss and gain effects

02 p0215 A71-12319

Quasi-Alfvén and acoustic wave coupling in inhomogeneous stratified plasma within intense magnetic field as function of directional pressure

02 p0292 A71-12627

Cyclotron electron beam transverse waves interaction in microwave amplifier resonant coupling element with double spiral

03 p0385 A71-13795

Solar wind microscopic structure, examining interplanetary wave-particle interactions

03 p0480 A71-14068

Baroclinic atmospheric model of interaction between zonal circulation and long waves, discussing motion instability and oscillation

04 p0620 A71-14636

Acoustic plane waves transient interaction with cylindrical elastic shell, using Volterra integral equations

04 p0668 A71-15189

Gravitational waves collision analysis using coordinate system for general relativity

04 p0658 A71-15832

Nonlinear interaction between three longitudinal plasma waves, calculating dissipation effect on coupling coefficients

04 p0635 A71-15902

Rotating electron beam cyclotron and space charge waves interaction with fast electromagnetic waves

05 p0719 A71-16002

Asynchronous spatial harmonics effect on O-type interaction in comb-type slow wave structure, obtaining transcendental dispersion equation

05 p0728 A71-16011

Nonself-similar wave type gas dynamic equations solutions, considering flow fields due to Riemann waves interaction in polytropic gas

05 p0693 A71-16376

Multiple wave intersections at marginal detonation front, determining dynamic behavior by soot technique

05 p0833 A71-16508

Detonation wave with finite reaction velocity interaction with rarefaction wave from behind, noting oscillations development associated with attenuation

05 p0834 A71-16511

Nonlinear interaction between waves with random phases in magnetoactive plasma of solid body, discussing weak turbulence theory

06 p0930 A71-17404

Electromagnetic wave trapping by nonlinear resonant interactions involving ion sound wave and two electromagnetic waves in isotropic plasma

06 p0869 A71-17988

Lamb wave interaction with current carriers in cubic symmetry piezosemiconductors, obtaining amplification factor

06 p0942 A71-18352

Extraordinary waves propagating perpendicularly to uniform magnetic field in hot electron plasma, discussing wave interaction

07 p1166 A71-18884

Magnetoactive cold plasma wave interaction theory, investigating energy transfer

07 p1167 A71-19230

Stress wave propagation in plates from explosive loading, discussing wave front interaction and scab formation

07 p1215 A71-20091

Ring laser two mode operation combination interaction and beat phasing, determining mode mismatch regions at synchronized frequencies

07 p1127 A71-20380

Artificial solar wind experiments, describing interaction between hydrogen plasma shock wave and simulated geomagnetic field

08 p1354 A71-21010

Three diffracting light beams parametric interaction, applying variational method to theory of backward wave parametric oscillator

08 p1334 A71-21181

Plane light wave interactions with moving dispersive dielectric medium, considering electron UV or ion IR resonant oscillation in regions of anomalous dispersion

08 p1253 A71-21278

Wave interference effects and energy transfer in coupled thin film optical waveguides

09 p1460 A71-22159

Naturally generated electromagnetic waves interaction with electron flux in magnetoplasma, noting gyroresonance

09 p1501 A71-22304

Ion acoustic and helicon waves nonlinear interactions in plasma, evaluating whistler buildup rate

09 p1501 A71-22336

Magnetized inhomogeneous plasma nonlinear wave coupling near hybrid resonances

09 p1503 A71-22868

Electromagnetic and electrostatic waves direct nonlinear coupling in plasma, describing experimental measurements of interacting waves frequency, wavelength, field configuration and power levels

09 p1504 A71-23254

Production rates for beat and sum frequencies mixing from interaction of two parallel laser beams with free electrons, using nonrelativistic radiation theory

09 p1465 A71-23546

Atmospheric Kelvin waves interaction with mean zonal flow in westerly shear zone, noting momentum flux divergence distribution correlation with observed zonal accelerations

09 p1489 A71-23552

Weak turbulence analysis of Maxwellian plasma waves nonlinear interactions effects on two stream instability with Gaussian momentum distribution

10 p1647 A71-23886

Electrostatic waves high order interaction in collisionless plasma, deriving coupling constants from energy conservation and invariance under time reversal

10 p1647 A71-23888

Transverse spatial particle diffusion in plasma under random oscillations, examining interaction between collisionless plasma and longitudinal wave

10 p1649 A71-24318

Sound generation by frontal collision of double pair vortices, showing pressure proportional to Mach number

10 p1641 A71-24346

Radiation and gas-dust interactions, examining dispersion relation and instability for cosmological models

10 p1675 A71-24490

Homogeneous wave turbulence-MHD tangential discontinuity structures interaction, resulting in shear stress across discontinuity surface

10 p1652 A71-24663

Waking and sleeping EEG signals bispectrum analysis, correlating component waves interactions with alpha activity, lead placement and state of consciousness

11 p1722 A71-26378

Charge particle motion and radiation in strong plane and spherical electromagnetic waves with nonthermal astrophysical applications

12 p1877 A71-26616

Magnetoactive cold electron plasma wave interaction theory, investigating energy transfer

12 p1934 A71-26748

Time and space variable echo waves in electron plasma by wave packets interaction, considering spectral line width finiteness influence

12 p1937 A71-27038

Electromagnetic wave propagation on uniform transmission line network, discussing passivity and stability notions concerning energy exchange between waves and material

12 p1879 A71-27039

Nonlinear waves in weakly dispersing media, discussing packet self-focusing and -compression, electromagnetic radiation with acoustic oscillations, geometric optics and HF-LF interactions

12 p1929 A71-27166

Cosmic rays resonant interaction with hydromagnetic waves, determining turbulent source for confining high energy radiation to Galactic disk

12 p1948 A71-27366

Nonself-similar wave type gas dynamic equations solutions, considering flow fields due to Riemann waves interaction in polytropic gas

12 p1898 A71-27453

Ionospheric wave/particle interactions under controlled electron beam energy and flux conditions, using Aerobee rocket for experimental investigation

12 p1902 A71-27668

Nonlinear interaction between three weakly coupled waves with well defined phases in dissipative media (fluids, plasmas or crystals)

13 p2106 A71-28453

MHD wave coupling in homogeneous plasma in field dependent on single coordinate, obtaining modified Alfvén and acoustic waves stability conditions

13 p2106 A71-28498

MHD waves nonlinear interaction in magnetosonic, calculating transverse Alfvén and magnetosonic and longitudinal acoustic wave decay instabilities

13 p2106 A71-28562

Combustion instability with wave motion coupling in solid propellant rocket motors due to energy gain and loss mechanisms within chamber

14 p2296 A71-30787

Electromagnetic waves in interplanetary space and effects on magnetosphere, considering solar wind characteristics due to wave interactions

14 p2202 A71-30956

Gain improvement in TWT parametric amplifiers based on slow space charge waves interaction with slow wave structure field by electron beam modulation

15 p2378 A71-32625

Gravity waves over flow with nonuniform velocity distribution, investigating neutral stability problem of generation and momentum transport

16 p2557 A71-32984

Sporadic E layer enhancement by horizontal transport within layer, considering gravity waves interaction effect on ion density horizontal redistribution

16 p2573 A71-33960

Traveling ionospheric disturbances due to gravity wave interactions during solar eclipse of 7 March 1970, confirming electron content variations from ATS 3 polarization data

16 p2575 A71-33975

Signal waves amplifier in medium of high nonlinear electric polarization, considering reflected waves effect on amplification

16 p2544 A71-34131

Two-stream instability for magnetically confined pure electron gas column resulting from surface wave interaction

18 p2950 A71-35864

Large amplitude whistler as collisionless laminar shock model, showing instability for oblique perturbation propagation

18 p2950 A71-35865

Transverse wave tubes with cyclotron and synchronous wave interactions as microwave amplifiers, analyzing energy exchange mechanism and alpha beam velocity spread

18 p2888 A71-36128

Hall fields effect on interaction of MHD waves in inhomogeneous plasma, considering MHD wave dispersion

19 p3109 A71-37134

Electron wave coupling in plasma column, determining exact resonance and field configurations of frequencies

19 p3111 A71-37635

Pressure wave interaction with orifices inside ducts, calculating reflection and transmission characteristics relationship to orifice geometry and initial steady flow conditions

19 p3044 A71-37642

Debye potential well formation in collisionless current carrying plasma, noting wave-particle resonant interaction role

19 p3115 A71-38216

Longitudinal wave interaction and excitation by current instability in equatorial jet, considering energy transfer mechanism

19 p3057 A71-38363

Nonlinear equations for traveling wave amplifiers using transverse wave interaction modes /cyclotron and synchronous electron beam waves/, calculating saturation characteristics

20 p3203 A71-39003

Electromagnetic wave transmission through conducting plasma slab, reducing nonlocal wave interaction two point boundary value problem to Cauchy system

20 p3274 A71-39080

Artificial solar wind experiments, describing interaction between hydrogen plasma shock wave and simulated geomagnetic field

20 p3279 A71-39590

Gravitational radiation interaction with uniform incompressible inviscid fluid in simple motion, considering response in linearized approximation to general relativity

21 p3446 A71-40421

Sound waves interaction in piezoelectric semiconductors under pumping, deriving basic equations for parametric amplification investigation

21 p3430 A71-41216

Elastic continuous medium with nonlocal interactions, calculating surface waves dispersion equations with boundary solutions

21 p3417 A71-41366

Nonlinear waves in weakly dispersing media, discussing packet self-focusing and compression, electromagnetic radiation with acoustic oscillations, geometric optics and HF-LF interactions

22 p3576 A71-42621

Rotating electron beam cyclotron and space charge waves interaction with fast electromagnetic waves

22 p3515 A71-42751

Asynchronous spatial harmonics effect on O-type interaction in comb-type slow wave structure, obtaining transcendental dispersion equation

22 p3524 A71-42759

Triggered whistler emissions in magnetosphere, considering nonlinear interaction between whistler wave and resonating particles

23 p3643 A71-43175

Three dimensional transient interaction of spherical acoustic waves with cylindrical elastic shell, using integral transform techniques

23 p3775 A71-43207

Differential equation solution for plane self focusing and one dimensional self modulation of waves interacting in nonlinear media

23 p3704 A71-43408

Traveling wave pair interaction with three energy level medium at resonance frequencies, deriving coupled differential equations for amplitude variations

24 p3833 A71-44662

Wave interference phenomena associated with elastic scattering of atoms, considering differential inelastic scattering cross sections anomalies

24 p3851 A71-45166

Electrostatic waves nonlinear interactions in uniform plasma in presence of external constant magnetic field, deriving coupling coefficients by coupled mode theory

24 p3858 A71-45276

WAVE MOTION

U WAVES

WAVE OSCILLATORS

U OSCILLATORS

WAVE PROPAGATION

NT DIFFRACTION PROPAGATION

NT GROUND WAVE PROPAGATION

NT IONOSPHERIC F-SCATTER PROPAGATION

NT IONOSPHERIC PROPAGATION

NT LIGHT SCATTERING

NT SCATTER PROPAGATION

NT SHOCK WAVE PROPAGATION

NT TRANSEQUATORIAL PROPAGATION

Longitudinal acceleration and distinct transverse waves propagation in Hadamard and Green hypoelastic materials

01 p0165 A71-10025

Arterial branches pulsating flow and wave propagation in large blood vessels, considering flow measurements from simulated model experiments

01 p0008 A71-10111

Compression shock wave development in compressible media, deriving wave amplitude/time relationship via velocity distribution approximation by discontinuous Mach wave series

01 p0069 A71-10122

Helical TWT direct wave propagation constants calculation method

01 p0052 A71-10475

Frequency correlation between amplitude and phase fluctuations of different-frequency spherical waves propagating in turbulent medium

01 p0073 A71-10545

Rayleigh wave propagation in stochastically inhomogeneous elastic medium

01 p0169 A71-10637

Bar impact against rigid obstacle, using method of characteristics for elastoplastic waves propagation and interaction

01 p0171 A71-10651

Structure and propagation of large amplitude modulated isolated compression waves in cold three component plasma with negatively charged ions

01 p0132 A71-10676

Wave propagation in plane neutral electron beam near interface with semiconductor

01 p0139 A71-10782

Acceleration waves propagation in elastoplastic materials based on nonlinear thermodynamic theory

01 p0173 A71-10873

Torsional and compressional hydromagnetic wave propagation in inhomogeneous magnetic fields

01 p0134 A71-11001

Uniaxial strain waves propagation across nonlinear strain hardening slab, deriving expressions for stress, strain, particle velocity and shock path

01 p0175 A71-11013

EM wave propagation along radially inhomogeneous dielectric cylinders, considering permittivity variation

01 p0037 A71-11170

Shear wave propagation into heat conducting viscoelastic fluids, considering steady one dimensional flow stability

01 p0181 A71-11188

Electron beam nonlinear interaction with plasma, considering electrostatic wave propagation, instability and dispersion equation

01 p0135 A71-11209

Transverse surface wave propagation in piezosemiconducting body with electron damping, formulating boundary conditions

01 p0140 A71-11287

Trapped LF ion wave propagation along warm plasma cylinder imbedded in dielectric, obtaining dispersion relation

01 p0136 A71-11476

Particle acceleration by coherent electrostatic wave propagation through plasma, producing monoenergetic particle beam

01 p0131 A71-11513

Electromagnetic potentials and Lorentz relation in anisotropic medium, considering Bromwich function and plane wave propagation

02 p0211 A71-11719

Pure shear mode propagation in sapphire, determining acoustic axes velocity

02 p0294 A71-11947

Plane and cylindrical MHD wave propagation in conducting compressible fluid under Hall effect, examining flow perturbation

02 p0291 A71-12533

Stochastic wave propagation in continuous randomly inhomogeneous media, surveying analytical methods

02 p0219 A71-12545

Longitudinal elastic wave propagation equations of motion in cone with small apex angle, using perturbation theory

03 p0456 A71-12974

Continuous filament composite materials fabrication and tests for dynamic deformation, fracture and wave propagation properties, considering axially reinforced cylindrical body compression

03 p0508 A71-13768

Periodic beam structure vibration response, using formulation for flexural wave propagation groups [ASME PAPER 70-WA/DE-3]

03 p0511 A71-14139

Pressure wave propagation through annular and mist flow patterns, noting virtual mass effects in interphase momentum transport of rarefaction and compression waves

03 p0405 A71-14418

Nonpotential ion cyclotron waves propagation at very large angles to unperturbed magnetic field, obtaining dispersion relation numerical solutions

03 p0420 A71-14530

Soviet monograph on visible and IR waves atmospheric propagation covering monochromatic radiation absorption and scattering, laser light beams under turbulence, etc

04 p0551 A71-14800

Monograph on helicon and Alfvén wave propagation in nonmagnetic semiconductors and semimetals covering active and passive waves

04 p0635 A71-14808

Plastic wave propagation of combined stresses due to longitudinal impact of pretorqued tube

04 p0668 A71-15190

Plane wave propagation in layer direction in fiber reinforced viscoelastic materials

04 p0669 A71-15202

Transient axisymmetrical rotary shear wave propagation in nonhomogeneous viscoelastic media with cylindrical hole

04 p0671 A71-15752

Semicircular canal ducts dynamic behavior, using mathematical model for wave transmission of elastic fluid-filled toroidal shell in rigid channel

04 p0547 A71-15772

Conducting and ferromagnetic liquids thermoconvective waves, considering disturbance propagation process in equilibrium state with constant entropy gradient

04 p0628 A71-15809

Light propagation in gas filled pipe with uniform heat flux through wall under forced convection, determining lens efficiency relation to length

04 p0628 A71-15811

Decimeter radio wave propagation in Venusian atmosphere, determining refraction and absorption coefficients height dependence based on Venera spacecraft data

05 p0718 A71-15993

Refractive index equation for oblique wave propagation in inhomogeneous compressible electron plasmas

05 p0786 A71-16287

Shock initiated detonation wave propagation in combustible hydrogen oxygen flow in constant area duct, considering wave initiation Mach number and ignition temperature

05 p0834 A71-16519

Viscous incompressible fluid flow with free boundary at large Reynolds numbers, deriving asymptotic expansion solution for wave motion

05 p0737 A71-16989

Spiral structure of galaxies identified with growing wave propagation in finite thickness axisymmetric disk hydrodynamic theory

05 p0813 A71-17036

Rayleigh wave propagation in anisotropic substrates, using light diffraction by surface acoustic waves

05 p0783 A71-17078

Internal gravity wave propagation in neutral wind stratified atmospheric model

06 p0888 A71-17274

Ultrasound propagation visualization in solids, describing sensitive schlieren apparatus

06 p0903 A71-17323

Short elastic sine waves propagation in cylindrical shells, applying nonclassical equations

06 p0982 A71-17359

Multimode ionization wave growth and saturation in finite length positive plasma column of gas discharge, investigating feedback and external driving signal effects

06 p0933 A71-17469

Cylindrical structure longitudinal stress wave propagation characteristics, analyzing wave induced structural instability and destruction process

06 p0991 A71-17801

Magnetospherically reflecting nonducted whistler mode waves propagation noting dispersion, hybrid frequencies, ray curvature and field lines

06 p0868 A71-17983

Whistler wave packet propagating in ambient magnetic field direction, computing nonlinear particle trajectories

06 p0869 A71-17987

Stress wave propagation from spherical cavity in isotropic nonhomogeneous elastic medium in contact with vacuum at infinity, obtaining closed form solution

06 p1001 A71-18228

Short rotor blade span supersonic fan for pressure wave forward propagation elimination, obtaining acoustic and aerodynamic characteristics [AIAA PAPER 71-182]

06 p0885 A71-18621

One component system gas wave propagation kinetic theory, calculating monatomic gas and plasma oscillations by discrete ordinate method

07 p1165 A71-18876

Unstable electrostatic waves propagating in uniform infinite plasma with weak beam, Fourier transforming space dependent variables

07 p1166 A71-18881

Upstream discrete wave packets propagation interplanetary medium from Ogo 5 observation

07 p1197 A71-19656

Equatorial westward propagating wave disturbance model for diagnosing atmosphere response to known diabatic heating distribution

07 p1152 A71-19755

Hydromagnetic wave propagation with coupled isotropic and guided modes, obtaining steady state solution with toroidal, plasma resonance induced period dependent reflecting barrier

07 p1197 A71-19767

Axisymmetric wave propagation in semiinfinite hollow elastic circular cylinders subjected to pressure step loading, obtaining asymptotic solutions for strains by double integral transforms

07 p1214 A71-19954

Torsional wave propagation in elastic circular composite cylinders, introducing correction factors for approximate theory

07 p1214 A71-19955

Elastic harmonic waves propagation in composite circular elastic cylinder

07 p1214 A71-19956

Plane compression waves propagation into constant state nonviscous fluid, considering shock formation of pressure pulses and overpressure as function of time

07 p1091 A71-19961

Stress wave propagation in plates from explosive loading, discussing wave front interaction and scab formation

07 p1215 A71-20091

WAVE PROPAGATION

Collision free ionizing wave propagation into cold low density ionized gas, showing wave oscillations damping due to ion velocities phase mixing
07 p1171 A71-20289

Magnetoplasma modulated waves nonlinear instability, taking into account relativistic effects
07 p1171 A71-20296

Dominant diagrams of renormalization method in coherent random wave propagation
07 p1065 A71-20322

Coupled electroacoustic and electromagnetic wave propagation in inhomogeneous compressible and lossy plasma
07 p1065 A71-20324

Multiple wave propagation in acoustic duct with winds, using perturbation Lagrangian for ideal fluid flow
08 p1276 A71-21651

Jacobian calculation in kinematic theory of wave propagation, using ray equation
08 p1276 A71-21652

Short radio wave propagation over single jump lines in F 2 critical frequency gradient presence, examining maximum usable frequency increase
09 p1405 A71-22439

Elastic waves in isotropic body, calculating initial deformation effect on propagation rate based on finite deformation theory
09 p1537 A71-22515

Wave propagation through random inhomogeneous media, discussing mean wave profile modification due to scattering from density inhomogeneities
09 p1434 A71-23168

MHD wave propagation in magnetoplasma perturbed by LF magnetoacoustic waves, considering wave scattering and polarization
09 p1505 A71-23566

Concentric shield for surface wave propagation loss at bend in open waveguide, using Airy function
09 p1410 A71-23570

Wave propagation in elastoviscoplastic medium in temperature field under complex dynamic and thermal conditions, considering mathematical models and mechanical properties changes
09 p1543 A71-23611

Ultrasonic waves propagation in hydraulic and lubricating oils, testing shear resistance
09 p1484 A71-23673

Wave propagation with frequency inferior to gyrofrequency of ions in collisionless hydrogen plasma, showing Alfvén wave reflection on discontinuity surface parallel to magnetic field
10 p1599 A71-23846

Pc1 propagation in magnetosphere model accounting for ionization gradients aligned along geomagnetic field
10 p1599 A71-23849

Rapidly rotating fluid flows, calculating inertia waves by geometrical optics method
10 p1591 A71-23854

Nondestructive evaluation of ultrasonic wave propagation in adhesively bonded test specimens, using schlieren method
10 p1616 A71-24104

Ionospheric irregularities two fluid model, using nonlinear differential equations for longitudinal waves propagating in hot collisional magnetoplasma
10 p1648 A71-24294

Ion acoustic waves propagation and structure measurements with metal electrode technique and continuous channel electron multiplier in plasma wind tunnel
10 p1611 A71-24517

Infinitely small flexural oscillations of initially stretched incompressible elastic circular cylinder, showing stretch effect on wave propagation velocity
10 p1689 A71-24521

Higher approximations of spherical harmonic method and moment method applied to propagation of periodic disturbances in radiating gas
10 p1696 A71-24545

Magnetoacoustic wave propagation in magnetic plasma traps by geometrical optics methods, considering annular traps existence
10 p1651 A71-24638

Surface layer-bulk body interaction and Rayleigh wave propagation in elastic solid, using two dimensional continuum theory
10 p1691 A71-24645

Spatially uniform external periodic magnetic field effect on wave propagation perpendicular to hot electron plasma, obtaining dispersion relation from hydrodynamic equations
10 p1578 A71-24655

HF and VHF radio propagation on earth surface, describing launchers used for generation and detection
10 p1579 A71-24950

Age, obliterating arteriopathy and peripheral arterial sclerosis effects on rheographic wave propagation speed to lower limbs
10 p1566 A71-24976

Geomagnetic Pc1 pulsations propagation in F region, deriving hydromagnetic waves equations by ray tracing method and waves refractivity index in extraordinary mode
10 p1607 A71-25118

Midlatitude whistlers propagation paths during minimum solar activity for estimating magnetospheric electron density profile
10 p1580 A71-25135

Frequency equation for harmonic waves with circumferential nodes traveling in composite traction free circular cylindrical shells, using IBM 7094 computer
11 p1847 A71-25461

Magnetospheric cold plasma dispersive and amplifying combined effects on pearl elements spectral shape, considering wave packet propagation applications
11 p1730 A71-25543

Nonlinear beam plasma interactions theory review, using plasma column circuit equation models
11 p1805 A71-25629

Italian book on microwave propagation covering electromagnetic wave attenuation, rainfall space-time structure and radioelectrical/meteorological data recording
11 p1731 A71-25650

Homogeneous Gaussian beam propagation in inhomogeneous negative absorption media, noting amplification of plane wave
11 p1798 A71-25665

Atmospheric wave dynamics in equatorial region, obtaining approximate solution with Coriolis force within perturbation theory
11 p1795 A71-25921

Traveling wave propagation, modal vibrations and elastic transmission medium studies from theoretical seismograms for realistic gravitating heterogeneous spherical earth model
11 p1760 A71-26148

Longitudinal, flexural and elastic waves propagation in infinite orthotropic circular cylinders
11 p1850 A71-26176

Mechanical waves propagation in elastic viscoplastic medium in presence of temperature field, using mechanical and mathematical models
11 p1850 A71-26177

Longitudinal waves propagation in viscoelastic semiinfinite rod under constant velocity impact, solving by characteristics and finite difference methods
11 p1850 A71-26178

Phase and log amplitude spectral and angular covariance of scintillation for propagation of two differing plane waves in randomly inhomogeneous medium
11 p1800 A71-26297

Viscous model for stress wave propagation perpendicular to plates of bilaminate composite material
11 p1851 A71-26381

Rellich uniqueness theorem for Helmholtz equation for steady state wave propagation in inhomogeneous anisotropic media subject to Sommerfeld radiation
12 p1929 A71-26865

Limiting absorption principle and Schroedinger nonelliptic spectral theory for steady state wave propagation in inhomogeneous anisotropic media
12 p1929 A71-26866

Heat conduction effects on small amplitude plane harmonic wave propagation in transversely isotropic elastic Zn single crystals
12 p1985 A71-26925

Rayleigh wave propagation along edge of thin plate, calculating velocity dependence on frequency
12 p1929 A71-26929

Large amplitude wave propagation in arteries, deriving aorta mathematical model consistent with heart pressure and flow pulses and wavefront velocity
12 p1870 A71-26937

Pulse wave velocity measurements in human veins by transcutaneous ultrasonic flow detectors, noting respiration and Valsalva effects
12 p1874 A71-27136

Soviet papers on wave propagation in viscoelastic and elastoplastic media covering shock wave interaction, magnetoelastic waves, etc
12 p1980 A71-27444

Elastoplastic and elastic-viscoplastic waves propagation, considering longitudinal wave resonance, plane load waves and loading and unloading criteria
12 p1980 A71-27446

Asymptotic solutions of improved equations for elastic and elastoplastic waves in rods, considering longitudinal waves propagation
12 p1980 A71-27449

Laser beam propagation in turbulent atmosphere studied for alignment survey applications, discussing development, construction and testing of centering detectors
12 p1915 A71-27538

Collisionless plasma with thermal ions in magnetic field absence, investigating stationary ion shock wave propagation
12 p1941 A71-27767

Axial wave propagation in linearly elastic membrane shells of revolution, using dynamic finite element technique
13 p2147 A71-27786

One dimensional wave propagation at low temperatures in thermoelastic half space under step strain at free surface
13 p2148 A71-27828

Numerical solution of current distribution, wave propagation constant and propagation mode cut-off frequencies on periodic linear array
13 p2028 A71-28001

Propagation of 26-month oscillations in meridional component of wind velocity in stratosphere at extratropical latitudes from hydrothermodynamic equations solution
13 p2057 A71-28021

Surface waves propagation in initially deformed elastic body, using elastic potential to define half space mechanical properties
13 p2150 A71-28131

Constant space curvature perturbations, considering density, rotational and propagation of gravitational waves with Lipschitz method
13 p2137 A71-28479

Longitudinal wave propagation in ideal elastic bar with viscous stress, calculating approximation to nonlinear wave equations
13 p2153 A71-28483

Magnetosphere transmittance for fast magnetosonic waves, considering refraction, reflection and earth surface intersection
13 p2060 A71-28531

Propagation constant relation to frequency for waveguide filled with simple moving medium, presenting dispersion curves set
13 p2030 A71-28607

Plane longitudinal stress waves propagation in plane-parallel viscoelastic partition of finite thickness dividing two linear half spaces with different elastic properties
13 p2155 A71-28655

Soviet book on detonation waves in condensed media covering excitation and propagation in compacted explosives, liquid/solid explosives and pulsations
13 p2161 A71-28737

Conical bar with yield point lag, investigating elastoplastic wave propagation with Rabotnov model
13 p2155 A71-29064

Soviet monograph on EM waves in solid state plasma covering propagation, amplification, generation and penetration
13 p2112 A71-29078

Elastic wave propagation in infinite elastic medium due to explosion at spherical cavity center, considering material properties thermal change as function of radial distance
13 p2165 A71-29104

Relativistic thermo-magnetoelastic wave propagation, considering elastic solid under magnetic and thermal fields
13 p2101 A71-29105

Wave propagation near upper hybrid frequency in mirror-confined hot electron unstable plasma
13 p2109 A71-29242

Moliere high energy solution of Schroedinger scattering equation for optical propagation in turbulent atmosphere, noting inconsistency of Born-Rytov approximation
13 p2102 A71-29441

Stellar wind flow models associating energy transport with propagation and dissipation of hydrodynamic waves and heat conduction
14 p2297 A71-29586

Atmospheric models of partially trapped waves propagation in layer above tropopause with large stratospheric Scorer parameter
14 p2268 A71-29763

High coupling low diffraction loss cut for acoustic surface wave propagation on lithium niobate
14 p2283 A71-29796

Soviet monograph on wave propagation in cold and hot magnetoplasmas covering particle collisions, plasma control and instability and plasma-particle interactions
14 p2280 A71-30246

Low temperature plasma MHD waves propagation in inhomogeneous magnetic fields, comparing numerical solutions with experimental results
14 p2282 A71-30559

Millimeter and visible waves propagation through clear atmosphere and precipitation
14 p2204 A71-30971

Linear elastokinetics dynamic problems, emphasizing elastic wave propagation in infinite micropolar medium
15 p2502 A71-31153

Asymptotic theory of wave propagation extended to slightly inhomogeneous and slowly varying anisotropic media exhibiting spatial and temporal dispersion
15 p2449 A71-31476

Thermodynamic properties effects on transverse acceleration wave propagation in inhomogeneous isotropic elastic bodies with internal state variables
15 p2504 A71-31729

Magnetoactive plasma layer in strong constant magnetic field, computing dispersion equation for large amplitude thermomagnetic wave propagation
15 p2456 A71-31745

Propagation angle effect on time harmonic wave dispersion in periodically laminated medium, using two dimensional equations of elasticity [ASME PAPER 70-WA/APM-47]

Book on viscoelasticity covering isothermal stress-strain relations, wave propagation, mechanical properties, thermodynamics and nonisothermal effects 15 p2506 A71-32010

Stochastic wave propagation in continuous randomly inhomogeneous media, surveying analytical methods 15 p2509 A71-32438

Coupled radiative transfer-gas dynamic interactions in unsteady wave propagation, two dimensional steady flows and atmospheric motions 15 p2373 A71-32501

Small monochromatic disturbances propagation in stable ideal MHD fluid by geometric optics method, solving point source radiation at short wavelengths 15 p2515 A71-32562

Relativistic kinetic theory of large amplitude transverse Alfvén wave, discussing propagation in collisionless plasma 15 p2459 A71-32652

Nonlinear interaction between three resonant modified ordinary electromagnetic waves propagating perpendicular to static magnetic field in homogeneous electron plasma, studying relativistic effects 15 p2459 A71-32653

Magnetic stabilization of transverse plasma instabilities, considering waves propagating transversely to plasma direction in presence of uniform external magnetic field 15 p2460 A71-32658

Pulsed laser double exposure holographic interferometry for measuring transverse wave propagation in beams 15 p2413 A71-32790

Internal gravity waves vertical propagation in lower ionosphere from temperature and wind profiles measurements 16 p2561 A71-32802

Temporal and spatial flow velocity profiles produced by shock tube generated pressure wave propagation in open-end pipe 16 p2556 A71-32921

Unsteady waves in parallel shear flows, noting viscous and nonlinear effects 16 p2558 A71-33011

Gases refractive behavior, discussing constitutive properties, wave propagation, Lorentz electron theory of dispersion, spectral interferometry and hook method 16 p2608 A71-33156

Plane and cylindrical waves three dimensional propagation, investigating finite electrical fluid conductivity and radiation effects in MGD 16 p2618 A71-33172

Plasma flow wave propagation, investigating compressibility, radiation and finite electrical conductivity effects with plane asymptotic solution combinations 16 p2618 A71-33173

Wave fronts in Einstein-Maxwell theory, showing perturbation propagation along background spacetime metric field 16 p2609 A71-33261

Bounded sources gravitational waves generation and propagation, noting refraction phenomenon in matter presence 16 p2612 A71-33282

Weak discontinuity unloading wave propagation in semiinfinite slender prismatic bar of elastoplastic material 16 p2656 A71-33356

Tunguska explosion of 30 June 1908, determining air waves propagation velocity 16 p2639 A71-33696

Neutral atmosphere density profile data from satellite-borne accelerometer experiment, observing gravity waves propagating in north-south direction at high latitudes 16 p2570 A71-33825

Initial strains effect on propagation rate of elastic waves, applying finite deformation theory 16 p2658 A71-33902

Electron beam nonlinear interaction with plasma, considering electrostatic wave propagation, instability and dispersion equation 17 p2786 A71-34261

Book on optical holography covering basic concepts, Fourier transform, propagation and diffraction, pulsed lasers, interferometry, geometric analysis of point source hologram, etc 17 p2738 A71-34450

Dynamical thermal expansion effect on plane elastic-plastic stress wave propagation, using classical heat conduction equation 17 p2819 A71-34507

Anisotropy instabilities of hydromagnetic wave propagation at small angle perpendicular to magnetic field above ion cyclotron frequency, calculating dispersion relation 17 p2788 A71-34664

Communications systems using carbon dioxide laser wave propagation, considering wave extinction by absorption and scattering, scintillations due to atmospheric turbulence, etc 17 p2700 A71-34749

Electromagnetic wave propagation into time varying medium, considering boundary value transmission problems 17 p2701 A71-34760

High latitude sudden impulses, calculating transverse hydromagnetic waves propagation from magnetosphere equatorial plane 17 p2733 A71-34777

Steady wave propagation in laminated media, developing mechanical theory for composite response with hydrodynamic, thermodynamic and strength effects 17 p2823 A71-34808

Orthotropic laminated plates dynamic response to impulse loads, detailing flexural wave propagation 17 p2823 A71-34809

Time dependent multidimensional axisymmetric computations for extended extragalactic radio sources propagation into intergalactic media having different densities and temperatures 17 p2806 A71-35411

TE modes propagation in rectangular guide partially filled with dielectric slab, considering two waveguides junction equivalent circuit 17 p2708 A71-35481

Traveling waves propagation in elastic shell of revolution subjected to bending moment 17 p2833 A71-35618

Transverse wave structure of two-dimensional detonation waves propagating in narrow channel, considering longitudinal instabilities 17 p2841 A71-35708

Complex wave structure development upon underexpanded jet impact on plane obstruction at small incidence angles, determining gas dynamics parameters of supersonic jet 18 p2903 A71-36120

Double exposure pulsed laser holographic interferometry application to transverse wave propagation in Al plate 18 p2977 A71-36233

Asymptotic expansions for solution of wave motions of viscous incompressible fluid flow with free boundary at large Reynolds number 18 p2909 A71-36789

Plasmapause Alfvén, ion-acoustic, electron and ion drift wave modes coupling, calculating instability condition and growth rate 19 p3110 A71-37371

Oswatitsch expansion method of characteristics for weak perturbations in nonlinear propagation processes 19 p2992 A71-37452

Pressure wave interaction with orifices inside ducts, calculating reflection and transmission characteristics relationship to orifice geometry and initial steady flow conditions 19 p3044 A71-37642

Wave propagation in three layered plates, giving frequency spectrum 19 p3158 A71-37884

Book on active and nonlinear wave propagation in electronics covering transmission lines, wave systems stability, quasi-harmonic active propagation, equivalent circuits, etc 19 p3029 A71-38018

Detonation propagation through tubes with thin fuel film coated walls, obtaining heat transfer coefficients, friction, evaporation rate, reaction zone length and propagation velocity 19 p3171 A71-38129

Transverse waves and electromagnetic instabilities propagating along magnetic field in homogeneous plasma, discussing ions and electrons energy losses and plasma dispersion 19 p3114 A71-38206

Ion and electron drift waves propagation and stability in nonhomogeneous plasma containing impurity ions 19 p3115 A71-38214

Pressure wave propagation through one and two component annular and mist flows, showing importance of inertial interphase momentum transfer 19 p3171 A71-38293

H wave propagation in waveguide consisting of two parallel plates with longitudinal rectangular grooves, determining electric and magnetic fields by reduction method 19 p3019 A71-38331

Thermal motion effects on space charge waves propagation along plasma columns in weak magnetic field, comparing measured wavelength/frequency relationship with theoretical prediction 20 p3273 A71-38879

Small pressure wave transmission in abdominal venae cavae of dogs in mathematical model development for viscoelastic behavior of large veins 20 p3187 A71-38987

Cosserat continuum elastic tensor potentials applied to Kirchhoff theory of wave diffraction 20 p3269 A71-39033

Transverse waves propagation in vibrating orthotropic rectangular beams, noting inexact information regarding shear distribution 20 p3307 A71-39037

Coherent small amplitude hydromagnetic wave propagation in magnetic field with time independent random component 20 p3274 A71-39057

Atmospheric wave dynamics in equatorial region, obtaining approximate solution with Coriolis force within perturbation theory 20 p3256 A71-39212

Short periodical pulsations in solar atmosphere related to magnetosound propagation in area of temperature minimum with directed perpendicular magnetic field 20 p3290 A71-39305

Narrow flare angle low permittivity conical dielectric waveguide antenna, examining radiation patterns and propagation characteristics by approximate theory 20 p3196 A71-39380

Polar mesosphere internal gravity waves generation and propagation, using temperature and wind profiles from rocket granade method 20 p3221 A71-39693

GBR wavefield above winter nighttime ionosphere, noting latitudinal profile due to D region spatial variations and signal fading with F region structure 20 p3197 A71-39744

Finite amplitude entropic waves with propagated acoustic radiation-fluid particle motion energy coupling, using thermodynamic J function methods 20 p3315 A71-39772

Superposed plastic deformation and plane wave propagation in elastic-plastic media applied to circular bar twisting 20 p3310 A71-39780

Submillimeter plane monochromatic waves propagation in ground layer of turbulent atmosphere, deriving received signals levels fluctuations 20 p3198 A71-39804

Weak discontinuities propagation speeds, equations and eigenvectors in uniform collisionless plasma 21 p3421 A71-40209

Outwardly propagating coronal Alfvén waves pressure exertion on solar wind, using one fluid polytropic model 21 p3438 A71-40423

Universal dispersion curve for steady state sinusoidal flexural wave propagation in plates and bars, using Poisson ratio as single parameter 21 p3463 A71-40535

Plane waves propagation in viscoelastic body representing parallel union of Kelvin and Maxwell bodies in magneto-thermal field 21 p3463 A71-40577

Plastic wave propagation along rods and through slabs, describing finite deformation elastic-plastic theory 21 p3464 A71-40785

Elastic-plastic stress wave attenuation, applying theory of wave propagation in single crystals to flow field numerical solution 21 p3465 A71-40786

Electromagnetic stress gage for wave propagation study in nonconducting materials, discussing calibration, design and accuracy 21 p3379 A71-40793

Binary computer holograms construction, discussing two and three dimensional objects, wave propagation, plotter instrumentation, photographic reduction and diffusers 21 p3380 A71-40921

Fiber reinforced elastic materials steady state plane wave propagation by modeling constituents as continua undergoing individual motions 21 p3469 A71-41004

Singularities of Green matrix in steady state wave propagation in homogeneous anisotropic media 21 p3416 A71-41245

Soviet monograph on radio wave propagation in fluctuating parameters media covering ionosphere /fluctuating electron concentration/ and troposphere /fluctuating inhomogeneities and refractive index values/ 21 p3349 A71-41372

Electromagnetic HF wave field pressure effects on slow transverse magnetic wave propagation along plasma layer, noting dispersion equations difference from linear theory 21 p3426 A71-41400

Time harmonic waves oblique propagation in periodically laminated composite, using coupled thermoelasticity theory for plane strain 22 p3613 A71-41433

Backward propagation method for ultrasonic image reconstruction, examining resolution in near field for high contrast objects 22 p3541 A71-41784

Temporal frequency spectra for spherical wave propagating through atmospheric turbulence, using covariance functions and Taylor hypothesis 22 p3575 A71-41788

Magnetospheric VLF transverse wave propagation along geomagnetic field, examining dispersion relation 22 p3533 A71-41797

Fundamental derivative γ and other thermodynamic variables in gas dynamics, considering

WAVE RADIATION

transonic passage variation, Prandtl-Meyer wave, adiabatic flow and nonlinear wave propagation 22 p3530 A71-41887

LF wave propagation in weakly ionized plasma under magnetic field, observing forward and backward waves dispersions near cathode 22 p3582 A71-41905

Plane wave propagation following thin elastic rectangular plate impact against smooth rigid obstacle, using difference scheme 22 p3531 A71-41910

One dimensional propagation and multiple reflection of plane thermoelastic wave in Lame elastic isotropic plate with finite heat transmission 22 p3615 A71-41911

Acoustic wave propagation and heating in solar atmosphere, using Harvard Smithsonian reference atmosphere and Stein frequency spectra 22 p3601 A71-42170

Ferrite and dielectric element waveguide phase shifters with rectangular hysteresis loop, deriving differential phase and attenuation constants for wave propagation 22 p3512 A71-42308

Flexural wave propagation in thin curved rod oscillating in plane, calculating frequency and velocity from boundary conditions according to Saint Venant 22 p3617 A71-42574

Decimeter radio wave propagation in Venusian atmosphere, determining refraction and absorption coefficients height dependence based on Venera spacecraft data 22 p3515 A71-42742

Wave equations for motion in stochastic medium, using linear random operator theory 23 p3699 A71-43115

Frequency dependence of Rayleigh wave propagation velocity along rough surfaces, based on smooth surface mass loading 23 p3703 A71-43203

Equations of elastic wave propagation in isotropic materials in presence of static surface stresses and body forces 23 p3775 A71-43205

Coherent acoustic wave propagation speed and attenuation coefficient in turbulent flow 23 p3703 A71-43209

Electron periodic energization by magnetospheric RF wave propagation, examining cyclotron resonant interaction 23 p3644 A71-43321

Sporadic E layer ionization relation to thunderstorm surface pressure disturbance, considering gravity wave propagation 23 p3670 A71-43322

Steady nonlinear waves propagation along ring electron beam axis analogous to ionospheric E layer 23 p3711 A71-43412

Elastic surface wave amplitude and propagation velocity in lunar rocks, calculating Poisson ratio 23 p3761 A71-43784

Arbitrary multipole structure spherical wave propagation in Schwarzschild metric, using Bondi coordinate system and negative powers of r 23 p3704 A71-43826

Sound waves propagation in fully ionized gas, considering electron plasma frequency 23 p3705 A71-44001

Nonlinear wave packet and modulated beam propagation description in approximate heuristic theories, considering chimeras as neoclassical approximation for equations solution 23 p3705 A71-44122

Open waveguide field expansion in orthogonal wave system with proper and improper modes 23 p3647 A71-44332

Nonlinear ion acoustic soliton wave propagation and dissipation in nonhomogeneous nonisothermal weakly absorbing plasma 23 p3714 A71-44333

Spatial characteristics based difference scheme application to axisymmetric problems of elastic wave propagation, allowing for solid or hollow circular cylinder boundary conditions 24 p3885 A71-45221

Stress wave propagation in rod consisting of viscoelastic finite and semiinfinite elastic parts during pulsed sinusoidal load at end 24 p3885 A71-45223

Ultrasonic flaw detection analytical and experimental wave propagation procedure including dynamic photoelasticity and elastic wave computer codes in nondestructive testing 24 p3831 A71-45282

WAVE RADIATION

U ELECTROMAGNETIC RADIATION

WAVE REFLECTION

Electromagnetic wave reflection from ferrite moving domain wall, considering wave separation and permittivity and magnetic susceptibility tensors 01 p0138 A71-10435

Oblique reflection of horizontally and vertically polarized electromagnetic waves from isotropic media with limiting Epstein stratifications 01 p0031 A71-10775

Tropospheric layers radio reflectivity as function of refractivity index and thickness/wavelength ratio 01 p0040 A71-11607

Shadow photography applied to Mach reflections in argon, carbon dioxide and Freon 12 in shock tube, using Huygens principle for transfer mechanism 02 p0239 A71-11635

Ionospheric absorption of radio waves reflected from sporadic E layer, noting attenuation frequency dependence 02 p0211 A71-11768

Background noise in optical communication system, considering direct, reflected and scattered radiation sources in atmosphere 02 p0213 A71-12015

Point source acoustic radiation field in presence of absorbing plane, presenting solutions and approximations based on plane wave reflection and modified image method 03 p0456 A71-13276

Free wave reflection measurements of normal acoustic impedance of ground surfaces in relation to shock waves from large supersonic commercial aircraft 03 p0347 A71-13278

Ion reflection and whistler trace shapes as function of magnetic latitude from satellite observations 03 p0408 A71-13389

Topside ionosphere plasma resonance due to electrostatic wave echoes, comparing electron temperature dependent beat pattern with ray tracing calculations 03 p0421 A71-14540

Hemispherical imploding shock wave reflection, noting cold wall presence and gas density effects 04 p0568 A71-14682

Reflected shock wave interaction with boundary layer and contact surface in shock tube, examining flow uniformity 04 p0568 A71-14703

Transient pulse plane wave reflection from ionospheric model with linear electron density profile 04 p0553 A71-15218

Inviscid nonheat conducting gas flow parameters behind shock wave reflection from solid wall at obtuse angle using linear approximation from variable separation method 04 p0572 A71-15554

Holographic interferometry of diffusely reflecting surfaces, analyzing homologous rays concept 05 p0747 A71-16192

Reflection point slide velocity of traveling F region ionospheric disturbance by receivers amplitude focusing and echo phase path changes 05 p0741 A71-16440

Strong shock wave Mach reflection, determining pressure and temperature at wedge surface by shock tube experiment 05 p0835 A71-16526

Single pulse shock tube in high temperature chemical reaction kinetics, considering shock reflection theory 05 p0836 A71-16527

Plane EM waves at two dimensional periodic media boundary, obtaining reflection and refraction for harmonics 05 p0723 A71-17029

Light reflection during plane cloud layer light scattering, studying zenith angles and angular brightness distribution 06 p0923 A71-17510

VHF/UHF satellite transmission, predicting multiple ground reflection effects on signal fading and effective antenna gain by computerized method 06 p0868 A71-17732

Plane sound waves incident on flat plate airfoils lattice, obtaining transmitted and reflected pressure amplitudes [AIAA PAPER 71-181] 06 p0885 A71-18620

Magnetoreflexion of helicon wave from n-InSb semiconductor in microwave range 07 p1176 A71-19270

Alfven wave transformation into magnetoacoustic wave during passage across boundary between two media in strong magnetic field, considering reflection and refraction laws 07 p1195 A71-19381

Thin single layer orthotropic circular cylindrical shell shear coupled traveling wave reflections, determining stresses in terms of particle velocities 07 p1216 A71-20134

Plane electromagnetic wave propagation and reflection in presence of substances with arbitrary complex permittivity 07 p1066 A71-20543

Interaction between perfect gas ionizing shock wave and transverse magnetic field in coaxial channel, indicating incident wave attenuation and reflected shock wave formation 09 p1498 A71-22128

Curved shock reflection from straight rigid boundary, calculating relationship between incident and reflected wave curvatures 09 p1433 A71-22855

Electromagnetic HF potential effect on reflection of waves obliquely incident on plasma with gas kinetic pressure nonlinearity 09 p1406 A71-22886

Electromagnetic wave propagation through bounded time-space periodic cold plasma under plane wave incidence, calculating transmitted and reflected components 09 p1503 A71-22986

Electromagnetic waves reflection and transmission from weakly ionized moving plasma, noting dependence on medium velocity and nonlinearity effect 09 p1505 A71-23519

Reflected radiative shock wave propagation velocity under transverse magnetic field, taking into account radiation pressure and energy 09 p1506 A71-23588

Wave propagation with frequency inferior to gyrofrequency of ions in collisionless hydrogen plasma, showing Alfven wave reflection on discontinuity surface parallel to magnetic field 10 p1599 A71-23846

Transonic aircraft jet exhaust wave structure, examining reflection geometry at shear layer and shock diamond train 10 p1553 A71-24867

MHD waves incident at density step, calculating reflection, refraction and transmission coefficients and coupling modes 11 p1807 A71-26429

Flowfields behind reflected shock waves, predicting end-wall pressure, radiative heat transfer and radiative gas dynamic coupling effects [AIAA PAPER 70-774] 12 p1986 A71-27562

Magnetoionic component with fluctuating elliptical polarization during wave reflection from F 2 layer, discussing suppression mechanism 13 p2030 A71-28537

Electron concentration profiles in D region from radio wave partial reflection coefficients 13 p2030 A71-28558

Electromagnetic wave reflection from interface between moving and stationary electron plasma, giving boundary conditions at velocity discontinuity surface 13 p2108 A71-28855

Nonlinear skin effects in gas discharge plasma during electromagnetic wave propagation with dissipation, obtaining wave amplitude and carrier temperature dependence on reflection parameters 13 p2108 A71-29042

Electromagnetic wave reflection by rough surfaces based on geometrical optics, discussing reflected power density reflection coefficient and frequency limit 13 p2033 A71-29240

Reflection, diffraction and transmission of plane microwave incident on conducting screen perforated periodically with circular holes, using transmission line analysis and dipole moments method 14 p2192 A71-29568

Vertically incident radio waves reflection from horizontally stratified ionosphere with random electron density irregularities 14 p2192 A71-29718

Jupiter reflected light, examining model having elliptical polarization by surface layer scattering 14 p2306 A71-29730

Reflection and refraction patterns of various wave number media vertical electromagnetic dipole fields at even and uneven interfaces 14 p2192 A71-29805

Point and large sources acoustic free field measurement, predicting reflecting ground surface effects on accuracy 14 p2274 A71-30066

Differential equation describing nonstationary reflection of symmetrical shock front from spherical and cylindrical blunt bodies 14 p2170 A71-30216

Incident sonic boom shock wave reflection factors off smooth surface, discussing pressure rise and flight near threshold Mach number 14 p2177 A71-30610

VHF and UHF ground reflection measurements for antenna site layout, showing feasible operations at short ranges 14 p2217 A71-31050

Internal reflection of VLF whistlers incident from above on model nighttime lower ionosphere 15 p2369 A71-31433

Shock wave reflection process model in magnetic fields, describing time development of interaction process 16 p2616 A71-32901

Ultrasound reflection from defects, using method of similarity and approximation of ray acoustics 16 p2584 A71-33560

Plane uniform waves reflected from layer with random permittivity inhomogeneities, determining distribution function and scattered wave propagation direction 16 p2543 A71-33568

Daytime occurrence of maximum wave reflection frequency and blanketing frequency for period of two solar cycles at Rarotonga and Christchurch stations

16 p2574 A71-33970

Microwave reflection factor analytical and graphical dependences on resistivity of variable thickness semiconductor layers

16 p2544 A71-34032

Impulsive time variation plane wave reflection from ionospheric sech squared electron density profile, comparing full wave and WKB solutions

17 p2701 A71-34769

Reflection and transmission on plane parallel layers of planetary atmospheres with strongly anisotropic scattering, examining three eigenvalue problems

17 p2736 A71-35567

Absorption spectra formation by diffuse reflection from semiinfinite plane parallel scattering planetary atmosphere, using asymptotic expressions for higher order scattering

17 p2736 A71-35568

Mirror-contained collisional plasmas, deriving wave reflection and absorption from equilibrium density and temperature profile equations

18 p2950 A71-35860

Oblique shock wave incident on plane boundary of nonlinear homogeneous elastic solid, proving wave reflection pattern uniqueness

18 p2982 A71-36813

Electromagnetic wave propagation through magnetoplasma disturbed by acoustic wave, calculating transmitted and reflected waves amplitude modulation

19 p3110 A71-37480

Variable stars atmospheric radiation, investigating unsteady light reflection

19 p3133 A71-37505

Pressure wave interaction with orifices inside ducts, calculating reflection and transmission characteristics relationship to orifice geometry and initial steady flow conditions

19 p3044 A71-37642

Alfven wave transformation into magnetoacoustic wave during passage across boundary between two media in strong magnetic field, considering reflection and refraction laws

19 p3138 A71-37806

Transmitted and reflected waves dispersion and structure in waveguide loaded by semiinfinite series of equidistant homogeneous scattering bodies

19 p3019 A71-38329

Anisotropic plasma half space moving normal to interface, investigating incident H waves reflection and transmission coefficients

19 p3024 A71-38610

Sound reflection by dense doubly periodic lattice parallel to rigid screen, describing asymptotic characteristics by double lattice virtual mass including mirror image

20 p3268 A71-38807

Shock fronts diffraction and reflection with vortices generation at discontinuities, predicting wave shape and strength distribution in two dimensional or axisymmetric situations

21 p3365 A71-40016

Ionospheric irregularities and reflection points calculation, developing simple ray interference model from large antenna array data

21 p3372 A71-40042

Stereo viewing transmission/reflection display by producing stereopair image on CRT screen with polarizing polaroid sheets

21 p3376 A71-40126

Plane sound waves transmission and reflection through finite plates single cascade by Wiener Hopf technique

21 p3437 A71-40537

Soviet monograph on unsteady motion of compressible fluids covering acoustic and shock wave reflection from solid boundaries, impact penetration and pressure propagation

21 p3369 A71-40869

Rayleigh wave reflection from crack tip after propagation along open crack faces in elastic solid, determining surface wave energy loss

21 p3468 A71-41003

Electromagnetic wave reflection from interface between moving and stationary electron plasmas, giving boundary conditions at velocity discontinuity surface

21 p3426 A71-41288

One dimensional propagation and multiple reflection of plane thermoelastic wave in Lamé elastic isotropic plate with finite heat transmission

22 p3615 A71-41911

Monte Carlo method calculation for light pulse reflection from clouds for all orders of multiple scattering

22 p3576 A71-42562

Near-normal plane shock wave reflection from rigid impermeable wall, obtaining nonstationary flow parameters in terms of Jacobi polynomials convergent series

22 p3531 A71-42865

Plane electromagnetic waves reflection and transmission at boundary of semiinfinite magnetoelectric medium

23 p3642 A71-42918

Infinite plane elastic wave reflection and refraction coefficients at fluid-solid interface, noting reflected beam lateral displacement at critical angles

23 p3703 A71-43202

Electromagnetic wave reflection from ferrite plate in external alternating magnetic field, showing frequency change due to moving domain wall

23 p3645 A71-43568

Hypersonic shock wave front motion into air at one atmosphere, measuring reflectivity and curvature for comparison with theory

23 p3626 A71-43929

Reflection and scattering properties of two dimensional periodic arrays of loaded dipoles with bandpass filter characteristics as function of frequency

23 p3654 A71-44159

Pressure and flow direction defects behind Mach reflected shock near three shock intersection, considering steady flow theoretical model

24 p3820 A71-44953

Airborne measurement of directional variation in reflected solar radiation over soil surface and vegetation, using scanning radiometer

24 p3826 A71-44984

Multicomponent meteoritic composition effects on meteor trails radio wave reflections, obtaining ionospheric electron concentration distribution

24 p3804 A71-45033

Inhomogeneous rarefied plasma, investigating non-local, linear and nonlinear effects on electromagnetic wave reflection and transmission

24 p3857 A71-45117

Jones reflection and transmission matrices representation for beam splitters, investigating reversibility and action on incident light amplitude and/or phase

24 p3849 A71-45210

Circularly polarized ultrashort radio wave reflection from lunar and planetary surfaces, determining angular scattering spectrum

24 p3805 A71-45313

Two dimensional reflection supersonic nozzle shock wave initiated unsteady starting process, presenting shadowgraphs from shock tube investigation

24 p3821 A71-45367

WAVE SCATTERING

NT ACOUSTIC SCATTERING

NT ATMOSPHERIC SCATTERING

NT ELECTROMAGNETIC SCATTERING

NT HALOS

NT IONOSPHERIC F-SCATTER PROPAGATION

NT LIGHT SCATTERING

NT MICROWAVE SCATTERING

NT MIE SCATTERING

NT RAMAN SPECTRA

NT RAYLEIGH SCATTERING

NT REVERBERATION

NT TROPOSPHERIC SCATTERING

NT X RAY SCATTERING

Breaking waves and resulting CAT characteristics from ultrahigh resolution FM-CW radar observation, using model of unstable waves at sheared inversion layer

01 p0116 A71-10565

Diffraction frequency splitting of opposed waves produced by diaphragm in He-Ne laser resonator

02 p0260 A71-11938

Radar scattering from turbulent underdense ionized wakes, showing relationship between Doppler spectrum and wake characteristics

04 p0551 A71-15011

Lunar seismic waves scattering as two dimensional random walk process, taking crust and rock compositions into account

04 p0650 A71-15544

Seismic waves scattering mechanism in heterogeneous medium from lunar seismograms

04 p0650 A71-15546

Stress wave scattering in fiber reinforced composite material, using model of parallel elastic cylinders embedded in unbounded elastic medium

05 p0826 A71-16719

Spherical wave scattering on thin conducting truncated bodies of revolution, deriving equations system for field pattern

08 p1254 A71-21460

Plane TM wave scattering by systems of two parallel conducting elliptical cylinders, metal tapes and combinations

09 p1407 A71-23106

MHD wave propagation in magnetoplasma perturbed by LF magnetoacoustic waves, considering wave scattering and polarization

09 p1505 A71-23566

Observation range determination numerically for cyclotron resonances of effective scattering cross section of light wave by collisionless plasma in magnetic field

10 p1646 A71-23848

High beta turbulent plasmas radiation scattering due to magnetic field strength and direction fluctuations from optical Faraday rotation observation

10 p1652 A71-24660

S wave scattering from H and He positron systems at low energies, applying Kohn and Harris variational methods

11 p1803 A71-26373

Cosmic radio waves scattering in outer solar corona, considering refraction and gradients in electron density fluctuations

12 p1970 A71-27706

Steady state scattering of cylindrical magnetoacoustic waves traveling along axis of rigid ideally conducting static cylinder

13 p2105 A71-28281

Infinite radially nonuniform thin plasma cylinder wave scattering with electrical field component along inhomogeneity gradient

14 p2191 A71-29512

Electromagnetic wave scattering on inhomogeneities by Born approximation, estimating maximum error for small correlation radius

14 p2194 A71-30100

Electromagnetic and gravitational waves scattering by static gravitational field, comparing classical general relativistic and quantum field theoretic results

14 p2275 A71-30861

Communications systems using carbon dioxide laser wave propagation, considering wave extinction by absorption and scattering, scintillations due to atmospheric turbulence, etc

17 p2700 A71-34749

Radio wave scattering from ionosphere, considering plasma experiments in E and F region

19 p3018 A71-38247

Transmitted and reflected waves dispersion and structure in waveguide loaded by semiinfinite series of equidistant homogeneous scattering bodies

19 p3019 A71-38329

Monostatic plane wave scattering by semiinfinite perfectly conducting wedge with rounded edge for line source excitation in far field

19 p3023 A71-38593

Numerical solution of two dimensional scattering by waveguide bifurcation, using transmission line matrix impulse analysis

22 p3511 A71-42282

Transport properties of low density gas of rotating diatomic molecules, deriving quantum mechanical expression for relaxation time via restricted distorted wave approximation method

23 p3706 A71-42908

Boundary value problem for plane wave scattering by spherical cap, obtaining scattering cross section for Helmholtz resonator and hemispherical shell

23 p3703 A71-43208

Reflection and scattering properties of two dimensional periodic arrays of loaded dipoles with bandpass filter characteristics as function of frequency

23 p3654 A71-44159

Characteristic modes theory for radiation and scattering by conducting bodies, considering electric and magnetic fields

23 p3660 A71-44161

Characteristic modes computation for conducting bodies of revolution, discussing radiation and scattering patterns convergence

23 p3654 A71-44162

Numerical solution for plane wave scattering by dielectric sheet with imbedded periodic array of conducting strips

23 p3654 A71-44164

WAVE SUPERHEATERS

U HYPERVELOCITY WIND TUNNELS

U SHOCK TUBES

WAVEFORMS

NT PULSE AMPLITUDE

NT PULSE DURATION

NT SAWTOOTH WAVEFORMS

NT SQUARE WAVES

Auto and cross correlation function computation from waveform polarity by flexible one bit digital correlator for frequencies to 25 MHz

02 p0211 A71-11644

Horizontal aperture equalization for desired waveform response, describing scanning methods and quantitative effect on noise

02 p0211 A71-11645

Pulsar PSR 1237 plus 25, noting correlated subpulse structure with Fourier analysis method

02 p0318 A71-12951

Single phase static inverter module with voltage waveform synthesis by time optimal response /bang-bang/ closed loop technique

04 p0535 A71-15287

Crab Nebula pulsar PSR 0531 plus 21 at 410-1664 MHz, noting mean pulse profiles and spectral indices

05 p0812 A71-16697

Bandpass limiter output envelope fluctuations dependence on input form and bandwidth

05 p0730 A71-17061

ECG beat-to-beat variation reduction using digital computer wave recognition

07 p1049 A71-19839

Primary T wave derived from ECG waveform dependent intrinsic ventricular recovery properties

07 p1050 A71-19840

Tunnel diode output voltage converter circuit diagram and waveforms

07 p1080 A71-20360

Frequency agile waveforms effects on detection and tracking radars performance, decorrelating distributed clutter echoes

08 p1253 A71-20798

Transistor circuit constant current technique for wave generation and shaping involving triangular, trapezoid and staircase waveforms

08 p1264 A71-21223

Si step-junction avalanche diodes conduction current pulse waveforms during large signal operation, using numerical calculation

08 p1265 A71-21290

Short N wave refraction and diffraction by gas-filled soap bubble, discussing measurements to explain peaking and rounding in sonic boom pressure signature

10 p1642 A71-24811

Transonic aircraft jet exhaust wave structure, examining reflection geometry at shear layer and shock diamond train

10 p1553 A71-24867

Supersonic compressor performance, discussing shock and dump losses and wave structure model errors

10 p1553 A71-24869

Pulsed optical range finders, predicting transmitter pulse wave shape effects on calibration, precision and efficiency by probability density function

12 p1903 A71-26792

Electrical waveform sampling circuits without switched feedback amplifiers, discussing advantages of open loop configuration with circuit diagrams

12 p1891 A71-26997

Waveform and spectral analysis program for electronic system designs, discussing fast Fourier transform modular staging and noise control applications

12 p1884 A71-27148

Turbomachine blade cascades in supersonic flow, noting wave configurations, entropy and counter pressure variations

12 p1864 A71-27475

Inhomogeneous plasma, describing linear wave transformation with fourth order differential equation with variable coefficients

12 p1942 A71-27768

Respiratory wave basic pattern during cat diaphragm artificial activation by electric rectangular stimulus to phrenic nerves

14 p2185 A71-30412

Triangular pulse shaper using transistors and dynistors, obtaining pulse duration, rise time and maximum repetition frequency

14 p2213 A71-30581

Computer quantitation of ST segment response to graded exercise in untrained and trained subjects, continuously recording amplitude of selected points on ECG waveform

15 p2358 A71-31452

Arbitrary shape pulsed AM systems prediction technique improvement, using time-domain signal

15 p2373 A71-32371

Rectangular pulse formation in nonlinear homogeneously distributed systems, discussing energy conversion efficiency

15 p2382 A71-32626

Pulsar polarization characteristics and pulse profile observations in 250-450 MHz range

17 p2807 A71-35417

Surface wave patterns created by constant velocity pressure point on inviscid plasma bounded by magnetic field

19 p3111 A71-37637

Stability conditions for square wave sustaining voltage, including complex rectangular waveforms with pulsed discharges in plasma display

20 p3233 A71-39060

Transverse hydromagnetic shock structure in partially ionized gas, calculating ions, electrons and atoms temperatures, velocities and momentum

21 p3444 A71-40239

Elastic viscous plastic waves profiles of finite uniaxial strain, obtaining constitutive equations

21 p3465 A71-40788

Flash light angular size, adaptation luminance, pulse shape and color effects on Blondel-Rey constant tested on observers with good binocular vision

22 p3498 A71-41483

Mathematical model for pulse waveform identical with single integrator delta modulator, using analog techniques of angle modulation and sampling

22 p3522 A71-42276

Power spectral density of N-ary orthogonal continuous phase FSK waveforms for ELF/VLF communications

22 p3513 A71-42385

Bonding conditions effect on wave mode formation at explosive bonded interface in bullet experiments on thin metal targets

22 p3617 A71-42495

Unmodulated and step-modulated HF pulse signal envelope calculation and diagram plotting

23 p3644 A71-43319

Large amplitude high efficiency TRAPATT oscillation mode in Si avalanche diodes, using resonant cavity for voltage and current waveforms analysis

23 p3650 A71-43352

Damped exponential cosine probability distribution function for clipped waveforms of voiced speech signal

23 p3645 A71-43439

Binary parabolic phase coded waveform generation from analog signals by pi-quantization

23 p3645 A71-43440

Airborne radar sea return averaged pulse shape measurements over various water surfaces, noting clear distinction between specular and scattered reflection components

24 p3824 A71-45083

SHF resonator small resonant frequency shift and Q factor changes measurement based on FM signal envelope shape analysis

24 p3858 A71-45237

WAVEGUIDE ANTENNAS

Plane infinite horn antenna with small aperture angle coupled to waveguide, considering wave excitation

01 p0038 A71-11207

Directional dielectric loaded waveguide antenna for probing electromagnetic field oscillations, discussing design and performance tests

04 p0560 A71-15880

Axial slits circular array pattern in large conducting cylinders fed by waveguides

09 p1419 A71-23497

Modal superpositions for mutual coupling on cylindrical array of waveguide elements

09 p1420 A71-23513

Y-shaped microwave power splitter, using dielectric wedge partially extending into rectangular metallic waveguide

11 p1733 A71-26349

Computerized design of optimally efficient dual-series feed microwave networks for waveguide phased arrays

14 p2209 A71-29566

Flush mounted aeronautical waveguide antennas with dielectric plug for 5GHz operation

14 p2216 A71-31043

Marconi 90 ft space communication antennas and waveguide components, using feed horn radiation patterns to compute gain

15 p2374 A71-31141

Plane infinite horn antenna with small aperture angle coupled to waveguide, discussing wave excitation and field strength

17 p2697 A71-34259

Reflection and transmission coefficients of nonresonant slots in rectangular waveguide antenna with comb type slow wave structure

19 p3019 A71-38334

Narrow flare angle low permittivity conical dielectric waveguide antenna, examining radiation patterns and propagation characteristics by approximate theory

20 p3196 A71-39380

Edge effects in finite linear arrays of uniform slits fed by parallel plate waveguides terminated on ground plane

23 p3653 A71-44156

WAVEGUIDE FILTERS

Waveguide and stripline bandstop filters for pass-band loss minimization, using Chebyshev response curves

09 p1418 A71-23158

WAVEGUIDE TUNERS

Waveguide microwave load element with separate adjustment for reflection coefficient phase and magnitude

03 p0378 A71-13397

Frequency saturation effects in transferred electron /Gunn/ microwave oscillators mechanical tuning characteristics in conventional waveguide cavities

07 p1072 A71-19105

Postcoupled waveguide cavity Gunn effect microwave oscillator equivalent circuit analysis, using lumped constant elements

07 p1072 A71-19106

Magnetically tunable microwave bandpass and bandstop filters with yttrium-iron garnet /YIG/ single crystal

11 p1737 A71-25625

WAVEGUIDES

NT BEAM WAVEGUIDES

NT PLASMAGUIDES

Electric potential and field distribution in dielectric plate insert of rectangular waveguide calculated by net point method using computer program

01 p0051 A71-10149

Signal detection processes selection and components sizing for stand for echometric measurement of attenuation in long distance waveguide connection

01 p0029 A71-10309

Round dielectric waveguides dominant mode radiation losses calculation

01 p0052 A71-10467

Open barrel shaped resonators in plasma diagnostics, using waveguide concepts

01 p0133 A71-10683

Wall loss influence on energy flow center velocity of rectangular carrier pulses in circular waveguide for long distance transfer

01 p0056 A71-11195

Circulation adjustment of m-port waveguide single junction circulator by scattering matrix eigenvalues

01 p0056 A71-11197

Variational bounds on phase shifts for electromagnetic wave scattering by dielectric obstacles in waveguides

01 p0056 A71-11199

Radiator systems field calculation based on waveguide and resonator excitation method, noting field amplitudes in two and three dimensional arrays

01 p0038 A71-11202

Whistler ducts as enhanced ionization fromOGO 3 satellite observations near magnetic equator, noting magnetospheric ionization hydrostatic model and predicted cut-off

01 p0076 A71-11499

Integrated optical communication circuit technology adaptable to batch processing, considering encapsulated planar arrays of rectangular dielectric waveguides

02 p0231 A71-12008

Uniform periodic waveguide mode coupling, obtaining mode transducer design

02 p0216 A71-12342

Waveguide feeder system design for antenna receive path of Intelsat 3 satellite ground station, considering system noise temperature

02 p0223 A71-12800

Quasi-optical waveguide components for millimeter and submillimeter waves, considering couplers, attenuators, isolators, bandpass and bandstop filters

02 p0235 A71-12907

Propagation modes and circularly polarized wave production in circular waveguides with anisotropic walls

03 p0384 A71-13317

Nonautonomous operation of reflex klystron coupled to multifrequency waveguide, noting response to microwave signal

03 p0385 A71-13792

Resonant excitation of plane dielectric waveguide by plane monochromatic wave

03 p0378 A71-13798

Wideband amplitude modulator for quasi-optical waveguide channels, featuring one dimensional rotating wire grating

03 p0378 A71-13804

Polarization control of emission from cross-shaped slots on square and circular waveguide walls via phase and amplitude adjustment

03 p0386 A71-13809

Transient waveform distortion of arbitrarily modulated signal propagating through ideal waveguide

04 p0553 A71-15219

Rectangular waveguide with T junction, deriving characteristic impedance, maximum power and damping constant

05 p0719 A71-15997

Irregular waveguide and horn construction using asymptotic two beam sum theory

05 p0719 A71-15998

Electromagnetic waves phase velocity in helical waveguides in magnetodielectric medium with cylindrical void interspace

05 p0722 A71-16827

Waveguide cavity CW Gunn microwave oscillator bias voltage controlled amplitude and frequency modulation

07 p1073 A71-19110

Antenna feed waveguides interconnection for compensation of cross coupling between elements of two dimensional array

07 p1079 A71-20072

Optimal nonreciprocal waveguide phase shifters using ferrites with rectangular hysteresis loop, considering electromagnetic wave propagation

07 p1079 A71-20074

Open barrel shaped resonators in plasma diagnostics, using waveguide concepts

07 p1170 A71-20145

Single mode oversize optical waveguide fabrication and components

07 p1162 A71-20423

Satellite-borne long wave transmitting antenna excitation, calculating electromagnetic field near earth surface by earth-ionosphere waveguide model

08 p1252 A71-20744

Arbitrarily shaped waveguide analysis computer program EHPOL for polynomial approximation to eigenfunctions of Helmholtz equation, considering homogeneous Neumann and Dirichlet boundary conditions

08 p1261 A71-20752

Infinitely long dielectric rod waveguide HE sub 11 surface wave mode launching efficiency, using Fourier integral

08 p1262 A71-20754

- Short-slot waveguide latching ferrite switch structure, operation principle, phase constants calculation and isolation characteristics 08 p1262 A71-20756
- Dual channel rotary joint combining Tm and Te modes in circular waveguide for X band antenna high average power operation 08 p1252 A71-20758
- Four-cavity elliptic waveguide microwave bandpass filter design and performance prediction from mathematical model 08 p1262 A71-20762
- Dielectric loaded waveguide electromagnetic field and coupling matrix derivation by finite element computer program, presenting dispersion curves and field plots 08 p1262 A71-20765
- Book on electromagnetic fields and waves covering vectors, current density, flux integral, Coulomb law, Laplace equation, magnetomotive force, waveguides, etc 08 p1335 A71-21459
- Holographic spectrum analyzer for plasma diagnostics in microwave band, deriving formulas for emission spectrum based on interference patterns intensities in waveguide 09 p1499 A71-22150
- Wave interference effects and energy transfer in coupled thin film optical waveguides 09 p1460 A71-22159
- External SHF signal effects on multifrequency spectrum of reflex klystron coupled with long waveguide 09 p1414 A71-22221
- Electromagnetic wave propagation in circular waveguide loaded with coaxial dielectric cylinders, calculating band pass characteristics 09 p1406 A71-23039
- Concentric shield for surface wave propagation loss at bend in open waveguide, using Ayrton function 09 p1410 A71-23570
- Azimuthal surface waves launching on cylindrical impedance boundary using waveguide open end as excitation aperture 09 p1410 A71-23571
- Book on lasers and masers covering electric and magnetic dipole transitions, electron oscillator, collision broadening, optical resonators, waveguides, etc 09 p1466 A71-23725
- Lower ionosphere RF whistlers polarization and electromagnetic structure, determining earth-ionosphere waveguide resonance frequency 10 p1575 A71-23828
- EM wave excitation in plane parallel waveguide by rotating relativistic electron flux, deriving dispersion relation and interaction solutions 10 p1577 A71-24323
- Rough circular rod effective surface impedance and propagation constant, discussing guided electromagnetic wave attenuation on structure 10 p1578 A71-24399
- Pi-section waveguide with narrow slot in broad wall, calculating reflection and transmission coefficients as function of design parameters 10 p1584 A71-24719
- Wideband gas discharge duplexer as transmitter receiver microwave antenna switch in H₀₁/mode circular waveguide 10 p1584 A71-24720
- Earth-ionosphere spherical waveguide, calculating mean and differential phase velocities and field amplitude of low frequency waves 11 p1731 A71-25774
- Eigenvalues of axially uniform fluid waveguide with eccentric annulus cross section and acoustically hard boundaries 12 p1928 A71-26700
- Electric and magnetic surface current coefficients of antenna radiating elements in metallic waveguides and resonators by harmonics expansion applied to circular-cylindrical array 12 p1885 A71-26839
- EM wave scattering in waveguide by active regular shape bodies, using integrodifferential equations 12 p1881 A71-27337
- Differential equations for wave propagation in irregular electromagnetic waveguides 12 p1888 A71-27530
- Cylindrical waveguide with three differential phase shift sections, deriving microwave output magnitude and polarization for comparison with ferrite experiment 13 p2037 A71-28604
- Circular waveguides containing pure dielectrics, examining propagation mode inversion criteria via TE and TM characteristic equations 13 p2037 A71-28606
- Propagation constant relation to frequency for waveguide filled with simple moving medium, presenting dispersion curves set 13 p2030 A71-28607
- Spherical waveguide eigenvalues calculation from two layer model of earth with radially inhomogeneous atmosphere, using Airy functions 14 p2209 A71-29515
- Radiation field description with spatial complex variables, considering application to scattering and waveguide problems 14 p2209 A71-29567
- Millimeter wave waveguide time delay distortion characteristics equalization using directional filter cascades 14 p2210 A71-29572
- Dielectric loaded waveguides electromagnetic fields solution by finite element method for cutoff modes determination 14 p2212 A71-30509
- Millimeter wave semiconductor isolator using circular waveguide with coaxial n-type InSb in longitudinal magnetic field 14 p2212 A71-30510
- Microwave scattering by DC magnetized ferrimagnetic circular cylinder in rectangular waveguide 14 p2212 A71-30512
- Iris-type discontinuity problems in waveguides and periodic structures, investigating numerical solutions convergence 14 p2212 A71-30513
- Electromagnetic wave propagation on Yagi-Uda structure, obtaining current distribution, free space vs guided wavenumbers diagram and cutoff frequencies 14 p2196 A71-30514
- Schwarz-Christoffel conformal transformation inversion for electrostatic field integral equation formulation, applying to stepped-guide junction 14 p2212 A71-30515
- Ridged waveguide complete eigenvalue solution by integral equation formulation and Ritz-Galerkin method 14 p2212 A71-30516
- Earth-ionosphere waveguide excitation by satellite-borne horizontal dipole antenna, deriving fields at earth surface based on idealized model 14 p2196 A71-30562
- Radar duct surface interference phenomena and focusing effects on radar beam energy propagation 14 p2201 A71-30936
- Miniature 20-watt CW TWT with samarium cobalt focusing magnets for fitting X-band waveguide, comparing performance, size and weight with conventional design 15 p2375 A71-31206
- Modified method of cross sections applied to scalar Helmholtz equation solution in infinite symmetrical waveguides 15 p2449 A71-31711
- Wideband four probe waveguide impedance meters design for standing wave structure measurement 15 p2378 A71-32634
- Multimode coaxial feed with circular cross section waveguide and concentric ring shaped radiator for parabolic antennas 16 p2546 A71-33480
- Radiator system field calculation based on waveguide and resonator excitation method, noting field amplitudes in two and three dimensional arrays 17 p2697 A71-34254
- Fence guide waveguide on dielectric substrate for millimeter wave, applying to power dividers, directional couplers, hybrid rings and resonators 17 p2713 A71-34444
- Low loss surface oriented waveguide for millimeter IC, using high permittivity rectangular dielectric image line 17 p2714 A71-34603
- Wall impedance method application to long distance transmission elliptical, parabolic and circular waveguides 17 p2707 A71-35480
- Uniform inhomogeneous waveguides with linear time invariant passive medium, determining functional behavior in frequency domain of electromagnetic waves propagation constant 17 p2708 A71-35492
- Avalanche diode microwave oscillator design, comparing coaxial lumped, lumped element, microstrip and waveguide circuits 18 p2893 A71-36600
- Waveguide mounted X band CW Gunn effect oscillators load impedance characteristics, proposing lumped equivalent circuit 18 p2894 A71-36830
- Telecommunication developments covering coaxial cables, waveguides, error elimination, information theory, sound transmission and radars 19 p3016 A71-37340
- Perturbations effects on ELF propagation in inhomogeneous anisotropic ionospheric waveguide 19 p3017 A71-37867
- High-power high-efficiency CW X band Gunn oscillators on diamond heat sinks, noting operation in waveguide cavities 19 p3029 A71-38219
- Transmitted and reflected waves dispersion and structure in waveguide loaded by semiinfinite series of equidistant homogeneous scattering bodies 19 p3019 A71-38329
- Electromagnetic wave scattering on single ellipsoidal inhomogeneity in cylindrical waveguide, obtaining relationship for electric and magnetic waves reflection coefficient 19 p3019 A71-38330
- H wave propagation in waveguide consisting of two parallel plates with longitudinal rectangular grooves, determining electric and magnetic fields by reduction method 19 p3019 A71-38331
- Wave diffraction at step junction of two rectangular waveguides and symmetrical diaphragm with dielectric fillers 19 p3019 A71-38332
- Design algorithm for gyrotropic waveguide consisting of symmetrical rectangular coaxial with magnetized ferrite rods 19 p3019 A71-38333
- Natural oscillations existence in cross section of cylindrical waveguide with resonant cavity based on Hilbert space operators, solving boundary value problem 19 p3019 A71-38336
- Waveguide systems coupled through slots in lattice partition approximated by anisotropic dielectric layer 19 p3019 A71-38338
- Green tensor function for waveguides, resonators and radiating devices with boundaries coinciding with orthogonal cylindrical coordinate systems surfaces 19 p3104 A71-38339
- Electromagnetic wave propagation in comb type waveguides, obtaining boundary value electrodynamic problem rigorous solution 19 p3020 A71-38342
- VLF fields of horizontal dipole in waveguide formed between ice covered ground and anisotropic ionosphere of Antarctica 19 p3024 A71-38595
- Liquid nitrogen cooled microwave low temperature noise standard in WR-51 waveguide 20 p3202 A71-38832
- Reflection and transmission coefficients of long lossy single-wave waveguide line with random inhomogeneities 20 p3198 A71-39805
- Microwave waveguide semiconductor modulator with p-n-n diode as control element, taking into account semiconductor control element conductivity change along waveguide wall 20 p3206 A71-39813
- Voltage-polarization induced optical waveguide using electrooptical lithium niobate crystal 21 p3393 A71-41039
- Hollow dielectric waveguide gas laser with He-Ne mixtures at 6328 Å 21 p3393 A71-41040
- Waveguide structure effect on electron beam pumped GaAs laser characteristics, considering diffraction losses and laser threshold reduction 21 p3394 A71-41233
- Earth-ionosphere spherical waveguide, calculating mean and differential phase velocities and field amplitude of LF waves 22 p3509 A71-41542
- Waveguide simulator study of blindness/resonance or surface wave/effect in phased array antennas 22 p3509 A71-41631
- Electromagnetic field distributions and far field radiation patterns of three layer waveguide GaAs heterostructure injection lasers, using Maxwell equations 22 p3555 A71-41688
- Dielectric articles thickness and flaw control by microwave magic tee junction waveguide, describing instrument design and operating characteristics 22 p3521 A71-41772
- Thin film optical waveguide TE-TM mode converters, using gyrotropic or anisotropic substrate material 22 p3556 A71-41806
- Electromagnetic wave propagation and radiation pattern of circular corrugated waveguide antenna feeds, considering unity azimuthally dependent modes 22 p3511 A71-42278
- Field configuration of TM mode in elliptical waveguide, showing inaccuracy of microwave theory 22 p3522 A71-42279
- Numerical solution of two dimensional scattering by waveguide bifurcation, using transmission line matrix impulse analysis 22 p3511 A71-42282
- Ferrite and dielectric element waveguide phase shifters with rectangular hysteresis loop, deriving differential phase and attenuation constants for wave propagation 22 p3512 A71-42308
- Experimental observation of 10.6 micron guided waves in Ge thin films, noting application to carbon dioxide laser communication 22 p3587 A71-42568
- Rectangular waveguide with T shaped pedestal, deriving characteristic impedance, maximum power and damping constant 22 p3515 A71-42746
- Irregular waveguide and horn construction using asymptotic two beam sum theory 22 p3515 A71-42747

WAVELENGTHS

Quasi-optical waveguide system for measuring electrical properties of dielectric and magnetic materials in submillimeter band
23 p3677 A71-43530

Waveguide system for measuring semiconductors electrical and photoelectric properties at SHF, observing temperature effects
23 p3652 A71-43531

PAM signal transmission through statistically rough waveguide, calculating wall roughness effects on transient response by multiple scattering theory
23 p3645 A71-43566

Normal wave scattering on random permittivity inhomogeneities of stratified waveguide dielectric layer, calculating beam width and energy loss by perturbation procedure
23 p3645 A71-43567

Low loss microwave iris-loaded circular TE mode waveguide delay line for pulse compression at X band
23 p3653 A71-43963

Nonlinear theory for synchrotron emission of tubular electron flux in cylindrical waveguide, discussing wave-electron interactions optimization
23 p3653 A71-44058

Wideband phase-matched carbon dioxide laser second harmonic generation in GaAs thin film waveguide through dielectric dispersion
23 p3687 A71-44136

Critical frequencies of higher order modes in circular waveguides with arbitrary thick dielectric sleeve
23 p3647 A71-44319

Approximate calculation of cut-off frequencies of H- and Pi-section waveguides using corrugated plane surface theory
23 p3655 A71-44323

Open waveguide field expansion in orthogonal wave system with proper and improper modes
23 p3647 A71-44332

Spectral representation and propagation mode of microwave transmission line on circular waveguides at great distance
24 p3803 A71-44361

Plasma microwave harmonic generation conversion efficiency, applying field gradient theory to case of positive column placed through rectangular waveguide
24 p3803 A71-44648

VLF day and night waveguide modes attenuation coefficients and phase velocities, using moving secondary source formed by mode conversion at sunrise and sunset shadow line
24 p3803 A71-44650

Long distance atmospheric propagation in earth-ionosphere waveguide, obtaining phase velocities and damping factors
24 p3804 A71-45030

Microstrip line on silicon-silicon oxide system, investigating propagation modes and fringing effect by parallel-plate waveguide model
24 p3809 A71-45091

Plane TEM wave propagation in free space using rectangular waveguide partially filled with two dielectric slabs
24 p3809 A71-45093

Movable metal iris with nearly frequency independent susceptance, relating characteristics to centered capacitive obstacle in waveguide
24 p3809 A71-45095

Point source radiation in stratified waveguide system with magnetoplasma slab, evaluating transverse field by Fourier integral representation
24 p3857 A71-45181

HF dispersion, power and energy storage in periodic slow wave waveguides of resonator chains coupled through openings
24 p3805 A71-45257

Composite quasi-optical-broad waveguide transmission lines for millimeter and submillimeter waves with spectrum phase correction
24 p3810 A71-45258

WAVELENGTHS

High pressure rare gas UV emission spectra, examining wavelength cut-offs and flux ratios
04 p0549 A71-15691

Thorium wavelength measurements by interferometry, noting weighted averages as secondary standards of length
04 p0627 A71-15697

Optical beam scintillation dependence on wavelength in strong refractive index turbulence
04 p0609 A71-15694

Solar line spectra wavelength improvement in 7780 to 7925 A range, using carbon dioxide bands
05 p0803 A71-16020

Two wavelength nondiffuse holography for interferometry of transparent media
05 p0748 A71-16264

CdS laser wavelength and relative threshold excitation levels as function of temperature based on band edge absorption effects
05 p0763 A71-16498

Compact nebulae IC 4997, VV 8 and FG Sge observed at 3.5 and 11.0 microns, noting IR wavelength energy
05 p0812 A71-16696

EEG wave phase durations over human brain surface, examining asymmetry distribution level
05 p0709 A71-16801

Thermocompensated cavity resonator for SHF wavelength measurements
07 p1075 A71-19302

Self preserving solutions of Stewart-Townsend and Ogura-Meakoda equations for isotropic turbulence decay, discussing asymptotic nature for small and large wavenumbers
07 p1091 A71-20027

Photocathode area sensitivity contours-wavelength relationship from photomultiplier absolute intensity and near IR spectrum laser research
08 p1291 A71-21408

Lidar wavelength optimization for Raman scatter atmospheric studies, taking into account aerosol and weak signal statistical effects
08 p1254 A71-21458

Holographic interferometry at two wavelengths for phase objects dispersion characteristics
08 p1292 A71-21487

Brightness temperature measurement in high pressure Ar plasma by comparing reference lamp to plasma radiation intensities
10 p1646 A71-23833

Frequency stabilized lasers as absolute wavelength standards, discussing perturbation causes for optical resonant cavities and atomic transitions
10 p1621 A71-24581

Large angle Rayleigh light scattering for density fluctuations determination in dilute gases with wavelength comparable to mean free path
10 p1642 A71-24835

Longitudinal magnetic field effect on output power, polarization and lasing frequency of He-Ne laser operating at 0.63 micron wavelength
11 p1774 A71-26003

Temperature dependent isophote wavelength in Brill and Planck formulas, comparing uvby and UVB photometric systems
13 p2068 A71-28512

Microwave power transmission from satellite solar energy station to earth, discussing atmospheric attenuation mechanisms and wavelength and power density optimization
13 p2000 A71-28670

Chromospheric flare on 11 July 1966, comparing solar radio emissions at 10 cm and 1.5 m wavelengths
14 p2298 A71-29976

Aberration-free wave front reconstruction from holograms illuminated at wavelengths differing from forming wavelength
14 p2240 A71-30130

Two-wavelength holographic interferometry for phase objects dispersion characteristics, noting plasma diagnostics application
14 p2248 A71-30675

Frequency stabilized He-Ne laser wave secondary length standard for automatic measurements, discussing electronic control, accuracy, line width, pressure, current and magnetism effects
16 p2588 A71-34119

Carbon dioxide laser single wavelength operation in TEM mode without intracavity dispersive elements
17 p2751 A71-34379

Wavelength table for determination of stellar radial velocities in spectral classes F6-M2, including Hyades cluster and Coma Berenices
19 p3144 A71-38168

Wavelength discrimination from color naming by young adults with normal visual acuity and color vision
19 p3004 A71-38285

Solar atmosphere oscillatory component observations at 3 mm wavelengths with two radio telescopes, obtaining power spectra
21 p3447 A71-40424

Liquid laser output wavelength dependence on rhodamine dye concentration, comparing experimental data with Stepanov theory
23 p3684 A71-43417

Illumination wavelength effect and supply voltage dependence of photomultiplier area sensitivity map
23 p3676 A71-43505

Seyfert galaxies optical polarization, investigating time and wavelength dependences by multicolor polarimetric and photometric observations
24 p3873 A71-45078

Low loss mode selection and wavelength regulation of gas lasers with electro-optical intracavity resonator
24 p3834 A71-45163

WAVES

Rotating inviscid incompressible fluids in tubes, investigating axisymmetric nonlinear waves motion in relation to vortex breakdown
01 p0072 A71-11224

Crosshatched wave patterns in liquid films, discussing supersonic wind tunnel experiments aimed at elimination of sublimation or vaporization as pattern generating mechanisms
15 p2389 A71-31551

WAXES

Atomization drop size distributions in sprays from convergent pneumatic nozzles for molten wax and polyethylene mixtures
13 p2049 A71-29007

WEAPON SYSTEM MANAGEMENT

Computer simulation for evaluating equipment effect on weapon mission success, considering failure time, repair cycle, operational and maintenance parameters
03 p0431 A71-13090

Defense management efficiency improvement concepts for weapon systems programs, discussing elimination of bureaucracy, communication between organizational levels, mission instead of function orientation, etc
12 p1988 A71-27246

Weapons R and D flexible economical response to defense needs by emphasis on component and subsystem experimentation
14 p2341 A71-31130

Cost control over changes in major weapons systems between letting of contract and final hardware delivery
14 p2342 A71-31134

WEAPON SYSTEMS

NT GROUND OPERATIONAL SUPPORT SYSTEM

NT MISSILE SYSTEMS

USAF weapons and support systems, discussing military R and D funding and resulting constraints
05 p0839 A71-16285

F-15 air superiority fighter, describing military requirements, program management and procedures in terms of speed, maneuverability, acceleration and weaponry
07 p1018 A71-19078

Fluidics application to weapon systems safety and arming devices, investigating reliability and immunity to environmental conditions
07 p1025 A71-20561

Worldwide aeronautical charts maintenance for weapon systems support, discussing data sources
08 p1281 A71-21254

Performance test methods and equipment for aircraft avionics and weapons systems, discussing computer integration with radar and phototherdolite range instrumentation system
08 p1260 A71-21660

Weapons systems design for logistics supportability, discussing operational availability at minimal life cycle cost as function of reliability, maintainability and MIL Spec documentation
09 p1429 A71-23476

Cheyenne attack helicopter weapons system, discussing night vision capability, armament, fire control and navigation equipment integration
14 p2178 A71-31091

Weapons delivery computer for attack helicopters, using planar distributed function generator for general closed form instantaneous solution capability
14 p2209 A71-31092

One man Jaguar aircraft navigation, weapon aiming system and pilot operational tasks, noting inertial platform alignment, displays and target attack modes
20 p3261 A71-39825

WEAPONS

NT GUNS [ORDNANCE]

NT NUCLEAR WARHEADS

NT NUCLEAR WEAPONS

NT WARHEADS

Operational research for decision making in weapons procurement and deployment, considering military effectiveness, weapon assessment criteria, local conflict conditions, cost and operational environment
07 p1206 A71-19418

Millimeter wave holographic imaging for concealed weapon detection by phase-only hologram, discussing recording and reconstruction systems configurations
22 p3546 A71-42485

WEAPONS DEVELOPMENT

Operational research in designing ground-to-air launch weapons, considering model, effectiveness measure, decision and experiment
09 p1532 A71-22992

Remotely piloted vehicles development and limitations, considering air superiority, weapons delivery, sensors and survivability
18 p2849 A71-35899

WEAR

Oscillatory motion effects on bonded solid film lubricants wear life, discussing oscillation arc and frequency, surface finish and load
02 p0258 A71-12593

Dimensional analysis of wear by solid particle impact in fluid flows in pumps and ducts
19 p3046 A71-38273

Aircraft parts lubrication friction and wear problems, discussing failure modes, solid and liquid lubricants, component damage and lubrication systems
21 p3389 A71-40902

WEAR INHIBITORS

Friction coefficient in antifriction polytetrafluoroethylene compounds with lead, bronze or graphite

02 p0275 A71-12600

Synthesized hydrocarbon oil antiwear and extreme pressure additives effects on bearing spinning torque and endurance

06 p0904 A71-17580

Nitriding effect on hardness and wear resistance of Mo alloys

06 p0912 A71-17936

Mechanical property modifications of polytetrafluoroethylene by filler additions, noting improved wear resistance [PLASTICS INST. PAPER 13]

09 p1482 A71-22346

Mechanized ultrasonic inspection probes with high stable dynamic acoustic coupling coefficient, high sensitivity and wear resistance and low coupling fluid expenditure

09 p1450 A71-22897

Solid additives, graphite and molybdenum disulfide concentration effects on liquid lubricants and greases antiwear performance

14 p2251 A71-29827

Lead bronze and Babbit metal composite material, detailing antifriction efficiency and wear resistance in bearings

15 p2417 A71-32666

Chromium carbides or borides high melting wear resistant surfacing material for machine components subjected to abrasive wear

15 p2418 A71-32669

Refractory tungsten boride with iron or nickel for powdery surfacing mixtures, showing hardness and wear resistance dependence on low melting component

15 p2438 A71-32675

WEAR TESTS

Boride coatings for Fe-Si alloy, testing corrosion and wear resistances in aqueous salt, acid and alkali solutions

01 p0097 A71-10039

Liquid droplet diameter effect on solid surface erosive wear

01 p0072 A71-11242

Ni and Fe alloys for tooling materials, examining die life and wear at elevated temperatures [SME PAPER MF-70-121]

01 p0090 A71-11266

Test time and contact stresses effect on jet fuels antiwear properties under rolling friction

02 p0298 A71-12570

Sliding friction and wear of metal pairs under vacuum, using gravimetric and electron optical methods

03 p0432 A71-13366

Bearing vibration monitoring for wear and damage detection

04 p0603 A71-15671

Counterface nature effect on friction and wear processes of carbon fiber reinforced polymers, discussing formation of transfer film of wear debris

05 p0773 A71-17245

Device for jet fuels antiwear properties measurement under rolling friction

07 p1111 A71-19493

Steel coatings produced by boriding, investigating structure and wear resistance properties

07 p1118 A71-19583

Chemical composition effect of low carbon alloys metallic matrix on wear resistance in abrasive medium, showing austenitic manganese alloys superiority to martensitic or ferritic alloys

07 p1136 A71-19630

Wet and dry lubricated slip ring systems long term application testing in ion pumped vacuum chambers

07 p1120 A71-20274

High melting compound tools wear resistance during Ti and Ni continuous microcutting

08 p1297 A71-21065

Friction and wear tests on materials of various speeds, loads and temperatures at high relative humidity

09 p1426 A71-22325

Tribological characteristics of carbon fiber reinforced thermoplastics, noting improved sliding wear against metal surfaces [PLASTICS INST. PAPER 12]

09 p1481 A71-22344

Friction and wear of steels, Ti, Al, Cu and copper beryllium in sliding over hardness range of steel plates in vacuum and air

11 p1771 A71-26143

Jet fuels deoxygenation effects on steels antiwear properties and critical loading under vibrational and gliding friction

12 p1945 A71-27662

Disintegration energy of hard compounds/carbides, nitrides and borides/ related to wear resistance and microhardness of alloys

13 p2072 A71-27818

Friction coefficient and wear of steel in vacuum and air at low and room temperatures

13 p2072 A71-27870

Plastics contact strength test apparatus, describing wear test machine for contact load resistance of epoxides used in automobile engine bearings

15 p2383 A71-31656

Jet fuel dissolved oxygen concentration effects on plunger antiwear properties

15 p2464 A71-31677

Jet fuel antiwear properties relation to viscosity and adsorption tar and mercaptans content

15 p2464 A71-31678

Mathematical models for boundary lubrication, computing specific liquid lubricant/surface wear rates in machine element design

15 p2414 A71-31950

Surfacing materials based on transition metal borides with boron carbide additions, testing brittleness, hardness and abrasive wear resistance

15 p2431 A71-32163

Antiwear properties of jet fuels as function of dissolved oxygen, resin and heteroorganic compound content and temperature, considering antioxidant additives

16 p2623 A71-33579

Chemical composition effect of low carbon alloys metallic matrix on abrasive wear resistance, showing austenitic manganese alloys superiority to martensitic or ferritic alloys

16 p2593 A71-33626

Antiwear property assessment of piston engine and aviation jet fuels under point contact conditions, recommending ball and cylinder test technique

17 p2792 A71-34447

Temperature effects on wear and failure of titanium and niobium carbides, using electron microscopy

19 p3076 A71-37114

Friction, wear and adhesion of filler and matrix polymer composite bearing materials including glass, carbon, lamellar solids, metal powders, carbons, nylons, PTFE, polyimides, etc

21 p3405 A71-40602

Mo, W and Al alloying additives effects on mechanical properties and wear resistance of austenitic high Mn electroslog melted steel

21 p3403 A71-41106

Static joint wear role in overall machine reliability and service life under working loads from mathematical prediction

22 p3619 A71-42852

Diboride-nitride system dry friction and wear resistance at room temperature

23 p3681 A71-43254

Boron silicide coatings wear resistance in vacuum and air, determining slipping rate and working medium influence on friction process in active surface layers

24 p3830 A71-44859

Solid lubricant-epoxy compounds shear modulus measurement by cantilever beam specimens dynamic testing, calculating wear life coefficients for molybdenum disulfide in epoxy resin [ASLE PREPRINT 71LC-1]

24 p3842 A71-45284

WEATHER

NT COLD WEATHER

Weather effects on pilot performance

03 p0369 A71-13021

VFR flying under adverse weather conditions, discussing radio navigational aid equipment and communication with ground stations

08 p1330 A71-20683

VFR flying under bad weather conditions, discussing flight through and above cloud layers, need for radiotelephone communication and ground radar support

08 p1231 A71-21767

Weather influence on long range radio navigation aids, considering supersonic aircraft operation and inertial navigation

10 p1640 A71-29463

Weather minimum standards for civil aircraft, considering cloud ceilings, visibility, wind velocity and direction, onboard and ground-based flight control equipment and aircraft characteristics

12 p1924 A71-27141

Venus rotation observations during 1964 eastern spring elongation, noting weather period and wind velocities

13 p2136 A71-28386

Nondeveloping synoptic weather systems description by isentropic structural analysis, studying particle motion and dynamic behavior using models

18 p2944 A71-36219

Weather interruption effects on air transportation operations and economics, considering fog, snow, freezing rain, thunderstorms, winds, CAT and runway conditions

24 p3845 A71-44983

WEATHER CHARTS

U METEOROLOGICAL CHARTS

WEATHER CONDITIONS

U WEATHER

WEATHER CONTROL

U WEATHER MODIFICATION

WEATHER FORECASTING

NT LONG RANGE WEATHER FORECASTING

NT NUMERICAL WEATHER FORECASTING

NT STATISTICAL WEATHER FORECASTING

Severe thunderstorm warning by single pulse Doppler radar plan shear indicator

01 p0117 A71-10572

Soviet book on nephanalysis for synoptic forecasting covering meteorological satellite observations and network characteristics, photointerpretation, data processing, cloud identification, weather charts, etc

02 p0278 A71-12842

Satellite meteorology, discussing system, observational data, weather prediction, communications sensors, TV imaging and global atmospheric research program

04 p0621 A71-15308

Terrain and frictionally induced vertical velocity analysis for local and regional forecasting operations, considering low level air flow effects

05 p0777 A71-16674

Planetary boundary layer forecast model, determining horizontal and vertical wind components, temperature, pressure and moisture with numerical variational objective analysis

05 p0778 A71-17049

All-weather aircraft operations, discussing takeoff, landing, safety and forecasting

06 p0847 A71-17923

Probabilistic weather forecasts reliability estimation

07 p1150 A71-18871

Atmospheric circulation integral characteristics prediction from wind intensity, kinetic energy and angular momentum

07 p1150 A71-18873

Meteorological network design, analysis and forecast errors, optimum interpolation and station density and distance

08 p1327 A71-21717

World Meteorological Organization global weather observing, discussing coordinate function, developing countries technical assistance, observing systems planning and UN relations

08 p1327 A71-21718

Meteorological observing program execution legal and legislative aspects, noting social adjustment to weather effects

08 p1329 A71-21731

Linear vector differential Fridman equations for cosmic and telluric effects on earth atmosphere facilitating dynamic climate forecasts

10 p1639 A71-25115

Second order probabilities and strictly proper scoring rules in weather forecasting, discussing subjective judgment role in forecasting processes

11 p1793 A71-25376

Aircraft hazards due to frequent low cloud occurrences at Kenya airport, forecasting weather with statistical analysis and radiosounding

13 p2097 A71-29106

Thunderstorm, CAT, weather and mountain wave induced turbulence forecasting and analysis for transport aircraft

14 p2268 A71-29764

Stochastic dynamic meteorological prediction depicted in graphical formats

14 p2269 A71-29947

World Weather Watch global telemetry system including observing stations, and rockets, balloons and satellite-borne sensors, determining atmospheric states on ground and sea

14 p2199 A71-30913

Local short term mesoscale weather forecasting by finite difference solution of hydrothermodynamic equations

15 p2443 A71-31222

Soviet papers on analysis and forecasting of meteorological conditions for aircraft flying in troposphere and stratosphere

15 p2443 A71-31358

Height sign change prediction for lower cloud boundary from pressure Laplacian sign at earth surface

15 p2443 A71-31359

Atmospheric primitive equation prediction model, discussing four processor version

15 p2374 A71-31516

Meteorological satellite system for weather forecasting in Mediterranean area, including visible and IR ranges survey and automatic stations and buoys interrogation

16 p2604 A71-32846

Canadian observational sites for solar eclipse of 10 July 1972, describing expected weather conditions, totality time/duration and location accessibility

16 p2630 A71-33125

Numerical integration of quasi-static system of hydrodynamic equations, considering economical production of short range high resolution meteorological forecasts

16 p2604 A71-33532

Manned orbital research modules design for atmospheric physics, weather and earth resources observations and stellar astronomy [AIAA PAPER 71-815]

17 p2814 A71-35426

Meteorological objectives, radiometry and ground stations for Meteosat weather prediction system using geostationary satellite

18 p2878 A71-36527

WEATHER FRONTS

Baric levels determination for weather forecasting from statistical analysis of atmospheric numerical model

21 p3410 A71-40823

Soviet book on long wavelength radiative heat exchange in atmosphere covering radiation relationship to circulation, cloud formation and weather prediction

21 p3411 A71-40873

Water vapor-droplet transitional state and halo observation around light sources in radiative fog formation, applying to flight weather forecasts

24 p3844 A71-44866

Radar vs visual observation of cloudiness and hazardous weather phenomena, emphasizing storm warnings

24 p3845 A71-44885

Climatological studies and weather forecast support for Apollo 14 mission prelaunch, launch, emergency landing and terminal areas

24 p3845 A71-44981

French-American Eole project for meteorological prediction systems development, discussing balloon sounding and satellite data transmission

24 p3876 A71-45274

WEATHER FRONTS

U FRONTS [METEOROLOGY]

WEATHER MAPS

U METEOROLOGICAL CHARTS

WEATHER MODIFICATION

NT CLOUD SEEDING

Spatial correlations between inside cumulus cloud conditions and precipitation onset and intensity for modification experiments from aircraft penetration measurements

08 p1326 A71-21450

Meteorological observations for terminal weather modification in aviation, noting airport fog dispersal

08 p1329 A71-21732

Warm fog modification by condensation nucleus seeding, discussing droplet concentrations, cloud height and aerosol content effects on salt seeding material optimal size and dosage

09 p1488 A71-23253

Ice crystal and cloud drop nuclei origins and physical characteristics, discussing nucleation pollution products, weather modification and microphysical processes

14 p2270 A71-30496

Rain and fog modification concerning natural and artificial nuclei role, warm fog clearing and supercooled cloud experimentation

17 p2769 A71-34545

Fog dissipation programs by commercial and military agencies

18 p2944 A71-36450

Helicopter experimental fog clearing by downwash mixing at Greenbrier Valley Airport, Lewisburg, West Virginia

20 p3256 A71-39206

Weather and climate modification, reviewing techniques for meteorological processes control, cloud and precipitation modification, ascending flow stimulation, etc

23 p3701 A71-43450

SST operation climatic impact assessment program, considering carbon dioxide, water vapor, contrails, particulates, nitrogen oxides and carbon monoxide

24 p3823 A71-44982

WEATHER RADAR

U METEOROLOGICAL RADAR

WEATHER RECONNAISSANCE AIRCRAFT

Airborne severe storm surveillance, including radar detection hurricane model

07 p1058 A71-18826

Oklahoma and Malaysia thunderstorms comparison based on weather reconnaissance aircraft measurements, considering turbulence patches

14 p2266 A71-29752

High power 10 cm radar as CAT detector, comparing with radar and aircraft data coincident in space and time

14 p2267 A71-29761

WEATHER STATIONS

Kennedy Space Center Meteorological Tower Facility, describing equipment and data acquisition mission

02 p0277 A71-12528

Operational uniformity requirements for large meteorological station networks, emphasizing data acquisition and processing

08 p1327 A71-21716

Meteorological network design, analysis and forecast errors, optimum interpolation and station density and distance

08 p1327 A71-21717

World Weather Watch plan, discussing upper air, surface and satellite observations, telecommunication and data processing

08 p1328 A71-21719

Ionosonde stations world distribution for vertical incidence soundings during IQSY and comparison with IGY

15 p2396 A71-31610

Meteosat satellite for taking earth photographs and relaying between weather stations

19 p3154 A71-38474

Mobile monitoring and testing meteorological laboratory design and equipment for automated station network, considering pressure sensors, thermohygrostat and wind measurement

21 p3365 A71-41381

WEATHERING

Na and Mn homogeneity in chondritic meteorites, discussing accretion processes, metamorphisms, weathering effects and specimens size

04 p0659 A71-15855

Weather stress tests for determining optimum adhesive system for bonding reinforced fiberglass panels to Al extrusions held by steel beams

10 p1616 A71-24114

Apollo 12 lunar dust sample 12070,128, determining response to effective agents of earth-type chemical weathering

23 p3746 A71-43669

WEAVING

Three dimensional orthogonally woven reinforced felt-yarn composite for low density thermal insulation and chemical vapor deposition

14 p2262 A71-29651

WEBER-FECHNER LAW

Cat retina ganglion cell /YCC-1/ threshold intensity, obeying reversed Weber law

01 p0009 A71-10234

Human eye optimum information reception assessment by Weber-Fechner law, threshold amount constancy and minimum continuous signal energy

07 p1043 A71-20110

World four dimensional and space three dimensional characters and psychophysical sensations dependence on Weber-Fechner law and trisimulus principle in psychology

09 p1530 A71-23730

WEBS [MEMBRANES]

U MEMBRANES

WEBS [SHEETS]

Thin web shear test device demonstrated on aluminum foil and glass fiber composites

03 p0508 A71-13765

WEBS [SUPPORTS]

Shear modulus, flexure and buckling of web stiffened sandwich structures, using core layer model based on continuum theory [ASME PAPER 71-APM-8]

16 p2656 A71-33217

WEDGE FLOW

Turbulent boundary layer recovery factor for wedge model in hypersonic helium flow at high Reynolds and Mach numbers

03 p0517 A71-13461

Rarefied gas low speed slip flow over wedge, solving for velocity profiles and skin friction [ASME PAPER 70-WA/APM-26]

03 p0344 A71-14158

Hypersonic rarefied nitrogen flow over wedge, investigating density field

04 p0570 A71-15033

Strong shock wave Mach reflection, determining pressure and temperature at wedge surface by shock tube experiment

05 p0835 A71-16526

Shock wave interaction with wedge moving at supersonic speed, calculating geometry of regions formed intersecting wavefronts

07 p1014 A71-19741

Ideal gas jet sonic flow past wedge according to Kirchhoff scheme, testing sine series solution for convergence

07 p1016 A71-20085

Particle motion behind oblique shock wave in two phase supersonic wedge flow, deriving expressions for particle trajectories and velocity equalization time

08 p1227 A71-21754

Collisionless plasma steady flow past thin symmetrical semiinfinite wedge, considering dispersion due to finite Larmor radius

09 p1504 A71-23052

Laminar incompressible boundary layer flow over thin Joukowski, parabolic and slender wedge airfoils, using small perturbation and quasi-similar theories

10 p1549 A71-23957

Uniform surface blowing effects on hypersonic boundary layer with viscous interaction, calculating heat transfer on flat plate and slender wedge

10 p1598 A71-25096

Compressible turbulent boundary layer interaction with wedge or corner induced oblique shock waves, using transformation methods

11 p1750 A71-25481

Mach reflection of strong shock waves by sharp compressive corner in real gas in hypersonic tube, using laser Mach-Zehnder interferometer

11 p1752 A71-26190

Small surface curvature effect on unsteady hypersonic flow over thin oscillating wedge, using perturbation theory

11 p1705 A71-26197

Pitching stability derivatives of sharp oscillating wedges at zero incidence in viscous hypersonic flow

from perturbation method, including thickness and wave reflection effects

14 p2171 A71-31023

Plane transonic gas flows through Laval nozzle and symmetrical wedge-shaped profile, solving boundary value problem by reduction to singular integral equation

19 p2991 A71-37101

Wall effects and correction rules for cavitation flow past wedge in closed water tunnel, deriving drag coefficient from various theoretical models

23 p3663 A71-43442

Forced convection steady heat transfer across laminar incompressible constant-property boundary layers over wedges with step discontinuity in surface temperature

23 p3784 A71-44196

WEDGES

Plane shock wave diffraction at wedge, analyzing role of gas specific heats ratio

01 p0070 A71-10664

Two dimensional diffraction of plane wave by perfectly conducting wedge using straightforward scattering approach

03 p0456 A71-13347

Far field diffraction of unidirectional surface wave by conducting rectangular wedge in cold anisotropic plasma, showing frequency dependent transmission coefficient

03 p0465 A71-13953

Plane electromagnetic wave scattering, arbitrarily polarized and normally impinging on wedge tapered absorbing structure

09 p1409 A71-23501

Near field asymptotic solution for electromagnetic wave diffraction by perfectly conducting wedge, using steepest descent method

09 p1411 A71-23679

Shock wave incidence on wedge moving at supersonic speed, considering uniform flow region on upper wedge surface for specific values of Mach number and vertex angle

12 p1897 A71-27445

Hypersonic wakes of two dimensional slender wedges and flat plate, testing stability in transition region in wind tunnel

12 p1866 A71-27561

Particle interaction with wedge surface in supersonic two phase flow, determining incidence coordinates and collision frequency as function of initial conditions

12 p1866 A71-27665

Electromagnetic wave diffraction by ideally conducting wedge of finite radius, deriving asymptotic formula for plane wave scattering

13 p2029 A71-28360

Mutual impedance of interacting dipoles at wedge tip, determining errors for short spacing distances

13 p2036 A71-28370

Base pressure measurement behind wedge-parallelepipeds and cone-cylinder models of variable geometry

13 p2049 A71-29199

Multiple-beam interference effects in Fabry-Perot interferometer with small wedge between mirrors, deriving expressions for light beams path

14 p2243 A71-30273

Plane shock wave diffraction at wedge, analyzing role of gas specific heats ratio

14 p2228 A71-30997

Hypersonic wakes behind wedges for various angles of attack, determining near and far wakes [AIAA PAPER 71-563]

15 p2344 A71-31558

Plane oblique shock wave diffraction on wedge moving in homogeneous gas flow at supersonic speed, reducing boundary value problem to Hilbert problem

16 p2519 A71-32930

Potential energy minimization for elastic elements with integral loads applied to bending of bar and wedge, using variational method

16 p2659 A71-33995

Thermal stresses distribution in wedge shaped solids with cracks, solving elastic equilibrium equations

16 p2661 A71-34158

Electromagnetic wave diffraction by moving wedge with surface impedance, evaluating Doppler shifts and scattered field in shadow region

17 p2698 A71-34429

Inclined wedges in rarefied hypersonic flow conditions, investigating base and wake pattern geometrical and aerodynamic characteristics

18 p2849 A71-36756

Monostatic plane wave scattering by semiinfinite perfectly conducting wedge with rounded edge for line source excitation in far field

19 p3023 A71-38593

Electron beam fluorescence probe with modulation technique for measuring density disturbance near sharp wedge in rarefied hypersonic flow

22 p3529 A71-42052

Particle interaction with wedge surface in supersonic two phase flow, determining incidence coordinates and collision frequency as function of initial conditions

24 p3790 A71-44930

WEIBULL DENSITY FUNCTIONS

Weibull density functions applied to fracture location distribution in brittle solids

01 p0167 A71-10294
Statistical analysis of neutron induced gain degradation of silicon power transistors, determining failures distribution fit to Weibull function

07 p1070 A71-19063
Failure criteria percentages for bipolar transistors, determining adequacy of Weibull distribution for low gamma ray dose survival probability

07 p1071 A71-19064
Peak structural response to nonstationary random excitations, approximating by Weibull distribution and Monte Carlo technique
[AIAA PAPER 71-347]

11 p1843 A71-25326
Two-line all-equipment test and aeronautic systems division reliability testing, analyzing by Weibull Monte Carlo simulation

12 p1909 A71-26657
Bayesian time to failure distribution for graphical estimation of component burn-in time and reliability prediction, comparing with Weibull technique failure rates

12 p1911 A71-26686
Weibull distribution analysis of saccadic eye movements interval during visual task

17 p2688 A71-34366
Location and scale parameters estimation from ordered statistical samples with numerical applications to Gumbel and Weibull distributions

19 p3088 A71-38471
Steels, aluminums and titaniums ultimate and yield strength statistical distributions in Weibull parameter form, presenting stimulus-response potential failure model

21 p3396 A71-40307
[ASME PAPER 71-VIBR-64]
Stress corrosion testing of Al alloy in NaCl bath under tensile stress, using Weibull distributions

WEIERSTRASS FUNCTIONS

Conflicting and relaxed minimax controls for Weierstrass E condition or Pontryagin maximum principle

11 p1792 A71-25752
Weierstrass condition for optimality in coplanar elliptic orbit transfer involving velocity impulse control variables, discussing switching relations at corner of optimal trajectory

12 p1963 A71-27061
Soviet book on theory of elliptic functions covering analytic functions, Jacobi and Liouville theorems, modular functions, Weierstrass functions, theta and Jacobi functions

17 p2767 A71-35200
Geometrically nonlinear integral solutions to equilibrium equations of curvilinear beam under uniform pressure, using Weierstrass functions

WEIGHT [MASS]

NT BODY WEIGHT
NT STRUCTURAL WEIGHT

Material stiffness/weight ratio effects on helicopter blades uncoupled flapwise, chordwise and torsional natural frequencies by rapid estimation

06 p0985 A71-17691
Optimal motion of multistage body of variable mass during vertical climb with allowance for weight limitations

10 p1683 A71-24845
Space shuttle thermal protection system optimal weight by numerical parameterization, discussing temperature constraints and material rearrangement effects
[AIAA PAPER 71-444]

WEIGHT ANALYSIS

Parachute weight, configuration and strength correlations for tradeoffs and design

07 p1017 A71-18900
Aircraft wings automated preliminary structural design and weight determination procedures based on external shape, aerodynamic loads and fuel mass interaction

09 p1541 A71-23274
Automated optimal weight fully stressed large scale structural design of aircraft, using matrix-mathematical programming technique
[AIAA PAPER 71-361]

11 p1844 A71-25340
Thermionic reactor electric spacecraft propulsion system for unmanned outer planets missions, investigating voltage and radiator temperature effects on weight

11 p1811 A71-25872
Sex differences in rat body weight regulation due to lateral hypothalamic lesions

11 p1720 A71-26074
Performance prediction of fixed wing leading edges radiative, ablative and active cooling thermal protection systems and system weights comparison for space shuttle entry mission
[AIAA PAPER 71-445]

11 p1839 A71-26230
Thin shallow annular radiating fins for heat removal from sphere or polyhedron with isothermal surfaces, determining optimal weight and geometrical parameters

12 p1986 A71-27331

Landing load estimation methods for preliminary design weight prediction for military aircraft

13 p1995 A71-28211
Optimal structural design of minimum weight trusses and beam cross sections for given load using computerized nonlinear programming method

14 p2321 A71-29541
L-1011 Tristar antenna arrangement test results, considering weight, aerodynamic and structural design requirements

14 p2218 A71-31060
Size effects on large rotor systems design, considering weight, blade loading, tip speed, etc
[AHS PREPRINT 552]

14 p2180 A71-31104
Composite materials application to V/STOL prop/rotors, determining material properties parametric effect on frequencies and weight by Southwell coefficients
[AHS PREPRINT 554]

14 p2180 A71-31106
Concorde lightweight disk brakes, discussing operating costs, weight and volume factors, design philosophy, structural materials, component life, maintenance and reliability

16 p2522 A71-33226
Sequential analysis and Bayesian demonstration in hypothesis testing, considering weight ratios based on objective lower level program reliability test information

16 p2582 A71-33289
VTOL aircraft gross weight and direct operating costs penalties from additionally installed control power
[AIAA PAPER 71-768]

16 p2524 A71-34005
Airborne display and electric management system, discussing weight reduction, protective function coordination, power quality, onboard maintenance, data processing and reliability

17 p2739 A71-34617
Aircraft loading system consisting of onboard weight and balance equipment and fully mechanized cargo pallet transfer, using computerized simulation model for parametric evaluation
[SAWE PAPER 900]

17 p2676 A71-35811
Statistical analysis of error sources and magnitudes in Boeing 747 weight values obtained by onboard aircraft weighing system and by manual calculations
[SAWE PAPER 897]

17 p2676 A71-35813
Boron-epoxy composite wing box beam design, describing preliminary weight estimation from layouts
[SAWE PAPER 891]

17 p2834 A71-35815
Weight reduction potential of composite materials in aerospace structures, proposing weight estimation technique
[SAWE PAPER 887]

17 p2834 A71-35819
Strut pressure and axle strain gage systems testing for balance and weighing onboard De Havilland C-7A aircraft
[SAWE PAPER 881]

17 p2676 A71-35827
Wing group weight prediction for subsonic aircraft design, taking into account root bending moments due to lift

18 p2976 A71-35925
Book on optimum structural design covering single element optimizations, load transmission, slender columns, cost-weight tradeoffs and statically indeterminate structures

18 p2977 A71-36249
Parts qualification and acceptance for outer planet mission spacecraft, minimizing random and wear-out failures to meet weight and other constraints
[AAS PAPER 71-161]

19 p3153 A71-37958
Real weight formula for shell fuselages based on theoretical similarity considerations

20 p3178 A71-39411
Cold gas rocket propulsion systems design parameters, determining performance and weight formulae
21 p3437 A71-41050

WEIGHT FACTORS

U WEIGHT [MASS]

WEIGHT INDICATORS

NT STRAIN GAGE BALANCES

NT THERMOBALANCES

Wind tunnel apparatus for reproducing coning and spinning motions of bodies of revolution, using six-component strain gage balance for aerodynamic forces

01 p0002 A71-10930
Supersonic wind tunnel electromagnetic balance with superconducting coils

07 p1084 A71-20151
Aerospace dynamic balancing machine for measuring unbalance forces of small objects and components, using AI construction to minimize inertial masses

17 p2725 A71-35823
[SAWE PAPER 878]

WEIGHT MEASUREMENT

Ventricular mass estimation using electrocardiographic parameters

13 p2021 A71-29302
Onboard weighing system for gross weight determination and center of gravity location of Alouette helicopter, using load sensors, electrical circuits and visual indicators

14 p2175 A71-30320
Aircraft weighing in place during maintenance operations, describing load cell equipped jacks design for time saving weight determination
[SAWE PAPER 898]

STAN/MASS system aircraft weight and balance determination, discussing basic concepts, design requirements and applications
[SAWE PAPER 896]

17 p2834 A71-35816
Mass, center of gravity and moment of inertia measurements curtailment by tolerance and regression analyses and Monte Carlo method
[SAWE PAPER 883]

17 p2834 A71-35820
Center of gravity and moment of inertia measurement system based on standards of comparison principle

17 p2835 A71-35822
[SAWE PAPER 880]
Mass and center of gravity determining system model, describing equipment, operation principle, calibration data and techniques accuracy and errors

17 p2725 A71-35824
[SAWE PAPER 879]
Analytical weight determination of articulated shaft driven helicopter main rotor blades, presenting computer program

17 p2835 A71-35826
[SAWE PAPER 893]
Celestial body mass determination in many body problem, using Kalman-Bucy filtering for Taylor series approximation linearized problem

18 p2960 A71-35935

WEIGHTING FUNCTIONS

Eigenvalue errors in applying method of weighted residuals to linear nonself adjoint problems of structural analysis

01 p0174 A71-10944
Video MTI pulse radar Doppler filter optimum symmetrical weighting factors in clutter-plus-noise environment

07 p1059 A71-18847
Lower bounds for minimum weight of binary cyclic code vectors of composite length, using factorization

08 p1324 A71-21321
Nonstationary automatic control systems analysis using frozen coefficients and weighting functions

08 p1270 A71-21978
Optimal trajectory measurement program for orbit parameter determination, assuming random errors and nondegenerate weighting matrix of normal equations

09 p1519 A71-22542
Aerial photographs orientation point location, relating measurement weight of transverse parallax

09 p1451 A71-23178
Weighted distribution functions of normal processes, calculating stochastic mixture components in Borel sets

10 p1637 A71-24903
Explicit formulas for Euclidean geometry and Berlekamp subcodes weight enumerators for second order binary Reed-Muller codes

14 p2209 A71-30828
Weighted finite incidence systems construction using nonnegative integer functions and column vectors

16 p2603 A71-33591
Rotationally symmetric quasi-cylindrical viscous incompressible vortex flow, using method of weighted residuals approximating axial velocity and circulation profiles by series of exponentials

21 p3369 A71-40951
Gaussian errors effect in maximal ratio diversity combiner weighting factors on probability distribution of output SNR

22 p3513 A71-42384
Anisotropically weighted smoothing theoretical interpretation based on numerical variational analysis for upstream and downstream observations in weather forecasting

22 p3569 A71-42415
Astronomical observations weighted estimation based on smoothing Pearson curves empirical distribution

23 p3771 A71-44257
Dynamic system optimal weighting function determination, using variational methods for statistical criteria

24 p3813 A71-44677
Linear control system optimal weighting function determination from maximum probability for system error

24 p3814 A71-44687

WEIGHTLESS FLUIDS

Supercavitating bounded flow of weightless fluid past slender bodies, deriving singular integral equations in terms of pressure gradient and cavern thickness derivative

20 p3213 A71-39787

WEIGHTLESSNESS

Proportionate role in perception of arm bending and extension during weightlessness and accelerations in aircraft flight along parabolic trajectory

01 p0014 A71-11143
Bipropellant droplet supercritical steady combustion temperature measurements in zero gravity near critical point, comparing high and low pressures models for ambient gas solubility

01 p0141 A71-11309
Boiling under weightlessness, examining gravitational effects on bubbles formation frequency and diameters

02 p0331 A71-11922

WEIGHTLESSNESS SIMULATION

Capillary ball game phenomenon under weightlessness, showing photographs of mercury droplet reflection from fluid boundary 02 p0239 A71-11925

Differential equations for control and adaptation of hand motion in cubital joint under weightlessness and accelerations 03 p0357 A71-12990

Soyuz 9 prolonged space flight biomedical effects on human organism, emphasizing weightlessness 03 p0365 A71-14392

Vestibular problems in long manned space flight, discussing weightlessness and rotating environment for artificial gravity 04 p0541 A71-14753

Space station experiments fine pointing and stability, discussing attached or coorbiting free flying mode with zero G conditions [AIAA PAPER 71-62] 06 p0980 A71-18521

Weightlessness effects on muscular reflexes, tonus and contractibility in Soyuz 9 astronauts 09 p1389 A71-22202

Soyuz 9 astronaut vertical posture control after 18 day orbital flight, considering cardiovascular disturbances caused by reduced muscle tone and changed interaction between analyzers 09 p1389 A71-22203

Weightlessness, high acceleration and aerospace vehicle maneuvering effects on cardiovascular and vestibular systems, discussing disorientation, space sicknesses and blood circulation 09 p1398 A71-22357

Space travel genetic effects, discussing radiation, weightlessness, vibration and acceleration 09 p1394 A71-23149

Biosatellite 3 onboard camera time lapse photography of monkey sleep/wake activity patterns during weightlessness 09 p1394 A71-23240

Long term zero gravity effects on mammal physiologic rhythms characteristics, studying rats in biosatellite orbits 10 p1565 A71-24611

Psychobiological stress of prolonged weightlessness /bed rest/ in man in terms of adaptive homeostatic state and decreased sensory-motor-muscular input 11 p1725 A71-26120

Astronaut selection and training, considering acceleration, hypoxia, weightlessness and temperature variation tolerance 12 p1873 A71-26951

Space flight factors effects on human physiology and psychology, discussing spacecraft gaseous medium control, food supply, closed ecological systems and weightlessness effects 13 p2016 A71-27876

Boiling under weightlessness, examining gravitational effects on bubbles formation frequency and diameters 13 p2159 A71-28209

Isothermal flow under capillary forces in heat pipe with zero gravity, deriving relation between flow rate and duct parameters 13 p2050 A71-29219

Space crew members muscle tone, determining weightlessness effect by rigidity and bioelectric activity 15 p2357 A71-31317

Radiative heat transfer effects on small fires in zero gravity spacecraft and free falling chamber environments from diffusion flame models 15 p2514 A71-32084

Cardiovascular and respiratory systems, motor and muscular activity, metabolism and body energetics functional changes due to prolonged weightlessness 16 p2531 A71-33676

Human energy requirements in weightless environments, correlating metabolic data from Gemini and Apollo missions with food consumption and energy balance measurements 16 p2532 A71-33778

Life support systems test under weightlessness environment in Nike Tomahawk sounding rockets launched from Wallops Island 16 p2537 A71-33816

Gas bubble in liquid under surface tension, weightlessness and rotation, determining angular velocity for fluid system disintegration 16 p2560 A71-34142

Zero gravity whole body shower system for space station, describing air drag and vacuum methods for water collection [ASME PAPER 71-AV-2] 18 p2865 A71-36369

Zero-gravity circulating water electrolysis system prototype design for metabolic and leakage makeup oxygen supply in 12-man space station regenerative life support system [ASME PAPER 71-AV-20] 18 p2867 A71-36387

Zero-g propellant tank quantity gaging methods, suggesting large cryogenic propellant tanks for space shuttle orbiter stage 18 p2922 A71-36455

Manned earth-orbital missions performance assessment experiments, studying effects of artificial and zero gravity spacecraft environments on humans [AIAA PAPER 71-891] 18 p2857 A71-36641

Chemically activated electroadhesive pads on spacecraft surface, allowing astronauts to maneuver or work in zero gravity environments 18 p2872 A71-36645

Artificial gravity selection by rats in centrifugal acceleration fields superimposed on weightlessness during sounding rocket flights [AIAA PAPER 71-854] 18 p2857 A71-36646

Astronaut orthostatic tolerance loss due to weightlessness, describing compensation by periodic lower body negative pressure [AIAA PAPER 71-859] 18 p2872 A71-36648

Weightless environment effects on fluid behavior and heat transfer in life support systems, obtaining analytical models [AIAA PAPER 71-864] 18 p2909 A71-36652

Engineering aspects of zero gravity personal hygiene and waste management systems, noting controlled air flows, surface tension and artificial gravity use [AIAA PAPER 71-865] 18 p2872 A71-36653

Dielectrophoresis force measurements and wedge shaped capacitor separation properties in satellite zero gravity conditions 19 p3103 A71-37278

Human response to space environment, discussing prolonged weightlessness, extravehicular work and lunar surface activity 19 p3002 A71-37492

Free fuel droplet spherical combustion in freely falling chamber under zero gravity condition 19 p3169 A71-38111

Physicotechnical and biomedical aspects of human efficiency under weightlessness, discussing physical exercise role in adaptation 20 p3192 A71-39217

Liquid He containment in space zero-g environment, proposing use of high thermal conductivity porous plug operating in superfluid regime 20 p3184 A71-39280

Biosatellite 2 onboard experiments studying weightlessness effects on biological processes and interaction with radiation from Sr 85 gamma ray source 21 p3341 A71-40007

Weightlessness effect on vestibular apparatus from bullfrogs vestibular nerve single fibers spike train data during orbital flight 22 p3598 A71-41689

Transient heart rate response to square wave breathing in man under zero G parabolic flight 22 p3501 A71-41828

Biomedical effects of Apollo 14 space flight, considering weightlessness adaptation 22 p3487 A71-41985

Human orthostatic and vestibular stability responses to weightlessness during extended space flights noting acceleration tolerance, physical efficiency, infection resistance and medication sensitivity 22 p3495 A71-42790

WEIGHTLESSNESS SIMULATION

Horizontal clinostat rotation rate for optimal and acceptable weightlessness simulation in plants, comparing with wheat seedlings growth in Biosatellite 2 05 p0712 A71-16150

Permanent magnets for footwear restraint and mobility in zero gravity spacecraft, testing neutral buoyancy and six degree of freedom simulation effects [IEEE PAPER 2.2] 07 p1048 A71-19607

Weightlessness simulation for aerospace mechanisms, using tower release and gyrometric system for testing stage separation, satellite perturbation, yo-yos, probes and mast development [ONERA-TP-940] 18 p2971 A71-36018

Orbital cargo transfer simulation techniques involving zero-g aircraft and water immersion 18 p2899 A71-36469

Structural development in rat bone under earth gravity, hypergravity and simulated weightlessness, discussing physical dimensions, density, rigidity, microhardness and ash content [AIAA PAPER 71-895] 18 p2856 A71-36640

Intravehicular manual cargo transfer, using water immersion technique for zero gravity simulation [AIAA PAPER 71-851] 18 p2871 A71-36642

Weightlessness simulation for orbital man machine experimentation, discussing telerboard and cargo transfer examples [AIAA PAPER 71-850] 18 p2871 A71-36643

Mathematical model for underwater simulation of astronaut extravehicular activities in weightless conditions, using computer program [AIAA PAPER 71-852] 18 p2872 A71-36644

Pinto beans circadian leaf movements in simulated weightless environment, relating rotational treatment time to rhythm phase 21 p3341 A71-40006

Water immersion or bed rest effects on basic metabolism and external respiration under simulated weightlessness 22 p3495 A71-42794

WEIGHTS [COEFFICIENTS]

U COEFFICIENTS

WELD STRENGTH

Welded joints ductile and brittle static tensile strength at low temperatures, allowing for mechanical inhomogeneities 01 p0085 A71-10085

Low temperature steel welded joints resistance to brittle fracture, discussing Niblink dynamic loading, deep notch static loading and Charpy V tests 03 p0433 A71-14585

Residual and mean stresses effects on fatigue strength of specimens with longitudinal nonload-carrying fillet welds 04 p0613 A71-15763

Ti alloys welded joints in annealed state and after heat treatment strengthening, noting welding conditions, filler wire composition and edge preparation 05 p0757 A71-16173

Porosity in gas tungsten arc aluminum weldments and elimination by hydrogen reduction 07 p1119 A71-19969

Strength, toughness and hardness of gas tungsten arc multipass welds in titanium alloy plates 07 p1119 A71-19970

Fatigue strength of butt, lap and tee welded joints in aluminum alloys under axial stress and repeated bending loads 07 p1119 A71-19971

Low carbon steel welds, investigating low cycle deformation and rupture resistance as function of weld zones 08 p1316 A71-21609

Complex Al brazing alloy for honeycomb core joining to Ti alloy face sheets, discussing fillet formation and strength optimization 08 p1299 A71-21686

Impact strength decrease of welded joints in Ti alloys due to air cooling rate after aging 09 p1478 A71-23421

Hot strain cycle recording in single and multipass welds for C-Mn steel using welding simulation, surface pressed plug and microscopic techniques 09 p1459 A71-23455

Minimum strength of groove and fillet welded joints in heat treated Al alloy tubular members 11 p1769 A71-25745

Optimal electron beam welding of Nb alloy to bronze, showing high mechanical properties due to deep Cu diffusion 14 p2253 A71-30491

Creep rupture behavior and high temperature exposure effects on room temperature properties of Ni-Cr-Mo maraging steel plates and welds 15 p2434 A71-32256

Multipass low alloy steel weld metal strength dependence on microstructural changes due to thermal effects 15 p2437 A71-32614

Stress rupture ductility of electron beam, gas tungsten arc and gas metal arc welds, considering creep crack initiation 15 p2437 A71-32617

High temperature Ti alloys welding, discussing strength, ductility, beta stabilizing elements and chemical compositions 17 p2758 A71-34806

Tensile properties and notch toughness of Al alloys at low temperature, considering fracture toughness and weld strength 20 p3251 A71-39266

Strength, ductility and notch toughness research on base materials and welds of nickel maraging steel rocket motor cases 21 p3389 A71-40913

Explosive peening effects on weld fatigue in Ni maraging steel, Fortiwell and Al-Zn-Mg alloy 23 p3682 A71-43877

WELD TESTS

Electrical resistance spot weld penetration measurement by ultrasonic method using shear waves 01 p0086 A71-10305

Laser vs electron beam welding, examining high and partial vacuum and atmospheric pressure environments, penetration and ionization and dissociation processes [SME PAPER MR-70-523] 01 p0090 A71-11269

High strength steel weldability with shielded and gas metal arc processes, discussing hardness, tensile, bend, impact and fatigue tests 04 p0603 A71-14922

High alloy weldability evaluation methods - Conference, Philadelphia, April 1969 04 p0616 A71-15906

Ti and Ni base high temperature alloys welded joints efficiency, discussing fatigue, storage, long time heat and corrosion tests 05 p0765 A71-16172

Postweld heat treatment cracking of high Ni alloys using mechanical testing and metallography 13 p2087 A71-29092

Electron beam welding of martensitic turbine grade steel thick sections, showing accelerating voltage and focus coil current effect on weld profile 19 p3070 A71-38314

Stress relief, temper and creep embrittlement effects on ferrous alloy welds 19 p3082 A71-38317
Co, Mo, Ti and Cr effect on mechanical properties and microstructure of maraging weld metals 19 p3083 A71-38491
High temperature properties of weld metals formed by electrodes for welding of low alloy heat resistant Cr-Mo and Cr-Mo-V steels 20 p3249 A71-39014

WELDABILITY

Carbon dioxide laser vs electron beam welding, examining weldability of high thermal conductivity metals 01 p0087 A71-10452
Microstructure and mechanical properties of weldable heat resistant Ni alloy containing carbon and boron 01 p0103 A71-11068
High strength steel weldability with shielded and gas metal arc processes, discussing hardness, tensile, bend, impact and fatigue tests 04 p0603 A71-14922
High alloy weldability evaluation methods - Conference, Philadelphia, April 1969 04 p0616 A71-15906
Maraging steel weldability, examining crack origin and fracture toughness 05 p0770 A71-17246
Spacecraft propellant tank development from Al alloy providing excellent weldability, propellant compatibility and strength to weight ratio 07 p1116 A71-18899
Microstructure and mechanical properties of weldable heat resistant Ni alloy containing carbon and boron 08 p1305 A71-21035
Anisotropy and weldability, considering through-thickness tension decohesion cracking under static nonload conditions in corner and tee joints 09 p1459 A71-23454
Fracture-safe design, discussing strength transition, ratio analysis diagram, R-curve resistance, weldability and computer techniques 11 p1778 A71-25747
Heat affected zone crack filling and weld metal-base metal interactions of high strength alloys in dissimilar gas arc welding 11 p1769 A71-25749
Ferritic steels weldability, establishing relations between transition points and cold crack formation 15 p2417 A71-32662
Heat resistant weldable dispersion hardened Ni base alloy, discussing intermetallic phase hardening 16 p2594 A71-33715
Soviet book on austenitic boron steels and alloys for welded structures, covering boron influence on steels and alloys structure and properties, with special reference to weldability 20 p3251 A71-39090
Heat treatment for weldability and formability improvement of Udimet 700, evaluating by bend, hardness and tensile tests 21 p3388 A71-40622
Electron beam hearth refined ferritic stainless steel, presenting weldability with gas tungsten arc process 21 p3388 A71-40623
Tungsten and tungsten alloys weldability by gas tungsten arc, electron beam and chemical vapor deposition techniques 21 p3388 A71-40624

WELDED JOINTS

NT SPOT WELDS
Materials and welded joints brittle fracture resistance estimation from impact bending tests 01 p0085 A71-10084
Welded joints ductile and brittle static tensile strength at low temperatures, allowing for mechanical inhomogeneities 01 p0085 A71-10085
Ni maraging steel weldments stress corrosion cracking characteristics in air and pentaborane by electron microscopy 02 p0262 A71-11707
High strength steel weld metal, determining gaseous impurities effects on mechanical properties degradation 02 p0262 A71-11710
Inconel 718 arc welding procedures and weldments mechanical properties, discussing impact strength and ductility improvement by heat treatment 02 p0255 A71-11711
Welded joint structural stability determination by measuring decarburized steel layer thickness after carbon diffusion into lower activity region 03 p0432 A71-13690
Welded joints triaxial residual stress measurement by scanner 03 p0433 A71-14587
High strength steel butt welds surface geometry effect on fatigue durability under cyclic loads, using photoelastic analysis 04 p0602 A71-14881
Stainless steel-Al joining techniques, describing gas tungsten arc process 04 p0603 A71-14920

Solar cell module joints welding technology development under ESRO sponsorship, emphasizing resistance welding and process optimization 05 p0704 A71-16095
Ti and Ni base high temperature alloys welded joints efficiency, discussing fatigue, storage, long time heat and corrosion tests 05 p0765 A71-16172
Ti alloys welded joints in annealed state and after heat treatment strengthening, noting welding conditions, filler wire composition and edge preparation 05 p0757 A71-16173
Residual stress measurement in Hastelloy N gas tungsten arc welds by Sachs boring-out method, permitting stress distribution determination over short distance increments 06 p0912 A71-18043
Mechanical properties, crack formation sensitivity, corrosion resistance and stress cracking behavior of Al-Zr-Mg alloys welded joints 07 p1136 A71-19633
Fatigue strength of butt, lap and tee welded joints in aluminum alloys under axial stress and repeated bending loads 07 p1119 A71-19971
Structure and mechanical properties of Mo alloy weld metal as function of Re concentration, using metallography, electron microscopy, X ray analysis and autoradiography 07 p1120 A71-20245
Metals and welded joints corrosion resistance at high temperatures and pressures, describing tests in autoclave with pneumatic loading 09 p1429 A71-23050
Polymer adhesive protective coatings for improving fatigue resistance of butt and lap welded joints in thin Al sheet construction 09 p1478 A71-23355
Arc weld metal carbon content effects on welded joints mechanical properties in Ni at low and high temperatures, noting crack reduction 09 p1479 A71-23422
Anisotropy and weldability, considering through-thickness tension decohesion cracking under static nonload conditions in corner and tee joints 09 p1459 A71-23454
Diffusion bonding for vacuum tight heat resistant and oscillation proof large area joints 09 p1459 A71-23584
Metals ultrasonic welding, discussing welded elements interactions in terms of thermal and diffusive phenomena, sample preparation, transducers, electric generators and process control systems 10 p1617 A71-24134
Weld heat affected zone transient thermal stresses examined by weld joint model constrained system 10 p1617 A71-24533
Minimum strength of groove and fillet welded joints in heat treated Al alloy tubular members 11 p1769 A71-25745
Structural stability degradation mechanisms in welded joint of plain and low alloy steels, deriving equation for carbon diffusing 11 p1771 A71-26158
Mechanical properties of welded joints in Ti alloys with high oxygen content 13 p2072 A71-27875
Al-Zn-Mg alloy plates welded with Al-Mg filler metals, observing ghost defects in radiographs 13 p2074 A71-28524
Beta stabilizing Mo and Cr effects on mechanical properties of welded and heat treated Ti alloys 14 p2260 A71-30490
Thin sheet Nb-Zr alloy welds, detailing residual stresses in butt joints 15 p2413 A71-31204
Al alloy spot welding, investigating defects effects on welded joint fatigue strength under dynamic tests by metallographic and X ray examinations 15 p2436 A71-32467
Pressed or sintered steel powder joining to wrought mild steel parts, evaluating welded joints with torsion test 15 p2417 A71-32615
Hydrogen and nitrogen pores formation in welds, considering gas concentration redistribution between liquid and solid metal 15 p2417 A71-32663
Optimum heat treatment for welds, investigating residual stress relief with higher harmonics method 15 p2417 A71-32664
Steel joint weld decay mechanism, observing intergranular corrosion initiation and development in nitric acid solutions 15 p2417 A71-32665
Ti alloys argon TIG welding to Nb alloys, detailing joint impact strength, fusion zone ductility and bending tests 15 p2418 A71-32668
Mechanical properties, crack formation sensitivity, corrosion resistance and stress cracking behavior of Al-Zr-Mg alloys welded joints after prolonged heating 16 p2593 A71-33629

Materials and welded joints low temperature operation reliability prediction by estimating brittle fracture resistance from impact bending tests 16 p2584 A71-33640
Welded joints ductile and brittle static tensile strength at low temperatures, allowing for mechanical inhomogeneities 16 p2584 A71-33641
Corrosion resistance of Ar TIG welded joints in Ti alloys, discussing chemical and mechanical slag film removal effects 17 p2757 A71-34804
Electroslag welding of large pressed Al-Mg alloys sections, using electrodes to reduce weld grain size and obtain high mechanical properties 17 p2748 A71-34807
Monograph on tensile tests of welded joint structural properties as function of introduced heat, applying method to Cu-Ni alloyed steel 17 p2748 A71-34825
Ti alloys diffusion bonding and forging, discussing joints testing and material utilization improvement through die forging process [SME PAPER AD-71-244] 18 p2927 A71-36656
Aluminum alloy gas tungsten arc welds, determining defect size and distribution effects on fracture strength 18 p2929 A71-36857
Argon arc welding of Ti VT5-L alloy to Ti VT5-L and to wrought alloys OT4 and OT4-1, noting ductile, tough and stress raiser insensitive joints 19 p3070 A71-38421
Manual pulsed and continuous arc TIG welding in controlled atmosphere chamber, examining joint quality 19 p3070 A71-38422
AMg6M alloy hot rolling butt joints, showing ductility and strength of welds 19 p3070 A71-38424
Al-Zn-Mg alloy welded joints under repeated static loads, determining shape, filler wire composition and aging effects on fatigue strength 19 p3083 A71-38425
Structural stability and creep properties of heat resistant steel weld joints, considering substitutional and precipitation hardening and dislocation effects 20 p3249 A71-39015
Tensile, impact and fatigue properties of welded Ti alloys, determining joint quality and friction welding sensitivity in highly stressed gas turbine components 21 p3387 A71-40619
Isotopic X ray photography application to welded joint flaw detection in atomic power plant with radiation background 22 p3540 A71-41763
Basic parameters of echo and mirror shadow methods for ultrasonic defectoscopy of welded joints, considering standardization principles 24 p3829 A71-44784
Ultrasonic method for measuring poor root penetration zone width in welded T joints without reference standard, suggesting practical applications 24 p3829 A71-44785

WELDED STRUCTURES
Maraging steel welded plates edge displacements under linear multilayer burner heating, determining temporal deformations by heat distribution from additional source 01 p0088 A71-11098
Portable xerographic unit construction and electric circuitry, discussing application for welded seams X ray imagery 09 p1450 A71-22895
Welded steel structures fracture safe design, considering continuity conditions responsible for catastrophes resulting from crack initiation 09 p1458 A71-23453
Copper wire laser welding to film on Cr substrate exhibiting nonhomogeneous columnar structure and recrystallization 12 p1912 A71-27779
Monograph on tensile tests of welded joint structural properties as function of introduced heat, applying method to Cu-Ni alloyed steel 17 p2748 A71-34825
Soviet book on austenitic boron steels and alloys for welded structures, covering boron influence on steels and alloys structure and properties, with special reference to weldability 20 p3251 A71-39090
Copper wire laser welding to film on Cr substrate, exhibiting nonhomogeneous columnar structure and recrystallization 21 p3389 A71-41104
Random loading parameters adjustment in fatigue tests of welded aircraft structures 22 p3528 A71-41692

WELDING
NT ARC WELDING
NT BRAZING
NT DIFFUSION WELDING
NT ELECTRIC WELDING
NT ELECTRON BEAM WELDING
NT ELECTROSLAG WELDING
NT EXPLOSIVE WELDING

WELDING MACHINES

- NT FLASH WELDING
 NT FUSION WELDING
 NT GAS TUNGSTEN ARC WELDING
 NT GAS WELDING
 NT PLASMA ARC WELDING
 NT PRESSURE WELDING
 NT ULTRASONIC SOLDERING
 NT ULTRASONIC WELDING
 Continuous Nd-YAG laser welding, considering power, penetration depth and applications
 01 p0087 A71-10453
 Soviet book on friction welding of metals covering theory, equipment and quality control
 02 p0255 A71-11849
 Soviet book on welding fillers based on high melting point compounds covering alloy selection, surfacing techniques, working machine maintenance, etc
 03 p0432 A71-13689
 Hot ductility curves for cracking sensitivity prediction during welding
 04 p0617 A71-15907
 Ti alloy plate multipass welding process, describing temperature measurement techniques for multiple thermal cycles
 04 p0604 A71-15910
 Lasers applications to materials working including welding, cutting, machining, etc
 06 p0908 A71-18069
 Optically pumped pulsed ruby laser welding unit, noting joining and hole drilling problems
 07 p1119 A71-19968
 Welding rods chemical composition and welding procedures for heat resistant austenitic and martensitic steels for gas turbines, considering maraging steels heat treatment influence
 09 p1456 A71-23291
 Al-Mg alloy positional welding for porosity elimination
 09 p1457 A71-23356
 Laser welding, machining and safety - Conference, Pennsylvania State University, July 1969
 09 p1457 A71-23401
 Laser microwelding, discussing focusing properties, high power radiation interactions, metal working, machining and microelectronic applications
 09 p1458 A71-23407
 Low alloy steels and superalloys inertia welding in gas turbine field, discussing microstructure tensile strength and stress rupture
 [ASME PAPER 71-GT-21]
 11 p1770 A71-25965
 Welding of maraging steels, discussing metallurgical aspects of weldments and advantages/disadvantages of various techniques
 12 p1918 A71-27465
 Dissimilar metals welding, emphasizing melting point, linear expansion coefficient, thermal conductivity, electrical resistivity and polymorphic transformation
 13 p2072 A71-27887
 Cooling during welding of Ti for prevention of deleterious overheating, discussing safe temperature range for water cooling during butt welding of tubes
 15 p2413 A71-31221
 German book on welding conditions and material composition effects on structural changes and heat-affected zone mechanical properties of high strength structural steels
 17 p2748 A71-34851
 Aluminum bronze alloy forming dies fabrication and repair, discussing surfacing, hot working grinding, machining and welding methods
 18 p2928 A71-36855
 Austenitic stainless steels susceptibility to intergranular corrosion under unwelded, welded and heat treated conditions in process environments
 20 p3241 A71-39341
 Closed form solution for quasi-static thermal stress field due to moving point heat source in circular disk, noting application to welding problems
 21 p3467 A71-40966
 Thermocouple measurements of thermal gradients in steel during automatic welding
 23 p3679 A71-43892
 Ni-base superalloys metallography, investigating catastrophic cracking in weld heat affected zones by electron microscopy
 24 p3839 A71-45139

WELDING MACHINES

- Electron beam welding system, discussing solid state controls, programmed operation and type and thickness of welded materials
 01 p0087 A71-10451
 High speed light gage Al welding, discussing plasma arc system
 01 p0087 A71-10454
 Gas tungsten arc, manual, machine and resistance welding in assembly of gas turbine parts
 [SME PAPER AD-70-147]
 01 p0089 A71-11258
 Long pulse glass laser welder-driller, determining mean energy densities and spot sizes
 09 p1464 A71-23404
 Production welding and annealing, investigating low heat input, intermetallics formation, atmospheric contamination, hot short cracking, speed and cost
 09 p1458 A71-23408

Jet engine components inertia welding, discussing process, equipment, low weight-cost advantage and mechanical properties reproducibility
 11 p1770 A71-25970
 [ASME PAPER 71-GT-33]

Book on electron beam welding covering generation and control, thermal effects, techniques and equipment, metallurgical and mechanical properties, etc
 13 p2074 A71-28736

Arc welding apparatus for chemically active high-melting metals in controlled superpure He atmosphere
 14 p2253 A71-30486

Local shielding chambers for welding circumferential and longitudinal seams in Ti alloys with minimum residual oxygen concentrations
 14 p2253 A71-30489

Ruby laser microwelding machine for simultaneous welding of several points with one discharge suitable for micromechanics, computer manufacturing, watchmaking, etc
 19 p3069 A71-38232

Ti alloys semiautomatic pulsed arc MIG welding, showing increased productivity and reduced distortion
 19 p3070 A71-38423

WENTZEL-KRAMER-BRILLOUIN METHOD

WKB wave functions for one dimensional non-relativistic problems by simple transformation derivation, solving by application of Liouville substitution to Schroedinger equation
 12 p1923 A71-27666

Oscillations excited by pulsed dipole antenna at upper hybrid resonance in weakly inhomogeneous plasma investigated by Wentzel-Kramer-Brillouin approximation
 15 p2460 A71-32656

Impulsive time variation plane wave reflection from ionospheric sech squared electron density profile, comparing full wave and WKB solutions
 17 p2701 A71-34769

French monograph on ULF geomagnetic field variations covering plasmapause, geomagnetic pulsations, WKB limit and magnetospheric density
 17 p2735 A71-35248

WEST GERMANY

U GERMANY

WESTLAND AIRCRAFT

Westland WG 13 Lynx helicopter, discussing design features, performance characteristics and civil and military applications
 14 p2175 A71-30301

WETNESS

U MOISTURE CONTENT

WETTABILITY

High modulus carbon fiber wettability by matrix resin
 [PLASTICS INST. PAPER 21]
 08 p1322 A71-20928

WETTING

Metal coatings and thin films wetting by soldering materials, emphasizing oxide removal
 06 p0903 A71-17426

Alloying addition effects on wetting of carbon by liquid metals, using sessile drop technique
 [PLASTICS INST. PAPER 19]
 08 p1296 A71-20911

Room temperature evaporating water drop shape history on cooper, lucite, stainless steel and Teflon, observing wetting dynamics effects
 21 p3476 A71-40903

WHEATSTONE BRIDGES

Precision temperature controller using resistive sensor and Wheatstone bridge in heater loop, discussing prototype design for gyroscope application
 08 p1287 A71-20986

Wheatstone bridge with thermistors, discussing linearity, sensitivity and applications for temperature difference and flow velocity measurements /anemometers/
 13 p2071 A71-29278

Thermistor bolometer characteristics, considering resistance-performance relationship, radiation and Wheatstone bridge potentials
 20 p3233 A71-38969

WHEEL BRAKES

Concorde lightweight disk brakes, discussing operating costs, weight and volume factors, design philosophy, structural materials, component life, maintenance and reliability
 16 p2522 A71-33226

WHEELS

NT FLYWHEELS
 NT NOSE WHEELS
 NT REACTION WHEELS
 NT TURBINE WHEELS
 NT VEHICLE WHEELS

External-internal gear stages contact ratio on basis of gear wheels working drawing geometrical quantities
 03 p0431 A71-13025

Transition curve equation for end cross section of slant-toothed wheel cut by rack type instrument with protuberance and rounded edge
 07 p1117 A71-19360

WHIRL

U ROTATION

WHIRL INSTABILITY

U ROTARY STABILITY

WHIRLING

U ROTATION

WHIRLING TESTS

U SPIN TESTS

WHISKER COMPOSITES

Cadmium-copper fibrous eutectic alloy morphology, describing sample preparation and crystallographic examinations by optical and electron microscopes
 01 p0103 A71-11018

Whisker technology developmental history and current state, discussing composite material production and whisker testing methods
 04 p0611 A71-14941

Whisker composites mechanical properties analysis, discussing stiffness and strength under static loads, elastic moduli, stress analysis, statistical tensile failure model, etc
 04 p0667 A71-14947

Interfacial wetting, bonding and chemical and mechanical stabilities in whisker composites, discussing system stability
 04 p0611 A71-14948

Whisker reinforced composites fabrication principles and methods, discussing constituents, mechanical, geometrical, physical and chemical requirements
 04 p0603 A71-14949

Metal whisker composite technology based on unidirectionally solidified eutectics, discussing mechanical behavior of whisker phase isolated from matrix
 04 p0611 A71-14950

Whisker composites tensile and fatigue properties, fracture toughness and mechanical properties at high temperatures
 04 p0611 A71-14951

Whisker composites applications, considering aerospace technology, turbine components, deep submergence structures, dental ceramics, electronics and wear resistant materials
 04 p0611 A71-14952

Plastics reinforcement by combining high plastic deformation and fracture resistances with stiffness, discussing ceramics, whiskers, carbon and glass fibers
 11 p1788 A71-25654

Boron filaments and whiskers as reinforcements in high strength composite materials
 11 p1790 A71-26336

Fiber reinforcements for structural composites, considering glass, polycrystals, vapor deposition, whiskers and metals
 12 p1922 A71-27636

Nickel and cobalt pseudobinary eutectic alloys reinforced by refractory metal monocarbides whiskers, studying mechanical properties, solidification and phase equilibria
 15 p2432 A71-32169

Carbon and boron fibers and whisker reinforced plastics fabrication, properties and costs, noting materials and optimum matrix combination
 21 p3405 A71-40600

WHISKERS [SINGLE CRYSTALS]

High temperature annealing effect on sapphire single whiskers structure, using electron microscopy
 01 p0106 A71-10276

Papers on whisker technology covering mechanical properties, crystal growth, composite materials, etc
 04 p0611 A71-14940

Whisker technology developmental history and current state, discussing composite material production and whisker testing methods
 04 p0611 A71-14941

Whisker growth by vapor phase reactions, detailing thermodynamics, kinetics and supersaturation in aluminum oxide whisker formation
 04 p0635 A71-14942

Crystal growth mechanism involving vapor, liquid and solid phases, discussing Si whiskers and impurities effects
 04 p0636 A71-14943

Sapphire whiskers production by melt growth technique, describing process and whiskers mechanical properties
 04 p0636 A71-14944

Testing methods for mechanical properties of individual whiskers, describing tensile machines, shear stress measurement torsion device and Young modulus measurement method
 04 p0603 A71-14945

Ceramic and metallic whiskers mechanical properties, discussing failure and deformation mechanisms
 04 p0611 A71-14946

Gravitationally induced electric field shielding using whisker model with conducting metal surface for reducing strain dependence on altitude
 05 p0792 A71-16315

Liquid drop role in aluminum nitride whisker growth by aluminum oxide reduction in nitrogen or by direct nitriding
 05 p0768 A71-16820

Field ionization yield with single graphite whisker lateral surface as ionizer, using helium, ammonia, carbon monoxide and carbon dioxide
 07 p1164 A71-19855

Composite morphology and mechanical properties relationship, considering reinforcing effect, filament-

tous systems, whisker growth ladder molecules synthesis and material production

10 p1635 A71-24768

Composite materials reinforced by brittle sapphire and ductile copper whisker crystals, noting surface defects effect on mechanical properties

16 p2601 A71-33917

Beta rhombohedral boron whiskers production from hydrogen reduction of boron bromide and chloride by vapor-liquid-solid mechanism

22 p3564 A71-42533

In-Bi whisker growth by squeeze technique, measuring crystal structure by X ray analysis and melting point method

23 p3689 A71-42956

WHISTLERS

Stability analysis of magnetosphere whistler amplification, discussing energetic electron interaction with background plasma

01 p0038 A71-11308

Whistler ducts as enhanced ionization fromOGO 3 satellite observations near magnetic equator, noting magnetospheric ionization hydrostatic model and predicted cut-off

01 p0076 A71-11499

Ion reflection and whistler trace shapes as function of magnetic latitude from satellite observations

03 p0408 A71-13389

Thermal magnetospheric plasma densities from hydromagnetic whistlers dispersion characteristics by normalized dispersion curve method

03 p0419 A71-14521

Whistler-mode waves circular polarization measurement byOGO 6 satellite, noting application to hiss, chorus and ion density studies

03 p0421 A71-14538

Magnetospheric whistlers, deriving group refractive index and velocity, propagation time and various L values

05 p0721 A71-16443

Proton whistlers damping compared to predictions by cyclotron damping theory, discussing proton density

06 p0949 A71-17262

Magnetospherically reflecting nonducted whistler mode waves propagation noting dispersion, hybrid frequencies, ray curvature and field lines

06 p0868 A71-17983

Whistler wave packet propagating in ambient magnetic field direction, computing nonlinear particle trajectories

06 p0869 A71-17987

Subprotonospheric and ion cyclotron whistlers generated by same lightning discharge observed by OVI-10 satellite

06 p0869 A71-17995

Whistler indicator generation, relating VLF emissions to iano-acoustic oscillations in magnetosphere

07 p1099 A71-19387

Electron and proton whistlers polarization reversal and magnetic coupling, explaining magnetic latitude dependence

07 p1062 A71-19667

Whistler wave propagation along bell shaped ducts of enhanced ionization in magnetosphere

07 p1064 A71-20321

Whistlers with harmonic bands caused by multiple stroke lightning, using Injun 5 VLF data

08 p1283 A71-21649

Electron loss by resonant interaction with whistlers in nonuniform magnetic field, taking Fokker-Planck equation as distribution function

09 p1513 A71-22423

Ion acoustic and helicon waves nonlinear interactions in plasma, evaluating whistler buildup rate

09 p1501 A71-22536

Complex ray theory for ion cyclotron whistlers of proton and helium type in topside ionosphere

09 p1437 A71-22927

Magnetoionic theory for drifting plasma whistler mode propagation, deriving magnetic field effects on imaginary and real parts of complex refractivity

09 p1505 A71-23385

Lower ionosphere RF whistlers polarization and electromagnet structure, determining earth-ionosphere waveguide resonance frequency

10 p1575 A71-23828

Midlatitude whistlers occurrence rates, dispersion and structural features sampled recording over North Italy

10 p1579 A71-25002

Riser whistlers observed at low latitude ground station, noting time delay increase with frequency

10 p1579 A71-25009

Midlatitude whistlers propagation paths during minimum solar activity for estimating magnetospheric electron density profile

10 p1580 A71-25135

Multicomponent whistler spectra due to discrete ionization inhomogeneities and complex structure nonuniformities forming diffuse whistlers in outer ionosphere

11 p1758 A71-25789

F region ion and temperature effects on VLF and ELF wave absorption in whistler mode propagation at midlatitudes during solar minimum

12 p1879 A71-27049

Plasma turbulent electron and ion heating by large amplitude whistler resonant excitation, investigating mechanisms

12 p1937 A71-27182

Earth plasmasphere annual and sunspot cycle variations, considering observations with respect to whistler paths and Pc4 pulsations mean period variations

12 p1902 A71-27669

Ionospheric anisotropic plasma with mixture of different ions, deriving refractivity at whistler frequencies

13 p2058 A71-28027

Electron thermal anisotropy effect on oblique whistlers preceding strong collisionless shock waves, using linear Vlasov theory

13 p2064 A71-29168

Particle collisions effects on whistler ray paths, considering penetration through lower boundary of ionosphere

14 p2193 A71-29917

LF whistler mode radio noise emissions observations in polar regions with Alouette 2, noting association with energetic particles influx into ionosphere

14 p2300 A71-30036

Whistlers propagation through ionosphere, considering coupling conditions between whistler mode signals magnetospheric trajectories and earth-ionosphere waveguide

14 p2203 A71-30963

Height variations of ionospheric absorption of downgoing whistler waves during nighttime at moderate and low latitudes

15 p2369 A71-31426

Internal reflection of VLF whistlers incident from above on model nighttime lower ionosphere

15 p2369 A71-31433

Linear and nonlinear whistler mode cyclotron instability, discussing VLF emissions generation mechanism in magnetosphere

16 p2615 A71-32803

Normal angle determination by rocket observations for whistler mode waves propagation through magnetosphere and ionosphere from conjugate VLF ground station signals

16 p2569 A71-33805

Discrete VLF emissions triggered by naturally occurring whistler trains or man-made signals of constant frequency

16 p2544 A71-33950

Nonnose whistlers nose frequency and minimum group delay measurements

17 p2732 A71-34323

Large amplitude whistler as collisionless laminar shock model, showing instability for oblique perturbation propagation

18 p2950 A71-35865

Asteroid magnetospheres effects on magnetic moments and whistler mode noise propagation in solar wind

18 p2964 A71-36292

Diurnal distribution, latitudinal occurrence and intensity patterns of ELF, VLF and LF whistler-mode noise emissions from Alouette 2 satellite observation

19 p3016 A71-37364

Magnetospheric whistler mode signal propagation paths and amplification, investigating echoes of ground to satellite transmission

19 p3016 A71-37400

Whistler indicator generation, relating VLF emissions to iano-acoustic oscillations in magnetosphere

19 p3052 A71-37812

Whistlers as diagnostic tools in space plasma, measuring electron densities at large distances in earth outer atmosphere within magnetosphere

19 p3116 A71-38246

Drifting whistler frequency cutoff phenomena /striations/ observation in low latitude by POGO satellites, discussing interpretation based on propagation effect

20 p3198 A71-39746

Multicomponent whistler spectra due to discrete ionization inhomogeneities and complex structure nonuniformities forming diffuse whistlers in upper ionosphere

22 p3532 A71-41557

Plasma turbulent electron and ion heating by large amplitude whistler resonant excitation, investigating mechanisms

22 p3583 A71-42459

Atmospheric triggered VLF emissions theory, examining magnetospheric whistler Morse pulses

23 p3643 A71-43135

Triggered whistler emissions in magnetosphere, considering nonlinear interaction between whistler wave and resonating particles

23 p3643 A71-43175

Low latitude whistler propagation characteristics associated with magnetic storms in March 1970 at Sugadaira /Japan/

23 p3644 A71-43364

Whistling atmospherics generation mechanism, showing ionic sound excitation by hydromagnetic wave propagation through magnetospheric rapid plasma concentration change regions

24 p3823 A71-45035

WHITE DWARF STARS

Photon-neutrino coupling theory of weak interactions, noting exclusion by astrophysical data for white dwarfs

01 p0130 A71-11272

Neutrino synchrotron radiation for relativistic gas applied to white dwarfs and neutron stars

01 p0145 A71-11337

White dwarfs, investigating spectral classification, clusters, motions and location on H-R diagram

04 p0647 A71-15243

White dwarf data, examining continuous energy distribution, degenerate star theory, mass-radius relation, spectra, radial velocities and Einstein shift

04 p0648 A71-15244

DA and DB white dwarf atmospheres convection effect on structure based on mixing length theory and constant flux model

04 p0658 A71-15841

Evolutionary cooling sequences and lifetimes for low mass white dwarfs in Hyades cluster, considering near surface convection in models with hydrogen envelopes

07 p1190 A71-18856

He shell burning termination in solar mass stars evolution to white dwarf stage

07 p1198 A71-19823

White dwarf G195-19 circular polarization measurements of continuum radiation in broad band, using electro-optically switched polarimeter

07 p1198 A71-19832

Magnetic white dwarf G195-19 circularly polarized light, confirming handedness and approximate magnitude

07 p1199 A71-19833

White dwarfs, neutron stars and black holes origin and characteristics, discussing density, mass radius, gravitation and structure

07 p1199 A71-19999

Circular polarization in white dwarf G99-37 continuum radiation as function of wavelength

12 p1956 A71-26609

Periodic variations in circular polarization of continuum radiation of white dwarf G195-19 from 3800 to 5400 A

12 p1956 A71-26610

Relativity and neutronization effects on radial pulsations and density decrease of rotating cold white dwarfs near stability loss, using energetic method

12 p1966 A71-27236

Helium-rich white dwarfs convective envelopes, acoustic noise generation and corona formation

12 p1970 A71-27746

Rapid differential rotation in completely degenerate white dwarfs, using perturbation method

13 p2135 A71-28300

Double and triple stars common proper motion, discussing white dwarf or degenerate components

14 p2310 A71-30360

Strong magnetic fields effects on neutron stars or white dwarfs, considering Thomson scattering in fully ionized collisionless plasma

14 p2315 A71-30858

White dwarfs - Conference, Fife, Scotland, August 1970

14 p2316 A71-31004

White dwarf discovery method and properties, discussing color, spectra, parallaxes, luminosities, masses, red shifts, cluster and frequency distribution

14 p2316 A71-31005

Trigonometric white dwarf star parallax measurements, using astrometric reflector to derive H-R diagram

14 p2316 A71-31007

White dwarf identification with Lowell proper motion program, detailing color classes, tangential velocity and UVB values

14 p2317 A71-31008

White dwarfs from Catalog of Nearby Stars, indicating radial and tangential velocities, proper motions, positions luminosity and UVB spectra

14 p2317 A71-31009

HF stellar radiation oscillations based on photoelectric monitoring of southern white dwarfs power spectra

14 p2317 A71-31010

Spectroscopic criteria for strong lined white dwarf stars identification on low dispersion objective prism plates

14 p2317 A71-31012

White dwarf stars effective temperature measurements, matching absolute spectral energy distributions with fluxes from model atmospheres

14 p2317 A71-31013

White dwarf model atmosphere, discussing DA and non-DA spectral types, surface gravity, mass-radius relation, composition and convection effects

14 p2317 A71-31014

- White dwarf line spectra, constructing atmospheric models and effective temperatures
14 p2317 A71-31015
- Hydrogen deficient white dwarf atmospheres, computing line free flux constant models for He rich compositions with varied metal abundances
14 p2318 A71-31016
- White dwarf coronas convection zones thermodynamic calculations, considering high electron degeneracy, and He I and He II ionization
14 p2318 A71-31017
- White dwarf star gravity mode stability, considering hydrogen-helium transition sorting zone
14 p2318 A71-31018
- White dwarf stars equilibrium models, discussing vibrational stability and radial pulsations eigenvalues and eigenfunctions
14 p2318 A71-31019
- Collapsing white dwarf stars, investigating detonation wave formation for thermonuclear explosion
16 p2631 A71-33228
- White dwarf and neutron stars magnetic field generation, noting system in metastable Lofler state
18 p2963 A71-36242
- Rotating isothermic radially pulsating white dwarf evolution, considering neutronization and general relativistic effects
19 p3134 A71-37511
- Rotating magnetic white dwarf stars possibility as X ray sources with thermal spectrum, considering evidence based on Sco X-1 emission relationship to bremsstrahlung
19 p3127 A71-38010
- White dwarfs production in small mass binary systems, deriving formulas for final mass and orbital velocity with application to blue stragglers
19 p3143 A71-38160
- White dwarf stars broadband circular polarization and normal/quadratic Zeeman effect
20 p3304 A71-39940
- Cen X-3 source X ray flux periodic variations due to white dwarf star radial vibrations based on nonrotating model
21 p3449 A71-40613
- Cosmic rays origin, discussing nuclear, electron and electromagnetic components, supernovae, pulsars, white dwarfs and gas motions in Galactic Center
22 p3594 A71-42550
- White dwarfs EG 248, GR 289 and EG 250 spectra with circular polarization, detailing violet lines, absolute magnitudes, color and luminosity
23 p3733 A71-43079
- Ellipticity of weakly rotating configurations, determining 5m/4 delta ratio for white dwarfs
23 p3770 A71-44063
- Sirius B white dwarf star effective temperature, radius and gravitational red shift determination from H-alpha and H-gamma line profile analysis
24 p3871 A71-44908

WHITE NOISE

NT THERMAL NOISE

- Linear information feedback methods for white Gaussian noise channels
01 p0064 A71-10904
- Forced random oscillations of nonholonomic systems about equilibrium positions, deriving stability conditions in white noise disturbances
01 p0176 A71-11042
- Prewhitening technique for acoustic turbulent flow data recording and analysis
04 p0600 A71-15598
- Optimal and nonoptimal signal reception under conditions of incomplete a priori information based on approximation by Markov processes in white noise
05 p0730 A71-16000
- FM discriminator with nonideal limiting, calculating signal to noise ratio under white Gaussian noise input
05 p0730 A71-17071
- Coherent communication link pseudonoise synchronization error due to white Gaussian noise and amplitude jitter produced by reference carrier phase error, discussing digital simulation
05 p0725 A71-17072
- Pulsed phase locked automatic phase control system linear model, discussing optimal white noise filtration with integrating filter
06 p0867 A71-17377
- Optimal temporal and spatial temporal resolution for unknown parameter of interfering signal on white noise background
09 p1404 A71-22219
- Woodward ambiguity function generalization for case of radar signal reflection from rapidly fluctuating target, mixed with white Gaussian noise
09 p1404 A71-22292
- Noise effects on characteristics of automatic radar rangefinder with logarithmic receiver, showing discrimination curve deformation with increasing SNR
09 p1415 A71-22297
- Signal-white noise mixture filtration, determining maximum SNR position and magnitude and filter bandwidth
09 p1416 A71-22466

- Current spectral noise density in nonlinear element transmitter stage, examining vacuum tube frequency multiplier phase and amplitude fluctuations
09 p1405 A71-22469
- Nonstationary colored noise linear shaping filter to transform white noise into nonstationary random process with specified covariance function
09 p1424 A71-23100
- Rate distortion over band limited feedback channels, considering capacity of additive Gaussian white noise channel
09 p1407 A71-23104
- Diversified frequency radio data transmission and reception by linear modulation, considering error rate in white noise and selective/flat fading
10 p1580 A71-25109
- Coding for feedback communication system with additive white Gaussian noise, using mean-square estimation error
13 p2034 A71-29379
- Optimal detection of rectangular radio signal pulse envelope distortions by multiplex fluctuations over white noise background
14 p2195 A71-30113
- Planar and nonplanar transistors noise factor dependence on signal source impedance and emitter current, considering amplification and frequency conversion application
14 p2213 A71-30628
- Pin-ended column stability and random behavior under white noise excitation, using analog simulation and application to vertical earthquake and aerospace vibration environments
14 p2330 A71-30683
- LF white Gaussian noise generator with continuously variable output, describing transistorized circuitry and output characteristics
15 p2371 A71-31851
- Bandlimiting effects on coherent detection of PSK, ASK and FSK signals in presence of white Gaussian noise, using SNR as performance criterion
17 p2704 A71-35085
- Probability density function of optimum phase locked loop synchronizer of sinusoidal signal with white Gaussian noise in partially coherent receiver
20 p3195 A71-38858
- Critique of paper on additional signal power for optimum performance of PCM binary signal detection under channel band limiting effect in white noise
20 p3196 A71-38870
- Noise variance maximum likelihood estimate based on order statistics for first order Reed-Muller code transmission over zero-mean white Gaussian noise channel
20 p3202 A71-38875
- Optimal and nonoptimal signal reception under conditions of incomplete a priori information based on approximation by Markov processes in white noise
22 p3527 A71-42749
- WHITHAM RULE**
Three dimensional convergence for spherical shock wave by linear pinch wall shaping based on Whitham ray-shock theory
11 p1752 A71-26191
- Near field flow pattern of inclined slender body of revolution, using Whitham far field theory of supersonic flow
15 p2344 A71-31554
- [AIAA PAPER 71-626]
- WHITTAKER FUNCTIONS**
Periodicity solutions of Whittaker-Hill equation in trigonometric series form by three term recurrence relations
03 p0450 A71-13372
- WICKS**
Fluid mechanics of shallow liquid fuel layer near burning wick, deriving continuity, momentum and convective diffusion equations to obtain extinction condition
02 p0334 A71-12855
- Vaporization heat transfer mechanism from capillary wick covered heated surface, considering applicability to heat pipes
03 p0353 A71-13615
- Cryogenic heat pipes with parallel capillary channel wicks
[ASME PAPER 70-WA/ENER-1]
03 p0520 A71-14106
- Elemental maximum energy transport formula for wick heat pipe evaporators under artificial gravity and external acceleration, testing by laboratory centrifuge
11 p1857 A71-26210
- Noncondensable gas temperature controlled heat pipe systems design, considering working fluid, reservoir wicks and ambient thermal environment
11 p1857 A71-26211
- Design and performance testing of arterial wick circular heat pipes for OAO-C spacecraft
18 p2868 A71-36393
- [ASME PAPER 71-AV-26]
- WIDE ANGLE LENSES**
Interference passband filters with wide angle lenses for multispectral photography, discussing design and applications
01 p0081 A71-10827

- Optical transfer function measurement and computation test applications to aerial camera wide angle lens standard design, using interlaboratory comparisons
09 p1494 A71-23001
- Fabrication technology limitations effect on use of dielectric interference filters in wide angle optical receivers
18 p2946 A71-35847
- High aperture wide angle lens design for compact electro-optical systems of airborne moving map projection navigational instruments
18 p2947 A71-36605

WIDEBAND

U BROADBAND

WIDEBAND COMMUNICATION

- Machine-to-machine compatibility in wideband magnetic tape recording, discussing record-head gap width variations effects on record transfer characteristics
01 p0033 A71-10895
- Frequency division multiplexing methods for wideband optical communications systems, calculating approximate information capacity
02 p0214 A71-12022
- Ultrawide bandwidth optical data relay link between earth satellites, discussing system design concept
02 p0214 A71-12024
- Ultrawide bandwidth laboratory laser communication link for high fidelity signal transmission, discussing system configuration, components and preliminary test results
02 p0214 A71-12025
- Earth station mixers design as wideband millimeter wave up- and down-converters for satellite communication systems
02 p0234 A71-12818
- Linear low noise wideband frequency modulator for Intelsat 4 satellite telephony communication, considering channel capacity
02 p0234 A71-12819
- Intelsat system earth station on-site planning considerations for integration with existing wideband communication system and traffic growth demand
03 p0380 A71-14343
- Wideband interdigital microwave circuits using lithium niobate crystals for electro-optic modulation of light, discussing design and performance tests
05 p0762 A71-16336
- Wideband FSK system involving direct and reflected path transmission, predicting diversity performance from mathematical model
05 p0724 A71-17057
- Monopole antenna with continuous resistive loading, studying broadband characteristics over frequency range by thin film evaporation techniques
06 p0867 A71-17710
- Wideband radar array antenna system with suppressed grating lobes
06 p0867 A71-17712
- Wideband mixer for Intelsat 3 satellite, describing design, operation and performance
06 p0877 A71-18401
- Wideband microwave nonpulsed radar direction finding techniques, discussing concept, operation theory, characteristic equations and error analysis
07 p1059 A71-18846
- Cross couplings in wideband antenna arrays, determining scattering coefficients, self/mutual impedances and admittances of two radiating elements
11 p1738 A71-26344
- Dipole elements input impedance of wideband linear antenna arrays, using coupled circuits and induced emf
11 p1738 A71-26345
- Malfunction probabilities in presence of wideband noise for tunnel diode binary logic element /flip-flop/ pulse triggered into either of two output states
11 p1740 A71-26543
- Broadband FM systems behavior, calculating transmission deviations via transfer functions obtained from measurements and linear network analysis
12 p1878 A71-26993
- Integrated wideband low-noise X-band sweeping superheterodyne receiver, demonstrating advantages of microwave IC techniques application
16 p2547 A71-33553
- European telecommunication and TV distribution satellite system, including telephony, telegraphy, telex and wideband data transmission
17 p2696 A71-34232
- Parametric up-converters for low noise broadband microwave receivers, discussing electronically tunable pump frequency accuracy and stability
17 p2714 A71-34606
- Superheterodyne wideband microwave receiver requirements, design and performance
17 p2699 A71-34607
- Wideband Cassegrain microwave antenna for space communication, discussing reflecting horn for maximum radiation gain
17 p2715 A71-34686
- SPADE system digital channel unit applicability to services other than voice transmission, discussing nar-

row- and wide-band data transmissions and bit-error-rate performance
17 p2706 A71-35104

Optical wideband digital communication system performing operational space-ground link functions
18 p2878 A71-36520

IR CdTe-HgTe detectors for laser space communications at 10.6 microns, using directivity of light waves in vacuo for wideband transmission
18 p2892 A71-36566

Wideband fiber waveguide communication systems for optical frequencies, considering information carrying capacity limitation by components available for repeaters and terminal equipment
18 p2883 A71-36995

Wideband communications theory applied to continuous /analog/ signals using frequency and amplitude modulation
19 p3015 A71-37254

Broadband point-to-point communication satellite systems for 1970s, discussing R and D effort, economics and international and domestic applications
20 p3197 A71-39606

Electronic broad banding of VLF/LF antennas for FSK radio communication through switched magnetically coupled reactor, determining antenna transient response
22 p3513 A71-42388

Uniform signal energy distribution in wideband synchronous data transmission channels using linear sequential filters with scramblers
23 p3647 A71-44345

Wideband transistorized active dipole antenna for reception at 100-1000 MHz, calculating impedance and effective height by linear theory
24 p3807 A71-44360

WIDMANSTATTEN STRUCTURE
Microstructural variables effects on fracture stress in alpha beta Ti alloy having Widmanstatten structure
07 p1139 A71-19992

WIENER FILTERING
Power gyrostatizer optimal controlling section with random base frame oscillations, solving filtration problem as function of platform structure by Wiener method
01 p0079 A71-10427

Pole path deconvolution by optimum Wiener filter for acausal and causal cases, considering earthquake excitation
06 p0890 A71-17884

French book on optimal inertial navigation and statistical filtering covering Wiener and Kalman filters, gyroscopes, accelerometers, inertial platforms, data processing, computer programming, etc
14 p2271 A71-29940

Kalman-Bucy filter construction as true time varying Wiener filter with covariances independent of signal generation, applying to data smoothing problem
14 p2220 A71-30460

WIENER HOPF EQUATIONS
Book on antenna admittance problem covering iterative solution of integral equations, Fourier series solution, Wiener Hopf methods, transmission line theory, etc
14 p2193 A71-29932

Closed linear systems optimal stabilization, determining transfer function from Wiener Hopf equation
16 p2550 A71-33900

Plane sound waves transmission and reflection through finite plates single cascade by Wiener Hopf technique
21 p3437 A71-40537

Iterative solution for radiant energy transport equation by Wiener Hopf operator equations, investigating convergence conditions
23 p3699 A71-43573

WIGHTMAN THEORY
U FIELD THEORY (PHYSICS)
U QUANTUM THEORY
U RELATIVISTIC THEORY

WIND [METEOROLOGY]
NT GEOSTROPHIC WIND
NT GROUND WIND
NT GUSTS
NT JET STREAMS [METEOROLOGY]
NT MONSOONS
NT SQUALLS
NT WINDS ALOFT

Land breeze fronts observed by X and S band radars at Wallops Island
01 p0116 A71-10563

Stratospheric thermal structure and circulation, considering temperature, wind and composition fields
01 p0122 A71-11358

Exponential thermal wind spiral equations, discussing planetary boundary layer flow over Antarctic Plateau
03 p0452 A71-33228

Urban heat island induced circulation without synoptic winds, using two dimensional atmospheric model
03 p0453 A71-13232

Equatorial electric field generation by ionosphere dynamo region neutral wind meridional component
07 p1101 A71-19409

Nighttime airflow deviations over urban areas from radar tracked tetoron flights, discussing effects as function of atmospheric wind and temperature
11 p1793 A71-25377

Neutral air winds and ionospheric continuity equation, calculating midlatitude electron concentration longitudinal variations
11 p1754 A71-25605

Three dimensional quasi-stationary problem of local winds in neutrally stratified atmosphere in low latitudes, analyzing Coriolis force role
13 p2096 A71-28016

Neutral fluctuations of zonal winds in stratosphere and mesosphere from flow equations, noting flow instability role in generation mechanism
13 p2057 A71-28020

Nongeostrophic wind behavior in free atmosphere during cyclogenesis, noting maximum development during cyclone lifetime middle stage
15 p2400 A71-31969

Joule heating and winds in upper atmosphere due to geomagnetic disturbances at 140 km altitude, deriving set of nonlinear partial differential equations
16 p2564 A71-33726

Neutral winds in F region from traveling ionospheric disturbance data, investigating gravity wave hypothesis
16 p2570 A71-33828

Thermospheric circulation and temperature changes due to global scale winds flow through F region ionization anomalies, using time independent dynamic model
16 p2571 A71-33836

COSPAR international reference atmosphere containing seasonal variations, solar flux and altitude models for density, temperature, pressure and wind
16 p2572 A71-33851

Upper atmosphere mean temperature, pressure, density and wind distributions as functions of altitude, season and latitude, discussing planetary, infrasonic and internal gravity wave effects
17 p2735 A71-35236

Equatorial electric field generation by ionosphere dynamo region neutral wind meridional component
19 p3053 A71-37833

Midlatitude ionospheric data comparison to F 2 critical frequency from continuity equation and neutral air winds
21 p3372 A71-40043

WIND CIRCULATION
U ATMOSPHERIC CIRCULATION

WIND DIRECTION
Atmospheric boundary layer nonlinear equations of motion numerical integration for eddies structure and wind direction and latitude effects on turbulence intensities
01 p0113 A71-10351

Wind speed field estimations from wind direction, using satellite cloud photographs
01 p0119 A71-10851

Free nonlinear air convective motion in two dimensional cloud banks along vertical wind shift
02 p0277 A71-11690

Midlatitude wind vector longitudinal and transverse components correlation functions for different isobaric surfaces in summer and winter
06 p0924 A71-17647

Vertical velocity effects on ionospheric horizontal wind magnitude and direction, solving integral equations system by successive approximations
09 p1435 A71-22428

Atmospheric wind velocity radial components measurements for meteor drift as function of wind direction, using transmitter and receiver antennas synchronized orientation method
11 p1758 A71-25791

Cold front zone meteorological elements, calculating temperature gradients, dew point deficit, and wind vector vertical distribution
11 p1795 A71-26558

Stratospheric seasonal wind reversals morphological classification for comparing atmospheric processes over different rocket sounding stations
12 p1900 A71-27065

Stratospheric wind seasonal reversals over Polish coast of Baltic Sea in 1967-1969 from rocket sounding and upper air synoptic analysis
12 p1900 A71-27067

Solar wind rotational to tangential discontinuities ratio determination and hypothesis concerning origin in interplanetary magnetic field
16 p2628 A71-33942

Ionospheric wind velocity, direction and diffusion coefficient measurements using artificial aluminum oxide luminescent clouds
19 p3091 A71-38629

Atmospheric wind velocity radial components measurements for meteor drift as function of wind direction, using transmitter and receiver antennas synchronized orientation method
22 p3533 A71-41559

Wind velocities and directions, air temperature and visibility range in atmospheric boundary layer under fog conditions
22 p3569 A71-42846

Upwind/downwind differential Doppler spectra of radar sea echo for P, L and C bands
23 p3646 A71-44173

WIND EFFECTS
Skyнет satellites earth stations design, structure, transportation and erection ease, considering operational and stowed position survivability in high velocity winds
02 p0223 A71-12804

Soviet book on meteorological conditions and supersonic aircraft flight covering atmospheric composition and structure, temperature distribution, wind effects, etc
02 p0278 A71-12840

F region diurnal behavior, comparing neutral winds and electric field effects
03 p0408 A71-13383

Wind compensation method for launching sounding rockets susceptible to nonlinear wind effects, using data generated by six degree of freedom trajectory digital simulation program
03 p0498 A71-13672

Topside ionosphere O-H ions transition level altitude variation due to atmospheric winds
03 p0416 A71-14030

Cylindrical cantilever shells /sloes/ under wind loads by semimembrane analysis, discussing cross section distortion and stress prediction
04 p0667 A71-15182

Internal gravity wave propagation in neutral wind stratified atmospheric model
06 p0888 A71-17274

Ionization disturbances caused by gravity waves in neutral air propagating through ionosphere in electrostatic field and background wind
06 p0888 A71-17278

Flight range and optimum angle of attack under wind conditions of constant velocity and direction, considering fuel consumption for given distance
06 p0847 A71-18325

Inertial aircraft lateral guidance system limitations in stochastic gust environment, comparing configurations using aileron or differential spoilers
06 p0925 A71-18489

Magnetospheric convection and polar wind influence on outer radiation belt energetic electron loss, subjecting previously large fluxes of lower energy electrons to trapping limit
07 p1186 A71-19661

Dissipative effects on tidal winds at ionospheric heights concerning Lorentz force, molecular viscosity and heat conductivity
08 p1278 A71-21201

Multiple wave propagation in acoustic duct with winds, using perturbation Lagrangian for ideal fluid flow
08 p1276 A71-21651

Linear coastal hydrostatic boundary layers of lake with no horizontal motion, discussing flow conditions under wind stress and interior velocity
10 p1600 A71-23961

Electric field, neutral air winds and atmospheric composition changes effects on electron concentration diurnal variation in midlatitude F layer
10 p1607 A71-24922

Wind gradient effect on flight characteristics during aircraft landing approach, particularly path deviation
11 p1706 A71-25194

Ionospheric drift mechanism in midlatitude F region, discussing ground level magnetic field, E region side effects, horizontal winds and polarization fields
11 p1753 A71-25550

Second order longitudinal variations of vertical ionospheric drift by middle latitude horizontal neutral air winds, showing maxima at universal time
11 p1754 A71-25604

Neutral wind effects on redistribution of E region ionization and recombination, comparing electron density profiles to vertical ion drift velocities
11 p1755 A71-25613

Neutral winds produced vertical ion drift toward electric polarization in equatorial F region, discussing field discharge through E region and atmospheric superrotation effects
12 p1900 A71-26890

Wind gust tracking on autotracking antenna servosystem feedback error, evaluating torque disturbance admittance
12 p1868 A71-27002

F layer vertical drifts due to winds at midlatitudes, computing longitudinal variations
13 p2054 A71-27793

Lake Erie steady state wind driven currents numerical solutions, using shallow lake model for velocity as function of depth and horizontal position
13 p2054 A71-27857

Nonzonal atmospheric motion effects on meteorological elements 26-month oscillations stability in equatorial zone from linear hydrothermodynamic equations
13 p2057 A71-28022

Wind noise reduction by windshields, considering effect of mean flow velocity, turbulence, flow

direction, windscreens shape and size, covering material and microphone location 13 p2040 A71-29283

Wind transport effect on redistribution of ionization produced by geocoronal and interplanetary UV emissions in nighttime ionosphere, using electron density sounding rocket data 14 p2230 A71-29709

Extreme turbulence measurement during low level flights of Mirage A3-76 fighter aircraft, determining true gust velocities and power spectral energy distributions 14 p2267 A71-29756

Aircraft with T tail configuration, examining dynamic response to lateral gusts 14 p2174 A71-29786

Aircraft design and fatigue life monitoring, investigating effects of gust velocity frequency distribution in patches of atmospheric turbulence 14 p2174 A71-29789

Steady state wind driven currents velocity in Lake Erie, using shallow lake level model in numerical calculation 14 p2231 A71-29935

Spores released from solids interiors by aeolian erosion on planetary surface, noting application to microbes in planetary quarantine 16 p2537 A71-33796

Thermospheric dynamics, including global compositional structure, winds and temperature response to solar radiation and vertical mass diffusion 16 p2571 A71-33838

F region plasma phenomena discoveries by U.S. researchers /1967-1970/, considering thermal structure, ion composition, conjugate photoelectrons effects, wind effects, etc 17 p2732 A71-34465

Gust loading on two dimensional thin airfoil in compressible flow, deriving closed-form lift expression 17 p2671 A71-35285

Case histories of aircraft damage due to wind acting on airport surfaces, discussing wind and hail protection 17 p2675 A71-35442

Undisturbed ionospheric ion and electron temperature warming, investigating frictional heating effect by neutral winds 19 p3048 A71-37399

Cold climate clothed human windchill tables, considering various heat transfer modes and skin temperature 20 p3192 A71-39205

Seasonal stratospheric wind effects on infrasound propagation to U.S. northeast coast from rockets launched at Cape Kennedy 20 p3306 A71-39762

Climatic changes periodicity in Italy, considering cause by sirocco enhancement 21 p3411 A71-40827

Atmospheric wind, temperature, turbulence, hydrometeors, ozone, cosmic radiation and radio activity effects on commercial SST Concorde flight 21 p3325 A71-40829

WIND MEASUREMENT

NT WIND VELOCITY MEASUREMENT

Clear air radar structures temperature, wind components and true gust velocities combined with radar data for observed traveling wave features 01 p0030 A71-10560

Wind flow patterns in severe thunderstorms structures, using Doppler radar 01 p0117 A71-10573

Lower atmosphere turbulence model derivation from data obtained by Doppler radar windfield measurements in snowfall environment 01 p0117 A71-10578

Tower turbulence characteristics, using surface wind and temperature measurements to estimate horizontal velocity and dissipation rate variances at top 03 p0452 A71-13226

Neutral atmospheric wind measurements at 75-110 km by radar observation of meteor trail drift, discussing diurnal variations 03 p0407 A71-13308

Sounding rocket dispersion reduction using optimum wind filter for impact prediction based wind statistics and measurement [ALIA PAPER 70-1394] 03 p0499 A71-13675

Rocket probe launched by aircraft for measuring pressure, temperature, magnetic field and wind velocity around tornado vortex through radio telemetry 05 p0778 A71-17140

Wind field from macroscale atmospheric whirlpools /typhoons/ pressure fields by nonlinear hydrodynamic equations 06 p0923 A71-17514

Upper atmosphere wind measurement by meteor trails radar sounding, discussing seasonal variations, amplitudes and phases of harmonic components 09 p1487 A71-22302

Ionospheric drifts at 64-108 km at Birdlings Flat, New Zealand, comparing with meteor wind measure-

ments, chemical release trails and general circulation models 09 p1440 A71-23631

Crosswind components measurement for different runways of important German civil airports 10 p1639 A71-25041

Upper level wind measurements by Doppler equipped aircraft and jimsphere balloon radar tracking, presenting measured data rms variation and power spectral density 11 p1794 A71-25384

Rocketsonde instrumentation noise separation from stratospheric variability, discussing paired soundings based large scale discrepancies in temperature and wind observations 11 p1794 A71-25386

Rocket sonde prototype for wind and temperature measurements, discussing electrical circuits, mechanical design and operation 12 p1972 A71-27064

Stratospheric and mesospheric wind measurements over Leba sounding rocket station 12 p1900 A71-27066

Rocket-borne wind measurements at 40-70 km by glass fiber and Cu chaff clouds 12 p1901 A71-27068

Microwave emission from North Sea and North Atlantic at surface wind speeds of 5-25 m/sec, measuring brightness temperature 12 p1902 A71-27199

Upper atmospheric winds measurements at 160 and 275 km, finding upward motion difficult to relate to intrinsic atmospheric motions 13 p2056 A71-27930

Aircraft instrumentation and data analysis for clear air turbulence, including orthogonal components and temperature and wind distributions 14 p2267 A71-29753

Single anemometer wind measurement required for aircraft landing, comparing data from different sampling periods 14 p2270 A71-30395

Thermospheric wind measurement by chemical releases, observing artificial cloud motion and growth 16 p2565 A71-33735

German monograph on lower atmospheric turbulence and gustiness coefficients in connection with large scale parameters, deriving climatological flow characteristics from wind measurements 17 p2770 A71-35233

Portable run-of-wind recorder featuring variable gear changes to facilitate range adjustments 18 p2925 A71-36960

Thermospheric winds measurement during geomagnetic storms with Fabry-Perot interferometer from Doppler shift of two 6300 A fringe profiles 19 p3047 A71-37366

Ionospheric E region nighttime model from rocket soundings, obtaining electron density profiles by Langmuir probe and wind measurements by glowing vapor release 19 p3055 A71-38036

Gust factor variation as function of height and atmospheric stability, deriving simple power law expression from meteorological tower wind measurements 19 p3091 A71-38289

Wind velocity vertical component determination through meteor trail drift observation, presenting mean diurnal measurements data 19 p3059 A71-38393

Geostrophic wind measurements by radiosondes at various altitudes over British Isles, relating deviations from geostrophic equilibrium to vertical motions near tropospheric trough 20 p3258 A71-39551

Winds and diffusion measurements in lower thermosphere using sodium vapor cloud release from Centaur IIB rocket 20 p3221 A71-39692

E region wind and temperature measurements from Nancay incoherent scatter experiments, observing prevailing semidiurnal oscillation with phase propagating downwards 21 p3372 A71-40041

Mountain induced lee waves, turbulence and wind measurements in Colorado, using aircraft flight data 22 p3569 A71-42548

WIND PRESSURE

Static wind loading on large radar antenna structures from wind tunnel tests, considering forces and moments reduction by perforated reflectors and shallow curved cover 10 p1591 A71-23757

Correlation coefficient between winds at 850-30 mb pressure levels over Italy in winter, proposing theoretical model 21 p3411 A71-40825

WIND PROFILES

CAT wind structure and velocity dynamics, using Doppler radar techniques 01 p0116 A71-10564

Snow storms wind field and turbulent region detection, using Doppler VAD pattern and mapping 01 p0117 A71-10576

Wind speed difference quotient conversion to gradients at atmospheric surface layer geometric mean height, considering wind and temperature profiles 03 p0452 A71-13229

Rocket-borne Na-K vapor release for upper atmosphere winds profiles and diffusion measurements by ballistic camera photography 03 p0415 A71-14027

Semiannual atmospheric wind and pressure oscillations relation to seasonal meridional baric systems displacements, considering cosinusoidal wave motion variations between Northern and Southern Hemispheres 04 p0621 A71-14639

Annual and diurnal variations of temperature inversion over antarctic plateau, discussing wind field structure and ice crystal precipitation 05 p0778 A71-17043

Wind field from macroscale atmospheric whirlpools /typhoons/ pressure fields by nonlinear hydrodynamic equations 06 p0923 A71-17514

Atmospheric circulation integral characteristics prediction from wind intensity, kinetic energy and angular momentum 07 p1150 A71-18873

Atmospheric surface layer wind and temperature profile measurements over horizontally uniform flat terrain 09 p1489 A71-23554

Baroclinic instability problem analytical solutions for models with linear wind profiles, presenting growth rate variations and unstable waves phase velocity 10 p1638 A71-23962

Balance equation solution in spherical coordinate form, applying vector alterations to geostrophic wind field from pressure-height observations grid point analysis 10 p1638 A71-23964

Upper level wind measurements by Doppler equipped aircraft and jimsphere balloon radar tracking, presenting measured data rms variation and power spectral density 11 p1794 A71-25384

Venus water, discussing polar seas, acidity, temperature, wind patterns and clouds 11 p1824 A71-25700

Wind structure in boundary layer pilot-balloon observation, discussing baseline data processing for digital computer 11 p1796 A71-26560

Wind structure and atmospheric disturbances, noting resolution of pilot-balloon data 11 p1796 A71-26561

Wind structure in atmospheric boundary layer, outlining semiempirical laws for mean wind speed variation with height and statistical properties of turbulent fluctuations 13 p2097 A71-29266

Wind profile data in Cape Kennedy area from FPS-16 radar/Jimsphere master tapes 13 p2098 A71-29346

Monograph on persistent radio meteor echoes fading relation to upper atmosphere wind structure 14 p2192 A71-29579

Time and frequency statistics of turbulent fluctuations of wind, temperature and humidity in atmospheric surface layer 14 p2266 A71-29706

Meteorological research on upper atmosphere energy sinks/sources, composition, density, turbulence, winds and thermal structure 14 p2236 A71-30494

Stratospheric turbulence induced aircraft buffeting dependence on horizontal temperature and wind distribution 15 p2444 A71-31366

Wind profile determinations at 90-100 km from meteor trail drift and ionosphere inhomogeneity radar data, noting semidiurnal harmonics in wind components 15 p2395 A71-31450

Summertime meridional wind component profile construction and hydrodynamic model for semidiurnal fluctuations in upper atmosphere 15 p2399 A71-31962

Internal gravity waves vertical propagation in lower ionosphere from temperature and wind profiles measurements 16 p2561 A71-32802

Upper atmospheric winds viscous damping energy deposition calculation for midlatitude profiles 16 p2568 A71-33789

Earth atmosphere wind field motion calculation from displacement of longitudinally elongated cyclones 20 p3277 A71-38736

Dynamo theory for ionospheric thin shell model, considering wind fields determination from diurnal geomagnetic variations 20 p3218 A71-39522

- Woomera /Australia/ meteorological rocket firings, using temperature and wind profiles to assess sensors and parachutes performance 20 p3221 A71-39691
- Longitudinal, transverse and vertical wind distribution microstructure during convection from airborne experiments 21 p3412 A71-41388
- Upper atmosphere rotation rate decrease at altitudes above 350 km, determining zonal wind variations by satellite orbits analysis from Hewitt camera observations 23 p3667 A71-43140
- Rocket and radio wave wind profiles from 60 km to E region near 53N, presenting partial reflections and zonal winds time cross section 23 p3700 A71-43343
- WIND SHEAR**
- Weather radar signals decorrelation times due to vertical wind shear and azimuth scanning 01 p0030 A71-10598
- Vorticity generation or suppression using scale analysis with vorticity equation, considering wind shear in jet stream 02 p0241 A71-12744
- Venus atmosphere rotational model, considering nonlinear instability due to wind shear from solar heat induced convection 03 p0489 A71-13607
- High latitude E region plasma irregularities based on wind velocity shear fields 07 p1153 A71-19760
- Vector wind shears statistical analysis at various altitudes, using balloon sounding measurements 08 p1327 A71-21457
- Flow equations of vertical shear modes in inertial waves on rotating earth, comparing chemical release ionospheric wind profiles 09 p1489 A71-23449
- Aircraft approach and landing under low altitude wind shear conditions, discussing flying hazards and glide path correction procedures 11 p1708 A71-26364
- Sporadic E wind shear theory, discussing time variation in metallic ion content 13 p2055 A71-27923
- Sporadic E layer formation, using wind shear theory and drift data 13 p2059 A71-28257
- Nonadiabatic convection parameters calculation allowing for vertical wind shear, determining effect on thunderstorm maximum possible duration, gusts and precipitation quantity 15 p2444 A71-31361
- Storm clouds tops maximum height and vertical velocity calculation, allowing for entrainment and vertical wind shear 15 p2444 A71-31362
- Vertical wind shear calculation in atmospheric surface layer, studying layer thickness effect 15 p2444 A71-31363
- Vertical wind shears distribution in atmospheric boundary layer, noting features due to differences in synoptic processes 15 p2444 A71-31364
- Stratospheric turbulence induced aircraft buffeting dependence on vertical wind shear, Richardson number and thermal stability change from underlying to overlying layer 15 p2444 A71-31365
- Atmospheric structure near large amplitude Kelvin-Helmholtz billows in upper troposphere, deriving static stability, vertical wind shear and Richardson number 19 p3089 A71-37498
- Midlatitude sporadic E layer formation mechanism, considering wind shear theory 19 p3061 A71-38630
- Numerical model of three dimensional convection in atmosphere with vertical wind shear, solving system of differential equations 21 p3411 A71-41385
- Lower boundary condition effects on quasi-geostrophic baroclinic instability, showing vertical wind shear as function of pressure and wavelength 22 p3569 A71-42544
- Ageostrophic deviations and advection corrections to geostrophic wind velocity and shear stresses above water surface 22 p3570 A71-42849
- Blanketing sporadic E layer diurnal and seasonal variations from equatorial stations ionosonde data obtained during IGY, discussing wind shear mechanism 23 p3667 A71-43134
- WIND TUNNEL APPARATUS**
- NT WIND TUNNEL DRIVES**
- NT WIND TUNNEL NOZZLES**
- Wind tunnel apparatus for reproducing coning and spinning motions of bodies of revolution, using six-component strain gage balance for aerodynamic forces 01 p0002 A71-10930
- Hypersonic low pressure wind tunnel design and operation, describing instrumentation 06 p0880 A71-18045
- Supersonic wind tunnel electromagnetic balance with superconducting coils 07 p1084 A71-20151
- Schlieren visualization for supersonic annular fixed cascade and freon compressor wind tunnels, using vane holding cylinder devices [ONERA-TP-948] 12 p1867 A71-27717
- Gun tunnel free flight testing system and components, discussing model dropping, magnetic suspension and light beam and RF tracing [DFVLR-SONDDR-136] 21 p3362 A71-40382
- Lightweight free oscillating cone shaped model design for intermittent wind tunnel facilities, discussing dynamic stability derivatives measuring techniques 21 p3363 A71-40390
- WIND TUNNEL BALANCES**
- U WEIGHT INDICATORS**
- U WIND TUNNEL APPARATUS**
- WIND TUNNEL CALIBRATION**
- Return circuit rectangular wind tunnel design, construction, instrumentation and calibration, discussing drive, jet inclination, velocity distribution, etc 08 p1272 A71-21305
- Pulsed air gust generator for sinusoidal streamwise perturbation of wind tunnel test stream, describing upstream blowing air jet array, flow calibration and mathematical model [AIAA PAPER 71-281] 08 p1275 A71-22005
- Hot wire signal interpretation using universal calibration law, studying yaw and incidence angles effects 09 p1453 A71-23694
- Wind tunnel test models and force measuring balances design, fabrication, inspection and calibration 15 p2413 A71-31440
- Dual scatter laser Doppler velocimeters for transonic wind tunnel measurements and calibration applied to simulated helicopter downwash, high lift wing and jet crossflow 21 p3364 A71-40399
- Miniature wind tunnel velocity field calibration for testing anemometers, using null method with spherical probe 21 p3384 A71-41380
- Low speed wind tunnel measurements correction for acoustic effects due to fan noise propagation 24 p3790 A71-44763
- WIND TUNNEL DRIVES**
- Return circuit rectangular wind tunnel design, construction, instrumentation and calibration, discussing drive, jet inclination, velocity distribution, etc 08 p1272 A71-21305
- End wall sampling of high pressure shock tube, using abrupt pressure rise to drive test gas flow through duct to sample bottle [WSS/CI PAPER 71-18] 15 p2383 A71-31627
- WIND TUNNEL MODELS**
- Reentry lifting body hypersonic and subsonic flight enhancement by configuration modifications with compound curvatures minimization, giving wind tunnel model data 02 p0319 A71-11974
- Sonic boom problem, investigating pressure signature of large models in supersonic wind tunnels [AIAA PAPER 71-184] 06 p0886 A71-18623
- Space shuttle technology, discussing wind tunnel studies, aerothermal and operational flight mechanics, model characteristics, orbiter configurations and booster-orbiter separation 07 p1209 A71-20227
- Ground boundary layer effects of fixed ground plane for powered STOL wind tunnel model, discussing flow breakdown criteria, contraction lag, strut fairing interference, etc 08 p1232 A71-21992
- [AIAA PAPER 71-266] 08 p1274 A71-21993
- Single and multiple sting support evaluation for unmodified interference free wind tunnel data over 0.85 to 2.2 M range using image method [AIAA PAPER 71-267] 08 p1274 A71-21993
- Wind tunnel testing of base pressure model attached to long cylindrical body extended and supported far upstream 08 p1274 A71-21994
- [AIAA PAPER 71-268] 08 p1274 A71-21995
- Rocket/launcher aerodynamic interference effects investigation by wind tunnel simulation, determining interference coefficients for rockets ballistic dispersion calculations 08 p1274 A71-21995
- [AIAA PAPER 71-269] 08 p1275 A71-22004
- Three degree of freedom gas bearing for wind tunnel dynamic measurements, allowing models simultaneous spin, pitch and yaw motions [AIAA PAPER 71-279] 08 p1275 A71-22004
- Captive trajectory techniques for six degree of freedom external store separation wind tunnel testing, noting capability for missile guidance system simulation [AIAA PAPER 71-282] 08 p1275 A71-22007
- Airfoil profile drag measurements, correlating full scale flight tests and scale model tests in transonic and high Reynolds number wind tunnels [AIAA PAPER 71-289] 08 p1229 A71-22012
- High speed aircraft external store separation testing and prediction techniques, considering flow field survey, dynamically similar drop models and captive trajectory methods [AIAA PAPER 71-294] 08 p1229 A71-22014
- Wind tunnel boundary interference on V/STOL model calculated in test section with solid vertical and slotted horizontal walls, using image method and Fourier transforms [AIAA PAPER 70-575] 08 p1229 A71-22029
- Static aerodynamic data correlation for high subsonic speed transport aircraft model in transonic wind tunnels, including relative buoyancy and turbulence effects [AIAA PAPER 71-291] 09 p1429 A71-23423
- Static wind loading on large radar antenna structures from wind tunnel tests, considering forces and moments reduction by perforated reflectors and shallow curved cover 10 p1591 A71-23757
- Double oblique shock inlet scramjet model development as test bed for instrumentation and hydrogen fuel supersonic combustion experiments 10 p1590 A71-24862
- Plenum chamber with nozzle wind tunnel model, noting jet flow phenomena at various angles of attack 10 p1590 A71-24865
- Wind tunnel evaluation of analytical method for predicting longitudinal stability and aerodynamic characteristics of large flexible aircraft applied to supersonic transport configuration [AIAA PAPER 71-343] 11 p1707 A71-25322
- Pressure orifices inclination in low density flow from experiments with cooled flat plate model in hypersonic low density wind tunnel 11 p1751 A71-25490
- Rocket engine exhaust jet simulation in wind tunnel tests, discussing principles derived from aerodynamic geometrical and physical similarity laws 12 p1945 A71-27466
- Crosshatched ablation patterns on conical bodies, presenting wind tunnel test results on Mach number, local static pressure and temperature ratio effects 12 p1987 A71-27591
- Ballistic wind tunnel for drag measurement on models during free flight at supersonic speeds 13 p2045 A71-29201
- Wind tunnel model trajectory simulation system with closed loop control by digital computer, describing instrumentation, system servoamplifiers and testing procedures 14 p2208 A71-30334
- Miniature pressure transducers for wind tunnel aircraft models buffet phenomena measurements, discussing calibration, frequency and pressure range, sensitivity and accuracy 14 p2245 A71-30335
- Miniature integrated sensor pressure transducers for inlet air flow distortion and buffet studies of wind tunnel models 14 p2245 A71-30336
- Wind tunnel test models and force measuring balances design, fabrication, inspection and calibration 15 p2413 A71-31440
- Externally blown flap powered transport high lift wind tunnel model visual flow field investigation with multiple filament smoke streamlines [AIAA PAPER 71-577] 15 p2345 A71-31567
- Lee side air flow from cone-cylinder model, determining vortex core regions from subsonic wind tunnel smoke visualization techniques 15 p2346 A71-32117
- Wing installed VTOL coaxial drive lift fan model in wind tunnel test, investigating performance in cross-wind environment [AIAA PAPER 71-742] 15 p2469 A71-32284
- Helicopter rotor model testing in water tunnel, discussing advantages over wind tunnel testing due to Reynolds number scaling and avoidance of wall interference effects 16 p2526 A71-34151
- Critical forward speed effects on two dimensional peripheral jet ground effect support systems, comparing theoretical analysis with wind tunnel model data [AIAA PAPER 71-908] 19 p2995 A71-37159
- Augmentor wing high-lift aerodynamics, discussing results of wind tunnel tests and simulation studies [CASI PAPER 72/20] 19 p2993 A71-37606
- Free flight hypersonic wind tunnel model testing in Ludwig tube, discussing launching device and recording setup 21 p3362 A71-40381
- Gun tunnel free flight testing system and components, discussing model dropping, magnetic suspension and light beam and RF tracing [DFVLR-SONDDR-136] 21 p3362 A71-40382
- Lightweight free oscillating cone shaped model design for intermittent wind tunnel facilities, discussing dynamic stability derivatives measuring techniques 21 p3363 A71-40390

- On-line digital dampometer for free oscillation wind tunnel model study under varying Mach number and stagnation pressure avoiding flutter destruction
21 p3363 A71-40391
- Nonlinear flight dynamic simulation using wind tunnel and aircraft model as analog function generator and computer for motion equation processing and command orientation
21 p3363 A71-40392
- Conical ablation surface models in hypersonic wind tunnel tests, describing Mach number and nosetip bluntness effects on cross hatching
21 p3476 A71-40965
- Two dimensional and three dimensional wakes in supersonic and hypersonic rarefied gas wind tunnels, comparing cone and dihedron configurations
23 p3625 A71-43357
- WIND TUNNEL NOZZLES**
- Curvature matching method for two dimensional flexible plate nozzle contour of trisonic wind tunnel, obtaining overdetermined simultaneous equations
01 p0068 A71-10970
- Axisymmetric hypersonic wind tunnel nozzle design by determining inviscid contour and correcting for turbulent boundary layer growth
[AIAA PAPER 69-337] 01 p0003 A71-11578
- Air flow turbulence generating grids at nozzle outlet in wind tunnel for measuring turbulence levels
04 p0577 A71-15618
- Supersonic wind tunnel design, discussing flexible nozzle flow aspects
06 p0880 A71-17700
- Heater and nozzle design of ONERA/S4MA hypersonic wind tunnel for supersonic combustion ramjet tests
[ONERA-TP-924] 18 p2956 A71-36017
- Gas flows with thermodynamic relaxation, considering expanding flows in hypersonic wind tunnel nozzles
19 p3162 A71-37458
- Plasma wind tunnels for high enthalpy flows of low density, considering plasma arc heaters and expansion nozzles with diffusers
19 p3040 A71-37461
- WIND TUNNEL STABILITY TESTS**
- Sounding rockets nonlinear aerodynamic characteristics from full scale and supersonic wind tunnel free flight data, using wobble analysis
[AIAA PAPER 70-1383] 03 p0498 A71-13666
- Airfoil profiles with flaps at medium Reynolds numbers, determining performance characteristics in wind tunnel tests
04 p0526 A71-15025
- Wind tunnel tests for measuring aerodynamic interaction forces between two tandem lifting surfaces
[ONERA-TP-890] 04 p0526 A71-15354
- Low speed wind tunnel stability tests of small guide surface, slotted solid, ring slot, cross and streamer decelerators, considering parachutes and drag measurement
07 p1022 A71-20310
- Wind tunnel dynamic stability testing of unconventional aircraft configurations without sting support
[AIAA PAPER 71-276] 08 p1274 A71-22001
- Aerodynamic support interference in wind tunnel testing of configurations involving bulbous base, mass addition, transition near base and hypersonic low density flows
[AIAA PAPER 71-277] 08 p1228 A71-22002
- Launch and data reduction in supersonic wind tunnel free flight testing of high fineness ratio bodies
[AIAA PAPER 71-278] 08 p1228 A71-22003
- Wind tunnel stability tests of wing with different blowing nozzle arrangements on bottom overpressure surface at 18 and 30 m/sec air speeds
09 p1384 A71-23663
- F-8D aircraft transonic flight and wind tunnel tests for buffet onset prediction, considering effects of g level and fluctuation amplitude and frequency
[AIAA PAPER 70-341] 10 p1557 A71-24863
- Nonlinear aerodynamic stability coefficients from free angular motion of rigid bodies, using three degrees of freedom subsonic wind tunnel tests on Apache model
11 p1837 A71-25515
- Sounding rockets aerodynamic characteristics, comparing wind tunnel and flight test data
12 p1864 A71-27474
- Hypersonic wakes of two dimensional slender wedges and flat plate, testing stability in transition region in wind tunnel
12 p1866 A71-27561
- Yak 40 aircraft flight test program, discussing airworthiness requirements, static structural, vibration and wind tunnel tests
14 p2174 A71-29911
- Frequency response of five component strain gage oscillating balance for dynamic wind tunnel stability testing
14 p2221 A71-30333
- Wind tunnel force test program design for jet aircraft configurations, including propulsion system simulation
14 p2176 A71-30605

- Multimission strategic aircraft installation effects testing in propulsion and aerodynamic wind tunnels, yielding flowfield definition, inlet internal performance, drag, forebody shape and orientation
[AIAA PAPER 71-759] 14 p2171 A71-30792
- Flightworthy 25-foot diameter propotor wind tunnel test, considering civil and military need for VTOL transportation
[AHS PREPRINT 501] 14 p2177 A71-31077
- Forward flight performance of coaxial rigid rotor in NASA wind tunnel, comparing to aerodynamic stability with conventional rotors
[AHS PREPRINT 524] 14 p2178 A71-31090
- Rotor stability derivatives determination from instrumented OH-6A prototype helicopter wind tunnel tests, comparing data with analytical results obtained by digital computing technique
[AHS PREPRINT 543] 14 p2179 A71-31100
- Boeing 347 helicopter program consisting of analysis, vibration simulation, wind tunnel, whirl tower and bench tests
[AHS PREPRINT 571] 14 p2180 A71-31112
- Wing installed VTOL coaxial drive lift fan model in wind tunnel test, investigating performance in crosswind environment
[AIAA PAPER 71-742] 15 p2469 A71-32284
- Two dimensional wind tunnel tests on airfoil fastened between tunnel walls, investigating variable chord concept applicability in sailplane design
15 p2350 A71-32294
- Low speed testing of VTOL models in wind tunnels, describing method for estimating free air approach velocity and angle of attack
15 p2386 A71-32724
- Free flight static and dynamic stability tests on lightweight cone shaped models in longshot tunnel at hypersonic speeds, using spark recording
16 p2519 A71-32879
- Lightweight free oscillating cone shaped model design for intermittent wind tunnel facilities, discussing dynamic stability derivatives measuring techniques
21 p3363 A71-40390
- WIND TUNNEL WALLS**
- Transonic wind tunnel wall interference effects experimental determination, investigating porous and slotted walls
[AIAA PAPER 71-292] 08 p1229 A71-22013
- Wind tunnel boundary interference on V/STOL model calculated in test section with solid vertical and slotted horizontal walls, using image method and Fourier transforms
[AIAA PAPER 70-575] 08 p1229 A71-22029
- Turbulent skin friction and heat transfer prediction on flat plates and wind tunnel walls at supersonic and hypersonic Mach numbers, using Van Driest theory
14 p2334 A71-29868
- WIND TUNNELS**
- NT BLOWDOWN WIND TUNNELS**
- NT CASCADE WIND TUNNELS**
- NT HYPERVELOCITY WIND TUNNELS**
- NT LOW DENSITY WIND TUNNELS**
- NT LOW SPEED WIND TUNNELS**
- NT PLASMA JET WIND TUNNELS**
- NT RECTANGULAR WIND TUNNELS**
- NT SHOCK TUNNELS**
- NT SLOTTED WIND TUNNELS**
- NT SUBSONIC WIND TUNNELS**
- NT SUPERSONIC WIND TUNNELS**
- NT TRANSONIC WIND TUNNELS**
- Cambered and symmetric wing profiles and flap configurations, discussing wind tunnel tests at moderate Reynolds numbers
02 p0185 A71-11950
- Performance characteristics of horizontal and vertical stabilizers at medium Reynolds number from wind tunnel measurements, considering air foil and flap effects
06 p0842 A71-18249
- Transient and turbulent flow structure in wake behind thin plates in wind tunnel, noting velocity fields, temperature and initial boundary layers
07 p1089 A71-19750
- Three degree of freedom gas bearing for wind tunnel dynamic measurements, allowing models simultaneous spin, pitch and yaw motions
[AIAA PAPER 71-279] 08 p1275 A71-22004
- Sonic boom wind tunnel testing techniques at high Mach numbers, giving sample pressure signatures
[AIAA PAPER 71-280] 08 p1229 A71-22006
- Schlieren system conversion to holographic visualization in operational wind tunnels and test facilities
09 p1449 A71-22788
- Cylinder vibration due to wake force in wind tunnel, discussing self exciting force induction
09 p1540 A71-23057
- Flow with time harmonic function velocity in wind tunnel, controlling rate by sonic striction of varying cross section
10 p1552 A71-24454
- Trisonic wind tunnel calibration tests results including second throat effects, Mach number and static

- pressure distributions, flow inclination and aerodynamic characteristics
10 p1590 A71-24819
- High temperature aerodynamics with electromagnetic radiation, considering thermally radiating shock layers, electric arc driven wind tunnels and gas dynamic lasers
12 p1940 A71-27277
- Transonic airfoil testing techniques in two dimensional flow, discussing wind tunnel conditions at various Reynolds numbers
12 p1864 A71-27467
- Supersonic inlet turbojet engine compatibility tests in wind tunnels, using light panels and Summation Device analysis
13 p2114 A71-28032
- Wind tunnel tests of geometrically compatible airfoils for variable chord sailplane
13 p1994 A71-29257
- Heat transfer within resonant cavities at subsonic and supersonic flow, discussing wind tunnels, test procedures and data reduction
[ASME PAPER 71-FE-9] 13 p2166 A71-29450
- Noise production during aerodynamic tests on helicopter rotor in wind tunnel
14 p2176 A71-30519
- Holographic interferometry for flow visualization within aerodynamic wind tunnels with retrodiffuser apparatus
15 p2405 A71-31276
- German monograph on accelerating grids in wind tunnel and axial flow turbine, covering plane/secondary flows past cascades and stator/rotor blading
15 p2347 A71-32303
- German monograph on pressure changes as boundary layer effect in tube wind tunnels covering test equipment and experimental design, Becker theory, pipe flow, etc
17 p2670 A71-34792
- Space flight aerodynamic problems and wind tunnel simulation, considering satellites, maneuverability for landing and synergetic orbit rotation, hypersonic problems of reentry, etc
18 p2846 A71-36408
- Allen and Vincenti blockage corrections for drag coefficients on circular cylinder in wind tunnel
19 p3041 A71-37888
- Turbulent boundary layer response to step change in surface roughness, discussing wind tunnel measurements of pressure and velocity profiles
20 p3212 A71-39505
- Fluctuating aerodynamic force measurement on stationary circular cylinder spanning wind tunnel, using direct method without support interference
21 p3363 A71-40393
- Trailing vortices behind wing tip with vortex dissipator, using wind tunnel flow visualization and flight tests
21 p3319 A71-40496
- WIND VARIATIONS**
- Sporadic E layer formation based on wind shift theory with drift data
05 p0746 A71-17202
- Equatorial region stratospheric and upper tropospheric circulation, examining relationships between time variations of winds at both levels
08 p1327 A71-21455
- Mixing length theory of near ground Ekman boundary layer in stationary and diurnal conditions, determining surface drag and wind rotation
09 p1487 A71-22638
- Diurnal variations of meridional winds by dynamo electric field in troposphere, comparing with Thomson scattering
09 p1490 A71-23646
- Wind resonance in ionosphere under pressure fluctuations, noting turbulent friction factor above 110 km
13 p2060 A71-28533
- Neutral upper atmosphere properties, discussing temperature, density and wind variations during disturbed conditions associated with geomagnetic storms
16 p2565 A71-33727
- Martian surface topography effects on mean wind from time independent and frictionless thermal wind equation solution for radiative-convective atmospheres at scaling analysis level
18 p2964 A71-36287
- Synoptic and microscale variance spectrum of horizontal wind velocity at 50 m above ground, comparing with perturbations models
20 p3257 A71-39439
- Spectral statistics of seasonal tropospheric wave disturbances in tropical Western Pacific, observing synoptic and planetary scale wind field
21 p3374 A71-41177
- WIND VELOCITY**
- CAT wind structure and velocity dynamics, using Doppler radar techniques
01 p0116 A71-10564
- Wind speed field estimations from wind direction, using satellite cloud photographs
01 p0119 A71-10851

Air temperature and wind speed role in finger-freezing time 02 p0197 A71-11669

Wind speed difference quotient conversion to gradients at atmospheric surface layer geometric mean height, considering wind and temperature profiles 03 p0452 A71-13229

Venus atmosphere wind velocity calculation based on radial velocity fluctuations measurements of instrument packages parachuted from Venera 5 and 6 satellites 03 p0486 A71-13288

Simple two fluid solar wind speed and proton temperature model, discussing nonthermal energy dissipation 03 p0481 A71-14504

Stochastic analysis of wind gusts applied to prediction of long term maximum velocities 04 p0621 A71-15168

Unstable atmospheric surface layer wind speed and temperature profiles mathematical representation 05 p0777 A71-16664

Forced convection over infinite periodically over-heated plane on basis of mesometeorological vertical wind velocity 06 p0923 A71-17515

Solar wind velocity relationship with F 2 layer electron density 06 p0950 A71-17991

High latitude E region plasma irregularities based on wind velocity shear fields 07 p1153 A71-19760

Tropical hurricane central pressure drop to maximal wind velocity ratio, discussing thermal to mechanical energy transfer as function of ocean surface temperature 08 p1330 A71-21873

Book on atmospheric boundary layer dynamics considering theoretical models of vertical distribution of wind velocity, temperature and humidity 09 p1488 A71-23175

Venus atmosphere wind velocity calculation based on radial velocity fluctuations measurements of instrument packages parachuted from Venera 5 and 6 satellites 09 p1525 A71-23261

Electric field, neutral wind velocities and ion collision frequency from artificial ionic clouds motion and deformation in ionospheric E and F regions 10 p1602 A71-24549

Wind speed and potential temperature vertical profile in day/night planetary atmospheres estimated by similarity theory of boundary layer parameters 11 p1826 A71-25719

Atmospheric boundary layer refractive index fluctuations structural characteristics determined from summer vertical wind velocity and temperature profiles 11 p1795 A71-25922

Unsteady solution of simplified atmospheric dynamics equations, reducing to system of Volterra integral equations of second kind for complex horizontal wind velocity 12 p1924 A71-26734

Propagation of 26-month oscillations in meridional component of wind velocity in stratosphere at extra-equatorial latitudes from hydrothermodynamic equations solution 13 p2057 A71-28021

Venus rotation observations during 1964 eastern spring elongation, noting weather period and wind velocities 13 p2136 A71-28386

Time variable effect on synthetic wind speed and air temperature profiles based on sensible heat flux density and stress at surface layer 14 p2266 A71-29705

Seasonal variations in semidiurnal tidal wind velocities in upper atmosphere for Northern Hemisphere radio meteor observations 14 p2231 A71-29720

Anemometer measurement optimum averaging time of wind speed for conventional aircraft landings 14 p2270 A71-30394

Single anemometer wind measurement required for aircraft landing, comparing data from different sampling periods 14 p2270 A71-30395

Venusian atmosphere circulation modeling, calculating temperature differences, thermal inertia and wind velocity 15 p2496 A71-32729

Tidal theory comparison with lower thermospheric wind observations, taking into consideration dissipation and excitation effects 16 p2565 A71-33736

Atmospheric stability at 30-90 km based on wind and temperature data from grenade experiments 16 p2568 A71-33788

Thermospheric convective instability as interpretation of north polar cap high speed winds observed by satellite at 200 km altitude during magnetic storm of May 1967 16 p2572 A71-33847

Northern Hemisphere atmospheric vertical velocity computation for all seasons compatible with climatological heating functions, using time averaged thermodynamic energy equation 17 p2770 A71-34803

Combustion systems ionic wind velocities, investigating gauze parameters, magnetic fields and mixture inhomogeneity effects 17 p2785 A71-35703

CAT physical model and formation mechanism, using turbulent zone characteristics and wind velocity spectra 19 p3049 A71-37448

Wind velocity vertical component determination through meteor trail drift observation, presenting mean diurnal measurements data 19 p3059 A71-38393

Atmospheric boundary layer refractive index fluctuations structural characteristics determined from summer vertical wind velocity and temperature profiles 20 p3256 A71-39213

Synoptic and microscale variance spectrum of horizontal wind velocity at 50 m above ground, comparing with perturbations models 20 p3257 A71-39439

Mesoscale perturbations in wind velocity field in jet streams, interpreting data in terms of hydrodynamic stability theory 21 p3412 A71-41392

Ocean surface condition correlation to radar backscattering cross sections and wind velocity from scatterometer data 22 p3569 A71-42545

Wind velocities and directions, air temperature and visibility range in atmospheric boundary layer under fog conditions 22 p3569 A71-42846

Ageostrophic deviations and advection corrections to geostrophic wind velocity and shear stresses above water surface 22 p3570 A71-42849

Venusian atmosphere circulation modeling, calculating temperature differences, thermal inertia and wind velocity 23 p3735 A71-43298

Atmospheric wind velocity time variations at 80-100 km altitudes from ionospheric drift data, finding planetary oscillation periodicities relationship to solar activity cycle 24 p3822 A71-44349

WIND VELOCITY MEASUREMENT

Maximum wind speed estimation in tornadoes and waterspouts, using cloud deck height and funnel cloud photographs 03 p0453 A71-14203

LF boundary of inertial range in lowest atmospheric layer, comparing turbulence scale and wind velocity components 04 p0622 A71-15632

Wind speed measurement by cup and sonic anemometers, considering errors due to tower structure effect 05 p0752 A71-16663

Rawinsonde reported extreme wind speed in arctic stratosphere at SST altitudes 05 p0777 A71-16700

Stratospheric wind field determination at extreme vertical velocity, noting basic field asymmetry 06 p0923 A71-17512

Neutral wind and ion velocity determination under quiet and disturbed geomagnetic conditions in auroral zone, noting electric field measurements 09 p1440 A71-23600

Wind velocity data processing technique for azimuthal radar observations in meteor zone, using least squares method 10 p1600 A71-24035

Mean wind velocity and turbulence remote measurement with laser anemometry, using intensity modulation technique 10 p1623 A71-25091

Atmospheric wind velocity radial components measurements for meteor drift as function of wind direction, using transmitter and receiver antennas synchronized orientation method 11 p1758 A71-25791

Ultrasonic rotameter for turbulent wind velocity circulation measurement, using cylindrical electroacoustic capacitor converter with solid dielectric for radiators and receivers 15 p2444 A71-31447

Sea surface slope distribution and wind velocity determination by sun glitter photography from synchronous satellite 17 p2734 A71-35215

Fast response anemometer for measuring atmospheric wind speeds and turbulence components 17 p2745 A71-35327

Antenna azimuthal radiation patterns and meteor radiant distribution effects on wind velocity measurement by radar observation of meteor trains 19 p3145 A71-38372

Ionospheric wind velocity, direction and diffusion coefficient measurements using artificial aluminum oxide luminescent clouds 19 p3091 A71-38629

Laser system for atmospheric wind velocity and turbulence, using Doppler frequency shift undergone by radiation beam scattered by particles suspended in flows 21 p3319 A71-40490

Correlation functions characteristics of wind velocity field in troposphere and stratosphere up to 25 km based on bihourly radiosonde data 21 p3412 A71-41390

Atmospheric wind velocity radial components measurements for meteor drift as function of wind direction, using transmitter and receiver antennas synchronized orientation method 22 p3533 A71-41559

Optical phase variations, temperature structure and wind velocity measurements in atmosphere using He-Ne laser beam on 70 m propagation path 22 p3509 A71-41787

Lower atmosphere wind and cloud velocity measurements by combined stereophotogrammetry and balloon visual observation 22 p3542 A71-41862

Ion anemometer for measuring wind velocity magnitude and direction in rarefied Martian atmosphere 22 p3600 A71-41960

Atmospheric wind speed estimation, using ATS geostationary satellite cloud photographs 22 p3535 A71-42411

Detailed wind velocities and temperature profile measurements by FPS-14 radar/lidsphere technique for space vehicle and SST applications 22 p3569 A71-42543

WINDING

NT FILAMENT WINDING

NT HELICAL WINDINGS

NT WIRE WINDING

Elasticity and strength anisotropy changes of unidirectional fiberglass reinforced plastics during winding 05 p0759 A71-16372

Automatic regulators of wire tension during coil winding 07 p1108 A71-19310

Odesa observatory automatic film winding photoelectric system, discussing construction and accuracy 23 p3680 A71-44266

WINDMILLING

U AUTOROTATION

WINDOWS

Spacecraft windows optical degradation from contamination with condensed particles, presenting light scatter measurement results [AIAA PAPER 71-472] 11 p1833 A71-26252

WINDOWS [APERTURES]

Carbon dioxide laser with Ge Brewster windows equipped sealed gas discharge tube, comparing with NaCl and KBr windows 06 p0908 A71-18080

Carbon dioxide laser Ge windows thermal runaway characteristics 08 p1302 A71-21391

Plate and acoustic finite elements simulation of window-room system coupled transient response to sonic booms, discussing equations of motion and cavity depth effect 12 p1981 A71-27481

Visual detection of stars in spacecraft environment, considering window cleanliness and antireflection coating effect on light scattering 18 p2864 A71-36278

Flat modulation transfer functions obtained by spatial filtering of high aspect ratio annular apertures images in coherent optical processor 22 p3549 A71-42552

WINDOWS [INTERVALS]

NT LAUNCH WINDOWS

WINDOWS ALOFT

NT GEOSTROPHIC WIND

NT JET STREAMS [METEOROLOGY]

Lidar observations of visually clear troposphere compared with simultaneous rawinsonde data for relationship between lidar echoes and atmospheric winds aloft 05 p0721 A71-16670

Thermospheric wind induction by auroral electrojet heating, considering effects of Joule dissipation of magnetospheric electric fields 20 p3215 A71-38744

WINDSCREENS

U WINDSHIELDS

WINDSHIELDS

Vision loss from windshield tinting in night visual flying accident 08 p1247 A71-20824

Wind noise reduction by windshields, considering effect of mean flow velocity, turbulence, flow direction, windshield shape and size, covering material and microphone location 13 p2040 A71-29283

Polycarbonates transparency applications in aircraft windshield design, discussing heat resistance, mechanical, chemical and optical properties
20 p3253 A71-38751

WINDWARD

U WIND (METEOROLOGY)

WING FLAPS

NT LEADING EDGE SLATS

NT TRAILING-EDGE FLAPS

Upwash interference on two dimensional jet flap wing in slotted wall tunnel, using small disturbance theory
02 p0187 A71-12690

Two dimensional flow around wing sections with slats and slotted flaps in various positions, presenting surface pressure and boundary layer measurements [AIAA PAPER 71-96]
06 p0844 A71-18551

Airplane wing high lift and flap designs by interactive computer graphics system [AIAA PAPER 71-227]
07 p1019 A71-19705

Power augmented lift STOL aircraft operating costs reduction by channel wing concept, discussing aerodynamic theory and structural applications to high lift flaps aircraft
09 p1385 A71-22592

Automatic gust alleviation system employing inertial sensors and feedback devices with wing flaps and elevators, considering linkage control, noninteracting control and split control
11 p1706 A71-25195

Lifting force of wing with rotating flap, deriving lift increase due to circulation redistribution at surface
12 p1865 A71-27491

Noise measurement data on various types of blown flap configurations for STOL aircraft, discussing integration effects between jet and flap assembly [AIAA PAPER 71-745]
14 p2171 A71-30785

WING FLOW METHOD TESTS

Laminar-turbulent boundary layer transition point on wing, using hot-wire anemometer and oscilloscope
02 p0186 A71-12555

Two dimensional flow around wing sections with slats and slotted flaps in various positions, presenting surface pressure and boundary layer measurements [AIAA PAPER 71-96]
06 p0844 A71-18551

Wind tunnel stability tests of wing with different blowing nozzle arrangements on bottom overpressure surface at 18 and 30 m/sec air speeds
09 p1384 A71-23663

WING LOADING

Civil aircraft aspect ratio relationship to commercial viability, considering need for minimum induced drag at wing loading to improve payloads, speeds and ranges
01 p0905 A71-11628

Integral relation between boundary conditions and aerodynamic loads on straight and inverted wings, using reversibility theory for arbitrary time dependences
03 p0345 A71-14566

Wing representation by lifting line lattice as computation method for complex configurations unsteady aerodynamic forces, presenting numerical program for wings in two parallel planes [ONERA-TP-891]
04 p0526 A71-15356

Sailwing aerodynamic characteristics, obtaining aerodynamic loading by two dimensional flexible airfoil and Prandtl lifting line theories
07 p1017 A71-20303

Thin rectangular wing load distribution in nonstationary incompressible flow, using downwash integral equation Fourier transform
09 p1383 A71-22946

Aircraft wings automated preliminary structural design and weight determination procedures based on external shape, aerodynamic loads and fuel mass interaction
09 p1541 A71-23274

Wing structure fatigue substantiation procedures under fail-safe concept for general aviation aircraft [SAE PAPER 710404]
10 p1555 A71-24264

Aircraft wing fatigue test procedures for gust, maneuver, ground-air-ground, taxi and landing impact loads [SAE PAPER 710403]
10 p1694 A71-25133

Loads induced on infinite aspect ratio wing by straight infinite free vortex in subsonic compressible freestream, using planar lifting surface theory
11 p1702 A71-25474

Wing-jet interference effects in cross wind on thrust and aerodynamic characteristics at large distance from and near ground
13 p1993 A71-29207

Gust transfer functions relating lift and moments to upwash in single sinusoidal wave for large aspect ratio rectangular wings in turbulent incompressible flow
14 p2176 A71-30604

Helicopter rotor blade airload by applying lifting surface solution [AHS PREPRINT 510]
14 p2171 A71-31081

Size effects on large rotor systems design, considering weight, blade loading, tip speed, etc [AHS PREPRINT 552]
14 p2180 A71-31104

Aerodynamic free vortex loading on two dimensional wing at zero incidence at low speeds in incompressible flow
16 p2521 A71-33420

Self induction function and stability for vortex with finite core at aircraft wing, confirming Crow theory
21 p3320 A71-40502

Aerodynamic aspect ratio effects on drag and aircraft performance, noting span loading as major force on wing lifting function
21 p3325 A71-41246

Convergence proof for chordwise vorticity equation for discrete panel wing loading
22 p3481 A71-42840

WING OSCILLATIONS

Critical flutter of wing with rigid aileron studied by analog computer modeling
01 p0169 A71-10606

Three dimensional wings harmonic oscillation with arbitrary frequency in subsonic flow, presenting approximation method for singular integral equation
01 p0173 A71-10844

Aerodynamic forces on control surfaces in subsonic range, investigating pressure distribution on harmonically oscillating wing
03 p0344 A71-14347

Unsteady motion of finite span wing in ideal incompressible liquid near solid surface by integral operator method in potential acceleration space
06 p0846 A71-18701

Solid foil small oscillations in unsteady incompressible flow, mapping physical plane and corresponding complex potential region onto curvilinear half strip
07 p1092 A71-20088

Oscillating airfoil wake interaction with fixed cascade, considering two dimensional incompressible inviscid small perturbation flow theory
09 p1511 A71-22943

Aerodynamic forces on harmonically oscillating wing in subsonic flow of ideal gas
09 p1384 A71-23615

Wing aperiodic motion during change from one frequency to another, using Laplace and Fourier transforms to reduce partial to ordinary differential equation
10 p1688 A71-24353

Instantaneous aerodynamic force measurements and flow visualization on flapping wing, showing increase of thrust force mean value over maximum steady state value
10 p1550 A71-24362

Comparative vertical turbulence and loss restrictive stochastic models for threshold crossing rotor blade flapping vibrations at low lift high advance ratio [AIAA PAPER 71-389]
11 p1846 A71-25351

Small surface curvature effect on unsteady hypersonic flow over thin oscillating wedge, using perturbation theory
11 p1705 A71-26197

Oscillating thin wing with control surfaces in two dimensional compressible subsonic flow, calculating aerodynamic forces based on kernel function method [DFVLR-SONDDR-132]
16 p2519 A71-33013

Active feedback wing/store flutter control for fighter aircraft, using computer programs based on frequency and time domains for linear analysis
23 p3630 A71-44109

WING PANELS

Ball forming technique application to Al alloys structural part contouring, discussing L-1011 wing panel forming and prestress tooling
08 p1299 A71-21681

Structural and inertial nonlinearities influence on flat or curved panel flutter
14 p2331 A71-30825

Wing structural elements ballistic damage tolerance and residual fracture strength characteristics, discussing projectile velocity, impact angle and target thickness effects
17 p2827 A71-35161

Boron-epoxy composite wing box beam design, describing preliminary weight estimation from layouts [SAWE PAPER 891]
17 p2834 A71-35815

Convergence proof for chordwise vorticity equation for discrete panel wing loading
22 p3481 A71-42840

WING PLANFORMS

NT DELTA WINGS

NT INFINITE SPAN WINGS

NT SWEPTBACK WINGS

NT VARIABLE SWEEP WINGS

Sectional drag relationships in linearized wing theory, examining lifting and thickness problems for various planforms
03 p0344 A71-14240

Thin plane wings with mixed leading edges, applying linearized supersonic flow theory
03 p0344 A71-14241

Integral relation between boundary conditions and aerodynamic loads on straight and inverted wings, using reversibility theory for arbitrary time dependences
03 p0345 A71-14566

Unsteady coefficient measurements to corroborate theory for coefficient distribution about little elongated two dimensional wings with control surfaces
05 p0694 A71-16737

Incompressible boundary layers with specific velocity distribution, studying stability on straight and yawing wings
05 p0736 A71-16849

Three dimensional boundary layer with Pohlhausen velocity distribution, examining stability on yawing wing
05 p0736 A71-16850

High lift nose slats generation for arbitrary airfoil, using conformal transformations and computer program [AIAA PAPER 71-11]
06 p0842 A71-18485

Hypersonic minimum drag slender wing leading edge shape for given airfoil section, using Newtonian theory
08 p1229 A71-20309

Aerodynamic characteristics of arbitrary planform wing moving near screen, ground or water surface, using vortex model
16 p2521 A71-33596

Canard space shuttle reusable launch vehicle wing geometry variations effect on flyback systems weight, noting influence of aspect ratio and wing area
18 p2974 A71-36484

Vortex-induced heating alleviation to lee side of slender wings in hypersonic flow by contouring leading edge planform
19 p2993 A71-37892

Three dimensional nonlinear subsonic flow over finite wings of arbitrary planform, solving transonic small disturbance equation by integral method
20 p3177 A71-39568

Turbulent skin friction drag for tapered wings as function of root chord Reynolds number
22 p3481 A71-42839

WING PROFILES

NT WING SPAN

Cambered and symmetric wing profiles and flap configurations, discussing wind tunnel tests at moderate Reynolds numbers
02 p0185 A71-11950

Transonic wing profiles analog determination by hodograph method
05 p0694 A71-16735

Constant curvature wing contours in transonic flow, determining stream function by approximation
06 p0842 A71-18227

Two dimensional flow around wing sections with slats and slotted flaps in various positions, presenting surface pressure and boundary layer measurements [AIAA PAPER 71-96]
06 p0844 A71-18551

Pressure distribution on arbitrary finite symmetrical wings with rounded leading edges at zero incidence in subsonic flow
09 p1383 A71-22945

Solid profile wing motion near solid wall or free surface, using acceleration potential method
12 p1863 A71-27174

Unsteady flow measurement around wing sections during rapid angle of attack variations, emphasizing helicopter rotor blades
12 p1864 A71-27468

Wing thickness optimal distribution for minimum wave drag in supersonic flow at zero angle of attack for given planform, using Ritz method at lower Mach numbers
13 p1994 A71-29222

Heat conduction role in leading edge heating of wing in hypersonic flight, using conducting plate theory
13 p2165 A71-29282

Wing models development by tangent milling on jig-borer, approximating cross section by hand finish smoothened polygon
15 p2413 A71-31439

Laminar boundary layer on wing profiles and bodies of revolution, calculating flow characteristics based on integral momentum relation
17 p2670 A71-34424

Supersonic flow past V-shaped wings with leading edges, applying method of establishment to space variable for pressure distribution
17 p2673 A71-35647

V shaped conical wing in supersonic and hypersonic flow with shock attached to leading edge, investigating complex wave system with time dependent and analytical methods
18 p2845 A71-36339

Two dimensional jet flapped symmetric wing in subsonic flow, assuming irrotational flow inside jet bounded by vortex sheets
21 p3318 A71-40172

Shock wave diffraction at symmetric lenticular wing profile with free stream critical Mach number of 0.87, using Godunov difference scheme
21 p3322 A71-40679

Wing group weight prediction for subsonic aircraft design, taking into account root bending moments due to lift
18 p2976 A71-35925

WING SLATS

U LEADING EDGE SLATS
WING SLOTS

Two dimensional flow around wing sections with slats and slotted flaps in various positions, presenting surface pressure and boundary layer measurements [AIAA PAPER 71-96] 06 p0844 A71-18551

Wind tunnel stability tests of wing with different blowing nozzle arrangements on bottom overpressure surface at 18 and 30 m/sec air speeds 09 p1384 A71-23663

WING SPAN

Spanwise distribution of induced drag in subsonic flow by vortex lattice method, noting applicability to rotary derivatives in stability analysis 02 p0187 A71-12691

Incompressible fluid motion in laminar boundary layer on blade rotating uniformly about axis perpendicular to wing span 14 p2170 A71-30218

Constrained torsion of spar box fastened along isolated parts of wing span, noting structural failure due to tangential stress distribution 17 p2830 A71-35313

Hybrid V/STOL jet lift aircraft design, examining wing area-lift engine bypass ratios relation [AIAA PAPER 71-767] 18 p2850 A71-36273

Critique of paper on spanwise distribution of induced drag in subsonic flow by vortex lattice method, noting infinities in downwash across all vortex lines 19 p2991 A71-37297

Spanwise lift distribution over wings and wake formation in thin airfoils of finite aspect ratio in linear subsonic potential flow 21 p3319 A71-40495

Minimum drag and lifting line characteristics of large aspect ratio wing in uniform shear flow with velocity variations along span 23 p3625 A71-43312

WING STALL

U BOUNDARY LAYER SEPARATION
WING TANKS

Transverse and torsional vibrations of fuselage-wing combination with wing tip fuel tanks, calculating mass and stiffness matrix for elastic beam 07 p1022 A71-20364

WING TIPS

Pressure distribution singularity at tip of thin lifting parabolic wing in subsonic flow [AIAA PAPER 71-10] 06 p0842 A71-18484

Heating effects on wing tip vorticity diffusion rate in gas vortex, causing outward radial convection and increased kinematic viscosity [AIAA PAPER 71-616] 15 p2512 A71-31556

Wing tip vortex control device, discussing design, operation and effectiveness 20 p3175 A71-39084

Straight or moderately sweptback wings tip shape effect on vortex sheet roll, using detachment laws 20 p3176 A71-39418

Aircraft wing tip vortex air motion measurements, utilizing Doppler radar techniques 21 p3318 A71-40489

Drooped wing tip effects on trailing vortex sheet structure and position from spanwise load distribution determination by vortex lattice theory 21 p3319 A71-40493

Trailing vortices behind wing tip with vortex dissipator, using wind tunnel flow visualization and flight tests 21 p3319 A71-40496

WING-FUSELAGE STORES

Interference loading linear prediction on aircraft stores at supersonic speeds, considering flow field due to jet fighter bomber 19 p2996 A71-37290

WINGED ROCKET BOOSTERS

U LAUNCH VEHICLES
U WINGED VEHICLES

WINGED VEHICLES

Winged lifting body quasi-optimal reentry trajectory for minimum flight time, taking into account angle of attack control and angular motion inertia 08 p1367 A71-22038

Time optimal control for distributed systems with random properties, considering integral relations and flying wing vehicle torsional vibration problems 19 p2994 A71-37094

WINGS

NT CAMBERED WINGS

NT CARET WINGS

NT CRUCIFORM WINGS

NT DELTA WINGS

NT FIXED WINGS

NT FLEXIBLE WINGS

NT INFINITE SPAN WINGS

NT LIFTING ROTORS

NT LOW ASPECT RATIO WINGS

NT PARAWINGS

NT RECTANGULAR WINGS

NT RIGID ROTORS

NT RIGID WINGS

NT RING WINGS

NT ROTARY WINGS

NT SLENDER WINGS

NT SWEEP WINGS

NT SWEEPBACK WINGS

NT THIN WINGS

NT TILTING ROTORS

NT TIP DRIVEN ROTORS

NT TWISTED WINGS

NT UNSWEEP WINGS

NT VARIABLE SWEEP WINGS

Circular cone with cross shaped wings in supersonic flow, determining flow characteristics, velocities and pressure 02 p0185 A71-11958

Two dimensional axisymmetric laminar boundary layer on blown wing and body of revolution, using sixth-order polynomial for velocity distribution 02 p0186 A71-12554

Wing computation in steady or unsteady supersonic flow, using network, inverse discrete and numerical inversion methods [ONERA-TP-896] 03 p0339 A71-13129

Vortex sheet behavior in inviscid subsonic flow of lifting wing with nonzero trailing edge angle 03 p0342 A71-13738

Linear airfoil theory applicability for wings aerodynamic characteristics, considering high lift, ground effect, angle of attack and aspect ratio 04 p0525 A71-14593

Wing upper surface air suction influence on aircraft longitudinal controllability, considering control stick forces for deflected flaps and angle of attack 04 p0528 A71-14594

Finite supercavitating wings numerical calculation using acceleration potential method 04 p0526 A71-15210

Wings with control surfaces in unsteady subsonic flow, applying lifting surface theory [ONERA-TP-889] 04 p0526 A71-15355

Trailing vortex generation behind jet flapped wing at high wing lift coefficients 04 p0527 A71-15413

Aerodynamics of wing immersed in propeller slipstreams, presenting calculation method for lift, drag, pitching moment, normal force distribution and wake characteristics [DGLR-70-057] 05 p0693 A71-15947

Jet interference effects on rectangular and swept wings, presenting wind tunnel test data for range of jet locations, inclinations and velocity ratios [DGLR-70-052] 05 p0693 A71-15951

Lightning induced voltages in aircraft wing structures, examining induced voltage across load impedances in electric circuits 06 p0874 A71-17581

Three dimensional inviscid supersonic flow fields with primary and embedded shock and expansion waves determined over and behind wings and wing-body configurations [AIAA PAPER 71-99] 06 p0844 A71-18554

Filament winding manufacturing methods using unidirectional glass reinforcements for design and fabrication of aircraft wing structure [SME PAPER EM-70-406] 07 p1120 A71-20546

High lift wing characteristics with/without additional devices, emphasizing lift control and load distribution 12 p1864 A71-27476

Interference analysis of wing with overlapping multirotors in uniform velocity stream confined in elliptical cross section cylinder [AIAA PAPER 71-614] 15 p2346 A71-31583

Probabilistic approach to prolonged lifetime design and static strength of structures of monocoque and multispar wings, using fatigue characteristics of individual elements 16 p2657 A71-33604

Fatigue crack initiation and growth and residual strength of F-100 wing, comparing service failure data with full scale fatigue test results 17 p2827 A71-35159

Two dimensional flow over two dimensional finite wing without correction for downwash, assuming known pressure distribution 21 p3318 A71-40173

WINTER

Wintertime Arctic F region critical frequency secondary maxima, discussing UT control hypothesis 03 p0408 A71-13386

Auroral oval continuity during winter/1969-1970/ from jet aircraft ionospheric instrumentation, showing band distribution along geomagnetic pole 03 p0419 A71-14526

Ionospheric absorption winter anomaly observation based on Loran-A pulse signals during IQSY, noting diurnal variation 06 p0889 A71-17685

Anomalous winter ionospheric radio wave absorption related to amplitude increases of microbarometric oscillations at ground level 10 p1606 A71-24919

Winter day absorption variability of HF radio waves reflected at oblique incidence from ionosphere, using ray tracing method 13 p2027 A71-27799

Ionospheric absorption winter anomaly including temporal and local variations and frequency depen-

dence, examining possible correlations with stratospheric and mesospheric phenomena 14 p2237 A71-30943

Midlatitude D region electron density winter variability causes consideration based on enhancements, absorption and ionization changes data during stratospheric warming 14 p2237 A71-30944

D region winter anomaly causes from coordinated rocket measurements, discussing electron density profiles and electron-ion recombination 17 p2731 A71-34315

GBR wavefield above winter nighttime ionosphere, noting latitudinal profile due to D region spatial variations and signal fading with F region structure 20 p3197 A71-39744

Correlation coefficient between winds at 850-30 mb pressure levels over Italy in winter, proposing theoretical model 21 p3411 A71-40825

Day to day fluctuations of winter anomaly in ionospheric absorption, showing regular and irregular trends 23 p3666 A71-42974

WIRE

NT ELECTRIC WIRE

NT EXPLODING WIRES

NT GUY WIRES

Thin wires mechanical properties compared for epoxy resin reinforcement applications, considering ductility, temperature and aging effects, cost, etc 01 p0108 A71-10694

Tungsten wire reinforced brass composites, studying multiple necking phenomena during tensile tests 04 p0615 A71-15794

Mo wire annealing with degassing, investigating temperature effect on mechanical properties 04 p0616 A71-15802

Steel wire reinforced Al manufacture and properties, discussing wire-matrix bonding 05 p0764 A71-15922

Automatic regulators of wire tension during coil winding 07 p1108 A71-19310

Plated wire storage element for military and aerospace scratch pad, main and mass memories of various speeds [IEEE PAPER 7.6] 07 p1077 A71-19608

Mo-Re alloy wire structure and properties, observing heat treatment effect with metallographic techniques and X ray analysis 07 p1141 A71-20242

Stainless steel wire fibers in refractory castables, noting flexural and compressive strength improvements 13 p2093 A71-28663

Vibration effect on heat transfer by natural convection from oscillating horizontal wire in air 13 p2164 A71-28984

Wire connection damage due to high vibration, examining termination and joining techniques 18 p2852 A71-36837

Water aerosol flux interaction and drop capture with particles of solid reagent, considering agaroid films and precipitation on thin wires 19 p3094 A71-38699

High purity Ni wire hardening by lunacae agglomeration during tempering, using comparative tension curves 22 p3562 A71-42245

Residual resistance measurements for studying recovery of high purity potassium wires deformed at/below 4.2 K, discussing anomalous difference with sodium 24 p3861 A71-45195

WIRE BRIDGE CIRCUITS

NT WHEATSTONE BRIDGES

Thermal conductance measurement in electroexplosive device by self balancing wire bridge, considering quality control or design applications 09 p1493 A71-22732

WIRE CLOTH

Ideal reflector simulation of periodically supported infinite plane metallic wire gratings with rectangular mesh showing small sag 09 p1409 A71-23503

WIRE MESH

U WIRE CLOTH

WIRE WINDING

Symmetrical hysteretic micromotors stator structure with windings around unilateral crowned teeth, calculating maximum EM power in starting mode 13 p1999 A71-28631

WIRELESS COMMUNICATIONS

AM crosstalk in unified carrier telemetry system, studying implications for carrier false lock and tracking 22 p3514 A71-42390

WIRING

Single thermocouple temperature measurement, discussing millivoltmeters wiring method with resistance matching to ensure accuracy 03 p0430 A71-14329

- Europa 1 multistage booster rocket interstage electric circuit connection, discussing specifications and compatibility tests 05 p0697 A71-15955 [DGRL-70-059]
- Retinal electronic model with about 700 photoreceptors and output cells and new interconnections technique 05 p0715 A71-17079
- Automated design system producing wire format data for cabling avionics subsystem of light attack aircraft [AIAA PAPER 69-976] 06 p0874 A71-17698
- Computerized automatic control of aircraft electrical system using remote power controllers and multiplexed data bus for wiring reduction and reliability improvement 17 p2677 A71-34700
- High voltage DC electric power transmission systems with ground return, reducing aircraft wiring weight and energy dissipation 17 p2678 A71-35771
- Remote power controller as static circuit protection device for aircraft and spacecraft automatically controlled electrical wiring system, discussing performance improvement 17 p2678 A71-35782

WIRING SYSTEMS

- U WIRING
- WKB APPROXIMATION
- U WENTZEL-KRAMER-BRILLOUIN METHOD
- WOMEN
- U FEMALES
- WOOD AIRCRAFT CONSTRUCTION
- U AIRCRAFT STRUCTURES
- U WOODEN STRUCTURES
- WOODEN STRUCTURES
- Nonmetallic aircraft construction materials, discussing wood epoxy and polyester resins 02 p0273 A71-12299
- WORDS [LANGUAGE]
- NT SYLLABLES
- Biological memory and perception processes electronic simulation by keyboard structure reenacting word reception, storage and delivery 07 p1051 A71-20118
- Unique word detection in digital burst communication, determining effects on voice quality from analytic study and digital simulation 08 p1255 A71-21595
- In-flight target reporting, analyzing quantitative meaning of ambiguous general modifier terminology as used by pilots in verbal sighting reports 12 p1875 A71-27251
- Communication satellites unique word coding with algorithm, reducing false detection probability by error correlation technique 14 p2201 A71-30926

WORK

- NT PHYSICAL WORK
- Human spinal reflex effects during static work, suggesting cord segmental chiasmatic connections interaction with spinobulbar-spinal tract 08 p1249 A71-21973
- Plastic deformation work derivation, taking into account deviation from similarity of stress deviators 15 p2501 A71-31150
- First law of thermodynamics implications to general theory of work and energy for material systems 18 p2986 A71-36811

WORK CAPACITY

- Human survivability and work capacity in aerospace environments, discussing sudden unprotected exposure to vacuum 01 p0022 A71-10512
- Human work level adjustment to specific energy expenditures during hard work on servocontrolled treadmill 02 p0202 A71-11665
- Oxygen debt after steady state work in submaximal physical exercise 02 p0202 A71-11668
- Mathematical model for optimizing observational data sampling and working time losses by scientific research personnel 02 p0336 A71-11859
- Respiratory features for conscious or unconscious warning of impending exhaustion, noting work load-performance decrement relation 04 p0545 A71-15159
- Physical fitness in prolonged muscular work tolerance evaluation by oxygen consumption for 170 beat/min heart rate, considering age, sex and occupation 05 p0708 A71-16614
- Human work capacity in hot environment irrelevance to normal conditions, considering physiological reactions to exercise in heat by heart rate criterion 05 p0709 A71-16621
- Human physical exercise with stepwise increasing load noting working capacity, cardiovascular and respiratory system performance and blood composition interrelations 05 p0709 A71-16805

Human valvular heart disease, examining work load effects on oxygen demand 06 p0849 A71-17294

Human work capacity measurements by graded step test and bicycle ergometer, considering heart rate and oxygen uptake 07 p1046 A71-19457

Human work load assessments by time study of officers and physiologists, noting disagreeing values 07 p1047 A71-19466

Redundancy effects on human memorization working capacity, noting application to memory systems design 07 p1043 A71-20113

Psychological aspects influencing aircrewman capacity to perform useful work, detailing selection, training, operational environment and global factors 08 p1245 A71-20724

Oxygen deficiency and body temperature effects on work capacity of human subjects in hot humid environment 09 p1399 A71-22922

Furosemide effect on physical work capacity, studying recovery pulse response, oxygen extraction during exercise and altitude acclimatized subjects oxygen uptake 09 p1394 A71-23237

High altitude submaximal and maximal work by humans, noting time required for steady state oxygen consumption, ventilation and heart rate 09 p1401 A71-23368

On-line computer technique for pulmonary ventilation continuous/automatic measurement of cardiac patients exercise and work tolerances 11 p1734 A71-25255

Cardiovascular responses to submaximum and maximum effort cycling and running on bicycle ergometer and motor driven treadmill, using carbon dioxide rebreathing method 12 p1873 A71-27128

Engineering management, discussing technical men work effort, time/intellectual changes, performance measurements, motivational factors and relationship to company 13 p2167 A71-28799

High altitude aerobic working capacity limitations, examining oxygen transport system and circulator factors 14 p2183 A71-30276

Human muscle blood flow measurement by Xe 133 clearance method during rhythmic exercise, noting work load effects 15 p2358 A71-31455

Skylab habitability facilities for astronaut work effectiveness and physical well being 15 p2363 A71-31456

Work load and maximum physical exercise duration relationship for forearm reciprocating flexion and extension, cranking of both arms and bicycle pedalling 17 p2688 A71-34359

Subjective fatigue feeling correlation to symptoms based on bank clerks and broadcasting workers work load assessment ratings 17 p2688 A71-34367

Maximal sweat evaporative heat loss and permitted work load measurements as function of temperature and clothing insulation 18 p2872 A71-36861

Pilot workload reduction in steep approach landing of light aircraft from flight test data analysis [AIAA PAPER 71-904] 19 p3095 A71-37155

Mental work capacity investigation methodology, including Kekcheev, Kosilov, Zinchenko, Pratushevich and Kraepelin tests 19 p3006 A71-37446

Astronaut work capacity and adaptation during long term flight of space vehicle Soyuz 9 21 p3342 A71-40259

Computerized simulation of maintenance man hour loading for communication system based on repair, failure and availability distributions 22 p3554 A71-42113

WORK DECREMENT

U WORK CAPACITY

WORK FUNCTIONS

- Schottky diode bipolar IC and silicon gate MOS LSI techniques in manufacturing 02 p0228 A71-11652
- Tungsten cathode current partitioning in dense Ar plasma, noting electron emitter work function reduction due to ion space charge field 02 p0289 A71-11940
- Titanium and niobium monocarbides electron work function relation to homogeneity region composition, considering electron structure and thermal emission 02 p0263 A71-12199
- Thermionic emitter work function extrapolation and interpolation, noting correlation to surface temperature and Cs pressure 02 p0294 A71-12202
- Langmuir S curves for W 110/-Cs and Mo 100/-Sr adsorption determined by thermionic electron emission microscope, noting minimum work function 02 p0295 A71-12203

Electropolished and single crystal surface effects on work function of macroscopic tungsten emitter in cesiated converter 02 p0295 A71-12204

Bare and cesiated work function of covapor deposited tungsten-rhenium electrodes from vacuum emission vehicle Schottky plots 02 p0295 A71-12205

Vacuum work function of thermionic converter using planar monocrystalline rhenium emitter over temperature range 02 p0192 A71-12206

Cesiated work functions of directed monocrystalline Re thermionic emitter from saturated electron emission currents over temperature range 02 p0295 A71-12207

High work function stable faceted W thermionic emitter surface preparation by electroetching and vapor deposition 02 p0295 A71-12209

Electron emission formulation for cesiated metal surfaces in thermionic converter in terms of work function, using Swanson-Strayer correlation 02 p0295 A71-12210

Thermionic dispenser cathodes with emitter surfaces covered and replenished from inside by high work function material 02 p0295 A71-12213

Performance tests of identical cylindrical thermionic converters with W emitters and Nb collectors, using X ray diffraction and work function measurements 02 p0193 A71-12217

Volt-ampere characteristics dependence on collector temperature in thermionic converters compared with collector work function 02 p0195 A71-12235

Thermionic diode with integral guard ring, measuring emitter and collector work functions and heat transfer 02 p0195 A71-12236

Vapor deposited W impurities effect on crystal structure and preferred orientation, considering work function increase 02 p0296 A71-12241

Nitrogen chemisorption on Ta by field emission microscopy, taking into account work function changes 06 p0940 A71-17299

Diffusion varactor and Schottky barrier semiconductor diodes for frequency multiplication at millimeter wave frequency range 06 p0873 A71-17545

Au-Ba intermetallic compound electron work function temperature dependence 07 p1179 A71-19922

Noise behavior of Schottky barrier gate FET at microwave frequencies, discussing effects of carrier velocity saturation and parasitic resistances on noise parameters and measurement method 08 p1261 A71-20741

Microwave diode technology, discussing Schottky barrier, p-n junction, varactor, tunnel, bulk effect and avalanche diodes performance and applications 08 p1266 A71-21622

Contact potential measurements of work function dependence on adsorption of alkali metals on Ta(110) and W(100) crystals under ultrahigh vacuum 09 p1497 A71-22701

Mo fibers surface state and reactions under uniaxial stress from electron work function measurements 09 p1471 A71-23080

X band Schottky barrier diodes RF impedance mismatch and noise factor, calculating dependence on microwave oscillator voltage-standing wave ratio 09 p1421 A71-23723

Junction diameter reduction approaches for low noise generation, using Schottky diode parameters 11 p1737 A71-25675

Macroscopic working model for CVD tungsten assuming change of substrate work function and preferential crystal orientation by impurity adsorbed molecules 11 p1808 A71-25861

Thermionic emitter CVD W layer on Mo, investigating work function change due to Mo diffusion and crystal structure dependence on heat treatment 11 p1808 A71-25863

Thermionic converters surface physics theory, discussing work functions, desorption energy and rates relationship to atomic and crystallographic properties 11 p1711 A71-25878

Thermionic collector work function measurements, considering error sources and I-V characteristics 11 p1711 A71-25881

Variable spacing thermionic converter consisting of fluoride vapor deposited W emitter and Nb collector, considering cesiated work function of electrode pair 11 p1714 A71-25905

Power gain of Q-band GaAs FET with Schottky-barrier gate, giving amplifier and oscillator designs 14 p2210 A71-29800

Thermal characteristics of emission and work functions of spherical Ta single crystal faces by Martin microscope measurements
15 p2453 A71-32644

Molybdenum-niobium alloys single crystals electron work function in vacuum from emission patterns and anisotropy
16 p2595 A71-33881

Ti adsorption on W and Re, measuring field emission average work function at various Ti layer thicknesses
17 p2791 A71-34855

Oxygen adsorption study on polycrystalline W through work function variation and adhesion coefficient measurements, using mass spectrometry
18 p2874 A71-35974

Schottky barrier, point contact and Ge back diodes for microwave mixers and detectors, noting burnout characteristics
18 p2894 A71-36979

Fabrication and noise performance of high power Schottky barrier GaAs IMPATT diodes with double epitaxial layer structure on low-etch-pit density substrates
18 p2895 A71-36982

Photolithographic fabrication and electrical characteristics of GaAs Schottky barrier diodes for pulse operation
19 p3027 A71-37259

Photovoltaic and electron-voltaic properties of diffused and Schottky barrier GaAs diodes, considering irradiance in 0.001-10,000 microwatt/sq cm range
19 p3027 A71-37484

Schottky barrier diodes as photodetectors in hot electron mode, deriving ballistic transport model for scattering mechanisms effects
20 p3236 A71-39191

Nitrogen adsorption on single crystal W planes by flash desorption experiment, noting work function change dependence on planes
21 p3345 A71-40539

Silicon Schottky tunnel MOS diodes, discussing effect of thin interfacial film between metal and semiconductor on I-V characteristics
23 p3652 A71-43936

Polycrystalline Nb and Ta and Ta-on-Nb thin film thermionic emission surface barrier analysis from periodic deviations in Schottky effect
24 p3862 A71-45346

Surface potential barrier models for thermionic and photoelectric emissions from semiconductors in Schottky deviation region
24 p3862 A71-45350

WORK HARDENING

NT STRAIN HARDENING

Elastoplastic constitutive laws with nonassociated flow laws and work hardening, nonhardening and softening behavior
01 p0174 A71-10999

Thin cylindrical work hardening shell under nonuniform heating and external stresses, determining elastoplastic deformation by flow theory
02 p0323 A71-11744

Axisymmetrically loaded shells of revolution made of work hardening materials, determining inelastic finite deformations and buckling loads by incremental variational method
03 p0505 A71-13543

Work hardening model for grain size effects on metals flow stress, discussing dislocation density as stress-strain function
03 p0447 A71-14494

Grain size effects on metal fatigue, considering work hardening and crack initiation and propagation
03 p0447 A71-14495

Atomic ordered alloy compressive strengthening for fcc and bcc lattices in terms of yielding, work hardening and no hardening stages
07 p1132 A71-19438

Pure vs dispersion hardened Ni plastic deformation, noting flow stress and temperature effects on work hardening
08 p1311 A71-21544

W fibers reinforced Cu matrix work hardening rates as function of fiber diameter and volume fraction, using isolated tension pile-up model
09 p1535 A71-22279

Crystal structure alterations in work hardened surface layers of W, Nb and Mo during thermocyclic treatment, using X ray micrography
09 p1477 A71-23329

LiF single crystals temperature, strain rate and positive Mg ionic impurity effects on work hardening characteristics
11 p1809 A71-26478

Work hardening material planar frame inelastic load deformation and buckling, using finite difference method and variational principle
14 p2330 A71-30693

Deformable thermally work hardenable Al-Mg-Li alloy, detailing phase composition changes during aging
16 p2594 A71-33711

Critical growth work hardening germination and recrystallization of oriented compression deformed Nb, Mo and W refractory cubic centered crystals
18 p2935 A71-36200

Prestrain directional effects in steel tension and compression test specimens, noting Bauschinger and work hardening effects
18 p2937 A71-36834

Work hardening materials yield criterion derivation from mathematical model for inclusions embedded in elastoplastic matrix
19 p3078 A71-37644

Copper single crystals fatigue as statistical work hardening phenomenon
19 p3081 A71-38072

Hydrogen content effect on annealed and work hardened palladium wire tensile properties, determining yield/tensile stress and elongation
20 p3247 A71-38765

Finite elastoplastic deformation thermodynamic theory based on isotropic work hardening, excluding Bauschinger effect or localized modification of yield surface due to plastic flow
20 p3308 A71-39486

Alpha Ti at blue brittle temperature, observing strain rate dependent work hardening effects on necking strain
21 p3398 A71-40464

Elastoplastic work hardening material characteristics, using microhardness analysis
21 p3468 A71-41001

Plastic work hardening produced by pressure application to spherical cavity surface in infinite elastoplastic medium, considering spherical elastic wave attenuation
23 p3775 A71-43147

Fatigue strength of two phase Ti alloys, considering work hardening, electrochemical finishing, electropolishing and protective media
23 p3694 A71-44232

Ni-Cr single crystals plastic deformation, presenting work hardening characteristics and critical resolved shear stress
23 p3694 A71-44278

WORK-REST CYCLE

Resting oxygen consumption in exercise-trained and nontrained normal, hypophysectomized and thyroidectomized rats
01 p0016 A71-11408

Circadian work-rest cycles in isolated humans
01 p0017 A71-11411

Visual task vigilance deterioration under hypoxia, considering work-rest schedule effect and IQ scores
01 p0017 A71-11418

Oxygen uptake kinetics in human submaximal exercise during work load transitions and work-rest cycle
02 p0202 A71-11663

Human strength decrement and recovery for repetitive maximal muscular exertions with various intertrial intervals
04 p0540 A71-15846

Human sleep deprivation research, discussing task performance, man machine interaction and work-rest cycles
04 p0540 A71-15848

Tolerance time for hot humid conditions, considering acclimatized and unacclimatized men at rest and at work with moderate rate of energy expenditure
05 p0705 A71-16153

Knowledge of results and rest pauses effect on sensorimotor skills at different training conditions
05 p0714 A71-16618

Operator reliability control models, discussing rational work-rest schedule for man machine systems
05 p0731 A71-17017

Neuroendocrine and metabolic responses to rotating workshift schedules, using urinalysis to assess physiological disturbances and adaptive changes
08 p1239 A71-20817

Diurnal rhythm of adrenaline secretion in subjects with different working habits, comparing catecholamine excretion under relaxation conditions
11 p1721 A71-26355

Serotonin role in central nervous system activity, stressing sleep/wakefulness cycle regulation
12 p1869 A71-26651

Diurnal rhythms of human physiological functions and performance during frequently alternating sleep-work cycles
13 p2006 A71-28410

Astronauts work-rest schedule principles during space flight, discussing circadian rhythms and desynchronization
15 p2363 A71-31315

Lactic and succinic acids and creatine phosphates content in rat hind leg muscles during swimming and at rest
16 p2532 A71-33897

Human fatigue with emphasis on chronic conditions unrelieved by rest or sleep, recommending elimination of conditions resulting in excessive stress, anxiety or boredom
17 p2687 A71-34353

Electroencephalographic evaluation of brain functions disturbances in response to stress in flying personnel, relating fatigue and rest periods allocation
19 p3008 A71-38223

Trace processes as basis for efficiency change during exercise and active rest
21 p3337 A71-41061

In-flight study of work/rest cycle effects on double crew performance and fatigue in flying transport missions
22 p3501 A71-41829

WORKING FLUIDS

Liquid volume deformation effect on hydraulic drive under continuous or jumpwise pressure
01 p0007 A71-11243

Isothermal irradiators of neon filled stainless steel heat pipes with Na as working fluid, discussing laboratory and reactor feasibility tests
02 p0280 A71-12250

Reciprocating organic single cylinder Rankine cycle engine using thiophene working fluid
03 p0351 A71-13034

Radiative properties of construction properties and working media, noting importance to radiative heat transfer calculation
03 p0519 A71-13747

Fluoro-alkyl s-triazines as high temperature lubricants and energy transfer fluids for aerospace systems [ASLE PREPRINT 70LC-5]
08 p1322 A71-21155

Space vehicles dimensions effects on working fluid mass and power required for orientation
09 p1532 A71-23133

Gas agent temperature measurement by sodium spectral line reversal method using MHD generators experimental research
09 p1512 A71-23671

Gas dynamic CW laser with supersonic hot moist carbon dioxide-nitrogen as working fluid, discussing laser gain vs water content
10 p1619 A71-23760

Life tests and properties of organic working fluids heat pipes for electronic component cooling [AIAA PAPER 71-408]
11 p1856 A71-26203

Noncondensable gas temperature controlled heat pipe systems design, considering working fluid, reservoir wicks and ambient thermal environment [AIAA PAPER 71-420]
11 p1857 A71-26211

Working fluid /Ar/ purity and stability effects on fatigue life and creep of Nb and Mo alloys using gas analysis, microstructure and microhardness data
14 p2256 A71-29622

Rankine cycle turboelectric nuclear space power conversion system with liquid K as working fluid, discussing current technology status [GESP-623]
16 p2526 A71-33525

Vacuum pump fluids spectral absorption coefficient measurement, using variable UV cell
17 p2784 A71-35141

Variable thermal conductance wall based on working fluid evaporation and condensation [ASME PAPER 71-HT-39]
19 p3166 A71-38001

Component performance of three loop Rankine cycle test rig using lithium, potassium and NaK-78 as working fluids
20 p3263 A71-38923

Working gas parameter determination for valve supply main system during feed opening, explaining heating effect for second valve by shock wave theory
24 p3793 A71-45021

WORLD

U EARTH [PLANET]

WORLD DATA CENTERS

Book on sources and availability of IQSY data, Volume 7, covering stations, sounding rockets, satellites, space probes and World Data Centers catalog
15 p2395 A71-31518

Ionosonde stations world distribution for vertical incidence soundings during IQSY and comparison with IGY
15 p2396 A71-31610

WOUND HEALING

High-mountain altitudes inhibition of inflammation and wound healing in rabbits
16 p2531 A71-33522

WRINKLING

Strain analysis based on thin metallic film optical measurements, determining principal strain directions from wrinkle and microfracture patterns [SESA PAPER 1828A]
17 p2820 A71-34551

WROUGHT ALLOYS

Tensile-compressive yield strengths of wrought Mg alloy, noting plastic deformation by slip on basal plane
04 p0614 A71-15786

Wrought high strength Al alloy nonequilibrium second phase particles formation effect on mechanical behavior during solidification
07 p1137 A71-19978

Pressed or sintered steel powder joining to wrought mild steel parts, evaluating welded joints with torsion test
15 p2417 A71-32615

Wrought precipitation hardened Co-base alloy, investigating Ti and Al additives effects on tensile and

stress rupture strengths, microstructure and fabricability

17 p2758 A71-35147

Argon arc welding of Ti VT5-L alloy to Ti VT5-L and to wrought alloys OT4 and OT4-1, noting ductile, tough and stress raiser insensitive joints

19 p3070 A71-38421

X

X BAND

U SUPERHIGH FREQUENCIES

X RAY ABSORPTION

Solar hard X ray absorption in D region, calculating integral flux radiation

01 p0145 A71-11076

Earth atmosphere X ray absorption, determining photon flux, energy and angular distribution as function of altitude by Monte Carlo method

02 p0299 A71-11776

Atmospheric absorption models of solar X-rays at occultation times, using Solrad satellites

03 p0480 A71-14048

High atmosphere X ray absorption grazing scale height variations from satellite measurement of solar X-ray flux during sunrise and sunset

03 p0480 A71-14049

Pyrolytic graphite microcalorimeter for X ray absorbed dose measurement, exploiting for calibration self heating

10 p1608 A71-23742

X ray absorption and atomic number corrections in quantitative microprobe analysis of metals

14 p2277 A71-30476

Atmospheric scattering and absorption effects on balloon altitude spectra observations of auroral X ray penetration into atmosphere

23 p3720 A71-43130

X RAY ANALYSIS

Temperature dependence curves and X ray spectrum analyses of different ferrite compositions, indicating absorption band K-edge shift toward shorter wave region

01 p0139 A71-11111

Photogrammetry in precision three dimensional X ray stereoradiography, comparing doses with Kymography, Tomography and Seriescopy

02 p0203 A71-11951

High purity hafnium titanate, discussing preparation and DTA, electron microscopy wet chemical and X ray analyses

02 p0275 A71-12595

X ray films in emulsion chambers, discussing electron-photon cascades

03 p0426 A71-13839

Limitations of electron and X ray microscopy concerning damage of biological molecules by observation

04 p0596 A71-15140

Fatigue damage detection by X ray diffraction method, testing different steel specimens with Co-K-alpha radiation to obtain characteristic diffraction patterns

05 p0749 A71-16295

Stony meteorite fragments, using X ray powder method for diamond detection

06 p0967 A71-17900

Laser produced plasma temperature measurements using X ray detectors

06 p0938 A71-18459

Chest and cardiovascular system optimal radiologic facilities, discussing X ray examination, catheterization-angiographic and nuclear radiology laboratories

07 p1053 A71-20354

X ray analysis of oxide film structure, oxygen concentration and residual stresses at surface of oxidized Ti and Ti alloy

08 p1317 A71-21760

Primary, secondary and combinatory recrystallization kinetics and textures in tungsten wire of different compositions over 900-2300 C using X ray analysis and metallography

09 p1476 A71-23323

Subgrain growth kinetics for tungsten deformed by rolling and polygonizing annealing, using metallography, X ray microradiography and crystal spectrometry

09 p1476 A71-23324

Thermal, microstructural and X ray analyses of Al-Ti alloys phase diagrams, measuring hardness and conductivity

09 p1480 A71-23704

Phase diagram isothermal cross sections of Ti-Zr-Nb alloys for various temperatures and heating periods by X ray and microstructural analysis

09 p1480 A71-23705

Semiquantitative X ray nondestructive analysis of metal alloys, noting critical nature of sampling

13 p2074 A71-28438

Mo-Ni-C ternary alloy X ray analysis, determining solidus temperature from phase diagrams

15 p2424 A71-31237

Gallium antimonide-germanium system solid solution lattice constant determination, using X ray and microstructural analysis and microhardness measurements

17 p2791 A71-34566

Gages using X radiation for measuring thickness range, linearity and response time, noting application of absorption and fluorescence techniques

17 p2744 A71-35287

Electrolytic behavior of yttria-hafnia solid solutions from X ray analysis and electroconductivity measurements

18 p2874 A71-37001

Eutectoidal decomposition of tantalum dicarbide, noting X ray phase identification during carburization of tantalum ribbons

20 p3252 A71-39961

X ray films in emulsion chambers, discussing electron-photon cascades

22 p3550 A71-42640

X ray analysis of scale formation in precipitation hardened nickel, investigating thermal resistance and oxidation rates

23 p3691 A71-43520

X ray probe, scanning electron microscopy and spectral reflectance analysis of lunar environment effects on Apollo 12 returned Surveyor 3 materials surface cratering

23 p3766 A71-43818

Zone refined Be crystals under room temperature compression, examining lattice defects with X ray synergy method

23 p3695 A71-44287

Mo-W, Ta-W and Nb-W alloys X ray analysis at high temperatures, calculating interdiffusion coefficients and temperature effects on W concentration

24 p3836 A71-44671

X RAY APPARATUS

X ray Debye chambers and diffractometer cameras for high temperature investigations of metal systems phase equilibrium

07 p1112 A71-19620

X RAY ASTRONOMY

Radio sources, cosmic rays and X ray background origin, discussing synchrotron mechanism Compton scattering and red shifts

01 p0144 A71-10770

Gas-Cerenkov balloon-borne detector for low energy gamma rays, calculating efficiency and angular response by Monte Carlo program

01 p0083 A71-11222

Background emission characteristics, discussing cosmic electrons, X rays and radiation sources

02 p0300 A71-12092

Diffuse cosmic X ray spectrum obtained from telescope aboard OSO 3 satellite

02 p0300 A71-12580

Diffuse cosmic X rays observation by telescope aboard OSO 3 satellite, determining isotropy

02 p0301 A71-12581

Scorpius X-1 X ray and optical variations observation by Vela 5 satellites

02 p0315 A71-12662

Worldwide geophysical observatories network for observing solar optical, radio, particle X rays and geomagnetic and ionospheric effects [AIAA PAPER 70-1354]

02 p0239 A71-12692

European X ray astronomy lunar occultation satellite, providing high resolution cosmic X ray source observation

02 p0303 A71-12952

X ray sources location and grouping into supernova remnants and loose cluster categories, accounting for galactic background

03 p0483 A71-13187

X ray sources at various flux levels, evaluating contribution to background radiation

03 p0481 A71-14269

X ray background angular structure comparison with optical galaxies spatial distribution, ruling out universe models with sources following cosmological mass distribution

04 p0657 A71-15826

Extragalactic pulsars visible and X ray detection and luminosity

05 p0801 A71-15928

Balloon-borne observation of X ray sources in northern sky, including Sco, Cyg and SN 1572

05 p0797 A71-15931

Pulsars optical and X ray luminosity secular decrease, examining emission close to velocity of light radius

05 p0807 A71-16209

Nova-like X ray source near or in Centaurus constellation, presenting energy spectra measured by sounding rockets in Japan during August 1969

05 p0808 A71-16452

X ray source Sco X-1 gamma radiation due to Compton synchrotron process, comparing flux observation for synchrotron origin validity

05 p0799 A71-16476

North Galactic Pole soft X ray flux measurements, using Teflon windowed proportional counter

05 p0799 A71-16699

OAO continuous observation capability, Project STAR telescopes, solar and X ray instruments and resupply missions based on space shuttle concept

05 p0818 A71-17132

X ray sources identification and position measurements near galactic center on basis of rocket experiments

05 p0814 A71-17234

HF modulation of optical, X ray and gamma radiation of Crab pulsar, discussing radiation production mechanisms

06 p0970 A71-18033

Double star system with neutron star in pair with matter-losing star, discussing X ray sources variability causes

06 p0976 A71-18455

Rotating modulation collimator as astronomical X ray camera, discussing data reduction techniques for image synthesis

07 p1109 A71-19455

X ray and far IR measurement inconsistency from Centaurus A, discussing metagalactic submillimeter background

07 p1185 A71-19546

Isotropic component of diffuse gamma ray background, discussing possible dense intergalactic medium coexistence with universal cosmic ray flux

07 p1185 A71-19549

Soft X rays from supernova remnants Pup A and Vel X complex observed by X ray astronomy payload on Nike-Tomahawk rocket

07 p1187 A71-19817

H I and H beta emission, Sco-Cen association stellar members near Sco X-1, discussing X ray heating and ionization

07 p1187 A71-19818

Scorpius X-1 X ray emission temporal behavior on 3 March 1969

07 p1198 A71-19831

X ray observations of NP0532 and other radio pulsars and galactic X ray sources

07 p1200 A71-20052

Low energy cosmic X ray observations, examining diffuse background and absolute flux values

08 p1349 A71-20936

Crab Nebula and pulsar NP 0532 X ray spectra discussing pulse profile, emission and interstellar absorption

08 p1353 A71-20984

Scorpius XR-1 simultaneous radio and optical measurements, discussing correlation of fluxes

08 p1360 A71-20985

Background emission characteristics, discussing cosmic electrons, X rays and radiation sources

08 p1355 A71-21142

X ray astronomy, discussing measurement methods and equipment, radiation mechanism and cosmic sources, with particular reference to hot rarefied plasma and pulsar types

09 p1516 A71-22058

X ray source in Perseus region, studying Aerobee rocket proportional counters measurements

09 p1512 A71-22348

X ray spectrum measurement of Scorpius X-1 by Bragg spectrometer, explaining emission or absorption absence by source model with line weakened by electron scattering

09 p1518 A71-22349

Cosmic X ray astronomy by upper atmosphere research vehicles, noting collimators, detectors, high resolution crystal spectrometers and X ray telescopes

09 p1450 A71-22892

Cosmic X ray astronomy, discussing supernova, variable and extragalactic radiation sources, diffuse background radiation and Crab Nebula measurements

09 p1522 A71-22976

Variable stars, quasars and X ray source ScoXR-1 UBVI light photoelectric data, examining optical emissions and brightness variations

09 p1524 A71-23186

Stellar X ray sources as close binary stars and old novae, calculating radiation by deceleration process

09 p1528 A71-23544

OSO 3 satellite observations of diffuse X ray emission from galactic plane, eliminating straight line interpolation of spectrum between 3-10 keV X ray range and 100 MeV energy range

10 p1665 A71-23750

Intensity variations of Cygnus X ray sources, analyzing high resolution results of Adelaide and Tasmania universities

10 p1661 A71-23882

Flux and shape variability of X ray emission from M87 using proportional counters onboard Aerobee-Hi rocket

10 p1661 A71-24421

Galactic X ray thermal emission model, discussing origin and location of sources

10 p1662 A71-24675

X ray astronomy, including celestial sources emission, discrete cosmic sources, recording techniques, isotropic background and shielding

10 p1681 A71-25117

Galactic plane X ray scan by NASA small astronomy satellite Uhuru, discussing satellite instrumentation, detector and sensor sensitivity and preliminary measurements

Cygnus X-1 and X-2 X ray source location from Uhuru satellite measurements

Seyfert galaxies NGC 1275 and NGC 4151 X ray flux detection, determining position and emission intensity

M87, Cen A NGC 5128 and 3C 273 X ray emission observations in Virgo cluster, using Uhuru satellite

X ray astronomy orthogonal mirror telescopes, noting collecting efficiency, angular resolution and focusing

Binary system of neutron star paired with matter-losing star, discussing X ray emission variability

Milky Way Galaxy X ray sources, discussing bremsstrahlung, synchrotron radiation, Compton effect optical objects, supernova remnants and X ray astronomy

X ray flux variability of massive elliptical galaxy M87 from rocket flight measurement, considering synchrotron, inverse Compton and thermal bremsstrahlung

Quasars and X ray sources, observing UVB magnitude variation with photoelectric data

X ray and gamma ray astronomy, considering intensity monotonic decline in cosmic electromagnetic spectrum

X ray pulsations from Cygnus X-1 observed from Uhuru satellite, suggesting exstar discovery

Line emission in X ray background in galactic plane and at galactic pole based on rocket flight data

X ray evidence of limit amount of hot intracuster gas for gravitational binding of Coma cluster of galaxies

OSO-G satellite instrumentation for solar and celestial X ray detection, exploring spectral distribution, temporal intensity variations, sources and atmospheric albedo

Cosmic X ray background observations, using rocket-borne proportional counter

Pulsar signature on diffuse X ray background, converting fraction of luminosity into k series photons

Soft X ray background source, discussing north polar galactic spur as supernova outburst remnant

Extragalactic X ray sources from Explorer 42 flight, confirming explosive nature of Seyfert galaxies revealed by optical telescopes

Aries-Taurus region as soft X ray source, determining energy flux and source

Multiple periodicity of Cygnus X-1 X ray emission from rocket sounding

High energy X ray flux from source in Centaurus Crux detected by balloon sounding

Rapid fluctuations in high energy X ray flux from source in Centaurus Crux from balloon sounding

Galactic discrete X ray sources identification with black nebulae, H II regions, close binary stars, Wolf-Rayet stars and planetary nebulae

Neutron stars with pulsar characteristics in binary systems, discussing matter accretion relationship to X ray source evolution

Thermal X ray sources associated with rotating collapsed stars with surrounding plasma shells, discussing plasma density profile and electron distribution in stellar magnetosphere

Cygnus X-1 distance estimate based on low energy X ray spectrum obtained by sounding rocket

Extragalactic cosmic X ray sources at high galactic latitude from sounding rocket experiments, correlating with galactic clusters

Balloon X ray astronomy techniques and observations, noting collimated scintillation counter instrumentation and PCM telemetry

Australian space research 1970 report to COSPAR covering rocket sounding, X ray and gamma ray astronomy, tracking stations and international cooperation

Cyg X-1 X ray intensity and energy spectrum variation data, using balloon-borne telescope

Large amplitude periodic X ray pulsations from Centaurus X-3, observing abrupt source intensity and pulse rate changes

Galactic weak X ray sources observation in Southern Hemisphere for flux and energy spectrum

Coma cluster X ray source data from Uhuru satellite, observing size, luminosity, spectra, thermal bremsstrahlung mass and stability

OSO satellites observations, studying X ray flare phases, temperatures and spectra

Cyg X-1 X ray pulsar age determination and emission model speculations based on observation data for supernova remnant and radio counterpart absence explanation

Papers on elementary particle and cosmic ray physics, covering neutron monitor, fireball models, radio pulses and X ray astronomy

Cosmic X ray astronomy by rocket and balloon soundings and discrete emission source measurements, considering energy spectra

X ray astronomy with SAS-A satellite, discussing proportional counters, detectors and short period pulsation discovery

Pulsed X ray emission from NP 0532 at 20-200 keV measured by balloon flown sun sensor controlled azimuth stabilized detectors

Excess intensities of diffuse cosmic X rays related to characteristic line spectrum excitation and element abundances in interstellar region and nebulae

Scorpius X-1 cocoon pulsar thermal X ray emission model, describing hot gaseous region around rotating neutron star

Virgo XR-1 X rays observation with rocket-borne proportional counters, noting photo index or bremsstrahlung temperature consistency with spectrum

Magellanic clouds X rays observation, interpreting spectrum analysis data as due to few strong sources

X ray source Cygnus X-1 location measurement by balloon, noting agreement with Uhuru data

X ray source Cygnus X-1 position determination by Aerobee rocket-borne rotating modulation collimator

GX 17 X ray observation, noting exponential spectrum characteristic of thermal bremsstrahlung and resemblance with Sco X-1 radiation

Pulsed emission of hard X rays from Crab Nebula pulsar NP 0532, using balloon-borne telescope

Quasars and X ray sources, observing UVB magnitude variation with photoelectric data

Outer planets Grand Tour X ray investigation of planetary magnetospheres to obtain flux and energy spectrum of electrons precipitated from Jovian magnetosphere

Rotating magnetic white dwarf stars possibility as X ray sources with thermal spectrum, considering evidence based on Sco X-1 emission relationship to bremsstrahlung

Extragalactic background soft X ray diffuse flux consistent with absorption by Small Magellanic Cloud

Cygnus X-1 X ray data with temporal resolution, examining pulsations and flare activity

Cygnus XR-1 X ray intensity fluctuations, discussing time scales and periodicities

Hard X ray pulsations limits in higher energy range from Cyg X-1, comparing with Crab Nebula pulsar

Cosmic soft X ray detection by proportional counters with thin polypropylene windows onboard sounding rocket, considering galactic emission possibility

X ray rocket observations of Sco X-1 on 7-8 August 1969 compared to simultaneous optical observation, interpreting in terms of hot plasma model

X RAY DENSITY MEASUREMENT

Diffuse background 0.1-1 MeV gamma ray component observed by balloon-borne counter system, finding no positive evidence for cosmic component existence

X ray observations in Crab Nebula, including angular size, location, energy spectra, time variability, line emission, interstellar absorption and polarization

Taurus X-1 X ray emission polarization from rocket-borne polarimeter measurements, utilizing incoherent scattering

Continuous injection models for secular X ray and radio emission from supernova remnants in Crab Nebula, Cas A and Tycho

Scorpius X-1 radio emission detection at 1415 MHz, discussing brightness distribution

Bright star at radio source and X ray observations evaluation from optical identification of Cygnus X-1, taking into account spectrum and energy distribution characteristics

Cosmic X and gamma radiation, discussing galactic and extragalactic sources, generation processes and spectrometric characteristics

Spectrum and galactic isotropy of diffuse cosmic X rays by balloon-borne detector

Coma cluster X ray observations implying limits on gas density in intergalactic space and Friedmann models

X ray variable source GX 1 plus 4 balloon observations in sky region near galactic center

Circinus pulsating X ray source spectrum analysis, considering bremsstrahlung and black body models

UK 5 spacecraft experiments in X ray astronomy, investigating spatial distribution and energy spectra of emissions in space, polarization and pulsar periodicities

Balloon obtained Crab pulsar gamma ray emission data searched for pulsation above 50 MeV

Cosmic soft X rays in energy range 0.14-7 keV from rocket soundings with thin polypropylene window proportional counters, covering field of view in Cygnus-Cassiopeia region

Galactic discrete X ray sources identification with black nebulae, H II regions, close binary stars, Wolf-Rayet stars and planetary nebulae

Pulsar characteristics suppression in neutron stars of binary systems, discussing matter accretion relationship to X ray source evolution

Scorpius X-1 optical and X ray flux transient short period oscillations correlation from Aerobee sounding rocket data

X ray astronomy, considering emissions and intensities of various classes of sources

Cosmic X ray astronomy, considering discrete sources and isotropic background X radiation

Diffuse cosmic X rays small scale structure, comparing Wolfe-Burbridge theoretical autocorrelation functions for galaxies clusters and superclusters with experimental value

Balloon flight detected gamma ray source Lib gamma-1, discussing possible identification with PKS 1514-24 radio galaxy

Galactic radio spur association with soft X ray emission

Vela X and Puppis A soft X ray observations using rocket-borne methane counter

X ray sources pulsation limits and locations determination by rocket-borne rotating modulation collimator

Galactic nucleus X ray source observations by Uhuru satellite, discussing emission and absorption spectra

X RAY DENSITY MEASUREMENT

Quiet corona temperature from solar equator soft X ray flux measurement by satellite-borne heliograph

Scorpius X-1 high energy X ray flux variations from balloon-borne scanner data

X RAY DIFFRACTION

Bremsstrahlung X rays-radar echoes relation in southern auroral zone, discussing electron precipitation role 03 p0408 A71-13388

X ray sources at various flux levels, evaluating contribution to background radiation 03 p0481 A71-14269

Quiet corona temperature from solar equator soft X ray flux measurement by satellite-borne heliograph 08 p1361 A71-21127

Debye-Waller factors for Nb and Sn atoms in intermetallic niobium stannide by X ray intensity measurements on single crystal 10 p1655 A71-23770

Morphology, dynamics and time variations of auroral zone electron precipitation events from balloon measurements of bremsstrahlung X rays 10 p1662 A71-24535

Galactic and albedo X rays measurement by balloon-borne instruments and sounding rockets 12 p1949 A71-27371

Auroral 1.2-4 second periodicity X ray pulsations during magnetic storms, using omnidirectional detector at balloon altitude 15 p2474 A71-31775

Expanding metal vapor density-radius measurements in wire explosions, using twin tube flash X ray unit 20 p3311 A71-38827

Scorpius X-1 X ray flux observations, noting high frequency oscillations responsible for radiation production 23 p3733 A71-43078

X RAY DIFFRACTION

Liquid Fe, Co and Ni atomic distributions investigation by X ray diffraction 04 p0612 A71-15036

Fatigue damage detection by X ray diffraction method, testing different steel specimens with Co-K-alpha radiation to obtain characteristic diffraction patterns 05 p0749 A71-16295

Ti-Zr-O alloys cross sections investigation by neutron and X ray diffraction, discussing stoichiometry deviation 06 p0911 A71-17382

Metastable Al-rich Al-Fe solid solutions decomposition during isothermal and isochronal annealing, from X ray diffraction patterns 07 p1137 A71-19979

Carbon fibers and composites nondestructive testing, discussing defect detection problems in ultrasonics, X ray diffraction and X radiography methods [PLASTICS INST. PAPER 52] 08 p1296 A71-20918

Rolled metals crystallographic texture and pole figure determination using X ray diffractometer 09 p1467 A71-22307

Fe-Si alloy with pronounced texture and large grain size, determining lattice period from X ray diffractogram obtained by reverse response method 09 p1467 A71-22308

Cut metal crystal orientation planes and dislocation structure determination, using Bragg reflection of monochromatic X ray beam 09 p1452 A71-23319

Apollo 12 clinopyroxenes exsolution and epitaxy by electron microprobe and single crystal X ray diffraction 10 p1672 A71-24391

Ti-Al-Cr-Fe alloys microstructure, investigating alpha and beta phases with X ray diffraction 10 p1627 A71-24531

High resolution X ray diffraction patterns of yeast phenylalanyl transfer RNA crystals, discussing double helical regional distribution characteristics 11 p1727 A71-25834

Stacking fault formation in Nb deformed by filing, determining coherent scattering regions with X ray diffraction 12 p1917 A71-27299

Residual stresses rapid X ray diffraction measurement, noting faster operation in go-no-go mode for nondestructive testing 12 p1912 A71-27533

Antiprismatic intergrowths from single crystal X ray studies of lunar rock plagioclase 13 p2142 A71-29140

X ray diffraction lines diffusion of deformed Ni and Nb, attributing absence to small block dispersion 17 p2755 A71-34415

Residual stress measurement in thin contoured Ti alloy sheets by X ray diffraction, using stress camera in normal incident beam mode 17 p2757 A71-34537

Laser drilled holes in alumina substrates, studying structure by scanning electron microscopy and X ray diffraction patterns analysis 17 p2763 A71-35738

Recrystallization behavior of thorium dispersion hardened W-Re alloy compared to pure W by X ray diffraction, hardness tests, metallographic and electron microscopy methods 20 p3247 A71-38763

Cell structure development during room temperature tensile deformation of beryllium after prism slip by combined X ray diffraction-transmission electron microscopy 20 p3249 A71-39002

Thin gold films strain distribution determination from X ray diffraction peaks, noting elasticity theory 20 p3276 A71-39012

Kinematic theory of resonant gamma rays diffraction by single crystals, calculating differential cross sections of Bragg scattering for total degeneracy and Zeeman splitting 21 p3420 A71-41123

X RAY FLUORESCENCE

Solar stimulated X ray fluorescence by photoelectric ionization in upper atmosphere, discussing effects on X ray astronomy experiments 06 p0949 A71-17268

X RAY FLUORESCENCE ANALYSIS

U X RAY ANALYSIS

U X RAY FLUORESCENCE

X RAY INSPECTION

Submerged arc welding process, observing arc motion and metal transfer with X ray high speed photography 06 p0905 A71-18090

Portable xerographic unit construction and electric circuitry, discussing application for welded seams X ray imagery 09 p1450 A71-22895

Nondestructive testing, discussing visual, liquid penetrant, thermal, X and gamma rays, ultrasonics, magnetic, electrical and eddy currents methods 13 p2073 A71-28218

Multidirectional reinforced resin matrix composites inspection and nondestructive analysis by film/neutron radiography and X ray Vidicon 14 p2263 A71-29659

X ray monitoring process optimization with pnb-6 betatron, discussing intensifying screens thickness and composition effects on defects detectability 22 p3553 A71-41762

Isotopic X ray photography application to welded joint flaw detection in atomic power plant with radiation background 22 p3540 A71-41763

Flash X ray technique for imaging of cavities formation during electron beam welding of Al alloy 23 p3681 A71-43195

Rheological factors and error sources in X ray measurements of lubricant film thickness in rolling contact 24 p3830 A71-44947

X RAY IRRADIATION

C 14 incorporation from labeled glucose into cerebral glycogen of normal and X ray irradiated rats 01 p0011 A71-10850

X ray effects on dogs with and without UV preexposure, determining blood protein and chemical composition, hemoglobin content and thermostability 03 p0364 A71-13524

X ray influence on protein and mineral content of blood serum in dogs 06 p0858 A71-18728

Radiosensitizer and radioprotector action mode in altering X ray effects on DNA in biological systems of different complexity 07 p1032 A71-18928

DNA modification in *Escherichia coli* exposed to X rays and sensitized by triacetoneamine N-oxyl and oxygen 07 p1033 A71-18939

Cysteine incorporation in *Escherichia coli* B, noting X ray sensitivity and radioprotection 07 p1034 A71-18942

Cysteamine protection of hydroxyurea sensitized Chinese hamster lung cells during X ray exposure 07 p1034 A71-18947

Polycation effect on tumor cells, describing growth rate inhibitions, X ray sensitivity and DNA interference 07 p1035 A71-18951

Methylhydrazine radiosensitization of Ehrlich ascites tumor cells, investigating X radiation enhanced cell killing effect via deoxyribonucleic acid strand breakage 07 p1035 A71-18955

Chemical radioprotective effectiveness modification by open skin wounds, discussing results with whole body X ray irradiated mice 07 p1037 A71-18964

Short and long term radiation effects reduction by chemical radioprotectors mixtures, noting improved survival and decrease in leukemia and cancer incidence in X ray irradiated mice 07 p1037 A71-18970

Aminoethylisothiuronium and methoxy-tryptamine synergism quantitative analysis by pharmacological methods of radioprotective effect in X irradiated mice 07 p1038 A71-18971

Long term IR X ray irradiation effects on complementary MOS logic networks with several p and n channels on single silicon, determining radiation induced failure modes 07 p1174 A71-19054

X irradiation induced currents across aluminum oxide films sandwiched between thin metal electrodes as function of voltage and time 07 p1174 A71-19056

Dinitrophenol inhibition of rejoining of X ray induced DNA breaks by L cells 07 p1045 A71-20447

Chromosome radiation injury preservation in generations of X ray irradiated cells of human diploid strains 08 p1242 A71-21966

Radiation induced visual phosphores observed by dark adapted human subjects in fast neutron, X ray and positive pion beams at Berkeley comparative to primary cosmic ray effects 12 p1871 A71-27675

Interstellar gas heating by soft X rays and cosmic rays for electron production, calculating heating rate with Boltzmann equation and Monte Carlo method 14 p2302 A71-30642

X ray flare regions structure, temperature and density, showing directed electron beams presence 19 p3126 A71-37622

Combined and individual effects of UV light, X ray irradiation and freezing-thawing cycles on ribonuclease 22 p3496 A71-42830

X RAY PHOTOGRAPHY

U PHOTOGRAPHY

U RADIOGRAPHY

X RAY SCATTERING

Diffuse galactic X ray background intensity as function of galactic scattering and discrete sources 01 p0145 A71-11345

Low alloy Mo sheet recovery and aging characteristics studied by X ray scattering 08 p1305 A71-21031

Solar soft X-rays scattering in upper atmosphere, providing background against cosmic X rays 23 p3721 A71-43363

X RAY SPECTROGRAPHY

U X RAY SPECTROSCOPY

X RAY SPECTROMETRY

U X RAY SPECTROSCOPY

X RAY SPECTROSCOPY

K-beta and L-alpha X ray spectral emission bands of high melting vanadium compounds, considering chemical bonds 02 p0263 A71-11892

L-alpha X ray spectral band and K absorption edges in vanadium silicides and high temperature superconductors, obtaining energy bands electron distribution 02 p0294 A71-11893

Hard solar X-ray spectra measurements, reinterpreting OSO 3 scintillation counter response due to pulse pile-up 02 p0302 A71-12766

Solar X-ray resonance, intercombination and forbidden lines variations of O VII emission 06 p0968 A71-17910

Zirconium nitride electronic structure from X ray emission spectra, analyzing chemical bonds 08 p1305 A71-21061

X ray spectrum measurement of Scorpius X-1 by Bragg spectrometer, explaining emission or absorption absence by source model with line weakened by electron scattering 09 p1518 A71-22349

Condensed state Ni and Pd atoms X ray emission spectra and electron structure 09 p1474 A71-23233

Al-Co alloys, investigating Al and Co intermediate phases formation effect on X ray emission K spectra 09 p1474 A71-23234

Model for relativistic electrons diffusion from IR sources, determining injected electron spectrum distortion due to inverse Compton losses and X ray spectrum 11 p1814 A71-25294

Plasma focus hard X ray spectrum, using electron sensitive nuclear emulsions 12 p1936 A71-26920

Soft X ray spectra measurements of vanadium carbides in homogeneity range on ultralong wave spectrometer, showing three zone energy structure of valence band 15 p2430 A71-32151

Solar X-ray line emission, using crystal spectrometers during large chromospheric flare 19 p3130 A71-38672

Auroral X rays passage through atmosphere, discussing integral spectral measurements with collimated and omnidirectional detectors 22 p3593 A71-42399

X RAY STRESS ANALYSIS

Elastic stresses during local deformation in Nb-Mo, Ni-Cr, Cu-Al and pure bcc metals, using X ray analysis 13 p2085 A71-28225

X ray interference lines widening in Al-Mo alloy foil obtained from melt by rapid cooling attributed to stress relieving 14 p2258 A71-30008

Peak shifts evaluation errors in X ray stress analysis using diffractometer and three point parabola fitting method
12 p2260 A71-30479

X RAY TELESCOPES

Balloon-borne telescopes to detect pulsed gamma rays from Crab Nebula, graphing data and diagramming telescope

06 p0950 A71-18034

Hot coronal components of solar active regions observations with satellite-borne grazing incidence X ray telescope, discussing emission dependency on photospheric magnetic field

12 p1954 A71-27707

X ray telescopes and neutron cameras telephoto lenses for satellites and space stations, discussing optical design and correction methods

14 p2246 A71-30391

Cosmic ray secondary background of balloon-borne X ray scintillation astronomical telescopes for equatorial latitudes with reference to shutter technique and NaI/Tl crystal

15 p2406 A71-31751

Crab Nebula pulsar NP 0532 pulsed gamma emission from balloon flight measurements with spark chamber equipped gamma ray telescope

20 p3283 A71-39754

X RAY TESTING

U X RAY INSPECTION

X RAYS

NT SOLAR X-RAYS

Galactic soft X rays role in interstellar dust grains alignment producing starlight polarization

01 p0145 A71-11344

Daytime stratospheric X ray bursts, examining occurrence time, duration, cosmic radio noise and magnetic activity relationship

02 p0299 A71-11775

Pulsar radio signal characteristics, examining pulse profiles, nulls interstellar scintillation and optical and X ray bursts

02 p0318 A71-12914

Organic compounds carbon K emission spectra, using light element X ray spectrometer for aliphatic, aromatic and partly ionic substances spectral analysis

03 p0375 A71-13200

Supernova remnant X ray and radio emission secular behavior, considering hot plasma and synchrotron models and continuous injection

04 p0640 A71-14874

Intense X radiation source in Cetus region observation by Black Brant rocket

04 p0640 A71-15049

Navy X ray research and utilization, discussing generation and interaction, radiography, radiation damage, dosimetry, spectroscopy, fluorescence analysis, etc

04 p0625 A71-15095

Cosmic objects relativistic plasma X ray and gamma ray background radiation increase, considering bremsstrahlung effect on radiation spectrum

04 p0657 A71-15747

Metagalactic background X rays origin, hypothesizing electron leakage from radio galaxy

04 p0657 A71-15748

Transition metal diborides X ray emission K alpha band, establishing asymmetry index, bandwidth and maximum power shift deviations from B

05 p0770 A71-17169

Auroral luminosity and X ray bremsstrahlung quasi-periodic pulsations data analysis by power spectrum and cross correlation methods

06 p0949 A71-17265

Anoxic fern spores X ray sensitization, observing diacetyl and isatin effects

07 p1036 A71-18961

Isotropic diffuse cosmic X rays and gamma radiation background origin

07 p1184 A71-19321

Soft galactic X rays role in interstellar grains alignment

07 p1188 A71-20056

Hydrogen and helium photoionization, calculating total cross section and transitions for soft X ray region

08 p1350 A71-20948

Radiative transfer theory extended to cosmological red shift and expansion effects on uniform isotropic X rays and gamma rays in homogeneous intergalactic medium

09 p1512 A71-22333

X ray emission from optical and inner shell transitions of multiply ionized Cu, Fe, and Ti in low pressure discharge dense plasma

09 p1501 A71-22414

Diffuse cosmic X ray observations, discussing balloon and OSO-3 data

09 p1514 A71-22934

Auroral X radiation at magnetocumulative points Kerguelen/Archangel region, using balloon-borne spectrometers

09 p1438 A71-23146

Soft X ray radiation correlations to radio emission flux at various frequencies in 20th solar activity cycle

09 p1515 A71-23529

Balloon sonde for auroral luminosity measurements and comparison of auroral emissions, X rays and ionospheric absorptions

10 p1602 A71-24530

Magnetic mirror confined plasma diagnostics, considering hot electron density, X ray pulse height and synchrotron radiation measurement techniques

10 p1651 A71-24651

Line emission in diffuse cosmic X ray continuum, discussing probable interstellar or intergalactic matter source

11 p1817 A71-26317

Cosmic soft X rays diffuse component dependence on galactic latitude related to interstellar absorption

12 p1949 A71-27370

Auroral zone X ray events due to electron precipitation, considering relationship to polar magnetic substorms

13 p2119 A71-27797

Midnight sector balloon measurements of X ray bremsstrahlung from electrons precipitating in auroral zone during polar magnetic substorms

13 p2119 A71-27798

Electron flux rigidities in polar aurora region, using stratospheric nighttime X ray and cosmic radio noise absorption measurements

14 p2302 A71-30595

Line emission in diffuse X ray background at high galactic latitudes, interpreting rocket observations

15 p2480 A71-32760

Diffuse low energy cosmic X rays rocket measurements, noting excess over extrapolated power law valid for higher energies

15 p2480 A71-32761

Background phonon X ray and gamma quanta intensities dependence on solar activity from Geiger counter recordings in outer space

16 p2626 A71-33675

Holographic analysis of periodic microobjects at X ray wavelengths, obtaining high contrast

17 p2737 A71-34292

Soft optical, radio and X ray emission during accretion of interstellar gas by neutron star with magnetic dipole moment

17 p2800 A71-34570

Local time dependence of auroral zone electron precipitation X ray events from balloon measurements of bremsstrahlung

18 p2911 A71-35894

Nitrogen X ray emission K alpha band behavior in zirconium mononitride in entire range of ZrN homogeneity

19 p3083 A71-37280

Soft galactic X rays role in interstellar grains alignment, taking into account interstellar absorption

19 p3124 A71-37336

Nighttime D region behavior under ionization by X ray spectrum of Scorpius source

19 p3017 A71-37864

Flare stars X ray emission by fast electrons nonthermal bremsstrahlung

19 p3128 A71-38157

X ray background model based on photons bremsstrahlung emission by subcosmic metagalactic electrons or protons

20 p3279 A71-39296

Auroral zone X ray events in midnight sector associated with substorm and electron precipitation following electrojet, using balloon-borne detector measurements

20 p3284 A71-39851

Power spectral analyses of auroral light and X ray pulsations, discussing damping due to velocity dispersions of electrons with various energies

21 p3373 A71-40069

Cen X-3 source X ray flux periodic variations due to white dwarf star radial vibrations based on nonrotating model

21 p3449 A71-40613

Gangliosides and cerebroside content in rat brain under normal conditions, during hypoxia and under small X ray doses action

21 p3337 A71-41057

Diffuse 0.2-2 keV cosmic X ray flux, discussing energy spectrum and spatial distribution

22 p3591 A71-41914

Auroral X rays passage through atmosphere, discussing integral spectral measurements with collimated and omnidirectional detectors

22 p3593 A71-42399

White rats resistance to acute anoxic, anemic and histotoxic hypoxia during various phases of X radiation sickness, studying adrenal cortex histophysiological state

22 p3494 A71-42731

Highly compact X ray source spectrum fitted by black body model at 15 million K

23 p3732 A71-43076

Cygnus X1 short term X ray flux pulsation variability from Southern Hemisphere sounding rocket flight

24 p3865 A71-44445

Metagalactic X ray and cosmic electrons power spectra explanation by electron acceleration and scat-

tering in turbulent plasma with frozen-in magnetic field

24 p3865 A71-44568

Auroral X ray radiation measurements in midnight sector during solar storm of 8 March 1970

24 p3823 A71-45034

X-Y PLOTTERS

Touch sensitive X-Y position encoder for computer display input using surface wave piezoelectric transducer

01 p0047 A71-10214

Three dimensional graphics software package for CRT and storage tube displays and plotters, describing coordinate transformation

21 p3347 A71-40133

Isodensity mapping with digital computer symbol selection and cathode ray X-Y plotter, showing photographic image display and enhancement of density or height information

24 p3826 A71-44787

X-15 AIRCRAFT

Manned space flight escape systems evolution, examining requirements and devices from X-15 to Apollo program

02 p0320 A71-11977

Static and dynamic stability characteristics of X-15 aircraft, lifting body and trapezoidal and delta wing reentry body

18 p2971 A71-36434

X-24 AIRCRAFT

Lifting body vehicle handling qualities, considering X-24A, M2-F3 and HL-10 reentry vehicles flight characteristics and simulation requirements

09 p1532 A71-22622

XB-70 AIRCRAFT

U B-70 AIRCRAFT

XC-142 AIRCRAFT

Aerodynamic design of VTOL propellers, demonstrating possibility of cyclic control of XC-142 experimental propeller

15 p2347 A71-32784

XENON

NT XENON ISOTOPES

NT XENON 137

Shock tube generated Xe plasma electron density measurements by spectroscopy and laser interferometry, deriving ionization relaxation time

01 p0134 A71-10995

Electron density profiles in ruby laser generated Xe plasma, using differential interferometry

01 p0134 A71-10996

Cylindrical Xe filled thermionic diodes breakdown and low voltage arcs at various pressures and interelectrode distances

02 p0190 A71-11942

Ionized Xe laser lines in spontaneous emission, establishing correlation with unidentified lines

03 p0438 A71-13887

Laser action on six lines of ionized Xe spectrum, discussing discharge tube, optical resonator and spectrograph characteristics

03 p0438 A71-13895

CW ion laser transitions in Ar, Kr and Xe, tabulating threshold data

03 p0438 A71-13896

Temperature measurements for xenon plasma diagnostics in high output pulsed mode

05 p0786 A71-16223

Primordial Kr and Xe trapping as possible cause of element abundance trend reversal in Apollo 11 and 12 fines

10 p1673 A71-24428

Mixed plasmas transport properties at one atmosphere and 5000-35,000 K, considering helium-nitrogen, argon-nitrogen and xenon-nitrogen plasmas

12 p1986 A71-27188

Pulsed Xe ion laser properties, considering emission divergence, coherence and cross section

13 p2080 A71-29028

Radiative heat transfer effects behind reflected and incident shock waves in high temperature air and xenon respectively

16 p2662 A71-32888

Continuous light absorption, emission and ionization relaxation behind shock front in xenon

16 p2613 A71-32890

Liquid Xe filled single wire proportional and multiple wire ionization chambers, measuring gain and time/spatial resolution properties

19 p3065 A71-38178

Brayton cycle power conversion system using He-Xe gas mixture, discussing compressor net engine and turbine static efficiencies

20 p3180 A71-38908

Protective xenon atmospheres in sealed silicon-germanium alloy thermoelectric generators, discussing leakage and pressure levels

20 p3265 A71-38934

Periodic current pulse and superradiant radiation pulsing in DC excited xenon plasma with increased cathode-anode capacitance

21 p3424 A71-41046

Molecular nitrogen ions collisions with He and Xe gas atoms, discussing processes based on atomic N ion

XENON ISOTOPES

fragment velocity distribution measurements at varying electron energies 21 p3421 A71-41405

Effective flashes by scintillating Xe arc flash tube, considering perception by human eye 22 p3499 A71-41492

Ar, Kr and Xe emanation during stepwise heating of lunar rocks under slow neutron irradiation in pile, using mass spectroscopy 23 p3754 A71-43726

XENON ISOTOPES

NT XENON 133

Apollo 12 lunar rock 12013 petrologic and mineralogic characteristics, discussing data on isotopic Xe and Gd composition 03 p0494 A71-14217

Solar temperature after formation, using isotopic composition differences in terrestrial and extraterrestrial xenon 10 p1668 A71-23871

Xe and Kr isotopes gas extraction and mass spectrometer analyses of Apollo 11 lunar soil, Murray carbonaceous chondrite and atmospheric Xe 10 p1661 A71-24410

Meteoritic Xe isotopes production mechanism covering spallation, neutron absorption, extinct I 129 and Pu 244 radiative decay and Xe component trapping 11 p1819 A71-25223

Galactic and solar cosmic ray effects on Apollo 11 lunar soil and rock samples, analyzing Xe isotopic anomalies 23 p3722 A71-44016

XENON LAMPS

Toulouse space environment simulator artificial sun assembly consisting of xenon lamp and projection optics for cylindrical light beam production 02 p0239 A71-12748

Xenon resonance lamp with high spectral purity, discussing construction, life and refilling ease 04 p0600 A71-15599

Pulsed xenon solar simulator system for testing single and group cells and panels for flight spacecraft programs 05 p0733 A71-16098

High intensity vacuum UV solar simulator, using high pressure jet pinched xenon arc lamp with magnesium fluoride envelope 11 p1747 A71-26515

Aircraft flash light designs, discussing tandem oscillating lights, fixed lamp rotating reflectors and lamps, xenon flashtube, quartz-iodine lamp and flash frequencies 22 p3483 A71-41494

Visible and near UV spectra of vacuum Ar, Kr and Xe microwave discharge lamps with magnesium fluoride windows 24 p3849 A71-45211

XENON 133

Xe 133 elimination from anterior tibial muscles in dry and water immersed sitting subjects, discussing effects of air and oxygen breathing 13 p2022 A71-29358

XEROGRAPHY

Portable xerographic unit construction and electric circuitry, discussing application for welded seams X ray imagery 09 p1450 A71-22895

Y

Y AXIS

U COORDINATES

YAG [GARNET]

U YTTRIUM-ALUMINUM GARNET

YAGI ANTENNAS

Electromagnetic wave propagation on Yagi-Uda structure, obtaining current distribution, free space vs guided wavenumbers diagram and cutoff frequencies 14 p2196 A71-30514

Computerized numerical optimization for Yagi-Uda antenna array gain, noting nonoptimum in standard traveling-wave design methods 21 p3349 A71-41410

Turnstile loop Yagi and hexafilar contrawound spiral antennas for microwave telemetry rocket data reception, describing design and radiation patterns 23 p3643 A71-43095

YAK 40 AIRCRAFT

Soviet book on Yak-40 passenger transport aircraft configurational design and aerodynamic characteristics covering stability, controllability and flight under special conditions 08 p1230 A71-20750

Yak 40 aircraft flight test program, discussing airworthiness requirements, static structural, vibration and wind tunnel tests 14 p2174 A71-29911

YARNS

Carbon base multifiber yarns for metal matrix composites reinforcement, considering fiber strength degradation minimization methods 03 p0449 A71-14419

Three dimensional orthogonally woven reinforced felt-yarn composite for low density thermal insulation and chemical vapor deposition 14 p2262 A71-29651

YAW

Roll moment of inertia to static margin ratio effect on yaw of repose angle magnitude in ballistic match of projectiles 14 p2325 A71-29890

Transfer function system relating cornering force and aligning torque of rolling pneumatic aircraft tire to yaw angle and lateral displacement 21 p3324 A71-40167

YAWING MOMENTS

Projectiles yawing and rolling over long flight paths, describing onboard solar aspect sensor and telemetry link to ground stations [AIAA PAPER 70-538] 11 p1761 A71-25513

YAWMETERS

U ATTITUDE INDICATORS

U YAW

YEAST

Radioreistant yeast strain *Saccharomyces cerevisiae*, discussing cycloheximide and gamma irradiation treatment influence on growth 07 p1034 A71-18943

High resolution X ray diffraction patterns of yeast phenylalanyl transfer RNA crystals, discussing double helical regional distribution characteristics 11 p1727 A71-25834

Bacteria and yeast strains, fungus specimens and seaweed species high vacuum resistance, noting microorganisms interplanetary transport in outer space 13 p2009 A71-28689

Acetyl-coenzyme A synthetase in aerobic yeast cells localization in microsomal fraction by density gradients 14 p2187 A71-31003

Yeasts growth on synthetic carbohydrates with crude formose sugars, discussing application as regenerating food in long term closed life support system 19 p3011 A71-37576

YHU-1 HELICOPTER

U UH-1 HELICOPTER

YIELD POINT

Iron single crystal wavy slip pattern of plastic deformation under tension at room temperature, noting relation between yield point and crystal orientation 01 p0105 A71-11621

Stability loss of circular cylindrical shells under bending beyond elastic limit 02 p0325 A71-12287

Incompressible fluid filled circular cylindrical shells loaded by pressure ring at center, obtaining yield point load 03 p0500 A71-13022

Elastic and perfectly plastic plane stress problems yield point load lower bounds by finite element method, considering weakened slabs 03 p0505 A71-13541

Yield point in metals, using Cottrell theory of atmospheres of foreign atoms near dislocations 04 p0612 A71-15062

Composite material of ductile matrix and straight reinforcing fibers, deriving yield condition 04 p0669 A71-15196

Test stand for endurance and creep testing of plastics, glazed ceramics and other brittle materials 04 p0567 A71-15645

Plasticity theory isotropic and anisotropic yield conditions for various stresses 04 p0672 A71-15774

Alloy melting technique and heat treatment effects on elastic limit and modulus of elasticity 06 p0912 A71-17947

Plastic deformation of circular plates and shells from material with different yield and strengthening moduli in tension and compression 07 p1211 A71-19164

Ni-Mn, Ni-Fe and Ni-Fe-Al alloys yield behavior and microstructure as result of ordering and disordering treatments, using center annealing technique 07 p1132 A71-19434

Ni-Ti alloy structural modulation during aging, examining effect on yield stress by X ray diffraction and tensile tests 07 p1143 A71-20494

Book on yield point phenomena in metals and alloys covering Fe, V, Cr, Ni, Mo, Ta, W, Al and alloys, hydrogen in metals and fcc lattices 08 p1304 A71-20999

Ta and W single crystals yield stress temperature dependence, confirming asymmetric Peierls barrier 08 p1307 A71-21507

Portevin-Le-Chatelier effect and sharp yield point in zone refined Ni, discussing internal friction and pinning effect on dislocations by hydrogen atoms at low temperatures 08 p1310 A71-21533

Radiation-anneal hardening and radiation effects on yield stress temperature dependence in bcc metals 08 p1312 A71-21550

Strain rate effects on Ta flow stress, examining yield and postyield behavior models and stress-strain diagrams 08 p1313 A71-21562

Optimum tip vertex angles measurement for determining steels tensile strength and yield point from hardness 09 p1467 A71-22314

Yield point temperature dependence in heat resistant austenitic alloys, showing tendency to brittle failure under short term overloads 09 p1468 A71-22598

Prolonged storage effect on polycarbonates mechanical properties, measuring tensile strength, elastic modulus, yield point and breakdown strains under uniaxial tension 09 p1483 A71-22825

Annealed Al-Mg alloys mechanical measurement, noting low temperature tensile strength and yield point variations with specimen composition and temperature 09 p1473 A71-23230

Failure/yield points, stiffness and failure energy from adhesive shear stress elongation curves, using computer assisted thick adherend tests 10 p1631 A71-24071

Rigid plastic media dynamic model, showing yielding time delay effect on residual deflection as function of load duration 12 p1982 A71-27515

Fiber reinforced composite materials plastic behavior shear stress theory, determining yield criteria and plastic strain rates associated with various failure modes 12 p1984 A71-27773

Local plastic deformation analysis of spherical and cylindrical shells subjected to yield point loads through rigid boss, using nonlinear programming 13 p2147 A71-27787

Load bearing capacity of thin walled box shaped rod of strain hardening material during bending beyond elastic limit 13 p2153 A71-28294

Elastically and plastically anisotropic single crystals randomly oriented in polycrystalline aggregate, noting initial yield surface in fcc lattice 13 p2155 A71-29063

Conical bar with yield point lag, investigating elastoplastic wave propagation with Rabotnov model 13 p2155 A71-29064

Polycrystalline Nb cyclic yield point behavior under strain softening and hardening, noting stable hysteresis loop 13 p2087 A71-29123

Thermally activated plastic deformation of metals at low temperatures, determining stress flow, creep properties and upper yield limit 14 p2258 A71-30007

Elastic rods and rings stability under compression beyond elasticity limit, determining equilibrium branching characteristics near bifurcation point 16 p2647 A71-32927

Fatigue S-N curves discontinuities associated with plastic yield and crack path tested on mild steel notched specimens 16 p2591 A71-33346

Ordered structure recovery in Fe-Co-V alloy from elasticity limit behavior, studying duration effect on mechanical properties of strain hardened samples 16 p2591 A71-33370

Yield point thermal component in bcc metals at low temperatures as function of hydrostatic compression, noting interionic reaction potential nonspphericity 16 p2596 A71-33889

Yield surface approximations for thin shell made of material obeying von Mises yield criterion, considering transverse shear effect 16 p2661 A71-34118

Plastic deformation of circular plates and shells of material with different yield and hardening moduli in tension and compression from creep theory relationships 17 p2834 A71-35660

Orthotropic annular plate plastic flow law, establishing yield conditions with plane stress-strain state equations 19 p3155 A71-37527

Work hardening materials yield criterion derivation from mathematical model for inclusions embedded in elastoplastic matrix 19 p3078 A71-37644

Prestressing effect on yield surfaces of Al and Cu thin walled tubes 19 p3079 A71-37705

Yield conditions and flow rules derivation from hypoelasticity, regarding constitutive equation as linear transformation on six dimensional inner product space of symmetrical tensors 21 p3455 A71-40090

Temperature and strain rate effects on yield and flow stress of bcc Ti-Mo alloy over 77-824 K range 21 p3404 A71-41414

Orthotropic shells of revolution limit analysis, considering yield conditions and flow rules 22 p3614 A71-41605

Bending strain diagram conversion into tensile strain diagram, considering elastic limit values correlation for Cu-Ni-Al alloy 22 p3561 A71-41698

Microstructure, yield point and creep rupture strength of Nb-Ti alloy, investigating oxygen concentration and temperature effects 22 p3563 A71-42365

Crack model with strain rate dependent yield stress, calculating stress intensity factor variation with fracture propagation velocity 23 p3774 A71-43145

YIELD STRENGTH

Discontinuous yielding in annealed Al alloy resulting from negative slope in flow stress-strain rate relationship, discussing impurities diffusion role 01 p0105 A71-11606

High purity Nb and Nb-O solid solution single crystals, investigating temperature dependence of yield stress 02 p0263 A71-11866

Three phase particulate epoxy composite compressive yield strength, considering strain rate filler content, porosity and voids effect 03 p0442 A71-13538

Tensile-compressive yield strengths of wrought Mg alloy, noting plastic deformation by slip on basal plane 04 p0614 A71-15786

Thin plates and shell with various yield stress materials, observing limiting equilibrium under tension and compression loads 06 p0992 A71-17810

Anisotropic tubular Ti alloy samples, noting yield strength and crystal structure dependence on stress-strain state 06 p0912 A71-17937

Energy dissipation-fatigue strength relationships during vibrations for prestrained metals and alloys 08 p1369 A71-21118

Dislocation pinning point flow stress decrease in superconducting-normal transition 08 p1345 A71-21536

Tensile data for dispersion hardened iron containing thorium spherulites analyzed in terms of Orowan theory, considering bcc materials yield strength 09 p1466 A71-22172

Fracture toughness relationship to microstructure in alpha-beta Ti alloy heat treated to constant yield strength, considering crack propagation 09 p1472 A71-23126

Yield strength theories of heterophase systems with precipitates surrounded by elastic strain fields, considering dislocation precipitation interaction mechanism 09 p1510 A71-23321

Strengthening processes in precipitation hardened and dispersion hardened alloys produced by powder metallurgy 10 p1614 A71-23903

Tensile yield and ultimate strength and elongation of Al after unidirectional and reversed torsional prestrain 10 p1624 A71-23940

Variational formulation for minimum weight of structures with given yield stress, considering homogeneous isotropic material, plasticity condition and collapse mechanism 10 p1685 A71-23977

Stress redistribution and static inelastoelastic instability of rotating beams and disks of low modulus high yield strength materials 11 p1848 A71-25495

Intermetallic compound precipitation processes in Ti-Cu alloys for high yield strengths, using electron microscopy 11 p1779 A71-26017

Modified interaction equation for biaxially bent beam columns of hollow tubular sections yielding satisfactory prediction of ultimate strength 12 p1973 A71-26699

Approximate limiting loads with minimum yield stress for axisymmetric rigid-plastic body of arbitrary shape, using computerized static equilibrium method 13 p2150 A71-28137

Be sheet plastic bend ductility and yield strength, considering purity and processing effects 13 p2088 A71-29403

Yield pressure, starting torque, consistency and rheology of lubricating greases at low temperature in ball bearings [ASLE PREPRINT 71AM 1B-2] 13 p2076 A71-29489

Thermally induced residual stresses effect on yield behavior of unidirectionally solidified eutectic composites 15 p2432 A71-32171

Guinier-Preston zone size and volume fraction effects on polycrystalline Al-Zn alloys yield strength, discussing precipitation strengthening and thermally activated plastic flow 15 p2433 A71-32182

Yield condition and stability of elastoplastic bodies with large deformations, using Gibbs method of thermodynamics 16 p2650 A71-33015

Cold hardened Cr-Si steels strength/plasticity thermal dependence and brittleness from short torsion and compression tests, identifying low temperature failure mechanisms 16 p2593 A71-33638

Limit analysis of dissipation power and collapse load of rigid perfectly plastic continua with piecewise linear yield surface, using linear programming 17 p2816 A71-34324

German monograph on structural steels tensile and yield strength, detailing strain rate and testing machine effects 17 p2818 A71-34483

Dynamic yield and absorptivity of steel during brittle fracture propagation under neutron irradiation 18 p2934 A71-35987

Linear-elastic fracture mechanics limits concerning toughness based on elastic-plastic rupture model for yielding materials 19 p3161 A71-38726

Fatigue crack propagation in high yield strength steels at room temperature in air environments, considering primary influence of applied stress intensity range 20 p3248 A71-38769

Plasticity with noncoincident yield and loading surfaces, noting isothermal isotropic hardening 20 p3309 A71-39565

Maximum yielding tensile stress envelope curves as function of structural load index based on compression tests of Al alloy stiffened plane panels 20 p3309 A71-39570

Steels, aluminums and titaniums ultimate and yield strength statistical distributions in Weibull parameter form, presenting stimulus-response potential failure model [ASME PAPER 71-VIBR-64] 21 p3396 A71-40307

High purity Be single crystal transverse bending tests, plotting yield stress and bending angle vs temperature 24 p3836 A71-44673

YIG [GARNET]

U YTTRIUM-IRON GARNET

YJ-85 ENGINE

U J-85 ENGINE

YO-YO DEVICES

Azur satellite structure and mechanism requirements, design and tests, noting damping characteristics and Yo-Yo system [DGLR-71-014] 15 p2501 A71-32783

YOUNG MODULUS

U MODULUS OF ELASTICITY

YTTRIUM

Cr specimens containing Y, investigating microscopic breakdown at high temperatures as function of deformation during vacuum rolling 09 p1474 A71-23235

Cr plastic properties, investigating recovery and recrystallization effects from La and Y additions 09 p1476 A71-23316

Temperature dependent diffusion coefficient of yttrium in refractory metal single crystals of Mo, W, Nb and Ta, using radiometric analysis 14 p2258 A71-30005

High efficiency room temperature lasing operation assisted by energy transfer in holmium doped yttrium lithium fluoride 20 p3247 A71-39761

YTTRIUM ALLOYS

Mg-Y alloy age hardening due to coherent metastable phase precipitation 08 p1312 A71-21548

Yttrium effect on phase composition of V-Ga alloys from microstructural, X ray structural and microdilatometric analysis 16 p2622 A71-33909

Age hardenable Mg-Y alloys, investigating impurity phase in solution heat treatment 23 p3696 A71-44292

YTTRIUM COMPOUNDS

NT YTTRIUM OXIDES

NT YTTRIUM-ALUMINUM GARNET

NT YTTRIUM-IRON GARNET

Fe 57 nuclei longitudinal and transverse relaxation in yttrium iron oxide sublattices at various temperatures and magnetic field strengths 05 p0794 A71-16878

YTTRIUM OXIDES

Alkoxy derived yttria stabilized hafnia composition, using DTA, X ray diffraction, electron microscopy and emission spectrographic analysis 02 p0275 A71-12596

Temperature dependent ionic domain for yttrium oxide doped thoria as solid electrolytes at low oxygen activities 09 p1480 A71-22114

Compressive creep behavior of yttria rare earth stabilized zirconia storage heater refractories, determining stress time to failure 09 p1484 A71-23686

Point defects relation to thermoelectric emission at high temperatures in yttrium oxide 15 p2462 A71-32714

Electrolytic behavior of yttria-hafnia solid solutions from X ray analysis and electroconductivity measurements 18 p2874 A71-37001

YTTRIUM-ALUMINUM GARNET

Continuous Nd-YAG laser welding, considering power, penetration depth and applications 01 p0087 A71-10453

Mode locked continuously pumped Nd-YAG laser pulse shape, using optical correlation technique 02 p0262 A71-12730

Nd-YAG laser with intracavity lithium niobate phase modulator, investigating frequency sweeping /modulation/ mode operation 03 p0437 A71-13878

Nd-YAG pulsed laser, comparing Kr and Xe flash lamps for pumping performance 03 p0437 A71-13880

Nd-YAG pulsed laser mode locking with internal FM modulation 03 p0437 A71-13883

Vibrating mirror for continuously pumped Nd/YAG laser repetitive Q switching 03 p0438 A71-13888

Pulsed laser threshold measurements in YAG activated by Ho, Er and Tm isotopes, noting temperature dependence 03 p0438 A71-13890

Input-output properties of Nd-YAG rods in W pumped continuous lasers 04 p0606 A71-14715

Pulse repetition rate of Q switched YAG-Nd oscillator-amplifier laser systems 05 p0762 A71-16479

Nd-YAG laser branching ratios measurement for all transitions during oscillations at room temperature 05 p0764 A71-16912

High repetition rate Q switched Nd-YAG lasers, graphing theoretical Q switching from rate equations of ideal four-level laser 05 p0764 A71-17076

YAG-Nd laser rods CW pumping by cooled and room temperature GaAsP diodes, determining threshold temperature dependence 07 p1129 A71-20621

Controllable pulse length Q switched Nd-YAG laser using lithium iodate doubling crystal 09 p1463 A71-22757

Continuously pumped Q switched neodymium doped YAG laser micromachining tool for resistor trimming, resonator/filter frequency tuning and diode/transistor vaporizing 09 p1457 A71-23402

Nd-YAG laser cavity dumping for continuously pumped efficient pulsing at various repetition rates 11 p1773 A71-25797

Nd-YAG folded center lasers Q switching and cavity dumping, using fused silica and Brewster cut intracavity acousto-optic modulator 11 p1773 A71-25798

Laser parameters of Nd-doped hydrated phosphorus oxychloride-stannic chloride liquid system compared with YAG and Nd-doped glass, studying optical evolution and losses 13 p2078 A71-28400

Spectral filter effects on Nd-YAG laser performance stability and output 14 p2254 A71-30155

Optimal pulsed power output of continuously pumped Q switched Nd-YAG laser as function of mode parameters 15 p2423 A71-32603

Nd-YAG laser spatial hole burning effects, considering number of oscillating modes, transverse mode degeneracy and sinusoidal phase perturbation influence 15 p2423 A71-32604

Krypton arc lamps of high conversion efficiency for optical pumping of neodymium lasers, setting lamp and Nd-YAG rod in prolate ellipsoidal cavity 16 p2585 A71-33140

Short pulse Nd-YAG direct detection laser system for space communications, noting RF links complementation, high data rates, practical size, weight and power requirements 17 p2705 A71-35093

Papers on quantum electronics, Volume 1, covering carbon dioxide and YAG lasers, quantum counter action and interference holography 18 p2930 A71-36144

Solid state laser with Nd ions in YAG, discussing crystal growth and structure, optical pumping continuous and Q switched operation and mode locking 18 p2930 A71-36146

Nd-YAG laser optimum single frequency output operation, discussing two-component-mode filters methods using intracavity tilted Fabry-Perot and metallic film reflector etalons 18 p2932 A71-37005

Solid state lasers, considering ruby and YAG-Nd ion materials pumped at room temperature 19 p3074 A71-38229

Lutetium effects on UV absorption strength of Nd-YAG laser materials 20 p3244 A71-39104

YTTRIUM-IRON GARNET

Pulse shape of mode locked frequency doubled Nd-YAG laser, using single crystal for second harmonic generation and phase modulation 22 p3558 A71-42348

YTTRIUM-IRON GARNET

YIG with thin piezosemiconductor coating, investigating transverse surface wave amplification and velocity 01 p0140 A71-11288

YIG C band microwave amplifier using longitudinal pumping, comparing to other systems 02 p0228 A71-11692

Yttrium-iron garnet single crystals angle between variable and constant fields influence on spin wave thresholds 05 p0794 A71-16883

Absorption peaks mode numbers and separation using magnetostatic spin waves in axially magnetic YIG rods 07 p1180 A71-20172

Microwave oscillators with Gunn effect device resonant circuit and YIG tuning, discussing design and performance 08 p1263 A71-20992

Electronically tunable compact X band triplexer, consisting of four port nonreciprocal directional YIG filters in cascade 09 p1418 A71-23416

Optimal location of nonreciprocal disk shaped YIG element of traveling wave quantum ruby paramagnetic amplifier for weak magnetic field levels 10 p1585 A71-24883

Magnetically tunable microwave bandpass and bandstop filters with yttrium-iron garnet (YIG) single crystal 11 p1737 A71-25625

Fe ion photodetachment cross section polarization dependence on a sites in YIG-Si to explain photoinduced uniaxial anisotropy, using crystal field theory 12 p1943 A71-26858

One magnon Raman scattering induced by light magnetic dipole coupling with YIG coherent spin waves 12 p1913 A71-26860

Grain scattering in unstable spin wave region of parametrically excited magnons in polycrystalline YIG 21 p3428 A71-41047

YUH-1 HELICOPTER

U UH-1 HELICOPTER

YUKAWA POTENTIAL

Three particle elastic scattering amplitudes calculation using local Yukawa potentials 14 p2277 A71-30862

Z

Z AXIS

U COORDINATES

Z TRANSFORM

U LAPLACE TRANSFORMATION

ZEEMAN EFFECT

Linearly polarized light measurements of solar spectral lines Zeeman effects, describing calibration method based on Fraunhofer lines broadening due to magnetic fields 04 p0642 A71-14903

Galactic magnetic field observation, investigating cluster polarization, Zeeman effect, pulsar rotation and signal dispersion, interstellar cloud elongation and models 06 p0972 A71-18331

Taurus dust cloud magnetic field line of sight component observations and M17 and Cyg A absorption spectra data noting Zeeman splitting at 21 cm H lines 12 p1957 A71-26623

Magnetic field strength measurements from Zeeman splittings of sunspots molecular lines, considering saturation effects 13 p2140 A71-29047

Xe plasma flash tubes with very low discharge current magnetic field for spectroscopic and laser applications in presence of Zeeman effect 14 p2243 A71-30272

Optically pumped magnetometers for earth and interplanetary magnetic fields measurement, using Zeeman effect 15 p2405 A71-31409

High resolution quiescent and active solar prominences and magnetic field observations, discussing Zeeman effect and line spectrum polarization 17 p2806 A71-35393

Atmospheric noise temperature variation with frequency in 2.53 mm molecular oxygen rotation line, considering Zeeman effect 19 p3048 A71-37402

Solar prominences magnetic fields, determining strength and orientation with Zeeman effect 19 p3146 A71-38572

White dwarf stars broadband circular polarization and normal/quadratic Zeeman effect 20 p3304 A71-39940

ZENER DIODES

U AVALANCHE DIODES

ZENER EFFECT

Correlation coupling matrix elements for one electron transfer and ion-ion recombinations in Landau-Zener calculations 18 p2948 A71-35839

ZENITH

Automatic instrument for star detection and azimuth derivation, scanning nighttime zenith star field [AIAA PAPER 69-861] 01 p0126 A71-11584

Latitude observations at Pulkovo from 1948 through 1967 with zenith telescope 07 p1194 A71-19327

Geographical latitude from azimuths and zenithal measurements of two stars on hour circle 09 p1438 A71-23180

Obliquely incident radio wave absorptions measurements from January-October 1968 vertical ionospheric soundings, correlating diurnal variations with solar zenith angular changes 11 p1732 A71-25787

Zenith angular air shower distribution by Monte Carlo method, discussing muons horizontal component separation from background events 12 p1951 A71-27385

Zenith angle distribution of atmospheric muons at Mt. Chalcaltaya, considering differential intensity of cosmic ray mesons and horizontally incident cosmic rays 12 p1952 A71-27400

Sea level muon spectra at 83 degrees zenith angle up to 1 TeV, using Kiel spectrometer 12 p1952 A71-27404

Zenith sky brightness and color change during total solar eclipse of 12 November 1966 at Santa Ines, Peru, using interference filter photometers 14 p2309 A71-30118

Zenith sky intensity and spectral distribution changes during solar eclipse of 12 November 1966, discussing dependence on height and terrain 14 p2309 A71-30119

Zenith skylight spectral intensity distribution measurement during total solar eclipse of 7 March 1970, using optical scanning spectrometer 14 p2309 A71-30121

Extensive air showers detection by correlation of optical and radio pulses at 60 deg zenith angle 15 p2472 A71-31199

Ultrahigh energy muons intensity distribution as function of zenith angle at fixed slant depth of rock 15 p2476 A71-31793

Atmospheric muons anomalous zenithal distribution at extremely high energy regions 15 p2477 A71-31794

Stellar proper motions in photographic zenith tubes programs for time service clocks correction, examining catalogs used for astronomical data processing 18 p2962 A71-36110

Polarization measurement of cosmic ray muons at sea level as function of energy and zenith angle 19 p3124 A71-37284

Obliquely incident radio wave absorptions measurements from January-October 1968 vertical ionospheric soundings, correlating diurnal variations with solar zenith angular changes 22 p3509 A71-41555

Astronomical telescopes stellar image motion dependence on zenith distance, determining RMS value of jitter 23 p3771 A71-44259

International zenith telescopes micrometer value, determining correction for ocular screw from latitude observations 23 p3680 A71-44261

ZERO ANGLE OF ATTACK

Heat transfer on spheres and sharp cones in rarefied hypersonic gas flow at zero angles of attack in wind tunnel vacuum 13 p1992 A71-29176

Wing thickness optimal distribution for minimum wave drag in supersonic flow at zero angle of attack for given planform, using Ritz method at lower Mach numbers 13 p1994 A71-29222

Flow field measurement about sharp and slightly blunted slender cone at hypersonic speed and zero angle of attack [AIAA PAPER 71-625] 15 p2344 A71-31553

Inviscid incompressible flow past thin circular arc airfoil at zero incidence, expanding for complex potential or velocity in powers of thickness ratio 17 p2670 A71-34674

ZERO CROSSINGS

U ROOTS OF EQUATIONS

ZERO GRAVITY

U WEIGHTLESSNESS

ZERO LIFT

Boundary layer higher order effects on zero-lift drag of short slender bodies, emphasizing shock generated vorticity 04 p0569 A71-15029

Reacting and nonreacting gases laminar boundary layer flows over two dimensional and axisymmetric bodies at zero lift, comparing numerical methods 07 p1015 A71-19860

ZERO-ZERO WEATHER

U WEATHER

ZETA AURIGAE STAR

Zeta Aurigae chromospheric lines observed radial velocities mean variations, taking into account H ion gas acceleration, K star mass ejection and rotation 08 p1364 A71-21417

ZINC

Zinc single crystals plastic deformation and dislocations movement enhancement under pulsating direct current, noting stress peaks-voltage relationship 02 p0296 A71-12297

Zn deposition on Zn single crystals in KOH solution, examining time and potential effects on deposit morphology 02 p0210 A71-12956

Zinc reduced di(4-pyridyl) ketone methiodides, examining electronic and electron spin resonance spectrum 03 p0377 A71-14301

Noise spectra of CW hollow cathode zinc ion laser comparison with conventional discharges, noting gain per unit length on transitions 06 p0910 A71-18662

Zinc electrode kinetics noting exchange reactions, anodic behavior in alkaline solutions and capacitance 08 p1233 A71-21080

Zinc morphology electrodeposited from alkaline electrolyte, investigating charging and cell failure 08 p1233 A71-21081

Zinc electrodes performance improvement, discussing electrochemical corrosion rate, current density and temperature effects 08 p1233 A71-21082

He-Ne-Zn laser oscillations in red, yellow or blue spectral regions with total output power of nearly 10 mW 22 p3558 A71-42344

Neutron irradiation effects on dissociative high temperature zinc diffusion in indium and gallium arsenides 23 p3716 A71-43480

Elastoplastic deformation of Zn single crystals under uniaxial tensile loads, noting critical stresses relationship to current pulses 24 p3838 A71-45100

Surface oxide, organic and lead film effects on friction and plastic deformation of Zn single crystal during sliding [ASLE PREPRINT 71ILC-6] 24 p3839 A71-45288

ZINC ALLOYS

AlZnMgCu alloys fracture behavior, examining aging conditions, rolling, forging, cracking, tensile strength and chemical composition 04 p0613 A71-15745

High temperature creep in Al-Zn solid solution, using isothermal tests 15 p2429 A71-31997

Guinier-Preston zone size and volume fraction effects on polycrystalline Al-Zn alloys yield strength, discussing precipitation strengthening and thermally activated plastic flow 15 p2433 A71-32182

Zinc and misch metal in Mg alloys, detailing rare earth metals distributions in various phases 16 p2594 A71-33714

Storing and plastic deformation effects on artificial aging of Al-Zn-Mg alloy, using thin foil electron microscopy and hardness measurements 17 p2755 A71-34417

Dezincification of Al-Zn alloys, creating loops and dislocations due to vacancies from Zn evaporation 18 p2935 A71-36199

Al-Zn-Mg alloy welded joints under repeated static loads, determining shape, filler wire composition and aging effects on fatigue strength 19 p3083 A71-38425

Formation and interdependence of quenched induced defect structure in Al-Zn, discussing nucleated loops and screw dislocation developed helical dislocations 20 p3249 A71-39001

Morphological change of spherical G.P. zones and solute diffusion coefficient in binary Al-Zn alloy during dissolution, using X ray small angle scattering 21 p3395 A71-40022

Weldable Al-Zn-Mg alloys with cathodic polarization protection, noting decrease in stress corrosion crack propagation rate 22 p3560 A71-41625

Accelerated intergranular corrosion tests under high humidity on Zn-Al alloy with lamellar eutectoid microstructure due to postforming heat treatment 22 p3564 A71-42534

Mn-Zn ferrite for pulse transformers, discussing permeability and temperature range 23 p3650 A71-43348

Al-Zn solid solution mean effective and internal stresses and activation area during high temperature creep 23 p3691 A71-43900

ZINC COMPOUNDS

NT ZINC OXIDES

NT ZINC SELENIDES

NT ZINC SULFIDES

NT ZINC TELLURIDES

NT ZINCBLLENDE

- Zinc chalcogenides core electron energy levels measurement by X ray induced photoemission, noting agreement with observed auger transitions 05 p0792 A71-16318
- Zinc-hydroxy system spectrum analysis, using laser source Raman spectrometer and modified IR reflectance accessory 08 p1233 A71-21079
- Space radiation environmental effects on reactively encapsulated zinc orthotitanates and paints [AIAA PAPER 71-449] 12 p1920 A71-26762
- Zinc arsenide-zinc telluride ternary system phase diagram investigation by X ray, differential thermal and microstructural analyses and microhardness measurements 16 p2621 A71-33564
- Raman and IR reflection spectra of zinc tungstenate single crystals 17 p2790 A71-34201
- Lithium magnesium zinc silicates crystallization phase equilibria, noting temperature effects, structure, melting and solubility 20 p3253 A71-38818

ZINC NICKEL BATTERIES

U NICKEL ZINC BATTERIES

ZINC OXIDES

- Zinc-zinc oxide electrode chemistry, describing interaction with strongly alkaline solution of alkaline battery system 08 p1233 A71-21078
- Space stable thermal control coatings, noting reflectance optical spectroscopy of zinc oxide based paints and zinc orthotitanate 11 p1747 A71-26520
- Stimulated emission of ZnO laser by electron beam excitation at 82-250 K near A-L-O line, considering exciton interactions 16 p2589 A71-34121
- UV photoemission measurements on hexagonal ZnO cleaved in vacuum, determining Zn 3d states location 17 p2791 A71-34854

ZINC SELENIDES

- Semiconductor zinc selenide and zinc cadmium selenide crystals two photon absorption coefficients, noting forbidden bandwidth relation 13 p2077 A71-27954
- Two photon absorption coefficients of ZnSe and zinc cadmium selenide crystals for ruby laser radiation, showing energy gap reduction effect 21 p3395 A71-41340

ZINC SILVER BATTERIES

U SILVER ZINC BATTERIES

ZINC SILVER OXIDE BATTERIES

U SILVER ZINC BATTERIES

ZINC SULFIDES

- NT ZINCBLLENDE
- Activator Mn impurity effect of carrier redistribution and partial photoionization of photoconductivity spectra of ZnS single crystals 21 p3430 A71-41218

ZINC TELLURIDES

- P-n junction formation in zinc mercury telluride samples, using heat treatment to control carrier concentration 01 p0140 A71-11464
- Photorecombination model explaining kinetics of negative photoconductivity effect during illumination of impurity region in high resistivity p-type ZnTe-CdTe single crystals at room temperatures 23 p3717 A71-43948

ZINC-OXYGEN BATTERIES

- Zinc air battery, evaluating materials capable of peroxide decomposition as low cost oxygen electrodes 03 p0351 A71-13040

ZINCBLLENDE

- Semiconductor defects, including stoichiometric vacancies in sphalerite lattices, epitaxial interfaces and dislocations in Ge 18 p2953 A71-35870

ZIRCALOY 2 [TRADEMARK]

- Zr and zircaloy 2 fracture mode, examining grain boundaries and strain rates effects 02 p0268 A71-12887

ZIRCALOYS [TRADEMARK]

NT ZIRCALOY 2 [TRADEMARK]

- Anomalous thermal diffusivity measurements of Hf, Nb and Zircaloys, using modulated electron beam technique 10 p1624 A71-23909
- Water cooled reactor Zircaloy brazing filler metals, investigating corrosion resistance, joint strength and brazing capability 18 p2928 A71-36856

ZIRCONATES

NT STRONTIUM ZIRCONATES

- Curie point of solid solutions in ternary system of zirconate-titanate and lead metaniobate, using maxima on temperature dependence curve of permittivity 13 p2111 A71-28152
- Lead zirconate-titanate point defects crystal chemistry, interpreting sintering and grain growth behavior 13 p2093 A71-28992

ZIRCONIUM

- Polycrystalline Zr extremely low temperature tensile deformation, discussing prestraining effects, stress-displacement relations, strain distribution, twinning, etc 02 p0267 A71-12878
- Zr and zircaloy 2 fracture mode, examining grain boundaries and strain rates effects 02 p0268 A71-12887
- Zr surface nitriding process in purified and high purity nitrogen respectively, comparing results 04 p0616 A71-15806
- Zr solid state solubility in Mo as function of quenching temperature, using optical microscopy and microhardness testing techniques 07 p1130 A71-19300
- Zirconium droplet combustion in oxygen-rare gas mixtures, observing transient burning phenomena, oxidation conditions and luminosity-time records 07 p1223 A71-19623
- Zr effect on Ti-Mo beta alloy stability, considering Zr suppression and retardation of omega precipitation on basis of TTT diagram and tensile tests 10 p1625 A71-24007
- Fiber textures formation in polycrystalline Zr from cold forging and cold drawing, observing fully developed recrystallization 10 p1629 A71-25028
- Mg-Al eutectic alloy and commercial-purity Zr stress relaxation tests and mechanical behavior 11 p1780 A71-26022
- Solid state reaction of titanium carbide with Ti, Zr and V in vacuum at high temperatures 13 p2082 A71-27821
- Zirconium oxidation kinetics at 500-1200 C under low oxygen pressure 14 p2257 A71-29843
- Transition metals addition effects on cast Zr grain size, microhardness and electrical resistivity, explaining results in terms of solid state electron theory 15 p2424 A71-31239
- Optimum temperature for Zr and Mo soldering of graphite materials with formation of carbide interlayer for ensuring maximum heat resistance 15 p2439 A71-32145
- Liquid Zr drops combustion in oxygen-nitrogen atmospheres, examining critical conditions for sac formation with homogeneous bubble nucleation theory 17 p2837 A71-34511
- Strain hardened zirconium alpha tensile stress analysis, explaining inelastic phenomena by dislocation motion blocking with oxygen in lattice structure 21 p3397 A71-40432
- Pressure sensors thermal protection by porous Zr disk as heat shield, considering acoustic transparency, linearity, transient response and air flow resistance [ONERA-TP-957] 22 p3547 A71-42501
- Zirconium liquid-crystal distribution in phase ilmenite of Apollo 11 and 12 lunar rocks 23 p3739 A71-43618

ZIRCONIUM ALLOYS

NT ZIRCALOY 2 [TRADEMARK]

NT ZIRCALOYS [TRADEMARK]

- Zr-Ga phase diagram eutectoid region metallographic analysis, discussing solubility, reactions and compound formation 04 p0614 A71-15779
- Nb-N and Nb-Zr-N alloys phase composition, examining microconstituents at various temperatures after quenching 04 p0616 A71-15905
- Electrodeposition of coherent coatings of zirconium diboride from solution of zirconium tetrafluoride and boron oxide in molten eutectic mixture of NaF-KF-LiF 07 p1118 A71-19567
- Mechanical properties, crack formation sensitivity, corrosion resistance and stress cracking behavior of Al-Zr-Mg alloys welded joints 07 p1136 A71-19633
- Alloying elements, mechanical working and heat treatment effects on vibration damping of Mg-Zr alloys, using Fastov device 07 p1136 A71-19634
- Phase equilibria in Zr-Mo-Re and Zr-W-Re systems, studying isothermal section diagrams via X ray and metallographic techniques 07 p1140 A71-20234
- Fe-Cr-Zr ternary alloys, investigating Zr effect on high temperature hardness and heat resistance 09 p1473 A71-23228
- Ti-Zr alloy phase diagram from vacuum melting, using high purity wafers and apparatus similar to McQuillan 11 p1780 A71-26028
- Ti-Zr alloying in for microstructural hardness and mechanical strength increases, discussing Zr concentrations at Nb granular boundaries 11 p1782 A71-26470
- Equilibrium diagrams for Nb-Zr-B alloys, establishing solidus surface, Zr/B isothermal and vertical sections 11 p1782 A71-26474

- Mo-Zr-Cr alloy samples cast annealed and quenched at 1500 C, calculating phase equilibrium diagram 12 p1918 A71-27528
- Temperature dependent absorption line width and secondary moments of nuclear magnetic resonance spectra of Ti-Zr-H system 14 p2258 A71-30009
- Thin sheet Nb-Zr alloy welds, detailing residual stresses in butt joints 15 p2413 A71-31204
- Niobium-zirconium system alloys Debye-Waller factor temperature and concentration dependence, noting nonmonotonicities due to phonon spectra 15 p2437 A71-32625
- Mechanical properties, crack formation sensitivity, corrosion resistance and stress cracking behavior of Al-Zr-Mg alloys welded joints after prolonged heating 16 p2593 A71-33629
- Alloying elements, mechanical working and heat treatment effects on vibration damping of Mg-Zr alloys 16 p2593 A71-33630
- Superconducting transition temperature measurement of cast and solution treated Nb-Zr alloys, substantiating dependence on density of states at Fermi surface 17 p2759 A71-35221
- High temperature strengthening of vacuum melted W-Ti alloys with Mo and Zr additions 19 p3076 A71-37267
- Vertical phase diagrams of Ti-Al-Zr-Mo-Fe alloy system at varying Fe concentrations, showing structural hardening after quenching 19 p3078 A71-37471
- Two temperature region oxidation of zirconium diboride, showing formation of continuous surface film and quadratic crystallized discontinuous layer 22 p3563 A71-42246
- Oxygen concentration and heat treatment effects on structure and mechanical properties of Nb-Zr alloys 22 p3563 A71-42366
- Ni-Zr alloy crystallization at large cooling rates obtained by melt droplets blowing with compressed He jet onto rotating Cu cylinder surface 24 p3840 A71-45374

ZIRCONIUM CARBIDES

- TiC and ZrC samples with different porosities, examining bending strength at various temperatures 01 p0102 A71-10786
- Secondary recrystallization of Ti, Zr and Nb carbides within homogeneity ranges, determining activation energies as function of carbon deficiency in carbide lattice 04 p0609 A71-14749
- Zirconium carbide fiber insulating materials, examining heat conductivity coefficient 05 p0838 A71-16781
- Temperature dependence of Vickers pyramid hardness for Ti, Zr and Hf carbides at wide temperature range in vacuum 07 p1142 A71-20483
- Molybdenum doped zirconium monocarbide, investigating Hall coefficient, thermal emf and resistivity measurements 15 p2460 A71-31284
- Niobium and zirconium carbides enthalpy and specific heat dependence on temperature and composition 15 p2431 A71-32156
- Zirconium monocarbide congruent vaporization rate and temperature dependence for nonstoichiometric compositions 15 p2431 A71-32157
- ZrC vaporization at high temperatures, investigating dissociation into components by mass spectroscopy 15 p2431 A71-32158
- Cast ZrC hot hardness measurement by static tests at high temperatures, comparing with hot-pressed samples 15 p2431 A71-32161
- Heat conductivity coefficient of thermal insulation material made from zirconium carbide fibers, giving measurement procedure 16 p2662 A71-33033
- High temperature vaporization of titanium, zirconium, hafnium and thorium carbides by Knudsen effusion mass spectrometry, measuring ion intensities, formation enthalpies and dissociation energies 16 p2540 A71-33251
- Plastic deformation in hot compressed Ti, Zr and Nb carbides during diamond grinding, studying fine structure on diffractometer 16 p2584 A71-33896
- Cast electron-beam remelted Mo, investigating carbon and zirconium carbide additions effects on structure and low-temperature plasticity 18 p2937 A71-36723
- Age hardening of Mo alloys with titanium and zirconium carbides at high temperatures after quenching 19 p3077 A71-37268
- Nonstoichiometric zirconium niobium carbide thermodynamic properties, deriving components activity equations from statistical considerations based on pairwise interaction energies [ECS PAPER 120] 20 p3252 A71-39554

Zirconium uranium carbide and zirconium hafnium carbide thermodynamic properties, using time-of-flight mass spectrometer
[ECS PAPER 120] 20 p3252 A71-39555

Zirconium monocarbide electrical conductivity, Hall coefficient, thermal emf and magnetic susceptibility measurements for temperature dependence at 500-1000 C in homogeneity region 23 p3692 A71-44021

Zirconium carbide eutectic and supraeutectic alloys preparation with graphite addition, determining heat resistance under thermal cycling tests 23 p3697 A71-44025

Ti, Zr and Nb carbides alloying effects on deformed and annealed Mo alloys cellular structure and mechanical properties 24 p3836 A71-44672

TaC-WC, ZrC-WC and refractory compounds thermal expansion coefficient measurements 24 p3838 A71-44738

ZIRCONIUM COMPOUNDS

NT STRONTIUM ZIRCONATES

NT ZIRCONATES

NT ZIRCONIUM CARBIDES

NT ZIRCONIUM HYDRIDES

NT ZIRCONIUM IODIDES

NT ZIRCONIUM NITRIDES

NT ZIRCONIUM OXIDES

Rare earth element concentrations in zircons and apatites separated from dacites and granites, explaining partition coefficients between phenocrysts and groundmass by crystal structure 03 p0407 A71-13338

Hafnium and zirconium sulfides, determining partial molar free energy of sulfur at metal saturation with electromotive force cell 09 p1387 A71-23129

Galvanomagnetic properties of solid refractory zirconium and titanium compounds in two-band representation, measuring Hall effect and reluctance vs external magnetic field 15 p2426 A71-31512

Chemical properties of titanium, zirconium and hafnium germanides exposed to acids, oxidizers, complex salts, alkaline solutions and water 19 p3075 A71-37106

ZIRCONIUM HYDRIDES

Safe disposal for nuclear zirconium hydride reactors for manned space base mission 20 p3263 A71-38921

PbTe thermoelectric converter for ZrH reactor space power supply, discussing operational performance, design and materials technology 20 p3265 A71-38951

Delta-zirconium hydride hydrogen engassing experiment, investigating hydrogen absorption rate and diffusion constant temperature dependence 23 p3688 A71-42929

Zirconium hydride phases density determination from lattice parameters, comparing results with direct measurement 23 p3689 A71-42930

ZIRCONIUM IODIDES

Zirconium iodide vapor deposition kinetics, determining activation temperature 15 p2425 A71-31395

ZIRCONIUM NITRIDES

Zr surface nitriding process in purified and high purity nitrogen respectively, comparing results 04 p0616 A71-15806

Zirconium nitride electronic structure from X ray emission spectra, analyzing chemical bonds 08 p1305 A71-21061

Hall effect and reluctance of TiN and ZrN specimens obtained by hot compression 15 p2427 A71-31515

Nitrogen X ray emission K alpha band behavior in zirconium mononitride in entire range of ZrN homogeneity 19 p3083 A71-37280

ZIRCONIUM OXIDES

Oxygen diffusion in monoclinic zirconia as function of equivalent pressure, using oxygen 18 gas-solid exchange techniques 05 p0769 A71-17096

Phase equilibria, microstructure and physical properties of high temperature vacuum sintered oxygen deficient zirconia and thorium 08 p1304 A71-20697

Compressive creep behavior of yttria rare earth stabilized zirconia storage heater refractories, determining stress time to failure 09 p1484 A71-23686

Monoclinic, stabilized and metastable tetragonal and cubic zirconias, noting IR and Raman spectra 13 p2093 A71-28991

Zirconium dioxide reactions with chromium, molybdenum and tungsten carbides, studying reaction products, phase composition, sintering temperatures and chemical separation 15 p2432 A71-32166

Semiconductor behavior of zirconium oxide formed on Zr substrate with n-type below 685 C and p-type above 17 p2759 A71-35222

Zirconium oxide-lanthanum oxide systems near melting point, plotting solidification and phase diagrams 20 p3254 A71-39962

ZODIACAL DUST

Three body gravitational capture of interstellar dust in solar system, examining zodiacal cloud 01 p0158 A71-10771

Outer planets missions combined zodiacal experiment, examining meteoric, asteroidal and satellite particles distribution and orbits [AAS PAPER 71-127] 19 p3064 A71-37919

ZODIACAL LIGHT

Zodiacal light polarized component observation at ecliptic longitudes and latitudes compared to zodiacal cloud model 01 p0158 A71-10773

Zodiacal light theoretical models, considering interplanetary particles optics, Mie theory and multicolor polarization 03 p0491 A71-14011

Zodiacal light interpretation based on ground-based, satellite and deep space probe Helios observations, considering particle flux measurements 03 p0491 A71-14012

Zodiacal light IR spectroscopy by rocket-borne detector, providing information on interplanetary dust properties 03 p0491 A71-14013

Zodiacal light brightness measurement in three mutually perpendicular directions, tabulating data 06 p0966 A71-17677

Sky brightness broadband measurements by Skylark sounding rocket, noting relationship to zodiacal light 16 p2575 A71-32842

Gegenschein as zodiacal light illuminated lunar dust ejected from meteorite impacts 20 p3286 A71-38730

Pioneer 8 and 9 micrometeorite measurements of particles kinetic energy, momentum, velocity and direction, correlating measured particle flux rates with predictions based on zodiacal light 20 p3297 A71-39634

Zodiacal light lines in interplanetary dust particle flux diagram, suggesting agreement with micrometeorite data 23 p3695 A71-44287

Two-parametric models of interplanetary dust distribution predictions involving zodiacal light scattering measurements from space probes for in- and out-of-ecliptic missions 20 p3298 A71-39636

20 p3219 A71-39637

ZONAL HARMONICS

External geopotential expansion coefficients and zonal harmonics estimation 06 p0976 A71-18453

NonKeplerian intermediate orbit of artificial earth satellite motion with account of zonal harmonics, using fixed centers 11 p1829 A71-25807

External geopotential zonal harmonics expansion coefficients estimate 12 p1898 A71-26603

Condition equations for zonal harmonics using low inclination DIAL satellite interferometric measurements over perigee revolution 20 p3300 A71-39664

ZOND SPACE PROBES**NT ZOND 3 SPACE PROBE**

Zond 4 and 5 space probes proton flux measurements at 1.5-50 MeV, describing instrument equipment used and results obtained 06 p0953 A71-18120

Biological experiments on plants, animals and bacteria aboard Zond 5, 6 and 7 space probes 20 p3187 A71-39134

Proton recording equipment onboard automatic interplanetary stations Zond 4 and 5 at 1.5-50 MeV using silicon drift counters 23 p3675 A71-43274

ZOND 3 SPACE PROBE

Photometric maps of reverse side lunar surface from AIM Zond 3 material 03 p0484 A71-13215

ZOND 5 SPACE PROBE

Lethal recessive point mutation in *Drosophila melanogaster* eggs on Zond 5 spacecraft 01 p0187 A71-11552

Space flight effects on survival, mutation and cell development of *Chlorella* cells suspensions onboard Zond 5 spacecraft 01 p0019 A71-11554

ZOND 7 SPACE PROBE

Earth surface characteristics relationship to meteorological elements based on interpretation of color space photographs from automated Zond 7 station 20 p3260 A71-39687

Postflight histological analysis of turtles aboard Zond 7, noting decrease in cell nuclei size due to space flight conditions adaptation 21 p3334 A71-40568

ZONE MELTING

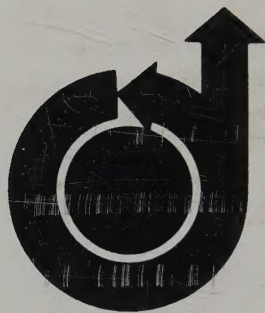
Ni maraging steels weld heat-affected zone, showing liquid grain boundary film formation due to titanium sulfide inclusions constitutional liquidation 04 p0603 A71-14921

Tumor theory of crust formation and moon-earth consolidation, showing fractional crystallization of basaltoid silicate melts 10 p1681 A71-25112

Pure W single crystals grown by electron beam zone melting technique, noting rolling workability 12 p1919 A71-27761

Nb alloy ingots electron beam melting, investigating reverse zone liquation intensity and behavior dependence on melting parameters 15 p2424 A71-31241

Zone refined Be crystals under room temperature compression, examining lattice defects with X ray synergy method 23 p3695 A71-44287



AIAA TECHNICAL INFORMATION SERVICE

750 THIRD AVENUE

NEW YORK, N. Y. 10017